Semiempirical HAM/3 calculation of valence-electron shake-up satellite bands in the ionization spectra of CO_2, N_2O, and C_2F_4

DELANO P. CHONG

Department of Chemistry, University of British Columbia, Vancouver, B.C., Canada V6T 1Y6

Received April 26, 1982

DELANO P. CHONG. Can. J. Chem. **61**, 1 (1983).

Valence-electron shake-up satellite bands in the ionization spectra of carbon dioxide, nitrous oxide, and tetrafluoroethene have been calculated with a modified version of the HAM/3 program. The results are compared with experiment and with the computations based on two-particle-hole Tamm-Dancoff approximation Green's function method. Because of the limitation of such Green's function procedures for inner-valence electrons, the results can often be inferior to those from the present HAM/3 calculations.

DELANO P. CHONG. Can. J. Chem. **61**, 1 (1983).

Utilisant une version modifiée du programme HAM/3 on a calculé les bandes satellites d'agitation de l'électron de valence dans les spectres d'ionisation du bioxyde de carbone, de l'oxyde nitreux et du tétrafluoroéthène. On a comparé ces résultats avec ceux obtenus expérimentalement et avec ceux obtenus par les calculs basés sur l'approximation de Tamn-Dancoff de la particule à deux trous de la méthode de fonction de Green. A cause de la limitation de telles méthodes de fonction de Green pour les électrons de valence internes, les résultats peuvent être inférieurs à ceux obtenus actuellement par les calculs de HAM/3.

[Traduit par le journal]

Can. J. Chem. Downloaded from www.nrcresearchpress.com by 210.87.254.5 on 09/06/12
For personal use only.

1. Introduction

Ionization processes have been studied extensively by photoelectron (PE) spectroscopy with ultraviolet photon sources, X-rays, and synchrotron radiation. Recently, both binary and dipole (e,2e) binding energy spectra have been obtained for a number of molecules. The importance of valence-electron shake-up (VESU) satellite bands in ionization spectra is well recognized, especially for inner-valence electrons. Such VESU structure will even dominate the ionization spectra of many larger molecules to such an extent that there is often a complete breakdown of the molecular orbital model.

In the past few years, Cederbaum and co-workers (1–4) have used the two-particle-hole Tamm-Dancoff approximation (2ph-TDA) in their Green's function (GF) calculation of inner-valence ionization spectra. Because of the large dimension of the matrices to be diagonalized, the atomic orbital basis set is usually limited to double-ζ quality and the molecular orbital space is often truncated. Consequently, the 2ph-TDA results thus far are not as accurate as those from the outer-valence Green's function method (5).

Another *ab initio* method used to analyze VESU in ionization spectra is limited configuration interaction (CI) (6, 7).

On the other hand, Lindholm and Åsbrink (8) simplified the complex problem of VESU, incorporating the treatment into the semi-empirical HAM method (9, 10) and obtaining reasonable agreement with the observed PE spectra of ethene and benzene. Unfortunately, minor errors were inadvertently allowed into their simple treatment. These errors have been corrected (11) and the HAM/3 program (12) has been modified in our laboratory to perform VESU calculations.

In this paper, we wish to report semiempirical HAM/3 computations of the VESU bands in the ionization spectra of CO_2, N_2O, and C_2F_4 and compare the results with those from 2ph-TDA GF calculations as well as with experiment. Experimental geometries (13) are used throughout. The method is reported elsewhere (11). Suffice it to say that the relative intensities are estimated by the sum of the squared amplitudes (multiplied by the degeneracy factor). In other words, we assume uniform in-phase non-interfering photoionization cross-section matrix elements (4).

2. Carbon dioxide

Experimental studies (4, 14–19) of the ionization of CO_2 were reviewed by Domcke *et al.* (4) in 1979. Since then, another binary (e,2e) spectrum has been recorded (20). These results are summarized in Table 1. In Fig. 1, we present some of them (4, 15, 20) to show the uncertainty in the locations of the VESU satellite bands.

The results of the present calculations are summarized in Table 2 and compared with those of 2ph-TDA GF (4) in Fig. 1. In the GF method, the low-energy region is more accurately calculated by the outer-valence GF procedure than by 2ph-TDA. For different reasons, the original HAM/3 method without VESU is in better agreement with experiment for the primary PE bands than the present inclusion of VESU. Consequently, only the inner-valence region of 20–45 eV is shown in Fig. 1 (*d*) and (*e*). There is qualitative agreement between the two sets of calculations, although there are some differences in the vertical ionization potentials (VIP) and the relative intensities. The first VESU band of appreciable intensity is due to a $^2\Pi_u$ state at 25.68 eV according to HAM/3. This VIP is closer to the binary (e,2e) value of 25 eV (20) and the dipole (e,2e) result of 26.5 eV (4). The 2ph-TDA GF result of 28.33 eV (4), on the other hand, agrees better with the HeII value of 27.2 eV (16) and the synchrotron VIP of 27.3 eV (18). That this state is a Π state has been confirmed by momentum distribution measurements (20). At higher energies, the most intense band is at 37 eV according to HAM/3 (35.3 eV by 2ph-TDA GF (4)), with a strong line also predicted at 38.8 eV. These results are in excellent agreement with the experimental ones summarized in Table 1.

0008-4042/83/010001-06$01.00/0

©1983 National Research Council of Canada/Conseil national de recherches du Canada

TABLE 1. Observed vertical ionization potentials (in eV) of CO_2

Orbital	1970 HeI (14)	1972 MgKα (15)	1974 HeII (16)	1977 Binary (e,2e) (17)	1978 Synchrotron (18)	1978 ZrMζ (19)	1979 Dipole (e,2e) (4)	1981 Binary (e,2e) (20)
$1\pi_g$	13.82	13.8	13.79					
$1\pi_u$	17.60	17.6	17.59					
$3\sigma_u$	18.11	18.1	18.08					
$4\sigma_g$	19.43	19.4	19.40					
—			22.6		22.8		23.5	
—			27.2		27.3		26.5	25
—			31.4		31.3		30.0	
—		32		33.0		32.5	32.0	33
—			35.3		35.1		35.5	
$2\sigma_u$		37.6		37.0		37.5		
$3\sigma_g$			38.5	39.0	38		38.0	38

TABLE 2. Vertical ionization potentials (in eV) of CO_2 calculated with HAM/3 method

State	No VESU	With VESU	Relative intensity	Mainly from	Observed (14)
$^2\Pi_g$	13.79	13.15	1.93	$(1\pi_g)^{-1}$	13.82
		31.22	0.05	$(1\pi_g)^{-1}$	
$^2\Pi_u$	17.73	16.71	1.78	$(1\pi_u)^{-1}$	17.60
		21.11	0.01	$(1\pi_u)^{-1}$	
		25.68	0.19	$(1\pi_u)^{-1}$	
$^2\Sigma_u$	18.01	17.26	0.95	$(3\sigma_u)^{-1}$	18.11
		30.27	0.03	$(3\sigma_u)^{-1}$	
		31.31	0.02	$(2\sigma_u)^{-1}$	
		34.24	0.10	$(2\sigma_u)^{-1}$	
	36.81	37.02	0.89	$(2\sigma_u)^{-1}$	
		44.67	0.02	$(2\sigma_u)^{-1}$	
$^2\Sigma_g$	19.50	18.57	0.93	$(4\sigma_g)^{-1}$	19.43
		30.42	0.05	$(4\sigma_g)^{-1}$	
		32.29	0.05	$(3\sigma_g)^{-1}$	
		34.35	0.03	$(3\sigma_g)^{-1}$	
		37.06	0.46	$(3\sigma_g)^{-1}$	
	37.64	38.79	0.48	$(3\sigma_g)^{-1}$	

TABLE 3. Observed VIP (in eV) of N_2O

Orbital	1969 HeI (21)	1973 XPS (22)	1974 HeII (16)	1974 AlKα (23)	1979 Dipole (e,2e) (4)	1982 Binary (e,2e) (24)
2π	12.89	12.9	12.89			
7σ	16.39	16.4	16.39			
1π	18.24	18.1	18.24			
			19.5			
6σ	20.11	20.1	20.11			
			22.6	23.5	23.7	23
			24.1		24.5	26
			28.7	28.5	28.5	29
			33.7	33	33.5	
5σ		35.5		35.5	36	35
			37.3			
4σ		39.0		38.5	38.5	39

Can. J. Chem. Downloaded from www.nrcresearchpress.com by 210.87.254.5 on 09/06/12
For personal use only.

Can. J. Chem. Downloaded from www.nrcresearchpress.com by 210.87.254.5 on 09/06/12
For personal use only.

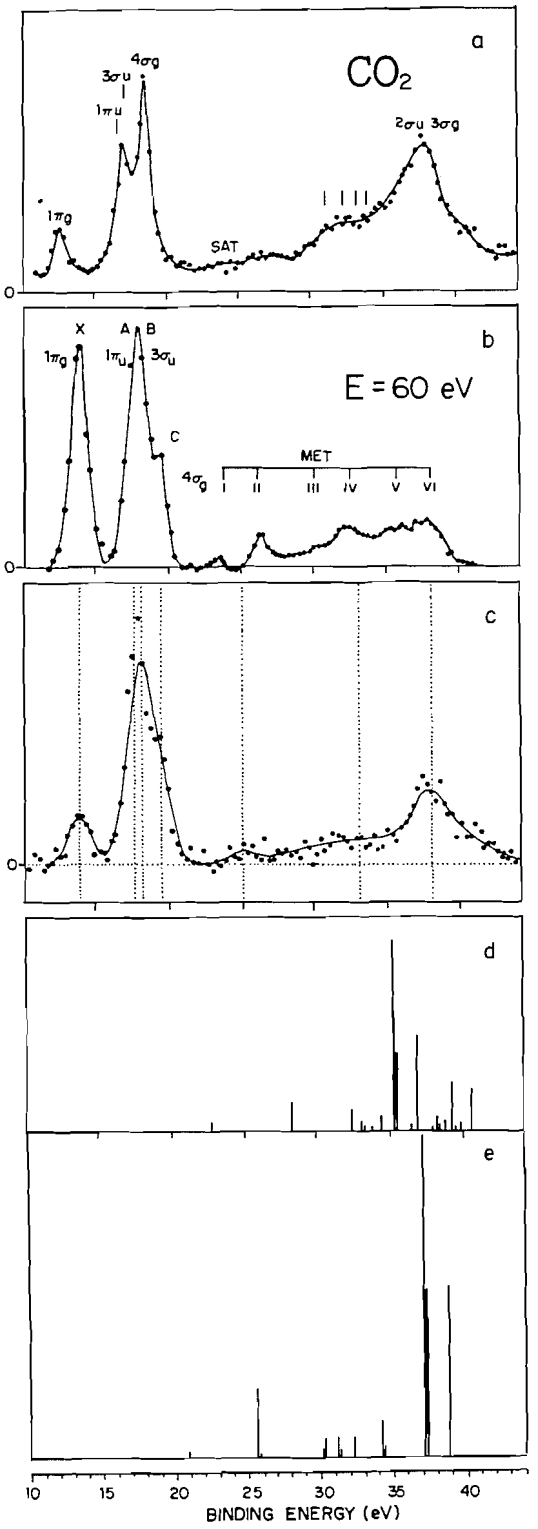

FIG. 1. Comparison of ionization spectra of CO_2: (*a*) ESCA (15), (*b*) dipole (e,2e) (4), (*c*) binary (e,2e) (20), (*d*) calculated by 2ph-TDA GF (4), (*e*) calculated by HAM/3.

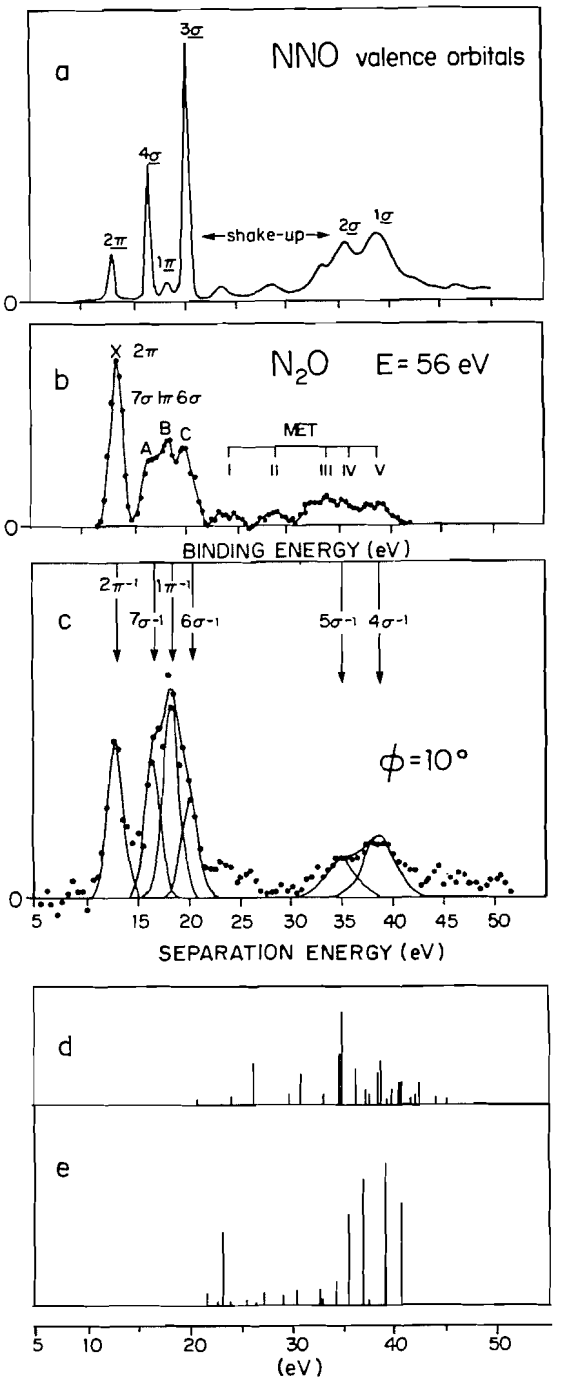

FIG. 2. Comparison of ionization spectra of N_2O: (*a*) ESCA (23), (*b*) dipole (e,2e) (4), (*c*) binary (e,2e) (24), (*d*) calculated by 2ph-TDA GF (4), (*e*) calculated by HAM/3.

3. Nitrous oxide

As in the case of CO_2, we first summarize the experimental results on N_2O in Table 3 and compare some of them (4, 23, 24) in Fig. 2. The uncertainty in the positions of the VESU bands is about 0.5 eV (4).

The results of our HAM/3 computations are displayed in Table 4 and compared with those of 2ph-TDA GF (4) in Fig. 2. Again, only the interesting region of 20–45 eV is displayed in Fig. 2 (*d*) and (*e*), and the agreement between the two sets of calculations is only qualitative. The VESU satellites calculated by HAM/3 to be at 21.6 and 23.2 eV agree better with the observed spectra in UPS (16), XPS (23), and dipole (e,2e) studies (4). The VIP of 23.8 and 26.2 eV from 2ph-TDA GF calculations (4), on the other hand, show better agreement with the recent binary (e,2e) experiment (24).

TABLE 4. VIP (in eV) of N_2O calculated with HAM/3 method

State	No VESU	With VESU	Relative intensity	Mainly from	Observed (21)
$^2\Pi$	12.48	11.85	1.93	$(2\pi)^{-1}$	12.89
	18.67	17.09	1.06	$(1\pi)^{-1}$	18.24
		17.93	0.51	$(1\pi)^{-1}$	
		18.20	0.05	$(1\pi)^{-1}$	
		19.70	0.02	$(1\pi)^{-1}$	
		22.87	0.01	$(1\pi)^{-1}$	
		23.16	0.29	$(1\pi)^{-1}$	
		23.91	0.01	$(1\pi)^{-1}$	
		25.52	0.02	$(1\pi)^{-1}$	
		30.48	0.06	$(2\pi)^{-1}$	
$^2\Sigma$	16.50	15.54	0.91	$(7\sigma)^{-1}$	16.39
	20.68	19.49	0.90	$(6\sigma)^{-1}$	20.11
		21.57	0.04	$(7\sigma)^{-1}$	
		26.52	0.01	$(7\sigma)^{-1}$	
		27.16	0.04	$(7\sigma)^{-1}$	
		29.03	0.04	$(5\sigma)^{-1}$	
		32.85	0.06	$(6\sigma)^{-1}$	
		32.91	0.03	$(6\sigma)^{-1}$	
		34.28	0.08	$(5\sigma)^{-1}$	
		35.53	0.37	$(5\sigma)^{-1}$	
	36.06	36.89	0.51	$(5\sigma)^{-1}$	
		37.58	0.02	$(5\sigma)^{-1}$	
	39.57	39.24	0.56	$(4\sigma)^{-1}$	
		40.72	0.42	$(4\sigma)^{-1}$	

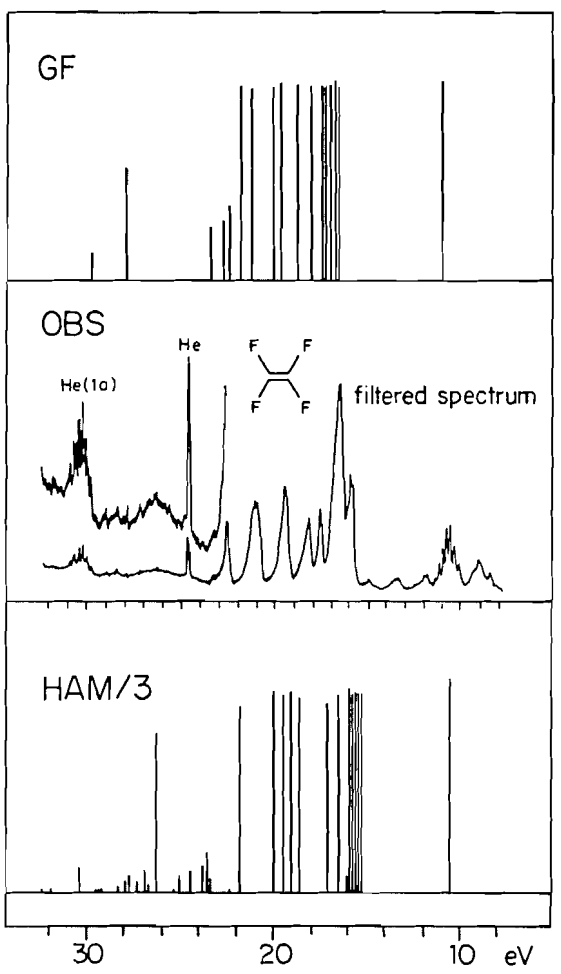

FIG. 3. Comparison of ionization spectra of C_2F_4.

4. Tetrafluoroethene

The VESU satellite bands of C_2F_4 have been studied both experimentally and theoretically (with 2ph-TDA GF method) by Bieri and co-workers (5, 25).

Our HAM/3 calculations are given in Table 5 and compared with the previous results (5, 25) in Fig. 3. The VESU band observed at 22.5 eV is very sharp. It corresponds to the intense band at 21.8 eV in the HAM/3 results. In contrast, the 2ph-TDA GF calculations predict three bands in this energy region, at 22.5, 22.7, and 23.4 eV, with relative intensities of 0.35, 0.28, and 0.25, respectively. The $(2a_g)^{-1}$ band at 26.3 eV is closer to the HAM/3 value of 26.25 eV than to the VIP of 27.94 eV predicted by 2ph-TDA GF (5, 25).

5. Discussions

From the examples given above, one sees that the HAM/3 program, after modifications to include VESU, is capable of producing results which can compete with those from 2ph-TDA GF calculations in terms of reliability at a small fraction of the computing cost. Results of similar quality have also been obtained for formamide (11), N_2O_4, CH_3NO (26), N_2, C_2H_2, CO, O_3, and other molecules (27).

Because the parameters in the HAM/3 program were obtained without considering VESU, the VIP of the outer-valence electrons are more reliably calculated excluding VESU than including. One could partially correct this deficiency by shifting the orbital energies so that the VIP for the primary hole states calculated with VESU match the experimental values. However, this procedure is completely empirical and the HAM/3 parameters used are not the best set. In principle, one should reoptimize the entire set of parameters in the HAM/3 method. In practice, the reoptimization will be carried out in Version 4 of the HAM method (28).

Can. J. Chem. Downloaded from www.nrcresearchpress.com by 210.87.254.5 on 09/06/12
For personal use only.

TABLE 5. VIP (in eV) of C_2F_4 calculated with HAM/3 method

State[a]	No VESU	With VESU	Relative intensity	Mainly from	Observed (25)
$^2A''$	10.67	10.53	0.99	$(2b_{3u})^{-1}$	10.69
	16.27	15.60	0.93	$(1a_u)^{-1}$	16.6
	16.32	15.67	0.93	$(1b_{1g})^{-1}$	16.6
		15.81	0.07	$(1b_{2g})^{-1}$	
	17.68	17.25	0.88	$(1b_{2g})^{-1}$	18.2
	19.33	18.68	0.91	$(1b_{3u})^{-1}$	19.4
		22.32	0.01	$(1b_{3u})^{-1}$	
		23.41	0.06	$(1b_{1g})^{-1}$	
		23.47	0.06	$(1a_u)^{-1}$	
		24.98	0.07	$(1b_{3u})^{-1}$	
		26.64	0.04	$(1b_{2g})^{-1}$	
		32.28	0.01	$(1b_{3u})^{-1}$	
$^2A'$	15.96	15.29	0.93	$(4b_{3g})^{-1}$	15.9
	16.08	15.41	0.93	$(4b_{2u})^{-1}$	16.6
	16.22	15.73	0.95	$(6a_g)^{-1}$	16.6
	17.29	16.60	0.92	$(5b_{1u})^{-1}$	17.6
	19.62	19.08	0.94	$(3b_{3g})^{-1}$	19.4
	20.19	19.56	0.92	$(3b_{2u})^{-1}$	21.0
	20.48	20.01	0.94	$(5a_g)^{-1}$	21.0
	22.43	21.80	0.87	$(4b_{1u})^{-1}$	22.5
		23.33	0.07	$(4b_{2u})^{-1}$	
		23.49	0.07	$(4b_{3g})^{-1}$	
		23.74	0.12	$(4b_{1u})^{-1}$	
		24.45	0.10	$(4a_g)^{-1}$	
		25.25	0.02	$(4a_g)^{-1}$	
	26.61	26.25	0.74	$(4a_g)^{-1}$	26.3
		26.79	0.10	$(4a_g)^{-1}$	
		27.24	0.04	$(3b_{2u})^{-1}$	
		27.70	0.04	$(4b_{1u})^{-1}$	
		27.70	0.02	$(3b_{2u})^{-1}$	
		27.78	0.02	$(4a_g)^{-1}$	
		27.90	0.05	$(3b_{3g})^{-1}$	
		28.23	0.02	$(4b_{1u})^{-1}$	
		29.19	0.02	$(3b_{2u})^{-1}$	
		29.30	0.01	$(5b_{1u})^{-1}$	
		29.43	0.01	$(4b_{3g})^{-1}$	
		30.37	0.11	$(4a_g)^{-1}$	
		31.74	0.02	$(4b_{1u})^{-1}$	

[a]Simplified state symbols for reduced C_s symmetry.

Can. J. Chem. Downloaded from www.nrcresearchpress.com by 210.87.254.5 on 09/06/12
For personal use only.

Acknowledgements

The author wishes to thank the Natural Sciences and Engineering Research Council of Canada for financial support, and Professors E. Lindholm and C. E. Brion for valuable discussions.

1. L. S. CEDERBAUM and W. DOMCKE. Adv. Chem. Phys. **36**, 205 (1977).
2. J. SCHIRMER and L. S. CEDERBAUM. J. Phys. B, **11**, 1889 (1978).
3. L. S. CEDERBAUM, J. SCHIRMER, W. DOMCKE, and W. VON NIESSEN. Int. J. Quantum Chem. **14**, 593 (1978).
4. W. DOMCKE, L. S. CEDERBAUM, J. SCHIRMER, W. VON NIESSEN, C. E. BRION, and K. H. TAN. Chem. Phys. **40**, 171 (1979).
5. G. BIERI, W. VON NIESSEN, L. ÅSBRINK, and A. SVENSSON. Chem. Phys. **60**, 61 (1981).
6. S. IWATA. Chem. Phys. Lett. **83**, 134 (1981); K. KIMURA, S. KATSUMATA, Y. ACHIBA, T. YAMAZAKI, and S. IWATA. Handbook of HeI photoelectron spectra of fundamental organic molecules. Halsted, New York. 1981.
7. N. HONJOU, T. SASAJIMA, and F. SASAKI. Chem. Phys. **57**, 475 (1981).
8. E. LINDHOLM and L. ÅSBRINK. J. Electron Spectrosc. **18**, 121 (1980).
9. L. ÅSBRINK, C. FRIDH, and E. LINDHOLM. Chem. Phys. Lett. **52**, 63 (1977); **52**, 69 (1977); **52**, 72 (1977).
10. L. ÅSBRINK, C. FRIDH, E. LINDHOLM, S. DE BRUIJN, and D. P. CHONG. Phys. Scr. **22**, 475 (1980).
11. L. ÅSBRINK, D. P. CHONG, C. FRIDH, and E. LINDHOLM. To be published.
12. L. ÅSBRINK, C. FRIDH, and E. LINDHOLM. QCPE, **12**, No. 393 (1980).
13. K. H. HELLWEGE. Landolt–Börnstein numerical data and functional relationships in science and technology. New Series, Group II, Vol. 7. Springer, Berlin. 1976.
14. D. W. TURNER, C. BAKER, A. D. BAKER, and C. R. BRUNDLE. Molecular photoelectron spectroscopy. Wiley, New York. 1970.
15. C. J. ALLAN, U. GELIUS, D. A. ALLISON, G. JOHANSSON, H. SIEGBAHN, and K. SIEGBAHN. J. Electron Spectrosc. **1**, 131 (1972).
16. A. W. POTTS and T. A. WILLIAMS. J. Electron Spectrosc. **3**, 3 (1974).
17. A. GIARDINI-GUIDONI, R. TIRIBELLI, D. VINCIGUERRA, R. CAMILLONI, and G. STEFANI. J. Electron Spectrosc. **12**, 405 (1977).

18. T. GUSTAFSON, E. W. PLUMMER, D. E. EASTMAN, and W. GUDAT. Phys. Rev. A**17**, 175 (1978).
19. D. A. ALLISON and R. G. CAVELL. J. Chem. Phys. **68**, 593 (1978).
20. J. P. D. COOK and C. E. BRION. Chem. Phys. **69**, 339 (1982).
21. C. R. BRUNDLE and D. W. TURNER. Int. J. Mass Spectrosc. Ion Phys. **2**, 195 (1969).
22. C. J. ALLAN, U. GELIUS, D. A. ALLISON, G. JOHANSSON, H. SIEGBAHN, and K. SIEGBAHN. Unpublished results; J. W. D. CONNOLLY, H. SIEGBAHN, U. GELIUS, and C. NORDLING. J. Chem. Phys. **58**, 4265 (1973).
23. U. GELIUS. J. Electron Spectrosc. **5**, 983 (1974).
24. A. MINCHINTON, I. FUSS, and E. WEIGOLD. J. Electron Spectrosc. **27**, 1 (1982).
25. G. BIERI, L. ÅSBRINK, and W. VON NIESSEN. J. Electron Spectrosc. **23**, 281 (1981).
26. D. P. CHONG, D. C. FROST, W. M. LAU, and C. A. MCDOWELL. Chem. Phys. Lett. **90**, 332 (1982).
27. D. P. CHONG. Unpublished results.
28. E. LINDHOLM. Private communications.

Can. J. Chem. Downloaded from www.nrcresearchpress.com by 210.87.254.5 on 09/06/12
For personal use only.

Synthesis of indeno[1,2,3-*ij*]isoquinolines

HEMANT A. PATEL AND DAVID B. MACLEAN[1]
Department of Chemistry, McMaster University, Hamilton, Ont., Canada L8S 4M1

Received August 26, 1982

HEMANT A. PATEL and DAVID B. MACLEAN. Can. J. Chem. **61**, 7 (1983).

1-Methyl and 1-benzyl-1,2,3,10b-tetrahydro-5,6,8,9-tetramethoxyindeno[1,2,3-*ij*]isoquinoline have been synthesized from the corresponding 8-phenyl-3,4-dihydro-1(2*H*)isoquinolinones by treatment with $POCl_3$ under Vilsmeier conditions followed by borohydride reduction. The isoquinolinones were prepared in six steps from 2-(2,3,4-trimethoxyphenyl)-4,4-dimethyl-2-oxazoline. This sequence of reactions provides a new route to dihydro and tetrahydroindeno[1,2,3-*ij*]isoquinolines.

HEMANT A. PATEL et DAVID B. MACLEAN. Can. J. Chem. **61**, 7 (1983).

On a synthétisé la méthyl-1 et la benzyl-1 tétrahydro-1,2,3,10b tétraméthoxy-5,6,8,9 indéno[1,2,3-*ij*] isoquinoléine à partir des phényl-8 dihydro-3,4 (2*H*) isoquinolinones-1 que l'on traite par du $POCl_3$ dans les conditions de Vilsmeier suivi d'une réduction par un borohydrure. On a préparé les isoquinolinones en 6 étapes à partir de la (triméthoxy-2,3,4 phényl)-2 diméthyl-4,4 oxazoline-2. Cette suite de réactions fournit une nouvelle voie d'accès aux dihydro et aux tétrahydro-indénol[1,2,3-*ij*] isoquinoléines.

[Traduit par le journal]

Indeno[1,2,3-*ij*]isoquinoline (2-azafluoranthene) **1** was reported in 1948 as a constituent of coal tar and its structure established through degradation to known compounds (1). The synthesis of **1** from a fluorenone precursor was reported in 1958 by Campbell and Reid who, at the same time, described further physical properties and several reactions of this system (2). In 1972 Cava *et al.* (3) isolated the alkaloids, rufescine **2** and imeluteine **3**, from *Abuta rufescens* and *Abuta imene* and demonstrated, through spectral examination and by synthesis, that they were methoxylated derivatives of **1**. A few years later Huls *et al.* (4) isolated another alkaloid of this class from *Triclisia gilletii* to which they assigned structure **4** on spectral grounds and confirmed this structure through an unambiguous synthesis. More recently Menachery and Cava (5) isolated the alkaloids, norrufescine and telitoxine, from *Telitoxicum peruvianum* for which they proposed the structures **4***a* and **4***b*, respectively, on the basis of spectroscopic data.

Fluorenones (2, 6), 1-(2-aminophenyl)-3,4-dihydroisoquinolines (3, 4), and 1-(2-aminophenyl)-1,2,3,4-tetrahydroisoquinolines (7) have been used as starting materials to prepare the ring system present in **1**. In the synthesis beginning with the isoquinolines the five membered ring was generated by diazotization followed by Pschorr cyclization (3, 4, 7). This procedure worked well in the synthesis of rufescine and imeluteine (3) but gave low yields in the synthesis of **4** (4). In the third case (7) the ring system of **1** was formed in unspecified yield but products expected from a simple cyclization were not obtained. Here we report the synthesis of 1,2,3,10b-tetrahydro-5,6,8,9-tetramethoxy-1-methylindeno[1,2,3-*ij*]isoquinoline **5** and its 1-benzyl analogue **6** in which the ring system is generated by a new route from the corresponding 8-phenyl-1(2*H*)isoquinolinone. In the course of this work we have prepared some previously unreported 8-phenylisoquinoline derivatives.

Only a few syntheses of 8-phenylisoquinolines have been reported. The classical routes, namely the Bischler–Napieralski, Pictet–Spengler, and the Pomeranz–Fritsch cyclizations, when applied to this task have proved unrewarding. Our experience with the Pomeranz–Fritsch reac-

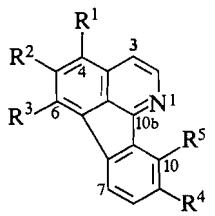

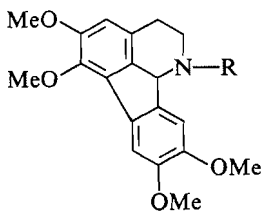

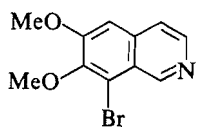

12

1, $R^1 = R^2 = R^3 = R^4 = R^5 = H$

2, $R^1 = R^2 = R^3 = R^4 = OCH_3$; $R^5 = H$

3, $R^1 = R^2 = R^3 = R^4 = R^5 = OCH_3$

4, $R^1 = R^4 = R^5 = H$; $R^2 = R^3 = OCH_3$

4*a*, $R^1 = R^2 = R^3 = OCH_3$, $R^4 = OH$, $R^5 = H$

4*b*, $R^1 = H$, $R^2 = R^3 = OCH_3$, $R^4 = OH$, $R^5 = H$

5, $R = CH_3$

6, $R = CH_2C_6H_5$

[1]Author to whom correspondence may be addressed.

0008-4042/83/010007-07$01.00/0

©1983 National Research Council of Canada/Conseil national de recherches du Canada

Can. J. Chem. Downloaded from www.nrcresearchpress.com by 210.87.254.5 on 09/06/12
For personal use only.

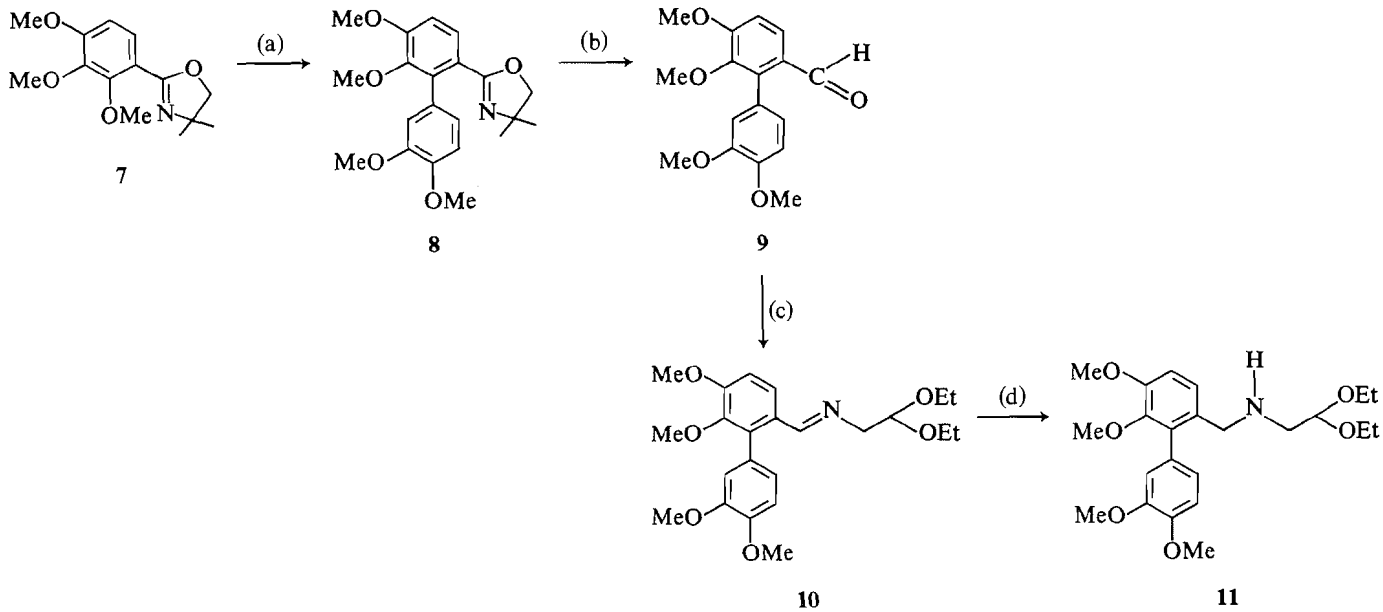

(a) MeO–C$_6$H$_3$(MeO)–MgBr, THF, reflux
(b) *i*, CH_3I; *ii*, $NaBH_4$; *iii*, H_2O, H_3O^+
(c) $NH_2CH_2CH(OEt)_2$, benzene, reflux
(d) H_2/Pt

SCHEME 1

tion (*vide infra*) and its various modifications confirms the experience of earlier workers. The first successful synthesis of 8-phenylisoquinoline was reported by Ahmad and Hey (8) who prepared the parent compound and a few derivatives. In 1979 Dyall and Pullin (9) used a related phenylation procedure to prepare 8-phenylisoquinoline and its six isomers. In the same year Ellefson (10) published a method that promises to be generally applicable to the preparation of a range of substituted 8-phenylisoquinolines or 8-phenyl-1-(2*H*)isoquinolines. Pridgen (11) has shown that haloisoquinolines will couple with aryl magnesium halides in the presence of dichloro[1,3-bis(diphenylphosphino)propane]nickel II (Ni dppp) and has prepared two 8-phenylisoquinolines by this route, both in good yield. More recently Hara *et al.* (12) have shown that a *p*-quinolacetate derived from a 6,7-dioxygenated tetrahydroisoquinoline will react with aralkylethers in the presence of trifluoracetic acid to give 8-phenyltetrahydroquinolines.

We were interested, like earlier workers, in the 8-phenylisoquinolines as precursors of aporphine alkaloids and set out to prepare derivatives of 6,7-dimethoxy-8-(3,4-dimethoxyphenyl)isoquinoline. In the course of our work we made the related 1-(2*H*)isoquinolinones and observed that they underwent cyclization and reduction to indeno[1,2,3-*ij*]isoquinoline derivatives.

Our first approach to the 8-phenylisoquinolines was through the Pomeranz–Fritsch reaction. We expected that recent modifications of the reaction might be successful even though earlier attempts gave negative results. To this end we set out to prepare 3,4-dimethoxy-2-(3,4-dimethoxyphenyl)benzaldehyde. The Ullman reaction gave very poor yields but the route outlined in Scheme 1 was suitable. 2,3,4-Trimethoxybenzoic acid was converted by established procedures to the oxazoline **7** and that in turn in excellent yield to the biphenyl **8** by the method of Meyers and Mihelich (13). The aldehyde **9** was prepared from **8** by the procedure developed by Nordin (14) which involved quaternization at nitrogen, borohydride reduction, and hydrolysis. The aldehyde **9** was converted to the Schiff's base **10** and that in turn to its reduction product **11**, the two compounds required to test the various modifications of the Pomeranz–Fritsch ring closure reaction for the formation of the isoquinoline system. In the case of **10**, cyclization was attempted with polyphosphoric acid (15), 70% H_2SO_4 (16), and $BF_3 \cdot Et_2O/(CF_3CO)_2O$ (17) with a singular lack of success. The same was true when **11** was treated with 6 *M* HCl (18) or its tosyl derivative with 6 *M* HCl in dioxane (19). The reasons for the failure of this cyclization in this seemingly highly activated system are not apparent. A possible explanation may be that the oxonium ion generated from the acetal readily complexes with the π electrons of the *ortho* phenyl group and decomposes to products other than those of normal cyclization. Models show that the interaction would be favourable geometrically.

The next approach to our target molecule was based on the method of Pridgen (11). We prepared the previously unreported 8-bromo-6,7-dimethoxyisoquinoline **12** from 2-bromo-3,4-dimethoxybenzaldehyde (20, 21) via the modified Pomeranz–Fritsch procedure developed by Bewis *et al.* (17). Treatment of isoquinoline **12** with 3,4-dimethoxyphenylmagnesium bromide according to Pridgen's procedure in the presence of "Ni dppp" did not yield the expected 8-phenylisoquinoline.

Finally we turned to the method of Ellefson (10) (Scheme 2) which proved to be successful. The oxazoline **8** was lithiated with *n*-BuLi (22, 23) and treated with an excess of ethylene oxide to give compound **13** which was hydrolysed (24) in 3 *M* HCl to the isocoumarin **14**; the yield was found to be sensitive

Can. J. Chem. Downloaded from www.nrcresearchpress.com by 210.87.254.5 on 09/06/12
For personal use only.

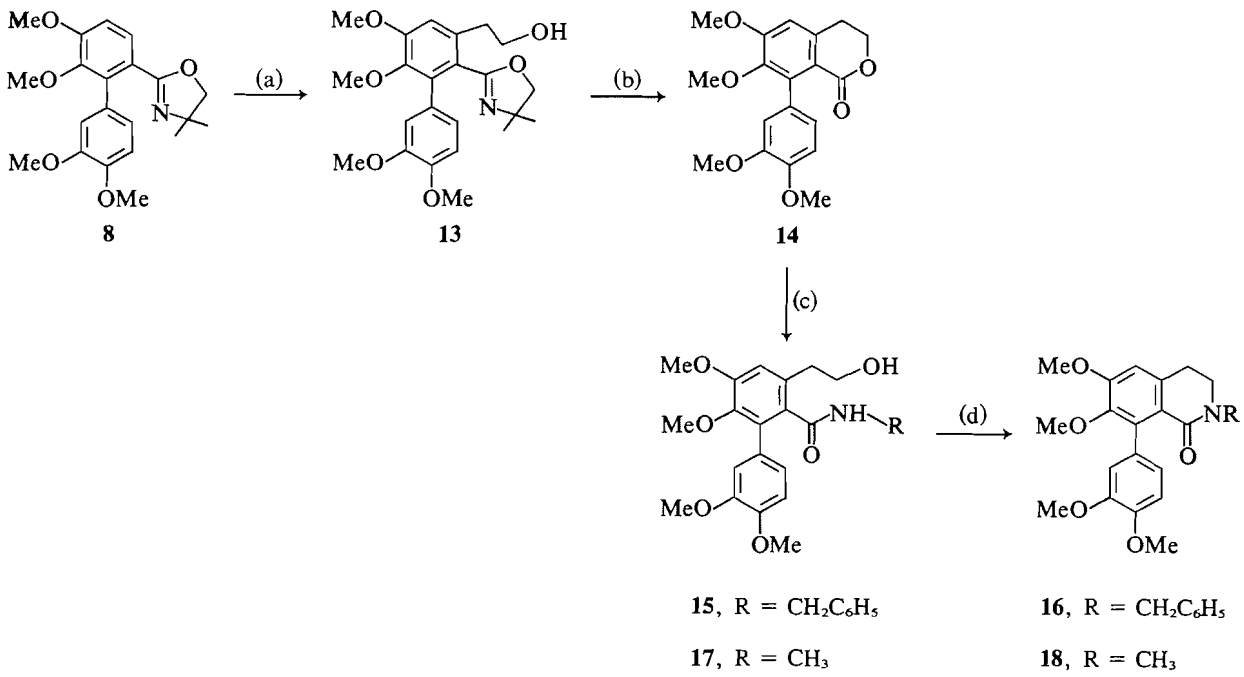

8 **13** **14**

15, R = $CH_2C_6H_5$ **16**, R = $CH_2C_6H_5$

17, R = CH_3 **18**, R = CH_3

(a) *i*, n-BuLi, THF; *ii*,
(b) 3 *M* HCl, 20 min
(c) **14** → **15**, benzylamine, benzylammonium chloride, 125°C, 24 h.
14 → **17**, CH_3NH_2, CH_3OH, H_2O, reflux
(d) *i*, mesylchloride, pyridine; *ii*, NaH, THF

SCHEME 2

both to the acid concentration and the time of reflux. The amide **15** was obtained by treating **14** with a mixture of benzylamine and benzylammonium chloride under reflux for 24 h. Esterification of the primary hydroxy group of **15** was effected with mesyl chloride in pyridine and the mesylate treated with sodium hydride in THF to afford the lactam **16**.

2-Methyl-3,4-dihydro-6,7-dimethoxy-8-(3,4-dimethoxyphenyl)-1(2*H*)isoquinolinone **18** was prepared in an analogous series of reactions by the sequence **14** → **17** → **18**.

The indeno[1,2,3-*ij*]isoquinolines were formed from the lactams **16** and **18** by treatment with $POCl_3$ as shown in Scheme 3. The tetrahydro compounds **5** and **6** were obtained in good yield by reduction of the isoquinolinium salts, **20** and **19**, respectively with sodium borohydride.

The structures of the compounds discussed above are based upon their composition and their spectroscopic properties, particularly the ^1H nmr spectra. It is not the intention to give a detailed analysis of the spectra but several features are noteworthy. In all the biphenyls and 8-phenylisoquinolines prepared in this study, one methoxy group appears in the vicinity of 3.5 + 0.1 ppm, in contrast to the other three which appear in the region 3.9 + 0.2 ppm. We assign the low field signal to the methoxy group *ortho* to the phenyl group by which it must be shielded because of the nonplanarity of the biphenyl system. In the indeno[1,2,3-*ij*]isoquinolines none of the four methoxy signals occurs near 3.5 ppm, presumably because the molecule is forced into near planarity by the constraints of the ring system. The chemical shifts of other protons in the indenoisoquinoline systems are more or less in accord with expectations based on analogy with the spectra of aporphine alkaloids (25).

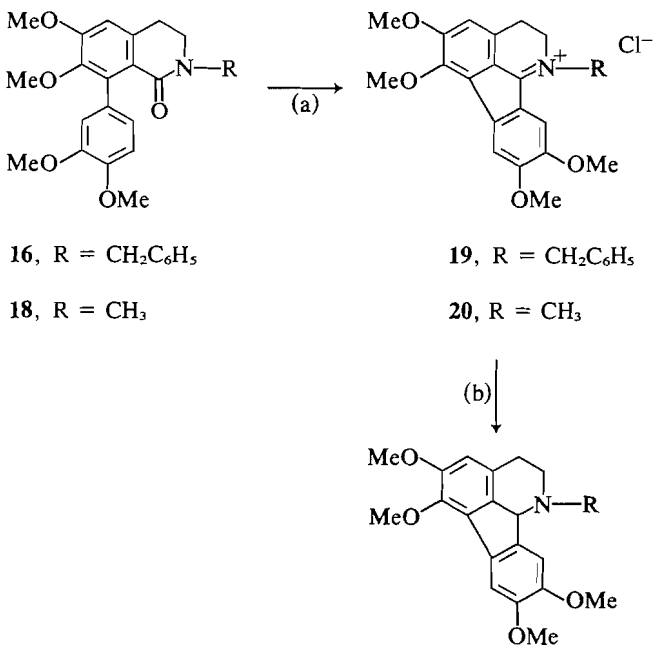

16, R = $CH_2C_6H_5$ **19**, R = $CH_2C_6H_5$

18, R = CH_3 **20**, R = CH_3

6, R = $CH_2C_6H_5$

5, R = CH_3

(a) $POCl_3$, toluene, reflux
(b) $NaBH_4$, EtOH

SCHEME 3

Can. J. Chem. Downloaded from www.nrcresearchpress.com by 210.87.254.5 on 09/06/12
For personal use only.

Can. J. Chem. Downloaded from www.nrcresearchpress.com by 210.87.254.5 on 09/06/12
For personal use only.

It is noteworthy that compound **5** shows only three aromatic protons in its ^{1}H nmr spectrum and only three aromatic carbon atoms bound to hydrogen in its ^{13}C nmr spectrum. Both the ^{13}C and ^{1}H spectra indicate that there are only two methylene groups and one methine group in the molecule. Similar results are observed for **6** but the ^{1}H spectrum is more complex because of the presence of the *N*-benzyl group.

This study provides a new approach to the indeno-[1,2,3-*ij*]isoquinoline system. The precursor 8-phenyl-1-(2*H*)-isoquinolinones may be conveniently prepared from 2-(2-methoxyphenyl)-4,4-dimethyloxazolines by the method of Ellefson (10). Two key steps in this synthesis involve oxazoline chemistry, the first, directed displacement of the methoxy group *ortho* to the oxazoline by the method of Meyers and Mihelich (13), and the second, *ortho* lithiation of the oxazoline followed by alkylation with ethylene oxide (10, 22, 23).

Experimental

Apparatus, materials, and methods

The continuous wave ^{1}H nmr spectra were run on a Varian EM 390 or T-60 spectrometer. The Fourier transform spectra were run on either a Bruker WP 80 or WH 90 or WM 250 spectrometer. Unless otherwise specified, the samples were dissolved in chloroform-*d* using tetramethylsilane (TMS) as the internal standard. Chemical shifts, quoted as δ values, were measured in relation to TMS. The symbols s, singlet, d, doublet, t, triplet, q, quartet, bs, broad singlet, and m, multiplet are used in reporting spectra. The ^{13}C nmr spectra were run at 62.9 MHz on a Bruker WM 250 FT spectrometer at 22.7°C. Mass spectra were recorded on a V.G. Micromass 7070 F mass spectrometer, at 70 eV.

Infrared spectra were recorded on a Perkin–Elmer 283 spectrometer in chloroform solution. Melting points were determined on a Kofler micro hot stage and are uncorrected. The microanalyses were performed by the Guelph Chemical Laboratories Ltd., Guelph, Ontario.

Thin layer chromatography (tlc) was performed using polygram Sil G/UV$_{254}$ and Al_2O_3 N/UV$_{254}$ plates. Gravity columns were run using Merck SiO_2 60, and "flash" columns prepared as described in the literature (26).

THF was dried by distillation from Na in a N_2 atmosphere, just prior to use. The following compounds were prepared by standard methods and gave satisfactory physical and spectral data: 2-bromoisovanillin (20), 2-bromo-3,4-dimethoxybenzaldehyde (21), 4-iodoveratrole (27), triethyloxonium fluoroborate (28).

2-(2,3,4-Trimethoxyphenyl)-4,4-dimethyl-2-oxazoline 7

$SOCl_2$ (44 mL; 0.6 mol) was added in one lot to 2,3,4-trimethoxybenzoic acid (42.4 g; 0.2 mol) and the dark brown mixture was stirred at ambient temperature for 24 h. The excess $SOCl_2$ was distilled off leaving a dark brown oil which was dissolved in CH_2Cl_2 (150 mL). The resulting solution was added dropwise to a stirred solution of 2-amino-2-methyl-1-propanol (36.8 g; 0.4 mol) in CH_2Cl_2 (150 mL) at 0°C during 1 h and the reaction mixture was left to stir overnight. After filtration, the filtrate was washed with H_2O, 5% HCl, 5% NaOH, and H_2O and dried. Removal of the solvent furnished the trimethoxybenzamide as a white solid (42.5 g; 75%), which was pure enough for the next step. To the above amide (42.5 g; 0.15 mol), $SOCl_2$ (16 mL) was added and the mixture stirred. After the solid had dissolved, the yellow solution was further stirred for 25 min and poured into anhydrous ether (150 mL). The precipitated hydrochloride was washed with ether and dried (43.4 g; 96%). The solid hydrochloride was dissolved in a minimum of H_2O, neutralized with cold 50% NaOH, extracted with ether, washed, and dried. Removal of the solvent gave a pale yellow oil which was crystallized from a small amount of cold petroleum ether, giving the required oxazoline as colorless crystals (35.5 g; 93%), mp 43–44°C; ir ($CHCl_3$): 2935, 1650, 1602, 1461, 1392, 1358, 1320, 1112, 1090, 970 cm^{-1}; ^{1}H nmr: 1.35 (6H, s, CH_3), 3.87 (9H, s, OCH_3), 4.05 (2H, s, CH_2), 6.67 (1H, d, J = 9 Hz, Ar-H), 7.50 (1H, d, J = 9 Hz, Ar-H) ppm; ms m/z: 265 (M^+ 46%), 250 (75%), 222 (31%), 204 (25%), 192 (33%), 179 (61%), 178 (100%), 165 (20%), 151 (21%). *Anal.* calcd. for $C_{14}H_{19}NO_4$: C 63.38, H 7.10; found: C 63.42, H 7.10%. *Mol. Wt.* calcd. for $C_{14}H_{19}NO_4$: 265.131; found (hrms): 265.128.

2-[2-(3,4-Dimethoxyphenyl)-3,4-dimethoxyphenyl]-4,4-dimethyl-2-oxazoline 8

To the stirred solution of Grignard reagent (prepared from 4-bromoveratrole (26.04 g; 0.12 mol) and Mg (3.0 g; 0.12 mol) in refluxing THF (100 mL)) was added the oxazoline **7**, (26.5 g; 0.1 mol in THF (50 mL)) at 10°C during 10 min. The reaction mixture was allowed to stir at room temperature for 20 h, slowly decomposed with saturated NH_4Cl (50 mL), extracted with CH_2Cl_2, washed with brine, and dried. Evaporation of the solvent furnished a red viscous liquid which was triturated with petroleum ether to give yellow crystals of the required product (34.1 g; 92%), mp 97–99°C; ir ($CHCl_3$): 2940, 2840, 1650, 1600, 1572, 1488, 1462, 1355, 1320, 1300, 1120, 1010, 970, 940, 860 cm^{-1}; ^{1}H nmr: 1.22 (6H, s, C—CH_3), 3.52 (3H, s, OCH_3), 3.77 (2H, s, CH_2), 3.85 (3H, s, OCH_3), 3.92 (6H, s, OCH_3), 6.84–7.10, 7.27–7.45 (5H, m, Ar-H) ppm; ms m/z: 371 (M^+ 37%), 370 (100%), 356 (14%), 285 (13%). *Anal.* calcd. for $C_{21}H_{25}NO_5$: C 67.91, H 6.79; found: C 67.92, H 6.70%. *Mol. Wt*: calcd. for $C_{21}H_{25}NO_5$: 371.173; found (hrms): 371.174.

2-[2-(3,4-Dimethoxyphenyl)-3,4-dimethoxyphenyl]-3,4,4-trimethyl-2-oxazolinium iodide

A solution of the product **8**, prepared above (3.71 g; 0.01 mol) and MeI (1.9 g; 0.015 mol) in nitromethane (7 mL) was heated at 70°C overnight. The cooled red reaction mixture was diluted with an equal volume of ether, ice-cooled, and filtered to furnish yellow crystals of the required quarternary salt (4.9 g; ~96%), mp 190–192°C; ir ($CHCl_3$): 3310, 2937, 1632, 1580, 1480, 1360, 1280, 1108, 918 cm^{-1}; ^{1}H nmr: 1.53 (6H, s, C—CH_3), 2.88 (3H, s, $=\overset{+}{N}$—CH_3), 3.57 (3H, s, OCH_3), 3.90 (3H, s, OCH_3), 3.93 (3H, s, OCH_3), 4.00 (3H, s, OCH_3), 5.03 (2H, s, CH_2), 6.70–7.30 (4H, m, Ar-H), 8.29 (1H, d, J = 7.5 Hz, Ar-H). *Anal.* calcd. for $C_{22}H_{28}NO_5I$: C 51.47, H 5.50; found: C 51.54, H 5.41%.

2-(3,4-Dimethoxyphenyl)-3,4-dimethoxybenzaldehyde 9

(A) To a stirred solution of the quarternary salt prepared above (5.1 g; 0.01 mol) in EtOH (40 mL) was added $NaBH_4$ (0.378 g; 0.01 mol) in portions at 0°C, and the mixture was stirred at 0°C for 4 h. The yellow reaction mixture was then diluted with 2 *M* HCl (80 mL) to give a red solution that was extracted with CH_2Cl_2, washed with brine, and dried. Removal of the solvent yielded a red oil which was purified by flash chromatography giving the required aldehyde as a white solid (2.1 g; 66%). A portion was recrystallized from 95% EtOH to give colorless crystals, mp 119–120°C; ir ($CHCl_3$): 2840, 1680, 1582, 1460, 1322, 1122, 940, 900 cm^{-1}; ^{1}H nmr: 3.57 (3H, s, OCH_3), 3.89 (3H, s, OCH_3), 3.95 (3H, s, OCH_3), 3.99 (3H, s, OCH_3), 7.20–7.43 (4H, m, Ar-H), 7.85 (1H, d, J = 9 Hz, Ar-H), 9.74 (1H, s, CHO) ppm; ms m/z: 302 (M^+, 100%), 287 (11%), 259 (14%), 229 (14%). *Anal.* calcd. for $C_{17}H_{18}O_5$: C 67.54, H 6.00%; found: C 67.51, H 6.28%. *Mol. Wt.* calcd. for $C_{17}H_{18}O_5$: 302.114; found (hrms): 302.108.

(B) A mixture of 2-bromo-3,4-dimethoxybenzaldehyde (1.22 g; 0.05 mol) and 4-iodoveratrole (2.64 g; 0.01 mol) was warmed on a steam bath to form a homogenous solution to which copper powder (30 g) was added in several portions according to the procedure of Brown and Robin (29). After each addition, the reaction mixture was centrifuged to form a compact mass which was then heated at 220–230°C for 1 h. After cooling, it was thoroughly washed with CH_2Cl_2 and filtered. The filtrate on evaporation furnished a red oil which was purified by flash chromatography, giving the required aldehyde as a white solid (0.2 g; 13%), mp 119–120°C.

2-(3,4-Dimethoxyphenyl)-3,4-dimethoxybenzylideneaminoacetaldehyde diethyl acetal 10

A mixture of aminoacetaldehyde diethyl acetal (0.732 g; 0.055 mol) and the aldehyde **9** (1.51 g; 0.005 mol) in dry benzene (25 mL)

Can. J. Chem. Downloaded from www.nrcresearchpress.com by 210.87.254.5 on 09/06/12
For personal use only.

was refluxed under a Dean–Stark trap until no further water was separated (14 h); removal of the solvent under vacuum then gave the required Schiff's base **10** as an oil (2.0 g; ~96%) which was used without further purification for either cyclization or reduction; ^{1}H nmr: 1.17 (6H, t, J = 6 Hz, CH_3), 3.53 (3H, s, OCH_3), 3.47–3.73 (6H, m, CH_2), 3.85 (3H, s, OCH_3), 3.93 (6H, s, 2 × OCH_3), 4.73 (1H, t, J = 5 Hz, CH_2—C*H*—O), 6.67–7.06 (4H, m, Ar-H), 7.86 (1H, d, J = 9 Hz, Ar-H), 7.97 (1H, s, CH=N) ppm.

N-[2-(3,4-Dimethoxyphenyl)-3,4-dimethoxy]benzylaminoacetaldehyde diethyl acetal ***11***

The benzylideneaminoacetal **10** (2.09 g; 0.005 mol) was dissolved in absolute ethanol (25 mL) and platinum dioxide (30 mg) was added. The solution was hydrogenated at 45 psi and 25°C for 16 h. The catalyst was filtered and the solvent evaporated under vacuum to yield the required benzylamino acetal **11** as a viscous oil (2.0 g; ~98%) which was used without further purification for attempted cyclization reactions; ^{1}H nmr: 1.13 (6 H, t, J = 6 Hz, CH_2CH_3), 2.53 (2H, d, J = 6 Hz, CH_2), 2.75 (2H, s, CH_2), 3.23–3.70 (5H, m, 2 × CH_2—O, NH), 3.57 (3H, s, OCH_3), 3.87 (3H, s, OCH_3), 3.90 (3H, s, OCH_3), 3.93 (3H, s, OCH_3), 4.45 (1H, t, J = 6 Hz, C*H*—O), 6.70–7.18 (5H, m, Ar-H) ppm.

8-Bromo-6,7-dimethoxyisoquinoline ***12***

A mixture of aminoacetaldehydediethylacetal (2.39 g; 0.018 mol) and 2-bromo-3,4-dimethoxybenzaldehyde (4.0 g; 0.0163 mol) in C_6H_6 was refluxed under a Dean–Stark trap until no further H_2O separated (6 h). The solvent was removed and the oily Schiff base was treated at 5°C with trifluoroacetic anhydride (17 mL).

This solution was added to the stirred solution of $BF_3 \cdot AcOH$ complex (40% BF_3; 12.3 g; 3 mol) in trifluoroacetic anhydride (20 mL) at 5°C. The solution was stirred for 48 h at room temperature and the deep cherry red mixture was poured into ice-water, basified with aqueous NH_3, and extracted with $CHCl_3$. The combined $CHCl_3$ extract was extracted with 4 *M* HCl, basified with aqueous NH_3 and extracted with CH_2Cl_2, washed, and dried. Evaporation of the solvent gave the required isoquinoline as a solid (1.26 g; 29%), mp 135–137°C; ir ($CHCl_3$): 2944, 2840, 1620, 1550, 1480, 1460, 1390, 1335, 1142, 995, 870, 850, cm^{-1}; ^{1}H nmr: 3.97 (3H, s, OCH_3), 4.03 (3H, s, OCH_3), 7.03 (1H, s, H-5), 7.43, (1H, d, J = 5 Hz, H-4), 8.43 (1H, d, J = 5 Hz, H-3), 9.45 (1H, s, H-1) ppm; ms m/z: 269 (M^+, 98%), 267 (100%), 254 (24%), 252 (25%), 226 (28%), 224 (34%), 173 (11%), 117 (16%), 102 (15%), 75 (20%). *Anal.* calcd. for $C_{11}H_{10}NO_2Br$: C 49.27, H 3.76; found: C 49.25, H 3.74%. *Mol. Wt.* calcd. for $C_{11}H_{10}NO_2{}^{79}Br$: 266.989; found (hrms): 266.993.

2-[2-(3,4-Dimethoxyphenyl)-3,4-dimethoxy-6-(2-hydroxyethyl)-phenyl]-4,4-dimethyl-2-oxazooline ***13***

To the stirred solution of the oxazoline (11.13 g; 0.03 mol) in dry THF (125 mL) under argon at −10°C was added n-BuLi (30 mL of 1.5 *M* in hexane; 0.045 mol) and the mixture further stirred at −5 to −10°C for 6 h. The resulting deep red solution was treated with ethylene oxide (12 mL) at −10°C and immediately a balloon (5 L capacity) was fixed at the top of the reflux condenser to keep the ethylene oxide atmosphere under slight pressure throughout the reaction time. The mixture was stirred for 3 h at −5 to −10°C and allowed to warm up to room temperature overnight. Water (40 mL) was added, the THF evaporated, and the aqueous phase extracted with CH_2Cl_2, washed with brine, and dried. Distillation of the solvent gave a red oil which was purified by flash chromatography, giving a yellow oil (7.6 g; 61%) which was crystallized from ethyl acetate – petroleum ether to furnish the required alcohol as a white solid (5.5 g; 44%) mp 131–132°C; ir ($CHCl_3$): 3200, 2940, 2840, 1650, 1582, 1460, 1355, 1320, 1135, 1070, 1000, 965, 858 cm^{-1}; ^{1}H nmr: 1.23 (6H, s, C—CH_3), 2.91 (2H, t, J = 6 Hz, CH_2) 3.48 (3H, s, OCH_3), 3.63 (2H, s, CH_2), 3.85 (3H, s, OCH_3), 3.90 (6H, s, OCH_3), ca. 3.9 (2H, t, CH_2OH, obscured by OMe signal), 5.06 (1H, bs, OH), 6.83–6.93 (4H, m, Ar-H) ppm; ms m/z: 415 (M^+, 30%), 414 (30%), 397 (83%), 384 (100%), 369 (30%). *Anal.* calcd. for $C_{23}H_{29}NO_6$: C 66.49, H 7.04; found: C 66.52, H, 7.01%. *Mol. Wt.* calcd. for $C_{23}H_{29}NO_6$: 415.200; found (hrms): 415.198.

3,4-Dihydro-6,7-dimethoxy-8-(3,4-dimethoxyphenyl)isocoumarin ***14***

A mixture of the oxazoline prepared above (8.3 g; 0.02 mol) and 3 *M* HCl (250 mL) was stirred under reflux for 20 min. The solid that separated from the hot red reaction mixture was filtered after cooling, washed with H_2O, and dried to furnish the required isocoumarin as a white solid (6.88 g; 79%), a portion of which was crystallized from 95% EtOH giving colorless, long needles, mp 194–195°C; ir ($CHCl_3$): 2940, 2840, 1725, 1585, 1455, 1386, 1352, 1260, 1136, 1090, 1010, 990 cm^{-1}; ^{1}H nmr: 3.00 (2H, t, J = 6 Hz, CH_2), 3.48 (3H, s, OCH_3), 3.85 (3H, s, OCH_3), 3.91 (3H, s, OCH_3), 3.95 (3H, s, OCH_3), 4.45 (2H, t, J = 6 Hz, CH_2O), 6.67–6.95 (4H, m, Ar-H) ppm; ms m/z: 344 (M^+, 100%), 329 (12%), 165 (12%). *Anal.* calcd. for $C_{19}H_{20}O_6$: C 66.27, H 5.86%; found: C 66.21, H 5.92%.

N-*Benzyl-6-(2-hydroxyethyl)-2-(3,4-dimethoxyphenyl)-3,4-dimethoxybenzamide* ***15***

A mixture of the isocoumarin (5.1 g; 0.0148 mol) and benzylamine hydrochloride (3.05 g; 0.0213 mol) in benzylamine (20 mL) was stirred at 120–125°C for 24 h. The red solution was cooled, poured into 5% HCl (200 mL), and extracted with CH_2Cl_2. The combined CH_2Cl_2 extract was washed with 5% HCl, H_2O, and dried. Removal of the solvent furnished a red oil which was purified by flash chromatography giving the required benzamide as a white solid (5.85 g; ~88%), mp 58–60°C; ir ($CHCl_3$): 3440, 3350, 2940, 2840, 1736, 1640, 1580, 1460, 1315, 1135, 1000 cm^{-1}; ^{1}H nmr: 2.83 (2H, t, J = 6 Hz, $PhCH_2$), 3.40 (3H, s, OCH_3), 3.73 (3H, s, OCH_3), 3.87 (6H, s, OCH_3), ca. 3.9 (2H, CH_2OH, obscured by OMe signal), 4.30 (2H, d, J = 6 Hz, CH_2—N), 5.22 (1H, s, OH), 5.69 (1H, t, J = 6 Hz, NH), 6.86–7.50 (9H, m, Ar-H) ppm, ms m/z: 451 (M^+, 30%), 433 (72%), 432 (42%), 342 (37%), 327 (23%), 315 (28%), 297 (33%), 91 (100%). *Mol. Wt*: calcd. for $C_{26}H_{29}NO_6$: 451.196; found (hrms): 451.200.

N-*Benzyl-6-[2-(methylsulfonyloxy)ethyl]-2-(3,4-dimethoxyphenyl)-3,4-dimethoxybenzamide*

A solution of the alcohol **15** (6.76 g; 0.015 mol) and mesyl chloride (3.44 g; 0.03 mol) in dry pyridine (50 mL) was left in the refrigerator overnight. The resulting yellow solution was poured into cold H_2O (100 mL) and extracted with CH_2Cl_2. The combined CH_2Cl_2 extract was washed with 5% HCl, H_2O, and dried. Removal of the solvent gave the required mesylate as a yellow oil (7.66 g; 97%), which was pure enough for the next step.

2-Benzyl-3,4-dihydro-6,7-dimethoxy-8-(3,4-dimethoxyphenyl)-1-(2H)isoquinolinone ***16***

A mixture of the above mesylate (7.66 g; 0.0145 mol) and NaH (50% suspension in oil; 1.738 g; 0.036 mol) in dry THF (150 mL) was stirred under reflux overnight. The mixture was cooled and the excess of NaH was decomposed with H_2O. The THF was removed and the residue was taken up in CH_2Cl_2, washed with H_2O, and dried. Evaporation of the solvent yielded a red viscous liquid which was thoroughly washed with petroleum ether (to remove paraffin oil) to give a yellow solid, which was crystallized from ethyl acetate – petroleum ether to furnish the required isoquinolinone as a white solid (3.82 g; 71%), mp 140–141°C; ir ($CHCl_3$): 2940, 2840, 1668, 1590, 1464, 1385, 1350, 1318, 1135, 1095, 1010 cm^{-1}; ^{1}H nmr: 2.92 (2H, t, J = 6 Hz, $PhCH_2$) 3.47 (3H, s, OCH_3), 3.79 (3H, s, OCH_3), 3.92 (6H, s, OCH_3), 4.30 (2H, t, J = 6 Hz, N—CH_2), 4.37 (2H, s, $PhCH_2$—N), 6.67–7.2 (9H, m, Ar-H) ppm; ms m/z: 433 (M^+, 49%), 432 (100%), 418 (13%), 341 (26%), 326 (10%), 91 (30%). *Anal.* calcd. for $C_{26}H_{27}O_5N$: C 72.04, H 6.28, N 3.23%; found: C 72.08, H 6.40, N 3.01%.

N-*Methyl-6-(2-hydroxyethyl)-2-(3,4-dimethoxyphenyl)-3,4-dimethoxybenzamide* ***17***

A mixture of the isocoumarin **14** (2.55 g; 0.074 mol) and methyl amine (40% aqueous solution; 10 mL) in CH_3OH (35 mL) in a round-bottom flask fitted with a reflux condenser and balloon (5 L capacity) at the top (to prevent the escape of methyl amine gas) was heated under reflux with stirring for 24 h. Upon cooling, the green reaction mixture was diluted with H_2O (10 mL), the CH_3OH evaporated, and the

Can. J. Chem. Downloaded from www.nrcresearchpress.com by 210.87.254.5 on 09/06/12
For personal use only.

aqueous phase extracted with CH_2Cl_2, washed with brine, and dried. Removal of the solvent gave a red oil which was purified by flash chromatography, giving the required *N*-methylbenzamide as a white solid (2.40 g; 86.3%), mp 71–73°C; ir ($CHCl_3$): 3460, 2940, 2840, 1640, 1582, 1462, 1315, 1138, 1000 cm^{-1}; ^1H nmr: 2.57 (3H, d, J = 4.5 Hz, NHC*H*$_3$), 2.88 (2H, t, J = 6 Hz, Ar-CH_2), 3.47 (3H, s, OCH_3), 3.88 (3H, s, OCH_3), 3.95 (6H, s, OCH_3), 3.95 (2H, *C*H_2OH, obscured by OMe signal), 6.85–6.97 (4H, m, Ar-H) ppm; ms *m/z*: 375 (M^+, 47%), 357 (100%), 356 (68%), 345 (73%), 342 (23%), 328 (22%), 327 (32%), 315 (33%). *Anal.* calcd. for $C_{20}H_{25}NO_6$: C 63.98, H 6.71; found: C 63.93, H 6.61%. *Mol. Wt.* calcd. for $C_{20}H_{25}NO_6$: 375.168; found (hrms): 375.167.

N-Methyl-6-[2-(methylsulfonyloxyethyl)]-2-(3,4-dimethoxyphenyl)-3,4-dimethoxybenzamide

A solution of the alcohol prepared above (1.875 g; 0.005 mol) and mesyl chloride (1.145 g; 0.01 mol) in dry pyridine (10 mL) was left in the refrigerator overnight. The resulting yellow solution was poured into cold H_2O (20 mL) and extracted with CH_2Cl_2. The combined CH_2Cl_2 extract was washed with 5% HCl, H_2O, and dried. Removal of the solvent gave the required mesylate as a yellow oil (2.6 g; 97%) which was used directly in the next step.

2-Methyl-3,4-dihydro-6,7-dimethoxy-8-(3,4-dimethoxyphenyl)-1(2H)isoquinolinone ***18***

A mixture of the mesylate prepared above (2.60 g; 0.0057 mol) and NaH (50% suspension in oil, 0.688 g; 0.0143 mol) in dry THF (50 mL) was stirred under reflux overnight. Upon cooling, the excess of NaH was decomposed with H_2O, the THF evaporated, and the residue taken up in CH_2Cl_2, washed with H_2O, and dried. Removal of the solvent yielded a red viscous liquid which was thoroughly washed with petroleum ether (to remove paraffin oil) to give a yellow oil which slowly solidified but failed to crystallize from a solvent (1.56 g; 76%), mp 53–55°C; ir ($CHCl_3$): 2940, 2480, 1730, 1668, 1590, 1458, 1380, 1350, 1315, 1270, 1132, 1082, 1004, 970, 945 cm^{-1}; ^1H nmr: 2.73 (3H, s, N*CH*$_3$), 2.87 (2H, t, J = 6 Hz, CH_2), 3.47 (3H, s, OCH_3), , 3.85 (3H, s, OCH_3), 3.90 (6H, s, OCH_3), 4.27 (2H, t, J = 6 Hz, *CH*$_2$—N), 6.62–6.98 (4H, m, Ar-H) ppm; ms *m/z*: 357 (M^+, 35%), 356 (100%), 342 (7%), 340 (13%), 326 (22%), 298 (7%). *Anal.* calcd. for $C_{20}H_{23}NO_5$: C 67.21, H 6.49; found: C 66.69, H 6.42%. *Mol. Wt.* calcd. for $C_{20}H_{23}NO_5$: 357.156; found (hrms): 357.156.

2,3-Dihydro-5,6,8,9-tetramethoxy-1-methylindeno[1,2,3-ij]-isoquinolinium chloride ***20***

A mixture of *N*-methylisoquinolinone prepared above (1.5 g; 0.0042 mol) and $POCl_3$ (1.3 g; 0.0085 mol) in dry toluene (25 mL) was refluxed under argon for 4 h. The dark brown reaction mixture was cooled, diluted with an excess of petroleum ether, ice-cooled, and filtered to give brown crystals of the cyclized product (1.5 g; 96%), mp 117–120°C; ir ($CHCl_3$) 2940, 1670, 1594, 1464, 1402, 1280, 1100, 994 cm^{-1}; ^1H nmr: (CF_3COOH): 3.23 (2H, t, J = 7.5 Hz, CH_2), 3.97 (3H, s, $=\overset{+}{N}CH_3$), 4.08 (6H, s, OCH_3), 4.17 (6H, s, OCH_3), 4.33 (2H, t, J = 7.5 Hz, *CH*$_2$—N), 6.67 (1H, s, Ar-H), 7.50 (1H, s, Ar-H), 7.60 (1H, s, Ar-H) ppm.

1,2,3,10b-Tetrahydro-5,6,8,9-tetramethoxy-1-methylindeno-[1,2,3-ij]isoquinoline ***5***

To a stirred solution of the quarternary salt prepared above (0.751 g; 0.002 mol) in EtOH (20 mL) was added $NaBH_4$ (0.228 g; 0.006 mol) in small portions (10 min) and further stirred for 2 h at room temperature. During this time the deep brown reaction mixture became colorless. The excess of $NaBH_4$ was destroyed by adding glacial acetic acid, the CH_3OH evaporated, and the residue treated with H_2O (10 mL), basified to pH >10 with NaOH, and extracted with CH_2Cl_2. The combined CH_2Cl_2 extract was washed with brine and dried. Evaporation of the solvent furnished a gum (0.412 g; 61%). The base was recovered from the purified hydrochloride (*vide infra*) for spectroscopic analysis; ir ($CHCl_3$): 2940, 2840, 1605, 1580, 1462, 1400, 1320, 1290, 1260, 1100, 998 cm^{-1}; ^1H nmr (250 MHz): 2.30 (3H, s, NCH_3), 2.8 (2H, m, H's at C-3), 3.2 (2H, m, H's at C-2), 3.85 (3H, s, OCH_3), 3.90 (3H, s, OCH_3), 3.93 (3H, s, OCH_3), 3.96 (3H, s, OCH_3), 4.27 (1H, s, H-10b), 6.51 (1H, s, Ar-H), 7.18 (1H, s, Ar-H), 7.52 (1H, s, Ar-H) ppm; ^{13}C nmr: 24.03 (t, C-3), 38.74 (q, N—Me), 54.31 (t, C-2) 56.35 (q, 3 × OCH_3), 60.64 (q, 1 × OCH_3), 67.56 (d, C-10b) 107.17, 109.23, 109.57 (all d's, C-4, C-7, C-10) 127.53, 131.95, 133.27, 135.06, 137.51, 142.56, 148.66, 149.60, 153.82 (all s's, other aromatic C-atoms); ms *m/z*: 341 (M^+, 45%), 340 (68%), 326 (24%), 310 (100%), 296 (10%), 283 (25%). *Mol. Wt.* calcd. for $C_{20}H_{22}NO_4$ (M − 1): 340.155; found (hrms): 340.152.

The free base was dissolved in ethanol and treated with dry HCl. Upon addition of ether the hydrochloride crystallized as a white solid. Recrystallization from ethanol–ether gave colorless crystals, mp 207–209°C. The hydrochloride was highly solvated and failed to give satisfactory analysis even after prolonged drying at 70°C at 1.0 Torr. The ^1H nmr ($CDCl_3$, 250 MHz) of the hydrocloride showed that the crystals contained roughly 5 moles of water. The following signals were observed: −1.75 (ca. 10H, H_2O), 2.24 (d, N—Me, J = 5 Hz), 2.9–3.7 (m, 4H, H's at C-2 and C-3), 3.90, 3.96, 3.97, 3.98 (4s, 3H each, 4 × OCH_3), 5.20 (s, 1H, H-10b), 6.58, 7.47, 8.01 (3s, 1H each, 3 × Ar-H) ppm.

2,3-Dihydro-5,6,8,9-tetramethoxy-1-benzylindeno[1,2,3-ij]-isoquinolinium chloride ***19***

A mixture of *N*-benzylisoquinolinone **16** (0.866 g; 0.002 mol) and $POCl_3$ (0.616 g; 0.004 mol) in dry toluene (15 mL) was refluxed under argon for 4 h. The dark brown reaction mixture was cooled, diluted with an excess of petroleum ether, ice-cooled, and filtered to give brown crystals of the cyclized product (0.8 g; 92%) mp 134–136°C; ir ($CHCl_3$): 2940, 2840, 1660, 1610, 1595, 1500, 1464, 1408, 1350, 1282, 1164, 1086, 1005 cm^{-1}; ^1H nmr (CF_3COOH): 3.13 (2H, t, J = 7.5 Hz, CH_2), 3.75 (3H, s, OCH_3), 3.97 (3H, s, OCH_3), 4.05 (6H, s, OCH_3), 4.18 (2H, t, J = 7.5 Hz, CH_2), 5.35 (2H, s, CH_2), 6.55 (1H, s, Ar-H), 7.18–7.55 (7H, m, Ar-H) ppm.

1,2,3,10b-Tetrahydro-5,6,8,9,-tetramethoxy-1-benzylindeno-[1,2,3-ij]isoquinoline **6**

To a stirred solution of the quarternary salt **19** (0.451 g; 0.001 mol) in EtOH (10 mL) was added $NaBH_4$ (0.114 g; 0.003 mol) in small portions (10 min) and the solution further stirred for 2.5 h at room temperature. During this time the deep brown reaction mixture became faint yellow. The excess of $NaBH_4$ was destroyed by adding glacial acetic acid, the CH_3OH evaporated, and the residue treated with H_2O (5 mL), basified to pH >10 with NaOH, and extracted with CH_2Cl_2. The combined CH_2Cl_2 extract was washed with brine and dried. Removal of the solvent furnished the required indenotetrahydroisoquinoline as a gum (0.30 g; 74%). The base was recovered from the purified hydrochloride (*vide infra*) before spectroscopic analysis; ir ($CHCl_3$): 2940, 2840, 1610, 1500, 1468, 1400, 1290, 1108, 1090, 1002 cm^{-1}; ^1H nmr (250 MHz): 2.66–2.94 (2H, m, H's at C-3), 3.15–3.32 (2H, m, H's at C-2), 3.35 (2H, s, N—CH_2—Ph), 3.90 (3H, s, OCH_3), 3.93 (3H, s, OCH_3), 4.01 (3H, s, OCH_3), 4.02 (3H, s, OCH_3), 4.77 (1H, s, H-10b), 6.59 (1H, s, Ar-H), 7.17 (1H, s, Ar-H), 7.20–7.35 (5H, m, Ar-H), 7.59 (1H, s, Ar-H) ppm; ms *m/z*: 417 (M^+, 65%), 416 (52%), 402 (37%), 387 (29%), 386 (64%), 325 (11%), 298 (43%), 283 (15%), 91 (100%), 65 (47%). *Mol. Wt.* calcd. for $C_{26}H_{27}NO_4$: 417.194; found (hrms): 417.194. The free base was converted to its hydrochloride in ether solution and recrystallized from ethanol, mp 185–187°C. The hydrochloride was highly solvated and failed to give satisfactory elemental analysis even after prolonged drying at 70°C and 1.0 Torr. In the nmr (250 MHz) spectrum, peaks were present at 1.23 (t) and 3.72 (q) attributed to ethanol of solvation and at 1.58 (s) attributed to water of solvation. The signals attributed to the compound itself appeared as follows: 2.80–3.45 (4H, complex m, H's at C-2 and C-3), 3.7 (1H, underlying CH_2 of EtOH, one H from the N—*CH*$_2$—Ph), 3.94 (3H, s, OCH_3), 3.98 (3H, s, OCH_3), 4.02 (6H, s, 2 × OCH_3), 4.11–4.18 (1H, dd, one H from N—*CH*$_2$Ph), 5.41 (1H, s, H-10b), 6.61 (1H, s, Ar-H), 7.35 and 7.58 (5H, 2 multiplets, aromatic H's of benzyl group), 7.50 (1H, s, Ar-H), 8.31 (1H, s, Ar-H), 13.85 (1H, bs, NH) ppm.

Acknowledgement

We thank the Natural Sciences and Engineering Research Council of Canada for financial support of this work.

1. O. KRUBER. Chem. Ber. **82**, 199 (1949).
2. N. CAMPBELL and K. F. REID. J. Chem. Soc. 4743 (1958).
3. M. P. CAVA, K. T. BUCK, and A. I. DA ROCHA. J. Am. Chem. Soc. **94**, 5931 (1972); M. P. CAVA, K. T. BUCK, I. NOGUCHI, M. SRINIVASAN, M. G. RAO, and A. I. DA ROCHA. Tetrahedron, **31**, 1667 (1975).
4. R. HULS, J. GASPERS, and R. WARIN. Bull. Soc. R. Sci. Liege, **45**, 40 (1976).
5. M. D. MENACHERY and M. P. CAVA. J. Nat. Prod. **44**, 320 (1981).
6. T. J. SCHWAN. U. S. Patent No. 3,971, 788, July 27, 1976; Chem. Abstr. **85**, 192589y. (1976).
7. T. KAMETANI, S. SHIBUYA, R. CHARUBALA, M. S. PREMILA, and B. R. PAI. Heterocycles, **3**, 439 (1975).
8. Y. AHMAD and D. H. HEY. J. Chem. Soc. 3882 (1961).
9. L. R. DYALL and C. J. PULLIN. Aust. J. Chem. **32**, 345 (1979).
10. C. R. ELLEFSON. J. Org. Chem. **44**, 1533 (1979).
11. L. N. PRIDGEN. J. Heterocycl. Chem. **17**, 1289 (1980).
12. H. HARA, O. HOSHINO, and B. UMEZAWA. Heterocycles, **15**, 911 (1981).
13. A. I. MEYERS and E. D. MIHELICH. J. Am. Chem. Soc. **97**, 7383 (1975).
14. I. C. NORDIN. J. Heterocycl. Chem. **3**, 531 (1966).
15. M. J. BEWIS, E. J. FORBES, and B. C. UFF. Tetrahedron, **25**, 1585 (1969).
16. R. H. F. MANSKE and M. KULKA. Can. J. Res. B, **27**, 161 (1949).
17. M. J. BEWIS, E. J. FORBES, N. N. NAIK, and B. C. UFF. Tetrahedron, **27**, 1253 (1971).
18. J. M. BOBBIT, J. M. KIELY, K. L. KHANNA, and R. EBERMAN. J. Org. Chem. **30**, 2247 (1965).
19. A. J. BIRCH, A. H. JACKSON, and P. V. R. SHANNON. J. Chem. Soc. Perkin Trans. I, 2185 (1974).
20. T. A. HENRY and T. M. SHARP. J. Chem. Soc. 2279 (1930).
21. L. C. RAIFORD and R. P. PERRY. J. Org. Chem. **7**, 355 (1942).
22. H. W. GSCHWEND and A. HAMDEN. J. Org. Chem. **40**, 2008 (1975).
23. A. I. MEYERS and E. D. MIHELICH. J. Org. Chem. **40**, 3158 (1975).
24. A. I. MEYERS, D. L. TEMPLE, R. L. NOLEN, and E. D. MIHELICH. J. Org. Chem. **39**, 2778 (1974).
25. M. SHAMMA. The Isoquinoline Alkaloids. Academic Press, New York. 1972. Chapt. 10, and references therein.
26. W. C. STILL, M. KAHN, and A. MITRA. J. Org. Chem. **43**, 2923 (1978).
27. D. E. JANSSEN and C. V. WILSON. Org. Synth. Coll. Vol. IV, *Edited by* N. Rabjohn. Wiley, New York. 1962. p. 547.
28. H. MEERWEIN. Org. Synth. Coll. Vol. V, *Edited by* H. E. Baumgarten. Wiley, New York. 1973 p. 1080.
29. E. BROWN and J. P. ROBIN. Tetrahedron Lett. 2015 (1977).

Can. J. Chem. Downloaded from www.nrcresearchpress.com by 210.87.254.5 on 09/06/12
For personal use only.

Theory for electronic Raman activity of chlorophyll dimers[1]

L. V. HALEY AND J. A. KONINGSTEIN
The Ottawa-Carleton Graduate Institute for Research and Graduate Studies in Chemistry, Carleton University, Ottawa, Ont., Canada K1S 5B6

Received April 27, 1982

L. V. HALEY and J. A. KONINGSTEIN. Can. J. Chem. **61**, 14 (1983).

We present a modification of a supermolecule model of a general chlorophyll dimer, and calculate the excited state electronic Raman selection rules between the various singlet states. The model utilizes the electronic part of the total wavefunction within the strong intermolecular coupling scheme. Under this condition and the neglect of underlying orbitals, the electronic wave function of the dimer is reduced to a four orbital function with each monomer contributing one HOMO and one LUMO. Using a Hückel type molecular orbital calculation, the one electron orbital energies and coefficients of the ground and excited state wavefunctions of the dimer are obtained and are shown to depend explicitly on the ground and excited state intermolecular interaction terms. The resulting Raman activity calculation between the various excited state configurations yields two types of tensor elements: (*1*) contains only coordinates of the individual monomer α_1 (molecule 1) and α_2 (molecule 2) and are called spatially localized elements and (*2*) labelled spatially delocalized and contains coordinates of both monomer molecules simultaneously (α_3 and α_4).

L. V. HALEY et J. A. KONINGSTEIN. Can. J. Chem. **61**, 14 (1983).

Nous présentons une modification d'un modèle de super molécule pour un dimère général de la chlorophylle et nous calculons les règles de sélection Raman électronique de l'état excité entre les divers états singulets. Le modèle utilise la partie électronique de la fonction d'onde globale à l'intérieur du schéma de couplage intermoléculaire fort. Dans ces conditions et en négligeant les orbitales soulignées, on réduit la fonction d'onde électronique du dimère à 4 fonctions d'orbitales; chaque monomère contribuant une fonction HOMO et une base vacante. Faisant appel à un calcul d'orbitale moléculaire de type Hückel, on a obtenu les énergies de l'orbitale à un électron et les coefficients des fonctions d'onde des états fondamental et excité du dimère et on montre qu'elles dépendent explicitement des termes de l'interaction intermoléculaire des états fondamental et excité. Le calcul de l'activité Raman résultant entre les diverses configurations de l'état excité donne deux types d'éléments de tension: (*1*) il contient uniquement les coordonnées du monomère individuel α_1 (molécule 1) et α_2 (molécule 2) et on les appelle des éléments localisés spatialement et (*2*) des éléments marqués délocalisés spatialement qui contiennent simultanément les coordonnées des deux monomères (α_3 et α_4).

[Traduit par le journal]

I. Introduction

In the past, laser-induced electronic Raman transitions have been induced and recorded from many types of systems like rare earth (1) or transition metal ions (2) in solids, of molecules (3) or molecular complexes (4) and recently also of optical-pumped excited electronic states (5). The selection rules — and in some cases the theory (6) for the intensity (3, 6) — of the electronic Raman effect are well understood and in this paper we consider the case of an electronic Raman effect between excited states of chlorophyll dimers. The structure of such dimers is dynamic and monomeric chlorophyll molecules assume the roles of donor and acceptors (7). The frequency associated with the change in roles is smaller than the duration of a Raman transition, hence one expects a well-defined light scattering spectrum. Using time-resolved fluorescence spectroscopy, an insight has been obtained of the excited state separation of a chlorophyll dimer in pyridine (8). An energy level diagram (9, 10) of the excited states of dimers has been published; however, in the present work a more complete analysis is made. The position of excited state discussed here is based on various excited state configurations which arise from the occupation of orbitals, related to the highest occupied and lowest unoccupied molecular orbital levels of monomeric chlorophyll molecules. A series of excited level electronic Raman transitions are predicted and an insight is obtained of the selection rules. The lifetime of these excited states is such that sufficient populations can be created during optical pumping with pulsed lasers. That part of the laser radiation not used for pumping may then be employed as a Raman probe to induce the electronic transitions, this method has been shown to yield good results for other systems (11–14).

II. Ground and excited state wavefunctions for chlorophyll dimers

Presently, there are several publications containing information on the process which governs the intensity of the fluorescence transitions of dimeric Chl *a* in solution (9, 10). These transitions originate from a number of excited states, and they are derived from various possible excited electronic configurations. In the present study, we are primarily concerned with Raman scattering between some of these excited states and the details of the electronic scattering process will be given in the next section.

Our starting point is centered around the occupation of the two sets of orbitals of a general dimer which are related to the highest occupied molecular orbital (HOMO) and the lowest unoccupied molecular orbital levels (LUMO) of the monomer (see Fig. 1*a*) where the individual chromophor molecules 1 and 2 are not necessarily identical. The monomer levels for molecule 1 are separated by Δm cm^{-1}, and for molecule 2, the splitting is $\Delta m'$ cm^{-1}. In the dimer, the orbital splitting is δ_g for the ground state and δ_{ex}

[1]Research supported by the Natural Sciences and Engineering Research Council of Canada.

0008-4042/83/010014-07$01.00/0
©1983 National Research Council of Canada/Conseil national de recherches du Canada

Can. J. Chem. Downloaded from www.nrcresearchpress.com by 210.87.254.40 on 09/06/12
For personal use only.

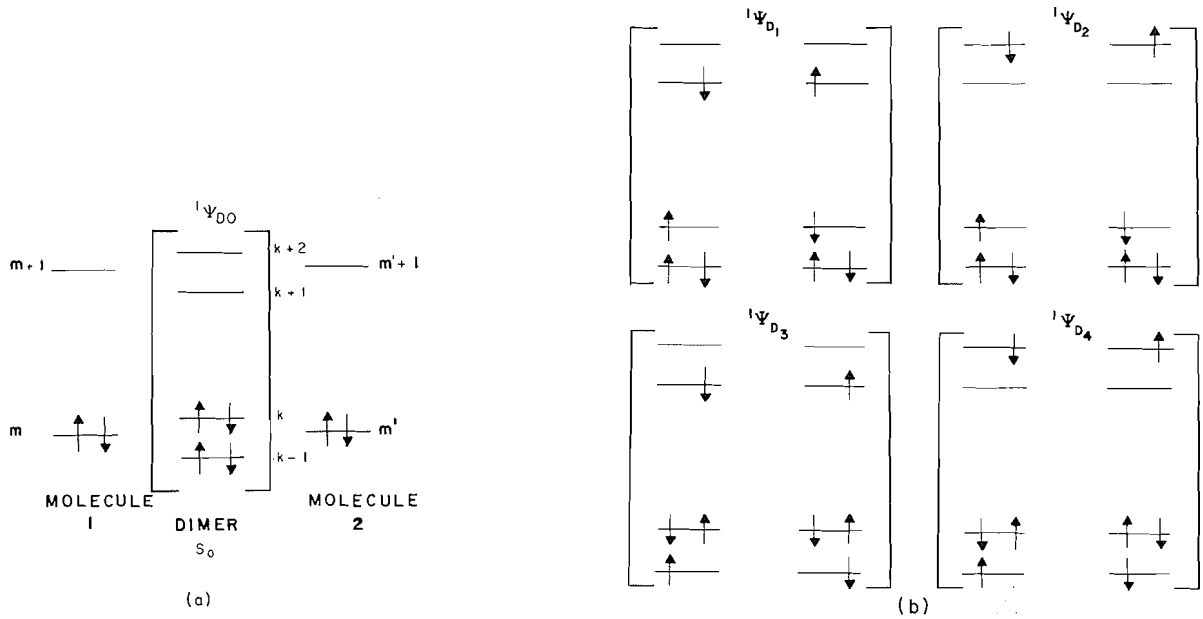

FIG. 1. (*a*) Ground state orbital schematic of a four orbital chlorophyll dimer model, (m, m') and (m + 1, m' + 1) are the monomer HOMO and LUMO respectively. $k-1$, k, k + 1, and k + 2 represent the HOMO − 1, HOMO, LUMO, and LUMO + 1 of the dimer respectively. (*b*) Configuration of the various excited states of the dimer. Orbital labelling is the same as in (*a*).

for the excited state (see below for definitions of δ_g and δ_{ex}). In general, the $S_1 \rightarrow S_0$ fluorescence of the monomer occurs in the 660–730 nm spectral region (8, 15), and with $\delta_g \neq \delta_{ex} \ll \Delta m, \Delta m'$ cm^{-1}, we expect the fluorescence of the dimer also to occur in this region. It is well known that dimeric Chl *a* units assume the role of donor and acceptor molecules with a dynamic structure (7), and we assume this phenomenon is also active in the general case. The frequency of this process is slower than the duration of the Raman transition between electronic levels of the dimer, consequently the dimer may be considered as an asymmetric donor–acceptor molecule.

In the theory of the transfer of electronic energy between two or more molecules (16), the amount of interaction between the molecules is characterized by an intermolecular potential energy term. The size of this term determines the strength of the coupling among the molecules. For chlorophyll molecules with an intermolecular distance less than or equal to the usual van der Waals contact distance (3.4–3.6 Å) (17), a supermolecule formation can be expected with a large interaction between the monomer molecules. In the exciton model theory (16), this situation would be the strong interaction or strong coupling limiting case. Under these conditions and within the Born–Oppenheimer approximation, the wave function for the singlet ground state of the dimer is

$$[1] \quad {}^1\Psi_{ev} = {}^1\Psi_{D0}\,\theta_v$$

where $^1\Psi_{D0}$ is the electronic wave function and θ_v the vibrational wave function. In the present study, we will only consider the electronic part of the total wave function for the derivation of the selection rules for the Raman transitions.

Recent *ab initio* calculations (18) predict a π type HOMO for chlorophyllide *a* and related molecules, therefore we can reduce the formal $2N_T$ electron description of the dimer where N_T is the total number of π electrons in a monomer molecule to a four π electron problem if we assume that neglected molecular orbitals are not significantly involved in the stabilization of the dimer. Under this condition, the electronic ground state wave function for the dimer is

$$[2] \quad {}^1\Psi_{D0} = N_0 \mid \psi_{k-1}\bar{\psi}_{k-1}\psi_k\bar{\psi}_k \mid$$

where N_0 is a normalization constant and the subscripts k and $k-1$ are the HOMO and HOMO − 1 respectively. Since the individual chlorophyll molecules of the dimer are highly conjugated systems of carbon, nitrogen, and oxygen atoms, a simple Hückel type model will be adequate for the present calculation.

The monomer HOMO's ϕ_m and $\phi_{m'}$, denoted as (m) and (m') in Fig. 1*a*, are taken to be Hückel-type molecular orbitals with $\langle\phi_m \mid \phi_{m'}\rangle = 0$. In order to calculate the dimer molecular orbitals ψ_k and ψ_{k-1} in a modification of a supermolecule model (19), the following effective one electron Hamiltonian is used:

$$[3] \quad \hat{\mathcal{H}} = \hat{\mathcal{H}}_1 + \hat{\mathcal{H}}_2$$

where $\hat{\mathcal{H}}_1$ and $\hat{\mathcal{H}}_2$ are the monomer Hamiltonians. Diagonalization of the appropriate secular equation yields the eigenvalue results

$$[4] \quad \epsilon'_D(\pm) = \left(\frac{\epsilon_m + \epsilon_{m'}}{2}\right) \pm \frac{1}{2}\sqrt{(\epsilon_m - \epsilon_{m'})^2 + 4H^2_{m,m'}}$$

where ϵ_m and $\epsilon_{m'}$ are the one electron orbital energies of molecules 1 and 2 respectively, and $H_{m,m'}$ is the one electron intermolecular interaction term. In terms of the notation given in eq. [2], the eigenvalue for the HOMO of the dimer is $\epsilon'_D(+) = \epsilon_k$ with the eigenvector

Can. J. Chem. Downloaded from www.nrcresearchpress.com by 210.87.254.40 on 09/06/12
For personal use only.

[5] $$\psi_k = \frac{1}{\sqrt{2}}[{}^gC_{11}\phi_m + {}^gC_{12}\phi_{m'}]$$

with

[6] $${}^gC_{11} = \left\{1 + \frac{(\epsilon_m - \epsilon_{m'})}{[(\epsilon_m - \epsilon_{m'})^2 + 4H^2_{m,m'}]^{1/2}}\right\}^{1/2}$$

[7] $${}^gC_{12} = \left\{1 - \frac{(\epsilon_m - \epsilon_{m'})}{[(\epsilon_m - \epsilon_{m'})^2 + 4H^2_{m,m'}]^{1/2}}\right\}^{1/2}$$

For the HOMO − 1, $\epsilon'_D(-) = \epsilon_{k-1}$ and the resulting eigenvector is

[8] $$\psi_{k-1} = \frac{1}{\sqrt{2}}[{}^gC_{21}\phi_m - {}^gC_{22}\phi_{m'}]$$

and

[9] $${}^gC_{21} = \left\{1 - \frac{(\epsilon_m - \epsilon_{m'})}{[(\epsilon_m - \epsilon_{m'})^2 + 4H^2_{m,m'}]^{1/2}}\right\}^{1/2}$$

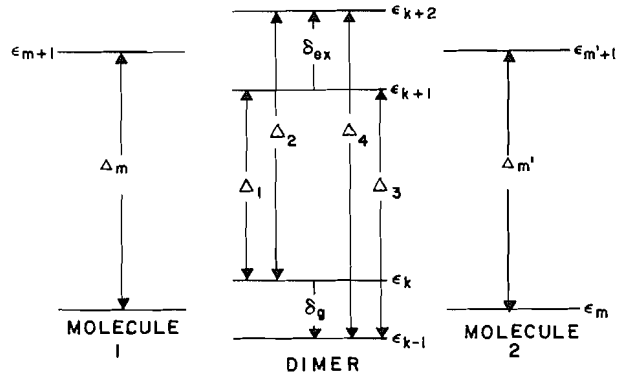

FIG. 2. One electron energy schematic for the monomer and dimer molecules. Terms are defined in the text.

[10] $${}^gC_{22} = \left\{1 + \frac{(\epsilon_m - \epsilon_{m'})}{[(\epsilon_m - \epsilon_{m'})^2 + 4H^2_{m,m'}]^{1/2}}\right\}^{1/2}$$

To obtain the LUMO and LUMO + 1 of the dimer, let the monomer levels $(m + 1)$ and $(m' + 1)$ in Fig. 1*a* be represented by the Hückel type wave functions ϕ_{m+1} and $\phi_{m'+1}$ respectively. Also, $\langle\phi_{m+1}|\phi_{m'+1}\rangle = 0$. Using eq. [3], the ϕ_{m+1} and $\phi_{m'+1}$ wave functions, and standard matrix algebra, we obtain the following eigenvalues:

[11] $$\epsilon''_D(\pm) = \left(\frac{\epsilon_{m+1} + \epsilon_{m'+1}}{2}\right) \pm \frac{1}{2}\sqrt{(\epsilon_{m+1} - \epsilon_{m'+1})^2 + 4H^2_{m+1,m'+1}}$$

The corresponding dimer wave functions of $\epsilon''_D(-) = \epsilon_{k+1}$ and $\epsilon''_D(+) = \epsilon_{k+2}$ (LUMO and LUMO + 1 respectively) are

[12] $$\psi_{k+1} = \frac{1}{\sqrt{2}}[{}^cC_{11}\phi_{m+1} - {}^cC_{12}\phi_{m'+1}]$$

[13] $$\psi_{k+2} = \frac{1}{\sqrt{2}}[{}^cC_{21}\phi_{m+1} + {}^cC_{22}\phi_{m'+1}]$$

with

[14] $${}^cC_{11} = {}^cC_{22} = \left\{1 - \frac{(\epsilon_{m+1} - \epsilon_{m'-1})}{[(\epsilon_{m+1} - \epsilon_{m'+1})^2 + 4H^2_{m+1,m'+1}]^{1/2}}\right\}^{1/2}$$

[15] $${}^cC_{12} = {}^cC_{21} = \left\{1 + \frac{(\epsilon_{m+1} - \epsilon_{m'+1})}{[(\epsilon_{m+1} - \epsilon_{m'+1})^2 + 4H^2_{m+1,m'+1}]^{1/2}}\right\}^{1/2}$$

Using the four electron model described in the above calculation, the expression for the orbital splitting between ψ_k and ψ_{k-1} is found to be

[16] $$\delta_g = \sqrt{(\epsilon_m - \epsilon_{m'})^2 + 4H^2_{m,m'}}$$

and

[17] $$\delta_{ex} = \sqrt{(\epsilon_{m+1} - \epsilon_{m'+1})^2 + 4H^2_{m+1,m'+1}}$$

for the ψ_{k+1} and ψ_{k+2} orbital splitting. In the present discussion, we assume that the $\delta_{ex} > \delta_g$ due to a geometry change of the chlorophyll molecules in their excited state. The above results are collected and shown in Fig. 2.

Within the four orbital model of chlorophyll dimers, four single excited state configurations can be derived from the orbitals shown in Fig. 1*a*. They give rise to four state functions:

[18] $${}^1\Psi_{D1} = N_1[\,|\,\psi_{k-1}\bar{\psi}_{k-1}\psi_k\bar{\psi}_{k+1}\,| - |\,\psi_{k-1}\bar{\psi}_{k-1}\bar{\psi}_k\psi_{k+1}\,|\,]$$

[19] $${}^1\Psi_{D2} = N_1[\,|\,\psi_{k-1}\bar{\psi}_{k-1}\psi_k\bar{\psi}_{k+2}\,| - |\,\psi_{k-1}\bar{\psi}_{k-1}\bar{\psi}_k\psi_{k+2}\,|\,]$$

[20] $${}^1\Psi_{D3} = N_1[\,|\,\psi_{k-1}\bar{\psi}_k\psi_k\bar{\psi}_{k+1}\,| - |\,\bar{\psi}_{k-1}\psi_k\bar{\psi}_k\psi_{k+1}\,|\,]$$

[21] $${}^1\Psi_{D4} = N_1[\,|\,\psi_{k-1}\bar{\psi}_k\psi_k\bar{\psi}_{k+2}\,| - |\,\bar{\psi}_{k-1}\psi_k\bar{\psi}_k\psi_{k+2}\,|\,]$$

Schematic representations of the excited singlet state configurations are shown in Fig. 1*b*.

Before discussing the selection rules for the Raman processes in the dimer system, the calculation of the excitation energies and energy differences among the excited state configurations will be necessary. Four excitation energies can be found to arise from

Can. J. Chem. Downloaded from www.nrcresearchpress.com by 210.87.254.40 on 09/06/12
For personal use only.

the ground state level to the levels described by the wave functions given in eqs. [18]–[21]. For the excitation energy between $^1\Psi_{D1}$ and $^1\Psi_{D0}$, we can use the following calculation

[22] $\langle {}^1\Psi_{D1} \mid \hat{\mathcal{H}} \mid {}^1\Psi_{D1}\rangle - \langle {}^1\Psi_{D0} \mid \hat{\mathcal{H}} \mid {}^1\Psi_{D0}\rangle = \epsilon_{k+1} - \epsilon_k = \Delta_1$

where $\epsilon_{k+1}$and ϵ_k are the one electron energies given by eqs. [4] and [11]. The analogous expressions for the remaining transitions are

[23] $\langle {}^1\Psi_{D2} \mid \hat{\mathcal{H}} \mid {}^1\Psi_{D2}\rangle - \langle {}^1\Psi_{D0} \mid \hat{\mathcal{H}} \mid {}^1\Psi_{D0}\rangle = \epsilon_{k+2} - \epsilon_k = \Delta_2$

[24] $\langle {}^1\Psi_{D3} \mid \hat{\mathcal{H}} \mid {}^1\Psi_{D3}\rangle - \langle {}^1\Psi_{D0} \mid \hat{\mathcal{H}} \mid {}^1\Psi_{D0}\rangle = \epsilon_{k+1} - \epsilon_{k-1} = \Delta_3$

and

[25] $\langle {}^1\Psi_{D4} \mid \hat{\mathcal{H}} \mid {}^1\Psi_{D4}\rangle - \langle {}^1\Psi_{D0} \mid \hat{\mathcal{H}} \mid {}^1\Psi_{D0}\rangle = \epsilon_{k+2} - \epsilon_{k-1} = \Delta_4$

If eqs. [4] and [11] are substituted into eqs. [22]–[25], the excitation energies can be obtained in terms of the individual monomer transition energies, ground and excited state interaction energy terms. We find that

[26] $\Delta_1 = \frac{1}{2}[\Delta m + \Delta m'] - \frac{1}{2}[\delta_{ex} + \delta_g]$

[27] $\Delta_2 = \frac{1}{2}[\Delta m + \Delta m'] + \frac{1}{2}[\delta_{ex} - \delta_g]$

[28] $\Delta_3 = \frac{1}{2}[\Delta m + \Delta m'] - \frac{1}{2}[\delta_{ex} - \delta_g]$

[29] $\Delta_4 = \frac{1}{2}[\Delta m + \Delta m'] + \frac{1}{2}[\delta_{ex} + \delta_g]$

where

[30] $\Delta m = \epsilon_{m+1} - \epsilon_m$

[31] $\Delta m' = \epsilon_{m'+1} - \epsilon_m$

The ϵ_{m+1}, $\epsilon_{m'+1}$, ϵ_m, and $\epsilon_{m'}$ are the one electron orbital energies of the LUMO and HOMO of the respective monomers. With the given condition of $\delta_{ex} > \delta_g$, the following order is found $\Delta_4 > \Delta_2 > \Delta_3 > \Delta_1$.

Using eqs. [26]–[31], the energy differences between the excited states can be calculated and the six differences are

[32] $\Delta_4 - \Delta_3 = \delta_{ex}$

[33] $\Delta_2 - \Delta_1 = \delta_{ex}$

[34] $\Delta_4 - \Delta_2 = \delta_g$

[35] $\Delta_3 - \Delta_1 = \delta_g$

[36] $\Delta_4 - \Delta_1 = \delta_{ex} + \delta_g$

[37] $\Delta_2 - \Delta_3 = \delta_{ex} - \delta_g$

The results shown in eqs. [32]–[37] predict four first order Raman transitions eqs. [32]–[35], with accidental degeneracies encountered in the difference pairs eqs. [32], [33] and eqs. [34], [35]. The sum and difference of the interaction energies in eqs. [36] and [37] will be observed as second order Raman transitions; consequently we will not consider this type of transition in the following discussions.

III. Theory for excited state Raman scattering

Let us assume the following experimental conditions: (*1*) a chlorophyll dimer solution with a concentration of approximately 10^{-4} *M* is prepared for irradiation with a pulsed laser; (*2*) the laser radiation has a wavelength and sufficient power necessary to populate the first singlet state $^1\Psi_{D1}$; and (*3*) within the time of the laser pulse, there is the necessary energy remaining to produce a light scattering process among the excited states. Once the above conditions have been satisfied, the Raman spectrum of the chlorophyll dimer can be observed if the Raman activity between the excited states is allowed. To determine the electronic Raman activity, we start with an expression similar to that of the case for resonance enhancement of vibrational Raman scattering (20). The resulting expectation value of the dimer Raman operator α_D between the $^1\Psi_{D1}$ and $^1\Psi_{D2}$ states is

$$\langle {}^1\Psi_{D1} \mid \hat{\alpha}_D \mid {}^1\Psi_{D2}\rangle$$

where

[38] $$\hat{\alpha}_D = \frac{1}{h}\sum_{s_D}\left\{\frac{[\,\langle \hat{r}_\sigma(D) \mid s_D\rangle\langle s_D \mid \hat{r}_\rho(D)\,\rangle]}{\nu_{s_D} - \nu_0} + \frac{[\rho \leftrightarrow \sigma]}{\nu_{s_D} + \nu_0}\right.$$

for the non-resonant case. Here $\hat{r}_\sigma(D)$ and $\hat{r}_\rho(D)$ are the dimer dipole moment operators and s_D are the virtual state wave functions of the dimer. If we let

[39] $\hat{r}_\sigma(D) = \hat{r}_\sigma + \hat{r}'_\sigma$

Can. J. Chem. Downloaded from www.nrcresearchpress.com by 210.87.254.40 on 09/06/12
For personal use only.

[40] $\hat{r}_\rho(D) = \hat{r}_\rho + \hat{r}'_\rho$

where the dipole moment operators $(\hat{r}_\sigma, \hat{r}_\rho)$ and $(\hat{r}'_\sigma, \hat{r}'_\rho)$ are defined with respect to the coordinates of molecule 1 and molecule 2 of the dimer respectively. Substitution of eqs. [39] and [40] into eq. [38] yields

$$[41]\quad \hat{\alpha}_D = \frac{1}{h}\sum_{s_D}\frac{1}{\nu_{s_D} - \nu_0}\Big\{[\,|\,\hat{r}_\sigma\,|\,s_D\rangle\langle s_D\,|\,\hat{r}_\rho\,|\; + \;|\,\hat{r}'_\sigma\,|\,s_D\rangle\langle s_D\,|\,\hat{r}'_\rho\,|\; + \;|\,\hat{r}_\sigma\,|\,s_D\rangle\langle s_D\,|\,\hat{r}'_\rho\,|$$

$$+\;|\,\hat{r}'_\sigma\,|\,s_D\rangle\langle s_D\,|\,\hat{r}_\rho\,|\,] + [\rho\leftrightarrow\sigma]\Big\}$$

therefore, using eqs. [18], [19], and [41],

$$[42]\quad \langle {}^1\Psi_{D1}\,|\,\hat{\alpha}_D\,|\,{}^1\Psi_{D2}\rangle = K_1[\langle\psi_{k+1}\,|\,\hat{\alpha}_1\,|\,\psi_{k+2}\rangle + \langle\psi_{k+1}\,|\,\hat{\alpha}_2\,|\,\psi_{k+2}\rangle + \langle\psi_{k+1}\,|\,\hat{\alpha}_3\,|\,\psi_{k+2}\rangle + \langle\psi_{k+1}\,|\,\hat{\alpha}_4\,|\,\psi_{k+2}\rangle]$$

where K_1 is a constant and

$$[43]\quad \langle\psi_{k+1}\,|\,\hat{\alpha}_1\,|\,\psi_{k+2}\rangle = \frac{1}{h}\sum_{s_D}\left\{\frac{[\langle k+1\,|\,\hat{r}_\sigma\,|\,s_D\rangle\langle s_D\,|\,\hat{r}_\rho\,|\,k+2\rangle]}{\nu_s - \nu_0} + \frac{[\rho\leftrightarrow\sigma]}{\nu_s + \nu_0}\right\}$$

$$[44]\quad \langle\psi_{k+1}\,|\,\hat{\alpha}_2\,|\,\psi_{k+2}\rangle = \frac{1}{h}\sum_{s_D}\left\{\frac{[\langle k+1\,|\,\hat{r}'_\sigma\,|\,s_D\rangle\langle s_D\,|\,\hat{r}'_\rho\,|\,k+2\rangle]}{\nu_s - \nu_0} + \frac{[\rho\leftrightarrow\sigma]}{\nu_s + \nu_0}\right\}$$

$$[45]\quad \langle\psi_{k+1}\,|\,\hat{\alpha}_3\,|\,\psi_{k+2}\rangle = \frac{1}{h}\sum_{s_D}\left\{\frac{[\langle k+1\,|\,\hat{r}_\sigma\,|\,s_D\rangle\langle s_D\,|\,\hat{r}'_\rho\,|\,k+2\rangle]}{\nu_s - \nu_0} + \frac{[\rho\leftrightarrow\sigma]}{\nu_s + \nu_0}\right\}$$

$$[46]\quad \langle\psi_{k+1}\,|\,\hat{\alpha}_4\,|\,\psi_{k+2}\rangle = \frac{1}{h}\sum_{s_D}\left\{\frac{[\langle k+1\,|\,\hat{r}'_\sigma\,|\,s_D\rangle\langle s_D\,|\,\hat{r}_\rho\,|\,k+2\rangle]}{\nu_s - \nu_0} + \frac{[\rho\leftrightarrow\sigma]}{\nu_s + \nu_0}\right\}$$

If the dimer orbitals ψ_{k+1} and ψ_{k+2} in eqs. [43]–[46] are replaced by their equivalent in terms of monomer orbitals (eqs. [12] and [13]), we obtain

$$[47]\quad \langle\psi_{k+1}\,|\,\hat{\alpha}_1\,|\,\psi_{k+2}\rangle = \frac{1}{2}\,{}^cC_{11}\,{}^cC_{21}\langle\phi_{m+1}\,|\,\hat{\alpha}_1\,|\,\phi_{m+1}\rangle$$

$$[48]\quad \langle\psi_{k+1}\,|\,\hat{\alpha}_2\,|\,\psi_{k+2}\rangle = -\frac{1}{2}\,{}^cC_{12}\,{}^cC_{22}\langle\phi_{m'+1}\,|\,\hat{\alpha}_2\,|\,\phi_{m'+1}\rangle$$

$$[49]\quad \langle\psi_{k+1}\,|\,\hat{\alpha}_3\,|\,\psi_{k+2}\rangle = \frac{1}{2}\,{}^cC_{11}\,{}^cC_{22}\langle\phi_{m+1}\,|\,\hat{\alpha}_3\,|\,\phi_{m'+1}\rangle$$

$$[50]\quad \langle\psi_{k+1}\,|\,\hat{\alpha}_4\,|\,\psi_{k+2}\rangle = -\frac{1}{2}\,{}^cC_{12}\,{}^cC_{21}\langle\phi_{m'+1}\,|\,\hat{\alpha}_4\,|\,\phi_{m+1}\rangle$$

Inspecting eqs. [41] and [47]–[50] reveals the following: (*1*) the operator $\hat{\alpha}_1$ and the monomer wave functions ϕ_{m+1} of eq. [47] are defined with respect to the coordinates of molecule 1; (*2*) similarly, the operator $\hat{\alpha}_2$ and monomer wave function $\phi_{m'+1}$ of eq. [48] contain only the coordinates of molecule 2, consequently we can identify these electronic Raman activity tensor elements as spatially localized elements; (*3*) in eqs. [49] and [50], both the operators $(\hat{\alpha}_3, \hat{\alpha}_4)$ and the wave functions $(\phi_{m'+1}, \phi_{m+1})$ contain the coordinates of molecule 1 and molecule 2 simultaneously. Hence, we can label such tensor elements as spatially delocalized. In a final form, eq. [42] is written as

$$[51]\quad \langle {}^1\Psi_{D1}\,|\,\hat{\alpha}_D\,|\,{}^1\Psi_{D2}\rangle = \frac{K_1}{2}\,[{}^cC_{11}\,{}^cC_{21}\langle\phi_{m+1}\,|\,\hat{\alpha}_1\,|\,\phi_{m+1}\rangle - {}^cC_{12}\,{}^cC_{22}\langle\phi_{m'+1}\,|\,\hat{\alpha}_2\,|\,\phi_{m'+1}\rangle + {}^cC_{11}\,{}^cC_{22}\langle\phi_{m+1}\,|\,\hat{\alpha}_3\,|\,\phi_{m'+1}\rangle$$

$$- {}^cC_{12}\,{}^cC_{21}\langle\phi_{m'+1}\,|\,\hat{\alpha}_4\,|\,\phi_{m+1}\rangle]$$

Thus eq. [51] contains four terms which contribute to the Raman activity of a general dimer and this result predicts a nonzero intensity at δ_{ex} cm^{-1} in the Raman spectrum. See Fig. 3*a* for the schematic representation of the process. Several general remarks can be made about the results of eq. [51]. First, the value of the individual coefficients ${}^cC_{11}$, ${}^cC_{21}$, ${}^cC_{12}$, and ${}^cC_{22}$ are different from unity because the individual molecules for the general case are different (i.e. Chl *a* – Chl *b*) but the products ${}^cC_{11}\,{}^cC_{21} = {}^cC_{12}\,{}^cC_{22}$ and ${}^cC_{11}\,{}^cC_{22} \neq {}^cC_{12}\,{}^cC_{21}$. Second, the most trivial case that can be encountered would be a dimer composed of identical molecules such as Chl *a* – Chl *a* and each component molecule would be placed in a mirror image configuration. Under these conditions, the coefficients ${}^cC_{11} = {}^cC_{21} = {}^cC_{12} = {}^cC_{22} = 1$ and the interaction terms $\delta_{ex} = \delta_g$. Since experimental data (7, 20) do not predict such a dimer configuration, we do not include this situation in our results in view of the fact that two of the excited states would be degenerate and configuration interaction calculations would be needed to eliminate the degeneracy. Third, the results of eq. [51] would be valid for skewed dimers as predicted from present data (7, 20), and this includes identical component molecules as well as hybrid dimers. The difference of δ_{ex} and δ_g can be expected from a geometry change in the excited state of the individual

Can. J. Chem. Downloaded from www.nrcresearchpress.com by 210.87.254.40 on 09/06/12
For personal use only.

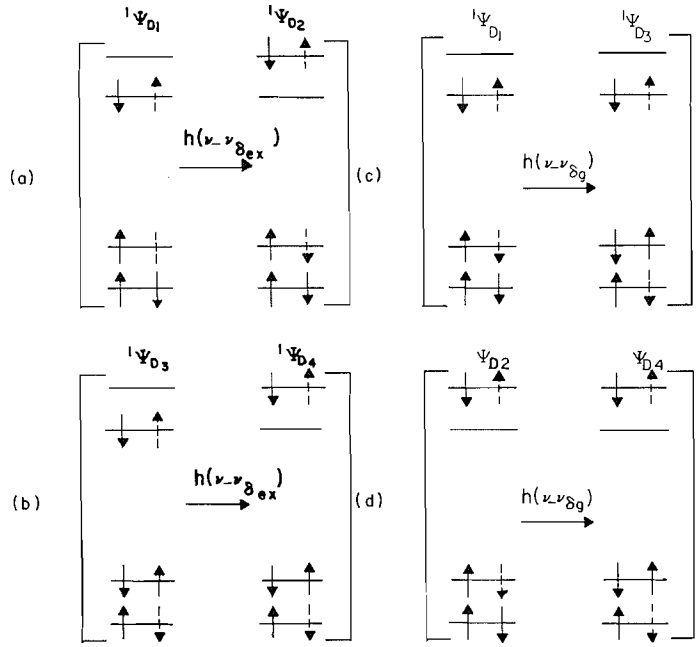

FIG. 3. (*a*, *b*) A representation of the Stokes excited state electronic Raman transitions which yield a transition at $h\nu_{\delta_{ex}}$ cm^{-1}. (*c*, *d*) Stokes transition at $h\nu_{\delta_g}$ cm^{-1}.

molecules of the dimer.

Finally, the Raman activity of the process described in eq. [51] originates from four terms: $\langle\phi_{m+1}|\hat{\alpha}_1|\phi_{m+1}\rangle$, $\langle\phi_{m'+1}|\hat{\alpha}_2|\phi_{m'+1}\rangle$, $\langle\phi_{m+1}|\hat{\alpha}_3|\phi_{m'+1}\rangle$, and $\langle\phi_{m'+1}|\hat{\alpha}_4|\phi_{m+1}\rangle$. Each of the terms is a Rayleigh-type process centered on either molecule 1 or molecule 2 (spatially localized) or between molecules 1 and 2 (spatially delocalized). In eq. [51] part of the expression for the activity is represented as a difference of the Rayleigh terms between molecule 1 and molecule 2. At first thought, these two terms would seem to cancel each other (at least for identical component molecules), but experimental data (7) show that a chlorophyll dimer exhibits an exchange of donor–acceptor roles at a frequency lower than the time scale of optical experiments. Therefore, at any point in time during the Raman experiment molecule 1 will be different from molecule 2 due to the donor–acceptor exchange, consequently $\langle\phi_{m+1}|\alpha_1|\phi_{m'+1}\rangle \neq \langle\phi_{m+1}|\alpha_2|\phi_{m'+1}\rangle$ and $\langle\phi_{m+1}|\alpha_3|\phi_{m'+1}\rangle \neq \langle\phi_{m'+1}|\alpha_4|\phi_{m+1}\rangle$. Also, a second transition $^1\Psi_{D3} \rightarrow {}^1\Psi_{D4}$ can give a Raman spectrum with a band at δ_{ex} cm^{-1} and $^1\Psi_{D3}|\alpha_D|{}^1\Psi_{D_4}\rangle$ yields the same results as eq. [51] for the selection rule. An orbital schematic for this process is shown in Fig. 3*b*.

In addition to the possibility of observing a Raman transition between states that are separated by δ_{ex} cm^{-1}, a similar calculation between the states $^1\Psi_{D1} \rightarrow {}^1\Psi_{D3}$ and $^1\Psi_{D2} \rightarrow {}^1\Psi_{D4}$ predicts a nonzero Raman activity at the frequency of δ_g cm^{-1}. Therefore,

$$[52]\quad \langle {}^1\Psi_{D1} \mid \hat{\alpha}_D \mid {}^1\Psi_{D3}\rangle = \langle {}^1\Psi_{D2} \mid \hat{\alpha}_D \mid {}^1\Psi_{D4}\rangle = \frac{K_2}{2}\,[{}^gC_{21}{}^gC_{11}\langle\phi_m \mid \hat{\alpha}_1 \mid \phi_m\rangle - {}^gC_{12}{}^gC_{22}\langle\phi_{m'} \mid \hat{\alpha}_2 \mid \phi_{m'}\rangle$$
$$+ {}^gC_{11}{}^gC_{22}\langle\phi_m \mid \hat{\alpha}_3 \mid \phi_{m'}\rangle - {}^gC_{12}{}^gC_{21}\langle\phi_{m'} \mid \hat{\alpha}_4 \mid \phi_m\rangle]$$

An inspection of the coefficients and Raman activity terms reveals that similar conditions are predicted from eq. [52] as in the above calculation of eq. [51]. Besides the obvious difference that the coefficients in eq. [52] contain the ground state interaction term, the results predict Raman activity based on Rayleigh terms which contain the HOMO's of the individual molecules. From the schematic representation of the transitions shown in Fig. 3*c* and *d*, the transitions predicted by eq. [52] can be seen to originate between the dimer orbitals ψ_{k-1} and ψ_k which have their parentage in the monomer HOMO's ϕ_m and $\phi_{m'}$. Thus, the calculation yields the expected results of depending on the spatially localized and delocalized terms.

IV. Conclusive remarks

In the present study, we have developed a model of a general chlorophyll dimer system within a modified supermolecule type of approximation. This model differs from the exciton theory model in that the present calculations yield explicitly the molecular orbitals of the dimer. The usual approach describes the dimer system only in terms of state functions. In addition, the calculations presented in sections II and III define and use the interaction energy δ_g between the HOMO and HOMO − 1 of the dimer. This specific formalism (supermolecule) was necessary to develop the selection rules for the Raman activity between excited states but it can also be used to obtain such rules governing the fluorescence transitions between all excited states and the ground state.

The inclusion of the ground state interaction energy δ_g besides the excited state interaction δ_{ex} terms results in a more complete prediction of excited state electronic (but also fluorescence) Raman transitions. The lifetime of these excited states is related to that of the monomers and for chlorophyll *in vitro* one finds that these lifetimes are in the order of nanoseconds. Such excited levels are readily populated using radiation of pulsed lasers and Raman probing can then take place with the part of the radiation not used for pumping or using another laser operating at a different wavelength. Such types of experiments may also yield information on

Can. J. Chem. Downloaded from www.nrcresearchpress.com by 210.87.254.40 on 09/06/12
For personal use only.

the position of absorption bands of the dimeric species and would allow one to distinguish a symmetric dimer from an asymmetric dimer.

1. J. A. KONINGSTEIN. J. Chem. Phys. **46**(7), 2811 (1967).
2. A. AZIMA *et al.* Chem. Phys. Lett. **7**(6), 565.
3. D. W. LEPARD. Can. J. Phys. **48**, 1664 (1970).
4. B. F. GACHTER *et al.* J. Chem. Phys. **62**(12), 4628 (1975).
5. L. V. HALEY *et al.* Chem. Phys. Lett. **54**(2), 389 (1978).
6. O. S. MORTENSEN and J. A. KONINGSTEIN. J. Chem. Phys. **48**(9), 3971 (1968).
7. J. J. KATZ and J. R. NORRIS, JR. Curr. Topics Bioenerg. **5**, 41 (1974).
8. (*a*) M. ASANO and J. A. KONINGSTEIN. Chem. Phys. **57**(1, 2), 1 (1980); (*b*) A. DE WILTON *et al.* Can. J. Chem. **60**, 2198 (1982).
9. (*a*) L. L. SHIPMAN *et al.* J. Am. Chem. Soc. **98**(25), 8222 (1976); (*b*) F. K. FONG. Appl. Phys. **6**, 151 (1975).
10. K. F. FREED. J. Am. Chem. Soc. **102**(9), 3130 (1980).
11. M. ASANO *et al.* J. Chem. Phys. **73**(2), 688 (1980).
12. G. H. ATKINSON and L. R. DOSSER. J. Chem. Phys. **72**, 2195 (1980).
13. R. F. DALLINGER and W. H. WOODRUFF. J. Am. Chem. Soc. **101**, 4391 (1979).
14. M. FOSTER and R. E. HESTER. Chem. Phys. Lett. **81**, 42 (1981).
15. (*a*) J. C. HINDMAN *et al.* Chem. Phys. Lett. **53**(1), 197 (1978); (*b*) M. J. YUEN *et al.* Photochem. Photobiol. **32**, 281 (1980).
16. M. KASHA. Rad. Res. **20**, 55 (1963).
17. G. M. MAGGIORA. Int. J. Quant. Chem. **16**, 331 (1979).
18. J. D. PETKE *et al.* Photochem. Photobiol. **30**, 203 (1979).
19. A. K. CHANDRA and E. C. LIM. J. Chem. Phys. **48**(6), 2589 (1968).
20. I. TOBIAS. J. Chem. Phys. **75**(10), 5210 (1981).

Can. J. Chem. Downloaded from www.nrcresearchpress.com by 210.87.254.40 on 09/06/12
For personal use only.

Synthèse et étude chimique préliminaire des pentadiényl-2,4-phosphines

CATHERINE C. SANTINI ET FRANÇOIS MATHEY
Laboratoire CNRS–SNPE, 2–8 rue Henry Dunant, 94320 Thiais, France

Reçu le 9 juin 1982

CATHERINE C. SANTINI et FRANÇOIS MATHEY. Can. J. Chem. **61**, 21 (1983).

La réaction du magnésien de l'iodure de méthyle avec un oxa-1-phospha-2-cycloheptadiène-4,6 fournit facilement un oxyde de pentadiényl-2,4-phosphine après deux étapes intermédiaires conventionnelles. La phosphine correspondante peut être obtenue par réduction directe de l'oxyde au trichlorosilane ou par réduction–complexation du sulfure correspondant par le nickelocène. Elle ne semble pas pouvoir jouer le rôle de chélatant diène-phosphore pour un métal par suite de facteurs stériques. L'oxyde est un précurseur valable pour les triènes conjugués par réaction de Wittig–Horner avec un dérivé carbonylé.

CATHERINE C. SANTINI and FRANÇOIS MATHEY. Can. J. Chem. **61**, 21 (1983).

A penta-2,4-dienylphosphine oxide is easily obtained by reaction of methylmagnesium iodide with 1-oxa-2-phosphacyclohepta-4,6-diene followed by two more intermediate steps. The corresponding phosphine may be obtained either by trichlorosilane reduction of the oxide or nickelocene reduction–complexation of the sulfide. It seems that the dienic part of penta-2,4-dienylphosphines cannot be involved in a η^4-complexation for steric reasons. The oxides are valuable precursors for conjugated trienes through Wittig–Horner reactions with carbonyl compounds.

Introduction

Depuis quelques années nous avons lancé un programme d'investigation systématique sur la synthèse et les propriétés coordinantes des diénylphosphines de structure générale

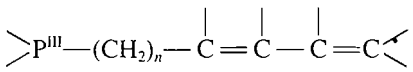

Nous avons ainsi préparé les butadiényl-1,3-phosphines de stéréochimie *E* (1) aptes à se coordonner sur deux centres métalliques disposés à une distance de l'ordre de 3,5 Å convenable pour l'activation bimétallique de petites molécules (2). Nous avons également préparé les hexadiényl-3,5-phosphines de stéréochimie *Z* (3) théoriquement capables de chélater un métal entre le phosphore trivalent et le diène. La longueur et la difficulté de cette dernière synthèse nous ont toutefois interdit l'étude systématique des propriétés coordinantes des phosphines correspondantes. Recherchant toujours un chélatant potentiel diène-phosphore trivalent, nous décrivons maintenant la préparation et quelques propriétés des pentadiényl-2,4-phosphines de stéréochimie *Z* d'accès beaucoup plus facile.

Synthèse des pentadiényl-2,4-phosphines

Nous avons découvert il y a quelques années (4) la double extension de cycle des phospholes par les chlorures d'acides aromatiques qui fournit facilement les cycles à 7 chaînons du type **2**. Ces cycles, par simple hydrolyse, donnent les cétones **3**

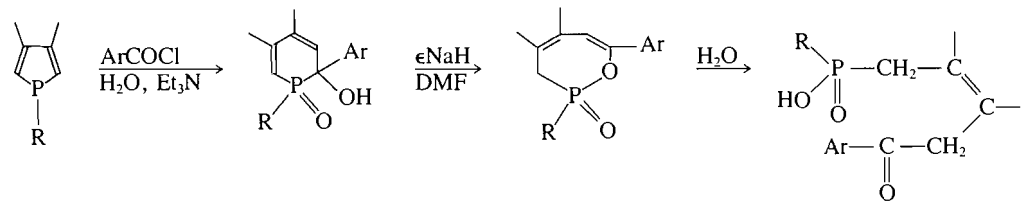

1 **2** **3**

présentant la stéréochimie *Z* désirée au niveau de la double liaison et offrant la possibilité de créer une seconde double liaison à partir du groupement carbonyle. Nous avons donc logiquement choisi d'utiliser les cycles du type **2** comme point de départ de nos synthèses.

Nous avons, tout d'abord, rencontré quelques difficultés dans la reproduction de la conversion **1** → **2**, la présence de traces d'eau dans le solvant utilisé ayant tendance à provoquer l'ouverture immédiate de **2** en **3**. Nous avons définitivement réglé ce problème en utilisant la triéthylamine au reflux du toluène comme catalyseur de l'extension de cycle; l'absence totale d'eau dans ce cas évitant toute ouverture malencontreuse de **2**, le rendement en **2** est alors quantitatif.

L'attaque d'un nucléophile B^- sur un cycle du type **2** peut, suivant les cas, se produire sur le CH_2 en α du P=O (métallation) ou sur le phosphore (ouverture) (5):

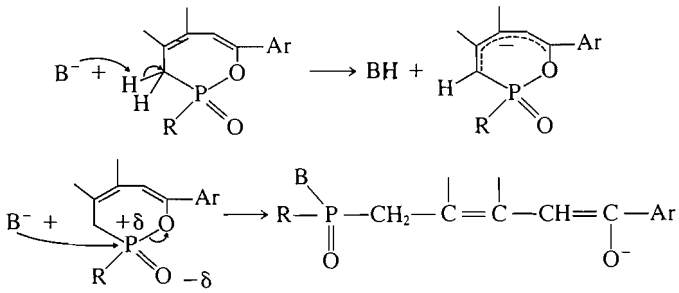

L'accroissement de la nucléophilie et de l'encombrement de B^- favorisent la métallation, leurs diminutions favorisent l'ouverture. En fonction de notre objectif, nous avons donc étudié l'action de MeMgI dans l'éther (nucléophile carboné peu encombré et peu basique) sur **2***a*.

0008-4042/83/010021-05$01.00/0
©1983 National Research Council of Canada/Conseil national de recherches du Canada

Can. J. Chem. Downloaded from www.nrcresearchpress.com by 210.87.254.105 on 09/06/12
For personal use only.

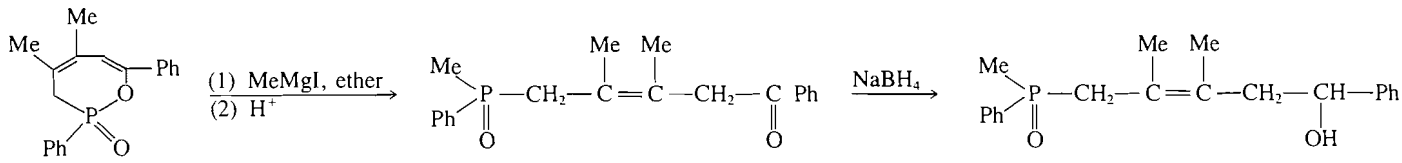

2a **4** **5**

Nous avons ainsi obtenu l'oxyde de phosphine **4** avec un bon rendement. Sa réduction par le borohydrure de sodium dans le méthanol pour donner **5** ne pose aucun problème. L'alcool **5** est un mélange de deux diastéréoisomères comme l'indique le spectre de rmn ^{31}P. En ir, le groupe hydroxyle présente une fréquence très basse (3250 cm^{-1}) indépendante de la concentration et du solvant. D'un autre côté, **5** est élué plus facilement que **4** sur une colonne de gel de silice. Tout ceci suggère l'existence d'une liaison hydrogène intramoléculaire forte entre les groupes OH et PO. La déshydratation de **5** pour donner le diène **6** est classique dans son principe mais nécessite des précautions expérimentales car **6** est peu stable à haute température. Alors que la stéréochimie de la double liaison C(Me)=C(Me) est *Z* dans **6** comme dans **5** par suite du choix d'un précurseur cyclique, au contraire la nouvelle double liaison CH=CH de **6** est de stéréochimie *E* comme l'atteste la constante de couplage ^3J(H—H) observée (16 Hz). Ce résultat est logique pour une élimination E1. Le spectre de masse de **6** (70 eV, 180°C) indique comme schéma de décomposition pratiquement unique le clivage en oxyde de phosphine secondaire Ph(Me)P(O)H (*m/e* 140, 100%) et en hydrocarbure $C_{13}H_{15}$ (*m/e* 171, 100%). Nous avons effectivement constaté que **6** se décomposait par simple chauffage à partir de 170°C pour fournir un hydrocarbure non identifié (M = 196) et un résidu phosphoré pouvant être identifié comme $MePhPO_2H$ ($\delta^{31}P$ = 40 ppm dans l'eau).

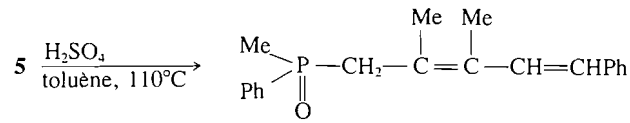

(*Z*) (*E*)

6

Malgré son instabilité à chaud, la préparation de **6** est assez satisfaisante puisque les produits de départ sont simples et accessibles et que le rendement global à partir du phosphole est supérieur à 30%. Le diène **6** est donc un synthon intéressant. En conséquence, nous avons étudié sa chimie de façon assez approfondie. Sa conversion en phosphine **7** a été réalisée de deux façons. Tout d'abord, nous avons utilisé une classique réduction au trichlorosilane. Dans ce cas on n'observe aucune hydrogénation du système diénique contrairement à ce qui est noté avec les oxydes de butadiényl-1,3-phosphines (1). L'éloignement du phosphoryle supprime la possibilité d'hydrogénation nucléophile du diène. La phosphine **7** ainsi obtenue a été caractérisée par son signal en rmn ^{31}P ($\delta^{31}P$(**7**) = −35,64 ppm dans C_6D_6) et complètement authentifiée par complexation à température ambiante par $Fe(CO)_4THF$.

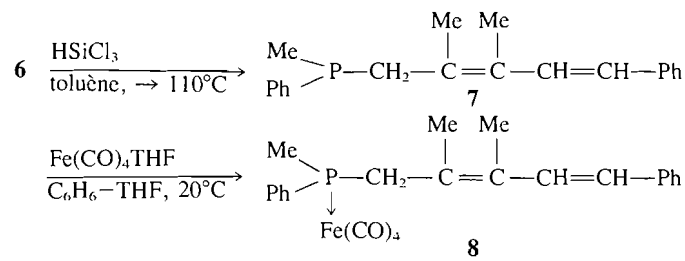

7 **8**

Le rendement modeste de cette réduction (~30%) nous a incité à étudier une autre voie d'accès. La conversion de l'oxyde **6** en sulfure **9** est aisément réalisée par le réactif de Lawesson et coll. (6)[1] avec un rendement de 84%:

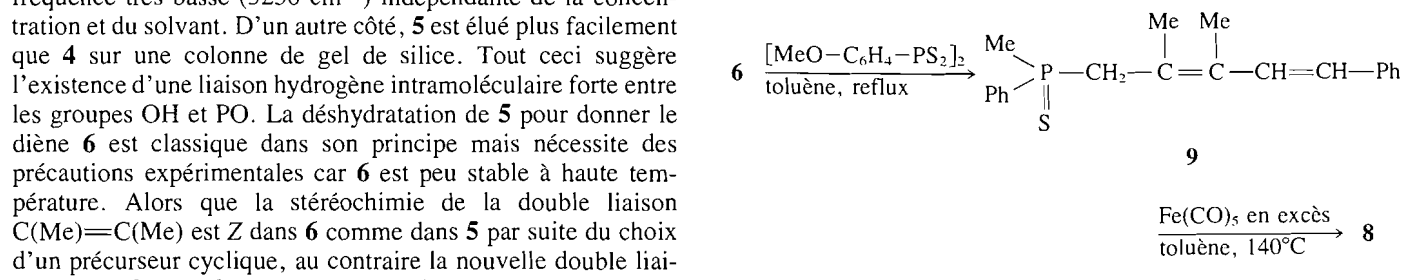

9 **8**

Ce sulfure **9** a été soumis à deux types de réductions—complexations. Tout d'abord chauffé en autoclave à 140°C avec un excès de fer pentacarbonyle, il conduit directement au complexe **8** avec un bon rendement (72%). Ce type de réduction—complexation des sulfures de phosphines a déjà été décrit dans la littérature (7). Il est à remarquer qu'il est plus simple et plus efficace de préparer **8** à partir de **6** en passant par le sulfure **9** que par la phosphine **7** (Rdt global 60% contre 15%). Mais le point le plus intéressant concerne l'absence de complexation de la partie diénique de **7** dans ces conditions énergiques. Cette absence jette un doute sur la capacité de **7** à jouer le rôle de coordinat chélatant et ce doute est confirmé par toute une série d'essais négatifs en ce sens sur les complexes **8** et **11**. A priori, cette incapacité peut être liée à deux causes: (1) une substitution inadaptée de la partie diénique de **7**; (2) un blocage stérique de la complexation du diène par le substituant phosphoré —CH_2P(Me)Ph dû à la géométrie *Z* de la double liaison en 2,3.

Une désactivation électronique du diène par le substituant phosphoré est exclue puisque nous avons montré que les butadiényl-1,3-phosphines avec une jonction directe P—diène sont capables de jouer le rôle de coordinats à 6 électrons (1). L'étude attentive du spectre de masse du complexe **8** apporte un élément de réponse à cette question. La perte de 4 carbonyles conduit à l'ion de *m/e* 350 (*I* = 100%). Cet ion perd classiquement son atome de fer pour donner la phosphine **7** (*m/e* 294, *I* = 7%). Mais le schéma de décomposition principal comporte une migration du fer du phosphore sur la partie diénique combinée avec une perte du substituant phosphoré analogue à celle observée sur l'oxyde **6**. Cette décomposition conduit à l'ion de *m/e* 226 ($C_{13}H_{14}Fe$, *I* = 56%) et est confirmée par la présence du métastable correspondant à *m/e* = 145.9. Il semble donc

[1]Nous avons déjà utilisé plusieurs fois ce réactif pour effectuer la conversion P=O → P=S dans des cas délicats, voir la référence 12: cas d'un phosphinate cyclique; la sulfuration s'effectue avec respect de la liaison P—O—C; Nief *et al.* (13): cas d'un oxyde d'hydroxy-2-dihydro-1,2-phosphorine; la sulfuration s'effectue avec respect de la fonction alcool; Santini *et al.* (14): cas d'un dimère d'oxyde de phosphole; la sulfuration s'effectue sans perte du pont phosphore. Récemment Horner et Lindel (15) ont décrit ce même type de conversion P=O → P=S sur des oxydes de phosphines plus simples.

Can. J. Chem. Downloaded from www.nrcresearchpress.com by 210.87.254.105 on 09/06/12
For personal use only.

clair que la substitution de la partie diénique n'est pas en cause et que l'incapacité de **7** à jouer le rôle de coordinat à 6 électrons est liée à la géométrie *Z* de l'enchaînement P—CH_2—diène, ce que l'étude du modèle de Dreiding de **7** tend à confirmer.

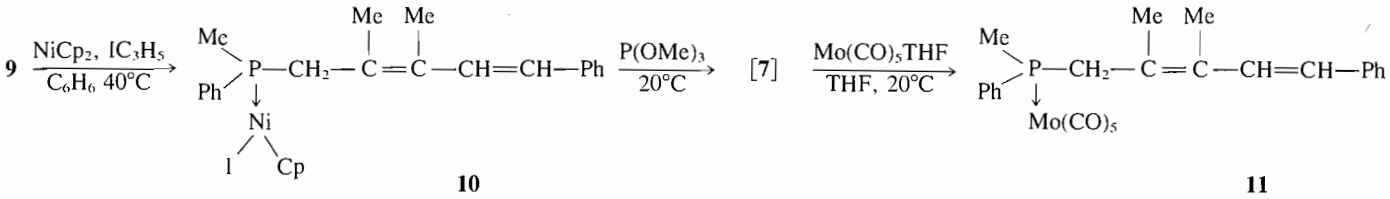

10 **11**

complexe du molybdène **11**. Cette séquence classique ne justifie aucun commentaire particulier. Comme annoncé précédemment, tous les essais de complexation de la partie diénique de **11** par $Fe(CO)_3$ ont échoué. Les phosphines du type **7** ne semblent donc pas présenter les possibilités attendues en chimie de coordination.

Disposant d'un accès commode à l'oxyde diénique **6**, nous avons voulu tester quelques possibilités synthétiques plus conventionnelles offertes par ce produit. La métallation de **6** par le tertiobutylate de potassium suivie d'un chauffage avec le benzaldéhyde conduit au triène attendu **12** de stéréochimie *E,Z,E* avec un rendement de 60%:

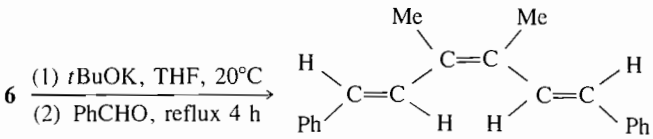

12

La structure symmétrique de **12** est confirmée par la présence d'un seul type de méthyle dans les spectres de rmn ^1H et ^{13}C de ce composé. Cette réaction est analogue à la dernière étape du mécanisme d'une synthèse des triènes à partir des sels de phospholéniums imaginée par Lednicer (9). Cependant, contrairement à Lednicer, nous pouvons ici obtenir des triènes dont les extrémités sont substituées différemment. Nous avons ensuite voulu transposer cette méthode pour obtenir des triènes fonctionnels. À titre d'exemple, nous avons donc préparé dans une première étape le produit phosphoré fonctionnel **13** par réaction de l'anion de **6** sur le diphényldisulfure:

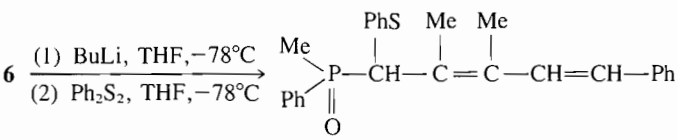

13

Le composé **13** est un mélange de deux diastéréoisomères (rmn ^{31}P) dont l'un est fortement majoritaire et peut être obtenu à l'état quasiment pur. L'anion de **13**, préparé par réaction du tertiobutylate de potassium, ne réagit malheureusement pas avec le benzaldéhyde certainement à cause de son encombrement stérique. Au lieu du triène fonctionnel attendu, les seuls produits obtenus sont des hydrocarbures résultant de la décomposition thermique de l'anion. Ces hydrocarbures, préparés en petite quantité, n'ont pas pu être complètement identifiés. Cependent leur étude par spectrométrie de masse (ionisation chimique) semble montrer qu'ils résultent de l'oxydation et du couplage de la partie hydrocarbonée de **13**:

La réduction−complexation de **9** par le nickelocène suivant une technique maintenant bien rodée (8) conduit, quant à elle, au complexe **10** qui est détruit par le triméthylphosphite pour fournir la phosphine **7**. Cette dernière est convertie *in situ* en

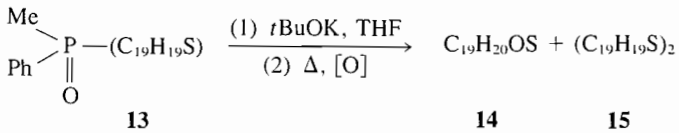

13 **14** **15**

Ce type de dégradation oxydante d'anions α-phosphorylés a déjà été décrit dans la littérature (10).

Partie expérimentale

Toutes les réactions sont effectuées sous courant d'argon. Les points de fusion ont été déterminés au banc Kofler. Les spectres ir ont été enregistrés à l'aide d'un spectrophotomètre Perkin−Elmer 457; les spectres de masse ont été réalisés sur un appareil Nermag R10-10 par M. Charré de la S.N.P.E. (Vert-le-Petit) et sur un appareil AEI MS-30. Les spectres de rmn pour tous les noyaux ont été enregistrés sur un appareil Bruker WP−80. Les chromatographies sont effectuées sur colonne de gel de silice (70−230 mesh).

L'oxyde d'hydroxy-2-diméthyl-4,5-diphényl-1,2-dihydro-1,2-phosphorine **1***a* a été préparé à quelques modifications près comme décrit dans la littérature (4).

*Oxyde de diméthyl-4,5-diphényl-2,7-oxa-1-phospha-2-cycloheptadiène-4,6 (***2**a)

L'oxyde de phosphorine **1***a* (4 g, 3.7×10^{-2} *M*) et 25 cm^3 de Et_3N dans 250 cm^3 de toluène sont chauffés au reflux du solvant durant la nuit. Après refroidissement de la solution à la température ambiante le solvant est évaporé conduisant à 4 g de **2** (rendement quantitatif) qui cristallise lorsque 5 cm^3 d'éther éthylique sont ajoutés.

*Oxyde de (diméthyl-2,3-phényl-5-oxo-5-penténYl-2)méthylphénylphosphine (***4**)

On ajoute 15 cm^3 d'une solution de MeMgI (1.5 *N*) dans l'éther éthylique en 30 min à une solution de **2** (7 g, 2.6×10^{-3} *M*) dans l'éther. Un abondant précipité blanc apparaît. L'agitation est maintenue 2 heures à la température ambiante. Le milieu réactionnel est hydrolysé avec une solution diluée d'acide chlorhydrique, jusqu'à neutralisation du milieu. Les solvants sont évaporés, le résidu est repris au chloroforme (200 cm^3), puis lavé à l'eau. La phase organique est séchée, puis évaporée. Le résidu est chromatographié (éluant acétate d'éthyle) ce qui permet d'isoler 1.9 g de **2***a*, R_f 0.7, et **4** (5,3 g, ρ 72.6%), R_f 0.15. Le produit **4** ne cristallise pas; ir (film) ν(C=O): 1675, ν(C=C): 1590, 1572, ν(P=O): 1165 cm^{-1}; rmn ^1H ($CDCl_3$): 1.73 (d, $^2J_{PH}$ = 12 Hz, Me—P), 1.76 (s, CH_3—C), 2.8 (d, $^2J_{PH}$ = 14.5 Hz, CH_2—P), 3.7 (s, large, CH_2—C), 7.4 (m, Hmp Ph—P), 7.70 (m, Ho Ph—P); rmn ^{31}P ($CDCl_3$): 32.37 ppm.

Oxyde de (hydroxy-5-diméthyl-2,3-phényl-5-pentenyl-2)méthylphénylphosphine

À 5.3 g (1.62×10^{-2} M) de **4** dans 80 cm^3 de méthanol fraîchement distillé sur Mg sont ajoutés 0.2 g de $NaBH_4$ par portion. Le milieu réactionnel est agité 2 heures à la température ambiante. Le solvant est évaporé et le résidu est dissout dans du chloroforme, puis

Can. J. Chem. Downloaded from www.nrcresearchpress.com by 210.87.254.105 on 09/06/12
For personal use only.

Can. J. Chem. Downloaded from www.nrcresearchpress.com by 210.87.254.105 on 09/06/12
For personal use only.

lavé à l'eau jusqu'à neutralisation du milieu. La phase organique est sechée ($MgSO_4$), puis évaporée permettant d'isoler 5.0 g (ρ 93%) d'une huile jaune qui cristallise lorsque 5 cm^3 d'éther éthylique sont ajoutés; pf 163°C, R_f 0.45 ($MeCO_2Et$–MeOH 95:5); ir (KBr) ν (OH): 3240, ν (C=C): 1597 et 1585, ν (P=O): 1140 cm^{-1}; ir (CH_2Cl_2) ν (OH): 3250 cm^{-1} fréquence de vibration indépendante de la concentration; rmn ^1H ($CDCl_3$): 1.2 (s.large, Me—C), 1.77 (d, ^2J(H—P) = 12.6 Hz, Me—P), 1.82 (m, 2 isomères, Me—C), 2.15–3.5 (m, CH_2P + CH_2C—OH), 4.90 (dd, CH—OH), 7.2–7.9 (m, Ph); rmn ^{31}P ($CDCl_3$): 33.62 et 32.10 ppm (majoritaire); sm (70 eV, 130°C): 329 (M + 1, 1%), 310 (M − H_2O, 6%), 140 (PhMePOH, 100%).

Oxyde de (diméthyl-2,3-phényl-5-pentadiényl-2,4)méthylphénylphosphine (6)

Dix grammes de l'alcool **5** sont déshydratés par l'acide sulfurique en traces catalytiques dans le toluène anhydre au reflux en 2 heures. Après refroidissement à la température ambiante, le milieu réactionnel est lavé avec une solution saturée de carbonate, puis la phase organique est décantée, séchée conduisant à 6,5 g (ρ 68,7%) d'une huile incolore qui cristallise lorsque quelques gouttes d'éther sont ajoutées, pf 188°C, R_f = 0.27 ($MeCO_2Et$–MeOH 95:5); ir (KBr) ν(C=C): 1615, 1590 et 1570 faible, ν(P=O): 1160–1172 ep fort; rmn ^1H ($CDCl_3$): 1.73 (d, $^2J_{PH}$ = 12,7 Hz, Me—P), 1.86 (s, MeC=), 1.93 (s, MeC=), 3.07 (d, $^2J_{PH}$ = 16 Hz, CH_2—P), δ_A: 6.37 δ_B: 6.87 (J_{AB} = 16.02 Hz, HC=CH), rmn ^{31}P ($CDCl_3$): 32.7 ppm; sm (70 eV, 180°C): 310 (M, 77%), 171 ($C_{13}H_{15}$, 100%), 140 (PhMePH(O), 100%). *Anal.* calc. pour $C_{20}H_{23}OP$: C 77.39, H 7.47, P 9.98, trouvé: C 76.85, H 7.50, P 9.74.

(Diméthyl-2,3-phényl-5-pentadiényl-2,4)méthylphénylphosphine (7)

Dans un ballon monocol muni d'un réfrigérant à Carboglace, l'oxyde de phosphine **6** (0.8 g, 2.58 × 10^{-3} *M*) et le chlorosilane $HSiCl_3$ sont chauffés au reflux du toluène pendant 2 heures. Après évaporation du solvant et de l'excès de $HSiCl_3$, le résidu est repris au benzène et avec une solution saturée de bicarbonate. La phase organique est ensuite séchée et évaporée. L'huile incolore obtenue est étudiée en rmn ^{31}P (C_6D_6), δ: −35.64; +29.52 (oxyde de phosphine). Rendement environ 30% (déterminé par rmn). Tous les solvants utilisés sont dégazés.

Diméthyl-2,3-phényl-5-pentadiényl-2,4)méthylphénylphosphine fer tetracarbonyle (8)

La phosphine **7** (10^{-3} *M*) en solution dans 50 cm^3 de benzène est ajoutée à une solution de $Fe(CO)_4THF(Fe_2(CO)_9$, 0.4 g; THF, 100 cm^3, 25°C) après une heure d'agitation à la température ambiante, les solvants sont évaporés et le résidu chromatographié (éluant hexane–benzène 75:25) permettant d'isoler 0.25 g, ρ ≃ 50% du complexe **8**, R_f 0.33, pf 132°C; ir (hexane) ν(CO): 2050, F 1980 F, 1944, 1935 TF; rmn ^1H (C_6D_6): 1.28 (m, Me—C=), 1.47 (d, J_{PH} = 9.2 Hz, Me—P), 1.67 (deux massifs, Me—C=), 3.0 (d, J_{PH} = 10 Hz, CH_2—P), 6.3 et 6.5 (partie A de système AB, J_{AB} = 15.3 Hz); rmn ^{31}P (toluène): +56.24 ppm; sm (70 eV, 120°C): 462 (M, 1%), 434 (M—CO, 10%), 406 (M—2CO, 21%), 376 (M—3CO, 20%), 350 (M—4CO, 100%), 294 (L, 7%), 226 (350 − PhP(H)Me, 56%), 171 ($C_{13}H_{15}$, 24%).

Préparation de 8 à partir du sulfure de phosphine 9

Un mélange de 0.54 g (1.74 × 10^{-3} *M*) de sulfure de phosphine **9** et 2 g (10^{-2} *M*) de fer pentacarbonyle dans 100 cm^3 de toluène sont chauffés en autoclave à 140°C (*P* ≃ 5 bars) pendant 24 h. Après filtration du précipité noir sur Celite le filtrat est concentré, chromatographié sur silice (100 g, éluant toluène) conduisant à 0.45 g (ρ ≃ 72%) de complexe **8**; 0.1 g de sulfure de départ **9** élué avec le mélange toluène − acétate d'éthyle 90:10 sont recouvrés.

Sulfure de (diméthyl-2,3-phényl-5-pentadiényl-2,4)méthylphénylphosphine (9)

Un mélange de 1.24 g (4 × 10^{-3}*M*) d'oxyde de phosphine **6** et 0.88 g (2 × 10^{-3} *M*) de $[MeOC_6H_4PS_2]_2$ sont chauffés au reflux dans 100 cm^3 de toluène pendant 2 heures. Après refroidissement du milieu réactionnel à la température ambiante, le solvant est évaporé conduisant à une huile jaune-marron qui est chromatographiée (éluant toluène − acétate d'éthyle 95:5). Après le trimère $[MeOC_6H_4POS]_3$ R_f 0.7, 1.1 g (ρ 84%) de sulfure R_f 0.33 sont isolés sous forme d'une huile incolore qui cristallise lorsque 5 cm^3 d'éther éthylique sont ajoutés, pf (Et_2O) 135°C; R_f 0.57 dans CH_2Cl_2; ir (KBr) ν(C=C): 1625, 1600, 1580 cm^{-1}; rmn ^1H ($CDCl_3$): 1.6 (m, CH_3—C=), 1.73 (d, $^2J_{PH}$ = 12 Hz, CH_3P), 3.06 (d, $^2J_{PH}$ = 15Hz, CH_2—P), système AB δ_A: 6.08 δ_B: 6.52 (J_{AB} = 16 Hz, CH=CH); rmn ^{31}P: +34.8 ppm; sm (70 eV, 200°C): 326 (M, 10%), 171 ($C_{13}H_{15}$, 100%).

Iodure de (diméthyl-2,3-phényl-5-pentadiényl-2,4)méthylphénylphosphine cyclopentadiényl nickel (10)

Un mélange de 1.2 g (3.68 × 10^{-3} *M*) de sulfure de phosphine **9**, 2 g de nickelocène et 0.5 cm^3 d'iodure d'allyle sont chauffés à 40°C dans 100 cm^3 de benzène pendant 2 heures. Après filtration sur Célite des insolubles, le milieu réactionnel est concentré, puis chromatographié (éluant benzène), conduisant à 0.86 g (ρ 50%) d'une huile rouge sombre (R_f 0.7) qui cristallise lentement sous vide; rmn ^{31}P (C_6D_6): +13.8 ppm; sm (70 eV, 160°C, ^{58}Ni): 544 (M, 1%), 417 (M − I, 1%), 310 (LO, 35%), 294 (L, 20%), 171 ($C_{13}H_{14}$, 47%), 130 (100%).

(Diméthyl-2,3-phényl-5-pentadiényl-2,4)méthylphénylphosphine pentacarbonyl molybdène (11)

À 7 g (12.9 × 10^{-3} *M*) de complexe **10** dissous dans du benzène (100 cm^3) sont ajoutés 2 cm^3 de triméthylphosphite. La couleur du milieu réactionnel passe du rouge sombre au vert marron. L'agitation est maintenue 30 min. Puis le milieu réactionnel filtré sur silice (50 g) est ajouté à une solution de $Mo(CO)_5THF$ ($Mo(CO)_6$ 3.43 g; 1000 cm^3 de THF) à la température ambiante. L'agitation est maintenue 1 heure à cette température puis les solvants sont évaporés et le résidu est chromatographié (éluant hexane − toluène 80:20) ce qui permet d'isoler 3 g (ρ 53%) de complexe **11** (R_f 0.5) qui doit être recristallisé dans l'hexane (ρ 30%); ir (hexane) ν(CO): 2065 f, 1952 m, 1947 TF; rmn ^1H (C_6D_6): 1.21 (m, CH_3—C=), 1.37 (d, J_{PH} = 5.6 Hz, CH_3—P), 1.52 (m, CH_3—C=), 2.75 (d, J_{PH} = 7 Hz, CH_2—P), 6.3 et 6.57 (partie A du système AB, J_{AB} = 16 Hz, CH=CH); rmn ^{31}P: 6.87 ppm; sm (130°C, 70 eV, ^{98}Mo): 532 (M, 10%), 392 (*M* − 5CO, 47%), 294 (L, 53%), 171 ($C_{13}H_{15}$, 100%).

(E-Z-E) diméthyl-3,4-diphényl-1,6-hexatriène-1,3,5 (12)

On ajoute 0.23 g de tertiobutylate de potassium par portion à une solution d'oxyde de phosphine **6** (0.5 g, 1.6 × 10^{-3} *M*) dans 100 cm^3 de THF à la température ambiante. Dès l'addition de *t*BuOK il y a apparition d'une couleur rouge orangé sombre. L'agitation est maintenue 15 min après l'addition, puis 0.17 g (1.6 × 10^{-3} *M*) de benzaldéhyde sont ajoutés. Il y a décoloration spontanée du milieu réactionnel, puis ce dernier est chauffé pendant 4 heures à reflux du solvant. Après refroidissement à la température ambiante, 50 cm^3 d'eau sont ajoutés puis le milieu est extrait à l'éther éthylique (3 × 100 cm^3). La phase organique est décantée, séchée sur $MgSO_4$, puis concentrée conduisant à 0.25 g (ρ 60%) de **12**, solide jaune, F 175°C (pentane); rmn ^1H ($CDCl_3$): 2.2 (s, CH_3), 6.73 et 6.93 (partie A d'un système AB, J_{AB} = 16 Hz, CH=CH); rmn ^{13}C: 14.2 (s, CH—C=), 126.4–128.9 (m, Ph), 132.15 (s, C sec du phényl), 138.26 (s, $C(H)$=H); sm (70 eV, 150°C): 260 (M, 53%), 169 (M − $PhCH_2$, 66%), 91 ($PhCH_2$, 100%). D'après les points de fusion, **12** est différent du triène de même formule déjà décrit dans la littérature (11) qui est probablement de structure (*E,E,E*).

Oxyde de (diméthyl-2,3-phényl-5-phénylthio-1-pentadiényl-2,4)-méthylphénylphosphine (13)

On ajoute 3 cm^3 de BuLi (1.4 *N* dans l'hexane) goutte à goutte à une solution de 1 g (3.22 × 10^{-3} *M*) d'oxyde de phosphine **6** dans 50 cm^3 de THF refroidie à −78°C. Une coloration rouge sombre apparaît spontanément. En fin d'addition, l'agitation est maintenue 15 min à cette température, puis 0.7 g de diphényldisulfure dissous dans 25 cm^3 de THF sont ajoutés. En fin d'addition de ce réactif la couleur du milieu réactionnel est passée du rouge sombre à l'orange. L'agitation est maintenue 30 min à cette température, puis 50 cm^3 d'une solution

saturée en carbonate de sodium sont ajoutés et la température du milieu revient à l'ambiante. Le milieu réactionnel est extrait avec 4 × 25 cm^3 de CH_2Cl_2. Après décantation la phase organique est lavée avec 50 cm^3 d'acide chlorhydrique dilué, puis 50 cm^3 d'une solution aqueuse saturée en NaCl, puis est séchée sur $MgSO_4$. Après évaporation des solvants le résidu est chromatographié (éluant acétate d'éthyle) conduisant à 0.4 g (R_f 0.72) de $(PhS)_2$, 0.5 g (R_f 0.4, ρ 52%) de **13** et 0.3 g (R_f 0.1) de l'oxyde **6**. Composé **13**, solide blanc, pf 157−158°C; rmn ^1H ($CDCl_3$): 1.3 (s large, CH_3—C═), 2.01 (d, J_{PH} = 12.7 Hz, CH_3—P), 2.15 (s large, CH_3—C═), 4.5 (d, SPh | J_{PH} = 10.7 Hz, P—C*H*), 6.26 et 6.46 (partie A d'un système AB, J_{AB} = 16 Hz, CH═CH), 7.06 et 7.26 (partie B d'un système AB); rmn ^{31}P ($CDCl_3$): 34.51 (majoritaire) et 33.36 ppm; sm (IC): 419 (M + 1, 100%).

Décomposition thermique de l'anion de l'oxyde de phosphine 13

On ajoute 0.214 g de *t*BuOK par portion à une solution de **13** (0.8 g, 1.91 × 10^{-3} *M*) dans 50 cm^3 de THF à la température ambiante. Dès l'addition de *t*BuOK le milieu devient rouge sombre. En fin d'addition, le milieu réactionnel est chauffé pendant 2.5 h au reflux du solvant. Après refroidissement à la température ambiante, 50 cm^3 d'eau saturée en NH_4Cl sont ajoutés. Le milieu est extrait avec 3 × 25 cm^3 de CH_2Cl_2; la phase organique après décantation et lavage (50 cm^3 HCl 1 *N*, puis 50 cm^3 d'eau saturée en NaCl) est séchée sur $MgSO_4$. Après concentration le résidu est une première fois chromatographié sur silice (éluant CH_2Cl_2) conduisant à une huile jaune (0.46 g) éluant en tête. Cette huile est à nouveau chromatographiée (éluant hexane − CH_2Cl_2 80:20) permettant d'isoler 0.15 g (R_f 0.4) de **14** et 0.2 g (R_f 0.2) de **15**. Composé **14**: sm (ionisation chimique NH_3): 297 (M + 1, 100%), 279 (M − OH, 16%), 187 (M − PhS, 16%), 171 ($C_{13}H_{15}$, 22%). Composé **15**: sm (ionisation chimique NH_3): 560 (M + 2, 100%), 449 (M − PhS, 43%); 339 (449 − PhSH, 14%), 279 (M/2, 100%), 170 ($C_{13}H_{14}$, 20%). Les spectres rmn ^1H de **14** et **15** sont complexes et laissent supposer que **14** et **15** sont des mélanges de diastéréoisomères. On ne voit pas de bande OH sur le spectre ir de **14**.

1. F.MATHEY, F. MERCIER et C. SANTINI. Inorg. Chem. **19**, 1813 (1980).
2. R. POILBLANC. Nouv. J. Chim. **2**, 145 (1978).
3. F. MATHEY et C. SANTINI. Can. J. Chem. **57**, 723 (1979).
4. F. MATHEY. Tetrahedron, **29**, 707 (1973); F. MATHEY, D. THAVARD et B. BARTET. Can. J. Chem. **53**, 855 (1975).
5. F. MATHEY. Bull. Soc. Chim. Fr. 2783 (1973).
6. B. S. PEDERSEN, S. SCHELBYE, N. H. NILSSON et S. O. LAWESSON. Bull. Soc. Chim. Belg. **87**, 223 (1978).
7. F. MATHEY et G. MULLER. J. Organometal. Chem. **136**, 241 (1977); F. MERCIER, F. MATHEY, J. ANGENAULT, J. C. COUTURIER et Y. MARY. J. Organometal. Chem. **231**, 237 (1982).
8. F. MATHEY et F. MERCIER. J. Organometal. Chem. **177**, 255 (1979).
9. D. LEDNICER. J. Org. Chem. **36**, 3473 (1971).
10. L. HORNER, H. HOFFMANN, G. KLAHRE, V. G. TOSCANO et H. ERTEL. Chem. Ber. **94**, 1987 (1961).
11. F. MATHEY et D. THAVARD. C. R. Acad. Sci. Paris, Ser. C, **281**, 243 (1975).
12. F. MATHEY et F. MERCIER. J. Chem. Soc. Chem. Commun. 191 (1980).
13. F. NIEF, C. CHARRIER, F. MATHEY et M. SIMALTY. Tetrahedron Lett. **21**, 1441 (1980).
14. C. C. SANTINI, J. FISCHER, F. MATHEY et A. MITSCHLER. J. Am. Chem. Soc. **102**, 5809 (1980).
15. L. HORNER et H. LINDEL. Phosphorus Sulfur, **12**, 259 (1982).

Can. J. Chem. Downloaded from www.nrcresearchpress.com by 210.87.254.105 on 09/06/12
For personal use only.

The planar conformation of 2-methylthiobenzaldehyde in solution

TED SCHAEFER AND RUDY SEBASTIAN
Department of Chemistry, University of Manitoba, Winnipeg, Man., Canada R3T 2N2

Received June 30, 1982

TED SCHAEFER and RUDY SEBASTIAN. Can. J. Chem. **61**, 26 (1983).

The ^{1}H nmr spectral parameters are extracted for a 4 mol% solution of 2-methylthiobenzaldehyde in CCl_4 at 305 K. The long-range spin–spin coupling constants involving the aldehydic and methyl protons are consistent only with a preferred conformation in which all heavy atoms are coplanar, as are the chemical shifts of the ring and methyl protons. This conclusion contradicts previous interpretations of the dipole moment, the nmr parameters, and of the infrared data for CCl_4 solutions. The present data show that the *O-syn* and *O-anti* forms of the compound are present in roughly equal proportions.

TED SCHAEFER et RUDY SEBASTIAN. Can. J. Chem. **61**, 26 (1983).

On a déduit les paramètres spectraux de la rmn du ^{1}H d'une solution à 4 mol% de méthyl-2 thiobenzaldéhyde à 305 K. Les constantes de couplages à longue distance impliquant les protons aldéhydiques et ceux du méthyle sont en accord uniquement avec une conformation préférentielle dans laquelle tous les atomes lourds sont coplanaires. Il en est de même pour les déplacements chimiques des protons du cycle et du méthyle. Cette conclusion contredit les interprétations antérieures du moment dipolaire, des paramètres de la rmn et des données infrarouges des solutions dans le CCl_4. Les données actuelles montrent que les formes *O-syn* et *O-anti* du composé sont présentes approximativement en proportions égales.

Introduction

The stereospecificity of the long-range coupling over five bonds, $^5J_m^{H,CHO}$, between the aldehydic proton and the ring proton in the *meta* position of benzaldehyde is documented (1–6). For example, in conformation **1***a* of 2-methylthiobenzaldehyde, **1**, the available evidence from a host of other *ortho* substituted benzaldehyde derivatives implies that ^5J vanishes for H-5 and may approach 1 Hz for H-3; with a corresponding reversal in **1***b*. In benzaldehyde itself, $^5J_m^{H,CHO}$ is 0.38 Hz (7), implying ^5J as 0.76 Hz to H-3 and 0.00 Hz to H-5 in the hypothetical rigid form **1***a*.

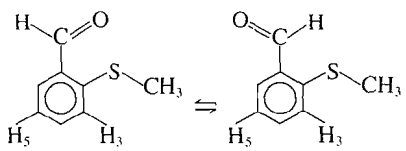

1*a* **1***b*

Small intrinsic substituent perturbations of $^5J_m^{H,CHO}$ may occur (5). Thus, in 2-methoxybenzaldehyde, $^5J_m^{H,CHO}$ to H-5 is 0.83 Hz (4), indicating also that the *O-anti* conformer is by far the most abundant in solution.

Because the barrier to internal rotation of the aldehyde group in benzaldehyde is at least 31 kJ/mol in solution (8), discussion in terms of a planar conformation is an adequate approximation. It follows that experimental values for $^5J_m^{H,CHO}$ in nonplanar conformations are not available. By analogy to other (9–11) $^5J_m^{H,XH}$ magnitudes and their theoretical conformational dependence, however, a finite $^5J_m^{H,CHO}$ is anticipated for all nonplanar aldehydic conformations.

If $^6J_p^{H,CHO}$ contains a substantial $\sigma-\pi$ component, then its magnitude will increase as $\sin^2\theta$ where θ is the angle by which the CHO plane twists out of the benzene plane. Indeed, significant magnitudes are observed for *ortho* disubstitution by chlorine or nitro moieties (12).

In view of these remarks, it is puzzling that no $^5J_m^{H,CHO}$ was observed for **1** in CCl_4 or acetone (13, 14) and that the apparent absence of the coupling was interpreted as evidence for a nonplanar conformation of **1**. A discussion (13) of the dipole moment and infrared spectrum of **1** came to the same conclusion.

It is shown below that **1** exists in CCl_4 solution in similar proportions of **1***a* and **1***b* and that *all* heavy atoms are effectively coplanar.

Experimental

Compound **1** was prepared from 2-methylthiobenzyl alcohol (Maybridge) by the method of Pratt and van de Castle (15) as adumbrated by Traynelis and Borgnaes (16). A 4 mol% solution of **1** in CCl_4, containing ca. 4 mol% of tetramethylsilane (TMS), was filtered into a 5 mm od nmr tube. The solution was thoroughly degassed by the freeze–pump–thaw procedure and was then flame-sealed into the nmr sample tube.

The ^{1}H nmr spectrum was calibrated in the frequency sweep mode on an HA100 spectrometer at a probe temperature of 305 K. The calibration procedure was recently described (17) and gave root-mean-square deviations of $\leq$0.02 Hz for the peak frequencies. Calibrations of the ring and aldehydic protons were carried out while decoupling the methyl protons, which couple to all ring protons.

Results and discussion

Spectral analysis

The LAME (18, 19) procedure, in which 80 of 84 calculated transitions with relative intensities above 0.05 were assigned to observed peaks, gave the spectral parameters in Table 1. As an example of the spectral quality, the observed and calculated spectrum of the aldehydic proton is displayed in Fig. 1. No coupling between the aldehydic and the methyl protons could be detected by double irradiation.

The conformation of the carbonyl group

The sum of the $^5J_m^{H,CHO}$ values in Table 1 is 0.82 Hz. If it is assumed that $^5J_m^{H,CHO}$ is solely determined by the stereospecificities discussed above, then the equilibrium constant for **1***b*/**1***a* is $^5J_5^{H,CHO}/^5J_3^{H,CHO}$ or 0.486/0.335. Hence, the population ratio is 59:41 to the advantage of **1***b*, the *O-anti* conformer.

An alternative, somewhat extreme, assumption has $^5J_3^{H,CHO}$ as the intrinsically perturbed parameter (the SCH_3 group is attached to the coupling pathway). That is, if **1** existed as **1***a*, $^5J_5^{H,CHO}$ would be 0.38 Hz, as in benzaldehyde; and if **1** were in

0008-4042/83/010026-03$01.00/0
©1983 National Research Council of Canada/Conseil national de recherches du Canada

Can. J. Chem. Downloaded from www.nrcresearchpress.com by 210.87.254.105 on 09/06/12
For personal use only.

TABLE 1. The ^{1}H nmr spectral parameters for a 4 mol% solution of 2-methylthiobenzaldehyde in CCl_4 at 305 K

Parameter[a]	Value	Parameter[a]	Value
ν_{CHO}	1026.722(2)[b,c]	$^5J_3^{H,CHO}$	0.335(4)
ν_{CH_3}	245.025	$^5J_5^{H,CHO}$	0.486(3)
ν_3	727.620(3)	$^6J_p^{H,CHO}$	−0.032(4)
ν_4	743.104(3)	$^5J_o^{H,CH_3}$	−0.341
ν_5	720.149(3)	$^6J_4^{H,CH_3}$	±0.04 ± 0.01
ν_6	773.884(2)	$^7J_5^{H,CH_3}$	±0.05 ± 0.01
$^3J_{34}$	8.026(4)	$^6J_6^{H,CH_3}$	±0.06 ± 0.01
$^3J_{45}$	7.323(4)	Peaks observed	63
$^3J_{56}$	7.674(4)	Peaks calculated	84
$^3J_{35}$	1.078(3)	Peaks assigned	80
$^4J_{46}$	1.614(4)	Largest difference	0.02 Hz
$^5J_{36}$	0.476(4)	Root-mean-square	
$^4J_o^{H,CHO}$	−0.175(3)	deviation	0.008 Hz

[a]Chemical shifts are in Hz at 100.001 MHz to low field of internal TMS.
[b]The numbers in parentheses are the standard deviations in the last significant figures.
[c]An analysis based on peak positions obtained while decoupling the methyl protons.

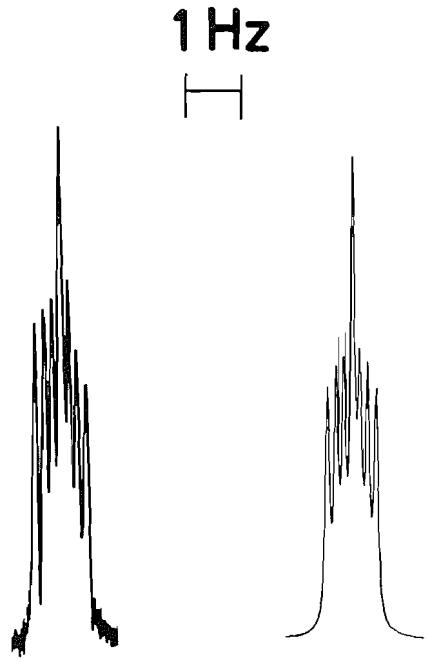

FIG. 1. The observed ^{1}H nmr spectrum at 100 MHz of the aldehydic proton of 2-methylthiobenzaldehyde is compared with that calculated with the parameters in Table 1. It is quite clear that the aldehydic proton couples to at least three ring protons. Decoupling experiments indicate very small or zero couplings between the methyl and aldehydic protons.

form **1***b*, $^5J_3^{H,CHO}$ would be 0.44 Hz. The sum of the two couplings would then equal 0.82 Hz as observed for **1**. In that event, one would write the equilibrium constant above as 0.38/0.335 or as 0.486/0.44, yielding the population ratio of **1***b* to **1***a* as 53:47.

The two approaches represent the limits of this ratio, suggesting an estimate of 56 ± 3:44 ± 3. The measurement errors themselves fall within the suggested range.

The question of the coplanarity of the carbonyl and benzene planes can be approached as follows. $^6J_p^{H,CHO}$ in **1** is apparently −0.03 Hz, the same as quoted for benzaldehyde (7). Whether these numbers are significant or not, if benzaldehyde is considered a planar molecule, then **1** must also have the aldehydic function in the benzene plane. As the carbonyl group takes on nonplanar conformations $^6J_p^{H,CHO}$ increases in magnitude, becoming −0.21(2) Hz in 2,6-dinitrobenzaldehyde and −0.15 (2) Hz in the 2,6-dichloro derivative (12). Whatever the twist angle in the latter two compounds, it is clear that **1** behaves more like benzaldehyde itself.

The conformation of the thiomethyl group

A detailed investigation of the long-range couplings of the methyl protons in 2,5-dichlorothioanisole (20) yields −0.35(1) Hz for the coupling to the *ortho* ring proton, $^5J_o^{H,CH_3}$. This coupling originates in a proximate manner, involving spin polarization via interactions of the electrons in the bonds containing the coupled nuclei. Its magnitude drops off rapidly as the SCH_3 group twists out of the benzene plane. In fact, in 2-hydroxythioanisole, where the C—S—C plane is held roughly perpendicular to the benzene plane by stereospecific hydrogen bonding to the 3*p* lone pair on sulfur, no $^5J_o^{H,CH_3}$ is observable (21). In **1**, $^4J_o^{H,CH_3}$ is −0.34(1) Hz, implying an effectively coplanar orientation of the benzene and SCH_3 skeletons.

Additional evidence comes from the ring proton shifts in **1**. The 3*p*. . .π conjugation in thioanisole and thiophenol is not very strong, the barrier to internal rotation about the C1—S bond being only about 3.3 kJ/mol (22, 23). The ring proton shifts reflect the extent of conjugation and are the same for the two compounds to within 0.02 ppm (24, 25). In **1**, the coplanar conformation of the SCH_3 group will be favored by the presence of the carbonyl function. Hence the π electron densities at C-3 and C-5 in **1** should increase, reflecting the increased π electron donation by SCH_3. On an additive basis, the observed shifts in benzaldehyde (26) and thioanisole (25), together with δ_H as 7.25 for benzene in CCl_4, imply δ_3, δ_4, δ_5, and δ_6 as 7.36, 7.43, 7.24, and 7.70 respectively. The observed shifts display excess high field shifts of 0.08 and 0.04 ppm at H-3 and H-5, respectively, consistent with increased π electron density at the sites *ortho* and *para* to SCH_3 and therefore with an increased tendency towards planarity of this substituent. The additive scheme predicts δ_4 as 7.43, observed as 7.43; and δ_6 as 7.70, whereas the observed value is 7.74. In view of concentration differences for the three compounds in CCl_4, it may be concluded that the ring proton shifts are consistent with a preferred coplanar conformation of the SCH_3 fragment.

The chemcial shift of the methyl protons in **1** is 2.45 ppm, is 2.44 ppm in thioanisole (25), and 2.43 ppm in 2,5-dichlorothioanisole (20). In contrast, it is 2.27 ppm in 2-hydroxythioanisole and, as shown previously (21), reflects the upfield shift caused by the magnetic anisotropy of the benzene nucleus in the perpendicular conformation. Accordingly, and allowing for small shifts caused by electronic perturbations by the substituent (21), δ_{CH_3} in **1** is consistent with a coplanar conformation of the SCH_3 group.

Other long-range couplings to methyl protons

In 2,5-dichlorothioanisole, in which the SCH_3 group prefers the benzene plane, the methyl protons couple significantly to all the ring protons. In 2-hydroxythioanisole, the SCH_3 fragment prefers a plane perpendicular to that of the ring and the methyl protons are appreciably coupled to H-3 and H-5 only (21). In **1**, the methyl protons do couple to all ring protons (Table 1), indicating a preferred planar conformation.

Can. J. Chem. Downloaded from www.nrcresearchpress.com by 210.87.254.105 on 09/06/12
For personal use only.

Carbonyl–sulfur interactions

The relative populations of the *O-syn* and *O-anti* conformers of **1** are very similar to those for 2-methylbenzaldehyde at the same temperature and in the same solvent (6). By way of contrast, there is no evidence for other than the *O-anti* conformation in 2-methoxybenzaldehyde, and 2-chlorobenzaldehyde appears to be at least 96% in the *O-anti* form (4). Considering the sizes of these substituents and the dipole moments of the C—Cl and C—O bonds in these two compounds, it appears reasonable that the significant population of the *O-syn* form of **1** can be attributed to a favorable dipole–dipole attraction of the C=O and C—S bonds which, to some extent, may overcome unfavorable steric repulsions. Because the sulfur atom is relatively polarizable, the favorable interaction may be predominantly of the dipole-induced dipole kind. In the corresponding tellurium compound, the *O-anti* form apparently predominates (14), suggesting steric repulsions as predominant.

Acknowledgments

We are grateful to the Natural Sciences and Engineering Research Council of Canada for financial assistance.

1. G. J. KARABATSOS and F. M. VANE. J. Am. Chem. Soc. **85**, 3886 (1963).
2. S. FORSÉN and R. A. HOFFMAN. J. Mol. Spectrosc. **20**, 168 (1966).
3. D. G. DEKOWALEWSKI and V. J. KOWALEWSKI. Mol. Phys. **9**, 331 (1965).
4. D. G. KOWALEWSKI and S. CASTELLANO. Mol. Phys. **16**, 567 (1969).
5. R. WASYLISHEN and T. SCHAEFER. Can. J. Chem. **49**, 3216 (1971).
6. T. SCHAEFER, S. R. SALMAN, and T. A. WILDMAN. Can. J. Chem. **58**, 2364 (1980).
7. R. J. KOSTELNIK, M. P. WILLIAMSON, D. E. WISNOSKY, and S. M. CASTELLANO. Can. J. Chem. **47**, 3313 (1969).
8. F. A. L. ANET and M. AHMAD. J. Am. Chem. Soc. **86**, 119 (1964).
9. R. WASYLISHEN and T. SCHAEFER. Can. J. Chem. **50**, 1852 (1972).
10. T. SCHAEFER, T. A. WILDMAN, and S. R. SALMAN. J. Am. Chem. Soc. **102**, 107 (1980).
11. T. SCHAEFER, T. A. WILDMAN, and R. SEBASTIAN. Can. J. Chem. **60**, 1924 (1982).
12. C. L. BELL, S. S. DANYLUK, and T. SCHAEFER. Can. J. Chem. **47**, 3529 (1969).
13. C. G. ANDRIEU and A. RUWET. Bull. Soc. Chim. Fr. 1008 (1972).
14. G. LLABRES, M. BAIVIR, L. CHRISTIAENS, and J.-L. PIETTE. Bull. Soc. R. Sci. Liege, **49**, 178 (1980).
15. E. F. PRATT and J. F. VAN DE CASTLE. J. Org. Chem. **26**, 2973 (1961).
16. V. J. TRAYNELIS and D. M. BORGNAES. J. Org. Chem. **37**, 3824 (1980).
17. T. SCHAEFER and R. SEBASTIAN. J. Magn. Reson. **41**, 395 (1980).
18. S. CASTELLANO and A. A. BOTHNER-BY. J. Chem. Phys. **41**, 3863 (1964).
19. C. W. HAIGH. Annu. Rep. Nucl. Magn. Reson. Spectrosc. **4**, 311 (1971).
20. T. SCHAEFER, R. SEBASTIAN, and S. R. SALMAN. J. Magn. Reson. **46**, 325 (1982).
21. T. SCHAEFER, S. R. SALMAN, T. A. WILDMAN, and P. D. CLARK. Can. J. Chem. **60**, 342 (1982).
22. A. SCHWEIG and N. THON. Chem. Phys. Lett. **38**, 482 (1976).
23. N. W. LARSEN and F. M. NICOLAISEN. J. Mol. Struct. **22**, 29 (1974).
24. W. J. E. PARR and T. SCHAEFER. Can. J. Chem. **25**, 171 (1977).
25. G. LLABRES, M. BAIWIR, L. CHRISTIAENS, J. DENVEL, L. LAITEM, and J.-L. PIETTE. Can. J. Chem. **56**, 2008 (1978).
26. S. CASTELLANO and C. SUN. J. Am. Chem. Soc. **88**, 4741 (1967).

Can. J. Chem. Downloaded from www.nrcresearchpress.com by 210.87.254.105 on 09/06/12
For personal use only.

Some unique properties of $^4J_o^{F,CH_3}$ in 2-fluorotoluene derivatives. Conformational dependence

TED SCHAEFER, RUDY SEBASTIAN, RICHARD P. VEREGIN, AND REINO LAATIKAINEN[1]
Department of Chemistry, University of Manitoba, Winnipeg, Man., Canada R3T 2N2

Received July 5, 1982

TED SCHAEFER, RUDY SEBASTIAN, RICHARD P. VEREGIN, and REINO LAATIKAINEN. Can. J. Chem. **61**, 29 (1983).

A complete analysis of the ^{1}H nmr spectrum of 2-fluorotoluene yields $^4J_o^{F,CH_3}$, the spin–spin coupling constant between ^{19}F and the methyl protons, as 1.99 Hz. Analysis of nmr spectra of 21 other derivatives of 2-fluorotoluene shows that $^4J_o^{F,CH_3}$ can vary between 1.69 and 2.55 Hz. This strong dependence on substitution contrasts with the near invariance of other long-range couplings such as $^4J_o^{H,CH_3}$, $^6J_p^{H,CH_3}$, and $^5J_m^{F,CH_3}$. The substituent dependence is discussed in terms of coupling mechanisms. INDO MO FPT calculations of $^4J_o^{F,CH_3}$ are inadequate. By means of appropriate model compounds, an adequate empirical conformational dependence is deduced for $^4J_o^{F,CH_3}$, which can be used to reproduce some observed couplings. INDO MO FPT computations, in which certain off-diagonal Fock matrix elements are suppressed, are used to show that spin polarization via interacton of the methyl hydrogen orbitals is a major source of the discrepancy between theory and experiment. Some STO 3G MO calculations are reported for 2-fluorotoluene conformations.

TED SCHAEFER, RUDY SEBASTIAN, RICHARD P. VEREGIN et REINO LAATIKAINEN. Can. J. Chem. **61**, 29 (1983).

Une analyse complète du spectre de rmn du ^{1}H du fluoro-2 toluène fournit la constante de couplage spin–spin entre le ^{19}F et les protons du méthyle, $^4J_o^{F,CH_3}$ = 1,99 Hz. L'analyse des spectres de rmn de 21 autres dérivés du fluoro-2 toluène montre que $^4J_o^{F,CH_3}$ peut varier entre 1,69 et 2,55 Hz. Cette forte influence de la substitution contraste avec la quasi invariance des autres couplages à longue distance tels: $^4J_o^{H,CH_3}$, $^6J_p^{H,CH_3}$ et $^5J_m^{F,CH_3}$. On discute de l'influence des substituant en fonction des mécanismes de couplage. Les calculs INDO MO FPT de $^4J_o^{F,CH_3}$ ne sont pas adéquats. Au moyen d'un composé modèle approprié, on a déduit une influence conformationnelle empirique adéquate pour $^4J_o^{F,CH_3}$ qui peut être utilisée pour reproduire quelques-uns des couplages observés. On a utilisé des calculs INDO MO FPT dans lesquels on a supprimé certains éléments de la matrice de Fock hors diagonale pour montrer que cette polarisation de spin par l'intermédiaire des orbitales des hydrogènes du méthyle est la cause principale de cette différence entre la théorie et l'expérience. On rapporte quelques calculs d'OM STO 3G sur les conformations du fluoro-2 toluène.

[Traduit par le journal]

Introduction

Some of the spin–spin coupling constants between ring protons or ^{19}F nuclei and methyl protons are satisfactorily interpreted in terms of σ and σ–π electron coupling mechanisms (1–8). For example, $^6J_p^{H,CH_3}$ is a σ–π coupling, is insensitive to intrinsic (electronic) perturbations by ring substituents, and has a simple conformational dependence (1). In consequence, $^6J_p^{H,CH}$ has proved useful in deductions of conformational preferences, and of small barriers, about the exocyclic C—C bond in benzyl and benzal compounds (9). $^6J_p^{F,CH_3}$ can also be discussed in terms of a predominant σ–π mechanism (3), while $^5J_m^{F,CH_3}$ can be rationalized as a composite of σ and σ–π coupling mechanisms (8).

$^4J_o^{F,CH_3}$ is relatively large in magnitude (6), positive in sign (6), and may contain a third component, the so-called "through-space" contribution (10–14). Here this mechanism for the transmission of nuclear spin state information will be called the proximate component. INDO MO FPT computations (12), although in decent agreement with experiment for $^6J_p^{F,CH_3}$ (3) and $^5J_m^{F,CH_3}$ (8), apparently (14) overemphasize the proximate and/or σ mechanisms in 2-fluorotoluene.

In this paper, precise analyses of the ^{1}H nmr spectra of 2-fluorotoluene and 21 of its derivatives are reported. The results are examined for evidence concerning the relative importance of the three coupling mechanisms, the qualitative veracity of the INDO prediction of the conformational dependence of $^4J_o^{F,CH_3}$, and the reliability of some unexpected coupling magnitudes in the literature (15).

It turns out that, among the couplings mentioned above, $^4J_o^{F,CH_3}$ is unique in its large sensitivity to substituent perturbations and in that standard INDO MO FPT approaches fail in the reproduction of its conformational dependence. The latter is observed for defined dihedral angles by the use of 2,6-difluoroisopropylbenzene, 2-chloro-6-fluoroisopropylbenzene, and of 2,6-difluoroethylbenzene. The coupling mechanism is examined within the INDO MO approximation by the approach of Barfield (16), in which the development of spin polarization is repressed for certain nonbonded pathways.

Experimental

The compounds were mainly of commercial origin. The 3,5-dibromo, the 4,6-dibromo, and the 5-amino-4,6-diiodo derivatives of 2-fluorotoluene were prepared from the amino precursors in the obvious way. The deamination of the diiodo compound proved unsuccessful. The 4,5-dinitro and the 4,6-dinitro derivatives were made by nitration of 4-nitro-2-fluorotoluene. The synthesis of the 4-carbonyl fluoride derivative has been described (17). The 6-nitro and 6-amino derivatives were obtained via standard diazotization and reduction procedures from 2-amino-6-nitrotoluene. The 6-fluoro derivative appeared on reduction of 2,6-difluorobenzyl bromide with tri-n-butyl tin hydride. The 2,6-difluoroisopropylbenzene and 2-chloro-6-fluoroisopropylbenzene were synthesized from the corresponding carboxylic acids by methods recently described (18, 19), as was 2,6-difluoroethylbenzene from the acetophenone precursor (18). All compounds gave satisfactory mass spectra and characteristic ^{1}H nmr spectra.

The compounds were prepared as dilute solutions (see tabular data),

[1]Research associate from the Department of Chemistry, University of Jyväskylä, SF-40100, Jyväskylä 10, Finland.

0008-4042/83/010029-08$01.00/0
©1983 National Research Council of Canada/Conseil national de recherches du Canada

Can. J. Chem. Downloaded from www.nrcresearchpress.com by 210.87.254.105 on 09/06/12
For personal use only.

TABLE 1. Spectral parameters for a 9.9 mol% solution of 2-fluorotoluene, **1**, in CS_2 at 305 K

Parameter	Value[a]		Parameter	Value	
ν_{CH_3}[b]	—	220.205(2)	$^5J_{5F}$	−0.250(17)	−0.233(4)
ν_3	684.042(8)[c]	683.732(2)	$^4J_o^{H,CH_3}$	—	−0.779(2)
ν_4	701.940(9)	701.601(2)	$^5J_{m3}^{H,CH_3}$	—	0.401(2)
ν_5	689.940(10)	689.602(2)	$^5J_{m5}^{H,CH_3}$	—	0.352(2)
ν_6	703.917(9)	703.624(2)	$^6J_p^{H,CH_3}$	—	−0.603(2)
$^3J_{3F}$	9.748(14)	9.731(3)	$^4J_o^{F,CH_3}$	—	1.990(3)
$^3J_{34}$	8.188(13)	8.195(3)	$^3J_{45}$	7.423(13)	7.432(3)
$^4J_{35}$	1.226(11)	1.220(2)	$^3J_{56}$	7.529(13)	7.520(3)
$^4J_{46}$	1.782(10)	1.780(2)	Transitions		
$^4J_{4F}$	5.159(15)	5.186(4)	Calculated	86	646
$^4J_{6F}$	7.738(16)	7.723(4)	Assigned	76	581
$^5J_{36}$	0.344(13)	0.343(3)	rms deviation	0.028	0.017

[a]The first column refers to a calibration for which the CH_3 protons are decoupled.
[b]The shifts are in Hz at 100.001 MHz to low field of internal tetramethylsilane; the Bloch–Siegert shift is evident for the decoupled spectrum.
[c]The numbers in parentheses are the standard deviations in the least squares LAME analysis.

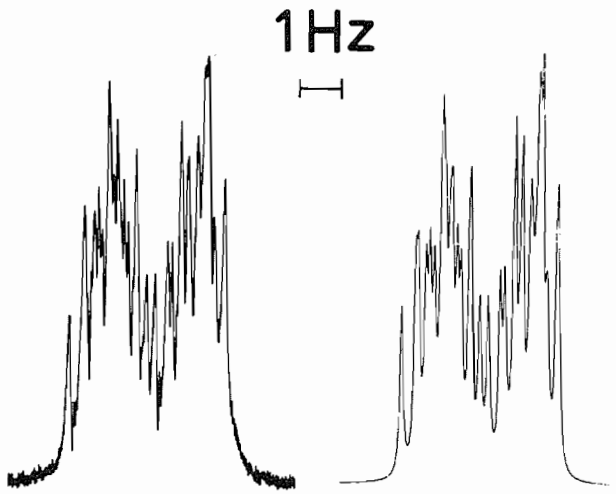

FIG. 1. The observed and calculated methyl proton ^{1}H nmr spectrum at 100 MHz of a 10 mol% solution of 2-fluorotoluene in CS_2 solution at 305 K. The calculated spectrum assumes the parameters in Table 1.

preferably in CS_2, containing ca. 4 mol% tetramethylsilane. The solutions were degassed by the freeze–pump–thaw technique and were flame-sealed into 5 mm od nmr tubes.

The ^{1}H nmr spectra were recorded in the frequency sweep mode on an HA100 spectrometer at a probe temperature of 305 K. Calibration procedures followed those described in detail recently (20). Interpolated peak frequences relative to TMS had standard deviations ≤0.02 Hz. Relative signs of coupling constants were found by weak multiple irradiation experiments (21). The spectral acquisitions for 2,6-difluoroisopropylbenzene and 2,6-difluoroethylbenzene have been described (18), those for 2-chloro-6-fluoroisopropylbenzene being done in the same way.

Calculations at the STO 3G (22) and INDO MO FPT (23) levels of molecular orbital theory were performed on an Amdahl 470/V7 system.

Results and discussion

Spectral analyses

Using the computer program LAME (24, 25), the spectral parameters for 2-fluorotoluene were extracted and are given in Table 1. Figure 1 displays the calculated and observed spectra for the methyl protons in 2-fluorotoluene. The program NUMARIT (26) was employed in the analysis of the spectra from the large spin systems, e.g., from the 6-methyl and 3-methyl derivatives and from 2,6-difluoroisopropylbenzene. The computer program MAOCON (27) was also utilized in some instances. The number of assigned transitions was as large as 1125 in one of these analyses.

In Table 2, the coupling constants of immediate interest in this paper are reported for 22 compounds. If an accuracy of 3 times the standard deviation in the parameters is assumed (99% confidence limits), the long-range couplings are known to an accuracy of at least 0.02 Hz and to 0.01 Hz in a substantial number of instances.

The couplings from ^{19}F to the methine and methylene protons in the isopropyl and ethyl compounds are quoted at the appropriate points in the text, and do not appear in Table 2.

It may be noted that $^5J_p^{H,F}$ in 4-iodo-2-fluorotoluene is −0.66 Hz, not 0.46 Hz as previously (15) reported and that, in the 6-chloro derivative $^5J_m^{H,CH_3}$ is 0.45 Hz for H-3 and 0.40 Hz for H-5, while $^6J_p^{H,CH_3}$ is −0.62 Hz. These three numbers are unexceptional and quite different from those in the literature (15), where they are given as <0.06 Hz in magnitude.

The substituent dependence of $^4J_o^{F,CH_3}$

First, note that $^6J_p^{H,CH_3}$ for the compounds in Table 2 is essentially the same as the −0.62 Hz in toluene (28). This coupling is calculated (1) and observed (2, 7) to be proportional to $\langle\sin^2\theta\rangle$, the expectation value of $\sin^2\theta$, where θ is the angle by which the methyl C—H bond twists out of the ring plane. In other words, $^6J_p^{H,CH_3}$ is dominated by a σ−π mechanism which is insensitive to the presence of the ring substituents. Second, $^4J_o^{H,CH_3}$ for the compounds in Table 2 is also remarkably insensitive to the ring substituents and scarcely different from the −0.75 ± 0.03 Hz in toluene (28). $^4J_o^{H,CH_3}$ is also predominantly a σ−π coupling although a small σ component is likely (1).

The near invariance of these two couplings contrasts with $^4J_o^{F,CH_3}$, which ranges from 1.69 Hz in the 6-amino to 2.55 Hz in the 5-amino-4,6-diiodo dervative. In terms of the coupling model, there arises the question whether the variation in $^4J_o^{F,CH_3}$ can be attributed to a substituent perturbation of one or more of the three coupling mechanisms. In this paper, the aim is not the establishment of correlations between $^4J_o^{F,CH_3}$ and the plethora of

Can. J. Chem. Downloaded from www.nrcresearchpress.com by 210.87.254.105 on 09/06/12
For personal use only.

Can. J. Chem. Downloaded from www.nrcresearchpress.com by 210.87.254.105 on 09/06/12
For personal use only.

TABLE 2. Some spectral parameters for the methyl protons in 2-fluorotoluene derivatives

	Compound[a,b]	$^4J_o^{F,CH_3}$	δ_{CH_3}	$-^4J_o^{H,CH_3}$	$-^6J_p^{H,CH_3}$
1	(9, 9)	1.990(3)[i]	2.202	0.779(2)	0.603(2)
2	4-NH_2 (10)[c]	1.845(7)	2.058	0.753(2)	—
3	4-NO_2 (10)	2.166(4)	2.373	0.794(2)	—
4	4-CFO[d]	2.119(3)	2.345	0.782(2)	—
5	4-I (9.8)	2.023(4)	2.173	0.782(2)	—
6	3-CH_3 (10)	2.190(2)	2.173	0.719(10)[j]	0.641(10)[j]
7	3,5-diBr (15)	2.326(3)	2.248	0.778(1)	0.617(1)
8	5-Br (10)	2.080(3)	2.201	0.779(2)	0.620(2)
9	5-NH_2 (1.4)[e]	2.006(7)	2.109	0.757(4)	0.590(4)
10	5-NO_2 (10)	2.157(4)	2.353	0.797(2)	0.603(2)
11	4,5-diNO_2 (10)	2.246(5)	2.446	0.778(5)	—
12	4-I-5-NH_2[f]	1.961(3)	2.209	0.786(2)	—
13	6-CH_3(10)	2.044(3)	2.092	—	0.602(2)
14	6-Cl (10)	2.275(4)	2.241	—	0.617(1)
15	6-NO_2 (10)	2.277(5)	2.392	—	0.608(4)
16	6-NH_2 (10)	1.693(5)	1.931	—	0.584(2)
17	6-F (8)	1.836(2)	2.146	—	0.623(5)
18	4,6-diNO_2 (10)	2,398(6)	2.549	—	—
19	4,6-diBr (10)[g]	2.407(7)	2.249	—	—
20	5-NH_2-4,6-diI[h]	2.550(3)[k]	2.304	—	—
21	3,5,6-tri F (10)	2.231(1)[l]	2.232	—	0.620(1)
22	3,4,5,6-tetra F (7)	2.255(6)[m]	2.248	—	—

[a]Compound **1** is 2-fluorotoluene, positions of *additional* substituents being indicated for subsequent entries.

[b]The parentheses give the mol% concentration in CS_2 solution, also containing about 4 mol% of TMS.

[c]A 6 mol% solution in C_6D_{12} had δ_{CH_3} as 2.068 and $^4J^{F,CH_3}$ as 1.858(5) Hz.

[d]For a 5 mol% solution in C_6D_6, full analysis of ^{19}F nmr spectrum included.

[e]A 4.5 mol% solution CCl_4 gave the coupling parameters as listed and δ_{CH_3} as 2.146.

[f]For a 9.5 mol% solution in $CDCl_3$.

[g]11.7 mol% in CCl_4.

[h]5 mol% in CCl_4.

[i]Numbers in parentheses are standard deviations in the last significant figure.

[j]Because of the nature of the spin system, the sum of $^4J^{H,CH_3}$ and $^6J^{H,CH_3}$ is the reliable parameter.

[k]A 5 mol% solution in $CDCl_3$ gave 2.569(3) Hz. A 2 mol% solution in $CDCl_3$ gave 2.54 Hz at 400 MHz.

[l]$^5J_m^{F,CH_3}$ is −0.232(1) Hz. A full analysis of the ^{19}F spectrum for a 10 mol% solution in $(CD_3)_2C{=}O$ gave $^5J_m^{F,CH_3}$ as −0.212(1) Hz, $^4J_o^{F,CH_3}$ as 2.231(1) Hz, and $^5J_p^{H,CH_3}$ as −0.622(1) Hz.

[m]$^5J_m^{F,CH_3}$ is −0.251(5) Hz and $^5J_p^{F,CH_3}$ is 1.384(5) Hz. The ^{19}F nmr spectrum was not analyzed.

substituent parameters which have been used in many attempts at the interpretation of nmr chemical shifts (see, for example, refs. 29, 30, and 31). Rather, certain chemical shifts may be useful as indicators of an approach to the rationalization of the variation of $^4J_o^{F,CH_3}$ and to an eventual use of this coupling in conformational problems.

Now δ_{CH_3} in *para*, *meta*, and *ortho* derivatives of toluene is sensitive to the usual substituent parameters meant to describe the changes induced in σ and π electron distributions in benzene derivatives (32, 33), and is *not* sensitive to peculiar "ortho" or "heavy-atom" parameters (33). Figure 2 displays an illustrative plot[2] of $^4J_o^{F,CH_3}$ versus δ_{CH_3} for 18 of the compounds in Table 2.

Given that δ_{CH_3} is a rough measure of the electron density at the methyl site or at its contiguous carbon atom, the changes in δ_{CH_3} and $^4J_o^{F,CH_3}$ caused by *ortho* and *para* amino or nitro substituents are indicative of an electron density dependence of these parameters (points 2, 3, 11, 15, 16, 18, and Fig. 2). An amino group causes a negative shift in $^4J_o^{F,CH_3}$ and a nitro substituent causes a positive shift. Now, it is known that the hyperfine interaction parameter, Q_{CCH}, in radicals depends on the electron density (charge) on the contiguous carbon atom, decreasing as the electron density increases (34). The σ−π component of $^4J_o^{F,CH_3}$ is proportional to Q_{CCH} in the spin polarized molecule (1, 3). Because the amino group is a π electron donor, the decrease of $^4J_o^{F,CH_3}$ in the 4- and 6-amino derivatives (points 2 and 16) is consistent with the apparent properties of Q_{CCH}, as are the increases in the 4- and 6-nitro derivatives (points 3, 15, and 18).

However, the situation is really more complicated because $^4J_o^{H,CH_3}$ and $^6J_p^{H,CH_3}$ are also proportional to Q_{CCH} and would be expected to reflect the changes in Q_{CCH} suggested by the magnitudes of $^4J_o^{F,CH_3}$. As can be seen in Table 2, this expectation is not confirmed. Of course, the σ−π component of $^4J_o^{F,CH_3}$ is also proportional to the hyperfine parameter Q_{CF}, which may vary with the amount of formal double bond character in the C—F bond (6). The coupling is less sensitive to an amino substituent placed *para* to fluorine rather than *para* to methyl. However, 4-nitro and 5-nitro substituents cause the same increase in $^4J_o^{F,CH_3}$.

The σ−π contribution to $^4J_o^{F,CH_3}$ is also proportional to the reciprocal of a mean excitation energy to appropriate triplet states (35). Again, it is difficult to see why substituent-induced

[2]δ_{CH_3} should really be measured at infinite dilution, not at the roughly 10 mol% concentration in CS_2 of most of the compounds. For our purposes the present values are sufficiently accurate (see footnotes in Table 2).

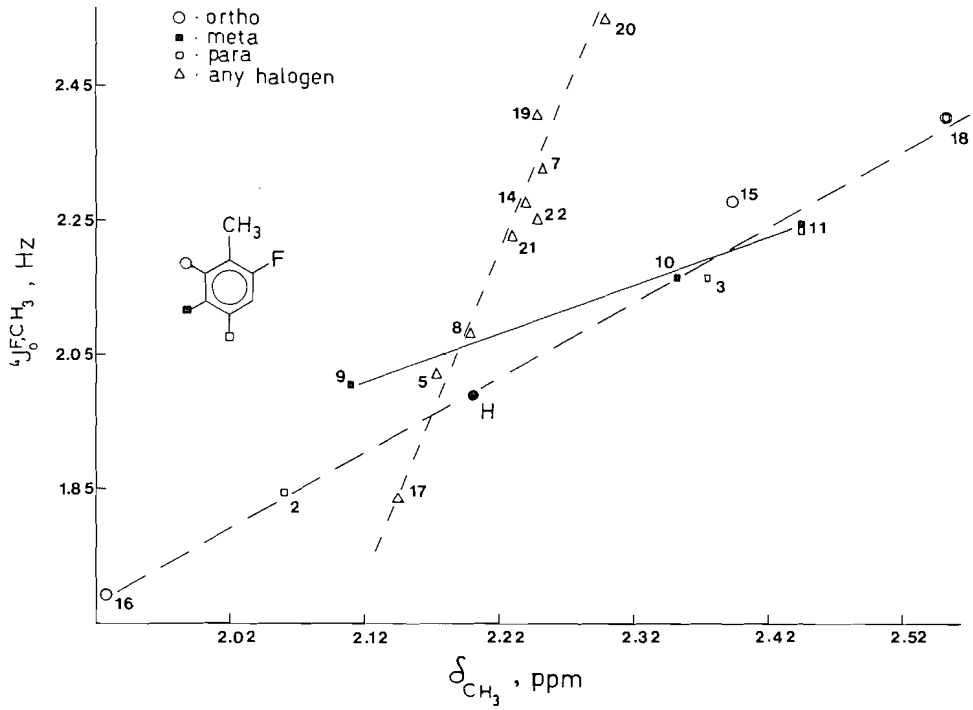

FIG. 2. $^4J_o^{F,CH_3}$ is plotted versus the chemical shift of the methyl protons for a series of 2-fluorotoluene derivatives. The substituents indicated as *ortho*, *meta*, or *para* are amino and nitro groups. The triangles identify *any* derivative containing one or more halogen substituents and may also contain other substituents. Note that a substituent placed *meta* to methyl is *para* to fluorine. Point 8 is for 5-Br, so that it could also be indicated as a solid square. The points are numbered as in Table 2.

changes in this excitation energy should leave $^6J_p^{H,CH_3}$ or $^4J_o^{H,CH_3}$ relatively constant, while perturbing $^4J_o^{F,CH_3}$ substantially.

The situation is further complicated by the trends in $^4J_o^{F,CH_3}$ for the halogen-substituted 2-fluorotoluene derivatives (Fig. 2). Over a range of only 0.15 ppm in δ_{CH_3}, $^4J_o^{F,CH_3}$ changes by 0.7 Hz. Part of this variation is probably conformationally determined (see below). Some of the variation must surely be an intrinsic electronic perturbation, unique to halogen substituents. Yet the perturbation is again such that Q_{CCH} and Q_{CH} and their associated triplet energies do not change much or do so in a compensatory manner. For example, $^6J_p^{H,CH_3}$ in symtetrafluorotoluene remains at -0.62 Hz, its value in toluene. However, in pentafluorotoluene (point 22 in Table 2) $^6J_p^{F,CH_3}$ is 1.38 Hz, about 0.25 Hz larger than in 4-fluorotoluene (3, 36), the amount by which $^4J_o^{F,CH_3}$ increases in the former compound relative to 2-fluorotoluene. These comparisons suggest variations in Q_{CF} as a cause of the changes in $^4J_o^{F,CH_3}$ in the halo derivatives.

No doubt $^4J_o^{F,CH_3}$ would correlate with other shift parameters for related molecules. For example, $^4J_o^{F,CH_3}$ for compounds **14**, **17**, **19**, and **20** (containing F, Cl, Br, and I *ortho* to CH_3) correlates well with $\delta_{C\text{-}1}$ in 2-halotoluenes (37). The latter also correlate well with "virtually all measureable liquid and/or vapor phase properties of halogen-containing molecules" (30). As indicated by Bailey and Wiberg (30), this fact may be related to the dominant role of the polarizability of the halogen containing molecules. Note that the largest $^4J_o^{F,CH_3}$ is found for compound **20**, containing two iodine substituents.

A partial resolution of these puzzles is provided by our previous data on methyl derivatives of the fluoropyridines (38). In these compounds $^6J_p^{H,CH_3}$ retains its value in toluene and the heteroatom also perturbs $^6J_p^{F,CH_3}$ only slightly. A good example among the eleven compounds is 2,6-dimethyl-3-fluoropyridine. Here $^6J_p^{H,CH_3}$ is $-0.59(2)$ Hz and $^6J_p^{F,CH_3}$ is 1.21(2) Hz. These two π electron dominated couplings are not appreciably perturbed by nitrogen. However, $^4J_o^{H,CH_3}$ is -0.52 Hz, substantially lower in magnitude than in toluene, and $^4J_o^{F,CH_3}$ is 3.03 Hz, 50% larger than in 2-fluorotoluene. The discussion in ref. 38 concluded that substantial polarization of the σ-core near C-2 and C-6 by the electronegative heteroatom caused changes in the σ electron contributions to $^4J_o^{H,CH_3}$ and $^4J_o^{F,CH_3}$.

With these facts in mind, comparison of all the long-range coupling data in Table 2 strongly suggests that much of the variation in $^4J_o^{F,CH_3}$ arises from changes in the σ electron contribution and/or in the proximate mechanism. It would be difficult and perhaps pointless to attempt a disentanglement of these two mechanisms. The data do indicate that changes in the π electron distribution will cause changes in, i.e. polarize, the σ-electron distribution. The latter are then reflected in changes in $^4J_o^{F,CH_3}$, as for the amino and nitro derivatives.[3]

In addition, $^4J_o^{F,CH_3}$ must also display a conformational dependence, unless the θ dependence of the σ electron/proximate component is independent of θ or behaves like the $\sigma-\pi$ component. The conformational dependence is now to be demonstrated. This will show that some of the changes in $^4J_o^{F,CH_3}$ for the 6-substituted derivatives very likely arise from the latter.

Empirical conformational dependence of $^4J_o^{F,CH_3}$

$^6J_p^{H,CH_3}$ in toluene is given by $-1.24\ \langle\sin^2\theta\rangle$ Hz (1, 9). Because the sixfold barrier is only 59 J/mol (41), the expectation value of $\sin^2\theta$ is 0.5 and $^6J_p^{H,CH_3}$ is observed and

[3]It appears that the nitro group withdraws "a constant amount of electron density from the ring regardless of what substituent is attached to the *meta* and *para* position" (39). Compare points 3 and 10 in Fig. 2, but see also ref. 40.

Can. J. Chem. Downloaded from www.nrcresearchpress.com by 210.87.254.105 on 09/06/12
For personal use only.

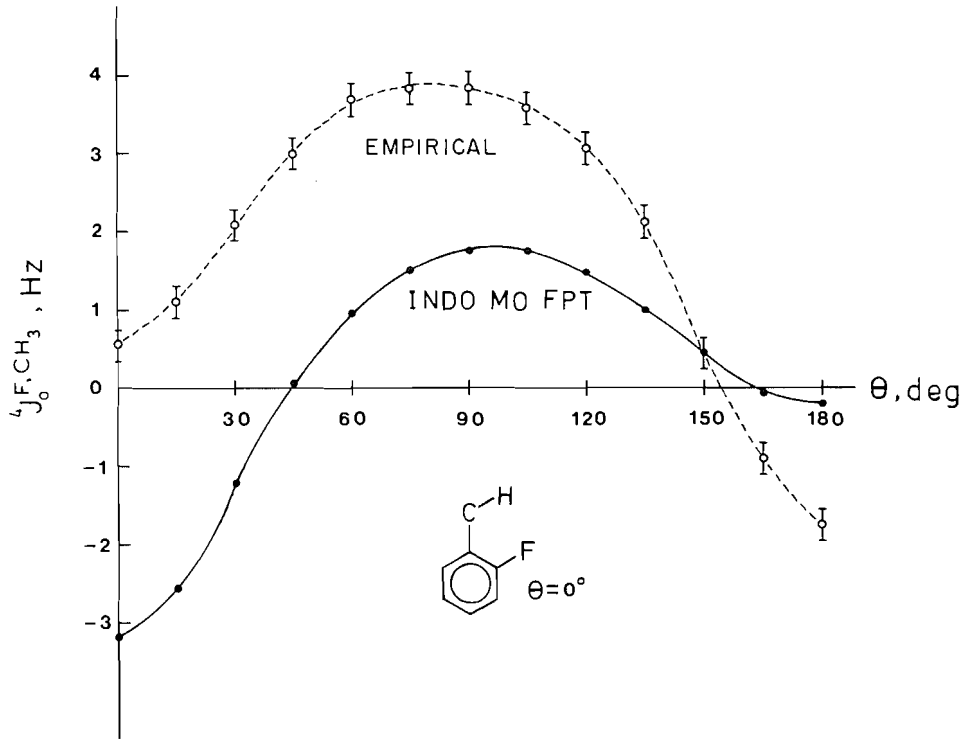

FIG. 3. The INDO MO FPT values for $^4J_o^{F,CH_3}$ in 2-fluorotoluene (14) are plotted versus the angle θ, as defined in the figure. At θ = 180° the C—H bond lies *trans* to the C—F bond and in the benzene plane. The upper curve shows the empirical couplings given in Table 3. This curve gives the correct "observed" couplings at θ = 0°, 30°, 150°, and 180° and also the experimental average value of $^4J_o^{F,CH_3}$. The error bars are meant to indicate that a coupling for a given conformation is reliable to about 0.2 Hz.

calculated by INDO MO FPT to be −0.62 Hz. The angle θ measures the out-of-plane twist of the C—H bond in the methyl group. This σ−π coupling mechanism yields $^6J_p^{H,CH_3}$ as −0.62 Hz, whatever the conformational preference of the methyl group, as follows from an average of $\sin^2\theta$ for the three C—H bonds in the methyl group. In 2-fluorotoluene, for example, **1**

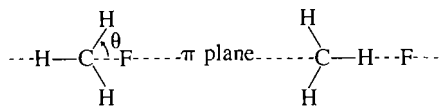

1 **2**

is favored over **2** (threefold barrier) by 2.7 ± 0.6 kJ/mol (42) but $^6J_p^{H,CH_3}$ remains the same as in toluene (Table 2).

In 4-fluorotoluene, $^6J_p^{F,CH_3}$ is also dominated by a σ−π mechanism (1, 3). The INDO values (1) agree with this mechanism but underestimate its magnitude by about 0.2 Hz or 20%.

Now, the INDO MO FPT curve in Fig. 3 clearly suggests the presence of a σ−π component, varying as $\sin^2\theta$, but that other components cause a distortion. The average of the computed values is only 0.13 Hz. In 2,6-difluorotoluene, $^4J_o^{F,CH_3}$ is 1.84 Hz and, because the internal barrier is now sixfold and therefore very small, is near the number expected from a faithful theoretical value. Naturally, as follows from the discussion in the previous section, an intrinsic substituent perturbation from the good π donor fluorine (compare amino in Table 2) should reduce the average coupling somewhat (ca. 0.1 Hz) from its magnitude in a hypothetical 2-fluorotoluene with a vanishing internal rotational barrier.

An empirical approach to the θ dependence of $^4J_o^{F,CH_3}$ is provided by the measurement of $^4J_o^{F,CH}$ in **3**, **4**, and **5**. In **3** the twofold barrier to rotation about the sp^2-sp^3 carbon–

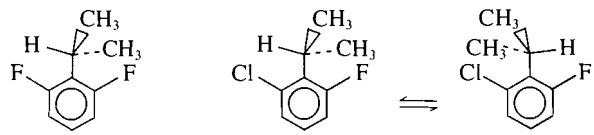

3 **4*a*** **4*b***

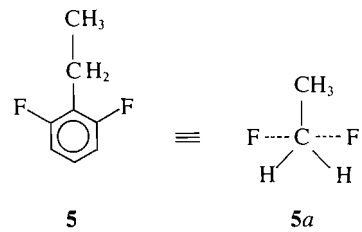

5 **5*a***

carbon bond is not less than 24 kJ/mol (18) and $^4J_o^{F,CH}$ is −0.60(1) Hz. At 180 K, rotation about the exocyclic carbon–carbon bond in **4** is slow enough so that two ^{19}F peaks can be observed. If it is assumed that there is no entropy difference between **4*a*** and **4*b***, admittedly somewhat unlikely, then the population of **4*a*** at 305 K can be extrapolated as 12%. If the stereospecific five-bond couplings, $^5J_m^{H,CH}$, in **4** at 305 K are used to obtain the populations of **4*a*** and **4*b*** as recently done for another molecule (43), then the population of **4*a*** is 24%. The latter is an overestimate, for reasons to be discussed in future. The free energy barrier to interconversion of **4*a*** and **4*b*** is not less than 41 kJ/mol (unpublished work in this laboratory). $^4J_o^{F,CH}$ in **4** is −1.33(1) Hz.

Because the internal barriers in both **3** and **4** are substantially larger than *kT* at 305 K, it is reasonable to derive $^4J_o^{F,CH}$ values for θ = 0° and 180° from the coupling data above. Assuming

Can. J. Chem. Downloaded from www.nrcresearchpress.com by 210.87.254.105 on 09/06/12
For personal use only.

Can. J. Chem. Downloaded from www.nrcresearchpress.com by 210.87.254.105 on 09/06/12
For personal use only.

the population of **4***a* as 18%, yields $^4J^{F,CH}$ as 0.54 Hz at $\theta = 0°$ and as -1.74 Hz at $\theta = 180°$. The extremes in the population estimates suggest errors of ca. 0.25 Hz in these numbers.

Again, **5***a* is the preferred conformation of **5** to the extent of 25 ± 8 kJ/mol (18) and $^4J_o^{F,CH_2}$ is +1.29(1) Hz. Therefore, the latter can be taken as a reasonable estimate of the average of $^4J_o^{F,CH_2}$ at $\theta = 30°$ and 150°.

Unfortunately, there appears to be no clear procedure by which $^4J_o^{F,CH}$ can be measured for other angles θ, particularly at 90°. Nevertheless, the average value of $^4J_o^{F,CH_3}$ for essentially free rotation is known to within about 0.1 Hz and a $\sin^2\theta$ component is no doubt present. Accordingly, an empirical θ dependence of $^4J_o^{F,CH_3}$ is displayed in Fig. 3. The average value for this curve is 1.90 Hz, approximately midway between the values of 1.99 Hz for 2-fluorotoluene and 1.84 Hz for 2,6-difluorotoluene. The mean of the points at 30° and 150° is in fact within 0.01 Hz of the observed +1.29(1) Hz. The numbers at $\theta = 0°$ and 180° reproduce the experimental values. To allow for uncertainties in $^4J_o^{F,CH_3}$ introduced by, for example, distortions of bond angles caused by methyl substitution or by the bulky sidechain chlorine substituent in **4**, error bars are introduced into the empirical curve. Polarization of the α C—H bond by the methyl groups is apparently rather small (9, 44, 45). That $^4J_o^{F,CH}$ is indeed negative at $\theta = 180°$ is confirmed by previous work on the analogue of **4** in which the methyl groups are replaced by chlorine atoms (46).

Other tests of the empirical curve can be made as follows. A bulky substituent at position 6 should favor conformation **2** for the methyl group, although probably only by amounts comparable to *kT* (47). The mean of the couplings at $\theta = 0°$ and $\theta = 120°$ (weighted twice) is 2.22 Hz, an increase of 0.32 Hz over the value for free rotation. The data in Table 2, when allowance is made for the intrinsic electronic perturbations discussed above,[4] support this change in $^4J_o^{F,CH_3}$. In *cis* 1-fluoropropene $^4J_o^{F,CH_3}$ is +2.6 Hz (48). In this molecule the conformation analogous to **2** is favored rather strongly and, allowing for the difference in the nature of the intervening bonds, the curve in Fig. 3 can be said to be consistent with observation. The numbers defining this curve are given in Table 3.

It is clear that $^4J_o^{F,CH}$ has applications in the study of conformational preferences. It is also clear that the empirical curve in Fig. 3 should be used carefully with due attention being paid to nonconformational perturbations by substituents on the ring and/or sidechain. The latter may well amount to about 0.5 Hz in extreme cases and for certain conformations. For example, in 2,6-difluorobenzylbromide, $^4J_o^{F,CH_2}$ is 1.14(2) Hz (unpublished work in this laboratory). This value is 0.15 Hz smaller than in 2,6-difluoroethylbenzene. Part of this difference arises from the difference in electronegativity of the methyl and bromine substituents (9). Another part may be caused by the expected larger barrier to rotation about the sp^2-sp^3 carbon–carbon bond in the bromine compound. A larger barrier implies a sharper pair of θ values at 30° and 150°, implying in turn that the empirical values at these angles are in error by about 0.1 Hz.

One other test of the empirical curve in Fig. 3 is possible. The conformational dependence of four coupling constants in 2-fluorobenzyl alcohol is sufficiently well known for a comparison with conformational energy predictions from molecular orbital methods (48*a*). Such calculations were performed for 18 conformations and the prediction by STO-3G of these couplings is in good agreement with experiment. The same approach to $^4J_o^{F,CH_2}$ in 2-fluorobenzyl alcohol, observed to be 1.22(3) Hz in CS_2 solution (48*a*), yielded 1.51 Hz for the numbers in Table 3. It is very probable (48*b*) that the $\sigma-\pi$ parameter, Q_{CCH}, for a CH_2OH group lies between 85 and 90% of Q_{CCH} for a methyl group. Most of the significantly populated conformations have a significant $\sigma-\pi$ contribution to $^4J_o^{F,CH_2}$ so that a reduction of 0.1 to 0.2 Hz might well occur. Further, the weighting of coupling constants by "rigid" conformations is not rigorous (9). In any event, the present number is in much better agreement with experiment than the −0.16 Hz calculated in the same manner from the INDO curve in Fig. 3.

The empirical curve in Fig. 3 is well-defined at $\theta = 0$, 30, 150, and 180°. The area under the curve is also correct to within 0.2 Hz. The other points on the curve follow from the assumption that it be smooth and are *not* experimental points, except insofar as their average is constrained to an experimental value. The error bars are estimated by a consideration of intrinsic substituent effects, and possible distortions of geometry caused by substituents on the ring or on the methyl group. If considerations of this kind are made for a particular compound, it does seem that significant conformational deductions will be possible, but it should be noted that a referee has expressed doubts on this point.

TABLE 3. Some INDO MO FPT computations of $^4J_o^{F,CH_3}$ in Hz in 2-fluorotoluene

θ[a]	Emp[b]	INDO[c]	Fsp/CH_3[d]	Fsp/Csp[e]	Fs/CH_3[f]
0°	0.54	−3.15	0.08	−3.39	−0.07
15	1.14	−2.56	0.11	−2.77	−0.01
30	2.12	−1.23	0.20	−1.43	−0.11
45	3.00	0.05	0.38	−0.19	0.31
60	3.69	0.95	0.72	0.61	0.56
75	3.82	1.51	0.90	1.07	0.83
90	3.83	1.77	1.08	1.28	1.00
105	3.57	1.76	1.07	1.29	1.01
120	3.06	1.48	0.86	1.14	0.80
135	2.11	0.99	0.50	0.84	0.45
150	0.48	0.41	0.09	0.47	0.04
165	−0.90	−0.06	−0.22	0.16	−0.29
180	−1.74	−0.24	−0.33	0.04	−0.41

[a]The conformational angle θ is defined in Fig. 3 and is zero when the C—H and C—F bonds are *cis*.

[b]These define the empirical curve in Fig. 3.

[c]Taken from ref. 14 for a standard geometry.

[d]Here the off-diagonal Fock matrix elements involving the 2*s* and 2*p* orbitals of fluorine and the 1*s* orbital of the methyl protons are set to zero. The C—F bond length is 1.35(7) Å, the sp^2-sp^3 carbon–carbon length is 1.53(2) Å, and $\angle C_2C_1CH_3$ is 119° (see text).

[e]Fock matrix elements involving fluorine and carbon valence orbitals are set to zero.

[f]No interaction between 2*s* orbitals on fluorine and the methyl hydrogen 1*s* orbitals.

Modified INDO MO FPT calculations

Because the calculated values of $^4J_o^{F,CH_3}$ are clearly deficient, it is of interest to examine the origin of the large computed negative values near $\theta = 0°$. This examination involved the procedure of Barfield (16), in which off-diagonal elements of Fock matrices associated with orbitals centered on certain nonbonded atoms were set equal to zero. This approach prevented

[4]A reliable disentanglement of the conformational from the intrinsic electronic perturbations for the 6-substituted derivatives seems impossible at present.

Can. J. Chem. Downloaded from www.nrcresearchpress.com by 210.87.254.105 on 09/06/12
For personal use only.

the transmission of spin–spin coupling via overlap of those orbitals. Some of these calculations are given in Table 3.

The numbers in Table 3 imply that it is the overlap of the hydrogen orbital with the 2*s* orbital on fluorine which is the primary interaction causing the large negative computed contributions to $^4J_o^{F,CH_3}$ near $\theta = 0°$. Furthermore, these calculations suggest that the observed negative value at $\theta = 180°$ arises via spin polarization of the orbitals on the methyl carbon. Finally, the computations clearly imply the expected $\sigma-\pi$ contributions to $^4J_o^{F,CH_3}$. If the Fock matrix elements involving direct overlap between the fluorine orbitals and the hydrogen orbitals are forced to vanish, then the computed curve qualitatively resembles the empirical curve in Fig. 2 but underestimates the average magnitude by a factor of about five.

It appears that the source of the qualitative discrepancy between calculated and observed couplings resides in the σ electron/proximate component of the computation. It is likely that 2-trifluoromethyl benzaldehyde is another example where a similar discrepancy occurs (11). Here $^5J_o^{CH,CF_3}$ is +2.2 Hz and is computed as negative (11). Yet, for the *cis* arrangement of the OH bond and the other substituent in 2-fluorophenol and 2-trifluoromethylphenol, $^4J_o^{OH,F}$ and $^5J_o^{OH,CF_3}$ lie near −4.5 Hz and are reproduced in a sensible way by INDO MO FPT approaches (49–51). Elucidation of these matters would be of interest; perhaps there exist other than contact mechanisms for some of these couplings (52).

Further MO calculations

The standard INDO MO FPT calculations assumed (14) a standard geometry (53). Because proximate coupling mechanisms are very sensitive to interatomic distances, a possible reason for discrepancies between theory and experiment lies in the difference between actual and standard geometries.

The geometry used by Schwoch and Rudolf (42) in their microwave work assumes a regular hexagon (r_{cc} = 1.391, r_{CH} = 1.084, r_{CF} = 1.348, r_{C-CH_3} = 1.520 Å) with tetrahedral angles at the methyl group. STO 3G MO calculations for such a geometry gave the eclipsed conformation, **2**, as 0.029 kJ/mol more stable than the staggered form, **1**. The latter is actually 2.7 ± 0.6 kJ/mol more stable than the former. INDO found 2.1 kJ/mol.

Partial optimization of bond angles and bond lengths at the STO 3G level yielded the following geometries (staggered, eclipsed):

$\angle C_2C_1C_7$(118.8°, 119.7), $\angle C_5C_6H_{12}$(120.4, 120.4)
$\angle C_1C_7H_{13}$(110.7, 110.7), $\angle C_1C_2F$(119.7, 120.1);
C_6—H_{12}(1.083 Å, 1.083), C_6—H(1.087, 1,087),
C—F(1.357, 1.357), C_1—C_7(1.532, 1.531).

All other bonds were kept at 120°, C—C lengths were 1.391 Å, and C—H lengths were 1.084 Å. For these geometries the staggered form was preferred by 0.10 kJ/mol.

For this partially optimized geometry, the INDO MO FPT calculations gave the staggered conformer a preference of 0.66 kJ/mol but did not encourage a belief that geometry accounts for the difficulties with the theoretical spin polarization mechanisms. Further STO 3G MO optimization procedures, in which all bond angles and bond lengths except for the regular hexagon were allowed to vary, did not alter the geometry or the conformational preferences in a significant way. It may be that optimization of the geometry of the benzene nucleus would lead to a more reliable result. It would also be very expensive (the details of the optimized structures are available from the authors).

INDO MO FPT calculations on derivatives of 2-fluorotoluene

Remarkably, the average over rotation for the calculated values of $^4J_o^{F,CH_3}$ in 2,6-difluorotoluene was 0.03 Hz and was 0.41 Hz in sym-tetrafluorotoluene. These *changes* from the calculated 0.13 Hz in 2-fluorotoluene reproduce the *trends* in Table 2 rather well. In addition, the average of $^6J_p^{H,CH_3}$ is calculated as -0.59_5 Hz, very close to the value in toluene and those observed (Table 2). Again, in the 4-nitro and 5-nitro derivatives an increase of 0.1 Hz is calculated for $^4J_o^{F,CH_3}$, roughly as observed. However, similar increases are also calculated for the corresponding amino compound, contrary to observation.

Summary and conclusions

In contrast to $^4J_o^{H,CH_3}$, $^6J_p^{H,CH_3}$, and $^6J_p^{F,CH_3}$, the magnitude of $^4J_o^{F,CH_3}$ in 2-fluorotoluene has a marked dependence on ring substituents. A large part of the substituent-induced changes in $^4J_o^{F,CH_3}$ is attributed to perturbations of the σ electron/proximate mechanisms, which are not easily distinguishable. The $\sigma-\pi$ contribution to $^4J_o^{F,CH_3}$ is relatively insensitive to intrinsic substituent perturbations. The conformational dependence of $^4J_o^{F,CH_3}$ is marked with a positive value for a planar *cis* orientation of the C—H and C—F bonds and a substantial negative value for a planar *trans* arrangement. These latter facts are not reproduced by standard INDO MO FPT computations. Further, examination of these calculations suggests that much of the disagreement with experiment originates in large negative contributions from 1*s*/2*s* overlaps between methyl hydrogens and fluorine. Judicious use of the empirical conformational dependence of $^4J_o^{F,CH}$ can be of value in stereochemical investigations.

Acknowledgments

We are grateful to the Natural Sciences and Engineering Research Council of Canada for financial assistance. R. L. thanks the Research Council for the Natural Sciences of the Academy of Finland for support. We thank Dr. G. Kotovych for the 400 MHz ^{1}H nmr spectrum of one of the compounds.

1. R. WASYLISHEN and T. SCHAEFER. Can. J. Chem. **50**, 1852 (1972).
2. C. J. MACDONALD and W. F. REYNOLDS. Can. J. Chem. **48**, 1002 (1970).
3. R. WASYLISHEN and T. SCHAEFER. Can. J. Chem. **49**, 94 (1971).
4. R. A. HOFFMAN. Mol. Phys. **1**, 326 (1958).
5. M. BARFIELD and B. CHAKRABARTI. Chem. Rev. **69**, 757 (1969).
6. D. J. BLEARS, S. S. DANYLUK, and T. SCHAEFER. J. Chem. Phys. **47**, 5037 (1967).
7. J. B. ROWBOTHAM and T. SCHAEFER. Can. J. Chem. **52**, 489 (1974).
8. T. SCHAEFER, W. DANCHURA, and W. NIEMCZURA. Can. J. Chem. **56**, 2233 (1978).
9. W. J. E. PARR and T. SCHAEFER. Acc. Chem. Res. **13**, 400 (1980).
10. J. HILTON and L. H. SUTCLIFFE. Prog. Nucl. Magn. Reson. **10**, 27 (1975).
11. T. SCHAEFER, S. R. SALMAN, and T. A. WILDMAN. Can. J. Chem. **58**, 2364 (1980).
12. M. BARFIELD and M. KARPLUS. J. Am. Chem. Soc. **91**, 1 (1969).
13. M. BARFIELD, A. M. DEAN, C. J. FOLLICK, R. J. SPEAR, S. STERNHELL, and P. W. WESTERMAN. J. Am. Chem. Soc. **97**, 1482 (1975).
14. R. E. WASYLISHEN and M. BARFIELD. J. Am. Chem. Soc. 4545 (1975).
15. P. ALBRIKTSEN and G. HANSEN. Acta Chem. Scand. **26**, 2511 (1972).

16. M. BARFIELD. J. Am. Chem. Soc. **102**, 1 (1980).
17. T. SCHAEFER, K. MARAT, K. CHUM, and A. F. JANZEN. Can. J. Chem. **55**, 3936 (1977).
18. T. SCHAEFER, R. P. VEREGIN, R. LAATIKAINEN, R. SEBASTIAN, K. MARAT, and J. L. CHARLTON. Can. J. Chem. **60**, 2611 (1982).
19. R. P. VEREGIN. M.Sc. thesis, University of Manitoba, 1982.
20. T. SCHAEFER and R. SEBASTIAN. J. Magn. Reson. **41**, 395 (1980).
21. R. FREEMAN and W. A. ANDERSON. J. Chem. Phys. **37**, 2053 (1962).
22. W. J. HEHRE, W. A. LATHAN, R. DITCHFIELD, M. D. NEWTON, and J. A. POPLE. Quantum Chemistry Program Exchange, **11**, 236 (1979).
23. P. A. DOBOSH. Quantum Chemistry Program Exchange, **11**, 1414 (1979).
24. S. CASTELLANO and A. A. BOTHNER-BY. J. Chem. Phys. **41**, 3863 (1964).
25. C. W. HAIGH. Ann. Rep. Nucl. Magn. Reson. Spectrosc. **4**, 311 (1971).
26. A. R. QUIRT and J. S. MARTIN. J. Magn. Reson. **5**, 318 (1971); J. S. MARTIN, A. R. QUIRT, and K. F. WORVILL. The nmr program library. Daresbury Laboratory, Daresbury, U.K.
27. R. LAATIKAINEN. J. Magn. Reson. **27**, 169 (1970); Doctoral thesis, University of Jyväskylä, Finland, 1979.
28. M. P. WILLIAMSON, R. KOSTELNIK, and S. M. CASTELLANO. J. Chem. Phys. **49**, 2218 (1968).
29. W. F. REYNOLDS, P. DAIS, G. K. HAMER, and I. R. PEAT. J. Magn. Reson. **43**, 81 (1981).
30. W. F. BAILEY and K. B. WIBERG. J. Org. Chem. **46**, 4225 (1981).
31. N. B. CHAPMAN and J. SHORTER (*Editors*). Correlation analysis in chemistry. Plenum Press, New York. 1978.
32. S. H. MARCUS, W. F. REYNOLDS, and S. I. MILLER. J. Org. Chem. **31**, 1872 (1966).
33. W. B. SMITH and T. W. PROULX. Org. Magn. Reson. **8**, 567 (1976).
34. R. HULME and M. C. R. SYMONS. J. Chem. Soc. (London), 1120 (1965).
35. H. M. MCCONNELL. J. Chem. Phys. **30**, 126 (1959); J. Mol. Spectrosc. **1**, 11 (1957).
36. T. SCHAEFER, W. DANCHURA, W. NIEMCZURA, and J. PEELING. Can. J. Chem. **56**, 2442 (1978).
37. W. F. BAILEY, E. A. CIOFFI, and K. B. WIBERG. J. Org. Chem. **46**, 4219 (1981).
38. J. B. ROWBOTHAM and T. SCHAEFER. Can. J. Chem. **50**, 2344 (1972).
39. K. B. LIPKOWITZ. J. Am. Chem. Soc. **104**, 2647 (1982).
40. W. F. REYNOLDS, P. DAIS, R. W. TAFT, and R. D. TOPSOM. Tetrahedron Lett. **22**, 1795 (1981).
41. H. RUDOLPH, H. DREIZLER, A. JAESCHKE, and P. WENDLING. Z. Naturforsch. Part A, **22**, 940 (1967).
42. D. SCHWOCH and H. D. RUDOLPH. J. Mol. Spectrosc. **57**, 47 (1975).
43. T. SCHAEFER, B. M. ADDISON, R. SEBASTIAN, and T. A. WILDMAN. Can. J. Chem. **59**, 1656 (1981).
44. T. SCHAEFER, L. KRUCZYNSKI, and W. NIEMCZURA. Chem. Phys. Lett. **38**, 498 (1976).
45. T. SCHAEFER, W. J. E. PARR, and W. DANCHURA. J. Magn. Reson. **25**, 167 (1977).
46. H. M. HUTTON, J. B. ROWBOTHAM, B. H. BARBER, and T. SCHAEFER. Can. J. Chem. **49**, 2033 (1971).
47. P. DIEHL, P. M. HENRICHS, W. NIEDERBERGER, and J. VOGT. Mol. Phys. **21**, 377 (1971).
48. R. A. BEAUDET and J. D. BALDESCHWIELER. J. Mol. Spectrosc. **9**, 30 (1962).
48. (*a*) T. SCHAEFER and W. J. E. PARR. J. Chem. Phys. **65**, 1197 (1976); (*b*) T. SCHAEFER, W. DANCHURA, W. NIEMCZURA, and W. J. E. PARR. Can. J. Chem. **56**, 1721 (1978).
49. T. SCHAEFER and J. B. ROWBOTHAM. Chem. Phys. Lett. **29**, 633 (1974).
50. J. B. ROWBOTHAM, M. SMITH, and T. SCHAEFER. Can. J. Chem. **53**, 986 (1975).
51. T. SCHAEFER and J. B. ROWBOTHAM. Can. J. Chem. **54**, 2243 (1976).
52. J. KOWALEWSKI. Prog. Nucl. Magn. Reson. Spectrosc. **11**, 1 (1977).
53. J. A. POPLE and M. GORDON. J. Am. Chem. Soc. **89**, 4253 (1967).

Can. J. Chem. Downloaded from www.nrcresearchpress.com by 210.87.254.105 on 09/06/12
For personal use only.

The system sulfur dioxide – *N*-methyl-2-pyrrolidinone

WILLIAM A. ADAMS
Defence Research Establishment Ottawa, Department of National Defence, Ottawa, Ont., Canada K1A 0Z4

AND

PEETER KRUUS and TIMOTHY J. PATRABOY
Department of Chemistry, Carleton University, Ottawa, Ont., Canada K1S 5B6

Received July 20, 1982

WILLIAM A. ADAMS, PEETER KRUUS, and TIMOTHY J. PATRABOY. Can. J. Chem. **61**, 37 (1983).

Solubility and freezing point data are presented for the system sulfur dioxide – *N*-methyl-2-pyrrolidinone (NMP). The enthalpy and entropy of solution are determined as -33.7 kJ mol^{-1} and -94.6 J K^{-1} mol^{-1}, respectively. The freezing point diagram shows maxima at $X_{SO_2} = 0.33$ (-14.0°C) and $X_{SO_2} = 0.50$ ($+2.6$°C), suggesting the presence of 2:1 and 1:1 NMP:SO_2 complexes. The existence of such complexes in the liquid state is supported by viscosity and permittivity data. Nuclear magnetic resonance and Raman spectroscopic data suggest an overall shift of electron density from the nitrogen and the carbonyl carbon of NMP to the O of SO_2, with weakening of the CO bond of NMP.

WILLIAM A. ADAMS, PEETER KRUUS et TIMOTHY J. PATRABOY. Can. J. Chem. **61**, 37 (1983).

On présente les données relatives à la solubilité et au point de congélation du système bioxyde de soufre/*N*-méthylpyrrolidinone-2 (NMP). On a déterminé l'enthalpie et l'entropie de solution qui sont respectivement de $-33,7$ kJ mol^{-1} et $-94,6$ J K^{-1} mol^{-1}. Le diagramme du point de congélation montre des maxima à $X_{SO_2} = 0,33$ ($-14,0$°C) et $X_{SO_2} = 0.50$ ($+2,6$°C) suggérant ainsi la présence de complexes NMP:SO_2 du type 2:1 et 1:1. Les données de viscosité et de permitivité témoignent de l'existence de tels complexes à l'état liquide. Les données de la spectroscopie de la rmn et Raman suggèrent un glissement global de la densitè électronique de l'atome et du carbone du carbonyle du NMP vers l'oxygène du SO_2 avec un affaiblissement de la liaison CO du NMP.

[Traduit par le journal]

Introduction

Solutions of sulfur dioxide in organic solvents are of current interest for several reasons. Non-aqueous solvents can be effective absorbers of SO_2 for the purposes of pollution control (1), and are vital in lithium–SO_2 high energy density primary batteries (2).

The solvent *N*-methyl-2-pyrrolidinone (NMP) has several industrial uses such as in the extraction of various petroleum fractions and as a solvent in the plastics industry (3). It has also been proposed as a potential adsorbent for SO_2 and H_2S in pollution control systems (4). As seen in Table 1, it has many desirable properties. A thorough study of this system was undertaken in order to give background information needed to assess its usefulness for various applications. The nature of the SO_2–NMP molecular level interactions giving rise to the macroscopic properties was also investigated.

TABLE 1. Some properties of NMP and SO_2

Property	NMP (3)	SO_2 (5)
Molecular weight/g mol^{-1}	99.13	64.06
Freezing point/°C	−24	−75.5
Boiling point/°C	204	−10.07
Density/g cm^{-3}	1.027 (25°C)	1.46 (−10°C)
Viscosity/cP	1.65	0.403 (0°C)
Dipole moment/D	4.09	1.62
Relative permittivity	32.0	15.4 (0°C)
ΔH^{θ}_{vap}/ kJ mol^{-1}	52.8	24.9

Experimental

The NMP (Aldrich reagent grade or Fisher purified grade) was vacuum distilled (at 60 to 65°C) from a calcium hydride slurry. The infrared spectrum of the liquid showed no discernible peak at 3200 cm^{-1} corresponding to the OH stretch of water and gas chromatography showed water content to be less than 100 ppm. The purified liquid was stored under dried nitrogen and was degassed immediately before use on a vacuum line by at least three freeze–pump–thaw cycles. All manipulations were carried out under anhydrous conditions.

Matheson anhydrous SO_2 was used. For high pressure solubility experiments, it was not further purified, but for the remaining experiments it was subjected to a distillation.

Gas solubility measurements were made by introducing a known amount of SO_2 gas (up to 250 cm^3) to a known amount of NMP (typically of the order of 0.5 g) and noting the pressure above the solution after equilibration (typically 1 h). Constant stirring in the solubility flask was provided by a magnetic stirrer with temperatures maintained to better than ±0.05°C by a circulating bath. The pressure above the solution was measured by either a mercury manometer or an MKS Baratron pressure meter. Corrections to the mass of SO_2 dissolved were made assuming the gas in the space above the solution to follow the ideal gas equation of state.

Solubility measurements were made in sets with either the temperature or the total amount of SO_2 (in gas and solution phase) held constant. The latter method had to be used for solution temperatures greater than ambient. In such cases, only higher pressure solubility measurements were possible, as at low SO_2 content the NMP would have condensed out into the gas lines above the solution.

For some studies, e.g. viscosity, ultrasonics, relative permittivity, solutions were made up by diluting a concentrated solution of SO_2 in NMP with NMP. The SO_2 content was in such cases obtained by mixing the solution into standardized sodium hydroxide solution and then back titrating with hydrochloric acid, using bromcresol green as indicator. For other studies, e.g. freezing points, nmr, Raman, solutions were made up by weight.

Freezing point measurements were obtained from cooling and heating curves using apparatus similar to that in ref. 6, density using a pycnometer, viscosity using a Cannon Fenske viscometer, permittivity using a General Radio bridge operating at 2.5 to 10 kHz, and

0008-4042/83/010037-08$01.00/0
©1983 National Research Council of Canada/Conseil national de recherches du Canada

Can. J. Chem. Downloaded from www.nrcresearchpress.com by 210.87.254.42 on 09/06/12
For personal use only.

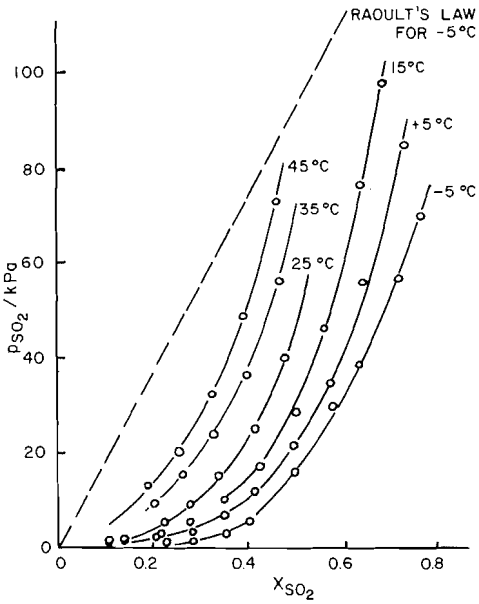

FIG. 1. Partial pressure of SO_2 above SO_2–NMP solutions.

ultrasonic absorption using the apparatus described in ref. 7.

Raman spectra were taken on a Jobin-Yvon HG2S spectrometer using the 514.5 nm line from a CR-12 argon ion laser at 300 mW power. Detection was by photon counting with a cooled R928 or R936 Hamamatsu PM tube with digital aquisition on a Nicolet 1180 computer. Curve resolution was done using the Nicolet 1180 CAP program with a Lorentzian–Gaussian distribution.

Nuclear magnetic resonance spectra were obtained on the following spectrometers: Varian T-60 for ^1H with tetramethylsilane as a reference, $T = 20 \pm 2°C$; Varian XL-100-12 with a Nicolet TT-100 Fourier transform data system for ^{13}C at 25.16 MHz with methanol-d_1 as reference, $T = 32 \pm 1°C$; Varian XL-200 for ^{17}O at 27.12 MHz with D_2O as reference, $T = 29°C$; Varian XL-200 for ^{15}N at 20.27 MHz with 2.9 *M* ammonium chloride in 1.0 *M* hydrochloric acid as reference, $T = 20.3°C$.

Results

(a) High pressure gas solubility

The high pressure solubility data are shown in Fig. 1.[1] There is a large negative deviation from Raoult's law ($p_{SO_2} = X_{SO_2} p^*_{SO_2}$) at all temperatures from −5 to 45°C, as illustrated by comparison of the −5°C curves. At the high X_{SO_2} values shown in Fig. 1, the partial pressure of NMP is negligible compared to the experimental uncertainty in the data.

Data displayed in Fig. 1 was used to calculate the excess free energy of mixing, ΔG^e_{mix}, of the solution. This quantity is defined as

$$[1]\quad \Delta G^e_{mix} = \Delta G_{mix} - \Delta G^{id}_{mix}$$
$$= \Delta G_{mix} - RT(X_{SO_2} \ln X_{SO_2} + X_{NMP} \ln X_{NMP})$$
$$= -RT(X_{SO_2} \ln \gamma_{SO_2} + X_{NMP} \ln \gamma_{NMP} \ln \gamma_{NMP})$$
$$= -RT\left\{X_{SO_2} \ln\left(\frac{p_{SO_2}}{X_{SO_2} p^*_{SO_2}}\right) + X_{NMP} \ln\left(\frac{p_{NMP}}{X_{NMP} p^*_{NMP}}\right)\right\}$$

For this calculation, the total measured pressure must be divided into the two partial pressures p_{SO_2} and p_{NMP}, even though p_{NMP} is very small.

[1]Tables of numerical data are available from P.K. at Carleton University.

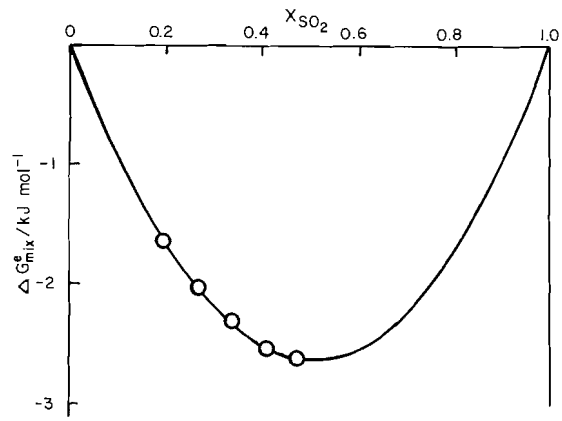

FIG. 2. Excess Gibbs free energy of mixing for SO_2–NMP, 25.0°C.

TABLE 2. Partial pressures and activities for the system SO_2–NMP, $T = 25.0°C$

X_{SO_2}	P_{tot}*	P_{SO_2}*	γ_{SO_2}†	P_{NMP}*	γ_{NMP}†	ΔG^e_{mix}‡
0.	0.034	—	—	0.034	1.00	—
0.20	4.069	4.062	0.07	0.023	0.83	−1.64
0.27	8.249	8.239	0.10	0.018	0.75	−2.03
0.33	14.600	14.586	0.15	0.014	0.64	−2.31
0.41	25.176	25.076	0.21	0.010	0.53	−2.52
0.47	38.529	38.522	0.28	0.007	0.44	−2.63
1.00	292.243	292.243	1.00	—	—	—

*kPa.
†$\gamma_i \rightarrow 1$ as $X_i \rightarrow 1$.
‡ kJ mol^{-1}.

This was done by a method similar to that used in ref. 9. The ΔG^e_{mix} was assumed to be described by an equation

$$[2]\quad \Delta G^e_{mix} = RTX_{SO_2}X_{NMP} \sum_{r=1}^{4} c_r(X_{SO_2} - X_{NMP})^{r-1}$$

The activity coefficients and partial pressures are related to the coefficients c_r by the Gibbs–Duhem relation:

$$[3]\quad X_{SO_2} d \ln \gamma_{SO_2} + X_{NMP} d \ln \gamma_{NMP} = 0$$

This gives the relation:

$$[4]\quad \ln \gamma_{SO_2} = X^2_{NMP}\left\{c_1 + \sum_{r=2}^{4} c_r(2rX_{SO_2} - 1)(X_{SO_2} - X_{NMP})^{r-2}\right\}$$

A non-linear least-squares program was used to obtain the best values of the coefficients c_1 to c_4 using these relations and all the available experimental data. In the case of higher temperatures, only five data points were available.

Table 2 shows the results for the 25°C data, with Fig. 2 showing the ΔG^e_{mix} obtained. Table 3 gives a listing of the c_r for all temperatures studied. There is relatively little variation of the ΔG^e_{mix} curves with temperature, with the minimum varying only from −2.5 kJ mol^{-1} to −3.2 kJ mol^{-1}.

The data in Fig. 1 are well above the Henry's law region, where $p_{SO_2} = K_H X_{SO_2}$. A limiting value of K_H can be obtained by extrapolating p_{SO_2}/X_{SO_2} to $X_{SO_2} \rightarrow 0$, but this introduces considerable uncertainty.

(b) Low pressure gas solubility

Figure 3 shows the gas solubility data at low pressures.[1] Two methods were used to obtain the data: (*a*) series of measurements at constant temperature, varying the total SO_2 and

Can. J. Chem. Downloaded from www.nrcresearchpress.com by 210.87.254.42 on 09/06/12
For personal use only.

TABLE 3. Coefficients describing the excess Gibbs free energy of mixing for SO_2–NMP (eq. [2])

T/°C	c_1	c_2	c_3	c_4
−5.0*				
+5.0	−4.93	−0.89	+0.78	−1.77
+15.0	−4.99	−1.22	+1.13	−0.35
+25.0	−4.27	−0.28	+0.09	−0.60
+35.0	−5.02	+1.06	+3.48	+6.97
+45.0	−3.82	−1.01	−0.28	−0.22

*No reasonable fit possible with four coefficients.

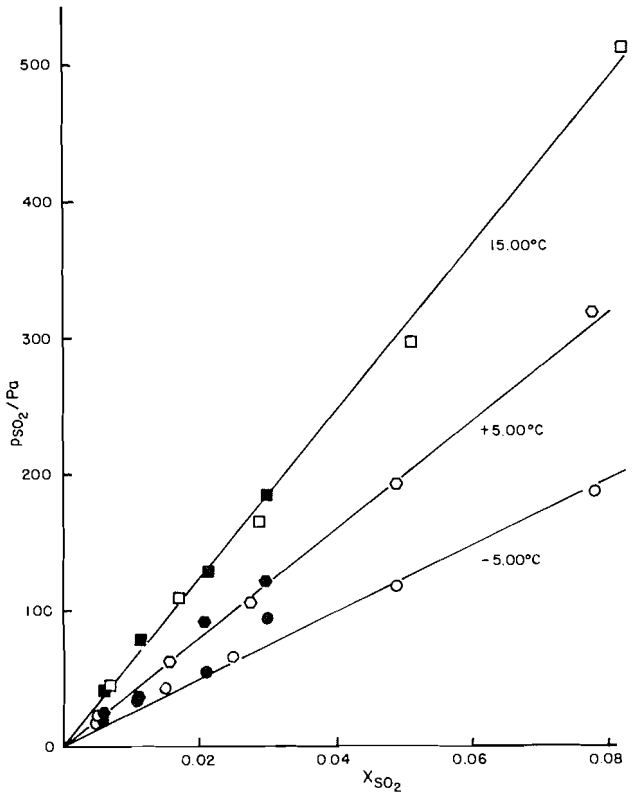

FIG. 3. Partial pressure of SO_2 above SO_2–NMP solutions in Henry's law range. Open symbols, method (*a*); closed symbols, method (*b*).

using the Baratron pressure meter, and (*b*) series of measurements at constant total SO_2, varying the temperature and obtaining pressure from a manometer aided by a cathetometer. These data are consistent with each other and are in the linear Henry's law region.

A free energy of solution can be obtained from such data. This is for the reaction:

[5] $SO_2(g) \rightleftharpoons SO_2(\text{NMP solution})$

The standard free energy of solution is defined as:

$$[6] \quad \Delta G^{\theta}_{sol} = -RT \ln K_a = -RT \ln \left(\frac{a_{SO_2(sol)}}{a_{SO_2(g)}} \right)$$

The activity equilibrium constant K_a approaches the ratio $X_{SO_2}/p_{SO_2} = 1/K_H$ as $X_{SO_2}, p_{SO_2} \rightarrow 0$ with the conventions

$$a_{SO_2(g)} = \gamma^{p}_{SO_2} p_{SO_2} \rightarrow p_{SO_2} \text{ as } p_{SO_2} \rightarrow 0$$

and

$$a_{SO_2(sol)} = \gamma^{l}_{SO_2} X_{SO_2} \rightarrow X_{SO_2} \text{ as } X_{SO_2} \rightarrow 0$$

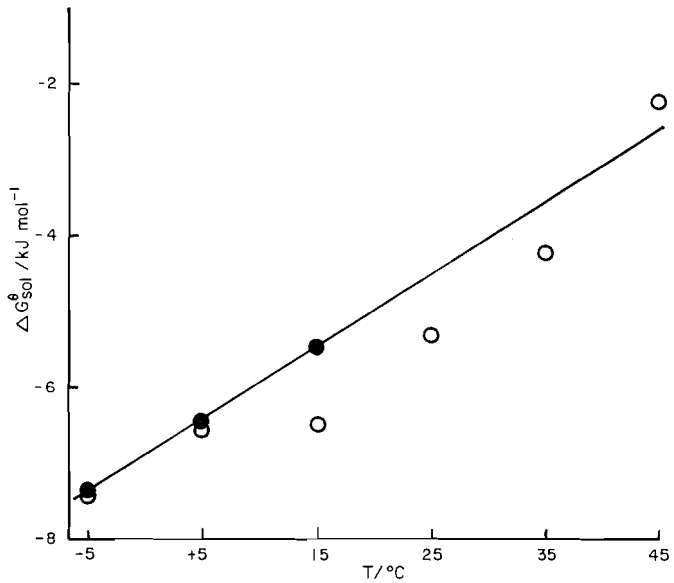

FIG. 4. ΔG^{θ}_{sol} for SO_2 in NMP ($X_{SO_2} \rightarrow 0$). ●, low pressure data (Fig. 3); ○, extrapolation from high pressure data (Fig. 1).

This latter convention commonly used in discussions of gas solubility differs from the convention in part (*a*), where $\gamma_{SO_2} \rightarrow 1$ as $X_{SO_2} \rightarrow 1$, even though composition is expressed in the same units (mol fraction).

Figure 4 shows the ΔG^{θ}_{sol} as a function of temperature. Points obtained from the extrapolation of high pressure data are also included, even though they are not considered very reliable. The entropy and enthalpy of solution can be obtained from such a plot as

$$[7] \quad \Delta S^{\theta}_{sol} = -\partial(\Delta G^{\theta}_{sol})/\partial T$$
$$\Delta H^{\theta}_{sol} = \Delta G^{\theta}_{sol} + T\Delta S^{\theta}_{sol}$$

The analysis using only low-pressure points gives values of

$$\Delta S^{\theta}_{sol} = -94.6 \pm 0.7 \text{ J K}^{-1} \text{ mol}^{-1}$$
$$\Delta H^{\theta}_{sol} = -33.7 \pm 0.2 \text{ kJ mol}^{-1}$$

(c) Freezing point diagram

The freezing point diagram for the system SO_2–NMP is shown in Fig. 5.[1] The accuracy of the data is estimated to be ±0.2°C, except for points near $X_{SO_2} \simeq 0.7$, where error limits are indicated. Eutectic temperatures of −29.6, −14.7, and −87.9°C are clearly present in some of the mixtures. The melting points of the pure components are close to, but somewhat higher, than literature values (Table 1), indicating that the NMP and SO_2 used were of high purity.

Both 1:1 and 1:2 complexes of SO_2 and NMP appear to be present in the solid, as indicated by the freezing point maxima at $X_{SO_2} = 0.33$ and $X_{SO_2} = 0.50$.

(d) Viscosity and density

The viscosity data[1] shown in Fig. 6 suggest that the 1:2 complex is also present in the liquid mixtures. The deviation of the actual viscosity from the ideal viscosity shows a maximum near $X_{SO_2} = 0.33$. The "ideal" viscosity η^{id} is taken here to be

$$[8] \quad \eta^{id} = \phi_{SO_2}\eta_{SO_2} + \phi_{NMP}\eta_{NMP}$$

where ϕ is the volume fraction. Values for the (hypothetical) viscosity of pure liquid SO_2 were obtained by extrapolation of data from ref. 10.

Can. J. Chem. Downloaded from www.nrcresearchpress.com by 210.87.254.42 on 09/06/12
For personal use only.

Can. J. Chem. Downloaded from www.nrcresearchpress.com by 210.87.254.42 on 09/06/12
For personal use only.

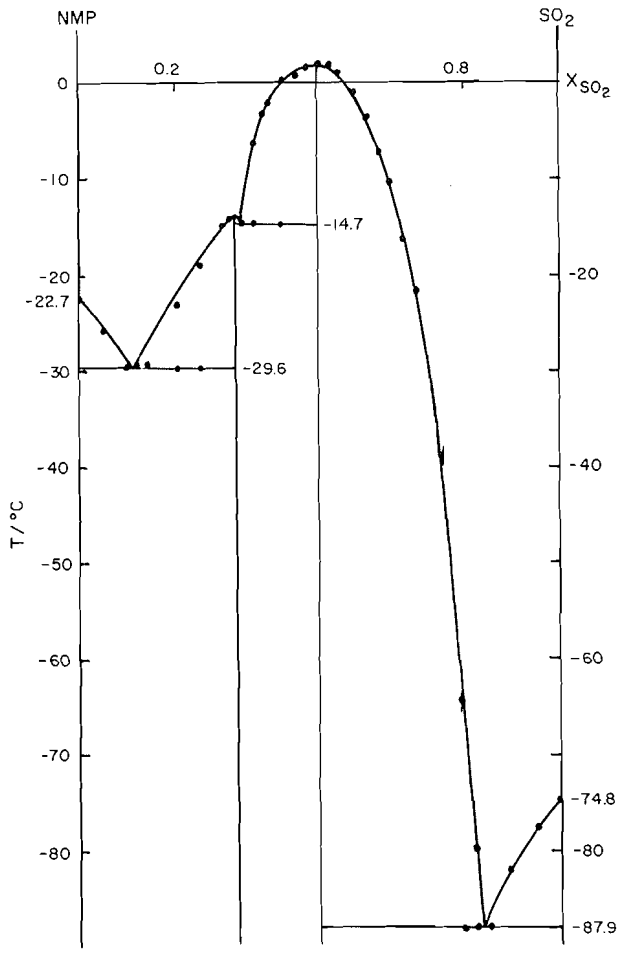

FIG. 5. Freezing point diagram for SO_2–NMP.

Density measurements were made of the solutions at 25°C. The results indicate negligible deviation from ideality, at least for the purpose of calculation of dynamic viscosity from flow times. The partial molar volume of the solutions is linear with X_{SO_2} (slope -55.5 cm^3 mol^{-1}, correlation coefficient 0.9997) in the experimentally investigated range ($X_{SO_2} < 0.5$). For pure NMP, the molar volume measured is 96.4 ± 0.1 cm^3 mol^{-1}, as compared to 96.5 cm^3 mol^{-1} obtained from data in Table 1. The corresponding values for pure (hypothetical) SO_2 are 40.9 ± 0.4 cm^3 mol^{-1} (from extrapolation of experimental data) and 43.9 cm^3 mol^{-1} (Table 1). The densities of the mixtures at 5°C were assumed to be ideal. The density of NMP was measured to be 1.044 g cm^{-3} and that of SO_2 was interpolated to be 1.42 g cm^{-3} (10).

(d) Relative permittivity

Reliable permittivity values could be obtained only for $X_{SO_2} < 0.25$. At 20 ± 2°C, ϵ increase approximately linearly from 33.4 (pure NMP) to 74 ± 1 ($X_{SO_2} = 0.248$).[1] At higher X_{SO_2} values, the conductivity was too high to make reasonably accurate permittivity measurements at the frequencies available. There was a considerable further increase of ϵ with X_{SO_2}; at $X_{SO_2} = 0.41$, the value of ϵ is estimated to be 170 ± 10.

(e) Ultrasonic absorption

NMP has ultrasonic absorption characteristic of associated liquids (11). In the frequency range 10.5 MHz to 52.5 MHz at 25°C it has a low absorption, $\alpha/\nu^2 = (40 \pm 5) \times 10^{-15}$ s^2 m^{-1}, with no consistent decrease with frequency. At 0°C, α/ν^2 increases to $(55 \pm 5) \times 10^{-15}$ s^2 m^{-1}.

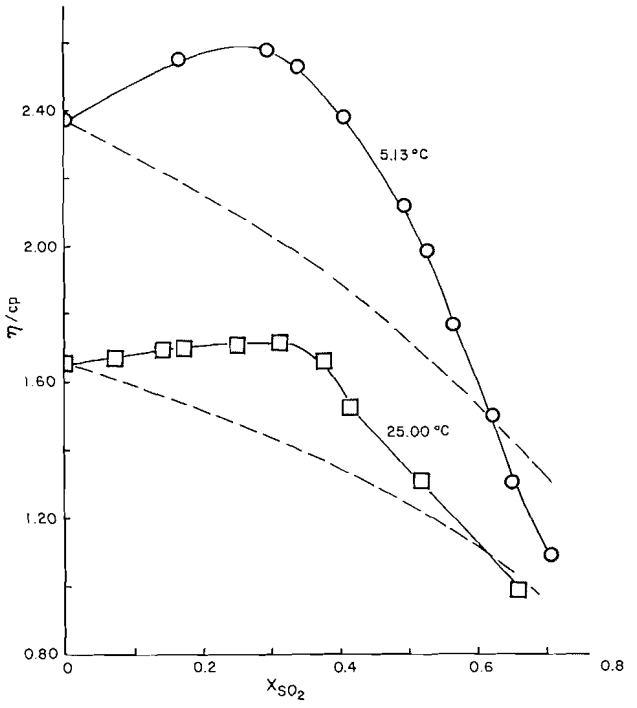

FIG. 6. Viscosity of SO_2–NMP solutions --- η^{id} (eq. [8]).

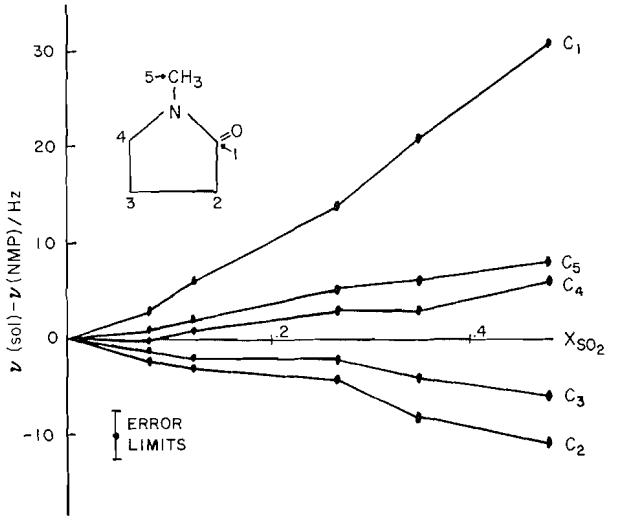

FIG. 7. Relative shifts of ^{13}C resonances in SO_2–NMP solutions, T = 32°C, 25.16 MHz.

When SO_2 is added to NMP at 25°C, the absorption follows the behaviour of the viscosity (Fig. 6). At 31.7 MHz, there is a small increase (from 40 to 50 units) to $X_{SO_2} \simeq 0.2$, and then a levelling off (data were taken to $X_{SO_2} = 0.47$). There is no evidence of any relaxation, i.e. decrease of α/ν^2 with ν, in the frequency range 10.5 to 52.5 MHz for a solution $X_{SO_2} = 0.27$ at 25°C or at 0°C.

(f) Nuclear magnetic resonance

Figure 7 shows the ^{13}C resonance shifts of the NMP carbons as SO_2 is added.[1] The resonances were assigned following ref. 12.

Similar data were taken using ^{1}H nmr.[1] The only identifiable shifts noted were for hydrogens on C_1 (methyl) and C_4; the frequency of both resonances decreased by 6 ± 2 Hz as X_{SO_2}

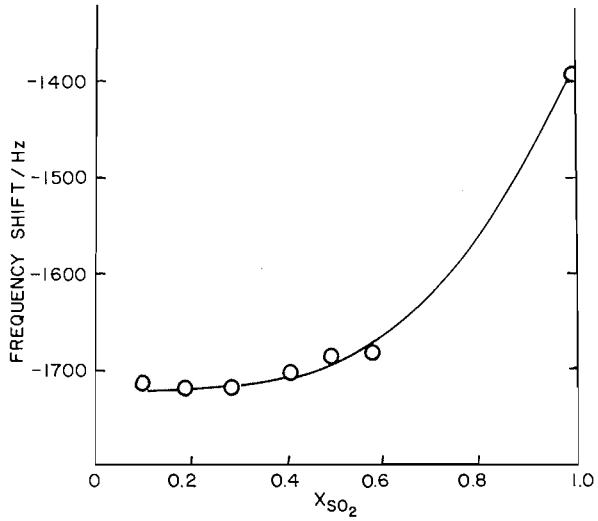

FIG. 8. Shifts of ^{17}O resonances of SO_2 oxygens in SO_2–NMP solutions relative to $D_2{}^{17}O$.

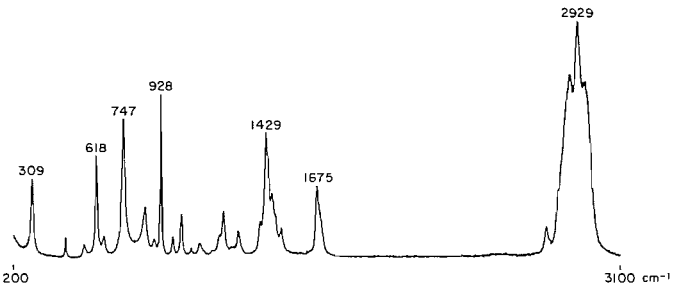

FIG. 9. Raman spectrum of NMP, 20°C. Slits 2, 4, 4, 2 cm^{-1}; one scan at 2 cm^{-1} s^{-1}. CH region at 2929 cm^{-1}, CO at 1675 cm^{-1}, CN at 1429 cm^{-1}.

increased from 0 to 0.45. The ^{15}N resonance frequency shifted from 1713 Hz (pure NMP) to 1834 Hz (X_{SO_2} = 0.58) on addition of SO_2. The frequencies quoted are relative to the reference (NH_4Cl in HCl solution). If this reference is assumed to be 29.43 ppm from ammonia, then pure NMP has its ^{15}N resonance at 113.9 ppm, somewhat different from the value 108.7 ppm previously reported (13).

Oxygen-17 nmr resonances were investigated for the oxygens both in the NMP and in SO_2. The NMP ^{17}O resonance showed no consistent trend in freqnency as SO_2 was added. The frequency was at +8240 Hz relative to D_2O, in reasonable agreement with the data for other amides such as dimethyl formamide (14). The ^{17}O resonance is broad, especially in NMP, so that its position is accurate to at best +20 Hz. This contrasts to the large shift of the NMP ^{17}O when water is added. The signal (at 24°C) shifts from 8257 Hz (X_{H_2O} = 0) to 7574 Hz (X_{H_2O} = 0.635) to 7184 Hz (X_{H_2O} = 0.792). Large ^{17}O shifts of oxygens in C=O bonds on adding water have been noted previously (14).

Figure 8 shows the shift in the SO_2 ^{17}O resonance as a function of X_{SO_2}.[1] There is considerable decrease in the ^{17}O resonance as NMP is initially added to SO_2, but at $X_{SO_2} < 0.33$, it no longer changes. The pure SO_2 value is taken from ref. 15; it is misquoted in ref. 16.

(g) Raman spectroscopy

Figure 9 shows the Raman spectrum of NMP from 200 to 1700 cm^{-1}, indicating the assignments of various modes. The

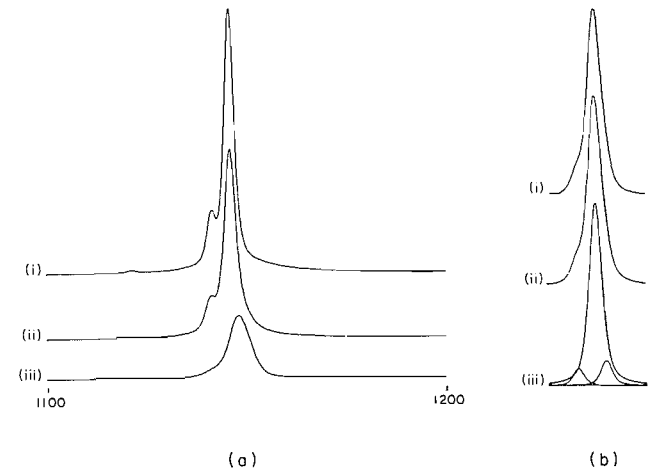

FIG. 10. (*a*) Raman spectra of the SO_2 stretch region, 25°C. Slits 2, 4, 4, 2 cm^{-1}; two scans at 1 cm^{-1} s^{-1}. (*i*) X_{SO_2} = 1, (*ii*) X_{SO_2} = 0.86, (*iii*) X_{SO_2} = 0.37. (*b*) Curve resolution of the SO_2 stretch region, X_{SO_2} = 0.51. (*i*) experimental, (*ii*) calculated, (*iii*) component bands (see Table 4). 40% Gaussian, 60% Lorentzian.

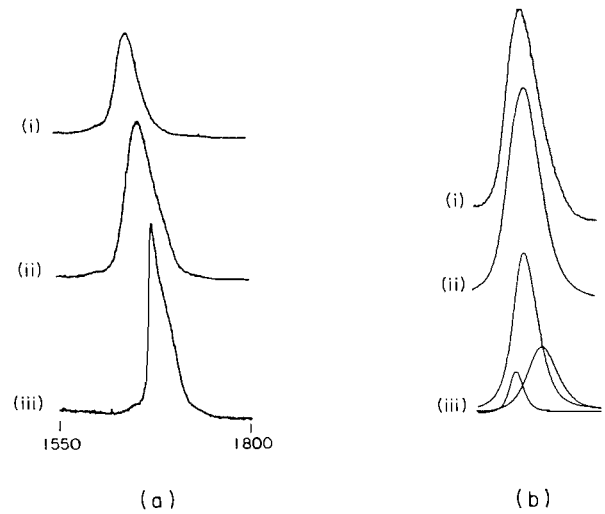

FIG. 11. (*a*) Raman spectra of the carbonyl region, 25°C. Slits 2, 4, 4, 2 cm^{-1}; four scans at 1 cm^{-1} s^{-1}. (*i*) X_{SO_2} = 0.86, (*ii*) X_{SO_2} = 0.37, (*iii*) X_{SO_2} = 0.00. (*b*) Curve resolution of the carbonyl region, X_{SO_2} = 0.51. (*i*) experimental, (*ii*) calculated, (*iii*) component bands (see Table 5). 40% Gaussian, 60% Lorentzian.

SO_2 bending (530 cm^{-1}) and asymmetric stretch (1320 cm^{-1}) regions overlap NMP bands, but the symmetric stretch (1148 cm^{-1}) can be seen without interference.

More detailed spectra of the NMP carbonyl and the SO_2 symmetric stretching regions are shown in Figs. 10 and 11. As can be seen there and in Tables 4 and 5 it is necessary to use at least two lines to resolve the carbonyl band properly, even for the pure NMP. Three lines are required for the SO_2 band. The low frequency shoulder (1140 cm^{-1}) is due to an isotopic shift (17). There are no significant changes in spectra recorded for the systems at 10°C and 5°C.[1]

Discussion

The system NMP–SO_2 contains several reasonably strong, specific interactions. The high Trouton constant (Table 1) and the C=O band shape (Fig. 10) suggest that NMP has a strong tendency to be in a dimer form as a liquid. There is consid-

Can. J. Chem. Downloaded from www.nrcresearchpress.com by 210.87.254.42 on 09/06/12
For personal use only.

TABLE 4. Raman spectral data for SO_2 symmetric stretch band, T = 25°C (intensities are relative to the intensity of the 459 cm^{-1} band of CCl_4)

	Line 1		Line 2		Line 3	
X_{SO_2}	Position/ width cm^{-1}	Relative intensity $\times 10^3$	Position/ width cm^{-1}	Relative intensity $\times 10^3$	Position/ width cm^{-1}	Relative intensity $\times 10^3$
0.12	1140.5	0.62_4	1148.1	12.13	1150.6	0.48_4
	34.6		31.8		11.9	
0.24	1140.5	1.10	1147.4	21.33	1150.1	2.74
	23.2		30.2		22.4	
0.37	1140.9	1.62	1147.4	28.79	1150.3	3.02
	22.4		29.7		22.4	
0.51	1140.6	3.57	1146.6	38.20	1150.0	5.39
	23.6		25.7		25.2	
0.86	1140.6	7.55	1145.8	40.09	1149.4	5.39
	18.9		16.8		33.8	

TABLE 5. Raman spectral data for NMP carbonyl band, T = 25°C (intensities are relative to the intensity of the 459 cm^{-1} band of CCl_4)

X_{SO_2}	Position/ width cm^{-1}	Relative intensity $\times 10^3$	Position/ width cm^{-1}	Relative intensity $\times 10^3$	Position/ width cm^{-1}	Relative intensity $\times 10^3$
0	—	—	1675.0	3.93	1688.1	10.18
			21.0		63.3	
0.12	1648.7	1.29	1673.2	11.97	1694.5	2.72
	50.7		63.9		50.1	
0.24	1646.2	1.45	1664.6	14.10	1689.7	3.15
	47.4		73.9		55.0	
0.37	1646.9	2.13	1660.6	13.02	1685.0	3.72
	52.3		69.3		65.2	
0.51	1642.3	1.69	1653.5	11.53	1670.3	5.49
	39.4		65.2		77.6	
0.8	1637.0	0.39	1646.1	5.54	1663.1	1.32
	21.8		55.3		58.8	

erable evidence of dimerization in similar compounds (18). Sulfur dioxide is also believed to associate substantially, in spite of its low boiling point (9).

It is evident from the freezing point diagram (Fig. 5) that there is a strong 1:1 complex formed between NMP and SO_2. Several other organic compounds form such complexes with SO_2 (19, 20). There is also evidence of a complex $(NMP)_2:SO_2$ in the freezing point diagram. A diagram such as Fig. 5 is also obtained for the system dimethylsulfoxide–SO_2, except that in that case, a complex $DMSO:(SO_2)_2$ is apparent (21). The presence of such complexes gives an explanation for the viscosity and permittivity data obtained.

Viscosity data has been interpreted to give sizes of the aggregates present in solutions (22). The data in Fig. 6 can be used to estimate the activation energy for viscous flow. For pure NMP it is 12.4 kJ mol^{-1}, for X_{SO_2} = 0.33, 13.9 kJ mol^{-1}, and for X_{SO_2} = 0.50, 15.2 kJ mol^{-1}. An analysis following the suggestions in ref. 22 would suggest that pure NMP is to a large extent in a dimer form, and that at a mole fraction of 0.5, a 2:2 rather than a 1:1 complex could be present.

In principle, the equilibrium constants, K, for such complexation reaction can be obtained from thermodynamic and/or spectroscopic data. The ΔG^e_{mix} data can be fitted by various statistical-mechanical models, and the equilibrium constants obtained (9). The ΔH^θ of the equilibria can then be obtained from the temperature variation of the K's. Such an analysis of the ΔG^e_{mix} data (Table 3) was attempted using a model allowing for NMP dimers and NMP–SO_2 1:1 complexes. The results obtained showed no consistency. This may be because of an oversimplified model or because the experimental data are insufficiently extensive and accurate.

Spectroscopic evidence such as that in Figs. 10 and 11 is difficult to use for quantitative calculations of K values as resolution of such band into components is difficult and subjective. Tables 4 and 5 show no trends which could properly be used for such calculations. Molar scattering coefficients of the band components would also have to be estimated. Many additional Raman spectra would be required if "Job's method" (23) were to be attempted for an analysis.

The value ΔH^θ_{sol} = −33.7 kJ mol^{-1} obtained from the temperature dependence of Henry's law plots (Figs. 2, 3) refers to the enthalpy of solution of SO_2 at infinite dilution. The ΔH^θ_{sol} and ΔS^θ_{sol} values obtained for NMP are closest to the values for acetonitrile and propylene carbonate obtained by Benoit and Milanova (24), and considerably less negative than DMSO. There seems to be little correlation between the NMP ΔH^θ_{sol} and the Gutmann donor or acceptor numbers (25).

A simple classical calculation predicts an energy of this order of magnitude. The energy of two permanent, non-polarizable dipoles 4.1 D (NMP) and 1.6 D (S—O bond in SO_2) parallel and 0.3 nm apart is −15 kJ mol^{-1}. Attraction due to polarization and dispersion forces would lower this value, i.e. in-

Can. J. Chem. Downloaded from www.nrcresearchpress.com by 210.87.254.42 on 09/06/12
For personal use only.

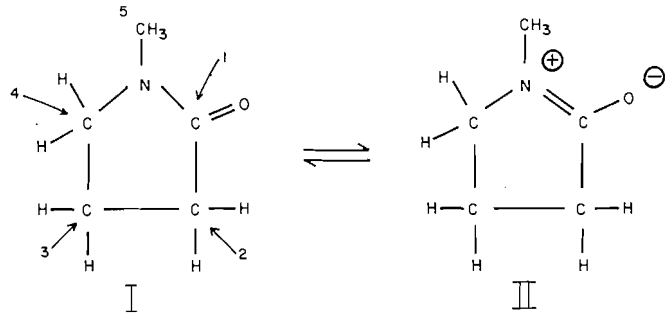

FIG. 12. Resonance structures of NMP.

crease the attraction. There is obviously a considerable distortion of the electronic distribution as indicated by the nmr and Raman results. The yellowish tinge of the solutions also suggests that some charge transfer is present.

An enthalpy value of -33 kJ mol^{-1} for complex formation gives an explanation for the kinetic effects observed. The kinetics are obviously more rapid than nmr time scales (10^{-2} s) as no new resonances are seen, only shifts. The lack of excess ultrasonic absorption at 10 MHz is likely due to the fact that the kinetics is slower than that time scale (10^{-7} s). An activation energy of 33 kJ mol^{-1} for a rate-controlling step in a reaction suggests a rate constant of the order of $10^{12} \exp[-33/(8.3 \times 0.3)] \simeq 10^6$ s^{-1} or a relaxation time τ of 10^{-6} s. This value of τ is a lower limit considering the nature of the assumptions made in this crude model.

The distortions of the electron distributions which occur on interactions of the SO_2 and the NMP can be inferred from the nmr and Raman spectra. The nmr results suggest that there is an overall electron shift from the carbonyl π system of NMP to the lowest unoccupied molecular orbital of SO_2. There seems to be little net change of the electon density near the O in NMP, but there is a decrease of electron density at the N and the carbonyl C. The C=O bond is weakened by these changes and shifts to lower frequencies (Fig. 11). Qualitatively this can be thought of as a shift of the NMP towards resonance structure **II** (Fig. 12), as in the case of other amides (14).

The SO_2 stretching frequency increases slightly as NMP is added. Any electron charge transferred to the SO_2 is thought to go into an orbital which is S—O antibonding but O—O bonding (26). Thus the first approximation would predict the opposite effect, i.e. a weakening of the S—O bond and a decrease in frequency. This is indeed what happens when Br^- ions interact with SO_2. Intense broad lines appear at 1135, 1120, and 1110 cm^{-1} (27). When pyridine is added to SO_2, both effects take place: the SO_2 frequency increases slightly from 1145 cm^{-1} and a broad intense absorption appears at 1130 cm^{-1} (8).

On the basis of the directions of the bond dipoles, it would be expected that the S of SO_2 is close to the O of NMP and the O of SO_2 close to the N of NMP (Fig. 12). X-ray diffraction experiments in the solid complex formed at $X_{SO_2} = 0.50$ would give a definitive structure for the complex.

Conclusion

Solubility and freezing point data for the system NMP–SO_2 shows that the large negative Raoult's law deviation is due to the formation of 1:1 and 2:1 NMP:SO_2 complexes. Viscosity and permittivity data support the existence of these complexes. The ΔH^{θ}_{sol} and ΔS^{θ}_{sol} for solution of SO_2 in NMP are -33.7 kJ mol^{-1} and -94.6 J K^{-1} mol^{-1} respectively, as determined from the temperature dependence of Henry's law constants.

The interaction of SO_2 with NMP seems to occur by electron density transferred from the nitrogen and the carbonyl carbon of NMP to the O of SO_2 by way of the —N—C=O π electron system of NMP. When complexed by SO_2, the NMP resembles more its resonance structure **II** (Fig. 12) with a reduced C—O bond order.

Acknowledgements

The authors are indebted to Dr. G. W. Buchanan and Ms. M. J. Bell (Carleton University) for providing ^{13}C, ^{15}N, and ^{17}O nmr spectra using the XL-100 and XL-200 machines; to Miss C. H. Hayes and Dr. C. L. Gardner (Defence Research Establishment, Ottawa) for providing Raman spectra and aid with permittivity, density, and viscosity measurements; and to Mr. L. Page for glassblowing. The project was financially supported by an NSERC grant to P. K.

1. K. SEMARU. Sulfur removal and recovery from industrial processes. *Edited by* J. B. Pfeiffer. Adv. Chem. Ser. **139** (1975).
2. J. O. BESENHARD and G. EICHINGER. J. Electroanal. Chem. **68**, 1 (1976).
3. M-Pyrol Handbook. GAF Corp., New York. 1972.
4. W. GROENENDAAL and M. W. LENZ. Ger. Offen. 2,207,515 (Aug. 31, 1972); Chem. Abstr. **77**, 168339*f* (1972).
5. T. C. WADDINGTON (*Editor*). Non-aqueous solvent systems. Academic Press, New York. 1965.
6. H. S. BOOTH and D. R. MARTIN. J. Am. Chem. Soc. **64**, 2198 (1942).
7. R. J. FANNING and P. KRUUS. Can. J. Chem. **48**, 2052 (1970).
8. L. A. DIERKER. A Raman spectroscopy study of the pyridine SO_2 system. Work report for the University of Waterloo prepared at Defence Research Establishment Ottawa, 1982.
9. J. W. LORIMER, B. C. SMITH, and G. H. SMITH. J. Chem. Soc. Faraday Trans. I, **71**, 2232 (1975).
10. R. C. WEAST (*Editor*). Handbook of chemistry and physics. 48th ed. CRC Press. 1967.
11. P. KRUUS. Liquids and solutions: structure and dynamics. Marcel Dekker, New York. 1977.
12. I. D. RAE. Aust. J. Chem. **32**, 567 (1979).
13. G. FRONZA, R. MONDELLI, E. W. RANDALL, and G-P. GARDINI. J. Chem. Soc. Perkin II, 1746 (1977).
14. M. I. BURGAR, T. E. ST. AMOUR, and D. FLAT. J. Phys. Chem. **85**, 502 (1981).
15. B. N. FIGGIS, R. G. KIDD, and R. S. NYHOLM. Proc. R. Soc. A**269**, 469 (1962).
16. R. K. HARRIS and B. E. MANN. NMR and the periodic table. Academic Press, London. 1978.
17. M. H. BROOKER and H. H. EYSEL. Proc. 8th Int. Conf. Raman Spectroscopy, Ottawa 1980. *Edited by* W. S. Murphy. North-Holland. 1980. p. 266.
18. G. MONTAUDO, S. CACCAMESE, and A. RECCA. J. Phys. Chem. **79**, 1554 (1975).
19. K. R. HOFFMAN and C. A. VANDER WERF. J. Am. Chem. Soc. **68**, 997 (1946).
20. N. F. ALBERTSON and W. C. FERNELIUS. J. Am. Chem. Soc. **65**, 1687 (1943).
21. W. D. HARRISON, J. B. GILL, and D. G. GOODALL. J. Chem. Soc. Dalton, 1431 (1978).
22. F. KOEHLER, H. ATROPS, H. KALALI, E. LIEBERMANN, E. WILHELM, F. RATKOVICS, and T. SALAMON. J. Phys. Chem. **85**, 2520 (1981).
23. A. SALAMA, S. B. SALAMA, M. SOBEIR, and S. WASIF. J. Chem. Soc. A, 1112 (1971).
24. R. L. BENOIT and E. MILANOVA. Can. J. Chem. **57**, 1319 (1979).

Can. J. Chem. Downloaded from www.nrcresearchpress.com by 210.87.254.42 on 09/06/12
For personal use only.

25. V. GUTMANN. The donon–acceptor approach to molecular interactions. Plenum, New York. 1978.
26. P. D. DACRE and M. ELDER. Theoret. Chim. Acta, Berl. **25**, 254 (1972).
27. J. W. EATOCK. A study of lithium salt effects on the NMP–SO_2 system. B.Sc. Honours report, Carleton University. 1982.

Can. J. Chem. Downloaded from www.nrcresearchpress.com by 210.87.254.42 on 09/06/12
For personal use only.

Molecular orbital treatment of substituent effects. I. Structures of some carbon acids and their conjugate bases

KENNETH E. EDGECOMBE AND RUSSELL J. BOYD
Department of Chemistry, Dalhousie University, Halifax, N.S., Canada B3J 4J3

Received April 30, 1982

KENNETH E. EDGECOMBE and RUSSELL J. BOYD. Can. J. Chem. **61**, 45 (1983).

The STO-3G optimized structures of three series of carbon acids, CH_nX_{4-n}, where n = 1, 2, or 3 and X = F, CN, or NO_2 and their corresponding conjugate bases are compared with the limited number of experimentally determined structures. The 6-31G* equilibrium geometries of CH_3^-, CH_2F^-, CHF_2^-, CF_3^-, CH_2CN^-, and $CH_2NO_2^-$ are included as a check on the reliability of the STO-3G structures of the anions. Although the effects of successive substitutions on the STO-3G structures are generally systematic, a few apparent anomalies are readily explained in terms of resonance stabilization. Calculations at the 3-21G level, on the STO-3G optimized structures, indicate that the stabilization energy associated with increasing the number of orbitals in the basis set is approximately additive. The stabilization energies are 0.865 ± 0.007 au per fluorine substituent, 0.661 ± 0.008 au per cyano substituent, and 1.561 ± 0.027 au per nitro substituent.

KENNETH E. EDGECOMBE et RUSSELL J. BOYD. Can. J. Chem. **61**, 45 (1983).

On a comparé les structures optimisées par des calculs STO-3G de trois séries d'acides carbonés CH_nX_{4-n} où n = 1, 2 ou 3 et X = CN ou NO_2 ainsi que les bases conjuguées correspondantes avec un nombre limité de structures déterminées expérimentalement. On a exclu les géométries d'équilibre 6-31G* de CH_3^-, CH_2F^-, $CF_3^-CH_2CN^-$ et $CH_2NO_2^-$ comme moyen de vérification des structures de STO-3G des anions. Bien que les effets des substitutions successives sur les structures de STO-3G sont généralement systématiques, on a expliqué facilement quelques anomalies apparentes en fonction de la stabilisation de la résonance. Les calculs au niveau 3-21G des structures améliorées en STO-3G indiquent que l'énergie de stabilisation associée à l'augmentation du nombre d'orbitales de l'ensemble de base est approximativement additive. Les énergies de stabilisation sont de 0,865 ± 0,007 ua par substituant fluor, de 0,661 ± 0,08 ua par substituant cyano et de 1,561 ± 0,027 par substituant nitro.

[Traduit par le journal]

Introduction

The effect of substituents on the properties of carbanions is usually based on thermodynamic and kinetic studies in solution (1). More recently gas-phase data have become available from flowing afterglow (2), high-pressure mass spectrometric (3) and ion cyclotron resonance experiments (4). As Hehre and co-workers (5) have stressed, the solution-phase results do not reflect the inherent properties of the anions so much as they reflect the effects of solvation. Alternatively *ab initio* molecular orbital (MO) theory may be used to obtain useful data appropriate to isolated molecules and ions in the gas phase (6). Although many *ab initio* MO calculations on monosubstituted methyl anions have been reported (5, 7), the effects of multiple substitutions have not been discussed. Accordingly, the results of a systematic study of three series of carbon acids, CH_nX_{4-n}, where n = 1, 2, or 3 and X = F, CN, or NO_2, and their corresponding conjugate bases, $CH_{n-1}X_{4-n}^-$, are presented in this paper.

Method and results

Standard single determinant *ab initio* MO calculations were carried out by use of the GAUSSIAN 76 program (8*a*) on a Control Data CYBER 170-720 system.[1] Complete geometry optimizations, subject only to specified symmetry constraints, were performed at the STO-3G level (9). Several of the anions have been optimized at the 6-31G* level. In order to improve energy calculations, charge distributions, and other properties, 3-21G calculations (10) were carried out on the STO-3G optimized structures.

The STO-3G equilibrium geometries of some carbon acids and their conjugate bases are compared with the available experimental structural data in Table 1. For each species the point group of the equilibrium geometry is listed. The equilibrium conformations of the nitromethanes and their conjugate bases are illustrated in Fig. 1. In all cases lower symmetries were included in the optimization procedure but only the data pertinent to the lowest energy structures are included in this paper. A few of the smaller molecules and ions which have been optimized at the STO-3G level by Pople's group (11) are listed for completeness.

Table 2 lists the STO-3G//STO-3G and 3-21G//STO-3G total energies. The stabilization of the total energy gained by replacing the minimal basis set by the small split-valence basis set is shown in the fourth column of Table 2.

Discussion

The point group symmetries of the STO-3G equilibrium conformations of the fluorine-containing species agree with the available experimental data. Where direct comparison of the geometries is possible, the agreement is quite typical for calculations at the STO-3G level (10, 19). Successive fluorination of CH_4 lengthens the C—H bond by 0.012 ± 0.002 Å at the STO-3G level. Within the carbanion series a similar but more pronounced effect is observed. Successive fluorination of CH_4 decreases the C—F bond by 0.007 Å at the STO-3G level.[2] The more pronounced shortening of the C—F bond at the 3-21G level: 1.404, 1.372, and 1.345 Å in CH_3F, CH_2F_2, and

[1] For a few of the larger calculations an expanded version of Gaussian 76 was used. The expanded version has been described in ref. 8*b*.

[2] See ref. 7*i* and references therein for further discussion of these effects.

0008-4042/83/010045-05$01.00/0
©1983 National Research Council of Canada/Conseil national de recherches du Canada

Can. J. Chem. Downloaded from www.nrcresearchpress.com by 210.87.254.6 on 09/06/12
For personal use only.

TABLE 1. Equilibrium geometries[a] of some carbon acids and their conjugate bases

Species[b]	Parameter[c]	STO-3G[d]	Expt.	Species[b]	Parameter[c]	STO-3G[d]	Expt.
CH_4 (T_d)	r(C—H)	1.083	1.092[e]	CH_3NO_2 (C_s)	r(C—N)	1.530	1.489[j]
CH_3^- (C_{3v})	r(C—H)	1.117			r(N—O)	1.276	1.224
	∠(HCH)	99.8			r(C—H_1)	1.088	1.088
CH_3F (C_{3v})	r(C—F)	1.384	1.383[f]		r(C—H_2)	1.089	
	r(C—H)	1.097	1.10		∠(O_1NC)	117.7	
	∠(HCF)	110.6	110.6		∠(O_2NC)	117.5	
CH_2F^- (C_s)	r(C—F)	1.436			∠(ONO)	124.8	125.3
	r(C—H)	1.133			∠(H_1CN)	107.7	107.2
	∠(HCF)	101.1			∠(H_2CN)	108.2	
	∠(HCH)	98.8			∠(H_2CNO_2)	59.7	
CH_2F_2 (C_{2v})	r(C—F)	1.377	1.357[f]	$CH_2NO_2^-$ (C_{2v})	r(C—N)	1.352	
	r(C—H)	1.109	1.093		r(N—O)	1.336	
	∠(FCF)	108.7	108.3		r(C—H)	1.071	
	∠(HCF)	109.9	108.7		∠(ONC)	120.3	
CHF_2^- (C_s)	r(C—F)	1.429			∠(HCN)	119.1	
	r(C—H)	1.152		$CH_2(NO_2)_2$ (C_s)	r(C—N_1)	1.541	
	∠(FCF)	100.2			r(C—N_2)	1.531	
	∠(HCF)	99.9			r(N_1—O_2)	1.273	
CHF_3 (C_{3v})	r(C—F)	1.371	1.332[f]		r(N—O)	1.275	
	r(C—H)	1.119	1.098		r(C—H)	1.095	
	∠(HCF)	110.3	110.1		∠(NCN)	109.3	
CF_3^- (C_{3v})	r(C—F)	1.425			∠(HCN_1)	108.3	
	∠(FCF)	99.2			∠(O_1NC)	115.9	
CH_3CN (C_{3v})	r(C—C)	1.486	1.462[g]		∠(O_2NC)	117.8	
	r(C—N)	1.154	1.157		∠(O_3NC)	116.9	
	r(C—H)	1.088	1.095		∠(HCH)	112.4	
	∠(HCC)	109.9	109.9	$CH(NO_2)_2^-$ (C_1)	r(C—N)	1.451	
CH_2CN^- (C_s)	r(C—C)	1.413			r(N—O)	1.295	
	r(C—N)	1.168			r(C—H)	1.083	
	r(C—H)	1.086			∠(NCN)	115.7	
	∠(NCC)	180.0			∠(HCN_1)	110.5	
	∠(HCC)	111.3			∠(HCN_2)	110.8	
	∠(HCH)	109.9			∠(O_1NC)	117.1	
$CH_2(CN)_2$ (C_{2v})	r(C—C)	1.492	1.460[h]		∠(O_2NC)	122.1	
	r(C—N)	1.155	1.158		∠(O_3NC)	117.1	
	r(C—H)	1.094	1.09		∠(O_4NC)	122.2	
	∠(CCC)	111.5	113.6		∠(O_1NCN)	209.9	
	∠(HCC)	109.3			∠(O_2NCN)	35.1	
	∠(NCC)	180.0			∠(O_3NCN)	151.9	
$CH(CN)_2^-$ (C_{2v})	r(C—C)	1.397			∠(O_4NCN)	−32.8	
	r(C—N)	1.166		$CH(NO_3)_3$ (C_3)	r(C—N)	1.542	1.505[k]
	r(C—H)	1.073			r(C—H)	1.100	1.13
	∠(CCC)	122.3			r(N—O_1)	1.274	1.219
	∠(HCC)	118.8			r(N—O_4)	1.275	
	∠(NCC)	180.0			∠(NCH)	110.0	
$CH(CN)_3$ (C_{3v})	r(C—C)	1.499			∠(O_1NC)	116.5	
	r(C—N)	1.156			∠(O_4NC)	116.0	
	r(C—H)	1.100			∠(O_1NCH)	39.8	
	∠(HCC)	108.3		$C(NO_3)_3^-$ (C_3)	r(C—N)	1.526	
	∠(NCC)	180.0			r(N—O_1)	1.283	
$C(CN)_3^-$ (D_{3h})	r(C—C)	1.420	1.40[i]		r(N—O_4)	1.280	
	r(C—N)	1.162	1.15		∠(NCN)	106.4	
					∠(O_1NC)	121.3	
					∠(O_4NC)	116.6	
					∠(O_1NCN)	119.1	
					∠(O_4NCN)	−65.7	

[a]Bond lengths in angstroms and angles in degrees.
[b]Point group of equilibrium conformation is indicated by the symbol in parentheses.
[c]Bond angles are defined by three nuclei whereas torsional or dihedral angles are defined by four nuclei.
[d]The STO-3G optimized structures of CH_4, CH_3^-, CH_3F, CH_2F_2, and CHF_3 are from ref. 11.
[e]Reference 12. [f]Reference 13. [g]Reference 14.
[h]Reference 15. [i]Reference 16. [j]Reference 17.
[k]Reference 18.

Can. J. Chem. Downloaded from www.nrcresearchpress.com by 210.87.254.6 on 09/06/12
For personal use only.

Can. J. Chem. Downloaded from www.nrcresearchpress.com by 210.87.254.6 on 09/06/12
For personal use only.

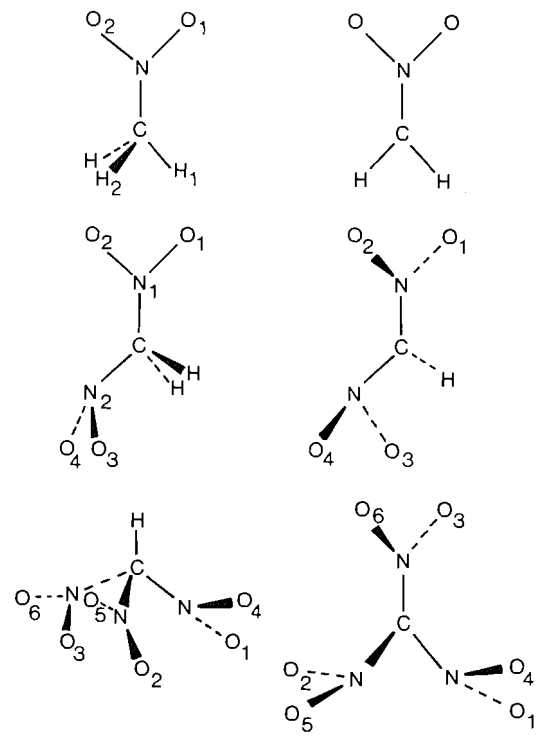

FIG. 1. STO-3G equilibrium conformations of nitromethanes and their conjugate bases.

TABLE 2. Total energies[a] of some carbon acids and their conjugate bases

Species	Total energy STO-3G	Total energy 3-21G[b]	Difference
CH_4	−39.72686	−39.97688	−0.25002
CH_3^-	−38.83473	−39.23842	−0.40369
CH_3F	−137.16905	−138.28097	−1.11192
CH_2F^-	−136.31158	−137.57325	−1.26167
CH_2F_2	−234.62754	−236.60705	−1.97951
CHF_2^-	−233.80581	−235.93267	−2.12686
CHF_3	−332.10006	−334.94766	−2.84760
CF_3^-	−331.31656	−334.31560	−2.99904
CH_3CN	−130.27154	−131.19060	−0.91906
CH_2CN^-	−129.48005	−130.54247	−1.06242
$CH_2(CN)_2$	−220.80623	−222.39033	−1.58410
$CH(CN)_2^-$	−220.10334	−221.82348	−1.72014
$CH(CN)_3$	−311.33295	−313.57922	−1.24627
$C(CN)_3^-$	−310.70066	−313.07445	−2.37379
CH_3NO_2	−240.42469	−242.25139	−1.82670
$CH_2NO_2^-$	−239.66726	−241.65993	−1.99267
$CH_2(NO_2)_2$	−441.10987	−444.50195	−3.39208
$CH(NO_2)_2^-$	−440.43323	−443.97079	−3.53756
$CH(NO_2)_3$	−641.78744	−646.73470	−4.94726
$C(NO_2)_3^-$	−641.16189	−646.23324	−5.07135

[a]All energies are in atomic units: 1 au = 27.2116 eV.

[b]According to the convention of Pople and co-workers (ref. 10) these results should be labelled as 3-21G//STO-3G since the calculations have been performed with the 3-21G basis set at the STO-3G optimum geometries.

CHF_3, respectively, is consistent with the 0.025 Å decrease observed experimentally (13). The 3-21G results for the C—H bond lengths are qualitatively opposed to the STO-3G results: 1.083, 1.080, 1.073, and 1.066 Å in CH_4, CH_3F, CH_2F_2, and CHF_3, respectively (11).

With two exceptions the point group symmetries of the cyano-substituted species match those of the fluorine analogues. The exceptions occur for $CH(CN)_2^-$ and $C(CN)_3^-$ which have higher symmetries than CHF_2^- and CF_3^-, respectively. These differences are readily explained in terms of resonance stabilization of the negative charge in the cyano cases. For CH_2CN^- resonance stabilization is not sufficient at the STO-3G level to produce the C_{2v} symmetry observed in the isoelectronic diazomethane, CH_2N_2 (20). At the 4-31G level, the planar C_{2v} structure is favoured (5). As observed in other compounds (21), the STO-3G C—N bond lengths agree extraordinarily well with experiment. This is due to cancellation of basis set and electron correlation errors (22). Successive CN substitutions lengthen the C—H bonds by about half as much as in the CH_nF_{4-n} series. In contrast to the $CH_{n-1}F_{4-n}^-$ series, the C—H bonds of the anions are predicted to be shortened by CN substitution. The C—C bond length increases with each additional CN substitution, except in $CH(CN)_2^-$ where there is a substantial shortening due to the resonance stabilization of the C_{2v} geometry. Once again the experimental data is too incomplete to test the reliability of these conclusions.

The symmetries of the equilibrium conformations of the nitromethanes are lower than those of the cyanomethanes. The effect of successive substituents on C—H bond lengths is systematic in the nitromethanes. For the anions the substituent effects are unique. The short C—H bond length in $CH_2NO_2^-$ is consistent with a principal resonance form which places a dou-

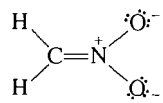

ble bond between C and N. This suggestion is consistent with the short C—N and long N—O bonds. Except for $CH_2NO_2^-$, the N—O bonds are remarkably constant. The C—N bond lengths of the nitromethanes appear to be overestimated by about 0.04 Å and are not strongly influenced by the number of nitro groups. In the anions, resonance stabilization leads to a large shortening of the C—N bond of $CH_2NO_2^-$, a smaller effect in $CH(NO_2)_2^-$, and a very small effect in $C(NO_2)_3^-$. Despite the scarcity of experimental structural data on the nitromethanes, we note that the observation that the NO_2 groups of $CH(NO_2)_3$ appear to be rotated by 26° around the CN bonds away from a coplanar HCNO arrangement (18) is consistent with the C_3 propeller structure obtained at the STO-3G level. In contrast to the cyanomethanes, loss of a proton from $CH(NO_2)_3$ does not lead to a more symmetrical anion. Thus $C(NO_2)_3^-$ has a C_3 propeller structure whereas $C(CN)_3^-$ has the planar D_{3h} structure at the STO-3G level. The latter is consistent with a resonance-stabilized structure and the substantial shortening of the C—C bond, in agreement with experiment (16). And finally to conclude this part of the discussion, we note that ∠CCN equals 180° in all of the cyano-substituted methanes and carbanions, whereas planar NO_2 groups are predicted only for CH_3NO_2, $CH_2NO_2^-$, $CH_2(NO_2)_2$, and $CH(NO_2)_3$.

It is well-known that one-electron properties calculated at the Hartree-Fock level are correct to first order (23–25) and that the equilibrium geometry may be regarded as a one-electron property (26). Although this does not imply any absolute accuracy, extensive calculations on neutral molecules and cations have shown that single-determinant molecular orbital theory produces geometries in close agreement with experimental val-

TABLE 3. Comparison of 4-31G and 6-31G* equilibrium geometries with the STO-3G results for selected anions

Anion[a]	Parameter	Value		
		STO-3G	4-31G[b]	6-31G*[c]
CH_3^- (C_{3v})	r(C—H)	1.117	1.119	1.119
	∠(HCH)	99.8	114.5	116.4
CH_2F^- (C_s)	r(C—F)	1.436	1.561	1.492
	r(C—H)	1.133	1.117	1.119
	∠(HCF)	101.1	104.4	100.1
	∠(HCH)	98.8	102.5	101.0
CHF_2^- (C_s)	r(C—F)	1.429		1.447
	r(C—H)	1.152		1.115
	∠(FCF)	100.2		100.3
	∠(HCF)	99.9		99.4
CF_3^- (C_{3v})	r(C—F)	1.425	1.438	1.412
	∠(FCF)	99.2	99.3	96.2
CH_2CN^- (C_{2v})	r(C—C)	1.413	1.366	1.390
	r(C—N)	1.168	1.174	1.164
	r(C—H)	1.086	1.073	1.075
	∠(HCC)	111.3	120.8	120.2
	∠(HCH)	109.9	118.5	119.6
$CH_2NO_2^-$ (C_{2v})	r(C—N)	1.352	1.290	1.313
	r(N—O)	1.336	1.315	1.255
	r(C—H)	1.071	1.066	1.071
	∠(ONC)	120.3	120.4	120.3
	∠(HCN)	119.1	118.6	118.1

[a]At the STO-3G level, CH_2CN^- is predicted to have a C_s equilibrium conformation.

[b]All data from ref. 5, except CF_3^- which has been optimized at the 3-21G level (ref. 11).

[c]The results for CH_3^- are from ref. 11. The 6-31G* geometry optimizations are less extensive than the STO-3G results: the latter are believed to be within ±0.002 Å and ±0.2° of the true theoretical values whereas the former are estimated to be within ±0.005 Å and ±0.5° of the true 6-31G* values. The 6-31G* total energies are −39.44616, −138.32889, −237.21287, −336.11754, −131.28630, and −243.05770 au, respectively.

ues (27, 28). Even though anions have received less attention due to the lack of experimental data and to the problems associated with Hartree–Fock calculations on anions (6, 29), it appears that extended basis sets are necessary to obtain an accuracy comparable to the small basis set results for neutral molecules and cations (30). With this in mind we have carried out 6-31G* geometry optimizations for a few of the smaller anions included in this paper. The results are compared with the STO-3G and 4-31G geometries in Table 3. Relative to the 6-31G* basis set, the STO-3G basis set tends to overestimate the bond lengths between heavy atoms. We have noticed a similar effect in several electron-rich systems (31). CH_2F^- and, to a lesser extent, CHF_2^- are notable exceptions. Two major discrepancies between the STO-3G and 6-31G* angles are apparent: the extended basis set favours a nearly planar methyl anion and a planar cyanomethyl anion. With reference to the STO-3G results, the 4-31G angles are closer to the 6-31G* values, but the bond lengths are not consistently closer to the 6-31G* values. In the case of the C—F bond in CH_2F^-, the 4-31G basis set appears to over-correct the inadequacy of the STO-3G basis set. In general, the agreement between the STO-3G and 6-31G* anion geometries is only slightly poorer than comparable data for neutral species. On the basis of these calculations and previous studies of anion geometries (5, 32), we have carried out geometry optimizations for all anions and molecules at the STO-3G level and then for the calculation of properties we have carried out single point calculations at the 3-21G level. The size of some of the species included in this paper precludes geometry optimizations with extended basis sets for the entire set of molecules and anions. In a later paper we will show that the use of the STO-3G geometries has only a minor effect on our discussion of substituent effects.

The total energies (Table 2) obtained with the STO-3G and 3-21G basis sets at the STO-3G optimized geometries (Table 1) indicate that the stabilization associated with increasing the number of orbitals in the basis set is approximately additive. With reference to the differences between the 3-21G//STO-3G and STO-3G//STO-3G total energies, as listed in the fourth column of Table 2, successive differences of the stabilization energies within the series CH_4, CH_3F, CH_2F_2, CHF_3 and within the series CH_3^-, CH_2F^-, CHF_2^-, CF_3^- lead to an average value of 0.865 ± 0.007 au per fluorine substituent. This observation applies equally well to the neutral species and to the anions. The corresponding values are 0.661 ± 0.008 and 1.561 ± 0.027 au per cyano and nitro substituent, respectively. These stabilizations are not determined solely by the size of the substituent since the stabilization per fluorine atom is greater than that per cyano group.

The requirements for computer time were reduced by carrying out the 3-21G calculations at the STO-3G geometries. On the basis of the available data (11), the energy lowering associated with geometry optimization is expected to be small relative to the differences listed in Table 2. For CH_4 there is no change, while the lowering is 0.00092, 0.00205, 0.00406, and 0.00120 au for CH_3F, CH_2F_2, CHF_3, and CH_3CN, respectively. For properties such as proton affinities, which depend on differences between an acid and its conjugate base, there will be a substantial cancellation of errors. In such cases we believe that the 3-21G//STO-3G energies and wavefunctions provide a reliable indication of the consequences of extending a minimal basis set by increasing the number of orbitals while keeping the number of primitive Gaussians fixed.

In a later paper we will discuss the effect of substituents on the proton affinities and the charge distributions of the series of carbon acids included in this work and on the same properties of a number of simple carboxylic acids.

Acknowledgements

We are grateful to the Dalhousie University Computer Centre for generous amounts of computing time and to the Natural Sciences and Engineering Research Council of Canada for financial assistance. One of us (K. E. E.) is grateful for a Dalhousie Graduate Scholarship.

1. (*a*) D. J. CRAM. Fundamentals of carbanion chemistry. Academic Press, New York. 1965; (*b*) F. G. BORDWELL, J. E. BARTMESS, and J. A. HAUTALA. J. Org. Chem. **41**, 2786 (1976).
2. (*a*) J. H. STEWART, R. H. SHAPIRO, C. H. DEPUY, and N. M. BIERBAUM. J. Am. Chem. Soc. **99**, 7650 (1977); (*b*) G. I. MACKAY, R. S. HEMSWORTH, and D. K. BOHME. Can. J. Chem. **54**, 1624 (1976).
3. (*a*) J. B. CUMMING and P. KEBARLE. Can. J. Chem. **56**, 1 (1978); (*b*) P. KEBARLE. Ann. Rev. Phys. Chem. **28**, 445 (1978).
4. (*a*) J. E. BARTNESS, J. A. SCOTT, and R. T. MCIVER, JR. J. Am. Chem. Soc. **101**, 6046 (1979); (*b*) R. GYGAX, H. L. MCPETERS, and J. I. BRAUMAN. J. Am. Chem. Soc. **101**, 2567 (1979); (*c*) R. FARID and T. B. MCMAHON. Can. J. Chem. **58**, 2307 (1980).
5. A. PROSS, D. J. DEFREES, B. A. LEVI, S. K. POLLACK, L. RADOM, and W. J. HEHRE. J. Org. Chem. **46**, 1693 (1981).

Can. J. Chem. Downloaded from www.nrcresearchpress.com by 210.87.254.6 on 09/06/12
For personal use only.

6. L. RADOM. *In* Modern theoretical chemistry. Vol. 4. *Edited by* H. F. Schaeffer. Plenum Press, New York. 1977.
7. (*a*) J. CHANDRASEKHAR, J. G. ANDRADE, and P. v. R. SCHLEYER. J. Am. Chem. Soc. **103**, 5609 (1981); (*b*) J. K. WILMSHURST and C. E. DYKSTRA. J. Am. Chem. Soc. **102**, 4668 (1980); (*c*) G. I. MACKAY, M. H. LIEN, A. C. HOPKINSON, and D. K. BOHME. Can. J. Chem. **56**, 131 (1978); (*d*) P. G. MEZEY, M. A. ROBB, K. YATES, and I. G. CSIZMADIA. Theor. Chim. Acta, **49**, 277 (1978); (*e*) D. W. BOERTH and A. STREITWIESER. J. Am. Chem. Soc. **100**, 750 (1978); (*f*) J.-M. LEHN and G. WIPFF. J. Am. Chem. Soc. **98**, 7498 (1976); (*g*) F. BERNARDI, I. G. CSIZMADIA, A. MANGINI, H. B. SCHLEGEL, M. H. WHANGBO, and S. WOLFE. J. Am. Chem. Soc. **97**, 2209 (1975); (*h*) J. N. MURRELL, B. VIDAL, and M. F. GUEST. J. Chem. Soc. Faraday Trans. II, **71**, 1577 (1975); (*i*) A. PROSS and L. RADOM. J. Comp. Chem. **1**, 295 (1980).
8. (*a*) J. S. BINKLEY, R. A. WHITEHEAD, P. C. HARIHARAN, R. SEEGER, and J. A. POPLE. QCPE, **11**, 241 (1974); (*b*) R. J. BOYD and K. E. EDGECOMBE, QCPE Bulletin, **2**, 10 (1982).
9. W. J. HEHRE, R. F. STEWART, and J. A. POPLE. J. Chem. Phys. **51**, 2657 (1969).
10. J. S. BINKLEY, J. A. POPLE, and W. J. HEHRE. J. Am. Chem. Soc. **102**, 939 (1980).
11. R. A. WHITESIDE, M. J. FRISCH, J. S. BINKLEY, D. J. DEFREES, H. B. SCHLEGEL, K. RAGHAVACHARI, and J. A. POPLE. Carnegie-Mellon Quantum Chemistry Archive, 2nd ed. July 1981.
12. K. KUCHITSU and L. S. BARTELL. J. Chem. Phys. **36**, 2470 (1962).
13. M. D. HARMONY, U. W. LAURIE, R. L. KUCZKOWSKI, R. H. SCHWENDEMAN, D. A. RAMSAY, F. J. LOVAS, W. J. LAFFERTY, and A. G. MAKI. J. Phys. Chem. Ref. Data, **8**, 619 (1979).
14. J. DEMAISON, A. DUBRULLE, D. BOUCHER, J. BURIE, and V. TYPKA. J. Mol. Spectrosc. **76**, 1 (1979).
15. N. MULLER and D. E. PRITCHARD. J. Am. Chem. Soc. **80**, 3483 (1958).
16. P. ANDERSEN and B. KLEWE. Nature, **200**, 464 (1963).
17. A. P. COX and S. WARING. Trans. Faraday Soc. **68**, 1060 (1972).
18. N. I. SADOVA, N. I. POPIK, and L. V. VILKOV. Zh Struckt. Khim. **17**, 298 (1976).
19. M. D. NEWTON, W. A. LATHAN, W. J. HEHRE, and J. A. POPLE. J. Chem. Phys. **52**, 4064 (1970).
20. W. H. FLETCHER and T. P. GARRETT. J. Chem. Phys. **25**, 50 (1956); A. P. COX, L. F. THOMAS, and J. SHERIDAN. Nature, **181**, 1000 (1958).
21. R. J. BOYD, W. E. JONES, and K. W. LING. Chem. Phys. **58**, 203 (1981).
22. D. J. DEFREES, B. A. LEVI, S. K. POLLACK, W. J. HEHRE, J. S. BINKLEY, and J. A. POPLE. J. Am. Chem. Soc. **101**, 4085 (1979).
23. M. COHEN and A. DALGARNO. Proc. Phys. Soc. London, **77**, 748 (1961).
24. C. W. KERN and M. KARPLUS. J. Chem. Phys. **40**, 1374 (1964).
25. R. J. BOYD. Chem. Phys. Lett. **44**, 363 (1976); A. GUPTA and R. J. BOYD. J. Chem. Phys. **68**, 1951 (1978).
26. K. F. FREED. Chem. Phys. Lett. **2**, 255 (1968).
27. J. A. POPLE. *In* Modern theoretical chemistry. Vol. 4. *Edited by* H. F. Schaeffer. Plenum Press, New York. 1977 and references therein.
28. W. J. HEHRE. *In* Modern theoretical chemistry. Vol. 4. *Edited by* H. F. Schaeffer. Plenum Press, New York, 1977 and references therein.
29. L. RADOM. J. Chem. Soc. Chem. Commun. 403 (1974); R. AHLRICHS. Chem. Phys. Lett. **34**, 570 (1975).
30. P. CARSKY and M. URBAN. Lecture notes in chemistry. No. 16. Springer-Verlag, Berlin. 1980.
31. K. E. EDGECOMBE and R. J. BOYD. In preparation; S.-C. CHOI and R. J. BOYD. Unpublished results.
32. A. C. HOPKINSON and M. H. LIEN. Intern. J. Quantum Chem. **18**, 1371 (1980).

Can. J. Chem. Downloaded from www.nrcresearchpress.com by 210.87.254.6 on 09/06/12
For personal use only.

The structure and conformation of 1-phenyl-2-methylcyclopropene-3-carboxylic acid and *cis*-2-(*m*-nitrophenyl)cyclopropanecarboxylic acid

JAMES D. KORP, IVAN BERNAL, AND RICHARD FUCHS
Department of Chemistry, University of Houston, Houston, TX 77004, U.S.A.

Received July 6, 1982

JAMES D. KORP, IVAN BERNAL, and RICHARD FUCHS. Can. J. Chem. **61**, 50 (1983).

The structures of *cis*-2-(*m*-nitrophenyl)cyclopropanecarboxylic acid (**1**) and 1-phenyl-2-methylcyclopropene-3-carboxylic acid (**2**) have been determined by X-ray methods. Crystals of **1** are triclinic, space group $P\bar{1}$, with $a = 7.422$, $b = 8.615$, $c = 9.499$ Å, $\alpha = 60.24$, $\beta = 63.76$, $\gamma = 71.36°$, and two molecules in the unit cell. Crystals of **2** are monoclinic, space group $P2_1/c$, with four molecules in a unit cell of dimensions $a = 9.345$, $b = 13.286$, $c = 8.187$ Å, and $\beta = 98.22°$. The carboxyl group of **1** approaches the bisecting conformation. The phenyl group is 37° from this conformation, by contrast with the unhindered compound 2-(*p*-nitrophenyl) cyclopropyl methyl ketone. In **2** the carboxyl group bisects the three-membered ring, indicating that carbonyl-cyclopropene π interactions can occur if sterically allowed. The two rings are essentially coplanar, permitting maximum interaction of the phenyl group and the double bond. In both compounds, the carbonyl oxygen of the carboxyl is the nearer oxygen to the three-membered ring.

JAMES D. KORP, IVAN BERNAL et RICHARD FUCHS. Can. J. Chem. **61**, 50 (1983).

On a déterminé par cristallographie de rayons-X les structures de l'acide (*m*-nitrophényl)-2 cyclopropanecarboxylique (**1**) et de l'acide phényl-1 méthyl-2 cyclopropène-3 carboxylique (**2**). Les cristaux de l'acide (**1**) sont tricliniques et appartiennent au groupe d'espace $P\bar{1}$ avec $a = 7{,}422$, $b = 8{,}615$, $c = 9{,}499$ Å, $\alpha = 60{,}24$, $\beta = 63{,}76$, $\gamma = 71{,}36$. La maille élémentaire contient deux molécules. Les cristaux de l'acide (**2**) sont monocliniques et appartiennent au groupe d'espace $P2_1/c$ avec $a = 9{,}345$, $b = 13{,}286$, $c = 8{,}187$ Å, $\beta = 98{,}22°$ avec quatre molécules dans la maille élémentaire. Le groupe carboxyle de **1** s'approche de la conformation bisectrice. Le groupe phényle est à 37° de cette conformation contrairement à sa position dans le composé non encombré, (*p*-nitrophényl)-2 cyclopropyle méthyle cétone. Dans l'acide (**2**), le groupe carboxyle bisecte le cycle à trois chainons indiquant ainsi que des interactions entre le carboxyle et les électrons π du cyclopropène peuvent se produire si elles sont permises stériquement. Les deux cycles sont essentiellement coplanaires permettant ainsi une interaction maximale entre le groupe phényle et la double liaison. Dans les deux composés, l'oxygène du carbonyle du groupe carboxyle est celui qui est le plus près du cycle à trois chaisons.

[Traduit par le journal]

The presently available experimental thermochemical data on simple cyclopropane derivatives (1) (cyclopropane, 1,1-dimethylcyclopropane, cyclopropylamine, cyclopropyl cyanide, and cyclopropylbenzene) demonstrate appreciable stabilization only in the case of cyclopropylbenzene. This is surprising, in light of the well-established ability of π acceptor groups such as cyano and carbonyl to alter ring geometry (the substituent at C_1 shortens the distal C_2—C_3 bond, and lengthens the two vicinal bonds) (2), and the tendency of π donor groups to affect geometry in the opposite (F, Cl) or same (NH_2) direction. The phenyl group also appears to affect ring bond lengths (2). Crystal studies indicate the two rings are generally not in the bisected conformation required for electron release from cyclopropane to phenyl. As the inter-ring angle approaches 90° from the bisected conformation, electron donation from phenyl to the $4e'$ orbital of cyclopropane may be possible (3), but the interaction is not strong enough to require this conformation in the crystal of 1,1-dibromo-*trans*-2,3-diphenylcyclopropane (3). The carboxyl group of 2,2-diphenylcyclopropanecarboxylic acid bisects the cyclopropane ring, but the phenyl groups are at 87° and 71° to the bisected conformation (4). By contrast, *trans*-2-(*p*-nitrophenyl)cyclopropyl methyl ketone exists with both the aromatic ring and acetyl groups essentially bisecting the cyclopropane ring (5).

It is interesting to speculate whether the preferred conformation of the phenyl group is dependent on the electronic properties of other substituents, or on steric factors in the molecule. With this question in mind we have undertaken an X-ray study of the hindered compound *cis*-2-(*m*-nitrophenyl)cyclopropanecarboxylic acid (6), containing the same conjugating groups (phenyl, carbonyl) as the unhindered compound *trans*-2-(*p*-nitrophenyl)cyclopropyl methyl ketone.

From the sparse data on cyclopropene derivatives with phenyl and carbonyl substituents a somewhat different question arises. The structure of 3,3-dimethoxycarbonyl-1-methyl-2-phenylcyclopropene (7) has the two rings coplanar, for maximum interaction of phenyl with the cyclopropene double bond. However, the carbonyl groups deviate substantially from the ring-bisecting conformation, and conjugation is uncertain (8). This may result from mutual repulsion of the two carbomethoxy groups. 1-Phenyl-2-methylcyclopropene-3-carboxylic acid (9) has now been examined to determine whether the unhindered carbonyl substituent prefers the bisecting conformation.

Experimental

Synthesis

cis-*2-(*m*-Nitrophenyl)cyclopropanecarboxylic acid*

This compound was synthesized by the addition of ethyl diazoacetate to *m*-nitrostyrene, ester hydrolysis, and separation of the *cis*- and *trans*-acids by repeated fractional crystallization (6), mp 178.7−179.7°C. A crystal for X-ray study was formed by slow partial evaporation at room temperature of an acetonitrile solution.

1-Phenyl-2-methylcyclopropene-3-carboxylic acid

Ethyl diazoacetate was added to 1-phenylpropyne, and the resulting ester was hydrolyzed to the acid, mp 137.2−137.9°C (9). A crystal was grown from benzene solution by partial evaporation at room temperature.

X-ray structure determination

Data collections for the two different compounds were similar,

0008-4042/83/010050-07$01.00/0
©1983 National Research Council of Canada/Conseil national de recherches du Canada

Can. J. Chem. Downloaded from www.nrcresearchpress.com by 210.87.254.105 on 09/06/12
For personal use only.

TABLE 1. Summary of data collection and processing parameters

Parameter	Value	
	Cyclopropene	Cyclopropane
Space group	$P2_1/c$	$P\bar{1}$
Cell constants	a = 9.345(5)	7.422(4) Å
	b = 13.286(5)	8.615(4)
	c = 8.187(3)	9.499(5)
	β = 98.22(4)	α = 60.24(4)°
		β = 63.76(5)
		γ = 71.36(4)
	V = 1006	469 Å^3
Molecular formula	$C_{11}H_{10}O_2$	$C_{10}H_9NO_4$
Molecular weight	174.19	207.18
Molecules per cell	Z = 4	2
Density (calcd)	ρ = 1.15	1.47 g cm^{-3}
Absorption coefficient	μ = 0.4	0.7 cm^{-1}
Collection range	$4° \leq 2\theta \leq 50°$	$4° \leq 2\theta \leq 60°$
Scan width	1.20 + 0.35 tan θ	1.00 + 0.35 tan θ
Maximum scan time	240	240 s
Scan speed range	0.5 to 5.0	0.4 to 5.0° min^{-1}
Total data collected	1973	2265
Data with $I \geq 3\sigma(I)$	928	1075
Total variables	150	172
$R = \Sigma\|\|F_o\| - \|F_c\|\|/\Sigma\|F_o\|$	0.036	0.038
$R_w = [\Sigma_w(\|F_o\| - \|F_c\|)^2/\Sigma_w\|F_o\|^2]^{1/2}$	0.031	0.030
Weights	$w = \sigma(F)^{-2}$	$\sigma(F)^{-2}$

except as noted below. An Enraf-Nonius CAD-4 automatic diffractometer was used with MoKα radiation which was monochromatized by a dense graphite crystal, assumed for all purposes to be ideally imperfect. Final cell constants, as well as other pertinent data, are given in Table 1. For the monoclinic cyclopropene the data were collected from the quadrant of reciprocal space having k and l non-negative while h assumes all values, whereas for the triclinic cyclopropane the hemisphere of data having l non-negative was used. Intensities were measured using the $\theta-2\theta$ scan technique, with the scan rates depending directly on the net count obtained in rapid prescans of each reflection. The standard reflections monitored every 2 h during both experiments showed no unusual aberrations. In reducing the data, Lorentz and polarization factors were applied, but no corrections for absorption were made.

Both structures were solved using MULTAN (10), with the cyclopropane being a somewhat more difficult problem due to the lack of translational symmetry in the space group. The usual sequence of isotropic and anisotropic refinement was followed, after which all hydrogens were located in difference density Fourier maps. In the case of the cyclopropene, the hydrogen temperature factors refined poorly and thus were held fixed at reasonable values in the final refinement. After all shift/esd ratios were less than 0.1, the full-matrix least-squares refinement converged to the agreement factors listed in Table 1. The atomic scattering factors for C, O, and N were computed from numerical Hartree–Fock wave functions (11); for hydrogen those of Stewart, Davidson, and Simpson were used (12). All calculations were made with the SHELX-76 series of crystallographic programs (13). No unusually high correlations were noted in either refinement. Final positional and thermal parameters for the cyclopropene are listed in Table 2, while those for the cyclopropane are in Table 3. Bond lengths, angles, least-squares planes, and torsion angles are given in Tables 4–7 based on these positions. The numbering schemes for the molecules are shown in the stereoviews of Figs. 1 and 2.

Discussion

cis-2-(m-Nitrophenyl)cyclopropanecarboxylic acid

The bond lengths and angles in the two substituents are as expected based on previous structural determinations. The six phenyl ring distances average 1.383 Å, with the bond of attachment (C4—C5) = 1.494 Å. These values compare quite well with the averages of 1.387 Å and 1.502 Å reported in the survey by Allen (2). The nitro group is twisted less than 4° with respect to the phenyl ring and exhibits the characteristic deviation from trigonality caused by the nonbonded electron pair repulsions of the oxygens (14–16). The carboxyl group adopts the preferred (17, 18) conformation having the carbonyl oxygen near the cyclopropane center. The OH group is in the *syn*-planar conformation, and the overall geometry agrees quite well with the averages reported in the exhaustive study of carboxylic acids made by Leiserowitz (19). The C1—C2 length is shorter than would be expected for a C_{sp^2}—C_{sp^3} bond (1.505 Å) (20), and is indicative of conjugation between the cyclopropane and the C=O group. Both cyclopropane ring substituents are approximately in the *cis gauche* (cg3) position, according to the terminology of Allen (2), although the carboxyl is considerably closer to the *cis* bisecting (cb) position than is the phenyl (as shown by the torsion angles C3—C2—C1—O2 = 16°, C6—C5—C4—C3 = 6°).

The cyclopropane ring itself shows substantial bond asymmetry, having a maximum difference of 0.060 Å. Compared to the bond length of 1.510 Å found in unsubstituted cyclopropane (21), C3—C4 is seen to be somewhat shorter while C2—C4 is considerably longer. The variation of bond lengths with exocyclic substituents has been examined theoretically (22, 23) and experimentally (2, 4, 17, 24), and it is now well established that both carboxyl and phenyl substituents have the effect of shortening the distal cyclopropane bond while lengthening the vicinal ones. Furthermore, the absolute amount of the shortening is correlated with the positioning of the substituent group, with the maximum effect occurring at the bisecting position (2, 3) where the substituent π system has the greatest overlap with the occupied $3e'$ orbital of cyclopropane (3).

Can. J. Chem. Downloaded from www.nrcresearchpress.com by 210.87.254.105 on 09/06/12
For personal use only.

TABLE 2. Cyclopropene atomic coordinates and thermal parameters (×1000)

Atom	X/A	Y/B	Z/C	U_{11}	U_{22}	U_{33}	U_{12}	U_{13}	U_{23}
O1	0.9314(2)	0.0785(1)	0.3316(2)	74(1)	61(1)	86(1)	11(1)	0(1)	−4(1)
O2	0.8958(2)	0.0825(1)	0.3885(2)	83(1)	60(1)	90(1)	8(1)	−7(1)	−15(1)
C1	0.8723(3)	0.0077(2)	0.2961(3)	48(2)	61(2)	77(2)	0(2)	15(1)	2(2)
C2	0.7734(3)	0.0145(2)	0.1404(4)	68(2)	62(2)	71(2)	2(2)	10(2)	−8(2)
C3	0.7608(3)	0.1135(2)	0.0477(3)	85(2)	66(2)	70(2)	3(2)	17(2)	5(2)
C4	0.6546(3)	0.0914(2)	0.1229(3)	66(2)	65(2)	63(2)	4(2)	5(2)	4(2)
C5	0.5165(3)	0.1115(2)	0.1766(3)	57(2)	79(2)	55(2)	5(2)	0(1)	−1(2)
C6	0.4452(3)	0.2006(2)	0.1353(4)	74(2)	96(3)	81(2)	18(2)	10(2)	0(2)
C7	0.3131(4)	0.2198(3)	0.1855(5)	98(3)	126(4)	98(3)	36(3)	2(2)	−16(3)
C8	0.2538(4)	0.1498(5)	0.2775(5)	72(3)	197(5)	85(3)	22(3)	13(2)	−28(3)
C9	0.3216(5)	0.0621(4)	0.3197(4)	86(3)	158(4)	83(3)	−17(3)	19(2)	11(3)
C10	0.4556(3)	0.0407(2)	0.2707(4)	70(2)	108(3)	71(2)	−1(2)	7(2)	6(2)
C11	0.8414(5)	0.1772(3)	−0.0551(6)	142(4)	103(4)	137(4)	−6(3)	68(3)	25(3)
H1	1.000(3)	−0.084(2)	0.433(3)	110(0)					
H2	0.761(2)	−0.046(2)	0.084(3)	69(8)					
H6	0.490(3)	0.247(2)	0.073(3)	110(0)					
H7	0.271(3)	0.291(2)	0.151(3)	110(0)					
H8	0.160(3)	0.165(2)	0.307(3)	110(0)					
H9	0.284(3)	0.011(2)	0.375(4)	110(0)					
H10	0.513(3)	−0.026(2)	0.303(3)	110(0)					
H11A	0.927(3)	0.204(2)	0.004(4)	130(0)					
H11B	0.795(3)	0.242(2)	−0.063(4)	130(0)					
H11C	0.867(3)	0.141(2)	−0.132(4)	130(0)					

TABLE 3. Cyclopropane atomic coordinates and thermal parameters (×1000)

Atom	X/A	Y/B	Z/C	U_{11}	U_{22}	U_{33}	U_{12}	U_{13}	U_{23}
O1	0.9495(3)	0.2396(2)	0.9331(2)	58(1)	44(1)	64(1)	−12(1)	−34(1)	−19(1)
O2	0.7911(3)	0.0465(2)	0.9500(2)	58(1)	34(1)	63(1)	−6(1)	−33(1)	−18(1)
O3	0.5804(3)	−0.1789(3)	0.7064(3)	98(2)	52(1)	78(2)	−27(1)	−24(1)	−25(1)
O4	0.7653(3)	−0.1525(3)	0.4466(3)	103(2)	75(2)	95(2)	−2(1)	−42(1)	−60(2)
N	0.6893(4)	−0.0964(3)	0.5595(4)	64(2)	44(2)	73(2)	3(1)	−39(2)	−30(2)
C1	0.8000(4)	0.1990(4)	0.9210(3)	48(2)	43(2)	29(2)	−11(1)	−13(1)	−14(1)
C2	0.6513(4)	0.3572(3)	0.8698(3)	51(2)	39(2)	48(2)	−3(1)	−22(1)	−24(1)
C3	0.4464(5)	0.3284(4)	0.8955(4)	44(2)	52(2)	53(2)	−2(2)	−16(2)	−29(2)
C4	0.5890(4)	0.4077(4)	0.7150(3)	48(2)	33(2)	43(2)	−1(1)	−22(2)	−15(1)
C5	0.6883(4)	0.3143(3)	0.5970(3)	37(2)	34(1)	37(2)	−3(1)	−20(1)	−11(1)
C6	0.6446(4)	0.1495(3)	0.6374(4)	41(2)	35(2)	40(2)	−6(1)	−16(1)	−13(1)
C7	0.7370(4)	0.0800(3)	0.5150(4)	47(2)	37(2)	50(2)	0(1)	−27(2)	−20(1)
C8	0.8698(4)	0.1689(4)	0.3524(4)	52(2)	60(2)	46(2)	4(2)	−23(2)	−30(2)
C9	0.9118(5)	0.3337(4)	0.3126(4)	51(2)	55(2)	42(2)	−12(2)	−12(2)	−14(2)
C10	0.8225(4)	0.4055(4)	0.4336(4)	50(2)	41(2)	47(2)	−10(1)	−20(2)	−14(2)
H1	1.056(4)	0.117(4)	0.975(3)	94(10)					
H2	0.656(3)	0.466(3)	0.884(3)	44(7)					
H3A	0.430(4)	0.195(3)	0.950(3)	60(8)					
H3B	0.321(4)	0.418(3)	0.936(3)	62(8)					
H4	0.564(3)	0.545(3)	0.650(2)	38(6)					
H6	0.557(3)	0.079(3)	0.748(3)	46(8)					
H8	0.935(4)	0.108(3)	0.274(3)	52(8)					
H9	1.007(4)	0.403(3)	0.195(3)	57(8)					
H10	0.852(3)	0.526(3)	0.403(3)	56(8)					

Although it would seem reasonable to expect some alteration of the bond shortening by adding substituents such as a nitro group to the phenyl ring, this can effectively be ruled out in light of the reported results of Jason and Ibers (3).

Our cyclopropane ring distance pattern is in complete accord with the above observations, and, in fact, provides additional evidence to support the "additivity principle" suggested for π-acceptor substituents (25). This proposes that "bond length asymmetry in multiply-substituted cyclopropanes should approximate a summation of the asymmetries induced by each individual substituent." Our ring values can be thought of as the composite of the following two effects: (*1*) The carboxyl group shortens the distal bond C3—C4 by an amount δ_c and lengthens each of C2—C3 and C2—C4 (by $\sim\delta_c/2$). (*2*) The phenyl ring shortens C2—C3 by δ_p and lengthens C2—C4 and C3—C4 (by $\sim\delta_p/2$).

According to Allen (2), reasonable values to expect for δ_c and δ_p are 0.023 Å and 0.018, and when applied to the value

Can. J. Chem. Downloaded from www.nrcresearchpress.com by 210.87.254.105 on 09/06/12
For personal use only.

Can. J. Chem. Downloaded from www.nrcresearchpress.com by 210.87.254.105 on 09/06/12
For personal use only.

TABLE 4. Intramolecular bond distances (Å)

Bond	Distance	
	Cyclopropene	Cyclopropane
C1—O1	1.286(3)	1.330(3)
C1—O2	1.249(3)	1.219(3)
C1—C2	1.466(3)	1.472(3)
C2—C3	1.515(4)	1.512(4)
C2—C4	1.500(3)	1.550(3)
C3—C4	1.275(3)	1.490(4)
C4—C5	1.446(3)	1.494(3)
C5—C6	1.377(3)	1.382(3)
C5—C10	1.388(3)	1.393(3)
C6—C7	1.380(4)	1.380(3)
C7—C8	1.364(5)	1.380(4)
C8—C9	1.347(5)	1.379(4)
C9—C10	1.397(4)	1.382(4)
O1—H1	0.98(3)	1.10(3)
C2—H2	0.93(2)	1.02(2)
C3—C11	1.474(4)	—
C7—N	—	1.479(3)
N—O3	—	1.221(3)
N—O4	—	1.228(3)

TABLE 5. Intramolecular bond angles (deg)

Bonds	Angle	
	Cyclopropene	Cyclopropane
O1—C1—O2	122.6(3)	122.4(2)
O1—C1—C2	116.7(3)	112.4(2)
O2—C1—C2	120.7(3)	125.2(2)
C1—C2—C3	118.9(3)	119.0(2)
C1—C2—C4	119.4(3)	121.1(2)
C3—C2—C4	50.0(2)	58.2(2)
C2—C3—C4	64.4(2)	62.1(2)
C2—C3—C11	140.8(3)	—
C4—C3—C11	154.8(3)	—
C3—C4—C2	65.6(2)	59.6(2)
C3—C4—C5	153.4(3)	124.6(2)
C2—C4—C5	141.0(3)	123.4(2)
C4—C5—C6	120.3(6)	123.6(2)
C4—C5—C10	119.9(3)	117.3(2)
C6—C5—C10	119.8(3)	118.9(3)
C5—C6—C7	120.5(3)	118.9(3)
C6—C7—C8	119.4(4)	122.9(3)
C7—C8—C9	121.2(4)	118.0(3)
C8—C9—C10	120.7(4)	120.3(3)
C9—C10—C5	118.5(3)	121.1(3)
C6—C7—N	—	118.5(3)
C8—C7—N	—	118.7(3)
C7—N—O3	—	118.4(3)
C7—N—O4	—	117.7(3)
O3—N—O4	—	124.0(3)

of 1.510 Å for normal cyclopropane the predicted values of our ring bond distances would be:

$$\text{C2—C3} = 1.510 + \frac{0.023}{2} - 0.018 = 1.504 \text{ Å}$$

$$\text{C2—C4} = 1.510 + \frac{0.023}{2} + \frac{0.018}{2} = 1.531 \text{ Å}$$

$$\text{C3—C4} = 1.510 - 0.023 + \frac{0.018}{2} = 1.496 \text{ Å}$$

These predictions agree remarkably well with the observed values of 1.512, 1.550, and 1.490 Å, especially taking into account that the phenyl and carboxyl groups in our compound are not in the ideal bisecting conformations. Also, the application of $\delta/2$ to each vicinal bond is overly simplistic and has been shown to be the non-preferred case in the compilation by Allen (2). The overly long C2—C4 bond might also imply some synergy between the two exocyclic substituent effects.

The fact that the C2—C3 value is longer than predicted while the C3—C4 value is shorter fits in well with the earlier remark (*vide supra*) about the greater deviation of the phenyl ring from the bisecting position. It is not at all clear, however, why *both* the phenyl and the carboxyl groups deviate — the closest contact between the two groups is O2···H6 = 2.98 Å, which is longer than the O2···H8′ intermolecular contact (2.77 Å), and so steric hindrance alone does not seem to be the answer. In the unhindered *trans* methyl ketone analog investigated by Bordner *et al.* (5), both substituents are near the bisecting position, with the phenyl ring somewhat closer to ideal than the carbonyl. Their ring bond length pattern is the same as ours, although the values are much lower and subject to some suspicion due to the higher R value and standard deviations. Also, the maximum difference between ring bonds in the *trans* compound is only 0.030 Å, half of the value which we observe in the *cis* where less difference would be expected due to the angles of the substituents.

The packing of the molecules in the unit cell is shown in Fig. 3. Pairs of molecules are mutually hydrogen bonded across crystallographic inversion centers, while the π clouds of the phenyl ring are in staggered opposition in planes parallel to the b axis. The hydrogen bonding parameters are: O···O = 2.674(3) Å, O···H = 1.57(3) Å, and O—H···O = 172(3)°. These values agree well with those found in other cyclopropanecarboxylic acids having similar hydrogen bonding (4, 17, 26).

1-Phenyl-2-methylcyclopropene-3-carboxylic acid

In the cyclopropene compound, the bond lengths and angles of the substituents are not in such good agreement with literature values as are those in the cyclopropane. The six phenyl ring distances average 1.376 Å with a bond of attachment (C4—C5) = 1.446 Å. There is large variation among the individual bond lengths due to the high thermal motion of the more distant ring carbons, the magnitude of which can be clearly seen in Fig. 2. The carboxyl group shows a much smaller difference between C—O bond lengths, possibly due to more extensive conjugation with the three-membered ring. The bond of attachment (C1—C2) is again much shorter than that of a pure C_{sp^2}—C_{sp^3} (20), and the whole system may be somewhat more delocalized than in the cyclopropane case. The carboxyl group is in the preferred conformation (17, 18) having the carbonyl oxygen nearer the cyclopropene center, and with a *syn*-planar hydrogen. The orientation is *cis* bisecting with respect to the cyclopropene, while the phenyl ring, on the other hand, is practically co-planar with it.

The cyclopropene ring has an exceedingly short double bond, shorter than those found in ethylene (27) and in allene (28). The explanation for this is increased s character in the σ component of the bond, together with strong $p\pi$ overlap (8).

Can. J. Chem. Downloaded from www.nrcresearchpress.com by 210.87.254.105 on 09/06/12
For personal use only.

TABLE 6. Least-square planes

(*A*) Coefficients of $Ax + By + Cz = D$

		A	*B*	*C*	*D*
Plane *1*:	O1,C1,O2 (carboxyl)				
	Cyclopropene:	0.844	0.259	−0.470	5.486
	Cyclopropane:	0.140	−0.234	−0.962	−6.557
Plane *2*:	C2,C3,C4 (C_3 ring)				
	Cyclopropene:	−0.333	−0.469	−0.818	−3.373
	Cyclopropane:	−0.100	0.994	−0.034	4.798
Plane *3*:	C5−C10 (phenyl)				
	Cyclopropene:	−0.348	−0.422	−0.837	−3.434
	Cyclopropane:	−0.873	0.348	−0.342	−7.349
Plane *4*:	N,O3,O4 (nitro)				
	Cyclopropane:	−0.892	0.353	−0.281	−7.217

(*B*) Dihedral angles (deg)

	Dihedral angle			
Compound	*1/2*	*1/3*	*2/3*	*3/4*
Cyclopropene	91.1	90.6	3.1	—
Cyclopropane	102.4	82.8	63.6	3.7

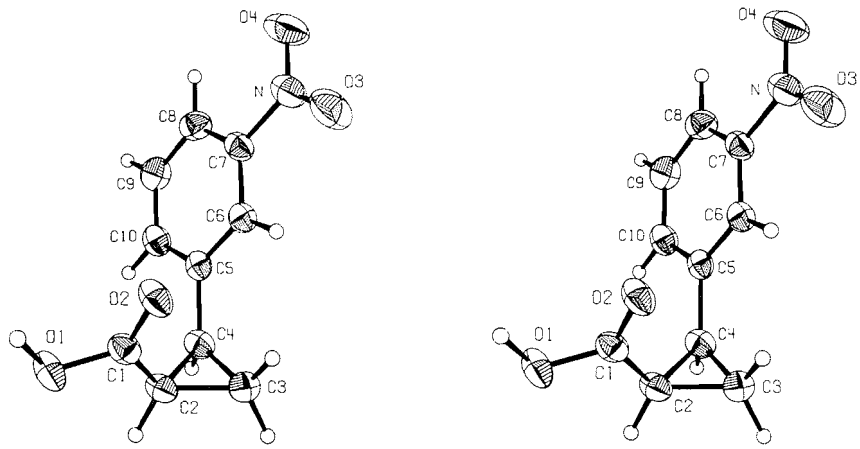

FIG. 1. Stereoscopic view of the atom-labeling scheme for *cis*-2-(*m*-nitrophenyl)cyclopropanecarboxylic acid. The thermal ellipsoids are 40% equiprobability envelopes, with hydrogens as spheres of arbitrary diameter.

TABLE 7. Torsion angles (deg)[a]

	Torsion angle	
Bonds	Cyclopropene	Cyclopropane
C3—C2—C1—O1	−148.8	−163.9
C3—C2—C1—O2	31.6	16.0
C4—C2—C1—O2	−26.4	−52.4
C4—C2—C1—O1	153.2	127.7
C4—C3—C2—C1	−105.6	−110.6
C5—C4—C2—C1	−73.4	−6.7
C5—C4—C3—C11	−2.1	—
C6—C5—C4—C3	−0.5	6.0
C6—C5—C4—C2	175.5	79.6

[a]The average esd is 0.3°.

The ring geometry is in reasonably good agreement with electron diffraction results for cyclopropene itself (29), although the strong conjugation with the exocyclic substituents tends to weaken the comparison. In fact, the only structural report in the literature which lends itself to close comparison is that of the 3,3-dimethoxycarbonyl analogue (7). Those values are in remarkably good agreement with ours, with the exception of the C—O bonds. The cyclopropene ring bond patterns are identical, with the longer of the two C_{sp^2}—C_{sp^3} bonds being opposite the phenyl substituent. Our double bond is slightly shorter, which could be due to the more favorable positioning of the carboxyl group with respect to orbital overlap of the π system. Obviously, the answer to the question that provided the impetus for this investigation is that the unhindered carbonyl substituent does indeed prefer the *cis* bisecting conformation, but it remains to be shown whether or not any perturbations to the cyclopropene caused by π-acceptor substituents can be quantified as in the case of the cyclopropanes.

The molecular packing in the unit cell is shown in Fig. 4. As in the case of the cyclopropane compound, pairs of molecules are mutually hydrogen bonded across inversion centers, although the arrangement of the pairs is completely different.

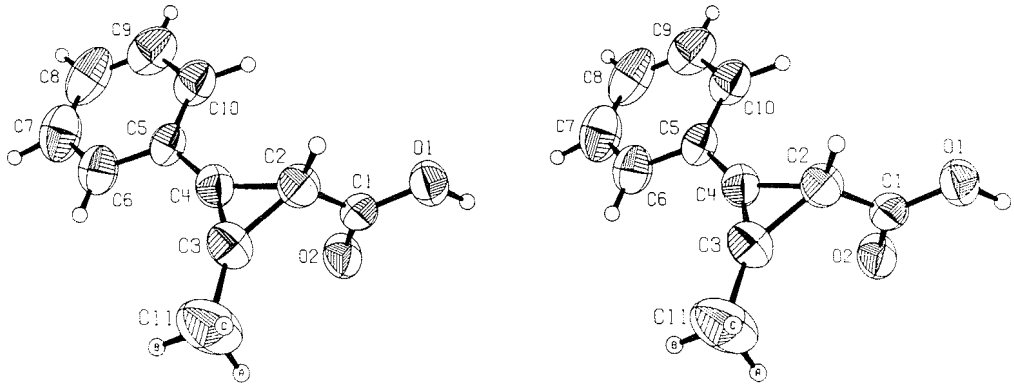

FIG. 2. Stereoscopic view of the atom-labeling scheme for 1-phenyl-2-methylcyclopropene-3-carboxylic acid. The thermal ellipsoids are 40% equiprobability envelopes, with hydrogens as spheres of arbitrary diameter.

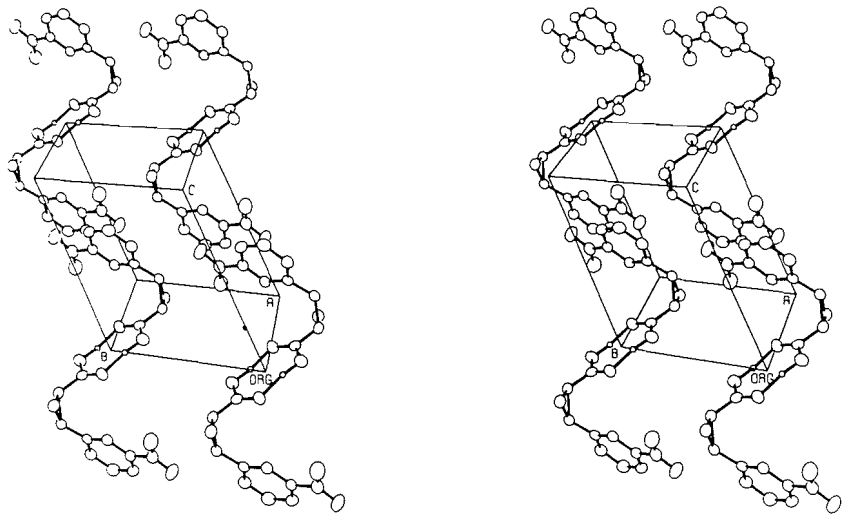

FIG. 3. Stereoscopic view of the molecular packing of the cyclopropane compound, as viewed along the *a* axis. Hydrogens are omitted for clarity, and the hydrogen bonds between pairs of molecules are included.

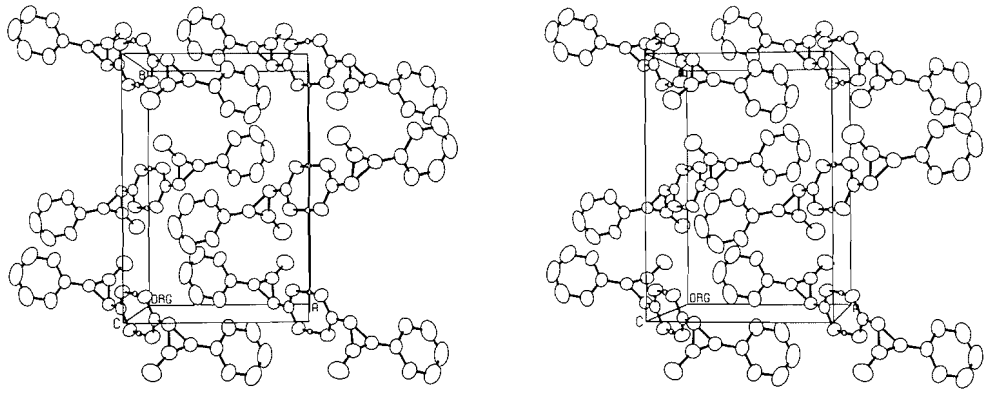

FIG. 4. Stereoscopic view of the molecular packing of the cyclopropene compound, as viewed into the *c* axis. Hydrogens are omitted, and hydrogen bonds between pairs of molecules across inversion centers are included.

The O···O separation is 2.609(3) Å, O···H = 1.63(3) Å, and the O—H···O angle is 173(3)°. There are no unusually close intermolecular contacts.

Acknowledgements

Acknowledgement is made to the donors of The Petroleum Research Fund, administered by the American Chemical Society, for partial support of this research, and to The Robert A. Welch Foundation (J.D.K. and I.B., Grant E-594, R.F., Grant E-136) for additional support.

1. R. FUCHS, J. H. HALLMAN, and M. O. PERLMAN. Can. J. Chem. **60**, 1832 (1982).
2. F. H. ALLEN. Acta Crystallogr. B**36**, 81 (1980), and references therein.
3. M. E. JASON and J. A. IBERS. J. Am. Chem. Soc. **99**, 6012 (1977).

Can. J. Chem. Downloaded from www.nrcresearchpress.com by 210.87.254.105 on 09/06/12
For personal use only.

4. C. C. CHIANG, C.-T. LIN, A. H.-J. WANG, D. Y. CURTIN, and I. C. PAUL. J. Am. Chem. Soc. **99**, 6303 (1977).
5. J. BORDNER, L. A. JONES, and R. L. JOHNSON. Cryst. Struct. Commun. **1**, 389 (1972).
6. R. FUCHS, C. A. KAPLAN, J. J. BLOOMFIELD, and L. F. HATCH. J. Org. Chem. **27**, 733 (1962).
7. C. ROMMING and A. S. BERG. Acta Chem. Scand. Ser. A, **33**, 271 (1979).
8. F. H. ALLEN. Tetrahedron, **38**, 645 (1982), and references therein.
9. R. FUCHS and A. B. THIGPEN, JR. J. Org. Chem. **34**, 505 (1969).
10. G .GERMAIN, P. MAIN, and M. M. WOOLFSON. Acta Crystallogr. A**27**, 368 (1971).
11. D. T. CROMER and J. B. MANN. Acta Crystallogr. A**24**, 321 (1968).
12. R. F. STEWART, E. R. DAVIDSON, and W. T. SIMPSON. J. Chem. Phys. **42**, 3175 (1965).
13. G. M. SHELDRICK. SHELX-76 Programs for crystal structure determination. Univ. of Cambridge. 1976.
14. J. L. RICCI and I. BERNAL. J. Am. Chem. Soc. **91**, 4078 (1969).
15. J. D. KORP, I. BERNAL, R. F. MILLER, J. C. TURLEY, L. WILLIAMS, and G. E. MARTIN. J. Cryst. Mol. Struc. **8**, 127 (1978).
16. J. D. KORP, I. BERNAL, and G. E. MARTIN. J. Cryst. Mol. Struc. **11**, 11 (1981).
17. M. A. M. MEESTER, H. SCHENK, and C. H. MACGILLAVRY. Acta Crystallogr. B**27**, 630 (1971).
18. D. J. BRAUER, C. KRUGER, and P. J. ROBERTS. J. Chem. Soc. Perkin II Trans. 533 (1976).
19. L. LEISEROWITZ. Acta Crystallogr. B**32**, 775 (1976).
20. L. S. BARTELL and R. A. BONHAM. J. Chem. Phys. **32**, 824 (1960).
21. O. BASTIANSEN, F. N. FRITSCH, and K. HEDBERG. Acta Crystallogr. **17**, 538 (1964).
22. R. HOFFMANN. Proc. XXIII Intl. Congr. Pure Appl. Chem. **2**, 233 (1971).
23. R. HOFFMANN. Tetrahedron Lett. **33**, 2907 (1970).
24. J. W. LAUHER and J. A. IBERS. J. Am. Chem. Soc. **97**, 561 (1975).
25. R. HOFFMANN and W.-D. STOHRER. J. Am. Chem. Soc. **93**, 6941 (1971).
26. P. A. LUHAN and A. T. MCPHAIL. J. Chem. Soc. Perkin II Trans. 2372 (1972).
27. K. KUCHITSU. J. Chem. Phys. **44**, 906 (1966).
28. A. G. MAKI and R. A. TOTH. J. Mol. Spectrosc. **17**, 136 (1975).
29. J. F. CHIANG. J. Chin. Chem. Soc. Taipei, **17**, 65 (1970).

Can. J. Chem. Downloaded from www.nrcresearchpress.com by 210.87.254.105 on 09/06/12
For personal use only.

Mononuclear and binuclear copper(II) complexes of some polyfunctional pyridyl phthalazines

GRAHAM BULLOCK, FREDERICK W. HARTSTOCK, AND LAURENCE K. THOMPSON[1]
Department of Chemistry, Memorial University of Newfoundland, St. John's, Nfld., Canada A1B 3X7

Received June 24, 1982

GRAHAM BULLOCK, FREDERICK W. HARTSTOCK, and LAURENCE K. THOMPSON. Can. J. Chem. **61**, 57 (1983).

Mononuclear and binuclear copper(II) complexes of the potentially tetradentate binucleating ligands 1,4-di(3′-methyl-2′-pyridyl)aminophthalazine (PAP3Me) and 1,4-di(5′-methyl-2′-pyridyl)aminophthalazine (PAP5Me) are reported. In the case of the ligand 1,4-di(4′,6′-dimethyl-2′-pyridyl)aminophthalazine (PAP46DiMe) only binuclear derivatives were obtained. The mononuclear complexes, involving protonated ligand, result from the sensitivity of these ligands to mildly acidic conditions in aqueous solutions of certain copper salts. Binuclear, neutral ligand, complexes are also formed when the pH increases. Hydroxy bridged binuclear structures exist in all the binuclear complexes described with the exception of one acetate bridged derivative. Sub normal magnetic moments are observed for all the binuclear complexes (<1.74 BM) indicating spin coupled systems with very low values (<0.88 BM) for binuclear complexes of PAP46DiMe, indicating the possibility of strong antiferromagnetic exchange between the metal centres.

GRAHAM BULLOCK, FREDERICK W. HARTSTOCK et LAURENCE K. THOMPSON. Can. J. Chem. **61**, 57 (1983).

On rapporte les complexes mononucléaires et binucléaires de cuivre (II) des ligands binucléaires potentiellement tétradentates, di(méthyl-3′ pyridyl-2′)-1,4 aminophthalazine (PAP3Me) et di(méthyl-5′ pyridyl-2′)-1,4 aminophthalazine (PAP5Me). On a obtenu uniquement des dérivés binucléaires dans le cas du ligand di(diméthyl-4′,6′ pyridyl-2′) aminophthalazine (PAP4DiMe). Les complexes mononucléaires, impliquant un ligand protoné, proviennent du fait que ces ligands sont sensibles aux conditions acides douces des solutions aqueuses de certains sels de cuivre. Il se forme également des complexes binucléaires de ligand neutre, lorsque le pH augmente. Des structures binucléaires, ayant un hydroxy en position de pont, existent dans tous les complexes binucléaires décrits à l'exception d'un dérivé ayant un pont acétate. On a observé des moments magnétiques sub-normaux pour tous les complexes binucléaires (<1,74 BM) indiquant ainsi des systèmes à spin couplé avec de très faibles valeurs (<0,88 BM) pour les complexes binucléaires de PAP46DiMe et également la possibilité d'un fort échange antiferromagnétique entre les centres métalliques.

[Traduit par le journal]

Introduction

Binuclear copper centres are found in the oxygen breathing protein hemocyanin and in a number of enzymes which have oxidase or oxygenase function (Type III centres). Magnetic studies have shown that strong antiferromagnetic exchange exists between the two copper(II) centres in Megathura crenulata oxyhemocyanin ($-2J \geq 1250$ cm^{-1}) (1, 2) and Rhus vernicifera laccase ($-2J \geq 1000$ cm^{-1}) (2). Antiferromagnetic coupling is usually mediated by a superexchange pathway which would imply the presence of a bridging group or groups between the two copper atoms and that the metal centres would be in close proximity in the protein. Resonance Raman studies on oxyhemocyanins have indicated a peroxide bridge between the copper(II) centres (3, 4) and EXAFS studies by Spiro *et al.* on Busycon canaliculatum oxyhemocyanin have suggested a copper–copper separation of 3.67 Å in a proposed structure with three imidazoles bound to each copper centre, a peroxide bridge, and another endogenous protein ligand bridge (5). Hodgson *et al.* studied the oxyhemocyanin binuclear centres in Megathura crenulata and Helix pomatia and found the two copper atoms to be separated by 3.55 Å in a proposed structure involving two imidazoles per copper, a peroxide bridge and a protein ligand bridge in an approximately square planar structure (6). Further studies by Solomon *et al.* suggest two copper centres bridged by peroxide and some endogenous ligand with two imidazoles and a water molecule at each five-coordinate copper centre in various mollusc and arthropod oxyhemocyanins. They also point out the similarity, based on chemical and spectroscopic studies, of the Type III centre in tyrosinase with that in oxyhemocyanin (7, 8). Reporter probe studies involving substitution of copper(II) by cobalt(II) in squid (Sepioteuthis lessoniana) hemocyanin suggest that in the deoxy form, three histidine imidazoles are bound to each copper(I) centre in a structure involving one pseudo-tetrahedral copper site and a tetragonally distorted site with a possible endogenous bridge. A double bridged five-coordinate structure involving three imidazoles per copper, a bridging peroxide, and another bridge group was proposed for the oxy form (9).

In previous papers we have described the copper coordination chemistry of some polyfunctional binucleating pyridylphthalazines, which present the two copper centres with two nitrogen donor groups in multibridged structures involving, in many cases, hydroxy bridges between the metal centres (10–13). The ligands have included PAP(1,4-di(2′-pyridyl)-aminophthalazine) and PAP4Me and PAP6Me which have methyl substituents on the 4- and 6-positions of the pyridine rings respectively. X-ray structures have shown that the binuclear centre in a series of hydroxy bridged species can be tuned by varying a third bridging group (Fig. 1) (10, 12–14). In general, systems of this sort have low room temperature magnetic moments, signalling exchange-coupled copper centres and in cases where exchange integrals were measured the exchange was observed to increase with increasing oxygen bridge angle.

In this report we describe the copper coordination chemistry of three other related pyridyl phthalazines: 1,4-di(3′-methyl-2′-pyridyl)aminophthalazine (PAP3Me), 1,4-di(5′-methyl-2′-pyridyl)aminophthalazine (PAP5Me), and 1,4-di(4′,6′-di-

[1]To whom all correspondence should be addressed.

0008-4042/83/010057-06$01.00/0
©1983 National Research Council of Canada/Conseil national de recherches du Canada

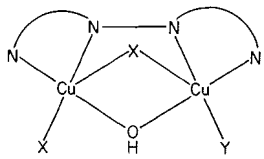

FIG. 1. Dimensions and magnetic exchange at the binuclear centre in some binuclear copper phthalazine complexes

Ligand	X	Y	Cu—O—Cu (deg)	Cu---Cu (Å)	$-2J$ (cm^{-1})	References
PAP	Cl	Cl	101.8, 100.1	3.001, 2.972	201	10, 14
PAP	Br	Br	101.3, 102.9	3.010, 2.986	186	10, 13
PAP	IO_3	IO_3	113.4	3.166	335	10, 13
PAP4Me	NO_3	$(H_2O)_2$	115.3	3.138	—	12, 13

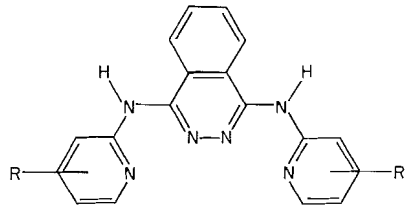

FIG. 2. PAP3Me (R = 3-methyl), PAP5Me (R = 5-methyl), PAP46DiMe (R = 4,6-dimethyl).

methyl-2′-pyridyl)aminophthalazine (PAP46DiMe) (Fig. 2). These ligands are previously unreported. Protonated ligand mononuclear complexes and neutral ligand binuclear complexes are obtained for PAP3Me and PAP5Me while for PAP46DiMe only binuclear complexes have been synthesized so far. In many cases low room temperature magnetic moments suggest antiferromagnetically-coupled copper(II) centres and in most of the binuclear complexes hydroxy bridges are implicated.

Experimental

Electronic spectra were recorded with a Cary 17 spectrometer and infrared spectra with a Perkin-Elmer Model 283 spectrometer. Magnetic susceptibilities were obtained at room temperature by the Faraday method using a Cahn Model #7600 Faraday Magnetic Susceptibility system, coupled to a Cahn gram electrobalance. Microanalyses were carried out by Canadian Microanalytical Service, Vancouver (C, H, N). Metal analyses were determined by atomic absorption with a Varian Techtron AA-5, after digestion of the samples in concentrated HNO_3 or aqua regia.

Ligands

PAP3Me (mp 257°C), PAP5Me (mp 114°C), and PAP46DiMe (mp 288–289°C) (Fig. 2) were prepared by the same methods used for the synthesis of other previously reported pyridylphthalazines (10, 12). Further details on their syntheses and the general properties of these and other pyridylphthalazines will be published elsewhere. Satisfactory elemental analyses were obtained for these three ligands (Table 1).[2]

Copper complexes (LH = protonated ligand)

$[Cu_2(PAP3Me)(OH)X_3]\cdot yH_2O$ (I) (X = Cl, y = 1.5), (II) (X = Br, y = 0); $[Cu_2(PAP5Me)(OH)X_3]$ (IX) (X = Cl), (X) (X = Br)

$CuCl_2\cdot 2H_2O$ (1.50 g, 8.80 mmol) was dissolved in water (50 mL), PAP3Me (1.50 g, 4.39 mmol) added, and the mixture refluxed until the ligand dissolved. After 10–15 min a green crystalline powder (**I**) formed which was filtered off, washed with water, and dried under vacuum. The other compounds were prepared similarly and obtained as green crystalline solids.

$[Cu_2(PAP46DiMe)(OH)Cl_3]\cdot EtOH$ (XVII)

$CuCl_2\cdot 2H_2O$ (0.920 g, 5.40 mmol) was dissolved in water (150 mL), PAP46DiMe (1.00 g, 2.70 mmol) added, and the mixture refluxed for 4 h. The hot solution was filtered to remove a small amount of orange impurity and the volume of the green solution reduced by half. Addition of ethanol (30 mL) led to the formation of dark green crystals (**XVII**) on standing.

$[Cu(PAP3MeH)_2](ClO_4)_4\cdot 2H_2O$ (IV), $[Cu_2(PAP3Me)(OH)(H_2O)_2](ClO_4)_3$ (V), $[Cu(PAP5MeH)_2](ClO_4)_4\cdot H_2O$ (XII)

$Cu(ClO_4)_2\cdot 6H_2O$ (1.50 g, 3.98 mmol) was dissolved in water (100 mL), PAP3Me (0.690 g, 2.01 mmol) added, and the mixture refluxed for $1\frac{1}{2}$ h. A brown precipitate (**IV**) was filtered off and the green mother liquor reduced in volume. On standing a green crystalline powder (**V**) was obtained. Compound **XII** was obtained similarly as a buff solid, but the corresponding binuclear complex could not be obtained in a pure enough state and so is not reported.

$[Cu(PAP3MeH)_2](NO_3)_4\cdot 3H_2O$ (VI), $[Cu_2(PAP3Me)(OH)(H_2O)_2(NO_3)_2]NO_3$ (VII), $[Cu_2(PAP3Me)(OH)(NO_3)_2](NO_3)$ (VIII), $[Cu(PAP5MeH)_2(H_2O)_2](NO_3)_4\cdot 5H_2O$ (XIII), $[Cu_2(PAP5Me)(OH)(H_2O)_2(NO_3)_2](NO_3)$ (XIV), $[Cu_2(PAP5Me)(OH)(NO_3)_2](NO_3)$ (XV)

$Cu(NO_3)_2\cdot 3H_2O$ (1.00 g, 4.14 mmol) was dissolved in water (100 mL), PAP3Me (0.680 g, 1.99 mmol) was added, and the mixture refluxed for 1 h. The green solution was filtered and allowed to stand. A light brown crystalline powder (**VI**) was obtained which was filtered off and the mother liquor reduced in volume. On standing blue crystals (**VII**) were obtained. Compounds **XII** (buff) and **XIV** (dark blue) were prepared similarly while **VIII** and **XV** (green) were obtained by heating **VII** and **XIV** respectively at 80°C under vacuum for several hours. Compound **XIX** was obtained as green crystals by a procedure similar to that of **VII**, using ethanol as solvent. No protonated complex was obtained in this case.

$[Cu(PAP3Me)(OH)(SO_4)(H_2O)_2](SO_4)_{0.5}\cdot 5H_2O$ (III), $[Cu_2(PAP5Me)(OH)(SO_4)(H_2O)](SO_4)_{0.5}$ (XI)

$CuSO_4\cdot 5H_2O$ (1.00 g, 4.00 mmol) was dissolved in warm water (100 mL), PAP3Me (0.680 g, 1.99 mmol) added, and the mixture refluxed for $1\frac{1}{2}$ h. The green product **III** was filtered off and recrystallized from water to given bright green crystals. Compound **XI** was prepared similarly and obtained as green crystals.

$[Cu_2(PAP5Me)(CH_3COO)_3]\cdot 0.5CHCl_3$ (XVI), $Cu_2(PAP46DiMe)(OH)(CH_3COO)_2]\cdot 1.5H_2O$ (XVIII)

$[Cu(CH_3COO)_2\cdot H_2O]_2$ (1.00 g, 2.51 mmol) was dissolved in methanol (100 mL), PAP5Me (0.800 g, 2.34 mmol) added, and the mixture refluxed for $1\frac{1}{2}$ h. A khaki-green powder formed (**XVI**) which was filtered off and recrystallized from chloroform/hexane. Compound **XVIII** was prepared similarly using ethanol as solvent and obtained as a sparingly soluble khaki-brown product which was used without further purification.

Satisfactory analytical data have been obtained for all the complexes and are reported in Table 1 which is available from the Depository of Unpublished data.[2]

Results and discussion

Characterization of the complexes

Tetradentate pyridylphthalazines (PAPR; R = H, 4Me, 6Me) (Fig. 2) have shown a preference for the formation of binuclear complexes in which two metals are bound to the same ligand in a multiple bridged structural arrangement (10–17). Polynuclear derivatives involving three copper centres have also been reported (11, 12) and in some cases protonated, mononuclear derivatives are found in which the formation of a protonated ligand is seen as the result of the sensitivity of these ligands to even mildly acidic conditions which are common in

[2]Photocopies may be obtained at a nominal charge, upon request, from the Depository of Unpublished Data, CISTI, National Research Council of Canada, Ottawa, Canada K1A 0S2.

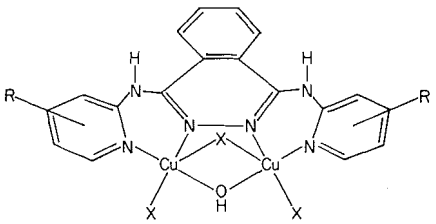

FIG. 3. Proposed structures for the complexes $[Cu_2(PAP3Me)(OH)X_3]$ (X = Cl, Br), $[Cu_2(PAP5Me)(OH)X_3]$ (X = Cl, Br), and $[Cu_2(PAP46DiMe)(OH)Cl_3]$.

aqueous solutions of transition metal salts (11, 12, 17).

Magnetic and X-ray structural studies have shown that in binuclear copper complexes of PAP (R = H), in which a constant structural feature involves the double bridge including a hydroxide and the phthalazine N—N group, variation in size of the third bridging group (e.g. $Cl \rightarrow IO_3$) can dramatically alter the spin exchange between the metal centres as a result of a concomitant increase in the oxygen bridge angle (13). This change is also reflected in the room temperature magnetic moments. While modifications in the bridging groups can tune the binuclear centre, structural variations in the ligand itself appear also to be capable of altering the geometry at the binuclear centre by imposing certain steric constraints. The complexes $[Cu_2(PAP6Me)(OH)X_3]$ (X = Cl, Br) (12) were shown to have very low room temperature magnetic moments (<0.7 BM) possibly indicating stronger exchange than that observed in the complex $[Cu_2(PAP)(OH)(IO_3)_3]\cdot 4H_2O$ (10, 13) and an increased oxygen bridge angle.

In this report we have examined the ligands PAP3Me, PAP5Me, and PAP46DiMe (Fig. 2) in which steric constraints imposed by the substituent methyl groups on the pyridine rings are likely to differ from those of the previously reported systems. Earlier studies indicate that the pK_a of PAP is close to 3.8 and that the ligand can behave as a neutral, anionic, or cationic entity (10–12). In its neutral form $\pi-\pi^*$ charge transfer absorptions were found to occur in the range 27400–29600 cm^{-1}, while for anionic systems the lowest energy charge transfer band was found to occur between 24000 and 25600 cm^{-1} (10). In the uncomplexed ligand this band occurs at 26200 cm^{-1}. Criteria of this sort will be used to assess the charged state of the methylated ligands. The nuetral ligands PAP3Me, PAP5Me, and PAP46DiMe have $\pi-\pi^*$ absorptions in methanol in the range 26700–27800 cm^{-1} (Table 2).

The chloro-complexes **I**, **IX**, and **XVII** and the bromo-complexes **II** and **X** appear to have similar five-coordinate structures, in which, as in the PAP analogues (10–12) the two metals are bridged by a phthalazine moiety, a hydroxide, and a halide (Fig. 3, X = Cl, Br). Reduced magnetic moments (Table 2) are observed for all the halide complexes indicating exchange coupled copper centres. However, the very low moment observed for the PAP46DiMe complex suggests strong exchange with the possibility of a quite large oxygen bridge angle. As in the case of the PAP6Me complexes (12) this may be attributable to steric effects associated with the 6-methyl substituents on the pyridine rings.

The sulfato-complexes of PAP3Me (**III**) and PAP5Me (**XI**) are both neutral ligand systems involving hydroxy bridges between the copper centres. Very rich infrared absorption is observed for both systems in the range 950–1200 cm^{-1} (Table 2) where the ν_1 and ν_3 vibrations associated with sulfate are observed. The sulfate ion (T_d) exhibits one broad band (ν_3) at about 1100 cm^{-1} but on reducing the symmetry through C_{3v} to C_{2v} two and three bands respectively associated with the ν_3 vibration are observed in the range 1000–1200 cm^{-1} (18). It seems likely that a bidentate sulfato bridge occurs in both systems and the most obvious place for it to occur would be as a bridge between the two copper centres. The other sulfate could be ionic or perhaps behave as a bidentate bridge between two binuclear centres.

An X-ray structural study (13) of the analogous system $[PAPCu_2(OH)Cl(SO_4)]\cdot 2H_2O$ reveals a sulfate bridge and a hydroxy bridge between two five-coordinate copper centres (Fig. 1, X = SO_4; Y = Cl). However, the sulfate group is in fact tridentate, bridging a third copper atom from the binuclear centre in an adjacent molecule. The Cu—O(H)—Cu bond angle was found to be 115.6° and the Cu—Cu separation 3.211 Å. A low magnetic moment (1.01 BM) was found, indicative of fairly strong magnetic exchange between the copper centres. Details of this structure will be published elsewhere. An immediate structural analogy between this compound and **III** and **XI** may not be reasonable because of the presence of an additional half sulfate in each case. However, these systems both clearly contain binuclear hydroxy bridged copper(II) centres. The magnetic moment for **III** is close to the spin-only value for copper(II), implying a small exchange, while the low moment for **XI** suggests significant spin exchange between the copper(II) centres and a much larger oxygen bridge angle.

As with other PAP-type ligands, protonated mononuclear complexes are formed with certain copper salts in addition to neutral ligand polynuclear derivatives (11, 12). PAP3Me reacts with copper perchlorate in aqueous solution to give a buff solid (**IV**) initially which appears to be a four-coordinate square planar derivative involving two bidentate protonated ligands. The high magnetic moment for this system is typical of a mononuclear copper(II) complex. A typical feature of these protonated complexes is a rich CN-stretching region of the infrared spectrum with, in some case, in excess of four distinguishable bands. The neutral systems usually only exhibit two such bands. The site of protonation is assumed to be the pyridine nitrogen (11). Compound **IV** exhibits just two CN-stretching bands which may indicate protonation at a different ligand nitrogen site.

The perchlorate complex **V** is a binuclear system involving neutral ligand and although a hydroxide absorption cannot be clearly seen in the infrared it is implied that such a group bridges the two metal centres. A rather broad perchlorate band is observed in the infrared at 1080 cm^{-1} but the lack of structure of this absorption suggests that the perchlorate group is ionic. However, a weakly associated perchlorate bridge between the two copper centres should not be ruled out. The low magnetic moment for **V** indicates significant spin exchange and a fairly large oxygen bridge angle, which can be associated with a bulky third bridge between the metal centres (e.g. ClO_4).

With PAP5Me only the protonated mononuclear perchlorate complex **XII** could be isolated satisfactorily and as with **IV** appears to have a speudo-square planar structure. Four CN-stretching bands are observed in the infrared, in general agreement with other such systems, suggesting protonation at the pyridine nitrogen sites.

As with copper perchlorate two pairs of complexes are obtained in each case in the reactions between PAP3Me and PAP5Me with copper nitrate in aqueous solution. The protonated mononuclear complex **VI** has a high energy $d-d$ absorption, perhaps more typical of a pseudo-square system,

TABLE 2. Electronic spectra (mull transmittance), infrared spectra, and magnetism

	Compound	$d-d$ (cm^{-1})	CT (cm^{-1})	Infrared (cm^{-1})	μ $(BM)_{Cu}$ (room temp.)
	PAP3Me		26700*		
	PAP5Me		27800*		
	PAP46DiMe		27800*		
I	$[Cu_2(PAP3Me)(OH)Cl_3]\cdot 1.5H_2O$	14900	[25900]	265, 303(Cu—Cl), 3620(OH)	1.64
II	$[Cu_2(PAP3Me)(OH)Br_3]$	15400	[24700], [29000]	250(Cu—Br), 3600(OH)	1.25
III	$[Cu_2(PAP3Me)(OH)(SO_4)(H_2O)_2](SO_4)_{0.5}\cdot 5H_2O$	13700	[28900]	950, 1020, 1100, 1130, 1180 (SO_4^{2-}), 3630(OH)	1.70
IV	$[Cu(PAP3MeH)_2](ClO_4)_4\cdot 2H_2O$	[22000]	27800	1080(ClO_4^-)	2.19
V	$[Cu_2(PAP3Me)(OH)(H_2O)_2](ClO_4)_3$	15400	28600	1080(ClO_4^-), 3550(OH,H_2O)	1.13
VI	$[Cu(PAP3MeH)_2](NO_3)_4\cdot 3H_2O$	19000	27800	1745($\nu_1 + \nu_4$, NO_3^-)	2.02
VII	$[Cu_2(PAP3Me)(OH)(H_2O)_2(NO_3)_2](NO_3)$	15900	[29400]	1728, 1744, 1756($\nu_1 + \nu_4$, NO_3^-), 3500(OH, H_2O)	1.24
VIII	$[Cu_2(PAP3Me)(OH)(NO_3)_2](NO_3)$	15600	[25000] [28600]	1716, 1743, 1752($\nu_1 + \nu_4$, NO_3^-), 3490(OH)	1.28
IX	$[Cu_2(PAP5Me)(OH)Cl_3]$	15300	28600	260, 280, 290(Cu—Cl), 3610(OH)	1.49
X	$[Cu_2(PAP5Me)(OH)Br_3]$	14900	28200	250(Cu—Br), 3590(OH)	1.35
XI	$[Cu_2(PAP5Me)(OH)(SO_4)(H_2O)](SO_4)_{0.5}$	14300	[27800]	962, 1030, 1085, 1130(sh), 1150(SO_4^{2-}), 3530(OH, H_2O)	1.17
XII	$[Cu(PAP5MeH)_2](ClO_4)_4\cdot H_2O$	[23000]	27800	1040, 1100(ClO_4^-)	1.98
XIII	$[Cu(PAP5MeH)_2(H_2O)_2](NO_3)_4\cdot 5H_2O$	[14900], [19000]	[28600]	1757($\nu_1 + \nu_4$, NO_3^-)	1.98
XIV	$[Cu_2(PAP5Me)(OH)(H_2O)_2(NO_3)_2](NO_3)$	15600	29000	1748, 1756, 1769($\nu_1 + \nu_4$, NO_3^-), 3500(OH, H_2O)	1.18
XV	$[Cu_2(PAP5Me)(OH)(NO_3)_2](NO_3)$	16700	[28200]	1711, 1742, 1765($\nu_1 + \nu_4$, NO_3^-), 3570(sh)(OH)	1.60
XVI	$[Cu_2(PAP5Me)(CH_3COO)_3]\cdot 0.5CHCl_3$	13800	[23500]	1360, 1400, 1576(CH_3COO^-)	1.74
XVII	$[Cu_2(PAP46DiMe)(OH)Cl_3]\cdot EtOH$	15200	27800	268, 280(Cu—Cl), 3520 (OH, EtOH)	0.88
XVIII	$[Cu_2(PAP46DiMe)(OH)(CH_3COO)_2]\cdot 1.5H_2O$	[15200]	24100	1360, 1370, 1570, 1585, 1605 (CH_3COO^-)3400(OH, H_2O)	0.78

*Methanol solution.

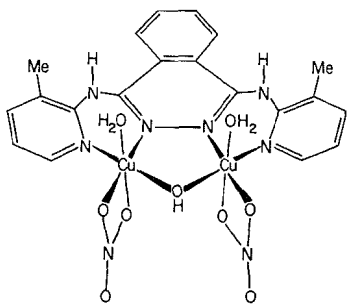

FIG. 4. Proposed structure for the cation in $[Cu(PAP3Me)(OH)(H_2O)_2(NO_3)_2](NO_3)$.

although a tetragonally distorted six-coordinate system involving loosely bound water should not be ruled out. A high magnetic moment for this complex typifies a mononuclear entity and, as with other protonated PAP3Me systems, only two CN-stretching bands are observed (1604, 1630 cm^{-1}). **XIII** exhibits five prominant CN-stretching bands, typical of a protonated ligand, and a high magnetic moment. A shoulder at 14900 cm^{-1} in the electronic spectrum suggests a tetragonally distorted six-coordinate system involving axially bound water molecules.

The binuclear dark blue nitrate complex **VII** has a hydroxy bridge and infrared absorption associated with coordinated water. Three nitrate combination bands ($\nu_1 + \nu_4$) are observed at 1728, 1744, and 1756 cm^{-1}. The absorption at 1744 cm^{-1} can be associated with ionic nitrate while the other two bands suggest the presence of bidentate chelating nitrate. There is no infrared evidence to support the presence of a bidentate bridging nitrate between the two copper centres (19), which was found to be the case in the blue six-coordinate complex $[Cu_2(PAP4Me)(OH)(H_2O)_2(NO_3)_2]NO_3$ according to X-ray studies (12, 13). The low magnetic moment for this system indicates significant exchange between the metal centres and a large oxygen bridge angle. The $d-d$ absorption at 15900 cm^{-1} is comparable with that observed for the PAP4Me analogue (16300 cm^{-1}) and so a six-coordinate structure is suggested for this system (Fig. 4).

On heating **VII** under vacuum a colour change from blue to green occurs (**VIII**). Two water molecules are clearly lost but the role of the nitrate groups appears to be the same. If the $\nu_1 + \nu_4$ nitrate band at 1743 cm^{-1} can be associated with ionic nitrate the other two bands suggest the presence of bidentate chelating nitrate. A five-coordinate structure involving a hydroxy bridge is suggested for this system (Fig. 4, water molecules removed from both copper centres). Since the magnetic moment does not change appreciably on dehydration the hydroxy bridge angle in both systems is presumed to be comparable.

The blue PAP5Me complex **XIV** has similar spectral and magnetic features to **VII** and a similar structure is proposed for this system (Fig. 4). On heating this compound under vacuum a colour change from blue to green also occurs (**XV**). A shift in the $d-d$ absorption of 1100 cm^{-1} to higher energy was

observed in addition to an increase in the magnetic moment from 1.18 to 1.60 BM. It is clear from the microanalysis that two water molecules are lost on heating and coupled with nitrate combination band data, indicating the presence of both ionic and chelating bidentate nitrate, a five-coordinate binuclear hydroxy bridged structure is again proposed (Fig. 4; water molecules removed from both copper centres). The increase in magnetic moment on dehydration can be interpreted in terms of a decrease in the oxygen bridge angle which may result from the steric constraints associated with the pyridine ring methyl substituents occupying different ring positions.

Copper acetate complexes have been obtained with PAP5Me (**XVII**) and PAP46DiMe (**XVIII**) and a comparison of their spectral and magnetic properties reveals some substantial structural differences. A low energy charge transfer absorption indicates the presence of anionic ligand in **XVI** and infrared absorptions due to carboxylate suggest the presence of both terminal and bridging acetate, although there is no significant absorption associated with the asymmetric vibration of a terminally bound carboxylate (10, 12). Structurally **XVI** appears to be similar to a series of copper carboxylate complexes of the pyridylphthalazine PAP (10) which were assumed to have a carboxylate bridge between the two copper centres and two terminally bound carboxylates. The absence of an asymmetric terminal carboxylate vibration was seen as a result of an intermolecular association where the terminal carboxylates form weak bridges to adjacent molecules thus forming effectively five-coordinate systems. The magnetic moment of 1.74 BM does not necessarily indicate a non-exchanged system but that the spin exchange is likely to be small. Low temperature magnetic studies by the Gouy method have shown an exchange integral $-2J = 114$ cm^{-1} for the analogous complex $[Cu_2(PAP)(CH_3COO)_3]$ (20) which has a room temperature moment of 1.66 BM (10).

The copper acetate complex of PAP46DiMe (**XVIII**) has a low energy charge transfer absorption implying the presence of anionic ligand and a very low room temperature magnetic moment indicating a strongly coupled system with a hydroxy bridge. A strong broad infrared absorption at 3400 cm^{-1} is associated with a hydroxide bridge which may be hydrogen bonded to either a neighbouring carboxylate or a water molecule. Infrared absorptions associated with both terminal and bridging carboxylate can be identified and suggest a carboxylate bridge between the two copper centres. Since the molecule contains just two acetate groups a terminal acetate is assigned to one copper atom with the possibility of a water molecule occupying the fifth coordination site at the other copper centre (Fig. 3, X = CH_3COO^-, one terminal X = H_2O). The $d-d$ absorption for this system is consistent with five-coordinate copper(II).

Binucleating pyridyl phthalazines (PAPR) present the two copper centres each with two nitrogen donor groups (mimetic of histidine imidazole) in mainly five-coordinate systems involving in most cases hydroxy bridges. Metal–metal separations have approached 3.2 Å with Cu—O—Cu bridge angles of up to around 115° (12–14) and very low room temperature magnetic moments have been observed, indicative of antiferromagnetic exchange. The largest exchange integral so far was found to be 335 cm^{-1} ($-2J$) for the complex $[Cu_2PAP(OH)(IO_3)_3]\cdot 4H_2O$ (10, 13) which has an oxygen bridge angle of 113.4°. It is expected that enhanced exchange will be observed for those systems with increased bridge angles. The maximum metal–metal separation, and hence Cu—O—Cu bridge angle in these binuclear phthalazine complexes, will perhaps be determined by the dimensions of the Cu_2N_2 (phthalazine) unit and assuming a limit of 120° in the Cu—N—N angle a limit of ~3.4 Å would be placed on this separation. However, in other pyridyl phthalazine and pyridyl pyridazine complexes involving nickel and copper, respectively, the M—N—N (diazine) angle has been shown to exceed 120° (21–23). In the complex $[Ni_2(dhph)_2(H_2O)_4]Cl_4\cdot 2H_2O$ (dhph = 1,4-dihydrazinophthalazine) Ni—N—N (phthalazine) angles of 124.8° and 125.6° are found with a metal–metal separation of 3.791 Å (21) while for the complex $[Cu_2LCl_3(OH)(H_2O)]$ (L = 3,6-bis(2′-pyridyl)pyridazine), Cu—N—N (pyridazine) angles of 120.7° and 120.9° are found with a metal–metal separation of 3.376 Å and a Cu—O—Cu bridge angle of 126.5° (no exchange data are quoted for this system) (23). Clearly, therefore, diazine systems, including phthalazines, pyridazines, and pyrazoles, should be capable of generating binuclear copper systems with metal–metal separations in the range anticipated for hemocyanin and the Type III centres. The implication of this and other studies (10, 12–14) involving binuclear phthalazine complexes is that the Cu—O(R)—Cu unit is a reasonable proposition for the exchange coupled part of the biological chromophore in these binuclear protein centres. The ubiquity of the $[Cu—O(H)—Cu]^{3+}$ unit suggests that the oxygen bridge may simply be a hydroxide and not part of a protein side chain.

Acknowledgement

We thank the Natural Sciences and Engineering Research Council of Canada for financial support for this study.

1. E. I. SOLOMON, D. M. DOOLEY, R.-H. WANG, H. B. GRAY, M. CERDONIO, F. MOGNO, and G. L. ROMANI. J. Am. Chem. Soc. **98**, 1029 (1976).
2. D. M. DOOLEY, R. A. SCOTT, J. ELLINGHAUS, and E. I. SOLOMON. Proc. Natl. Acad. Sci. U.S.A. **75**, 3019 (1978).
3. T. B. FREEDMAN, J. S. LOEHR, and T. M. LOEHR. J. Am. Chem. Soc. **98**, 2809 (1976).
4. T. J. THAMANN, J. S. LOEHR, and T. M. LOEHR. J. Am. Chem. Soc. **99**, 4187 (1977).
5. J. M. BROWN, L. POWERS, B. KINCAID, J. A. LARRABEE, and T. G. SPIRO. J. Am. Chem. Soc. **102**, 4210 (1980).
6. M. S. CO, K. O. HODGSON, T. K. ECCLES, and R. LONTIE. J. Am. Chem. Soc. **103**, 984 (1981).
7. R. S. HIMMELWRIGHT, N. C. EICKMAN, C. D. LUBIEN, and E. I. SOLOMON. J. Am. Chem. Soc. **102**, 5378 (1980).
8. R. S. HIMMELWRIGHT, N. C. EICKMAN, C. D. LUBIEN, K. LERCH, and E. I. SOLOMON. J. Am. Chem. Soc. **102**, 7339 (1980).
9. S. SUZUKI, J. KINO, M. KIMURA, W. MORI, and A. NAKAHARA. Inorg. Chim. Acta, **66**, 41 (1982).
10. L. K. THOMPSON, V. T. CHACKO, J. A. ELVIDGE, A. B. P. LEVER, and R. V. PARISH. Can. J. Chem. **47**, 4141 (1969).
11. J. C. DEWAN and L. K. THOMPSON. Can. J. Chem. **60**, 121 (1982).
12. D. V. BAUTISTA, J. C. DEWAN, and L. K. THOMPSON. Can. J. Chem. In press.
13. A. W. HANSON. Personal communication.
14. G. MARONGUI and E. C. LINGAFELTER. Acta Crystallogr. B. **38**, 620 (1982).
15. A. B. P. LEVER, L. K. THOMPSON, and W. M. REIFF. Inorg. Chem. **11**, 104 (1972).
16. A. B. P. LEVER, L. K. THOMPSON, and W. M. REIFF. Inorg. Chem. **11**, 2292 (1972).
17. J. A. DOULL and L. K. THOMPSON. Can. J. Chem. **58**, 221 (1980).

18. K. NAKAMOTO. Infrared spectra of inorganic and coordination compounds. Wiley-Interscience. 1970.
19. A. B. P. LEVER, E. MONTOVANI, and B. S. RAMASWAMY. Can. J. Chem. **49**, 1957 (1971).
20. A. B. P. LEVER. Ph.D. thesis, London. 1959.
21. J. E. ANDREW and A. B. BLAKE. J. Chem. Soc. A, 1408 (1969).
22. D. A. SULLIVAN and G. J. PALENIK. Inorg. Chem. **16**, 1127 (1977).
23. M. GHEDINI, G. DE MUNNO, G. DENTI, A. M. MANOTTI LANFREDI, and A. TIRIPICCHIO. Inorg. Chim. Acta, **57**, 87 (1982).

Crystal structures of an α-cyclobutyl tricyclic enone and its *p*-bromobenzoate derivative

RICHARD A. PAUPTIT AND JAMES TROTTER

Department of Chemistry, University of British Columbia, Vancouver, B.C., Canada V6T 1Y6

Received April 20, 1982

RICHARD A. PAUPTIT and JAMES TROTTER. Can. J. Chem. **61**, 63 (1983).

Crystals of the enone, $C_{22}H_{32}O_3$, are monoclinic, $P2_1/n$, a = 15.722(4), b = 7.463(2), c = 17.213(1) Å, β = 104.67(1)°, Z = 4. The structure was solved by direct methods and was refined to R = 0.040 for 656 reflections with $I/\sigma(I) \geq 3.0$. Crystals of the *p*-bromobenzoate derivative are triclinic, $P\bar{1}$, a = 11.023(1), b = 11.877(1), c = 10.900(1) Å, α = 90.461(8), β = 111.57(1), γ = 80.51(1)°, Z = 2. The structure was solved by Patterson and Fourier methods and refined to R = 0.032 for 2715 reflections with $I/\sigma(I) \geq 3.0$. The X-ray studies were carried out in order to investigate a possible highly strained *trans*-fused 4- and 5-membered ring system in a photoadduct obtained as an intermediate in the projected syntheses of stemodin and aphidicolin. The ring system was, however, *cis*-fused.

RICHARD A. PAUPTIT et JAMES TROTTER. Can. J. Chem. **61**, 63 (1983).

Les cristaux de l'énone, $C_{22}H_{32}O_3$, sont monocliniques, $P2_1/n$, a = 15.722(4), b = 7.463(2), c = 17.213(1) Å, β = 104.67(1)°, Z = 4. On a résolu la structure par les méthodes directes et on a l'affinée jusqu'à une valeur de R = 0.040 pour 656 réflexions avec $I/\sigma(I) \geq 3.0$. Les cristaux de la derivée de *p*-bromobenzoate sont tricliniques, $P\bar{1}$, a = 11.023(1), b = 11.877(1), c = 10.900(1) Å, α = 90.461(8), β = 111.57(1), γ = 80.51(1)°, Z = 2. On a résolu la structure par les méthodes de Patterson et de Fourier et on l'a affinée jusqu'à une valeur de R = 0.032 pour 2715 réflexions avec $I/\sigma(I) \geq 3.0$. On a fait les études par X-rayon pour réchercher une système des cycles a 4 et 5 membres possiblement *trans*-fusée et très constraindu dans un photoproduit obtenu comme une intermediaire dans une synthèse projetée de stemodin et de aphidicolin. La système des cycles était, néanmoins, *cis*-fusée.

Introduction

Recent work by Piers and co-workers (1) directed towards the total synthesis of the tetracyclic diterpenoids aphidicolin (**1**, Scheme 1) and stemodin (**2**) included the photoaddition of allene to the tricyclic enone **3**. The latter reaction produced, as major products, two isomeric photoadducts which could be separated by column chromatography on silica gel. The isomer first eluted (39% yield) was shown by X-ray crystallography to possess structure **4** (2), and, therefore, the second product (42% yield) was presumed to be the isomeric photoadduct **5**. Subjection of the keto olefin 4 to ozonolysis (O_3, CH_2Cl_2/MeOH, −78°C; Me_2S) (see Scheme 2) followed by treatment of the resultant cyclobutanone with NaOMe/MeOH (room temperature, 2.5 h), produced the expected keto ester **6** (see Scheme 2), in 88% yield. However, surprisingly, when the second photoadduct (presumed to be **5**) was subjected to an identical sequence of reactions, the product (obtained in excellent yield) proved to be the *same* keto ester **6**, rather than the expected substance **7**. This unexpected result implied either (*a*) that the second photoaddition product was not **5** but possessed the (unlikely) *trans*-fused structure **8**, or (*b*) that a novel and facile rearrangement reaction had occurred in the transformation of **5** into **6**.

In order to provide conclusive evidence regarding the structure of the second photoadduct, an X-ray study was undertaken. Described herein are the results of this study, which unequivocally establishes that the second photoaddition product possesses structure **5**.[1]

X-ray crystal structure of compound 5

Unfortunately, compound **5** did not crystallize as easily as the isomeric substance **4**, and the quality of the crystals even after various recrystallizations was poor. Considerable effort was required in selecting a crystal which was suitable for analysis. Crystals that were apparently well-formed were shown to be multiple platelets by examination on a polarizing microscope, or if this failed, by X-ray photography. Eventually, by selecting a sufficiently thin platelet (0.05 × 0.42 × 0.35 mm^3), a single crystal was located.

Experimental

Crystal data are as follows:

$C_{22}H_{32}O_3$ fw = 344.5

Monoclinic, a = 15.722(4), b = 7.463(2), c = 17.213(1) Å, β = 104.67(1)°, V = 1953.8 Å^3, Z = 4, space group = $P2_1/n$, $F(000)$ = 752, λ = 0.71073 Å, D_c = 1.17 g/cm^3, μ = 0.7 cm^{-1}.

The intensity data were collected on an Enraf-Nonius CAD4 diffractometer using an ω–(1/3)θ scan technique and graphite-monochromatized MoKα radiation. The ω-scan angle was (1.2 + 0.35 tan θ)° and the aperture was (2.50 + tan θ) mm wide and 4 mm high. The intensities of three standard reflections were measured every hour and showed no variation. Another three reflections were checked every 100 reflections for orientation, and reorientation occurred if the difference between observed and calculated scattering vectors was greater than 0.06°.

Of the 3836 reflections collected within the range $0 < \theta \leq 25°$, only 749 (19.5%) had $I/\sigma(I) \geq 3.0$, and so all reflections with a θ value greater than 19.5° were removed from the data set. Of the remaining data, 656 out of 1708 (38%) reflections have $I/\sigma(I) \geq 3.0$ and were considered observed. The unit cell parameters were refined by least-squares methods with sin θ/λ values of 18 reflections in the θ range 9 to 18°, and they appear above with other crystal data. Absorption effects were negligible, and Lorentz and polarization corrections were applied.

The structure was solved by direct methods. 342 E's > 1.2 were obtained from a K-curve and, together with the 50 lowest E's, were input into the MULTAN (3) programme, and from the correct E-map

[1]Some of the details regarding the pathway via which **5** is converted into **6** have been elucidated (see ref. 1).

0008-4042/83/010063-06$01.00/0

©1983 National Research Council of Canada/Conseil national de recherches du Canada

Can. J. Chem. Downloaded from www.nrcresearchpress.com by 210.87.254.40 on 09/06/12
For personal use only.

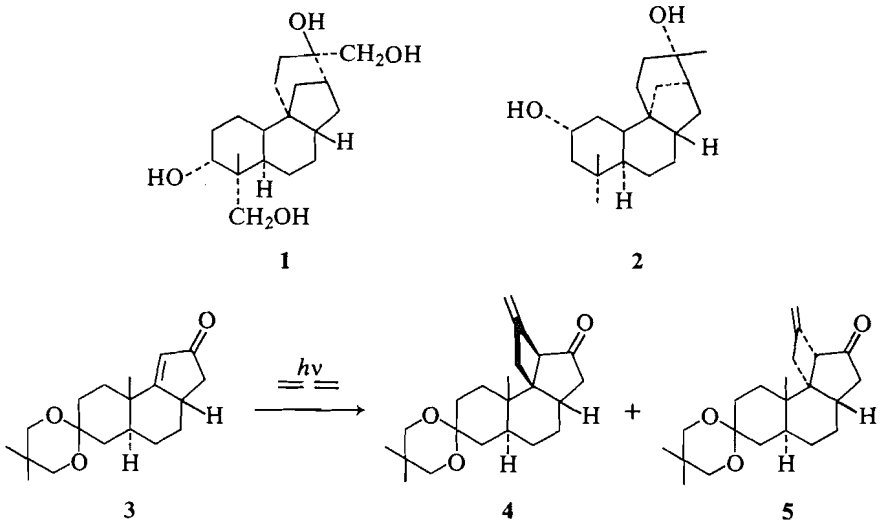

SCHEME 1

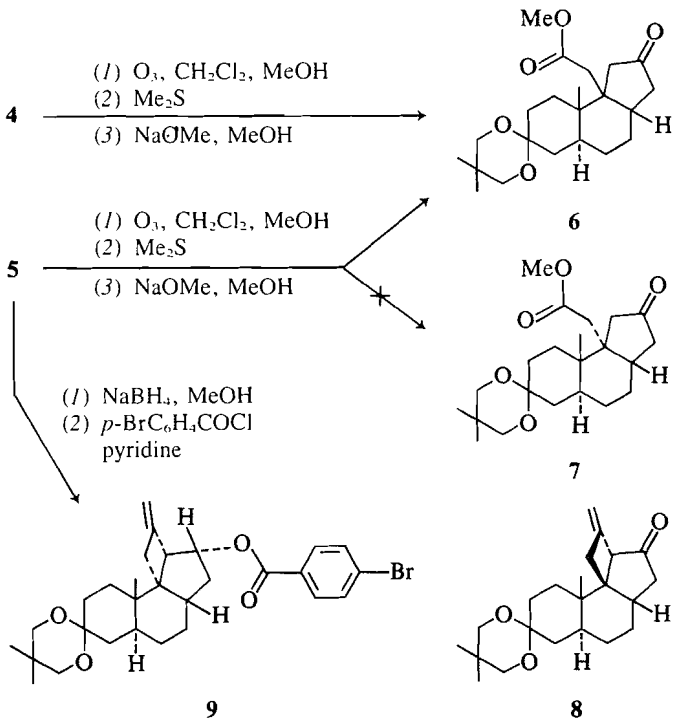

SCHEME 2

the positions of all 25 non-hydrogen atoms could be determined.

After three isotropic and seven anisotropic least-squares refinement cycles, all the hydrogen atoms could be located on a difference map; however, the use of calculated positions for the hydrogen atoms produced a significantly lower R value. Attempts to refine the hydrogen thermal parameters proved unsuccessful, and each hydrogen was assigned a temperature factor 10% greater than that of the carbon to which it is bound (25% for methyl hydrogens). The structure converged after three more least-squares cycles using a Hughes' weighting scheme (4) where $(w)^{1/2} = 1.0$ for $|F_o| < F^*$ and $(w)^{1/2} = F^*/|F_o|$ for $|F_o| > F^*$, and $F^* = 21.0$. The weighting scheme could be slightly improved so three more cycles were run with $F^* = 20.0$. The final R values are $R = 0.040$ (0.169 including the unobserved reflections to $\theta = 19.5$) and $R_w = 0.053$. The scattering factors of ref. 5 were used for non-hydrogen atoms and those of ref. 6 for the hydrogen atoms. Final positional and isotropic thermal parameters[2] appear in Table 1.

Results

It can be concluded from the X-ray study summarized above that the structure of the second photoadduct is as shown in structural formula **5**. A stereoview of the molecule with the atomic labelling is shown in Fig. 1. Bond lengths and angles[2] of the non-hydrogen atoms appear in Tables 2 and 3. There are no unusually short intermolecular distances.[2]

[2]Anisotropic thermal parameters, bond lengths and angles of the hydrogen atoms and the *p*-bromobenzoate group, mean plane calculations, packing diagrams, and the structure factor tables for both structures are available, at a nominal charge, from the Depository of Unpublished Data, CISTI, National Research Council of Canada, Ottawa, Ont., Canada K1A 0S2.

Can. J. Chem. Downloaded from www.nrcresearchpress.com by 210.87.254.40 on 09/06/12
For personal use only.

Can. J. Chem. Downloaded from www.nrcresearchpress.com by 210.87.254.40 on 09/06/12
For personal use only.

TABLE 1. Atomic positional and isotropic thermal parameters of molecule **5** (fractional × 10^4, H × 10^3, U × 10^3 Å^2)

Atom	x	y	z	U_{eq}/U_{iso}
O(1)	1489(4)	755(9)	2764(4)	82
O(2)	3008(3)	2381(8)	−1409(3)	53
O(3)	4525(3)	1907(8)	−1025(3)	56
C(1)	3037(5)	3008(12)	324(5)	54
C(2)	3814(5)	3193(12)	−42(5)	58
C(3)	3738(5)	1937(14)	−756(5)	53
C(4)	3586(6)	41(12)	−533(5)	55
C(5)	2813(5)	−154(11)	−153(5)	46
C(6)	2625(6)	−2089(13)	13(5)	65
C(7)	1812(6)	−2312(13)	342(5)	64
C(8)	1933(5)	−1105(12)	1072(5)	55
C(9)	2057(5)	847(12)	855(4)	44
C(10)	2909(5)	1083(12)	588(4)	46
C(11)	1874(5)	1946(12)	1578(5)	52
C(12)	1514(5)	561(12)	2062(6)	59
C(13)	1247(5)	−1075(14)	1567(5)	66
C(14)	1206(5)	1708(12)	300(5)	59
C(15)	1079(6)	2827(12)	1000(5)	59
C(16)	524(6)	4058(13)	1109(6)	81
C(17)	3708(5)	572(12)	1285(5)	66
C(18)	3112(5)	4039(14)	−1790(5)	61
C(19)	3949(5)	4064(14)	−2107(5)	60
C(20)	4691(5)	3521(13)	−1393(5)	61
C(21)	4092(6)	5927(15)	−2390(6)	85
C(22)	3880(6)	2690(15)	−2778(5)	85
H(011)	312	387	80	70
H(012)	251	345	−4	70
H(021)	437	302	36	65
H(022)	386	442	−25	65
H(041)	348	−81	−100	74
H(042)	410	−54	−15	74
H(051)	227	26	−55	65
H(061)	256	−283	−48	75
H(062)	314	−261	39	75
H(071)	129	−203	−4	81
H(072)	174	−360	49	81
H(081)	248	−156	145	72
H(111)	235	272	188	66
H(131)	65	−110	117	87
H(132)	124	−226	185	87
H(141)	132	235	−16	73
H(142)	75	85	6	73
H(161)	46	535	161	100
H(162)	−13	506	59	100
H(171)	366	−66	145	99
H(172)	425	71	115	99
H(173)	373	131	176	99
H(181)	259	444	−220	99
H(182)	317	511	−138	99
H(201)	475	453	−99	68
H(202)	525	351	−152	68
H(211)	418	677	−192	106
H(212)	459	607	−260	106
H(213)	358	639	−277	106
H(221)	372	153	−260	104
H(222)	339	301	−324	104
H(223)	439	257	−296	104

X-ray crystal structure of compound 9

In view of the difficulty in selecting a suitable crystal of **5**, it seemed possible that the crystal chosen for examination might have been one of an impurity — a minor third product. The validity of such a suggestion is always difficult to establish. A structure determination on another crystal in the batch would be expensive, time consuming, and only conclusive if it produced different results. Also, the crystals were sufficiently poor that locating another single crystal of reasonable quality would have been a major task in itself.

An X-ray analysis of a derivative of the second eluted isomer that produces high quality crystals should solve this ambiguity. Therefore, compound **5** was reduced with sodium borohydride in methanol and the resultant alcohol was allowed to react with *p*-bromobenzoyl chloride in pyridine. The resultant *p*-bromobenzoate **9** yielded crystals of high quality (recrystallization from ethanol, 0.42 × 0.33 × 0.37 mm^3).

Experimental

Crystal data are as follows:

$C_{29}H_{37}BrO_4$ fw = 529.5

Triclinic, a = 11.023(1), b = 11.877(1), c = 10.900(1) Å, α = 90.461(8), β = 111.57(1), γ = 80.51(1)°, Z = 2, space group = $P\bar{1}$, $F(000)$ = 556, λ = 0.71073 Å, D_c = 1.32 g/cm^3, V = 1306.8 Å^3, μ = 15.86 cm^{-1}.

Preliminary photography showed that the crystal is triclinic and, as the derivative is a racemate, of the centrosymmetric space group $P\bar{1}$.

The data were collected on an Enraf-Nonius CAD4 diffractometer using an ω–(4/3)θ scan technique and graphite-monochromatized MoKα radiation. The ω-scan angle was (0.70 + 0.35 tan θ)° and the aperature was (2.50 + tan θ) mm wide and 4 mm high. The intensities of three standard reflections were meaured every hour and showed a linear decay of 2% over the data collection. The data were scaled accordingly. Three reflections out of every 100 were checked for orientation, and reorientation occurred if the difference between observed and calculated scattering vectors was greater than 0.05°.

Of the 4549 reflections collected in the range $0 < \theta \leq 25°$, 2715 (59.7%) had $I/\sigma(I) \geq 3.0$ and were considered observed. The cell parameters were refined by least-squares methods with the sin θ/λ values of 24 reflections in the θ range 15 to 19°, and appear together with other crystal data above. The large value of the linear absorption coefficient μ suggests that an absorption correction is in order. 144 sampling points were used with an average spacing of 0.076 mm for a crystal volume of 0.0568 mm^3, and the resulting transmission factors varied from 0.569 for the −12 −4 4 reflection to 0.631 for 5 −1 9. The intensities were thus corrected for absorption, as well as for Lorentz and polarization effects.

The structure was solved by Patterson techniques: the Patterson map contains one outstanding non-origin peak at (0.1542, 0.3450, 0.9215) which establishes the position of the bromines at ±(0.0771, 0.1725, 0.4608).

Other atomic positions (including hydrogens) were then located by Fourier methods, and the structure was refined by least-squares methods, with a polynomial weighting scheme (7) and an anomalous dispersion correction for Br (8), to final R and R_w values of 0.032 and 0.036 (0.083 and 0.076 including the unobserved reflections) respectively. The final coefficients used in the polynomial weighting scheme were A = 0.3074, B = 0.0464, C = −0.00511, and D = 0.000129. In the last cycle, the mean and maximum parameter shifts were 0.046 and 0.474σ, respectively. A final difference map was calculated and showed two peaks of 0.4 electrons/Å^3. One is in the vicinity of the bromine and could perhaps be due to a lone pair interaction, but the other is near the ring containing the two oxygens for no obvious reason. Interestingly enough, bond lengths and bond angles involving O(2) and C(18) show some slight deviations from normal values. Final positional and isotropic thermal parameters[2] are listed in Table 4.

Results

A stereoview of the molecule is presented in Fig. 2. With the exception of the *p*-bromobenzoate group, the atomic labelling is as before.

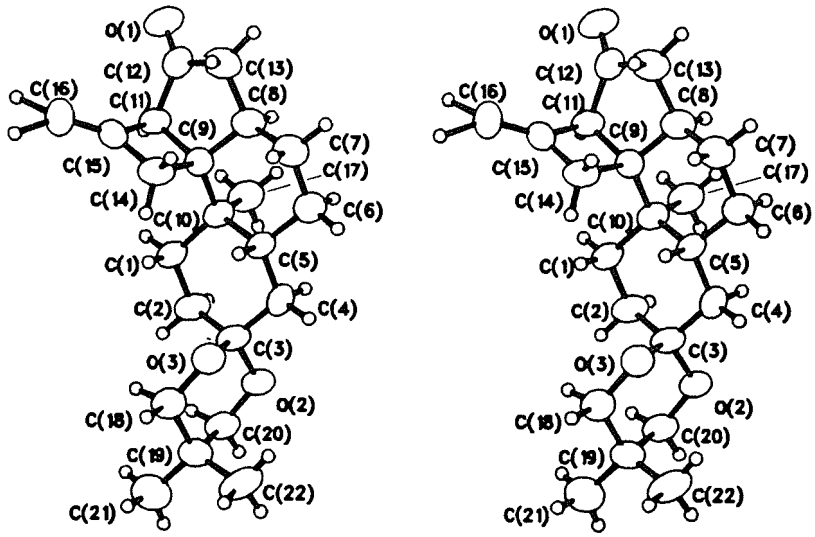

FIG. 1. A stereoview of molecule **5**.

TABLE 2. Comparisons of equivalent bond lengths (Å) in molecules **4**, **5**, and **9**

Bond	Length		
	4	**5**	**9**
O(1)—C(12)	1.199(3)	1.229(09)	—
O(2)—C(3)	1.420(2)	1.428(09)	1.430(3)
O(2)—C(18)	1.428(3)	1.428(10)	1.406(4)
O(3)—C(3)	1.424(2)	1.427(08)	1.429(3)
O(3)—C(20)	1.423(3)	1.415(09)	1.431(3)
C(1)—C(2)	1.524(3)	1.515(10)	1.530(4)
C(1)—C(10)	1.538(3)	1.536(11)	1.533(4)
C(2)—C(3)	1.509(3)	1.526(11)	1.508(4)
C(3)—C(4)	1.523(3)	1.501(11)	1.521(5)
C(4)—C(5)	1.529(3)	1.526(10)	1.530(4)
C(5)—C(6)	1.529(3)	1.516(11)	1.537(4)
C(5)—C(10)	1.546(3)	1.550(10)	1.560(4)
C(6)—C(7)	1.514(3)	1.533(10)	1.533(5)
C(7)—C(8)	1.528(3)	1.519(11)	1.520(5)
C(8)—C(9)	1.544(3)	1.528(11)	1.532(4)
C(8)—C(13)	1.528(3)	1.538(11)	1.521(4)
C(9)—C(10)	1.544(3)	1.532(10)	1.542(4)
C(9)—C(11)	1.571(3)	1.577(10)	1.571(4)
C(9)—C(14)	1.563(3)	1.571(10)	1.566(4)
C(10)—C(17)	1.538(3)	1.549(10)	1.540(4)
C(11)—C(12)	1.515(4)	1.523(10)	1.529(4)
C(11)—C(15)	1.515(4)	1.534(11)	1.520(4)
C(12)—C(13)	1.511(4)	1.487(12)	1.521(5)
C(14)—C(15)	1.496(4)	1.521(11)	1.507(4)
C(15)—C(16)	1.324(4)	1.312(11)	1.315(5)
C(18)—C(19)	1.521(3)	1.546(10)	1.515(4)
C(19)—C(20)	1.521(3)	1.520(11)	1.513(4)
C(19)—C(21)	1.525(3)	1.510(13)	1.531(5)
C(19)—C(22)	1.518(4)	1.529(12)	1.529(5)

The *p*-bromobenzoate derivative contains the four-membered ring *cis*-fused to the cyclopentanone ring. Therefore the previous structure solved was not an impurity, but was indeed the second eluted isomer. Bond lengths and angles of the non-hydrogen atoms[2] for the bulk of the molecule[2] are listed in Tables 2 and 3. The crystal is held together by van der Waals forces.[2]

Discussion

Whenever the structures of three molecules (**4**, **5**, and **9**; ref. 2 plus this paper) as similar as those presented so far are solved, it is of interest to compare derived quantities, e.g. bond lengths, bond angles, and molecular geometry.

Those data for **5** are included for completeness, although this structure is less accurately determined.

Bond lengths for these three structures are compared in Table 2. Upon inspection of this table, it is immediately obvious that the estimated standard deviations in molecule **5** are about three times as great as those in molecules **4** and **9**. This is not surprising; the crystal structure of **5** is the least accurate of the three, mainly as the crystal was so poor that only 20% of the collected reflections could be considered observed (as opposed to 60% in the other two structures). Consistent with this, the *R* values for the structure of molecule **5** are slightly larger than those for **4** and **9**, especially when the unobserved reflections are included.

The bond lengths compare extremely well with each other. Only one pair shows a significant difference (i.e., has a difference greater than 3.0σ): O(2)—C(18) has lengths 1.428(3) (in **4**) and 1.406(4) Å (in **9**), a difference of only 0.022 Å (about 4.5σ) and so of little importance. The largest absolute difference is for C(18)—C(19), which has lengths 1.546(10) (in **5**) and 1.515(4) Å (in **9**), a difference of 0.031 Å, but this only corresponds to about 3.0σ.

More interesting trends may be found by comparing the bond angles (Table 3). Because of the larger esd's in **5**, the closest match is most often found between the values from **4** and **9**. However, bond angles involving O(2) and C(18) in **9** again show significant but most probably unimportant deviations. This might be related to the slight electron density (0.4 electrons/Å^3) located near this ring. Important deviations do occur when we examine bond angles in the vicinity of the four-membered ring. Angles involving atoms in the six-membered ring closest to the cyclobutyl ring are very similar in **5** and **9** but very different in **4**. It seems very likely that the magnitudes of these angles are affected by the orientation of the four-membered ring. This effect is especially pronounced in the angles marked with an asterisk (*) in Table 1. In examining the angles in the five-membered ring, one notices that this time

Can. J. Chem. Downloaded from www.nrcresearchpress.com by 210.87.254.40 on 09/06/12
For personal use only.

Can. J. Chem. Downloaded from www.nrcresearchpress.com by 210.87.254.40 on 09/06/12
For personal use only.

TABLE 3. Comparison of bond angles (deg) in molecules **4**, **5**, and **9**

Bonds	Angle		
	4	**5**	**9**
C(3) —O(2)—C(18)	114.3(1)	113.6(6)	116.1(2)
C(3) —O(3)—C(20)	114.3(2)	113.9(7)	114.6(2)
C(2) —C(1)—C(10)	112.8(2)	112.9(8)	113.2(3)
C(1) —C(2)—C(3)	112.4(2)	111.8(7)	112.6(3)
O(2) —C(3)—O(3)	110.2(1)	109.7(6)	110.3(2)
O(2) —C(3)—C(2)	105.8(2)	112.0(7)	105.4(2)
O(2) —C(3)—C(4)	112.0(2)	105.8(7)	112.2(2)
O(3) —C(3)—C(2)	105.1(2)	112.0(7)	105.5(2)
O(3) —C(3)—C(4)	112.2(2)	106.0(8)	111.9(2)
C(2) —C(3)—C(4)	111.2(2)	111.0(7)	111.1(3)
C(3) —C(4)—C(5)	112.3(2)	113.3(7)	112.6(2)
C(4) —C(5)—C(6)	111.7(2)	112.7(7)	112.4(2)
C(4) —C(5)—C(10)	113.1(2)*	112.0(6)	112.0(2)
C(6) —C(5)—C(10)	111.4(2)*	113.3(6)	113.0(3)
C(5) —C(6)—C(7)	110.5(2)*	113.2(8)	113.1(3)
C(6) —C(7)—C(8)	115.3(2)*	107.5(7)	109.5(3)
C(7) —C(8)—C(9)	111.5(2)	111.1(7)	110.9(3)
C(7) —C(8)—C(13)	108.3(2)*	120.7(8)	121.8(3)
C(9) —C(8)—C(13)	104.6(2)	105.9(7)	103.5(2)+
C(8) —C(9)—C(10)	114.7(2)*	111.0(7)	111.0(2)
C(8) —C(9)—C(11)	104.5(2)	104.0(6)	105.9(2)+
C(8) —C(9)—C(14)	114.3(2)	113.4(7)	112.9(2)
C(10)—C(9)—C(11)	118.8(2)*	121.7(7)	121.1(2)
C(10)—C(9)—C(14)	113.7(2)*	116.4(7)	115.7(2)
C(11)—C(9)—C(14)	88.0(2)	88.3(6)	88.3(2)
C(1) —C(10)—C(5)	107.7(2)	107.8(6)	108.4(2)
C(1) —C(10)—C(9)	111.1(2)*	112.8(7)	112.8(2)
C(1) —C(10)—C(17)	109.7(2)	108.6(7)	108.0(3)
C(5) —C(10)—C(9)	109.3(2)*	105.6(6)	105.3(2)
C(5) —C(10)—C(17)	111.2(2)*	112.4(6)	112.7(3)
C(9) —C(10)—C(17)	107.8(2)*	109.8(6)	109.6(2)
C(9) —C(11)—C(12)	105.1(2)*	104.2(7)	104.1(2)
C(9) —C(11)—C(15)	88.3(2)	89.6(6)	88.6(2)
C(12)—C(11)—C(15)	110.8(2)	106.9(7)	114.3(3)
O(1) —C(12)—C(11)	125.0(2)	124.5(9)	—
O(1) —C(12)—C(13)	126.1(2)	125.9(8)	—
C(11)—C(12)—C(13)	108.9(2)	109.5(7)	106.7(3)+
C(8) —C(13)—C(12)	103.0(2)	101.1(7)	102.4(3)
C(9) —C(14)—C(15)	89.3(2)	90.3(6)	89.2(2)
C(11)—C(15)—C(14)	92.6(2)	91.7(6)	92.5(2)
C(11)—C(15)—C(16)	131.9(4)	132.0(9)	132.2(3)
C(14)—C(15)—C(16)	135.2(4)	136.3(9)	134.1(3)
O(2) —C(18)—C(19)	111.6(2)	113.4(7)	112.8(3)
C(18)—C(19)—C(20)	105.6(2)	105.1(7)	105.4(3)
C(18)—C(19)—C(21)	110.3(2)	109.6(9)	110.5(3)
C(18)—C(19)—C(22)	109.6(2)	110.8(8)	109.0(3)
C(20)—C(19)—C(21)	110.3(2)	111.1(8)	111.2(3)
C(20)—C(19)—C(22)	109.5(2)	109.0(8)	110.2(3)
C(21)—C(19)—C(22)	111.4(2)	111.2(8)	110.3(3)
O(3) —C(20)—C(19)	111.5(2)	112.2(8)	111.2(2)

the odd angles seem to come from the *p*-bromobenzoate derivative, **9**. This is not too surprising as the hybridization of C(12) is different in **9**. The angles that are affected by this are marked with a plus sign (+) in Table 1. The cyclobutyl angles are all fairly similar and do not deviate greatly from the free cyclobutyl angle (9), 89.3°.

Mean plane calculations[2] were performed for planes in the vicinity of the cyclobutyl ring for all three structures. The envelope tip of the five-membered ring, C(13), is always oriented in the same direction as the cyclobutyl ring. The change of hybridization at C(12) in the *p*-bromobenzoate deriv-

TABLE 4. Atomic positional and isotropic thermal parameters for molecule **9** (fractional × 10^4, Br × 10^5, H × 10^3, U × 10^3 Å^2)

Atom	*x*	*y*	*z*	U_{eq}/U_{iso}
Br	92418(5)	−17003(4)	−46120(4)	88
O(1)	7636(2)	653(2)	389(2)	54
O(2)	1527(2)	4669(2)	1602(2)	54
O(3)	2222(2)	5980(2)	3229(2)	52
O(4)	8288(2)	2182(2)	−211(2)	61
C(1)	4149(4)	4344(3)	1408(3)	47
C(2)	3501(4)	5345(3)	1976(4)	53
C(3)	2636(3)	4983(2)	2644(3)	47
C(4)	3389(4)	4000(3)	3666(3)	50
C(5)	4020(3)	2991(2)	3094(3)	45
C(6)	4697(4)	1968(3)	4103(3)	60
C(7)	5298(4)	935(3)	3533(4)	61
C(8)	6175(3)	1316(3)	2874(3)	52
C(9)	5397(3)	2278(2)	1814(3)	41
C(10)	4943(3)	3359(2)	2435(3)	41
C(11)	6229(3)	2327(3)	921(3)	43
C(12)	7333(4)	1283(3)	1419(3)	52
C(13)	6879(4)	485(3)	2181(4)	60
C(14)	4296(3)	1874(3)	601(3)	47
C(15)	5031(3)	2124(2)	−261(3)	46
C(16)	4722(5)	2227(3)	−1545(4)	66
C(17)	6161(4)	3777(4)	3434(4)	58
C(18)	407(3)	4606(3)	1909(4)	58
C(19)	−65(3)	5692(2)	2462(3)	48
C(20)	1131(3)	5914(3)	3622(3)	53
C(21)	−574(4)	6684(3)	1412(4)	66
C(22)	−1163(5)	5491(5)	2932(5)	79
C(23)	8092(3)	1209(3)	−366(3)	48
C(24)	8330(3)	492(2)	−1404(3)	46
C(25)	8391(4)	1023(3)	−2502(3)	62
C(26)	8636(4)	377(3)	−3464(4)	68
C(27)	8857(3)	−794(3)	−3307(3)	57
C(28)	8811(3)	−1334(3)	−2222(4)	59
C(29)	8527(3)	−684(3)	−1278(3)	53
H(011)	473(3)	462(2)	102(3)	54(8)
H(012)	349(3)	410(2)	71(3)	47(8)
H(021)	294(3)	593(3)	126(3)	55(8)
H(022)	416(3)	570(3)	259(3)	63(10)
H(041)	409(3)	430(2)	438(3)	52(8)
H(042)	287(3)	370(3)	404(3)	66(10)
H(051)	331(3)	275(2)	239(3)	35(7)
H(061)	545(3)	225(3)	491(3)	63(9)
H(062)	400(4)	176(3)	446(4)	84(11)
H(071)	460(3)	59(3)	293(3)	63(10)
H(072)	581(3)	36(3)	424(3)	69(10)
H(081)	688(3)	162(3)	351(3)	61(10)
H(111)	657(3)	302(2)	85(2)	42(7)
H(121)	806(3)	154(3)	192(3)	56(10)
H(131)	624(4)	4(3)	155(4)	75(11)
H(132)	757(4)	−1(3)	275(3)	65(10)
H(141)	426(3)	105(3)	73(3)	55(8)
H(142)	345(3)	228(2)	38(2)	35(7)
H(161)	534(3)	245(3)	−194(3)	69(10)
H(162)	386(4)	210(3)	−215(3)	71(10)
H(171)	653(4)	334(4)	426(5)	103(15)
H(172)	597(4)	459(4)	359(4)	92(12)
H(173)	684(4)	373(3)	312(3)	73(11)
H(181)	−33(3)	443(2)	108(3)	59(8)
H(182)	67(3)	390(3)	264(4)	83(11)
H(201)	133(3)	528(2)	432(3)	50(8)
H(202)	91(3)	666(3)	399(3)	68(9)
H(211)	−83(4)	481(4)	351(4)	89(14)
H(212)	−147(5)	619(4)	335(5)	119(16)
H(213)	−186(5)	522(4)	217(5)	109(15)

TABLE 4 (*Concluded*)

Atom	*x*	*y*	*z*	U_{eq}/U_{iso}
H(221)	19(4)	682(3)	113(3)	79(11)
H(222)	−88(3)	728(3)	184(3)	57(9)
H(223)	−133(4)	651(3)	62(4)	89(12)
H(251)	821(3)	182(3)	−256(3)	61(9)
H(261)	871(3)	73(3)	−419(4)	82(11)
H(281)	896(3)	−213(3)	−210(3)	68(10)
H(291)	854(3)	−106(2)	−52(3)	54(9)

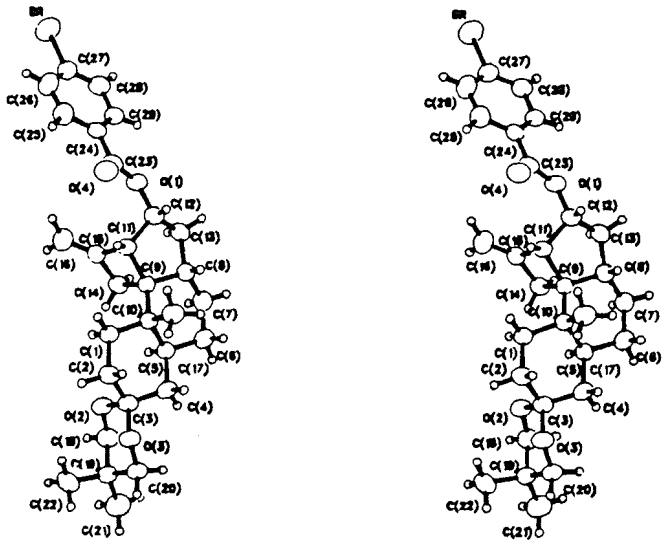

FIG. 2. A stereoview of molecule **9**.

ative affects the geometry of the five-membered ring only slightly — the envelope tip is bent down 35 and 36° in **4** and **5**, and 39° in **9**. When O(1) is doubly bound to C(12) it is on the opposite side of the five-membered ring to the envelope tip. The cyclobutyl ring is folded away from the envelope tip along the C(11)...C(14) axis in every structure, although the degree of folding varies — 14°, 4.3°, and 12.7° in **4**, **5**, and **9** respectively. The angle between the cyclobutyl and five-membered rings is about 109° for all three structures. For the *p*-bromobenzoate derivative, the phenyl group is oriented at 22° to the carboxyl moiety. The bromine lies in the phenyl plane. The other six-membered rings all have chair conformations.

Acknowledgements

We thank the Natural Sciences and Engineering Research Council Canada for financial support and the University of British Columbia Computing Centre for assistance. We also thank Dr. Piers for the crystals, background material, and helpful discussion.

1. E. PIERS, B. ABEYSEKERA, D. J. HERBERT, and I. D. SUCKLING. J. Chem. Soc. Chem. Commun. In press.
2. R. A. PAUPTIT and J. TROTTER. Can. J. Chem. **59**, 524 (1981).
3. G. GERMAIN, P. MAIN, and M. M. WOOLFSON. Acta Crystallogr. A**27**, 368 (1971).
4. E. W. HUGHES. J. Am. Chem. Soc. **63**, 1737 (1941).
5. D. T. CROMER and J. B. MANN. Acta Crystallogr. A**24**, 321 (1968).
6. R. F. STEWART, E. R. DAVIDSON, and W. T. SIMPSON. J. Chem. Phys. **42**, 3175 (1965).
7. D. W. J. CRUICKSHANK. *In* Computing methods in crystallography. *Edited by* J. S. Rollett. Pergamon Press. 1965. p. 14.
8. D. T. CROMER and D. LIBERMAN. J. Chem. Phys. **53**, 1891 (1970).
9. C.-H. CHANG, R. F. PORTER, and S. H. BAUER. J. Molec. Struct. **7**, 89 (1971).

Can. J. Chem. Downloaded from www.nrcresearchpress.com by 210.87.254.40 on 09/06/12
For personal use only.

Crystal structures of optically active naphthidine (4,4′-diamino-1,1′-binaphthyl) and 1,1′-binaphthyl

RICHARD A. PAUPTIT AND JAMES TROTTER
Department of Chemistry, University of British Columbia, Vancouver, B.C., Canada V6T 1Y6

Received August 3, 1982

RICHARD A. PAUPTIT and JAMES TROTTER. Can. J. Chem. **61**, 69 (1983).

Crystals of optically active naphthidine and of binaphthyl are tetragonal, $P4_12_12$ (or $P4_32_12$), a = 7.945(1), 7.164(2), c = 24.264(5), 27.70(1) Å, respectively, Z = 4. The structures were solved by direct methods and refined by full-matrix least-squares techniques to respective R = 0.068 and 0.030 for 548 and 562 reflexions. The dihedral angles between the planes of the naphthalene residues are 87 and 102°, respectively. Bond lengths and angles are normal.

RICHARD A. PAUPTIT et JAMES TROTTER. Can. J. Chem. **61**, 69 (1983).

Les cristaux de naphtidine et de binaphtyle actifs optiquement sont tetragonals, $P4_12_12$ (ou $P4_32_12$), a = 7.945(1), 7.164(2), c = 24.264(5), 27.70(1) Å, respectivement, Z = 4. On a résolu les structures par les méthodes directes et on les a affinées par la méthode des moindres carrés (matrice entière) jusqu'à des valeurs respectives de R = 0.068 et 0.030 pour 548 et 562 réflexions. Les angles dièdres entre les plans des residus naphtaléniques sont 87 et 102°, respectivement. Les longeurs de liaison et les angles sont normales.

Introduction

When maintained at temperatures just below the melting point, racemic 1,1′-binaphthyl undergoes spontaneous resolution to the higher-melting optically active form (1–4). In contrast, for the 4,4′dimethyl derivative rapid racemization of the active form is observed (5, 6). 4,4′-Diamino-1,1′-binaphthyl (naphthidine) also exhibits racemization, although in a narrow temperature range (197–202°C) just below the melting point active naphthidine has been obtained from the racemate by seeding (7). In a continuing study of these phenomena the crystal structure of optically active naphthidine has now been investigated. Since the crystal structure of optically active 1,1′-binaphthyl was unknown, its structure has also been determined; after completion of the work two other independent studies of binaphthyl appeared (8, 9), and our results are presented briefly for completeness and for comparison.

Experimental

Crystal and intensity data for both compounds were measured on an Enraf-Nonius CAD4 diffractometer.

I. 4,4′-Diamino-1,1′-binaphthyl, naphthidine (optically active form)
Crystal data:
$C_{20}H_{16}N_2$, mp = 204°C fw = 284.4
Tetragonal, $P4_12_12$ (or $P4_32_12$), a = 7.945(1), c = 24.264(5) Å, V = 1532 Å^3, Z = 4, ρ_c = 1.23 g cm^{-3}, CuKα, λ = 1.5418 Å, μ = 5.3 cm^{-1}.

The crystals were well-formed brown tetragonal bipyramids, but they were weakly diffracting and appeared to decompose (or racemize (7)), becoming opaque, often with liquified surfaces. Three separate data sets were collected. An initial set with MoKα radiation had too small a proportion of observed reflections, a second set with CuKα radiation and $\theta \leq 45°$ was used to solve the structure, and a final set, CuKα and $\theta \leq 65°$, was used in the refinement. In the final set an $\omega - (2/3)\theta$ scan was used, with an ω scan angle of (0.7 + 0.14 tan θ) deg extended by 25% on either side for background counts, and an aperture (2.5 + tan θ) mm wide and 4 mm high. Three check reflections were used for orientation control and scaling. 548 of 826 reflections (66%) with $\theta \leq 65°$ had $I/\sigma(I) \geq 3.0$, where $\sigma^2(I) = S + B + (0.04S)^2$, S and B being the scan and background counts, and were used in the analysis.

The structure was solved by direct methods with use of MULTAN (10) and refined by full-matrix least-squares techniques. Difficulty was encountered in locating the hydrogen atoms; the ring H atoms were placed in ideal calculated positions, and the two amino hydrogen atoms were assigned to the most chemically plausible peaks near the nitrogen atom on a difference map. Refinement of C and N parameters was then completed to final R = 0.068 and R_w = 0.075 for 548 reflections. Scattering factors of refs. 11 and 12 were used, with the weighting scheme $\sqrt{w} = 1$ for $|F_o| \leq 19$, $\sqrt{w} = 19/|F_o|$ for $|F_o| > 19$.

TABLE 1. Positional (fractional, × 10^4) and equivalent isotropic thermal parameters (Å^2, × 10^3) for optically active naphthidine and 1,1′-binaphthyl

Atom	x	y	z	U_{eq}
		Naphthidine		
C(1)	1070(6)	193(7)	2412(2)	68
C(2)	2654(8)	250(10)	2640(2)	95
C(3)	3852(8)	1496(12)	2452(3)	113
C(4)	3430(10)	2615(9)	2053(3)	108
C(5)	1381(12)	3705(9)	1369(4)	116
C(6)	−133(13)	3595(12)	1125(4)	136
C(7)	−1340(12)	2458(11)	1312(3)	117
C(8)	−954(8)	1363(8)	1734(2)	80
C(9)	653(7)	1385(7)	1992(2)	68
C(10)	1846(8)	2616(8)	1803(3)	87
N	4680(9)	3775(11)	1878(3)	166
		Binaphthyl		
C(1)	4852(3)	3743(3)	2582(1)	45
C(2)	4660(4)	2074(3)	2347(1)	60
C(3)	3353(4)	740(4)	2493(1)	69
C(4)	2253(4)	1070(3)	2878(1)	63
C(5)	1299(4)	3116(3)	3556(1)	64
C(6)	1483(4)	4729(4)	3807(1)	71
C(7)	2744(4)	6096(4)	3652(1)	65
C(8)	3831(3)	5813(3)	3254(1)	50
C(9)	3702(3)	4117(3)	2989(1)	42
C(10)	2397(3)	2755(3)	3141(1)	49

II. 1,1′-Binaphthyl (optically active form)
Crystal data:
$C_{20}H_{14}$ fw = 254.4
Tetragonal, P_42_12 (or $P4_32_12$), a = 7.164(2), c = 27.70(1) Å, V = 1422 Å^3, Z = 4, ρ_c = 1.19 g cm^{-3}, MoKα, λ = 0.71073 Å, μ = 0.6 cm^{-1}.

0008-4042/83/010069-03$01.00/0
©1983 National Research Council of Canada/Conseil national de recherches du Canada

Can. J. Chem. Downloaded from www.nrcresearchpress.com by 210.87.254.40 on 09/06/12
For personal use only.

Can. J. Chem. Downloaded from www.nrcresearchpress.com by 210.87.254.40 on 09/06/12
For personal use only.

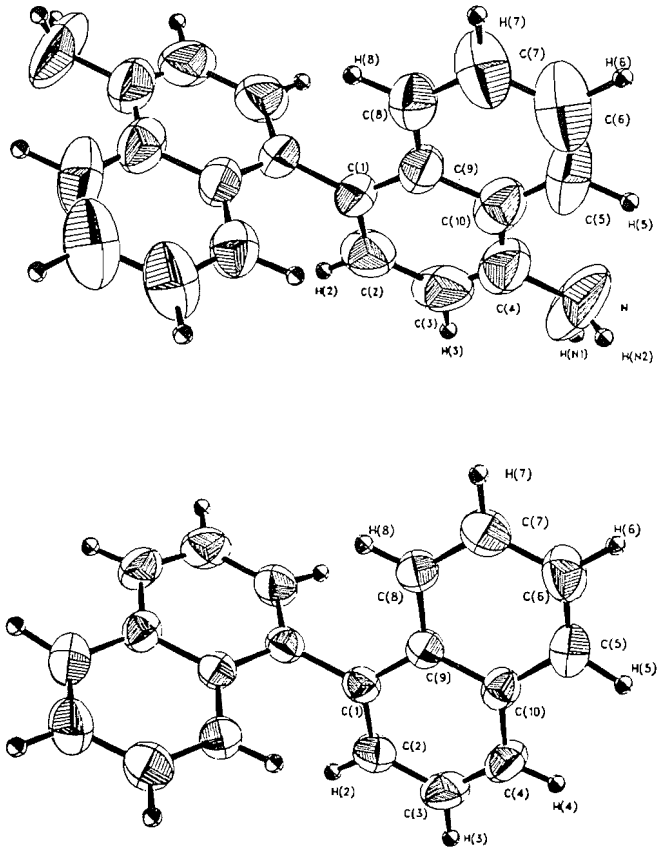

FIG. 1. Views of optically active naphthidine (top) and 1,1′-binaphthyl (bottom).

The intensity data were collected with MoKα radiation, ω−θ scan, ω scan angle (1.0 + 0.35 tan θ) deg, aperture (2.75 + tan θ) × 4 mm, and 562 of 812 reflexions (69%) with $\theta \leq 25°$ had $I \geq 3\sigma(I)$. The structure was solved by direct methods, the hydrogen atoms being located from a difference map and included in the refinement. A polynomial weighting scheme was used (13), with $A = -0.0201$, $B = 0.0372$, $C = -0.004211$, and $D = 0.000169$, and final R and R_w were 0.030 and 0.037, respectively, for 562 reflections.

The atomic positional parameters for the two structures are given in Table 1.[1]

Results and discussion

For each structure the asymmetric unit is one half of the molecule, the other half being generated by rotation about a crystallographic twofold axis which bisects the C(1)—C(1′) bond (Fig. 1). The naphthalene residues are approximately at right angles to each other in both molecules, although the arrangement in naphthidine is slightly "*cis*" (dihedral angle 87°) while in binaphthyl it is slightly "*trans*" (102°). The naphthalene residues show small folds along C(9)—C(10), 2.5° in naphthidine and 1.6° in binaphthyl.[1] The positions derived from the difference map for the amino hydrogen atoms suggest a pyramidal NH_2 group about 60° out of the naphthalene plane (Fig. 1); however, the positions should not be considered too reliable, in view of the difficulty in locating these atoms. Bond lengths and valency angles (Table 2[1]) are normal.

TABLE 2. Bond lengths (Å) and valency angles (degrees) in optically active naphthidine and 1,1′binaphthyl

	Length (Å)	
Bond	Naphthidine	Binaphthyl
C(1)—C(2)	1.375(7)	1.369(3)
C(1)—C(9)	1.430(7)	1.421(3)
C(1)—C(1)′	1.481(9)	1.494(4)
C(2)—C(3)	1.447(9)	1.398(4)
C(3)—C(4)	1.357(10)	1.347(3)
C(4)—C(10)	1.396(9)	1.415(3)
C(4)—N	1.420(8)	—
C(5)—C(6)	1.344(11)	1.354(4)
C(5)—C(10)	1.411(9)	1.417(3)
C(6)—C(7)	1.394(11)	1.400(4)
C(7)—C(8)	1.378(9)	1.364(3)
C(8)—C(9)	1.423(7)	1.424(3)
C(9)—C(10)	1.438(8)	1.416(3)
	Angle (deg)	
Bonds	Naphthidine	Binaphthyl
C(2)—C(1)—C(9)	118.4(5)	119.0(2)
C(2)—C(1)—C(1)′	121.8(5)	120.7(2)
C(9)—C(1)—C(1)′	119.7(4)	120.4(2)
C(1)—C(2)—C(3)	119.9(6)	121.8(2)
C(2)—C(3)—C(4)	120.7(7)	120.1(2)
C(3)—C(4)—C(10)	122.2(7)	121.0(2)
C(3)—C(4)—N	117.7(9)	—
C(10)—C(4)—N	120.0(8)	—
C(6)—C(5)—C(10)	121.6(7)	121.2(3)
C(5)—C(6)—C(7)	120.9(8)	120.2(2)
C(6)—C(7)—C(8)	119.9(9)	120.8(2)
C(7)—C(8)—C(9)	121.3(7)	120.5(2)
C(1)—C(9)—C(8)	120.9(5)	122.2(2)
C(1)—C(9)—C(10)	121.7(5)	119.3(2)
C(8)—C(9)—C(10)	117.3(6)	118.5(2)
C(4)—C(10)—C(5)	124.1(7)	122.3(2)
C(4)—C(10)—C(9)	117.0(6)	118.8(2)
C(5)—C(10)—C(9)	118.9(7)	118.9(2)

In both structures the molecules spiral around the fourfold screw axes along c, and packing forces are of van der Waals type. In naphthidine the closest intermolecular N . . . N distance is 3.48(2) Å, considerably longer than the N . . . N range of 2.9−3.3 Å normally found in N—H . . . N type hydrogen bonds.

Five binaphthyls have been the subjects of recent crystal structure studies, two racemates (binaphthyl and the 4,4′-dimethyl derivative) and three optically active forms (binaphthyl, the 4,4′-dimethyl, and 4,4′-diamino derivatives) (present paper and refs. 6, 8, 9, 14). The molecules in the racemic forms have dihedral angles between the two naphthalene residues of about 68° (i.e. a *cis* conformation); in the optically active forms this dihedral angle is 80−102°. The molecules in the racemic forms are thus slightly more compact and pack to give a higher density for the racemic form in each case. Both racemates crystallize in space group $C2/c$, although the unit cells are not of similar shape. All three chiral forms crystallize in space group $P4_12_12$, with $a = 7-8$, $c = 24-27$ Å. The crystallographic results shed little light on the dif-

[1]Anisotropic thermal parameters, hydrogen atom positional and thermal parameters, bond lengths and angles involving hydrogen atoms, details of mean planes, packing diagrams, and structure factors are available, at a nominal charge, from the Depository of Unpublished Data, CISTI, National Research Council of Canada, Ottawa, Ont., Canada K1A 0S2.

Can. J. Chem. Downloaded from www.nrcresearchpress.com by 210.87.254.40 on 09/06/12
For personal use only.

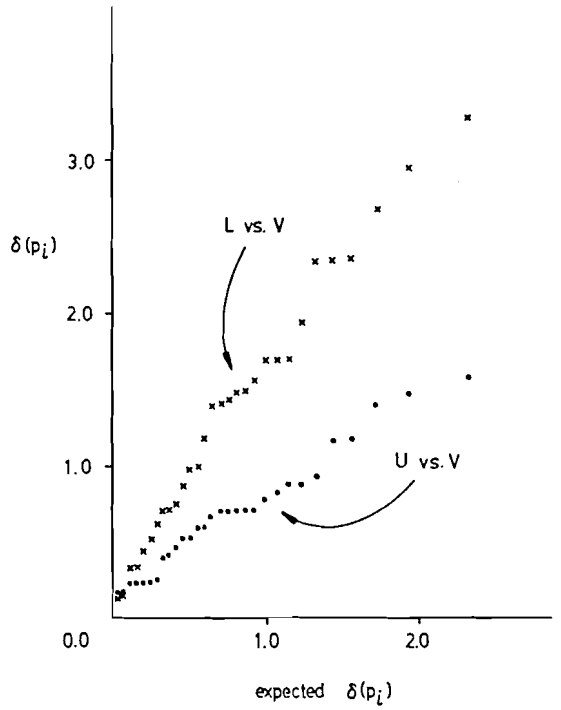

FIG. 2. Half-normal probability plots comparing the carbon positional parameters for 1,1′-binaphthyl from three studies: U = ref. 8, L = ref. 9, V = present paper.

ferences in stereochemical behaviour (resolution vs. racemization), which appear to arise from the different ranges in temperature in which racemic and eutectic phases are stable (7); and, as ref. 7 comments, "a crystallographically based explanation of relative stabilities of polymorphic phases does not seem possible as yet". In addition, under the conditions of ref. 8, the major reaction pathway in the spontaneous resolution of binaphthyl appears to be a solid−vapour−solid process and not a solid−solid transformation.

The bond distances in the five structures generally do not differ much from the lengths of the corresponding bonds in naphthalene. The shortest bonds are those of type C(1)—C(2) (and 3—4, 5—6, 7—8) with mean values in the range 1.360−1.369 (σ = 0.003−0.009 Å), the value in naphthalene being 1.357(4) Å (15). Mean values for the other types of bond are all in the range 1.40−1.44 Å. The central C(1)—C(1′) bonds are in the range 1.481−1.511 Å, the differences probably not being significant.

Finally a comparison may be made between the three independent sets of results for optically active 1,1′-binaphthyl (present paper and refs. 8 and 9). The present (V = Vancouver) and ref. 8 (U = Urbana) results agree very closely. The *a* cell parameters (7.164(2) and 7.181(2) Å) differ by about 6σ, which probably indicates slightly optimistic estimates of the standard deviations. A more detailed comparison by use of half-normal probability plots (16) confirms the good agreement. For example, a plot of differences between the two sets of positional parameters for the ten carbon atoms (Fig. 2, U vs. V) is approximately linear, with close-to-zero intercept, and slope slightly less than unity, suggesting that the estimated standard deviations are slightly too large (by about 30%). The agreement with the ref. 9 (L = London) results is not quite so close, with differences in cell parameters of about 20σ, and half-normal probability plot with slope of about 1.5 (Fig. 2, L vs. V).

Acknowledgements

We thank the Natural Sciences and Engineering Research Council of Canada and the Natural, Applied, and Health Sciences Committee, University of British Columbia, for financial support, the University of British Columbia Computing Centre for assistance, and Dr. R. E. Pincock for crystals and helpful discussion.

1. R. E. PINCOCK and K. R. WILSON. J. Chem. Ed. **50**, 455 (1973).
2. R. E. PINCOCK, R. P. BRADSHAW, and R. R. PERKINS. J. Mol. Evol. **4**, 67 (1974).
3. R. E. PINCOCK and K. R. WILSON. J. Am. Chem. Soc. **97**, 1474 (1975).
4. R. E. PINCOCK and K. R. WILSON. Can. J. Chem. **55**, 889 (1977).
5. R. E. PINCOCK, M. D. LU, and F.-N. FUNG. *In* Origin of life. *Edited by* Y. Wolman. D. Reidel Publishing Company. 1981.
6. R. A. PAUPTIT and J. TROTTER. Can. J. Chem. **59**, 1149 (1981).
7. M. D. LU and R. E. PINCOCK. J. Org. Chem. **43**, 601 (1978).
8. R. B. KRESS, E. N. DUESLER, M. C. ETTER, I. C. PAUL, and D. Y. CURTIN. J. Am. Chem. Soc. **102**, 7709 (1980).
9. R. KURODA and S. F. MASON. J. Chem. Soc. Perkin Trans II, 167 (1981).
10. P. MAIN, S. E. HULL, L. LESSINGER, G. GERMAIN, J. P. DECLERCQ, and M. M. WOOLFSON. MULTAN78. A system of computer programs for the automatic solution of crystal structures from X-ray diffraction data. Univs. of York, England, and Louvain, Belgium. 1978.
11. D. T. CROMER and J. B. MANN. Acta Crystallogr. A**24**, 321 (1968).
12. R. F. STEWART, E. R. DAVIDSON, and W. T. SIMPSON. J. Chem. Phys. **42**, 3175 (1965).
13. D. W. J. CRUICKSHANK. *In* Computing methods in crystallography. *Edited by* J. S. Rollett. Pergamon Press. 1965.
14. K. A. KERR and J. M. ROBERTSON. J. Chem. Soc. B, 1146 (1969).
15. D. W. J. CRUICKSHANK. Acta Crystallogr. **10**, 504 (1957).
16. S. C. ABRAHAMS and E. T. KEVE. Acta Crystallogr. A**27**, 157 (1971).

Phthalocyanines: electrolyte Schottky-junction devices

R. O. LOUTFY AND L. F. MCINTYRE

Xerox Research Centre of Canada, 2480 Dunwin Drive, Mississauga, Ont., Canada L5L 1J9

Received April 20, 1982

R. O. LOUTFY and L. F. MCINTYRE. Can. J. Chem. **61**, 72 (1983).

The photoelectrochemical properties of phthalocyanine coated tin-oxide (SnO_2) electrodes in the presence of several redox couples were investigated. The photovoltaic performances were optimized for $Fe(CN)_6^{4-/3-}$ and I_2/I_3^- redox couples with respect to concentration, pH, counter electrode, and back contact. Under AM2 solar illumination the SnO_2/x-H_2Pc $Fe(CN)_6^{4-/3-}$ cells developed a photocurrent of 0.63 mA/cm^2, photovoltage of 0.33 volts, fill factor of 0.25, and a power conversion efficiency of 0.07% to white light irradiation of 75 mW/cm^2. The low efficiency of carrier collection was attributed to the high series resistance, surface recombination of carriers, and slow charge exchange at the counter electrode.

R. O. LOUTFY et L. F. MCINTYRE. Can. J. Chem. **61**, 72 (1983).

On a étudié les propriétés photoélectrochimiques d'une électrode de phtalocyamine recouverte d'oxyde d'étain (SnO_2) en présence de plusieurs couples rédox. On a maximisé les performances photovoltaiques des couples redox $Fe(CN)_6^{4-/3-}$ et I_2/I_3^- en ce qui a trait à la concentration, au pH, à l'électrode opposé et au contact de retour. Sous la lumière solaire de type AM2, les cellules de SNO_2/x-H_2Pc $Fe(CN)_6^{4-/3-}$ développement un courant photoélectrique de 0,63 mA/cm^{-2}, un photovoltage de 0,33 volt, un facteur de remplissage de 0,25 et un pouvoir de conversion efficace de 0,07% en irradiation de lumière blanche de 75 mW/cm^{-2}. On attribue la faible efficacité du transporteur de réception à une grande série résistance, à la surface de recombinaison des transporteurs et à un échange lent à l'électrode opposé.

[Traduit par le journal]

1. Introduction

Photoelectrochemical solar cells are the analog of a metal–semiconductor junction, with the metal replaced by an electrolyte. The junction formed at the interface between the semiconductor and the electrolyte serves in the photoconversion. Many of the electrochemical photovoltaic cells can convert light energy directly to electricity as well as store the energy internally as chemical products. In electrochemical cells the conductivity and charge injection characteristics of the space charge layer are easily altered by the use of surfactants and by adjusting the chemical potential and composition of the electrolyte. These features make electrochemical photovoltaic cells an attractive alternative to the expensive solid state solar cells. The major problem with photoelectrochemical cells has been photocorrosion processes which are observed with most inorganic semiconductors in aqueous electrolyte. However, recently Heller and Vadimsky (1) have shown that a stable and efficient semiconductor–electrolyte solar cell based on *p*-type InP can be made. The resistance of the *p*-type semiconductor to photocorrosion was attributed to cathodic protection of the semiconductor against surface oxidation.

The goal of this work is to evaluate the feasibility and practicality of solar cells consisting of organic semiconductors in contact with an electrolyte. Two organic semiconductors, x-metal free phthalocyanine (x-H_2Pc) and vanadyl phthalocyanine (VOPc), which are well matched to the solar spectrum were investigated. Several redox couples were used; the performance of $Fe(CN)_6^{4-/3-}$ and I_2/I_3^-, in particular, was optimized. The principle element of the photoelectrochemical cell is a thin organic film of microcrystalline particles of phthalocyanines (x-H_2Pc or VOPc) dispersed in a polymer binder coated onto a conductive tin-oxide (SnO_2) substrate. These films functioned as photocathodes in electrochemical cells in contact with aqueous electrolyte containing the $Fe(CN)_6^{4-/3-}$ or I_2/I_3^-. The effects of electrolyte, pH, redox couple concentration, counter electrodes, and back electrodes are discussed. The action spectra and capacitance–voltage behaviour are presented. The stability of these systems both in the dark and under illumination is also described.

2. Experimental

Materials

x-H_2Pc was prepared as described before (2). The process involves dissolving commercial H_2Pc in concentrated sulfuric acid kept at 5°C, then pouring the mixture, while stirring, into ice-water. The blue flaky precipitation (α-H_2Pc) is then filter washed with ammonia solution, water, acetone, then methanol, and dried. The solid α-H_2Pc is then dry milled for three weeks in a plastic bottle using flint stones; this process induces the conversion of α-H_2Pc to x-H_2Pc. Finally, methyl ethyl ketone is added and milling is continued for 16 h to form a slurry before filtering, then washing with acetone and methanol. Vanadyl phthalocyanine (VOPc) was obtained from the reaction of phthalonitrile and vanadium tetrachloride. The deep blue product was acid pasted in sulfuric acid to give submicron (25 nm) particles. The x-H_2Pc pigment particle size, determined by scanning electron microscopy, averaged 80 nm in diameter. All other matierals were from common commercial sources, used without further purification. The polymer used throughout this study was Makrolon 5705 (MK), a polycarbonate from Bayer. Other polymers used were polyester PE-200 and polyvinylacetate (PVA).

The phthalocyanine films were prepared as described previously (3). All films contained approximately 60 weight percent of the phthalocyanine dispersed in polymer binder coated onto precleaned heavily doped SnO_2 (NESA glass, PPG Company, Pittsburg Pennsylvania). The thickness of the pigmented films was measured using a Talystep and on average was 1 μm.

Apparatus

The experimental setup of a typical electrochemical cell was described previously (4). The cell body was made of Plexiglas. The phthalocyanine-coated SnO_2 electrodes were pressure sealed to the cell body using a rubber gasket. The electrolyte was contained in a cylindrical cavity made in the cell, with a thin window on one side and the phthalocyanine electrode on the other. A platinum or ruthenized titanium ring was used as counter electrode. The sample electrode was

0008-4042/83/010072-06$01.00/0

©1983 National Research Council of Canada/Conseil national de recherches du Canada

Can. J. Chem. Downloaded from www.nrcresearchpress.com by 210.87.254.5 on 09/06/12
For personal use only.

Can. J. Chem. Downloaded from www.nrcresearchpress.com by 210.87.254.5 on 09/06/12
For personal use only.

illuminated through the electrolyte with an Oriel 1 KW Xenon Solar simulator. Monochromatic light was obtained through a set of narrow band pass filters, each of which had a transmitting band of half width of 8–10 nm. The radiant intensity was measured with a Karl Lambrecht calibrated light probe. The photoelectrochemical current and voltage were measured using a Keithley electrometer (model 616). The dark and light current–voltage characteristics of the electrochemical cells were determined using Polarographic analyser EG&G, model 174A.

In preliminary experiments it was shown that the same photovoltage and current were observed using either the two-electrode arrangement or by measuring potential relative to a reference electrode (which was $Ag/AgNO_3$ or calomel reference electrode). For this reason the simpler arrangement was used, involving only two electrodes. The light source for action spectrum measurements consisted of a 150-W Xe lamp and a $\frac{1}{4}$-m Jarrel Ash monochromator. All photocurrent action spectra have been normalized against the photon flux of the lamp and monochromator (3).

The capacitance of the cells was measured using the low frequency oscillographic technique described in ref. 5 at 10 Hz.

3. Results

3.1 Current–voltage behaviour of the phthalocyanine coated SnO_2 electrode

The current–voltage characteristics of all films investigated showed strong rectifying behaviour (Fig. 1(a)) with large anodic current arising in the positive potential region, typical of *p*-conducting material. In the presence of oxidizing agents, e.g. $Fe(CN)_6^{3-}$ or I_2, a large cathodic photocurrent was observed. The electrochemical current–voltage behaviour of SnO_2/x-H_2Pc electrodes in the presence of 0.1 *M* $K_4Fe(CN)_6$/0.01 *M* $K_3Fe(CN)_6$ in solution at pH 8 is shown in Fig. 1(b) under solar illumination (85 mW/cm^2). The cell generated a V_{oc} of 0.2 volts while J_{sc} was 135 μA/cm^2. The fill factor had a value of 0.28. The power conversion efficiency for solar light is 0.01%. Using 620 nm light at a power density of 2.5 mW/cm^2, the quantum efficiency in terms of incident radiation is 10^{-2}. The efficiency in terms of absorbed photon is about 10^{-1}. This low efficiency is due to considerable recombination of carriers in the junction as indicated by the high reverse saturation current, J_0, (1.7×10^{-6} A/cm^2) and to the high series resistance. The performance characteristics of SnO_2/x-H_2Pc electrodes in the presence of 0.1 *M* KI/0.003 *M* I_2 at pH 7 was quite similar and is shown in Fig. 1(c). The V_{oc} = 0.15 volts, J_{sc} = 84 μA/cm^2, ff = 0.26, and the power conversion efficiency = 0.0035%.

The photoelectrochemical behaviour of the SnO_2/VOPc electrode in the presence of $Fe(CN)_6^{4-/3-}$ at pH 8.0 under solar illumination was quite similar to that of SnO_2/x-H_2Pc. The V_{oc} = 0.22 volts, J_{sc} = 270 μA/cm^2, and ff = 0.28.

3.2 Effect of redox couples concentration

The output power of the SnO_2/x-H_2Pc photocathodes was found to depend strongly on the concentration of the redox couples. Figure 2 shows the dependence of the short circuit photocurrent, J_{sc}, and open circuit photovoltage, V_{oc}, on the concentration of $Fe(CN)_6^{4-/3-}$ and I_2/I_3^-. The addition of a small amount of $K_4Fe(CN)_6$ to the $K_3Fe(CN)_6$ solution or I_2 to KI solution sharply increases the cathodic photocurrent of SnO_2/x-H_2Pc electrodes as shown in Figs. 2(a) and (b), respectively. After the initial sharp increase at low concentration, the current tends to level off, then drop at high concentration, suggesting that internal electron–hole pair recombination, rather than the solution reduction, is governing the current. The open circuit voltage monotonically decreases with increasing the concentration of $K_4Fe(CN)_6$ or I_2. The optimum redox

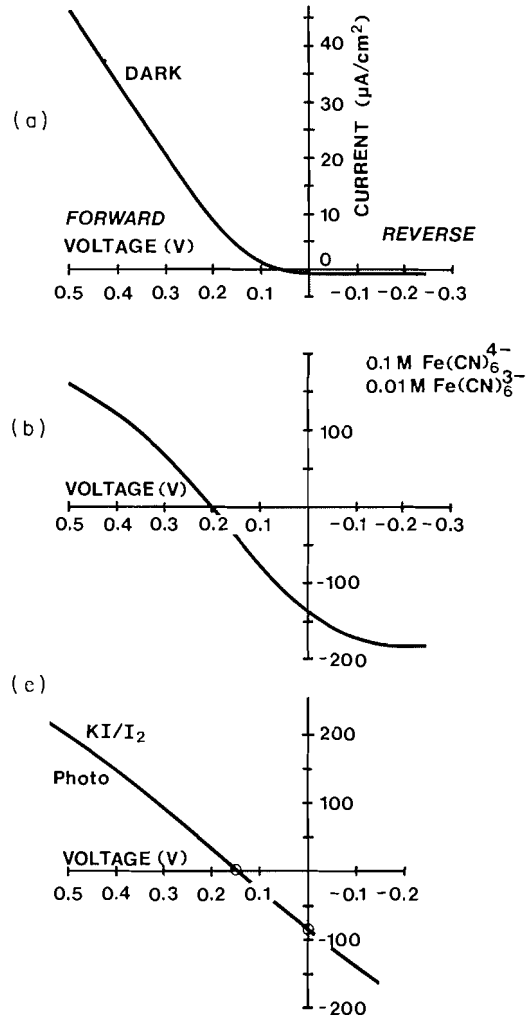

FIG. 1. Current–voltage characteristics of the SnO_2/x-H_2Pc electrode (a) in the dark; and under illumination (150 mW/cm^2) in presence of (b) 0.1 *M* $Fe(CN)_6^{4-}$/0.01 *M* $Fe(CN)_6^{3-}$ (pH 8) and (c) 0.1 *M* KI/0.003 *M* I_2 (pH 7). The sign of the potential is that applied to the SnO_2/Pc.

couple concentrations were found to be: 0.1 *M* $K_4Fe(CN)_6$/0.01 *M* $K_3Fe(CN)_6$ and 1 *M* KI/0.003 *M* I_2.

3.3 Effect of pH

Figures 3(a) and (b) show the influence of pH of the electrolyte on the magnitude of short circuit current and open circuit voltage for the 0.1 *M* $Fe(CN)_6^{4-}$/0.01 *M* $Fe(CN)_6^{3-}$ and 1 *M* KI/0.003 *M* I_2 solutions using platinum as counter electrode. The photocurrent and voltage reach a maximum at pH 8 for the $Fe(CN)_6^{4-/3-}$ and at pH 7 for the I_2/I_3^- redox system. The electrochemical redox potential of these couples at that pH is +0.2 volts vs. SCE (6).

3.4 Dependence of photocurrent and voltage on light intensity

The photocurrent of the system SnO_2/x-H_2Pc/$Fe(CN)_6^{4-/3-}$ pH 8/Pt varied linearly with light intensity with a light intensity exponent near unity. Similar results were obtained for the I_2/I_3^- system, however, the light intensity exponent was 0.56. Information on the junction parameters *n* and J_0, diode quality factor and reverse saturation current, respectively, can be obtained using the simple diode equation:

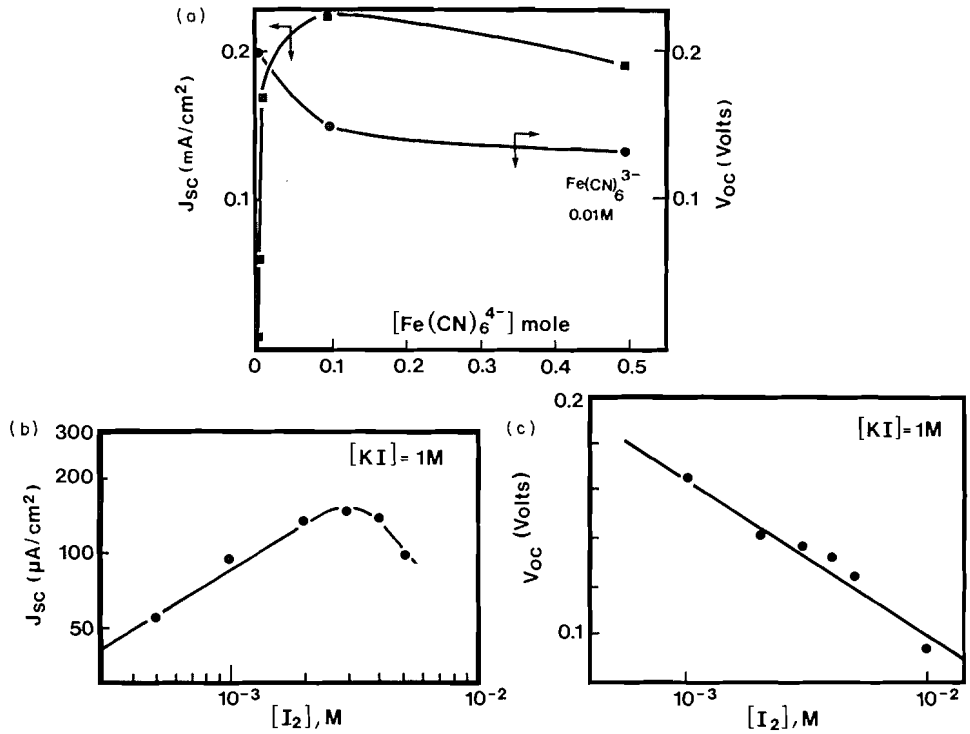

FIG. 2. The dependence of short circuit current, J_{sc} and open circuit voltage, V_{oc} on the concentration of (a) $K_4Fe(CN)_6$ (pH 8) and (b, c) I_2 (pH 7).

$$V_{oc} = \left(\frac{nRT}{e}\right) \ln\left[\frac{J_{sc}}{J_0} + 1\right]$$

Plots of V_{oc} against $\ln J_{sc}$ determined at different light intensities give a straight line, the slope is nkT/e and the intercept is $\ln J_0$. Values of 1.2 and 1.7×10^{-6} A/cm^2 for n and J_0, respectively, were obtained for the $Fe(CN)_6^{4-/3-}$ redox couples. Similar n and J_0 values of 1.3 and 8.6×10^{-7} A/cm^2 were obtained for the I_2/I_3^- system. The relatively large reverse saturation current indicates that surface recombination of carrier is a significant energy wasting process.

3.5 *Action spectrum*

The spectral dependence of the cathodic photocurrent of SnO_2/x-H_2Pc/$Fe(CN)_6^{4-/3-}$ system is shown in Fig. 4, which is essentially the same as the absorption spectrum of x-H_2Pc film if the light is incident through the electrolyte side. For light incident on the SnO_2 electrode, the action spectrum resembled the transmission spectrum of x-H_2Pc film. This behaviour indicates the presence of a Schottky junction at the semiconductor–electrolyte interface.

3.6 *Dependence of photocurrent and voltage on electrode materials*

The back contact has a significant effect on the performance of the device. We varied the back electrode using Pt, Au, Ag, ITO, Cr, Cu, and In and compared the device performance to that of the standard SnO_2 electrode. The photocurrent, J_{sc}, increased with the increase of the work function of the back electrode, see Table 1. The function of the back electrode is to provide an ohmic contact to the *p*-type x-H_2Pc. The results indicate that the contact between x-H_2Pc and the back electrode becomes more ohmic as the work function increases. The performance characteristics of SnO_2/x-H_2Pc/$Fe(CN)_6^{4-/3-}$ cells were found to depend strongly on the counter electrode. Table

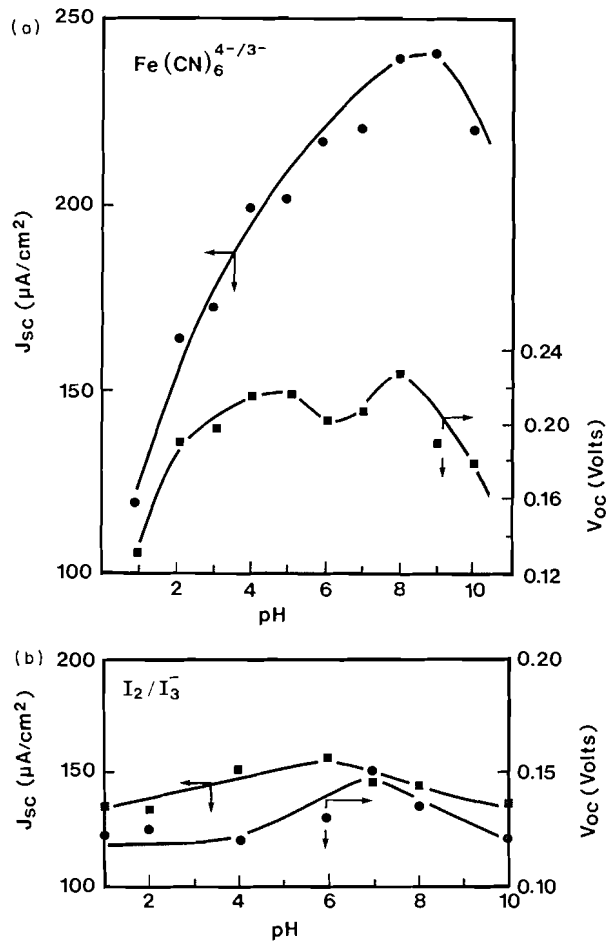

FIG. 3. The dependence of J_{sc} and V_{oc} of SnO_2/x-H_2Pc electrode on the pH for (a) $Fe(CN)_6^{4-/3-}$ and (b) I_2/I_3^- solutions.

Can. J. Chem. Downloaded from www.nrcresearchpress.com by 210.87.254.5 on 09/06/12
For personal use only.

Can. J. Chem. Downloaded from www.nrcresearchpress.com by 210.87.254.5 on 09/06/12
For personal use only.

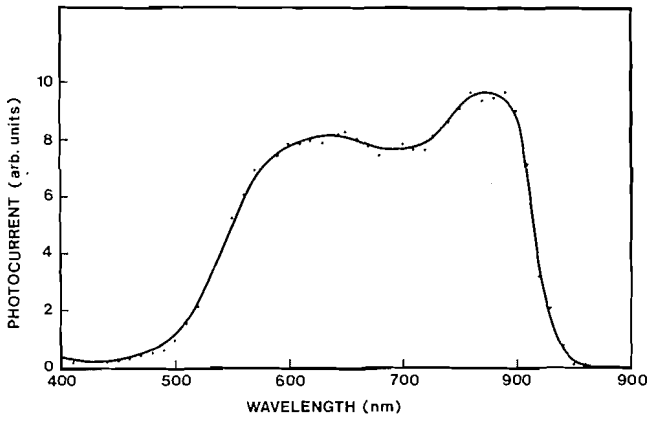

FIG. 4. The action spectrum of the SnO_2/x-H_2Pc/$Fe(CN)_6^{4-/3-}$/Pt cell. Light incident from the solution side.

TABLE 1. Effect of back contact (electrode x-H_2Pc, $Fe(CN)_6^{4-/3-}$ 0.01:0.1 *M* pH 8/Pt)

Electrode	J_{sc} (A/cm^2)	V_{oc} (Volts)
SNO_2/Pt	220	0.17
Pt	195	0.17
Au	195	0.16
Ag	170	0.15
ITO	155	0.15
SnO_2	100	0.15
Cu	44	0.14
Cr	40	0.12
In	−2.3	−0.13

TABLE 2. Effect of counter electrode on SnO_2/x-H_2Pc/ $Fe(CN)_6^{4-/3-}$ cell performance

Counter electrode	J_{sc} (mA/cm^2)	V_{oc} (Volts)
Al	0.63	0.33
Fe	0.48	0.16
In	0.40	0.20
Cu	0.38	0.32
Sn	0.27	0.19
Ag	0.21	0.22
Pt	0.21	0.21
Ti	0.15	0.25
Pb	0.08	0.10
Au	0.03	0.22

2 lists the photocurrent and voltage for the above cell as a function of the counter electrode. Cathodic photocurrent as high as 0.63 mA/cm^2 and photovoltage of 330 mV were observed with aluminum counter electrodes. The power conversion efficiency of this device approaches 0.1%. In these cells the dark current was in the order of a few nanoamps. The strong dependence of the photocurrent on the counter electrode materials could be due to oxidation of the metal electrode by a photoassisted electrochemical catalytic mechanism.

3.7 Capacitance measurements

Application of a sinusoidal voltage across the space charge region of a semiconductor electrode leads to a periodic redistribution of charge, which manifests itself as a capacitance. Figure 5 shows the current−voltage curve of the SnO_2/x-H_2Pc

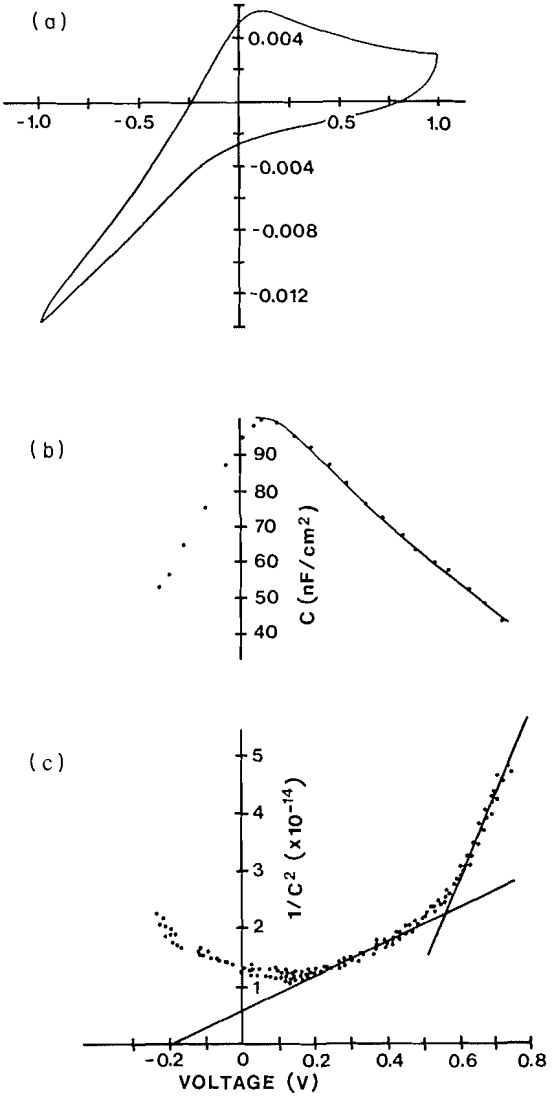

FIG. 5. Low frequency oscillogram of the SnO_2/x-H_2Pc/ $Fe(CN)_6^{4-/3-}$ (pH 8)/Pt cell (a); capacitance vs. voltage (b); and $1/C^2$ vs. *V* plot (c).

electrode immersed in a phosphate buffer solution (pH 8) containing $Fe(CN)_6^{4-/3-}$. The observed hysteresis gives the junction capacitance (5). The zero bias capacitance is 110 nF/cm^2 which gives a barrier width ($C = \epsilon\epsilon_0/W$) of 300 Å. A plot of $1/C^2$ vs. *V* is shown in Fig. 5. The plot can be fitted to two straight lines intersecting at +0.50 volts. The discontinuity in the $C-V$ plot is due to interfacial states localized 0.7 eV above the Fermi level (4). The slope of the $1/C^2$ vs. *V* plot at low bias gives the density of hole traps and ionized states which approached 1×10^{17} cm^{-3}; the intercept gives the barrier potential V_b which is 0.2 volts.

3.8 Time dependence

The stability of the SnO_2/x-H_2Pc electrode in solution is quite remarkable. The photocurrent−time and photovoltage−time dependence for SnO_2/x-H_2Pc in the presence of $Fe(CN)_6^{4-/3-}$ at pH 8 and I_2/I_3^- and pH 7 were found to be stable for hours.

4. Discussion

Results presented here (particularly the action spectrum and

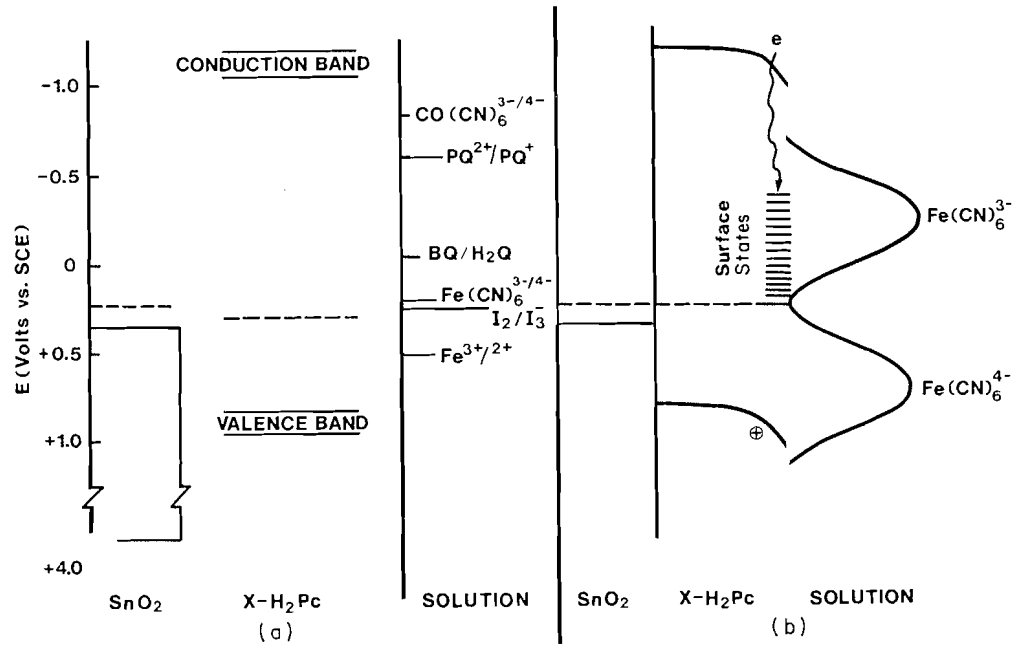

FIG. 6. Energy level diagram of SnO_2, x-H_2Pc, and redox couple potentials (a) and energy scheme of x--$H_2Pc/Fe(CN)_6^{4-/3-}$ at pH 8 (b).

capacitance−voltage data) give considerable support to the idea that phthalocyanine pigment is capable of forming a Schottky junction with various electrolyte containing redox couples. The Schottky barrier width determined from the $C-V$ data is about 300 Å. This value gives a solar light collection efficiency of x-H_2Pc/electrolyte devices of 29% (3). If the photogeneration efficiency within the barrier region is 100%, the 75 mW/cm^2 light would generate a short circuit current of 11 mA/cm^2. We obtained instead between 0.11 to 0.63 mA/cm^2 depending on the back and counter electrodes, indicating that the generation efficiency for x-H_2Pc is 1 to 6×10^{-2}. Recently Bard and co-workers (7) reported on the spectral sensitization of several single-crystal n-type semiconductors by various phthalocyanine thin films in photoelectrochemical cells using hydroquinone/benzoquinone (H_2Q/BQ) redox couples. Both anodic and cathodic sensitized photocurrent could be observed depending upon the applied potential. The photoelectrochemical efficencies of these systems ranged from 1.3×10^{-5} to 1.1×10^{-3} per absorbed photon and under external potential bias. Similarly, Armstrong and co-workers (8) reported on the sensitization of SnO_2 electrodes by thin films of phthalocyanines (GaPcCl, GaPcF, AlPcF, AlPcCl, and silicon phthalocyanine) in PEC using H_2Q. Efficiencies for the dye-sensitized photoelectrolysis of H_2Q of 10^{-2} per absorbed photon (monochromatic) and under potential bias were reported (8). In our systems the cathodic photocurrents reported above were obtained under short circuit conditions. A much larger anodic and cathodic photocurrent can be obtained under forward and reverse bias potenital, respectively. However, for solar energy applications, interest lies in cells which can operate without external bias.

In Fig. 2 the dependence of SnO_2/x-H_2Pc photocurrent and voltage on the concentration of the $Fe(CN)_6^{4-/3-}$ and I_2/I_3^- redox couples is shown. The open circuit voltage (V_{oc}) changes by the expected 60 mV due to a 10-fold change in the ratio of oxydant/reductant. However, the dependence of the photoreduction current on the redox couples concentration is quite surprising. The highest photoreduction currents were obtained at relatively low concentration of oxydant and very high concentration of reductant. These results suggest that the performance of these cells is limited by the discharge rate of the reductant at the counter electrode.This hypothesis is corroborated by the strong dependence of the photocurrent on the counter electrode materials (Table 2). In these cases the discharge at the counter electrode might involve, in addition to the oxidation of the reductant, an oxidation of the metal electrode by photoassisted electrochemical catalytic mechanism. It should be noted that in these cells the dark current was very small, in the order of a few nanoamps. We found, however, platinum, gold, and ruthenized titanium to be sufficiently inert under our experimental conditions.

TABLE 3. Effect of redox couples formal potential on the performance of SnO_2/x-H_2Pc cathodes

Redox system	E^0 (volts vs. SCE)	V_{ph} (volts)	J_{sc} (A/cm^2)
$Co(CN)_6^{4-/3-}$	−0.83	0.44	80
$Cr^{3+/2+}$	−0.65	0.25	1.0
PQ^{2+}/PQ^{+}	−0.66	0.21	37
BQ/QH_2	−0.05	0.21	120
$Fe(CN)_6^{4-/3-}$	0.20	0.165	200
I_2/I_3^-	0.26	0.15	120
$Fe^{3+/2+}$	+0.52	0.15	30
$Co(CH_3COCHCOCH_3)_3^{3+/2+}$	1.84	0.24	8

Surface state model

When a photon of light is absorbed at the semiconductor electrode, an electron−hole pair is created. The electron and hole separate under the influence of the junction field. The electrons (minority carriers) are driven to the surface and reduce an acceptor in solution. The holes are conducted through the bulk of the material and the back electrode to the anode where they oxidize a donor (reductant) in solution. Electron transfer from the semiconductor to an electroactive species in the electrolyte theoretically is feasible if the Gaussian energy

Can. J. Chem. Downloaded from www.nrcresearchpress.com by 210.87.254.5 on 09/06/12
For personal use only.

distribution of the solution redox species overlaps the conductance band of the *p*-type semiconductor (9).

It is usual to determine the potential of the band edges of a semiconductor in a particular electrolyte experimentally and then select an appropriate redox system. Energy band models can be a useful starting point to indicate the potential region for a practical choice of redox couple. Figure 6 shows the energy-band diagram for the interface between x-H_2Pc and electrolyte solution. The upper edge of the valence band of x-H_2Pc lies at $+0.9 \mp 0.1$ volts vs. SCE and the lower edge of the conduction band lies at -1.1 ∓ 0.1 volts vs. SCE (10). The Fermi level is 0.6 eV from the valence band (11) and, therefore, the flat band potential, V_{fb}, for x-H_2Pc is near +0.3 volts vs. SCE. In order to realize the maximum open circuit voltage V_{max} ($V_{max} = V_{fb} - E^0$), where E^0 is the equilibrium redox potential, one should select in our case a redox couple with sufficient negative potential ($E^0 \leq -0.8$ volts vs. SCE). Table 3 shows the dependence of the open circuit voltage and short circuit photocurrent of SnO_2/x-H_2Pc electrodes on the standard potential of a series of redox couples. One notes a weak dependence of V_{oc} on E^0 and strong dependence of photocurrent on E^0. Surprisingly, the highest photoactivity was observed with redox couples with energies located within the x-H_2Pc forbidden gap region (E^0 between -0.1 to $+0.3$ volts vs. SCE). These results suggest that the simple idealized model for a semiconductor–electrolyte interface must be modified. It has been shown previously that surface states present in sufficient density in the forbidden band gap of a semiconductor can mediate electron transfer processes across the interphase (6, 12), even for couples with energies located within the forbidden gap. The experimental results presented here lead to the conclusion that charge exchange between x-H_2Pc and $Fe(CN)_6^{4-/3-}$ or I_2/I_3^- must occur via surface states as shown in Fig. 6b.

This surface-controlled model is consistent with recent results by Fan and Faulkner (10) who studied charge transfer between *p*-type phthalocyanine electrodes and various iron complexes.

Although interfacial states were important in mediating electron transfer from x-H_2Pc to $Fe(CN)_6^{4-/3-}$ and I_2/I_3^- systems, they limit the open circuit voltage. They also constitute a path for loss of the photogenerated carriers by surface recombination. The nature of surface states in phthalocyanines is not clear at the present time, however, adsorbed oxygen or surface dislocation are very likely candidates. Attempts to eliminate or influence the energetics of the surface state by adsorption of ionic species or by surfactants is under way. The behaviour of SnO_2/x-H_2Pc as a photocathode makes possible the use of a photoanode as the counter electrode to increase power output. Cadmium sulfide was successfully used as counter electrode, increasing the photovoltage of the SnO_2/x-H_2Pc/$Fe(CN)_6^{4-/3-}$/CdS cell to 0.95 volts and photocurrent to 0.5 mA/cm^2.

In summary, we feel that the phthalocyanine coated tin-oxide electrode is a good candidate for future investigation as photocathode. Reduction of surface recombination of photogenerated carriers should be the major focus of future development.

1. A. HELLER and R. G. VADIMSKY. Phys. Rev. Lett. **46**, 1153 (1981).
2. J. F. BYRNE and P. F. KURZ. U.S. Patent No. 3,357,989 (1967).
3. R. O. LOUTFY and J. H. SHARP. J. Chem. Phys. **71**, 1211 (1979); R. O. LOUTFY, J. H. SHARP, C. K. HSIAO, and R. HO. J. Appl. Phys. **8**, 5218 (1981).
4. R. O. LOUTFY and L. F. MCINTYRE. Sol. Energy Mater. **6**, 467 (1982).
5. Y. SHING and R. O. LOUTFY. J. Appl. Phys. **52**, 6961 (1981).
6. J. GOBRECHT, H. GERISCHER, and H. TRIBUTSCH. Ber. Bunsenges Phys. Chem. **82**, 1331 (1978).
7. C. D. JAEGER, F.-R. F. FAN, and A. J. BARD. J. Am. Chem. Soc. **102**, 2592 (1980); A. GIRANDEAU, F.-R. F. FAN, and A. J. BARD. J. Am. Chem. Soc. **102**, 5137 (1980).
8. T. M. MEZZA, C. L. LINKOUS, V. R. SHEPARD, N. R. ARMSTRONG, R. NOHR, and M. KENNEY. J. Electroanal. Chem. **124**, 311 (1981), and references therein.
9. H. GERISCHER. Physical chemistry, an advanced treatise. Vol. 1XA. *Edited by* H. Eyring. Academic Press, New York, NY. 1970. p. 492.
10. R. O. LOUTFY and J. H. SHARP. J. Appl. Electrochem. **1**, 315 (1977); F. R. FAN and L. R. FAULKNER. J. Am. Chem. Soc. **101**, 4779 (1979); A. GIRANDEAU, F. R. FAN, and A. J. BARD. J. Am. Chem. Soc. **102**, 5137 (1980).
11. R. O. LOUTFY. Phys. Status Solidi A, **65**, 659 (1981).
12. A. J. BARD, A. B. BOCARSLY, F. R. FAN, E. G. WALTON, and M. S. WRIGHTON. J. Am. Chem. Soc. **102**, 3671 (1980); R. MEMMING. J. Electrochem. Soc. **125**, 117 (1978).

Can. J. Chem. Downloaded from www.nrcresearchpress.com by 210.87.254.5 on 09/06/12
For personal use only.

Nucleophilic and acid-catalyzed cleavage of the cyclopropane rings of β,γ-unsaturated α-spirocyclopropyl ketones[1]

FOR ERRATA SEE
V.62 #12 1984 P.2748

PETER YATES, PATRICK HUGH HELFERTY,[2] AND PAUL MAHLER

Lash Miller Chemical Laboratories, University of Toronto, Toronto, Ont., Canada M5S 1A1

Received July 12, 1982

PETER YATES, PATRICK HUGH HELFERTY, and PAUL MAHLER. Can. J. Chem. **61**, 78 (1983).

Treatment of isophorone (**8**) with sodium amide and 1,2-dibromomethane gives 6,6-dimethyl-8-methylenespiro[2.5]octan-4-one (**9**) and 6,6,8-trimethylspiro[2.5]oct-7-en-4-one (**10**); similar treatment of 3-methylcyclohex-2-en-1-one (**5**) gives analogous spiro compounds **6** and **7** together with 8-methylenedispiro[2.1.2.3]decan-4-one (**11**) and 8-methyldispiro[2.1.2.3]dec-8-en-4-one (**12**). The spiro ketones **6**, **7**, **9**, and **10** undergo homoconjugate nucleophilic addition on being heated in morpholine with cleavage of the cyclopropane rings to give 2-[2-(4-morpholinyl)ethyl]cyclohex-2-en-1-ones. The rates of reaction are much greater for the *exo* methylene compounds **6** and **9** than for their *endo* isomers **7** and **10**, but the rate of reaction of **10** is only slightly greater than that of the corresponding saturated compound, 6,6,8-trimethylspiro[2.5]octan-4-one (**15**). A corresponding rate differential between **9** and **10** is observed in their reactions with isophorone (**8**) and sodium hydride to give 2,2′-(ethanediyl)bis[3,5,5-trimethylcyclohex-2-en-1-one] (**18**). The acceleration in the cases of **6** and **9** relative to that of **15** is attributed to spiroactivation by both the carbonyl and exocyclic ethylenic groups; the much smaller effect of the endocyclic ethylenic groups in the cases of **7** and **10** is ascribed to torsional strain in the transition states for ring opening. The spiro ketones **6**, **7**, **9**, and **10** also undergo acid-catalyzed cyclopropane ring cleavage in ethanol, giving 2-(2-ethoxyethyl)cyclohex-2-en-1-ones. Again the *exo* methylene compounds **6** and **9** react much more rapidly than their *endo* isomers **7** and **10**; this is considered to be due to factors analogous to those operative in the nucleophilic addition reactions and/or the more rapid protonation of the *exo* methylene compounds.

PETER YATES, PATRICK HUGH HELFERTY et PAUL MAHLER. Can. J. Chem. **61**, 78 (1983).

L'isophorone (**8**) réagit avec l'amidure de sodium et le dibromo-1,2 éthane en donnant la diméthyl-6,6 méthylène-8 spiro[2.5] octanone-4 (**9**) et la triméthyl-6,6,8 spiro[2.5] octène-7 one-4 (**10**). Dans les mêmes conditions, la méthyl-3 cyclohexène-2 one-1 (**5**) donne les composés spiro analogues **6** et **7** ainsi que la méthylène-8 dispiro[2.1.2.3] décanone-4 (**11**) et la méthyl-8 dispiro[2.1.2.3] décène-8 one-4 (**12**). Lorsqu'on les chauffe dans la morpholine, les spiro cétones **6**, **7**, **9** et **10** subissent une addition nucléophile homoconjuguée avec une rupture des cycles cyclopropane en donnant des [(morpholinyl-4)-2 éthyl]-2 cyclohexène-2 ones-1. Les vitesses de réaction sont plus élevées pour les composés ayant une méthylène *exo* (**6** et **9**) que pour le cas des isomères *endo* (**7** et **10**); la vitesse de réaction du composé **10** est légèrement plus grande que celle du composé saturé correspondant: la triméthyl-6,6,8 spiro[2.5] octanone-4 (**15**). On a observé une différence de vitesse correspondante entre les composés **9** et **10** lorsqu'ils réagissent avec l'isophorone (**8**) et l'hydrure de sodium en donnant la (éthanediyl)-2,2′ bis(triméthyl-3,5,5 cyclohexène-2 one-1) (**18**). On attribue l'accélération dans le cas des composés **6** et **9** par rapport à celle du composé **15** a une spiro-activation à la fois par le groupe carbonyle et les groupes éthylèniques *exo*-cycliques; on attribue l'effet beaucoup plus faible du groupe éthylénique *endo*-cyclique, dans le cas des composés **7** et **10**, à une contrainte de torsion dans l'état de transition de l'ouverture du cycle. Les cétones **6**, **7**, **9** et **10** subissent également un clivage acido-catalysé du cyclopropane dans l'éthanol en donnant les (éthoxy-2 éthyl)-2 cyclohexène-2 ones-1. Là encore les composés ayant un méthylène *exo*-cyclique **6** et **9** réagissent plus rapidement que leurs isomères *endo*-cycliques **7** et **10**. On considère que ce fait est dû à des facteurs semblables à ceux que l'on rencontre dans les réaction d'addition nucléophile et/ou la protonation plus rapide des composés à méthylène *exo*.

[Traduit par le journal]

The term "spiroactivation" has been coined by Danishefsky and Singh (2) to describe the remarkable facilitation of homoconjugate addition of nucleophiles to cyclopropanes with geminal activating groups when these groups are incorporated into a spirocyclic system as in **1**. They have proposed that in such spiro compounds the carbonyl groups are held in an optimal orientation for delocalization of the developing carbanion in the transition state (**2**) for opening of the cyclopropyl ring by a nucleophile (Nu).

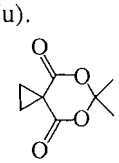

1

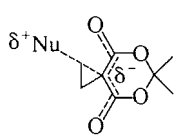

2

We have investigated the homoconjugate addition of nucleophiles to β,γ-unsaturated α-spirocyclopropyl ketones of types **3** and **4** to determine whether spiroactivation is involved in these cases and, if so, whether its magnitude is dependent on the relative disposition of the carbonyl and ethylenic double bonds, *exo*–*exo* in **3** and *exo*–*endo* in **4**. We have also investigated the acid-catalyzed fission of the cyclopropane ring of such spiro ketones.

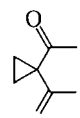

3

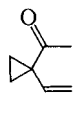

4

Preparation of β,γ-unsaturated and saturated α-cyclopropyl ketones

Newman *et al.* (3) found that treatment of 3-methylcyclohex-2-en-1-one (**5**) with sodium amide and 1,2-dibromoethane

[1]For a preliminary account of part of this work, see ref. 1.

[2]Present address: Research Department, Imperial Oil Ltd., Sarnia, Ont.

0008-4042/83/010078-08$01.00/0

©1983 National Research Council of Canada/Conseil national de recherches du Canada

Can. J. Chem. Downloaded from www.nrcresearchpress.com by 210.87.254.42 on 09/06/12
For personal use only.

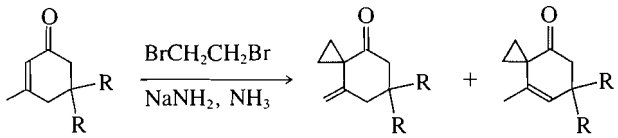

SCHEME 1

in liquid ammonia gave a mixture of 8-methylenespiro[2.5]-octan-4-one (**6**, 26%) and 8-methylspiro[2.5]oct-7-en-4-one (**7**, 15%) together with unconsumed **5** (47%) and 1,2-dibromoethane (12%). The mixture was separated by preparative gas chromatography since distillation failed to separate **6** and **7** from **5**. We have found that treatment of isophorone (**8**) under analogous conditions gave a mixture of 6,6-dimethyl-8-methylenespiro[2.5]octan-4-one (**9**, 35%) and 6,6,8-trimethylspiro-[2.5]oct-7-en-4-one (**10**, 19%) together with **8** (46%) (Scheme 1).[3] Again the starting ketone could not be separated from the spiro ketones by distillation. However, it was found possible to free the spiro ketones from **8** by treatment of the mixture with alkaline hydrogen peroxide, which oxidized **8** to an acidic product (5) that was removed as its salt. This procedure led to an 83% recovery of a mixture of **9** and **10** from which a pure sample of **9** was obtained by column chromatography. Heating a mixture of **9** and **10** in dioxane containing *p*-toluenesulfonic acid completely converted the *exo* compound **9** to the more stable *endo* compound **10** (*vide infra*) and permitted the isolation of the latter in pure form. The assignments of structures **9** and **10**, like those of the other reaction products discussed in the sequel, are based on spectroscopic data. The ir and ^{1}H nmr spectra of **10** corresponded to those previously reported by Ofune *et al.* (6). These workers prepared **10** from the photoadduct of **8** and ethylene in an overall yield of 48% from **8**, whereas our yield was 27%; however, their route did not provide **9**.

Having prepared **9** and **10** from **8**, we reinvestigated the preparation of the analogous spiro ketones **6** and **7** from **5**. Alkylation of **5** with 1,2-dibromoethane as before gave a mixture of **6** (19%) and **7** (19%) together with unconsumed **5** (54%) and the dispiro ketones **11** (2%) and **12** (6%). Unfortunately, attempted removal of **5** by treatment of the product mixture with alkaline hydrogen peroxide resulted in concomitant destruction of **6** and **7**, although the dispiro ketones **11** and **12** were stable under the reaction conditions; the survival of the

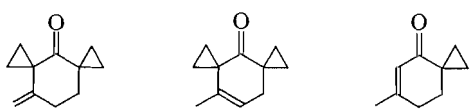

11 **12** **13**

latter and of **9** and **10** is ascribed to steric hindrance to attack of hydroperoxide anion at the carbonyl group in these compounds. Chromatography of the product mixture allowed the separation of unconsumed **5** and provided a mixture of the dispiro ketones **11** and **12**, a mixture of the spiro ketones **6** and

[3]Resubmission of mixtures of this type to the original alkylation conditions led to a product mixture containing an increased proportion of **9** and **10**, but this was offset by reduction in overall recovery. Alkylation with the use of powdered potassium hydroxide in dimethyl sulfoxide (4) returned 81% of **8** and gave only 19% of **9** and **10**.

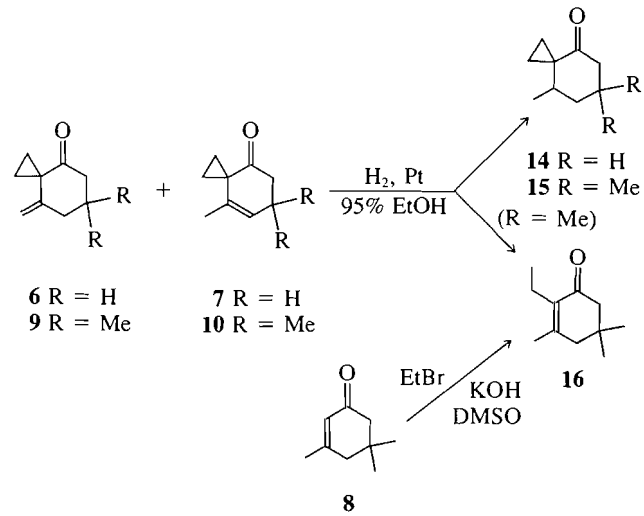

SCHEME 2

7, and pure 8-methylenespiro[2.5]octan-4-one (**6**). Treatment of the mixtures of spiro ketones and of dispiro ketones with *p*-toluenesulfonic acid in dioxane gave pure samples of 8-methylspiro[2.5]dec-7-en-4-one (**7**) and 8-methyldispiro-[2.1.2.3]dec-8-en-4-one (**12**), respectively. The other dispiro ketone, **11**, could not be separated from its mixture with **12**. Compounds **6** and **7** were identified by comparison of their ir and ^{1}H nmr spectra with those reported by Newman *et al.* (3)[4] and the structural assignments were confirmed by these and other spectroscopic data. The assignment of structure **12** is based on spectroscopic data and that of **11** on comparison of the spectra of the mixture of **11** and **12** with the corresponding spectra of **12**.

The dispiro compounds are considered to be formed via alkylation of **6** and **7** rather than of **13**, since none of the latter was detected in the product mixture and its formation would be expected to involve the kinetic enolate while the reaction conditions favor formation of the thermodynamic enolates (7). There was no evidence for the formation of the analogous dispiro compounds from **8**. While **8** has been methylated at C-6 with lithium isopropylcyclohexylamide and methyl iodide (8), unfavorable steric interaction between the more bulky 1,2-dibromoethane and one of the geminal methyl groups must prevent the introduction of a bromoethyl group at C-5 in **9** and **10**.

Newman *et al.* (3) reported that hydrogenation of a mixture of **6** and **7** in 95% ethanol over platinum gave 8-methylspiro-[2.5]octan-4-one (**14**) (Scheme 2). Similar treatment of a 4:1 mixture of **9** and **10** resulted in the rapid uptake of 0.8 molar equivalent of hydrogen, after which the rate of uptake slowed considerably. Analysis of the product mixture by ^{1}H nmr spectroscopy and gas chromatography showed that it consisted mainly of 6,6,8-trimethylspiro[2.5]octan-4-one (**15**) together with 2-ethyl-3,5,5-trimethylcyclohex-2-en-1-one (**16**) and unconsumed **10**. Further hydrogenation of the mixture under analogous conditions gave a mixture of **15** (85%) and **16** (15%) (Scheme 2), which was separated by column chromatography. The structural assignment for **15** is based on spectroscopic data and that for **16** on direct comparison with an authentic sample prepared by ethylation of **8** with ethyl bromide and potassium hydroxide in dimethyl sulfoxide (cf. ref. 4).

[4]Compound **7** has also been obtained from the photoadduct of **5** and ethylene in an overall yield of 12% (6).

Can. J. Chem. Downloaded from www.nrcresearchpress.com by 210.87.254.42 on 09/06/12
For personal use only.

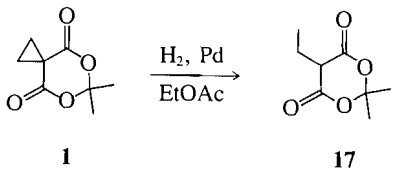

1 17

SCHEME 3

The persistence of **10** after uptake of 0.8 molar equivalent of hydrogen, although it represents only 20% of the mixture of **9** and **10**, reveals that hydrogenation of the *endo* isomer proceeds much more slowly than that of the *exo* isomer, presumably because of increased steric hindrance. The hydrogenolysis of the cyclopropane ring to give **16**, which may involve 1,4 addition to **9**, finds analogy in the reduction of **1** to **17** (2*a*) (Scheme 3). The fact that such hydrogenolysis was not observed in the case of **6** and **7** (3) is attributable to more ready hydrogenation of the ethylenic double bond in the absence of the geminal dimethyl group.

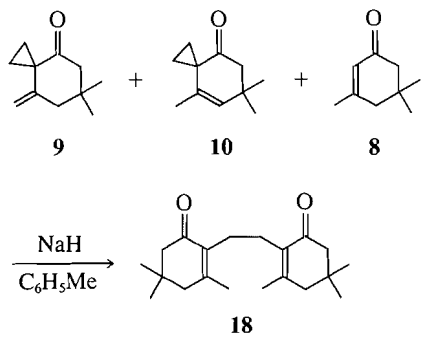

9 10 8

18

SCHEME 4

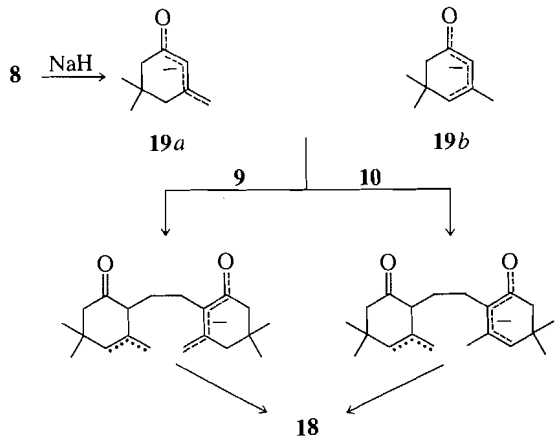

18

SCHEME 5

Homoconjugate nucleophilic addition

Heating of a 3.5:1 mixture of **9** and **10** with **8** and sodium hydride in toluene for 10 h gave 2,2′-(ethanediyl)bis[3,5,5-trimethyl-2-cyclohexen-1-one] (**18**) together with unconsumed **8** and **10**. Similar treatment of pure **10** and **8** again gave **18**, together with unconsumed **8** and **10** (Scheme 4). Heating of a 3:1 mixture of **9** and **10** in toluene with sodium hydride did not result in any change in the isomer ratio. The fact that interconversion of **9** and **10** does not occur under the reaction conditions establishes that **18** must be formed by attack of the anions **19***a* and **19***b* on both **9** and **10** (Scheme 5). That all of

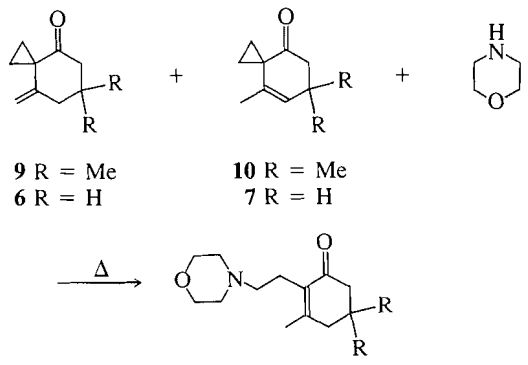

9 R = Me
6 R = H

10 R = Me
7 R = H

20 R = Me
21 R = H

SCHEME 6

9 but not all of **10** was consumed after 10 h when the 3.5:1 mixture of these compounds was subjected to the reaction demonstrates that the rate of ring opening of **9** is significantly greater than that of **10**.

Heating of a mixture of **9** and **10** in morpholine gave 3,5,5-trimethyl-2-[2-(4-morpholinyl)ethyl]cyclohex-2-en-1-one (**20**) (Scheme 6), which was also formed when **10** alone was heated in morpholine. Again the rate of ring opening of **9** was greater than that of **10**: while 95% conversion of **10** into **20** required 110 h, conversion of **9** into **20** was complete within 3 hours under similar conditions. An analogous difference in reaction rates was observed when a mixture of **6** and **7** was heated in morpholine: both gave 3-methyl-2-[2-(4-morpholinyl)ethyl]-cyclohex-2-en-1-one (**21**) (Scheme 6), but while the *exo* isomer **6** was completely consumed in 3 hours, reaction of the *endo* isomer **7** was incomplete after 80 h. Heating of a mixture of the two *endo* isomers **7** and **10** in morpholine gave a mixture of **20** and **21** and revealed that the rate of consumption of **10** was slower than that of **7**.

Heating of **15**, the saturated analogue of **9** and **10**, with morpholine gave *trans*-3,5,5-trimethyl-2-[2-(4-morpholinyl)-ethyl]cyclohexan-1-one (**22**) (Scheme 7). The gross structure of **22** is assigned on the basis of spectroscopic data and its independent synthesis by hydrogenation of **20**. The relative configuration is assigned on the basis of the observations that the compound is unchanged on being heated for 18 h with methanolic sodium methoxide and that, on treatment with sodium methoxide in methanol-*O*-*d*, deuterium is introduced into both the C-2 and C-6 positions; these observations taken together show that it has the more stable *trans* configuration as in **22**. The formation of the *trans* product via the hydrogenation

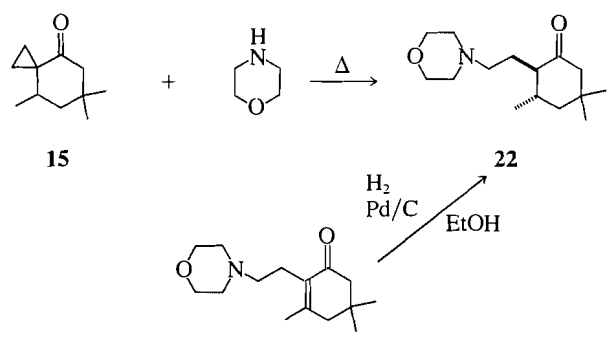

15 22

20

SCHEME 7

Can. J. Chem. Downloaded from www.nrcresearchpress.com by 210.87.254.42 on 09/06/12
For personal use only.

Can. J. Chem. Downloaded from www.nrcresearchpress.com by 210.87.254.42 on 09/06/12
For personal use only.

of **21** is attributable to either 1,4-addition followed by ketonization of the resulting enol or to 1,2-addition to give the *cis* isomer of **22** followed by self-catalyzed epimerization of this to **22**.

In its reaction with morpholine, consumption of **15** required ~240 h, whereas that of **10** required 110 h and that of **9** <3 hours. In summary, the order of rates of nucleophilic ring opening of the spiro compounds studied is **6** ≃ **9** ≫ **7** > **10** > **15**. The very much greater rates for the β,γ-unsaturated ketones **6** and **9** relative to the rate for the saturated ketone **15** are attributed to spiroactivation involving both the *exo* ethylenic double bond and the carbonyl group, although the conditions required for homoconjugate addition are still much more vigorous than in the case of the spiro acylal **1** since only one of the activating groups is a carbonyl group and the other is the much more weakly activating ethylenic double bond.

Of considerable interest is the observation that the β,γ-unsaturated ketones **7** and **10** are considerably less reactive than **6** and **9** and only slightly more reactive than the saturated ketone **15**. It seems unlikely that this is simply related to a variation of spiroactivation resulting from the change from an *exo*–*exo* disposition of the carbonyl and ethylenic double bonds to an *exo*–*endo* disposition and we propose the following interpretation. Full delocalization of the anions formed from the *endo* compounds **7** and **10** requires coplanarity of all of the six-membered ring atoms with concomitant angle strain at C-5 and C-6 and eclipsing of the C-5 hydrogen atoms or methyl groups with the C-6 hydrogen atoms (cf. **23**). In contrast, full delocalization of the anions formed from the *exo*-methylene compounds **6** and **9** requires coplanarity of only five of the six-membered ring atoms with C-5 out of plane (cf. **24**). While this difference will only be partially developed in the transition states it seems likely that it can account for the very much more rapid reaction of the *exo*-methylene compounds. In these terms the greater reactivity of **7** in comparison with **10** can be attributed to the smaller torsional strain in a transition state related to **23** when R = H than when R = CH_3.

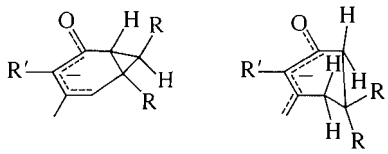

23 **24**

R = H, Me

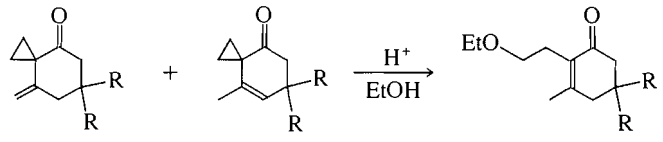

6 R = H, **9** R = Me **7** R = H, **10** R = Me **25** R = H, **26** R = Me

SCHEME 8

Acid-catalyzed cyclopropane ring cleavage

Newman *et al.* (3) have reported that the *exo*-methylene spiro ketone **6** was cleanly isomerized to its *endo* isomer **7** when a mixture containing both **6** and **7** was heated in ethanol containing *p*-toluenesulfonic acid. Although we were able to effect such a clean isomerization when the reaction was carried out in dioxane (*vide supra*), we found that when a 1:1 mixture of **6** and **7** was heated in boiling ethanol containing *p*-toluenesulfonic acid for 6 hours a 3:1 mixture of **7** and 2-(2-ethoxyethyl)-3-methylcyclohex-2-en-1-one (**25**) was formed with almost complete consumption of **6**. Further treatment of this mixture under the same conditions led to its complete conversion to **25** after 109 h (Scheme 8). These results show clearly that acid-catalyzed fission of the cyclopropane ring occurs much more rapidly in the *exo* compound **6** than in the *endo* compound **7**. Analogous observations were made in the cases of **9** and **10**. Treatment of a 3:1 mixture of these compounds under the same reaction conditions led to complete conversion to 2-(2-ethoxyethyl)-3,5,5-trimethylcyclohex-2-en-1-one (**26**) after 150 h (Scheme 8). Again, examination of the reaction mixture at earlier stages of the reaction showed that conversion of the *exo* compound **9** to **26** was much more rapid than that of the *endo* compound **10**.

The formation of **25** and **26** from the spiro compounds can be interpreted in the terms depicted for **25** in Scheme 9. One pathway could involve protonation of the ethylenic double bond to give **27**. Alternatively, the transformations could be initiated by protonation of the carbonyl group to give **28** or **29**.

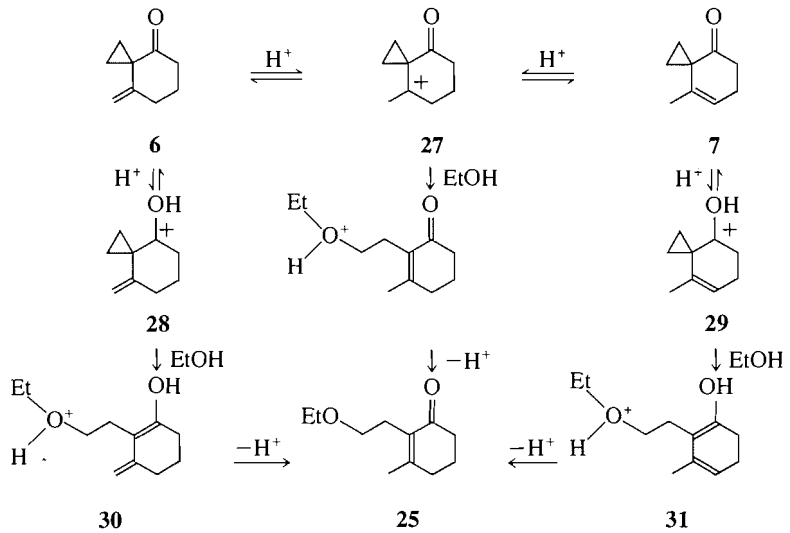

6 **27** **7**

28 **29**

30 **25** **31**

SCHEME 9

The more rapid ring fission of the *exo* compounds relative to the *endo* compounds may involve two factors. First, formation of ions of type **27** from the *exo* compounds is more ready than from the *endo* compounds because of the greater stability of the latter. Second, in analogy with our previous proposal to account for the rate differences in the corresponding homoconjugate nucleophilic addition reactions, we suggest that the rate differences here may reflect that planarity, and therefore maximum delocalization of the developing diene system in the transition states leading to **30** or **31** can be more readily achieved by the *exo* isomer (cf. **32**) than the *endo* isomer (cf. **33**).

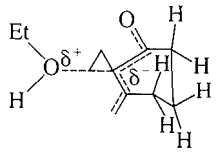

32

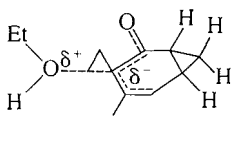

33

Experimental

Melting points were determined on a Fisher–Johns apparatus and are uncorrected. The ir spectra were taken in $CHCl_3$ solution and the ^1H and ^{13}C nmr spectra in $CDCl_3$ solution unless otherwise specified. The uv spectra were taken in 95% ethanol and/or hexane solution as indicated. Gas chromatography (gc) analyses were carried out on a Varian 2700 gas chromatograph, equipped with a flame ionization detector. The temperatures of the in-column injector and detector were set at 260°C and 335°C, respectively; oven temperatures of 90–120°C were used, unless otherwise noted. The flow rate of the carrier gas (nitrogen) was maintained at 30 mL/min. Unless otherwise indicated, a 6-ft glass column (od 1/8 in., id 2 mm) packed with 3% OV-101 on Chromosorb G(HP), 80/100 was utilized. The only other column used was a 6-ft glass column (od 1/8 in., id 2 mm) packed with 3% OV-17 on Chromosorb W(HP), 80/100. The relative intensities and retention times were determined with a Varian Chromatography Data System 111C; since in some cases there was peak overlap and the relative intensities are uncorrected for variation in the response factors the relative product yields given are approximate only. Analytical thin-layer chromatography (tlc) was carried out on 70 × 20 × 0.25 mm silica gel LK6F plates from Whatman Inc. Preparative tlc was carried out on 20 × 20 cm plates coated with a 1-mm or 2-mm layer of silica gel and activated at 150°C for 30 min prior to use. Column chromatography was performed on silica gel (Grace–Davison, grade 923, 100/200). Organic solutions were dried over anhydrous $MgSO_4$ and concentrated on a rotary evaporator under water aspirator pressure.

*Alkylation of isophorone (**8**) with 1,2-dibromoethane. Formation of **9** and **10***

Liquid ammonia (~50 mL) was distilled into a 100-mL three-necked flask containing sodium amide (4.00 g, 108 mmol) and a magnetic stirring bar and fitted with a Dry-Ice condenser with a soda-lime guard tube. Isophorone (**8**) (4.98 g, 36.0 mmol) was added and the solution was boiled under reflux for 1 h after which 1,2-dibromoethane (20.3 g, 108 mmol) was added dropwise over 30 min. The solution was boiled under reflux for 4 h, ammonium chloride (5.5 g) was added, and the ammonia was allowed to evaporate. The products were taken up in methylene chloride (150 mL) and the solution was washed with water (100 mL) and aqueous 20% ammonium chloride (75 mL). The organic layer was dried, evaporated, and fractionally distilled to give a mixture of **8** (46%), 6,6-dimethyl-8-methylenespiro[2.5]octan-4-one (**9**, 35%), and 6,6,8-trimethylspiro-[2.5]oct-7-en-4-one (**10**, 19%), bp 80–89°C (12 Torr), as shown by gc analysis. The yields of **9** and **10** based on consumed starting material were 55% and 30%, respectively. Attempted separation of **8** from **9** and **10** by spinning band distillation was unsuccessful.

*Oxidative removal of isophorone (**8**) from a mixture of **8**, **9**, and **10**. Isolation of 6,6-dimethyl-8-methylenespiro[2.5]octan-4-one (**9**)*

To an ice-cooled solution of a mixture of **8**, **9**, and **10** (21.3 g; 26% **9** and 9% **10**), prepared as above, in methanol (785 mL), was added 1 *N* aqueous sodium hydroxide (440 mL). Over 30 min 30% hydrogen peroxide (200 mL) was added at a rate such that the solution temperature did not exceed 20°C. The solution was stirred overnight at room temperature, poured into water (500 mL), and extracted with methylene chloride (3 × 500 mL). The extracts were washed with saturated aqueous ferrous sulfate (400 mL) and water (400 mL), dried, and evaporated. Distillation through a Vigreux column gave a 3:1 mixture of **9** and **10** (6.20 g, 83%), bp 87–89°C (12 Torr). This mixture (1.25 g) was chromatographed on silica gel (130 g) with 5% ether in hexanes. The eluate was analyzed by gc. Initially a mixture of **9** and **10** was eluted, but the proportion of **10** decreased in later fractions until only **9** was present. Combination of the fractions containing both **9** and **10** followed by solvent removal gave 1.08 g of the isomer mixture. Evaporation of the solvent from the fractions containing only **9** yielded a pale yellow oil (156 mg) which was molecularly distilled at 105°C (12 Torr) to give pure **9** (124 mg); ir λ_{max}: 3.43 (m), 5.95, 6.10 (m) μm; uv λ_{max} (ε) (hexanes): 214 (2220), 218 (2200), 278 (37), 287 (37) nm; ^1H nmr δ: 1.05 (s, 6H), 1.12 (m, 2H), 1.50 (m, 2H), 2.30 (s, 2H), 2.40 (br s, 2H), 4.52 (m, 1H), 4.63 (m, 1H); ^{13}C nmr δ: 209.1, 146.5, 105.8, 53.4, 47.6, 32.9, 31.7, 28.4, 22.1; *m/e*: 164 (100). *Anal.* calcd. for $C_{11}H_{16}O$: C 80.44, H 9.82; found: C 80.21, H 9.85.

*Isomerization of **9** to **10**. Isolation of 6,6,8-trimethylspiro[2.5]oct-7-en-4-one (**10**)*

A mixture of **9** and **10** (250 mg, 1.52 mmol) obtained as above was dissolved in dioxane (5.0 mL) containing *p*-toluenesulfonic acid (25 mg) and the solution was boiled under reflux for 1 h. After cooling, the solution was poured into saturated aqueous sodium bicarbonate (25 mL) and the mixture was extracted with methylene chloride (4 × 15 mL). The combined organic extracts were dried and filtered and the solvent was removed. Molecular distillation at 110°C (12 Torr) gave 6,6,8-trimethylspiro[2.5]oct-7-en-4-one (**10**) (208 mg, 84%); ir λ_{max}: 3.40 (m), 5.91, 6.03 (w) μm; uv λ_{max} (ε) (95% ethanol): 214 (3230), 239 (766) nm; uv λ_{max} (ε) (hexanes): 217 (2170), 232 (sh, 1070), 284 (43) nm; ^1H nmr δ: 1.08 (s, 6H), 1.13 (m, 2H), 1.35 (m, 2H), 1.48 (d, J = 2 Hz, 3H), 2.37 (s, 2H), 5.55 (m, 1H), ^{13}C nmr δ: 210.5 (s), 133.5 (d), 131.2 (s), 53.3 (t), 33.4 (s), 31.1 (s), 29.2 (q), 17.6 (q), 16.8 (t); *m/e*: 164 (14), 149 (100). *Mol. Wt.* calcd. for $C_{11}H_{16}O$: 164.1201; found (ms): 164.1194. *Anal.* calcd. for $C_{11}H_{16}O$: C 80.44, H 9.82; found: C 80.17, H 9.89.

*Alkylation of 3-methylcyclohex-2-en-1-one (**5**) with 1,2-dibromoethane. Formation of **6**, **7**, **11**, and **12** and isolation of 8-methylenespiro[2.5]octan-4-one (**6**)*

Liquid ammonia (~1500 mL) was distilled into a 3-L three-necked flask containing sodium amide (117 g, 3.00 mol) and a magnetic stirring bar and fitted with a soda-lime guard tube. 3-Methylcyclohex-2-en-1-one (**5**) (110 g, 1.00 mol) was added and the solution was boiled under reflux for 1 h after which 1,2-dibromoethane (564 g, 3.00 mol) was added dropwise over 30 min. The solution was boiled under reflux for 4 h, ammonium chloride (161 g) was added, and the ammonia was allowed to evaporate. The products were taken up in methylene chloride (500 mL) and the solution was washed with water (500 mL) and aqueous 20% ammonium chloride (250 mL). The organic layer was dried, evaporated, and fractionally distilled to give a mixture of **5** (54%), 8-methylenespiro[2.5]octan-4-one (**6**; 19%), 8-methylspiro[2.5]oct-7-en-4-one (**7**; 19%), 8-methylenedispiro-[2.1.2.3]decan-4-one (**11**; 2%), and 8-methyldispiro[2.1.2.3]dec-8-en-4-one (**12**; 6%) (46 g), bp 35–60°C (0.25 Torr). The yields of **6**, **7**, **11**, and **12** based on consumed starting material were 8.3%, 8.3%, 0.73%, and 2.2%, respectively.

Attempted oxidative removal of **5** from the spiro compounds (as in the case of isophorone) resulted in concomitant consumption of **6** and **7**. Chromatography of the distillate (9.0 g; Waters Associates Prep. LC/System 500, silica gel) with 2% ether in hexanes gave a 1:3

Can. J. Chem. Downloaded from www.nrcresearchpress.com by 210.87.254.42 on 09/06/12
For personal use only.

Can. J. Chem. Downloaded from www.nrcresearchpress.com by 210.87.254.42 on 09/06/12
For personal use only.

mixture of dispiro ketones **11** and **12** (0.66 g) followed by a 1:1 mixture of spiro ketones **6** and **7** (3.2 g); **5** (4.60 g) was recovered by elution with ethyl acetate. Compound **11** could not be separated from its isomer **12** by column chromatography on silica gel or by analytical hplc on μ Porasil or μ Bondapak C_{18}. Comparison of the ^{1}H nmr spectrum of the mixture of **11** and **12** with that of pure **12** (*vide infra*) revealed multiplets at δ 2.47, 4.43, and 4.63, assigned to **11**.

The mixture of spiro compounds **6** and **7** (2.00 g) was chromatographed on silica gel (250 g) with 10% ether in hexanes. The eluate was analyzed by gc. Initially a mixture of **6** and **7** was eluted, but the proportion of **7** decreased in later fractions until only **6** was present. Combination of the fractions containing **6** and **7** followed by solvent removal gave 1.82 g of the isomer mixture. Evaporation of the solvent from the fractions containing only **6** yielded an oil (158 mg) which was molecularly distilled at 85°C (12 Torr) to give pure **6** (145 mg); ir λ_{max}: 3.41 (m), 5.92, 6.10 μm; uv λ_{max} (ε) (hexanes): 217 (1730), 284 (58.2) nm; ^{1}H nmr δ: 1.12 (m, 2H), 1.48 (m, 2H), 1.7−2.2 (m, 2H), 2.3−2.8 (m, 4H), 4.50 (s, 1H), 4.67 (s, 1H); ^{13}C nmr δ: 209.3 (s), 147.8 (s), 105.0 (t), 39.7 (s), 34.1 (t), 33.6 (t), 22.3 (t), 22.0 (t). The ir and ^{1}H nmr spectra corresponded with those previously reported for **6** (3).

*Isomerization of **6** to **7**. Isolation of 8-methylspiro[2.5]oct-7-en-4-one (**7**)*

A mixture of **6** and **7** (285 mg, 2.10 mmol) obtained as above was dissolved in dioxane (6.0 mL) containing *p*-toluenesulfonic acid (29 mg) and the solution was boiled under reflux for 1 h. After cooling, the solution was poured into saturated aqueous sodium bicarbonate (25 mL) and the mixture was extracted with methylene chloride (4 × 15 mL). The combined organic extracts were dried and filtered and the solvent was removed. Molecular distillation at 90°C (12 Torr) gave 8-methylspiro[2.5]oct-7-en-4-one (**7**) (202 mg, 71%); ir λ_{max}: 3.44 (m), 5.88 μm; uv λ_{max} (ε) (hexanes): 222 (1150), 232 (sh, 941), 275 (78) nm; uv λ_{max} (ε) (95% ethanol): 218 (1130), 235 (576), 285 (sh, 79) nm; ^{1}H nmr δ: 1.15 (m, 2H), 1.36 (m, 2H), 1.53 (m, 3H), 2.48 (m, 4H), 5.73 (m, 1H); ^{13}C nmr δ: 210.5, 133.9, 122.0, 38.5, 31.9, 22.7, 17.8, 16.8. The ir and ^{1}H nmr spectra corresponded with those previously reported for **7** (3).

*Isomerization of **11** to **12**. Isolation of 8-methyldispiro[2.1.2.3]dec-8-en-4-one (**12**)*

A 1:3 mixture of **11** and **12** (1.16 g, 7.16 mmol) obtained as above was dissolved in dioxane (25 mL) containing *p*-toluenesulfonic acid (40 mg) and the solution was boiled under reflux for 4 h. After cooling, the solution was poured into saturated aqueous sodium bicarbonate (100 mL) and the mixture was extracted with methylene chloride (4 × 70 mL). The combined organic extracts were dried and filtered and the solvent was removed. Molecular distillation at 105°C (12 Torr) gave 8-methyldispiro[2.1.2.3]dec-8-en-4-one (**12**) (1.05 g, 91%); ir λ_{max}: 3.46 (w), 5.98 μm; uv λ_{max} (ε) (hexanes): 221 (1470), 230 (sh, 1150), 280 (75) nm; ^{1}H nmr δ: 0.68 (m, 2H), 0.9−1.5 (m, 6H), 1.53 (m, 3H), 2.35 (m, 2H), 5.72 (m, 1H); ^{13}C nmr δ: 210.4 (s), 133.0 (s), 121.0 (d), 32.6 (t), 31.8 (s), 26.4 (s), 18.9 (t), 18.5 (q), 17.2 (t); *m/e*: 162 (31), 134 (100). *Anal.* calcd. for $C_{11}H_{14}O$: C 81.44, H 8.70; found: C 81.44, H 8.73.

*Reduction of **9** and **10**. Preparation of 6,6,8-trimethylspiro[2.5]-octan-4-one (**15**) and formation of **16***

A 4:1 mixture of **9** and **10** (504 mg, 3.07 mmol) in 95% ethanol (20 mL) was stirred with platinum oxide (30.6 mg) under hydrogen (1 atm) for 14 h. The catalyst was allowed to settle and the supernatant solution was transferred to a flask containing fresh platinum oxide (2.10 mg) in 95% ethanol (5.0 mL). The spent catalyst was washed with 95% ethanol (2 × 30 mL) and the washings were combined with the solution containing fresh catalyst, which was stirred under hydrogen for 11 h. The catalyst was filtered and washed with ethanol and ether and the solvent was evaporated from the combined filtrate and washings. Gas chromatographic analysis (OV-17) showed that the crude product (441 mg, 86%) was a mixture of **15** (85%) and **16** (15%). This material was chromatographed on silica gel (80 g) with 10% ether in hexanes. The second band eluted (48.1 mg, 9%) was shown to be **16** by comparison of its ^{1}H nmr and ir spectra with those of an authentic sample (*vide infra*). The first fraction was molecularly distilled at 90°C (12 Torr) to provide 6,6,8-trimethylspiro[2.5]octan-4-one (**15**; 345 mg, 68%); ir λ_{max}: 3.42 (m), 5.91 μm; ^{1}H nmr δ: 0.4−0.9 (m) and 0.73 (d, J = 5 Hz) (5H), 0.9−1.3 (m) and 1.05 (s) (8H), 1.3−1.7 (m, 3H), 2.1−2.3 (m, 2H); ^{13}C nmr δ: 211.8 (s), 53.3 (t), 46.7 (t), 32.3 (s), 32.0 (d), 31.9 (s), 29.3 (q), 27.2 (q), 16.4 (q), 13.6 (t), 10.0 (t); *m/e*: 166 (20), 82 (100). *Anal.* calcd. for $C_{11}H_{18}O$: C 79.46, H 10.91; found: C 79.30, H 10.84.

*Preparation of 2-ethyl-3,5,5-trimethylcyclohex-2-en-1-one (**16**) (4)*

To a stirred solution of isophorone (**8**) (1.38 g, 10.0 mmol) and ethyl bromide (1.09 g, 10.0 mmol) in dimethyl sulfoxide (15 mL) was added over 3 h powdered potassium hydroxide (840 mg, 15.0 mmol). The mixture was stirred for a further 8 h at room temperature, poured into water, neutralized with 0.1 *N* hydrochloric acid, and extracted with ether. The combined organic solutions were washed with water, dried, and evaporated to provide a reddish oil (1.95 g). Gas chromatographic analysis of this oil revealed the presence of **8** (25%), **16** (45%), and three other components (8−12% each). Preparative tlc of this material (259 mg) with 50% ether in hexanes gave pure 2-ethyl-3,5,5-trimethylcyclohex-2-en-1-one (**16**; 110 mg); ir λ_{max}: 3.41 (m), 6.03, 6.14 (m) μm; uv λ_{max} (ε) (95% ethanol): 244 (9040) nm (lit. (9) 246 (9400) nm): ^{1}H nmr δ: 0.92 (t, J = 8 Hz) and 1.02 (s) (9H), 1.92 (s, 3H), 2.22 (s) and 2.28 (br q, J = 9 Hz) (6H); ^{1}H nmr δ (C_6D_6): 0.77 (s, 6H), 0.98 (t, J = 7 Hz, 3H), 1.52 (s, 3H), 1.73 (br s, 2H), 2.07 (s, 2H), 2.36 (br q, J = 7 Hz, 2H); ^{13}C nmr δ: 198.7 (s), 151.9 (s), 136.1 (s), 51.4 (t), 47.0 (t), 32.7 (s), 28.2 (q), 21.0 (q), 18.2 (t), 13.4 (q); *m/e*: 166 (48), 110 (100).

*Reaction of isophorone (**8**) with sodium hydride and a mixture of **9** and **10**. Preparation of 2,2′-(ethanediyl)bis[3,5,5-trimethylcyclohex-2-en-1-one] (**18**)*

To a mixture of isophorone **8** (67%) and spiro ketones **9** (26%) and **10** (7%) (5.00 g, 10.1 mmol) in toluene (15 mL) was added a 50% dispersion of sodium hydride in mineral oil (870 mg, 18.1 mmol). The resulting mixture was boiled under reflux under nitrogen for 10 h, allowed to cool to room temperature,and quenched with 0.5 *N* hydrochloric acid (40 mL). The two layers were separated and the aqueous layer was extracted with methylene chloride (3 × 25 mL). The combined organic solutions were washed with saturated aqueous sodium bicarbonate, dried, and evaporated. The remaining solid, dispersed in oil, was collected by vacuum filtration and washed with the minimum volume of petroleum ether (bp 30°−60°C). The ^{1}H nmr and gc analyses of the oil obtained on evaporation of the solvent from the washings revealed the presence of unconsumed **8** and **10**. None of the *exo* isomer **9** was present. The solid, 2,2′-(ethanediyl)bis[3,5,5-trimethylcyclohex-2-en-1-one] (**18**; 1.37 g, 45%), was ~99% pure by gc analysis.[5] A sample for elemental analysis was obtained by recrystallization from acetone; mp 181°−182.5°C; ir λ_{max}: 3.40 (m), 6.03, 6.11 (sh) μm; uv λ_{max} (ε) (95% ethanol): 244.5 (16600) nm; ^{1}H nmr δ: 1.02 (s, 12H), 2.02 (s, 6H), 2.22 (s) and 2.27 (s) (12H); ^{1}H nmr δ (C_6H_6): 0.80 (s, 12H), 1.68 (s, 4H), 1.88 (s, 6H), 2.08 (s, 4H), 2.58 (s, 4H); ^{13}C nmr δ: 199.0 (s), 153.5 (s), 134.0 (s), 51.5 (t), 47.1 (t), 32.8 (s), 28.3 (q), 24.6 (t), 21.3 (q); *m/e*: 302 (78), 152 (100), 96 (100). *Anal.* calcd. for $C_{20}H_{30}O_2$: C 79.42, H 10.00; found: C 79.16, H 9.89.

*Reaction of isophorone (**8**) with sodium hydride and **10**. Formation of **18***

To a mixture of isophorone **8** (78%) and **10** (22%) (2.50 g, 3.35 mmol of **10**) in toluene (7.5 mL) was added a 50% dispersion of sodium hydride in mineral oil (433 mg, 9.02 mmol). The resulting mixture was boiled under reflux under nitrogen for 10 h and poured into water (13 mL), and the basic solution was neutralized with dilute hydrochloric acid. The layers were separated and the aqueous phase

[5]The oven temperature for the gc analysis was 240°C.

Can. J. Chem. Downloaded from www.nrcresearchpress.com by 210.87.254.42 on 09/06/12
For personal use only.

was extracted with methylene chloride (3 × 16 mL). The combined organic solutions were washed with saturated aqueous sodium bicarbonate and dried, and the solvent was evaporated to give a suspension of a solid in oil. The solid was collected by vacuum filtration and washed with a minimum volume of petroleum ether (bp 30°−60°C). The ^{1}H nmr and gc analyses[5] of the oil obtained on evaporation of the solvent from the washings revealed the presence of unconsumed **8** and **10**. The solid (403 mg, 40%) was shown by ^{1}H nmr, ir, and gc analyses to be **18**.

*Treatment of a mixture of **9** and **10** with sodium hydride in toluene*

To a 1:2 mixture of **9** and **10** (150 mg, 0.915 mmol) in toluene (1.5 mL) was added a 50% dispersion of sodium hydride in mineral oil (43.5 mg, 0.906 mmol). The resulting mixture was boiled under reflux under nitrogen for 10 h and poured into water (5.0 mL), and the basic solution was neutralized with dilute hydrochloric acid. The layers were separated and the aqueous phase was extracted with methylene chloride (3 × 15 mL). The combined organic solutions were washed with saturated aqueous sodium bicarbonate and dried, and the solvent was evaporated. The oil thus obtained (126 mg) consisted of **9** and **10** in a 1:2 ratio and a small amount of mineral oil.

*Reaction of a mixture of **9** and **10** with morpholine. Preparation of 3,5,5-trimethyl-2-[2-(4-morpholinyl)ethyl]cyclohex-2-en-1-one (**20**)*

A mixture of spiro ketones **9** (79%) and **10** (21%) (549 mg, 3.34 mmol) was dissolved in morpholine (distilled from calcium hydride; 6.0 mL) and the solution was boiled under reflux under nitrogen for 28 h. Gas chromatographic analysis of aliquots showed that while all of **9** was consumed within 3 h, **10** was still present when the reaction was stopped after 28 h. Evaporation of the morpholine gave a viscous oil which was molecularly distilled at 55°C (0.025 Torr) to provide a liquid which was shown by ^{1}H nmr spectroscopy to be a mixture of **20** and unconsumed **10**. Further molecular distillation at 100°C (0.025 Torr) yielded 3,5,5-trimethyl-2-[2-(4-morpholinyl)-ethyl]cyclohex-2-en-1-one (**20**; 520 mg, 62%) as a colorless liquid; ir λ_{max}: 3.47 (m), 3.53 (m), 6.07, 6.14 (sh), 8.97 (m) μm; uv λ_{max} (ϵ) (95% ethanol): 245.5 (9400) nm; ^{1}H nmr δ: 1.00 (s, 6H), 1.93 (s, 3H), 2.22 (s, 4H), 2.3−2.6 (m, 8H), 3.70 (m, 4H); ^{1}H nmr δ (C_6D_6): 0.80 (s, 6H), 1.53 (s, 3H), 1.72 (s, 2H), 2.07 (s, 2H), 2.2−2.8 (m, 8H), 3.57 (m, 4H); ^{13}C nmr δ: 198.5 (s), 153.3 (s), 132.5 (s), 67.1 (t), 57.7 (t), 53.7 (t), 51.2 (t), 47.1 (t), 32.7 (s), 28.2 (q), 22.4 (t), 21.3 (q); *m/e*: 251 (0.6), 100 (100). *Mol. Wt.* calcd. for $C_{15}H_{25}NO_2$: 251.1885; found (ms): 251.1891. *Anal.* calcd. for $C_{15}H_{25}NO_2$: C 71.67, H 10.02, N 5.57; found: C 71.62, H 10.12, N 5.65.

*Reaction of **10** with morpholine. Formation of **20***

Spirooctenone **10** (300 mg, 1.83 mmol) was dissolved in morpholine (3.0 mL) and the solution was boiled under reflux. After 43, 64, 88, and 110 h the ^{1}H nmr spectrum of the crude product mixture was obtained. Integration of the first spectrum indicated 72% conversion of **10** to amine **20**. After 88 h, ~10% of **10** was observed, but none was detected after 110 h. The crude product was dissolved in ether (30 mL) and extracted with 0.6 *N* hydrochloric acid (3 × 25 mL). The organic solution was washed with saturated aqueous sodium bicarbonate (15 mL) and water (15 mL), dried, and evaporated, leaving a yellow oil (18 mg) which was <50% **10** (by ^{1}H nmr analysis). The combined aqueous extracts were basified with potassium hydroxide and extracted with ether (3 × 40 mL). The combined organic extracts were washed with water (50 mL), dried, and evaporated to give **20** (268 mg, 58%).

*Reaction of a mixture of **6** and **7** with morpholine. Preparation of 2-methyl-2-[2-(4-morpholinyl)ethyl]cyclohex-2-en-1-one (**21**)*

A 1:1 mixture of spiro ketones **6** and **7** (302 mg, 2.22 mmol) in morpholine (5.0 mL) was boiled under reflux under nitrogen for 80 h. Gas chromatographic analysis of aliquots revealed that while all of **6** was consumed within 3 h, **7** was still present after 80 h. Evaporation of the morpholine gave a viscous oil which was molecularly distilled at 55°−95°C (0.05 Torr) to give a mixture of **21** and unconsumed **7** (38 mg). Further molecular distillation at 105°C (0.05 Torr) gave 3-methyl-2-[2-(4-morpholinyl)ethyl]cyclohex-2-en-1-one (**21**; 277 mg, 56%); ir λ_{max}: 3.44 (m), 6.03, 6.15 (m) μm; uv λ_{max} (ϵ) (95% ethanol): 243 (9300) nm; ^{1}H nmr δ: 1.97 (s) and 1.8−2.2 (m) (5H), 2.2−2.6 (m, 12H), 3.72 (m, 4H); ^{13}C nmr δ: 198.3, 156.1, 133.4, 67.0, 57.7, 53.6, 37.7, 32.8, 22.5, 22.2, 21.1; *m/e*: 223 (13), 100 (27), 99 (100). *Anal.* calcd. for $C_{13}H_{21}NO_2$: C 69.92, H 9.48, N 6.27; found: C 69.79, H 9.46, N 6.41.

*Reaction of a mixture of **7** and **10** with morpholine*

A 1.5:1 mixture of **7** and **10** in morpholine was boiled under reflux for 90 h. Gas chromatographic analysis revealed that after 24, 38, and 64 h the ratios of **10**:**7** were 1.9:1, 2.2:1, and 3.0:1, respectively. While some of **10** was present after 90 h, **7** was not detected. Evaporation of the morpholine followed by ^{1}H nmr and ir analyses showed that **7** and **10** had been converted to **21** and **20**.

*Hydrogenation of **20**. Preparation of 3,5,5-trimethyl-2-[2-(4-morpholinyl)ethyl]cyclohexan-1-one (**22**)*

Amine **20** (230 mg, 0.916 mmol) in 95% ethanol (10 mL) was stirred with 10% palladium on carbon (30 mg) under hydrogen (1 atm). The catalyst was filtered and washed with ethanol and ether and the solvent was evaporated from the combined filtrate and washings. Molecular distillation at 110°C (0.05 Torr) gave 3,5,5-trimethyl-2-[2-(4-morpholinyl)ethyl]cyclohexan-1-one (**22**; 193 mg, 83%); ir λ_{max}: 3.52 (m), 5.88 μm; ^{1}H nmr δ: 0.87 (s) and 1.05 (s) (9H), 1.53 (br s, 2H), 1.6−2.0 (m, 3H), 2.07−2.25 (m, 3H), 2.25−2.63 (m, 6H), 3.67 (t, J = 4.5 Hz, 4H); ^{13}C nmr δ: 211.8 (s), 67.0 (t), 57.0 (t), 54.9 (t), 54.4 (d), 53.8 (t), 48.3 (t), 35.5 (s), 34.4 (d), 32.1 (q), 25.6 (q), 22.5 (t), 20.9 (q); *m/e*: 253 (5), 100 (100). *Anal.* calcd. for $C_{15}H_{27}NO_2$: C 71.10, H 10.74, N 5.53; found: C 70.67, H 10.65, N 5.72.

*Reaction of **15** with morpholine. Formation of **22***

Spirooctanone **15** (165 mg, 0.994 mmol) was dissolved in morpholine (3.0 mL) and the solution was boiled under reflux. After 47, 89, 137, 200, and 240 h the ^{1}H nmr spectrum of the crude product mixture was obtained. While peaks attributable to unconsumed **15** were observed in the first four spectra, no evidence for its presence was detected in that taken after 240 h. A solution of the crude product in ether (20 mL) was washed with 0.6 *N* hydrochloric acid (3 × 15 mL) and water (15 mL), dried, and evaporated to provide an oil (17 mg), which was shown by ^{1}H nmr spectroscopy to be primarily **15**. The combined acidic washings were neutralized with potassium hydroxide and extracted with ether (3 × 20 mL). The combined organic extracts were washed with water, dried, and evaporated to give amine **22** (53 mg, 21%) having ir, ^{1}H nmr, and ^{13}C nmr spectra identical to those described above.

*Treatment of **22** with methanolic sodium methoxide*

Amine **22** (66 mg, 0.261 mmol) in methanol (3.0 mL) containing sodium methoxide (340 mg) was boiled under reflux for 18 h. After cooling, the mixture was poured into water and extracted with ether. The combined organic extracts were washed with water, dried, and evaporated to return **22** (64 mg, 97% recovery) which was shown by ir and ^{1}H nmr spectroscopy to be identical to the starting material.

*Treatment of **22** with sodium methoxide in methanol*-O-d. *Formation of deuterated **22***

A solution of amine **22** (193 mg, 0.763 mmol) in methanol-*O-d* (5.0 mL) containing sodium methoxide (200 mg) was boiled under reflux for 18 h. After cooling, the mixture was poured into ether (25 mL) and extracted with water (2 × 10 mL). The organic layer was dried and evaporated to give an oil (135 mg, 70% recovery), the ir spectrum of which was very similar to that of the starting material. In its ^{1}H nmr spectrum the relative area of the multiplets at δ 2.07−2.25 and 3.54 was 1.1:4.0; in unlabelled **22** it was 3.0:4.0. Its fully decoupled ^{13}C nmr spectrum corresponded to that of unlabelled **22** except for the absence of the peaks at δ 54.9 and 54.4 and the presence of several very weak peaks at δ ~54.5. Its mass spectrum had peaks at *m/e*: 256 (1.6), 255 (2.9), 254 (2.3), 253 (1.1), and 100 (100).

Reaction of a mixture of ***6*** *and* ***7*** *with acidic ethanol. Preparation of 2-(2-ethoxyethyl)-3-methylcyclohex-2-en-1-one (****25****)*

A 1:1 mixture of **6** and **7** (219 mg, 1.61 mmol) in ethanol (3.0 mL) containing *p*-toluenesulfonic acid (25 mg) was boiled under reflux. After 6 h, gc analysis showed that the ratio of **7** to **6** was 45:1. The reaction mixture was poured into water (15 mL) and extracted with methylene chloride (3 × 15 mL). The combined organic extracts were dried and evaporated. ^{1}H nuclear magnetic resonance spectroscopy showed that the crude material was a 3:1 mixture of **7** and the product **25**. This mixture was dissolved in ethanol containing *p*-toluenesulfonic acid as above and the solution was boiled under reflux for 63 h (total = 69 h). ^{1}H nuclear magnetic resonance spectroscopy of the material obtained after work-up as above revealed that the ratio of **7** to **25** was 1:7. Further treatment of this mixture with boiling acidic ethanol for 46 h (total = 115 h), followed by work-up as above and molecular distillation at 100°C (12 Torr), gave 2-(2-ethoxyethyl)-3-methylcyclohex-2-en-1-one (**25**; 166 mg); ir λ_{max}: 3.40 (m), 6.02, 6.13 (m) μm; uv λ_{max} (ϵ) (95% ethanol): 244 (10 900), 310 (64) nm; ^{1}H nmr δ: 1.17 (t, J = 7 Hz, 3H), 2.00 (s) and 1.7–2.2 (m) (5H), 2.37 (br t, J = 6 Hz) and 2.58 (t, J = 7 Hz) (6H), 3.36 (t, J = 7 Hz) and 3.45 (q, J = 7 Hz) (4H); ^{13}C nmr δ: 198.5, 157.3, 132.2, 69.3, 66.0, 37.8, 33.0, 26.0, 22.3, 21.4, 15.3; *m/e*: 182 (42), 136 (100). *Anal.* calcd. for $C_{11}H_{18}O_2$: C 72.49, H 9.95; found C 72.31, H 9.86.

Reaction of a mixture of ***9*** *and* ***10*** *with acidic ethanol. Preparation of 2-(2-ethoxyethyl)-3,5,5-trimethylcyclohex-2-en-1-one (****26****)*

A 3:1 mixture of **9** and **10** (500 mg, 3.05 mmol) in ethanol (7.0 mL) containing *p*-toluenesulfonic acid (50 mg) was boiled under reflux. Gas chromatographic analysis showed that **9** was consumed within 10 h. However, complete consumption of **10** required 150 h. After 150 h the reaction mixture was poured into saturated aqueous sodium bicarbonate (40 mL) and extracted with methylene chloride (3 × 40 mL). The combined organic extracts were dried, evaporated, and molecularly distilled at 135°C (12 Torr) to give 2-(2-ethoxyethyl)-3,5,5-trimethylcyclohex-2-en-1-one (**25**; 412 mg, 64%); ir λ_{max}: 6.06, 6.16 (m) μm; uv λ_{max} (ϵ) (95% ethanol): 245 (10 500), 310 (69) nm; ^{1}H nmr δ: 1.03 (s, 6H), 1.17 (t, J = 7 Hz, 3H), 1.97 (s, 3H), 2.24 (s, 4H), 2.60 (br t, J = 7 Hz, 2H), 3.37 (t, J = 7 Hz) and 3.46 (q, J = 7 Hz) (4H); ^{1}H nmr δ (C_6H_6): 0.82 (s, 6H), 1.12 (t, J = 7 Hz, 3H), 1.67 (br s, 3H), 1.80 (m, 2H), 2.12 (s, 2H), 2.75 (br t, J = 7 Hz, 2H), 3.30 (t, J = 7 Hz) and 3.43 (q, J = 7 Hz) (4H); ^{13}C nmr δ: 198.7, 154.6, 131.1, 69.3, 66.0, 51.3, 47.2, 32.7, 28.2, 25.8, 21.6, 15.3; *m/e*: 210 (21), 164 (100). *Anal.* calcd. for $C_{13}H_{22}O_2$: C 74.24, H 10.54; found: C 74.10, H 10.42.

Acknowledgements

We thank the Natural Sciences and Engineering Research Council of Canada for support of this work and Messrs. Baldev Gambhir, Nick Plavac, and Leo Dugbe for technical assistance.

1. P. H. HELFERTY, P. MAHLER, and P. YATES. J. Chem. Soc. Chem. Commun. 1084 (1979).
2. (*a*) S. DANISHEFSKY and R. K. SINGH. J. Am. Chem. Soc. **97**, 3239 (1975); (*b*) S. DANISHEFSKY and R. K. SINGH. J. Org. Chem. **40**, 3807 (1975); R. K. SINGH and S. DANISHEFSKY. J. Org. Chem. **40**, 2969 (1975); **41**, 1668 (1976).
3. M. S. NEWMAN, V. DEVRIES, and R. DARLAK. J. Org. Chem. **31**, 2171 (1966).
4. H. TSUKASA and S. SAITO. Nippon Kagaku Kaishi, 1555 (1974); Chem. Abstr. **81**, 135501g (1974).
5. R. D. TEMPLE. J. Org. Chem. **35**, 1275 (1970).
6. Y. OFUNE, S. MISUMI, A. FURUSAKI, H. SHIRAHAMA, and T. MATSUMOTO. Tetrahedron Lett. 279 (1977).
7. J. D'ANGELO. Tetrahedron, **32**, 2979 (1976).
8. R. W. MOUK, K. M. PATEL, and W. REUSCH. Tetrahedron, **31**, 13 (1975).
9. M. A. KAZI, I. H. KHAN, and M.Y. KHAN. J. Chem. Soc. 1511 (1964).

Can. J. Chem. Downloaded from www.nrcresearchpress.com by 210.87.254.42 on 09/06/12
For personal use only.

Ullmann condensation using copper or copper oxide as the reactant. Arylation of active hydrogen compounds (imides, amides, amines, phenol, benzoic acid, and phenylacetylene)

TAKAKAZU YAMAMOTO[1] AND YASUNDO KURATA

Research Laboratory of Resources Utilization, Tokyo Institute of Technology, 4259 Nagatsuta, Midori-ku, Yokohama 227, Japan

Received April 26, 1982

TAKAKAZU YAMAMOTO and YASUNDO KURATA. Can. J. Chem. **61**, 86 (1983).

Ullmann condensation using Cu or copper oxide as the reactant and using no base has been studied. Reactions of active N—H, O—H, and C—H compounds, RZH (imides, amides, amines, phenol, benzoic acid, and phenylacetylene), with mixtures of aryl halides and more than a stoichiometric amount of Cu or copper oxide (Cu_2O or CuO) without addition of base lead to facile arylation of the active hydrogen compounds. In the arylation reaction Cu and copper oxides serve not only as the catalyst but also as the acceptor of halogen from aryl halide. The reactivity of phenyl halide, PhX, increases in the order PhCl < PhBr < PhI. Cu generally gives higher yields than Cu_2O and CuO and, of the two copper oxides, Cu_2O has the higher activity. The stronger the acidity of the active hydrogen compound (RZH), the more easily the compound is phenylated by the mixture of PhX and Cu; a roughly linear correlation between T_i, the temperature where the phenylation starts, and the pK_a value of the active hydrogen compound has been observed. A mechanism involving initial formation of an RZ—Cu species by the reaction between RZH and Cu or copper oxide and ensuing attack of organic halide at the RZ—Cu species is proposed.

TAKAKAZU YAMAMOTO et YASUNDO KURATA. Can. J. Chem. **61**, 86 (1983).

On a étudié la condensation de Ullman qui utilise le cuivre ou l'oxyde de cuivre comme réactif en l'absence de base. Les réactions des composés ayant des hydrogènes actifs N—H, O—H et C—H, RZH (imides, amides, amines, phénol, acide benzoique et phénylacétylène) avec des mélanges d'halogénures aryliques en présence d'un excès de cuivre ou d'oxyde de cuivre (Cu_2O ou CuO) et en l'absence de base conduit à une arylation facile des composés ayant un hydrogène actif. Dans les réactions d'arylation le Cu et les oxydes de cuivre servent non seulement de catalyseur mais également d'accepteur d'halogène des halogénures aryliques. La réactivité de l'halogénure de phényle PhX augmente dans l'ordre: PhCl < PhBr < PhI. Le cuivre donne généralement de meilleurs rendements que le Cu_2O ou le CuO et des deux oxydes de cuivre le CuO_2 est le plus actif. Si l'acidité du composé hydrogène actif (RZH) est élevée il est plus facile de le phényler avec le mélange de PhX et de Cu; on a observé une corrélation linéaire approximatique entre T_i, la température de départ de la phénylation, et la valeur de pK_a du composé à hydrogène actif. On propose un mécanisme impliquant la formation initiale d'espèces du type RZ—Cu par suite de la réaction entre RZH et le cuivre ou l'oxyde de cuivre et l'attaque subséquente de l'halogénure organique sur RZ—Cu.
[Traduit par le journal]

Introduction

Copper promoted arylation of O—H (e.g., phenol) and N—H (e.g., diphenylamine) compounds by aryl halides (Ullmann condensation) has been widely applied to the preparation of aromatic compounds (1).

$$[1]\quad RZH + ArX \xrightarrow{Cu} RZ—Ar$$

ZH = OH, NH

Addition of bases such as K_2CO_3 and KOH as the acceptor of HX released is necessary for the reaction to proceed, and sometimes, instead of the O—H and N—H compounds, use of their salts (e.g., C_6H_5OK) as the starting material is required. In almost 80 years of study of the Ullmann condensation, reactions using copper metal (2*a*) or copper oxide (2) catalyst themselves as the acceptor of halogen, and thus using no base,

$$[2]\quad RZH + ArX + Cu \text{ (or Cu oxide)} \longrightarrow RZ—Ar + CuX$$

have also been reported, but the reported examples of this type of reaction (especially reactions using Cu metal as the reactant) are limited and no systematic study of the reaction has been reported. We have made a systematic study of the reactions expressed by eq. [2], and in this paper we wish to report several features of the reactions, including some advantages of the reaction over the usual Ullmann condensation using base. Part of the results were briefly reported previously in communication form (3).

Results and discussion

Table 1 shows typical data of the present Ullmann condensation using Cu or copper oxide as the reactant. As shown in Table 1, a variety of active hydrogen compounds are arylated by simply heating them with mixtures of the aryl halides and Cu metal or copper oxide. Thus, the condensation reaction proceeds smoothly without addition of solvent, and this is regarded as one of the merits of the present condensation reaction since removal of solvent from the reaction mixture is not necessitated in the present reaction and consequently isolation of products becomes easy. It is known that the yield of the usual Ullmann condensation using base depends on the solvent, and employment of special solvents (usually polar solvents) such as 2,4,6-collidine and quinoline is required in order to get a reasonably good yield. Good miscibility of RZH with ArX in the present system seems to account for the occurrence of the facile condensation reaction in the absence of solvent; in the usual Ullmann condensation only ArX is a liquid material and both the salt of RZH or base and the copper catalyst are generally

[1]Author to whom all correspondence should be addressed.

0008-4042/83/010086-06$01.00/0
©1983 National Research Council of Canada/Conseil national de recherches du Canada

Can. J. Chem. Downloaded from www.nrcresearchpress.com by 210.87.254.5 on 09/06/12
For personal use only.

TABLE 1. Ullmann condensation using copper or copper oxide as the reactant[a]

Expt.	Active hydrogen compound (RZH)	Aryl halide (ArX)	Copper species	Temp. (°C)	Yield of product (% RZH) RZ—Ar	Others
	RZH = imide					
1	Phthalimide	PhBr	Cu	240	100	
2	Phthalimide	p-$CH_3C_6H_4Br$	Cu	240	100	
3	Phthalimide	p-FC_6H_4Br	Cu	240	98	
4	Phthalimide	p-$CH_3OC_6H_4Br$	Cu	240	86	
5	Phthalimide	PhBr	Cu_2O	210	99	
6	Phthalimide	PhBr	CuO	240	30	
7	Succinimide	PhI	Cu	150	97	
8	Succinimide	PhBr	Cu	210	100	
9	Succinimide	PhBr	Cu_2O	210	77	
10	Succinimide	PhCl	Cu	210	58	
	RZH = amide					
11	Benzamide	PhI	Cu	180	64	$PhCONPh_2$ (5)
12	Benzamide	PhBr	Cu	210	79	$PhCONPh_2$ (12), Ph_2NH (1)
13	Acetamide	PhI	Cu	150	65	
14	Acetamide	PhBr	Cu	180	58	$MeCONPh_2$ (18), Ph_2NH (13)
15	2-Pyrrolidinone	PhBr	Cu	180	100	
16	2-Pyrrolidinone	PhBr	Cu_2O	210	100	
17	2-Pyrrolidinone	PhBr	CuO	240	21	
	RZH = amine					
18	Ph_2NH	PhI	Cu	210	86	
19	Ph_2NH	PhBr	Cu	270	87	
20	$PhNH_2$	PhI	Cu	180	31	Ph_3N (46)
21	$PhNH_2$	PhI[b]	Cu	220	0	Ph_3N (86)
22	$PhNH_2$	PhBr	Cu	270	21	Ph_3N (4)
	RZH = O—H compound					
23	PhOH	PhI	Cu	220	94	
24	PhOH	PhBr	Cu	240	94	
25	PhCOOH	PhI	Cu	180	55	Ph—Ph (7)
26	PhCOOH	PhBr	Cu	240	79	Ph—Ph (4)
	RZH = C—H compound					
27	Phenylacetylene	PhI	Cu	155	66	

[a]Reaction time = 12 h; RZH = 10 mmol; ArX/RZH = 1.9–2.3 unless otherwise noted; Cu or CuO/RZH = 4.7; Cu_2O/RZH = 2.4.
[b]$PhI/PhNH_2$ = 29.

insoluble in ArX, whereas in the present reaction system RZH and ArX mix well with each other and Cu or copper oxide is the only insoluble material.

Yields of the arylation reactions of phthalimide (4), succinimide (4), diphenylamine (5), phenol (1, 2), and benzamide (6) are comparable to, or higher than, those attained by the usual Ullmann condensation. For 2-pyrrolidinone, acetamide, and phenylacetylene, arylation of these compounds by the usual Ullmann condensation has no precedents. As for aniline, its arylation by active aryl halides such as halobenzoic acid (6) has some precedents, but phenylation of aniline by simple phenyl halides, PhX, has not been reported. Details of the arylation reactions of each class of active hydrogen compounds are described below.

Imides

Among the active hydrogen compounds tested, imides (phthalimide and succinimide) are most easily phenylated by phenyl halides. In the phenylation of phthalimide, substitution of the p-hydrogen of phenyl bromide by an electron-donating group (CH_3, OCH_3) or electron-withdrawing element (F) has only a minor effect on the yield (Expts. 2–4 in Table 1). Figure 1 shows the temperature dependence of the yield in the phenylation reaction of phthalimide by the mixture of PhBr and Cu or copper oxide.

As shown in Fig. 1, the reaction starts at about 145°C when Cu or Cu_2O is employed as the reactant. The yield increases on raising the temperature and almost a quantitative yield is attained at about 210°C but, when Cu_2O is employed, further raising of the temperature causes degradation of the product and thus the yield decreases. In contrast to the high yield attained by using the mixture of PhBr and Cu or Cu_2O, only a poor yield was obtained in the arylation reaction of phthalimide by a mixture of PhBr and CuO.

Can. J. Chem. Downloaded from www.nrcresearchpress.com by 210.87.254.5 on 09/06/12
For personal use only.

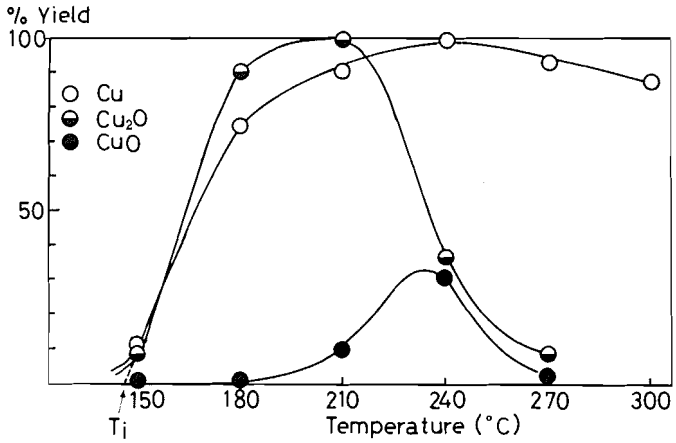

FIG. 1. Temperature dependence of the yield of *N*-phenylphthalimide in the phenylation reaction of phthalimide by the mixture of PhBr (2 mol/mol of phthalimide) and Cu (4.7 mol/mol of phthalimide, ○), Cu_2O (2.4 mol/mol of phthalimide, ◒), or CuO (4.7 mol/mol of phthalimide, ●). Time = 12 h.

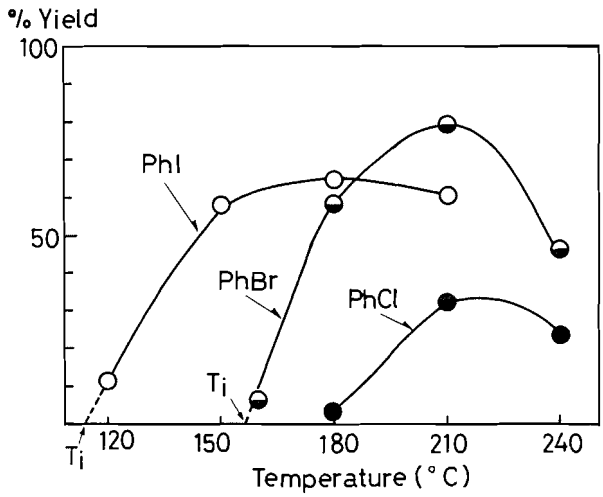

FIG. 2. Temperature dependence of the yield of PhCONHPh in the phenylation reaction of benzamide by the mixture of Cu (4.7 mol/mol of benzamide) and PhI (○), PhBr (◒), or PhCl (●). PhX = 2 mol/mol of benzamide. Time = 12 h.

The trends (temperature dependence of yield and relative activities of Cu, Cu_2O, and CuO) observed for the phenylation of phthalimide are also observed for the phenylation of succinimide. It is reported that PhCl is inactive for phenylation of imides in the usual Ullmann condensation (4), but in the present condensation reaction PhCl is also active if it is used in combination with Cu metal, and thus *N*-phenylsuccinimide is obtained in a medium yield (Expt. 10). Since *N*-arylimides are easily converted into arylamines, the present method seems to be applicable to the preparation of arylamines from imides and aryl halides.

Amides

Amides of both aromatic and aliphatic acids (benzamide and acetamide) are phenylated by mixtures of PhX and Cu or copper oxide, and the present method is also applicable to the phenylation of the cyclic amide, 2-pyrrolidinone.

Figure 2 shows the temperature dependence of the yield of the phenylation reaction of benzamide by PhX and Cu. When

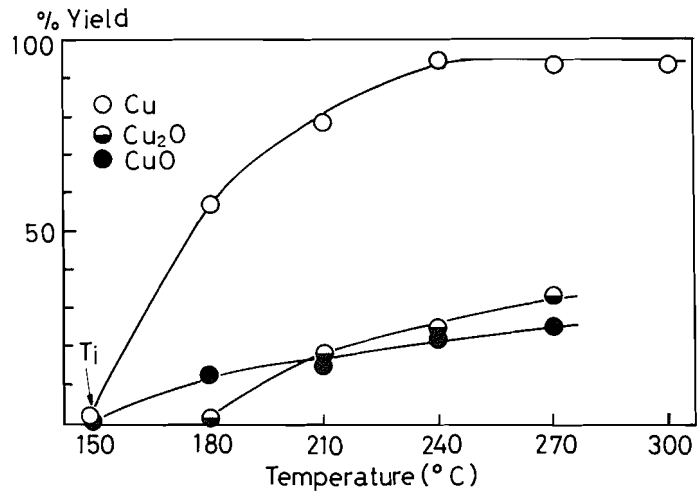

FIG. 3. Temperature dependence of the yield of PhOPh in the phenylation reaction of PhOH by the mixture of PhBr (2 mol/mol of PhOH) and Cu (4.7 mol/mol of PhOH, ○), Cu_2O (2.4 mol/mol of PhOH, ◒), or CuO (4.7 mol/mol of PhOH, ●). Time = 12 h.

a mixture of PhBr and Cu is employed, the coupling reaction starts at about 160°C and the yield of PhCONHPh reaches 79% at 210°C, but the yield decreases at higher temperature due to occurrence of a perphenylation reaction to give $PhCONPh_2$ and a deamination reaction from $PhCONPh_2$ to give $HNPh_2$ (cf. Table 1). A similar dependence of the yield on temperature was observed for phenylation of acetamide by PhX and Cu; the yield of the reaction using PhBr reaches a maximum at 180°C and decreases due to the perphenylation and deamination reactions. Formation of $HNPh_2$ in the usual Ullmann condensation between $CH_3CONHPh$ and PhX has been reported (1*d*). At lower temperatures (below 150°C, 170°C, and 210°C for PhI, PhBr, and PhCl, respectively), perphenylation and deamination are negligible.

The phenylation of 2-pyrrolidinone by the mixture of PhBr and Cu proceeds quantitatively in a temperature range of 180–210°C. A mixture of Cu_2O and PhBr needs somewhat higher temperature to provide a quantitative yield. The yield of the phenylation reaction of 2-pyrrolidinone by a mixture of PhBr and Cu or Cu_2O decreases to ca. 70% at 240°C, presumably due to a deamination reaction similar to that observed in the phenylation reaction of benzamide and acetamide, although in this case products of the deamination reaction have not been identified. CuO gives only a low yield.

Amines

In the phenylation of Ph_2NH, the reactivity of PhX increases in the order PhCl < PhBr < PhI; PhCl gives only a low yield even at 270°C. Among the copper species, only Cu gives a reasonably high yield and copper oxides give only poor yields (e.g., a mixture of Cu_2O and PhBr phenylates Ph_2NH in only 1% yield at 210°C). As shown in Table 1 (Expts. 20–22) phenylation of aniline gives a mixture of Ph_2NH and Ph_3N, but in the presence of excess PhI the reaction gives Ph_3N exclusively. An aralkyl amine, $(PhCH_2)_2NH$, was also phenylated by the mixture of PhX and Cu or copper oxide, but the yield (e.g., 38% by a mixture of PhBr and CuO, which has the highest activity among the copper species in this phenylation reaction, in contrast to the other phenylation reaction where CuO generally has the lowest activity) was low.

The phenylation reactions of amines were retarded by addi-

Can. J. Chem. Downloaded from www.nrcresearchpress.com by 210.87.254.5 on 09/06/12
For personal use only.

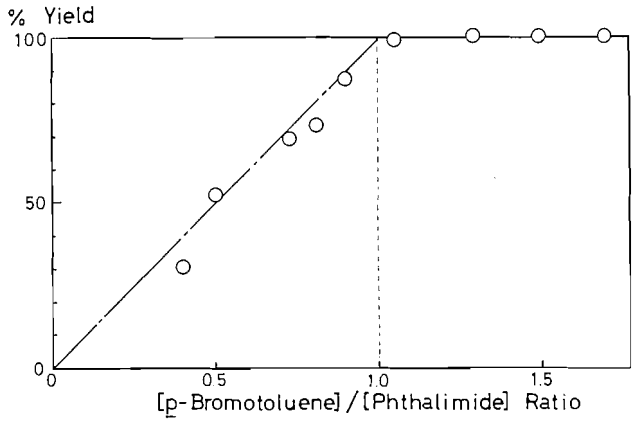

FIG. 4. Effect of the amount of *p*-bromotoluene on the yield of the arylation reaction of phthalimide at 240°C. Cu = 4.7 mol/mol of phthalimide. Time = 12 h.

tion of basic ligand such as pyridine and *o*-phenanthroline.

Phenol

Figure 3 shows the temperature dependence of the yield of the arylation reaction. As shown in Fig. 3, the phenylation of PhOH by the mixture of PhBr and Cu starts at ca. 150°C and the yield increases on raising the temperature. Phenylation by the mixture of PhI and Cu starts at a lower temperature and among the copper species only Cu gives good yields in the phenylation reactions of phenol.

Benzoic acid

Phenylation of PhCOOH by the mixture of PhBr and Cu starts at 130°C, and among the copper species only Cu gives good yields. Formation of biphenyl (Expts. 25 and 26) seems to be due to an Ullmann coupling reaction of PhX or to a copper catalyzed decarbonylative coupling between PhCOOH and PhX as reported by Nilsson (7).

Besides the phenylation reaction of PhCOOH by the mixture of PhX and Cu, alkylation reactions of PhCOOH by mixtures of alkyl halides and Cu also proceed to give the corresponding esters in good yields (e.g., 83% by a mixture of EtBr and Cu at 210°C). In this alkylation reaction, in contrast to the phenylation reaction, Cu_2O and CuO also have high activities, and yields comparable to those attained by Cu are obtained.

Compounds having active C—H bond

The present method is applicable to the phenylation of phenylacetylene, a compound having an active C—H bond. Attempts to arylate other active C—H compounds such as diethyl malonate and acetophenone, however, have not been successful. Heating of diethyl malonate with a mixture of PhX and Cu led to the evolution of CO_2. Bjorklund and Nilsson (8) reported arylation of 1,3,5-trinitrobenzene, having the active C—H bond, by aryl iodide and Cu_2O. Hagihara and coworkers (9) reported substitution of the acetylenic hydrogen by reaction with aryl halides and Et_3N in the presence of catalytic amounts of Pd–phosphine complex and CuI.

Reaction conditions and relative reactivities of the reactants

Amount of aryl halide

Among the arylation reactions tested, the arylation of imides by a mixture of aryl halide and Cu proceeds most cleanly and the yield of the reaction between phthalimide and the mixture of *p*-bromotoluene and Cu (3.0 mol/mol of phthalimide) increases linearly with increase in the amount of

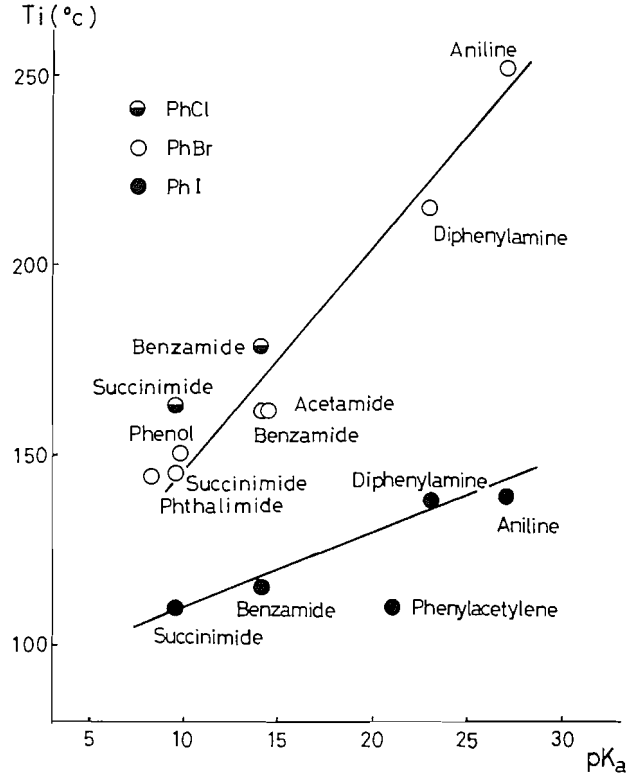

FIG. 5. Plots of the initiation temperature, T_i, against pK_a value of the active hydrogen compound.

p-bromotoluene (Fig. 4). The data shown in Fig. 4 indicate that 1 mol of *p*-bromotoluene arylates 1 mol of phthalimide. Although similar increases in the yield with increase in the amount of organic halide are observed in the other arylation reactions described above, such a clean 1:1 correlation between the amount of aryl halide and the yield as shown in Fig. 4 was not obtained, and generally addition of more than ca. 1.5 mol of ArX per mol of RZH is necessitated in order to get maximum yields. When the acidity of the active hydrogen compound is weak, as in the case of aniline, addition of a large excess of organic halide is desirable.

Amount of Cu and relative reactivities of Cu species

In the 1:1 reaction between phthalimide and *p*-bromotoluene the yield of the reaction increases with an increase in the amount of Cu (yield = 58%, 86%, and 100% at 1.0, 2.0, and 3.0 mol of Cu per mol of phthalimide, respectively). Generally, addition of 3 mol of Cu is sufficient for the phenylation of RZH employed in the present study.

Among the copper species, Cu metal gives higher yields than Cu_2O and CuO in most cases and, of the two copper oxides, Cu_2O usually has the higher activity.

Relative activities of ArX and RZH

The reactivity of PhX increases in the order PhCl < PhBr < PhI as judged from the reaction temperature and the yield. PhF has no activity in the phenylation reaction. Weingarten (10) reported a similar trend concerning the usual $CuCl_2$-catalyzed Ullmann condensation between PhOK and PhX.

Since the present condensation reaction is applicable to various RZH compounds under simple common reaction conditions using neither solvent nor base, a direct comparison of the reactivity of RZH is possible. Figure 5 shows plots of initiation temperature, T_i, where the phenylation of the RZH starts (for

Can. J. Chem. Downloaded from www.nrcresearchpress.com by 210.87.254.5 on 09/06/12
For personal use only.

Can. J. Chem. Downloaded from www.nrcresearchpress.com by 210.87.254.5 on 09/06/12
For personal use only.

some examples, see Figs. 1–3), against the pK_a value of RZH. As shown in Fig. 5, a roughly linear correlation between pK_a value and T_i holds for the phenylation of phenol and N—H compounds (imides, amides, and amines). The data point for phenylacetylene, however, deviates from the linearity, indicating that the acetylenic compound has a higher reactivity against Cu than expected from its pK_a value.

Although it has been recognized (1) that phenol and aryl amine having more acidic O—H and N—H bonds generally have higher reactivities in the usual Ullmann condensation, such a relationship as shown in Fig. 5 has not been demonstrated, since each of the usual Ullmann condensation reactions has been carried out under different reaction conditions (different solvent and catalyst).

Usually the yield of the reaction exceeds 70–80% at a temperature higher than T_i by 50°C.

Reaction mechanism

One of the conceivable reaction mechanisms of the present condensation reaction includes initial formation of a Cu—N, Cu—O, or Cu—C intermediate by the reaction of the active hydrogen compound with Cu or copper oxide; the ensuing coupling reaction between the Cu—N, Cu—O, or Cu—C intermediate and the organic halide gives the product

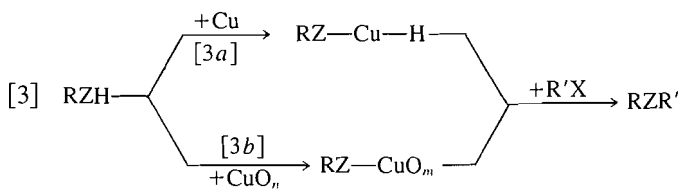

It is reported that isolated Cu—N (11*a*), Cu—O (11*b*, *c*), and Cu—C (12) species give corresponding N-, O-, and C-aryl compounds on treating them with aryl halides. In the case of PhCOOH, $Cu(OCOPh)_2(PhCOOH)$ (13) was actually isolated from a mixture of PhCOOH and CuO heated at 240°C, and reactions of Cu(II) benzoates such as $Cu(OCOPh)_2(PhCOOH)$ and Cu(OH)(OCOPh) (14) with aryl halides afforded the corresponding esters. The reaction mechanism expressed by eq. [3] is consistent with the trend that the O—H and N—H compound having higher acidity has a higher reactivity, since a more acidic compound is expected to react with Cu more easily.

Experimental

Material

Cu was prepared by reducing Cu^{2+} with Zn (15). The powder X-ray diffraction spectrum of the copper showed contamination with a small amount of Cu_2O. Use of commercially available Cu gave a somewhat lower yield. Copper oxide (Cu_2O and CuO), active hydrogen compounds, and organic halides were used as purchased from Tokyo Kasei or Wako Co., Ltd.

Condensation reactions

Phthalimide (1.5 g, 10 mmol), phenyl bromide (3.0 g, 19 mmol), and Cu (1.9 g, 30 mmol) were placed in a 50 cm^3 simple type stainless steel autoclave purchased from Taiatsu Glass Co., Ltd. (Type VS-1). The autoclave was heated at 240°C (temperature at the outside of the autoclave) for 12 h. Gas chromatographic analysis of the gas phase showed evolution of a small amount of H_2 during the reaction. Most of the *N*-phenylphthalimide formed was obtained as white needles which were scraped up from the reaction vessel by a spatula. After extracting products further with ethyl alcohol, the needles of *N*-phenylphthalimide and 1 mmol of *p*-methylbiphenyl (standard for glc) were dissolved in the extract. The glc analysis using a Shimadzu GC-3BT gas chromatograph (column SDC-410, 300°C, carrier gas = He) indicated consumption of all phthalimide and formation of 10 mmol (100%) of *N*-phenylphthalimide (cf. Expt. 1). Use of a glass autoclave instead of the stainless steel autoclave gave almost the same results. When the reaction temperature is not high, use of the usual glass tube is also possible.

Other condensation reactions were carried out analogously in the simple type autoclave. Throughout the text, Table 1, and Figs. 1–5 the reaction temperature indicates the temperature at the outside of the autoclave. The temperature at the inside of the autoclave was found to be lower by 10–15°C than the temperature outside the autoclave. All the reactions listed in Table 1, including the reactions using Cu, were carried out in the stainless steel autoclave filled with air (1 atm) containing ca. 0.5 mmol of O_2. For the phenylation of phthalimide, 2-pyrrolidinone, and phenol with the mixture of Cu and PhBr (Expts. 1, 15, and 24, respectively), carrying out the phenylation reactions under N_2 gave almost the same yields but, in the case of the phenylation of less acidic Ph_2NH (Expt. 19) with the mixture of Cu and PhBr (Expt. 19), carrying out the reaction under N_2 gave a considerably lower yield (ca. 40%) than that given in Table 1, indicating the importance of the activation of Ph_2NH and/or Cu by O_2 in the phenylation reaction of Ph_2NH.

Isolation of $Cu(OCOPh)_2(PhCOOH)$ and reactions of Cu(II) benzoates with aryl halides

Heating a mixture of PhCOOH (1.8 g, 15 mmol) and CuO (3.7 g, 47 mmol) in the simple type autoclave at 240°C for 12 h gave H_2O and a solid containing a blue material. Extraction of the blue material with acetone gave a blue solution. Acetone was evaporated in vacuum and the remaining blue material was washed with ether repeatedly to obtain a blue complex, which was characterized as $Cu(OCOPh)_2(PhCOOH)$ (13) by comparing its ir spectrum with that of an authentic sample.

Heating a mixture of $Cu(OCOPh)_2(PhCOOH)$ (1.0 g, 2.3 mmol) and PhBr (0.74 g, 4.7 mmol) in the simple type stainless steel autoclave at 240°C for 12 h gave 1.7 mmol of PhCOOPh, and heating 0.06 mmol of Cu(OH)(OCOPh) (14) with aryl halides gave PhCOOAr in medium yields.

Acknowledgement

The authors would like to express their grateful acknowledgement to Professor A. Yamamoto for his helpful discussions.

1. (*a*) F. Ullmann. Chem. Ber. **36**, 2382 (1903); **37**, 2001 (1904); (*b*) F. Ullmann and H. Kipper. Chem. Ber. **38**, 2120 (1905); (*c*) R. G. R. Bacon and H. A. O. Hill. Q. Rev. **19**, 95 (1965); (*d*) A. A. Goldberg and W. Kelly. J. Chem. Soc. 102 (1946); (*e*) M. Hida. J. Synth. Org. Chem. Jpn. **37**, 207 (1979); (*f*) T. Cohen and A. H. Lewin. J. Am. Chem. Soc. **88**, 4521 (1966); (*g*) H. Weingarten. J. Org. Chem. **29**, 3624 (1964); (*h*) C. P. Whittle. Aust. J. Chem. **33**, 1545 (1980); (*i*) T. D. Tuong and M. Hida. J. Chem. Soc. Perkin Trans. II, 676 (1974); (*j*) H. King. J. Chem. Soc. 1157 (1939).
2. (*a*) R. G. R. Bacon and H. A. O. Hill. J. Chem. Soc. 1109 (1964); (*b*) R. G. R. Bacon and O. J. Stewart. J. Chem. Soc. 4953 (1965); (*c*) R. G. R. Bacon, S. G. Seeterram, and O. J. Stewart. Tetrahedron Lett. 2003 (1967).
3. (*a*) T. Yamamoto. Synth. Commun. **9**, 219 (1979); (*b*) T. Yamamoto and Y. Kurata. Chem. Ind. London, 737 (1981).
4. R. G. R. Bacon and A. Karom. J. Chem. Soc. Perkin Trans. I, 272 (1973); 278 (1973).
5. F. D. Hager. Org. Synth. Coll. Vol. I, 545 (1953).
6. I. Goldberger. Chem. Ber. **39**, 1691 (1906).
7. M. Nilsson. Acta Chem. Scand. **20**, 423 (1966).
8. C. Bjorklund and M. Nilsson. Acta Chem. Scand. **22**, 2581 (1968).

9. K. SONOGASHIRA, Y. TOHDA, and N. HAGIHARA. Tetrahedron Lett. 4469 (1975).
10. H. WEINGARTEN. J. Org. Chem. **29**, 977 (1964).
11. (*a*) T. YAMAMOTO, Y. EHARA, M. KUBOTA, and A. YAMAMOTO. Bull. Chem. Soc. Jpn. **53**, 1299 (1980); (*b*) T. KAWAKI and H. HASHIMOTO. Bull. Chem. Soc. Jpn. **45**, 1499 (1972); (*c*) T. KAWAKI and H. HASHIMOTO. Bull. Chem. Soc. Jpn. **45**, 3130 (1972).
12. (*a*) M. NILSSON. Tetrahedron Lett. 679 (1966); (*b*) P. E. FANTA. Synthesis, 9 (1974); (*c*) A. MIYASHITA and A. YAMAMOTO. Bull. Chem. Soc. Jpn. **50**, 1102 (1977); (*d*) C. E. CASTRO and R. D. STEPHENS. J. Org. Chem. **28**, 2163 (1963).
13. F. EPHRAIM and A. PFISTER. Helv. Chim. Acta, **8**, 369 (1925).
14. S. F. PAVKOVIC. J. Inorg. Nucl. Chem. **33**, 1475 (1971).
15. P. H. GORE and G. K. HUGHES. J. Chem. Soc. 1615 (1959).

Can. J. Chem. Downloaded from www.nrcresearchpress.com by 210.87.254.5 on 09/06/12
For personal use only.

Experimental study of the structure I clathrate hydrate of trimethylene oxide by adiabatic calorimetry

JOHN COMPER, ANDRÉ QUESNEL, COLIN A. FYFE, AND ROBERT K. BOYD
Department of Chemistry, University of Guelph, Guelph, Ont., Canada N1G 2W1
Received October 14, 1981[1]

JOHN COMPER, ANDRÉ QUESNEL, COLIN A. FYFE, and ROBERT K. BOYD. Can. J. Chem. **61**, 92 (1983).

The structure I clathrate hydrate of trimethylene oxide (TMO), of composition $6TMO:46H_2O$, has been studied by adiabatic calorimetry over the temperature range 85–270 K. A thermal anomaly, with the appearance of a classical λ-transition, was observed between about 140–170 K. This anomaly was reproducible, provided precautions were taken against supercooling. No evidence for such a transition has been observed in previous studies using dynamic relaxation techniques (dielectric and nmr relaxation). The temperature range of this anomaly is close to the melting point of a known TMO-rich eutectic, but evidence is presented which argues against interpretation of the present observations in these terms. The previous relaxation measurements indicated a transition involving mobility of the TMO guest, centred at about 100 K. In the present work, the only evidence of this transition consisted of a much worse (order of magnitude) precision in the measured heat capacities in this temperature range. Thermal equilibration is known to be extremely slow in this system. The transition observed in the present work at higher temperatures must therefore correspond to some restructuring of the water host, and this may be connected with anomalous results obtained previously for the far infrared absorptions of water in the TMO clathrate hydrate.

JOHN COMPER, ANDRÉ QUESNEL, COLIN A. FYFE et ROBERT K. BOYD. Can. J. Chem. **61**, 92 (1983).

On a étudié la structure I du clathrate de l'hydrate de l'oxyde de triméthylène (OTM) de composition $6(OTM):46(H_2O)$, par calorimétrie adiabatique dans un intervalle de température allant de 85 à 270 K. On a observé une anomalie thermique avec l'apparition d'une transition λ classique environ entre 140–170 K. Cette anomalie est reproductible et on a pris de précautions pour prévenir la surfusion. On n'a pas obtenu la preuve de l'existence d'une telle transition dans les études antérieures utilisant les techniques de relaxation dynamique (relaxation rmn et diélectrique). Le domaine de température de cette anomalie est voisin du point de fusion d'un eutectique connu riche en OTM, mais on présente des preuves qui vont à l'encontre de l'interprétation des observations actuelles dans ces termes. Les mesures antérieures de relaxation suggèrent la présence d'une transition centrée autour de 100 K impliquant la mobilité du OTM hôte. Dans ce travail, la seule preuve de cette transition consiste en une très mauvaise précision (un ordre de grandeur) dans les capacités calorifiques mesurées dans ce domaine de température. On sait que l'équilibration thermique est très lente dans ce système. La transition que l'on observe dans ce travail à température plus élevée doit cependant correspondre à une certaine restructuration de l'eau hôte et ceci doit être relié aux résultats anormaux obtenus antérieurement par les absorptions, dans l'infrarouge lointain, de l'eau dans le clathrate de l'hydrate du OTM.
[Traduit par le journal]

Introduction

Molecular clathrate solids are crystals in which one species, the "host", forms a strongly-bonded structure which provides cages for individual molecules of a second "guest" species. The guests are firmly held in these cages, although there is seldom anything resembling a chemical bond formed between host and guest. A clathrate hydrate is a special case in which the host consists of an ice-like hydrogen-bonded structure (1) of water molecules. Current understanding of the structures of clathrate hydrates relies upon the work of von Stackelberg (2, 3). Apart from their inherent chemical interest, the practical importance of clathrate hydrates lies in the existence of large natural deposits of clathrate hydrates of methane (1). For the present calorimetric study, however, we chose to work with a system which is more readily handled than the methane case.

Trimethylene oxide (TMO) forms two distinct hydrates. That melting incongruently at about 264 K has been identified (4–6) as a clathrate hydrate of von Stackelberg's structure II (2) with a composition close to $TMO:17H_2O$. The hydrate melting incongruently near 252 K was identified as having von Stackelberg's structure I (3) by dielectric and proton nmr linewidth studies (4, 7) and X-ray powder diffraction measurements.[2] These studies (4,7)[2] suggested a composition, for this structure I hydrate, of $TMO:7\frac{2}{3}H_2O$, i.e. $6TMO:46H_2O$. This composition is consistent with a structure I hydrate in which each of the six larger tetrakaidecahedral cages, in the unit cell, is occupied by a TMO guest, while the two smaller dodecahedral cages are empty. As emphasised previously (7, 9), such a conclusion is reasonable in view of the fairly large size of the TMO molecule (van der Waals diameters of 0.55 nm, and 0.62 nm through the diagonally opposed methylene groups) compared with the mean free diameter (0.51 nm) of the dodecahedral cages. The cubic cell lattice parameter of the TMO structure I hydrate was found[2] to be slightly larger than the range of values found for a range of other structure I hydrates (3), as expected from the anticipated tight fit of TMO guest into even the larger cages (mean free diameter 0.58 nm).

However, a study (6, 10) of the TMO–water phase diagram, using thermal analysis, suggested a composition $TMO:6\frac{1}{2}H_2O$ for the structure I hydrate. Such a composition implies that more than 50% of the smaller cages are occupied by TMO guests. It was emphasised previously (7) that equilibration in the TMO–water system is extremely slow, so that erroneous results could easily arise if insufficient equilibration time were allowed. This discrepancy in the literature was one reason for undertaking the present work. In addition, comparison (9) of the far infrared spectra of structure I hydrates of ethylene oxide, cyclopropane, and TMO, between about 100 and 200 cm^{-1} at 4.3 K, indicates that TMO modifies the absorption by the water

[1]Revision received July 6, 1982.
[2]L. D. Calvert, quoted in ref. 6.

0008-4042/83/010092-05$01.00/0
©1983 National Research Council of Canada/Conseil national de recherches du Canada

Can. J. Chem. Downloaded from www.nrcresearchpress.com by 210.87.254.5 on 09/06/12
For personal use only.

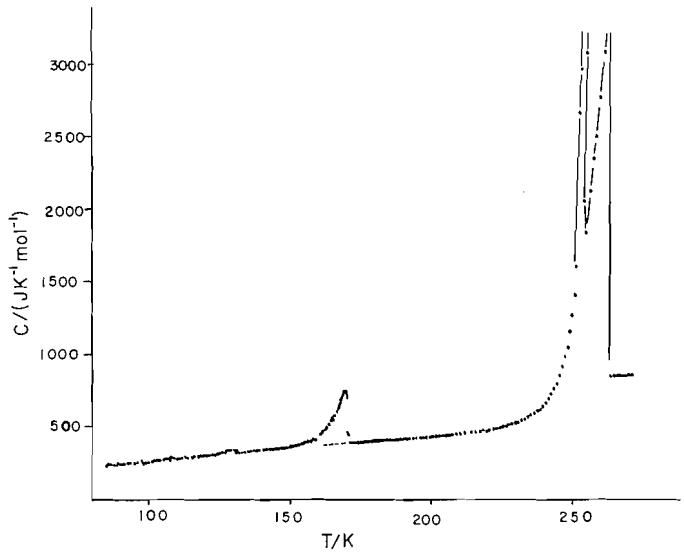

FIG. 1. Heat capacities (C/J K^{-1} mol^{-1}) obtained for structure I hydrate of trimethylene oxide. On this scale, most individual data points cannot be resolved (average temperature rise per determination ~0.5 K). Dashed curve between 162 and 170 K represents supercooling (Series 5 experiments).

molecules in a fashion qualitatively different from that of either of the other two guest species. There appeared (9) to be no unambiguous explanation for this discrepancy. It was hoped that the present work might shed some light on this problem also.

Experimental

The TMO used in these experiments was a product of Columbia Organic Chemicals Co., and was used without further purification other than a single distillation from which the middle third of the distillate was used for the work described here. Analysis by gc/ms (10% SE 30 on 80/100 mesh Chromosorb W-HMDS, 6 foot column, 2 mm id, in Perkin-Elmer Sigma III GC, interfaced to VG Analytical 7070F mass spectrometer with VG 2025 datasystem) revealed *no* impurities attributable to the distilled TMO sample. Several sets of temperature programming/carrier flow-rate conditions were tried, but all yielded a single gc peak corresponding to TMO. This procedure should easily have detected impurities at the 0.1% level, and probably at even lower levels. The calorimeter vessel was loaded by weighing out 20.3955 g of TMO plus 48.5024 g of triply distilled water, a molar ratio of 1:7.664. Both liquids were de-aerated immediately before weighing by bubbling helium gas through them for 1 h. Following loading of the calorimeter via syringes through small tubes of solder attached to the lid, the residual air was flushed out by a stream of helium which was first bubbled through a TMO–water mixture of the same composition. The calorimeter vessel was then sealed off by fusing closed the solder tubes. The vessel was reweighed, and the residual solder was weighed separately. No discrepancy attributable to loss or gain of sample was detected. The calorimeter and peripheral equipment have been described previously (11). After mounting the cryostat, the calorimeter vessel was maintained at 240 ± 2 K continuously for 17 days, in an attempt to ensure complete transformation to structure I solid from structure II plus TMO-rich liquid (7). The vessel was then maintained at 130 ± 5 K for a further 28 days. This conditioning temperature was chosen in the light of the findings (7) of long-term drift in the dielectric properties at temperatures between 40 and 100 K. The subsequent thermal history of the present sample is described with the experimental results.

Results and discussion

In all, 300 independent determinations of heat capacity were made, in the temperature range 85 to 272 K. It is neither convenient nor necessary to tabulate this large quantity of data in detail here,[3] since most of it falls in regions of little interest with no thermal anomalies. Accordingly, a gross overview of the results obtained is shown in Fig. 1, while regions of more immediate interest are plotted in more detail in Fig. 2. A summary of the thermal history of the sample, following its original conditioning (see Experimental section), is shown in Table 1. Following Series 19 (Table 1), the sample was again conditioned at 240 ± 2 K for 14 days, then at 135 ± 5 K for 7 days, and finally at 85 ± 5 K for 16 days. The experiments of Series 20 (Table 1) were then begun. The heat capacities, obtained under pressure of helium of ~1 atm at room temperature, were corrected for the empty calorimeter vessel plus solder and grease, but the precision was such that helium correction was not justifiable.

It is clear from Fig. 2(*b*) that the quality of the data obtained between 85 and 130 K, in Series 20–28 (Table 1), is signifi-

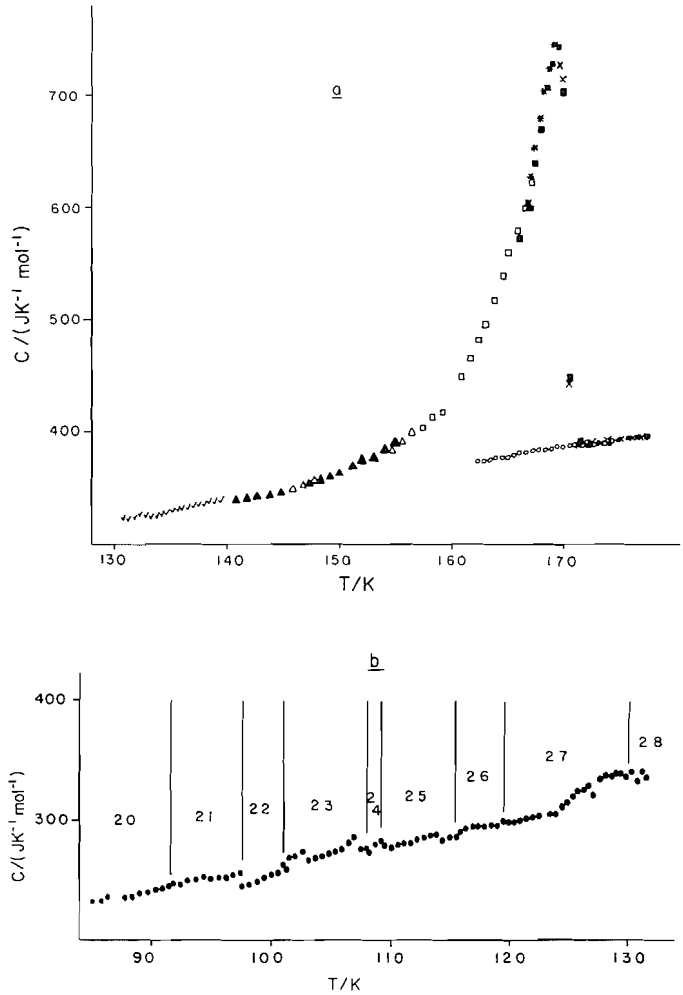

FIG. 2. Details of data obtained in regions of interest. (*a*) Thermal anomaly observed between 140 and 170 K. ⁄, Series 1 and 2; *, Series 3; ×, Series 4; ○, Series 5; △, Series 7; □, Series 8; ■, Series 9; ●, Series 10. (*b*) Data obtained between 85 and 135 K. Series numbers (Table 1) are indicated in the appropriate ranges.

[3]The complete set of data (C vs. temperature) are available at a nominal charge from the Depository of Unpublished Data, CISTI, National Research Council of Canada, Ottawa, Ont., Canada K1A 0S2.

Can. J. Chem. Downloaded from www.nrcresearchpress.com by 210.87.254.5 on 09/06/12
For personal use only.

TABLE 1. Summary of thermal history of sample in calorimeter subsequent to initial conditioning (see Experimental section)

Series	No. of determinations	Temperature range (K)	Wait before next series (h)	Temperature during waiting period (K)
1	5	130–133	18	133
2	14	133–140	65	140–160
3	7	166–169	18	169
4	16	169–179	18	179 (17 h); 162 (1 h)
5	23	162–174	48	140
6	14	140–155	48	145
7	6	145–156	18	156
8	13	157–167	40	165
9	10	166–171	18	171
10	16	172–186	18	186
11	9	186–196	85	196
12	15	197–215	18	215
13	11	216–227	18	227
14	9	228–238	320	238
15	10	238–248	18	248
16	8	248–253	18	253
17	3	253–255	18	255
18	10	255–263	40	263
19	11	264–272		See text
20	10	85–91	18	91
21	10	91–97	18	97
22	7	97–101	40	101
23	14	101–108	115	108
24	3	108–109	18	109
25	12	109–115	18	115
26	8	116–120	115	120
27	22	120–130	18	130
28	4	130–132		

cantly worse than that of any other Series in the present work. The importance of this temperature range lies in the fact that the dielectric and nmr linewidth studies (7) indicate that an ordering transition, in which TMO dipoles assume parallel alignment along the $\bar{4}$ axes of the large cages, occurs below about 105 K. On the other hand, no evidence for such a transition was found in the thermal analysis experiments (6, 10), which covered the range from 77 K to room temperature. Unfortunately, the present work does not significantly clarify the situation in the temperature range 80–120 K. The unexpectedly large scatter in the data of Fig. 2(*b*) might possibly reflect an order–disorder transition of the type proposed (7) if the preconditioning period of 16 days at 85 K (see above) were insufficient. It is known (7) that the dielectric behaviour below 100 K changes on a timescale of weeks, though the present conditioning period was chosen with this in mind. Alternatively, it is possible that the present conditioning *did* suffice to establish the ordered phase at 85 K, but the disordering process is sufficiently slow that thermal equilibrium was not, in fact, established thereafter in our experiments. The experiments of Series 24 (Table 1) were conducted to test whether waiting a longer time for the final temperature measurement, after the heat input, would make any difference to the quality of the data. This was found to not be the case. Thus the outcome of those of the present experiments conducted between 85 and 130 K is disappointing, and merely indicates that some thermal process was not fully equilibrated.

The results obtained between about 240 and 265 K appear to be generally consistent with the published phase diagram (6). The maximum in the heat capacity curve (Fig. 1) observed near 253 K corresponds to the peritectic temperature of 252.5 K observed (6) for the transition (structure I hydrate → structure II hydrate plus TMO-rich liquid). Above this temperature the structure II hydrate progressively melts; a mixture of composition 1TMO:$7\frac{2}{3}H_2O$ should be completely melted (6) at temperatures above about 262 K, in good agreement with the present observations (Fig. 1). Thus, the present work appears to be entirely consistent with the earlier thermal analysis data (6) in this temperature range.

The results obtained in the temperature range 140–175 K (Fig. 2(*a*)) have the appearance of a classical λ-transition. The results of Series 5 (Table 1) show that it is possible to supercool the system below this transition. The baselines above and below the transition extrapolate well into one another, and through the data of Series 5. If the measured heat capacities are taken to be C_P values, the excess enthalpy of the transition ΔH_{excess} is 2360 J mol^{-1}, while the excess enthropy ΔS_{excess} is 13.9 J K^{-1} mol^{-1}. If the transition does, in fact, correspond to a simple order–disorder transition, so that ΔS_{excess} can be interpreted (12) as $R \ln (W_a/W_b)$ where W_a and W_b are the numbers of distinguishable configurations above and below the transition, respectively, then $(W_a/W_b) = 5.3$. If such an interpretation is valid, it is pertinent to note here that the nmr linewidth results (7) indicate that, at the temperature of the thermal transition (169 K at peak), the TMO guest molecules are already reorienting extremely fast, indicated by the closeness of the second moments to the limiting value calculated on the assumption of isotropic rotation of the TMO molecules (7). Thus, if the thermal transition observed here is indeed of this type, it cannot correspond to an ordering of the TMO guests within the cages, but must involve the host lattice in some way.

However, it remains to be established that the observed

Can. J. Chem. Downloaded from www.nrcresearchpress.com by 210.87.254.5 on 09/06/12
For personal use only.

Can. J. Chem. Downloaded from www.nrcresearchpress.com by 210.87.254.5 on 09/06/12
For personal use only.

transition (Fig. 2 (*a*)) is genuine. In particular, it is disturbing that the temperature of this transition is close to that of an eutectic point observed (6) at 172 K. While it is true that the thermal analysis results (6) are somewhat suspect due to insufficient thermal conditioning (for example, only 1 h at 248 K (6), with no other conditioning process), the establishment of this eutectic point from the TMO-rich side should be relatively unambiguous. Temperature measurements in the present work were made using a Leeds and Northrup platinum resistance thermometer calibrated by the National Research Council of Canada. The discrepancy between 172 K (6) and 169 K (present work) could represent uncertainties in the thermal analysis results (6).

The composition of the TMO–water mixture used in the present work was almost exactly that for the structure I hydrate. In principle, therefore, there should be *no* observable effect from this eutectic. However, the well-documented difficulties (7) in equilibrating this system do raise the possibility of localised inhomogeneities within the sample used in this work. At the simplest conceptual level, there might possibly have existed one region which was TMO-rich, relative to the structure I hydrate composition. (Of course, this would imply the existence of a corresponding water-rich region elsewhere.)

We now examine in more detail the possible interpretation of the thermal transition, observed in the present work (Fig. 2 (*a*)), in terms of eutectic melting. The eutectic point at 172 K involves (6) co-equilibrium of almost pure solid TMO, a liquid phase containing 93% (by mass) of TMO, and solid structure I hydrate. If such an eutectic did in fact occur in the present experiments, the postulated TMO-rich region buried within the structure I hydrate must have given rise to the first two phases mentioned in the preceding sentence, i.e., must have been >93% TMO. This conclusion permits the following rough estimate of the amount of TMO locked up in this postulated inhomogeneity. The enthalpy of fusion of TMO does not appear to have been measured, but that of the homologue ethylene oxide has been found (13) to be 5173 J mol^{-1}. On this basis, the enthalpy of fusion of TMO is estimated to be 5500 J mol^{-1}. The observed eutectic is 80 mol% of TMO, so that 1 mol of TMO in the liquid eutectic is associated with 0.24 mol of H_2O; for this liquid to have been formed by the postulated eutectic melting, 0.97 mol of solid TMO plus 0.03 mol of structure I hydrate must have melted. The enthalpy of fusion of the structure I hydrate, under these conditions, is not known. We estimate this quantity as the sum of the values for the separate components; this should not give rise to gross error, in view of the small amount (3%) of the hydrate involved in the eutectic melt. Thus, finally, our rough estimate for the enthalpy of fusion of 0.97 mol solid TMO plus 0.03 mol structure I hydrate, to form the postulated eutectic liquid containing 1 mol TMO (at 172 K), is $(\Delta H_{fusion}(TMO) + 0.24x\Delta H_{fusion}(H_2O)) =$ 6950 J/(mol of TMO in liquid eutectic). The observed excess enthalpy associated with the observed transition (Fig. 2(*a*)) was 2360 J/(mol of TMO assumed to be present as TMO: $7\frac{2}{3}H_2O$), and 0.3512 mol of TMO were present. The *actual* observed excess enthalpy was thus 829 J. If this observation is interpreted as eutectic melting, approximately 0.12 mol of TMO, or 34% of the TMO in the sample, must have melted to eutectic. This estimate is somewhat crude but the implication, that 30–40% of the TMO in the present sample existed as essentially pure solid TMO, seems unlikely in view of the precautions taken in conditioning the sample. Such an interpretation also implies that a corresponding proportion of the water was present as essentially pure ice, a proposal not borne out by Fig. 1 which shows that melting was complete at temperatures above 263 K or so.

A further consideration which supports this view concerns the baseline values for the heat capacities immediately above and below the transition (Fig. 2(*a*)). As noted above, these extrapolate well into one another, and through the data of Series 5. If, immediately above the transition, the sample did indeed contain a large proportion of liquid as required by the interpretation in terms of eutectic melting, the heat capacity above the transition would be expected to be appreciably higher than predicted by extrapolation of the low-temperature data. The undercooled system investigated in Series 5 was the result (Table 1) of only one hour's equilibration after cooling below the transition; these data are in excellent agreement with the extrapolated baseline. Much more extreme examples of undercooling below higher-order transitions are known (14). On the other hand, the fact that undercooling occurs so readily also presents some difficulties for the eutectic melting theory. It is, of course, possible to undercool a liquid below its freezing point in the absence of nuclei for crystallisation. However, the eutectic interpretation of the observed transition requires that above the transition the liquid eutectic exists in intimate contact, and in equilibrium, with large amounts of one of the solids which solidify out on cooling (structure I hydrate). There should thus have been no shortage of sites to initiate solidification on cooling the sample. An interpretation in terms of host lattice reorganisation meets no such difficulties.

If it is tentatively accepted that the transition near 169 K is indeed a genuine effect, reflecting some change in the host lattice of the structure I hydrate, the earlier data must be re-examined. First, the dynamic relaxation studies (dielectric and nmr) (7) are not always sensitive to minor structural changes. It is conceivable that, if genuine, the transition near 169 K did not show up in these results (7). The X-ray powder diffraction patterns were obtained[2] both at 240 K and at 140 K. In both cases, the cubic lattice characteristic of structure I hydrates was observed, with a slight decrease in the unit cell dimension at the lower temperature.[2] Assuming that the sample used in the X-ray work[2] was not supercooled through the transition near 169 K, although our experience indicates that this is easily done, these results indicate that only a minor structural change can be involved. This is consistent with the fairly small excess enthalpy and entropy changes associated with the transition. It is conceivable that this transition is connected in some way with the anomalous water vibrations in the far infrared, observed (9) for the structure I TMO clathrate hydrate.

Finally the implications, of accepting the thermal anomaly near 169 K as a genuine transition, for the TMO–water phase diagram obtained (6) by thermal analysis must be investigated. As pointed out previously (7), this phase diagram is almost certainly in error, at least in part, in view of the composition TMO:$6\frac{1}{2}H_2O$ deduced (6, 10) for the structure I hydrate. The compositions of the incongruently melting compounds were determined (6, 10) as the compositions giving maximum duration of thermal arrest during the conversion of one solid to another while in equilibrium with a liquid phase (8). As noted previously (7), erroneous analysis may have resulted (6, 10) from the lack of proper equilibration. It is also signifcant that interpretation of the durations of thermal arrest as a function of composition assumed (6, 10) that these plots are triangular, with the composition of the incongruently melting compound given by the apex. Clearly this is not necessarily so (8), and

indeed the plots for the TMO–water system (6, 10) are quite poorly defined near the structure I hydrate composition, being fairly flat there. Since a composition TMO:$7\frac{2}{3}H_2O$ corresponds to 29.6% of TMO by mass, not too different from 33.1% for TMO:$6\frac{1}{2}H_2O$, the possibility of erroneous interpretation from this cause is also real.

Also significant, from the point of view of the present work, is the earlier finding (6, 10) of a "thermal arrest" at 165 K. This thermal arrest was not reproducible, in accord with the present finding of ready supercooling through the transition near 169 K. The original authors (6, 10) interpreted their findings in terms of an eutectic point involving solid TMO, structure II hydrate, and liquid containing about 81% by mass of TMO. Such an eutectic point would be observable only in mixtures in which lack of proper equilibration at ~240 K had prevented structure I hydrate from being formed. In view of the very long equilibration times used in the present work (about three times longer than that used in the dielectrics and nmr work (4)), we do not consider it likely that structure II hydrate played any significant role in the present work at these temperatures. However, an alternative explanation of these earlier observations (6, 10) would involve a real higher-order transition in the structure I hydrate, as postulated here. In the absence of more experimental details of the thermal arrest studies, it does not seem possible to examine this proposal further.

In summary, the most suggestive finding of the present calorimetry studies is the proposed existence of a λ-transition in the structure I hydrate of TMO, peaking near 169 K. The most likely interpretation of such a transition appears to involve changes in the host lattice. While it is not possible to entirely rule out an interpretation of the observations in terms of eutectic melting in localised TMO-rich inhomogeneities, the evidence does appear, on balance, to oppose such a view. If genuine, the observed transition might be connected with anomalous results obtained (9) for the far infrared absorptions of the water in this system, and with a non-reproducible thermal arrest observed (6, 10) near 165 K. On the other hand, it is disturbing that dielectric and nmr measurements (7) did not find any evidence for this transition. At the very least, the present work re-emphasises the necessity for extreme care in the preparation and conditioning of this system.

Acknowledgements

We are indebted to Dr. J. A. Ripmeester for suggesting this work, and for helpful criticisms. The work was supported by NSERC operating grants and by the University of Guelph Research Advisory Board.

1. D. W. DAVIDSON. *In* Water: a comprehensive treatise; Vol. 2. *Edited by* F. Franks. Plenum Press, New York. 1973. p. 115.
2. M. VON STACKELBERG and H. R. MULLER. Z. Elektrochem. **58**, 25 (1954).
3. M. VON STACKELBERG and W. JAHNS. Z. Elektrochem. **58**, 162 (1954).
4. R. E. HAWKINS and D. W. DAVIDSON. J. Phys. Chem. **70**, 1889 (1966).
5. D. F. SARGENT and L. D. CALVERT. J. Phys. Chem. **70**, 2689 (1966).
6. J.-C. ROSSO and L. CARBONNEL. Compt. Rend. Acad. Sci Paris, **274**C. 1108 (1972).
7. S. R. GOUGH, S. K. GARG, and D. W. DAVIDSON. Chem. Phys. **3**, 239 (1974).
8. A. FINDLAY. The phase rule and its applications. 7th ed. Longmans, Green and Co., London. 1931. p. 114.
9. J. E. BERTIE and S. M. JACOBS. Can. J. Chem. **55**, 1777 (1977).
10. L. CARBONNEL and J.-C. ROSSO. J. Solid State Chem. **8**, 304 (1973).
11. J. A. RIPMEESTER, D. A. WRIGHT, C. A. FYFE, and R. K. BOYD. J. Chem. Soc. Faraday Trans. II, **74**, 1164 (1978).
12. E. F. WESTRUM, JR. and J. P. MCCULLOUGH. *In* Physics and chemistry of the solid state. *Edited by* D. Fox, M. M. Labes, and A. Weissberger. Interscience. 1963. Chapt. 1.
13. W. F. GIAUQUE and J. GORDON. J. Am. Chem. Soc. **71**, 2176 (1949).
14. H. L. FINKE, M. E. GROSS, J. F. MESSERLY, and G. WADDINGTON. J. Am. Chem. Soc. **76**, 854 (1954).

Can. J. Chem. Downloaded from www.nrcresearchpress.com by 210.87.254.5 on 09/06/12
For personal use only.

A comparison of methyl and phenyl substituent effects on the gas phase basicities of amines and phosphines

S. IKUTA[1] AND P. KEBARLE[2]

Department of Chemistry, University of Alberta, Edmonton, Alta., Canada T6G 2G2

Received June 2, 1982

S. IKUTA and P. KEBARLE. Can. J. Chem. **61**, 97 (1983).

The proton affinities of phenyl phosphine and cyclohexylphosphine were measured by determining the equilibrium constants of proton transfer equilibria with a pulsed electron beam high ion source pressure mass spectrometer. These proton affinities combined with values for methyl and phenyl phosphines and the analogous amines provide an interesting comparison of the methyl and phenyl substituent effects on the basicities of phosphine and ammonia. Methyl substitution increases the basicity of both ammonia and phosphine; however, the increase is significantly larger for the phosphine. Phenyl substitution increases the basicity of ammonia and phosphine and the increase for phosphine is very much larger. Calculations at the STO-3G, 4-31G, STO-3G*, and 4-31G* (* with *d* orbitals) for PH_3, $MePH_2$, $PhPH_2$, the protonated species, and the nitrogen analogues predict proton transfer reaction energies in good agreement with the experimental results. A shortening of the C—P bond is predicted for protonation of $MePH_2$ and particularly $PhPH_2$, while a lengthening of the C—N bond is predicted for the corresponding nitrogen compounds. The much stronger increase in proton affinity of the phosphines caused by phenyl substitution is due to the stabilization of the phenyl phosphonium ion by π donation from the phenyl group to the empty orbitals of phosphorus in the PH_3^+ group; in contrast, in the amines, it is the free base aniline which is stabilized by conjugation of the nitrogen lone pair with the aromatic ring. This stabilization of the free base is less important in phenyl phosphine. The participating empty orbitals of phosphorus in the conjugation of phenyl with PH_3^+ in phenyl phosphonium are mostly π^* with some πd participation. The stabilization of the aniline free base contributes considerably more than the conjugation in the phosphonium ion, to the phenyl substituent difference for the amines and phosphines. The factors involved in the bigger substituent effect of methyl in the phosphines are somewhat similar to those for phenyl: stabilization of the methyl amine by conjugation of the nitrogen lone pair with empty orbitals of CH_3 and stabilization of the $CH_3PH_3^+$ by hyperconjugation. An alternate description can be given in terms of hybridization changes.

S. IKUTA et P. KEBARLE. Can. J. Chem. **61**, 97 (1983).

On a mesuré les affinités pour le proton de la phénylphosphine et de la cyclophosphine en déterminant les constantes des équilibres de transfert du proton à l'aide d'un spectromètre de masse à faisceau d'électrons pulsés avec une source d'ions à haute pression. Ces affinités pour le proton combinées aux valeurs des méthyl- et phényl-phosphines et des amines analogues fournissent une comparaison intéressante des effets des substituants méthyle et phényle sur les basicités de la phosphine et de l'ammoniac. La substitution du méthyle augmente la basicité de la phosphine et de l'ammoniac; l'augmentation est plus forte pour la phosphine. La substitution du phényle augmente la basicité de l'ammoniac et de la phosphine et l'augmentation dans le cas de la phosphine est de beaucoup plus forte. Les calculs aux niveaux STO-3G, 4-31G, STO-3G* (avec les orbitales *d*) pour le PH_3, le $MePH_2$, le $PhPH_2$, les espèces protonées et les analogues azotés prédisent des énergies de réaction de transfert du proton en parfait accord avec les résultats expérimentaux. On a prédit un racourcissement de la liaison C—P pour la protonation de $MePH_2$ et particulièrement celle du $PhPH_2$ tandis que l'on prédit un élongation de la liaison C—N dans le cas des composés azotés correspondants. L'augmentation beaucoup plus forte de l'affinité des phosphines pour le proton provoquée par le substituant phényle est due à la stabilisation de l'ion phénylphosphonium par transfert π du phényle aux orbitales vacantes du phosphore du groupe PH_3^+; au contraire dans le cas des amines, c'est la base libre aniline qui est stabilisée par la conjugaison du doublet libre de l'azote avec le noyau aromatique. Cette stabilisation de la base libre est moins importante dans le cas de la phénylphosphine. Les orbitales vacantes du phosphore participant dans la conjugaison du phényle avec PH_3^+ du phénylphosphonium sont principalement du type π^* avec une participation occasionnelle des orbitales πd. La stabilisation de l'aniline sous forme de base libre contribue d'avantage que la conjugaison dans l'ion phosphonium à la différence du substituant phényle pour les amines et les phosphines. Les facteurs impliqués dans le plus grand effet de substituant du méthyle dans les phosphines sont quelque peu semblables à ceux du phényle. Ce sont la stabilisation de la méthylamine par conjugaison du doublet libre de l'azote avec les orbitales vides du CH_3 et la stabilisation du $Ch_3PH_3^+$ par hyperconjugaison. On peut faire alterner une description en fonction des changements d'hybridation.

[Traduit par le journal]

Introduction

We reported recently (1) measurements of the gas phase basicities of Me_2PhP, $MePh_2P$, and Ph_3P. The present work gives experimental determinations of the basicities of phenyl phosphine $PhPH_2$ and cyclohexyl phosphine. The basicities of PH_3, $MePH_2$, Me_2PH, and Me_3P (2–4) as well as the basicities of almost all analogously substituted amines (3) are available in the literature. On the basis of these data it is possible to make an interesting comparison between the methyl and phenyl substituent effects in ammonia and phosphine. In order to obtain additional insights, molecular orbital calculations for some key bases and their onium ions were also performed.

Experimental

The gas phase basicity measurements were performed with a pulsed electron beam high ion source pressure mass spectrometer. The measurements of the proton transfer equilibria were similar to those described in the preceding publication (1).

[1]Permanent address: Department of Chemistry, Tokyo Metropolitan University, Fukasawa, Setagaya-ku, Tokyo 158, Japan.

[2]To whom all correspondence should be addressed.

0008-4042/83/010097-06$01.00/0

©1983 National Research Council of Canada/Conseil national de recherches du Canada

Can. J. Chem. Downloaded from www.nrcresearchpress.com by 210.87.254.6 on 09/06/12
For personal use only.

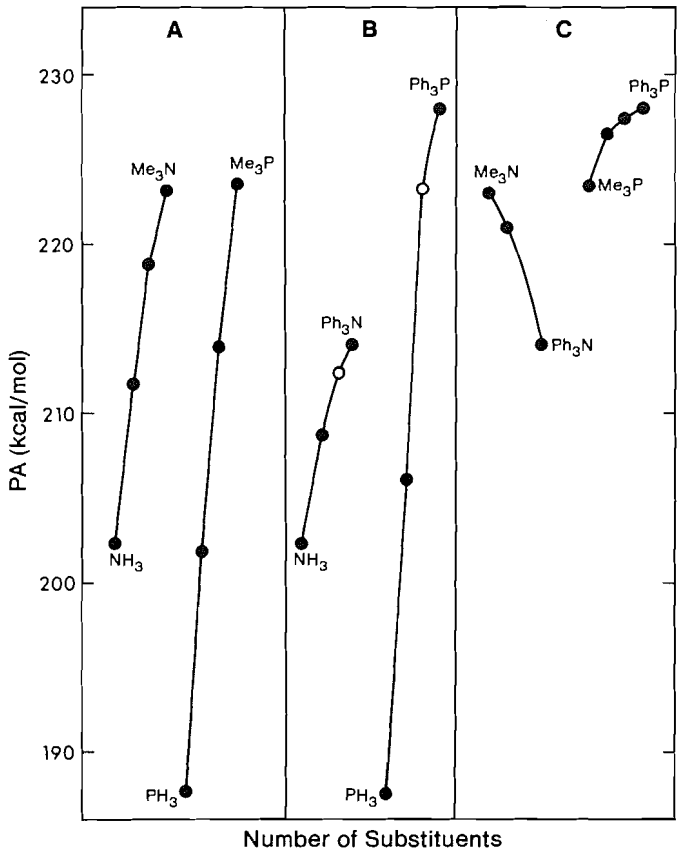

FIG. 1. Changes of proton affinities of amines and phosphines with methyl and phenyl substitution. (*A*) Methyl increases the proton affinity of both ammonia and phosphine but the increase for the phosphine is larger. (*B*) Phenyl increases the proton affinity of ammonia and phosphine but the increase for the phosphine is much larger. (*C*) Progressive replacement of methyl by phenyl decreases the proton affinity of trimethylamine while an increase for trimethylphosphine is observed. ●, experimental results from Table 1. ○, interpolated values.

The proton equilibria measured were:

[1] $PhPH_3^+ + PhNH_2 = PhPH_2 + PhNH_3^+$
$\Delta G_1^0 = -2.7 \pm 0.2$ kcal/mol

[2] $PhPH_3^+ + cyclo\text{-}C_6H_{11}PH_2 = PhPH_2 + cyclo\text{-}C_6H_{11}PH_3^+$
$\Delta G_2^0 = -2.5 \pm 0.5$ kcal/mol

Measurements were made at temperatures between 70 and 300°C. The free energy changes observed at different temperatures were fairly close and showed no consistent trend with temperature which indicates that the entropy change in both reactions is small, i.e. $\Delta G^0 \approx \Delta H^0$. Equilibrium [2] showed some dependence of the equilibrium constant on the ratio of the neutral bases. The cause for this was not discovered. The larger error limit for that determination was selected in order to given an indication of that problem.

Calculations

The total energies of the various compounds were obtained after geometry optimizations. The PH_3 and PH_4^+ geometries were completely optimized using the energy gradient method (6) with the STO-3G (7), STO-3G* (8), 4-31G (9), and 4-31G* basis set. A *d* polarization function with $\zeta = 0.43$ (10) was added to obtain 4-31G*. The CH_3PH_2 and $CH_3PH_3^+$ were fully optimized with the energy gradient method in the STO-3G and STO-3G* calculations. Parabolic 3 point fitting was used in the optimized geometry in the 4-31G calculation. For 4-31G* the 4-31G geometry was used.

TABLE 1. Proton affinities of methyl and phenyl phosphines and the corresponding amines

Compound	PA (kcal/mol) P	PA (kcal/mol) N
XH_3	187[b]	202.3[a]
XH_2Me	201.8[b]	212[d]
$XHMe_2$	214.0[b]	218.9[d]
XMe_3	223.5[b]	223.1[d]
XH_2, $c\text{-}C_6H_{11}$	208.6[c]	219.5[d]
XH_2Ph	206.1[c]	208.8[d]
XMe_2Ph	226[d]	221.5[d]
$XMePh_2$	226.7[d]	
XPh_3	~227[d]	214[e]
	228[e]	

[a]Proton affinities based on $PA(NH_3) = 202.3$ kcal/mol Kebarle (5) Beauchamp (3). This values is not well established; however, only the relative proton affinities are of interest in this work.
[b]Staley and Beauchamp (2, 3).
[c]This work.
[d]Kebarle (5), see also Beauchamp (3).
[e]Munson (4).

The energy gradient method was used in $C_6H_5PH_2$ and $C_6H_5PH_3^+$ optimizations to obtain the STO-3G geometries; however, the benzene ring was taken as invariant with r(C—C) = 1.397 Å, r(C—H) = 1.084 Å.

NH_3 and NH_4^+ were optimized completely with the energy gradient method, CH_3NH_2 and $CH_3NH_3^+$ were optimized by the energy gradient method when STO-3G was used while parabolic fitting was used with 4-31G. $C_6H_5NH_2$ and $C_6H_5NH_3^+$ were optimized in the same manner as the corresponding phosphorus compounds.

The calculations were performed with the Gaussian 70 (11), HONDO 5 (12), and Monster Gauss 81 (13) programs.

Results and discussion

The effect of methyl and phenyl substitution on the basicities of ammonia and phosphine is shown in Fig. 1. The proton affinity of phosphine is some 15 kcal/mol lower than that of ammonia. Methyl substitution increases the basicities of both compounds (see Fig. 1*A*); however, the effect of methyl is much larger for the phosphines. Thus, while the proton affinity of phosphine is 15 kcal/mol lower than the proton affinity of ammonia, after triple methyl substitution, the proton affinity of trimethylphosphine has caught up with and even slightly surpassed the proton affinity of trimethylamine. The difference between the substituent effects in ammonia and phosphine is even more dramatic for the phenyl substituent. Substitution with phenyl increases the basicities of both ammonia and phosphine; however, the increase for the proton affinity of phosphine is so much larger that the proton affinity of the phosphine almost catches up with the proton affinity of the amine after the first phenyl substitution. By the time the third phenyl has been put on, the proton affinity of the phosphines is found to exceed that of the amine by some 14 kcal/mol (Fig. 1*B*). A comparison of the replacement of methyl by phenyl is shown in Fig. 1*C*. In the amines, replacement of methyl by phenyl lowers the basicity, for the phosphines the opposite is true. Thus, tri-

Can. J. Chem. Downloaded from www.nrcresearchpress.com by 210.87.254.6 on 09/06/12
For personal use only.

TABLE 2. Total energies E obtained from *ab initio* calculations[a]

Compound	E			
	STO-3G	STO-3G*[d]	4-31G	4-31G*[e]
PH_3	−338.6364	−338.7071	−342.0257	−342.0895
PH_4^+	−339.0250	−339.1048	−342.3244	−342.4051
CH_3PH_2	−377.2238	−377.2979	(−381.0125)[g]	(−381.0716)[f]
$CH_3PH_3^+$	−377.6316	−377.7198	(−381.3330)[g]	(−381.4113)[f]
$C_6H_5PH_2$	(−565.3921)[b]	(−565.4462)[c]	(−571.2458)[c]	
$C_6H_5PH_3^+$	(−565.8053)[b]	(−565.8778)[c]	(−571.5753)[c]	
NH_3	−55.4554		−56.1067	
NH_4^+	−55.8689		−56.4589	
CH_2NH_2	−94.0329		(−95.0703)[g]	
$CH_3NH_3^+$	−94.4606		(−95.4397)[g]	
$C_6H_5NH_2$	(−282.2117)[b]		(−285.3171)[g]	
$C_6H_5NH_3^+$	(−282.6384)[b]		(−285.6792)[g]	

[a]To calculate the total energies fully optimized geometries were used except for the systems whose energies are shown in parentheses. The total energies are given in atomic units 1 au = 627.2 kcal/mol.
[b]The geometry except that of the benzene ring was optimized.
[c]STO-3G geometries were used.
[d]The exponent for the polarization function was 0.39.
[e]The exponent for the polarization function was 0.43.
[f]4-31G geometries were used.
[g]Optimized geometry parameters given in Table 3.

methylamine and trimethylphosphine have about the same proton affinity, while the proton affinity of triphenylphosphine is very much larger than that of triphenylamine.

The proton affinities used in Fig. 1 were obtained from Table 1, some are literature values (1−4), others are results of the present work (see Experimental). The proton affinity of cyclohexylphosphine (Table 1) can be compared with that of the corresponding amine. The cyclohexyl substituent increases the basicities of NH_3 and PH_3, the increase being larger for the phosphine. The effect is similar to that observed for methyl substitution.

In order to obtain additional insights on the differences between the amine and phosphine basicities described above, we performed *ab initio* calculations for the neutral and protonated bases: ammonia, methylamine, aniline, and the corresponding phosphines. Some details about the calculations are given in the Calculations section. The total energies $E(B)$ and $E(BH^+)$ obtained from the calculations are shown in Table 2. The geometries are given in Table 3. The proton affinities predicted by the calculation can be obtained from the difference: $E(B) - E(BH^+)$. The resulting proton affinities are not very close to the experimental values, even for the best basis set used (4-31G, 4-31G*). The major source of error, when a good basis set is used, is the neglect of zero point energy, which can be as large as 10 kcal/mol (14). Much more useful are the energy changes ΔE for the (isodesmic) proton transfer reactions, shown in Table 4. Fairly good agreement with the experimental enthalpy change is observed with nearly all basis sets. For the phosphines, use of the more extensive 4-31G and 4-31G* leads to a small improvement of the agreement between theory and experiment. One important benefit from the data in Table 4 is the clarification of the site of protonation that they provide. It has been shown that protonation of the nitrogen in aniline is more favorable (by ~1 kcal/mol) than protonation of the ring (15, 16). Without the present calculations for the phenyl phosphine it would not have been completely straightforward to decide whether ring or substituent protonation is more favorable. The agreement of the calculated ΔE with the experimental result demonstrates that phosphorus protonation has occurred.

There has been considerable discussion in the literature (3, 17) of the methyl and phenyl substituent effects in ammonia. Thus, it has been recognized that the dominant effect causing the increase of basicity with methyl substitution is the stabilization of the onium ion by the polarizability due to methyl. Probably the most satisfactory proof of that effect is given by the protonation energy decomposition method of Morokuma (18). Interestingly, the polarizability contribution in the series $NH_3 \rightarrow Me_3N$ was properly assessed only at the 4-31G level of calculation, STO-3G did not adequately predict this effect.

The fact that methyl provides an increase of basicity in the $PH_3 \rightarrow Me_3P$ series that is larger than the increase in the ammonia series can not be explained by larger polarizability increases in the phosphine series since these changes, if anything, should be smaller. Beauchamp (2) has pointed out the essential factors responsible for the stronger methyl effect in the phosphines. Conversion of the H—N bonds of ammonia to C—N bonds requires an increase of the bond length and this is achieved by an increase of the p character of the C—N bond(s) at the expense of the p character of the lone pair. The latter corresponds to a shrinkage of the lone pair and leads to a decrease of the dipole moment in the series NH_3-Me_3N. The lone pair becomes less suited for protonation and a partial rehybridization to increase the p character of the lone pair occurs on protonation. This has an adverse effect on the proton affinity of the methylated species. The situation is different for the phosphines, since already in PH_3 rather long bonds are required, these have strong p character which leaves the lone pair with strong s character. Therefore, methylation can induce only a very minor decrease of the p character of the lone pair. Thus, the differential effect of larger and larger increases of p character on protonation is mostly absent in the series PH_3, Me_3P.

Calculated p/s ratios of the lone pair orbital obtained with localized orbital analysis by Boys (19) method using the STO-3G basis set are shown below. They follow all the qualitatively

Can. J. Chem. Downloaded from www.nrcresearchpress.com by 210.87.254.6 on 09/06/12
For personal use only.

TABLE 3. Geometries from calculations[a]

Compound	Parameter	Value STO-3G	STO-3G*	4-31G	4-31G*	Expt.Q[b]
PH_3	r(P—H)	1.380	1.378	1.434	1.416	1.415
	θ(HPH)	93.7	92.9	95.3	93.9	93.3
	Dipole	0.60	0.13	1.074	0.56	0.56
PH_4^+	r(P—H)	1.382	1.380	1.403	1.392	
CH_3PH_2	r(C—H)[c]	1.083(1)	1.084(1)			
		1.084(2)	1.086(2)	(1.081)		
	r(C—P)	1.842	1.832	1.93		
	r(P—H)	1.382	1.379	1.43		
	θ(HCH)[c]	107.8(2)	107.9(2)			
		107.1(2)	107.3(2)	(109.5)		
	θ(HPH)	93.8	96.7	95		
	θ(cPHp)	96.6	95.3	97		
	Dipole	0.55	0.12	1.18		1.1
$CH_3PH_3^+$	r(C—H)	1.085	1.089	(1.081)		
	r(C—P)	1.831	1.798	1.90		
	r(P—H)	1.381	1.379	1.40		
	θ(HCH)	109.9	109.4	(109.5)		
	θ(HPH)	107.6	107.0	108.7		
CH_3NH_2	r(C—H)[c]	1.089(2)		(1.081)		1.093
		1.093(1)				
	r(C—N)	1.485		1.48		1.474
	r(N—H)	1.033		1.00		1.014
	θ(HCH)[c]	107.9(2)		(109.5 fixed)		109.5
		108.5(1)				
	θ(HNH)	104.4		118.7		105.8
	θ(CNH)	107.3		114		
	Dipole	1.62		1.54		1.3
$CH_3—NH_3^+$	r(C—H)	1.091		(1.081)		
	r(C—N)	1.531		1.53		
	r(N—H)	1.043		1.02		
	θ(HCH)	111.0		110		
	θ(HNH)	107.4		109		

Compound	Parameter	Value STO-3G	Compound	Parameter	Value STO-3G
$C_6H_5NH_2$	r(C—N)	1.446	$C_6H_5—PH_2$	r(C—P)	1.834
	r(N—H)	1.028		r(P—H)	1.381
	θ(HNH)	110.8		θ(HPH)	94.3
	θ(CNH)	110.4		θ(CPH)	96.3
$C_6H_5—NH_3^+$	r(C—N)	1.510	$C_6H_5—PH_3^+$	r(C—P)	1.817
	r(N—H)	1.043		r(P—H)	1.380
	θ(HNH)	107.3		θ(HPH)	106.3
	θ(CNH)	111.5		θ(CPH)	112.2

[a]Bond distances in angstrom, dipole moments in Debye units.
[b]Experimental dipole moments from ref. 20*a* and experimental bond distances and bond angles from ref. 20*b*.
[c]C—H hydrogen 1 is in the plane of the C—P resp. C—N bond.

	p/s			
X	XH_3	XH_4^+	$MeXH_2$	$MeXH_3^+$
N	1.12	1.48	0.79	1.52
P	0.79	1.33	0.80	1.28

predicted changes of the rehybridization argument. An approximate estimate of the energy cost of the rehybridization can be made from Morokuma's (18) energy decomposition scheme, by assuming that the lone pair hybridization change will show up mostly in the term ES corresponding to the electrostatic energy of attraction between the proton and the base. The change of this term from NH_3 to $MeNH_2$ is found (18) to be ~+3 kcal/mol while for the corresponding phosphines the change should be much less, i.e. ~0.5 kcal/mol. The difference of ~2.5 kcal/mol is close to the experimentally and theoretically calculated differences of the proton transfer reactions, see Table 4. This suggests that rehybridization changes are the major cause for the smaller methyl effect on the basicity of the amines as compared to the phosphines.

The large difference in the phenyl substituent effect for NH_3

Can. J. Chem. Downloaded from www.nrcresearchpress.com by 210.87.254.6 on 09/06/12
For personal use only.

TABLE 4. Energy changes for proton transfer reactions from calculation and experiment[a]

Reaction	ΔE (STO-3G)	STO-3G*	4-31G	4-31G*	ΔH
$PH_3 + CH_3PH_3^+ = PH_4^+ + CH_3PH_2$	12.0	15.2	13.4	14.8	14.4
$PH_3 + C_6H_5PH_3^+ = PH_4^+ + C_6H_5PH_2$	16.5	21.3	19.2	—	18.7
$NH_3 + CH_3NH_3^+ = NH_4^+ + CH_3NH_2$	9.0	—	10.8	—	9.6
$NH_3 + C_6H_5NH_3^+ = NH_4^+ + C_6H_5NH_2$	8.3, 6.5[b]	—	6.2	—	6.5

[a]All values in kcal/mol, experimental ΔH from Table 1.
[b]Hehre and Taft (15).

and PH_3 can arise mostly from two factors. It has long been recognized that aniline is stabilized by conjugation as shown below (structure **I**). Since this stabilization of the base does not

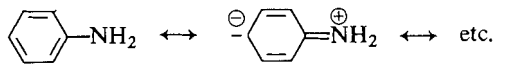

I

occur in the protonated onium ion, a reduction of basicity results. Due to a mismatch between the bonding orbitals of the phosphorus and the π orbitals of the aromatic ring the stabilization in **I** is expected to be much less in phenyl phosphine. A second factor is conjugation which stabilizes specifically the phosphonium ion as shown in structure **II**. This conjugation

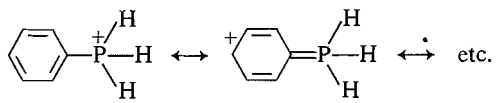

II

will not be important in the anilinium ion, since nitrogen does not have suitable empty orbitals to accept π donation from the aromatic system.

Results pertinent to the discussion above are given in Table 5, which gives the calculated electron transfer between occupied and unoccupied orbitals in RX where R is either methyl or phenyl and X is NH_2, NH_3^+ or PH_2, PH_3^+. Examining first aniline, we find a large electron transfer (0.088) from NH_2 to phenyl which should correspond to the conjugation **I**. The corresponding transfer in phenyl phosphine is much smaller, i.e., only about one third the aniline effect. The transfer of electrons from phenyl to PH_3^+ corresponding to conjugation **II** is also a relatively large effect, the analogous transfer from phenyl to NH_3^+ is predicted to be only half as big. Thus, the results in Table 5 are supportive of the differential effect of conjugation **I** in reducing the basicity of aniline but not of phenyl phosphine and conjugation **II** in selectively increasing the stability of the phenyl phosphonium ion. The numbers in Table 5, if taken at face value, indicate that the difference of the phenyl substituent effect between ammonia and phosphine is much more due to the selective stabilization of aniline by conjugation **I** than to the selective stabilization of the phenyl phosphonium ion by conjugation **II**.

The conjugative stabilization **II** of the phenyl phosphonium ion may be thought to involve significant phosphorus *d* orbital participation. Since the STO-3G basis set does not include *d* orbitals for phosphorus, the importance of conjugation **II** in Table 5 may be thought to be grossly underestimated. Very probably this is not the case. We saw earlier in Table 4 that the 4-31G calculation gives very good agreement with the experimentally measured enthalpy change for reaction [2]. The 4-31G also does not contain *d* orbitals. It is true that in Table 4, STO-3G*, with *d* orbitals, gives better agreement with the ΔH than STO-3G, but in the case of STO-3G, addition of *d* orbitals provides an important increase of the flexibility of the basis set and needs not to mean true *d* orbital participation. The conjugation **II** seems to be due mostly to the empty π^* orbitals of the phosphorus which happen to match somewhat with the π orbitals of benzene.

The results in Table 5 for methyl substitution in NH_3 and PH_3 run parallel to the discussed effects for phenyl substitution. Thus, there is a significant stabilization of the neutral base, methyl amine, by conjugation of empty orbitals on methyl with occupied orbitals on NH_2, just as was the case for aniline, and there is a noticeable stabilization by conjugation of occupied orbitals of methyl with unoccupied orbitals in PH_3^+, for the methyl phosphonium ion, just as was the case for phenyl phosphonium, only the effects for methyl are considerably smaller than those for phenyl. The respective C—N and C—P bond length changes with protonation are also parallel for methyl and phenyl. The C—N bonds for both methyl and phenyl increase in length, while the C—P bonds decrease in length, with pro-

TABLE 5.
(*a*) Electron transfer between occupied orbitals of R and unoccupied orbitals of X and vice versa from PMO STO-3G analysis[a]

R—X	CT(ϕ(R) → ϕ^*(X))	CT(ϕ^*(R) ← ϕ(X))
C_6H_5—NH_2	0.007 (−2.4)	0.088 (−19.1)
C_6H_5—PH_2	0.008 (−1.8)	0.027 (−4.3)
C_6H_5—NH_3^+	0.014 (−3.5)	0.014 (−2.3)
C_6H_5—PH_3^+	0.032 (−6.6)	0.006 (−1.0)
CH_3—NH_2	0.005 (−1.3)	0.027 (−6.3)
CH_3—PH_2	0.009 (−1.25)	0.008 (−1.25)
CH_3—NH_3^+	0.009 (−2.5)	0.008 (−1.25)
CH_3—PH_3^+	0.022 (−3.8)	0.003 (−0.5)

(*b*) Total electron transfer from R to X (X = NH_2 and PH_2) upon protonation

	Energy transfer		
R—X	STO-3G	4-31G	4-31G*
CH_3NH_2	0.270	0.266	
$C_6H_5NH_2$	0.328	0.347	
CH_3PH_2	0.279	0.294	0.269
$C_6H_5PH_2$	0.335	0.342	

[a]Numbers given in parentheses correspond to energies in kcal/mol.

Can. J. Chem. Downloaded from www.nrcresearchpress.com by 210.87.254.6 on 09/06/12
For personal use only.

TABLE 6.
(*a*) Bond length changes on protonation of C—N and C—P bonds

Compound	Bond length change STO-3G	4-31G
$MeNH_2$	+0.005	+0.07
$PhNH_2$	+0.07	—
$MePH_2$	−0.01	−0.03
$PhPH_2$	−0.02	—

(*b*) STO-3G, Mulliken electron population of bonds between C—N resp. C—P

Compound	Electron population Neutral	Cation
$MeNH_2$	0.219	0.076
$MePH_2$	0.266	0.260
$PhNH_2$	0.246	0.080
$PhPH_2$	0.184	0.228

tonation. Table 6 summarizes these bond lengths as predicted by STO-3G. The bond length changes predicted by 4-31G, where available (Table 3), support the same trends. The Mulliken electron populations between C—N resp. C—P are also given in Table 6. Comparing the changes in these bond populations with the changes in Table 5 one finds that the changes of Table 5, outlined in the discussion above, make an important contribution also to the total Mulliken bond population changes. This indicates that the dominant conjugations of Table 5 are largely responsible for the opposite C—N resp. C—P bond length changes on protonation of the bases.

Earlier in this discussion, the smaller basicity increasing effect of methyl on ammonia, as compared to phosphine, was explained on the basis of rehybridization, i.e. a decrease of *p* character of the lone pair in methyl amine. The data in Table 5 for methyl amine predict conjugation between the NH_2 group as electron donor and CH_3 as acceptor. The two explanations appear different only because they are cast in the different language of two bonding models that chemists use. The situation is analogous regarding the stabilization of the methyl phosphonium ion. There is (a small) stabilization by conjugation with CH_3 acting as electron donor and PH_3^+ as the acceptor (Table 5). This is recognized as hyperconjugation, but it can also be described as a rehybridization.

1. S. IKUTA, P. KEBARLE, G. M. BANCROFT, T. CHAN, and R. J. PUDDEPHATT. J. Am. Chem. Soc. To be published.
2. R. H. STALEY and J. L. BEAUCHAMP. J. Am. Chem. Soc. **96**, 6252 (1974).
3. J. F. WOLF, R. H. STALEY, I. KOPPEL, M. TAAGEPERA, R. T. MCIVER, J. L. BEAUCHAMP, and R. W. TAFT. J. Am. Chem. Soc. **99**, 5417 (1977).
4. V. T. TRAN and B. MUNSON. Paper presented at 27th Conference of the American Society for Mass Spectrometry, Seattle, 1979.
5. R. YAMDAGNI and P. KEBARLE. J. Am. Chem. Soc. **95**, 3504 (1973); **98**, 1320 (1976).
6. P. PAULAY. Mol. Phys. **17**, 197 (1969).
7. W. J. HEHRE, R. T. STEWART, and J. A. POPLE. J. Chem. Phys **51**, 2657 (1969).
8. J.B. COLLINS, P. V. R. SCHLEYER, J. S. BINKLEY, and J. A. POPLE. J. Chem. Phys. **64**, 5142 (1976).
9. R. DITCHFIELD, W.J. HEHRE, and J.A. POPLE. J. Chem. Phys. **54**, 724 (1971).
10. B. ROOS and P. SIEGBAHN. Theoret. Chim. Acta, **17**, 199 (1970).
11. W. J. HEHRE, W. A. LATHAN, R. DITCHFIELD, M. D. NEWTON, and J. A. POPLE. QCPE, **11**, 236 (1973).
12. M. KING, M. DUPUIS, and J. RYS. Nat. Resour. Comput. Chem. Software Cat., Vol. 1, Prog. No. QHOS, HONDO 5. 1980.
13. M. PETERSON and R. POIRIER. Monstergauss. Chemistry Department, University of Toronto, Toronto, Ont., Canada. 1981.
14. J. E. DEL BENE, M. J. IRISH, K. RAGHARACHAR, J. A. POPLE, and P. V. R. SCHLEYER. J. Am. Chem. Soc. To be published.
15. S. K. POLLACK, J. L. DEVLIN, K. D. SUMMERHAYS, R. W. TAFT, and W. J. HEHRE. J. Am. Chem. Soc. **99**, 4583 (1977).
16. Y. K. LAU, K. NISHIZAWA, A. TSE, R. S. BROWN, and P. KEBARLE. J. Am. Chem. Soc. **103**, 6291 (1981).
17. R. W. TAFT. *In* Proton transfer reactions. *Edited by* E. F. Caldin and V. Gold. Chapman and Hall, London. 1975.
18. H. UMEZAMA and K. MOROKUMA. J. Am. Chem. Soc. **98**, 4400 (1976).
19. J. M. FOSTER and S. F. BOYS. Rev. Mod. Phys. **32**, 300 (1960).
20. (*a*) A. L. MCCLELLAN. Tables of experimental dipole moments. W. H. Freeman and Co. 1963; (*b*) CRC handbook of Chemistry and Physics. 59th ed.

Can. J. Chem. Downloaded from www.nrcresearchpress.com by 210.87.254.6 on 09/06/12
For personal use only.

The oxidation of a nickel(II) oxime complex by polypyridine iron(III) ions in acidic aqueous media. Formation of a Ni(IV) species

D. H. MACARTNEY[1] AND A. MCAULEY[2]
Department of Chemistry, University of Victoria, Victoria, B.C., Canada V8W 2Y2

Received December 29, 1981

D. H. MACARTNEY and A. MCAULEY. Can. J. Chem. **61**, 103 (1983).

The kinetics of the oxidation of a nickel(II) oxime complex by a series of iron(III) phenanthroline and bipyridine cations, $Fe(LL)_3^{3+}$, have been investigated. The overall reaction

$$Ni(II)(H_2L)^{2+} + 2Fe(LL)_3^{3+} \rightarrow Ni(IV)L^{2+} + 2Fe(LL)_3^{2+} + 2H^+$$

is considered to take place via two one-electron steps, the first (rate-determining) process yielding $Ni(III)(H_2L)^{3+}$ being followed by very rapid oxidation to the nickel(IV) product. The second order rate constants at 25°C in 0.50 *M* *p*-toluenesulphonic acid are: $Fe(dmbpy)_3^{3+}$, $1.32 \times 10^3\ M^{-1}\ s^{-1}$; $Fe(dmphen)_3^{3+}$, $3.73 \times 10^3\ M^{-1}\ s^{-1}$; $Fe(bpy)_3^{3+}$, $3.20 \times 10^4\ M^{-1}\ s^{-1}$; $Fe(mphen)_3^{3+}$, $6.83 \times 10^4\ M^{-1}\ s^{-1}$; $Fe(phen)_3^{3+}$, $9.16 \times 10^4\ M^{-1}\ s^{-1}$; and $Fe(cphen)_3^{3+}$, $5.6 \times 10^5\ M^{-1}\ s^{-1}$. The reactions are outer-sphere in character. The rate of the corresponding cross reaction of nickel(II) species with $Ru(bipy)_3^{3+}$ ($k_{12} = 1.1 \times 10^6\ M^{-1}\ s^{-1}$) has also been measured. Activation parameters have been incorporated in a Marcus theory correlation to yield information ($k_{11} \sim 3 \times 10^3\ M^{-1}\ s^{-1}$) for the $Ni^{II}(H_2L)^{2+}/Ni^{III}(H_2L)^{3+}$ electron exchange reaction. This value is compared with exchange parameters for Ni^{II}/Ni^{III} tetraaza-macrocycle and other similar systems.

D. H. MACARTNEY et A. MCAULEY. Can. J. Chem. **61**, 103 (1983).

On a étudié la cinétique de l'oxydation d'un complexe oxime de nickel(II) par une série de cations phénanthroline et bipyridine de fer(III), $Fe(LL)_3^{3+}$. On considère que la réaction globale suivante:

$$Ni(II)(H_2L)^{2+} + 2Fe(LL)_3^{3+} \rightarrow Ni(IV)L^{2+} + 2Fe(LL)_3^{2+} + 2H^+$$

se fait par l'intermédiaire de deux étapes à un électron, la première (qui est l'étape déterminante) donne le Ni(III) $(H_2L)^{3+}$ est suivie de l'oxydation rapide en un composé de nickel(IV). Les constantes de vitesse d'ordre deux à 25°C dans l'acide *p*-toluènesulfonique 0,50 *M* sont de $Fe(dmphen)_3^{3+}$, $1,32 \times 10^3\ M^{-1}\ s^{-1}$; $Fe(dmphen)_3^{3+}$, $3,73 \times 10^3\ M^{-1}\ s^{-1}$; $Fe(bpy)_3^{3+}$, $3,20 \times 10^4\ M^{-1}\ s^{-1}$; $Fe(mphen)_3^{3+}$, $6,83 \times 10^4\ M^{-1}\ s^{-1}$; $Fe(phen)_3^{3+}$, $9,16 \times 10^4\ M^{-1}\ s^{-1}$ et $Fe(cphen)_3^{3+}$, $5,6 \times 10^5\ M^{-1}\ s^{-1}$. Les réactions ont un caractère périférique. On a également mesuré la vitesse de la réaction croisée des espèces de nickel(II) avec le $Ru(bipy)_3^{3+}$ ($k_{12} = 1,1 \times 10^6\ M^{-1}\ s^{-1}$). On a incorporé les paramètres d'activation dans une corrélation de la théorie de Marcus pour obtenir l'information sur la réaction d'échange d'électron du $Ni^{II}(H_2L)^{2+}/Ni^{III}(H_2L)^{3+}$ ($k_{11} \sim 3 \times 10^3\ M^{-1}\ s^{-1}$). On a comparé cette valeur avec les paramètres d'échange du tétraazamacrocycle Ni^{II}/Ni^{III} et d'autres systèmes semblables.

[Traduit par le journal]

Introduction

Investigations of metal complexes containing nickel in oxidation states greater than +2 have been of considerable interest recently (1–4). Significant progress has been made in the stabilisation and description of nickel(III) complexes, with primary attention being paid to compounds containing tetraaza-macrocyclic ligands (5–7). In the case of nickel(IV) there are fewer reported complexes (8). However, compounds containing dioxime ligands have been prepared and studied (3, 8–11).

For the stabilisation of nickel(IV), a hexadentate dioxime ligand of type **I** has been employed (9). This ligand,

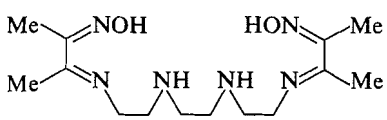

I

3,14-dimethyl-4,7,10,13-tetraazahexadeca-3,13-diene-2,15-dioxime (H_2L), forms pseudo-octahedral NiN_6 complexes with nickel(II), (III), and (IV). The preparative oxidation of the nickel(II) oxime complex, $Ni(H_2L)^{2+}$, to the nickel(IV) species has been accomplished both electrochemically ($E°(Ni^{IV}/Ni^{II}) = 0.95$ V) (10) or chemically with nitric acid (9).

With the exception of a recent study (12) in these laboratories of the oxidation of $Ni(H_2L)^{2+}$ by Co^{3+}, no kinetic data on the oxidation of nickel(II) oximes in aqueous solution have been reported previously.

In the present investigation the kinetics of the oxidation of $Ni^{II}(H_2L)^{2+}$ by a series of substituted polypyridine (1,10-phenanthroline and 2,2′-bipyridine) complexes of iron(III), $Fe(LL)_3^{3+}$, were examined. These complexes have been used in a number of rate studies with a variety of reductants, including Fe^{2+} (13), I^- (14), and ascorbic acid (15). The insolubility of the $Fe(LL)_3^{3+}$ species in non-coordinating perchlorate media prevents their use with a number of reductants. In the present study, however, both the reductant, $Ni(H_2L)^{2+}$, and the oxidants are soluble in the *p*-toluenesulphonate medium employed.

The activation parameters for this reaction system may be used in an estimation of the self-exchange parameters of the Ni^{II}/Ni^{III} oxime couple by means of Marcus theory correlations. These parameters are of interest for comparison with the values determined for the Ni^{II}/Ni^{III} tetraaza-macrocycle exchange reactions (16, 17), where there is an increase in coor-

[1]Present address: Chemistry Department, Brookhaven National Laboratories, Upton, Long Island, New York.

[2]To whom all correspondence should be addressed.

0008-4042/83/010103-06$01.00/0

©1983 National Research Council of Canada/Conseil national de recherches du Canada

Can. J. Chem. Downloaded from www.nrcresearchpress.com by 210.87.254.42 on 09/06/12
For personal use only.

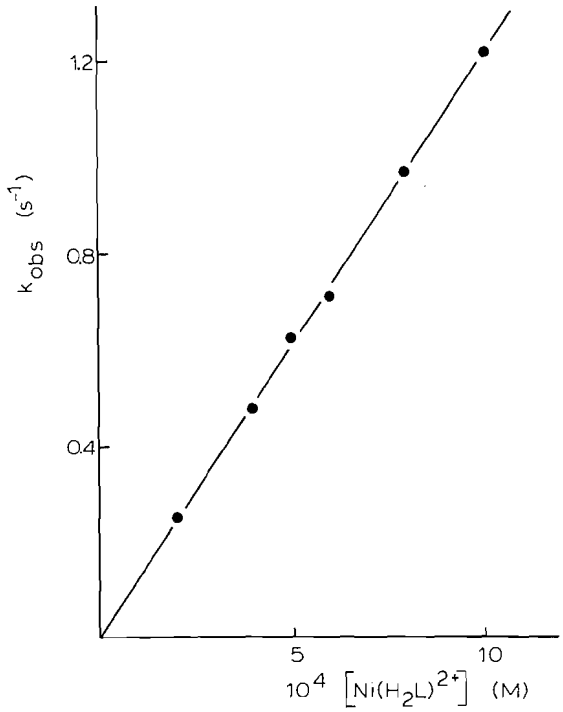

FIG. 1. Dependence of k_{obs} on $[Ni(H_2L)^{2+}]$ in the reaction with $Fe(dmbpy)_3^{3+}$ at 25°C, $[H^+] = 0.50\ M$, $I = 1.00\ M$ (H^+/Li^+ *p*-toluenesulphonate).

dination number on oxidation similar to the axial solvent interactions seen to be of importance in the attainment of nickel(III) for deprotonated peptide complexes (18).

Experimental

Reagents

The nickel(II) oxime complex $Ni(H_2L)(ClO_4)_2$, was prepared (9) by the addition of the ligand H_2L (H_2L = 3,14-dimethyl-4,7,10,13-diene-2,15-dione dioxime (19) to a methanol solution of nickel(II) perchlorate, followed by recrystallization from water. Analysis of the product, performed by the Canadian Microanalytical Service, was satisfactory; obsd. (calcd.) C 29.71 (29.49), H 5.02 (4.91), N 14.75 (14.70).

The iron(II) complexes, $[Fe(LL)_3](ClO_4)_2$, containing substituted 1,10-phenanthroline and 2,2′-bipyridine ligands (LL) were prepared by mixing solutions of ammonium ferrous sulphate and the polypyridine ligands (G. F. Smith) in methanol. The perchlorate salts of the iron(II) complexes were precipitated by the addition of an excess of sodium perchlorate. The iron(III) species, $Fe(LL)_3^{3+}$, were prepared in situ by the addition of 0.75 equivalents of Co^{3+} (in 4 *M* $HClO_4$) to acidic aqueous solutions of $Fe(LL)_3^{2+}$ ($2-4 \times 10^{-5}\ M$).

The reactions were studied in *p*-toluenesulphonate media, in which both the reductant and oxidants are soluble. The acid concentration was maintained at 0.50 *M* with recrystallized *p*-toluenesulphonic acid (Fisher). The ionic strength was constant at 1.00 *M* using lithium *p*-toluenesulphonate, prepared by neutralisation of the acid with lithium carbonate.

Kinetic studies

The kinetic experiments were carried out using a stopped-flow apparatus described previously (20). Reactions were studied at temperatures between 16.4 and 31.0°C with thermostating to ±0.05°C. Pseudo-first-order conditions of excess $[Ni(H_2L)^{2+}]$ were employed and the reactions were monitored at 500 nm where both $Ni^{IV}L^{2+}$ and $Fe(LL)_3^{2+}$ absorb strongly. Absorbance data derived from photomultiplier output were collected by a PCM-12 mini-computer. Plots of ln $(A_\infty - A_t)$ against time were linear for three or more half-lives.

Cyclic voltammetry

The reduction potentials of the $Fe(LL)_3^{2+}$ complexes in 1.00 *M* *p*-toluenesulphonic acid were determined by cyclic voltammetry. A Princeton Applied Research Model 173 instrument with a PAR Model 175 Universal Programmer were employed in conjunction with platinum working and counter electrodes and a saturated calomel electrode. Similar measurements were also made on the nickel(II) and nickel(IV) species. In this case the cyclic voltammograms observed were dependent on the pH of the solution. For runs at high acidity the Ni(IV) complex was used owing to possible hydrolysis of the nickel(II) species under these conditions. At higher pH's where two one-electron transfer reactions were observed, acetate and phosphate buffered solutions were employed.

Results

Reaction in solution of nickel(II) complex with the oxidants studied produced an immediate change in spectrum consistent with the formation of the nickel(IV) cation. In solutions of 0.5 *M* $[H^+]$, the products were stable for at least several hours. The stoichiometry of the oxidation is represented (to ±4%) by the reaction

$$[1]\quad Ni(II)(H_2L)^{2+} + 2Fe(LL)_3^{3+} \rightarrow Ni(IV)L^{2+} + 2Fe(LL)_3^{2+} + 2H^+$$

Oxidants used in this study may be represented by the following: $Fe(dmbpy)_3^{3+}$, (dmbpy) = 4,4′-dimethyl-2,2′-bipyridine; $Fe(dmphen)_3^{3+}$, (dmphen) = 4,7-dimethyl-1,10-phenanthroline; $Fe(bpy)_3^{3+}$, (bpy) = 2,2′-bipyridine; $Fe(mphen)_3^{3+}$, (mphen) = 5-methyl-1,10-phenanthroline; $Fe(phen)_3^{3+}$, (phen) = 1,10-phenanthroline; and $Fe(cphen)_3^{3+}$, (cphen) = 5-chloro-1,10-phenanthroline.

Owing to the insolubility of the reactants in perchlorate media, the investigation was carried out using $I = 1.0\ M$ *p*-toluenesulphonate, pts^-, with Lipts = Hpts = 0.50 *M*. Under the pseudo-first-order conditions of excess reductant, the order of reaction was established as unity with respect to each reagent. In Fig. 1 is shown the first-order dependence of k_{obs}, the observed rate constant, on the concentration of $Ni(H_2L)^{2+}$ for the reaction of $Fe(dmbpy)_3^{3+}$ at 25°C. Although solid samples of some of the iron(III) complexes were prepared and used, it was found more convenient to prepare $Fe(LL)_3^{3+}$ ions in situ in most cases by oxidation of the corresponding $Fe(LL)_3^{2+}$ complex by a stoichiometric deficiency of Co_{aq}^{3+}. No dependence of k_{obs} on either Co^{2+} or $Fe(LL)_3^{2+}$ concentrations was observed. In the reaction with $Fe(phen)_3^{3+}$, for example, the rate constant for the $Fe(phen)_3^{3+}$ solution prepared by Co^{3+} oxidation ($9.16 \times 10^4\ M^{-1}\ s^{-1}$) is in agreement with the value obtained with a solution prepared from solid $[Fe(phen)_3](ClO_4)_3$ ($8.95 \times 10^4\ M^{-1}\ s^{-1}$).

There was also no hydrogen ion dependence observed in this reaction system. The rate constant measured for $Fe(dmbpy)_3^{3+}$ at $[H^+] = 0.10\ M$ ($1.32 \times 10^3\ M^{-1}\ s^{-1}$) agrees with the value obtained at $[H^+] = 0.50\ M$ ($1.25 \times 10^3\ M^{-1}\ s^{-1}$). The rate expression may therefore be written as

$$[2]\quad d[Ni^{IV}L^{2+}]/dt = k[Ni(H_2L)^{2+}][Fe(LL)_3^{3+}]$$

The second-order rate constants for the six oxidants, measured at several temperatures together with the corresponding activation parameters are presented in Table 1.

Cyclic voltammetry of $Fe(LL)_3^{2+/3+}$

The reduction potentials of the $Fe(LL)_3^{3+}$ complexes in 1.00 *M* *p*-toluenesulphonic acid were measured using cyclic voltammetry. Reversible one-electron traces were observed in

Can. J. Chem. Downloaded from www.nrcresearchpress.com by 210.87.254.42 on 09/06/12
For personal use only.

Can. J. Chem. Downloaded from www.nrcresearchpress.com by 210.87.254.42 on 09/06/12
For personal use only.

TABLE 1. Rate and activation parameters for reactions of $Ni(II)(H_2L)^{2+}$ with various $Fe(LL)_3^{3+}$ oxidants; $[Ni(II)(H_2L)]^{2+} = (2-8) \times 10^{-4}$ *M*; $[Fe(III)] = (1-3) \times 10^{-5}$ *M*; $[H^+] = 0.50$ *M*, $[I] = 1.00$ *M* (H^+/Li^+ *p*-toluenesulphonate)

Oxidant	T (°C)	10^{-4} k (M^{-1} s^{-1})	ΔH^* (kcal mol^{-1})	ΔS^* (cal deg^{-1} mol^{-1})
$Fe(dmbpy)_3^{3+}$	16.9	0.104	4.8±0.5	−28±2
	21.3	0.115		
	25.0	0.125		
	25.0	0.132[a]		
	31.0	0.153		
$Fe(dmphen)_3^{3+}$	16.4	0.239	8.7±0.5	−13±2
	21.3	0.330		
	25.0	0.373		
	31.0	0.530		
$Fe(bpy)_3^{3+}$	16.9	2.53	5.2±0.5	−20±2
	21.3	2.65		
	25.0	3.20		
	31.0	4.07		
$Fe(mphen)_3^{3+}$	16.9	5.72	3.4±0.5	−25±2
	21.3	6.05		
	25.0	6.83		
	31.0	7.78		
$Fe(phen)_3^{3+}$	16.8	7.22	4.0±0.5	−22±2
	21.3	8.04		
	25.0	8.95[b]		
	25.0	9.16		
	31.0	10.4		
$Fe(cphen)_3^{3+}$	16.7	44	1.9±0.5	−26±2
	21.3	51		
	25.0	56		

[a] $[H^+] = 0.10$ *M*.
[b] Solid $[Fe(phen)_3](ClO_4)_3$ used in place of $Fe(phen)_3^{3+}$ oxidised by Co^{3+}.

TABLE 2. Thermodynamic parameters for the oxidation of Ni(II) $(H_2L)^{2+}$ by $Fe(LL)_3^{3+}$

Oxidant	E° (V)[a]	ΔG°_{12}[b]	ΔG^*_{12}[b]	α	ΔG^{**}_{11}[c]
$Fe(dmbpy)_3^{3+}$	0.96	6.69	10.7	0.138	9.86
$Fe(dmphen)_3^{3+}$	1.00	5.77	10.1	0.119	9.81
$Fe(bpy)_3^{3+}$	1.09	3.69	8.7	0.079	9.49
$Fe(mphen)_3^{3+}$	1.13	2.77	8.4	0.056	9.94
$Fe(phen)_3^{3+}$	1.14	2.54	8.1	0.053	9.53
$Fe(cphen)_3^{3+}$	1.24	0.23	7.2	0.005	10.24

[a] Measured in 1.0 *M* *p*-toluenesulphonic acid.
[b] In kcal mol^{-1}.
[c] Derived using eq. [17], $\Delta G^*_{22} = 3.5$ kcal mol^{-1} and work terms quoted in text. Average $\Delta G^{**}_{11} = 9.88 \pm 0.19$ kcal mol^{-1}.

each case, with separations between cathodic and anodic peaks in the range 60−70 mV at a scan rate of 50 mV s^{-1}. The E° values (vs. NHE) are listed in Table 2. These reduction potentials are about 60−100 mV more positive than the values measured in 0.50 *M* H_2SO_4 (e.g. $Fe(phen)_3^{2+/3+}$, $E^\circ = 1.14$ V in *p*-toluenesulphonic acid and $E^\circ = 1.06$ V in H_2SO_4) (13).

One inference from the lower value of E° in sulphate media compared to the much more weakly coordinating pts^- ion is that ion-pairing $[Fe(LL)_3^{3+} \cdot SO_4^{2-}]$ takes place in solution. From the ΔE° values obtained, assuming no outer-sphere interaction with pts^-, an estimate of K_{ip} $(Fe(LL)_3^{3+} \cdot SO_4^{2-})$ ~10−15 *M* may be derived dependent on the individual complexes. If such is the case, then for many previous studies, normally carried out in 0.5 *M* SO_4^{2-}, there is a reasonable concentration (40−50%) of the ion-pair present in the solution.

TABLE 3. Cyclic voltammetry of nickel oxime complexes in various solutions; $I = 0.100(pts^-)$ $Ni(II)(H_2L)^{2+} = 5 \times 10^{-4} - 5 \times 10^{-3}$ *M*; saturated calomel reference electrode

pH[d]	E (vs. NHE)	$E_a - E_c$ (V)
1.00	0.880	0.045[a]
2.38	0.800	0.045
3.70	0.720	0.060
4.81	0.665	0.060−0.080[b]
6.83	0.655	0.060[c]
	0.460	0.060
7.85	0.660	0.070[c]
	0.430	0.080
9.22	0.650	0.090
	0.410	0.140

[a] Scan rates 2−5 mV/s. Using higher scan rates (50−100 mV/s) peak separations of 50−60 mV were observed.
[b] Peaks overlapping.
[c] Scan rates 5−20 mV/s.
[d] At $[H^+] = 1.00$ *M*, $E^\circ_{obs} = 0.94$ V.

Previous authors (14) have attempted to take effects of such interactions into account and have estimated (21) a value of K_{ip} $[Fe(LL)_3^{3+} \cdot I] = 4.1$ *M* for the iodide complex, in reasonable agreement with the present data. More information on these interactions is needed before any differences in reactivities can be ascribed.

Cyclic voltammetry of the Ni(IV)/Ni(II) complexes

The observed redox potentials of the nickel species were found to be significantly pH-dependent (Table 3). At higher

Can. J. Chem. Downloaded from www.nrcresearchpress.com by 210.87.254.42 on 09/06/12
For personal use only.

acid concentrations ($I = 0.1\ M$ pts^-) only a single two-electron wave (peak-to-peak separation ~45 mV) was observed at scan rates of 2–5 mV/s. The potentials observed are similar to those observed in chloride media (8) although in that study a 30 mV separation was observed. Above pH ≈ 4 (Table 3), two processes were discernible, each of which at pH > 7 showed separations of 60 mV. The higher potential was acid independent whereas the position of the lower moved, up to pH ~ 7.8, where pH independence was noted. These findings, including a marked departure from 60 mV reversible separation at higher pHs, are in excellent agreement with extensive studies in nitrate media completed by Lappin (22).

At pH = 0, the data are consistent with a single process (E° vs. NHE)

[3] $Ni(IV)L^{2+} + 2H^+ + 2e \leftrightharpoons Ni(H_2L)^{2+}$ $\quad E^\circ = 0.94$ V

where the product formed is the (oxime-) protonated nickel(II) species. Above pH ~ 5, the Ni(III)/(II) couple is acid dependent, owing to the protonation (10) of the nickel(II) species ($pK_1 = 7.69$, $pK_2 = 5.91$) and of the nickel(III) complex ($pK_3 = 3.91$) (22) where only a single acid–base equilibrium is observed.

[4] $Ni(III)L^+ + 2H^+ + e \rightleftharpoons Ni(II)(H_2L)^{2+}$ $\quad E^\circ = 1.23$ V

[5] $Ni(III)L^+ + H^+ + e \rightleftharpoons Ni(HL)^+$ $\quad E^\circ = 0.87$ V

[6] $Ni(III)L^+ + e \rightleftharpoons Ni(II)L^+$ $\quad E^\circ = 0.41$ V

[7] $Ni(III)HL^{2+} + e \rightleftharpoons Ni(HL)^+$ $\quad E^\circ = 0.64$ V (22)

The redox process for the nickel(IV) ion is independent of acidity.

[8] $Ni(IV)L^2 + e \rightleftharpoons Ni(III)L^+$ $\quad E^\circ = 0.65$ V

Discussion

The results of the kinetic study are consistent with a mechanism of the form

[9] $Ni(II)(H_2L)^{2+} + Fe(LL)_3^{3+} \xrightarrow{k} Ni(III)(H_2L)^{3+} + Fe(LL)_3^{2+}$

[10] $Ni(III)L + Fe(LL)_3^{3+} \xrightarrow{\text{fast}} Ni(IV)L + Fe(LL)_3^{2+}$

where a rate-determining one-electron outer-sphere reaction is proposed. Both $Fe(LL)_3^{3+}$ and $Ni(H_2L)^{2+}$ are relatively substitution-inert, and the large rate constants (10^3–10^5 $M^{-1}\ s^{-1}$) observed are considered to preclude any inner-sphere mechanism.

Since, under the reaction conditions, the reductant is in the form $Ni(II)(H_2L)^{2+}$ and the electron transfer rate is independent of acidity, the appropriate reductant redox couple is $Ni(II)(H_2L)^{2+}/Ni(III)(H_2L)^{3+}$. There is preliminary X-ray crystal (23) and solution (22) evidence for protonation of only one of the oxime groups in the nickel(III) complex. If, for the reaction

$$Ni(III)HL^{2+} + H^+ \rightleftharpoons Ni(III)(H_2L)^{3+}$$

$pK_4 < 0$ then $E^\circ(Ni(III)(H_2L)^{3+}/Ni(II)(H_2L)^{2+} \geq 0.98$ V. We have attempted to derive a more accurate assessment of this reduction potential by reaction in similar conditions with $Ru(bipy)_3^{3+}$. The overall process exhibits the same second order dependence (first with respect to both [Ni(II)] and [Ru(III)]). For nickel(III)/(II) complexes of this type the self-exchange rate (k_{11}) is ~1–3 × 10^3 $M^{-1}\ s^{-1}$. Combination of this parameter with that k_{22} for the $Ru(bipy)_3^{3+/2+}$ couple ($10^9\ M^{-1}\ s^{-1}$) (21) and the observed second order rate constant for the cross reaction, $k_{12} = 1.1 \times 10^6\ M^{-1}\ s^{-1}$ leads to a reduction potential $E^\circ(Ni(III)/(II)(H_2L)) \sim 1.23$ V. We have used this value in free-energy calculations. A consequence of this value is that pK_4 may be computed as −3 to −4 in keeping with only one observed protonation of the nickel(III) complex.

Although in most instances the net free energy changes for the first step are unfavourable, there is no evidence for any reaction reversibility. This is, in part, the result of reaction conditions where a large excess of reductant nickel(II) (15–80-fold over the iron(III) present) was used and also from a very favourable second step ($E^\circ(Ni(IV)/(III)) = 0.65$ V). In the case of $Fe(bipy)_3^{3+}$, for example, the free energy change leads to an equilibrium constant $K = 4 \times 10^{-3}$ and hence a reverse rate of $7 \times 10^6\ M^{-1}\ s^{-1}$. The subsequent reaction to yield $Ni(IV)L^{2+}$, however, has a rate calculated as $6 \times 10^8\ M^{-1}\ s^{-1}$. Even in the least favourable system, $Fe(dmbpy)_3^{3+}$, no evidence was found for reversibility, with a first-order dependence on [Ni(II)] confirmed over a wide concentration range (See Fig. 1).

The Marcus theory (24) for outer-sphere electron transfer reactions predicts a relationship between the free energy of reaction (ΔG°_{12}), the free energy of activation for the cross reaction (ΔG^*_{12}), and the free energies of activation for the reductant and oxidant self-exchange reactions (ΔG^*_{11} and ΔG^*_{22}). The relationship may be expressed in the form

[11] $$\Delta G^*_{12} = w + \lambda_{12}/4 + \Delta G^\circ_{12}/2 + (\Delta G^\circ_{12})^2/4\lambda_{12}$$

where $\lambda_{12} = 2(\Delta G^*_{11} + \Delta G^*_{22})$ and w is a parameter encompassing work terms associated with each of the free energy parameters.

Consideration has recently been given to the work term contributions in systems analysed using this approach (25–27). The relationship [11] may be rewritten in a modified form

[12] $$\Delta G^{**}_{12} = 0.5(\Delta G^{**}_{11} + \Delta G^{**}_{22}) + 0.5\Delta G^\circ_c(1 + \alpha)$$

where

[13] $$\Delta G^{**}_{12} = \Delta G^*_{12} - w_{12}$$

[14] $$\Delta G^{**}_{11} = \Delta G^*_{11} - w_{11}$$

[15] $$\Delta G^{**}_{22} = \Delta G^*_{22} - w_{22}$$

and

[16] $$\Delta G^\circ_c = \Delta G^\circ_{12} + w_{21} - w_{12}$$

The single and double asterisks refer to measured and corrected free energies of activation, the subscripts 1 and 2 relate to the nickel and iron couples, and w represents the corresponding Coulombic term. ΔG° and ΔG°_c are the measured and corrected reaction free energies.

In these systems, the distance between the centres in the activated complex is taken as 12 Å. Within the error of measurement, there is no detectable difference in the Fe—N bond lengths between $Fe(phen)_3^{2+}$ and $Fe(phen)_3^{3+}$ (26, 28). In the case of the nickel complexes, a recent study has compared the Ni—N, oxime, imine, and amine bond lengths in a similar species (11) where the ligand is a tridentate "half" of that considered here. For bis-2-(2-aminoethyl)imino-3-butanone oximato nickel(IV), the metal ion coordination geometry is distorted octahedral with the two tridentate ligands in a meridional arrangement, no significant changes in stereochemistry having occurred during oxidation from the nickel(II) ion. Val-

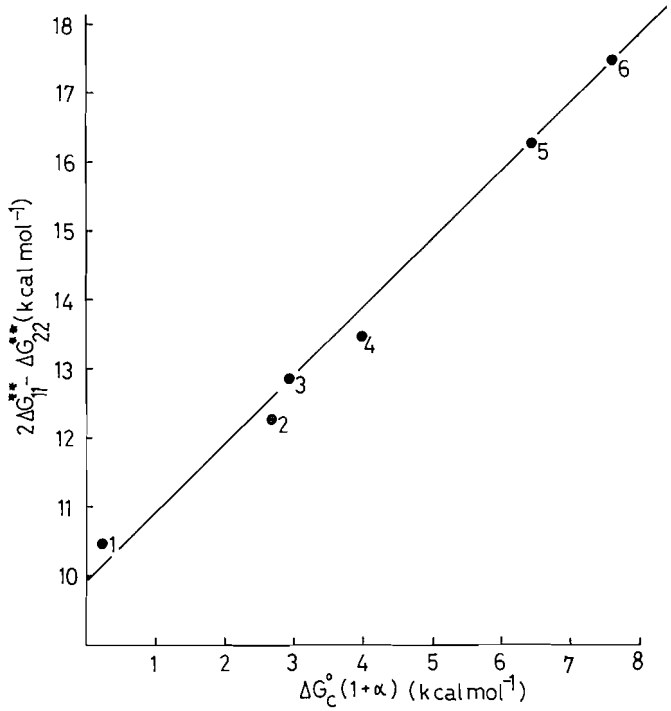

FIG. 2. Marcus plot for the oxidation of $Ni^{II}(H_2L)^{2+}$ with various $Fe(LL)_3^{3+}$ complexes: $Fe(cphen)_3^{3+}$ (*1*), $Fe(phen)_3^{3+}$ (*2*), $Fe(mphen)_3^{3+}$ (*3*), $Fe(bpy)_3^{3+}$ (*4*), $Fe(dmphen)_3^{3+}$ (*5*), and $Fe(dmbpy)_3^{3+}$ (*6*). Line drawn is of slope 0.96 (eq. [17]).

ues for the Ni(III)—N (oxime, imine, and amine) bond lengths were derived by averaging the appropriate Ni(IV)—N and Ni(II)—N distances (11).

In order to estimate the self-exchange rate constants for the $Ni(II)(H_2L)^{2+}/Ni(III)(H_2L)^{3+}$ electron exchange reaction, a Marcus plot was made according to the equation

$$[17] \quad (2\Delta G_{12}^{**} - \Delta G_{22}^{**}) = \Delta G_{11}^{**} + \Delta G_c^{\circ}(1 + \alpha)$$

where

$$[18] \quad \alpha = \Delta G_c^{\circ}/4(\Delta G_{11}^{**} + \Delta G_{22}^{**} - w_{11} - w_{22})$$

Initial values of ΔG_{11}^{**} were calculated using $\alpha = 0$ and using these in [18] an iterative approach led to limiting values of α. Thermodynamic data used are presented in Table 2. The reported value ($k_{22} = 3 \times 10^8\ M^{-1}\ s^{-1}$) (29) was used for the rate of $Fe(LL)_3^{2+/3+}$ self exchange. In Fig. 2 is shown a plot of $(2\Delta G_{12}^{**} - \Delta G_{22}^{**})$ against $\Delta G_c^{\circ}(1 + \alpha)$. The line drawn is of unit slope (eq. [17]) and the intercept yields a value of $\Delta G_{11}^{**} = 9.88 \pm 0.2$ kcal mol^{-1} ($k_{11} \sim 2.7 \times 10^3\ M^{-1}\ s^{-1}$). This value is very similar to those derived recently by Lappin (22). In the reactions (pH = 4–7) of $Ni(III)HL^{2+}$ and $Ni(III)L^{+}$ with $Co(phen)_3^{2+}$, rates of $10^3\ M^{-1}\ s^{-1}$ and $2 \times 10^3\ M^{-1}\ s^{-1}$) respectively were found for the nickel(II)/(III) exchanges.

Although complete structural and vibrational spectroscopic data are not yet available, the exchange rate derived in the present study is consistent with relatively small changes in bond lengths within the Ni complexes on electron transfer. The rate-determining process involves exchange between d^8 and d^7 octahedral species, the latter with an unpaired electron likely residing in the d_z^2 orbital. Where large structural changes are involved in outer-sphere reactions, exchange is generally slow, e.g. in the $Co(phen)^{2+/3+}$ (30) or $Co(sepulchrate)^{2+/3+}$ (31) systems the rates are 45 and 5 $M^{-1}\ s^{-1}$ respectively, and Co(II)/Co(III)–nitrogen bond length differences are of the order of 0.19 Å respectively (31). For the $Fe(phen)^{3+/2+}$ exchange where the M—N bond lengths are essentially the same, rates are $\sim 10^8\ M^{-1}\ s^{-1}$ (26–28). It would appear that for the octahedral Ni(II)/(III) complexes under consideration, the Ni—N distances change by ≤ 0.1 Å on electron transfer. Structural studies currently being undertaken will hopefully confirm this suggestion.

Unfortunately attempts to prove the existence of Ni(III)L species as intermediates were unsuccessful. Both uv–visible and esr methods were used but no firm evidence of any transient species was obtained.

The Ni(II)/Ni(III) oxime self-exchange parameters are similar to those found for Ni(II)/(III) cyclam complexes. Recent measurements of the $Ni(cyclam)^{2+/3+}$ exchange rate constant using ^{61}Ni esr (16) in 1.0 M $HClO_4$ yielded a $k_{11} = 1 \pm 0.3 \times 10^3\ M^{-1}\ s^{-1}$. Some variation might be expected for other macrocyclic systems, however, as is shown in the range of rates observed for cobalt(II)/(III) systems (32).

The oxime complexes have an octahedral configuration in both the Ni(II) and Ni(III) species, whereas a change from square-planar $Ni^{II}L^{2+}$ to octahedral $Ni^{III}L(H_2O)_2^{3+}$ occurs when L is a tetraaza-macrocycle.The similarity in the self-exchange parameters suggests there is only a small reorganisational energy associated with the change in geometry. Kinetic studies on the oxidation of other nickel(II) complexes with cyclic and non-cyclic ligands will be useful in further determining the effect of ring size, substituents, and geometry on thermodynamics of electron exchange.

Acknowledgements

We thank the Natural Sciences and Engineering Research Council of Canada and the University of Victoria for support. This work was carried out during the tenure of a University of Victoria graduate Fellowship (to D.H.M.) which is acknowledged.

1. J. C. BRODOVITCH and A. MCAULEY. Inorg. Chem. **20**, 1667 (1981).
2. J. M. T. RAYCHEBA and D. W. MARGERUM. Inorg. Chem. **20**, 1441 (1981).
3. A. F. LAPPIN, M. C. M. LARANJEIRA, and L. YOUDE-OWEI. J. Chem. Soc. Dalton Trans. 721 (1981).
4. F. P. BOSSU and D. W. MARGERUM. Inorg. Chem. **16**, 1210 (1977).
5. A. BENCINI, L. FABBRIZZI, and A. POGGI. Inorg. Chem. **20**, 2544 (1981).
6. R. I. HAINES and A. MCAULEY. Coord. Chem. Rev. **39**, 77 (1981).
7. E. ZEIGERSON, G. GINSBURG, N. SCHWARTZ, Z. LUZ, and D. MEYERSTEIN. J. Chem. Soc. Chem. Commun. 241 (1979).
8. K. NAG and A. CHAKRAVORTY. Coord. Chem. Rev. **33**, 87 (1980).
9. J. G. MONANTY, R. P. SINGH, and A. CHAKRAVORTY. Inorg. Chem. **14**, 2178 (1975).
10. J. G. MOHANTY and A. CHAKRAVORTY. Inorg. Chem. **15**, 2912 (1976).
11. H. SAARINEN, J. KORVENRANTA, and E. NASAKKALA. Acta Chem. Scand. A**34**, 443 (1980).
12. D. H. MACARTNEY and A. MCAULEY. To be published.
13. M. H. FORD-SMITH and N. SUTIN. J. Am. Chem. Soc. **83**, 1830 (1961).

Can. J. Chem. Downloaded from www.nrcresearchpress.com by 210.87.254.42 on 09/06/12
For personal use only.

14. C. O. ADEDINSEWO and A. ADEGITE. Inorg. Chem. **18**, 3597 (1979).
15. E. PELIZZETTI, E. MENASTI, and E. PRAMAURO. Inorg. Chem. **15**, 2898 (1976); **17**, 1181 (1978).
16. D. H. MACARTNEY, A. MCAULEY, and T. OSWALD. J. Chem. Soc. Chem. Commun. 274 (1982).
17. J. C. BRODOVITCH, A. MCAULEY, and T. OSWALD. Inorg. Chem. **21**, 3442 (1981).
18. M. P. YOUNGBLOOD and D. W. MARGERUM. Inorg. Chem. **19**, 3072 (1980).
19. A. M. BLATT (*Editor*). Organic synthesis. Coll. Vol. 2. Wiley, New York. p. 204.
20. K. J. ELLIS and A. MCAULEY. J. Chem. Soc. Dalton Trans. 1533 (1973).
21. R. G. WILKINS. Kinetics and mechanism of reactions of transition metal complexes. Allyn and Bacon, Boston, MA. 1974. p. 183.
22. A. G. LAPPIN. Private communication.
23. G. W. BUSHNELL, D. H. MACARTNEY, and A. MCAULEY. Unpublished results.
24. R. A. MARCUS. Ann. Rev. Phys. Chem. **15**, 155 (1964).
25. M. J. WEAVER and E. L. YEE. Inorg. Chem. **19**, 1936 (1980).
26. G. M. BROWN and N. SUTIN. J. Am. Chem. Soc. **101**, 883 (1979).
27. J. PHILIPS and A. HAIM. Inorg. Chem. **19**, 76 (1980).
28. A. ZALKIN, D. H. TEMPLETON, and T. UEKI. Inorg. Chem. **12**, 1641 (1973); J. BAKER, L. M. ENGLEHARDT, B. N. FIGGIS, and A. H. WHITE. J. Chem. Soc. Dalton. Trans. 530 (1975).
29. I. RUFF and M. ZIMANYI. Electrochem. Acta, **18**, 515 (1973).
30. R. FARINA and R. G. WILKINS. Inorg. Chem. **7**, 514 (1968).
31. A. M. SARGESON. Chem. Br. **15**, 23 (1979).
32. J. F. ENDICOTT and B. DURHAM. *In* Coordination chemistry of macrocyclic compounds. *Edited by* G. A. Melson. Plenum, New York. 1979. p. 420.

Can. J. Chem. Downloaded from www.nrcresearchpress.com by 210.87.254.42 on 09/06/12
For personal use only.

Nuclear magnetic resonance characterization of the ring conformations of monosubstituted derivatives of 1,3-dioxa-5,6-benzocycloheptene

R. ST-AMOUR AND M. ST-JACQUES

Département de Chimie, Université de Montréal, C.P. 6210, Succ. A, Montreal (Que.), Canada H3C 3V1

Received May 21, 1982

R. ST-AMOUR and M. ST-JACQUES. Can. J. Chem. **61**, 109 (1983).

The conformational properties of 2-alkyl (Me, Et, i-Pr, and *t*-Bu) and 2-phenyl derivatives of 1,3-dioxa-5,6-benzocycloheptene (**1**) were studied by ^{13}C dnmr. Analysis of slow exchange spectra at 100.6 MHz indicates that all derivatives except *tert*-butyl exist in an equilibrium of chair (major) and twist-boat (minor) conformations. Substituent effects on the position of the equilibrium are rationalized in terms of steric effects.

R. ST-AMOUR et M. ST-JACQUES. Can. J. Chem. **61**, 109 (1983).

Faisant appel à la rmn du ^{13}C, on a étudié les propriétés conformationnelles des dérivés alkyl-2 (Me, Et, i-Pr et *t*-Bu) et phényl-2 du dioxa-1,3 benzo-5,6 cycloheptène (**1**). L'analyse des spectres d'échange lent à 100,6 MHz indique que tous les dérivés, à l'exception du *tert*-butyl, existent dans des conformations à l'équilibre de la forme chaise (majoritaire) et de la forme bateau croisé (minoritaire). On rationalise les effets des substituants sur la position de l'équilibre en fonction des effets stériques.

[Traduit par le journal]

Present knowledge of the conformational properties of derivatives of 1,3-dioxa-5,6-benzocycloheptene (**1**; also called 2,4-benzodioxepin) indicates that they can exist either in the chair conformation (C) the twist-boat form (TB), or as a mixture of both. For example, ^1H and ^{13}C dnmr results have shown that **1** exists as a mixture of C (79%) and TB (21%) forms in CHF_2Cl at $-130°C$. Furthermore, whereas the low temperature ^{13}C nmr spectra of the 2-methyl derivative (**4**) were interpreted in terms of a highly dominant chair conformation (**2**; R = CH_3), the 2-methoxy derivative was shown (1) to adopt the TB form exclusively (**3**; R = OCH_3).

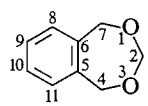

1

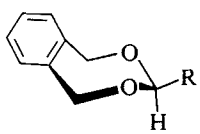

2

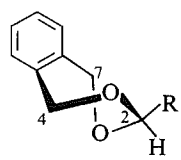

3

More recently, infrared and dipole moment studies on compound **1** and the series of 2-substituted derivatives **4** to **11** suggested that most of these derivatives adopt two conformations in solution at room temperature (2, 3). Quantitative determinations were not made for all compounds because of the inherent limitations of the experimental techniques used, although it was possible to suggest that the *tert*-butyl derivative (**8**) exists solely in the C form (2) and that the aryl derivatives (**9**–**11**) exist as a mixture with a C/TB ratio approximately 2:3 (3).

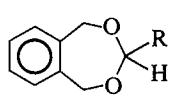

4

4	R = CH_3	**9**	R = C_6H_5
5	CH_2CH_3	**10**	C_6H_4Cl
6	$CH(CH_3)_2$	**11**	$C_6H_4NO_2$
7	$CH_2CH_2CH_3$	**12**	OCH_3
8	$C(CH_3)_3$		

Our continuing work on this system had led us to investigate compounds **4**, **5**, **6**, **8**, and **9** by ^{13}C nmr at high field (100.6 MHz) which, because of increased sensitivity, clearly reveals signals for the less populated conformation thus permitting a complete and quantitative conformational characterization of the 2-monosubstituted derivatives. Furthermore, the ^{13}C nmr parameters obtained for the various forms provide useful parameters for conformational and stereochemical diagnostic purposes.

Results

Compounds **4**, **5**, **6**, and **9** were found to give pertinent temperature dependent ^{13}C nmr spectra. For example, the 100.6 MHz ^{13}C nmr spectra of **4** (2-CH_3 derivative) are shown in Fig. 1 where it is seen that each of the various lines splits into two lines of unequal intensity, the more intense one is labelled c and the less intense one is labelled b in the spectrum recorded at $-115°C$. The spectrum at $-83°C$ shows the characteristic line broadening. Table 1 contains a summary of the chemical shifts for all the pertinent signals at high and low temperatures. Integration of the two lines for the various signals in the low temperature spectra reveals that the ratios of c/b are 87:13 for a CH_3OCH_3 solution and 96:4 in the more polar CHF_2Cl solvent. Published data (1, 2) indicate that the c lines are associated with the chair form and the b lines with the TB form; this assignment is confirmed in the next section. Consequently the free energy difference (ΔG^0) between these two conformations can be calculated in a straightforward manner taking into account the existence of two equivalent TB forms (see discussion in the next section). Table 2 contains a summary of the thermodynamic data obtained for all the compounds studied in both solvents.

Free energies of activation ($\Delta G^{\ddagger}$) can most easily be obtained from the changing spectra of compound **9** (2-phenyl) for which the 2-site approximation yields 7.9 kcal/mol (33.4 kJ/mol) at $-98°C$, the coalescence temperature determined at 20.15 MHz for a solution in CHF_2Cl; because of the appreciable intensity of both lines, this value is a reasonable approximation for $\Delta G^{\ddagger}$ which turns out to be similar to the reported

0008-4042/83/010109-07$01.00/0

©1983 National Research Council of Canada/Conseil national de recherches du Canada

Can. J. Chem. Downloaded from www.nrcresearchpress.com by 210.87.254.40 on 09/06/12
For personal use only.

Can. J. Chem. Downloaded from www.nrcresearchpress.com by 210.87.254.40 on 09/06/12
For personal use only.

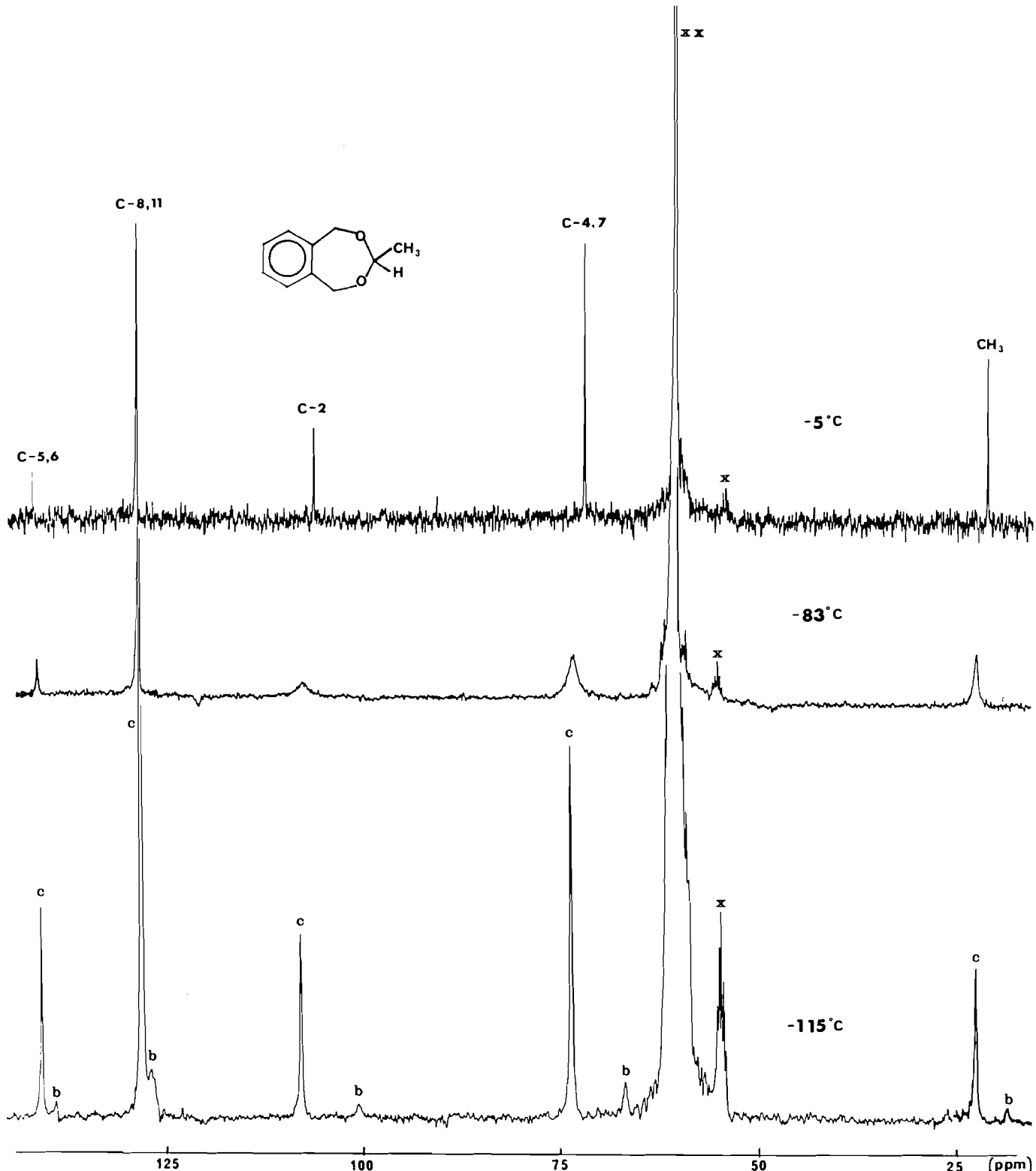

FIG. 1. The 100.6 MHz ^{13}C nmr spectra of **4** (2-CH_3 derivative) in CH_3OCH_3 solution at several temperatures. The lock (CD_2Cl_2) and solvent signals are labelled × and ×× respectively.

value for **1** (1).

Finally, compound **8** (2-*tert*-butyl) does not show a spectral change for the seven-membered ring carbon-13 signals but instead shows a spectral change of the methyl signal which splits into a characteristic doublet owing to slowing down of the C—C bond rotation at low temperatures. A similar observation was noted for 2-*tert*-butyl-1,3-dioxa-5,6-cycloheptene (4).

Discussion

Ring conformations

The data reported in Table 1 provide direct evidence for the existence of a mixture of two ring conformations for compounds **4**, **5**, **6**, and **9** whereas for **8** (2-*tert*-butyl) the signals of only one conformation are detected at low temperatures. Earlier work (1) on **4** had shown that the predominant con-

TABLE 1. ^{13}C nuclear magnetic resonance chemical shifts for compounds **1**, **4**–**6**, and **8** and **9** at high and low temperatures[a]

Compound	T(°C)	C-5,6	C-8,11	C-2	C-4,7	Other signals	
	25	141.03	128.55	100.54	73.96		
1	−130[b] (c)	140.72	129.59, 129.37	103.09	76.25		
	(b)	139.64	128.08, 127.86	96.84	70.38		
	25	141.09	128.74	107.04	72.72	21.51 (CH_3)	
4	−115 (c)	140.53	129.30	109.33	74.71	22.49	
	(b)	139.36	127.97	101.57	67.55	18.78	
	25	142.16	129.59, 129.45	112.18	73.31	29.16 (CH_2)	9.33 (CH_3)
5	−115 (c)	140.77	129.36	113.78	74.98	29.91	9.73
	(b)	140.00	128.32	106.25	67.66	25.36	
	25	142.31	129.60, 129.45	115.64	73.83	34.24 (CH)	18.36 (CH_3)
6	−115 (c)	140.92	129.30	116.30	75.17	34.61	17.96
	(b)	139.44	128.17	109.91	67.96	30.53	
	25	141.89	129.04	118.46	75.47	36.10 (C)	25.69 (CH_3)
8	−115	140.90	129.35	118.56	75.39	36.98	25.54
	25	140.91	128.79	107.26	71.93	140.91, 129.96, 129.60 127.92 (C_6H_5)	
9	−115 (c)	140.71	129.62	111.83	75.48	140.41, 130.34, 129.88,	
	(b)	139.51	127.87	102.49	68.06	126.92.	

[a]Data obtained for CHF_2Cl solutions containing TMS and CD_2Cl_2 (15%) for field lock.
[b]Data obtained from ref. 1. The letters (c) and (b) refer to the more intense and less intense lines observed at low temperatures.

TABLE 2. Conformer populations for compounds **1**, **4**–**6**, and **8** and **9** at −115°C

Compound	Solvent	C(%)	TB(%)	$-\Delta G^{0}$[a]	$-\Delta G^{0}_{corr}$[b]
1	CHF_2Cl	79	21	0.38	0.38
	CH_3OCH_3	67	33	0.21	0.21
4	CHF_2Cl	96	4	1.00	1.22
	CH_3OCH_3	87	13	0.60	0.82
5	CHF_2Cl	94	6	0.87	1.09
	CH_3OCH_3	88	12	0.63	0.85
6	CHF_2Cl	91	9	0.73	0.95
	CH_3OCH_3	92	8	0.77	0.99
8	CHF_2Cl	>99	—	>1.54	>1.67
9	CHF_2Cl	77	23	0.38	0.60
	CH_3OCH_3	56	44	0.08	0.30

[a]In kcal/mol, calculated from measurements on the C-4,7 signals and using the equation $\Delta G^{0} = -RT \ln K$ where $K = [C]/[TB]$.
[b]In kcal/mol calculated from $\Delta G^{0}_{corr} = \Delta G^{0} + RT \ln 2$ for the monosubstituted derivative.

former is the equatorially substituted chair (C-e) and the dynamic spectral results shown in Fig. 1 clearly reveal the existence of a minor conformer whose chemical shift parameters are labelled (b) in Table 1.

Although it appears most probable that this second conformer is the TB form (1−4), the ^{13}C chemical shifts determined at −115°C confirm this identification. In fact it has been reported (1) that the C and TB forms of the parent compound **1** show characteristic chemical shift differences for the C-5,6 (1.1 ppm) and C-8,11 (1.5 ppm) signals which are relatively insensitive to the substitution pattern on C-2 for several alkyl substituents. The observations that the less intense C-5,6 signal of **4** is 1.2 ppm upfield from the more intense one and that the C-8,11 signal is 1.3 ppm upfield for the minor conformer are in accord with the expectation that the TB form is less abundant.

Supporting arguments are also provided from the analysis of the C-4,7 chemical shifts in terms of the so-called γ-effect of the substituents (7), which is discussed in detail later in the text.

Similar arguments for compounds **5** and **6** lead to the conclusion that the minor conformer ((b) signals in Table 1) is also the TB form.

The low temperature spectrum for **8** shows that the *tert*-butyl group has a stronger conformational preference than the methyl (**4**), ethyl (**5**), and isopropyl (**6**) groups. Indeed the ^{13}C chemical shifts show that for **8** only the C-e form is detected in the low temperature ^{13}C nmr spectrum. A similarly strong C-e preference was noted previously for the analogous 2-*tert*-butyl derivative of 1,3-dioxacycloheptene (4).

Finally, a similar analysis of the C-5,6, C-8,11, and C-4,7 signals of each of the two forms observed for **9** leads to the association of the (c) lines of Table 1 with the C-e conformation and the (b) lines with the TB form. Interestingly, the phenyl group favours the TB form to a greater extent than the alkyl groups as the data in Table 2 show.

It is also important to point out that while the C-e ⇌ TB interconversion in Scheme 1 has been slowed down sufficiently on the nmr time scale to lead to distinct signals for each form, the inversion process of the minor TB form (TB ⇌ TB*,

Can. J. Chem. Downloaded from www.nrcresearchpress.com by 210.87.254.40 on 09/06/12
For personal use only.

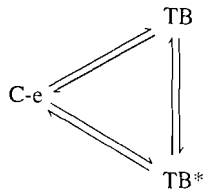

SCHEME 1

where the * indicated mirror image conformations) of **4**, **5**, **6**, and **9** has not been slowed down. If it had been, then the benzylic C-4 and C-7 would give distinct signals as was found to be the case for the 2-methoxy derivative (1).

The conformational effect of the 2-substituents

The low temperature conformational populations determined in two solvents are summarized in Table 2. Coupled with the results for the 2-methoxy group (1), it is seen that the conformational preference for the TB form in the more polar solvent (CHF_2Cl) is OCH_3(~100%), C_6H_5 (23%), $(CH_3)_2CH$ (9%), CH_3CH_2 (6%), and CH_3 (4%). Comparison with the parent compound **1** for which 21% of TB exist, however, indicates that alkyl substitution actually destabilized the TB form relative to C-e while phenyl substitution has relatively little overall effect. The distinct behaviour of the 2-methoxy derivative was ascribed to stereoelectronic effects (1) and for this reason this compound will not be compared further with the other monosubstituted derivatives in Table 2.

The solvent change to the less polar dimethyl ether increases the amount of TB for all compounds except for **6** (2-isopropyl). Nevertheless the overall qualitative picture is still retained.

In order to express the measured conformer populations in terms of thermodynamic parameters, consideration must be given to the statistical weight (or symmetry number) of the C and TB forms for the parent compound and for the monosubstituted derivatives. Differences in symmetry numbers for the C and TB forms are important when one wishes to use the approximation $\Delta H^0 \approx \Delta G^0$. In Table 2, the statistical contribution to entropy, namely R ln 2, must then be taken into account for the monosubstituted derivatives by means of the equation $\Delta G^0_{corr} = \Delta G^0 + RT$ ln 2. This effectively corresponds to the removal of entropic contributions from purely statistical effects, which is required prior to any attempt to relate thermodynamic data to structural parameters such as steric effects, nonbonded interactions, etc. (8, 9).

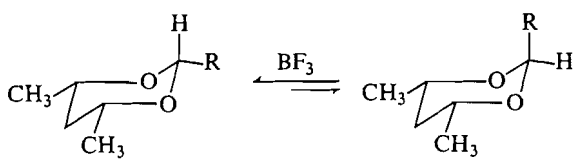

13	R = CH_3	ΔG^0 = 3.98 kcal/mol
14	= CH_3CH_2	= 4.04
15	= $(CH_3)_2CH$	= 4.17
16	= $(CH_3)_3C$	> 4.9
17	= C_6H_5	= 3.12

It is interesting to compare the trends for ΔG^0_{corr} in Table 2 with ΔG^0 values obtained for BF_3 catalysed equilibrations of derivatives **13** to **17** of 4,6-dimethyl-1,3-dioxane in diethyl ether at 25°C (10). Although these values correspond to the C-e ⇌ C-a process, there exists a remarkable parallel to the trend of ΔG^0_{corr} listed in Table 2 for solutions in dimethyl ether for the C-e ⇌ TB process of the analogously 2-substituted seven-membered acetals. Such an observation suggests that similar factors could be responsible in large part for the shifts in equilibria. Thus it is pertinent to point out that steric (nonbonded) interactions between the 2-alkyl substituent of the dioxanes with the two *syn*-axial protons on C-4 and C-6 (as in **18** where the R groups are either H or CH_3) were deemed responsible for the observed ΔG^0 values.

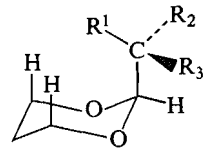

18

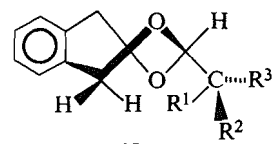

19

Structure **19** shows that a similar nonbonded interaction can exist in the TB form of the seven-membered acetals between only one of the benzylic protons and the alkyl substituent. Furthermore, for **4**, **5**, and **6** repulsive CH_3---H nonbonding interaction is avoided in the conformation with R^1 = H whereas for the *tert*-butyl derivative (**8**) R^1 = CH_3 and nonbonding CH_3---H repulsion is present. Consequently greater destabilization of conformation **19** occurs for **8** so that only the C-e form is effectively detected by the nmr methods.

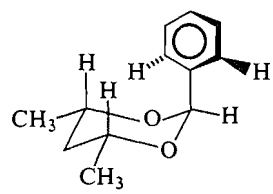

20

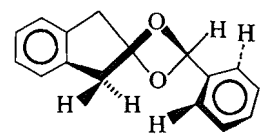

21

The conformational effect of the phenyl group in **9** and **17** is more subtle and for **17** was found to reflect a substantial difference in the freedom of internal rotation about the C-2 to phenyl bond in the axial and equatorial isomers (11, 12). In fact, it was shown that the equatorial phenyl is an effectively free rotor whereas the axial phenyl librates about an average perpendicular orientation which is illustrated by structure **20**. An unusually large conformational entropy results (ΔS^0 = 3.9 eu) so that ΔH^0 = −2.0 kcal/mol, a value significantly smaller than ΔG^0 = −3.12 kcal/mol.

It therefore appears that the phenyl group in the TB form can take up a position which effectively minimizes nonbonded interaction with the axial-like benzylic proton. Structure **21** represents a possible favored orientation. Thus, the phenyl group would not significantly destabilize the TB form as the results in Table 2 seem to indicate. Alternatively, if a significant stereoelectronic (or anomeric) effect were operational, it would most likely perturb the C ⇌ TB equilibrium which ought to be a probe for this kind of stabilizing effect as indicated by the fact that the 2-methoxy derivative exists exclusively in the TB form (1).

The nmr results reported in Table 2 therefore constitute reliable quantitative conformational information at the temperatures of measurement which are relatively low. But in order to compare them with results obtained from other methods (albeit less precise than nmr) such as the interpretation of

Can. J. Chem. Downloaded from www.nrcresearchpress.com by 210.87.254.40 on 09/06/12
For personal use only.

TABLE 3. Carbon-13 substituent effects at the α, γ, and δ positions[a]

Compound	Conformation	α	γ	δ
4 (2-CH_3)	C-e	6.24	−1.54	−0.19
	TB	4.73	−2.83	−0.29
5 (2-CH_2CH_3)	C-e	10.69	−1.27	0.05
	TB	9.41	−2.72	0.36
6 (2-$CH(CH_3)_2$)	C-e	13.21	−1.08	0.20
	TB	13.07	−2.42	−0.20
8 (2-*t*-Bu)	C-e	15.47	−0.86	+0.18
9 (2-C_6H_5)	C-e	8.74	−0.77	−0.01
	TB	5.65	−2.32	−0.13
12 (2-OCH_3)	TB	17.51	γ_g[b] −7.81	−1.33
			γ_a −2.59	

[a]Calculated as the difference between the chemical shift of each signal with the corresponding one in the parent compound **1**. A negative sign means an upfield shift.
[b]Values taken from ref. 1. Here $\gamma_g = \gamma_{gauche}$ and $\gamma_a = \gamma_{anti}$ effects.

dipole moments and ir studies (2, 3), at significantly higher temperatures, it is necessary to extrapolate from the data obtained at low temperatures (13).

Firstly, it is possible to obtain approximate conformer populations at about +25°C from the analysis of averaged chemical shifts at room temperature which actually represent a weighted average of the individual chemical shifts observed below the coalescence temperature. Mole fractions of the C and TB forms for the compounds listed in Table 2 can easily be calculated (14, 15).

It is well known that the accuracy of this averaged chemical shift method is reduced when the temperature dependences of the chemical shifts are not taken into account. Although this question was not resolved through chemical shift measurements below coalescence for an appreciable temperature range, the data for the *tert*-butyl derivative **8**, which exists only in the C-e form, may be pertinent. Table 1 shows that C-2 and C-4,7 signals of the C-e form of **8** have the same chemical shift at 25° and −115°C, whereas the published data for the 2,2-dimethyl derivative (1) shows that the C-2 and C-4,7 TB signals undergo very little change from 25° to −120°C, namely 0.1 and 0.6 ppm respectively. But because it has been shown that the chemical shift of TMS exhibits a temperature gradient (16), this method must be considered as very approximative. For example, the C/TB ratios are calculated as 61:39 for **1**, 51:49 for **9** in CHF_2Cl and 57:43 for **1**, 45:55 for **9** in CH_3OCH_3.

Secondly, it is interesting to note that a simple extrapolation of the experimentally determined K values (Table 2) to higher temperature using the equation $\Delta G^0 = -RT \ln K$, while assuming that $\Delta S^0 \approx 0$ and that ΔH^0 is temperature independent, yields relative amounts for the two conformers which are quite similar to those obtained by the chemical shift method. For example, the C/TB ratio is 65:35 for **1**, 58:42 for **9** in CHF_2Cl and 59:41 for **1**, 45:55 for **9** in CH_3OCH_3. Of course, such closeness could be fortuitous since the ΔS^0 and ΔH^0 effects could cancel each other in large part. The uncertainty associated with this second method can be appreciated from a consideration of results published for six-membered cyclic acetals where it is seen that the ΔS^0 measured are small (17, 18). On the other hand, the case of the phenyl derivative (**9**) is different because a large ΔS^0 value exists, as was pointed out earlier (11).

It is therefore interesting to compare the extrapolated nmr results with those obtained from dipole moment studies (2) which gave a C/TB ratio of 44:56 in CCl_4 at room temperature for the parent compound **1**. The nmr value in CH_3OCH_3 is 57:43 and the difference in polarity between these two solvents might not be sufficient to account for the observed difference between the two sets of values. Nevertheless, it is significant that both methods converge in indicating nearly equal amounts for both conformers.

For the 2-phenyl derivative (**9**), dipole moments (3) yielded a C/TB ratio of 40:60 while the nmr results indicate a 45:55 ratio. Agreement is therefore quite good. Unfortunately, the dipole moment approach did not permit quantification for **4**, **5**, and **6** (2-alkyl derivatives) so that the nmr results constitute the sole source of quantitative information.

Carbon-13 chemical shifts

The observation of individual ^{13}C nmr signals for the C-e and TB forms, as given in Table 1, permits the determination of the stereodependent effect of substituent on the chemical shifts of carbons C-2, C-4,7, and C-5,6 which are commonly termed α, γ, and δ effects respectively (7). These parameters are summarized in Table 3.

Whereas for six-membered cyclic acetals it is difficult to obtain reference parameters for the TB form, in this family of seven-membered rings it is the C-a form which has not yet been observed. Accordingly, only the C-e form is common to similar derivatives of both ring sizes.

Furthermore, it must be recognized that the seven-membered TB form is still undergoing rapid inversion through a pseudorotation process. Hence, some of the ^{13}C nmr signals represent averages at −115°C as was clearly demonstrated previously (1) for **12**, whose ^{13}C nmr spectrum at −150°C shows two benzylic carbon signals (i.e. C-4 and C-7 are no longer made equivalent by rapid inversion as shown in structure **22**). Unfortunately, the inversion barrier is lower when the substituent is nonpolar so that TB averaging is still rapid even at −150°C for the compounds listed in Table 1.

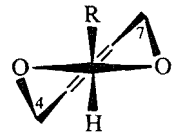

22

The α and δ effects in Table 3 reveal similar magnitudes for C-e and TB for a given substituent. By comparison, methyl

Can. J. Chem. Downloaded from www.nrcresearchpress.com by 210.87.254.40 on 09/06/12
For personal use only.

Can. J. Chem. Downloaded from www.nrcresearchpress.com by 210.87.254.40 on 09/06/12
For personal use only.

substitution on C-2 of 1,3-dioxane produced α_e and α_a parameters of 5.06 and −1.02 ppm respectively (5).

The γ effect is most interesting since it is this parameter which is most useful for stereochemical and conformational assignments. Whereas γ_e for 2-methyl substitution of 1,3-dioxane is −0.14 (5), a significant difference is found for **4** for which γ_e is −1.54 ppm, possibly because of differences in ring puckering as will be discussed shortly. Part of the difference may also originate from temperature effects on chemical shifts. It is therefore pertinent to compare the above value of −1.54 ppm for **4** with the −1.63 ppm at 25°C and −1.24 ppm at −85°C for 5-methylbenzocycloheptene (19). Finally, the trend for γ_e values observed for **4**, **5**, **6**, and **8** may be indicative of some ring deformation as the substituent size increases.

The γ_{TB} upfield shifts in Table 3 are also fairly constant, being −2.83 ppm for methyl substitution in **4**. This value actually represents the average of a small γ_{anti} effect (C-4 in **22**) and a larger γ_{gauche} effect (C-7 in **22**). Here again differences in ring puckering prevent simple comparison with six-membered ring parameters for γ_{anti} and γ_{gauche}.

Recently, a successful attempt to correlate the γ effect with dihedral angles has been reported (20) and it is useful to consider our results from that point of view. Although both steric and electronic factors have been considered in the past to explain the γ effect, it now appears acceptable to consider that a linear relationship with dihedral angles exists for CH_2 groups in substituted cycloalkanes.

Assuming that a similar linear relationship also existed for CH_2 carbons of acetals, the γ_e and γ_a effects of six-membered acetals substituted at C-2 with a methyl group then should provide useful reference values for dihedral angles of ~180° and ~60°. The average of two sets of published γ_e and γ_a values are used for this purpose, −0.14 and −7.76 ppm (5) and 0.1 and −7.3 ppm (6). Now, if we consider that the γ_e effect for **4** corresponds to a dihedral angle of about 160° (as measured from Dreiding models of the C-e form), we find that these three reference points on a γ vs. angle plot fall on a straight line. Therefore, the existence of a linear relationship for CH_2 carbons next to oxygen in acetals appears verified.

Examination of the TB form (**22**) for **4** shows that the measured dihedral angles for the C(4)—O—CH—CH_3 and C(7)—O—CH—CH_3 moities depend on the exact geometry of the ring conformation. Because the TB conformation is rather flexible, it is a priori impossible to select the minima on the energy profile of the pseudorotation cycle. Nevertheless, it appears reasonable to assume that the C(4)—O—CH—CH_3 dihedral angle is close to 180°; molecular models then show that the C(7)—O—CH—CH_3 angle is about 85 ± 5°. Using the straight line obtained above for acetals, γ effects of about 0.0 and −6.0 ppm are found to correspond to these two dihedral angles (i.e. 180° and 85°) so that their average (−3.0 ppm) is reasonably close to the value of −2.8 ppm determined experimentally for the TB form of **4**. Even though the quality of such linear relationships is not sufficient to permit the determination of accurate dihedral angles (20), it appears adequate to rationalize the γ parameters summarized in Table 3. Hence the differences between six and seven-membered acetals are due mainly to different ring geometries.

The γ_{TB} parameter (−2.8 ppm) determined for **4** is most useful to reassess the conformational situation of 2-methyl-1,3-dioxa-5,6-cycloheptene (**4***a*) for which the benzo group of **4** is replaced by a double bond. The reported upfield shift for the C-4,7 signal of **4***a* relative to the parent compound is −1.68 ppm (4); this value is significantly less than the −2.8 ppm determined for **4**. It would therefore appear that the predominant conformation of **4***a* is TB, as previously concluded (4), but that a significant amount of the C-e form does exist in rapid equilibrium even at −150°C.

Experimental

Melting points are uncorrected and were determined using a Buchi melting point apparatus.

Routine ^1H nmr spectra were recorded at 90 MHz on a Bruker WH-90 spectrometer. The room temperature ^{13}C nmr spectra were recorded at 20.15 MHz on a Bruker WP-80 spectrometer as were the variable temperature spectra of **9**. The lower temperature ^{13}C nmr spectra used for population determination were taken at 100.6 MHz using a Bruker WH-400 spectrometer equipped with a variable temperature unit (B-VT-1000) and located at the "Laboratoire Régional de rmn à haut champ" in Montreal.

The ^{13}C nmr spectra were recorded with proton decoupling for solutions in CHF_2Cl or CH_3OCH_3 using from 75 to 150 mg of sample in about 2.5 mL of solvent containing a little Me_4Si and about 15% of CD_2Cl_2 (for locking purposes) in standard 10 mm tubes which had been degassed and sealed. The temperatures of the spectra recorded at 20.15 MHz were determined after calibration with a thermocouple and are believed to be accurate to at least ±3°C.

The following instrumental conditions are typical for the low temperature ^{13}C nmr spectra at 100.6 MHz: flip angle: 65−70°; SW = 17 000−25 000 Hz; data size: 16K; acquisition time = 0.328 s or 0.482 s; pulse repetition time = 0.428 or 0.582 s. Temperatures were determined directly using the B-VT-100 unit. Calibration using a thermocouple inside a solvent-containing nmr tube indicates that the low temperatures reported are known within ±3°C. Results published by Booth and Jozefowicz (21) indicate that integrations of the c and b signals for a given carbon should not suffer from differential T_1 and nOe effects at −115°C. In fact, a check was carried out for compound **9** at −115°C and the T_1 values obtained are: 0.19 s for C-4,7 of C, 0.18 for C-4,7 of TB, 0.38 for C-2 of C, and 0.35 for C-2 of TB. Furthermore, variations in the flip angle did not significantly change the results for conformer populations.

Compound preparation

All compounds were prepared from recrystallized 1,2-benzenedimethanol (Aldrich) using a published procedure (22). In all cases, the work-up included removal of most of the benzene solvent by distillation at atmospheric pressure and distillation of the compounds at reduced pressure (~1 Torr). Yields varied from 45% to 75%. All melting points agreed with those reported in the literature (2, 3).

The ^1H nmr spectra of compounds **4** and **9** were identical to those reported previously (1, 2) while those for compounds **5**, **6**, and **8** show the following characteristics for $CDCl_3$ solutions. Compound **5**: 7.2 (s, 4H), 4.9 (s, 4H), 4.8 (t, 1H), 1.7 (m, 2H), 1.0 (t, 3H). Compound **6**: 7.2 (s, 4H), 4.9 (s, 4H), 4.5 (d, 1H), 1.9 (m, 1H), 1.0 (d, 6H). Compound **8**: 7.2 (s, 4H), 4.9 (s, 4H), 4.4 (s, 1H), 1.0 (s, 9H).

Finally, the ^{13}C nmr spectra reported in Table 1 confirmed the identity of each of the compounds prepared.

Acknowledgements

We wish to acknowledge the valuable contribution of Dr. M. T. Phan Viet of the "Laboratoire Régional de rmn à haut champ" in Montréal. We thank the Natural Sciences and Engineering Research Council of Canada and the Ministère de l'Education du Québec for their financial assistance.

1. A. Blanchette, F. Sauriol-Lord, and M. St-Jacques. J. Am. Chem. Soc. **100**, 4055 (1978).
2. B. A. Arbusov, E. N. Klimovitskii, A. B. Remisov, and G. N. Sergeeva. Bull. Soc. Chim. USSR, **29**, 211 (1980).

3. B. A. ARBUSOV, E. N. KLIMOVITOKII, A. B. REMISOV, and G. N. SERGEEVA. Bull. Soc. Chim. USSR, **28**, 1873 (1979).
4. (*a*) R. ST-AMOUR AND M. ST-JACQUES. Can. J. Chem. **59**, 2283 (1981); (*b*) Unpublished results.
5. K. PIHLAJA and T. NURMI. Isr. J. Chem. **20**, 160 (1980).
6. G. M. KELLIE and F. G. RIDDELL. J. Chem. Soc. (B), 331 (1971).
7. F. W. WEHRLI and T. WIRTHLIN. Interpretation of carbon-13 nmr spectra. Heyden, London. 1976.
8. W. F. BAILEY and A. S. MONAHAN. J. Chem. Educ. **55**, 489 (1978).
9. F. A. L. ANET and I. YAVARI. J. Chem. Soc. Chem. Commun. 58 (1978).
10. F. W. NADER and E. L. ELIEL. J. Am. Chem. Soc. **92**, 3050 (1970).
11. W. F. BAILEY, H. CONNON, E. L. ELIEL, and K. B. WIBERG. J. Am. Chem. Soc. **100**, 2202 (1978).
12. E. L. ELIEL, W. F. BAILEY, K. B. WIBERG, H. CONNON, and F. W. NADER. Justus Liebigs Ann. Chem. 2240 (1976).
13. F. R. JENSEN and C. H. BUSHWELLER. *In* Advances in alicyclic chemistry.Vol. 3. *Edited by* H. Hart and G. J. Karabatsos. Academic Press, New York. 1971.
14. F. A. L. ANET and R. ANET. *In* Determination of organic structures by physical methods. Vol. 3. *Edited by* F. C. Nachod and J. J. Zuckerman. Academic Press, New York. 1971.
15. H.-J. SCHNEIDER, W. FREITAG, and V. HOPPEN. Org. Magn. Reson. **13**, 266 (1980).
16. F.G. MORIN, M. S. SOLUM, J. D. WITHERS, D. M. GRANT, and D. K. DALLING. J. Magn. Reson. **48**, 138 (1982).
17. K. PIHLAJA. J. Chem. Soc. Perkin Trans. II, 890 (1974).
18. F. G. RIDDEL and M. J. T. ROBINSON. Tetrahedron, **23**, 3417 (1967).
19. (*a*) D. MÉNARD. M.Sc. Thesis, Université de Montréal, 1978; (*b*) D. MÉNARD and M. ST-JACQUES. Unpublished results.
20. J. B. LAMBERT and A. R. VAGENAS. Org. Magn. Reson. **17**, 265 (1981).
21. H. BOOTH and M. L. JOSEFOWICZ. J. Chem. Soc. Perkin Trans. II, 895 (1976).
22. K. C. BRANNOCK and G. R. LAPPIN. J. Org. Chem. **21**, 1366 (1956).

Can. J. Chem. Downloaded from www.nrcresearchpress.com by 210.87.254.40 on 09/06/12
For personal use only.

Kinetic β-deuterium isotope effects for solvolysis of 1-methyl cyclopentyl chloride in an ethanol + water mixture

ROSS ELMORE ROBERTSON AND EDWARD WONG
Department of Chemistry, University of Calgary, Calgary, Alta., Canada T2N 1N4

JOHN MARSHALL WILLIAM SCOTT
Department of Chemistry, Memorial University, St. John's, Nfld., Canada A1C 5S7

AND

MICHAEL JESSE BLANDAMER, REHMAT KHAN, AND CLIVE JOHNSON
Department of Chemistry, University of Leicester, Leicester LE1 7RH, England

Received March 3, 1982[1]

ROSS ELMORE ROBERTSON, EDWARD WONG, JOHN MARSHALL WILLIAM SCOTT, MICHAEL JESSE BLANDAMER, REHMAT KHAN, and CLIVE JOHNSON. Can. J. Chem. **61**, 116 (1983).

Kinetic data are reported for the solvolysis of 1-methyl cyclopentyl chloride in a 50% by volume ethanol + water mixture. These data are combined with kinetic data for solvolysis of three deuterated analogues; 1-methyl-d_3 cyclopentyl chloride, 1-methyl-2,2,5,5-d_4 cyclopentyl chloride, and 1-methyl-d_3-2,2,5,5-d_4 cyclopentyl chloride, being the d_3, d_4, and d_7 derivatives respectively. The kinetic data are used to calculate the kinetic deuterium isotope effect, k_H/k_D. For these systems, the d_7-isotope effect is close to the product of the d_3 and d_4 effects.

ROSS ELMORE ROBERTSON, EDWARD WONG, JOHN MARSHALL WILLIAM SCOTT, MICHAEL JESSE BLANDAMER, REHMAT KHAN et CLIVE JOHNSON. Can. J. Chem. **61**, 116 (1983).

On rapporte les données cinétiques de la solvolyse du chlorure de méthyl-1 cyclopentyle dans un mélange à 50% en volume d'éthanol et d'eau. On a combiné ces données aux données cinétiques de la solvolyse de trois analogues deutérés: le chlorure de méthyl-1-d_3 cyclopentyle, le chlorure de méthyl-1 cyclopentyl-2,2,5,5-d_4 et le chlorure de méthyl-1-d_3 cyclopentyl-2,2,5,5-d_4, ces composés ayant respectivement 3,4 et 7 atomes de deutérium. On a utilisé les données cinétiques pour calculer l'effet isotopique du deutérium, k_H/k_D. Pour ces systèmes, l'effet isotopique-d_7 est voisin du produit des effets d_3 et d_4.
[Traduit par le journal]

Quite generally, β-deuterium substitution leads to a decrease in rate constant for a solvolytic S_N reaction (1). We have measured the kinetic deuterium isotope effects for solvolysis of 1-methyl cyclopentyl chloride deuterated at the 1-methyl group, d_3, at the methylene groups in the 2 and 5 positions, d_4, and at both methyl and 2- and 5-methylene groups, d_7.

Results

The solvent was a 50% mixture of ethyl alcohol and water. The kinetics of solvolysis, followed by measuring the change in electrical conductance (2), obeyed first order kinetics (Table 1).

TABLE 1. Kinetic data for the solvolysis of 1-methylcyclopentyl chloride in 50:50 by volume ethyl alcohol + water mixture

T (K)	$10^4 k$ (s^{-1})	T (K)	$10^4 k$ (s^{-1})	T (K)	$10^4 k$ (s^{-1})
1-Methylcyclopentyl chloride		1-Methyl(d_3)-derivative		1-Methyl(d_3)-2,2,5,5-d_4-derivative	
268.147	3.636	268.147	2.740	268.141	1.219
273.105	7.173	273.101	5.413	273.101	2.429
274.150	8.211	277.155	9.200	277.147	4.200
276.150	10.67	279.161	11.88	279.160	5.457
277.158	12.22	281.155	15.25	281.153	7.033
278.151	13.84	283.155	19.42	283.151	9.021
279.157	15.76			288.150	16.67
280.152	17.79	1-Methyl-2,2,5,5-d_4-derivative			
281.154	20.20	268.150	1.615		
282.147	22.66	273.103	3.212		
283.159	25.87	277.145	5.523		
288.143	47.07	279.157	7.185		
		281.153	9.204		
		283.162	11.81		
		288.153	21.65		

[1]Revision received September 8, 1982.

0008-4042/83/010116-02$01.00/0
©1983 National Research Council of Canada/Conseil national de recherches du Canada

Can. J. Chem. Downloaded from www.nrcresearchpress.com by 210.87.254.105 on 09/06/12
For personal use only.

Can. J. Chem. Downloaded from www.nrcresearchpress.com by 210.87.254.105 on 09/06/12
For personal use only.

Discussion

In the solvolysis of 1-methyl cyclopentyl chloride, nucleophilic displacement of chloride occurs at a tertiary carbon centre and the most obvious comparison is with the kinetic data for *tert*-butyl chloride in the same solvent mixture (3). Indeed the isotope effect per *d*-atom on the 1-methyl(d_3) cyclopentyl compound is 1.099 at 283 K (i.e. $\sqrt[3]{1.329}$), which is close to that calculated for *tert*-butyl chloride, 1.11 (i.e. $\sqrt[9]{2.505}$). The corresponding value for the *d*-atoms at the 2 and 5 positions is quite different, 1.23, and must reflect the constraint imposed by the cyclopentyl ring on the conformational changes during the displacement process. It is noteworthy, however, that the overall isotope effect in the d_7-derivative is, over the measured temperature range, within 4% of that predicted by the products of the d_3 and d_4 kinetic isotope effects. In other words, the isotope effects are additive with respect to their contributions to the activation Gibbs function, $\Delta G^{\neq}$ (see Fig. 1).

Experimental

1-Methylcyclopentanol was prepared from cyclopentanone using the Grignard reaction. The chloride was prepared by passing dry HCl through the solution at 263 K. The 2,2,5,5-d_4 derivatives were prepared from cyclopentanone-d_4. The latter was prepared by warming together cyclopentanone and D_2O in the presence of a trace amount of K_2CO_3. The deuterated cyclopentanone was reduced to the alcohol (4) with 82% yield and better than 93% isotopic substitution. The 1-methyl(d_3) derivatives were prepared by well-established modifications to the above synthetic methods.

1. V. J. SHINER, JR. *In* Isotope effects in chemical reactions. *Edited by* C. J. Collins and N. S. Bowman. Van Nostrand Reinhold Co., New York, NY. 1970. Chapt. 8.
2. R. E. ROBERTSON. Prog. Phys. Org. Chem. **4**, 213 (1967).
3. L. HAKKA, A. QUEEN, and R. E. ROBERTSON. J. Am. Chem. Soc. **87**, 161 (1965).
4. A. STREITWEISER, JR., R. H. JAGOW, R. C. FAHEY, and S. SUZUKI. J. Am. Chem. Soc. **80**, 2326 (1958).

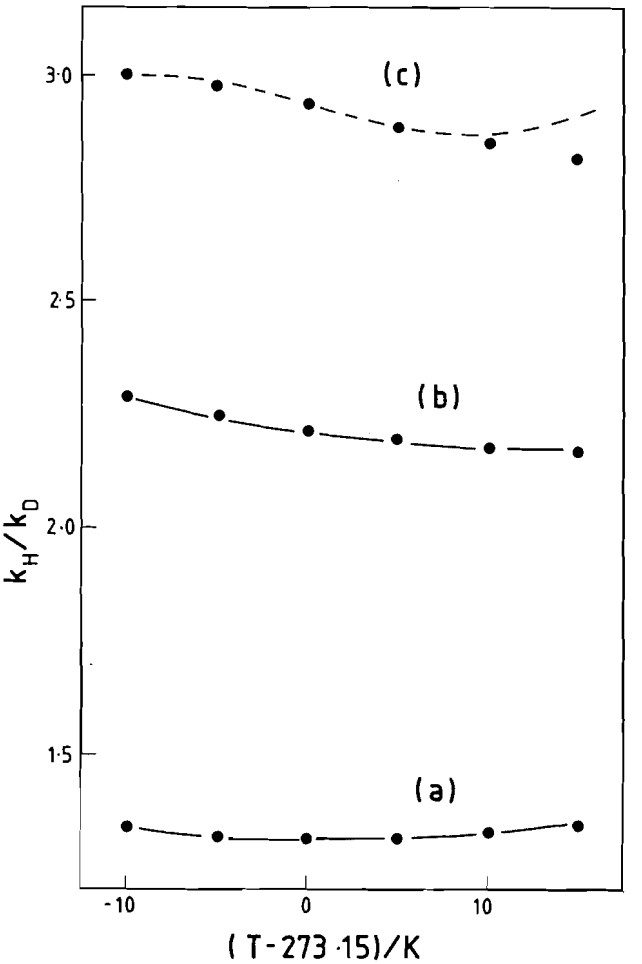

FIG. 1. Kinetic deuterium isotope effects for 1-methyl cyclopentyl chloride; (a) 1-methyl(d_3) derivative, (b) -2,2,5,5-d_4 derivative, and (c) 1-methyl(d_3)-2,2,5,5-d_4 derivative. Curve c is drawn through the points predicted by the products of values given by curves a and b.

Alkylation of ambident ions derived from phosphoric–carboxylic imides. *N*-Benzoyl-*O*,*O*-dimethyl-*O*-ethylphosphorimidate and *E*/*Z* *O*-ethyl-*N*-(dimethylphosphoryl)benzimidate

VALERIE MIZRAHI, THEODORE HENDRICKSE, AND TOMASZ A. MODRO
Department of Organic Chemistry, University of Cape Town, Rondebosch, South Africa

Received April 16, 1982

VALERIE MIZRAHI, THEODORE HENDRICKSE, and TOMASZ A. MODRO. Can. J. Chem. **61**, 118 (1983).

The sodium salt of *N*-benzoyldimethylphosphoramidate was ethylated using triethyloxonium ion or ethyl iodide as alkylating agents. The former reaction gave two oxygen-alkylated products: *N*-benzoyldimethylethylphosphorimidate and *O*-ethyl-*N*-(dimethylphosphoryl)benzimidate. The latter reaction yielded only the carbonyl oxygen ethylation product as a pair of the geometrical (*E*/*Z*) isomers. The nmr spectra and fragmentation patterns of the obtained products are discussed.

VALERIE MIZRAHI, THEODORE HENDRICKSE et TOMASZ A. MODRO. Can. J. Chem. **61**, 118 (1983).

Utilisant l'ion triéthyloxonium ou l'iodure d'éthyle comme agent alkylant, on a éthylé le sel de sodium du *N*-benzoyl-diméthylphosphoramidate. La première réaction a donné deux produits alkylés contenant de l'oxygène; le *N*-benzoyl-diméthyléthylphosphorimidate et le O-éthyl-*N*-(diméthylphosphoyl)benzimidate. La dernière réaction a donné uniquement les isomères géométriques (*E*/*Z*) du produit d'éthylation de l'oxygène du carbonyle. On discute des spectres de rmn et des modes de fragmentation des produits obtenus.

[Traduit par le journal]

Can. J. Chem. Downloaded from www.nrcresearchpress.com by 210.87.254.42 on 09/06/12
For personal use only.

The Gabriel synthesis of primary amines is based on the nucleophilicity of the nitrogen of the imide salt. Following our interest in the reactivity of *N*-acylphosphoramidates,[1] we have investigated the nucleophilicity of the sodium salt of *N*-benzoyldimethylphosphoramidate (**1**) in alkylation reactions. The detailed charge distribution in the ion **1** is not known

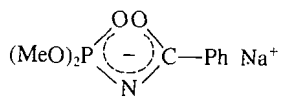

1

and the system can, in principle, give rise to the *N*-alkylated and two *O*-alkylated products. Zwierzak (1) recently reported the synthetic utility of *N*-alkylation of the similar salt $(EtO)_2P(O)NNaC(O)OBu^t$ under conditions of phase transfer catalysis. In this work, we report our results on the ethylation of **1** and the structural characteristics of the products formed.

Results and discussion

Ethylation of **1** with triethyloxonium tetrafluoroborate in methylene chloride gives two products which were identified by ^{1}H nmr and ir spectroscopy as the phosphoryl oxygen-ethylated (**2**) and carbonyl oxygen-ethylated (**3**) derivatives:

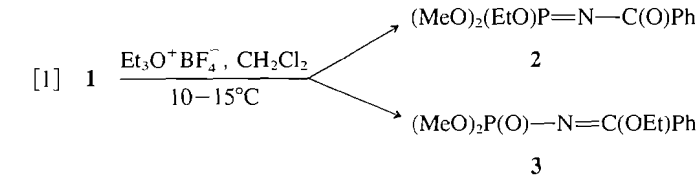

Products **2** and **3** are initially formed in about equimolar proportions, which probably corresponds to the kinetic control of the reaction. The concentration of **2** diminishes from 50% to zero between 5 and 20 h of the reaction, indicating greater stability of the benzimidate structure (**3**). The structure of *N*-benzoyl-*O*,*O*-dimethyl-*O*-ethylphosphorimidate (**2**) was established according to the following spectroscopic data. The methylene protons of the ethyl group resonate in the ^{1}H nmr spectrum as a low field quintet ($J_{H,H} = J_{H,P} = 7.5$ Hz), characteristic of the P^{IV}—OCH_2CH_3 function and indicate unambiguously the location of the ethyl moiety.

The ir spectrum of **2** showed a band for the carbonyl group at 1611 cm^{-1} and a new band at 1347 cm^{-1} due to the presence of a P=N bond. The positions of these bands remain in excellent agreement with the positions of the C=O (str.) and P=N (str.) bands of the trialkyl-*N*-acylphosphorimidates observed by other authors (1608–1620 cm^{-1} and 1346–1380 cm^{-1}, respectively) (2, 3).

In contrast to **2**, the methylene protons in **3** resonate as a quartet ($J_{H,H} = 7.5$ Hz), indicating no coupling with the ^{31}P nucleus. The ir spectrum of **3** showed the disappearance of the C=O band and retention of the band at 1271 cm^{-1} (P=O str.), as well as the appearance of a new band at 1657 cm^{-1}, characteristic of a C=N bond.[2]

In an attempt to prepare the *N*-alkylated derivative of **1**, this substrate was alkylated under similar conditions to those described by Zwierzak (1). However, we observed no alkylation at nitrogen, as indicated by the absence of a signal expected for the P(O)NEt group in the ^{1}H nmr spectrum of the product mixture. The reaction mixture consisted of two products having very similar R_f values on a tlc plate. The ^{1}H nmr spectrum of the reaction mixture also indicated the presence of two closely related compounds (Fig. 1). Both compounds exhibit a quartet at δ 4.0–4.5, characteristic of the methylene protons of the Et group, *not* coupled with the ^{31}P nucleus. In fact the spectrum of product A was found to be identical with that of the benzimidate (**3**) prepared above. The great similarity in the ^{1}H nmr spectra of these two compounds led us to believe that

[1]Papers concerning our results on the molecular structure, fragmentation patterns, and solvolytic behavior of *N*-acylphosphoramidates are being submitted for publication.

[2]Kabachnik *et al.* (4) report C=N (str.) at 1642–1644 cm^{-1} for *O*-methyl-*N*-(diethylphosphoryl)acetimidate.

0008-4042/83/010118-06$01.00/0
©1983 National Research Council of Canada/Conseil national de recherches du Canada

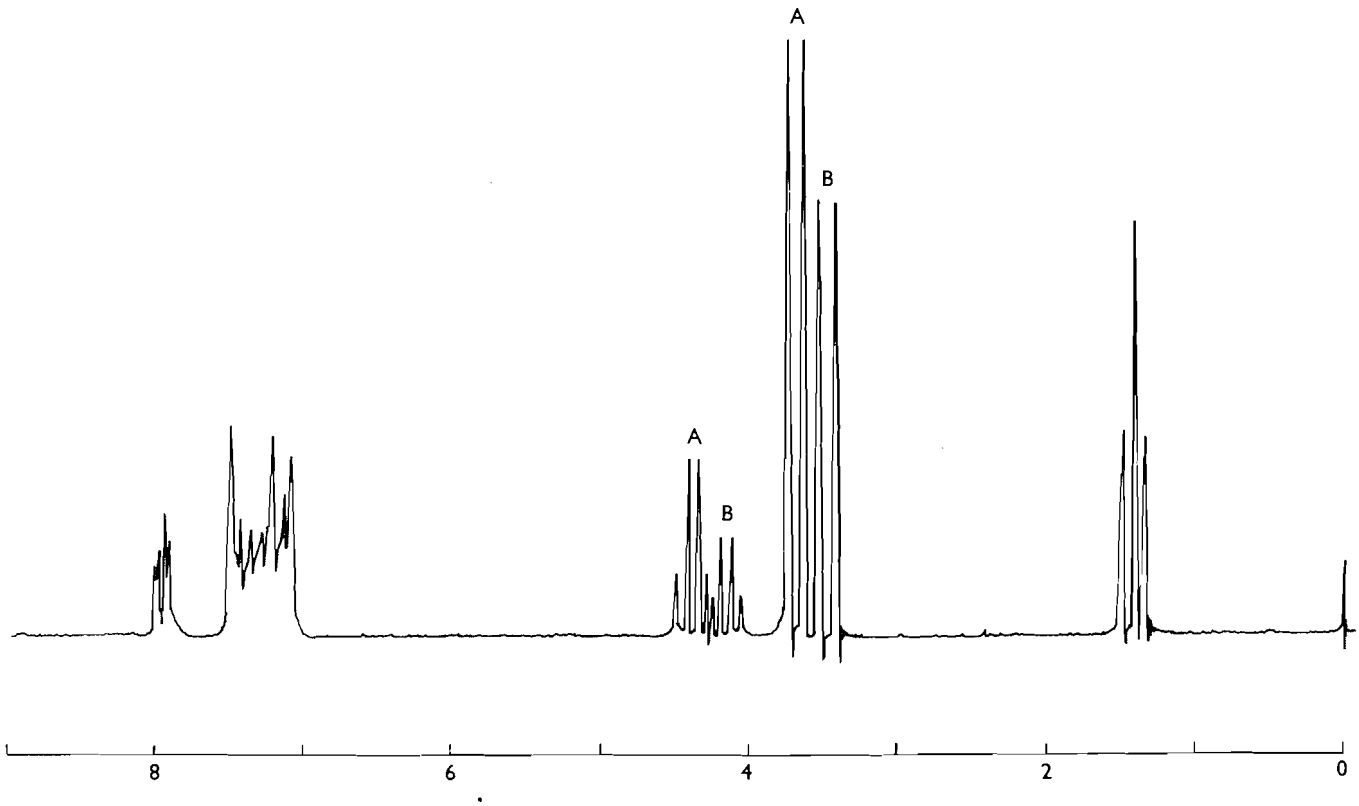

FIG. 1. The ^1H nmr spectrum ($CDCl_3$) of the reaction mixture obtained by ethylation of **1** with ethyl iodide.

they are the geometrical isomers of *O*-ethyl-*N*-(dimethylphosphoryl)-benzimidate, **3***a* and **3***b*:

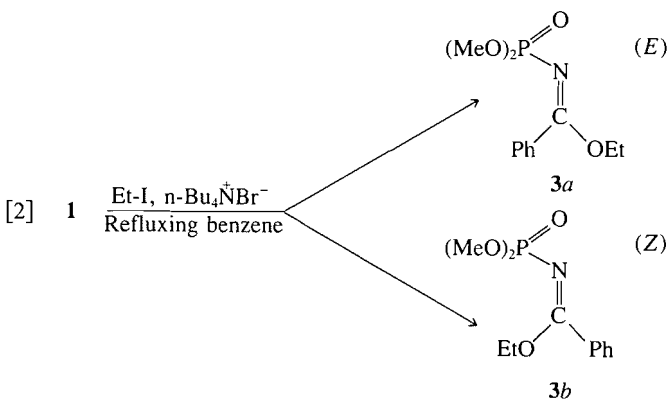

The benzimidates (**3**) were separated by column chromatography, and their structures determined by ^1H and ^{13}C nmr, ir, and mass spectrometry. The ^{13}C nmr spectra of the individual compounds are very similar, both showing five low field signals of the sp^2 carbon atoms (four aromatic and one of the C=N group), one high field signal of the β-methyl carbon of the ethyl group, and two midfield signals: a doublet ($J_{C,P}$ = 7.0 Hz) of the dimethylphosphoryl Me groups, and a singlet of the OCH_2 carbon of the *O*-imidate function. The most obvious difference between the ^{13}C nmr spectra of the two compounds lies in the chemical shift of the latter signal; the δ_{OCH_2} value of compound A is ca. 20 Hz more positive (more deshielded) than the δ_{OCH_2} value of the other isomer. Since the α-methylene carbons of **3***a* and **3***b* differ significantly in through-space distance to the phosphoryl group and to the pair of nonbonding electrons on nitrogen (*E*/*Z* relation), large differences in the shielding parameters of these atoms are expected. The infrared spectra of the alkylation products are extremely similar; both contain a prominent P=O (str.) band and a characteristic C=N (str.) band of frequency 1654–1657 cm^{-1}, in good agreement with literature values.

Although the nmr and ir spectroscopic results fully confirmed the postulated structures of the geometrical isomers **3***a* and **3***b*, the assignment of absolute configuration to the individual compounds was possible by analyzing and comparing their mass spectra. The ms of the ethylation products of **1** were recorded and fragmentation patterns of each of the isomeric compounds are proposed. The ions observed in the ms of compounds **2**, **3***a*, and **3***b* are given in Table 1.

The principal fragmentation pathway in the ms of **2** involves loss of a phenyl radical to give the resonance stabilized ion of *m*/*e* 180 (Scheme 1). Subsequent loss of ethylene via a MacLafferty rearrangement gives rise to the base peak of *m*/*e* 152, which can then fragment as indicated. It is unlikely that the loss of 28 mass units in going from *m*/*e* 180 to *m*/*e* 152 is due to CO expulsion since the resulting ion would be of much lower stability. The molecular ion also undergoes homolytic N—C bond fission to give the stable benzoylium ion of *m*/*e* 105 which further fragments in the characteristic way. Two pathways of minor importance but supported by metastable peaks involve loss of ethylene and water from the molecular ion to give fragments of *m*/*e* 229 and *m*/*e* 239 respectively. The fragments of *m*/*e* 212, *m*/*e* 154, *m*/*e* 127, and *m*/*e* 103 can be accounted for by an initial rearrangement of the parent ion, in which intramolecular nucleophilic attack by carbonyl oxygen at tetrahedral phosphorus occurs to give a tbp intermediate, which may collapse by loss of ethoxy radical to *m*/*e* 212, by loss of benzonitrile to the mixed phosphate ester of *m*/*e* 154, or by loss of ethyldimethylphosphate to benzonitrile radical ion of *m*/*e*

Can. J. Chem. Downloaded from www.nrcresearchpress.com by 210.87.254.42 on 09/06/12
For personal use only.

Can. J. Chem. Downloaded from www.nrcresearchpress.com by 210.87.254.42 on 09/06/12
For personal use only.

TABLE 1. Mass spectra of ethylation products

	Relative intensity		
m/e	**2**	**3***a*	**3***b*
Molecular ion	4	2	6
41	—	10	—
47	—	4	—
51	10	27	17
77	14	75	31
78	—	13	8
79	7	6	9
80	—	—	9
95	—	8	10
96	7	10	7
103	8	9	11
104	—	12	31
105	15	100	50
106	—	13	5
109	28	20	41
110	—	32	57
118	—	12	14
121	7	8	5
126	—	10	30
127	10	6	15
131	—	8	11
149	—	55	100
152	100	20	47
154	6	3	6
180	44	—	—
201	—	7	—
212	10	15	21
228	—	3	—
229	5	14	8
239	5	—	—
255	—	12	19

103. Loss of $C_2H_3\cdot$ from *m/e* 154 (via a double hydrogen shift mechanism (5)) yields the stable quasi-phosphonium ion of *m/e* 127. An alternative explanation of the presence of fragments of *m/e* 154 and 127 is based on the observation by Kirsanov *et al.* (6) that *N*-acyltriarylphosphorimidates (**4**) release nitriles when heated:

[3] $(ArO)_3P{=}N{-}\overset{\overset{O}{\|}}{C}{-}R \xrightarrow{\Delta} O{=}P(OAr)_3 + RCN$

4

No mechanism was proposed for reaction [3], but the most likely intermediate is identical to that shown in Scheme 1. In light of the above, it is conceivable that ethyldimethylphosphate and benzonitrile are formed prior to entering the ionization chamber. Direct loss of EtO· from the parent ion would yield fragment **5** of *m/e* 212, a nitrogen analogue of the commonly observed phosphorylium ions (**6**).

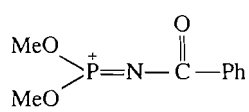

5

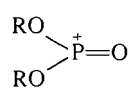

6

Very little information is available on the mass spectral characteristics of *N*-substituted phosphorimidates. Goldwhite *et al.* (7) discussed the possible origin of the most significant ions in the mass spectra of $(RO)_3PNEt$ (R = Me, Et); comparison with the ms of **2** shows that the nature of the fragment ions is determined exclusively by the substituent on nitrogen (ethyl vs. benzoyl) rather than by the substituents on phosphorus.

The most important fragmentation pathways available to the geometrical isomers **3***a* and **3***b* are given in Scheme 2. As can be seen from Table 1, the mass spectra of the isomers are specific for the type of isomer (*E* vs. *Z*), not in the nature of the ions, but in their abundance.

The two principal fragmentation pathways both involve the migration of a hydrogen from either the methoxyl or ethoxyl group to the nitrogen atom (pathways a, b). In the *E* isomer (**3***a*), loss of ethylene via a MacLafferty rearrangement is the most favoured pathway yielding the radical ion of *m/e* 229 (pathway a). This species is *N*-benzoyldimethylphosphoramidate, the precursor to the sodium salt (**1**), and its ms has recently been recorded (5). The second important H-migration fragmentation involves expulsion of a molecule of $C_2H_5O_3P$ and formation of *O*-ethylbenzimidate radical ion *m/e* 149 (pathway b). We have recently observed expulsion of the same neutral species in the ms of $(MeO)_2P(O)NHPh$ (5) and believe its structure is that of methyl methylene phosphite. This constitutes the principal fragmentation route of **3***b* (base peak *m/e* 149); it is also operative in the fragmentation of **3***a*, although to a lesser degree. The ms of independently synthesized ethylbenzimidate was recorded and we found the molecular ion to be remarkably stable (base peak). However, isomerization to *N*-ethyl benzamide does take place and subsequent fragmentation occurs as expected (8).

Loss of ethoxy radical from the molecular ion to yield *N*-dimethylphosphoryl benzonitrilium ion *m/e* 212 is a third minor pathway common to both isomers (pathway e). Loss of hydrogen from the molecular ion to yield the *O*-vinyl derivative *m/e* 255 is another minor pathway, again common to both isomers (pathway c). However, loss of benzonitrile from the molecular ion and from *m/e* 255 to yield the mixed phosphate esters *m/e* 154 and 152, respectively (pathways d, f), is more predominant in the fragmentation pattern of the *Z* isomer (**3***b*) than the *E* isomer (**3***a*). This is reasonable, since loss of benzonitrile from such a parent ion requires a *cis* orientation of the *N*-dimethylphosphoryl substituent and the migrating *O*-alkyl group (eq. [4]).

[4] 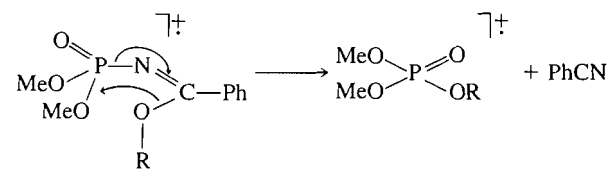

R = Et (*m/e* 257)
R = $CH_2{=}CH$ (*m/e* 255)

Mixed phosphate ester formation appears to be the best explanation for the peaks observed at *m/e* 110, *m/e* 121, and *m/e* 127.

The main difference in the mass spectra of the geometrical isomers is a consequence of the stereospecificity of pathways a, d, and f, the former requiring a *trans* orientation and the latter two requiring a *cis* orientation of the *N*-dimethylphosphoryl and *O*-alkyl groups. The observation that all peaks are common to both spectra, but the peaks arising from initial loss of ethylene from the molecular ion (*m/e* 229, 228, 201, 105, 77, and 51) are noticeably more abundant in the ms of **3***a* than **3***b*, indicates a certain degree of interconversion of the

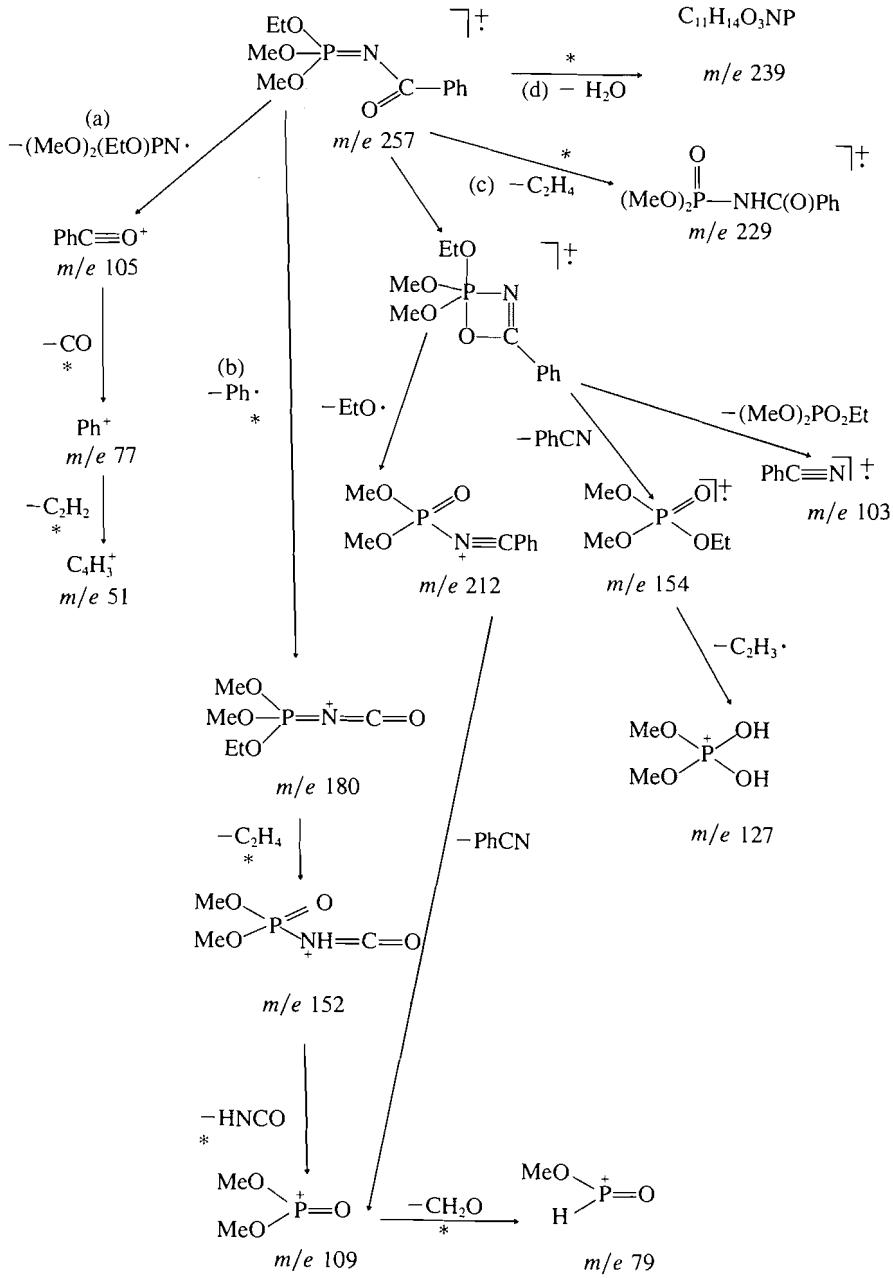

SCHEME 1. Proposed fragmentation pattern of **2**. NOTE: Pathways supported by metastable peaks are indicated by an asterisk.

isomers prior to fragmentation. The ion source temperature of 200°C thus appears to be sufficiently high to cause rotation about the carbon−nitrogen bond. The value of the C—N rotational barrier in benzimidates **3** is not known; however, it should not differ significantly from that determined for other N-substituted *O*-alkyl imidates. For a number of imidates R(R′O)CNR″, the inversion barrier has been found (9) to be of the order of 16−21 kcal mol^{-1}, sufficiently low to enable $E \rightleftharpoons Z$ interconversion at the ion source temperature.[3]

In conclusion, mass spectrometry is clearly a useful tool for distinguishing positional isomers. However, in accordance with the observation made by Natalis (10), a more detailed analysis of comparative ion peak intensities is required when using ms to differentiate geometrical isomers.

It is worthwhile to point out that in contrast to the literature report concerning a similar system (1), we were never able to detect any ethylation occuring at the nitrogen atom of ion **1**. This selectivity indicates that the kinetic and thermodynamic factors governing the nucleophilic behaviour of the carboxylic/phosphoric imide system are a sensitive function of the substrate and alkylating agent structures, as well as of the reaction conditions.

Experimental

The ^{1}H nmr spectra were recorded on a 100 MHz Varian XL100 spectrometer with TMS as internal standard. The ^{13}C nmr spectra were recorded on a WH90 Bruker spectrometer operating in the FT mode with TMS as internal standard. Infrared spectra were recorded on a Model 180 Perkin−Elmer ir spectrometer. Mass spectra were recorded on a VG Micromass 16F spectrometer operating at 70 eV and

[3]For all imidates reported in ref. 9, the coalescence temperature necessary to determine $\Delta G^{\neq}$ (E/Z) values by dynamic nmr spectroscopy was 90−150°C.

Can. J. Chem. Downloaded from www.nrcresearchpress.com by 210.87.254.42 on 09/06/12
For personal use only.

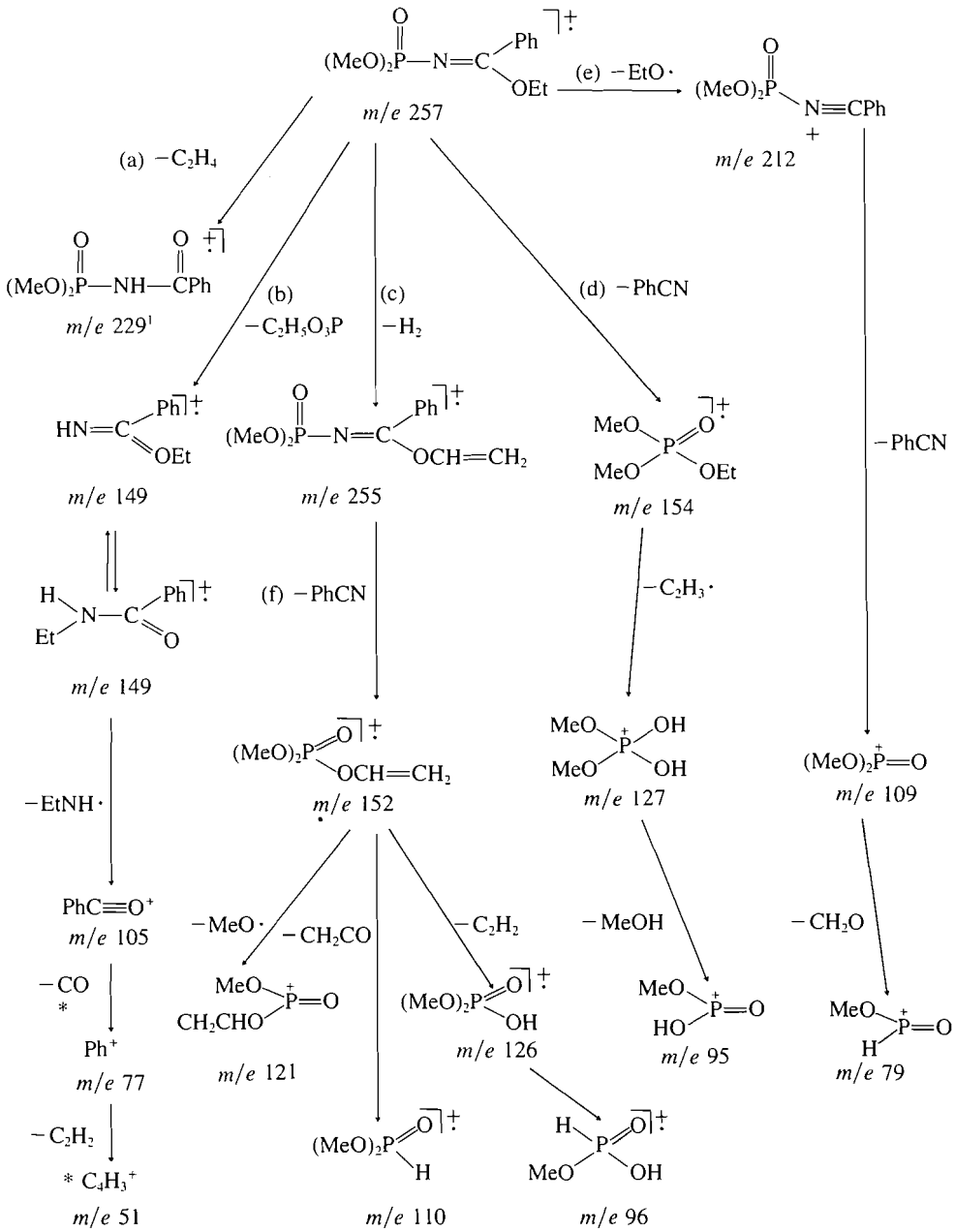

[1]NOTE: Radical ion *m/e* 229 further fragments to give species of *m/e* 228, 201, 152, 126, 105, 77, and 51 (5)

SCHEME 2. Proposed fragmentation pattern of **3***a* and **3***b*.

an ion source temperature of 200°C. Silica gel plates were used for thin-layer chromatography and Silica gel 60 (Merck, Art. 9385, 230–400 mesh) was used for column chromatography.

Ethylation of ***1*** *with triethyloxonium tetrafluoroborate*

A solution of 2.3 g (10 mmol) of *N*-benzoyldimethylphosphoramidate in 50 cm^3 dry benzene was added dropwise to a stirred suspension of 0.3 g (10 mmol) sodium hydride, forming a white jelly-like suspension of the sodium salt. The benzene was removed under reduced pressure leaving a white solid; ir (5% CCl_4 soln): 1205 (m, s), 1370 (s, s), 1550 (s, s), 1595 (m, s) cm^{-1}; ^1H nmr (DMSO-d_6), δ: 3.55 (6H, d, OCH_3, $J_{H,P}$ = 11 Hz), 7.4–7.5 (3H, m, *m*-, *p*-aryl H), 8.0–8.15 (2H, m, *o*-aryl H).

To a stirred suspension of 2.5 g (10 mmol) of the sodium salt in 50 cm^3 dry dichloromethane was added a solution of 1.9 g (10 mmol) triethyloxonium tetrafluoroborate in 10 cm^3 dry dichloromethane, maintaining the temperature at 10–15°C. The mixture was stirred for a fixed length of time (5–20 h), transferred to a separating funnel, and washed with 25 cm^3 water. The solution was dried over anhydrous magnesium sulfate and the solvent removed under reduced pressure, leaving a yellow oily product (1.82 g; 71% yield). Thin-layer chromatography (10% acetone in chloroform (v/v)) revealed two products of R_f values 0.40 and 0.56 respectively. After a reaction time of 5 h, the nmr spectrum of the product showed the formation of two compounds in 1 : 1 proportion (as measured from the integrated areas of the individual signals). The mixture was separated by column chromatography, eluting with the same solvent system, giving the following products.

First fraction

The pale yellow oil collected (**2**) showed the following spectral characteristics: ir (5% CCl_4 soln): 1187 (m, s, δ CH_3 of P—O—CH_3), 1347 (s, s, ν P=N), 1611 cm^{-1} with shoulder at 1624 (s, s, ν C=O) cm^{-1}; ^1H nmr ($CDCl_3$), δ: 1.39 (3H, t, CH_3, $J_{H,H}$ = 7 Hz), 3.92 (6H,

Can. J. Chem. Downloaded from www.nrcresearchpress.com by 210.87.254.42 on 09/06/12
For personal use only.

d, CH_3O, $J_{H,P}$ = 11 Hz), 4.30 (2H, quint., CH_2, $J_{H,H} = J_{H,P}$ = 7 Hz), 7.20–7.50 (3H, m, *m*-, *p*-aryl H), 8.12–8.24 (2H, pair of doublets, *o*-aryl H).

Second fraction

The yellow waxy solid (**3***a*) showed the following spectral characteristics: ir (5% CCl_4 soln): 1187 (m, s, δ CH_3 of P—O—CH_3), 1271 (s, s, ν P=O), 1657 (s, s, ν C=N) cm^{-1}; ^1H nmr ($CDCl_3$), δ: 1.42 (3H, t, CH_3, $J_{H,H}$ = 7.5 Hz), 3.67 (6H, d, CH_3O, $J_{H,P}$ = 11 Hz), 4.42 (2H, quart., $J_{H,H}$ = 7.5 Hz), 7.40–7.50 (3H, m, *m*-, *p*-aryl H), 7.87–7.98 (2H, pair of doublets, *o*-aryl H); ^{13}C nmr ($CDCl_3$, Hz downfield from TMS): 14.2 (s, β-CH_3 of the Et group), 53.2 (d, OCH_3, $J_{C,P}$ = 7.0 Hz), 64.0 (s, α-methylene of the OEt group), 125–135 (m, aromatic C and imidate C).

*Ethylation of **1** with ethyl iodide*

To a mixture of 0.02 mol of the sodium salt **1** (prepared as above) in 100 cm^3 dry benzene, was added a 10-fold excess of ethyl iodide (16.3 cm^3) together with a catalytic amount of tetra-n-butylammonium bromide (0.34 g, 5 mol%). The mixture was refluxed with stirring for 21 h. The supernatant benzene solution was decanted off and the solid white residue washed with 20 cm^3 benzene. The benzene was evaporated under reduced pressure to yield 3.00 g (58%) of crude product. This product was dissolved in 20 cm^3 chloroform and the solution was washed with water (2 × 5 cm^3). The organic layer was dried ($MgSO_4$) and the chloroform removed under reduced pressure, leaving a clear yellow oil. The product was subjected to column chromatography and eluted with 33% ethyl acetate in dichloromethane to yield the following compounds.

First fraction

The yellow waxy solid showed the same spectral characteristics as **3***a*.

Second fraction

The yellow oil (**3***b*) showed the following spectral characteristics: ir (5% CCl_4 soln): 1187 (m, s, δ CH_3 of P—O—CH_3), 1268 (s, s, ν P=O), 1654 (s, s, ν C=N) cm^{-1}; ^1H nmr ($CDCl_3$), δ: 1.42 (3H, t, CH_3, $J_{H,H}$ = 7.5 Hz), 3.48 (6H, d, OCH_3, $J_{H,P}$ = 11 Hz), 4.16 (2H, quart., CH_2, $J_{H,H}$ = 7.5 Hz), 7.10–7.30 (5H, m, aryl H), ^{13}C nmr ($CDCl_3$, Hz downfield from TMS): 14.0 (s, β-CH_3 of the OEt group), 44.2 (s, α-methylene of the OEt group), 53.2 (d, OCH_3, $J_{C,P}$ = 7.0 Hz), 125–135 (m, aromatic C, imidate C).

Acknowledgments

The financial assistance of the University of Cape Town and the Council for Scientific and Industrial Research is gratefully acknowledged. V. Mizrahi thanks African Explosives and Chemical Industries for a postgraduate grant.

1. A. ZWIERZAK. Phosphorus chemistry. *Edited by* L. D. Quin and J. G. Verkade. ACS Symposium Series. Vol. 171. p. 169.
2. C. GLIDEWELL. J. Organomet. Chem. **108**, 335 (1976).
3. M. I. KABACHNIK, V. A. GILYAROV, and E. M. POPOV. Zh. Obshch. Khim. **32**, 1598 (1962).
4. M. I. KABACHNIK, V. A. GILYAROV, and C. CHENG-TIEH. Izv. Akad. Nauk SSSR, Ser. Khim. 665 (1965).
5. V. MIZRAHI and T. A. MODRO. J. Org. Chem. **47**, 3533 (1982).
6. (*a*) A. V. KIRSANOV, G. I. DERKACH, and R. G. MAKITRA. Zh. Obshch. Khim. **28**, 1227 (1958); (*b*) A. V. KIRSANOV and G. I. DERKACH. Zh. Obshch. Khim. **26**, 2631 (1956).
7. H. GOLDWHITE, P. GYSEGEM, S. SCHOW, and C. SWYKE. J. Chem. Soc. Dalton Trans. 12 (1975).
8. A. M. DUFFIELD, G. DE MARTINO, and C. DJERASSI. Org. Mass Spectrom. **9**, 137 (1974).
9. (*a*) C. O. MEESE, W. WALTER, and M. BERGER. J. Am. Chem. Soc. **96**, 2259 (1974); (*b*) W. WALTER and C. O. MEESE. Chem. Ber. **110**, 2463 (1977).
10. P. NATALIS. Mass spectrometry. NATO Adv. Study Inst. Glasgow, 1964. p. 379.

Can. J. Chem. Downloaded from www.nrcresearchpress.com by 210.87.254.42 on 09/06/12
For personal use only.

Preparation, characterization, and antioxidant properties of polystyrenes with 4-methoxyphenol end groups

BRIAN K. HUNTER, KENNETH E. RUSSELL, AND ATAA K. ZAGHLOUL[1]
Department of Chemistry, Queen's University, Kingston, Ont., Canada K7L 3N6

Received August 20, 1982

BRIAN K. HUNTER, KENNETH E. RUSSELL, and ATAA K. ZAGHLOUL. Can. J. Chem. **61**, 124 (1983).

Polystyrenes with 4-methoxyphenol end groups have been prepared by the cationic polymerization of styrene in the presence of the phenol. The products range from 1:1 adduct to polymer of number-average molecular weight close to 3000. The 1:1 adduct separated from the reaction mixture was shown by nuclear Overhauser effect studies to be 2-(1-methylbenzyl)-4-methoxyphenol. Only about half of the polymer molecules have 4-methoxyphenol end groups. ^{13}C nmr studies indicate that the polystyrene chains are attached principally at the 2-position of the phenol. The activity of the polymer as an antioxidant is comparable to that of corresponding low molecular weight methoxyphenols including butylated hydroxyanisole.

BRIAN K. HUNTER, KENNETH E. RUSSELL et ATAA K. ZAGHLOUL. Can. J. Chem. **61**, 124 (1983).

On a préparé des polystyrènes ayant le méthoxy-4 phénol-4 comme groupe terminal par polymérisation cationique du styrène en présence du phénol. Les produits vont de l'adduit 1:1 à un polymère d'un poids moléculaire moyen voisin de 3000. L'adduit 1:1 isolé du mélange réactionnel se révèle être le (méthyl-1 benzyl)-2 méthoxy-4 phénol d'après les études de eOn. Seulement la moitié des molécules de polymère aurait le méthoxy-4 phénol en position terminal. Les études de la rmn du ^{13}C indiquent que les chaînes de polystyrène sont attachées principalement en position 2 du phénol. L'activité du polymère comme antioxydant est comparable à celle des méthoxyphénols correspondants de faibles poids moléculaires incluant l'hydroxyanisole butylé.

[Traduit par le journal]

Introduction

Cationic polymerization of styrene in the presence of alkylphenols leads to polystyrenes with alkylphenols incorporated as a significant fraction of the end groups (1, 2). The growing polystyrene carbenium ion attacks the 4-position of the phenol if it is free, or the 6-position if there is an alkyl substituent at the 4-position. Products such as 2-*t*-butyl-4-methylphenol with a polystyrene chain attached at the 6-position show antioxidant activity comparable to that of 2,6-di-*t*-butyl-4-methylphenol, BHT.

Butylated hydroxyanisole, BHA, a mixture of 2- and 3-butyl-4-methoxyphenol, is a more reactive antioxidant than BHT. Replacement of the butyl group by a polystyrene chain should yield a phenol with comparable antioxidant activity to BHA but with different physical properties. The volatility of the phenol would be reduced, enabling the antioxidant to be used at higher temperatures without loss through vaporization. The compatibility of the antioxidant with polymers and with fats would be affected. The objectives of this research were thus to prepare polystyrenes with 4-methoxyphenol end groups, to characterize materials ranging from a 1:1 adduct to 4-methoxyphenols with attached polymer chains, and to determine whether these products had the anticipated high antioxidant activity.

Experimental

Styrene (Dow Chemical of Canada) was distilled under reduced pressure and dried over molecular sieves. 4-Methoxyphenol was recrystallized from benzene – petroleum ether. Dichloromethane was dried over molecular sieves. Aluminum chloride solutions were prepared in dichloromethane and allowed to stand in the dark for at least one day. *N*,*N*-Dimethylformamide was vacuum distilled from phosphorus pentoxide.

Polymerization mixtures were prepared containing styrene (3.7 *M*) and 4-methoxyphenol (0.1–0.5 *M*) in dichloromethane at the reaction temperature (−78°C to 20°C). Polymerization was initiated by the slow addition of aluminum chloride solution to the reaction mixture and terminated with methanol (1 mL) after a sufficient yield of polystyrene had been obtained. Polystyrene was precipitated by the dropwise addition of the solution to stirred methanol. It was reprecipitated twice from dichloromethane–methanol solutions and dried in a vacuum oven at 40°C.

The solution remaining after the first precipitation contained free 4-methoxyphenol and a number of low molecular weight derivatives. Dichloromethane and methanol were removed by means of a rotary evaporator and the residue distilled at reduced pressure. The fraction boiling in the range 40–60°C (at approximately 1 Torr) consisted mainly of 4-methoxyphenol and residual styrene monomer. The fraction boiling from 90–100°C was recrystallized from petroleum ether to give a white solid, mp 61–61.5°C. Mol. wt. (vapor pressure osmometry), 241 (calcd. for $C_{15}H_{16}O_2$, 228). *Anal.* calcd. for $C_{15}H_{16}O_2$: C 78.95, H 7.02; found: C 79.46, H 7.02. ^1H nmr ($CDCl_3$) δ: 1.56 (d, 3H, CH_3), 3.69 (s, 3H, OCH_3), 4.35 (q, 1H, CH), 4.92 (s, 1H, OH), 6.77 (s, 2H, aryl), 6.93 (s, 1H, aryl), and 7.35 (m, 5H, aryl).

The fraction boiling from 150–170°C in the low pressure distillation consisted largely of 1:2 4-methoxyphenol–styrene adducts together with some unsaturated oligomer. Two 1:2 adducts were separated by means of hplc (either a C_{18} analytical column with a 65:35 methanol–water as solvent, or a C_8 preparative column with 80:20 methanol–water as solvent). The main component appears to contain styryl groups at both the 2- and 6-positions.

Polymer characterization

Number-average molecular weights were determined by means of a Wescan vapor pressure osmometer with chloroform as solvent. Molecular weight distributions were obtained using a Waters 244 chromatograph with μ-styragel columns (100, 500, 1000, and 10 000 Å). The ratio of weight-average to number-average molecular weight is typically 1.5 for polymers prepared at 0–20°C but this is a minimum value because some low molecular weight polymer is lost during isolation. The presence of phenolic end groups over the whole range of polymer molecular weights is demonstrated through the use

[1]Present address: Technical Development Division, Polysar Ltd., Sarnia, Ont., Canada N7T 7M2.

0008-4042/83/010124-04$01.00/0
©1983 National Research Council of Canada/Conseil national de recherches du Canada

Can. J. Chem. Downloaded from www.nrcresearchpress.com by 210.87.254.6 on 09/06/12
For personal use only.

Can. J. Chem. Downloaded from www.nrcresearchpress.com by 210.87.254.6 on 09/06/12
For personal use only.

of simultaneous refractive index and uv (280 nm) detection (1). The absorbance is a measure of phenol end group content because the polystyrene absorbs only weakly at 280 nm, and the change in refractive index is a measure of polymer concentration except at very low molecular weights. Removal of monomer, free phenol, and 1:1 adduct from the polymer is readily monitored by size exclusion chromatography since these materials are well resolved by the low porosity μ-styragel columns.

The fraction of polystyrene molecules with 4-methoxyphenol end groups was first estimated by uv analysis. The phenol-terminated polymer shows an absorbance maximum at 294 nm in chloroform solution as compared with 291 nm (ε, 3100 L mol^{-1} cm^{-1}) for 4-methoxyphenol and 292 nm (ε, 3700 L mol^{-1} cm^{-1}) for the 1:1 adduct. The molar absorptivity for the phenolic end groups was assumed to be equal to that for the 1:1 adduct in calculations of the phenol content of polymer samples. A direct estimate of the acidic OH groups in the polymer was obtained by potentiometric titration (3). The solvent was *N*,*N*-dimethylformamide and the base tetra-*n*-butyl ammonium hydroxide diluted with anhydrous isopropanol; titrations were performed under dry N_2.

The nmr spectra were obtained on a Bruker CXP-200 spectrometer (200 MHz for ^1H and 50.3 MHz for ^{13}C). With the exception of the nuclear Overhauser effect (nOe) difference spectra of the 1:1 adduct, samples were dissolved in $CDCl_3$ and run with pulse times and relaxation delays which give reliable intensity data for similar compounds. The nOe difference spectra were run in acetone-d_6 in which the spectrum of the aromatic protons of the phenol is well dispersed and easily analysed. Three spectra were run under identical conditions with a 1 s irradiation to establish the nOe, followed by a 5 ms delay and then by data acquisition. In one case, the irradiation was "off resonance" in order to provide a blank and in the other two cases the OH or the OCH_3 protons were irradiated. The spectra were Fourier transformed, phase corrected using the same phase parameters, and the difference taken between the blank and each of the specific irradiations.

Antioxidant studies were conducted with styrene (10 mL) as substrate and azobisisobutyronitrile (0.010 *M*) as initiator (4). The volume of oxygen absorbed was determined as a function of time at a reaction temperature of 65°C.

Results and discussion

Polymerization of styrene by aluminum chloride at 20°C in the presence of 0.3 *M* 4-methoxyphenol leads to polymer of $\bar{M}_n \sim 2800$ and to significant amounts of 1:1 and 1:2 phenol–styrene adducts. An increase of 4-methoxyphenol concentration from 0.1 *M* to 0.3 *M* causes a decrease in $\bar{M}_n$ of the isolated polystyrene from about 3600 to 2800 and an increase in phenolic end groups from 23% to 45%. Increasing the temperature from −78°C to 20°C results in a decrease in $\bar{M}_n$ and an increase in the fraction of phenolic end groups from about 16% to 46%. Typical conditions of 0.3 *M* methoxyphenol and 20°C were chosen to yield a relatively high fraction of 4-methoxyphenol end groups.

The 1:1 adduct

Size exclusion chromatography of the precipitated polymer and of the mixture isolated from the remaining solution suggests the presence of 1:1 adduct in the reaction product. The material isolated by distillation is not a single compound but recrystallization yields a solid whose molecular weight and ^1H nmr spectrum correspond to the structure:

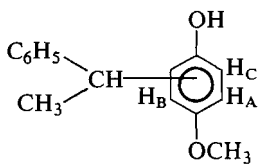

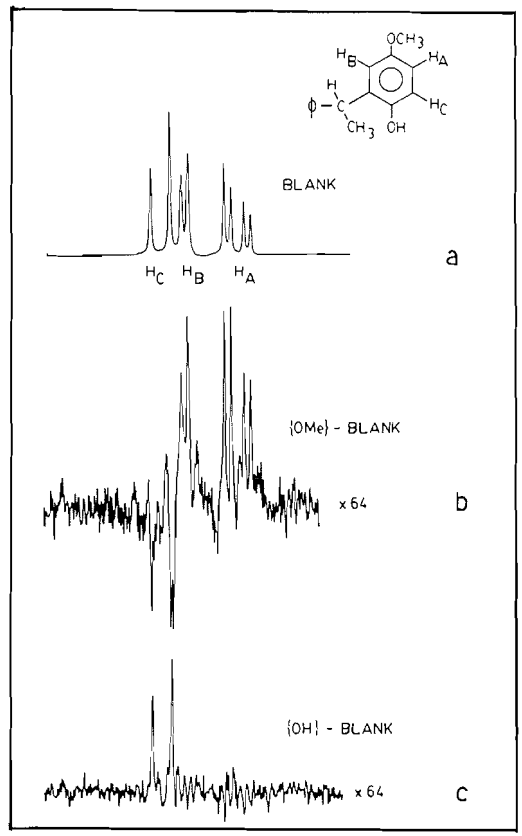

FIG. 1. Nuclear Overhauser effect study of the three protons of the phenolic ring of the 1:1 phenol–styrene adduct. Solvent: $(CD_3)_2CO$.

In particular the doublet at 1.56 ppm and the quartet at 4.35 ppm confirm the presence of the $CH_3CH\langle$ segment in the adduct. As anticipated, the resonance at 4.92 ppm almost disappears when D_2O is added, confirming the assignment to OH in chloroform-*d* solution. The ^1H nmr spectrum of the 1:1 compound in acetone-d_6 is similar to that obtained in chloroform-*d* solution except that the aromatic protons are well resolved and the OH resonance has moved upfield to 2.93 ppm.

The ^1H and ^{13}C nmr spectra of the adduct indicate that it is a single isomer. The preferred position of attack of the styryl carbenium ion on the phenol was investigated by means of nOe studies. Figure 1(*a*) shows the ^1H nmr spectrum in acetone-d_6 solution of the three protons of the aromatic ring of the phenol; (*b*) is a difference spectrum giving the effect of irradiating the methoxy resonance at 3.69 ppm and (*c*) the difference spectrum obtained on irradiating the hydroxy resonance at 2.93 ppm. Irradiation at OCH_3 increases the intensities of the resonances of two protons (H_A and H_B) whereas irradiation at OH increases the intensity of the resonance of one proton (H_C). The styryl group in the 1:1 adduct isolated in this work is consequently *ortho* to the OH rather than the OCH_3. The compound is therefore 2-(1-methylbenzyl)-4-methoxyphenol.

It is notable that in addition to the expected positive nOe's to the protons *ortho* to the methoxyl group, there is a large negative nOe to the proton *meta* to the methoxyl. This indirect negative nOe is transmitted via the intervening *ortho* proton and has been described in detail by Mersh and Sanders (5, 6).

^{13}C chemical shifts for the aromatic carbon atoms of 4-methoxyphenol are given in Table 1, together with those of the corresponding carbon atoms in the 1:1 adduct and

TABLE 1. ^{13}C nmr chemical shifts for derivatives of 4-methoxyphenol

	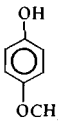	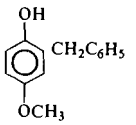	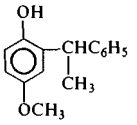	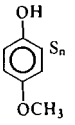
C-1	149.8	149.3*	147.4	147.8
C-2	116.4	129.4	133.4	133.3
C-3	115.3	116.2	114.5	114.0
C-4	153.4	153.6	153.8	153.6
C-5	115.3	112.4	111.9	111.6
C-6	116.4	116.9	116.7	116.2

*Solvent, $(CD_3)_2CO$ (7).

2-benzyl-4-methoxyphenol. In a general study of derivatives of benzylphenols (7) it was shown that introduction of a benzyl group at C-2 causes a 13 ppm downfield shift at C-2 and a 2.7 ppm upfield shift at C-5. The main effects of 1-methylbenzyl substitution are quite comparable — a 17 ppm downfield shift at C-2, and a 3.4 ppm upfield shift at C-5. Similar results are anticipated if a polystyrene chain is attached to C-2 of the 4-methoxyphenol.

Polystyrene with 4-methoxyphenol end groups

The main samples of polystyrenes prepared at 0°C in the presence of 0.3 *M* 4-methoxyphenol possess number-average molecular weights ($\bar{M}_n$) close to 3000. Simultaneous monitoring by uv (280 nm) and refractive index detectors showed that 4-methoxyphenol end groups are present in these samples over the whole range of molecular weights (approximately 500−8000). There is a maximum in the uv spectrum of the polymer at 294 nm compared with 292 nm for the 1:1 compound. The molar absorptivity of the 1:1 compound is 3700 L mol^{-1} cm^{-1} at λ_{max}, and if the phenolic end groups in the polymer possess the same molar absorptivity, the fraction of such end groups in the polystyrene samples is estimated to be at least 60%. Potentiometric titration yields a value of only 45%. The assumed molar absorptivity of the phenolic end groups in the polymer may be low and some of the polystyrene chains may be attached to the phenol at C-1 instead of C-2 or C-3.

The position on the phenol at which substitution occurs was investigated by means of ^{13}C nmr. The weaker resonances associated with the end groups do not overlap appreciably with the resonances arising from the phenyl groups in the polystyrene chain. Chemical shifts of the larger peaks originating from phenolic end groups are recorded in Table 1. The signal from the C-1 carbon bearing the OH group undergoes an upfield shift of about 2 ppm while the signal from the C-4 carbon bearing the OCH_3 group is unchanged. This implies that the preferred position of attachment of the polystyrene chain is at C-2 of the phenol. Such substitution leads to a 3.7 ppm upfield shift at C-5; the assignments at C-3 and C-6 are possibly interchanged.

The ^{13}C spectrum shows additional resonances close to 152 and 150 ppm and these indicate that attack can also occur at C-3 of the phenol. A fair proportion of the phenol is converted to the 1:1 adduct and some of it is incorporated as an end group, particularly if the yield of polymer is not kept low. The polystyrene thus contains a mixture of phenolic end groups and attachment at C-2 is merely a preferred rather than an exclusive chain-breaking process.

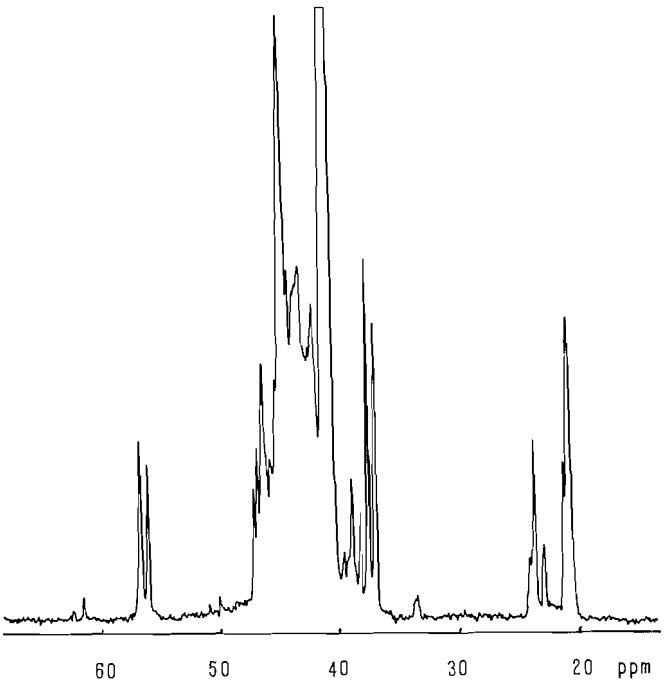

FIG. 2. Aliphatic region of ^{13}C nmr spectrum of polystyrene prepared in presence of 0.3 *M* 4-methoxyphenol. Solvent: $CDCl_3$.

Some of the aromatic carbon atoms in the phenolic end groups, e.g. C-2, give rise to more than one peak in the ^{13}C spectrum. This is presumably the result of variations in tacticity in the polymer chain, since model compounds of polystyrene show effects of similar magnitude (8). The effect is more striking in the aliphatic region of the spectrum (see Fig. 2). A pattern of peaks at 20.9, 21.3, 23.0, and 23.5 ppm is similar to that observed with other low molecular weight styrenes prepared in the presence of alkylphenols. These resonances are found in the spectra of model compounds and have been assigned to a terminal methyl group in the polymer chain (8); the methyl group may be formed either by proton transfer (e.g. from a co-initiator in the initiation step) or as a result of hydrolysis of a Cl_2AlCH_2-group introduced in an alternative mode of initiation. Tacticity effects are probably also the cause of there being two methine peaks at 36.9 and 37.5 ppm. These are present in spectra of alkylphenol-terminated polystyrenes and are assigned to the CH carbon of the methylbenzyl end group. The strong resonances in the 40−46 ppm region arise from backbone CH and CH_2 groups in the polystyrene chain.

Incorporation of 4-methoxyphenol into polystyrene can be represented by the equation

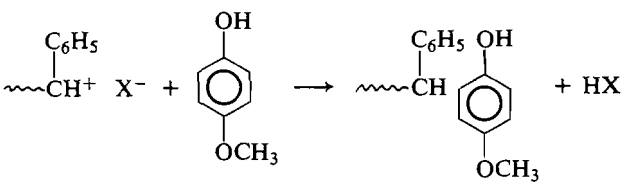

Alternatively, chain breaking may occur by proton transfer from the carbenium ion to the negative ion or to monomer. The resulting end groups may be unsaturated (—CH=CHC_6H_5) or saturated indane derivatives (9, 10). A weak band at 965 cm^{-1} in the infrared spectrum of the polymer suggests the presence of some unsaturated end groups. It is also possible that some

Can. J. Chem. Downloaded from www.nrcresearchpress.com by 210.87.254.6 on 09/06/12
For personal use only.

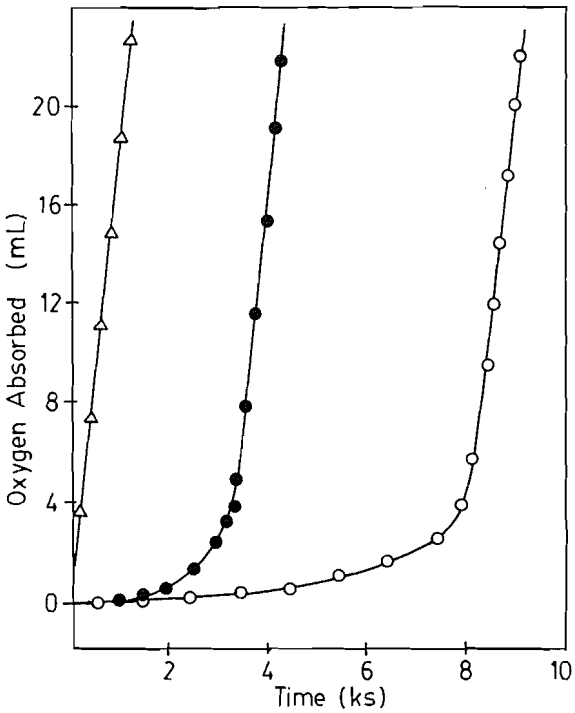

FIG. 3. Autoxidation of styrene at 65°C in the presence of various phenols. Δ, in the absence of phenol; ●, with 0.001 *M* polystyrene with phenol end groups; ○, with 0.001 *M* 1:1 adduct.

isomerization of unsaturated end groups may have occurred (11), resulting in methyl and methine groups in cyclic isomers which contribute to the patterns noted above. In each case, however, firm quantitative evidence has not been obtained.

Antioxidant activity of the phenol-terminated polystyrene

The 1:1 adduct and the phenol-terminated polymer were used as antioxidants for the autoxidation of styrene initiated by azobisisobutyronitrile at 65°C. Figure 3 shows the volume of oxygen absorbed as a function of time in the absence of phenol and in the presence of phenol-terminated polymer and of 1:1 phenol–styrene adduct at concentrations close to 0.001 *M*. In other experiments it was shown that the induction period is proportional to the concentration of phenol-terminated polymer in the range 0.00068 *M* to 0.0020 *M*. Assuming that the 1:1 adduct is pure, the fraction of phenolic end groups in the polystyrene sample was found to be 41%.

The behaviour of these materials as antioxidants is quite comparable to that of BHA under similar experimental conditions. At a concentration of 0.001 *M*, BHT reduces the initial rate of autoxidation of styrene to a much less extent than the 4-methoxyphenol derivatives. The rates of absorption of oxygen allow a rough estimate to be made of the ratio of rate constants for hydrogen abstraction by the peroxy radical from these phenols to that for its reaction with styrene. This ratio is close to 1000 at 65°C, confirming that the activity of these phenols is comparable to that of the more conventional antioxidant, 2-*t*-butyl-4-methoxyphenol (4, 12).

Acknowledgements

This research was supported by an operating grant from the Natural Sciences and Engineering Research Council of Canada. The CXP-200 nmr spectrometer was purchased with the aid of grants from the Council and Queen's University. We are grateful to L. Rose and P. Mulligan for technical assistance.

1. K. E. RUSSELL, L. G. M. C. VAIL, and M. E. WOOLSTON. Eur. Polym. J. **15**, 969 (1979).
2. K. E. RUSSELL and L. G. M. C. VAIL. U. S. Patent No. 4 107 144, Aug. 15, 1978.
3. A. J. WNUK, T. F. DAVIDSON, and J. E. MCGRATH. J. Appl. Polym. Sci. Appl. Polym. Symp. **34**, 89 (1978).
4. J. A. HOWARD and K. U. INGOLD. Can. J. Chem. **41**, 2800 (1963).
5. J. D. MERSH and J. K. M. SANDERS. Tetrahedron Lett. **22**, 4029 (1981).
6. J. D. MERSH and J. K. M. SANDERS. Org. Magn. Res. **18**, 122 (1982).
7. Y. NAKAI and F. YAMADA. Org. Magn. Res. **11**, 607 (1978).
8. B. JASSE, F. LAUPRÊTRE, and L. MONNERIE. Makromol. Chem. **178**, 1987 (1977).
9. S. BYWATER and D. J. WORSFOLD. Can. J. Chem. **44**, 1671 (1966).
10. T. HIGASHIMURA and H. NISHII. J. Polym. Sci., Polym. Chem. Ed. **15**, 329 (1977).
11. M. SAWAMOTO and T. HIGASHIMURA. Macromolecules, **14**, 467 (1981).
12. J. A. HOWARD and K. U. INGOLD. Can. J. Chem. **43**, 2729 (1965).

Can. J. Chem. Downloaded from www.nrcresearchpress.com by 210.87.254.6 on 09/06/12
For personal use only.

A constrained Roothaan–Hartree–Fock method

G. D. ZEISS AND M. A. WHITEHEAD

Chemistry Department, McGill University, 801 Sherbrooke Street West, Montreal, P.Q., Canada H3A 2K6

Received May 12, 1982

G. D. ZEISS and M. A. WHITEHEAD. Can. J. Chem. **61**, 128 (1983).

Nonperturbational and perturbation–iteration procedures for determining constrained Roothaan–Hartree–Fock wavefunctions are described and compared. The perturbation–iteration procedure most rapidly converges, the secant-parameterization method requires less computation and is less sensitive to numerical errors.

G. D. Zeiss et M. A. WHITEHEAD. Can. J. Chem. **61**, 128 (1983).

On décrit et on compare les procédés de non perturbation et de perturbation–répétition pour la détermination des fonctions d'onde de contrainte de Roothaan–Hartree–Fock. La méthode de perturbation–répétition converge plus rapidement alors que la méthode de mise en paramètre séquentielle requiert moins de calcul et elle est moins sensible aux erreurs numériques.

[Traduit par le journal]

Can. J. Chem. Downloaded from www.nrcresearchpress.com by 210.87.254.40 on 09/06/12
For personal use only.

Introduction

The constrained variational Roothaan–Hartree–Fock (RHF) method (1–6) requires the wavefunction to satisfy one or more one-electron expectation value constraints (7–10). Non-variational calculations (11–19) used sufficient constraints to determine the wavefunction without the minimum energy principle.

Some of the constrained variational procedures considered here are applicable to this type of calculation. The variational calculations use several different procedures based on the parameterization (7), perturbation, perturbation–iteration methods (9), and pattern-search techniques in conjunction with the constrained density matrix methods (16). No calculation involved more than two free variational parameters. For larger systems computing the constrained RHF equations becomes significant, therefore several constraint procedures, with particular reference to computation, are developed. A rapid parameterization procedure, the *secant-parameterization method*, applicable to both singly and multiply constrained calculations, is described, and compared with several nonperturbational numerical methods, and perturbation theory methods. Computational difficulties, specific to multiply constrained calculations, are discussed.

Two questions arise: (*1*) how do constraints affect approximate wavefunctions, and (*2*) to what extent is a constrained wavefunction improved over a free variational wavefunction? Previous studies (7–9, 20–26) considered the effect of constraints on property expectation values, populations (27), and electron density distribution maps (7, 27, 28). In a constrained RHF calculation on HF (7), the expectation values of the dipole moment and the proton (deuteron) electric field gradient were constrained to experimental values; the constrained wavefunction significantly improved the expectation values of the diamagnetic shielding constant and the electric field at the proton and worsened the expectation values of the diamagnetic susceptibility and the electric field at the fluorine. The electron density distributions derived from the free variational and constrained wavefunctions compared with a distribution obtained from Nesbet's extended basis set RHF wavefunction (29) showed the gross characteristics of the exact wavefunction to be better represented by the constrained wavefunction. Two constrained RHF calculations using the N_2 wavefunction of Scherr (30), satisfied the molecular virial theorem (31) or yielded the experimental value (32) of the molecular quadrupole moment, the latter impaired the wavefunction, giving poorer expectation values for several one-electron properties, but (28) the virial theorem constraint improved the wavefunction.

The constrained Roothaan–Hartree–Fock equation for a closed shell system

The constrained Hartree–Fock method is a special case of the constrained variational theory in which, for a closed shell system, the wavefunction is required to have the form of an equivalence restricted (33) Slater determinant with $2n$ electrons and ϕ_ν linearly independent spatial one-electron functions to be determined. Each Hartree–Fock one-electron function ϕ_ν is expanded in terms of a finite number of known one-electron functions χ_i where $m > n$, and the coefficients $c_{i\nu}$ are to be

$$[1] \quad \phi_\nu = \sum_i^m \chi_i c_{i\nu}$$

determined. Substituting ϕ_ν into the free variational principle gives the constrained Roothaan–Hartree–Fock equations, which in canonical form are represented by the pseudo-eigenvalue equation

$$[2] \quad \sum_j^m F'_{ij} c_{j\nu} = \sum_j^m S_{ij} c_{j\nu} \epsilon'_\nu$$

and the associated constraint conditions

$$[3] \quad 2 \sum_\nu^n \sum_{ij}^m \langle \chi_i | M_q - \mu_q/2n | \chi_j \rangle c_{i\nu} c_{j\nu} = 0; \quad q = 1, \ldots, s$$

where M_q is a Hermitian operator and μ_q is the known expectation value of the operator, hence

$$[4] \quad F'_{ij} = F_{ij} + \sum_q^s \lambda_q \langle \chi_i | M_q - \mu_q/2n | \chi_j \rangle$$

and S_{ij} and F_{ij} are elements of the overlap matrix and Fock matrix, respectively. The quantities ϵ'_ν, $\nu = 1, \ldots, m$ are the roots of the secular equation

$$[5] \quad |F'_{ij} - \epsilon'_\nu S_{ij}| = 0$$

In the absence of constraints, when all $\lambda_q = 0$, eq. [3] reduces to the free variational RHF equation (3).

0008-4042/83/010128-07$01.00/0

©1983 National Research Council of Canada/Conseil national de recherches du Canada

Can. J. Chem. Downloaded from www.nrcresearchpress.com by 210.87.254.40 on 09/06/12
For personal use only.

Equations analogous to [3]–[5] for open shell systems in either the unrestricted (34) or restricted (35) formulations are easily formulated.

Procedures for solving the constrained variational RHF equations

Solving the constrained RHF equations [3] and [4] requires simultaneous determination of the s Lagrange multipliers λ_q, and the nm variational parameters c_i of the trial wavefunction.

The secant-parameterization procedure (36)

In the parameterization method (22), the constraint conditions (4) are treated as a system of nonlinear equations in the independent variables λ_q, obtained by iteration. After each iteration a set of λ_q values is estimated and substituted into eq. [3], which is solved in the usual iterative self-consistent manner. The coefficients evaluate the expectation value of each constraint operator. The process is continued until each of the constraint conditions is satisfied to within a predetermined tolerance.

The secant-parameterization procedure requires two initial estimates of the Lagrange multiplier, $\lambda^{(0)}$ and $\lambda^{(1)}$, and the corresponding expectation values of the constraint operator, $\Delta\mu^{(0)}$ and $\Delta\mu^{(1)}$, where

$$[6] \quad \Delta\mu^{(i)} = \langle\psi^{(i)}|M - \mu|\psi^{(i)}\rangle$$

and $\psi^{(i)}$ is obtained by solving eq. [3] for $\lambda = \lambda^{(i)}$. $\lambda^{(0)}$ is chosen zero, and $\psi^{(0)}$ is the free variational RHF wavefunction: $\lambda^{(1)}$ is $\lambda^{(0)} \pm h$ (the sign is the sign of $\Delta\mu^{(0)}$), where h is a positive number sufficiently large that ($\Delta\mu^{(1)} = \Delta\mu^{(0)}$) possesses at least two or three significant digits, but small enough that only a few iterations are required for self-consistency when the coefficients $c_{i\nu}^{(0)}$ are used as an initial approximation to the $c_{i\nu}^{(1)}$. A new estimate $\lambda^{(2)}$ is

$$[7] \quad \lambda^{(i+1)} = \lambda^{(i)} - \frac{\lambda^{(i)} - \lambda^{(i-1)}}{\Delta\mu^{(i)} - \Delta\mu^{(i-1)}}\Delta\mu^{(i)}$$

Equation [3] is solved for $\lambda = \lambda^{(2)}$ and the process is repeated using $\lambda^{(1)}$ and $\lambda^{(2)}$. The coefficients determined for the previous value of λ initiate the iterative self-consistence procedure for solving eq. [3]. The iterative process terminates if (a)

$$[8] \quad |\delta\mu^{(i)}| < \epsilon_M$$

where ϵ_M is a predetermined tolerance; the procedure has converged, if (b)

$$[9] \quad |\Delta\mu^{(i)}| < \epsilon\Delta P_{\max}|M|$$

and the process is terminated. Here $\Delta P_{\max}$ is the largest absolute change in any element of the first order density matrix in the last iteration of the preceding self-consistency procedure, $|M| = \sum_{ij}|\langle\chi_i|M|\chi_j\rangle|$, and ϵ is a positive number ~1. This criterion terminates the process when the number of significant digits in ($\Delta\mu^{(i)} - \Delta\mu^{(i-1)}$) in eq. [7] becomes so small that the λ values estimated using eq. [7] become erratic, and if (c) after a pre-selected maximum allowed number of iterations, neither criterion (a) nor (b) is satisfied, the process is terminated.

For multiple constraints there are s constraint conditions, eq. [4] to be satisfied and s Lagrange multipliers λ_q to be determined. The cyclic procedure treats each constraint independently (25), while the remaining Lagrange multipliers are held constant. This procedure converges most rapidly when the constraint conditions are weakly coupled (37).

Nonperturbational procedures for determining constrained RHF wavefunctions

The approaches are: (*1*) direct energy minimization with respect to the variational parameters of the wavefunction subject to one or more nonlinear constraints, (*2*) solution of a system of nonlinear equations in the variables λ_q, (*3*) maximization of the expectation value of the fictitious Hamiltonian H' with respect to the parameters λ_q, and (*4*) application of the perturbation theory.

(1) Direct energy minimization (38–41) procedures for determining (unconstrained) RHF wavefunctions converge slowly.

(2) Two procedures (9, 22, 25, 42–44) are (a) the secant-parameterization method, and (b) a numerical procedure (45–47) for solving nonlinear equations.

(3) The derivative of the expectation value of the fictitious Hamiltonian H' with respect to the Lagrange multiplier λ_q is the expectation (22) value eq. [6] of the qth constraint operator, and this approach is well-suited to extremalization requiring the gradient of the function being extremalized (48).

The three numerical methods iterate to give a new set of λ_q values. Solve eq. [3] and use the wavefunction to calculate new expectation values of H' and the constraint operators. These expectation values determine new estimates of the λ_q's. The time-consuming part is the iterative SCF solution of the RHF equations. Therefore, a good comparative measure of the computation to solve the constrained RHF equations is the sum $\sum_i{}' N_{\text{SCF}}^{(i)}$ (the prime indicates that the iterations required initially to solve the unconstrained RHF equations are not included) of the number of iterations $N_{\text{SCF}}^{(i)}$ to achieve self-consistency in the ith step of the constraint procedure. The number of SCF iterations at each step depends on the SCF convergence criterion. The SCF procedure terminates if the energy change between SCF iterations is less than a predetermined value ϵ_E; for large ϵ_E, the number of SCF iterations is small, but ϵ_E must be small enough that the expectation values eq. [6] of the constraint operators are computed with sufficient precision for rapid convergence of the constraint procedure. Since the maximum change in any first order density matrix element between iterations is proportional to the square root of the corresponding energy change, this can be used to estimate an appropriate value of ϵ_E.

LiH constrained RHF calculations (Table 1) used these three numerical constraint procedures. The basis set was a minimum set of STO-4G functions (49) with Ransil's BLMO exponents (50). The constraints were the kinetic energy T, the diple moment x_n, and the electric field, E_{Li}^{c} and E_{H}^{c}, at the lithium and hydrogen nuclei, respectively, due to the electronic charge distribution. The SCF convergence criterion used was $\epsilon_E = 10^{-8}$ hartrees. For each constraint or combination of constraints the final values of the Lagrange multipliers from the three procedures agree to four significant figures. The secant procedure converges with much less computation (measured by $\Sigma' N_{\text{SCF}}^{(i)}$). The kinetic energy constraint calculations, Table 2, reveal that for the Fletcher–Powell method the initial rapid convergence rate becomes slow and erratic as the maximum is approached, because the E' hypersurface is very flat.

Rapid convergence requires a high precision in E' and in the expectation values of the constraint operators, achieved by making the SCF convergence criterion more stringent but thereby increasing the amount of computation. Brown's (45–47) method requires precise partial derivatives of the ex-

TABLE 1. LiH. *Different procedures for constraining RHF wavefunctions.* Final values of the Lagrange multiplier(s), the remaining errors in the constrained properties, and the total number of SCF iterations required are given. The calculations used BLMO exponents. The SCF convergence criterion was 10^{-8} *hartrees*

Constraint(s)	Method	$\Sigma' N_{SCF}^{(i)}$	Final Lagrange multipliers $\lambda_{(1)}$	$\lambda_{(2)}$	Remaining errors in constrained properties $\Delta_{(1)}$	$\Delta_{(2)}$
T	Secant	12	−0.12499		-9×10^{-6}	
	Brown	20	−0.12495		5×10^{-5}	
	Fletcher–Powell	26	−0.12501		6×10^{-6}	
x_n	Secant	12	0.00084		2×10^{-5}	
	Brown	17	0.00087		3×10^{-5}	
	Fletcher–Powell	31	0.00086		7×10^{-6}	
E^e_{Li}, E^e_H	Secant	68	0.25640	0.69162	4×10^{-6}	-6×10^{-6}
	Brown	118	0.25678	0.69158	-7×10^{-5}	-4×10^{-6}
	Fletcher–Powell	174	0.25641	0.69150	5×10^{-6}	3×10^{-6}
T, x_n	Secant	143	−0.16540	0.02115	-5×10^{-5}	-5×10^{-5}
	Brown	124	−0.16537	0.02111	4×10^{-7}	4×10^{-4}
	Fletcher–Powell	157	−0.16539	0.02112	-2×10^{-6}	-3×10^{-5}

TABLE 2. LiH. *Different procedures for kinetic energy, T, constraint of RHF wavefunctions.* The remaining error Δ in T, the Lagrange multiplier λ, and the number of SCF iterations required are given for each step. The calculations were performed using BLMO exponents. The SCF convergence criterion was 10^{-8} *hartrees*

	Secant-parameterization			Brown			Fletcher–Powell		
Iteration	$N_{SCF}^{(i)}$	$\lambda^{(i)}$	$\Delta^{(i)}$	$N_{SCF}^{(i)}$	$\lambda^{(i)}$	$\Delta^{(i)}$	$N_{SCF}^{(i)}$	$\lambda^{(i)}$	$\Delta^{(i)}$
0	12	0.0	−0.13090	12	0.0	−0.13090	12	0.0	−0.13090
1	6	−0.12901	0.00400	6	−0.13764	0.01262	5	−0.06545	−0.06033
2	3	−0.12519	0.00020	5	−0.12174	−0.00326	5	−0.13089	0.00588
3	2	−0.12499	-8×10^{-6}	4	−0.12527	0.00025	3	−0.12917	0.00419
4				3	−0.12495	−0.00005	3	−0.12518	0.00019
5				1	−0.12495	-5×10^{-5}	3	−0.12119	−0.00380
6							3	−0.12513	0.00011
7							1	−0.12502	0.00003
8							1	−0.12490	−0.00008
9							1	−0.12501	-6×10^{-6}

pectation values of the constraint operators with respect to the Lagrange multipliers λ_q, but the partial derivatives are evaluated numerically, and the method is very sensitive to imprecision in the calculated expectation values of constraint operators. The secant method is relatively *insensitive* to numerical errors in the calculated expectation values of constraint operators, and this is responsible for the rapid convergence.

The convergence criterion, $\epsilon_E = 10^{-8}$ hartrees, ensures convergence to 9–10 significant figures in the energy and about 5 significant figures in property expectation values. The computation is reduced by choosing a more lenient SCF convergence criterion; Table 3 contains results where ϵ_E was 10^{-5} hartrees: property expectation values are correct to at least 3–4 significant figures. Tables 1 and 3 show the Lagrange multipliers to agree to three significant figures. Table 4 shows the rate of convergence to be very rapid. The total number of SCF iterations in the constraint procedure is less than the number of iterations to solve the initial unconstrained RHF equations.

Sometimes no reasonable wavefunction satisfies a particular constraint condition (11–13, 25); the electric field or electric field gradient constraint at the proton on a minimum basis set LiH wavefunction with Slater exponents were unsuccessful, since the wavefunction lacks flexibility in regions weighted by the constraint operator (25, 27): a minimum basis set for LiH does not include a polarization function on the proton and cannot satisfy constraints of properties depending on the wavefunction near the proton.

Perturbation–iteration methods to determine constrained RHF wavefunctions

Three approximate forms of the first order RHF perturbation theory (8, 9, 20–24) are now applied to the constrained RHF method, and compared with calculations using the secant-parameterization procedure.

Perturbation theory (51–58) directly determines constrained variational wavefunctions, or is combined with a finite difference procedure (59–64), since for small basis set wavefunctions the perturbation expansion converges slowly (9, 22, 23, 65). In the iterative approach (66–74) each new estimate of the Lagrange multiplier is obtained using only the first term in the perturbation expansion. Both procedures were applied (8, 9) in the fully coupled CRHF form to a minimum basis set RHF calculation on N_2 in which the wavefunction was constrained to give the experimental molecular quadrupole mo-

Can. J. Chem. Downloaded from www.nrcresearchpress.com by 210.87.254.40 on 09/06/12
For personal use only.

TABLE 3. LiH. *Different procedures for determining constrained RHF wavefunctions.* Final values of the Lagrange multipliers, the remaining errors in the constrained properties, and the total number of SCF iterations required are given. The calculations were performed using BLMO exponents. The SCF convergence criterion was 10^{-5} *hartrees*

Constraint(s)	Method	$\Sigma' N_{SCF}^{(i)}$	Final Lagrange multipliers			Remaining errors in constrained properties		
			$\lambda_{(1)}$	$\lambda_{(2)}$	$\lambda_{(3)}$	$\Delta_{(1)}$	$\Delta_{(2)}$	$\Delta_{(3)}$
T	Secant	6	−0.1254			7×10^{-4}		
	Brown	11	−0.1260			7×10^{-4}		
	Fletcher–Powell	12	−0.1249			7×10^{-4}		
x_n	Secant	5	0.0010			-2×10^{-3}		
	Brown	20	0.0004			5×10^{-3}		
	Fletcher–Powell	7	0.0004			-3×10^{-4}		
E_{Li}^{c}, E_{H}^{c}	Secant	36	0.2564	0.6919		-7×10^{-6}	3×10^{-5}	
	Brown	60	0.2565	0.6931		-5×10^{-6}	-7×10^{-5}	
	Fletcher–Powell	87	0.2567	0.6914		-7×10^{-5}	-2×10^{-5}	
r_{Li}^{-1}, r_{H}^{-1}, x_n	Secant	140	−0.3333	−0.1279	0.0317	-3×10^{-4}	3×10^{-4}	3×10^{-3}
	Brown	*						
	Fletcher–Powell	*						

*Convergence was not achieved within the maximum allowed number of iterations.

TABLE 4. LiH. Secant-parameterization procedure to a singly constrained RHF wavefunction. The constrained property is the *kinetic energy T*. The value of the Lagrange multiplier, the remaining error in T, the number of SCF interactions required, and the total electronic energy are given for each iteration. The calculation was performed using BLMO exponents. The SCF convergence criterion was 10^{-5} *hartrees*

Iteration	$N_{SCF}^{(i)}$	$\lambda^{(i)}$	$\Delta^{(i)}$	$E^{(i)}$
0	8	0.0	−0.1309	−8.93653
1	4	−0.1278	0.0025	−8.92821
2	1	−0.1254	7×10^{-4}	−8.92843

ment (32). The convergence of the perturbation expansion was fast in the iterative perturbation procedure. The computation difficulties with solving the CRHF equations are not apparent for a minimum basis set N_2 wavefunction because of symmetry; less symmetrical systems and larger basis sets show the computational disadvantages of the CRHF method.

Three computationally less time-consuming first order RHF perturbation methods are examined in the context of the iterative perturbation procedure; the finite perturbation, FPT, and two uncoupled RHF methods.

To first order the Lagrange multiplier is

$$[10]\quad \lambda = \frac{\Delta\mu}{2E^{(2)}} + O(\Delta\mu^2)$$

where

$$[11]\quad E^{(2)} = \frac{d^2E}{d\lambda^2}$$

Using the generalized Hellman–Feynman theorem, $E^{(2)}$ is

$$[12]\quad E^{(2)} = \frac{d}{d\lambda}\langle\phi|\hat{M} - \mu|\phi\rangle$$

In the FPT method $E^{(2)}$ is evaluated using the finite difference analogue of eq. [12]. The "zeroeth order" RHF equations are solved for two values of λ where the difference h between them is small (64), and the method is capable of reproducing the exact CRHF value of $E^{(2)}$ to any desired accuracy.

The singly excited configuration obtained by replacing occupied ϕ_κ by virtual RHF orbitals ϕ_σ in the ground state RHF wavefunction are used as the zeroeth order wavefunction and the Rayleigh–Schrodinger perturbation theory applied giving an approximate sum-over-states expression for $E^{(2)}$

$$[13]\quad E^{(2)} \simeq -2\sum_{\kappa\phi}\frac{|\langle\phi_\kappa|M|\phi_\sigma\rangle|^2}{\epsilon_\sigma - \epsilon_\kappa - (\sigma\sigma|\kappa\kappa) + 2(\sigma\kappa|\sigma\kappa)}$$

ϵ_κ and ϵ_σ are the eigenvalues, and $(\sigma\sigma|\kappa\kappa)$ and $(\sigma\kappa|\sigma\kappa)$ are electron repulsion and exchange integrals. Neglecting these, a simple approximate expression is (71, 72)

$$[14]\quad E^{(2)} = 2\sum_{\kappa\sigma}\frac{|\langle\phi_\kappa|M|\phi_\sigma\rangle|^2}{\epsilon_\sigma - \epsilon_\kappa}$$

Equations [13] and [14] give different variants of the uncoupled RHF theory, I and II. Method I closely resembles the uncoupled RHF method of Langhoff *et al.* (57).

Constrained RHF calculations using these three perturbation methods, in conjunction with an iterative procedure, were perfomed on N_2, using a minimum basis set STO-4G function with Slater exponents (9). The constraint is the experimental molecular quadrupole moment (32). The SCF convergence criterion is $\epsilon_E = 1\times10^{-8}$ hartrees, and the corresponding value of ΔP_{max} is $\sim1\times10^{-4}$. The increment h in the finite perturbation theory was 1×10^{-3} to give $E^{(2)}$ to three significant figures, and was used to obtain the initial Lagrange multiplier in the secant-parameterization calculation. The Lagrange multiplier converged to five significant figures, Table 5 (the difference between the value of λ, 0.14148, and Bjørn's (9) value 0.14167, is because of different basis sets and the remaining errors in the quadrupole moment are all $\sim1\times10^{-4}$). The most rapid convergence is the finite perturbation method, the secant-parameterization and UCRHF method I are poorer, and UCRHF method II requires twice as many iterations, due to the poor estimates of $E^{(2)}$ obtained by the UCRHF method II (57, 75); the initial estimate of $E^{(2)}$ differs from the FPT value by 22% compared to a 5% discrepancy for the UCRHF method I

Can. J. Chem. Downloaded from www.nrcresearchpress.com by 210.87.254.40 on 09/06/12
For personal use only.

TABLE 5. N_2. *Comparison of different perturbation–iteration procedures for constraining RHF wavefunctions.* The property constrained is the molecular quadrupole moment $-\theta_n^e$. The remaining error Δ in $-\theta_n^e$, the Lagrange multiplier λ, and the number of SCF iterations required are given for each step. The calculations were performed using Slater exponents. The SCF convergence criterion was 10^{-8} *hartrees*

	FPT			UCRHF I			UCRHF II			Secant-parameterization		
Iteration	$N_{SCF}^{(i)}$	$\lambda^{(i)}$	$\Delta^{(i)}$	$N_{SCF}^{(i)}$	$\lambda^{(i)}$	$\Delta^{(i)}$	$N_{SCF}^{(i)}$	$\lambda^{(i)}$	$\Delta^{(i)}$	$N_{SCF}^{(i)}$	$\lambda^{(i)}$	$\Delta^{(i)}$
0	13	0.0	0.8558	13	0.0	0.8558	13	0.0	0.8558	13	0.0	0.8558
1	10	0.16897	−0.1890	7	0.16083	−0.1327	7	0.21539	−0.5148	10	0.16897	−0.1890
2	10	0.14144	0.0002	5	0.14264	−0.0080	6	0.12237	0.1282	6	0.13843	0.0206
3	7	0.14147	-6×10^{-5}	4	0.14152	−0.0003	6	0.14725	−0.0393	4	0.14143	0.0003
4				1	0.14147	-8×10^{-5}	5	0.13985	0.0109	2	0.14148	-4×10^{-5}
5							4	0.14193	−0.0030			
6							3	0.14135	0.0008			
7							2	0.14150	-1×10^{-4}			

estimate. The errors in $E^{(2)}$ using the approximate UCRHF methods varies with the property constrained. The secant-parameterization procedure requires the least computation per iteration.

A disadvantage of the finite perturbation method is that eq. [3] must be solved for two values of λ at each step. In the secant-parameterization procedure eq. [3] is solved once per iteration after the initial step. In UCRHF method I $n(m-n)$ electron repulsion integrals are evaluated at each step and the same number of exchange integrals between RHF orbitals, significantly increasing the computation time per iteration. The UCRHF method II involves the least computation per iteration. Unfortunately, it also gives the slowest convergence. The secant-parameterization calculation required ~30 s on an IBM 360/75; the other calculations required 35–40 s.

The finite perturbation method uses numerical derivatives and is sensitive to calculated expectation value errors due to the SCF convergence criterion; values of $E^{(2)}$ calculated using eq. [3] or [4] are insensitive to the SCF convergence criterion. The secant-parameterization method is not sensitive to errors in constraint operator expectation values. Near convergence, when $(\lambda^{(i)} - \lambda^{(i-1)})$ becomes small, the correction $\Delta\lambda = (\lambda^{(i+1)} - \lambda^{(i)})$ to $\lambda^{(i)}$ obtained using eq. [7] is also small and very few significant digits are required (36).

Constrained RHF calculations with multiple constraints

The constrained RHF calculations on LiH in Tables 1 and 3 show the computation required to solve the constrained RHF equations increases dramatically with the number of constraints and hence the present calculations involve only two, or three, constraints. The combination of constraints influences the labour to determine multiple constrained wavefunctions.

A double constraint RHF calculation on LiH, in which the Hellman–Feynman electric field, E_A^e, at each nucleus is required to vanish, is given in Table 6. The expectation value of each constraint operator is independent of the Lagrange multiplier associated with the other constraint operator, the two constraint operators are only weakly coupled, and a cyclic multiple constraint procedure converges (37); the final Lagrange multipliers do not differ greatly from the values, 0.2411 and 0.7050, determined in singly constrained RHF calculations. An appropriate choice of the initial estimate $\lambda_q^{(0)}$ is the value in the corresponding singly constrained calculation (25, 37).

Table 7 contains results of a doubly constrained RHF calculation to CO; the wavefunction is constrained to give the experimental and theoretical values of the electric field gradient,

TABLE 6. LiH. *Determination of a doubly constrained RHF wavefunction using the cyclic secant-parameterization procedure.* The constrained properties are E_{Li}^e and E_H^e. Values of the Lagrange multipliers, the remaining errors in E_{Li}^e and E_H^e, and the total electronic energy are given for each cycle. The calculation was performed using BLMO exponents. The SCF convergence criterion was 10^{-5} *hartrees*

	Lagrange multipliers		Remaining errors in E_{Li}^e and E_H^e		
Cycle	$\lambda_1^{(i)}$	$\lambda_2^{(i)}$	$\Delta_1^{(i)}$	$\Delta_2^{(i)}$	$E^{(i)}$
0	0.0	0.0	0.0504	0.0298	−8.93653
1	0.2411	0.7449	0.0030	−0.0021	−8.91973
2	0.2574	0.6873	−0.0002	0.0001	−8.92054
3	0.2564	0.6919	7×10^{-6}	3×10^{-5}	−8.92052

TABLE 7. CO. *Determination of a doubly constrained RHF wavefunction using the cyclic secant-parameterization procedure.* The constrained properties are $-q_C^e$ and $-q_O^e$. Values of the Lagrange multipliers, the remaining errors in $-q_C^e$ and $-q_O^e$, and the total electronic energy are given for each cycle. The calculation was performed using a PL-4G (r^{-1}) basis set with Clementi and Raimondi's best atom exponents. The SCF convergence criterion was 10^{-6} *hartrees*

	Lagrange multipliers		Remaining errors in $-q_C^e$ and $-q_O^e$		
Cycle	$\lambda_1^{(i)}$	$\lambda_2^{(i)}$	$\Delta_1^{(i)}$	$\Delta_2^{(i)}$	$E^{(i)}$
0	−0.0268	−0.2236	−1.2831	−0.1433	−134.6281
1	−0.0853	−0.3570	−0.5267	−0.0023	−134.3466
2	−0.1103	−0.3824	−0.0775	−0.0007	−134.4981
3	−0.1151	−0.3877	0.0069	0.0009	−134.4380
4	−0.1151	−0.3876	0.0077	−0.0009	−134.4886
5	−0.1147	−0.3872	0.0007	−0.0017	−134.4897

$-q_A^e$, at each nucleus. The initial $\lambda_q^{(0)}$ were the values obtained in singly constrained RHF calculations. The expectation value of each constraint operator is strongly dependent on the value of the Lagrange multiplier of the other constraint operator, Table 7. This coupling between the constraint operators is stronger than in LiH, convergence is slower, and the final Lagrange multipliers values are quite different from the singly constrained values.

Constrained calculations with large basis sets show (24) the coupling between property operators to be greatest when the operators weight the same region, particularly if the basis set is relatively inflexible in these regions. In constrained minimum basis set calculations there is considerable coupling between

Can. J. Chem. Downloaded from www.nrcresearchpress.com by 210.87.254.40 on 09/06/12
For personal use only.

Can. J. Chem. Downloaded from www.nrcresearchpress.com by 210.87.254.40 on 09/06/12
For personal use only.

constraint operators, even when they weight different regions of space. In some cases the wavefunction is unable to simultaneously satisfy two or more constraint conditions involving strongly coupled constraint operators (25), as in N_2, where the minimum basis set wavefunction posesses only two free variational degrees of freedom.

The expectation values of four of the seven properties of N_2, namely the molecular quadrupole moment, $-\theta_n^c$, the diamagnetic contribution to the diamagnetic susceptibility r_n^2, the total one-electron energy $T + V_{ne}$, and the electric field gradient $-q_N^c$, all depend on one of the two variational parameters, and it is impossible for the wavefunction to simultaneously satisfy two constraint conditions involving any two of these four properties.

Conclusion

Of the several procedures to determine constrained RHF wavefunctions the nonperturbational procedures included Brown's method (45–47), a general numerical procedure for solving systems of nonlinear algebraic equations, the Fletcher–Powell method (48) for extremalizing functions of several variables, and the secant-parameterization procedure, several procedures based on the RHF perturbation theory including the finite perturbation method (59–64), and two uncoupled RHF perturbation methods (57, 71, 72), the most rapidly converging was a constraint procedure based on the finite perturbation method; however, the secant-parameterization procedure, converging more slowly, required less computation and was less sensitive to numerical errors.

Therefore, the secant-parameterization method should be used to calculate constrained variational RHF wavefunctions.

The results from the method for an extensive series of constrained RHF calculations on N_2, FH, LiH, and CO are being published and analyzed (76, 77) using property expectation values, populations and electron density distribution profiles (78). The trends are very encouraging, and should advance the field from the dead-end surveyed in 1976 (79).

Acknowledgements

This research was supported by the National Research Council of Canada.

1. D. R. HARTREE. Proc. Cambridge Phil. Soc. **24**, 89 (1920).
2. V. FOCK. Z. Phys. **61**, 126 (1930).
3. C. C. J. ROOTHAAN. Rev. Mod. Phys. **23**, 69 (1951).
4. S. FRAGA and F. W. BIRSS. Theoret. Chim. Acta, **5**, 398 (1966).
5. W. L. CLINTON, A. J. GALLI, G. A. HENDERSON, G. B. LAMERS, L. J. MASSA, and J. ZARUR. Phys. Rev. **177**, 27 (1969).
6. N. BJØRNA. J. Phys. B, **4**, 424 (1971).
7. A. MUKHERJI and M. KARPLUS. J. Chem. Phys. **38**, 44 (1963).
8. N. BJØRNA. J. Phys. B, **5**, 732 (1972).
9. N. BJØRNA. Mol. Phys. **24**, 1 (1972).
10. R. K. ZIMMERMAN, JR. M.Sc. Thesis. Southern Illinois University. 1975.
11. R. F. W. BADER and G. A. JONES. Can. J. Chem. **41**, 586 (1963).
12. R. F. W. BADER and G. A. JONES. J. Chem. Phys. **38**, 2791 (1963).
13. R. F. W. BADER and G. A. JONES. Can. J. Chem. **41**, 2251 (1963).
14. R. F. W. BADER and H. J. T. PRESTON. Theoret. Chim. Acta, **17**, 384 (1970).
15. W. L. CLINTON, J. NAKHLEH, and F. WUNDERLICH. Phys. Rev. **177**, 1 (1969).
16. W. L. CLINTON, A. J. GALLI, and L. J. MASSA. Phys. Rev. **177**, 7 (1969).
17. W. L. CLINTON, G. A. HENDERSON, and J. V. PRESTIA. Phys. Rev. **177**, 13 (1969).
18. W. L. CLINTON and L. J. MASSA. Int. J. Quantum Chem. **VI**, 519 (1972).
19. G. A. HENDERSON and M. A. LEE. J. Chem. Phys. **58**, 2388 (1973).
20. Y. RASIEL and D. R. WHITMAN. J. Chem. Phys. **42**, 2124 (1965).
21. W. BYERS BROWN. J. Chem. Phys. **44**, 567 (1966).
22. D. P. CHONG and Y. RASIEL. J. Chem. Phys. **44**, 1819 (1966).
23. D. P. CHONG and W. BYERS BROWN. J. Chem. Phys. **45**, 392 (1966).
24. C. P. YUE and D. P. CHONG. Theoret. Chim. Acta, **12**, 431 (1968).
25. R. J. LOEB and Y. RASIEL. J. Chem. Phys. **52**, 4995 (1970).
26. D. R. WHITMAN and R. N. CARPENTER. J. Chem. Phys. **53**, 3830 (1970).
27. C. W. KERN and M. KARPLUS. J. Chem. Phys. **40**, 1374 (1964); **43**, 2926 (1965).
28. N. BJØRN. Phys. Norv. **6**, 81 (1972).
29. R. K. NESBET. J. Chem. Phys. **36**, 1518 (1962).
30. C. W. SCHERR. J. Chem. Phys. **23**, 569 (1955).
31. J. C. SLATER. J. Chem. Phys. **1**, 687 (1933).
32. A. D. BUCKINGHAM, R. L. DISCH, and D. A. DUNMUR. J. Am. Chem. Soc. **90**, 3104 (1968).
33. R. K. NESBET. Proc. R. Soc. A**230**, 312 (1955).
34. J. A. POPLE and R. K. NESBET. J. Chem. Phys. **22**, 571 (1954).
35. C. C. J. ROOTHAAN. Rev. Mod. Phys. **32**, 179 (1960).
36. A. RALSTON. A first course in numerical analysis. McGraw-Hill. 1965.
37. D. P. CHONG and M. L. BENSTON. Theoret. Chim. Acta, **12**, 175 (1968).
38. R. MCWEENY. Proc. R. Soc. A**235**, 496 (1956).
39. R. FLETCHER. Mol. Phys. **19**, 55 (1970).
40. T. CLAXTON and W. SMITH. Theoret. Chim. Acta, **22**, 399 (1971).
41. B. T. SUTCLIFFE. Theoret. Chim. Acta, **33**, 201 (1974).
42. D. P. CHONG and M. L. BENSTON. J. Chem. Phys. **49**, 1302 (1968).
43. C. P. YUE and D. P. CHONG. Theoret. Chim. Acta, **13**, 159 (1969).
44. J. THORHALLSON, J. F. LARCHER, and D. P. CHONG. Theoret. Chim. Acta, **16**, 51 (1970).
45. K. M. BROWN. Comm. ACM, **10**, 728 (1967).
46. K. M. BROWN. SIAM J. Numer. Anal. **6**, 560 (1969).
47. K. M. BROWN. *In* Numerical solution of systems of nonlinear algebraic equations. *Edited by* G. D. Byrne and C. A. Hall. Academic Press. 1973. p. 281.
48. R. FLETCHER and M. J. D. POWELL. Computer J. **6**, 163 (1963).
49. W. J. HEHRE, R. F. STEWART, and J. A. POPLE. J. Chem. Phys. **51**, 2657 (1969).
50. B. J. RANSIL. Rev. Mod. Phys. **32**, 245 (1960).
51. H. PENG. Proc. R. Soc. A**178**, 499 (1941).
52. A. DALGARNO. Proc. R. Soc. A**251**, 282 (1959).
53. S. KANEKO. J. Phys. Soc. Jpn. **11**, 1600 (1959).
54. L. C. ALLEN. Phys. Rev. **118**, 167 (1960).
55. R. M. STEVENS, R. M. PITZER, and W. N. LIPSCOMB. J. Chem. Phys. **38**, 550 (1963).
56. A. DALGARNO and H. A. J. MCINTYRE. Proc. Phys. Soc. **85**, 47 (1965).
57. P. W. LANGHOFF, M. KARPLUS, and R. P. HURST. J. Chem. Phys. **44**, 505 (1966).
58. W. N. LIPSCOMB. *In* Theoretical chemistry. *Edited by* W. Byers Brown. Butterworths. 1972. p. 167.
59. H. D. COHEN and C. C. J. ROOTHAAN. J. Chem. Phys. **43**, 534 (1965).
60. H. D. COHEN. J. Chem. Phys. **43**, 3558 (1965).
61. H. D. COHEN. J. Chem. Phys. **45**, 10 (1966).
62. A. SCHWEIG. Chem. Phys. Lett. **1**, 163 (1967).

63. A. SCHWEIG. Chem. Phys. Lett. **1**, 195 (1967).
64. J. A. POPLE, J. W. MCIVER JR., and N. S. OSTLUND. J. Chem. Phys. **49**, 2960 (1968).
65. D. P. CHONG. Theoret. Chim. Acta, **12**, 337 (1968).
66. R. M. STERNHEIMER. Phys. Rev. **96**, 951 (1954).
67. R. M. STERNHEIMER. Phys. Rev. **107**, 1565 (1957).
68. R. M. STERNHEIMER. Phys. Rev. **115**, 1198 (1959).
69. T. P. DAS and R. BERSOHN. Phys. Rev. **102**, 733 (1956).
70. A. TEMKIN. Phys. Rev. **107**, 1004 (1957).
71. A. DALGARNO and J. M. MCNAMEE. J. Chem. Phys. **35**, 1517 (1961).
72. A. DALGARNO. Adv. Phys. **11**, 281 (1962).
73. M. KARPLUS and H. J. KOLKER. J. Chem. Phys. **38**, 1263 (1963).
74. M. KARPLUS and H. J. KOLKER. J. Chem. Phys. **39**, 2011 (1963).
75. H. NAKATSUJI. J. Chem. Phys. **61**, 3728 (1974).
76. M. A. WHITEHEAD. J. Mol. Struct. **58**, 375 (1980).
77. M. A. WHITEHEAD and G. D. ZEISS. Quantum chemistry — the state-of-the-art, 181, SRS England. 1975.
78. G. D. ZEISS and M. A. WHITEHEAD. Int. J. Quantum Chem. In press.
79. A. HINCHCLIFFE and D. G. BOUNDS. Special Periodical Reports, The Chemical Society. Theoretical chemistry, Vol. 3. 1976. p. 85.
80. R. HUBY. Proc. Phys. Soc. **78**, 529 (1961).

Appendix

Explicit expressions for Rayleigh–Schrödinger perturbation energies through seventh order

H_1 is a perturbation Hamiltonian and H_0 a zeroeth order Hamiltonian with eigenfunctions ϕ_n and energies E_n: Q_0 is the projection operator into the subspace spanned by the eigenfunctions of H_0 which are orthogonal to the eigenfunction ϕ_0 of the lowest eigenvalue E_0. The operator $Q_0/(E_0 - H_0)$ is defined so that for any operators A and B, the matrix element with respect to eigenfunctions ϕ_i and ϕ_j is

$$[4] \quad \langle\phi_i|A\frac{Q_0}{E_0 - H_0}B|\phi_j\rangle = \sum_{k\neq 0}\frac{\langle\phi_i|A|\phi_k\rangle\langle\phi_k|B|\phi_j\rangle}{E_0 - E_k}$$

Q_0 is idempotent, hence

$$[5] \quad \langle\phi_i|A\left(\frac{Q_0}{E_0 - H_0}\right)^n B|\phi_j\rangle = \langle\phi_i|A\frac{Q_0}{(E_0 - H_0)^n}B|\phi_j\rangle$$

In the Rayleigh–Schrödinger perturbation theory the perturbation expansion coefficients $E^{(n)}$ involve matrix elements which can be simplified being eqs. [4] and [5]

$$[6] \quad \langle\phi_0|H_1\frac{Q_0}{(E_0 - H_0)^{n_1}}H_1\frac{Q_0}{(E_0 - H_0)^{n_2}}H_1 \ldots H_1|\phi_0\rangle$$

For simplicity, eq. [6] is abbreviated as $\langle n_1 n_2 \ldots\rangle$.

The expressions for the $E^{(n)}$ were derived using Huby's prescription (80)

$$[7] \quad E^{(1)} = \langle\phi_0|H_1|\phi_0\rangle$$

$$[8] \quad E^{(2)} = \langle\phi_0|H_1\frac{Q_0}{E_0 - H_0}H_1|\phi_0\rangle = \langle 1\rangle$$

$$[9] \quad E^{(3)} = \langle 11\rangle - E^{(1)}\langle 2\rangle$$

$$[10] \quad E^{(4)} = \langle 111\rangle - 2E^{(1)}\langle 21\rangle + (E^{(1)})^2\langle 3\rangle - E^{(2)}\langle 2\rangle$$

$$[11] \quad E^{(5)} = \langle 1111\rangle - E^{(1)}(2\rangle 211\rangle + \langle 121\rangle) + (E^{(1)})^2(2\langle 31\rangle + \langle 22\rangle) - (E^{(1)})^3\langle 4\rangle + 2E^{(1)}E^{(2)}\langle 3\rangle - 2E^{(2)}\langle 21\rangle - E^{(3)}\langle 2\rangle$$

$$[12] \quad E^{(6)} = \langle 11111\rangle - E^{(1)}(2\langle 2111\rangle + 2\langle 1211\rangle) + (E^{(1)})^2(2\langle 221\rangle + \langle 212\rangle + 2\langle 311\rangle + \langle 131\rangle) - (E^{(1)})^3(2\langle 41\rangle + 2\langle 32\rangle) + (E^{(1)})^4\langle 5\rangle - E^{(2)}(2\langle 211\rangle + \langle 121\rangle) + E^{(1)}E^{(2)}(4\langle 31\rangle + 2\langle 22\rangle) - (E^{(1)})^2E^{(2)}\langle 4\rangle + (E^{(2)})^2\langle 3\rangle - 2E^{(3)}\langle 21\rangle + 2E^{(1)}E^{(3)}\langle 3\rangle - E^{(4)}\langle 2\rangle$$

$$[13] \quad E^{(7)} = \langle 111111\rangle - E^{(1)}(2\langle 21111\rangle + 2\langle 12111\rangle + \langle 11211\rangle) - (E^{(1)})^3(2\langle 411\rangle + 2\langle 321\rangle + 2\langle 312\rangle + 2\langle 231\rangle + \langle 222\rangle + \langle 141\rangle) + (E^{(1)})^4(2\langle 51\rangle + 2\langle 42\rangle + \langle 33\rangle) - (E^{(1)})^5\langle 6\rangle - E^{(2)}(2\langle 2111\rangle + 2\langle 1211\rangle) + (E^{(2)})^2(2\langle 31\rangle + \langle 22\rangle) + E^{(1)}E^{(2)}(4\langle 311\rangle + 4\langle 221\rangle + 2\langle 212\rangle + 2\langle 131\rangle) - (E^{(1)})^2E^{(2)}(6\langle 41\rangle + 6\langle 32\rangle) + 4(E^{(1)})^3E^{(2)}\langle 5\rangle - 3(E^{(2)})^2E^{(1)}\langle 4\rangle - E^{(3)}(2\langle 211\rangle + \langle 121\rangle) + E^{(1)}E^{(3)}(4\langle 31\rangle + 2\langle 22\rangle) - 3(E^{(1)})^2E^{(3)}\langle 4\rangle + 2E^{(2)}E^{(3)}\langle 3\rangle - 2E^{(4)}\langle 21\rangle + 2E^{(1)}E^{(4)}\langle 3\rangle - E^{(5)}\langle 2\rangle$$

The expressions were checked by repeating the LiH calculation of Chong (65). The perturbation energies and Lagrange multipliers agreed with Chong's to five places.

Can. J. Chem. Downloaded from www.nrcresearchpress.com by 210.87.254.40 on 09/06/12
For personal use only.

1-Iodoacétylènes. IV. Relations structure–réactivité pour la complexation des 1-iodoacétylènes substitués avec des bases de Lewis

CHRISTIAN LAURENCE, MICHÈLE QUEIGNEC-CABANETOS ET BRUNO WOJTKOWIAK

Laboratoire de Spectrochimie Moléculaire, U.E.R. de Chimie, Université de Nantes, 2, rue de la Houssinière, 44072 Nantes, France

Reçu le 25 mars 1982[1]

CHRISTIAN LAURENCE, MICHÈLE QUEIGNEC-CABANETOS et BRUNO WOJTKOWIAK. Can. J. Chem. **61**, 135 (1983).

Les constantes de l'équilibre de formation des complexes de Ph_3PO et Ph_3AsO avec les iodoacetylènes **1**–**8** ainsi que les déplacements des fréquences de vibration de bases de Lewis sont reliées aux constantes électroniques du substituant. Les déplacements chimiques du ^{13}C de la triple liaison constituent également des paramètres structuraux utiles pour prévoir l'acidité de Lewis des iodoalcynes.

CHRISTIAN LAURENCE, MICHÈLE QUEIGNEC-CABANETOS, and BRUNO WOJTKOWIAK. Can. J. Chem. **61**, 135 (1983).

The equilibrium constants for complex formation between the substituted 1-iodoacetylenes **1**–**8** and the vibrational frequency shifts induced by complex formation are related to the electronic substituent constants. The ^{13}C chemical shifts of the triple bond are also useful structural parameters for predicting the Lewis acidity of iodoalkynes.

Can. J. Chem. Downloaded from www.nrcresearchpress.com by 210.87.254.5 on 09/06/12
For personal use only.

Nous avons vu que l'acidité de Lewis de l'atome d'iode des 1-iodoacétylènes substitués **1**–**8** augmente considérablement en passant du substituant n-propyle au substituant cyano (1, 2). Le substituant modifie en effet le pouvoir accepteur d'électrons

$$IC{\equiv}C\ X$$

	X		X
1	n-Pr	**5**	I
2	Ph	**6**	*p*-$NO_2C_6H_4$
3	$SiEt_3$	**7**	COOEt
4	CH_2Br	**8**	CN

de l'atome d'iode par effets inductif et de résonance. Ces effets sont bien mesurés en série benzénique par les facteurs de Hammett (3) ou par les facteurs de Taft σ_I et σ_R (4). D'autres paramètres structuraux susceptibles de traduire les effets de substituant sont les déplacements chimiques $\delta^{13}C$ des carbones de la triple liaison. On a en effet souvent affirmé (5, 6) que $\delta^{13}C$ pouvait traduire les variations de densité électronique autour de l'atome de carbone.

L'objet de ce travail est d'analyser les corrélations pouvant exister entre la variation d'acidité des 1-iodoacétylènes substitués et ces deux types de paramètres structuraux. En effet l'application à la série acétylénique des facteurs σ définis en série benzénique n'a fait l'objet que de travaux limités (7) et est encore discutée (8). Par ailleurs à la lumière de la corrélation précédemment établie (9) entre l'acidité des alkylacétylènes et le déplacement chimique du carbone attaché au proton acétylénique, il semble intéressant de généraliser cette corrélation aux iodoacétylènes, substitués d'une manière plus diversifiée.

Résultats

Les propriétés corrélées sont les déplacements de fréquence $\Delta\nu$ d'un vibrateur du partenaire basique engagé dans le complexe moléculaire avec les iodoacétylènes, publiés dans un travail précédent (1), et les constantes d'équilibre de formation des complexes de Ph_3PO et Ph_3AsO avec $IC{\equiv}CX$, dont la détermination fait l'objet d'une publication séparée (2) et qui sont rappelées dans le tableau 1. Les constantes σ_I mesurant les effets inductifs des substituants X, σ_R^0 mesurant ses effets de résonance, et la constante globale[2] $\sigma_p = \sigma_I + \sigma_R^0$ sont également reportées dans ce tableau.

Les spectres de ^{13}C des iodoacétylènes **1**–**8** et des alcynes-1 correspondants (dont l'origine est indiquée dans la référence 1) ont été enregistrés sur un appareil Varian XL 100 pour des solutions approximativement molaires dans $CDCl_3$, ce solvant permettant le blocage champ-fréquence. Les déplacements des raies du ^{13}C sont mesurés à partir de la raie du TMS (référence interne) et sont comptés positivement du TMS vers les champs faibles. Ils sont rassemblés dans le tableau 2. L'influence de la concentration est pratiquement nulle pour δC_β et déplace légèrement δC_α vers les champs faibles, comme le montre le tableau 3.

Dans les spectres de 1-iodoacétylènes $IC_\alpha{\equiv}C_\beta X$ la raie C_α est toujours nettement plus intense que la raie C_β. Bien qu'une relaxation du carbone α par couplage scalaire avec le noyau quadrupolaire de l'iode soit plausible, il semble plutôt que ce fait soit lié aux conditions d'enregistrement: l'intervalle de temps (environ 3 s) séparant deux impulsions successives du champ magnétique permettrait une relaxation déjà efficace du carbone α, le temps de relaxation T_1 spin-réseau de ce carbone étant de cet ordre de grandeur. Au contraire celui du carbone β est beaucoup plus grand.[3]

Les spectres des alcynes-1 ont été enregistrés sous découplage total des protons. L'égalisation des populations des niveaux d'énergie du proton acétylénique conduit à une intensification très marquée de la raie de résonance du carbone α car la relaxation de ce carbone est dominée par un mécanisme dipôle–dipôle carbone–hydrogène.

[1]Revision reçue le 14 juillet 1982.

[2]$\sigma_p = \sigma_I + \sigma_R$ par définition. Mais pour les substituants étudiés ici $\sigma_R = \sigma_R^0$ (3).

[3]Pour $MeC{\equiv}CI$, T_1 (C_α) = 7 s et T_1 (C_β) = 33 s. On peut s'attendre dans la série $IC{\equiv}CX$ à des temps de relaxation du même ordre de grandeur.

0008-4042/83/010135-04$01.00/0

©1983 National Research Council of Canada/Conseil national de recherches du Canada

Can. J. Chem. Downloaded from www.nrcresearchpress.com by 210.87.254.5 on 09/06/12
For personal use only.

TABLEAU 1. Constantes d'équilibre[a] des complexes des iodoacétylènes IC≡CX et constantes électroniques[b] des substituants X

		Log K				
N°	X	$Ph_3AsO-IC{\equiv}CX$	$Ph_3PO-IC{\equiv}CX$	σ_I	σ_R^e	σ_p
1	n-Pr	1,65	0,44	−0,01	−0,15	−0,17
2	Ph	2,69	0,90	0,12	−0,11	0,01
3	$SiEt_3$[c]	2,56	0,96	−0,11	0,12	0,01
4	CH_2Br	3,57	—	0,20	−0,10	0,10
5	I[d]	3,89	1,50	0,40	−0,16	0,24
6	$C_6H_4NO_2$	4,11	2,01	0,23	0,03	0,26
7	COOEt	5,24	2,39	0,30	0,11	0,41
8	CN	6,93	3,74	0,57	0,08	0,65
—	IC≡N	7,93	4,80			

[a]Tirées de la référence 2.
[b]On a adopté les valeurs récentes de la référence 3.
[c]Les valeurs σ de $SiEt_3$ sont prises égales à celles de $SiMe_3$.
[d]Les valeurs log K du diiodoacétylène sont corrigées par le facteur statistique log 2.
[e]Pour cet échantillonnage de substituants $\sigma_R = \sigma_R^0$ (3).

TABLEAU 2. Déplacements chimiques $\delta^{13}C$ des iodoalcynes $XC_\beta{\equiv}C_\alpha I$ et des alcynes $XC_\beta{\equiv}C_\alpha H$

		IC≡CX						HC≡CX	
N°	X	δC_α	δC_β	δC_1	δC_2	δC_3	δC_4	δC_α	δC_β
8	—C≡N	13,05	68,60	105,20				72,98	57,55
9	—COOH[a]	16,43	87,67	152,70				76,25	75,90
7	—$COOCH_2CH_3$ (1 2 3)	13,02	87,26	152,20	62,34	14,00		74,30	74,90
6		13,80	92,45	130,00	133,10	123,47	14,60	82,10	81,60
5	—I	0,7						—	—
4	—CH_2Br	4,59	88,12	15,07				74,78	78,75
3	—$Si(CH_2CH_3)_3$ (1 2)	20,20	102,10	7,60	4,80			94,10	87,40
2		6,50	94,50	123,50	132,20	128,10	128,60	77,10	83,64
1	—$CH_2CH_2CH_3$ (1 2 3)	−7,45	94,60	22,04	28,80	13,40		68,10[b]	84,53[b]

[a]Solution 2 M dans dioxanne.
[b]Radical $CH_2CH_2CH_2CH_3$.

TABLEAU 3. Influence de la concentration sur les déplacements chimiques δC_α et δC_β de $IC_\alpha{\equiv}C_\beta$ COOEt et de $IC_\alpha{\equiv}C_\beta$ nPr

	Concentration[a]	δC_α[b]	δC_β[b]
IC≡C COOEt	0,1	12,70±0,05	87,23±0,08
	0,53	13,02±0,05	87,20±0,08
	1,0	13,02±0,05	87,26±0,08
	1,7	13,68±0,05	87,20±0,05
IC≡C nPr	0,2	−7,6 ±0,05	94,7 ±0,05
	1,2	−7,45±0,05	94,6 ±0,05
	2,05	−7,28±0,05	94,55±0,05

[a]Molaire dans $CDCl_3$.
[b]ppm/TMS.

Corrélations avec les paramètres σ

L'équation de corrélation la plus simple est celle de Hammett (3, 4, 7)

$$\log K \text{ ou } \Delta\nu = \rho(\sigma_I + \sigma_R) + h = \rho\sigma_p + h$$

où K est la constante d'équilibre de formation des complexes (Tableau 1), $\Delta\nu$ le déplacement d'un vibrateur de la base par complexation (Tableau 1 de la référence 1), ρ est le coefficient de sensibilité aux effets électroniques du substituant mesurés par σ_p et h est l'ordonnée à l'origine (voisine de log K ou $\Delta\nu$ du composé non substitué IC≡CH). Les résultats des corrélations sont reportés dans le tableau 4 et illustrés sur la figure 1. La plupart des corrélations ont un coefficient de corrélation supérieur à 0,95: pour le phénomène et l'échantillonnage de substitutants étudiés, on peut donc en conclure que les facteurs σ_p de la série benzénique (3) sont transposables en série acétylénique. Ces corrélations montrent comment croît le caractère accepteur d'électrons de l'atome d'iode des 1-iodoacétylènes substitués quand le pouvoir électroattracteur du substituant augmente. Elles permettent de prévoir qu'un des iodoacétylènes les moins acides sera $Me_2NC{\equiv}CI$ puisque $\sigma_p(NMe_2) = -0,71$ (3), qu'un des plus acides sera $IC{\equiv}CSO_2CF_3$ puisque $\sigma_p(SO_2CF_3) = +0,92$ (3) et que ce dernier formera avec Ph_3AsO des complexes plus stables (log $K_{calculé} = 8,49$) que l'iodure de cyanogène (log $K = 7,93$).

Un nombre trop limité de substituants ne permet pas de

TABLEAU 4. Corrélations log K ou $\Delta\nu = \rho\sigma_p + h$ pour les complexes des iodoacétylènes

Log K^a ou $\Delta\nu^b$	ρ	h	R^c	n^d
Log K ($Ph_3AsO-IC\equiv CX$)	6,4	2,6	0,994	8
Log$K$ ($Ph_3PO-IC\equiv CX$)	4,0	0,9	0,982	7
$\Delta\nu$(AsO) ($Ph_3AsO-IC\equiv CX$)	17	17	0,975	8
$\Delta\nu$(SO) ($(CH_2)_4SO-IC\equiv CX$)	12	14	0,964	7
$\Delta\nu$(CO) ($Et_2NCOMe-IC\equiv CX$)	15	19	0,960	7
$\Delta\nu$(NO) ($PyNO-IC\equiv CX$)	9	16	0,914	8
$\Delta\nu$(PO) ($Ph_3PO-IC\equiv CX$)	17	17	0,982	7
$\Delta\nu$(PS) ($Ph_3PS-IC\equiv CX$)	6	4	0,976	7
$\Delta\nu$(6a) (3-picoline$-IC\equiv CX$)	4	5	0,980	7
$\Delta\nu$(NH) ($PhNHMe-IC\equiv CX$)	36	51	0,957	5

[a]Tirées de la référence 2.
[b]Tirées de la référence 1.
[c]Coefficient de corrélation.
[d]Nombre de points.

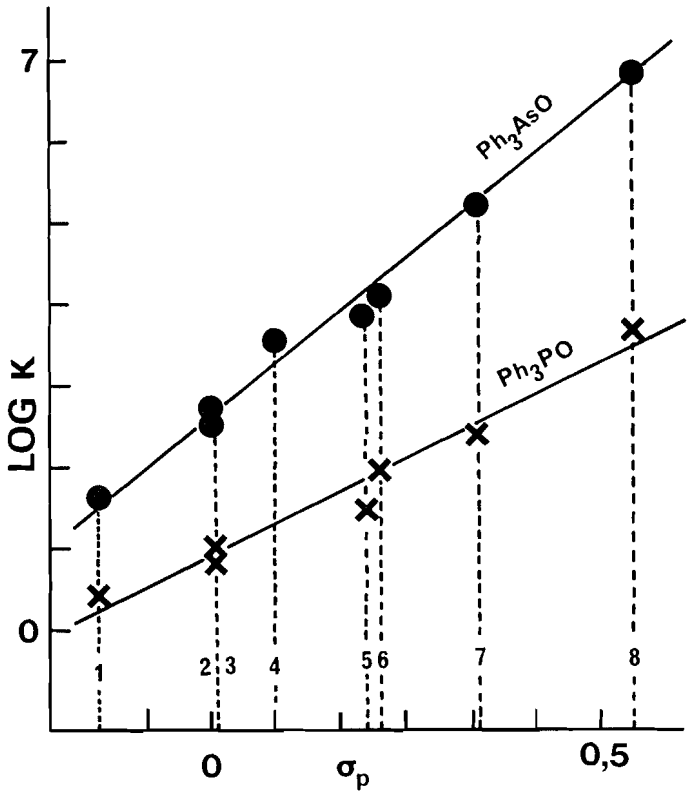

FIG. 1. Corrélation entre log K des complexes de Ph_3AsO et Ph_3PO, avec $IC\equiv CX$ et les facteurs de Hammett des substituants X. (**1**) n-Pr, (**2**) Ph, (**3**) $SiEt_3$, (**4**) CH_2Br, (**5**) I, (**6**) $C_6H_4NO_2$, (**7**) COOEt et (**8**) CN.

calculer de manière sûre les coefficients de sensibilité ρ_I et ρ_R aux effets inductif et de résonance, à l'aide de l'équation de Taft, log K ou $\Delta\nu = \rho_I\sigma_I + \rho_R\sigma_R + h$, dont l'avantage sur celle de Hammett est de ne pas imposer $\rho_I = \rho_R = \rho$ et de permettre d'utiliser diverses échelles $\sigma_R(\sigma_R^0, \sigma_R^-$ ...) selon la nature de l'interaction de résonance entre le groupe fonctionnel et le substituant.[4] On observe cependant des deplacements de

[4]Pour $IC\equiv CX$ on peut hésiter entre l'échelle σ_R^0 correspondant aux formules limites de résonance $I-{}^+C=C=\overline{X}$ ou $I-\overline{C}=C=\overset{+}{X}$ et l'échelle σ_R^- pour les substituants $-R$ correspondant à la formule limite + $I=C=C=X$ −.

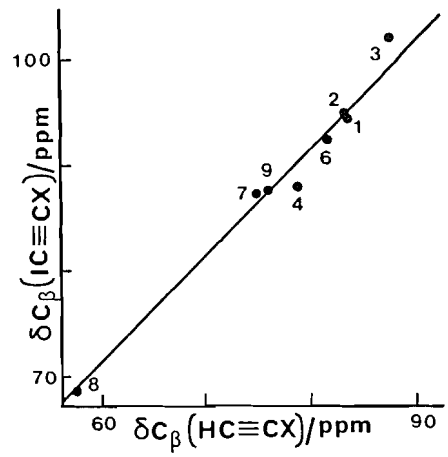

FIG. 2. Relation linéaire entre les déplacements chimiques δC_β des dérivés homologues $HC\equiv CX$ et $IC\equiv CX$. Même numérotation que Fig. 1; (**9**) COOH.

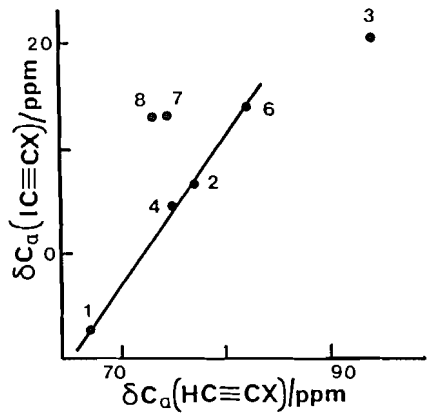

FIG. 3. Relation entre les déplacements chimiques δC_α des dérivés homologues $HC\equiv CX$ et $IC\equiv CX$. Même numérotation que Fig. 1.

fréquence (voir référence 2) et des constantes d'équilibre (Tableau 1) très voisins pour $PhC\equiv CI$ et $Et_3SiC\equiv CI$. Puisque pour les substituants Ph et Et_3Si $\sigma_I(Ph) = \sigma_R(Et_3Si)$ et $\sigma_I(Et_3Si) = \sigma_R(Ph)$, il est probable que ρ_I doit peu différer de ρ_R et que la variation de l'acidité de Lewis des iodoalcynes substituées dépend d'une manière quasiment égale des effets inductif et de résonance des substituants.

Corrélations avec les déplacements chimiques des ^{13}C de la triple liaison. Additivité des effets de substituant

Il existe une excellente relation linéaire de pente unité entre $\delta C_\beta(HC\equiv CX)$ et $\delta C_\beta(IC\equiv CX)$ (Fig. 2).

$$\delta C_\beta(IC\equiv CX) = 1{,}0(\delta C_\beta(HC\equiv CX) + 9);\ R = 0{,}986\quad n = 8$$

Cette relation prouve l'additivité des effets de l'iode et du groupement X sur δC_β (10). Cette additivité n'est plus respectée pour δC_α (Fig. 3). Une relation linéaire, déviant cependant sensiblement de l'additivité (pente 1,5 au lieu de 1), est observée pour les substituants +R (n—Pr (**1**), CH_2Br (**4**) et Ph (**2**)) et $C_6H_4NO_2$ (**6**) dont l'effet $-R$ est voisin de zéro tandis que les substituants $-R$ (CN (**8**), COOEt (**7**) et $SiEt_3$ (**3**)) dévient beaucoup plus. Cette non-additivité des effets de l'iode et des substituants X électroattracteurs sur δC_α s'explique probablement par une contribution significative des formes

Can. J. Chem. Downloaded from www.nrcresearchpress.com by 210.87.254.5 on 09/06/12
For personal use only.

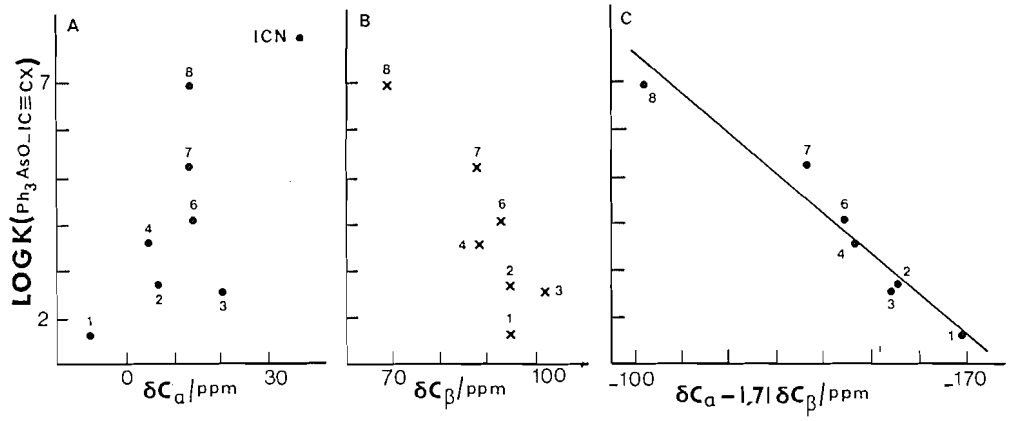

FIG. 4. Relations entre l'acidité de Lewis des iodoacétylènes et (A) δC_α, (B) δC_β et (C) une combinaison linéaire de δC_α et δC_β. Même numérotation que Fig. 1.

limites de résonance à la fonction d'onde décrivant l'environnement électronique du carbone α.

$$+ I{=}C{=}C{=}C{=}N^-, \quad + I{=}C{=}C{=}C\begin{matrix}\diagup O^- \\ \diagdown OEt\end{matrix}, \quad + I{=}C{=}C{=}\bar{S}iEt_3$$

Corrélations de δC_α et δC_β avec les constantes électroniques de substituant

Elles donnent les résultats suivants (le diiodoacétylène est exclu des corrélations):

$$\delta C_\alpha = 10 - 4\,\sigma_I + 71\,\sigma_R^0 \quad R = 0{,}90 \quad n = 7 \quad (R = 0{,}80 \text{ avec } \sigma_R^-)$$

$$\delta C_\beta = 98 - 46\,\sigma_I + 7\,\sigma_R^0 \quad R = 0{,}953 \quad n = 7$$

Elles montrent clairement que l'effet de résonance joue un rôle prédominant sur les variations de δC_α tandis que c'est l'effet inductif qui gouverne principalement les variations de δC_β. La faiblesse de notre échantillonnage de substituants (aucun halogène, aucun substituant fortement $+R$ tel que OMe et NMe_2) ne permet cependant pas de conclure définitivement. Il est en effet évident que les variations des déplacements chimiques des carbones de la triple liaison dans les iodoalcynes ne dépendent pas uniquement des effets électroniques des substituants: ainsi seulement 81% ($R^2 = 0{,}81$) de la variance de δC_α sont expliqués (64% si on remplace σ_R^0 par σ_R^-).

Corrélations entre δC_α, δC_β et l'acidité de Lewis des iodoacétylènes

δC_α et δC_β seuls ne permettent que grossièrement d'estimer la variation d'acidité des iodoacétylènes (et de ICN avec δC_α) comme le montre la figure 4. Cependant une combinaison linéaire de ces deux paramètres pourrait permettre de mieux pondérer les effets inductif et de résonance et peut-être d'éliminer partiellement les contributions non électroniques aux variations des déplacements chimiques. Les équations

$$\log K\,(Ph_3PO{-}IC{\equiv}CX) = 10 + 0{,}05\,\delta C_\alpha - 0{,}09\,\delta C_\beta \quad R = 0{,}982 \quad n = 6$$

$$\log K\,(Ph_3AsO{-}IC{\equiv}CX) = 16 + 0{,}09\,\delta C_\alpha - 0{,}15\,\delta C_\beta \quad R = 0{,}976 \quad n = 7$$

dont la seconde est illustrée sur la figure 4, sont effectivement obéies avec une précision satisfaisante et pourraient permettre de prévoir l'acidité de Lewis des iodoacétylènes à partir de leurs spectres rmn.

Remerciements

Nous remercions Mme Martin, Professeur à l'Université de Nantes, des discussions dont elle nous a fait bénéficier et M. Berry et Mme Mabon pour l'enregistrement des spectres rmn.

1. C. LAURENCE, M. QUEIGNEC-CABANETOS, T. DZIEMBOWSKA, R. QUEIGNEC et B. WOJTKOWIAK. J. Am. Chem. Soc. **103**, 2567 (1981).
2. C. LAURENCE, M. QUEIGNEC-CABANETOS et B. WOJTKOWIAK. J. Chem. Soc. Perkin Trans. II. Sous presse.
3. M. CHARTON. Prog. Phys. Org. Chem. **13**, 119 (1981).
4. S. EHRENSON, R. T. C. BROWNLEE et R. W. TAFT. Prog. Phys. Org. Chem. **10**, 1 (1973).
5. W. J. EHRE, R. W. TAFT et R. D. TOPSOM. Prog. Phys. Org. Chem. **12**, 159 (1976).
6. G. L. NELSON et E. A. WILLIAMS. Prog. Phys. Org. Chem. **12**, 229 (1976).
7. M. CHARTON. Prog. Phys. Org.Chem. **10**, 81 (1973).
8. C. LAURENCE, J. GUILLEME et B. KIRSCHLEGER. J. Chem. Soc. Perkin Trans. II, 1341 (1981).
9. J. CHRISMENT et J. J. DELPUECH. J. Chem. Res. (S), 340 (1978).
10. O. EXNER. Collect. Czech. Chem. Commun. **41**, 1516 (1976).

Can. J. Chem. Downloaded from www.nrcresearchpress.com by 210.87.254.5 on 09/06/12
For personal use only.

Rôle de l'alcool dans les microemulsions. II. Volumes et capacités calorifiques molaires apparents du système eau + dodécylsulfate de sodium + isopropanol à 298,15 K

VLADIMIR MAJER,[1] ALAIN-HENRI ROUX, GENEVIÈVE ROUX-DESGRANGES ET ANDRÉ VIALLARD

Laboratoire de Thermodynamique et Cinétique Chimique, Université de Clermont-Ferrand 2, B.P. 45-F, 63170 Aubière, France

Reçu le 4 mai 1982

VLADIMIR MAJER, ALAIN-HENRI ROUX, GENEVIÈVE ROUX-DESGRANGES et ANDRÉ VAILLARD. Can. J. Chem. **61**, 139 (1983).

Les masses volumiques et les capacités calorifiques par unité de volume du système ternaire: eau + dodécylsulfate de sodium (NaDS) + isopropanol (iPrOH) ont été mesurés en fonction de la concentration en alcool et en tensioactif à 298,15 K. Les volumes et les capacités calorifiques molaires apparents ou partiels de l'alcool dans le système ternaire en sont dérivés. Leur évolution en fonction de la composition reflète le comportement de l'alcool. En milieu dilué, il se solubilise partiellement dans les micelles et contribue à la formation de micelles mixtes. En milieu concentré, il se solubilise dans des microagrégats de nature très proche de celle de l'alcool. La variation de la capacité calorifique molaire apparente à dilution infinie de l'isopropanol en fonction de la concentration en NaDS, révèle l'existence d'une transition dans la structure micellaire vers 0,3 *m*.

VLADIMIR MAJER, ALAIN-HENRI ROUX, GENEVIÈVE ROUX-DESGRANGES, and ANDRÉ VAILLARD. Can. J. Chem. **61**, 139 (1983).

Densities and heat capacities per unit volume of the ternary system: water + sodium dodecylsulfate (NaDS) + isopropanol (iPrOH) have been measured as a function of concentration of alcohol and surfactant at 298.15 K. Apparent and partial molar volumes and heat capacities of isopropanol have been derived therefrom. These quantities reflect the behavior of alcohol in the solution. The results confirm that in the dilute region, iPrOH is partially solubilized in the micelles and contributes to the formation of mixed micelles, and that in the concentrated alcohol region, iPrOH is solubilized in microaggregates of alcohol. The variation of apparent heat capacity at infinite dilution of iPrOH as a function of NaDS concentration shows the existence of a transition in the micellar structure around 0.3 *m*.

Introduction

Depuis quelques années, un intérêt croissant est porté à l'étude des microémulsions, du fait de leurs applications dans des domaines variés (1, 2) et plus particulièrement en Récupération Assistée du Pétrole (3) et dans l'extraction d'hydrocarbures à partir des sables bitumineux (4). La présence d'un alcool est indispensable pour la formation et la stabilité de ces microémulsions, mais son rôle n'est pas encore clair.

En milieu micellaire, l'action des alcools apparaît complexe. Ils affectent la structure de l'eau et perturbent la constante diélectrique du milieu (5), mais ils se solubilisent aussi partiellement dans les micelles. De ce fait, ils interviennent sur la formation (6), la structure et la stabilité des micelles (7−12). Tous ces effets sont simultanés et difficiles à séparer (13, 14). L'étude des propriétés thermodynamiques des systèmes eau + tensioactif + alcool est un moyen d'investigation du comportement des alcools. Dans un travail précédent, nous avons étudié le système ternaire eau − dodécylsulfate de sodium − n-butanol (15).

Ce système est utilisé pour solubiliser le toluène et la microémulsion formée est une microémulsion modèle qui a déjà fait l'objet de nombreuses études (16−18), thermodynamiques entre autres (19, 20). Dans ce système ternaire, au-delà d'une certaine concentration en tensioactif, le butanol, peu soluble dans l'eau, devient totalement miscible. L'interprétation des résultats (15) conduit à considérer un partage de l'alcool entre phase aqueuse et phase micellaire et la formation de micelles mixtes alcool−tensioactif. Lorsque la concentration en alcool augmente, l'évolution des propriétés thermodynamiques permet de penser qu'il y a alors formation de "microphases" à caractère alcool proche de celui du corps pur.

Il nous a alors semblé nécessaire d'étudier le comportement d'un alcool totalement soluble dans l'eau, mais possédant un faible caractère hydrophobe. Nous avons choisi l'isopropanol qui a été particulièrement étudié dans l'eau (21). Son influence sur les propriétés des solutions micellaires reste encore controversée (22, 23). L'étude des propriétés volumiques et calorifiques du système ternaire eau + dodécylsulfate de sodium + isopropanol doit permettre de mieux comprendre les interactions de l'isopropanol avec le milieu et ses effets sur la structure micellaire.

Conditions expérimentales

Les solutions sont préparées par pesée avec de l'eau déionisée et distillée. Le dodécylsulfate de sodium (NaDS) est un produit Touzart et Matignon recristallisé deux fois dans l'éthanol et séché sous vide.[2] L'isopropanol (iPrOH) (Merck pour analyses 99,7%) conservé sur tamis moléculaires est utilisé sans purification ultérieure.

Les masses volumiques ρ des solutions sont déterminées à l'aide d'un densimètre à écoulement liquide permanent (Sodev 02D −

[1]Department of Physical Chemistry, Institute of Chemical Technology, Suchbatarova 5, 166 28 Prague 6, Czechoslovakia.

[2]La pureté du dodécylsulfate de sodium recristallisé dans les mêmes conditions a été vérifiée par des mesures de tension de surface. Aucun minimum n'apparaît au voisinage de la cmc indiquant l'absence d'impuretés. Nous remercions O. Dusart qui a bien voulu réaliser ces mesures.

0008-4042/83/010139-08$01.00/0

©1983 National Research Council of Canada/Conseil national de recherches du Canada

Can. J. Chem. Downloaded from www.nrcresearchpress.com by 210.87.254.105 on 09/06/12
For personal use only.

TABLEAU 1. Volumes et capacités calorifiques molaires apparents de l'isopropanol dans le mélange binaire H_2O + NaDS à 298.15 K*

m_3	ρ	$V_{\phi,3}$	c_p	$C_{\phi,3}$	m_3	ρ	$V_{\phi,3}$	c_p	$C_{\phi,3}$	m_3	ρ	$V_{\phi,3}$	c_p	$C_{\phi,3}$
	m_2 = 0,002945					m_2 = 0,006334					m_2 = 0,010046			
0	0,997195		4,1788		0	0,997366		4,1781		0	0,997537		4,1766	
0,1265	0,995765	71,74	4,1927	361,8	0,1299	0,995898	71,72	4,1929	366,2	0,1227	0,996145	71,74		
0,2228	0,994721	71,61	4,2034	362,8	0,2158	0,994965	71,61	4,2030	368,1	0,2084	0,995200	71,68	4,1990	360,0
0,3186	0,993714	71,50	4.2137	362,6	0,3263	0,993806	71,48	4,2149	366,2	0,3080	0,994144	71,56	4,2098	360,9
0,4408	0,992481	71,36	4,2269	363,0	0,4625	0,992433	71,33	4,2289	364,1	0,4317	0,992880	71,42	4,2226	360,4
0,8693	0,988509	70,93	4,2733	365,4	1.0959	0,986734	70,76	4,2956	365,4	1,0099	0,987566	70,87	4,2833	363,1
2,0344	0,979729	70,13	4,3890	367,1	2,0330	0,979815	70,17	4,3870	366,4	2,0156	0,980026	70,21	4,3826	365,6
3,1396	0,972797	69,79	4,4777	364,3	3,0732	0,973228	69,84	4,4727	364,7	3,1146	0,973040	69,86	4,4724	363,8
4,1509	0,966654	69,80	4,5216	354,3	4,0646	0,967187	69,83	4,5186	355,3	4,2619	0,965995	69,89	4,5177	351,6
5,3115	0,959335	70,09	4,5105	333,5	5,3242	0,959263	70,13	4,5095	333,3	5,4304	0,958146	70,31	4,4974	329,4
	m_2 = 0,04916					m_2 = 0,1979					m_2 = 0,2632			
0	0,999012		4,1488							0	1,006746		4,0104	
0,1310	0,997492	71,89	4,1618	349,1	0	1,004488		4,0502		0,1837	1,004417	72,37	4,0277	335,8
0,2175	0,996524	71,80	4,1707	351,5	0,3234	1,000589	72,06	4,0810	340,4	0,3723	1,002174	72,14	4,0440	333,1
0,3184	0,995427	71,69	4,1815	353,8	0,4789	0,998840	71,92	4,0952	340,1	0,5209	1,000465	72,04	4,0571	333,3
0,4544	0,994005	71,56	4,1957	355,4	1,0071	0,993439	71,49	4,1446	342,8	1,0085	0,995342	71,66	4,1008	336,0
1,0920	0,988072	70,97	4,2614	359,2	1,6216	0,987962	71,10	4,2003	345,0	1,5260	0,990526	71,33	4,1474	339,0
2,1402	0,980099	70,34	4,3616	361,6	1,9246	0,985517	70,94	4,2265	345,6	2,0325	0,986248	71,09	4,1908	340,6
3,0708	0,973969	70,08	4,4347	359,6	2,3605	0,982137	70,79	4,2617	345,7	2,4923	0,982610	70,95	4,2250	340,0
4,0977	0,967421	70,10	4,4794	349,9	2,8927	0,978230	70,67	4,2955	342,9	2,9825	0,978918	70,86	4,2554	337,9
5,0238	0,961432	70,30	4,4752	333,9	3,9829	0,970543	70,66	4,3375	332,8	3,7593	0,973235	70,85	4,2853	330,6
					4,9018	0,964121	70,84	4,3355	318,7	4,9888	0,964416	71,05	4,2834	312,1
					5,9164	0,957232	71,09	4,2975	300,1	5,9571	0,957623	71,31	4,2508	295,8
	m_2 = 0,3475					m_2 = 0,4261					m_2 = 0,5132			
0	1,009555		3,9661		0	1,012035		3,9246		0	1.014747		3,8794	
0,2268	1,006629	72,40	3,9820	309,4	0,07374	1,011028	72,79	3,9290	295,1	0,2516	1,011334	72,64	3,8929	287,6
0,4888	1,003462	72,19	4,0022	314,4	0,1675	1,009798	72,59	3,9347	296,9	0,4881	1,008313	72,48	3,9079	293,3
0,9758	0,998118	71,84	4,0433	322,1	0,2490	1,008744	72,53	3,9398	297,9	1,0236	1,002078	72,14	3,9470	303,3
1,6403	0,991703	71,47	4,1001	328,1	0,3538	1,007424	72,44	3,9468	300,0	1,4274	0,997939	71,85	3,9777	308,0
1,9871	0,988652	71,33	4,1270	329,0	0,5734	1,004749	72,31	3,9633	305,7	1,9591	0,992697	71,71	4,0179	312,2
2,4753	0,984600	71,18	4,1617	329,1	1,0529	0,999413	71,98	4,0023	314,3	2,4960	0,987936	71,54	4,0521	312,7
2,934	0,980988	71,09	4,1827	327,3	2,1108	0,989349	71,48	4,0846	321,2	2,8894	0,984554	71,50	4,0732	311,9
3,752	0,974754	71,08	4,2177	320,5	2,974	0,982150	71,30	4,1349	319,2	3,9257	0,976117	71,50	4,1031	303,6
4,833	0,966712	71,25	4,2199	305,9	4,388	0,971145	71,36	4,1657	305,3	4,7219	0,969872	71,62	4,1024	293,8
5,674	0,960623	71,45	4,2087	295,6	5,017	0,966400	71,47	4,1589	296,6	5,9546	0,960561	71,90	4,0699	276,6
	m_2 = 0,09845					m_2 = 0,3984					m_2 = 0,3064			
0	1,000884		4,1168		0	1,011149		3,9382		0	1,008177		3,9877	
0,2082	0,998437	71,95	4,1365	343,7	0,2203	1,008252	72,50	3,9521	300,2	0,08817	1,007031	72,48	3,9956	329,5
0,4192	0,996117	71,74	4,1573	346,6	0,4350	1,005571	72,37	3,9674	305,3	0,1792	1,005883	72,37	4,0027	323,9
0,7154	0,993103	71,45	4,1868	349,5	0,6670	1,002854	72,19	3,9858	310,9	0,2990	1,004414	72,26	4,0118	321,6
0,8040	0,992254	71,37	4,1957	350,3	0,8979	1,000289	72,04	4,0050	315,0	0,5955	1,000952	72,06	4,0364	324,3
0,9947	0,990483	71,22	4,2148	351,8	1,3035	0,996135	71,77	4,0386	319,7	1,0264	0,996396	71,74	4,0741	329,0
1,128	0,989309	71,11	4,2275	352,2	1,6009	0,993282	71,62	4,0639	322,7	1,5041	0,991845	71,45	4,1161	332,7
2,063	0,981915	70,56	4,3143	355,0	2,2024	0,987937	71,38	4,1087	324,3	1,9125	0,988262	71,26	4,1512	335,0
3,265	0,973665	70,28	4,4000	351,2	3,0871	0,980727	71,22	4,1596	321,7	2,5330	0,983219	71,06	4,1969	334,8
6,254	0,953870	70,88	4,3700	303,1	4,4138	0,970519	71,30	4,1850	307,4	2,9360	0,979990	71,04	4,2205	332,9
10,096	0,931072	71,97	4,1496	252,6	6.234	0,957233	71,72	4.1365	280,4	3,8851	0,973038	70,98	4,2508	323,2
12,568	0,918956	72,48	4,0224	234,2	12,984	0,918683	73,08	3,8239	221,0	5,0005	0,964900	71,18	4,2486	307,5
25,592	0,877560	73,97	3,6038	196,5	20,670	0,890802	73,93	3,5875	198,6	5,5780	0,960810	71,31	4,2327	298,3
36,262	0,858517	74,57	3,4181	186,1	42,61	0,850962	74,99	3,2537	179,5					
59,71	0,835434	75,25	3,1987	176,9	73,94	0,827391	75,60	3,0521	171,4					
112,18	0,813923	75,88	2,9889	169,6	261,72	0,796687	76,45	2,7683	161,9					

*Unités: m = mol kg $^{-1}$. ρ = g cm^{-3}; $V_{\phi,3}$ = cm^3 mol^{-1}; c_p = J K^{-1} g^{-1}; $C_{\phi,3}$ = J K^{-1} mol^{-1}.

Canada) (24). Les mesures de capacités calorifiques volumiques σ sont réalisées à l'aide d'un calorimètre à écoulement pour chaleur spécifique type Picker. Cet appareil, ainsi que les procédures mises en oeuvre, ont été déjà décrits dans la littérature (25). L'appareil utilisé (Sétaram − France) est équipé de cellules en or. Les mesures sont effectuées avec une puissance de base de 21 mW, un débit liquide de 0,5 cm^3 min^{-1}, l'élévation de température est alors environ de 0,6 K. Les mesures de ρ et σ sont effectuées à 298,15 K, la température de référence est régulée à ±0,005 K et contrôlée à l'aide d'un thermomètre à quartz. Dans ces conditions, la précision des mesures est de 3×10^{-6} g cm^{-3} pour les masses volumiques et 7×10^{-5} J K^{-1} cm^{-3} pour les capacités calorifiques volumiques. Selon le domaine de concentration étudié, deux procédures de détermination de σ sont utilisées: soit par rapport à une référence fixe pour les solutions diluées, soit suivant la méthode des "références successives" pour les solutions concentrées.

Résultats

Les grandeurs expérimentales ρ et σ sont traitées sous la forme de grandeurs molaires apparentes $Y_{\phi,i}$ de la propriété Y pour un soluté i. Pratiquement, les volumes ($V_{\phi,i}$) et capacités calorifiques ($C_{\phi,i}$) molaires apparents du soluté i dans le système ternaire sont calculés à partir des différences ($\rho - \rho_0$) et ($\sigma - \sigma_0$) à l'aide des relations bien connues:

$$[1] \quad V_{\phi,i} = \frac{M_i}{\rho} - \frac{1000(\rho - \rho_0)}{m_i \rho \rho_0}$$

$$[2] \quad C_{\phi,i} = M_i c_p + \frac{1000(c_p - c_{p_0})}{m_i}$$

dans lesquelles M_i est la masse molaire du soluté i et m_i sa

Can. J. Chem. Downloaded from www.nrcresearchpress.com by 210.87.254.105 on 09/06/12
For personal use only.

Can. J. Chem. Downloaded from www.nrcresearchpress.com by 210.87.254.105 on 09/06/12
For personal use only.

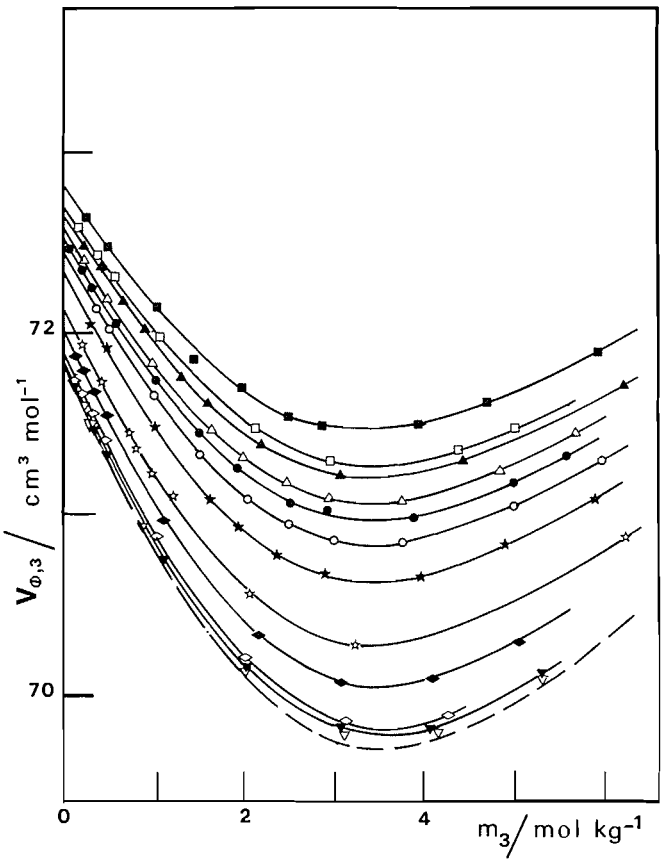

FIG. 1. Volumes molaires apparents de l'isopropanol à 298,15 K en fonction de la molalité en isopropanol m_3, à différentes molalités en NaDS (m_2) du solvant mixte H_2O + NaDS:
m_2 = 0 (41) ——; 0,0029, ▽; 0,0063, ▼; 0,0100, ◇; 0,0499, ◆; 0,0985, ☆; 0,1979, ★; 0,2632, ○; 0,3064, ●; 0,3475, △; 0,3984, ▲; 0,4261, □; 0,5132, ■.

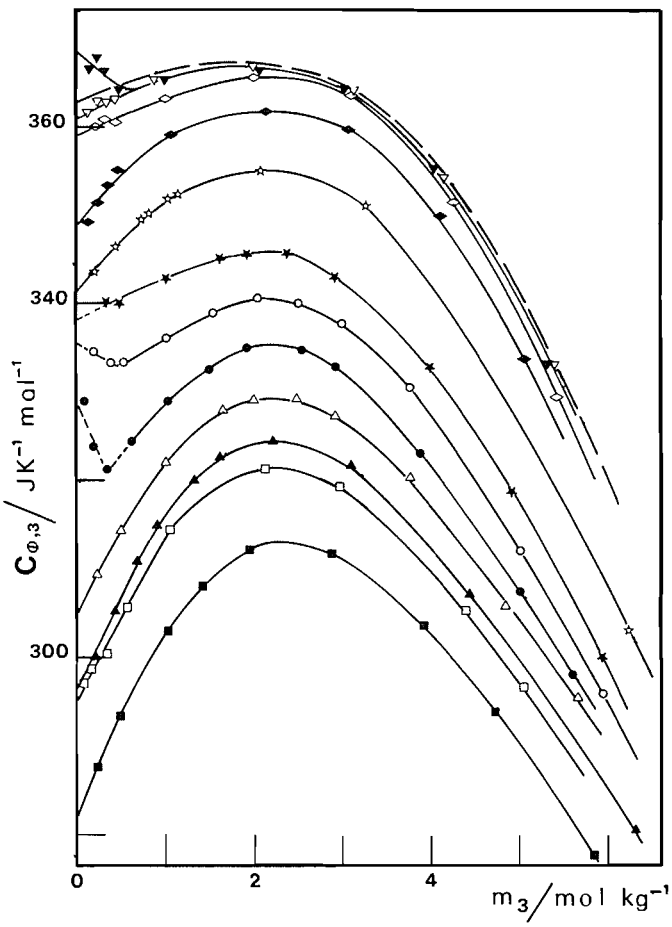

FIG. 2. Capacités calorifiques molaires apparentes de l'isopropanol à 298,15 K, en fonction de la molalité en isopropanol m_3 à différentes molalités en NaDS (m_2) du solvant mixte H_2O + NaDS:
m_2 = 0 (41) ——; 0,0029, ▽; 0,0063, ▼; 0,0100, ◇; 0,0499, ◆; 0,0985, ☆; 0,1979, ★; 0,2632, ○; 0,3064, ●; 0,3475, △; 0,3984, ▲; 0,4261, □; 0,5132, ■.

molalité par rapport au solvant de référence; ρ_0 et c_{p_0} sont les masses volumiques et capacités calorifiques du solvant de référence; dans le cas d'un système ternaire, le solvant de référence est le système binaire dans lequel est ajouté le soluté i. Les différences $(c_p - c_{p_0})$ sont calculées à partir des capacités calorifiques volumiques mesurées $(\sigma - \sigma_0)$, à l'aide de la relation:

$$[3] \quad c_p - c_{p_0} = c_{p_0}\left(\frac{\sigma - \sigma_0}{\sigma_0} + 1\right)\frac{\rho_0}{\rho} - c_{p_0}$$

dans laquelle $\sigma_0 = c_{p_0}\rho_0$ et $\sigma = c_p\rho$.

Le soluté i est l'isopropanol (i = 3), le solvant de référence est le mélange binaire H_2O (1) + NaDS (2). Les valeurs ρ_0 et c_{p_0} du binaire sont déterminées par rapport à l'eau (26, 27). Les masses volumiques et capacités calorifiques déterminées en fonction de la molalité en isopropanol, ainsi que les grandeurs apparentes $V_{\phi,3}$ et $C_{\phi,3}$ qui en résultent sont indiquées tableau 1.

Les variations de $V_{\phi,3}$ et $C_{\phi,3}$ sont représentées respectivement sur les figures 1 et 2. L'erreur estimée sur $V_{\phi,3}$ est de 0,1 cm^3 mol^{-1} à m_3 = 0,1 mol kg^{-1}, mais diminue très rapidement pour de plus fortes concentrations (elle est de 0,03 cm^3 mol^{-1} pour m_3 = 0,5 mol kg^{-1} par exemple). Pour les mêmes molalités, l'erreur sur $C_{\phi,3}$ est respectivement 1 et 0,2 J K^{-1} mol^{-1}. Les valeurs à dilution infinie $V^0_{\phi,3}$ et $C^0_{\phi,3}$ sont obtenues par extrapolation à partir des courbes $V_{\phi,3} = f(m_3)$ et $C_{\phi,3} = f(m_3)$ quand $m_3 \rightarrow 0$. Pour le domaine dilué en alcool, une équation du type Redlich–Meyer peut être utilisée pour répresenter les variations de $V_{\phi,3}$ et $C_{\phi,3}$:

$$[4] \quad Y_\phi = Y^0_\phi + A_Y m + B_Y m^2 + \ldots$$

avec $Y = V$ ou C. Une méthode de moindres carrés (premier ou second degré) permet l'évaluation des paramètres Y^0_ϕ et A_Y, ainsi que leur incertitude dans le domaine de molalité $0-m_{3,\max}$ en isopropanol. Ces différentes valeurs sont données dans le tableau 2. Cependant, pour les molalités en NaDS comprises entre 0,2 et 0,3 m, la forme particulière des courbes $C_{\phi,3} = f(m_3)$ dans leur partie initiale n'autorise pas l'utilisation d'une méthode de moindres carrés aussi simple. Les valeurs de $C^0_{\phi,3}$ et $A_{c,3}$ sont alors obtenues graphiquement; elles sont entâchées d'une erreur relativement importante.

Discussion

Les grandeurs molaires partielles ou apparentes d'un soluté sont caractéristiques de l'environnement moléculaire du soluté dans le milieu. Ces grandeurs traduisent non seulement la contribution propre du soluté, mais aussi la contribution des interactions subies par le soluté et des perturbations subies par le solvant. Ainsi, l'examen des variations des grandeurs molaires apparentes d'un soluté apporte des informations sur les change-

TABLEAU 2. Volumes et capacités calorifiques molaires apparents à dilution infinie de l'isopropanol dans le mélange binaire H_2O + NaDS à 298,15 K (les incertitudes sont entre parenthèses)

m_2 (mol kg^{-1})	m_3 max	$V^0_{\phi,3}$ (cm^3 mol^{-1})	$A_{v,3}$ (cm^3 mol^{-2} kg)	m_3 max	$C^0_{\phi,3}$ (J K^{-1} mol^{-1})	$A_{c,3}$ (J K^{-1} mol^{-2} kg)
iPrOH (0)†	4,5	71,87	−1,22	4,5	362,5	+5,9
		(0,02)	(0,02)		(0,8)	(1,2)
0,00295	4,5	71,87	−1,20	4,5	360,5	+8,0
		(0,01)	(0,02)		(0,4)	(1,0)
0,00633	4,5	71,85	−1,16		[368]*	[−18]*
		(0,01)	(0,02)			
0,01005	4,5	71,90	−1,16	4,5	357,6	+9,1
		(0,01)	(0,01)		(0,9)	(1,3)
0,04916	4,5	72,04	−1,14	4,5	349,0	+12,7
		(0,01)	(0,01)		(0,7)	(1,1)
0,09846	4,5	72,18	−1,13	4,5	341,4	+13,3
		(0,01)	(0,01)		(0,3)	(0,5)
0,19786	4,5	72,37	−1,03		[338,5]*	[+4]*
		(0,01)	(0,01)			
0,26321	4,5	72,50	−0,98		[337,0]*	[−6]*
		(0,01)	(0,01)			
0,30638	4,5	72,54	−0,92		[329,0]*	[−22]*
		(0,02)	(0,02)			
0,34753	4,5	72,60	−0,90	4,5	305,2	21,1
		(0,01)	(0,01)		(0,5)	(0,6)
0,39837	4,5	72,71	−0,88	4,5	296,6	23,4
		(0,01)	(0,02)		(1,0)	(1,2)
0,42615	4,5	72,73	−0,84	4,5	293,3	23,1
		(0,01)	(0,01)		(0,7)	(1,0)
0,51325	4,5	72,85	−0,84	4,5	282,3	24,8
		(0,03)	(0,03)		(0,6)	(0,7)

*Valeurs extrapolées graphiquement.
†Référence 41.

ments de structure de la solution qui résultent de l'addition du soluté.

A. *Evolution des grandeurs molaires apparentes de l'alcool dans le système ternaire*

1. *Examen des variations de* $V_{\phi,3}$ *et* $C_{\phi,3}$

L'allure des différentes courbes $V_{\phi,3} = f(m_3)$ (Fig. 1) d'une part, et $C_{\phi,3} = f(m_3)$ (Fig. 2) d'autre part, est comparable à celle de V_ϕ et C_ϕ de l'isopropanol dans l'eau pure (21).

Lorsque la concentration en NaDS augmente, pour une même concentration en alcool, $V_{\phi,3}$ croît et $C_{\phi,3}$ décroît. Les pentes initiales $A_{v,3}$ et $A_{c,3}$ varient peu (tableau 2). Les variations particulières observées au voisinage de la cmc (0,008 *m*), et entre 0,2 et 0,3 *m*, traduisent des changements de structure à propos desquels nous reviendrons au paragraphe B-2.

Les variations des grandeurs molaires partielles $\bar{V}_3$ et $\bar{C}_{p_3}$ sur tout le domaine de fraction molaire en isopropanol sont données (Fig. 3) pour différentes compositions du binaire H_2O + NaDS. $\bar{V}_3$ et $\bar{C}_{p_3}$ ont été déterminés à partir des variations de $V_{\phi,3}$ et $C_{\phi,3}$ selon la procédure utilisée par Desnoyers *et al.* (28). Les variations de $\bar{V}_3$ et $\bar{C}_{p_3}$ sont comparables à celles de $\bar{V}$ et $\bar{C}_p$ de l'isopropanol dans l'eau pure. Au-delà des extremums situés dans le domaine dilué, $\bar{V}_3$ et $\bar{C}_{p_3}$ tendent très rapidement vers le volume et la capacité calorifique molaire de l'isopropanol pur. Pour les fractions molaires en alcool supérieures à 0,15, quelle que soit la concentration en NaDS dans le domaine étudié, $\bar{V}_3$ et $\bar{C}_{p_3}$ apparaissent confondus avec $\bar{V}$ et $\bar{C}_p$ de l'alcool dans l'eau.

2. *Interprétation*

A l'examen de ces différentes variations, une remarque générale s'impose: le comportement de l'isopropanol en solution micellaire est similaire à son comportement dans l'eau pure.

En système binaire eau + isopropanol (21), l'isopropanol se comporte comme d'autres solutés organiques dans l'eau tels que le terbutanol (29), des alkoxyéthanols (30), des amines (21), des amines oxydes (31), etc. La similitude observée entre les variations de V_ϕ et C_ϕ en fonction de la molalité pour ces solutés et celles pour des tensioactifs vrais (32), suggère que de tels solutés ont la propriété de s'agréger pour former des microhétérogénéités dans l'eau. La formation de ces agrégats se traduit par une variation rapide de V_ϕ et C_ϕ (et surtout $\bar{V}$ et $\bar{C}_p$) dans un étroit domaine de concentration en soluté. Ensuite $\bar{V}$ et $\bar{C}_p$ ont sensiblement les valeurs du corps pur V_0 et C_{p_0}. Ceci indique que les molécules de soluté sont essentiellement localisées au sein d'un microenvironnement organique de nature proche de celui qui leur est offert dans le corps pur.

En système ternaire H_2O + NaDS + iPrOH, on constate (Figs. 1 et 2) que les variations de $V_{\phi,3}$ et $C_{\phi,3}$ en fonction de la concentration en alcool, pour différentes concentrations en tensioactif ont toutes la même allure générale, même à des concentrations élevées en tensioactif. Dans le domaine dilué en alcool, les variations de $V_{\phi,3}$ sont essentiellement représentatives des interactions soluté−soluté dans la phase aqueuse: elles traduisent les interactions hydrophobes de l'alcool. Avec l'augmentation de la concentration en tensioactif du binaire (H_2O + NaDS) à même teneur en alcool, les faibles variations de $V_{\phi,3}$ et $C_{\phi,3}$ conduisent à admettre que la quantité d'isopropanol solubilisée dans les micelles est faible. En effet, le caractère hydrophile de la molécule d'isopropanol fait qu'en solution diluée, en présence de tensioactif, il est pour l'essentiel dans la phase aqueuse. Les propriétés apparentes sont alors

Can. J. Chem. Downloaded from www.nrcresearchpress.com by 210.87.254.105 on 09/06/12
For personal use only.

Can. J. Chem. Downloaded from www.nrcresearchpress.com by 210.87.254.105 on 09/06/12
For personal use only.

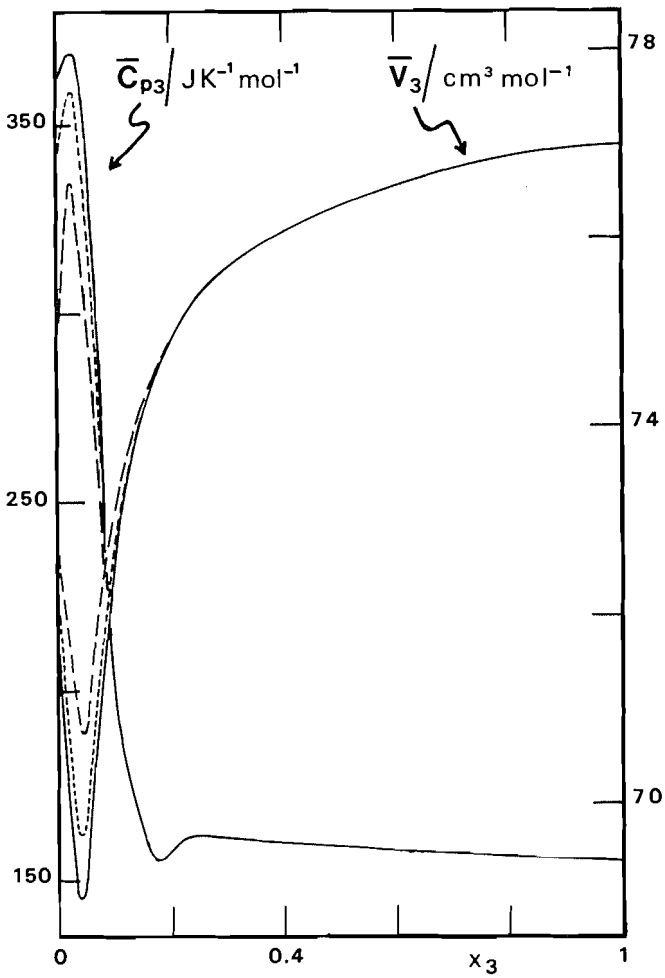

FIG. 3. Volumes et capacités calorifiques molaires partiels de l'isopropanol à 298,15 K, en fonction de la fraction molaire en isopropanol x_3, à différentes molalités en NaDS du solvant mixte H_2O + NaDS: ——— m_2 = 0 (41); --------- 0,0985; — — —, 0,3984.

assez peu différentes de celles dans l'eau pure, et ce, d'autant plus que certains auteurs (12−14) ont suggéré qu'il serait solubilisé dans la partie la plus externe de la micelle.

Dans le domaine plus concentré en alcool, au-delà du minimum de $V_{\phi,3}$ (du maximum de $C_{\phi,3}$) la contribution du phénomène d'agrégation de l'isopropanol l'emporte; le tensioactif serait susceptible de stabiliser ces agrégats sous forme de "micelles mixtes". Les variations de $V_{\phi,3}$ et $C_{\phi,3}$ traduisent la résultante des interactions entre molécules d'alcool en phase aqueuse et celle de l'alcool solubilisé dans les micelles ou sous forme d'agrégats. Pour des valeurs de x_3 supérieures à 0,15 (Fig. 3), l'alcool est presque entièrement sous forme de micro-agrégats et l'isopropanol se solubilise dans un milieu ressemblant à un milieu alcool pur. L'existence de ces micro-hétérogénéités est encore discutée, mais de récents travaux sur les systèmes eau + iPrOH + benzène (33) et eau + iPrOH + hexane (34) confortent cette hypothèse, les auteurs qualifiant même l'isopropanol de composant actif d'une "micro-émulsion sans détergent".

B. *Grandeurs à dilution infinie* $V^0_{\phi,3}$ *et* $C^0_{\phi,3}$

1. *Volumes*

La variation de $V^0_{\phi,3}$ en fonction de la molalité m_2 en NaDS est représentée (Fig. 4). $V^0_{\phi,3}$ reste constant avant la cmc, puis ensuite augmente régulièrement sur tout le domaine de concentration en NaDS étudié. Dans le domaine prémicellaire, l'isopropanol est en phase aqueuse et $V^0_{\phi,3}$ résulte des interactions de l'alcool avec les monomères de NaDS et l'eau; en milieu micellaire, comme il est réparti entre la phase aqueuse et les micelles sa propriété molaire apparente est une moyenne pondérée de celles dans chacune des deux phases. Les valeurs de $V^0_{\phi,3}$ très proches de celle de l'isopropanol à dilution infinie dans l'eau pure et la très faible variation de $V^0_{\phi,3}$ dans tout le domaine de concentration étudié montrent que la contribution de l'alcool dans la phase micellaire est très faible; l'isopropanol est donc solubilisé dans une très large proportion en phase aqueuse. Ce résultat est en accord avec ceux de Manabe *et al.* (35); ces auteurs ont étudié $V^0_{\phi,a}$ de part et d'autre de la cmc dans un étroit domaine de concentration en NaDS pour la série des alcools linéaires; ils n'observent pas de variation de cette grandeur pour les alcools inférieurs à C_4, ce qui va dans le sens d'une solubilisation de ces alcools, essentiellement en phase aqueuse. Pour des alcools à longue chaîne, peu solubles dans l'eau, $V^0_{\phi,a}$ est alors très proche du volume molaire de l'alcool pur, en raison de la solubilisation quasi totale de l'alcool dans la phase micellaire de nature organique (23, 35).

2. *Capacités calorifiques*

L'évolution de $C^0_{\phi,3}$ en fonction de la molalité m_2 en NaDS, représentée Fig. 4, apparaît plus complexe que celle de $V^0_{\phi,3}$. Au voisinage de la cmc $C^0_{\phi,3}$ semble tendre vers une valeur maximum. Pour m_2 compris entre 0,2 et 0,35 *m*, $C^0_{\phi,3}$ reste d'abord à peu près constant, puis décroît rapidement. Dans ce domaine, compte-tenu de l'incertitude sur les valeurs extrapolées de $C^0_{\phi,3}$, la forme de la courbe $C^0_{\phi,3}$ reste significative et traduit l'existence d'un phénomène réel. Ce phénomène observé à dilution infinie est encore là pour des concentrations finies en alcool, mais disparaît progressivement lorsque la concentration en alcool augmente, comme en témoigne la forme des courbes $C_{\phi,3}$ (m_2) pour différentes valeurs de m_3 (Fig. 4). Bien que le partage de l'isopropanol se fasse préférentiellement en faveur de la phase aqueuse, la contribution à $C^0_{\phi,3}$ des interactions de l'alcool solubilisé dans les micelles permet de mettre en évidence vers 0,3 *m* un changement dans la structure micellaire du binaire H_2O + NaDS. Ce changement observé lors de l'étude du binaire H_2O + NaDS (36) a aussi été mis en évidence dans l'étude du système ternaire H_2O + NaDS + n-BuOH (15). Des changements de même type ont également été observés avec des carboxylates de sodium (37) et, si l'on admet l'existence de "pseudo-phases" (37), ils correspondraient à des transitions entre des structures stables différentes.

Les variations particulières de $C^0_{\phi,3}$ au voisinage de la cmc et vers 0,3 *m* en NaDS, sont liées aux déplacements des équilibres chimiques, par suite de l'élévation de température provoquée pour l'évaluation de la capacité calorifique (38). Ainsi, les équilibres du tensioactif entre phase aqueuse et phase micellaire au voisinage de la cmc et entre les structures différentes vers 0,3 *m* sont modifiés. Il en résulte une perturbation du partage de l'alcool entre les différentes structures évoquées et, corrélativement, des valeurs de $C^0_{\phi,3}$.

C. *Grandeurs molaires apparentes relatives à NaDS en milieu eau + isopropanol*

Les mesures de masses volumiques et de capacités calorifiques réalisées dans le système ternaire permettent, au moyen d'interpolations, de calculer les grandeurs molaires apparentes $V_{\phi,2}$ et $C_{\phi,2}$ associées au tensioactif dans des solvants mixtes H_2O + iPrOH de composition donnée lorsque varie la

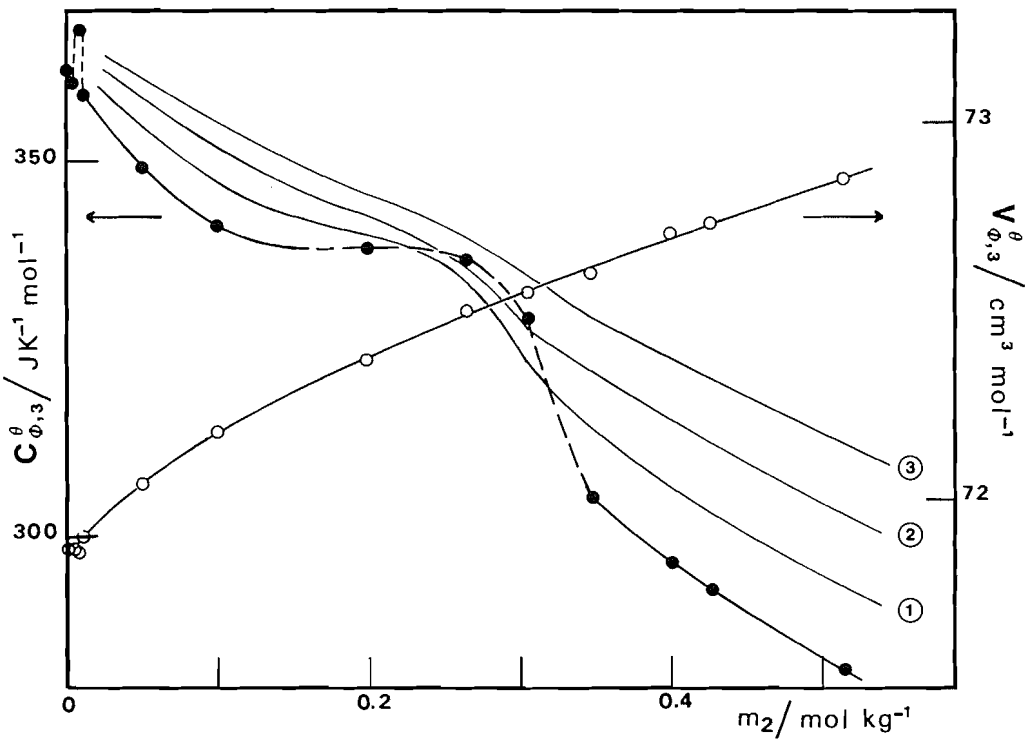

FIG. 4. Volumes et capacités calorifiques molaires apparents de l'isopropanol à 298,15 K, en fonction de la molalité en NaDS m_2 du solvant mixte H_2O + NaDS.
●○ valeurs extrapolées à dilution infinie $m_3 = 0$; ① valeurs interpolées à $m_3 = 0{,}5$; ② valeurs interpolées à $m_3 = 1$; ③ valeurs interpolées à $m_3 = 2$.

concentration en NaDS. Les courbes représentant les variations de $V_{\phi,2}$ et $C_{\phi,2}$ en fonction de m_2 pour des solutions 0,5, 1, 2, 3 et 4 *m* en iPrOH sont données respectivement figs. 5 et 6.

Il est bien connu que l'isopropanol abaisse la cmc du dodécylsulfate de sodium (11); à l'examen de ces courbes, on remarque que l'augmentation rapide de $V_{\phi,2}$ et la décroissance de $C_{\phi,2}$ se produisent pour des concentrations en tensioactif de plus en plus faibles, au fur et à mesure que la quantité d'alcool augmente dans le solvant mixte.

Dans la région prémicellaire, étant donné la très faible valeur de la cmc de NaDS ($8{,}3 \times 10^{-3}$ *m* (39)), il est difficile d'effectuer l'étude quantitative de l'influence de l'alcool sur les propriétés molaires du monomère de tensioactif, comme l'ont réalisée Vikingstad et Kvammen (14) avec la série des alcools à chaîne courte dans les solutions de décanoate de sodium ou Güveli *et al.* (40) avec les mêmes alcools dans le système H_2O – bromure de dodécyltriméthylammonium. Qualitativement, lorsque la quantité d'isopropanol augmente, on observe que le volume apparent du monomère NaDS augmente et sa capacité calorifique décroît, en accord avec les résultats précités. Ces auteurs expliquent ces variations à la fois par une diminution de l'hydratation hydrophobe de la partie hydrocarbonée du tensioactif et par une diminution de l'hydratation hydrophile de sa tête ionique, le monomère se trouvant dans un environnement de plus en plus organique.

Dans la région post-micellaire, les valeurs de $V_{\phi,2}$ augmentent et celles de $C_{\phi,2}$ diminuent lorsque la quantité de l'alcool croît dans le solvant mixte H_2O + iPrOH. L'effet de l'alcool doit être relié à des changements de la couche superficielle micellaire par suite de la solubilisation de l'alcool dans les micelles (12). Vikingstad et Kvammen (14) considèrent que l'augmentation de volume apparent du tensioactif est due à une réduction de l'électrostriction des molécules d'eau sur la surface micellaire.

Les courbes $V_{\phi,2}$ (m_2) passent par un maximum (un minimum pour $C_{\phi,2}$) puis tendent vers la valeur du volume apparent (et de la capacité calorifique apparente) de NaDS dans les micelles. Il semble que ces extremums soient d'autant plus prononcés que la composition du binaire H_2O + iPrOH est proche de celle pour laquelle il se forme des microhétérogénéités dans le binaire.

Conclusion

L'étude des volumes et capacités calorifiques du système ternaire H_2O + NaDS + iPrOH contribue à une meilleure connaissance du rôle de l'alcool dans les solutions micellaires. La nature de l'isopropanol, de par son caractère légèrement amphiphile, fait qu'il est susceptible de former des microagrégats dans l'eau, aussi certains auteurs ont-ils évoqué le "rôle actif de l'isopropanol dans les microémulsions sans détergent" (33, 34). Dans les solutions micellaires, l'isopropanol agit à la fois sur la structure du solvant et sur les propriétés micellaires provoquant un abaissement de la cmc du tensioactif. Nos résultats corroborent l'hypothèse selon laquelle l'isopropanol s'incorpore dans la micelle à l'interface micelle–solvant pour former des micelles mixtes, sans pénétrer profondément dans le coeur micellaire. En jouant un rôle d'écran entre les têtes ioniques du tensioactif, il abaisserait la densité superficielle de charge et contribuerait ainsi à stabiliser la micelle. Les alcools à plus longue chaîne, leur caractère hydrophobe augmentant, pénètrent alors plus à l'intérieur de la micelle et perturbent de façon plus importante la structure de la micelle (12, 40).

L'étude des capacités calorifiques molaires apparentes à di-

Can. J. Chem. Downloaded from www.nrcresearchpress.com by 210.87.254.105 on 09/06/12
For personal use only.

Can. J. Chem. Downloaded from www.nrcresearchpress.com by 210.87.254.105 on 09/06/12
For personal use only.

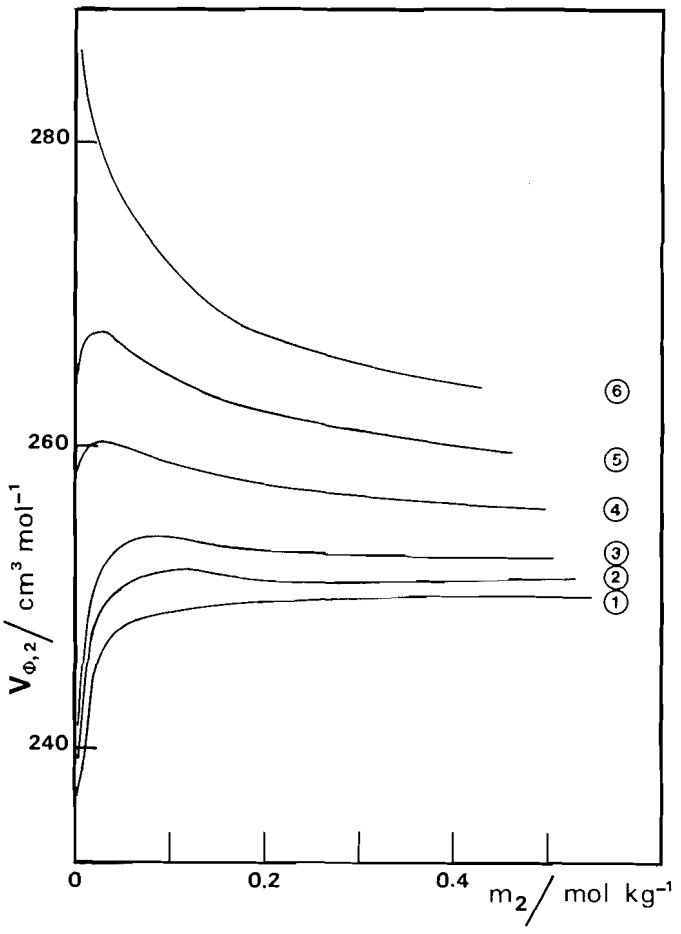

FIG. 5. Volumes molaires apparents de NaDS à 298,15 K en fonction de la molalité en NaDS m_2 à différentes molalités en isopropanol dans le solvant mixte H_2O + iPrOH:
m_3 = 0 (36), ①; 0,5, ②; 1, ③; 2, ④; 3, ⑤; 4, ⑥.

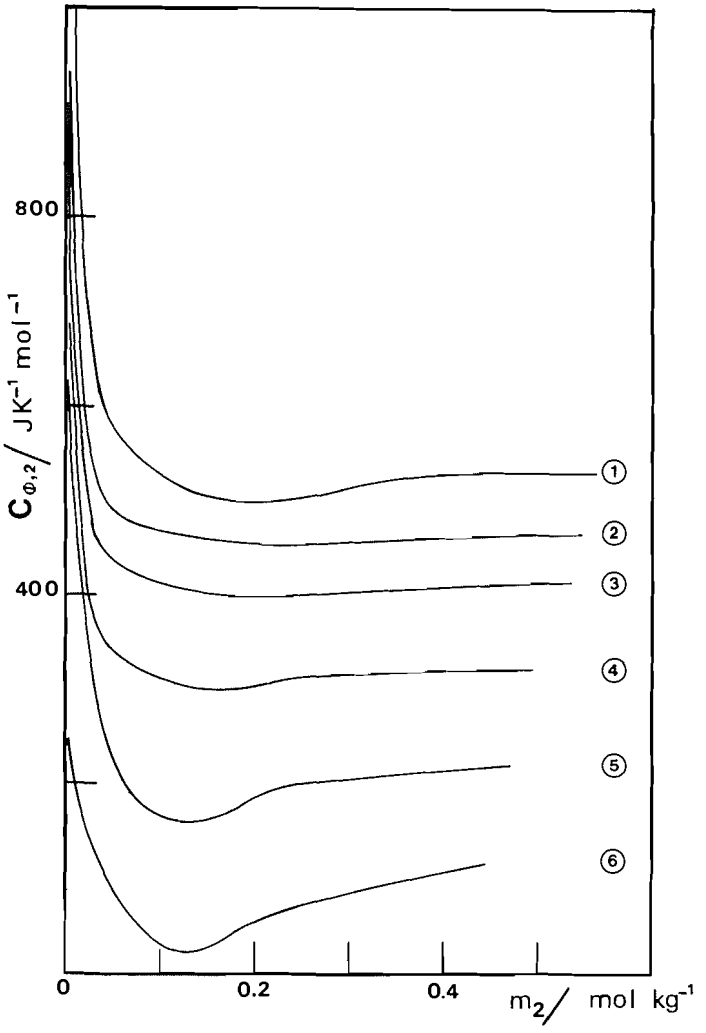

FIG. 6. Capacités calorifiques molaires apparentes de NaDS, à 298,15 K, en fonction de la molalité en NaDS m_2, à différentes molalités en isopropanol dans le solvant mixte H_2O + iPrOH:
m_3 = 0 (36), ①; 0.5, ②; 1, ③; 2, ④; 3, ⑤; 4, ⑥.

lution infinie de l'isopropanol (ou dans le domaine très dilué en alcool) a permis de mettre en évidence des changements de structure dans le binaire H_2O + NaDS. En plus de la transition correspondant à la concentration critique micellaire du tensioactif, l'existence d'une seconde transition pourrait être responsable des changements observés vers 0,3 *m* en NaDS (plus clairement mise en évidence que lors de l'étude du seul binaire H_2O + NaDS (36)). Cette transition semblerait jouer un rôle essentiel pour la solubilisation de molécules organiques telles que le butanol (15) et pour la solubilisation des hydrocarbures en milieu microémulsion (19, 20).

Remerciements

L'un de nous (V. M.) tient à exprimer ses remerciements pour l'obtention d'une bourse de la D.G.R.C.S.T., Ministère des Relations Extérieures, dans le cadre des échanges France–Tchécoslovaquie. Nous remercions aussi M. le Professeur J. E. Desnoyers (Université de Sherbrooke, Canada) pour les discussions fructueuses et l'intérêt qu'il a bien voulu porter à ce travail.

1. K. L. MITTAL (*Editeur*). Micellization, solubilization and microemulsions. Vols. 1 et 2. Plenum Press, New York. 1977.
2. L. M. PRINCE (*Editeur*). Microemulsions. Theory and practice. Academic Press, New York. 1977.
3. R. L. BERG, L. A. NOLL et W. O. GOOD. Chemistry of oil recovery. *Edité par* R. T. Johansen et R. L. Berg. A.C.S. Symposium Séries N° 91. Washington, DC. 1979. p. 81.
4. J. E. DESNOYERS, F. QUIRION, D. HETU et G. PERRON. Fuel. Sous presse.
5. F. FRANKS et D. J. G. IVES. Q. Rev. **20**, 1 (1966).
6. H. N. SINGH et S. SWARUP. Bull. Chem. Soc. Jpn. **51**, 1534 (1978).
7. B. D. FLOCKART et A. R. UBBELOHDE. J. Colloid. Sci. **8**, 428 (1953).
8. K. SHINODA. J. Phys. Chem. **58**, 1136 (1954).
9. M. F. EMERSON et A. HOLTZER. J. Phys. Chem. **71**, 3320 (1967).
10. A. S. C. LAURENCE et J. T. PARSON. Trans. Faraday Soc. **63**, 495 (1967).
11. K. SHIRAHAMA et T. KASHIWABARA. J. Colloid Interface Sci. **36**, 65 (1971).
12. R. ZANA, S. YIV, C. STAZIELLE et P. LIANOS. J. Colloid Interface Sci. **80**, 208 (1981).
13. J. W. LARSEN et L. B. TEPLEY. J. Colloid Interface Sci. **49**, 113 (1974).
14. E. VIKINGSTAD et O. KVAMMEN. J. Colloid Interface Sci. **74**, 16 (1980).
15. G. ROUX-DESGRANGES, A. H. ROUX, J. P. E. GROLIER et A. VIALLARD. J. Solution Chem. **11**, 357 (1982).
16. A. M. BELLOCQ, J. BIAIS, B. CLIN, P. LALANNE et

B. LEMANCEAU. J. Colloid Interface Sci. **70**, 524 (1979).
17. J. LANG, A. DJAVANBAKHT et R. ZANA. J. Phys. Chem. **84**, 1541 (1980).
18. A. GRACIAA. Thèse Doctorat d'Etat, Université de Pau, France. 1978.
19. A. H. ROUX, G. ROUX-DESGRANGES, J. P. E. GROLIER et A. VIALLARD. J. Colloid Interface Sci. **84**, 250 (1981).
20. G. ROUX-DESGRANGES, A. H. ROUX, J. P. E. GROLIER et A. VIALLARD. J. Colloid Interface Sci. **84**, 536 (1981).
21. G. ROUX, D. ROBERTS, G. PERRON et J. E. DESNOYERS. J. Solution Chem. **9**, 629 (1980).
22. K. S. BIRDI, S. BACKLUND, K. SØRENSEN. T. KRAG et S. DALSAGER. J. Colloid Interface Sci. **66**, 118 (1978).
23. E. VIKINGSTAD. J. Colloid Interface Sci. **72**, 75 (1979).
24. P. PICKER, E. TREMBLAY et C. JOLICOEUR. J. Solution Chem. **3**, 377 (1974).
25. P. PICKER, P. A. LEDUC, P. R. PHILIP et J. E. DESNOYERS. J. Chem. Thermodyn. **3**, 631 (1971).
26. G. S. KELL. J. Chem. Eng. Data, **12**, 66 (1977).
27. H. F. STIMSON. Am. J. Phys. **23**, 614 (1955).
28. J. E. DESNOYERS, R. DE LISI, C. OSTIGUY et G. PERRON. Solution chemistry of surfactants. *Edité par* K. L. Mittal et A. S. Kertes. Plenum Press, New York. 1979.
29. C. DE VISSER, G. PERRON et J. E. DESNOYERS. Can. J. Chem. **55**, 856 (1977).
30. G. ROUX, G. PERRON et J. E. DESNOYERS. J. Solution Chem. **7**, 639 (1978).
31. J. E. DESNOYERS, D. ROBERTS, R. DE LISI et G. PERRON. Solution behaviour of surfactants: theoretical and applied aspects. *Edité par* E. J. Fendler et K. L. Mittal. Plenum Press, New York. Sous presse.
32. G. M. MUSBALLY, G. PERRON et J. E. DESNOYERS. J. Colloid Interface Sci. **48**, 494 (1974).
33. J. LARA, G. PERRON et J. E. DESNOYERS. J. Phys. Chem. **85**, 1600 (1981).
34. G. D. SMITH, C. E. DONELAN et R. E. BARDEN. J. Colloid Interface Sci. **60**, 488 (1977).
35. M. MANABE, K. SHIRAHAMA et M. KODA. Bull. Chem. Soc. Jpn. **49**, 2904 (1976).
36. V. MAJER, A. H. ROUX, G. ROUX-DESGRANGES et A. VIALLARD. En préparation.
37. G. DOUHERET et A. VIALLARD. J. Chim. Phys. **78**, 85 (1981).
38. J. E. DESNOYERS, R. DE LISI et G. PERRON. Pure Appl. Chem. **52**, 433 (1980).
39. P. MUKERJEE et K. J. MYSELS. Critical micelle concentrations of aqueous surfactant systems. Natl. Stand. Ref. Data Ser. N.B.S. (US) Washington, DC. 1971.
40. D. E. GÜVELI, J. B. KAYES et S. S. DAVIS. J. Colloid Interface Sci. **22**, 307 (1981).
41. A. H. ROUX, J. P. E. GROLIER et E. WILHELM. En préparation.

Can. J. Chem. Downloaded from www.nrcresearchpress.com by 210.87.254.105 on 09/06/12
For personal use only.

The synthesis of α-*N*,*N*-dimethyl-1′-diphenylphosphinoferrocenylethylamine and related ligands

IAN R. BUTLER AND WILLIAM R. CULLEN

Chemistry Department, University of British Columbia, Vancouver, B.C., Canada V6T 1Y6

Received July 15, 1982

IAN R. BUTLER and WILLIAM R. CULLEN. Can. J. Chem. **61**, 147 (1983).

Routes to the title compound were explored based on the cleavage of [1]-ferrocenophanes with aryllithium. Thus the cleavage of $(\eta^5\text{-}C_5H_4)Fe(\eta^5\text{-}C_5H_3(CHMeNMe_2)PPh)$ with phenyllithium affords $(\eta^5\text{-}C_5H_4Li)Fe(\eta^5\text{-}C_5H_3(CHMeNMe_2)PPh_2)$ and $\eta^5\text{-}C_5H_4PPh_2)Fe(\eta^5\text{-}C_5H_3Li(CHMeNMe_2))$ in the ratio 15:85. Hydrolysis of this mixture affords the title compound **4**. The lithio-ferrocenes can be treated with XER_2 to yield other mixed ligands (E = As, P).

A route to **4** via $(\eta^5\text{-}C_5H_4PPh_2)Fe(\eta^5\text{-}C_5H_4C(O)Me)$ was also established but it is complicated by low yields and many side products such as $[(\eta^5\text{-}C_5H_4PPh_2)Fe(\eta^5\text{-}C_5H_4)]_2C{=}CH_2$.

IAN R. BUTLER et WILLIAM R. CULLEN. Can. J. Chem. **61**, 147 (1983).

On a exploré des voies d'accès au composé mentionné dans le titre qui fait appel au clivage des ferrocénophanes [*1*] avec l'aryllithium. Ainsi le clivage $(\eta^5\text{-}C_5H_4)Fe(\eta^5\text{-}C_5H_3(CHMeNMe_2)PPh$ avec le phényllithium conduit au $(\eta^5\text{-}C_5H_4Li)Fe(\eta^5\text{-}C_5H_3(CHMeNMe_2)PPh_2)$ et au $(\eta^5\text{-}C_5H_4PPh_2)Fe(\eta^5\text{-}C_5H_3Li(CHMeNMe_4))$ dans un rapport de 15:85. L'hydrolyse de ce mélange permet d'obtenir le composé **4** mentionné dans le titre. On peut traiter le lithio-ferrocène avec XER_2 pour obtenir d'autres ligands mixtes (E = As, P).

On a également établi une voie d'accès au composé **4** par l'intermédiaire de $(\eta^5\text{-}C_5H_4PPh_2)Fe(\eta^5\text{-}C_5H_4C(O)Me)$ mais dans ce cas le rendement est faible et on obtient plusieurs produits secondaires, tel le $[(\eta^5\text{-}C_5H_4PPh_2)Fe(\eta^5\text{-}C_5H_4)]_2C{=}CH_2$.

[Traduit par le journal]

Introduction

It is well known that cationic rhodium(I) complexes of formula $[Rh(L{-}L')(NBD)]^+[ClO_4]^-$ ((L—L′) = symmetrical, unsymmetrical, or asymmetric bidentate ligand; NBD = norbornadiene) are catalyst precursors for the effective hydrogenation and hydrosilylation of a range of olefins and ketones (1–3).

In our laboratories we have been particularly interested in derivatives where L—L′ is a ferrocenylphosphine such as **1** or **2** where the catalyst precursor is bound to the rhodium through both the N and P atoms (2). These ligands which possess both a chiral carbon atom and a plane of chirality can be prepared in their optically pure form reasonably easily (4). The cationic

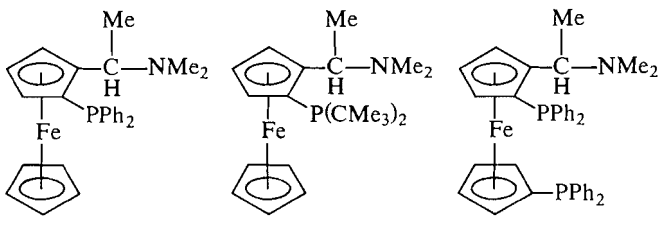

1 **2** **3**

rhodium(I) complex of **1** is an effective catalyst for the hydrogenation of amino acid precursors such as acylaminocinnamic acid in high optical yield, reaction [1].

The rhodium(I) complex of the 2-*tert*-butylphosphinoferrocenylamine **2** is also a good hydrogenation catalyst precursor with respect to reaction [1], affording higher optical yields at a faster rate than the complex of **1**. The absolute configuration of the product, however, is reversed. These results cannot be easily rationalized using any of the models currently employed to predict the course of these reactions. Thus, it is important to obtain more insight into the nature of the discrimination step. With this in mind, we have been interested in studying the effects of spatial modification of the ligand **1** and have set out to prepare 1,1′-substituted derivatives such as **4**.

[1]

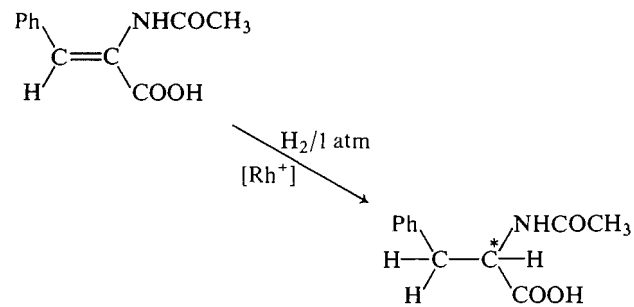

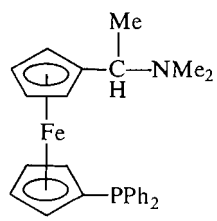

4

The present paper describes the synthesis of **4** from [1]-ferrocenophanes utilizing the synthetically useful cleavage reaction of 5 with alkyl- and aryllithium reagents as reported by Seyferth and Withers (5), reaction [2]. We also show how a modification of this reaction can be applied to the preparation of new ligands related to **3** which can also afford metal complexes for further studies of catalytic hydrogenation.

0008-4042/83/010147-07$01.00/0

©1983 National Research Council of Canada/Conseil national de recherches du Canada

Can. J. Chem. Downloaded from www.nrcresearchpress.com by 210.87.254.105 on 09/06/12
For personal use only.

TABLE 1. Analytical data for new compounds

	Compound	Color	Melting point (°C)	Found (%) C	H	N	Calcd. (%) C	H	N
4	$(\eta^5\text{-}(C_6H_5)_2PC_5H_4)Fe(\eta^5\text{-}(CH_3C(H)NMe_2)C_5H_4)$	Yellow	69	70.72	6.31	3.08	70.76	6.39	3.17
7	$(\eta^5\text{-}(C_6H_5)_2PC_5H_4)Fe(\eta^5\text{-}CH_3C(O)C_5H_4)$	Orange	116	69.91	5.29	—	69.92	5.13	—
8	$[(\eta^5\text{-}(C_6H_5)_2PC_5H_4)Fe(\eta^5\text{-}C_5H_4)]C(C_6H_5)=CH_2$[a]	Yellow	109	Characterised by mass spectroscopy and ^{1}H nmr					
9	$[(\eta^5\text{-}(C_6H_5)_2PC_5H_4)Fe(\eta^5\text{-}C_5H_4)]_2C=CH_2$	Cream	138	72.39	5.28	—	72.27	5.01	—
10	$(\eta^5\text{-}(C_6H_5)_2PC_5H_4)Fe(\eta^5\text{-}CH_3C(H)OHC_5H_4)$	Yellow	89	69.82	5.51	—	69.58	5.61	—
11	$[(\eta^5\text{-}(C_6H_5)_2PC_5H_4)Fe(\eta^5\text{-}(CH=CH_2)C_5H_4)$[b]	Yellow	Oil	Characterised by mass spectroscopy and ^{1}H nmr					
16 and **17**	$(\eta^5\text{-}(C_6H_5)_2EC_5H_4)Fe(\eta^5\text{-}(C_6H_5)_2E'(Me_2NC(H)Me)C_5H_3$[c]	Yellow	—	68.23	5.83	2.02	68.18	5.57	2.09
19 and **20**	$(\eta^5\text{-}(C_6H_5)_2PC_5H_4)Fe(\eta^5\text{-}(C_4H_9)_2P(Me_2NC(H)Me)C_5H_3$ $(\eta^5\text{-}(C_4H_9)_2PC_5H_4)Fe(\eta^5\text{-}(C_6H_5)_2P(Me_2NC(H)Me)C_5H_3$	Yellow	Oil	Characterised by ^{1}H nmr only					

[a]Always obtained with trace impurities formed during recrystallisation.
[b]Product obtained in very low yield as oily solid.
[c]Mixture of isomers E = As, E′ = P or E = P, E′ = As.

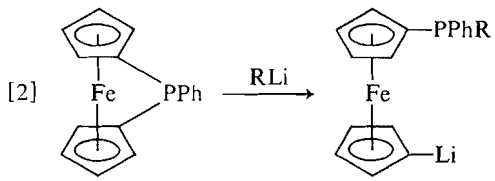

5 **6**

Experimental

All manipulations were carried out under a nitrogen atmosphere. Solvents were predried and freshly distilled. ^{1}H nmr chemical shifts are given in ppm from TMS and were recorded on a Bruker W.P.80 operating at 80 MHz, a Varian XL100 at 100 MHz, or a Bruker WM400 at 400 MHz. Elemental analyses were performed by Mr. Peter Borda of this department and are reported in Table 1. Spectroscopic data are given in Table 2. The ferrocenophanes **5** and **14** were prepared as previously described (6, 7).

1. Preparation of 1-acetyl-1′-diphenylphosphinoferrocene, 7

The ferrocenophane **5** (2.92 g, 10 mol), in the minimum volume of ether required for dissolution, was added dropwise to an ethereal solution (100 mL) of phenyllithium (15 mmol) maintained at −78°C. The solution was warmed slowly to room temperature. A clear orange solution resulted which was then rechilled to −78°C. Acetyl chloride (1.20 g, 15.3 mmol) in ether (10 mL) was added dropwise. The solution was warmed to room temperature and was stirred for a further 10 min. Water (10 mL) was added dropwise. The ethereal layer was separated, dried over anhydrous $MgSO_4$, and the solvent volume reduced under vacuum to approximately 5 mL. The residual oil was ehromatographed on neutral alumina by eluting with progressively polar mixtures of hexane/diethyl ether. A yellow fraction which eluted first (later shown to contain a mixture of **8**, **9**, and diphenylphosphinoferrocene following a second chromatographic separation) was followed by the orange product band. The product **7** was crystallised from hexane at −20°C to give an orange crystalline solid (1.6 g, 39% yield).

2. Preparation of 1,1′-bis-(1′-diphenylphosphinoferrocenyl)ethylene, 9

The reaction of **5** (5.0 g, ~17 mmol) with phenyllithium (17 mmol) at room temperature using a similar procedure to **1** above gave 1,1′-bis-(1′-diphenylphosphinoferrocenyl) ethylene **9** as the major isolated product as a cream-coloured solid (orange in solution). This compound was isolated following column chromatography, eluting with diethyl ether (yield, 2.8 g, 43%).

3. Preparation of 1-(α-hydroxyethyl)-1′-diphenylphosphinoferrocene, 10

A solution of **7** (1.0 g, 2.92 mmol) in benzene (10 mL) was added slowly to a well-stirred suspension of $LiAlH_4$ (0.1 g, 2.7 mmol) in benzene (50 mL). After complete addition, the solution was stirred for 1 h at room temperature. Ethyl acetate (5 mL) was then added dropwise followed by water (30 mL). The organic layer was separated and dried over anhydrous $MgSO_4$. The solvent volume was reduced under vacuum to a few mL and the remaining oil was chromatographed on neutral alumina to give a single yellow band. Solvent removal under vacuum gave a yellow oil which on further drying (~50°C) *in vacuo* gave a solid product (crude yield ~95%). The solid was crystallised from hexane to give crystalline **10**, 70% yield.

4. Reaction of 10 with HBr and $HNMe_2$

Gaseous HBr was slowly bubbled through a rapidly stirred solution of **10** (0.8 g, 1.93 mmol) in benzene (50 mL). A pale yellow precipitate was observed after saturating the solution. Excess anhydrous dimethylamine was added dropwise and the precipitate, which had become orange, was filtered. The benzene solution was then treated with diethyl ether to give a pale yellow precipitate which was also filtered off. The solvent volume of the residual ether/benzene solution was reduced to a few mL and the resulting orange oil was chromatographed on neutral alumina. Two bands were isolated, the first was eluted with a 50/50 hexane/ether mixture and was identified as **4** by ^{1}H nmr spectroscopy, the second was identified as **11** by ^{1}H nmr and mass spectroscopy (Table 2). The precipitated fractions were combined and redissolved in chloroform, ether was added as a top layer, and the solution left to crystallise overnight. This gave an orange/yellow solid (0.6 g).

5. Reaction of 10 with acetic anhydride in pyridine, and acetic acid in benzene

The alcohol **10** (100 mg, 0.24 mmol) in pyridine was stirred with an excess of acetic anhydride (50 mg, 0.49 mmol) for 20 h. The solution was filtered and the solvent removed under vacuum. The residual oil was redissolved in methanol, 10 mL, and dimethylamine (50 mg, 1.1 mmol (excess)) was added. The solution was stirred for 2 h. Again the solvent was removed under vacuum and the residual oil chromatographed on neutral alumina. Two yellow bands were isolated (by elution with diethyl ether). The first was identified as unreacted **10** and the second as the product **4** (52 mg, ~49%) by ^{1}H nmr spectroscopy.

In a similar reaction **10** (300 mg, 0.725 mmol) and acetic acid (60 mg, 1.0 mmol) were refluxed in benzene (70 mL) for a 3.5 h period in an apparatus fitted with a Dean and Stark trap. After cooling, excess dimethylamine (90 mg, 2.0 mmol) was added. The reaction solution was then examined by tlc; this showed only a minor trace of product **4** with a large excess of the starting material **10**.

6. Direct preparation of 1-(α-dimethylaminoethyl)-1′-diphenylphosphinoferrocene, 4

To an ethereal solution (30 mL) of phenyllithium (0.5 mmol) maintained at −78°C, a solution of **14** (100 mg, 0.275 mmol), in the

Can. J. Chem. Downloaded from www.nrcresearchpress.com by 210.87.254.105 on 09/06/12
For personal use only.

TABLE 2. Spectroscopic data for new compounds

Compound No.	^{1}H nmr ($CDCl_3$) δ values		Mass spectra	
	Ferrocenyl protons	Aromatic protons	Aliphatic protons	*m/e* (relative intensity)
4	4.35(m,2) 4.05(m,6)	7.25–7.50(m,10)	1.30(d,3); CH_3 2.05(s,6); $N(CH_3)_2$ 3.50(q,1); CH	[c]441($M^{+\cdot}$)(35.0)396(64.9) 212(49.5)183(27.9)169(26.1) 165(36.0)152(27.7)121(45.5) 69(68.9)56(100)
7	4.68(t,2) 4.40(t,2) 4.37(q,2) 4.14(q,2)	7.20–7.60(m,10)	2.30(s,3); CH_3	[c]413(27.5)412($M^{+\cdot}$)(100) 321(64.0)262(22.7) 183(43.3)171(38.4)170(31.0) 105(20.7)77(19.3)56(33.2)
8	3.98–4.40(m,8)	7.20–7.50(m,15)	5.13(d,1)CH 5.45(d,1)CH	[c]473(35.1)472($M^{+\cdot}$)(100) 471(14.8)470(9.3)395(8.1) 370(8.0)236(4.4)223(7.2) 171(9.9)120(5.7)
9	4.00–4.60(m,16)	7.40(bs,20)	5.40(s,2)CH_2	[c]766(16.5)765(53.7) 764($M^{+\cdot}$)(100)763(12.4) 762(14.2)516(18.9)515(51.6) 382(10.0)330(30.5)328(23.9)
10	4.43(m,2) 4.33(m,6)	7.25–7.55(m,10)	1.80(d,3); CH_3 2.10(m,1); OH 4.60(m,1); H[q,D_2O]	[c]414($M^{+\cdot}$)(100)322(18.7) 321(24.4)245(11.4)244(31.7) 226(26.0)197(18.7)171(15.5) 170(15.5)121(11.5)
11	4.00–4.50(m,10)[a]	7.25–7.70(m,10)	5.10(m) 5.36(m) 5.48(m)	[d]396($M^{+\cdot}$),364, 321,283,268
16 and **17**	3.75–4.35(m,8)	7.15–7.60(m,20)	3.68, 3.66 (q,1); CH 1.76, 1.77 (s,6); $N(CH_3)_2$ 1.15, 1.19 (d,3); CH_3	—
19 and **20**[b]	4.12–4.52(m,8)	7.30–7.90(m,10)	2.06(s,6); $N(CH_3)_2$ 1.30(d,3); CH_3 3.44(q,1); CH (d,9); CH_3	—
7b[e]	3.80–4.45(m,8)	7.00–7.80(m,15)	1.70(s,3); CH_3 2.70(bs,1); OH[f]	—

[a]Includes signal from overlap of vinyl proton resonances.
[b]The isomers are indistinguishable by nmr.
[c]Mass spectra with high resolution.
[d]Low resolution mass spectral data.
[e]Spectral comparison of alcohol derived from hydrolysis of the reaction mixture of phenyllithium with acetylferrocene was used.
[f]bs = broad singlet.

minimum quantity of ether necessary for dissolution, was added dropwise. The solution was stirred for 5 min at −78°C before it was warmed slowly to room temperature. A clear orange solution resulted. This solution was then hydrolysed by careful dropwise addition of water (10 mL). The ethereal layer was separated, dried over anhydrous $MgSO_4$, and finally the volume was reduce to a few mL. The ^{1}H nmr spectrum of this mixture is shown in Fig. 1*c*. Column chromatography of the redissolved residual orange oil (chloroform, 2 mL) gave initially a fraction which eluted with hexane/ether, 50/50, containing **1** of known ^{1}H nmr spectrum, followed by a fraction containing **4** which eluted with diethyl ether. The solvent was removed to give the pure product, 55% yield which crystallised at −20°C from hexane over a period of 3 days to give a yellow–orange crystalline solid.

*7. Preparation of the isomers **16** and **17***

The initial procedure employed was identical with that used in the preparation of **4** but on a 10 mmol scale. Instead of hydrolysis, however, excess chlorodiphenylarsine (20 mmol) in diethyl ether was added dropwise to the chilled solution. The resulting suspension was warmed slowly to room temperature and was stirred for a further 30 min before hydrolysis (H_2O, 20 mL). The ethereal layer was separated, dried over anhydrous $MgSO_4$, and the filtered solution volume reduced to ~5 mL under vacuum. Chromatography on neutral alumina gave a single broad yellow band eluting with progressively polar mixtures of hexane and ether. On complete solvent removal a yellow oily solid remained, which when crystallised (hexane, −20°C), gave yellow nodules. ^{1}H nmr spectroscopy showed these to be a mixture of the positional isomers **16** and **17**.

These two isomers are separable by tlc (hexane eluant, aluminum backed Kieselgel plates) and preparative tlc. Long columns of alumina are required for large scale separation (there is slight decomposition on silica gel columns).

Can. J. Chem. Downloaded from www.nrcresearchpress.com by 210.87.254.105 on 09/06/12
For personal use only.

Can. J. Chem. Downloaded from www.nrcresearchpress.com by 210.87.254.105 on 09/06/12
For personal use only.

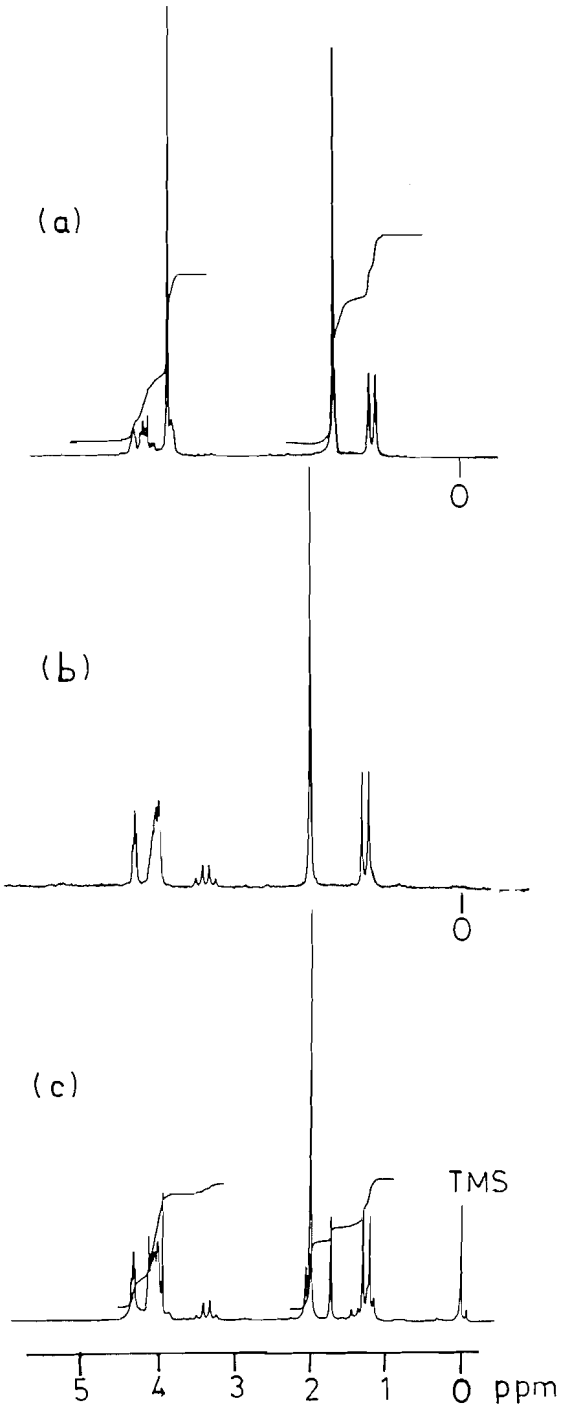

FIG. 1. The 80 MHz proton nmr spectra of (0–5 ppm) (a) PPFA **1**, (b) **4**, (c) the crude reaction mixture following reaction of **14** with phenyllithium followed by H_2O.

*8. The reaction of **14** with phenyllithium and di-*tert*-butylchlorophosphine*

To an ethereal solution (100 mL) of phenyllithium (2.0 mmol) maintained at −78°C, a solution of **14** (400 mg, 1.1 mmol) in ether was added dropwise. After warming to room temperature and recooling to −78°C an excess of di-*tert*-butylchlorophosphine (450 mg, ~2.5 mmol) was added dropwise. The solution was warmed to room temperature and was refluxed for 30 min. Following workup by an identical procedure to that in the previous preparations the resultant oil was chromatographed on Brockman Grade I neutral alumina. Two bands were isolated eluting with a mixture of diethyl ether/chloroform. The first orange band decomposed during recrystallisation and the second gave a deep-coloured oil on attempted crystallisation from hexane. This was identified as a mixture of the isomers **19** and **20** by ^{1}H nmr.

9. Reaction of 7 with phenyllithium

A solution of **7** (100 mg, 2.43 mmol) with phenyllithium (2.00 mL of 1.9 *M* solution; excess) in dry diethyl ether (10 mL) was stirred for 4 h. The solution was hydrolysed (H_2O, 5 mL) and the ethereal layer separated, dried over anhydrous $MgSO_4$. Following filtration the resultant solution was chromatographed on neutral alumina. A yellow fraction eluting with 15% diethyl ether in hexane was obtained. The solvent was removed and the ^{1}H nmr of the residual oily solid was recorded. The product was thus characterised spectroscopically as the methylphenyl alcohol derivative *7b*. A solution of the product in chloroform was observed to decompose with the formation of a small quantity of the vinyl derivative **8**.

Results and discussion

The preparation of **4** was initially approached via the ring cleavage reaction (reaction [2]) of **5** reported by Seyferth and Withers (5). The subsequent synthetic route involved the reaction of the intermediate 1′-monolithio-derivative **6** with acetyl chloride to give the 1′-acetyl derivative **7** (Scheme 1, *a*).

The procedure used was to add **5** to a solution of phenyllithium in diethyl ether since the reaction product, the 1′-monolithidiphenylphosphinoferrocene **6**, could conceivably react with **5** to give a monolithiobisferrocenyl derivative *7a*. The optimum yield of **6** is therefore achieved using an excess of phenyllithium, and a 1.5 molar excess was typically employed. On addition of acetyl chloride to the resultant solution of **6** the desired product **7** was obtained in moderate yield. However, the vinylferrocene derivative, **8**, is also produced. It is likely that the excess phenyllithium attacks the carbonyl group of **7** to give the lithium salt of the tertiary alcohol. This could give rise to **8** by acid-catalysed dehydration of an intermediate alcohol (Scheme 1, *b*) or deacetylation of the ester formed by reaction of the intermediate lithium derivative with acetyl chloride (Scheme 1, *c*).

The reaction of excess phenyllithium with **7** was carried out independently. The product formed following hydrolysis was the alcohol *7b* which was observed to decompose in chloroform solution on prolonged standing to give **8**.

When a 1:1 ratio of phenyllithium to **5** is used the major isolated product is the bisferrocenylethylene derivative **9**; presumably formed by the result of an analogous sequence to the one which afforded **8**; however, in this case the lithiating agent is **6** instead of phenyllithium (Scheme 1, *d*). Column chromatography on an alumina support can be used to separate the products **7**, **8**, and **9**. All products were identified by elemental analysis and spectroscopy.

The reduction of **7** with lithium aluminum hydride in benzene gave **10** in high yield in a relatively clean reaction (reaction [3]).

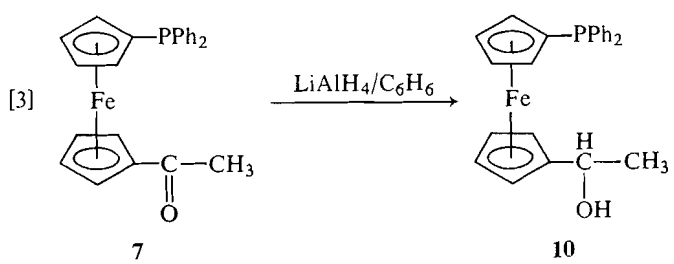

7 10

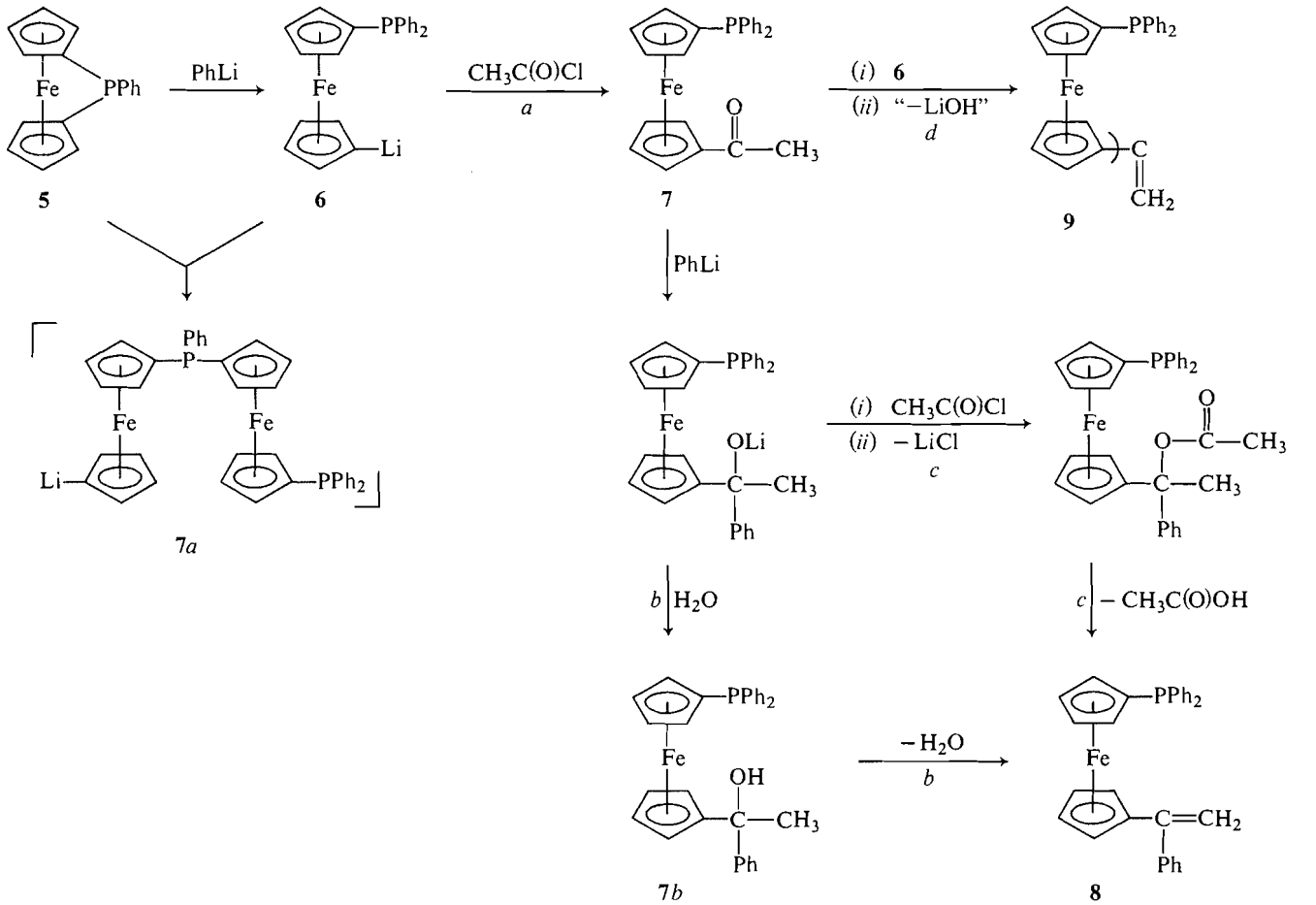

SCHEME 1

The conversion of **10** to **4** was explored by several routes: treatment of **10** with acetic anhydride in pyridine followed by the reaction of the crude product (without isolation) with dimethylamine gave **4** in approximately 50% yield although **10** was the only other compound isolated. Appreciably lower yields of **4** were obtained by a similar route using acetic acid in benzene.

The reaction of α-ferrocenylethyl alcohols with HBr followed by treatment of the crude product mixture with secondary amines is known to give the corresponding ferrocenylamines in moderate yield, reaction [4] (8).

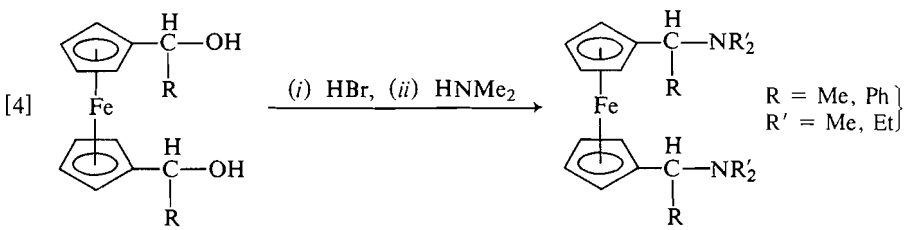

The reaction of **10** with HBr followed by treatment of the crude reaction mixture with anhydrous dimethylamine also gave **4** but in very low yield. The major product consisted of a mixture of compounds which are probably phosphonium salts formed by the reaction of the diphenylphosphino substituent with HBr. These products were found to be difficult to obtain in a pure form, thus further study was not pursued. Another minor product obtained was the 1′-vinyl compound **11** identified by ^1H nmr and mass spectroscopy. This product is presumably formed by the acid-catalysed dehydration of **10**, reaction [5]; similar reactions are known to occur under very mild conditions (9, 10).

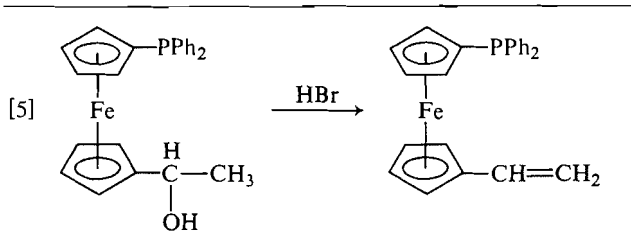

The overall synthetic utility of the foregoing procedures is small because of the low yields achieved. This prompted us to seek an alternate route to **4**, especially since we ultimately

Can. J. Chem. Downloaded from www.nrcresearchpress.com by 210.87.254.105 on 09/06/12
For personal use only.

Can. J. Chem. Downloaded from www.nrcresearchpress.com by 210.87.254.105 on 09/06/12
For personal use only.

desired a resolved sample for asymmetric hydrogenation studies.[1]

The alternate preparation of **4** was approached via a synthetic pathway beginning with the easily resolvable α-*N*,*N*-dimethylferrocenylethylamine **12** (11). It is also well established that the lithiation of **12** is stereoselective (12). Thus treatment of an ethereal solution of **12** with butyllithium is known to form the 2-lithio derivative **13**. The *R*-isomer shown affords the (*R*,*S*)-isomer of **13** in 96% yield. The substitution in the ring introduces an element of planar chirality. The selectivity arises because of the stabilizing influence of the lone-pair on the adjacent nitrogen atom reaction [6]).

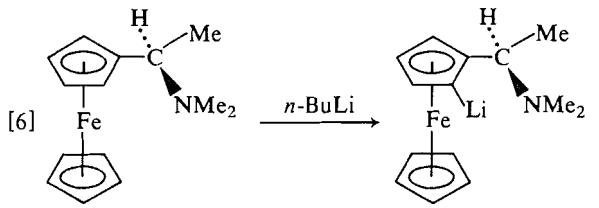

12 **13**

We have previously prepared the ferrocenophane **14** (7) which would be expected to undergo a cleavage reaction (reaction [2]) with phenyllithium to give predominantly the monolithio derivative **15***a* at the expense of its isomer **15***b* (reaction [7]) because **15***a* would be stabilized due to the interaction of the lithium with the adjacent amino function. Furthermore, compound **15***a* would appear to be sterically less crowded than **15***b*.

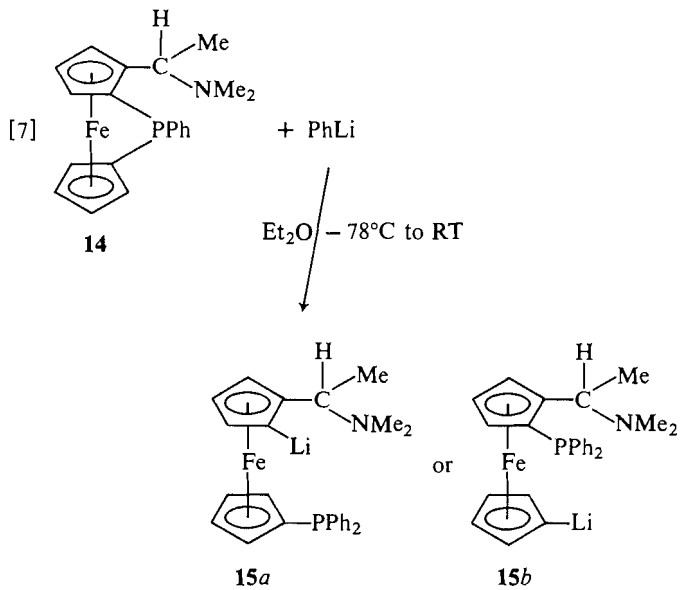

14 **15***a* **15***b*

This explanation is well founded since treatment of **14** with phenyllithium at low temperatures followed by hydrolysis does give **4** as the major product. Figure 1 shows the ratio of the products **4** to **1** as 85 to 15. Treatment of **14** with phenyllithium at room temperature followed by hydrolysis was found to give substantially higher yields of **1** at the expense of **4**.

The reaction of **14** with phenyllithium at low temperature followed by treatment of the crude solution with chlorodiphenylarsine gave, on recrystallisation, approximately equal quantities of the positional isomers **16** and **17**. Presumably **17**,

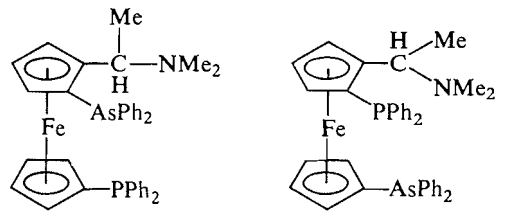

16 **17**

which should be formed in lower yield, is less soluble than **16**, and the crystals of the mixture obtained on crystallisation (hexane, −20°C) become enriched in **17**. These compounds are separable by tlc and by careful column chromatography on a neutral alumina support. They are of interest in hydrogenation reactions since the cationic rhodium(I) complex of **1**, in its resolved form, is an effective asymmetric hydrogenation catalyst precursor while its arsine analogue **18** is ineffective (2).

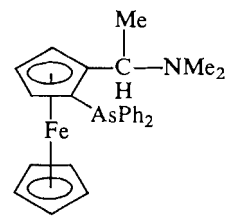

18

In a similar manner the reaction of **14** with phenyllithium followed by treatment with di-*tert*-butylchlorophosphine gives the isomers **19** and **20**, isolated as an oily mixture. In this case separation has not yet been achieved. This oil was found to be considerably more air-sensitive than the compounds **16** and **17** possibly because of trace impurities.

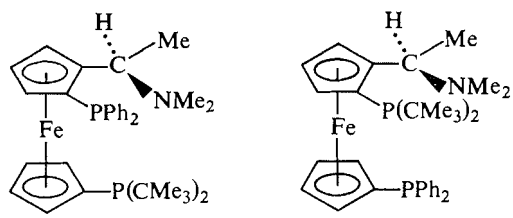

19 **20**

The preparation and use in catalytic reactions of various metal complexes of the ligands described in this paper will be the subject of a later communication.

Acknowledgement

Financial assistance from the Natural Sciences and Engineering Research Council of Canada is gratefully acknowledged.

1. W. R. CULLEN and J. D. WOOLINS. Can J. Chem. **60**, 1793 (1982).
2. W. R. CULLEN, F. W. B. EINSTEIN, C-H. HUANG, A. C. WILLIS, and E-S YEH. J. Am. Chem. Soc. **102**, 998 (1980).
3. T. HAYASHI, K. YAMAMOTO, and M. KUMADA. Tetrahedron Lett. **49–50**, 4405 (1974).
4. T. HAYASHI, T. MISE, M. FUKUSHIMA, M. KAGOTANI, N. NAGASHIMA, Y. HAMADA, A. MATSUMOTO, S. KAWAKAMI,

[1]It should be noted that all syntheses described are of racemic compounds; however, optically active samples of **4** may be prepared from the resolved amine **12**.

M. KONISHI, K. YAMAMOTO, and M. KUMADA. Bull. Chem. Soc. Jpn. **53**, 1138 (1980).
5. D. SEYFERTH and H. P. WITHERS. J. Organomet. Chem. **185**, C1-C5 (1980).
6. A. G. OSBORNE and R. H. WHITELY. J. Organomet. Chem. **194**, 91 (1980).
7. I. R. BUTLER, W. R. CULLEN, F. W. B. EINSTEIN, A. C. WILLIS, and S. J. RETTIG. Organometallics. To be published.
8. I. R. BUTLER and W. R. CULLEN. Unpublished results.
9. S. C. CHEN, C. C. LEE, and R. G. SUTHERLAND. Synth. React. Inorg. Met.-Org. Chem. **7**, 565 (1977).
10. F. S. ARIMOTO and A. C. HAVEN. J. Am. Chem. Soc. **77**, 6259 (1955).
11. D. MARQUARDING, H. KLUSACEK, G. GOKEL, P. HOFFMAN, and I. UGI. J. Am. Chem. Soc. **92**, 5389 (1970).
12. L. F. BATTELLE, R. BAU, G. W. GOKEL, R. T. OYAKAWA, and I. K. UGI. J. Am. Chem. Soc. **95**, 482 (1973).

Can. J. Chem. Downloaded from www.nrcresearchpress.com by 210.87.254.105 on 09/06/12
For personal use only.

Reactions of sydnones. Part III.[1] Bromination of 3-[*p*-(1′-pyrazolyl)]phenylsydnone

SHAMBHULING B. HAVANUR, BHARATI V. BADAMI, AND GURUBASAV S. PURANIK[2]

Department of Chemistry, Karnatak University, Pavate Nagar, Dharwad-580003, Karnataka, India

Received January 11, 1982[3]

SHAMBHULING B. HAVANUR, BHARATI V. BADAMI, and GURUBASAV S. PURANIK. Can. J. Chem. **61**, 154 (1983).

3-[*p*-(1′-Pyrazolyl)]phenylsydnone (**2**) and its derivatives have been subjected to bromination in order to study the relative reactivities of the sydnone and pyrazole moieties. The products have been confirmed by their elemental analysis and their spectral data.

SHAMBHULING B. HAVANUR, BHARATI V. BADAMI et GURUBASAV S. PURANIK. Can. J. Chem. **61**, 154 (1983).

On a bromé la [*p*-(pyrazolyl)-1′]-3 phénylsydnone (**2**) et ses dérivés dans le but d'étudier les réactivités relatives des unités sydnone et pyrazole. On a identifié des produits en faisant appel à l'analyse élémentaire et aux données de la rmn.

[Traduit par le journal]

Sydnones unsubstituted at the 4-position undergo electrophilic substitution reactions and because of this behaviour they are classified as aromatic. The degree of aromaticity of the sydnone ring has been expected to be about the same order as that of the furan ring (3). In 3-phenylsydnone (**1**) the phenyl ring is less susceptible to electrophilic substitution reactions because of the positive charge, which is substantially localized on the N-3 atom (4).

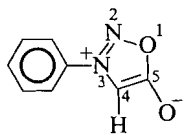

1

Electrophilic substitution in 1-phenylpyrazole leads to initial attack at the 4-position of the pyrazole and hence a method was developed to prepare 5-substituted pyrazoles through 4-substituted sydnones (5).

In an earlier work, 3-[*p*-(1′-pyrazolyl)]phenylsydnone (**2**) and its derivatives were synthesized to study the variation in biological properties (2, 6). Structure **2** is a combination of three aromatic moieties, viz., the phenyl, the sydnone, and the pyrazole rings, with a number of replaceable hydrogen atoms which are expected to undergo electrophilic substitution reactions.Since the phenyl ring is less susceptible to electrophilic substitution reactions in this system, it provides an opportuniy to compare the reactivities of sydnone and pyrazole rings.

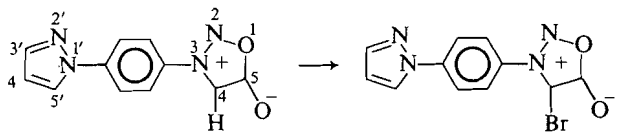

2 **2*a***

In the present study, the bromination of **2** and its derivatives has been dealt with. Bromination has been carried out with bromine in aqueous ethanol in the presence of sodium bicarbonate (7). On bromination with one mole of bromine, **2** gives 3-[*p*-(1′-pyrazolyl)]phenyl-4-bromosydnone (**2*a***).

On the other hand, when the dimethyl derivative (**3**) is brominated with one mole of bromine, the product is 3-[*p*-(4′-bromo-3′,5′-dimethyl-1′-pyrazolyl)]phenylsydnone (**3*a***).

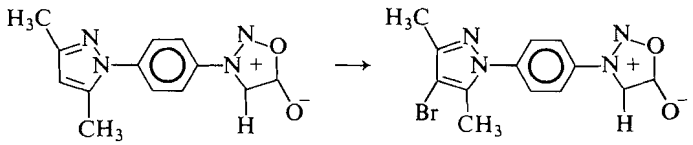

3 **3*a***

Further bromination of **2*a*** and **3*a*** gives 3-[*p*-(4′-bromo-1′-pyrazolyl)]phenyl-4-bromosydnone (**2*b***) and 3-[*p*-(4′-bromo-3′,5′-dimethyl-1′-pyrazoyl)]phenyl-4-bromosydnone (**3*b***) respectively.

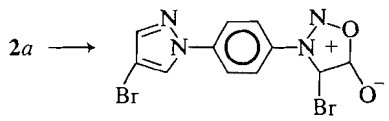

2*b*

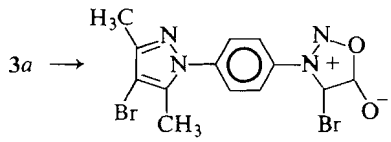

3*b*

From the above results it can be concluded that in this phenyl-linked system the sydnone ring is more reactive towards bromination than the pyrazole ring. The reactivity of the pyrazolyl-4 position is enhanced when electron-donating groups are introduced adjacent to the reactive site.

Bromination of pyrazolyl phenylsydnones with a CH_3 or C_6H_5 group in the 4-position of the sydnone ring has also been carried out to get the corresponding 4′-bromopyrazolyl phenylsydnone derivatives.

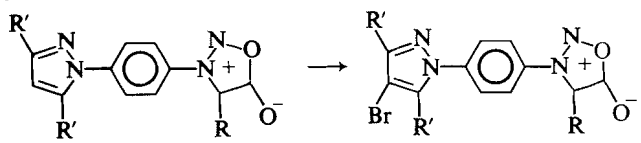

4 **5**

a R = CH_3; R′ = H
b R = C_6H_5; R′ = H
c R = CH_3; R′ = CH_3
d R = C_6H_5; R′ = CH_3

[1]For Part II, see ref. 1.
[2]Author to whom correspondence may be addressed.
[3]Revision received April 29, 1982.

0008-4042/83/010154-02$01.00/0
©1983 National Research Council of Canada/Conseil national de recherches du Canada

Can. J. Chem. Downloaded from www.nrcresearchpress.com by 210.87.254.5 on 09/06/12
For personal use only.

TABLE 1. Nuclear magnetic resonance spectral data

Structure	R	δ ppm	R′	δ ppm	Phenyl protons centered at δ ppm
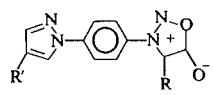	H	6.7(s)	H	6.5(t)	7.9(m)
	Br	—	H	6.6(t)	7.9(m)
	Br	—	Br	—	7.9(m)
	CH_3	2.2	H	6.6(t)	7.8(m)
	CH_3	2.2	Br	—	7.8(m)
	C_6H_5	7.2	H	6.4(t)	7.7(m)
	C_6H_5	7.3	Br	—	7.6(m)
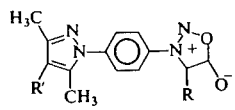	H	6.85(s)	H	6.1(s)	7.85(s)
	H	6.7(s)	Br	—	7.75(m)
	Br	—	Br	—	7.8(s)
	CH_3	2.15	H	6.05(s)	7.7(m)
	CH_3	2.15	Br	—	7.7(m)
	C_6H_5	7.3	H	6.05(s)	7.65(m)
	C_6H_5	7.3	Br	—	7.65(m)

TABLE 2. Analytical data for bromo derivatives

Compound	Yield (g)	Melting point •(°C)	Molecular formula	Analysis Found C	Found H	Calculated C	Calculated H
2*a*	1.38 (89%)	161–162	$C_{11}H_7BrN_4O_2$	43.25	2.24	43.00	2.28
3*a*	1.52 (90%)	188–189	$C_{13}H_{11}BrN_4O_2$	46.56	3.29	46.57	3.28
2*b*	0.89 (91%)	158–159	$C_{11}H_6Br_2N_4O_2$	34.26	1.56	34.20	1.55
3*b*	0.94 (91%)	149–150	$C_{13}H_{10}Br_2N_4O_2$	37.65	2.43	37.68	2.42
5*a*	0.74 (92%)	163–164	$C_{12}H_9BrN_4O_2$	44.90	2.86	44.86	2.80
5*b*	0.89 (93%)	204–205	$C_{17}H_{11}BrN_4O_2$	53.26	2.92	53.24	2.94
5*c*	0.84 (95%)	132–133	$C_{14}H_{13}BrN_4O_2$	48.20	3.73	48.14	3.72
5*d*	0.98 (91%)	148–149	$C_{19}H_{15}BrN_4O_2$	54.52	3.63	54.50	3.66

The structures of the compounds have been confirmed by elemental analysis and spectral data. The nmr data proved to be very helpful, since the sydnone-4 and pyrazole-4 protons cannot be distinguished in the infrared spectra.

The nmr spectrum of **2** shows a singlet of the sydnone-4 proton at 6.7 δ and a triplet of the pyrazolyl-4 proton at 6.5 δ. Absence of the signal at 6.7 δ in the spectrum of **2***a* confirms the bromination in the sydnone-4 position. On the other hand, in the spectrum of **3**, the sydnone-4 and pyrazolyl-4 protons appear as singlets at 6.8 δ and 6.1 δ, respectively. Disappearance of the signal at 6.1 δ in the spectrum of **3***a* suggests that the bromination has taken place at the pyrazolyl-4 position. In the case of compounds **2***b* and **3***b*, absence of both the respective signals due to the sydnone-4 and pyrazolyl-4 protons is observed. The nmr spectral details are given in Table 1.

Experimental

Melting points are uncorrected. The nmr spectra were determined at 60 MHz on a Varian A-60 nmr spectrophotometer with TMS as an internal reference.

The compounds **2**, **3**, **4***a*, **4***b*, **4***c*, and **4***d* were prepared following the procedures mentioned earlier (6).

Bromination

Bromination has been carried out with 0.005 mol of compounds **2** and **3**. In the case of **2***a*, **3***a*, **4***a*, **4***b*, **4***c*, and **4***d*, 0.0025 mol of the compound has been used.

To a suspension of the compound (0.005 mol), in 50 mL of ethanol, was added sodium bicarbonate (2.00 g, 0.024 mol) in 25 mL of water at room temperatures. The resultant cloudy solution was clarified on addition of bromine (0.005 mol) in 25 mL of ethanol. The reaction mixture was stirred further for 30 min and diluted with 200 mL of water. The separated solid was filtered and dried in air.

All of the bromo derivatives were crystallized from ethanol and the results are set out in Table 2.

Acknowledgements

We wish to thank Dr. E. S. Jayadevappa, Professor and Head, for encouragement. One of us (S.B.H.) thanks U.G.C. New Delhi for the fellowship.

1. B. V. BADAMI and G. S. PURANIK. Rev. Roum. Chim. **20**, 981 (1975).
2. S. B. HAVANUR. Ph.D. Thesis, Karnatak University, Dharwad, India. 1979.
3. M. OHTA and H. KATO. Nonbenzenoid aromatics. Vol. I. *Edited by* J. P. Snyder. Academic Press, New York. 1969. p. 146.
4. C. TIN-LOK, J. MILLER, and F. STANSFIELD. J. Chem. Soc. 1213 (1964).
5. B. V. BADAMI and G. S. PURANIK. Can. J. Chem. **53**, 913 (1975).
6. S. B. HAVANUR, B. V. BADAMI, and G. S. PURANIK. J. Heterocycl. Chem. **17**, 1049 (1980).
7. C. V. GRECO, M. PESCE, and J. M. FRANCO. J. Heterocycl. Chem. **3**, 391 (1966).

Can. J. Chem. Downloaded from www.nrcresearchpress.com by 210.87.254.5 on 09/06/12
For personal use only.

Simulation of edge effects in electroanalytical experiments by orthogonal collocation. Part 3. Application to chronoamperometric experiments

BERND SPEISER AND STANLEY PONS
Department of Chemistry, University of Alberta, Edmonton, Alta., Canada T6G 2G2

Received April 5, 1982

BERND SPEISER and STANLEY PONS. Can. J. Chem. **61**, 156 (1983).

The theory of two-dimensional collocation has been employed to simulate a model describing chronoamperometric experiments under conditions where edge diffusion has to be taken into account. The influence of the dimensionless parameters, β and β′, the initial integration stepwidth, $\Delta T_0'$, the number of collocation points, N, and the kind of polynomial used to approximate the real solution are investigated and discussed. An additional transformation of the radial coordinate is introduced. The numerical values for a large number of simulations with different sets of the above parameters are compared to reference values.

BERND SPEISER et STANLEY PONS. Can. J. Chem. **61**, 156 (1983).

On a utilisé la théorie de collocation bidimensionnelle pour simuler un modèle décrivant des expériences de chronoampérométrie dans des conditions où l'on doit tenir compte de la diffusion par l'arête. On discute de l'influence des paramètres sans dimension β et β′, de l'étendue de l'intégration initiale $\Delta T_0'$, du nombre de points de collocation, N, et du type de polymère utilisé pour faire une approximation de la solution réelle. On a introduit une transformation additionnelle de la coordonnée radicale. On a comparé les valeurs numériques d'un grand nombre de simulations avec des ensembles différents des paramètres ci-dessus avec des valeurs de référence.

[Traduit par le journal]

Introduction

In parts 1 and 2 (1) of this series we derived the theory for the application of orthogonal collocation to the simulation of two-dimensional models. These are described by partial differential equations with *two independent space variables* and the time variable t. Let us consider a two-dimensional diffusion situation at a flat, circular electrode, where diffusion *not only perpendicular* to the surface may occur. This additional diffusion is called edge diffusion. The concentration c of each species is given by a partial differential equation of the form

$$[1] \quad \frac{\partial c}{\partial t} = D\left[\frac{\partial^2 c}{\partial x^2} + \frac{1}{r}\frac{\partial c}{\partial r} + \frac{\partial^2 c}{\partial r^2}\right] - f(c)$$

where x is the distance perpendicular to the surface and r is the radial distance from the centre of the electrode. The "kinetic term" $f(c)$ is determined by chemical reactions of the given species.

Our goal is to calculate c as a function of x and r at any time t under a set of initial and boundary conditions. The *initial conditions* model the experimental starting conditions, i.e. in general only the starting compound is present in a homogeneous solution. The *boundary conditions* specify the particulars of the experiment performed, e.g. chronoamperometry, cyclic voltammetry, or another electroanalytical method.

Orthogonal collocation (2, 3) approximates the real solution of partial differential equations, e.g. [1], by orthogonal polynomials, such that the differential equation is fulfilled at certain points, the collocation points. This provides a method to reduce the partial differential equations to a system of coupled ordinary differential equations.

In part 1 of this series (1) we used a product of two polynomials in x and r respectively as approximation function to the real solution of our two-dimensional model for edge effects. We solved a system of three equations of type [1] describing an EC mechanism

$$[2] \quad \mathrm{A} \underset{+ne^-}{\overset{-ne^-}{\rightleftharpoons}} \mathrm{B} \qquad E^\circ, n$$

$$[3] \quad \mathrm{B} \xrightarrow{k} \mathrm{C}$$

under the boundary conditions valid for chronoamperometric experiments.

This third part of our series demonstrates the application of the derived theory to chronoamperometry. We examine the influence of several parameters on the numerical solutions of the simulations: the dimensionless parameters β and β′, the integration stepwidth $\Delta T_0'$, the number of collocation points N, and the type of polynomial we are using to approximate the real solution. Also, we investigate the effect of choosing a different dimensionless coordinate system.

The calculations herein have been performed using only the concentration of the substrate A at the collocation points, because the current through the electrode may be calculated from the concentration profiles of A only. The concentration profiles of species B and C, however, may be calculated from the formulae in part 1 (1*a*).

We compare our numerical simulations to the results derived by an exact solution of a related problem by Oldham (4). These numbers compare very well with solutions calculated by Aoki and Osteryoung (5) and Kakihana *et al.* (6), all using different approaches to compute values for the current at a finite disc electrode under chronoamperometric conditions with consideration of edge effects. All these approaches, however, are restricted to a very simple mechanism, the reversible electron transfer. The method of orthogonal collocation on the other hand is — once derived for a specific type of model, e.g. a two-dimensional model — very easily used to simulate all possible kinds of electrode mechanism. We only have to change the kinetic terms $f(c)$ in our partial differential equations [1]. Equations describing species other than A, B, or C

0008-4042/83/010156-05$01.00/0
©1983 National Research Council of Canada/Conseil national de recherches du Canada

Can. J. Chem. Downloaded from www.nrcresearchpress.com by 210.87.254.40 on 09/06/12
For personal use only.

Can. J. Chem. Downloaded from www.nrcresearchpress.com by 210.87.254.40 on 09/06/12
For personal use only.

are very similar in form to those already derived (1). This has been shown in part 2 of this series (*1b*) for the boundary conditions of cyclic voltammetry. Also, changes in mechanisms require only minor changes of the computer code used to calculate numerical data. Thus, orthogonal collocation proves to be a flexible method to generate simulated values for electrochemical experiments modelled by two-dimensional diffusion equations.

The dimensionless parameters β and β′

To perform the method of orthogonal collocation we have to normalize our problem into a space [0,1] in both directions x and r. Also, we have to divide the r-space into an inner and an outer segment, simulated by two different functions. We denote the new distance coordinate perpendicular to the electrode as X, and refer to the normalized inner radial segment as R while using R' for the outer coordinates. The dimensionless simulation time is T'.

After substituting the transformation equations given in part 1 (*1a*) we arrive at normalized differential equations which contain two dimensionless parameters, β and β′:

$$[4] \quad \beta = r_0^2/L^2$$

$$[5] \quad \beta' = r_0^2/(M - r_0)^2$$

Here r_0 is the radius of the electrode disc, imbedded in an insulator. The quantity L is a distance in the X-direction from the electrode at which no diffusion occurs during the simulated experiment, while M is an analogous distance in the r-direction. Thus, L and M define a region in real space which is simulated in the calculations. The real points corresponding to our N collocation points are distributed within this space. We consider two limiting cases for L. An analogous discussion may be applied to M.

First, L may be very large. Then the points corresponding to the collocation points in real space, i.e. those points at which the concentration of the species involved is calculated, are spread over a large distance. The diffusion layer in which the concentration of a species is depleted or increased, however, is very narrow in the beginning of the simulation. It increases with $t^{1/2}$. Thus, at short times, corresponding to small values of the dimensionless simulation time T', the diffusion may have reached none or only a few of the points at which the concentration is calculated. Consequently, the numerical values calculated may not represent a good approximation to the real solution of our model and yield erroneous results.

On the other hand, if L is very small, we are looking at a very narrow layer of solution in real space. Even after a short time the diffusion layer may have reached all of our points and the boundary condition that no diffusion occurs at $X = 1$ (corresponding to $x = L$) is no longer true. We are using the mathematical formulation of this boundary condition ($c_A^*(X = 1) = 1$) in our calculations and thus the numerical values may deviate from the real solution after this is happening.

We expect that the approximation solution given by orthogonal collocation is valid only in a certain time range and that this range depends on the values of β and β′ chosen.

For all calculations referred to in this paper we used the condition β = β′. We simulate a square space adjacent to the insulator, because

$$[6] \quad \beta/\beta' = 1 = (M - r_0)^2/L^2$$

or

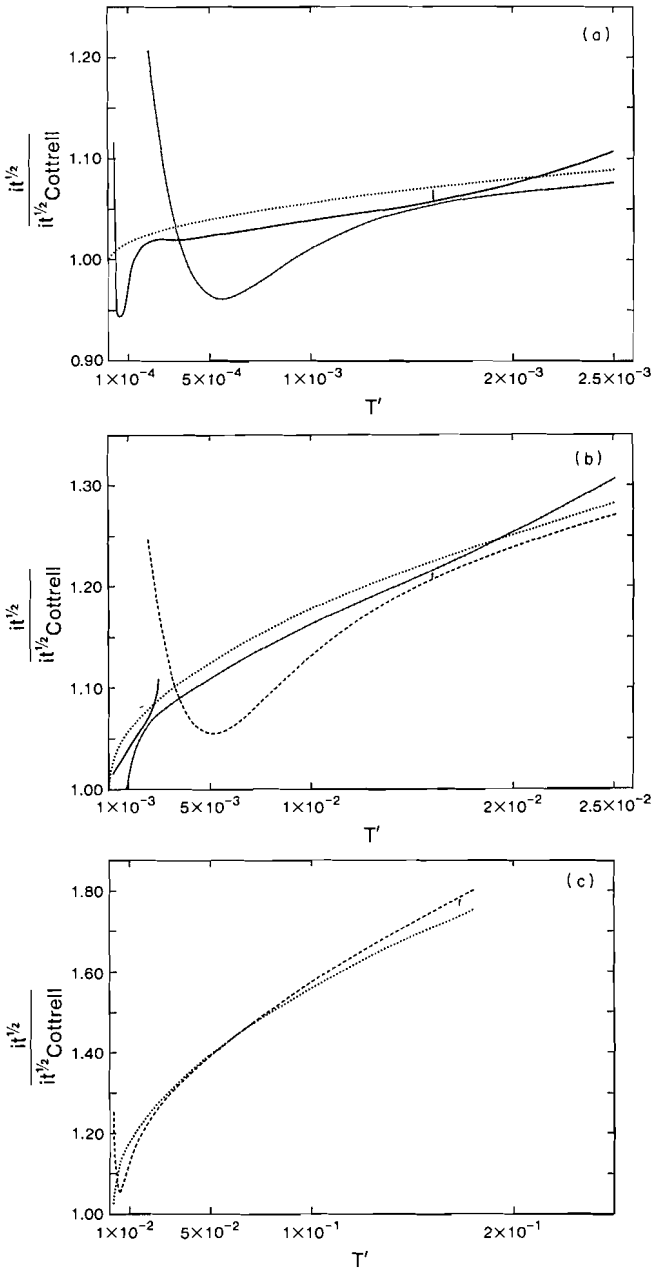

FIG. 1. Simulations of chronoamperometric experiments including edge effects with orthogonal collocation; simulation parameters: number of collocation points in each dimension $N = 6$, initial integration stepwidth $\Delta T_0' = 1 \times 10^{-4}$, Legendre polynomials in both dimensions, (—) β = 100, (·····) β = 10, (---) β = 1; (···) values calculated according to Oldham (4). The arrows indicate T', when the concentration at one of the outmost collocation points reaches 0.98.

$$[7] \quad L = (M - r_0)$$

Figure 1*a*–*c* shows calculated values for the current obtained including edge effects divided by the ideal Cottrell current. Comparing simulations using Legendre polynomials of degree $N = 6$ in both dimensions but different values for β = β′ with the reference curve given by Oldham (4), we see that the above analysis is correct. For β = 1 good agreement over a wide range of the dimensionless simulation time is found ($2 \times 10^{-2} < T' < 1.1 \times 10^{-1}$). To give a specific example ($D = 1 \times 10^{-5}$ cm²/s, $r_0 = 0.1$ cm), this range corresponds

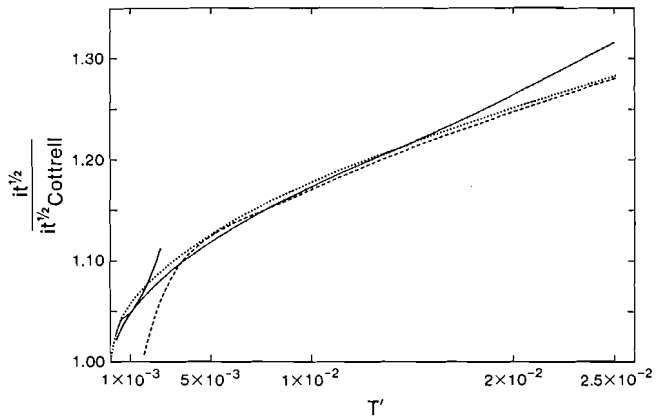

FIG. 2. Simulations of chronoamperometric experiments including edge effects with orthogonal collocation; simulation parameters: number of collocation points in each dimension $N = 9$, other parameters as in Fig. 1. The arrow indicates T', when the concentration at one of the outmost collocation points reaches 0.996.

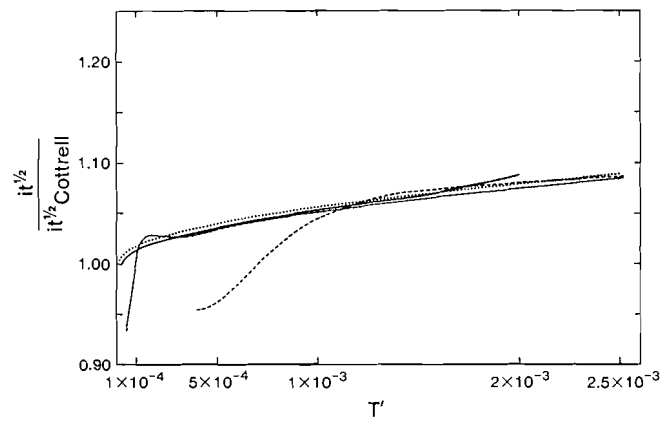

FIG. 3. Simulations of chronoamperometric experiments including edge effects with orthogonal collocation; simulation parameters: number of collocation points in each dimension $N = 12$, other parameters as in Fig. 1.

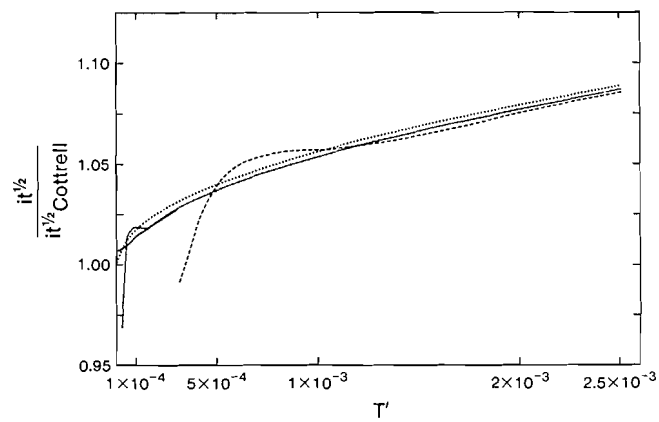

FIG. 4. Simulations of chronoamperometric experiments including edge effects with orthogonal collocation; simulation parameters: number of collocation points in each dimension $N = 15$, other parameters as in Fig. 1. The ordinate scale is expanded compared to the other figures.

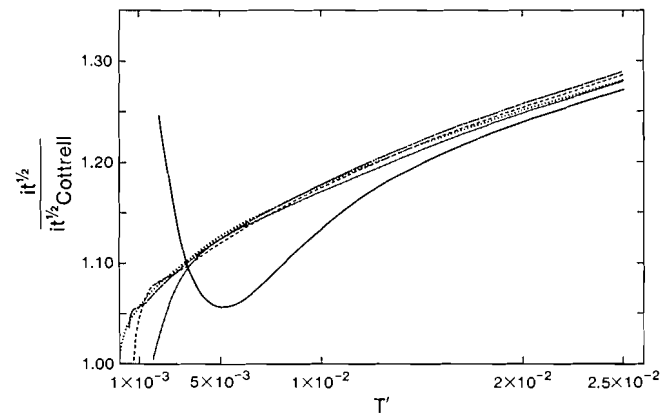

FIG. 5. Simulations of chronoamperometric experiments including edge effects with orthogonal collocation; simulation parameters: (—) $N = 6$, (·····) $N = 9$, (---) $N = 12$, (·-·-·) $N = 15$; initial integration stepwidth $\Delta T'_0 = 1 \times 10^{-4}$, Legendre polynomials in both dimensions, dimensionless parameters $\beta = \beta' = 1$, (···) values calculated according to Oldham (4).

to real times t between 2×10^1 and 1.1×10^2 s according to the transformation equation relating t and T' (1). At short times the error is considerable and it can be seen that the solution needs a number of integration steps to become stable. At longer times the collocation simulation result increases faster than Oldham's curve. This simulation needed 60 s cpu-time to calculate the entire curve ($10^{-4} \leq T' \leq 1.8 \times 10^{-1}$).

More accurate simulations for shorter times may be obtained using larger values for β. For example, with $\beta = 10$ in a range between $T' = 2 \times 10^{-3}$ and 1.2×10^{-2} good agreement with Oldham's curve is found, while $\beta = 100$ gives a reasonable approximation for $2 \times 10^{-4} \leq T' \leq 1.3 \times 10^{-3}$. In the latter cases significant deviation from Oldham's curve is seen at a time when our numerical values increase. This occurs at the same time as the calculated concentration at *one* of the outmost collocation points in the X-direction becomes smaller than about 0.98, thus confirming our conclusions drawn above. With increasing β, however, the oscillating deviations at the beginning occur in a narrower time frame, again in accordance with our analysis.

The same behavior may be seen if we use polynomials with a larger number of collocation points ($N = 9$, 12, 15; Figs. 2–4). Now the "critical concentration" at the outmost collocation points moves nearer to unity, being about 0.996 for $N = 9$. The time T' at which the deviations occur, however, is almost the same as for $N = 6$. This leads to the empirical conclusion, that the upper time limit of the simulations is only determined by β. An analogous approach has been used by Whiting and Carr (2). They defined the maximum simulation time which is accessible with a certain β as $T'_{max} \leq 0.15/\beta$. In our case we have the condition

$$[8] \quad T'_{max} \leq 0.1/\beta$$

to be within the usable time range.

The number of collocation points N

In the preceding paragraph we have seen that the number of collocation points N has a marked influence on the simulated numerical values. Thus, we compare curves obtained with different numbers N but using the same other parameters in Fig. 5.

Can. J. Chem. Downloaded from www.nrcresearchpress.com by 210.87.254.40 on 09/06/12
For personal use only.

TABLE 1. Numerical values for simulation of a chronoamperometric experiment with edge effects: current with edge effects divided by Cottrell current; simulation parameters: $N = 6$, $\beta = \beta' = 1$, Legendre polynomials in both dimensions, $\Delta T_0'$ as indicated

T'	$\Delta T_0' = 10^{-2}$	$\Delta T_0' = 10^{-3}$	$\Delta T_0' = 10^{-4}$	$\Delta T_0' = 10^{-5}$
0.01	1.13249*	1.13256	1.13256	1.13256
0.02	1.23883*	1.23884	1.23886	1.23886
0.03	1.29817*	1.29816*	1.29817	1.29817
0.04	1.34786*	1.34787*	1.34787	—
0.05	1.39292*	1.39292	1.39292	—
0.06	1.43443*	1.43444	1.43444	—
0.07	1.47305	1.47303*	1.47305	—
0.08	1.50926	1.50926	1.50926	—
0.09	1.54348	1.54350*	1.54349	—
0.1	1.57606	1.57607	1.57607	—

*Values calculated by interpolation.

TABLE 2. Numerical values for simulation of a chronoamperometric experiment with edge effects: current with edge effects divided by Cottrell current; simulation parameters: $N = 9$, $\beta = \beta' = 1$, Legendre polynomials in both dimensions, $\Delta T_0'$ as indicated

$T'/\Delta T_0'$	10^{-2}	10^{-3}	10^{-4}	10^{-5}
0.01	1.17081*	1.17080	1.17082	1.17082
0.02	1.24847*	1.24848*	1.24848	—
0.03	1.30911	1.30911*	1.30911	—
0.04	1.36075	1.36075*	1.36076	—
0.05	1.40674	1.40672	1.40673	—
0.06	1.44862*	1.44864	1.44864	—
0.07	1.48748	1.48748*	1.48748	—
0.08	1.52387	1.52387	1.52387	—
0.09	1.55826*	1.55826	1.55826	—
0.1	1.59100	1.59100*	1.59100	—

*Values calculated by interpolation.

As N increases, the net of collocation points becomes more narrow, forcing the approximation function to fulfill the differential equation at more and more points exactly. This has two effects: first, the overall solution becomes more accurate but we also have more simulation points near the boundaries (using Legendre polynomials, the collocation points are more densely spaced near $X = 0$ and $X = 1$ than around $X = 0.5$). Thus, for short times, we have more points to represent the steep concentration profile exhibited shortly after applying the potential pulse and we expect the range within which the oscillating deviations from the reference solution occur to be more narrow. With increasing N, the overall solutions should reach a common limiting value which should be a good approximation to the real solution.

Comparing the results given in Fig. 5 we see that this is true. By increasing the number of collocation points from $N = 6$ to $N = 15$, the range in which no useful results are to be obtained because oscillations occur decreases by a factor of about 10; one gets very good approximations from $2 \times 10^{-3} - > 3 \times 10^{-2}$ dimensionless time units. The upper limit of the useful range is not affected, as Figs. 1–4 show.

Also, the results differ only little (~0.4% when increasing N from 12 to 15) with increasing N. This shows the consistency of the calculations. The "limiting" values reached are very close to Oldham's solution (4).

Increasing the number of collocation points gives more and more accurate results as is to be expected. However, the cpu-time used to perform the simulations in a given range also increases considerably. While integrating a system of $2 \times 6 \times 6 = 72$ ordinary differential equations in the case of $N = 6$ we have to deal with 162, 288, and 450 such equations if we use 9, 12, or 15 interior collocation points, respectively. The average cpu-time needed to calculate one concentration profile increases by a factor of 10 when N is increased from 6 to 15.

The integration stepwidth

The next parameter we want to discuss is the initial integration stepwidth, $\Delta T_0'$. This is an input parameter for the subroutine performing the integrations of our system of ordinary differential equations. The value chosen is used by the subroutine to calculate the first concentration profiles at $\Delta T_0'$. The subroutine DHPCGL (in the SSP library package) used by us then "decides" if sufficient accuracy is available with this value. If not, the stepwidth is divided by 2 and the calculation is repeated. Other integration subroutines, e.g. STIFF3 (3), also have the option to increase the initial stepwidth if the error is below a specific margin.

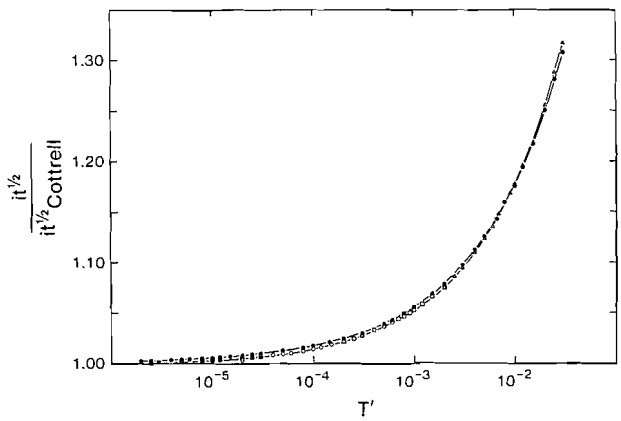

FIG. 6. Simulations pieced together from four calculations with $N = 15$ and different β compared to Oldham's solution (●); points calculated with $\beta = \beta' = 1000$ (■), $\beta = \beta' = 100$ (○), $\beta = \beta' = 10$ (□), $\beta = \beta' = 1$(Δ). The dimensionless time T covers the entire experimentally accessible range of t for an example with $D = 10^{-5}$ cm²/s and $r_0 = 0.1$ cm.

To evaluate the influence of $\Delta T_0'$ on the accuracy and performance of the edge effect calculations we run simulations with $N = 6$ and 9 using $\Delta T_0'$ values ranging from 10^{-2} to 10^{-5}. Results for $\beta = \beta' = 1$ are given in Tables 1 and 2. We see immediately that the actual value of $\Delta T_0'$ has only a very small effect on the numerical simulation results. Deviations are 0.00007 in the worst case, this corresponds to 0.007%. However, for a small $\Delta T_0'$ (10^{-5} dimensionless time units), the cpu-time needed to simulate the model up to a certain time increases considerably. The savings using $\Delta T_0'$ values $>10^{-3}$ are only about 10–20%. With large initial integration stepwidths there is not enough accuracy at the beginning of the simulation, thus causing DHPCGL to cut down $\Delta T'$ to smaller values. The actual choice of $\Delta T_0'$, however, seems not to be critical.

Complete simulations using Legendre polynomials

After discussing three of the parameters used in simulations of chronoamperometric experiments with consideration of edge

Can. J. Chem. Downloaded from www.nrcresearchpress.com by 210.87.254.40 on 09/06/12
For personal use only.

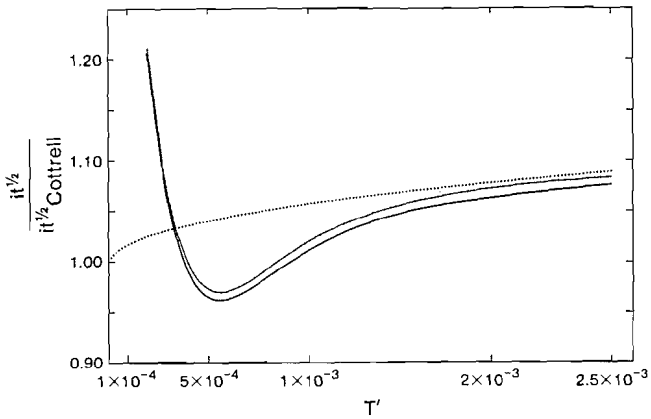

FIG. 7. Comparison of simulations using the model system given in part 1 of this series (1*a*) and the formulae derived from the transformation [13]; $N = 6$, $\beta = \beta' = 10$; (—) before transformation, (·····) after transformation, (···) Oldham's curve.

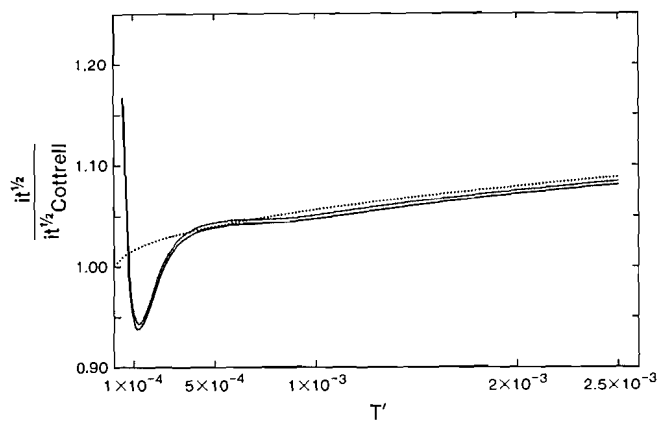

FIG. 8. Comparison of simulations using the model system given in part 1 of this series (1*a*) and the formulae derived from the transformation [13]; $N = 9$, $\beta = \beta' = 10$; (—) before transformation, (·····) after transformation, (···) Oldham's curve.

effects, we may now choose sets of parameters to obtain an approximate solution of the differential equations over a large range of the dimensionless simulation time. The number of interior collocation points will be 15. We will piece together the curve from solutions calculated with different β's, choosing the appropriate initial integration stepwidth. The trial functions will be Legendre polynomials.

The result is given in Fig. 6, where the calculated current divided by the "ideal" Cottrell current is plotted against T' (in logarithmic scale). Four different values for β (1000, 100, 10, 1) have been used and the entire curve compares very well with Oldham's results (4). The total cpu-time needed to calculate our curve was about 1340 s on an Amdahl 470/V6 computer. We cover, however, more than four orders of magnitude of the dimensionless simulation time. Using the same constants for D and r_0 as above, we simulated the response of an electrode with edge effects from 4 ms up to 30 s. At the lower limit ($T' \approx 2.5 \times 10^{-6}$) the current with edge effects deviates only by about 0.05% from the Cottrell current, while at the upper limit ($T' \approx 3 \times 10^{-2}$) the current in real experiments may be affected by convection, thus giving rise to another kind of nonideal behavior. Therefore, we can cover the entire accessible time range in which edge effects contribute to the experimental current with this simulation.

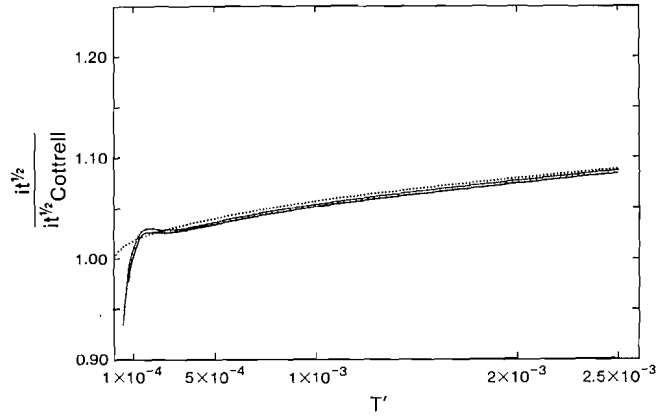

FIG. 9. Comparison of simulations using the model system given in part 1 of this series (1*a*) and the formulae derived from the transformation [13]; $N = 12$, $\beta = \beta' = 10$; (—) before transformation, (·····) after transformation, (···) Oldham's curve.

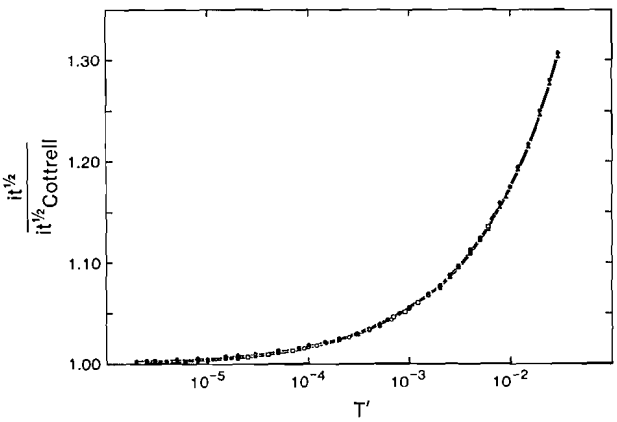

FIG. 10. Simulations to cover the entire time range $2 \times 10^{-6} < T' < 4 \times 10^{-2}$, pieced together from four calculations with $N = 15$ and different β, using the transformed system of equations, compared to Oldham's solution (●), points calculated with $\beta = \beta' = 1000$ (■), $\beta = \beta' = 100$ (○), $\beta = \beta' = 10$ (□), and $\beta = \beta' = 1$ (Δ).

Other polynomials

Orthogonal collocation may be performed using a variety of trial functions as long as we have a set of complete and linearly independent functions (7). A certain class of sets fulfilling these conditions are the Jacobi polynomials $P_N^{(\delta,\epsilon)}(x)$ given by (3)

$$[9] \quad P_N^{(\delta,\epsilon)}(x) = \sum_{i=0}^{N} (-1)^{N-i}\gamma_i x^i \qquad \gamma_0 = 1$$

with the orthogonality condition

$$[10] \quad \int_0^1 x^{\epsilon}(1-x)^{\delta} P_j(x)P_N(x)\mathrm{d}x = 0 \quad j = 0, 1, \ldots, N-1$$

The two terms x^{ϵ} and $(1-x)^{\delta}$ are "weight factors" which determine the behavior of the function at the boundaries (3). For $\epsilon \neq 0$ the function goes to zero at $x = 0$, for $\delta \neq 0$ zero is reached for $x = 1$. In our case the radial functions have nonzero values at both boundaries. Also, the x-functions in our

Can. J. Chem. Downloaded from www.nrcresearchpress.com by 210.87.254.40 on 09/06/12
For personal use only.

TABLE 3. Numerical values for simulation of a chronoamperometric experiment with edge effects: current with edge effects divided by Cottrell current; transformed simulation model vs. nontransformed system, $N = 15$, $\beta = \beta' = 10$, Legendre polynomials in both dimensions

T'	Oldham's solution (4)	Transformed model	Nontransformed model
1×10^{-4}	1.0175	1.0206	1.0192
2	1.0249	1.0223	1.0210
3	1.0305	1.0291	1.0278
4	1.0353	1.0338	1.0326
5	1.0395	1.0380	1.0367
6	1.0433	1.0416	1.0405
7	1.0468	1.0452	1.0441
8	1.0500	1.0485	1.0473
9	1.0531	1.0515	1.0504
1×10^{-3}	1.0560	1.0544	1.0534
2	1.0792	1.0776	1.0770
3	1.0970	1.0954	1.0953

outer space have a finite value at $x = 0$ (the insulator).

Thus, we would expect the best set of trial functions to be Legendre polynomials, $P_N^{(0,0)}(x)$ with $\delta = \epsilon = 0$. We used Legendre polynomials in all previous calculations in this paper, but tried also several other polynomials for the radial discretization function (e.g. $\delta = 0$, $\epsilon = 2$ which yielded good results for problems with spherical symmetry (8)).

The calculations showed that in all these cases the simulation results gave poorer agreement with Oldham's solution. We conclude therefore that the use of Jacobi type functions other than Legendre polynomials cannot be recommended in our case, due to the form of the boundary value problem.

Additional transformation of the radial variable *R*

After having simulated the concentration profile in our model we wish to calculate the current through the electrode as a function of time. In order to compare this current to the "ideal" Cottrell current we derived the expression [11] (1):

$$[11]\quad \frac{it^{1/2}}{it^{1/2}_{\text{Cottrell}}} = 2\sqrt{\beta\pi T'}\int_0^1 R\left(\frac{\partial c^*_{\text{Al}}}{\partial X}\right)_{X=0} dR$$

where we have to integrate the product of R and the flux to the electrode surface over the entire radius of the circular electrode.

This integration may be performed by a quadrature formula

$$[12]\quad \int_0^1 y(r)w_k(r)\,dr = \sum_{l=1}^{N_r+2} Q_l Y_l$$

where the Q_l's depend on the trial function used (see eq. [117] in part 1 (1*a*)).

The form of the integral in eq. [11] would suggest a trial function with $\delta = 0$ and $\epsilon = 1$. We have seen in the last paragraph, however, that the only suitable trial functions for our problem are Legendre polynomials with $\delta = \epsilon = 0$. Thus, it is desirable to bring [11] into a form with $\delta = \epsilon = 0$ by a variable transformation.

This may be done by the substitution

$$[13]\quad \mathcal{R} = R^2$$

Then

$$[14]\quad dR = \frac{1}{2\mathcal{R}^{1/2}}d\mathcal{R}$$

and

$$[15]\quad dR^2 = \frac{1}{4\mathcal{R}}d\mathcal{R}^2$$

The integral in eq. [11] reduces to

$$\frac{1}{2}\int_0^1 \left(\frac{\partial c^*_{\text{Al}}}{\partial X}\right)_{X=0} d\mathcal{R}$$

thus having a form consistent with $\delta = \epsilon = 0$.

We have to apply tranformations [13]–[15] to the differential equation describing the inner part of our model (see eq. [26], part 1 of this series (1*a*)) and to the boundary condition at $R = 1$ ($R' = 0$), where we piece together the inner and outer function (eq. [50] in part 1 (1*a*)).

The result for species A is

$$[16]\quad \frac{\partial c^*_{\text{Al}}}{\partial T'} = \beta\frac{\partial^2 c^*_{\text{Al}}}{\partial X^2} + 2\frac{\partial c^*_{\text{Al}}}{\partial \mathcal{R}} + 4\mathcal{R}\frac{\partial^2 c^*_{\text{Al}}}{\partial \mathcal{R}^2}$$

and the boundary condition changes to

$$[17]\quad \left(\frac{\partial c^*_{\text{Al}}}{\partial \mathcal{R}}\right)_{\mathcal{R}=1} = \frac{\sqrt{\beta'}}{2}\left(\frac{\partial c^*_{\text{A2}}}{\partial R'}\right)_{R'=0}$$

If we substitute these equations for eqs. [26] and [50] in part 1 (1*a*) and repeat the derivation of the discretized formulae [98] and [104] in part 1 (1*a*) we find a new, very similar system of ordinary differential equations.

In fact, we only have to change the definition of the matrix elements $E_{l,k}$ to

$$[18]\quad E_{l,k} = 2C_{l,k} + 4\mathcal{R}D_{l,k}$$

and substitute $\sqrt{\beta'/2}$ for $\sqrt{\beta'}$ in the definitions of the vector elements G_l, the matrix elements $L'_{l,k}$ and the discretized expression [98].

We calculated numerical values for this system. The results are given and compared to the nontransformed system in Figs. 7–9 for $N = 6$, 9, 12. Values for $N = 15$ are compared in Table 3, while Fig. 10 gives a curve pieced together using four calculations performed with $N = 15$ and different β values. The numerical values are consistent with changes <0.2% with N increasing by 3 in a region, where the oscillatory behavior at the beginning has stopped. Comparing to the nontransformed system and to Oldham's reference values, we find that the new equations give better values for a given number of collocation points. For $N = 15$ deviation from the reference values is in the range of 0.16% (Table 3).

Figure 10 also shows how well our numerical values compare to Oldham's model over more than four orders of magnitude in T'. While the nontransformed equations gave rise to a curve which was lower than Oldham's at shorter times and higher at longer times (Fig. 6), we see that our transformed system gives values which are slightly lower than the reference over the entire range.

This example clearly shows that the choice of trial functions and transformations has an influence on the exact numerical solutions calculated. Good approximations, however, may be available with the "standard" method also (i.e. without consideration of the type of functions used). A more detailed investigation on the effect of using different sets of trial functions is currently under way.

Conclusions

Our two-dimensional diffusion model using orthogonal col-

Can. J. Chem. Downloaded from www.nrcresearchpress.com by 210.87.254.40 on 09/06/12
For personal use only.

location has proved to provide good approximations for the current expected at a flat, circular electrode imbedded into an insulator over several orders of magnitude for the dimensionless time variable T'. The discussion of parameters in this paper shows that even with only 6 interior collocation points, i.e. a grid of $2 \times 6 \times 6 = 72$ collocation points in the entire simulation space, reliable numerical values may be obtained. With increasing number of collocation points the simulations are consistent and give even better approximations. However, longer cpu-times and costs to perform the calculations are necessary. We again like to point out that changes to different mechanisms require only the exchange or addition of a few statements in the computer code. Thus, orthogonal collocation may be recommended as a fast and powerful method to simulate edge effects at electrodes.

1. B. SPEISER and S. PONS. Can. J. Chem. (*a*) **60**, 1352 (1982); (*b*) **60**, 2463 (1982).
2. L. F. WHITING and P. W. CARR. J. Electroanal. Chem. **81**, 1 (1977).
3. J. VILLADSEN and M. L. MICHELSON. Solution of differential equation models by polynomial approximation. Prentice Hall, Englewood Cliffs. 1978.
4. K. B. OLDHAM. J. Electroanal. Chem. **122**, 1 (1981).
5. K. AOKI and J. OSTERYOUNG. J. Electroanal. Chem. **122**, 19 (1981).
6. M. KAKIHANA, H. IKEUCHI, G. P. SATO, and K. TOKUDA. J. Electroanal. Chem. **108**, 381 (1980).
7. B. A. FINLAYSON. *In* Mathematics in science and engineering. Vol. 87. *Edited by* R. Bellman. Academic Press, New York and London. 1972. (*a*) p. 34. (*b*) p. 99 f.

Can. J. Chem. Downloaded from www.nrcresearchpress.com by 210.87.254.40 on 09/06/12
For personal use only.

On the use of the rotational isomeric state approximation in studies of internal rotation

VICTOR M. S. GIL
Department of Chemistry, University of Aveiro, 3800 Aveiro, Portugal
ANTONIO J. C. VARANDAS
Department of Chemistry, University of Coimbra, 3000 Coimbra, Portugal
AND
JOHN N. MURRELL
School of Chemistry and Molecular Sciences, University of Sussex, Brighton BN1 9QJ

Received May 6, 1982

VICTOR M. S. GIL, ANTONIO J. C. VARANDAS, and JOHN N. MURRELL. Can. J. Chem. **61**, 163 (1983).

A critical appraisal is made of the validity of the rotational isomeric state (RIS) approximation in studies of rotational isomerism, especially as far as the determination of energy differences for the stable conformers is concerned. By using simple model potential energy functions for internal rotation appropriate to some ethane derivatives, a comparison is made between the thermodynamic parameters that can be extracted from such potential functions and those obtained by applying the RIS method to continuum averaged values of conformation dependent properties. The effects due to the form of this conformation dependence, to the features of the potential energy curve, and to the temperature are discussed. The errors can be very large for realistic situations, and variable with temperature and with the property being studied; cases for which the errors are small are usually accidental.

VICTOR M. S. GIL, ANTONIO J. C. VARANDAS et JOHN N. MURRELL. Can. J. Chem. **61**, 163 (1983).

On a fait une évaluation critique de la validité de l'approximation de l'état isomérique rotationnelle (EIR) lors de l'étude de l'isomère rotationnelle. Cette évaluation concerne surtout la détermination des différences d'énergie des conformères stables. En utilisant un modèle simple des fonctions d'énergie potentielle pour la rotation interne appropriée à quelques dérivés de l'éthane, on a comparé les paramètres thermodynamiques que l'on peut tirer de telles fonctions de potentiel avec ceux obtenus en appliquant la méthode de EIR aux valeurs moyennes du continuum des propriétés qui dépendent de la conformation. On discute des effets de la forme de cette influence de la conformation des caractéristiques de la courbe d'énergie potentielle et de la temperature. Les erreurs peuvent être très grandes pour des situations réelles; elles varient avec la température et la propriété étudiée. Les cas où les erreurs sont faibles sont habituellement acidentelles.

[Traduit par le journal]

Can. J. Chem. Downloaded from www.nrcresearchpress.com by 210.87.254.40 on 09/06/12
For personal use only.

Introduction

Molecular properties that are conformation dependent have long been used in studies of hindered internal rotation, aiming especially at an approximate determination of the energy differences between the minima in the potential energy function for internal rotation (1, 2).

The usual procedure — often called the rotational isomeric state approximation (RIS) — consists of describing the internal rotation in terms of an equilibrium mixture of the most stable rotational isomers. Equilibrium constants are then determined, based on the observed property and its temperature dependence, and $\Delta H^{\ominus}$ and $\Delta S^{\ominus}$ values obtained.

The method obviously requires that temperature variations of medium effects are either negligible or properly accounted for (3). Even so, some recent model calculations have shown that the RIS approach can lead to quite large errors (4–7). Also, it has previously been found that when more than one type of data are available for analysis, the RIS method in its pure form may lead to inconsistent results (3, 8). Here we give a discussion of the basic sources of such discrepancies, associated with the neglect of conformations other than those of minimum energy.

Results and discussion

Two limiting situations can be identified, depending on the energy barriers to internal rotation (angle θ, potential energy $V(\theta)$), on the temperature, and on the property being measured $A(\theta)$: (*a*) The "equilibrium" is slow in the time scale of the measurement, hence distinct A values can be observed and assigned to each conformer. (*b*) The "equilibrium" is fast and only a rotational averaged A value is measured.

The terms "fast" and "slow" are defined with respect to the frequency spectrum of the observable A (9, 10)

$$[1] \quad A(\omega) = \int_0^\infty \exp(-i\omega t)\langle A(0)A(t)\rangle \, dt$$

where $\langle A(0)A(t)\rangle$ is the correlation function. This will contain periodic components with characteristic frequencies ω_i and, typically, decay components with a time constant ω_d. If ω_d is much less than all differences between frequencies ω_i, the spectrum will consist of distinguishable peaks at ω_i; if ω_d is much greater than all differences only a weighted average of the ω_i will be seen as a single frequency. We shall only examine these limiting cases. If ω_d is of the order of some ω_i differences, then a complicated (generally broadened) spectrum of A will be observed. For a criticism of the RIS method applied to dynamic properties see Vaughan (7).

In both the fast and slow cases, analysis of the data requires some knowledge about the functional form of $A(\theta)$. Even in the case of slow equilibrium this is necessary to assign separately measured properties to separate structures. Moreover, although

0008-4042/83/010163-08$01.00/0
©1983 National Research Council of Canada/Conseil national de recherches du Canada

observation may suggest slow equilibrium (case *a*), this may be due to a special form for $A(\theta)$, as Honegger and Heilbronner (5) have shown is possible for photoelectron spectral bands. The attribution of distinct A quantities to stable conformers presupposes that the distribution of A values (e.g. ionization energies (5)) is determined mainly by the conformer distribution density $P(\theta,T)$, therefore $V(\theta)$, and not by the way A varies with θ. Those authors showed that, even in the case of free rotation, multiple spectral bands may occur.

If practically only the lowest energy conformations are populated (the case of sufficiently deep potential troughs), then distinct A results can be attributed to the various rotational isomers and the ratio a_i/a_j of the intensities with which A_i and A_j occur is proportional to the equilibrium constant $K = C_i/C_j$:

$$[2] \quad a_i/a_j = \alpha_i C_i/\alpha_j C_j$$

α_k being the value of the intensity a_k for unit concentration of conformer k (e.g. molar extinction coefficient).

In general, however, such a proportionality will not hold, either because A_k may not arise entirely from conformer k or the coefficients α_k are temperature dependent and only accidentally can the ratio α_i/α_j be temperature independent. Braun and Liittke have attributed inconsistent results obtained from different ir bands of an internally rotating species to variation of α_i/α_j with temperature (8), and examined the consequences of such variation (11).

When only an averaged A value is observed, we have

$$[3] \quad \langle A \rangle = \int_0^{2\pi} A(\theta)P(\theta,T)\mathrm{d}\theta$$

with

$$[4] \quad P(\theta,T) = \exp\left[-V(\theta)/RT\right]/N$$

or

$$[5] \quad P(\theta,T) = \sum_\mu \phi_\mu^2(\theta) \exp\left(-E_\mu/RT\right)/N'$$

for the classical and quantum-mechanical approaches, respectively; N and N' are (temperature-dependent) normalizing factors and ϕ_μ is the μth torsional eigenfunction of energy E_μ.

Except when RT is much smaller than the energy barriers, [4] and [5] will be approximately identical (this has been confirmed in a few examples; see also refs. 12, 13). However, it will not in general be possible to associate a sub-set of ϕ_μ to each potential trough. Accordingly, the notion of equilibrium between any two stable conformers i, j becomes less clear. An equilibrium constant can then be defined as

$$[6] \quad K = \int_i P(\theta,T)\,\mathrm{d}\theta \Big/ \int_j P(\theta,T)\,\mathrm{d}\theta$$

where the integrals are calculated in the sub-domains of θ corresponding to troughs i and j. In a classical treatment, [6] is equal to the ratio of the partition functions for oscillations in each potential well: f_i/f_j.

The observed value $\langle A \rangle$ given by [3] can be partitioned into contributions from each well:

$$[7] \quad \langle A \rangle = \sum_k \bar{A}_k p_k$$

with

$$[8] \quad p_k = f_k/N$$

$$[9] \quad \sum_k p_k = 1$$

where $\bar{A}_k$ is the (temperature-dependent) weighted average value of $A(\theta)$ for well k. However, the usual procedure in the RIS method is to write

$$[10] \quad \langle A \rangle = \sum_k A_k^0 p_k^*$$

A_k^0 referring to the conformation of minimum energy in well k and p_k^* being an effective (temperature dependent) population (for sufficiently deep troughs, $p_k^* \approx p_k$) subject to the condition

$$[11] \quad \sum_k p_k^* = 1$$

From [7], [8], and [10] it is clear that any equilibrium constant defined by $K^* = p_i^*/p_j^*$ will differ from the true value $K = f_i/f_j = p_i/p_j$ in so far as the set of $\bar{A}_k$ values differs from the set of A_k^0 values. Such a difference depends on $V(\theta)$, T, and $A(\theta)$.

A similar discussion applies to the case when distinct A values are detected for each stable conformer. Then we can write

$$[12] \quad a_i = \alpha_i^0 C_i^* = \bar{\alpha}_i C_i$$

in parallel with [7] and [10], and $K = C_i/C_j$ will differ from $K^* = C_i^*/C_j^*$ to the extent the ratio $\bar{\alpha}_i/\bar{\alpha}_j$ differs from α_i^0/α_j^0.

But the basic criticism that can be made to the use of eqs. [10] and [11] is that, unless $\bar{A}_k \approx A_k^0$, the normalizing condition [11] does not necessarily hold. It is quite possible, for example, that all $\bar{A}_k$ values are larger (or smaller) than the corresponding A_k^0 values; therefore, in order to reproduce $\langle A \rangle$ with eq. [10], $\sum_k p_k^*$ must be greater (smaller) than 1. It may even happen that, by forcing eq. [11] to hold, negative populations are deduced. Examples of this are given further below.

As a consequence, the $(\Delta H^\ominus)^*$ and $(\Delta S^\ominus)^*$ values which are deduced from a study of K^* given by the RIS method, as a function of T^{-1}, will in general deviate from the "true" thermodynamic values as defined in terms of $K = p_i/p_j$. This will be most evident when different properties A lead to different thermodynamic parameters (3, 8).

In addition, even if $\Delta H^\ominus$ may be equated to $\Delta U^\ominus$, i.e. Δ(pressure $\times$ volume) = 0, the latter, which is a difference between weighted averages that take all possible conformations associated with each potential well into account, is not necessarily equal to the difference ΔV^0 between the corresponding minima in the potential energy function; nor, for that matter, to ΔU^0 which allows for zero-point energy. Unless the depths of the potential wells are similar and/or the temperature is sufficiently low, we expect $\Delta H_{ij}^\ominus \neq \Delta U_{ij}^0$, according to the thermodynamic relationship

$$[13] \quad \Delta H_{ij}^\ominus = \Delta U_{ij}^0 - \mathrm{d}\left[\ln f_i^0/f_j^0\right]/\mathrm{d}\,(1/T)$$

where f_k^0 are partition functions defined for each well by taking the origin of U at the respective minima.

Whereas the difference between $\Delta H^\ominus$ and ΔU^0 depends only on $V(\theta)$ and T, that between $\Delta H^\ominus$ and $(\Delta H^\ominus)^*$ depends also on the property $A(\theta)$.

We shall now consider some numerical examples in order to illustrate especially how $(\Delta H^\ominus)^*$ obtained by the RIS method can differ from the "true" $\Delta H^\ominus$ value, and how the latter differs from ΔU^0 or ΔV^0 (the quantity one usually aims to determine by the RIS method).

Can. J. Chem. Downloaded from www.nrcresearchpress.com by 210.87.254.40 on 09/06/12
For personal use only.

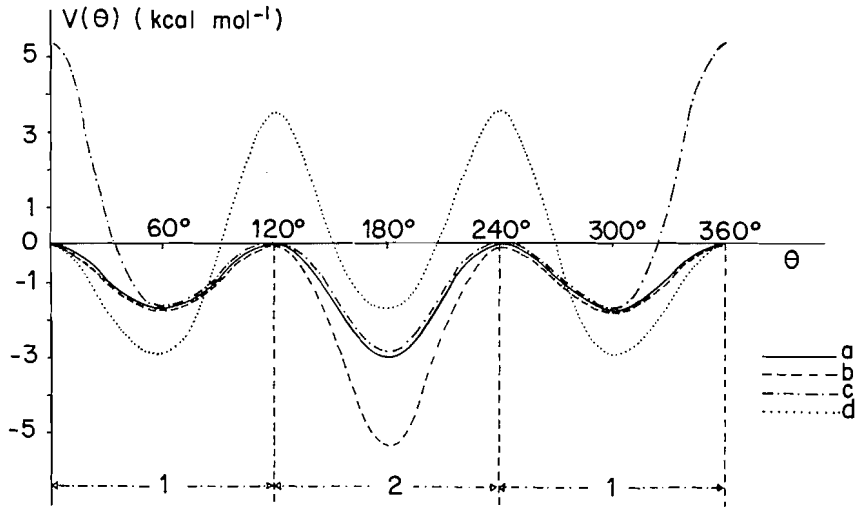

FIG. 1. Types of potential energy functions used.

(a) The difference between $(\Delta H_{ij}^{\ominus})^*$ determined by the RIS approach and the true $\Delta H_{ij}^{\ominus}$

For reasons of simplicity, we shall only deal with cases when $V(\theta)$ is a potential with three minima occurring at $\theta = 60°$, 180°, and 300°, with only one ΔV_{ij}^0 value, as shown in Fig. 1 (see also refs. 4 and 6). The troughs 0−120° and 240−360° are associated with conformer **1** and 120−240° with conformer **2**. Molecules having this type of potential function for internal rotation would, for example, be some substituted ethanes; e.g., curve *c* resembles that calculated for 1,2-dichloroethane, apart from a small displacement of the minima at 60° and 300° (16). Whereas curves *a* and *b* presuppose eclipsed conformations of equal energy, this is not the case with *c* and *d*. The actual form of $V(\theta)$ in the intervals 0−60°, 60−120°, 120−180°, etc. is that of the leading term in the potential energy function for ethane (14): proportional to $(1 - \cos 3\theta)$. The main qualitative conclusions, however, are not expected to be greatly influenced by the detailed form of $V(\theta)$ in these intervals.

As far as the θ-dependence of the property A is concerned, we have examined in particular $A(\theta) = \cos\theta$ and $A(\theta) = \cos^2\theta$. These are appropriate functions for expressing, for example, the dipole moment of $CH_2X—CH_2X$ and $CHX_2—CHX_2$ molecules as a function of θ (the squared dipole moment for each θ is proportional to $1 + \cos\theta$ provided the dipole is given as a sum of two local dipole vectors), for the square value of the distance between two vicinal nuclei (of the form $m + n\cos\theta$) and for vicinal HH nuclear spin coupling constants ($a' + b'\cos\theta + c'\cos^2\theta$ (15)). We note that any property or term varying with $\sin\theta$ gives zero with the $V(\theta)$ functions above.

The calculations have been performed for temperatures ranging from 150 to 1000 K.

For the $V(\theta)$ functions of Fig. 1, we have from [7] and [9]:

$$[14]\quad \langle A\rangle = 2p_1(\bar{A}_1 - \bar{A}_2) + \bar{A}_2$$

If [11] is assumed to be true, then from [10] and [11] we can also write

$$[15]\quad \langle A\rangle = 2p_1^*(A_1^0 - A_2^0) + A_2^0$$

Example 1

$$V(\theta) = \tfrac{1}{2}V_1^0(1 - \cos 3\theta) \qquad 0 \leqslant \theta \leqslant 120° \text{ and } 240° \leqslant \theta \leqslant 360°$$

$$= \tfrac{1}{2}V_2^0(1 - \cos 3\theta) \qquad 120° \leqslant \theta \leqslant 240°$$

$$A(\theta) = \cos\theta;\ \cos^2\theta;\ \mu\cos\theta + \lambda\cos^2\theta$$

We first take $V_1^0 = -1.8$ kcal mol^{-1} and $V_2^0 = -3.0$ kcal mol^{-1} (curve *a* in Fig. 1), noting that V^0 for ethane is ca. −3.0 kcal mol^{-1}. For $A(\theta) = \cos\theta$, [15] becomes

$$[16]\quad \langle\cos\theta\rangle = 3p_1^* - 1$$

For low temperatures, $\langle\cos\theta\rangle$ approaches −1, p_1^* and p_1 become very small, $\bar{A}_2$ tends to −1 and $\bar{A}_1$ to 1/2. As the temperature increases, so do $\langle\cos\theta\rangle$ and $\bar{A}_2$, whereas $\bar{A}_1$ decreases; p_1 and p_1^* increase and become closer ($p_1 < p_1^*$) and so do the equilibrium constants $K_{1,2}$ and $K_{1,2}^*$ ($K_{1,2} < K_{1,2}^*$). Figure 2 compares $\ln K_{1,2}$ with $\ln K_{1,2}^*$ as a function of T^{-1}. A small deviation from linearity is apparent. $\Delta H_{1,2}^{\ominus}$ is larger than $(\Delta H_{1,2}^{\ominus})^*$ but only by 5−6%. Depending on the temperature range, $\Delta H^{\ominus}$ varies from 1070 at the higher to 1210 at the lower temperatures, whereas $(\Delta H^{\ominus})^*$ goes from 1020 to 1160 cal mol^{-1}.

This difference becomes even smaller as $\Delta V_{1,2}^0$ decreases. For $\Delta V_{1,2}^0 = 0$ it vanishes, because $(\Delta H^{\ominus})^*$ and $\Delta H^{\ominus}$ are both zero. On the contrary, as the depth of trough 2 in Fig. 2 increases (curve *b*), the deviations are expected to increase, because $\bar{A}_2$ decreases and approaches A_2^0 especially at low temperatures; accordingly (see [15] and [16]), p_1^* deviates more from p_1 ($p_1 < p_1^*$). Figure 3, which is the equivalent of Fig. 2 except that trough 2 has been changed so as to make $\Delta V_{1,2}^0 = 3 \times 1.2$ kcal mol^{-1} (curve *b*, $V_1^0 = -1.8$ kcal mol^{-1}, $V_2^0 = -5.4$ kcal mol^{-1}), shows how large the difference between $(\Delta H^{\ominus})^*$ and $\Delta H^{\ominus}$ can be depending on the temperature. In particular, the variation of $-\ln K^*$ with T^{-1} is far from linear. For $\Delta H^{\ominus} = 3280 - 3580$ cal mol^{-1} $(\Delta H^{\ominus})^*$ varies from 440 cal mol^{-1} at low temperatures to 3230 cal mol^{-1} at high temperatures.

For $A(\theta) = \cos^2\theta$, $\bar{A}_1$ and $\bar{A}_2$ deviate more from A_1^0 ($\bar{A}_1 > A_1^0$) and A_2^0 ($\bar{A}_2 < A_2^0$) (see eqs. [14] and [15]) and p_1^* becomes greater than in the case $A(\theta) = \cos\theta$, hence deviating more from p_1, especially at low temperatures. For example, for $V(\theta)$ given by curve *a* (Fig. 1) and $T = 300$ K, we get $p_1 = 0.133$ and $p_1^* = 0.138$ for $A(\theta) = \cos\theta$ and $p_1^* = 0.152$ for $A(\theta) =$

Can. J. Chem. Downloaded from www.nrcresearchpress.com by 210.87.254.40 on 09/06/12
For personal use only.

Can. J. Chem. Downloaded from www.nrcresearchpress.com by 210.87.254.40 on 09/06/12
For personal use only.

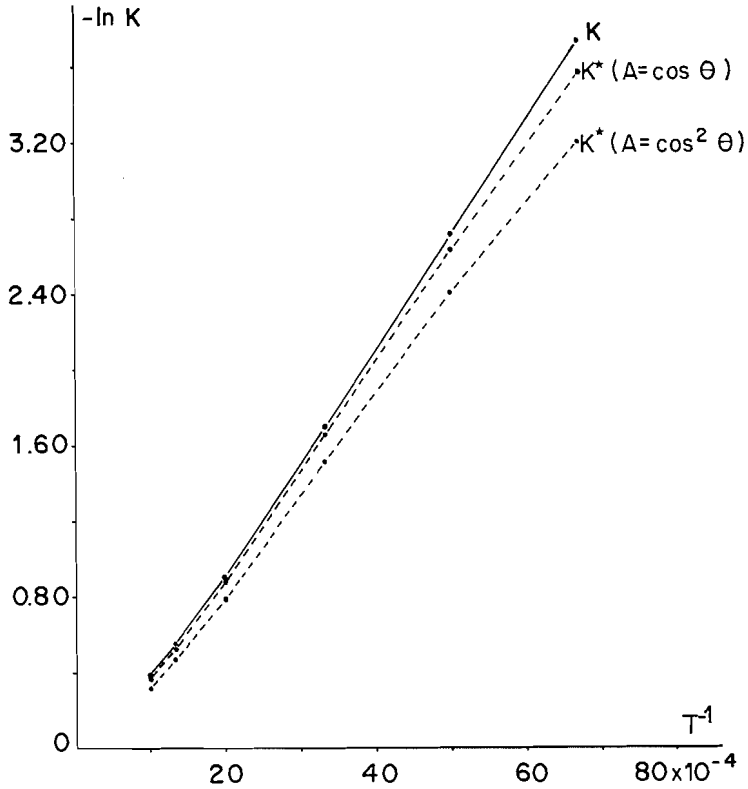

FIG. 2. Equilibrium constants – temperature plots, using $V(\theta)$ given by curve *a* in Fig. 1 (ΔV^0 = 1200 cal mol^{-1}) and $A(\theta) = \cos\theta$ (leading to $(\Delta H^{\ominus})^*$ = 1020−1160 cal mol^{-1}) and $A(\theta) = \cos^2\theta$ (leading to $(\Delta H^{\ominus})^*$ = 950−1090 cal mol^{-1}). The full line ($\Delta H^{\ominus}$ = 1070−1210 cal mol^{-1}) is obtained using eq. [6].

$\cos^2\theta$; accordingly, $K^* = 0.191$ and $K^* = 0.218$, respectively. K in comparison has the value $K = 0.182$. Again, the difference becomes more marked when $V(\theta)$ is given by curve *b*. The corresponding plots of $-\ln K^*$ against T^{-1} are shown in Figs. 2 and 3.

For $A(\theta) = \mu\cos\theta + \lambda\cos^2\theta$, p_1^* can be related to the corresponding values obtained with $A(\theta) = \cos\theta$ and $A(\theta) = \cos^2\theta$ by using [15]:

$$[17]\quad p_1^* = \left(\mu p^*_{1,\cos\theta} - \frac{\lambda}{2}\,p^*_{1,\cos^2\theta}\right) \Big/ \left(\mu - \frac{\lambda}{2}\right)$$

In Karplus' equation for HH coupling constants (15), $\lambda \gg \mu$ and the deviations are approximately those obtained with $A(\theta) = \cos^2\theta$. With $\mu = \lambda = 1$, $p_1^* = 2p^*_{1,\cos\theta} - p^*_{1,\cos^2\theta}$; since $p_1 < p^*_{1,\cos\theta} < p^*_{1,\cos^2\theta}$, p_1^* now approaches p_1. In other cases, however, the differences can be much bigger; p_1^* may even become negative. For $A(\theta) = 1.1\cos\theta + 2.0\cos^2\theta$, for example, the p_1^* values obtained for several temperatures and $V_1^0 = -1.8$, $V_2^0 = -5.4$ kcal mol^{-1}, are as follows:

T (K)	p_1^*
150	−0.0619
200	−0.0841
300	−0.124
500	−0.142
750	−0.0700
1000	+0.0160

For $A(\theta) = \cos\theta + 2\cos^2\theta$, p_1^* given by [17] would become $-\infty$! $A(\theta)$ functions like the latter giving $A_1^0 = A_2^0$ (= 1 in the present case) render the RIS method inoperative and clearly serve to demonstrate that the satisfactory results sometimes obtained with the method are purely accidental. In the case just considered, the average value $\langle A\rangle$ is not very much different from the common value $A_1^0 = A_2^0 = 1$. But in other cases when the RIS procedure is not applicable, the difference can be large. For example, with $A(\theta) = \cos 3\theta$ and T = 500 K, we have $\langle A\rangle = -0.515$ for curve *a* and −0.752 for potential *b*, whereas $A_1^0 = A_2^0 = -1$.

Example 2

$$V(\theta) = [-3.6(1 - \cos 3\theta) + 5.4] \text{ kcal mol}^{-1} \quad 0 \leqslant \theta \leqslant 60° \text{ and } 300° \leqslant \theta \leqslant 360°$$

$$= -0.9(1 - \cos 3\theta) \text{ kcal mol}^{-1} \quad 60° \leqslant \theta \leqslant 120° \text{ and } 240° \leqslant \theta \leqslant 300°$$

$$= -1.5(1 - \cos 3\theta) \text{ kcal mol}^{-1} \quad 120° \leqslant \theta \leqslant 240°$$

$A(\theta) = \cos\theta;\ \cos^2\theta$

The potential function used now is that corresponding to curve *c* in Fig. 1; it differs from curve *a* in that the energy of the conformations close to $\theta = 0°$, 360° is increased. As a consequence, for $A(\theta) = \cos\theta$, $\langle A\rangle$, p_1^*, and $\bar{A}_1$ all decrease, whereas $\bar{A}_2$ remains the same as, of course, do A_1^0 and A_2^0. According to [14] and [15], p_1^* decreases more than p_1; eventually $p_1 > p_1^*$ and $K^*_{1,2}$. This occurs at higher temperatures, because it is then that $\bar{A}_1$ obtained with curve *c* shows the greatest differences from $\bar{A}_1$ calculated using curve *a*. This is illustrated in Fig. 4. With respect to potential *a*, the difference between $\Delta H^{\ominus}$ (= 1140−1180 cal mol^{-1}) and $(\Delta H^{\ominus})^*$ (= 980−1080 cal mol^{-1}) increases and the $\Delta S^{\ominus}$ and $(\Delta S^{\ominus})^*$

Can. J. Chem. Downloaded from www.nrcresearchpress.com by 210.87.254.40 on 09/06/12
For personal use only.

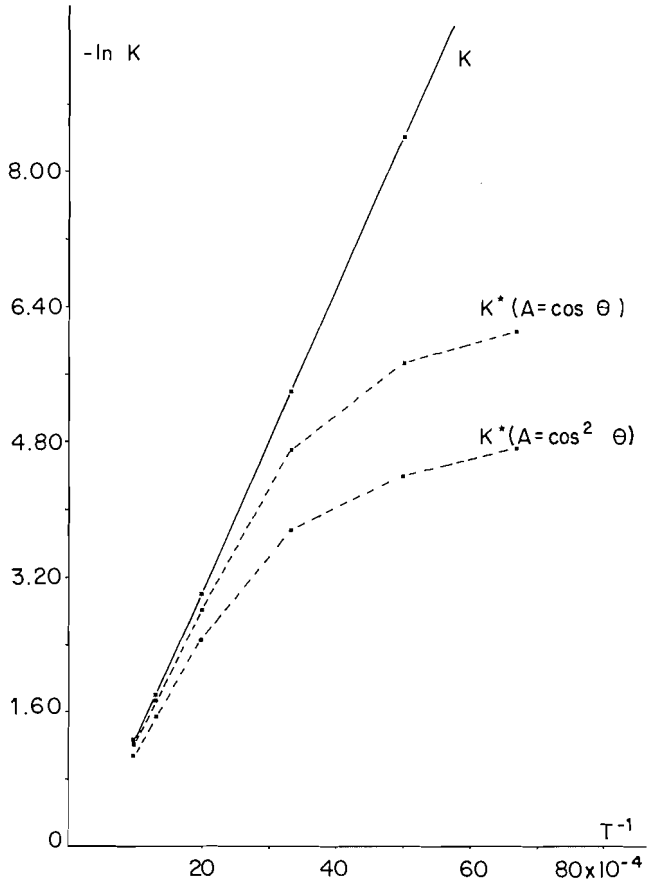

FIG. 3. The same as Fig. 2, with curve b (ΔV^0 = 3600 cal mol^{-1}); $(\Delta H^{\ominus})^*$ = 3230−440 cal mol^{-1} for $A(\theta)$ = cos θ and $(\Delta H^{\ominus})^*$ = 2780−400 cal mol^{-1} for $A(\theta)$ = cos^2 θ; $\Delta H^{\ominus}$ = 3280−3580 cal mol^{-1}.

values are now also significantly different.

For the case $A(\theta) = \cos^2\theta$, p_1^* becomes greater than for $A(\theta)$ = cos θ, as in Example 1. For example, at 300 K, p_1 = 0.105 and p_1^* = 0.103 with $A(\theta)$ = cos θ and p_1^* = 0.144 with $A(\theta) = \cos^2\theta$: accordingly, K^* = 0.129 and K^* = 0.202 respectively, in comparison with K = 0.132.

Example 3

$$V(\theta) = [-1.5(1 - \cos 3\theta)] \text{ kcal mol}^{-1} \quad 0 \leqslant \theta \leqslant 60° \text{ and } 300° \leqslant \theta \leqslant 360°$$

$$= [-3.3(1 - \cos 3\theta) + 3.6] \text{ kcal mol}^{-1} \quad 60° \leqslant \theta \leqslant 120° \text{ and } 240° \leqslant \theta \leqslant 300°$$

$$= [-2.7(1 - \cos 3\theta) + 3.6] \text{ kcal mol}^{-1} \quad 120° \leqslant \theta \leqslant 240°$$

$A(\theta)$ = cos θ; cos^2 θ

With $V(\theta)$ given by curve d, ⟨cos θ⟩ decreases from 0.519 for 150 K to 0.271 for 1000 K. $\bar{A}_2$ increases with temperature; $\bar{A}_1$ also increases up to a certain temperature and then decreases, corresponding to the population of conformations with θ approaching 120°. Both p_1 and p_1^* decrease on increasing T, with $p_1^* > p_1$. The logarithms of $K_{1,2}$ and $K_{1,2}^*$ are plotted in Fig. 5 against T^{-1}. Now $\Delta H_{2,1}^{\ominus}$ = 1320−1180 cal mol^{-1} and $(\Delta H_{2,1}^{\ominus})^* \simeq$ 1650 cal mol^{-1}; the error is 20−40%, with $(\Delta H^{\ominus})^* > \Delta H^{\ominus}$. It is noted that for T < 200 K, ⟨cos θ⟩ > A_1^0 = 0.5, hence $p_1^* > 0.5$ and p_2^* becomes negative; the higher the barrier in trough 2, the higher the temperature at which this occurs, thus making the RIS method of no value.

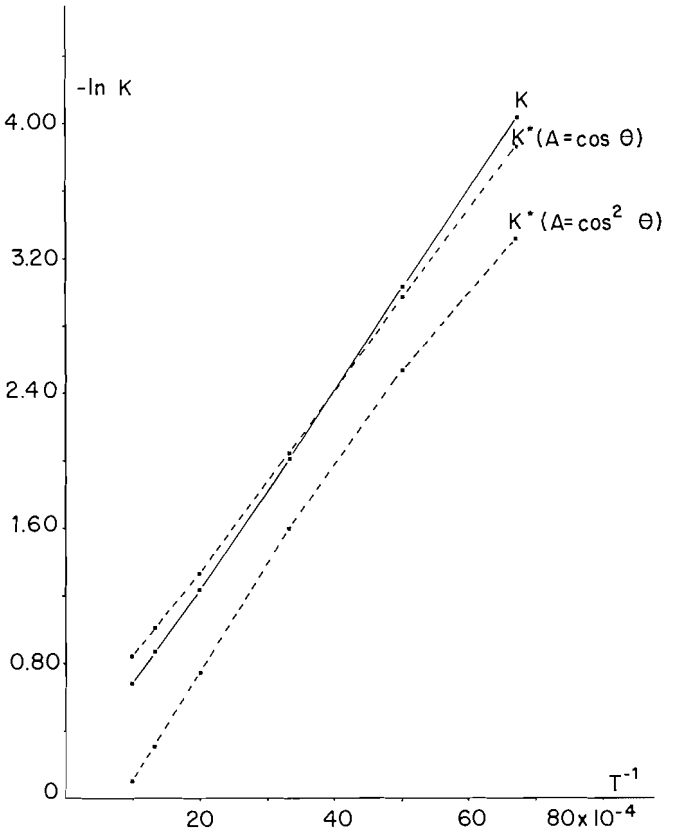

FIG. 4. The same as Fig. 2, with curve c (ΔV^0 = 1200 cal mol^{-1}); $(\Delta H^{\ominus})^*$ = 980−1080 cal mol^{-1} for $A(\theta)$ = cos θ and $(\Delta H^{\ominus})^*$ = 1290−920 cal mol^{-1} for $A(\theta) = \cos^2\theta$; $\Delta H^{\ominus}$ = 1140−1180 cal mol^{-1}.

In the case of $A(\theta) = \cos^2\theta$, $p_1^* < p_1$ especially at higher temperatures. For T = 300 K, $K_{1,2}$ = 8.57 and $K_{1,2}^*$ = 2.91; for $A(\theta)$ = cos θ, $K_{1,2}^*$ = 19.4. As seen from Fig. 5, $(\Delta H_{2,1}^{\ominus})^*$ ranges from 420 to 900 cal mol^{-1}.

(b) The difference between $\Delta H_{ij}^{\ominus}$ *and* ΔV_{ij}^0

From the plots of $-\ln K$ and $-\ln K^*$ against T^{-1}, we have obtained $\Delta H^{\ominus}$ and $(\Delta H^{\ominus})^*$ values that depend on the temperature; it was assumed that $\Delta S^{\ominus}$ and $(\Delta S^{\ominus})^*$ remain approximately constant in the temperature interval considered: 150−1000 K. Figures 2−5 show that for lower temperatures $\Delta H^{\ominus} \simeq \Delta V^0$ as would be expected. For higher temperatures, some small deviations can be observed.

In order to ascertain how big these deviations can be, we have performed analytical calculations of $\Delta H^{\ominus}$ taken equal to $\Delta U^{\ominus}$, for V-shape potentials resembling the potential curves of Fig. 1. $\Delta U_{1,2}^{\ominus}$ is defined as the difference of average values for wells 1 and 2, in a classical manner:

$$[18] \quad \Delta U_{1,2}^{\ominus} = \frac{\int_1 V(\theta) \exp[-V(\theta)/RT]d\theta}{\int_1 \exp[-V(\theta)/RT]d\theta} - \frac{\int_2 V(\theta) \exp[-V(\theta)/RT]d\theta}{\int_2 \exp[-V(\theta)/RT]d\theta}$$

(the integrals extend to all angles θ for each well).

Figure 6 shows the variation of $\Delta U^{\ominus}$ with temperature. For temperatures around 300 K and below the differences between

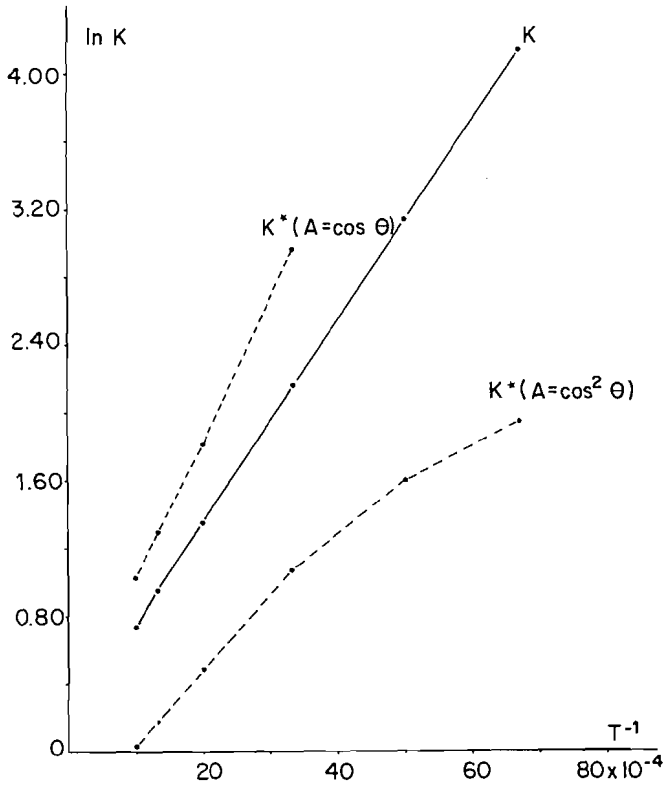

FIG. 5. The same as Fig. 2, with curve d (ΔV^0 = 1200 cal mol^{-1}); $(\Delta H^{\ominus})^*$ = 1650 cal mol^{-1} for $A(\theta) = \cos\theta$ and $(\Delta H^{\ominus})^*$ = 900−420 cal mol^{-1} for $A(\theta) = \cos^2\theta$; $\Delta H^{\ominus}$ = 1320−1180 cal mol^{-1}.

$\Delta U^{\ominus}$ and ΔV^0 are small, but for temperatures approaching 1000 K the deviations reach −25 to −30% for potentials a' and b' and +40% for curve c'. Comparing the results for potentials a' and a'' it is clear that for a given ΔV^0 value, the deviations become smaller the deeper the potential wells, as would be anticipated.

Conclusion

We have discussed two basic sources of difference between ΔV^0 for the minima in a potential energy curve appropriate to the internal rotation of ethane derivatives and the enthalpy change $(\Delta H^{\ominus})^*$ for the rotational isomers as determined by the rotational isomeric state approach. One depends only on the shape of the potential $V(\theta)$ and on the temperature; this leads to a difference between ΔV^0 and $\Delta H^{\ominus}$, $\Delta H^{\ominus}$ being the true enthalpy change. The other varies also with the conformation-dependent property $A(\theta)$ used leading to a difference between $\Delta H^{\ominus}$ and $(\Delta H^{\ominus})^*$. Other sources of error are known to exist and have been considered elsewhere (3). The following are the main conclusions:

(*1*) As would be expected, the difference between $\Delta H^{\ominus}$ and ΔV^0 depends not only on the value of ΔV^0 but also on the maxima of the potential energy function, which occur close to the eclipsed conformations. Such a difference is smaller the lower the temperature and the deeper the potential troughs. For temperatures up to 400 K and for realistic energy barriers, the deviation is ±10% at the most, increasing to about ±30% at 1000 K.

(*2*) Despite the changes of $\Delta H^{\ominus}$ with temperature, the plot of ln K against $1/T$ gives almost a straight line (passing near the origin) if K is the true equilibrium constant. However, when the equilibrium constant K^* given by the RIS method is used, a substantial and consistent deviation from linearity can be observed, especially at intermediate and low temperatures. We note that: (*a*) If the eclipsed conformations have approximately the same energy, then K and K^* approach each other at high temperatures. At low temperature, the deviation is more marked for a property varying as $A(\theta) = a \pm b\cos^2\theta$ than for $A(\theta) = c \pm d\cos\theta$ and it increases with ΔV^0. With the first $A(\theta)$ function and in the temperature range 200−300 K, $(\Delta H^{\ominus})^*$ is smaller than ΔH^0 by about 10% for ΔV^0 = 1.2 kcal mol^{-1} and up to 80% for ΔV^0 = 3.6 kcal mol^{-1}. (*b*) If the eclipsed conformations have different energies K^* can be very different from K at any temperature. This is particularly true for $A(\theta) = a \pm b\cos^2\theta$, and a significant apparent $(\Delta S^0)^*$ results.

For a system like 1,2-dichloroethane (potential of type c in Fig. 1 (16)), both $A(\theta)$ functions lead to $(\Delta H^{\ominus})^*$ in the interval 200−300 K that is only ca. 10% less than $\Delta H^{\ominus}$. This (together with conclusion 1 above) explains why Mark and Sutton (16) found good agreement between the dipole moments calculated using the continuum average and the RIS method for this compound (see also ref. 5). However, for systems in which the least stable staggered conformation occurs at θ = 180° and the least stable eclipsed conformations are those for θ = 120°, 240°, the results are quite different. In fact, for potential d in Fig. 1, the $(\Delta H^{\ominus})^*$ values at room temperature deviate in magnitude from $\Delta H^{\ominus}$ by +40% with $A(\theta) = c \pm d\cos\theta$ and by −35% with $A(\theta) = a \pm b\cos^2\theta$. Systems to which this conclusion is likely to apply semi-quantitatively are 1,2-difluoroethane (17, 18) and 1,1,2,2-tetrachloroethane (in solution or as pure liquid) (3). It is therefore anticipated that the $(\Delta H^{\ominus})^*$ values obtained, in the same conditions, from dipole moments and from HH spin couplings will be very different, the former being larger and the latter smaller than the true $\Delta H^{\ominus}$. We could not find data to confirm this prediction, but it is interesting that the RIS method based on nuclear spin coupling constants for 1,2-difluoroethane vapour gives 0.6 kcal mol^{-1} (19) whereas the value obtained from electron diffraction is 0.93 kcal mol^{-1} (17). For the pure liquid the estimated $(\Delta H^{\ominus})^*$ value is 2 kcal mol^{-1} (19), the conformation for θ = 180° being the least stable of the staggered conformations.

(*3*) The relative energies of eclipsed conformations cannot be ignored. This is demonstrated by the points (*a*) and (*b*) above. It is also a possible explanation for the unexpected stability of some conformations deduced from the RIS method. For example, succinic acid and its salts (20) and also methylsuccinic acid and its esters (21) show a surprisingly high stability of the *syn−clinal* conformations when the RIS method is applied to HH nuclear spin coupling constants. This result may just reflect the high energies of the *cis* conformations. In particular, the pair of vicinal H nuclei, for which a curve of type c (Fig. 1) would be expected to apply, should show a smaller coupling than if all eclipsed conformations had approximately the same energy.

(*4*) Cases may occur for which the RIS approach would lead to negative populations for the higher energy conformers.

Although, according to our calculations, some of the ΔV^0 values obtained by the RIS method may be approximately correct (e.g. 1,2-dichloroethane, perhaps the most studied ethane derivative from the point of view of conformation and internal rotation), many others may be in substantial error due to the interpretation of observed properties in terms of the

Can. J. Chem. Downloaded from www.nrcresearchpress.com by 210.87.254.40 on 09/06/12
For personal use only.

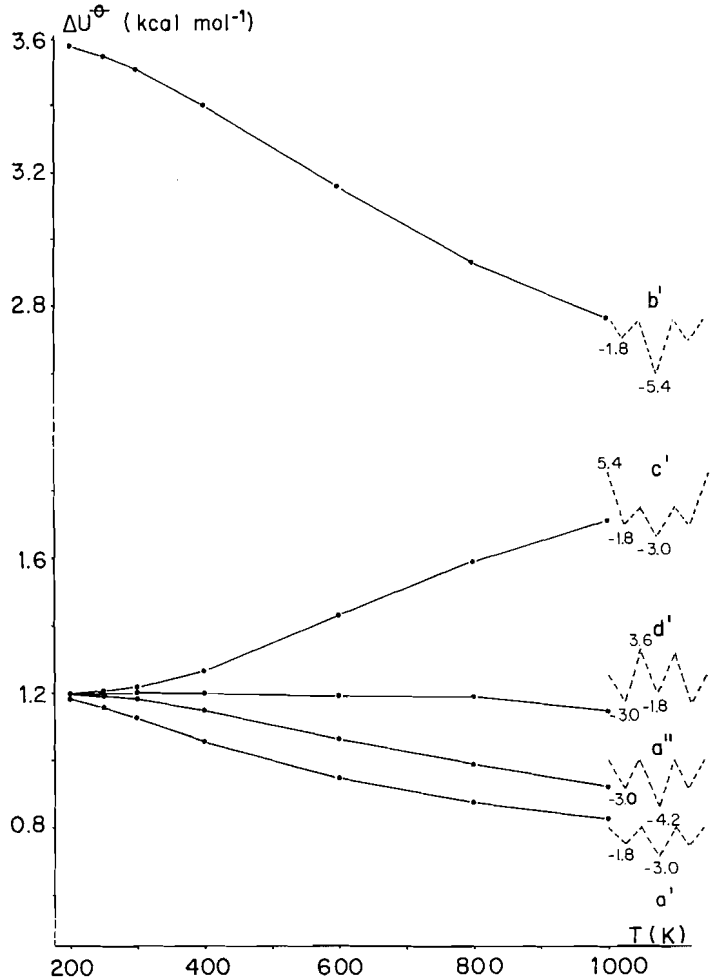

FIG. 6. Plot of $\Delta U^{\ominus}$ given by eq. [18] as a function of T for V-shape functions related to those of Fig. 1.

stable conformers only. Provided some knowledge exists on the type of potential function for internal rotation, it is possible to estimate the sign and roughly the magnitude of such errors and to decide on the conditions, namely the temperature range, for which the errors are minimized. For example, if all eclipsed conformations have approximately the same energy, then for lower temperatures the deviation between $(\Delta H^{\ominus})^*$ and $\Delta H^{\ominus}$ increases. On the other hand, for high temperatures it is the difference between ΔV^0 and $\Delta H^{\ominus}$ that is large. There will then be a minimum deviation, not necessarily negligible, between $(\Delta H^{\ominus})^*$ and ΔV^0 at some intermediate temperature. This, apart from an entropy factor which was deliberately ignored, was found by Gil and Varandas in previous calculations using vicinal HH nuclear spin coupling constants (4) and electric dipole moments (6) as conformation-dependent properties. They actually compared directly ΔV^0 with a $\Delta E'$ value which is, in fact, $(\Delta G^{\ominus})^*$.

An approximate correction to the ΔV^0 value given by the RIS approach is helpful if one is trying to fit the parameters of a potential energy function to observed properties and their temperature dependence. Obviously the study will gain much from using more than one conformation-dependent property. Apart from the values of the various energy barriers, a parameter that may be of some importance is the exact position of the minima (eventually also the maxima) in the potential energy curve (16). Work is in progress along these lines including an extension to non-symmetrical potentials.

Information on energy differences between rotational isomers can also be obtained from data in various solvents coupled with a theory of solvent effects on ΔV^0 values. This has been developed with some success by Abraham and co-workers (3). We note that, when fitting experimental data for variable dielectric constants (e.g. nuclear spin coupling constants), in terms of ΔV^0 for the vapour (in fact $\Delta G^{\ominus}$) and the coupling constants of the rotational isomers, these are effective averaged couplings appropriate to each potential well and not just the coupling constant for a specific angle of rotation. Accordingly, the equilibrium constants and the energy differences (actually $\Delta G^{\ominus}$) determined should be approximately correct, at least in so far as the values taken for the vapour are correct. We note that the approximate constancy of those couplings in various solvents must require changes in the energy of the eclipsed conformations with solvent that offset the effect of changes in the minimum energy conformations. Also, the orientation-dependent substituent effects on coupling constants demonstrated by those studies must partly arise from the features of each potential well.

Acknowledgements

V.M.S.G. thanks the School of Chemistry and Molecular Sciences, University of Sussex, for hospitality during his sabbatical leave and the NATO Scientific Affairs Division for a Fellowship (Senior Scientist Award No. B 180, 1981).

Can. J. Chem. Downloaded from www.nrcresearchpress.com by 210.87.254.40 on 09/06/12
For personal use only.

1. S. MIZUSHIMA. The structure of molecules and internal rotation. Academic Press, New York. 1954.
2. W. J. ORVILLE-THOMAS (*Editor*). Internal rotation in molecules. Wiley, London. 1974, and references therein.
3. R. J. ABRAHAM and E. BRETSCHNEIDER. *In* Internal rotation in molecules. *Edited by* W. J. Orville-Thomas. Wiley, London. 1974. p. 481.
4. V. M. S. GIL and A. J. C. VARANDAS. J. Magn. Reson. **43**, 28 (1981).
5. E. HONEGGER and E. HEILBRONNER. Chem. Phys. Lett. **81**, 615 (1981).
6. V. M. S. GIL and A. J. C. VARANDAS. Can. J. Chem. **60**, 2049 (1982).
7. W. E. VAUGHAN. Adv. Mol. Relaxation Interaction Processes, **13**, 171 (1978).
8. H. BRAUN and W. LÜTTKE. J. Mol. Struct. **28**, 391 (1975).
9. R. G. GORDON. Adv. Magn. Reson. **3**, 1 (1963).
10. P. J. D. PARK, R. A. PETHRICK, and B. H. THOMAS. *In* Internal rotation in molecules. *Edited by* W. J. Orville-Thomas. Wiley, London. 1974. p. 57.
11. H. BRAUN and W. LÜTTKE. J. Mol. Struct. **28**, 415 (1975).
12. A. HAALAND and J. E. NILLSON. Acta Chem. Scand. **22**, 2653 (1968).
13. T. A. WILDMAN. Chem. Phys. Lett. **75**, 383 (1980).
14. E. B. WILSON. Chem. Soc. Rev. **1**, 293 (1972) and references therein.
15. M. KARPLUS. J. Am. Chem. Soc. **85**, 2870 (1963).
16. J. E. MARK and C. SUTTON. J. Am. Chem. Soc. **94**, 1083 (1972).
17. L. FERNHOLT and W. KVESETH. Acta Chem. Scand. A**34**, 163 (1980).
18. R. J. ABRAHAM and R. STÖLEVIK. Chem. Phys. Lett. **77**, 181 (1981).
19. R. J. ABRAHAM and R. H. KEMP. J. Chem. Soc. B, 1240 (1971).
20. M. T. NUNES, V. M. S. GIL, and J. ASCENSO. Tetrahedron, **37**, 611 (1981).
21. J. RÉTEY, W. E. HULL, F. SNATZKE, G. SNATZKE, and U. WAGNER. Tetrahedron, **35**, 1845 (1979).

Can. J. Chem. Downloaded from www.nrcresearchpress.com by 210.87.254.40 on 09/06/12
For personal use only.

The retroaldol reaction of 3-methyl-2-butenal

J. PETER GUTHRIE[1] AND BRIAN A. DAWSON

Department of Chemistry, University of Western Ontario, London, Ont., Canada N6A 5B7

Received June 11, 1982

J. PETER GUTHRIE and BRIAN A. DAWSON. Can. J. Chem. **61**, 171 (1983).

In aqueous sodium hydroxide solutions at 25°C, 3-methyl-2-butenal, **1***c*, undergoes retroaldol cleavage to acetone and acetaldehyde. The kinetics of the retroaldol reaction were followed spectrophotometrically at 242 nm and showed simple first order behavior. When 3-methyl-3-hydroxybutanal, **2***c*, was added to aqueous sodium hydroxide solutions at 25°C, there was an initial increase in absorbance at 242 nm, attributed to formation of **1***c*, followed by a 20-fold slower decrease; the rate of the slow decrease matches the rate of disappearance of **1***c* under the same conditions. Analysis of the kinetics allows determination of the three rate constants needed to describe the system: $k_{hyd} = 0.00342$; $k_{dehyd} = 0.00832$; $k_{retro} = 0.0564$; all M^{-1} s^{-1}. The equilibrium constant for enone hydration is 0.41. Rate constants for the analogous reactions for acrolein and crotonaldehyde could be obtained from the literature. There is a reasonable rate–equilibrium correlation for the retroaldol step. For the enone hydration step, rate and equilibrium constants respond differently to replacement of hydrogen by methyl. It is proposed that this results from release of strain after the rate-determining step by rotation about a single bond; this decrease in strain is reflected in the equilibrium constant but not in the rate constant.

J. PETER GUTHRIE et BRIAN A. DAWSON. Can. J. Chem. **61**, 171 (1983).

Le méthyl-3 buténal-2 (**1***c*), dans des solutions aqueuses d'hydroxyde de sodium à 25°C, subit un clivage rétroaldolique conduisant à l'acétone et l'acétaldéhyde. On a suivi spectrophométriquement à 242 nm la cinétique de cette réaction simple d'ordre un. Lorsqu'on ajoute du méthyl-3 hydroxy-3 butanal (**2***c*) à des solutions aqueuses d'hydroxyde de sodium à 25°C, il y a une augmentation initiale de l'absorption à 242 nm que l'on attribue à la formation du composé **1***c* suivie d'une diminution qui est 20 fois plus lente; le taux de la faible diminution correspond au taux de disparition du produit **1***c* dans ces mêmes conditions. L'analyse des données cinétiques permet de déterminer les trois constantes de vitesse nécessaires à la description du système: $k_{hyd} = 0{,}00342$; $k_{déhyd} = 0{,}00832$; $k_{rétro} = 0{,}564$; tous M^{-1} s^{-1}. La constante d'équilibre de l'hydratation de l'énone est égale à 0,41. On peut obtenir dans la littérature les constantes de vitesse des réactions analogues de l'acroléine et du crotonaldéhyde. Il y a corrélation raisonnable entre vitesse et équilibre pour l'étape de rétroaldol. Dans l'étape d'hydratation de l'énone, les constantes de vitesse et d'équilibre répondent différemment au remplacement d'un hydrogène par un méthyle. On propose que ceci provient d'une diminution de contrainte, après l'étape déterminante, provenant de la rotation autour d'une liaison simple. Cette diminution de contrainte se réflète dans les constantes d'équilibre mais pas dans les constantes de vitesse.

[Traduit par le journal]

Can. J. Chem. Downloaded from www.nrcresearchpress.com by 210.87.254.42 on 09/06/12
For personal use only.

Introduction

We have reported a study (1) of the equilibrium constants for aldol condensation reactions. It seemed highly desirable to look for rate–equilibrium correlations for these synthetically important reactions, particularly since equilibrium constants were now available. However, there have been comparatively few kinetics investigations of aldol reactions. This is in large measure due to the great potential for complexity for most aldol reactions, with various modes of reaction, competing equilibria, and polymerization leading to hopelessly complicated mixtures. We have shown that much of this complexity can be avoided by studying the retroaldol reaction at low concentrations, in a study of the reaction of crotonaldehyde in dilute aqueous base (2). We now wish to report a study of a closely related compound with one additional carbon methyl group, namely 3-methyl-2-butenal, **1***c*. These new results, combined with data from the literature, allow a detailed comparison of the kinetic behavior of compounds **1***a–c*.

Results and discussion

The retroaldol reaction of **1***c* can be followed spectrophotometrically; when **1***c*, as a solution in acetonitrile, is injected into aqueous sodium hydroxide solution there is a smooth disappearance of the absorbance at 242 nm, which

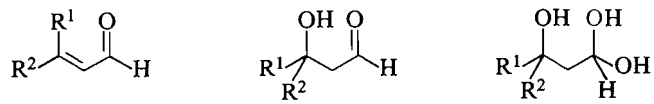

1*a–c* **2***a–c* **3***a–c*

a: R' = R^2 = H
b: R' = H, R^2 = CH_3
c: R' = R^2 = CH_3

SCHEME 1

follows a simple first order rate law. Thus one can see no sign of the two stages which are believed to be essential for this reaction (eqs. [1] and [2])

$$[1]\quad (CH_3)_2C{=}CH{-}CHO \underset{k_{21}}{\overset{k_{12}}{\rightleftharpoons}} (CH_3)_2COO + CH_3{-}CHO \qquad K_1$$

$$[2]\quad (CH_3)_2COH{-}CH_2{-}CHO \underset{k_{23}}{\overset{k_{23}}{\rightleftharpoons}} (CH_3)_2CO + CH_3{-}CHO \qquad K_2$$

The two phases of the reaction are quite apparent when the aldol, 3-methyl-3-hydroxybutanal, **2***c*, is injected into aqueous sodium hydroxide solution; the absorbance at 242 nm first rises and then, about 20 times more slowly, falls again; see Fig. 1. The rate of the slow fall in absorbance is essentially identical to the rate of disappearance of the absorbance of **1***c* when the

[1]E. W. R. Steacie Fellow, 1980–1982, and author to whom correspondence may be addressed.

0008-4042/83/010171-08$01.00/0

©1983 National Research Council of Canada/Conseil national de recherches du Canada

Can. J. Chem. Downloaded from www.nrcresearchpress.com by 210.87.254.42 on 09/06/12
For personal use only.

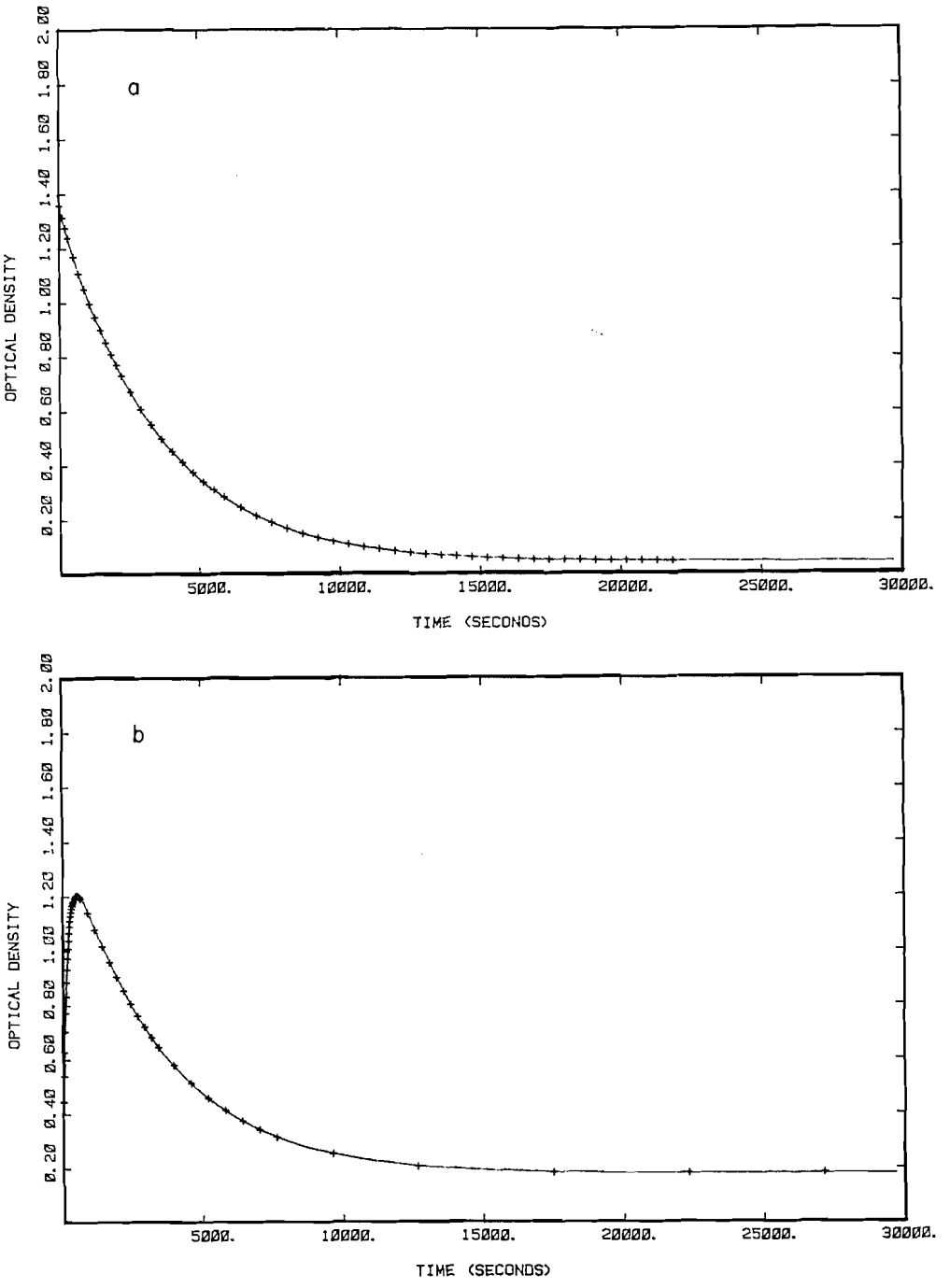

FIG. 1. Absorbance vs. time curves for reactions of 3-methyl-2-butenal (a) and 3-hydroxy-3-methylbutanal (b) with 0.1 *N* NaOH in water at 25°C. The lines are calculated using parameters determined by least squares. At the maximum in (b) 11% of the starting material had been converted to 3-methyl-2-butenal.

latter is used to initiate reaction. Analysis of the two-phase kinetics data permits evaluation of the rate constants. For the system of interest, where a low concentration of aldol product undergoes retroaldol cleavage, the rate of the second order aldol formation process, k_{32}, is negligible. A rigorous solution of the kinetics equations is possible following the procedure described in Moore and Pearson (3), and leads to eq. [3] which gives the absorbance as a function of time.

$$[3] \quad A = A_\infty + \alpha \exp(-\lambda_2 t) + \beta \exp(-\lambda_3 t)$$

where: A = absorbance, A_∞ = absorbance at infinite time, $\lambda_{2,3} = (p \pm q)/2$, $p = k_{12} + k_{21} + k_{23}$, and $q = (p^2 - 4k_{12}k_{23})^{1/2}$. When reaction starts with **1***c*,

$$\alpha = C_1^0 k_{12}\epsilon_1(\lambda_2 - k_{23})\{1 - \epsilon_2\lambda_2/\epsilon_1(\lambda_2 - k_{23}) - \epsilon_3 k_{23}/\epsilon_1(\lambda_2 - k_{23})\}/\lambda_2(\lambda_2 - \lambda_3)$$

$$\beta = C_1^0 k_{12}\epsilon_1(k_{23} - \lambda_3)\{1 - \epsilon_2\lambda_2/\epsilon_1(k_{23} - \lambda_3) - \epsilon_3 k_{23}/\epsilon_1(k_{23} - \lambda_3)\}/\lambda_3(\lambda_2 - \lambda_3)$$

When reaction starts with the aldol,

$$\alpha = C_2^0 k_{21}\epsilon_1\{-1 + \epsilon_2(\lambda_2 - k_{12})/\epsilon_1 k_{21} - \epsilon_3 k_{23}(\lambda_2 - k_{12})/\epsilon_1 k_{21}\lambda_2\}/(\lambda_2 - \lambda_3)$$

TABLE 1. Kinetic results for 3-methyl-2-butenal and 3-methyl-3-hydroxybutanal[a]

[NAOH]	α	$10^3 \times \lambda_2$	β	$10^4 \times \lambda_3$	$10^4 \times k_{21}$	$10^3 \times k_{23}$	$10^4 \times k_{12}$	K_{app}
3-Methyl-2-butenal as substrate[b]								
1.0[c]			1.353±0.002	31.54±0.039				
0.6[c]			1.295±0.001	16.85±0.012				
0.3[c]			1.314±0.001	7.922±0.004				
0.1[c]			1.324±0.0003	2.325±0.001				
0.1			1.312±0.0004	2.901±0.001				
3-Hydroxy-3-methylbutanal as substrate								
0.098[d]	−1.209±0.002	5.506±0.018	1.276±0.001	2.928±0.004	7.31±0.37	4.73±0.04	3.41±0.03	0.467±0.020
0.0588[e]	−1.203±0.001	3.429±0.012	1.232±0.001	1.727±0.002	4.29±0.22	3.04±0.03	1.99±0.02	0.463±0.020
0.0291[f]	−0.995±0.0003	1.800±0.002	1.016±0.0003	0.863±0.0004	2.28±0.12	1.56±0.01	1.00±0.01	0.437±0.019
0.01[g]	−1.147±0.001	0.651±0.016						

[a]In aqueous solution, 1% (v/v) acetonitrile, at 25°C, ionic strength 0.1 (KCl) unless otherwise noted.
[b]Initial substrate concentration was 1.143×10^{-5} *M*.
[c]Ionic strength was 1.0 (KCl).
[d]Initial substrate concentration was 7.65×10^{-5} *M*.
[e]Initial substrate concentration was 8.01×10^{-5} *M*.
[f]Initial substrate concentration was 6.41×10^{-5} *M*.
[g]Initial substrate concentration was 8.01×10^{-5} *M*.

$$\beta = C_2^0 k_{21}\epsilon_1\{1 - \epsilon_2(\lambda_3 - k_{12})/\epsilon_1 k_{21} + \epsilon_3 k_{23}(\lambda_3 - k_{12})/\epsilon_1 k_{21}\lambda_3\}/(\lambda_2 - \lambda_3)$$

where in either case: ϵ_1 = extinction coefficient for **1***c*, ϵ_2 = extinction coefficient for aldol, ϵ_3 = extinction coefficient for the products (acetaldehyde plus acetone), and C_i^0 = initial concentration of **1***c* ($i = 1$) or aldol ($i = 2$). These equations can be usefully simplified by noting that $\epsilon_1 \gg \epsilon_2, \epsilon_3$, so that for reaction starting with **1***c*:

$$\alpha \simeq C_1^0 k_{12}\epsilon_1(\lambda_2 - k_{23})/\lambda_2(\lambda_2 - \lambda_3)$$

$$\beta \simeq C_1^0 k_{12}\epsilon_1(k_{23} - \lambda_3)/\lambda_3(\lambda_2 - \lambda_3)$$

and for reaction starting with the aldol, **2***c*:

$$\beta \simeq -\alpha \simeq C_2^0 k_{21}\epsilon_1/(\lambda_2 - \lambda_3)$$

For reactions starting with the aldol, **2***c*, the individual rate constants can now be calculated using:

$$k_{21} = (\lambda_2 - \lambda_3)\beta/C_2^0\epsilon_1$$

$$k_{23} = \{(p - k_{21}) + \sqrt{[(p - k_{21})^2 - 4\lambda_2\lambda_3]}\}/2$$

$$k_{12} = \{(p - k_{21}) - \sqrt{[(p - k_{21})^2 - 4\lambda_2\lambda_3]}\}/2$$

The equilibrium constant for the first step can be calculated using:

$$K_1 = k_{12}/k_{21}$$

We were concerned that k_{12} might be subject to error because it is the result of a subtraction of larger quantities. k_{12} can also be calculated from the steady state rate equation,

$$\lambda_3 \simeq k_{12}k_{23}/(k_{21} + k_{23})$$

which can also be derived from the above rigorous solution when $k_{12} \ll k_{21}, k_{23}$. Error analysis showed that both methods led to comparable uncertainty in k_{12} and that this uncertainty was no greater than for the other rate constants. There is of course an ambiguity in the quadratic solution, so that chemical intuition must be used to assign the identity of the larger and smaller roots. In the present case the assignment can be made as follows. The value of β is about 0.14 of the value expected if all of the aldol, **2***c*, were converted into **1***c*, requiring that k_{21} and k_{23} be in approximately this ratio. Since k_{21} is about 0.15 of the larger root of the quadratic, this larger root must be k_{23}, and the smaller root of the quadratic equation, which is smaller

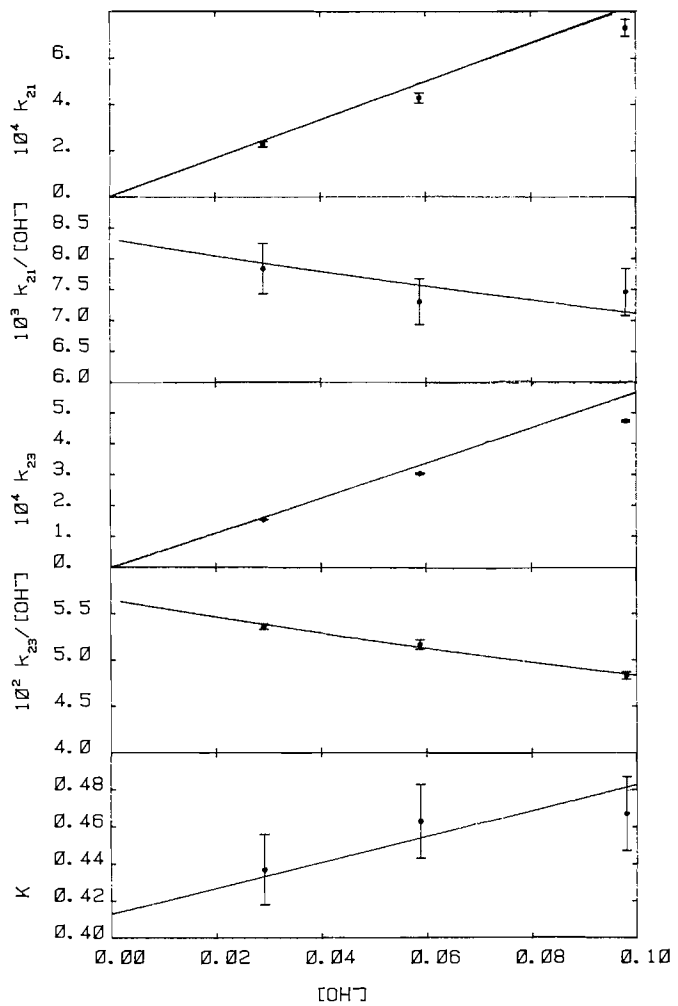

Fig. 2. Hydroxide dependence for rate and equilibrium constants derived from the kinetic parameters for **1***c* and **2***c*.

Can. J. Chem. Downloaded from www.nrcresearchpress.com by 210.87.254.42 on 09/06/12
For personal use only.

TABLE 2. Second order rate constants and equilibrium constant for **1***c* extrapolated to zero hydroxide concentration[a]

Rate constant	Value
k_{12}	$3.42\pm0.05 \times 10^{-3}$[b]
k_{21}	$8.32\pm0.34 \times 10^{-3}$[b]
k_{23}	$5.64\pm0.03 \times 10^{-2}$[b]
K_1	0.413 ± 0.011[c]

[a]In aqueous solution at 25°C, μ = 0.1 (KCl).
[b]M^{-1} s^{-1}.
[c]Dimensionless; $K_1 = k_{12}/k_{21}$.

TABLE 3. pK_a results for formaldehyde hydrate

Temperature (°C)	pK_a	Reference
0	14.0	20
15	12.92	21
20	13.4	22
23	12.79	23
25	13.29	9
25	12.80	Calculated from results in ref. 6
25	12.92	Calculated from results in ref. 11
30	12.89	24
40	12.69	10
50	12.48	25

than k_{21}, must be k_{12}. That apparently single exponential kinetics were observed when reaction began with **1***c* is consistent with the rate constants derived from the analysis just described; the amplitude of the unobserved fast exponential process is calculated to be only about 5% of the amplitude of the observed slow exponential process when the rate constants derived from the analysis are substituted in eq. [3].

Table 1 shows the results of applying this analysis to the experimental data for **1***c* and the corresponding aldol, **2***c*. The rate constants refer to the *total* aldol concentration including the aldehyde, the carbonyl hydrate, and the anion of the carbonyl hydrate. The individual rate constants show the expected first order dependence upon the hydroxide concentration, but there may be a more complex dependence for some; see Fig. 2. We had previously (2) found that for crotonaldehyde, **2***b*, k_{21}, k_{23}, and $1/K_1$ showed a dependence upon hydroxide concentration of the form:

$$k_i = k_i^0/(1 + a[OH^-])$$

Similar behavior appears to be shown here, although one cannot be very confident because the variation with changing hydroxide concentration is only clearly greater than experimental error for k_{21}. Table 2 shows the second order rate constants for the individual steps evaluated in this work, corrected where appropriate to zero hydroxide ion concentration.

Another source of concern is that there appears to be a slight dependence of the second order rate constants for breakdown of **1***c* upon the hydroxide concentration. This seems most improbable because there is no obvious mechanistic path allowing two equivalents of hydroxide to be involved in the transition state. The curvature, if such there is, is slight and close to the limits of detection. The possibility that it is an artefact caused by imperfect matching of salt effects between KCl and NaOH must be kept in mind.

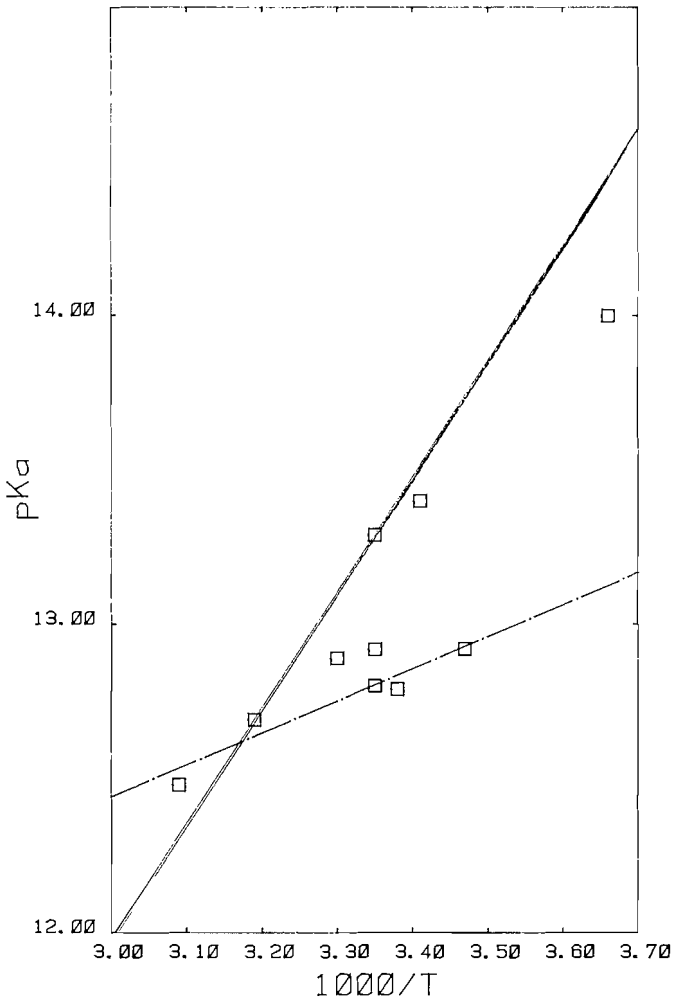

FIG. 3. Temperature dependence for the pK_a of formaldehyde hydrate (——) line based on assumption 1; (–·–·–) line based on assumption 2.

The enone hydration[2] of **1***c* has been studied in acidic solution by Lucas *et al.* (4). In experiments at 25°C and ionic strength 1.04, these authors report a hydration constant of 0.39, which is in reasonable accord with our value at ionic strength of 0.1 of 0.41.

Comparison with lower homologs

It is now possible to compare the kinetic and thermodynamic behavior of the three aldehydes of general structure **1**, with R^1, R^2 = H or CH_3. We have previously reported equilibrium constants for the aldol addition reactions and the enone dehydration steps (1). For crotonaldehyde, **1***b*, we have reported kinetics for the enone hydration, enone dehydration, and retroaldol steps (2). Ogata *et al.* (5) and Vik (6) have reported studies of the aldol addition reaction of acetaldehyde and formaldehyde, and Vik (7) has reported a study of the base catalyzed enone hydration of acrolein, **1***a*. The acid catalyzed enone hydration of acrolein had been studied earlier by Pressman and Lucas (8). From these results it has proven possible to extract the rate constants needed in the present context.

[2]We will use "carbonyl hydration" to refer to addition of water to a carbonyl group, and "enone hydration" to refer to the 1,4-addition of water to an α,β-unsaturated carbonyl compound to give the β-hydroxy carbonyl compound.

Can. J. Chem. Downloaded from www.nrcresearchpress.com by 210.87.254.42 on 09/06/12
For personal use only.

Can. J. Chem. Downloaded from www.nrcresearchpress.com by 210.87.254.42 on 09/06/12
For personal use only.

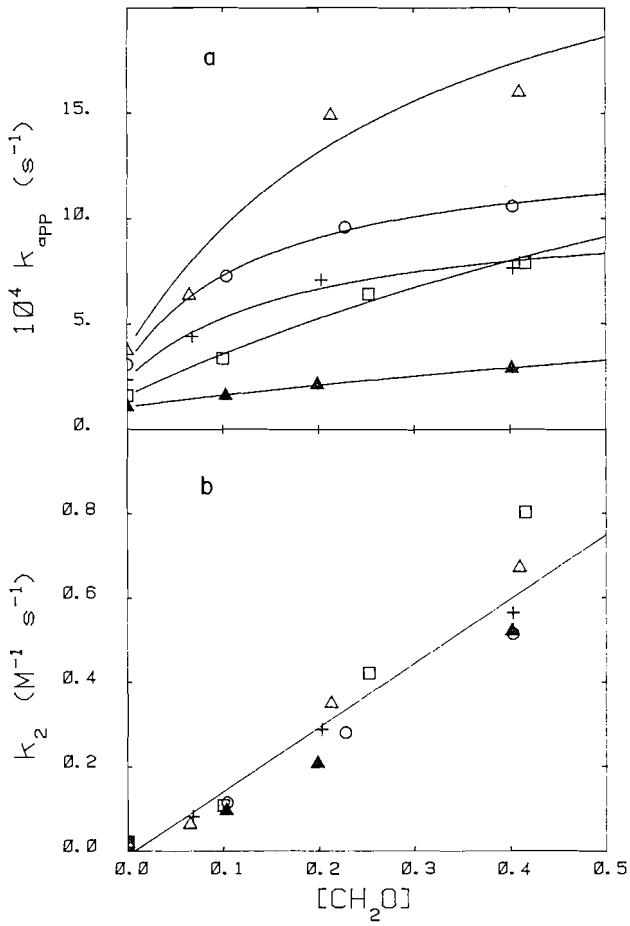

FIG. 4. Rate constants for aldol formation from formaldehyde and acetaldehyde. (a) Relationship between observed rate constants and the total formaldehyde concentration for various hydroxide concentrations: data from ref. 5, curves calculated as described in the text. (▲) 0.005 *M* NaOH; (□) 0.009 *M* NaOH; (+) 0.012 *M* NaOH; (○) 0.018 *M* NaOH; (△) 0.021 *M* NaOH. (b) Relationship between rate constants, corrected as described in the text for consumption of hydroxide by neutralization of formaldehyde hydrate, and the total formaldehyde concentration; data from ref. 5.

Unfortunately, upon critical examination of the paper by Ogata *et al.* (5), it became clear that it was necessary to reanalyse their data. Ogata *et al.* reported that the pseudo first order rate constant at fixed hydroxide concentration showed a nonlinear dependence upon formaldehyde concentration, levelling off at high formaldehyde concentration. They interpreted this as a change in rate-determining step from the aldol addition step to the proton transfer step. However, as Vik (6) had pointed out, the concentration of hydroxide in the kinetics solutions is not the same as the titrimetric concentration of base, which is what Ogata *et al.* assumed, because of partial neutralization of the weakly acidic formaldehyde hydrate (pK_a13.29 at 25°C (9). So long as the aldol addition step is rate limiting, it is the concentration of hydroxide ion, and not the total base concentration, which controls the concentration of the enolate of acetaldehyde, and thus the rate of reaction. Vik (6) carried the study to still higher formaldehyde concentrations where there was an actual decrease in apparent second order rate constant, which almost certainly indicates that there was a change in rate-determining step from addition to proton transfer. Unfortunately Vik (6) only reports apparent second order rate constants obtained by dividing the pseudo first order rate constants by the total base concentration, and does not report the base concentration used, so that the rate constants needed for our purposes cannot be extracted from his data. Since Ogata *et al.* (5) report their data in more detail it is possible to extract an approximate value of the rate constant which we require. The first step is to obtain basicity constants for formaldehyde hydrate as a function of temperature. Martin (10) has reviewed the early literature and reports a carefully determined value at 40°C. Bell and Onwood (9) report a value of 13.29 at 25°C. The data when plotted show considerable scatter; see Table 3 and Fig. 3. Bell's value, which is widely quoted in literature, is not in agreement with the trend of most values at comparable temperatures. Furthermore Vik (6) reports pH values which lead to a pK_a value of 12.8 ± 0.1 for 25°C. Other workers (11) have reported data leading to a value of 12.92.[3] To assess the uncertainty introduced by this discrepancy in pK_a values we have tried two approaches: (1) to choose Bell's value at 25°C and Martin's value at 40°C as two recent and reliable values and use them as the basis for estimates at lower temperatures; (2) to discard Bell's value at 25°C and two other discordant values and fit the remaining data by least squares. The K_b values resulting from both methods are given in Table 4, and Fig. 3 shows the relationship of the two hypotheses to the data. It should be noted that although either hypothesis leads to a similar ΔH for pK_a, the two hypotheses lead to opposite signs for the temperature dependence of pK_b. It is straightforward to derive eq. [4] which gives the true hydroxide concentration as

TABLE 4. Rate constants for aldol addition of acetaldehyde to formaldehyde[a]

Temperature (°C)	Assumption 1 K_b	Assumption 1 Rate constant (M^{-2} s^{-1})	Assumption 2 K_b	Assumption 2 Rate constant (M^{-2} s^{-1})
5	2.8	0.042±0.008	46.	0.505±0.079
10	3.3	0.087±0.034	33.	0.683±0.169
15	3.9	0.198±0.045	27.	1.038±0.212
20	4.4	0.433±0.122	20.	1.516±0.400
25	5.1	(0.876)	16.	(2.10)

[a]Rate constants derived from data in ref. 5 as described in the text. K_b values calculated from K_a values estimated as described in the text, and K_w values from ref. 26.

TABLE 5. Equilibrium constants for carbonyl hydration of aldehydes[a]

Compound	K_h
CH_2O	2280[b]
CH_3CHO	1.06[c]
HO—CH_2-CH_2-CHO	2.28[d]
HO-CH(CH_3)—CH_2-CHO	2.15[d]
HO-C(CH_3)$_2$-CH_2-CHO	2.03[d]

[a]K_h = [hydrate]/[carbonyl compound], in water at 25°C.
[b]Reference 27.
[c]Reference 28.
[d]Estimated as described in text.

[3]This value was obtained by correcting the pK_a values in ref. 11 for ionic strength effects using the Davies equation (12) and then plotting the corrected pK_a values as a function of ionic strength in order to extrapolate to zero ionic strength. A reasonably straight line (r = 0.986) was obtained.

TABLE 6. Rate and equilibrium constants for the retroaldol reactions of **1***a–c*[a]

Compound	k_{12}[b]	k_{21}[b]	K_1[c]	k_{23}[b]	k_{32}[d]	K_2[e]
Acrolein, **1***a*[f]	0.305	0.0987	3.09	7×10^{-5}	4100.	6×10^{7}
Crotonaldehyde, **1***b*[g]	0.035	0.110	0.318	0.0088	4.71	396.
3-Methyl-2-butenal, **1***c*[h]	0.0034	0.025	0.136	0.171	0.043	0.4

[a]In aqueous solution at 25°C; corrected for carbonyl hydration of aldehydes.
[b]M^{-1} s^{-1}.
[c]Dimensionless; K_1 = [**2**]/[**1**].
[d]M^{-2} s^{-1}.
[e]M^{-1}; K_2 = [**2**]/[acetaldehyde] [carbonyl compound].
[f]Rate constants derived from data in refs. 5 and 6, as described in the text; K_1 from ref. 7, corrected as described in the text; K_2 from ref. 1.
[g]Rate constants derived from data in ref. 2 as described in the text.
[h]This work.

a function of the basicity constant K_b, the total base concentration B, and the formaldehyde concentration F.

$$[4]\quad K_b[OH^-]^2 + \{1 + K_b(F—B)\}[OH^-] - B = 0$$

This equation may readily be solved, but it must be borne in mind that the hydroxide concentrations so calculated are subject to considerable error because of the uncertainties in K_b. Nevertheless they permit a closer approximation to the actual conditions and convert the leveling off in pseudo first order rate constant with increasing formaldehyde concentration reported by Ogata to a simple linear dependence of the apparent second order rate constants upon formaldehyde concentration. Figure 4 shows the data for 20°C plotted as discussed by Ogata *et al.* (5), with curves derived by fitting Ogata's equation (eq. 14a of ref. 5) to the data at a particular hydroxide concentration, and also the second order rate constants obtained by dividing the observed pseudo first order rate constant by the calculated hydroxide concentration (hypothesis 2). The scatter is severe but there is a roughly linear correlation (r = 0.967) with no sign of a change in rate-determining step. By carrying out this procedure at each temperature for both hypotheses concerning pK_a, we obtained two sets of third order rate constants given in Table 4, each of which could be extrapolated to give a rate constant at 25°C. Of the two estimates we prefer the one based on hypothesis 2, which uses concordant data from various laboratories. Hypothesis 1 puts great weight on Bell and Onwood's value (9), which was a conductimetric determination. Although conductimetry is a very precise technique, it is subject to systematic errors if there is an unexpected ionic contaminant.

The apparent third order rate constant for hydroxide catalyzed reaction of acetaldehyde with formaldehyde, 2.10 M^{-2} s^{-1}, can now be corrected for the fraction of acetaldehyde and formaldehyde present as the hydrate, since the carbonyl compounds are the actual reactive species. The carbonyl hydration constants for compounds discussed in this paper are found in Table 5. When this is done the rate constant becomes 9900.M^{-2} s^{-1}. Then using the equilibrium constant which we evaluated for the free carbonyl species, i.e. 6×10^7 M^{-1} (1), we can calculate the rate constant for the reverse reaction, i.e. the breakdown of 3-hydroxypropanal, **2***a*, to be 2×10^{-4} M^{-1} s^{-1}. Vik (7) has reported rate constants for the enone hydration of acrolein, **1***a*, and the enone dehydration of **2***a*. The latter rate constant must be corrected for the carbonyl hydration of **2***a*; since no equilibrium constant for this carbonyl hydration has been reported, we estimate a value by use of a linear free energy relation (13) as previously reported (1); see Table 5. All of the rate constants so derived are found in Table 6.

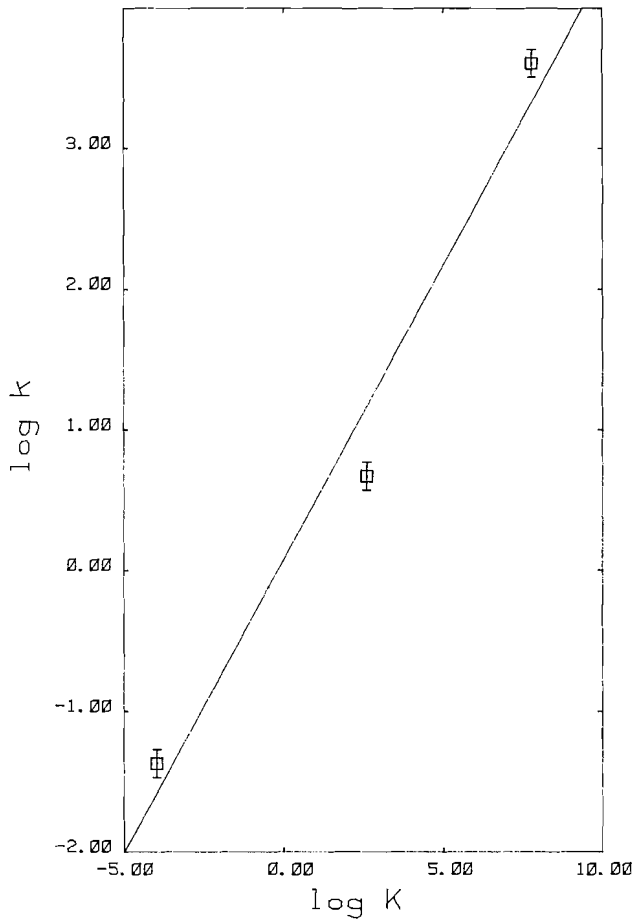

FIG. 5. Relationship between rate and equilibrium constants for the aldol addition of acetaldehyde to formaldehyde, acetaldehyde, and acetone, log k = 0.08 + 0.42 log K; r = 0.985.

The apparent rate constants for the enone hydration and retroaldol reactions of crotonaldehyde, **1***b*, have been reported (2); in a manner analogous to that just described, they can be corrected for carbonyl hydration of the aldehydes to give the values found in Table 6. Similarily the results found in this work may be corrected for aldehyde carbonyl hydration, and the corrected rate constants are given in Table 4.

Examining the results in this table we see that the aldol addition step shows the expected qualitative dependence upon reactivity of the carbonyl group to which addition takes place. Furthermore there is the expected quantitative relationship between the rate and equilibrium constants, as shown by Fig. 5.

Can. J. Chem. Downloaded from www.nrcresearchpress.com by 210.87.254.42 on 09/06/12
For personal use only.

Can. J. Chem. Downloaded from www.nrcresearchpress.com by 210.87.254.42 on 09/06/12
For personal use only.

No simple interpretation can be put upon the nature of this correlation because the rate and equilibrium constants are composite quantities; the equilibrium constant includes enolate formation, the actual C—C bond-forming step, and protonation of the initially formed alkoxide ion. Assuming the C—C bond formation is rate limiting, the apparent rate constant reflects both this step and pre-equilibrium enolate formation. In fact the slope of the least-squares line ($r = 0.985$) is 0.42, which is close to the value of 0.5 expected for $\log K = 0$ on the basis of Marcus theory (14). For the three reactions considered here one expects very similar equilibrium constants for the pre- and post-equilibria, so that the observed correlation will reflect the behavior of the microscopic constants for the rate-determining step. The slope of the correlation line suggests a transition state midway along the reaction coordinate for C—C bond formation. The rate constants for enone hydration show a very regular decrease of about an order of magnitude per methyl group as the terminal hydrogens in acrolein are replaced by methyls.[4] Curiously, this regularity is less apparent in the equilibrium constants; although the first methyl group produces a tenfold decrease in the equilibrium constant for enone hydration, the second methyl produces a much more modest decrease. It is not the deviation from regularity which is curious, but the fact that it shows up only in the equilibrium constant and not in the rate constant. The second methyl would be expected to stabilize the double bond, but also introduces steric crowding; with two opposing effects, the net effect must be smaller than if only the stabilizing effect were present. The fact that the substituent effect is almost the same for rate and equilibrium constants for the first two compounds implies a late transition state; this is apparently inconsistent with the divergent behavior seen for the second methyl group. A plausible rationale is that the equilibrium constant which governs the rate constant is not that for formation of the stable conformation of the hydroxyaldehyde, but that for formation of the initial conformation of the enolate which is the immediate product. In the initial enolate corresponding to **2***c* the crowding between methyl and aldehydic hydrogen is still largely present; see Scheme 2. Thus, as far as the rate constant is concerned, thermodynamics of the enone hydration are affected only by the stabilizing effect of the methyl; the fact that a simple bond rotation will eventually offset most of this stabilization by relieving crowding is irrelevant. We see in this set of reactions an illustration of what we suspect will be a very general pattern; rate–equilibrium correlations must refer to the reactants and products of the microscopic rate-determining process and not to any more stable conformations or tautomers which may be reached by exceedingly fast transformations before or after the rate-determining step.

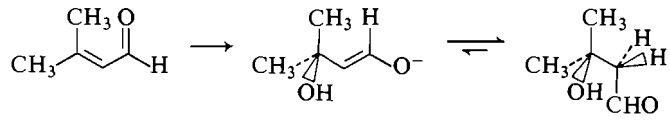

SCHEME 2

Experimental

Methods

Solutions of sodium hydroxide were made up starting with Fisher concentrates, diluting with glass-distilled water which had been boiled to drive out carbon dioxide. Ionic strength was maintained with KCl.

Kinetics were carried out using a Cary 210 spectrophotometer with a thermostatted 10 cm cell holder. A Neslab Exacal circulating bath was used to maintain the temperature at 25.0 ± 0.1°C. Reactions were initiated by adding a suitable amount of a solution of substrate in acetonitrile to the cell containing sodium hydroxide solution, which had been in the thermostatted cell holder for at least 15 min. Digital absorbance data were taken from the Digital Interface Port of the Cary 210 and stored in a Dynabyte BC2 controller board, which supplied time values, until the end of the experiment, when absorbance–time data were transferred to a Xitan microcomputer for permanent storage and processing. Data were fitted to the appropriate equation using weighted least squares by means of programs essentially the same as those previously described (1, 16). For every run direct, semi-log, and residual plots of the experimental data and the calculated line were drawn on an HP6225A plotter.

Preparation of 3-methyl-2-butenal, **1***c*

Oxidation of 3-methyl-2-butenol (Aldrich) was carried out using Ratcliffe's method (17). To a solution of pyridine (9.5 g) in dry methylene chloride (passed through Grade 1 neutral alumina) (150 mL) was added chromium trioxide (6 g). After stirring for ca. 15 min, 3-methyl-2-buten-1-ol (0.86 g) was added and stirring was continued for another 15 min. The organic solvent was decanted off and the tarry residue was washed with ether (2 × 100 mL). The combined organic solvents were washed with 5% NaOH (3 × 100 mL), 5% HCl (100 mL), 5% $NaHCO_3$ (100 mL), and saturated NaCl (100 mL). After drying over $MgSO_4$, the solvent was removed and the oil left behind was distilled, bulb-to-bulb, (bp 100–110°C) under nitrogen at atmospheric pressure. Proton nmr showed the product (0.7 g) to be pure 3-methyl-2-butenal.

Preparation of 3-hydroxy-3-methylbutanal, **2***c*

This compound was prepared by addition of a masked acetaldehyde equivalent to acetone using the procedure devised by Meyers *et al.* (18). To a solution of 2-methyl-2-thiazoline (2.8 g) in dry THF (Karl Fisher titration showed less than 100 μg/mL) (15 mL) at −78°C under a nitrogen atmosphere was added 14.4 mL of n-butyllithium (2.2 *M* in hexanes). After stirring for 2 hours, acetone (2.5 mL) in dry THF (15 mL) was slowly added and stirring was continued as the flask was allowed to come to room temperature (ca. 2.5 hours). The contents of the flask were poured into ice-water and acidified to ca. pH 2 with 6 *N* HCl and then extracted with ether–pentane (1:1). The aqueous layer was made alkaline by adding 20% NaOH, and then extracted with ether (3 × 50 mL). The combined ether extracts were dried over anhydrous potassium carbonate and the solvent removed to give an hydroxythiazoline compound. The proton nmr of this crude product showed that there was a small amount of impurity present.

This crude hydroxythiazoline compound was dissolved in ether which had been previously saturated with water. This solution was treated with freshly prepared aluminum-amalgam (19) (ca. 4 g) by refluxing for 2 hours. The solids were removed by filtration and washed with ether. The combined ether solutions were dried (K_2CO_3) and the ether removed. The proton nmr of this product showed two singlets (δ 1.2 and 1.4) in the region where methyl groups are expected to absorb, indicating that there was more than one product.

This crude product was dissolved in acetonitrile and the solution was slowly added to a solution of mercuric chloride in 80% acetonitrile–water. The mixture was stirred for ca. 15 min and then diluted with water and filtered. The filtrate was extracted with ether–pentane (1:1) and the organic layer was dried (K_2CO_3) and the solvent removed. This crude product was distilled, bulb-to-bulb, to give ca. 0.15 g of a clear oil which proton nmr showed to be 3-hydroxy-3-methylbutanal. A solution of this final product in $CDCl_3$ gave an nmr spectrum which changed with time, reaching an apparent equilibrium (50:50) with what is presumed to be its dimer within 20 h; no further change in the nmr spectrum was seen at 40 h.

[4]That replacement of hydrogens by alkyl groups stabilizes carbonyl groups or alkenes is a well-recognized empirical fact, for which various explanations have been offered (15).

Acknowledgement

We thank the Natural Sciences and Engineering Research Council of Canada for generous financial support.

1. J. P. GUTHRIE. Can. J. Chem. **56**, 962 (1978).
2. J. P. GUTHRIE. Can. J. Chem. **52**, 2037 (1974).
3. J. W. MOORE and R. G. PEARSON. Kinetics and mechanism. 3rd ed. Wiley, New York. 1981. p 296.
4. H. J. LUCAS, W. T. STEWART, and D. PRESSMAN. J. Am. Chem. Soc. **66**, 1818 (1944).
5. Y. OGATA, A. KAWASAKI, and K. YOKOI. J. Chem. Soc. (B), 1013 (1967).
6. J.-E. VIK. Acta Chem. Scand. **26**, 3165 (1972).
7. J.-E. VIK. Acta Chem. Scand. **27**, 251 (1973).
8. D. PRESSMAN and H. J. LUCAS. J. Am. Chem. Soc. **64**, 1953 (1942).
9. (*a*) R. P. BELL and P. T. MCTIGUE. J. Chem. Soc. 2983 (1960); (*b*) R. P. BELL and D. P. ONWOOD. Trans. Faraday Soc. **58**, 1557 (1962).
10. R. J. L. MARTIN. Aust. J. Chem. **7**, 400, (1954).
11. V. V. BUDANOV and V. D. KIBENKO. Izv. Vyssh. Uchebn. Zaved. Khim. Khim. Tekhnol. **13**, 1536 (1970).
12. C. H. DAVIES. J. Chem. Soc. 2093 (1938).
13. P. GREENZAID, Z. LUZ, and D. SAMUEL. J. Am. Chem. Soc. **89**, 749 (1967).
14. A. O. COHEN and R. A. MARCUS. J. Phys. Chem. **72**, 4249 (1968); R. A. MARCUS. J. Am. Chem. Soc. **91**, 7224 (1969); R. A. MARCUS. Annu. Rev. Phys. Chem. **15**, 155 (1964), and references cited therein; A. J. KRESGE. Rev. Chem. Soc. **2**, 475 (1973); J. R. MURDOCH. J. Am. Chem. Soc. **94**, 4410 (1972).
15. J. HINE. Structural effects on equilibria in organic chemistry. Wiley, New York. 1975. Chapt. 8.
16. P. R. BEVINGTON. Data reduction and error analysis for the physical sciences. McGraw–Hill, New York. 1969.
17. R. RATCLIFFE and R. RODEHORST. J. Org. Chem. **35**, 4000 (1970).
18. A. I. MEYERS, J. L. DURANDATTA, and R. MUNAVU. J. Org. Chem. **40**, 2025 (1975).
19. A. L. MEYERS and J. L. DURANDATTA. J. Org. Chem. **40**, 2021 (1975).
20. H. EULER and A. EULER. Ber. Dtsch. Chem. Ges. **38**, 2551 (1905).
21. R. SAUTEREY. Ann. Chem. (12) **7**, 1 (1949).
22. K. VESELY and R. BRDICKA. Coll. Trav. Chim. Tchecosl. **12**, 313 (1947).
23. M. WADANO. Ber. Dtsch. Chem. Ges. **67**, 191 (1934).
24. M. LEVY. J. Biol. Chem. **105**, 157 (1934).
25. H. EULER and T. LOVGREN. Z. Anorg. Chem. **147**, 123 (1925).
26. R. C. WEAST (*Editor*). Handbook of Chemistry and Physics. 48th ed. Chemical Rubber Co., Cleveland, OH. 1967. p. D-92.
27. P. LEHENAFF. Bull. Soc. Chim. Fr. 4687 (1968).
28. J. L. KURZ. J. Am. Chem. Soc. **89**, 3524 (1967).

Can. J. Chem. Downloaded from www.nrcresearchpress.com by 210.87.254.42 on 09/06/12
For personal use only.

Synthesis of 4-hydroxy-3,4-dihydro-1,2,3-benzotriazines via 2-(3-alkyl-1-triazeno)benzaldehydes and 2-(3-alkyl-1-triazeno)benzophenones

PATRICIA L. FAYE AND KEITH VAUGHAN[1]
Department of Chemistry, Saint Mary's University, Halifax, N.S., Canada B3H 3C3

AND

DONALD L. HOOPER
Department of Chemistry, Dalhousie University, Halifax, N.S., Canada B3H 4J3

Received July 26, 1982

PATRICIA L. FAYE, KEITH VAUGHAN, and DONALD L. HOOPER. Can. J. Chem. **61**, 179 (1983).

Diazotization of *o*-aminobenzaldehyde, followed by immediate coupling of the diazonium salt with primary alkylamines, affords unstable 1-aryl-3-alkyltriazenes which immediately cyclize to the 4-hydroxy-3-alkyl-1,2,3-benzotriazines. Analogous reaction of *o*-aminobenzophenones affords stable 4-aryl-4-hydroxy-3-alkyl-1,2,3-benzotriazines. The 4-hydroxytriazine derived from *o*-anthraniloylbenzoic acid undergoes further cyclization spontaneously to a novel spiro-1,2,3-triazine-furan. Diazotization of *o*-aminopropiophenone and coupling to methylamine affords a surprisingly stable 4-alkyl-4-hydroxytriazine. Preliminary assay of the biological activity of the 4-hydroxytriazines shows significant cytotoxicity of two members of the series towards M21 melanoma cells in vitro.

PATRICIA L. FAYE, KEITH VAUGHAN et DONALD L. HOOPER. Can. J. Chem. **61**, 179 (1983).

La diazotization du *o*-aminobenzaldéhyde, suivie par le couplage immédiat du sel de diazonium avec les alkylamines primaires, fournit les aryl-1 alkyl-3 triazènes instables qui se cyclisent immédiatement en hydroxy-4 alkyl-3 benzotriazines-1,2,3. La réaction analogue des *o*-aminobenzophénones conduit aux aryl-4 hydroxy-4 alkyl-3 benzotriazines-1,2,3 stables. L'hydroxy-4 triazine provenant de l'acide *o*-anthranylbenzoïque subit spontanément une cyclisation plus poussée en un nouveau spiro-triazine-1,2,3 furanne. La diazotization de l'*o*-aminopropiophénone et le couplage avec la méthylamine donne d'une façon surprenante l'alkyl-4 hydroxy-4 triazine stable. Un essai préliminaire de l'activité biologique des hydroxy-4 triazines montre une cytoxicité *in vitro* significative de deux composés de la série vis-à-vis les cellules mélanoma M21.

[Traduit par le journal]

Introduction

The coupling reaction of arenediazonium salts with primary alkylamines affords good yields of the monoalkyltriazenes (ArN=N·NHR) (1), which have attracted wide interest not only because of their chemistry, but also for their pharmacological importance (2). 1-Aryl-3-alkyltriazenes, with reactive substituents in the *ortho*-position of the aryl nucleus, are useful precursors of a variety of heterocyclic triazines (3). For example, coupling the diazonium salt (**1**) derived from *o*-aminoacetophenone with alkylamines leads to the novel 4-methylene-1,2,3-benzotriazines (**4**) (4). The 4-methylenetriazines presumably arise by spontaneous cyclization of the triazene (**2**) and dehydration of the intermediate 4-hydroxytriazine (**3**); neither **2** or **3** could be isolated from this reaction. The instability of the intermediate hydroxytriazine (**3**) derives from the presence of protons on the 4-methyl carbon, which are suitably situated for β-elimination to give the methylenetriazine (**4**).

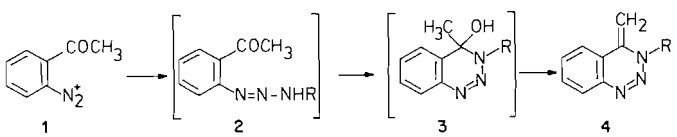

The apparent ease of cyclization of the *o*-acetylphenyltriazenes (**2**) suggests that 4-hydroxytriazines of type **3** might be isolable and stable if the dehydration step **3** → **4** could be prevented. Stable 4-hydroxytriazines analogous to **3** would be expected to arise from *o*-triazenoaryl carbonyl compounds without α-hydrogens, in which case the final dehydration step is structurally impossible. This paper describes this approach to the synthesis of such 4-hydroxy-1,2,3-triazines using *o*-aminobenzophenones and *o*-aminobenzaldehyde as starting materials.

[1]Author to whom all correspondence should be addressed.

Experimental

Melting points were obtained on a hot-stage apparatus and are uncorrected. Infrared spectra were recorded with liquid paraffin mulls on a Perkin–Elmer Model 299 spectrophotometer. Nuclear magnetic resonance spectra were recorded in deuteriochloroform or dimethyl sulfoxide-d_6, using tetramethylsilane as internal standard, with Varian EM360 and CFT-20 spectrometers. Microanalysis was performed by the Canadian Microanalytical Laboratory, Vancouver, B.C. *o*-Aminobenzophenones and *o*-nitrobenzaldehyde were obtained from Aldrich Chemical Company and were used without further purification.

4-Hydroxy-3-alkyl (aryl)-1,2,3(4H)-benzotriazines (7)

General procedure

o-Aminobenzaldehyde (**5**) was prepared immediately before use by reduction of *o*-nitrobenzaldehyde with ammonia and ferrous sulphate according to the method of Smith and Opie (5).

o-Aminobenzaldehyde (1.44 g, 0.012 mol) was ground in a mortar with solid sodium nitrite (0.83 g, 0.012 mol) to a fine homogeneous powder. The solid mixture was slurried with water (4 mL) and added slowly with constant agitation to a mixture of concentrated hydrochloric acid (2.1 mL) and ice (5 g). Transfer of the slurry to the acid/ice mixture was facilitated by several washings with small amounts of water (total volume 10 mL). The temperature of the mixture was maintained below 5°C during this process. The mixture was filtered onto ice (~8 g) and the clear filtrate/ice mixture (containing the diazonium salt) was mixed with a cold solution of the appropriate amine (0.025 mol) in water (2 mL) or 2 *M* hydrochloric acid

0008-4042/83/010179-05$01.00/0
©1983 National Research Council of Canada/Conseil national de recherches du Canada

Can. J. Chem. Downloaded from www.nrcresearchpress.com by 210.87.254.105 on 09/06/12
For personal use only.

Can. J. Chem. Downloaded from www.nrcresearchpress.com by 210.87.254.105 on 09/06/12
For personal use only.

TABLE 1. Physical and spectroscopic data of the 4-hydroxy-3-alkyl(aryl)-1,2,3(4*H*)-benzotriazines (**7**)[a]

No.	R	% Yield	Melting point (°C)	Crystal type	Solvent	Infrared spectrum (cm^{-1})	Nuclear magnetic resonance spectrum DMSO-d_6			
							Arom. (m)	OH	H(C-4)	N^3—R
7*a*	Me	30	95–97	White needles	Hexane/benzene	3170(br)	7.25–7.55(4H)	6.65(1H, d, J=8 Hz)	5.80(1H, d, J=8 Hz)	3.60(3H, s)
7*b*	Et	38	88–90	White prisms	Hexane/benzene	3150(br)	7.35–7.60(4H)	6.65(1H, d, J=8 Hz)	5.90(1H, d, J=8 Hz)	3.95(2H, q, J=7 Hz) 1.35(3H, t, J=7 Hz)
7*c*	$PhCH_2$	37	121–122	Buff prisms	Hexane/benzene	3100(br)	7.30–7.70(9H)	6.87(1H, d, J=8 Hz)	5.73(1H, d, J=8 Hz)	5.20(2H, S)
7*d*	Ph	42	117–119	Yellow needles	Hexane/benzene	3180(br)	7.20–7.90(9H)	6.97(1H, d, J=8.5 Hz)	6.53(1H, d, J=8.5 Hz)	

[a]All compounds gave satisfactory C, H, and N analyses (±0.3%).

(12 mL). The resulting mixture was stirred in the cold for 2.5 h and then filtered to afford the solid product, which was recrystallized from hexane/benzene mixture. The yields and physical data of these 4-hydroxytriazines are given in Table 1.

*4-Aryl-4-hydroxy-3-methyl-1,2,3-benzotriazines (**9**)*

General procedure

The *o*-aminobenzophenone (**8**) (0.01 mol) was suspended in 2 *M* hydrochloric acid (24 mL) and the mixture heated to boiling. Concentrated hydrochloric acid (1.6 mL) was added to take the amine into solution, which was then diluted with water (32 mL) and cooled to below 5°C, whereupon the hydrochloride salt precipitated. The cold slurry was diazotized with sodium nitrite (0.77 g) in water (10 mL) and stirred until a clear solution was obtained (usually no more than 1 h). Aqueous methylamine (40%, 7.2 mL) was added in one portion to the cold diazonium salt solution, which raised the pH of the mixture to approximately 9–10. The product precipitated immediately and was filtered, usually at once, dried, and recrystallized from an appropriate solvent to afford the 4-aryl-4-hydroxy-3-methylbenzo-1,2,3-triazine (**9**) (Table 2). *Note:* In some instances, the *o*-aminobenzophenone did not dissolve readily in hot hydrochloric acid, resulting in low yields. In the case of 2-amino-2′,5-dichlorobenzophenone, the diazotization was carried out in concentrated nitric acid without diffuculty and the remaining procedure carried out as described above. Diazotization of 2-amino-3-nitrobenzophenone was also carried out in nitric acid, but coupling with methylamine was only partially successful; in one instance a violent reaction occurred when methylamine was added to the diazonium salt in one portion and in another, under more controlled conditions, a low yield of a very impure product was obtained.

*3′,4′-Benzo-5,6-benzo-3-methyl-5′-oxo-spiro[1,2,3-triazine-4,2′-furan] (**12**)*

o-Anthraniloylbenzoic acid (**10**) (2.47 g) was suspended in 2 *M* hydrochloric acid (24 mL) and concentrated hydrochloric acid (4.2 mL) was added. The mixture was diluted with water (32 mL), and then cooled to below 5°C. The suspension was diazotized with sodium nitrite (0.71 g) in a minimum volume of water and stirred for 1 h. The mixture was filtered and the clear filtrate (diazonium salt solution) was treated with 40% aqueous methylamine (7.4 mL) in one portion. The pH of the solution rose to ~10 and an off-white precipitate appeared almost immediately. The product was filtered and recrystallized from absolute alcohol to afford the spiro-lactone (**12**) (yield 0.47 g, 17.5%), mp 175–176°C (EtOH) (buff needles); ν_{max}: 1765 cm^{-1}; δ($CDCl_3$): 3.3 (s, 3H), 6.5–8.2 (m, 8H). *Anal.* calcd. for $C_{15}H_{11}N_3O_3$: C 67.92, H 4.18, N 15.84%; found: C 67.69, H 4.33, N 15.76.

*4-Ethyl-4-hydroxy-3-methyl-1,2,3-benzotriazine (**14**)*

o-Nitropropiophenone was prepared by nitration of propiophenone according to the method of Zenitz and Hartung (6). Reduction of the *o*-nitropropiophenone by a modification of the method of Simpson *et al.* (7) afforded a good yield of *o*-aminopropiophenone, which was purified by steam distillation before use.

o-Aminopropiophenone (**13**) (1.5 g) was dissolved in 2*M* hydrochloric acid (24 mL), to which concentrated hydrochloric acid (1.6 mL) was added to facilitate dissolution. The solution was diluted with water (32 mL) and then cooled to 0°C in an ice/salt bath. The cold solution was stirred while a solution of sodium nitrite (0.75 g) in water was added slowly with constant stirring. The mixture was stirred in the cold for 0.75 h and the resulting diazonium salt solution treated with a cold solution of methylamine (40%, 6.8 mL), stirred in the cold for a further 0.75 h, and filtered to afford the 4-ethyl-4-hydroxy-3-methyl-1,2,3-benzotriazine (**14**), 1.4 g (80%), mp 108°C (from benzene): ν_{max}: 2600–3300 cm^{-1}; δ (DMSO d_6): 0.65 (3H, t, J = 7.4 Hz, C—CH_3), 2.20 (2H, q, J = 7.4 Hz, —CH_2-), 3.59 (3H, s, N—CH_3), 6.84 (1H, s, OH), and 7.3–7.6 (4H, m, aromatic). *Anal.* calcd. for $C_{10}H_{13}N_3O$: C 62.81, H 6.85, N 21.97%; found: C 62.93, H 6.76, N 22.12%.

Can. J. Chem. Downloaded from www.nrcresearchpress.com by 210.87.254.105 on 09/06/12
For personal use only.

Discussion

A minor problem encountered in the experimental approach to the 4-hydroxytriazines was the diazotization of *o*-aminobenzaldehyde (**5**). The tendency of *o*-aminobenzaldehydes to form polymeric products when treated with acid (8) makes diazotization by addition of aqueous sodium nitrite to an acidic solution of the amine (**5**) unfeasible. Successful

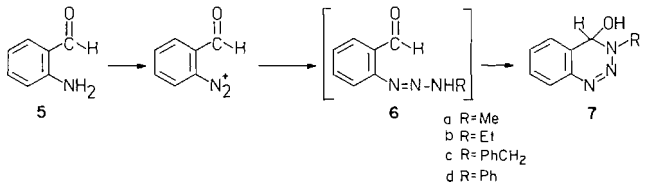

diazotization of **5** has been achieved by slurrying a solid mixture of the amine and sodium nitrite in water and treating the slurry with hydrochloric acid and ice (9). The latter method has been employed in the present work to prepare the diazonium salt of **5**. However, significant material loss results during the filtration step necessary to achieve a clear solution of diazonium salt before further treatment, which probably accounts for the poor yields of the final products.

Treatment of the diazonium salt of **5** with an aqueous solution of the primary alkylamine affords the 4-hydroxy-3-alkyl-1,2,3-benzotriazine (**7**). The spectroscopic properties of the products of these reactions are consistent with the cyclic benzotriazine structure (**7**) rather than the open-chain triazene valence tautomer (**6**). The cyclization of the diazonium-coupling product (**6**) appears to be spontaneous and the cyclic hydroxytriazines (**7**) are stable crystalline solids. The method is equally applicable to the synthesis of 3-alkyl- and 3-aryl-4-hydroxytriazines. A significant feature of the ir spectra of these 4-hydroxy triazines (**7**) is the absence of carbonyl absorption, which rules out the open-chain structure (**6**) in favour of **7**. The cyclic structure is further corroborated by the presence in the ir spectra of hydroxyl absorption in the range 3100–3180 cm^{-1}; these OH bands are relatively sharp and readily observed in Nujol mulls. Aside from the characteristic hydroxyl band, the ir spectra show no other outstanding features.

The nmr spectra (Table 1) of the 4-hydroxytriazines in DMSO-d_6 provide unequivocal evidence of the cyclic triazine structure (**7**). All compounds exhibit an aromatic multiplet in the range 7.20–7.90 ppm and the predicted signals for the alkyl group at N-3: a singlet at 3.60 ppm for the N—Me group of **7***a*; a triplet at 1.35 ppm and quartet at 3.95 ppm for the N—Et group of **7***b*; and a singlet at 5.20 ppm for the benzylic *N*-methylene group of **7***c*. The most striking features of these spectra are the two one-proton doublets arising from the vicinal coupling (J = 8–8.5 Hz) between the methine proton at C-4 and the hydroxylic proton of the OH group attached to C-4. The hydroxylic proton is observed at 6.65 ppm in the spectra of the *N*-methyl (**7***a*) and *N*-ethyl (**7***b*) derivatives and is shifted downfield to 6.87 ppm in the *N*-benzyl derivative (**7***c*) and to 6.97 ppm in the *N*-phenyl analogue (**7***d*). The C-4 methine proton appears in the range 5.7–5.9 ppm in the *N*-alkyl triazines (**7***a*, *b*, and *c*) and is also shifted downfield to 6.53 ppm in the *N*-phenyl triazine (**7***d*). In each case (**7***a–d*) the addition of D_2O to the DMSO-d_6 solution resulted in the disappearance of the OH resonance and the collapse of the C-4 methine proton doublet to a singlet, providing confirmation of the assignments of these signals.

Diazotization of the *o*-aminobenzophenones (**8**) by addition

TABLE 2. Physical and spectroscopic data of the 4-aryl-4-hydroxy-3-methyl-1,2,3-benzotriazines (**9**)[a]

No.	R^1	R^2	R^3	% Yield	Melting point (°C)	Crystal type	Solvent	Infrared spectrum (cm^{-1})	Nuclear magnetic resonance spectrum DMSO-d_6			
									Arom. (m)	OH(s)	N—Me(s)	R^3
9*a*	**H**	**H**	H	96	140–142	White needles	EtOH	2600–3300	6.8–7.6(9H)	7.40(1H)	3.20(3H)	—
9*b*	Cl	**H**	H	55	144–146	White needles	CH_3CN/ EtOH	2560 –3250	7.4–7.7(8H)	7.70(1H)	3.27(3H)	—
9*c*	Cl	Cl	**H**	96	139–140	White prisms	Hexane/ benzene	2800–3300	7.3–8.3(7H)	7.90(1H)	3.15(3H)	—
9*d*	H	H	Me	85	144–145	White needles	EtOH	2600–3300	6.8–7.6(8H)	7.40(1H)	3.20(3H)	2.30(3H)
9*e*	**H**	F	H	92	134.5–136	White prisms	Benzene/ pet. ether	2700–3400	6.8–8.2(8H)	7.65(1H)	3.25(1H)	—

[a]All compounds gave satisfactory elemental analysis.

of sodium nitrite to an acidic solution of the amine, followed by coupling with methylamine, afforded good yields of the 4-aryl-4-hydroxy-3-methyl-1,2,3-benzotriazines (**9**). Like the

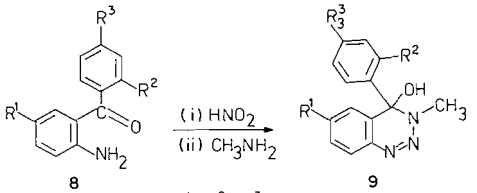

8 9

a $R^1 = R^2 = R^3 = H$
b $R^1 = Cl$; $R^2 = R^3 = H$
c $R^1 = R^2 = Cl$; $R^3 = H$
d $R^1 = R^2 = H$; $R^3 = Me$
e $R^1 = R^2 = H$; $R^3 = F$

4-hydroxy-1,2,3 (4*H*)-triazines (**7**), the 4-aryl-4-hydroxytriazines (**9**) are apparently formed by spontaneous, irreversible cyclization of the intermediate monomethyltriazenes, which could not be isolated or observed. The cyclic products are stable crystalline solids which show spectroscopic features consistent with the assigned triazine structure (**9**). The ir spectra show similar characteristics to the C-4 unsubstituted analogues (**7**). Carbonyl absorption is absent in the spectra of compounds **9***a*–*e* and hydroxyl absorption is evident, but much broader (2560–3400 cm^{-1}) than in the spectra of compounds **7***a*–*d*.

The nmr spectra of **9** provide further evidence for the assigned cyclic structure. The aromatic multiplets, in the range 6.8–8.4 ppm, integrate for the respective number of aromatic protons depending on the number of aryl substituents; the *p*-tolyl derivative (**9***d*) exhibits a signal at 2.30 ppm arising from the protons of the *C*-methyl group. The *N*-methyl protons consistently give rise to a signal in the range 3.15–3.27 ppm. The hydroxylic proton, in the range 7.40–7.90, was in each case partially obscured by a component of the aromatic multiplet, but the assignment was confirmed by addition of D_2O to the DMSO-d_6 solution, which caused the OH resonance to disappear from the multiplet and the HOD signal at ca. 4.10 ppm to appear.

A further confirmation of the assignment of the 4-hydroxytriazine structure (**9**) to these products came somewhat unexpectedly from the analogous reaction of *o*-anthraniloylbenzoic acid (**10**). Diazotization of **10** was accomplished by the

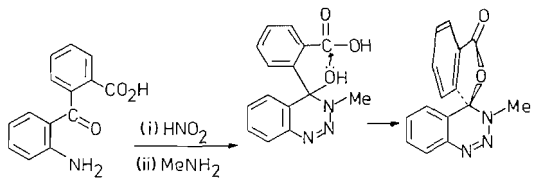

10 11 12

normal procedure and coupling with methylamine afforded a low yield of a crystalline product, which was identified as the spiro-triazinofuran (**12**) on the basis of elemental analysis and spectroscopic data. The nmr spectrum of **12** shows an N—Me group at 3.3 ppm and an eight-proton aromatic multiplet at 6.5–8.2 ppm. The infrared spectrum is devoid of absorption in the NH or OH stretching region but shows a strong band at 1765 cm^{-1} confirming the presence of the lactone carbonyl group. The formation of the lactone presumably arises from spontaneous cyclization of the intermediate 4-hydroxytriazine (**11**) and provides further striking evidence for the 4-hydroxytriazine structures (**7** and **9**) proposed above.

A surprising result was observed when the diazonium salt from *o*-aminopropiophenone (**13**) was treated with methylamine. A stable, white, crystalline product was obtained which

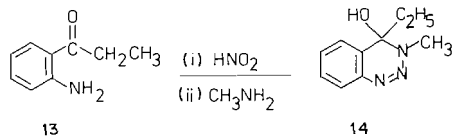

13 14

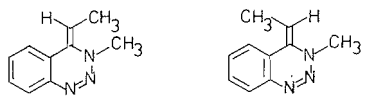

15 16

displays spectroscopic properties of the 4-hydroxy-4-ethyl-1,2,3-triazine (**14**). The surprising feature of this compound is not its formation, presumably via an acyclic methyltriazene, but that it survives the reaction and recrystallization conditions without undergoing dehydration to a methylenetriazine (e.g. **15** or the geometric isomer **16**). By analogy with our previously reported observations of the same reaction with *o*-aminoacetophenone (4), the dehydration of **14** would be expected to be relatively facile. The stability of **14** contradicts the apparent instability of the intermediate **3** in the conversion **1** → **4**. A possible explanation for this different behaviour may be the greater barrier to dehydration as a result of the steric hindrance introduced by the ethyl group at C-4.

However, the stability of **14** may not extend to prolonged exposure in solution. The ^1H nmr spectrum of a fresh solution of **14** in DMSO-d_6 shows that this compound exists exclusively as the ring-closed form (**14**); the C-4 ethyl group gives rise to signals at 0.65 (triplet) and 2.20 (quartet) ppm as expected and the *N*-methyl group resonance is observed at 3.59 ppm. In addition to the aromatic multiplet at ca. 7.5 ppm, a sharp singlet at 6.84 ppm arises from the hydroxylic proton; this assignment was confirmed by the disappearance of the OH signal upon the addition of D_2O. When the solution of **14** in DMSO-d_6 is left standing, additional signals grow into the spectrum which suggest that dehydration to the methylene triazine (**15**) is occurring in the solution. The additional signals are observed at 2.03 (3H, d, J = 7.4 Hz), 3.40 (3H, s), and 5.07 (1H, q, J = 7.4 Hz) ppm, consistent with the vinylic $=C\begin{matrix}H\\CH_3\end{matrix}$ system in **15**. The observation of only one set of signals suggests a preference during the dehydration of **14** to give the less sterically hindered methylenetriazine, i.e. **15**.

A more complex situation prevails when a freshly prepared $CDCl_3$ solution of **14** is examined by ^1H nmr, with no less than six different C—CH_3 signals observed. Two of these signals at 1.95 (d, J = 8.0 Hz) and 1.92 (d, J = 7.9 Hz) ppm are assigned to the *C*-methyl groups of the dehydration products, the methylenetriazine geometric isomers (**15** and **16**). Two others at 1.18 (t, J = 7.3 Hz) and 1.11 (t, J = 7.4 Hz) ppm are assigned to the tautomeric forms of the linear triazene ($ArN{=}N{-}NHCH_3 \rightleftharpoons ArNH{-}N{=}N{-}CH_3$; Ar = *o*-$CH_3CH_2CO\cdot C_6H_4$); tautomerism of this nature in $CDCl_3$ has been well defined (10). This observation of ring opening of **14** in chloroform is clearly an effect of the solvent and not due to the presence of impurities; in other respects (i.e. mp, ir spec-

Can. J. Chem. Downloaded from www.nrcresearchpress.com by 210.87.254.105 on 09/06/12
For personal use only.

Can. J. Chem. Downloaded from www.nrcresearchpress.com by 210.87.254.105 on 09/06/12
For personal use only.

trum, and tlc) compound **14** exhibits properties of a single species, the heterocyclic 4-hydroxytriazine. The two remaining C—CH_3 signals in the $CDCl_3$ spectrum of **14**, 0.61 (t, J = 7.5 Hz) and 0.76 (t, J = 7.6 Hz) ppm, have chemical shifts close to that observed for the ring-closed form **14** in DMSO-d_6 solution. However, it is difficult to envisage different diastereomeric forms of **14**, since this would require postulation of slow inversion at a ring nitrogen, in contrast with the expected rapid inversion at such centres.

These observations of the transformations of **14** in solution in dimethyl sulfoxide and chloroform suggest that further studies of the chemistry of **14** may be fruitful on a preparative scale, and encourage a further study of the resolution of the stereoisomers of the 4-hydroxytriazines (**7**, **9**, and **14**) and the spiro triazine (**12**) reported here; all these compounds have a chiral centre at C-4 of the triazine ring. A second promising extension of the work reported here will be the preparative conversion of **14** to the novel methylenetriazines (**15** and **16**); the separation of these geometric isomers is a challenging prospect.

Aside from the previous preliminary report of the 4-phenyl-4-hydroxytriazine (**9***a*) (4), this paper is the first account of the general synthesis of 4-hydroxytriazines of types **7** and **9**. The stability of these 4-hydroxytriazines is significant and relevant to the chemistry of the parent 4-alkyl- and 4-aryltriazines (**17**), which have been extensively studied by

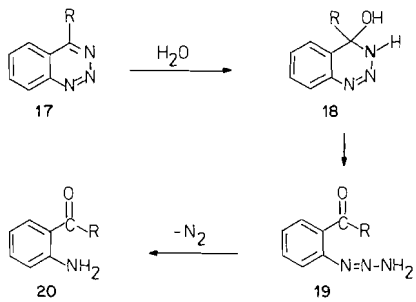

Rees and co-workers (11). Hydrolysis of **17** results in degradation to the respective *o*-aminophenyl ketone or aldehyde (**20**); the proposed mechanism of hydrolysis involves nucleophilic addition at C-4 of **17** to give the unstable 4-hydroxytriazine (**18**), which undergoes ring opening to the triazine (**19**) followed by N_2 elimination to give **20**. The intermediate **18** is the N-3 unsubstituted parent compound of the series of 4-hydroxytriazines (**7** and **9**) reported here.

In addition to the wealth of chemistry associated with these 4-hydroxytriazines, there is considerable potential in this ring system for pharmacological application. This potential derives from the antineoplastic properties of arylmonoalkyl triazenes (Ar·N=N·NHR) (12); the monomethyltriazenes have been implicated as the active metabolites of the extensively studied anti-tumour dimethyltriazenes (Ar·N=N·NMe_2) (2). Although the 4-hydroxytriazines exist almost exclusively in the ring-closed form, it is feasible that these compounds would undergo enzymatic or nonenzymatic ring-opening in vivo, or intracellularly, and thereby act as pro-drugs for the potentially cytotoxic open-chain triazene, e.g. **6**.

We have recently developed an assay for assessing the cytotoxicity of various triazenes against the M21 melanoma cell line in culture (in vitro) (13). A prepliminary assay of two of the 4-hydroxytriazines reported here indicates significant biological activity. 4-Hydroxy-3-methyl-4-phenyl-1,2,3-benzotriazine (**9***a*) was administered to M21 cells in culture at a dose of 50 μg/mL; the rate of growth of cells was inhibited by 58% compared to controls. The inhibitory effect of 4-hydroxy-3-methyl-1,2,3(4*H*)-benzotriazine (**7***a*) was even more striking; **7***a* was administered at a dose of 100 μg/mL (**7***a* is more soluble in the cell-growth medium than **9***a*; **9***a* precipitates out at concentrations above 50 μg/mL) and inhibition of cell growth was virtually 100%. Within 48 hours of addition of **7***a* to the cell culture, almost all the cells had become detached from the cell culture dishes and had ceased to divide. Further studies are underway to determine definitive inhibitory properties of the 4-hydroxytriazines and to assess their in vivo antitumour activity.

Acknowledgements

The authors are grateful for financial support from the Natural Sciences and Engineering Research Council of Canada, the Saint Mary's University Senate Research Fund, and the Research Development Fund for the Sciences, Dalhousie University. Special thanks are due to the Department of Pathology at Dalhousie University for providing the facilities to carry out preliminary biological screening.

1. T. P. AHERN, H. FONG, and K. VAUGHAN. Can. J. Chem. **55**, 1701 (1977).
2. K. VAUGHAN and M. F. G. STEVENS. Chem. Soc. Rev. **7**, 377 (1978).
3. R. J. LEBLANC and K. VAUGHAN. Can. J. Chem. **50**, 2544 (1972).
4. H. FONG and K. VAUGHAN. Can. J. Chem. **53**, 3714 (1975).
5. L. I. SMITH and J. W. OPIE. Org. Synth. Coll. Vol. **III**, *Edited by* E. C. Horning. 56 (1955).
6. B. L. ZENITZ and W. H. HARTUNG. J. Org. Chem. **11**, 444 (1946).
7. J. C. SIMPSON, C. M. ATKINSON, K. SCHOFIELD, and O. STEPHENSON. J. Chem. Soc. 646 (1945).
8. P. CALUWE. Tetrahedron (Special Report No. 92), **36**, 2361 (1980).
9. H. E. BAUMGARTEN and M. R. DEBRUNNER. J. Am. Chem. Soc. **76**, 3489 (1954).
10. D. L. HOOPER and K. VAUGHAN. J. Chem. Soc. Perkin Trans. II, 1161 (1981).
11. B. M. ADGER, S. BRADBURY, M. KEATING, C. W. REES, R. C. STORR, and M. T. WILLIAMS. J. Chem. Soc. Perkin Trans. I, 31 (1975).
12. A. GESCHER, J. A. HICKMAN, R. J. SIMMONDS, M. F. G. STEVENS, and K. VAUGHAN. Biochem. Pharmacol. **30**, 89 (1981).
13. D. J. KOHLSMITH, S. J. LUNER, and K. VAUGHAN. Unpublished results.

Hydrazonium(2+) hexafluorosilicate, $N_2H_6SiF_6$: a NaCl-type structure with two-dimensional hydrogen-bonding networks

T. Stanley Cameron, Osvald Knop,[1] and Laura Ann Macdonald
Department of Chemistry, Dalhousie University, Halifax, N.S., Canada B3H 4J3

Received June 7, 1982

T. Stanley Cameron, Osvald Knop, and Laura Ann Macdonald. Can. J. Chem. **61**, 184 (1983).

Hydrazonium(2+) hexafluorosilicate, $N_2H_6SiF_6$, at room temperature has an orthorhombic (*Pbca*, $Z = 4$), pseudotetragonal unit cell ($a = 7.605(1)$ Å, $b = 7.586(2)$ Å, $c = 8.543(1)$ Å). The structure consists of centrosymmetric $N_2H_6^{2+}$ and SiF_6^{2-} ions arranged in a NaCl-type packing and connected by hydrogen bonds to two-dimensional $N_2H_6-SiF_6$ layers parallel to (001). All H atoms are engaged in hydrogen bonding. Four of the six H···F bonds to each cation are normal but significantly bent; the other two are trifurcated, N—H···3 F, but the out-of-layer component of the trifurcated bond is relatively unimportant. The $N_2H_6SiF_6$ structure is compared in some detail with the structures of other hydrazonium(2+) salts, with particular attention to the N—N bond length, to the "effective" size of the $N_2H_6^{2+}$ ion, and to the tendency of this ion to form bent hydrogen bonds.

T. Stanley Cameron, Osvald Knop et Laura Ann Macdonald. Can. J. Chem. **61**, 184 (1983).

A la température ambiante l'hexafluorosilicate d'hydrazonium(2+), $N_2H_6SiF_6$, a une maille élémentaire orthorhombique (*Pbca*, $Z = 4$), pseudotétragonale ($a = 7{,}605(1)$ Å, $b = 7{,}586(2)$ Å, $c = 8{,}543(1)$ Å). La structure consiste en des ions $N_2H_2^{2+}$ et SiF_6^{2-} centrosymétriques disposés selon un arrangement identique à celui du NaCl et reliés par des liaisons hydrogène à des couches bidimensionnelles de N_2H_6—SiF_6 parallèles à (001). Tous les atomes hydrogène participent dans les liaisons hydrogène. Quatre des six liaisons H···F de chaque cation sont normales mais assez coude'es. Les deux autres liaisons sont trifurquées, N—H···3F, mais la composante hors couche de la liaison trifurquée est relativement peu importante. On a comparé en détail la structure du $N_2H_6SiF_6$ avec celles d'autres sels d'hydrazonium (2+) en s'attardant particulièrement sur la longueur de liaison N—N, sur la dimension effective de l'ion $N_2H_6^{2+}$ et sur la tendance de cet ion à former des liaisons hydrogène coude'es.

[Traduit par le journal]

There are very few inorganic cations that can act as effective donors to form hydrogen bonds: $H(H_2O)_n^+$ ($n \leq 4$), NH_4^+, PH_4^+, $HONH_3^+$, $N_2H_5^+$, $N_2H_6^{2+}$. Of these, $N_2H_6^{2+}$ (abbreviated in the following to Hy) is the only such cation carrying a double charge.[2] At the same time it is a counterpart of NH_4^+ as regards the equivalence of all its hydrogens (at maximum symmetry) and their ability simultaneously to engage in hydrogen bonding. Thus if NH_4^+ may be viewed, from the point of view of crystal chemistry of ionic solids, as a size match of Rb^+ with hydrogen-bonding ability added, Hy might be considered as the corresponding companion of a large divalent simple ion, say Ba^{2+}. This analogy is given credence, albeit only within the very limited scope of the structural information available to date, when the Hy salts listed in Table 1 are compared with the corresponding Ba compounds and features specific to the cation structure and the presence of hydrogen bonding in the former are disregarded.

Table 1 presents crystallographic data of all the Hy compounds we have been able to find in the literature. This set contains only 14 compounds, the selection of which owes more to accidents of history than to premeditation, and the quality of the structural information varies widely from compound to compound. Nevertheless, the *symmetry* of the Hy ion[3] in the crystals can be ascertained (uniquely except in two cases) regardless of the details and accuracy of the structure determination, simply by comparing Z with the equipoint multiplicities of the respective space group, provided only that Z and the space group are correct.

Examination of Table 1 reveals a remarkable variety of Hy symmetries in this handful of compounds: $\bar{3}\,m$ (the maximum point group of the ion) and five of its nine subgroups are represented. This variety in turn is reflected in a diversity of hydrogen-bonding situations, characterized by the occurrence of highly-bent, bifurcated or trifurcated N—H···X bonds. The present study was undertaken to explore further the full extent of the structural behaviour of the Hy ion, the available information being quite inadequate compared with what is known, for example, about the NH_4^+ ion in crystals.

$HySiF_6$ was chosen in part to clear up the *a priori* uncertainty about the cation/anion packing in this compound. If the composite nature of Hy is disregarded, $HyTiF_6$ (and almost certainly also $HyTcF_6$, $HyReF_6$, and $HyMoF_6$) is isostructural with $KSbF_6$ and $AgSbF_6$, both reported (29, 30) to be superstructure variants (*Ia*3, $Z = 8$) of the CsCl arrangement found in $BaTiF_6$ and $BaSiF_6$ ($TlSbF_6$ type, $R\bar{3}\,m$, $Z = 1$).[4] This would suggest that the packing in $HySiF_6$, too, is of this type. However, a survey of the known ABF_6 structures (Fig. 1) shows that for a BF_6^{2-} ion as small as SiF_6^{2-} a NaCl-type packing is a distinct possibility.

[1]To whom all correspondence should be addressed.

[2]And in fact one of the very few doubly-charged composite cations, if one disregards doubly protonated amines (although Hy itself may be considered to be the initial member of the $^+H_3N(CH_2)_nNH_3^+$ series). As for the hypothetical tetrahedral H_4O^{2+} ion, *ab initio* MO calculations at the 6-31G* level (R. J. Boyd, unpublished results) predict that the isolated ion is unstable with respect to loss of a proton by about 59 kcal/mol; a more elaborate treatment might reduce this estimate by possibly as much as 15 kcal/mol. Similar calculations predict that the removal of a proton from an isolated H_3O^+ ion would require ca. 175 kcal/mol. Conditions can be envisaged under which H_4O^{2+} might be stabilized by the electrostatic potential at a crystal site.

[3]I.e. the symmetry at the midpoint of the N—N bond.

[4]It is noteworthy than no $M^{2+}X^{2-}$ compound of the CsCl type is known for simple M and X ions.

0008-4042/83/010184-05$01.00/0
©1983 National Research Council of Canada/Conseil national de recherches du Canada

Can. J. Chem. Downloaded from www.nrcresearchpress.com by 210.87.254.6 on 09/06/12
For personal use only.

TABLE 1. Crystallographic data of previously reported $N_2H_6^{2+}$ compounds

Symmetry of Hy	Compound	Space group	Z	d(N—N), Å	Reference[a]
$\bar{3}m$	HyF_2	$R\bar{3}m$	1	1.42(2)	1; 2–5
$\bar{3}$	$HyCl_2$	$Pa3$	4	1.42(2)	6, 7; 2, 4, 5, 8, 9
$\bar{3}$	$HyTiF_6$	$Ia3$	8	1.474(7)	10
$(\bar{3})$	$HyTcF_6$, $HyReF_6$, $HyMoF_6$[b]	$(Ia3)$	(8)		11
3	$HyNa[Co(NO_2)_6]$	$P23$	4		12
2	$HyZrF_6$, $HyHfF_6$	$C2/m$	4	1.41(3)	13
$\bar{1}$	$Hy(H_2PO_4)_2$	$P2_1/c$	2	1.432(6)	14
$\bar{1}$	$Hy(NbOF_5)(H_2O)$	$Pnma$	4	1.4394(34)[c]	15, 16
1	$HyBeF_4$	$P2_1/c$	4	1.417(16)	17
1	$HySO_4$	$P2_12_12_1$	4	1.418(2),[d] 1.426(3)[c]	18–20; 5, 8, 21–23
1	$Hy_2(NbOF_5)F_2$	$P2_1$	4		24

[a]Where two sets of references are given, the first set concerns crystallographic information, the second set refers to other physical measurements. In addition to the compounds listed in the table, a ^1H nmr study of $Hy(NO_3)_2$ is reported in ref. 21; $HyBr_2$ and $HyPF_6$ have been studied by inelastic neutron scattering (5); and normal coordinate analysis of Hy has been reported (25). $HyBr_2$ is probably isostructural with $HyCl_2$ (5).

[b]These three fluorides have been reported as bcc, a = 10.48–10.55 Å. It is probable that they are isostructural with $HyTiF_6$.

[c]Neutron diffraction.

[d]X-ray diffraction.

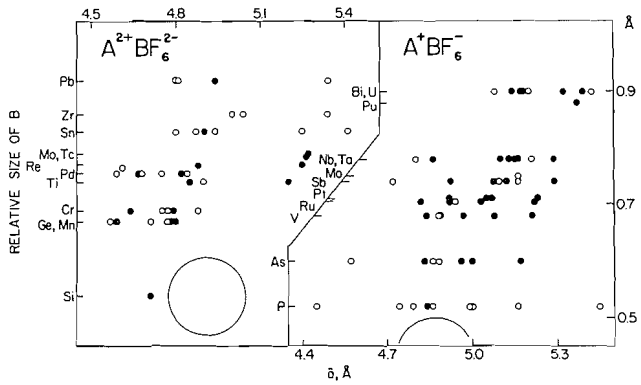

FIG. 1. Distribution of the NaCl- and CsCl-type packing arrangements among the hexafluorometallates ABF_6 (room-temperature structures; data assembled from refs. 26–28). $\bar{a}$ is the mean linear unit-cell dimension $(V/Z)^{1/3}$; the relative size of B = Shannon's crystal radius of B for 6-coordination. Open circles, NaCl type; full circles, CsCl type. On estimates from size similarity the point for $HySiF_6$ would be expected to fall within the circled areas, where the packing type is difficult to predict.

Experimental

Preparation

A calculated amount of anhydrous hydrazine was added dropwise to a vigorously stirred 23% aqueous solution (commercial) of H_2SiF_6 in a teflon beaker. Well-developed colourless crystals of the salt began to form even before the addition was completed. On removal from the saturated mother liquor the crystals were pressed between layers of filter paper, washed quickly with 95% EtOH, and dried in air. They showed pronounced cleavage. The compound is very soluble in water, somewhat soluble in EtOH.

Crystal data

$F_6H_6N_2Si$ fw = 176.14

Orthorhombic, *Pbca* (systematic absences: $0kl$, $k = 2n + 1$; $h0l$, $l = 2n + 1$; $hk0$, $h = 2n + 1$); a = 7.605(1) Å, b = 7.586(2) Å, c = 8.543(1) Å, V = 492.8 Å^3, Z = 4, ρ_c = 2.374 g/cm^3; Mo $K\alpha_1$, λ = 0.70926 Å (graphite monochromator), μ_{Mo} = 9.07 cm^{-1}, $F(000)$ = 704 e.

Structure determination

The crystal used in the determination was 0.3 × 0.3 × 0.6 mm^3 in size. A total of 870 reflections in the range $2° < \theta < 28°$ were measured on a CAD-4 four-circle diffractometer; of the 718 unique reflections 591 had $I > 3\sigma(I)$ and were used in the refinements. The unit-cell dimensions were determined from 25 general reflections with $14° < \theta < 24°$.[5] The intensities were reduced by routine procedures (31). Lorentz and polarization corrections were applied but no absorption or extinction corrections. The scattering factors for neutral atoms were taken from ref. 32. The structure was solved by the heavy atom method using the SHELX system (33).

Full-matrix least-squares ($u\Delta F^2$ = min.) refinement was carried out with isotropic temperature factors on heavy atoms until R = 0.06. The hydrogen atoms were clearly visible in a difference Fourier map calculated at this stage. The N—H bond lengths were constrained to 1.06 ± 0.02 Å and the HNH angles to tetrahedral (through a constraint on the H···H distances, 1.68 ± 0.03 Å), and refinement was continued with anisotropic temperature factors on the nonhydrogen atoms and isotropic factors on the hydrogens until R = 0.029, based on all 591 reflections. The least-squares weights were calculated from $w^{-1} = \sigma^2|F_o| + 0.000381F_o^2$, where σ is the weight for an individual reflection derived from the diffractometer counting statistics. The atomic and thermal parameters are given in Table 2, interatomic distances and bond angles in Tables 3 and 4.[6]

Description of the structure

Space-group constraints require both ions to be centrosymmetric. The centres of the cations are in equipoint 4(a) and those of the anions in equipoint 4(b) of *Pbca*. Each set thus constitutes a lattice complex *Fmmm*, the two complexes being displaced by $(\boldsymbol{a} + \boldsymbol{b} + \boldsymbol{c})/2$. Since *Pbca* ⊂ *Pa*3, the complex *Fmmm* is an orthorhombic distortion of the cubic complex *Fm*3*m*, i.e. the packing of Hy and SiF_6 is of the NaCl type (Fig. 2), the first such packing to be reported for a Hy compound.

[5]It was necessary to go to a high angle along one axis in order to find a reflection suitable for determining the unit-cell dimension.

[6]Copies of Table 5 (structure factors) are available, at a nominal charge, from the Depository of Unpublished Data, CISTI, National Research Council of Canada, Ottawa, Ont., Canada K1A 0S2.

Can. J. Chem. Downloaded from www.nrcresearchpress.com by 210.87.254.6 on 09/06/12
For personal use only.

Can. J. Chem. Downloaded from www.nrcresearchpress.com by 210.87.254.6 on 09/06/12
For personal use only.

TABLE 2. Positional and thermal parameters of atoms in $N_2H_6SiF_6$ at room temperature[a]

Atom	x y z	Temperature factor	U_{11} U_{22} U_{33}	U_{12} U_{13} U_{23}
Si	½		147(3)	8(2)
	½	135(3)	104(3)	2(2)
	0		154(3)	5(2)
N	4873(2)		293(7)	−8(5)
	0140(2)	228(7)	200(7)	18(5)
	0819(2)		189(6)	−4(5)
F(1)	3677(2)		302(5)	−59(5)
	3570(2)	314(6)	233(5)	93(5)
	0939(1)		408(6)	87(5)
F(2)	3342(1)		232(5)	76(5)
	5590(2)	314(6)	442(7)	−63(4)
	−1194(1)		269(5)	55(5)
F(3)	5598(2)		501(7)	102(5)
	3434(2)	322(6)	201(5)	46(5)
	−1269(1)		265(5)	−63(4)
H(1)	4391(34)			
	1384(18)	537(97)		
	1063(37)			
H(2)	6089(18)			
	−0020(35)	497(93)		
	1341(34)			
H(3)	4018(29)			
	−0801(28)	498(90)		
	1254(33)			

[a]All values except x(Si) and y(Si) have been multiplied by 10^4. The temperature factor values represent mod(U) for the nonhydrogen atoms and the isotropic temperature factor U for the hydrogens. The anisotropic temperature factor is defined as $T = \exp[-2\pi^2(U_{11}h^2a^{*2} + U_{22}k^2b^{*2} + U_{33}l^2c^{*2} + 2U_{23}klb^*c^* + 2U_{13}hla^*c^* + 2U_{12}hka^*b^*)]$.

TABLE 3. Bond distances (Å) and angles (deg) in $N_2H_6SiF_6$

Bond	Distance	Bonds	Angle
Si—F(1)	1.683(1)	F(1)—Si—F(2)	90.7(1)
Si—F(2)	1.682(1)	F(1)—Si—F(3)	90.8(1)
Si—F(3)	1.671(1)	F(2)—Si—F(3)	90.0(1)
N—N	1.428(2)	N—N—H(1)	112(1)
		N—N—H(2)	107(1)
		N—N—H(3)	110(1)

TABLE 4. N···F and H···F distances (Å) and NHF angles (deg) in $N_2H_6SiF_6$[d]

H	F	N(B′)···F[a]	H···F[b]	N(B′)—H—F[c]
1B	1B′	2.758	1.748	165
	3D	2.768	2.461	96
	3B	3.119	2.689	105
2B	2C	2.714	1.771	150
	3D	2.768	2.399	100
	1	3.210	2.569	120
3B	3F	2.761	2.018	126
	1G	2.952	2.122	136
	2D	2.859	2.245	116
—	1F	3.375		
	1C′	3.403		
	3C	3.447		

[a]To 3.5 Å; esd = 0.004 Å.
[b]To 2.7 Å; esd = 0.024 Å.
[c]esd = 1°.
[d]Symmetry code: B, $\bar{x}$, ½ + y, ½ − z;
B′, 1 − x, ½ + y, ½ − z;
C, ½ − x, $\bar{y}$, ½ + z;
C′, x, 1 − y, ½ + z;
D, $\bar{x}$, $\bar{y}$, $\bar{z}$;
F, x, ½ − y, ½ + z;
G, ½ + x, y, ½ − z.

The closeness of the distortion to tetragonal, with $2c/(a + b) \sim 1.12$, is a consequence of the orientation of the N—N groups. They are almost parallel to the c-axis, so that the dimension effective in determining the a and b values is the *smallest* dimension of the Hy ion. If the SiF_6 groups were assumed spherical and in contact, the effective size of the Hy ion normal to the N—N bond would be of the order of 1.1 Å; taking the effective length of the ion to be twice the N—N distance, 2.86 Å, the $2c/(a + b)$ ratio would be 1.08, in reasonable agreement with observation. This means the the effective size of Hy in a crystal would be within the limits 1.1−2.9 Å, depending on the orientation of the ion. The mean $(2.86 + 2 \times 1.1)/3 \sim 1.7$ Å would indicate a rough size similarity to the Ba^{2+} ion in 12-coordination, $r^{xii}(Ba^{2+}) \sim 1.61$ Å (Shannon).

Viewed as an assembly of spherical SiF_6 and elongated N—N groups the packing arrangement in $HySiF_6$ shows formal similarity to the *Pbca* structures of PdS_2 and β-HgO (both related to the *Pa*3 pyrite structure), and an even closer similarity to the tetragonal CaC_2-type structure, in which the c/a ratio (for MO_2 peroxides) ranges from 1.15 to 1.31. Still more conspicuous is the similarity to the tetragonal $MeNH_3Br$ and $MeNH_3I$ structures, with $c/a = 1.22$ and 1.24 respectively (34, 35). The only essential difference between these two halides and $HySiF_6$ is in the hydrogen-bonding scheme: Hy can engage in hydrogen bonding at both ends of the ion but $MeNH_3^+$ only at one end.[7]

The hydrogen bonds in $HySiF_6$ are shown in Fig. 2 and in more detail in Fig. 3. All hydrogens are bonded to F atoms. The H(1)···F(1) and H(2)···F(2) bonds are normal (i.e. to a single F each) but appreciably bent (Table 4). H(3) participates in an asymmetrically trifurcated N—H···3 F bond to F(1), F(2), and F(3) (Fig. 3), the mean H···F being 2.13(4) Å and the mean NHF angle, 126(4)°. With the exception of H(3)···F(2) the H···F bond vectors are practically parallel to (001). They are located within slabs about 0.4 Å thick, one such slab being at a mean distance of about 1 Å on each side of a layer of Si atoms parallel to (001). The hydrogen bonds thus form two-dimensional networks parallel to (001), with only a minor interlayer component H(3)···F (2), which corresponds to the longest H···F distance in the structure that may still be considered as involved in hydrogen bonding, 2.25(3) Å, N—H(3)—F(2) = 116(1)°. The NaCl packing of ions in $HySiF_6$ is thus associated with an unusual feature, viz. a layer-type hydrogen-bonding scheme reflected in the pseudotetragonal symmetry of the structure and a most pronounced cleavage along (001).

The formation of two normal but bent and one quasi-

[7]The spectroscopic and other consequences of this contrast have been explored in a number of investigations (see for example refs. 5 and 36).

Can. J. Chem. Downloaded from www.nrcresearchpress.com by 210.87.254.6 on 09/06/12
For personal use only.

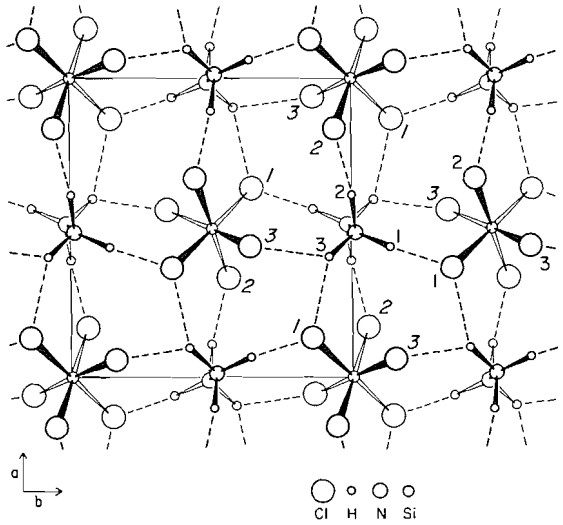

FIG. 2. Projection of the lower half of the $HySiF_6$ unit cell on (001). The Si atoms are at $z = 0$. F and H atoms with the Roman numerals have coordinates as in Table 2; the numbers in italic designate the *type* of F atom. The origin is in the lower right-hand corner of the unit-cell outline.

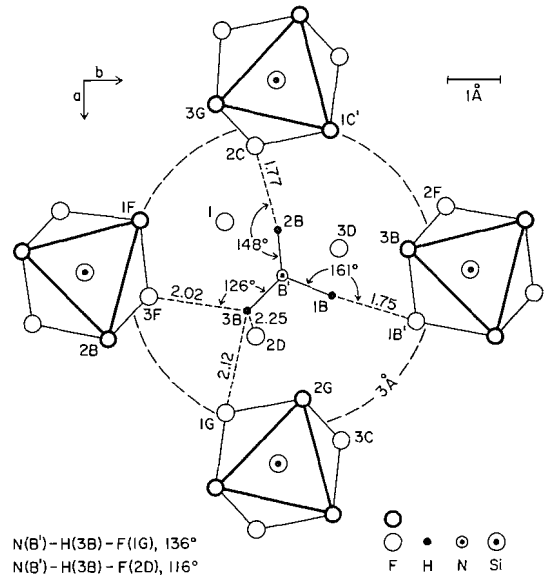

FIG. 3. Environment of a nitrogen atom in $HySiF_6$. The H···F distances (up to 2.3 Å) and NHF angles of the hydrogen bonds are shown. For longer H···F distances and symmetry code, see Table 4.

bifurcated hydrogen bond may appear surprising. In fact, this is the normal situation. In $HySiF_6$ the triplet of H atoms bonded to a nitrogen may be viewed as approximately coplanar and concentric with a quadrangle of F acceptor atoms (1B′, 1G, 2C, and 3F in Fig. 3). In an equilibrium configuration of minimum energy of an equilateral triangle of positive unit charges located within a coplanar, concentric square of negative unit charges one of the vertices of the triangle is on the bisector of a side of the square. If the positive charges are represented by H atoms at 1 Å from the centre *C* and the negative charges by fluorines at 2.8 Å (the mean of the observed N···F distances involving the four F) from *C*, the two normal H···F bonds in an equilibrium configuration will have a length of ca. 1.9 Å each, with a *C*HF angle of ca. 157°, and the symmetrically bifurcated bond will have an H···F distance of ca. 2.2 Å, with a *C*HF angle of ca. 117°. While in $HySiF_6$ these assumptions are realized only very approximately, this model accounts for the geometry actually observed better than qualitatively.[8] It is also of interest to note that much the same local hydrogen-bonding geometry as in $HySiF_6$ is observed for N(1) in $HyBeF_4$ (17) and also in $Hy(NbOF_5)(H_2O)$ (16), except that in the latter one of the two normal bonds is to an H_2O oxygen and the trifurcated bond is to two fluorines and an anion oxygen; the H···X distances and NHX angles are very similar to those in $HySiF_6$.

The two shortest H···F distances in $HySiF_6$, 1.75(3) and 1.77(3) Å, are appreciably larger than the H···F distances in HyF_2, 1.54(1) Å (3),[5] but comparable to the shortest H···F distances in $HyBeF_4$, 1.70(7) and 1.77(7) Å (19), and in $Hy(NbOF_5)(H_2O)$, 1.70(1) Å (16). They are also of the same order as the H···O distances in the last-named compound, 1.77 (1) Å, and in $HySO_4$, 1.642(4), 1.715(5), and 1.774(5) Å (20). A feature common to all these normal N—H···X bonds is the fairly constant deviation of about 15° of the NHX angle from 180°; in this the N—H(2)···F(2) bond, with its unusually small NHF angle of 150°, is an exception.

Apart possibly from $HyCl_2$ and $HyBr_2$, HyF_2 to date appears to be the only Hy compound in which the NHX angle is close to 180°. The bent normal N—H···X bonds in Hy salts are evidently the result of the staggered cation adopting the energetically most favourable orientation, with respect to hydrogen bonding, in an acceptor environment generally of unfavourable geometry forced upon the cation by the Coulombic forces which dominate the structure of the ionic crystal. It is difficult to say to what extent linearity of a normal N—H···F bond is affected by the presence of acceptor atoms at H···F distances greater than say 2.3 Å (cf. Fig. 3 and Table 4).

The N—H bond length in $HySiF_6$, 1.428(2) Å, is indistinguishable from the weighted mean of the nine d(N—N) values of Table 1, 1.426(13) Å (1.427(10) Å if $HySiF_6$ is included). This raises the question of the validity of the unusually high d(N—N) value reported for $HyTiF_6$, this value being 0.047(12) Å larger than the mean, i.e. 0.01 Å outside 3σ and 0.027 Å if $HyTiF_6$ is not included in the mean. Aware of the difficulty, the authors (10) suggest that the lengthening may be due to the strength of the six N—H···F bonds, N···F = 2.612(6) Å (as against ≥2.71 Å in $HySiF_6$). However, this may not be the explanation. In HyF_2 the six equivalent N···F distances are of comparable length, 2.62(2) Å, as found by X-ray diffraction (1) and nmr (3); assuming N, H, and F to be collinear, the H···F distance obtained from the ^{19}F resonance spectrum is 1.542(10) Å. It is unlikely that the hydrogen bonding to F^- in HyF_2 would be weaker than in $HyTiF_6$, yet d(N—N) in the fluoride is quoted as 1.42(2) Å (1).[9]

[8]It should be possible to verify the validity of this model by locating the N-hydrogens in the tetragonal $MeNH_3X$ (X = Cl, Br, I) structures, in which the model requirements are more closely satisfied. In the chloride at room temperature (34, 37) the calculated approximate H···Cl distances and NHCl angles would be 2.16 Å and 166° for the normal and 2.51 Å and 123° for the symmetrically bifurcated N—H···Cl bonds; in the bromide (35) the corresponding values would be 2.45 Å and 159°, and 2.86 Å and 120°, respectively. Nuclear magnetic resonance studies (38–40) suggest that the NH_3 triplet in the room-temperature phases undergoes spontaneous reorientations, by 90° rotations about the N—C (= C_4) axis, between the four equivalent positions resulting from the tetragonal symmetry of the non-hydrogen portion of the crystal structure.

[9]This value may be too low (cf. ref. 5).

In spite of the low overall symmetry of the structure the SiF_6 octahedron in $HySiF_6$ is only very slightly distorted (Table 3). The mean Si—F bond length, 1.678(2) Å, is shorter than the Si—F distance in $BaSiF_6$, 1.71 Å (41). However, the accuracy of this early determination is uncertain: a decrease of the stated x(F) and z(F) by 0.002 would be sufficient to reproduce the mean d(Si—F) in $HySiF_6$.

It is not clear at present why $HySiF_6$ adopts the NaCl-type and $HyTiF_6$ the CsCl-type packing. If anion size is a factor, the difference of about 0.2 Å between the Si—F and Ti—F distances must be critical, which invites examination of $HyGeF_6$.

Acknowledgment

This investigation was supported by grants from the Natural Sciences and Engineering Research Council of Canada to the two first-named authors.

1. M. L. KRONBERG and D. HARKER. J. Chem. Phys. **10**, 309 (1942).
2. C. M. DEELEY, P. LEWIS, and R. E. RICHARDS. Trans. Faraday Soc. **50**, 556 (1954).
3. C. M. DEELEY and R. E. RICHARDS. Trans. Faraday Soc. **50**, 560 (1954).
4. R. G. SNYDER and J. C. DECIUS. Spectrochim. Acta, **13**, 280 (1959).
5. C. J. LUDMAN, C. I. RATCLIFFE, and T. C. WADDINGTON. J. Chem. Soc. Faraday 2, **72**, 1741 (1976).
6. R. W. G. WYCKOFF. Am. J. Sci. **5**, 15 (1923).
7. J. DONOHUE and W. N. LIPSCOMB. J. Chem. Phys. **15**, 115 (1947).
8. R. ANANTHAKRISHNAN. Proc. Ind. Acad. Sci. A, **5**, 87 (1937).
9. L. COUTURE and J.-P. MATHIEU. Ann. Phys. (Paris), **9**, 255 (1954).
10. B. KOJIĆ-PRODIĆ, B. MATKOVIĆ, and S. ŠĆAVNIČAR. Acta Crystallogr. B, **27**, 635 (1971).
11. B. FRLEC, H. SELIG, and H. H. HYMAN. Inorg. Chem. **6**, 1775 (1967).
12. A. FERRARI and M. NARDELLI. Gazz. Chim. Ital. **77**, 422 (1947).
13. B. KOJIĆ-PRODIĆ, S. ŠĆAVNIČAR, and B. MATKOVIĆ. Acta Crystallogr. B, **27**, 638 (1971).
14. R. LIMINGA. Acta Chem. Scand. **20**, 2483 (1966).
15. YU. E. GORBUNOVA, V. I. PAKHOMOV, V. G. KUZNETSOV, and E. S. KOVALEVA. Zh. Strukt. Khim. **13**, 165 (1972); (Engl. transl.) **13**, 154 (1972).
16. V. A. SARIN, V. YA. DUDAREV, L. E. FYKIN, YU. E. GORBUNOVA, E. G. IL'IN, and YU. A. BUSLAEV. Dokl. AN SSSR (fiz. khim.) **236**, 393 (1977); (Engl. transl.) **236**, 892 (1977).
17. M. R. ANDERSON, S. VILMINOT, and I. D. BROWN. Acta Crystallogr. B, **29**, 2961 (1973).
18. I. NITTA, K. SAKURAI, and Y. TOMIIE. Acta Crystallogr. **4**, 289 (1951).
19. P.-G. JÖNSSON and W. C. HAMILTON. Acta Crystallogr. B, **26**, 536 (1970).
20. L. F. POWER, K. E. TURNER, J. A. KING, and F. H. MOORE. Acta Crystallogr. B, **31**, 2470 (1975).
21. L. PRATT and R. E. RICHARDS. Trans Faraday Soc. **49**, 744 (1953).
22. M. GUAY, J. WEBER, and R. SAVOIE. Can. J. Spectrosc. **19**, 127 (1974).
23. C. CAVILLE. Can. J. Spectrosc. **20**, 123 (1975).
24. V. I. PAKHOMOV, T. A. KAIDALOVA, E. G. IL'IN, and YU. A. BUSLAEV. Koordin. Khim. **1**, 37 (1975); Soviet J. Coord. Chem. **1**, 28 (1975).
25. Z. MIELKE and H. RATAJCZAK. J. Mol. Struct. **19**, 751 (1973).
26. R. W. G. WYCKOFF. Crystal structures. 2nd ed. Vols. 1–3. Interscience, New York. 1963–1965.
27. LANDOLT-BÖRNSTEIN. Zahlenwerte und Funktionen aus Naturwissenschaft und Technik. Neue Serie, Bd. 7a. *Edited by* W. Pies and A. Weiss. Springer–Verlag, Berlin. 1973.
28. A. F. WELLS. Structural inorganic chemistry. 4th ed. Clarendon Press, Oxford. 1975.
29. H. BODE and E. VOSS. Z. Anorg. Allg. Chem. **264**, 144 (1951).
30. H. BODE. Z. Anorg. Allg. Chem. **267**, 62 (1951).
31. T. S. CAMERON and R. E. CORDES. Acta Crystallogr. B, **35**, 748 (1979).
32. International tables for X-ray crystallography. Vol. IV. The Kynoch Press, Birmingham, England. 1974.
33. G. SHELDRICK. X-ray system report. University Chemical Laboratories, Lensfield Road, Cambridge, England. 1976.
34. S. B. HENDRICKS. Z. Kristallogr. **67**, 106 (1928).
35. E. J. GABE. Acta Crystallogr. **14**, 1296 (1961).
36. C. J. LUDMAN, C. I. RATCLIFFE, and T. C. WADDINGTON. J. Chem. Soc. Faraday 2, **72**, 1759 (1976).
37. M. STAMMLER. J. Inorg. Nucl. Chem. **29**, 2203 (1967).
38. J. TSAU and D. F. R. GILSON. Can. J. Chem. **48**, 717 (1970).
39. J. TEGENFELDT and L. ÖDBERG. J. Phys. Chem. Solids, **33**, 215 (1972).
40. S. ALBERT and J. A. RIPMEESTER. J. Chem. Phys. **58**, 541 (1973).
41. J. L. HOARD and W. B. VINCENT. J. Am. Chem. Soc. **62**, 3126 (1940).

Can. J. Chem. Downloaded from www.nrcresearchpress.com by 210.87.254.6 on 09/06/12
For personal use only.

A pulse radiolysis study of trapped electrons in aqueous ethylene glycol glasses[1]

ZHENNAN WU,[2] NORMAN V. KLASSEN, HUGH A. GILLIS, AND GEORGE G. TEATHER
Division of Physics, National Research Council of Canada, Ottawa, Ont., Canada K1A 0R6

Received June 4, 1982

ZHENNAN WU, NORMAN V. KLASSEN, HUGH A. GILLIS, and GEORGE G. TEATHER. Can. J. Chem. **61**, 189 (1983).

The yield and reaction kinetics of trapped electrons, e^-_{ir} and e^-_{vis}, in several ethylene glycol/D_2O glasses have been studied from 6–72 K by pulse radiolysis. An increased D_2O concentration is believed to increase the concentration of IR-traps thereby leading to a greater $G(e^-_{ir})$ and to decrease the concentration of VIS-traps thereby increasing the stability of e^-_{ir}. The yield and stability of e^-_{ir} are also increased by lowering the temperature. A redetermination of $\epsilon(e^-_{ir})$ ($1.3 \times 10^4\ M^{-1}\ cm^{-1}$ at 1800 nm) confirms earlier values.

ZHENNAN WU, NORMAN V. KLASSEN, HUGH A. GILLIS et GEORGE G. TEATHER. Can. J. Chem. **61**, 189 (1983).

Le rendement et les cinétiques des électrons piegés, e^-_{ir} ct e^-_{vis}, dans quelques verres de glycol d'éthylène/D_2O ont été étudiés de 6–72 K par radiolyse pulsée. Une augmentation en concentration de D_2O augmente la concentration des pièges-IR, qui entraine une valeur plus elevée pour $G(e^-_{ir})$, et baisse la concentration des pièges-VIS augmentant la stabilité de e^-_{ir}. Le rendement et la stabilité de e^-_{ir} sont aussi augmenté par une baisse de température. Une redétermination de $\epsilon(e^-_{ir})$ ($1.3 \times 10^4\ M^{-1}\ cm^{-1}$ à 1800 nm) confirme la valeur précédente.

Introduction

Aqueous ethylene glycol glass has proven to be a useful matrix in which to study the behaviour of infrared-absorbing trapped electrons, e^-_{ir}, and visible-absorbing trapped electrons, e^-_{vis} (1–7). The pulse radiolysis of pure ethylene glycol (EG) glass, even at 6 K, shows no evidence of e^-_{ir} whereas both e^-_{ir} and e^-_{vis} are produced in 50/50 (vol/vol) EG/D_2O and EG/H_2O glasses (3, 4). Thus the presence of water permits the production of e^-_{ir}.

In publications from this laboratory, pulse radiolysis experiments have been interpreted as indicating that e^-_{ir} and e^-_{vis} are electrons trapped in two distinctly different molecular environments both in certain aqueous glasses (1–4, 8, 9) and in crystalline ice (10, 11), although the conversion of e^-_{ir} into e^-_{vis} is readily observable in some aqueous glasses (1, 8, 12) including aqueous EG glasses (1). Dolivo and Kevan (13), on the other hand, have argued that the essential difference between the two types of electron is that e^-_{ir} has a first solvation shell of water molecules which are not at equilibrium, whereas the water molecules immediately adjacent to e^-_{vis} are at equilibrium. The present results continue to favour two distinctly different molecular environments for e^-_{ir} and e^-_{vis}.

In this study, the pulse radiolysis of EG/D_2O glasses of varied composition provides new insight into the production and decay of e^-_{ir} and e^-_{vis} and the interdependence of the two species. A redetermination of $\epsilon(e^-_{ir})$ was made to insure the reliability of the calculated values of $G(e^-_{ir})$ and $G(e^-_{vis})$.

Experimental

Ethylene glycol and sodium salicylate (NaSal) (Fisher Certified), D_2O (99.7 atom % Merck, Sharp and Dohme), and argon (Airco Superpurified) were used as received. EG/D_2O glasses are designated by the parts by volume used to make up the solution, e.g. 45/55 EG/D_2O, as well as by mol% D_2O. In practice all solutions were made by weighing because of the extreme sensitivity of $G(e^-_{ir})/G(e^-_{vis})$ to glass composition and the difficulty in accurately pipetting EG.

Windowless, crack-free glasses with a 3 mm optical path were prepared from argon-saturated solutions (4). Samples were irradiated between 6 K and 72 K in a Janis model 8DT liquid helium cryostat with a temperature control of ±1 K or at 72 K in liquid nitrogen (helium bubbled) in a quartz dewar (2). Optical windows were Suprasil.

Irradiations were carried out with single 40 ns pulses of 35 MeV electrons from a linear accelerator. The dose per pulse was about 8 krad. Dosimetry was based on oxygen-saturated $5 \times 10^{-3}\ M$ KSCN for which $OD(SCN)_2^-$ was extrapolated to mid-pulse and $G\epsilon_{475}$ was taken to be 2.2×10^4. Each pulse was monitored with a secondary emission chamber.

Optical absorption measurements were made at $350 \leq \lambda \leq 800$ nm with a Philips XP-1003 photomultiplier, at $450 \leq \lambda \leq 1000$ nm with an EG&G SHS-100 Si photodiode and at $\lambda \geq 900$ nm with a Barnes A-100 InAs detector (14). Spectra were measured by the split light beam technique. Measurements were made and stored with a Tektronix R7912/computer system (15).

Results

Spectra and kinetics of e^-_{ir} and e^-_{vis} at 72 K and 6 K

The 100 ns spectra for 45/55, 50/50, and 55/45 EG/D_2O are shown in Fig. 1 for 72 K and in Fig. 2 for 6 K. The band due to e^-_{vis} has $\lambda_{max} \simeq 650$ nm but the apparent maximum shifts to higher wavelengths for spectra dominated by the infrared band due to e^-_{ir}. The maximum for e^-_{ir} has been estimated to be 3600 nm in $MgCl_2/D_2O$ (1).

By taking $\epsilon_{max}(e^-_{vis}) = 2.0 \times 10^4$ and $\epsilon_{1800}(e^-_{ir}) = 1.3 \times 10^4$ (see below) the values of $G(e^-_{vis})$ and $G(e^-_{ir})$ were calculated for 100 ns, 400 ns, and 835 ns and for the extrapolation to mid-pulse. These data are given in Table 1.

Where it is indicated that the irradiation was done at 6 K the temperature of the sample was stabilized at 6 (±1) K before the electron pulse. The analyzing light and the electron pulse may have caused a substantial (but undetermined) rise in the temperature of the sample. All experiments were carried out in the same manner so that the temperature rise was similar each time. The spectrum labeled "6 K" is clearly very different from the 72 K spectrum but is similar to the spectrum determined by γ-radiolysis of EG/H_2O at 4 K (6). The discussion of these results does not depend on knowing accurately the temperature of the "6 K" sample.

[1]NRCC No. 20689.

[2]Permanent address: University of Science and Technology of China, Hefei, The People's Republic of China.

0008-4042/83/010189-05$01.00/0

©1983 National Research Council of Canada/Conseil national de recherches du Canada

Can. J. Chem. Downloaded from www.nrcresearchpress.com by 210.87.254.105 on 09/06/12
For personal use only.

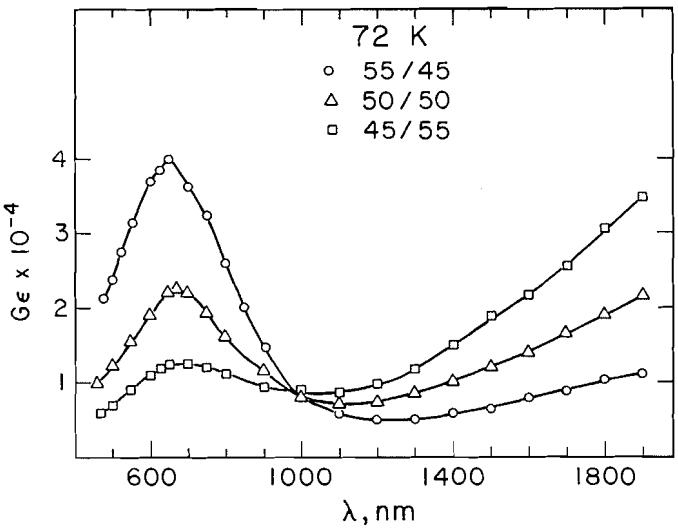

FIG. 1. The 100 ns spectra of EG/D_2O glasses at 72 K.

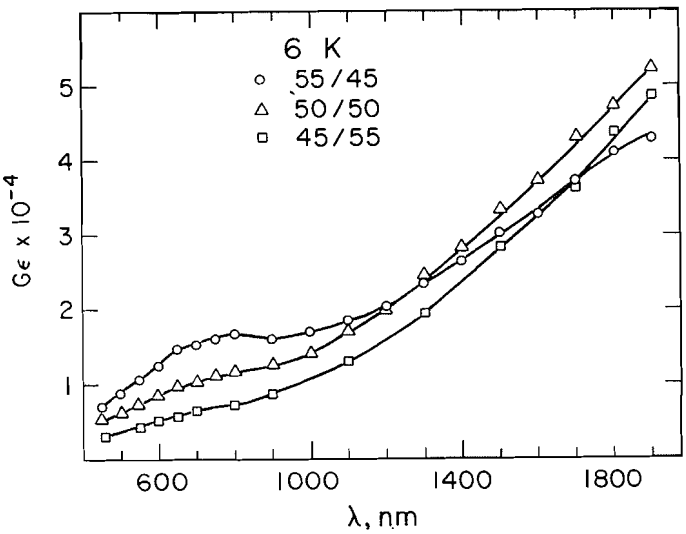

FIG. 2. The 100 ns spectra of EG/D_2O glasses at 6 K.

Determination of $\epsilon_{1800}(e_{ir}^-)$

Both the yield and stability of e_{ir}^- are increased by high D_2O concentrations and low temperatures. Advantage was taken of these factors to redetermine $\epsilon(e_{ir}^-)$. Sodium salicylate was used to scavenge electrons according to the reaction:

$$Sal^- + e^- \rightarrow Sal^{2-}$$

EG/D_2O glasses containing Sal^- were irradiated and the absorption at 460 nm and 650 nm (due to Sal^{2-}, e_{vis}^-, and e_{ir}^-) and at 1800 nm (due to e_{ir}^-) was measured and compared to the absorption in the absence of Sal^-. $G(Sal^{2-})$ was equated to the reduction of $G(e_{ir}^- + e_{vis}^-)$ estimated at mid-pulse.

The spectrum of Sal^{2-} was measured at 8 μs, 72 K, for 50/50 EG/D_2O containing 0.3 *M* Sal^-. It was found to be very similar to that reported by Singh, Chase, and Hunt (16) for Sal^{2-} in a room-temperature D_2O solution of 2 *M* NaSal (λ_{max} = 460 nm). Accordingly we adopted their value of $\epsilon_{460}(Sal^{2-}) = 4500$. Other ε's and ratios of ε's that were used are as follows: (*a*) $\epsilon_{460}(Sal^{2-})/\epsilon_{650}(Sal^{2-}) = 6.0$ from our spectrum of Sal^{2-}; (*b*) $\epsilon_{460}(e_{vis}^-)/\epsilon_{650}(e_{vis}^-) = 0.5$ from the spectrum for 55/45 EG/D_2O at 72 K (Fig. 1); (*c*) $\epsilon_{650}(e_{vis}^-) = 2.0 \times 10^4$ from ref. 17; (*d*) $\epsilon_{650}(e_{ir}^-)/\epsilon_{1800}(e_{ir}^-) = 0.08$ and $\epsilon_{460}(e_{ir}^-)/\epsilon_{1800}(e_{ir}^-) = 0.05$ estimated from the spectrum for 45/55 EG/D_2O at 6 K (Fig. 2). Absorption measurements were made at 460, 650, and 1800 nm from 100 ns to 835 ns and the concentrations of e_{ir}^-, e_{vis}^-, and Sal^{2-} at mid-pulse were estimated. The extrapolation to mid-pulse was larger for e_{ir}^- than for e_{vis}^- or Sal^{2-} but more straightforward since only e_{ir}^- absorbs at 1800 nm whereas all three species absorb at 650 and 460 nm. The uncertainty due to these extrapolations results in a large uncertainty in the calculated values of $\epsilon(e_{ir}^-)$.

The calculated values of $\epsilon_{1800}(e_{ir}^-)$ are 1.2×10^4 and $1.7 \times 10^4\ M^{-1}\ cm^{-1}$ for 45/55 EG/D_2O containing 0.01 *M* Sal^- at 6 K and 72 K, respectively, and $1.5 \times 10^4\ M^{-1}\ cm^{-1}$ for 50/50 EG/D_2O containing 0.02 *M* Sal^- at 6 K. The 45/55 matrix with 0.01 *M* Sal^- at 6 K was probably best suited for this determination because $G(e_{vis}^-)/G(e_{ir}^-)$ is small, the ratio of the extrapolated mid-pulse yield of e_{ir}^- to the yield at 100 ns is relatively small at 1.33, and because it involves the lower of the two Sal^- concentrations (which reduces the risk that Sal^- scavenges electrons which otherwise would have recombined very rapidly and therefore would not have been accounted for in the extrapolated yields of e_{ir}^- and e_{vis}^- in the absence of Sal^-). We take $\epsilon_{1800}(e_{ir}^-) = 1.3\ (\pm 0.3) \times 10^4\ M^{-1}\ cm^{-1}$ as the best value.

Concentration dependence of $G(e_{ir}^-)$ *and* $G(e_{vis}^-)$

In order to present as complete a picture as possible of the role of matrix composition on the distribution of trapped electrons at early times, measurements were made on EG/D_2O matrices at 6 K over the whole range of concentrations which were easily glassed. These results, extrapolated to mid-pulse, are plotted in Fig. 3.

Accuracy of the data

The absolute values of $G\epsilon$ reported here are believed to be accurate to ±10%. Each value is the result of several determinations on different days. Scatter in the results can result from our inability to reproduce exactly the sample composition, position, temperature, and structure (e.g. strains, which develop during glassing) as well as electron beam wander and many other parameters common to pulse radiolysis experiments. There are, however, three types of results presented here which are internally consistent to better than ±10%. They are the spectral shapes (Figs. 1 and 2), the decays (Table 1), and the relative yields at 72 K and 6 K for the same composition (Table 1). Spectra were measured by the split light beam technique in which the analyzing light is split into two beams with a partially reflecting mirror after passing through the sample. With one beam $G\epsilon_{ref}$ is measured at a reference wavelength for each pulse. The other beam is used to measure $G\epsilon_\lambda$ at different wavelengths. A spectrum made up from $G\epsilon_\lambda/G\epsilon_{ref}$ is much less sensitive to many of the experimental variables than is the absolute value of $G\epsilon$. No significant effect of accumulated dose on $G\epsilon(e_{vis}^-)$ and $G\epsilon(e_{ir}^-)$ was noticed. The decays given in Table 1 are much more accurate than ±10% because each corresponds to the same electron pulse. In addition, the decays were verified by similar results obtained on several occasions. The values of $G\epsilon_{72K}/G\epsilon_{6K}$ for a given sample composition (Table 1) are more accurate than ±10% because they were determined on the same sample after changing only the temperature.

Discussion

The values of $G(e_{ir}^-)$ and $G(e_{vis}^-)$ in this report have been calculated using a single value for $\epsilon_{1800}(e_{ir}^-)$ of $1.3 \times 10^4\ M^{-1}$

Can. J. Chem. Downloaded from www.nrcresearchpress.com by 210.87.254.105 on 09/06/12
For personal use only.

TABLE 1. Yields of e_{ir}^- and e_{vis}^- in EG/D_2O glasses at 6, 72 K[a]

Glass	T (K)	Species	G Mid-pulse[b]	G 100 ns	G 400 ns	G 835 ns
45/55	72	e_{ir}^-	2.95	2.35	1.98	1.79
		e_{vis}^-	0.38	0.49	0.57	0.63
		$e_{ir}^- + e_{vis}^-$	3.33	2.84	2.55	2.42
50/50	72	e_{ir}^-	2.38	1.65	1.20	1.02
		e_{vis}^-	0.97	1.10	1.24	1.30
		$e_{ir}^- + e_{vis}^-$	3.35	2.75	2.44	2.32
55/45	72	e_{ir}^-	1.44	0.80	0.48	0.38
		e_{vis}^-	1.92	2.01	2.09	2.14
		$e_{ir}^- + e_{vis}^-$	3.36	2.81	2.57	2.52
45/55	6	e_{ir}^-	3.56	3.36	3.23	3.13
		e_{vis}^-	0.20	0.12	0.07	0.06
		$e_{ir}^- + e_{vis}^-$	3.76	3.48	3.30	3.19
50/50	6	e_{ir}^-	3.88	3.62	3.35	3.24
		e_{vis}^-	0.31	0.30	0.29	0.27
		$e_{ir}^- + e_{vis}^-$	4.19	3.92	3.64	3.51
55/45	6	e_{ir}^-	3.48	3.16	2.90	2.78
		e_{vis}^-	0.50	0.58	0.60	0.60
		$e_{ir}^- + e_{vis}^-$	3.98	3.74	3.50	3.38

[a]Values of $G(e_{ir}^-)$ and $G(e_{vis}^-)$ are quoted here to a precision greater than warranted for their absolute yields in order to show the changes which occur with time which do warrant the precision indicated.

[b]Values of G at mid-pulse were estimated by extrapolation.

cm^{-1} and a single value for $\epsilon_{max}(e_{vis}^-)$ of $2.0 \times 10^4\ M^{-1}\ cm^{-1}$ regardless of glass composition, temperature, or time after the pulse. This is clearly an approximation since $\lambda_{max}(e_{vis}^-)$ in EG/H_2O glasses is known to depend on the temperature (6) and on the composition of the glass (18). After γ-radiolysis of EG/H_2O glasses at 77 K, $\lambda_{max}(e_{vis}^-)$ varies from 502 nm for the 100/0 glass to 585 nm for 20/80 EG/H_2O (18). However, there are no strong reasons to believe that $\epsilon_{max}(e_{vis}^-)$ changes significantly over the range of conditions in this report. Spectral variations of e_{ir}^- are difficult to assess since all measurements have been limited to wavelengths below λ_{max} due to strong absorption bands of water. We have used D_2O, rather than H_2O, to extend our measurements as far as practical into the infrared. Table 2 lists values of $\epsilon_{1900}/\epsilon_{1500}$ at 100 ns for EG/D_2O glasses at 6 and 72 K. If the spectrum of e_{ir}^- were constant and if e_{vis}^- did not contribute to the absorption above 1500 nm, all the values in Table 2 would be the same (at 72 K the differences are close to the estimated experimental uncertainties). Two trends are indicated; the ratio $\epsilon_{1900}/\epsilon_{1500}$ decreases with decreasing temperature and with decreasing yield of e_{ir}^-. These effects could be partly accounted for by a long wavelength tail of e_{vis}^- extending into the infrared at 6 K. For example, the 100 ns spectrum of trapped electrons in 8 M NaOD/D_2O glass at 6 K shows no prominent band due to e_{ir}^- but e_{vis}^- seems to have a very broad spectrum with $G\epsilon_{1500}/G\epsilon_{650} = 0.30$ and $G\epsilon_{1900}/G\epsilon_{650} = 0.26$ (19). On the other hand, $G\epsilon_{1900}/G\epsilon_{650}$ is only 0.05 at 100 ns 6 K for pure EG glass. We conclude that there may be a significant variation in $\epsilon_{1800}(e_{ir}^-)$ over the range of temperature and EG/D_2O concentrations in this study but no reasonable alternative to adopting a single value for the present calculations is evident.

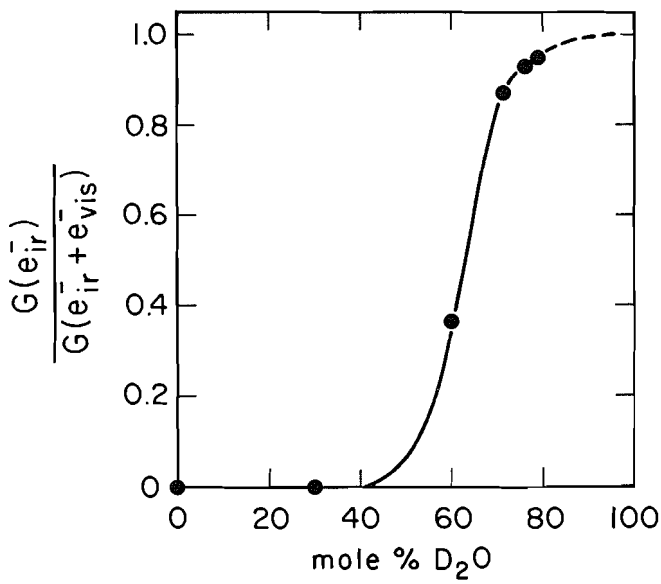

FIG. 3. The variation of $G(e_{ir}^-)/G(e_{vis}^- + e_{ir}^-)$ with EG/D_2O composition at 6 K as calculated for mid-pulse.

In this study we determined $\epsilon_{1800}(e_{ir}^-)$ to be 1.3 (±0.3) × $10^4\ M^{-1}\ cm^{-1}$ using Sal^- as an electron scavenger. We were able to take advantage of the large yield of e_{ir}^- in 45/55 EG/D_2O and its slow decay at 6 K. A previous measurement using Ag^+ as an electron scavenger in 50/50 EG/D_2O at 72 K yielded $\epsilon_{1400}(e_{ir}^-) = 0.57\ (\pm 0.08) \times 10^4\ M^{-1}\ cm^{-1}$ (1) which becomes $\epsilon_{1800}(e_{ir}^-) = 1.08\ (\pm 0.15) \times 10^4\ M^{-1}\ cm^{-1}$ when applied to the 50/50 EG/D_2O spectrum in Fig. 1. Another determination (2),

Can. J. Chem. Downloaded from www.nrcresearchpress.com by 210.87.254.105 on 09/06/12
For personal use only.

TABLE 2. Effect of temperature and matrix on the spectrum of e_{ir}^-

	$\frac{\epsilon_{1900}}{\epsilon_{1500}}$, 100 ns	
EG/D_2O	6 K	72 K
45/55	1.71±0.06	1.86±0.06
50/50	1.57±0.06	1.79±0.07
55/45	1.41±0.06	1.72±0.08

$\epsilon_{2500}(e_{ir}^-) = 3.5 \times 10^4\ M^{-1}\ cm^{-1}$ in 9.5 M $LiCl/D_2O$ containing 10^{-4} M tryptophan, is convertible into $\epsilon_{1800}(e_{ir}^-) = 1.3 \times 10^4$.

We believe that the spectrum reported for trapped electrons in 50/50 EG/H_2O after γ-radiolysis at 4 K with $OD_{1900}/OD_{700} = 1.4$ (6) had probably evolved considerably from its initial value when we compare it to the 100 ns spectrum of 50/50 EG/D_2O at 6 K, for which $OD_{1900}/OD_{700} = 5$ (Fig. 2). The evolution was probably due largely to decay of e_{ir}^- (see Table 1).

Figures 1–3 and Table 1 show that at both 6 and 72 K, $G(e_{ir}^-)$ increases with the concentration of D_2O in the matrix. A small extrapolation of the data in Fig. 3 (see dashed line) indicates that in a pure D_2O glass at 6 K probably all of the trapped electrons would be e_{ir}^- initially. These observations are qualitatively similar to the finding (9) that for $LiCl/D_2O$ glasses at 72 K electron yields fit the expression

$$\frac{G(e_{ir}^-)}{G(e_{vis}^-)} \propto \frac{[\text{Free } D_2O]}{[LiCl \cdot 4D_2O]}$$

This expression implies that e_{vis}^- is an electron trapped in a cluster of $LiCl \cdot 4D_2O$ molecules, whereas e_{ir}^- resides in an environment of only water molecules, which are thought to be incorporated interstitially at the interfaces between the clusters of $LiCl \cdot 4D_2O$ (20). Similarly the trapped electron yields for BeF_2/D_2O glasses (12) and the present results for EG/D_2O glasses suggest that e_{vis}^- is an electron trapped in clusters of $BeF_2 \cdot nD_2O$ or in clusters of $EG \cdot nD_2O$, respectively, and that e_{ir}^- is found in a pure D_2O environment. It is important to note that, at least in LiCl glasses and probably also in BeF_2 and EG glasses, the water molecules are packed differently than in ice (20, 21), so the conclusion that e_{vis}^- is found in clusters of $LiCl \cdot 4D_2O$ (or $BeF_2 \cdot nD_2O$ or $EG \cdot nD_2O$) molecules is not inconsistent with the observation that irradiation of crystalline ice at low temperatures results in a significant yield of e_{vis}^- as well as large yields of e_{ir}^- (10).

On the basis of the above picture one might expect the ratio $G(e_{ir}^-)/G(e_{vis}^-)$ to remain constant with temperature below the glass transition temperature since the structure of the glass and therefore the ratio of concentrations of the two kinds of traps should not change with temperature. However, Figs. 1 and 2 and Table 1 indicate that this ratio increases considerably for EG/D_2O glasses when the temperature is lowered from 72 to 6 K. Similarly, for $LiCl/D_2O$ glasses $G(e_{ir}^-)/G(e_{vis}^-)$ increases as the temperature is lowered from 72 to 6 K, especially for 12 and 14 M glasses in which very little free D_2O is expected (22). This could be due at least in part to a slightly higher activation energy for the process of trapping to give e_{vis}^- than for trapping to give e_{ir}^-, so that at 6 K the rate constant for trapping to give e_{ir}^- is much greater than for trapping to give e_{vis}^-. This possibility has been suggested earlier for alcohols (23–25) and for EG/D_2O (4) and EG/H_2O glasses (5).

Recently, Bartczak, Hilczer, and Kroh (26) have offered an explanation for the correlation between D_2O concentration and the ratio $G(e_{ir}^-)/G(e_{vis}^-)$ for $LiCl/D_2O$ glasses at 72 K which is very different than the one discussed above; they regard the $LiCl/D_2O$ glass as a distorted crystal lattice and suggest that e_{ir}^- and e_{vis}^- are electrons trapped in cation and anion vacancies, respectively. As the authors have stated, this treatment obviously cannot be extended to EG/D_2O glasses.

Recently, experiments were reported of a study of both temperature and concentration effects in ethanol/water glasses (27). As the water concentration was increased, the measured spectra became less like pure ethanol and more like the e_{vis}^- plus e_{ir}^- spectra of $LiCl/D_2O$ and EG/D_2O. At the highest water concentration reported (26 mol%) e_{vis}^- decreased and e_{ir}^- increased as the temperature was lowered from 72 K to 6 K. This result parallels those for $LiCl/D_2O$ and EG/D_2O. The similar results for these three systems suggest that the mechanism responsible for the proportions of e_{ir}^- and e_{vis}^- are also similar. If so, this argues against the explanation of Bartzcak, Hilczer, and Kroh, which can apply only to $LiCl/D_2O$.

An nmr study of ethanol/water solutions at 20°C (28) showed that ethanol present in small amounts is structure-making whereas, above 20 mol%, ethanol hinders the water molecules from organizing into three dimensional structures and, instead, water–ethanol hydrogen bonds are formed. Li and Kevan (29) have shown that silver ions in frozen ethanol/H_2O solutions exist in a water environment from 0–13 mol% ethanol, but above 13 mol% ethanol there is an abrupt change to an ethanol environment. It may be that above ~20 mol% EG three dimensional water structures are replaced by hydrogen bonded water–EG so that trapping sites for e_{ir}^- are replaced by trapping sites for e_{vis}^-.

The results of this study are more consistent with the model in which e_{ir}^- and e_{vis}^- are trapped in two distinctly different molecular environments than the model of Dolivo and Kevan (13) in which e_{ir}^- is the presolvated form of e_{vis}^-, with e_{ir}^- having a nonequilibrium orientation of first solvent shell molecules and e_{vis}^- having an equilibrium orientation of first solvent shell molecules. The spectra in Fig. 1 show no sign of any intermediate states between e_{ir}^- and e_{vis}^- as would be expected from the latter model. In an earlier publication (4) we showed that some published results of γ-radiolysis experiments were incorrectly interpreted in favour of the latter model.

Within the limitations of the accuracy placed on the absolute values of $G\epsilon$ reported here there are two clear trends in Table 1. They are: (*1*) $G(e_{vis}^- + e_{ir}^-)$ at a given time and temperature does not change with changes in EG/D_2O sufficient to cause large variations in $G(e_{vis}^-)/G(e_{ir}^-)$; (*2*) $G(e_{vis}^- + e_{ir}^-)$ increases on going from 72 K to 6 K. Trend (*1*) also holds for $LiCl/D_2O$ glasses as well as trend (*2*) which is less pronounced (9). As can be seen from Table 1, the most important factor in maintaining $G(e_{ir}^- + e_{vis}^-)$ independent of the matrix from mid-pulse to 835 ns is that the absolute decay of e_{ir}^-, $\Delta G(e_{ir}^-)$, is independent of the matrix. Also there is a delicate balance between the decay of e_{ir}^- and e_{vis}^- and the conversion of e_{ir}^- into e_{vis}^-. The conversion of e_{ir}^- into e_{vis}^- represents about 23% of the e_{ir}^- decay from mid-pulse to 835 ns in all three matrices at 72 K if e_{vis}^- is assumed not to decay at all. If we assume the concentration of visible traps to be proportional to $G(e_{vis}^-)$ at 6 K, mid-pulse, which implies no decay of e_{vis}^- before mid-pulse at 6 K, we find that the absolute decay of e_{ir}^-, $\Delta G(e_{ir}^-)$, between 100 ns and 400 ns can be described by

Can. J. Chem. Downloaded from www.nrcresearchpress.com by 210.87.254.105 on 09/06/12
For personal use only.

$$\Delta G(e_{ir}^-) = k[e_{ir}^-][\text{visible traps}]$$

where k varies by ±5% over the three glasses. Thus, it seems that the decay rate of e_{ir}^- at 72 K is proportional to the concentration of visible traps or the structure in which they exist. This implies that the species (or structures) with which e_{ir}^- reacts at 72 K (including the 23% converted into e_{vis}^-) are also to be found mostly in the region containing visible traps. Perhaps ethylene glycol molecules scavenge D_2O^+ and OD efficiently to produce ethylene glycol cations and free radicals which might then become the major electron scavengers. $G(e_{ir}^- + e_{vis}^-)$ at 100 ns, 6 K, averages 3.7 for 45/55, 50/50, and 55/45 EG/D_2O (Table 1). Thus EG/D_2O matrices trap electrons very efficiently. This might be due in part to rapid reaction of EG with D_2O^+ which is potentially a very mobile species.

Changing EG/D_2O at 72 K or at 6 K has little effect on the overall efficiency for trapping electrons. However, the increase in $G(e_{ir}^- + e_{vis}^-)$ at mid-pulse on going from 72 K to 6 K suggests that the trapping efficiency, relative to competing electron reactions, increases with decreasing temperatures.

At 6 K (Table 1) a decay of e_{vis}^- was observed in 45/55 and 50/50 glasses but a growth was measured in the 55/45 glass. This suggests that e_{vis}^- reacts on the 10^{-8} to 10^{-7} s time scale but that a net growth of e_{vis}^- is observed when a sufficiently high rate of conversion of e_{ir}^- into e_{vis}^- occurs as is found in the 55/45 matrix.

1. G. V. BUXTON, H. A. GILLIS, and N. V. KLASSEN. Can. J. Chem. **54**, 367 (1976).
2. N. V. KLASSEN, G. G. TEATHER, and F. KIEFFER. Can. J. Chem. **57**, 1488 (1979).
3. G. J. TRUDEL, H. A. GILLIS, N. V. KLASSEN, and G. G. TEATHER. Can. J. Chem. **59**, 1235 (1981).
4. J. CYGLER, H. A. GILLIS, N. V. KLASSEN, and G. G. TEATHER. Radiat. Phys. Chem. **17**, 379 (1981).
5. J. W. VAN LEEUWEN, M. G. J. HEIJMAN, and H. NAUTA. Radiat. Phys. Chem. **17**, 367 (1981).
6. H. HASE, M. NODA, and T. HIGASHIMURA. J. Chem. Phys. **54**, 2975 (1971).
7. S. A. RICE, G. DOLIVO, and L. KEVAN. J. Chem. Phys. **70**, 18 (1979).
8. N. V. KLASSEN, R. J. ADAMS, G. G. TEATHER, and C. K. ROSS. J. Phys. Chem. **84**, 3609 (1980).
9. H. A. GILLIS, G. G. TEATHER, and G. V. BUXTON. Can. J. Chem. **56**, 1889 (1978).
10. G. V. BUXTON, H. A. GILLIS, and N. V. KLASSEN. Can. J. Chem. **55**, 2385 (1977).
11. H. A. GILLIS, G. G. TEATHER, and C. K. ROSS. J. Phys. Chem. **84**, 1248 (1980).
12. T. Q. NGUYEN, D. C. WALKER, and H. A. GILLIS. J. Chem. Phys. **69**, 1038 (1978).
13. G. DOLIVO and L. KEVAN. J. Chem. Phys. **70**, 5489 (1979).
14. G. G. TEATHER, N. V. KLASSEN, and H. A. GILLIS. Int. J. Rad. Phys. Chem. **8**, 477 (1976).
15. C. K. ROSS, K. H. LOKAN, and G. G. TEATHER. Computers Chem. **3**, 89 (1979).
16. A. SINGH, W. J. CHASE, and J. W. HUNT. J. Chem. Soc. Faraday Discuss. **63**, 28 (1977).
17. H. HASE and L. KEVAN. J. Chem. Phys. **54**, 908 (1971).
18. B. G. ERSHOV, I. E. MAKAROV, and A. K. PIKAEV. High Energy Chem. **1**, 414 (1967).
19. N. V. KLASSEN and G. G. TEATHER. Unpublished results.
20. I. C. BAIANU, N. BODEN, D. LIGHTOWLERS, and M. MORTIMER. Chem. Phys. Lett. **54**, 169 (1978).
21. C. A. ANGELL and E. J. SARA. J. Chem. Phys. **52**, 1058 (1970).
22. G. V. BUXTON, K. KAWABATA, and G. A. SALMON. Chem. Phys. Lett. **60**, 48 (1978).
23. M. TACHIYA and A. MOZUMDER. J. Chem. Phys. **60**, 3037 (1974).
24. R. L. BUSH and K. FUNABASHI. J. Chem. Soc. Faraday Trans. II, **73**, 274 (1977).
25. W. M. BARTCZAK and J. KROH. Chem. Phys. **44**, 251 (1979).
26. W. M. BARTCZAK, M. HILCZER, and J. KROH. Radiat. Phys. Chem. **17**, 431 (1981).
27. G. V. BUXTON, G. A. SALMON, C. STRADOWSKI, and J. KROH. Radiat. Phys. Chem. **17**, 361 (1981).
28. A. COCCIA, P. L. INDOVINA, F. PODO, and V. VITI. Chem. Phys. **7**, 30 (1975).
29. A. S. W. LI and L. KEVAN. J. Phys. Chem. **84**, 2862 (1980).

Can. J. Chem. Downloaded from www.nrcresearchpress.com by 210.87.254.105 on 09/06/12
For personal use only.

Solvation of aminopyridines by water and methanol

J. N. SPENCER, S. W. BARTON, K. A. SMITH, W. S. WOLBACH, J. F. POWELL, M. R. KIRSHENBAUM, AND D. W. FIRTH

Department of Chemistry, Franklin and Marshall College, Lancaster, PA 17604, U.S.A.

Received June 24, 1982

J. N. SPENCER, S. W. BARTON, K. A. SMITH, W. S. WOLBACH, J. F. POWELL, M. R. KIRSHENBAUM, and D. W. FIRTH. Can. J. Chem. **61**, 194 (1983).

The hydrogen-bonded interactions by water and methanol in the first solvation shell of 2-aminopyrimidine, 2-, 3-, and 4-aminopyridine were determined by calorimetric analysis. The aminopyridines are enthalpically more stable in methanol than in water. This is due to methanol interactions at the amino nitrogen which do not seem to occur in water. The transfer enthalpies from water to methanol are determined primarily by the making and breaking of hydrogen bonds in the two solvents.

J. N. SPENCER, S. W. BARTON, K. A. SMITH, W. S. WOLBACH, J. F. POWELL, M. R. KIRSHENBAUM et D. W. FIRTH. Can. J. Chem. **61**, 194 (1983).

Faisant appel à l'analyse calorimétrique, on a déterminé les interactions de liaisons d'hydrogène avec l'eau et le méthanol dans la première couche de solvatation de l'amino-2 pyrimidine, des amino-2, amino-3 et amino-4 pyridines. Les aminopyridines sont enthalpiquement plus stables dans le méthanol que dans l'eau. Ceci est dû aux interactions entre le méthanol et l'azote du groupe amino qui ne semblent pas se manisfester dans l'eau. On a déterminé initialement les enthalpies de transfert de l'eau au méthanol principalement par la formation et la suppression des liaisons hydrogène dans les deux solvants.

[Traduit par le journal]

Introduction

A previous article (1) reported the solvation of heterocyclic nitrogen-containing compounds by water and methanol. The present work is a continuation of that study for the aminopyridines and 2-aminopyrimidine. Of particular interest is the interaction of the amino group of these compounds with solvent water. These amino–water solvation interactions may be used as a model for the solvation of amino groups on more complex compounds such as adenine and guanine.

Experimental

The calorimeters and methods of analysis have been previously described (2, 3). Purifications of water and methanol have been reported (1). The aminopyridines, 2- and 4-dimethylaminopyridine, and 2-aminopyrimidine were Aldrich Analyzed compounds and were vacuum sublimed. Chloroform was refluxed over P_2O_5 and fractionally distilled under nitrogen atmosphere. No absorption in the hydroxyl stretching region was observed.

Spectra were recorded on a Beckman 5240 UV-VIS-near IR spectrophotometer. For the pure base calorimetric analysis, 4-dimethylaminopyridine and 2-dimethylaminopyridine were used as model compounds for 4-aminopyridine and 2-aminopyridine, respectively.

Results

Enthalpies of solution are given in Table 1. Enthalpies of hydrogen bond formation by the amino group of 4-aminopyridine with water and methanol, and the hydrogen bond enthalpy of the amino group of 2-aminopyridine with methanol were calculated by the pure base calorimetric method (4) and are given in Table 2.

Pure base method calculations for the hydrogen bonding of the amino groups of 2-aminopyridine and 4-aminopyridine with methanol gave -3.5 and -4.0 kcal mol^{-1} of the pyridine, respectively. The frequency shifts for the 2- and 4-aminopyridine amino groups hydrogen bonded to dimethylformamide in chloroform solvent are 165 and 192 cm^{-1}, respectively. These shifts show that in agreement with the pure base calculations, the amino group of 4-aminopyridine is a better proton donor than that of 2-aminopyridine. The corresponding frequency shift for 3-aminopyridine is 174 cm^{-1} which gives an enthalpy of hydrogen bond formation for the amino group of 3-aminopyridine with methanol to be -3.7 kcal mol^{-1}. It was not possible to use the pure base method to calculate this enthalpy for 3-aminopyridine because a suitable model compound for use in the pure base calculations was not available.

The interactions of the amino groups with water of 2- and 3-aminopyridine could not be determined by the pure base method for reasons just noted for 3-aminopyridine and because of the insolubility of the model compound for 2-aminopyridine in water. The ratio of the enthalpies in water and methanol for 4-aminopyridine was used to calculate the interaction enthalpy for 2- and 3-aminopyridine in water. It was assumed that the relative strengths of the hydrogen bonds formed by the amino groups with water and methanol by 2- and 3-aminopyridine would be the same as the relative strengths of the hydrogen bonds formed by 4-aminopyridine with water and methanol. Thus the hydrogen bonds formed with methanol by the amino group were taken to be 1.25 times as strong as the hydrogen bonds to water. The results of these calculations are given in Table 2.

The enthalpy of vaporization of 2-dimethylaminopyridine (5), 12.26 kcal mol^{-1}, was combined with the enthalpy of solution of 2-dimethylaminopyridine in methanol to give the enthalpy of solvation of this compound. Corrections for the enthalpy due to interactions at the two methyl groups attached to the amino nitrogen were made (1, 4) and the enthalpy of solvation of 2-dimethylaminopyridine was compared to the enthalpy of solvation of pyridine (1). These transfers from gas phase to methanol give the interaction at the ring nitrogen of 2-aminopyridine to be -3.2 kcal mol^{-1}. Previous work (1) has shown a correlation between the proton affinity of the ring nitrogens of pyridine and the diazines with enthalpies due to interactions at the ring nitrogens. The proton affinities of pyridine, 2-, 3-, and 4-aminopyridine are 222, 228, 225, and 234 respectively (6, 7). These proton affinities were used with the

0008-4042/83/010194-03$01.00/0

©1983 National Research Council of Canada/Conseil national de recherches du Canada

Can. J. Chem. Downloaded from www.nrcresearchpress.com by 210.87.254.6 on 09/06/12
For personal use only.

TABLE 1. Enthalpies of solution at 298 K (kcal mol^{-1})

Solute	Solvent		
	H_2O	CH_3OH	$CHCl_3$
4-Aminopyridine	+4.11±0.22	+1.68±0.07	+5.09±0.14
4-Dimethylaminopyridine	+3.38±0.25	+3.08±0.14	+2.52±0.20
3-Aminopyridine	+3.26±0.16	+2.11±0.05	
2-Aminopyridine	+3.61±0.18	+2.60±0.17	+4.50±0.29
2-Dimethylaminopyridine		−0.27±0.10	−1.87±0.03
2-Aminopyrimidine	+4.18±0.12	+4.59±0.26	

TABLE 2. Enthalpies due to interactions

Compound		ΔH (kcal mol^{-1})	
		H_2O	CH_3OH
2-Aminopyridine	(NH_2)	−2.8	−3.5
	(C_2—N)		−1.7
	(N_1)	−4.6	−3.2
3-Aminopyridine	(NH_2)	−3.0	−3.7
	(C_3—N)		−1.9
	(N_1)	−4.5	−3.1
4-Aminopyridine	(NH_2)	−3.2	−4.0
	(C_4—N)		−3.0
	(N_1)	−4.8	−3.4
2-Aminopyrimidine	(NH_2)	−2.8	−3.5
	(N_1)	−4.6	−3.2
	(N_3)	−4.6	−3.2
	(C_2—N)		−1.7
Pyridine	(N)	−4.3	−2.9
Imidazole	(N_1H)	−2.7	−3.8
	(N_1)		−1.6
	(N_3)	−4.3	−2.9

interaction enthalpies of pyridine (1) (Table 2) and 2-aminopyridine to assign enthalpies due to interactions by methanol at the ring nitrogens for 3- and 4-aminopyridine. These enthalpies are given in Table 2. Frequency shifts, determined in CCl_4 solvent, for pyridine, 2-dimethylaminopyridine, and 4-dimethylaminopyridine complexing with methanol were used to derive a $\Delta H-\Delta\nu$ relation. The enthalpy calculated for the interaction at the ring nitrogen of 4-dimethylaminopyridine was identical to that estimated from the proton affinities for 4-aminopyridine.

Enthalpies due to interactions with water by the ring nitrogen of 2- and 3-aminopyridine were determined by using transfer enthalpies. The transfer enthalpies of the ring nitrogens of pyridine, 1,2-diazine, 1,3-diazine, and 1,4-diazine from water to methanol were found to be +1.4 kcal mol^{-1} (1). It was assumed that the ring nitrogen of 3-aminopyridine would transfer from water to methanol as +1.4 kcal mol^{-1}. Furthermore, because transfer enthalpies of 2- and 3-aminopyridine, −1.01 and −1.15 kcal mol^{-1}, respectively, are nearly the same, the thermodynamic states of 2-aminopyridine and 3-aminopyridine must be comparable in water and methanol. Thus a transfer enthalpy of +1.4 kcal mol^{-1} for the ring nitrogen was also assumed for 2-aminopyridine. These assumptions then allow a calculation of the interaction enthalpy of water at the ring nitrogens of 2-aminopyridine and 3-aminopyridine. The interaction enthalpies at the ring nitrogens for 2- and 3-aminopyridine were found to be −4.6 and −4.5 kcal mol^{-1} respectively.

In a previous study, the interaction of water with N_3 of imidazole was found to be −4.3 kcal mol^{-1}; the same interaction enthalpy was found for the pyridine nitrogen interaction with water (1). The interaction of the imidazole N_1 and N_3 nitrogens with methanol was found to be −4.1 kcal mol^{-1} relative to pyrrole (1). The pyrrole nitrogen − methanol interaction was taken to be −0.4 kcal mol^{-1}. Thus, an interaction by methanol at the amino nitrogen seems likely. All interaction enthalpies except those which might be due to methanol interactions at the amino group nitrogen have now been assigned. These assigned enthalpies and transfer enthalpies may be used to identify and quantify any interactions not accounted for. The transfer enthalpy of 2-aminopyridine from water to methanol is −1.01 kcal mol^{-1}. This transfer is considered to be made up of the following group contributions:

$$\Delta H_{tr} = \Delta H_{tr}^{NH_2} + \Delta H_{tr}^{N_1} + \Delta H_{tr}^{C_4\text{—}N}$$

where subscripts refer to the group being transferred. $\Delta H_{tr}^{N_1}$ was taken to be +1.4 kcal mol^{-1} and $\Delta H_{tr}^{NH_2}$ to be −0.7 (Table 2), which then gives $\Delta H_{tr}^{C_4\text{—}N} = -1.7$ kcal mol^{-1}. For reasons to be discussed later, the enthalpy of interaction with methanol at the amino nitrogen of 2-aminopyridine was taken to be −1.7 kcal mol^{-1}. This means that no corresponding interaction at the amino group nitrogen is considered to occur with water. Similar calculations gave −1.9 kcal mol^{-1} for the interaction of the amino group nitrogen of 3-aminopyridine with methanol.

The interaction enthalpies assigned to each group should be consistent with the interactions for similar groups on other compounds. The transfer enthalpy from water to methanol for 2-aminopyrimidine is +0.41 kcal mol^{-1}. This transfer is considered to consist of the sum of group transfers:

$$\Delta H_{tr} = \Delta H_{tr}^{NH_2} + \Delta H_{tr}^{C_2\text{—}N} + \Delta H_{tr}^{N_3} + \Delta H_{tr}^{N_1}$$

By using the group transfers for 2-aminopyridine found from data given in Table 2, ΔH_{tr} is found to be:

$$\Delta H_{tr} = -0.7 - 1.7 + 1.4 + 1.4 = +0.4 \text{ kcal mol}^{-1}$$

Thus it appears that the group contributions for the aminopyridines will give reasonable estimates for similar interactions

Can. J. Chem. Downloaded from www.nrcresearchpress.com by 210.87.254.6 on 09/06/12
For personal use only.

by other compounds.

The parameters given in Table 2 may be used with the transfer enthalpy to calculate the interaction enthalpy at the amino nitrogen of 4-aminopyridine. This interaction is −3.0 kcal mol^{-1}, about twice as large as the corresponding interactions for the 2- and 3-aminopyridines. The transfer of 4-dimethylaminopyridine, when corrected for the transfer enthalpy of the two methyl groups and the ring nitrogen, gives the interaction enthalpy for the amino group nitrogen to be −3.3 kcal mol^{-1}, which is in reasonable agreement with that assigned in Table 2.

Discussion

The tautomeric imino and amino forms of these pyridines were considered, but no consistent interpretation of the data could be found if imino forms were assumed to be present. All pyridines were assumed to exist as the amino form.

The transfer enthalpy for benzene from water to methanol is −0.13 kcal mol^{-1} (1). This small transfer enthalpy indicates that the cavity and interaction terms for benzene in these two solvents must nearly cancel. If the benzene transfer is taken as a model for the transfer of the ring portion of the pyridines of this study, it must be concluded that the transfers of these pyridines are primarily determined by the solvent interactions at the ring nitrogens and amino groups. These interactions are largely due to hydrogen bonding, thus the transfer enthalpies of the compounds of this study are determined by the making and breaking of hydrogen bonds of the first solvation shell.

The methanol interactions at the amino nitrogen of these pyridines is probably due to hydrogen bonding. The site of interaction is most likely from above and below the plane of the ring. The larger interaction enthalpy found for the amino nitrogen of 4-aminopyridine in methanol may involve two methanol molecules while only one may bond to the amino nitrogen of the 2- and 3-aminopyridine. The interaction by methanol at the amino nitrogen site was assigned by considering that no hydrogen bonding by water occurred at this site. This may not be the case but these interactions, if they occur in both solvents, are nearly 2 kcal mol^{-1} more exothermic with methanol than with water. Because water is a better proton donor than methanol (1), it does not seem likely that such interactions occur at the amino nitrogen by water. The transfer enthalpies of pyridine, 1,2-diazine, 1,3-diazine, and 1,4-diazine from water to methanol are all positive and in excess of 1 kcal mol^{-1} (1). The pyrrole, imidazole, and aminopyridine transfer enthalpies are all more negative than 1 kcal mol^{-1}. The better proton-accepting ability of methanol over water accounts for some of the heat observed in the transfer process but only about 1 kcal mol^{-1} can be attributed to stronger N—H hydrogen bonding in methanol. The additional heat found for the solvation of the aminopyridines, over that of pyridine, and the diazines must result from the formation of more hydrogen bonds with methanol than with water. Absolute values of the interaction enthalpies for the ring nitrogen of 4-aminopyridine with methanol and water are different from those for the pyridine nitrogen but the transfer enthalpy of the ring nitrogen from water to methanol should be quite similar for 4-aminopyridine and pyridine. The large exothermic transfer of 4-aminopyridine can best be rationalized by strong interactions by methanol at the amino nitrogen.

The transfer enthalpies for the aminopyridines are exothermic, meaning that the aminopyridines are enthalpically more stable in methanol than in water. Methanol is a better proton acceptor than water and correspondingly the amino group is enthalpically stabilized in methanol relative to water. Water, however, is a better proton donor than methanol and the ring nitrogens correspondingly interact with water more strongly than with methanol. For 2-aminopyrimidine the methanol interaction enthalpies at the ring and amino nitrogen sites are not sufficient to compensate for the stronger water interactions at the N_1 and N_3 positions. Hence the transfer enthalpy of 2-aminopyrimidine is positive.

Acknowledgements

This material is based upon work supported by the National Science Foundation under Grant No. PRM-8102879. Additional support for this work was provided by the Research Corporation through the Cottrell College Science Grants program and by Franklin and Marshall College.

1. J. N. SPENCER, E. S. HOLMBOE, M. R. KIRSHENBAUM, S. W. BARTON, K. A. SMITH, W. S. WOLBACH, J. F. POWELL, and C. CHORAZY. Can. J. Chem. **60**, 1183 (1982).
2. J. N. SPENCER, J. E. GLEIM, M. L. HACKMAN, C. H. BLEVINS, and R. C. GARRETT. J. Phys. Chem. **82**, 536 (1978).
3. J. N. SPENCER, S. K. BERGER, C. R. POWELL, B. D. HENNING, G. S. FURMAN, W. M. LOFFREDO, E. M. RYDBERG, R. A. NEUBERT, C. E. SHOOP, and D. N. BLAUCH. J. Phys. Chem. **85**, 1236 (1981).
4. J. N. SPENCER, J. E. GLEIM, C. H. BLEVINS, R. C. GARRETT, and F. J. MAYER. J. Phys. Chem. **83**, 1249 (1979).
5. C. H. ROCHESTER and J. A. WATERS. J. Chem. Soc. Faraday Trans 1, **78**, 631 (1982).
6. M. MEOT-NER. J. Am. Chem. Soc. **101**, 2396 (1979).
7. D. H. AUE, H. M. WEBB, M. T. BOWERS, C. L. LIOTTA, C. J. ALEXANDER, and H. P. HOPKINS. J. Am. Chem. Soc. **98**, 854 (1976).

Can. J. Chem. Downloaded from www.nrcresearchpress.com by 210.87.254.6 on 09/06/12
For personal use only.

Charge distributions and chemical effects. XXXI. Molecular energies of ethylenic compounds

M.-T. BÉRALDIN AND S. FLISZÁR
Department of Chemistry, University of Montreal, Montreal, P.Q., Canada H3C 3V1

Received May 27, 1982

M.-T. BÉRALDIN and S. FLISZÁR. Can. J. Chem. **61**, 197 (1983).

The energy formula describing bond contributions in terms of the charges carried by the bond-forming atoms is applied to ethylenic compounds. It is shown in what manner σ and π electrons can be treated within the framework of the bond energy theory giving the atomization energy of the vibrationless molecule at 0 K. Proper consideration of zero-point and thermal vibrational energies leads to standard enthalpies of formation. These calculations, which are carried out on the basis of ^{13}C nuclear magnetic resonance spectra, agree with their experimental counterparts, within experimental uncertainties (~0.3 kcal mol^{-1} average deviation).

M.-T. BÉRALDIN et S. FLISZÁR. Can. J. Chem. **61**, 197 (1983).

La formule décrivant l'énergie contribuée par un lien chimique en fonction des charges portées par les atomes du lien est appliquée à une série d'éthyléniques. Le traitement des électrons σ et π est illustré dans le cadre de la théorie conduisant à l'énergie d'atomisation de la molécule à 0 K, sans énergie vibrationnelle. Une considération des énergies vibrationnelles conduit aux enthalpies de formation standard. Ces calculs, entièrement basés sur les spectres de résonance magnétique nucléaire du ^{13}C, sont en accord avec leurs contreparties expérimentales, avec une déviation moyenne de 0.3 kcal mol^{-1}.

Can. J. Chem. Downloaded from www.nrcresearchpress.com by 210.87.254.105 on 09/06/12
For personal use only.

Introduction

The energy of a molecule in its hypothetical vibrationless state at 0 K is conveniently described in terms of bond energy contributions depending on the charges of the bond-forming atoms (1). The appropriate expressions were successfully tested (1–3) in comparisons with experimental atomization energies, ΔE^*_a, given by eq. [1] (see Appendix I: glossary).

$$[1] \quad \Delta E^*_a = \Sigma_i n_i[\Delta H^0_f(A_i) - 5\,RT/2] + \mathrm{ZPE} + H_T - H_0 - \Delta H^0_f$$

These verifications were made for linear and branched paraffins, including saturated hydrocarbons constructed from chair and/or boat cyclohexane rings (1, 2), as well as for ethers, aldehydes, and ketones (3). The present study offers a test for simple alkenes C_nH_{2n}.

The basic formula

$$[2] \quad \epsilon_{ij} = \epsilon^0_{ij} + a_{ij}\Delta q_i + a_{ji}\Delta q_j$$

gives the energy contribution of an *ij* bond to ΔE^*_a. Neglecting the nonbonded contributions (in the usual chemical sense), which are very small indeed (1–3), we use the approximation $\Delta E^*_a \simeq \Sigma\epsilon_{ij}$, i.e.,

$$[3] \quad \Delta E^*_a \simeq \Sigma\epsilon^0_{ij} + \Sigma_i\Sigma_j a_{ij}\Delta q_i$$

in which the $\Sigma_i\Sigma_j a_{ij}\Delta q_i$ term is responsible for the energy differences between structural isomers. The ϵ^0_{ij}'s are reference bond energies (1) (Appendix II) in kcal mol^{-1},

$\epsilon^0_{CH} = 106.806$ (CH in ethane)

$\epsilon^0_{CC} = 69.633$ (CC in ethane)

$\epsilon^0_{C=C} = 139.27$ (C=C in ethylene)

and Δq_i is the increment in net charge at atom *i* relative to the charge in the molecule selected for defining ϵ^0_{ij}. The reference net charges are (1) (Appendix III), in me = 10^{-3} electron units,

$q^0_C = 35.1$ me (C atom in ethane)

$q^0_H = -11.7$ me (H atom in ethane)

$q^0_{C\alpha} = 7.7$ me (C atom in ethylene)

Finally, the a_{ij}'s are given by the expression (1) (Appendix I)

$$a_{ij} = \frac{1}{\nu_i}\frac{K^{mol}_{Av}}{K^{mol}_i}\left[\left(\frac{\partial E^{vs}_i}{\partial N_i}\right)^0 - \frac{1}{2}\left(\frac{\partial^2 E^{vs}_i}{\partial N_i^2}\right)^0 \Delta q_i\right] - K^{mol}_{Av}\, Z^{eff}_j \langle r^{-1}_{ij}\rangle^0$$

which enables their theoretical evaluation. The second-order derivative can be safely neglected in the present case because the Δq_i's turn out to be sufficiently small. The a_{ij}'s required in this study and the parameters from which they were derived are indicated in Table 1.

For the CH and CC bonds involving sp^3 carbon atoms, the average inverse distance between nucleus *i* and the center of electronic charge on atom *j* (i.e., $\langle r^{-1}_{ij}\rangle^0$) is approximated in the usual manner (1) by the inverse of the internuclear distance, $r_{CH} = 1.08$ and $r_{CC} = 1.53$ Å. This approximation locates the centroids of σ charges at the nuclear positions. For sp^2 carbons, however, we consider that the center of π atomic charge is shifted by ~0.04 Å from the center of σ charge, toward the other carbon engaged in the double bond. The corresponding $\langle r^{-1}_{ij}\rangle^0$ parameters (Table 1) reflect this hypothesis which is justified *a posteriori* by the results obtained in this fashion.

A complication arises when atomic electron populations vary at different energy levels. Consider, for example, vinyl carbons with charges varying at the σ and π levels, i.e.,

$$\Delta q_i = \Delta q_{i\sigma} + \Delta q_{i\pi}$$

In this case, the term $a_{ij}\Delta q_i$ of eq. [2] becomes

$$a_{ij}\Delta q_i = a^\sigma_{ij}\Delta q_{i\sigma} + a^\pi_{ij}\Delta q_{i\pi}$$

indicating that a_{ij} represents now the appropriately weighted average of a^σ_{ij} and a^π_{ij}, i.e.,

$$a_{ij} = (a^\sigma_{ij}\Delta q_{i\sigma} + a^\pi_{ij}\Delta q_{i\pi})/(\Delta q_{i\sigma} + \Delta q_{i\pi})$$

0008-4042/83/010197-09$01.00/0
©1983 National Research Council of Canada/Conseil national de recherches du Canada

TABLE 1. Calculation of a_{ij} (eq. [4])[a]

Atom	$(\partial E_i^{vs}/\partial N_i)^0$ (au)	r_{ij} (Å)	a_{ij} (au)
H(1*s*)	−0.195	1.08 (CH)	$a_{HC} = -1.007$
C(2*s*)	−0.735	1.08 (CH)	$a_{CH} = -0.394$ (sp^3—H)
		1.53 (CC)	$a_{CC} = -0.777$ (sp^3—sp^3)
C_σ	−0.375	1.34 (C=C)	$a^{\sigma}_{C=C} = -0.802$ (sp^2—sp^2)
C_π	−0.244	1.30 (C=C)	$a^{\pi}_{C=C} = -0.779$ (sp^2—sp^2)
C_σ	−0.375	1.08 (CH)	$a^{\sigma}_{C\alpha H} = -0.335$ (sp^2—H)
C_π	−0.244	1.10 (CH)	$a^{\pi}_{C\alpha H} = -0.2874$ (sp^2—H)
C_σ	−0.375	1.53 (CC)	$a^{\sigma}_{C\alpha C} = -0.718$ (sp^2—sp^3)
C_π	−0.244	1.55 (CC)	$a^{\pi}_{C\alpha C} = -0.666$ (sp^2—sp^3)

[a] We sincerely thank Professor D. Salahub and Drs. B. N. McMaster and N. A. Baykara for carrying out the SCF-Xα calculations of the derivatives. They were made as indicated in ref. 1, using α = 0.686 for H and α = 0.75928 for carbon. The results for σ and π electrons are deduced from a calculation of ethylene.

Taking advantage of the relationship $\Delta q_\sigma = m\Delta q_\pi$ ($-1 < m < 0$) describing the inverse variations in σ and π charges at vinyl carbon atoms (4), it appears that the appropriate average is simply

$$[5] \quad a_{ij} = (ma^{\sigma}_{ij} + a^{\pi}_{ij})/(m + 1)$$

The difficulty comes from the fact that calculated σ charges are considerably more basis set dependent than π charges, rendering a reliable theoretical evaluation of *m* illusory. Present numerical analyses suggest that $m \simeq -0.955$, a value which is consistent with the general conclusions drawn from the study of correlations between ^{13}C nuclear magnetic resonance shifts and atomic charges of sp^2 carbons (4). So far we have collected the theoretical information required for using eq. [3]. Now we can look at the olefins and inquire about the appropriate charges for use in this energy expression.

Charge normalization

The total (σ + π) net charge $q^0_{C\alpha}$ of the ethylene-C atom (relative to 6 e) is also its net σ charge (relative to 5 e) because its net π charge (relative to 1 e) is 0. Hence, a vinyl carbon whose net σ and π charges are q_σ and q_π, respectively, differs from the ethane carbon by $\Delta q_C = q_\sigma + q_\pi - q^0_C = (q_\sigma - q^0_{C\alpha}) + (q^0_{C\alpha} - q^0_C) + (q_\pi - 0)$, i.e.,

$$[6] \quad \Delta q_C = \Delta q_\sigma + \Delta q_\pi + \Delta q^0_{C\alpha}$$

where

$$[7] \quad \Delta q^0_{C\alpha} = q^0_{C\alpha} - q^0_C = -27.4 \text{ me}$$

is the difference in net charge between the ethylene and the ethane carbon atoms. The ethylene net charge ($q^0_{C\alpha}$), of course, is used in the evaluation of C=C double bonds, i.e.,

$$\epsilon_{C=C} = \epsilon^0_{C=C} + a_{C=C}\Sigma\Delta q_{C\alpha}$$

where $\Delta q_{C\alpha} = q_{C\alpha} - q^0_{C\alpha}$ refers to sp^2 carbons, relative to ethylene. The CH and CC simple bonds, however, *including those formed by the* sp^2 *carbon atoms* (identified as α-carbons), are expressed with reference to the ethane CH and CC bond energies. This implies that the charge increments $\Delta q_H = q_H - q^0_H$ and $\Delta q_C = q_C - q^0_C$ are also to be taken relative to the ethane net charges, namely, $q^0_C = 35.1$ me for carbon.

The hydrogen net charges appear in the final result (from eq. [3]) as the sum $\Sigma\Delta q_H$. The calculation of $\Sigma\Delta q_H = \Sigma q_H - 2nq^0_H$ is straightforward. From charge normalization, i.e., $\Sigma q_H = -(\Sigma q_{C\alpha} + \Sigma q_{C\neq\alpha})$, it follows that

$$[8] \quad \Sigma\Delta q_H = -(\Sigma\Delta q_{C\neq\alpha} + \Sigma\Delta q_{C\alpha}) - 2\Delta q^0_{C\alpha} + nq^0_H$$

where *n* is the number of C atoms in the C_nH_{2n} alkene. In this fashion, it becomes possible to express ΔE^*_a (eq. [3]) by means of a general formula requiring only the charges of the carbon atoms.

General formula for C_nH_{2n} alkenes

The sum of the $\Sigma_i\Sigma_j a_{ij}\Delta q_i$ terms (eq. [3]) referring to CC bonds gives

$$\sum_i^{\text{CC bonds}}\sum_j a_{ij}\Delta q_i = a_{CC}\Sigma N_{CC}\Delta q_{C\neq\alpha} + a_{C=C}\Sigma\Delta q_{C\alpha} + a_{C\alpha C}\Sigma N_{C\alpha C}\Delta q_C$$

Similarly, we find for the CH bonds that

$$\sum_i^{\text{CH bonds}}\sum_j a_{ij}\Delta q_i = 4a_{CH}\Sigma\Delta q_{C\neq\alpha} - a_{CH}\Sigma N_{CC}\Delta q_{C\neq\alpha} + 2a_{C\alpha H}\Sigma\Delta q_C - a_{C\alpha H}\Sigma N_{C\alpha C}\Delta q_C + a_{HC}\Sigma\Delta q_H$$

A distinction is made between CC and CH bonds involving sp^3 carbons (≠ α, described by a_{CC} and a_{CH}) and bonds formed by sp^2 carbons (α-C, described by $a_{C\alpha C}$ and $a_{C\alpha H}$, respectively). Similarly, $N_{C\alpha C}$ is the number of CC bonds formed by α carbons with

Can. J. Chem. Downloaded from www.nrcresearchpress.com by 210.87.254.105 on 09/06/12
For personal use only.

sp^3 C atoms and N_{CC} is the number of CC bonds formed by sp^3 carbon atoms. Using now eq. [8], the final sum over all the CC and CH bonds becomes

$$[9]\quad \Sigma_i\Sigma_j a_{ij}\Delta q_i = \lambda_1 \Sigma N_{CC}\Delta q_{C\neq\alpha} + \lambda_2 \Sigma \Delta q_{C\neq\alpha} + n a_{HC} q_H^0 + (a_{C=C} - a_{HC})\,\Sigma\Delta q_{C\alpha} + (a_{C\alpha C} - a_{C\alpha H})\sum^{\alpha} N_{C\alpha C}\Delta q_C + 2a_{C\alpha H}\sum^{\alpha}\Delta q_C - 2a_{HC}\Delta q_{C\alpha}^0$$

where

$$\lambda_1 = a_{CC} - a_{CH} = -0.383 \text{ au}$$

$$\lambda_2 = 4a_{CH} - a_{HC} = -0.569 \text{ au}$$

The $\lambda_1 \Sigma N_{CC}\Delta q_{C\neq\alpha} + \lambda_2 \Sigma \Delta q_{C\neq\alpha} + n a_{HC} q_H^0$ part of eq. [9] is well known from the study of saturated hydrocarbons (1). By means of the charge – ^{13}C nmr shift correlation $\Delta q_C = -0.148\delta_C$ me (1) we can write this part in terms of nmr shifts relative to ethane (taken at ~5.8 ppm from TMS), i.e. (with 1 au = 627.51 kcal mol^{-1}), $0.0356\Sigma N_{CC}\delta_C + 0.0529\Sigma\delta_C + 7.393n$ kcal mol^{-1}. The term in $\Sigma\Delta q_{C\alpha}$ creates no problem because the charges are expressed with respect to ethylene and can be easily resolved. The terms in Δq_C, however, which are for vinyl carbons with respect to that of ethane, require special attention.

Let us first consider the term $F = (a_{C\alpha C} - a_{C\alpha H})\sum^{\alpha} N_{C\alpha C}\Delta q_C$ of eq. [9]. The difference $a_{C\alpha C} - a_{C\alpha H}$ is λ_1^σ or λ_1^π, depending on whether it relates to σ or to π charge variations at the vinyl carbons. Of course, λ_1^σ is simply the λ_1 value indicated above and $\lambda_1^\pi = a_{C\alpha C}^\pi - a_{C\alpha H}^\pi = -0.379$ au is deduced from Table 1. Instead of using net charges, $q = Z - N$, we begin this calculation in terms of the numbers of electrons, remembering that $\Delta N = -\Delta q$. The $\sigma - \pi$ separation gives

$$F = -\lambda_1^\sigma \sum^{\alpha} N_{C\alpha C}\,(N_{\sigma v} - N_{\sigma e}) - \lambda_1^\pi \sum^{\alpha} N_{C\alpha C}(N_{\pi v} - N_{\pi e})$$

where the subscripts v and e stand for vinyl and ethane carbon, respectively. The following transformations are self-explanatory, remembering that σ net charges are expressed with respect to 5, viz. 6 e for vinyl and sp^3 carbons, respectively, while π net charges are expressed relative to 1 electron.

$$\begin{aligned}
F &= -\lambda_1^\sigma \sum^{\alpha} N_{C\alpha C}(N_{\sigma v} - 5 - 1 + 6 - N_{\sigma e}) - \lambda_1^\pi \sum^{\alpha} N_{C\alpha C}(N_{\pi v} - 1 + 1 - 0)\\
&= -\lambda_1^\sigma \sum^{\alpha} N_{C\alpha C}(-q_\sigma - 1 + q_C^0) - \lambda_1^\pi \sum^{\alpha} N_{C\alpha C}(-q_\pi + 1)\\
&= -\lambda_1^\sigma \sum^{\alpha} N_{C\alpha C}(-q_\sigma + q_{C\alpha}^0 - q_{C\alpha}^0 + q_C^0 - 1) - \lambda_1^\pi \sum^{\alpha} N_{C\alpha C}(-q_\pi + 1)\\
&= -\lambda_1^\sigma \sum^{\alpha} N_{C\alpha C}(-\Delta q_\sigma - \Delta q_{C\alpha}^0 - 1) - \lambda_1^\pi \sum^{\alpha} N_{C\alpha C}(-\Delta q_\pi + 1)\\
&= \lambda_1^\sigma \sum^{\alpha} N_{C\alpha C}\Delta q_\sigma + \lambda_1^\pi \sum^{\alpha} N_{C\alpha C}\Delta q_\pi + (\lambda_1^\sigma \Delta q_{C\alpha}^0 + \lambda_1^\sigma - \lambda_1^\pi)\sum^{\alpha} N_{C\alpha C}
\end{aligned}$$

The first two terms of this last expression combine to give $\lambda_{1_\alpha}\Sigma N_{C\alpha C}\Delta q_{C\alpha}$, with λ_{1_α} defined as follows, from eq. [5],

$$[10]\quad \lambda_{1_\alpha} = (m\lambda_1^\sigma + \lambda_1^\pi)/(m+1)$$

On the other hand, using the results given in Table 1, it is found that

$$(\lambda_1^\sigma \Delta q_{C\alpha}^0 + \lambda_1^\sigma - \lambda_1^\pi)\sum^{\alpha} N_{C\alpha C} = 4.19 \sum^{\alpha} N_{C\alpha C} \text{ kcal mol}^{-1}$$

With these results, we can now write eq. [9] as follows, in kcal mol^{-1},

$$[11]\quad \Sigma_i\Sigma_j a_{ij}\Delta q_i = 0.0356\,\Sigma N_{CC}\delta_C + 0.0529\,\Sigma\delta_C + 7.393n + (a_{C=C} - a_{HC})\,\Sigma\Delta q_{C\alpha} + \lambda_{1_\alpha}\sum^{\alpha} N_{C\alpha C}\Delta q_{C\alpha} + 4.19\sum^{\alpha} N_{C\alpha C} + 2a_{C\alpha H}\sum^{\alpha}\Delta q_C - 2a_{HC}\Delta q_{C\alpha}^0$$

The calculation of $(a_{C\alpha C} - a_{C\alpha H})\sum^{\alpha} N_{C\alpha C}\Delta q_C$ has presented no difficulty because λ_1^σ and λ_1^π are constants, depending only upon molecular geometry and the location of the centers of charge. The important point is that the derivatives $(\partial E_i^{vs}/\partial N_i)^0$ which are part of the a_{ij}'s (eq. [4]) cancel exactly in λ_1^σ and λ_1^π. This is no longer the case with the $2a_{C\alpha H}\sum^{\alpha}\Delta q_C$ term of eq. [11].

The $\sigma-\pi$ separation of $a_{C\alpha H}\sum^{\alpha}\Delta q_C$ gives, by means of eq. [6],

$$a_{C\alpha H}^\sigma \sum^{\alpha}\Delta q_\sigma + a_{C\alpha H}^\pi \sum^{\alpha}\Delta q_\pi + 2\langle a_{C\alpha H}\rangle \Delta q_{C\alpha}^0$$

The first two terms are now well defined with reference to ethylene, and enter the final sum as $2a_{C\alpha H}^\sigma\sum^{\alpha}\Delta q_\sigma + 2a_{C\alpha H}^\pi\sum^{\alpha}\Delta q_\pi$. The $a_{C\alpha H}^\sigma$ and $a_{C\alpha H}^\pi$ values can be calculated from eq. [4] and are indicated in Table 1. The $\langle a_{C\alpha H}\rangle$ parameter, however, represented here loosely as an appropriately chosen average, remains to be clarified. On the physical side, $\langle a_{C\alpha H}\rangle \Delta q_{C\alpha}^0$ appears to describe the gain

Can. J. Chem. Downloaded from www.nrcresearchpress.com by 210.87.254.105 on 09/06/12
For personal use only.

in stability of a CH bond in going from ethane to ethylene due to (*i*) an increase in electron population of 27.4 me and (*ii*) to the shift of the center of charge (by ~0.04 Å along the C=C axis) for 1 electron, which destabilizes the CH bond by $\sim(3/7)0.529[(1/1.08) - (1/1.10)]$ au $\simeq$ 2.395 kcal mol^{-1}. As regards the gain in electronic charge in going from ethane to ethylene, the appropriate a_{CH} values are (from Table 1) −0.394 au for ethane and −0.335 au for ethylene. Tentatively taking the average of these values, we obtain in this approximation that

$$[12]\quad \langle a_{C\alpha H}\rangle \Delta q^0_{C\alpha} = [(a_{CH} + a^{\sigma}_{C\alpha H})/2]\Delta q^0_{C\alpha} - (3/7)0.529[(1/1.08) - (1/1.10)] \text{ au}$$
$$= 3.872 \text{ kcal mol}^{-1}$$

The validity of this estimate can be evaluated as follows. The 3.872 term represents the gain in stability of a CH bond due to the change C(sp^3) → C(sp^2) from ethane to ethylene. Leaving the ethane-H charge as reference for the $a_{HC}\Delta q_H$ part, the new ϵ^0_{CH} (sp^2-H) reference energy becomes 106.806 + 3.872 = 110.68 kcal mol^{-1}. Using now the ethylene-H net charge, −3.85 me (corresponding to its C charge of 7.7 me), i.e., Δq_H = 7.85 me, it results that $a_{HC}\Delta q_H$ = −4.96 and ϵ_{CH} = 105.72 kcal mol^{-1}. Four of these CH bonds plus the theoretical $\epsilon^0_{C=C}$ = 139.27 double bond contribution lead to ΔE^*_a(ethylene) = 562.15 kcal mol^{-1}, which compares favorably with its experimental counterpart, 562.22 kcal mol^{-1}. Similarly, remembering that the gain for a C(sp^2)—C(sp^3) bond is 4.19 kcal mol^{-1} larger than that for a C(sp^2)—H bond, i.e., $\langle a_{C\alpha C}\rangle \Delta q^0_{C\alpha} = \langle a_{C\alpha H}\rangle \Delta q^0_{C\alpha}$ + 4.19 kcal mol^{-1}, we can define a new ϵ^0_{CC} (sp^2–sp^3) reference as 69.633 + 3.872 + 4.19 = 77.70 kcal mol^{-1}, where the Δq_C's are taken relative to ethylene and ethane for the sp^2 and sp^3 carbons, respectively.

The $\langle a_{C\alpha H}\rangle \Delta q^0_{C\alpha}$ term appears twice for $a_{C\alpha H}\overset{\alpha}{\Sigma}\Delta q_C$ which, in turn, enters eq. [11] with a factor 2. Hence, taking now also into account the $-2a_{HC}\Delta q^0_{C\alpha}$ term of eq. [11], the constant term appearing in this equation is

$$[13]\quad 4\langle a_{C\alpha H}\rangle \Delta q^0_{C\alpha} - 2a_{HC}\Delta q^0_{C\alpha} = -19.14 \text{ kcal mol}^{-1}$$

In comparisons with experimental atomization energies deduced from eq. [1], this result, combined with the theoretical $\epsilon^0_{C=C}$ = 139.27 kcal mol^{-1} energy, leads to a systematic deviation of ~0.08 kcal mol^{-1}. Of course, it is not possible to decide which of eq. [13] or $\epsilon^0_{C=C}$ is "wrong" because each term appears once for a C=C double bond system. At this level of accuracy, however, this question is academic.[1] Tentatively, assuming the $\epsilon^0_{C=C}$ value to be correct, we modify the result indicated in eq. [13] from −19.14 to −19.06 kcal mol^{-1}. Incidentally, it is noteworthy that the location of the π center of charge which has been postulated affects both the result given in eq. [13] and the 4.19 kcal mol^{-1} coefficient of $\overset{\alpha}{\Sigma}N_{C\alpha C}$. Moreover, it enters the calculation of $a_{C=C}$. This ~0.04 Å parameter satisfies thus three numerical values which play important roles in the final energy formula.[2]

This analysis of the $a^{\sigma}_{C\alpha H}\overset{\alpha}{\Sigma}\Delta q_C$ term still leaves us with $2a^{\sigma}_{C\alpha H}\overset{\alpha}{\Sigma}\Delta q_\sigma + 2a^{\pi}_{C\alpha H}\overset{\alpha}{\Sigma}\Delta q_\pi$ which are part of eq. [11]. Combining now these terms with $(a_{C=C} - a_{HC})\overset{\alpha}{\Sigma}\Delta q_{C\alpha}$ which is easily separated to give $(a^{\sigma}_{C=C} - a_{HC})\overset{\alpha}{\Sigma}\Delta q_\sigma + (a^{\pi}_{C=C} - a_{HC})\overset{\alpha}{\Sigma}\Delta q_\pi$, we define

$$\lambda^{\sigma}_3 = a^{\sigma}_{C=C} + 2a^{\sigma}_{C\alpha H} - a_{HC} = -0.465 \text{ au}$$
$$\lambda^{\pi}_3 = a^{\pi}_{C=C} + 2a^{\pi}_{C\alpha H} - a_{HC} = -0.347 \text{ au}$$

and obtain from eq. [5] that

$$[14]\quad \lambda_3 = (m\lambda^{\sigma}_3 + \lambda^{\pi}_3)/(m + 1)$$

In this manner, eq. [11] reduces to

$$[15]\quad \Sigma_i\Sigma_j a_{ij}\Delta q_i = 0.0356\Sigma N_{CC}\delta_C + 0.0529\Sigma\delta_C + \lambda_{1_\alpha}\overset{\alpha}{\Sigma}N_{C\alpha C}\Delta q_{C\alpha}$$
$$+ \lambda_3\Sigma\Delta q_{C\alpha} + 4.19\overset{\alpha}{\Sigma}N_{C\alpha C} + 7.393n - 19.06 \text{ kcal mol}^{-1}$$

The important point is that the $\Delta q_{C\alpha}$'s are expressed with respect to the proper reference, which is ethylene, in terms of increments in total (σ + π) net charge. Moreover, the participation of σ and π charges is also accounted for in eq. [15].

The final step consists in translating this formula into an equivalent one in which the $\Delta q_{C\alpha}$'s are expressed in terms of ^{13}C nmr shifts relative to ethylene. Recent studies (4, 5) indicate that, indeed, this is possible. If we write for vinyl carbons

$$\delta_{C\alpha} = k\Delta q_{C\alpha}$$

[1]Moreover, it must be considered that this type of uncertainty may possibly be due to a systematic error in the estimates of the zero-point plus heat content energies which are described further below.

[2]Overlapping *p* electrons forming a π bond are expected, in keeping with current views, to displace their respective centers of charge inwards, as bonding orbitals tend to collect the charge between the bonded atoms, whereas populated corresponding antibonding orbitals would have the opposite effect. It is, therefore, fair to say that the proposed model is certainly in qualitative accord with the accepted understanding of π bonds. It remains that the shift of ~0.04 Å which is assumed here is a product of trial and error analysis. Its appropriateness can be illustrated as follows. If no shift is considered (which would clearly represent an arbitrary assumption), the coefficient $\lambda^{\sigma}_1\Delta q^0_{C\alpha} + \lambda^{\sigma}_1 - \lambda^{\pi}_1$ of $\overset{\alpha}{\Sigma}N_{C\alpha C}$ and the constant term (eq. [13]) would amount to 6.59 and −9.56 kcal mol^{-1}, respectively. With a shift of 0.06, instead of 0.04 Å, these two parameters would become 2.87 and −23.80 kcal mol^{-1}, respectively. These examples and inspection of eq. [16] indicate that any choice other than ~0.04 Å leads to two distinct and important sources of systematic errors. While, of course, we would prefer to obtain this result from strict theoretical considerations, it is obvious from the present calculations that there is not much room left for error in locating the "effective" center of charge of *p* electrons engaged in a vinyl π bond.

Can. J. Chem. Downloaded from www.nrcresearchpress.com by 210.87.254.105 on 09/06/12
For personal use only.

TABLE 2. Zero-point and $H_T - H_0$ energies of selected olefins (kcal mol^{-1})[a]

Molecule	ZPE (References)	$H_T - H_0$
Ethene	30.83 (8)	2.53
	30.54 (9)	
Propene	48.58 (10)	3.24
1-Butene	65.62 (11)	4.11
2-Butene *cis*	65.97 (10)	3.94
2-Butene *trans*	65.51 (10)	4.19
Isobutene	65.57 (10, 12)	4.08
	65.41 (13)	

[a]The $H_T - H_0$ values are taken from ref. 7. The ZPE values are deduced from vibrational analyses given, references in parentheses.

and use the relationships $\Delta q_\sigma = m\Delta q_\pi$ and $\Delta q_{C\alpha} = \Delta q_\sigma + \Delta q_\pi = (m + 1)\Delta q_\pi$ it follows that

$$d\delta_{C\alpha}/dq_\alpha = k(m + 1)$$

Consequently, it is (4)

$$\Delta q_{C\alpha} = [(m + 1)/(d\delta_{C\alpha}/dq_\pi)]\delta_{C\alpha}$$

It is now possible to express λ_{I_α} (eq. [10]) and λ_3 (eq. [14]) in kcal mol^{-1} ppm^{-1} units, using also the conversion factor 1 au = 627.51 kcal mol^{-1}. In this manner we obtain

$$\lambda_{I_\alpha} = (m\lambda_I^\sigma + \lambda_I^\pi)627.51/(d\delta_{C\alpha}/dq_\pi) \text{ kcal mol}^{-1} \text{ ppm}^{-1}$$

$$\lambda_3 = (m\lambda_3^\sigma + \lambda_3^\pi)627.51/(d\delta_{C\alpha}/dq_\pi) \text{ kcal mol}^{-1} \text{ ppm}^{-1}$$

where λ_I^σ, λ_I^π, λ_3^σ, and λ_3^π are in atomic units and the derivative in ppm/electron. Within the limits of validity of the charge shift relationship, eq. [15] becomes

[16] $$\Sigma_i\Sigma_j a_{ij}\Delta q_i = 0.0356\Sigma N_{CC}\delta_C + 0.0529\Sigma\delta_C + \lambda_{I_\alpha}\Sigma N_{C\alpha C}\delta_{C\alpha} + \lambda_3\Sigma\delta_{C\alpha} + 4.19\Sigma N_{C\alpha C} + 7.393n - 19.06 \text{ kcal mol}^{-1}$$

The real difficulty rests with the "true" values of m and $d\delta_{C\alpha}/dq_\pi$ because atomic charges calculated from Mulliken's scheme are strongly basis set dependent, particularly as regards σ charges. Charge separations are invariably larger when increasingly larger basis sets are used in *ab initio* calculations, to the point that unrealistic results are obtained (6). Charge analyses carried out at the STO-3G level (5) suggest a value of ~250 ppm/e for the $d\delta_{C\alpha}/dq_\pi$ slope, which is probably also a result of slightly overestimated π charges. In selecting tentatively $d\delta_{C\alpha}/dq_\pi \simeq 300$ ppm/e for vinyl C atoms, we regard this value only as a reasonable estimate but cannot attach any precision to it. This holds also for the $m \simeq -0.955$ value which is tentatively selected. With these premises, we deduce $\lambda_{I_\alpha} \simeq -0.028$ and $\lambda_3 \simeq 0.20$ kcal mol^{-1} ppm^{-1}, but it is clear that similar values can also be obtained from alternate choices for m and $d\delta_{C\alpha}/dq_\pi$. The important point is that λ_{I_α} is small and negative, whereas λ_3 is relatively large and positive. The approximate validity of our rough estimates for m and $d\delta_{C\alpha}/dq_\pi$ is best illustrated by comparisons with experimental results. Indeed, using $\lambda_{I_\alpha} = -0.028$ and $\lambda_3 = 0.20$ kcal mol^{-1} ppm^{-1} in applications of eq. [16], it turns out that ethylene, 1-alkenes, *trans*-alkenes, and tetramethylethylene are calculated with an average error of ~0.2 kcal mol^{-1}. Numerical applications indicate that the following simplified expression (eq. [17]), in which $\lambda_{I_\alpha} = 0$, gives equally satisfactory results, within the limits of uncertainties set by the precision of the experimental data. This simplification seems reasonable, considering the uncertainties associated with λ_{I_α} and λ_3.

[17] $$\Sigma_i\Sigma_j a_{ij}\Delta q_i = 0.0356\Sigma N_{CC}\delta_{C\neq\alpha} + 0.0529\Sigma\delta_{C\neq\alpha} + 0.18\Sigma\delta_{C\alpha} + 7.393n + 4.19\Sigma N_{C\alpha C} - 19.06 \text{ kcal mol}^{-1}$$

This is the basic formula which is used in the forthcoming comparisons with experimental results.

Comparison with experimental energies

The atomization energies of olefins can now be readily deduced from their ^{13}C nmr spectra, using eqs. [3] and [17]. The calculation of the corresponding enthalpies of formation, however, also requires a realistic estimate of zero-point and heat-content energies, i.e., of ZPE + $H_T - H_0$, for use in eq. [1]. Spectroscopic information is unfortunately scarce for this class of compounds. The appropriate ZPE's, calculated in the harmonic oscillator approximation (ZPE = $\Sigma_i h\nu_i/2$) from literature data are indicated in Table 2. Fortunately, however, we can profit from a detailed study on a representative variety of saturated hydrocarbons indicating, namely, that one CH_2 added to an alkyl group increases ZPE + $H_T - H_0$ by 18.213 kcal mol^{-1} whereas branching lowers this energy by 0.343 kcal mol^{-1} (2). (Situations of extreme steric crowding, such as those arising with the presence of two *tert*-butyl groups attached to a same carbon atom are not represented by these rules.) It seems reasonable to assume a similar pattern for the normal and branched ethylenic hydrocarbons. This approximation is expressed by eq. [18].

[18] $$\text{ZPE} + H_T - H_0 \simeq 33.35 + 18.213(n - 2) - 0.343n_{\text{branch}}$$

The experimental results given in Table 2 certainly support eq. [18] although, evidently, additional vibrational energy data would

Can. J. Chem. Downloaded from www.nrcresearchpress.com by 210.87.254.105 on 09/06/12
For personal use only.

TABLE 3. Comparison between calculated and experimental enthalpies of formation of unsaturated hydrocarbons (kcal mol^{-1})[a]

Molecule	$\Sigma\epsilon_{ij}^{0}$	$\Sigma_i\Sigma_j a_{ij}\Delta q_i$	ΔE_a^*	ΔH_f^0(298.15, gas) Calcd.	Benson (15)	Exptl.
Ethene	568.62	−6.40	562.22	12.38	12.22	12.50
Propene	851.87	6.77	858.64	4.80	4.78	4.88
1-Butene	1135.11	17.44	1152.55	−0.27	−0.01	−0.03
(*Z*)2-Butene	1135.11	18.71	1153.83	−1.54	−1.97	−1.67
(*E*)2-Butene	1135.11	19.88	1154.99	−2.71	−2.97	−2.67
2-Me-Propene	1135.11	21.39	1156.51	−4.22	−3.56	−4.04
1-Pentene	1418.36	28.05	1446.41	−5.28	−4.96	−5.00
(*Z*)2-Pentene	1418.36	29.52	1447.88	−6.75	−6.73	−6.71
(*E*)2-Pentene	1418.36	30.36	1448.72	−7.60	−7.73	−7.59
2-Me-1-Butene	1418.36	31.81	1450.17	−9.05	−8.32	−8.68
3-Me-1-Butene	1418.36	29.30	1447.66	−6.87	−6.78	−6.92
2-Me-2-Butene	1418.36	32.95	1451.31	−10.19	−10.30	−10.17
1-Hexene	1701.60	38.15	1739.76	−9.80	−9.88	−9.96
(*Z*)2-Hexene	1701.60	39.99	1741.60	−11.64	−11.68	−12.51
(*E*)2-Hexene	1701.60	40.96	1742.57	−12.61	−12.68	−12.88
(*Z*)3-Hexene	1701.60	40.25	1741.86	−11.90	−11.49	−11.38
(*E*)3-Hexene	1701.60	40.97	1742.58	−12.62	−12.49	−13.01
2-Me-1-Pentene	1701.60	42.22	1743.82	−13.86	−13.27	−14.19
3-Me-1-Pentene	1701.60	39.62	1741.22	−11.60	−11.73	−11.82
4-Me-1-Pentene	1701.60	39.91	1741.52	−11.90	−11.17	−12.24
(*Z*)3-Me-2-Pentene	1701.60	43.68	1745.29	−15.33	−15.06	−15.08
(*E*)3-Me-2-Pentene	1701.60	43.11	1744.71	−14.75	−15.06	−14.86
(*Z*)4-Me-2-Pentene	1701.60	41.56	1743.16	−13.54	−15.53	−13.73
(*E*)4-Me-2-Pentene	1701.60	42.40	1744.00	−14.38	−14.53	−14.69
2-Et-1-Butene	1701.60	41.31	1742.91	−12.95	−13.18	−13.38
2, 3-diMe-1-Butene	1701.60	43.34	1744.95	−15.33	−14.65	−15.85
3, 3-diMe-1-Butene	1701.60	41.28	1742.89	−13.61	−13.71	−14.70
2, 3-diMe-2-Butene	1701.60	45.14	1746.74	−16.78	−16.74	−16.68
(*Z*)2-Heptene	1984.85	50.44	2035.29	−16.49	−16.6	−16.9
(*E*)2-Heptene	1984.85	51.40	2036.25	−17.44	−17.6	−17.6
(*Z*)3-Heptene	1984.85	50.73	2035.58	−16.77	−16.4	−16.90
(*E*)3-Heptene	1984.85	51.56	2036.40	−17.60	−17.4	−17.60
(*Z*)3-Me-3-Hexene	1984.85	53.82	2038.66	−19.86	−19.83	−18.60
(*E*)3-Me-3-Hexene	1984.85	53.89	2038.74	−19.93	−19.83	−19.22
2, 4-diMe-1-Pentene	1984.85	54.35	2039.19	−20.74	−19.50	−20.27
4, 4-diMe-1-Pentene	1984.85	52.62	2037.47	−19.35	−18.17	−19.20
(*E*)4, 4-diMe-2-Pentene	1984.85	54.85	2039.70	−21.58	−21.47	−21.46
(*E*)2, 2-diMe-3-Hexene	2268.09	65.42	2333.52	−26.56	−26.23	−26.16
3-Et-2-Me-1-Pentene	2268.09	64.03	2332.12	−24.82	−24.55	−24.40

[a]The assignment of the *Z* and *E* isomers of 3-Me-3-Hexene and of 3-Me-2-Pentene are those given by de Haan and van de Ven (14). The experimental ΔH_f^0 values are taken from ref. 15. The nmr data are taken from refs. 14 and 16 (C_2H_4 to C_4H_8, ref. 16*a*; trimethylethylene, ref. 16*b*; 1-olefins, ref. 16*c*).

FOR ERRATA SEE v. 61 #619, 83 P. 1291

Can. J. Chem. Downloaded from www.nrcresearchpress.com by 210.87.254.105 on 09/06/12
For personal use only.

be desirable. It is noteworthy, in any case, that numerous enthalpies of formation calculated from the appropriate ΔE_a^* atomization energies (eqs. [3] and [13]), and eqs. [1] and [18], are in satisfactory agreement with their experimental counterparts, as indicated in Table 3.

The results deduced from eq. [17] concern only monoalkyl-, *trans*-dialkyl-substituted ethylenes and tetramethylethylene. They agree within ~0.2 kcal mol^{-1} (average deviation) with their experimental counterparts. Before proceeding with the study of *cis* and *gem* disubstituted and of trialkyl-substituted ethylenes, it becomes important to examine the geometries of the compounds investigated here. *Ab initio* calculations (5) indicate the results given below.

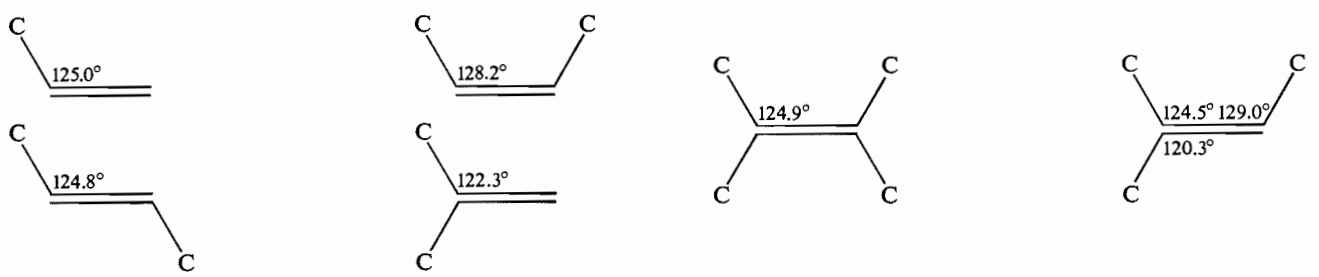

These results correspond well to what one would anticipate in a first place and it appears reasonable to assume that the hybridization of the sp^2 carbons is the same (or nearly so) in all the compounds described by eq. [17]. Indeed, a change in local geometry about the vinyl carbons would cause an additional difficulty linked to the $\sigma-\pi$ charge separation, affecting the relationship (4) $q_\sigma = mq_\pi$ + constant. This point must be considered in the evaluation of *cis* olefins. If we write $q_\sigma^{cis} = mq_\pi^{cis} + c^{cis}$ for the latter and describe their Δq_σ and Δq_π charge increments with respect to reference charges taken from the relationship $q_\sigma^{trans} = mq_\pi^{trans} + c^{trans}$ (which describes *trans*- or 1-olefins), a nonzero difference $c^{cis} - c^{trans}$ introduces a modification in the coefficient of $\Sigma N_{C\alpha C}$ and in the constant term of eq. [17]. Small effects of this sort resist their theoretical evaluation because $c^{cis} - c^{trans}$ cannot be evaluated in a reliable manner. On the other hand, an empirical assessment is presently also difficult because it is not known how accurately eq. [18] approximates the ZPE + $H_T - H_0$ values of *cis* olefins. It appears, however, that the approximation

[19] $\Sigma_i\Sigma_j a_{ij}\Delta q_i \simeq 0.0356\Sigma N_{CC}\delta_{C\neq\alpha} + 0.0529\Sigma\delta_{C\neq\alpha} + 0.18\Sigma\delta_{C\alpha} + 7.393n + 4.0\Sigma N_{C\alpha C} - 18.12$ kcal mol^{-1}

combined with eqs. [18] and [1] yields satisfactory standard enthalpies of formation for *cis* olefins. The results for trisubstituted ethylenes are deduced in the same manner (Table 3). The overall average deviation (0.30 kcal mol^{-1}) is certainly acceptable and it appears fair to conclude that, in spite of some difficulties and uncertainties, the charge dependence of the bond energy contributions which is predicted by theory has been verified at a very demanding level, that of experimental accuracy.

Conclusions

In a first place it is appropriate to assess the significance of the final results used in comparisons between theory and experiment. For saturated hydrocarbons (1), the "experimental" ΔE_a^* results were deduced entirely from experimental data, namely, the ZPE, $H_T - H_0$, and ΔH_f^0 energies required for solving eq. [1]. Nonbonded interaction energies, whose sums turn out to be small at the molecular level, were also estimated, thus permitting comparisons between theory and experiment at the best possible level (average deviation = 0.16 kcal mol^{-1}). It has appeared that *differences in nonbonded interactions cannot be made responsible for energy differences between isomers*. An approximation (2) not requiring the explicit calculation of nonbonded interactions suffers only a small loss in precision (average deviation = 0.23 kcal mol^{-1}). This approximation is exploited in ref. 2 leading eventually to simple rules for evaluating reliable ZPE + $H_T - H_0$ energies in hydrocarbons, except in situations of extreme steric crowding. Application of these rules to ethylenic compounds, for which only scarce spectroscopic information is presently available, enables a reasonable evaluation of numerous ΔE_a^* energies of olefins from their enthalpies of formation and "constructed" ZPE + $H_T - H_0$ energies. The quality of the comparisons offered for the olefins (Table 3) should be judged accordingly, also keeping in mind that nonbonded energies were not calculated explicitly. Results derived from the group additivity scheme for the estimation of thermochemical properties, as originally proposed by Benson and Buss (17), are also indicated. The quality of this additivity scheme certainly justifies Benson's statement that sufficient data are available for hydrocarbons to render suspect any data which deviate from the value predicted by the scheme, by more than ~1 kcal mol^{-1} in ΔH_f^0. It is noteworthy that in the four cases showing the largest discrepancies (0.71–1.26 kcal mol^{-1}) between our theoretical ΔH_f^0's and their experimental counterparts, Benson's values are, indeed, very similar to the present theoretical results. Under these circumstances it appears fair to conclude that the overall agreement (0.30 kcal mol^{-1} average deviation) between theory and experiment is similar in quality to that relating to the saturated hydrocarbons.

The $\lambda_1\Sigma N_{CC}\Delta q_C + \lambda_2\Sigma\Delta q_C$ term, which plays the leading role in the calculation of saturated hydrocarbons and differentiates isomers from one another, appears in the calculation of any molecule containing alkyl substituents. Its precise evaluation is, therefore, most important in all cases involving large alkyl parts. In kcal mol^{-1} ppm^{-1} units, both λ_1 and λ_2 are positive quantities. Since ^{13}C shifts of saturated hydrocarbon-C atoms are farther downfield as carbon atoms are closer to electroneutrality (i.e., have gained electronic charge), we can express the overall conclusion as a thumb rule: "*in comparisons between isomers, the more stable compound is one whose carbon skeleton best approaches electroneutrality, i.e., gains electronic charge from the hydrogen atoms, which is reflected by larger (downfield)* δ_C *values*". This, of course, is the echo of a conclusion reached earlier (1–3) describing alkyl hydrogen atoms as electron reservoirs releasing electrons toward carbon in isomerizations leading to more stable compounds. On the other hand, the fact that λ_3 is positive (as it is the case for λ_1 and λ_2) indicates that *downfield* ^{13}C *shifts at* sp^2 *carbons also reflect in a gain in molecular stability*. Contrasting with sp^3 carbons, however, a downfield shift observed for a sp^2 carbon indicates a decrease of its total electron population. Now we know (4) that such a decrease consists in a lowering in π population prevailing over an almost equally important increase in σ population. *The gain in stability accompanying downfield shifts at* sp^2 *carbons is thus traced back to a prevailing role of* σ *charges,* whose population increases, *in promoting the stability of an alkene molecule.*

Finally, *the 4.19* $\Sigma N_{C\alpha C}$ *term indicates an* a priori *gain in stability of 4.19 kcal mol*$^{-1}$ *for each CC bond formed by a vinyl carbon, in replacement for a CH bond*. This aspect is, of course, included in the calculations presented in Table 3. It appears, however, that *this gain in stability is somewhat reduced by electron redistributions*. For example, in going from 2-Me-1-pentene ($\Sigma N_{C\alpha C} = 2$) to 3-Me-1-pentene ($\Sigma N_{C\alpha C} = 1$), the decrease in ΔE_a^* is not 4.19 but only 2.6 kcal mol^{-1} because of compensating electronic rearrangements, but the leading term is clearly given by $4.19\Sigma N_{C\alpha C}$. On these grounds it is easy to predict that methylenecyclohexane ($\Sigma N_{C\alpha C} = 2$) is less stable than 1-methylcyclohexene ($\Sigma N_{C\alpha C} = 3$).

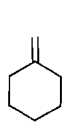

Methylenecyclohexane
ΔH_f^0(298.15, gas) = −7.2 kcal mol^{-1} (15). Calcd. (15) −8.1 kcal mol^{-1}.

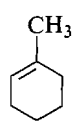

1-Methylcyclohexene
ΔH_f^0(298.15, gas) = −10.0 kcal mol^{-1} (15). Calcd. (15) −9.7 kcal mol^{-1}.

This rationale is relevant in the discussion of the relative thermochemical stabilities of *exo*- vs. *endo*-cyclic double bonds. Of course, the fact alone that a double bond is exocyclic does

Can. J. Chem. Downloaded from www.nrcresearchpress.com by 210.87.254.105 on 09/06/12
For personal use only.

not necessarily imply a loss in stability. For example, ethylidenecyclohexane and 1-ethylcyclohexene, for which $\Sigma N_{C\alpha C} = 3$ in both cases, are similar as regards their thermochemical stabilities.

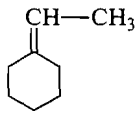

Ethylidenecyclohexane
ΔH_f^0(298.15, gas) = −14.7 kcal mol^{-1} (18).

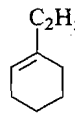

1-Ethylcyclohexene
ΔH_f^0(298.15, gas) = −15.0 kcal mol^{-1} (15). Calcd. (15) −14.5 kcal mol^{-1}.

These theoretical expectations, based on the $4.19\Sigma N_{C\alpha C}$ term, fully confirm similar views expressed by Fuchs and Peacock (18), suggesting that the cyclic compounds differ in double bond substitution rather than conformational stability. These aspects are currently under detailed investigation.

It is certainly pleasing that this insight is gained from basic and clearly identified physical concepts, namely from a reduction of the problem of molecular energies to its electrostatic aspects, featuring the role of local charges (1). It is also clear, however, that efforts in the study of atomic charges are worth pursuing because, so far, we had to carry on with barely the minimum of information as regards sp^2 carbons.

Acknowledgement

We express our gratitude to the National Research Council of Canada for financial assistance.

1. S. Fliszár. J. Am. Chem. Soc. **102**, 6946 (1980).
2. S. Fliszár and J.-L. Cantara. Can. J. Chem. **59**, 1381 (1981).
3. S. Fliszár and M.-T. Béraldin. Can. J. Chem. **60**, 792 (1982).
4. S. Fliszár, G. Cardinal, and M.-T. Béraldin. J. Am. Chem. Soc. **104**, 5287 (1982).
5. H. Henry and S. Fliszár. J. Am. Chem. Soc. **100**, 3312 (1978).
6. S. Fliszár, G. Kean, and R. Macaulay. J. Am. Chem. Soc. **96**, 4353 (1974), and references therein.
7. F. D. Rossini. Selected values of physical and thermodynamic properties of hydrocarbons and related compounds. Carnegie Press, Pittsburgh, PA. 1952.
8. B. L. Crawford, J. E. Lancaster, and R. G. Inskeep. J. Chem. Phys. **21**, 678 (1953).
9. J. E. Kilpatrick and K. S. Pitzer. J. Res. Natl. Bur. Stand. **38**, 191 (1948).
10. A. J. Baines and J. D. R. Howells. J. Chem. Soc. Faraday Trans. II, **69**, 532 (1973).
11. N. Sheppard. J. Chem. Phys. **17**, 74 (1979).
12. W. C. Harris and I. W. Levin. J. Chem. Phys. **54**, 3227 (1971).
13. W. C. Harris and I. W. Levin. J. Mol. Spectrosc. **39**, 441 (1971).
14. J. W. de Haan and L. J. M. van de Ven. Org. Magn. Reson. **5**, 147 (1973).
15. S. W. Benson, F. R. Cruickshank, D. M. Golden, G. R. Haugen, H. E. O'Neal, A. S. Rodgers, R. Shaw, and R. Walsh. Chem. Rev. **69**, 279 (1969).
16. (*a*) J. B. Stothers. Carbon-13 nmr spectroscopy. Academic Press, New York, NY. 1972; (*b*) G. J. Abruscato, P. D. Ellis, and T. T. Tidwell. J. Chem. Soc. Chem. Commun. 988 (1972); (*c*) J. W. de Haan, L. J. M. van de Ven, A. R. N. Wilson, A. E. van der Hout-Lodder, C. Altona, and D. H. Faber. Org. Magn. Reson. **8**, 477 (1976).
17. S. W. Benson and J. H. Buss. J. Chem. Phys. **29**, 546 (1958).
18. R. Fuchs and L. A. Peacock. Can. J. Chem. **57**, 2302 (1979).
19. D. R. Stull and G. C. Sinke. Adv. Chem. Ser. No 18 (1956).
20. S. Fliszár, M. Foucrault, M.-T. Béraldin, and J. Bridet. Can. J. Chem. **59**, 1074 (1981).

Appendix I
Glossary

ΔE_a^*	Atomization energy of a molecule in its vibrationless state at 0 K
$\Delta H_f^0(A_i)$	Standard enthalpy of formation of atom A_i: ΔH_f^0(C) = 170.89, ΔH_f^0(H) = 52.09 kcal mol^{-1} (19)
ΔH_f^0	Standard enthalpy of formation of the molecule (gas, 298.15 K)
ZPE	Zero-point energy
$H_T - H_0$	Heat content
K_i^{at}	Constant for an isolated atom = total/nuclear-electronic energy. $K_H^{at} = 1/2$, $K_C^{at} = 0.4276$ (20)
K_i^{mol}	Constant for an atom in a molecule, similar to K_i^{at}. $K_H^{mol} = 1/2$, $K_C^{mol} = 0.4287$ (20)
K_{Av}^{mol}	Molecular average of the K_i's, approximated as 3/7 (refs. 1, 20, and references therein)
ν_i	Number of atoms attached to atom i
$(\partial E_i^{vs}/\partial N_i)^0$	Derivative of the total energy of atom i, considered in its valence state, with respect to its electron population
Z_i^{eff}	Effective nuclear charge of atom i, e.g., 1 for H and 4 for carbon (ref. 1 and references therein)
$\langle r_{ij}^{-1}\rangle^0$	Average inverse distance between nucleus i and the center of charge of the N_j electrons allocated to atom j

Appendix II

The total (nuclear–electronic and nuclear–nuclear) potential energies V(C, mol) were derived from Hartree–Fock calculations at the $(9s5p|6s) \rightarrow [5s3p|3s]$ level for methane (−88.5540), ethane (−88.4670), and ethylene (−88.4168 au) as well as the nuclear potential energy V_{ne}(C, at) = −87.9315 au for the isolated carbon atom. From the equation (1)

$$V_{ne}(\text{C, at}) - V(\text{C, mol}) = Z_C \Sigma_j (\partial \epsilon_{Cj}/\partial Z_C)$$

in which Z_C is the nuclear charge of carbon and ϵ_{Cj} the energy associated with the bond C forms with atom j, we obtain $\partial \epsilon_{CH}/\partial Z_C \simeq 0.026$ au. Using this result and the V(C, mol)'s given above, we calculate $\partial \epsilon_{CC}/\partial Z_C$ for the ethane and the ethylene carbon–carbon bonds. In this fashion we obtain from the equation (1)

$$\epsilon_{ij} = K_i^{mol} Z_i \frac{\partial \epsilon_{ij}}{\partial Z_i} + K_j^{mol} Z_j \frac{\partial \epsilon_{ij}}{\partial Z_j} + (K_i^{at} - K_i^{mol})\, V_{ne}(\text{at. } i)/\nu_i + (K_j^{at} - K_j^{mol})\, V_{ne}(\text{at. } j)/\nu_j$$

that ϵ_{CC} = 66.7 for ethane and 133.7 kcal mol^{-1} for ethylene, i.e., a ratio of 1:2.00. While this basis cannot match experimental accuracy, it remains that comparisons on a relative scale can be regarded as being meaningful. Using, therefore, the value 69.633 kcal mol^{-1} determined earlier (1) for ethane we can estimate ϵ_{CC} = 139.27 kcal mol^{-1} for the ethylene CC bond. A rescaling of the potential and Hartree–Fock energies along the lines given in ref. 1 gives $\partial \epsilon_{C=C}/\partial Z_C \simeq 0.0305$ au and $\epsilon_{C=C}$ = 139.20 kcal mol^{-1}.

Appendix III

The ethylene-C net charge, $q_{C\alpha}^0$, is best evaluated using tetramethylethylene as a starter. Its methyl-C nmr shift is 14.3 ppm from ethane, giving (1) $\Delta q_C = -0.148\delta_C = -2.12$ me relative to the ethane carbon atom, i.e., $q_C = 35.1 - 2.12 = 32.98$ me. From the correlation (described in ref. 3, Appendix

Can. J. Chem. Downloaded from www.nrcresearchpress.com by 210.87.254.105 on 09/06/12
For personal use only.

II) between q_H and q_C in methyl groups, q_H is estimated at -12.29 me. The net charge of the methyl group is, therefore, -3.89 me and that of the sp^2 carbon is 7.77 me. Assuming $m = -0.955$ and $d\delta_{C\alpha}/dq_\pi \simeq 300$ ppm/e, as described in the text, we find $\Delta q_{C\alpha} \simeq 0.15\delta_{C\alpha}$ me. Tetramethylethylene (δ 123.2 ppm from TMS) and ethylene (δ 122.8 ppm from TMS) differ only by ~0.4 ppm, so that the difference in net charge is ~0.06 me, ethylene being thus only marginally electron-richer than tetramethylethylene. The final estimate is $q^0_{C\alpha} \simeq 7.7$ me and, of course, $q_H \simeq -3.85$ me.

Can. J. Chem. Downloaded from www.nrcresearchpress.com by 210.87.254.105 on 09/06/12
For personal use only.

Structural studies of organoboron compounds. XIII.[1] Preparation and crystal and molecular structure of bis[(salicylaldoximato(2−))phenylboron]

STEVEN J. RETTIG AND JAMES TROTTER

Department of Chemistry, University of British Columbia, 2036 Main Mall, Vancouver, B.C., Canada, V6T 1Y6

Received July 6, 1982

STEVEN J. RETTIG and JAMES TROTTER. Can. J. Chem. **61**, 206 (1983).

The reaction of $(C_6H_5)_2BOH$ with salicylaldoxime yielded $[(C_7H_5NO_2)BC_6H_5]_2$ via a boron−carbon bond cleavage reaction. Crystals of bis[(salicylaldoximato(2−))phenylboron] are triclinic, a = 9.219(1), b = 11.240(1), c = 12.086(1) Å, α = 100.682(7), β = 112.224(6), γ = 92.189(7)°, Z = 2, space group $P\bar{1}$. The structure was solved by direct methods and was refined by full-matrix least-squares procedures to R = 0.036 and R_w = 0.049 for 3433 reflections with $I \geq 3\sigma(I)$. The molecule, which has approximate C_2 symmetry, contains a system of five fused six-membered rings including the first crystallographically characterized $B_2N_2O_2$ ring. The compound is stabilized both by intramolecular N → B coordination and by resonance delocalization and contains boron atoms in a distorted tetrahedral environment. Bond lengths (corrected for libration) are: O—B, 1.469(2)−1.488(2), N—B, 1.602(2) and 1.575(2), C—B, 1.598(2) and 1.599(2) Å.

STEVEN J. RETTIG et JAMES TROTTER. Can. J. Chem. **61**, 206 (1983).

La réaction du $(C_6H_5)_2BOH$ avec la salicylaldoxime conduit au composé $[(C_7H_5NO_2)BC_6H_5]_2$ via une réaction de clivage de la liaison bore−carbone. Les cristaux de bis[(salicylaldoximato(2−))phénylbore] sont tricliniques, a = 9,219(1), b = 11,240(1), c = 12,086(1) Å, α = 100,682(7), β = 112,224(6), γ = 92,189(7)°, Z = 2, groupe d'espace $P\bar{1}$. On a résolu la structure par des méthodes directes et on l'a affinée par la méthode des moindres carrés (matrice complète) jusqu'à des valeurs de R = 0,036 et de R_w = 0,049 pour 3433 réflexions avec $I \geq 3\sigma(I)$. La molécule qui a approximativement une symétrie C_2 contient un système de 5 cycles à 6 chaînons condensés incluant le premier cycle $B_2N_2O_2$ caractérisé par cristallographie. Le composé est stabilisé à la fois par une coordination intramoléculaire N → B et par une délocalisation de la résonance et contient des atomes de bore dans un environnement tétraédrique déformé. Les longueurs de liaison (corrigées pour la libration) sont: O—B, 1,469(2)−1,488(2), N—B, 1,602(2) et 1,575(2), C—B, 1,598(2) et 1,599(2) Å.

[Traduit par le journal]

Introduction

Organoboron compounds containing four-coordinate boron and stabilized by intramolecular N→B or O→B interactions have been extensively studied for the past 30 years (e.g. refs. 2, 3). In addition to the unusual hydrolytic and oxidative stability of these compounds, which prompted much of the earlier work, many of these molecules have biologically and medically useful applications (ref. 3, pp. 223, 224). As part of a continuing study[1] of the molecular structures of compounds of this type, we report here the isolation and molecular structure of bis[(salicylaldoximato(2−))phenylboron], **1**.

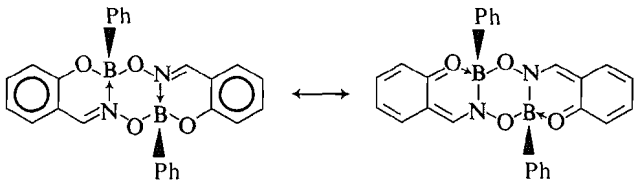

1*a* **1***b*

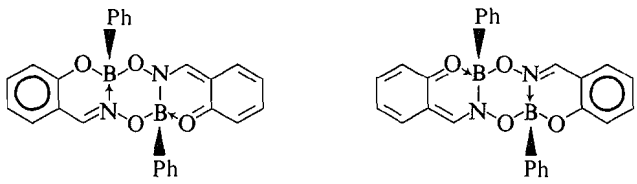

1*c* **1***d*

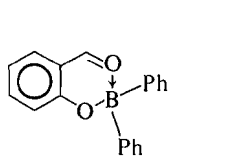

2

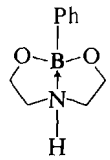

3

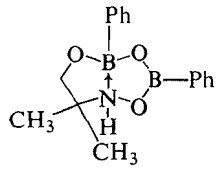

4

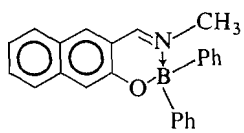

5

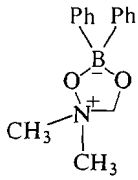

6

An attempt to prepare the salicylaldoxime ester of diphenylborinic acid (in which there are several possible modes of chelation to the Ph_2B moiety) by a procedure analogous to that employed for related esters (4) resulted in the isolation of **1**. The overall reaction

$$2C_7H_7NO_2 + 2(C_6H_5)_2BOH \rightarrow [(C_7H_5NO_2)BC_6H_5]_2 + 2C_6H_6 + 2H_2O$$

proceeds via a carbon−boron bond cleavage reaction (3, 5−7) to produce the dimeric ester of phenylboronic acid. The above stoichiometry indicates that the same product could be obtained by a reaction of phenylboronic acid with salicylaldoxime.

Experimental

A solution of salicylaldoxime (0.34 g, 2.5 mmol) in 50 mL of ethanol was added to a solution of diphenylborinic acid (from the acid hydrolysis of 2-aminoethyldiphenylborinate, 0.59 g, 2.6 mmol) in

[1]Previous paper in this series: ref. 1.

0008-4042/83/010206-05$01.00/0

©1983 National Research Council of Canada/Conseil national de recherches du Canada

Can. J. Chem. Downloaded from www.nrcresearchpress.com by 210.87.254.40 on 09/06/12
For personal use only.

TABLE 1. Final positional (fractional × 10^5, H × 10^4) and isotropic thermal parameters ($U \times 10^3$ Å^2) with estimated standard deviations in parentheses

Atom	x	y	z	U_{iso}/U_{eq}
O(1)	54784(11)	123722(9)	87520(9)	41
O(2)	36651(11)	96710(8)	62966(9)	40
O(3)	60500(11)	87335(9)	66618(9)	41
O(4)	44990(11)	103758(9)	87964(9)	39
N(1)	41859(13)	108936(10)	68318(10)	35
N(2)	54673(13)	96400(10)	84065(10)	35
C(1)	57262(16)	131560(13)	81049(14)	39
C(2)	51849(16)	128327(13)	68243(14)	39
C(3)	54819(20)	136637(15)	61869(17)	50
C(4)	63141(23)	147883(17)	68018(21)	61
C(5)	68890(22)	150842(16)	80676(20)	60
C(6)	66092(19)	142843(15)	87183(17)	50
C(7)	45440(16)	115848(13)	62247(14)	38
C(8)	74144(16)	84638(13)	74489(14)	39
C(9)	78321(16)	87982(12)	87229(14)	38
C(10)	92649(18)	85126(15)	95209(17)	49
C(11)	102675(20)	79194(17)	90616(21)	62
C(12)	98645(22)	76273(18)	78070(22)	64
C(13)	84594(20)	78924(16)	70057(19)	54
C(14)	68328(16)	95255(13)	91704(13)	36
C(15)	24678(16)	117799(13)	80105(13)	39
C(16)	10964(20)	109859(18)	72906(18)	59
C(17)	−3899(21)	113459(21)	70895(20)	69
C(18)	−5306(22)	125104(20)	76156(19)	64
C(19)	7940(22)	132982(18)	83488(20)	61
C(20)	22814(20)	129384(15)	85467(16)	48
C(21)	37337(16)	76429(13)	69254(14)	39
C(22)	39730(19)	70843(16)	79069(18)	51
C(23)	32246(21)	59339(17)	77495(21)	62
C(24)	22241(24)	53118(18)	66166(23)	67
C(25)	19410(25)	58410(19)	56342(22)	71
C(26)	26700(21)	69973(18)	57873(18)	57
B(1)	41642(19)	113880(15)	81533(14)	36
B(2)	47039(18)	88977(15)	70440(15)	36
H(3)	5077(20)	13453(16)	5323(18)	58(5)
H(4)	6508(23)	15354(19)	6365(19)	72(6)
H(5)	7510(21)	15849(17)	8491(17)	64(5)
H(6)	7034(20)	14455(16)	9643(17)	57(5)
H(7)	4417(18)	11280(14)	5388(16)	48(4)
H(10)	9499(19)	8780(15)	10404(17)	52(5)
H(11)	11229(23)	7734(17)	9616(18)	69(6)
H(12)	10581(26)	7237(20)	7507(20)	89(7)
H(13)	8164(22)	7730(17)	6100(19)	70(6)
H(14)	7171(18)	9960(14)	10037(15)	45(4)
H(16)	1170(22)	10208(18)	6911(18)	66(6)
H(17)	−1334(29)	10766(23)	6543(23)	88(8)
H(18)	−1615(25)	12772(18)	7460(19)	79(6)
H(19)	712(25)	14165(21)	8750(20)	91(7)
H(20)	3229(20)	13546(15)	9027(15)	52(5)
H(22)	4728(23)	7547(18)	8755(19)	76(6)
H(23)	3479(24)	5528(19)	8468(20)	76(6)
H(24)	1732(23)	4450(19)	6483(19)	73(6)
H(25)	1215(27)	5459(20)	4847(22)	90(7)
H(26)	2442(23)	7373(19)	5101(19)	71(6)

ethanol/diethyl ether. A fine white powder began to precipitate almost immediately. The reaction mixture was refluxed for 6 h, allowed to cool, filtered, and was washed with water and then with ethanol. The product was dried, yielding 0.72 g (1.61 mmol, 65% yield) of product. *Anal.* calcd. for $[(C_7H_5NO_2)BC_6H_5]_2$: C 70.01, H 4.52, N 6.28; found: C 69.96, H 4.54, N 6.31. Mp (decomp.) 254−256°C.

Crystals suitable for X-ray analysis were obtained by recrystallization from a large (500 mL) volume of acetone. A crystal ca. 0.22 × 0.26 × 0.31 mm in size was mounted in a general orientation. Unit-cell parameters were refined by least-squares on 2 sin θ/λ values for 50 reflections measured on a diffractometer with Mo-Kα_1 radiation (λ = 0.70930 Å). Crystal data at 22°C are:

$C_{26}H_{20}B_2N_2O_4$ fw = 446.08

Triclinic, a = 9.219(1), b = 11.240(1), c = 12.086(1) Å, α = 100.682(7), β = 112.224(6), γ = 92.189(7)°, V = 1131.0(2) Å^3,

Can. J. Chem. Downloaded from www.nrcresearchpress.com by 210.87.254.40 on 09/06/12
For personal use only.

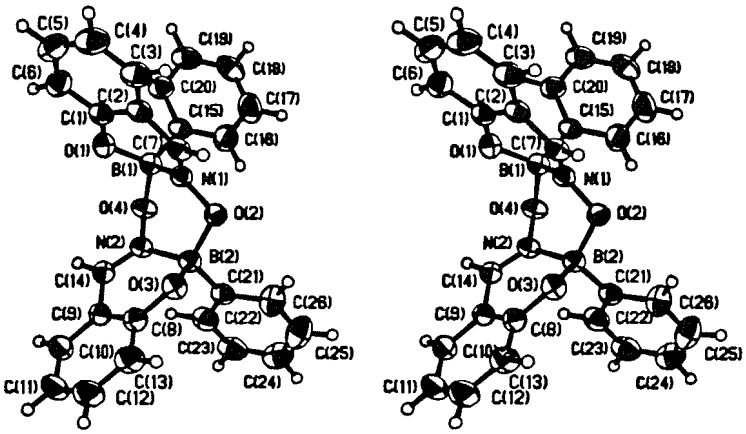

FIG. 1. Stereoscopic view of the bis[(salicylaldoximato(2−))phenylboron] molecule, 50% thermal ellipsoids are shown for the non-hydrogen atoms.

ρ_m = 1.30 (by flotation in aqueous KI), Z = 2, ρ_c = 1.310 g cm^{-3}, $F(000)$ = 464, μ(Mo-Kα) = 0.81 cm^{-1}. Absent reflections: none, space group $P\bar{1}$ (C_i^1, No. 2, reduced cell) from structure analysis. The crystal was bounded by the 6 faces: (0 ±1 0), (±1 0 0), and (0 0 ±1) (in order of increasing separation of the parallel faces).

Intensities were measured with graphite-monochromated Mo-Kα radiation (λ = 0.71073 Å) on an Enraf-Nonius CAD4-F diffractometer. An ω−1.33θ scan at 1.12−6.71° min^{-1} over a range of (0.58 + 0.35 tan θ) degrees in ω (extended by 25% on both sides for background measurement) was employed. Data were measured to 2θ = 55°. The intensities of three check reflections, measured every 3600 s throughout the data collection, remained constant to within 3%. After data reduction,[2] no absorption correction was made in view of the low value of μ. Of the 5169 independent reflections measured, 3433 (66.4%) had intensities greater than $3\sigma(I)$ above background where $\sigma^2(I) = S + 2B + (0.04(S - B))^2$ with S = scan count and B = background count.

The centrosymmetric space group $P\bar{1}$ was chosen on the basis of the E-statistics. The structure was solved by direct methods, the positions of all non-hydrogen atoms being determined from an E-map. After full-matrix least-squares refinement of the non-hydrogen atoms with anisotropic thermal parameters to R = 0.077, all 20 hydrogen atoms were positioned from a difference map and were refined with isotropic thermal parameters in subsequent least-squares cycles. The scattering factors of ref. 8 were used for non-hydrogen atoms and those of ref. 9 for hydrogen atoms. The weighting scheme, $w = 1/\sigma^2(F)$, where $\sigma^2(F)$ is derived from the previously defined $\sigma^2(I)$ gave uniform average values of $w(|F_o| - |F_c|)^2$ over ranges of both $|F_o|$ and sin θ/λ and was employed in the final stages of refinement. Convergence was reached at R = 0.036 and R_w = 0.049 for 3433 reflections with $I \geq 3\sigma(I)$. For all 5169 reflections R = 0.065. The function minimized was $\Sigma w(|F_o| - |F_c|)^2$, $R = \Sigma||F_o| - |F_c||/\Sigma|F_o|$ and $R_w = (\Sigma w(|F_o| - |F_c|)^2/\Sigma w|F_o|^2)^{1/2}$.

On the final cycle of refinement the mean and maximum parameter shifts corresponded to 0.16 and 0.94σ respectively. The maximum parameter shift was associated with the temperature factor of a hydrogen atom. The mean error in an observation of unit weight was 1.696. A final difference map showed no unusual features. The final positional and thermal parameters appear in Tables 1 and 2[3] respectively. Measured and calculated structure factors have been placed in the Depository of Unpublished Data.[3]

The ellipsoids of thermal motion for the non-hydrogen atoms are shown in Fig. 1. The thermal motion has been analysed in terms of the rigid-body modes of translation, libration, and screw motion (10). The rms standard error in the temperature factors σU_{ij} (derived from the least-squares analysis) is 0.0009 Å^2. Analysis of all 34 non-hydrogen atoms gave rms ΔU_{ij} = 0.0058 Å^2 and indicated significant independent motion of the phenyl groups. Three separate smaller fragments of the molecule were analysed, the two C_6H_5B groups and the five fused rings plus the two phenyl carbon atoms bonded to B (rms ΔU_{ij} = 0.0014, 0.0018, and 0.0038 Å^2 respectively). The appropriate bond distances have been corrected for libration (10, 11), using shape parameters q^2 of 0.08 for all atoms involved. Corrected bond lengths appear in Table 3 along with the uncorrected values; corrected bond angles do not differ by more than 1σ from the uncorrected values given in Table 4. Intra-annular torsion angles defining the conformations of six-membered heterocyclic rings are listed in Table 5. Bond lengths and angles involving hydrogen and a complete listing of torsion angles (Tables 6−8) are included as supplementary material.

Results and discussion

The boron atoms in **1** are chiral, the crystal structure consisting of *RR* and *SS* pairs linked across centres of symmetry by weak C—H···O interactions (C(7)—H(7)···O(3) (1 − x, 2 − y, 1 − z), H···O = 2.35(2), C···O = 3.267(2) Å, C—H···O = 159(1)°). All other intermolecular distances correspond to normal van der Waals contacts. No attempt has been or will be made ro resolve the racemic modification. The presence of a *meso* form has not been verified although during the recrystallization only part of the material used was recovered in a crystalline state. It is quite possible that the initial product was a mixture of the *rac* and *meso* forms.

The molecule (Fig. 1) contains a linear system of five fused six-membered rings, including two C_3BNO rings and the first crystallographic example of a $B_2O_2N_2$ ring although others are known (12−14). The central $B_2N_2O_2$ ring has a slightly distorted twist-boat conformation while the two C_3BNO rings each have distorted B-envelope conformations (see Table 5), the boron atoms being displaced from the approximate planes de-

[2]The computer programs used include locally written programs for data processing and locally modified versions of the following: MULTAN 80, multisolution program by P. Main, M. M. Woolfson, L. Lessinger, G. Germain, and J. P. Declerq; ORFLS, full-matrix least-squares, and ORFFE, function and errors, by W. R. Busing, K. O. Martin, and H. A. Levy; FORDAP, Patterson and Fourier syntheses, by A. Zalkin; ORTEP II, illustrations, by C. K. Johnson.

[3]The structure factor table, Table 2 (anisotropic thermal parameters) and other material mentioned in the text are available, at a nominal charge, from the Depository of Unpublished Data, CISTI, National Research Council of Canada, Ottawa, Ont., Canada K1A 0S2.

Can. J. Chem. Downloaded from www.nrcresearchpress.com by 210.87.254.40 on 09/06/12
For personal use only.

TABLE 3. Bond lengths (Å) with estimated standard deviations in parentheses

Bond	Length		Bond	Length	
	Uncorr.	Corr.		Uncorr.	Corr.
O(1)—C(1)	1.347(2)	1.349	C(8)—C(13)	1.392(2)	1.393
O(1)—B(1)	1.467(2)	1.469	C(9)—C(10)	1.400(2)	1.401
O(2)—N(1)	1.3865(14)	1.388	C(9)—C(14)	1.442(2)	1.444
O(2)—B(2)	1.479(2)	1.481	C(10)—C(11)	1.380(3)	1.381
O(3)—C(8)	1.345(2)	1.347	C(11)—C(12)	1.387(3)	1.389
O(3)—B(2)	1.486(2)	1.488	C(12)—C(13)	1.376(3)	1.377
O(4)—N(2)	1.3903(14)	1.392	C(15)—C(16)	1.395(2)	1.404
O(4)—B(1)	1.472(2)	1.474	C(15)—C(20)	1.390(2)	1.402
N(1)—C(7)	1.275(2)	1.277	C(15)—B(1)	1.596(2)	1.599
N(1)—B(1)	1.599(2)	1.602	C(16)—C(17)	1.388(2)	1.391
N(2)—C(14)	1.277(2)	1.279	C(17)—C(18)	1.379(3)	1.390
N(2)—B(2)	1.572(2)	1.575	C(18)—C(19)	1.367(3)	1.376
C(1)—C(2)	1.403(2)	1.406	C(19)—C(20)	1.390(2)	1.393
C(1)—C(6)	1.392(2)	1.393	C(21)—C(22)	1.393(2)	1.401
C(2)—C(3)	1.396(2)	1.397	C(21)—C(26)	1.391(2)	1.402
C(2)—C(7)	1.441(2)	1.443	C(21)—B(2)	1.594(2)	1.598
C(3)—C(4)	1.373(3)	1.375	C(22)—C(23)	1.388(2)	1.391
C(4)—C(5)	1.384(3)	1.387	C(23)—C(24)	1.362(3)	1.373
C(5)—C(6)	1.375(3)	1.377	C(24)—C(25)	1.368(3)	1.377
C(8)—C(9)	1.409(2)	1.412	C(25)—C(26)	1.387(3)	1.391

TABLE 4. Bond angles (deg) with estimated standard deviations in parentheses

Bonds	Angle (deg)	Bonds	Angle (deg)
C(1)—O(1)—B(1)	119.48(11)	C(8)—C(13)—C(12)	120.0(2)
N(1)—O(2)—B(2)	110.21(10)	N(2)—C(14)—C(9)	118.27(13)
C(8)—O(3)—B(2)	119.38(11)	C(16)—C(15)—C(20)	117.01(14)
N(2)—O(4)—B(1)	110.33(10)	C(16)—C(15)—B(1)	121.04(14)
O(2)—N(1)—C(7)	119.34(12)	C(20)—C(15)—B(1)	121.89(13)
O(2)—N(1)—B(1)	117.37(11)	C(15)—C(16)—C(17)	121.6(2)
C(7)—N(1)—B(1)	123.08(12)	C(16)—C(17)—C(18)	119.8(2)
O(4)—N(2)—C(14)	119.80(11)	C(17)—C(18)—C(19)	119.8(2)
O(4)—N(2)—B(2)	115.73(10)	C(18)—C(19)—C(20)	120.3(2)
C(14)—N(2)—B(2)	124.21(11)	C(15)—C(20)—C(19)	121.4(2)
O(1)—C(1)—C(2)	121.30(13)	C(22)—C(21)—C(26)	116.21(15)
O(1)—C(1)—C(6)	119.54(14)	C(22)—C(21)—B(2)	123.20(14)
C(2)—C(1)—C(6)	119.06(15)	C(26)—C(21)—B(2)	120.42(15)
C(1)—C(2)—C(3)	119.64(14)	C(21)—C(22)—C(23)	121.7(2)
C(1)—C(2)—C(7)	118.25(13)	C(22)—C(23)—C(24)	120.5(2)
C(3)—C(2)—C(7)	121.45(14)	C(23)—C(24)—C(25)	119.3(2)
C(2)—C(3)—C(4)	120.6(2)	C(24)—C(25)—C(26)	120.4(2)
C(3)—C(4)—C(5)	119.3(2)	C(21)—C(26)—C(25)	121.7(2)
C(4)—C(5)—C(6)	121.2(2)	O(1)—B(1)—O(4)	109.75(11)
C(1)—C(6)—C(5)	120.0(2)	O(1)—B(1)—N(1)	104.64(11)
N(1)—C(7)—C(2)	118.52(14)	O(1)—B(1)—C(15)	115.37(12)
O(3)—C(8)—C(9)	120.80(12)	O(4)—B(1)—N(1)	106.59(11)
O(3)—C(8)—C(13)	119.78(15)	O(4)—B(1)—C(15)	110.20(12)
C(9)—C(8)—C(13)	119.37(14)	N(1)—B(1)—C(15)	109.82(11)
C(8)—C(9)—C(10)	119.55(14)	O(2)—B(2)—O(3)	108.01(12)
C(8)—C(9)—C(14)	118.61(12)	O(2)—B(2)—N(2)	107.98(11)
C(10)—C(9)—C(14)	121.60(14)	O(2)—B(2)—C(21)	110.66(11)
C(9)—C(10)—C(11)	120.1(2)	O(3)—B(2)—N(2)	104.84(11)
C(10)—C(11)—C(12)	119.8(2)	O(3)—B(2)—C(21)	113.32(11)
C(11)—C(12)—C(13)	121.1(2)	N(2)—B(2)—C(21)	111.73(12)

fined by the remaining ring atoms. The C_3BNO ring conformations are very similar to that observed in the related C_3BO_2 rings of (salicylaldehydato)diphenylboron, **2** (15), and (acetylacetonato)diphenylboron (1). Each of the four aromatic rings displays statistically, but not chemically, significant deviations from planarity (maximum deviation from mean plane = 0.015 Å). The geometry of the B-substituted phenyl rings is as expected (16, 17).

The molecule has approximate C_2 symmetry, all symmetry-related bond lengths and angles except those involving B and N atoms being equal within experimental error. The molecule is stabilized both by intramolecular N→B coordination and by

Can. J. Chem. Downloaded from www.nrcresearchpress.com by 210.87.254.40 on 09/06/12
For personal use only.

TABLE 5. Intra-annular torsion angles (deg) with standard deviations in parentheses

Atoms	Value (deg)
B(1)—O(1)—C(1)—C(2)	−23.6(2)
O(1)—C(1)—C(2)—C(7)	−8.3(2)
C(1)—C(2)—C(7)—N(1)	14.6(2)
B(1)—N(1)—C(7)—C(2)	9.6(2)
C(7)—N(1)—B(1)—O(1)	−35.9(2)
C(1)—O(1)—B(1)—N(1)	41.41(15)
B(2)—O(3)—C(8)—C(9)	−25.5(2)
O(3)—C(8)—C(9)—C(14)	−5.2(2)
C(8)—C(9)—C(14)—N(2)	13.2(2)
B(2)—N(2)—C(14)—C(9)	8.8(2)
C(14)—N(2)—B(2)—O(3)	−34.2(2)
C(8)—O(3)—B(2)—N(2)	41.2(2)
O(2)—N(1)—B(1)—O(4)	33.17(15)
B(2)—O(2)—N(1)—B(1)	−63.23(14)
N(1)—O(2)—B(2)—N(2)	26.66(15)
O(4)—N(2)—B(2)—O(2)	36.77(15)
B(1)—O(4)—N(2)—B(2)	−67.57(14)
N(2)—O(4)—B(1)—N(1)	30.60(14)

resonance delocalization, the molecular geometry indicating that forms **1***a*−*d* are the major contributors to the structure.

The boron atoms are tetrahedrally coordinated, bond angles ranging from 104.6(1)−115.4(1)° (see Table 4). Both of the two significantly different N—B distances (1.575(2) and 1.602(2) Å) are considerably shorter than those in the closely related molecules **3** (18) and **4** (19) (N—B = 1.666(3) and 1.692(2) Å respectively). The N—B bonds in **1** occur at the junction of two six-membered rings while those in **3** and **4** occur at the junction of two five-membered rings and are subject to a greater degree of ring strain. The N(sp^3)—B bonds in **3** and **4** are expected to be longer than the N(sp^2)—B bonds in **1** as a result of hybridization effects. The longer N—B bond in **1**, 1.602(2) Å, is the same as the corresponding N(sp^2)—B distance of 1.601(4) Å in **5** (20) while the shorter N—B bond of 1.575(2) Å is the shortest yet observed in this type of compound. The four O—B distances also differ significantly, ranging from 1.469(2) to 1.488(2) Å, the two chemically different types of O—B bond being roughly of the same strength. The mean[4] O—B distance of 1.478(8) Å is in agreement with the mean O—B distance of 1.477(5) Å observed in the ethanolamine esters of diarylborinic acids (15, 21, 22), but slightly longer than the corresponding value of 1.463(9) Å in **3** and **4** (which compensates for the longer N—B distances in **3** and **4**). The phenolic O—B distances of 1.500(4) and 1.506(3) Å in **2** and **5** respectively as well as those of 1.530(2)−1.565(2) Å in the acetylacetone and tropolone esters of diphenylborinic acid (1) are significantly longer than those in **1**. The two equal C—B distances (mean 1.599(1) Å) are the same as that in **4** (1.599(2) Å), but shorter than those in other compounds containing tetrahedral boron, which range from 1.603(5) Å in **2** to 1.639(8) Å in **6** (23). The bonds C(2)—C(7), C(9)—C(14), C(1)—O(1), and C(8)—O(3) are all significantly longer than their counterparts in **2** and **5** indicating a lesser contribution from resonance form **1***b* than from comparable forms contributing to the structures of **2** and **5**.

[4]Here and elsewhere in this report mean values refer to weighted means with rms deviations from the mean in parentheses.

The statistically significant differences in corresponding C_2 related N—B and O—B bond lengths noted above must arise from asymmetric perturbation of the central part of the molecule. σ-Hybridization effects arise from the deviation of the molecule from true C_2 symmetry; calculations (24) predicting equivalence of the N—O and B—O bond lengths in the central ring, and that B(1)—O(1) < B(2)—O(3) and B(1)—N(1) > B(2)—N(2), both by 0.01 Å. In addition to the possible contribution of resonance forms to the overall structure in which the B, N, and O atoms are not equivalent; such a perturbation may also be attributed to the C—H···O interaction which is the only non-bonded interaction of any significance. The B(1)—O(1) distance of 1.469(2) Å is significantly shorter than the B(2)—O(3) distance of 1.488(2) Å, the latter bond being involved in the C—H···O interaction.

Acknowledgments

We thank the Natural Sciences and Engineering Research Council Canada for financial support and the University of British Columbia Computing Centre for assistance. Microanalysis was performed by Mr. P. Borda.

1. S. J. RETTIG and J. TROTTER. Can. J. Chem. In press.
2. H. K. ZIMMERMAN. Adv. Chem. Ser. **42**, 23 (1964).
3. T. ONAK. Organoborane chemistry. Academic Press, New York. 1975.
4. F. UMLAND and C. SCHLEYERBACH. Angew. Chem. **77**, 426 (1965).
5. K. LANG, K. NUTZEL, and F. SCHUBERT. Ger. Pat. 1130445 (1962).
6. J. N. COOPER and R. E. POWELL. J. Am. Chem. Soc. **85**, 1590 (1963).
7. G. BAUM. J. Organometal. Chem. **23**, 269 (1970).
8. D. T. CROMER and J. B. MANN. Acta Crystallogr. Sect. A, **24**, 321 (1968).
9. R. F. STEWART, E. R. DAVIDSON, and W. T. SIMPSON. J. Chem. Phys. **42**, 3175 (1965).
10. V. SCHOMAKER and K. N. TRUEBLOOD. Acta Crystallogr. Sect. B, **24**, 63 (1968).
11. D. W. J. CRUICKSHANK. Acta Crystallogr. **9**, 747 (1956); **9**, 754 (1956); **14**, 896 (1961).
12. L. P. KUHN and M. INATOME. J. Am. Chem. Soc. **85**, 1206 (1963).
13. H. J. ROTH and B. MILLER. Arch. Pharm. Weinheim, **297**, 744 (1964).
14. W. MARINGGELE and A. MELLER. Monatsch. Chem. **106**, 1369 (1975).
15. S. J. RETTIG and J. TROTTER. Can. J. Chem. **54**, 1168 (1976).
16. S. J. RETTIG and J. TROTTER. Can. J. Chem. **54**, 3130 (1976).
17. A. DOMENICANO, A. VACIAGO, and C. A. COULSON. Acta Crystallogr. Sect. B, **31**, 221 (1975); **31**, 1630 (1975).
18. S. J. RETTIG and J. TROTTER. Can. J. Chem. **53**, 1393 (1975).
19. S. J. RETTIG, J. TROTTER, W. KLIEGEL, and H. BECKER. Can. J. Chem. **54**, 3142 (1976).
20. O. E. KOMPAN, N. G. FURMANOVA, YU. T. STRUCHKOV, L. M. SITKINA, V. A. BREN', and V. I. MINKIN. Zh. Strukt. Khim. **21**(2), 90 (1980).
21. S. J. RETTIG and J. TROTTER. Can. J. Chem. **51**, 1288 (1973).
22. S. J. RETTIG and J. TROTTER. Acta Crystallogr. Sect. B, **30**, 2139 (1974).
23. S. J. RETTIG, J. TROTTER, and W. KLIEGEL. Can. J. Chem. **52**, 2531 (1974).
24. S. J. RETTIG. Ph.D. Thesis. University of British Columbia. 1974.

Can. J. Chem. Downloaded from www.nrcresearchpress.com by 210.87.254.40 on 09/06/12
For personal use only.

Crystal structure of *N,N'*-dimethyl-2-imidazolidinethione, a by-product from the reaction of $Na_2(CH_2N(CH_3)CS_2)_2$ and $HgCl_2$

CHUNG CHIEH AND SING KWEN CHEUNG

Guelph-Waterloo Centre for Graduate Work in Chemistry, University of Waterloo, Waterloo, Ont., Canada N2L 3G1

Received June 9, 1981[1]

CHUNG CHIEH and SING KWEN CHEUNG. Can. J. Chem. **61**, 211 (1983).

The reaction between mercury (II) chloride and *N,N'*-dimethylethylenebisdithiocarbamate gave a white precipitate. In an attempted recrystallization from an aqueous–ethanol solution, a cyclic thiourea-type compound, *N,N'*-dimethyl-2-imidazolidinethione, was obtained. The crystals of this compound are monoclinic, $a = 10.388(2)$, $b = 6.139(1)$, $c = 12.291(4)$ Å, $\beta = 118.64(2)$, and space group $P2_1/c$. The non-hydrogen atoms of the molecule are planar and the C=S bond length is 1.673(4) Å. The structure was refined by full-matrix least-squares from 642 independent reflections measured on an automatic diffractometer to R and R_w of 0.053 and 0.068, respectively.

CHUNG CHIEH et SING KWEN CHEUNG. Can. J. Chem. **61**, 211 (1983).

Le chlorure mercurique réagit avec le *N,N'*-diméthyléthylènebisdithiocarbamate en donnant un précipité blanc. En essayant de recristallisé le produit obtenu dans une solution aqueuse d'éthanol on obtient un composé de type thiourée cyclique, la *N,N'*-diméthylimidazolinethione-2. Les cristaux de ce composé sont monocliniques et appartiennent au groupe d'espace $P2_1/c$ avec $a = 10{,}388(2)$, $b = 6{,}139(1)$, $c = 12{,}291(4)$ Å, $\beta = 118{,}64(2)$. Les atomes de la molécule qui ne sont pas des atomes d'hydrogène, sont plans et la longueur de liaison C=S est de 1,673(4) Å. On a affiné la structure par la méthode des moindres carrés (matrice entière) jusqu'à des valeurs de R et de R_w de 0,053 et 0,068 respectivement pour 642 réflexions mesurées à l'aide d'un diffractromère automatique.

[Traduit par le journal]

Introduction

For the study of complexation between dithiocarbamates and metal ions, *N,N'*-dimethylethylenebisdithiocarbamate was prepared (1). However, the reaction between this bisdithiocarbamate and mercury(II) chloride led to a cyclic by-product *N,N'*-dimethyl-2-imidazolidinethione. Its crystal structure as determined by X-ray method and the possible reason for its formation are reported.

Result and discussion

The *N,N'*-dimethylethylenebisdithiocarbamate were prepared by the reaction of *N,N'*-dimethylethylenediamine and carbon disulfide in the presence of NaOH by methods similar to the one given in ref. 2. This bisdithiocarbamate reacted with mercury(II) chloride in an aqueous-ethanol solution giving a white precipitate. This precipitate turned to a creamy color on standing. In an attempt to recrystallize this product, the precipitate was stirred in an aqueous-ethanol solution for an hour to obtain a saturated solution so that the filtrate would yield crystals suitable for structural analysis. This filtrate was allowed to evaporate in a cold room (273 K) giving colorless crystals, whose nmr spectrum and elemental analysis suggested a thiourea-type compound, *N,N'*-dimethyl-2-imidazolidinethione. Furthermore, the X-ray structure determination confirmed the same result.

Spectroscopic evidences showed that the bisdithiocarbamate sample was pure, and the slow color change of the precipitate when $HgCl_2$ was added might be due to the elemental sulfur generated during the reaction. Although the oxidation of the bisdithiocarbamate might lead to these products:

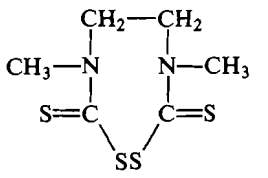

I

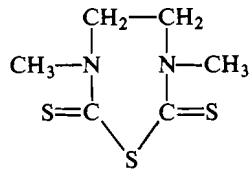

II

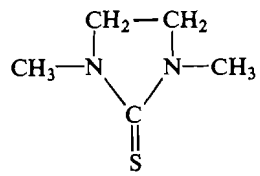

III

only **III** has been detected and confirmed as a by-product. The lack of a detectable amount of **I** or **II** is probably due to the instability of the 8- or 7-membered ring respectively. However, a compound with H instead of CH_3 in **II** was obtained by vigorous aeration of dilute solutions of disodium ethylenebisdithiocarbamate (3).

The reaction leading to **III** can be formulated as:

$$Na_2(CH_2N(CH_3)CS_2)_2 \rightarrow (CH_2N(CH_3))_2CS + CS_2 + S + 2Na^+$$

via a ring-closure mechanism. Similar ring-opening or -closure reactions were reported for many cyclic thiourea-type compounds (4), for example $(CH_2NH)_2CS$ was reported to give an orange crystal adduct

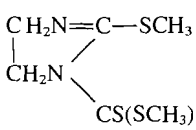

which, when treated by dry H_2S in an ethanol solution, gave

[1]Revision received September 8, 1982.

0008-4042/83/010211-03$01.00/0

©1983 National Research Council of Canada/Conseil national de recherches du Canada

Can. J. Chem. Downloaded from www.nrcresearchpress.com by 210.87.254.5 on 09/06/12
For personal use only.

two products, one as a bisdithiocarbamate, a ring-opening process, and the other the original cyclic thiourea, a reverse reaction from the adduct. Apparently, the addition of —CS—SCH_3 to the cyclic thiourea is promoted by the *n*-C_4H_9Li, and $HgCl_2$ seems related to the ring closure in the formation of **III** from the bisdithiocarbamate.

One of the referees pointed out that a non-oxidation process could lead to the formation of **III** by

$$Na_2\begin{matrix}CH_2—N(CH_3)CS_2\\ |\\ CH_2—N(CH_3)CS_2\end{matrix} \rightarrow \begin{matrix}CH_2—N(CH_3)\\ |\quad\quad >CS\\ CH_2—N(CH_3)\end{matrix} + CS_2 + Na_2S$$

but the Na_2S would react with Hg^{2+} to give a black product; such was not the case as indicated by tests even on partially decomposed solutions of disodium *N,N'*-dimethylethylenebisdithiocarbamate.

The synthesis and properties of **III** were reported by Sakai, Fujimura, and Ishii (5) by the reaction of 1,3-dimethyl-2,2-dibutyl-1,3-diaza-2-stannacyclopentane and carbon disulfide at 273 K. The Zn(II) and Cd(II) complexes of the title compound were studied by Devillanova and Verani (6), but there has not been any structural study of **III**.

Crystal data

$C_5H_{10}N_2S$ fw = 130.8

Monoclinic, a = 10.388(2), b = 6.139(1), c = 12.291(4) Å, β = 118.64(2)°. V = 688(1) Å^3, space group $P2_1/c$ (from systematic absences), Z = 4, D_c = 1.262, D_m = 1.265 g cm^{-3} (by flotation), $F(000)$ = 280. μ(Mo Kα) = 3.60 cm^{-1}, (Mo Kα) = 0.71069 Å.

The non-hydrogen atoms of the molecule lie in a plane with a maximum deviation (N(2)) of 0.05 Å. Bond lengths and angles are shown in Fig. 1; the value of 1.673(4) Å for C=S is in agreement with those of similar compounds, for example 1.673 and 1.702 Å for dithiobiurea (7). The average angle for a regular pentagon is 108°; however, the two CNC angles of the 5-membered ring are significantly larger than the NCN or NCC angles. This may result from the partial double bond character of the (S=)C—N bonds, in agreement with their lengths. However, there are significant differences between the observed values and those composed purely from theoretical considerations in a recent CNDO/S calculation for the interpretation of $\pi-\pi^*$ transition (8).

Only van der Waals force is present in the intermolecular packing diagram shown in Fig. 2. The methyl hydrogens were not located from the difference Fourier map, but the small circles are the methylene hydrogens. The four molecules in the unit cell can be divided into two pairs, each consists of two molecules related by a center of symmetry.

Experimental

Preparation of disodium N,N'*-dimethylethylenebisdithiocarbamate*

To 30 mL aqueous solution containing 0.03 mol *N,N'*-dimethylethylenediamine, 0.06 mol (3.7 mL) of carbon disulfide and 20 mL aqueous solution of 0.06 mol NaOH were added dropwise. The mixture was stirred at 315 K until all CS_2 had reacted (~3 h). After the solvent evaporated, the solid was collected and recrystallized from water to afford a white powder. The yield was 54% and the mp, 613 K. *Anal.* Calcd. for $Na_2C_6H_{10}N_2S_4$: C 24.74, H 4.17, N 9.72; found: C 25.35, H 3.55, N 9.86. The ^{1}H nmr (60 MHz, D_2O) spectrum consisted of $\delta(CH_3$, s), 3.5 and $\delta(CH_2$, s), 4.45 ppm.

In another preparation, 15 mL of the THF was used instead of water, a precipitate immediately formed after CS_2 was added. This solid was filtered and washed with THF and then recrystallized from water.

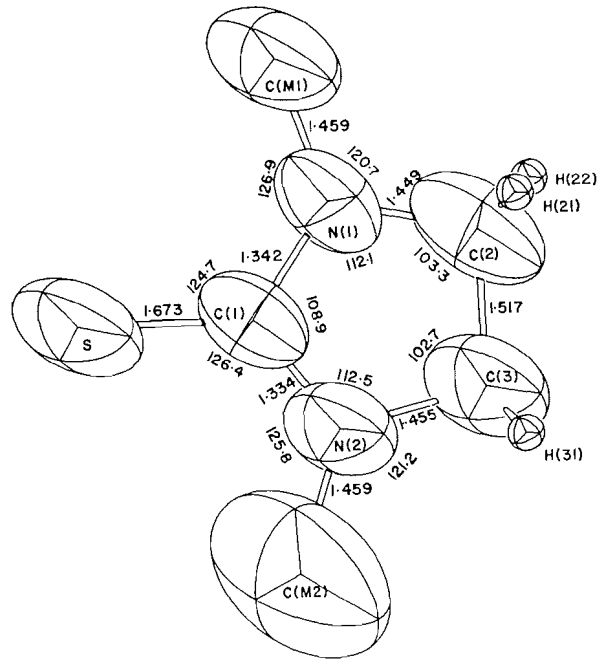

FIG. 1. An OETEP plot of the molecule with atomic numbering, bond lengths, and angles (standard deviations for bond lengths, 0.005 Å and angles 0.4°).

Reaction of disodium N,N'*-dimethylethylenebisdithiocarbamate and mercury(II) chloride*

When 20 mL ethanol solution containing 1 m*M* $HgCl_2$ was added to 20 mL aqueous-ethanol solution of 1 m*M* bisdithiocarbamate, a white precipitate immediately formed. This precipitate turned to a creamy color gradually and the solid was collected by filtration. It was then stirred in an aqueous-ethanol solution for an hour; the clear filtrate from this evaporated in a cold room (273 K) and gave colorless crystals. *Anal.* Calcd. for $C_5H_{10}N_2S$: C 46.15, H 7.62, N 21.15; found: C 45.12, H 7.81, N 21.61. The ^{1}H nmr (60 MHz, D_2O) consisted of $\delta(CH_3$, s) 3.05 and $\delta(CH_2$, s) 3.6 ppm.

Further tests indicated that a 1:1 complex was formed between $HgCl_2$ and the bisdithiocarbamate. and the creamy colored solid formed was not soluble in DMSO, DMF, pyridine, acetone, chloroform, or ethanol. The ir spectrum of this solid showed characteristic peaks of the bisdithiocarbamate, but none of the solvents mentioned above dissolved enough of the complex to give an nmr spectrum, other than that of the thione as indicated above.

Crystallographic study

Crystals of *N,N'*-dimethyl-2-imidazolidinethione are colorless and preliminary X-ray photographs gave estimates of cell constants and space group. A cubic crystal with edges of ~0.2 mm was then selected and mounted on a Syntex $P2_1$ automatic diffractometer, on which 642 independent reflections, ($\pm h$, k, l), with $2\theta \leq 40°$ were collected and the structure factor amplitudes were derived by applying the Lorentz and polarization but not the absorption corrections. Structural analysis was carried out by using the SHELX system (7). The methylene hydrogen positions were found in a difference Fourier which had no clear indication of the methyl hydrogen atoms. Anisotropic thermal parameters were given to all non-hydrogen atoms and isotropic thermal parameters were assumed for the H atoms. These were refined as well as their positions with a total of 89 variables. Using all reflections, the final R and R_w were 0.053 and 0.068 respectively, the weighting scheme being $1/(\sigma^2(F) + 0.0001F^2)$ in the function, $\sum w(|F_o| - |F_c|)^2$, minimized. The difference Fourier at the end had

Can. J. Chem. Downloaded from www.nrcresearchpress.com by 210.87.254.5 on 09/06/12
For personal use only.

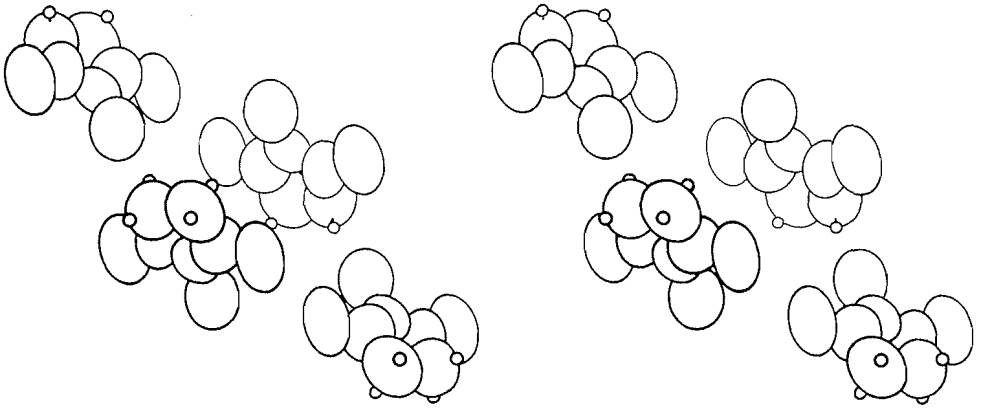

FIG. 2. Arrangement of the four molecules per unit cell — a stereo pair.

TABLE 1. Atomic coordinates ($\times 10^4$ for S, N, C and $\times 10^3$ for H)

Atom	x/a	y/b	z/c	B*
S	7573(1)	6779(2)	2748(1)	5.92
N(1)	6624(2)	3393(6)	1189(3)	5.20
N(2)	8267(4)	5361(6)	1025(3)	5.02
C(1)	7485(4)	5158(7)	1621(3)	3.63
C(2)	6769(6)	2334(9)	199(5)	5.47
C(3)	8002(6)	3590(10)	156(5)	5.57
C(M1)	5549(5)	2630(9)	1546(5)	6.04
C(M2)	9413(5)	6951(8)	1298(5)	6.04
H(21)	584(6)	242(8)	−5(5)	7(1)
H(22)	706(6)	64(9)	40(5)	8(1)
H(31)	760(7)	450(11)	−7(7)	10(2)
H(32)	890(6)	270(10)	44(5)	8(2)

*$B = 8\pi^2 \sum_{i=1}^{3} U_{ii}/3$ for non-hydrogen atoms.

a background of 0.5 e Å^{-3} and the maximum shift was 0.3 of its standard deviation. The final atomic coordinates are given in Table 1.[2]

1. C. CHIEH and S. K. CHEUNG. Can. J. Chem. **59**, 2746 (1981).
2. H. L. KLOPPING and G. J. M. VAN DER KERK. Recueil, **70**, 949 (1951).
3. G. D. THORN and R. A. LUDWIG. Can. J. Chem. **32**, 872 (1954).
4. M. YOKOYAMA, K. HOSI, and T. IMAMOTO. Synthesis, 908 (1981).
5. S. SAKAI, Y. FUJIMURA, and Y. ISHII. J. Organomet. Chem. **50**, 113 (1973).
6. R. A. DEVILLANOVA and G. VERANI. J. Inorg. Nucl. Chem. **42**, 623 (1980).
7. W. A. SPOFFORD and E. L. AMMA. J. Cryst. Mol. Struct. **2**, 151 (1972).
8. D. BOUIN-ROUBAUD, J. KISTER, T. AVIGNON, and L. BOUSCASSE. Can. J. Chem. **60**, 1295 (1982).
9. G. M. SHELDRICK. Private communication.

[2]A complete set of data is available, at a nominal charge, from the Depository of Unpublished Data, CISTI, National Research Council of Canada, Ottawa, Ont., Canada K1A 0S2.

Can. J. Chem. Downloaded from www.nrcresearchpress.com by 210.87.254.5 on 09/06/12
For personal use only.

COMMUNICATION

Stereoselective cyclization of epoxy allylsilanes. A synthesis of karahana ether

ROSEMARY J. ARMSTRONG AND LARRY WEILER[1]
Department of Chemistry, University of British Columbia, Vancouver, B.C., Canada V6T 1Y6

Received October 1, 1982

ROSEMARY J. ARMSTRONG and LARRY WEILER. Can. J. Chem. **61**, 214 (1983).

Epoxy allylsilanes can be cyclized with Lewis acids to give cyclic alcohols in a biomimetic synthesis of mono and bicyclic compounds. The allylsilane has a pronounced effect on activating an olefin in this cyclization and producing the exocyclic methylene regioselectively. A short synthesis of karahana ether (**5**) is reported.

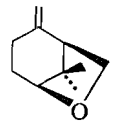

5

ROSEMARY J. ARMSTRONG et LARRY WEILER. Can. J. Chem. **61**, 214 (1983).

On peut cycliser les époxyallylsilanes avec des acides de Lewis pour obtenir des alcools cycliques dans une synthèse biomimétique de composés mono- et bicycliques. L'allylsilane a un effet marqué en activant l'oléfine dans cette cyclisation et en produisant d'une façon régiosélective le méthylène exocyclique. On rapporte une courte synthèse de l'éther karahana (**5**).
[Traduit par le journal]

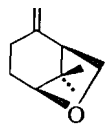

5

In 1955, Stork and Burgstahler (1) and Eschenmoser *et al.* (2) independently developed the hypothesis that many cyclic terpenoid natural products may arise via electrophilic cyclization of appropriate polyolefins. Both groups illustrated the hypothesis with laboratory examples. Since then several groups have extended and applied the cyclization of polyolefins in natural products chemistry. Most notable have been the contributions from W. S. Johnson's laboratory (3). In these cases cyclization is initiated by either protons or Lewis acids to produce products with few, if any, functional groups other than alkenes.

Following the pioneering work by Goldsmith (4*a*), several groups recognized that terminal epoxides of polyolefins might well serve as precursors in electrophilic cyclizations (4*b*). In 1966, Corey *et al.* (5) and van Tamelen *et al.* (6) showed that squalene 2,3-oxide was efficiently converted into cholesterol *in vivo*. However, *in vitro* experiments using acid catalyzed cyclizations of epoxyolefins and epoxypolyolefins usually were much less efficient. These cyclizations frequently produced a plethora of products which detracted from the synthetic utility of this reaction.[2]

In 1976, Fleming *et al.* (8) found that an allylsilane can have a dramatic effect in controlling the regiochemistry of olefin cyclizations and several groups since have reported the synthetic utility of allylsilane cyclizations (9). Recently we described the electrophilic cyclization of polyolefin allylsilanes (10). We would now like to report that the incorporation of an allylsilane moiety in an epoxyolefin has a marked effect on the cyclization of these compounds. The diene **1** can be regioselectively epoxidized in good yield to give the epoxy allylsilane **2** (Scheme 1). We found that cyclization of **2** with two equivalents of boron trifluoride etherate in *dry* methylene chloride gave a good yield of cyclized material. Vapor phase chromatographic analysis indicated that the crude product contained approximately 80% of **3**, 10% of **2**, and 10% of two other products. We did experience some losses in the column chromatographic purification of **3**. However, when the crude cyclization mixture was treated with lithium aluminum hydride, the diol **4** could be isolated in 68% yield from **2**. The spectral and chromatographic properties of **3** and **4** indicated that each was a single diastereomer. The spectral properties of the diol **4** were identical to those reported by Coates and Melvin (11). Finally, the structure and stereochemistry of the diol **4** was confirmed by its conversion to (±)-karahana ether (**5**) (12) following the procedure of Coates and Melvin (11). Two other syntheses of karahana ether (**5**) have recently been reported (13).

The trimethylsilyl group again had a marked effect on activating the olefin in this electrophilic cyclization and in controlling the regiochemistry of the product to yield the exocyclic olefin (8, 10). This is one of the first examples of an efficient

[1]Author to whom correspondence may be addressed.

[2]For some recent examples of the limitations of these reactions in organic synthesis, see refs. 4*b* and 7.

0008-4042/83/010215-02$01.00/0
©1983 National Research Council of Canada/Conseil national de recherches du Canada

Can. J. Chem. Downloaded from www.nrcresearchpress.com by 210.87.254.40 on 09/06/12
For personal use only.

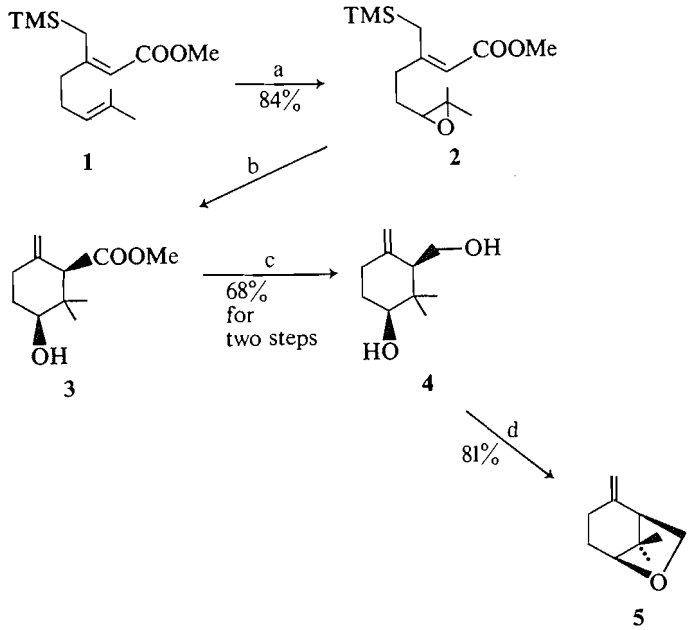

SCHEME 1. (a) MCPBA, CH_2Cl_2, 0°C; (b) 2 equiv. $BF_3 \cdot Et_2O$, dry CH_2Cl_2, −56°C; (c) $LiAlH_4$, Et_2O, 0° → 25°C; (d) TsCl, py, 0° → 25°C, 5 h.

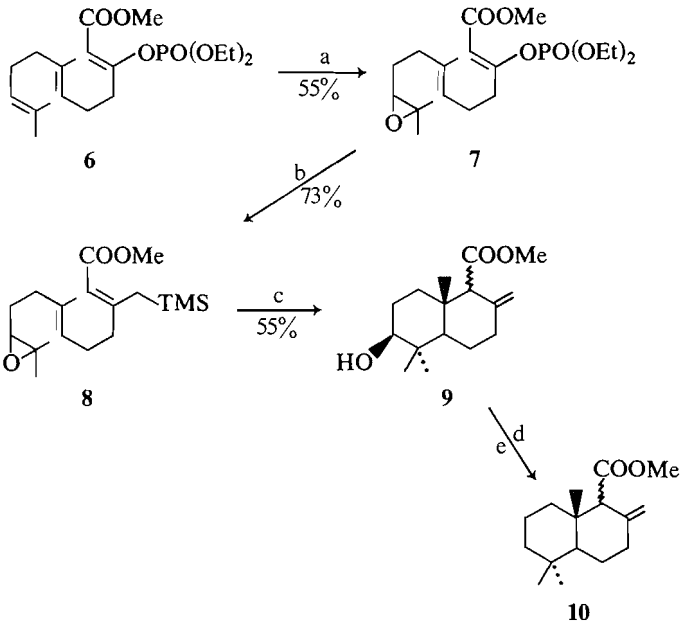

SCHEME 2. (a) MCPBA, CH_2Cl_2, −50° → 0°C; (b) $TMSCH_2MgCl$, $Ni(acac)_2$, Et_2O; (c) $SnCl_4$, CH_2Cl_2, 0 → 25°C; (d) PCC, NaOAC, 4 Å sieves, CH_2Cl_2; (e) $TsNHNH_2$ then 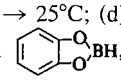 , $CHCl_3$, 0°C.

cyclization of an olefinic epoxide and it illustrates the utility of an allylsilane in cyclizations of epoxyolefins. The stereochemistry of **3** can be interpreted as the outcome of a chair-like transition state for cyclization (1−4, 14).

We have also extended this cyclization to bicyclic systems as shown in Scheme 2. The triene **6** (10) was epoxidized with fair regioselectivity (C-10,11/C-6,7 ≃ 4:1) using *m*-chloroperbenzoic acid. The enol phosphate **7** was coupled with trimethylsilylmethylmagnesium chloride (10) to give **8** which was cyclized with stannic chloride to give a 55% yield of two products in a ratio of ca. 2:1 after purification (15). The two products **9** were shown to be epimeric at C-9 by oxidation of the C-3 alcohol (16), conversion to the tosyl hydrazone, and reduction with catecholborane (17) to give the 9α- and 9β-isomers of **10** (10) in the same ratio as the products in the cyclization step. The 9β-isomer is the major product. Thus the path appears open to utilize the cyclization of epoxy allylsilanes in the synthesis of functionalized polycyclic compounds.

Acknowledgements

We are grateful to Professor R. M. Coates and Professor Y. Yamada for the spectral data of karahana ether and to the Natural Sciences and Engineering Research Council of Canada for financial support. One of us (R.J.A.) is grateful to the Canadian Commonwealth Scholarship and Fellowship Plan for the award of a graduate scholarship.

1. G. STORK and A. W. BURGSTAHLER. J. Am. Chem. Soc. **77**, 5068 (1955).
2. A. ESCHENMOSER, L. RUZICKA, O. JEGER, and D. ARIGONI. Helv. Chim. Acta, **38**, 1890 (1955).
3. W. S. JOHNSON, C. E. WARD, S. G. BOOTS, M. B. GRAVESTOCK, R. L. MARKEZICH, B. E. MCCARRY, D. A. OKORIE, and R. J. PARRY. J. Am. Chem. Soc. **103**, 88 (1981), and references therein.
4. (*a*) D. J. GOLDSMITH. J. Am. Chem. Soc. **84**, 3913 (1962); (*b*) *In* Fortschritte der chemie organischer naturstoffe. Vol. 29. *Edited by* W. Herz, H. Grisebach, and G. W. Kirby. Springer-Verlag, Vienna, Austria. 1971. p. 363.
5. E. J. COREY, W. E. RUSSEY, and P. R. ORTIZ DE MONTELLANO. J. Am. Chem. Soc. **88**, 4750 (1966).
6. E. E. VAN TAMELEN, J. D. WILLETT, R.B. CLAYTON, and K. E. LORD. J. Am. Chem. Soc. **88**, 4752 (1966).
7. (*a*) N. H. CHISHTI, S. M. COPPELL, and R. RAMAGE. Tetrahedron Lett. 1025 (1975); (*b*) E. E. VAN TAMELEN. Acc. Chem. Res. **1**, 111 (1968); (*c*) J. K. SUTHERLAND. Chem. Soc. Rev. **9**, 265 (1980), and references therein; (*d*) E. E. VAN TAMELEN and T. M. LEIDEN. J. Am. Chem. Soc. **104**, 2061 (1982); (*e*) E. E. VAN TAMELEN, A. STORNI, E. J. HESSLER, and M. A. SCHWARTZ. Bioorg. Chem. **11**, 133 (1982); (*f*) E. E. VAN TAMELEN and R. M. COATES. Bioorg. Chem. **11**, 171 (1982).
8. I. FLEMING, A. PEARCE, and R. L. SNOWDEN. J. Chem. Soc. Chem. Commun. 182 (1976).
9. (*a*) T. K. SARKAR and N. H. ANDERSEN. Tetrahedron Lett. 3513 (1978); (*b*) L. R. HUGHES, R. SCHMID, and W. S. JOHNSON. Bioorg. Chem. **8**, 513 (1979); (*c*) I. FLEMING and A. PEARCE. J. Chem. Soc. Perkin Trans. 1, 251 (1981).
10. R. J. ARMSTRONG, F. L. HARRIS, and L. WEILER. Can. J. Chem. **60**, 673 (1982).
11. R. M. COATES and L. S. MELVIN, JR. J. Org. Chem. **35**, 865 (1970).
12. Y. NAYA and M. KOTAKE. Tetrahedron Lett. 1645 (1968).
13. (*a*) Y. YAMADA, H. SANJOH, and K. IGUCHI. Tetrahedron Lett. 1323 (1979); (*b*) T. MUKAIYAMA, N. IWASAWA, T. TSUJI, and K. NARASAKA. Chem. Lett. 1175 (1979).
14. E. E. VAN TAMELEN and D. R. JAMES. J. Am. Chem. Soc. **99**, 950 (1977).
15. W. C. STILL, M. KAHN, and A. MITRA. J. Org. Chem. **43**, 2923 (1978).
16. E. J. COREY and J. W. SUGGS. Tetrahedron Lett. 2647 (1975).
17. G. W. KABALKA, J. D. BAKER, JR., and G. W. NEAL. J. Org. Chem. **42**, 512 (1977).

Can. J. Chem. Downloaded from www.nrcresearchpress.com by 210.87.254.40 on 09/06/12
For personal use only.

Synthèse de cyclopropanes électrophiles à fonction aldéhyde libre ou masquée[1]

HASSAN ABDALLAH,[2] RENÉ GRÉE ET ROBERT CARRIÉ

Groupe de Recherches de Physicochimie Structurale, ERA n° 389 au C.N.R.S., Laboratoire n° 3, Université de Rennes, 35042 Rennes Cedex, France

Reçu le 3 mai 1982

HASSAN ABDALLAH, RENÉ GRÉE et ROBERT CARRIÉ. Can. J. Chem. **61**, 217 (1983).

Le diméthylacétal du diazoacétaldéhyde **2** d'une part et l'oléfine **3** d'autre part permettent l'accès, dans d'excellentes conditions, à des cyclopropanes électrophiles possédant une fonction aldéhyde supplémentaire.

HASSAN ABDALLAH, RENÉ GRÉE, and ROBERT CARRIÉ. Can. J. Chem. **61**, 217 (1983).

Electrophilic cyclopropanes **1** bearing an extra aldehyde function are conveniently prepared starting either from the diazoacetal **2** or from the olefin **3**.

Can. J. Chem. Downloaded from www.nrcresearchpress.com by 210.87.254.105 on 09/06/12
For personal use only.

Les cyclopropanes électrophiles sont des intermédiaires très utiles en synthèse organique et il semble que de nouvelles voies d'accès à ces composés méritent d'être développées (2). Dans le cadre de travaux concernant l'utilisation en synthèse de la réaction de cycloaddition 1,3 dipolaire, nous nous sommes intéressés à la préparation des cyclopropanes électrophiles **1** possédant en outre une fonction aldéhyde supplémentaire, ce

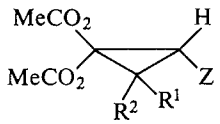

Z = CHO ou $CH(OCH_3)_2$

1

qui offre de nouvelles potentialités synthétiques notamment pour la préparation de produits naturels ou de leurs analogues (2).

Différents cyclopropanes de type **1** ont déjà été préparés par action de bromomalonates sur des aldéhydes insaturés, en présence de base (3) ou dans les conditions de catalyse par transfert de phase (4, 5). Cette réaction présente un certain nombre de limitations car l'oléfine utilisée doit être suffisamment électrophile et peu encombrée (4).

L'objet de ce mémoire est de montrer que l'utilisation du diméthylacétal du diazoacétaldéhyde **2** d'une part et de l'oléfine **3** d'autre part permet d'obtenir, dans d'excellentes conditions, les cyclopropanes recherchés **1**.

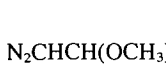

2

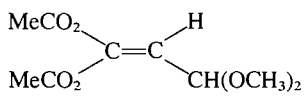

3

I. Synthèse et réactions du diméthylacétal du diazoacétaldehyde 2

Deux diazoacétals ont été préparés par Kirmse et Buschhoff afin d'étudier les aptitudes migratrices des groupes OR dans les carbènes correspondants (6) mais, à notre connaissance, aucune étude de ces composés en tant que dipôles 1,3 n'a été effectuée.

Le diazoacétal **2** utilisé au cours de ce travail présente un certain nombre d'avantages qui lui permettent d'occuper, tant par ses propriétés physiques que chimiques, une place assez unique dans la chimie des diazocomposés: il est assez facile d'accès et peut être isolé; il présente une bonne stabilité thermique et également une excellente réactivité en cycloaddition dipolaire 1,3; enfin, les pyrazolines-1 obtenues ne s'isomérisent pas en pyrazolines-2 par migration de l'hydrogène en α du groupe acétal.

A. Synthèse de 2

Le diazoacétal **2** est préparé selon la méthode décrite pour son homologue diéthylique (6). L'aminoacétal **4**, commercial, conduit de façon pratiquement quantitative à l'urée **5** qui est

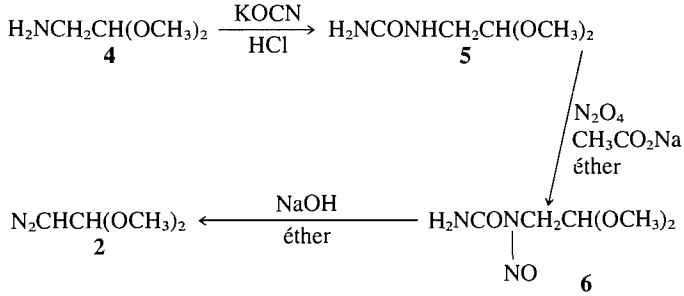

ensuite nitrosée pour donner **6**. Le traitement de cette nitrosourée par la soude diluée conduit au diazoacétal **2**. Le diazocomposé brut obtenu peut être utilisé directement pour les cycloadditions ultérieures. Il est également possible de le distiller sous pression réduite (distillation "trap to trap": $E_{0,05}$ = 15−20°C). Le rendement global en diazoacétal **2** par rapport à **4** est de 45%. Le composé **2** peut être conservé plusieurs mois à −15°C sous atmosphère inerte.

B. Synthèse des cyclopropanes électrophiles

Le diazocomposé **2** réagit avec les oléfines **7**, en quelques heures, dans l'éther à 0°C, pour conduire de façon quasi quantitative aux pyrazolines **8** caractérisées à l'aide de la rmn (un seul diastéréoisomère dans chaque cas). Par photolyse (en solution dans le toluène à température ambiante, avec un filtre Pyrex) ces pyrazolines conduisent aux cyclopropanes **9** qui après traitement à l'acide formique pur (7) donnent les formylcyclopropanes **10** (un seul diastéréoisomère, contrôle rmn).

[1]Une partie de ce travail a fait l'objet d'une communication préliminaire (1).

[2]Boursier du Conseil National de la Recherche Scientifique Libanais.

0008-4042/83/020217-07$01.00/0

©1983 National Research Council of Canada/Conseil national de recherches du Canada

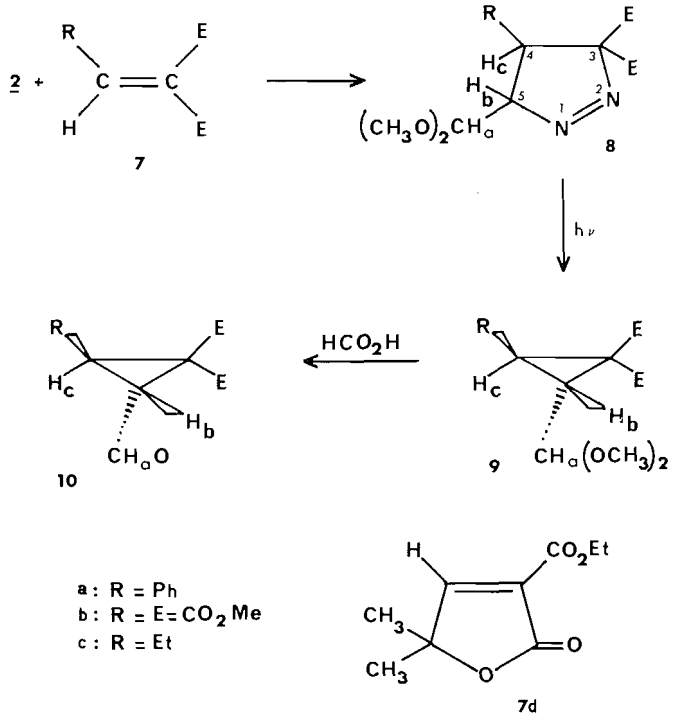

SCHÉMA 1

Toutes ces étapes ont des rendements excellents puisque les cyclopropanes **10** ont été obtenus purs après distillation au four tubulaire avec des rendements compris entre 65 et 94% à partir des oléfines **7**. Lors de la photolyse de **8***c* on observe à côté de **9***c* la formation de 15% de **11***c*; de même à partir de **8***d*, 18% de **11***d* sont obtenus. Dans les deux cas, ces composés sont

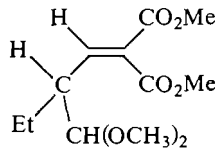

11*c*

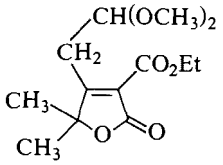

11*d*

séparés par chromatographie sur gel de silice. Les caractéristiques spectroscopiques des composés **8** à **10** figurent aux tableaux 1, 2 et 3.

(a) Structure des pyrazolines 8

L'étude rmn apporte les éléments suivants. (*i*) La multiplicité des signaux correspondant aux différents protons cycliques confirme l'orientation des cycloadditions. (*ii*) L'attribution des signaux correspondant à H_a et H_c a été effectuée sans ambiguité dans le cas de **8***a* après utilisation de l'oléfine deutériée **7***'a*. Pour les autres pyrazolines, l'attribution a été effectuée par analogie: le déplacement chimique de H_a variant

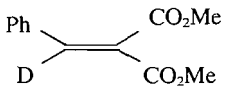

7*'a*

peu avec la structure. (*iii*) Sauf pour **8***d* (J_{bc} = 3,0 Hz; H_b et H_c en *trans*) la configuration relative au niveau des atomes de carbone 4 et 5 n'est pas établie: les constantes de couplage observées peu différentes de 7 Hz ne pouvant être considérées comme caractéristiques (8).

(b) Structure des cyclopropanes 9

La détermination de la configuration relative des carbones 2 et 3 des cyclopropanes électrophiles pose un problème généralement délicat en raison des valeurs élevées observées pour les constantes de couplage: elles sont par exemple de 9,2 Hz et

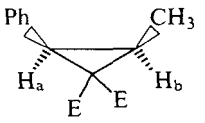

12

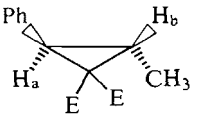

13

E = CO_2Me

8,0 Hz pour le couple de diastéréoisomères **12** et **13** (9).

Nous avons attribué aux cyclopropanes **9** et **10** obtenus une stéréochimie *trans* sur la base des éléments suivants. Pour les composés bicycliques **9***d* et **10***d*, les constantes de couplage observées (4,7 et 4,1 Hz) indiquent sans ambiguité une position *trans* des deux protons cycliques.[3] Dans le cas de **10***b*, son diastéréoisomère **14***a* a été préparé par une autre voie et une constante J_{bc} = 9,0 Hz a été observée (10). La stéréochimie

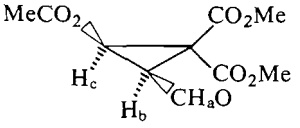

14

des autres composés **9***a*, **9***c*, **10***a* et **10***c* a été attribuée par analogie; leurs constantes J_{bc} étant proches de celles de **9***b* et **10***b*.

Remarque: Ces formylcyclopropanes présentent une bonne réactivité. Par action du carbomethoxymethylenetriphénylphosphoranne dans le benzène à température ambiante on obtient les vinylcyclopropanes **15***a* (Rdt 68%) et **15***b* (Rdt 80%).

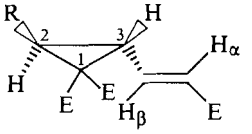

a R = Ph
b R = E = CO_2Me

15

Un seul isomère, de stéréochimie *E*, est obtenu ($J_{\alpha\beta}$ = 15,0 et 16,0 Hz).

II. Synthèse et réactions de l'oléfine 3

L'oléfine **3**, dont nous avons mis au point la synthèse, offre une voie d'accès complémentaire aux cyclopropanes électrophiles **1**. Le diazoacétal **2** est très peu réactif vis à vis d'oléfines tétrasubstituées telles que **16**; seule l'utilisation du composé **3**

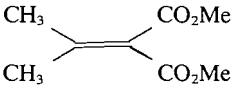

16

[3]Le cyclopropane analogue à **9***d* et **10***d* pour lequel le groupement acétal (ou aldéhyde) est remplacé par un hydrogène (J. Martelli et R. Grée, travaux non publiés) présente des constantes ^3J = 7,9 et 5,5 Hz respectivement attribuables à J_{cis} et J_{trans}.

Can. J. Chem. Downloaded from www.nrcresearchpress.com by 210.87.254.105 on 09/06/12
For personal use only.

TABLEAU 1. Caractéristiques rmn (C_6D_6) des pyrazolines **8** (δ ppm/TMS, J en Hz)

	δ(H_a)	δ(H_b)	δ(H_c)	δ(OCH_3)	J_{ab}	J_{bc}	δ(R)
8*a*	4,70	5,30	4,50	2,84 3,07 3,02 3,42	4,0	7,0	7,35–6,80
8*b*	4,72	5,57	4,15	3,06 3,30 3,10 3,33 3,45	3,7	7,0	—
8*c*	4,67	4,54	3,08	3,16 3,30 3,19 3,50	3,5	7,0	CH_2 1,45 CH_3 0,95
8*d*	4,80	5,17	3,20	3,28 3,15	2,5	3,0	OCH_2 4,06 CH_3 1,05 $C(CH_3)_2$ 1,40 et 1,08

TABLEAU 2. Caractéristiques rmn* des cyclopropanes **9**

	δ(H_a)	δ(H_b)	δ(H_c)	δ(OCH_3)	J_{ab}	J_{bc}	δ(R)
9*a*	4,39	2,78	3,40	3,30 (9H) 3,72 (3H)	6,0	8,0	7,19
9*b*	4,34	2,65	2,85	3,32 (6H) 3,66 3,71 3,73	6,7	7,3	—
9*c*	4,40	2,31	2,19	3,20 3,25 3,45 3,51	5,4	7,4	CH_2 1,35 CH_3 0,91
9*d*	4,57	1,83	2,70	3,32 (6H)	5,3	4,7	OCH_2 4,22 CH_3 1,32 $C(CH_3)_2$ 1,40 et 1,52

*Solvant $CDCl_3$ sauf **9***c* (C_6D_6).

TABLEAU 3. Caractéristiques rmn* des cyclopropanes **10**

	δ(H_a)	δ(H_b)	δ(H_c)	δ(OCH_3)	δ(R)	J_{ab}	J_{bc}
10*a*	9,25	3,36	3,70	3,00 3,36	7,00	3,9	7,4
10*b*	9,43	3,12	3,27	3,78 3,75 3,72	—	4,3	6,9
10*c*	9,40	2,67	2,47	3,76 3,74	CH_2 1,50 CH_3 1,02	4,3	6,8
10*d*	9,55	2,45	3,17	—	OCH_2 4,27 CH_3 1,32 $C(CH_3)_2$ 1,42 et 1,60	4,3	4,1

*Solvant $CDCl_3$ sauf **10***a* (C_6D_6).

permet la préparation, dans de bonnes conditions, des cyclopropanes **1** disubstitués sur le carbone 2 (R^1 et $R^2 \neq H$).

*A. Synthèse de **3***

Elle s'effectue en deux étapes (11): l'aldéhyde **17** est préparé par condensation du mésoxalate de méthyle avec le formylméthylène triphénylphosphoranne.

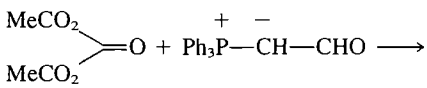

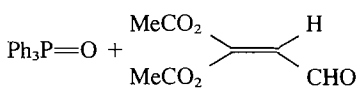

17

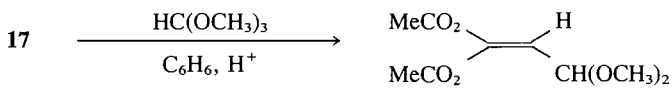

3

Cette oléfine, fragile, est isolée par distillation sous vide poussé (Rdt 70%).[4] L'acétalisation de **17** au moyen de l'orthoformiate de méthyle et à la température ambiante, conduit à l'oléfine **3** avec un rendement de 84%.[5]

B. Synthèse des cyclopropanes disubstitués en position 2

Les principaux résultats sont résumés dans le schéma 2: la

[4]Cette oléfine constitue en outre un intermédiaire clef pour la synthèse de cyclopropanes chiraux (12).

[5]Cette oléfine, ainsi que le cyclopropane **18**, ont étés préparés indépendamment par le Professeur Krief, en utilisant d'autres réactions (13).

Can. J. Chem. Downloaded from www.nrcresearchpress.com by 210.87.254.105 on 09/06/12
For personal use only.

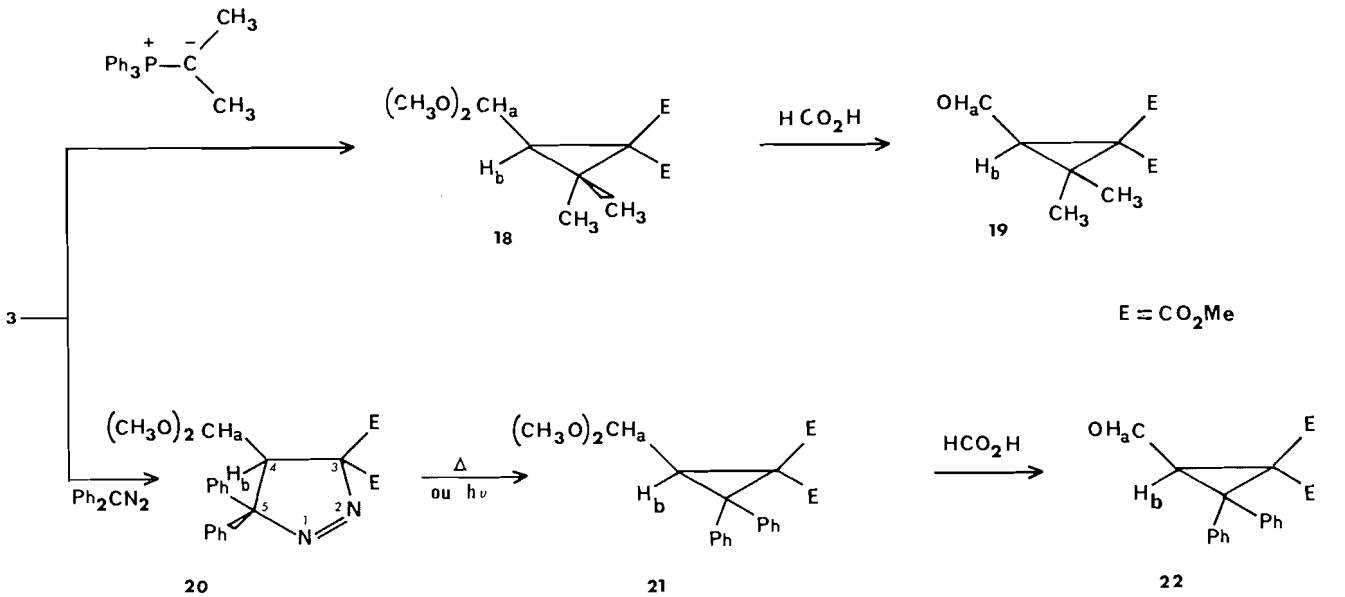

SCHÉMA 2

TABLEAU 4. Caractéristiques rmn ($CDCl_3$) des produits de réaction de **3** avec l'isopropylidène phosphoranne ou le diphényldiazométhane

	$\delta(H_a)$	$\delta(H_b)$	$\delta(OCH_3)$	$\delta(C(CH_3)_2)$ ou $\delta(C(C_6H_5)_2)$	J_{ab}
18	4,51	2,05	3,75 et 3,37	1,40 et 1,20	7,8
19	9,57	2,58	3,79 et 3,77	1,49 et 1,34	4,5
20	4,10 et 3,85		3,82 3,24 3,78 2,67	7,85–6,85	8,8
21	4,52 (d)	3,21 (d)	3,62 3,40 3,47 3,33	7,55–7,05	8,0
22	9,37 (d)	3,45 (d)	3,71 3,41	7,55–7,05	6,0

réaction de l'isopropylidène phosphoranne (13) sur **3** conduit au cyclopropane **18**, puis après formolyse à **19** (Rdt 75% par rapport à **3**). Avec le diphényldiazométhane en solution éthérée à température ambiante, les cyclopropanes **21** puis **22** (Rdt 90% par rapport à **3**) sont obtenus.

La pyrazoline intermédiaire **20** peut être isolée et caractérisée à l'aide de la rmn mais elle évolue lentement dès la température ambiante pour conduire à **21**. L'orientation de la cycloaddition 1,3 dipolaire est établie à l'aide de la rmn ^{13}C: le déplacement chimique du carbone 4 qui porte un hydrogène (47,9 ppm) est nettement différent de ceux des carbones quaternaires 3 et 5 (106,0 et 104,7). Les caractéristiques spectroscopiques des composés **18** à **22** figurent au tableau 4.

C. Réaction de 3 avec le diazoacétal 2

Elle permet la préparation de cyclopropanes électrophiles possédant cette fois deux fonctions aldéhydes (schéma 3).

La cycloaddition de **2** au composé **3** conduit quantitativement (contrôle rmn) à la pyrazoline **23** qui par photolyse donne le cyclopropane **24** (rendement 93% à partir de **3**). Le traitement de **24** par HCO_2H pur en excès conduit au cyclopropane bisaldéhyde **25**. Il est possible de libérer sélectivement l'une des fonctions aldéhydes; par traitement avec de l'acide trifluoroacétique (4 équivalents) dans le chloroforme pendant 20 heures à température ambiante, on obtient un mélange 70:30 (intégration rmn) de **26** et **25**. Les caractéristiques spectroscopiques de ces différents composés figurent au tableau 5.

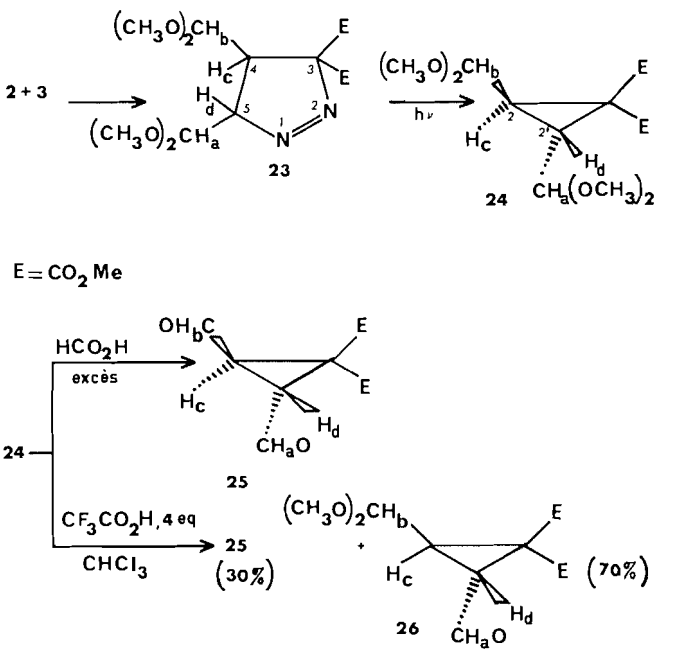

SCHÉMA 3

(a) Structure de la pyrazoline 23

La multiplicité des signaux en rmn (double doublets pour H_4 et H_5) permet de connaître l'orientation de la cycloaddition. Par

Can. J. Chem. Downloaded from www.nrcresearchpress.com by 210.87.254.105 on 09/06/12
For personal use only.

TABLEAU 5. Caractéristiques rmn ($CDCl_3$) des composés obtenus à partir de **2** et **3**

	$\delta(H_a)$	$\delta(H_b)$	$\delta(H_c)$	$\delta(H_d)$	$\delta(OCH_3)$	J_{ad}	J_{bc}	J_{cd}
23	4,67	4,41	3,50	5,33	3,56 3,20 3,51 3,17 3,25 3,12	3,0	6,6	4,1
24	4,40 (2H)		2,45 (2H)		3,80 (6H) 3,38 (6H) 3,36 (6H)		Système non analysé	
25	9,52 (2H)		3,36 (2H)		3,83 (6H)		Système non analysé	
26	9,40	4,45	2,76	3,01	3,37 3,33	4,0	5,1	7,0

ailleurs, l'attribution du signal à 5,31 ppm au proton H_d a été confirmée par l'utilisation du diazocomposé deutérié **2'**; ceci permet donc une attribution non ambigüe de la constante de couplage J_{45} = 4,1 Hz. Cette faible valeur indique que les deux protons 4 et 5 sont en position *trans* (8).

(b) Structure des cyclopropanes

Nous avons attribué pour ces composés **24** et **25** une position relative *trans* des hydrogènes H_c et H_d en raison de l'équivalence des deux groupements esters, observée à l'aide des rmn ^1H et ^{13}C.

Les caractéristiques de **26** sont identiques à celles d'un échantillon préparé au laboratoire par une autre voie (12) et très voisines de celles décrites par Kucherov et coll. (5) (esters éthyliques).

Conclusion

L'utilisation du diazoacétal **2** ou de l'oléfine acétal **3** permet de préparer avec d'excellents rendements et de façon stéréospécifique les cyclopropanes électrophiles fonctionnalisés recherchés **1**. Ces composés apparaissent comme des intermédiaires susceptibles d'être très intéressants pour la synthèse de produits élaborés tels que les produits naturels.

Partie expérimentale

Indications générales

Les points de fusion, non corrigés, sont déterminés au banc chauffant Kofler. Les spectres ir ont été enregistrés sur spectrophotomètre Perkin–Elmer 225 en suspension dans le Nujol ou en film liquide. Les fréquences d'absorption sont exprimées en cm^{-1}. Les spectres de rmn ^1H ont été enregistrés à 100 MHz sur un appareil JEOL MH 100 ou à 80 MHz sur un appareil Bruker WP 80. Les spectres de rmn ^{13}C sont enregistrés à 20,115 MHz sur un appareil à transformée de Fourier Bruker WP 80 DS. Les déplacements chimiques δ sont donnés en ppm (référence interne TMS); les constantes de couplage sont en Hz. Les chromatographies sur colonne ont été effectuées avec du gel de silice 60 Merck (230–400 mesh). Les chromatographies sur couches minces (épaisseur 2 mm) sont effectuées avec du gel de silice 60 G Merck. Les photolyses sont effectuées dans une cellule en Pyrex à refroidissement par circulation d'eau. La lampe utilisée est une Hanau HQ 80 (puissance 80 W); après dégazage de la solution par barbottage d'azote, les produits sont irradiés en solution (température 25–30°C) dans le benzène ou le toluène anhydres (200 cm^3). Les analyses sont effectuées au laboratoire central de Microanalyses du C.N.R.S. (Lyon).

Urée 5

Elle est préparée selon la méthode décrite pour son homologue diéthylique (15). Composé **5** (huile), ir (film liquide): 3340 (NH), 1650 (C=O); rmn ($CDCl_3$) δ: 6,16 (t, N*H*, J = 5,7), 5,31 (s, NH_2), 4,36 (t, C*H* $(OCH_3)_2$, J = 5,1), 3,37 (s, 6H, OCH_3), 3,30 (m, CH_2).

N-*nitrosourée 6 et diazoacétal 2*

Ils sont préparés selon la méthode décrite pour leurs homologues diéthyliques (6). Composé **6**, F = 68–69°C (éther); ir (Nujol): 3329–3395 et 3177–3230 (NH), 1732 (C=O), 1602 (NO); rmn ($CDCl_3$) δ: 6,80 (s large, NH_2), 4,52 (t, C*H*, J = 5,7), 4,00 (d, CH_2), 3,30 (s, 6H, OCH_3). *Anal.* calc. pour $C_5H_{11}N_3O_4$: C 33,90, H 6,21, N 23,73; trouvé: C 33,6, H 6,3, N 23,9. Composé **2** (huile), ir (film liquide): 2078 (C=N_2); rmn (C_6D_6) δ: 4,90 (d, $(CH_3O)_2CH$, J = 2,7), 3,21 (d, N_2CH), 3,02 (s, 6H, OCH_3).

Diazoacétal deutérié 2'

Dans un Erlenmeyer, on introduit une solution de 200 mg de K_2CO_3 dans 5 cm^3 de D_2O. Sous agitation magnétique et à 0°C, on ajoute une solution de 300 mg de diazoacétal **2** dans 10 cm^3 d'éther anhydre. On abandonne 6 heures à 0°C, la phase éthérée est alors décantée, séchée sur pastilles de KOH. Après distillation du solvant, on obtient le diazoacétal deutérié (200 mg). Le taux de deutériation est supérieur à 90% (contrôle rmn).

Pyrazolines-1 8

À une solution de 10^{-2} mol d'oléfine dans 15 cm^3 d'éther anhydre, on ajoute à 0°C un léger excès (1,1 équivalent) de diazoacétal. Après 6 heures, les réactions sont terminées et l'éther est distillé sous pression réduite. La rmn montre la présence d'un seul isomère.

Les caractéristiques de rmn ^{13}C (C_6D_6) du composé **8***a* confirment l'orientation: 166,7 (m, CO_2CH_3, J = 3 et 4), 164,9 (m, CO_2CH_3, J = 4 et 5), 137, 1–127,0 (m, C_6H_5), 107,2 (d, C_3, J = 5), 103,8 (d.m, $CH(OCH_3)_2$, ^1J = 162, ^3J = 5), 98,4 (d, C_5, ^1J = 139), 55,6 et 55,3 (2q.d, $CH(OCH_3)_2$, ^1J = 143 et 142, ^3J = 6 et 5), 53,4 et 52,8 (2q, $COCH_3$, ^1J = 148), 44,6 (dd, C_4, ^1J = 137 et J = 3).

À l'exception de **8***d* qui cristallise et peut être purifiée, la photolyse est effectuée avec les produits bruts de cycloaddition. Composé **8***d*, F = 95°C (éther); ir (Nujol): 1720 et 1760 (C=O). *Anal.* calc. pour $C_{13}H_{20}N_2O_6$: C 52,00, H 6,67, N 9,33, trouvé: C 51,8, H 6,9, N 9,6.

Le composé **7***'a* est préparé par condensation du benzaldéhyde deutérié (16) avec le malonate de méthyle; **7***b* est préparé selon la référence 11 ou 17.

Cyclopropanes 9

On photolyse pendant 18 h une solution de 10^{-2} mol de pyrazoline dans 200 cm^3 de benzène ou toluène anhydre. Le solvant est ensuite distillé sous pression réduite.

(a) Composé **9***a* 66°C (éther); ir (Nujol): 1736 et 1723 (C=O). *Anal.* calc. pour $C_{16}H_{20}O_6$: C 62,34, H 6,49; trouvé: C 62,2, H 6,6.

(b) Le composé **9***b* est distillé au four tubulaire: 105°C (0,01 Torr); ir (film liquide): 1732 (large) (C=O). *Anal.* calc. pour $C_{12}H_{18}O_8$: C 49,65, H 6,21; trouvé: C 49,8, H 6,1.

(c) Le cyclopropane **9***c* et l'oléfine **11***c* sont séparés par chromatographie sur couche mince (SiO_2, éluant éther – éther de pétrole 2:3, 2 élutions). Les R_f sont respectivement de 0,65 et 0,60. Ces deux composés sont purifiés par distillation au four tubulaire. Composé **9***c* 100°C (0,05 Torr); ir (film liquide): 1728 (large) C=O. *Anal.* calc. pour $C_{12}H_{20}O_6$: C 55,38, H 7,69; trouvé: C 55,5, H 7,7. Composé **11***c* 95°C (0,003 Torr); ir (film liquide): 1724 (C=O) et 1640 (C=C); rmn ($CDCl_3$) δ: 6,87 (d, *H*C=, J = 10,8), 4,23 (d, $(CH_3O)_2CH$,

Can. J. Chem. Downloaded from www.nrcresearchpress.com by 210.87.254.105 on 09/06/12
For personal use only.

Can. J. Chem. Downloaded from www.nrcresearchpress.com by 210.87.254.105 on 09/06/12
For personal use only.

J = 5,6), 3,80 (3H), 3,76 (3H), 3,32 (6H) (OCH_3), 2,79 (m, $HC—C_2H_5$), 1,49 (m, $CH_2—CH_3$), 0,84 (t, $CH_2—CH_3$). *Anal.* calc. pour $C_{12}H_{20}O_6$: C 55,38, H 7,69; trouvé: C 55,3, H 7,7.

(d) Le cyclopropane **9***d* et l'oléfine **11***d* sont également séparés par chromatographie sur couche mince (SiO_2, éluant éther − éther de pétrole 1:1, 2 élutions). R_f = 0,3 pour **9***d* et 0,25 pour **11***d*. Ces deux composés sont purifiés par distillation au four tubulaire. Composé **9***d* 125°C (0,05 Torr); ir (film liquide): 1768 et 1728 (C=O). *Anal.* calc. pour $C_{13}H_{20}O_6$: C 57,35, H 7,35; trouvé: C 57,1, H 7,4. Composé **11***d* (également obtenu quantitativement par thermolyse de **8***d*, deux heures dans le toluène à reflux); 130°C (0,004 Torr); ir (film liquide): 1766 et 1714 (C=O); rmn ($CDCl_3$) δ: 4,69 (t, $(CH_3O)_2CH$, J = 5,6), 4,34 (q, OCH_2CH_3), 3,37 (s, 6H (OCH_3)$_2$), 2,92 (d, $—CH_2—C=$), 1,50 (s, 6H, $(CH_3)_2C$), 1,36 (t, $OCH_2—CH_3$). *Anal.* calc. pour $C_{13}H_{20}O_6$: C 57,35, H 7,35; trouvé: C 57,1, H 7,2.

Cyclopropanes ***10***

À 10^{-2} mol du cyclopropane acétal brut, on ajoute le même poids d'acide formique pur. On abandonne une nuit à température ambiante. Après distillation sous vide (15 Torr) de HCO_2H et HCO_2CH_3, les formylcyclopropanes sont purifiés par distillation au four tubulaire. Les rendements indiqués correspondent aux cyclopropanes distillés; ils sont calculés par rapport aux oléfines de départ **7**. Composé **10***a* 145°C (0,05 Torr). Rendement 94%; ir (film liquide): 1732 et 1712 (C=O). *Anal.* calc. pour $C_{14}H_{14}O_5$: C 64,12, H 5,34; trouvé: C 64,4, H 5,4. Composé **10***b* 145°C (0,05 Torr). Rendement 93%; ir (film liquide): 1736 (large) (C=O). *Anal.* calc. pour $C_{10}H_{12}O_7$: C 49,18, H 4,92; trouvé: C 48,9, H 5,0. Composé **10***c* 90°C (0,05 Torr). Rendement 80%; ir (film liquide): 1728 et 1708 (C=O). *Anal.* calc. pour $C_{10}H_{14}O_5$: C 56,07, H 6,54; trouvé: C 55,9, H 6,7. Composé **10***d* 130°C (0,05 Torr). Rendement 65%; ir (film liquide): 1772, 1720 et 1712 (C=O). *Anal.* calc. pour $C_{11}H_{14}O_5$: C 58,41, H 6,19; trouvé: C 58,2, H 6,1.

Vinylcyclopropanes ***15***

À 10^{-2} mol des cyclopropanes **10***a* ou **10***b* dissous dans 15 cm^3 de benzène anhydre sous azote, on ajoute un équivalent de carbométhoxyméthylène triphénylphosphoranne. Après 4 heures à température ambiante, le solvant est distillé sous vide. La majeure partie de l'oxyde de phosphine est d'abord précipité par addition d'éther au réfrigérateur. Le reste est éliminé par chromatographie sur une courte colonne de gel de silice (éluant: éther − éther de pétrole 1:1). Composé **15***a*, F = 72−73°C (méthanol). Rendement 68%; ir (Nujol): 1725 (C=O), 1644 (C=C); rmn ($CDCl_3$) δ: 7,30 (5H, arom), 6,80 (H_β, dd, $J_{\beta\alpha}$ = 16,0, $J_{\beta 3}$ = 8,2), 6,25 (d, H_α), 3,86 (3H), 3,78 (3H), 3,49 (3H) (OCH_3), 3,60 à 3,40 (m, H_2, H_3). *Anal.* calc. pour $C_{17}H_{18}O_6$: C 64,15, H 5,66; trouvé: C 64,2, H 5,7. Le composé **15***b* est purifié par distillation au four tubulaire 155°C (0,01 Torr). Rendement 80%. ir (film liquide): 1730 (C=O) et 1650 (C=C); rmn ($CDCl_3$) δ: 6,60 (H_β, dd, $J_{\beta\alpha}$ = 15,0, $J_{\beta 3}$ = 8,0), 6,10 (H_α, d), 3,75 (s, 3H), 3,73 (s, 3H), 3,70 (s, 6H) (OCH_3), 3,03 (H_3, dd, J_{23} = 6,8), 2,98 (H_2, d). *Anal.* calc. pour $C_{13}H_{16}O_8$: C 52,00, H 5,33; trouvé: C 52,2, H 5,6.

Oléfine 17

Dans un tricol de 100 cm^3 on introduit sous azote 4,4 g (3×10^{-2} mol) de mésoxalate de méthyle (18) dissous dans 60 cm^3 de benzène anhydre. A cette solution, refroidie dans un bain d'eau glacée, on ajoute par petites fractions sous agitation magnétique et sous courant d'azote un équivalent (9,1 g) de formylméthylènetriphénylphosphoranne (19). La réaction est instantanée. Après distillation sous vide du benzène, l'oxyde de triphénylphosphine est précipité par addition d'éther à 0°C. Il est séparé par filtration et l'éther est distillé; l'huile obtenue est ensuite fractionnée sous vide. On obtient 3,63 g de **17**, $Eb_{0,0005}$ = 60−65°C. Rendement 70%. Ce composé fragile doit être utilisé rapidement. Ses caractéristiques sont les suivantes: ir (film liquide): 1686 et 1726 (C=O), 1622 (C=C); rmn ($CDCl_3$) δ: 9,96 (d, J = 6,7, CHO), 6,86 (d, $HC=$), 3,92 et 3,86 (s, OCH_3).

Oléfine 3

À 1,70 g (10^{-2} mol) de l'oléfine **17** dissoute dans 20 cm^3 de benzène anhydre et refroidie dans un bain d'eau froide on ajoute quelques cristaux d'acide paratoluène sulfonique (~100 mg) puis un léger excès (1,2 g) d'orthoformiate de méthyle. Il y a décoloration quasi immédiate de la solution; on ajoute quelques grains de tamis moléculaire 3 Å. Un contrôle à l'aide de la rmn montre que la réaction est terminée. Après une filtration rapide sur une courte colonne de silice, le solvant est distillé. L'oléfine est purifiée par distillation au four tubulaire, 100°C (0,05 Torr); 1,83 g, rendement 84%, ir (film liquide): 1726 (C=O) et 1648 (C=C); rmn ($CDCl_3$) δ: 6,82 (d, J = 4,8, $=CH$), 5,15 (d, $CH(OCH_3)_2$), 3,84 (s, 3H) et 3,81 (s, 3H) (CO_2CH_3), 3,35 (s, 6H, $CH(OCH_3)_2$). *Anal.* calc. pour $C_9H_{14}O_6$: C 49,54, H 6,42; trouvé: C 49,5, H 6,5.

Le composé **3** peut être préparée sans isoler l'oléfine intermédiaire **17**: le produit brut de la réaction conduite à partir de 2,2 g de mésoxalate de méthyle et de 4,58 g de phosphoranne est traité par un excès (2,0 équivalents) d'orthoformiate de méthyle avec 350 mg d'acide paratoluène sulfonique et du tamis moléculaire 3 Å. Le mélange réactionnel est porté 1 heure à 45°C. Après distillation du benzène, l'oxyde de phosphine est précipité avec de l'éther. Après filtration sur une courte colonne de silice (éluant éther − éther de pétrole 2:3) l'oléfine **3** est purifiée par distillation. On obtient 2,63 g de produit (rendement 80% par rapport au mésoxalate de méthyle).

Cyclopropanes ***18*** *et* ***19***

À une solution de 2,18 g (10^{-2} mol) de **3** dans 20 cm^3 de THF anhydre on ajoute goutte à goutte et sous agitation magnétique un équivalent d'isopropylidènephosphoranne (14) dissous dans 50 cm^3 de THF. La réaction est effectuée sous atmosphère d'azote à température ambiante. L'addition terminée l'agitation est maintenue pendant une heure. Après distillation du THF sous pression réduite, le produit brut cristallisé est repris avec 60 cm^3 de chloroforme et porté à reflux pendant une heure. Après distillation sous vide du solvant, le résidu est chromatographié sur gel de silice: l'élution avec un mélange CH_2Cl_2 − éther de pétrole 3:1 donne la triphénylphosphine. On élue ensuite avec un mélange éther − éther de pétrole 1:1, ce qui permet d'isoler **18**. Ce cyclopropane est purifié par distillation au four tubulaire 100°C (0,02 Torr); 2,10 g, rendement 81%; ir (film liquide): 1724 (C=O). *Anal.* calc. pour $C_{12}H_{20}O_6$: C 55,38, H 7,69; trouvé: 55,4, H 7,7.

Ce cyclopropane, traité avec un large excès (10 equiv.) d'acide formique pur pendant 3 heures à la température ambiante conduit au cyclopropane **19** purifié par distillation au four tubulaire 105°C (0,02 Torr); 1,61 g (rendement 75% par rapport à **3**); ir (film liquide): 1728 et 1702 (C=O). *Anal.* calc. pour $C_{10}H_{14}O_5$: C 56,07, H 6,54; trouvé: C 56,3, H 6,5.

Cyclopropanes ***21*** *et* ***22***

À 2,18 g (10^{-2} mol) d'alcène **3** dissous dans 3 cm^3 d'éther anhydre, on ajoute un équivalent (1,95 g) de diphényldiazométhane. Le mélange réactionnel est abandonné à température ambiante à l'abri de la lumière. Après deux jours on obtient des cristaux de pyrazoline **20**, F = 106−107°C (déc.); ir (Nujol): 1744 et 1722 (C=O), 1590 et 1560 (N=N, C_6H_5); rmn ^{13}C ($CDCl_3$) δ: 166,5 (m, ^3J = 4) et 165,8 (m, ^3J = 4, $—CO_2CH_3$); 141,2 à 127,3 (m, C_6H_5); 106,0 (m, ^3J = 3, $C(CO_2CH_3)_2$), 104,7 (d, ^3J = 4, C $(C_6H_5)_2$), 102,1 (d.m, ^1J = 168, ^3J = 4−5, $CH(OCH_3)_2$), 55,8 (d.q, ^1J = 143, ^3J = 4) et 50,9 (d.q., ^1J = 143, ^3J = 6, $CH—OCH_3$), 53,9 (q, ^1J = 148) et 53,4 (q, ^1J = 148, $CO_2—CH_3$), 47,9 (d, ^1J = 136, $HC—CH(OCH_3)_2$).

La photolyse de cette pyrazoline pendant 16 h conduit quantitativement au cyclopropane **21**, F = 128−129°C (éther); ir (Nujol): 1754 et 1722 (C=O). *Anal.* calc. pour $C_{22}H_{24}O_6$: C 68,75, H 6,25; trouvé: C 68,5, H 6,3.

Abandonné durant quatre semaines à la température ambiante, **20** conduit également quantitativement à **21**.

Ce cyclopropane (1,9 g) traité par 2,3 g (10 équiv.) d'acide formique pur sans solvant à température ambiante (5 h) conduit quasi quantitativement à **22** purifié par distillation au four tubulaire 185°C (5×10^{-4} Torr); ir (film liquide): 1728, 1712, 1696 (C=O). *Anal.* calc. pour $C_{20}H_{18}O_5$: C 71,01; H 5,33; trouvé: C 71,3, H 5,5.

Dans les conditions décrites ci-dessus: cycloaddition, évolution

thermique de la pyrazoline puis traitement à l'acide formique du produit brut de réaction, on obtient après distillation l'aldéhyde **22** avec un rendement de 90% par rapport à l'oléfine **3**.

Cyclopropanes 24, 25 et 26

A 2,18 g (10^{-2} mol) de **3** dissous dans 15 cm^3 d'éther anhydre à 0°C, on ajoute un léger excès (1,2 g) de diazoacétal **2**. La réaction est pratiquement immédiate. Après distillation du solvant, on obtient la pyrazoline **23** sous forme d'une huile. Celle-ci est photolysée pendant 20 h. Après distillation du toluène, le cyclopropane **24** est purifié par distillation au four tubulaire 140°C (0,05 Torr); 2,88 g (rendement 94% par rapport à **3**); ir (film liquide): 1724 (C=O). *Anal.* calc. pour $C_{13}H_{22}O_8$: C 50,98, H 7,19; trouvé: C 51,2, H 7,3.

On traite 1,5 g de **24** par 10 équivalents d'acide formique pur (2,3 g) sans solvant pendant une nuit à température ambiante. Après distillation de l'acide formique et du formiate de méthyle, **25** est purifié par distillation au four tubulaire: 120°C (0,05 Torr); 1,0 g, rendement 96% par rapport à **24**; ir (film liquide): 1728, 1708 (C=O). *Anal.* calc. pour $C_9H_{10}O_6$: C 50,47, H 4,67; trouvé: C 50,7, H 4,8.

Le traitement de **24** par l'acide trifluoroacétique (4 équiv.) dans le chloroforme (20 h, temp. amb.) conduit au mélange 30:70 (intégration rmn) de **25** et **26**. Ce dernier composé a été caractérisé uniquement à l'aide de la rmn. Les différents essais de séparation de **25** et **26** par chromatographie sur couche mince ont échoué.

1. H. ABDALLAH et R. GRÉE. Tetrahedron Lett. **21**, 2239 (1980).
2. S. DANISHEFSKY. Acc. Chem. Res. **12**, 66 (1979).
3. G. BONAVENT, M. CAUSSE, M. GUITARD et R. FRAISSE-JULLIEN. Bull. Soc. Chim. Fr. 2462 (1964).
4. J. M. MCINTOSH et H. KHALIL. Can. J. Chem. **56**, 2134 (1978).
5. N. I. SHTEMENKO, V. F. KUCHEROV et L. A. YANOVSKAYA. Izv. Akad. Nauk SSSR, Ser. Khim. 1444 (1978).
6. W. KIRMSE et M. BUSCHHOFF. Chem. Ber. **100**, 1491 (1967).
7. A. GORGUES. Bull. Soc. Chim. Fr. 529 (1974).
8. R. DANION-BOUGOT et R. CARRIÉ. Org. Magn. Reson. **5**, 453 (1973).
9. N. KAWABATA et M. TANIMOTO. Tetrahedron, **36**, 3517 (1980).
10. A. MONPERT, J. MARTELLI, R. GRÉE et R. CARRIÉ. Tetrahedron Lett. **22**, 1961 (1981).
11. M.S. OUALI, M. VAULTIER et R. CARRIÉ. Synthesis, 626 (1977).
12. H. ABDALLAH, R. GRÉE et R. CARRIÉ. Tetrahedron Lett. **23**, 503 (1982).
13. A. KRIEF. Tetrahedron, **36**, 2538 (1980).
14. P.A. GRIECO et R. S. FINKELHOR. Tetrahedron Lett. 3781 (1972).
15. R. DUSCHINSKY et L. A. DOLAN. J. Am. Chem. Soc. **68**, 2350 (1946).
16. A. W. BRUGSTAHLER, D. E. WALKER JR., J. P. KUEBRICH et R. L. SHOWEN. J. Org. Chem. **37**, 1272 (1972).
17. H. K. HALL JR. et P. YKMAN. J. Am. Chem. Soc. **97**, 800 (1975).
18. E. GILMAN et T. B. JOHNSON. J. Am. Chem. Soc. **50**, 3344 (1928).
19. S. TRIPPETT et D. M. WALKER. J. Chem. Soc. 1266 (1961).

Can. J. Chem. Downloaded from www.nrcresearchpress.com by 210.87.254.105 on 09/06/12
For personal use only.

The probable planarity of 1,2-dimethoxybenzene in solution

TED SCHAEFER AND REINO LAATIKAINEN[1]
Department of Chemistry, University of Manitoba, Winnipeg, Man., Canada R3T 2N2

Received June 7, 1982

TED SCHAEFER and REINO LAATIKAINEN. Can. J. Chem. **61**, 224 (1983).

A precise analysis of the ^{1}H nmr spectrum of 1,2-dimethoxybenzene in benzene solution yields an accurate value for the proximate spin–spin coupling constant, $^5J_o^{H,CH_3}$, between the *ortho* ring proton and the methyl protons. The latter also couple to other ring protons and these couplings are assessed. Comparison with some values in other anisole derivatives and with a variety of INDO MO FPT calculations of $^5J_o^{H,CH_3}$ strongly implies the predominance of a planar conformation in solution. This implication disagrees with the interpretation of some other experimental and theoretical data. The mechanism of this proximate coupling is examined by the procedure of Barfield. It seems that the magnitude of the coupling is dominated by interactions involving the orbitals on the carbon atom of the methyl group.

TED SCHAEFER et REINO LAATIKAINEN. Can. J. Chem. **61**, 224 (1983).

Une analyse précise du spectre de rmn du diméthoxy-1,2 benzène en solution dans le benzène donne une valeur exacte de la constante de couplage de spin voisin $^5J_o^{H,CH_3}$ entre le proton en position *ortho* du cycle et les protons du méthyle. Ces derniers se couplent également avec les autres protons du cycle et on a évalué ces couplages. La comparaison avec certaines valeurs obtenues pour d'autres dérivés de l'anisole et avec différents calculs du type INDO, OM, FPT de $^5J_o^{H,CH_3}$ laisse supposer la prédominance d'un conformation plane en solution. Cette supposition ne s'accorde pas avec l'interprétation de certaines autres données expérimentales et théoriques. On examine le mécanisme de ce couplage voisin selon le procédé de Barfield. Il semble que l'ordre de grandeur de ce couplage est influencé par les interactions qui font intervenir les orbitales de l'atome de carbone du groupe méthyle.

[Traduit par le journal]

Introduction

The conformational preferences of the methoxy groups in 1,2-dimethoxybenzene (*o*-DMB) and its derivatives have been discussed in detail (1, 2), perhaps because the psychotomimetic activity of some of these compounds is related to the orientations of the methoxy groups relative to the benzene plane. Aromatic 1,2-dimethoxy substituents are fairly common in natural products, for example, in isoquinoline alkaloids (2*b*).

In the solid state, *o*-DMB prefers a planar orientation of the heavy atoms, possibly due to crystal packing forces. In the vapor phase, the photoelectron spectrum can be interpreted as arising from a conformation in which one methoxy group is planar and the other is perpendicular with respect to the benzene plane. Partial geometry optimization procedures in MO

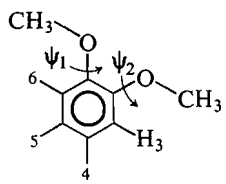

1

STO 3G calculations (1) for **1** find that the conformations defined by $\psi_1 = \psi_2 = 0°$ and by $\psi_1 = 0°$, $\psi_2 = 90°$ differ by only 0.1 kJ/mol in energy. In that situations, entropy terms will favor the nonplanar forms in the conformational equilibrium. The STO 3G results also imply unfavorable electronic, rather than steric, interactions in the planar form, as the reason for the nonplanar preferences.

In solution the observed dipole moment, partition coefficients, and dielectric relaxation times apparently require nonplanar forms of *o*-DMB. It has been suggested (1) that ^{1}H (3) and ^{13}C (4) nmr chemical shifts may have similar implications, but it seems that the ^{13}C shifts are also consistent with a planar conformation of the methoxy group if it has only one *ortho* substituent. Spin-lattice relaxation times of the carbon nuclei in the methoxy groups of some *o*-DMB derivatives (2) provide evidence for planar conformations of two *ortho* methoxy substituents.

One observable, whose potential as a conformational indicator has not been fully exploited, is $^5J_o^{H,CH_3}$ in **1**. Early measurements (5) of this long-range spin–spin coupling constant between the methoxy protons and the *ortho* ring protons yielded a magnitude of 0.30 ± 0.03 Hz for 2-X-anisoles (X = Cl, Br, I, NO_2). For X = OH or OCH_3 the coupling was not resolved, suggesting a small magnitude and perhaps a rotational averaging process (5). The determination of $^5J_o^{H,CH_3}$, as −0.33 (2) Hz in 2,4-dibromoanisole (6) stimulated the suggestion of a proximate or through-space mechanism for this coupling, arising from overlap of orbitals centered on the proximate nuclei and on the carbon atoms to which the protons are bonded. INDO-MO-FPT calculations on anisole (7) reproduced the sign of $^5J_o^{H,CH_3}$, and emphasized its sensitivity to internuclear distances. Furthermore, a complete analysis of the ^{1}H spectrum of 2-hydroxyanisole in benzene solution (8) gave $^5J_o^{H,CH_3}$, as (−)0.29 Hz.[2] The observed $^5J_m^{H,OH}$ indicated that the intramolecularly hydrogen bonded form existed to the extent of at least 95% in CCl_4 or C_6D_6 solution at 305 K, implying that the methyl group lies *trans* to the hydroxyl group.

Recent INDO MO FPT calculations of $^5J_o^{H,CH_3}$ confirm the through-space mechanism and the sensitivity to interproton

[1]Research associate from the Department of Chemistry, University of Jryväskylä, SF-40100, Jyväskylä 10, Finland.

[2]In CCl_4 solution the chemical shift between H-3 and H-4 is only 0.02 ppm (8). This tight coupling probably accounts for the observations at 60 MHz (5).

0008-4042/83/020224-06$01.00/0
©1983 National Research Council of Canada/Conseil national de recherches du Canada

Can. J. Chem. Downloaded from www.nrcresearchpress.com by 210.87.254.42 on 09/06/12
For personal use only.

Can. J. Chem. Downloaded from www.nrcresearchpress.com by 210.87.254.42 on 09/06/12
For personal use only.

distances (9*a*). In this paper, a complete analysis of the ten-spin ^{1}H nmr spectrum of *o*-DMB in benzene solution yields a reliable value of $^5J_o^{H,CH_3}$. Its conformational implications are discussed in connection with further INDO MO FPT computations and with the coupling observed in related compounds.

Experimental

A 10 mol% solution of *o*-dimethoxybenzene (K & K Laboratories) in benzene-d_6 was degassed by the freeze–pump–thaw method and was flame-sealed into a 5 mm od nmr sample tube, which also contained a small amount of tetramethylsilane (TMS). In the same way, 5 mol% solutions in CCl_4 of 3,5-dichloroanisole, 1,2,4-trimethoxybenzene, 1,2-dimethoxy-4-formylbenzene, and 1,2,3-trimethoxybenzene (all from Aldrich) were prepared as samples for nmr measurements. A 10 mol% solution of the formyl compound in benzene-d_6 was also prepared.

The ^{1}H nmr spectra of the latter four samples were calibrated on an HA100 spectrometer at a probe temperature of 305 K in the manner described recently in detail (9*b*). The ^{1}H nmr spectrum of 1,2-dimethoxybenzene was obtained on a WH90 (^{2}H internal lock), again at 305 K and in the manner described before (9*b*) for another molecule (see also the caption to Fig. 1).

Results and discussion

Spectral analyses

In CCl_4 solution, the ring protons of *o*-DMB resonate within 0.02 ppm of each other, thereby accounting for the small reported $^5J_o^{H,CH_3}$ (5). In benzene solution the internal shift increases to about 0.1 ppm and a proper 10-spin analysis becomes feasible with the program NUMARIT (10). There is no doubt that the methyl protons are coupled to all the ring protons. Most of these couplings are rather small but they do influence the spectral appearance. The spectrum was analyzed by iteration for all coupling larger than 0.1 Hz in magnitude, followed by visual optimization of the smaller couplings. When these smaller couplings were varied, the other couplings were always optimized. The number of calculated transitions with observable intensity was ca. 850 in the ring region and ca. 550 in the methyl proton region, while the number of non-degenerate transitions (separated by more than 0.002 Hz) was 250 and 46, respectively. The number of observed peaks or shoulders was only 55 and 3 in the two regions. These complications necessitated the procedure above. The very small couplings were varied in a systematic way in a series of some 90 trials. With hindsight it was clear that a seven-spin analysis (four ring protons and three sidechain protons), based on the six-line multiplet at high field and a few singlets at lower field, would yield the correct magnitude of $^5J_o^{H,CH_3}$. However, this analysis could not reproduce the detailed appearance of the whole spectrum.

The final parameters are given in Table 1. In Figs. 1 and 2 some calculated and observed spectra are displayed.

The 5 mol% solution of 3,5-dichloroanisole in CCl_4 had $^5J_o^{H,CH_3}$ as (−)0.158(7) Hz by a MAOCOON analysis (11). The actual observed splittings were 0.144 Hz, but a correction[3] for incomplete resolution was applied.

The 5 mol% solution of 1,2,4-trimethoxybenzene gave $^5J_o^{H,CH_3(1)}$, $^5J_o^{H,CH_3(2)}$, $^5J_o^{H,CH_3(4)}$, and $^5J_o^{H,CH_3(4)}$ as −0.232(5), −0.281(5), −0.120(20), and as −0.170(20) Hz, respectively.

TABLE 1. The ^{1}H nmr spectral parameters for 1,2-dimethoxybenzene, *o*-DMB, as a 10 mol% solution in benzene-d_6 and 305 K

Parameter	Value	Parameter	Value
ν_{CH_3}[a]	3.454(1)	$^5J_o^{H,CH_3}$	−0.280(10)
ν_3	6.6691(1)	$^6J_m^{H_4,OCH_3}$	0.060(10)[b]
ν_4	6.8305(1)	$^6J_m^{H_6,OCH_3}$	−0.010(10)[b]
$^3J_{34}$	8.005(4)	$^7J_p^{H,OCH_3}$	−0.009(10)[b]
$^3J_{45}$	7.547(4)	$^7J_p^{CH_3,CH_3}$	0.000(10)[c]
$^4J_{35}$	1.520(4)		
$^5J_{36}$	0.235(6)	Root mean square error	0.018

[a]In ppm from internal tetramethylsilane at 90.020 MHz, centerband.
[b]A fit to the spectrum demands nonzero magnitudes, i.e., these couplings *cannot* be set to zero.
[c]The spectrum was relatively insensitive to this parameter but appeared to be most compatible with a zero coupling.

Again, a 10 mol% solution of 1,2-dimethoxy-4-formylbenzene in benzene-d_6 had $^5J_o^{H,CH_3(1)}$ as −0.292(15) Hz and $^5J_o^{H,CH_3(2)}$ as −0.308(5) Hz, somewhat larger in magnitude than those recently reported (9).

For 1,2,3-trimethoxybenzene in CCl_4, $^5J_o^{H,CH_3}$ was −0.250(20) Hz and $^6J_m^{H_5,OCH_3}$ was 0.075(10) Hz. The peak arising from the methoxy protons at position 2 was sharp. Irradiation of this peak did not lead to a noticeable decrease in linewidth of the peaks from the ring protons.

The dihedral angle dependence of $^5J_o^{H,CH_3}$

Previous INDO MO FPT calculations (7, 9) encourage the belief that $^5J_o^{H,CH_3}$ is a proximate coupling whose magnitude has a strong dependence on the distance between the methyl and the *ortho* ring protons. The present detailed computations are based on the following geometry.

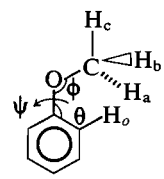

$\phi = 112° + 3.0°|\cos\psi|$
$\theta = 125° + 5.0°\cos\psi$
$r(O—CH_3) = 142.5$ pm
$r(O\text{-}C_1) = 136.0$ pm

2

The benzene fragment had a standard geometry (12), while the other bond lengths and bond angles were assigned on the basis of X-ray data[4] and of extensive MO STO 3G calculations (1, 13, and footnote 5). The torsion angle ψ is zero for the indicated "planar" conformation, **2**. The ψ dependence of the bond angles θ and ϕ is theoretical and the C—O bond lengths were kept constant. Because $^5J_o^{H,CH_3}$ is appreciable only for small values of ψ, the constancy of the C—O bond lengths is not a critical assumption.

The chosen geometry yields the following couplings in Hz for ψ = 0°, 90°, and 180°:

	ψ=0°	ψ=90°	ψ=180°
$^5J(H,OCH_a)$	−0.338	0.023	−0.010
$^5J(H,OCH_b)$	−0.338	0.087	−0.010
$^5J(H,OCH_c)$	−0.199	−0.002	0.132

[3]Tables of correction factors for overlapping lorentzians are available from R.L.

[4]Reference 1 gives an extensive survey of crystal structure data.
[5]T. A. Wildman, private communication.

Can. J. Chem. Downloaded from www.nrcresearchpress.com by 210.87.254.42 on 09/06/12
For personal use only.

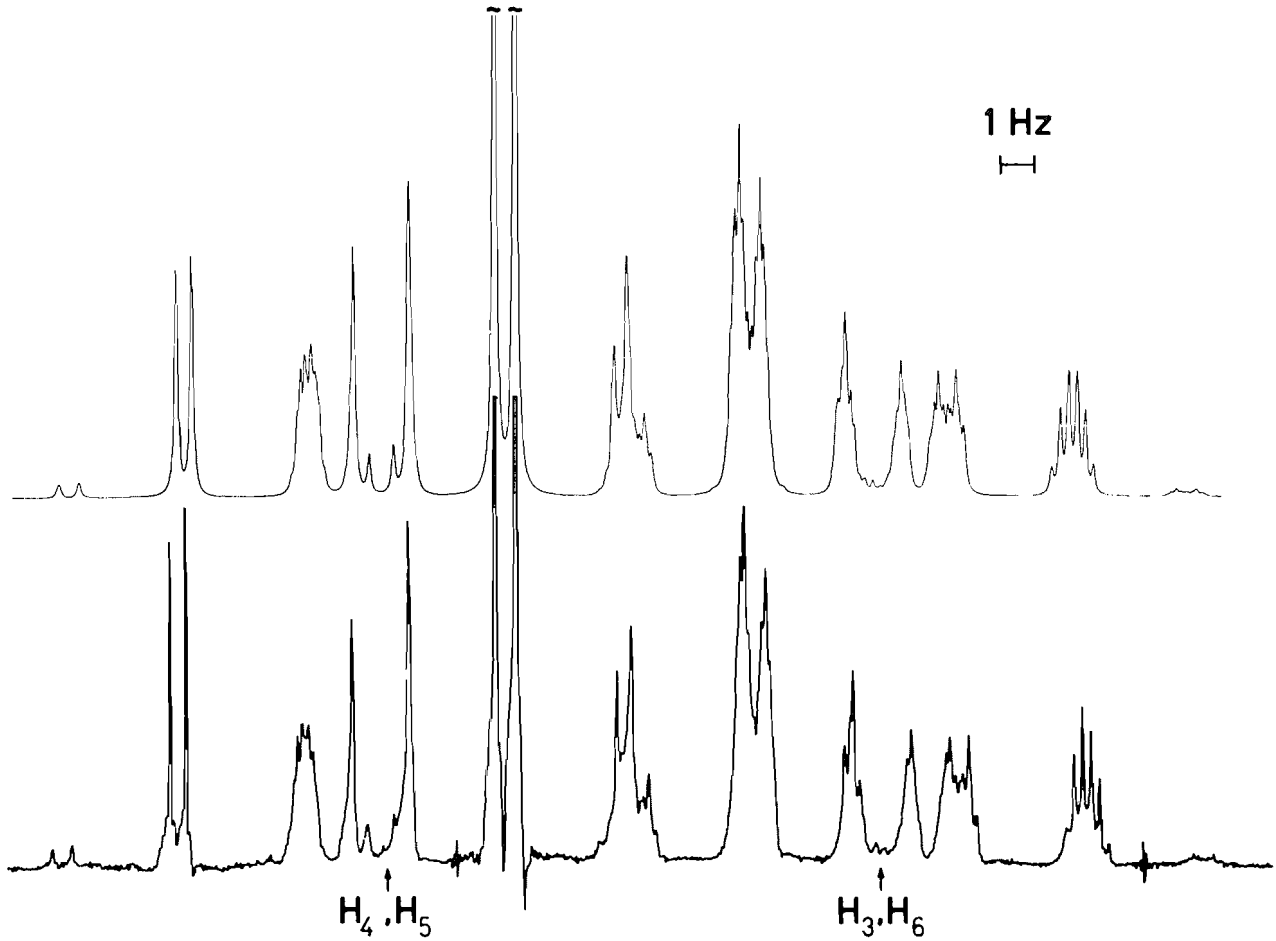

FIG. 1. The calculated and observed ring ^{1}H nmr spectra at 90 MHz of a 10 mol% solution of 1,2-dimethoxybenzene in benzene-d_6 at 305 K. The calculated spectrum assumes the parameters in Table 1 and a linewidth at half-heights of 0.10 Hz. The experimental spectrum contains some distortions near the baseline in some regions, particularly near the arrow indicating the chemical shifts of H-4 and H-5. It was accumulated with twelve free induction decays with an acquisition time of 35 s and 45° pulses.

For the planar form, **2**, the average value is −0.292 Hz. In these calculations the methyl group was not rotated about the O—CH_3 bond.

More detailed sets of computations were also undertaken, involving many more choices of the torsion angle ψ. In one set the CH_3 group was not rotated about the O—C(H_3) bond. In a second set the H_a—H_o and H_b—H_o distances were kept constant by allowing a torsion about this bond. This correlated torsion reduced the total energy relative to the first set up to ψ = 45°, after which the noncorrelated motion appeared to be favored.

The calculations of the first set were repeated in a manner first described by Barfield (14). In order to assess the importance of "coupling paths", off-diagonal elements of Fock matrices associated with orbitals centered on certain *nonbonded* atoms were set equal to zero. This procedure prevented the transmission of spin–spin coupling via overlap of those orbitals. In particular, in one calculational sequence all matrix elements involving *s* orbitals of H_o and CH_3 moiety were forced to vanish, yielding a rough estimate of the coupling transmitted via the intervening five-bond path. In another sequence, this was done for *all* orbitals centered on the coupled protons. In the last sequence, the elements involving the *s* orbitals of H_o and of the *carbon* atom of the methyl group were set equal to zero. The results of the calculations are summarized in Table 2 and Fig. 3.

Conformational deductions from $^5J_o^{H,CH_3}$

The striking aspect of the standard INDO calculations of $^5J_o^{H,CH_3}$ in Table 2 is the strong dependence of its magnitude on the torsional angle, ψ, for both the correlated and uncorrelated torsional motions. On the basis of these numbers and the relative energies of the partially optimized STO 3G conformations in ref. 1 the average $^5J_o^{H,CH_3}$ in *o*-DMB can be calculated as in Table 3. The average is -0.14_6 Hz. The planar conformation is only 10% abundant according to the STO 3G energies for the isolated molecule. In other words, the observed and calculated $^5J_o^{H,CH_3}$ values for *o*-DMB suggest negligible populations of nonplanar conformations in solution. Of course, the molecule is not rigid and some torsional motions occur (15). These can be as large as 20° in ψ without altering substantially the predicted $^5J_o^{H,CH_3}$.

If the planar form of anisole is predominant in solution, then the numbers in Table 2 suggest $^5J_o^{H,CH_3}$ in anisole as (−0.292 + 0.037)/2 or −0.13 Hz, i.e., the mean of the values for ψ = 0° and 180°. In 3,5-dichloroanisole $^5J_o^{H,CH_3}$ is (−)0.16(1) Hz, providing support for the quantitative reliability of the computed numbers and consistent with a substantial barrier to internal rotation, so that the methyl carbon atom does not sample substantially the out-of-plane conformations at 305 K. Judging from calculations for 3-fluorophenol (16), the internal barrier in 3,5-dichloranisole is larger than in anisole.

Can. J. Chem. Downloaded from www.nrcresearchpress.com by 210.87.254.42 on 09/06/12
For personal use only.

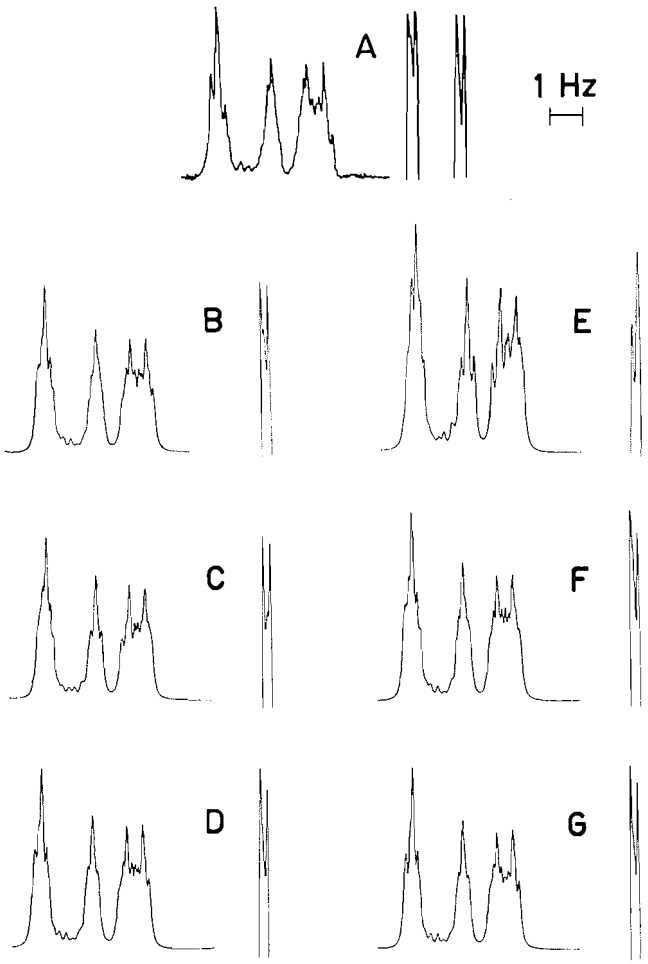

FIG. 2. In A the observed ring proton region near the chemical shifts of H-3 and H-6 (Fig. 1) and the methoxy ^{1}H nmr are displayed. The two methoxy signals are obtained by the use of different window compositions and are, of course, obtained from the same free induction decay. In B the calculated spectrum arises from the preferred spectral parameters of Table 1. In C all the long-range couplings, except for $^5J_o^{H,CH_3}$, are set equal to zero. In D all couplings less than 0.1 Hz in magnitude are zero, except for $^6J_m^{H_4,OCH_3} = {}^6J_m^{H_5,OCH_3} = +0.060$ Hz. In E the parameters in Table 1 are used except that $^6J_m^{H_4,OCH_3} = {}^6J_m^{H_5,OCH_3} = -0.060$ Hz. In F the signs of $^6J_m^{H_6,OCH_3}$ and $^6J_m^{H_3,OCH_3}$ have been changed to give +0.01 Hz. In G the values of $^7J_p^{H,OCH_3}$ have been changed to +0.01 Hz. The spectrum is *relatively* insensitive to $^7J^{CH_3,CH_3}$ but appears to be most compatible with a zero magnitude.

Because the formyl substituent has a π-electron-acceptor ability comparable to that of the nitro group (17), one might expect somewhat increased magnitudes for $^5J_o^{H,CH_3}$ in the 4-formyl derivative of *o*-DMB (smaller out-of-plane torsions). In CCl_4 solution, both $^5J_o^{H,CH_3}$ magnitudes do appear to be *somewhat* larger than in *o*-DMB. In the corresponding 4-methoxy derivative, the concomitant decrease in conjugation of the 1-methoxy group could be adduced as the reason for its $^5J_o^{H,CH_3}$ of −0.23 Hz; indeed smaller in magnitude than in *o*-DMB, whereas $^5J_o^{H,CH_3}$ for the 2-methoxy group is −0.28 Hz, the same as in *o*-DMB. The sum of the two unequal $^5J_o^{H,CH_3}$ values involving the 4-methoxy substituent is −0.29(4) Hz. The individual values are somewhat uncertain, yet their difference is large enough to suggest that the 4-methoxy group prefers the orientation remote from the 2-methoxy substituent to some extent.

$^5J_o^{H,CH_3}$ is −0.25(2) Hz in 1,2,3-trimethoxybenzene and indicates preferred planar conformations for the 1,3-methoxy substituents, whose preference for planarity, however, may be somewhat smaller than in *o*-DMB. The central methoxy group no doubt takes up a nonplanar conformation (2) and the absence of any observable coupling to the ring protons in the *meta* or *para* positions may prove useful as a conformational hint.

More indirect evidence for the ψ dependence of $^5J_o^{H,CH_3}$ comes from its sign and magnitude in 2,5-dichlorothioanisole (18) and 2-hydroxythioanisole (19). In the former, $^5J_o^{H,CH_3}$ is −0.35(1) Hz and is very likely a proximate coupling (19). In the latter, a stereospecific OH···S hydrogen bond constrains the methyl group to a plane roughly perpendicular to the benzene ring and $^5J_o^{H,CH_3}$ is ≤ 0.02 Hz in magnitude. These data are consistent with a very small $^5J_o^{H,CH_3}$ when ψ lies near 90°, as given by the INDO calculations on the analogous molecule, anisole.

Coupling mechanisms for $^5J_o^{H,CH_3}$

The rapid decrease in the magnitude of $^5J_o^{H,CH_3}$ as ψ increases, in the standard INDO calculations in Table 2, implies the importance of the proximity of the bonds containing the coupled nuclei. When the Fock matrix elements involving overlap of the *s* orbitals on H_o and on the atoms of the methyl group are set equal to zero, what remains of $^5J_o^{H,CH_3}$ in Table 2 might be termed the through-bond contribution. This contribution is ca. +0.1 Hz for ψ > 45° (see Table 2 and Fig. 3). Again, when only the *s* orbital overlaps between H_o and the hydrogen atoms of the methyl group are eliminated, one has $TS(H,H) = {}^5J^I - {}^5J(H, CH_3)$ as given in Table 2 ($^5J^I$ is the standard INDO value) and plotted in Fig. 3. In other words, the two calculations yield very similar numbers (their difference is near zero), indicating that direct overlap of *s* orbitals on the hydrogen atoms does not give rise to a negative coupling. However, if direct interaction between *s* orbitals on H_o and on the *carbon* atom of the methyl group is prevented, then $TS(H, CH) = {}^5J^I - {}^5J(H, CH_3)$. The substantial negative numbers between ψ = 0° and ψ = 60° imply a negative proximate contribution to $^5J_o^{H,CH_3}$ via the carbon orbitals. As pointed out by Barfield (14), even though certain elements of the Fock matrices are kept zero, interactions with other atoms can still lead to transmission of coupling by a particular atom (alternative coupling pathways). That is, the calculated results need not be precisely additive. Nevertheless, the present calculations may be taken to mean that it is proximate interactions via the methyl carbon atom which determine the sign of $^5J_o^{H,CH_3}$ and that they dominate over positive contributions from proximate interactions between the hydrogen atoms themselves. It may also be noted that choosing certain nonbonded interactions as zero in these calculations will not drastically alter the electronic structure of the molecule.

Calculations of $\partial(^5J)/\partial X$, where *X* is a bond length or bond angle, were done for ψ = 0°, 90°, 180° on **2**. This quantity was negligible for ψ = 90° and 180° for all reasonable changes in *X*. For ψ = 0°, changes of 1 pm in the C_1—O, O—$C(H_3)$, and C—H bond lengths cause ≤0.005 Hz changes in $^5J_o^{H,CH_3}$. A decrease of φ by 1° causes a decrease in $^5J_o^{H,CH_3}$ of 0.018 Hz. If θ decreases by 1°, the coupling decreases by 0.031 Hz, whereas it increases by 0.025 Hz if θ increases by 1°. A torsion of 10° about the O—$C(H_3)$ bond decreases $^5J_o^{H,CH_3}$ by 0.02 Hz. In other words, as expected for a proximate coupling, com-

TABLE 2. INDO MO FPT Calculations of $^5J_o^{H,CH_3}$ in anisole[a]

Dihedral angle, ψ°	INDO MO FPT		INDO MO FPT (B)		
	1[b]	2[c]	via-bond[d]	TS(H,H)[e]	TS(H,CH)[f]
0	−0.292	−0.292	0.124	−0.022	−0.490
7.5	−0.283	−0.283	0.114	−0.008	−0.483
15.0	−0.258	−0.257	0.087	0.013	−0.462
30.0	−0.182	−0.167	0.010	0.067	−0.369
45.0	−0.112	−0.064	−0.035	0.063	−0.228
60.0	−0.051	0.010	−0.021	0.021	−0.100
75.0	0.011	0.044	0.013	0.002	−0.024
90.0	0.036	0.050	0.033	−0.004	0.002
120.0	0.037	0.039	0.034	−0.001	0.003
150.0	0.037	0.038	0.036	−0.001	0.002
180.0	0.037	0.037	0.037	0.000	0.000
ΔE(kJ)[g]	2.7	7.1	−2.1	2.2	−2.2

[a]The anisole geometry is given in **2**, see text.
[b]As the O—C(H_3) bond twists out-of-plane there is no rotation of the methyl group.
[c]As the O—C(H_3) bond twists the methyl group rotates so as to keep two H—H_{ortho} distances equal (correlated rotation).
[d]All Fock matrix elements between H_o and the *s* orbitals of the atoms in the methyl group are set equal to zero, in the manner of Barfield (14).
[e]All direct interactions involving the *s* orbitals of the four hydrogen atoms are made to vanish. The ensuing ^5J values are subtracted from the standard INDO MO FPT numbers in the second column.
[f]As in [c] but for the *s* orbitals on H_o and the carbon atom of the methyl group.
[g]The value of ΔE is $E(\psi = 90°) - E(\psi = 0°)$.

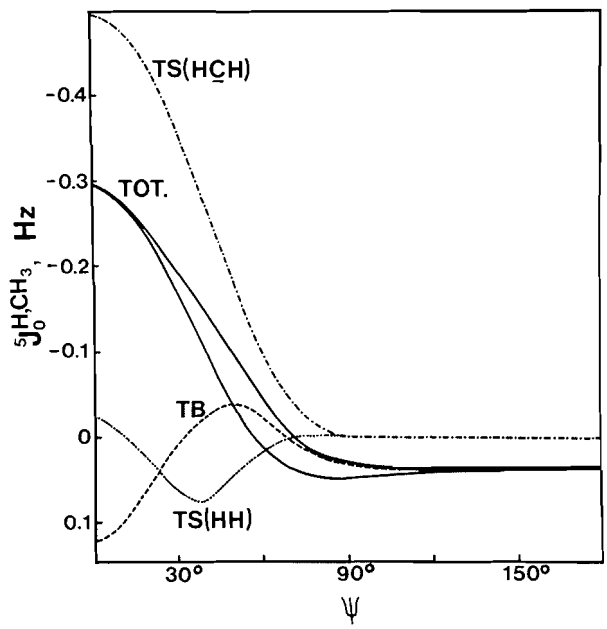

FIG. 3. $^5J_o^{H,CH_3}$ in anisole, as computed by INDO MO FPT, is shown for the standard calculation, column 2 of Table 1, for a calculation in which the methoxy group is rotated about the C_1—O bond by angle ψ (upper solid line). The lower solid line represents the data of column 3 of Table 2 for correlated rotation, in which the distance between the *ortho* hydrogen atom and two methyl hydrogen atoms is kept constant as ψ increases. The curve marked TB (through-bond) is that calculated by the method of Barfield (14) and described in the text. The curve marked TS(HH) (through-space) represents what remains of the solid curves when the coupling, obtained by elimination of interactions between the hydrogen atoms containing the coupled protons, is subtracted. Similarly, the curve marked TS(H*C*H) is obtained by subtraction of the coupling, calculated in the absence of interactions between the *ortho* hydrogen *s* orbital and the methyl carbon *s* orbital, from the solid curve.

TABLE 3. Calculations for $^5J_o^{H,CH_3}$ in *o*-dimethoxybenzene for the partially optimized conformations according to STO 3G computations (1)

Conformer	ψ_1°	ψ_2°	E (kJ/mol)	g_i[b]	P_i[c]	J_i[d,e]
1[a]	0	90	0	4	0.438	−0.128
2	0	0	0.13	1	0.100	−0.292
3	90	90	0.92	2	0.153	0.036
4	0	30	1.92	4	0.206	−0.237
5	0	60	3.68	4	0.103	−0.172

[a]The torsional angles ψ_1 and ψ_2 refer to rotation about the C_1—O and C_1—O bonds; $\psi_1 = \psi_2 = 0$ is the planar conformation, $\psi_1 = \psi_2 = 90°$ has the CH_3 groups on opposite sides of the benzene plane.
[b]Degeneracy of the conformation.
[c]Calculated from $P_i = g_i \exp(-\Delta E/RT) / \sum_i g_i \exp(-\Delta E/RT)$.
[d]According to column 1 of Table 2. The proviso, that conformational interconversion is rapid on this time scale, yields $\langle J \rangle = \sum P_i J_i = -0.14_6$ Hz as the predicted coupling for *o*-DMB.
[e]The calculated dipole moments of the nonplanar conformers 1, 4, and 5 are larger than that of the planar form, 2. Accordingly, dielectric solvent interactions would be expected to increase their relative populations, leading to larger discrepancies between observed and calculated couplings in *d*. The dipole moments of 1 to 5 are 2.06, 0.96, 0.43, 1.29, and 1.75 D in that order (1).

pression of the geometry around the methoxy group and the *ortho* C—H bond in **2** increases the magnitude of $^5J_o^{H,CH_3}$.

Summary and conclusions

The magnitude and sign of $^5J_o^{H,CH_3}$ in 1,2-dimethoxybenzene, when compared with some model compounds, imply a predominantly planar conformation in solution. The strong computed dependence of $^5J_o^{H,CH_3}$ on the torsion angle, ψ, about the C_1—O bond indicates that, if the expectation value, $\langle\psi\rangle$, were much larger than about 20°, then the magnitude of $^5J_o^{H,CH_3}$ would be much smaller than observed, suggesting in turn that the planar conformation is preferred by an energy substantially larger than kT (15).

Can. J. Chem. Downloaded from www.nrcresearchpress.com by 210.87.254.42 on 09/06/12
For personal use only.

Again, if 3,5-dichloroanisole is predominantly planar in solution, then the observed $^5J_o^{H,CH_3}$ is explicable in terms of its calculated ψ dependence. Similar remarks hold for 1,2,4-trimethoxybenzene and for 1,2-dimethoxy-4-formylbenzene.

The available T_1 data are consistent with these conclusions. In our opinion, chemical shift data need not disagree with these conclusions because nonadditivity exists for many *ortho* substituted benzene derivatives, not only for those in which the substituents are free to take on a number of orientations. We cannot judge the cogency of other physical data cited as evidence for nonplanar conformations in solution.

Recently, Caillet (20) has computed crystal lattice energies for some *o*-DMB derivatives and suggests that planar conformations exist due to steric interactions, arising when nonplanar molecules are stacked. Our results are for dilute solutions of *o*-DMB in benzene (the spectrum is very tightly coupled in other solvents). It may be that nonplanar solvent molecules would give a different result, but we doubt that. It may also be relevant that the STO 3G calculations refer to the gas phase, of course, and give a barrier of only 6 to 7 kJ for the rotation about the C—O bond in anisole. In a series of preliminary experiments on anisole in solution we have shown that this barrier can hardly be smaller than about 15 kJ (the measurements involve long-range coupling constants, T_2 and $T_{1\rho}$, and will be reported in due course). Perhaps, then, the planarity of *o*-DMB in solution arises from solvent-induced changes in the C—O barrier.

Acknowledgments

We are grateful to T. A. William for advice on the structure of anisole and to the Natural Sciences and Engineering Research Council of Canada and the Research Council for the Natural Sciences of the Academy of Finland for support.

1. G. M. ANDERSON III, P. A. KOLLMAN, L. N. DOMELSMITH, and K. N. HOUK. J. Am. Chem. Soc. **101**, 2344 (1979), and references therein.
2. (*a*) J. J. KNITTEL and A. MAKRIYANNIS. J. Med. Chem. **24**, 906 (1981), and references therein; (*b*) M. SHAMMA and J. L. MONIOT. Isoquinoline alkaloids research 1972–77. Plenum Press, New York. 1978.
3. J. S. MARTIN and B. P. DAILEY. J. Chem. Phys. **39**, 1722 (1963).
4. K. S. DHAMI and J. B. STOTHERS. Can. J. Chem. **44**, 2855 (1966).
5. R. W. CRECELY, K. W. MCCRACKEN, and J. H. GOLDSTEIN. Tetrahedron, **25**, 877 (1969).
6. H. A. GAUR, J. VRIEND, and W. G. B. HUYSMANS. Tetrahedron Lett. 1999 (1969).
7. T. SCHAEFER, H. D. GESSER, and J. B. ROWBOTHAM. Can. J. Chem. **54**, 2235 (1976).
8. T. SCHAEFER and T. A. WILDMAN. Can. J. Chem. **57**, 450 (1979).
9. (*a*) D. G. DE KOWALEWSKI, R. H. CONTRERAS, A. R. ENGELMANN, J. C. FACELLI, and J. C. DURAN. Org. Magn. Reson. **17**, 199 (1981); (*b*) T. SCHAEFER and R. SEBASTIAN. J. Magn. Reson. **41**, 395 (1980).
10. A. R. QUIRT and J. S. MARTIN. J. Magn. Reson. **5**, 318 (1971); J. S. MARTIN, A. R. QUIRT, and K. F. WORVILL. The nmr program library. Daresbury Laboratory, Daresbury, U.K.
11. R. LAATIKAINEN. J. Magn. Reson. **27**, 169 (1977); Ph.D. Thesis, University of Jyväskylä, Finland, 1979.
12. J. A. POPLE and M. S. GORDON. J. Am. Chem. Soc. **89**, 4253 (1967).
13. H. KONSCHIN, H. TYLLI, and C. GRUNDFELT-FORSIUS. J. Mol. Struct. **77**, 51 (1981).
14. M. BARFIELD. J. Am. Chem. Soc. **102**, 1 (1980).
15. T. A. WILDMAN. Chem. Phys. Lett. **75**, 383 (1980); **80**, 210 (1981).
16. A. PROSS and L. RADOM. Prog. Phys. Org. Chem. **13**, 1 (1981).
17. G. KEMISTER, A. PROSS, L. RADOM, and R. W. TAFT. J. Org. Chem. **45**, 1056 (1980).
18. T. SCHAEFER, R. SEBASTIAN, and S. R. SALMAN. J. Magn. Reson. **46**, 325 (1982).
19. T. SCHAEFER, S. R. SALMAN, T. A. WILDMAN, and P. D. CLARK. Can. J. Chem. **60**, 342 (1982).
20. J. CAILLET. Acta Crystallogr. Sect. B, **38**, 1786 (1982).

Can. J. Chem. Downloaded from www.nrcresearchpress.com by 210.87.254.42 on 09/06/12
For personal use only.

Application of the Hammett equation in the esterification of substituted benzoic acids, catalyzed by $AlPO_4$ in the gas phase

J. V. SINISTERRA[1] AND J. M. MARINAS

Organic Chemistry Department, Faculty of Science, University of Cordoba, Cordoba, Spain

AND

A. LLOBERA

Organic Chemistry Department, Faculty of Science, University of Palma de Mallorca, Balearic Islands, Spain

Received September 21, 1981[2]

J. V. SINISTERRA, J. M. MARINAS, and A. LLOBERA. Can. J. Chem. **61**, 230 (1983).

The Hammett equation has for the first time been applied to the esterification in the gas phase of *m*-MeO, *p*-MeO, *m*-Me, *p*-Me, H, *m*-NO_2, *m*-Cl, and *m*-Br benzoic acids, catalyzed by $AlPO_4$ of the F type. It is shown that the Hammett equation could be applied to the adsorption equilibrium constant, K_A, and to the apparent kinetic constant, $\vec{K}$. The K_A and $\vec{K}$ values used in this paper have been taken from a study by the same authors. The *m*-NO_2 benzoic acid is in disagreement with the general behavior of the other acids in the application of the Hammett equation to the adsorption process. The *p*-MeO benzoic acid is in disagreement with the behavior of the acids in the application of the equation to the surface reaction. In these cases, the ρ values were negative. It can be deduced that a positive charge is generated in the adsorption process and in the surface reaction. The $A_{Ac}2$ mechanism is discussed according to the values of ρ, and a more detailed mechanism is proposed. The separation of the enthalpic and entropic contributions to the substituent effect is carried out. $\bar{\rho}_s$ and $\bar{\rho}_H$ are nearly 50% in the adsorption process. In the surface reaction, the entropic contribution is greater (72.5%) than the enthalpic (27.5%).

J. V. SINISTERRA, J. M. MARINAS et A. LLOBERA. Can. J. Chem. **61**, 230 (1983).

On a appliqué pour la première fois l'équation de Hammett à l'estérification en phase gazeuse des acides *m*-MeO, *p*- MeO, *m*-Me, *p*-Me, H, *m*-NO_2, *m*-Cl et *m*-Br benzoïques catalysées par le $AlPO_4$ de type F. On a montré que l'équation de Hammett peut s'appliquer à la constante d'équilibre d'adsorption K_A et à la constante cinétique apparente $\vec{K}$. Les valeurs de K_A et de $\vec{K}$ utilisées proviennent d'une étude que nous avons réalisée antérieurement. L'acide *m*-NO_2 benzoïque se distingue du comportement général des autres acides lorsqu'on applique l'équation de Hammett au processus d'adsorption. L'acide *p*-MeO benzoïque se distingue des autres acides lorsqu'on applique l'équation à la réaction de surface. Dans ces cas, les valeurs de ρ sont négatives. On peut déduire qu'il y a production d'une charge positive dans le processus d'adsorption et dans la réaction de surface. On discute du mécanisme $A_{Ac}2$ selon la valeur de ρ et on propose un mécanisme plus détaillé. On a effectué une séparation de la contribution de l'enthalpie et de l'entropie à l'effet de substituant. Les valeurs de $\bar{\rho}_s$ et de $\bar{\rho}_H$ sont voisines de 50% dans le processus d'adsorption. Dans la réaction de surface, la contribution de l'entropie est supérieure (72,5%) à celle de l'enthalpie (27,5%).

[Traduit par le journal]

Introduction

A problem that has challenged chemists for years is the determination of the electronic influence that substituents exert on the rate and stereochemistry of a reaction. This problem (structure–reactivity relationship) is usually discussed by organic chemists within the context of the lineal free energy relationship (LFER). The most popular example of LFER in organic chemistry is the Hammett equation (1). It has been used in many organic reactions in homogeneous media, e.g. bromination of monosubstituted benzenes or esterification of monosubstituted benzoic acids. It has been used rarely, however, in reactions of aromatic compounds in the heterogeneous phase, e.g. intrinsic acidities of substituted benzoic acids (2), and in the adsorption of arenes on $AlPO_4$ and $AlPO_4$–SiO_2 catalysts (3).

We have recently studied the esterification of substituted benzoic acids with ethanol (4) in the vapour phase along the lines of investigation followed for the application of $AlPO_4$ to the different organic reactions: catalytic cracking, Beckmann rearrangement, etc. The kinetic runs were carried out in this study in order to elucidate the mechanism of the esterification of these acids on $AlPO_4$. We concluded that the pathway was a typical bimolecular acyl–oxygen cleavage mechanism ($A_{Ac}2$) in all cases. The rate-controlling step was not the adsorption process but the surface reaction between an adsorbed molecule of acid on the catalyst and a nonadsorbed molecule of alcohol. The application of the Hammett equation to the esterification of these acids in the vapour phase is studied in the present paper. The separation of enthalpic and entropic contributions to the substituent effect is also analyzed. The mechanism of the esterification of the substituted benzoic acids catalyzed by means of $AlPO_4$ is discussed according to the kinetic runs (4) and the Hammett equation.

Experimental

The method of synthesis, in ammoniacal medium, of the catalyst called F(100% $AlPO_4$) used in this work has been published in a previous paper (5). From adsorption–desorption isotherms of nitrogen at liquid nitrogen temperature, the surface area (S_{BET}) and accumulated pore volume (ΣV_p) were determined by the BET method (6). The results obtained were: S_{BET} = (109 ± 4) m^2/g, ΣV_p = (0.23 ± 0.09) mL/g. The acidity of the catalyst and the density of acidic sites were measured by titration in nonaqueous medium by applying the alteration to the original method (7) proposed by Balikova (8) using n-butylamine (0.0253 *M* in benzene) as the titrating agent and *p*-dimethylaminoazobenzene as the Hammett indicator (pK_a = +3.3).

[1]Author to whom correspondence may be addressed.

[2]Revision received September 17, 1982.

0008-4042/83/020230-05$01.00/0

©1983 National Research Council of Canada/Conseil national de recherches du Canada

Can. J. Chem. Downloaded from www.nrcresearchpress.com by 210.87.254.42 on 09/06/12
For personal use only.

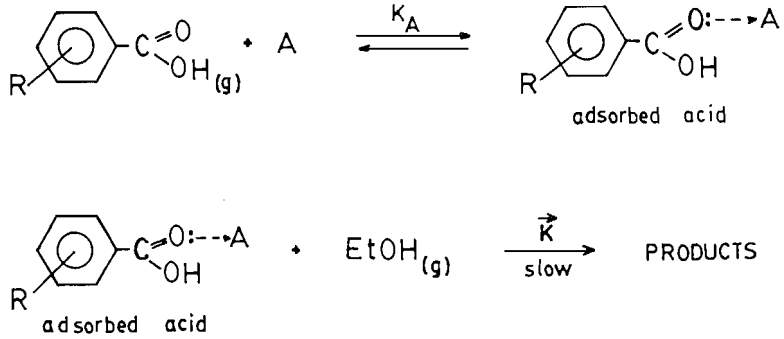

SCHEME 1

TABLE 1. Adsorption constant (K_A), apparent rate constant ($\vec{K}$), and activation parameters of esterification of substituted benzoic acids with ethanol in the gas phase, catalyzed by $AlPO_4$ (F)[a]

R—C_6H_4—CO_2H R	K_A (atm^{-1})	$\vec{K} \times 10^4$ (mol atm^{-1} g^{-1} s^{-1})	ΔH^* (kcal mol^{-1})	ΔS^* (cal mol^{-1} K^{-1})	ΔG^* (kcal mol^{-1})
H	85±7	10.1±0.8	10 ±2	−53±10	35±5
m-CH_3	84±7	8.7±0.7	5.8±0.4	−62±4	35±2
p-CH_3	97±8	10.7±0.9	3.6±0.7	−66±13	35±6
m-NO_2	82±7	6.7±0.5	9 ±1	−56±9	35±4
m-OCH_3	48±5	9.1±0.9	7.7±0.5	−58±3	35±6
p-OCH_3	130±12	2.7±0.2	17 ±4	−40±9	35±6
m-Cl	51±4	8.2±0.7	9.3±0.7	−54±5	35±3
m-Br	53±4	7.6±0.6	9.3±0.9	−54±5	35±3

[a]T = 200°C, W = 0.3 g of catalyst, $F_{N_2} = 5.6 \times 10^{-5}$ mol s^{-1} (carrier gas flow).

In this way the results were: total acidity = (0.49 ± 0.04) mequiv/g and density of acidic sites = (4.5 ± 0.4) × 10^{-3} mequiv/m^2. Ethanol, benzoic acid, and *m*-Me, *p*-Me, *m*-NO_2, *m*-MeO, *p*-MeO, *m*-Cl, and *m*-Br-benzoic acid were provided by Merck. Panreac anhydrous dioxane (99.98% purity) was used as an inert solvent to dissolve the reagents. This product vaporizes quickly at reaction temperature and it is inert in the reaction (4).

The kinetic runs were carried out in a conventional fixed bed reactor. The experimental results are described in the literature (4).

Results and discussion

In a previous study (4) we have shown that the esterification of substituted benzoic acids on $AlPO_4$ in the gas phase is carried out by a typical $A_{Ac}2$ mechanism where A is an active site of the catalyst (Lewis or Brönsted) (see Scheme 1).

The rate-controlling step is the surface reaction between an adsorbed molecule of acid and an unadsorbed ethanol molecule. The kinetic equation of the process is [1]

$$[1] \quad r_0 = \frac{\vec{k} \cdot s \cdot L \cdot K_A}{(1 + K_A P_{Ac})^2} P_{Ac} P_{Al}$$

where r_0 = initial reaction rate, S = number of adjacent active sites that act in the rate-controlling step, L = total number of active sites, P_{Ac} = acid pressure, and P_{Al} = alcohol pressure. From the kinetic runs, Langmuir's adsorption constants, K_A (atm^{-1}), apparent kinetic constants $\vec{K} = \vec{k} \cdot s \cdot L$(mol atm^{-1} g^{-1} s^{-1}), and the activation parameters ΔH (kcal mol^{-1}), ΔS^* (cal mol^{-1} K^{-1}), and ΔG^* (kcal mol^{-1}) were obtained for each substituent studied. Results are shown in Table 1. The adsorption parameters, ΔH^*_{ads}, ΔS^*_{ads}, and ΔG^*_{ads} were not accessible from the kinetic runs because the Yang and Hougen method (9) was used. In this method we must suppose that the adsorption constant, K_A, does not change within the range of temperatures used (160−240°C) and this is not exactly true. For this reason the precision of the constants K_A and $\vec{K}$ is not great (Table 1) but it is enough to get the sign of the slope of the Hammett equation and to study the mechanism of the organic reaction in a qualitative manner.

TABLE 2. Values of σ constants for the substituted benzoic acids studied

R—C_6H_4—CO_2H R	σ(10)	σ_H(15)	σ_S(15)
H	0.000	0.000	0.000
m-CH_3	−0.069	0.029	−0.077
p-CH_3	−0.170	−0.103	−0.055
m-NO_2	0.170	−0.198	0.942
m-OCH_3	0.115	0.045	0.068
p-OCH_3	−0.268	−0.359	0.079
m-Cl	0.373	−0.066	0.437
m-Br	0.391	−0.051	0.446

Application of the Hammett equation to the adsorption process

The values of the σ constants (10) are given in Table 2. In Fig. 1 the fitting of the experimental data with the Hammett equation, [2], for the σ constant is shown. The equation obtained was [3]

$$[2] \quad \log K_{ARBZ} = \rho\sigma \pm \log K_{AHBZ}$$

$$[3] \quad \log K_{ARBZ} = -(0.58 \pm 0.012)\,\sigma + (1.9 \pm 0.4) \quad (>99\%)$$

for r = 0.90, s = 0.078, and $F_{1,5}$ = 21.4.[3] K_{AHBZ} is the adsorption constant for benzoic acid, while K_{ARBZ} is the same

[3]Theoretical values of Snedecor's F constant: $F_{1,5}$ = 6.61 (α = 0.05); $F_{1,5}$ = 16.3 (α = 0.01).

Can. J. Chem. Downloaded from www.nrcresearchpress.com by 210.87.254.42 on 09/06/12
For personal use only.

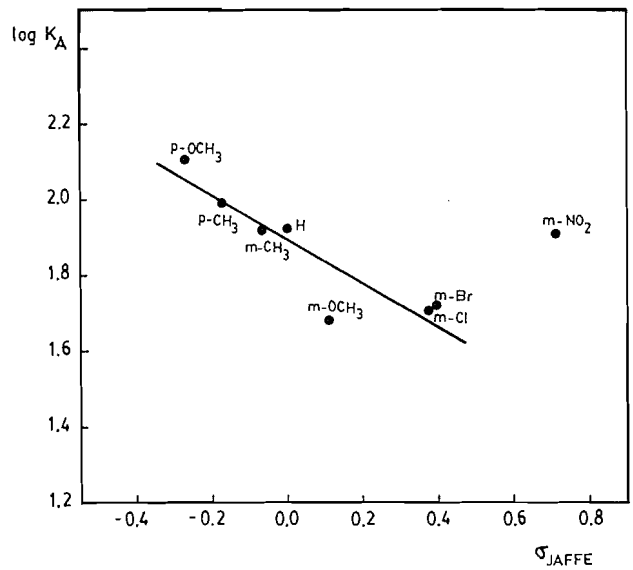

FIG. 1. Hammett plot for the Langmuir adsorption constant, catalyst $AlPO_4(F)$; $T = 200°C$.

constant for the substituted benzoic acid. The value for the m-NO_2 is in disagreement with the general trend and it has not been included in the fitting of the experimental data to the Hammett equation [2]. This disagreement could be explained considering that this molecule will be adsorbed for the NO_2 group better than for the CO_2H group because of the greater negative charge of the NO_2 group. Thus the fundamental adsorption of this molecule[4] will not drive the esterification process to completion and the adsorption constant determined by the Yang and Hougen method will not be the true adsorption constant of this acid by the oxygen of the C=O bond (Scheme 2).

The negative sign of the ρ constant (−0.58) obtained indicates that a positive charge is produced on the substituted benzoic acid when the adsorption takes place. Because of this, the electron-donating groups favour the adsorption process: $K_{p\text{-MeO}} > K_{p\text{-Me}} > K_{m\text{-Me}} > K_H$, and electron-withdrawing groups do not favour the adsorption: $K_{m\text{-Cl}} < K_{m\text{-Br}} < K_{m\text{-MeO}} < K_H$. This agrees with the assumption that the adsorption process takes place on an acid site of the catalyst by means of a polar interaction between this active site and the point of greatest negative charge of the acid, the oxygen of the C=O group of carboxylic acid, except in the case of the m-NO_2 benzoic acid.

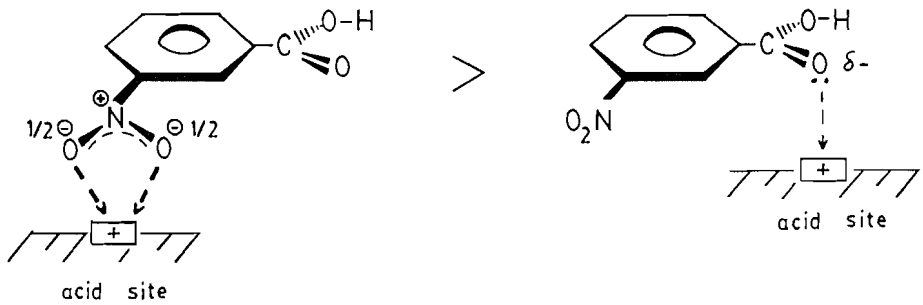

SCHEME 2

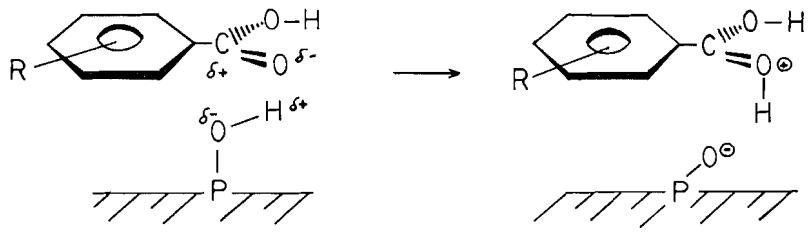

SCHEME 3

This kind of adsorption could describe the "activated adsorption" of carboxylic acid on the active site of the $AlPO_4$, probably a σ^*_{OH} bond of a P—OH alone (11). $AlPO_4$ would transfer a H^+ to the oxygen of C=O. The positive charge of this atom would be transmitted by the π conjugation to the aromatic ring. This would agree with the negative sign of the constant ρ. Thus, the adsorption process of these acids on $AlPO_4$ may be written as in Scheme 3.

Application of the Hammett equation to the surface reaction

The values of the apparent kinetic constant, $\vec{K}$, (Table 1) were adjusted to σ values of Table 2. The equation obtained was [4]

$$[4] \quad \log \vec{K}_{RBZ} = -(0.21 \pm 0.04)\,\sigma - (3.02 \pm 0.52) \quad (>99\%)$$

for $r = 0.93$, $s = 0.028$, and $F_{1,5} = 31.9$.[3] The Hammett plot is shown in Fig. 2. The p-MeO group is in disagreement with the other acids. Thus it has not been considered in the fit. This discordance could be explained by the strong +K effect of the group which makes it different from the other substituents studied. Its behaviour as an "abnormal" group has been reported in the organic literature for several reactions in homogeneous phase (12). Another explanation could be according to Yamdagni *et al.* (2) that the structure (I) (Scheme 4), being charge-separated, could be important in the "normal" solvents where the σ values are obtained. Therefore it cannot be important in the adsorbed state on the catalyst surface, where the separation of charges will probably be hindered by the electrical structure of the $AlPO_4$ catalytic surface. The σ constant of this group, for this reason, cannot be used in the gas phase.

The values of the ρ constant (−0.21) is smaller than the values obtained by the other workers in the esterification of

[4]This has been proved by F.O. theory (4).

Can. J. Chem. Downloaded from www.nrcresearchpress.com by 210.87.254.42 on 09/06/12
For personal use only.

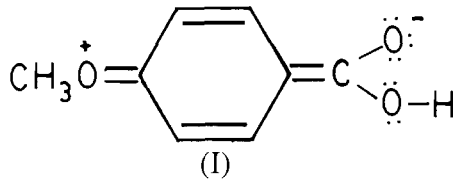

(I)

SCHEME 4

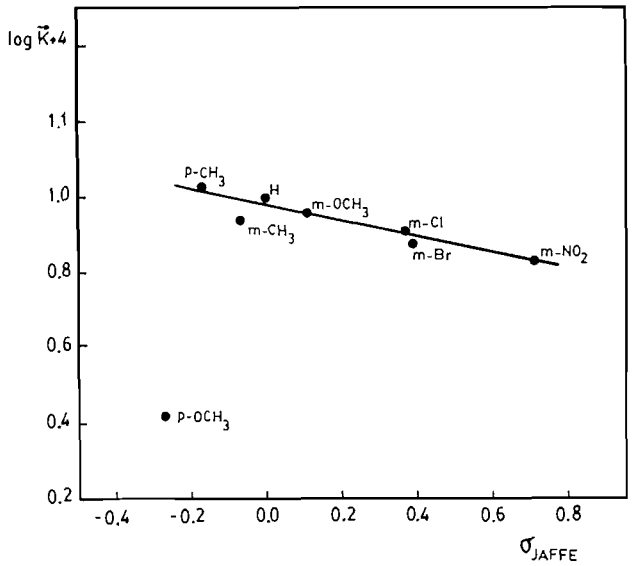

FIG. 2. Hammett plot for the apparent kinetic constant, catalyst $AlPO_4$(F); T = 200°C.

substituted benzoic acids with several alcohols, e.g. −0.58 with MeOH and HCl as the catalyst (13) and −0.48 with F_3B as the catalyst (14). This low value indicates that in our case the transition state is nearer the initial state (adsorbed acid) than the tetrahedral intermediate of a $A_{Ac}2$ mechanism. The negative sign of the ρ constant indicates that a positive charge is produced on the substituted benzoic acid when the surface reaction takes place and the activating groups: *p*-Me, *m*-Me, etc. favour the process. It only can be explained by means of an $A_{Ac}2$ mechanism if the electron donation from the lone oxygen pair of alcohol is very poor and if the C=O bond is practically broken by means of the $AlPO_4$ in the transition state. In this

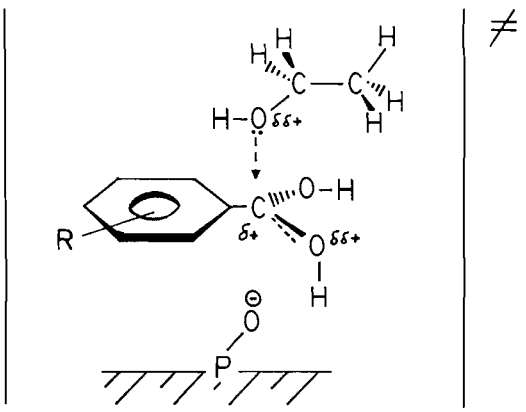

SCHEME 5

case the positive charge of the carbon of the CO_2H group would increase and this positive charge would be transferred to the aromatic ring. This supposition is in agreement with the mechanism proposed from the kinetic data (4) where the rate-controlling step is the surface reaction between an adsorbed molecule of benzoic acid and an unadsorbed alcohol molecule. This also agrees with the postulates of the Frontier Orbital theory (F.O.) that say a small value of ρ indicates a very poor gap between the HOMO of the ethanol and the LUMO of the adsorbed acid. So, the transition state must be near the initial state. The transition state of the esterification of substituted benzoic acids with ethanol in the vapour phase, catalyzed by $AlPO_4$, may be pictured as in Scheme 5.

Separation of enthalpic and entropic contributions to substituent effects

In order to know if the separation of enthalpic and entropic contributions to substituent effects could be valid in a reaction in the gas phase, the Krygowski equation [5], (ref. 15), was applied

$$[5] \quad \log K = \log K_0 + \rho_H\sigma_H + \rho_S\sigma_S$$

where σ_H and σ_S are independent substituent constants for the enthalpic and entropic contributions (Table 2), ρ_H and ρ_S are the corresponding reaction constants, and K can be K_A or $\vec{K}$ according to the process under study.

The values of K_A and $\vec{K}$ (Table 1) were fitted to eq. [5]

$$[6] \quad \log K_{ARBZ} = 1.87 - 0.83\,\sigma_H - 0.49\,\sigma_S \quad (<70\%) \quad (<70\%)$$

for r = 0.93, s = 0.064, and $F_{2,4}$ = 14.0

$$[7] \quad \log \vec{K}_{RBZ} = -3.02_5 - 0.38_5\sigma_H - 0.23\sigma_S \quad (<30\%) \quad (<70\%)$$

for r = 0.93, s = 0.024, and $F_{2,4}$ = 17.5.[5] As in the Hammett equation, the *m*-NO_2 group was not considered in the adsorption process and the *p*-MeO was not considered in the surface reaction. The fit of the experimental data is acceptable but the significance level is minor compared to the other cases (only 95%), see Snedecor's F constant.

The ρ_s and ρ_H values were negative in both cases because a positive charge is created in the aromatic compound. The values of ρ_s(−0.49 and −0.23) are approximately equal to the Hammett reaction constants (−0.58 [3] and −0.21 [4]) according to the literature (15). The percentage of the enthalpic and entropic contributions $\bar{\rho}_H$ and $\bar{\rho}_S$ (15), respectively, to the substituent effect, was determined. The values obtained were by the adsorption process

$$\bar{\rho}_H = 51\% \qquad \bar{\rho}_S = 49\%$$

and by the reaction on the surface of the catalyst

$$\bar{\rho}_H = 27.5\% \quad \bar{\rho}_S = 72.5\%$$

We can say then that in the adsorption process the enthalpic and entropic contributions are equal, but not in the surface reaction, where $\bar{\rho}_S$ is greater than $\bar{\rho}_H$. These results confirm that there is a high interaction in the rate-controlling step between the molecule of benzoic acid and the environment (in our case the active surface of the catalyst $AlPO_4$). This is in agreement with the mechanism proposed in which the benzoic acid is adsorbed on the catalytic surface before the rate-controlling step.

Conclusions

From the results of this work we can deduce that the Hammett equation can be applied to the esterification process of

[5] Theoretical values of Snedecor's F constant: $F_{2,4}$ = 6.94 (α = 0.05); $F_{2,4}$ = 18 (α = 0.01).

Can. J. Chem. Downloaded from www.nrcresearchpress.com by 210.87.254.42 on 09/06/12
For personal use only.

substituted benzoic acids with ethanol in the vapour phase by means of $AlPO_4$ as catalyst.

On the other hand, the Hammett equation has been used to analyze the mechanism of the organic reaction. The mechanism, $A_{Ac}2$, seems to be the same for all substituted benzoic acids. The adsorption process and the rate-controlling step (surface reaction) take place creating a positive charge on the aromatic compound ($\rho < 0$). The small value of the ρ constant indicates a poor HOMO/LUMO gap and a preponderance of the electrostatic interaction in both processes. On the other hand, we could say that the transition state of the esterification of all acids studied is nearer the adsorption state than the tetrahedral state of the $A_{Ac}2$ mechanism, due to the small value of the ρ constant in the surface reaction. This is in agreement with the mechanism where the rate-controlling step is the reaction between an adsorbed molecule of acid and an unadsorbed ethanol molecule.

1. L. P. HAMMETT. J. Am. Chem. Soc. **59**, 96 (1937).
2. R. YAMDAGNI, T. B. MCMAHON, and R. KEBARLE. J. Am. Chem. Soc. **96**, 4035 (1974).
3. P. DEYA, A. COSTA, J. V. SINISTERRA, and J. M. MARINAS. Proc. VII[th] Iberoamerican Symposium of Catalysis. La Plata, Argentina. July, 1980, p. 44.
4. A. LLOBERA. PhD Thesis, Science Faculty of Palma de Mallorca, Spain. July, 1981.
5. J. V. SINISTERRA, J. M. MARINAS, and R. PEREZ-OSSORIO. An. Quim. **70**, 371 (1974).
6. S. BRUNAUER, P. H. EMMETT, and E. TELLER. J. Am. Chem. Soc. **60**, 309 (1938).
7. O. JOHNSON. J. Phys. Chem. **59**, 827 (1955).
8. H. BALIKOVA. React. Kinet. Catal. Lett. **2**, 323 (1975).
9. K. H. YANG and O. A. HOUGEN. Chem. Eng. Prog. **46**, 146 (1950).
10. H. H. JAFFE. Chem. Rev. **53**, 191 (1953).
11. M. A. ALARIO. PhD Thesis, Faculty of Science, Universidad Complutense, Madrid, Spain. Ser. A. No 110. 1970.
12. L. P. HAMMETT. Physical Organic Chemistry. 2nd ed. McGraw Hill, New York. 1970.
13. R. J. HARTMAN and A. M. BORDERS. J. Am. Chem. Soc. **59**, 2107 (1937).
14. GY. DEAK, L. FENICHEL, and A. MESZAROS. Acta Chim. Hung. **29**, 111 (1958).
15. T. M. KRYGOWSKI and W. R. FAWCETT. Can. J. Chem. **53**, 3622 (1975).

Can. J. Chem. Downloaded from www.nrcresearchpress.com by 210.87.254.42 on 09/06/12
For personal use only.

Betylates. 4. The synthesis and preparative nucleophilic substitution reactions of alkyl *S*-[3]betylates[1]

JAMES FREDERICK KING, STANISLAW SKONIECZNY,[2] AND GARY ALLAN POOLE
Department of Chemistry, University of Western Ontario, London, Ont., Canada N6A 5B7

Received August 18, 1982

JAMES FREDERICK KING, STANISLAW SKONIECZNY, and GARY ALLAN POOLE. Can. J. Chem. **61**, 235 (1983).

Alkyl *S*-[3]betylates (*S*,*S*-dialkyl-*S*-3[(alkyloxy)sulfonyl]propylsulfonium salts), the first examples of *S*-betylates (sulfonioalkanesulfonic esters), have been synthesized by two routes, and their suitability as intermediates in the transformation of alcohols by nucleophilic substitution reactions examined. They have been found to react readily in stoichiometric phase transfer processes, including substrate–reagent ion-pair reactions, like their previously studied nitrogen analogues, with the following particular features: (a) they may be used with basic nucleophiles (unlike [2]betylates), (b) they are more simply made from commercially available starting materials than [3]betylates, and (c) they can be made by a route that avoids a final alkylation step.

JAMES FREDERICK KING, STANISLAW SKONIECZNY et GARY ALLAN POOLE. Can. J. Chem. **61**, 235 (1983).

On a utilisé deux méthodes pour synthétiser les *S*-[3]bétylates d'alkyles, les sels de *S*,*S*-dialkyl-*S*[(alkyloxy)sulfonyl]-3-propylsulfonium, les premiers exemples de *S*-bétylates (esters de l'acide sulfonioalcanesulfonique) et on a étudié leur utilité comme intermédiaire lors de la transformation des alcools par des réactions de substitutions nucléophiles. On a trouvé qu'ils réagissent facilement par des processus de transfert de phase stoechiométriques, incluant des réactions de paire d'ions substrat–réactif, comme ceux de leurs analogues azotés étudiés antérieurement, ayant les caractéristiques particulières suivantes: (a) ils peuvent être utilisés avec des nucléophiles basiques (contrairement aux [2]bétylates), (b) ils sont obtenus plus facilement à partir de produits de départ disponibles commercialement que les [3]bétylates et (c) ils peuvent être préparés par une méthode qui évite l'étape finale d'alkylation.

[Traduit par le journal]

We have recently pointed to the merits of betylates (**1**) and norbetylates (**2**) as intermediates in the conversion of alcohols into other classes of compounds by way of nucleophilic substitution (1–5). Their application was illustrated by examples

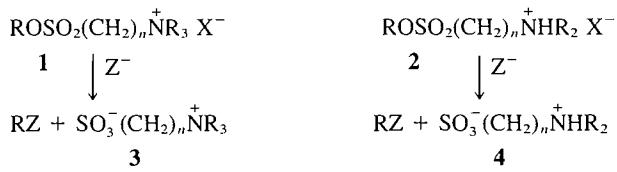

involving ten primary or secondary alkyl groups and more than thirty different nucleophiles, leading to such varied products as halides, azides, thiocyanates, sulfonium salts, and carboxylate, sulfonate, and perchlorate esters. The particular advantages of betylates stem largely from their ability to undergo stoichiometric phase transfer, either in the form of (a) substrate phase transfer in two-phase aqueous–organic or simple aqueous systems, or (b) substrate–reagent ion-pair (SRIP) reactions in nonpolar media. One difficulty with [2]betylates (**1**, $n = 2$), however, is that under basic conditions, instead of undergoing nucleophilic displacement with formation of RZ and the betaine (**3**), they are converted back to the alkyl ethenesulfonate, which may either fail to react or simply give a product other than RZ. In practice this reaction is observed in aqueous solution when the pH is greater than about 6.5, or, in nonaqueous media with such reagents as alkylamines, alkoxides, and thiophenoxides. [3]Betylates (**1**, $n = 3$) do not suffer from this difficulty but at present their preparation from commercially available materials is rather inconvenient. In addition, current syntheses of [2]- and [3]betylates (**1**, $n = 2$ and 3, respectively) require quaternization of a tertiary amine as their final step, a procedure which may not be suitable if certain reactive groups (e.g. tertiary amino functions) are present in the original alcohol component. The formation of norbetylates (**2**), of course, does not require this alkylation step, but since these species are readily deprotonated by bases they too are obviously unsuited for general use with such reagents. Accordingly, in the hope of finding a betylate species which (a) could be used with basic reagents, (b) could be made readily from commercially available materials, and (c) did not require an alkylation step after the esterification of the alcohol, we explored – and now describe – the preparation and reactions of "*S*-[3]betylates" (**11**–**15**), the sulfur analogues of [3]betylates (**1**, $n = 3$).

S-[3]Betylates are prepared from the commercially available sultone (**5**) by either of the two routes shown in Scheme 1. All steps can be carried out in good yield, with the conversion of the alcohol (ROH) to the desired *S*-[3]betylate (**12**, **13**, **14**, or **15**) giving better than 85% yields based on the alcohol. Elemental analyses or an exact mass value were obtained for compounds **6** and **7** and representative esters (**10***b* and *e*, and **15***a*, $X^- =$ picrate), but the properties of the sulfonyl chlorides prevented full characterization; their nmr and infrared spectra taken with their mode of synthesis and conversion to esters clearly establish their identity. 3-Ethylthio-1-propanesulfonyl chloride (**8**) was readily prepared from **6** by *brief*, mild treatment with thionyl chloride in carbon tetrachloride; longer reactions times or more vigorous conditions led to poorer yields. The sulfonyl chloride (**8**) is reasonably stable in solution, showing significant decomposition only after more than two weeks at room temperature; it is distillable ($bp_{0.001}$ 62–63°C) but even with a good vacuum a good deal of decomposed stillpot residue is formed and the neat distillate so obtained turns brown after only a few hours at room temperature. Because of the short

[1]For part 3 of this series see ref. 5.
[2]On leave from the Technical University of Gdańsk, Poland.

0008-4042/83/020235-09$01.00/0
©1983 National Research Council of Canada/Conseil national de recherches du Canada

Can. J. Chem. Downloaded from www.nrcresearchpress.com by 210.87.254.42 on 09/06/12
For personal use only.

Can. J. Chem. Downloaded from www.nrcresearchpress.com by 210.87.254.42 on 09/06/12
For personal use only.

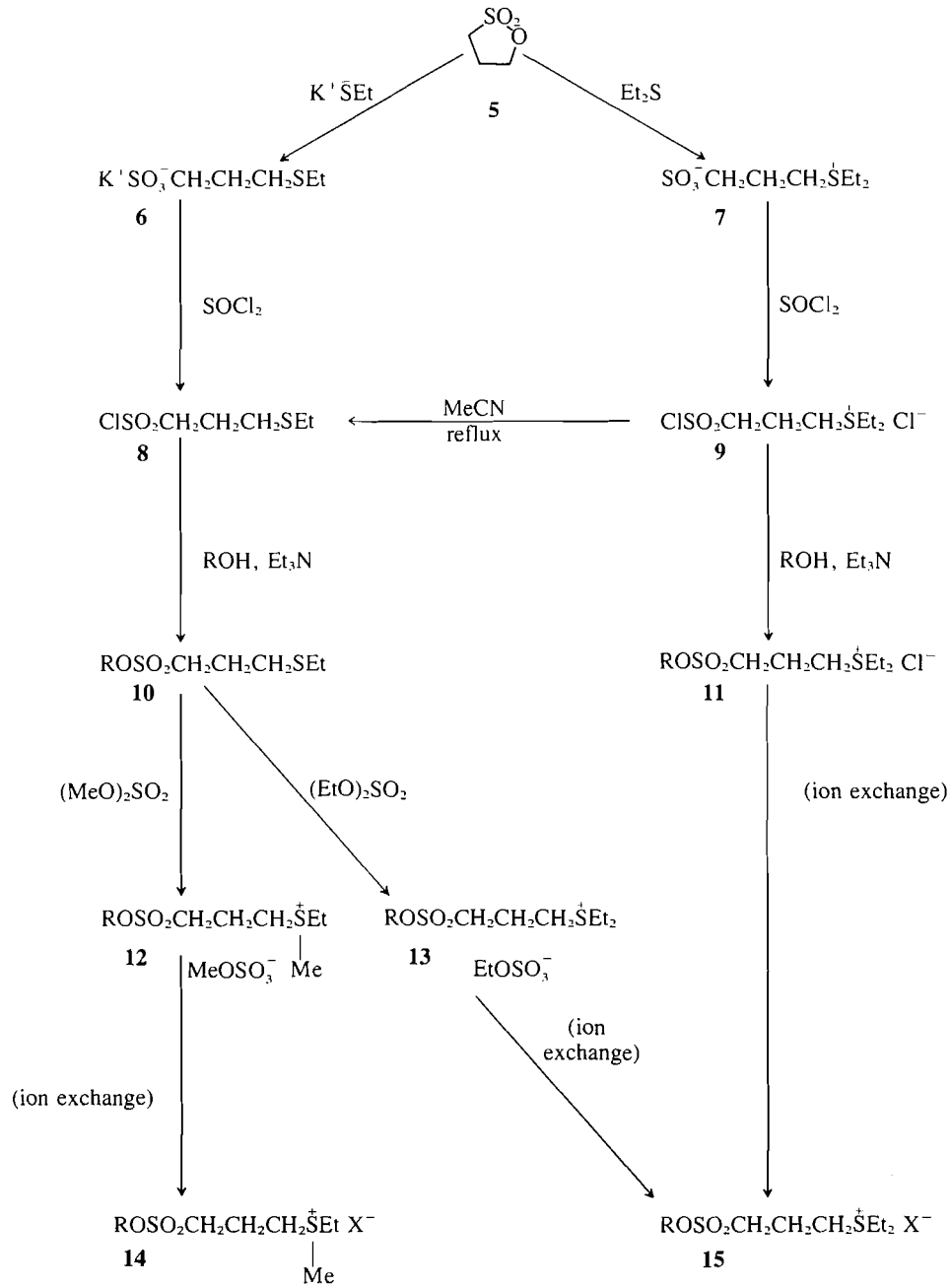

a) R = $CH_3(CH_2)_{15}$
b) R = $CH_3(CH_2)_3$
c) R = $(CH_3)_3CCH_2$
d) R = $CH_2{=}CHCH_2CH_2$
e) R = $CH_3(CH_2)_5CH(CH_3)$

SCHEME 1

shelf-life of the neat sulfonyl chloride (**8**), the preparation of 3-ethylthio-1-propanesulfonate esters (**10**) was carried out by using a freshly prepared solution of **8**, which is readily obtained from **6** in about 30 min in a laboratory scale preparation. The use of excess alcohol, excess sulfonyl chloride, and equimolar amounts of each, has been tried and found to give satisfactory results in all cases. The esters (**10**) so obtained appear to behave as conventional sulfonic esters. Whereas the analogous esters of aminosulfonic acids are rapidly converted by intermolecular alkyl transfer to betaines (6, 7),

$$R'_2N(CH_2)_nSO_2OR \longrightarrow RR'^{+}_2N(CH_2)_nSO_3^-$$

the corresponding reaction of the sulfide-esters (**10**) is evidently slow, distillation of the butyl ester (**10**, R = butyl) at 83–84°C (0.001 Torr) having been carried out with >80% recovery. Fortunately, however, alkylation of the sulfide

Can. J. Chem. Downloaded from www.nrcresearchpress.com by 210.87.254.42 on 09/06/12
For personal use only.

grouping in **10** to form the *S*-betylates (**12**) and (**13**) is effected in good yield by using the somewhat more reactive alkyl transfer agents diethyl and dimethyl sulfate at somewhat higher temperatures, respectively 110°C (for 1 h) and 100°C (for 0.5 h).

The alternative route to *S*-[3]betylates proceeds by way of "*S*-[3]betyl chloride" (**9**) which was obtained as an oil which in our hands did not crystallize, but which appeared from its ^{1}H nmr spectrum to be reasonably pure. A freshly prepared solution of **9** in D_2O showed no sign of the betaine (**7**) in its nmr spectrum, but after a short time peaks due to **7** appeared and those due to **9** diminished; a half-life of about 40 min (at 37°C) indicates a rate constant[3] of roughly 3×10^{-4} s^{-1}. Under ordinary storage conditions, neat **9**, in contrast to **8**, appears to keep about as well as other liquid sulfonyl chlorides. In refluxing acetonitrile **9** is converted to **8**, with ethyl chloride the presumed coproduct; such SRIP reactions of sulfonium halides are well-precedented (10).

Conversion of the *S*-betyl chloride (**9**) to hexadecyl *S*-[3]betylate chloride (**11**) was easily effected by reaction of an excess of **9** with the alcohol in the presence of triethylamine. The betylate chloride (**11**) was converted by ion extraction to the betylate picrate and camphor-10-sulfonate (**15**, X^- = picrate and camphor-10-sulfonate), the yields based on the alcohol being 97% and 88% respectively. To avoid contamination of the final product with the alkyl chloride it is apparently prudent to remove all unreacted thionyl chloride from the sulfonyl chloride (**9**) and to avoid heating of the betylate chloride (**11**) (see Experimental for details).

The reactions of some *S*-[3]betylates with a number of nucleophiles are summarized in Table 1. These reactions were found to occur under mild conditions to give clean products in respectable yields. With respect to reactions with such basic reagents as sodium ethoxide, sodium thiophenoxide, methylamine, and potassium cyanide, the behavior of *S*-[3]betylates was like that of their nitrogen analogues, the [3]betylates (**1**, $n = 3$), and much more satisfactory from a preparative viewpoint than that of the [2]betylates (**1**, $n = 2$).

Perhaps the chief difficulty with *S*-[3]betylates derives from the ease with which sulfonium salts transfer alkyl groups to nucleophiles; this reaction has already been encountered in the formation of **8** from **9** and is illustrated with *S*-[3]betylates by the SRIP reaction of the methyl ethyl picrate **14***a* (X^- = picrate). The product contained, in addition to the expected hexadecyl picryl ether, about 15% of a material which appeared from its ^{1}H nmr spectrum to be methyl picryl ether. As would be expected from the lower S_N2 reactivity of ethyl vs. methyl groups, the use of the diethyl sulfonium picrate (**15***a*, X^- = picrate) gave hexadecyl picryl ether with no sign of any ethyl picryl ether. But the alkyl transfer capability of an alkylsulfonium salt is still present even with the diethyl salts (**15**) and shows up when the alkyl group, R, is relatively unreactive; **13***c*, on treatment with sodium thiophenoxide gave roughly equivalent amounts of thiophenetole (PhSEt) and the ethylthio ester (**10***b*) together with a smaller amount of a previously unknown compound, neopentyl 3-phenylthio-1-propanesulfonate (**18***b*), the identity of which was shown by independent synthesis from **5** by the standard route (Scheme 2). Thio-

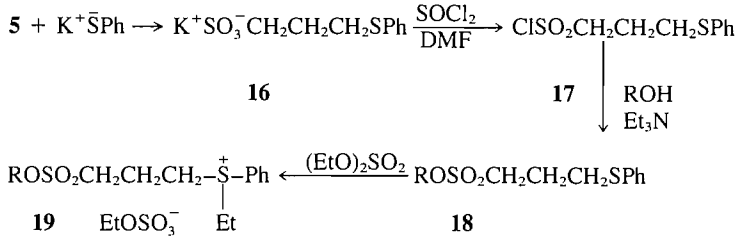

a) R = hexadecyl
b) R = neopentyl

SCHEME 2

phenetole and **10** were obviously formed by transfer of one of the *S*-ethyl groups, whereas **18** presumably arose (along with an equivalent amount of diethyl sulfide which evaporated during work-up) by reaction at the remaining carbon attached to the positively charged sulfur, i.e. C-1 of the propylsulfonium system. The comparative ease of this latter substitution at C-1 is of interest because it shows that regardless of the nature of the other two alkyl groups on the sulfonio sulfur, the undesired *S*-dealkylation will compete with *O*-alkyl transfer in the simple *S*-[3]betylate system when difficultly transferable alkyl groups such as neopentyl are attached to the sulfonyl oxygen.

The preparation of **17** and **18***b* as in Scheme 2 prompted us to take a brief look at the properties of an arylalkylsulfonic betylate (**19**) to see if such *S*-betylates possessed any advantages over their diethyl analogues (**15**). Arylalkyl sulfides are known to be more difficult to alkylate than dialkyl sulfides (11), presumably because of delocalization of the nonbonded electrons on the sulfur into the aromatic system, and we found in fact that the formation of **19***a* from **18***a* was distinctly less conveniently carried out than the preparation of **13** from **10**; after 2.5 h the reaction of **10***a* with diethyl sulfate at 80°C was nearly finished whereas that of **18***a* was less than 20% complete. By the same token, ethyl transfer *from* the positively charged sulfur was faster from **19***a* than from **13***a*; whereas the latter with aqueous sodium thiophenoxide gave phenyl hexadecyl sulfide in 81% yield, **19***a* afforded little or none of this product but rather almost entirely reverted to **18***a* (see Table 1). Evidently incorporation of one aryl group into the sulfonic grouping leads to a betylate which is less useful for the synthetic purposes studied in this paper than the dialkyl analogues **14** and **15**. A second aryl group, as in $Ar_2\overset{+}{S}CH_2CH_2CH_2SO_2OR$ X^-, would presumably not be any better since it would proba-

[3]For the corresponding hydrolysis of methanesulfonyl chloride (37°C, D_2O) a rate constant of 4.4×10^{-4} s^{-1} may be estimated from the work of Robertson and Laughton (8, 9) and the assumption that the kinetic solvent isotope effect is much the same at 37° and 20°C.

Can. J. Chem. Downloaded from www.nrcresearchpress.com by 210.87.254.42 on 09/06/12
For personal use only.

Table 1. Nucleophilic reactions of *S*-[3]betylates, 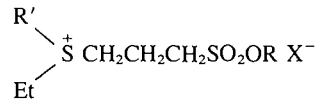

Substrate				Conditions						
R	R′	X^-	mmol	Procedure[a]	Reagent	Medium	Temp(°C)	Time(h)	Isolated product	Yield[b]
Butyl	Ethyl	$EtOSO_3^-$	0.33	A	KSCN	H_2O	37	1.5	R—SCN	(87)
Butyl	Ethyl	$EtOSO_3^-$	0.14	A	$(NH_2)_2CS$	H_2O	37	5	$[R—SC(NH_2)_2]^+EtOSO_3^-$	(80)
Hexadecyl	Methyl	$MeOSO_3^-$	1.0	A[c]	NaSPh	H_2O	25	6	Ph—S—R	81
Hexadecyl	Methyl	$MeOSO_3^-$	1.0	B[c]	NaSPh	CCl_4-H_2O	25	6	Ph—S—R	70
Hexadecyl	Methyl	$MeOSO_3^-$	4	C	$MeNH_2$	$DME-H_2O$[d]	~2	24	Me—NH—R	89
Hexadecyl	Methyl	$MeOSO_3^-$	1	C	NaOEt	EtOH(abs)	25	1.5	Et—O—R	90
Hexadecyl	Methyl	F^-	1	D	—	PhMe	110	2	R—F	67
Hexadecyl	Methyl	Picrate	1	D	—	PhMe	110	5	2,4,6-Trinitrophenyl—OR	(68)
									2,4,6-Trinitrophenyl—OMe	(13)
Hexadecyl	Ethyl	$EtOSO_3^-$	2	A	KCN	H_2O	80	2	R—CN	83
Hexadecyl	Ethyl	$EtOSO_3^-$	1	A[c]	NaSPh	H_2O	25	18	Ph—S—R	74
Hexadecyl	Ethyl	$EtOSO_3^-$	1	C	NaOEt	EtOH(abs)	25	48	Et—O—R	94
Hexadecyl	Ethyl	$EtOSO_3^-$	1.5	B	NaN_3	$CH_2Cl_2-H_2O$	25	18	$R—N_3$	83
Hexadecyl	Ethyl	$EtOSO_3^-$	4	C	$MeNH_2$	$DME-H_2O$[d]	~2	24	R—NH—Me	69
Neopentyl	Ethyl	$EtOSO_3^-$	1	A[c]	NaSPh	H_2O	25	6	Ph—S—Et	(27)[e]
									10*c*	(27)
									18*b*	(52)
1-Methylheptyl	Ethyl	$EtOSO_3^-$	1	A[c]	NaSPh	H_2O	25	6	Ph—S—R	93
Hexadecyl	Ethyl	F^-	1	D	—	PhMe	110	2	R—F	69
Hexadecyl	Ethyl	Picrate	1	D	—	PhMe	110	6	2,4,6-Trinitrophenyl—OR	70
Hexadecyl	Ethyl	Picrate	1.5	B	NaN_3	$CH_2Cl_2-H_2O$	25	18	$R—N_3$	72
Hexadecyl	Ethyl	Picrate	2	A	KCN	H_2O	80	2	R—CN	76
Hexadecyl	Ethyl	Camphor-10-sulfonate	2	A	KCN	H_2O	80	2	R—CN	81
Hexadecyl	Phenyl	$EtOSO_3^-$	1	A[c]	NaSPh	H_2O	25	6	**18***a* + Ph—S—Et	68

[a]Procedures: A, a suspension (or solution) of the substrate was stirred with an aqueous solution of the reagent used in tenfold excess; B, a solution of the substrate in CH_2Cl_2 (50 mL) is stirred with an aqueous solution of the reagent (50 mL); C, reaction in the organic solvent; D, reflux in toluene with no other reagents added (SRIP reaction).

[b]Yields without parentheses refer to isolated products; those within parentheses were estimated from nmr spectra.

[c]Reaction was carried out under nitrogen. In the presence of oxygen Ph—S—S—Ph was formed (as judged by tlc).

[d]50 mL of 1,2-dimethoxyethane and 4 mL of 40% aqueous $MeNH_2$.

[e]Product composition was determined by comparison of nmr spectrum with that of an authentic mixture; in addition peaks at 1.03 (s), 3.25 (s), and 7.1–7.2 (m) are consistent with the presence of a small amount (~6%) of neopentyl phenyl sulfide.

bly suffer attack at C-1 of the propylsulfonium system analogous to the formation of **18***b* from **13***c*. Alkyl transfer from sulfur could, of course, be avoided with **20**, for example, but the preparation and reactions of such materials, in our view, constitute another project,

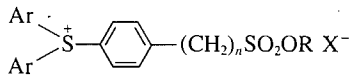

20 (n = 0, 1, 2 ...)

The conclusion of this initial exploration is that *S*-[3]-betylates are (a) good alkyl transfer agents for unhindered primary and secondary alkyl groups, and (b) readily prepared from a stable species (**6** or **7**) which is in turn easily made from a commercially available starting material (**5**). As such they should find, in conjunction with the other betylates (**1**) and the norbetylates (**2**), a useful part in the transformation of alcohols into other species.

Experimental

Reagent grade chemicals and solvents were used without additional purification unless otherwise noted. Melting points are uncorrected and were determined on a Kofler Hot Stage. Infrared spectra were obtained with Perkin–Elmer 621 Grating and Beckman 4250 spectrophotometers and unless otherwise noted refer to $CHCl_3$ solutions in 0.1 mm cells. Proton magnetic resonance spectra were obtained using Varian T60 and Varian XL100 spectrometers; all chemical shifts reported were obtained with the latter instrument; the ^{13}C nmr spectrum was determined on a Varian XL 200 instrument.

Potassium 3-ethylthio-1-propanesulfonate (6)

1,3-Propane sultone (**5**) (Aldrich, purified by distillation, $bp_{0.3}$ 94°C, 12.2 g, 100 mmol) in absolute ethanol (70 mL) was added dropwise during 20 min to a solution of ethanethiol (11.16 g, 180 mmol) and KOH (8.4 g, 150 mmol) in absolute ethanol (150 mL). Heat was evolved and a white precipitate formed immediately. After 1 h the reaction mixture was cooled in ice and the crystalline product **6** (20.0 g, 91%) collected by filtration; concentration of the filtrate gave a second crop (0.67 g, 3%). Recrystallization from absolute ethanol yielded white, hygroscopic crystals which decomposed without melting at 250–260°C; ir (KBr) ν_{max}: 2950 (m), 2900 (m), 1440 (m), 1410 (w), 1250 (s), 1185 (vs, br), 1040 (s) cm^{-1}; ^1H nmr (D_2O)δ: 1.24 (t, 3H), 2.02 (quintet, 2H), 2.68 (quartet, 2H), 2.74 (t, 2H), 3.02 (t, 2H). *Anal.* calcd. for $C_5H_{11}O_3S_2K$: C 27.03, H 4.95, S 28.83; found: C 27.21, H 5.02, S 28.61.

3-Ethylthio-1-propanesulfonyl chloride (8)

Recrystallized potassium 3-ethylthio-1-propanesulfonate (**6**) (4.44 g, 20 mmol) was suspended in carbon tetrachloride (20 mL). Thionyl chloride (22 mL) was added dropwise with stirring. After about 15 min of stirring at room temperature all the substrate had dissolved. After another 15 min the solution was diluted with CCl_4 (20 mL) and poured onto ice. The organic layer was washed with ice-water (100 mL) and then with five 100 mL portions of water. Each water portion was additionally washed with 5 mL of CCl_4. The organic layer was then dried with anhydrous $MgSO_4$ and the solvent evaporated giving **8** as a colourless oil (3.52 g, 87%); $bp_{0.001}$ 62–63°C. The purified compound **8** decomposed in a few hours at room temperature but was found to be stable in CCl_4 solution for at least 2 weeks; ir ν_{max}: 2960 (m), 2920 (m), 1450 (m), 1375 (vs), 1345 (m), 1300 (w), 1165 (vs), 1050 (w), 995 (w), and 840 (w) cm^{-1}; ^1H nmr ($CDCl_3$) δ: 1.27 (5, 3H), 2.30 (quintet, 2H), 2.58 (quartet, 2H), 2.74 (t, 2H), 3.88 (t, 2H); ^{13}C nmr ($CDCl_3$) δ: 14.61, 23.96, 25.54, 28.91, 63.84.

Alkyl 3-ethylthio-1-propanesulfonates (10)

(a) *Hexadecyl 3-ethylthio-1-propanesulfonate (10a)*

A solution of triethylamine (5.05 g, 50 mmol) in CCl_4 (100 mL) was added dropwise during 45 min (very slowly at the beginning) to a solution of 3-ethylthio-1-propanesulfonyl chloride (**8**) (3.64 g, 18 mmol) and 1-hexadecanol (3.0 g, 12.4 mmol) in CCl_4 (100 mL). The mixture was stirred at room temperature for 0.5 h longer and washed, twice with 100 mL portions of 1 *M* HCl, 100 mL of H_2O, 100 mL of 5% Na_2CO_3, and three other 100 mL portions of H_2O. The water layer was washed each time with an additional 5 mL of CCl_4. The organic layer was then dried over $MgSO_4$ and the solvent evaporated under reduced pressure yielding 4.7 g (94%) of the product (**10***a*) which was recrystallized from pentane (50 mL) at −20°C. The white needles were collected by filtration and washed with cold pentane, mp 40°C; ir ν_{max}: 3020 (w), 2920 (vs), 2850 (s), 1465 (w), 1450 (w), 1355 (m), 1340 (m), 1160 (s), and 940 (m) cm^{-1}; ^1H nmr ($CDCl_3$) δ: 0.88 (t, 3H), 1.19–1.33 (m, 29H), 1.75 (t, 2H), 2.14 (quintet, 2H), 2.55 (quartet, 2H), 2.68 (t, 2H), 3.26 (t, 2H), 4.23 (t, 2H). *Anal.* calcd. for $C_{21}H_{44}O_3S_2$: C 61.66, H 10.77, S 15.66; found: C 61.63, H 10.80, S 15.70. The following esters were prepared similarly.

(b) *Butyl 3-ethylthio-1-propanesulfonate (10b)*

3-Ethylthio-1-propanesulfonyl chloride (**8**) (3.04 g, 15 mmol) and 1-butanol (1.11 g, 150 mmol) in 80 mL of CCl_4 and triethylamine (4.04 g, 40 mmol) in 80 mL of CCl_4 gave a colourless liquid (3.45 g, 96%) which was purified by distillation at reduced pressure, $bp_{0.001}$ 83–84°C (2.81 g, 78%); ir ν_{max}: 2960 (vs), 2930 (vs), 2875 (s), 1450 (s), 1410 (m), 1350 (vs, br), 1300 (s), 1260 (s), 1165 (vs), 1055 (m), 1010 (s), 990 (s), 950 (vs, br), 885 (vs), 850 (s), and 820 (s) cm^{-1}; ^1H nmr ($CDCl_3$) δ: 0.96 (t, 3H), 1.27 (t, 3H), 1.38–1.92 (m, 4H), 2.14 (m, 2H), 2.44–2.80 (m, 4H), 3.28 (t, 2H), 4.26 (t, 2H); ms M^+ calcd.: 240.0854; found: 240.0857.

(c) *Neopentyl 3-ethylthio-1-propanesulfonate (10c)*

3-Ethylthio-1-propanesulfonyl chloride (**8**) (6.1 g, 30 mmol) and neopentyl alcohol (2.2 g, 25 mmol) in 150 mL of CCl_4 and triethylamine (8.08 g, 80 mmol) in 100 mL of CCl_4 gave a slightly yellow liquid (6.05 g, 95%). The compound **10***c* was recrystallized from pentane in Dry Ice to give white needles, mp ~0°C; ir (neat) ν_{max}: 2950 (vs), 2910 (s), 2855 (m), 1470 (m), 1445 (m), 1350 (vs), 1335 (s), 1260 (w), 1160 (vs), 955 (vs), 930 (s), 850 (m), and 825 (m) cm^{-1}; ^1H nmr ($CDCl_3$) δ: 1.00 (s, 9H), 1.26 (t, 3H), 2.12 (quintet, 2H), 2.54 (quartet, 2H), 2.68 (t, 2H), 3.27 (t, 2H), 3.87 (s, 2H).

(d) *3-Buten-1-yl 3-ethylthio-1-propanesulfonate (10d)*

3-Ethylthio-1-propanesulfonyl chloride (**8**) (2.43 g, 12 mmol) and 3-buten-1-ol (0.86 g, 12 mmol) in CCl_4 (50 mL) and triethylamine (4.04 g, 40 mmol) in CCl_4 (80 mL) gave a colourless liquid (2.5 g, 89%); ir (neat) ν_{max}: 3070 (w), 2960 (s), 2920 (s), 2860 (m), 1640 (w), 1445 (m), 1425 (m), 1355 (vs), 1340 (vs), 1265 (s), 1165 (vs), 950 (vs, br), 900 (vs), and 845 (m) cm^{-1}; ^1H nmr ($CDCl_3$) δ: 1.25 (t, 3H), 2.06 (quintet, 2H), 2.38–2.71 (m, 6H), 3.22 (t, 2H), 4.22 (t, 2H), 5.07–5.27 (m, 2H), 5.60–6.00 (m, 1H).

(e) *1-Methylheptyl 3-ethylthio-1-propanesulfonate (10e)*

3-Ethylthio-1-propanesulfonyl chloride (**8**) (2.43 g, 12 mmol) and 2-octanol (1.56 g, 12 mmol) in CCl_4 (50 mL) and triethylamine (3.03 g, 30 mmol) in CCl_4 (60 mL) gave a colourless liquid (3.25 g, 91%); ir ν_{max}: 2960–2910 (vs), 2860 (vs), 1460–1450 (s), 1370–1320 (br, vs), 1265 (m), 1170–1160 (vs), 1115 (m), 1025 (w), 960 (m), 910 (vs), and 875 (s) cm^{-1}; ^1H nmr ($CDCl_3$) δ: 0.89 (t, 3H), 1.18–1.64 (m, 16H), 2.13 (quintet, 2H), 2.55 (quartet, 2H), 2.68 (t, 2H), 3.23 (t, 2H), 4.74–4.92 (m, 1H); ms M^+ calcd.: 269.1479; found: 269.1478.

S-Ethyl-S-3-[(hexadecyloxy)sulfonyl] propyl-S-methylsulfonium methylsulfate (12a)

Hexadecyl 3-ethylthio-1-propanesulfonate (**10***a*) (2.04 g, 5 mmol) was dissolved in dimethyl sulfate (10 mL, BDH, redistilled, bp_2 56°C), heated for 0.5 h at 100°C, cooled to 60°C, and the excess of Me_2SO_4 distilled off under reduced pressure. The residue was dissolved in anhydrous ether (15 mL), stirred for 5 min, and cooled to give **13***a* as white hygroscopic crystals. The recrystallization from

Can. J. Chem. Downloaded from www.nrcresearchpress.com by 210.87.254.42 on 09/06/12
For personal use only.

Can. J. Chem. Downloaded from www.nrcresearchpress.com by 210.87.254.42 on 09/06/12
For personal use only.

anhydrous ether was repeated several times. Yield 2.40 g (90%); ir ν_{max}: 2970 (s), 2930 (s), 1700 (w, br), 1635 (w), 1445 (w), 1415 (w), 1385 (w), 1340 (s), 1250–1200 (vs, br), 1160 (vs), 1005 (vs), 950 (w) and 910 (vs) cm^{-1}; ^1H nmr ($CDCl_3$) δ: 0.88 (t, 3H), 1.26 (s, 26H), 1.50 (t, 3H), 1.64–1.73 (m, 2H), 2.34 (quintet, 2H), 2.99 (s, 3H), 3.42–3.56 (m, 6H), 3.70 (s, 3H), 4.25 (t, 2H).

S-*Ethyl*-S-*methyl*-S-*3-[(neopentyloxy)sulfonyl] propylsulfonium methylsulfate (**12**c)*

Neopentyl 3-ethylthio-1-propanesulfonate (**10***c*) (1.02 g, 4 mmol) was methylated with 10 mL of dimethylsulfate as described for the preparation of **12***a* yielding 1.44 g (96%) of **12***c*; ir (neat) ν_{max}: 2950 (vs), 2865 (m), 1480 (w), 1455 (w), 1425 (w), 1350 (vs), 1240 (vs), 1220 (vs), 1165 (vs), 1055 (m), 1005 (s), 955 (s), 930 (s), 910 (vs), and 855 (m) cm^{-1}; ^1H nmr ($CDCl_3$) δ: 0.99 (s, 9H), 1.51 (t, 3H), 2.35 (quintet, 2H), 3.01 (s, 3H), 3.42–3.57 (m, 6H), 3.68 (s, 3H), 3.93 (s, 2H).

S-*3-[(3-Buten-1-yl)oxysulfonyl] propyl*-S-*ethyl*-S-*methylsulfonium methylsulfate (**12**d)*

Compound **10***d* (2.4 g, 10 mmol) was methylated with 8 mL of dimethyl sulfate as described for the preparation of **12***a* yielding 2.83 g (79%) of **12***d*; ir (neat) ν_{max}: 2970 (s), 2930 (s), 1700 (w, br), 1635 (w), 1445 (w), 1415 (w), 1385 (w), 1340 (s), 1250–1200 (vs, br), 1160 (vs), 1005 (vs), 950 (w), and 910 (vs) cm^{-1}; ^1H nmr ($CDCl_3$) δ: 1.51 (t, 3H), 2.28–2.60 (m, 4H), 3.00 (s, 3H), 3.44–3.57 (m, 6H), 3.69 (s, 3H), 4.32 (t, 2H), 5.08–5.29 (m, 2H), 5.61–6.02 (m, 1H).

S,S-*Diethyl*-S-*3-[(hexadecyloxy)sulfonyl] propylsulfonium ethylsulfate (**13**a)*

Hexadecyl 3-ethylthio-1-propanesulfonate (**10***a*) (3.3 g, 8 mmol) was dissolved in 10 mL of diethyl sulfate (BDH, redistilled, $bp_{0.2}$ 95°C), heated for 1 h at 110°C, and the excess of Et_2SO_4 distilled off under reduced pressure. The residue was dissolved in anhydrous ether and cooled. White crystals were precipitated and washed several times with anhydrous ether at −20°C to yield 4.4 g (99%) of **13***a*; ir ν_{max}: 3000 (vs), 2920 (vs), 2850 (m), 1455 (m), 1420 (w), 1385 (m), 1370 (m), 1345 (s), 1250–1200 (vs, br), 1165 (vs), 1105 (m), 1055 (m), 1015 (vs), and 915 (vs) cm^{-1}; ^1H nmr ($CDCl_3$) δ: 0.88 (t, 3H), 1.14–1.34 (m, 3H), 1.27 (s, 26H), 1.43 (t, 6H), 1.48–1.67 (m, 2H), 2.36 (quintet, 2H), 3.46–3.72 (m, 8H), 4.04 (quartet, 2H), 4.26 (t, 2H).

S-*3-(Butoxysulfonyl) propyl*-S,S-*diethylsulfonium ethylsulfate (**13**b)*

Butyl 3-ethylthio-1-propanesulfonate (**10***b*) (0.24 g, 1 mmol) was ethylated with diethyl sulfate (20 mL, 153 mmol) as described for the preparation of **13***a*, yielding **13***b* as a clear colourless liquid (0.33 g, 84%); ir ν_{max}: 2965 (vs), 2940 (vs), 2880 (s), 1455 (s), 1420 (m), 1350 (vs), 1260 (vs, br), 1160 (vs, br), 1055 (s), 1010 (vs), 940 (vs, br), 885 (s), 860 (s), and 830 (s) cm^{-1}; ^1H nmr ($CDCl_3$) δ: 0.95 (t, 3H), 1.1–1.9 (m, 13H), 2.37 (m, 2H), 3.57 (m, 8H), 4.3 (m, 4H).

S,S-*Diethyl*-S-*3-[(neopentyloxy)sulfonyl] propylsulfonium ethylsulfate (**13**c)*

Neopentyl 3-ethylthio-1-propanesulfonate (**10***c*) (1 g, 4 mmol) was ethylated with diethyl sulfate (10 mL, 75 mmol) as described for the preparation of **13***a* to yield **13***c* as a viscous liquid (1.435 g, 89%); ir (neat) ν_{max}: 2960 (vs), 2865 (m), 1480 (w), 1455 (w), 1425 (w), 1350 (vs), 1240 (vs), 1220 (vs), 1165 (vs), 1055 (m), 1005 (s), 995 (s), 930 (s), 910 (vs), and 855 (m) cm^{-1}; ^1H nmr ($CDCl_3$) δ: 0.99 (s, 9H), 1.28 (t, 3H), 1.53 (t, 6H), 2.38 (quintet, 2H), 3.41–3.79 (m, 8H), 3.94 (s, 2H), 4.04 (quartet, 2H).

S,S-*Diethyl*-S-*3-[(1-methylheptyloxy)sulfonyl]propylsulfonium ethylsulfate (**13**e)*

1-Methylheptyl 3-ethylthio-1-propanesulfonate (**10***e*) (2.96 g, 10 mmol) was ethylated with diethyl sulfate (15 mL, 110 mmol) as described for the preparation of **13***a* to yield **13***d* as a viscous liquid (3.96 g, 82%); ir ν_{max}: 2940–2900 (br, vs), 2840 (s), 1340–1310 (br, s), 1270–1135 (br, vs), 1000 (vs), and 900 (vs) cm^{-1}; ^1H nmr (CD_3CN) δ: 1.19–1.60 (m, 25H), 2.38 (quintet, 2H), 3.21 (t, 2H), 3.32–3.60 (m, 6H), 4.07 (quartet, 2H), 4.15–4.45 (m, 1H).

3-(Diethylsulfonio)propane-1-sulfonate (7)

1,3-Propane sultone (**5**) (Aldrich, purified by distillation $bp_{0.3}$ 94°C, 12.2 g, 0.1 mol) was refluxed with diethyl sulfide (45 g, 0.5 mol) for 40 min, cooled, and the abundant white precipitate filtered off (16.1 g, 76%). The filtrate was refluxed for an additional 2 h yielding 2.2 g (10%) of a second crop. The betaine (**7**) was recrystallized from absolute ethanol–ether, mp 260°C (dec.); ir (KBr) ν_{max}: 2970 (s), 2950 (s), 2920 (s), 1450 (s), 1425 (m), 1385 (m), 1305 (m), 1290 (s), 1265 (m), 1215 (vs), 1200–1180 (vs, br), 1055 (m), 1030 (vs) cm^{-1}; ^1H nmr (D_2O) δ: 1.45 (t, 6H), 2.26 (quintet, 2H), 3.09 (t, 2H), 3.36 (quartet, 4H), 3.47 (t, 2H). *Anal.* calcd. for $C_7H_{16}O_3S_2$: C 39.60, H 7.60, S 30.20; found: C 39.61, H 7.71, S 30.11.

S,S-*Diethyl*-S-*3-(chlorosulfonyl)propylsulfonium chloride (**9**)*

3-(Diethylsulfonio)propane-1-sulfonate (**7**) (1.06 g, 5 mmol) was dissolved in thionyl chloride (15 mL) and refluxed gently for 8–10 min. Most of the excess $SOCl_2$ was then evaporated under reduced pressure. Residual $SOCl_2$ was removed as follows. The residue was dissolved in freshly dried acetonitrile (20 mL) and evaporated; CH_3CN (20 mL) was again added and evaporated; freshly dried nitromethane (20 mL) was added and evaporated. The oily product **9** dissolves easily in water ($t_{1/2}$ for hydrolysis ~40 min at 37°C, with betaine (**7**) being the product), easily in CH_3NO_2 and in CH_3CN, and slightly in CH_2Cl_2; ir (neat) ν_{max}: 2960 (s), 2920 (s), 1445 (s), 1415 (m), 1370 (vs, br), 1270 (s), 1160 (vs), 1030 (s), 970 (m) cm^{-1}; ^1H nmr (CD_3CN) δ: 1.40 (t, 6H), 2.46 (quintet, 2H), 3.48 (quartet, 4H), 3.67 (t, 2H), 4.34 (t, 2H); ^1H nmr (D_2O) δ: 1.44 (t, 6H), 2.55 (quintet, 2H), 3.42 (quartet, 4H), 3.53 (t, 2H), 4.26 (t, 2H).

A separate nmr experiment showed that the maximum amount of the product **9** (ca. 80%) was observed after 10 min of gentle reflux of **7** in $SOCl_2$. The formation of **9** was accompanied by decomposition so that after 20 min of the reflux only ca. 50% of **9** was observed and after another 20 min almost 90% of the product was gone. In another nmr experiment purified **9** was refluxed in freshly dried acetonitrile for 10 h and the spectrum showed the product to be entirely **8**. In the presence of $SOCl_2$, however, no signals characteristic of **8** were observed.

S,S-*Diethyl*-S-*3-[(hexadecyloxy)sulfonyl] propylsulfonium chloride (**11**a)*

S,S-Diethyl-*S*-3-(chlorosulfonyl)propylsulfonium chloride (**9**) (1.34 g, 5 mmol) dissolved in freshly dried acetonitrile (15 mL) was cooled in a CCl_4 – Dry Ice bath (−23°C) and 1-hexadecanol (315 mg, 1.3 mmol) in dried methylene chloride (25 mL) added. A cold solution of freshly dried triethylamine (0.6 g, 6 mmol) in CH_2Cl_2 (20 mL) was then added dropwise (very slowly at the beginning). When the addition was complete (30–40 min) the solution was stirred for another 0.5 h while the temperature of the reaction mixture was allowed to rise to 0°C. The excess of NEt_3 was then washed out with two portions of dilute hydrochloric acid (1 *M*, 50 mL) with some ice added to bring the temperature of the solution to ca. 0°C and the organic solution was washed three times with water (50 mL each). A small sample of the reaction mixture was taken and the solution evaporated under reduced pressure at as low a temperature as possible. The ^1H nmr spectrum of the crude product showed peaks at 0.89 (t, 3H), 1.27 (s, 26H), 1.54 (t, 6H), 1.6–1.8 (m, 2H), 2.44 (quintet, 2H), 3.50 (t, 2H), 3.58 (quartet, 4H), 3.81 (t, 2H), 4.26 (t, 2H), characteristic of **11***a*.

S,S-*Diethyl*-S-*3-[(hexadecyloxy)sulfonyl] propylsulfonium picrate (**15**a, X^- = picrate)*

The CH_2Cl_2–CH_3CN solution of **11***a* was extracted twice with potassium picrate (1.1 g, 4 mmol, 150 mL of H_2O) and the excess of potassium picrate washed out with water (5–7 portions, 100 mL each). Each water layer was additionally washed with CH_2Cl_2 (10 mL); compound **15***a*, X^- = picrate, was found to be partly soluble in H_2O making the aqueous solutions milky. The organic layer was then

Can. J. Chem. Downloaded from www.nrcresearchpress.com by 210.87.254.42 on 09/06/12
For personal use only.

filtered twice through a paper filter and the solvent evaporated yielding an orange crude product **15***a* (X^- = picrate) (819 mg, 97%). The product was recrystallized from ethanol giving sticky crystals (730 mg, 86%), mp 82–85°C; ir (KBr) ν_{max}: 2900 (vs), 2835 (s), 1625 (m), 1605 (w), 1545 (w), 1460 (w), 1340 (s), 1300 (m), 1255 (m), 1230 (m), 1205 (m), 1155 (m) cm^{-1}; ^1H nmr ($CDCl_3$) δ: 0.88 (t, 3H), 1.27 (s, 26H), 1.55 (t, 6H), 1.6–1.8 (m, 2H), 2.42 (quintet, 2H), 3.49 (t, 2H), 3.57 (quartet, 4H), 3.81 (t, 2H), 4.26 (t, 2H), 8.79 (s, 2H). *Anal.* calcd. for $C_{29}H_{51}O_{10}S_2N_3$: C 52.33, H 7.67, S 9.62, N 6.32; found: C 52.48, H 7.83, S 9.62, N 6.31.

Compound **15***a* (X^- = picrate) was also obtained in the same manner in 83% yield from **13***a*.

S,S-*Diethyl*-S-*3-[(hexadecyloxy)sulfonyl] propylsulfonium camphor-10-sulfonate (15*a, *X^- = camphor-10-sulfonate)*

d,l-Camphor-10-sulfonic acid (0.93 g, 4 mmol, 100 mL) was used to obtain **15***a* (X^- = camphor-10-sulfonate) from a similar amount of the CH_2Cl_2–CH_3CN solution of **11***a* and using the same work-up as described for preparation of **15***a* (X^- = picrate). White sticky crystals of **15***a* (X^- = camphor-10-sulfonate) were obtained (768 mg, 88%); ir ν_{max}: 2970 (vs), 2850 (s), 1730 (m), 1350 (vs), 1240 (vs), 1165 (vs), 1045 (m), 950 (s), and 910 (vs) cm^{-1}; nmr ($CDCl_3$) δ: 0.82 (s, 3H), 0.88 (t, 3H), 1.07 (s, 3H), 1.26 (s, 26H), 1.49 (t, 6H), 1.43–3.40 (m, 15H), 3.55 (quartet, 4H), 3.52–4.00 (m, 2H), 4.28 (t, 2H).

S,S-*Diethyl*-S-*3-[(hexadecyloxy)sulfonyl] propylsulfonium fluoride (15*a, *X = F)*

A modification of the literature procedure (16) was used to prepare the F^--resin: Rexyn 203(OH) resin (7 g, 6.3 mequiv./g, 44 mmol) was treated with an excess of hydrofluoric acid (49.2% HF, 10 mL, diluted with H_2O, 190 mL) and the excess of aqueous HF was washed out with excess of distilled water to make the resin neutral and then the resin was washed with methanol (100 mL). A solution of **12***a* (2.3 g, 4 mmol) in methanol (50 mL) was then passed through the column (30 drops a minute) and the column washed with 100 mL of methanol; the methanol fractions were collected and the solvent evaporated under reduced pressure at ca. 0°C. Compound **15***a* (X = F) was found to be very hygroscopic and fragile so even gentle warming gave a product which showed, among other peaks, a doublet of triplets at δ 4.4 (J_{HF} = 48 Hz) in the ^1H nmr spectrum, characteristic of 1-fluorohexadecane. This decomposition product was easily washed out with cold hexane.

Reactions of S-*[3]betylates*

Reactants, quantities, reaction conditions, and yields are summarized in Table 1 and the spectra and mode of identification of products in Table 2. Examples of each of the four procedures referred to in Table 1 are given below.

Procedure A

S,S-Diethyl-3-[(hexadecyloxy)sulfonyl]propylsulfonium picrate (**15***a*, X^- = picrate; 1.33 g, 2 mmol) was suspended in water (50 mL) and potassium cyanide added (1.3 g, 20 mmol). A white precipitate (apparently **15***a*, X = CN) was formed after a few minutes; the suspension was heated at 80°C for 2 h. After cooling, the reaction mixture was extracted three times with methylene chloride (50 mL each), the organic layers pooled, dried over $MgSO_4$, and the solvent evaporated. The residue was dissolved in benzene (30 mL) and purified by filtration through a short column of silica gel; evaporation of the solvent gave hexadecyl cyanide as a colourless oil (381 mg, 76%) (see Table 2).

Procedure B

S,S-Diethyl-*S*-3-[(hexadecyloxy)sulfonyl]propylsulfonium ethylsulfate (**13***a*, 0.84 g, 1.5 mmol) was dissolved in methylene chloride (50 mL) and added to a solution of sodium azide (0.98 g, 15 mmol) in water (50 mL) and stirred at room temperature for 18 h. The organic layer was separated and the aqueous phase extracted with another portion of CH_2Cl_2 (30 mL); the organic solutions were pooled, dried over $MgSO_4$, the solvent evaporated, the residue dissolved in benzene (30 mL) and purified by filtration through a short column of silica gel to give hexadecyl azide as a colourless oil (332 mg, 83%) (see Table 2).

Procedure C

Sodium metal (560 mg, 20 mmol) was dissolved in absolute ethanol (20 mL) and then *S*-ethyl-*S*-methyl-*S*-3-[(hexadecyloxy) sulfonyl]propylsulfonium methylsulfate (**12***a*, 535 mg, 1 mmol) was added and the mixture stirred at room temperature for 1.5 h. The reaction mixture was then diluted with CCl_4 (40 mL) and washed with 3 portions of water (50 mL each). The organic layer was dried over sodium sulfate and the solvent evaporated to give ethyl hexadecyl ether as a colourless oil (240 mg, 90%) (see Table 2).

Procedure D

A sample of *S,S*-diethyl-3-[(hexadecyloxy)sulfonyl]propylsulfonium picrate (**15***a*, X^- = picrate; 665 mg, 1 mmol) was refluxed in toluene (15 mL) for 8 h. On cooling, a white precipitate of betaine was formed. This was filtered off and the toluene solution diluted with methylene chloride (50 mL), washed with water (three times, 50 ml each), dried over $MgSO_4$, and the solvent evaporated to dryness giving yellowish crystals of crude product (492 mg), which after two recrystallizations from petroleum ether gave hexadecyl picryl ether as white crystals, mp 64–65°C, 319 mg, 70% (see Table 2).

Potassium 3-phenylthio-1-propanesulfonate (16)

1,3-Propane sultone (**5**) (6.1 g, 50 mmol) in absolute ethanol (40 mL) was added dropwise during 15 min to a solution of benzenethiol (7.7 g, 70 mmol) and KOH (4 g, 70 mmol) in absolute ethanol (80 mL). After 0.5 h the precipitate was filtered off (12.7 g; 94%) and recrystallized from ethanol giving white fine crystals (11.5 g, 85%), mp 280°C (dec.); ir (KBr) ν_{max}: 3040 (w), 2940 (m), 2900 (w), 1565 (w), 1470 (m), 1430 (m), 1255–1245 (s), 1220–1200 (vs), 1180–1170 (vs), 1150 (m), 1090 (m), and 1045 (vs) cm^{-1}; ^1H nmr (D_2O) δ: 2.03 (quintet, 2H), 3.03 (2t, 4H), 7.18 (m, 5H).

3-Phenylthio-1-propanesulfonyl chloride (17)

Recrystallized potassium 3-phenylthio-1-propanesulfonate (**16**), (5.4 g, 20 mmol) was suspended in thionyl chloride (20 mL) and one drop of DMF was added. The suspension was refluxed for 10 min, cooled, diluted with methylene chloride (50 mL), and poured onto ice. The organic layer was washed with ice-water and then with five 100 mL portions of water. Each water portion was additionally washed with 5 mL of CH_2Cl_2. The organic layer was then dried with anhydrous $MgSO_4$ and the solvent evaporated to give an oily product (4.8 g, 96%) which was stable for at least 2 weeks at room temperature in the neat state and 1 month in $CDCl_3$ solution; ir ν_{max}: 3060 (m), 3050 (m), 2950 (s), 1580 (s), 1480 (s), 1435 (s), 1375–1350 (br, vs), 1300 (s), 1255 (s), 1170–1150 (br, vs), 1090 (m), 1020 (s), and 1000 (m) cm^{-1}; ^1H nmr ($CDCl_3$) δ: 2.30 (quintet, 2H), 3.09 (t, 2H), 3.86 (t, 2H), 7.26–7.42 (m, 5H).

Alkyl 3-phenylthio-1-propanesulfonates (18)

The following esters were obtained following the general procedure for preparing **10***a*.

(a) *Hexadecyl 3-phenylthio-1-propanesulfonate (18*a*)*

3-Phenylthio-1-propanesulfonyl chloride (**17**) (5.01 g, 20 mmol) and 1-hexadecanol (4.36 g, 18 mmol) in CCl_4 (150 mL) and triethylamine (4.04 g, 40 mmol) in 80 mL of CCl_4 gave a white solid (7.76 g, 95%), which was recrystallized from pentane, mp 40°C; ir ν_{max}: 2910 (s), 2840 (s), 1465 (w), 1430 (w), 1345 (m), 1150 (s), and 955 (w) cm^{-1}; ^1H nmr ($CDCl_3$) δ: 0.88 (t, 3H), 1.26 (s, 26H), 1.45–1.76 (m, 2H), 2.15 (quintet, 2H), 3.07 (t, 2H), 3.27 (t, 2H), 4.19 (t, 2H), 7.27–7.41 (m, 5H); ms M^+ calcd.: 456.2731; found: 456.2723.

(b) *Neopentyl 3-phenylthio-1-propanesulfonate (18*b*)*

3-Phenylthio-1-propanesulfonyl chloride (**17**), (5.01 g, 20 mmol) and neopentyl alcohol (1.32 g, 15 mmol) in 150 mL of CCl_4 and triethylamine (6.06 g, 60 mmol) in 80 mL of CCl_4 gave slightly brown liquid (4.4 g, 97%); ir ν_{max}: 3040 (w), 2945 (br, vs), 2850 (m),

Can. J. Chem. Downloaded from www.nrcresearchpress.com by 210.87.254.42 on 09/06/12
For personal use only.

TABLE 2. Characterization of products listed in Table 1

Product	Infrared maxima (cm^{-1})	^1H nmr (δ)	Further characterization
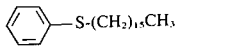	(KBr) 2950 (m), 2910 (vs), 2840 (s), 1580 (w), 1480 (w), 1470 (w), 1460 (w), 1435 (w), 1020 (w)	0.88 (t, 3H), 1.26 (s, 26H), 1.37–1.52 (m, 2H), 2.91 (t, 2H), 7.18–7.33 (m, 5H)	mp 48–49°C; ^1H nmr and ir spectra identical to those of an authentic sample[a,b]
$CH_3—\overset{+}{N}H_2—(CH_2)_{15}CH_3\ Cl^-$	(KBr) 2955 (s), 2930 (vs), 2855 (s), 2740 (m, br), 2450 (w, br), 1590 (w), 1460 (m), 1130 (s, br), 1030 (w), 940 (w), 920 (w), 860 (w), 825 (w)	0.88 (t, 3H), 1.26 (s, 26H), 1.75–1.95 (m, 2H), 2.68 (s, 3H), 2.93 (t, 2H), 9.45 (s, 2H)	mp 169–170°C (lit.[c] 169–170°C), mixture mp with an authentic sample 170°C; ^1H nmr and ir spectra identical to those of an authentic sample[b]
$CH_3CH_2—O—(CH_2)_{15}CH_3$	2930 (s), 2860 (s), 1470 (w), 1380 (m), 1355 (w), 1265 (m), 1165 (m), 1105 (s), 1015 (m), 940 (w)	0.88 (t, 3H), 1.19 (t, 3H), 1.26 (s, 26H), 1.4–1.7 (m, 2H), 3.40 (t, 2H), 3.46 (q, 2H)	^1H nmr and ir spectra identical to those of an authentic sample prepared from hexadecyl bromide and sodium ethoxide[b,d]
$CH_3(CH_2)_{15}F$	2930 (s), 2860 (s), 1465 (w), 1045 (w), 995 (w)	0.88 (t, 3H), 1.27 (s, 26H), 1.80 (t, 2H), 4.43 (d of t, J_{HF} = 48 Hz)	^1H nmr and ir spectra identical to those of an authentic sample[b,d]
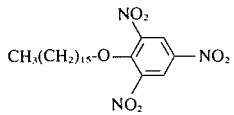	2930 (m), 2860 (m), 1610 (w), 1550 (s), 1350 (s)	0.88 (t, 3H), 1.27 (s, 26H), 1.84 (t, 2H), 4.26 (t, 2H), 8.87 (s, 2H)	mp 64–65°C, mixture mp with an authentic sample 64–65°C; ^1H nmr and ir spectra identical to those of an authentic sample[d,e]
$CH_3(CH_2)_{15}—CN$	2930 (s), 2860 (s), 2250 (m), 1470 (m)	0.88 (t, 3H), 1.26 (s, 26H), 1.60 (m, 2H), 2.33 (t, 2H)	^1H nmr and ir spectra identical to those of an authentic sample prepared from hexadecyl iodine and sodium cyanide[b,d]
$CH_3(CH_2)_{15}—N_3$	2930 (s), 2860 (s), 2100 (s), 1465 (m), 1360 (m), 1165 (m), 1020 (m), 945 (m), 925 (m)	0.87 (t, 3H), 1.25 (s, 26H), 1.56 (m, 2H), 3.22 (t, 2H)	^1H nmr and ir spectra identical to those of an authentic sample[b,f]
$CH_3(CH_2)_3—SCN$	2990 (vs), 2900 (s), 2180 (s), 1460 (s), and 1380 (m)	0.93 (t, 3H), 1.45 (m, 2H), 1.79 (m, 2H), 2.93 (t, 2H)	Calcd. M^+ for C_5H_9NS: 115.0456; found: 115.0456; ^1H nmr and ir spectra identical to those of an authentic sample[d,e]
$CH_3(CH_2)_5CH(CH_3)—SPh$	3080–3060 (w), 2960 (vs), 2930 (vs), 2850 (vs), 1585 (m), 1475 (s), 1440 (s), 1375 (m), 1090 (m), 1020 (m)	0.88 (t, 3H), 1.24–1.60 (m, 13H), 3.17 (m, 1H), 7.18–7.56 (m, 5H)	^1H nmr and ir spectra identical to those of an authentic sample[g]

[a]Reference 12.
[b]Prepared by J. D. Lock.
[c]Reference 13.
[d]Reference 5.
[e]Prepared by M. Aslam.
[f]Reference 14.
[g]Reference 15.

1580–1570 (w), 1435 (m), 1350–1320 (br, s), 1260 (w), 1150 (s), 950–920 (br, s), and 850–830 (s) cm^{-1}; ^1H nmr ($CDCl_3$) δ: 0.95 (s, 9H), 2.14 (quintet, 2H), 3.06 (t, 2H), 3.27 (t, 2H), 3.82 (s, 2H), 7.24–7.35 (m, 5H); ms M^+ calcd.: 302.1010; found: 302.1009.

S-*Ethyl*-S-*3*-[*(hexadecyloxy)sulfonyl*]*propyl*-S-*phenylsulfonium ethylsulfate (**19**a)*

Hexadecyl 3-phenylthio-1-propanesulfonate (**18***a*) (4.56 g, 10 mmol) was dissolved in diethyl sulfate (20 mL, freshly redistilled), heated for 10 h at 85°C, and the excess of Et_2SO_4 distilled off under reduced pressure. The residue was dissolved in anhydrous ether (20 mL), stirred for a few minutes, and cooled at −20°C to give **19***a* as white hygroscopic crystals. The recrystallization from anhydrous ether was repeated 3 times. Yield 3.1 g (52%); ir ν_{max}: 3000–2980 (m), 2930 (s), 2860 (m), 1445 (m), 1350 (m), 1265–1230 (s), 1170 (vs), 1050 (br, m), 1010–1000 (s), and 915 (s) cm^{-1}; ^1H nmr ($CDCl_3$) δ: 0.88 (t, 3H), 1.13–1.68 (m, 34H), 2.18 (quintet, 2H), 3.38–4.46 (m, 10H), 7.74–7.78 (m, 2H), 8.04–8.15 (m, 3H).

Acknowledgement

We thank the Natural Sciences and Engineering Research Council of Canada for support of this work.

1. J. F. KING, S. M. LOOSMORE, J. D. LOCK, AND M. ASLAM. J. Am. Chem. Soc. **100**, 1637 (1978).
2. J. F. KING, M. ASLAM, AND J. D. LOCK. Tetrahedron Lett. 3615 (1979).
3. J. F. KING AND M. ASLAM. Synthesis, 285 (1980).
4. J. F. KING AND M. ASLAM. Tetrahedron Lett. **22**, 3573 (1981).
5. J. F. KING, S. M. LOOSMORE, M. ASLAM, J. D. LOCK, AND M. J. MCGARRITY. J. Am. Chem. Soc. In press.
6. A. LE BERRE, A. ÉTIENNE, AND B. DUMAITRE. Bull. Soc. Chim. Fr. 946 (1970).
7. J. F. KING AND M. J. MCGARRITY. J. Chem. Soc. Chem. Commun. 1140 (1979).
8. R. E. ROBERTSON AND P. M. LAUGHTON. Can. J. Chem. **35**, 1319 (1957).
9. R. E. ROBERTSON. Prog. Phys. Org. Chem. **4**, 213 (1967).
10. A. C. KNIPE. *In* The chemistry of sulphonium salts. *Edited by* C. J. M. Stirling. John Wiley and Sons, Chichester and New York. 1981. pp 313–385 esp. pp 322–323.
11. P. A. LOWE. *In* The chemistry of sulphonium salts. *Edited by* C. J. M. Stirling. John Wiley and Sons, Chichester and New York. 1981. pp 267–312, esp. pp 273–274.
12. K. TAKAHASHI, K. OHKI, T. MIZUMA, AND S. TOYOSHIMA. Chem. Pharm. Bull. **8**, 757 (1960).
13. O. WESTPHAL AND D. JERCHEL. Ber. **73**, 1002 (1940).
14. E. LIEBER, T. S. CHAO, AND C. N. R. RAO. J. Org. Chem. **22**, 238 (1957).
15. E. L. ELIEL AND R. S. RO. J. Am. Chem. Soc. **79**, 5995 (1957).
16. J. M. MILLER, S. R. CATER, K-H SO, AND J. H. CLARK. Can. J. Chem. **57**, 2629 (1979).

Can. J. Chem. Downloaded from www.nrcresearchpress.com by 210.87.254.42 on 09/06/12
For personal use only.

Setchenow coefficients for naphthols by distribution method

M. BALÓN ALMEIDA, A. MAESTRE ALVAREZ,[1] E. MUÑOZ DE MIGUEL, AND E. SORIA DEL HOYO
Departamento de Química Física, Facultad de Ciencias Químicas, Universidad de Sevilla, Sevilla, Spain

Received December 11, 1981[2]

M. BALÓN ALMEIDA, A. MAESTRE ALVAREZ, E. MUÑOZ DE MIGUEL, and E. SORIA DEL HOYO. Can. J. Chem. **61**, 244 (1983).

Salting constant measurements have been made on 1-naphthol, 2-naphthol, and 1-NO-2-naphthol using a distribution method at 298 K. In general, the order of the salting effect is similar to that for other acidic nonelectrolytes. However, a net salting-in is observed in the pair 1-NO-2-naphthol − NaF, and such an effect is interpreted by postulating hydrogen bonding. A comparison of results with those found for benzene, naphthalene, phenol, etc..., reveals that salt effects for organic nonelectrolytes depend upon the solute size for a given salt.

Experimental k_s are compared with those calculated using various salting theories. The agreement is not quantitative.

M. BALÓN ALMEIDA, A. MAESTRE ALVAREZ, E. MUÑOZ DE MIGUEL et E. SORIA DEL HOYO. Can. J. Chem. **61**, 244 (1983).

Utilisant une méthode de distribution à 298 K, on a déterminé les constantes de salage du naphtol-1, du naphtol-2 et du NO-1 naphtol-2. En général, l'ordre de l'effet de sel est semblable à celui des autres acides non électrolytes Cependant on observe un relargage inverse net de la paire NO-1 naphtol-2 − NaF et on interprète un tel effet en supposant l'existence de liaisons hydrogène. Une comparaison des résultats avec ceux trouvés pour le benzène, la naphtalène, le phénol etc..., révèle que les effets de sel pour les non électrolytes organiques dépendent de la dimension de soluté pour un sel donné.

On a comparé les k_s expérimentaux avec ceux calculés en utilisant diverse théories de sel. L'accord n'est pas quantitatif.

[Traduit par le journal]

Introduction

A great amount of work has been done on the behavior of nonelectrolytes in aqueous electrolyte solutions (1−6). At present, the interest in the influence of electrolytes on the activity coefficients of nonelectrolytes in water and mixed solvents continues because of the increasing interest in the structural behavior of water and related problems (ion−nonelectrolyte−solvent interactions). The Setchenow coefficients, or salting constants, k_s, quantify direct interactions between the nonelectrolyte and the added salt (7).

A variety of theories have been used to calculate k_s (8); the McDevit and Long theory (MLT) and the scaled particle theory (SPT) have been the most useful in this context. The MLT and SPT were developed to describe salting effects of nonpolar solutes. Cross (9, 10) has expanded upon MLT to calculate activity coefficients of polar nonelectrolytes in salt solutions with reasonable success. For practical and theoretical reasons, most of the nonelectrolytes employed have been nonpolar solutes, but recent studies on the salting behavior of alcohols (11), tetrahydrofuran and acetonitrile (12), and cyclohexanone (13) have shown that SPT is actually the most successful theory for the prediction of the Setchenow constant of a polar solute in an inorganic salt solution.

It seemed interesting to us to study the salting effect in a series of naphthols because they present a polar character, great size, and a considerable hydrophobic group. Their comparison with benzene and naphthalene would help us to understand ion−nonelectrolyte−solvent interactions a little better. A comparison between experimental values and those predicted by the above theories may be interesting.

Experimental

The nonelectrolytes, 1-naphthol, 2-naphthol and 1-NO-2-naphthol were of the best commercially available quality (Merck, p.a., min. 99% GC) and they were purified by repeated recrystallization from water−methanol (mp, 1-naphthol 95−97°C, 2-naphthol 122−123°C, 1-NO-2-naphthol 106−108°C).

The salts employed LiCl, NaCl, KCl, NH_4Cl, HCl, Me_4NCl, $MgCl_2$, $BaCl_2$, NaF, KF, NaBr, NaI, and KI were purchased from Merck (p.a.) or Fluka (p.a.). They were purified by standard recrystallization procedures and kept in a vacuum desiccator. The organic solvents (extractants) were purchased from Merck (p.a.) and employed without being purified. Doubly distilled water was used in every experiment.

Distribution measurements

Distribution ratios of naphthols between water or salt solutions and inert organic solvent were determined by vigorous agitation of small aliquots. After equilibrium had been reached (15 min) the agitation was stopped and the systems were left in the bath for at least 2 hours. Aliquots of the aqueous phase were taken and after suitable dilution the concentrations of 1-naphthol, 2-naphthol, and 1-NO-2-naphthol were determined by measuring the optical density at 295, 320, and 380 nm respectively on a Beckman DBGT spectrophotometer equipped with digital readout. At each salt concentration 3−4 concordant replicate experiments were performed. All measurements were done at 25 ± 0.1°C.

The distribution method makes the study of very dilute solutions under identical conditions of both sparingly and readily soluble substances possible. Korenman proposed this method to obtain true Setchenow coefficients (14).

Results and discussion

The salt effect at high dilution can be estimated from the distribution of a nonelectrolyte between water, or aqueous electrolyte solutions, and an immiscible solvent (extractant) from the Setchenow equation:

$$[1] \quad \log \frac{K}{K_0} = k_s C_s$$

where K_0 and K are distribution constants of nonelectrolyte in water and aqueous electrolyte solutions respectively, C_s is the concentration of the salt, and k_s the Setchenow coefficient.

[1]Author to whom correspondence may be addressed.
[2]Revision received July 21, 1982.

0008-4042/83/020244-05$01.00/0
©1983 National Research Council of Canada/Conseil national de recherches du Canada

Can. J. Chem. Downloaded from www.nrcresearchpress.com by 210.87.254.105 on 09/06/12
For personal use only.

Can. J. Chem. Downloaded from www.nrcresearchpress.com by 210.87.254.105 on 09/06/12
For personal use only.

TABLE 1. Comparison of k_s for 1-naphthol by NaCl from solubility method and distribution method (25°C)

Extractant	k_s ($mol^{-1}dm^3$)	K_0[a]	$10^3\ S_0$ (mol dm^{-3})
Solubility method			
	0.237±0.002		9.39±0.05
Distribution method			
CCl_4	0.209±0.008	15.922	
$CHCl_3$	0.218±0.007	4.034	
C_6H_6	0.195±0.011	76.170	
C_6H_{12}	0.209±0.007	70.232	

[a]K_0 = distribution constant for 1-naphthol without salt.

TABLE 2. Setchenow coefficients for naphthols[a]

	k_s (mol^{-1} dm^3)		
Salt	1-Naphthol	2-Naphthol[b]	1-NO-2-Naphthol[c]
LiCl	0.193±0.008		
NaCl	0.209±0.008	0.186±0.006	+0.108±0.006
KCl	0.179±0.007		
NH_4Cl	0.101±0.005		
HCl	0.054±0.006		
Me_4NCl	−0.360±0.025[d]	−0.399±0.008[e]	−0.087±0.008[d]
$MgCl_2$	+0.332±0.021		+0.158±0.006
$BaCl_2$	0.352±0.015		
NaF	0.224±0.008		−0.533±0.037
KF	0.212±0.007		
NaBr	0.155±0.005		0.027±0.004
KBr	0.129±0.006		
NaI	0.191±0.006		−0.586±0.031
KI	0.174±0.013		

[a]Extractant CCl_4.
[b]K_0 = 9.011 in CCl_4; K_0 = 48.465 in $CHCl_3$.
[c]K_0 = 123.609 in CCl_4; K_0 = 4.035 in C_6H_{12}.
[d]Extractant C_6H_{12}.
[e]Extractant $CHCl_3$.

In Table 1, k_s values obtained by the solubility and distribution methods for 1-naphthol are compared. We observe that the distribution method produces a smaller k_s value than the solubility method. In the solubility method the concentration of 1-naphthol is 9.39×10^{-2} M and in the distribution method the concentration employed is 10^{-4} M. In a saturated solution solute−solute interactions may be observed; on the contrary, if the distribution method is used, we work with very dilute solutions and self-interaction may be avoided. Differences in k_s when applying the solubility and distribution methods have been observed for other solutes (1*a*). In Table 1 the effect on k_s when the organic solvent is changed in a given nonelectrolyte system is also shown. It seems that extractant does not affect the salting constants. In Table 2 the k_s values for 1-naphthol, 2-naphthol, and 1-NO-2-naphthol with various salts are given. In Figs. 1, 2, and 3 values of log K/K_0 are plotted against C_s. The slopes of the lines on these plots give the Setchenow constants for the various salts used.

A comparison of the k_s values (Table 1) shows that the salt orders for 1-naphthol are:

(*a*) $Ba^{2+} > Mg^{2+} > Na^+ > Li^+ > K^+ > NH_4^+ > H^+ > Me_4N^+$ (as chlorides)

(*b*) $F^- > Cl^- > I^- > Br^-$ (sodium and potassium)

These sequences reveal a behavior similar to other acidic nonelectrolytes (1). Setchenow coefficients for a series of nonelectrolytes are given in Table 3. Several comments can be made on various aspects: k_s increases with increasing size of the solutes (increase in hydrophobicity) for a given salt. So the

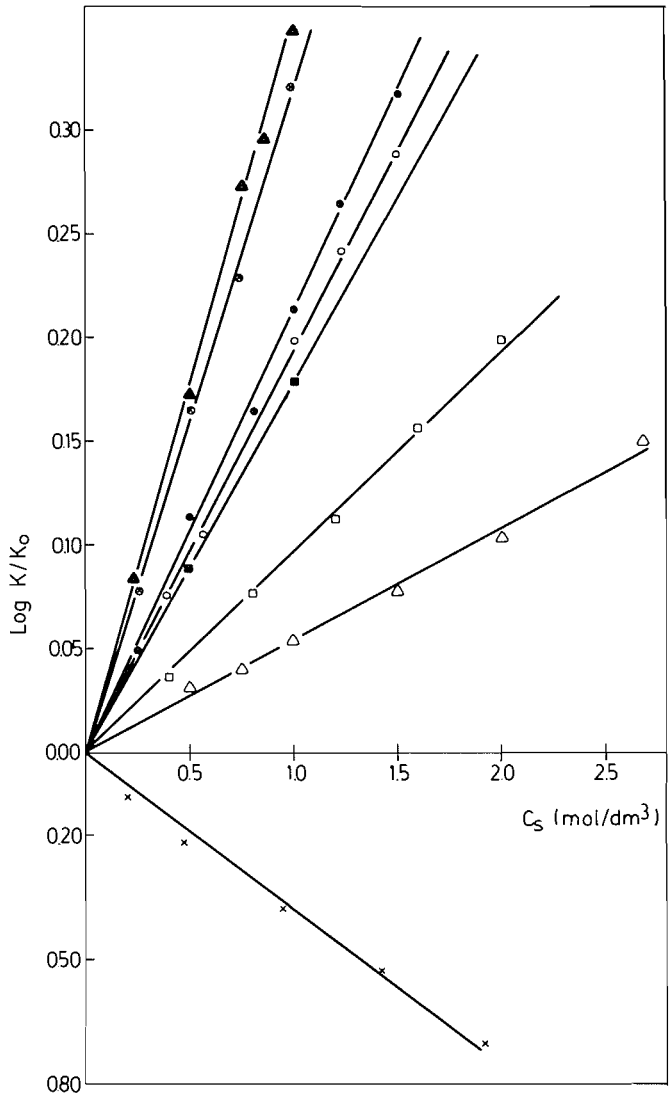

FIG. 1. Variation of log K/K_0 with salt molarity, C_s, for 1-naphthol at 25°C. ▲, $BaCl_2$; ⊗, $MgCl_2$; ●, NaCl; ○, LiCl; ■, KCl; □, NH_4Cl; △, HCl; ×, Me_4NCl.

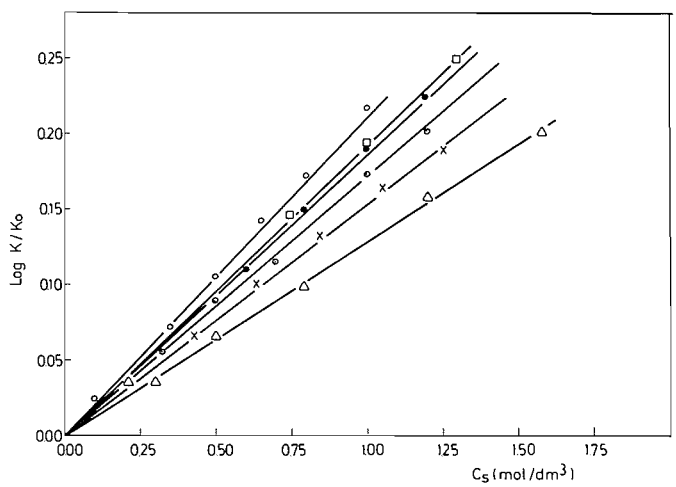

FIG. 2. Variation of log K/K_0 with salt molarity, C_s, for 1-naphthol at 25°C. ○, NaF; □, KF; ●, NaI; ⊙, KI; ×, NaBr; △, KBr.

Can. J. Chem. Downloaded from www.nrcresearchpress.com by 210.87.254.105 on 09/06/12
For personal use only.

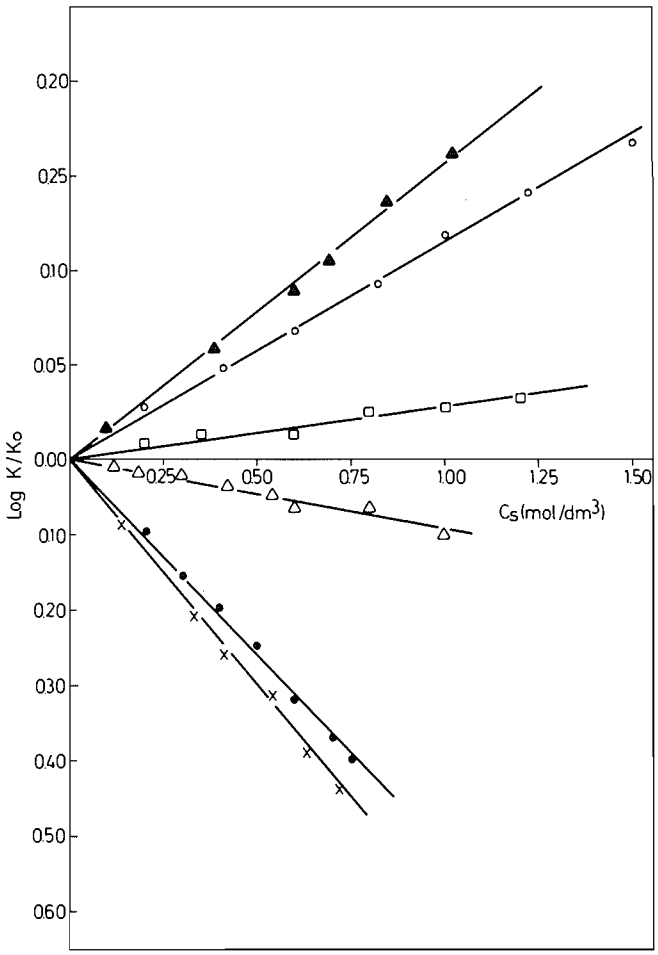

FIG. 3. Variation of log K/K_0 with salt molarity, C_s, for 1-NO-2-naphthol at 25°C. ▲, $MgCl_2$; ○, NaCl; □, NaBr; △, Me_4NCl; ●, NaF; ×, NaI.

pairs benzene−naphthalene, naphthalene−biphenyl, and phenol − 1-naphthol exhibit this behavior. In this sense, Treiner (15) has recently observed for some organic solutes (nonpolar and polar) that the k_s is a monotonic function of the solute size and the nonelectrolyte dipole moment plays no role. Korenman and Bortnikova (16) have found identical results in a series of alkylphenols in various salt solutions (k_s increases systematically with the number of carbon atoms in the alkyl group). The inclusion of an OH group in benzene (Table 3) leads to more negative Setchenow coefficients, the salting-in becoming more favorable. The same pattern is observed in the pair naphthalene − 1-naphthol or 2-naphthol. The salting constants for naphthols depend on the position of the hydroxyl group. It is a general phenomenon that the location and kind of substituent in an isomer series affect k_s in different ways. Table 3 shows how k_s is affected by different salts in a mononitrophenol series; with all the salts studied, k_s diminishes in the sequence *para* > *ortho* > *meta*. This decrease could even produce a net salting-in on *meta*-nitrophenol with alkali metal chlorides and bromides. The inclusion of a NO group in the 2-naphthol molecule leads to more negative Setchenow coefficients (Table 2). It is known that the interaction of organic compounds in water or salt solutions is essentially an entropic phenomenon (8). This interaction may involve an increase or decrease of entropy depending on whether hydrophilic or hydrophobic interactions predominate. The lowering of k_s for 1-NO-2-naphthol in relation to other naphthols studied could be interpreted as a balance between hydrophilic and hydrophobic groups in each particular molecule. The NO group will be able to increase the hydrophilic interactions to a greater extent than other naphthols will. This effect produces an increase of entropy greater than other naphthols do, and, therefore, k_s will be more negative.

The large salting-in effect of Me_4NCl on 1-naphthol and 2-naphthol is remarkable. The hydrophobic interactions are important when tetraalkylammonium salts are involved (17). These interactions will be more important when the solutes are large nonelectrolytes with a predominantly hydrophobic exterior, and this is the present case. At this point, we note the influence of NaF on 1-NO-2-naphthol. This salt exhibits a large salting-out with organic solutes, but its anomalous salting-in in the present case could involve hydrogen bonding to a fluoride ion by the hydroxyl group of the 1-NO-2-naphthol, because the NO group in the molecule weakens the adjacent OH bond and this makes hydrogen bonding easier. This increases the solubility of 1-NO-2-naphthol and produces a net salting-in effect.

It is interesting to consider theoretical values of k_s. McDevit and Long (18) proposed a theory based on a thermodynamic approach that relates the changes in solubility of nonelectrolytes to the electrostriction of the solvent and the partial molal volume of the nonelectrolytes. The expression given for k_s is:

$$[2] \quad k_s = \lim_{C_s \to 0} \frac{V_i^0 \, dP_e}{2.3RT \, dC_s} = \frac{V_i^0 (V_s - V_s^0)}{2.3RT \, \beta_0}$$

where V_i^0 is the partial molar volume of the solute at infinite dilution and may reasonably be taken as the molar volume of the pure solute, V_m, when V_i^0 data are lacking, since V_i^0 and V_m are frequently similar in magnitude. V_s^0 is the partial molar volume of the salt at infinite dilution, V_s is the volume occupied by the salt as a liquid (the intrinsic volume). The difference, $V_s - V_s^0$ is the electrostriction of the solvent caused by the salt and is proportional to the effective pressure, P_e, exerted by the salt in solution; β_0 is the compressibility of water. We will limit our study to 1-naphthol. For this nonelectrolyte, V_i^0 is taken as V_m which we have determined from the molecular weight M and the density ρ of the crystal (19). We have calculated k_s using effective pressure, P_e, of the electrolytes where these are known (18) and $V_s - V_i^0$ for those where P_e, is lacking (18) (KBr and $MgCl_2$). In the case of Me_4NCl and KI, V_s has been equated to the molar volume of the crystalline salt and V_i^0 is taken from ref. 20. The values of k_s calculated are compared with experimental values in Table 4.

The scaled-particle theory (SPT) has been applied to some systems to calculate Setchenow coefficients in order to predict the salting effect of nonpolar solutes in aqueous solutions (3). However, a few researchers have applied the SPT to salting effects on polar solutes with reasonable agreement (11, 13). Desrosiers and Desnoyers (21) have applied it to the transfer functions of But_4N^+ from water to *tert*-butylalcohol + water and urea + water mixtures and the agreement with experiment is good.

We have employed the equations of Masterton and Lee (3) to calculate k_s. In order to find k_s it is necessary to know diameters, σ, of nonelectrolytes, cation, and anion and polarizabilities, α, of nonelectrlytes, cation, and anion as well as the apparent molal volume, ϕ_v^0, of the salt at infinite dilution and the energy parameter of the nonelectrolyte (ϵ/k). These parameters are given in Table 5 and the calculated k_s values for 1-naphthol are reported in Table 4.

TABLE 3. Setchenow coefficients for some nonelectrolytes in aqueous salt solutions at 298 K

	LiCl	NaCl	KCl	NaBr	NaF	NaI	Ref.
Benzene	0.141	0.198	0.166	0.155	0.254	0.095	5,18
Naphthalene	0.180	0.260	0.204	0.169			32
Biphenyl	0.218	0.276	0.295	0.209			32
Phenol	0.143	0.172	0.133	0.111			1
1-Naphthol	0.193	0.209	0.179	0.155	0.224	0.191	[a]
1-NO-2-naphthol		0.108		0.027	−0.533	−0.586	[a]
o-Nitrophenol	0.138		0.094	0.076	0.244		16[b]
m-Nitrophenol	−0.152		−0.208	−0.278	0.202		16[b]
p-Nitrophenol	0.176		0.158	0.132	0.209		16[b]

[a]This work
[b]Reference 16 at 293 K.

TABLE 4. Experimental and calculated values of k_s for 1-naphthol

	LiCl	NaCl	KCl	NH_4Cl	HCl	Me_4NCl	$MgCl_2$
Experimental	0.193	0.209	0.179	0.101	0.054	−0.369	0.032
MLT	0.396	0.529	0.429	0.186	0.107	−0.584	1.092
SPT	0.223	0.306	0.268	0.012	—	−0.120	0.012
Cross	0.139	0.207	0.191	—	—	—	—

	$BaCl_2$	NaF	KF	NaBr	KBr	NaI	KI
Experimental	0.352	0.224	0.212	0.155	0.129	0.191	0.174
MLT	1.263	0.837	0.672	0.441	0.410	0.343	0.243
SPT	0.327	0.375	0.294	0.262	0.225	0.282	0.243
Cross	—	—	—	—	0.142	—	—

TABLE 5. Parameters used in SPT

		Electrolytes										
Parameter	1-Naphthol	Li^+	Na^+	K^+	NH_4^+	Me_4N^+	Mg^{2+}	Ba^{2+}	F^-	Cl^-	Br^-	I^-
ϵ/k (K)	123.3[a]											
σ(Å)	7.06[b]	1.88[d]	2.34[d]	2.98[d]	2.86[c]	5.02[c]	1.30[f]	2.70[f]	2.32[d]	3.28[d]	3.60[d]	4.10[d]
$10^{24}\cdot\alpha(cm^3)$	18.07[c]	0.075[d]	0.21[d]	0.87[d]	1.43[g]	9.55[h]	0.094[i]	1.55[i]	1.04[d]	3.02[d]	4.17[d]	6.28[d]

[a]Calculated from eq. 18 in ref. 3 and commented on in ref. 22.
[b]Calculated from density of crystal (19).
[c]Obtained by adding bond refraction given in ref. 20.
[d]Values for σ taken from Gourary and Adrian, where these are known (26).
[e]For NH_4^+ and Me_4N^+ from ref. 23.
[f]Reference 24.
[g]Reference 11.
[h]Reference 25.
[i]Reference 26; ϕ_v°, ref. 27.

TABLE 6. Sensitivity of k_s obtained from SPT to ionic size (σ) and intrinsic volume of salt (V_s) respectively

SPT (1-naphthol + NaCl)				
σ (cation and anion)[a]	P	W	G	G−A
k_s	0.335	0.427	0.393	0.306
Expanded MLT (1-naphthol + NaCl) (eq. [3])				
V_s[b] 26.9	27.5	28.9	29.1	30.4
k_s 0.163	0.170	0.198	0.207	0.237

[a]Values for σ from P = Pauling; W = Waddington; G = Goldsmidt; G−A = Gourary and Adrian; ref. 27.
[b]Reference 10.

From Table 4 we see that the values calculated from MLT are too large. In general, this is observed in many systems with MLT. However, the theory is able to predict the salting-in of Me_4NCl and gives the qualitative order of the salt effect. The values for k_s from SPT agree better with the experimental values than those from MLT, except for NH_4Cl. But SPT is very dependent on the various parameters chosen, particularly σ (cation and anion). In Table 6 we have calculated k_s for 1-naphthol with NaCl employing various σ from different sources. It is clear from Table 6 that the quantitative agreement may be very sensitive to σ.

Cross and McTigue (10) have extended the MLT to enable the calculation of activity coefficients of polar nonelectrolyte solutions. The relative mole fraction activity coefficients for the distribution of a nonelectrolyte between an organic phase and an aqueous phase are given by

Can. J. Chem. Downloaded from www.nrcresearchpress.com by 210.87.254.105 on 09/06/12
For personal use only.

$$[3]\quad \lim_{\eta_{nc}\to 0}(\log f_{nc}) = \frac{V_m \cdot C_s(V_s - \phi_s)}{2.3\,RT\,\beta} \times \left[1 - \frac{C_s}{2}(V_s - \phi_s) - \frac{C_s^2}{3}(V_s - \phi_s)^2 - \ldots\right] \frac{r_h}{r_h + r_{nc}}$$

where: ϕ_s = apparent molar volume of salt in C_s molar salt solution; β = isothermal compressibility of a C_s molar salt solution: r_h = distance of closest approach to the non-electrolyte molecule. We have calculated log γ_{nc} (molar scale) at various concentrations of salt for LiCl, NaCl, and KBr and we have then obtained k_s from the plot of log γ_{nc} vs. C_s. The parameters used in eq. [3] in testing this approximation were taken in the following manner: V_m was taken at the same value as in MLT, ϕ_s from ref. 27, β from refs. 28 and 29, V_s from ref. 30, r_{nc} values have been calculated from $V_m = 4/3\pi r_{nc}^3$, and r_h were calculated from the individual ion radii, as determined from density measurements and tabulated in ref. 31.

The results obtained from eq. [3] are compiled in Table 4. Equation [3] produces the best agreement with the experimental values. It is important to notice that the values calculated from eq. [3] are also dependent on the V_s chosen. In Table 6 we have calculated k_s for the 1-naphthol − NaCl system employing various V_s. The possible general utility of eq. [3] lies in the prediction of activity coefficients, or k_s, for polar nonelectrolytes in salt solutions if an appropriate value of V_s has been found. Moreover, the treatment requires no precise mathematical description of interaction between particles or structural aspects of water.

In short, all present theories on salt effect give no quantitative agreement with experimental values. It is evident that more theoretical and practical work must be done on this problem.

1. (*a*) F. A. Long and W. F. McDevit. Chem. Rev. **51**, 119 (1952); (*b*) V. F. Sergeeva. Russ. Chem. Rev. **34**, 309 (1965).
2. S. K. Shoor and K. E. Gubbins. J. Phys. Chem. **73**, 498 (1968).
3. W. L. Masterton and T. P. Lee. J. Phys. Chem. **74**, 1776 (1970).
4. B. E. Conway, D. M. Novak, and L. Laliberté. J. Solution Chem. **3**, 683 (1974).
5. C. V. Krishnan and H. L. Friedman. J. Solution Chem. **3**, 727 (1974).
6. G. Perron, D. Joly, and J. E. Desnoyers. Can. J. Chem. **56**, 552 (1978).
7. N. C. Deno and C. H. Spink. J. Phys. Chem. **67**, 1347 (1963).
8. B. E. Conway and D. M. Novak. Chem. and Phys. Aqueous Gas Solutions (Proc. Symp.), 115 (1975).
9. R. F. Cross. J. Phys. Chem. **79**, 1822 (1975).
10. R. F. Cross and P. McTigue. J. Phys. Chem. **80**, 814 (1976).
11. R. Aveyard and R. Heselden. J. Chem. Soc. Faraday Trans. I, **71**, 312 (1975).
12. M. Fromon and C. Treiner. J. Chem. Soc. Faraday Trans. I, **75**, 1837 (1979); **76**, 1062 (1980).
13. Z. Sir, L. Strnadova, and V. Rod. Collect. Czech. Chem. Commun. **45**, 679 (1980).
14. Ya I. Korenman. Russ. J. Phys. Chem. **52**(6), 841 (1978).
15. C. Treiner. Can. J. Chem. **59**, 2518 (1981).
16. Ya I. Korenman and R. N. Bortnikova. Russ. J. Phys. Chem. **53**(4), 545 (1979).
17. J. M. Blandamer. Adv. Phys. Org. Chem. **14**, 204 (1977).
18. W. F. McDevit and F. A. Long. J. Am. Chem. Soc. **74**, 1773 (1952).
19. B. Robinson and A. Hargreaves. Acta. Crystallogr. **17**, 944 (1964).
20. R. C. Weast (*Editor*). Handbook of chemistry and physics. CRC Publishing Co., Cleveland, OH. 1979.
21. N. Desrosiers and J. E. Desnoyers. Can. J. Chem. **54**, 3800 (1976).
22. Y. L. Tien, M. Y. Schier, and E. Schrier. J. Phys. Chem. **78**, 165 (1974).
23. W. L. Masterton, D. Bolocofsky, and Tei Pei Lee. J. Phys. Chem. **75**, 2809 (1971).
24. L. Pauling. The nature of the chemical bond. 3rd ed. Cornell University Press, Ithaca, NY. 1960. p. 514.
25. B. E. Conway, D. M. Novak, and Laliberté. J. Solution Chem. **3**, 683 (1974).
26. Tables Landolt−Bornstein. I band: Atom and Molecularphysik; 1 teil: Atome und Ione. Berlin. 1950. p. 401.
27. F. J. Millero. *In* Water and aqueous solutions: structure, thermodynamics and transport process. *Edited by* E. A. Horne. Wiley−Interscience, New York. 1972.
28. H. S. Harned and B. B. Owen. The physical chemistry of electrolytic solutions. 3rd ed. Reinhold Publishing Corporation, New York. 1958.
29. F. J. Millero. *In* Activity coefficients in electrolyte solutions. Vol II. *Edited by* R. M. Pytkowicz. CRC Press Inc., Boca Raton, FL. 1979. Chapt. 2.
30. A. F. Scott. J. Phys. Chem. **35**, 3379 (1931).
31. B. E. Conway, J. E. Desnoyers, and A. C. Smith. Phil. Trans. R. Soc. London Ser. A, **256** (1074), 389 (1964).
32. M. A. Paul. J. Am. Chem. Soc. **74**, 5274 (1952).

Can. J. Chem. Downloaded from www.nrcresearchpress.com by 210.87.254.105 on 09/06/12
For personal use only.

Extrapolation from concentrated to dilute aqueous acids

A. J. KRESGE,[1] H. J. CHEN, G. L. CAPEN, AND M. F. POWELL

Department of Chemistry, University of Toronto, Scarborough College, West Hill, Ont., Canada M1C 1A4 and Department of Chemistry, Illinois Institute of Technology, Chicago, IL 60616, U.S.A.

Received June 15, 1981[2]

A. J. KRESGE, H. J. CHEN, G. L. CAPEN, and M. F. POWELL. Can. J. Chem. **61**, 249 (1983).

The location and the manner of union of the H_0 and H_R acidity functions with $-\log C_{H^+}$ have been determined for aqueous $HClO_4$, HCl, and H_2SO_4 (H_0 only) through particularly careful and extensive indicator measurements in dilute and moderately concentrated solutions of these acids. These data were also used to evaluate and compare a number of different ways of extrapolating measurements made in concentrated acids down to dilute solution; over the limited range of acidity investigated, the traditional acidity function method, as commonly applied in the absence of an appropriate acidity function (i.e. in the form of mH_0), was found to be the least satisfactory of these extrapolative methods, and the Cox–Yates technique was found to be the best.

A. J. KRESGE, H. J. CHEN, G. L. CAPEN et M. F. POWELL. Can. J. Chem. **61**, 249 (1983).

On a déterminé la position et le mode d'union des fonctions d'acidité de H_0 et de H_R avec $-\log C_{H^+}$ pour des solutions aqueuses de $HClO_4$, de HCl et de H_2SO_4 (H_0 seulement); on a effectué ces déterminations avec un soin particulier grâce à des mesures extensives d'indicateurs dans des solutions diluées et modérément concentrées de ces acides. On a également utilisé ces données pour évaluer et comparer un nombre de méthodes différentes de mesures par extrapolation faites à partir de solutions concentrées d'acide jusqu'à des solutions diluées dans les limites de l'intervalle d'acidité étudié. On a trouvé que la méthode traditionnelle de fonction d'acidité, i.e. telle qu'appliquée couramment en l'absence d'une fonction appropriée d'acidité sous la forme de mH_0, est la moins satisfaisante des méthodes par extrapolation et on a trouvé que la technique de Cox–Yates est la meilleure.

[Traduit par le journal]

One of the principal uses of acidity functions is to provide a means of extrapolating measurements made in concentrated acids down to dilute solution. For example, when the quantity of interest is the ratio of protonated to unprotonated forms of a weak base, C_{BH^+}/C_B ($\equiv I$), this operation gives I in a medium within the normal pH region from which a dilute solution pK_a may readily be estimated.

Such extrapolations have traditionally been performed on the assumption that $\log I$ is directly proportional to an appropriate acidity function, H_x, eq. [1] (1).

$$[1] \quad \log I = a + H_x$$

When the correct acidity function is not available, the further assumption that different acidity functions are linearly related to one another (2), and therefore to H_0, $H_x = mH_0$, is sometimes made, and the extrapolation is then performed down mH_0, eq. [2].

$$[2] \quad \log I = a + mH_0$$

This method, however, runs into the difficulty that m, though different from unity in concentrated acid solutions, must eventually become one when the H_x acidity function joins the $-\log C_{H^+}$ scale. This makes accurate extrapolation difficult, for the way in which m changes is not generally known.

An alternative method of extrapolation which avoids this problem was proposed some time ago by Bunnett and Olsen (3), who assumed that activity coefficient (f) functions of the form $\log (f_B f_{H^+}/f_{BH^+})$ rather than acidity functions are proportional to one another, eq. [3].

$$[3] \quad \log (f_B f_{H^+}/f_{BH^+}) = (1-\phi) \log (f_{B'} f_{H^+}/f_{B'H^+})$$

This hypothesis leads to the expression shown as eq. [4], which has the advantage that the extrapolation is now made down a

$$[4] \quad \log I + H_0 = pK_a + \phi(H_0 + \log C_{H^+})$$

quantity, $H_0 + \log C_{H^+}$, which becomes zero in dilute acids; this provides a simple solution to the problem of where the extrapolation should be terminated. Equation [4] was tested extensively by Bunnett and Olsen (3) and also by Marziano and Passerini (4) and was found to be generally valid. Marziano and Passerini also used the hypothesis of linearly proportional activity coefficient terms (eq. [3]) to construct a generalized activity coefficient function based upon a large number of different kinds of indicators, M_c, whose use they advocated in eq. [4] in place of ($H_0 + \log C_{H^+}$). More recently this method was extended to an even larger data base with further mathematical refinements by Cox and Yates, who called their result the excess acidity function, X (5).

We have for some time been concerned with accurate extrapolation of both kinetic and equilibrium data from concentrated to dilute acid solution. A number of years ago we therefore made extensive and careful determinations of the H_0 and H_R acidity functions in dilute and moderately concentrated aqueous acids. These data, which we present here in full,[3] show how these two acidity functions run into the $-\log C_{H^+}$ scale, and they also allow comparison of the newly developed methods of extrapolation.[4]

Results

Three H_0 indicators and three H_R indicators, chosen to give good regions of overlap, were used in this study. Extents of protonation of these indicators were measured spec-

[1]To whom all correspondence should be addressed at the University of Toronto.

[2]Revision received September 2, 1982.

[3]Some of this work was published in preliminary form (6).

[4]For a different examination of this problem, see ref. 7.

0008-4042/83/020249-08$01.00/0

©1983 National Research Council of Canada/Conseil national de recherches du Canada

Can. J. Chem. Downloaded from www.nrcresearchpress.com by 210.87.254.6 on 09/06/12
For personal use only.

TABLE 1. Indicator acidity constants

Indicator	pK_a[a]		
	$HClO_4$	HCl	H_2SO_4[b]
4-Nitroaniline	1.003±0.002	0.995±0.002	—
3,5-Dinitroaniline	—	0.205±0.004	0.220±0.020
2-Nitroaniline	−0.242±0.006	−0.263±0.006	−0.303±0.017
4,4′,4″-Trimethoxytriphenylmethanol	0.763±0.008	0.724±0.007	—
4,4′-Dimethoxy-4″-methyltriphenylmethanol	−0.270±0.013	−0.441±0.008	—
4,4′-Dimethoxytriphenylmethanol	−0.928±0.007	−1.163±0.008	—

[a]Error limits are standard deviations of mean values based upon experimental deviations; as such, they are an index of precision only and probably overestimate the accuracy.

[b]The pK_a of the most basic indicator, 4-nitroaniline, could not be determined by extrapolation in this medium because H^+ concentrations of sulfuric acid solutions are not known accurately enough. The pK_a of this indicator was therefore taken to be the average of the values determined in $HClO_4$ and HCl solutions, and this was used with the method of overlap to determine pK_a's for the two remaining indicators in H_2SO_4 solution.

Can. J. Chem. Downloaded from www.nrcresearchpress.com by 210.87.254.6 on 09/06/12
For personal use only.

trophotometrically, making use of the large changes in ultraviolet or visible spectra which accompany their protonation. Measurements were made with both sets of indicators in perchloric and hydrochloric acids and with the H_0 indicators only in sulfuric acid. For each acid–indicator combination, values of log I were determined in triplicate at three different wavelengths for 20 to 40 solutions whose concentrations were chosen to distribute the log I values evenly over the interval log $I = -1.5$ to $+1.5$, which is the range where this quantity can be determined most accurately (8). These log I values were then transformed into H_0 and H_R functions using the wholly analytical method which we developed in constructing an H_0 function for ethanolic sulfuric acid (9). In this method the usual graphical techniques for extrapolating to infinitely dilute solution and interpolating in regions of overlap are replaced by the more objective and accurate evaluation of analytical functions generated by weighted least-squares fitting of the data to appropriate mathematical expressions.[5]

The indicator pK_a's obtained in this way are listed in Table 1. The values for the most basic indicator in each set, 4-nitroaniline and 4,4′,4″-trimethoxyphenylmethanol, are based upon extrapolation to infinite dilution; the others are averages of pK_a's determined by such extrapolation and by overlap with more basic indicators. The results obtained for 4-nitroaniline in the two acids in which the pK_a of this indicator was determined are in good agreement; the pK_a's of the other indicators, however, show differences from acid to acid.[6] These differences increase with decreasing indicator basic strength, and therefore with increasing concentration of the acid in which the measurements were made, which suggests that they are the result of different medium effects, i.e. different interactions of the indicator base and its conjugate acid with the different acid solvents. This implies a breakdown of the extrapolative and comparative procedures upon which acidity functions are based. Effects of this kind are not uncommon among bases of different structure, but they are somewhat more rare for indicators belonging to structurally homogeneous classes (see, however, refs. 4, 5, and 10).

Since there is no reason to expect medium effects to be the same in different acids, these pK_a differences were retained in constructing the present H_0 and H_R scales, i.e. the pK_a's determined in a given acid were used to build the acidity function for that acid. Representative H_0 and H_R values over the regions of acid concentration covered in this study are listed in Table 2.

TABLE 2. Acidity function values determined in this study (25°C)

wt% acid	H_0			H_R	
	$HClO_4$	HCl	H_2SO_4	$HClO_4$	HCl
0.25	1.60	1.15	1.43	1.59	1.15
0.50	1.29	0.83	1.15	1.27	0.82
0.75	1.10	0.64	0.98	1.07	0.61
1.00	0.97	0.50	0.85	0.92	0.44
2.00	0.64	0.15	0.53	0.53	−0.01
3.00	0.44	−0.08	0.32	0.27	−0.33
4.00	0.29	−0.26	0.16	0.06	−0.61
5.00	0.16	−0.41	0.03	−0.11	−0.86
6.00	0.06	−0.55	−0.09	−0.27	−1.09
7.00	−0.04	−0.68	−0.19	−0.42	−1.31
8.00	−0.13	−0.80	−0.25	−0.56	−1.52
9.00	−0.21	−0.92	−0.33	−0.69	−1.73
10.00	−0.28	−1.03	−0.41	−0.81	−1.94
12.00	−0.43	−1.25	−0.56	−1.05	−2.35
14.00	−0.56	−1.47	−0.70	−1.28	—
16.00	−0.69	—	−0.82	−1.51	—
18.00	−0.81	—	−0.95	−1.74	—
20.00	−0.93	—	−1.07	−1.97	—
22.00	—	—	−1.21	−2.21	—
24.00	—	—	−1.34	−2.46	—

These new results compare well, on the whole, with previous determinations. For example, the Long and Paul (11) – Jorgenson and Hartter (12) H_0 scale for H_2SO_4 as compiled by Boyd (1*b*) is only 0.10 more positive than ours, and the Bascombe and Bell (13) H_0 scale for H_2SO_4 is also more positive but by a smaller amount: 0.02 to 0.05. More recent determinations of H_0 in H_2SO_4 were made by Tickle, Briggs, and Wilson (14), whose scale is 0.07 to 0.14 more positive than ours, and also by Johnson, Katritzky, and Shapiro (15), whose scale is 0.01 and 0.07 more positive than ours.

Fewer determinations of H_0 in other acids have been made, but here again agreement of modern work with the present results is good. This is especially true of the Arnett and Mach (16) H_0 scale for HCl, which never differs from ours by more than 0.01. The Yates and Wai (17) H_0 scale for $HClO_4$, as well as the closely similar Attiga and Rochester (18) scale, are also

[5]Tables of the complete log I values determined here are available, at a nominal charge, from the Depository of Unpublished Data, CISTI, National Research Council of Canada, Ottawa, Ont., Canada K1A 0S2.

[6]A referee has asked us to emphasize that these differences impair the thermodynamic significance of these pK_a's.

Can. J. Chem. Downloaded from www.nrcresearchpress.com by 210.87.254.6 on 09/06/12
For personal use only.

consistent with ours; the former runs 0.05 to 0.13 more negative than ours.

The literature contains only one determination of H_R for each of the two acids studied with this kind of indicator here. The Arnett and Mach (16) H_R scale for HCl is only 0.10 to 0.13 more positive than ours from 0.1 to 8 wt% acid, but the difference then jumps to 0.20 at 10 wt% and 0.26 at 14 wt%. For $HClO_4$, the present scale is in essential agreement with the early work of Deno, Barkheimer, Evans, and Peterson (19) at 0.5 wt% acid, but above that point the latter runs progressively more negative than our scale until at 20 wt% acid the difference amounts to 0.47.

The present results cover only a limited range of acid concentrations, and they were therefore fused with selected literature scales to provide more extensive acidity functions in the following more or less arbitrary way. Because the Johnson, Katritzky, and Shapiro (15) H_0 scale for H_2SO_4 agrees with ours to within 0.01 over the region 20–22 wt% acid, we simply joined these two scales at this point, i.e. the resulting H_0 scale for H_2SO_4 uses our values for 0.25 to 22 wt% acid and the Johnson, Katritzky, and Shapiro data from 22 to 95 wt% acid. We also joined the Arnett and Mach (16) H_0 scale for HCl to ours in the same way, i.e. with no adjustment, since it also agrees with ours to within 0.01. The Yates and Wai (17) H_0 scale for $HClO_4$, however, is more negative than ours by 0.06 at 20 wt% acid, and we therefore used our scale up to this point and the Yates and Wai scale plus 0.06 from 20 to 78 wt% acid. We also made adjustments to literature H_R scales in joining them to our results. For H_R in HCl, we used our scale up to 14 wt% acid and the Arnett and Mach (16) scale minus 0.26 from 14 to 38 wt% acid, and for H_R in $HClO_4$, we used our scale up to 24 wt% and then the Deno, Berkheimer, Evans, and Peterson (19) scale plus 0.50 from 24 to 60 wt%.

We have not supplied tables of the resulting acidity functions because we find it more convenient to store values in mathematical form. We have found that an acidity function can usually be represented quite well, to 0.01 to 0.02, by a sixth order polynomial plus a logarithmic term, eq. [5], and we therefore fitted our data to such functions by least-squares pro-

$$[5]\quad H_x = a_1 \ln x + a_2 + a_3x + a_4x^2 + a_5x^3 + a_6x^4 + a_7x^5 + a_8x^6;\ x = \text{wt\% acid}$$

cedures. The coefficients of such expressions for H_0 in $HClO_4$ and HCl[7] and for H_R in $HClO_4$ and HCl are listed in Table 3 together with those of other functions which interconvert wt% and molar concentration scales for these acids. These functions are easily programmed into small calculators and therefore provide an especially useful way of retrieving and interpolating data.

TABLE 3. Mathematical functions relating properties of concentrated aqueous acids (25°C)

		Coefficients[a]							
y	x	a_1	a_2	a_3	a_4	a_5	a_6	a_7	a_8
wt% $HClO_4$	M $HClO_4$ (0.1 to 11.5M)	0.000+00	0.000+00	1.008+01	−5.698−01	3.301−02	−2.473−03	1.543−04	−3.854−06
M $HClO_4$	wt% $HClO_4$ (1 to 70 wt%)	0.000+00	0.000+00	9.993−02	3.943−04	1.600−05	−4.508−07	8.291−09	−5.042−11
wt% HCl	M HCl (1 to 9.5M)	0.000+00	0.000+00	3.655+00	−6.370−02	1.879−03	−5.787−05	−1.551−06	2.649−07
M HCl	wt% HCl (1 to 30 wt%)	0.000+00	0.000+00	2.737−01	1.274−03	7.214−06	−4.472−07	1.877−08	−2.907−10
wt% H_2SO_4	M H_2SO_4 (0.1 to 18M)	0.000+00	0.000+00	9.787+00	−5.781−01	3.749−02	−1.710−03	3.145−05	2.654−07
M H_2SO_4	wt% H_2SO_4 (1 to 95 wt%)[b]	0.000+00	0.000+00	1.017−01	6.255−04	5.574−06	−7.226−08	−2.201−10	2.782−11
H_0	wt% $HClO_4$ (0.1 to 78 wt%)	−4.397−01	9.956−01	−2.262−02	−3.680−04	−8.645−06	6.961−07	−1.841−08	1.169−10
H_0	wt% HCl (0.1 to 38 wt%)	−4.450−01	5.474−01	−4.164−02	−1.184−03	−5.720−05	5.681−06	−1.932−07	2.192−09
H_R	wt% $HClO_4$ (0.1 to 60 wt%)	−4.433−01	1.001+00	−8.248−02	4.246−04	4.379−06	−1.881−06	3.718−08	−2.547−10
H_R	wt% HCl (0.1 to 36 wt%)	−4.186−01	6.093−01	−1.673−01	2.733−03	−2.206−04	3.796−06	−4.384−09	−1.814−10

[a]Coefficients of the function $y = a_1 \ln X + a_2 + a_3x + a_4x^2 + a_5x^3 + a_6x^4 + a_7x^5 + a_8x^6$; the last two digits of a coefficient and the sign preceding them denote the power of ten. These equations reproduce wt% acid to 1/1000, M to 0.01 and H_0 and H_R to 0.01–0.02. The relationships between M and wt% are based on densities given by ref. 22*a* for $HClO_4$, ref. 22*b*, p. 54 for HCl, and p. 56 for H_2SO_4.
[b]An additional term in $(\text{wt\%})^7$ is needed whose coefficient is −2.179−13.

Discussion

Union of H_x *and* $-log\ C_{H^+}$ *scales*

Examination of Table 4, in which the presently determined H_0 and H_R scales are compared with $-\log C_{H^+}$, shows that sizeable differences exist between these acidity functions and $-\log C_{H^+}$ at the point where the latter is equal to zero (C_{H^+} =

[7]We could not find a set of coefficients which reproduced the H_0 data for H_2SO_4 well, and we therefore do not include an expression for this scale in Table 3. Our scale for this acid from 0.25 to 24 wt% is listed in Table 2; above 24 wt% acid we recommend the values of ref. 15.

TABLE 4. Comparison of H_x and log C_{H^+}

wt% acid	C_{H^+}	$-\log C_{H^+}$	H_0	H_R
$HClO_4$				
9.54	1.00	0.00	−0.25	−0.76
6.59	0.68	0.17	0.00	−0.36
4.34	0.44	0.35	0.24	0.00
1.00	0.100	1.00	0.97	0.92
0.500	0.050	1.30	1.29	1.27
0.250	0.025	1.60	1.60	1.59
0.100	0.010	2.00	2.01	2.01
HCl				
3.59	1.00	0.00	−0.19	−0.50
2.62	0.73	0.14	0.00	−0.22
1.98	0.55	0.26	0.16	0.00
0.365	0.100	1.00	0.98	0.97
0.183	0.050	1.30	1.30	1.29
0.091	0.025	1.60	1.61	1.60
0.037	0.010	2.00	2.01	1.99
H_2SO_4				
7.82	1.00[a]	0.00	−0.22	—
5.42	0.68[a]	0.17	0.00	—
0.775	0.100[a]	1.00	0.91	—
0.368	0.050[a]	1.30	1.27	—
0.162	0.025[a]	1.60	1.61	—

[a]Interpolated using the data of Table II in ref. 5.

1.00 *M*) for all three acids investigated. These differences diminish as C_{H^+} drops through the region where the acidity functions themselves pass through zero, but even at C_{H^+} = 0.100 the differences are still significant; for example H_R measures 0.100 *M* $HClO_4$ as 0.08 more acidic than does $-\log C_{H^+}$, and H_0 measures 0.78 wt% H_2SO_4 (0.079 *M*), in which C_{H^+} = 0.100 *M*, to be 0.09 more acidic than does $-\log C_{H^+}$. These, of course, are differences on a logarithmic scale; their antilogs correspond to factors of 1.20 and 1.23, respectively. It is not until C_{H^+} drops to ca. 0.025 *M* that differences between H_0 and H_R and $-\log C_{H^+}$ reach a value, 0.01, which is experimentally indistinguishable from zero.

This point of union of H_x with $-\log C_{H^+}$ is understandable in terms of the definition of H_x, eq. [6], and the behavior of activity coefficients as represented, for example, by the Debye–Hückel equation, eq. [7]. In the Debye–Hückel formulation, activity coefficients of different ions have dissimilar

$$[6] \quad H_x = -\log C_{H^+} - \log f_x f_{H^+}/f_{xH^+}$$

$$[7] \quad -\log f = A\sqrt{\mu}/(1 + aB\sqrt{\mu})$$

values at the same ionic strength, μ, because of differences in the ion-size parameter, *a*. The H^+ ion, because it is so strongly hydrated in aqueous solution, has an unusually large value of this parameter: 8–9 Å; *a* for other ions is generally much smaller (20). This difference gives the quantity $\log f_{H^+}/f_{xH^+}$ a non-zero value and makes H_x different from $-\log C_{H^+}$ in moderately concentrated acids. The difference, however, diminishes as ionic strength decreases, and, with values of *a* recommended by Bates (20) and the condition that f_x = 1.00, the activity coefficient term $\log f_x f_{H^+}/f_{xH^+}$ drops to within 0.01 of unity when μ = ca. 0.025 *M*.

Extrapolation to dilute solution

As the data of Table 4 show, the union of H_0 and H_R with $-\log C_{H^+}$ is achieved only very gradually. This means that the coefficient *m* in the expression relating one acidity function to another, $H_x = mH_0$, begins to change from its constant concentrated-solution value in acids which are still not very dilute. This makes extrapolation down an "inappropriate" acidity function in the manner of eq. [2] difficult.

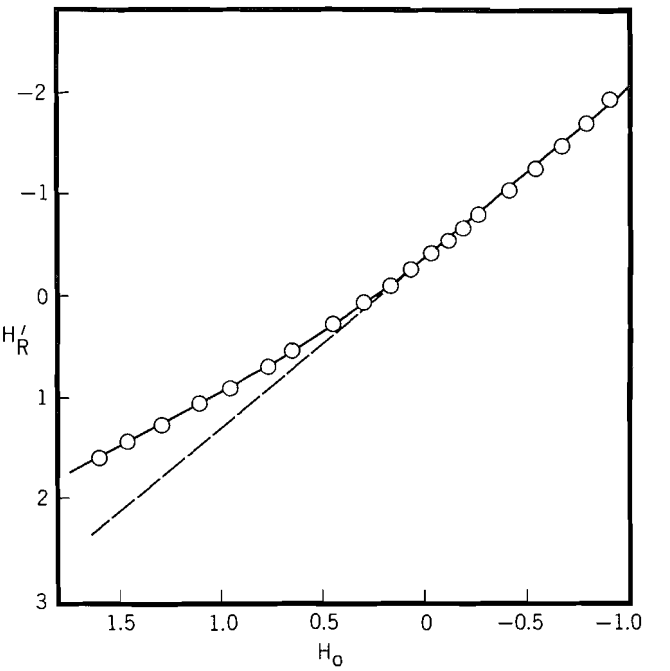

FIG. 1. Relationship between H_0 and H'_R acidity functions in aqueous $HClO_4$ at 25°C.

For example, an H'_R scale constructed from our H_R function[8] for $HClO_4$ is a good linear function of H_0 over the region 5–20 wt% acid (Fig. 1): $H'_R = (-0.343 \pm 0.009) + (1.654 \pm 0.018)H_0$; *r*(correlation coefficient) = 0.9995.[9] At 5% acid (0.51 *M*), however, *m* begins to decrease gradually, dropping from 1.654 to its dilute solution value of unity, which it reaches in 0.025 wt% $HClO_4$. This means that linear extrapolations from acids more concentrated than 5 wt% down to dilute solution (down the broken line of Fig. 1) will produce erroneous values of the quantity extrapolated. Take, for example, the case of a hypothetical H'_R base with $pK_a = 0.00$, $K_a = 1.00$, for which, by definition, $\log I = -H'_R$. Extrapolation of the linear relationship $H_R = -0.343 + 1.654H_0$ down to 0.25 wt% acid, the point where H_0 and H'_R unite with $-\log C_{H^+}$ and all three quantities have the value 1.60, gives $\log I = -2.30$. This, when combined with $\log C_{H^+}$ according to eq. [8], coupled with

$$[8] \quad pK_a = \log I + H_R = \log I - \log C_{H^+} + -\log f_x f_{H^+}/f_{xH^+}$$

the condition that in 0.25 wt% $HClO_4$ $\log f_x f_{H^+}/f_{xH^+} = 0$, produces $pK_a = -0.70$. This result differs from the true value $pK_a = 0.00$ by 0.70 log unit, which corresponds to a factor of 5 in K_a. Similar treatment of the data for HCl gives $pK_a = -0.96$, which corresponds to an acidity constant that is too high by a factor of 9.

Linear extrapolations continued to more dilute solutions lead

[8]Because H_R indicators ionize by combining with a molecule of water, $R^+ + H_2O \rightleftarrows ROH + H^+$, the H_R function differs from other acidity functions by an activity of water term: $H_R = -\log (A_{H^+} f_{ROH}/f_{R^+}) + \log (A_{H_2O})$ whereas $H_x = -\log (A_{H^+} f_B/f_{BH^+})$; conversion to H'_R removes this difference: $H'_R = H_R - \log (A_{H_2O})$.

[9]A similar good linear relationship exists in HCl from 4 to 12 wt% acid: $H'_R = (-0.145 \pm 0.012) + (1.680 \pm 0.014)H_0$, $r = 0.9997$.

Can. J. Chem. Downloaded from www.nrcresearchpress.com by 210.87.254.6 on 09/06/12
For personal use only.

Can. J. Chem. Downloaded from www.nrcresearchpress.com by 210.87.254.6 on 09/06/12
For personal use only.

to even greater errors. Extrapolations terminated in less dilute acids, on the other hand, would give better values of log I, but they would run into the additional difficulty that in these media $\log f_x f_{H^+}/f_{xH^+}$ is not zero and pK_a is therefore no longer simply equal to log I − log C_{H^+}. For example, the least concentrated $HClO_4$ solution in which the linear relationship between H_R and H_0 still holds reasonably well is 5 wt% acid with $C_{H^+} = 0.51$ M and $H_0 = +0.16$. In this medium, a pK_a estimated from the linear relationship and log I − log C_{H^+} has the value 0.37, which corresponds to an acidity constant, $K_a = 0.43$, lower than the true value of unity by a factor of 2.3. At the ionic strength of this medium, 0.51 M, estimation of the activity coefficient term needed to obtain a better value, $\log f_x f_{H^+}/f_{xH^+}$, would of course be very difficult.

The pK_a's of bases which protonate only in concentrated acids may of course be calculated without extrapolating to dilute solution by using the relationshiop log I = pK_a − H_x, which leads to the condition p$K_a = H_x$ at the point where log $I = 0$. In the event that the acidity function appropriate to the base under consideration is not available, H_x may be replaced by mH_0, but the present data show that this technique is not entirely satisfactory either. For our H'_R base with p$K_a = 0.00$, log I will be zero when $H'_R = 0.00$. In $HClO_4$ solution, this occurs at 4.5% acid where $H_0 = 0.22$ and $mH_0 = 1.654 \times 0.22 = 0.36$; this corresponds to $K_a = 0.43$, which is low by a factor of 2.3. Similar treatment of the data for HCl gives p$K_a = 0.25$, which corresponds to an acidity constant too low by a factor of 1.8. These erroneous results may be traced back to the fact that deviations from ideal behavior, i.e. from $H'_R = H_0 = -\log C_{H^+}$, begin to occur in solutions more dilute than $C_{H^+} = 1.00$ M, and that these deviations are different for different acidity functions; H_0 is consequently not equal to zero when $H'_R = 0$.

The problem of where extrapolations from concentrated to dilute acids should be terminated does not arise in the Bunnett–Olsen method and its derivatives, for here the quantity down which the extrapolation is made, $H_0 + \log C_{H^+}$, M_c, or X, becomes zero in dilute solution. These methods, however, still require the extrapolations to be truly linear. This assumption has been tested and has been found to be generally valid (3–5). However, the presently determined highly accurate values of H_0 and H'_R allow a more detailed examination of this point than was possible before.

For our hypothetical H'_R base with p$K_a = 0.00$, log I is equal to $-H'_R$ and the Bunnett–Olsen expression, eq. [4], becomes $H_0 - H'_R = \phi(H_0 + \log C_{H^+})$. Figure 2 shows that the present data for $HClO_4$ solution conform to this expression only moderately well: there are systematic deviations which suggest that the relationship between the two variables is actually curved rather than linear. The best straight line through all of the data, however, does produce a good pK_a: least-squares analysis gives $(H_0 - H'_R) = (0.024 \pm 0.009) - (1.733 \pm 0.037)(H_0 + \log C_{H^+})$, $r = 0.9960$, and this leads to p$K_a = -0.02$ and $K_a = 0.95$ which differs from the true value by only 5%. The data for the more concentrated solutions (10–20 wt% $HClO_4$) give a much better straight line, $(H_0 - H'_R) = (0.127 \pm 0.008) - (1.477 \pm 0.019)(H_0 + \log C_{H^+})$, $r = 0.9996$, but now p$K_a = -0.13$ and $K_a = 0.75$ which is 25% too low (Fig. 2, broken line). The situation in HCl is much the same: the data over the entire range investigated give a curved relationship in the manner of Fig. 2 but they produce a good acidity constant, $K_a = 1.02$, whereas the data for the more concentrated solutions (5–12 wt%) are more nearly linear but give the poorer acidity constant $K_a = 0.80$.

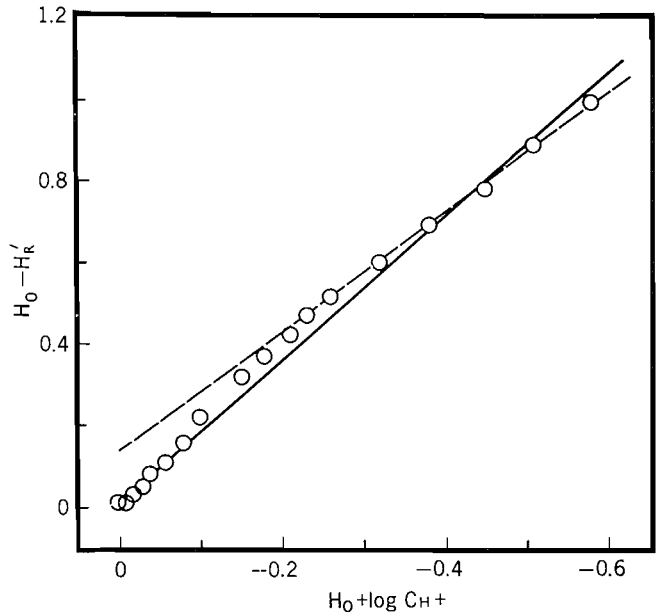

FIG. 2. Bunnett–Olsen plot for a hypothetical H'_R base with pK_a = 0.00 in $HClO_4$ at 25°C.

In the Marziano–Passerini and Cox–Yates methods, (log I − log C_{H^+}) rather than (log $I - H_0$) is used as the independent variable, and this is plotted against either M_c or X. There is an alternative formulation of the Bunnett–Olsen method which uses the same independent variable. This leads to the relationship of eq. [9], whose right-hand side differs from that of the previous Bunnett–Olsen expression, eq. [4], only in that

$$[9] \quad \log I - \log C_{H^+} = pK_a + (\phi - 1)(H_0 + \log C_{H^+})$$

the slope parameter is now $\phi - 1$ rather than ϕ. Such a Bunnett–Olsen plot using the present data for $HClO_4$ is shown in Fig. 3, for the purpose of comparison with Marziano–Passerini and Cox–Yates plots using the same data to be shown below. It is gratifying that least-squares analysis of this plot gives intercepts which are the same as those obtained with eq. [4] (Fig. 2) and slopes which are exactly one unit lower, as demanded by mathematics: from 0–20 wt% $HClO_4$, $(-H'_R - \log C_{H^+}) = (0.024 \pm 0.009) - (2.733 \pm 0.037)(H_0 + \log C_{H^+})$, $r = 0.9960$; from 10–20 wt% $HClO_4$, $(-H'_R - \log C_{H^+}) = (0.127 \pm 0.008) - (2.477 \pm 0.019)(H_0 + \log C_{H^+})$, $r = 0.9998$.

Figure 4 shows that a Marziano–Passerini plot using the present data for $HClO_4$ solutions is somewhat curved in the same manner as the Bunnett–Olsen plots. Again, the best straight line through all of the data, $(-H'_R - \log C_{H^+}) = (0.040 \pm 0.012) + (1.529 \pm 0.027)M_c$, $r = 0.9972$, gives a reasonably good estimate of the acidity constant, $K_a = 0.91$, and a better straight line through the points for the more concentrated solutions, $(-H'_R - \log C_{H^+}) = (0.144 \pm 0.010) + (1.377 \pm 0.015)M_c$, $r = 0.9984$, gives the poorer acidity constant $K_a = 0.71$.

A Cox–Yates plot using the present $HClO_4$ data is even more strongly curved, Fig. 5, and the best line through all of the points, $(-H'_R - \log C_{H^+}) = (0.089 \pm 0.022) + (2.798 \pm 0.097)X$, $r = 0.9895$, affords an acidity constant, $K_a = 0.81$, which is only moderately good. The better straight line through the data for the more concentrated solutions, $(-H'_R - \log C_{H^+}) = (0.319 \pm 0.012) + (2.199 \pm 0.029)X$, $r = 0.9996$ gives $K_a = 0.48$, which is a factor of two too low. Very recently,

Can. J. Chem. Downloaded from www.nrcresearchpress.com by 210.87.254.6 on 09/06/12
For personal use only.

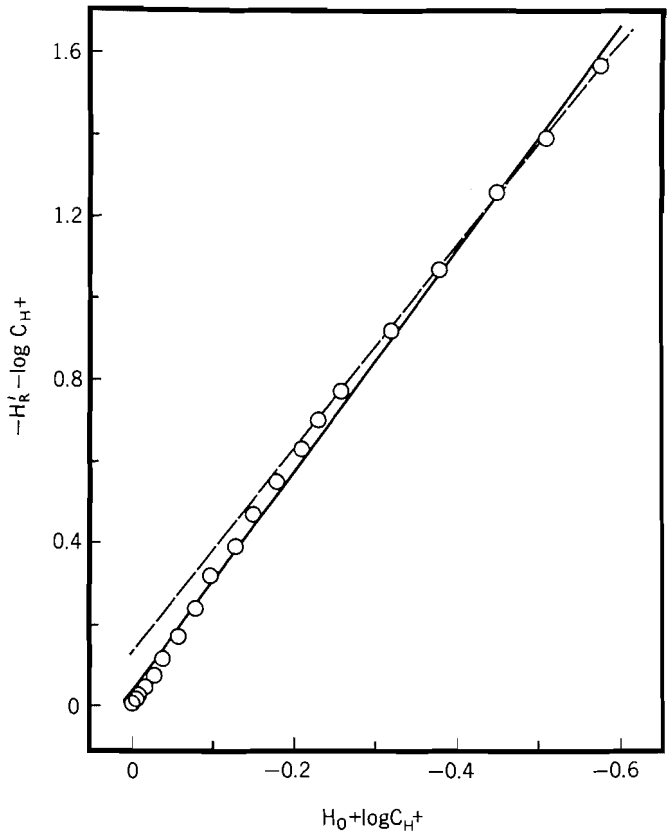

FIG. 3. Alternative formulation of the Bunnett–Olsen relationship for a hypothetical H'_R base with $pK_a = 0.00$ in $HClO_4$ at 25°C.

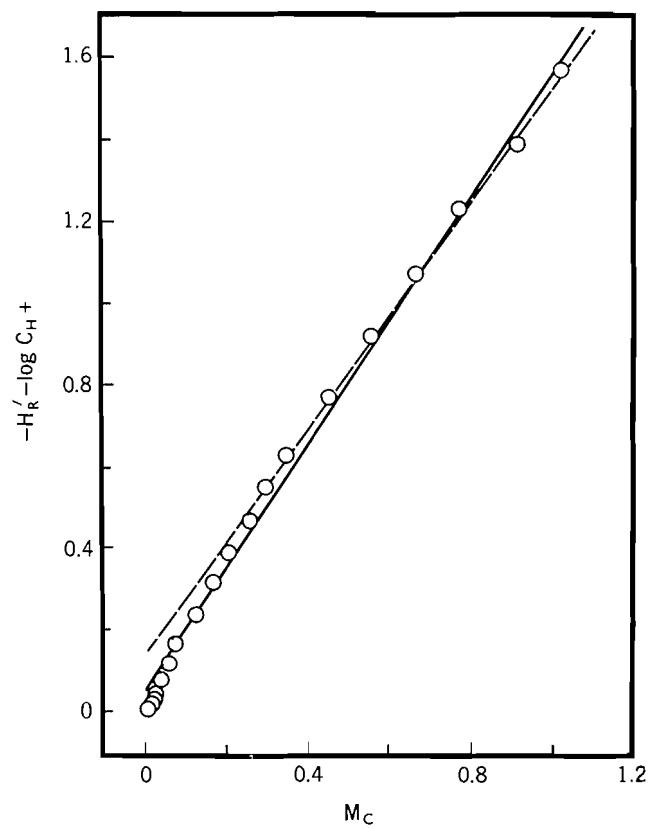

FIG. 4. Marziano–Passerini plot for a hypothetical H'_R base with $pK_a = 0.00$ in $HClO_4$ at 25°C.

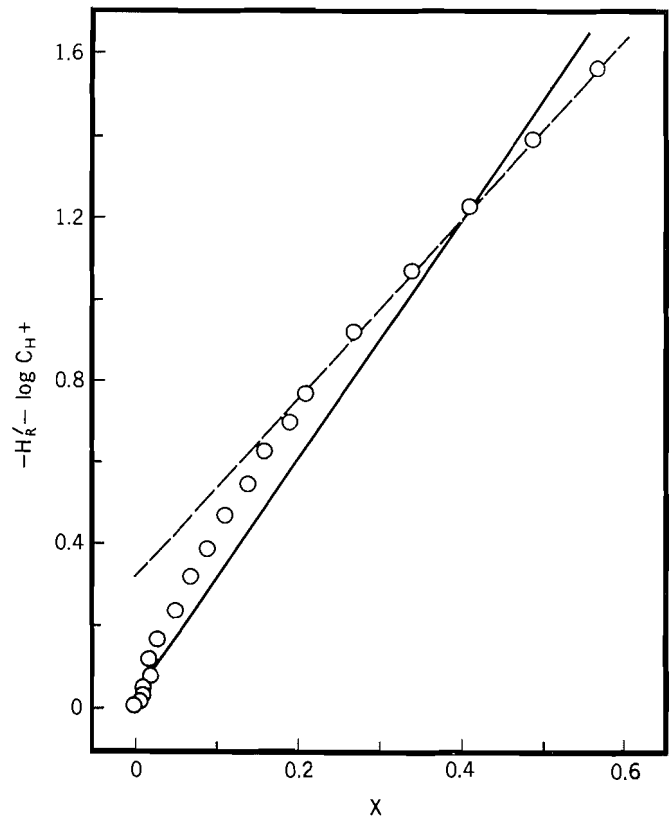

FIG. 5. Cox–Yates plot using the excess acidity function X for a hypothetical H'_R base with $pK_a = 0.00$ in $HClO_4$ at 25°C.

however, Cox and Yates have produced a revised excess acidity function for $HClO_4$ based on primary aniline indicators only, X_0 (5*b*), and this scale correlates the present data very well. As Fig. 6 shows, the Cox–Yates plot using X_0 is accurately linear over the entire range of the present data, $(-H'_R - \log C_{H^+}) = -(0.022 \pm 0.005) + (2.854 \pm 0.020)X_0$, $r = 0.9996$, and it also gives a good value of the acidity constant, $K_a = 1.05$. In HCl solution, on the other hand, Cox–Yates plots using the X and X_0 functions are equally good; both plots show only a slight hint of curvature, and the best straight lines in both cases, $(-H'_R - \log C_{H^+}) = (0.024 \pm 0.012) + (2.005 \pm 0.028)X$, $r = 0.9985$ and $(-H'_R - \log C_{H^+}) = (0.030 \pm 0.014) + (2.654 \pm 0.044)X_0$, $r = 0.9979$, give respectably good acidity constants: $K_a = 0.95$ and 0.93 using X and X_0 respectively.

Conclusions

Of the four techniques for extrapolating data from concentrated acids down to dilute solution considered here, the traditional acidity function method as applied when an appropriate acidity function is not available (eq. [2]) gives the poorest results; it produces significant errors, several fold large in the quantity extrapolated, when the extrapolation is terminated at $C_{H^+} = 0.025\ M$, the point at which H_0 first becomes equal to $-\log C_{H^+}$. Better results are obtained with protonation equilibrium data if the pK_a is taken to be equal to mH_0 at the point where $\log I = 0$, but even so errors of the order of a factor of two are produced, and the method cannot be used with kinetic data. These shortcomings of course do not apply when the appropriate acidity function is available and is used in the manner of eq. [1].

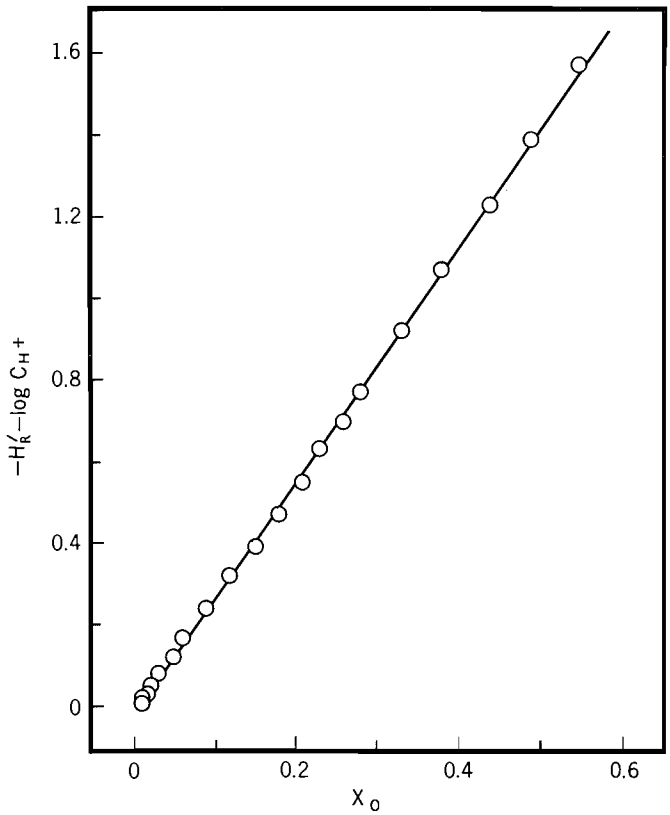

FIG. 6. Cox–Yates plot using the excess acidity function X_0 for a hypothetical H_R' base with $pK_a = 0.00$ in $HClO_4$ at 25°C.

The other three methods produce consistently better results, although the data often do give gently curved relationships where linear correlations are to be expected. Plots using the newly produced Cox–Yates function X_0 for $HClO_4$ are a notable exception: here the data are accurately linear over the entire range studied and give an extrapolated value in dilute solution which is correct to 5%. The Cox–Yates method also affords the best results in HCl solution from the point of view of both providing linear correlations and giving good extrapolated values; here, however, the functions X and X_0 appear to be equally effective.

Experimental

Materials

Triarylmethanols were prepared by standard methods and were purified as their picrates (21). Although the nmr spectra of these preparations showed no detectable impurities, only 4,4′,4″-trimethoxytriphenylmethanol could be obtained in crystalline form. The carbinols were therefore converted to their solid perchlorate salts and these were used for the indicator measurements.

The aniline indicators were obtained commercially and were purified by recrystallization until their melting points were constant and in agreement with literature values. The nmr spectra of these materials were consistent with their structures.

Acid solutions were prepared from reagent grade acids and deionized water which had been purified further by distillation from alkaline potassium permanganate. Acid concentrations were determined by titration of weighed amounts with standard sodium hydroxide.

Indicator measurements

Absorbance determinations for a given indicator–acid pair were made on series of solutions of varying acidity but accurately constant total indicator concentration. These solutions were prepared in two ways: (*1*) by combining carefully pipetted 10.00-mL aliquots of wholly aqueous stock indicator solution with similarly obtained aliquots of acid solutions of appropriate concentration, or (*2*) by adding 10.00-mL aliquots of indicator solution to 25.00-mL volumetric flasks and making up to the mark with acid and water. The second method was always used for the more strongly acidic solutions where there was danger that simple mixing of indicator and acid solutions might produce a density change and result in a final volume which was not accurately the sum of the volumes of the two pipetted aliquots. Pipetting was always done with the same pipette throughout a given series of measurements.

Since the triarylcarbinols used here are only very sparingly soluble in water, special care was taken in preparing their stock solutions. Excess carbinols or their perchlorate salts were shaken with water overnight, the saturated solutions were filtered twice, and the second filtrate was then diluted with additional water to about 90% saturation.

All volumetric manipulations were done on solutions which had equilibrated with a 25.0°C constant temperature bath, and the cell compartments of the spectrometers were also thermostatted at 25.0 ± 0.05°C. Measurements on the aniline indicators were made with a Beckman DK-2 instrument and those on the triarylcarbinols with a Cary 16 spectrometer. Reduced absorbance scales were used for the measurements with triarylcarbinols on the Cary instrument (0.06 to 0.2 *A* full scale deflection), but the greater solubility of the aniline indicators allowed the standard 0–1 *A* scale to be used for measurements with these indicators on the Beckman instrument. All measurements were made in the differential mode using reference solutions prepared exactly as the sample solutions except that pure water was substituted for the stock indicator solution.

Absorbance readings were made three times for each solution at three different wavelengths: at the absorption maximum and at wavelengths 5 nm to either side of the maximum. These nine values were then averaged and indicator ratios were calculated using the formula $I = (A_B - A)/(A - A_{BH^+})$. Absorbances of the basic forms of the indicators, A_B, were measured either in pure water or dilute alkali, and absorbances of the acidic forms, A_{BH^+} were measured in solutions whose acidity function values, H_0 or H_R as appropriate, were at least three units more acidic than the indicator pK_a's. Complete tables of all of the indicator data so obtained are available from the Depository of Unpublished Data.[5]

Acknowledgements

We are grateful to Dr. Robin Cox for many helpful discussions and to the Natural Sciences and Engineering Research Council of Canada and the Petroleum Research Fund of the American Chemical Society for their financial support of this research.

1. (*a*) L. P. HAMMETT. Physical organic chemistry. McGraw Hill, New York. 1st ed. 1940. p. 267; 2nd ed. 1970. p. 267; E. M. Arnett. Prog. Phys. Org. Chem. **1**, 223 (1963); (*b*) R. H. BOYD. *In* Solute–solvent interactions. *Edited by* J. F. Coetzee and C. D. Ritchie. Marcel Dekker, New York. 1969. Chapt. 3; (*c*) C. H. ROCHESTER. Acidity functions. Academic Press, New York. 1970.
2. K. YATES and R. A. MCCLELLAND. J. Am. Chem. Soc. **89**, 2086 (1967); L. P. HAMMETT. Physical organic chemistry. 2nd ed. McGraw Hill, New York. 1970. Chapt. 9.
3. J. F. BUNNETT and F. P. OLSEN. Can. J. Chem. **44**, 1899 (1966); **44**, 1917 (1966).
4. N. C. MARZIANO, G. M. CIMINO, and R. C. PASSERINI. J. Chem. Soc. Perkin II, 1915 (1973); N. C. MARZIANO, P. G. TRAVERSO, and R. C. PASSERINI. J. Chem. Soc. Perkin II, 306 (1977); N. C. MARZIANO, P. G. TRAVERSO, A. TOMASIN, and R. C. PASSERINI. J. Chem. Soc. Perkin II, 309 (1977); N. C. MARZIANO, A. TOMASIN, and P. G. TRAVERSO. J. Chem. Soc. Perkin II, 1070 (1981).
5. (*a*) R. A. COX and K. YATES. J. Am. Chem. Soc. **100**, 3861

Can. J. Chem. Downloaded from www.nrcresearchpress.com by 210.87.254.6 on 09/06/12
For personal use only.

(1978); (*b*) R. A. COX and K. YATES. Can. J. Chem. **59**, 2116 (1981); (*c*) V. LUCCHINI, G. MODENA, G. SCORRANO, R. A. COX, and K. YATES. J. Am. Chem. Soc. **104**, 1958 (1982).
6. A. J. KRESGE, H. J. CHEN, and Y. CHIANG. J. Chem. Soc. Chem. Commun. 969 (1972).
7. U. L. HALDNA and H. J. KUUS. Org. Reactivity, **16**, 5 (1979); U. HALDNA. Org. Reactivity, **16**, 129 (1979).
8. A. J. KRESGE and H. J. CHEN. Anal. Chem. **41**, 74 (1969).
9. A. J. KRESGE and H. J. CHEN. J. Am. Chem. Soc. **94**, 8192 (1972).
10. E. M. ARNETT and G. SCORRANO. Adv. Phys. Org. Chem. **13**, 83 (1976).
11. M. A. PAUL and F. A. LONG. Chem. Rev. **57**, 1 (1957).
12. M. J. JORGENSON and D. R. HARTTER. J. Am. Chem. Soc. **85**, 878 (1963).
13. K. N. BASCOMBE, and R. P. BELL. Discuss. Faraday Soc. **24**, 158 (1957).
14. P. TICKLE, A. G. BRIGGS, and J. M. WILSON. J. Chem. Soc. B, 65 (1970).
15. C. D. JOHNSON, A. R. KATRITZKY, and S. A. SHAPIRO. J. Am. Chem. Soc. **91**, 6654 (1969).
16. E. M. ARNETT and G. W. MACH. J. Am. Chem. Soc. **88**, 1177 (1966).
17. K. YATES and H. WAI. J. Am. Chem. Soc. **86**, 5408 (1964).
18. S. A. ATTIGA and C. H. ROCHESTER. J. Chem. Soc. Perkin II, 1624 (1974).
19. N. C. DENO, H. E. BERKHEIMER, W. L. EVANS, and H. J. PETERSON. J. Am. Chem. Soc. **81**, 2344 (1959).
20. R. G. BATES. Determination of pH. John Wiley, New York. 1973. p. 49.
21. N. C. DENO, J. J. JARUZELSKI, and A. SCHRIESHEIM. J. Am. Chem. Soc. **77**, 3044 (1955).
22. (*a*) J. C. SCHUMACHAR (*Editor*). Perchlorates. Reinhold, New York. 1960. p. 16; (*b*) International critical tables. Vol. 3. McGraw Hill, New York. 1928.

Can. J. Chem. Downloaded from www.nrcresearchpress.com by 210.87.254.6 on 09/06/12
For personal use only.

Structural studies of steric effects in phosphine complexes. Part XI.[1,2] Synthesis, characterization, crystal and molecular structure of the dinitrato(trimesitylarsine)mercury(II) dimer

ELMER C. ALYEA, SHELTON A. DIAS, GEORGE FERGUSON, AND PIK Y. SIEW

Guelph-Waterloo Centre for Graduate Work in Chemistry, Guelph Campus, Department of Chemistry, University of Guelph, Guelph, Ont., Canada N1G 2W1

Received July 23, 1982

ELMER C. ALYEA, SHELTON A. DIAS, GEORGE FERGUSON, and PIK Y. SIEW. Can. J. Chem. **61**, 257 (1983).

The synthesis and crystal and molecular structure of the dinitrato(trimesitylarsine)mercury(II) dimer are reported. The compound $[HgAs(mesityl)_3(NO_3)_2]_2$ belongs to the monoclinic space group $P2_1/c$ (C_2^5h, No. 14) with $a = 20.001(2)$, $b = 17.591(5)$, $c = 16.553(2)$, $\beta = 99.991(6)$, and $Z = 4$; the asymmetric unit contains two independent half dimers. The structure was refined to a final R of 0.0458 for 2631 observed reflections measured by diffractometer with $2 < \theta < 20°$. The crystal structure consists of discrete centrosymmetric dimeric molecules of $[HgAs(mesityl)_3(NO_3)_2]_2$ separated by normal van der Waals distances. The mercury coordination in both dimers **I** and **II** is characterized by three strong, nearly coplanar bonds (in **I** Hg—As 2.476(3), Hg—O 2.41(2) and 2.20(2), and in **II** Hg—As 2.482(3), Hg—O 2.28(2) and 2.39(2), and three weaker Hg—O bonds in the range 2.55–2.90 Å. Both independent trimesitylarsine ligands have the same regular propeller conformation (Hg—As—C—C torsion angles of 45 to 50°) and the largest C—As—C angles (mean value 112.5(8)°) yet determined. The As(mesityl)$_3$ cone angle is 202°. The two independent dimers differ primarily in the orientation of the non-bridging nitrato groups. Nitrato vibrational and arsine ^{1}H nmr data are also presented for $[HgAs(mesityl)_3(NO_3)_2]_2$, which becomes monomeric in dichloroethane solution.

ELMER C. ALYEA, SHELTON A. DIAS, GEORGE FERGUSON et PIK Y. SIEW. Can. J. Chem. **61**, 257 (1983).

On rapporte la synthèse et les structures cristalline moléculaire du dimère du dinitrano(trimésitylarsine)mercure(II). Le composé $[HgAs(mésityl)_3(NO_3)_2]_2$ appartient au groupe d'espace monoclinique $P2_1/c$ (C_2^5h, No. 14) avec $a = 20,001(2)$, $b = 17,591(5)$, $c = 16,553(2)$, $\beta = 99,991(6)$ et $Z = 4$. L'unité asymétrique contient deux demi dimères indépendants. On a affiné la structure jusqu'à une valeur finale de $R = 0,0458$ pour 2631 réflexions observées et mesurées à l'aide d'un diffractomètre avec $2 < \theta < 20°$. La structure du cristal consiste en des molécules dimères centrosymétriques discrètes de $[HgAs(mesityl)_3(NO_3)_2]_2$ séparées par des distances normales de van der Waals. La coordination du mercure dans les deux dimères **I** et **II** est caractérisée par trois liaisons quasi coplanaires fortes (dans **I**, Hg—As = 2,476(3), Hg—O = 2,41(2) et 2,20(2), dans **II**, Hg—As = 2,482(3), Hg—O = 2,28(2) et 2,39(2) et trois liaisons Hg—O plus faibles de l'ordre de 2,55 à 2,90 Å. Les deux ligands trimésitylarsine indépendants ont la même conformation du type hélice régulière (Hg—As—C—C angles de torsion de 45 à 50°) et les plus grands angles C—As—C (valeur moyenne 112,5(8)°) observés jusqu'à maintenant. L'angle du cone As(mésityl)$_3$ est de 202°. Deux dimères indépendants diffèrent initialement par l'orientation des groupes nitrato qui ne sont pas en position de pont. On présente également les données relatives à la vibration du groupe nitrato et à la rmn du ^{1}H de l'arsine pour le composé $[HgAs(mesityl)_3(NO_3)_2]_2$ qui devient un monomère en solution dans le dichloroéthane.

[Traduit par le journal]

Introduction

A systematic study of metal complexes of tertiary phosphines containing bulky substituents is in progress in our laboratories (1). X-ray analysis of complexes of tricyclohexylphosphine, tris(*tert*-butyl)phosphine, tri(*o*-tolyl)phosphine, and trimesitylphosphine have provided a range of experimental cone angle values (2) in good agreement with those estimated from space-filling molecular models (3). The development of the concept of a "ligand profile" (2) allowed precise comparison of the conformations of the groups bonded to phosphorus. As an extension of the use of maximum cone angles and ligand profiles derived from X-ray structural data in describing the steric effects of bulky ligands we have chosen to study an arsine with sterically demanding substituents. This paper reports the preparation, characterization, crystal and molecular structure determination of $[HgAs(mesityl)_3(NO_3)_2]_2$ (mesityl = $C_6H_2(CH_3)_3$), the first complex of trimesitylarsine to be so characterized. The compound is isomorphous with the corresponding phosphine complex (4).

[1]For Part X, see ref. 1.

[2]Presented in part at the International Conference on Phosphorus Chemistry, Durham, NC, June 1–5, 1981, Abstract 235.

Experimental

Spectroscopic and other physical measurements were performed as previously described (5). Trimesitylarsine was prepared by an appropriate modification of the literature method for trimesitylphosphine (6).

Preparation of the dinitrato(trimesitylarsine)mercury(II) dimer, $[HgAs(mesityl)_3(NO_3)_2]_2$

A solution of As(mesityl)$_3$ (0.433 g, 1.00 mmol) in absolute ethanol (50 mL) was added to a suspension of $Hg(NO_3)_2 \cdot H_2O$ (0.343 g, 1.00 mmol) in the same solvent (25 mL). The mixture was refluxed under dinitrogen for 0.5 h, giving a clear solution, from which a white crystalline solid was deposited on cooling to room temperature. The product was isolated by filtration, washed with dry ether, and dried *in vacuo*. Recrystallization from absolute ethanol afforded suitable crystals for X-ray analysis; yield 56%; mp 181–183 (decomp.). *Anal.* calcd. for $[HgAs(mesityl)_3(NO_3)_2]_2$: C 42.84, H 4.39, N 3.70; found: C 42.31, H 4.23, N 3.66.

X-ray crystallographic analysis

Weissenberg and precession photographs provided approximate unit cell dimensions; accurate lattice parameters were obtained by a least-squares treatment of the diffractometer setting angles for 12 reflections for which θ_{hkl} (Mo-K_α) was between 10 and 20°. Crystal data (at 21°C) are

0008-4042/83/020257-06$01.00/0

©1983 National Research Council of Canada/Conseil national de recherches du Canada

Can. J. Chem. Downloaded from www.nrcresearchpress.com by 210.87.254.105 on 09/06/12
For personal use only.

TABLE 1. Final fractional coordinates ($\times 10^4$) and isotropic temperature factors ($Å^2 \times 10^3$) with estimated standard deviations in parentheses*

Atom	x/a	y/b	z/c	U_{iso}	Atom	x/a	y/b	z/c	U_{iso}
Hg(1)	4(1)	860(1)	1006(1)	54(1)*	Hg(2)	4968(1)	714(0)	1028(1)	49(1)*
As(1)	−636(1)	700(1)	2148(1)	38(1)*	As(2)	4416(1)	708(1)	2261(1)	40(2)*
N(11)	1232(14)	129(13)	743(16)	95(7)	N(21)	4432(11)	1167(12)	−591(14)	81(6)
N(12)	411(12)	2314(14)	332(16)	98(7)	N(22)	6239(10)	1377(11)	807(12)	70(5)
O(11)	651(8)	18(8)	291(9)	67(4)	O(21)	4858(8)	673(8)	−364(9)	69(4)
O(12)	1258(10)	518(11)	1384(14)	109(6)	O(22)	4160(10)	1520(10)	−103(13)	104(6)
O(13)	1706(12)	−218(12)	573(14)	126(7)	O(23)	4235(11)	1281(12)	−1362(15)	128(7)
O(14)	157(17)	2496(17)	972(23)	194(11)	O(24)	5773(9)	1833(9)	775(11)	86(5)
O(15)	211(10)	1688(12)	87(12)	107(6)	O(25)	6157(7)	688(8)	1001(9)	64(4)
O(16)	630(9)	2783(9)	−79(11)	35(4)	O(26)	6806(10)	1544(9)	639(12)	98(5)
C(111)	56(9)	499(10)	3107(12)	43(5)	C(211)	5150(9)	900(10)	3197(11)	42(5)
C(112)	618(10)	1000(11)	3238(13)	54(5)	C(212)	5073(10)	1503(10)	3748(12)	52(6)
C(113)	1192(10)	802(11)	3864(13)	56(6)	C(213)	5649(11)	1711(12)	4328(14)	62(6)
C(114)	1122(12)	154(13)	4317(15)	70(6)	C(214)	6258(10)	1364(11)	4338(13)	50(5)
C(115)	608(13)	−286(13)	4232(15)	76(7)	C(215)	6292(12)	774(12)	3801(15)	73(7)
C(116)	28(11)	−112(11)	3642(14)	60(6)	C(216)	5736(10)	532(10)	3229(12)	45(5)
C(117)	676(11)	1721(13)	2767(14)	69(7)	C(217)	4393(13)	1870(14)	3873(16)	81(7)
C(118)	1780(15)	−21(16)	4991(19)	103(9)	C(218)	6895(15)	1632(16)	4965(19)	100(9)
C(119)	−562(11)	−635(12)	3652(14)	63(6)	C(219)	5849(11)	−118(12)	2713(14)	62(6)
C(121)	−1077(9)	1665(9)	2260(11)	39(5)	C(221)	4039(9)	−298(10)	2327(12)	44(5)
C(122)	−1391(10)	2023(10)	1518(12)	47(5)	C(222)	3648(9)	−596(10)	1608(12)	43(5)
C(123)	−1594(11)	2791(12)	1550(14)	65(6)	C(223)	3381(11)	−1310(12)	1603(14)	60(6)
C(124)	−1542(11)	3158(12)	2295(14)	65(6)	C(224)	3506(10)	−1764(11)	2291(13)	54(6)
C(125)	−1306(11)	2775(12)	3025(14)	66(6)	C(225)	3867(10)	−1466(11)	3029(13)	54(6)
C(126)	−1068(9)	2018(10)	3008(12)	45(5)	C(226)	4125(10)	−737(10)	3034(12)	48(5)
C(127)	−1499(11)	1647(12)	680(14)	65(6)	C(227)	3463(11)	−128(11)	815(14)	60(6)
C(128)	−1814(13)	4000(15)	2309(17)	90(8)	C(228)	3223(12)	−2566(13)	2302(15)	76(7)
C(129)	−880(12)	1622(13)	3856(16)	75(7)	C(229)	4469(14)	−402(15)	3864(18)	90(8)
C(131)	−1244(8)	−149(8)	1870(10)	28(4)	C(231)	3740(10)	1474(11)	2113(12)	51(5)
C(132)	−1930(10)	−101(10)	1854(13)	52(5)	C(232)	3892(11)	2173(11)	1803(13)	56(6)
C(133)	−2362(11)	−710(11)	1485(14)	64(6)	C(233)	3386(12)	2763(12)	1582(14)	68(6)
C(134)	−2087(12)	−1322(12)	1168(15)	69(7)	C(234)	2750(11)	2598(12)	1689(13)	61(6)
C(135)	−1380(11)	−1373(11)	1191(14)	60(6)	C(235)	2582(12)	1933(13)	1964(15)	69(7)
C(136)	−963(9)	−794(9)	1552(11)	38(5)	C(236)	3065(11)	1371(11)	2228(13)	59(6)
C(137)	−2270(11)	542(12)	2274(15)	69(6)	C(237)	4610(11)	2458(11)	1742(14)	61(6)
C(138)	−2543(18)	−1925(19)	691(24)	134(12)	C(238)	2160(15)	3221(17)	1381(19)	108(9)
C(139)	−197(11)	−942(12)	1619(13)	62(6)	C(239)	2832(14)	638(15)	2613(17)	94(8)

*These atoms were refined anisotropically. The value given above is the mean of the U_{ii} values; the anisotropic values ($Å^2 \times 10^4$) are given below

Atom	U_{11}	U_{22}	U_{33}	U_{23}	U_{12}	U_{13}
Hg(1)	541(7)	558(6)	510(7)	33(5)	168(5)	39(5)
As(1)	379(14)	442(12)	390(16)	26(10)	65(12)	19(10)
Hg(2)	487(7)	575(6)	553(7)	−40(5)	131(5)	43(5)
As(2)	404(15)	412(12)	484(18)	2(10)	52(13)	5(10)

$C_{54}H_{66}As_2Hg_2N_4O_{12}$ fw = 1514.2
Monoclinic, $a = 20.001(2)$, $b = 17.591(5)$, $c = 16.553(2)$, $\beta = 99.991(6)$, $V = 5735.6$ Å^3, $Z = 4$, $D_c = 1.75$ g cm^{-3}, $F(000) = 2960$, μ(Mo-K$_\alpha$) = 44.8 cm^{-1}. On the basis of systematic absences ($h0l$, l odd; and $0k0$, k odd) the crystals were uniquely assigned to space group $P2_1/c$ (C_2^5h, No. 14).

The intensity data for a unique quadrant within the limit $2 < \theta < 20$ were collected with a small crystal (0.21 × 0.21 × 0.25 mm) as described for the isomorphous phosphine complex (4), and were corrected for Lorentz and polarization factors and a numerical absorption correction was applied. Maximum and minimum values of transmission coefficients are 0.39 and 0.23 respectively. Of the 5377 measured reflections, 2631 reflections with $I > 3\sigma(I)$ were used in the final refinement of the structure parameters.

The asymmetric unit consists of two independent half dimers situated about independent symmetry centres. A first Fourier summation was phased with mercury and arsenic atom contributions, their coordinates being obtained from the phosphine complex. All non-hydrogen atoms were located in this first electron density map. The structure was then refined by full-matrix least-squares calculations with anisotropic thermal parameters for the Hg and As atoms and isotropic for the remaining non-hydrogen atoms to a final R value of 0.046. Unit weights were used in the refinement and scattering factors were taken from ref. 7 and anomalous dispersion corrections were applied (8) for Hg and As atoms. A final difference synthesis showed a few peaks in positions expected for some of the protons and no other chemically significant features.

The maximum shift/error ratios in the final cycle were 0.080 (for the z-coordinate of C(239)), and 0.028 (for U_{iso} of C(218)). The final fractional coordinates with estimated standard deviations are given in Table 1 and selected molecular dimensions are in Table 2. A listing of the observed and calculated structure factors has been deposited in the Depository of Unpublished Data.[3]

The mercury coordination and our numbering scheme are shown in

[3]A complete set of tabular data is available, at a nominal charge, from the Depository of Unpublished Data, CISTI, National Research Council of Canada, Ottawa, Ont., Canada K1A 0S2.

Can. J. Chem. Downloaded from www.nrcresearchpress.com by 210.87.254.105 on 09/06/12
For personal use only.

Can. J. Chem. Downloaded from www.nrcresearchpress.com by 210.87.254.105 on 09/06/12
For personal use only.

TABLE 2. Interatomic distances (Å) and angles (deg) for $[HgAs(mesityl)_3(NO_3)_2]_2$*

(*a*) Interatomic distances

Atoms	Distance	Atoms	Distance	Atoms	Distance	Atoms	Distance
Hg(1)—As(1)	2.476(3)	Hg(2)—As(2)	2.482(3)	N(11)—O(13)	1.20(4)	N(21)—O(23)	1.28(3)
Hg(1)—O(11)	2.41(2)	Hg(2)—O(21)	2.28(2)	N(12)—O(14)	1.29(5)	N(22)—O(24)	1.22(3)
Hg(1)—O(12)	2.55(2)	Hg(2)—O(22)	2.66(2)	N(12)—O(15)	1.22(3)	N(22)—O(25)	1.27(2)
Hg(1)—O(14)	2.90(3)	Hg(2)—O(24)	2.62(2)	N(12)—O(16)	1.20(3)	N(22)—O(26)	1.25(3)
Hg(1)—O(15)	2.20(2)	Hg(2)—O(25)	2.39(2)	As(1)—C(111)	1.95(2)	As(2)—C(211)	1.97(2)
Hg(1)—O(11)^{I}	2.78(2)	Hg(2)—O(21)^{II}	2.72(2)	As(1)—C(121)	1.94(2)	As(2)—C(221)	1.94(2)
N(11)—O(11)	1.28(3)	N(21)—O(21)	1.23(3)	As(1)—C(131)	1.93(2)	As(2)—C(231)	1.90(2)
N(11)—O(12)	1.25(3)	N(21)—O(22)	1.22(3)				

(*b*) Bond angles

Bonds	Angle	Bonds	Angle	Bonds	Angle	Bonds	Angle
As(1)—Hg(1)—O(11)	134.3(4)	As(2)—Hg(2)—O(21)	148.6(4)	C(111)—As(1)—C(121)	110.6(8)	C(211)—As(2)—C(221)	110.9(7)
As(1)—Hg(1)—O(11)^{I}	106.9(4)	As(2)—Hg(2)—O(21)^{II}	115.7(4)	C(111)—As(1)—C(131)	112.4(7)	C(211)—As(2)—C(231)	113.4(8)
As(1)—Hg(1)—O(12)	113.7(5)	As(2)—Hg(2)—O(22)	106.2(5)	C(121)—As(1)—C(131)	115.0(7)	C(221)—As(2)—C(231)	112.4(8)
As(1)—Hg(1)—O(14)	101.4(8)	As(2)—Hg(2)—O(24)	120.5(4)	Hg(1)—O(11)—N(11)	97(1)	Hg(2)—O(21)—N(21)	103(2)
As(1)—Hg(1)—O(15)	142.0(5)	As(2)—Hg(2)—O(25)	127.0(4)	Hg(1)—O(12)—N(11)	92(2)	Hg(2)—O(22)—N(21)	85(1)
O(11)—Hg(1)—O(11)^{I}	60.1(6)	O(21)—Hg(2)—O(21)^{II}	63.8(6)	Hg(1)—O(14)—N(12)	80(2)	Hg(2)—O(24)—N(22)	89(1)
O(11)—Hg(1)—O(12)	52.1(6)	O(21)—Hg(2)—O(22)	50.5(6)	Hg(1)—O(15)—N(12)	117(2)	Hg(2)—O(25)—N(22)	99(1)
O(11)—Hg(1)—O(14)	122.3(8)	O(21)—Hg(2)—O(24)	79.4(5)	Hg(1)—O(11)—Hg(1)^{I}	120(1)	Hg(2)—O(21)—Hg(2)^{I}	116(1)
O(11)—Hg(1)—O(15)	83.5(7)	O(21)—Hg(2)—O(25)	84.3(5)	Hg(1)—O(11)^{I}—N(11)^{I}	143(2)	Hg(2)—O(21)^{II}—N(21)^{I}	129(2)
O(12)—Hg(1)—O(11)^{I}	111.8(6)	O(22)—Hg(2)—O(21)^{II}	107.2(6)	O(11)—N(11)—O(12)	118(2)	O(21)—N(21)—O(22)	122(2)
O(12)—Hg(1)—O(14)	97.8(8)	O(22)—Hg(2)—O(24)	78.6(5)	O(11)—N(11)—O(13)	117(2)	O(21)—N(21)—O(23)	119(2)
O(12)—Hg(1)—O(15)	91.8(7)	O(22)—Hg(2)—O(25)	118.8(6)	O(12)—N(11)—O(13)	124(3)	O(22)—N(21)—O(23)	119(2)
O(14)—Hg(1)—O(11)^{I}	125.0(7)	O(24)—Hg(2)—O(21)^{II}	118.9(7)	O(14)—N(12)—O(15)	110(3)	O(24)—N(22)—O(25)	120(2)
O(14)—Hg(1)—O(15)	45.1(9)	O(24)—Hg(2)—O(25)	50.9(5)	O(14)—N(12)—O(16)	122(3)	O(24)—N(22)—O(26)	124(2)
O(15)—Hg(1)—O(11)^{I}	87.6(7)	O(25)—Hg(2)—O(21)^{II}	77.3(7)	O(15)—N(12)—O(16)	124(3)	O(25)—N(22)—O(26)	116(2)
Hg(1)—As(1)—C(111)	104.8(6)	Hg(2)—As(2)—C(211)	105.6(6)				
Hg(1)—As(1)—C(121)	106.2(6)	Hg(2)—As(2)—C(221)	106.5(6)				
Hg(1)—As(1)—C(131)	107.1(5)	Hg(2)—As(2)—C(231)	107.5(7)				

(*c*) Intermolecular contacts

Atoms	Distance	Atoms	Distance	Atoms	Distance	Atoms	Distance
O(13)...C(127)^{I}	3.24	O(16)...C(113)^{III}	3.35	O(22)...C(138)^{I}	3.29	O(23)...C(217)^{III}	3.29
O(15)...C(139)^{I}	3.11	O(16)...C(129)^{III}	3.39	O(22)...C(217)^{III}	3.38	O(25)...C(227)^{II}	3.37
				O(23)...C(219)^{II}	3.01	O(26)...C(127)^{IV}	3.38

*The superscripts on the second atom refer to the following transformations: I, $-x, -y, -z$; II, $1 - x, -y, -z$; III, $x, 1/2 - y, -1/2 + z$; IV, $1 + x, y, z$.

Can. J. Chem. Downloaded from www.nrcresearchpress.com by 210.87.254.105 on 09/06/12
For personal use only.

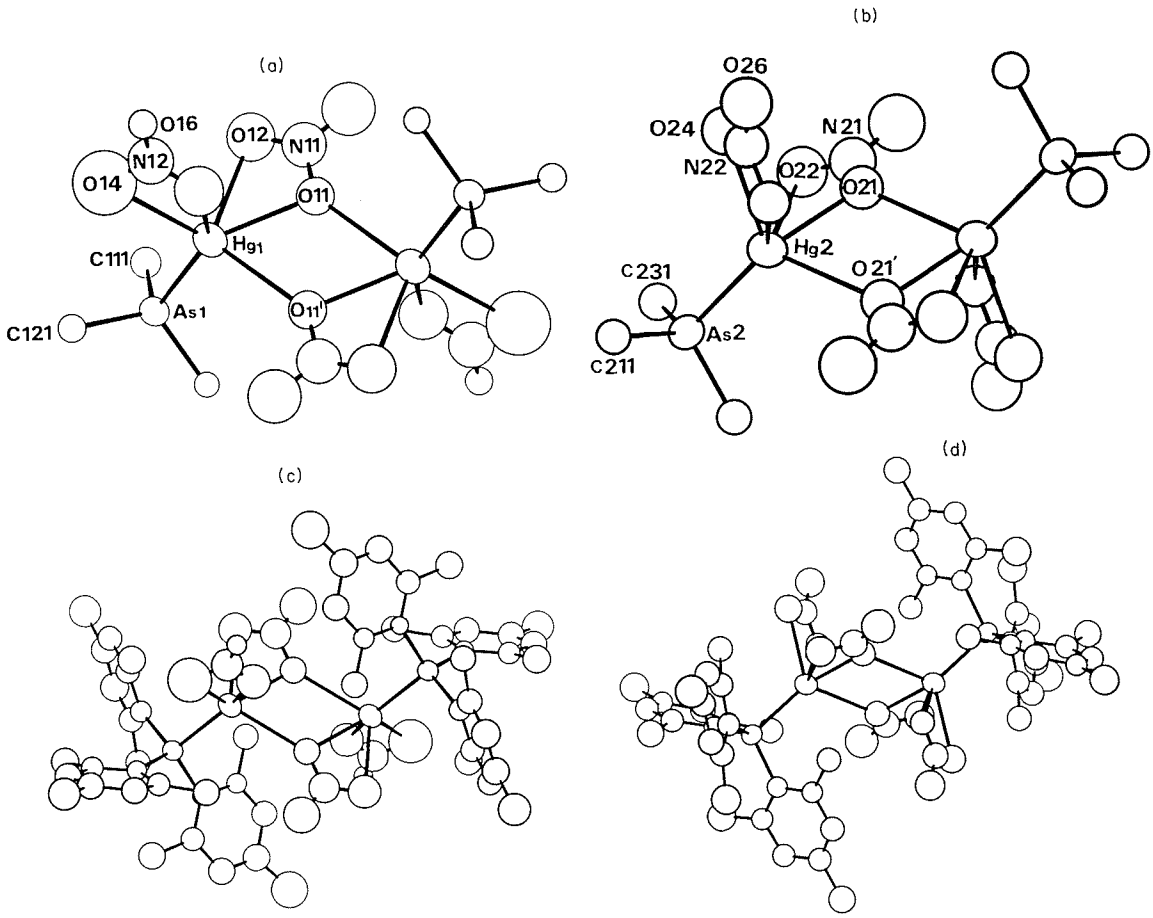

FIG. 1. Views with 50% probability ellipsoids of (*a*) and (*c*) dimer **I**, and (*b*) and (*d*) dimer **II**, of $[HgAs(mesityl)_3(NO_3)_2]_2$ showing molecular geometry and details of our numbering schemes. For simplicity, only the mesityl carbons bonded to arsenic are shown in (*a*) and (*b*).

Fig. 1 for both dimers; for simplicity only the mesityl carbons bonded to arsenic are shown in Fig. 1 *a* and *b*. The orientations of the mesityl groups may be seen in Fig. 1 *c* and *d*.

Discussion

Description of the steric effects of phosphorus ligands in terms of cone angles has found wide applicability (3) but the concept has not been developed for other ligands. In order to extend our use (1, 2) of a "ligand profile" to yield precise maximum cone angle data based on X-ray structural results, we wished to examine an arsine complex. The title compound involving the bulkiest known arsine ligand allows a direct comparison with the previously characterized analogous $P(mesityl)_3$ complex (4).

$[HgAs(mesityl)_3(NO_3)_2]_2$ has a molecular weight by osmometry in dichloroethane (ca. 10^{-3} *M* solution) of 757, which corresponds to the monomer. The complex is a non-electrolyte in dichloroethane, and the slight conductance in nitromethane (Λ26.0 ohm^{-1} cm^2 mol^{-1}, 10^{-3} mol dm^{-3}) can be attributed to partial dissociation. The ^1H nmr spectrum of the complex for a $CDCl_3$ solution at ambient temperature showed a pseudosinglet at δ2.26 ppm due to the methyl groups and a singlet at δ6.93 ppm assigned to the aromatic protons. For the free arsine, a $CDCl_3$ solution shows methyl resonances at 2.13 and 2.23 ppm in a 2:1 ratio and an aromatic proton resonance at 6.85 ppm. In contrast, splitting of both types of resonance peaks in the case of the analogous $P(mesityl)_3$ complex attested to the restricted rotation of the mesityl groups (4).

The vibrational spectrum of $[HgAs(mesityl)_3(NO_3)_2]_2$ clearly shows the absence of ionic nitrate and the presence of more than one kind of coordinated nitrato group in the solid state. Nitrato infrared spectral bands (in cm^{-1}, Nujol mull) can be identified at 1498(vs), 1265(vs), 1250(s, sh), 1080(m, br), 1040(m), 1015(s), 980(m), 922(mw), 835(m), 829(m), 810(m), 735(m), 715(mw), and 705(m). The large number of ir nitrato bands and the observation of two Raman spectral bands at 1013 cm^{-1} (s) and 1023 cm^{-1} (s, sh) attributable to the symmetric stretching mode of the nitrato group suggest the presence of at least two types of coordinated nitrato group. By analogy with our previous assignments (4, 5, 9), Raman bands at 76 cm^{-1} (vs) and 152, 176 cm^{-1} (m) might tentatively be assigned to ν(Hg—As) and ν(Hg—O), respectively.

The crystal structure contains discrete well-resolved molecules of $[HgAs(mesityl)_3(NO_3)_2]_2$, with the unit cell having four dimeric molecules, half of each of the dimers **I** and **II** corresponding to the asymmetric unit. The two independent centrosymmetric dimers differ from each other in the orientations of the nitrato groups and the configuration of the trimesityl arsine moieties at each mercury.

In both dimers (Fig. 1) the mercury coordination is essentially trigonal planar with three strong bonds (Hg—As 2.476(3) in **I** and 2.482(3) Å in **II**, Hg—O 2.41(2) and 2.20(2) in **I** and 2.28(2) and 2.39(2) Å in **II**); similar geometries are found in $[HgPCy_3(OAc)_2]_2$, $[HgP(o\text{-tolyl})_3(OAc)_2]_2$ (10), and

TABLE 3. Mean plane equations and dihedral angles (deg) within $[HgAs(mesityl)_3(NO_3)_2]_2$

Plane	Atoms in plane	Equation
1	Hg(1), As(1), C(111)	$0.085x + 0.980y + 0.181z = 1.784$
2	C(111)–C(116)	$-0.394x + 0.559y + 0.729z = 4.223$
3	Hg(1), As(1), C(121)	$0.796x + 0.315y + 0.517z = 1.341$
4	C(121)–C(126)	$0.914x + 0.332y - 0.234z = -1.982$
5	Hg(1), As(1), C(131)	$0.707x - 0.620y + 0.339z = -0.368$
6	C(131)–C(136)	$0.099x - 0.462y + 0.881z = 3.000$
7	Hg(2), As(2), C(211)	$-0.166x + 0.983y - 0.076z = -0.385$
8	C(211)–C(216)	$0.259x + 0.652y - 0.712z = 1.162$
9	Hg(2), As(2), C(221)	$0.857x - 0.306y + 0.416z = 7.989$
10	C(221)–C(226)	$0.842x - 0.361y - 0.401z = 5.879$
11	Hg(2), As(2), C(231)	$0.668x + 0.668y + 0.328z = 7.369$
12	C(231)–C(236)	$0.204x + 0.367y + 0.908z = 4.463$

Planes	Dihedral angle (deg)
1,2	49.7
3,4	44.6
5,6	49.1
7,8	49.3
9,10	48.3
11,12	47.2

$[HgP(mesityl)_3(NO_3)_2]_2$ (4). Centrosymmetric dimer formation involves oxygen atoms O(11) in **I** and O(21) in **II** making longer contacts (2.78 and 2.72 Å respectively) with adjacent mercury atoms. Each mercury completes its six-fold coordination by virtue of two further weak contacts involving the nitrato oxygen atoms (Hg—O 2.55–2.90 Å).

The nitrato groups have N—O bond lengths in the range 1.20(4)–1.29(5), which are not significantly different but the groups differ markedly in their orientations (Fig. 1). The Hg—O distances (Table 2) show the same degree of asymmetry as was found in the phosphine complex (4).

The coordination about arsenic is distorted tetrahedral in both dimers with Hg—As—C angles averaging 106.1 and 106.5(6)° and C—As—C angles 112.7(7) and 112.2(8) in **I** and **II** respectively. In the free $As(mesityl)_3$ (11) the C—As—C angles are 107.6(2)°. The Hg—As—C and C—As—C angles show slightly less distortion from tetrahedral than the analogous angles found in the isostructural $P(mesityl)_3$ dimers (105.2, 105.6(4) and 113.3, 113.1(5)° respectively (4) but are comparable to the Hg—P—C and C—P—C angles (106.8 and 112.0(7)°) found in $HgP(t\text{-}Bu)_3(OAc)_2$ (12). The Hg—As bond lengths (2.476 and 2.482(3) Å) are about 0.08 Å longer than the Hg—P bond distances found in the related isostructural phosphine complexes (4, 10), which corresponds to the difference in covalent radii of P and As atoms (13). There are few structural comparisons possible for mercury complexes of arsines; for example, Hg—As (2.557 Å) in trigonal $Hg(SCN)_2AsPh_3$ (14) and Hg—As (2.60, 2.82 Å) in tetrahedral $HgBr_2QAS$ (QAS = tris(diphenylarsino)phenylarsine) (15). The mean bond lengths As—C (1.94(2) Å), aromatic C—C (1.39(2) Å and CH_3—C(sp^2) (1.54(3) Å) are in agreement with values found for the free arsine (11).

Steric crowding in the bulky $As(mesityl)_3$ moieties is relieved by out-of-plane displacements of arsenic and methyl groups and by increases of (As)C—Ĉ—CH_3 angles. The angle deformations at the *o*-methyl groups are similar to those reported for the mesityl groups in $As(mesityl)_3$ (11) and in $[HgP(mesityl)_3(NO_3)_2]_2$ (4). To gauge the steric bulk of the $As(mesityl)_3$ ligands we have prepared ligand profile diagrams and computed maximum semi-cone angles θ/2 as described previously (2, 4). In dimer **I** maximum θ/2 values are 101.3, 103.4, and 100.1° with a mean value of 101.6° leading to a maximum cone angle θ of 203°. For dimer **II** equivalent θ/2 values are 100.2, 101.5, and 100.0°, giving θ = 201°. As anticipated, the calculated cone angles are less than that found (208° (4)) for P(mesityl) in the isostructural $[HgP(mesityl)_3(NO_3)_2]_2$ as a result of the longer Hg—As bond lengths. A similar decrease (5°) in cone angle has been previously noted (16) for the PPh_3 and $AsPh_3$ moieties (cone angles 145 and 140° respectively). One consequence of the lower steric bulk of the arsine ligand is its lower rate of metallation with palladium and platinum (17). Both $As(mesityl)_3$ ligands adopt regular propeller conformations with dihedral angles between the appropriate Hg—As—C and mesityl plane in the range 45–50° (Table 3).

Acknowledgement

We are grateful to the Natural Sciences and Engineering Research Council for operating grants (to E.C.A. and G.F.).

1. E. C. ALYEA, G. FERGUSON, and A. SOMOGYVARI. Inorg. Chem. **21**, 1369 (1982).
2. G. FERGUSON, P. J. ROBERTS, E. C. ALYEA, and M. KHAN. Inorg. Chem. **17**, 2965 (1978).
3. C. A. TOLMAN. Chem Rev. **77**, 313 (1977).
4. E. C. ALYEA, S. A. DIAS, G. FERGUSON, and M. PARVEZ. Inorg. Chim. Acta, **37**, 45 (1979).
5. E. C. ALYEA and S. A. DIAS. Can. J. Chem. **57**, 83 (1979).
6. B. I. STEPANOV, E. N. KARPOVA, and A. I. BOKANOV. J. Gen. Chem. USSR, **39**, 1514 (1969).
7. D. T. CROMER and J. B. MANN. Acta Crystallogr. A**24**, 321 (1968).
8. D. T. CROMER. Acta Crystallogr. **18**, 17 (1965).
9. E. C. ALYEA, S. A. DIAS, G. FERGUSON, and M. A. KHAN. J. Chem. Res. Synop. 360; Miniprint 4101 (1979).
10. E. C. ALYEA, S. A. DIAS, G. FERGUSON, M. A. KHAN, and

Can. J. Chem. Downloaded from www.nrcresearchpress.com by 210.87.254.105 on 09/06/12
For personal use only.

P. J. ROBERTS. Inorg. Chem. **18**, 2433 (1979).
11. A. N. SOBOLEV, I. P. ROMM, N. YU. CHERNIKOVA, V. K. BELSKY, and E. N. GURYANOVA. J. Organomet. Chem. **219**, 35 (1981).
12. P. J. ROBERTS, G. FERGUSON, R. G. GOEL, W. O. OGINI, and R. J. RESTIVO. J. Chem. Soc. Dalton, 253 (1978).
13. L. PAULING. The nature of the chemical bond. 3rd ed. Cornell University Press, Ithaca, New York. 1960. p. 203.
14. J. HUBERT, A. L. BEAUCHAMP, and R. RIVEST. Can. J. Chem. **53**, 3383 (1975).
15. G. DYER, D. C. GOODALL, R. H. B. MAIS, H. M. POWELL, and L. M. VENANZI. J. Chem. Soc. A, 1110 (1966).
16. C. GAGNON and A. L. BEAUCHAMP. Acta Crystallogr. B**35**, 166 (1979).
17. S. A. DIAS and E. C. ALYEA. Transition Met. Chem. **4**, 205 (1979).

Can. J. Chem. Downloaded from www.nrcresearchpress.com by 210.87.254.105 on 09/06/12
For personal use only.

Force field of acetic acid: use of CNDO/force calculations

A. ANNAMALAI AND SURJIT SINGH[1]

Structural Chemistry Group, Department of Chemistry, Indian Institute of Technology, Madras 600 036, India

Received May 25, 1982

A. ANNAMALAI and SURJIT SINGH. Can. J. Chem. **61**, 263 (1983).

The redundancy-free internal valence force field of monomeric acetic acid is evaluated using CNDO/force calculations and least-squares refinement. The initial force field is set up by taking the interaction and bending force constants from CNDO force field and transferring the stretching force constants from the force fields of chemically related molecules. Vibrational frequencies of monomeric CH_3COOH, CH_3COOD, CD_3COOH, and CD_3COOD are used to refine the force constants. The experimental force field thus obtained is found to be reasonable when compared to the force fields of related molecules as well as on the basis of the frequency fits and potential energy distributions.

A. ANNAMALAI et SURJIT SINGH. Can. J. Chem. **61**, 263 (1983).

Utilisant des calculs de force/CNDO et des ajustements par la méthode des moindres carrés, on a évalué le champ de force de valence interne sans répétition de l'acide acétique sous forme monomère. On a établi le champ de force initial en prenant l'interaction et les constantes de force de courbure du champ de force CNDO et en transferrant les constantes de force de tension à partir des champs de force de molécules chimiquement apparentées. On a utilisé les préférences de vibration des acides monomères: CH_3COOH, CH_3COOD, CD_3COOH et CD_3COOD pour ajuster les constantes de force. On a trouvé que le champ de force expérimental ainsi obtenu est raisonnable quand lon le compare aux champs de force des molécules apparentées ainsi que sur la base des agréments des fréquences et des distributions d'énergie potentielle.

[Traduit par le journal]

Can. J. Chem. Downloaded from www.nrcresearchpress.com by 210.87.254.42 on 09/06/12
For personal use only.

Introduction

A number of papers (1–7) deal with the ir and Raman spectroscopic studies of acetic acid monomer and its deuterated derivatives. Considering point mass models, force field calculations were carried out by Thomas (8), and Nakamoto and Kishida (9). Other force field calculations for acetic acid were carried out by Fukushima and Zwolinski (10) using a modified Urey–Bradley force field, and by Brooks and Haas (11), Alfheim and Cyvin (12), and Meyer *et al.* (5) using valence force fields. In the widely used least-squares method of force field refinement, an initial force field matrix ($\mathbf{F}_0$) is set up by transferring the force constants from chemically related molecules, and then refined using experimental data such as vibrational frequencies. The diagonal force constants can reasonably be transferred among chemically related molecules but in the case of interaction force constants, such a transfer is not justified as it very much depends on the geometry of the molecule. In the previous studies (13–17) it is found that the CNDO/force MO calculations predict reasonably well the signs of interaction force constants. The magnitudes of bending as well as stretch–bend and bend–bend interaction force constants are also reasonably estimated by these calculations. The stretch–stretch interaction constants are about 50% higher than the experimental values and the stretching force constants are overestimated by a factor of 2 to 3.5. CNDO/force calculations provide us with a reasonable way of choosing the bending and interaction force constants for the $\mathbf{F}_0$ matrix in order to perform least-squares refinement. It was pointed out by IUPAC (18) that the force constants corresponding to the coordinates expressed by redundancy conditions are indeterminate and recommendations were made that redundancy-free coordinates should be used in order to have meaningful force fields. In the present work, initial force field is set up by taking interaction and bending force constants from CNDO force field and transferring stretching force constants from the force fields of chemically related molecules from literature. Redundancy-free internal valence force field (RFIVFF) is then calculated by refining this force field using vibrational frequency data on various isotopic species of acetic acid.

Computational details and results

The CNDO/force calculations are carried out using a modified form (15) of Pople's computer program CNINDO (19). The molecular geometry is optimised as described earlier (13, 15) using the steepest descent method. The forces are then calculated by distorting the molecule from the optimised reference geometry in the positive and negative directions of redundancy-free internal coordinates. The distortions considered are 1 pm, 1°, and 2° respectively for stretching, bending, and torsional coordinates. The CNDO force constants are then derived from the forces using the relationships given earlier (15). The redundancy-free internal coordinates[2] are expressed below in terms of the internal coordinates given in Fig. 1. The CNDO/force field is given in Table 1.

In-plane:

1. $\nu_{C=O} = R$
2. $\nu_{C-C} = D$
3. $\nu_s(CH_3) = (1/\sqrt{3})\,(r_1 + r_2 + r_3)$
4. $\nu_s'(CH_3) = (1/\sqrt{6})\,(2r_1 - r_2 - r_3)$
5. $\nu_{C-O} = L$
6. $\nu_{O-H} = d$
7. $\delta_{C-C-O} = (1/\sqrt{6})\,(2\delta_1 - \delta_2 - \delta_3)$
8. $\rho_{C=O} = (1/\sqrt{2})\,(\delta_2 - \delta_3)$
9. $\delta_s(CH_3) = [3(1 + b^2)]^{-1/2}[b(\alpha_1 + \alpha_2 + \alpha_3) - (\beta_1 + \beta_2 + \beta_3)]$
   $(b = -3 \sin\beta \cos\beta/\sin\alpha)$

[1]To whom all correspondence should be addressed.

[2]The corresponding redundancy coordinates are $(1/\sqrt{3})\,(\delta_1 + \delta_2 + \delta_3)$ and $[3(1 + b^2)]^{-1/2}[(\alpha_1 + \alpha_2 + \alpha_3 + b(\beta_1 + \beta_2 + \beta_3)]$, where $b = -3\sin\beta \cos\beta/\sin\alpha$.

0008-4042/83/020263-04$01.00/0

©1983 National Research Council of Canada/Conseil national de recherches du Canada

10. $\delta_s'(CH_3) = (1/\sqrt{6})\,(2\alpha_1 - \alpha_2 - \alpha_3)$
11. $\rho_{\parallel}(CH_3) = (1/\sqrt{6})\,(2\beta_1 - \beta_2 - \beta_3)$
12. $\delta_{C-O-H} = \theta$

Out-of-plane:

13. $\nu_a(CH_3) = (1/\sqrt{2})\,(r_2 - r_3)$
14. $\delta_a(CH_3) = (1/\sqrt{2})\,(\alpha_2 - \alpha_3)$
15. $\rho_{\perp}(CH_3) = (1/\sqrt{2})\,(\beta_2 - \beta_3)$
16. $\gamma_{C=O} = \phi$
17. $\tau(CH_3) = (1/\sqrt{6})\,(\tau_1 + \tau_2 + \tau_3 + \tau_1' + \tau_2' + \tau_3')$
18. $\tau(OH) = (1/\sqrt{2})\,(\tau_4 + \tau_5)$

The initial force field is constructed according to the procedure given above. The stretch–stretch interaction force constants of the CNDO force field are scaled down by a factor of 0.65 (17) before being included in the $\mathbf{F}_0$ matrix. Schachtschneider's FPERT program (20) is used to carry out the refinement after including the damped least-squares subroutines. The force field is refined using absolute weighting factors (21) for the frequency parameters. All the calculations were performed on an IBM 370/155 computer. The vibrational frequencies of CH_3COOH, CH_3COOD, CD_3COOH, and CD_3COOD listed by Meyer *et al.* (5) with the revised assignments for a few bands are employed in the calculations. Since the CH and OH stretching frequencies were not given by Meyer *et al.*, they are taken from ref. 4. The **G** matrices are calculated on the basis of the geometry obtained by Derissen (22) from the electron diffraction data. The bond angles around the methyl C atom are assumed to be 109.47°. Based on C_s symmetry of acetic acid the 18 fundamental modes can be distributed as $12A' + 6A''$ vibrations. Calculations for A' and A'' vibrations were carried out separately. Since the number of independent force constants of acetic acid exceeds the number of available vibrational frequencies, some reasonable constraints on the force field are imposed. For the experimental force fields 38 significant parameters were considered for A' species whereas 9 force constants were considered for A'' species. The force constants are refined using 46 frequencies for A' species and 19 frequencies for A'' species. In the case of A' vibrations, the parameters *F8,9* and *F8,11* corresponding to the interactions $\rho_{C=O}/\delta_s(CH_3)$ and $\rho_{C=O}/\rho_{\parallel}(CH_3)$ respectively are constrained to zero, since the trial calculations carried out indicate negligibly small values for these constants. The force constant *F17,17* corresponding to the methyl group torsional mode is kept fixed at 0.004×10^{-18} N m rad^{-2} based on similar values obtained for acetaldehyde and acetone (17). The experimental force field obtained is also included in Table 1. In Table 2 the calculated and observed frequencies are given along with the potential energy distributions (PED).

Discussion

The force field reported in this work is rather too elaborate and includes all the diagonal and off-diagonal force constants. Meyer *et al.* (5) reported a value of 8.048×10^2 N m^{-1} for the carbonyl stretching force constant ($F_{C=O}$) of acetic acid which is considerably different from the present value (12.692×10^2 N m^{-1}). In a redundancy valence force field obtained by Ha, Meyer, and Gunthard (23) employing the *ab initio* results as the initial force constants and refining the force field using vibrational frequency data, the $F_{C=O}$ of formic acid was found to be 13.05×10^2 N m^{-1}. The estimate of Meyer *et al.* for acetic acid makes a difference of 5×10^2 N m^{-1} between the $F_{C=O}$ values of formic acid and acetic acid. For these two acids, the

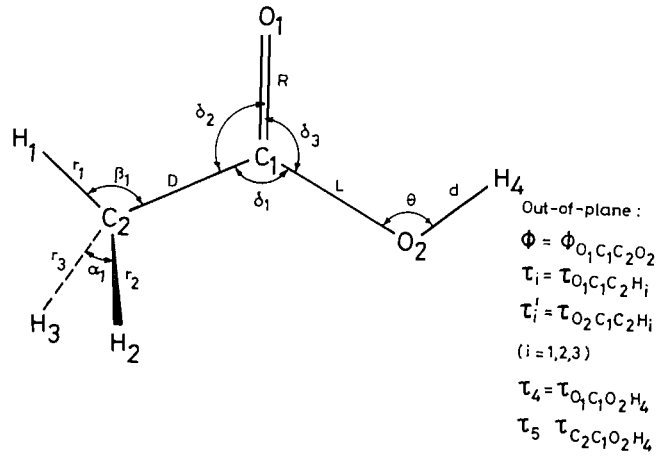

FIG. 1. Internal coordinates of acetic acid.

TABLE 1. Force fields of acetic acid[a]

Force constant	Theoretical CNDO/force	Exp.	Force constant	Theoretical CNDO/force	Exp.
F1,1	30.305	12.692	F 5,12	0.504	0.441
F1,2	1.312	0.778	F 6,6	16.472	7.225
F1,5	2.282	1.327	F 6,7	0.029	—
F1,7	−0.534	−0.533	F 6,8	−0.023	—
F1,8	−0.115	−0.149	F 6,12	0.341	0.201
F1,9	−0.066	−0.182	F 7,7	0.865	1.129
F1,10	0.022	—	F 7,8	0.148	0.087
F1,11	−0.098	−0.067	F 7,10	0.011	—
F1,12	0.075	0.117	F 7,11	0.125	0.001
F2,2	16.058	4.525	F 7,12	0.097	0.295
F2,3	0.566	0.396	F 8,8	1.060	1.085
F2,5	0.896	0.444	F 8,9	−0.047	—
F2,7	0.195	0.350	F 8,11	−0.054	—
F2,8	0.436	0.460	F 9,9	0.720	0.583
F2,9	−0.398	−0.413	F 9,10	−0.015	—
F2,10	−0.034	—	F 9,11	−0.042	−0.073
F2,11	0.099	0.128	F10,10	0.730	0.516
F2,12	0.083	0.076	F10,11	−0.048	—
F3,3	12.273	5.061	F11,11	0.752	0.716
F3,8	0.035	—	F11,12	0.025	—
F3,9	0.179	0.108	F12,12	0.818	0.729
F4,4	11.803	4.955	F13,13	11.771	4.798
F4,7	0.054	—	F13,14	−0.255	−0.014
F4,8	−0.024	—	F13,15	0.281	0.114
F4,10	−0.252	−0.059	F13,16	−0.032	—
F4,11	0.286	0.037	F14,14	0.757	0.533
F5,5	21.742	6.065	F14,15	−0.035	—
F5,6	0.628	0.188	F15,15	0.501	0.522
F5,7	0.086	0.199	F15,16	−0.128	−0.118
F5,8	−0.548	−0.189	F16,16	0.619	0.669
F5,9	−0.051	—	F17,17	0.0003	0.004[b]
F5,11	0.049	—	F18,18	0.0562	0.0805

[a]Units: stretch–stretch, 10^2 N m^{-1} (mdyn Å^{-1}), stretch–bend, 10^{-8} N rad^{-1} (mdyn rad^{-1}), and bend–bend, 10^{-18} N m rad^{-2} (mdyn Å rad^{-2}).
[b]Constrained force constant values.

$F_{C=O}$ values obtained using CNDO/force calculations are found to differ only by about 1.6×10^2 N m^{-1} (24). Hence, it is felt that the value of $F_{C=O}$ reported in the present work for acetic acid is more reasonable. The almost insignificant decrease in $F_{C=O}$ value ($\sim 0.04 \times 10^2$ N m^{-1}) from formic acid to acetic acid due to the substituent CH_3 is parallel to the similar observations made when the $F_{C=O}$ values of formaldehyde,

Can. J. Chem. Downloaded from www.nrcresearchpress.com by 210.87.254.42 on 09/06/12
For personal use only.

TABLE 2. Observed and calculated frequencies (in cm^{-1}) and PED for acetic acid[a]

	ν				ν			
	Obs.	Calcd.	Δν	PED	Obs.	Calcd.	Δν	PED
CH_3COOH					CD_3COOH			
A′	3583	3594	−11	F6,6(100)	3582	3594	−12	F6,6(100)
	3051	3047	4	F4,4(100)	2285	2278	7	F4,4(99)
	2944	2949	−5	F3,3(101)	2118	2116	2	F3,3(101)
	1779	1779	0	F1,1(93)	1774	1777	−3	F1,1(94) F5,5(26) F11,11(15)
	1439	1466	−7	F10,10(56) F9,9(17) F11,11(12)	1332	1326	6	F5,5(37) F12,12(28) F8,8(19) F2,2(13) F5,12(13)
	1380	1381	−1	F9,9(48) F10,10(35)				
	(1280)	1293	−13	F9,9(40) F5,5(27) F2,2(22) F12,12(20) F8,8(12) F2,9(−15)	(1182)	1178	4	F12,12(55) F5,5(33) F5,12(−18)
					1070	1067	3	F9,9(93) F2,2(28) F2,9(−26)
	1181	1194	−13	F12,12(54) F5,5(22) F11,11(11) F5,12(−14)	1034	1027	7	F10,10(93)
					817	820	−3	F2,2(39)
	987	986	1	F11,11(72) F5,5(22)	(774)	774	0	F11,11(66) F2,2(20) F7,7(11)
	847	855	−8	F2,2(80) F5,5(13)	563	560	3	F8,8(70)
	581	576	5	F8,8(75)	408	399	9	F7,7(92) F12,12(18) F7,12(−26)
	428	434	−6	F7,7(100) F12,12(21) F7,12(−30)				
A″	2996	2996	0	F13,13(100)	2230	2235	−5	F13,13(99)
	1434	1431	3	F14,14(95)	1034	1035	−1	F14,14(97)
	1044	1047	−3	F15,15(62) F16,16(20) F15,16(19)	919	920	−1	F16,16(41) F15,15(40) F15,16(16)
	639	648	−9	F18,18(55) F16,16(34) F15,15(20) F15,16(−10)	610	613	−3	F18,18(82) F15,15(16)
					479	474	5	F16,16(57) F15,15(46) F18,18(16) F15,16(−20)
	535	528	7	F16,16(50) F18,18(45) F15,15(18) F15,16(−11)	—	85	—	F17,17(100)
	—	116	—	F17,17(100)				
CH_3COOD					CD_3COOD			
A′	3039	3047	−8	F4,4(100)	2642	2626	16	F6,6(100)
	2952	2949	3	F3,3(101)	2275	2277	−2	F4,4(99)
	2642	2626	16	F6,6(100)	2116	2116	0	F3,3(101)
	1770	1768	2	F1,1(97)	1766	1766	0	F1,1(98)
	1436	1441	−5	F10,10(65) F9,9(14) F11,11(12)	(1282)	1278	4	F5,5(61) F8,8(25) F2,2(24) F2,8(−10)
	1377	1375	2	F9,9(64) F10,10(27)	1073	1068	5	F9,9(93) F2,2(27) F2,9(−25)
	1267	1265	2	F5,5(49) F2,2(32) F9,9(28) F8,8(19) F2,8(−10) F2,9(−15)	1035	1033	2	F10,10(80)
					1001	988	13	F12,12(55) F10,10(12) F5,5(10) F7,12(10) F5,12(−10)
	—	1031	—	F11,11(44) F12,12(26)	818	809	9	F11,11(41) F5,5(22) F2,2(20)
	956	958	−2	F12,12(35) F5,5(32) F11,11(32) F5,12(−14)	(747)	750	−3	F11,11(38) F2,2(36) F12,12(17)
					535	536	−1	F8,8(73)
	835	826	9	F2,2(72) F12,12(15)	—	386	—	F7,7(96) F12,12(26) F7,12(−33)
	545	551	−6	F8,8(78)				
	418	416	2	F7,7(103) F12,12(32) F7,12(−37)	2240	2235	5	F13,13(99)
CH_3COOD					—	1035	—	F14,14(97)
A″	2996	2996	0	F13,13(100)	919	919	0	F15,15(41) F16,16(41) F15,16(16)
	1429	1431	−2	F14,14(95)	531	534	−3	F15,15(48) F16,16(39) F18,18(28) F15,16(−17)
	1051	1047	4	F15,15(62) F16,16(20) F15,16(14)	409	403	6	F18,18(71) F16,16(23) F15,15(13)
	604	608	−4	F16,16(70) F15,15(33) F18,18(14) F15,16(−19)	—	85	—	F17,17(100)
	422	417	5	F18,18(86) F16,16(14)				
	—	116	—	F17,17(100)				

[a]Values in parentheses are estimated by Meyer *et al.* (5).

acetaldehyde, and acetone are considered (17). Force constants of C—O and O—H stretching, and COH bending modes of acetic acid are very close to the corresponding force constants of formic acid (23). The C=O/C—O interaction force constant obtained in this work (1.327×10^2 N m^{-1}) is in good agreement with the *ab initio* value reported by Ha *et al.* (23) for formic acid (1.3×10^2 N m^{-1}). The C—O stretching force constant of acetic acid (6.065×10^2 N m^{-1}) is greater than the corresponding force constants of methyl alcohol (5.4×10^2 N m^{-1}) (25) and diethyl ether (5.04×10^2 N m^{-1}) (26). In both the studies (25, 26), the initial force fields were transferred from chemically related molecules and not obtained from MO calculations and whereas the force field obtained for methanol was redundancy free, the force field for ether had redundant force constants. However, a greater C—O stretching force constant in acetic acid in comparison to methyl alcohol and ether, to some extent, may be in order because of π electron delocalisation in acetic acid. This is also reflected in the C=O/C—O interaction force constant which has a very high positive value in the case of acetic acid. The force constants corresponding to the methyl group vibrations do not differ significantly from those obtained for acetaldehyde and acetone in similar calculations (17). The observed frequencies are well reproduced by the calculated force field. The potential energy

Can. J. Chem. Downloaded from www.nrcresearchpress.com by 210.87.254.42 on 09/06/12
For personal use only.

distributions in the present work are found to be in general similar to those reported by Meyer *et al.* (5).

Acknowledgements

A. A. thanks DAE and CSIR, India for the award of research fellowships.

1. W. WELTNER. J. Am. Chem. Soc. **77**, 3941 (1955).
2. J. K. WILMSHURST. J. Chem. Phys. **25**, 1171 (1956).
3. M. HAURIE and A. NOVAK. J. Chim. Phys. **62**, 137 (1965).
4. C. V. BERNEY, R. L. REDINGTON, and K. C. LIN. J. Chem. Phys. **53**, 1713 (1970).
5. R. MEYER, T.-K. HA, H. FREI, and HS. H. GUNTHARD. Chem. Phys. **9**, 393 (1975).
6. J. LAANE. J. Chem. Phys. **55**, 2514 (1971).
7. R. W. REDDING. J. Chem. Phys. **57**, 3729 (1972).
8. W. J. O. THOMAS. Discuss. Faraday Soc. **9**, 339 (1950).
9. K. NAKAMOTO and S. KISHIDA. J. Chem. Phys. **41**, 1554 (1964).
10. K. FUKUSHIMA and B. J. ZWOLINSKI. J. Chem. Phys. **50**, 737 (1969).
11. W. V. F. BROOKS and C. M. HAAS. J. Phys. Chem. **71**, 650 (1967).
12. I. ALFHEIM and S. J. CYVIN. Acta Chim. Scand. **24**, 3043 (1970).
13. P. PULAY and F. TOROK. Mol. Phys. **25**, 1153 (1973).
14. K. KOZMUTZA and P. PULAY. Theoret. Chim. Acta (Berl.), **37**, 67 (1975).
15. M. KANAKAVEL, J. CHANDRASEKHAR, S. SUBRAMANIAN, and S. SINGH. Theoret. Chim. Acta (Berl.), **43**, 185 (1976).
16. A. ANNAMALAI, M. KANAKAVEL, and S. SINGH. Proc. Indian Acad. Sci. Sec. A, **87**, 337 (1978).
17. A. ANNAMALAI and S. SINGH. J. Mol. Struct. Theochem. **87**, 169 (1982) and J. Chem. Phys. In press.
18. IUPAC. Appl. Spectrosc. **31**, 569 (1977).
19. J. A. POPLE and D. L. BEVERIDGE. Approximate molecular orbital theory. McGraw-Hill, New York. 1970.
20. J. H. SCHACHTSCHNEIDER. Technical Reports No. 57-65. Shell Development Co., CA. 1964.
21. J. OVEREND and J. R. SCHERER. J. Chem. Phys. **32**, 1720 (1960).
22. J. L. DERISSEN. J. Mol. Struct. **7**, 67 (1971).
23. T.-K. HA, R. MEYER, and HS. H. GUNTHARD. Chem. Phys. Lett. **59**, 17 (1979).
24. A. ANNAMALAI. Ph.D. thesis, Indian Institute of Technology, Madras. 1981.
25. P. D. MALLINSON and D. C. MCKEAN. Spectrochim. Acta, Part A, **30**, 1133 (1974).
26. H. WIESER, W. G. LAIDLAW, P. J. KRUEGER, and H. FUHRER. Spectrochim. Acta, Part A, **24**, 1055 (1968).

Can. J. Chem. Downloaded from www.nrcresearchpress.com by 210.87.254.42 on 09/06/12
For personal use only.

Conductimetric studies on aqueous solutions of electrolytes. I. Conductivities of copper sulphate

VICTOR HUGO ACEVEDO, JUANA ALBARRACÍN DE MORÁN, AND LEOPOLDO ARMANDO SALES
Instituto de Química Inorgánica, Facultad de Bioquímica, Química y Farmacia, Universidad Nacional de Tucumán, Ayacucho 491, 4000-Tucumán, República Argentina

Received December 11, 1981[1]

VICTOR HUGO ACEVEDO, JUANA ALBARRACÍN DE MORÁN, and LEOPOLDO ARMANDO SALES. Can. J. Chem. **61**, 267 (1983).

The specific conductivities and pH values of copper sulphate solutions in water were measured in the temperature range from 10°C to 50°C. The data, previously corrected by hydrolysis, were analyzed by means of the Lee Wheaton theory.

This fit, for the evaluation of Λ_0, R, and K_A parameters, is quite satisfactory up to a maximum concentration of 25×10^{-4} mol dm^{-3} and the agreement between experimental data and the literature value for 25°C is acceptable.

VICTOR HUGO ACEVEDO, JUANA ALBARRACÍN DE MORÁN et LEOPOLDO ARMANDO SALES. Can. J. Chem. **61**, 267 (1983).

On a mesuré les conductivités spécifiques et le pH de solutions de sulfate de cuivre dans l'eau dans un intervalle de température allant de 10 à 50°C. Utilisant la théorie de Lee Wheaton, on a analysé les données, corrigées antérieurement par hydrolyse. Cet ajustement, pour l'évaluation des paramètres Λ_0, R et k_A, est assez satisfaisant jusqu'à une concentration maximum de 25×10^{-4} mol.dm^{-3} et l'accord entre les données expérimentales et celles de la littérature à 25° est acceptable.

[Traduit par le journal]

Introduction

For high charge electrolytes such as $CuSO_4$, the dual effects of hydrolysis and strong ion association makes the detailed interpretations of the conductance data rather difficult. The 2:2 sulphates, by contrast with 1:1 salts, show large, although non-specific negative deviations from the Debye Onsager limiting law. These deviations are usually ascribed to the formation of non-conducting ion pairs between oppositely charged ions which have approached each other quite closely. The K_A calculated for $CuSO_4$ is very strongly dependent on the particular theory applied and markedly dependent on the parameters used in the data fitting (1).

As part of an extensive investigations of the conductance of aqueous solutions of salts, we have obtained precise data for $CuSO_4$, up to a maximum concentration of 25×10^{-4} mol dm^{-3}, in the temperature range 10°C to 50°C.

In this paper we discuss the fitting of these data to the Lee Wheaton equation (2).

Experimental

The techniques used including the preparation of high purity conductivity water have been described elsewhere (3). Merck reagent grade copper sulphate pentahydrate was recrystallized three times from conductivity water. The purified salt was dried over a mixture of the penta- and trihydrates. All solutions were made up in volumetric flasks by weight. Taking into account the temperature dependence of the concentration, the weights of solute and solvent were calculated on the basis of the $d = f(c,t)$ values. The corresponding demalities were checked by gravimetric analysis.

For measurement of electrical conductivity, the Digital Conductimeter Tacussel CD 78 and immersion type cells with smooth Pt electrodes calibrated (for the different temperatures of the programme) with KCl solutions were used. Each concentration was measured at four frequencies and the conductivity extrapolated to infinite frequency.

For pH measurements the Orion 701 A Digital pH-meter with an accuracy of ±0.001 pH units was used.

The temperature of the bath was checked against two N.P.L. calibrated thermometers and was held constant to 0.005°C. In order to attain temperature equilibrium rapidly and avoid the polarization effect during measurements, the solution in the cell was stirred.

The computer analysis of the conductance data was performed in a TI 59 Microcomputer.

Results

The variation of the pH with total salt concentration is due to hydrolysis of Cu^{2+} ion, and can be expressed as follows:

[1] $Cu^{2+} + H_2O \leftrightarrow Cu(OH)^+ + H^+$

[2] $SO_4^{2-} + H_2O \leftrightarrow HSO_4^- + OH^-$

The formation of H_2SO_4 and $Cu(OH)_2$ was assumed to be negligible in dilute solutions.

The hydrolysis correction was carried out in the usual way (4), taking into account the activity coefficients and temperature dependence of the equilibrium constants.

The limiting ionic conductances for H^+, and the dissociation constants for H_2SO_4 were taken from the literature (5) while the values of conductances for $Cu(OH)^+$ and HSO_4^- and of hydrolysis constant were based on our data (9). The corrected conductivities of $CuSO_4$ solutions are given in Table 1.

Values of the molar conductivity, Λ, are quoted for the (1/2 $CuSO_4$) molar unit and in international ohms. Concentrations are given in terms of the $CuSO_4$ molar unit.

Discussion

The best-known conductance equations are one due to Pitts (6) (P equation) and those due to Fuoss (7, 8) (F 75, F 78). Lee and Wheaton have proposed, in 1978, a new conductance equation (L.W.), based on the Gurney co-sphere model, which describes charge transport in solutions containing any number of ionic species, of any valence type. For the specific case of solutions containing only a single symmetrical electrolyte, this equation has the general form:

[3] $\Lambda = f(\Lambda_0, R, K_A)$

where Λ_0 is the equivalent conductance at infinite dilution, K_A

[1]Revision received September 10, 1982.

0008-4042/83/020267-02$01.00/0
©1983 National Research Council of Canada/Conseil national de recherches du Canada

Can. J. Chem. Downloaded from www.nrcresearchpress.com by 210.87.254.5 on 09/06/12
For personal use only.

TABLE 1. Corrected conductivities of $CuSO_4$ solutions

$C \times 10^4$ (mol dm^{-3})	Conductivity								
	10°C	15°C	20°C	25°C	30°C	35°C	40°C	45°C	50°C
2	84.86_7	97.25_0	110.3_9	123.7_2	137.6_9	152.2_4	167.2_7	182.7_1	198.9_1
3	82.78_8	94.88_0	107.7_0	120.7_2	134.3_5	148.5_6	163.2_4	178.3_2	194.1_2
4.5	80.22_0	91.96_0	104.3_8	117.0_2	130.2_4	144.0_3	158.2_7	173.9_1	188.2_4
6	78.08_8	89.52_0	101.6_3	113.9_5	126.8_3	140.2_7	154.1_6	168.4_4	183.3_8
8	75.70_4	86.80_0	98.56_0	110.5_2	123.0_3	136.0_8	149.5_8	163.4_5	177.9_7
12.5	71.55_0	82.07_5	93.20_0	104.5_6	116.4_1	128.8_0	141.6_1	154.7_8	168.5_7
18	67.82_0	77.82_0	88.40_0	99.16_0	110.4_7	122.2_6	134.7_4	147.0_3	160.1_5
24.5	64.50_0	74.04_0	84.12_0	94.43_0	105.1_9	116.4_6	128.1_3	140.1_4	152.7_0

TABLE 2. Results of analysis of data for $CuSO_4$ in water*

t (°C)	Λ_0 (Ω^{-1} cm^2 mol^{-1})	K_A (dm^3 mol^{-1})
10	92.83	267
15	106.3_6	265
20	120.7_2	264
25	135.3_0	262
30	150.6_0	261
35	166.5_3	260
40	182.9_7	258
45	199.8_9	257
50	217.6_5	256.5

*R = 9.64 Å; $\sigma(\Lambda) = 0.04$, $C_{max} = 25 \times 10^{-4}$ mol dm^{-3}.

the pairwise ion association constant, and R the distance parameter.

The simplified equation could be put into the form:

$$[4]\quad \Lambda = \gamma\Lambda_0[1 + C_1(\beta\kappa) + C_2(\beta\kappa)^2 + C_3(\beta\kappa)^3] - \frac{(\rho\kappa)}{(1 + KR)}[1 + C_4(\beta\kappa) + C_5(\beta\kappa)^2 + KR/12]$$

where C_1–C_5 are complex functions of (K,R), $\rho = |z|Fe/(299.79 \times 3\pi n)$, $\beta = z^2e^2/DkT$, R is the distance parameter, and all other symbols have their usual meanings.

Here,

$$[5]\quad K_A = \frac{1 - \alpha}{\alpha^2 c f_{\pm}^2}$$

and the Debye Hückel equation is used for the activity coefficient of dissociated species.

Table 2 shows the parameters obtained when fitting our results with the Lee–Wheaton equation. For low concentration results the equation provides a good fit of data. This is reflected in the standard deviation for data up to a maximum concentration of 25×10^{-4} mol dm^{-3} ($\sigma_\Lambda\% \cong 0.04$). When all data below a concentration of 50×10^{-4} mol dm^{-3} are analysed, $\sigma_\Lambda\%$ rises to 0.065.

The R value obtained is very reasonable in terms of the model proposed. It indicates that copper and sulphate ions separated by two water molecules or less should be treated as paired.

Finally we have analysed the equilibrium constant. Using the Fuoss nomenclature (7, 8) the ion pairs are divided as below,

TABLE 3. Corrected conductivities at 25°C

$C \times 10^3$ (mol dm^{-3})	Conductivity
3	91.06
3.5	88.3
4	86.22
4.5	84.21
5	82.40

with two equilibrium constants

$$[6]\quad K_A = K_R(1 + K_S)$$

$$[7]\quad K_R = (1 - \alpha)(1 - \gamma)/c\gamma^2 f^2 = (4\pi NR^3/3000)\exp(z^2e^2/D\kappa TR)$$

K_R is the association constant for the formation of solvent separated ion pairs. γc is the concentration of unpaired ions,

$$[8]\quad K_S = \alpha/(1 - \alpha)$$

is the association constant for the formation of contact ion pairs.

For this system, at 25°C the results are the following: $K_S = 5.68$, $\alpha = 8.5 \times 10^{-1}$, $K_R = 46.12$. For the lowest concentration (2×10^{-4} M), the proportion of the solvent-separated pairs would be very small: 0.88% at 25°C. However, the validity of applying these theoretical calculations is still questionable.

Acknowledgement

The authors gratefully acknowledge the assistance of Mrs. Lore S. de Zuccardi in the preparation of this paper.

1. W. G. DAVIES and J. E. OTTER. Discuss. Faraday Soc. **24**, 103 (1957).
2. W. H. LEE and R. J. WHEATON. J. Chem. Soc. Faraday II, **74**, 1456 (1978).
3. A. D. PETHYBRIDGE and D. J. SPIERS. J. Electroanal. Chem. **66**, 231 (1975).
4. B. B. OWEN and R. W. GURRY. J. Am. Chem. Soc. **60**, 3074 (1938).
5. S. ROBINSON. Electrolyte solutions. Butterworths. 1965.
6. E. PITTS. Proc. R. Soc. A, **217**, 43 (1953).
7. R. M. FUOSS. J. Phys. Chem. **79**, 1983 (1975).
8. R. M. FUOSS. J. Phys. Chem. **82**, 2427 (1978).
9. L. SALES, J. MORÁN, and V. ACEVEDO. To be published.

Can. J. Chem. Downloaded from www.nrcresearchpress.com by 210.87.254.5 on 09/06/12
For personal use only.

Total synthesis of the stemodane-type diterpenoids, (±)-2-desoxystemodinone, (+)-2-desoxystemodinone, and (±)-stemodinol

RONALD B. KELLY, MARY LOU HARLEY, SANDRA J. ALWARD, RABINDRA N. REJ, GOPALA GOWDA, AND ASISH MUKHOPADHYAY

Department of Chemistry, University of New Brunswick, P.O. Box 5050, Saint John, N.B., Canada E2L 4L5

AND

PERCY S. MANCHAND

Chemical Research Department, Hoffman-La Roche Inc., Nutley, NJ, 07110 U.S.A.

Received July 26, 1982

RONALD B. KELLY, MARY LOU HARLEY, SANDRA J. ALWARD, RABINDRA N. REJ, GOPALA GOWDA, ASISH MUKHOPADHYAY, and PERCY S. MANCHAND. Can. J. Chem. **61**, 269 (1983).

Stereospecific total syntheses of (±)-2-desoxystemodinone, (+)-2-desoxystemodinone, and (±)-stemodinol are described. Also described are the isolation of (+)-2-desoxystemodinone from *S. maritima* and its characterization. A strategy for the elaboration of the C/D ring systems of the stemodane diterpenoids, stemarin and aphidicolin, from a common 6-hydroxybicyclo[2.2.2]octan-2-one system is delineated and its efficacy is demonstrated by the synthesis of the stemodane diterpenoids and our previous synthesis of stemarin.

RONALD B. KELLY, MARY LOU HARLEY, SANDRA J. ALWARD, RABINDRA N. REJ, GOPALA GOWDA, ASISH MUKHOPADHYAY et PERCY S. MANCHAND. Can. J. Chem. **61**, 269 (1983).

On décrit des synthèse totales stéréospécifiques de la (±) désoxy-2 stémodinone, de la (+) désoxy-2 stémodinone et du (±) stémodinol. On décrit également l'isolation de la (+) désoxy-2 stémodinone à partir de la *S. maritima* ainsi que sa caractérisation. On trace une stratégie pour l'élaboration des systèmes cycliques C/D du diterpène stémodane, de la stémarine et de l'aphidicoline à partir d'un système commun, l'hydroxy-6-bicyclo[2.2.2] octanone-2, et on prouve son efficacité par la synthèse des diterpènes stémodanes et par notre synthèse antérieure de la stémarine.

[Traduit par le journal]

Introduction

By virtue of their unique carbon skeleton and alleged medicinal properties of *Stemodia maritma* L. from which they have been isolated (1), the stemodane group of diterpenoids has received considerable attention as targets for syntheses. Recently, three brief reports of total syntheses of representatives of this group have appeared, viz. the synthesis of stemodin (**3**) and stemodinone (**4**) (2*a*), the synthesis of maritimol (**5**) (2*b*), and the synthesis of 2-desoxystemodinone (**1**) and stemodinol (**2**) (3).

More than two years ago we revealed (ref. 4, see also ref. 3) a simple strategy for the construction of the C/D ring systems of the diterpenoids of the stemodane group (**1**–**5**) (1, 5), stemarin **6** (5), and aphidicolin (**7**) (6) from a common, readily obtainable 6-hydroxybicyclo[2.2.2]octan-2-one system represented by **8**. We proposed that the functionality of **8** could be modified to give intermediates such as **9**, **10**, and **11** (L = leaving group) which could be induced to undergo skeletal rearrangement to **12**, **13**, and **14** possessing the C/D ring systems of the stemodane diterpenoids, stemarin and aphidicolin, respectively. In each case, the leaving group (L) is aligned *anti* and periplanar to the migrating bond so that the desired C/D ring system should result from a Wagner-type rearrangement (Scheme 1). It should be pointed out that the rearrangement of bicyclo[2.2.2]octane systems to bicyclo-[3.2.1]octane systems has been employed by Wiesner *et al.* (7) in the synthesis of the delphinine and aconite alkaloids and by van Tamelen *et al.* (2*b*) in a recently reported synthesis of maritimol (**5**).

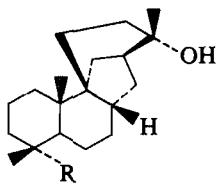

1 R = CH_3
2 R = CH_2OH
2a R = CH_2OTs

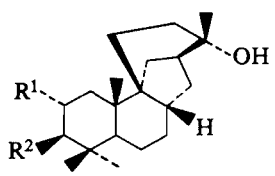

3 R^1 = OH; R^2 = H
4 R^1 = O; R^2 = H
5 R^1 = H; R^2 = OH

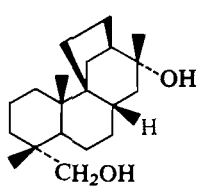

6

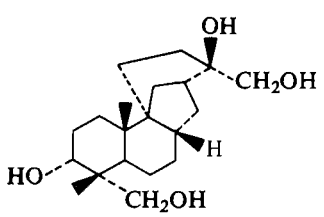

7

We have demonstrated the efficacy of our strategy by the completion of total syntheses of (±)-stemarin (**6**) (4), (±)-stemodinol (**2**) (3), (±)-2-desoxystemodinone (**1**) (3), and the naturally occurring enantiomer (+)-2-desoxystemodinone (**1**) (described in this article). The essential features of this strategy were adopted very recently by others (8) in some model studies which resulted in the synthesis of noraphidicolane and norstemodane skeleta but not in the synthesis of any naturally occurring diterpenoids.

We now wish to present the details of our syntheses of the stemodane type diterpenoids. We also wish to take this opportunity to describe the isolation of (+)-2-desoxystemodinone from *Stemodia maritima* L., the structure of which was deduced by spectral means (5) and confirmed by correlation with stemodinone (**4**) (see Experimental); the structure of the latter

0008-4042/83/020269-07$01.00/0
©1983 National Research Council of Canada/Conseil national de recherches du Canada

Can. J. Chem. Downloaded from www.nrcresearchpress.com by 210.87.254.42 on 09/06/12
For personal use only.

Can. J. Chem. Downloaded from www.nrcresearchpress.com by 210.87.254.42 on 09/06/12
For personal use only.

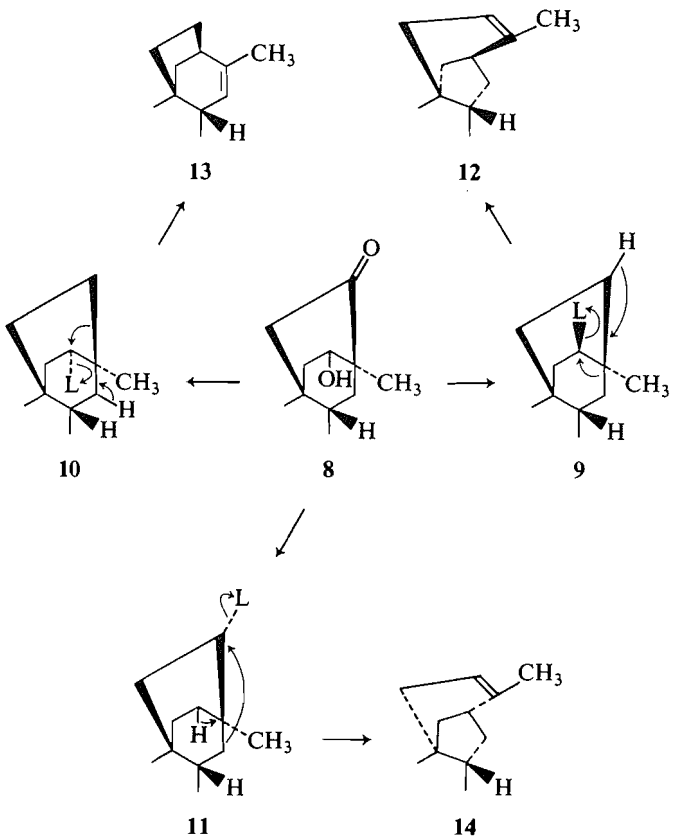

SCHEME 1

was unambiguously determined by single crystal X-ray analysis (1*a*).

Discussion and results[1]

Total synthesis of (±)-2-desoxystemodinone and (±)-stemodinol

An outline of the synthesis of these racemic diterpenoids is given in Scheme 2 (Series *a*). With the possible exception of steps where stereospecificity was of no consequence, the synthesis proceeds stereospecifically from the starting material (**15***a*) to the final products.

Photoaddition of allene to the totally synthetic (9) racemic unsaturated ketone **15***a* afforded, as expected (10), the adduct **16***a* in 78% yield.[1] The configuration of **16***a* was assigned on the basis of Wiesner's (10) definitive studies on the stereochemical course of such photoadditions; the eventual conversion of **16***a* into 2-desoxystemodinone (**1**) provides yet another example of the validity of his deductions in this regard. Treatment of the adduct **16***a* with CH_3I in THF in the presence of LDA gave the methylated ketone **17***a* (74%) which was converted to the ketal **18***a* in 90% yield.

Oxidation of **18***a* with OsO_4/IO_4^- (11) gave the cyclobutanone **19***a* (77%) which was reduced quantitatively with $NaBH_4$ to the cyclobutanol **20***a*.

Having obtained the cyclobutanol **20**, we had arrived at the stage for the execution of the first two skeletal rearrangements featured in this synthetic sequence. The rearrangement, for which there is ample precedent (7, 12) was achieved by refluxing **20***a* with HCl in aqueous THF, whereupon it underwent deketalization followed by retroaldolization, then spontaneous aldol condensation to produce the keto alcohol **21***a* (72%) and its C-12 epimer (23%). The major epimer, which was chosen for the continuation of the synthetic sequence for stereochemical reasons (*vide infra*) was assigned (4) the configuration shown in **21***a* which, unlike its C-12 epimer, permits stabilization by hydrogen bonding between the OH group and the ketone (7).

We now disgress briefly to report a phenomenon of ancillary interest which was encountered with regard to the rearrangement of **20***a* (*vide supra*). When **20***a* was treated with HCl in aqueous THF under mild conditions (room temperature, 3 h) there was obtained a crystalline compound in 60% yield whose spectral properties were inconsistent with those of the expected products, **21***a* and its C-12 epimer.The ir spectrum was devoid of a band attributable to a ketone function and, furthermore, the nmr spectrum exhibited a 3-proton doublet at δ 1.00 due to a secondary methyl and two one-proton doublets (J = 6.0 Hz for each) at δ 4.76 (secondary splitting) and δ 6.42. These spectral properties prompted us to assign to this compound the unsaturated hemiacetal structure **28**. This assignment was corroborated by the discovery that the compound in question could be

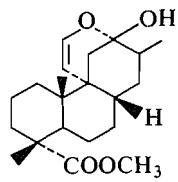

28

converted quantitatively into the same mixture of **21***a* and its C-12 epimer as was obtained above by subjecting it to the more vigorous acidic conditions employed in the direct rearrangement of **20***a* (*vide supra*).

Returning to the main theme, we now describe the transformation of the keto alcohol **21***a* into the skeletally rearranged olefin **25***a*, thence to (±)-stemodinol (**2**) and (±)-2-desoxystemodinone (**1**). Accordingly, **21***a* was converted quantitatively into the thioketal **22***a* which was reduced in 97% yield to the alcohol **23***a*. This alcohol was converted into the tosylate **24***a* in which the tosylate group (leaving group) was aligned *anti* and periplanar to bond (m), the required stereoalignment for the subsequent rearrangement which was now performed as follows. The tosylate (**24***a*) was heated at 60°C in DMSO in the presence of methyl sulfinyl carbanion (13) whereupon it was transformed, by migration of bond (m) and elimination of hydrogen, into the olefin **25***a* (60% from **23***a*). Thus, the second skeletal rearrangement was achieved to produce an intermediate possessing the stemodane carbon skeleton.

The ester group of **25***a* was reduced quantitatively with $LiAlH_4$ to provide the olefinic alcohol **26***a*. The latter, on oxidation with *m*-chloroperbenzoic acid, afforded the epoxide **27***a* which, finally, was reduced with $LiAlH_4$ to stemodinol (**2**).[2]

The synthetic diterpenoid **2** was clearly *not identical* to a

[1]Yields refer to compounds which were uncontaminated as judged by silica gel tlc and which, in the majority of cases, had been purified by column chromatography. No special effort was made to optimize yields.

[2]This synthesis of stemodinol was included as part of a plenary lecture given by R. B. K. on September 30, 1980 at the IUPAC 12th International Symposium on the Chemistry of Natural Products at Puerto de la Cruz, Tenerife, Canary Islands.

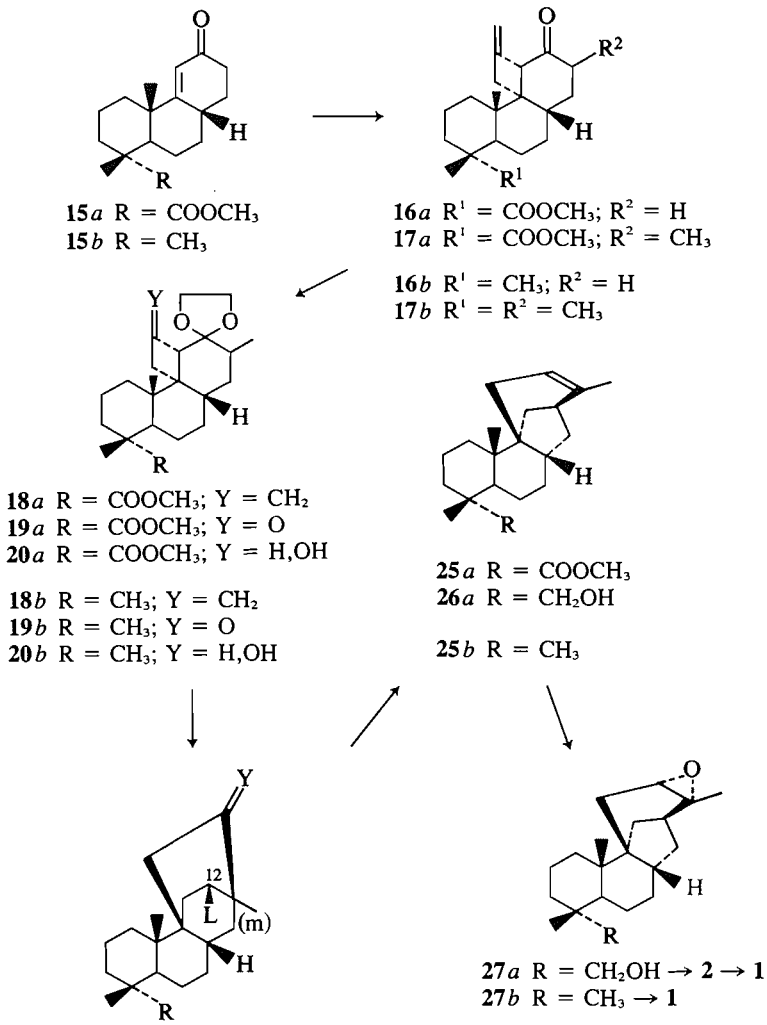

Series *a* refers to the synthesis of (±)-2-desoxystemodinone (**1**) and (±)-stemodinol (**2**)
Series *b* refers to the synthesis of (+)-2-desoxystemodinone from podocarpic acid

SCHEME 2

sample of "stemodinol" obtained from natural sources. Eventually it was discovered, by comparison with an authentic sample of stemarin, that the sample of naturally occurring stemodinol which we received was in fact stemarin (**6**) to which structure **2** had been erroneously assigned in the literature (1*b*). To the best of our knowledge, the diterpenoid having structure **2** has not been isolated from natural sources.[3]

We were now faced with the problem of demonstrating the validity of structure **2** for our synthetic diterpenoid. This task was complicated by our inability, despite the expenditure of a great deal of time and effort, to produce crystals of **2** or its derivatives amenable to X-ray crystallographic analysis. Eventually a solution was realized in the following manner. The tosylate **2***a* of **2** was reduced with $LiAlH_4$ and the product was shown to be identical (ir, nmr, ms, and silica gel tlc) to an authentic sample of the naturally occurring (5) 2-desoxystemodinone, the structure of which has been unequivocally shown to be (**1**) (*vide supra*). The assignment of the CH_2OH group in **2** to the α-orientation follows from the fact that **2** and stemarin (**6**) have been synthesized from common intermediates (4). Thus, the conversion of **2** into **1** proves that structure **2** is correct for our synthetic diterpenoid (stemodinol) and constitutes a stereospecific total synthesis of 2-desoxystemodinone (**1**).

[3]Professor C. D. Hufford, University of Mississippi, University, Mississippi, concurs with these conclusions.

Can. J. Chem. Downloaded from www.nrcresearchpress.com by 210.87.254.42 on 09/06/12
For personal use only.

Can. J. Chem. Downloaded from www.nrcresearchpress.com by 210.87.254.42 on 09/06/12
For personal use only.

Synthesis of (+)-2-desoxystemodinone from podocarpic acid

While searching for a means of resolving the difficulties surrounding our synthesis of stemodinol (**2**) (*vide supra*), we embarked upon a synthesis of the naturally occurring (+)-2-desoxystemodinone (**1**) from podocarpic acid. This synthesis was undertaken to demonstrate conclusively that the strategy described in the Introduction could be applied efficiently and stereospecifically to the synthesis of the stemodane group of diterpenoids. This objective was realized by the completion of the synthesis of **1** as described in the sequel and outlined in Scheme 2 (Series *b*).

The unsaturated ketone **15***b* was prepared in 43% overall yield from podocarpic acid by previously described procedures (14). Photoaddition of allene to **15***b* afforded the adduct **16***b*, the configuration of which was assigned as explained in the previous section.

Methylation of the photoadduct **16***b* was accomplished by a procedure different from that used in the previous synthesis. Thus, treatment of the adduct with NaH in dioxane followed by dimethylcarbonate gave the methyl ester **29** (97%) which, on treatment with NaH followed by CH_3I in dioxane, gave **30** in 90% yield. Saponification of the ester **30** with concomitant

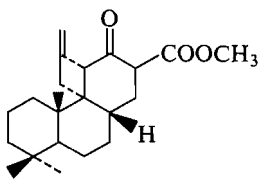

29

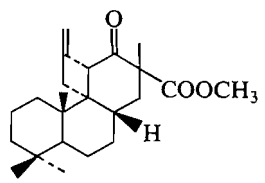

30

decarboxylation produced, in 89% yield, the methylated photoadduct **17***b*.

The sequence from **17***b* to the olefin 25*b* now paralleled exactly that employed in the preceding section (**17***a* → **25***a*). Consequently, a full amount of this portion of the present synthesis would be unnecessarily repititious and will not be given here: details are given in the experimental section. A few comments, however, are in order.

From the intermediate (**15***b*) to the synthetic diterpenoid (**1**), the synthesis required fourteen steps, eight of which were achieved in yields of over 80% and three in yields of 75% to 80%. Since skeletal rearrangements are important features of this synthesis, it should be mentioned here that the first rearrangement (**20***b* → **21***b*) yielded 76% of the desired keto alcohol **21***b* along with 20% of its C-12 epimer. It should also be mentioned that the second rearrangement proceeded smoothly to give the olefin **25***b* in 70% yield (**23***b* → **24***b* → **25**b).

In the penultimate step, the olefin **25***b* was converted into the epoxide **27***b* by oxidation with *m*-chloroperbenzoic acid. Finally, reduction of **27***b* with $LiAlH_4$ afforded the diterpenoid **1** in 75% yield. The synthetic diterpenoid **1** was identical to a sample of (+)-2-desoxystemodinone obtained from *Stemodia maritima* L. (mixture mp (145°C); nmr, ir, and mass spectra, silica gel tlc). Since a synthesis of (+)-podocarpic acid, the starting material, has been accomplished (15), the completion of this synthesis represents a formal, stereospecific synthesis of (+)-2-desoxystemodinone, the naturally occurring enantiomer; it also confirms the absolute stereochemistry of the stemodane group of diterpenoids which had been assigned on the basis of optical rotatory dispersion and circular dichroism studies (1*a*).

Experimental

Instrumentation, methods, and materials

Melting points were determined on a Fisher–Johns apparatus and are uncorrected.

Unless otherwise stated, ir spectra were determined as Nujol mulls with either a Digilab FTS-14 instrument or a Perkin–Elmer 297 instrument. Proton nmr were recorded in $CDCl_3$ on either a Varian XL-100 instrument or a Varian T-60 instrument; chemical shifts are expressed in ppm (δ-values) relative to TMS as an internal standard. The ms were recorded on a Vacuum Generator VG-ZAB-1F instrument.

Silica gel G-60 was used for column chromatography and silica gel GF-240 for tlc (E. Merck, Darmstadt.). The neutral alumina used for column chromatography was Brockman Act. II aluminum oxide (Camag).

Petroleum ether refers to the fraction with boiling point range 30–60°C. Brine refers to a saturated solution of NaCl.

*Photoadduct 16*a

A solution of 1.31 g of **15***a* and 14.5 g of allene in 500 mL of CH_2Cl_2 was irradiated at −70°C for 2 h, then left at room temperature overnight to allow excess allene to escape. Evaporation of the solvent *in vacuo*, crystallization of the residue from ether – petroleum ether, and chromatography of the mother liquor on 100 g of neutral alumina in ether – petroleum ether afforded 1.17 g (78%) of **16***a*, mp 121°C; ir: 1720 (ester), 1695 (ketone), 1662 and 900 (olefin) cm^{-1}; nmr δ: 0.88 and 1.14 (3-proton singlets, tertiary methyls), 3.63 (s, 3H, OCH_3), and 4.90 (m, 2H, exocyclic methylene). *Anal.* calcd. for $C_{21}H_{33}O_3$: C 76.33 H 9.15; found: C 76.44, H 9.16.

*Methylated photoadduct 17*a

The following reaction was carried out in a dry nitrogen atmosphere. A solution of 0.30 mL of disopropylamine in 2.4 mL of dry THF was cooled to 0°C and treated with 1.54 mL of a 1.5 M hexane solution of n-butyllithium. A solution of 668 mg of **16***a* in 3.5 mL of THF was then added to the cooled solution over 5 min. The resulting solution was cooled to −10°C, treated with 0.14 mL of CH_3I, and allowed to come to room temperature over 1 h. The reaction solution was diluted with 50 mL of benzene and washed with 25 mL of water and two 25-mL portions of brine. The aqueous washings were extracted with two 75-mL portions of ether. The combined extracts were dried over $MgSO_4$ and evaporated *in vacuo*. Separation of the product from unreacted starting material on 76 g of neutral alumina in ether–petroleum ether and recyclization of the latter afforded 518 mg (74%) of **17***a*, mp 124°C; ir: 1715 (ester), 1695 (ketone), 1665 and 890 (olefin) cm^{-1}: nmr δ: 0.88 and 1.13 (3-proton singlets, tertiary methyls), 1.16 (d, J = 6.5 Hz, 3H, secondary methyl), 3.65 (s, 3H, OCH_3), and 4.90 (m, 2H, exocyclic methylene). *Anal.* calcd. for $C_{22}H_{32}O_3$: C 76.70 H 9.36; found: C 76.63, H 9.52.

*Ketal 18*a

Under a nitrogen atmosphere, a toluene (250 mL) solution of 1.01 g of **17***a*, 80 mg of *p*-toluenesulfonic acid monohydrate, and 2.2 mL of ethylene glycol was refluxed for 5 h. During this period water was separated in a Dean–Stark adaptor and hourly additions of 1.0-mL portions of ethylene glycol were made. The cooled solution was washed with 100 mL of cold saturated Na_2CO_3 solution and 100 mL of cold brine and the aqueous washings were extracted with three 300-mL portions of ether. The combined extracts were dried over Na_2SO_4 and evaporated *in vacuo*. Crystallization of the residue from ether – petroleum ether, followed by chromatography of the mother liquor on 37 g of neutral alumina in ether – petroleum ether, afforded 1.03 g (90%) of **18***a*, mp 131°C; ir: 1732 (ester), 1675 and 913 (olefin) cm^{-1}; nmr δ: 0.91 (d, J = 6.5 Hz, 3H, secondary methyl), 0.95 and 1.14 (3-proton singlets, tertiary methyls), 3.97 (br s, 4H, ethylene of ketal), and 4.89 (m, 2H, exocyclic methylene). *Anal.* calcd. for $C_{24}H_{36}O_4$: C 74.19, H 9.34; found: C 74.18, H 9.13.

*Cyclobutanone 19*a

A solution of 58 mg of OsO_4, 1.9 mL of pyridine, and 3.9 mL of

Can. J. Chem. Downloaded from www.nrcresearchpress.com by 210.87.254.42 on 09/06/12
For personal use only.

water was treated with a solution of 572 mg of **18***a* in 48 mL of dioxane. After stirring in the dark for 15 min, the solution was treated dropwise over 1 h with a solution of 546 mg of $NaIO_4$ in 5.5 mL of water and the resulting mixture was stirred in the dark for 45 h. Solid material was removed by filtration and the filtrate was diluted with ether and washed with two 37-mL portions of cold 10% Na_2S solution and 75 mL of cold water. The aqueous washings were extracted with three 225-mL portions of ether. The extracts were dried over K_2CO_3 and evaporated *in vacuo*. Crystallization of the residue from ether – petroleum ether, followed by chromatography of the mother liquor on 10 g of neutral alumina in ether – petroleum ether, afforded 442 mg (77%) of **19***a*, mp 155°C; ir: 1779 (cyclobutanone) and 1733 (ester) cm^{-1}; nmr δ: 0.88 (d, J = 6.5 Hz, 3H, secondary methyl), 1.05 and 1.17 (3-proton singlets, tertiary methyls), 3.63 (s, 3H, OCH_3), and 3.96 (m, 4H, ethylene of ketal). *Anal.* calcd. for $C_{23}H_{34}O_5$: C 70.74, H. 8.78; found: C 70.85, H 9.13.

Cyclobutanol ***20***a

A solution of 282 mg of **19***a* in 17 mL of ethanol was treated with 172 mg of $NaBH_4$. After stirring for 1 h the reaction mixture was filtered and the filtrate was evaporated *in vacuo*. The residue was dissolved in 100 mL of ether and the solution was washed with two 75-mL portions of brine. The aqueous washings were extracted with two 100-mL portions of ether. The combined extracts were dried ($MgSO_4$) and evaporated *in vacuo* to give 283 mg (quantitative yield) of **20***a*, mp 164°C; ir: 3450 (OH) and 1722 (ester) cm^{-1}; nmr δ: 0.86 (d, J = 6.5 Hz, 3H, secondary methyl), 0.87 and 1.12 (3-proton singlets, tertiary methyls), 3.60 (s, 3H, OCH_3), 3.86 (m, 4H, ethylene of ketal), and 4.22 (m, 1H, *H*C—OH). *Anal.* calcd. for $C_{23}H_{36}O_5$: C 70.38, H 9.24; found: C 70.47, H 9.31.

Keto alcohol ***21***a *and its C-12 epimer*

Directly from ***20***a

A solution of 98 mg of **20***a* in 10 mL of THF containing 5 mL of 1 *M* aqueous HCl was refluxed under nitrogen for 20.5 h. The cooled reaction solution was diluted with 100 mL of ether and the ethereal solution was worked up with 50 mL of saturated aqueous $NaHCO_3$ solution, then with two 40-mL portions of brine. The aqueous washings were extracted with two 100-mL portions of ether. The combined extracts were dried ($MgSO_4$), evaporated *in vacuo*, and the residue was chromatographed on 10 g of silica gel in ether – petroleum ether.

The first fraction eluted from the column comprised 20 mg (23%) of the *C-12 epimer* of **21***a*, mp 197°C: ir: 3520 (OH), 1718 (ester) and 1700 (ketone) cm^{-1}; nmr δ: 0.98 (s, 6H, superimposed signals for two tertiary methyls), 1.20 (s, 3H, tertiary methyl), 3.63 (S, 3H, OCH_3), and 3.65 (m, 1H, *H*C—OH). *Anal.* calcd. for $C_{21}H_{32}O_4$: C 72.38, H 9.26; found: C 72.16, H 9.23.

The slower moving fraction from the column afforded 63 mg (72%) of **21***a*, mp 192°C; ir: 3498 (OH), 1720 (ester), and 1702 (ketone) cm^{-1}; nmr δ: 1.01 (s, 6H, superimposed signals for two tertiary methyls), 1.21 (s, 3H, tertiary methyl), 3.63 (s, 3H, OCH_3), 3.73 and 3.88 (dd, J = 3.5 Hz, 1H, *H*C—OH).

From the unsaturated hemiacetal ***28***

The unsaturated hemiacetal **28** (*vide infra*) was converted into **21***a* (80%) and its C-12 epimer (20%) by the procedure detailed above. The two epimers were identical (mixture mp, ir, and nmr spectra, silica gel tlc) to the corresponding epimers obtained directly from **20***a* (*vide supra*).

Unsaturated hemiacetal **28**

A solution of 75 mg of **20***a* in the 5 mL of THF and 4 mL of 1 *M* aqueous HCl was stirred in a nitrogen atmosphere at room temperature for 3 h. The reaction solution was diluted with 50 mL of brine and extracted with the three 50-mL portions of chloroform. The extracts were washed with 50 mL of saturated $NaHCO_3$ solution and 50 mL of brine, combined, dried over $MgSO_4$, and evaporated *in vacuo*. Column chromatography on 7.0 g of silica gel in ether – petroleum ether afforded 40 mg (60%) of **28**, mp 146°C; ir: 3340 (OH), 1725 (ester) and 1640 (olefin) cm^{-1}; nmr δ: 1.00 (d, J = 6.5 Hz, 3H, secondary methyl), 1.06 and 1.22 (3-proton singlets, tertiary methyls), 3.63 (s, 3H, OCH_3), 4.76 and 6.42 (doublets, J = 6.0 Hz, 1H each, vinylic protons). *Anal.* calcd. for $C_{21}H_{32}O_4$: C 72.38, H 9.26; found: C 72.38, H 9.24.

Thioketal ***22***a

Under a nitrogen atmosphere, a solution of 180 mg of **21***a* in 1 mL of ethane dithiol was cooled to 0°C and treated with 0.41 mL of boron trifluoride etherate. After stirring 9 min, a cold mixture of 50 mL each of CH_2Cl_2 and 1 *M* aqueous NaOH was added and the organic phase was separated and washed with two 100-mL portions of 1 *M* NaOH. The aqueous phases were extracted with three 100-mL portions of CH_2Cl_2. Evaporation *in vacuo* of the combined and dried ($MgSO_4$) extracts afforded 219 mg (quantitative yield) of **22***a*, mp 177–178°C; ir: 3435 (OH) and 1718 (ester) cm^{-1}; nmr δ: 0.90, 1.12 and 1.17 (3-proton singlets, tertiary methyls), 3.17 (m, 4H, ethylene of ketal), 3.61 (s, 3H, OCH_3), and 3.76 (m, 1H, *H*C—OH). *Anal.* calcd. for $C_{23}H_{36}S_2O_3$: C 65.05, H. 8.54; found: C 65.02, H 8.55.

Alcohol ***23****a*

A solution of 165 mg of **22**a in 70 mL of absolute alcohol was stirred with 3.0 g of Raney nickel, W-2 (16), under a nitrogen atmosphere for 22 h. The catalyst was removed by filtration, the alcohol was evaporated *in vacuo*, and the residue taken up in ether. The ether solution was filtered and evaporated *in vacuo* to give 126 mg (97%) of **23***a*, mp 130°C; ir: 3500 (OH) and 1705 (ester) cm^{-1}; nmr δ: 0.78, 0.93 and 1.20 (3-proton singlets, tertiary methyls), 3.56 (m, 1H, *H*C—OH), and 3.66 (s, 3H, OCH_3). *Anal.* calcd. for $C_{21}H_{34}O_3$: C 75.41, H 10.25; found: C 75.58, H 10.14.

Olefinic ester ***25***a

A solution of 76 mg of **23***a* in 1.1 mL of pyridine containing 134 mg of *p*-toluenesulfonyl chloride was left in the dark at 3°C for 66.5 h. The cold solution was diluted with 4 mL of ice water and, after stirring for 15 min, 50 mL of cold ether was added. The ethereal solution was washed with 50 mL of cold 2 *M* aqueous HCl solution and two 50-mL portions of cold brine. The aqueous washings were extracted with three 50-mL portions of ether. Evaporation of the combined, dried (K_2CO_3) extracts *in vacuo* afforded 106 mg of the tosylate **24***a* which was used immediately for the next step.

The following reaction was performed under a dry nitrogen atmosphere. A solution of 106 mg of **24***a* in 2.3 mL of dry DMSO was treated with 0.59 mL of a 0.5 *M* DMSO solution of methylsulfinyl carbanion (13). The resulting solution was stirred at 60°C for 1.5 h, then cooled, treated with 1 mL of water, and diluted with 50 mL of ether. The ethereal solution was washed with three 30-mL portions of brine and three 30-mL portions of water and the washings were extracted with five 50-mL portions of ether. Evaporation *in vacuo* of the combined, dried ($MgSO_4$) extracts and chromatography of the residue on 7.0 g of silica gel in ether – petroleum ether afforded 43 mg (60%) of the oily olefin **25***a*, ir (film): 1730 (ester) and 1650 (olefin) cm^{-1}; nmr δ: 0.97 and 1.23 (3-proton singlets, tertiary methyls), 1.55 (d, J = 2 Hz, 3H, vinylic methyl), 3.61 (s, 3H, OCH_3), and 4.94 (m, 1H, vinylic proton). *Mol. Wt.* calcd. for $C_{21}H_{32}O_2$: 316; found (ms): 316.

Olefinic alcohol ***26***a

A mixture of 43 mg of **25***a*, 100 mg of $LiAlH_4$, and 4 mL of ether was refluxed for 1 h, then treated with a few drops of saturated aqueous Na_2SO_4 solution, followed by anhydrous Na_2SO_4. Solid material was removed by filtration and washed with ether. Evaporation *in vacuo* of the combined filtrate and ether washings afforded 39 mg (quantitative yield) of oily **26***a*, ir (film): 3350.(OH) and 1625 (olefin) cm^{-1}; nmr δ: 0.83 and 1.00 (3-proton singlets, tertiary methyls), 1.62 (d, J = 2.0 Hz, 3H, vinylic methyl), 3.07 and 3.38 (dd, J = 11 Hz, 1 H each, CH_2OH), and 4.96 (m, 1H, vinylic proton). *Mol. Wt.* calcd. for $C_{20}H_{32}O$: 288; found (ms): 288.

Epoxide ***27***a

A solution of 38 mg of **26***a* in 2 mL of benzene was treated with 34 mg of *m*-chloroperbenzoic acid and stirred in the dark at room temperature for 2 h, then 10 mL of 10% aqueous Na_2SO_3 was added and stirring was continued for 10 min. Ether (60 mL) was added, the

Can. J. Chem. Downloaded from www.nrcresearchpress.com by 210.87.254.42 on 09/06/12
For personal use only.

layers were separated, and the ether phase was washed with two 50-mL portions of 5% aqueous Na_2CO_3 and 50 mL of brine. The aqueous washings were extracted with two 60-mL portions of ether. Evaporation of the combined and dried (K_2CO_3) extracts *in vacuo* and chromatography of the residue over 5.0 g of basic alumina in ether – petroleum ether afforded 28 mg (70%) of oily **27***a*, ir (film): 3350 (OH) cm^{-1}; nmr δ: 0.97 and 0.95 (3-proton singlets, tertiary methyls), 1.27 (s, 3H, methyl attached to oxirane ring), 3.03 and 3.34 (dd, J = 11 Hz, 1 H each, CH_2—OH). *Mol. Wt.* calcd. for $C_{20}H_{32}O_2$: 304; found (ms): 304.

(±)-Stemodinol (**2**)

A mixture of 21 mg of **27***a*, 80 mg of $LiAlH_4$, and 4 mL of THF was refluxed for 2 h. A few drops of saturated aqueous Na_2SO_4 solution was added to the cooled reaction mixture, followed by anhydrous Na_2SO_4. The solid material was removed by filtration and washed with CH_2Cl_2. Evaporation of the combined filtrate and washings afforded 17 mg (63%) of **2**, mp 160°C; ir: 3510 and 3350 (OH) cm^{-1}; nmr δ: 0.82, 1.00 and 1.11 (3-proton singlets, tertiary methyls), 3.07 and 3.37 (dd, J = 11 Hz, 1 H each, CH_2OH). *Anal.* calcd. for $C_{20}H_{34}O_2$: C 78.38, H 11.18; found: C 78.21, H 11.32.

Photoadduct **16**b

The unsaturated ketone **15***b* (14) was converted into the photoadduct **16***b* by the procedure described above for the preparation of **16***a*. From 2.04 g of **15***b* there was obtained 2.03 g (86%) of **16***b*, mp 90°C; ir: 1700 (ketone), 1672 and 895 (olefin) cm^{-1}; nmr δ: 0.83 (s, 3H, tertiary methyl), 0.85 (s, 6H, superimposed signals for two tertiary methyls), and 4.82 (m, 2H, exocyclic methylene). *Anal.* calcd. for $C_{20}H_3O$: C 83.85, H 10.56; found: C 84.06, H 10.64.

Ester **30**

The following reactions were performed under a dry nitrogen atmosphere. To a well-stirred mixture of 432 mg of NaH, 3.24 g of dimethylcarbonate, and 5 mL of dry dioxane at 80–85°C there was added a solution of 2.05 g of **16***b* in 10 mL of dry dioxane over 2 h. Stirring was continued at the elevated temperature for a further 2.5 h. The reaction mixture was cooled on an ice bath, acidified with 1 *M* HCl, and extracted with three 150-mL portions of ether. The ether extracts were washed with three 10-mL portions of brine and 10 mL of water, combined, dried ($MgSO_4$), and evaporated *in vacuo*. The residue was chromatographed on 55 g of silica gel in ether – petroleum ether to give 2.39 g (97%) of **29** as an oil, ir (film): 1660 and 1615 (enolized β-keto ester) cm^{-1}.

To a stirred mixture of 432 mg of NaH and 6 mL of dry dioxane there was added over 20 min a solution of 2.50 g of **29** in 10 mL of dioxane. After a further 10 min, 2.5 mL of CH_3I was added and the reaction solution was kept at 40°C for 2.5 h, then cooled on an ice bath and acidified with 1 *M* HCl. The resulting acidic mixture was extracted with three 150-mL portions of ether and the extracts were washed with 10 mL of saturated aqueous $NaHCO_3$, then with two 15-mL portions of brine. The extracts were combined, dried over $MgSO_4$, and evaporated *in vacuo*. Chromatography of the residue over 45 g of silica gel in ether – petroleum ether afforded 2.33 g (90%) of **30**, mp 101°C; ir: 1705 (ketone) and 1745 (ester) cm^{-1}; nmr δ: four methyl singlets between 0.80 and 0.84 and 4.88 (m, 2H, exocyclic methylene). *Anal.* calcd. for: $C_{23}H_{34}O_3$: C 77.05, H 9.56; found: C 77.12, H 9.65.

Methylated photoadduct **17**b

A mixture of 2.33 g of **30**, 35 mL of 10% aqueous KOH, and 12 mL of ethanol was refluxed under nitrogen for 5.5 h. The cooled solution was acidified with 1 *N* HCl and extracted with three 200-mL portions of ether. The extracts were washed with 10 mL of saturated aqueous $NaHCO_3$ solution, then with two 15-mL portions of brine. The combined extracts were dried over $MgSO_4$ and evaporated *in vacuo*. Chromatography of the residue over 45 g of silica gel in ether – petroleum ether gave 1.73 g (89%) of **17***b*, low melting; ir (film): 1700 (ketone), 1675 and 890 (olefin) cm^{-1}; nmr δ: 0.81 (s, 3H, tertiary methyl), 0.85 (s, 6H, superimposed signals for two tertiary methyls), 1.03 and 1.15 (doublets, secondary epimeric methyls). *Anal.* calcd. for $C_{21}H_{32}O$: C 83.94, H 10.74; found: C 83.58, H 10.57.

Ketal **18**b

The ketone **17***b* was converted into the ketal **18***b* by the procedure described above for the preparation of **18***a*. From 1.05 g of **17***b* there was obtained 1.06 g (87%) of **18***b*, mp 139°C; ir: devoid of bands attributable to carbonyl; nmr δ: 0.81, 0.83 and 0.92 (3-proton singlets, tertiary methyls), 0.88 (d, J = 6.5 Hz, 3H, secondary methyl), 3.98 (m, 4H, ethylene of ketal), and 4.90 (m, 2H, exocyclic methylene). *Anal.* calcd. for $C_{23}H_{36}O_2$: C 80.18, H 10.53; found: C 79.90, H 10.53.

Cyclobutanone **19**b

The ketal **18***b* was converted into the cyclobutanone **19***b* by the procedure described above for the preparation of **19***a*. From 1.00 g of **18***b* there was obtained 777 mg (77%) of **19***b*, mp 157°C, ir: 1773 (cyclobutanone) cm^{-1}; nmr δ: 0.83, 0.85 and 1.01 (3-proton singlets, tertiary methyls), 1.00 (d, J = 6.5, 3H, secondary methyl), and 3.96 (m, 4H, ethylene of ketal). *Anal.* calcd. for $C_{22}H_{34}O_3$: C 76.26, H 9.89; found: C 76.01, H 9.87.

Cyclobutanol **20**b

The cyclobutanone **19***b* was converted into the cyclobutanol **20***b* by the procedure described above for the preparation of **20***a*. From 537 mg of **19***b* there was obtained 537 mg (99%) of **20***b*, mp 149°C; ir: 3350 (OH) cm^{-1}; nmr δ: 0.83 (br s, 9H, three tertiary methyls), 0.95 (d, J = 6.5 Hz, 3H, secondary methyl), 4.08 (dd, 1H, J = 8 Hz, *H*C—OH), and 3.91 (m, 4H, ethylene of ketal). *Anal.* calcd. for $C_{22}H_{36}O_3$: C 75.81, H 10.41; found: C 76.10, H 10.63.

Keto alcohol **21**b *and its C-12 epimer*

The cyclobutanol **20***b* was converted into the keto alcohol **21***b* and its C-12 epimer by the procedure described above for the preparation of **21***a* and its epimer. From 700 mg of **20***b* there was obtained 126 mg (20%) of the epimer, mp 215°C; spectral properties similar to **21***b*. There also was obtained 468 mg (76%) of **21***b*, mp 149°C; ir: 3420 (OH) and 1690 (ketone) cm^{-1}; nmr δ: 0.89 (s, 6H, superimposed singlets for two tertiary methyls), 1.00 (s, 3H, tertiary methyl), and 3.80 (dd, J = 3 Hz, 1H, *H*C—OH). *Anal.* calcd. for $C_{20}H_{32}O_2$: C 78.89, H 10.60; found: C 78.74, H 10.64.

Thioketal **22**b

The keto alcohol **21***b* was converted into the thioketal **22***b* by the procedure described above for the preparation of **22***a*. From 200 mg of **21***b* there was obtained 212 mg (85%) of **22***b*, mp 142°C; ir: 3500 (OH) cm^{-1}; nmr δ: 0.84 (s, 6H, superimposed singlets for two tertiary methyls), 0.91 and 1.13 (singlets, 3H each, tertiary methyls), 3.20 (m, 4H, ethylene of ketal), and 3.68 (m, 1H, *H*C—OH). *Anal.* calcd. for $C_{32}H_{36}S_2O$: C 69.41, H 9.53; found: C 69.67, H 9.65.

Alcohol **23**b

The thioketal **22***b* was converted into the alcohol **23***b* by the procedure described above for the preparation of **23***a*. From 150 mg of **22***b* there was obtained 94 mg (83%) of **23***b*, mp 128°C; ir: 3350 cm^{-1}; nmr δ: 0.78 and 0.91 (singlets, 3H each, tertiary methyls), 0.85 (s, 6H, superimposed singlets for two tertiary methyls), and 3.54 (m, 1H, *H*C—OH). *Anal.* calcd. for $C_{20}H_{34}O$: C 82.69, H 11.80; found: C 82.80; H 11.89.

Olefin **25**b

The alcohol **23***b* was converted into the olefin **25***b* via the tosylate **24***b* by the procedure described above for the preparation of **25***a*. From 61 mg of **23***b* there was obtained 40 mg (70%) of **25***b* as an oil having spectral properties (nmr δ: 1.60 (s, 3H, vinylic methyl and 5.00 (m, 1H, vinylic proton)) identical to those reported for the same olefin obtained from stemodinone (**1***a*).

Epoxide **27**b

The olefin **25***b* was converted into the epoxide **27***b* by the procedure described above for the preparation of **27***a*. From 28 mg of **25***b* there was obtained 21 mg (75%) of **27***b* as an oil, nmr δ: 0.87 (s, 6H, superimposed singlets for two tertiary methyls), 1.21 (s, 3H, methyl attached to oxirane ring), and 2.73 (m, 1H, proton attached to oxirane

ring). *Mol. Wt.* calcd. for $C_{20}H_{32}O$: 288; found (ms): 288.

(+)-2-Desoxystemodinone (1)

A mixture of 28 mg of **27***b*, 100 mg of $LiAlH_4$, and 10 mL of THF was refluxed under nitrogen for 2 h. The cooled mixture was treated with a few drops of saturated aqueous Na_2SO_4 solution, followed by anhydrous Na_2SO_4. The mixture was filtered and the solid material was washed with 100 mL each of ether and CH_2Cl_2. The combined filtrate and washings were evaporated *in vacuo* and the residue was chromatographed on 5 g of silica gel in ether – petroleum ether to give 21 mg (75%) of **1**. The synthetic diterpenoid was identical with a sample of (+)-2-desoxystemodinone obtained from *Stemodia maritima* L. (mixture mp (145°C), nmr and ir spectra, ms and silica gel tlc).

(±)-2-Desoxystemodinone (1) from (±)-stemodinol (2)

A solution of 7 mg of **2** in 1 mL of pyridine was treated with 7 mg of *p*-toluenesulfonyl chloride and left at room temperature overnight. The solution was diluted with 10 mL of cold 0.1 *M* HCl and extracted twice with 20-mL portions of ethyl acetate. The extracts were washed with brine, dried over $MgSO_4$, and evaporated to give 9 mg of the tosylate **2***a* as a gum. This was immediately refluxed for 4 h in 10 mL of THF containing 10 mg of $LiAlH_4$. The reaction mixture was cooled to 0°C, acidified with 10 mL of 0.1 *M* HCl and extracted with two 15-mL portions of ethyl acetate. The combined extracts were dried over $MgSO_4$ and evaporated *in vacuo* to a gum which was purified by silica gel tlc with 20% ethyl acetate in hexane as solvent. There was obtained 4.5 mg of amorphous, racemic **1**, identical to 2-desoxystemodinone (5) isolated from *Stemodia maritima* L. (tlc, ir, nmr, and mass spectra).

Isolation of (+)-2-desoxystemodinone (1) from Stemodia maritima *L.*

Dried leaves (1.50 kg) of *S. maritima* (17), collected along the Palisadoes Peninsula of Jamaica in August 1973, were steeped in 10.0 L of hexane for 65 h. The mixture was filtered and the filtrate was concentrated to 1.50 L, diluted with 1.50 L of 95% methanol, and stirred at 50°C for 3 h. The hexane layer was separated and evaporated *in vacuo* to a yellow gum (11.3 g) which was dissolved in 50 mL of hexane and left overnight at 0°C. Crystalline stemodin (**3**) (1*a*) which had precipitated (1.6 g) was collected by filtration and the filtrate was evaporated *in vacuo*. The residue was chromatographed on 250 g of neutral alumina with 15% of ethyl acetate in hexane as eluent. Fractions containing **1**, as ascertained by silica gel tlc with the same solvent, were combined and evaporated *in vacuo*. Rechromatography of the residue on 40 g of neutral alumina as above afforded 173 mg of material which, on crystallization from aqueous methanol at 0°C, afforded 130 mg of **1**, mp 140–142°C; $[\alpha]_D^{25}$ + 6.5° (*c* 1.0, $CHCl_3$); ir ($CHCl_3$): 3590 and 3430 (OH) cm^{-1}; nmr δ: 0.88 (s, 6H, superimposed singlets for two tertiary methyls), 0.96 and 1.12 (singlets, 3H each, tertiary methyls). *Anal.* calcd. for $C_{20}H_{30}O$: C 82.76, H 11.72; found: C 82.81, H 11.67.

This material was identical to the product obtained by Huang–Minlon reduction of stemodinone (**4**) (1*a*) (mixture mp, optical rotation, ir, nmr, and mass spectra).

Acknowledgements

We are grateful to the Natural Sciences and Engineering Research Council of Canada for a grant to R. B. K. and for a post graduate scholarship awarded to M. L. H.

1. (*a*) P. S. MANCHAND, J. D. WHITE, H. WRIGHT, and J. CLARDY. J. Am. Chem. Soc. **95**, 2705(1973); (*b*) C. D. HUFFORD, R. GUERRO, and N. J. DOORENBOS. J. Pharm. Sci. **65**, 778 (1976).
2. (*a*) E. J. COREY, M. A. TIUS, and J. DAS. J. Am. Chem. Soc. **102**, 7613 (1980); (*b*) E. E. VAN TAMELEN, J. G. CARLSON, R. K. RUSSELL, and S. R. ZAWACKY. J. Am. Chem. Soc. **103**, 4615 (1981).
3. R. B. KELLY, M. L. HARLEY, S. J. ALWARD, and P. S. MANCHAND. Can. J. Chem. **60**, 675 (1982).
4. (*a*) M. L. HARLEY. PhD Thesis, University of New Brunswick. February, 1980; (*b*) R. B. KELLY, M. L. HARLEY, and S. J. ALWARD. Can. J. Chem. **58**, 755 (1980).
5. P. S. MANCHAND and J. F. BLOUNT. J. Chem. Soc. Chem. Commun. 894 (1975).
6. W. DALZIEL, B. HESP, K. M. STEVENSON, and J. A. J. JARVIS. J. Chem. Soc. Perkin Trans. I, 2841 (1973).
7. (*a*) K. WIESNER. Chem. Soc. Rev. **6**, 413 (1977), and references cited; (*b*) S. P. SETHI, K. S. ATWAL, R. MARINI-BETTOLO, T. Y. TSAI, and K. WIESNER. Can. J. Chem. **58**, 1889 (1980).
8. D. BRAVETTI, R. MARINI-BETTOLO, and A. LUPI. Helv. Chim. Acta, **65**, 371 (1982).
9. T. A. SPENCER, T. D. WEAVER, R. M. VILLARICA, R. J. FRIARY, J. POSLER, and M. A. SCHWARTZ. J. Org. Chem. **33**, 712 (1968).
10. (*a*) K. WIESNER. Tetrahedron, **31**, 1655 (1975); (*b*) R. MARINI-BETTOLO, S. P. SAHOO, G. A. POULTON, T. Y. R. TSAI, and K. WIESNER. Tetrahedron, **36**, 719 (1980); (*c*) J. F. BLOUNT, G. D. GRAY, K. S. ATWAL, T. Y. R. TSAI, and K. WIESNER. Tetrahedron Lett. 4413 (1980).
11. R. PAPPO, D. S. ALLEN, R. U. LEMIEUX, and W. S. JOHNSON. J. Org. Chem. **21**, 478 (1956).
12. (*a*) R. B. KELLY, J. ZAMECNIK, and B. A. BECKETT. Can. J. Chem. **50**, 3455 (1972); (*b*) R. B. KELLY, J. EBER, and H. K. HUNG. Can. J. Chem. **51**, 2534 (1973).
13. E. J. COREY and M. CHAYKOVSKY. J. Am. Chem. Soc. **87**, 1345 (1965).
14. E. WENKERT, V. I. STENBERG, and P. BEAK. J. Am. Chem. Soc. **83**, 2320 (1961).
15. E. WENKERT and A. TAHARA. J. Am. Chem. Soc. **82**, 3299 (1960).
16. R. MOSINGO. Org. Synth. Coll. Vol. **3**, 181 (1967).
17. C. D. ADAMS. Flowering plants of Jamaica. University of West Indies Press. 1972. p. 662.

Can. J. Chem. Downloaded from www.nrcresearchpress.com by 210.87.254.42 on 09/06/12
For personal use only.

Selective transformations of secologanin: epoxidation

GAVIN N. SAUNDERS, JOHN R. PURDY, AND STEWART MCLEAN
Department of Chemistry, University of Toronto, Toronto, Ont., Canada M5S 1A1

Received August 24, 1982

GAVIN N. SAUNDERS, JOHN R. PURDY, and STEWART MCLEAN. Can. J. Chem. **61**, 276 (1983).

The oxidation of tetraacetylsecologanin dimethyl acetal (**7**) by *m*-chloroperbenzoic acid has been studied and the results have been compared with those obtained when tetraacetylsweroside was oxidized by the same reagent. Complete site selectivity for the vinyl side chain and a relatively low stereoselectivity leading to the formation of a small excess (7:2) of the epoxide with the 3-*R* configuration was observed with the sweroside derivative. These results parallel those in the osmium tetraoxide oxidation, and the configurations of the glycols produced have been correlated chemically with those of the epoxides. In contrast, there is little site selectivity in the oxidation of the secologanin derivative; in fact, it is the β-alkoxyacrylate site that appears to be oxidized faster to produce an epoxide (**9**) that then undergoes a second epoxidation at the vinyl side chain. Stereoselectivity is complete in the first epoxidation and is high in the epoxidation of the vinyl side chain, leading to the isomer with the 3-*R* configuration as the major product. The site selectivity appears to parallel that observed in dihydroxylation of the secologanin derivative, but the stereoselectivity of oxidations at the vinyl side chain is opposite in the two series; the configurations of the glycols and epoxides have been correlated chemically. A rational explanation can be advanced for the observed stereoselectivity in every case, but no convincing argument to explain the observed differences in site selectivity has been found.

GAVIN N. SAUNDERS, JOHN R. PURDY et STEWART MCLEAN. Can. J. Chem. **61**, 276 (1983).

On a étudié l'oxydation de l'acétal diméthylique de la tétraacétylsécologanine (**7**) par l'acide *m*-chloroperbenzoique et on a comparé les résultats avec ceux obtenus lorsqu'on oxyde la tétraacétylswéroside avec le même réactif. Dans le cas du dérivé de la swéroside, on a observé une sélectivité de site complète pour la chaîne latérale vinylique et une stéréosélectivité relativement faible conduisant à la formation d'un léger excès (7:2) d'époxyde avec une configuration 3-*R*. Ces résultats rejoignent ceux obtenus lors de l'oxydation par le tétraoxyde d'osmium et permet de faire une corrélation chimique de la configuration des glycols obtenus avec celle des époxydes. Dans le cas de l'oxydation du dérivé de la sécologanine, au contraire, il y a peu de sélectivité de site; en fait c'est le site β-alkoxyacrylate qui semble s'oxyder plus rapidement en produisant un époxyde (**9**) qui subit alors une deuxième oxydation au niveau de la chaîne latérale vinylique. La stéréosélectivité est complète lors de la première oxydation et elle est élevée lors de l'époxydation de la chaîne latérale vinylique, conduisant à l'isomère avec la configuration 3-*R* comme produit majoritaire. La sélectivité de site semble rejoindre celle observée lors de la déhydroxylation du dérivé de la sécologanine, mais la stéréosélectivité des oxydations au niveau de la chaîne latérale vinylique est opposée dans les deux séries; on a établi une corrélation chimique entre les configurations des glycols et celles des époxydes. On peut avancer une explication rationnelle pour la stéréosélectivité observée dans chaque cas, mais on n'a pas trouvé d'argument convaincant pour expliquer les différences observées dans la sélectivité de site.

[Traduit par le journal]

We have been studying selective chemical transformations of the biosynthetically important iridoid glycoside secologanin (**1**), and we have previously reported (1) on the dihydroxylation reaction resulting from oxidation with osmium tetraoxide. We report now on the epoxidation by *m*-chloroperbenzoic acid (MCPBA).

In the early stages of our investigation we had assumed that the closely related iridoid sweroside (**2***a*) would serve as a useful model compound in these studies, but we learned from the dihydroxylation study that the reactions of the two series differed in site selectivity and stereoselectivity, and we have now found that the secologanin and sweroside derivatives also behave quite differently on treatment with MCPBA. Inouye *et al.* (2) had previously reported that the MCPBA oxidation of tetraacetylsweroside (**2***b*) produced a single epoxide, **3**, in a yield of about 35%. In our hands this oxidation led to a 52% yield of a product that was shown to be a mixture of the epimeric epoxides **3** and **4** in a ratio of about 7:2 based on its ^{1}Hmr spectrum. The mixture was not separated, but each epimer was prepared separately from the corresponding glycol (**5***a*, **6***a*) obtained by dihydroxylation of **2***b* (1). Each glycol was monotosylated at the primary hydroxyl and the tosylates **5***b* and **6***b* were converted to the epoxides **3** and **4**, respectively, by the action of potassium carbonate in dimethylformamide. This procedure, in which configuration at C-3 is retained, correlates the configurations of the dihydroxylation and epoxidation products, major epimer with major epimer and minor with minor. No evidence for the oxidation of the β-alkoxyacrylate moiety was seen, even on prolonged treatment with MCPBA, of any of these sweroside derivatives, or of any others examined, such as the 3,4-dihydro derivative. The MCPBA and osmium tetraoxide oxidations of tetraacetylsweroside show the same site selectivity for the vinyl side chain; stereoselectivity is not high in either oxidation, but both show some preference for forming the product with the 3-*R* configuration, and this preference is higher in epoxidation (7:2) than in dihydroxylation (3:2).

When tetraacetylsecologanin dimethyl acetal (**7**) was treated with MCPBA under the same conditions, oxidation took place more rapidly, and three identifiable products were obtained. The most abundant product, mp 167.5–169.5°C, isolated in 44% yield after chromatography and careful recrystallization, had the formula $C_{27}H_{38}O_{17}$, corresponding to a dioxide of **7**. Its spectroscopic properties indicated that both carbon–carbon double bonds (3,4 and 8,9) had been oxidized, and the data were compatible with the assignment of a bisepoxide structure to this product. The epoxidation of the vinyl side chain was, of course, expected, but the epoxidation of the β-alkoxyacrylate

0008-4042/83/020276-06$01.00/0
©1983 National Research Council of Canada/Conseil national de recherches du Canada

Can. J. Chem. Downloaded from www.nrcresearchpress.com by 210.87.254.40 on 09/06/12
For personal use only.

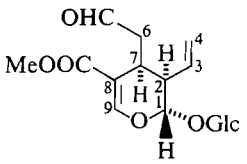

1

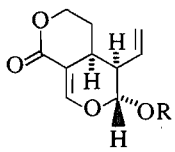

2*a* R = Glc
b R = $GlcAc_4$

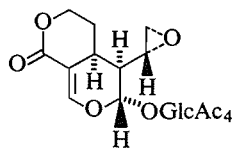

3

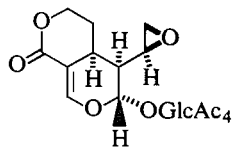

4

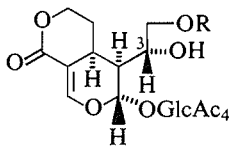

5*a* R = H
b R = Ts

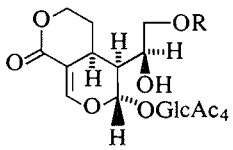

6*a* R = H
b R = Ts

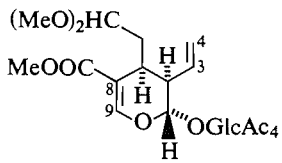

7

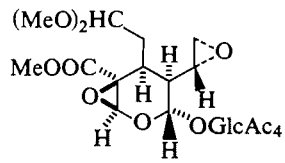

8

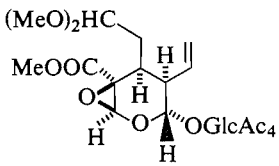

9

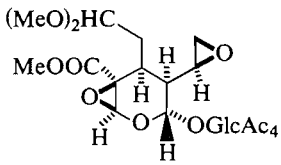

10

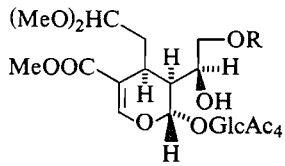

11*a* R = H
b R = Ts

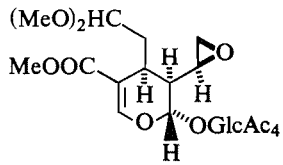

12

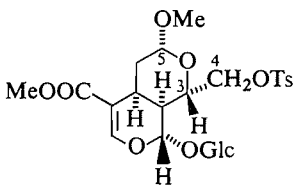

13

Glc = β-D-glucopyranosyl
$GlcAc_4$ = tetraacetyl-β-D-glucopyranosyl

moiety had little precedent; the only example we have found of an epoxidized β-alkoxyacrylate appeared in a recent report (3), where it was obtained unexpectedly from the related unsaturated ketone which underwent both Baeyer–Villiger oxidation and epoxidation when treated with MCPBA. Because it would be difficult to adduce unequivocal chemical evidence for the bisepoxide structure, and because a rigorous definition of its stereochemistry was of particular importance to us, the product was subjected to X-ray crystal structure analysis (4). This analysis established that the product was, indeed, the proposed bisepoxide, and that its configuration, both relative and absolute (by internal reference to the glucose moiety), is represented by **8**.

The second product of MCPBA oxidation of **7**, isolated in 19% yield as crystals, mp 137–139.5°C, proved to be the monoepoxide **9**. The ^{1}Hmr spectrum showed that the vinyl side chain was still intact, but that the characteristic signal of the proton at C-9 (near τ 2.6) had been replaced by a singlet at τ 5.20, and the uv spectrum confirmed that the β-alkoxyacrylate chromophore was no longer present. Further MCPBA oxidation of **9** produced bisepoxide **8**, establishing the structure and stereochemistry of the monoepoxide. The third product of oxidation of **7** was not isolated from this source, but was shown from the ^{1}Hmr spectrum to be a minor constituent (~9%) of the chromatographic fraction that afforded the bisepoxide **8**; in the same way it was found in the same abundance in the product of MCPBA oxidation of **9**. It was shown to be the bisepoxide **10**, the C-3 epimer of **8**, by synthesis.

Dihydroxylation of **7** produces the glycol **11***a* with a high degree of stereoselectivity (1). This glycol was converted to the monoepoxide **12**, mp 84–86°C, by the route through the monotosylate **11***b* described for the sweroside derivatives **3** and **4**; the modification of employing DBU in benzene as the base for the final step was found to be much superior. It is pertinent to note that, while it was presumed that monotosylation of the glycols took place selectively at the primary hydroxyl group, in keeping with well-established precedents, none of the tosylates (**5***b*, **6***b*, **11***b*) was stable enough to be characterized completely; however, **11***b* was readily converted by the action of acid to a product from which the crystalline cyclic acetal **13** was isolated, and characterization of **13** confirmed the expected site selectivity of the tosylation reaction. Oxidation of the monoepoxide **12** with MCPBA converted it in 76% yield to the bisepoxide **10**, mp 154–156°C. The ^{1}Hmr and ^{13}Cmr spectra and the tlc characteristics of **10** prepared in this manner were identical with those of the minor component of the mixture of bisepoxides obtained by MCPBA oxidation of **7** or **9**. Furthermore, when a sample of a 6:1 mixture of the glycols **11***a* and its C-3 epimer (1) was subjected to the same sequence of reactions, the intermediate monoepoxides **12** and its C-3 epimer were obtained in a 6:1 ratio (based on the ^{1}Hmr spectrum), and MCPBA oxidation of this mixture led to a 6:1 mixture of the same epoxides obtained by direct MCPBA oxidation of **7** or **9**, but with the major epimer from one sequence being the

Can. J. Chem. Downloaded from www.nrcresearchpress.com by 210.87.254.40 on 09/06/12
For personal use only.

TABLE 1. Nuclear magnetic resonance data of new compounds[a]

	Sweroside epoxides				Secologanin side chain epoxides			
	3		**4**		**12**		3-epi-**12**[e]	
Proton[b]	A[c]	B[d]	A	B	A	B	A	B
1	4.34	d, 2.4*	4.57	d, 1.9	4.63	d, 6.3	4.46	d, 4.6
2	8.32	n.r.*	8.10	n.r.	8.38	n.r.*		
3	7.28	n.r.	7.09	n.r.	7.12	m, 7.5,* 5, 2.7†		
4a	7.43	dd, 4.9,† 3.1	7.39	n.r.	7.42	dd, 5, 2.7†		
4b	7.12	m, 4.9,† 4.9	7.20	n.r.	7.16	m, 5, 5		
5a	5.65	n.r.	5.55	n.r.	5.42	dd, 7.6, 3.6		
5b	5.50	n.r.	5.55	n.r.	—	—		
6a	8.13	n.r.	8.20	n.r.	8.02	n.r.		
6b	8.13	n.r.	8.20	n.r.	7.96	n.r.		
7	7.04	n.r.§	7.06	n.r.	7.03	m, 6.4, 6		
9	2.38	d, 2.4§	2.43	d, 2.5	2.67	s		
COOMe	—	—	—	—	6.33	s	6.34	s
OMe	—	—	—	—	6.73	s	6.70	s
OMe	—	—	—	—	6.68	s	6.66	s
1′	5.07	d, 9	5.1–4.7 complex		5.12	d, 9		
2′	5.02	dd, 9, 9			5.01	dd, 9, 9		
3′	4.75	dd, 9, 9			4.79	dd, 9, 9		
4′	4.93	dd, 9, 9			4.89	dd, 9, 9		
5′	6.24	n.r.			6.28	n.r.		
6a′	5.84	dd, 12.2, 1.8	5.75	n.r.	5.88	dd, 12.3, 1.9		
6b′	5.67	dd, 12.2, 4.8	5.75	n.r.	5.75	dd, 12.3, 3.4		
OAc	8.02	s	8.03	s	8.05	s		
OAc	7.99	s	8.00	s	8.01	s		
OAc	7.97	s	7.97	s	7.99	s		
OAc	7.89	s	7.91	s	7.93	s		

[a]At 400 MHz, except **4** at 100 MHz; $CDCl_3$.
[b]Numbering system shown in structural formulae. 1′, 2′, etc. are glucosidic protons.
[c]Columns A: Chemical shifts on τ scale.
[d]Columns B: Apparent multiplicities: s, singlet; d, doublet; n.r., not resolved; coupling constants (Hz); *, †, § indicate decoupling experiments.
[e]Signals that were resolved and identified in the spectrum of the epimeric mixture.
[f]Tosyl signals: 2.22, d; 2.67, d; 7.57, s.

minor epimer from the other. These results establish that the bisepoxides **8** and **10** differ only in the configuration at C-3; they also confirm our previous assignment (1) of the stereochemistry of glycol **11** (as well as the sweroside and secogalioside derivatives with which it has been correlated (1)), and place the relative and absolute configuration of **11** on the secure foundation of the X-ray analysis of **8** and the demonstrated relationship of **8** with **11**. This result is of importance to us since we have used **11** as a key intermediate in the synthesis of the dihydrocadambine alkaloids (5).

The results of our studies of the oxidation of sweroside and secologanin derivatives can now be summarized and, to a considerable extent, rationalized. Both dihydroxylation (1) and epoxidation show complete site selectivity for the vinyl side chain in the sweroside series. Stereoselectivity is not high in either oxidation, but the formation of a product with the 3-*R* configuration is favored in both. In contrast, in the secologanin series the oxidations showed little site selectivity; this could only be deduced (1) from the study of osmium tetraoxide oxidation of **7**, since products of oxidation at the β-alkoxyacrylate site could not be characterized, but the present study explicitly shows that both olefinic sites undergo epoxidation. In fact, it appears that the β-alkoxyacrylate site reacted faster than the vinyl side chain since substantial amounts of the monoepoxide **9** were isolated after a relatively short reaction period, but no monoepoxides resulting from oxidation of the side chain were observed in this reaction. The stereoselectivity of the dihydroxylation reaction was much higher in the secologanin series than in the sweroside series, and led preferentially to the glycol with the 3-*S* configuration, opposite to that of the major sweroside glycol. The stereoselectivity of epoxidation of the side chain is also high, but the major product has the 3-*R* configuration; however, as we have just pointed out, it is almost certainly the epoxidation of the monoepoxide **9**, not the precursor **7**, that shows this stereoselectivity. The stereoselectivity of epoxidation at the β-alkoxyacrylate centre, leading to **9** as the immediate product, appears to be complete since we have seen no evidence for the formation of any epoxidation product differing in the stereochemistry at this site.

We previously rationalized (1) that the difference between the sweroside and secologanin series in the stereoselectivity of the dihydroxylation reaction at the vinyl side chain could be attributed to a difference between the two series in conformational mobility. Sweroside adopts a conformation with the vinyl side chain axial, and this does not change in derivatives in which the bulk of this two-carbon unit has been increased; in contrast, secologanin is more conformationally mobile and, when the bulk of the side chain is increased, a conformation with this side chain equatorial becomes dominant. These conformations are most easily recognized from the value of the coupling constant, $J_{1,2}$, between the protons at C-1 and C-2. Models indicate that the dominant rotamer for an axial

Can. J. Chem. Downloaded from www.nrcresearchpress.com by 210.87.254.40 on 09/06/12
For personal use only.

TABLE 1. (*Concluded*)

	Secologanin ring epoxide **9**		Secologanin bisepoxides **8**		**10**		Acetal tosylate **13**[f]	
Proton	A	B	A	B	A	B	A	B
1	5.07	d, 0.5	4.75	d, 1.8*	4.92	d, 1.5	4.52	d, 4.5*
2	7.36	n.r.*	8.39	ddd, 10,†, 7,§ 1.8*	8.38	m, 6.4,* 6.4,† 1.5	8.02	n.r.*†
3	4.05	m, 10, 7*	6.76	n.r.†	6.75	n.r.*	6.12	ddd, 8,† 5, 5
4a	4.82	n.r.	7.43	dd, 5.5, 3.5	7.53	dd, 4.5, 3.4	5.8	n.r.
4b	4.78	n.r.	7.12	dd, 4.5, 3.5	7.23	dd, 4.5, 4.5	5.8	n.r.
5a	5.54	dd, 7.5, 3.5	5.52	dd, 5.5, 5.5	5.33	dd, 5.6, 5.6	5.65	dd. 8, 3
5b	—	—	—	—	—	—	—	—
6a	8.27	n.r.	8.12	n.r.	8.11	n.r.	8.1	n.r.
6b	8.15	n.r.	8.12	n.r.	8.11	n.r.	8.1	n.r.
7	6.95	n.r.	6.85	n.r.§	6.83	n.r.†	7.03	n.r.
9	5.20	s	5.17	s	5.17	s	2.67	n.r.
COOMe	6.25	s	6.23	s	6.23	s	6.27	s
OMe	6.71	s	6.72	s	6.70	s	6.64	s
OMe	6.71	s	6.67	s	6.66	s	—	—
1′	5.10	d, 8.5	5.07	d, 8	5.09	d, 9	5.14	d, 8
2′	4.98	dd, 8.5, 8.5	5.00	dd, 8, 8	5.01	dd, 9, 9	5.00	dd, 9, 8
3′	4.80	dd, 8.5, 8.5	4.80	dd, 8, 8	4.80	dd, 9, 9	4.77	dd, 9, 9
4′	4.89	dd, 8.5, 8.5	4.90	dd, 8, 8	4.90	dd, 9, 9	4.93	dd, 9, 9
5′	6.25	n.r.	6.26	n.r.	6.16	n.r.	6.27	n.r.
6a′	5.90	dd, 11, 2	5.92	dd, 12.5, 2.3	5.86	dd, 12.8, 1.8	5.9	n.r.
6b′	5.71	dd, 11, 4.3	5.69	dd, 12.5, 5.3	5.72	dd, 12.8, 5.1	5.7	n.r.
OAc	8.05	s	8.05	s	8.04	s	8.10	s
OAc	8.00	s	8.00	s	8.00	s	8.03	s
OAc	7.97	s	7.97	s	7.98	s	8.00	s
OAc	7.91	s	7.90	s	7.91	s	7.95	s

vinyl substituent should be that with C-3 → C-4 pointing away from the ring, and the large $J_{2,3}$ values observed support this proposal. In this conformation of a sweroside derivative there is relatively little difference between the two faces of the olefin with respect to steric hindrance to the approach of the oxidizing agent, but what there is favors approach from the face that leads to a 3-*R* product; this is what is observed in dihydroxylation and epoxidation, and steric interactions appear to have a somewhat greater directing influence on epoxidation than on dihydroxylation. It has been shown that, in the reaction of osmium tetraoxide with an alkene, the formation of the osmate ester is preceded by a series of complexes formed reversibly between the alkene and the osmium reagent (6). Consequently, steric hindrance to approach of the reagent is not the only factor determining the stereoselectivity, and it is in dihydroxylation in the secologanin series that this point is clearly demonstrated. Here, as soon as the vinyl side chain forms the initial complex with the osmium reagent, the increased bulk forces the side chain to become equatorial, and in this conformation, with the bulky glucose moiety also equatorial, there is a clear steric preference for the productive development of the complex into the osmate ester on that face of the side chain that leads finally to the observed 3-*S* glycol. Since a corresponding reversible complexation is not believed to occur in epoxidation and direct steric factors control the stereoselectivity, it would have been of considerable interest to compare the outcome of the epoxidation and dihydroxylation at the same vinyl side chain in the secologanin series. However, our evidence shows that epoxidation at the vinyl side chain of **7**, the substrate in the dihydroxylation reaction, is not observed since the monoepoxide **9** is formed first, and it is the side chain of **9** that is subsequently epoxidized. The presence of an 8,9 epoxide very considerably alters the conformational preference of the iridoid ring, and forces the two-carbon side chain at C-2 to become axial; the X-ray study (4) shows this clearly in the case of the crystalline bisepoxide **8**, the $J_{1,2}$ value of 1.8 Hz shows that this is also the conformation of **8** in solution and, wherever they can be compared, the spectroscopic properties of **8** and **9** show that they both have the same conformation. The axial vinyl group of **9** has a steric environment similar to that of the side chain of sweroside except that the steric hindrance to approach to the more hindered face is markedly increased by the presence of the 8,9 epoxide and by the effect of the side chain at C-7 which is not tied back in a lactone, as in sweroside. The MCPBA oxidation consequently leads preferentially to the formation of the epoxide with the 3-*R* configuration, as it does in the sweroside case, but with a significantly higher degree of stereoselectivity.

It is difficult to find a convincing explanation for the difference between the two series of compounds in the site selectivity of the oxidations. It seems clear that it results from the difference in reactivity of the two β-alkoxyacrylate moieties and that it has its origin in the unusually high reactivity of the secologanin derivative. In simplest terms, the olefinic double bond is activated towards electrophilic attack by the presence of oxygen at C-9 and deactivated by the carbonyl at C-8. The latter effect is greatest when the carbonyl and olefin components are coplanar, and this condition is more closely met in sweroside by the constraints of the fused lactone ring than in secologanin where steric effects tend to cause the carbomethoxyl group to rotate. This argument places the two series in the correct order of reactivity, but we feel that it is not sufficient to explain the magnitude of the difference. We have looked for other arguments that would predict an augmented

Can. J. Chem. Downloaded from www.nrcresearchpress.com by 210.87.254.40 on 09/06/12
For personal use only.

Can. J. Chem. Downloaded from www.nrcresearchpress.com by 210.87.254.40 on 09/06/12
For personal use only.

difference in reactivity, but have found none without flaws. We feel intuitively that the complete stereoselectivity observed in the epoxidation of the β-alkoxyacrylate site in the secologanin derivative **7** should be related to the unusual reactivity of the site, but we can not point to a feature that should both facilitate the reaction and direct the approach of the reagent. The steric constraints associated with epoxidation by peracids are generally conceded to be severe, and it might be supposed that these might be felt most strongly in the approach of MCPBA to the relatively rigid sweroside derivative with axial substituents at C-1 and C-2, while the more mobile secologanin derivative could react through the alternative conformation with these substituents equatorial. However, the available evidence shows that the preferred conformation of the secologanin derivative **7** has these substituents axial (1) and that they remain axial in the product epoxide **9**, so it appears probable that this conformation is at least approximated in the transition state. The experimental evidence shows that MCPBA has avoided approach from the side of the iridoid ring carrying the bulky glucoside moiety and, provided that epoxidation from this side of the molecule had the same conformational requirements as those above, the unfavorable steric interaction between the MCPBA and the glucoside unit as the transition state is approached could provide an explanation for the failure of the molecule to undergo epoxidation from this side and so account for the observed stereoselectivity. However, this proposal can not be extended to explain the increased rate of epoxidation at the other side of the molecule (relative to sweroside), and so fails to account for the site selectivity.

Experimental

Melting points were determined on a calibrated Thomas–Kofler micro hot stage. Infrared spectra were measured on a Unicam SP. 1000 spectrometer; the wavelengths (μ) of selected absorption peaks of solutions in chloroform are reported. Ultraviolet spectra were measured on a Unicam SP.800A spectrometer; the λ_{max} values (nm) of peaks followed by the log ε values in parentheses for solutions in methanol are reported; where end absorption was observed, log ε at 215 nm is reported. Proton nmr spectra were recorded on a Bruker WH-400 or a Varian XL-100 spectrometer; solutions in $CDCl_3$ were used, and data showing chemical shifts (τ scale) and apparent multiplicities and coupling constants are collected in Table 1.

Sweroside derivatives

Epoxide 3

The glycol **5***a* (600 mg; 1.07 mmol) (1) and *p*-toluenesulfonyl chloride (227 mg; 1.19 mmol) were dissolved in 30 mL of dry pyridine and stirred with 2 g of freshly activated 4A molecular sieves for 36 h at room temperature. The mixture was poured into water, and extracted with chloroform; the extract was washed with water, dried, and evaporated to dryness. Chromatography of the residue (silica gel with 10:1 ether–methanol) afforded the amorphous tosylate **5***b* (263 mg; 0.37 mmol); unchanged **5***a* (120 mg) was also recovered. The tosylate was dissolved in 5 mL of anhydrous dimethylformamide and stirred with anhydrous potassium carbonate (100 mg) for 58 h at room temperature. The mixture was poured into water and extracted with chloroform; the extract afforded an oil that was chromatographed (silica gel with 12:1 ether–methanol) and epoxide **3** (118 mg; 0.22 mmol) was obtained, after recrystallization from ethanol, as crystals, mp 199–203°C; ir: 5.70, 5.85, 6.15; uv: 241 (3.95). *Anal.* calcd. for $C_{24}H_{30}O_{14}$: C 53.14, H 5.57; found: C 53.28, H 5.42.

Epoxide 4

In the manner just described, the glycol **6***a* (295 mg; 0.53 mmol) (1) was converted through its tosylate **6***b* (135 mg; 0.19 mmol) to epoxide **4** (56 mg; 0.10 mmol), which was obtained from ethanol as crystals, mp. 154–156°C; ir: 5.70, 5.85, 6.15. *Anal.* calcd. for $C_{24}H_{30}O_{14}$: C 53.14, H 5.57; found: C 53.31, H 5.68.

*MCPBA epoxidation of tetraacetylsweroside 2*b

A solution of tetraacetylsweroside (75 mg; 0.14 mmol) and purified MCPBA (20 mg; 0.12 mmol) in 2 mL of dry benzene was stirred at 50°C under argon for 48 h. Further MCPBA (20 mg) was added and the conditions were maintained for a further 24 h. The solution was cooled, diluted with 50 mL of chloroform, washed with 5% aqueous sodium hydroxide, then brine, and dried. Evaporation afforded a crystalline material (58 mg), which was subjected to flash chromatography (silica gel with 3:2 ether–dichloromethane). Unchanged starting material (12 mg; 0.02 mmol) was recovered from early fractions; subsequent fractions afforded a crystalline material (31 mg; 0.06 mmol), mp 174–177°C, that appeared to correspond to the material described by Inouye *et al.* (2). The ^{1}Hmr spectrum of this material showed that it consisted of a 7:2 mixture of epoxides **3** and **4** (see above).

Secologanin derivatives

MCPBA epoxidation of 7

A solution of **7** (500 mg; 0.83 mmol) and purified MCPBA (428 mg; 2.48 mmol) in 5 mL of dry benzene was stirred at 50°C under argon for 6 h. The mixture was poured into aqueous sodium bicarbonate and extracted with dichloromethane. The extract afforded an oil (586 mg) which was subjected to flash chromatography (silica gel with ether). The first major fraction (252 mg; 0.40 mmol) consisted of a crystalline mixture of the bisepoxides **8** and **10** in a 10:1 ratio (based on ^{1}Hmr spectrum). Repeated recrystallization of this material from ether–dichloromethane provided a pure sample of bisepoxide **8**, mp 167.5–169.5°C (used for X-ray analysis (4)); ir: 5.70, 5.73 (sh); uv end absorption (2.20). *Anal.* calcd. for $C_{27}H_{38}O_{17}$: C 51.10, H 6.04; found: C 51.08, H 6.09. The second major chromatographic fraction (95 mg; 0.16 mmol) consisted of the epoxide **9**, which, on recrystallization from ethanol, was obtained as crystals, mp 137–139.5°C; ir: 5.70, 5.75; uv end absorption (2.44). *Anal.* calcd. for $C_{27}H_{38}O_{16}$: C 52.42, H 6.19; found: C 52.37, H 5.90.

Further treatment of **9** with MCPBA under the conditions described converted it to the 10:1 mixture of **8** and **10**.

Epoxide 12

In the manner described above for **3**, glycol **11***a* (4.93 g; 7.75 mmol) was converted to its amorphous monotosylate **11***b* (4.46 g; 5.65 mmol), which was dissolved in 25 mL of benzene containing 1,5-diazobicyclo[5.4.0]undec-5-ene (2.57 g; 16.9 mmol) and stirred at room temperature for 2.5 h. The mixture was poured into water and extracted with dichloromethane; the extract was washed with *N* hydrochloric acid and then worked up. Epoxide **12** (3.42 g; 5.53 mmol) was obtained and recrystallized from ether, to provide material mp 84–86°C; ir: 5.70, 5.85, 6.15; uv: 230 (3.91). *Anal.* calcd. for $C_{27}H_{38}O_{16}$: C 52.42, H 6.19; found: C 52.38, H 6.23. A sample recrystallized from toluene–hexane formed crystals, mp 42.5–44.5°C. *Anal.* calcd. for $C_{27}H_{38}O_{16}\cdot 0.5(C_7H_8)$: C 55.11, H 6.37; found: C 55.49, H 6.16. (The ^{1}Hmr spectrum confirmed the presence of one-half of an equivalent of toluene).

When a 6:1 mixture of the glycol **11** and its C-3 epimer was carried through this sequence the ^{1}Hmr spectrum showed that the product was a 6:1 mixture of **12** and its C-3 epimer.

Bisepoxide 10

A solution of the monoepoxide **22** (343 mg; 0.55 mmol) and purified MCPBA (190 mg; 1.10 mmol) in 10 mL of benzene was stirred at 50°C; after 2 h and 10 h further MCPBA (2 × 190 mg) was added and heating was continued for a total of 14 h. The mixture was worked up as before and bisepoxide **10** (267 mg; 0.42 mmol) was obtained, on recrystallization from ethanol, as crystals, mp 154–156°C; ir: 5.70, 5.73 (sh); uv end absorption (2.19). *Anal.* calcd. for $C_{27}H_{38}O_{17}$: C 51.10, H 6.04; found: C 51.31, H 6.05.

When the 6:1 mixture of **12** and its C-3 epimer described above was carried through this epoxidation, the ^{1}Hmr spectrum of the product showed it to be a 6:1 mixture of the bisepoxides **10** and **8**.

Cyclic acetal tosylate ***13***

Glycol **11***a* (1.58 g; 2.48 mmol) was tosylated in the manner described for **3** except that the reaction mixture was poured into *N* hydrochloric acid (instead of into water) before extraction with chloroform. The extract provided a product which was chromatographed and recrystallized from ethanol to afford **13** (670 mg; 0.88 mmol), mp 123.5–125.5°C; ir: 5.70, 5.85, 6.13. *Anal.* calcd. for $C_{33}H_{42}O_{18}S$: C 52.24, H 5.58, S 4.23; found: C 52.16, H 5.56, S 4.11.

Acknowledgements

The nmr spectra were obtained at the Southwestern Ontario N.M.R. Center, funded by a Major Installation grant from the Natural Sciences and Engineering Research Council of Canada, who also provided financial support for this research.

1. J. R. PURDY, R. G. HAMILTON, L. AKHTER, and S. MCLEAN. Can. J. Chem. **59**, 210 (1981).
2. H. INOUYE, T. YOSHIDA, Y. NAKAMURA, and S. TOBITA. Chem. Pharm. Bull. **18**, 1889 (1970).
3. W. J. ROSS, A. TODD, B. P. CLARK, S. E. MORGAN, and J. E. BALDWIN. Tetrahedron Lett. **22**, 2207 (1981).
4. S. C. NYBURG, P. Y. SIEW, G. N. SAUNDERS, J. R. PURDY, and S. MCLEAN. Can. J. Chem. **61**, 282 (1983).
5. G. N. SAUNDERS, R. G. HAMILTON, and S. MCLEAN. Tetrahedron Lett. **23**, 2359 (1982); R. G. HAMILTON, G. N. SAUNDERS, and S. MCLEAN. Can. J. Chem. **61**, 284 (1983).
6. S. G. HENTGES and K. B. SHARPLESS. J. Am. Chem. Soc. **102**, 4263 (1980).

Can. J. Chem. Downloaded from www.nrcresearchpress.com by 210.87.254.40 on 09/06/12
For personal use only.

X-ray crystal structure analysis of a bisepoxide derived from secologanin: the structure and absolute configuration

STANLEY C. NYBURG, PIK Y. SIEW, GAVIN N. SAUNDERS, JOHN R. PURDY, AND STEWART MCLEAN
Department of Chemistry, University of Toronto, Toronto, Ont., Canada M5S 1A1

Received August 24, 1982

STANLEY C. NYBURG, PIK Y. SIEW, GAVIN N. SAUNDERS, JOHN R. PURDY, and STEWART MCLEAN. Can. J. Chem. **61**, 282 (1983).

The structure and absolute configuration of a bisepoxide (**2**) produced by oxidation of tetraacetylsecologanin dimethyl acetal (**1**) with *m*-chloroperbenzoic acid have been established by X-ray crystal structure analysis. Epoxidation of the vinyl side chain is unexceptional; epoxidation of the β-alkoxyacrylate moiety is novel. This determination represents a valuable bench mark for configurational assignments, since the bisepoxide has been correlated by chemical transformations with a number of synthetic and naturally-occurring derivatives of secologanin.

STANLEY C. NYBURG, PIK Y. SIEW, GAVIN N. SAUNDERS, JOHN R. PURDY et STEWART MCLEAN. Can. J. Chem. **61**, 282 (1983).

Faisant appel à la diffraction des rayons-X, on a établi la structure et la configuration absolue du bisépoxyde (**2**) produit lors de l'oxydation du diméthylacétal de tétraacétylsécologanine (**1**) par l'acide *m*-chloroperbenzoique. L'époxydation de la chaîne latérale vinylique est normale; toutefois l'époxydation de la portion β-alkoxyacrylate est nouvelle. Cette détermination est une étape importante dans les attributions de configuration, puisque des transformations chimiques ont permis d'établir une corrélation entre le bisépoxyde et un certain nombre de dérivés synthétiques et d'origine naturelle de la sécologanine.
[Traduit par le journal]

Can. J. Chem. Downloaded from www.nrcresearchpress.com by 210.87.254.40 on 09/06/12
For personal use only.

As part of our study of selective oxidations of derivatives of the biosynthetically important iridoid secologanin (1, 2), we investigated the reaction of *m*-chloroperbenzoic acid wth tetraacetylsecologanin dimethyl acetal (**1**). Oxidation took place readily, and a substance, mp 167.5−169.5°C, was the principal product isolated (2). The molecular formula, $C_{27}H_{38}O_{17}$, showed it to be the dioxide of the precursor **1**, and spectroscopic evidence indicated that both olefinic double bonds had undergone reaction. The data were compatible with the assignment of a bisepoxide structure to this product; however, while the epoxidation of the vinyl side chain was expected, the epoxidation of the β-alkoxyacrylate unit was not. Normally, such a unit is expected to resist electrophilic attack by oxidizing agents, and our own study of the closely related iridoid sweroside shows that it fails to undergo oxidation at its β-alkoxyacrylate site under the same conditions; in fact, the only example we have found of an epoxidized β-alkoxyacrylate was reported recently (3), and this was obtained unexpectedly when the corresponding ketone underwent both Baeyer−Villiger oxidation and epoxidation when treated with *m*-chloroperbenzoic acid.

Besides the structural question arising from the novel oxidation of the β-alkoxyacrylate centre, there is a stereochemical question of considerable interest to us concerning the epoxidation of the vinyl side chain. There are obvious difficulties in investigating these questions by ordinary chemical and spectroscopic methods, but both the structure and stereochemistry of the product can be established simultaneously and unambiguously by the X-ray method. Furthermore, this method would establish the stereochemistry of the whole molecule, not merely the configuration induced in the oxidized side chain, and define its absolute configuration by internal reference to the glucosidic moiety. Consequently, an X-ray crystal structure analysis of the oxidation product was undertaken.

Experimental

The oxidation of the secologanin derivative **1** has been described (2); the dioxide, mp 167.5−169.5°C, was obtained as colorless rectangular plates from hexane−dichloromethane. A 0.25 × 0.17 × 0.15-mm specimen was used for structure analysis. Unit cell dimensions were obtained from eleven reflections centred on the diffractometer. *Crystal data*:

$C_{27}H_{28}O_{17}$ M = 634.60

Monoclinic, $P2_1$, a = 11.29(3), b = 12.86(2), c = 11.2(3) Å, β = 97.50(5)°, U = 1600(6) Å^3, D_c (Z = 2) = 1.33 g cc^{-1}; μ(MoKα) = 1.20 cm^{-1}.

Intensity data were collected on the automated Picker four-circle diffractometer using Zr-filtered MoKα radiation. Reflections were measured in θ−2θ scan mode at 2° min^{-1} out to 2θ = 50°. The sample was stable to X-irradiation. Of 2960 unique reflections recorded, 1878 had $F_o > 2\sigma(F)$ and were used for structure refinement; $\sigma(F)$ was taken as $\{[\sigma(I)\cdot Lp]^2 + 0.02F_o^4\}^{\frac{1}{2}}/2F_o$, where $\sigma(I)$ = (scan + Σbackground)$^{\frac{1}{2}}$ and Lp is the Lorentz-polarization factor. No absorption corrections were applied.

The structure was solved by direct methods using 470 $|E|$ values >1.3 as input to the SHELX package (4). The first pass revealed the glucose fragment and the remaining atoms were found from the ΔF map. Most of the hydrogen atoms were found in the final ΔF map. These were included in the refinement in calculated positions (C-H, 1.08 Å) with a refined overall temperature factor. Full matrix least-squares refinement gave weighted and unweighted residuals of 0.074 and 0.087 respectively. Fractional atomic coordinates are listed in Tables 1(a) and (b). Bond lengths and angles have been deposited;[1] none deserve special comment. Figure 1 shows the molecule and the atomic numbering system used here.[2] The absolute configuration shown is that which assigns the β-D-glucose unit its correct configuration. The chirality at C(3), introduced by epoxidation of the side chain, was established by unambiguously identifying the attached atoms; not only were the hydrogen atoms associated with C(4) found

[1]These tables, along with tables of observed and calculated structure factors and of temperature factors are available, at a nominal charge, from the Depository of Unpublished Data, CISTI, National Research Council of Canada, Ottawa, Ont., Canada K1A 0S2.

[2]This numbering system is arbitrary and does not correspond to that normally used for secologanin derivatives.

0008-4042/83/020282-02$01.00/0
©1983 National Research Council of Canada/Conseil national de recherches du Canada

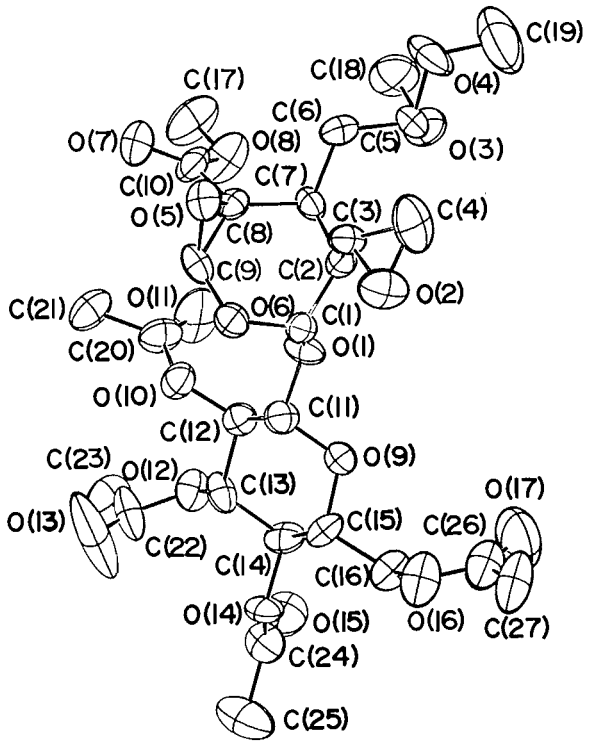

Fig. 1. ORTEP plot of molecule **2** showing atomic numbering.

on the ΔF map, but also it was demonstrated that, if two hypothetical hydrogen atoms were assigned to O(2) as if it were part of a methylene group, one of these hypothetical atoms clashed badly with a hydrogen atom attached to C(23) of another molecule.

Results and discussion

It can be seen from Scheme 1 that the oxidation product is the bisepoxide **2**, incorporating the novel epoxidized β-alkoxyacrylate component. The relative configuration follows unequivocally from the X-ray analysis and the absolute configuration can be assigned with confidence since there is no doubt that the integrity of the β-D-glucose moiety is maintained in the synthesis of **2**.

We have now a valuable bench mark for configurational

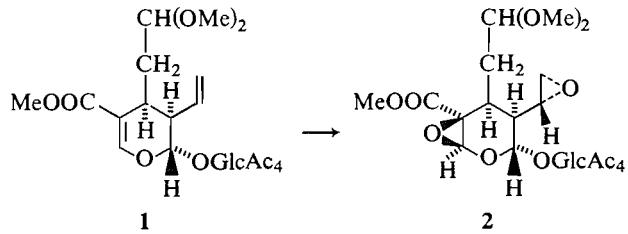

SCHEME I

assignments to related compounds. We have correlated **2** by chemical methods with the glycols derived from **1** (2), one of which was a key intermediate in the synthesis of the dihydrocadambine alkaloids (5). We had previously assigned the configuration of this glycol by chemical correlation with a glycol derived from sweroside (1), which had in turn been correlated with the iridoid secologanin, the configuration of which depended ultimately on a nuclear Overhauser enhancement experiment (6). Reciprocally now, the configuration of all of these synthetic intermediates and natural products (and of any others that can be correlated with them) are placed on the secure basis of an X-ray crystal structure analysis by their demonstrated relationship with **2**.

Acknowledgement

This research was supported by grants from the Natural Sciences and Engineering Research Council of Canada.

1. J. R. PURDY, R. G. HAMILTON, L. AKHTER, and S. MCLEAN. Can. J. Chem. **59**, 210 (1981).
2. G. N. SAUNDERS, J. R. PURDY, and S. MCLEAN. Can. J. Chem. **61**, 276 (1983).
3. W. J. ROSS, A. TODD, B. P. CLARK, S. E. MORGAN, and J. E. BALDWIN. Tetrahedron Lett. **22**, 2207 (1981).
4. G. M. SHELDRICK. Computing in crystallography. *Edited by* H. Schenk *et al.* Delft University Press. 1978.
5. G. N. SAUNDERS, R. G. HAMILTON, and S. MCLEAN. Tetrahedron Lett. **23**, 2359 (1982); R. G. HAMILTON, G. N. SAUNDERS, and S. MCLEAN. Can. J. Chem. **61**, 284 (1983).
6. K. BOCK, S. R. JENSEN, and B. J. NIELSEN. Acta Chem. Scand. Ser. B, **30**, 743 (1976).

Can. J. Chem. Downloaded from www.nrcresearchpress.com by 210.87.254.40 on 09/06/12
For personal use only.

The synthesis of 3α- and 3β-dihydrocadambine from secologanin

RAYMOND G. HAMILTON, GAVIN N. SAUNDERS, AND STEWART MCLEAN
Department of Chemistry, University of Toronto, Toronto, Ont., Canada M5S 1A1

Received August 24, 1982

RAYMOND G. HAMILTON, GAVIN N. SAUNDERS, and STEWART MCLEAN. Can. J. Chem. **61**, 284 (1983).

Secologanin, protected as the dimethyl acetal of its tetraacetate, had previously been dihydroxylated at the vinyl side chain with high stereoselectivity to provide the glycol (**4**) of the correct configuration for the synthesis of 3α- and 3β-dihydrocadambine. The glycol was converted to the cyclic acetal **5** to protect the secondary alcohol, the primary alcohol was oxidized to provide the aldehyde **6**, and this was reductively coupled with tryptamine. Treatment of the coupled intermediate (**8**) with 90% formic acid followed by deacetylation of the glycoside led to the formation of a mixture of 3α- and 3β-dihydrocadambine (40% and 33%, respectively). The synthesis confirms the structure assigned to these alkaloids, and establishes the configuration, relative and absolute, at all centres except C-3 (where it provides no new stereochemical information).

RAYMOND G. HAMILTON, GAVIN N. SAUNDERS et STEWART MCLEAN. Can. J. Chem. **61**, 284 (1983).

On a antérieurement dihydroxylé avec une haute stéréosélectivité la chaîne latérale vinylique de la sécologanine, protégée sous forme d'acétate diméthylique de son tétraacétate, pour obtenir le glycol (**4**) ayant la bonne configuration en vue de la synthèse des 3α- et 3β-dihydrocadambines. On a transformé le glycol en l'acétal cyclique (**5**) pour protéger l'alcool secondaire, et on a oxydé l'alcool primaire pour obtenir l'aldéhyde (**6**) et on a couplé ce dernier de façon réductrice avec la tryptamine. Le traitement de l'intermédiaire couplé (**8**) par l'acide formique à 90% suivi de la désacétylation du glycoside conduit à la formation d'un mélange de 3α- et de 3β-déhydrocadambine (40% et 33% respectivement). La synthèse confirme la structure attribuée à ces alcaloides et établit la configuration relative et absolue de tous les centres à l'exception de C-3 (où elle ne fournit aucune nouvelle information stéréochimique).

[Traduit par le journal]

We assigned the structure and relative configuration **1***a* to an alkaloid of *Nauclea diderrichii* (1); the same alkaloid was isolated from *Anthocephalus cadamba* by Brown and Fraser (2), who named it 3α-dihydrocadambine and independently assigned structure **1***a* to the alkaloid, citing circular dichroism studies of the alkaloid and its congener, cadambine (**2**), and biogenetic considerations as evidence that the relative and absolute configuration is that shown in **1***a*. Subsequently, Brown and Chapple (3) isolated the isomeric alkaloid 3β-dihydrocadambine (**1***b*), from the same extract, and demonstrated its relationship to **1***a* and **2**.

A reasonable hypothesis for the biogenesis of the dihydrocadambines involves the stereospecific oxidation of the vinyl side chain of strictosidine or vincoside to an epoxide or its equivalent, followed by internal opening of the epoxide by the nitrogen of the secondary amine, closing the seven-membered ring, and producing the secondary alcohol. Strictosidine and vincoside are, themselves, products of the biosynthetic equivalent of a Pictet–Spengler condensation of a tryptamine unit and secologanin (**3**). We have undertaken to synthesize the alkaloids from these precursors, tryptamine and secologanin, but we felt that a completely biomimetic strategy would face severe difficulties in vitro at the step requiring internal opening of the epoxide, both because the regioselectivity of this reaction is uncertain and because it can be expected that the nitrogen would more readily attack the carbomethoxy group and form a stable lactam. We chose, therefore, a strategy which essentially reverses the order of bond-forming reactions. A preliminary report of the synthesis of **1***a* has been communicated (4); more recently, improvements in our experimental procedure have significantly improved the yield of **1***a* and have also led to the isolation of its 3β epimer, **1***b*, in comparable yield.

The glycol **4**, which we prepared stereoselectively from secologanin (5), was quantitatively converted by the action of Amberlite IR 120 resin in methanol at room temperature to a crystalline substance,[1] mp 145–146°C, which was shown to be, at least in solution, a 5:2 mixture of the epimeric acetals **5**. (The configuration at C-5 is not of synthetic significance since its chirality is lost in a subsequent step.) Both **4** and **5** formed the same bridged bicyclic acetal **6** if treated with dilute acid. With the cyclic acetal function of **5** serving to protect both the aldehyde and secondary hydroxyl groups, the primary alcohol was selectively oxidized with pyridinium chlorochromate on Celite in dichloromethane with sodium acetate present (6) to provide the aldehyde **7**. The progress of the reaction was followed by ^{1}Hmr spectroscopy but **7** was not completely characterized because of its instability. As soon as it was isolated, **7** was reductively coupled with tryptamine hydrochloride in the presence of sodium cyanoborohydride without further characterization. The product **8** was isolated as a 5:2 mixture of epimers, from which the major isomer was separated chromatographically for characterization purposes.

The operations now required to complete the synthesis of the alkaloidal framework are the deprotection of the aldehyde function at C-5 and its coupling with the tryptamine moiety in an intramolecular Pictet–Spengler reaction. Both operations require acidic conditions, but it is clear that these conditions must provide a high degree of selectivity since the C-5 acetal is to be hydrolyzed in the presence of a dense array of sensitive functional groups, including several cryptoaldehydes; furthermore, there is ample evidence to indicate that hydrolysis of the acetal will be more difficult in the presence of the neighboring basic nitrogen. There was also some question concerning the effec-

[1]In preparative runs, since it was difficult to separate **4** from the small amount of its C-3 epimer produced in the dihydroxylation step (5), the mixture of epimers was carried through to this stage, where purification was more conveniently carried out.

0008-4042/83/020284-04$01.00/0
©1983 National Research Council of Canada/Conseil national de recherches du Canada

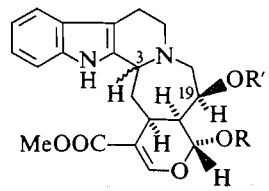

1*a* 3α H; R = Glc, R′ = H
b 3β H; R = Glc, R′ = H
c 3α H; R = $GlcAc_4$, R′ = Ac
d 3β H; R = $GlcAc_4$, R′ = Ac

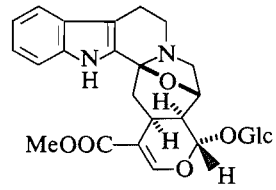

2

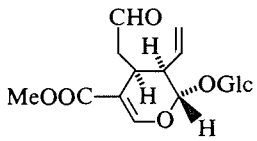

3

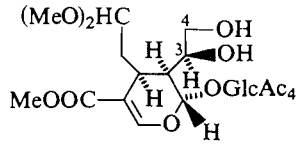

4

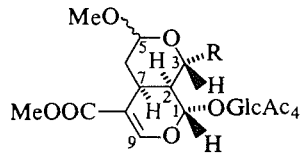

5 R = CH_2OH
7 R = CHO

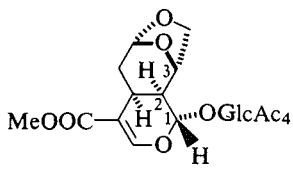

6

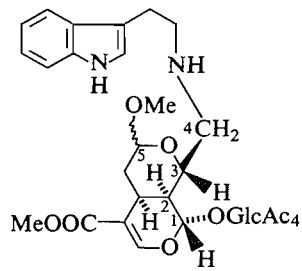

8

Glc = β-D-glucopyranosyl
$GlcAc_4$ = tetraacetyl-β-D-glucopyranosyl

tiveness of the Pictet–Spengler step since, although there is some precedent for such a reaction (7), comment has been made (8) about the possible difficulty of forming a seven-membered ring in a Pictet–Spengler reaction. The final question concerned the stereochemical outcome of the Pictet–Spengler condensation; we had maintained stereochemical control at all of the chiral centres up to this point, but we could see no good reason for anticipating stereoselectivity in this condensation and the generation of the 3α and 3β configurations in the alkaloids seemed equally probable.

Most of these concerns or reservations proved, in fact, to be well founded. We investigated the effect of many acidic systems on **8**, and found that either the starting material was recovered or an uncharacterizable mixture, apparently of degradation products, was obtained. We were delighted, therefore, to find that, when **7** was treated with 90% formic acid, derivatives of the target alkaloid were recognized in the product mixture. Optimization of the reaction conditions (95°C for 18 hours) and isolation procedure (deacetylation with potassium carbonate in methanol and chromatography) eventually gave very satisfactory yields of both 3α- and 3β-dihydrocadambine (40% of **1***a* and 33% of **1***b*). Clearly the Pictet–Spengler reaction has formed the seven-membered ring in good yield, but with little stereoselectivity. For characterization purposes, the alkaloids were converted to their pentaacetates **1***c* and **1***d*, which were identical in every respect, including optical activity, with materials prepared from the natural alkaloids.

This synthesis serves to confirm the structure assigned to 3α- and 3β-dihydrocadambine (1–3) and, more importantly, it provides unequivocal proof for the configurational assignments, both relative and absolute, at all centres except C-3, where it adds nothing to the evidence available from the natural alkaloids themselves. We note that the original assignments of relative configurations were based on ^{1}Hmr coupling constants (a procedure not without hazards, particularly when applied to a flexible molecule incorporating a seven-membered ring), while absolute configurations were assigned on the basis of circular dichroism and biogenetic assumptions.

Since our stereochemical conclusions are of significance, it is appropriate that we should provide more detail concerning the stereochemistry of our synthetic intermediates. It is clear that the alkaloids have the same relative and absolute configuration as secologanin at all of the chiral centres that they have in common, since none of the synthetic steps introduced the risk of isomerizing any of these centres. The configuration at C-19 in the synthetic alkaloids had its origin in the stereoselective dihydroxylation that led to **4**. We assigned (5) the configuration at C-3 of **4** by chemical correlation with the corresponding sweroside glycol, which in turn had been correlated with secogalioside, the configurational assignment of which ultimately rested on a nuclear Overhauser enhancement experiment (9). More recently we have provided conclusive proof for the stereochemistry of **4** by correlation (10) with a derivative, the structure and stereochemistry of which has been established by an X-ray crystal structure analysis (11); this procedure unequivocally establishes the relative configuration

TABLE 1. Nuclear magnetic resonance data of new compounds[a]

	5 (Major epimer)		**5** (Minor epimer)		**6**		**8** (Major epimer)[e]	
Proton[b]	A[c]	B[d]	A	B	A	B	A	B
1	4.72	d, 6	4.60	d, 4	4.57	d, 9.2*	4.63	d, 2.5
2	7.96	n.r.	7.96	n.r.	8.29	dd, 9.2*, 6**	8.04	n.r.*
3	6.28	n.r.	6.23	n.r.	5.23	d, 5.5	6.42	ddd, 9*, 9, 3.3
4a	6.36	dd, 11.5, 5.5	6.35	n.r.	6.12	dd, 7.3, 5.5	~7.15	n.r.
4b	6.18	dd, 11.5, 3.5	6.17	12, 3	6.03	d, 7.3	~7.15	n.r.
5	5.22	t, 5	5.60	dd, 5.5, 2	4.51	n.r.	5.83	dd, 9.2, 1.8
6a	7.88	n.r.	7.67	ddd, 14, 5.5, 2	7.79	dd, 12.5, 6	7.53	dm, 13
6b	8.12	n.r.	8.30	n.r.	8.64	dd, 12.5, 12	8.49	ddd, 13, 9.2, 5.2
7	7.22	n.r.	6.90	n.r.	6.88	n.r.**	~7.15	n.r.
9	2.40	d, <1	2.20	d, <1	2.57	s	2.60	d, 1.9
COOMe	6.28	s	6.27	s	6.30	s	6.30	s
1′	5.11	d, 8.5	5.14	d, 8.5	5.05	d, 8.1	5.18	d, 8.1
2′	4.95	dd, 9.5, 8.5	5.01	dd, 9.5, 8.5	4.93	dd, 9.5, 8.1	5.03	dd, 9.5, 8.1
3′	4.77	t, 9.5	4.78	t, 9.5	4.73	t, 9.5	4.80	t, 9.5
4′	4.90	t, 9.5	4.90	t, 9.5	4.88	t, 9.5	4.91	t, 9.5
5′	6.28	n.r.	6.28	n.r.	6.22	ddd, 9.5, 5.0, 2.3	6.30	n.r.
6a′	5.85	dd, 12, 2.5	5.87	dd, 12.5, 2.5	5.89	dd, 12.1, 2.3	5.89	dd, 12.1, 2.2
6b′	5.70	dd, 12.5, 4.5	5.69	n.r.	5.64	dd, 12.1, 5.0	5.69	dd, 12.1, 4.5
OAc	8.08	s	7.99	s	7.98	s	8.12	s
OAc	8.03	s	7.98	s	7.97	s	8.01	s
OAc	7.97	s	7.90	s	7.95	s	7.98	s
OAc	7.96	s	7.87	s	7.92	s	7.94	s
OMe	6.69	s	6.53	s	—	—	6.85	s
OH	6.94	n.r.	7.67	n.r.	—	—	—	—

[a]**5** at 360 MHz; **6** and **8** at 400 MHz; $CDCl_3$.
[b]Numbering system shown in structural formulae; 1′, 2′, etc. are glucosidic protons.
[c]Columns A: Chemical shifts on τ scale.
[d]Columns B: Apparent multiplicities; s, singlet; d, doublet; t, triplet; n.r., not resolved. Coupling constants (Hz); asterisks indicate decoupling experiments.
[e]Iridoid numbering system. Tryptamine-derived protons not listed.

at all chiral centres, including C-3, and provides the absolute configuration by internal reference to the glucose moiety.

Even though the configuration at all centres in **4** is secure, the possibility remains that the configuration at C-3 could undergo change during the formation or subsequent reaction of **7**, while C-4 is at the oxidation level of an aldehyde, but careful examination of the intermediates provides evidence against this. We have noted previously (5) that the dihydropyran ring of secologanin and a number of its derivatives is conformationally mobile and that the coupling constant, $J_{1,2}$, between the protons at C-1 and C-2 provides valuable information regarding the conformation of the ring. The cyclic acetals **5** have intermediate values of $J_{1,2}$ (see Table 1), indicating that they have sufficient conformational mobility to make $J_{2,3}$ values of little value for assigning the relative configuration at C-3; the appearance of the signal associated with the C-5 proton, an apparent triplet (5 Hz spacings) in the major isomer, indicates that the methoxyl group is axial at this centre, while the minor epimer has an equatorial methoxyl group. Only one bridged bicyclic acetal, **6**, was obtained; here the $J_{1,2}$ value of 9.2 Hz shows that the bridged system has reduced conformational mobility and that the molecule adopts the conformation with the corresponding protons diaxial. (In cadambine, **2**, with a similar bridged bicyclic structure, the corresponding coupling constant is 9.5 Hz, indicating a very similar rigid conformation (2), while the dihydrocadambines are more flexible.) The configuration at C-3 can not be deduced with confidence from the $J_{2,3}$ value associated with **6**, but the configuration at this centre in both **5** and **6** is secure since it can not have undergone epimerization under the reaction conditions used up to this stage. (Tietze and Henke (12) have assigned the structure and configuration **6** to a compound produced in a similar manner.) The decisive configurational question now concerns **8**, the first characterized derivative following oxidation at C-4. In this case the mixture of C-5 epimers was separated, and the ^{1}Hmr spectrum of the major isomer was examined carefully. The conformational preference of this compound is distinctly different from that of its precursors since the $J_{1,2}$ value of 2.5 Hz indicates that the corresponding protons are diequatorial on the dihydropyran ring. Although the configuration at C-5 is not of significance with respect to the configuration of the target alkaloids, it is of interest to note that the C-5 methoxyl group is equatorial in this isomer (the C-5 proton shows coupling constants of 9.2 and 1.8 Hz) and axial in the minor isomer, and that these epimers were formed in the same ratio (5:2 as judged by ^{1}Hmr spectra) that existed in the precursor **5**. The dominance of the epimer with an axial methoxyl group in **5**, formed under equilibrating conditions, probably results from an anomeric effect, while the change to an equatorial methoxyl group in the major epimer of **8** indicates that no equilibration at C-5 took place in its formation, so that the configuration at C-5 is unchanged, but the conformation of the ring is inverted. It appears that the conformation of **8** is governed by the requirement that the extended substituent at C-3 be equatorial to the tetrahydropyran ring. This leads to the fortunate result that the C-3 hydrogen is axial to this ring, as is the C-2 hydrogen, and the $J_{2,3}$ value of 9 Hz (confirmed by decoupling experiments) clearly establishes their *trans*-diaxial

relationship. The relative configuration at C-3 is, therefore, established, and the formation of **8** from **5** with retention of configuration at C-3 is thus verified; there is no doubt that the configuration is also retained at this centre, which becomes C-19 in the alkaloids, under the reaction conditions used to convert **8** to **1***a* and *b*. Consequently, the synthesis provides unequivocal confirmation for the assignment (1−3) of all structural and stereochemical features depicted by **1***a* and *b* (apart from the configuration at the centre where they are epimeric) to 3α- and 3β-dihydrocadambine.

Experimental

Melting points were determined on a calibrated Thomas−Kofler micro hot stage. Infrared spectra were measured on a Perkin−Elmer 337 spectrometer; the wavelengths (μ) of selected absorptions of solutions in chloroform are reported. Ultraviolet spectra were measured on a Unicam SP. 800A spectrometer; the λ_{max} values (nm) followed by the log ε values in parentheses for solutions in methanol are reported. Proton nmr spectra were recorded on a Nicolet 360 (at 360 MHz) or a Bruker WH-400 (at 400 MHz) spectrometer; solutions in $CDCl_3$ were used, and data showing chemical shifts (τ scale) and apparent multiplicities and coupling constants are collected in Table 1.

The cyclic acetals ***5***

A solution of the epimeric glycols (90 mg; ~90% **4**) described previously (5) in 4 mL of methanol was stirred at room temperature with 300 mg of Amberlite IR 120 resin for 12 h. The resin was removed by filtration and the solvent was evaporated providing a quantitative yield of the acetals. Recrystallization from ether provided crystalline **5**, mp 145−146°C; ir: 5.68, 5.85, 6.12; uv: 233 (3.78). *Anal.* calcd. for $C_{26}H_{36}O_{16}$: C 51.65, H 5.99; found: C 51.73, H 5.94.

The bicyclic acetal ***6***

A solution of **5** (59 mg; 0.09 mmol) in 7 mL of tetrahydrofuran containing 60 mg of concentrated hydrochloric acid was stirred at room temperature for 16 h. The solvent was removed under vacuum, and the residue was purified by chromatography on silica gel with elution by ether. The product **6** (37 mg; 0.06 mmol) was obtained as a glass; ir: 5.68, 5.85, 6.10.

The tryptamine-coupled product ***8***

A mixture of pyridinium chlorochromate (1.4 g; 6.5 mmol), sodium acetate (135 mg; 1.65 mmol), and 5 g of Celite (6) was dried at 100°C under vacuum for 2 h. The dried powder was slurried with 30 mL of dry dichloromethane, a solution of **5** (1.00 g; 1.66 mmol) in 10 mL of dichloromethane was added, and the mixture was stirred at room temperature for 14 h. The solvent was removed on a rotary evaporator, and the powder that remained was loaded on a silica gel chromatography column and eluted with dichloromethane. The aldehyde **7** was obtained as an unstable orange oil (ca. 730 mg; 1.2 mmol) which was dissolved in a mixture of 20 mL of methanol and 5 mL of tetrahydrofuran. Tryptamine hydrochloride (570 mg; 2.9 mmol), sodium cyanoborohydride (75 mg; 1.2 mmol), and 10 g of 4 Å molecular sieves were added, and the mixture was stirred at room temperature for 14 h. Solid material was removed on a rotary evaporator, and the residue was well triturated with dichloromethane. The dichloromethane solution was filtered and the solvent was removed by evaporation. The residue was chromatographed on silica gel with elution by 5:1 chloroform−methanol and the oily product **8** (581 mg; 0.78 mmol) was obtained as a 5:2 mixture of epimers. An aliquot was subjected to further chromatography on silica gel with elution by 9:1 dichloromethane−methanol and the major epimer was isolated from early fractions as an amorphous but homogeneous substance; ir: 2.87, 5.70, 5.85, 6.13; uv: 225 (4.39). *Anal.* calcd. for $C_{36}H_{46}O_{15}N_2$: C 57.90, H 6.20; found: C 57.81, H 6.18.

*The 3α- and 3β-dihydrocadambines (***1***a, b)*

A solution of the epimeric compounds **8** (164 mg; 0.22 mmol) in 10 mL of 90% formic acid was heated to 95°C for 18 h. The solvent was removed by vacuum distillation, and the residue (165 mg) was stirred with potassium carbonate (20 mg) in 5 mL of methanol at room temperature for 1 h, and then filtered. The solvent was removed on a rotary evaporator, and the residue was chromatographed on silica gel with methanol−chloroform elution. 3α-Dihydrocadambine (48 mg; 0.088 mmol) was eluted first, followed by the 3β isomer (40 mg; 0.073 mmol); other fractions afforded material (13 mg) that was a mixture of at least five uncharacterized compounds. The 3α-dihydrocadambine (**1***a*) was recrystallized from ether−chloroform, and obtained as crystals, mp 182−187°C (dec.), which showed spectroscopic characteristics (ir, uv, ^{1}Hmr) and tlc behavior identical with those of the natural alkaloid (1). Acetylation of the synthetic alkaloid provided a pentaacetate (**1***c*), mp 193−195°C (lit. (2) mp 197−199°C), recrystallized from hexane−acetone; this material was identical in every respect, including optical activity (cd in methanol, 350−205 nm), with a sample of **1***c* prepared from natural 3α-dihydrocadambine. Synthetic 3β-dihydrocadambine (**1***b*) was not obtained crystalline; it was characterized as its amorphous pentaacetate (**1***d*), which was identical with a sample of **1***d* (amorphous) derived from natural **1***b* (amorphous) (2) in spectroscopic characteristics (ir, uv, ^{1}Hmr), tlc behavior, and optical activity (cd in methanol, 350−205 nm).

Acknowledgements

We are grateful to Dr. R. T. Brown, University of Manchester, for kindly providing the reference sample of authentic pentaacetyl-3β-dihydrocadambine. We thank Dr. K. J. Dorrington, University of Toronto, for cd measurements. The nmr spectra were obtained at the Southwestern Ontario N.M.R. Center, funded by a Major Installation grant from the Natural Sciences and Engineering Research Council of Canada, and at the Toronto Biomedical NMR Centre, supported by a grant from the Medical Research Council of Canada. This research received financial support from the Natural Sciences and Research Council of Canada.

1. G. I. DMITRIENKO, D. G. MURRAY, and S. MCLEAN. Tetrahedron Lett. 1961 (1974); S. MCLEAN, G. I. DMITRIENKO, and A. SZAKOLCAI. Can. J. Chem. **54**, 1262 (1976).
2. R. T. BROWN and S. B. FRASER. Tetrahedron Lett. 1957 (1974).
3. R. T. BROWN and C. L. CHAPPLE. Tetrahedron Lett. 2723 (1976).
4. G. N. SAUNDERS, R. G. HAMILTON, and S. MCLEAN. Tetrahedron Lett. **23**, 2359 (1982).
5. J. R. PURDY, R. G. HAMILTON, L. AKHTER, and S. MCLEAN. Can. J. Chem. **59**, 210 (1981).
6. P. A. GRIECO, E. WILLIAMS, and T. SUGAHARA. J. Org. Chem. **44**, 2194 (1979).
7. G. H. BÜCHI. Chimia, **29**, 172 (1975).
8. S. F. MARTIN and P. J. GARRISON. J. Org. Chem. **46**, 3567 (1981).
9. K. BOCK, S. R. JENSEN, and B. J. NIELSEN. Acta Chem. Scand. Ser. B, **30**, 743 (1976).
10. G. N. SAUNDERS, J. R. PURDY, and S. MCLEAN. Can. J. Chem. **61**, 276 (1983).
11. S. C. NYBURG, P. Y. SIEW, G. N. SAUNDERS, J. R. PURDY, and S. MCLEAN. Can. J. Chem. **61**, 282 (1983).
12. L.-F. TIETZE and S. HENKE. Angew. Chem. **93**, 1005 (1981).

Five-membered ring spiro-annulation via thermal rearrangement of enol silyl ethers of 2-(cyclopropylmethylene)cycloalkanones. A formal total synthesis of some spirovetivane-type sesquiterpenoids

EDWARD PIERS, CHEUK KUN LAU, AND ISAO NAGAKURA

Department of Chemistry, University of British Columbia, 2036 Main Mall, University Campus, Vancouver, B.C., Canada V6T 1Y6

Received July 5, 1982

EDWARD PIERS, CHEUK KUN LAU, and ISAO NAGAKURA. Can. J. Chem. **61**, 288 (1983).

Treatment of the 2-(iodomethylene)cycloalkanones **10** and **11** with lithium (phenylthio)(cyclopropyl)cuprate provided good yields of the corresponding β-cyclopropyl enones **12** and **13**, respectively. Thermolysis of the latter substances produced relatively poor yields of the desired spiro-annulation products **14** and **15**. However, conversion of **12** and **13** into the corresponding enol silyl ethers **24** and **25**, followed by thermal rearrangement of the latter materials and acid hydrolysis of the resulting products, provided synthetically useful yields of the spiro enones **14** and **15**. Cuprous iodide-catalyzed addition of methyl magnesium iodide to 2-cyclohexen-1-one, followed by trapping of the resultant enolate anion with cyclopropanecarboxaldehyde, provided the ketols **38**, which could be converted readily into the mixture of enol silyl ethers **34** and **35**. Thermal rearrangement of the latter substances gave, after acid hydrolysis of the crude thermolysate, the spiro enones **42** and **43** in a ratio of ~2.5:1 (57% yield). Treatment of **42** with methyllithium in ether gave the tertiary alcohols **44** and **45** (ratio ~4:1). Hydroboration (disiamylborane, tetrahydrofuran; H_2O_2, NaOH) of **44**, followed by oxidation of the resultant diol **46** with pyridinium chlorochromate, provided the ketol **47**. A similar sequence of reactions converted the olefinic alcohol **45** into the ketol **49**. Dehydration (*p*-toluenesulfonic acid in benzene) of **47** gave the spiro enones **28** and **48**, in a ratio of ~9:1. Compound **28**, also prepared previously from the ketol **49**, had been converted earlier into the spirovetivane-type sesquiterpenoids (±)-α-vetispirene (**29**), (±)-β-vetivone (**30**), (±)-hinesol (**31**), (±)-hinesol acetate (**32**), and (±)-agarospirol (**33**).

EDWARD PIERS, CHEUK KUN LAU et ISAO NAGAKURA. Can. J. Chem. **61**, 288 (1983).

Les (iodométhylène)-2 cycloalcanones **10** et **11** réagissent avec le (phénylthio)(cyclopropyle)cuprate de lithium en donnant respectivement les β cyclopropylénones **12** et **13** avec de bons rendements. La thermolyse de ces derniers composés permet d'acéder aux produits de spiro-annellation **14** et **15** attendus mais avec des rendements relativement faibles. Cependant la transformation des composés **12** et **13** en éthers énoliques silylés **24** et **25** correspondants suivie d'une transposition thermique de ces derniers et d'une hydrolyse acide des produits résultants conduit aux spiro énones **14** et **15** avec des rendements intéressants pour la synthèse. L'addition d'iodure de méthyle magnésium, catalysée par l'iodure cuivreux, sur la cyclohexène-2 one-1, suivie du piégeage de l'anion énolate résultant par le cyclopropanecarboxaldéhyde permet d'obtenir les cétols **38** que l'on peut transformer rapidement en un mélange d'éthers énoliques silylés, **34** et **35**. La transposition thermique de ces éthers, suivie de l'hydrolyse acide des produits bruts de thermolyse donne les spiro énones **42** et **43** dans un rapport d'environ 2.5:1 (rendement de 57%). Le composé **42** réagit avec le méthyllithium dans l'éther en donnant les alcools tertiaires **44** et **45** (rapport de 4:1). L'hydroboration (disiamylborane, tétrahydrofuranne; H_2O_2, NaOH) du composé **44** suivie de l'oxydation du diol **46** qui en résulte par le chlorochromate de pyridinium conduit au cétol **47**. Par une série analogue de réactions, l'alcool oléfinique **45** donne le cétol **49**. La déshydratation (acide *p*-toluènesulfonique dans le benzène) du composé **47** permet d'obtenir les spiro énones **28** et **48**, dans un rapport d'environ 9:1. Antérieurement on a transformé le composé **28** préparé à partir du cétol **49**, en sesquiterpènes du type spirovétivane, soit le (±)-α-vétispirène **29**, la (±)-β-vétivone **30**, le (±)-hinésol (**31**), l'acétate du (±)-hinésol (**32**) et le (±)-agarospirol (**33**).

[Traduit par le journal]

Introduction

A recent paper from this laboratory (1) described a new five-membered ring annulation method based on the preparation and thermal rearrangement of β-cyclopropyl α,β-unsaturated ketones.[1] For example, treatment of 3-iodo-2-cyclohexen-1-one (**1**) with lithium (phenylthio)(cyclopropyl)cuprate[2] provided efficiently the corresponding β-cyclopropyl enone **2** which, upon thermolysis at ~425°C, followed by elution of the crude thermolysate (containing mainly the isomeric enones **3** and **4**) through a column of the basic alumina, provided the annulation product **4** in 72% overall yield (eq. [1]). Similarly, thermolytic rearrangement of

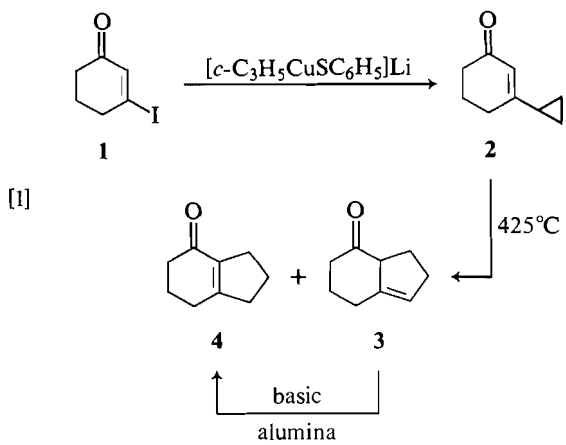

[1]

3-(1-methylcyclopropyl)-2-cyclohexen-1-one (**5**) afforded, in 87% yield, the bicyclic enone **6** which served as a convenient

[1]For a brief discussion of the vinylcyclopropane → cyclopentene rearrangement, along with appropriate literature citations, see ref. 1.

[2]For a report regarding the reaction of β-halo enones with a variety of organocuprate reagents, see ref. 2.

0008-4042/83/020288-10$01.00/0

©1983 National Research Council of Canada/Conseil national de recherches du Canada

Can. J. Chem. Downloaded from www.nrcresearchpress.com by 210.87.254.42 on 09/06/12
For personal use only.

Can. J. Chem. Downloaded from www.nrcresearchpress.com by 210.87.254.42 on 09/06/12
For personal use only.

[2] 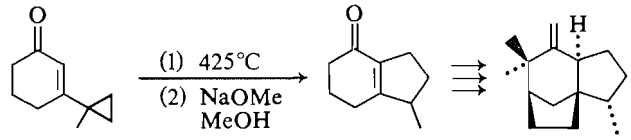

5 **6** **7**

starting material for a new formal total synthesis of the tricyclic sesquiterpenoid (±)-zizaene (**7**) (eq. [2]).

In an earler report (3) we had described, *inter alia*, efficient conversions of 2-(hydroxymethylene)cyclohexanone (**8**) and the analogous cyclopentanone derivative **9** into the corresponding (*E*)-2-(iodomethylene)cycloalkanones **10** and **11**, respectively. It is clear that successful use of the latter substances as starting materials in a sequence of reactions similar to that outlined in eq. [1] would constitute a new five-membered ring

[3] 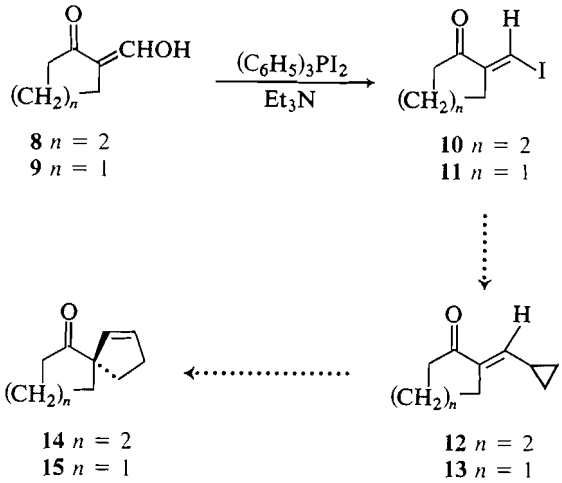

8 *n* = 2
9 *n* = 1

10 *n* = 2
11 *n* = 1

14 *n* = 2
15 *n* = 1

12 *n* = 2
13 *n* = 1

spiro-annulation method (see eq. [3]). Thus, treatment of compounds **10** and **11** with lithium (phenylthio)(cyclopropyl)-cuprate should provide the β-cyclopropyl enones **12** and **13** which, upon successful subjection to thermal vinylcyclopropane → cyclopentene rearrangement, would afford the spiro olefinic ketones **14** and **15**, respectively. Since spiro ring systems are quite commonly found in natural products, particularly in the sesquiterpenoid family, we wished to extend our earlier studies (1) in order to determine whether or not the spiro-annulation sequences outlined in eq. [3] are viable processes.[3] This paper describes the results of this investigation. In addition, we report the application of this new annulation method to a formal total synthesis of a number of spirovetivane sesquiterpenoids.[4]

Results and discussion

(a) *Preparation and thermal rearrangement of* (E)*-2-(cyclopropylmethylene)cyclohexanone (12) and* (E)*-2-(cyclopropylmethylene)cyclopentanone (13) (see Chart 1)*

As expected on the basis of our earlier work (1), the β-cyclopropyl enones **12** and **13** could be prepared smoothly and efficiently from the corresponding β-iodo enones **10** and **11**

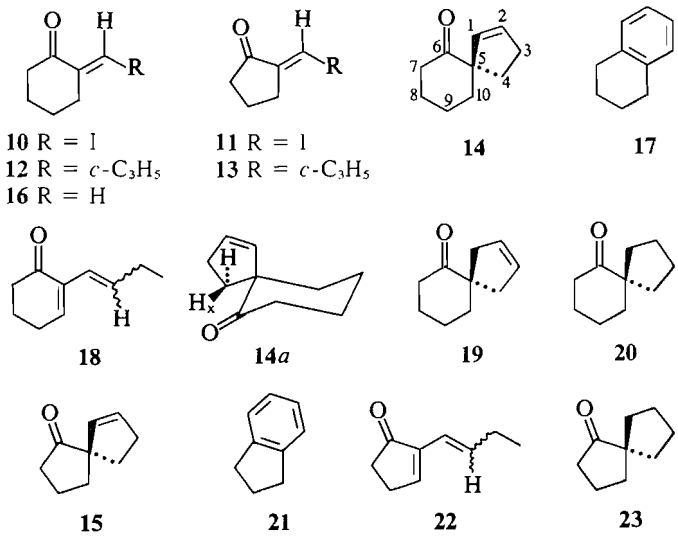

10 R = I
12 R = *c*-C_3H_5
16 R = H

11 R = I
13 R = *c*-C_3H_5

14 **17**

18 **14a** **19** **20**

15 **21** **22** **23**

CHART 1

(3). Thus, when the latter substances were allowed to react with lithium (phenylthio)(cyclopropyl)cuprate in ether–tetrahydrofuran (THF), the desired compounds **12** and **13** were obtained in yields of 82 and 65%, respectively. The stereochemistry of these products was shown to be as indicated on the basis of proton nuclear magnetic resonance (^{1}H nmr) spectroscopy. The chemical shifts of the two olefinic protons of 2-methylenecyclohexanone (**16**) have been shown to be δ 5.04 (proton *trans* to carbonyl) and δ 5.72 (proton *cis* to carbonyl) (11). Since the olefinic protons of the enones **12** and **13** resonate at δ 6.04 and 5.95, respectively, it seems appropriate to conclude that these protons are geometrically *cis* to the carbonyl group. Furthermore, in work to be described in a subsequent section of this paper (*vide infra*), we isolated the two geometric isomers of 2-(cyclopropylmethylene)-3-methylcyclohexanone. The alkene proton of the (*Z*) isomer resonated at δ 4.84, while the signal of the corresponding proton of the (*E*) isomer appeared at δ 5.98. These data unambiguously show that compounds **12** and **13** both possess the (*E*) geometry and since the stereochemistry of the starting materials (β-iodo enones **10** and **11**) had also been established (3), it is clear that, in an overall sense, the substitution reactions **10** → **12** and **11** → **13** had occurred with retention of configuration.

Thermolysis of the β-cyclopropyl enone **12** was carried out by passing a *n*-hexane solution of this material through a vertically-held, heated (~450°C) glass tube (1.2 × 32 cm) filled with glass helices. Gas–liquid chromatographic analysis of the distilled thermolysate, obtained in 74% yield, showed that it consisted of a mixture of three main components, the desired spiro ketone **14** (~44%), tetralin (**17**) (~38%), and the dienones **18** (~9%, mixture of geometric isomers), along with a number of very minor, unidentified compounds. A small sample of each of the major components was obtained by preparative glc. Tetralin was identified by comparison with commercially available material. Only a small amount of the mixture of dienones **18** was obtained and full characterization of the individual substances was not carried out. However, the fact that this material consisted of a mixture of geometric isomers was shown by the ^{1}H nmr spectrum which exhibited two signals (triplets) at high field due to the terminal methyl groups. Hydrogenation (H_2, Pd–C, methanol) of the two double bonds present in **18** afforded 2-*n*-butylcyclohexanone, which exhibited spectra identical with those of an authentic sample.

[3] For review articles related to the synthesis of spiro compounds, see ref. 4. For more recent studies, the reader is referred to refs. 5–8, and references therein (particularly the second citations in refs. 7 and 8).

[4] For preliminary reports regarding some of the work described herein, see refs. 9 and 10.

Can. J. Chem. Downloaded from www.nrcresearchpress.com by 210.87.254.42 on 09/06/12
For personal use only.

The ^{1}H nmr spectrum of the major thermolysis product, the desired spiro[4.5]dec-1-en-6-one (**14**), was deceptively simple. Although the high field region of the spectrum (7-proton and 5-proton multiplets at δ 1.40–2.03 and δ 2.18–2.60, respectively)[5] was relatively unexceptional, one might well have expected the olefinic protons of **14** to be magnetically nonequivalent. In fact, however, the alkene region of the ^{1}H nmr spectrum exhibited only a 2-proton singlet at δ 5.76.[6] On the other hand, when the spectrum was taken in the presence of an appropriate amount of the shift reagent Eu(FOD)$_3d_{27}$, the two olefinic protons did exhibit different chemical shifts (δ 6.06, 6.42) and each gave rise to a doublet of triplets with coupling constants of 6 Hz and ~2 Hz. Furthermore, the 5-proton multiplet (δ 2.18–2.60) had been transformed into two distinct signals, a 3-proton multiplet at δ 3.16–3.56 and a 2-proton multiplet at δ 2.50–2.86. In a decoupling experiment (in the presence of the shift reagent), irradiation at δ 2.70 (allylic methylene signal) caused the signals due to the olefinic protons to collapse to an AB pair of doublets (J = 6 Hz).

The proton decoupled ^{13}C nmr spectrum of the spiro ketone **14** exhibited the presence of two nonequivalent olefinic carbon atoms (δ 132.5 and 133.4). Other signals appeared at δ 211.5 (carbonyl carbon), 64.1 (quaternary carbon), 39.9 (2 carbon atoms), 32.3, 31.3, 27.7, and 23.0.

In order to obtain conclusive chemical evidence for the fact that the major thermolysis product did indeed possess the desired carbon skeleton, compound **14** was subjected to hydrogenation over palladium-on-carbon in methanol. The spectra (infrared, ^{1}H nmr) of the product, spiro[4.5]decan-6-one (**20**), were identical with those obtained from an authentic sample of this material, prepared by the method of Naro and Dixon (13).

Thermal rearrangement of (*E*)-2-(cyclopropylmethylene)-cyclopentanone (**13**) under conditions similar to those employed for the cyclohexanone analog **12** gave, in 90% yield, a colorless oil (distilled). Analysis of this material by glc revealed the presence of a number of components. Spectral data derived from small samples of the major products (collected by preparative glc) showed that they were the desired spiro[4.4]non-6-en-1-one (**15**) (~29% of the mixture), indan (**21**) (~11%), and a mixture of the geometrically isomeric dienones **22** (~44%). The olefinic region of the ^{1}H nmr spectrum of the spiro ketone **15**, in contrast to that of the homolog **14**, was found to be "normal", exhibiting two distinct multiplets at δ 5.30–5.53 and 5.73–5.97. Subjection of **15** and the mixture of dienones **22** to hydrogenation over palladium-on-carbon in methanol provided spiro[4.4]nonan-1-one (**23**) (14) and 2-*n*-butylcyclopentanone, respectively.

Although thermolysis of the β-cyclopropyl enones **12** and **13** did produce the spiro-annulation products **14** and **15**, respectively, the results summarized above show that the yields of these desired products are, from a synthetic point of view, less than satisfactory. However, even without going into a detailed mechanistic discussion, it is clear that the formation of the aromatic side products tetralin (**17**) and indan (**21**) involves, in each case, chemical reaction of the carbonyl group. Furthermore, it is not unreasonable to propose that the carbonyl groups in **12** and **13** also assist in the formation of the other major side products of these thermolysis reactions, the dienones **18** and **22**, respectively. That is to say, if the transition states involved in hydrogen migration from the C-3 carbons of **12** and **13** to produce the α,β-unsaturated ketone systems present in **18** and **22** have any degree of product-like character, they might well be expected to experience stabilization from the presence of the carbonyl groups. This mode of reasoning led us to attempt the conversion of **12** and **13** into the spiro-annulation products **14** and **15**, respectively, via thermolysis of derivatives of **12** and **13** in which the carbonyl groups were masked. The results of this study are described in the next section of this paper.

(b) *Preparation and thermal rearrangement of the enol silyl ethers 24 and 25 (see Chart 2)*

Treatment of the β-cyclopropyl enone **12** with lithium diisopropylamide in dimethoxyethane, followed by trapping of the resultant enolate anion with trimethylsilyl chloride, provided in 91% yield the enol silyl ether **24**. In identical fashion, (*E*)-2-(cyclopropylmethylene)cyclopentanone (**13**) was transformed into the enol silyl ether **25** (90% yield).

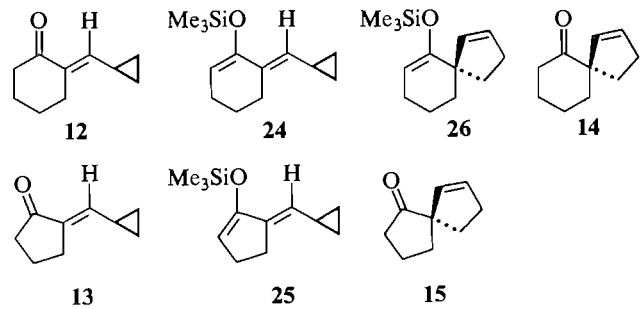

CHART 2

Rearrangement of compounds **24** and **25** was carried out via a procedure similar to that employed for the parent enones **12** and **13**, with the main differences being that the glass thermolysis tube was longer (100 cm instead of 32 cm) and the thermolysis temperature was slightly lower (~425°C instead of ~450°C).[7] In each case, the product mixture was much "cleaner" than that acquired from direct rearrangement of the corresponding β-cyclopropyl enone **12** or **13**. Thus, gas–liquid chromatographic analysis of the distilled product obtained in 85% yield from thermolysis of **24** showed that it consisted very largely (~84%) of one component, along with a number of minor unidentified materials. A small sample of the major product, collected by preparative glc, provided spectral data in accord with that expected from the spiro compound **26**. In practice, it was more convenient to subject the crude thermolysate to hydrolysis (hydrochloric acid, methanol) and purify the resultant material by column chromatography on silica gel. By means of this procedure, pure spiro[4.5]dec-1-en-6-one (**14**) could be obtained from **24** in overall yields of 50–60%.[8]

Although the distilled product obtained by sequential thermolysis and hydrolysis of the enol ether **25** consisted largely of

[5]The 5-proton multiplet at δ 2.18–2.60 presumably includes the allylic protons at C-3, the methylene protons at C-7, and one of the methylene protons at C-4. In the most stable conformation of **14** (cf. **14***a*), the C-4 proton which is *cis* to the carbonyl carbon (H_x in **14***a*) is in an orientation in which it would be expected to experience notable deshielding from the carbonyl group.

[6]It should be noted that the olefinic protons of the symmetrical, isomeric spiro[4.5]dec-2-en-6-one (**19**), kindly supplied by Dr. R. D. Sands (see ref. 12), gave rise to a singlet at δ 5.50.

[7]When the enone **13** was rearranged under these somewhat modified conditions, the results were very similar to those described previously.

[8]The fact that these yields were not higher was probably due at least in part to mechanical losses related to the volatile nature of the products.

Can. J. Chem. Downloaded from www.nrcresearchpress.com by 210.87.254.42 on 09/06/12
For personal use only.

one component, the yield (56%) was not particularly high.[8] Purification of this material by column chromatography on silica gel allowed for the isolation of pure spiro[4.4]non-6-en-1-one (**15**) in an overall yield of 40%.[8]

The results summarized above indicate that 2-(cyclopropylmethylene)cycloalkanones can indeed serve as convenient starting materials for a new spiro-annulation sequence, based on thermal vinylcyclopropane → cyclopentene rearrangement of derived enol silyl ethers. The next section of this paper describes an application of this method to the formal total synthesis of some spirovetivane-type sesquiterpenoids.

(c) *Formal total synthesis of some spirovetivane-type sesquiterpenoids*

The spirovetivane-type sesquiterpenoids possess the substituted spiro[4.5]decane carbon skeleton **27** (see Chart 3).[9] Members of this family of terpenoids have been isolated from a variety of sources and some of them have been shown to possess interesting biological activity. The latter fact, along with the structural novelty associated with the spirovetivanes, has led to a great deal of activity related to the synthesis of a number of these natural products. Indeed, since the important pioneering work in this area by Marshall *et al.* (16), a fairly large number of reports have appeared in the literature (17–34).[10]

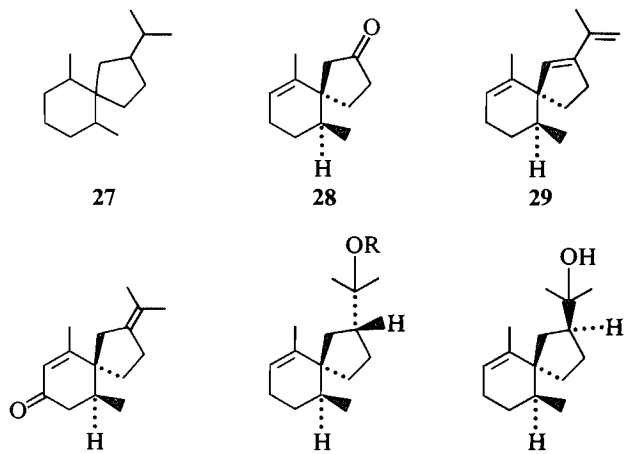

CHART 3

Of the impressive number of elegant synthetic routes which have been employed to prepare various members of the spirovetivane family of sesquiterpenoids, those described by Caine *et al.* (19), Buchi *et al.* (27), and Inubushi and co-workers (31)[11] have involved the use of the spiro enone **28** as a key synthetic intermediate. Thus far, the latter substance has been converted into (±)-α-vetispirene (**29**) (19), (±)-β-vetivone (**30**) (27, 31), (±)-hinesol (**31**) (31), (±)-hinesol acetate (**32**) (27), and (±)-agarospirol (**33**) (31).

Taking into account the work outlined in the previous section of this discussion, it seemed reasonable to propose that the new spiro-annulation method might serve as a convenient vehicle for a synthesis of the spiro enone **28** quite different from those reported previously (19, 27). More explicitly, our plan called for the synthesis and thermal rearrangement of the enol silyl ethers **34** and/or **35** (see eq. [4]). On the basis of steric considerations, it seemed likely that the secondary methyl group on the six-membered ring of **34** and/or **35** would, during the thermal rearrangement, direct bond formation at the adjacent center in the required stereochemical sense. Thus, one might expect the stereoselective formation of the desired spiro diene **36**. Conversion of the latter substance into the target molecule **28** would appear to be straightforward.

[4]

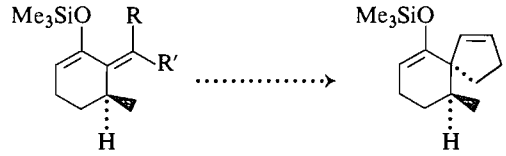

34 R = H, R′ = *c*-C_3H_5
35 R = *c*-C_3H_5, R′ = H
36

Cuprous iodide-catalyzed addition of methyl magnesium iodide to 2-cyclohexene-1-one (**37**) in ether at 0°C, followed by trapping (35) of the resultant enolate anion with cyclopropanecarboxaldehyde (36) afforded, after appropriate work-up, the ketol **38** which appeared to be a mixture of two diastereomers (97% yield)[12] (see Scheme 1). It should be noted that, when the aldehyde was added to the solution of enolate anion, a precipitate formed immediately. Presumably this material consisted of the magnesium alkoxides of the aldol products and the high regioselectivity and efficiency of this reaction can thus be attributed at least partially to the insolubility of these intermediates.

Dehydration of the ketols **38** could be accomplished by treatment of this mixture with a small amount of *p*-toluenesulfonic acid in refluxing benzene. Interestingly, monitoring of the progress of the reaction by thin-layer chromatography (tlc) revealed that one of the diastereomers of **38** dehydrated more rapidly than the other. When the reaction was allowed to proceed until the starting materials had been totally consumed, it was found that the yield of the desired β-cyclopropyl enones **39** and **40** was only 58%. Also isolated was a considerable amount (26%) of 3-methylcyclohexanone, clearly formed as the result of a retro-aldol process. The ^{1}H nmr spectra obtained from small samples of the geometrically isomeric enones **39** and **40** (isolated by preparative glc) clearly corroborated the stereochemical assignments. Thus, the signal due to the alkene proton of the (*E*) isomer **39** appeared, as expected, at lower field (δ 5.98) than the analogous resonance (δ 4.84) of the (*Z*) isomer.

In attempts to improve the efficiency of the conversion of **38** into **39** and/or **40**, it was found that transformation (acetic anhydride, pyridine) of the ketols **38** into the corresponding

[9] For an excellent review, see ref. 15.

[10] For citations related to the structural eludication of the increasing number of spirovetivane-type sesquiterpenoids, see refs. 15–34, inclusive.

[11] The work of Inubushi and co-workers (31) was published after the appearance of our preliminary report (10).

[12] Attempted trapping (cyclopropanecarboxaldehyde) of the enolate anion derived from the addition of lithium dimethylcuprate to **37** failed to provide the regioisomerically correct product(s). The cyclopropane-containing products in this case were the two geometric isomers of 2-(cyclopropylmethylene)-5-methylcyclohexanone, both of which were different from the desired products **39** and/or **40**. A number of alternative potential methods for conversion of 2-cyclohexene-1-one (**37**) into the β-cyclopropyl enones **39** and/or **40** were investigated, but all proved to be unsatisfactory. For details of these attempts, see ref. 37.

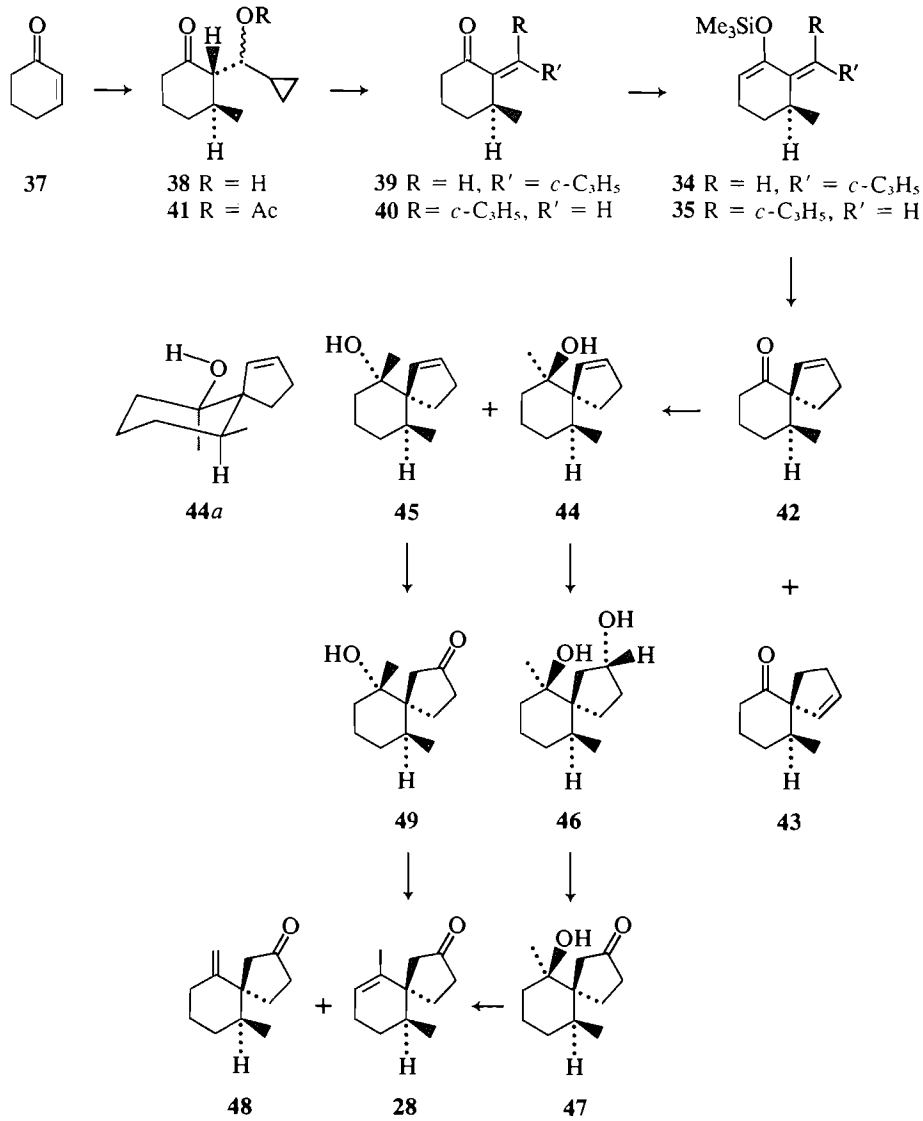

SCHEME 1

acetates **41**, followed by treatment of the latter substances with 1,5-diazabicyclo[4.3.0]non-5-ene in refluxing benzene, afforded, in 78% yield, a mixture of the desired enones **39** and **40**, in a ratio of ~13:1, respectively.

The mixture of enones **39** and **40** was converted (lithium diisopropylamide, dimethoxyethane; trimethylsilyl chloride) into a mixture of the corresponding enol silyl ethers **34** and **35**. Thermolysis of the latter material at 380°C, followed by acid hydrolysis of the resulting crude product afforded, in 57% yield, a mixture of the two spiro enones **42** and **43**, in a ratio of ~2.5:1, respectively. Thus, although the major product **42** (mp 35–38°C) of this key step did possess the desired stereochemistry (*vide infra*), the stereoselectivity of the rearrangement process was not particularly high.[13] Nevertheless, the two diastereomeric products could be separated quite readily by column chromatography on silica gel, and, therefore, the overall sequence of reactions involving the conversion of **37** into **42** + **43** provides a convenient route for the acquisition of appreciable quantities of the desired substance **42**.

Treatment of the spiro enone **42** with methyllithium in ether at 0°C gave a mixture of epimeric alcohols **44** and **45** (ratio ~4:1, respectively), which could be separated by column chromatography on silica gel. The major isomer **44** was found to be identical with a sample of the same alcohol prepared earlier by Buchi *et al.* (27).[14] Hydroboration of compound **44** with disiamylborane in THF, followed by oxidation of the resultant trialkylborane with alkaline hydrogen peroxide, provided a single crystalline diol **46** in 77% yield. The stereochemistry of this substance, although not of crucial importance to the overall synthetic scheme, was assigned on the basis of steric considerations. In the most stable conformation of **44** (cf. **44***a*), the double bond is "protected" on one side by the rather small hydroxyl function and on the other side by the more bulky methyl group. Therefore, if the hydroboration process takes place by way of conformation **44***a*, the reagent should

[13] Although different samples of **34** + **35**, containing varying relative amounts of the two geometric isomers, were subjected to thermolysis, the ratio of products was essentially invariant. Thus, in this rearrangement, there does not appear to be a relationship between the stereochemistry of the reactants (**34**, **35**) and that of the products (**42**, **43**).

[14] We are very grateful to Professor G. Buchi for small samples of the alcohol **44** and the enone **28**, and to Professor D. S. Caine for copies of ir and ^{1}H nmr spectra of compounds **28** and **49**.

Can. J. Chem. Downloaded from www.nrcresearchpress.com by 210.87.254.42 on 09/06/12
For personal use only.

Can. J. Chem. Downloaded from www.nrcresearchpress.com by 210.87.254.42 on 09/06/12
For personal use only.

approach the double bond from the less hindered side to produce, predominantly, the spiro diol **46**.

Oxidation of the diol **46** with pyridinium chlorochromate in methylene chloride afforded the crystalline keto alcohol **47** (27) in 88% yield. Dehydration of this material by treatment with *p*-toluenesulfonic acid in refluxing benzene provided, in 90% yield, a mixture of the two spiro enones **28** and **48**, in a ratio of ~9:1, respectively. A pure sample of the major product **28**, obtained by means of preparative tlc, was shown to be spectrally identical with the same substance prepared earlier by Caine *et al.* (19)[14] and by Buchi *et al.* (27).[14] As mentioned previously, compound **28** has been converted into (±)-α-vetispirene (**29**) (19), (±)-β-vetivone (**30**) (27, 31), (±)-hinesol (**31**) (31) (±)-hinesol acetate (**32**) (27), and (±)-agarospirol (**33**) (31) and, therefore, our preparation of this intermediate constitutes a new formal total synthesis of these natural products.

The olefinic alcohol **45** can also serve as a precursor for the spiro enone **28**. Thus, subjection of **45** to hydroboration–oxidation gave a crude diol which, upon treatment with pyridinium chlorochromate in methylene chloride, provided the keto alcohol **49** (19).[14] The latter substance had previously been converted into the spiro enone **28** (19).

Experimental

General

Melting points and distillation temperatures are uncorrected. Ultraviolet (uv) spectra were recorded on a Cary 15 spectrophotometer, while infrared (ir) spectra were taken on Perkin–Elmer models 710 or 710 B spectrophotometers. Proton magnetic resonance (^{1}H nmr) spectra (deuterochloroform solution) were measured using Varian Associates spectrometers, models T-60 and/or HA-100 or XL-100. Tetramethylsilane was employed as the internal standard. High resolution mass spectrometric measurements were recorded on a Kratos MS-50 mass spectrometer. Gas–liquid chromatography (glc) was carried out with a Hewlett–Packard model 5832 A gas chromatograph (analytical) or with a Varian Aerograph model 90-P instrument (preparative). Microanalyses were performed by Mr. P. Borda, Microanalytical Laboratory, University of British Columbia, Vancouver, B.C.

(E)-2-(Cyclopropylmethylene)cyclohexanone (12)

A stirred slurry of phenylthiocopper (38) (779 mg, 4.5 mmol) in dry THF (30 mL), under an atmosphere of argon, was cooled to −78°C and a solution of freshly prepared cyclopropyllithium (39, 40) (4.5 mmol) in ether was added. The mixture was warmed to −20°C and stirred at this temperature for 20 min. The resulting light brown solution of lithium (phenylthio)(cyclopropyl)cuprate was cooled to −78°C and a solution of (*E*)-2-(iodomethylene)cyclohexanone (**10**) (3) (708 mg, 3.0 mmol) in 6 mL of dry THF was added. The reaction mixture was allowed to warm to 0°C and was stirred at this temperature for 2.5 h. After addition of methanol (2 mL) and ether (20 mL), the mixture was warmed to room temperature and then was filtered through a short column of Florisil (30 g, 80–100 mesh). The column was eluted with an additional 300 mL of ether. Removal of the solvent from the combined eluate, followed by distillation (air-bath temperature ~80°C/0.2 Torr) of the residual oil, gave 369 mg(82%) of a colorless oil which, on the basis of analysis by glc, consisted very largely (>96%) of one component. An analytical sample of the β-cyclopropyl enone **12**, obtained by preparative glc, exhibited mp ~15°C; uv (methanol) λ_{max}: 265 nm (ε 11 750); ir (film): 1680, 1600 cm^{-1}; ^{1}H nmr δ: 0.49–1.10 (m, 4H), 1.18–2.03 (m, 5H), 2.26–2.50 (m, 2H), 2.50–2.76 (m, 2H), 6.04 (d of t, 1H, J = 11, 2 Hz). *Anal.* calcd. for $C_{10}H_{14}O$: C 79.96, H 9.39; found: C 79.69, H 9.35.

(E)-2-(Cyclopropylmethylene)cyclopentanone (13)

This compound was prepared via a procedure identical with that described above, except that the reaction was carried out at −78°C for 1 h and then at −20°C for an additional 2.5 h. From 666 mg (3 mmol) of (*E*)-2-(iodomethylene)cyclopentanone (**11**) (3) there was obtained a crude product which, upon distillation (air-bath temperature ~90°C/0.35 Torr) afforded 265 mg (65%) of a colorless oil which was shown by gas–liquid chromatographic analysis to consist very largely (~95%) of one component. An analytical sample of compound **13**, obtained by preparative glc, exhibited mp ~18°C; uv (methanol) λ_{max}: 267 nm (ε 14 800); ir (film): 1706, 1640 cm^{-1}; ^{1}H nmr δ: 0.54–1.10 (m, 4H), 1.16–1.70 (m, 1H), 1.76–2.14 (m, 2H), 2.18–2.42 (m, 2H), 2.58–2.82 (m, 2H), 5.95 (d of t, 1H, J = 11, 2.5 Hz). *Exact Mass* calcd. for $C_9H_{12}O$: 136.0887; found: 136.0902.

Preparation of the enol silyl ether 24

To a stirred, cold (0°C) solution of lithium diisopropylamide (4.0 mmol) in dry dimethoxyethane (4 mL) was added 450 mg (3.0 mmol) of (*E*)-2-(cyclopropylmethylene)cyclohexanone (**12**). Meanwhile, a mixture prepared by addition of 0.2 mL (~2 mmol) of triethylamine and 0.6 mL (5.1 mmol) of trimethylsilyl chloride to 2 mL of dry dimethoxyethane was centrifuged to remove any insoluble triethylamine hydrochloride. By means of a dry syringe, the resultant solution was added rapidly to the cold (0°C) solution containing the enolate anion of **12**. The resulting mixture (containing a precipitated white solid) was stirred at 0°C for 15 min, and then was treated with saturated aqueous sodium bicarbonate (10 mL) and pentane (30 mL). The aqueous layer was extracted with three 30-mL portions of pentane and the combined organic extract was dried over anhydrous magnesium sulfate. Removal of the solvent, followed by distillation (air-bath temperature ~125°C/16 Torr) of the crude oil, gave 606 mg (91%) of the enol silyl ether **24**; ir (film): 1620 cm^{-1}; ^{1}H nmr δ: 0.13 (s, 9H), 0.26–0.48 (m, 2H), 0.56–1.05 (m, 2H), 1.36–1.80 (m, 4H), 2.04–2.28 (m, 2H), 2.36–2.60 (m, 1H), 4.96 (t, 1H, J = 4.5 Hz), 5.08 (d, 1H, J = 9.5 Hz). *Exact Mass* calcd. for $C_{13}H_{22}OSi$: 222.1439; found: 222.1438.

Preparation of the enol silyl ether 25

This compound was prepared from (*E*)-2-(cyclopropylmethylene)-cyclopentanone (**13**) via a procedure identical with that decribed for the conversion of **12** into **14** (see above). From 408 mg (3 mmol) of **13** there was obtained, after distillation (air-bath temperature ~90–100°C/14 Torr) of the crude product, 562 mg (90%) of the enol silyl ether **25**; ir (film): 1615 cm^{-1}; ^{1}H nmr δ: 9.86 (s, 9H), 2.2–2.8 (m, 4H), 4.7–5.1 (m, 2H). Due to the instability of this material, it was subjected to thermolysis without further characterization.

Thermal rearrangement of (E)-2-(cyclopropylmethylene)-cyclohexanone (12)

A vertically held Pyrex tube (1.2 × 32 cm), filled with glass helices and placed inside a vertical, tubular furnace, was washed successively with saturated aqueous sodium bicarbonate, water, acetone, and *n*-hexane. The tube was heated to ~450°C and kept at this temperature for ~3 h. During this time, the tube was thoroughly purged with a stream of nitrogen. A solution of (*E*)-2-(cyclopropylmethylene)cyclohexanone (**12**) (200 mg) in *n*-hexane (20 mL) was added dropwise to the top of the heated tube. During this time, a slow flow of nitrogen (~3–5 mL/min) was passed through the tube. The thermolysate was passed through a water condensor and collected in a cold (−78°C) two-necked flask equipped with a drying tube. After the solution of **12** had been added, the hot tube was treated slowly with an additional 30 mL of *n*-hexane. Removal of the solvent from the combined thermolysate, followed by distillation (air-bath temperature ~110°C/16 Torr) of the residual oil, gave 148 mg (74%) of a colorless oil. Gas–liquid chromatographic analysis of this material showed that it contained, in addition to a number of minor unidentified components, spiro[4.5]dec-1-en-6-one (**14**) (~44%), tetralin (**17**) (~38%), and the dienones **18** (~9%). A small sample of each of these substances was obtained by preparative glc.

Tetralin (**17**) was identified by comparison (ir, ^{1}H nmr) with a sample of commercially available material.

Dienones **18**: ir (film): 1678, 1610 cm^{-1}. The fact that this material

consisted of a mixture of geometric isomers was shown by the ^{1}H nmr spectrum, which exhibited two triplets (δ 0.98, 1.01, J = 7 Hz in each case) due to terminal methyl groups and a series of multiplets between δ 5.46 and 7.04 due to the olefinic protons. Hydrogenation (10% Pd–C, methanol, room temperature, atmospheric pressure) of this material gave 2-*n*-butylcyclohexanone.

Spiro[4.5]dec-1-en-6-one (**14**): ir (film): 1710 cm^{-1}; ^{1}H nmr δ: 1.40–2.03 (m, 7H), 2.18–2.60 (m, 5H), 5.76 (s, 2H, $w_{1/2}$ = 2 Hz); ^{1}H nmr after addition of 20 mg of the shift reagent Eu(FOD)$_3$, δ: 1.82–2.38 (m, 7H), 2.50–2.86 (m, 2H), 3.16–3.56 (m, 3H), 6.06 (d of t, 1H, J = 6, 2 Hz), 6.42 (d of t, 1H, J = 6, 2 Hz). In a decoupling experiment, irradiation at δ ~2.70 caused the two signals due to the olefinic protons (δ 6.06, 6.42) to collapse to an AB pair of doublets with J = 6 Hz; ^{13}C nmr (proton decoupled) δ: 23.0, 27.7, 31.3, 32.3, 39.9 (2 carbons), 64.1, 132.5, 133.4, 211.5. *Exact Mass* calcd. for $C_{10}H_{14}O$: 150.1044; found: 150.1027.

Hydrogenation (10% Pd–C, methanol, room temperature, atmospheric pressure) of compound **14** gave spiro[4.5]decan-6-one (**20**), which was shown by ir and ^{1}H nmr spectra to be identical with an authentic sample of **20** prepared by the method of Naro and Dixon (13).

*Thermal rearrangement of (*E*)-2-(cyclopropylmethylene)cyclo-pentanone (13)*

Thermolysis of compound **13** was carried out under conditions very similar to those described above. From 400 mg of **13** (added to the heated tube as a solution in 20 mL of *n*-hexane) there was obtained, upon distillation (air-bath temperature ~110°C/12 Torr) of the crude product, 360 mg (90%) of a pale yellow oil. Gas–liquid chromatographic analysis of this material showed the presence of a number of components. Small samples of the major products were collected by preparative glc.

Indan (**21**), ~11% of the mixture, was identified by comparison with a sample of commercially available material.

Dienones **22** constituted ~44% of the mixture. The ^{1}H nmr spectrum of this material clearly showed the presence of two geometric isomers, in a ratio of ~2:1 (*E* isomer predominant). At high field, the terminal methyl groups gave rise to two triplets (δ 1.01, 1.03, J = 6.5 Hz in each case), while the low-field region of the spectrum (δ 5.60–7.54) exhibited a series of signals due to the olefinic protons. *Exact Mass* calcd. for $C_9H_{12}O$: 136.0887; found: 136.0891.

Hydrogenation (10% Pd–C, methanol, room temperature, atmospheric pressure) of the dienones **22** produced 2-*n*-butylcyclopentanone.

Spiro[4.4]non-6-en-1-one (**15**), ~29% of the mixture, exhibited ir (film): 1740 cm^{-1}; ^{1}H nmr δ: ~1.3–2.7 (diffuse m, 10H), 5.30–5.53 (m, 1H), 5.73–5.97 (m 1H). *Exact Mass* calcd. for $C_9H_{12}O$: 136.0887; found: 136.0901.

Hydrogenation (10% Pd–C, methanol, room temperature, atmospheric pressure) of compound **15** gave spiro[4.4]nonan-1-one (**23**), the 2,4-dinitrophenylhydrazone derivative of which exhibited mp 153–155°C (lit. (14) mp 155–157°C).

Thermal rearrangement of the enol silyl ether 24

(a) *With isolation of the spiro enol ether 26*

Thermolysis of compound **24** was carried out under conditions similar to those described above, except that the thermolysis tube was longer (100 cm), the tube was heated by means of a heating tape rather than a tubular furnace, the "carrier gas" was argon instead of nitrogen, and the thermolysis temperature was ~425°C rather than ~450°C. From 200 mg of the enol silyl ether **24**, added to the heated tube as a solution in 20 mL of *n*-hexane, there was obtained, upon distillation (air-bath temperature ~105°C/56 Torr) of the crude thermolysate, 170 mg (85%) of a colorless oil. Analysis of this liquid by glc showed that it consisted very largely (~84%) of one component, along with a number of minor, unidentified compounds. A small sample of the major product **26**, obtained by preparative glc, exhibited ir (film): 1655 cm^{-1}; ^{1}H nmr δ: 0.09 (s, 9H), 1.46–1.68 (m, 6H), 1.90–2.12 (m, 2H), 2.14–2.44 (m, 2H), 4.75 (t, 1H, J = 4 Hz), 5.44–5.56 (m, 1H), 5.66–5.79 (m, 1H). *Exact mass* calcd. for $C_{13}H_{22}OSi$: 222.1440; found: 222.1443.

(b) *Followed by direct hydrolysis of the crude thermolysis product*

The crude thermolysis product obtained from 1.0 g of the enol silyl ether **24** (added to the heated tube as a solution in 100 mL of *n*-hexane) was dissolved in a mixture of methanol (2.5 mL) and 1 *N* hydrochloric acid (2.5 mL) and the resulting solution was stirred at room temperature for 30 min. The mixture was diluted with water and thoroughly extracted with pentane. The combined extract was dried over anhydrous magnesium sulfate. Removal of the solvent gave an oil which was subjected to column chromatography on silica gel (50 g, 70–270 mesh). Elution of the column with pentane, followed by distillation (air-bath temperature ~100°C/14 Torr) of the oil derived from the appropriate fractions gave 340 mg (50%) of pure spiro[4.5]dec-1-en-6-one (**14**), the spectra of which were identical with those recorded previously.

Thermal rearrangement of the enol silyl ether 25

Thermolysis of compound **25** was carried out under conditions identical with those described above for the rearrangement of **24**. The crude thermolysate obtained from 200 mg of **25** (added to the heated tube as a solution in 20 mL of *n*-hexane) was subjected to acid hydrolysis as described under (b), above. Distillation (air-bath temperature ~90°C/16 Torr) of the crude hydrolysis product gave 87 mg of colorless oil which was subjected to column chromatography on silica gel (10 g, 70–270 mesh). Elution of the column with 9:1 *n*-hexane–ether, followed by distillation of the oil obtained from the appropriate fractions, gave 52 mg (40%) of pure spiro-[4.4]non-6-en-1-one (**15**), which was spectrally identical with the material isolated previously (*vide supra*).

Preparation of the keto alcohols 38

To a cold (0°C) stirred solution of methyl magnesium iodide (18 mmol) in 25 mL of dry ether was added 60 mg (0.3 mmol) of cuprous iodide and the resulting mixture was stirred at 0°C for 5 min. After addition of 2-cyclohexen-1-one (**37**) (1.44 g, 15 mmol), the reaction mixture was stirred at 0°C for 30 min, and then was cooled to −78°C. Cyclopropanecarboxaldehyde (1.05 g, 15 mmol) was added dropwise, whereupon a gummy precipitate formed. The mixture was stirred at −78°C for an additional 10 min, at 0°C for 30 min, and at room temperature for 30 min. After addition of saturated aqueous ammonium chloride (30 mL), the mixture was stirred for 5 min, the layers were separated, and the aqueous solution was washed with four 30-mL portions of ether. The combined extract was washed twice with brine and dried over anhydrous magnesium sulfate. Removal of the solvent gave 2.65 g (97%) of the keto alcohols **38** which, on the basis of analysis by tlc, consisted of two diastereomers. This material exhibited ir (film): 3470, 1700 cm^{-1} and, upon attempted distillation, underwent partial decomposition (dehydration, retro-aldol reaction). Therefore, further purification and characterization was not carried out.

Preparation of the β-cyclopropyl enones 39 and 40

(a) *By direct dehydration of the ketol alcohols 38*

A solution of the crude ketols **38** (2.65, 14.6 mmol) in benzene (60 mL) containing 33 mg of *p*-toluenesulfonic acid was refluxed under a Dean–Stark water separator. The progress of the dehydration reaction was monitored by thin-layer chromatographic analysis of aliquots taken from the reaction mixture. It was found that one of the diastereomers of **38** had reacted completely within 3 h, while the other was completely transformed into product(s) only after a period of ~18 h. The cooled benzene solution was washed with saturated aqueous sodium bicarbonate and dried over anhydrous magnesium sulfate. Removal of the solvent, followed by distillation of the residual oil, gave two distinct fractions. The first (air-bath temperature up to ~50°C/0.3 Torr, 426 mg, 26%) was shown by ir and ^{1}H nmr spectra to be 3-methylcyclohexanone, while gas–liquid chromatographic analysis of the second fraction (air-bath temperature ~80°C/0.3 Torr, 1.40 g, 58%) showed that it consisted of two components in ratio of

Can. J. Chem. Downloaded from www.nrcresearchpress.com by 210.87.254.42 on 09/06/12
For personal use only.

Can. J. Chem. Downloaded from www.nrcresearchpress.com by 210.87.254.42 on 09/06/12
For personal use only.

~6:1. A small sample of each of these materials was collected by preparative glc. The major and minor components were shown to be the β-cyclopropyl enones **39** and **40**, respectively.

Enone **39**: uv (methanol) λ_{max}: 265 nm (ε 11 400); ir (film): 1680, 1600 cm^{-1}; ^1H nmr δ: 0.50–2.52 (diffuse m, 11H), 1.04 (d, 3H, J = 7 Hz), 3.02–3.42 (m, 1H), 5.98 (d of d, 1H, J = 11, 1 Hz). *Exact Mass* calcd. for $C_{11}H_{16}O$: 164.1201; found: 164.1205.

Enone **40**: uv (methanol) λ_{max}:263 nm (ε 11 700); ir (film): 1685, 1610 cm^{-1}; ^1H nmr δ: 0.20–2.70 (diffuse m, 12H), 1.04 (d, 3H, J = 7 Hz), 4.84 (d of d, 1H, J = 10.5, 2 Hz). *Exact Mass* calcd. for $C_{11}H_{16}O$: 164.1201; found: 164.1206.

(b) *By elimination of acetic acid from the keto acetates* ***41***

A solution of the crude ketols **38** (1.1 g, 6 mmol) in a mixture of pyridine (20 mL) and acetic anhydride (6 mL) was stirred at room temperature under an atmosphere of argon for 17 h. Ether (200 mL) and water (30 mL) were added and the mixture was stirred for 5 min. The ether layer was separated and washed successively with three 20-mL portions of 1 *N* hydrochloric acid, 20 mL of brine, two 30-mL portions of saturated sodium bicarbonate and 20 mL of brine, and then was dried over anhydrous sodium sulfate. Removal of the solvent (water aspirator, followed by vacuum pump) afforded 1.3 g (98%) of the keto acetates **41**, the ^1H nmr spectrum of which exhibited two signals (δ 2.02, 2.04) due to acetate methyl groups.

To a solution of the crude acetates **41** in 95 mL of dry benzene was added 1.1 g (0.9 mmol) of 1,5-diazabicyclo[4.3.0]non-5-ene and the resulting mixture was refluxed under an atmosphere of argon for 17 h. Ether (250 mL) was added to the cooled reaction mixture, the solution was washed successively with ice-cold 1 *N* hydrochloric acid (30 mL) and brine (20 mL) and then was dried over anhydrous magnesium sulfate. Removal of the solvent, followed by distillation (air-bath temperature 75–90°C/0.4 Torr) of the residual oil, provided 770 mg (78% from the ketols **38**) of a colorless oil. Analysis of this material showed that it was a mixture of the two β-cyclopropyl enones **39** and **40** (ratio ~13:1, respectively) along with a number of very minor impurities. Small samples of the two major products, collected by preparative glc, produced spectra identical with those obtained previously.

Preparation of the enol silyl ethers ***34*** *and* ***35***

Conversion of the mixture of enones **39** and **40** into the corresponding enol silyl ethers **34** and **35**, respectively, was carried out via a procedure identical with that described for the transformation of the enone **12** into the enol silyl ether **24** (*vide supra*). From 492 mg (3 mmol) of **39** + **40** (ratio ~6:1) there was obtained 670 mg (95%) of a mixture of the enol ethers **34** and **35**, which exhibited ir (film): 1650, 1625 cm^{-1}; ^1H nmr δ: 1.03 (d, 3H, J = 7 Hz), 2.88–3.24 (m, 1H), 4.89 (t, 1H, J = 3 Hz), 5.02 (d, 1H, J = 10 Hz). This material was quite unstable and therefore was used immediately for the next step.

Thermolysis of the enol silyl ethers ***34*** *and* ***35***. *Preparation of the spiro enones* ***42*** *and* ***43***

The thermal rearrangement of the mixture of enol silyl ethers **34** and **35** was carried out under conditions described previously for the conversion of **24** into **26**, except that the thermolysis tube was heated at ~380°C instead of at ~425°C. The crude thermolysate obtained from 8.44 g of **34** + **35** (added to the hot tube as a solution in 200 mL of *n*-hexane) was subjected to acid hydrolysis (20 mL 1 *N* hydrchloric acid, 20 mL methanol, room temperature, 30 min) as described previously. Distillation (air-bath temperature 70–80°C/0.4 Torr) of the crude hydrolysis product gave 4.8 g of an oil which, on the basis of analysis by glc, consisted of a mixture of the spiro enones **42** and **43** (ratio ~2.5:1) along with a number of minor unidentified components (~15% of the mixture). This material was subjected to column chromatography on silica gel (350 g). Elution of the column with 10% ether in hexane afforded 2.03 g (35%) of the spiro enone **42**, 0.85 g (14%) of the spiro enone **43**, and 0.47 g (8%) of a mixture of **42** and **43**.

Spiro enone **42**: ir (chloroform): 1705 cm^{-1}; ^1H nmr δ: 0.90 (d, 3H, J = 6 Hz), 1.40–2.84 (diffuse m, 11H), 5.62–5.98 (m, 2H). *Exact Mass* calcd. for $C_{11}H_{16}O$: 164.1201; found: 164.1212.

Spiro enone **43**: ir (film): 1705 cm^{-1}; ^1H nmr δ: 0.86 (d, 3H, J = 6 Hz), 1.40–2.20 (diffuse m, 7H), 2.20–2.57 (diffuse m, 4H), 5.60–5.80 (m, 1H), 5.80–5.98 (m, 1H). *Exact Mass* cacld. for $C_{11}H_{16}O$: 164.1201; found: 164.1195.

Reaction of the ketone ***42*** *with methyllithium. Preparation of the epimeric alcohols* ***44*** *and* ***45***

To a cold (0°C) solution of the spiro enone **42** (492 mg, 3 mmol) in dry ether (25 mL) was added dropwise a solution of methyllithium (4.5 mmol) in ether. The mixture was stirred at 0°C for 1 h and at room temperature for 1 h. After addition of brine (20 mL), the layers were separated and the aqueous solution was extracted with ether (3 × 30 mL). The combined extract was washed with brine and dried over anhydrous magnesium sulfate. Removal of the solvent, followed by distillation (air-bath temperature ~75°C/0.4 Torr) of the residual oil gave 513 mg (95%) of a colorless oil. Analysis of this material by glc indicated the presence of two components in a ratio of ~4:1. Separation was achieved by means of column chromatrography on silica gel (50 g). Elution of the column with hexane containing 15% ether provided 286 mg (53%) of the alcohol **44**, 78 mg (14.5%) of a mixture of **44** and **45**, and 62 mg (11.5%) of the alcohol **45**.

Olefinic alcohol **44**: ir (film): 3500 cm^{-1}; ^1H nmr δ: 0.58 (d, 3H, J = 6 Hz), 1.22 (s, 3H), 1.12–1.88 (diffuse m, 9H), 2.00–2.48 (diffuse m, 3H), 5.72 (d of t, 1H, J = 6, 2 Hz), 6.07 (d of t, 1H, J = 6, 2 Hz). *Exact Mass* calcd. for $C_{12}H_{20}O$: 180.1515; found: 180.1556. This compound exhibited spectra identical with those of a sample of the same substance obtained from Professor G. Buchi (see footnote 14).

Olefinic alcohol **45**: ir (film): 3490 cm^{-1}; ^1H nmr δ: 0.75 (d, 3H, J = 6.5 Hz), 1.04 (s, 3H), 1.34–2.46 (diffuse m, 12H), 5.52 (d of t, 1H, J = 6, 2 Hz), 5.81 (d of t, 1H, J = 6, 2 Hz). *Exact Mass* cacld. for $C_{12}H_{20}O$: 180.1515; found: 180.1515.

Hydroboration of the olefinic alcohol ***44***. *Preparation of the diol* ***46***

To a cold (0°C) solution of disiamylborane (10 mmol) in 10 mL of dry tetrahydrofuran was added 180 mg (1 mmol) of the olefinic alcohol **44**. The mixture was stirred at 0°C for 1 h and then at room temperature for 21 h. After the reaction mixture had been cooled to 0°C, it was treated successively with ethanol (1 mL), 3 *N* aqueous sodium hydroxide (7 mL), and 30% aqueous hydrogen peroxide (4 mL). The resulting mixture was heated under reflux for 2 h, cooled, treated with brine (5 mL), and extracted thoroughly with ether. The combined extract was washed with brine and dried over anhydrous magnesium sulfate. Removal of the solvent, followed by recrystallization (ether–hexane) of the resultant yellow solid, gave 153 mg (77%) of the diol **46** as white crystals which exhibited mp 153–155°C; ir (chloroform): 3640, 3480 cm^{-1}; ^1H nmr δ: 0.93 (d, 3H, J = 6 Hz), 1.18 (s, 3H), 1.10–2.16 (diffuse m, 15H), 4.05–4.45 (m, 1H). *Anal.* calcd. for $C_{12}H_{22}O_2$: C 72.68, H 11.18; found: C 72.54, H 11.10.

Oxidation of the diol ***46***. *Preparation of the keto alcohol* ***47***

To a slurry of pyridinium chlorochromate (324 mg, 1.5 mmol) in dry methylene chloride (3 mL) was added a solution of the diol **46** (198 mg, 1 mmol) in 10 mL of dry methylene chloride and the resulting red solution was stirred at room temperature for 1 h. After addition of ether (20 mL), the mixture was filtered through a short column of Florisil (10 g, 80–100 mesh). The column was eluted with a further 50 mL of ether. Removal of the solvent from the combined eluate, followed by distillation (air-bath temperature ~120°C/0.2 Torr) of the residual oil, afforded 176 mg (88%) of a colorless oil which crystallized in a refrigerator. Recrystallization of a small amount of this material from ether–hexane gave an analytical sample of the keto alcohol **47** (27), which exhibited mp 51–52°C; ir (chloroform): 3660, 3500, 1730 cm^{-1}; ^1H nmr δ: 0.82 (d, 3H, J = 6.5 Hz), 1.28 (s, 3H), 1.04–2.48 (diffuse m, 12H), 2.16, 2.64 (AB pair of d, 1H each, J = 19 Hz). *Anal.* calcd. for $C_{12}H_{20}O_2$: C 73.43, H 10.27; found: C 73.53, H 10.17.

Can. J. Chem. Downloaded from www.nrcresearchpress.com by 210.87.254.42 on 09/06/12
For personal use only.

Dehydration of the keto alcohol ***47****. Preparation of the olefinic ketones* ***28*** *and* ***48***

To a solution of the keto alcohol **47** (118 mg, 0.6 mmol) in benzene (20 mL) was added 15 mg of *p*-toluenesulfonic acid and the resulting solution was heated under reflux for 87 h. The solution was cooled, washed successively with saturated aqueous sodium bicarbonate (5 mL) and brine (5 mL), and dried over anhydrous magnesium sulfate. Removal of the solvent, followed by distillation (air-bath temperature 60–65°C/0.4 Torr) of the residual material gave 96 mg (90%) of a colorless oil. This material exhibited two spots by thin-layer chromatographic analysis and, on the basis of the ^{1}H nmr analysis, appeared to consist of a mixture of the olefinic ketones **28** and **48** (ratio ~9:1, respectively). A small sample of the major component **28**, obtained from the mixture by preparative tlc, exhibited ir (film): 1740 cm^{-1}; ^{1}H nmr δ: 0.88 (d, 3H, J = 6.5 Hz), 1.2–2.5 (diffuse m,11H), 1.66 (m, 3H, $w_{1/2} \approx 4$ Hz), 5.44 (m, 1H, $w_{1/2} \approx 8$ Hz). *Exact Mass* calcd. for $C_{12}H_{18}O$: 178.1358; found: 178.1360. Compound **28** exhibited spectra identical with those of the same compound prepared previously by Caine *et al.* (19) and by Buchi *et al.* (27) (see footnote 14).

Conversion the the alcohol ***45*** *into the keto alcohol* ***49***

Hydroboration of the olefinic alcohol **45** (72 mg) under conditions identical with those described above (hydroboration of **44**) provided a crude product which, on the basis of analysis by glc, contained ~30% of the starting material **45**. Distillation (air-bath temperature up to ~80°C/0.4 Torr) removed the latter substance (~15 mg). The residual material was subjected to oxidation with pyridinium chlorochromate in dichloromethane (see above, oxidation of diol **46**). Distillation (air-bath temperature ~120°C/1 Torr) of the crude product afforded 30 mg (48% based on unrecovered **45**) of the keto alcohol **49**, which exhibited ir (film): 3500, 1730 cm^{-1}; ^{1}H nmr δ: 0.84 (d, 3H, J = 6.5 Hz), 1.16 (s, 3H), 1.02–2.48 (diffuse m, 14H). This compound exhibited spectra identical with those obtained from a sample of the same material prepared earlier by Caine *et al.* (19) (see footnote 14). Conversion of **49** into the olefinic ketone **28** has been described by Caine *et al.* (19).

Acknowledgements

Financial support for this work from the Natural Sciences and Engineering Research Council of Canada (N.S.E.R.C.C.) and a N.S.E.R.C.C. postgraduate scholarship (to C.K.L.) are gratefully acknowledged.

1. E. Piers, J. Banville, C. K. Lau, and I. Nagakura. Can. J. Chem. **60**, 2965 (1982).
2. E. Piers, K. F. Cheng, and I. Nagakura. Can. J. Chem. **60**, 1256 (1982).
3. E. Piers, J. R. Grierson, C. K. Lau, and I. Nagakura. Can. J. Chem. **60**, 210 (1982).
4. A. P. Krapcho. Synthesis, 383 (1974); 425 (1976); 77 (1978).
5. M. F. Semmelhack and A. Yamashita. J. Am. Chem. Soc. **102**, 5924 (1980).
6. J. F. Ruppert and J. D. White. J. Am. Chem. Soc. **103**, 1808 (1981); J. D. White, J. F. Ruppert, M. A. Avery. S. Torii, and J. Nokami. J. Am. Chem. Soc. **103**, 1813 (1981).
7. S. D. Burke, C. W. Murtiashaw, M. S. Dike, S. M. Smith Strickland, and J. O. Saunders. J. Org. Chem. **46**, 2400 (1981).
8. J. Ficini, G. Revial, and J. P. Genêt. Tetrahedron Lett. **22**, 629 (1981).
9. E. Piers, C. K. Lau, and I. Nagakura. Tetrahedron Lett. 3233 (1976).
10. E. Piers and C. K. Lau. Synth. Commun. **7**, 495 (1977).
11. L. M. Jackman and S. Sternhell. Applications of nuclear magnetic resonance spectroscopy in organic chemistry. 2nd ed. Pergamon Press, New York, NY. 1969. p. 190.
12. R. D. Sands. J. Org. Chem. **32**, 3682 (1967).
13. P. A. Naro and J. A. Dixon. J. Am. Chem. Soc. **81**, 1681 (1959).
14. D. J. Cram and H. Steinberg. J. Am. Chem. Soc. **76**, 2753 (1954).
15. J. A. Marshall, S. F. Brady, and N. H. Andersen. *In* Progress in the chemistry of organic natural products. Vol. 31. Springer-Verlag, New York, NY. 1974. pp. 283–371.
16. J. A. Marshall, N. H. Andersen, and P. C. Johnson. J. Am. Chem. Soc. **89**, 2748 (1967); J. A. Marshall and P. C. Johnson. J. Am. Chem. Soc. **89**, 2750 (1967); J. A. Marshall, N. H. Andersen, and P. C. Johnson. J. Org. Chem. **34**, 186 (1969).
17. J. A. Marshall and P. C. Johnson. Chem. Commun. 391 (1968); J. Org. Chem. **35**, 192 (1970); J. A. Marshall and S. F. Brady. Tetrahedron Lett. 1387 (1969); J. Org. Chem. **35**, 4068 (1970).
18. M. Mongrain, J. LaFontaine, A. Bélanger, and P. Deslongchamps. Can. J. Chem. **48**, 3273 (1970); J. LaFontaine, M. Mongrain, M. Sergent-Guay, L. Ruest, and P. Deslongchamps. Can. J. Chem. **58**, 2460 (1980).
19. D. Caine and J. B. Dawson. Chem. Commun. 1232 (1970); D. Caine and C. -Y. Chu. Tetrahedron Lett. 703 (1974); D. Caine, A. A. Boncugnani, S. T. Chao, J. B. Dawson, and P. F. Ingwalson. J. Org. Chem. **41**, 1539 (1976); D. Caine, A. A. Boncugnani, and W. R. Pennington. J. Org. Chem. **41**, 3632 (1976).
20. P. M. McCurry, Jr., R. K. Singh, and S. Link. Tetrahedron Lett. 1155 (1973); P. M. McCurry, Jr. and R. K. Singh. Tetrahedron Lett. 3325 (1973).
21. G. Stork, R. L. Danheiser, and B. Ganem. J. Am. Chem. Soc. **95**, 3414 (1973).
22. K. Yamada, H. Nagase, Y. Hayakawa, K. Aoki, and Y. Hirata. Tetrahedron Lett. 4963 (1973); K. Yamada, K. Aoki, H. Nagase, Y. Hayakawa, and Y. Hirata. Tetrahedron Lett. 4967 (1973); K. Yamada, S. Goto, H. Nagase, and A. T. Christensen. J. Chem. Soc. Chem. Commun. 554 (1977).
23. G. Bozzato, J. -P. Bachmann, and M. Pesaro. J. Chem. Soc. Chem. Commun. 1005 (1974).
24. W. G. Dauben and H. Hart. J. Am. Chem. Soc. **97**, 1622 (1975); **99**, 7307 (1977).
25. M. Deighton, C. R. Hughes, and R. Ramage. J. Chem. Soc. Chem. Commun. 662 (1975).
26. D. Buddhasukh and P. D. Magnus. J. Chem. Soc. Chem. Commun. 952 (1975); D. A. Chase, D. Buddhasukh, and P. D. Magnus. J. Org. Chem. **43**, 1750 (1978).
27. G. Buchi, D. Berthet, R. Decorzant, A. Grieder, and A. Hauser. J. Org. Chem. **41**, 3208 (1976).
28. K. Uneyama, K. Okamoto, and S. Torii. Chem. Lett. 493 (1977); S. Torii, K. Uneyama, and K. Okamoto. Bull. Chem. Soc. Jpn. **51**, 3590 (1978).
29. E. Wenkert, B. L. Buckwalter, A. A. Craveiro, E. L. Sanchez, and S. S. Sathe. J. Am. Chem. Soc. **100**, 1267 (1978).
30. K. B. Subrahamanian and W. Reusch. Tetrahedron Lett. 3789 (1978).
31. T. Ibuka, K. Hayashi, H. Minakata, and Y. Inubushi. Tetrahedron Lett. 159 (1979); T. Ibuka, K. Hayashi, H. Minakata, Y. Ito, and Y. Inubushi. Can. J. Chem. **57**, 1579 (1979).
32. A. P. Johnson and V. Vajs. J. Chem. Soc. Chem. Commun. 817 (1979).
33. C. Iwata, T. Fusaka, T. Fujiwara, K. Tomita, and M. Yamada. J. Chem. Soc. Chem. Commun. 463 (1981).
34. A. Murai, S. Sato, and T. Masamune. Tetrahedron Lett. **22**, 1033 (1981).
35. F. Naf and R. Decorzant. Helv. Chim. Acta, **57**, 1317 (1974).
36. L. B. Young and W. S. Trahanovsky. J. Org. Chem. **32**, 2349 (1967).
37. C. K. Lau. Ph.D. Thesis, University of British Columbia, Vancouver, B.C., Canada, 1978.

38. G. H. POSNER, C. E. WHITTEN, and J. J. STERLING. J. Am. Chem. Soc. **95**, 7788 (1973); G. H. POSNER, D. J. BRUNELLE, and L. SINOWAY. Synthesis, 662 (1974).
39. D. SEYFERTH and H. M. COHEN. J. Organomet. Chem. **1**, 15 (1963).
40. H. GILMAN and F. K. CARTLEDGE. J. Organomet. Chem. **2**, 447 (1964).

Can. J. Chem. Downloaded from www.nrcresearchpress.com by 210.87.254.42 on 09/06/12
For personal use only.

Spin trapping of hydroxyl in water: decay kinetics for the ·OH and CO_2^- adducts to 5,5-dimethyl-1-pyrroline-*N*-oxide[1]

ARLINDO L. CASTELHANO, M. JOHN PERKINS,[2] AND DAVID GRILLER
Division of Chemistry, National Research Council of Canada, Ottawa, Ont., Canada K1A 0R6

Received May 14, 1982

ARLINDO L. CASTELHANO, M. JOHN PERKINS, and DAVID GRILLER. Can. J. Chem. **61**, 298 (1983).

A spin-trapping technique for distinguishing between free and "bound hydroxyl" radicals has been proposed in the literature. This technique relied upon observations of the steady-state concentrations of the spin-adducts of ·OH and CO_2^- (from formate) to 5,5-dimethyl-1-pyrroline-*N*-oxide. In the present work, it is shown that the steady-state approach was only qualitatively correct. An alternative procedure is demonstrated which involves monitoring the growth of the spin-adducts after the start of radical generation. The latter approach is found to be quantitative.

ARLINDO L. CASTELHANO, M. JOHN PERKINS et DAVID GRILLER. Can. J. Chem. **61**, 298 (1983).

Une technique de piégeage de spin a été proposée antérieurement pour distinguer les radicaux hydroxyles libres et les radicaux "hydroxyles liés". Cette technique est reliée aux observations des concentrations de l'état stationnaire des adduits de spin de ·OH et de CO_2^- (à partir du formiate) sur le *N*-oxyde de la diméthyl-pyrrolinne-1. Dans ce travail, on montre que l'approche de l'état stationnaire n'est que qualitativement correcte. On propose une méthode alternative qui fait intervenir l'enregistrement de l'augmentation des adduits de spin après le début de la génération du radical. On a trouvé que la dernière approche est quantitative.

[Traduit par le journal]

In a recent publication (1) Lown and Chen used the spin-trap 5,5-dimethyl-1-pyrroline-*N*-oxide (DMPO), (1–12), to distinguish between the reactions of the free hydroxyl radical and those of radicals which behave as hydroxylating reagents. The latter were referred to as "bound hydroxyl". Their scheme is summarized in equations [1–3], where X· represents ·OH or "bound hydroxyl".

[1] $X\cdot + DMPO \xrightarrow{k_1}$ 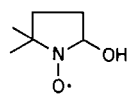

1

[2] $X\cdot + HCO_2^- \xrightarrow{k_2} CO_2^- + XH$

[3] $CO_2^- + DMPO \xrightarrow{k_3}$ 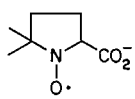

2

In principle, there should be a difference in the ratio k_1/k_2 between those cases where X· is free hydroxyl and those where it is "bound". Accordingly, in their experiments, Lown and Chen adjusted the concentrations of DMPO and HCO_2^- until the concentration of the spin-adducts **1** and **2** were equal (1). This was taken as evidence that the rates of formation of **1** and **2** were equal and hence, (1),

[4] $k_1[X\cdot][DMPO] = k_2[X\cdot][HCO_2^-]$

[5] $k_1/k_2 = [HCO_2^-]/[DMPO]$

Variations in the ratio k_1/k_2 were used to differentiate "bound" and free hydroxyl. However, this analysis could only have been correct if the rates of loss of **1** and **2** from the systems under study were *exactly* equal, since the steady-state radical concentrations observed depended not only upon the rates of formation of **1** and **2** but also upon their rates of destruction.

A suggestion that this kinetic scheme was flawed comes from the fact that $k_1/k_2 = 0.23 \pm 0.12$ for the case where free hydroxyl was generated by photolysis of hydrogen peroxide at pH 7. By contrast, measured values of the individual rate constants give $k_1 = k_2 = 2.7 \times 10^9\ M^{-1}\ s^{-1}$ and hence, $k_1/k_2 = 1.0$ (7, 13).

To resolve these problems, we have studied the decay kinetics of the spin-adducts **1** and **2**. In addition, we have measured k_1/k_2 for "free hydroxyl" using an approach which does not involve assumptions about the decay kinetics of these spin-adducts.

The methods used for sample preparation, measurement of radical concentrations, and kinetic analysis have been described in detail elsewhere (7).

Photolysis of an aqueous solution (pH 7.0; phosphate buffer) of hydrogen peroxide (1% v/v), containing DMPO (~0.1 *M*), in the cavity of an epr spectrometer gave a clean spectrum of radical **1**. Once a concentration of $2 \times 10^{-4}\ M$ had been attained, photolysis was stopped and the decay of the radical was followed with time. The decay followed second order kinetics until a concentration of $\sim 4 \times 10^{-5}\ M$ was reached. The rate constant for the second order decay, $2k_6$ (**1**), was found to be $17 \pm 3\ M^{-1}\ s^{-1}$. The decay process became first order below the concentration of $\sim 4 \times 10^{-5}\ M$ and the rate constant for this decay process, k_7 (**1**), was found to be $(8.4 \pm 1.0) \times 10^{-4}\ s^{-1}$, in exact agreement with the value of $8.4 \times 10^{-4}\ s^{-1}$ reported previously (7).

[6] $\mathbf{R}\cdot + \mathbf{R}\cdot \rightarrow$ products

[7] $\mathbf{R}\cdot \rightarrow$ products
$R \equiv$ **1** or **2**

Radical **2** was generated by photolysis of a solution similar

[1]NRCC no. 20691.

[2]Visiting scientist, 1980; permanent address: Department of Chemistry, Chelsea College, University of London, Manresa Road, London, England SW3 6LX.

0008-4042/83/020298-02$01.00/0
©1983 National Research Council of Canada/Conseil national de recherches du Canada

Can. J. Chem. Downloaded from www.nrcresearchpress.com by 210.87.254.6 on 09/06/12
For personal use only.

to that used to obtain **1** with the exception that it contained sodium formate, reactions [2 and 3]. The decay of **2** was second order in the concentration range $3 \times 10^{-4} \geq [\mathbf{2}] \geq 7 \times 10^{-5}$ *M* and $2k_6$ (**2**) = 12 ± 3 M^{-1} s^{-1}. Below a concentration of 7×10^{-5} *M* the decay became first order with $k_7 = (3.0 \pm 0.5) \times 10^{-4}$ s^{-1}.

These results show that the decay kinetics for radicals **1** and **2** are quite similar. Hence, the approach used by Lown and Chen is unlikely to be seriously in error if the reactions under study were carried out for the same lengths of time and the same absolute radical concentrations were obtained in each experiment. The fact that these conditions are unlikely to be realized probably accounts for the spread of a factor of 5 in the data obtained by Lown and Chen for the ratio k_1/k_2.

A more satisfactory approach to the measurement of rate constants for spin-trapping is to measure the growth of the spin-adducts from the time at which radical generation is started. We have used this approach to obtain an independent measure of the ratio k_1/k_2. The rate constant for attack by hydroxyl at methanol, reaction [8], was used as a standard so that k_1 and k_2 could be determined separately.

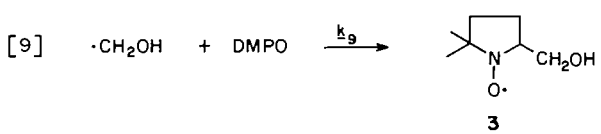

3

To measure the rates of growth of the spin-adducts, the light intensity at the sample was adjusted so that the radical concentrations grew over a convenient timescale for recording the spectra (ca. 3 min). This timescale was substantially shorter than that for the first order decay of the spin-adducts and the radical concentrations were sufficiently low that second order decay was insignificant. Under these conditions eq. [10] applied, subject to the further proviso that both $\cdot CH_2OH$ and $CO_2^{\cdot-}$ were efficiently trapped by DMPO, reactions [3 and 9].

$$[10] \quad \frac{k_2}{k_8} = \frac{d[\mathbf{2}]/dt}{d[\mathbf{3}]/dt} \cdot \frac{[CH_3OH]}{[HCO_2^-]}$$

Photolysis of an aqueous solution at pH 7 containing sodium formate (0.2 *M*), methanol (0.94 *M*), hydrogen peroxide (0.1 *M*), and DMPO (0.08 *M*) gave rise to the growth of spin-adducts **2** and **3**, Fig. 1. The ratio of the initial slopes, i.e. $(d[\mathbf{2}]/dt)/(d[\mathbf{3}]/dt)$, was 1.28 and hence $k_2/k_8 = 6.0$, eq. [10]. Taking $k_8 = 4.8 \times 10^8$ M^{-1} s^{-1} (13) yields $k_2 = 2.9 \times 10^9$ M^{-1} s^{-1}, in good agreement with the literature value of 2.7×10^9 M^{-1} s^{-1}. In a similar experiment k_1/k_8 was found to be 5.4 and hence $k_1 = 2.6 \times 10^9$ M^{-1} s^{-1}, which again is in excellent agreement with the value of 2.7×10^9 M^{-1} s^{-1} previously reported (7). Hence the ratio $k_1/k_2 = 0.90$ obtained in this work is in good agreement with the ratio of 1.0 obtained from literature data (7, 13), and is at variance with the value of 0.23 obtained by Lown and Chen in their steady-state approach.

To summarize, our results indicate that the ratio of rate constants for ·OH trapping by DMPO with respect to that for the reaction of ·OH with HCO_2^-, i.e. k_1/k_2, cannot be accurately determined by the steady-state technique (1). By contrast, an approach in which the growth of spin adducts as monitored directly gave a value for k_1/k_2 which was in excellent agreement with literature data.

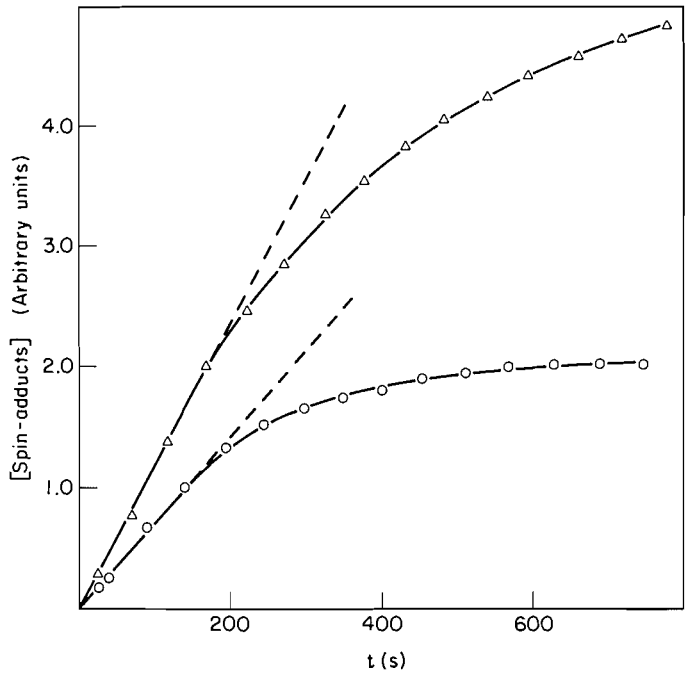

FIG. 1. Plots of the growth in concentration of spin adducts **2** (△) and **3** (○) vs. time after the start of radical generation ($t = 0$).

Acknowledgement

D.G. and M.J.P. wish to thank NATO for the award of a research grant which made this collaboration possible.

1. J. W. LOWN and H.-H. CHEN. Can. J. Chem. **59**, 390 (1981).
2. J. R. HARBOUR, V. CHOW, and J. R. BOLTON. Can. J. Chem. **52**, 3549 (1974); J. R. HARBOUR and J. R. BOLTON. Photochem. Photobiol. **28**, 231 (1978).
3. F. P. SARGENT and E. M. GARDY. Can. J. Chem. **54**, 275 (1976).
4. C.-S. LAI and L. H. PIETTE. Arch. Biochem. Biophys. **190**, 27 (1978).
5. G. R. BUETTNER and L. W. OBERLEY. Biochem. Biophys. Res. Commun. **83**, 69 (1978).
6. T. OZAWA and A. HANAKI. Chem. Pharm. Bull. **26**, 2572 (1978).
7. P. R. MARRIOTT, M. J. PERKINS, and D. GRILLER. Can. J. Chem. **58**, 803 (1980).
8. E. FINKELSTEIN, G. M. ROSEN, and E. J. RAUCKMAN. J. Am. Chem. Soc. **102**, 4994 (1980).
9. R. A. FLOYD and L. M. SOONG. Biochem. Biophys. Res. Commun. **74**, 79 (1977).
10. G. R. BUETTNER and L. W. OBERLEY. Biochem. Biophys. Res. Commun. **83**, 69 (1978).
11. A. T. BULLOCK, D. L. GAVIN, and M. D. INGRAM. J. Chem. Soc. Chem. Commun. 327 (1980).
12. A. L. CASTELHANO, D. GRILLER, and K. U. INGOLD. Can. J. Chem. **60**, 1501 (1982).
13. M. ANBAR and P. NETA. Int. J. Appl. Radiat. Isot. **18**, 493 (1967).

Can. J. Chem. Downloaded from www.nrcresearchpress.com by 210.87.254.6 on 09/06/12
For personal use only.

Photochromism of spiroindolinonaphthoxazine. I. Photophysical properties

NORI Y. C. CHU

Research and Development Laboratories, Vision Care and Safety Products Division, American Optical Corporation, Southbridge, MA 01550, U.S.A.

Received June 15, 1982

NORI Y. C. CHU. Can. J. Chem. **61**, 300 (1983).

A solution of spiroindolinonaphthoxazine in a common organic solvent shows profound photochromic effect. The colorless form in ethanol displays three absorption bands (~320, 235, 203 nm) in the ultraviolet region of the spectrum. The absorption spectrum of the colored metastable form shows two prominent absorption peaks at 612 and 578 nm. The triplet state energy level of the colorless form is estimated to be in the range from 2.4×10^4 to 2.1×10^4 cm^{-1} by the triplet–triplet energy-transfer method. There exists a thermal equilibrium between the colorless and colored forms. From the measurement of absorbance of the colored form at different temperatures, the standard enthalpy of equilibrium is obtained ($\Delta H^0 = 1500$ cm^{-1}). The thermal decay of the colored form to the colorless form depends strongly on temperature. The decay rate increases three times for every 10°C increase in temperature. From these temperature dependence studies of the thermal decay rate, the thermal energy barrier for the colored metastable state to decay to the colorless form is determined to be 6.9×10^3 cm^{-1}.

NORI Y. C. CHU. Can. J. Chem. **61**, 300 (1983).

La spiroindolinonaphthoxazine en solution dans un solvant organique ordinaire montre un effet photochimique marqué. La forme incolore dans l'éthanol présente trois bandes d'absorption (~320, 235, 203 nm) dans l'ultraviolet. Le spectre d'absorption de la forme métastable colorée montre deux pics de forte intensité à 612 et 578 nm. On évalue que le niveau d'énergie de l'état triplet de la forme incolore est de l'ordre de $2{,}4 \times 10^4$ à $2{,}1 \times 10^4$ cm^{-1} selon la méthode de transfert d'énergie triplet–triplet. Il existe un équilibre thermique entre les formes incolore et colorée. A partir des mesures d'absorption de la forme colorée à différentes températures, on obtient l'enthalpie standard d'équilibre ($\Delta H^0 = 1500$ cm^{-1}). La désintégration thermique de la forme colorée en la forme incolore dépend fortement de la température. La vitesse de désintégration augmente par un facteur de 3 pour chaque augmentation de température de 10°C. A partir des études de l'influence de la température sur la vitesse de désintégration thermique, on a déterminé la barrière d'énergie thermique de la désintégration de la forme métastable colorée en la forme incolore. Cette barrière est de $6{,}9 \times 10^3$ cm^{-1}.

[Traduit par le journal]

Can. J. Chem. Downloaded from www.nrcresearchpress.com by 210.87.254.42 on 09/06/12
For personal use only.

Introduction

The photochromism of spiroindolinobenzopyrans, **1**, is well known and has been thoroughly documented in a comprehensive review article by Bertelson (1). This review article integrates scattered information existing in technical reports, patent literature, and scientific journals to give a unified picture of the photochromism of spiroindolinobenzopyrans up to 1969. Since then, further understanding of the detailed mechanism of photocoloration has been greatly advanced by Russian workers (2, 3).

In contrast to spiroindolinobenzopyrans, of which hundreds have been synthesized, there is almost no information existing on a very closely related class of compound — spiro[indoline-2,3′-[3*H*]naphth[2,1-*b*][1,4]oxazine], **2**. The photochromism of this class of compound was first reported by Fox (4). He observed that the toluene solution of the parent compound — 1,3,3-trimethylspiro[indoline-2,3′-[3*H*]naphth[2,1-*b*][1,4]oxazine], **3** — and its 5-chloro derivative becomes blue in color upon irradiation by ultraviolet (uv) light at 10°C. Subsequently, 5-methyl, 5-methoxy, 1-carboxyethyl, and 1-cyanopropyl derivatives were reported to be photochromic in two patents by Ono *et al.* (5, 6).

The present work was undertaken with the aim of elucidation of the spectral properties and the electronic energy levels of **3** both in the colorless and colored form, the kinetics of the thermal decay of the colored form, and the thermodynamic parameters of **3**.

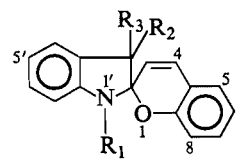

1, $R_1 = R_2 = R_3 = H$
5, $R_1 = R_2 = R_3 = CH_3$

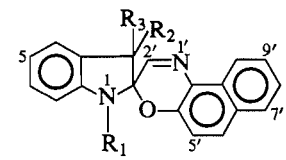

2, $R_1 = R_2 = R_3 = H$
3, $R_1 = R_2 = R_3 = CH_3$

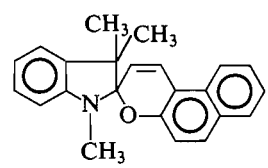

4

Experimental section

Materials

Compound **3** was prepared by reacting 1-nitroso-2-naphthol (18 g; Fisher) in MeOH (200 mL) under reflux with a solution of 1,3,3-trimethyl-2-methyleneindoline (17 g; Eastman) in MeOH (50 mL) which was added over a period of 10 min. After refluxing for 1 h, the reaction mixture was cooled. A brown solid precipitated, which was filtered and washed with plenty of methanol and yielded 15 g of product. The product was purified by repeated charcoal treatment and recrystallization from acetone, mp 124–125°C (lit. 122–124°C) (4);

0008-4042/83/020300-06$01.00/0

©1983 National Research Council of Canada/Conseil national de recherches du Canada

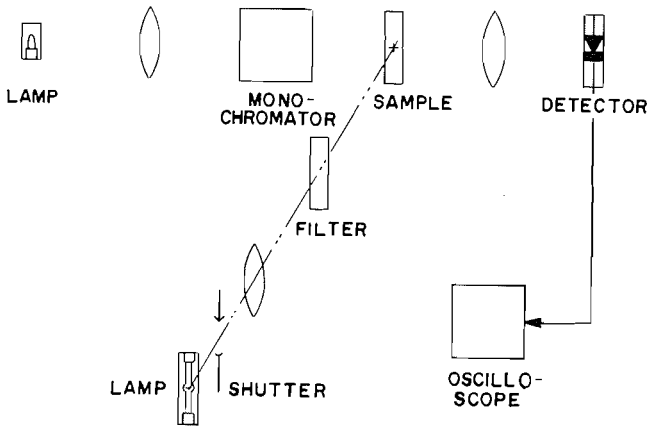

FIG. 1. Schematic diagram of the apparatus used for the kinetics measurements.

ir (KBr): 3054, 2961, 1619, 1605, 1589, 1506, 1484, 1452, 1438, 1421, 1381, 1358, 1297, 1271, 1242, 1073, 1028, 1000, 962, 813, 751, 740 cm^{-1}.

All the solvents used were either reagent or spectroscopy grade and were used without further purification.

The set-up for kinetics measurements

A schematic representation of the basic set-up is illustrated in Fig. 1. The light from the monitoring lamp (a 15 W microscope lamp) passed through a monochromator (Bausch & Lomb, 33-86-02) with the slit set at 610 nm for the maximum absorption of the colored form of **3**. The uv light from a 100 W Hg lamp was selected by using a Corning 7-37 glass filter and was used to activate the photocoloration of the photochromic solution. The variation in the monitoring light intensity due to the absorption by the colored form was detected by a Si photodiode. The output of the photodiode was displayed on an oscilloscope (Tektronix, Type 535A). The temperature of the sample in the water-jacketed cell was regulated by a Haake constant temperature bath unit.

General

The absorption spectra were recorded on a Cary 14 spectrophotometer. For low temperature measurements, either a Dry Ice – CH_2Cl_2 slush or liquid nitrogen was used. The absorption spectrum of the colored form was obtained by first irradiating the sample at low temperature with the uv from a 100 W Hg lamp filtering through a Corning 7-37 glass filter and then recorded the spectrum of the irradiated sample on a Cary 14 spectrophotometer. No error was introduced by this method since the thermal decay rate of the colored form at the Dry Ice – CH_2Cl_2 slush temperature (or lower) was negligible.

The infrared spectrum was recorded on a Perkin-Elmer 180 spectrophotometer and the melting point was determined on a Fisher-Johns melting point apparatus. The emission measurements were made on a Perkin-Elmer spectrophosphorimeter MPF-44B. In the determination of the triplet state energy levels of **3** by the triplet state sensitization, all the samples were degassed by the freeze–pump–thaw method.

Results

Absorption spectrum of the colorless form

A 3.26×10^{-5} *M* solution of **3** in ethanol is colorless and shows three groups of absorption bands in the ultraviolet region which are shown in Fig. 2. The first group in the region from 380 nm to 280 nm has moderate absorption intensity. There are three absorption peaks in this region: 345 nm ($\epsilon = 4.76 \times 10^3\ M^{-1}\ cm^{-1}$), 317 nm ($\epsilon = 6.78 \times 10^3\ M^{-1}\ cm^{-1}$), and 297 nm ($\epsilon = 6.53 \times 10^3\ M^{-1}\ cm^{-1}$). The other two absorption groups in the far ultraviolet reigon are very intense. The molar absorptivity of the absorption peak at 235 nm is $5.43 \times 10^4\ M^{-1}\ cm^{-1}$ and is $4.41 \times 10^4\ M^{-1}\ cm^{-1}$ for the peak at 203 nm.

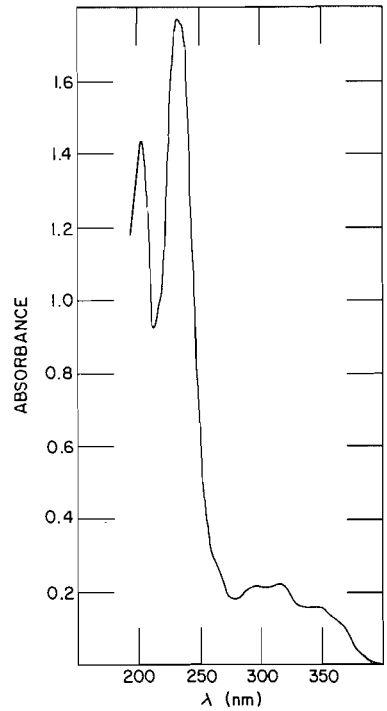

FIG. 2. The absorption spectrum of a 3.26×10^{-5} *M* solution of **3** in ethanol.

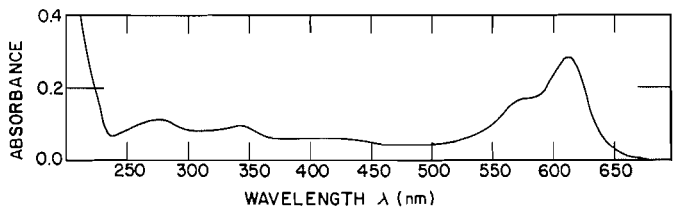

FIG. 3. The absorption spectrum of the colored form of **3** in ethanol at −75°C (3.47×10^{-6} *M*).

The positions of these absorption peaks do not change when a nonpolar solvent such as 3-methylpentane is used. On cooling to 77 K, the absorption spectrum does not show much increase in structure.

Absorption spectrum of the colored form

It is difficult to measure the complete absorption spectrum of the colored form at room temperature since its thermal decay is fairly rapid. Besides, the concentration of this metastable colored form cannot be measured. Fortunately, the thermal decay of the colored form decreases rapidly as the temperature is lowered. The decay can be completely stopped at a temperature below −60°C. Thus, a 3.47×10^{-6} *M* solution of **3** in ethanol was cooled by a Dry Ice – CH_2Cl_2 bath in a Dewar to −75°C. The solution was irradiated by a 100 W Hg lamp equipped with a Corning 7-37 glass filter for a period of 15 min to ensure the full conversion to the colored form. The measured absorption spectrum is given in Fig. 3.

The most prominent absorption peaks are at 612 nm and 578 nm with molar absorptivity of $8.1 \times 10^4\ M^{-1}\ cm^{-1}$ and $4.9 \times 10^4\ M^{-1}\ cm^{-1}$, respectively. In addition, three absorption bands at 410 nm ($\epsilon = 1.8 \times 10^4\ M^{-1}\ cm^{-1}$), 343 nm ($\epsilon = 2.7 \times 10^4\ M^{-1}\ cm^{-1}$), and 277 nm ($\epsilon = 3.2 \times 10^4\ M^{-1}\ cm^{-1}$) have been measured.

Can. J. Chem. Downloaded from www.nrcresearchpress.com by 210.87.254.42 on 09/06/12
For personal use only.

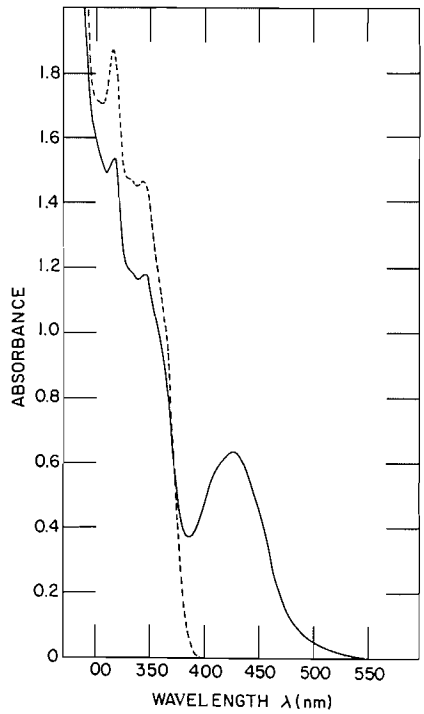

FIG. 4. The absorption spectrum of a degassed solution of **3** (1.79×10^{-4} *M*) in cyclohexane containing 2.24×10^{-3} *M* benzophenone before (- - -) and after (—) uv irradiation.

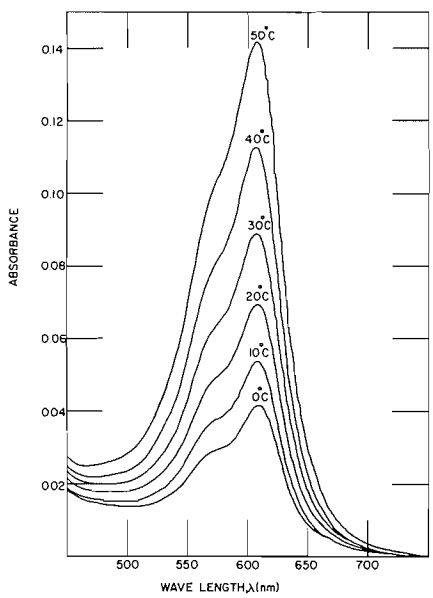

FIG. 5. The absorption spectrum of the colored form of **3** in ethanol (6.2×10^{-3} *M*) at several temperatures.

Triplet state desensitization

In a photosensitization experiment by the energy-transfer method, it was surprising to find that a degassed 1.79×10^{-4} *M* solution of **3** in cyclohexane containing 2.24×10^{-3} *M* benzophenone showed an additional absorption peak at 428 nm after 20 min uv irradiation by a 200 W Hg lamp filtered through a Corning 7-37 filter. This is shown in Fig. 4. In the meantime, the absorption peak height of **3** decreased. This new absorption peak at 428 nm was due to the photosensitized decomposition product of **3** by benzophenone since a control experiment containing either **3** or benzophenone alone did not show this additional peak under the same experimental conditions. As a matter of fact, no change in the absorption spectrum was observed for a solution of **3** or benzophenone in cyclohexane even after 8 h of irradiation. This photosensitized decomposition could still be observed even if the concentration of benzophenone was decreased by a factor of 10 to 2×10^{-4} *M*.

However, no photosensitized decomposition was observed when 2′-acetonaphthone (1.11×10^{-3} *M*) was used even after several hours of uv irradiation.

The compound responsible for the 428 nm absorption peak was a photosensitized decomposition product of **3**. This interpretation is further supported by the fact, that, besides the control experiment aforementioned, the peak height of the 428 nm absorption band increases in proportion to the decrease in height of the absorption peaks of **3**. Work is in progress trying to determine the precise nature of this compound and this will be reported in future.

Temperature dependence of the absorption of the colored form

There exists a thermal equilibrium between the ground states of the colorless and colored form. This is evident from the fact that the solution of **3** in ethanol becomes progressively bluer in color as the concentration is increased. Moreover, this thermal equilibrium is strongly temperature dependent. Thus, the ethanol solution of **3** is not only photochromic but also thermochromic. This thermochromic effect is illustrated in Fig. 5.

Kinetics of the thermal decay

The kinetics of photocoloration and thermal decay was measured by placing 0.50 mL solution of **3** in ethanol (1.35×10^{-4} *M*) in a 1 cm water-jacketed cell. By setting the slit of the monochromator at the maximum absorption of the colored form (610 nm), the change in the monitoring light intensity was easily followed by an oscilloscope. Before photocoloration, the zero absorption was recorded since the absorption of the colored form due to thermal equilibration at this concentration was negligible. Upon activation by the uv light of a Hg lamp, the absorption of the colored form increased and thus, decreased the monitoring light intensity. The thermal decay was then recorded after the photoequilibration was obtained by closing the shutter. An oscillograph representing a typical photocoloration and the thermal decay is shown in Fig. 6.

Discussion

The position of low-lying electronic excited states

The absorption spectrum of the colorless form of **3** in ethanol as displayed in Fig. 2 shows three major absorption bands. From the value of the molar absorptivity of these bands, they can be safely assigned as $\pi^* \leftarrow \pi$ transitions. This is supported by the fact that the absorption of the colorless form of III is very similar to that of 1,3,3-trimethylspiro[indoline-2,3′-[3]-naphtho-[2,1-*b*]pyran], **4**, the precise counterpart in the spiropyran series. The absorption transitions of **4** have been assigned by Tyer and Becker by comparing the spectral data of **4** with those of the appropriate chromene and indoline models (7). As in the case of **4**, the absorption peaks at 345 nm and 317 nm can be assigned to transitions localized on the oxazine half of the molecule. However, the transition at 297 nm could well have contributions from both oxazine and indoline halves of the molecule. Due to their high molar absorptivity and similarity to the indoline absorption, the transitions at 235 nm and

Can. J. Chem. Downloaded from www.nrcresearchpress.com by 210.87.254.42 on 09/06/12
For personal use only.

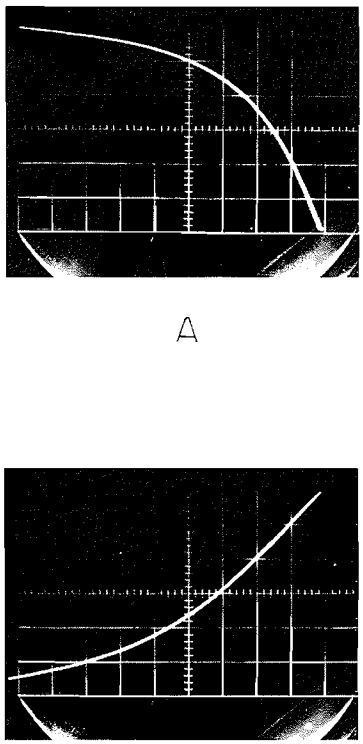

FIG. 6. The kinetics of photocoloration, *A*, and thermal decay, *B*, of a 1.35×10^{-4} *M* solution of **3** in ethanol at 20°C (20 mV/div, 1 s/div, V_0 = 270 mV).

203 nm are characteristically indoline transitions.

The absorption spectrum of the colored form of **3** in ethanol at −75°C is given in Fig. 3. The molar absorptivity of the 612 nm peak is 8.1×10^4 M^{-1} cm^{-1} (based on concentration measured at 20°C). If the contraction in volume of ethanol is corrected, then the molar absorptivity becomes 7.3×10^4 M^{-1} cm^{-1}. This is in good agreement with 6.7×10^4 M^{-1} cm^{-1} obtained for **4** (8). Upon further cooling to −196°C, the absorption spectrum of the colored form of **3** does not show any change. This is in contrast to **4** and many spiropyrans which show three distinct colored modification absorptions at low temperature (1, 9).

It is interesting to note that a hypsochromic effect of shifting the absorption maximum of the colored form of III to 555 nm occurs when cyclohexane is used as a solvent.

A well purified and freshly prepared sample of **3** in ethanol does not show any luminescence. Even at −77 K, the conversion to the colored form proceeds efficiently. Thus the location of the lowest triplet state cannot be directly measured. However, we are able to roughly measure the position of the triplet state of the colorless form from energy-transfer experiments. In a photosensitization experiment, it was surprisingly found that benzophenone (2.24×10^{-3} *M* in cyclohexane) catalyzes the photodecomposition of **3** drastically. However, no photosensitized decomposition can be detected when 2′-acetonaphthone (1.11×10^{-3} *M* in cyclohexane) is used, even after prolonged uv irradiation. Thus, the triplet state of the colorless form of **3** lies between 2.4×10^4 cm^{-1} and 2.1×10^4 cm^{-1} since the triplet state energy for benzophenone in a nonpolar solvent is 2.4×10^4 cm^{-1} and is 2.1×10^4 cm^{-1} for 2′-acetonaphthone (10).

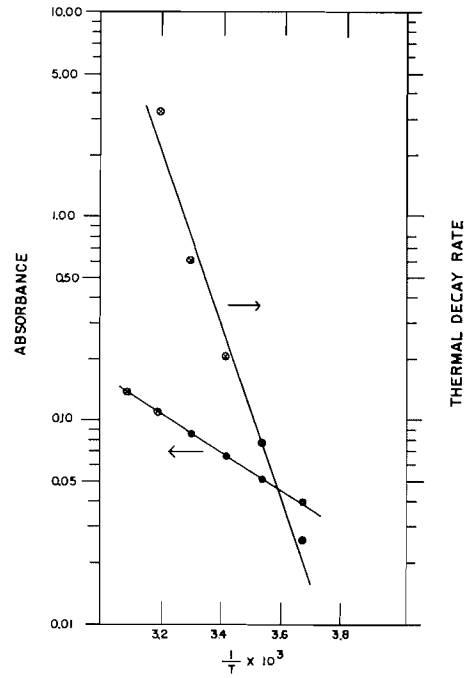

FIG. 7. A plot of the absorbance of the thermal equilibrated colored form and the thermal decay rate versus $1/T$.

The energy of the lowest triplet state of the colorless form of **4** is not known. An emission located at 720 nm from a solution of **4** in EPA at 77 K was assigned to a π,π^* triplet state of the colorless form of **4** (11), but later was reported to be a spurious one arising from an impurity (12).

The phosphorescence of 1′,3′,3′-trimethylspiro[2*H*-1-benzopyran-2,2′-indoline], **5**, in polystyrene and poly(methyl methacrylate), PMMA, has been observed and found to be located at 2.29×10^4 cm^{-1} in PMMA and 2.03×10^4 cm^{-1} in polystyrene (13). Since there is a bathochromic shift of 3.6×10^3 cm^{-1} of the singlet state energy when the conjugation is extended from **5** to **4**, the corresponding shift in the triplet state energy should not be greater than this amount. Therefore, the lowest triplet state of **3** and **4** is likely to be located in the vicinity of 2.0×10^4 cm^{-1}. This is a reasonable estimate since **3** and **4** are a perturbed phenanthrene system.

The energy diagram of the ground states

There exists a thermal equilibrium between the colorless form and the colored form of **3**. This is evident from the fact that a relatively concentrated solution of **3** is bluish in color, i.e. shows a colored form absorption. Furthermore, the intensity of the blue color increases as the temperature of the solution is increased. This phenomenon is shown in Fig. 5.

According to the law of thermodynamics, the standard enthalpy of this equilibrium reaction can be calculated using the following equation:

$$[1] \quad \log K_{eq}(T_2) - \log K_{eq}(T_1) = -\frac{\Delta H}{2.3R}\left(\frac{1}{T_2} - \frac{1}{T_1}\right)$$

A straight line should be obtained when the absorbance of the colored form is plotted against $1/T$ as shown in Fig. 7. In Table 1, the value of the absorbance at different temperatures is reported and from the least-square fitting the standard enthalpy of reaction, ΔH^0, is calculated to be 1.5×10^3 cm^{-1}.

By virtue of its photochromism, the metastable colored form

Can. J. Chem. Downloaded from www.nrcresearchpress.com by 210.87.254.42 on 09/06/12
For personal use only.

TABLE 1. The absorbance of the colored form in thermal equilibration (6.61×10^{-3} *M* solution of **3** in ethanol) and the thermal decay rate of the colored form at different temperatures

T (°C)	Absorbance	k (s^{-1})
0	0.0414	2.67×10^{-2}
10	0.0536	7.98×10^{-2}
20	0.0692	2.12×10^{-1}
30	0.0880	6.10×10^{-1}
40	0.1128	3.32
50	0.1414	

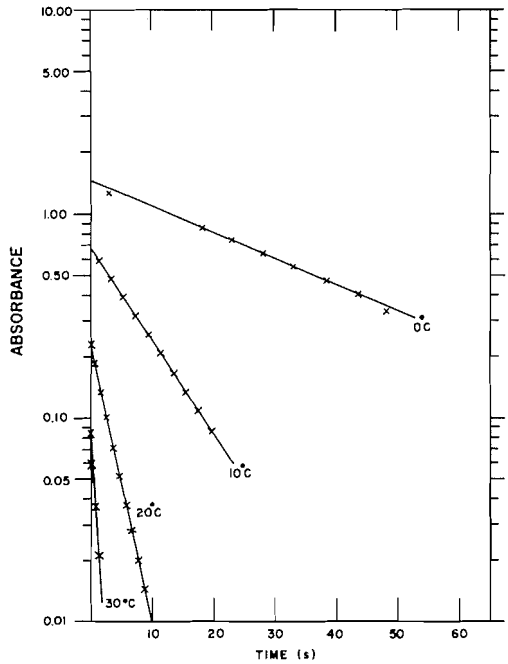

FIG. 8. The thermal decay of the colored form at different temperatures.

reverts to the colorless form upon removing the activating uv light. This is clearly illustrated in Fig. 6. This thermal decay follows a first order kinetics as shown in Fig. 8. The calculated

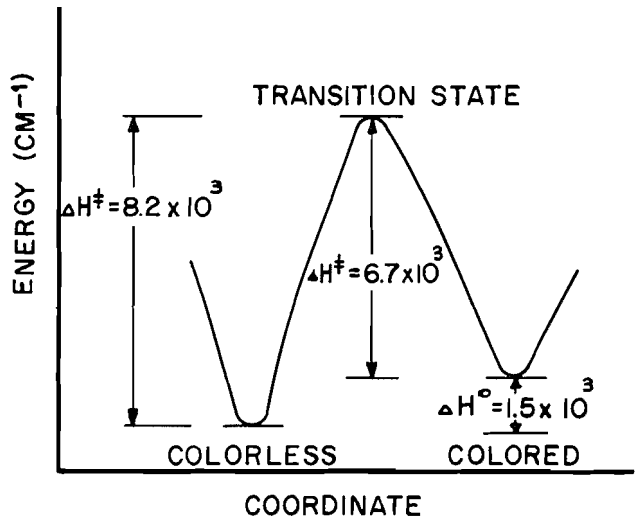

FIG. 9. The energy diagram of the ground states of **3**.

least-square fitting values at different temperatures are given in Table 1.

According to the Arrhenius Equation

$$[2] \quad \log k = -\frac{E_a}{2.3R}\left(\frac{1}{T}\right) + \log A$$

the activation energy for the transition, E_a, can be calculated. In eq. [2], A is the frequency factor. A plot of the thermal decay rate k versus $1/T$ is shown in Fig. 7. The calculated thermal barrier for this transition is 6.9×10^3 cm^{-1}.

The activation energy E_a is related to the activation enthalpy $\Delta H^{\ddagger}$ by the equation

$$[3] \quad \Delta H^{\ddagger} = E_a - RT$$

Thus, at $T = 293$ K, $\Delta H^{\ddagger} = 6.7 \times 10^3$ cm^{-1}.

In Fig. 9, an energy diagram of the ground states of the colored and colorless forms is given to illustrate their interrelations.

Finally, a comparison of the photophysical properties and thermodynamic functions of **3** and **4** is given in Table 2.

TABLE 2. The photophysical properties and thermodynamic functions of **3** and **4**

Compound	S_{Cl}^{1} [a]	S_{Cl}^{2} [a]	T_{Cl}^{1} [a]	S_{C}^{1} [a]	ΔH^{0}	E_a	k (s^{-1})
3	2.76×10^4	3.14×10^4	$2.4-2.1\times10^4$	1.64×10^4	1.5×10^3	6.9×10^3	2.7×10^{-2} [e]
4	2.73×10^4 [b]	3.17×10^4 [b]		1.72×10^4 [c]	1.1×10^3 [d]	6.7×10^3 [c]	4.7×10^{-2} [e]

[a] S_{Cl}^{1}, S_{Cl}^{2}, and T_{Cl}^{1} are the first and second excited singlet state and the first excited triplet state of the colorless form, respectively. S_{C}^{1} is the first excited singlet state of the colored form. All energies are in cm^{-1}.

[b] Reference 7.

[c] Reference 8.

[d] Reference 9.

[e] k is the thermal decay rate. For **3** the rate given is for the ethanol solution at 0°C. For **4** the rate is at −67.5°C and is taken from ref. 8.

Acknowledgements

The author is grateful to the American Optical Corporation for the support of this work and the permission for publication. The laboratory assistance in collecting the data by Messrs. N. R. Pelletier and J. W. Powers is appreciated.

1. R. C. BERTELSON. *in* Photochromism. *Edited by* G. H. Brown. Wiley-Interscience, New York. 1971. Chapt. III, p. 45, and references therein.
2. V. A. MURIN, V. F. MANDZHIKOV, and V. A. BARACHEVSKII. Opt. Spectrosc. **37**, 674 (1974), Engl. Transl. **42**, 43 (1977).
3. V. A. KUZMIN and Y. N. MALKIN. Photogr. Sci. Eng. **23**, 20 (1979).
4. R. E. FOX. Research reports and test items pertaining to eye protection of air crew personnel. Final Report on Contract AF41(657)-215, April 1961, AD440226.
5. H. ONO and T. OSADA. U.S. patent 3,562,172.

Can. J. Chem. Downloaded from www.nrcresearchpress.com by 210.87.254.42 on 09/06/12
For personal use only.

6. H. ONO, T. OSADA, and K. KOSUGE. U.S. Patent 3,578,602.
7. N. W. TYER, JR. and R. S. BECKER, J. Am. Chem. Soc. **92**, 1289 (1970).
8. Y. HIRSHBERG and E. FISCHER. J. Chem. Soc. 297 (1954).
9. R. HEILIGMAN-RIM, Y. HIRSHBERG, and E. FISCHER. J. Chem. Soc. 156 (1961).
10. W. G. HERKSTROETER, A. A. LAMOLA, and G. S. HAMMOND. J. Am. Chem. Soc. **86**, 4537 (1964).
11. R. S. BECKER and J. K. ROY. J. Phys. Chem. **69**, 1435 (1965).
12. N. W. TYLER, JR. and R. S. BECKER. J. Am. Chem. Soc. **92**, 1295 (1970).
13. D. A. REEVES and F. WILKINSON. Trans. Faraday Soc. II (London), **69**, 1381 (1973).

Can. J. Chem. Downloaded from www.nrcresearchpress.com by 210.87.254.42 on 09/06/12
For personal use only.

The use of localized and delocalized orbitals in a Rydberg expanded correlation analysis of the cycloaddition of ethylene

EARL M. EVLETH AND EMIL KASSAB

Centre de Mécanique Ondulatoire Appliquée, 23 rue du Maroc, Paris 75019, France

Received August 31, 1981[1]

EARL M. EVLETH and EMIL KASSAB. Can. J. Chem. **61**, 306 (1983).

Rydberg expanded orbital and state correlation diagrams are shown for the classical cycloaddition of ethylene. The diagrams are first developed at the localized valence MO level and the origins of the S^{**}-bitriplet correlations are shown. When extended to the Rydberg level, the localized state correlation diagram shows that the $\pi 3s$ Rydberg singlet state of ethylene can interact with the ground state of another ethylene to directly yield the same S^{**} surface as found in the valence-level-only diagram. In this manner the Rydberg state eventually derydbergizes.

EARL M. EVLETH et EMIL KASSAB. Can. J. Chem. **61**, 306 (1983).

Les diagrammes de corrélation des OM et ceux des états étendus au niveaux Rydberg sont montrés pour la cycloaddition classique de l'éthylène. Les diagrammes sont d'abord developpés au niveaux des OM localisées de valence et les origines de la corrélation de bitriplet-S^{**} sont montrées. Lorsque le diagramme des états est étendu aux états Rydberg, on montre que l'état Rydberg $\pi 3s$ de l'éthylène peut interagir avec l'état fondamental de l'éthylène à travers la même surface S^{**} produit directement et finira par acquérir un caractère de valence.

Can. J. Chem. Downloaded from www.nrcresearchpress.com by 210.87.254.6 on 09/06/12
For personal use only.

Introduction

Recently, there has been an expanded interest in theoretically rationalizing the photochemistry of small molecules whose lowest excited states are Rydberg in character (1–5). The theoretical methods used in these analyses are both computational and descriptive. Because of the expanded valence and Rydberg basis sets needed to adequately computationally treat excited state surfaces, *ab initio* computations are presently limited to small systems. To date, semi-empirical methods (6–8) either have failed to duplicate the known Rydberg characters of the excited states of small molecules (e.g. NH_3) or indicate (9) that there may not be a broadly applicable parameterization scheme extendable to large systems. Therefore, it is important to develop descriptive methods using Rydberg extended correlation diagrams which will permit analyzing systems too large for reliable computations. Even in those cases where computations are realizable, such analyses will permit establishing, *a priori*, the minimal Rydberg basis sets necessary to correlatively treat a particular excited state surface.

Here, we will develop the Rydberg extended correlation diagrams for the classic case of the $2s + 2s$ cycloaddition of two ethylenes to give cyclobutane. There are several reasons for this choice. First of all, the system is classic and familiar to both theoretical and non-theoretical chemists. Therefore, any Rydberg extension of orbital and state correlation diagrams will build on that previous knowledge. Secondly, we will demonstrate that in spite of previous work in this area, the actual relationship between the classical correlation diagrams and the real experimental situation needs considerable clarification. Thirdly, since Rydberg states are or may be the lowest lying singlet states for ethylene (10) and cyclobutane (1), it is obvious that the correlation diagrams must be Rydberg expanded if they are to contain some reality component at the final state level.

With regard to the general area of Rydberg extended correlation diagrams we recommend that the reader thoroughly study the simple but conceptually and methodologically complex NH bond rupture surfaces in the excited states of NH_3 (3, 4, 11, 12). In particular, the introduction of Rydberg orbitals into either computations or correlation diagrams generates a situation in which, depending on the symmetry of the molecular transformation, certain reactant Rydberg MO's (or molecular states) will evolve to product valence MO's (or molecular states). The MO derydbergizations (13) are an intrinsic feature of the united atom correlation diagrams (14). The concept of derydbergization is central in the rationalization of how a Rydberg excited reactant state adiabatically relaxes to a product valence excited or ground state.

We will develop our subject in the following manner. We will first review the known photochemical, energetic, and theoretical factors. Secondly, we will detail the conceptual traps that exist in the classical valence-level-only delocalized MO and state correlation diagrams. Next, we will show how these traps are avoided using localized MO's and how this modifies the state correlation diagrams. Finally, we will Rydberg expand both delocalized and localized MO diagrams and show a first order modification of the state correlation diagrams.

I. Known photochemical, energetic, and theoretical factors

We will mainly develop the subject from the viewpoint of the singlet photocycloaddition of two ethylenes (or simple olefins) to yield cyclobutane. In experimental fact, cyclobutanes represent a minor photoproduct in both the gas (especially) and condensed phase direct photolysis of ethylene and simple olefins (15–17). In the 2-butenes (18) the minor but stereospecific formation of various cyclobutanes is strongly perturbed by minor dilution of the neat systems. This indicates that the competitive photoprocesses are dominating these systems. In fact, the condensed phase photochemistry of a number of simple olefins is dominated by monomolecular events: *cis–trans* isomerization, 1,3-sigmatropic shifts, carbene formation, etc. (16).

In ethylene, experimental and theoretical work show that of the first two Franck–Condon singlet excited states to have $\pi 3s$ and $\pi\pi^*$ characters, respectively (7.1 and 7.4 eV (10, 19). The

[1]Revision received June 30, 1982.

0008-4042/83/020306-06$01.00/0

©1983 National Research Council of Canada/Conseil national de recherches du Canada

Can. J. Chem. Downloaded from www.nrcresearchpress.com by 210.87.254.6 on 09/06/12
For personal use only.

lowest state is fully Rydberg in character and even the classical $\pi\pi^*$ state has to be theoretically characterized as being partially Rydberg (intravalent (20)). Likewise, there are a series of $\pi 3p_{x,y,z}$ Rydberg states at only slightly higher energies (ca. 8 eV) (21, 22). Theoretically, there is an infinite number of Rydberg states merely in the energy region between these states and the ionization potential of the molecule. The possible role of any other valence excited states in this energy region becomes problematic since they may not theoretically exist, being submerged in a Rydberg sea. In any case, for practical reasons we will limit our discussion to the $\pi 3s$ and $\pi\pi^*$ monomer states. There is, however, an infinite separation dimer state which lies in the same energy region being conceptually described as two $\pi\pi^*$ triplets. Its Franck–Condon energy can also be estimated to be in the 8 eV region (23). Although the $\pi 3s$ state will retain near-planar geometry, both the $\pi\pi^*$ singlet and triplet states will relax to their more stable 90° twist configurations, having energies in the 5.6 and 2.8 eV regions, respectively (24). Therefore, for ultimate correlation purposes, the relaxed $\pi\pi^*$ singlet and bitriplet states have about the same energy.

Previous computational and correlative treatments (24–27) of the cycloaddition of ethylene have rationalized the photodimerization reaction in the following manner. The initial step, after photoexcitation of the monomer, yields the formation of an exciplex: $E_1^* + E_2 = S^*$, where E_1^* and E_2 represent the planar $\pi\pi^*$ excited state of ethylene 1 and the ground state on ethylene 2. The S^* potential energy surface eventually crosses with another "doubly excited" S^{**} exciplex surface which has a deep minimum in the region of the HOMO–LUMO crossing region (24). In this region, the ground state S_0 and the S^{**} state are probably in close proximity. These states also have the same symmetry and configurational properties and ought to be strongly coupled by the nuclear kinetic energy operator (27, 28). Therefore, it is in the HOMO–LUMO crossing region that the non-adiabatic excited state – ground state relaxation should take place (29, 30). The allowed Woodward–Hoffmann photocycloaddition depends on the existence of the S^{**} minimum and not on any possible direct overall correlation between the excited ethylene state and the excited cyclobutane state. A required feature in such a rationalization is that the energy of the S^{**} minimum lies below that of the excited ethylene monomer, E_1^*. However, knowledge of the shapes of the surfaces leading to the S^{**} minimum is also necessary. Unfortunately, calculations in this area (27) were not sufficiently accurate to state with any confidence the relative energies of the S^{**} minimum and the E_1^* state. Based on the above-discussed photochemistry of ethylene and simple olefins, we suspect that the S^{**} minimum is kinetically inaccessible from the 90° energy relaxed form of excited ethylene (31) either because the $S^{**} >$ 5.6 eV or the potential surface leading to S^{**} has a barrier and other monomolecular kinetic events dominate the relaxation. Therefore, one must hypothesize that the photodimerization surface is initiated from species having geometries and energies close to the Franck–Condon values.

This above hypothesis yields several additional complicating factors. First of all, in competition with extremely rapid monomolecular photochemical processes, the bimolecular photodimerization of olefins can only proceed in the condensed phase at very high concentrations (preferably neat). In the condensed phase, any energetic analysis based on gas phase spectroscopic measurements or isolated molecule computations, at whatever theoretical level, will be questionable. This is particularly true as to what are the characteristics of the $\pi 3s$ Rydberg states of olefins in condensed phase. Full resolution of these problems appears experimentally and theoretically inaccessible at this time. Even an adequate valence and Rydberg basis set CISD computation of critical portions of the dimer excited state surfaces, under partial geometry optimization, is not financially feasible at this time. However, given the possible role of $\pi 3s$ Rydberg states in the condensed phase photochemistry of olefins (16), a Rydberg extended correlation analysis of this system is a minimum necessity.

II. Comparison of the valence orbital delocalized and localized correlation diagrams

A. The delocalized view

There exists a major conceptual problem in attempting to visualize the photodimerization of ethylene in delocalized valence orbital terms. At large ethylene(E_1) – ethylene(E_2) separations four delocalized π-orbitals can be written using the localized π_1 and π_2 MO's. These are: $\pi_1 + \pi_2$, $\pi_1 - \pi_2$, $\pi_1^* + \pi_2^*$, and $\pi_1^* - \pi_2^*$, these having symmetries SS', SA', AS', and AA' in classical Woodward–Hoffmann terms (24). At large E_1–E_2 separations, the first two MO pairs are degenerate, as are the last two. Likewise, the monoexcited configurations that one can construct also *appear* diagramatically degenerate (24). Two separate state biconfigurational wavefunctions having different symmetries can be generated:

$$\Psi(AA') = c_1[SA' \rightarrow AS'] + c_2[SS' \rightarrow AA']$$

and

$$\Psi(AS') = c_3[SA' \rightarrow AA'] + c_4[SS' \rightarrow AS']$$

The total SS' state polyconfigurational function is even more complex

$$\Psi(SS') = c_1'[SS'^2SA'^2] + c_2'[SS'^2AS'^2] + c_3'[SA'^2AS'^2] + c_4'[SS'^2AA'^2] + c_5'[SA'^2AA'^2] + c_6''[SS'SA'AS'AA'] + c_6^b[SS'SA'AS'AA']$$

where c_6^a and c_6^b are two determinately different forms of the same four open shell configuration. At large E_1–E_2 separations the configurations c_2' through c_6^b all appear (deceptively) degenerate in a delocalized orbital correlation diagram. These pseudo-degeneracies all disappear as the distance between E_1 and E_2 diminishes. In the region of the HOMO–LUMO crossing ($SA' \rightleftarrows AS'$) the configurational form of the lowest singly excited surface, S^* (AA') is simple ($c_1 \rightarrow 1$) while the ground and "doubly" excited surfaces, S_0 and S^{**}, are the biconfigurational pairs: $c_1'[SS'^2SA'^2] \mp c_2'[SS'^2AS'^2]$, $c_1' = c_2'$.

There is no conceptual problem with the delocalized model at small E_1–E_2 distances. However, at large E_1–E_2 distances the delocalized model does not, without further analysis, indicate how the S^* and S^{**} surfaces correlate with real monomer or dimer states of excited ethylene. Furthermore, if the diagrams are to be used as computational guides, there are certain technical factors to consider if one wishes to impose delocalized symmetry orbitals on a particular system at large separations. Finally, from an aesthetic standpoint, one might wish to begin the analysis of this system from the standpoint of a localized excited ethylene initiating its interaction with a ground state ethylene at large distances and following the surface evolutions from this standpoint. Such an approach is computationally possible (27) by merely allowing the initial geometries of E_1 and E_2 to be different. In this case, the $2s + 2s$

Can. J. Chem. Downloaded from www.nrcresearchpress.com by 210.87.254.6 on 09/06/12
For personal use only.

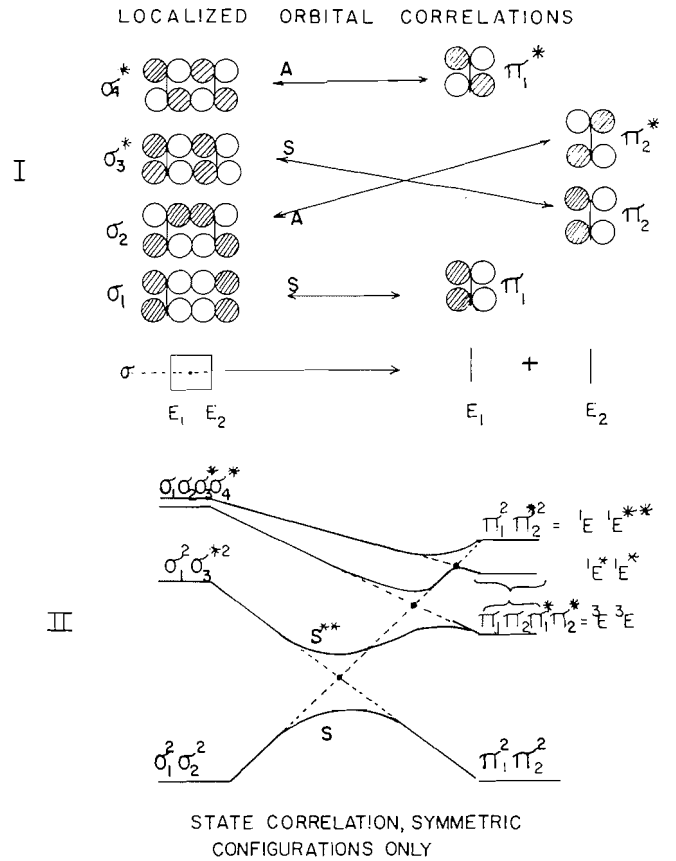

FIG. 1. I. Correlation between the delocalized cyclobutane and localized two ethylene molecular orbitals. See ref. 24 for the delocalized–delocalized correlation. II. Symmetric states only correlation diagram showing that the S^{**} state eventually terminates as two ethylene triplets by a second avoided crossing (•).

face-to-face cycloaddition would be initiated in C_{2v} symmetry at large E_1–E_2 separations, reach D_{2h} symmetry in the HOMO–LUMO crossing region, and terminate as D_{4h} at the planar cyclobutane configuration. This would require a passage from a localized to a delocalized model ($C_{2v} \rightarrow D_{2h}$) which we will now discuss.

B. The localized view

The localization procedure is a simple one and merely assumes that the CC distance in E_1 is smaller than E_2 at large E_1–E_2 separations. On the other hand, delocalized orbitals are retained on cyclobutane. This procedure will produce the following localizations at the E_1–E_2 large separation limit: $\pi_1 + \pi_2 \rightarrow \pi_1$, $\pi_1 - \pi_2 \rightarrow \pi_2$, $\pi_1^* + \pi_2^* \rightarrow \pi_2^*$, and $\pi_1^* - \pi_2^* \rightarrow \pi_1^*$. This localization will computationally occur because the absolute values of MO coefficients mixing the various localized π-orbitals will no longer be the same by symmetry (e.g. $c_1\pi_1 + c_2\pi_2$). The overall cyclobutane localized two ethylene MO correlation diagram is shown in Fig. 1, I. This MO correlation diagram appears similar to that obtained in the delocalized one in showing a required HOMO–LUMO inversion. It should be first noted under this localization procedure, all single excited configurations belong to the same representation, A. The general state function becomes: $\Psi(A) + c_1[\pi_1 \rightarrow \pi_1^*] + c_2[\pi_2 \rightarrow \pi_2^*] + c_3[\pi_1 \rightarrow \pi_2^*] + c_4[\pi_2 \rightarrow \pi_1^*]$. It is now clear that the four-fold-appearing diagrammatic degeneracy in the AA' and AS' delocalized states is deceptive. Actually two of these states are charge transfer pairs, $E_1^+E_2^- \mp E_1^-E_2^+$, which will lie at considerably higher energies than the excimer pairs, $E_1^*E_2 \mp E_1E_2^*$. The localized modified description of these excimer pairs merely decouples the two functions, giving $c_1E_1^*E_2 + c_2E_1E_2^*$. The amount of excitation localization on one of the ethylenes depends on the geometry difference between E_1 and E_2 and their separation distance. The most stable excimer state (B_{1g} in D_{2h}) results from a head-to-tail orientation of the individual ethylenes $\pi\pi^*$ transition dipoles ($\Updownarrow$). This excimer state is the one which eventually evolves along the S^* surface (27). The localized and delocalized views of the collapse of excited ethylene to the S^* exciplex are sufficiently similar that an overall state correlation diagram has not been displayed.

The diagrammatic behavior of the symmetric state surface is considerably modified at the large E_1–E_2 separation limit using the localized model. First of all, the lowest symmetric state of the dimer has a four open shell bitriplet configuration, $\pi_1\pi_2\pi_2^*\pi_1^*$, ($^3E_1{}^3E_2$), as shown in Fig. 1, II. The S^{**} surface must display two avoided crossings, one of which is that previously observed in delocalized diagram (24) between the $\sigma_1^2\sigma_2^2 \leftrightarrow \pi_1^2\pi_2^{*2}$ and $\sigma_1^2\sigma_3^{*2} \leftrightarrow \pi_1^2\pi_2^2$ correlations. The other avoided crossing exists between the former correlation and the $\sigma_1\sigma_2\sigma_3^*\sigma_4^* \leftrightarrow \pi_1\pi_2\pi_2^*\pi_1^*$ correlation. The overall first order configurational wavefunction of the S^{**} surface is tri- not bi- or polyconfigurational as implied either by a 2 × 2 CI (32) or the above-discussed diagrammatically deceptive delocalized SS' function. This triconfigurational form is:

$$\Psi(S, S^{**}) = c_1[H^2] + c_2[L^2] + c_3[(H\text{-}1)\cdot(H)\cdot(L)\cdot(L\text{-}1)]$$

where H = HOMO, L = LUMO. In the region of the HOMO–LUMO inversion, $|c_1| = |c_2|$, $c_3 \simeq 0$, while at the large separation limit, $c_3 \simeq 1$, c_1, $c_2 \simeq 0$. The ground state surface, S_0, will retain biconfigurational form in the region of the HOMO–LUMO crossing but is essentially monoconfigurational at either the cyclobutane or two ethylene limit. There are several additional nuances to the symmetric state correlation diagram shown in Fig. 1. All the features shown do not have to be physically real. None of the doubly excited cyclobutane configurations shown need to have real corresponding states, their diagrammatic role being to serve as correlation targets for other real states of the system. These real states are the ground state of cyclobutane, ethylene, and the bitriplet state. At the state correlation level, other avoided crossings can be proposed (e.g. with a bisinglet state $^1E_1^*{}^1E_2^*$). However, these other crossings are not of fundamental interest in determining the behavior of the S^{**} surface in either the HOMO–LUMO crossing region or at the E_1–E_2 separation limit. As we will now demonstrate, Rydberg additions to this state correlation will modify the S^{**} surface in an important manner.

III. A Rydberg expanded analysis

A. Construction of the orbital correlation diagrams

Because of the potentially infinite number of Rydberg product and reactant states, the construction of both the orbital and state correlation diagrams must be kept to as simple a level as possible to solve the problem raised. We will concentrate on the diagrammatic fate of the $\pi 3s$ monomer state of ethylene but will expand the subsequent discussion to include other Rydberg states. It is first stressed that the method used in the construction of Rydberg extended polyatomic MO correlation diagrams does not differ essentially from that employed in the united atom diagrams at either the diatomic or polyatomic level (14).

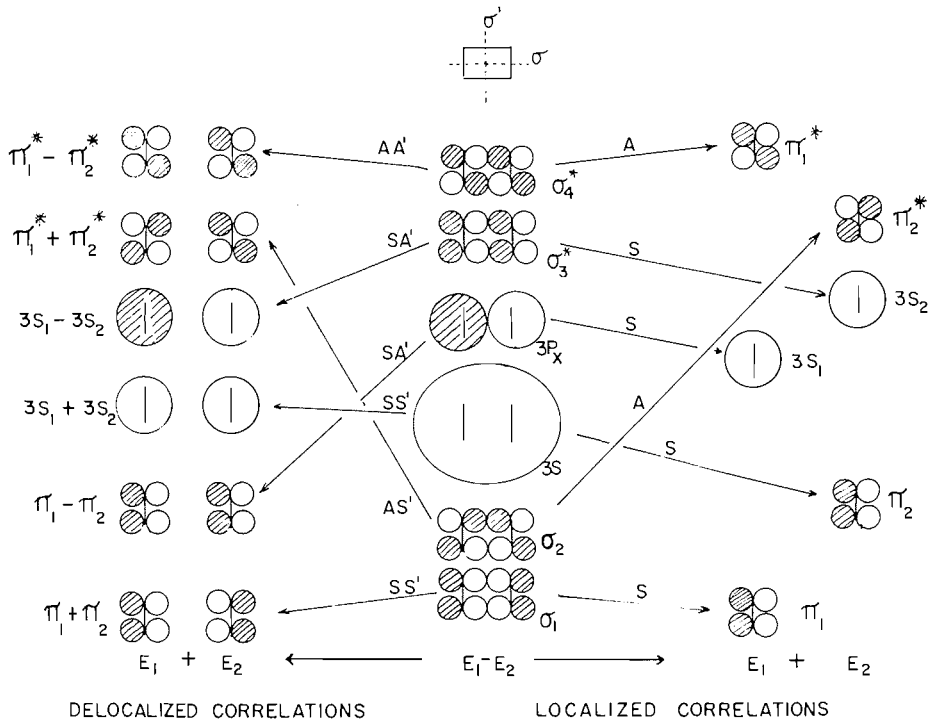

FIG. 2. Rydberg expanded delocalized and localized molecular orbital correlations. The right hand portion of this figure may be compared to Fig. 1, part I.

A recommended first step is to construct a conventional valence-orbital-only Woodward–Hoffmann type MO correlation diagram and subsequently analyze the behavior of the valence-orbital-only state correlation diagram. Next, add the Rydberg components as desired and repeat the sequence, examining the behavior of the state correlation diagram with respect to the real expected reactant and product states of interest. The added Rydberg components must be kept to a minimum, otherwise undue diagrammatic complications appear. In the case examined here, we have decided to keep the detailed analysis at the $3s$ Rydberg orbital level only. However, we will discuss the problem of variance of the diagrammatic behavior with Rydberg basis set.

The previous Rydberg extended orbital delocalized correlation diagram proposed for this system was developed by Wittel (33). Sandorfy did not specifically include Rydberg orbitals in the Woodward–Hoffmann delocalized MO correlation diagram but discussed the consequence of doing so (34). Neither authors constructed state correlation diagrams. At the minimal correlative and computational level, $3s$ orbital are placed on each ethylene, $3s_1$, $3s_2$. However, at the cyclobutane limit this basis set will generate two Rydberg MO's, $3s_1 + 3s_2$ and $3s_1 - 3s_2$, being, $3s$ and $3p_x$ by symmetry. An alternative decision to place only one $3s$ orbital at the molecular center of cyclobutane is insufficient since no Rydberg ethylene states can be generated at infinite separation. The placing of one $3s$ AO at each carbon atom will add a total of four Rydberg MO's ($3s$, $3p_{x,y}$, and $3d_{x,y}$) to the correlation diagram. Likewise, the specific addition of both $3s$ and $3p_{x,y,z}$ base orbitals will produce certain redundancies and overly complicate the final MO and, expecially, the state correlation diagrams. Finally, we have selected to diagrammatically place any Rydberg MO's energetically in between the valence bonding and antibonding MO's. This is generally what is encountered in any MO calculation on smaller systems. Rydberg MO's can be considered as having near-zero orbital energies, either at the closed shell or open shell RHF level of treatment (i.e. conceptually neither bonding nor antibonding.) Therefore our delocalized MO correlation diagram differs from that of Wittel in placing the cyclobutane $3p_x$ MO below the σ_3^* MO (Fig. 2). This placement is crucial in the sense that Wittel's diagram shows only direct Rydberg reactant – Rydberg product correlations without taking into account the possible derydbergization in the correlation diagrams, a factor which we will show is certainly important in the localized correlation.

The most important feature of Fig. 2 is that in both the delocalized and localized MO correlations certain MO's change Rydberg character in evolving from cyclobutane to two ethylenes ($3p_x \rightarrow \pi_1 - \pi_2$, $\sigma_3 \rightarrow 3s_1 - 3s_2$ or $3s \rightarrow \pi_2$, $3p_x \rightarrow 3s_1$, respectively). These Rydbergizations–derydbergizations are not diagrammatic artifacts and will also occur computationally (11, 12). For example, the MO function for the SA' delocalized correlation $3p_x \rightarrow \pi_1 - \pi_2$ will have the overall approximate form: $c_1 [2p_{1a} + 2p_{1b} - 2p_{2c} - 2p_{2d}] + c_2 [3s_1 - 3s_2]$, where the $2p$ valence orbitals are associated with carbons a and b on E_1 and c and d on E_2. At the cyclobutane configuration, $c_2 \gg c_1$ (i.e. the MO is Rydberg in character) and at the two ethylene limit, $c_1 \gg c_2$ (i.e. the same MO is valence in character). Such MO Rydbergizations are well-recognized phenomena in united atom correlation diagrams (14).

An important problem that must be pointed out is that certain portions of Rydberg expanded MO correlation diagrams may not be invariant with additional Rydberg components. For instance, if one decided to add another pair of higher energy $3p_y$ ethylene components, our previous orbital placement rules indicated that this would be inserted between the $3s_1 - 3s_2$ and the $\pi_1^* + \pi_2^*$ components. The two ethylene components would produce $3p_{y1} + 3p_{y2}$ ($3p_y$, AS'), and $3p_{y1} - 3p_{y2}$ ($3d$, AA'), in plane components. The $3p_y$ MO will correlate with σ_2 on

Can. J. Chem. Downloaded from www.nrcresearchpress.com by 210.87.254.6 on 09/06/12
For personal use only.

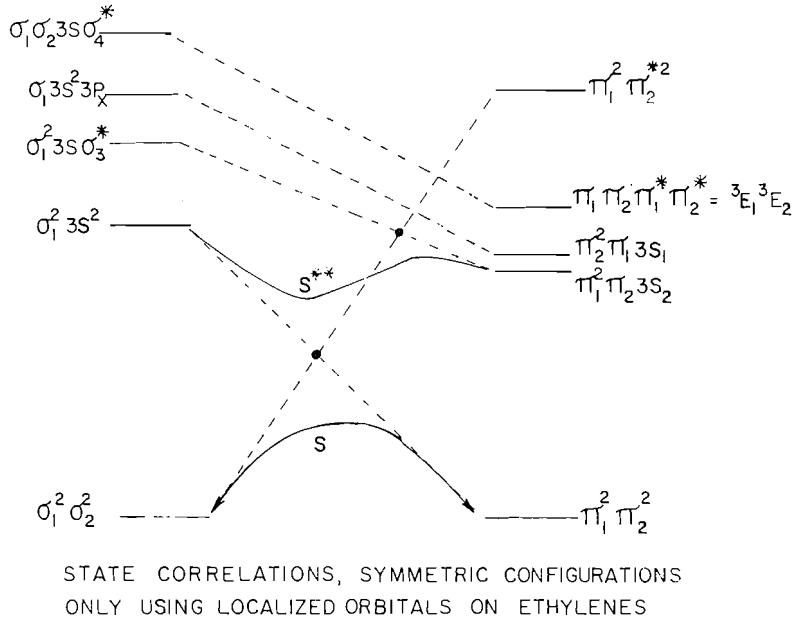

FIG. 3. Symmetric states only correlations showing that the S^{**} may correlate with a Rydberg state of the ethylene dimer.

cyclobutane. On the other hand, the additional higher energy Rydberg components will not affect the cyclobutane $3s$ localized or delocalized MO correlations. Similar variances and invariances are observed in normal united atom correlation diagrams. In a certain sense, it would appear that Fig. 2 is incomplete in not having included the $3p_{y1} + 3p_{y2} \rightarrow \sigma_2$ correlation. The AS' MO is involved in the HOMO–LUMO inversion and will eventually give rise, on the state correlation diagram, to the avoided crossing of the S_0 and S^{**} surfaces. However, this view is deceptive, since in the region of the HOMO–LUMO crossing the AS' MO will be valence and not Rydberg in character (having derydbergized before reaching this geometrical configuration). The AS' correlative behavior in this inversion region will be as if no Rydberg components had been added and the classical valence-orbital-only diagram was valid. Any interest in the Rydberg character of this AS' MO correlation would have to be retained, however, if we were interested in ethylene excited states having $3p_y$ (C—C axis directed) character. We will return to this point later.

B. Construction of the Rydberg expanded state correlation diagrams

Since, as we will show, the critical and most interesting part of the state correlation diagrams occurs using the localized Rydberg expanded MO correlation (Fig. 2) we will give a detailed discussion of Fig. 3. As is evident in Fig. 2, the lowest energy localized excitation has a $\pi 3s$ configuration. As in the previously discussed $\pi\pi^*$ valence-level-only diagram the excimer Rydberg excited states will be paired: $c_1\,[\pi_1^2\pi_2 3s_2] + c_2\,[\pi_2^2\pi_1 3s_1]$. The lowest energy excimer state will have a $\rightarrow\rightarrow$ orientation of the individual $\pi \rightarrow 3s$ transition dipoles (perpendicular to the ethylene plane). The symmetry of this state is S in the localized picture (A_1 in C_{2v}). In Fig. 3, the state configurations shown for these excimer states are considered real states as is the previously discussed bitriplet. However, on the cyclobutane part of the diagram, these doubly excited configurations do not represent real states and merely serve as correlation targets. As discussed just above, the doubly excited cyclobutane configuration, $\sigma_1^2 3s^2$, will derydbergize before reaching the minimum of the S^{**} surface, the avoided crossing region having a behavior just as if there were no Rydberg components in the correlation diagram.

The most important feature in Fig. 3 is that now the S^{**} surface evolves by a series of avoided crossings to the ethylene Rydberg monomer state, $\pi_1^2\pi_2 3s$. In the reverse direction, an ethylene $\pi 3s$ excited state will interact with an ethylene ground state to lead the system automatically onto the S^{**} surface. The critical early avoided crossing shown in Fig. 3 will be described by a configurational function having the conceptual form:

$$c_1[\pi_1^2\pi_2 3s_2] + c_2[\pi_2^2\pi_1 3s_1] + c_3[\pi_1\pi_2\pi_1^*\pi_2^*]$$

In this view, the initial portions of the S^{**} surface will have ethylene $\pi 3s$ character, the overall S^{**} surface wavefunction will derydbergize before reaching the S^{**} minimum. There is, therefore, no conceptual problem in rationalizing how an ethylene Rydberg state adiabatically evolves to the S^{**} minimum.

Analysis of the diagrammatic fate of a possible cyclobutane Rydberg state requires a further Rydberg expanded correlation diagram which we will not detail. However, the lowest A_g excited Rydberg cyclobutane state would probably have a $\sigma(e_u) \rightarrow 3p_{x,y}(e_u)$ configuration and not a doubly excited configuration A_g indicated in the classical correlation diagram. The Rydberg correlation would correlate upwards in energy and cross with the classical $\sigma_1^2\sigma_3^{*2}$ doubly excited configuration. These crossings would be avoided, and this initial cyclobutane $3p$ Rydberg state would also eventually adiabatically evolve into the S^{**} minimum.

Finally, it must be pointed out that attempts to analyze the correlative state behavior using the Rydberg expanded delocalized MO correlation diagram will lead to the same traps at the large E_1–E_2 separation that we discussed with regard to Fig. 1. Some avoidance of these conceptual traps can be accomplished by realizing that for each real monomer state there are pairs of excimer states. Even if one considers only the ethylene singlet monomer state, $\pi 3s$, $\pi\pi^*$, $\pi 3p_{x,y,z}$, this will generate 10 singlet dimer surfaces (plus the bitriplet dimer) having, initially, Franck–Condon energies all in the same energy region (7–8.5 eV). Our analysis indicates that one can limit the analysis to a simpler level in considering the probable evolution of only the S^{**} surface. Evolutions of the S^{**} hyper-

Can. J. Chem. Downloaded from www.nrcresearchpress.com by 210.87.254.6 on 09/06/12
For personal use only.

surfaces, however, will be made complicated by the fact that besides ending up in the region of the HOMO–LUMO minimum the system could also relax to give either the energy-relaxed 90° configuration of the singlet $\pi\pi^*$ state or two triplets. The latter relaxation, if it were efficient, would lead to *cis–trans* isomerization quantum yields in excess of unity.

Conclusions

We have demonstrated the utility of localized orbital and state correlation diagrams both at the valence and Rydberg extended level. The addition of Rydberg components to conventional Woodward–Hoffmann diagrams requires care because of the potentially large number of components that can be added and the redundancies in doing so. Finally, we have shown how a molecular Rydberg state can adiabatically evolve to a valence-excited state of the system.

1. M. B. ROBIN. Higher excited states in polyatomic molecules. Vols. I and II. Academic Press, New York. 1974, 1975.
2. C. SANDORFY. Topics in current chemistry. Vol. 86. Springer–Verlag. 1979. pp. 91–138.
3. E. M. EVLETH and E. KASSAB. Quantum theory of chemical activity. Vol. II. *Edited by* R. Daudel, A. Pullman, L. Salem, and A. Veillard. Reidel, Dordrecht. 1980. pp. 261–284.
4. E. M. EVLETH and E. KASSAB. Computational theoretical chemistry. *Edited by* I. G. Csizmadia and R. Daudel. Reidel, Dordrecht. 1981. pp. 379–395.
5. J.-P. MALRIEU. Theoret. Chim. Acta, Berlin, **59**, 251 (1981).
6. D. R. SALAHUB and C. SANDORFY. Theoret. Chim. Acta, Berlin, **20**, 227 (1971).
7. W. HAQUE. J. Chem. Phys. **67**, 3629 (1977).
8. A. N. SINGH and R. S. PRASAD. Chem. Phys. **49**, 267 (1980).
9. M. Z. D. HAMOUTAHRA. Thése, Elargissement de la base des états moléculaire pour des calculs C. N. D. O. par introduction d'orbitales de Rydberg; Université de Bordeaux, 1980.
10. R. S. MULLIKEN. J. Chem. Phys. **66**, 2448 (1978).
11. E. M. EVLETH, J. T. GLEGHORN, and E. KASSAB. Chem. Phys. Lett. **80**, 558 (1981).
12. E. M. EVLETH and E. KASSAB. Theoret. Chim. Acta, Berlin, **60**, 385 (1982).
13. R. S. MULLIKEN. Acc. Chem. Res. **9**, 7 (1976); Chem. Phys. Lett. **46**, 197 (1977).
14. G. HERZBERG. Molecular spectra and molecular structure. Vol. I. Van Nostrand, New York. 1950. pp. 328–329; Vol. 3, 1966. Figs. 123, 127, 129.
15. E. M. EVLETH and A. SEVIN. J. Am. Chem. Soc. **103**, 7414 (1981) and references therein.
16. P. KROPP. Org. Photochem. **4**, 1 (1979).
17. G. COLLIN, H. DESLAURIERS, and A. WIECKOWSKI. J. Phys. Chem. **85**, 944 (1981) and references therein.
18. H. YAMAZAKI, R. J. CVETANOVIĆ, and R. S. IRWIN. J. Am. Chem. Soc. **98**, 2198 (1976).
19. R. J. BUENKER and S. D. PEYERIMHOFF. Chem. Phys. **9**, 75 (1976).
20. R. J. BUENKER, S. D. PEYERIMHOFF, and S. K. SHIH. Chem. Phys. Lett. **69**, 7 (1980) and references therein.
21. L. E. MCMURCHIE and E. R. DAVIDSON. J. Chem. Phys. **67**, 5613 (1977).
22. A. GEDANKEN, N. A. KUEBLER, and M. B. ROBIN. J. Chem. Phys. **76**, 46 (1982).
23. B. R. BROOKS and H. F. SCHAEFFER III. J. Am. Chem. Soc. **101**, 307 (1979).
24. R. B. WOODWARD and R. HOFFMANN. The conservation of orbital symmetry. Verlag Chemie, Wienheim. 1970. pp. 19–21, 31–36.
25. S. SHAIK and N. D. EPIOTIS. J. Am. Chem. Soc. **100**, 18 (1978).
26. N. EPIOTIS, S. SHAIK, and W. ZANDER. Rearrangements in the ground and excited states. *Edited by* Paul de Mayo. Academic Press, New York. 1980. pp. 1–94.
27. E. KASSAB, E. M. EVLETH, J. J. DANNENBERG, and J. C. RAYEZ. Chem. Phys. **52**, 151 (1980).
28. C. GALLOY and J. C. LORQUET. J. Chem. Phys. **67**, 4672 (1977).
29. W. GERHARTZ, R. D. POSHUTA, and J. MICHL. J. Am. Chem. Soc. **98**, 6427 (1976); **99**, 4263 (1977).
30. J. D. GODDARD and I. G. CSIZMADIA. Chem. Phys. Lett. **43**, 73 (1976); **64**, 219 (1979).
31. R. J. BUENKER, V. BONACIC-KOUTECKY, and L. POGLIANI. J. Chem. Phys. **73**, 1936 (1980).
32. J. W. WRIGHT and L. SALEM. J. Am. Chem. Soc. **94**, 322 (1977).
33. K. WITTEL. Tetrahedron, **33**, 2687 (1977).
34. C. SANDORFY. Can. J. Chem. **58**, 2409 (1980); Int. J. Quant. Chem. **21**, 1147 (1981).

Can. J. Chem. Downloaded from www.nrcresearchpress.com by 210.87.254.6 on 09/06/12
For personal use only.

Chiral transformations of D-ribose to 2-(β-D-ribofuranosyl)-L and D-glycine and an anhydroallose hemiacetal used in C-nucleoside synthesis

MORRIS J. ROBINS AND J. M. ROBERT PARKER
Department of Chemistry, The University of Alberta, Edmonton, Alta., Canada T6G 2G2

Received May 19, 1982

MORRIS J. ROBINS and J. M. ROBERT PARKER. Can. J. Chem. **61**, 312 (1983).

Conversion of D-ribose to the epimeric 3,6-anhydro-4,5,7-tri-*O*-benzyl-D-*glycero*-D-(*allo* and *altro*)-heptonamides (**5**) followed published methods. Mesylation of **5** allowed convenient separation of the 2-*O*-methanesulfonyl D-*allo* (**6***a*) and D-*altro* (**6***b*) diasteromers. Individual treatment of **6***a* and *b* with lithium azide in DMF provided the inverted 2-azido D-*altro* (**7***a*) and D-*allo* (**7***b*) products. Acid catalyzed hydrolysis of the amide funciton of **7***a* and *b* followed by catalytic hydrogenolysis of the benzyl protecting and azide groups gave the target glycosyl amino acids, 2-(β-D-ribofuranosyl)-L-glycine (2-amino-3,6-anhydro-2-deoxy-D-*glycero*-D-*altro*-heptonic acid) (**9***a*) and its D-glycine (D-*allo*) epimer (**9***b*).

Deacylation of the known 2-(5-*O*-benzoyl-2,3-*O*-isopropylidene-β-D-ribofuranosyl)-1,3-diphenylimidazolidine (**10***a*) followed by mild acid catalyzed deprotection of the masked aldehyde function of **10***b* gave 3,4-*O*-isopropylidene-2,5-anhydro-D-allose (**11**), a compound prepared previously in racemic form and used in C-nucleoside synthesis.

MORRIS J. ROBINS et J. M. ROBERT PARKER. Can. J. Chem. **61**, 312 (1983).

Faisant appel à des méthodes connues, on a effectué la transformation du D-ribose en anhydro-3,6 tri-*O*-benzyl-4,5,7 D-*glycéro* D-(*allo* et *altro*) heptonamides (**5**). La mésylation du composé **5** permet une séparation convenable des diastéréoisomères *O*-méthanesulfonyl-2 D-*allo* (**6***a*) et D-*altro* (**6***b*). Les dérivés **6***a* et **6***b* réagissent chacun avec l'azoture de lithium dans le DMF en conduisant aux produits inversés azido-2 D-*altro* (**7***a*) et D-*allo* (**7***b*). L'hydrolyse de la fonction amide des composés **7***a* et **7***b*, catalysée par un acide, suivie de l'hydrogénolyse catalytique des groupes protecteurs benzyle et azoture permet d'accéder aux acides aminés glycosylés recherchés, soit l'acide (β-D-ribofurannosyl)-2 L-glycine (amino-2-anhydro-3,6 déoxy-2 D-*glycéro* D-*altro*-heptonique (**9***a*) et à son épimère, D-glycine (D-*allo*) (**9***b*).

L'élimination du groupe acyle de la (*O*-benzoyl-5 *O*-isopropylidène-2,3, β-D-ribofurannosyl)-2 diphényl-1,3 imidazolidine (**10***a*) connue, suivie de l'élimination acido catalysée du groupe protecteur de la fonction aldéhyde du composé **10***b*, donne le *O*-isopropylidène-3,4 anhydro-2,5 D-allose (**11**), un composé préparé antérieurement sous forme de mélange racémique et qui est utilisé dans la synthèse du nucléoside-C.

[Traduit par le journal]

A novel amino acid antibiotic named furanomycin (**1**) (see Scheme 1) was reported in 1967 (1). Assignment of the 2,5-*cis* stereochemistry for the glycyl and methyl substituents on the 2,5-dihydrofuran ring was made from ^{1}H nmr coupling constants. Circular dichroism data indicated an L configuration for the α-amino acid fragment. A multistep synthesis of racemic furanomycin that purported to confirm the proposed structure of the antibiotic was communicated in 1975 (2). However, no conclusions regarding the complete absolute configuration of the natural product were reached. We became interested in employing D-ribose as a chiral precursor to effect a stereodefined synthesis of the suggested *cis*-2(*R*),5(*R*)-dihydrofuran structure.

A modified Strecker-type synthesis of C-glycosyl amino acids was reported (3) for the preparation of the basic skeleton of the polyoxin group of nucleoside antibiotics (4) that have a C4′ derivatized sugar component (**2**). Other approaches were used to prepare carbohydrate analogues with an amino acid side chain at C3 (5) and C2 (6). Di-*O*-isopropylidene-D-mannono-1,4-lactone was treated with ethyl isocyanoacetate in the first step of the synthesis of the C1 linked β-D-mannofuranosylglycines (**3***a*) and β-D-lyxofuranosylglycines (**3***b*) (7). Treatment of acetobromoglucose and 3,4,6-tri-*O*-benzoyl-2,5-anhydro-D-allose with 2-phenyloxazolin-5-one gave intermediates that were converted to 2-(β-D-glucopyranosyl)-D,L-glycine and 3-(β-D-ribofuranosyl)-D,L-alanine, respectively (8). We now wish to report applications of the Strecker-type approach developed by Moffatt and coworkers to the synthesis of 2-(β-D-ribofuranosyl)-L-glycine, its

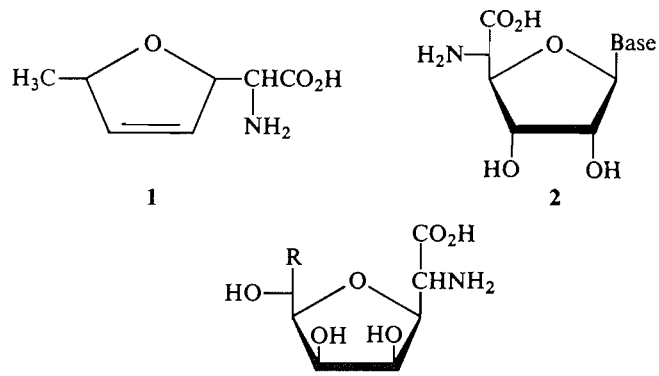

SCHEME 1

D-glycine epimer, and 3,4-*O*-isopropylidene-2,5-anhydro-D-allose.

Acid catalyzed deprotection of 2-(2,3,5-tri-*O*-benzyl-β-D-ribofuranosyl)-1,3-diphenylimidazolidine (**4**) (9) was followed immediately by *in situ* treatment of the resulting aldehyde with aqueous sodium cyanide/potassium carbonate, and then hydrogen peroxide as described (9, 10). The epimeric α-hydroxy amide products (**5**) were obtained in ~90% yield (see Scheme 2). Treatment of **5** with methanesulfonyl chloride in pyridine gave the diastereomeric 2-*O*-mesyl derivatives (**6**) as a solid. Trituration of this mixture with warm ether resulted

0008-4042/83/020312-05$01.00/0
©1983 National Research Council of Canada/Conseil national de recherches du Canada

Can. J. Chem. Downloaded from www.nrcresearchpress.com by 210.87.254.6 on 09/06/12
For personal use only.

Can. J. Chem. Downloaded from www.nrcresearchpress.com by 210.87.254.6 on 09/06/12
For personal use only.

in fractionation of the epimers. The insoluble residue (43%) was the more rapidly migrating isomer on thin layer chromatography (tlc, chloroform/ethyl acetate, 1:1, $R_f \sim 0.50$) and was later correlated as the 2(*R*) isomer (**6***a*). Chromatography of the ether supernatant solution gave **6***b* (38%, $R_f \sim 0.47$) contaminated with ~5% of **6***a*. These epimers were distinguished readily by ^{1}H nmr spectroscopy. The signal for the mesyl group appeared at δ 2.91 for **6***a* and 2.86 for **6***b*. The signal for H2 was centered at δ 4.90 (J_{2-3} = 5 Hz) for **6***a* and 4.91 (J_{2-3} = 4 Hz) for **6***b*. These H2 resonances were shifted downfield from those of their 2-hydroxy precursors (**5**). The pseudooctet centered at δ ~ 3.57 for the H7,7′ protons of **6***a* was clearly different from the corresponding multiplet at ~3.55 for **6***b* (see the Experimental).

Infrared (ir) spectra of **6***a* or *b* and all of the subsequently obtained α-substituted amides had the characteristic amide carbonyl stretching band at ~1650 cm^{-1}. Mass spectral fragmentation patterns for **6***a* and *b* were similar with parent ions at *m/z* 555 (M^+) and 556 (M + 1). The M + 1 ion was present in spectra of most of the other α-substituted amide derivatives. Other characteristic ions for **6***a*, *b* appeared at *m/z* 476 (M − SO_2CH_3) and 464 (M − $CH_2C_6H_5$).

Independent treatment of **6***a* and *b* with lithium azide[1] in hot *N*,*N*-dimethyl formamide (DMF) gave the diastereomeric α-azido amides **7***a* and *b* in ~90% yields. Moffatt and co-workers had utilized a parallel sequence in their synthesis of polyoxin compounds (3). They presented a chemical proof of inversion of configuration for the complementary α-azido amides. Indicative evidence supports parallel inversions in the present work. Loss of the mesyl singlet was accompanied by an upfield shift of the H2 nmr signal, and a strong band at 2120 cm^{-1} (R—N_3) appeared in the ir spectra of **7***a* and *b*. The splitting patterns for the H7 and 7′ nmr multiplets of **7***a* centered at δ 3.46 and 3.57 corresponded closely to those of **6***b*, and a similar correspondence of these patterns was observed for **7***b* and **6***a*. The order of melting behavior for **6***a* (mp 173−174°C) and **6***b* (114−115°C) also was inverted for **7***a* (93−94°C) and **7***b* (155−156°C).

Solvolysis of the amide function occurred smoothly (>90% yields) upon heating **7***a* or *b* with a strong acid resin in methanol (10). However, the subsequently obtained α-amino esters were unstable at room temperature and were slowly converted to unidentified (diketopiperazine?) products.

Hydrolysis of the amides **7***a* and *b* proceeded quantitatively in hot hydrochloric acid/dioxane solution to give the syrupy α-azido acids **8***a* and *b*. Hydrogenolysis of the azido function and benzyl protecting groups was effected at 100 psi in ethanol buffered at pH ~ 5 with aqueous ammonium acetate in the presence of an equal weight of 5% palladium on carbon. Complete deprotection was dependent on the efficiency of stirring as well as the quality of the catalyst.[2] The glycosyl amino acids **9***a* and *b* were isolated (in ~50% yields from **7***a* and *b*) by application of the hydrogenolysis residue to a strong acid resin and elution with aqueous ammonia. The L-amino acid (**9***a*) crystallized as a dihydrate that was partially dehydrated by heating *in vacuo* at 56°C. The D-epimer (**9***b*) did not crystallize and was isolated as an amorphous solid. Preliminary attempts to obtain more readily crystallized hydrochloride salts resulted in hygroscopic materials.

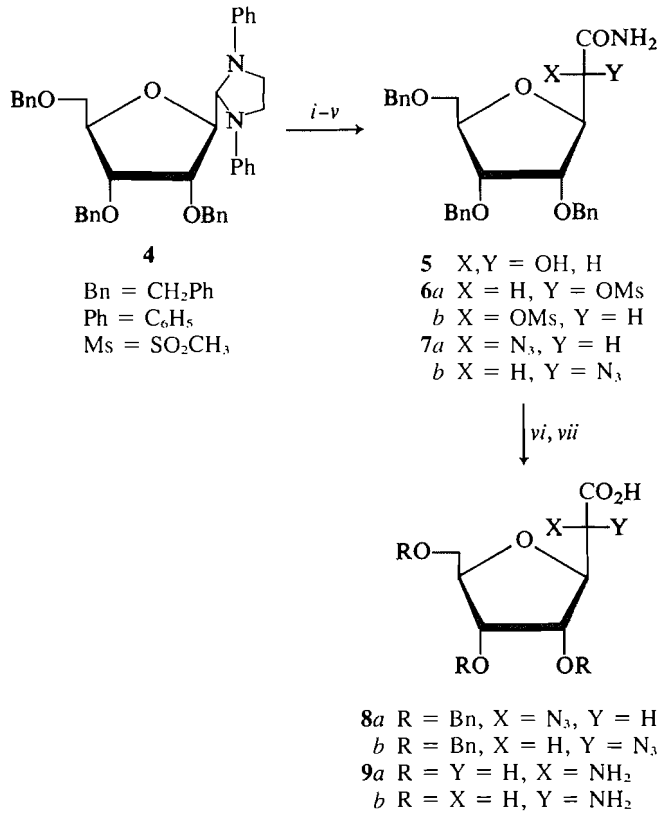

4
Bn = CH_2Ph
Ph = C_6H_5
Ms = SO_2CH_3

5 X,Y = OH, H
6*a* X = H, Y = OMs
b X = OMs, Y = H
7*a* X = N_3, Y = H
b X = H, Y = N_3

8*a* R = Bn, X = N_3, Y = H
b R = Bn, X = H, Y = N_3
9*a* R = Y = H, X = NH_2
b R = X = H, Y = NH_2

(*i*) *p*-$CH_3C_6H_4SO_3H \cdot H_2O$; (*ii*) $NaCN/K_2CO_3/H_2O$; (*iii*) H_2O_2/H_2O; (*iv*) MsCl/pyridine; (*v*) LiN_3/DMF; (*vi*) HCl/H_2O/dioxane; (*vii*) H_2(100 psi)/EtOH/NH_4OAc/H_2O.

SCHEME 2

The ir spectrum of **9***a* had strong bands at 1640 (CO_2^-), 1500 (NH_3^+), and 3100−3400 cm^{-1} (OH, NH) characteristic of α-amino acids. Assignments of the L and D amino configurations were made from ord and cd curves obtained from solutions of **9***a* and *b* in 6 *N* hydrochloric acid. Epimer **9***a* had $[\phi]_{225} = +2000$ and $[\theta]_{210} = +2010$. These positive effects are characteristic for L α-amino acids (11, 12). The D epimer (**9***b*) had $[\phi]_{225} = -2300$ and $[\theta]_{210} = -1850$.

During the course of our work on synthesis of C-glycosyl amino acids related to furanomycin (13, 14), 3,4-*O*-isopropylidene-2,5-anhydro-D-allose (**11**) (see Scheme 3) was prepared as an intermediate. This product had been synthesized in racemic form by Just and co-workers beginning from a Diels−Alder reaction with furan (15). Other anhydro derivatives of D-allose have been obtained beginning with D-glucose (16) or by diazotization of 2-amino-2-deoxyaltropyranose derivatives (17). Reviews of carbohydrate precursors and their elaboration to a variety of C-nucleosides are available (18). A facile route to **11** from D-ribose follows.

The readily prepared 2-(5-*O*-benzoyl-2,3-*O*-isopropylidene-β-D-ribofuranosyl)-1,3-diphenylimidazolidine (**10***a*) reported by Moffatt and co-workers (9) was deacylated with methanolic sodium methoxide to give **10***b* in 95% yield. Treatment of **10***b* with *p*-toluenesulfonic acid monohydrate resulted in hydrolysis of the imidazolidine ring within ten minutes. Participation of the primary alcohol function in the hydrolytic displacement of the *N*,*N*′-diphenylethylenediamine protecting group (19) is likely, since analogous deprotection (3, 9) of the aldehyde

[1]Analogous treatment with sodium azide (3) was ineffective.

[2]Activation of the catalyst by stirring with 1 *N* hydrochloric acid, washing with water, and drying and storage under vacuum proved useful.

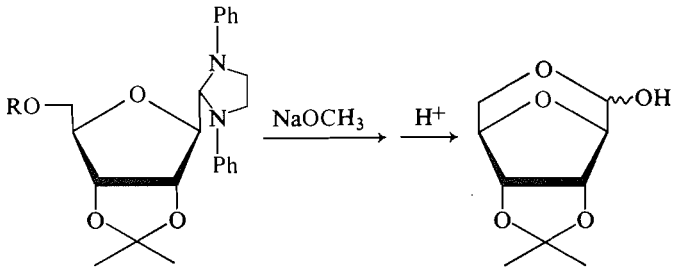

10*a* R = COPh
b R = H

11

SCHEME 3

function occurred much more slowly with the 6-*O*-benzyl or 6-*O*-benzoyl derivatives examined (13). Compound **11** was obtained in 84% yield after chromatography over silica. The tlc homogeneous solid was crystallized from chloroform/hexane to give an analytically pure product with ^{1}H nmr and mass spectral properties in agreement with the indicated structure. Exploratory reactions with **11** did not lead to promising routes for the synthesis of furanomycin (13). This sample of the epimeric hemiacetal (**11**) had a depressed melting point with respect to that of the reported racemate (15).

This study has demonstrated the convenient transformation of D-ribose to 3,4-*O*-isopropylidene-2,5-anhydro-D-allose (**11**), which was synthesized previously as a racemate and used to prepare C-nucleosides. Successful transformation of D-ribose to the target C-glycosyl amino acids 2-(β-D-ribofuranosyl)-L-glycine (2-amino-3,6-anhydro-2-deoxy-D-*glycero*-D-*altro*-heptonic acid) (**9***a*) and its 2-epimer (**9***b*) demonstrated the feasibility of this approach for the stereodefined synthesis of the structure proposed for furanomycin. Achievement of that goal and collaborative efforts that resulted in reassignment of the stereochemistry of the natural product structure are reported in the accompanying paper (14).

Experimental

General

Melting points were obtained on a Reichert microstage block and are uncorrected. Ultraviolet (uv) spectra were recorded on a Cary 15 spectrophotometer. Infrared (ir) spectra were recorded on a Nicolet 7199 FT (IR) spectrometer. Circular dichroism (cd) and optical rotatory dispersion (ord) spectra were determined on a Jasco ORD-UV-5 (CD-SS-20) spectrophotopolarimeter in H_2O or HCl/H_2O solutions. Optical rotations were measured using a Perkin–Elmer 241 polarimeter. The ^{1}H nmr spectra were recorded on a Varian HA-100 instrument by the nmr laboratory of this department using $CDCl_3$ with Me_4Si as internal standard unless otherwise specified. Mass spectra (ms) were obtained by the mass spectrometry laboratory of this department using an AEI MS-50 instrument with direct probe and computer averaging at 100–250°C and 70 eV for EI spectra or an AEI MS-12 instrument for chemical ionization (NH_3) spectra. Elemental analyses were determined by the microanalytical laboratory of this department.

All solvents were distilled prior to use. "Hexane" refers to the fraction of Skellysolve B boiling from 63–65°C. Solutions were dried over anhydrous sodium sulfate prior to filtration and evaporation using a Büchi rotary evaporator equipped with a Dewar Dry Ice condensor under water aspirator or oil vacuum pump (*in vacuo*) reduced pressure.

Thin layer chromatography (tlc) was performed on Eastman chromatogram sheets (silica gel #13181 with #6060 indicator) when uv (2537 Å) detection was used. Glass plates (coated with Merck silica gel PF-254 prepared as a slurry in $CHCl_3$) were used for detection by spraying with 5% H_2SO_4/EtOH and charring at 100–200°C. J. T. Baker #5-3405 (60–200 mesh) silica gel was used for column chromatography. J. T. Baker ANGC-244(H^+) strong acid resin was used for ion exchange chromatography and amide solvolysis catalysis. Paper chromatography (ascending) was performed on Whatman #2 Chroma sheets. Solvents used for chromatography were: (A) $CHCl_3$/EtOAc (1:1), (B) n-PrOH/H_2O (7:3), (C) n-BuOH/HOAc/H_2O (4:1:6) upper phase. The 5% palladium on carbon catalysts were purchased from Eastman or Apache Chemicals.

*3,6-Anhydro-4,5,7-tri-*O*-benzyl-*D-glycero-D-(allo *and* altro)*-heptonamide (**5**)*

A solution of *p*-toluenesulfonic acid monohydrate (5.9 g, 31 mmol) in Me_2CO (5 mL) was added to a stirred solution of 6.5 g (10.4 mmol) of 2-(2,3,5-tri-*O*-benzyl-β-D-ribofuranosyl)-1,3-diphenylimidazolidine (**4**) (9) in CH_2Cl_2 (100 mL) at 0°C. After stirring for 15 min at 0°C followed by 30 min at room temperature, an additional 500 mg of *p*-$CH_3C_6H_4SO_3H \cdot H_2O$ in Me_2CO (1 mL) was added. After a total reaction time of 1 h, the mixture was diluted with CH_2Cl_2 (100 mL), filtered using a Celite pad, washed with saturated brine (3 × 20 mL), dried, and evaporated. The residue was dissolved in dioxane, cooled to 10°C, and treated with NaCN (8.7 g) and K_2CO_3 (8.7 g) in H_2O (100 mL). After stirring at 0°C for 30 min the reaction was treated dropwise with 30% H_2O_2/H_2O (30 mL). After stirring for 1 h at 0°C the mixture was poured into H_2O (3 L). The precipitate was filtered and dried to give 4.5 g (91%) of **5** (10) contaminated with a trace impurity (tlc, A, impurity $R_f \sim 0.8$, product (**5**) $R_f \sim 0.2$).

*3,6-Anhydro-4,5,7-tri-*O*-benzyl-2-*O*-methanesulfonyl-*D-glycero-D-(allo *and* altro)*-heptonamides (**6**a *and* **6**b)*

A solution of the mixture of **5** (4.77 g, 10 mmol) in pyridine (25 mL) and CH_2Cl_2 (35 mL) at 0°C was treated dropwise with methanesulfonyl chloride (5.7 g, 4.05 mL, 50 mmol) in CH_2Cl_2 (15 mL). After 7 h at 0°C the reaction was diluted with CH_2Cl_2 (200 mL) and poured into ice-cold 1 *N* HCl/H_2O (100 mL). The organic layer was washed with 1 *N* HCl/H_2O (2 × 50 mL), saturated $NaHCO_3/H_2O$ (3 × 25 mL), saturated brine (3 × 25 mL), dried, and evaporated to a solid. This was triturated with warm Et_2O (100 mL) and filtered to give 2.4 g (43%) of **6***a* (tlc, A, $R_f \sim 0.50$). This product was recrystallized from MeOH to give 2.1 g (38%) of white needles, mp 173–174°C; $[\alpha]_D^{23}$ +65° (*c* 0.2, $CHCl_3$); ir (KBr): 1650 cm^{-1} ($CONH_2$); nmr δ: 2.91 (s, 3, SO_2CH_3), 3.44 & 3.71 (octet, $J_{7-7'} = 10$ Hz, $J_{7-6} = 3$ Hz, $J_{7'-6} = 2.5$ Hz, 2, H7,7′), 3.85–4.80 (m, 10, sugar and CH_2Ph), 4.90 (d, $J_{2-3} = 5$ Hz, 1, H2), 5.7 & 6.5 (bs, 2, $CONH_2$), 7.30 (m, 15, aromatic); ms *m/z*: 555.1954 (1.0, M^+, calcd for $C_{29}H_{33}NO_8S$: 555.1927), 476.2074 (0.6, M − SO_2CH_3), 465.1409 (26, M + 1 − CH_2Ph), 464.1374 (100, M − CH_2Ph), 449.1501 (2.4, M + 1 − OCH_2Ph), 448.1416 (2.7, M − OCH_2Ph), 358.0963 (M^+ − CH_2Ph − OCH_2Ph). *Anal.* calcd. for $C_{29}H_{33}NO_8S$: C 62.69, H 5.99, N 2.52, S 5.77; found: C 62.83, H 6.07, N 2.54, S 5.78.

The residual syrup from evaporation of the ether supernatant was chromatographed on silica (40 g, 3 × 14 cm). Elution with solvent A and evaporation of solvents gave 2.1 g (38%) of **6***b* as a white solid. This slower migrating isomer was crystallized from Et_2O (50 mL) to give a product (1.2 g) that contained a trace of **6***a* (tlc) and had mp 114–115°C; $[\alpha]_D^{23}$ +30° (*c*, 0.2, $CHCl_3$); nmr δ: 2.86 (s, 3, SO_2CH_3), 3.47 & 3.62 (m, $J_{7-7'} = 11$ Hz, $J_{7-6} = 4$ Hz, $J_{7'-6} = 3.5$ Hz, 2, H7,7′), 3.80–4.70 (m, 10, sugar and CH_2Ph), 4.91 (d, $J_{2-3} = 4$ Hz, 1, H2), 5.9 & 6.4 (bs, 2, $CONH_2$), 7.25 (m, 15, aromatic); ms *m/z*: 555.1928 (0.3, M^+, calcd. for $C_{29}H_{33}NO_8S$: 555.1927), 476.2049 (0.1, M − SO_2CH_3), 465.1426 (11; M + 1 − CH_2Ph), 464.1392 (42, M − CH_2Ph), 449.1481 (0.8, M + 1 − OCH_2Ph).

*3,6-Anhydro-2-azido-2-deoxy-4,5,7-tri-*O*-benzyl-*D-glycero-D-(altro *and* allo)*-heptonamides (**7**a *and* **7**b)*

A solution of **6***a* or **6***b* (1.11 g, 2 mmol) and LiN_3 (245 mg, 5 mmol) in DMF (40 mL) was heated at 100°C for 6 h, cooled, and poured into Et_2O (100 mL) and 5% $NaCl/H_2O$ (25 mL). The aqueous layer was extracted with Et_2O (3 × 25 mL). The combined organic layers were evaporated to a syrup and purified by chromatography on silica (20 g, 12 × 2.2 cm). Elution with solvent A gave the desired product.

Can. J. Chem. Downloaded from www.nrcresearchpress.com by 210.87.254.6 on 09/06/12
For personal use only.

Can. J. Chem. Downloaded from www.nrcresearchpress.com by 210.87.254.6 on 09/06/12
For personal use only.

"Faster" isomer (7a)

The yield after chromatography was 980 mg (98%). This solid was crystallized from EtOH with 50–70% recovery; mp 93–94°C; $[\alpha]_D^{23}$ +13° (*c* 0.2, $CHCl_3$); ir (KBr): 1670 ($CONH_2$), 2110 cm^{-1} (R—N_3); nmr δ3.46 & 3.57 (m, $J_{7-7'}$ = 10 Hz), J_{7-6} = 4 Hz, $J_{7'-6}$ = 3.5 Hz, 2, H7,7'), 3.80–4.20 (m, 11, sugar and CH_2Ph), 5.8 & 6.3 (bs, 2, $CONH_2$), 7.3 (s, 15, aromatic); ms *m/z*: 474.2157 (4.8, $M^+ - N_2$, calcd. for $C_{28}H_{30}N_2O_5$: 474.2155), 384.1646 (1.2, M + 1 − N_2 − CH_2Ph), 383.1610 (4.6, M − N_2 − CH_2Ph), 368.1734 (2.2, M + 1 − N_2 − OCH_2Ph). *Anal.* calcd. for $C_{28}H_{30}N_4O_5$: C 66.92, H 6.02, N 11.15; found: C 66.57, H 6.06, N 11.11.

"Slower" isomer (7b)

The yield after chromatography was 920 mg (92%). This solid was crystallized from Et_2O/hexane with ~70% recovery, mp 155–156°C; $[\alpha]_D^{23}$ +10° (*c* 0.2, $CHCl_3$); nmr δ: 3.92 & 3.60 (octet, $J_{7-7'}$ = 10 Hz, J_{7-6} = 3.5 Hz, $J_{7'-6}$ = 4 Hz, 2, H7,7'), 3.80–4.70 (m, 11, sugar and CH_2Ph), 6.0 & 6.4 (bs, 2, $CONH_2$), 7.3 (s, 15, aromatic); ms *m/z*: 503.2268 (2.1, M + 1), 502.2179 (0.2, M^+, calcd. for $C_{28}H_{30}N_4O_5$: 502.2189), 475.2211 (6.7, M + 1 − N_2), 474.2147 (11, M − N_2), 384.1645 (1.8, M − N_2 − CH_2Ph). *Anal.* calcd. for $C_{28}H_{30}N_4O_5$: C 66.92, H 6.02, N 11.15; found: C 66.96, H 6.11, N 10.97.

2-(β-D-Ribofuranosyl)-(L and D)-glycines or 2-amino-3,6-anhydro-2-deoxy-D-glycero-D-(altro and allo)-heptonic acids (9a and 9b)

A solution of **7***a* or **7***b* (502 mg, 1 mmol) in dioxane (10 mL) and 6 *N* HCl/H_2O (2 mL) was stirred at 80°C for 18 h, cooled, diluted with H_2O (20 mL), and extracted with $CHCl_3$ (3 × 20 mL). The combined organic layers were washed with saturated brine (3 × 10 mL), dried, and evaporated to give 510 mg (quantitative) of **8***a* or **8***b* as a colorless stiff syrup. This was dissolved in EtOH (40 mL) and 1 *M* NH_4OAc/H_2O (10 mL, adjusted to pH = 5 with HOAc) and hydrogenated over 5% Pd–C (500 mg) at 100 psi with vigorous stirring for 48 h. The mixture was filtered using a Celite pad and the filter cake was washed with 95% EtOH (25 mL) and H_2O (25 mL). The combined filtrate was evaporated to a syrup, dissolved in a small volume of H_2O, and applied to a column of ANGC(H^+) resin (20 g). The column was washed with H_2O until the eluate was neutral, followed by 0.5 *N* NH_3/H_2O. The ninhydrin positive fractions were collected and evaporated *in vacuo* to give ~110 mg (53%) of **9***a* or **9***b* as a tan colored solid that was homogeneous on paper chromatography (B, R_f 0.25; C, R_f 0.07). Crystallization of **9***a* from EtOH/H_2O gave fine colorless needles that gave analytical data in agreement with a dihydrate. This sample was dried *in vacuo* at 56°C for 3 days to give crystals that softened at ~125–130°C and melted with decomposition at ~208–210°C; $[\alpha]_D^{23}$ −12° (*c* 0.1, H_2O); ir (KBr): 1500 (NH_3^+), 1640 (CO_2^-), 3100–3400 cm^{-1} (OH, NH); ord (6 *N* HCl) $[\phi]_{225}$ = +2000; cd (6 *N* HCl) $[\theta]_{210}$ = +2010. *Anal.* calcd. for $C_7H_{13}NO_6 \cdot 0.75\ H_2O$: C 38.10, H 6.62, N 6.35; found: C 38.05, H 6.57, N 6.10.

The D-isomer (**9***b*) was isolated as an amorphous solid; mp ~120°C (dec.); $[\alpha]_D^{23}$ −4° (*c* 0.1, H_2O); ord (6 *N* HCl) $[\phi]_{225}$ = −2300; cd (6 *N* HCl) $[\theta]_{210}$ = −1850.

1,3-Diphenyl-2-(2,3-O-isopropylidene-β-D-ribofuranosyl)-imidazolidine (10b)

A solution of 10 g (20 mmol) of the 5-*O*-benzoyl derivative (**10***a*) (9) in $CHCl_3$ (150 mL) was added to a stirred solution of 0.1 *N* NaOMe/MeOH (150 mL) at room temperature. After 2.5 h the solution was poured into $CHCl_3$ (200 mL) and saturated NH_4Cl/H_2O (200 mL). The aqueous layer was extracted with $CHCl_3$ (3 × 25 mL). The combined organic layers were washed with saturated brine (3 × 20 mL), dried, and evaporated to a white solid. This residue was dissolved in hot MeOH (150 mL) and allowed to crystallize at room temperature to give 7.5 g (95%) of **10***b*, mp 170–171°C; $[\alpha]_D^{23}$ −50° (*c* 0.2, $CHCl_3$); uv (MeOH) max: 253 & 293 nm (ε 34 700 & 4400); nmr δ: 1.26 & 1.35 (s & s, 3 & 3, $C(CH_3)_2$), 2.2 (bs, 1, OH), 3.3–4.7 (m, 10, sugar and CH_2CH_2), 5.65 (s, 1, H1), 6.7–7.3 (m, 10, aromatic); ms *m/z*: 398.2159 (1.3, M + 2), 397.2124 (4.1, M + 1, calcd. for $C_{23}H_{29}N_2O_4$: 397.2127), 396.2029 (1.2, M^+), 395.1971 (2.4, *M* − 1), 382.1857 (0.9, M + 1 − CH_3), 381.1820 (3.0, M − CH_3). *Anal.* calcd. for $C_{23}H_{28}N_2O_4$: C 69.67, H 7.12, N 7.07; found: C 69.53, H 7.00, N 7.09.

2,5-Anhydro-3,4-O-isopropylidene-D-allose (11)

A stirred solution of **10***b* (396 mg, 1 mmol) in CH_2Cl_2 (15 mL) at room temperature was treated with *p*-toluenesulfonic acid monohydrate (570 mg, 3 mmol) in Me_2CO (1 mL). After 15 min the dense white mixture was diluted with Et_2O (25 mL) and filtered using a Celite pad. The filtrate was concentrated to a white gum, dissolved in EtOAc (25 mL), and washed with a small volume of saturated brine (5 mL). The aqueous layer was extracted with EtOAc (3 × 5 mL). The combined organic layers were dried and evaporated to a white solid (210 mg, quantitative). This product was rapidly chromatographed on silica gel with EtOAc/hexane (2:1) to give 170 mg (84%) of a white solid. An analytical sample was crystallized from $CHCl_3$/hexane to give **11** with mp 168–170°C (lit. (15) mp 185–186°C (racemate)); $[\alpha]_D^{23}$ +12° (*c* 1.0, $CHCl_3$); nmr (Me_2CO-d_6) δ: 1.30 & 1.38 (s & s, 3 & 3, $C(CH_3)_2$), 3.2–4.2 (m, 4, sugar protons), 4.6–5.0 (m, 3, sugar protons), 5.4 & 6.0 (d & d, 1, epimeric OH); ms *m/z*: 202.0843 (1.4, M^+, calcd. for $C_9H_{14}O_5$: 202.0841), 187.0608 (100, M − CH_3), 185.0815 (5.4, M − OH), 173.0813 (6.1, M − OH − CH_3). *Anal.* calcd. for $C_9H_{14}O_5$: C 53.46, H 6.98, O 39.56; found: C 53.24, H 7.00, O 39.69.

Acknowledgements

We thank the Natural Sciences and Engineering Research Council of Canada (A5890), the National Cancer Institute of Canada, and the University of Alberta for generous financial support. M.J.R. thanks Professor A. D. Broom for facilities and hospitality provided during a visiting professorship at the University of Utah 1981–1982.

1. K. KATAGIRI, K. TORI, Y. KIMURA, T. YOSHIDA, T. NAGASAKI, and H. MINATO. J. Med. Chem. **10**, 1149 (1967).
2. T. MASAMUNE and M. ONO. Chem. Lett. 625 (1975).
3. N. P. DAMODARAN, G. H. JONES, and J. G. MOFFATT. J. Am. Chem. Soc. **93**, 3812 (1971).
4. K. ISONO, K. ASAHI, and S. SUZUKI. J. Am. Chem. Soc. **91**, 7490 (1969).
5. (*a*) A. ROSENTHAL and B. CLIFF. J. Carbohydr. Nucleosides Nucleotides, **2**, 263 (1975); (*b*) A. J. BRINK, J. COETZER, O. G. DE VILLIERS, R. H. HALL, A. JORDAAN, and G. J. KRUGER. Tetrahedron, **32**, 965 (1976).
6. K. BISCHOFBERGER, A. J. BRINK, O. G. DE VILLIERS, R. H. HALL, and A. JORDAAN. J. Chem. Soc. Perkin Trans. I, 1472 (1977).
7. R. H. HALL, K. BISCHOFBERGER, S. J. EITELMAN, and A. JORDAAN. J. Chem. Soc. Perkin Trans. I, 743 (1977).
8. (*a*) A. ROSENTHAL and A. J. BRINK. J. Carbohydr. Nucleosides Nucleotides, **2**, 343 (1975); (*b*) A. ROSENTHAL and A. J. BRINK. Carbohydr. Res. **47**, 332 (1976).
9. H. P. ALBRECHT, D. B. REPKE, and J. G. MOFFATT. J. Org. Chem. **38**, 1836 (1973).
10. G. TRUMMLITZ and J. G. MOFFATT. J. Org. Chem. **38**, 1841 (1973).
11. J. C. CRAIG and S. K. ROY. Tetrahedron, **21**, 391 (1965).
12. B. W. BYCROFT. *In* Amino-acids, peptides and proteins. Chem. Soc. Spec. Periodical Report for 1971, Vol. **4**, 19 (1972).
13. J. M. R. PARKER. Ph.D. Dissertation, The University of Alberta. 1980.
14. M. J. ROBINS and J. M. R. PARKER. Can. J. Chem. **61**, 317 (1983).
15. (*a*) G. JUST and A. MARTEL. Tetrahedron Lett. 1517 (1973); (*b*) G. JUST, A. MARTEL, K. GROZINGER, and M. RAMJEESINGH. Can. J. Chem. **53**, 131 (1975).
16. T. OGAWA, Y. KIKUCHI, M. MATSUI, H. OHRUI, H. KUZUHARA,

and S. EMOTO. Agric. Biol. Chem. **35**, 1825 (1971).
17. C.-D. CHANG and JT. L. HULLAR. Carbohydr. Res. **54**, 217 (1977).
18. (*a*) S. HANESSIAN and A. G. PERNET. Adv. Carbohydr. Chem. Biochem. **33**, 111 (1976); (*b*) G. D. DAVES, JR. and C. C. CHENG. Prog. Med. Chem. **13**, 303 (1976).
19. H.-W. WANZLICK and W. LÖCHEL. Chem. Ber. **86**, 1463 (1953).

Can. J. Chem. Downloaded from www.nrcresearchpress.com by 210.87.254.6 on 09/06/12
For personal use only.

Chiral transformations of D-ribose to 2(*S*)-amino-2-[2,5-dihydro-5(*R*)-methylfuran-2(*R*)-yl]ethanoic acid, a diastereomer of the antibiotic (+)-furanomycin

MORRIS J. ROBINS AND J. M. ROBERT PARKER
Department of Chemistry, The University of Alberta, Edmonton, Alta., Canada T6G 2G2

Received May 19, 1982

MORRIS J. ROBINS and J. M. ROBERT PARKER. Can. J. Chem. **61**, 317 (1983).

The chain-extended 2-(2,3-*O*-isopropylidene-β-D-ribofuranosyl)-1,3-diphenylimidazolidine derivative (**3***a*) was prepared by a known sequence from D-ribose. Benzylation of the primary alcohol function of **3***a*, deprotection of the masked aldehyde, chain extension using a modified Strecker-type synthesis, and acetylation of the resulting epimeric 2-hydroxyl groups gave the appropriately blocked seven-carbon 3,6-anhydro compounds (**5***a*, *b*). The primary alcohol function was deprotected and then removed by mesylation, iodide replacement, and hydrogenolysis. The 2-hydroxyl group was deprotected, mesylated, and replaced by azide. Methanolysis of the amide and isopropylidene groups gave the α-azido ester diols (**13***a*, *b*). Treatment of **13***a* with thiocarbonyldiimidazole followed by the Corey–Winter reaction with trimethylphosphite effected concomitant reduction of the azide function and reductive elimination of the cyclic thionocarbonate group. Saponification of the ester intermediate gave the target α-amino acid, 2(*S*)-amino-2-[2,5-dihydro-5(*R*)-methylfuran-2(*R*)-yl]ethanoic acid (**1**). Comparison of the properties of **1** and (+)-furanomycin confirmed the necessity of revision of stereochemistry for the antibiotic.

MORRIS J. ROBINS et J. M. ROBERT PARKER. Can. J. Chem. **61**, 317 (1983).

Partant du D-ribose, on a allongé la chaîne par une série connue de réactions pour obtenir le dérivé (*O*-isopropylidène-2,3 β-D-ribofurannosyl)-2 diphényl-1,3 imidazolidine (**3***a*). La benzylation de la fonction alcool primaire du composé **3***a*, la déprotection de la fonction aldéhyde bloquée, l'extension de chaîne utilisant une synthèse modifiée de type Strecker et l'acétylation des groupes hydroxyle-2 épimères qui en résulte donne les composés anhydro-3,6 (**5***a*, *b*) à sept carbones protégés adéquatement. On a déprotégé la fonction alcool primaire et on l'a enlevé par une mésylation, suivie d'une substitution par l'iode et d'une hydrogénolyse. On a déprotégé le groupe hydroxyle-2 que l'on a mésylé puis substitué par un azide. La méthanolyse des groupes amides et isopropylidène donne les diols esters α-azido (**13***a*, *b*). Le traitement du composé **13***a* avec le thiocarbonyldiimidazole, suivi de la réaction de Corey–Winter avec le triméthylphosphite, conduit à une réduction concomitante de la fonction azide et à une élimination réductrice du groupe thiocarbonate cyclique. La saponification de l'ester intermédiaire permet d'obtenir l'acide α-aminé désiré: l'acide amino-2(*S*) [dihydro-2,5 méthyl-5(*R*) furannyl-2(*R*)]-2 éthanoique (**1**). La comparaison des propriétés du composé **1** avec celles de la (+)-furannomycine a confirmé la nécessité de revoir la stéréochimie de l'antibiotique.

[Traduit par le journal]

A new α-amino acid antibiotic, (+)-furanomycin, was reported by Katagiri and co-workers in 1967 (1). Chemical degradation and spectroscopic studies indicated an α-(5-methyl-2,5-dihydrofuran-2-yl)glycine structure. It was concluded from the large H2 to H5 proton coupling constant that the orientation of the methyl and glycyl substituents was *cis* on the dihydrofuran ring. The positive Cotton effects in circular dichroism spectra of the antibiotic and its dihydro derivative allowed assignment of the α-amino configuration. It was concluded that the natural product was "(+)-α(*R*)-amino(2,5-dihydro-5(*R*)-methyl)furan-2(*R*)-acetic acid or one of its [*cis*] diastereomers" (1).[1] In 1975 Masamune and Ono reported a multistep synthesis of racemic furanomycin. Their product, derived from an initial limited Birch reduction of 5-methyl-2-furoic acid, was assigned a *cis*-2,5-dihydrofuran structure that was "identical with the natural sample" (2). Since no data were presented to define the absolute stereochemistry of the antibiotic, we began studies involving chiral conversions of D-ribose to give 2(*S*)-amino-2-[2,5-dihydro-5(*R*)-methylfuran-2(*R*)-yl]ethanoic acid (**1**), the structure originally proposed (1).[1]

Modified Strecker-type syntheses of C-glycosyl glycine precursors were reported by Moffatt and co-workers in their preparation of the basic skeleton of the polyoxin group of

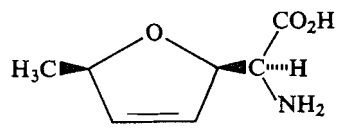

1

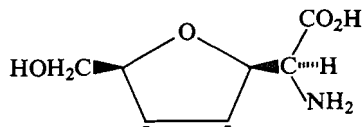

2

nucleoside antibiotics (3) and intermediates used in C-nucleoside syntheses (4). We successfully applied that approach to the construction of a 2-(β-D-ribofuranosyl)-L-glycine (**2**) model for furanomycin that possessed the requisite amino acid unit at position 2, a single carbon unit at position 5, and diol functionality at positions 3 and 4 suitable for elaboration to the target 2,5-dihydrofuran structure (**1**) (5, 6). Although conversion of **2** to **1** is presumably possible, the multifunctional hydrophilic nature of **2** suggested that a new approach from D-ribose using appropriately selected protecting groups would be more profitable. One sequence was pursued with tritylation of the primary alcohol, benzylation of the secondary alcohols, protection of the chain extended aldehyde with 1,2-di-(*N*-

[1]On page 1150 of ref. 1 it is stated that "these α-amino acids belong to the L-series." Therefore, their α(*R*) designation should have been α(*S*).

0008-4042/83/020317-06$01.00/0
©1983 National Research Council of Canada/Conseil national de recherches du Canada

Can. J. Chem. Downloaded from www.nrcresearchpress.com by 210.87.254.40 on 09/06/12
For personal use only.

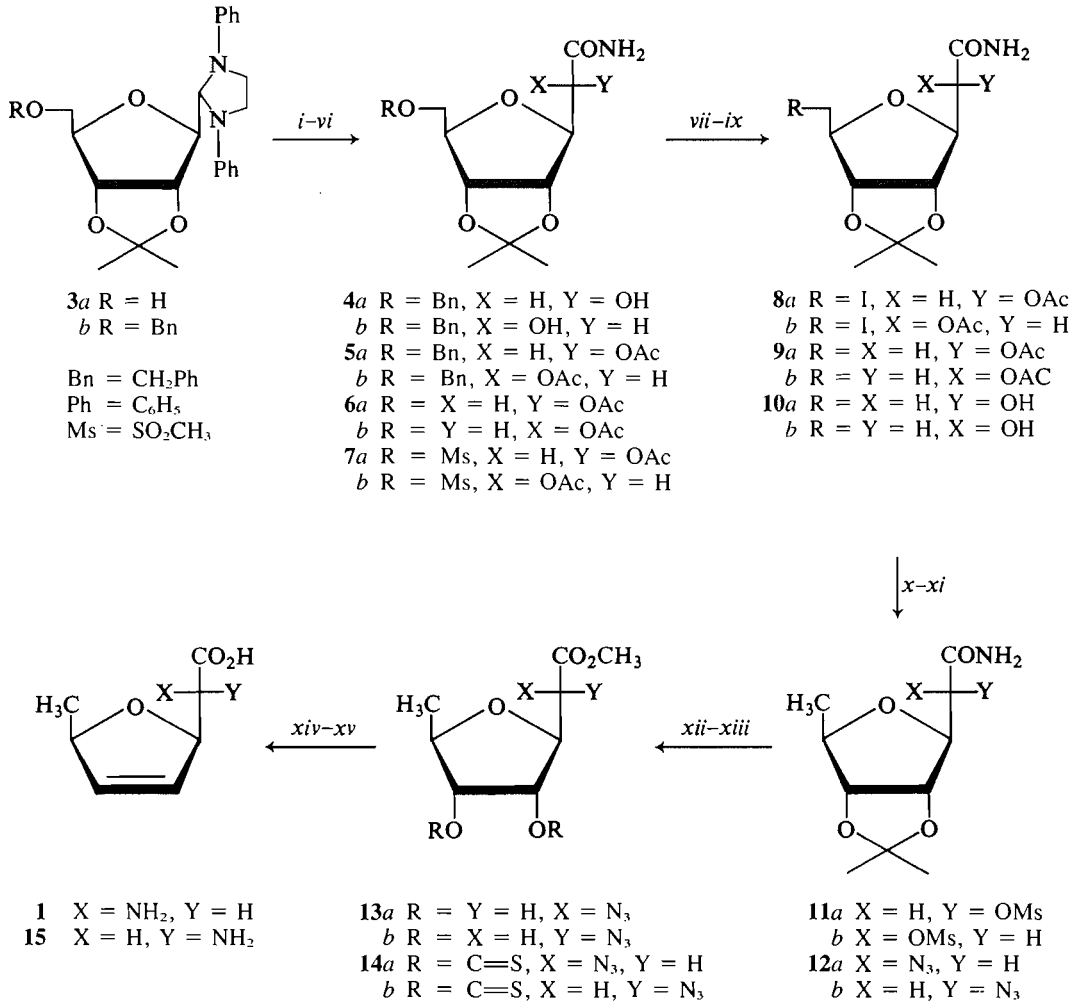

3*a* R = H
b R = Bn

Bn = CH_2Ph
Ph = C_6H_5
Ms = SO_2CH_3

4*a* R = Bn, X = H, Y = OH
b R = Bn, X = OH, Y = H
5*a* R = Bn, X = H, Y = OAc
b R = Bn, X = OAc, Y = H
6*a* R = X = H, Y = OAc
b R = Y = H, X = OAc
7*a* R = Ms, X = H, Y = OAc
b R = Ms, X = OAc, Y = H

8*a* R = I, X = H, Y = OAc
b R = I, X = OAc, Y = H
9*a* R = X = H, Y = OAc
b R = Y = H, X = OAC
10*a* R = X = H, Y = OH
b R = Y = H, X = OH

1 X = NH_2, Y = H
15 X = H, Y = NH_2

13*a* R = Y = H, X = N_3
b R = X = H, Y = N_3
14*a* R = C=S, X = N_3, Y = H
b R = C=S, X = H, Y = N_3

11*a* X = H, Y = OMs
b X = OMs, Y = H
12*a* X = N_3, Y = H
b X = H, Y = N_3

(*i*) *p*-$CH_3C_6H_4SO_3H \cdot H_2O$; (*ii*) $NaCN/K_2CO_3/H_2O$; (*iii*) H_2O_2/H_2O; (*iv*) Ac_2O/pyridine; (*v*) H_2/Pd-C/EtOH; (*vi*) MsCl/pyridine/CH_2Cl_2; (*vii*) NaI/2-butanone/Δ; (*viii*) H_2/Pd-C/EtOH; (*ix*) NH_3/MeOH; (*x*) MsCl/pyridine/CH_2Cl_2; (*xi*) LiN_3/DMF/Δ; (*xii*) MeOH/ANGC(H^+)/Δ; (*xiii*) Im_2CS/Me_2CO; (*xiv*) $(MeO)_3P$/Δ; (*xv*) NaOH/H_2O/Δ.

SCHEME I

anilino)ethane (7), and the derived α-hydroxy amide unit as a mixed *N,O*-isopropylidene derivative (5). We were concerned with the possible lability of the target dihydrofuran ring relative to strong acid conditions needed for hydrolysis of an α-substituted amide, and nucleophilic displacement of methanesulfonate by azide was unsuccessful with α-methanesulfonyloxy ester intermediates (5). Therefore, another sequence of reactions with different protecting groups was selected.

Benzylation of the primary hydroxyl function of 2-(2,3-*O*-isopropylidene-β-D-ribofuranosyl)-1,3-diphenylimidazolidine (**3***a*) (6) (see Scheme 1) gave the suitably protected precursor **3***b* (91%). Treatment of **3***b* under controlled acidic conditions (6, 8) unmasked the aldehyde function selectively. Immediate *in situ* treatment with aqueous sodium cyanide/potassium carbonate followed by 30% hydrogen peroxide to hydrolyze the cyanohydrin (3, 4) gave 3,6-anhydro-7-*O*-benzyl-4,5,-*O*-isopropylidene-D-*glycero*-D-(*allo* and *altro*)-heptonamides (**4***a* and *b*) in 86% yield from **3***b*. The more chromatographically mobile diastereomer crystallized selectively from ether solution (43% yield) and was later indicated to have been the *allo*-epimer **4***a*, based on the derived stereochemistry and analogy with prior studies (3, 6). Chromatography of the mother liquor on silica gave **4***b* (containing variable minor amounts of **4***a*) as a syrup (43%). Infrared and ^1H nmr spectral data were in harmony with the α-hydroxy amide structures of **4***a* and *b*, and a molecular ion was present in the mass spectrum of **4***a*. Each diastereomer was reacted independently in the parallel sequences that follow.

Acetylation of **4***a* and *b* in the usual manner gave the 2-*O*-acetyl derivatives (**5***a* and *b*) as viscous syrups in quantitative yields. These epimers were distinguished readily by ^1H nmr spectroscopy (see the Experimental). Hydrogenolysis of the 7-*O*-benzyl ether function from **5***a* and *b* occurred quantitatively at 60 psi over 5% palladium on carbon to give **6***a* and *b*. Mesylation of **6***a* and *b* gave the 7-*O*-methanesulfonyl products (**7***a* and *b*) in 88% yields after chromatographic purification. The more chromatographically mobile epimer **7***a* crystallized from chloroform/ether and was completely characterized.

Treatment of **7***a* and *b* with sodium iodide in hot 2-butanone gave the 7-iodo-7-deoxy compounds (**8***a* and *b*) in quantitative yields as colorless syrups that gave a characteristic mass spec-

Can. J. Chem. Downloaded from www.nrcresearchpress.com by 210.87.254.40 on 09/06/12
For personal use only.

Can. J. Chem. Downloaded from www.nrcresearchpress.com by 210.87.254.40 on 09/06/12
For personal use only.

tral fragmentation ion in high relative abundance. Hydrogenolysis of the iodo function gave the chromatographically purified 7-deoxy epimers (**9***a* and *b*) in over 90% yields. The ^{1}H nmr peak for the 7-protons appeared as the expected methyl doublet at δ 1.27 (**9***a*) and 1.33 (**9***b*).

Deacetylation of **9***a* and *b* with methanolic ammonia proceeded quantitatively. The resulting deprotected α-hydroxy amide products (**10***a* and *b*) were crystallized from chloroform/ether/hexane in over 80% yields and were fully characterized. Mesylation of **10***a* and *b* gave the crystalline 2-*O*-methanesulfonyl derivatives (**11***a* and *b*). Treatment of **11***a* and *b* with lithium azide in hot *N*,*N*-dimethylformamide (DMF) resulted in smooth displacement of the mesylate function (6) to give the chromatographically purified α-azido amides (**12***a* and *b*) in ~93% yields. These products were crystallized and fully characterized. It was assumed that the usual inversion of configuration had occurred at C2 (3, 6). Solvolysis of the amide function with concomitant removal of the isopropylidene group was effected by treatment of **12***a* and *b* with strong acid resin in hot methanol. The α-azido esters **13***a* and *b* were obtained as stiff syrups in 85% yields after chromatographic purification and were characterized by spectral properties.

Model reactions had demonstrated the feasibility of using the Corey–Winter (9) decomposition of furanose *cis*-glycol cyclic thionocarbonates to 2,5-dihydrofurans (5). We also anticipated that concomitant reductive displacement of dinitrogen from the α-azido function would be effected by heating in trimethylphosphite (10) to give the α-amino group after hydrolysis. Treatment of the α-azido esters (**13***a* and *b*) with *N*,*N*′-thiocarbonyldiimidazole in acetone at room temperature resulted in conversion to the cyclic thionocarbonates (**14***a* and *b*) in 92% purified yields. Epimer **14***a* was crystallized and both isomers were characterized by their spectroscopic properties. Compounds **14***a* and *b* were heated at reflux in trimethylphosphite for 14 hours followed by saponification of the resulting intermediates. The target 2(*S*)-amino-2-[2,5-dihydro-5(*R*)-methylfuran-2(*R*)-yl]ethanoic acid (**1**) and its 2(*R*) epimer (**15**) were isolated from a strong acid resin column in ~30% yields.

Comparison of the melting point, ^{1}H nmr, optical rotation, and circular dichroism (cd) data of compound **1** with those reported for (+)-furanomycin clearly revealed that the two were not identical. Compound **1** had a cd maximum with $[\theta]_{216} = +2200$ which was but slightly lowered by hydrogenation of the double bond to give the tetrahydrofuran product ($[\theta]_{215} = +2000$). In contrast, (+)-furanomycin was reported to have $[\theta]_{210} = +26\,000$ and its reduced product $[\theta]_{215} = +5000$ (1).

Simultaneously with completion of this sequence (5), a preliminary presentation alerted us to work by Joullié and coworkers (11) on the synthesis of *trans* diastereomers of **1**. Direct comparisons of chiroptical properties, high-field ^{1}H nmr spectra and chromatographic mobilities were made with our products and samples kindly provided by Professor M. M. Joullié. In their work (12), 2(*S*)-amino-2-[2,5-dihydro-5(*S*)-methylfuran-2(*R*)-yl]ethanoic acid (**16**) and its 2(*R*)-amino epimer were prepared by transformation chemistry from D-glucose. The value of the ellipticity measured at an inflection in the cd spectrum of **16** at 210 nm was $[\theta]_{210} = +26\,000$, in agreement with that reported for (+)-furanomycin ($[\theta]_{210} = +26\,000$) (1) and in marked contrast with those maxima measured for our *cis* isomers **1** ($[\theta]_{216} = +2200$) and **15** (calculated $[\theta]_{216} \sim -2500$). Our comparisons (5) also allowed assignment of absolute configurations for certain *cis* stereoisomers cleverly synthesized by Joullié and co-workers (13) from racemic 5-methyl-2,5-dihydrofurfural using the Ugi "four-component-condensation" approach to α-amino acids (14). Shiro *et al.* then reported an X-ray crystal structure of the *N*-acetyl derivative of (+)-furanomycin that corroborated the 2(*S*)-[5(*S*),2(*R*)] stereochemistry of **16** (15). Owing to the length of our classical Strecker-type approach and the demonstration that the natural product possessed the revised stereochemistry (**16**), the small quantities of compounds **1** and **15** obtained were characterized spectroscopically. No attempt was made to improve the rather poor yields of the last step (**14***a*, *b* → **1**, **15**) in our sequence.

It is interesting that (+)-furanomycin (**16**), isolated from a *Streptomyces* L-803 culture, has antibiotic activity against *Escherichia coli* H that is reversed by L-isoleucine (1). Some time ago racemic 2-amino-2-cyclopentylethanoic acid (cyclopentaneglycine) (16) and 2-amino-2-(cyclohex-3-enyl)-ethanoic acid (3-cyclohexene-1-glycine) (17) were prepared and also found to be isoleucine antagonists in *E. coli* cultures.

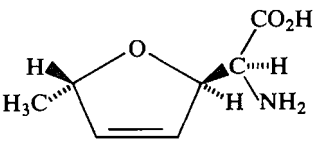

16

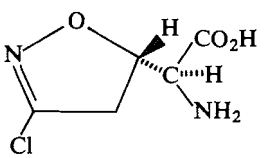

17

It was suggested that the planar rings attached to the α-carbon of glycine could approximate the β-branched alkyl chain of isoleucine (17). More recently another α-(heterocycle-substituted)glycine, 2(*S*)-amino-2-[3-chloro-4,5-dihydroisoxazol-5(*S*)-yl]ethanoic acid (**17**), was isolated from a *Streptomyces sviceus* culture (18) and synthesized (19) by the Upjohn group. Compound **17** was found to have significant activity against L1210 murine leukemia (20) and to inhibit a number of enzymes that catalyze amido transfer from L-glutamine (21). The activity of **17** was not reversed by L-isoleucine. Furanomycin was also detected in *Streptomyces* cultures examined by the Upjohn group and was found to have activity against the Walker 256 tumor (20). The Upjohn antibiotic (**17**) has a *threo*-α(*S*),β(*S*) configuration like L-*O*-methylallothreonine, whereas (+)-furanomycin (**16**) has the *erythro*-α(*S*),β(*R*) stereochemistry of L-*O*-methylthreonine. Incorporation of L-isoleucine into proteins of Ehrlich acites carcinoma was found to be inhibited by L-*O*-methylthreonine, but not by its α(*S*),β(*S*) *allo* diastereomer (22).

The present study has further demonstrated the viability of the modified Strecker-type approach for the stereodefined synthesis of *C*-glycosyl amino acids. The Corey–Winter conversion of furanose *cis*-glycol systems to 2,5-disubstituted-2,5-dihydrofurans of defined stereochemistry proceeds smoothly in most cases (5). The 2(*S*)-amino-2-[2,5-dihydro-5(*R*)-methylfuran-2(*R*)-yl]ethanoic acid (**1**) structure proposed for (+)-furanomycin (1) was synthesized. Collaborative efforts with Professor M. M. Joullié clearly demonstrated that a revised 2(*S*)-[5(*S*),2(*R*)] stereochemistry (**16**) exists for the natural antibiotic. No inhibition of proliferation of L1210 cells was observed with 2-(*S*)-amino-2-(β-D-ribofuranosyl)ethanoic acid (**2**) (6) at 0.1 m*M* concentration.[2] Biological evaluation of

[2]Private communication from Professor C. E. Cass, McEachern Cancer Research Laboratory, University of Alberta.

other diastereomers and analogues of furanomycin was pursued by Professor Joullié.

Experimental

General

Most general procedures are described in ref. 6 (and in more detail in ref. 5). The ^1H nmr spectra were determined at 100 MHz using $CDCl_3$ with Me_4Si as internal standard unless otherwise specified. High field (200 MHz) ^1H nmr spectra were determined on a Bruker WH200 instrument and the ^{13}C nmr spectra on a Bruker HFX90 spectrometer by the nmr laboratory of this department. Solvents used for chromatography are solvent A: hexane/ethyl acetate (1:1); solvent B: hexane/ethyl acetate (5:1).

*2-(5-O-Benzyl-2,3-O-isopropylidene-β-D-ribofuranosyl)-1,3-diphenylimidazolidine (**3**b)*

A solution of 2-(2,3,-*O*-isopropylidene-β-D-ribofuranosyl)-1,3-diphenylimidazolidine (**3***a*) (6) (3.96 g, 10 mmol) in DMF (20 mL) was added to a stirred suspension of NaH (960 mg, 50% oil suspension, 20 mmol) in DMF (5 mL) at 0°C under N_2. After 1 h at room temperature the solution was cooled to 0°C and treated dropwise with benzyl bromide (2.38 mL, 3.4 g, 20 mmol) in DMF (10 mL). The mixture was stirred at room temperature for 3 h, quenched with MeOH (2 mL), and poured into a mixture of CH_2Cl_2 (50 mL) and H_2O (50 mL). The aqueous layer was extracted with CH_2Cl_2 (3 × 25 mL). The combined organic phase was washed with saturated brine (10 mL), dried, and evaporated to a white solid. This solid was crystallized from MeOH/$CHCl_3$ to give 4.45 g (91%) of **3***b*, mp 148–149°C; $[\alpha]_D^{23}$ −14° (*c* 0.11, $CHCl_3$); uv (MeOH) max: 253 nm (ε 31 800), 293 (sh) (ε 4100); nmr δ: 1.24 & 1.38 (s & s, 3 & 3, $C(CH_3)_2$), 3.40–4.80 (m, 6, CH_2CH_2 and H6, H6′), 4.05 (q, $J_{5-6,6'}$ = 5 Hz, 1, H5), 4.25–4.40 (m, 2, H2 & H4), 4.50 (s, 2, CH_2Ph), 4.63 (d of d, *J* = 5 Hz, *J* = 6.5 Hz, 1, H3), 5.58 (d, J_{1-2} = 2 Hz, 1, H1), 6.60–7.40 (m, 15, aromatic); ms *m/z*: 486.2525 (0.5, M^+, calcd. for $C_{30}H_{34}N_2O_4$: 486.2518), 471 (M − CH_3), 380 (M − CH_3 − NPh). *Anal.* calcd. for $C_{30}H_{34}N_2O_4$: C 74.05, H 7.04, N 5.76; found: C 74.21, H 7.21, N 5.80.

*3,6-Anhydro-7-O-benzyl-4,5-O-isopropylidene-D-glycero-D-(allo and altro)-heptonamides (**4**a and **4**b)*

A stirred solution of **3***b* (12.15 g, 25 mmol) in CH_2Cl_2 (250 mL) at 0°C was treated with *p*-toluenesulfonic acid monohydrate (14.25 g, 75 mmol) in Me_2CO (20 mL). After 15 min an additonal 1 g of the acid in Me_2CO (5 mL) was added. After a total reaction time of 20 min the mixture was diluted with CH_2Cl_2 (200 mL) and filtered using a Celite pad. The filtrate was treated with solid $NaHCO_3$ (25 g), refiltered using Celite, and evaporated to a syrup. This residue was dissolved in dioxane (250 mL), cooled to 5°C, and treated with NaCN (18 g) and K_2CO_3 (18 g) in H_2O (250 mL). After 30 min at room temperature the solution was cooled to 0°C and treated dropwise with 30% H_2O_2/H_2O (125 mL) over a period of 30 min. The mixture was stirred at 0°C for an additional 30 min (the reaction temperature slowly rose to 35°C then subsided) and was then diluted with H_2O (600 mL) and EtOAc (250 mL). The aqueous phase was saturated with NaCl and extracted with EtOAc (3 × 50 mL). The combined organic phase was washed with saturated brine (3 × 20 mL), dried, concentrated to approximately 10 mL, and diluted with Et_2O (100 mL). The solid that crystallized was filtered to give 3.65 g (43%) of **4***a* (faster migrating isomer by tlc), mp 133–135°C; $[\alpha]_D^{23}$ +39° (*c* 0.1, $CHCl_3$); ir (KBr): 1650 cm^{-1} ($CONH_2$), 3300–3500 cm^{-1} (OH, NH_2); nmr δ: 1.31 & 1.50 (s & s, 3 & 3, $C(CH_3)_2$), 3.53 & 3.73 (ABX octet, J_{6-7} = 3.2 Hz, $J_{6-7'}$ = 2.7 Hz, $J_{7-7'}$ = 12 Hz, 2, H7 & H7′), 4.10–4.75 (m, 8, sugar and CH_2Ph), 5.7 & 6.7 (bs, 2, $CONH_2$), 7.3 (s, 5, Ph); ms *m/z*: 338.1599 (0.8, M + 1, calcd. for $C_{17}H_{24}NO_6$: 338.1604), 337.1539 (2.3, M^+), 323.1341 (1.6, M + 1 − CH_3), 322.1308 (7.5, M − CH_3), 263.1290 (12.2, M − $C_2H_4NO_2$). *Anal.* calcd. for $C_{17}H_{23}NO_6$: C 60.52, H 6.87, N 4.15; found: C 60.35, H 6.93, N 3.93.

The mother liquors were concentrated and purified by chromatography on silica (50 g, 3 × 15 cm). Elution with solvent A followed by EtOAc gave 3.67 g (44%) of **4***b* (as a syrup that contained a minor amout of **4***a*), $[\alpha]_D^{23}$ −10° (*c* 0.1, $CHCl_3$); nmr δ: 1.32 & 1.52 (s & s, 3 & 3, $C(CH_3)_2$), 3.56 & 3.76 (ABX octet, J_{6-7} = 3 Hz, $J_{6-7'}$ = 3 Hz, $J_{7-7'}$ = 12 Hz, 2, H7 & H7′), 4.10–4.75 (m, 8, sugar and CH_2Ph), 6.3 & 6.7 (bs, 2, $CONH_2$), 7.3 (s, 5, Ph).

*2-O-Acetyl-3,6-anhydro-7-O-benzyl-4,5-O-isopropylidene-D-glycero-D-(allo and altro)-heptonamides (**5**a and **5**b)*

A solution of **4***a* or **4***b* (11.8 g, 35 mmol) in pyridine (200 mL) at 0°C was treated with acetic anhydride (10 mL, 9.26 g, 91 mmol). After 1 h the solution was allowed to warm to room temperature for 12 h, treated with ice, and diluted with CH_2Cl_2 (250 mL). The organic phase was washed with 1 *N* HCl/H_2O, 5% $NaHCO_3/H_2O$, saturated brine (3 × 25 mL), dried, and evaporated to give **5***a* or **5***b* (13.6 g, quantitative).

The faster migrating isomer (**5***a*) was obtained as a viscous syrup, $[\alpha]_D^{23}$ −14° (*c* 0.1, $CHCl_3$); ir (film): 1700 cm^{-1} ($CONH_2$), 1750 cm^{-1} (OAc), 3300 cm^{-1} (NH_2); nmr δ: 1.33 & 1.52 (s & s, 3 & 3, $C(CH_3)_2$), 2.06 (s, 3, $COCH_3$), 3.48 & 3.69 (ABX multiplet, J_{6-7} = 5 Hz, $J_{6-7'}$ = 3.7 Hz, $J_{7-7'}$ = 11 Hz, 2, H7 & H7′), 4.05–4.30 (m, 1, H6), 4.28 & 4.33 (d of d, J_{3-2} = 5.5 Hz, J_{3-4} = 3.2 Hz, 1, H3), 4.52 (s, 2, CH_2Ph), 4.50–4.65 (d of d, J_{5-4} = 3.5 Hz, 1, H5), 4.78 & 4.81 (d of d, J_{4-3} = 3.2 Hz, J_{4-5} = 3.5 Hz, 1, H4), 5.23 (d, J_{2-3} = 5.5 Hz, 1, H2), 6.00–6.50 (bd, 2, $CONH_2$), 7.30 (s, 5, Ph); ms *m/z*: 379.1639 (0.3, M^+, calcd. for $C_{19}H_{25}NO_7$: 379.1631), 364.1393 (5.1, M − CH_3). *Anal.* calcd. for $C_{19}H_{25}NO_7$: C 60.15, H 6.64, N 3.69; found: C 59.91, H 6.57, N 3.62.

Isomer **5***b* was obtained as a viscous syrup, $[\alpha]_D^{23}$ +21° (*c* 0.1, $CHCl_3$); nmr δ: 1.33 & 1.52 (s & s, 3 & 3, $C(CH_3)_2$), 2.08 (s, 3, $COCH_3$), 3.00 (d, J_{6-7} = 4 Hz, 2, H7 & H7′), 4.00–4.25 (m, 1, H6), 4.20–4.40 (m, 1, H3), 4.52 (s, 2, CH_2Ph), 4.60–4.68 (m, 2, H4 & H5), 5.25 (d, J_{2-3} = 4.5 Hz, 1, H2), 5.90–6.40 (bd, 2, $CONH_2$), 7.31 (s, 5, Ph).

*2-O-Acetyl-3,6-anhydro-4,5-O-isopropylidene-D-glycero-D-(allo and altro)-heptonamides (**6**a and **6**b)*

A solution of **5***a* or **5***b* (4.0 g, 10.5 mmol) in 98% ethanol (100 mL) was hydrogenated over 5% Pd–C (2 g) at 60 psi. The reaction was monitored by tlc (EtOAc, **5***a*, *b*, R_f ~ 0.75; **6***a*, *b*, R_f ~ 0.25). After 8 h the mixture was filtered and evaporated to give 3.1 g (quantitative) of **6***a* or **6***b*, homogeneous by tlc, ms *m/z*: 290.1244 (3.5, M^+, calcd. for $C_{12}H_{20}NO_7$: 290.1248), 275.0966 (14.0, M + 1 − CH_3), 274.0933 (100, M − CH_3), 232.0824 (24.3, M + 1 − CH_3 − $COCH_3$).

*2-O-Acetyl-3,6-anhydro-4,5-O-isopropylidene-7-O-methanesulfonyl-D-glycero-D-(allo and altro)-heptonamides (**7**a and **7**b)*

A solution of **6***a* or **6***b* (5.0 g, 17.2 mmol) in pyridine (30 mL) and CH_2Cl_2 (30 mL) at 0°C, was treated dropwise with methanesulfonyl chloride (4.0 g, 35 mmol) in CH_2Cl_2 (10 mL). The solution was left at 0°C for 8 h, diluted with CH_2Cl_2, and poured into ice-water (25 mL). The organic phase was washed with saturated brine (3 × 10 mL), dried, and evaporated. This residue was chromatographed on silica (50 g, 3 × 20 cm). Elution with solvent A followed by EtOAc gave 5.6 g (89%) of **7***a* or **7***b* as a white foam. An analytical sample of the faster migrating isomer (**7***a*) was crystallized from $CHCl_3/Et_2O$. The slower isomer (**7***b*) was obtained as a white solid foam.

Isomer **7***a* had mp 133–134°C; $[\alpha]_D^{23}$ −11° (*c* 0.1, $CHCl_3$); ir (KBr): 1180, 1260 cm^{-1} (SO_2CH_3), 1750 cm^{-1} (OAc), 3400 cm^{-1} (NH_2); nmr δ: 1.35 & 1.54 (s & s, 3 & 3, $C(CH_3)_2$), 2.20 (s, 3, $COCH_3$), 3.06 (s, 3, SO_2CH_3), 4.10–4.40 (m, 4, H3, H6, H7, H7′), 4.58 (d of d, J_{5-6} = 4.5 Hz, J_{4-5} = 6.5 Hz, 1, H5), 4.93 (d of d, J_{4-5} = 6.5 Hz, J_{4-3} = 4 Hz, 1, H4), 5.32 (d, J_{2-3} = 4 Hz, 1, H2), 6.0–6.5 (bd, 2, $CONH_2$); ms *m/z*: 368.1006 (1.0, M + 1, calcd. for $C_{13}H_{22}NO_9S$: 368.1015), 352.0706 (100, *M* − 15), 323.0791 (0.9, M − $CONH_2$), 310.0604 (13.0, M + 1 − CH_3 − $COCH_3$), 308.0809 (3.5, M − CH_3 − $CONH_2$). *Anal.* calcd. for $C_{13}N_2NO_9S$: C 42.50, H 5.76, N

Can. J. Chem. Downloaded from www.nrcresearchpress.com by 210.87.254.40 on 09/06/12
For personal use only.

Can. J. Chem. Downloaded from www.nrcresearchpress.com by 210.87.254.40 on 09/06/12
For personal use only.

3.81, S 8.73; found: C 42.54, H 5.75, N 3.92, S 8.81.

Isomer **7***b* had $[\alpha]_D^{23}$ +14° (*c* 0.1, $CHCl_3$); nmr δ: 1.35 & 1.54 (s & s, 3 & 3, $C(CH_3)_2$), 2.18 (s, 3, $COCH_3$), 3.04 (s, 3, SO_2CH_3), 4.10–4.70 (m, 6, sugar), 5.22 (d, J_{2-3} = 4 Hz, 1, H2), 6.05–6.40 (bd, 2, $CONH_2$).

*2-O-Acetyl-3,6-anhydro-7-deoxy-4,5-*O*-isopropylidene-*D-glycero-D-(allo *and* altro)*-heptonamides (**9**a and **9**b)*

A solution of **7***a* or **7***b* (5.0 g, 13.6 mmol) in 2-butanone (200 mL) was treated with NaI (4.08 g, 27.2 mmol), stirred under N_2 at reflux for 2 h, cooled, and evaporated to a yellow paste. This residue was dissolved in EtOAc (200 mL) and 5% $NaHCO_3/H_2O$ (25 mL). The organic phase was washed with saturated brine (25 mL), dried, and evaporated to give 5.5 g (quantitative) of the 7-iodo-7-deoxy product (**8***a* or **8***b*) as a colorless syrup, ms *m/z*: 383.9952 (54.4, M − CH_3, calcd. for $C_{11}H_{15}INO_6$: 383.9946).

This syrup was dissolved in 98% ethanol (200 mL), treated with triethylamine (5 mL) and a chip of Dry Ice, and hydrogenated over 5% Pd–C (2.5 g) at 20 psi. After 10 h the reaction was filtered using a Celite pad and evaporated. The residue was dissolved in EtOAc (200 mL) and washed with saturated brine (25 mL) containing $NaHSO_3$ (500 mg). The aqueous phase was extracted with EtOAc (3 × 20 mL). The combined organic phase was dried, evaporated, and purified by chromatography on silica (50 g, 3 × 20 cm). Elution with solvent A followed by EtOAc gave the desired product as a syrup after removal of solvents.

The yield of "faster" isomer **9***a* was 3.5 g (94%), $[\alpha]_D^{23}$ −30° (*c* 0.1 $CHCl_3$); nmr δ: 1.27 (d, J_{7-6} = 6 Hz, 3, H7's), 1.36 & 1.56 (s & s, 3 & 3, $C(CH_3)_2$), 2.16 (s, 3, $COCH_3$), 3.98 (q, J_{6-7} = 6 Hz, J_{6-5} = 5 Hz, 1, H6), 4.10–4.30 (m, J_{5-6} = 5 Hz, J_{5-4} = 6.5 Hz, J_{3-2} = 4 Hz, J_{3-4} = 3.5 Hz, 2, H5 & H3), 4.88 (d of d, J_{4-5} = 6.5 Hz, J_{4-3} = 3.5 Hz, 1, H4), 5.28 (d, J_{2-3} = 4 Hz, 1, H2), 6.3–6.6 (bs, 2, $CONH_2$); ms *m/z*: 274.1290 (1.2, M + 1, calcd. for $C_{12}H_{20}NO_6$: 274.1292), 259.1015 (9.9, M + 1 − CH_3), 285.0981 (79.7, M − CH_3), 216.0874 (5.8, M + 1 − CH_3 − $COCH_3$), 215.0787 (5.4, M − CH_3 − $COCH_3$). *Anal.* calcd. for $C_{12}H_{19}NO_6$: C 52.74, H 7.00, N 5.13; found: C 52.37, H 7.11, N 4.80.

The yield of **9***b* was 3.4 g (91%), $[\alpha]_D^{23}$ −5° (*c* 0.1 $CHCl_3$); nmr δ: 1.33 (d, J_{7-6} = 6 Hz, 3, H7's), 1.36 & 1.56 (s & s, 3 & 3, $C(CH_3)_2$), 2.20 (s, 3, $COCH_3$), 4.00 (q, J_{6-7} ~ 6 Hz, J_{6-5} ~ 5 Hz, 1, H6), 4.15–4.35 (m, 2, H3 & H5), 4.64 (d of d, J_{4-5} ~ 6 Hz, J_{4-3} ~ 3 Hz, 1, H4), 5.25 (d, J_{2-3} = 4 Hz, 1, H2), 6.1–6.5 (bs, 2, $CONH_2$).

*3,6-Anhydro-7-deoxy-4,5-*O*-isopropylidene-*D-glycero-D-(allo *and* altro)*-heptonamides (**10**a and **10**b)*

A solution of **9***a* or **9***b* (4.0 g, 14.6 mmol) in MeOH (100 mL) was treated with saturated NH_3/MeOH (100 mL), left at 0°C for 16 h, and then evaporated to give 3.4 g (quantitative) of a white solid, homogeneous by tlc (EtOAc, **9***a*, *b*, R_f ~ 0.5; **10***a*, R_f ~ 0.26; **10***b*, R_f ~ 0.24).

The faster migrating product was crystallized from MeOH/hexane to give 2.95 g (87%) of **10***a*, mp 174–175°C; $[\alpha]_D^{23}$ −10° (*c* 0.1, $CHCl_3$); nmr (Me_2SO-d_6) δ: 1.19 (d, J_{7-6} ~ 7 Hz, 3, H7's), 1.22 & 1.41 (s & s, 3 & 3, $C(CH_3)_2$), 3.7–4.8 (m, 5, sugar), 5.70 (d, 1, OH), ~7.25 (bs, 2, $CONH_2$); ms *m/z*: 232.1186 (1.9, M + 1, calcd. for $C_{10}H_{18}NO_5$: 232.1185), 231.1111 (0.8, M^+), 217.0908 (8.9, M + 1 − CH_3), 216.0874 (84.2, M − CH_3), 188.1009 (2.5, M + 1 − $CONH_2$), 187.0978 (23.1, M − $CONH_2$). *Anal.* calcd. for $C_{10}H_{17}NO_5$: C 51.94; H 7.41, N 6.06; found: C 51.49, H 7.26, N 5.71.

The slower migrating product was crystallized from $CHCl_3$/hexane to give 2.76 g (82%) of **10***b*, mp 102–103°C; $[\alpha]_D^{23}$ −15° (*c* 0.1, $CHCl_3$); nmr (Me_2SO-d_6) δ: 1.16 (d, J_{7-6} ~ 7 Hz, 3, H7's), 1.24 & 1.42 (s & s, 3 & 3, $C(CH_3)_2$), 3.7–4.8 (m, 5, sugar), 5.5 (d, 1, OH), ~7.15 (bs, 2, $CONH_2$). *Anal.* calcd. for $C_{10}H_{17}NO_5$: C 51.94, H 7.41, N 6.06; found: C 51.90, H 7.63, N 5.99.

*3,6-Anhydro-7-deoxy-4,5-*O*-isopropylidene-2-*O*-methanesulfonyl-*D-glycero-D-(allo *and* altro)*-heptonamides (**11**a and **11**b)*

A solution of **10***a* or **10***b* (2.31 g, 10 mmol) in pyridine (25 mL) and CH_2Cl_2 (10 mL) at 0°C was treated dropwise with methanesulfonyl chloride (5.7 g, 50 mmol) in CH_2Cl_2 (10 mL). After 4 h at 0°C the solution was treated with a chip of ice, diluted with EtOAc (150 mL), washed with saturated brine (3 × 10 mL), dried, and evaporated to a syrup. This residue was chromatographed on silica (50 g, 3 × 20 cm). Elution with solvent B followed by EtOAc gave 2.6 g (84%) of **11***a* or **11***b*.

The faster migrating residue was crystallized from Et_2O/hexane to give 2.15 g (70%) of **11***a*, mp 104–105°C; $[\alpha]_D^{23}$ +9° (*c* 0.1, $CHCl_3$); nmr δ: 1.32 (d, J_{7-6} = 6 Hz, 3, H7's), 1.36 & 1.52 (s & s, 3 & 3, $C(CH_3)_2$), 3.15 (s, 3, SO_2CH_3), 4.00 (q, J_{6-7} ~ J_{6-5} ~ 6 Hz, 1, H6), 4.15–4.95 (m, 2, H3 & H5), 4.81 (d of d, J_{4-5} = 6.5 Hz, J_{4-3} = 4 Hz, 1, H4), 5.13 (d, J_{2-3} = 3.5 Hz, 1, H2), 6.25 & 6.7 (bs, 2, $CONH_2$); ms *m/z*: 295.0677 (10.3, M + 1 − CH_3, calcd. for $C_{10}H_{17}NO_7S$: 295.0716), 294.0651 (83.7, M − CH_3), 157.0860 (16.4, M − $C_3H_6NO_4S$). *Anal.* calcd. for $C_{11}H_{19}NO_7S$: C 42.71, H 6.19, N 4.53, S 10.36; found: C 42.60, H 6.08, N 4.27, S 10.25.

The slower migrating product was crystallized as above to give 2.4 g (78%) of **11***b*, mp 143–144°C; $[\alpha]_D^{23}$ −35° (*c* 0.1 $CHCl_3$); nmr δ: 1.32 (d, J_{7-6} = 6 Hz, 3, H7's), 1.36 & 1.52 (s & s, 3 & 3, $C(CH_3)_2$), 3.17 (s, 3, SO_2CH_3), 4.02 (m, J_{6-7} ~ J_{6-5} ~ 6 Hz, 1, H6), 4.20–4.35 (m, 2, H3 & H5), 4.80 (d of d, J_{4-5} = 6.5 Hz, J_{4-3} = 4 Hz, 1, H4), 5.00 (d, J_{2-3} = 4 Hz, 1, H2), 6.25 & 6.7 (bs, 2, $CONH_2$).

*3,6-Anhydro-2-azido-2,7-dideoxy-4,5-*O*-isopropylidene-*D-glycero-D-(altro *and* allo) *heptonamides (**12**a and **12**b)*

A solution of **11***a* or **11***b* (2.31 g, 7.5 mmol) in DMF was treated with LiN_3 (1.85 g, 38 mmol) and stirred at 80°C for 5 h. The mixture was concentrated to a yellow paste, dissolved in EtOAc (100 mL), washed with saturated brine (3 × 10 mL), dried, and evaporated. The residue was chromatographed on silica (25 g, 2.2 × 18 cm). Elution with solvent A followed by EtOAc gave the desired product.

The yield of the purified faster migrating isomer was 1.77 g (92%). A sample was crystallized from Et_2O/hexane to give **12***a*, mp 126–127°C; $[\alpha]_D^{23}$ −32° (*c* 0.1, $CHCl_3$); ir (KBr): 1600 cm^{-1} ($CONH_2$), 2120 cm^{-1} (RN_3), 3300–3400 cm^{-1} (NH_2); nmr δ: 1.31 (d, J_{7-6} = 6.5 Hz, 3, H7's), 1.34 & 1.52 (s & s, 3 & 3, $C(CH_3)_2$), 4.00 (q, J_{6-7} ~ J_{6-5} ~ 6.5 Hz, 1, H6), 4.26 (d, J_{2-3} = 4 Hz, 1, H2), 4.27 (t, J_{5-6} ~ J_{5-4} ~ 6.5 Hz, 1, H5), 4.42 (t, J_{3-2} ~ J_{3-4} = 4 Hz, 1, H3), 4.60 (d of d, J_{4-5} ~ 6.5 Hz, J_{4-3} ~ 4 Hz, 1, H4); ms *m/z*: 241.0934 (64.4, M − CH_3, calcd. for $C_9H_{13}N_4O_4$: 241.0937), 214.1081 (48.1, M − N_3), 199.0836 (1.2, M − N_3 − CH_3), 157.0863 (94, M − $C_2H_3N_4O$). *Anal.* calcd. for $C_{10}H_{16}N_4O_4$: C 46.87, H 6.29, N 21.86; found: C 46.59, H 6.50, N 22.06.

The slower migrating isomer was crystallized from Et_2O to give 1.8 g (94%) of **12***b*, mp 114–116°C. An analytical sample was recrystallized from Et_2O to give **12***b*, mp 119–120°C; $[\alpha]_D^{23}$ −84° (*c* 0.1, $CHCl_3$); nmr δ: 1.36 (d, J_{7-6} = 6.5 Hz, 3, H7's), 1.34 & 1.51 (s & s, 3 & 3, $C(CH_3)_2$), 3.90–4.90 (m, 4, H2, H3, H5, H6), 4.79 (d of d, J_{4-5} ~ 6.5 Hz, J_{4-3} ~ 3 Hz, 1, H4), 6.0 & 6.4 (bs & s, 2, $CONH_2$). *Anal.* calcd. for $C_{10}H_{16}N_4O_4$: C 46.87, H 6.29, N 21.86; found: C 47.23, H 6.55, N 21.50.

*Methyl 3,6-anhydro-2-azido-2,7-dideoxy-*D-glycero-D-(altro *and* allo)*-heptonamides (**13**a and **13**b)*

A solution of **12***a* or **12***b* (1.5 g, 5.9 mmol) in MeOH (50 mL, dried and distilled) was stirred at reflux with ANGC(H^+) resin (5 g). After 4.5 h an additional portion of resin (5 g) was added to the refluxing mixture. After a total reflux time of 9 h the mixture was filtered using a Celite pad, evaporated, and chromatographed over silica (20 g, 2.3 × 12 cm). Elution with solvent A followed by EtOAc gave 1.15 g (85%) of **13***a* or **13***b* as a stiff syrup.

The faster migrating isomer (**13***a*) had $[\alpha]_D^{23}$ −62° (*c* 0.1, $CHCl_3$); ir (film: 1740 cm^{-1} (CO_2CH_3), 2120 cm^{-1} (RN_3); nmr δ: 1.31 (d, J_{7-6} = 6 Hz, 3, H7's), 3.5–4.4 (m, 7, sugar, OH), 3.84 (s, 3, CO_2CH_3); ms *m/z*: 213.0749 (2.4, M − H_2O, calcd. for $C_8H_{11}N_3O_4$: 213.0749), 117.0549 (98.4, M − $C_3H_4N_3O_2$). *Anal.* calcd. for $C_8H_{13}N_3O_5$: C 41.56, H 5.67, N 18.17; found: C 41.08, H 5.72, N 18.08.

Isomer **13***b* had $[\alpha]_D^{23}$ +4° (*c* 0.1, $CHCl_3$); nmr δ: 1.31 (d, J_{7-6} = 6 Hz, 3, *H*7's), 3.5–4.4 (m, 7, sugar, OH), 3.82 (s, 3, CO_2CH_3).

*Methyl 3,6-anhydro-2-azido-2,7-dideoxy-4,5-*O*-thiocarbonato-*D-glycero-D-*(*altro *and* allo*)-heptonoates (**14***a and **14***b)*

A solution of **13***a* or **13***b* (1.15 g, 5 mmol) in Me_2CO (50 mL) was treated with *N*,*N*′-thiocarbonyldiimidazole (23) (1.78 g, 10 mmol) and stirred at room temperature. After 12 h, tlc (solvent A, **13***a*, *b*, R_f ~ 0.5; **14***a*, *b*, R_f ~ 0.7) indicated that reaction was complete. Solvent was evaporated, the residue was dissolved in EtOAc (100 mL) and washed with 1 N HCl/H_2O (2 × 10 mL), saturated brine (3 × 20 mL), dried, and evaporated. This residue was dissolved in Et_2O (50 mL) and rapidly filtered through silica (5 g). The silica was washed with Et_2O (20 mL) and the combined eluates were evaporated to give 1.25 g (91%) of **14***a* or **14***b*. The faster migrating isomer was isolated as a solid and was crystallized from Et_2O/hexane to give **14***a* with mp 95–96°C; ir (KBr): 1750 cm^{-1} (CO_2Me), 2120 cm^{-1} (RN_3); uv (MeOH) max: 238 nm; nmr δ: 1.43 (d, J_{7-6} = 6 Hz, 3, H7's), 3.84 (s, 3, CO_2CH_3), 4.07 (d, J_{2-3} ~ 3.5 Hz, 1, H2), 4.13 (m, J_{6-7} ~ J_{6-5} ~ 6 Hz, 1, H6), 4.55 (t, J_{3-4} = 3.0 Hz, J_{3-2} ~ 3.5 Hz, 1, H3), 4.85 (d of d, J_{5-4} = 8 Hz, J_{5-6} = 6.0 Hz, 1, H5), 5.32 (d of d, J_{4-5} = 8 Hz, J_{4-3} = 3.0 Hz, H4); ms *m*/*z*: 273.0420 (100, M^+, calcd. for $C_9H_{11}N_3O_5S$: 273.0420).

Isomer **14***b* was isolated as a viscous syrup with ir (Nujol): 1745 cm^{-1} (CO_2CH_3), 2120 cm^{-1} (RN_3); uv (MeOH) max: 238 nm; nmr δ: 1.44 (d, J_{7-6} = 6 Hz, 3, H7's), 3.84 (s, 3, CO_2CH_3), 4.14 (q, J_{6-7} ~ J_{6-5} ~ 6 Hz, 1, H6), 4.38 (d, J_{2-3} ~ 3.5 Hz, 1, H2), 4.51 (t, J_{3-4} = 3.0 Hz, J_{3-2} ~ 3.5 Hz, 1, H3), 4.82 (d of d, J_{3-4} = 8 Hz, J_{5-6} = 6.0 Hz, 1, H5), 5.34 (d of d, J_{4-5} = 8 Hz, J_{4-3} = 3.0 Hz, 1, H4); ms *m*/*z*: 273.0422 (100, M^+, calcd. for $C_9H_{11}N_3O_5S$: 273.0420).

*2(*S *and* R*)-amino-2-[2,5-dihydro-5(*R*)-methylfuran-2(*R*)-yl]ethanoic acids (**1** and **15**)*

A solution of **14***a* or **14***b* (273 mg, 1 mmol) in trimethylphosphite (25 mL) was stirred at reflux for 14 h under N_2, cooled, and evaporated to a syrup. This residue was saponified with 1 *N* $NaOH/H_2O$ (20 mL) at 90°C for 0.5 h, cooled to 0°C, and acidified to pH 2 with 1 *N* HCl/H_2O. This solution was applied to a column of ANGC(H^+) resin (20 g) and the column was washed with 0.1 *N* HCl/H_2O (100 mL) followed by H_2O (200 mL). The product was eluted with 0.5 *N* NH_3/H_2O and the ninhydrin positive fractions were collected and evaporated to give 50 mg (32%) of **1** or **15**. A solution of **1** in acetonitrile/MeOH was allowed to evaporate slowly to give a white microcrystalline solid with mp 175–178°C (dec.); $[\alpha]_D^{23}$ −50° (*c* 0.1, H_2O), $[\alpha]_D^{23}$ −8° (*c* 0.1, 1 *N* HCl/H_2O); ir (Nujol): 3000 cm^{-1} (NH_3^+), 1630 cm^{-1} (CO_2^-), 1590, 1460, and 1380 cm^{-1}; cd (*c* 1 mg/mL, 1 *N* or 6 *N* HCl/H_2O) $[\theta]_{216}$ = +2200; ord (*c* ~1 mg/mL), 6 *N* HCl/H_2O), $[\phi]_{210}$ = +1100; ^1H nmr (200 MHz) (D_2O) δ: 1.34 (d, J_{7-6} = 6.5 Hz, 3, H7's), 3.81 (d, J_{2-3} = 3 Hz, 1, H2), 4.95 (m, J_{6-7} = 6.5 Hz, J_{6-5} = 2 Hz, J_{6-4} = 0.5 Hz, J_{6-3} = 4.5 Hz, J_{6-2} ~ 0 Hz, 1, H6), 5.24 (m, J_{3-2} = 3.0 Hz, J_{3-4} = 2.5 Hz, J_{3-5} = 1 Hz, J_{3-6} = 4.5 Hz, 1 H3), 5.82 & 6.10 (ABX, J_{4-5} = 6 Hz, J_{4-3} = 2.5 Hz, J_{5-6} = 2 Hz, 2, H4 & H5); ^{13}C nmr (D_2O) δ: 21.2 (C7), 57.4 (C2), 83.6, 84.6 (C3, C6), 125.1, 136.0 (C4, C5), 172.0 (CO_2H).

Diastereomer **15** was recovered as a tan-colored solid with mp 185–190°C; $[\alpha]_D^{23}$ +21° (*c* 0.1, 1 *N* HCl/H_2O) (optical rotation calculated (5) for this particular mixture estimated from nmr to contain: **15** (82%) and **1** (18%) = +27°); cd (*c* ~ 1 mg/mL, 1 *N* HCl/H_2O) $[\theta]$ = −1700; ^1H nmr (200 MHz) (D_2O) δ: 1.28 (d, J_{7-6} = 7 Hz, 3 H7's), 3.99 (d, J_{2-3} = 4 Hz, 1, H2), 5.00 (m, J_{6-7} = 7 Hz, J_{6-5} = 2.5 Hz, J_{6-4} = 1 Hz, J_{6-3} = 4.5 Hz, J_{6-2} ~ 0 Hz, 1, H6), 5.30 (m, J_{3-2} = 4 Hz, J_{3-4} = 3 Hz, J_{3-5} = 1 Hz, J_{3-6} = 4.5 Hz, 1, H3), 5.70 & 6.12 (ABX, J_{4-5} = 6.5 Hz, J_{4-3} = 3 Hz, J_{5-6} = 2.5 Hz, 2, H4 & H5); ^{13}C nmr (D_2O) δ: 20.9 (C7), 56.9 (C2), 83.6, 84.0 (C3, C6), 122.9, 136.3 (C4, C5).

*2(*S*)-Amino-2-[tetrahydro-5(*R*)-methylfuran-2(*R*)-yl]ethanoic acid*

A solution of **1** (5mg) in H_2O (5 mL) was hydrogenated over 5% Pd–C (5 mg) at atmospheric pressure for 10 h, filtered using a Celite pad, and evaporated to give 5 mg of a solid with cd (*c* ~2 mg/mL, 6 *N* HCl/H_2O) $[\theta]_{215}$ = +2000; ^1H nmr (200 MHz) (D_2O) δ: 1.22 (d, 3, H7's), 1.40–2.20 (m, 4, H4's, H5's), 3.65 (d, 1, H2), 3.70–4.50 (m, 2, H3, H6).

Acknowledgements

We thank the National Cancer Institute of Canada, the Natural Sciences and Engineering Research Council of Canada (A5890), and the University of Alberta for generous financial support. M. J. R. thanks Professor A. D. Broom for facilities and hospitality provided during a visiting professorship at the University of Utah 1981–1982.

1. K. KATAGIRI, K. TORI, Y. KIMURA, T. YOSHIDA, T. NAGASAKI, and H. MINATO. J. Med. Chem. **10**, 1149 (1967).
2. T. MASAMUNE and M. ONO. Chem. Lett. 625 (1975).
3. N. P. DAMODARAN, G. H. JONES, and J. G. MOFFATT. J. Am. Chem. Soc. **93**, 3812 (1971).
4. G. TRUMMLITZ and J. G. MOFFATT. J. Org. Chem. **38**, 1841 (1973).
5. J. M. R. PARKER. Ph.D. Dissertation, The University of Alberta. 1980.
6. M. J. ROBINS and J. M. R. PARKER. Can. J. Chem. **61**, 312 (1983).
7. H.-W. WANZLICK and W. LÖCHEL. Chem. Ber. **86**, 1463 (1953).
8. H. P. ALBRECHT, D. B. REPKE, and J. G. MOFFATT. J. Org. Chem. **38**, 1836 (1973).
9. (*a*) E. J. COREY AND R. A. E. WINTER. J. Am. Chem. Soc. **85**, 2677 (1963); (*b*) A. H. HAINES. Carbohydr. Res. **1**, 214 (1965).
10. (*a*) W. S. MUNGALL, G. L. GREENE, G. A. HEAVNER, and R. L. LETSINGER. J. Org. Chem. **40**, 1659 (1975); (*b*) J. B. HOBBS and F. ECKSTEIN. J. Org. Chem. **42**, 714 (1977).
11. J. E. SEMPLE, P. C. WANG, Z. LYSENKO, and M. M. JOULLIÉ. Abstracts of Papers, 178th National Meeting of the American Chemical Society, Washington, DC. September, 1979; ORGN 124.
12. M. M. JOULLIÉ, P. C. WANG, and J. E. SEMPLE. J. Am. Chem. Soc. **102**, 887 (1980).
13. J. E. SEMPLE, P. C. WANG, Z. LYSENKO, and M. M. JOULLIÉ, J. Am. Chem. Soc. **102**, 7505 (1980).
14. R. URBAN and I. UGI. Angew. Chem. Int. Ed. Engl. **14**, 61 (1975).
15. M. SHIRO, H. NAKAI, K. TORI, J. NISHIKAWA, Y. YOSHIMURA, and K. KATAGIRI. J. Chem. Soc. Chem. Commun. 375 (1980).
16. W. M. HARDING and W. SHIVE. J. Biol. Chem. **206**, 401 (1954).
17. J. EDELSON, J. D. FISSEKIS, C. G. SKINNER, and W. SHIVE. J. Am. Chem. Soc. **80**, 2698 (1958).
18. D. G. MARTIN, D. J. DUCHAMP, and C. G. CHIDESTER. Tetrahedron Lett. 2549 (1973).
19. R. C. KELLY, I. SCHLETTER, S. J. STEIN, and W. WIERENGA. J. Am. Chem. Soc. **101**, 1054 (1979).
20. L. J. HAŇKA, D. G. MARTIN, and G. L. NEIL. Cancer Chemother. Rep. Part 1, **57**, 141 (1973).
21. (*a*) D. A. COONEY, H. N. JAYARAM, J. A. RYAN, and V. H. BONO. Cancer Chemother. Rep. Part 1, **58**, 793 (1974); (*b*) H. N. JAYARAM, D. A. COONEY, J. A. RYAN, G. NEIL, R. L. DION, and V. H. BONO. Cancer Chemother. Rep. Part 1, **59**, 481 (1975).
22. M. RABINOVITZ, M. E. OLSON, and D. M. GREENBERG. J. Am. Chem. Soc. **77**, 3109 (1955).
23. (*a*) H. A. STAAB and G. WALTHER. Justus Leibigs Ann. Chem. **657**, 98 (1962); (*b*) T. J. PULLUKAT and G. URRY. Tetrahedron Lett. 1953 (1967).

Can. J. Chem. Downloaded from www.nrcresearchpress.com by 210.87.254.40 on 09/06/12
For personal use only.

On the structure, chemistry, and ^{13}C nuclear magnetic resonance of ravidomycin

JOHN A. FINDLAY and JIA-SEN LIU
Department of Chemistry, University of New Brunswick, Fredericton, N.B., Canada E3B 6E2
AND
LAJOS RADICS
NMR Laboratory, Central Research Institute for Chemistry, P.O. Box 17, H-1525 Budapest, Hungary

Received May 17, 1982

JOHN A. FINDLAY, JIA-SEN LIU, and LAJOS RADICS. Can. J. Chem. **61**, 323 (1983).

Full spectral details in support of the earlier proposed structure **1***a* for the antitumor antibiotic ravidomycin are presented together with an account of chemical degradation products. A complete corroboration of structure is provided by cross correlation of ^{1}H and ^{13}C nmr for ravidomycin and its diacetate **1***b*.

JOHN A. FINDLAY, JIA-SEN LIU et LAJOS RADICS. Can. J. Chem. **61**, 323 (1983).

On présente toutes les données spectrales qui confirment la structure **1***a* proposé pour la ravidomycine l'antibiotique antituméreux, ainsi qu'une analyse des produits de dégradation. On obtient une corroboration complète de structure grâce à une corrélation croisée de la rmn du ^{1}H et du ^{13}C de la ravidomycine et de son diacétate **1***b*.

[Traduit par le journal]

In a recent preliminary report (1) we proposed structure **1***a* for ravidomycin, an antitumor antibiotic isolated (2) from the fermentation broth of *Streptomyces ravidus*. This proposal was based on analysis of ^{1}H nmr, infrared, and ultraviolet spectral data on **1***a*, its diacetate **1***b*, the alkali fusion derived aglycone **2***a* and tranformation products **3**, **4***a*, **4***b*, and **5**. We now provide full spectral characteristics for the latter together with appropriate mechanistic rationale for their formation. In addition, a detailed corroboration of structure is forthcoming from cross correlation of the ^{1}H and ^{13}C nmr spectra of ravidomycin **1***a* and ravidomycin diacetate **1***b*.

In our structural elucidation of ravidomycin the key chemical degradative products were the aglycone **2***a* and the optically inactive diastereomeric mixture (1 : 1) of hemiacetal carboxylic acids **4***a* which were obtained in 13% and 45% yield, respectively, from alkaline fusion of **1***a* in 50% KOH at reflux temperature for 6 h. Since our conclusions about the structures of these compounds led directly to the placement of the relative positions of the *C*-glycosidic moiety and the lactone ring ether oxygen on the phenyl naphthalene skeleton it is appropriate to account for their generation. Scheme 1 portrays a mechanistic proposal to rationalize the formation of aglycone **2***a* via a

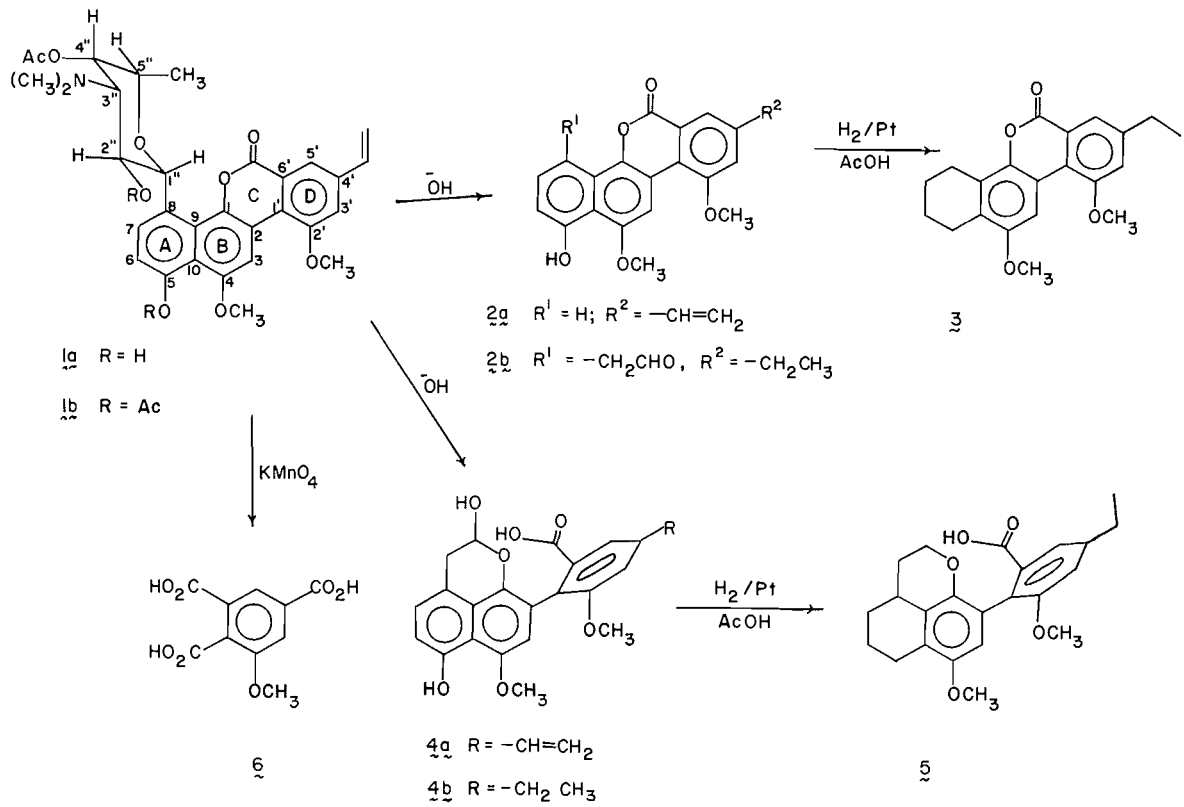

1*a* R = H
1*b* R = Ac

2*a* R^1 = H; R^2 = −CH=CH_2
2*b* R^1 = $-CH_2CHO$, R^2 = $-CH_2CH_3$

3

4*a* R = −CH=CH_2
4*b* R = $-CH_2CH_3$

5

6

0008-4042/83/020323-05$01.00/0
©1983 National Research Council of Canada/Conseil national de recherches du Canada

Can. J. Chem. Downloaded from www.nrcresearchpress.com by 210.87.254.6 on 09/06/12
For personal use only.

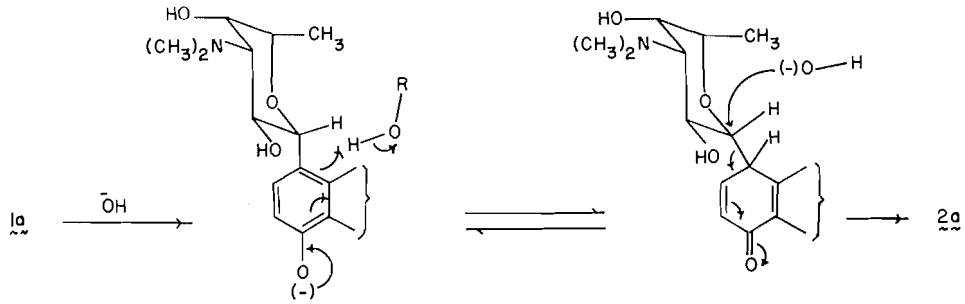

SCHEME 1

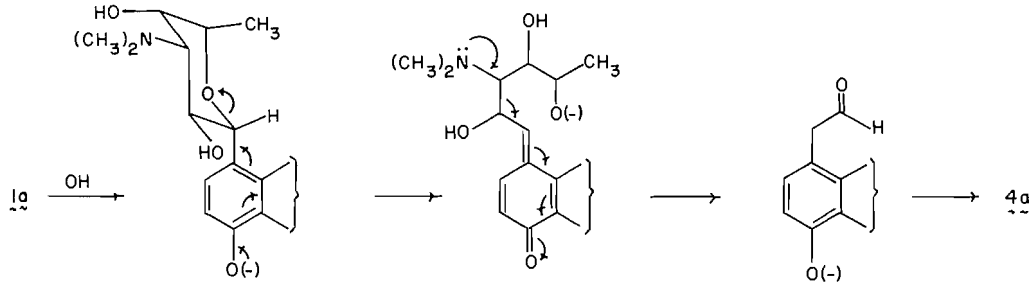

SCHEME 2

reverse electrophilic aromatic substitution in which the phenol is dealkylated at the *para* position via a quinonoid sigma complex. A possible mode of generation of the masked aldehyde **4***a* is portrayed in Scheme 2 in which the essential cleavage of the *C*-glycoside ether bond is accomplished by base catalysed generation of quinone methine **7** and followed by the rupture of the vinylogous β-aminoketone to provide the free aldehyde group which interacts with the B ring phenolate to produce the diastereomeric hemiacetals **4***a*.

The dihydro derivatives **4***b* were obtained from **4***a* in quantitative yield by catalytic (PtO) hydrogenation in ethanol and this mixture was transformed in 50% yield to the achiral isomeric lactone aldehyde **2***b* by heating in quinoline at 180°C in the presence of copper powder. The ir spectrum (KBr) of the latter gave no evidence of a carboxyl group but a strong absorption centred at 1710 cm^{-1} due to the conjugated lactone and aldehyde, while the ^1H nmr spectrum ($CDCl_3$) displayed the aldehyde proton as a singlet at δ 10.17 ppm.

It may be noted that the ready oxidative degradation of ravidomycin **1***a* to the known (5) anisole 2,3,5-tricarboxylic acid **6**, which affords corroboration of the juxtaposition of groups in ring D, is paralleled in the behaviour towards alkaline permanganate of the structurally related *C*-glycoside toromycin (3) which possesses the same aglycone as **1***a* but is devoid of nitrogen in its sugar moiety.

Complete corroborative evidence for the formulation of ravidomycin and its diacetate as in **1***a* and **1***b* is now available from our complementary ^{13}C nmr spectral analyses. The results are summarized in Table 1. To obtain these data, the following experiments were carried out. Broad band decoupled and off-resonance decoupled $^{13}C-\{^1H\}$ spectra were recorded to yield carbon chemical shifts and cross-correlations between proton-bearing carbons and their respective hydrogen atoms. The assignment of quaternary carbon signals was deduced from a series of single frequency selective (low power) $^{13}C-\{^1H\}$ double resonance experiments (correlating the quaternary carbon multiplets with individual protons in terms of long-range carbon–proton coupling constants), observed acetylation shifts, and the substantial differences in the $^{13}C-\{^1H\}$ (non-selective) nOe values of signals due to quaternary carbon atoms with and without proton(s) in *ortho* position (high and reduced nOe, respectively). Distinction between two-bond and three-bond coupling interactions (geminal vs. vicinal carbon–proton couplings) was usually based on the magnitude of the observed splittings (typical values: ^2J = 1 to 2 Hz and ^3J = 7 to 10 Hz). For couplings with 3 to 4.5 Hz moduli, the nature of the interaction was inferred either from SPT (selective population transfer) measurements (by selective inversion of one of the components of the pertinent proton satellites) affording the sign of the pertinent long-range coupling, or from the occurrence or absence of a selective $^{13}C-\{^1H\}$ nOe during selective proton decoupling experiments (the former case being characteristic of geminal coupling).

The formulation of the polycyclic backbone rests on the following evidence.

Single frequency selective $^{13}C-\{^1H\}$ decoupling experiments disclosed that the doublet splitting of the carbonyl carbon resonance of **1***b* at 160.3 ppm arises from three-bond coupling to H5′ (+4.2 Hz) and the *only* coupling exhibited by the quaternary carbon atom bearing the lactone oxygen (C1) was due to its three-bond spin–spin interaction (8.6 Hz) with H3. Selective decoupling experiments, furthermore, showed that C1′ was vicinally coupled to H5′, H3′, and H3. These findings, combined with other pertinent carbon-13 data (see Table 1), confirm that the arrangement of rings A, B, C, and D of the aglycone (as well as their respective patterns of substitution) must be as in formula **1***b*.

Low power selective irradiation of C4-OMe protons caused the C4 multiplet to collapse into a doublet due to the two-bond interaction with H3 (−4.5 Hz). This indicated the absence of vicinal interaction with ring A protons. Since the same conclusion has been reached for C1 (*vide supra*), both *peri* positions of ring A (i.e. C5 and C8) must be substituted.

Selective irradiation of the lower field *ortho*-coupled proton resonance (7.98 ppm, H-7 in **1***b*) caused the 8.4 Hz coupling of the signal at 125.16 ppm (C-9) to collapse, which showed the

Can. J. Chem. Downloaded from www.nrcresearchpress.com by 210.87.254.6 on 09/06/12
For personal use only.

TABLE 1. ^{13}C nuclear magnetic resonance data of ravidomycin **1***a* and its diacetate **1***b*[a]

Carbon	Chemical shift **1***a*	Chemical shift **1***b*	Multiplicity[b]	^nJ(C,H) Coupling constants[c]
C1	142.60	142.16	S,d	^3J(H3) = 8.6
C2	113.79	114.71	S,d	^2J(H3) = 1.6
C3	101.78	104.86	D,s	^1J(H3) = 164.55
C4	151.68	151.34	S,d,q	^2J(H3) = −4.5; ^3J(OCH$_3$) = 4.4
C5	154.67	146.64	S,d,d	^2J(H6) = −4.6; ^3J(H7) = 10.1
C6	112.24	121.25	D,s	^1J(H6) = 164.4
C7	129.48	127.85	D,d	^1J(H7) = 162.3; ^3J(H1″) = 4.1
C8	125.00	132.53	S,d,d,d	^2J(H7) = 2.1; ^3J(H6) = 4.8; ^3J(H2″) = 6.9
C9	125.14[e]	125.16[e]	S,d,d	^3J(H1″) = 1.7; ^3J(H7) = 8.4
C10	116.00[e]	120.89[e]	S,d,d	^3J(H3) = 6.2; ^3J(H6) = 5.7
C1′	123.10[e]	123.65[e]	S,d,d,d	^3J(H3) = 6.1; ^3J(H5′) = 6.2; ^3J(H3′) = 3.7
C2′	156.95	157.62	S,d,q	^2J(H3′) = −4.5; ^3J(OCH$_3$) = 4.4
C3′	113.72	114.38	D,d,d	^1J(H3′) = 156.8; ^3J(H5′) = 7.2; ^3J(=CH) = 4.9
C4′	138.49	139.14	S,d,d,d,d,d[d]	
C5′	119.46	120.17	D,d,d	^1J(H5′) = 166.14; ^3J(H3′) = 6.4; ^3J(=CH) = 4.9
C6′	122.00	122.79	S,s	
CO (lactone)	160.55	160.31	S,d	^3J(H5′) = +4.2
CH=	135.20	135.32	D,d,d,d	^1J(H) = 155.8; ^2J(H*cis*) = −2.5; ^3J(H3′) = 4.9; ^3J(H5′) = 4.9
=CH$_2$	116.28	116.71	T,s	^1J(H) = 158.01
C5-O*C*OCH$_3$	—	169.62	S,q,d	^2J(CH$_3$) = 7.4; ^4J(H6) = 0.8
C5-OCO*C*H$_3$	—	20.73	Q	
C4-OCH$_3$	55.87[f]	56.35[f]	Q	
C2′-OCH$_3$	55.80[f]	56.26[f]	Q	
C1″	80.48	78.60	D	
C2″	69.55	71.44	D	
C3″	65.35	67.30	D	
C4″	69.37	69.58	D	
C5″	74.97	75.47	D	
C6″	16.76	16.71	Q	
N(CH$_3$)	40.77	41.74	Q	
C2″-O*C*OCH$_3$	—	169.56	S,q,d	^2J(CH$_3$) = 6.8; ^3J(H2″) = 4.2
C2″-OCO*C*H$_3$	—	20.90	Q	
C4″-O*C*OCH$_3$	170.80	170.80	S,q,d	^2J(CH$_3$) = 7.2; ^3J(H4″) = 3.8
C4″-OCO*C*H$_3$	21.58	21.57	Q	

[a]Chemical shifts are in delta ppm relative to internal TMS, $CDCl_3$.
[b]Capital letters refer to multiplicity resulting from directly bonded protons and small letters to long range ^{13}C, ^1H couplings.
[c]Coupling constants (±0.2 Hz) were obtained from first-order treatment of the SFSD and undecoupled spectra run at 50.32 MHz. Four-bond and two-bond couplings with nearly zero moduli are not reported.
[d]Multiplet pattern not analyzed.
[e]Resonance with highly reduced nOe indicating the absence of α-CH proton(s).
[f]Assignments may be interchanged.

existence of a three-bond interaction between these nuclei. The lack of appreciable acetylation shift, on the other hand, indicated a *meta* relationship between this (low nOe) carbon and the C5-OAc (OH) substituent. Further selective decoupling experiments involving ring A and B protons revealed that the multiplet at 116.0 (ravidomycin) or 120.89 (diacetate) was due to the (low nOe) quaternary carbon atom (C10) which was vicinally coupled to H3 *and* the higher field (H6) ring A proton (7.22 ppm in **1***b*). The observed +5 ppm acetylation shift attested to the *ortho* relationship between the C10 carbon atom and the OAc (OH) function.

The ^{13}C chemical shift assignments for the ravidomycin nucleus are in close agreement with those of Takashima *et al.* (4) for the structurally related antitumor antibiotic gilvogarcin which possesses the same aglycone linked to a furanose moiety. In view of this the assignment of ^{13}C signals in the published inventory of chemical shifts for carbon atoms in the toromycin (3) aglycone is facilitated.

Experimental

All melting points were determined on a Kofler hot stage apparatus and are uncorrected.

High resolution mass spectra were recorded on an AE1 MS-50 spectrometer at the Mass Spectrometry Lab., University of Alberta. Low resolution mass spectra were recorded on an Hitachi Perkin–Elmer RMU-6D spectrometer. The infrared spectra were measured on a Perkin–Elmer 727B or 598 infrared spectrophotometer and ultraviolet spectra were obtained with a Beckman 25 instrument.

The ^1H spectra of compounds **2***a* to **6** inclusive were determined on a Nicolet NIC-360 spectrometer at Toronto Biomedical NMR Centre while ^1H and ^{13}C spectra of ravidomycin **1***a* and ravidomycin diacetate **1***b* were recorded on a disk-augmented Varian XL-100/15FT instrument. Proton-coupled and single frequency (low-power) selective ^{13}C–{^1H} double resonance spectra were run at 50.32–{200.13} MHz using a Bruker WP 200/SY spectrometer. The amplitude of the decoupling field in the SFSD experiments varied from 2.5 to 10 Hz and the decoupler power employed in selective population transfer measurements runs for relative sign determination was usually set to 2 Hz.

Can. J. Chem. Downloaded from www.nrcresearchpress.com by 210.87.254.6 on 09/06/12
For personal use only.

Can. J. Chem. Downloaded from www.nrcresearchpress.com by 210.87.254.6 on 09/06/12
For personal use only.

Purification of ravidomycin **1**a

The ravidomycin (1.1 g), supplied by Ayerst Research Laboratories, was dissolved in chloroform (10 mL) and applied to the top of a dry column of silica gel G (polyethylene pellicle column 2.6 × 46 cm), which was developed with choroform/methanol (8:1). As soon as the solvent reached the bottom of the column, the main yellow band was cut out of the column and eluted with chloroform/methanol (5:1) immediately . The eluate was concentrated and the residue was crystallized from ethyl acetate. Fine needles were obtained, mp 248–250°C; $[\alpha]_D$ −105.5° (*c* 0.20, $CHCl_3$); ir (KBr) ν_{max}: 3380 (OH), 1740, 1240 (acetate), 1720 (lactone), 1620, 1600, 1580 (aromatic ring) cm^{-1}; uv (MeOH)λ_{max} nm (log ϵ): 244 (4.68), 263 (4.54, sh), 277 (4.60), 285 (4.65), 308 (4.33), 320 (4.30), 335 (4.20), 350 (4.08), 392 (4.24); uv ($CHCl_3$) λ_{max} nm: 246, 265, 278, 288, 308, 322, 334, 350, 395; ms *m/e*: 563.2148 (52.09%, calcd. for $C_{31}H_{33}NO_9$: 563.2155, M^+); cd (*c* = 0.0081, $CHCl_3$) $[\theta]^{26}$ nm: −2659 (245), −1095 (264), −1877 (275), −2502 (288), −1870 (300), −1877 (310), −1880 (320), −1408 (330), −1410 (340), −1870 (400).

Ravidomycin acetate **1**b

Ravidomycin (20 mg) was acetylated in pyridine (1.5 mL) and acetic anhydride (1.5 mL) at room temperature for 2 days, affording its diacetate **1***b* in quantitative yield, a colloidal solid from dichloromethane/methanol, mp 238–239°C; $[\alpha]_D^{26}$ + 33.3° (*c* 0.072, $CHCl_3$); ir ($CHCl_3$) ν_{max}: 1740 (acetyl), 1725 (lactone), 1610, 1590 (aromatic ring) cm^{-1}, no hydroxyl; uv (MeOH) λ_{max} nm (log ϵ): 245 (4.50), 278 (4.48), 285 (4.51), 306 (4.17, sh), 323 (4.08), 335 (4.06), 346 (4.01, sh), 383 (4.13); ms *m/e*: 647.2361 (3.77%, calcd. for $C_{35}H_{37}NO_{11}$: 647.2367, M^+).

Aglycone **2**a *and hemiacetals* **4**a

Ravidomycin (0.5 g) in 50% potassium hydroxide (8 mL) was refluxed for 6 h under nitrogen. The reaction mixture was acidified with concentrated hydrochloric acid in an ice bath, and provided the yellow products which were chromatographed on a silica gel column eluting with chloroform, then chloroform/methanol (20:1). The early fractions eluted by chloroform gave the aglycone **2***a* (40 mg), yellow needles from chloroform/methanol, mp 265–266°C $[\alpha]_D^{20}$ 0° (*c* 0.50, $CHCl_3$). The middle fraction eluted by chloroform/methanol (20:1) yielded the yellow granular crystals (160 mg) **4***a*, mp 227–230°C after recrystallization with chloroform/methanol; $[\alpha]_D^{20}$ 0° (*c* 1.00, $CHCl_3$). The ^1H nmr spectrum indicates a mixture (1:1) of diastereomers.

Aglycone **2***a*: ir (KBr) ν_{max}: 3350 (br, OH), 1720 (lactone), 1625, 1600, 1580 (aromatic ring) cm^{-1}; uv (MeOH) λ_{max} nm (log ϵ): 243 (4.66), 263 (4.50), 273 (4.55), 283 (4.54), 307 (4.26), 386 (4.21); ^1H nmr ($CDCl_3/CD_3OD$) δ_{TMS}: 3.51 (br, 1H, OH), 4.12 (s, 6H, OCH_3 × 2), 5.47 (d, 1H, J_{cis} = 11.0 Hz, 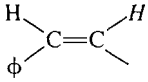), 5.96 (d, 1H, J_{trans} = 17.4 Hz, 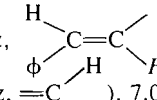), 6.81 (dd, 1H, J_{cis} = 11.0 Hz, J_{trans} = 17.4 Hz, 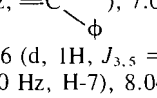), 7.00 (dd, 1H, $J_{6,7}$ = 8.0 Hz, $J_{6,8}$ = 0.8 Hz, H-6), 7.36 (d, 1H, $J_{3,5}$ = 1.6 Hz, H-3′), 7.50 (dd, $J_{6,7}$ = 8.0 Hz, $J_{7,8}$ = 8.0 Hz, H-7), 8.04 (dd, 1H, $J_{7,8}$ = 8.0 Hz, $J_{6,8}$ = 0.8 Hz, H-8), 8.10 (d, 1H, $J_{3',5'}$ = 1.6 Hz, H-5′), 8.31 (s, 1H, H-3); ms *m/e*: 348.0997 (100.00%, calcd. for $C_{21}H_{16}O_5$: 348.0998, M^+).

Hemiacetals **4***a*: ir (KBr) ν_{max}: 3600–2500, 1700 (OH, COOH), 1620, 1600, 1570 (aromatic ring) cm^{-1}; uv (MeOH) λ_{max} nm (log ϵ): 228 (4.76), 260 (4.38), 308 (4.07), 336 (4.01), 353 (4.11); ^1H nmr ($CDCl_3/CD_3OD$) δ_{TMS}: 2.82 (br, 3H, COOH, OH × 2), 3.00–3.30 (m, 2H, Ar-CH_2), 3.80, 3.79 (s, each 1.5 H, OCH_3-2′), 4.01 (s, 3H, OCH_3-4), 5.38 (dd, 0.5 H, *J* = 3.0/7.2 Hz, axial hemiacetal proton), 5.67 (dd, 0.5 H, *J* = 3.0/3.0 Hz, equatorial hemiacetal proton), 5.37 (d, 1H, J_{cis} = 11.0 Hz, 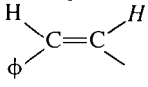), 5.86 (d, 1H, J_{trans} = 17.7 Hz, 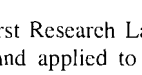), 6.77, 6.76 (dd, each 0.5 H, J_{trans} = 17.7 Hz, J_{cis} = 11.0 Hz, 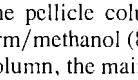), 6.73, 6.69 (s, each 0.5 H, H-3), 6.82 and 6.83, 7.08 and 7.10 (two pair of AB, each 0.5 H, $J_{6,7}$ = 8.0 Hz, H-7, H-6), 7.18, 7.19 (d, each 0.5 H, $J_{3',5'}$ = 1.5 Hz, H-3′), 7.51, 7.55 (d, each 0.5 H, $J_{3',5'}$ = 1.5 Hz, H-5′); ms *m/e*: 408.1205 (10.0%, calcd. for $C_{23}H_{20}O_7$: 408.1209, M^+).

Compound **3**

The aglyone **2***a* (5 mg) in acetic acid (20 mL) was hydrogenated in the presence of platinum oxide (20 mg) at 70–75°C for 4 h, giving colorless needles (3 mg) which were crystallized from methanol, mp 190–192°C; ir (KBr) ν_{max}: 1710 (lactone), 1610, 1585 (aromatic ring) cm^{-1}, no hydroxyl; uv (MeOH) λ_{max} nm (log ϵ): 212 (4.58, sh), 221 (4.61, sh), 232 (4.69, sh), 238 (4.70), 262 (4.29, infl), 274 (4.29), 350 (4.16); ^1H nmr ($CDCl_3$) δ_{TMS}: 1.30 (t, 3H, *J* = 7.6 Hz, CH_2CH_3), 2.78 (q, 2H, *J* = 7.6 Hz, CH_2CH_3), 1.82 (m, 4H, —CH_2—CH_2—), 2.73, 2.96 (m, each 2H, Ar-CH_2 × 2), 3.90 (s, 3H, OCH_3-4), 4.07 (s, 3H, OCH_3-2′), 7.16 (d, $J_{3',5'}$ = 1.5 Hz, H-3′), 7.95 (d, $J_{3',5'}$ = 1.5 Hz, H-5′), 8.30 (s, 1H, H-3); ms *m/e*: 338.1512 (100.00%, calcd. for $C_{21}H_{22}O_4$: 338.1518, M^+).

Compound **5**

The mixture of hemiacetals **4***a* (5 mg) was hydrogenated by the above-mentioned method and the reaction product was separated on tlc (solvent system: chloroform/methanol 30:1). The main product **5** was crystallized from methanol, plates (2 mg), mp 224–226°C; ir (KBr) ν_{max}: 3600–2500, 1690, 1670 (COOH), 1600 (aromatic ring) cm^{-1}; uv (MeOH) λ_{max} nm (log ϵ): 209 (4.60), 300 (3.78); ^1H nmr ($CDCl_3/CD_3OD$) δ_{TMS}: 1.29 (t, 3H, *J* = 7.5 Hz, CH_2CH_3), 2.70 (q, 2H, *J* = 7.5 Hz, CH_2CH_3), 1.60–2.05 (m, 7H, aliphatic CH_2 × 3 and COOH, covered), 2.50–2.90 (m, 3H, Ar-CH × 3), 3.73 (s, 3H, OCH_3-4), 3.76, 3.77 (s, each 1.5 H, OCH_3-2′), 4.05 (m, 1H, axial α-hydropyran proton), 4.24 (m, 1H, equatorial α-hydropyran proton), 6.55, 6.57 (s, each 0.5 H, H-3), 6.94 (d, 1H, $J_{3',5'}$ = 1.4 Hz, H-3′), 7.27 (d, $J_{3',5'}$ = 1.4, H-5′); ms *m/e*: 382.1780 (100.00%, calcd. for $C_{23}H_{26}O_5$: 382.1780, M^+).

4-Carboxyl-6-methoxyphthalic acid **6**

Ravidomycin (100 mg) in 1% potassium hydroxide (15 mL) was oxidized with an aqueous solution of potassium permanganate under stirring and refluxing until persistence of the pink color for half an hour. After filtration of the manganese dioxide the solution was concentrated in vacuum and then acidified with concentrated hydrochloric acid to pH 1 and extracted by ethyl acetate. The evaporated extract was chromatographed on silica gel with chloroform/methanol/acetic acid (6:1:1). The early fraction yielded 4-carboxyl-6-methoxylphthalic acid (25 mg), plates from dilute hydrochloric acid, mp 240–241°C, which were identical in ir spectra and mixture melting point with the authentic sample of **6** synthesized according to a known procedure (5). The acid was methylated in methanol with diazomethane, giving trimethyl ester, plates from chloroform/methanol, mp 145°C.

4-Carboxyl-6-methoxylphthalic acid: ir (KBr) ν_{max}: 3500–2500, 1700 (COOH), 1600, 1575 (aromatic ring) cm^{-1}; ^2H nmr (unisol) δ_{TMS}: 4.00 (s, 3H, OCH_3), 7.90 (d, 1H, *J* = 1.0 Hz, H-5), 8.25 (d, 1H, *J* = 1.0 Hz, H-3); ms *m/e*: 222 (M − H_2O), 194 (M − H_2O − CO), 164 (M-COOH-OCH_3).

Trimethyl ester: ir (KBr) ν_{max}: 1740, 1730, 1720 (—$COOCH_3$), 1600, 1580 (aromatic ring) cm^{-1}, no carboxyl; ^1H nmr ($CDCl_3$) δ_{TMS}: 3.97, 4.00 (s, each 6H, OCH_3, $COOCH_3$ × 3), 7.83 (d, 1H, *J* = 1.0 Hz, H-5), 8.30 (s, 1H, *J* = 1.0 Hz, H-3); ms *m/e*: 282 (M^+), 251 (M-OCH_3), 223 (M-$COOCH_3$), 192 (M-$COOCH_3$-OCH_3), 165.

Compound **4**b

The diastereomer mixture **4***a* (50 mg) in ethanol (10 mL) was hy-

drogenated in the presence of platinum oxide (20 mg) at room temperature, affording dihydro derivative **4***b* (45 mg), which was crystallized as yellow plates from methanol, mp 220–222°C; ir (KBr) ν_{max}: 3540 (OH), 3500–2400, 1690 (COOH), 1615, 1595 (aromatic ring) cm^{-1}; uv (MeOH) λ_{max} nm (log ϵ): 227 (4.63), 248 (sh, 4.22), 288–300 (plateau, 3.82), 317 (3.86), 336 (3.90), 351 (3.97); ^1H nmr ($CDCl_3/CD_3OD$) δ_{TMS}: 1.32, 1.33 (t, each 1.5 H, J = 7.5 Hz, $—CH_2—CH_3$), 2.74, 2.75 (q, each 1H, J = 7.5 Hz, $—CH_2CH_3$), 3.00–3.30 (m, 2H, Ar-CH_2), 3.76, 3.77 (s, each 1.5 H, OCH_3-2′), 4.00, 4.01 (s, each 1.5 H, OCH_3-4), 5.37 (dd, 0.5 H, J = 7.4/3.0 Hz, axial hemiacetal proton), 5.64 (dd, 0.5 H, J = 3.0/3.0 Hz, equatorial hemiacetal proton), 6.69, 6.73 (s, each 0.5 H, H-3), 6.80 and 6.81, 7.07 and 7.09 (two pair of AB, each 0.5 H, J = 7.9 Hz, H-7, H-6), 7.00, 7.01 (d, each 0.5 H, J = 1.4 Hz, H-3′), 7.31, 7.34 (d, each 0.5 H, J = 1.4 Hz, H-5′); ms m/e: 410.1367 (72.22%, calcd. for $C_{23}H_{22}O_7$: 410.1365, M^+).

Aldehyde lactone **2**b

The dihydro derivative **4***b* (100 mg) in quinoline (2 mL, freshly distilled) was heated at 180°C for 10 min in the presence of copper powder (250 mg) with stirring. After removal of copper powder, the reaction solution was mixed with ether (15 mL), then extracted with 1.5 *N* HCL and washed with water. The residue from the ethereal layer was chromatographed on a silica gel column eluting with chloroform and chloroform/methanol (20:1) in turn. The fractions eluted with chloroform/methanol gave the aldehyde lactone **2***b* (50 mg), which crystallized as yellow needles from chloroform/methanol, mp 220–222°C; ir (KBr) ν_{max}: 3300 (OH), 1715 (>C=O), 1620, 1610, 1590 (aromatic ring) cm^{-1}, no carboxyl; ^1H nmr ($CDCl_3$) δ_{TMS}: 10.17 (s, 1H, aldehyde proton), 9.73 (s, 1H, exchangeable with D_2O, OH), 8.47 (s, 1H, H-3), 7.92 (d, 1H, J = 1.5 Hz, H-5′), 7.22, 6.95 (AB, each 1H, J = 8.0 Hz, H-7, H-6), 7.19 (d, 1H, J = 1.5 Hz, H-3′), 4.50 (s, 2H, Ar-CH_2—CO—), 4.13, 4.08 (s, each 3H, OCH_3-2′, OCH_3-4), 2.80 (q, 2H, J = 7.6 Hz, $CH_3—CH_2$), 1.34 (t, 3H, J = 7.6 Hz, $CH_3—CH_2$); ms m/e: 392 (M^+), 363 (M − CHO).

Acknowledgements

The assistance of Ayerst Research Laboratories (Montreal) in providing ravidomycin and some financial support for this study is gratefully acknowledged. The authors are grateful to Dr. L. Szilágyi (Institute of Organic Chemistry, University of Debrecen, Hungary) for kind permission to use his WP-200/SY instrument. This work was supported, in part, by a grant from the Natural Sciences and Engineering Research Council of Canada.

1. JOHN A. FINDLAY, JIA-SEN LIU, LAJOS RADICS, and S. RAKHIT. Can. J. Chem. **59**, 3018 (1981).
2. (*a*) S. N. SEGHAL and CLAUDE VEZINA. Current chemotherapy and infectious disease. Proceedings of the 11th I.C.C. and the 19th I.C.A.C., American Society of Microbiology. 1980. p. 1553; (*b*) U.S. Patent No. 4,230,692 (1980).
3. SATOSHI HORII, HIROSHI FUKASE, EIJI MIZUTA, KAZUNORI HATANO, and KOMEI MIZUNO. Chem. Pharm. Bull. **28**, 3601 (1980).
4. KEIICHI TAKAHASHI, MAYUMI YOSHIDA, FUSAO TOMITA, and KUNIKATSU SHIRAHATA. J. Antibiot. **34**, 271 (1981).
5. (*a*) R. WALLACE, A. L. PORTE, and R. HODGES. J. Chem. Soc. 1445 (1963); (*b*) S. M. ADJANGBA and D. BILLET. Bull. Soc. Chim. 1970 (1962).

Can. J. Chem. Downloaded from www.nrcresearchpress.com by 210.87.254.6 on 09/06/12
For personal use only.

Basicité et structure de phosphoramides aliphatiques: dosage protométrique en solvants non-aqueux

JEAN-CLAUDE BOLLINGER, RENÉ FAURE ET THÉOPHILE YVERNAULT

Laboratoire de Chimie Générale et Analytique, Faculté des Sciences, 123 avenue Albert-Thomas, 87060 Limoges Cédex, France

Reçu le 25 juin 1982

JEAN-CLAUDE BOLLINGER, RENÉ FAURE et THÉOPHILE YVERNAULT. Can. J. Chem. **61**, 328 (1983).

Par des dosages potentiométriques à 25°C dans le nitrométhane ou le mélange sulfolane/benzène 98:2 p/p, on a déterminé la basicité selon Brönsted (potentiels de demi-neutralisation) de 19 phosphoramides aliphatiques OPXYZ, avec X, Y ou Z = Me; OEt; NMe_2; NEt_2; NHEt; $N(CH_2)_n$ (n = 3 ou 4); ou X + Y = —NMe—$(CH_2)_2$—NMe—. Ce sont des bases faibles, dont la plupart présentent un phénomène d'homoliaison hydrogène. Ceux qui contiennent des substituants Me ou $N(CH_2)_3$ se décomposent en milieu acide, ce qui a été confirmé par dosage en retour et par mesure de $E = f$(temps) au point équivalent. On compare les résultats dans les deux solvants, et on discute l'influence de la nature des substituants X, Y, Z sur les potentiels de demi-neutralisation et sur l'instabilité en milieu acide.

JEAN-CLAUDE BOLLINGER, RENÉ FAURE, and THÉOPHILE YVERNAULT. Can. J. Chem. **61**, 328 (1983).

Brönsted basicities (as half-neutralization potentials) have been determined at 25°C by potentiometric titrations in nitromethane or in the mixture sulfolane/benzene 98:2 p/p for 19 aliphatic phosphoramides OPXYZ, with X, Y, or Z = Me; OEt; NMe_2; NEt_2; NHEt; $N(CH_2)_n$ (n = 3 or 4); or X + Y = —NMe—$(CH_2)_2$—NMe—. Almost all of these weak bases give an homohydrogen bonding. Those with an Me or $N(CH_2)_3$ substituent are not stable in acidic medium, which is confirmed by back-titration and measure of E vs. time at the equivalent point. After comparing the results obtained in the two solvents, the effect of the nature of the substituents X, Y, Z on half-neutralization potentials and instability in acidic medium is analyzed.

Introduction

On sait que l'hexaméthylphosphotriamide $OP(NMe_2)_3$ ou HMPT est, parmi les solvants dipolaires aprotiques usuels, un des plus basiques au sens de Lewis; par contre il est une base de Brönsted très faible: non dosable par un acide fort dans l'eau, il se comporte comme l'urée ou le diméthylacétamide dans l'acide acétique (1), mais peut cependant être titré dans l'anhydride acétique (2); la valeur $pK_a = 0{,}15 \pm 0{,}10$ dans l'eau a été récemment déterminée par spectrophotométrie (3), et $pK_a = 7{,}0 \pm 0{,}1$ dans l'oxydipropionitrile par potentiométrie (4), à comparer à pK_a (H_2O) = −1,23 dans H_2O + H_2SO_4 par rmn du proton (5).

Depuis plusieurs années, notre laboratoire a entrepris des études en vue de mieux comprendre l'influence de la structure des composés organiques du phosphore(V) OPXYZ sur leur basicité et le mécanisme de leur coupure en milieu acide; nous avons ici utilisé une méthode de dosage potentiométrique pour évaluer la basicité selon Brönsted d'une série de phosphoramides voisins du HMPT (voir Tableau 1), en solvants non-aqueux.

Dans le nitrométhane, divers auteurs (6−11) ont étudié le dosage potentiométrique de composés organophosphorés de structures variées par une solution d'acide perchlorique. Nous avons utilisé les mêmes conditions pour doser nos phosphoramides; mais les propriétés acide−base du nitrométhane limitent son domaine d'utilisation (12, 13) et d'autre part le titrant y est partiellement aqueux.

C'est pourquoi nous avons adopté un solvant dipolaire aprotique, ni acide ni basique, le sulfolane; nous avons montré précédemment (14) que son mélange avec 2% pds de benzène permet d'obtenir à 25°C des caractéristiques très voisines de celles du sulfolane pur à 30°C (température habituellement utilisée) et qu'il convient bien pour le dosage de bases faibles, seules ou en mélanges, par le titrant $HClO_4$ dans le même mélange solvant. Les résultats du dosage de phosphoramides dans ce système sont plus particulièrement présentés dans ce mémoire, ainsi que les conclusions que l'on peut en tirer sur les basicités comparées de ces corps.

Partie expérimentale

L'origine, la purification et les propriétés physiques de plusieurs composés organophosphorés OPXYZ étudiés ici (voir Tableau 1) ont été précédemment décrites dans les références 15 (pour les composés **1** à **4**), 16 (pour **5** à **13**) et 17 (pour **17** à **21**).[1]

Les composés $OPMe(NMe_2)_2$, **23**, et $OPMe(NEt_2)_2$, **24**, ont été préparés à partir de $OPMeCl_2$[2] par action de l'amine correspondante, en solution benzénique en présence de triéthylamine, selon une méthode classique (16). Le mélange est laissé ensuite à température ambiante, 24 h pour **23** et 48 h pour **24** dont la formation est plus lente. Après élimination du sel précipité et évaporation du solvant, une première distillation sous pression réduite donne un produit riche en ions Cl^- et assez conducteur. Une deuxième distillation est effectuée en présence de soude aqueuse saturée (environ 1 mL pour 40 g) (16); on obtient alors des produits ne contenant plus d'ions Cl^- et ayant une résistivité de $10^5\ \Omega^{-1}$ cm environ. Rendements en produits purifiés: 59% pour **23**, 52% pour **24**.

On a observé les caractéristiques physiques suivants: $OPMe(NMe_2)_2$, **23**, $Eb_{0.8}$ = 60°C; F = −1,5°C; d^4_{25} = 1,016 (à comparer avec les valeurs assez nombreuses et peu concordantes de la littérature pour la température d'ébullition: réfs. 18−22); $OPMe(NEt_2)_2$, **24**, Eb_9 = 132°C (litt. (18) Eb_1 = 91°C); d^4_{25} = 0,960.

Les temps de rétention t_R ont été mesurés par chromatographie en phase gazeuse sur Carbowax 20M à 190°C, par comparaison avec HMPT, **1**: t_R(**23**) ≠ t_R(**1**); t_R(**24**) = 1,64 × t_R(**1**).

Pour les mesures dans le nitrométhane, nous avons utilisé un pH-mètre digital Beckman PHasar I (indiquant les potentiels à ±1 mV),

[1]Dans un souci de cohérence, nous avons adopté ici la même numérotation que celle utilisée dans notre précédent mémoire (17) consacré aux nombres donneurs d'une série de phosphoramides.

[2]Produit gracieusement fourni par le Prof. Dr. Klaus Weissermel (Hoechst A. G., Frankfurt/Main), à qui nous exprimons notre gratitude.

0008-4042/83/020328-06$01.00/0

©1983 National Research Council of Canada/Conseil national de recherches du Canada

Can. J. Chem. Downloaded from www.nrcresearchpress.com by 210.87.254.105 on 09/06/12
For personal use only.

TABLEAU 1. Liste des composés OPXYZ étudiés

Composé no.	X	Y	Z	Formule brute	No. Chem. Abstr.	Masse volumique ρ_{25} (g mL^{-1})
1	NMe_2	NMe_2	NMe_2	$C_6H_{18}N_3OP$	680-31-9	1,020
2	NMe_2	NMe_2	OEt	$C_6H_{17}N_2O_2P$	2404-65-1	1,025
3	NMe_2	OEt	OEt	$C_6H_{16}NO_3P$	2404-03-7	1,040
4	OEt	OEt	OEt	$C_6H_{15}O_4P$	78-40-0	1,064
5	NMe_2	NMe_2	NHEt	$C_6H_{18}N_3OP$	10159-47-4	1,017[a]
6	NMe_2	NHEt	NHEt	$C_6H_{18}N_3OP$	69981-36-8	1,027[a]
7	NHEt	NHEt	NHEt	$C_6H_{18}N_3OP$	19622-51-6	—
8	NMe_2	NMe_2		$C_8H_{20}N_3OP$	40725-71-1	1,057
9	NMe_2			$C_{10}H_{22}N_3OP$	53439-65-9	1,089
10				$C_{12}H_{24}N_3OP$	6415-07-2	1,115
11			NEt_2	$C_{12}H_{26}N_3OP$	69981-37-9	1,059
12		NEt_2	NEt_2	$C_{12}H_{28}N_3OP$	69981-38-0	1,009
13	NEt_2	NEt_2	NEt_2	$C_{12}H_{30}N_3OP$	2622-07-3	0,966
17	NMe_2	NMe_2		$C_7H_{18}N_3OP$	41657-48-1	1,061
18	NMe_2			$C_8H_{18}N_3OP$		1,103
19				$C_9H_{18}N_3OP$	3132-52-3	—
21	NMe_2	NMe—CH_2—CH_2—NMe		$C_6H_{16}N_3OP$	7778-06-5	1,082
23	Me	NMe_2	NMe_2	$C_5H_{15}N_2OP$	2511-17-3	1,016
24	Me	NEt_2	NEt_2	$C_9H_{23}N_2OP$		0,960

[a]Mesures à l'état surfondu.

équipé d'une électrode combinée verre/calomel (KCl 3 *M*) Metrohm EA121. Le pH-mètre est standardisé avant et après chaque dosage à l'aide de solutions tampons aqueuses pH = 4 et pH = 7 (ampoules Titrisol Merck). On opère dans une cellule thermostatée à 25°C où le titrant est introduit à l'aide d'une burette à piston Metrohm (au 1/100 mL).

Le nitrométhane Merck pour synthèse contient vraisemblablement comme impuretés principales, de l'eau et du propionitrile (23). Dans la mesure où le réactif titrant contiendra de l'eau (cf. ci-dessous), l'élimination de cette impureté n'a pas besoin d'être très poussée. C'est pourquoi nous avons simplement procédé à une distillation sous pression atmosphérique (Eb = 100°C).

Le titrant est une solution d'acide perchlorique $\simeq$ 0,1 *M* dans le nitrométhane (6, 9, 24−26) préparée à partir du produit RP p. anal. Prolabo (72% $HClO_4$ en poids). Son titre exact est déterminé selon la référence 27.

Les mesures conductométriques sont effectuées avec un conductomètre Tacussel CD7A, équipé d'électrodes en platine platiné.

Les techniques de purification et de récupération du sulfolane, la préparation du titrant ($HClO_4$ anhydre dans sulfolane/benzène 98:2 p/p) sont détaillés dans un précédent mémoire (14). Les mesures potentiométriques sont réalisées avec une électrode de verre Metrohm EA 109 et une électrode de référence Ag/$AgClO_4$ 0,05 *M*; $NaClO_4$ 0,05 *M* dans le mélange solvant; la réponse de l'électrode de verre et sa fatigue dans ce milieu, le comportement de $HClO_4$ ont également été précisés (14). Les dosages en retour sont réalisés avec une solution de pipéridine Fluka "puriss." dans le mélange solvant, dont le titre est déterminé par dosage potentiométrique avec $HClO_4$.

Résultats

Mesures dans le nitrométhane (NM)

Etant donné que le titrant ($HClO_4$ env. 0,1 *M* dans NM) n'est pas anhydre (au moins 4 g/L d'eau), nous avons étudié son comportement en suivant la variation de sa conductibilité équivalente Λ en fonction de la concentration. La courbe $\Lambda = f(\sqrt{C})$ n'est pas une droite, ce qui indique un comportement d'électrolyte faible; on en déduit, par la méthode de Fuoss et Kraus (28):

$$\Lambda_0 = 132{,}1\ \Omega^{-1}\ cm^2\ mol^{-1};\ pK_a = 2{,}40$$

Ces résultats sont comparables à ceux de la littérature (Λ_0 = 127 (29); pK_a = 2,23 (26*b*), 2,15 (cité par 13)), toutefois Wright *et al.* (29) affirment que $HClO_4$ est un électrolyte fort pour des concentrations inférieures à 10^{-3} *M* dans NM.

Afin de vérifier le bon fonctionnement de notre dispositif expérimental, nous avons effectué les dosages potentiométriques de quelques bases faibles (Fig. 1, Tableau 2); nous avons observé chaque fois que le saut de potentiel correspond bien à 100% de neutralisation. Dans le cas de la diphénylguanidine, la position du point équivalent a également été vérifiée par dosage conductométrique.

On doit signaler que, si la réponse de l'électrode de verre combinée est rapide lors de tous les dosages effectués, les potentiels mesurés sont instables dès que le milieu est acide, ce qui confirme les indications de Matrosov *et al.* (26*a*).

Nous avons ensuite opéré de façon similaire pour divers composés organophosphorés (Fig. 2; Tableaux 1 et 2). Ainsi que l'ont déjà indiqué divers auteurs (6−11), nous observons deux sauts de potentiel, correspondant à 50% et 100% de neutralisation (Fig. 2).

Ce phénomène met en évidence l'existence d'une homoliaison hydrogène[3] d'après le schéma réactionnel suivant (B = base organophosphorée):

[3]Selon la suggestion de Bordwell *et al.* (30), nous utilisons ce terme plutôt que "homoconjugaison", habituellement employé.

Can. J. Chem. Downloaded from www.nrcresearchpress.com by 210.87.254.105 on 09/06/12
For personal use only.

Can. J. Chem. Downloaded from www.nrcresearchpress.com by 210.87.254.105 on 09/06/12
For personal use only.

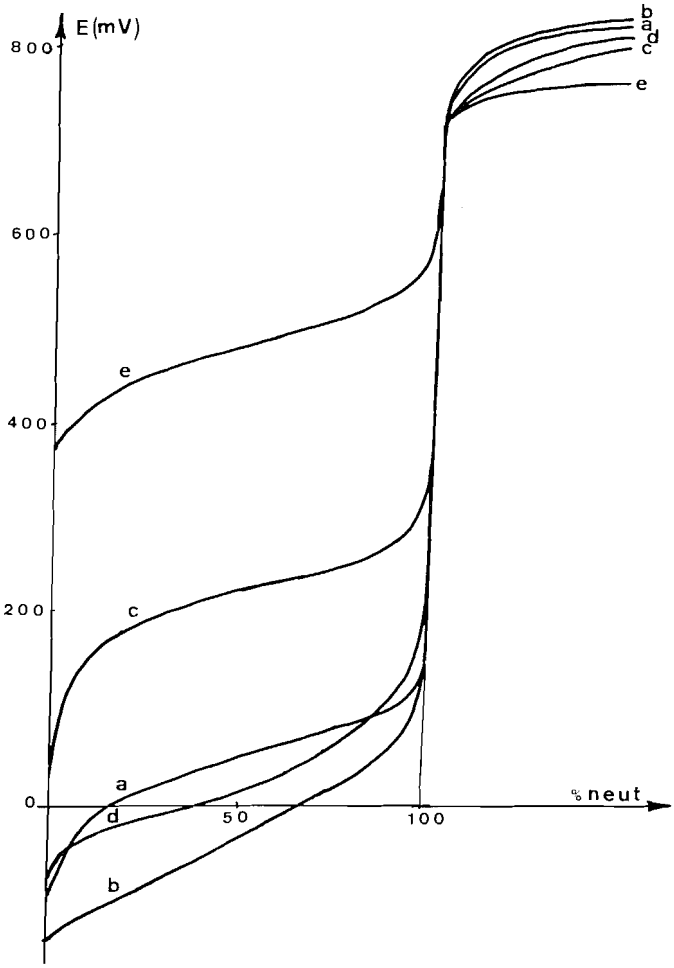

FIG. 1. Dosages protométriques de bases par $HClO_4$ 0,1 *M* dans le nitrométhane à 25°C. a: diphénylguanidine; b: triéthylamine; c: pyridine; d: morpholine; e: tétraméthylurée.

$$2\,B + H^+ \leftrightarrows BHB^+ \qquad K_1 = [B]^2[H^+]/[BHB^+]$$

$$H^+ + BHB^+ \leftrightarrows 2\,BH^+ \qquad K_2 = [BHB^+][H^+]/[BH^+]^2$$

$$2B + 2H^+ \leftrightarrows 2\,BH^+ \qquad K = [B][H^+]/[BH^+] = \sqrt{K_1 \cdot K_2}$$

Les calculs montrent (6, 26*b*) que l'on a alors, avec C = concentration stoechiométrique en base B, au quart de la neutralisation: $pH_{1/4} = pK_1 + \log C_{1/4}$; aux trois-quarts de la neutralisation: $pH_{3/4} = pK_2 - \log C_{3/4}$; à la demi-neutralisation: $pH = (pK_1 + pK_2)/2 \neq (pH_{1/4} + pH_{3/4})/2$ si la variation de la dilution est négligeable.

Quand le potentiel mesuré est fonction linéaire du pH:

$$E = E^0 + k \cdot pH$$

il vient:

$$E_{1/2} = (E_{1/4} + E_{3/4})/2 = E^0 + k \cdot pK$$

Ainsi, l'étalonnage de l'échelle des pK dans le NM n'est pas nécessaire pour comparer la basicité d'une série de composés donnant lieu à un phénomène d'homoliaison hydrogène, les potentiels de demi-neutralisation conviennent.

L'examen des courbes de dosage permet de constater qu'il est difficile d'avoir une bonne précision sur la valeur de $E_{1/2}$; il est donc préférable de la déduire des valeurs de $E_{1/4}$ et $E_{3/4}$, plus précises.

TABLEAU 2. Potentiels de demi-neutralisation de bases diverses par $HClO_4$ dans le nitrométhane à 25°C

Produits	$E_{1/4}$ (mV)	$E_{3/4}$ (mV)	$E_{1/2}$ (mV)
Triéthylamine	—	—	−38,5
Morpholine	—	—	+14,5
Diphénylguanidine	—	—	+50
Pyridine	—	—	+224
Tétraméthylurée	—	—	+485
1[a]	345	604	475±2
2	454	568	511±2
3			Non dosable
4			Non dosable
5	330	576	453±6
6	339	573	456±4
7	306	560	433±2
8	326	594	460±5
9	311	571	441±1
10	295	557	425±4
11	259	577	418±6
12	259	593	426±7
13	265	600	433±6
21			Se décompose

[a]Structures des organophosphorés **1** à **21**: voir Tableau 1.

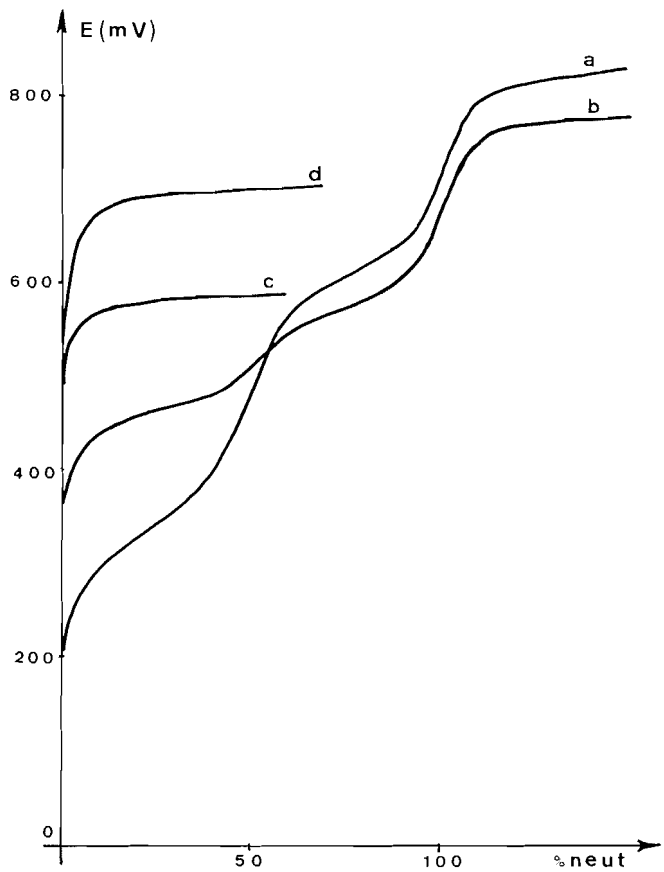

FIG. 2. Dosages protométriques de composés organophosphorés par $HClO_4$ 0,1 *M* dans le nitrométhane à 25°C. a: $OP(NMe_2)_3$ **1**; b: $OP(NMe_2)_2(OEt)$ **2**; c: $OP(NMe_2)(OEt)_2$ **3**; d: $OP(OEt)_3$ **4**.

Les résultats obtenus (Fig. 2; Tableau 2) indiquent que le monoamide **3** et le triester **4** ne sont pas dosés dans ces conditions, ce qui avait déjà été observé (7). D'autre part, le remplacement de groupements NMe_2 par des groupements NHEt

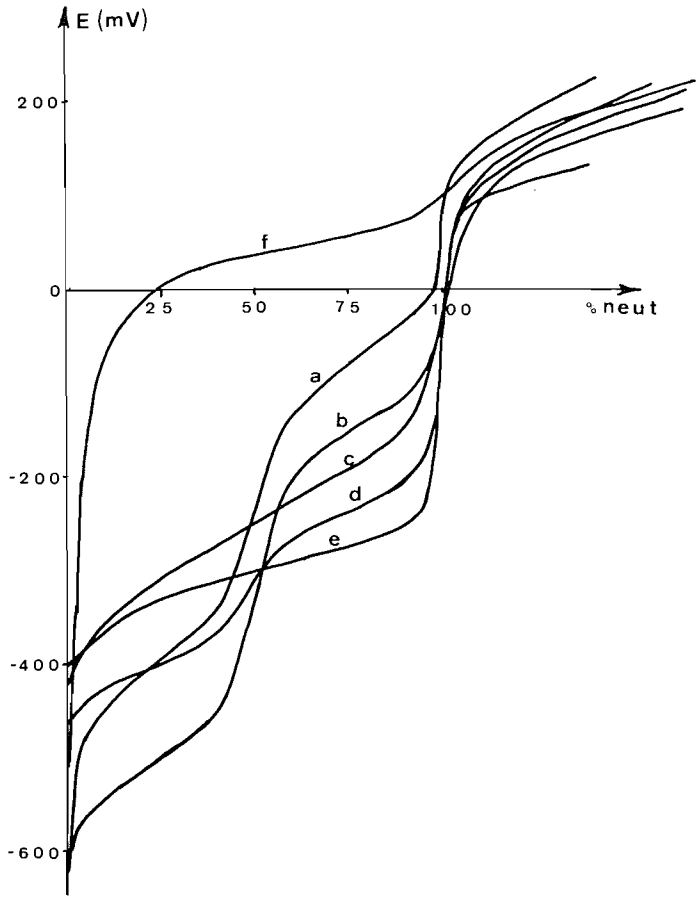

FIG. 3. Dosages protométriques de composés organophosphorés par $HClO_4$ 0,4 *M* dans le mélange sulfolane/benzène 98:2 p/p à 25°C. a: $OP(NMe_2)_3$ **1**; b: $OP(N\langle\rangle)_3$ **10**; c: $OP(NMe_2)_2(OEt)$ **2**; d: $OP(NHEt)(NMe_2)_2$ **5**; e: $OP(NMe_2)((NMe)_2(CH_2)_2)$ **21**; f: $OP(NMe_2)(OEt)_2$ **3**.

ou $N\langle\rangle$ augmente la basicité.

Mesures dans le mélange sulfolane/benzène 98:2 (p/p)

Nous avons suivi par potentiométrie le dosage de plusieurs phosphoramides OPXYZ par une solution d'acide perchlorique env. 0,4 *M*, dans le mélange solvant sulfolane/benzène 98:2 (p/p) (par la suite abrégé en S/B). Le point de neutralisation se manifeste par un brusque saut de potentiel et nous avons vérifié à chaque fois que ce point expérimental correspondait bien au point de neutralisation théorique (erreur inférieure à 2%). Dans le cas du HMPT, **1**, nous avons vérifié par conductométrie que le perchlorate formé est un électrolyte faible: $\Lambda_0 = 10{,}9\ \Omega^{-1}\ cm^2\ mol^{-1}$, $pK_a = 1{,}1$ selon la méthode (28).

En outre, comme dans le NM, la plupart des produits étudiés présentent un saut de potentiel intermédiaire à la demi-neutralisation, mettant ici encore en évidence l'existence d'une homoliaison hydrogène (Fig. 3).

Comme il a été montré dans notre précédent mémoire (14), il existe pour de nombreuses bases une relation linéaire entre le pK_a (H_2O) et le potentiel de demi-neutralisation $E_{1/2}$ dans S/B. Toutefois, les différentes catégories de bases étudiées (amines; pyridine *N*-oxydes) se placent sur des droites différentes; or nous ne disposons pas de valeurs de pK_a (H_2O) connues avec précision pour des composés OPXYZ, ce qui rend aléatoire toute estimation.

TABLEAU 3. Potentiels de demi-neutralisation des composés OPXYZ (structures: voir Tableau 1) par $HClO_4$ dans S/B à 25°C

Produits	$E_{1/2}$ (mV)
1[a]	−226±5
2[b]	−150±7
3[b]	+23±1
4	Non dosable
5[a]	−331±1
6[a]	−326±7
7[a]	−432±1
8[a]	−294±5
9[a]	−306±4
10[a]	−310±3
11[a]	−295±5
12[a]	−290±5
13[a]	−322±4
17	Se décompose
18	Se décompose
19	Se décompose
21[b]	−332±4
23	Se décompose
24[a]	−384

[a]Présence d'homoliaison hydrogène: $E_{1/2} = \frac{E_{1/4} + E_{3/4}}{2}$

[b]Pas d'homoliaison hydrogène.

Nous ne donnerons donc que des résultats en potentiels de demi-neutralisation dans S/B, ceux-ci variant dans le même sens que le pK_a. Les déterminations dans ce mélange solvant S/B sont rapportées aux potentiels de demi-neutralisation de la pyridine ($E_{1/2} = -415$ mV) et de la *p*-nitroaniline ($E_{1/2} = -70$ mV) (14).

Les résultats obtenus sont rassemblés dans le Tableau 3.

Dosage de composés instables en milieu acide

Lors du dosage du certains composés tels que **17**, **18**, **19** ou **23**, par $HClO_4$ 0,4 *M* dans S/B, les potentiels mesurés après chaque addition de titrant augmentent, puis diminuent et se stabilisent, donnant une courbe de dosage qui a toutefois l'allure habituelle.

Ce comportement est lié à une décomposition en milieu acide, qui vient d'être également signalée dans le cas de $OPMe(NMe_2)_2$, **23**, et de $OPMe_2NMe_2$, mais en solution dans NM (37). Pour notre part, afin de mettre en évidence cette décomposition, nous avons effectué des dosages en retour par une solution de base forte (pipéridine) dans S/B.

Pour le HMPT, **1**, le point équivalent correspond à celui du dosage direct, et on observe à nouveau le présence de l'homoliaison hydrogène (Fig. 4).

Par contre pour **23**, les deux points de neutralisation ne correspondent plus au dosage direct. Nous avons ici la preuve de la décomposition du produit initial (Fig. 5, courbes a, a'), ce qui est en accord avec les résultats récents de Matrosov *et al.* (37); Lelièvre et Plichon (20) avaient déjà noté que la dégradation de **23** dans l'acide acétique en présence de $HClO_4$ est suffisamment rapide pour empêcher toute détermination quantitative. Cette réaction est vraisemblablement une coupure de la liaison P—N (37) et libère de la diméthylamine qui est une

Can. J. Chem. Downloaded from www.nrcresearchpress.com by 210.87.254.105 on 09/06/12
For personal use only.

Can. J. Chem. Downloaded from www.nrcresearchpress.com by 210.87.254.105 on 09/06/12
For personal use only.

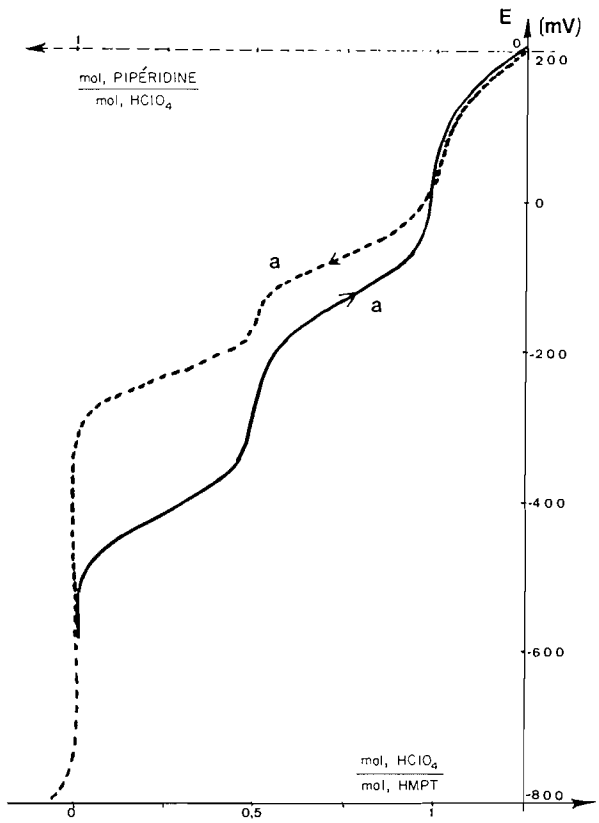

FIG. 4. Dosage protométrique direct (a: par $HClO_4$) et en retour (a': par la pipéridine) de $OP(NMe_2)_3$ **1** dans S/B à 25°C.

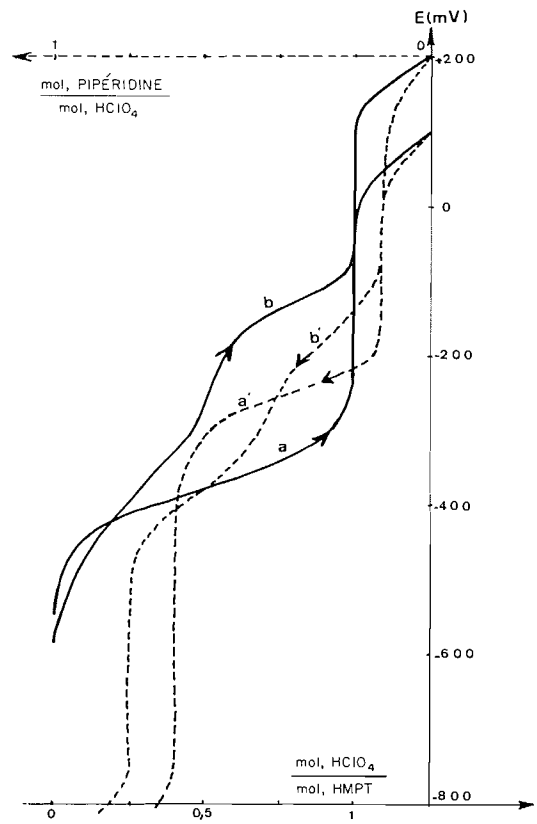

FIG. 5. Dosages protométriques directs (par $HClO_4$: a, b) et en retour (par la pipéridine: a', b') dans S/B à 15°C. a, a': $OPMe(NMe_2)_2$ **23**; b, b': $OP(NMe_2)_2$ (N◇) **17**.

base, ce qui explique le décalage entre le dosage direct et le dosage en retour.

Nous retrouvons le même phénomène de décomposition pour les dérivés azétidinylés **17**, **18** et **19** (cf. courbes bb', Fig. 5). Pour le composé **24** $OPMe(NEt_2)_2$, la décomposition est assez faible, ce qui permet de donner la valeur $E_{1/2} \simeq -384$ mV.

Cette décomposition en présence d'acide est confirmée par l'évolution du potentiel en fonction du temps, lorsque l'on mélange rapidement les deux réactifs (OPXYZ et $HClO_4$) en quantités stoechiométriques; la courbe $E = f(t)$ présente un maximum immédiatement après le mélange, puis le potentiel tend vers une valeur limite.[4]

Discussion

Comparaison des comportements dans NM et dans S/B

On peut tout d'abord constater (Tableaux 2 et 3) que, si la variation de la basicité se fait dans le même sens pour certains composés:

$$\left.\begin{array}{l} \mathbf{2 < 1 < 8 < 9 < 10} \\ \mathbf{1 < 6 < 5 < 7} \end{array}\right\} \quad \text{dans NM et S/B}$$

On a cependant plusieurs inversions dans les diverses "familles" d'organophosphorés OPXYZ:

$$\begin{cases} \mathbf{13 < 12 = 10 < 11} & \text{dans NM} \\ \mathbf{12 < 11 < 10 < 13} & \text{dans S/B} \end{cases}$$

$$\begin{cases} \mathbf{1 < 8 < 6 < 7 < 10 < 11} & \text{dans NM} \\ \mathbf{1 < 8 = 11 < 10 < 6 \ll 7} & \text{dans S/B} \end{cases}$$

Le NM est un solvant aprotique dipolaire faiblement protogène (12, 13); ce caractère, renforcé ici par la présence d'un nombre important de molécules d'eau, surtout en milieu $HClO_4$ (voir ci-dessus), facilite la formation de paires d'ions et la liaison-hydrogène entre acide et base conjugués. De fait, pour le composé **21** il y a bien présence d'homoliaison hydrogène, qui apparaît de façon éphémère si le dosage est assez rapide; mais le produit se décompose, vraisemblablement par ouverture du cycle en milieu acide. De même, le composé **2** présente le phénomène d'homoliaison hydrogène mais le composé **3** n'est pas dosable dans ce solvant.

Par contre dans le mélange S/B, qui présente un caractère dipolaire aprotique faiblement protophile, deux phénomènes nouveaux apparaissent: d'une part les composés **21** et **3** sont dosables, et d'autre part pour les composés **21**, **2** et **3** l'homoliaison hydrogène n'apparaît pas.

Influence de la structure de OPXYZ sur la coupure P—N en milieu acide dans S/B

Nous avons mis en évidence la décomposition de certains produits, par dosage en retour par une solution de base forte.

Pour les composés **17**, **18** et **19**, il s'agit probablement d'une réaction dûe à l'instabilité du cycle azétidine N◇;

[4]L'étude détaillée de cette réponse de l'électrode de verre en fonction du temps figure dans la Thèse de Doctorat de 3e Cycle de R. Faure (Poitiers, 19 Novembre 1982, no. d'ordre 861). Ce document sera envoyé aux personnes intéressées qui en feront la demande aux auteurs.

de même, les composés contenant des cycles aziridine: $OP(NMe_2)_x(N\langle\rangle)_{3-x}$ (x = 0, 1, 2) sont instables en milieu acide (31) et ne sont pas dosables dans S/B.

D'autre part, l'introduction d'un groupement méthyle parmi les substituants du phosphore(V) provoque une fragilité des liaisons P—N en milieu acide (voir ci-dessus, comportement du composé **23**). Ceci contraste avec la grande stabilité de la liaison P—N des phosphoramidates $OP(OR)_x(NMe_2)_{3-x}$ (x = 1, 2) en milieu acide, notée par Modro et coll. (32, 33) dans différents solvants et observée ici également (composés **2** et **3**). On peut rapprocher ces résultats de la diminution importante de la constante de force de la liaison de valence P—N et de l'ordre de liaison P—N quand on passe de $OP(NMe_2)_3$ à $OPMe(NMe_2)_2$ (21).

Toutefois **24** est nettement plus stable que **23**; cela peut être rapproché de la constatation que $OPCl(NEt_2)_2$ réagit beaucoup plus difficilement sur HNR_2 que $OPCl(NMe_2)_2$ (16, 34) et que HEPT **13** ne réagit pas sur $COCl_2$ ou $OPCl_3$ dans les mêmes conditions que HMPT (35).

Conclusion

Dans le mélange sulfolane/benzène 98:2 (p/p), le dosage potentiométrique des phosphoramides par une solution d'acide perchlorique est possible dans un domaine plus étendu que dans le nitrométhane. Ces composés organophosphorés se comportent comme des bases faibles, et donnent très souvent lieu à un phénomène d'autoassociation par liaison hydrogène avec l'acide conjugué.

Dans certains cas, et en particulier pour $OPMe(NMe_2)_2$, nous avons mis en évidence, notamment par dosages en retour, une décomposition du composé organophosphoré, probablement par coupure de la liaison P—N.

Toutefois, si nos mesures nous permettent de classer ces bases selon leur force, par les potentiels de demi-neutralisation dans chaque solvant, nous ne pouvons pas actuellement relier ces valeurs aux pK (H_2O). Rien ne nous permet non plus de préciser si cette protonation a lieu sur l'oxygène ou sur un atome d'azote; il est cependant généralement admis que la mono-protonation des phosphoramides se fait sur l'oxygène (36, 37), et donc la correction statistique qui serait nécessaire en cas de N-protonation n'a pas à être envisagée.

On ne peut mettre en évidence aucun incrément caractéristique des substituants; d'autre part, il n'y a pas de corrélation apparente entre les potentiels de demi-neutralisation dans NM et dans S/B. Ceci semble bien confirmer le fait que l'action spécifique des substituants n'est pas le facteur le plus important: la conformation, résultant de la rotation autour des liaisons P—N, et dans laquelle intervient également la nature du solvant, doit jouer un rôle prépondérant. Des conclusions analogues avaient été obtenues à partir de l'étude des propriétés diélectriques et de calculs CNDO/2 (31) ainsi que de la détermination calorimétrique des nombres donneurs (17).

1. J. Y. GAL, J. P. MARTINAT et T. YVERNAULT. C. R. Acad. Sci. (Paris) Ser. C, **277**, 1009 (1973).
2. D. C. WIMER. Anal. Chem. **30**, 77 (1958).
3. G. WADA, S. NAKAGO et Y. ABE. Bull. Chem. Soc. Jpn. **52**, 1381 (1979).
4. M. PERSIN et J. Y. GAL. Can. J. Chem. **59**, 2491 (1981).
5. N. K. SKVORTSOV, G. F. TERESHCHENKO, B. I. IONIN et A. A. PETROV. Zh. Obshch. Khim. **46**, 521 (1976).
6. B. I. STEPANOV, B. A. KOROLEV et A. I. BOKANOV. Zh. Obshch. Khim. **39**, 316 (1969).
7. E. P. BUCHIKHIN, V. V. YAKSHIN et V. I. MEDVEDEV. Zh. Obshch. Khim. **44**, 1354 (1974).
8. E. I. MATROSOV, E. N. TSVETKOV, Z. N. MIRONOVA, R. A. MALEVANNAYA et M. I. KABACHNIK. Izv. Akad. Nauk SSSR, Ser. Khim. 1333 (1975).
9. B. N. LASKORIN, V. V. YAKSHIN et L. I. SOKAL'SKAYA. Dokl. Akad. Nauk SSSR, **223**, 1405 (1975).
10. V. V. YAKSHIN, M. I. TYMONYUK, L. I. SOKAL'SKAYA et B. N. LASKORIN. Dokl. Akad. Nauk SSSR, **247**, 128 (1979).
11. V. V. YAKSHIN, M. I. TYMONYUK, L. I. SOKAL'SKAYA, I. A. VOLODIN et B. N. LASKORIN. Radiokhimiya, **22**, 517 (1980).
12. V. PLICHON. Bull. Soc. Chim. Fr. 2382 (1967).
13. M. BREANT et G. DEMANGE-GUERIN. Bull. Soc. Chim. Fr. 163 (1975).
14. J. C. BOLLINGER, R. FAURE et T. YVERNAULT. Analusis, **10**, 270 (1982).
15. J. C. BOLLINGER, G. YVERNAULT et T. YVERNAULT. J. Solution Chem. **7**, 317 (1978).
16. T. YVERNAULT, G. YVERNAULT et J. C. BOLLINGER. C. R. Acad. Sci. (Paris) Ser. C, **287**, 519 (1978).
17. J. C. BOLLINGER, G. YVERNAULT et T. YVERNAULT. Thermochim. Acta, 1982 (sous presse).
18. R. B. HARVEY et J. E. MAYHOOD. Can. J. Chem. **33**, 1552 (1955).
19. H. NORMANT et J. F. BRAULT. C. R. Acad. Sci. (Paris) Ser. C, **264**, 707 (1967).
20. D. LELIÈVRE et V. PLICHON. J. Electroanal. Chem. **45**, 99 (1973).
21. R. PANTZER, W. D. BURKHARDT, E. WALTER et J. GOUBEAU. Z. Anorg. Allg. Chem. **416**, 297 (1975).
22. E. I. MATROSOV, E. E. NIFANT'EV, A. A. KRYUCHKOV et M. I. KABACHNIK. Izv. Akad. Nauk SSSR, Ser. Khim. 530 (1976).
23. J. C. BARDIN. Analusis, **1**, 140 (1972).
24. C. A. STREULI. Anal. Chem. **31**, 1652 (1959).
25. L. G. CHATTEN et L. E. HARRIS. Anal. Chem. **34**, 1495 (1962).
26. (*a*) E. I. MATROSOV, A. G. KOZACHENKO et M. I. KABACHNIK. Izv. Akad. Nauk SSSR, Ser. Khim. 313 (1976); (*b*) 1470 (1976).
27. J. S. FRITZ. Acid–base titrations in nonaqueous solvents. Allyn and Bacon, Boston. 1973. p. 125.
28. R. M. FUOSS et C. A. KRAUS. J. Am. Chem. Soc. **55**, 476 (1933).
29. C. P. WRIGHT, D. M. MURRAY-RUST et H. HARTLEY. J. Chem. Soc. 199 (1931).
30. F. G. BORDWELL, J. C. BRANCA, D. L. HUGUES et W. N. OLMSTEAD. J. Org. Chem. **45**, 3305 (1980).
31. J. C. BOLLINGER, G. YVERNAULT, T. YVERNAULT, A. JULG et M. RAJZMANN. J. Mol. Struct. **69**, 273 (1980).
32. T. A. MODRO. J. Chem. Soc. Chem. Commun. 201 (1980).
33. T. A. MODRO et D. H. GRAHAM. J. Org. Chem. **46**, 1923 (1981).
34. Y. COUSTURES. Thèse 3e Cycle, Toulouse (1972).
35. S. POIGNANT, J. R. GAUVREAU et G. J. MARTIN. Can. J. Chem. **58**, 946 (1980).
36. B. DAVIDOWITZ et T. A. MODRO. S. Afr. J. Chem. **33**, 74 (1980).
37. E. I. MATROSOV, A. A. KRYUCHKOV, E. E. NIFANTYEV, A. G. KOZACHENKO et M. I. KABACHNIK. Phosphorus Sulfur, **13**, 69 (1982).

Can. J. Chem. Downloaded from www.nrcresearchpress.com by 210.87.254.105 on 09/06/12
For personal use only.

Synthesis and physical properties of the six furylpyridines

PIERRE RIBEREAU AND GUY QUEGUINER[1]

Laboratoire de Chimie Organique Hétérocyclique, Institut National Supérieur de Chimie Industrielle de Rouen, Faculté des Sciences et des Techniques de Rouen, 76130 Mont Saint Aignan, France

Received April 6, 1982[2]

PIERRE RIBEREAU and GUY QUEGUINER. Can. J. Chem. **61**, 334 (1983).

The 3-step synthesis of furylpyridines is described, using ethyl pyridinoylacetates as starting materials for 2-furyl compounds and chloroacetylpyridines for 3-furyl isomers. Furthermore, thesc last compounds were prepared by a convenient new method for 3-substituted furan synthesis. This synthesis starts from bromopyridines and proceeds through the key intermediates (2,2-diethoxyacetyl)pyridines and methyl 2-(*x*-pyridyl)-4,4-diethoxy-2-methoxy-2-butenoates. The physical properties of the furylpyridines have been determined. Structures and interactions between furan and pyridine rings have been discussed by comparing their uv spectra, basicity constants, and dipole moments with those of phenyl and thienylpyridines.

PIERRE RIBEREAU et GUY QUEGUINER. Can. J. Chem. **61**, 334 (1983).

Nous décrivons la synthèse des furylpyridines en trois étapes à partir des pyridoylacétates d'éthyle pour les dérivés en 2 du furanne et à partir des chloroacétylpyridines dans le cas des isomères en 3. Nous décrivons une nouvelle voie d'accès aux dérivés du furanne substitué en 3. La synthèse est réalisée à partir de bromopyridines et procède par l'intermédiaire des (diéthoxy-2,2 acétyl)pyridines et pyridyl-2 diéthoxy-4,4 méthoxy-2 butène-2 oates de méthyle. Les propriétés physiques des furylpyridines ont été déterminées. Leur structure et l'intéraction entre les cycles furanne et pyridine sont discutées en comparant leurs spectres uv, constantes de basicité et moments dipolaires avec ceux des phényl et thiénylpyridines.

Can. J. Chem. Downloaded from www.nrcresearchpress.com by 210.87.254.40 on 09/06/12
For personal use only.

In the last decade much interest has focussed on the properties and reactivity of biheterocycles which result from linking of "electrophilic" and "nucleophilic" rings (1).

A 2-(3-furyl)pyridine derivative was prepared as precursor in the synthesis of nupharamine (2). Derivatives of such naturally occurring compounds isolated from Nuphar and Castoreum (3) have been employed in pharmaceutical preparations (4). Furthermore, a methiodide derivative of 4-(3-furyl)pyridine has been found to display hypoglycemic activity (5). However, only a small number of papers dealing with the synthesis and the properties of furylpyridines have been published. Most routes adopted for the preparation of 3-(2-furyl)pyridine (6−10), 2-(2-furyl)pyridine (11), and 4-(3-furyl)pyridine (5) were either the construction of the nitrogen ring starting from furan derivatives, or the linkage of the two heterocycle units. But these syntheses gave rather low yields or can only be used for the preparation of one isomer. It seemed of interest to prepare furylpyridines by an improved general method. The synthesis of these compounds will be described, using a pyridine derivative as a substrate through the construction of the oxygen ring, as reported in a previous paper (12).

Furthermore, we describe a new synthetic procedure for 3-substituted furans, which are compounds of interest in the field of natural products but not easily accessible.

Synthesis of x-*(2-furyl)pyridines*

These have been prepared according to the method established by Lions and Ritchie (6) for the synthesis of 3-(2-pyrrolyl)pyridine. The cyclization step was modified to improve the yield of furyl derivative. Finally, the best yields of furan esters **3** were obtained when ethyl pyridoylacetates **1** were treated with 1,2-dichloroethyl acetate and 10% aqueous ammonia. In fact, thermolysis of the first reaction product was necessary in order to aromatize the compound. The intermediate product **2** was isolated under mild conditions and its structure was inferred from the spectral analyses. Its ir spectrum exhibits the characteristic absorption bands of the alcohol function at 3140 and 1100 cm^{-1}. The ^1H nmr spectrum presents a deshielded doublet of doublets at δ 5.37 ppm (J = 4 and 5.5 Hz) which is the resonance of a proton attached to an hydroxyl-bearing carbon of dihydrofuran (13, 14). The ^{13}C nmr spectrum of compound **2** presents no cyclic hemiacetal type carbon (about 100 ppm). In view of these observations, we identified compound **2** as ethyl 5-(*x*-pyridyl)-3-hydroxy-2,3-dihydro-4-furoate. Formation of this nondehydrated precursor of the furyl ring can be explained by a ketolization reaction between ketoester **1** and chloroacetaldehyde resulting from the hydrolysis of 1,2-dichloroethyl acetate. Subsequent cyclization gives a dihydrofuran derivative **2**. Thermolysis of this compound produced furan ester **3**. After saponification of the ester and decarboxylation of the acid **4** at 160−220°C the furylpyridine **5** was obtained. By this route 2-, 3-, and 4-(2-furyl)-pyridines were prepared in satisfactory overall yields, namely 40%, 50%, and 34%, respectively. These results compare favorably with the yields of the syntheses previously described (6, 11).

Synthesis of x-*(3-furyl)pyridines by cyclization of epoxyalkyne*

Among the several methods described in the literature to achieve the synthesis of 3-substituted furan, the only one which offered some interest was the route proceeding through an epoxide according to the sequence established by Miller (15) for the preparation of 3-phenylfuran. Following this method, chloroacetylpyridine hydrochlorides **6** (16) react with ethynylmagnesium bromide in tetrahydrofuran and give chlorhydrins **7**. The reaction of these compounds with sodium hydroxide proceeds smoothly to give the corresponding 3,4-epoxy-3-(*x*-pyridyl)-1-butynes **8**. Because of their instability, compounds **7** and **8** were not purified. They exhibited spectral data in accordance with their structural assignments and they were shown to have a purity of at least 95% by nmr.

When acetylenic α,β-epoxides **8***b* and **8***c* were heated with 2 *N* sulfuric acid containing a catalytic amount of mercuric

[1]Author to whom correspondence may be addressed.

[2]Revision received October 5, 1982.

0008-4042/83/020334-09$01.00/0

©1983 National Research Council of Canada/Conseil national de recherches du Canada

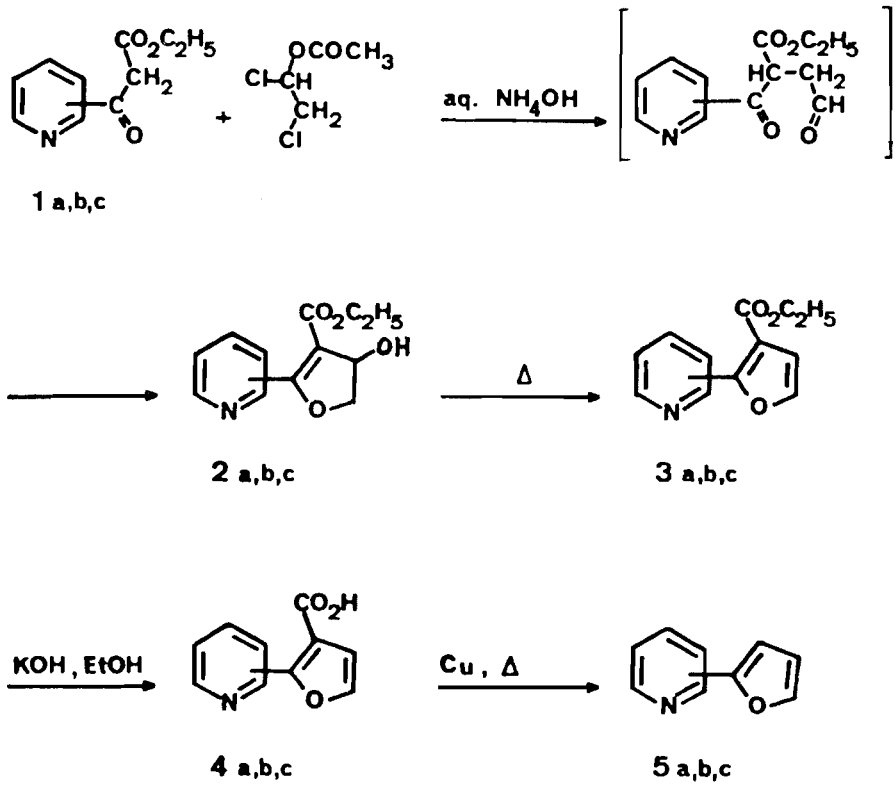

SCHEME 1

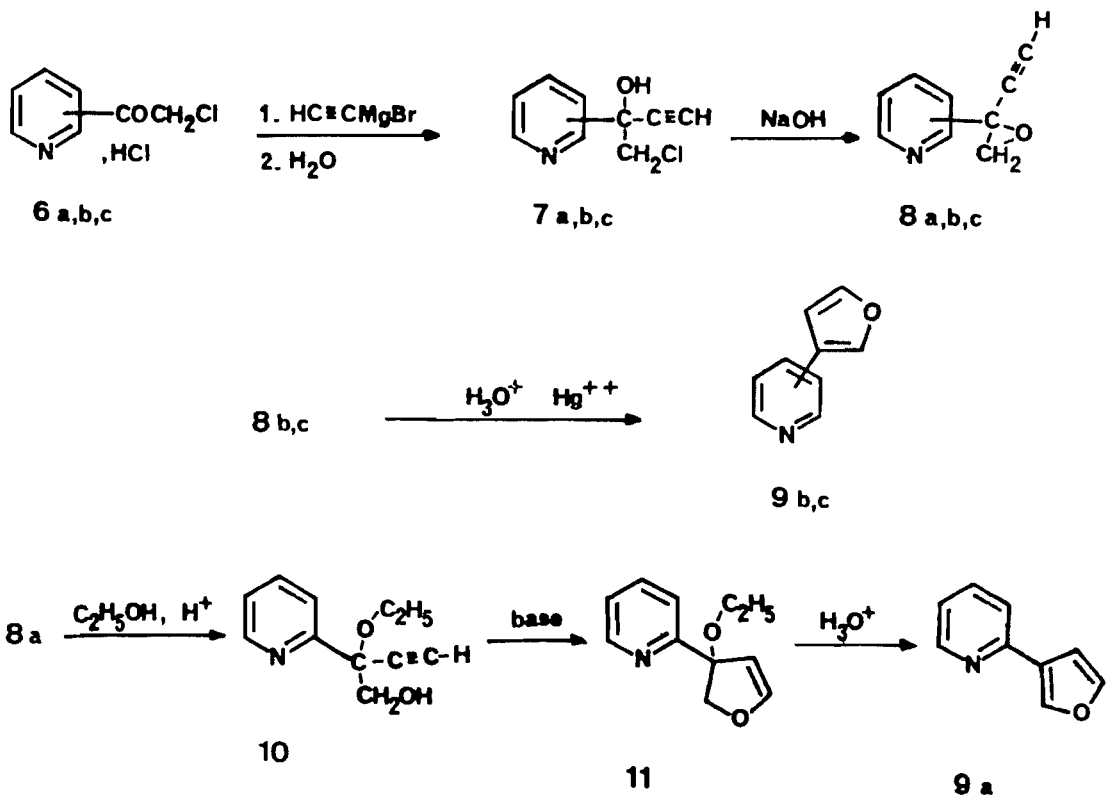

SCHEME 2

Can. J. Chem. Downloaded from www.nrcresearchpress.com by 210.87.254.40 on 09/06/12
For personal use only.

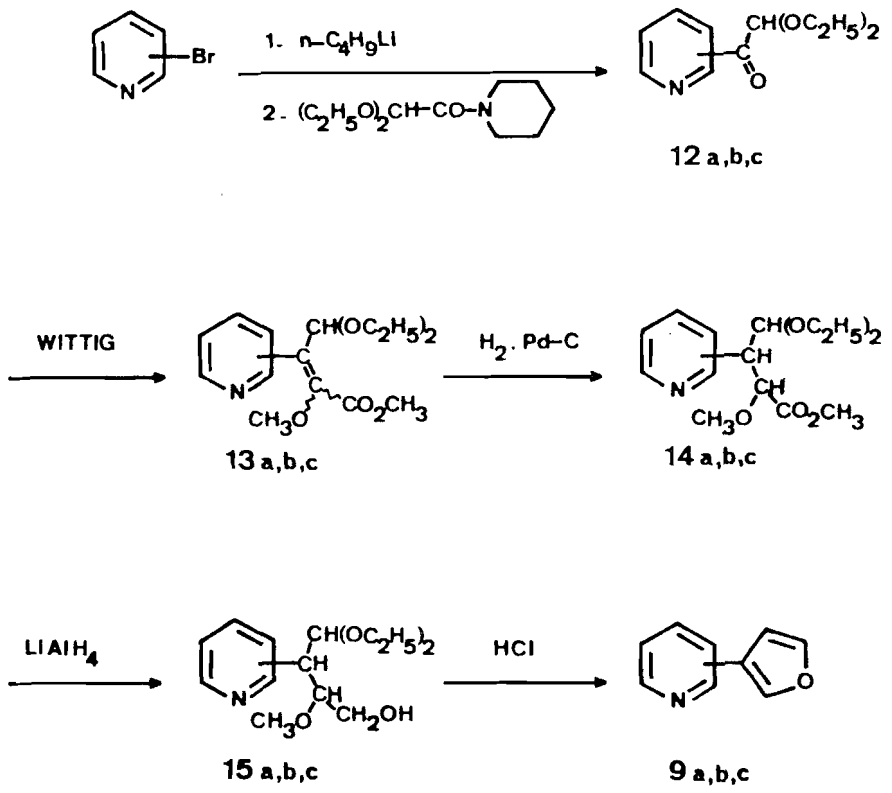

SCHEME 3

sulfate, cyclization occurred and gave furylpyridines **9***b* and **9***c* in rather low yields, 15% and 21%, respectively, from the corresponding chloroketones **6**. However under the same conditions, cyclization failed with the 2-pyridyl derivative. The acetylenic epoxide **8***a* also reacted but no 2-(3-furyl)pyridine could be isolated. Alternatively, this compound was prepared by a base-induced cyclization. The epoxide ring of compound **8***a* was opened with perchloric acid in ethanol to give 3-ethoxy-3-(2-pyridyl)-1-butyn-4-ol **10**. The structure was deduced from spectroscopic data similar to those of 3-ethoxy-3-phenyl-1-butyn-4-ol (15). Treatment of alcohol **10** with sodium ethoxide at 80°C gave the cyclized product **11** whose ir spectrum showed no hydroxy or acetylenic functions. The ^{1}H nmr spectrum exhibited two doublets at δ 6.70 and 5.21 ppm (J = 2.5 Hz) which were assigned to H-5 and H-4. The two protons on carbon 2 appeared as two singlets at δ 4.59 and 4.61 ppm. A base-induced intramolecular attack of oxygen on the acetylenic bond can easily explain this result. Such a reaction was previously used for cyclization of acetylenic diols (17) and enyne alcohols (18). Subsequent treatment of dihydrofuran derivative **11** with acid gave the expected 2-(3-furyl)pyridine (**9***a*) in a very low overall yield (9%) from chloroketone **6***a*. Since this method necessitates the prior synthesis of hard-to-obtain chloroacetylpyridines and since the yields were low, we sought another route to *x*-(3-furyl)pyridines. This new synthetic procedure was carried out using bromopyridines as starting material.

Synthesis of x-*(3-furyl)pyridines by cyclization of hydroxyacetal*

Lithiopyridines (19) were obtained from bromopyridines and n-butyllithium. The subsequent reaction with 1-(2,2-diethoxyacetyl)piperidine (20) at −70°C yields diethoxyacetylpyridines **12**. When methyl diethoxyphosphinylmethoxyacetate (21) was used in the Wittig–Horner reaction with ketones **12**, equivalent amounts of geometrical isomers of esters **13** were formed (nmr). The ethoxymethoxy series was chosen here because it offered the advantage of simple interpretation of nmr spectra of intermediates in the synthesis. Reduction of the ethylenic double bond with hydrogen and palladium catalyst provided the desired saturated esters **14**. The carbethoxy group was reduced to the hydroxymethyl group with lithium aluminium hydride. Finally, treatment of the alcohols **15** with hydrochloric acid in toluene gave the *x*-(3-furyl)pyridines. These compounds were obtained with an overall yield of 49%, 40%, and 42% from ketoacetals **12**. This easy access to the 3-furyl compounds offers an interesting potential entry to products of interest in biological or pharmaceutical problems.

Physical properties of furylpyridines

Because reactions carried out on these compounds gave results somewhat different from those obtained with analogues like thienyl and phenylpyridines (1), we have made some physical studies to clarify the interactions between the two rings.

The ultraviolet spectra of furylpyridines were obtained with absolute ethanol solution (see Table 1). 2-(2-Furyl)pyridine displays an absorption maximum at a longer wavelength than the other isomers, indicating that conjugation should be greater in this compound. From earlier studies (22–24), there is evidence that the differences between the characteristic spectral behaviour of arylpyridines and those of the corresponding pyridinium ions are related to the electronic interaction between the two rings. When the higher maximum wavelength of furyl, thienyl, and phenylpyridines (23) is compared with that of their

Can. J. Chem. Downloaded from www.nrcresearchpress.com by 210.87.254.40 on 09/06/12
For personal use only.

TABLE 1. Acidity constants, ultraviolet spectral data, and dipole moments of furylpyridines **5***a*–*c* and **9***a*–*c* and (thienyl-2)-2-pyridine **16**

		Ultraviolet		Dipole moment		
					μ^d	
Compounds	pK_a[a]	Solvent[b]	λ max, nm (log ε)	μ[c]	α = 0	α = 180
5*a*	4.18±0.05[e]	A	303 (4.16), 270 (4.12)	1.37±0.05	2.46	1.30
		B	332 (4.27)			
5*b*	4.62±0.06[f]	A	283 (4.21), 236 (3.72)	2.42±0.02	2.94	2.02
		B	290 (4.29), 236 (4.00)			
5*c*	5.60±0.08	A	294 (4.37), 235 (3.94)	3.04±0.08	2.94	
		B	332 (4.41), 237 (3.84)			
9*a*	4.65±0.03	A	285 (3.74), 255 (3.77) 227 sh[g]	2.27±0.02	2.50	1.80
		B	307 (3.99), 245 (3.86)			
9*b*	4.93±0.04	A	257 (3.86), 225 sh	2.23±0.03	2.45	1.68
		B	243 (4.03)			
9*c*	5.72±0.03	A	270 (4.01), 223 sh	2.35±0.03	2.09	
		B	304 (3.98), 250 sh, 239 (3.98)			
16	3.797±0.012[h]			2.06±0.02	2.49	1.42

[a]The acidity constants have been determined by spectrophotometry in water (I = 0.1, $NaClO_4$; 25°C).
[b]A, solution in absolute ethanol, B, solution in aqueous 0.01 M $HClO_4$, 0.1 M $NaClO_4$, and at 25°C.
[c]Dipole moments are measured in benzene solutions at 25°C.
[d]Calculated dipole moments respectively with the dihedral angle α between the planes of the two rings.
[e]Reference 8, pK_a = 4.17 ± 0.04.
[f]Reference 8, pK_a = 4.59 ± 0.011.
[g]sh, shoulder.
[h]Reference 25.

NOTE: 3-(2-Thienyl)pyridine: pK_a = 4.515; 4-(2-thienyl)pyridine: pK_a = 5.591; 2-(3-thienyl)pyridine: pK_a = 4.776; 3-(3-thienyl)pyridine: pK_a = 4.920; 4-(3-thienyl)pyridine: pK_a = 5.712; 2-phenylpyridine: pK_a = 4.735; 3-phenylpyridine: pK_a = 4.924; 4-phenylpyridine: pK_a = 5.488 (25); pyridine: pK_a = 5.33 (8).

protonated species, a bathochromic shift is apparent: 18 to 31 nm, −14 to 9 nm, and 32 to 40 nm for 2-, 3-, and 4-pyridyl derivatives respectively. These results show, as expected, that the interaction between the pyridine nuclei and the other aryl ring is weaker in the case of 3-substituted pyridines.

Acidity constants of furylpyridines are reported in Table 1. 4-Arylpyridines have similar pK_a and they are stronger bases than pyridine. This first result suggests that the mesomeric effect (+M) for all furyl, thienyl, and phenyl groups makes electrons available in the same order of magnitude. 3-Arylpyridines are slightly weaker bases than pyridine. This can be explained by the lack of conjugative interaction for the 3-substituted pyridines and by the weak electron-withdrawing due to the inductive effect of the aryl groups. For all the 2-substituted pyridines, the basicity is weaker than that of pyridine. It is evident that the +M effect of the aryl group is diminished by its greater hindrance and by the increased importance of its inductive effect. The pK_a values of 2-(3-furyl), 2-(3-thienyl), and 2-phenylpyridines are similar (24, 25), indicating that steric hindrance of the aryl groups is about the same because, as we have seen above, the mesomeric and inductive effects are of the same order of magnitude. 2-(2-Furyl)pyridine is a stronger base than 2-(2-thienyl)pyridine (**16**) and, apart from the −I effect which is presumed to be more important for oxygen than for sulfur, other parameters must influence the stability of the protonated species (coordination of the proton by the oxygen of the furyl compound may increase the stability of the protonated form).

The experimental dipole moments of furylpyridines are reported in Table 1. Ultraviolet spectra and basicity studies have shown that electron displacements within the molecules are similar in furyl, thienyl, and phenylpyridines. Thus there are good reasons to believe that the mesomeric moment induced in the furyl or thienyl groups by the primary moment associated with the pyridine ring is not so different from the dipole moment induced in the phenyl group of phenylpyridines (26). From the dipole moments of the unsubstituted parent compounds (26, 27) and the mesomeric moments deduced from phenylpyridine studies (26), we have determined, by vector analysis, a calculated moment for *trans*-planar (α = 0°) and *cis*-planar (α = 180°) conformations of furylpyridines (Table 1).

4-(2-Furyl)pyridine and 4-(3-furyl)pyridine yield calculated moments irrespective of the angle between the planes of the two rings and consistent with the experimentally determined values. These results show that the use of mesomeric moments of phenylpyridines is significant in the case of furylpyridines. 2-(2-Furyl)pyridine shows an experimental dipole moment in good agreement with the calculated value for the *trans*-planar geometry. The most preferred conformation of this compound is thus presumed to be planar. The other isomers of the series do not exhibit such an agreement. For these substances, the experimental dipole moments lie between the values calculated for *s-cis* and *s-trans* conformations, and suggest that the two rings are not coplanar. On the basis of the calculated and measured values of the dipole moment, 2-(2-thienyl)pyridine also appears to have a twisted equilibrium conformation (28), an indication of the difference between this compound and the corresponding furan derivative, as already implied from pK_a measurement. These physical properties of furylpyridines

Can. J. Chem. Downloaded from www.nrcresearchpress.com by 210.87.254.40 on 09/06/12
For personal use only.

Can. J. Chem. Downloaded from www.nrcresearchpress.com by 210.87.254.40 on 09/06/12
For personal use only.

TABLE 2. Yield, analytical, ^{1}H nmr, and infrared data for compounds **3***a*–*c* and **4***a*–*c*

Compounds	Boiling point (°C/Torr) *Melting point* (°C)	Yield %	Analysis (%) calcd. found C	H	N	^{1}H nmr[a] Pyridyl H-2	H-3	H-4	H-5	H-6	$J_{2,3}$ $_{5,6}$	$J_{2,4}$ $_{4,6}$	$J_{2,5}$ $_{3,6}$	$J_{3,4}$ $_{4,5}$	Furyl H-4	H-5	$J_{4,5}$	Others CH_2	CH_3	J	Infrared (cm^{-1})[b] ν(C=O)	ν(O—H)
3*a*	128/0.3	82	48.44	3.16	12.55	—	8.22	7.76	7.26	8.68	4.8	2.0	1.0	8.0	6.86	7.52	2.0	4.31	1.32	7	1709	—
			48.9	3.3	12.4		dt	td	ddd	ddd					d	d		q	t			
3*b*	120/0.1	60	48.44	3.16	12.55	9.12	—	8.35	7.36	8.58	4.8	2.0	1.0	8.0	6.87	7.48	1.8	4.31	1.32	7	1718	—
	27		48.3	3.2	12.4	dd		dt	ddd	dd					d	d		q	t			
3*c*	130/0.5	51	48.44	3.16	12.55	8.67	7.94	—	7.94	8.67	4.8		1.5		6.87	7.47	1.8	4.32	1.33	7	1721	—
	65		48.3	2.9	12.4	dd	dd		dd	dd					d	d		q	t			
4*a*	*170*	71	63.49	3.73	7.40	—	8.15	8.15	7.65	8.78	4.8	2	1	8	7.01	8.00	1.8				1701	3436
			63.6	3.5	7.2		m	m	m	m					d	d						
4*b*	229	93	63.49	3.73	7.40	9.10	—	8.30	7.50	8.63	4.8	2.0		8.0	6.89	7.83	1.8				1701	3486
			63.3	3.6	7.1	d		dt	dd	dd		1.8			d	d						
4*c*	*260*	80	63.49	3.73	7.40	8.63	7.92	—	7.92	8.63	4.5		1.5		6.91	7.82	1.8				1698	3436
			63.4	3.4	7.2	dd	dd		dd	dd					d	d						

[a]Abbreviations: d doublet, dd doublet of doublets, t triplet, q quartet, m multiplet. Solvent: compounds **3***a*–*c* in $CDCl_3$; compounds **4***a*–*c* in Me_2SO-d_6.
[b]In KBr except for compound **3***a*: neat.

show that interaction between the two rings is mainly inductive and steric in nature.

All of the furylpyridines show very similar mass spectra, with an intense peak for the molecular ion m/e = 145 and the same degradation fragments. Hydrogen abstraction leads to a fragmentation peak $M - 1$ with an intensity of 29% in the spectrum of 2-(2-furyl)pyridine and of only 10% in the case of 2-(3-furyl)pyridine (the results are somewhat different in the thiophene series (29)).

Experimental

Boiling points are uncorrected. Infrared (ir) spectra were determined on a Beckman IR 4250 grating infrared spectrometer. Ultraviolet (uv) spectra were obtained on a Beckman DK-2 spectrophotometer. Proton nuclearmagnetic resonance (^{1}H nmr) spectra were recorded using a Varian A 60 spectrometer and chemical shifts are reported as δ values in ppm relative to Me_4Si as internal standard; ^{13}C nmr spectra were obtained on a Brucker WH 90 spectrometer at 22.69 MHz and chemical shifts are reported in ppm downfield from internal Me_4Si. Mass spectra were recorded on a JEOL JMS D 100 spectrometer.

*Preparation of ethyl 2-(*x*-pyridyl)-3-furoates (**3**a–c)*

To a stirred and cooled (−5 to 0°C) solution of 116 g (0.6 mol) of ethyl 3-(*x*-pyridyl)-3-oxopropanoate (30) in 1 L of CH_2Cl_2 was added 300 mL of 10% aqueous ammonia. A solution of 100 g (0.64 mol) of 1,2-dichloroethyl acetate in 200 mL of CH_2Cl_2 was added over a 30 min period. The reaction mixture was stirred for an additional 2 h at 0°C and then allowed to come to room temperature overnight. After acidification with concentrated hydrochloric acid, the aqueous layer was extracted with $CHCl_3$. After removal of the solvents, the resulting oil was distilled, giving compounds **3***a*–*c* (Table 2).

*Ethyl 5-(3-pyridyl)-3-hydroxy-2,3-dihydro-4-furoate (**2**b)*

A solution of ketoester **1***b* was treated as described above in the preparation of compounds **3**. Decantation of the organic layer and removal of the solvent, at a temperature below 40°C to avoid dehydration, gave a residue which was recrystallized in CCl_4, giving 65 g (46%) of white crystals, mp 116°C; ir (KBr): 3140 (OH), 1690 (C=O), 1415, 1290, 1100 (OH) cm^{-1}; ^{1}H nmr ($CDCl_3$) δ: 1.12 (t, 3H, CH_3), 4.0 (m, 1H, OH), 4.11 (q, 2H, CH_2), 4.52 (d, 1H, J = 4 Hz, one H of CH_2—O), 4.53 (d, 1H, J = 5.5 Hz, one H of CH_2—O), 5.37 (2 doublets, 1H, HC(OH)), 7.25 (m, 1H, pyridyl H-5), 7.7 (m, 2H, pyridyl H-3 and H-4), 8.6 (m, 1H, pyridyl H-6); ^{13}C nmr ($CDCl_3$) δ: 13.7 (CH_3), 59.9 (CH_2—O), 73.5 (C—OH), 77.2 (ring CH_2—O), 122.2 (pyridyl C-5), 136.7 (pyridyl C-4), 149.9 (pyridyl C-2), 150.9 (pyridyl C-6). *Anal.* calcd. for $C_{12}H_{13}NO_4$: C 61.28, H 5.53, N 5.95; found: C 61.5, H 5.3, N 6.1.

*Preparation of 2-(*x*-pyridyl)-3-furoic acids (**4**a–c)*

To a stirred solution of 72 g (0.78 mol) of KOH in 300 mL of ethanol was added 70 g (0.32 mol) of ester **3**. The mixture was heated at 80°C for 16 h. After removal of the solvent the residue was dissolved in a minium quantity of water. The aqueous solution was washed with ether and then acidified to pH 4 with an aqueous solution of HCl. The precipitate was filtered, washed with cold water, and recrystallized from ethanol affording acids **4***a*–*c* (Table 2).

Preparation of x*-(2-furyl)pyridines (**5**a–c)*

A 10 g sample of **4** was mixed thoroughly with 10 g of red copper and the mixture was heated from 160°C to 220°C at reduced pressure (12 Torr). The resulting oil was dissolved in ether. The ether solution was washed with a 10% aqueous NaOH solution, then with water, and finally worked up as usual. Distillation offered compounds **5***a*–*c* (Table 3).

*2-(2-Chloroacetyl)pyridine hydrochloride (**6**a)*

A solution of 19.6 g (0.16 mol) of picolinic acid in 120 mL of freshly distilled sulfinyl chloride was heated at 80°C for 2 h. The excess of sulfinyl chloride was distilled off and, after addition of 20

Can. J. Chem. Downloaded from www.nrcresearchpress.com by 210.87.254.40 on 09/06/12
For personal use only.

mL of dry benzene, the solvents were removed under reduced pressure. A suspension of the residue in 100 mL of dry benzene was introduced in portions to a cooled (0−5°C) and stirred solution of about 22.5 g (0.54 mol) of diazomethane in 1.2 L of diethyl ether (dried 2 h on KOH pellets). The mixture was stirred and allowed to come to room temperature overnight. The solution was then filtered. In one run the solvent was removed using a rotary evaporator. Distillation of the residue afforded 20.7 g (88%) of 2-pyridyldiazoketone: bp 82°C/0.3 Torr; ir (CCl_4): 2110 (N_2), 1640 (C=O) cm^{-1}; ^1H nmr ($CDCl_3$) δ: 6.7 (s, 1H, CHN_2), 7.4 (m, 1H, C-5 H), 7.6−8.1 (m, 2H, C-3 H and C-4 H), 8.5 (dd, 1H, C-2 H). The cooled (0°C) and stirred solution of diazo ketone in ether was treated by a dry stream of hydrogen chloride. The precipitate was filtered and washed with dry ether. Drying under reduced pressure afforded 28.9 g of hydrochloride **6***a* (94%): ^1H nmr (DMSO-d_6) δ: 5.15 (s, 2H, CH_2Cl), 7.6 (m, 1H, C-5 H), 7.8−8.0 (m, 2H, C-3 H and C-4 H), 8.6 (m, 1H, C-6 H), 12.6 (m, 1H, N^+H). *Anal.* calcd. for C_7H_8NOCl: C 43.54, H 3.69, N 7.45; found: C 43.4, H 3.8, N 7.3.

*3-(2-Chloroacetyl)pyridine hydrochloride (**6**b)*

A solution of 41 g (0.33 mol) of nicotinic acid in 240 mL of sulfinyl chloride was heated at 80°C for 2 h. The excess of sulfinyl chloride was distilled and after addition of 20 mL of dry benzene the solvents were removed under reduced pressure. To the residue was added 32 g of freshly distilled pyridine. The mixture was distilled and the fraction collected at 91−95°C/13 Torr was redistilled offering 40 g of nicotinoyl chloride (85%), bp 90°C/12 Torr. A solution of 38.2 g (0.27 mol) of acid chloride in 100 mL of dry benzene was added dropwise to a cooled solution (0−5°C) of about 22.5 g (0.54 mol) of diazomethane in 1.2 L of ether (dried 2 h on KOH pellets). The mixture was treated as described above in the preparation of **6***a*. By this method was obtained 49 g of hydrochloride **6***b* (94%); ^1H nmr (DMSO-d_6) δ: 5.3 (s, 2H, CH_2Cl), 7.9 (ddd, 1H, J_{5-2} = 1 Hz, J_{5-4} = 8 Hz, J_{5-6} = 5 Hz, C-5 H), 8.7 (ddd, 1H, J_{4-2} = 2.5 Hz, J_{4-6} = 1.5 Hz, C-4 H), 9.0 (dd, 1H, C-6 H), 9.3 (dd, 1H, C-2 H), 11.4 (m, 1H, N^+H). *Anal.* calcd. for $C_7H_8NOCl_2$: C 43.54, H 3.69, N 7.45; found: C 43.7, H 3.6, N 7.3.

*4-(2-Chloroacetyl)pyridine hydrochloride (**6**a)*

According to the above method, the following were obtained from isonicotinic acid: 39 g (83%) of isonicotinoyl chloride, bp 81°C/13 Torr, and then 29 g (95%) of compound **6***c*: ^1H nmr (DMSO-d_6) δ: 5.45 (s, 2H, CH_2Cl), 8.3 (dd, 2H, J_{3-2} = 6.5 Hz, J_{5-2} = 1.5 Hz, C-3 H and C-5 H), 9.2 (dd, 2H, C-2 H and C-6 H), 11.2 (m, 1H, N^+H). *Anal.* calcd. for $C_7H_8NOCl_2$: C 43.54, H 3.69, N 7.45; found: C 43.6, H 3.5, N 7.2.

*Preparation of 4-chloro-3-(x-pyridyl)-1-butyn-3-ols (**7**a−c)*

Ethyl magnesium bromide, prepared in tetrahydrofuran (100 mL) from 35 g (0.32 mol) of ethyl bromide and 8 g (0.33 mol) of magnesium, was converted into ethynylmagnesium bromide by dropwise addition during 1 h to a saturated solution of acetylene in 100 mL of THF, while acetylene was passed continuously through the mixture. A suspension of 57.6 g (0.3 mol) of compound **6***a*−*c* in 250 mL of THF was added in portions to the Grignard reagent at 0−5°C. The mixture was stirred for 14 h at 20°C, cooled to 0−5°C, decomposed by addition of 16 mL of saturated aqueous ammonium chloride solution, and extracted with ether. Removal of the solvents left a dark oil which was used without further purification (Table 4).

*Preparation of 3,4-epoxy-3-(x-pyridyl)-1-butynes (**8**a−c)*

To a solution of compound **7***a*−*c* in 100 mL of dry ether was added 40 g of powdered sodium hydroxide. The mixture was stirred for 14 h, filtered, and the solvent removed. The residual oil was used without further purification (Table 4).

*3-(3-Furyl)pyridine (**9**b)*

A solution of 1.6 g of mercuric sulphate in 40 mL of 2 *N* sulphuric acid was added to a solution of compound **8***b* in 100 mL of 2 *N* sulphuric acid. The mixture was stirred 1 h at 90°C, cooled to 20°C,

TABLE 3. Yield, analytical, and ^1H nmr data for furylpyridines **5***a*−*c* and **9***a*−*c*

Compounds	Boiling point (°C/Torr)	Yield (%)	Analysis (%) found[a]			^1H nmr															
						Pyridyl								Furyl							
			C	H	N	H-2	H-3	H-4	H-5	H-6	$J_{2,3}$ $_{5,6}$	$J_{2,4}$ $_{4,6}$	$J_{2,5}$ $_{3,6}$	$J_{3,4}$ $_{4,5}$	H-2	H-3	H-4	H-5	$J_{2,3}$ $_{3,5}$	$J_{3,4}$	$J_{4,5}$	$J_{2,5}$
5*a*	58/0.3	80	74.4	4.9	9.8	—	7.58	7.58	7.05	8.56	4.5	1.2	1.2	8.0	—	7.03	6.48	7.48	0.8	3.3	1.8	
							m	m	m	dt						dd	dd	dd				
5*b*	67/0.4	86	74.4	4.9	9.8	8.91	—	7.79	7.25	8.45	4.9	1.9	1.0	8.0	—	6.65	6.50	7.43	0.8	3.5	1.9	
						dd		dt	ddd	dd						dd	dd	dd				
5*c*	110/0.6	83	74.5	4.8	9.6	8.60	7.47	—	7.47	8.60	4.5		1.5			6.83	6.48	7.52	0.8	3.5	1.8	
	69[b]					dd	dd		dd	dd						dd	dd	dd				
9*a*	112/13	84	74.6	4.9	9.6	—	7.2−7.7		7.10	8.56	4.7	2.0	1.0	6.7	7.96	—	6.82	7.32	0.8		1.8	1.5
							m		m	ddd	$J_{3,5}$ = 1.9				dd		dd	dd				
9*b*	120/13	83	74.6	5.0	9.5	8.76	—	7.68	7.20	8.48	4.7	2.0	0.8	8.0	7.72	—	6.66	7.46	0.8		1.8	1.6
						dd		dt	ddd	dd		1.7			dd		dd	dd				
9*c*	122/14	86	74.7	4.9	9.4	8.52	7.33	—	7.33	8.52	4.5		1.3		7.86	—	6.72	7.50	0.8		1.7	1.5
						dd	dd		dd	dd					dd		dd	dd				

[a]Analysis calculated for C_9H_7NO: C 74.47, H 4.86, H 9.65.
[b]Melting point (°C).

TABLE 4. ^{1}H nmr and infrared data for compounds **7***a*–*c* and **8***a*–*c*

Compounds	^{1}H nmr: Pyridyl H-2	H-3	H-4	H-5	H-6	$J_{2,3}$ $J_{5,5}$	$J_{2,4}$ $J_{4,6}$	$J_{2,5}$ $J_{3,6}$	$J_{5,4}$	Others: $C^{H_a}_{H_b}$	J_{ab}	≡CH	Infrared (cm^{-1}) ν(≡C—H)	ν(C≡C)
7*a*	—	7.7–7.9 m		7.3 m	8.5 m					3.90 s		2.70 s	3300	2120
7*b*	8.8 m	—	7.9 m	7.6 m	8.6 m					3.75 s		2.73 s	3300	2120
7*c*	8.6 dd	7.6 dd	—	7.6 dd	8.6 dd	4.8		1.5		3.75 s		2.75 s	3300	2120
8*a*	—	7.7 m		7.23 m	8.60 dt	4.8	1.8		8.5	3.43 s		2.62 s	3300	2120
8*b*	8.75 dd	—	7.75 dt	7.30 ddd	8.57 dd	4.8	2.0	1.0	8.0	3.05d 3.47d	6	2.60 s	3300	2120
8*c*	8.60 dd	7.40 dd	—	7.40 dd	8.60 dd	4.8		1.5		2.98d 3.48d	6	2.60 s	3300	2120

basified with $NaHCO_3$, and extracted with ether. Distillation afforded 7.2 g (15%) of **9***b*, bp 72°C/0.2 Torr.

*4-(3-Furyl)pyridine (**9**c)*

It was prepared as compound **9***b*. Distillation afforded 9.1 g (21%) of **9***c*, bp 80°C/0.3 Torr.

*3-Ethoxy-3-(2-pyridyl)-1-butyn-4-ol (**10**)*

To a solution of epoxide **8***a* in 50 mL of ethanol was added 0.5 mL of 70% perchloric acid. The mixture was stirred 1 h at 80°C, cooled, and treated with anhydrous sodium carbonate. After filtration, removal of the solvent left an oil which was used without further purification: ir (neat): 3650 and 3300 (O—H), 3310 (≡C—H), 2125 (C≡C) cm^{-1}; ^{1}H nmr ($CDCl_3$) δ: 1.1 (t, 3H, J = 6.5 Hz, CH_3—CH_2), 2.55 (s, 1H, ≡C—H), 3.1 (q, 2H, J = 6.5 Hz, CH_2—CH_3), 3.8 (s, 2H, CH_2), 4.0 (m, 1H, HO, signal disappeared on deuteriation), 7.2 (m, 1H, C-5 H), 7.8–7.6 (m, 2H, C-3 H and C-4 H), 8.5 (m, 1H, C-6 H).

*3-Ethoxy-3-(2-pyridyl)-4,5-dihydrofuran (**11**)*

A solution of sodium ethoxide (from 0.6 g of sodium in 150 mL of ethanol) was added to a solution of compound **10** in 50 mL of ethanol. The mixture was stirred at 80°C during 6 h. The solvent was removed and the residue was extracted with ether. Evaporation of the ether afforded an oil **11**: ^{1}H nmr ($CDCl_3$) δ: 1.20 (t, 3H, J = 6.5 Hz, CH_3—CH_2), 3.47 (q, 2H, J = 6.5 Hz, CH_2—CH_3), 4.60 and 4.58 (2s, 2H, furyl C-2 H_2), 5.21 (d, 1H, J = 2.5 Hz, furyl C-4 H), 6.70 (d, 1H, J = 2.5 Hz, furyl C-5 H), 7.10 (m, 1H, pyridyl C-5 H), 7.7–7.5 (m, 2H, pyridyl C-3 H and C-4 H), 8.53 (m, 1H, pyridyl C-6 H).

*2-(3-Furyl)pyridine (**9**a)*

A solution of compound **11** in 50 mL of 2 *N* sulphuric acid was stirred 1 h at 90°C, cooled to 20°C, treated with $NaHCO_3$, and extracted with ether. Distillation afforded 4.2 g (9.6%) of **9***a*, bp 68°C/0.2 Torr.

*2-(2,2-Diethoxyacetyl)pyridine (**12**a)*

A solution of 88.4 g (0.56 mol) of 2-bromopyridine in 100 mL of dry ether was added dropwise during 1 h to a cold (−20°C) and stirred solution of 450 mL (0.675 mol) of 1.5 *N* n-butyllithiun in hexane and 1.1 L of dry ether. The mixture was stirred for an additional 0.5 h and cooled to −25°C. A solution of 120.3 g (0.56 mol) of 1-(2,2-diethoxyacetyl)piperidine in 80 mL of dry ether was added during 1 h. The mixture was stirred at −25°C for 2 h and then allowed to come to room temperature overnight. A saturated aqueous solution of NH_4Cl (100 mL) was added slowly. Ether extraction followed by distillation of the residue afforded 98 g (84%) of ketone **12***a*, bp 95°C/0.03 Torr.

*3-(2,2-Diethoxyacetyl)pyridine (**12**b)*

A solution of 3-bromopyridine was treated according to the preparation of **12***a*, but at −70°C. By that method was obtained 91 g (78%) of ketone **12***b*, bp 90°C/0.05 Torr.

*4-(2,2-Diethoxyacetyl)pyridine (**12**c)*

A freshly prepared solution of 4-bromopyridine was treated as described above in the preparation of **12***b*. By this method was obtained 91.6 g (78.5%) of ketone **12***c*, bp 82°C/0.04 Torr.

*Preparation of methyl 3-(2-pyridyl)-4,4-diethoxy-2-methoxy-2-butenoates (**13**a–c)*

A stirred suspension of 3.0 g (0.126 mol) of sodium hydride (mineral oil free) in 120 mL dry THF was treated during 0.5 h with the dropwise addition of 30.2 g (0.126 mol) of methyl diethoxyphosphinylmethoxy acetate. Following the addition, the reaction mixture was stirred for an additional 0.5 h. After cooling to 0°C, a solution of 20.9 g (0.1 mol) of ketone **12***a*–*c* in 50 mL of dry THF was added dropwise to this solution over a 30 min period. Near the end of the addition, a gummy precipitate was formed. The reaction mixture was stirred overnight at 25°C and then treated with 75 mL of water. Benzene extraction, including an aqueous ammonium chloride wash, followed by distillation of the residue afforded a mixture (1:3) of unsaturated esters **13***a*–*c* (Table 5).

*Preparation of methyl 3-(x-pyridyl)-4,4-diethoxy-2-methoxy-butanoates (**14**a–c)*

To a solution of 11.8 g (0.04 mol) of the esters **13***a*–*c* in 50 mL of absolute ethanol was added 1.1 g of 10% palladium-on-carbon catalyst. The mixture was stirred under a hydrogen atmosphere until uptake of hydrogen ceased. The time required was approximately 20 min. Then the catalyst was removed by centrifugation and washed with ethanol. The organic fractions were combined and the solvent was evaporated. Distillation of the residue afforded esters **14***a*–*c* (Table 5).

*Preparation of 3-(x-pyridyl)-4,4-diethoxy-2-methoxy-1-butanols (**15**a–c)*

To a vigorously stirred suspension of 1.82 g (0.048 mol) of lithium aluminium hydride in 120 mL of dry THF was added 11.9 g (0.04 mol) of esters **14***a*–*c* in 30 mL of dry THF over a one-hour period. Following the addition, the reaction mixture was stirred for an additional hour before the excess hydride was destroyed by addition

Can. J. Chem. Downloaded from www.nrcresearchpress.com by 210.87.254.40 on 09/06/12
For personal use only.

Can. J. Chem. Downloaded from www.nrcresearchpress.com by 210.87.254.40 on 09/06/12
For personal use only.

TABLE 5. Yield, analytical, ^{1}H nmr, and infrared data for compounds **12***a*–*c*, **13***a*–*c*, **14***a*–*c*, and **15***a*–*c*

Compounds	Boiling point (°C/Torr)	Yield (%)	Analysis (%) calcd. found			^{1}H nmr																Infrared (cm^{-1}) ν(C=O) ν(O—H)
						Pyridyl								Acetal			Others					
			C	H	N	H-2	H-3	H-4	H-5	H-6	$J_{2,3}$ $J_{5,6}$	$J_{2,4}$ $J_{4,6}$	$J_{2,5}$ $J_{3,6}$	$J_{3,4}$ $J_{4,5}$	CH	CH_2	CH_3	CH_3—O	CH_3—O—CO	C—CH	CH_2	
12*a*	95/0.03	84	63.14 62.9	7.23 7.3	6.69 6.8	—	7.6–8.2 m		7.43 ddd	8.70 m	4.5	1.5	$J_{3,5}$ =2.5	6.5	6.17 s	3.75 dq	1.17 t					1725
12*b*	90/0.05	78	63.14 62.9	7.23 7.05	6.69 6.9	9.18 dd	—	8.31 dt	7.28 ddd	8.61 dd	4.5	2.0	1.0	7.0	4.95 s	3.69 m	1.21 t					1697
12*c*	82/0.04	78.5	63.14 63.2	7.23 7.1	6.69 6.8	8.58 dd	7.83 dd	—	7.83 dd	8.58 dd	4.5		1.5		4.95 s	3.65 m	1.18 t					1704
13*a*	120/0.04	87	61.00 60.8	7.17 7.0	4.74 4.8	—	7.3–7.7 m		7.0 m	8.4 m	4.5	1.5		6.5	5.58s 5.70s	3.6 m	1.1 m	3.47 s	3.62 2s			1735
13*b*	132/0.05	75	61.00 60.7	7.17 7.2	4.74 4.9	8.3 m	—	7.55 m	7.1 m	8.3 m	4.5	2.0	1.0	7.0	5.47s 5.50s	3.5 m	1.11 m	3.38 s	3.62 s			1733
13*c*	133/0.06	75	61.00 60.9	7.17 7.0	4.74 5.0	8.41 m	7.2 2dd	—	7.2 2dd	8.41 m	4.5		1.5		5.41s 5.51s	3.5 m	1.11 m	3.38 s	3.62 s			1733
14*a*	122/0.05	80	60.59 60.8	7.80 7.7	4.71 4.9	—	6.9–7.7 m			8.36 m					4.90d 5.02d	3.5 m	1.00 dt	3.17 s	3.57 s	4.1 m		1758
14*b*	120/0.03	87	60.59 60.9	7.80 7.9	4.71 4.5	8.45 m	—	7.7 dt	7.15 m	8.45 m		2.0	1.0	7.5	4.86d 4.95d	3.5 m	1.1 m	3.40 s	3.54 s	4.1 m		1768
14*c*	118/0.03	90	60.59 60.5	7.80 8.0	4.71 4.8	8.39 m	7.12 m	—	7.12 m	8.39 m	4.5		1.5		4.79d 4.88d	3.5 m	1.1 m	3.34 s	3.46 s	4.1 m		1755
15*a*	115/0.02	83	62.43 62.6	8.61 8.9	5.20 5.4	—	6.9–7.7		m	8.37 ddd	4.5	2.0		6.5	4.98d 4.99d	3.4 m	1.05 m	3.30 s	—	3.5 m	3.4 m	3400
15*b*	133/0.05	74	62.43 62.4	8.61 8.3	5.20 5.4	8.37 dd	—	7.70 dt	7.15 ddd	8.42 m	4.5	2.0	1.0	7.5	4.83 d	3.5 m	1.1 m	3.37 s	—	3.5 m	3.5 m	3400
15*c*	134/0.05	73	62.43 62.2	8.61 8.5	5.20 5.0	8.42 dd	7.28 dd	—	7.28 dd	8.42 dd	4.5		1.5		4.85 d	3.5 m	1.1 m	3.37 s	—	3.5 m	3.5 m	3300

of ethyl acetate. After work-up according to Fieser and Fieser (31) and benzene extraction, distillation afforded alcohols **15***a*–*c* (Table 5).

Preparation of x-*(3-furyl)pyridine (***9**a–c*) from compounds* ***15***a–c

To a stirred solution of 5.4 g (0.02 mol) of alcohols **15***a*–*c* in 150 mL of dry toluene was added 15 mL of a 1.6 *N* solution of hydrogen chloride in ether. The mixture was heated at 120°C for 24 h. After cooling, the mixture was base washed and distillation afforded compounds **9***a*–*c* (Table 3).

Acknowledgement

We wish to thank Professor Mollier (Université de Caen) for the dipole moments measurements.

1. T. KAUFFMANN. Angew. Chem. Int. Ed. Engl. **18**, 1 (1979).
2. J. SZYCHOWSKI, J. T. WROBEL, and A. LENIEWSKY. Can. J. Chem. **55**, 3105 (1977).
3. (*a*) J. T. WROBEL. The alkaloids. Vol. 9. *Edited by* R. H. F. Manske. Academic Press, New York, NY. 1967. p. 441; (*b*) B. MAURER and G. OHLOFF. Helv. Chim. Acta, **59**, 1169 (1976).
4. R. T. LALONDE, A. I. M. TSAI, C. J. WANG, and C. F. WONG. German Patent No. 2,603,176 (1976); Chem. Abstr. **85**, 177750a (1976).
5. E. WIEGAND, V. J. BAUER, and S. R. SAFIR. J. Med. Chem. **14**, 214 (1971).
6. F. LIONS and E. RITCHIE. J. Proc. R. Soc. W. S. Wales, **74**, 110 (1940).
7. H. S. RYANG and H. SAKURAI. J. Chem. Soc. Chem. Commun. **10**, 594 (1972).
8. L. FISERA, J. LESLO, J. KOVAK, J. HRABOVSKY, and J. SURA. Collect. Czech. Chem. Commun. **42**, 105 (1977).
9. F. ELOY and A. D. DERIJCKERE. Chim. Ther. **5**, 416 (1970); A. DERIJCKERE and F. ELOY. German Patent No. 2,052,536 (1971); Chem. Abstr. **75**, 35756b (1971).
10. R. FARAGHER and T. L. GILCHRIST. J. Chem. Soc. Chem. Commun. **8**, 252 (1977).
11. C. JUTZ, R. M. WAGNER, A. KROATZ, and H. G. LOBERING. Justus Liebigs Ann. Chem. **5**, 874 (1975).
12. P. RIBEREAU, G. NEVERS, G. QUEGUINER, and P. PASTOUR. C. R. Acad. Sci. Paris, **280**, 293 (1975).
13. E. BISAGNI, J. P. MARQUET, J. D. BOURZAT, J. J. PEPIN, and J. ANDRE-LOUISFERT. Bull. Soc. Chim. Fr. 4043 (1971).
14. L. M. JACKMANN and S. STERNHELL. Applications of nuclear magnetic resonance spectroscopy in organic chemistry. Pergamon Press, Oxford. 1969. pp. 182 and 188.
15. D. MILLER. J. Chem. Soc. C, 12 (1969).
16. (*a*) A. DORNOW. Ber. **3**, 185 (1940); (*b*) K. WINTERFELD and H. VON KOSEL. Arch. Pharm. **278**, 70 (1940).
17. (*a*) S. HOLAND and R. EPSZTEIN. C.R. Acad. Sci. Paris, **278**, 2876 (1964); (*b*) **261**, 4449 (1969).
18. A. J. DE JONG, L. BRANSMA, and J. F. ARENS. Recl. Trav. Chim. Pays-Bas, **93**, 15 (1974).
19. (*a*) H. GILMAN and S. M. SPATZ. J. Org. Chem. **16**, 1485 (1951); (*b*) A. MURRAY III and W. J. LANGHAM. J. Am. Chem. Soc. **74**, 6289 (1952).
20. K. SCHANK. Chem. Ber. **102**, 383 (1969).
21. (*a*) W. GRELL and H. MACHLEID. Ann. Chem. **699**, 53 (1966); (*b*) R. E. IRELAND, R. H. MULLER, and A. K. WILLARD. J. Org. Chem. **41**, 986 (1976).
22. P. KRUMHOLZ. J. Am. Chem. Soc. **73**, 3487 (1951); G. FAVINI. Gazz. Chim. Ital. **93**, 635 (1963).
23. H. WINBERG, T. J. VAN BERGEN, and R. M. KELLOG. J. Org. Chem. **34**, 3175 (1969).
24. E. BOUWHUIS and M. J. JANSSEN. Tetrahedron Lett. **3**, 233 (1972).
25. H. SIGEL, H. WYNBERG, T. J. VAN BERGEN, and K. KAHMANN. Helv. Chim. Acta, **55**, 610 (1972).
26. C. W. N. CUMPER, R. F. A. GINMAN, and A. I. VOGEL. J. Chem. Soc. 4518 (1962).
27. (*a*) A. L. MCCLELLAN. Tables of experimental dipole moments. W. H. Freeman and Co., London. 1963; (*b*) B. BAK, L. HANSEN-NYGAARD, and J. RASTRUP-ANDERSEN. J. Chem. Phys. **22**, 2013 (1954); (*c*) B. BAK, L. HANSEN, and J. RASTRUP-ANDERSEN. Discuss. Faraday Soc. **19**, 30 (1955); (*d*) B. BAK, D. CHRISTENSEN, J. RASTRUP-ANDERSEN, and E. TANNENBAUM. J. Chem. Phys. **25**, 892 (1956).
28. (*a*) V. GALASSO and G. DE ALTI. Tetrahedron, **27**, 4747 (1971); V. GALASSO, G. DE ALTI, and A. BIGOTTO. Tetrahedron, **27**, 991 (1971); (*b*) J. V. KNOP, N. TRINAJSTIC, M. MILUN, and S. PEJAKOVIC. Rev. Roum. Chim. **23**, 103 (1978).
29. S. GRONOWITZ and S. LIBJEFORS. Acta Chem. Scand. Ser. B, **31**, 771 (1977).
30. C. D. HURD and C. N. WEBB. J. Am. Chem. Soc. **49**, 551 (1927).
31. L. F. FIESER and M. FIESER. Reagents for organic synthesis. Vol. 1. John Wiley and Sons, New York, NY. 1967. p. 584.

Can. J. Chem. Downloaded from www.nrcresearchpress.com by 210.87.254.40 on 09/06/12
For personal use only.

Synthesis of 8,10- and 9,10-disubstituted camphor derivatives

WILLIAM M. DADSON, MAYDA LAM, THOMAS MONEY,[1] AND SUSAN E. PIPER
Department of Chemistry, University of British Columbia, Vancouver, B. C., Canada V6T 1Y6

Received June 3, 1982

WILLIAM M. DADSON, MAYDA LAM, THOMAS MONEY, and SUSAN E. PIPER. Can. J. Chem. **61**, 343 (1983).

Regiospecific bromination and debromination reactions have been used to provide a synthetic route from camphor to optically active 8,10- and 9,10-disubstituted camphor derivatives.

WILLIAM M. DADSON, MAYDA LAM, THOMAS MONEY et SUSAN E. PIPER. Can. J. Chem. **61**, 343 (1983).

On a utilisé des réactions de bromation et de débromation régiospécifiques pour transformer le camphre en dérivés optiquement actifs du camphre disubstitués respectivement en positions 8,10 et en position 9,10.

[Traduit par le journal]

Can. J. Chem. Downloaded from www.nrcresearchpress.com by 210.87.254.105 on 09/06/12
For personal use only.

The establishment of camphor (**1**) as a chiral starting material in natural product synthesis (1−17) is largely due to the availability of convenient methods for the regiospecific functionalization of camphor or simple derivatives at the C(5) (18), C(8) (19), C(9) (20), and C(10) (21, 22) positions. To increase the versatility of camphor as a starting material in terpenoid and steroid synthesis we have recently investigated various methods for the stereospecific synthesis of 8,10- and 9,10-disubstituted camphor derivatives.

Although 8,10-disubstituted camphor derivatives have not been described in the literature (22), Nishikawa and Hagiwara have reported (23) that treatment of 3,9-dichlorocamphor with fuming sulfuric acid yields a mixture of 6,9-dichlorocamphor and 3,9-dichlorocamphor-10-sulfonic acid while bromination ($Br_2/ClSO_3H$) provides 3,9-dichloro-10-bromocamphor. The synthetic potential of a direct C(10)-bromination process coupled with the prospect of its application to the synthesis of 8,10- and 9,10-disubstituted camphor derivatives prompted us to extend the earlier Japanese studies using the more readily available (+)-3,9-dibromocamphor (**3**) (20) in the bromination process. Treatment of **3** with bromine in chlorosulfonic acid for 5 days at room temperature produced a crystalline product (50% yield) which was identified as (+)-3,9,10-tribromocamphor (**4**) on the basis of spectroscopic evidence. Regiospecific debromination of **4** with zinc/acetic acid at 0°C provided (+)-9,10-dibromocamphor (**5**) in 62% yield. The nmr spectrum (400 MHz) of this compound indicated that the quartets normally expected for the C(9) and C(10) methylene groups overlap to a considerable extent. Confirmation for the identity of the reaction product as (+)-9,10-dibromocamphor (**5**) was obtained by X-ray crystallographic analysis.[2]

In similar fashion, (+)-3,8-dibromocamphor (**8**)[3] was converted, via the bromination/selective debromination sequence (Scheme 1), to (+)-8,10-dibromocamphor (**10**) (35% overall yield) and the structure of this compound was also confirmed by X-ray crystallographic analysis.[2] In the 270 MHz spectra of 3,8,10-tribromocamphor (**9**), one of the AB quartets expected for the C(8) and C(10) methylene groups appears as a singlet at 3.50 δ. By contrast, the C(8)-methylene groups in 8-bromocamphor (**7**), 3,8-dibromocamphor (**8**), and 8,10-dibromocamphor (**10**) appear as singlets in the 60 and 100 MHz spectra and as AB quartets (J_{AB} = 10−10.5 Hz) in the 270 MHz spectra.

The C(10)-bromination of 3,8-dibromocamphor (**8**) and 3,9-dibromocamphor (**3**) presumably occurs by a mechanism similar to that proposed to explain C(10)-sulfonation of camphor (24). Thus we presume that Wagner−Meerwein rearrangement provides an intermediate camphene derivative (**12**; X or Y = H, X or Y = Br) which can react with bromine and subsequently revert to the camphor framework (cf. Scheme 2). It is interesting to note that the reaction conditions used in this C(10)-bromination process are similar to those normally employed for stereospecific bromination of 3,3-dibromocamphor at the C(8)-position (19) and (+)-3-bromocamphor (**2**) at the C(9)-position (20). In the latter reaction the initial camphene intermediate (**12**; X = Y = H) undergoes a 2,3-*exo*-methyl shift to provide a second intermediate (**14**) which can be brominated (20*d*) (Scheme 2). Reversal of the Nametkin and Wagner−Meerwein rearrangements then produces (+)-3,9-dibromocamphor (**3**).[4] In the C(10)-bromination processes described above the presence of the C(8) or C(9)-bromomethyl group in the starting material probably inhibits the formation of intermediate (**14**) by Nametkin rearrangement (2,3-methyl shift) and therefore bromination occurs only at the C(10) position (cf. Scheme 2). In related investigations we have shown that 3,10-dibromocamphor (**17**) and 3-bromo-10-benzoyloxycamphor (**18**) do not readily brominate when treated with $Br_2/ClSO_3H$. In these cases the C(10) substituent may inhibit formation of a carbonium ion intermediate analogous to **11** (X = Y = H) (Scheme 2) and therefore C(9)-bromination does not occur.

In summary, the methodology described above provides a convenient route to a variety of optically pure 8,10- and 9,10-disubstituted camphor derivatives and the potential of these compounds as intermediates in steroid and terpenoid synthesis is currently being evaluated.

Experimental

(+)-3,9,10-Tribromocamphor (4)

A solution of bromine (5.0 mL) in chlorosulphonic acid (18 mL)

[1]Author to whom correspondence may be addressed.

[2]S. J. Rettig and J. Trotter, unpublished results.

[3](+)-3,8-Dibromocamphor (**8**) is prepared by bromination of (+)-8-bromocamphor (**7**) in acetic acid. It should be noted that earlier literature reports (22) describing "3,8-dibromocamphor" actually refer to the 3,9-isomer.

[4]In the C(8)-bromination proceeds (19) (not shown in Scheme 2) the corresponding intermediates undergo 2,3-*endo* methyl shifts (19*c*).

0008-4042/83/020343-04$01.00/0
©1983 National Research Council of Canada/Conseil national de recherches du Canada

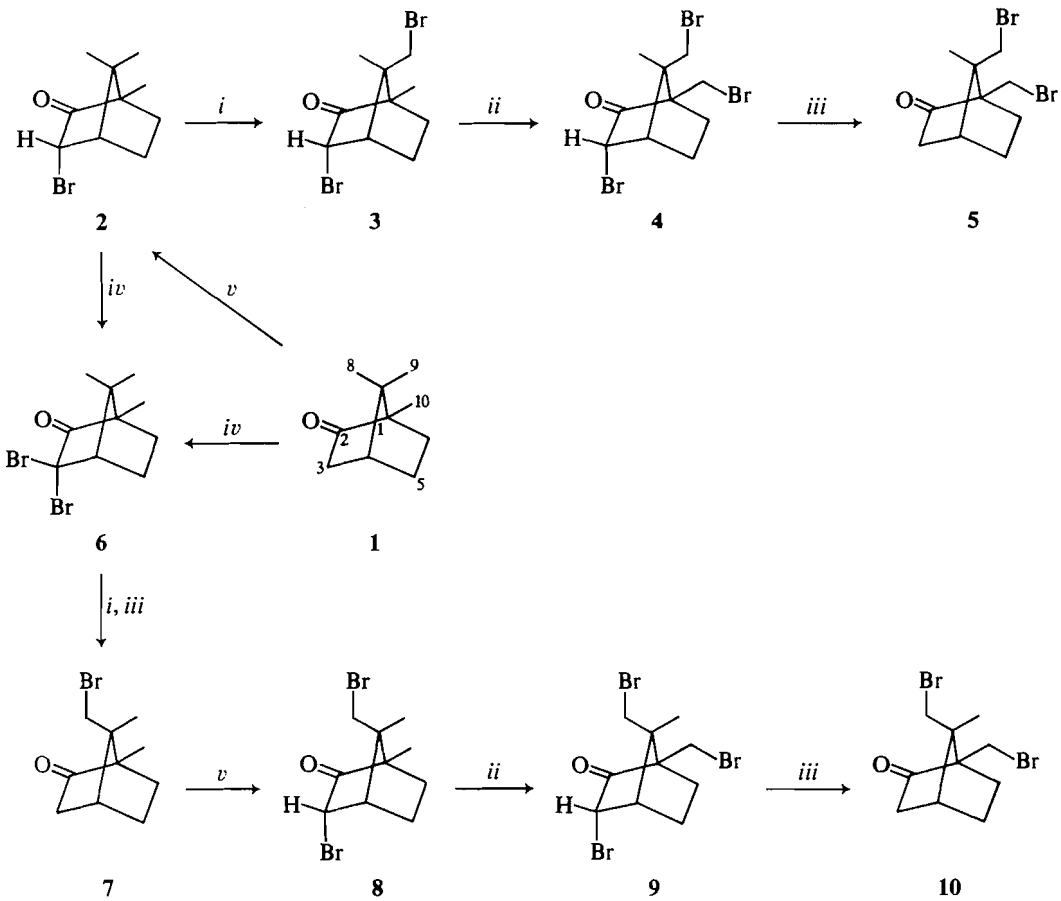

i $Br_2/ClSO_3H$/5 h ii $Br_2/ClSO_3H$/5 days iii Zn/HOAc iv Br_2
v Br_2/HOAc

SCHEME 1

was added to a stirred solution of (+)-3,9-dibromocamphor (**3**) (18 g) in chloroform (16 mL) at 0°C under nitrogen and the reaction mixture was left at room temperature for 5 days. The ether extract of the reaction mixture was washed with sodium bisulfite, sodium bicarbonate, and water. Removal of solvent produced a crude solid (22 g) which was crystallized from methanol to provide (+)-3,9,10-tribromocamphor (**4**) (12 g, 50% yield), mp 100–102°C; $[\alpha]_D$ +47.5 (*c* 1.0, MeOH); ν_{max} (CCl_3): 1760 cm^{-1}; nmr ($CDCl_3$, 400 MHz), δ: 1.21 (3H, s), 3.46 and 3.68 (2H, dd, J = 11.5 Hz), 3.64 and 3.73 (2H, AB quartet, J_{AB} = 10.5 Hz), 4.57 (1H, d, J = 4.5 Hz); *m/e*: 386/388/390/392 (M^+), 307/309/311 (M − Br), 228/230. *Anal.* calcd. for $C_{10}H_{13}Br_3O$: C 30.88, H 3.37, Br 61.64; found: C 30.87, H 3.44, Br 61.46.

(+)-9,10-Dibromocamphor (5)

A stirred solution of (+)-3,9,10-tribromocamphor (**4**) (11.5 g) in glacial acetic acid (150 mL) was treated with zinc powder (6.2 g) at room temperature for 3 hours. The reaction mixture was diluted with water, filtered through Celite, and extracted with ether. Work-up in the usual way provided a pale yellow solid (6.2 g) which was crystallized from methanol to provide (+)-9,10-dibromocamphor (**5**) (5.2 g, 62% yield), mp 98–100°C; $[\alpha]_D$ +69.75 (*c* 2.0, MeOH); nmr ($CDCl_3$, 400 MHz), δ: 1.10 (s, 3H), 3.48 (d) and 3.71 (d) (2H, AB quartet, J = 12 Hz), 3.59 (d) and 3.70 (d) (2H, AB quartet, J = 10.5 Hz); *m/e*: 312/310/308 (M^+), 231/229 (M − Br). *Anal.* calcd. for $C_{10}H_{14}Br_2O$: C 38.75, H 4.55, Br 51.55; found C 38.87, H 4.69, Br 51.33.

(+)-3,8-Dibromocamphor (8)

A solution of bromine (1.0 mL) in glacial acetic acid (50 mL) was added dropwise, at 80°C, over a period of 3.0 hours to a stirred solution of (+)-8-bromocamphor (**7**) (10.0 g) in glacial acetic acid (20 mL). After 24 h at 80°C the reaction mixture was added to ice and the ether extracts washed with sodium bisulfite, sodium bicarbonate, and water. Removal of solvent afforded a yellow oil (13.2 g) which was shown by glc to contain 80–85% 3,8-dibromocamphor. Distillation of the crude oil followed by crystallization from 95% ethanol provided (+)-3,8-dibromocamphor (**8**) (9.5 g, ~71% yield), mp 62°C; $[\alpha]_D$ +133.9 (*c* 2.0, MeOH); ν_{max} (CCl_4): 1770 cm^{-1}; nmr ($CDCl_3$, 270 MHz), δ: 0.98 (3H, s), 1.27 (3H, s), 2.64 (1H, t), 3.10 (d) and 3.20 (d) (2H, AB quartet, J = 10.1 Hz) 4.62 (1H, d, J = 4.0 Hz); *m/e*: 312/310/308 (M^+), 231/229 (M − Br). *Anal.* calcd. for $C_{10}H_{14}Br_2O$: C 38.75, H 4.55, Br 51.55; found: C 38.97, H 4.60, Br 51.33.

(+)-3,8,10-Tribromocamphor (9)

Chlorosulphonic acid (15 mL) was added dropwise at 0°C to a stirred mixture of (+)-3,8-dibromocamphor (**8**) (9.2 g), bromine (16.0 g; 5.13 mL), and chloroform (10 mL). The mixture was stirred at room temperature for 8 days before adding carefully to ice and washing the combined ether extracts with aqueous sodium bisulfite, aqueous sodium bicarbonate, and saturated NaCl solution. Removal of solvent afforded a viscous yellow oil (11.4 g) which was shown by glc to contain 75% 3,8,10-tribromocamphor and which could be used without further purification.

Purification by column chromatography (silica gel; petroleum ether (30–60°C)/ether 25:1) and crystallization from $MeOH/CH_2Cl_2$ provided (+)-3,8,10-tribromocamphor (**9**) (5.3 g, 51% yield based on recovered starting material), mp 63–66°C; $[\alpha]_D$ +126.1 (*c* 4.0, MeOH); ν_{max} (CCl_4): 1760 cm; nmr ($CDCl_3$, 270 MHz), δ: 1.39

Can. J. Chem. Downloaded from www.nrcresearchpress.com by 210.87.254.105 on 09/06/12
For personal use only.

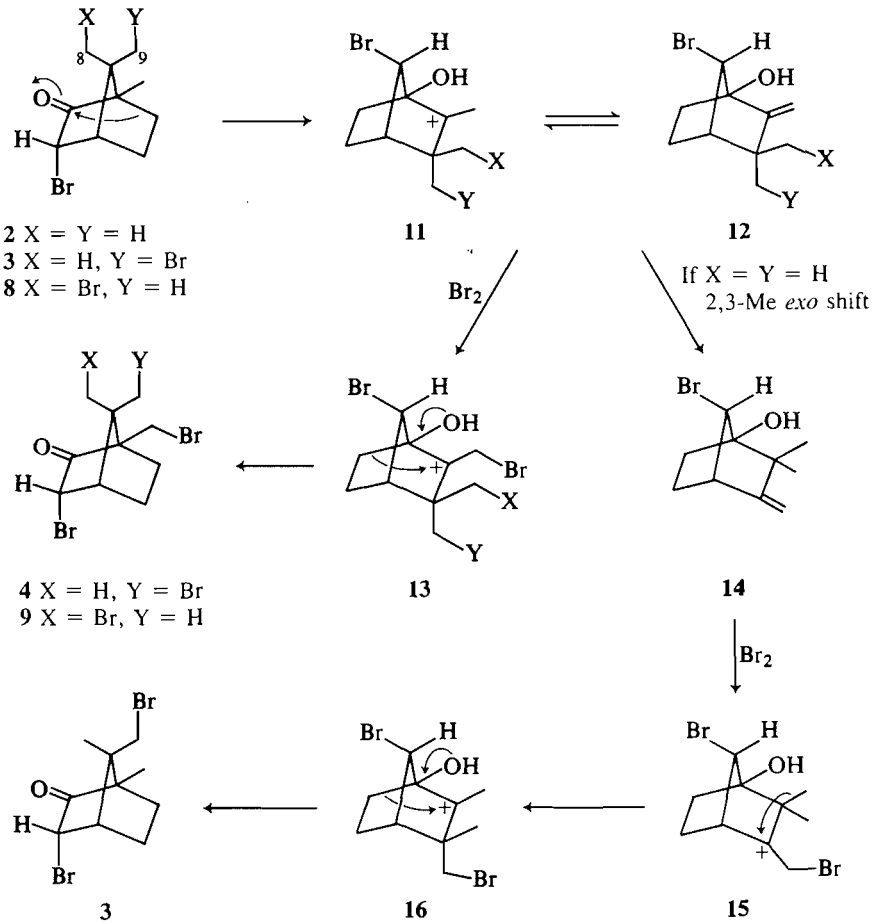

SCHEME 2

(3H, s), 2.71 (1H, t); 3.27 (d) and 3.52 (d) (2H, AB quartet, J = 10.1 Hz); 3.50 (2H, s), 4.62 (1H, d, J = 4.5 Hz); *m/e*: 392/390/388/386 (M^+), 311/309/307 (M − Br), 228/230; *Anal.* calcd. for $C_{10}H_{13}Br_3O$: C 30.88, H 3.37, Br 61.63; found: C 31.00, H 3.30, Br 61.44.

(+)-8,10-Dibromocamphor (10)

Zinc (1.0 g) was added to a stirred solution of 3,8,10-tribromocamphor (**9**) (2.0 g) in glacial acetic acid (10 mL) at 0°C. After stirring at 0°C for 10 min and at 25°C for 1 hour the mixture was added to ice. Work-up in the usual way provided 8,10-dibromocamphor (**10**) as a colorless solid (1.53 g, ~96% yield; 97% pure by glc). Crystallization from methanol yielded pure (+)-8,10-dibromocamphor (**10**), mp 76°C; $[\alpha]_D^{22}$ +63.45 (*c* 4.0, MeOH); ν_{max} (CCl_4): 1745 cm^{-1}; nmr ($CDCl_3$, 400 MHz), δ: 1.30 (3H, d, J = 1.5 Hz), 3.24 (1H, dd, J_{AB} = 10.1 Hz, J_{BX} = 1.5 Hz), 3.46 (1H, d, J_{AB} = 10.1 Hz), 3.47 (d), 3.52 (d) (2H, AB-quartet J = 10.15 Hz); *m/e*: 312/310/308 (M^+), 231/229 (M − Br). *Anal.* calcd. for $C_{10}H_{14}Br_2O$: C 38.74, H 4.55, Br 51.55; found: C 38.98, H 4.41, Br 51.38.

Acknowledgement

We acknowledge financial support for this research from N.S.E.R.C., Ottawa, Canada.

1. D. SEEBACH and H. O. KALINOWSKI. Nachr. Chem. Tech. **24**, 415 (1976).
2. W. A. SZABO and H. T. LEE. Aldrichimica Acta, **13**, 13 (1980).
3. R. B. WOODWARD, Pure Appl. Chem. **17**, 519 (1968); **25**, 283 (1971); **33**, 145 (1973).
4. S. Y. KAMAT, K. K. CHAKRAVARTI, and S. C. BHATTACHARYYA. Tetrahedron, **23**, 4487 (1967).
5. (*a*) E. J. COREY, S. W. CHOW, and R. A. SCHERRER. J. Am. Chem. Soc. **79**, 5773 (1957); (*b*) E. J. COREY and M. F. SEMMELHACK. J. Am. Chem. Soc. **89**, 2775 (1967).
6. (*a*) E. J. COREY, H. A. KIRST, and J. A. KATZENELLENBOGEN. J. Am. Chem. Soc. **92**, 6314 (1970); (*b*) E. J. COREY and H. YAMAMOTO. J. Am. Chem. Soc. **92**, 226 (1970).
7. J. COLONGE, G. DESCORTE, Y. BAHUREL, and A. MENET. Bull Soc. Chim. Fr. 374 (1966).
8. R. G. LEWIS, D. G. GUSTAFSON, and W. F. ERMAN. Tetrahedron Lett. 401 (1967).
9. C. R. ECK, G. L. HODGSON, D. F. MACSWEENEY, R. W. MILLS, and T. MONEY. J. Chem. Soc. Perkin Trans. I, 1938 (1974), and references cited therein.
10. R. V. STEVENS and F. C. A. GAETA. J. Am. Chem. Soc. **99**, 6105 (1977).
11. M. S. ALLEN, N. LAMB, and T. MONEY. J. Chem. Soc. Chem. Commun. 112 (1979).
12. N. DARBY, N. LAMB, and T. MONEY. Can. J. Chem. **57**, 742 (1979).
13. H.-J. LIU and W. H. CHAN. Can. J. Chem. **57**, 708 (1979); **60**, 1081 (1982).
14. P. CACHIA, N. DARBY, T. C. W. MAK, T. MONEY, and J. TROTTER. Can. J. Chem. **58**, 1172 (1980).
15. N. LAMB. Ph.D. Thesis, University of British Columbia, Vancouver, 1979; N. Lamb, T. Money, S. J. Rettig, and J. TROTTER. Can. J. Chem. **60**, 1055 (1982).
16. P. CACHIA. Ph.D. Thesis, University of British Columbia, Vancouver, 1980.
17. I. KITAGAWA, H. SHIBUYA, H. FUJIOKA, Y. YAMAMOTO,

Can. J. Chem. Downloaded from www.nrcresearchpress.com by 210.87.254.105 on 09/06/12
For personal use only.

A. KAJIWARA, K. KITAMURA, A. MIYAO, T. HAKOSHIMA, and K. TOMITA. Tetrahedron Lett. 1963 (1980).

18. (*a*) M. S. ALLEN, N. DARBY, P. SALISBURY, E. R. SIGURDSON, and T. MONEY. Can. J. Chem. **57**, 733 (1979), and references cited therein; (*b*) N. DARBY, N. LAMB, and T. MONEY. Can. J. Chem. **57**, 742 (1979).
19. (*a*) C. R. ECK, R. W. MILLS, and T. MONEY. J. Chem. Soc. Chem. Commun. 911 (1973); J. Chem. Soc. Perkin Trans. I, 251 (1975); (*b*) P. CACHIA, N. DARBY, C. R. ECK, and T. MONEY. J. Chem. Soc. Perkin Trans. I, 359 (1976); (*c*) W. M. DADSON and T. MONEY. J. Chem. Soc. Chem. Commun. 112 (1982); (*d*) W. L. MEYER, C. E. CAPSHEW, J. H. JOHNSON, A. R. KLUSENER, A. P. LOBO, and R. N. MCCARTY. J. Org. Chem. **42**, 527 (1977).
20. (*a*) H. NISHIMITSU, M. NISHIKAWA, and H. HAGIWARA. Proc. Jpn. Acad. **27** 285 (1951); Chem. Abstr. **46**, 6112 (1952); (*b*) E. J. Corey, S. W. Chow, and R. A. SCHERRER. J. Am. Chem. Soc. **79**, 5773 (1957); (*c*) W. L. MEYER, A. P. LOBO, and R. N. MCCARTY. J. Org. Chem. **32**, 1754 (1967); (*d*) J. H. JOHNSON. Diss. Abstr. B, **35**, 2657 (1974).
21. P. D. BARTLETT and L. H. KNOX. Org. Synth. **45**, 12 (1965), and references cited therein.
22. (*a*) E. JOSEPHY and F. RADT (*Editors*). Elsevier's encyclopaedia of organic chemistry. Vol 12A. Elsevier Publishing Co., Amsterdam. 1948; (*b*) J. L. SIMONSEN and L. N. OWEN. The terpenes. Vol II. Cambridge University Press. 1957; (*c*) A. PELTER and S. H. HARPER. *In* Rodd's chemistry of carbon compounds. Vol IIc. *Edited by* S. Coffey. Elsevier, Amsterdam. 1969.
23. M. NISHIKAWA and H. HAGIWARA. J. Pharm. Soc. Jpn. **74**, 76 (1954); **74**, 81 (1954); Chem. Abstr. **49**, 1596 (1955).
24. (*a*) Y. ASAHINA. Proc. Imp. Acad. Tokyo, **13**, 38 (1937); (*b*) P. LIPP and H. KNAPP. Ber. **73**, 915 (1940); (*c*) T. MIKI, M. NISHIKAWA, and H. HAGIWARA. Proc. Jpn. Acad. **31**, 718 (1955); (*d*) reference 6*b*, pp. 425–427; (*e*) A. M. T. FINCH and W. R. VAUGHAN. J. Am. Chem. Soc. **91**, 1416 (1969).

Can. J. Chem. Downloaded from www.nrcresearchpress.com by 210.87.254.105 on 09/06/12
For personal use only.

Solubilization of some related *para*-substituted benzenes in Type II DM mesophases

V. R. PAOLI-MONTEIRO, M. SUZUKI, AND J. A. VANIN
Instituto de Quimica, Universidade de Sao Paulo, Caixa Postal 20,780, Sao Paulo, Brazil

AND

L. W. REEVES[1]
Chemistry Department, University of Waterloo, Waterloo, Ont., Canada N2L 3G1

Received June 25, 1982

V. R. PAOLI-MONTEIRO, M. SUZUKI, J. A. VANIN, and L. W. REEVES. Can. J. Chem. **61**, 347 (1983).

A series of chemically related *para*-disubstituted aromatic solutes have been dissolved in two type II DM systems. The Saupe matrix elements of order have been determined for the solutes and the degrees of order of some segments in the amphiphiles have been derived from deuterium quadrupole splittings. The comparison of deuterium quadrupole splittings in uncontaminated mesophases with those containing the solutes leads to the conclusion that four solutes are located in the bilayer disk of the component micelles of one meosphase. A consideration of the structure and alignment of the disc micelles leads to absolute sign attribution for degrees of order of detergent segments and matrix elements for solute axes. A consideration of the orientations of the solute axes with respect to the mesophase director suggests the type of molecular interactions and motions which apply to solutes.

V. R. PAOLI-MONTEIRO, M. SUZUKI, J. A. VANIN et L. W. REEVES. Can. J. Chem. **61**, 347 (1983).

On a dissous une série de solutés aromatiques disubstituées en positions *para* reliés entre eux chimiquement dans deux systèmes du type II DM. On a déterminé les éléments d'ordres des matrices de Saupe pour les solutés et on a déduit le degré d'ordre de quelques segments d'amphiphiles à partir des dédoublements quadrupolaires du deutérium. La comparaison des dédoublements quadrupolaires du deutérium dans les mésophases non contaminées avec celles contenant les solutés permet de conclure que quatre solutés sont situés dans le disque de la couche double dans les micelles composantes d'une mésophase. En prenant en considération la structure et l'alignement des disques micellaires, on aboutit à une attribution du signe absolu des degrés d'ordre des segments de détergents et des éléments de matrice pour les axes de solutés. Une comparaison des orientations des axes du soluté par rapport à la mésophase directrice suggère le type d'interactions moléculaires et les mouvements qui s'appliquent aux solutés.

[Traduit par le journal]

Can. J. Chem. Downloaded from www.nrcresearchpress.com by 210.87.254.105 on 09/06/12
For personal use only.

Introduction

Type II DM nematic liquid crystals are used widely as a solvent matrix for small molecules (1−4) and ions (5, 6). The proton magnetic resonance spectra of the solutes in the magnetically aligned mesophase are used to determine molecular structures by standard techniques (7, 8). The interest in such studies of relative internuclear distances has, however, not been complemented in this context by considerations of the structure of the nematic solvent (8). The structure ot type II DM mesophases is now well established. It is therefore important to have some predictive notions of the location of solubilized material (9). Such knowledge of the location of solutes and the proper mesophase matrix to select is a considerable aid in achieving a high degree of order for a particular solute and in predicting the signs of the dipolar coupling constants to aid in the spectral analysis (7, 8).

The present study is designed to investigate the location and degrees of order of some simple chemically related solutes in two different mesophases. The emphasis of the work is not in the structure of the solutes because the *para*-substituted benzenes selected have rather well-known structures.

Experimental

Proton magnetic resonance spectra were detected at 100 MHz, usually in the continuous wave mode, while deuterium magnetic resonance was observed at 15.4 MHz in the Fourier transform mode; both observations were registered on a Varian XL-100 spectrometer, with the gyrocode option. Spectral analysis of the proton signals was achieved by use of the program EUAITR for both isotropic and aligned samples (10). The computer was a Burroughs model 3600 located in the electronic computer centre of the University of Sao Paulo. The spectrometer conditions were appropriately optimized in each case and accumulations for deuterium signals varied from 5000 to 30 000 transients.

1,1,9,9,10,10,10-Heptadeuteriodecylammonium chloride, 1,1-dideuterio potassium laurate, and potassium laurate-d_{23} were derived from a previous stock, the preparation of which has already been described (11). n-Decanol from J. T. Baker was twice distilled under reduced pressure. The effective pH in the lyomesophases was achieved by prior additions of hydrochloric acid or sodium hydroxide to the water utilized in their preparation. In this manner the water was mixed with other components at pH = 1 or pH = 13. In addition the water was doped with 0.1−0.5% D_2O as convenient for the mesophase under investigation. The solutes, all of analytical grade, were used without further purification. They were: parafluorobenzoic acid (Pierce Chem. Co.), parachlorobenozic acid (Eastmann), parabromobenzoic acid (B.D.H.), paraiodobenzoic acid (Eastmann), paracyanobenzoic acid (Eastmann), parahydroxybenzoic acid (B.D.H.), paraaminobenzoic acid (B.D.H.), parafluorophenol (Aldrich), parachlorophenol (Aldrich), parabromophenol (Aldrich), paraaminophenol (Aldrich), 4-pyridine carboxylic acid (B.D.H.), and paranitrophenol sodium salt (B.D.H.). In order to simplify notations these compounds have been nominated, in order, PFBA, PClBA, PBrBA, PIBA, PCNBA, POHBA, PNH_2BA, $PF\phi OH$, $PCl\phi OH$, $PBr\phi OH$, $PNH_2\phi OH$, PCaPyr, and $PNO_2\phi O^-$. Corresponding conjugate ions, present in basic media, are designated by merely adding a negative superscript, e.g. $PCNBA^-$ means paracyanobenzoate ion.

The mesophases were prepared in a manner previously reported

[1]Author to whom correspondence should be addressed. Visiting Professor, University of Sao Paulo, 1967 to 1981.

0008-4042/83/020347-09$01.00/0
©1983 National Research Council of Canada/Conseil national de recherches du Canada

TABLE 1. Mole percentages of components in various mesophases

A*	1	2	3	4	5	6	7	7	8	9	10	11	12	13
DAC-d_7	0.30	0.49	0.32	0.56	0.63	0.99	—	0.56	0.56	1.02	1.08	0.48	0.57	0.58
DAC	4.72	4.52	4.81	4.31	5.27	4.09	5.22	5.31	4.56	2.01	3.72	4.76	5.30	5.28
H_2O	93.35	93.09	92.84	92.86	91.38	93.67	92.45	91.16	93.07	94.61	93.57	91.35	92.25	91.38
KCl	1.08	1.62	1.86	2.13	2.41	0.99	2.01	2.65	1.22	0.77	1.33	3.05	1.56	2.37
Solute	0.55	0.28	0.17	0.14	0.31	0.26	0.32	0.32	0.59	0.59	0.30	0.36	0.32	0.39

B†								
DAC-d_7	0.57	0.56	0.56	0.55	0.54	0.53	0.52	0.50
DAC	4.70	4.66	4.60	4.53	4.46	4.36	4.28	4.18
KCl	3.05	3.02	2.99	2.94	2.90	2.83	2.78	2.72
H_2O	91.68	91.76	91.85	91.98	92.10	92.28	92.42	92.60

C‡	1	2	3	4	5	6	7	9	10
KL-d_2	0.10	—	—	—	0.34	0.25	0.54	—	—
KL-d_{23}	0.11	0.25	0.13	0.12	0.09	0.11	0.10	0.24	0.18
KL	4.15	3.74	3.90	3.98	3.69	3.81	3.30	4.05	4.31
KCl	2.53	2.46	2.61	2.18	2.03	1.94	1.83	2.27	2.49
DeOH	0.67	0.53	0.63	0.70	0.63	0.52	0.52	0.49	0.60
H_2O	91.90	92.51	92.34	92.61	92.83	93.00	93.39	92.13	91.86
Solute	0.54	0.51	0.39	0.41	0.39	0.37	0.32	0.82	0.56

D§							
KL-d_2	0.29	0.28	0.28	0.27	0.27	0.26	0.26
KL-d_{23}	0.08	0.08	0.08	0.08	0.07	0.07	0.07
KL	2.38	2.35	2.31	2.27	2.24	2.19	2.12
KCl	1.62	1.60	1.57	1.54	1.53	1.49	1.45
DeOH	0.79	0.78	0.77	0.75	0.74	0.72	0.70
H_2O	94.84	94.91	94.99	95.09	95.15	95.27	95.40

*A. Mole percentages of components in mesophases prepared from decylammonium chloride with different solutes. The water was acidified and kept at pH~1 before mixing the mesophase. The solutes may be identified by the numbers heading the columns as follows: 1 = PFBA, 2 = PClBA, 3 = PBrBa, 4 = PIBA, 5 = PCNBA, 6 = PNH_3^+BA (protonated form in the mesophase), 7 = POHBA, 8 = PFϕOH, 9 = PClϕOH, 10 = PBrϕOH, 11 = PNH_3^+ϕOH (protonated form in mesopahse), 12 = PNO_2ϕONa, 13 = PCaPyr (protonated form). The water also contained a small amount of D_2O.

†B. Mole percentages of components in uncontaminated DAC mesophases with varied water content. The water content increases as the columns progress to the right.

‡C. Mole percentages of components in mesophases prepared from potassium laurate with solutes. The solutes may be identified from the column heading numbers which are assigned in part A above. All solutes are in the deprotonated or conjugate base form at pH~13. DeOH = n-decanol.

§D. Mole percentages of components in uncontaminated KL mesophases with varied water content. The water content increases as columns progress to the right.

(11). The proton spectra were observed first, then the deuterium spectrum, followed by a repeat of the proton spectra to ensure an unaltered sample in each case.

For both isotropic samples and solutes in the Type II DM mesophase the spectral widths for protons varied between 100 and 500 Hz. Individual peaks were calibrated with a frequency counter and had a random error of position between 0.1 and 0.01 Hz. In a few cases the large H_2O peak did mask some transitions of the solute, but sufficient information was always available for the spectral analysis. The mol% of each component in all mesophases studied has been listed in two tables, Table 1A for phases with a host disc bilayer of decylammonium chloride (DAC) and Table 1C for a host disc bilayer of potasisum laurate (KL). Although the mole fraction of the detergent varies somewhat, as does that of the water and solute, the mesophases are considered to be dilute in solute. The maximum mole fraction of solute in the bilayer is 0.08 while the minimum is 0.03.The variation of composition is inevitable because of the range of chemical substances used as solutes and the sensitivity of the mesophase to different impurities.

This variation in water content and, to some extent, solute concentration is properly standardized by using ratios of degrees of order (12, 13), which are independent of water content (11, 12), and studying the dependence on solute, as we shall show. The Tables 1B and 1D list compositions for pure DAC and KL mesophases which were diluted with water over the range of stability of the Type II DM lyomesophase. These uncontaminated phases served as a standard for deviations in behaviour with solutes.

Results

(a) *Analysis of solute proton spectra in isotropic media*

The precise determination of the dipole–dipole "D_{ij}" direct coupling constants in anisotropic media requires good values of the corresponding scalar couplings J_{ij} and, hopefully, their sign. Solutes were dissolved in basic or acidic aqueous solution at 35°C in order to achieve the spectra required. The spectra are AA′BB′ and standard methods sufficed for the analysis. Table 2 summarizes the results. The chemical shift differences AA′ with BB′ are of course a strong function of solvent, but scalar couplings also vary, especially when comparing the present experiments with those of Cox (14) in DMSO. The signs of the coupling constants J_{ij} between the protons in the aromatic rings are positive. The pK_a values for all compounds investigated show that at pH = 1 the acid form is present and at pH = 13 the basic form predominates in at least 99% in all cases.

(b) *Analysis of proton spectra of solutes in aligned type II DM mesophases*

In DAC mesophases the pH of the component water cannot

Can. J. Chem. Downloaded from www.nrcresearchpress.com by 210.87.254.105 on 09/06/12
For personal use only.

Can. J. Chem. Downloaded from www.nrcresearchpress.com by 210.87.254.105 on 09/06/12
For personal use only.

TABLE 2. The scalar couplings and chemical shift differences for the solute species used in mesophases*

Solute	pH	$J_{12} = J_{34}$	J_{14}	J_{23}	δ
$PFBA^{-}$ [d]	13	8.8	2.8±0.1	2.9±0.1	0.717
PFBA[e]	1	8.1	4.9	4.4	0.822
$PClBA^{-}$	13	8.0	2.2	2.2	0.361
PClBA	1	8.4	3.2	3.2	0.649
$PBrBA^{-}$ [f]	13	7.4	5.1	5.1	0.123
PBrBA	1	8.3	0.1	0.1	0.116
$PIBA^{-}$ [g]	13	7.3	1.8	2.6	0.234
PIBA[h]	DMSO[a]	8.13	1.94	2.08	0.133
$PCNBA^{-}$	13	8.1	3.0	3.2	0.120
PCNBA[i]	DMSO[a]	8.02	1.71	1.74	0.158
PNH_2BA^{-}	13	8.30	2.60	2.60	0.921
$PNH_3^{+}BA$	DAC[b]	8.60	0	0	0.840
$POHBA^{-}$	13	8.60	2.36	2.36	0.900
POHBA[j]	1	8.0	1.6	1.6	0.969
$PCl\phi O^{-}$ [k]	13	7.9	1.1	2.5	0.402
PClφOH	1	8.3	0.3	0.7	0.401
$PBr\phi O^{-}$	13	8.5	2.9	2.9	0.610
PBrφOH	1	8.7	2.3	2.8	0.588
$PCaPyr^{+}$ [c, l]	1	6.3	0.7	0	

*The solvent is water at pH specified in column 2 except for (a) where the data of Cox is used (25) and for (b) which was a concentrated micellar solution of decylammonium chloride. The chemical shift difference in the AA′BB′ spectrum is listed in parts per million while scalar couplings are denoted in Hz, subscripts following the diagram given as Fig. 1 for the positions of protons. (c) Paracarboxylpyridinium ion. (d) The couplings to the fluorine are $J_{15} = 8.6$, $J_{25} = 5.5$. (e) Couplings to the fluorine are $J_{15} = 8.2$, $J_{25} = 8.1$. (f) Coupling $J_{13} = J_{24} = 0.8$. (g) $J_{13} = J_{24} = 1.0$. (h) $J_{13} = J_{24} = 0.37$. (i) $J_{13} = J_{24} = 0.56$. (j) $J_{13} = J_{24} = 0.6$. (k) $J_{13} = J_{24} = 0.7$. (l) $J_{13} = J_{24} = 0.6$. Couplings may be taken to have errors ±0.15 Hz.

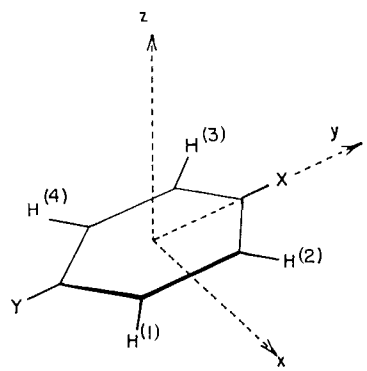

FIG. 1. The system of coordinates used for *para*-substituted benzenes. The axes, x, y, and z are equivalent to the principal axes of the order tensor 11, 22, and 33, respectively. The substituents Y are —COOH, —COO^{-}, —OH, or O while the substituents X are all other possibilities among the compounds chosen. The protons are enumerated in the diagram according to position and used as subscripts in the text, e.g. r_{12}, D_{23}, J_{24}, etc.

be raised to the basic region because the mesophase disintegrates and thus all the solutes are present in the acid form, which in the case of basic nitrogen solutes $PNH_2\phi OH$, PCaPyr, and PNH_2BA results in a protonated nitrogen. In the mesophases prepared from KL, the solutes are in the form of conjugate bases at pH = 13. The spectra of aligned solutes are also AA′BB′ except PFBA, $PFBA^{-}$, PFφOH, and $PF\phi O^{-}$ where the F-19 spin nucleus contributed to give two AA′BB′ subspectra. The values of J_{ij} obtained previously were introduced in order to compute by iteration the values D_{ij}. In the present work four spectra were averaged for the position of 10 to 12 peaks. The calculated spectra are insensitive to the relative changes of sign of D_{ij} provided a given set of parities is preserved, if the degree of order of the *para* axis is large. On the other hand, for PNH_3BA^{+} in DAC and the ions $PFBA^{-}$ and $PClBA^{-}$ in KL mesophases, the lower degree of order leads to a larger number of observable transitions and the absolute signs of D_{ij} become available from the spectral analysis. The dipole–dipole coupling $D_{14} = D_{23}$ ($D_{AA'} = D_{BB'}$) for all cases. The numbering of positions and labelling of axes are presented in Fig. 1.

The computed dipole–dipole couplings were converted into the defining ratios of distances for a rectangular arrangement of four protons (15) by using the three equations below and seeking the roots which are physically reasonable:

$$[1]\quad \left(\frac{r_{14}}{r_{23}}\right) = \left(\frac{D_{23}}{D_{14}}\right)^{1/3}$$

$$[2]\quad D_{12}\left(\frac{r_{12}}{r_{23}}\right)^{5} - D_{13}\left[\left(\frac{D_{23}}{D_{14}}\right)^{1/3} + \left(\frac{r_{12}}{r_{23}}\right)^{2}\right]^{5/2} = -D_{23}\left(\frac{D_{23}}{D_{14}}\right)^{1/3}$$

$$[3]\quad \left(\frac{r_{13}}{r_{23}}\right)^{2} = \left(\frac{D_{23}}{D_{14}}\right)^{1/3} + \left(\frac{r_{12}}{r_{23}}\right)^{2}$$

The two independent Saupe (16, 17) matrix elements of order were converted from the dipole–dipole couplings using the expressions:

$$[4]\quad S_{11} = -\frac{4\pi^2}{h\gamma_H{}^2} D_{23} r_{23}^3$$

$$[5]\quad S_{22} = -\left(\frac{4\pi^2}{h\gamma_H{}^2}\right) r_{12}^3 \left\{D_{12} - \left(\frac{D_{23}}{4}\right)\left(\frac{r_{12}}{r_{23}}\right)^{-5} \times \left[\left(\frac{D_{23}}{D_{14}}\right)^{1/3} - 1\right]^2\right\} \times \left\{1 - \frac{1}{4}\left(\frac{r_{12}}{r_{23}}\right)^{-2}\left[\left(\frac{D_{23}}{D_{14}}\right)^{1/3} - 1\right]^2\right\}^{-1}$$

Can. J. Chem. Downloaded from www.nrcresearchpress.com by 210.87.254.105 on 09/06/12
For personal use only.

TABLE 3. Ratios of internuclear distances desired for solutes in the present study

Solute	Mesophase	r_{12}/r_{14}		r_{13}/r_{14}	
PFBA	DAC	0.585 ±0.001	(1.32)§	1.1585±0.005	(0.33)
PFBA*	SDS†	0.587	(1.66)	1.1595	(0.42)
PFBA*	T‡	0.582	(0.80)	1.1572	(0.22)
$PFBA^-$	KL	0.563 ±0.004	(−2.49)	1.148 ±0.002	(−0.58)
PClBA	DAC	0.5824±0.0005	(0.87)	1.1572±0.0003	(0.22)
$PClBA^-$	KL	0.579 ±0.001	(0.28)	1.1555±0.0005	(0.07)
PBrBA	DAC	0.5817±0.0002	(0.74)	1.1569±0.0001	(0.19)
$PBrBA^-$	KL	0.590 ±0.001	(2.18)	1.1611±0.0005	(0.55)
PIBA	DAC	0.5795±0.0002	(0.36)	1.1558±0.0001	(0.1)
$PIBA^-$	KL	0.588 ±0.002	(1.84)	1.160 ±0.001	(0.47)
PCNBA	DAC	0.5867±0.0008	(1.61)	1.1584±0.0004	(0.41)
PNH_3^+BA	DAC	0.589 ±0.002	(2.01)	1.161 ±0.001	(0.55)
POHBA	DAC	0.595 ±0.004	(3.05)	1.164 ±0.002	(0.81)
PFϕOH	DAC	0.582 ±0.001	(0.80)	1.157 ±0.0005	(0.2)
PClϕOH	DAC	0.5795±0.0005	(0.36)	1.1558±0.0003	(0.1)
$PCl\phi O^-$	KL	0.5787±0.0003	(0.23)	1.1554±0.0002	(0.06)
PBrϕOH	DAC	0.587 ±0.001	(1.66)	1.1596±0.0005	(0.42)
$PBr\phi O^-$	KL	0.5784±0.0002	(0.17)	1.1552±0.0001	(0.04)
PNO_2BA¶	DAC	0.5895	(2.1)	1.1608	(0.53)

*Data of Den Otter and McLean (24).
†Mesophase of sodium decyl sulphate.
‡Thermotropic mesophase.
§Numbers in parentheses denote percentage error from the ideal regular hexagonal ring.
¶Data from ref. 22.
Some related compounds were studied as solutes by R. C. Long and J. M. Goldstein (25).

TABLE 4. The matrix elements of the Saupe order matrix for *para*-substituted solutes employed in this study*

Solutes	10^2S_{11}	10^2S_{22}	10^2S_{33}
PFBA†	±2.23	±10.4	±8.2
PClBA	±3.49	±12.8	±9.3
PBrBA	±3.32	±12.0	±8.7
PIBA	±3.98	±12.9	±9.0
PCNBA	±0.71	±7.03	±6.3
POHBA	−0.42	+4.64	−4.2
PNH_3^+BA	±3.3	±4.15	±7.5
PFϕOH	−1.29	−7.42	+8.7
PClϕOH	±0.20	±9.60	±9.4
PBrϕOH	±0.01	±8.30	±8.3
$PFBA^-$‡	−1.75	+4.50	−2.8
$PClBa^-$	−2.39	+6.45	−4.1
$PBrBA^-$	±2.16	±6.21	±4.1
$PIBA^-$	±2.33	±6.69	±4.4
$PCl\phi O^-$	±2.54	±6.35	±3.8
$PBr\phi O^-$	±4.61	±11.4	±6.8

*Random errors may be taken to be a maximum of ±0.6% and a minimum of ±0.05% in the table. Systematic errors in the internuclear distance chosen to derive the order parameters from dipole–dipole couplings are uncertain and larger, but they do not affect the arguments used in this paper.
†Molecular species and positive ions are present in mesophases of DAC.
‡Negative ions are present as solutes in KL mesophases.

TABLE 5. The quadrupole splittings determined in mesophases contaminated with solutes

	Quadrupole splittings (Hz)		
Solute	$\lvert\nu_{C_1D}\rvert$	$\lvert\nu_{C_9D}\rvert$	$\lvert\nu_{C_{10}D}\rvert$
PFBA*	12972	7044	1620
PClBA	13132	7084	1649
PBrBA	11940	6500	1469
PIBA	11568	6120	1422
PCNBA	12036	6168	1428
PNH_3^+BA	13740	7008	1608
POHBA	13404	6775	1558
PFϕOH	15936	7956	1764
PClϕOH	15744	7937	1747
PBrϕOH	12756	6528	1498
$PNH_3^+\phi ONa$	10944	5513	1270
$PNO_2\phi ONa$	16505	8261	1902
PCaPyr	13032	6586	1518
Solute	$\lvert\nu_{C_2D}\rvert$	$\lvert\nu_{C_{11}D}\rvert$	$\lvert\nu_{C_{12}D}\rvert$
$PFBA^-$†	17686	8894	2975
$PClBA^-$	14003	7101	2354
$PBrBA^-$	12691	6424	2160
$PIBA^-$	13232	6601	2196
$PCNBA^-$	16045	8351	2791
PNH_2BA^-	12285	6319	2153
$POHBA^-$	16124	8473	2830
$PCl\phi O^-$	11842	6219	2124
$PBr\phi O^-$	17991	9470	3246

*Molecular species and positive ions in mesophases of DAC.
†Negative ion solutes in KL mesophases. Random errors of measurement have a maximum of 1% and a minimum of 0.3% in the values cited.

The value of r_{12} was assumed to be 2.47 ± 0.01 Å. The third diagonal element of the order matrix was obtained by using the property that the trace is zero (17).

The results of these computations are listed in Tables 3 and 4. Table 3 lists the *ortho/meta* ratios and the *para/meta* ratios for the solutes studied in this investigation. The regular hexagon has an *ortho/meta* ratio of 0.5774 and a *para/meta* ratio 1.1547. The errors of corresponding experimental ratios for the solutes are expressed in columns 4 and 6 of Table 3. These errors arise from lack of vibrational corrections, which were not deemed important in a study which emphasizes the role of the nematic matrix. Many of the deviations are less than 1% while one result has a difference of 3.05%.

Can. J. Chem. Downloaded from www.nrcresearchpress.com by 210.87.254.105 on 09/06/12
For personal use only.

Table 4 is a composite of all values of S_{11}, S_{22}, and S_{33} obtained both in the present study and some previous similar determinations. In cases where only one sign is attributed the value is absolute, while all other cases have two relative sign assignments, leaving a choice to be made based on arguments to be presented in the discussion. A study of similar compounds without reference to the mesophase structure has recently appeared (18).

(c) *Deuterium magnetic resonance spectra*

The deuterium spectra contain the quadrupole splittings from which are derived the degree of order of C—D or O—D axes for deuteriated segments of the hydrocarbon chain and the water. The asymmetry parameter η is negligible, consequently the degrees of order can be derived from experiments using:

$$[6] \quad \Delta\nu_Q = 3/2\,\nu_Q S_{ZZ}\tfrac{1}{2}(3\cos^2\Omega - 1)$$

$\Delta\nu_Q$ is the measured quadrupole splitting in Hz, ν_Q is the quadrupole coupling for C—D bonds in hydrocarbon chains assigned as 170 ± 8.5 kHz (19). S_{ZZ} is the degree of order along the C—D bond and Ω is the angle ($\pi/2$) between the magnetic field and the director. The value of S_{ZZ} is determined from eq. [6] above, along the axis of the pseudo-extended hydrocarbon chain, which oscillates about the director of the mesophase.

The quadrupole splittings evaluated are listed in Table 5 for phases prepared from DAC and KL. The sign of the derived degrees of order along the extended chain axis is positive because the location of the chain axis with respect to the mesophase director is known from the structure of the Type II DM system and the action of the director under the dual influence of sample spinning about an axis perpendicular to the static magnetic field (9).

(d) *The dilution of uncontaminated mesophases with water*

In order to preserve mesophase stability the water content of Type II DM DAC mesophases remains unaltered with the addition of solutes, while the KL mesophases are affected considerably in their range of water content by the solute additions. Water content variations have been studied extensively in previous publications (11, 12) and for the present case it is sufficient to report that degrees of order of both water and —CD_2— segments decrease as water is added, but preserve their ratios of order in the chain segments to a high degree of experimental precision. The ratios measured for all water contents give 1.569 ± 0.0221 for S_1/S_8, i.e. first divided by eighth segment, 1.960 ± 0.013 for S_1/S_9, and 8.49 ± 0.199 for S_1/S_{10} for the DAC mesophases. The ratios of order for the uncontaminated laurate mesophases are S_2/S_{3-8} = 1.1833 ± 0.0036, S_2/S_{10} = 1.4640 ± 0.0137, S_2/S_{11} = 1.9154 ± 0.0162, and S_2/S_{12} = 5.7166 ± 0.082, independent of water content. The quadrupole splittings ν_{DOH} for water (DOH) are linear with those of the α-CD_2 group ν_{C_1D} of DAC and KL. A least-squares fit to the straight line has been obtained in the form:

$$[7] \quad \nu_{C_1D} = m\nu_{DOH} + \text{const.}$$

For DAC mesophases, m = 69.85 and const. = 116.00 Hz with a correlation 0.9986 while for KL mesophases, m = 36.783 and const. = 3097.12 Hz with a correlation 0.9929. The statistical errors are small compared to the systematic uncertainty in ν_Q. In direct comparisons of degrees of order from the same parameter, only the statistical error is of significance.

Discussion

(a) *General chemical considerations*

The effect of changes in water content on a pure host mesophase has previously been well characterized (9, 12). The decrease in absolute degrees of order of water and hydrocarbon chain segments is associated with the increased motional freedom of the micelles as a unit. The increase in motional freedom is to a large extent associated with the decrease in size of micelles as water is added. An estimate of the size range of disc micelles has recently been made (20). The basis of the discussion here depends on the preservation of ratios of degrees of order along C—D bonds in different segments of the host amphiphile in uncontaminated mesophases as water content changes. We can write this simply as (9):

$$[8] \quad (S_o)_n = (S_{t/g})_n \cdot S_c$$

and

$$[9] \quad \frac{(S_o)_n}{(S_o)_m} = \frac{(S_{t/g})_n}{(S_{t/g})_m} = \text{constant} = K$$

where S_o denotes observed degree of order of the C—D bond, subscripts m and n denote arbitrary segments of the amphiphile chains, $S_{t/g}$ denotes the contribution to the observed degree of order from intramolecular *trans/gauche* equilibria, and S_c represents the contribution derived from overall motion of the pseudo-rigid almost-extended hydrocarbon chain. Equation [8] is interpreted in terms of an internal structure of the micelle, which is independent of the water content (9). The object of the present study is to determine the locale of the small quantity of solute in terms of changes in the order parameters provoked by the additions. The variations in water content necessary to preserve the integrity of the Type II DM mesophase are not important, because in uncontaminated mesophases the ratios of segment order are preserved. It is the purpose of this discussion to bring more evidence to bear with respect to relative alignment of detergent chain axis and solute axes.

The quadrupole splittings of the first —CD_2— segment in Type II DM pure mesophases of DAC are plotted against the splittings of the ninth —CD_2— segment, adjacent to the terminal —CD_3 groups. This graph is used as the standard system uncontaminated by solutes. The slope of this line has been included in the results section and deviations are less than ±0.6% (standard deviation) for individual measurements. The measurements made on contaminated systems will be compared with the standard Type II DM mesophases. The graph reproduced as Fig. 2A corresponds to the DAC system, while Fig. 2C is a replicated treatment of the data for KL mesophases. In the latter case $\nu_{C_{11}D}$ is plotted against ν_{C_2D}, where carbon 2 is the first —CD_2— segment.

In order to leave no doubt as to the relative alignment of the disc–bilayer micelles, Fig. 3 has been designed to clarify this situation with respect to the axis of the nmr tube, axis of spinning, magnetic field direction, and the normal to the disk-like micelle (9).

(b) *Relationship between the deuterium quadrupole splittings of chain segment in mesophases containing solutes*

In Fig. 2A the experimental determinations of the quadrupole splittings ν_{C_1D} and ν_{C_9D} in mesophases containing solutes for DAC phases are plotted. The water content of these phases does vary, but of course they should follow the behaviour of the uncontaminated mesophase, if there is little insertion of impurity into the micelle. The points are identified according to

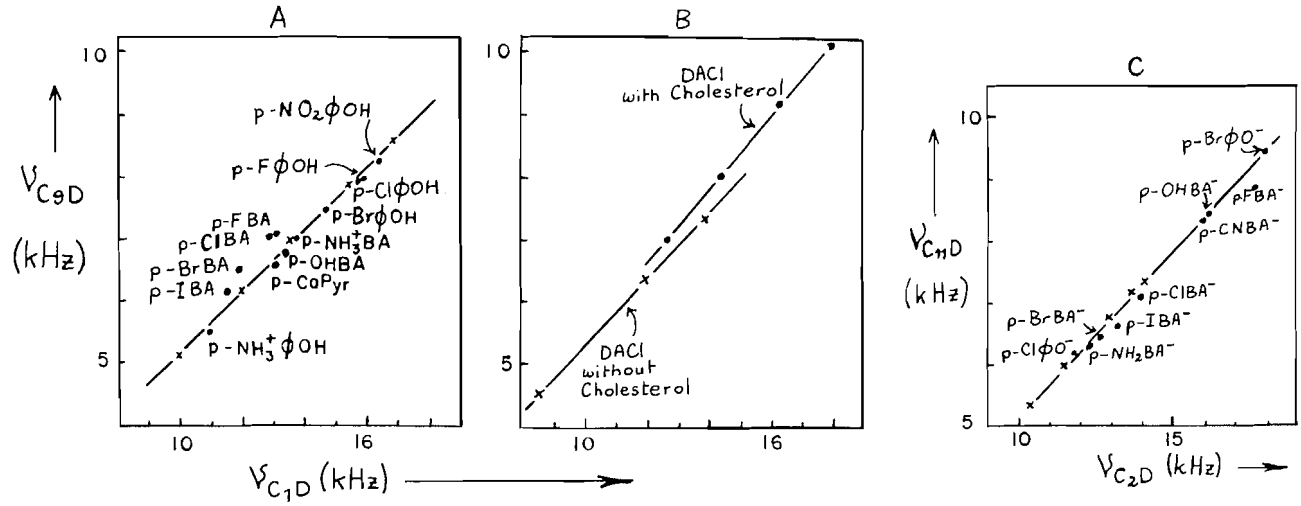

FIG. 2. A. Quadrupole splittings of the ninth segment plotted against the first segment —CD_2— for both contaminated and uncontaminated —DAC mesophases. The line corresponds to those phases which do not contain solutes or contain only solutes which do not change the ratio (ν_{C_1D}/ν_{C_9D}). Points derived from contaminated phases are identified by the name of the solute. The four points above the solid line are the four *p*-halo-substituted benzenes. Points set as crosses × are for uncontaminated mesophases. Solute points are identified by shortened names. B. Graph as in A for DAC mesophases with and without added cholesterol. Data taken from ref. 18. C. Graphs as in A for KL mesophases. Solid line corresponds to phases without solute. The mesophases which contain solutes are identified by shortened formulas given in the text.

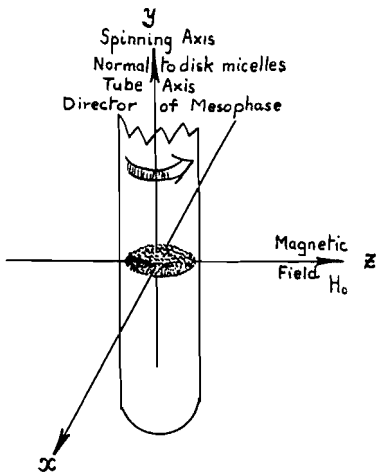

FIG. 3. The schematic arrangement of the alignments of magnetic field, disc micelle, and bilayer and the axis of the nmr tube. One micelle is diagrammatically represented at its mean position with the normal along the director of the mesophase. Relative sizes of objects are of course greatly distorted. If we take the magnetic field as a *z* axis, the director and glass tube axis as a *y* axis, then the micelle surface lies in the *xz* plane.

the impurity present and the concentrations can be obtained from the experimental section. The majority of solutes do not influence appreciably the ratio (ν_{C_1D}/ν_{C_9D}) and they give ratios which fall on or very close to the line for the mesophase without solutes. Taking the solutes, which do not perturb the ratio (ν_{C_1D}/ν_{C_9D}), i.e. PCNBA, POHBA, PNH_3BA^+, PFφOH, PClφOH, PBrφOH, $PNH_3\phi OH^+$, PCaPyr, and $PNO_2\phi O^-$, the value obtained from the experimental measurements is 1.977 ± 0.017, the deviation being given as the standard one over 9 points. This compares within the statistical error with 1.960 ± 0.013 for the same ratio over six data points for the uncontaminated mesophases reported in the experimental section. The conclusion on this evidence is clear, none of these solutes perturb (by eq. [8]) the *trans/gauche* equilibria of the host amphiphile in the micelle. This argument strongly suggests the absence of these solutes inside the micelle.

Four of the solutes do affect the ratio (ν_{C_1D}/ν_{C_9D}) appreciably and these are the chemically related *para*-halogen substituted benzoic acids. They appear in Fig. 2A above the line associated with uncontaminated phases. Although the concentrations of these perturbing solutes in the mesophase do differ, the systematic trend of their effect in increasing the ratio (ν_{D_1D}/ν_{C_9D}) qualifies their behaviour as indicating an inclusion among the solvent amphiphile chains in the micelle. The ratio of order in the first and ninth segments for the four perturbing solutes gives 1.842 for PFBA, 1.854 for PClBA, 1.836 for PBrBA, and 1.890 for PIBA. These values are substantially less than the value for standard uncontaminated phases of 1.960 ± 0.013. We conclude therefore that these solutes insert into the micelle deeper than the first —CD_2— segment but not as deep as the ninth —CD_2—. There is, of course, an equilibrium between aqueous solute and those solute molecules inserted into the micelle bilayer. The arguments above for molecular solutes in a cationic bilayer suggest that the coefficient of distribution is large compared to 1 for the solutes which perturb the host bilayer.

Since the micelle motion and other factors which influence S_c do not affect the ratios of order we can proceed to interpret changes in ratios as resulting from perturbed packing of amphiphile chains in the micelle. The ratios (ν_{C_1D}/ν_{C_9D}) are larger in uncontaminated mesophases and this indicates a larger difference in motional freedom between the head group segment and the last one (22). The interpretation of degrees of order in terms of motional freedom is complicated by constraint angle effects (23). In the present case, however, there is no ambiguity about the mean position of the pseudo-extended chains.

Having discussed the present case of solutes in DAC mesophases, it is possible to reconstruct the same argument from our previously published data (11). Cholesterol is soluble up to 9 mol% in the DAC bilayer and its location is in little doubt. In Fig. 2B the corresponding ratios of quadrupolar splittings for (ν_{C_1D}/ν_{C_9D}) are plotted as in 2A for this system. The ratio (ν_{C_1D}/ν_{C_9D}) is decreased on adding the hydrophobic solute, indicating the stiffening of solvent chains in a manner associ-

Can. J. Chem. Downloaded from www.nrcresearchpress.com by 210.87.254.105 on 09/06/12
For personal use only.

Can. J. Chem. Downloaded from www.nrcresearchpress.com by 210.87.254.105 on 09/06/12
For personal use only.

ated with biological membranes. The results from an earlier paper (11) were obtained by keeping the cholesterol content of the bilayer constant at 9.2 mol% but varying the water content (Fig. 3, ref. 18).

The results for KL mesophases are very similar (Fig. 2C). They show that no solute decreases the ratio ($\nu_{C_2D}/\nu_{C_{11}D}$) below the value 1.9154 ± 0.0162 quoted in the results section for the uncontaminated mesophase. We conclude therefore that the solutes are mostly located in the aqueous component or at the micelle interface of the liquid crystal. The values observed for the ratio ($\nu_{C_2D}/\nu_{C_{11}D}$) with solute are the following: $PFBA^-$ 1.989, $PClB^-$ 1.972, $PBrBA^-$ 1.976, PCNBA 1.922, PNH_2BA^- 1.944, $POHBA^-$ 1.903, $PCl\phi O^-$ 1.904, and $PBr\phi O^-$ 1.900. Four of these ratios are within the standard deviation for the uncontaminated mesophase, i.e. 1.915 ± 0.016, while the remaining five have somewhat higher values of the ratio. The solubility of the ionic solutes in water is of course higher than the conjugate acids and this has previously been shown to affect the deuterium quadrupole splitting of α-substituted carboxylates (21). Some small perturbation of the interface region is indicated in these cases.

(c) *Relationships between order parameters of solutes and those of detergent segments*

It is useful to consider the ratio of the matrix elements S_{11}, S_{22}, and S_{33}, defined by Saupe, for the solutes and compare them to the degree of order of the first —CD_2— segment of the detergent chains, taken along the axis of the pseudo-extended chain. This is the direction along which the included solutes will be most restricted in their motion because of the encasing bilayer. The geometry of the situation has been clarified in Fig. 3. The oscillatory motion of the pseudo-extended chain derives from both the motion of the micelle as a body and of the chain itself about the normal to the micelle interface (9). In Table 6 the ratios discussed in this section are listed. The uncertainty in the degree of order derived from the quadrupole splitting carries the uncertainty in ν_Q of eq. [6] of about ±5% but this is a systematic error which occurs in all ratios. The random error in the ratios cited may be taken to be a maximum of ±2%, these arising from the spectra AA′BB′, other errors being negligible in comparison. The direction of the axis S_{22} in the solute is the same as that of the S_{C_1D}, namely along a direction normal to the micelle disc interface if the solute is inserted into the bilayer with the *para* axis perpendicular to the plane of the disc. The magnitude of the solute degree of order along this 22 axis is always larger than the perpendicular axes, 11 and 33. The largest magnitudes of S_{22} occur for the series PFBA, PClBA, PBrBA, and PIBA in mesophases prepared from decylammonium chloride. This is consistent with the argument mounted in the last section. The ratios S_{22}/S_{C_1D} and S_{22}/S_{C_2D} in Table 6 are smaller than 1 for all other solutes, indicating greater freedom of movement for those solutes which, by previous argument, are located mainly in the aqueous layers.

The sign of the dipole–dipole coupling constant is the reverse of the sign of the degree of order, e.g. see eq. [4]. Since different relative sign combinations are possible for the different solutes used here, it is constructive to consider the implied orientations of the solutes in terms of the structure of the mesophase.

Taking into account the plane of the aromatic ring of the solute and the plane represented by the interface of the micelle, three limiting arrangements are possible. (a) The aromatic ring may lie flat on the interface, in which case the normal to the aromatic ring oscillates about the director of the mesophase. (b) The ring may be disposed with the *para* axis of substituents perpendicular to the interface, i.e. the *para* axis oscillates angularly about the mesophase director. (c) The plane of the ring may be in a plane perpendicular to the interface, with an axis perpendicular to the *para* axis oscillating about the director.

TABLE 6. Modulus of ratios of Saupe matrix elements of order for solutes to the degrees of order measured in segments of the hydrocarbon chains

Solutes	$\lvert S_{11}/S_{C_1D}\rvert$	$\lvert S_{22}/S_{C_1D}\rvert$	$\lvert S_{33}/S_{C_1D}\rvert$
PFBA*	0.219	1.022	0.806
PClBA	0.339	1.243	0.903
PBrBa	0.355	1.281	0.929
PIBA	0.439	1.422	0.992
PCNBA	0.075	0.745	0.667
POHBA	0.314	0.395	0.713
PNH_3^+BA	0.039	0.431	0.390
$PF\phi OH$	0.010	0.594	0.696
$PCl\phi OH$	0.016	0.777	0.761
$PBr\phi OH$	0.001	0.830	0.830
$PFBA^-$†	0.126	0.324	0.202
$PClBA^-$	0.218	0.587	0.373
$PBrBA^-$	0.217	0.624	0.412
$PIBA^-$	0.225	0.645	0.424
$PCl\phi O^-$	0.274	0.684	0.409
$PBr\phi O^-$	0.327	0.808	0.482

*Molecular and positive ion solutes in mesophases of DAC.

†Negative ion solutes in the KL mesophase. Errors in this ratio from random sources are ±1.0% at worst and ±0.4% at best.

The argument will be carried using the signs of the Saupe matrix elements S_{11}, S_{22}, and S_{33} since these are automatically derived from the relative signs of D_{ij}, the dipole–dipole couplings obtained by analysis of the spectra of solutes. An orientation of the benzene ring of solutes perpendicular to the mesophase director yields the following relative signs $S_{11} < 0$, $S_{22} < 0$, $S_{33} > 0$. If the aromatic ring is aligned with the *para*-substituted axis along the director, the relative signs become $S_{11} > 0$, $S_{22} < 0$, $S_{33} < 0$ while an orientation of the director in the plane of the aromatic ring along the direction perpendicular to the *para* axis leads to the sign combination $S_{11} > 0$, $S_{22} < 0$, $S_{33} < 0$.

It is important of course to understand that the degrees of order S_{11}, S_{22}, and S_{33} may be modulated by chemical exchange processes between the three fixed sites indicated and in principle others, including residence in the aqueous layer away from the interface. The residence time in the aqueous bath away from the influence of the interface does not impose orientational order on the solutes; indeed, for ions such as Cl^- or the D_2O, it has been shown that order is transferred at an adsorbed interface layer (11). The effect of residence time in the aqueous bath is to reduce the absolute degrees of order measured for the solute (9). In the sense that the degrees of order measured along the *para* axis for PFBA, PClBA, PBrBA, and PIBA exceed those of the detergent segment next to the ionic head group for DACl mesophases, we can expect negligible residence time for these species in the aqueous bath, a conclusion we have already drawn from other evidence cited earlier.

It is now interesting to suppose that the orientation of the aligned inserted species occurs in the manner with the director along the *para* axis, i.e. perpendicular to the interface of the micelle (see also Figs. 3 and 4). In this case the signs of order

Can. J. Chem. Downloaded from www.nrcresearchpress.com by 210.87.254.105 on 09/06/12
For personal use only.

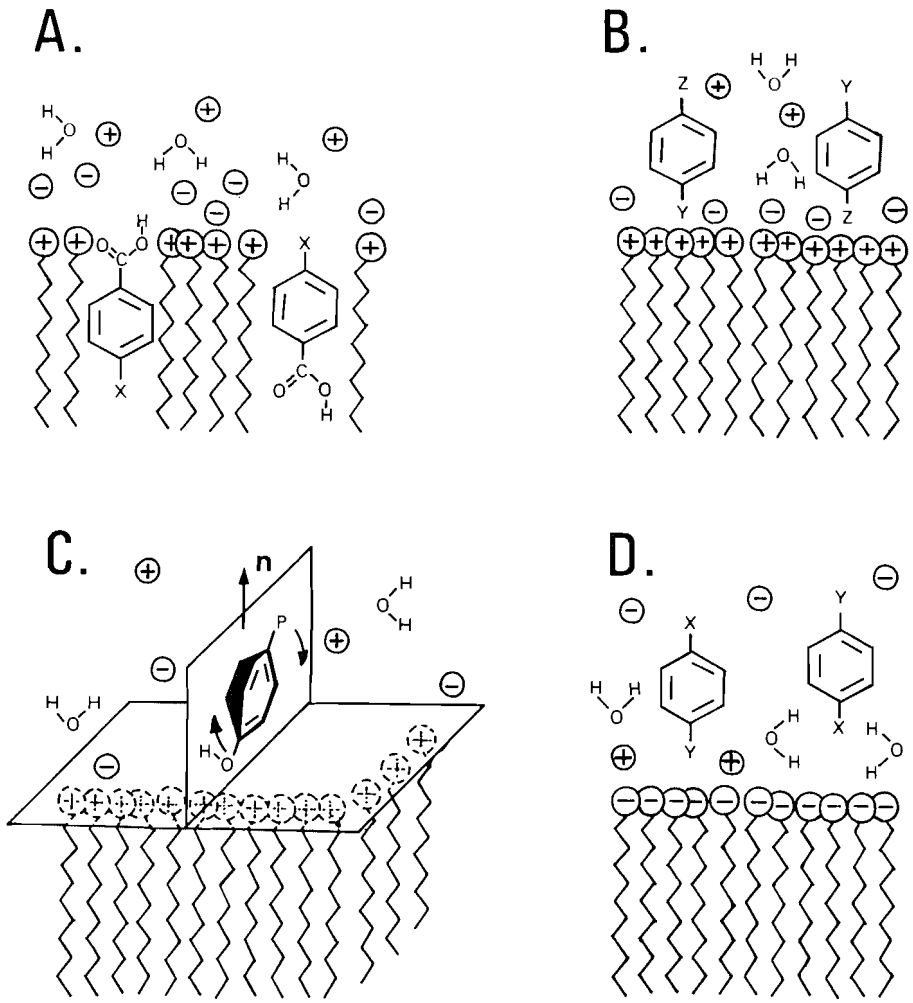

FIG. 4. A. Orientations of *para*-halobenzoic acids in the interface of the micelle following the evidence of sign attributions of S_{ii}'s and the evidence of insertion in the bilayer. The location of the carboxyl group in the interface is based on the polar chemical nature of this group. B. The two possible alignments of the compounds indicated with the alternate possibility of either *para* substituent in the interface. Some equilibrium with inserted situations in the bilayer is possible, though evidence points to attachment predominantly from the aqueous side. C. The alignment of parahydroxybenzoic acid and parafluorophenol in lyomesophases of DAC. The plane of the benzene ring is perpendicular to the interface plane of the micelle and the ring has freedom to rotate in this plane, probably with attachment to the interface by the *para*-substituted groups with water bridges. D. The alignment of *para*-substituted phenoxides and benzoates in mesophases of KL. In principle both *para* groups may attach to the ionic interface, perhaps with hydrogen bonded water bridges.

TABLE 7. Absolute signs of Saupe matrix elements determined using the mesophase structure and the relative signs available from the proton resonance spectra

Solute	S_{11}	S_{22}	S_{33}
PFBA	−	+	−
PClBA	−	+	−
PBrBA	−	+	−
PIBA	−	+	−
PCNBA	−	+	−
PNH_3^+BA	−	+	−
POHBA	−	−	+
PFϕOH	−	−	+
PClϕOH	−	+	−
$PFBA^-$	−	+	−
$PClBA^-$	−	+	−
$PBrBA^-$	−	+	−
$PIBA^-$	−	+	−
$PCl\phi O^-$	−	+	−
$PBr\phi O^-$	−	+	−

parameters are $S_{11} < 0$, $S_{22} > 0$, and $S_{33} < 0$. This is one of the two relative sign combinations derived from the experimental results, the other possibility being $S_{11} > 0$, $S_{22} < 0$, and $S_{33} > 0$, which we now discard. This is summarized in Table 7. The sign combination in itself leaves us still with the choice of alignments as in Figs. 4A or B, but obviously the prior evidence points to A being the correct assignment with the carboxyl group acting as a polar group in the interface and the *para*-halogen substituents inserted into, and perturbing the packing of, amphiphiles in the bilayer.

The values in Tables 4 and 6 for PCNBA, PNH_3BA^+, and PClϕOH also show that the value of S_{22} is somewhat larger than S_{11} and S_{33} in magnitude but the solute is considerably less ordered than the α detergent segment along this same direction. On the other hand, there is little perturbation (not detectable) of the order ratio in the detergent segments (ν_{C_1D}/ν_{C_9D}). The relative sign combination from the experiments indicates again the choice $S_{11} < 0$, $S_{22} > 0$, $S_{33} > 0$ rather than the inverse, which has no physical reality. We propose for these three solutes, therefore, an equilibrium between orientations 4A and 4B with

the polar groups —COOH, NH_3^+ or COOH and —OH in the interface. The equilibrium evidently favours attachment to the interface from the aqueous side with little insertion into the bilayer.

The situation with PBrϕOH is uncertain because the magnitude of S_{11} is very small and any sign attribution is within experimental error. Some inclined average orientation is indicated with more than one site in a chemical exchange, S_{22} and S_{33} having opposite signs.

The sign combination $S_{33} > 0$, $S_{22} < 0$ and $S_{11} < 0$ fits the cases of POHBA and PFϕOH (Table 5). The orientation corresponds to Fig. 4C with the plane of the aromatic ring perpendicular to the plane of the micelle interface. Presumably the polar *para* groups partake in hydrogen bonding, probably with water bridges to the interface head groups. It is interesting to recall that the phenolic —OH has stable configurations in the plane of the ring, as does the carboxyl group. Rotation of the plane of the aromatic ring about its perpendicular axis, in the perpendicular plane to the interface, is rather uninhibited as shown by the low values of S_{11} for both compounds. The rotation of the ring is indicated by arrows in Fig. 4C.

The solutes in KL mesophases all present the same relative signs for degrees of order so we can propose the only acceptable combination of absolute signs as $S_{11} < 0$, $S_{22} > 0$, and $S_{33} < 0$ (q.v.). Since we have previously argued that there is no detectable perturbation of the host bilayer packing, then a preponderance of the alignment of the *para* axis perpendicular to the interface, but from the aqueous side, is indicated. This corresponds to the situation in Fig. 5D, with the point of attachment to the interface being either *para* group, in principle.

Acknowledgements

We thank the Fundacao de Ampara a Pesquisa de Estado de Sao Paulo (FAPESP) for Equipment Grants and Scholarships, Conselho Nacional de Pesquisas (CNPq) for Scholarships, Banco Nacional de Desenvolvemento Economico for a large equipment grant, and the National Research Council of Canada for exchange scholarships (L.W.R.) and permission to bring compounds to Brazil which were provided from an operating grant to L.W.R. in Canada.

1. C. L. KHETRAPAL, A. KUNWAR, A. TRACEY, and P. DIEHL. *In* Lyotropic liquid crystals, NMR basic principles and progress. Vol. 9. *Edited by* P. Diehl, E. Fluck, and R. Kosfeld. Springer Verlag, West Berlin. 1975.
2. C. L. KHETRAPAL, A. C. KUNWAR, and A. V. PATANKAR. J. Magn. Reson. **15**, 219 (1974).
3. R. C. LONG and J. H. GOLDSTEIN. Mol. Cryst. Liq. Cryst. **23**, 137 (1973).
4. G. T. DEN OTTER, J. GERRITSEN, and C. MACLEAN. J. Mol. Struct. **16**, 379 (1973).
5. L. W. REEVES, J. SANCHEZ DE CARA, M. SUZUKI, and A. S. TRACEY. Mol. Phys. **25**, 1481 (1973).
6. L. W. REEVES, A. S. TRACEY, and M. M. TRACEY. J. Am. Chem. Soc. **95**, 3799 (1973).
7. A. SAUPE and G. ENGLERT. Phys. Rev. Lett. **11**, 462 (1963).
8. J. W. EMSLEY. *In* NMR spectroscopy using liquid crystal solvents. Pergamon Press, New York. 1975.
9. B. J. FORREST and L. W. REEVES. Chem. Rev. **1**, 1 (1981).
10. J. A. FERRITTI, R. K. HARRIS, and R. D. JOHANNESEN. J. Magn. Reson. **3**, 84 (1970).
11. F. Y. FUJIWARA and L. W. REEVES. J. Am. Chem. Soc. **98**, 6790 (1976).
12. F. Y. FUJIWARA, L. W. REEVES, M. SUZUKI, and J. A. VANIN. *In* Solution chemistry of surfactants. Vol. 1. *Edited by* K. L. Mittal. Plenum, Press, New York and London. 1979. p. 63.
13. L. W. REEVES and A. S. TRACEY. J. Am. Chem. Soc. **97**, 5729 (1975).
14. R. H. COX. Spectrochim. Acta Part A, **25**, 1189 (1969).
15. Y. LEE and L. W. REEVES. Can. J. Chem. **54**, 500 (1976).
16. G. ENGLERT and A. SAUPE. Z. Naturforsch. **199**, 172 (1962).
17. A. SAUPE. Z. Naturforsch. **199**, 161 (1964).
18. R. C. LONG and J. H. GOLDSTEIN. J. Magn. Reson. **34**, 361 (1979).
19. L. J. BURNETT and B. H. MULLER. J. Chem. Phys. **55**, 5829 (1971).
20. B. J. FORREST and L. W. REEVES. J. Am. Chem. Soc. **103**, 1641 (1981).
21. D. M. CHEN, F. Y. FUJIWARA, and L. W. REEVES. Can. J. Chem. **55**, 2404 (1977).
22. M. F. MANCONDES-HELENE and L. W. REEVES. J. Phys. Chem. **85**, 718 (1981).
23. B. J. FORREST, L. HECKER, and L. W. REEVES. J. Am. Chem. Soc. **102**, 1178 (1981).
24. G. T. DEN OTTER and C. MCLEAN. J. Mol. Struct. **31**, 57 (1976).
25. R. C. LONG and J. M. GOLDSTEIN. J. Magn. Reson. **34**, 361 (1979).

Can. J. Chem. Downloaded from www.nrcresearchpress.com by 210.87.254.105 on 09/06/12
For personal use only.

Organic solvents-induced difference spectra of bovine serum albumin

S. F. SUN, T. S. CHANG, AND G. M. LAM
Department of Chemistry, St. John's University, Jamaica, NY 11439, U.S.A.

Received July 15, 1982

S. F. SUN, T. S. CHANG, and G. M. LAM. Can. J. Chem. **61**, 356 (1983).

Difference spectra of tyrosyl residues in bovine serum albumin produced by three organic solvents (ethanol, *n*-propanol, and dioxane) have been studied at three different pH values (pH 2.2, pH 5.4–5.8, and pH 11.6). The measurements were taken at 25°C and ionic strength 0.03 and in a concentration of organic solvent from 5% to 25% by volume. The spectra are compared to those of a model chromophore, *N*-acetyl-L-tyrosine ethyl ester. Both *n*-propanol and dioxane cause a change in the conformation of the protein, while ethanol does not. Near the isoelectric point the difference spectra produced by *n*-propanol (at high concentration) and dioxane appear to be the results of a superposition of denaturation blue shifts on solvent-induced red-shifts; those produced by ethanol are characteristic of perturbation of tyrosyl and tryptophyl residues. An empirical equation which correlates $\Delta\epsilon$ (the molar difference absorption coefficient) with n (refractive index) and D (dielectric constant) is proposed to interpret the results qualitatively.

S. F. SUN, T. S. CHANG et G. M. LAM. Can. J. Chem. **61**, 356 (1983).

On a étudié à trois pH différents (pH 2,2, pH 5,4–5,8 et pH 11,6) les différences spectrales des unités tyrosyles de l'albumine du sérum de bovin produites par trois solvants organiques différents (éthanol, *n*-propanol et dioxanne). On a effectué les mesures à 25°C, à une force ionique de 0,3 et pour des concentrations de solvant organique allant de 5% à 25% en volume. On a comparé les spectres à ceux d'un chromophore modèle, l'ester éthylique de la *N*-acétyl L-tyrosine. Le *n*-propanol et le dioxanne provoquent un changement de conformation de la protéine, tandis que l'éthanol n'a aucun effet. Au voisinage du point isoélectrique, les différences dans les spectres des produits obtenus soit avec le *n*-propanol (à forte concentration) ou le dioxanne ne semblent être le résultat que de la superposition de glissements vers le bleu dû à une dénaturation sur les glissements vers le rouge induits par le solvant. Ceux produits par l'éthanol sont caractéristiques d'une perturbation des unités tyrosyle et tryptophyle. Pour interpréter qualitativement ces résultats, on propose une équation empirique qui établit une corrélation entre $\Delta\epsilon$ (le coefficient d'absorption de différence molaire) et n (indice de réfractions) et D (constante diélectrique).
[Traduit par le journal]

Introduction

Information has been accumulated through the years concerning the difference spectra of tyrosyl residues in proteins in different environments. The time seems ripe for us to draw some definite conclusions on the three major factors that influence the position, shape, and intensity of spectral lines. These factors are: burial and exposure, folding and unfolding, and ionization.

In order to achieve this goal, bovine serum albumin was selected for study. The abundance of literature on this protein (1–4) made the interpretation of data relatively simple. Bovine serum albumin is a model protein, important not only as a standard for calibration whenever a new experimental method is introduced in protein chemistry but also as a sample for testing new ideas regarding the structural properties of a protein or enzyme. Its behavior also commands attention: It is a very stable protein, easy to handle, and there is little fear of degradation. Its change in conformation as a function of pH is well known (1, 3). The three well-defined regions are: acidic region (below pH 4.3) where the protein unfolds due to ionization of glutamic and aspartic acids, basic region (above pH 10.5) where the protein almost completely unfolds due to ionization of basic groups such as lysine and arginine, and the region between 4.3 and 10.5 where the protein is in the folded, native stable state. Unless drastically disturbed, the change in conformation is reversible.

Ethanol, *n*-propanol, and dioxane were used as three probes. Both ethanol and *n*-propanol are hydroxy reagents, normally used for perturbation of tyrosyl residues in proteins. However, there is a pronounced difference between the two compounds. Although they are in the same homologous series, *n*-propanol is the first member that has a free rotational alkyl group. For that reason *n*-propanol's behavior in many ways is different from that of ethanol (5). Dioxane is known for its effect on hydrogen-bonding interactions (6–8). The presence of dioxane often causes pK shifts of charged groups in proteins (9). Even though solvent effects on differential spectra of bovine serum albumin have been reported in literature (4), the present study describes in a more conclusive way the subtle effect of environment on the physical and chemical states of aromatic residues, particularly tyrosine, in the three well-defined pH regions.

Experimental

Materials

Armour crystalline bovine serum albumin, Lot Nos. J 72003 and J 72105, was deionized by passing the concentrated aqueous solution through a mixed ion-exchange bed resin followed by dialysis against water in a cold room overnight. The model compound, *N*-acetyl-L-tyrosine ethyl ester, was purchased from the Schwartz-Mann Research Laboratories and was used as received. All the organic solvents used were reagent grade and were purified by fractionation distillation before use. Glass-distilled water was used throughout the experiments.

Preparation of solutions

A typical neutral protein solution (at a pH near the isoelectric point 5.3–5.8) was prepared as follows. To a calibrated 25-mL volumetric flask the following were added in order: 12.5 mL of 0.06 *M* KCl, 5 mL of the protein stock solution, a calculated amount of organic solvent, and water to the mark. An acid or basic protein solution was prepared in the same way as for a neutral solution, except that an additional calculated amount of KOH (0.22 *M*) or HCl (0.5 *M*) was added. To minimize the discrepancy in concentration the same two or three burets and the same two or three pipets were used for the

0008-4042/83/020356-06$01.00/0
©1983 National Research Council of Canada/Conseil national de recherches du Canada

Can. J. Chem. Downloaded from www.nrcresearchpress.com by 210.87.254.6 on 09/06/12
For personal use only.

Can. J. Chem. Downloaded from www.nrcresearchpress.com by 210.87.254.6 on 09/06/12
For personal use only.

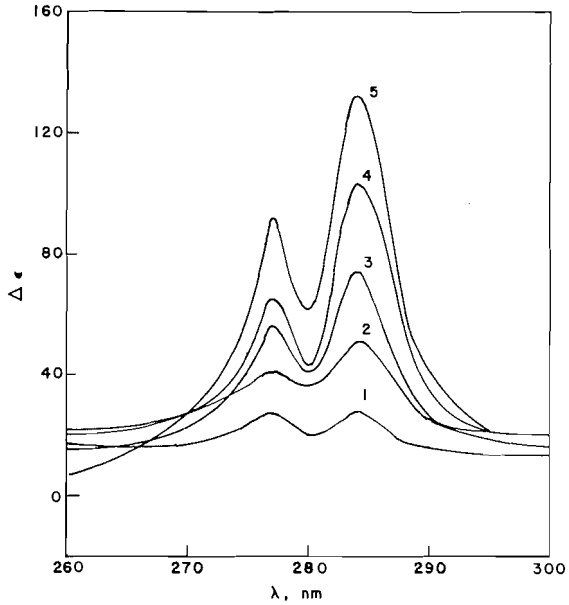

FIG. 1. Difference spectra of *N*-acetyl-L-tyrosine ethyl ester at pH 5.4, ionic strength 0.03 and 25°C produced by ethanol. Concentrations of ethanol (v/v): *1*, 5%; *2*, 10%, *3*, 15%; *4*, 20%; *5*, 25%.

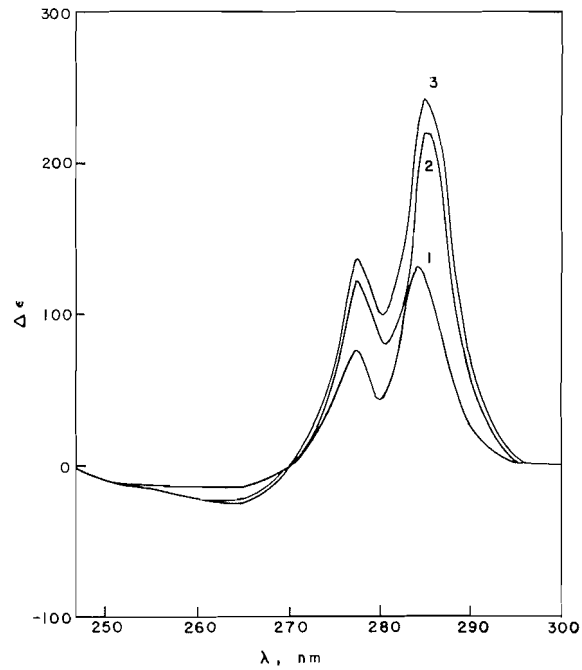

FIG. 2. Comparison of the difference spectra of *N*-acetyl-L-tyrosine ethyl ester produced by 25% organic solvent at pH 5.4–5.7, ionic strength 0.03 and 25°C. Curves: *1*, ethanol; *2*, *n*-propanol; *3*, dioxane.

preparation of all solutions. The reference solutions were prepared in the same way as the sample solutions except that no organic solvent was added. Since the ionization of acid or base in an aqueous solution is affected by the presence of an organic solvent, the amount of acid or base added to a reference solution was slightly different from that added to a sample solution. Similar methods were used for the preparation of solutions of the model compound.

Concentrations of the stock protein solution and of the model compound were determined spectrophotometrically, using $E^{1\%}_{1cm} = 6.67$ at 279 nm for albumin and 1340 for the molar extinction coefficient for tyrosyl ester at 274.5 nm. The molecular weight of bovine serum albumin used in calculations was 69 000. The protein concentrations used ranged from 2.5×10^{-5} to 3.2×10^{-5} *M*, while the concentrations of tyrosyl ester used ranged from 3.2×10^{-4} to 7.8×10^{-4} *M*.

Measurements

All the absorption measurements were done with a Cary model 14 recording spectrophotometer equipped with an expanded slide-wire in the range of 0–0.1 optical density units. A set of tandem double cells designed by Herskovits and Laskowski (10) with a 1.0 cm path length for each of the two components was used. The slit width was less than 0.2 mm for data obtained above 260 nm; it was more than 0.2 mm but not exceeding 1.0 cm for data obtained below 260 nm. We do not put much weight on the data below 260 nm. All difference spectra were obtained within 10 to 30 min after solutions were prepared. We did not find a time-dependent change in the spectrum, nor did we have any evidence for aggregation.

The pH of each solution was measured immediately after the absorption measurement with a Radiometer TTTIC equipped with a scale expander to check if the value was that planned. Usually the agreement was within 0.1 pH units. The pH values as read from the glass electrode pH meter were not corrected for the presence of organic solvent (6, 7, 9).

Results

(a) The model chromophore

Since serum albumin is rich in tyrosyl content (21 tyrosines and 2 tryptophans), only *N*-acetyl-L-tyrosine ethyl ester was used as a model. Difference spectra were obtained for the tyrosyl ester in organic solvent – water mixtures at ionic

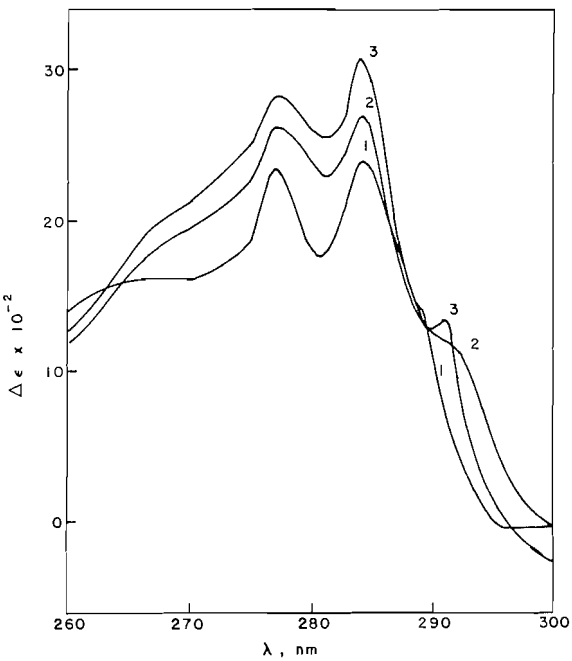

FIG. 3. Difference spectra of bovine serum albumin at pH 2.2, ionic strength 0.03 and 25°C produced by 25% organic solvent. Curves: *1*, dioxane; *2*, ethanol; *3*, *n*-propanol.

strength 0.03. The concentrations of organic solvents were selected: 5%, 10%, 15%, 20%, and 25% (v/v) respectively. Later the same concentrations were applied to serum albumin.

Figure 1 shows the representative difference spectra of tyrosyl ester produced by ethanol, curve *1* in 5% ethanol; curve *2*, 10% ethanol; curve *3*, 15% ethanol; curve *4*, 20% ethanol; and curve *5*, 25% ethanol. Each curve gives two peaks, one at 277–279 nm and the other at 284–286 nm, typical of tyrosine (11). As expected, the magnitudes of the two peaks are a linear

Can. J. Chem. Downloaded from www.nrcresearchpress.com by 210.87.254.6 on 09/06/12
For personal use only.

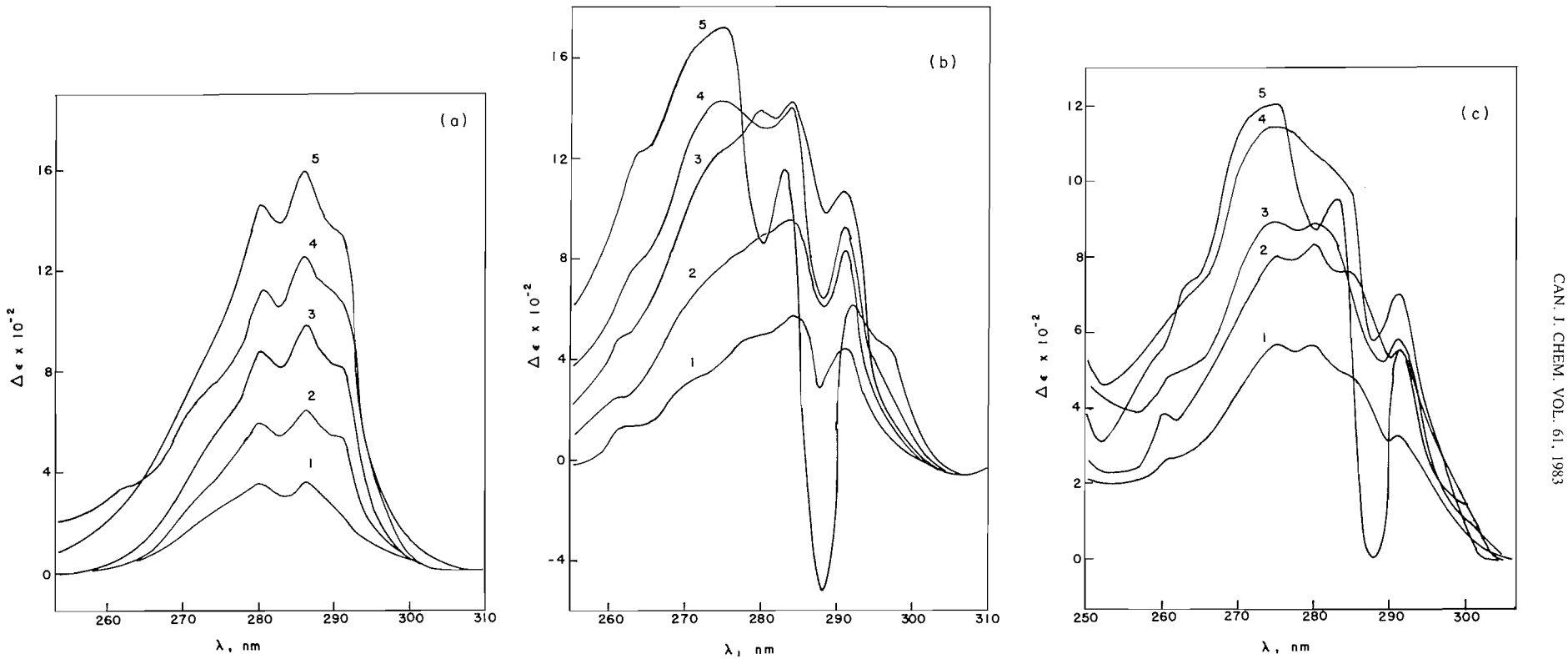

FIG. 4. (*a*) Difference spectra of bovine serum albumin at pH 5.2–5.4, ionic strength 0.03 and 25°C produced by ethanol. Concentrations of ethanol (v/v): *1*, 5%; *2*, 10%; *3*, 15%; *4*, 20%; *5*, 25%. (*b*) Difference spectra of bovine serum albumin at pH 5.2–5.4, ionic strength 0.03 and 25°C produced by *n*-propanol. Concentrations of *n*-propanol (v/v): *1*, 5%; *2*, 10%; *3*, 15%; *4*, 20%; *5*, 25%. (*c*) Difference spectra of bovine serum albumin at pH 5.2–5.4, ionic strength 0.03 and 25°C produced by dioxane. Concentrations of dioxane (v/v): *1*, 5%; *2*, 10%; *3*, 15%; *4*, 20%; *5*, 25%.

Can. J. Chem. Downloaded from www.nrcresearchpress.com by 210.87.254.6 on 09/06/12
For personal use only.

function of the concentration of ethanol. Similar difference spectra were obtained for tyrosyl ester produced by *n*-propanol and dioxane. For comparison, Fig. 2 gives the difference spectra of tyrosyl ester produced by 25% ethanol (curve *1*), 25% *n*-propanol (curve *2*), and 25% dioxane (curve *3*), at pH 5.4–5.7 and ionic strength 0.03. Under these experimental conditions (pH and ionic strength), the phenolic OH of tyrosine is not dissociated and the carboxylic and amino groups have no electric charge. The shapes of the three curves are almost identical. The differences lie mainly in intensities. The intensities of the two characteristic peaks reflect the strength of molecular interaction between the solvent and the solute. They are in the order: dioxane > *n*-propanol > ethanol. This is inversely proportional to the dielectric constant of the solvent medium, indicating the involvement of an electrostatic effect. The dielectric constants for the three solvents are: dioxane–water (25:75, v/v) 56.0; *n*-propanol – water (25:75, v/v), 61.5; and ethanol–water (25:75, v/v), 67.0 (12).

(b) Acidic serum albumin

The expansion of bovine serum albumin in acidic aqueous solutions reaches its maximum when the pH is 2.2 (2, 3). Our study of organic solvent effect in acidic region was, therefore, carried out at that pH value. In Fig. 3, difference spectra of serum albumin produced by three 25% organic solvents at pH 2.2 are compared: curve *1*, dioxane; curve *2*, ethanol; and curve *3*, *n*-propanol. The shapes of the three curves are similar to those of tyrosyl ester. However, the ratio of the height of the major peak at 284–286 nm over that of the minor peak at 277–278 nm is much smaller for the protein curve than for the tyrosyl ester curve. Furthermore, the values of $\Delta\epsilon$, the molar difference of absorption coefficient, at the 284–286 nm peak are in the order of *n*-propanol > ethanol > dioxane, not in correspondence with the increase or decrease of dielectric constant of the solvent medium as in the case of tyrosyl ester. Nor are they in correspondence with the increase or decrease in the refractive index of the solvent. The refractive indices of the solvents are $n_D^{25} = 1.3450$ for 25% ethanol, $n_D^{25} = 1.3499$ for 25% *n*-propanol, and $n_D^{25} = 1.3560$ for 25% dioxane. This clearly indicates that the presence of organic solvent involves more than the electrostatic effect. There must be something related to the neighboring groups of tyrosyl residues in the protein. Comparison of the difference spectra of tyrosyl residues in the protein at acidic pH with that of tyrosyl esters reveals that although the 21 tyrosyl residues are not all exposed to the surface (4), those which are exposed are completely accessible to the solvent. The estimate was based upon the choice of the model compound, the tyrosyl ester, as "100% exposed" (13).

(c) Isoelectric serum albumin

At pH near the isoelectric point, serum albumin is in its native state. Fig. 4 (*a*), (*b*), and (*c*) give the difference spectra of serum albumin as a function of the concentration of organic solvent at isoelectric pH. Concentrations of the organic solvent (v/v) in each figure are as follows: curve *1*, 5%; curve *2*, 10%; curve *3*, 15%; curve *4*, 20%; and curve *5*, 25%.

Figure 4 (*a*) shows that each curve contains the twin peaks and a shoulder. The twin peaks are unmistakably due to tyrosyls, while the shoulder is due to tryptophyls. The ratio of the heights of the two peaks increases as the concentration of ethanol increases. The values of $\Delta\epsilon$ of the major peak form a linear function with the concentration of ethanol indicating that there is no conformational change of the protein and ethanol serves as a perturbant to the tyrosyls.

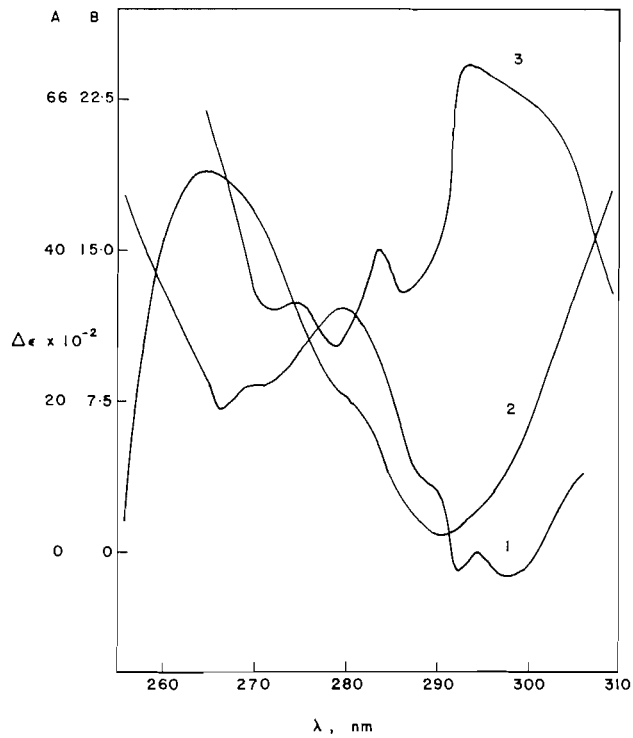

FIG. 5. Comparison of the difference spectra of bovine serum albumin at pH 11.6, ionic strength 0.03 and 25°C produced by 25% organic solvent. Curves: *1*, ethanol; *2*, dioxane; *3*, *n*-propanol. Scales: *A*, dioxane; *B*, ethanol and *n*-propanol.

The difference spectra of serum albumin produced by *n*-propanol shown in Fig. 4 (*b*) are more complicated than those shown in Fig. 4 (*a*). The curves in Fig. 4 (*b*) may be divided into two groups. The first group consists of three curves: 5%, 10%, and 15% *n*-propanol; the second group consists of two curves: 20% and 25% *n*-propanol. In the first group the values of $\Delta\epsilon$ at 284–286 nm form a linear function with the concentration of *n*-propanol as in the ethanol solutions, suggesting that *n*-propanol at these concentrations serves as a perturbant, but not as effectively as ethanol. The curves in the second group show a deep trough at 288 nm. The deep trough at 288 nm has been attributed to the red shift of the tryptophan trough and blue shift of the tyrosine trough, an indication of the change in tertiary structure of the protein (14).

Figure 4 (*c*) shows the difference spectra of serum albumin produced by dioxane at isoelectric pH. These curves are even more complicated than those produced by *n*-propanol. First, there are more peaks and troughs in the region between 240–270 nm, indicating more interference from phenylalanine residues. Second, the twin peaks of tyrosyls are obscure. There appears a deep and wide trough at 288 nm, suggesting some changes in the conformation of the protein.

(d) Basic serum albumin

The difference spectra of bovine serum albumin at pH 11.6 produced by 25% organic solvent are shown in Fig. 5. At such high pH the absorptions of chromophores interfere with each other and no peak can be assigned to a particular group unmistakably. The resolution of the *n*-propanol curve seems to be better than that of the ethanol curve. The curve of dioxane is markedly different from those of ethanol and *n*-propanol both in intensity and shape. A broad trough occurs at 290 nm and a

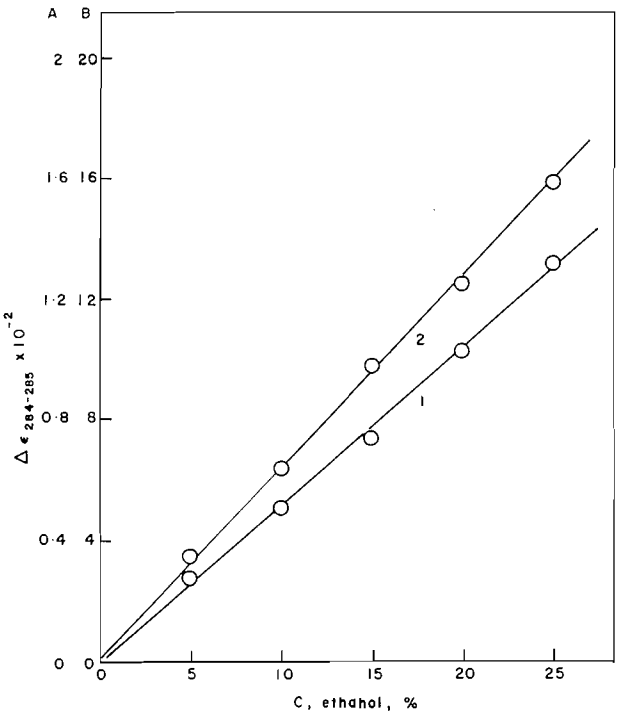

FIG. 6. Effect of the concentration of ethanol on the difference spectra of bovine serum albumin and that of *N*-acetyl-L-tyrosine ethyl ester at pH 5.4–5.7, ionic strength 0.03 and 25°C. Curve *1* and scale *A*, *N*-acetyl-L-tyrosine ethyl ester; curve *2* and scale *B*, bovine serum albumin.

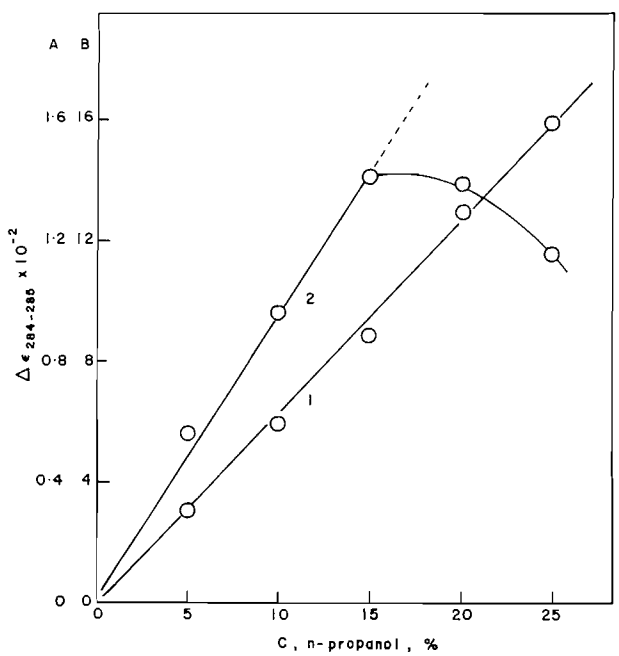

FIG. 7. Effect of the concentration of *n*-propanol on the difference spectra of bovine serum albumin and that of *N*-acetyl-L-tyrosine ethyl ester at pH 5.4–5.7, ionic strength 0.03 and 25°C. Curve *1* and scale *A*, *N*-acetyl-L-tyrosine ethyl ester; curve *2* and scale *B*, bovine serum albumin.

broad peak at 265 nm. The curve represents a complete ionization of the phenolic chromophores of bovine serum albumin (6).

Discussion

Tyrosyl residues in a protein are believed to involve three types of interactions: (*a*) tyrosyl–water interaction through hydrogen bonding, (*b*) tyrosyl–carboxylate (e.g. tyrosyl–glutamate) interaction also through hydrogen bonding (15, 16), and (*c*) the interaction between the methyl groups of non-polar side chains such as leucine or of polar side chains such as lysine and the benzene ring of tyrosine through hydrophobic bonds. The first type of interaction occurs on the surface of the protein molecule where the tyrosyl residues are accessible to the solvent. The second and third types of interaction occur in the interior of the protein molecule. The effect of an organic solvent depends on its ability to alter the relative strengths of the internal hydrogen and hydrophobic bonds in the native protein and of the hydrogen bond to water.

In acidic solution, e.g., pH 2.2, where the protein expands, the difference spectra produced by the three organic solvents are similar to those of tyrosyl esters, as shown in Figs. 2 and 3. This shows that the three organic solvents act mainly by solvent effect. However, the fact that the intensities of major peaks in the three organic solvent – water mixtures do not correlate with the dielectric constants of the solvents indicates that the polarity of the solvent is not the only factor to affect the absorption spectra. We attribute this fact to the different bonding strength of the three organic solvents. Dioxane seems to be stronger in interaction with water through hydrogen bonding than alcohols, but weaker in interaction with non-polar groups of side chains in a protein molecule than the two alcohols. Between the two alcohols, *n*-propanol is stronger than ethanol in hydrophobic bonding due to the additional alkyl group in the chain (5, 17).

At basic pH, e.g. 11.6, the protein molecule greatly expands. The value of the reduced viscosity is 3 times higher than that at pH 2.2 (3). Also, the tyrosyl residues are believed to be completely ionized. The spectral shift due to the solvent effect is cancelled by the conformational blue shift. The difference spectra we observed are a reflection of the change in pK values of the ionized tyrosyl residues. The pK shift for phenolic groups in 25% dioxane is 0.15 units (9); that in 25% *n*-propanol or in 25% ethanol is smaller than 0.15 units (our experimental results). That the spectrum in 25% ethanol is quite different from that in 25% propanol reflects the different chemical properties of the two alcohols as we described elsewhere (5).

At pH near isoelectric point (ca. 5.4), bovine serum albumin is in its native state. Here we observed the clear-cut influence of the three different environments produced by three different organic solvents on the physical and chemical states of the tyrosyl residues in a protein.

The value of $\Delta\epsilon$ (the molar difference absorption coefficient) depends upon the refractive index of the chromophore and the dielectric constant of the solvent medium. Parallel to the expression of $\Delta\nu/\nu$ (18) (where ν is the frequency of the absorption maxima), the parameter $\Delta\epsilon$ may be expressed by the equation

$$\Delta\epsilon = A + B[\mathrm{R}] + C[\mathrm{P}]$$

where

$$[\mathrm{R}] = \frac{n^2 - 1}{n^2 + 2}\frac{M}{P}$$

and

$$[\mathrm{P}] = \frac{D - 1}{D + 2}\frac{M}{P}$$

Can. J. Chem. Downloaded from www.nrcresearchpress.com by 210.87.254.6 on 09/06/12
For personal use only.

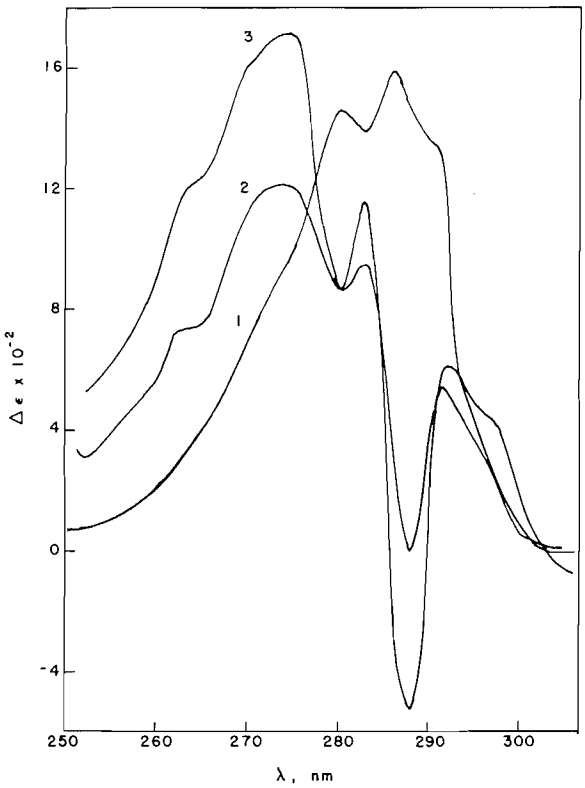

FIG. 8. Comparison of the difference spectra of bovine serum albumin at pH 5.4–5.7, ionic strength 0.03 and 25°C produced by 25% organic solvent. Curves: *1*, ethanol; *2*, dioxane; *3*, *n*-propanol.

In the above equations, n is the refractive index, M is the molecular weight, P is the density of the medium, and D is the dielectric constant. P is the molar polarization or distortion polarization which is related to the polarizability α of the chromophore by the equation $P = \frac{4}{3}\pi N\alpha$, N being the Avogadro's number. A, B, and C are constants: A is related to the dispersion force, B to the interaction between the chromophore as an oscillating dipole and the organic solvent molecule as an induced dipole, and C to the interaction between the oscillating dipole and the permanent dipole.

In Fig. 6 the values of $\Delta\epsilon$ at 284–285 nm are plotted against the concentration of ethanol for the model compound (curve *1*) and for serum albumin (curve *2*). The fact that a straight line was obtained for albumin just as it was for the model compound demonstrates that B is zero, that is, $\Delta\epsilon$ depends on the dielectric constant of the solvent medium alone. It is well known that $D = n^2$ for a molecule with no permanent dipole moment. There is obviously no change in conformation of the protein.

Figure 7 compares the values of $\Delta\epsilon$ at 284–285 nm of the tyrosyl ester with that of serum albumin as a function of the concentration of *n*-propanol. While a straight line was obtained for tyrosyl ester (curve *1*) in *n*-propanol–water mixtures as in ethanol–water mixtures, this was not so for serum albumin (curve *2*). The first three points (in 5%, 10%, and 15% *n*-propanol) are on the straight line, but the last two points (20% and 25% *n*-propanol) are off the line. This demonstrates that as the concentration of *n*-propanol increases to 20%, the conformation of the protein changes. That is, for tyrosyl residues in the protein, both B and C are not zero at higher concentrations of *n*-propanol. B is zero only for tyrosyl residues in the protein at low concentrations of *n*-propanol. It is zero for the model compound in both low and high concentrations.

Figure 8 compares difference spectra of serum albumin produced by the three organic solvents at the same concentration, 25%, and at the isoelectric pH. Among the differences are: the positions of the three peaks, the shapes of the curves, the intensities of the twin peaks of the tyrosyl residues, and the trough at 288 nm.

Spectral changes in the isoelectric pH region seem to correlate well with viscosity data. The intrinsic viscosity of bovine serum albumin in units of dl/g in 25% organic solvent – 75% H_2O, ionic strength 0.03, in the isoelectric pH region is: dioxane 0.019, *n*-propanol 0.061, and ethanol 0.037, in comparison with 0.037 when no organic solvent is present (9, 19). Thus the conformation of serum albumin remains the same in the presence of 25% ethanol, expands in the presence of 25% *n*-propanol, and shrinks in the presence of 25% dioxane.

The results lead us to the conclusion that for bovine serum albumin in its native state ethanol has no effect on the intermolecular forces that exist between tyrosyl residues and other polar or non-polar amino acid residues, but *n*-propanol and dioxane do. The presence of *n*-propanol has a strong impact on the hydrophobic region of the protein molecule. Possibly, the alkyl group in the side chain of *n*-propanol competes with the benzene ring of tyrosyl residues in forming hydrophobic bonds with the alkyl groups of polar and non-polar amino acid residues inside the protein molecule. That is, *n*-propanol has weakened the third type of interaction of tyrosyl residues, thereby causing the conformational change in protein. Dioxane has the ability of interrupting all three types of interactions of tyrosyl residues, though weaker than *n*-propanol in interrupting the third type of interaction. Because of this, the change in the conformation of the protein in the presence of dioxane is in the form of contraction (19).

1. C. TANFORD, S. A. SWANSON, and W. S. SHORE. J. Am. Chem. Soc. **77**, 6414 (1955).
2. J. T. YANG and J. F. FOSTER. J. Am. Chem. Soc. **76**, 1588 (1954).
3. S. F. SUN. Arch. Biochem. Biophys. **129**, 411 (1969).
4. T. T. HERSKOVITS and M. SORENSEN. Biochemistry, **7**, 2523 (1968).
5. S. F. SUN. J. Chem. Soc. Faraday Trans. 1, **78**, 2765 (1982).
6. S. F. SUN. Biochim. Biophys. Acta, **181**, 473 (1969).
7. S. F. SUN and N. O. DEL ROSARIO. J. Am. Chem. Soc. **92**, 1837 (1970).
8. K. E. VAN HOLDE and S. F. SUN. J. Am. Chem. Soc. **84**, 66 (1962).
9. S. F. SUN. Biochim. Biophys. Acta, **200**, 433 (1970).
10. T. T. HERSKOVITS and M. LASKOWSKI, JR. J. Biol. Chem. **237**, 2481 (1962).
11. D. B. WETLAUFER, J. T. EDSALL, and B. R. HOLLINGWORTH. J. Biol. Chem. **233**, 1421 (1958).
12. H. S. HARNED and B. B. OWEN. The physical chemistry of electrolytic solutions. Reinhold Publishing Co., 1943. p 161.
13. T. T. HERSKOVITS. Methods Enzynol. **11**, 748 (1967).
14. J. STEINHARDT, J. G. LEIDY, and J. P. MOONEY. Biochemistry, **11**, 1809 (1972).
15. A. Y. MOON, D. C. POLAND, and H. A. SCHERAGA. J. Phys. Chem. **69**, 2960 (1965).
16. D. A. CHIGNELL and W. B. GRATZER. J. Phys. Chem. **72**, 2934 (1968).
17. E. E. SCHRIER, R. T. INGWALL, and H. A. SCHERAGA. J. Phys. Chem. **69**, 298 (1965).
18. E. G. MCRAE. J. Phys. Chem. **61**, 562 (1957).
19. S. F. SUN. J. Phys. Chem. **76**, 128 (1972).

Can. J. Chem. Downloaded from www.nrcresearchpress.com by 210.87.254.6 on 09/06/12
For personal use only.

Structure et réactivité. V.[1] Étude par résonance magnétique nucléaire des produits d'halogénation des *tert*-butyl-3 methoxycarbonyl-4 cyclohexènes

JEANINE BOUTEILLER-PRATI, JEAN-CLAUDE BOUTEILLER ET JEAN-PIERRE AYCARD[2]

Laboratoire de Chimie Organique Structurale, Université de Provence, Centre de Saint-Jérôme, 13 rue Henri Poincaré, 13397 Marseille Cedex 13, France

Reçu le 5 juillet 1982

JEANINE BOUTEILLER-PRATI, JEAN-CLAUDE BOUTEILLER et JEAN-PIERRE AYCARD. Can. J. Chem. **61**, 362 (1983).

Les produits de la réaction de bromation (ou de chloration) des *tert*-butyl-3 carbométhoxy-4 cyclohexènes *cis* et *trans* sont étudiés par rmn. Les résultats montrent que la réaction sur l'isomère *cis* conduit à plus de 90% de la lactone de l'acide bromo-4 (chloro-4) *trans* hydroxy-3 *cis tert*-butyl-2 *trans* cyclohexane carboxylique alors que la réaction sur l'isomère *trans* conduit au dibromo (dichloro)-1,2 *trans tert*-butyl-3- *cis* carbométhoxy-4 *trans* cyclohexane qui adopte une conformation twist. Pour le composé dibromé ce produit cinétique se transpose en dibromo-1,2 *trans tert*-butyl-3 *trans* carbométhoxy-4 *cis* cyclohexane par un rearrangement dyotropique. La formation des produits cinétiques est expliquée par l'intervention des conformères diaxiaux des dérivés cyclohexéniques de départ.

JEANINE BOUTEILLER-PRATI, JEAN-CLAUDE BOUTEILLER, and JEAN-PIERRE AYCARD. Can. J. Chem. **61**, 362 (1983).

The product of the bromination (chlorination) reaction on *cis* and *trans* 3-*tert*-butyl 4-carbomethoxy cyclohexene is studied by nmr. The results show that the reaction of the *cis* isomer gives 90% of the *trans* 4-bromo (chloro) *cis* 3-hydroxy *trans* 2-*tert*-butyl cyclohexane 1-carboxylic acid lactone and the reaction of the *trans* isomer gives *trans* 1,2-dibromo (dichloro) *cis* 3-*tert*-butyl *trans* 4-carbomethoxy cyclohexane which adopts a twist conformation. For the dibromo compound this kinetic product gives the corresponding thermodynamically more stable isomer, *trans* 1,2-dibromo *trans* 3-*tert*-butyl *cis* 4-carbomethoxy cyclohexane, by a diotropic rearrangement. The formation of the kinetic product is explained by the reaction of the less stable diaxial conformer of the cyclohexene derivative.

Il est maintenant démontré que l'existence de fortes contraintes stériques dans les dérivés du *tert*-butyl-3 cyclohexène conduit à des données structurales (2), conformationnelles (3) et réactionnelles (4) particulières.

Ainsi, l'existence d'un équilibre conformationnel pour les dérivés 3,4 disubstitués conduit lors des réactions d'addition électrophile à des stéréosélectivités qui ne peuvent être expliqué que par l'intervention de conformères de haute énergie (5).

Dans le cadre d'une étude de réactivité de molécules fortement contraintes (5, 6), nous nous sommes intéressés aux réactions d'addition du brome et du chlore au *tert*-butyl-3 méthoxycarbonyl-4 cyclohexènes *cis* et *trans*, le choix de ces substrats nous ayant été dicté par la bonne connaissance des équilibres conformationnels des dérivés cyclohexéniques de départ et par les résultats de Bellucci *et al.* sur les réactions d'addition électrophile au méthoxycarbonyl-4 cyclohexène (7) et au *tert*-butyl-3 cyclohexène (8). Enfin, les cyclohexanes obtenus présentent un intérêt structural indéniable par le cumul des fortes contraintes stériques qu'ils comportent (9, 10).

Résultats expérimentaux

Afin de pouvoir étudier par rmn du proton la stéréochimie des produits de réaction, les additions sont effectuées (cf. partie expérimentale) sur les *tert*-butyl-3 méthoxycarbonyl-4 cyclohexènes *cis* et *trans*, et à titre de comparaison sur le méthoxycarbonyl-4 cyclohexène, spécifiquement deutériés en position allylique (3). Dans ces conditions, outre les signaux des groupements *tert*-butyl et méthoxycarbonyle, les spectres rmn se composent de deux systèmes de spins (deux et trois protons) indépendants facilement analysables. Les différents paramètres ainsi obtenus sont regroupés dans le tableau 1.

Addition au tert-*butyl-3 méthoxycarbonyl-4 cyclohexène* trans

Après addition du brome le spectre de rmn du mélange réactionnel montre un mélange de deux isomères du dibromo-1,2 *tert*-butyl-3 méthoxycarbonyl-4 cyclohexane **1** et **2** dans des proportions variant avec le temps d'analyse.

Ainsi, dans le spectre réalisé dans CCl_4 immédiatement après extraction, les signaux du composé majoritaire **1** (cf. Fig. 1) se composent essentiellement d'un spectre de type AB centré à $\delta = 4{,}55$ ($J = 4{,}8$ Hz) correspondant aux protons géminés des bromes, d'un triplet d'intensité 1 centré à 2,7 ($J = 6{,}5$ Hz) et d'un doublet correspondant aux deux protons du carbone 5 centré à $\delta = 1{,}91$. Le produit minoritaire **2** présente pour les protons géminés aux bromes, un singulet à $\delta = 4{,}69$. Les trois autres protons H_4, H_{5a} et H_{5b} (cf. schéma, Tableau 1) se présentent sous forme d'un spectre AMX dont les trois massifs sont centrés respectivement à $\delta = 2{,}75$, 1,71 et 2,20.

Après 48 h à température ambiante, on observe dans le milieu que le composé **2**; l'isomère **1** produit cinétique ayant quasiment disparu (**1** <5%).

Le spectre effectué dans le benzène permet par effet d'ASIS de transformer le spectre de type A_2 des protons géminés des bromes H_1 et H_2 en un spectre de type AB centré à $\delta = 4{,}44$ ($J = 3{,}5$ Hz).

Dans ce dernier solvant, l'observation de la constante de couplage à longue distance $^4J = 1{,}5$ Hz entre le proton résonnant à $\delta = 4{,}37$ et celui résonnant à $\delta = 1{,}43$ confirme la position équatoriale de H_{5a} et permet d'attribuer H_1. La situation axiale du proton résonnant à $\delta = 2{,}25$ est confirmée par la structure triplet de son signal (deux grandes constantes de couplage).

Après addition du chlore au *tert*-butyl-3 méthoxycarbonyl-4 cyclohexène *trans* on obtient un mélange invariant de **4** et de **5** (90% et 10% respectivement). Le spectre du produit majoritaire **4** se compose essentiellement d'un spectre de type AB relatif aux protons géminés des bromes et d'un spectre de type

[1]Pour la partie IV voir référence 1.

[2]Auteur à qui toute correspondance doit être adressée.

0008-4042/83/020362-04$01.00/0

©1983 National Research Council of Canada/Conseil national de recherches du Canada

Can. J. Chem. Downloaded from www.nrcresearchpress.com by 210.87.254.42 on 09/06/12
For personal use only.

TABLEAU 1. Paramètres RMN des composés d'addition*

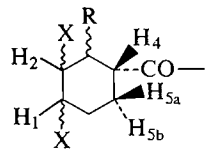

Paramètre	Composé 1	2		3		4	5	6	7	8
Solvant	a	a	b	a	b	c	c	c	a	b
$\delta(CH_3)_3C$	1,00	1,08	1,00	0,98	0,75	1,07	1,03	1,00	—	—
δCO_2CH_3	3,65	3,65	3,35	—	—	3,65	3,65	—	—	d
δ_1	4,52	4,69	4,37	4,44	4,05	4,00	4,36	4,38	4,30	4,21
δ_2	4,60	4,69	4,51	4,66	4,32	4,17	4,49	4,68	4,65	4,37
δ_4	2,70	2,75	2,79	2,57	2,34	2,39	2,85	2,64	2,50	2,71
δ_{5a}	1,91	1,71	1,43	1,91	1,52	2,35	—	1,97	1,80	1,61
δ_{5b}	1,91	2,20	2,25	1,91	1,52	1,72	—	1,97	1,80	1,86
J_{12}	4,8	—	3,5	4,2	4,0	6,8	3,2	4,5	4,0	3,6
J_{15a}	—	—	1,5	—	—	—	—	—	—	—
J_{42}	—	—	—	—	1,2	—	—	1,3	—	—
J_{45a}	6,5	3,5	3,5	3,7	3,6	5,4	3,6	3,5	3,0	3,9
J_{45b}	6,5	12,3	12,3	3,7	3,6	8,6	12,0	3,5	3,0	11,3
J_{5a5b}	—	−13,8	−13,7	—	—	−14,1	—	—	—	−13,5

* δ en ppm par rapport au TMS, J en Hz; T = 303 K; solvant: (a) CCl_4, (b) C_6H_6, (c) $CDCl_3$; (d) CO_2CH_2-CH_3: δ CH_2 = 3,95, δ CH_3 = 1,50, J = 7 Hz.

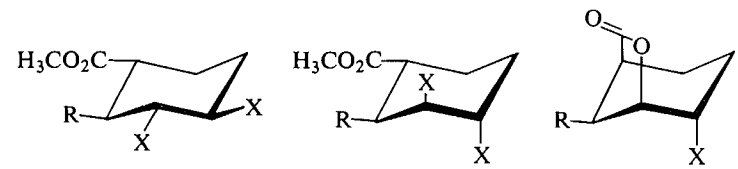

R = $C(CH_3)_3$

X = Br	**1**	**2**	**3**
= Cl	**4**	**5**	**6**

R = D

X = Br	**8**	**7**

FIG. 1

ABX relatif aux protons H_4, H_{5a} et H_{5b}. Le proton H_4, en α du groupement fonctionnel est attribué au signal résonnant à δ = 2,59 et H_{5b} à celui présentant deux grandes constantes de couplage. Pour **5** seuls les signaux des protons géminés des bromes et du groupement méthoxycarbonyl ont pu être analysés. Pour ce composé, l'attribution de H_1 et H_2 est faite par l'observation d'un élargissement des raies vraisemblablement dû à un couplage ^4J avec le proton H_{5a}.

Addition au tert-*butyl-3 méthoxycarbonyl-4 cyclohexène* cis

Après addition du chlore ou du brome sur l'isomère *cis*, la première observation que l'on puisse effectuer sur le spectre rmn des produits de réaction est l'absence totale ou quasi totale du signal correspondant au groupement méthoxycarbonyl.

En effet lors de l'addition du brome nous obtenons un mélange essentiellement composé de **3** (>95%) et d'environ 5% d'un produit minoritaire présentant encore la fonction ester.

Dans CCl_4, le spectre de **3** est essentiellement constitué d'un doublet centré à δ = 1,91 correspondant à deux protons et d'un triplet centré à δ = 2,57 attribuable à H_1. À δ = 4,44 et δ = 4,66 apparaissent deux doublets caractéristiques d'un spectre de type AX. Les raies centrées à 4,6 présentent un élargissement correspondant à une constante de couplage à longue distance (^4J = 1,2 Hz) avec le proton H_4. Cette dernière apparaît nettement dans le spectre enregistré dans C_6D_6 et permet d'attribuer le signal du proton H_2.

L'existence de cette constante et la présence dans le spectre ir d'une vibration d'élongation $\bar{\nu}$ (C=O) à 1785 cm^{-1} permet d'attribuer à ce composé la structure d'une lactone bicyclique correspondant à l'attaque du groupement méthoxycarbonyl sur le carbone 3. Dans une telle structure de type [3.2.1.]octane, le cycle à cinq et le cycle à six chainons sont dans des conformations favorables (enveloppe et chaise respectivement) et les protons H_4 et H_2 peuvent présenter un couplage à longue distance de type W.

La faible intensité des signaux de l'ester minoritaire et le fait que ceux ci soient partiellement recouvert par ceux de **3** ne permet pas de déterminer la totalité des paramètres rmn de ce composé. Néanmoins dans le spectre enregistré dans C_6D_6 il est possible d'observer deux doublets centrés à δ = 4,2 et δ = 3,81 (J = 3,8 Hz) correspondant vraisemblablement à une structure *trans* diaxiale des bromes, et centré à δ = 2,42 (J = 3,2 Hz)

Can. J. Chem. Downloaded from www.nrcresearchpress.com by 210.87.254.42 on 09/06/12
For personal use only.

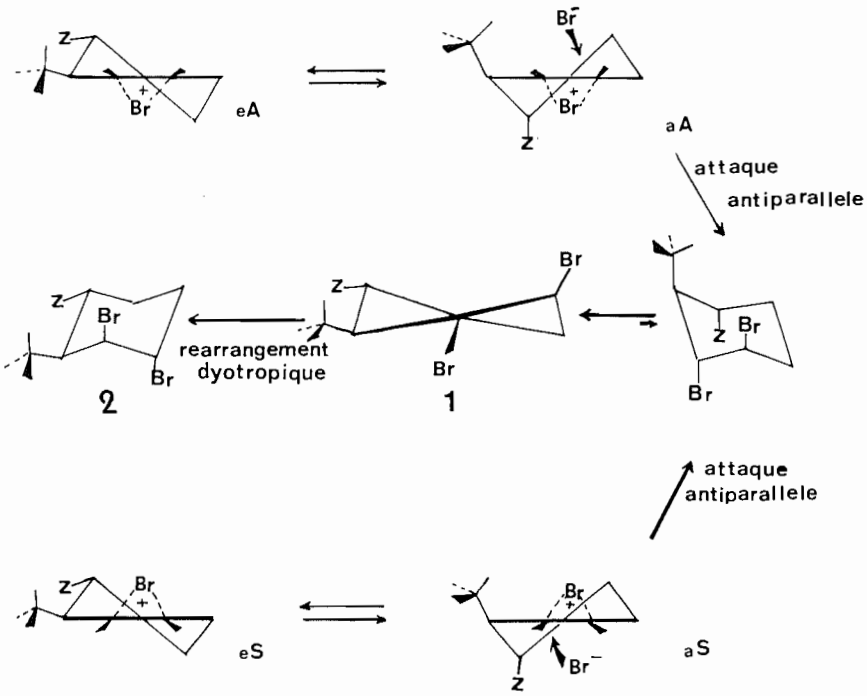

SCHÉMA 1

un triplet pouvant correspondre au signal du proton H_4 en α groupement fonctionnel.

Lors de l'addition du chlore nous n'observons qu'un seul composé **6** dont le spectre rmn est identique à celui obtenu par **3**. La présence pour ce composé d'une vibration $\bar{\nu}$(C=O) à 1785 cm^{-1} permet d'envisager pour **6** une structure de lactone bicyclique identique à celle de **3**.

Addition au carboxy-4 cyclohexène et à son ester d'éthyle

Afin de vérifier les résultats obtenus par nos molécules contraintes nous avons effectué l'addition du brome et du chlore sur l'acide carboxy-4 cyclohexène et sur son ester d'éthyle.

Nous avons ainsi obtenu en procédant selon la méthode de Bellucci *et al.* (7) la lactone **7** ou son homologue chlorée dont les paramètres rmn et ir sont comparables à ceux de **3** et **6**, alors que l'addition du brome sur l'ester conduit uniquement à l'ester **8**.

Discussion

L'obtention des lactones **3** et **6** s'explique aisément en considérant une attaque intramoléculaire du groupement méthoxycarbonyl sur l'ion bromonium ou chloronium résultant de l'entrée *anti* de l'halogène. Cette approche de l'halogène analogue à celle observée dans la réaction d'époxydation de ces dérivés (5) peut facilement s'interpréter en considérant la gène stérique engendrée par le groupement ester lors de l'entrée *syn* du chlore ou du brome.

Lors des réactions d'addition à l'ester *trans*, nous obtenons dans tous les cas un produit cinétique **1** ou **4** qui reste stable dans le cas de **4** ou qui évolue dans le cas du dérivé bromé **1** vers un produit thermodynamiquement plus stable **2**. Pour ce dernier la structure chaise à groupement méthoxycarbonyl équatorial et à bromes diaxiaux (analogue à celle de **8** et **5**) est aisément déterminée à partir des valeurs des constantes de couplage (cf. Tableau 1). Celles-ci sont en effet en tout point comparables à celles du diastéréoisomère le plus stable du *tert*-butyl-2 méthoxycarbonyl cyclohexane (11) (J_{45b} = 12 Hz et J_{45a} = 4 Hz). De plus il faut remarquer que la stéréochimie *cis* du *tert*-butyle et du brome vicinal correspond à celle du diastéréoisomère le plus stable du dibromo-1,2 *tert*-butyl-3 cyclohexane (4*b*).

Pour les produits cinétiques **1** et **4** les faibles valeurs des constantes de couplage J_{45b} et J_{12} (cf. Tableau 1) sont incompatibles avec une conformation chaise à substituants équatoriaux. Nous devons donc envisager l'existence d'un équilibre conformationnel entre cette conformation et une conformation croisée[3] analogue à celle envisagée lors de l'étude rmn des dibromo-1,2 *tert*-butyl-3 cyclohexane (10) et dont les angles dièdres sont voisins de ceux déterminés lors de l'étude cristallographique du dibromo-2 *cis*-3 *trans tert*-butyl-4 *cis* cyclohexyl *p*-nitrobenzoate (12).

Leur formation peut être envisagée à partir des quatre intermédiaires issus de l'addition *syn* ou *anti* sur les deux conformères du *tert*-butyl-3 méthoxycarbonyl-4 cyclohexène *trans* (3) (cf. Schéma 1). Dans ces conditions suivant le mécanisme généralement admis d'une addition *trans* diaxiale (13, 14), nous devons considérer que **1** (ou **4**) est issu d'une des espèces aA ou aS alors que les quelques pourcents de produits thermodynamiques obtenus proviendraient de eA ou eS (cas du chlore). Cette sélectivité est vraisemblablement due à la gène stérique des groupements *tert* butyle et carbométhoxy équitoriaux qui augmente trop l'énergie d'activation via eA ou eS.

Dans le cas des dérivés bromés le passage de **1** à **2** s'effectue suivant un mécanisme classique de transposition dyotropique des bromes (15, 16) qui minimise les interactions gauches *t*-Bu Br (4*a*).

Partie expérimentale

Toutes les synthèses ont été effectuées sur des stéréoisomères purs, préalablement séparés par chromatographie en phase gazeuse préparative. La synthèse des esters utilisés a déjà été décrite (5).

[3] D'apres les modèles Dreiding la structure la plus probable correspond à une conformation croisée possédant un pseudo axe propre d'ordre 2 entre les carbones C_2 et C_5 et ayant pour angle dièdre ϕ_{12} = +40, ϕ_{23} = +30, ϕ_{34} = −70, ϕ_{45} = +40, ϕ_{56} = +30, ϕ_{61} = −70.

Can. J. Chem. Downloaded from www.nrcresearchpress.com by 210.87.254.42 on 09/06/12
For personal use only.

Can. J. Chem. Downloaded from www.nrcresearchpress.com by 210.87.254.42 on 09/06/12
For personal use only.

Les mélanges réactionnels sont analysés par chromatographie en phase vapeur (cpv) dans les conditions suivantes: chromatographe Girdel Série 3000 équipé d'un détecteur à ionisation de flamme; gaz vecteur: azote, débit environ 10 mL/min; température du détecteur: 215°C; colonne en acier inoxydable de 1/8 po de diamètre et de 3 m de long, remplie de Chromosorb W(AW) 60/80 mesh, imprégné à 10% en poids de Réoplex 400.

Les spectres infrarouges sont effectués en solution dans CCl_4 sur un spectrographe Perkin–Elmer 577; les fréquences sont données en cm^{-1}. Les spectres rmn ont été réalisés sur un appareil Varian XL 100, en solution à 10% dans le CCl_4 avec du tétraméthylsilane comme étalon interne et avec irradiation du deutérium. Les microanalyses n'ont été effectuées que sur les composés non deutériés. Seuls les carbones et hydrogènes ont été analysés.

Les réactions de bromation ont été conduites suivant la méthode générale décrite ci-dessous.

On ajoute goutte à goutte, à 10^{-3} mol de dérivé cyclohexénique dissous dans 10 mL de tétrachlorure de carbone, $1{,}2 \times 10^{-3}$ mol de brôme provenant d'une solution 0,23 *M* de brome dans le tétrachlorure de carbone. Durant toute l'addition, puis durant 3 à 4 heures, le mélange réactionnel est maintenu à 0°C, sous agitation et à l'abri de la lumière. Puis l'excès de brôme et le solvant sont évaporés sous vide, le résidu est repris par du CCl_4, filtré sur laine de verre et évaporé de nouveau.

Bromo-4 tert-*butyl-8 one-7 oxa-6 bicyclo octane [3.2.1]*

On fait réagir 0,14 g ($0{,}7 \times 10^{-3}$ mol) de *tert*-butyl-3 carbométhoxy-4 cyclohexène *cis* avec 3,7 mL de la solution de brome ($0{,}85 \times 10^{-3}$ mol). Le rendement est de l'ordre de 97%, la lactone représentant 95% des produits formés. *Anal.* calc. pour $C_{11}H_{17}O_2Br$: C 50,59, H 6,56, Br 30,59; trouvée: C 50,31, H 6,49. On synthétise de la même manière le bromo-4 *tert*-butyl-8 one-7 oxa-6 bicyclo octane[3.2.1.] (D_3-3,3,8) à l'aide de l'ester correspondant; cpv: température 140°C, t_r: 2,70 min; ir (CCl_4) ν_{max}: 1785 (C=O), 2100 à 2200 (C—D) cm^{-1}.

Dibromo-1,2 tert-*butyl-3 méthoxycarbonyl-4 cyclohexane*

On opère sur 0,119 g ($0{,}6 \times 10^{-3}$ mol) de *tert*-butyl-3 carbométhoxy-4 cyclohexène *trans* et 3,2 mL de la solution de brôme. Rendement 96%. *Anal.* calc. pour $C_{12}H_{20}O_2Br_2$: C 40,47, H 5,66, Br 44,88; trouvée: C 40,16, H 5,52. On synthétise semblablement les dibromo-1,2 *tert*-butyl-3 méthoxy carbonyl-4 cyclohexanes (D_3-3,6,6) à partir de l'ester correspondant; cpv: température 140°C, t_r: 3,75 min; ir (CCl_4) ν_{max}: 1730 (C=O), 2100 à 2200 (C—D) cm^{-1}.

Bromo-4 one-7 oxa-6 bicyclo octane[3.2.1] (D_4*-3,3,8,8)*

On utilise la méthode décrite par Bellucci *et al.* (7) en faisant réagir 0,176 g d'acide cyclohexène carboxylique-4 (D_4-3,3,6,6). Les réactions de chloration ont été conduites de la manière suivante. Une solution de 10^{-3} mol de composé cyclohexénique dans 20 mL de tétrachlorure, maintenue à 0°C et à l'abri de la lumière, est saturée de chlore gazeux. Après une demie-heure, le mélange réactionnel est traité de la même manière que précédemment.

Chloro-4 tert-*butyl-8 one-7 oxa-6 bicyclo octane[3.2.1]*

Le rendement est de l'ordre de 98%. *Anal.* calc. pour $C_{11}H_{17}O_2Cl$: C 60,97, H 7,91, Cl 16,36; trouvée: C 60,65, H 7,80. On synthétise de la même manière le chloro-4 *tert*-butyl-8 one-7 oxa-6 bicyclo octane[3.2.1] (D_3-3,3,8); cpv: température 140°C, t_r = 1,76 min; ir (CCl_4) ν_{max}: 1735 (C=O), 2100 à 2200 (C—D) cm^{-1}.

Dichloro-1,2 tert-*butyl-3 méthoxycarbonyl-4 cyclohexane*

Anal. calc. pour $C_{12}H_{20}O_2Cl_2$: C 53,94, H 7,54, Cl 26,54; trouvée: C 53,65, H 7,42.

Dichloro-1,2 tert-*butyl-3 méthoxycarbonyl-4 cyclohexane (*D_3*-3,6,6)*

Chromatographie en phase vapeur: température 140°C, t_r: 2,35 min; ir (CCl_4) ν_{max}: 1735 (C=O), 2100 à 2200 (C—D) cm^{-1}.

1. J. P. AYCARD, R. LAFRANCE et B. BOYER. Can. J. Chem. **57**, 2823 (1979).
2. (*a*) R. VIANI et J. LAPASSET. Acta Crystallogr. Sect. B, **37**, 477 (1981); (*b*) R. VIANI, J. LAPASSET, J. P. AYCARD et H. BODOT. J. Org. Chem. **44**, 899 (1979).
3. J. P. AYCARD et H. BODOT. Org. Magn. Reson. **7**, 226 (1975).
4. (*a*) R. C. CAMBIE, P. S. RUTLEDGE, T. SMITH-PALMER et P. D. WOODGATE. J. Chem. Soc. Perkin Trans. I, 997 (1978); (*b*) P. L. BARILI, G. BELLUCCI, G. BERTI, F. MARIONI, A. MARSILI et I. MORELLI. Chem. Commun. 1437 (1970).
5. (*a*) L. PIZZALA, J. P. AYCARD et H. BODOT. J. Org. Chem. **43**, 1013 (1978); (*b*) J. BOUTEILLER-PRATI. Thèse de Spécialité, Marseille. 1979.
6. J. BOUTEILLER-PRATI, J. C. BOUTEILLER et J. P. AYCARD. Can. J. Chem. **59**, 859 (1981).
7. G. BELLUCCI, F. MARIONI et A. MARSILI. Tetrahedron, **28**, 3393 (1972).
8. G. BELLUCCI, G. BERTI, M. FERRETTI, G. INGROSSO et E. MASTRORILLI. J. Org. Chem. **43**, 423 (1978).
9. J. P. AYCARD et H. BODOT. Can. J. Chem. **51**, 741 (1973).
10. P. L. BARILI, G. BELLUCCI, G. INGROSSO, F. MARIONI et I. MORELLI. Tétrahedron, **28**, 4583 (1972); G. BELLUCCI, G. INGROSSO et E. MASTRORILLI. Tetrahedron, **34**, 387 (1978).
11. J. P. AYCARD et H. BODOT. Org. Magn. Reson. **7**, 35 (1975).
12. G. BELLUCCI, G. BERTI, M. COLAPIETRO, R. SPAGNA et L. ZAMBONELLI. J. Chem. Soc. 1213 (1976).
13. D. H. R. BARTON and R. C. COOKSON. Q. Rev. **10**, 67 (1956).
14. (*a*) J. WALLS et E. TOROMANOFF. Bull. Soc. Chim. Fr. 758 (1960); (*b*) O. EISEINSTEIN, J. KLEIN et J. M. LEFOUR. Tetrahedron, **35**, 225 (1979).
15. M. F. GRENIER-LOUSTALOT, A. LECTARD et F. METRAS. Org. Magn. Reson. **7**, 376 (1975).
16. M. T. REETZ. Tetrahedron, **29**, 2189 (1973).

Photochemically initiated addition of alcohols to ketones: facile photoketalization of cycloalkanones[1]

VINCENZO MALATESTA,[2] MICHAEL JENNINGS,[3] AND PETER HACKETT
Laser Chemistry Group, Division of Chemistry, National Research Council of Canada, Ottawa, Ont., Canada K1A 0R6
Received April 2, 1982

VINCENZO MALATESTA, MICHAEL JENNINGS, and PETER HACKETT. Can. J. Chem. **61**, 366 (1983).

Irradiation at 300 nm of cycloalkanones in methanol gives the corresponding ketals in good yields. The results indicate that an excited state of the cycloalkanone is responsible for the facile addition of methanol to the carbonyl group.

VINCENZO MALATESTA, MICHAEL JENNINGS et PETER HACKETT. Can. J. Chem. **61**, 366 (1983).

L'irradiation des cycloalcanones dans le méthanol à 300 nm donne les cétals correspondants avec de bons rendements. Les résultats indiquent qu'un état excité de la cycloalcanone est responsable de l'addition facile du méthanol sur le groupe carbonyle.

[Traduit par le journal]

The photochemistry of cycloalkanones has been dealt with in great detail in both gas phase and in solution. The Norrish type I α-cleavage has been established as the most prevalent photochemical process for non-conjugated cyclic ketones in solution (Scheme 1) (1–4). The secondary reactions of the alkylacyl diradical depend upon both structure and the conditions of the photolysis (5–8). For example, the ratio of aldehyde to ester is sensitive to conformational effects upon the transition states of enol and ketene formation (9).

When cyclobutanone is irradiated in methanol solution a moderate yield (8%) of 2-methoxytetrahydrofuran is observed in addition to those products reported from gas phase photolyses (ethylene, cyclopropane, carbon monoxide, and ketene) (10–12). We have observed a new reaction pathway. When methanolic solutions of cyclobutanone, cyclopentanone, and cyclohexanone were irradiated at 300 nm the corresponding dimethylketals were obtained in 80, 25, and 40% yield respectively. Ketals are normally prepared by acid-catalysed transketalization reactions between either orthoesters (13, 14) or 2,2-dimethoxypropane and ketones (15). The photo-induced addition of alcohols reported here could provide a useful alternative whenever acid-sensitive functional groups are present.

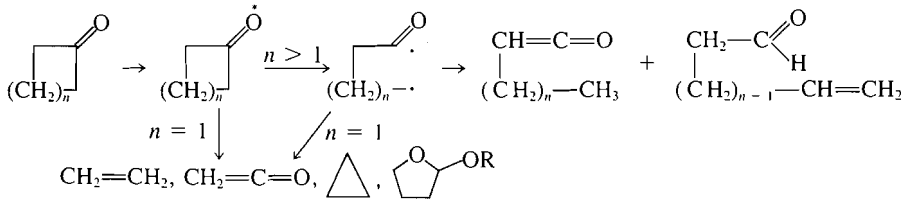

SCHEME 1

Typical runs involved the irradiation of 2 mL of 1.35 *M* solutions of cycloalkanones in methanol, using a Rayonet Srinivasan photochemical reactor. The reaction mixture was analysed by vpc on a 12 ft × 1/8 in., 12% OV-101 on chromasorb-WHP column, programmed between 25 and 135°C at 6°C/min. Authentic samples of the dimethylketals were prepared by acid-catalysed reaction between trimethylorthoformate and the corresponding ketones. Their nmr spectra and vpc retention times were identical to those of the reaction products.

During irradiation the presence of trace amounts of sodium acetate suppressed ketal formation. This result suggests that acetate ion removes any species responsible for acid catalysis; yet the reaction is still observed in dry, neutral methanol distilled from magnesium methoxide. Furthermore, those carboxylic acids which could form from ketenes by *in situ* reaction with moisture are not effective catalysts. This was shown in control experiments in which dark reaction between cyclobutanone and methanol in the presence of acetic acid gave only 0.5% conversion to 1,1-dimethoxycyclobutane after 1 week; this same solution rapidly yielded ketal upon irradiation. These observations all suggest that an excited state of the cycloalkanone is responsible for the facile addition of methanol to the carbonyl group, and that addition is itself acid-catalysed.

We suggest that irradiation in a protic solvent leads to carbonium ion intermediates which are susceptible to nucleophilic attack by solvent as shown in Scheme 2.

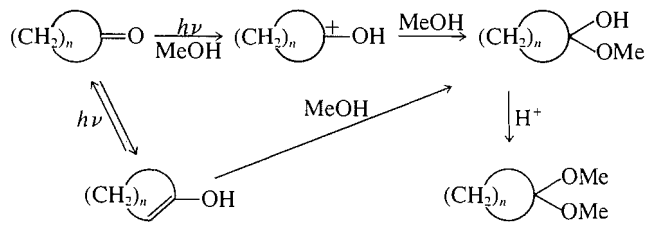

SCHEME 2

[1]NRCC No. 20589.
[2]To whom all correspondence should be addressed.
[3]NRC/Simon Fraser University Co-Op student.

0008-4042/83/020366-02$01.00/0
©1983 National Research Council of Canada/Conseil national de recherches du Canada

Can. J. Chem. Downloaded from www.nrcresearchpress.com by 210.87.254.42 on 09/06/12
For personal use only.

Neither the semiketal nor the enol ether are expected to absorb at the photolysing wavelength and their secondary photoreactions are hence precluded. This leads us to conclude that the final stage in ketal formation is catalysed by organic acids formed during the irradiation. The effect of acetate ion could then occur at two stages: by deprotonating the initial cation, reforming ketone; or by slowing the protonation of the hemiketal.

One might have expected that n—π* excitation of the carbonyl group would lead to decreased susceptibility to nucleophilic attack on carbon due to the influence of resonance structure **3** (16).

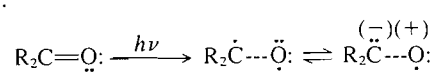

1 **2** **3**

However, this argument is only strictly applicable to gas phase systems (17) and may be extensively modified by hydrogen bonding in protic solvents.

Photochemically induced addition of alcohols to double bonds has been previously observed for cycloalkenones (18, 19), cyclic dienes (20–22), and olefins (23, 24). It was suggested that protonation of the triplet state of olefins (orthogonal or twisted) would relieve configurational strain, giving an intermediate with carbonium ion character (25). In the present case it is possible that protonation relieves the *ground state* ring strain and the variation in yield from cyclobutanone to cyclohexanone could reflect this.[4] However, there are many parallel reactions in these systems (cycloreversion, decarbonylation, and aldehyde and ketene formation) which complicate the mechanistic picture and make detailed interpretations premature. However, the reaction is of synthetic interest and studies of its scope and mechanism are in progress.

1. J. SWETON. J. Chem. Ed. **46**, 217 (1969).
2. R. SRINIVASAN. Advances in photochemistry. Vol. I. Wiley, New York. 1963. p. 83.
3. P. YATES. Pure Appl. Chem. **16**, 93 (1968).
4. G. QUINKERT. Angew. Chem. Intern. Ed. **4**, 211 (1965).
5. P. WAGNER and R. W. SPOERKE. J. Am. Chem. Soc. **91**, 4437 (1969).
6. J. C. DALTON, D. M. POND, D. S.WEISS, F. D. LEWIS, and N. J. TURRO. J. Am. Chem. Soc. **92**, 2564 (1970).
7. D. S. WEISS, N. J. TURRO, and J. C. DALTON. Mol. Photochem. **2**, 91 (1970).
8. J. C. DALTON, K. DAWES, N. J. TURRO, D. S. WEISS, J. A. BALTROP, and J. D. COYLE. J. Am. Chem. Soc. **93**, 7213 (1971).
9. J. A. BALTROP and J. D. COYLE. Chem. Commun. 390 (1970).
10. N. J. TURRO and R. M. SOUTHAM. Tetrahedron Lett. 545 (1967).
11. D. R. MORTON, E. LEE-RUFF, R. M. SOUTHAM, and N. J. TURRO. J. Am. Chem. Soc. **92**, 4349 (1970).
12. P. YATES and R. O. LOUFTY. Acc. Chem. Res. **75**, 209 (1975) and references therein.
13. C. A. MCKENZIE and J. H. STOCKER. J. Org. Chem. **20**, 1695 (1955).
14. R. B. WAGNER and H. D. LOOK. Synthetic organic chemistry. J. Wiley, New York. 1953. Chapt. 8.
15. N. B. LORETTE and W. L. HOWARD. J. Org. Chem. **25**, 521 (1959).
16. H. E. ZIMMERMANN. Science, **153**, 837 (1966).
17. D. E. FREEMAN and W. KLEMPERER. J. Chem. Phys. **40**, 604 (1964).
18. O. L. CHAPMAN, J. B. SEIJIA, and W. J. WELSTEAD JR. J. Am. Chem. Soc. **88**, 161 (1966).
19. T. MATSURRA and K. OGURA. J. Am. Chem. Soc. **88**, 2602 (1966).
20. W. G. DAUBER and W. T. WIPKE. Pure App. Chem. **9**, 539 (1964).
21. T. N. HUCKERBY, N. A. ROGERS, and A. SATTAR. Tetrahedron Lett. 1113 (1967).
22. G. BAUSLAGH, G. JUST, and E. LEE-RUFF. Can. J. Chem. **44**, 2837 (1966).
23. J. A. MARSHALL and R. D. CARROLL. J. Am. Chem. Soc. **88**, 4092 (1966).
24. P. J. KROPP. J. Am. Chem. Soc. **88**, 4091 (1966).
25. P. J. KROPP and H. J. KRAUSS. J. Am. Chem. Soc. **89**, 5199 (1967).
26. P. LIPP, J. BUCHKREMER, and H. SEELES. Ann. Chem. **499**, 1 (1932).

[4]Cyclopropanone is reported to give hemiketals by spontaneous reaction with alcohols. See ref. 26.

Can. J. Chem. Downloaded from www.nrcresearchpress.com by 210.87.254.42 on 09/06/12
For personal use only.

Syntheses of 1-trifluoromethyl-2-naphthalenols via a novel construction of the naphthalene nucleus

STEVEN FUNG, NEDUMPARAMBIL A. ABRAHAM, FRANCESCO BELLINI, AND KAZIMIR SESTANJ
Department of Chemistry, Ayerst Laboratories, P.O. Box 6115, Montreal, P.Q., Canada H3C 3J1

Received July 8, 1982

STEVEN FUNG, NEDUMPARAMBIL A. ABRAHAM, FRANCESCO BELLINI, and KAZIMIR SESTANJ. Can. J. Chem. **61**, 368 (1983).

A relatively simple and efficient synthesis of the hitherto unknown 1-trifluoromethyl-2-naphthalenols is described. Easily accessible benzenoid precursors **6** and **7** were converted to the oximino-ketones **8** and **9** by nitrosation. A novel cyclization and hydrolysis afforded surprisingly stable hydroxytetralones **12** and **13** which in turn were aromatized to the naphthalenols **1** and **15**.

STEVEN FUNG, NEDUMPARAMBIL A. ABRAHAM, FRANCESCO BELLINI et KAZIMIR SESTANJ. Can. J. Chem. **61**, 368 (1983).

On décrit une synthèse efficace relativement simple des trifluorométhyl-1 naphtalénols-2 inconnus jusqu'ici. On a transformé les précurseurs benzenoïdes **6** et **7** facilement accessibles en oximino cétones **8** et **9** par nitrosation. Une nouvelle cyclisation et une hydrolyse conduisent d'une façon surprenante aux hydroxytétralones **12** et **13** stables qui à leur tour sont aromatisés en naphtalénols **1** et **15**.

[Traduit par le journal]

We have recently been interested in general synthetic methods for the preparation of the hitherto unknown 1-trifluoromethyl-2-naphthalenol (**1**) and its congeners, which can serve as intermediates in the synthesis of compounds of potential therapeutic utility.

Demethylation of the methyl ether **2** would be the method of choice since **2** can be easily obtained from 1-iodo-2-methoxynaphthalene, iodotrifluoromethane, and copper powder under pressure (1). Unfortunately, the naphthalenol **1** belongs to a class of compounds generally known to be sensitive to demethylation reaction conditions (2, 3) and consequently has never been prepared by this route. In addition, the trifluoromethylation reaction itself becomes prohibitively expensive on a large scale due to costly trifluoromethyl iodide and special alloy pressure equipment.

Herein, we wish to report a relatively simple and efficient synthesis of the naphthalenols and their derivatives involving a *de novo* construction of the naphthalene ring and introduction of the trifluoromethyl group without application of high pressure reactions.

Our synthetic plan consisted, in principle (Retrosynthetic Scheme), of cyclization of a benzenoid precursor (**3**) containing a trifluoromethyl group and two carbonyl functions in the side chain. The percursor **3** in turn could be prepared from the inexpensive and easily available γ-halopropyl-benzene and trifluoroacetic acid.

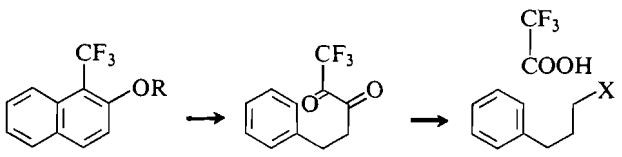

1 R = H
2 R = CH_3

3

Retrosynthetic Scheme

Reaction of organomagnesium compounds with trifluoroacetic acid results in the formation of trifluoromethyl ketones in reasonable yields. According to Dishart and Levine (4), the reaction is best performed with a threefold excess of the organomagnesium compound.

In the execution of the synthesis we used the Grignard reagent prepared from commercially available 3-bromopropylbenzene (**4**). In order to reduce the amount of starting material required, less expensive ethylmagnesium bromide was employed for the *in situ* conversion of the trifluoroacetic acid to the bromomagnesium salt. Subsequent addition of 1.5 moles of phenylpropylmagnesium bromide to the salt gave ketone **6** in 55% yield.

Introduction of the second functional group was initially attempted by selenium dioxide oxidation of the ketone **6**. The reaction, performed in methanol, ethanol, or acetic acid, did not give the expected diketone **3**. Better results were obtained by the nitrosation with sodium nitrite in water/acetic acid giving a 42% yield of keto-oxime **8**.

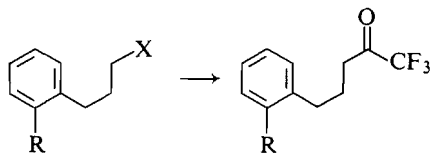

4 X = Br, R = H
5 X = Cl, R = CH_3

6 R = H
7 R = CH_3

However, the conversion of **8** to the diketone **3** proved quite troublesome. Acidic hydrolysis (dilute hydrochloric or sulfuric acids) and acid catalyzed carbonyl exchange reactions (e.g. with pyruvic acid, acetone, etc.) resulted in complex mixtures from which no diketone **3** could be isolated. A surprising result was obtained by treating **8** with 85% sulfuric acid. The cyclized oxime **10** was formed as the principal reaction product (69%

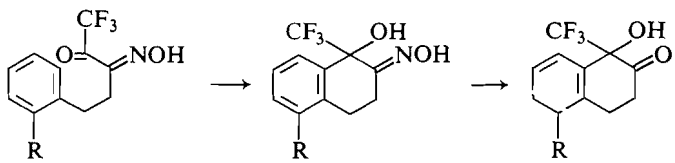

8 R = H
9 R = CH_3

10 R = H
11 R = CH_3

12 R = H
13 R = CH_3

0008-4042/83/020368-04$01.00/0
©1983 National Research Council of Canada/Conseil national de recherches du Canada

Can. J. Chem. Downloaded from www.nrcresearchpress.com by 210.87.254.40 on 09/06/12
For personal use only.

Can. J. Chem. Downloaded from www.nrcresearchpress.com by 210.87.254.40 on 09/06/12
For personal use only.

yield). Besides hydrolysis, several other reactions could be expected to occur, e.g. Beckmann rearrangement or scission between two sp^2 carbon atoms (8). Preferential cyclization in the case of **8** (and **9**) undoubtedly has to be ascribed to the presence of the strongly electronegative trifluoromethyl group. The electron deficiency of the neighbouring carbonyl carbon facilitates the intramolecular electrophilic substitution on the nearby aromatic system. Subsequent hydrolysis with concentrated hydrochloric acid gave the hydroxyketone **12** in 54% yield. Attempted conversion of **10** to **12** in the presence of sodium bisulfite effected ring cleavage to give the unwanted ketonitrile **14** (arising from a carbon–carbon bond scission and concomitant loss of water, **14***a*). Interestingly enough, the hydroxyketone **12** was not detected in the mixture of products obtained in the attempted preparation of **3** by hydrolysis of the oxime **8**.

Although a vinylogous dehydration of **10** or **12**, accompanied (or preceded) by enolization of the keto- or oximino-groups (**17**), would result in the formation of a fully aromatic

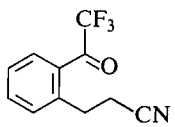

14

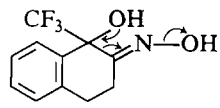

14*a*

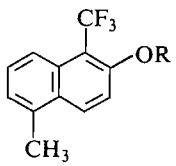

15 R = H
16 R = CH_3

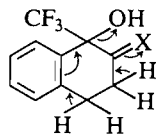

17

(**10** X = NOH
12 X = O)

system (e.g. **12** → **1**), it did not occur spontaneously or under the reaction conditions employed to prepare the compounds. Remarkable stability of the hydroaromatic system of these compounds is apparently due also to high electronegativity of the trifluoromethyl group which makes the hydroxyl tightly bound to the tertiary carbon atom. Removal of the elements of water requires more energetic treatment. The hydroxyketone **12** was thus aromatized to **1** by dehydration with either trifluoroacetic anhydride/pyridine and a catalytic amount of 4-dimethylaminopyridine at room temperature (75% yield of **1**) or with thionyl chloride/pyridine at 70°C (81% crude yield).

The applicability of the above method for the preparation of ring substituted 1-trifluoromethyl-2-naphthalenol analogs was demonstrated by the synthesis of the naphthalenol **15**. The required starting material, *o*-(3-chloropropyl)toluene (**5**) was prepared by chlorotricarbon homologation (5) of *o*-tolylmagnesium chloride with 1-bromo-3-chloropropane in excellent yield (90%).

Only a few nonessential modifications were applied in some of the steps. Instead of trifluoroacetic acid (or its halomagnesium salt), in the preparation of ketone **7**, the lithium salt

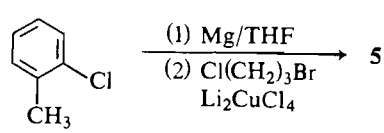

was employed (6). The yield was 85%. Nitrosation of **7** was performed with either sodium nitrite/acetic acid/isopropanol (51% yield) or with potassium nitrite/acetic acid/*tert*-butanol, giving an almost quantitative yield of the crude keto-oxime **9**. Cyclization of **9** to **11** was performed with cold concentrated sulfuric acid. Hydrolysis of **11** and dehydration of the resulting hydroxyketone **13** gave the naphthalenol **15** in an overall yield (from *o*-chlorotoluene) of 57%. The methyl ethers **2** and **16** were obtained by methylation of **1** and **15** with dimethylsulfate.

The synthesis, we believe, is one of general significance and, besides containing some new and unusual features, provides an inexpensive and efficient route to various substituted 1-trifluoromethyl-2-naphthalenols.

Experimental

Infrared spectra were recorded on a Perkin–Elmer 225 spectrophotometer, ultraviolet spectra on a Zeiss DMR-21 spectrophotometer, nmr spectra on a Varian CFT-20 spectrometer, and mass spectra on a LKB 9000S. Melting points were recorded on a Thomas Hoover capillary melting point apparatus and are uncorrected.

5-Phenyl-1,1,1-trifluoro-2-pentanone (6)

A solution of ethylmagnesium bromide (0.37 mol) in anhydrous ether (96 mL) was added dropwise under nitrogen to a stirred solution of trifluoroacetic acid (24.9 mL, 0.33 mol) in anhydrous ether (84 mL) at −5 to −10°C. The reaction mixture was allowed to warm to room temperature to produce the magnesium bromide salt of trifluoroacetic acid. A solution of 3-bromopropylbenzene (100 g, 0.50 mol, Eastman) in anhydrous ether (130 mL) was added dropwise with stirring to magnesium (13.4 g, 0.55 mol), iodine (catalytic amount), and anhydrous ether (~10 mL) at a rate to maintain a steady reflux. The mixture was refluxed until the reaction was complete (~2 h). To the resulting Grignard solution was added dropwise under nitrogen the trifluoroacetic acid salt suspension at ~5°C. The reaction mixture was stirred overnight at room temperature and cold HCl (8 *N*, 123 mL) was added dropwise at 0°C. The solid was separated by filtration and the aqueous layer extracted with ether. The organic layer was washed with brine, dried ($MgSO_4$), concentrated, and distilled (40°C/10 Torr) to give pure **6** (40 g, 55%)[1] as a colorless liquid; ir ($CHCl_3$): 1760, 1160, 1140 cm^{-1}; nmr ($CDCl_3$) δ: 7.2 (5H, m, ArH), 2.65 (4H, m, $ArCH_2$, $COCH_2$), 2.0 (2H, m, $ArCH_2CH_2$); ms *m/e*: 216 (M^+), 147, 136, 118, 104, 91 (100).

3-Oximino-5-phenyl-1,1,1-trifluoro-2-pentanone (8)

A solution of sodium nitrite (6.5 g, 94.2 mmol) in water (10 mL) was added dropwise to a stirred solution of **6** (10.0 g, 46.3 mmol) in acetic acid (10 mL) at 0°C. The reaction mixture was stirred overnight at room temperature, diluted with water, and extracted with ethyl acetate (2×). The combined organic layers were washed with brine, dried ($MgSO_4$), and concentrated under reduced pressure. Recrystallization (hexane) of the residue gave **8** as pale yellow crystals (4.75 g, 42%). An analytically pure sample of **8** was obtained as colorless prisms, mp 92–93°C by sublimation (60°C/0.05 Torr); ir ($CHCl_3$): 3540, 3350, 1730, 1160 cm^{-1}; nmr ($CDCl_3$) δ: 7.2 (5H, m, ArH), 2.85 (4H, m, CH_2); ms *m/e*: 245 (M^+), 228, 176, 148, 131, 104, 91 (100). *Anal.* calcd. for $C_{11}H_{10}F_3NO_2$: C 53.88, H 4.11, N 5.71; found: C 54.12, H 4.18, N 5.60.

1-Hydroxy-2-oximino-1-trifluoromethyl-1,2,3,4-tetrahydronaphthalene (10)

Sulfuric acid (85%, 80 mL) was added to **8** (1.6 g, 6.5 mmol), cooled in an ice–water bath. The reaction mixture was stirred and heated on a steam bath for 10 min, cooled, and extracted with ether. The ethereal extract was washed with brine, dried ($MgSO_4$), and concentrated under reduced pressure. The residue was recrystallized twice (hexane) to give **10** (1.1 g, 69%) as white crystals, mp 121–122°C; ir ($CHCl_3$): 3560, 3480, 1170 cm^{-1}; nmr ($CDCl_3$) δ: 7.75

[1]It was estimated (nmr) that the distillation forerun contained additional **6** (15.6 g).

Can. J. Chem. Downloaded from www.nrcresearchpress.com by 210.87.254.40 on 09/06/12
For personal use only.

(1H, m, ArH), 7.45 (1H, bs, OH), 7.2 (3H, m, ArH), 4.55 (1H, bs, OH), 2.9 (4H, m, CH_2); ms *m/e*: 245 (M^+), 176 (100), 158, 148, 131, 130, 103. *Anal.* calcd. for $C_{11}H_{10}F_3NO_2$: C 53.88, H 4.11, N 5.71; found: C 53.84, H 4.14, N 5.63.

1-Hydroxy-2-oxo-1-trifluoromethyl-1,2,3,4-tetrahydronaphthalene (12)

A solution of **10** (1.5 g, 6.1 mmol) in concentrated HCl (150 mL) was stirred at 65°C for 2 h. The product started to precipitate after 15 min. The reaction mixture was cooled, poured into ice, stirred, and filtered to give crude **12**. Ether extraction of the filtrate gave additional crude material. Recrystallization (hexane) of the crude product gave purified **12** (0.98 g, 70%) as pale yellow crystals, mp 87–88°C; ir ($CHCl_3$): 3460, 1730, 1175 cm^{-1}; nmr ($CDCl_3$) δ: 7.65 (1H, m, ArH), 7.25 (3H, m, ArH), 4.5 (1H, s, OH), 3.1 (4H, m, CH_2); ms *m/e*: 230 (M^+), 188, 161, 133, 119 (100), 105, 91. *Anal.* calcd. for $C_{11}H_9F_3O_2$: C 57.40, H 3.94; found: C 57.09, H 3.91.

3-(2-Trifluoroacetylphenyl)propionitrile (14)

A solution of **10** (603 mg, 2.45 mmol) and sodium bisulfite (1.02 g, 9.8 mmol) in ethanol (15 mL) and water (15 mL) was refluxed for 8 h and concentrated under reduced pressure. Water was added and the mixture extracted with chloroform. The extract was dried ($MgSO_4$) and concentrated under reduced pressure. The residue was recrystallized (hexane) to give **14** (300 mg, 54%) as flat needles, mp 48–49°C; ir ($CHCl_3$): 2240, 1715, 1185, 1150 cm^{-1}; nmr ($CDCl_3$) δ: 7.95 (1H, m, ArH), 7.5 (3H, m, ArH), 3.15 (2H, t, J = 7, $ArCH_2$), 2.7 (2H, t, J = 7, CH_2CN); ms *m/e*: 227 (M^+), 200, 187, 158 (100), 130, 103. *Anal.* calcd. for $C_{11}H_8F_3NO$: C 58.15, H 3.55, N 6.17; found: C 57.82, H 3.56, N 6.18.

1-Trifluoromethyl-2-naphthalenol (1)

Trifluoroacetic anhydride (2.0 mL, 14.2 mmol) was added dropwise under anhydrous conditions to a solution of **12** (0.4 g, 1.74 mmol) and 4-dimethylaminopyridine (5 mg) in pyridine (20 mL, 24.7 mmol). The reaction mixture was stirred overnight at room temperature, poured into ice, stirred, and extracted with ether. The ethereal extract was washed with dilute HCl, brine, sodium bicarbonate solution, and brine, dried ($MgSO_4$), and concentrated under reduced pressure. The residue was triturated with hexane and column chromatographed (silica gel, 20% ethyl acetate/toluene) to give **1** (0.28 g, 75%). An analytical sample was prepared by sublimation (25°C/0.05 Torr) to give **1** as white crystals, mp 55–56°C; ir ($CHCl_3$): 3620, 1235, 1210 cm^{-1}; uv (CH_3OH): 331 (2760), 319 (2440), 287 (3300), 276 (4470), 266 (3990), 223 nm (68 500); nmr ($CDCl_3$) δ: 7.9 (1H, m, H-8), 7.8 (1H, d, J = 9, H-4), 7.5 (3H, m, ArH), 7.05 (1H, d, J = 9, H-3); ms *m/e*: 212 (100) (M^+), 192, 170, 164. *Anal.* calcd. for $C_{11}H_7F_3O$: C 62.27, H 3.33, found: C 61.61, H 3.18.

Alternative preparation of 1

Thionyl chloride (0.20 mL, 2.74 mmol) was added dropwise to a solution of **12** (50 mg, 0.22 mmol) in pyridine (0.5 mL) at 0°C. The reaction mixture was heated at 70°C for 2 h and concentrated under reduced pressure. Ice was added and the mixture extracted with ether. The ethereal extract was washed with brine, dried ($MgSO_4$), and concentrated under reduced pressure to give **1** (37.5 mg, 81%), homogenous by tlc.

2-Methoxy-1-trifluoromethylnaphthalene (2)

A mixture of **1** (52 mg, 0.25 mmol), dimethyl sulfate (0.030 mL, 0.32 mmol), potassium carbonate (53 mg, 0.038 mmol), and acetone (1 mL) was stirred at room temperature for 20 h. The solvent was evaporated and the residue diluted with water and extracted with hexane (3×). The combined extracts were dried ($MgSO_4$) and concentrated under reduced pressure. The crude material was purified by preparative tlc (silica, 10% ethyl acetate/hexane) to give **2** as slightly yellow crystals (45 mg, 81%), mp 52–53°C; ir ($CHCl_3$); 1620, 1595, 1505, 1345, 1295, 1205, 1105, 1065 cm; uv (CH_3OH): 333 (2690), 319 (2430), 291 (3490), 279 (4455), 270 (3780), 224 nm (54 410). Compound **2** was identical (mp, tlc, ir, uv) with authentic material prepared according to ref. 1.

o-(γ-Chloropropyl)toluene (5)

A mixture of freshly distilled *o*-chlorotoluene (94.9 g, 0.75 mol), magnesium (18.23 g, 0.75 mol), and iodide (catalytic amount) was stirred in an oil bath kept at 145°C. Dry tetrahydrofuran (3 mL) was added. The reaction began within 1/2 h. More tetrahydrofuran (333 mL) was added dropwise over 2 h. The reaction temperature was not allowed to rise above 145°C by controlling the rate of addition of tetrahydrofuran. The oil bath temperature was decreased gradually to 120°C during the tetrahydrofuran addition and kept at 120°C for another 2 h. The *o*-tolylmagnesium chloride solution was decanted under anhydrous conditions into a cooled mixture (−78°C) of 1-bromochloropropane (94.4 g, 0.6 mol), Li_2CuCl_4 (0.1 *M* in tetrahydrofuran, 18 mL) (7), and tetrahydrofuran (210 mL). The mixture was stirred overnight at room temperature, cooled in ice, and a solution of NH_4Cl (30 g) in water (90 mL) was added. The mixture was extracted with ether. The organic layer was washed with brine, dried (Na_2SO_4), and concentrated under reduced pressure. The residue was distilled (58–60°C/0.05 Torr) to give **5** (91.1 g, 90%) as a colorless oil; ir ($CHCl_3$): 1600, 1490, 1455, 1440, 1375 cm^{-1}; nmr ($CDCl_3$) δ: 7.1 (4H, m, ArH), 3.55 (2H, t, J = 6, $ClCH_2$), 2.8 (2H, t, J = 7.5, $ArCH_2$), 2.35 (3H, s, CH_3), 2.05 (2H, m, $ArCH_2CH_2$); ms *m/e*: 168 (100) (M^+), 132, 117, 105.

5-(o-Tolyl)-1,1,1-trifluoro-2-pentanone (7)

The Grignard reagent was prepared from **5** (88.1 g, 0.522 mol), magnesium (12.6 g, 0.522 mol), and a catalytic amount of iodine in anhydrous ether (366 mL). It was reacted in a similar manner as described for the preparation of **6** with a suspension of lithium trifluoroacetate (50 g, 0.417 mol) (6) in anhydrous ether (366 mL) at −78°C. After the usual work-up, the crude liquid was distilled (68–70°C/1.55 Torr) to give **7**; ir ($CHCl_3$): 1760 cm^{-1}; nmr ($CDCl_3$) δ: 7.05 (4H, s, ArH), 2.65 (4H, m, $ArCH_2$, $COCH_2$), 2.3 (3H, s, CH_3), 2.0 (2H, m, $ArCH_2$—CH_2); ms *m/e*: 230 (M^+), 161, 150, 132, 118 (100), 105.

3-Oximino-5-(o-tolyl)-1,1,1-trifluoro-2-pentanone (9)

A solution of potassium nitrite (22.2 g, 261 mmol) in water (7.4 mL) was added in one portion to a stirred solution of **7** (20.0 g, 86.9 mmol) in acetic acid (25 mL) and *tert*-butanol (50 mL) at room temperature. After stirring for 2.5 h, additional potassium nitrite solution (7.5 g/2.5 mL) was added to the reaction mixture and stirred for 1.5 h. A work-up similar to that of **8** gave crude **9** as a yellow crystalline material (22.1 g, 98%). It was used as starting material for **11**. An analytically pure sample of **9** was prepared by recrystallization (hexane) to give white crystals, mp 80–81°C; ir ($CHCl_3$): 3540, 3340, 1730, 1165 cm^{-1}; nmr ($CDCl_3$) δ: 7.1 (4H, s, ArH), 2.8 (4H, s, CH_2), 2.35 (3H, s, CH_3); ms *m/e*: 259 (M^+), 242, 190, 145, 118, 105 (100). *Anal.* calcd. for $C_{12}H_{12}F_3NO_2$: C 55.60, H 4.67, N 5.40; found: C 55.41, H 4.60, N 5.42.

1-Hydroxy-5-methyl-2-oximino-1-trifluoromethyl-1,2,3,4-tetrahydronaphthalene (11)

Concentrated H_2SO_4 (12 mL) was added at 0°C to a stirred suspension of crude **9** (11.9 g, 45.9 mmol) in toluene (16 mL). The reaction mixture was allowed to warm to room temperature with stirring for 30 min. The reaction was worked up in a similar manner as described in the preparation of **10** to give crude **11** as an amber coloured solid (10.4 g, 87%). Crude **11** was used as starting material for **13**. Analytically pure **11** was prepared by recrystallization (ether/hexane) to give white crystals, mp 160.5–161.5°C; ir ($CHCl_3$): 3570, 3480, 1165, 1115 cm^{-1}; nmr ($CDCl_3$) δ: 7.6 (1H, m, ArH), 7.2 (2H, m, ArH), 4.6 (1H, bs, OH), 2.9 (4H, m, CH_2), 2.3 (3H, s, CH_3); ms *m/e*: 259 (M^+), 190 (100), 173, 172, 162, 145, 144, 117. *Anal.* calcd. for $C_{12}H_{12}F_3NO_2$: C 55.60, H 4.67, N 5.40; found: C 55.60, H 4.65, N 5.36.

1-Hydroxy-5-methyl-2-oxo-1-trifluoromethyl-1,2,3,4-tetrahydronaphthalene (13)

Concentrated HCl (220 mL) and crude **11** (10.2 g, 39.4 mmol) were employed in a similar manner as described in the preparation of **12** to

give crude **13** as a yellow solid (8.7 g, 91%). An analytically pure sample was prepared by recrystallization (hexane) to give white crystals, mp 122–123°C; ir ($CHCl_3$): 3460, 1730, 1170, 1115 cm^{-1}; nmr ($CDCl_3$) δ: 7.55 (1H, m, ArH), 7.2 (2H, m, ArH), 4.6 (1H, s, OH), 3.1 (4H, m, CH_2), 2.3 (3H, s, CH_3); ms *m/e*: 244 (M^+), 175 (100), 147, 105. *Anal.* calcd. for $C_{12}H_{11}F_3O_2$: C 59.02, H 4.54; found: C 59.22, H 4.44.

*5-Methyl-1-trifluoromethyl-2-naphthalenol (**15**)*

Thionyl chloride (0.33 mL, 4.52 mmol), **13** (1.04 g, 4.26 mmol), 4-dimethylaminopyridine (3.5 mg), and pyridine (0.73 mL) were reacted at room temperature for 30 min in a manner similar to that described in the alternative preparation of **1**. Crude **15** was obtained as yellow crystals (961 mg, 100%) homogenous by tlc. An analytically pure sample was prepared by sublimation (30–35°C/0.05 Torr) to give **15** as white crystals, mp 83–84°C; ir ($CHCl_3$): 3620, 1125 cm^{-1}; uv (CH_3OH): 335 (2770), 322 (2420), 293 (4050), 281 (4680), 222 nm (46 400); nmr ($CDCl_3$) δ: 8.05 (1H, d, J = 9, H-4), 7.85 (1H, m, H-8), 7.35 (1H, q, J = 8, H-7), 7.25 (1H, m, H-6), 7.1 (1H, d, J = 9, H-3), 6.55 (1H, m, OH), 2.65 (3H, s, CH_3); ms *m/e*: 226 (100 (M^+), 206, 178. *Anal.* calcd. for $C_{12}H_9F_3O$: C 63.72, H 4.01; found: C 63.47, H 3.96.

*2-Methoxy-5-methyl-1-trifluoromethylnaphthalene (**16**)*

In similar fashion to that described for **2**, dimethylsulfate (1.13 g, 8.75 mmol), **15** (1.8 g, 7.96 mmol), potassium carbonate (2.2 g, 15.9 mmol), and dimethylformamide (20 mL) were reacted for 2 h at room temperature. The usual work-up gave crude **16** (1.7 g, 90%). An analytical sample was prepared by trituration of the crude solid with pentane and sublimation (45°C/0.05 Torr) to give pure **16** as white crystals, mp 69–70°C; ir ($CHCl_3$): 1390, 1340, 1280, 1255, 1245, 1110, 1095, 1085, 1045 cm^{-1}; uv (CH_3OH): 336 (2910), 323 (2645), 297 (4440), 286 (4880), 236 (30 050), 224 nm (46 730); nmr ($CDCl_3$) δ: 8.1 (1H, d, J = 9, H-4), 8.0 (1H, m, H-8), 7.35 (1H, q, J = 8, H-7), 7.2 (2H, m, H-3, H-6), 3.95 (3H, s, OCH_3), 2.65 (3H, s, $ArCH_3$); ms *m/e*: 240 (100) (M^+), 225, 221, 209, 197, 171. *Anal.* calcd. for $C_{13}H_{11}F_3O$: C 65.00, H 4.62; found: C 64.90, H 4.38.

Acknowledgements

We wish to thank Mrs. S. Goulet, Mr. G. Marcoux, Ms. H. Venda, Mr. Y. S. Lin, Mr. M. Boni, Mr. P. Bouca, and Mr. M. Barron, who performed a large part of the experimental work, and Dr. G. Schilling and his staff for the analytical and spectral data. The authors would also like to thank Dr. L. Humber and Prof. Z. Valenta for their interest and support.

1. K. Hosokawa, S. Fujii, and K. Inukai. Nippon Kagaku Kaishi, 294 (1979); Y. Kobayashi *et al.* J. Chem. Soc. Perkin Trans. I, 2755 (1980), and references therein.
2. P. Seiler and J. Wirz. Helv. Chim. Acta, **55**, 2693 (1972).
3. H. J. Wirz. Eidg. Tech. Hochsch. Dissertation 4614, Zurich, 1970. p. 36.
4. K. T. Dishart and R. Levine. J. Am. Chem. Soc. **78**, 2268 (1955).
5. L. Friedman and A. Shani. J. Am. Chem. Soc. **96**, 7101 (1974).
6. D. A. Rausch, A. M. Lovelace, and L. E. Coleman, Jr. J. Org. Chem. **21**, 1328 (1956); G. W. Astrologes and J. C. Martin. J. Am. Chem. Soc. **98**, 2895 (1976).
7. M. Tamura and J. Koshi. Synthesis, 303 (1971).
8. L. G. Donaruma and W. Z. Heldt. Org. React. **11**, 35 (1960).

Can. J. Chem. Downloaded from www.nrcresearchpress.com by 210.87.254.40 on 09/06/12
For personal use only.

On the biosynthesis of some polyketide metabolites in *Alternaria solani*: ^{13}C and ^{2}Hmr studies[1,2]

ALBERT STOESSL AND C. H. UNWIN
Canada Agriculture, London Research Centre, University Sub Post Office, London, Ont., Canada N6A 5B7

AND

J. B. STOTHERS
Department of Chemistry, University of Western Ontario, University Sub Post Office, London, Ont., Canada N6A 5B7

Received July 29, 1982

ALBERT STOESSL, C. H. UNWIN, and J. B. STOTHERS. Can. J. Chem. **61**, 372 (1983).

^{13}C nuclear magnetic resonance spectroscopy has revealed that cultures of the fungus *Alternaria solani* incorporate [1,2-$^{13}C_2$]acetate into the anthraquinone macrosporin (**3**) and the tetrahydroanthraquinones altersolanol A (**4**) and dactylariol (**6**) from a single octaketide chain. The carbon skeleton of **4**-$^{13}C_x$ was incorporated *in toto* into **3**, with **6** as a probable intermediate; there is also evidence that **4** may be a precursor of altersolanol B (**5**). The ^{2}Hmr spectra show that deuterium from [1-$^{13}C_1$,2-$^{2}H_3$]acetate is retained to a considerable extent in the C-methyl groups and the 1, 6, and 8 positions of **3** and **4** but is completely lost from the 3-position in **4**. Zinniol (**7**), also a metabolite of the fungus, is a normal tetraketide.

ALBERT STOESSL, C. H. UNWIN et J. B. STOTHERS. Can. J. Chem. **61**, 372 (1983).

La spectroscopie de la rmn du ^{13}C a révélé que les cultures du champignon *Alternaria solani* incorporent l'acétate [$^{13}C_2$-1,2] dans l'anthraquinone macrosporine (**3**) et dans les tétrahydroanthraquinones altersolanol A (**4**) et dactylariol (**6**) à partir d'une chaîne simple d'octacétide. Le squelette carboné $^{13}C_x$-**4** est incorporé *in toto* dans le composé **3** utilisant probablement le composé **6** comme intermédiaire; on a aussi des données à l'effet que le composé **4** peut être un précurseur de l'altersolanol B (**5**). Les spectres de rmn du ^{2}H montrent que le deutérium de l'acétate [$^{13}C_1$-1-$^{2}H_3$-2] est retenu dans une grande proportion dans les groupes C-méthyle et au niveau des positions 1, 6 et 8 des composés **3** et **4** mais qu'il n'y a pas de deutérium en position 3 du composé **4**. Le zinniol (**7**), un métabolite du champignon est un tétracétide normal.

[Traduit par le journal]

Can. J. Chem. Downloaded from www.nrcresearchpress.com by 210.87.254.5 on 09/06/12
For personal use only.

The fungus *Alternaria solani* (Ell. & Mart.) Sorauer, the causative organism of early blight disease of tomato and potato (1), produces the following yellow and orange pigments: 2-methylxanthopurpurin-7-methyl ether (**1**), 7-methoxy-2-methyl-3,4,5-trihydroxyanthraquinone (**2**), macrosporin (**3**), altersolanol A (**4**), and altersolanol B (**5**) (2). The last two compounds are rare but not unique examples of naturally occurring tetrahydroanthraquinones (3, 4). Macrosporin, an anthraquinone, is known from several *Alternaria* spp. (5) and from two other, unrelated fungi, *Phomopsis juniperovora* (6) and *Dactylaria lutea* (5). It is significant that the latter fungi are also producers of **4**, and of **4** and **5**, respectively. The location of the hydroxyl group at the 3-position of macrosporin is anomalous for a polyketide-derived anthraquinone, as pointed out by Turner (7). Two further *A. solani* metabolites were discovered during the course of the present study, as reported in preliminary form (8). One is dactylariol (**6**),[3] which had been found previously as a congener of altersolanols A and B in *D. lutea* (5), and the other is zinniol (**7**), described earlier as phytotoxin from *A. zinniae* (9) and also, very recently, as a metabolite of *A. dauci* (10) and *A. carthami* (11).

The principal objective of the present study was to gain insight into the biosynthesis of these compounds by means of now well-established nmr methodology utilizing [1,2-$^{13}C_2$]- and [1-^{13}C,2-$^{2}H_3$]acetate as precursors. As a prerequisite, the

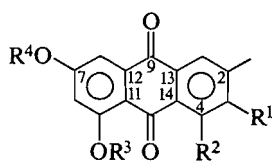

1–3

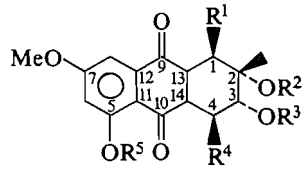

4–6

	R^1	R^2	R^3	R^4	R^5
1	H	H	H	Me	
1*a*	H	H	Ac	Ac	
2	OH	OH	OH	Me	
2*a*	OAc	OAc	Ac	Me	
3	OH	H	H	Me	
3*a*	OAc	H	Ac	Me	
4	OH	H	H	OH	H
4*a*	OAc	Ac	Ac	OAc	Ac
4*b*	OAc	H	Ac	OAc	Ac
4*c*	OAc	*		OAc	Ac
5	H	H	H	H	H
5*a*	H	Ac	Ac	H	Ac
6	OH	H	H	H	H

*isopropylidene group

^{13}Cmr spectra of the compounds and/or of pertinent derivatives were examined and the ^{13}C shielding data are collected in Table

[1]Part VII of the series, Metabolites of *Alternaria solani*; for Part VI, see ref. 20; Part V, ref. 8.

[2]Part 100 in the series ^{13}Cmr Studies; for Part 99, see ref. 21; for Part 98, see ref. 22; for Part 97, see ref. 23; for Part 96, see ref. 24.

[3]Through a most regrettable oversight, our preliminary report (8) refers to this compound as altersolanol C.

0008-4042/83/020372-06$01.00/0

©1983 National Research Council of Canada/Conseil national de recherches du Canada

Can. J. Chem. Downloaded from www.nrcresearchpress.com by 210.87.254.5 on 09/06/12
For personal use only.

1. The specific signal assignments were made through the usual methods (12)[4] primarily including detailed examination of the coupled spectra and, in a few cases, selective decoupling experiments. The relative intensities exhibited by the non-protonated carbons in both coupled and decoupled spectra are particularly informative for specific assignments since the number of neighboring protons governs the magnitude of the nuclear Overhauser enhancement experienced by these centres. In addition, data for several closely-related anthraquinones are readily available (13–16) from which it had been established that substitution in one of the aryl rings has relatively little effect on the ^{13}C shieldings for the other ring. For example, the shieldings for C-5 through C-13 in **1***a* were found to differ, on average, by 0.2 ppm from those for the corresponding centres in 1,3-diacetoxyanthraquinone (14). The same comparison revealed a −1.9 ppm upfield shift for C-14, readily attributable to the 2-methyl group to which it is *para*. The remaining aryl assignments followed from the results for 2-methylanthraquinone (15) with C-1 and -4 readily distinguished in a coupled spectrum because of the three-bond couplings for the former with H-3 and the methyl protons (16). Similarly, the signals for C-5 through C-13 in the spectra of **2***a* and **3***a* were easily identified by comparison with the results of 1-acetoxy-3-methoxyanthraquinone (14) and the assignments completed by consideration of the effects produced by the remaining substituents. Confirmation of the assignments for macrosporin diacetate (**3***a*) was provided by the spectra of the enriched samples obtained from incorporation experiments with doubly labelled [1,2-$^{13}C_2$]acetate.

Compounds **4**–**6** are 1,2,3,4-tetrahydroanthraquinone derivatives for which the C-5 through C-12 assignments could be made by comparison with the results for the corresponding centres in 1-acetoxy-3-methoxy or 1-hydroxy-3-methoxyanthraquinone (14). Although the data for the latter are reported for $CDCl_3$ solutions, the shieldings observed for **4** and **6** in DMSO-d_6 are not greatly different as was expected from the earlier comparison of the shieldings for the 1-hydroxy and 1-methoxyanthraquinone derivatives in both $CDCl_3$ and DMSO-d_6 (14). From the remarkable similarity of the shieldings of C-5 through C-12 for **4***a*–*c* and **5***a* it is apparent that differing substitution on the tetrahydro ring has little effect at these centres. With the exception of C-11 and -12, the observed shieldings are within 1 ppm of those for the corresponding carbons in 1-acetoxy-3-methoxyanthraquinone; C-11 and -12 apparently experience upfield shifts of −1 and −2 ppm in the tetrahydro derivatives. Assignments for the sp^3-carbons in the **4***a*–*c*, **5***a*, and **6** were essentially straightforward since C-3 in each could be identified by selective decoupling as could C-1 in **4***a*–*c* and **6**. Again, these assignments were confirmed by spectra of enriched **4**, **4***a*, and **6** obtained from the incorporation experiments.

For the biosynthetic studies, labelled precursors were administered to actively growing cultures of the fungus from which the labelled metabolites were isolated after an appropriate incubation period, as detailed in the Experimental. From the first set of experiments, the ^{13}Cmr spectra of the purified products (and/or their acetates) showed that [1,2-$^{13}C_2$]acetate was incorporated into macrosporin (**3**), altersolanol A (**4**), and dactylariol (**6**). The ^{13}C—^{13}C couplings in the spectra (Table 2) were similar and proved that the molecules arise from octa-

TABLE 1. ^{13}C shieldings of **1**–**6**[a]

Compound	Solvent[b]	C-1	C-2	C-3	C-4	C-5	C-6	C-7	C-8	C-9	C-10	C-11	C-12	C-13	C-14	OMe	Me	Other
1*a*	A	127.3	145.1	135.4	127.5	151.6	123.0	154.9	118.6	181.8	180.7	122.6	136.5	132.4	131.9		21.8	21.1(2) 169.2, 169.8
2*a*	A	127.2	138.6	147.3	142.4	152.3	116.4	164.1	109.4	181.5	179.2	119.3	135.9	131.1	124.8	56.2	16.8	20.2, 20.8, 21.2 167.4, 188.3, 169.2
3*a*	A	130.1	137.0	154.3	120.7	152.5	115.8	164.3	110.0	181.7	179.6	118.6	136.7	130.2	134.0	56.2	16.5	20.7, 21.1 168.2, 169.3
4	B	68.6	73.0	73.9	68.7	163.3	105.9	165.6	106.7	183.9	188.6	109.6	133.3	142.2	144.5	56.2	22.4	
4*a*	A	64.1	81.1	73.5	67.3	151.7	115.7	164.6	109.5	181.7	180.0	117.4	134.8	137.8	143.7	56.2	17.0	20.7(3), 21.0, 21.9 168.3, 169.2(2) 169.6, 170.4
4*b*	A	68.0	72.5	74.6	68.7	151.5	115.6	164.4	109.1	182.4	180.2	117.5	134.7	143.7	138.0	56.2	21.1	20.7, 20.9, 21.3(2) 169.1, 169.4, 170.0, 170.6
4*c*	A	64.0	81.5	81.0	66.4	152.0	115.8	164.5	109.8	181.9	179.6	117.0	135.1	142.2	141.6	56.2	24.2	25.0, 25.3(2), 27.0 27.7
5*a*	A	31.3	78.3	71.0	26.9	151.2	114.4	163.6	109.3	182.3	180.8	116.3	134.7	141.4	139.3	55.7	21.7	169.3(3), 109.6 20.6(2), 20.8 169.6(2), 168.7
6	B	69.3	72.0	66.8	29.0	163.4	105.6	165.6	107.0	182.9	188.2	109.1	133.5	143.0	144.0	56.3	21.9	

[a]Given in ppm from internal TMS.
[b]A = $CDCl_3$; B = DMSO-d_6.

[4] These references present discussion of signal assignments in polycyclic aryl systems.

TABLE 2. $^{13}C—^{13}C$ Coupling constants[a] as determined by [1,2-$^{13}C_2$]acetate incorporation into *A. solani* metabolites

Compound	$^{13}C—^{13}C$ Couplings						
	Me-2	1–13	9–12	8–7	6–5	11–10	14–4
3*a*	44	60	54	67	73	54	62
4	41	47	54	66	69	57	44
4*a*	40	48	55	68	72	60	50
6	41	47	56	65	69	53	42

[a]*J* values in Hz; estimated precision ±1 Hz.

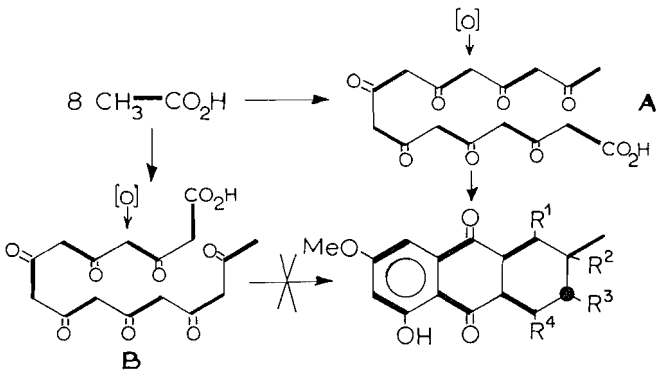

SCHEME 1. Biosynthesis of anthraquinoid metabolites.

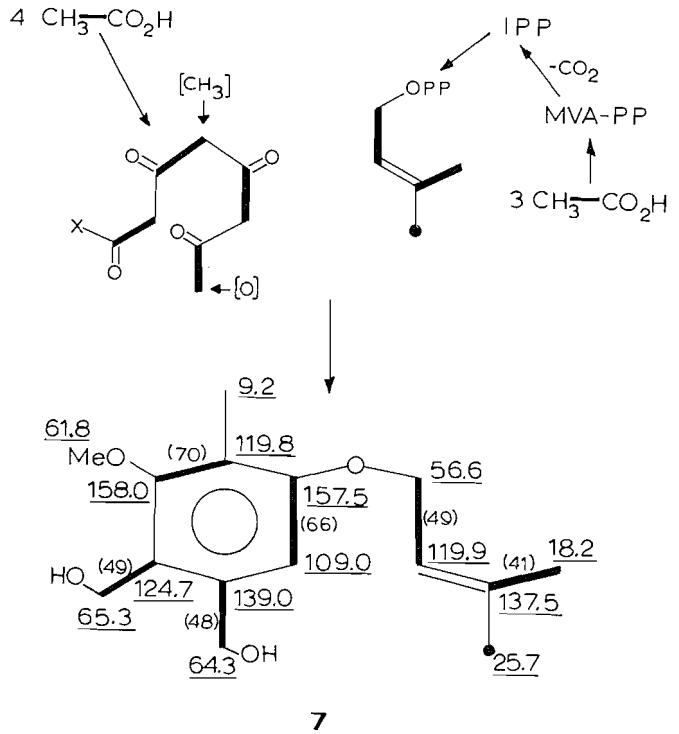

SCHEME 2. The ^{13}Cmr parameters and biosynthesis of zinniol (**7**). The black circles denote C-2 of acetate units which have lost C-1 by decarboxylation.

ketide chains without apparent skeletal rearrangement and without cleavage of acetate units, except for the loss of carboxyl carbon from the terminal unit, giving rise to an enhanced singlet for C-3. The octaketide apparently cyclizes from the folding pattern A as in Scheme 1, and not from the alternative pattern B. Derivation from a single polyketide chain is further supported by the near equality of incorporation levels at all positions except for the expected starter effects discernible in the C-2—Me units. The general incorporation levels were about 0.7% per site and were realized without attempts to optimize incorporation conditions. Altersolanol B (**5**) was also enriched, as indicated by mass spectrometry, but too little was obtained to allow measurement of its ^{13}Cmr spectrum. Finally, the identity of **6** with dactylariol from *D. lutea* (**5**) is assured by all available data (see Experimental).

The identity of zinniol (**7**) from *A. solani* with an authentic specimen from *A. zinniae* (9) was established by a direct comparison of their diacetates (**7***a*). The ^{13}Cmr spectrum of the specimen from *A. solani* showed that the aromatic moiety was assembled from a tetraketide as indicated in Scheme 2. The direction of assembly is revealed by the orsellinic acid-type substitution pattern. The incorporation level was about 1.5% per site. The dimethylallyl group was labelled as expected for its origin from acetate via mevalonic acid. The individual shieldings (underlined) and J_{CC} values in Hz (in parentheses) are given in **7**. The aryl methyl and methoxyl carbons were unlabelled, consistent with their expected origin from methionine.

When ^{13}C-labelled altersolanol A (**4**) from these experiments was administered to cultures of *A. solani*, it was slowly metabolized. The cultures used for this purpose were of a strain, ATCC 11078, which no longer produces detectable amounts of tetrahydroanthraquinones in culture media, although very small quantities of **1** and **3** can still be found in the mycelia. However, when extracted several days after addition of **4**, the culture filtrates were found to contain very small amounts of **5** and **6**, while the mycelia yielded nearly 3 times as much **3** as did untreated controls. The ^{13}Cmr spectrum of the diacetate **3***a*, prepared from the **3**, thus obtained, showed clearly that it was ^{13}C-enriched in precisely the same pattern as the administered **4**. The degree of enrichment at each site was about 70% of that at the corresponding site in starting material **4**. These results demonstrate that **4** was incorporated into **3** without prior degradation but with some dilution by endogenously formed material.

The small amount of **6** from the amended cultures decomposed during attempted isolation; it therefore remains formally unproved that it was significantly labelled. However, there seems little doubt that it is an intermediate on the pathway from **4** to **3**. The rapidity with which the postulated dehydration step takes place in culture makes it likely that it is enzyme-mediated; nevertheless, it is relevant that on tlc evidence, pure **6** is slowly transformed into **3** on standing in methanolic solution even at room temperature.

Altersolanol B (**5**) was isolated from the amended culture as the aromatized product **1**, which was more amenable to purification. The compound was obtained in insufficient amount for a ^{13}C spectrum, but its mass spectrum indicated it to be labelled. Unfortunately, however, small amounts of **5** tend to cochromatograph and cocrystallize with **4**, in which they are detectable only with difficulty at the 1% level. Because of this circumstance, and contrary to our earlier report (8), we are not certain that the small amount of **1** isolated from the experiment (<1 mg) was derived from **4** and not from **5**, traces of which (~0.9%) were, in fact, found to be present on a careful re-examination of a sample of the **4** which had been used in the experiment. In a duplicate experiment with very carefully purified altersolanol A-$^{13}C_x$, macrosporin-$^{13}C_x$ was isolated and found to be labelled in the same manner and to the same extent as before. Traces of **5** (and **6**) were also observed but in insuf-

Can. J. Chem. Downloaded from www.nrcresearchpress.com by 210.87.254.5 on 09/06/12
For personal use only.

Can. J. Chem. Downloaded from www.nrcresearchpress.com by 210.87.254.5 on 09/06/12
For personal use only.

ficient amounts to be isolable even after aromatization. Several preliminary runs with unlabelled **4** were attempted to intercept **5** and **6** at increased concentrations, by varying culture media and incubation periods, but these were unsuccessful. It is pertinent to note that very small amounts of **5** and **6** were observed in several of these experiments although the compounds could not be detected at equivalent levels in either starting material **4** or in untreated cultures. Thus, the evidence relating to the conversion of **4** to **5** remains inconclusive.

In another set of experiments [1-^{13}C,2-^{2}H$_3$]acetate was administered as the precursor and the resulting metabolites examined by both ^{13}C and ^{2}Hmr. For these doubly labelled acetate units, the ^{13}C nuclei experience upfield isotope shifts produced by their geminal deuterium neighbors. Thus, in the ^{13}C spectra of the metabolites, the presence of intact acetate units is revealed by the appearance of these shifted components accompanying the natural abundance signals. Since geminal ^{2}H—^{13}C spin coupling is very small (<1 Hz), these shifted signals are also singlets in proton-decoupled ^{13}C spectra. For acetate units in which the deuterium is lost, the ^{13}C label serves to enhance the intensity of the natural abundance signal with which it coincides. The ^{2}Hmr spectra provide a direct means for locating individual deuterium-labelled sites. The use of doubly labelled [1-^{13}C,2-^{2}H$_3$]acetate has been described for other biosynthetic studies (17).

Macrosporin (**3**-^{13}C$_x$,^{2}H$_y$) obtained from these experiments was diacetylated and the ^{13}C spectrum recorded. The signal for C-4 was significantly enhanced relative to those for the remaining protonated carbons, indicating an enrichment of ca. 7% for this centre. Isotopically shifted (0.03–0.07 ppm) components were apparent in the absorptions for C-2, -5, -7, and -13, establishing that these centres arise from intact acetate units bearing deuterium on the adjacent carbons, i.e. 2-CH$_3$, C-6, -8, and -1, respectively. Of the quinone carbonyl signals, that for C-10 was much more intense than that for C-9, while the C-12 signal was similarly enhanced relative to those for C-3 and -14. These results are fully in accord with acetate incorporation as in Scheme 1. The ^{2}Hmr spectrum of ***3a***-^{13}C$_x$,^{2}H$_y$ contained the three, expected (2*b*) aryl signals as well as methyl absorption, with the relative intensity of the aryl absorption almost equal to that for the methyl signal, indicating some deuterium loss from the methyl group (see Table 3).

The ^{13}Cmr spectra of **4**-^{13}C$_x$,^{2}H$_y$ and its pentacetate contained all of the features just described for **3**-^{13}C$_x$,^{2}H$_y$, with an additional benefit. The C-2 absorption pattern consisted of the normal signal at 81.1 ppm and three clearly resolved, isotope-shifted components at 0.05, 0.10, and 0.15 ppm higher field. This is definitive evidence for the presence of species with one, two, and three deuterium nuclei on the methyl carbon and establishes that significant deuterium loss occurred from this centre during the biogenesis of the metabolite, a feature noted for **3**-^{13}C$_x$,^{2}H$_y$ above from its ^{2}H spectrum. Unfortunately the isotope shifts are smaller in this compound and the shifted component in its C-2 absorption was too ill-defined to permit a definitive conclusion. The ^{2}Hmr spectrum of ***4a***-^{13}C$_x$,^{2}H$_y$ afforded one additional piece of evidence regarding its biosynthesis, namely, the complete absence, within the limits of detection, of deuterium at C-3. Again, the relative intensity of the absorption for deuterium at C-1, -6, and -8, an ill-resolved band because of the small shielding differences for these nuclei (2*a*), was found to be comparable to that for the methyl signal (Table 3), providing additional evidence of substantial deuterium loss from the methyl carbon. Thus during the generation of **4** there is substantial exchange at this methyl and complete loss of deuterium from C-3; the latter fact seems rather surprising, and probably has biosynthetic significance regarding the mode of oxygenation at this carbon. This aspect will require further study and experimentation.

TABLE 3. Incorporation of deuterium from [2-^{2}H$_3$-1-^{13}C]acetate into macrosporin (**3**) and altersolanol A (**4**)

		Position and enrichment[b] (atoms/mol)				
Compound[a]	Expt.	Me	1	8	6	3
3a	1[c]	Insufficient material obtained				
	2[d]	4.82	1.47	1.41	1.26	—
4a	1[c]	3.09		2.89		0
	2[d]	3.15		2.55		0

[a] Measurements were obtained after acetylation of **3** and **4** to their more soluble acetates ***3a*** and ***4a***.

[b] Calibrated by comparison to the natural abundance ^{2}H signal of the weighed solvent.

[c] Labelled acetate administered immediately after inoculation, with extraction 4 days later.

[d] Labelled acetate added 4 days after inoculation and extracted 2 days later.

Experimental

Solvents were reagent grade and redistilled before use. Ethanol was 96% EtOH. Agar was Difco Bacto-Agar; casein hydrolyzate was from ICN Pharmaceuticals, Cleveland, Ohio; V8 Juice (Campbell Soup Co.) was the canned product obtained from local groceries. Silica gel used for column chromatography was of tlc grade (Camag DF 5) but not activated. The same adsorbent, activated at 110°C, was used for preparative tlc. Analytical tlc was on precoated plates (Machery–Nagel Polygram SIL N-HR/UV$_{254}$ (0.2 mm)). Sodium [1,2-^{13}C$_2$]acetate (90% ^{13}C) and [1-^{13}C$_1$,2-^{3}H$_2$]acetate (90% ^{13}C, 98% ^{2}H) and deuterated solvents were from Merck, Sharp, and Dohme Canada Ltd., Pointe Claire – Dorval, Quebec.

Evaporations were done below 30°C at reduced pressure or under a slow stream of N_2. Ultraviolet spectra were measured on ethanolic solutions using Beckman DK 1 or Pye–Unicam SP-8000 spectrophotometers. Mass spectra were obtained with a Varian MAT 311A instrument. The ^{1}Hmr spectra were obtained with a Varian XL-100-12 system, operating in either the continuous wave or Fourier transform mode as appropriate, with TMS as internal reference and $CDCl_3$, CD_2Cl_2, or dimethylsulphoxide-d_6 as solvents. The majority of the ^{13}Cmr spectra were obtained with a Varian XL-100-15 system operating in the Fourier transform mode with either square wave modulated proton decoupling (for completely decoupled spectra) or gated decoupling for proton-coupled spectra. In the latter stages of the work, a Varian XL-200 system was employed, operating at 50.3 MHz for ^{13}C and 30.7 MHz for ^{2}H in the Fourier transform mode. In general the ^{13}C shielding data have an estimated precision of 0.05 ppm but, for the material obtained fom the [1-^{13}C,-^{2}H$_3$]acetate incorporation experiments, the precision of the isotope shifts is of the order of ± 0.01 ppm.

Fungal cultures

An altersolanol A-producing culture of *A. solani* was the gift of Dr. U. Matern, University of Freiburg, Germany. It was routinely maintained on V8-juice agar (V8 Juice, 350 mL; $CaCO_3$, 3.0 g; agar, 20 g; H_2O to 1 L) at 15°C in the dark. It has since been deposited at the American Type Culture Collection, Rockville, Maryland, as ATCC No. 44204 ("strain 44204" hereafter). This strain did not produce detectable amounts of alternaric acid (18) on the several occasions it was tested.

An alternaric acid-producing strain of the fungus, derived from one of Brian's original isolates (18), was freshly obtained from the Amer-

Can. J. Chem. Downloaded from www.nrcresearchpress.com by 210.87.254.5 on 09/06/12
For personal use only.

ican Type Culture Collection as ATCC No. 11078 ("strain 11078" below) and maintained similarly. In numerous experiments, liquid media supporting cultures of this strain appeared to remain free of **4** or other tetrahydroanthraquinonoid pigments. However, it should be noted that, in the earlier work in these laboratories (2*a*), substantial amounts of **4** and related pigments were obtained from cultures of the same parent strain.

Slants of these strains were used to inoculate Brian's Medium T (glucose, casein hydrolyzate, and mineral salts) (19) contained in Delong flasks (25 mL/flask; 4–6 flasks/slant) which were then incubated in the dark at 24°C. After 10–12 days, and using aseptic conditions throughout, the mycelia were collected, rinsed well with water, homogenized in water, diluted to a suitable volume, and inoculated into fresh Medium T in Roux bottles (100 mL/bottle; 3–5 bottles/flask) which were incubated as previously. Precursors were added to the cultures after the time intervals specified below, by injection of their aqueous solutions below the mycelia. Cultures were harvested by filtration through cheese cloth, the mycelia being rinsed well with H_2O. Further processing varied with the experiment. For reasons which are not understood, pigment production by *A. solani* strain 44204 has been characteristically variable both as regards quantity and timing. The timing of precursor addition was therefore decided on an *ad hoc* basis in each case.

Incorporation of sodium[1,2-$^{13}C_2$]acetate into metabolites of strain 44204

(a) Cultures of the fungus in 8 Roux bottles were supplemented 2 days after inoculation with 0.05 *M* sodium [1,2-$^{13}C_2$]acetate (10 mL/bottle) and with another 5 mL after another 5 days. The combined culture media were extracted with EtOAc (5 × 1 L) 9 days after inoculation. After evaporation, the extract (0.43 g) was distributed between $CHCl_3$/MeOH (9:1; 6 × 10 mL) and H_2O (6 × 10 mL), to furnish 6 lower phases (L1–L6) and 6 aqueous, upper phases. The latter were extracted in turn with EtOAc till almost colourless, the combined extracts evaporated, and the residue (129 mg) crystallized (EtOH) to give **4**-$^{13}C_x$ (52 mg after washing with hot EtOAc). Fractions L1 and L2 (239 mg) crystallized from EtOH to give **3**-$^{13}C_x$ (12.5 mg after washing with hot EtOAc) which was acetylated (2*a*) to the diacetate **3***a*-$^{13}C_x$. The mother liquors from the crystallizations of L1, L2, and **4** were chromatographed over a 300 g column in MeOH/$CHCl_3$/HOAc (10:90:0.1) ("solvent A") in 25-mL fractions. Fractions 24–26 were essentially pure **7**-$^{13}C_x$ (91 mg); fractions 27–30 on column rechromatography (iPrOH/MeOH/HOAc 5:95:0.1) and preparative tlc (solvent A) gave more **7** (6 mg) and **5**-$^{13}C_x$ (0.4 mg from EtOH). (The ms clearly indicated that the sample was enriched but because of the presence of impurities, the spectrum could not be quantitatively evaluated.) Fractions 34–38 and L3–L5 were rechromatographed (25 g SiO_2, solvent A), the main coloured band furnishing **6**-$^{13}C_x$ (5 mg) on recrystallization from EtOH. The compound, deep orange-red crystals, showing complex behavior on the Kofler block (rearrangement from plates to needles, 155–200°C; partial sublimation without melting, 235–290°C; decomposition, 290°C), had λ_{max}: 420, 284(sh), 269, 238, and 220 nm (ϵ 5500, 9810, 15 350, 9320, and 45 000) and *Exact Mass* calcd. for $C_{16}H_{16}O_7$: 320.0892; found (high resolution ms): 320.0892.

A direct comparison of ms and ^{1}Hmr spectra, kindly carried out by Dr. R. W. Rickards, Canberra, left no doubt that the *A. solani* metabolite and dactylariol (5) are identical. The identity of product **7** with zinniol was confirmed by treatment with Ac_2O/py (RT, 24 h) which on chromatography ($CHCl_3$) and recrystallization from light petrol gave the diacetate **7***a*, identical with an authentic specimen from *A. zinniae* (9) by tlc, ^{1}Hmr, ^{13}Cmr, mp, and mixture mp.

(b) Another 8 cultures initiated with the same inoculum were supplemented with the labelled acetate solution on day 7 only. Extraction of the cultures on day 9 and work-up as above furnished **4**-$^{13}C_x$ (28 mg).

(c) In a similar experiment, two 100-mL cultures of strain 44204 were supplemented with 0.054 *M* sodium [1,2-$^{13}C_2$]acetate (10 mL/bottle) 7 days after inoculation. The culture filtrates, collected after another 3 days and exceptionally heavily pigmented, yielded EtOAc extracts from which **4**-$^{13}C_x$ crystallized on concentration. Chromatography of the mother liquors gave **7**-$^{13}C_x$ (28 mg) and **6**-$^{13}C_x$ (2 mg; dissipated into several products upon acetylation).

The ^{13}Cmr spectra were obtained from the various samples of **4**-$^{13}C_x$ after acetylation to **4***a*. Measurements of the relative intensities of the satellites and central peaks in the absorption patterns for carbons from intact acetate units indicated general enrichment levels of 0.7–0.8% with 1.1–1.2% enrichment in the C-2 methyl group.

Incorporation of altersolanol A $^{13}C_x$ into macrosporin and altersolanol B

(d) Altersolanol A $^{13}C_x$ from (c) above was further purified by precipitation from DMSO-d_6 with H_2O and recrystallization from H_2O/EtOH. As shown by direct tlc comparison, the purified sample contained less than 1% of its weight of **5** and no detectable trace of **3**. The substance (22 mg in 8 mL EtOH) was administered in equal portions to four 11-day old cultures of strain 11078. Four similar cultures were treated with EtOH as controls. After a further 9 days' incubation, the cultures were harvested and the filtrates extracted as usual. The extracts were washed with 5% $NaHCO_3$ solution and H_2O, which removed acidic material (118 mg) consisting mostly of alternaric acid and indistinguishable by tlc from the corresponding fraction (115 mg) from the controls. The neutral fraction (55 mg; λ_{max} 402, $E^{1\%}_{1cm}$ 7.6) was chromatographed (50 g SiO_2, solvent A, 10 mL fractions) yielding 2 bands containing **5** ($\leq$1.5 mg from absorbance at λ_{max} 269 nm) and **6** respectively, the latter decomposing on attempted further purification. The fraction containing **5** was treated with $SOCl_2$ (3 microdrops) in ice-cold pyridine (0.5 mL) (2*a*) and the product chromatographed over SiO_2 (0.5 g) in $CHCl_3$ to give crystalline **1** (ca. 0.9 mg) on evaporation of the only coloured band. The neutral fraction from the controls (71 mg) had λ_{sh} 395 nm, $E^{1\%}_{1cm}$ 2.8, and contained at most a just detectable trace of **5** and no **6** (tlc; 2λ of a 5% solution).

The mycelia from the amended cultures were steeped in EtOH (200 mL) overnight, homogenized (Waring Blendor), filtered, and re-extracted similarly with EtOH (100 mL). Concentration of the filtrates till aqueous, extraction with EtOAc (3 × 50 mL), and chromatography of the extracts (300 g SiO_2, MeOH/$CHCl_3$ 5:95) gave crystalline **3**-$^{13}C_x$ (5.1 mg), identified by uv spectrum, mp and mp in admixture with an authentic specimen. This was converted into the diacetate with an enrichment level of ca. 0.8% at the C-2—Me and ca. 0.5% at the other sites (^{13}Cmr). The mycelia from the controls, on similar work-up, yielded only 1.9 mg of 3.

(e) In a similar experiment, **4**-$^{13}C_x$ (from (a)) was administered to 11-day old cultures of strain 11078 (2.5 mg/bottle), 8 of the cultures being extracted after 6, 7 after 11 days' further incubation. Altersolanol B (**5**) and dactylariol (**6**) were present in the extracts but in amounts too small to allow their isolation. Crystalline macrosporin (**3**) was isolated from the mycelia as the diacetate **3***a* (2.6 and 3.0 mg respectively) but incorporation levels were too low to allow a reliable spectroscopic comparison. After addition of a little more **3***a* from the culture filtrates, the combined material was shown by ^{13}Cmr to have an average enrichment of 0.5% with 0.8% in the C-2—Me group.

Incorporation of sodium [1-^{13}C,2-$^2H_3$]acetate into macrosporin and altersolanol A

(f) Four cultures of strain 44204 on potato-dextrose broth (100 mL/bottle) were treated with 0.05 *M* sodium [1-^{13}C,2-$^2H_3$]acetate (90%, ^{13}C; 98%, ^{2}H; 10 mL/bottle) immediately after inoculation and were extracted after 4 days, when the medium had turned orange. Another 4 cultures were treated with the acetate solution 4 days after inoculation and extracted 2 days later. Extraction of the mycelia from the first set of cultures furnished only a negligible trace of **3** but, after chromatography (solvent A), 8 mg of **3** was obtained from the second set. Direct crystallization of the EtOAc extracts from the culture filtrates afforded 20 mg of **4** from the first, and 25 mg from the second set of cultures. The ^{13}Cmr spectra of **4** were obtained in DMSO-d_6 and after acetylation, spectra of **3***a* and **4***a* were recorded in $CDCl_3$. The ^{2}Hmr spectra of **4** were measured in DMSO while **3***a* and **4***a* were examined in both $CHCl_3$ and CH_2Cl_2.

Acknowledgements

We wish to thank the Natural Sciences and Engineering Research Council of Canada for financial support of this work. We are very grateful to Dr. U. Matern for cultures of *A. solani*; Dr. R. W. Rickards for drawing our attention to the identity of dactylariol and "altersolanol C", and for comparing spectral data; Dr. A. N. Starratt for a gift of authentic zinniol diacetate; and we wish to acknowledge the skillful technical assistance of D. Hairsine, H. Schroeder, H. Bork, A. H. Hood, and G. L. Rock.

1. P. W. BRIAN, G. W. ELSON, H. G. HEMMING, and J. M. WRIGHT. Ann. Appl. Biol. **9**, 308 (1952).
2. (*a*) A. STOESSL. Can. J. Chem. **47**, 767 (1969); (*b*) Can. J. Chem. **47**, 777 (1969); (*c*) M. GORDON, A. STOESSL, and J. B. STOTHERS. Can. J. Chem. **50**, 122 (1972).
3. J. D. BU'LOCK and J. R. SMITH. J. Chem. Soc. C, 1941 (1968).
4. T. NODA, T. TAKE, T. WATANABE, and J. ABE. Tetrahedron, **26**, 1339 (1970); R. CHARUDATTAN and K. V. RAO. Appl. Environ. Microbiol. **43**, 846 (1982).
5. A. M. BECKER, R. W. RICKARDS, K. J. SCHMALZL, and H. C. YICK. J. Antibiot. **31**, 324 (1978).
6. M. M. WHEELER, D. M. WHEELER, and G. W. PETERSON. Phytochemistry, **14**, 288 (1975).
7. W. B. TURNER. Fungal metabolites. Academic Press, London and New York. 1971. p. 163.
8. A. STOESSL, C. H. UNWIN, and J. B. STOTHERS. Tetrahedron Lett. 2481 (1979).
9. (*a*) A. N. STARRAT. Can. J. Chem. **46**, 767 (1968); (*b*) G. N. WHITE and A. N. STARRATT. Can. J. Bot. **45**, 2087 (1967).
10. I. BARASH, H. MOR, D. NETZER, and Y. KASHMAN. Physiol. Plant Pathol. **19**, 7 (1981).
11. K. TIETJEN and U. MATERN. Conf. Abstract, Newsletter, Phytochemical Society North America. July, 1981. p. 12.
12. H. GOTTLIEB. Isr. J. Chem. **16**, 57 (1977); P. E. HANSEN. Org. Magn. Reson. **12**, 109 (1979).
13. Y. BERGER and A. CASTONGUAY. Org. Magn. Reson. **11**, 375 (1978).
14. Y. BERGER, A. CASTONGUAY, and P. BRASSARD. Org. Magn. Reson. **14**, 103 (1980).
15. Y. BERGER, M. BERGER-DEGUÉE, and A. CASTONGUAY. Org. Magn. Reson. **15**, 244 (1981).
16. G. HÖFLE. Tetrahedron, **33**, 1963 (1977).
17. C. ABELL and J. STAUNTON. J. Chem. Soc. Chem. Commun. 856 (1981); T. J. SIMPSON, A. E. DE JESUS, P. S. STEYN, and R. VLEGGAAR. J. Chem. Soc. Chem. Commun. 632 (1982).
18. P. W. BRIAN, P. J. CURTIS, H. G. HEMMING, E. G. JEFFERYS, C. H. UNWIN, and J. M. WRIGHT. J. Gen. Microbiol. **5**, 619 (1951).
19. P. W. BRIAN, P. J. CURTIS, and H. G. HEMMING. Proc. R. Soc. (London) Ser. B, **135**, 106 (1947).
20. A. STOESSL. Physiol. Plant Pathol. **20**, 263 (1982).
21. A. STOESSL and J. B. STOTHERS. J. Chem. Soc. Chem. Commun. 880 (1982).
22. J. L. JURLINA and J. B. STOTHERS. J. Am. Chem. Soc. **104**, 4677 (1982).
23. D. KAUFMANN, A. DEMEIJERE, K. LUK, K. OVERTON, and J. B. STOTHERS. Tetrahedron, **38**, 977 (1982).
24. A. STOESSL and J. B. STOTHERS. Org. Magn. Reson. In press (1982).

Can. J. Chem. Downloaded from www.nrcresearchpress.com by 210.87.254.5 on 09/06/12
For personal use only.

Tetrahydroaltersolanol B, a hexahydroanthronol from *Alternaria solani*[1,2]

A. STOESSL AND J. B. STOTHERS

Agriculture Canada, London Research Centre and the Department of Chemistry, University of Western Ontario, London, Ont., Canada N6A 5B7

Received September 13, 1982

A. STOESSL and J. B. STOTHERS. Can. J. Chem. **61**, 378 (1983).

The structure of a novel reduced anthraquinone, isolable in small amounts from culture filtrates of the fungus, *Alternaria solani*, is shown to be **6***a* mainly by spectroscopic methods. Detailed examination of the ^{1}Hmr spectra of **6***a* has defined its stereochemistry; the ^{13}Cmr spectral data for **6***a* and several derivatives are also reported.

A. STOESSL et J. B. STOTHERS. Can. J. Chem. **61**, 378 (1983).

À l'aide de méthodes spectroscopiques, on montre que la formule **6***a* correspond à la structure de la nouvelle anthraquinone réduite, isolée en petites quantités à partir du champignon *Alternaria solani*. Une étude poussée du spectre de rmn du ^{1}H a permis de définir sa stéréochimie; on rapporte également les données spectrales de la rmn du ^{13}C du composé **6***a* et de plusieurs dérivés.

[Traduit par le journal]

Can. J. Chem. Downloaded from www.nrcresearchpress.com by 210.87.254.42 on 09/06/12
For personal use only.

As described in the preceding paper (1), the fungus *Alternaria solani* (Ell. & Mart.) Sorauer produces the polyketide metabolites **1**–**5** as well as some anthraquinones related to **1**–**3**. One of these compounds, altersolanol A (**1**), is sometimes obtained in relatively large amounts (up to 0.25 mg/mL culture filtrate) but, at other times, the yields can be very much lower. Recently, in several instances of the latter sort, the altersolanol A-containing fractions were found to deposit colorless crystals which are even less soluble in common solvents than the sparingly soluble **1**.

The constitution of this new compound was established by precise mass determination as $C_{16}H_{20}O_6$. Recrystallization from methanol-d_4 replaced four hydrogen atoms with deuterium ($\Delta M^+ = +4$), indicating the presence of four hydroxyl groups. The uv spectrum (λ_{max}: 281 (35 300), 315 (14 900)) is almost identical to that for 2,4-dihydroxyacetophenone (λ_{max}: 277 (27 400), 315 (15 200)) and the presence in the ir spectrum of strong bands at ν_{max} 1600 and 1632 cm^{-1} is indicative of an aromatic nucleus and a conjugated chelated ketone, respectively. Acetylation gave a triacetate together with a small amount of a somewhat unstable diacetate. In the ir the triacetate showed the expected bands for aryl acetate (1779 cm^{-1}), two aliphatic acetates (1750, 1755 cm^{-1}), and conjugated, but not chelated, carbonyl absorption (1689 cm^{-1}).

The proton spectrum of the new metabolite in DMSO-d_6 contained four hydroxy absorptions, two singlets (3.81 and 12.91 ppm) and two doublets (4.45 and 5.63 ppm, J = 6.5 and 7.4 Hz, respectively); these signals disappeared upon addition of D_2O, confirming their facile exchange. A pair of *meta*-coupled protons were apparent at 6.35 and 6.70 ppm with J = 2.5 Hz as well as an aromatic methoxy signal at 3.82 ppm. These are features familiar from the spectra for **1**–**3** (1–4). However, the less shielded of the aryl protons also exhibited a second splitting of 1.1 Hz, indicating a long range coupling with a *peri*-proton. A one-proton multiplet at 4.29 ppm was shown to contain this 1.1 Hz splitting by decoupling, an experiment which also established that this multiplet was coupled to

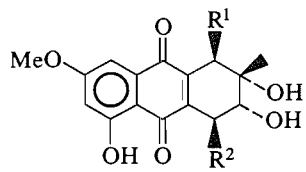

1 R^1 = R^2 = OH
2 R^1 = R^2 = H
3 R^1 = OH; R^2 = H

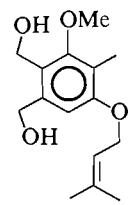

4

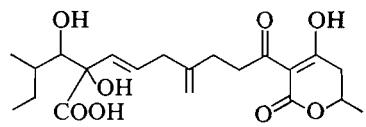

5

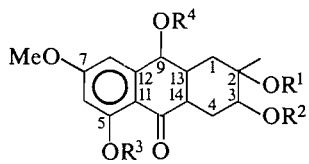

6

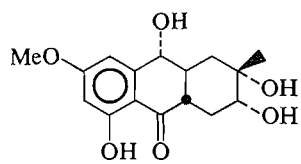

7

a R^1 = R^2 = R^3 = R^4 = H
b R^1 = R^3 = H; R^2 = R^4 = Ac
c R^1 = H; R^2 = R^3 = R^4 = Ac
d R^3 = R^4 = H; R^1, R^2 = C(CH$_3$)$_2$

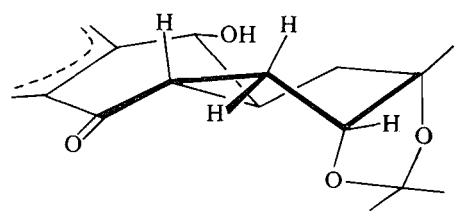

8

[1]Part VIII of the Series, "Metabolites of *Alternaria solani*"; for Part VII see ref. 1; for Part VI, see ref. 6.

[2]Part XXXVIII of NMR Studies; for Part XXXVII see ref. 7; for Part XXXVI see ref. 8; for Part XXXV see ref. 9; for Part XXXIV see ref. 10.

0008-4042/83/020378-05$01.00/0

©1983 National Research Council of Canada/Conseil national de recherches du Canada

Can. J. Chem. Downloaded from www.nrcresearchpress.com by 210.87.254.42 on 09/06/12
For personal use only.

the hydroxy absorption at 5.63 ppm. In DMSO-d_6/D_2O the 4.29 ppm multiplet shifted to 4.333 ppm and was collapsed to a sharp doublet, J = 11 Hz, upon irradiation of the less-shielded aryl proton. These results indicated that the quinone carbonyl, corresponding to that at C-9 in **1**−**3**, had been reduced to a hydroxy group in accord with the absence of color for this compound. Furthermore, this carbinyl proton has a vicinal proton. Other features similar to those in the spectra of **1**−**3** were the presence of a methyl singlet (1.160 ppm) and a carbinyl proton appearing as a doublet of doublets in DMSO-d_6/D_2O at 3.360 ppm (spacings of 4.6 and 10.7 Hz). An additional splitting of 6.5 Hz was evident in this multiplet in DMSO-d_6 and was shown to be common to the hydroxy signal at 4.45 ppm. From these data the new metabolite could be assigned structure **6***a* with the di- and triacetates as **6***b* and **6***c*. The sites of acetylation followed from (a) the appearance of a chelated hydroxy signal at 12.78 ppm in the spectrum of **6***b* and the absence of an analogous signal for **6***c*; (b) characteristic acylation shifts of ca. 1.5 ppm for the carbinyl protons, and (c) upfield shifts for H-8 of ca. −0.5 ppm (**6***b*) and −0.11 ppm (**6***c*). The relatively low field position for the carbinyl proton at C-9 is consonant with its benzylic nature. Hydrolysis of **6***c* to **6***a* confirmed that acetylation proceeds without skeletal rearrangement.

The question of stereochemistry for **6***a* was resolved by more detailed examination of the higher field region of its proton spectrum. As noted, the spectrum was simplified in DMSO-d_6/D_2O by the disappearance of the couplings with the hydroxy protons apparent in the spectrum in DMSO-d_6, which permitted us to correlate the individual hydroxy signals with specific carbinyl protons. (It should be mentioned that the addition of D_2O to the DMSO-d_6 solution produced minor shifts in position of the absorption patterns.) With the assignment of the carbinyl absorption at 4.333 ppm to H-9, the doublet of doublets at 3.360 ppm must arise from H-3 and the spacings of 4.6 and 10.7 Hz indicate an axial−axial and an axial−equatorial coupling for H-3 with its vicinal neighbors. A four-line multiplet at 1.495 ppm, which could be described as a doublet of triplets with comparable coupling constants for each of its three coupling interactions, ca. 12 Hz, was assigned to the axial proton at C-4 because irradiation of H-3 at 3.360 ppm collapsed the pattern to a 1:2:1 "triplet" with spacings of 12 Hz. It follows therefore that the H-3 carbinyl proton is axial.

A doublet of doublets centred at 1.296 ppm, having spacings of 12 and 13 Hz, was unaffected by this decoupling experiment but was collapsed to a clear doublet upon irradiation at 1.965 ppm which is the centre of another multiplet, a doublet of quartets with a total width of 38.5 Hz. This decoupling experiment also collapsed the H-9 carbinyl absorption at 4.333 ppm to a doublet with J = 1.1 Hz. Hence H-13 absorbs at 1.965 ppm and is most probably axial, displaying axial−axial spin coupling with H-9 and the proton absorbing at 1.296 ppm which can be assigned to the axial proton at C-1. In addition, the irradiation at 1.965 ppm resulted in the collapse of a "doublet of triplets" (spacings of 3.7 and 12 Hz) at 2.465 ppm to a "doublet of doublets" with the same splittings. The latter multiplet could, therefore, be directly assigned to H-14; the relatively large splitting of 12 Hz indicated that H-13 and -14 are both axial. Hence, **6***a* has a *trans* ring junction. Two overlapping multiplets near 2.2 ppm exhibited informative alterations during these decoupling experiments. A doublet of doublets, with spacings of 3.3 and 13 Hz, could be assigned to the equatorial proton at C-1, as the collapse of the larger splitting upon irradiation at 1.296 ppm (axial H-1) confirmed. The four-line pattern at 1.495 ppm (axial H-4) became a "triplet" upon irradiation near 2.2 ppm, thereby locating the obscured multiplet for the equatorial H-4. Thus, the protons at C-3, -9, -13, and -14, four of the five chiral centres, could be assigned axial orientations. Since the 2- and 3-hydroxyls are α as in **2** (4) and the 3-proton is axial, **6***a* must have the stereochemistry shown in **7**, with the 3-, 9-, and 14-protons β.

The proton data are collected in Table 1. The parameters listed for the protons on the saturated ring for **6***a* in DMSO-d_6/D_2O solution were obtained by spin simulation calculations using the program supplied with the XL-200 software. The patterns for the protons at C-3, -4, and -14 were calculated, including the coupling between H-14 and -13; in a similar manner the spectrum for the protons at C-1, -9, and -13 was obtained and the two results added to give a composite spectrum for comparison with that observed. Suitable adjustments of the parameters led to a good match for the simulated and observed spectra. A complete analysis was not attempted because of the size of the spin system and the presence of several small unresolved long range couplings. Nevertheless, the coupling constants listed in Table 1 are undoubtedly close to the true values and the key coupling constants are sufficiently large to render firm stereochemical conclusions. The ^{13}Cmr spectra of these compounds were also recorded and these data are listed in Table 2. The assignments were straightforward, following from the earlier data for **1**−**3** (1), and fully corroborate the structural elucidations discussed above.

On treatment with acetone in the presence of a trace of strong acid, **6***a* furnished an acetonide **6***d*, as confirmed by the presence in the ^{13}C spectrum of two new methyl signals and a strongly dishielded quaternary carbon at 107.5 ppm (Table 2). The proton spectrum (Table 1) similarly contained two new methyl singlets together with hydroxy peaks at 1.75 and 12.65 ppm. The absorptions for H-6, -8, and -9 were similar to those for **6***a* but the pattern for the remaining carbinyl proton was significantly different, appearing as a triplet with spacings of ca. 4 Hz at 4.14 ppm. Irradiation of this multiplet showed it to be coupled to a doublet of triplets (spacings, 4 and 15 Hz) at 2.74 ppm and to an eight-line pattern, total width 28 Hz, at 1.84 ppm. The latter multiplets must arise from the equatorial and axial protons, respectively, on C-4. A more detailed analysis of the spectrum was precluded, however, by severe overlapping of the multiplets for "equat" H-1, -13, and -14 in the region 2.2−2.45 ppm and partial masking of the remaining H-1 absorption near 1.85 ppm by the methyl signals. In any event, the relatively small couplings, ≤8 Hz, for H-3 indicate the absence of an axial−axial interaction for this proton, therefore signifying a conformational change for the saturated ring in **6***d*. While it is conceivable that the acid catalysis could change the ring junction geometry by epimerization at the α-carbon, C-14, the resulting *cis*-fusion should favor the chair conformer having an axial proton at C-3, contrary to the appearance of its absorption. We conclude, therefore, that the saturated ring in **6***d* exists as a non-chair ring or as a mixture of non-chair forms. The pronounced deshielding of one of the 4-protons indicates that it lies close to the plane of the carbonyl group, suggesting that **8** may be the favored conformer for **6***d*.

It is unclear at present whether **6***a* is biosynthetically a precursor of, or a metabolite derived from, altersolanol B (**2**) or indeed whether it is formed through a different pathway. The small amounts in which both compounds accrue currently present a bar to further examination of this question.

Can. J. Chem. Downloaded from www.nrcresearchpress.com by 210.87.254.42 on 09/06/12
For personal use only.

TABLE 1. Proton parameters for **6***a*–*d*

A. Shieldings (ppm from TMS)

		H-1				H-4								
Compound	Solvent[a]	ax	eq	2-Me	H-3	ax	eq	H-6	7-MeO	H-8	H-9	H-13	H-14	Other
6*a*	A	1.20	2.16	1.16	3.30	1.46	2.13	6.35	3.82	6.70	4.29	1.96	2.46	3.80 (2-OH) 4.45 (3-OH) 5.63 (9-OH) 12.91 (5-OH)
	A′	1.296	2.175	1.213	3.360	1.495	2.175	6.361	3.828	6.717	4.333	1.965	2.465	
6*b*	B			1.23	4.80			6.38	3.83	6.20	5.92			2.13 2.26
6*c*	B	1.40	2.03	1.23	4.76	~1.8	~2.4	6.57	3.87	6.59	6.00	~2.4	~2.4	2.11 2.28 2.38
6*d*	B	1.24	2.38	1.42	4.14	1.84	2.74	6.36	3.83	6.80	4.43	2.32	2.36	1.34 1.37

B. Coupling constants (Hz) for **6***a* in DMSO-d_6/D_2O

		H-1	H-3[b]	H-4 eq	H-6	H-9[c]	H-13	H-14
H-1	ax	13.5					12.3	
	eq						3.2	
H-4	ax		11.7	12.5				12.0
	eq		4.3					3.7
H-8					2.5	1.1		
H-13						11.0		12.0

[a]A = DMSO-d_6; A′ = DMSO-d_6/D_2O; B = $CDCl_3$.
[b]In DMSO-d_6, J_{HCOH} = 6.5 Hz.
[c]In DMSO-d_6, J_{HCOH} = 7.5 Hz.

Can. J. Chem. Downloaded from www.nrcresearchpress.com by 210.87.254.42 on 09/06/12
For personal use only.

TABLE 2. ^{13}C shieldings[a] for **6***a*–*d*

Compound	Solvent[b]	C-1	C-2	C-3	C-4	C-5	C-6	C-7	C-8	C-9	C-10	C-11	C-12	C-13	C-14	2-Me	7-Me	Other
6*a*	A	41.1	69.4	73.4	29.2	164.3	98.9	165.7	103.9	70.7	203.1	109.1	151.5	41.6	46.9	26.9	55.5	
6*b*	B	40.2	69.9	76.5	25.9	166.2	99.6	165.9	104.7	72.6	200.2	109.5	144.3	39.2	46.7	27.0	55.7	20.9, 21.1 170.0, 170.9
6*c*	B	40.5	69.8	76.4	26.2	152.5	109.4	163.9	108.9	73.0	193.0	114.1	145.3	39.0	47.8	26.9	55.7	20.9, 21.0, 21.1 169.6, 169.9, 171.0
6*d*	B	38.6	78.8	78.7	21.1	165.2	100.1	166.2	104.6	73.5	201.5	109.8	149.3	40.9	44.5	27.6	55.7	26.3, 28.1 107.5

[a]In ppm for TMS.
[b]A = DMSO-d_6; B = $CDCl_3$.

Experimental

Materials and the general techniques employed have been described previously (1). The ^{13}Cmr spectra were measured at 50.3 MHz with a Varian XL-200 instrument using 12 KHz spectral widths, 30° pulses, and 2 s repetition rates. Comparison of spectra obtained using the APT sequence (5) with usual proton decoupled spectra allowed distinction between methyl, methylene, methine, and fully-substituted carbons. The ^{13}C shieldings are reported relative to internal TMS with estimated precisions of ±0.05 ppm. Proton spectra were recorded at 200 MHz, generally using 3 KHz spectral widths and 32 K transforms. For **6***a*, the observed spectrum was compared with that obtained using the spin simulation program provided with the G-2 software for the XL-200. Since this program cannot handle an 8-spin system, the results for two 5-spin calculations were added to give a composite spectrum for the protons on sp^3-carbons. The best match of observed and calculated spectra was obtained with the parameters listed in Table 1 for **6***a* in DMSO-d_6/D_2O.

Isolation and properties of compound **6**a

The neutral EtOAc extracts of the filtrates obtained from 21 day-old cultures of *A. solani* ATCC 44204 on Brian's medium T (28 Roux bottles; 100 mL/bottle) were evaporated and the combined residues were triturated twice with a mixture of water (12.5 mL) and MeOH/$CHCl_3$ (1:9, 12.5 mL). The material which had remained undissolved was recrystallized from MeOH to furnish **6***a*, 7.5 mg, which contained traces of a compound containing an extra oxygen atom (ms) but could be purified through its triacetate **6***c*.

In a second run, the combined crude EtOAc extracts (534 mg) from 30 similar cultures, harvested in another connection at various time intervals, were chromatographed over SiO_2 (200 g) in MeOH/$CHCl_3$/HOAc (5:95:0.1; 25 mL/fraction). Fractions 112–131 (33 mg) consisted of **1**. Fractions 91–99 (33 mg) yielded pure **6***a* (16 mg) upon a single recrystallization from MeOH; mp 256–257°C, $[\alpha]_D^{25}$ −27.2° (*c* 0.18, MeOH); *m/e*: 308, 290, 272, 246, 232, 215, 203 (100%). *Exact Mass* calculated for $C_{16}H_{20}O_6$: 308.1258; found (high resolution ms): 308.1260. After recrystallization from methanol-d_4, *m/e*: 312, 292, 273, 248, 234, 216, 205 (100%). *Exact Mass* calculated for $C_{16}{}^1H_{16}{}^2H_4O_6$: 312.1508; found (high resolution ms): 312.1526.

Acetylation (Ac_2O/pyridine at room temperature overnight followed by evaporation *in vacuo*) gave the triacetate **6***c* together with a small amount of the diacetate **6***b*, which were separated by chromatography over SiO_2 (10 g) in Et_2O, **6***b* being eluted first.

Diacetate **6***b*, a crystalline solid when first isolated, had λ_{max} 279.5 (26 000) and 316 (11 400) and the nmr data recorded in Tables 1 and 2 when first measured. Subsequent examination of the solution indicated some decomposition and/or acyl migration. This material had *m/e*: 392, 350, 332, 314, 290, and 272 (100%).

Triacetate **6***c*, mp 168°C (from light petrol/Et_2O), $[\alpha]_D^{25}$ −16.1° (*c* 0.18, $CHCl_3$), had *m/e*: 434, 392, 350, 332, 314, 290, and 272 (100%) and λ_{max} 225 (14 100) and 273 (13 300). Hydrolysis of the compound (6.1 mg) in 0.05 *M* NaOH (2 mL) at room temperature for 2 days gave crystals of **6***a* (2.1 mg; mp 250–254°C) on acidification.

Acetonide **6***d*. Treatment of **6***a* (10 mg) with acetone (0.75 mL) containing H_2SO_4 (0.4% v/v) at ice temperature for 1.5 h, and at room temperature for another 1.5 h, gave **6***d* (6.6 mg) on extraction into EtOAc from $NaHCO_3$ solution; mp 150°C after recrystallization from CCl_4; *m/e*: 348, 333, 291 (100%), 273, 260, and 245. *Exact Mass* calculated for $C_{19}H_{24}O_6$: 348.15725; found (high resolution ms): 348.15705.

Acknowledgements

We thank G. L. Rock for excellent experimental support throughout, D. Hairsine for measuring the mass spectra, S. Pedras for optical rotation data, and the Natural Sciences and Engineering Research Council of Canada for financial support.

1. A. STOESSL, C. H. UNWIN, and J. B. STOTHERS. Can. J. Chem. **61**, 372 (1983).

2. A. STOESSL. Can. J. Chem. **47**, 767 (1969).
3. A. STOESSL. Can. J. Chem. **47**, 777 (1969).
4. M. GORDON, A. STOESSL, and J. B. STOTHERS. Can. J. Chem. **50**, 122 (1972).
5. S. L. PATT and J. N. SHOOLERY. J. Magn. Reson. **46**, 535 (1982).
6. A. STOESSL. Physiol. Plant Pathol. **20**, 263 (1982).
7. R. R. FRASER, A. J. RAGAUSKAS, and J. B. STOTHERS. J. Am. Chem. Soc. **104**, 6475 (1982).
8. A. STOESSL and J. B. STOTHERS. J. Labelled Compd. Radiopharm. **19**, 1111 (1982).
9. G. W. BUCHANAN and J. B. STOTHERS. Can. J. Chem. **60**, 787 (1982).
10. A. K. CHENG, A. K. GHOSH, I. SHEEPY, and J. B. STOTHERS. Can. J. Chem. **59**, 3379 (1981).

Can. J. Chem. Downloaded from www.nrcresearchpress.com by 210.87.254.42 on 09/06/12
For personal use only.

Formation equilibria of silver amminocomplexes at temperatures up to 453 K

BARBARA KOŁODZIEJ

Institute of Inorganic Chemistry and Metallurgy of Rare Elements, Technical University of Wrocław 50-370 Wrocław, Poland

Received January 26, 1982[1]

BARBARA KOŁODZIEJ. Can. J. Chem. **61**, 383 (1983).

The formation equilibria of silver amminocomplexes were investigated by potentiometric method over the temperature range 333 to 453 K. On the grounds of emf measurements of a concentration cell consisting of

$Ag|AgNO_3$, NH_4NO_3 (2 *M*)$\|AgNO_3$, NH_3, NH_4NO_3 (2 *M*)$|Ag$

the equilibrium concentrations of uncomplexed silver ions $[Ag^+]$ were determined in a $Ag-NH_3-H_2O$ system. The Leden method was followed and the mean number of ligands ($\bar{N}$) per silver atom bound in amminocomplexes as well as the equilibrium concentration of free ammonia $[NH_3]$ were calculated. From the values obtained above the stability constants of silver amminocomplexes β_1 and β_2 were determined over the temperature range 333 to 453 K. The dependence of log β_1 versus temperature was described by the equation: $\log \beta_1 = 6.89 - 1.16 \times 10^{-2}T$ whereas for log β_2 the linear equation: $\log \beta_2 = 14.10 - 2.41 \times 10^{-2}T$ is satisfied only up to 413 K. Above 413 K the nature of the dependence is changed.

BARBARA KOŁODZIEJ. Can. J. Chem. **61**, 383 (1983).

On a étudié la formation des équilibres des complexes aminés de l'argent en utilisant une méthode potentiométrique dans un intervalle de température allant de 333 à 453 K. En se basant sur les mesures de la fem d'une cellule de concentration de

$Ag|AgNO_3$, NH_4NO_3 (2 *M*)$\|AgNO_3$, NH_3, NH_4NO_3 (2 *M*)$|Ag$

on a déterminé les concentrations à l'équilibre des ions argent non complexés $[Ag^+]$ d'un système $Ag-NH_3-H_2O$. On a utilisé une méthode de calcul basée sur la méthode de Leden et on a ainsi calculé le nombre moyen de ligands ($\bar{N}$) par atome d'argent lié dans les complexes aminés ainsi que la concentration à l'équilibre de l'ammoniac libre $[NH_3]$. A partir des valeurs ainsi obtenues, on a déterminé les constantes de stabilité des complexes aminés de l'argent β_1 et β_2 sur un intervalle de température allant de 333 à 453 K. On décrit l'influence de la température sur le log β_1 par l'équation: $\beta_1 = 6{,}89 - 1{,}16 \times 10^{-2}T$ alors que pour le log β_2 l'équation linéaire: $\log \beta_2 = 14{,}10 - 2{,}41 \times 10^{-2}T$ est satisfaisante uniquement jusqu'à 413 K. Au dessus de 413 K la nature de la relation change.

[Traduit par le journal]

Introduction

In the present paper the formation equilibria of silver amminocomplexes were investigated using the potentiometric method in a temperature range from 303 to 453 K using an electrolytic cell of special design (1).

Bjerrum (2), Nasanen (3), and Koch (4) applied electrochemical methods for studies of the above equilibria at standard temperatures. The stability constants of silver amminocomplexes were also determined by means of potentiometric method at temperatures up to 373 K (5, 6).

In the present paper the emf of the following concentration cell was measured at suitable temperatures:

[1] $Ag|AgNO_3$, NH_4NO_3 (2 *M*)$\|AgNO_3$, NH_3, NH_4NO_3 (2 *M*)$|Ag$

I II

emf

In both semi-cells of the concentration cell [1] the concentration of $AgNO_3$ (0.01 *M*) and ionic strength of NH_4NO_3 (2 *M*) were kept constant, only the ammonia concentration in suitable electrolytes in semi-cell II was varied. Emf measurements of cell [1] at a specific temperature in the equilibrium enabled us to determine the uncomplexed silver ion concentration $[Ag^+]$ in solutions of semi-cell II according to eq. [2].

$$[2] \quad \log [Ag^+] = \log [Ag^+]_c - \frac{F}{2.303RT}\Delta E$$

Other values necessary for determination of the stability constants of silver amminocomplexes were found by means of a modified Leden method (7).

At each specific temperature in the $Ag-NH_3-H_2O$ system an equilibrium described by eq. [3] is established:

$$[3] \quad \frac{[Ag^+][NH_3]^{\bar{N}}}{[Ag(NH_3)^+_{\bar{N}}]} = \text{constant}$$

where $\bar{N}$, the mean number of ligands per silver atom bound in the amminocomplexes, is given by expression [4]:

$$[4] \quad \bar{N} = \frac{[Ag(NH_3)^+] + 2[Ag(NH_3)_2^+]}{[Ag(NH_3)^+] + [Ag(NH_3)_2^+]}$$

whose numerator and denominator may be presented as follows:

$$[5] \quad [Ag(NH_3)^+] + 2[Ag(NH_3)_2^+] = [NH_3]_c - [NH_3]$$

$$[6] \quad [Ag(NH_3)^+] + [Ag(NH_3)_2^+] = [Ag(NH_3)_{\bar{N}}^+] = [Ag^+]_c - [Ag^+]$$

Thus, on the grounds of eqs. [4], [5], [6], the equilibrium concentration of free ammonia, $[NH_3]$, is given by eq. [7]:

$$[7] \quad [NH_3] = [NH_3]_c - \bar{N}([Ag^+]_c - [Ag^+])$$

The value which is unknown in eq. [7] and is necessary to find $[NH_3]$ is the mean number of ligands $\bar{N}$. This value was determined by transforming eq. [2] into form [8] using eqs. [3] and [7].

[1]Revision received July 20, 1982.

0008-4042/83/020383-05$01.00/0

©1983 National Research Council of Canada/Conseil national de recherches du Canada

Can. J. Chem. Downloaded from www.nrcresearchpress.com by 210.87.254.40 on 09/06/12
For personal use only.

$$[8]\quad \Delta E = \frac{2.303RT}{F}\left\{\bar{N}\log\left[[NH_3]_c - \bar{N}([Ag^+]_c - [Ag^+])\right] + \log\frac{[Ag^+]_c}{[Ag^+]_c - [Ag^+]}\right\} + \text{constant}'$$

For the equilibrium free ion concentrations $[Ag^+]$ defined at a given temperature and determined from eq. [2] (other values in eq. [8] are present values), the trial-and-error method may be used to select such values of $\bar{N}$ so that eq. [9] would be a straight line whose slope is $2.303RT/F$.

$$[9]\quad \Delta E = f\left\{\bar{N}\log\left[[NH_3]_c - \bar{N}([Ag^+]_c - [Ag^+])\right] + \log\frac{[Ag^+]_c}{[Ag^+]_c - [Ag^+]}\right\}$$

The values of $\bar{N}$ found by this method at a given temperature together will the predetermined values of $[Ag^+]$ enable us to calculate the respective equilibrium concentrations of uncomplexed ammonia $[NH_3]$ (eq. [7]).

From the equilibrium concentrations $[Ag^+]$ and $[NH_3]$ which are established at a specific temperature in the $Ag-NH_3-H_2O$ system, one can determine the stability constants of silver amminocomplexes β_1 and β_2 defining them as coefficients of eq. [10]:

$$[10]\quad \frac{[Ag^+]_c - [Ag^+]}{[Ag^+][NH_3]} = \beta_1 + \beta_2[NH_3]$$

Equation [10] was derived from eqs. [5] and [6] taking into consideration the definitions of stability constants β_1 and β_2:

$$[11]\quad \beta_1 = [Ag(NH_3)^+]/[Ag^+][NH_3]$$

$$[12]\quad \beta_2 = [Ag(NH_3)_2^+]/[Ag^+][NH_3]^2$$

Experimental

Emf measurements of the concentration cell [1] were carried out in a specially designed and constructed electrolytic cell (1). Its design made it possible to measure the emf values at temperatures exceeding 373 K.

The electrolytic cell shown in Fig. 1 consists of a vertical cylindrical PTFE block (*1*) enclosed in a metal housing (*2*). The PTFE block contains four vertical cylindrical chambers (*3*) connected in their bottom parts through capillary holes (*4*) filled with asbestos to a profiled chamber (*5*) which, having been filled with electrolyte, acts as a salt-bridge. Cylindrical chambers (*3*) were filled completely with electrolyte solutions in order to eliminate any free space, and with electrodes installed in them, they function as respective semi-cells. Each of the four cylindrical chambers (*3*) is closed with a PTFE stopper (*6*) provided with an axially installed electrode. The holes closed with PTFE stoppers are made tight by means of sleeves (*7*) of setscrews (*8*) and (*9*). Setscrews (*8*) are screwed into a metal cover (*10*) pressed down to the metal housing by means of a nut (*11*). Chamber (*5*) for the salt-bridge solution is closed from the top by means of a PTFE stopper (*12*) tightened with a sleeve (*13*) and a screw (*14*) and from the bottom by means of a four-winged PTFE stopper (*15*) tightened with a set screw (*16*). In addition, the PTFE block is provided with four copper heating inlets (*17*) and a cylindrical hole (*18*) for a thermocouple and thermometer.

The cell was placed in an electric furnace whose temperature was adjusted by means of a thermoregulator. The temperature in the electrolytic cell was measured by means of a copper–constantan thermocouple using a KM-76 compensator and ekN/T12 recorder. After the temperature became stable, the emf of the respective cells was measured. Emf was measured by means of a KM-76 compensator accurate to 0.1 mV.

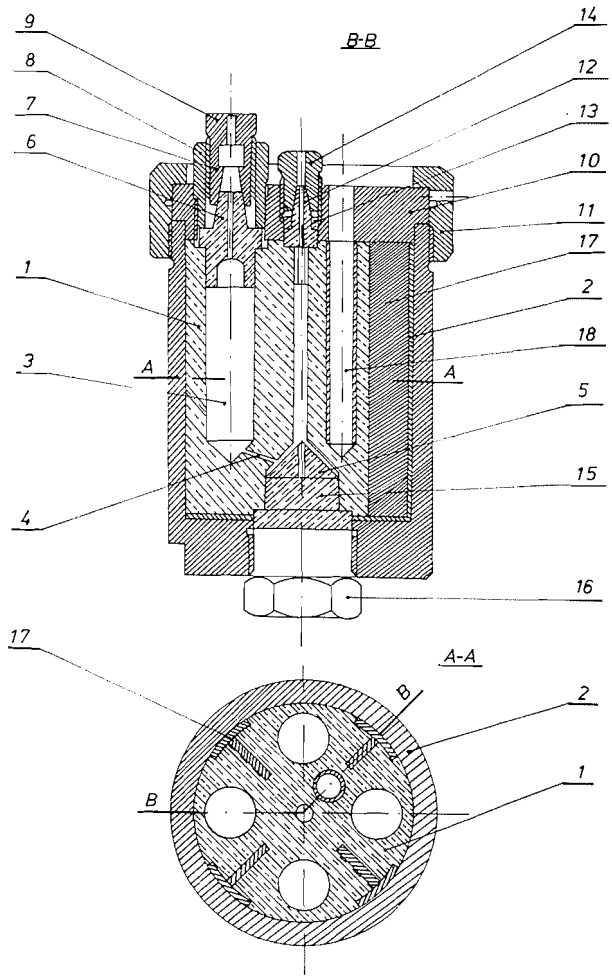

FIG. 1. Electrolytic cell for emf measurements at temperatures exceeding 373 K.

$AgNO_3$ solutions at suitable concentrations were prepared from weighed portions of crystalline silver nitrate after recrystallization of analytical grade $AgNO_3$. NH_4NO_3 solutions were prepared by the same method. Suitable ammonia solutions whose concentrations were determined by acid–base titrations were prepared by diluting concentrated NH_3 analytical grade.

Results and discussion

Emf measurements of cell [1] were carried out for the respective solutions in a temperature range from 303 to 453 K. In the solutions under investigation a constant ionic strength (2 *M* NH_4NO_3) and constant silver ion concentration $[Ag^+]_c$ was maintained. Only the concentration of ammonia $[NH_3]$ was varied.

Initial concentrations $[Ag]_c$, $[NH_3]_c$ in the electrolytes of cell [I] under investigation, their corresponding emf values at specific temperatures, and equilibrium concentrations of the uncomplexed silver ions $[Ag^+]$ calculated from eq. [2] are summarized in Table 1. In the values given, allowance was made for the change of the water density with temperature.

The values of $\bar{N}$ found for the respective temperatures by the trial-and-error method are presented in Table 2. Table 2 also contains a comparison of the slope coefficient for straight line [8] at the values of $\bar{N}$ assumed for specific temperatures with the actual value for a given temperature coefficient $2.303RT/F$. A satisfactory agreement between these coefficients enabled us, on the grounds of the selected values of $\bar{N}$, to determine the

Can. J. Chem. Downloaded from www.nrcresearchpress.com by 210.87.254.40 on 09/06/12
For personal use only.

TABLE 1. Initial concentrations $[Ag^+]_c$, $[NH_3]_c$, emf values and calculated equilibrium concentrations $[Ag^+]$ and $[NH_3]$ in solutions investigated over a temperature range from 333 to 453 K

Temperature (K)	$[Ag^+]_c 10^3$ (mol dm^{-3})	$[NH_3]_c 10^2$ (mol dm^{-3})	ΔE (V)	$[Ag^+]10^4$ (mol dm^{-3})	$[NH_3]10^3$ (mol dm^{-3})
333	9.832	2.274	0.0980	3.24	4.200
		2.550	0.1197	1.52	6.624
		3.032	0.1500	0.53	11.25
		3.308	0.1620	0.35	13.97
		3.515	0.1678	0.28	16.03
		3.642	0.1747	0.23	17.29
		4.066	0.1856	0.15	21.52
		4.518	0.1946	0.11	26.03
353	9.718	2.248	0.0836	6.23	5.381
		2.521	0.0991	3.74	7.643
		2.997	0.1262	1.54	11.98
		3.270	0.1373	1.07	14.63
		3.474	0.1438	0.86	16.63
		3.599	0.1472	0.77	17.86
		4.019	0.1620	0.47	22.01
		4.465	0.1712	0.35	26.44
373	9.584	2.216	0.0707	10.64	6.653
		2.486	0.0832	7.21	8.729
		2.956	0.1048	3.68	12.78
		3.225	0.1146	2.71	15.30
		3.426	0.1204	2.26	17.23
		3.549	0.1247	1.98	18.40
		3.964	0.1385	1.29	22.43
		4.404	0.1477	0.97	26.77
393	9.434	2.182	0.0595	16.29	8.083
		2.447	0.0697	12.06	9.988
		2.910	0.0875	7.13	13.91
		3.174	0.0950	5.74	16.14
		3.373	0.1011	4.77	17.96
		3.494	0.1044	4.33	19.10
		3.902	0.1162	3.05	22.95
		4.335	0.1247	2.38	27.16
413	9.264	2.143	0.0493	22.66	9.673
		2.403	0.0572	18.58	11.58
		2.857	0.0715	12.43	15.09
		3.117	0.0772	10.59	17.39
		3.312	0.0835	8.87	19.04
		3.431	0.0861	8.25	20.13
		3.831	0.0954	6.35	23.81
		4.257	0.1043	4.95	27.83
433	9.075	2.099	0.0401	31.00	11.25
		2.354	0.0456	26.75	13.11
		3.054	0.0625	17.01	18.52
		3.244	0.0665	15.28	20.13
		3.361	0.0705	13.73	21.06
		3.753	0.0780	11.23	24.57
		3.967	0.0800	10.64	26.61
		4.170	0.0865	8.94	28.36
453	8.866	2.051	0.0316	40.07	12.73
		2.299	0.0355	35.72	14.52
		2.983	0.0494	25.02	19.64
		3.169	0.0520	23.40	21.25
		3.284	0.0554	21.45	22.08
		3.667	0.0662	18.02	25.36
		4.074	0.0680	15.53	29.04

equilibrium concentrations of uncomplexed ammonia $[NH_3]$ (according to [7]). The values of $[NH_3]$ for the respective solutions are summarized in Table 1.

The calculated values of equilibrium concentrations $[Ag^+]$ and $[NH_3]$ as well as the total silver ion concentration $[Ag^+]_c$ enabled us, according to eq. [10], to determine the values of

Can. J. Chem. Downloaded from www.nrcresearchpress.com by 210.87.254.40 on 09/06/12
For personal use only.

TABLE 2. Values of $\bar{N}$ determined at suitable temperatures, comparison between the slope coefficient of straight line [8] and $2.303RT/F$ coefficient

Temperature (K)	$\bar{N}$	$\frac{2.303RT}{F}$	The slope coefficient [8]
333	1.95	0.066	0.065
353	1.88	0.070	0.071
373	1.82	0.074	0.073
393	1.76	0.078	0.077
413	1.68	0.082	0.082
433	1.63	0.086	0.087
453	1.60	0.090	0.088

stability constants β_1 and β_2 for silver amminocomplexes over the temperature range up to 453 K by the method of least squares.

The stability constants determined are presented in Table 3 and compared with the values determined by other authors.

Temperature dependences for the logarithms of stability constants β_1 and β_2 presented in Fig. 2 indicate that the stability of the respective silver amminocomplexes decreases with in-

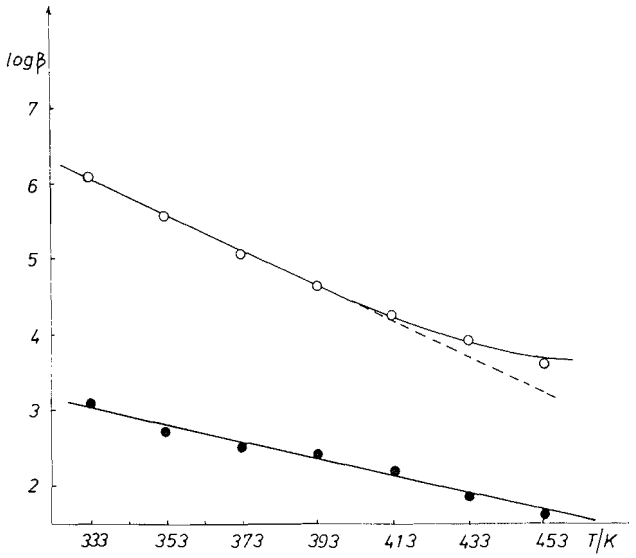

FIG. 2. Dependence of logarithms of silver amminocomplexes stability constants versus temperature. ●, log $\beta_1 = f(T)$; ○, log $\beta_2 = f(T)$.

TABLE 3. Logarithms of stability constants for silver amminocomplexes, their comparison with data provided by other authors

Temperature (K)	log β_1	log β_2	Medium	Method *	References
298	3.315	7.23	$I \rightarrow 0$	gl	2
	3.37	7.21	$I \rightarrow 0$	gl	2
	3.37	7.15	NH_4NO_3 1 *M*	gl	2
	3.31	7.21	KNO_3 1 *M*	AgΔ	3
	—	7.03	dil	M(Ag)	4
	3.35	7.23	NH_4NO_3 2 *M*	gl	5
	3.23	7.01	NH_4NO_3 2 *M*	gl	6
	3.44	6.92	NH_4NO_3 2 *M* (extr.)	M	This work
303	3.20	7.03	NH_4NO_3 2 *M*	gl	2
	3.24	7.05	NH_4NO_3 0.5 *M*	gl	2
	—	6.86	—		4
	3.27	6.93	NH_4NO_3 2 *M*	gl	5
	3.23	7.01	NH_4NO_3 2 *M*	gl	6
	3.38	6.80	NH_4NO_3 2 *M* (ext.)	M	This work
313	—	6.49	—		4
	3.10	6.58	NH_4NO_3 2 *M*	gl	5
	3.11	6.70	NH_4NO_3 2 *M*	gl	6
	3.26	6.56	NH_4NO_3 2 *M* (ext.)	M	This work
323	—	6.16	—		4
	2.81	6.17	NH_4NO_3 2 *M*	gl	5
	2.95	6.35	NH_4NO_4 2 *M*	gl	6
	3.15	6.32	NH_4NO_3 2 *M* (ext.)	M	This work
333	3.08	6.10	NH_4NO_3 2 *M*	M	This work
343	2.61	5.54	NH_4NO_3 2 *M*	gl	5
	2.74	5.87	NH_4NO_3 2 *M*	gl	6
353	2.71	5.58	NH_4NO_3 2 *M*	M	This work
363	2.25	4.95	NH_4NO_3 2 *M*	gl	5
	2.50	5.40	NH_4NO_3 2 *M*	gl	6
373	2.52	5.10	NH_4NO_3 2 *M*	M	This work
393	2.38	4.65	NH_4NO_3 2 *M*	M	This work
413	2.17	4.25	NH_4NO_3 2 *M*	M	This work
433	1.88	3.93	NH_4NO_3 2 *M*	M	This work
453	1.62	3.63	NH_4NO_3 2 *M*	M	This work

*gl = glass electrode, M = emf measurement with electrode of Ag.

Can. J. Chem. Downloaded from www.nrcresearchpress.com by 210.87.254.40 on 09/06/12
For personal use only.

creasing temperature. The temperature dependence for log β_1 over the entire temperature range under investigation follows eq. [13], while the dependence of log β_2 versus temperature is linear, according to eq. [14] only up to 413 K.

$$[13] \quad \log \beta_1 = 6.89 - 1.16 \times 10^{-2}T$$

$$[14] \quad \log \beta_2 = 14.10 - 2.41 \times 10^{-2}T$$

Acknowledgement

I thank Professor Z. Zembura, Academy of Mining and Metallurgy, Cracow, Poland, for valuable discussions.

1. F. ŁETOWSKI, B. KOŁODZIEJ, and J. LEŚNIAK. Polish Patent 45539. 1972.
2. J. BJERRUM. Metal ammine formation in aqueous solution. Copenhagen. 1957.
3. R. NASANEN. Acta Chem. Scand. **1**, 763 (1947).
4. F. K. V. KOCH. J. Chem. Soc. 2053 (1930).
5. B. KOZŁOWSKA, F. ŁETOWSKI, and J. NIEMIEC. Rocz. Chem. (Ann. Soc. Chim. Polonorum), **43**, 1597 (1969).
6. B. KOZŁOWSKA-KOŁODZIEJ. Doctoral Thesis, Wrocław. 1973.
7. J. LEDEN. Z. Phys. Chem. A**188**, 160 (1941).

Can. J. Chem. Downloaded from www.nrcresearchpress.com by 210.87.254.40 on 09/06/12
For personal use only.

The influence of the ionic strength on the adsorption of thiocyanate ions on mercury[1]

LUIS A. AVACA, ERNESTO R. GONZÁLEZ, AND ROMEU C. ROCHA FILHO[2]

Instituto de Física e Química de São Carlos, Universidade de São Paulo, C.P. 369, São Carlos, SP, 13560 Brasil

Received March 3, 1982

LUIS A. AVACA, ERNESTO R. GONZÁLEZ, and ROMEU C. ROCHA FILHO. Can. J. Chem. **61**, 388 (1983).

The adsorption of thiocyanate ions at mercury has been studied from aqueous solutions of two different and constant ionic strengths, namely, x *M* KSCN + $(0.5 - x)$ *M* KF and x *M* KSCN + $(1.0 - x)$ *M* KF, at 298 K. The surface excess due to thiocyanate ions was determined using the Hurwitz–Parsons analysis as well as using the surface pressure method. The amount of specifically adsorbed thiocyanate ion at a given electrode charge density and thiocyanate concentration is shown to depend on the ionic strength. For both ionic strengths, the adsorption process was found to be described by an isotherm congruent on the electrode charge density, to which virial isotherms were fitted with the following parameter values: B = 210 and 185 Å^2 ion^{-1}, and ΔG_0^0 = −93.05 and −92.88 kJ mol^{-1}, for ionic strengths 0.5 and 1.0 *M*, respectively. The properties of the inner layer are discussed based on the corresponding Christie plots.

LUIS A. AVACA, ERNESTO R. GONZÁLEZ et ROMEU C. ROCHA FILHO. Can. J. Chem. **61**, 388 (1983).

On a étudié l'adsorption des ions thiocyanates sur le mercure à partir de solutions aqueuses de deux forces ioniques différentes et constantes, soit: x *M* KSCN + $(0,5 - x)$ *M* KF et x *M* KSCN + $(1,0 - x)$ *M* KF à 298 K. On a déterminé la surface en excès due aux ions thiocyanates en utilisant l'analyse de Hurwitz–Parsons ainsi que la méthode de pression de surface. On montre que la quantité d'ions thiocyanates adsorbés spécifiquement à une densité de charge d'électrodes et à une concentration de thiocyanate données dépend de la force ionique. On a trouvé que pour les deux forces ioniques, le processus d'adsorption doit être décrit par une isotherme convergente sur la densité de charge d'électrode, sur laquelle on ajuste les isothermes viriaux à l'aide des valeurs des paramètres suivants: B = 210 et 185 Å ion^{-1} et ΔG_0^0 = 93,05 et −92,88 kJ mol^{-1} respectivement pour des forces ioniques de 0,5 et 1,0 *M*. On discute des propriétés de la couche interne en se basant sur les courbes correspondantes de Christie.

[Traduit par le journal]

Introduction

In recent years there has been a growing interest in the study of adsorption of ions at the mercury – aqueous solution interface from constant ionic strength solutions (1–6). In general, these studies included comparison with the results obtained from single salt solutions and, in some cases (3–5), comparisons between double-layer parameters for different values of the ionic strength were also carried out. Thus, Dutkiewicz (3) analyzed the adsorption of benzenesulphonate ions from solutions of 0.3 and 1.0 *M* ionic strength but, due to inherent complexities in the adsorption characteristics of this ion, the influence of the ionic strength on the adsorption process and on some electrical double-layer parameters was only partially discussed. On the other hand, Fawcett and Sellan (5) studied the adsorption of nitrate ions from 0.2 *M* ionic strength solutions and, by comparing the amounts of specifically adsorbed charges with those obtained by Payne (7) at 1.0 *M* ionic strength, were able to draw some conclusions regarding the dependence of the adsorption process on the ionic strength. A similar analysis was done previously for iodide adsorption (4).

Fawcett and Sellan (5) found that the nitrate ion is moderately adsorbed on Hg, that is, when the electrode charge density q^M is positive the interface shows an absolute value of the specifically adsorbed charge density $|q_-'|$ greater than q^M at high nitrate concentrations, while the opposite happens at low concentrations; a similar behavior was observed for azide ions (6). As a consequence, when a comparison between the specifically adsorbed charge densities obtained at two ionic strengths was carried out an interesting result was obtained: the adsorption is greater at the higher ionic strength for high nitrate concentrations, i.e., for $|q_-'| > q^M$, while the contrary becomes true at low concentrations. This behavior was explained in terms of the change in the potential at the outer Helmholtz plane (oHp), as pointed out previously by Randles (8). Studies of adsorption on mercury of the azide ion at different ionic strengths are being carried out in this laboratory to investigate further the adsorption behavior demonstrated by the nitrate ion study.

If an ion adsorbs strongly, $|q_-'|$ should be greater than q^M even at low bulk concentrations. This means that for a constant concentration of the ion its adsorption will be larger the greater the ionic strength, as has been shown by Fawcett and McCarrick (4) in the case of iodide. Previous studies of the adsorption of thiocyanate ions on mercury from single salt solutions have shown that this ion has characteristics of a pseudo-halide, with an adsorption only slightly weaker than that of iodide (10–13). Behr *et al.* (14) studied the adsorption of thiocyanate from aqueous solutions of constant ionic strength. However, as their aim was to analyze the effect of additions of acetone on the adsorption of SCN^-, a detailed study of the characteristics of the electrical double-layer was not made. The present work was undertaken to examine the influence of the ionic strength on the adsorption of a strongly adsorbing ion, thiocyanate. The influence of the ionic strength on the inner-layer properties was also analyzed. The systems studied were aqueous (KSCN + KF) solutions at 0.5 and 1.0 *M* ionic strengths.

Experimental

Data for differential capacity against electrode potential, for the

[1]Presented in part at the V Reunión Latinoamericana de Electroquímica y Corrosión, Concepción, Chile, Sept. 29 – Oct. 3, 1980.

[2]Permanent address: Departamento de Química, Universidade Federal de São Carlos, C.P. 676, São Carlos, SP, 13560 Brasil.

0008-4042/83/020388-07$01.00/0

©1983 National Research Council of Canada/Conseil national de recherches du Canada

Can. J. Chem. Downloaded from www.nrcresearchpress.com by 210.87.254.42 on 09/06/12
For personal use only.

Can. J. Chem. Downloaded from www.nrcresearchpress.com by 210.87.254.42 on 09/06/12
For personal use only.

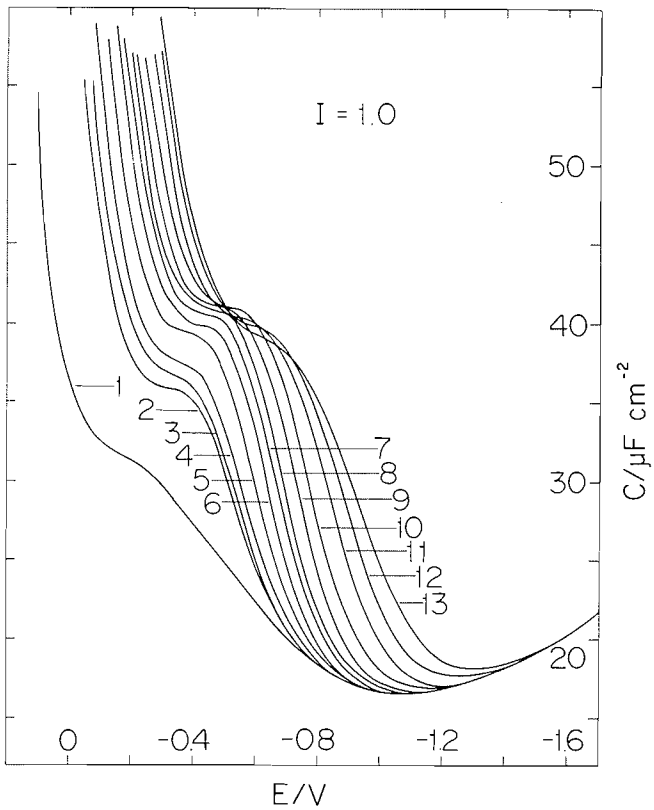

FIG. 1. Differential capacity of the electrical double layer for a mercury electrode in aqueous x *M* KSCN + $(1.0 - x)$ *M* KF solutions at 298 K. x = (*1*) 0, (*2*) 0.001, (*3*) 0.00125, (*4*) 0.0025, (*5*) 0.005, (*6*) 0.01, (*7*) 0.0175, (*8*) 0.025, (*9*) 0.05, (*10*) 0.1, (*11*) 0.25, (*12*) 0.5, (*13*) 1.0. Potentials with respect to a sce.

mercury – aqueous solution interface at 298 K, were obtained with 12 solutions of composition x *M* KSCN + $(0.5 - x)$ *M* KF, where x had the values 0, 0.001, 0.00125, 0.0025, 0.005, 0.01, 0.0175, 0.025, 0.05, 0.1, 0.25, and 0.5; and for 13 solutions of composition x *M* KSCN + $(1.0 - x)$ *M* KF, where x had the same values as before plus the additional value of 1.0. The experimental procedure has been described elsewhere (6). The calculated differential capacities were found to be independent of frequency in the range 50–800 Hz. Analytical grade salts, dried over P_2O_5, were used without further purification. The purity of KF was tested by comparing capacity curves of KF solutions at different concentrations with those from the literature (15), with good agreement. Water and mercury were purified as described previously (16). All potentials are referred to a saturated calomel electrode used as reference.

Results and discussion

Figure 1 shows the differential capacity against potential curves for an ionic strength of 1.0 *M*. As can be observed, the value of the differential capacity is independent of solution composition for potentials more negative than −1.5 V. The results obtained for the 0.5 *M* ionic strength were similar to those already shown, presenting the same behavior at large negative potentials.

The experimental values of the potential of zero charge, E^z, and the calculated values of the interfacial tension at this potential, γ^z, are shown in Table 1. The latter were calculated by back integration from the value at −1.70 V, which, in turn, was calculated through forward integration of the data for the KF electrolyte solution from the value 425.7 mN m^{-1} for γ^z (17), using a computer program described elsewhere (18).

The variation of ionic activity coefficients in mixed salt

TABLE 1. Potentials of zero charge E^z and respective interfacial tensions γ^z for aqueous solutions containing SCN^- at different concentrations, for the 0.5 and 1.0 *M* ionic strengths

	I = 0.5 *M*		I = 1.0 *M*	
x	E^z (V vs. sce)	γ^z (mN m^{-1})	E^z (V vs. sce)	γ^z (mN m^{-1})
0	−0.4344	425.7	−0.4288	425.7
0.001	−0.4630	425.0	−0.4616	424.9
0.00125	−0.4676	424.9	−0.4644	424.8
0.0025	−0.4820	424.5	−0.4798	424.3
0.005	−0.4989	423.8	−0.4981	423.5
0.01	−0.5181	422.8	−0.5174	422.5
0.0175	−0.5340	421.7	−0.5356	421.4
0.025	−0.5465	420.9	−0.5468	420.6
0.05	−0.5710	419.2	−0.5695	418.7
0.1	−0.5957	417.0	−0.5958	416.4
0.25	−0.6278	413.7	−0.6265	412.8
0.5	−0.6520	410.7	−0.6531	409.6
1.0	—	—	−0.6744	405.9

solutions containing, for example, a single cation has been considered in theoretical treatments of adsorption from such solutions (9, 19). As shown by Fawcett and McCarrick (4), the magnitude of this variation is a function of the nature of the system and, in some cases, can be disregarded. In this work, as a first approximation, the variation of the activity coefficient with composition was not taken into account and, so, the double-layer parameters were obtained on the basis of the treatment of Dutkiewicz and Parsons (20), as already described (6). Further below, the error in the values of the specifically adsorbed charge density q_-' due to this approximation will be estimated.

The adsorption isotherm

In each of the adsorption studies done from solutions containing only thiocyanate, a different isotherm was found to describe its adsorption on mercury. Thus, Wroblowa *et al.* (11) fitted their data to the Bockris–Devanathan–Müller isotherm (21) while Minc and Andrzejczak (12), applying the surface pressure method (22), found that the isotherm was congruent in charge density and were able to fit the data to the Frumkin equation; finally, Parsons and Symons (13) analyzed their data in terms of the virial isotherm.

Although the integral form of the iostherm (in terms of surface pressures) is not very sensitive, it is useful because it avoids the errors due to the differentiation necessary to obtain the specifically adsorbed charge q_-' (23). At the same time, it allows a comparison between the values of q_-' obtained from the isotherm and those calculated through differentiation of Parsons function ($\xi = \gamma + Eq^M$) against log c. Thus, the surface pressure method (22) was applied to the data obtained here, for both ionic strengths. The surface pressure Φ vs. log c curves for all charge densities q^M in the range −8 to 14 μC cm^{-2} were found to be congruent in the charge density; the composite curves shown in Figs. 2 and 3 were obtained as a result of this analysis. Both of these curves could be fitted to a virial isotherm, which may be written as

$$[1] \quad -q_-' = xF \exp\left(\frac{-\Delta G^0}{RT} + \frac{2Bq_-'}{F}\right)$$

where ΔG^0 is the standard free energy of adsorption at zero coverage which is a function only of q^M, B the second virial

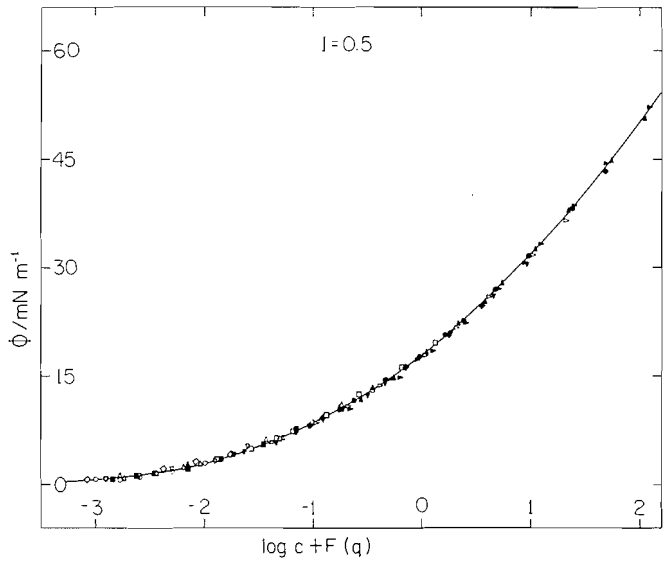

FIG. 2. Composite surface pressure curve at constant charge density for the adsorption of thiocyanate on Hg at 298 K from aqueous 0.5 M ionic strength solutions. (◇) $q^M = -8$, (▽) $q^M = -6$, (■) $q^M = -4$, (△) $q^M = -2$, (○) $q^M = 0$, (□) $q^M = 2$, (◆) $q^M = 4$, (▼) $q^M = 6$, (▷) $q^M = 8$, (●) $q^M = 10$, (▲) $q^M = 12$, (▶) $q^M = 14$ μC cm^{-2}. The solid line was calculated from a virial equation with the second virial coefficient $B = 210$ Å^2 ion^{-1}.

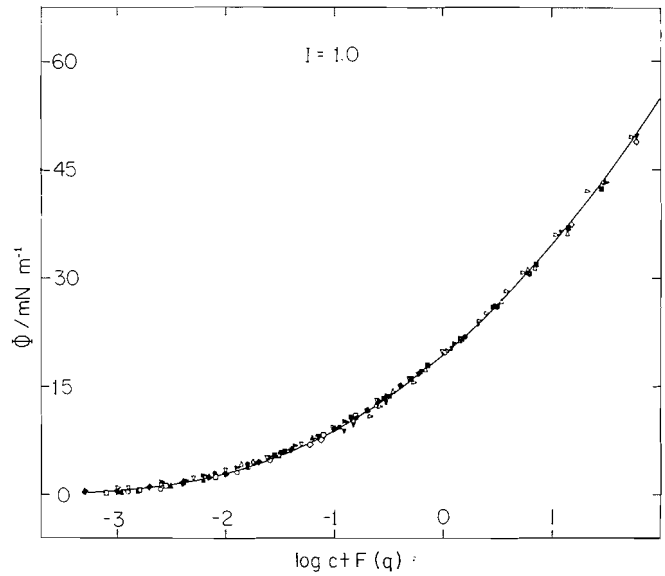

FIG. 3. Composite surface pressure curve at constant charge density for the adsorption of thiocyanate on Hg at 298 K from aqueous 1.0 M ionic strength solutions. (○) $q^M = -8$, (▲) $q^M = -6$, (□) $q^M = -4$, (◆) $q^M = -2$, (▽) $q^M = 0$, (▶) $q^M = 2$, (●) $q^M = 4$, (△) $q^M = 6$, (■) $q^M = 8$, (◇) $q^M = 10$, (▼) $q^M = 12$, (▷) $q^M = 14$ μC cm^{-2}. The solid line was calculated from a virial equation with the second virial coefficient $B = 185$ Å^2 ion^{-1}.

coefficient, x the SCN^- concentration, and R, F, and T have their usual significance.

The values found for the isotherm parameters were 210 and 185 Å^2 ion^{-1} for B, and −93.05 and −92.88 kJ mol^{-1} for the standard free energies of adsorption at zero coverage in the absence of electrical interaction between ion and electrode ΔG_0^0, for the ionic strengths 0.5 and 1.0 M, respectively. The standard states were 1 ion cm^{-2} on the surface and 1 mol L^{-1} in the solution.

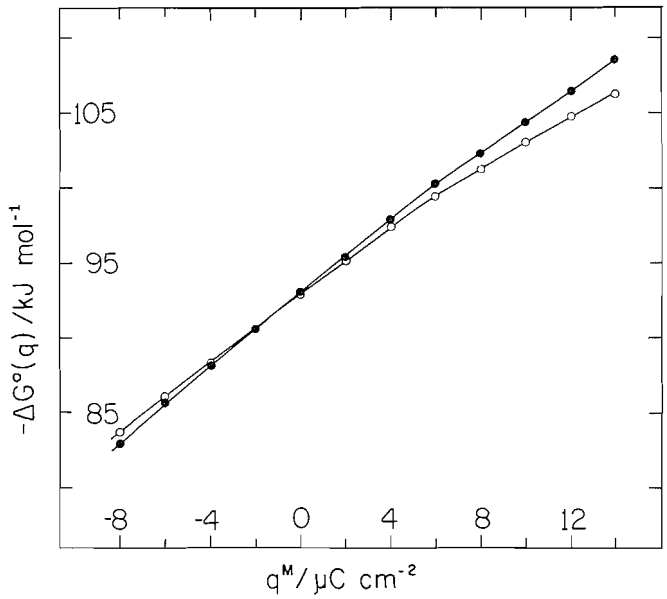

FIG. 4. Dependence of the standard free energy of adsorption at zero coverage on the electrode charge density, for the adsorption of thiocyanate on Hg at 298 K from aqueous (●) 0.5 and (○) 1.0 M ionic strength solutions.

The fact that the values of ΔG_0^0 are practically the same for both ionic strengths confirms the consistence of the analyses since this parameter should not depend on the ionic strength. Moreover, these values are very close to the one which can be estimated from the results of Minc and Andrzejczak (12) for pure KSCN solutions (−92.1 kJ mol^{-1} at 298 K). The different values of B obtained for the two ionic strengths are due to the fact that, as the ionic strength increases, the ionic atmosphere of each adsorbed SCN^- ion lowers the repulsive interaction between adsorbed SCN^- ions. Consequently, a smaller value of B is required for the isotherm which describes the adsorption process for the higher ionic strength. Parsons and Symons (13) found an apparent decrease of B from 1600 to 700 Å^2 ion^{-1} as the concentration of SCN^- increased in solutions of varying ionic strength. This variation and its range are consistent with the analysis above.

The values of the free energy of adsorption at zero coverage, ΔG^0, for each value of q^M were estimated from the displacements made along the log c axis in order to obtain the composite surface pressure curves of Figs. 2 and 3 (22). The dependence of ΔG^0 on q^M is shown in Fig. 4, for both ionic strengths. The behavior of each ionic strength is very similar in that the adsorption process becomes energetically favored as q^M increases. Starting from negative q^M values up to slightly positive ones the dependence of ΔG^0 on q^M is linear, which shows that in this range of q^M both systems behave as fixed parallel plate condensers in which one dielectric is replaced by another (24), while for high positive values of q^M this simple model no longer holds.

The specifically adsorbed charge

Figure 5 shows the specifically adsorbed charge density q_-', obtained via Parsons function, plotted against the electrode charge density for different SCN^- concentrations at the ionic strength 1.0 M. The curves are qualitatively similar to those presented by halide and pseudo halide ions in solutions of constant ionic strength, as well as in solutions containing one salt (2, 6, 13). For the 0.5 M ionic strength the results are

Can. J. Chem. Downloaded from www.nrcresearchpress.com by 210.87.254.42 on 09/06/12
For personal use only.

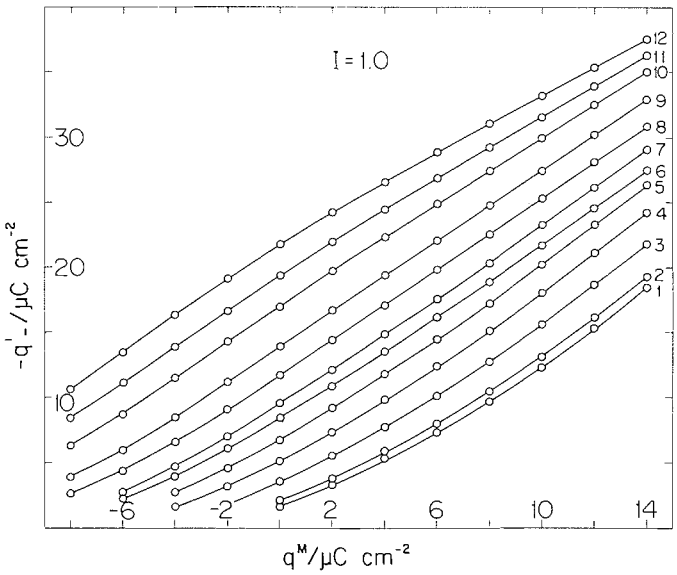

FIG. 5. Charge due to adsorbed thiocyanate ions on Hg at 298 K from aqueous x *M* KSCN + (1.0 − x) *M* KF solutions. x = (*1*) 0.001, (*2*) 0.00125, (*3*) 0.0025 (*4*) 0.005, (*5*) 0.01, (*6*) 0.0175, (*7*) 0.025, (*8*) 0.05, (*9*) 0.1, (*10*) 0.25, (*11*) 0.5, (*12*) 1.0.

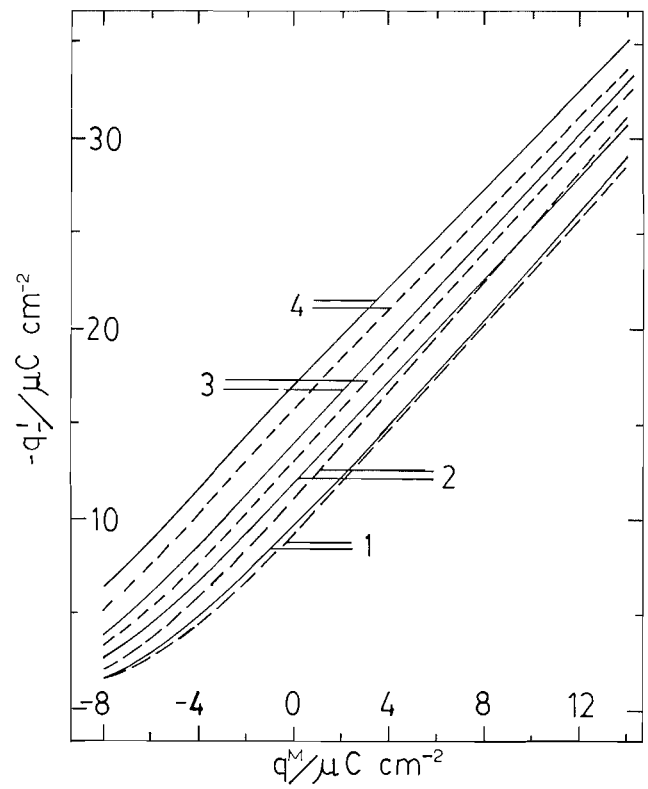

FIG. 6. Charge due to adsorbed thiocyanate ions on Hg at 298 K from aqueous x *M* KSCN + (1.0 − x) *M* KF (full lines) and x *M* KSCN + (0.5 − x) *M* KF solutions (broken lines). x = (*1*) 0.025, (*2*) 0.05, (*3*) 0.1, (*4*) 0.25.

similar to those in Fig. 5, showing smaller values of q_-' at the higher concentrations. It follows from Fig. 5 that the adsorption of SCN^- can be considered to be quite strong, since $|q_-'| > q^M$ even at low thiocyanate concentrations. This implies that the potential at the oHp, ϕ^2, should become less negative as the ionic strength is increased (8) and, consequently, for a fixed concentration of SCN^- its amount specifically adsorbed should increase accordingly. As can be seen in Fig. 6, the present results confirm this behavior, which has also been observed for iodide (4) and for nitrate ion adsorption (5) when the condition $|q_-'| > q^M$ is fulfilled. A comparison of the data in Fig. 6 with those for the adsorption of thiocyanate from pure salt solutions (11–13) again shows that for fixed concentrations of SCN^- the specifically adsorbed charge densities are larger the higher the ionic strength of the solution, as reported previously for other systems (2, 4–6). This behaviour has been qualitatively explained by Hills and Reeves (2) on the basis of charge imaging.

As mentioned before, the use of the surface pressure method to obtain the adsorption isotherm avoids the errors involved in the differentiation process to obtain the values of q_-', since they can be obtained from the isotherm by rewriting eq. [1] in the form (for standard states 1 ion cm^{-2} on the electrode surface and 1 mol L^{-1} in the solution)

$$[2] \quad \ln\left(-\frac{q_-'}{xe_0}\right) + \frac{\Delta G^0}{RT} - \frac{2Bq_-'}{e_0} = 0$$

where e_0 is the electronic charge. Once the values of ΔG^0 and B are known, eq. [2] can be used to obtain q_-' for the different values of x at different constant values of q^M. This was done iteratively, starting with the assumption that $q_-' = 0.01$ μC cm^{-2}, changing it in steps of 0.01 μC cm^{-2} up to the value for which eq. [2] was obeyed.

A comparison between the values of q_-' obtained through differentiation and those from the isotherm is shown in Fig. 7 for different concentrations of SCN^- at ionic strength 1.0 *M*. It can be seen that the two sets of values are in good agreement, except for the highest concentration (x = 0.5) and for highly positive values of q^M. The same type of behavior was observed for the results obtained at ionic strength 0.5 *M*. Before drawing any conclusions from the comparison above, it is interesting to estimate the error in q_-' obtained by differentiation without considering the variation of activity coefficients with solution composition.

Fawcett and co-workers (4, 5) have taken into account the variation of the activity coefficient with solution composition by introducing the parameter $\beta = (\beta_{KSCN} - \beta_{KF})I$, where β_{KX} is the interaction coefficient between K^+ and X^-, and I is the ionic strength. Thus, knowledge of the value of this parameter allows the calculation of q_-' through the equation (4)

$$[3] \quad \frac{F}{RT(1+\beta\mu)}\left(\frac{\partial\xi^+}{\partial \ln \mu}\right)_{q^M} = q_-' + q_-^{d}\frac{\beta\mu}{(1+\beta\mu)}$$

where q_-^d is the charge in the diffuse layer due to anions, ξ^+ the value of Parsons function for an electrode potential with respect to an electrode reversible to K^+, and $\mu = x/I$.

An examination of the values of $\gamma_\pm$(KSCN) and of $\gamma_\pm$(KF) in the literature (25), together with the works of Fawcett and McCarrick (4) and of Fawcett and Sellan (5), permits one to conclude that in the case of SCN^-, the values of q_-' obtained through differentiation without considering activity coefficient variation would be underestimated, as in the case of NO_3^- (5). One way of estimating the value of β is through the use of the equation (25)

$$[4] \quad \ln \gamma_\pm(KX) = -\frac{AI^{1/2}}{1 + BaI^{1/2}} + \beta_{KX}I$$

where A and B are the Debye–Hückel parameters, and a is the ion size parameter. This equation can be rewritten as

Can. J. Chem. Downloaded from www.nrcresearchpress.com by 210.87.254.42 on 09/06/12
For personal use only.

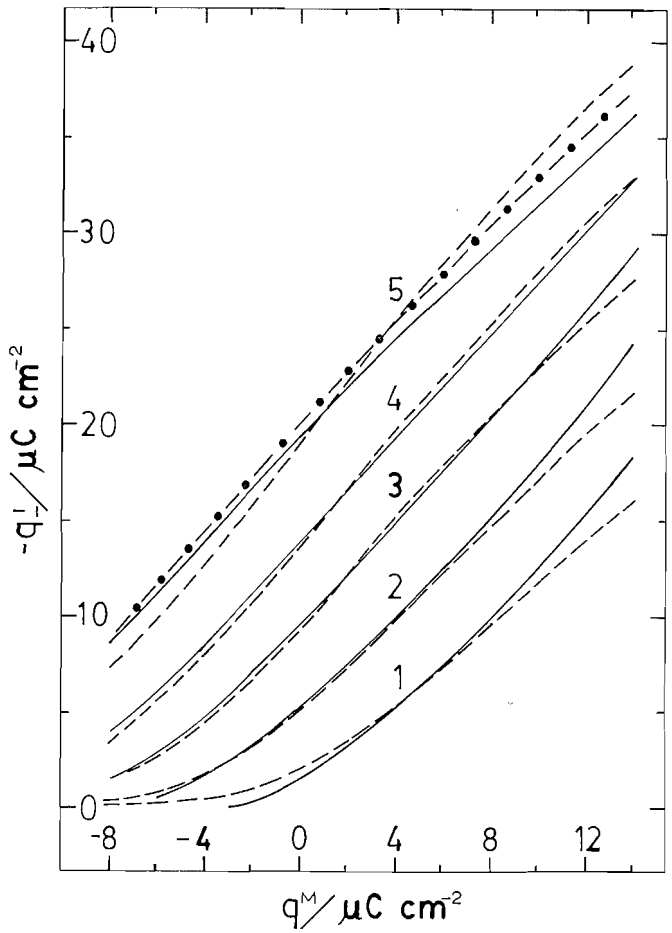

FIG. 7. Charge due to adsorbed thiocyanate ions on Hg at 298 K from aqueous x *M* KSCN + $(1.0 - x)$ *M* KF solutions. x = (*1*) 0.001, (*2*) 0.005, (*3*) 0.025, (*4*) 0.1, (*5*) 0.5. Full lines correspond to data obtained through differentiation; dashed lines correspond to data obtained from the isotherm fitted through the surface pressure method (see text); dotted dashed line corresponds to data obtained through differentiation and corrected because of activity coefficient variation (see text).

$$[5] \quad w = \ln \gamma_{\pm}(KX) + \frac{AI^{1/2}}{1 + BaI^{1/2}} = \beta_{KX} I$$

such that β_{KX} can be calculated through least squares from tabulated values of $\gamma_{\pm}(KX)$ (25), given the value of a for the salt. Least-squares fits were carried out for values of a in the range 2.5–6.0 Å, in steps of 0.1 Å, and the values of β_{KX} used to calculate β were those for the best fit (a_{KSCN} = 3.9 Å; a_{KF} = 3.9 Å). The value of β obtained was −0.072.

Assuming that this value of β is reasonable and considering that the maximum value of q_-^d is ~6 μC cm^{-2} for I = 1.0 *M* and ~4 μC cm^{-2} for I = 0.5 *M* (26), eq. [3] can be used to estimate errors in the values of q_-' of ca. 7% and 4% for μ = 1 for the ionic strengths 1.0 and 0.5 *M*, respectively. Hence, the values of q_-' for x = 0.5 and I = 1.0 *M* (full line No. 5 of Fig. 7) should be ~4% underestimated. When this is taken into consideration the dotted line No. 5 of Fig. 7 is obtained. If the following points are recalled: (*i*) the difference between the dotted line and the one for q_-' from the isotherm (dashed line No. 5 of Fig. 7) is at most ~10%; (*ii*) the values of q_-' obtained through differentiation for x = 0.5 are from one of the ends of the differentiation interval and, so, should be affected by a greater differentiation error; and (*iii*) the surface pressure

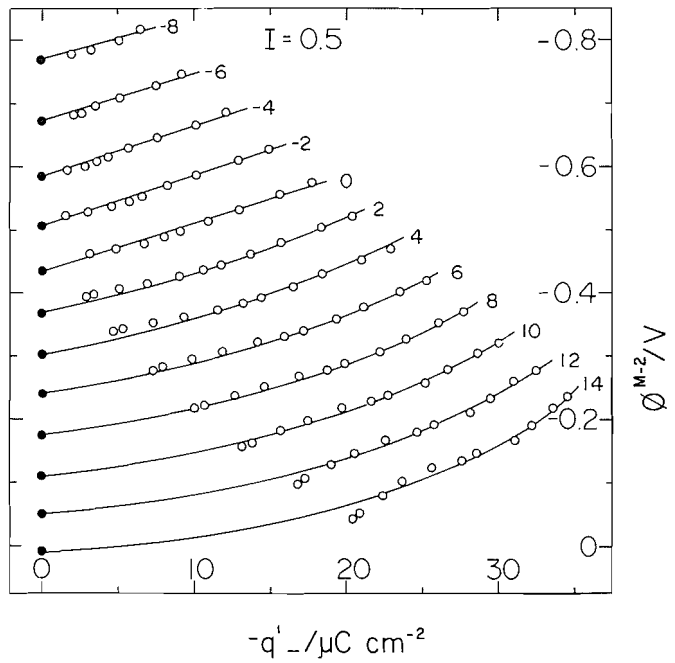

FIG. 8. Potential drop in the inner layer, ϕ^{M-2}, as a function of the specifically adsorbed charge due to SCN^-, q_-' at constant electrode charge density q^M (indicated by the integers adjacent to each curve) for adsorption from the system x *M* KSCN + $(0.5 - x)$ *M* KF. (●) values corresponding to the base solution (see text).

method lacks sensitivity (23); it seems that the difference between the two sets of values of q_-' for x = 0.5 and I = 1.0 *M* is not very significant.

Furthermore, from the value of β above, it can be concluded that there should be no significant error in the values of q_-' from the differentiation for values of $x < 0.25$ when the variation of the activity coefficient with solution composition is not taken into account. From Fig. 7 it can be seen that for $x < 0.25$ the values of q_-' from the differential and those from the isotherm are practically the same (such behavior was also found for I = 0.5 *M*). This indicates that the virial isotherms fitted to the composite surface pressure curves (Figs. 2 and 3) describe quite well the adsorption processes here studied. It would then be of interest to make the same type of comparison for other systems.

In principle, a congruent isotherm is not expected to be suitable to describe ionic adsorption, since the necessity of including a term in ϕ^2 has been demonstrated (27). However, as shown by Fawcett and Sellan (5), when ϕ^2 is small enough it can be expressed in terms of q^M and q_-'. Thus, even with a term in ϕ^2 the isotherm may still be congruent.

The inner layer

Plots of the potential drop across the inner layer, ϕ^{M-2}, against the specifically adsorbed charge density, q_-' at constant q^M (Christie plots) are usually employed to analyze the properties of the inner layer.

Such plots for the data obtained from differentiation are shown in Figs. 8 and 9 for the ionic strengths 0.5 and 1.0 *M*, respectively. From these figures it can be seen that a linear relationship between ϕ^{M-2} and q_-' exists only for $q^M \leq 0$; for positive values of q^M the plots are curvilinear. This latter type of relationship becomes clear by the inclusion of the value of ϕ^{M-2} for q_-' = 0, an important procedure previously called to attention by Fawcett and Sellan (5).

Can. J. Chem. Downloaded from www.nrcresearchpress.com by 210.87.254.42 on 09/06/12
For personal use only.

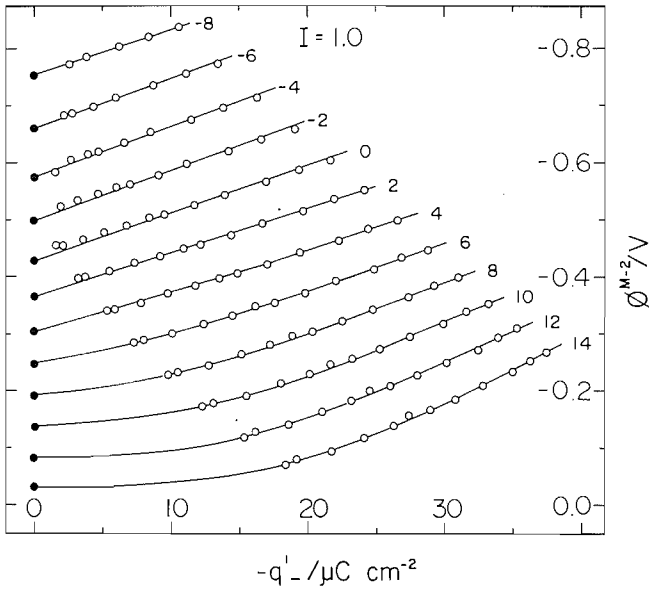

FIG. 9. Potential drop in the inner layer, ϕ^{M-2}, as a function of the specifically adsorbed charge due to SCN^-, q_-' at constant electrode charge density q^M (indicated by the integers adjacent to each curve) for adsorption from the system x *M* KSCN + $(1.0 - x)$ *M* KF. (●) values corresponding to the base solution (see text).

The potential drop across the inner layer, according to Grahame's model, is given by

$$[6] \quad \phi^{M-2} = \frac{q^M}{K_i} + \frac{q_-'}{K_2}$$

where K_i is the integral capacity of the inner layer, and K_2, that between the inner Helmholtz plane (iHp) and the oHp. If for a fixed value of q^M, K_i and K_2 are independent of q_-', then the slope of the Christie plots is equal to $1/K_2$. In general, the slope is given by

$$[7] \quad \left(\frac{\partial\phi^{M-2}}{\partial q_-'}\right)_{q^M} = \frac{1}{K_2} + q_-'\left(\frac{\partial(1/K_2)}{\partial q_-'}\right)_{q^M} + q^M\left(\frac{\partial(1/K_i)}{\partial q_-'}\right)_{q^M}$$

As the Christie plots (Figs. 8 and 9) are linear for $q^M \leq 0$ and curvilinear for $q^M > 0$, each one of these behaviors will be analyzed separately.

When the Christie plots are linear (for -8 μC cm$^{-2} \leq q^M \leq 0$), one may conclude that $\partial(1/K_2)/\partial q_-' \simeq 0$. Considering the fact that the plots are almost parallel but for $q^M = -8$ μC cm^{-2}, the contribution from the third term in eq. [7] must be small in magnitude. Hence, one may conclude that the slopes of the Christie plots are approximately equal to $1/K_2$ within the range of q^M under consideration. The values of K_2 obtained from the plots in Figs. 8 and 9 (Table 2) vary from 123 to 148 μF cm^{-2} at ionic strength 0.5 *M* and from 112 to 124 μF cm^{-2} at ionic strength 1.0 *M*. The smaller values of K_2 at the higher ionic strength may be explained by the increased adsorption which affects the nature of the predominant counter ion at the oHp and, consequently, the thickness of the inner layer. From the values of ϕ^{M-2} in the limit for $q_-' = 0$, one may calculate K_i as

$$[8] \quad K_i = \frac{q^M}{(\phi^{M-2})_{q_-' = 0}}$$

From the values so calculated (Table 2) it seems that K_i is independent of the ionic strength. The smaller variation in K_i with q^M when compared with that in K_2 can be explained by the fact that the nature of the counter ion, which changes when q^M increases, mainly affects the properties of the region of the inner layer between the iHp and oHp, and so, K_2 is expected to vary much more than K_i. If the values of K_i and K_2 here obtained for -8 μC cm$^{-2} \leq q^M < 0$ are compared with those obtained for solutions of one salt (Table 3 of ref. 12), it can be concluded that they are reasonably compatible notwithstanding the different concentration intervals studied. From this comparison it also becomes clear that K_i seems not to depend on the ionic strength.

TABLE 2. Inner-layer integral capacities in the presence of thiocyanate adsorbed on Hg from aqueous 0.5 *M* and 1.0 *M* ionic strength solutions (see text)

q^M (μC cm^{-2})	K_i (μF cm^{-2})		K_2 (μF cm^{-2})	
	I = 0.5 *M*	I = 1.0 *M*	I = 0.5 *M*	I = 1.0 *M*
−8	24	25	148	124
−6	25	26	135	112
−4	27	28	126	112
−2	28	29	123	112

Before analyzing the Christie plots for $q^M > 0$, it is of interest to compare the present results for $q^M < 0$ with those obtained for the adsorption of other ions on Hg from solutions of constant ionic strength (4, 6, 20). First, the comparison will be carried out for those ions whose adsorption was studied from solutions containing K^+ as the counter ion (4, 20) and, after, for those where Na^+ was the counter ion (4, 6), since, as Fawcett and Sellan (5) have pointed out, the nature of the counter ion determines the distance between the iHp and the oHp, χ_{ad}, thus changing the value of K_2. Dutkiewicz and Parsons (20) found K_2 to be approximately constant (60 μF cm^{-2}) in the x *M* KI + $(1.0 - x)$ *M* KF system at negative electrode charge densities ($-12 \leq q^M \leq -6$ μC cm^{-2}); Fawcett and McCarrick (4) found K_2 to be 50 μF cm^{-2} in the x *M* KI + $(0.25 - x)$ *M* KF system at $q_M = -8$ μC cm^{-2}; these values of K_2 are approximately half those obtained here, indicating that χ_{ad} decreases by approximately a factor of two when SCN^- is the adsorbing ion. Fawcett and McCarrick (4) found K_2 to be smaller than 50 μF cm^{-2} in the x *M* NaI + $(0.25 - x)$ *M* NaF system at $q^M = -8$ μC cm^{-2}; K_2 was found to be in the range $125 \leq K_2 \leq 137$ μF cm^{-2} in the x *M* NaN_3 + $(0.95 - x)$ *M* NaF system (6) at negative electrode charge densities ($-7 \leq q^M < 0$ μC cm^{-2}); again χ_{ad} decreases by approximately a factor of two. The fact that for the interfaces containing adsorbed SCN^- and N_3^-, respectively, χ_{ad} is ca. half that for the interfaces containing I^- adsorbed, strongly suggests that SCN^- as well as N_3^- behave as approximately cylindrical ions with their axes perpendicular to the electrode surface, as suggested previously in the case of SCN^- (13). Another important fact that should be pointed out is that the value of K_i for systems at constant ionic strength, besides having no dependence on the ionic strength, seems also not to depend on the nature of the system, as can be seen comparing the values presently obtained with those for I^- (20) and N_3^- (6) at $q^M = -8$ and -6 μC cm^{-2}. The value of K_i seems also not to depend on the nature of the counter ion, since N_3^- was adsorbed from constant ionic strength solutions containing Na^+ as counter ion (6) while I^- (20) and SCN^- were adsorbed from constant ionic strength solutions containing K^+ as counter ion; this same behavior was found before by Fawcett and Sellan (5) for NO_3^-. Such behavior is reasonable since K_i is calculated for $q_-' = 0$ and at $q^M < 0$

Can. J. Chem. Downloaded from www.nrcresearchpress.com by 210.87.254.42 on 09/06/12
For personal use only.

(eq. [8]); under this condition the potential drop across the inner layer seems to be very similar, independent of the nature of the cation at the oHp.

For $q^M > 0$ the Christie plots are curvilinear (Figs. 8 and 9) and present two different behaviors, i.e., their slopes decrease with increasing q^M at fixed q_-' for $|q_-'| < 20$ μC cm^{-2} and increase with increasing q^M at fixed q_-' for $|q_-'| > 20$ μC cm^{-2}. The following discussion will be made assuming that the derivatives defining changes in K_1 and K_2 with q_-' (see eq. [7]) are approximately constant for a given value of q^M (5). For $|q_-'| < 20$ μC cm^{-2}, since the slopes decrease with increasing q^M for constant q_-', it is possible to assume that $(\partial(1/K_1)/\partial q_-')_{q^M}$ is negative; thus, K_1 decreases with increasing adsorption. For $|q_-'| > 20$ μC cm^{-2}, the opposite is true; thus K_1 increases with adsorption. The fact that K_1 increases for $|q_-'| > 20$ μC cm^{-2} may be due to changes in the value of χ_{ad} or even in the value of the local dielectric constant, ϵ_i. A decrease in the value of χ_{ad} could be brought by fluoride coadsorption at the more positive electrode charge densities (28). If fluoride specific adsorption is significant, the specifically adsorbed charge density, neglecting variation of the activity coefficient with solution composition, is given by (19)

$$[9] \quad q_-' = q_-'(SCN^-) - \frac{x}{I - x} q_-'(F^-)$$

where $q_-'(SCN^-)$ and $q_-'(F^-)$ are the specifically adsorbed charge densities due to thiocyanate and fluoride ions, respectively, x is the SCN^- ion concentration, and I the ionic strength. Neglect of fluoride adsorption would result in an underestimation of $q_-'(SCN^-)$ and in the Christie plots being more curved. Furthermore, if, as suggested by Baugh and Parsons (29), fluoride ions retain their primary hydration shell when they become adsorbed at Hg, this could lead to an increase in the local dielectric constant. However, the subject of fluoride adsorption on Hg is still not settled and awaits further experimental evidence. For fixed values of q^M, the slopes of the Christie plots increase with increasing $|q_-'|$, indicating that $(\partial(1/K_2)/\partial q_-')_{q^M}$ is negative; thus, K_2 decreases with increasing adsorption.

Acknowledgements

Helpful discussions with Dr. W. R. Fawcett are gratefully acknowledged, as are the grants from the Fundação de Amparo à Pesquisa do Estado de São Paulo (FAPESP) and from the Conselho Nacional de Desenvolvimento Científico e Tecnológico (CNPq), Brasil, which made this work possible. The use of computer facilities of the Universidade Federal de São Carlos is also acknowledged.

1. R. PAYNE. J. Electroanal. Chem. **41**, 277 (1973).
2. G. J. HILLS and R. M. REEVES. J. Electroanal. Chem. **42**, 355 (1973).
3. E. DUTKIEWICZ. J. Electroanal. Chem. **50**, 221 (1974).
4. W. R. FAWCETT and T. A. MCCARRICK. J. Electrochem. Soc. **123**, 1325 (1976).
5. W. R. FAWCETT and J. B. SELLAN. Can. J. Chem. **55**, 3871 (1977).
6. E. R. GONZÁLEZ. J. Electroanal. Chem. **90**, 431 (1978).
7. R. PAYNE. J. Phys. Chem. **69**, 4113 (1965).
8. J. E. B. RANDLES. J. Electroanal. Chem. **41**, 272 (1973).
9. H. D. HURWITZ. J. Electroanal. Chem. **10**, 35 (1965).
10. N. TANAKA, T. TAKEUCHI, and R. TAMAMUSHI. Nippon kagaku zasshi. **85**, 846 (1964).
11. H. WROBLOWA, Z. KOVAK, and J. O'M. BOCKRIS. Trans. Faraday Soc. **61**, 1523 (1965).
12. S. MINC and J. ANDRZEJCZAK. J. Electroanal. Chem. **17**, 101 (1968).
13. R. PARSONS and P. C. SYMONS. Trans. Faraday Soc. **64**, 1077 (1968).
14. B. BEHR, J. DOJLIDO, and J. STROKA. Collection Czechoslov. Chem. Commun. **36**, 1317 (1971).
15. D. C. GRAHAME. J. Am. Chem. Soc. **76**, 4819 (1954).
16. C. V. D'ALKAINE, E. R. GONZÁLEZ, and R. PARSONS. J. Electroanal. Chem. **32**, 57 (1971).
17. A. W. M. VERKROOST, M. SLUYTERS-REBACH, and J. H. SLUYTERS. J. Electroanal. Chem. **24**, 1 (1970).
18. A. BATANA, R. C. ROCHA FILHO, L. A. AVACA, and E. R. GONZÁLEZ. J. Comp. Chem. **2**, 221 (1981).
19. S. LAKSHMANAN and S. K. RANGARAJAN. J. Electroanal. Chem. **27**, 127 (1970).
20. E. DUTKIEWICZ and R. PARSONS. J. Electroanal. Chem. **11**, 100 (1966).
21. J. O'M. BOCKRIS, M. A. V. DEVANATHAN, and K. MÜLLER. Proc. R. Soc. **274**A, 55 (1963).
22. R. PARSONS. Proc. R. Soc. **261**A, 79 (1961).
23. R. PAYNE. *In* Progress in surface and membrance science. Vol. 6. *Edited by* J. F. Danielli, M. D. Rosenberg, and D. A. Cadenhead. Academic Press, New York. 1972.
24. R. PARSONS. J. Electroanal. Chem. **5**, 397 (1963).
25. R. A. ROBINSON and R. H. STOKES. Electrolyte solutions. Butterworths, London. 1955.
26. D. C. GRAHAME. Chem. Rev. **41**, 441 (1947).
27. R. DE LEVIE. J. Electrochem. Soc. **118**, 185C (1971).
28. D. J. SCHIFFRIN. Trans. Faraday Soc. **67**, 3318 (1971).
29. L. M. BAUGH and R. PARSONS. J. Electroanal. Chem. **40**, 407 (1972).

Can. J. Chem. Downloaded from www.nrcresearchpress.com by 210.87.254.42 on 09/06/12
For personal use only.

The crystal structures of diaquatetra(β-picoline)M(II) perchlorate, $[M(H_2O)_2(C_6H_7N)_4](ClO_4)_2$ (M = Cu, Co)

SHENGZHI HU
Department of Chemistry, University of Amoy, Fujian, China

AND

RICHARD JAMES BARTON, KEITH JAMES JOHNSON, AND BEVERLY ELLIS ROBERTSON
Faculty of Science, University of Regina, Regina, Sask., Canada S4S 0A2

Received April 22, 1982

SHENGZHI HU, RICHARD JAMES BARTON, KEITH JAMES JOHNSON, and BEVERLY ELLIS ROBERTSON. Can. J. Chem. **61**, 395 (1983).

Crystals of the Cu(II), Co(II), and Ni(II) β-picoline complexes ($[M(H_2O)_2(C_6H_7N)_4](ClO_4)_2$, M = Cu, Co, Ni) all showed monoclinic rhombohedral morphology and were shown by diffraction methods to be isomorphous. The structures of the Cu(II) and Co(II) complexes have been determined in detail.

Atom	a (Å)	b (Å)	c (Å)	β (deg)	D_m	D_x	Colour
Cu(II)	15.292(4)	9.672(2)	20.579(5)	94.73(2)	1.45(1)	1.467	Blue
Co(II)	15.878(12)	9.374(3)	20.661(7)	96.50(4)	1.45(1)	1.448	Pink
Ni(II)	15.7	9.3	20.4	96.5	1.44(1)		Pale blue

The space group of crystals of the three complexes is $C2/c$. The structures were solved by the Patterson method. The structures of the Cu(II) and Co(II) complex were refined to a final R_w (on $|F|$) of 0.050 and 0.068 for 1918 and 2455 independent reflections, respectively, as measured with a modified Picker diffractometer. The structure of these complexes consists of coordination polyhedra with formulation $[M(H_2O)_2(\beta\text{-picoline})_4]^{2+}$ and perchlorate counterions. The ions are connected by hydrogen bonds of average length 2.76 Å in the Co(II) complex and 2.82 Å in the Cu(II) complex. The four N atoms of the β-picoline ligands form an equatorial plane with average [M—N] distances of 2.17 Å in the Co(II) complex and 2.03 Å in the Cu(II) complex. The water ligands are in apical positions with [M—O] distances of 2.124(6) Å and 2.493(10) Å in the Co(II) and Cu(II) complexes respectively. This large difference in bond lengths is manifested in marked differences in the appearance of crystals of the two compounds and is consistent with an expected Jahn–Teller effect. The thermal factors suggest that the perchlorate ion undergoes enhanced librational motion.

SHENGZHI HU, RICHARD JAMES BARTON, KEITH JAMES JOHNSON et BEVERLY ELLIS ROBERTSON. Can. J. Chem. **61**, 395 (1983).

Les cristaux des complexes ($[M(H_2O)_2(C_6H_7N)_4](ClO_4)_2$, M = Cu, Co, Ni) ont tous une forme rhomboédrique monoclinique et les méthodes de diffraction révèlent qu'ils sont isomorphes. On a déterminé en détail les structures des complexes du Cu(II) et de Co(II).

Atomie	a	b	c	β (deg)	D_m	D_x	Couleur
Cu(II)	15.292(4)	9.672(2)	20.579(5)	94.73(2)	1.45(1)	1.467	Bleu
Co(II)	15.878(12)	9.374(3)	20.661(7)	96.50(4)	1.45(1)	1.448	Rose
Ni(II)	15.7	9.3	20.4	96.5	1.44(1)		Bleu pale

Les cristaux des trois complexes appartiennent au groupe d'espace $C2/c$. On a résolu les structures par la méthode de Patterson et on a ajusté celles du Cu(II) et du Co(II) jusqu'à des valeurs conventionnelles de R_w (sur F) de 0,050 et 0,068 pour respectivement 1918 et 2455 réflexions indépendantes à l'aide d'un diffractomètre de Picker modifié. La structure de ces complexes consiste en une coordination polyédrique de formule $[M(H_2O)_2(\beta\text{-picoline})_4]^{2+}$ et des ions opposés de perchlorate. Les ions sont reliés par des liaisons hydrogène de longueur moyenne de 2,76 Å dans le complexe de Co(II) et de 2,82 Å dans le complexe de Cu(II). Les quatre atomes d'azote des ligands β-picoline forment un plan équatorial avec des distances moyennes [M—N] de 2,17 Å dans le complexe de Co(II) et de 2,03 Å dans le complexe du Cu(II). Les ligands eau sont disposés au sommet avec des distances [M—O] de 2,124(6) Å et de 2,493(10) Å dans les complexes de Co(II) et de Cu(II) respectivement. Cette grande différence au niveau des longueurs de liaison se manifeste dans les différences profondes d'apparence des cristaux des deux composés et elle est en accord avec l'effet de Jahn–Teller attendu. Les facteurs thermiques suggèrent que l'ion perchlorate subit un mouvement de libration accru.

[Traduit par le journal]

0008-4042/83/020395-05$01.00/0
©1983 National Research Council of Canada/Conseil national de recherches du Canada

Can. J. Chem. Downloaded from www.nrcresearchpress.com by 210.87.254.40 on 09/06/12
For personal use only.

Can. J. Chem. Downloaded from www.nrcresearchpress.com by 210.87.254.40 on 09/06/12
For personal use only.

Introduction

This research is part of a project to form a variety of mixed valence binuclear transition metal compounds by reacting anhydrous complexes with superoxides as has been done with DMSO (1). However, analyses of our products of the synthesis claimed by Brown *et al.* (2) to produce the anhydrous complexes were puzzling. Each of these complexes was found to consist of perchlorate ions and a metal atom coordination polyhedron with four β-picoline and two water ligands by X-ray crystal structure studies. These complexes imply that β-picoline does not substitute readily for all six water molecules in $M(H_2O)_6(ClO_4)_2$ as does DMSO.

Experimental

Preparation of the compounds

$[Cu(H_2O)_2(\beta\text{-pic})_4](ClO_4)_2$ (blue), $[Co(H_2O)_2(\beta\text{-pic})_4](ClO_4)_2$ (pink), and $[Ni(H_2O)_2(\beta\text{-pic})_4](ClO_4)_2$ (pale blue) were prepared by dissolving the appropriate hydrated metal perchlorate in a minimum of 1:1 diethyl ether:95% ethanol, the picoline complexes being formed by dropwise addition of a slight excess of the appropriate picoline, with stirring. All complexes precipitated on refrigeration at 0°C and were recrystallized twice from acetone, dried 14 h at 80°C under high vacuum, and stored in sealed bottles over indicating Drierite, in a desiccator.

Analyses of the β-picoline complexes suggested the general formula $M(\beta\text{-pic})_4(ClO_4)_2 \cdot xH_2O$. In addition, Karl Fisher titrations were carried out to measure the quantities of water present in all samples. Infrared spectra also revealed distinct bands in the region of 3400 cm^{-1} for all complexes, indicating the presence of water. However, it could not be rationalized as strictly complexed water, as in no case did the mole ratio of metal to unknown (assuming the unknown moiety to be water) take integral values.

X-ray crystallographic analysis

Precession photographs provided space groups and approximate unit cell dimensions. Accurate lattice parameters of the Cu(II) and Co(II) complexes wre obtained by a least-squares treatment of the diffractometer setting angles for ca. 20 reflections for which $2\theta_{hkl}$ (MoKα) was between 40 and 45°. Crystal data at 18(2)°C are:

$C_{24}H_{32}Cl_2CuN_4O_{10}$ fw = 670.3

TABLE 1. Fractional coordinates for $[M(H_2O)_2(\beta\text{-pic})_4](ClO_4)_2$ (M = Cu, Co) with estimated standard deviations in parentheses and isotropic thermal parameters, U (× 10^3) (Å)

	x		*y*		*z*		U_{eq}/U_{iso}*	
Atom	M = Cu	M = Co	M = Cu	M = Co	M = Cu	M = Co	M = Cu	M = Co
M	0.5000	0.5000	0.09707(15)	0.10262(9)	0.2500	0.2500	49	46
Cl	0.0879(2)	0.0832(1)	0.0989(3)	0.1010(2)	0.3870(1)	0.3790(1)	79	66
O(1)	0.1574(5)	0.1564(4)	0.1499(10)	0.1624(9)	0.4175(5)	0.4057(4)	254	237
O(2)	0.1076(7)	0.1036(4)	0.0228(10)	0.0066(6)	0.3361(4)	0.3317(3)	250	173
O(3)	0.0452(7)	0.0388(6)	0.2142(11)	0.2152(9)	0.3714(4)	0.3603(4)	265	260
O(4)	0.0461(7)	0.0496(6)	0.0262(9)	0.0342(6)	0.4270(5)	0.4268(3)	259	208
O(5)	0.5000	0.5000	−0.1584(9)	−0.1239(6)	0.2500	0.2500	69	67
O(6)	0.5000	0.5000	0.3571(12)	0.3295(6)	0.2500	0.2500	111	80
N(1)	0.3699(3)	0.3654(2)	0.1064(6)	0.1134(4)	0.2192(3)	0.2165(2)	55	51
C(1)	0.3340(4)	0.3283(3)	0.0228(8)	0.0320(5)	0.1727(3)	0.1680(2)	51	50
C(2)	0.2450(5)	0.2415(3)	0.0234(8)	0.0270(5)	0.1520(4)	0.1494(2)	58	57
C(3)	0.1952(6)	0.1927(4)	0.1157(11)	0.1121(8)	0.1846(5)	0.1858(3)	82	76
C(4)	0.2295(6)	0.2296(4)	0.2023(10)	0.1979(7)	0.2332(5)	0.2347(3)	86	78
C(5)	0.3184(5)	0.3152(4)	0.1951(9)	0.1966(6)	0.2486(4)	0.2480(3)	71	66
N(2)	0.4700(3)	0.4707(2)	0.0941(7)	0.0956(4)	0.3435(3)	0.3500(2)	56	51
C(6)	0.4141(5)	0.4125(3)	0.0005(9)	0.0038(5)	0.3650(4)	0.3691(2)	57	56
C(7)	0.3856(5)	0.3834(3)	−0.0004(9)	0.0045(6)	0.4271(4)	0.4288(2)	61	61
C(8)	0.4157(6)	0.4165(4)	0.1031(11)	0.1086(7)	0.4685(4)	0.4726(3)	70	69
C(9)	0.4731(6)	0.4756(4)	0.1996(10)	0.2025(6)	0.4476(5)	0.4546(3)	74	69
C(10)	0.4988(5)	0.5025(3)	0.1915(8)	0.1933(5)	0.3858(4)	0.3941(2)	55	54
C(11)(C(7))	0.3249(5)	0.3185(5)	−0.1127(9)	−0.1042(11)	0.4484(4)	0.4450(4)	91	90
C(12)(C(2))	0.2080(4)	0.2045(6)	−0.0689(9)	−0.0665(10)	0.1001(4)	0.0958(4)	91	89
H(1)(C(1))	0.370(2)	0.360(2)	−0.041(4)	−0.024(4)	0.152(2)	0.145(2)	0(12)	32(11)
H(3)(C(3))	0.141(4)	0.145(3)	0.112(7)	0.123(6)	0.176(3)	0.176(2)	69(24)	74(19)
H(4)(C(4))	0.187(4)	0.198(3)	0.268(8)	0.269(5)	0.260(3)	0.266(2)	119(30)	81(16)
H(5)(C(5))	0.342(4)	0.341(3)	0.259(7)	0.249(5)	0.286(3)	0.284(2)	116(31)	68(16)
H(6)(C(6))	0.397(3)	0.390(2)	−0.077(5)	−0.063(4)	0.338(2)	0.331(2)	32(16)	49(12)
H(8)(C(8))	0.395(3)	0.401(3)	0.104(7)	0.111(5)	0.516(3)	0.514(2)	83(23)	78(17)
H(9)(C(9))	0.492(4)	0.496(3)	0.264(5)	0.262(4)	0.476(2)	0.483(2)	46(21)	50(14)
H(10)(C(10))	0.528(3)	0.548(2)	0.255(4)	0.256(4)	0.369(2)	0.382(2)	0(14)	33(11)
H(11)(C(11))	0.294(6)	0.313(3)	−0.101(10)	−0.099(6)	0.476(5)	0.482(3)	230(43)	74(21)
H(12)(C(11))	0.348(5)	0.335(6)	−0.207(8)	−0.203(10)	0.439(4)	0.441(4)	150(30)	196(46)
H(13)(C(11))	0.269(5)	0.264(6)	−0.126(8)	−0.129(10)	0.417(4)	0.406(5)	149(31)	217(42)
H(14)(C(12))	0.241(4)	0.243(4)	−0.126(7)	−0.128(6)	0.079(3)	0.077(3)	121(27)	107(26)
H(15)(C(12))	0.194(4)	0.198(6)	−0.023(8)	−0.023(9)	0.059(3)	0.052(4)	137(29)	184(41)
H(16)(C(12))	0.158(4)	0.154(5)	−0.107(7)	−0.073(8)	0.106(3)	0.092(4)	108(23)	128(33)
H(17)(O(6))	0.491(5)	0.465(3)	0.384(8)	0.370(5)	0.219(3)	0.228(3)	74(31)	85(21)
H(18)(O(5))	0.472(5)	0.485(4)	−0.207(7)	−0.170(6)	0.223(3)	0.220(2)	89(30)	89(21)

*$U_{eq} = (1/3)\sum_i\sum_j U_{ij} a_i^* a_j^* \boldsymbol{a}_i \cdot \boldsymbol{a}_j$.

TABLE 2. Interatomic distances (Å), angles (deg), and mean plane data for $[M(H_2O)_2(\beta\text{-pic})_4](ClO_4)_2$ (M = Cu, Co), with estimated standard deviations in parentheses

Bond	Distance M = Cu	Distance M = Co	Bonds	Angle M = Cu	Angle M = Co
		(*a*) Coordination spheres			
M—N(1)	2.040(5)	2.173(4)	O(5)—M—O(6)	180	180
M—N(2)	2.015(5)	2.170(4)	N(1)—M—N(2)	90.3(2)	89.7(1)
M—O(5)	2.470(9)	2.123(5)	N(1)—M—O(5)	92.5(2)	92.7(1)
M—O(6)	2.515(12)	2.126(6)	N(2)—M—O(5)	89.2(2)	88.3(1)
		(*b*) Picolinyl groups			
N(1)—C(1)	1.336(9)	1.341(6)	C(1)—N(1)—C(5)	119.2(6)	117.4(4)
N(1)—C(5)	1.342(10)	1.336(7)	C(6)—N(2)—C(10)	116.6(6)	116.8(4)
N(2)—C(6)	1.344(10)	1.355(7)	C(1)—C(2)—C(12)	121.8(7)	121.6(5)
N(2)—C(10)	1.333(10)	1.349(6)	C(3)—C(2)—C(12)	123.4(7)	123.1(6)
Mean C—C	1.377(10)	1.375(8)	C(6)—C(7)—C(11)	121.1(7)	120.4(5)
Mean CH_3—C	1.495(11)	1.498(11)	C(8)—C(7)—C(11)	121.8(8)	123.0(6)
			Mean C—C—C	119.9(8)	120.0(5)
			Mean N—C—C	123.3(8)	123.5(5)
		(*c*) Perchlorate ion*			
	(*i*) (*ii*)	(*i*) (*ii*)			
Cl—O(1)	1.287(9) 1.472	1.358(7) 1.498	O(1)—Cl—O(2)	111.3(6)	107.4(4)
Cl—O(2)	1.335(10) 1.498	1.384(6) 1.530	O(1)—Cl—O(3)	99.6(6)	100.4(5)
Cl—O(3)	1.318(11) 1.544	1.314(9) 1.497	O(1)—Cl—O(4)	109.2(6)	107.1(5)
Cl—O(4)	1.291(10) 1.563	1.332(7) 1.557	O(2)—Cl—O(3)	114.6(6)	118.3(4)
Mean:	1.308(10) 1.519	1.347(7) 1.521	O(2)—Cl—O(4)	110.9(6)	111.6(4)
			O(3)—Cl—O(4)	110.8(7)	110.8(5)
			Mean:	109.4(6)	109.3(5)
		(*d*) Hydrogen bonds			
O(5)—H(18)	0.82(7)	0.78(5)	M—O(5)—H(18)	125(5)	124(4)
O(6)—H(17)	0.70(7)	0.78(5)	M—O(6)—H(17)	112(6)	120(4)
O(5)···O(3)	2.819(10)	2.746(8)			
O(6)···O(2)	2.819(11)	2.772(7)			

*(*i*) Uncorrected, (*ii*) corrected, TLS.

(*e*) Mean plane equations

Cu (II) complex:

(*i*) Plane through atoms N(1), C(1), C(2), C(3), C(4), C(5)
Plane equation: $-3.2143X - 6.7349Y + 14.4189Z = 1.2547$
Displacements (Å × 10^3): N(1)−1, C(1)8, C(2)−8, C(3)0, C(4)7, C(5)−8, C(12-16

(*ii*) Plane through atoms N(2), C(6), C(7), C(8), C(9), C(10)
Plane equation: $11.4380X - 5.6029Y + 5.3600Z = 6.6935$
Displacements (Å × 10^3): N(2)−4, C(6)−4, C(7)8, C(8)−6, C(9)−2, C(10)7, C(11)59

Co (II) complex:

(*i*) Plane through atoms N(1), C(1), C(2), C(3), C(4), C(5)
Plane equation: $-2.3932X - 6.9547Y + 13.7664Z = 1.3049$
Displacements (Å × 10^3): N(1)13, C(1)0, C(2)−13, C(3)13, C(4)0, C(5)−13, C(12)−19

(*ii*) Plane through atoms N(2), C(6), C(7), C(8), C(9), C(10)
Plane equation: $11.0207X - 5.9072Y + 5.5302Z = 6.5652$
Displacements (Å × 10^3): N(2)−7, C(6)−14, C(7)6, C(8)−25, C(9)−6, C(10)11, C(11)21

Monoclinic, $a = 15.292(4)$, $b = 9.672(2)$, $c = 20.579(5)$ Å, $\beta = 94.73(2)°$, $V = 3033.4$ Å^3, $\rho_o = 1.46(1)$ g cm^{-3}, $Z = 4$, $\rho_c = 1.467$ g cm^{-3}, $F(000) = 1388$, $\mu(MoK\alpha) = 9.85$ cm^{-1}. Absent reflections hkl, $h + k \neq 2n$; $h0l$, $l \neq 2n$, consistent with the space groups C_{2h}^6-$C2/c$ and Cs^4-Cc.

$C_{24}H_{32}Cl_2CoN_4O_{10}$ fw = 665.7

Monoclinic, $a = 15.878(12)$, $b = 9.374(3)$, $c = 20.661(7)$ Å, $\beta = 96.50(4)°$, $V = 3055.4$ Å^3, $\rho_o = 1.45(1)$ g cm^{-3}, $Z = 4$, $\rho_c = 1.448$ g cm^{-3}, $F(000) = 1380$, $\mu(MoK\alpha) = 8.19$ cm^{-1}. The absent reflections are the same as for the Cu(II) complex.

$C_{24}H_{32}Cl_2NiN_4O_{10}$

Monoclinic, $a = 15.7$, $b = 9.3$, $c = 20.4$ Å, $\beta = 96.5°$, $\rho_o = 1.44(1)$ g cm^{-3}. The absent reflections are the same as for the preceding two.

The intensity data of the crystals of the Cu(II) and Co(II) complexes were collected with a modified Picker diffractometer using graphite monochromated MoKα radiation within the limits $3 < 2\theta < 55°$ and $3 < 2\theta < 50°$ respectively for the Cu(II) and Co(II) complexes. The crystal of the Co(II) complex turned opaque gradually during data collection and the intensities of three standard reflections, monitored every 50 reflections, decreased by approximately 12%. The intensities of the standard reflections for the Cu(II) complex revealed no systematic trends during data collection. Data were corrected for the Lorentz and polarizations effects and scaled according to the changes in the standard reflections. Absorption was not considered to be important

Can. J. Chem. Downloaded from www.nrcresearchpress.com by 210.87.254.40 on 09/06/12
For personal use only.

Can. J. Chem. Downloaded from www.nrcresearchpress.com by 210.87.254.40 on 09/06/12
For personal use only.

because of the relatively small linear absorption coefficient and the small size of the crystals of both samples. The extinction condition (hkl, $h + k = 2n$; $h0l$, $l = n$) indicates the space group Cc or $C2/c$. The distribution of E values supports the latter. The structure of the Cu(II) complex was then solved by Patterson and heavy-atom methods in the space group $C2/c$. The structure of the Co(II) complex was assumed to be similar to that of the Cu(II) complex, as was verified by successful subsequent refinement. Of the 3508 and 2682 measured reflections for the Cu(II) and Co(II) complexes, 1918 and 2455 reflections with $|F_o| > 3\sigma(|F_o|)$ were used in the final refinement of the structure parameters respectively. In the Cu(II) complex the refinement converged to a conventional R factor of 0.099 and $R_w = [\Sigma\omega||F_o| - |F_c||^2/\Sigma\omega F_o^2]^{1/2} = 0.050$ with weighting factor $\sigma^{-2}(F_o)$, where $\sigma(F_o)$ is based on the counting statistics associated with the measurement of $|F_o|$ and an additional factor derived from the excess scatter in the standard reflections over that expected from counting statistics. In the final cycle of refinement the parameter shifts were less than 0.30 of the estimated standard deviations of the parameters for all atoms.

After completion of the initial refinement of the Co(II) structure, it was observed that the structure factors for the reflections 202 and 204 as measured by the diffractometer were in poor agreement with the calculated values of the structure factors. The diffractometer values were also inconsistent with approximate values obtained from film data. Therefore, it was assumed that an error had occurred during data collection, perhaps because of an attenuator malfunction, and the film data with appropriate weights were used to replace the diffractometer data for those reflections. Weighted full-matrix least-squares refinement with anisotropic temperature factors for all atoms except hydrogen yielded an R of 0.076 and $R_w = 0.068$. In the final cycle of refinement the parameter shifts were less than 0.20 of the estimated standard deviations of the parameters for the non-hydrogen atoms.

The data were collected using the National Research Council of Canada diffractometer control package, using the line profiling method. The preliminary solution of the structure was also obtained with this system of programs. Subsequent calculations were carried out using Xray 76 (3).

The atomic coordinates and their standard deviations for the Cu(II) and Co(II) complexes are given in Table 1. Bond distances and angles are reported in Table 2. The atoms are labelled in Fig. 1. A view of the Cu(II) complex is given in Fig. 2. Lists of calculated and observed structure factors and thermal parameters have been placed in the Depository of Unpublished Data.[1]

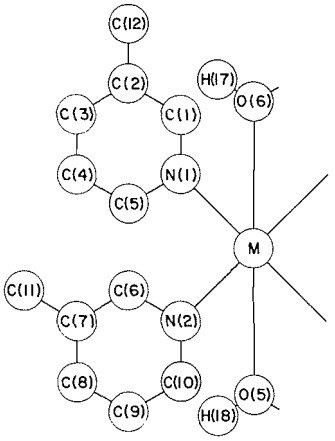

FIG. 1. Atom labelling sequence for the $[M(H_2O)_2(\beta\text{-picoline})_4]^{2+}$ ion.

[1]A complete set of tabular data is available at a nominal charge from the Depository of Unpublished Data, CISTI, National Research Council of Canada, Ottawa, Ont., Canada K1A 0S2.

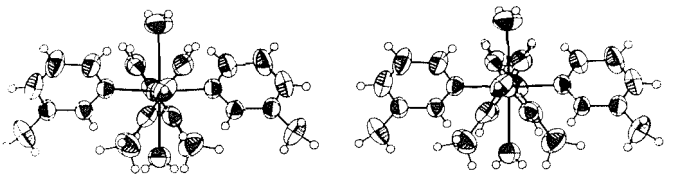

FIG. 2. View of the Cu(II) complex structure; 50% thermal ellipsoids are shown for the non-hydrogen atoms.

Discussion

In attempts to prepare the anhydrous complexes by the reaction of Cu(II), Co(II), and Ni(II) perchlorate with β-picoline, no products with consistent water content analyses were obtained. Consequently, the presently reported study was undertaken to determine the water composition and the coordination about the metal ion.

Both of the structures which we examined in detail show six-coordination about the cation in the form of an approximate octahedron in the case of the Co(II) complex and in the form of an octahedron with a strong tetragonal distortion in the case of the Cu(II) complex. Each coordination site has the symmetry 2. The geometry of the latter is similar to that of the Cu(II) ion in $Cu(NH_3)_4SO_4 \cdot H_2O$ (4), where the water molecule joins adjacent cations to form infinitive chains. In the structure of $[Cu(H_2O)_2(\beta\text{-pic})_4](ClO_4)_2$ the water molecules are hydrogen bonded to the perchlorate counterions.

The average length of the hydrogen bonds is 2.82 Å for the Cu(II) and 2.76 Å for the Co(II) complex. The four N atoms of the β-picoline ligands form an equatorial plane with [M—N] distances of 2.040(5) and 2.015(5) Å for the Cu(II) and 2.173(4) and 2.170(4) Å for the Co(II) complex. The former value is close to the sum of the covalent radii of Cu and N atoms and the latter is slightly longer than the sum of Co and N atoms (5). Conversely the average [Co—O] distance of 2.124(6) Å is close to that of a normal covalent bond whereas the average [Cu—O] distance of 2.493(10) Å is longer than the sum of covalent radii (5). It is of interest to note that the $[CuN_4O_2]$ chromophore provides strong corroboration of the Jahn–Teller predictions of elongation along the axial direction.

The perchlorate counterion undergoes enhanced librational motion in spite of the fact that it is hydrogen bonded to the water molecules. Bond length corrections for thermal motion using the procedure of Shomaker and Trueblood (6) lead to increases in bond length of ca. 0.2 Å. The corrected values are larger than expected for thermally corrected perchlorate bond lengths: 1.47 Å (7). They probably are a result of the inaccuracies in bond length corrections in cases of very large amplitude thermal motion.

The β-picoline ligands tilt from the basal plane of the nitrogen atoms by 40–44°. All the torsion angles as well as the other important parameters of the geometry are summarized in Table 3. The packing diagram of the Cu(II) complex is shown in Fig. 3. The two water molecules coordinated to the metal ions do not account for all of the water indicated to be present by the original quantitative analysis, particularly for the Cu(II) compound. The quantitative analysis of the products of this synthesis have shown variable and usually greater water content than that implied by this structural analysis. More than one product may have been produced in the synthesis. The materials produced showed variable degrees of crystallinity and it has not been possibile to verify this hypothesis by crystallographic examination.

TABLE 3. Some important mean parameters of the geometry of the complexes

Parameter	Value	
	M = Cu	M = Co
[M—N] (Å)	2.027(5)	2.171(4)
[M—O] (Å)	2.493(10)	2.124(6)
|<(L—M—L) − 90°| (L = O, N) (deg)	1.1	1.5
τ(O—M—N—C) (deg)	40	44
[Cl—O] (uncorrected) (Å)	1.31(1)	1.35(1)
[Cl—O] (corrected) (Å)	1.52(3)	1.52(2)
[O—H···O] (Å)	2.82(1)	2.76(1)
|<(O—Cl—O) − 109.47| (deg)	3.4	4.2

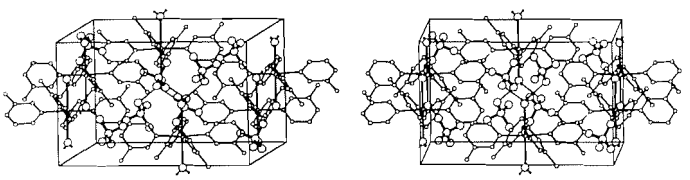

FIG. 3. Packing diagram of the Cu(II) complex. The hydrogen atoms except those associated with water are not shown for clarity.

The final difference map of the Cu(II) compound showed a negative peak corresponding to approximately 1.5 e $Å^{-3}$ at the location of the Cu(II) ion, and four smaller peaks in the vicinity corresponding to approximately 0.3 e $Å^{-3}$. These peaks may arise from the fact that the weights used in the least squares calculation were not constant which would be necessary in order that the difference Fourier map would give the same results as the least squares. The weighting scheme used gave greater significance to the low angle reflections, which reflect the outer electron density better than the higher angle reflections. The presence of a substantial Jahn–Tellar distortion may have perturbed the outer electron density such that the temperature factor of the Cu(II) ion as determined by least squares was lowered from that consistent with the difference Fourier map.

The validity of this hypothesis was investigated by altering the weighting scheme to lessen the significance of the low angle reflections. The changes in the temperature factor of the Cu(II) ion were consistent with the hypothesis but the standard deviations in the atom positions were increased. The difference electron density in the vicinity of the Cu(II) ion did not become completely flat which suggests that it cannot be accurately described by any generalized ellipsoid.

The crystal structure of the Ni(II) complex is isostructural with that of the Cu(II) and Co(II) complexes. The polyhedron around the nickel atom should be much closer to that of the Co(II) complex because of the d^8 configuration of Ni(II) as well as the similarity in lattice parameters between crystals of these two compounds.

Acknowledgements

We are grateful to the Natural Sciences and Engineering Research Council for support of this project. The support of the University of Amoy for Shengzhi Hu is also gratefully acknowledged. We thank Mr. Glen McDougall for his help in preparation of the crystals.

1. F. C. FREDERICK and K. E. JOHNSON. J. Electrochem. Soc. **128**, 2070 (1981); F. C. FREDERICK and K. E. JOHNSON. J. Inorg. Nucl. Chem. **43**, 1483 (1981); F. C. FREDERICK, M.Sc. Thesis, University of Regina. 1980.
2. D. H. BROWN, R. H. NUTTALL, J. MCAVOY, and D. S. A. SHARP. J. Chem. Soc. A, 892 (1966).
3. J. M. STEWART (*Editor*). X-ray system (1976). Tech. Rep. TR-446. Computer Science Centre, University of Maryland, College Park, MD 20742. U.S.A.
4. F. MAZZI. Acta Crystallogr. **8**, 137 (1955).
5. J. E. HUHEEY. Inorganic chemistry. 2nd ed. Harper and Row, Publishers. 1978.
6. V. SCHOMAKER and K. N. TRUEBLOOD. Acta Crystallogr. B**24**, 63 (1968).
7. G. J. M. IVARSSON. Acta Crystallogr. B**38**, 1831 (1982).

Can. J. Chem. Downloaded from www.nrcresearchpress.com by 210.87.254.40 on 09/06/12
For personal use only.

o-Nitrophenylethylene glycol as photoremovable protective group for aldehydes and ketones: syntheses, scope, and limitations

D. GRAVEL,[1] J. HEBERT, AND D. THORAVAL

Département de Chimie, Université de Montréal, C.P. 6210, Succ. A, Montréal (Qué.), Canada H3C 3V1

Received July 8, 1982

D. GRAVEL, J. HEBERT, and D. THORAVAL. Can. J. Chem. **61**, 400 (1983).

The preparation of *o*-nitrophenylethylene glycol is described along with its application as a photolabile protective group for aldehydes and ketones. Formation of the acetals and ketals is achieved in good to high yields in the usual manner and deprotection is carried out in fair to high yield, by photolysis at 350 nm in an inert solvent such as benzene. Because of the particular nature of the present protective group, its stability to basic and acidic conditions has been examined and is reported to complete the scope and limitations aspect. From a mechanistic point of view, the isolation and characterization of *o*-nitroso-α-hydroxyacetophenone as the spent reagent demonstrates a mechanistic link with the known *o*-nitrobenzaldehyde to *o*-nitrosobenzoic acid photorearrangement.

D. GRAVEL, J. HEBERT et D. THORAVAL. Can. J. Chem. **61**, 400 (1983).

La préparation de l'*o*-nitrophényléthylène glycol est décrite ainsi que son application comme groupe protecteur photolabile pour les aldéhydes et cétones. La formation des acétals et cétals est effectuée de la manière habituelle avec des rendements qui vont de bon à excellent. La déprotection, d'autre part, est effectuée avec des rendements, de moyen à excellent, par photolyse à 350 nm dans un solvant inerte tel que le benzène. À cause de la nature particulière du présent groupe protecteur, sa stabilité aux conditions basiques et acides a été étudiée et est rapportée afin de compléter l'aspect généralité et limitations de la réaction. Du point de vue mécanisme, l'isolement et la caractérisation de l'*o*-nitroso-α-hydroxyacétophénone comme réactif usé démontre un lien mécanistique entre cette réaction et le réarrangement photochimique connu de l'*o*-nitrobenzaldéhyde en acide *o*-nitrosobenzoïque.

Can. J. Chem. Downloaded from www.nrcresearchpress.com by 210.87.254.6 on 09/06/12
For personal use only.

Introduction

Over the years, the use of protective groups in organic synthesis has been refined to a high degree of sophistication and specificity, allowing chemists to synthesize some of the most complex organic structures known. There are at present a great number of protective groups available in the organic arsenal and these have been amply reviewed and organized (1, 2), making them a readily accessible tool even for the non-specialist.

The intrinsic role of a protective group requires that it possess some fundamental qualities such as: efficiency and specificity of introduction, stability under several reaction conditions, and efficiency, ease, and specificity of removal. In recent years, the need for more and more specific protective groups has prompted much research and one area which has been particularly fruitful is that of photochemistry, with the development of photochemically removable protective groups (3, 4) which can be released by irradiation at specific wavelengths.

At the beginning of the century, Ciamician and Silber (5) discovered the photochemical isomerization of *o*-nitrobenzaldehyde (**1**) to *o*-nitrosobenzoic acid (**2**) (eq. [1]) under solar light, a reaction which eventually, through works published in the literature (6), led to the discovery of a series of photoremovable protective groups having the same basic intramolecular rearrangement in common, i.e. the formal transfer of oxygen from the nitro group to the *o*-benzylic position (7).

[1] 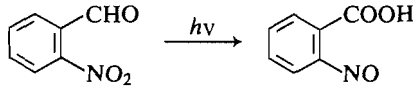

1 **2**

[1]Author to whom correspondence should be addressed.

Amongst the various new protective groups developed, many were designed for peptide (8), carbohydrate (9), and nucleoside synthesis (10). Upon examination of the pertinent literature, it became apparent that no photoremovable protective group had ever been developed for the protection of aldehydes and ketones and that such a tool might render important services in organic synthesis. It further appeared that such a group might easily be developed using the *o*-nitrobenzylic shift as its basis if *o*-nitrophenylethylene glycol (**3**) was available. This reagent should form nitrophenyl acetals and ketals **5** with carbonyl compounds **4** which should be labile under photolysis in aprotic solvents to yield the corresponding nitrosophenyl hemiketal derivative **6** by *o*-nitrobenzylic shift; the latter should then decompose in a ground state reaction to the starting aldehyde or ketone **4** and the spent reagent: *o*-nitroso-α-hydroxyacetophenone **7** (see Scheme 1) (a preliminary account of this work has been published, see ref. 11).

Synthesis of o-*nitrophenylethylene glycol (**3**)*

Although *o*-nitrophenylethylene glycol (**3**) was an unknown compound, its *meta* and *para* isomers were known and had been prepared by two different methods in 1960 (12). In the present case, the desired *ortho* isomer **3** was prepared by simple hydrolysis of *o*-nitrostyrene oxide (**8**) which is available by two known procedures namely: (*i*) from *o*-nitroacetophenone (**9**) via a bromination, reduction, epoxidation sequence reported by Guss (13), or (*ii*) simply by treating *o*-nitrobenzaldehyde (**1**) with diazomethane according to the method of Arndt *et al.* (14) (see Scheme 2).

In the first sequence, the α-bromination of *o*-nitroacetophenone (**9**) in acetic acid according to Guss (13) is reported without any mention of a yield and for that reason we preferred to adapt the method of Shevchuk and Dombrovskii (15) who report 98% yields for the *meta* and *para* isomers. In the present case, bromination is carried out using a bromine–dioxane

0008-4042/83/020400-11$01.00/0
©1983 National Research Council of Canada/Conseil national de recherches du Canada

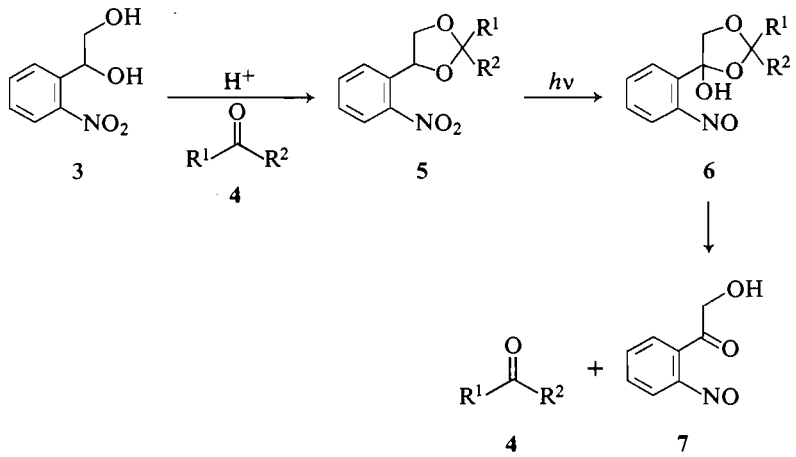

SCHEME 1

complex (16) which reacts almost instantaneously under cooling and in the somewhat more modest yield of 75% to give the desired α-bromo derivative **10**. It may be of interest to point out that, by fractional recrystallization, a small yield (6%) of the corresponding *gem*-dibromo derivative was isolated.

The next step in the sequence, which had also been reported by Guss (13), consisted in reducing the *o*-nitrophenacyl bromide with aluminum triisopropoxide to the corresponding bromohydrin which is isolated and then transformed into the desired epoxide by treatment with aqueous sodium hydroxide. In our particular case, for reasons of simplicity, we adapted the method of Fuchs (17) which uses sodium borohydride as the

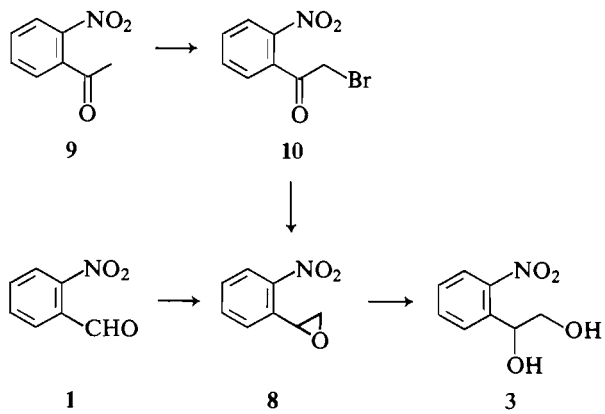

SCHEME 2

reducing agent followed by *in situ* generation of the epoxide by the addition of aqueous sodium hydroxide. The desired epoxide **8** is thus obtained in 89% yield and corresponds in all respects to that reported by Guss (13); the overall yield for the sequence starting from *o*-nitroacetophenone (**9**) is 67%.

The second method of preparing *o*-nitroepoxystyrene (**8**) is that first reported by Arndt and Partale in 1927 (14*a*) which describes the reaction of diazomethane on *o*-nitrobenzaldehyde (**1**). In a subsequent article (14*b*), the same group reports that epoxide **8** is the major product (67%) of the reaction, whereas *o*-nitroacetophenone (**9**) is obtained in a 16% yield. Because of its economical advantage and relative simplicity for small scale preparations, the reaction was repeated and found to yield a mixture of at least five products (tlc); however, a crystallization combined with a chromatography of the mother liquors yielded the desired *o*-nitroepoxystyrene (**8**) in a total yield of 61%. There was also obtained an 8% yield of unreacted *o*-nitrobenzaldehyde (**1**) along with 14% of *o*-nitroacetophenone (**9**).

The two methods of obtaining the epoxide **8** are therefore approximately equivalent in yield and whereas that starting from *o*-nitroacetophenone (**9**) is more costly in terms of time and materials it is on the other hand safer to carry out especially on relatively large scales. It is also important to note here that the *o*-nitroepoxystyrene (**8**) cannot be stored for long periods of time, even in the absence of light. Indeed, the epoxide **8**, after an induction period of a few months, decomposes rather rapidly to give a solid black mass.

The last step in the synthesis of the desired glycol **3** was attempted following the procedures used by Yagupolskii *et al.* (12) for the preparation of the *meta* and *para* isomers, namely, sulfuric acid catalyzed hydrolysis of the epoxide to the diol or preparation of the corresponding epichlorohydrin followed by treatment of the latter with an aqueous solution of potassium carbonate. In the event, it turned out that opening of the epoxide ring of **8** under various acidic conditions (sulfuric or hydrochloric) proved unsuccessful, giving rise to complex mixtures of products; on the other hand, since treatment by Yagupolskii *et al.* (12) of their epichlorohydrin with aqueous potassium carbonate yielded the desired diol, it was anticipated that the reaction proceeded via the epoxide which subsequently was hydrolyzed by base catalysis. This assumption proved correct or at least rewarding since, when *o*-nitroepoxystyrene (**8**) was treated with a 10% solution of aqueous potassium carbonate, *o*-nitrophenylethylene glycol (**3**) was obtained with a minimum[2] yield of 78%. The product crystallizes in the form of slightly yellow and hard needles with a melting point of 95–96°C.

It is important to note, although perhaps redundant here, that *o*-nitrophenylethylene glycol (**3**) is light sensitive and therefore must be protected accordingly. For instance, crystals exposed to daylight turned greenish after one week; however, when kept in a brown jar and in a drawer, the reagent can be preserved intact for years without any sign of alteration.

Protection–deprotection of carbonyl compounds

General method of ketalization

The general method chosen to introduce this new protective

[2]The mother-liquors of crystallization retained some of the glycol **3** and were not chromatographed in order to maximize the yield.

Can. J. Chem. Downloaded from www.nrcresearchpress.com by 210.87.254.6 on 09/06/12
For personal use only.

TABLE 1. Formation of acetals and ketals (**5**) with *o*-nitrophenylethylene glycol (**3**)

Carbonyl compound (**4**)	Reflux time (h)	% Yield of **5**	Remarks
Cyclohexanone	1	96	Oil
p-Nitrobenzaldehyde	2	97	60:40 Mixture *cis*−*trans*
Benzophenone	12	94	Melting point 115−116°C
Δ^5-Androsten-3β-ol-17-one acetate	3	92	Mixture of diastereoisomers
Δ^5-Pregnen-3β-ol-20-one acetate	10	80	Mixture of diastereoisomers
Testosterone	20	70	Mixture of diastereoisomers

group on various substrates is the following: the carbonyl compound **4** is treated with three equivalents of *o*-nitrophenylethylene glycol (**3**) in presence of a catalytic amount of *p*-toluenesulfonic acid in benzene under reflux and water separation conditions (see Experimental and footnote 5). After isolation and purification, the acetals and ketals **5** are protected from light until liberation by photolysis.

The results for a representative set of carbonyl compounds **4** are reported in Table 1.

General method of deprotection

In order to effect deprotection under the best possible conditions, i.e. liberating the carbonyl group under conditions such that the liberated carbonyl and other functional groups of the molecule are not affected, some preliminary irradiations were carried out using different set-ups and different solvents. The results show that a Rayonet apparatus equipped with a Pyrex vessel and 16 monochromatic lamps emitting at 350 nm is a very efficient set-up to effect deprotection since the photochemical reaction is generally "quantitative" after a reasonable time and since most functional groups are either stable or relatively stable at that wavelength. Concerning the choice of solvents for the deprotection reaction, various types were examined, such as carbon tetrachloride, chloroform, benzene, diethylether, dioxane, 1,2-dimethoxyethane, and methanol. Of these, a certain number were rejected for various reasons: methanol is not a good solvent for the ketals examined, carbon tetrachloride leaves a brown precipitate on the walls of the Pyrex vessel, thereby considerably reducing the amount of light transmitted to the solution, and finally, diethyl ether was rejected because of its too great volatility. Although all of the other solvents appeared equally efficient, we chose benzene for the preparative scale irradiations because it seems to have all of the necessary characteristics for this kind of photolysis: it is a good solvent for the ketals, its boiling point is in the right range, minimizing losses by evaporation during photolysis and being easy to evaporate after reaction, it is easy to purify and render anhydrous, it does not absorb light at 350 nm, and most importantly, it is aprotic and chemically inert.

The concentration of ketals in benzene was set at 10^{-3} − 10^{-4} *M* and the irradiations limited to 6 hours on the basis of preliminary trials which revealed only small amounts of unreacted material. Before presenting the various results of deprotection, it may be of importance to give a general description of the reaction as it proceeds: in every case studied, the solution under irradiation very early takes on a greenish color which then rapidly turns to yellow, then to red-brown, as the reaction progresses. Thin-layer chromatographic monitoring of the reaction reveals the appearance of many unstable intermediates, of which many are colored on the plate. Towards the end of the reaction, the photo by-products are all more polar than the starting acetals or ketals **5** and the liberated carbonyl compounds, which facilitates their recovery after reaction. Quite unfortunately, although many of these unstable intermediates were identical in all photolyses, every attempt to isolate any one of them by column chromatography failed (see, however, below under mechanistic aspects).

The results obtained in the photolyses of the six acetals and ketals **5** are reported in Table 2 which shows that after 6 hours of irradiation about 90% of the starting material has been deprotected, giving the liberated carbonyl compound in 80−90% isolated yield except in two cases where yields are fair to low.

As pointed out in Table 2, the case of the deprotection of the ketal of Δ^5-androsten-3β-ol-17-one acetate (**5**) under the standard conditions gave 65% of the liberated ketone but accompanied by a small percentage of its 13α epimer. Since the epimerization of this steroidal ketone is known in the literature (18), it was presumed that some light emitted at 313 nm by the lamps used was responsible for the epimerization of the liberated ketone (**4**). In an effort to control this side reaction, a filter solution composed of aqueous copper sulfate (19) was used in order to eliminate radiation under 320 nm, since the ketone carbonyl n-π^* absorption extends to 310 nm whereas that of the nitro group extends to 360 nm. Unfortunately, however, the results observed were much less impressive than hoped; the yield of the liberated ketone was raised to 71% but there was still a 7% yield of the 13α epimer which most probably came from sensitization by the spent reagent, i.e. *o*-nitroso-α-hydroxyacetophenone (**7**) (*vide infra*) or its reaction products, since a control experiment showed that the starting ketone irradiated for 9 hours through the filter solution remained intact.

In the case of testosterone, the ketal prepared and irradiated is the deconjugated ($\Delta^{5,6}$) isomer and the poor yields of recovered testosterone are again most probably attributable to the photoreactivity of the liberated $\Delta^{5,6}$ isomer of testosterone.[3] In fact, the photochemistry of β,γ-unsaturated ketones is well known (20) and could very well be one of the important limiting factors in this reaction, the other being possibly the instability of $\Delta^{5,6}$-testosterone, under chromatography condi-

[3]All our attempts to prepare the $\Delta^{4,5}$-3-ketal with *o*-nitrophenylethylene glycol **3** were unsuccessful.

Can. J. Chem. Downloaded from www.nrcresearchpress.com by 210.87.254.6 on 09/06/12
For personal use only.

TABLE 2. Deprotection of acetals and ketals (**5**) by photolysis in benzene at 350 nm

Protected carbonyl compounds (**5**)	Irradiation time (h)	% Yield of liberated carbonyl compound (**4**)	% Yield of unreacted starting material (**5**)
Cyclohexanone	6	85[a]	9
p-Nitrobenzaldehyde	6	86	11
Benzophenone	6	90	7
Δ^5-Androsten-3β-ol-17-one acetate	6	65[b] (71)[c]	14 (12)
Δ^5-Pregnen-3β-ol-20-one acetate	6	83	13
Testosterone	6	31[d] (37)[d,e]	14 —

[a]Identified as its 2,4-dinitrophenylhydrazone.
[b]Beside the expected 13β isomer there is also observed a small amount of epimer, the 13α isomer, arising most probably by photoisomerization of the liberated ketone.
[c]Same compound using Hanovia reactor and filter solution, does not prevent the formation of 7% 13α epimer.
[d]Isolated as the conjugated form.
[e]Same compound using Hanovia reactor and filter solution.

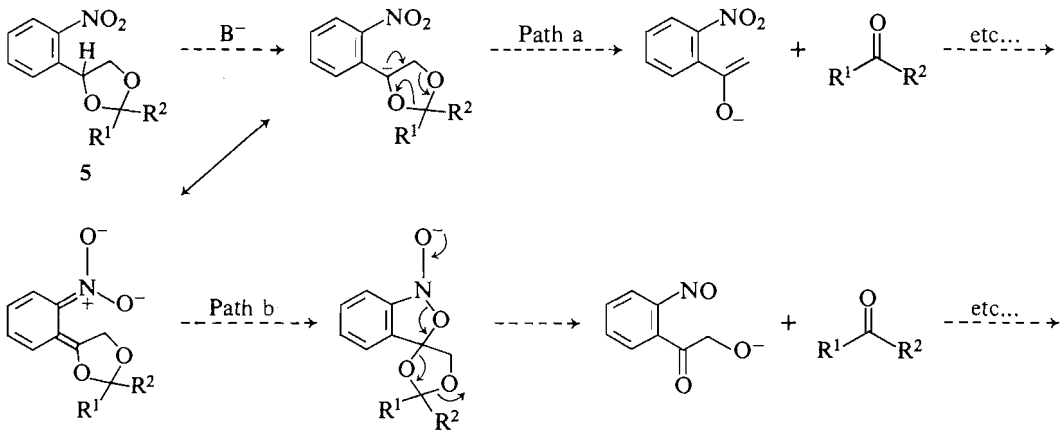

SCHEME 3

tions, which partly reconjugates but also decomposes. In order to attempt to rectify this situation we, also in this case, carried out the photolysis using the aforementioned filter solution and then treated the crude photolysis product with sodium methoxide in methanol in order to reconjugate the double bond before chromatography. After column chromatography on silica gel there was obtained a 37% yield of testosterone compared to 31% under the other conditions; it therefore appears that here again the limiting factor is the photochemical instability of the liberated ketone under the reaction conditions, possibly again due to sensitization, but this particular aspect was not verified with a pure sample of deconjugated testosterone.

Stability of the o*-nitrophenylethylenedioxy protective group in basic and reducing media*

As is most often the case in organic synthesis, acetals and ketals are used as protective groups for aldehydes and ketones when the substrate bearing such functional groups must be manipulated in basic or reducing media. However, the present group bearing the *o*-nitrobenzyl functionality should be quite susceptible to certain strongly basic conditions and certain specific reducing conditions. In fact, it could even be anticipated that a strong base might liberate the ketone from its protective group as depicted in Scheme 3.[4]

In order to evaluate the stability of the present group under these conditions we chose as representative substrate the *o*-nitrophenylethylenedioxyketal of benzophenone (**5**, $R^1 = R^2$ = Ph) because it is isomerically homogeneous and because it should be free of undesirable side reactions which would complicate analysis of the results. Table 3 shows the stability (or instability, as the case may be) of the title protective group under a series of typical basic conditions and typical reducing conditions. It is readily apparent from these results that the group shows good stability in the presence of sodium hydride in nonpolar solvents, sodium alkoxides in alcohol–dioxane mixtures at room temperature, and aqueous bases such as 10% sodium hydroxide or 10% sodium bicarbonate in dioxane or ethanol. It is also apparent that, under certain conditions, some strong bases (NaH, DME, reflux 20 h, gives 73% of the liberated ketone) can effect deprotection quite cleanly and lead to the liberated ketone, possibly by one of the paths represented in Scheme 3;[4] since no trace of *o*-nitroacetophenone could be found in this type of liberation, path a is eliminated and path b remains as most likely, which is interesting because of its analogy with the photochemical reaction and other *o*-sub-

[4]The *a priori* possible α-elimination path to yield a carbene is considered as unlikely and is not represented.

Can. J. Chem. Downloaded from www.nrcresearchpress.com by 210.87.254.6 on 09/06/12
For personal use only.

TABLE 3. Stability of *o*-nitrophenylethylenedioxy ketal of benzophenone in basic and reducing media

Reagent	Solvent	*T* (°C)	Time (h)	% Recovered starting material	% Liberated benzophenone
NaH	Benzene	Reflux	22	91	Trace
NaH	Toluene	Reflux	16	92	Trace
NaH	Ether	Reflux	6	96	Trace
NaH	DME	Room temp	17	88	8
NaH	DME	Reflux	20	10	73
NaH	DMF	Room temp	10	19	40
NaH	DMSO	Room temp	10	6	47
$NaHCO_3$ 10%	H_2O/EtOH	Reflux	9	95	0
NaOH 10%	H_2O/dioxane	Reflux	12	85	Trace
EtONa	EtOH/dioxane	Room temp	24	94	Trace
EtONa	EtOH/dioxane	Reflux	4	23	44
t-BuOK	*t*-BuOH/dioxane	Room temp	9	85	10
t-BuOK	*t*-BuOH/dioxane	Reflux	2	0	58
LDA	THF	(−78°C, 0°C 1 h, room temp 6 h)		61	32
$NaBH_4$	H_2O/dioxane	Room temp	1	95	0
$LiAlH_4$	Ether	0°C	0.5	0	0
Na/EtOH	DME	Room temp	1	56	0

TABLE 4. Approximate stability of *o*-nitrophenylethylenedioxy ketal of benzophenone under acidic conditions

Conditions	*T*	Result
5% aq. HCl−THF	Room temp	Almost completely stable for 10 h Almost completely hydrolyzed after 72 h
10% aq. AcOH−THF	Room temp	Completely stable after 72 h
2% aq. oxalic acid − THF	Room temp	Completely stable after 72 h
10% aq. H_2SO_4−THF	Room temp	Almost completely stable for 5 h Almost completely hydrolyzed after 48 h
3% aq. *p*-TsOH − THF	Room temp	Almost completely stable for 5 h

stituted nitrobenzene cyclization reactions (for a review of the generalized *o*-nitrobenzylic shift, see ref. 7*g*). This rather unusual method of liberating a protected ketone could perhaps even be useful in some particular situation! Concerning the stability under various typical reducing media, it turns out, as anticipated, that it is about comparable to that of aromatic nitro compounds (21).

Finally, although stability to acid hydrolysis is not a property usually sought in acetals and ketals, we had observed qualitatively that the *o*-nitrophenylethylenedioxy group is relatively more difficult to introduce than the simple ethylenedioxy group;[5] this then suggested that it could also be possibly, although not necessarily, more difficult to remove under acidic conditions, which would constitute a potentially useful bonus in the present context.

We therefore qualitatively determined the stability to acid hydrolysis of the same model ketal (benzophenone) using tlc monitoring to evaluate the approximate onset or completion of hydrolysis, in order to make the prospective user aware of another facet of the reactivity of this new protective group (see Table 4).

Considering the results of Table 4 and the fact that the ethylenedioxy ketal of benzophenone is completely hydrolyzed at room temperature after 30 min in 5% aqueous HCl−THF (1:1), it may be safely concluded that the *o*-nitrophenylethylenedioxy group shows relatively good resistance to acid hydrolysis.

Concerning the stability to various other reaction conditions, it may be of interest to the prospective user that, since the *o*-nitrophenylethylenedioxy group is made up of a 1,3-dioxolane moiety and an *o*-nitrobenzyl ether moiety, both of which are well known in protective group chemistry, one can glean useful information by consulting the reactivity charts at the end of ref. 1*b*.

Mechanistic aspects

As mentioned in the beginning (see Scheme 1), it was presumed that the ketals or acetals **5** would, upon photolysis, regenerate the carbonyl compound **4** and the spent reagent in the form of *o*-nitroso-α-hydroxyacetophenone (**7**); this prediction was based on the rather well accepted mechanistic scheme proposed (6*g*, 7*a*, 7*b*) for such *o*-nitrobenzylic shifts (Scheme 4). Although the various carbonyl compounds **4** were regenerated upon photolysis of the ketals and acetals **5** in accordance with the scheme, the structure of the spent reagent remained to be proven. As stated above, however, every attempt made to isolate the elusive nitroso compound **7** during the various deprotection photolyses proved unfruitful.

However, since Arndt and Partale (14*a*) had already reported the preparation of the nitroso compound **7** in question, by treatment of *o*-nitrostyrene oxide (**8**) with formic acid at 0°C,

[5]It has been found, however, by R. C. Kelly and his group at Upjohn (22) that for some labile aldehydes the introduction of the *o*-nitrophenylethylenedioxy group is facilitated by exchange with the more easily introduced dimethyl acetal. These authors have provided what is probably, to date, the best illustration of the usefulness of this reagent, in their work related to thromboxane A_2.

Can. J. Chem. Downloaded from www.nrcresearchpress.com by 210.87.254.6 on 09/06/12
For personal use only.

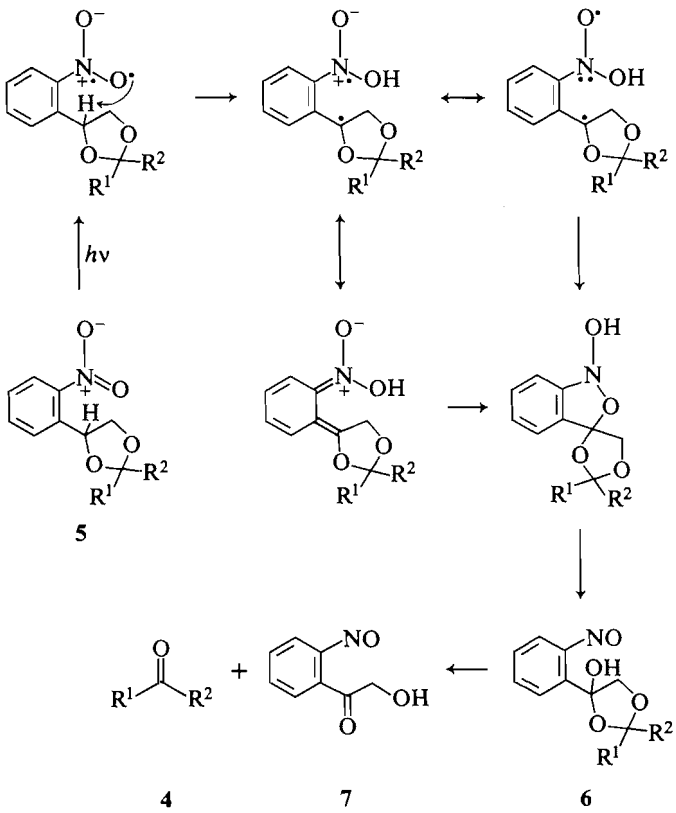

SCHEME 4

we repeated the procedure and obtained an authentic sample of **7** (mp 102–103°C, lit. (14*a*) mp 104°C), as also shown by nmr, ir, uv, and mass spectrometry (see Experimental). As mentioned by Arndt and Partale (14*a*), the nitroso compound **7** is very unstable and decomposes rapidly under the influence of heat or light.

Having then in hand an authentic sample of **7**, we could show by tlc analysis that, aside from the liberated ketone, the first product formed in the photolysis of every ketal or acetal **5** studied is *o*-nitroso-α-hydroxyacetophenone (**7**) and that the other products formed later result from its decomposition. This result, although rather convincing, did not bring absolute proof of the presence of **7** and therefore one last attempt was made at isolating **7** from a photolysis mixture, taking advantage of the experience acquired in manipulating authentic samples of the compound.

In order to carry out this delicate experiment we chose firstly to prepare and irradiate the *o*-nitrophenylethylenedioxy ketal of acetone because it shows good solubility and therefore hopefully would not interfere with the crystallization of *o*-nitroso-α-hydroxyacetophenone (**7**) and also because the liberated ketone is a solvent for the crystallization of **7**. Secondly, we chose ether as the solvent for photolysis since it does not dissolve the nitroso compound well and, finally, the photolysis was carried out at 0°C in order to minimize the thermal decomposition of **7**.

It was therefore under these conditions that the photolysis was undertaken and monitored by tlc; the reaction was stopped when the concentration of the presumed nitroso compound **7** appeared about at its maximum and the solution was still green. Evaporation of part of the ether allowed the crystallization of a small amount of the suspected *o*-nitroso-α-hydroxyacetophenone (**7**) as shown by comparison with an authentic sample (mp, mixture mp, ir, nmr). This result therefore demonstrates unambiguously the nature of the spent reagent as compound **7**.

Experimental

Melting points were taken on a Büchi apparatus and are uncorrected. The nmr spectra were recorded in $CDCl_3$ (unless otherwise specified) on a Varian model A-60 apparatus or a JEOL model C60-H apparatus using TMS as internal reference; the letters s, d, t, q, and m, meaning respectively singlet, doublet, triplet, quadruplet, and multiplet, are used in the description of the spectra. The ir spectra were recorded in $CHCl_3$ (unless otherwise specified) on a Beckman model IR-8 apparatus. The uv spectra were recorded in ethanol 95% on a Bausch and Lomb Spectronic 505 spectrophotometer. The mass spectra were obtained from AEI MS 902 and Hitachi–Perkin–Elmer RMU 6D mass spectrometers. Photolyses were carried out in a Rayonet photochemical reactor equipped with 350 nm lamps or in a homemade photochemical reactor, equipped with a single Hanovia lamp (450 watts) when the use of a filter solution was necessary. The latter, placed between the lamp and the irradiated solution, was 5 cm thick and prepared by dissolving 38 g of $CuSO_4 \cdot 5H_2O$ in 100 mL of water. Thin-layer chromatography was carried out using Eastman–Kodak 13181 Silica Gel plates. Column chromatography was carried out using 100 to 150 grams of J. T. Baker Silica Gel 60–80 mesh per gram of mixture. Finally, microanalyses were performed by Midwest Microlab Inc., Indianapolis, USA and by Dr. C. Daesslé, Organic Microanalyses, Montreal.

o-*Nitrophenacyl bromide* (***10***) (13, 15, 16)

A solution of bromine (134 g, 0.837 mol) in dioxane (1250 mL) is added dropwise over a 2 h period to a solution of *o*-nitroacetophenone (**9**) (Aldrich) (137.8 g, 0.835 mol) in dioxane (250 mL). The reaction may be monitored by tlc (hexane–ether 1:1) by following the appearance of a major compound, slightly less polar than the starting material. After the addition is completed, the solvent and hydrobromic acid formed are evacuated by evaporation. The oily residue thus obtained is dissolved in ether (1000 mL) and the solution washed successively with a 10% solution of sodium bicarbonate and brine until neutrality. The organic layer is dried over magnesium sulfate and evaporated.

Crystallization of the crude mixture in 95% ethanol affords pure *o*-nitrophenacyl bromide (**10**) (139 g, 0.572 mol) in 68% yield. Distillation under reduced pressure of the mother liquor furnishes 14% (18 g) of the unreacted material (**9**). Purification of the distillation residue by filtration through a silica gel column (eluent: CCl_4) gives a colorless oil which, upon treatment with 95% ethanol, yields pure crystalline dibromo derivative (3.2 g, 9.9 mmol), 6%. The nmr analysis of the noncrystalline residue shows equal proportions of mono and dibromo derivatives by the relative intensities of the signals at δ 4.37 and 6.31.

The pure *o*-nitrophenacyl bromide (**10**) has: mp 54–55°C (95% ethanol) (lit. (13) mp 55–56°C); ir: 1350, 1530, and 1715 cm^{-1}; uv, λ_{max}: 213.0 nm (ε = 10 000), 261.5 nm (ε = 6,000); nmr, δ: 4.37 (s, 2H), 7.40–8.15 (m, 4H). The dibromo derivative has: mp 85–86°C (95% ethanol); ir: 1350, 1530, and 1725 cm^{-1}; uv, λ_{max} 211.0 nm (ε = 11 800), 262.0 nm (ε = 5,900); nmr, δ: 6.31 (s, 1H) and 7.50–8.30 (m, 4H); ms, *m/e*: 242 and 244 (rel. int. 1:1) $M^+ - Br$, *m/e*: 171, 173 and 175 (rel. int. 1:2:1) $CHBr_2^+$.

o-*Nitroepoxystyrene* (***8***) (13, 14)

(a) *From* o-*nitrophenacyl bromide* (***10***) (13, 17)

A suspension composed of sodium borohydride (98%) (22.1 g, 0.580 mol) and water (200 mL) is added dropwise and under stirring to a cooled (ice bath) solution of *o*-nitrophenacyl bromide (**10**) (138.5 g, 0.567 mol) in dioxane (200 mL). The rate of addition (approx. 2 h) is adjusted so as to prevent the temperature from exceeding 5°C. The mixture is then stirred at room temperature for 30 min after which an aqueous solution of sodium hydroxide (30 g/200 mL) is added. After a stirring period of 15 min, a tlc (hexane–ether 6:4) of the crude mixture shows complete disappearance of the starting material and the presence of a less polar compound. After several

Can. J. Chem. Downloaded from www.nrcresearchpress.com by 210.87.254.6 on 09/06/12
For personal use only.

Can. J. Chem. Downloaded from www.nrcresearchpress.com by 210.87.254.6 on 09/06/12
For personal use only.

extractions with ether, the combined organic layers are washed with brine, dried over magnesium sulfate, and evaporated. Several crystallizations (95% ethanol) of the oily residue afford 83% (78 g, 0.473 mol) of the desired epoxide (**8**), while filtration through a silica gel column (eluent: CCl_4) of the mother liquors furnishes another 5% (5 g, 0.030 mol) of the same epoxide (**8**) for a total yield of 88%. The compound has: mp 63–64°C (95% ethanol) (lit. (13) mp 64–65°C); ir: 1345, 1525, 1580, and 1615 cm^{-1}; uv, λ_{max}: 206.5 nm (ϵ = 13 800), 261.5 nm (ϵ = 6,520); nmr, δ: 2.62 (q, 1H, portion A of AMX, J_{AM} = 6 Hz, J_{AX} = 2.5 Hz), 3.27 (q, 1H, portion M of AMX, J_{MX} = 4.5 Hz), 4.45 (q, 1H, portion X of AMX), and 7.26–8.17 (m, 4H).

(b) *From o-nitrobenzaldehyde (1)* (14)

To an ice-cold ethereal (50 mL) solution of *o*-nitrobenzaldehyde (**1**) (10.0 g, 0.066 mol) is added, over a 15 min period, an ice-cold ethereal solution of diazomethane (0.071 mol). The mixture is stirred at 0°C for 1 h, then at room temperature for 3 additional hours. The ether is partly distilled to eliminate the excess diazomethane and the remainder evaporated under vacuum. Thin-layer chromatography (hexane–ether 1:1) of the crude mixture shows 5 compounds in unequal proportions.

Several crystallizations (methanol) of the crude mixture afford 39% (4.3 g) of the epoxide (**8**), which is the less polar compound on tlc. Column chromatography (eluent: hexane–ether 8:2) of the concentrated mother liquors furnishes an additional 22% (2.4 g) of epoxide (**8**) (for a total yield of 61%), 8% (0.8 g) of the title compound (**1**), and 14% (1.5 g) of *o*-nitroacetophenone (**9**). Spectral data for epoxide (**8**) are identical to those presented in section (a).

o-*Nitrophenylethylene glycol (3)*

Mixed solutions of *o*-nitroepoxystyrene (**8**) (82.5 g, 0.5 mol) in dioxane (100 mL) and 10% aqueous potassium carbonate (800 mL) are heated under reflux and protected from daylight, for a 17 h period. Thin-layer chromatography of the mixture (hexane–ether 1:1) shows complete disappearance of the starting material and the presence of a new, much more polar substance. The cooled mixture is saturated with sodium chloride and extracted several times with chloroform. The combined organic layers are dried over magnesium sulfate and evaporated under vacuum. Several crystallizations in chloroform of the solid yellow residue yield 78% (71.3 g) of the desired diol (**3**). The latter can be stored "indefinitely" providing it is protected from daylight. It has: mp 95–96°C ($CHCl_3$); ir: 1350, 1525, 3615, and 3430 cm^{-1}; uv, λ_{max}: 206.0 nm (ϵ = 2,750), 259.0 nm (ϵ = 5,300); nmr (DMSO-d_6), δ: 3.43–3.63 (m, 2H), 4.93–5.33 (m, 2H), 5.78 (d, J = 4.5 Hz, 1H) and 7.50–8.20 (m, 4H); nmr (DMSO-d_6 + D_2O), δ: 3.60 (d, J = 6 Hz, 2H) and 5.25 (t, J = 6 Hz, 1H) *etc.*; nmr (CD_3COCD_3), δ: 3.42–3.95 (m, 2H), 4.15 (t, J = 5.5 Hz, 1H), 4.83 (d, J = 4.5 Hz, 1H), 5.15–5.50 (m, 1H), and 7.35–8.10 (m, 4H); nmr (CD_3COCD_3 + D_2O), δ: 3.50–4.02 (8 lines, AB portion of ABX, 2H) and 5.30–5.48 (q, X portion of ABX, 1H) *etc.*; ms, *m/e*: 152 (M^+ – CH_2OH). *Anal.* calcd. for $C_8H_9NO_4$: C 52.46, H 4.95, N 7.65; found: C 52.30, H 5.11, N 7.57.

Protection of carbonyl groups

General method of ketalization (see footnote 5)

A solution composed of the carbonyl compound (0.01 mol), *o*-nitrophenylethylene glycol (**3**) (5.49 g, 0.03 mol), *p*-toluenesulfonic acid (100 mg), and anhydrous benzene (125 mL) is heated under reflux in an apparatus protected from daylight and equipped with a Dean–Stark water separator or a Soxhlet extractor with the thimble filled with anhydrous magnesium sulfate. The reaction is monitored by tlc using an appropriate eluent. The reaction is stopped after all the starting material is consumed or when no noticeable change can be observed in the progress of the reaction. The mixture is then allowed to cool to room temperature and filtered to recover the excess diol **3**. The filtered solution is washed with a 10% solution of sodium bicarbonate and then with brine until neutrality. The organic layer is dried over magnesium sulfate and evaporated. The crude acetals or ketals are then purified by column chromatography or in certain cases by crystallization (*vide infra*).

Cyclohexanone ketal

The reaction can be monitored by tlc (hexane–ether 6:4) and is complete in one hour. The oily residue obtained after work-up is purified by column chromatography (eluent: benzene) to afford 96% (2.53 g) of pure ketal as a colourless oil, bp 142°C/0.25 Torr; ir: 1345, 1525, 1580, and 1610 cm^{-1}; uv, λ_{max}: 206.5 nm (ϵ = 12 500), 262.0 nm (ϵ = 5,500); nmr, δ: 1.2–2.0 (m, 10H), 3.74 (q, 1H, portion A of AMX, J_{AM} = 6.0 Hz, J_{AX} = 6.8 Hz), 4.66 (q, 1H, portion M of AMX, J_{MX} = 6.8 Hz), 5.62 (t, 1H, portion X of AMX) and 7.25–8.20 (m, 4H); ms, *m/e*: 263 (M^+).

p-*Nitrobenzaldehyde acetal*

The reaction is monitored by tlc (hexane–ether 1:1) and is complete in 2 h. The oily residue obtained after work-up is crystallized in hexane–dichloromethane to afford 72% (2.28 g) of a pure acetal, mp 118–119°C, shown below to be the *cis* isomer. Concentration of the mother liquors and column chromatography of the residue (eluent: benzene) yields a mixture of the *cis* and *trans* acetals which is recrystallized to afford 25% (0.78 g) of acetal. The nmr analysis shows, by comparing relative intensities of peaks at δ 6.10 and 6.42, that the mixture contains 60% of the *cis* isomer (less polar compound on tlc) and 40% of the *trans* isomer (more polar compound on tlc). Analytical samples of the two isomers are obtained either by fractional crystallization or column chromatography (eluent: benzene–ether 9:1).

cis Isomer, mp 118–119°C; yield, 58%; ir: 1345, 1520, and 1610 cm^{-1}; uv, λ_{max}: 203.0 nm (ϵ = 21 200), 261.0 nm (ϵ = 15 800); nmr, δ: 4.04 (q, 1H, portion A of AMX, J_{AM} = 8.2 Hz, J_{AX} = 5.3 Hz), 4.73 (t, 1H, portion M of AMX, J_{MX} = 8.2 Hz), 6.10 (s, 1H), and 7.4–8.6 (m, 8H); ms, *m/e*: 316 (M^+).

trans Isomer, mp 111–112°C; yield, 39%; ir: 1350, 1525, and 1610 cm^{-1}; uv, λ_{max}: 205.0 nm (ϵ = 20 000), 261.5 nm (ϵ = 16 600); nmr, δ: 3.92 (q, 1H, portion A of AMX, J_{AM} = 8.2 Hz, J_{AX} = 6.3 Hz), 4.82 (q, 1H, portion M of AMX, J_{MX} = 6.3 Hz), 5.84 (t, 1H, portion X of AMX), 6.42 (s, 1H), and 7.4–8.5 (m, 8H); ms, *m/e*: 316 (M^+).

Benzophenone ketal

The reaction is monitored by tlc (benzene) and is complete in 12 h. The oily residue obtained after work-up is crystallized from ether–methanol to afford 64% (2.21 g) of pure ketal. Concentration of the mother liquors and column chromatography (eluent: benzene) furnishes 30% (1.06 g) more of the same ketal, mp 115–116°C; yield, 94%; ir: 1350, 1525, 1575, and 1610 cm^{-1}; uv, λ_{max}: 202.5 nm (ϵ = 24 400), 261.0 nm (ϵ = 33 500); nmr, δ: 4.01 (q, 1H, portion A of AMX, J_{AM} = 7.5 Hz, J_{AX} = 5.3 Hz), 4.58 (t, 1H, portion M of AMX, J_{MX} = 7.5 Hz), 5.68 (q, 1H, portion X of AMX), and 7.2–8.2 (m, 14H); ms, *m/e*: 347 (M^+).

Δ^5-Androsten-3β-ol-17-one acetate ketals

The reaction is monitored by tlc (hexane–ether 1:1) and is complete in 3 h. The oily residue obtained after work-up is crystallized in methanol to afford 76% (3.75 g) of pure diastereoisomeric ketals. Concentration of the mother liquors and column chromatography (eluent: benzene–ether 9:1) furnishes 16% (0.81 g) more of ketals as a mixture of diastereoisomers. Yield, 92%; ir: 1725, 1350, 1525, 1580, and 1615 cm^{-1}; uv, λ_{max}: 202.5 nm (ϵ = 16 000), 260.0 nm (ϵ = 5,450); nmr, δ: 0.92 (s, 3H), 1.06 (s, 3H), 2.04 (s, 3H), 3.60–3.84 (m, 1H, portion A of AMX), 4.40–4.75 (m, 2H, H_3 and portion M of AMX), 5.30–5.65 (m, 2H, H_6 and portion X of AMX), and 7.30–8.20 (m, 4H); ms, *m/e*: 435 (M^+ – AcOH).

Δ^5-Pregnen-3β-ol-20-one acetate ketals

The reaction is monitored by tlc (hexane–ether 6:4) and is complete in 10 h. The oily residue obtained after work-up is crystallized in methanol to afford 51% (2.67 g) of pure diastereoisomeric ketals. Concentration of the mother liquors and column chromatography (eluent: benzene) furnishes 29% (1.53 g) more of ketals as a mixture of diastereoisomers. Yield, 80%; ir: 1725, 1350, 1525, 1580, and 1615 cm^{-1}; uv, λ_{max}: 205.5 nm (ϵ = 13 600), 260.5 nm (ϵ = 5,000); nmr, δ: 0.84 (s, 3H), 1.05 (s, 3H), 1.48 and 1.53 (2s, 3H), 2.05 (s, 3H), 3.52–3.88 (m, 1H, portion A of AMX), 4.40–5.00 (m, 2H, H_3 and portion M of AMX), 5.30–5.75 (m, 2H, H_6 and portion X of AMX),

Can. J. Chem. Downloaded from www.nrcresearchpress.com by 210.87.254.6 on 09/06/12
For personal use only.

and 7.30–8.20 (m, 4H); ms, *m/e*: 463 (M^+ – AcOH).

Testosterone ketals

The reaction is monitored by tlc (dichloromethane–ether 8:2) and is complete in 24 h. The oily residue obtained after work-up is crystallized from methanol to afford 1.75 g of diastereoisomeric ketals. Concentration of the mother liquors and column chromatography (eluent: dichloromethane–ether 19:1) furnishes an additional 1.45 g of ketals and 26% (0.75 g) of unreacted testosterone. Total yield of ketals: 70%; ir: 3630, 1350, 1525, 1580, and 1610 cm^{-1}; uv, λ_{max}: 203.5 nm (ϵ = 16 300), 262.0 nm (ϵ = 5,400); nmr, δ: 0.80 (s, 3H), 1.12 (s, 3H), 3.52–3.95 (m, 2H, H_1 and portion A of AMX), 4.50–4.90 (m, 1H, portion M of AMX), 5.30–5.80 (m, 2H, H_6 and portion X of AMX), and 7.30–8.25 (m, 4H); ms, *m/e*: 453 (M^+). The ketals obtained are therefore the $\Delta^{5,6}$ isomers because the ethylenic proton at C-6 appears as a multiplet centered at δ 5.44.

Removal of the protective group by irradiation

General method

The protective group is removed by irradiation at room temperature for 6 h of a 10^{-3} – 10^{-4} *M* solution of the ketal in benzene (200 mL). A Pyrex vessel and uv light of wavelength longer than 320 nm are used. The red-brown residue is chromatographed on silica gel. Yields of regenerated carbonyl compounds are generally good to excellent except in the case of androstenolone acetate and testosterone.

Irradiation of cyclohexanone ketal

A solution of cyclohexanone ketal (1.315 g, 5×10^{-3} mol) in anhydrous benzene (200 mL) is irradiated for 6 h at 350 nm. Thin-layer chromatography (hexane–ether 7:3) of the brownish solution shows complete disappearance of the starting material. The benzene is then slowly removed by distillation and 250 mL of water is added to the residue. Distillation is then pursued and the distillate collected into a freshly prepared solution of 2,4-dinitrophenylhydrazine. The precipitate is filtered; recrystallization in 95% ethanol affords pure cyclohexanone 2,4-dinitrophenylhydrazone (mp 159–162°C) in 85% (1.18 g) yield. This compound is identical (mixture mp, ir, nmr) with an authentic sample prepared from commercially available cyclohexanone.

Irradiation of p-*nitrobenzaldehyde acetals*

A solution of *p*-nitrobenzaldehyde acetals (1.58 g, 5 x 10^{-4} mol) (mixture of *cis* and *trans* isomers in a 60:40 ratio) in anhydrous benzene (200 mL) is irradiated for 6 h at 350 nm. Thin-layer chromatography (hexane–ether 1:1) shows almost complete disappearance of the starting material. The solvent is evaporated under vacuum and the residual mixture purified by column chromatography (hexane–ether 1:1) to yield 11% (0.18 g) of unreacted acetals (mixture of *cis* and *trans* isomers) and 86% (0.65 g) of *p*-nitrobenzaldehyde. Comparison of physical (mp) and spectral (ir, nmr) data of these two compounds with those of authentic samples proves identical.

Irradiation of benzophenone ketal

A solution of benzophenone ketal (1.735 g, 5×10^{-4} mol) in anhydrous benzene (200 mL) is irradiated for 6 h at 350 nm. Thin-layer chromatography (benzene) shows almost complete disappearance of the starting material. The solvent is evaporated under vacuum and the residual mixture purified by column chromatography (benzene) to yield 7% (0.13 g) of unreacted ketal and 90% (0.82 g) of benzophenone. These compounds prove identical (mp, ir, nmr) with authentic samples.

Irradiation of Δ^5*-androsten-3*β*-ol-17-one acetate*

A solution of androstenolone acetate (1.0 g) in anhydrous benzene (100 mL) is irradiated for 6 h at 350 nm. Thin-layer chromatography (dichloromethane–ether 19:1) shows, apart from the starting material, the presence of a less polar compound. The solvent is evaporated under vacuum and the residual mixture purified by column chromatography (dichloromethane–ether 19:1) to yield 30% (0.30 g) of a photoproduct identified as the 13α epimer of androstenolone acetate. An analytical sample is obtained by recrystallization (ether–hexane), mp 138–140°C (lit. (18) mp 140–141°C); ir: 1725 cm^{-1}; nmr, δ: 0.89 (s, 3H), 1.02 (s, 3H), 2.05 (s, 3H), 4.58 (m, 1H), and 5.44 (m, 1H). The second fraction eluted furnishes 56% (0.56 g) of androstenolone acetate, identified by comparison of its physical (mp) and spectral (ir, nmr) properties to authentic material.

Irradiation of Δ^5*-androsten-3*β*-ol-17-one acetate with a filter solution*

A solution of the title compound (0.30 g) in anhydrous benzene (500 mL) is irradiated with a Hanovia medium pressure lamp through 5 cm of a filter solution composed of 760 g of $CuSO_4 \cdot 5H_2O$ in 2 litres of water. Thin-layer chromatography (dichloromethane–ether 19:1) shows, after 9 h of irradiation, the sole presence of the starting material. The solvent is evaporated under vacuum to afford the unchanged 13 β epimer, mp 168–170°C (lit. (18) mp 168–170°C); nmr, δ: 0.89 (s, 3H), 1.08 (s, 3H), 2.05 (s, 3H), 4.58 (m, 1H) and 5.44 (m, 1H).

Irradiation of the ketal of Δ^5*-androsten-3*β*-ol-17-one acetate with the filter solution*

A solution of the title ketal (0.30 g, 6.2×10^{-4} mol) in anhydrous benzene (500 mL) is irradiated according to the conditions described above. After 5 h, tlc (dichloromethane–ether 19:1) shows almost complete consumption of the starting material. The solvent is evaporated under vacuum and the residue purified by column chromatography (dichloromethane–ether 19:1) to yield 12% (0.035 g) of unreacted ketal, 0.7% (0.012 g) of 13α epimer of androstenolone acetate and 71% (0.125 g) of the desired 13β epimer. The physical and spectral data of these compounds are identical to those described above.

Irradiation of the ketal of Δ^5*-pregnen-3*β*-ol-20-one acetate*

A solution of pregnenolone ketal acetate (2.615 g, 5×10^{-4} mol, mixture of diastereoisomers) in anhydrous benzene (200 mL) is irradiated for 6 h at 350 nm. Thin-layer chromatography (hexane–ether 6:4) shows almost complete consumption of the starting material. The solvent is evaporated under vacuum and the residue purified by column chromatography (dichloromethane) to afford 13% (0.33 g) of unreacted ketal and 83% (1.49 g) of pregnenolone acetate, crystallized from hexane–ether. The latter compounds are identical (mp, ir, and nmr) with authentic samples.

Irradiation of testosterone ketal

(a) *Under the standard conditions*

A solution of testosterone ketal (2.265 g, 0.5×10^{-3} mol, mixture of diastereoisomers) in anhydrous benzene (200 mL) is irradiated for 6 h at 350 nm. Thin-layer chromatography (dichloromethane–ether 9:1) shows, in order of increasing polarity: unreacted ketal, $\Delta^{5,6}$ testosterone as the major compound, and its $\Delta^{4,5}$ isomer. The solvent is evaporated under vacuum and the residue purified by column chromatography (dichloromethane) to afford 14% (0.33 g) of unreacted ketal, traces of $\Delta^{5,6}$ testosterone, and 31% (0.455 g) of $\Delta^{4,5}$ testosterone. The latter are identical (mp, ir, and nmr) with authentic samples, except $\Delta^{5,6}$ testosterone which was identified by tlc only.

Using a filter solution

A solution of testosterone ketal (0.50 g, 1.1×10^{-3} mol) in anhydrous benzene (800 mL) is irradiated using the filter solution and the conditions described above. After 4 h, tlc (dichloromethane–ether 9:1) shows almost complete consumption of the starting material. The solvent is evaporated under vacuum and the oily residue submitted to reconjugation conditions, i.e. dissolved in 200 mL of anhydrous methanol to which is added 3 mL (3×10^{-5} mol) of a 0.01 *M* sodium methoxide solution. The solution is stirred at room temperature for 4 h, then treated with a 20% HCl solution until neutrality. After the solvent has been evaporated, the residue is dissolved in dichloromethane (50 mL), washed with brine, dried over magnesium sulfate, and the solvent evaporated. The residue is then purified by column chromatography (dichloromethane) to afford 37% (0.117 g) of $\Delta^{4,5}$ testosterone, identical (mp, ir, and nmr) with an authentic sample.

Synthesis of α*-hydroxy* o-*nitrosoacetophenone (7)* (14*a*)

To 6 mL of ice-cold formic acid is added 1 g (6 mmol) of *o*-nitroepoxystyrene (**8**). The stirred suspension immediately turns to green,

Can. J. Chem. Downloaded from www.nrcresearchpress.com by 210.87.254.6 on 09/06/12
For personal use only.

then to yellow after 5 min. When all of the epoxide **7** has dissolved (20 min), ether (40 mL) is quickly added. The brownish solution becomes yellow again with a beginning of crystallization. After a 10 min stirring period, tlc (hexane–ether 6:4) shows complete disappearance of epoxide **8** and appearance of a much more polar compound. The solution is maintained at 0°C under stirring for 1 h and then filtered. The crystals are washed with ether and dried. The average yield of the reaction is 50%, depending at which time ether is added. The solid can be recrystallized by quickly dissolving it in hot acetone and then rapidly cooling down the solution in a Dry Ice-acetone bath. The compound has: mp 102–103°C (dec.) (lit. (14a) mp 104°C); ir (Nujol): 3430, 1705, and 1600 cm^{-1}; uv, λ_{max}: 286 nm (ϵ = 4,800), 310 nm (ϵ = 4,700); nmr (CD_3COCD_3), δ: 3.07 (m, 1H), 4.65 (s, 2H), and 7.2–8.0 (m, 4H); ms, *m/e*: 165 (M^+).

Detection of the nitroso derivative 7 during the photolysis of acetals, ketals, and diol 3

Detection of the nitroso derivative **7** is accomplished by simultaneously irradiating solutions of the acetals, the ketals, diol **3**, and nitroso derivative **7** (50 mg) in DME (10 mL) at 350 nm. The photolyses are monitored by tlc (ether) at 5 min intervals. The nitroso derivative **7** is readily detected (R_f = 0.6) in the acetals, the ketals, and the diol **3** photolysis solutions. Prolonged irradiation results in further decomposition of the nitroso derivative **7**, giving rise to polar and coloured compounds on tlc.

Synthesis of acetone ketal

A solution of acetone (20 mL), diol **3** (1.83 g, 10^{-2} mol), and *p*-toluenesulfonic acid (100 mg) in anhydrous benzene (125 mL) is heated under reflux in an apparatus protected from daylight and equipped with a Dean–Stark separator. After 30 min, another 20 mL of acetone is added to the reaction mixture. Thin-layer chromatography (hexane–ether 7:3) shows, after a 1 h period, complete disappearance of diol **3**. The mixture is allowed to cool, is then washed with a 10% solution of sodium carbonate and then with brine until neutrality. The organic layer is dried over magnesium sulfate and evaporated. The crude product is purified by distillation under reduced pressure to afford 95% (2.12 g) of ketal, bp 105°C/0.3 Torr; ir: 1345, 1525, and 1610 cm^{-1}; nmr, δ: 1.50 and 1.62 (2s, 6H), 3.76 (q, 1H, portion A of AMX, J_{AM} = 9 Hz, J_{AX} = 6 Hz), 4.69 (q, 1H, portion M of AMX, J_{MX} = 7 Hz), 5.63 (q, 1H, portion X of AMX) and 7.4–8.2 (m, 4H); ms, *m/e*: 223 (M^+).

Isolation of the nitroso derivative 7 during the acetone ketal irradiation

An ice-cold solution of acetone ketal (0.1 g) in ether (50 mL) is irradiated at 350 nm in a Pyrex tube at 0°C. After 1 h, tlc (ether) of the greenish solution shows a considerable amount of the nitroso derivative **7** with some traces of decomposition of the latter. The ethereal solution is concentrated (15 mL) at room temperature under vacuum and placed in the freezer (1 h) to allow crystallization. The precipitate is filtered, washed with ether, and dried. The collected solid (0.075 g) is identical (mixture mp, ir, nmr) with the nitroso derivative **7** prepared from *o*-nitroepoxystyrene (**8**).

Stability of ketals in basic and reductive media

1. *Treatment of benzophenone ketal with sodium hydride; general procedure*

A suspension composed of benzophenone ketal (347 mg, 1 mmol), sodium hydride (240 mg, 5 mmol), and anhydrous solvent (25 mL) is stirred (under reflux or at room temperature) for a certain period of time. Water (1 mL) is then added to quench the excess hydride. The solution is washed twice with water or extracted, then the organic layer dried over magnesium sulfate and evaporated. The reaction can be monitored by tlc (hexane–benzene 3:7) and the mixture separated by column chromatography (benzene).

(a) *In refluxing benzene* After a 22 h refluxing period, tlc shows mostly unreacted starting material and traces of benzophenone. Column chromatography affords 91% (315 mg) of unreacted benzophenone ketal (crystallization in methanol), identified by comparison with authentic material.

(b) *In refluxing toluene* After a 16 h refluxing period, tlc shows unreacted starting material and traces of benzophenone. Column chromatography affords 92% (320 mg) of unreacted ketal.

(c) *In refluxing ether* After a 6 h refluxing period and usual treatment, 96% (335 mg) of unreacted ketal is recovered by column chromatography.

(d) *In DME at 20°C* After a 17 h stirring period, ether (100 mL) and water (100 mL) are added to the mixture. The ethereal layer is decanted and treated in the usual manner. Column chromatography affords 88% (305 mg) of unreacted ketal and 8% (14 mg) of benzophenone.

(e) *In DMF at 20°C* After a 10 h stirring period, tlc shows consumption of nearly all the ketal, leading to benzophenone as the major product. Water (100 mL) is added to the mixture, followed by 2 extractions with dichloromethane. The organic layer is dried over magnesium sulfate and evaporated. Column chromatography affords 19% (65 mg) of unreacted ketal and 40% (70 mg) of benzophenone.

(f) *In DMSO at 20°C* After a 10 h stirring period, tlc shows consumption of nearly all the ketal, leading to benzophenone as the major product. Water (100 mL) is added to the mixture, followed by extraction with ether (100 mL). The organic layer is dried over magnesium sulfate and evaporated. Column chromatography affords 6% (20 mg) of unreacted ketal and 47% (85 mg) of benzophenone.

2. *Treatment of benzophenone ketal with sodium hydroxide*

A solution composed of ketal (347 mg, 1 mmol), dioxane (20 mL), and sodium hydroxide (20 mL of a 10% solution) is heated under reflux for a 12 h period. The solution is extracted with ether and the organic layer dried over magnesium sulfate and evaporated. Column chromatography affords 85% (295 mg) of unreacted ketal and traces of benzophenone (identified by tlc).

3. *Treatment of benzophenone ketal with sodium carbonate*

A solution composed of ketal (347 mg, 1 mmol), ethanol (20 mL), and sodium carbonate (20 mL of a 10% solution) is heated under reflux for a 9 h period. After evaporation of the ethanol, the mixture is extracted with dichloromethane. The organic layer is dried and evaporated. Column chromatography affords 95% (300 mg) of unreacted ketal.

4. *Treatment of benzophenone ketal with sodium ethoxide*

(a) *At 20°C* A solution of absolute ethanol (25 mL) and sodium (230 mg, 10 mmol) is added to a solution of ketal (347 mg, 1 mmol) in dioxane (5 mL). The mixture is stirred for a 24 h period, afterwards water (50 mL) is added, ethanol is evaporated, and the aqueous solution extracted with ether. The organic layer is dried over magnesium sulfate and evaporated. Column chromatography affords 94% (325 mg) of unreacted ketal.

(b) *Under reflux* After a 4 h refluxing period, the solution is treated as described above. Column chromatography affords 23% (80 mg) of ketal and 44% (80 mg) of benzophenone.

5. *Treatment of benzophenone ketal with potassium* tert-*butoxide*

(a) *At 20°C* A solution of anhydrous *tert*-butanol (25 mL) and potassium (195 mg, 5 mmol) is added to a solution of ketal (347 mg, 1 mmol) in dioxane (5 mL). The mixture is stirred for a 9 h period, afterwards water (50 mL) is added, *tert*-butanol evaporated, and the aqueous solution extracted with ether. The organic layer is dried over magnesium sulfate and evaporated. Column chromatography affords 85% (295 mg) of ketal and 10% (20 mg) of benzophenone.

(b) *Under reflux* After a 2 h refluxing period, the solution is treated as described above. Column chromatography affords 58% (106 mg) of benzophenone, the ketal being absent.

6. *Treatment of benzophenone ketal with sodium borohydride*

A solution of sodium borohydride (114 mg, 3 mmol) in ice-cold water (20 mL) is added, dropwise over a 15 min period, to a solution of ketal (347 mg, 1 mmol) in dioxane (10 mL). The mixture is stirred at room temperature for 1 h and extracted with ether (3 × 25 mL). The organic layer is dried over magnesium sulfate and evaporated. Thin-layer chromatography (benzene) shows that no reaction occurred and 95% (330 mg) of the ketal is recovered by crystallization in ether–methanol.

Can. J. Chem. Downloaded from www.nrcresearchpress.com by 210.87.254.6 on 09/06/12
For personal use only.

7. *Treatment of benzophenone ketal with lithium aluminium hydride*

A solution of ketal (347 mg, 1 mmol) in anhydrous ether (20 mL) is added, dropwise over a 15 min period, to an ice-cold suspension of lithium aluminium hydride (114 mg, 3 mmol) in anhydrous ether (10 mL). The mixture is stirred at 0°C for 15 min, afterwards ice-cold water (10 mL) is added cautiously to destroy the excess hydride. The filtered orange suspension is then extracted several times with ether. The organic layer is dried over magnesium sulfate and evaporated to afford 295 mg of a reddish oil. Thin-layer chromatography (benzene) shows complete disappearance of the ketal and two unidentified products contaminated with colored impurities.

8. *Treatment of benzophenone ketal with sodium in ethanol*

To a stirred solution of ketal (347 mg, 1 mmol) in anhydrous DME (5 mL) and absolute ethanol (20 mL) is added small pieces of sodium (460 mg, 20 mmol). The suspension is periodically cooled in an ice bath to maintain a temperature of 20°C. After all the sodium has reacted, stirring is maintained for 30 min at room temperature, afterwards water (100 mL) is cautiously added. The solvents are evaporated and the aqueous layer extracted with dichloromethane. The organic layer is dried over magnesium sulfate and evaporated. Column chromatography affords 56% (194 mg) of unreacted ketal. Other compounds were not investigated.

9. *Treatment of benzophenone ketal with lithium diisopropylamide*

To a solution of ketal (250 mg, 0.729 mmol) in THF (10 mL), cooled to −78°C, is added 2.5 mL (0.9 mmol) of a solution of lithium diisopropylamide (prepared from 0.138 mL diisopropylamine and 0.625 mL of butyllithium (1.6 *M*) in 2 mL of THF). The colour of the solution changes rapidly from orange to black at the beginning of the addition. The mixture is stirred at −78°C for one hour without any evidence of reaction as shown by tlc (benzene). The temperature is then raised gradually to 0°C for one hour and the formation of a new product (benzophenone) is observed by tlc. After 6 h at 25°C, the reaction is quenched with 10% HCl, diluted with 10 mL water, and extracted with 2 × 20 mL CH_2Cl_2. The organic phase is dried on anhydrous magnesium sulfate and evaporated to dryness to yield a brown oil which is chromatographed on silica gel (50 g, 200:1) (benzene−hexane 1:1) to yield 61% (153 mg, 0.446 mmol) of recuperated ketal and 32% (43 mg, 0.236 mmol) of liberated benzophenone.

Stability of ketals in acidic medium

General procedure

Samples of the benzophenone ketal (10 mg, 0.029 mmol) in 0.5 mL THF are treated with 0.5 mL of the appropriate acid in water at 25°C. The acids chosen are: HCl 5%, AcOH 10%, oxalic acid (10 mg/0.5 mL water), H_2SO_4 10%, and *p*-TsOH (15 mg/0.5 mL water). Progress of the reaction is monitored by tlc (benzene) and the results are reported in Table 4. These results are to be compared with that of the ethylenedioxy ketal of benzophenone which is *completely hydrolyzed after 30 min* in HCl 5% in THF (1:1) at room temperature.

Acknowledgements

Financial assistance from the Natural Sciences and Engineering Research Council of Canada, le Ministère de l'Éducation du Québec (FCAC), and Shell Canada Ltd. is gratefully acknowledged.

1. (*a*) J. F. W. McOMIE. (*Editor*). Protective groups in organic chemistry. Plenum Publishing Corporation, New York. 1973; (*b*) T. W. GREENE (*Editor*). Protective groups in organic synthesis. John Wiley and Sons, Inc., New York. 1981.
2. (*a*) Compendium of organic synthetic methods (Series). John Wiley and Sons, Inc., New York; (*b*) Annual reports in organic synthesis. Academic Press, New York.
3. B. AMIT, U. ZEHAVI, and A. PATCHORNIK. Israel J. Chem. **12**, 103 (1974).
4. V. N. R. PILLAI. Synthesis, 1 (1980).
5. G. CIAMICIAN and P. SILBER. Chem. Ber. **34**, 2040 (1901); **35**, 1992 (1902).
6. (*a*) F. SACHS and R. KEMPF. Chem. Ber. **35**, 2704 (1902); (*b*) F. SACHS and S. HILPERT. Chem. Ber. **37**, 3425 (1904); (*c*) E. BAMBERGER and F. ELGER. Justus Liebigs Ann. Chem. **371**, 319 (1909); (*d*) G. SCHULTZ and K. L. GANGULY. Chem. Ber. **58**, 702 (1925); (*e*) I. TANASESCU. Bull. Soc. Chim. Fr. **39**, 1718 (1926); (*f*) E. BAMBERGER and F. ELGER. Justus Liebigs Ann. Chem. **475**, 288 (1929); (*g*) J. A. BERSON and E. BROWN. J. Am. Chem. Soc. **77**, 447 (1955); (*h*) P. L. COE, A. E. JUKES, and J. C. TATLOW. J. Chem. Soc. C, 2020 (1966); (*i*) M. A. HEMS. Tetrahedron Lett. 375 (1969).
7. (*a*) P. A. LEIGHTON and F. A. LUCY. J. Chem. Phys. **2**, 756 (1934); (*b*) P. DE MAYO and S. T. REID. Q. Rev. **15**, 393 (1961); (*c*) H. MAUSER and H. HEITZER. Z. Naturforsch. Teil B, **21**, 109 (1966); (*d*) J. G. CALVERT and J. N. PITTS. Photochemistry. John Wiley and Sons, New York. pp. 478, 1966; (*e*) R. O. KAN. Organic photochemistry. McGraw−Hill, New York. 1966. p. 218; (*f*) D. C. NECKERS. Mechanistic organic photochemistry. Reinhold Publishing Corp., New York. 1967. p. 207; (*g*) P. N. PRESTON and G. TENNANT. Chem. Rev. **72**, 627 (1972).
8. (*a*) J. A. BARLTROP, P. J. PLANT, and P. SCHOFIELD. Chem. Commun. 822 (1966); (*b*) A. PATCHORNIK. *In* Pharmacology of hormonal polypeptides and proteins. Plenum Publishing Co., New York. 1968. p. 11; (*c*) A. PATCHORNIK, B. AMIT, and R. B. WOODWARD. *In* Peptides. North Holland Publishing Co., Amsterdam. 1969. p. 12; (*d*) A. PATCHORNIK, B. AMIT, and R. B. WOODWARD. J. Am. Chem. Soc. **92**, 6333 (1970); (*e*) S. M. KALBAG and R. W. ROESKE. J. Am. Chem. Soc. **97**, 440 (1975); (*f*) B. AMIT, E. HAZUM, M. FRIDKIN, and A. PATCHORNIK. Int. J. Peptide Protein Res. **9**, 91 (1977); (*g*) U. ZEHAVI and A. PATCHORNIK. J. Am. Chem. Soc. **95**, 5673 (1973); A. PATCHORNIK and M. A. KRAUS. Pure Appl. Chem. **46**, 183 (1976); (*h*) D. H. RICH and S. K. GURWARA. Chem. Commun. 610 (1973); (*i*) D. H. RICH and S. K. GURWARA. Tetrahedron Lett. 301 (1975); (*j*) D. H. RICH and S. K. GURWARA. J. Am. Chem. Soc. **97**, 1575 (1975); (*k*) B. AMIT and A. PATCHORNIK. Tetrahedron Lett. 2205 (1973); (*l*) B. AMIT, D. A. BEN-EFRAIM, and A. PATCHORNIK. J. Chem. Soc. Perkin Trans. I, 57 (1976).
9. (*a*) P. M. COLLINS and N. N. OPARAECHE. Chem. Commun. 532 (1972); (*b*) U. ZEHAVI, B. AMIT, and A. PATCHORNIK. J. Org. Chem. **37**, 2281 (1972); U. ZEHAVI and A. PATCHORNIK. J. Org. Chem. **37**, 2285 (1972); (*c*) B. AMIT, U. ZEHAVI, and A. PATCHORNIK. Israel Chem. Soc. 42nd Meeting. 1972. p. 60; (*d*) J. Org. Chem. **39**, 192 (1974); (*e*) U. ZEHAVI and A. PATCHORNIK. Israel Chem. Soc. 42nd Meeting. 1972. p. 61; (*f*) Am. Chem. Soc., Division of Carbohydrate Chemistry, 164th ACS National Meeting, New York. 1972.
10. (*a*) M. RUBINSTEIN, B. AMIT, and A. PATCHORNIK. Tetrahedron Lett. 1445 (1975); (*b*) D. G. BARTHOLOMEW and A. D. BROOM. Chem. Commun. 38 (1975).
11. J. HEBERT and D. GRAVEL. Can. J. Chem. **52**, 187 (1974).
12. L. M. YAGUPOLSKII, M. A. BUTLEROVSKII, R. V. BELINSKAYA, and V. I. IVANOVA. Zh. Obshch. Khim. **30**, 1288 (1960); Chem. Abstr. **55**, 441 (1961).
13. C. O. GUSS. J. Org. Chem. **17**, 678 (1952).
14. (*a*) F. ARNDT and W. PARTALE. Chem. Ber. **60**, 446 (1927); F. ARNDT, B. EISTERT, and W. PARTALE. Chem. Ber. **61**, 1107 (1928); **61**, 1949 (1928); (*b*) F. ARNDT, E. AMENDE, and E. ENDER. Monatsh. Chem. **59**, 202 (1932).
15. M. I. SHEVCHUK and A. V. DOMBROVSKII. Zh. Obshch. Khim. **33**, 1135 (1963); Chem. Abstr. **59**: 9921 (1963).
16. L. F. FIESER and M. FIESER. Reagents for organic chemistry. John Wiley and Sons, New York. 1967. p. 333.
17. R. FUCHS and C. A. VANDERWERF. J. Am. Chem. Soc. **76**, 1631 (1954).
18. H. WEHRLI and K. SCHAFFNER. Helv. Chim. Acta, **45**, 385 (1962).
19. M. KASHA. J. Opt. Soc. Am. **38**, 929 (1948).

20. S. S. HIXSON, P. S. MARIANO, and H. E. ZIMMERMAN. Chem. Rev. **73**, 531 (1973).
21. N. G. GAYLORD. Reduction with complex metal hydrides. Interscience Publishers, New York. 1956. p. 773; H. O. HOUSE. Modern Synthetic reactions. 2nd ed. W. A. Benjamin, Inc., Menlo Park, NJ. 1972.
22. R. C. KELLY. *In* Organic synthesis today and tomorrow (IUPAC). *Edited by* B. M. Trost and C. R. Hutchinson. Pergamon Press, Oxford and New York. p. 259. 1981.

Can. J. Chem. Downloaded from www.nrcresearchpress.com by 210.87.254.6 on 09/06/12
For personal use only.

1-(Dialkylaminomethyl)-azetidin-2-ones. Intermediates in a highly stereoselective preparation of *trans*-3,4-disubstituted azetidin-2-ones

A. BEVIN HAMLET AND TONY DURST
Department of Chemistry, University of Ottawa, Ottawa, Ont., Canada K1N 9B4

Received June 4, 1982

A. BEVIN HAMLET and TONY DURST. Can. J. Chem. **61**, 411 (1983).

The use of dialkylaminomethyl derivatives as a new β-lactam N—H protecting group is described. The group is stable to basic reagents but is readily removed with dilute aqueous acids. 1-Dialkylaminomethyl derivatives bearing a 4-substituent are converted in good yield and with high stereoselectivity into *trans*-3,4-disubstituted derivatives via reaction with LDA and subsequent addition of electrophiles. The products of several of these sequences are of interest as intermediates to thienamycin related substances.

A. BEVIN HAMLET et TONY DURST. Can. J. Chem. **61**, 411 (1983).

On décrit l'utilisation des dérivés dialkylaminométhyles comme un nouveau groupe protecteur du N—H des β-lactames. Le groupe est stable en présence de réactifs basiques mais s'élimine facilement en solutions diluées d'acides. On transforme les dérivés dialkylaminométhyles-1 portant un substituant en position 4 avec un bon rendement et avec une grande stéréosélectivité en dérivés disubstitués *trans* en positions 3,4 par l'intermédiaire d'une réaction avec la LDA et l'addition subséquente d'électrophiles. Les produits de plusieurs de ces séries de réaction sont intéressants comme intermédiaire de substances apparentées à la thiénamycine.

[Traduit par le journal]

Can. J. Chem. Downloaded from www.nrcresearchpress.com by 210.87.254.40 on 09/06/12
For personal use only.

In 1974 we showed that *N*-unsubstituted azetidin-2-ones (β-lactams) such as **1** reacted with two equivalents of *n*-BuLi at 0°C in THF to yield the dianion **2** (1). Subsequent trapping of **2** with a series of electrophiles furnished 3,4-disubstituted β-lactams in fair to good yield. The products were generally obtained as a mixture of *trans/cis* isomers in ratios varying between 3:1 and about 10:1 (eq. [1]).

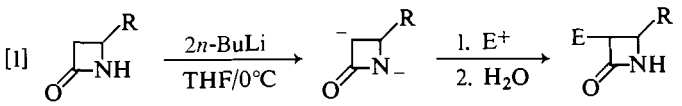

1 *R* = Ph

2

3 *cis*
4 *trans*

The discovery of the potent antibiotic thienamycin, **5** (2), has placed importance on highly stereoselective routes to *trans*-3,4-disubstituted azetidin-2-ones bearing a free N—H group. Of particular interest as potential starting points to thienamycin or derivatives thereof are *trans*-3(1′-hydroxyethyl)-4-vinyl-azetidin-2-one **6** and *trans*-3(1′-hydroxyethyl)-4-(3′-butenyl)-azetidin-2-one, **7**, since the corresponding 3-unsubstituted derivatives **6***a* and **7***a*, respectively, have been used to prepare thienamycin itself, from **6***a* (3) the Δ-1 carbapenem (4) and carbapenam ring systems (5), and carbacephems[1] from **7***a*.

We would like to report a facile synthesis of **6** and **7**, both as a 1:1 mixture of stereoisomers in the 3-hydroxyethyl side chain and as samples considerably enriched in the desirable *trans-R*-isomer (thienamycin stereochemistry), starting with the readily available 4-vinyl- and 4(3′-butenyl)azetidin-2-ones, **6***a* and **7***a*, respectively, and utilizing dialkylaminomethyl groups as new, base-stable N—H protecting groups.

Discussion and results

The *tert*-butyldimethylsilyl group has previously been used as an N—H protecting group in β-lactams (6, 7). This group is stable to alkyllithiums and allows the generation of the mono-anion **8** through which a variety of substituents can be introduced at position 3 of the β-lactam ring. Most recently, Bouffard and Christensen (7) have completed a careful study of introduction of the thienamycin side chain into the 1-*tert*-butyldimethylsilyl-4-vinylazetidin-2-one, **8**. These authors reported that, under a variety of conditions, the lithium enolate of **8** reacted with acetaldehyde to give an 85:15 mixture of *trans/cis* isomers. The *trans*-isomer was obtained as an approximately 1:1 mixture of *R* and *S* side chain isomers. Considerably higher ratios of the desirable *trans-R* isomer (thienamycin isomer) could be obtained by first acylating and then reducing the 3-acyl derivative **10** with K-selectride.

Testa and co-workers (8) have reported that β-lactams react readily with secondary amines such as pyrrolidine and morpholine in the presence of 37% formaldehyde solution to afford 1-dialkylaminomethyl β-lactams. We felt that the dialkylaminomethyl group might serve as a useful and inexpensive base-stable protecting group, thereby enabling us to introduce substituents into the 3-position with the desirable *trans*-stereochemistry. The protecting group should be removable under mildly acidic conditions.

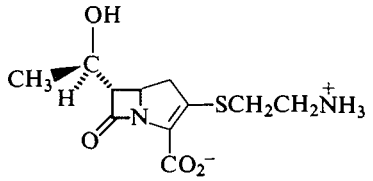

5

6 R = CH=CH$_2$ **6***a*
7 R = (CH$_2$)$_2$CH=CH$_2$ **7***a*

[1]B. Hamlet, D. Dugat, and T. Durst; unpublished observations

0008-4042/83/020411-05$01.00/0
©1983 National Research Council of Canada/Conseil national de recherches du Canada

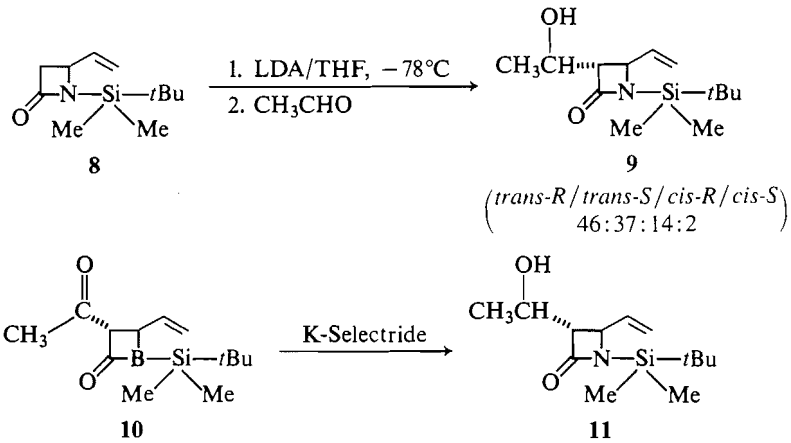

TABLE 1. Reaction of **13** and **14** with electrophiles

Reactant	Electrophile	Product (%)		Deprotection (5)	
13	CH_3CHO	[a]		**17**	(58)[b]
13	$(CH_3)_2CO$	[a]			(52)[b]
13	CH_3COEt	**19**	(63)	**21**	(72)[c]
13	PhCHO		(84)		(85)
13	Ph_2CO		(83)		(91)
13	I_2		(63)		
14	CH_3CHO	[a]			(74)
14	$(CH_3)_2CO$	[a]		**15**	(79)
14	CH_3CO_2Et	**20**	(68)	**22**	(71)[c]

[a]Not isolated.
[b]Overall yield.
[c]K-Selectride reduction and deprotection.

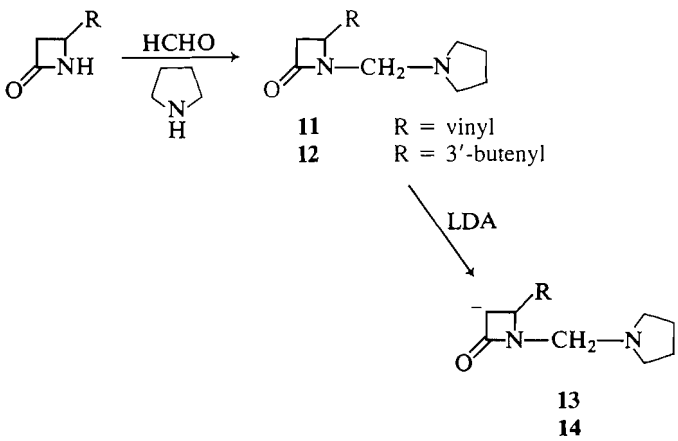

Reaction of **11** and **12**, prepared in 93 and 92% yield from 4-vinyl-, (**6***a*), and 4-(3′-butenyl)azetidin-2-one, (**7***a*), respectively, with LDA in THF at −78°C furnished, essentially instantaneously, the monanions **13** and **14**. These anions were combined with a number of electrophiles, among them acetaldehyde, acetone, ethyl acetate, benzaldehyde, benzophenone, and iodine. In each case the *trans*-3,4-disubstituted isomer was isolated as the sole product in yields varying from 63% for ethyl acetate to over 85% for benzophenone (Table 1).

In the case of the acetone adducts, we had available samples of the pure *cis*-isomers prepared by reaction of the dianion **2** (R = $CH{=}CH_2$ and R = $CH_2CH_2CH{=}CH_2$) with acetone. Thus, using nmr spectroscopy, we were able to place the upper limit of the *cis*-isomer in the reaction of **11** and **12** with acetone at less than 3%. Interestingly, the reaction of **1** (R = $CH_2CH_2CH{=}CH_2$) with acetone gave a 1:1 mixture of the *cis*- and *trans*-disubstituted isomers **15***a* and **15***b*, respectively.

The dialkylamino group, as expected, was readily removed under mildly acidic conditions such as refluxing in methanolic HCl (methanol − 1% aqueous HCl, 1:9) or 1:9 THF − 1% HCl for 4−6 h. The yields for this individual step were generally very good. In most cases, see Table 1, the initial adducts were not isolated but directly deprotected to yield the *N*-unsubstituted lactams.

The 1,3-dianion route appears to give greater amounts of the *cis*-3,4-disubstituted products than any of the monanion reactions (7, 9) and may therefore be of value in the preparation of carpetimycins, **16** (10), and derivatives. Generally the reactions of **2** show less selectivity than those of **13** and **14**, presumably due to the much higher reactivity of the dianions compared to the monanions.

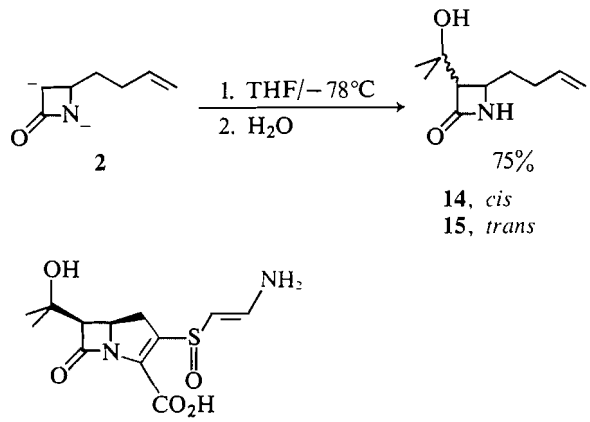

16, carpetimycin A

For the other adducts the *trans* structures were assigned on the basis of the 1.8−2.0 Hz coupling constant between the remaining H(3) and H(4) (7). In the particular case of the reaction of **11** with acetaldehyde, the absence of significant amounts of the *cis* product accompanying the desired *trans*-isomer **17** was ascertained by nmr using the reported chemical shift value of H(3) in *cis*-**18** as model. The overall yield of **17**, obtained as a 1:1 diastereomer mixture from **11**, was 58%.

Highly stereoselective reductions of the 3-acyl derivatives **19** and **20** were obtained using the K-Selectride reduction procedures of Bouffard and Christensen (7). Thus **19** and **20** gave reduction products in 72 and 71% yield, respectively, in which the isomers **21** and **22**, having the desired relative stereo-

Can. J. Chem. Downloaded from www.nrcresearchpress.com by 210.87.254.40 on 09/06/12
For personal use only.

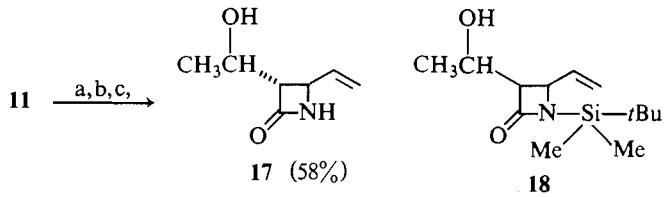

(a) LDA; (b) CH_3CHO; (c) H^+

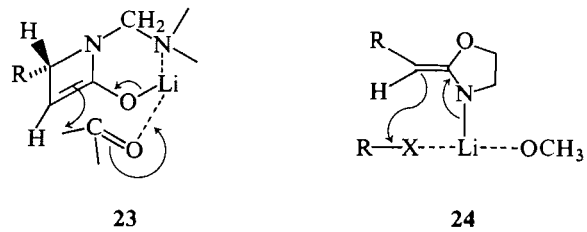

FIG. 1

chemistry of thienamycin, predominated in ratios of 4:1 and 9:1. Reduction of **19** with $NaBH_4$ in ethanol gave an isomeric mixture in which **21** represented the minor isomer (1:2 ratio).

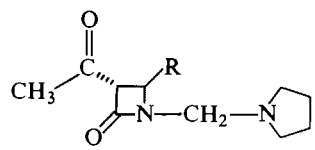

19 R = vinyl
20 R = 3′-butenyl

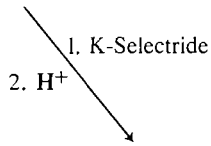

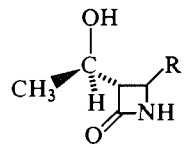

21 (4:1 diastereomer ratio)
22 (9:1 diastereomer ratio)

The higher *trans* selectivity shown in the reactions of the carbanions derived from **6** and **7** as compared with **8** is possibly related to an internal chelation invloving the pyrrolidine nitrogen (Fig. 1, **23**). Such a chelation, which should help deliver the electrophile from the same side as the chelating group, is similar to that proposed by Meyers *et al.* (11) as an explanation of the asymmetric induction observed in the alkylation of the carbanions obtained from optically active 2-alkyl-4-methoxyl-1,3-oxazolines (Fig. 1, **24**).

Experimental

Infrared spectra were recorded as films for liquids and in $CHCl_3$ solution for solids on a Unicam CP-1100 spectrophotometer. The nmr spectra were obtained using Varian HA-100 and T-60 spectrometers; peak positions are given in δ units. Melting points were taken on a Gallenkamp apparatus and are uncorrected. All reactions involving alkyl lithiums were carried out in freshly distilled anhydrous tetrahydrofuan (THF) and under N_2. Usual work-up refers to quenching the reaction with H_2O or aqueous NH_4Cl, extraction with CH_2Cl_2, drying the organic extracts over $MgSO_4$, and evaporation of the solvents under reduced pressure. For the sake of clarity the azetidin-2-one nomenclature is used through this section.

*1-Pyrrolidinomethyl-4(3′-butenyl)-azetidin-2-one, **12** (8)*

A solution of 4-(3′-butenyl)azetidin-2-one (3.0 g, 24 mmol), 2.01 mL of pyrrolidine, and 2.4 mL of 37% formaldehyde in 20 mL of ethanol was refluxed for 2 h. The solvent was evaporated and the crude yellowish oil was purified by distillation. The yield of colorless oil, bp 140–143°C/0.7 Torr, was 4.58 g (92%); ir: 1765 cm^{-1}; nmr: 1.5–2.2 (m, 8H), 2.4–2.7 (m, 5H), 3.05 (dd, J = 16, 5 Hz, 1H), 3.86 (d, J = 13.5 Hz, 1H), 4.12 (d, J = 13, 5 Hz, 1H), 4.9–6.2 (m, 3H): *Anal.* calcd. for $C_{12}H_{20}N_2O$: C 69.19, H 9.68; found: C 69.59, H 9.42.

*1-Pyrrolidinomethyl-4-vinylazetidin-2-one, **11** (8)*

Using the above procedure, 4.0 g (41 mmol) of 4-vinylazetidin-2-one, 4.1 mL of formaldehyde solution, and 3.44 g of pyrrolidine in 45 mL of ethanol afforded 6.87 g (93%) of **11** as a clear oil, bp 109–112°C/0.3 Torr; ir: 1760 cm^{-1}; nmr: 1.7–1.9 (m, 4H), 2.5–2.7 (m, 4H), 2.68 (dd, J = 16, 2 Hz, 1H), 3.23 (dd, J = 16, 5 Hz, 1H), 3.76 (d, J = 13.5 Hz, 1H), 4.14 (d, J = 13.5 Hz, 1H), 4.1 (m, 1H), 5.2–5.6 (m, 3H); *Anal.* calcd. for $C_{10}H_{16}N_2O$: C 66.23, H 8.95; found: C 66.68, H 9.25.

*Formation of lithio derivatives **13** and **14** and their reaction with electrophiles*

General procedure

Lithium diisopropylamide (LDA) was formed by addition of *n*-BuLi (2.4 *M* in hexane) to an equivalent amount of diisopropylamine in THF at −78°C. To the cold, well-stirred LDA solution (1.1 equiv.) was added 1.0 equiv. of the appropriate electrophile and the solution was kept at −78°C for an additional 10–20 min. Usual work-up gave the crude products which were purified by recrystallization on silica gel chromatography or hydrolyzed to the N–H lactams.

The hydrolysis of the 1-pyrroldinomethyl group was achieved by refluxing the protected lactams either with aqueous methanolic HCl or THF–aqueous HCl for 3 h. The hydrolyzed product was isolated by dilution with H_2O and extraction into CH_2Cl_2, drying the organic phase with $MgSO_4$, and evaporation of the solvent. Purification of the products was accomplished by recrystallization or column chromatography. Yields refer to purified materials (See also Table 1).

*Reactions of **13***

(a) *With benzophene*

To a solution containing 2.78 mmol of **13**, prepared from 500 mg of **11** in 10 mL of dry THF, was added 607 mg (3.3 mmol) of benzophenone. Work-up afforded 1.05 g of crude product which was recrystallized from ether–hexane to yield 830 mg (83%) of a white powder, mp 121–125°C.

The pyrrolidinomethyl group was removed by heating 400 mg (1.10 mmol) of the above product with 3 mL methanol and 18 mL of 1% HCl for 3 h. The crude product (280 mg) was recrystallized from ether–hexane to afford 200 mg (65%) of the *trans*-3,4-disubstituted products as fine white needles, mp 118–120°C; ir: 3450, 1760 cm^{-1}; nmr: 2.96 (O*H*), 3.98 (m, 2H), 4.8–5.8 (m, 3H), 6.1 (N*H*), 7.1–7.6 (m, 10H). *Anal.* calcd. for $C_{18}H_{17}NO_2$: C 77.40, H 6.13; found: C 77.37, H 6.12.

(b) *Benzaldehyde*

A solution of 2.8 mmol of **13** in 8 mL of dry THF was reacted with 3.3 mmol of freshly distilled benzaldehyde. Column chromatography (ethyl acetate – hexane 2:1) furnished 667 mg (85%) of a viscous oil which was hydrolyzed as above to yield 85% of a 2:1 isomeric mixture of *trans*-3,4-disubstituted product as pale yellow crystals, mp 93–98°C (CH_2Cl_2–hexane); nmr: 3.2 and 3.3 (2 dd, J = 6.0 and 2.0 Hz for each, ratio 2:1, 1H), 3.85–4.0 and 4.25–4.35 (m, 1H).

(c) *Acetone*

An excess of acetone (1.0 mL) was added to a solution of the monoanion **13** prepared from 400 mg of **11** at −78°C. Work-up gave

Can. J. Chem. Downloaded from www.nrcresearchpress.com by 210.87.254.40 on 09/06/12
For personal use only.

Can. J. Chem. Downloaded from www.nrcresearchpress.com by 210.87.254.40 on 09/06/12
For personal use only.

a crude product which was hydrolyzed by refluxing in a mixture of 5 mL THF and 25 mL of 1% HCl for 3 h. The deprotected 3,4-*trans* adduct (1) was obtained in 52% overall yield as an oil; ir: 3480, 1760 cm^{-1}; nmr: 1.23 and 1.40 (2s, 6H), 2.90 (d, J = 2 Hz, 1H), 3.4 (OH, exchangeable), 4.4–4.5 (m, 1H), 5.0–6.2 (m, 3H), 6.7 (N–H, exchangeable).

(d) *Acetaldehyde*

An excess of freshly distilled acetaldehyde (2.5 mL) was added to a stirred solution of **13** obtained from 2 g of **11** in 51 mL of THF at −78°C. This reaction sequence was continued as in the case of acetone. The crude deprotected product was purified on silica gel using 1:2 ethyl acetate – hexane. The yield of **17** was 58%; ir 3450, 1750 cm^{-1}; nmr: 1.26 and 1.32 (2d, J = 6 Hz, 3H), 2.91 (dd, J = 6, 2 Hz, 1H), 3.6 (OH, exchangeable), 4.0–4.3 (m, 2H), 2.1–6.1 (m, 3H), 6.9 (N—H, exchangeable); ms: $M^{+\cdot}$ 123 (M − H_2O). *Anal.* calcd. for $C_7H_{11}NO_2$: C 59.56, H 7.86, N 9.22; found: C 59.54, H 8.24, N 10.18.

(e) *Iodine*

trans-3-Iodo-4-vinylazetidin-2-one (1) was obtained in 63% overall yield from **11** using 500 mg **11** and 846 mg I_2. The crude initial adduct was immediately hydrolyzed in a 5 mL methanol – 25 mL 1% HCl mixture and the final product purified on column chromatography using 4:1 hexane – ethyl acetate as eluant; nmr: 4.33 (dd, J = 7, 2 Hz, 1H), 4.6 (m, H), 5.3–6.1 (m, 3H), 6.8 (NH, exchangeable).

(f) *Ethyl acetate*

Ethyl acetate (2.6 mL) was reacted with **13** prepared from 4.0 g of **11**. The crude product was purified on hplc (4:1 ethyl acetate – hexane). The 3-acetyl derivative **19** (3.10 g, 63%) thus obtained was quite labile and generally reduced immediately to the 3-hydroxyethyl derivative (see below); ir: 1760, 1712 cm^{-1}; nmr: 1.7–2.1 (m, 4H), 2.32 (s, 3H), 2.5–2.7 (m, 4H), 3.84 (d, J = 14 Hz, 1H), 4.22 (d, J = 14 Hz, 1H), 3.97 (d, J = 2 Hz, 1H), 4.54 (dd, J = 7, 2 Hz, 1H), 5.2–5.9 (m, 3H).

(*i*) *Reduction with sodium borohydride*

The 3-acetyl adduct (800 mg, 3.60 mmol) obtained above was dissolved in 25 mL of ethanol, cooled to −30°C, and reacted with 680 mg (5.2 equiv.) of sodium borohydride for 2 h. The reaction was quenched with saturated NH_4Cl solution, extracted once with 25 mL of ether and 4 times with 25 mL of CH_2Cl_2. The crude product was purified on silica gel using 2:1 ethyl acetate – hexane as eluent. Yield: 577 mg (72%); nmr: 1.26 and 1.35 (2d, J = 6 Hz, 3H), 1.7–1.9 (m, 4H), 2.5–2.8 (m, 4H), 2.93 (dd, J = 7, 2 Hz, 1H), 3.84 (d, J = 13 Hz, 1H), 4.2 (d, J = 13 Hz, 1H), 4.1–4.3 (m, 1H), 5.1–6.1 (m, 3H).

The pyrrolidino group was removed in the usual way using aqueous methanolic HCl. The yield of **17** was 60%; nmr spectroscopy indicated a 2:1 diastereomeric mixture in which the "thienamycin isomer" is disfavoured.

(*ii*) *K-Selectride reduction* (8)

To a solution of 450 mg (2.1 mmol) of 3-acyl derivative and 344 mg of KI in ether at 25°C was added 12.4 mL of K-Selectride (0.5 *M* in ether, 3 equiv.) The reaction mixture was worked up as usual to give 276 mg (60%) of reduced product. The relative intensities of the two methyl doublets indicated an approximately 4:1 diastereomer mixture favouring the "thienamycin isomer."

*Reaction of **14** with electrophiles*

(a) *Acetone*

To a solution of **14** prepared from 1.0 g of **12** in 10 mL of THF at −78°C was added 2.5 mL of reagent grade acetone. The crude adduct obtained after usual work-up was hydrolyzed in a 1:6 mixture of THF – 1% HCl to give, after purification, 694 mg (79%) of **15**. ir: 3450, 1755 cm^{-1}; nmr: 1.24 and 1.40 (2s, 6H), 1.6–2.2 (m, 4H), 2.76 (d, J = 2 Hz, 1H), 3.6 (m, 1H), 5.6–6.3 (m, 3H).

(b) *Acetaldehyde*

Compound **12** 1.86 g, 8.9 mmol) was converted in the usual way to its lithio derivative and reacted with acetaldehyde. The crude product thus obtained was immediately hydrolyzed in THF – aqueous HCl to yield, after chromatography (1:2 ethyl acetate – hexane), 1.12 g (74%) of *trans*-3(1′-hydroxyethyl)-4(3′-butenyl)azetidin-2-one as a 1:1 diastereomer mixture. Infrared: 3450, 1755 cm^{-1}; nmr: 1.27 and 1.32 (2d, J = 7 Hz, 3H), 1.64–1.85 (m, 2H), 2.0–2.4 (m, 2H), 2.81 (dd, J = 6.5, 2 Hz, 1H), 3.2 (OH, exchangeable), 3.4–4.8 (m, 1H), 3.9–4.3 (m, 1H), 5–6.1 (m, 3H), 6.7 (NH, exchangeable); ms: $M^{+\cdot}$ 151 (m − H_2O). *Anal.* calcd. for $C_9H_{15}NO_2$: C 63.88, H 8.93, N 8.28; found: C 63.63, H 9.34, N 7.92.

(c) *Ethyl acetate*

The protected lactam (5.0 g) was lithiated and acylated in the usual manner. The intermediate 3-acyl derivative **20** was purified by hplc using 4:1 ethyl acetate – hexane as eluant. Yield 4.37 g (73%); ir: 1744, 1715 cm^{-1}; nmr: 1.7–2.2 (m, 8H), 2.33 (s, 3H), 2.5–2.7 (m, 4H), 3.93 (d, J = 2Hz, 1H), 3.77 (d, J = 13.5 Hz, 1H), 4.27 (d, J = 13.5 Hz, 1H), 4.1 (m, 1H), 4.9–6.2 (m, 3H):

(*i*) *Reduction of **20** with sodium borohydride*

Acyl derivative **20** (750 mg, 3 mmol), was reduced with $NaBH_4$ (57 mg) in ethanol at −30°C for 2 hours. Work-up as in the case of **19** afforded 530 mg (71%) of the 3-hydroxyethyl derivative as a 1:2 diastereomer mixture (see also below). Hydrolysis in aqueous methanolic HCl gave **22** in 68% yield.

(*ii*) *K-Selectride reduction*

The 3-acyl lactam (4.6 g, 18.4 mmol) was reduced with 3 equivalents of K-Selectride as described for compound **19**. Purification of the crude product by chromatography on silica gel afforded 3.0 g (65%) of protected **22**; nmr: 1.26 (d, J = 6 Hz, only a single doublet could be seen), 1.6–2.13 (m, 8H), 2.76 (dd, J = 7, 2 Hz, 1H), 3.0 (OH, exchangeable), 3.76 (d, J = 13 Hz, 1H), 4.10 (J = 13 Hz, 1H), 3.6–4.2 (m, 2H), 4.8–6.1 (m, 3H).

Hydrolysis in refluxing aqueous HCl–methanol (6:1) afforded **22** essentially as a single diastereomer since only the δ 1.27 methyl doublet remained. The major isomer in the K-Selectride reaction has the same relative stereochemistry as thienamycin and is opposite to that obtained upon $NaBH_4$ reduction.

Reaction of 1,3-dilithio-4(3′-butenyl)azetidin-2-one with acetone

n-BuLi (8.0 mL, 2.0 *M* in hexane) was slowly added to a solution of 1.0 g of 4-vinylazetidin-2-one dissolved in THF at 0°C. After 30 min, the dark solution was quenched with excess acetone (2.5 mL). Usual work-up, followed by filtration through a short silica gel column, afforded 1.09 g (75%) of a 1:1 *cis*/*trans* diastereomer mixture. More careful chromatography gave a separation of the isomers. The *cis*-isomer was obtained as colorless crystals, mp 118–120°C. For the *cis*-isomer, ir: 1755, 3450 cm^{-1}; nmr: 1.35 and 1.46 (2s, 6H), 1.8–2.3 (m, 4H), 3.25 (d, J = 6 Hz, 1H), 3.6–3.9 (m, 1H), 4.9–6.0 (m, 3H). For the *trans*-isomer, ir: 3450, 1755 cm^{-1}; nmr: 1.24 and 1.40 (2s, 6H), 1.6–2.2 (m, 4H), 2.76 (d, J = 2 Hz, 1H), 3.6 (m, 1H), 5.0–6.3 (m, 3H). *Anal.* (for *cis*.) calcd. for $C_{10}H_{17}NO_2$: C 65.65, H 9.35, N 7.64; found: C 65.43, H 9.40, N 7.59.

Acknowledgement

Continued support by NSERC is gratefully acknowledged.

1. T. DURST, R. VAN DEN ELZEN, and R. LEGAULT. Can. J. Chem. **52**, 3206 (1974).
2. G. ALBERS-SCHÖNBERG, B. H. ARISON, O. D. HENSENS, J. HIRSCHFIELD, K. HOOGSTEEN, E. A. KACZKA, R. E. RHODES, J. S. KAHAN, M. F. KAHAN, R. W. RATCLIFFE, E. WALTON, L. J. RUSWINKLE, R. B. MORIN, and B. G. CHRISTENSEN. J. Am. Chem. Soc. **100**, 6491 (1978).
3. B. G. CHRISTENSEN, D. B. JOHNSTON, W. RANDOLPH, and S. M. SCHMITT. German Patent No. 2,751,596.
4. (*a*) B. VENUGOPALAN, A. B. HAMLET, and T. DURST. Tetrahedron Lett. **22**, 191 (1980); (*b*) R. SHARMA and R. STOODLEY. Tetrahedron Lett. **22**, 2025 (1981); (*c*) K. HIRAI, K. FUJIMOTO, Y. IWANO, T. HIRAOKA, T. HATA, and C. TAMURA. Tetrahedron Lett. **22**, 1021, 1981.
5. T. AIDA, D. DUGAT, R. LEGAULT, and T. DURST. Tetrahedron Lett. 4993 (1979).

6. R. W. RATCLIFFE, T. N. SALZMAN, and B. G. CHRISTENSEN. Tetrahedron Lett. **21**, 31 (1980).
7. F. A. BOUFFARD and B. G. CHRISTENSEN. J. Org. Chem. **46**, 2208 (1981).
8. C. CIGNARELLI, G. E. CRISTIANI, and E. TESTA. Ann. **661**, 181 (1963).
9. T. DURST and M. J. LEBELLE. Can. J. Chem. **50**, 3196 (1972).
10. M. NAKAYAMA, S. KIMURA, S. TANABE, T. MIZOGUCHI, I. WATANABE, T. MORI, K. MIYAHARA, and T. KAWASAKI. J. Antibiot. **34**, 818 (1981).
11. A. I. MEYERS, G. KNAUS, K. KAMATA, and M. E. FORD. J. Am. Chem. Soc. **98**, 567 (1976).

Can. J. Chem. Downloaded from www.nrcresearchpress.com by 210.87.254.40 on 09/06/12
For personal use only.

Fractionation of lignosulphonates released during the early stages of delignification

NORMAN G. LEWIS, DAVID A. I. GORING, AND ALFRED WONG
Pulp and Paper Research Institute of Canada, 570 St. John's Boulevard, Pointe Claire, P.Q., Canada H9R 5J9

Received August 3, 1982

NORMAN G. LEWIS, DAVID A. I. GORING, and ALFRED WONG. Can. J. Chem. **61**, 416 (1983).

High-yield spent bisulphite liquor (HY-SBL) from sulphonated black spruce wood (*Picea mariana*) was fractionated by gel permeation chromatography (GPC) and by high-performance liquid chromatography (HPLC). The GPC fractionation gave a wide bimodal distribution, whereas with HPLC, a more detailed resolution was seen with the bulk of the fraction giving several clearly defined peaks. The paucidisperse material was further concentrated by a bulk fractionation of the crude SBL which included complexing the lignosulphonates with dicyclohexylamine. The isolated paucidisperse material was found to be dialyzable and to constitute 90% of the lignosulphonate in the sample of SBL. If the bisulphite pulp obtained was recooked in fresh acid sulphite liquor to a lower yield, most of the lignosulphonate dissolved was widely polydisperse with no indication of the discrete components resolvable by HPLC. However, 25% of the lignin made soluble was in the form of the paucidisperse fractions. In all, we were able to obtain about 50% of the lignin in spruce wood as a relatively low molecular weight lignosulphonate resolvable into discrete fractions by HPLC.

NORMAN G. LEWIS, DAVID A. I. GORING et ALFRED WONG. Can. J. Chem. **61**, 416 (1983).

De la lessive résiduaire au bisulfite à haut rendement (LRB–HR) de bois d'épinette noire sulfoné (*Picea mariana*) a été fractionée par chromatographie de perméation en gel (CPG) et par chromatographie liquide à haute résolution (CLHR). Le fractionnement CPG a donné une large distribution bimodale, tandis que la CLHR a permis une résolution plus détaillée du matériel dont la principale fraction a été scindée en plusieurs pics bien distincts. Le matériel paucidispersé a été concentré ultérieurement au moyen d'un fractionnement grossier de la LRB d'origine comprenant la formation d'un complexe entre les lignosulfonates dans l'échantillon de LRB. Si la pâte au bisulfite obtenue subissait une nouvelle cuisson dans une lessive fraiche de bisulfite acide jusqu'à un rendement plus faible, la majeure partie des lignosulfonates dissous étaient polydispersés et la plupart des constituants ne semblaient pas séparés par CLHR. Cependant, 25% de la lignine rendue soluble l'était sous la forme de fractions polydispersées. Nous avons pu obtenir environ 50% de la lignine du bois d'epinette sous la forme de lignosulfonates de poids moléculaire relativement bas et pouvant être fractionnés par CLHP.

Introduction

Lignin removal by sulphonation under acidic conditions has been studied for many wood species. Unfortunately, despite numerous investigations, detailed chemical characterisation of these soluble, sulphonated lignin (or lignin-derived) materials have achieved only limited success. For example, an in-depth study of the lignosulphonates obtained from an acid sulphite treatment of the angiosperm, wattle wood (*Acacia mearnsii*) resulted in the isolation and identification of only six sulphonated compounds which were structurally related to sinapyl alcohol (1). Similar studies with the gymnosperms, western hemlock (*Tsuga heterophylla*), and white fir (*Abies lasiocarpa*) afforded materials presumably derived from coniferyl alcohol (2). However, in both studies, these identified components only constituted 1–2% of the original lignin content of the wood.

Previous attempts to fractionate the bulk of the lignosulphonic acids have been based largely upon separations according to molecular size differences by gel permeation chromatography (GPC). For these applications, however, poor resolution constitutes a severe disadvantage, as evidenced, for example, by the incomplete separation of a mixture reported to contain an homologous series of lignosulphonic acids (3). In a similar study, it was estimated that as much as 17% of the lignosulphonate obtained from mixed softwood species, existed as either discrete substances or groups of substances (4, 5). However, in more recent studies, lignosulphonates obtained by the partial delignification of western hemlock were compared with corresponding material derived from milled wood lignin (MWL) (6–8). GPC fractionation, as before, suffered from poor resolution of the lignin-derived components. Indeed, further fractionation and refractionation of such lignosulphonates, as their acetylated lignosulphonic methyl esters, led these authors to conclude that these materials were either in equilibrium with one another (7) or were unstable to further manipulations (8). It is apparent, therefore, that since limited chromatographic resolution has been achieved in previous work, there is a necessity for a rapid and reliable fractionating technique with enhanced resolution.

Experimental

GPC conditions are described in Fig. 1. Sephadex G-50F was obtained from Pharmacia Fine Chemicals. A peristaltic pump (Pharmacia P-1) was used to ensure flow stability.

HPLC analyses were carried out using a Hewlett-Packard liquid chromatograph, model HP 1084B, equipped with a variable wavelength detector set at 280 nm. Columns used were protein I-250, I-125, and I-60 purchased from Waters Associates. All analyses were carried out at pH = 3.0. Samples were adjusted to this pH by addition of 1.0 *M* citric acid or 1.0 *M* disodium hydrogen phosphate, as required.

All solvents (and dicyclohexylamine) were redistilled prior to use. The silica gel used was obtained from Merck, graded Keiselgel 60, 70–230 mesh ASTM.

All uv analyses were carried out using a Pye Unicam SP 8000 instrument. Samples were dissolved in buffer solution (pH = 7.8, 0.1 *M* KH_2PO_4/Na_2HPO_4).

Experiment 1. Preparation of pulp and HY-SBL

Spruce wood chips (2 kg, dry weight, Klason lignin content: 26.8 g/100 g) were steam pretreated (pressure = 138 kPa, 3 min, 3 cycles) in a 20 L batch digester. The wood was then exposed to a sodium-based bisulphite solution (10 L; total SO_2: 2.7%; free SO_2: 1.38%; pH = 3.0). Pulping conditions were as follows: (*i*) temperature raised

0008-4042/83/020416-05$01.00/0
©1983 National Research Council of Canada/Conseil national de recherches du Canada

Can. J. Chem. Downloaded from www.nrcresearchpress.com by 210.87.254.5 on 09/06/12
For personal use only.

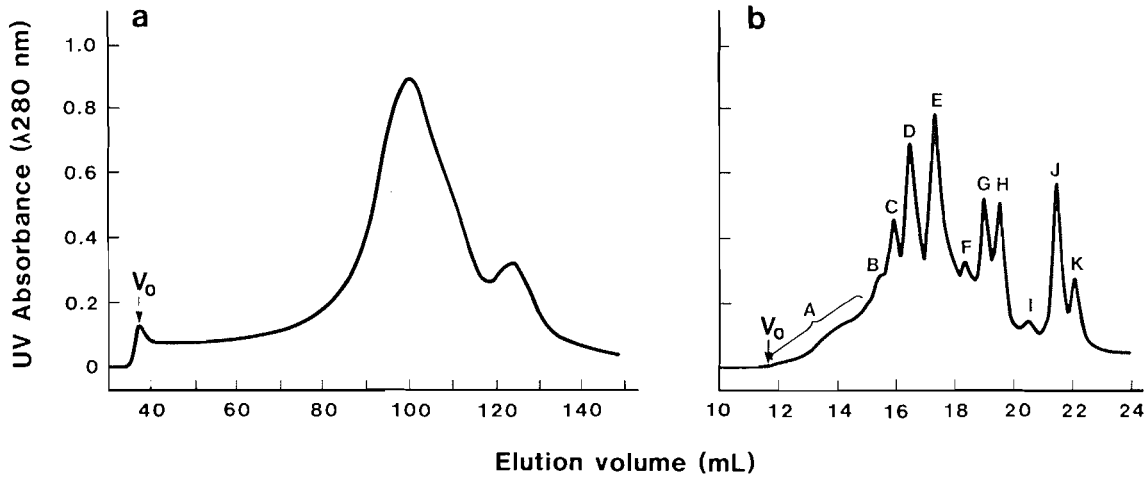

FIG. 1. Chromatograms of dissolved uv-absorbing materials present in an HY-SBL from spruce wood by (*a*) GPC and (*b*) HPLC. (*a*) Sephadex G-50F (10 g) in a glass column (dimensions 65 × 1.5 cm i.d.) and eluted with 0.2 mol/L Li_2SO_4. Flow 1 mL/min. (*b*) Waters I-125 and I-60 protein columns in series and eluted with 50 m*M* citric acid/Na_2HPO_4 buffer, pH 3.0. Flow = 1 mL/min. V_0 = void volume.

from 20°C to 85°C in 10 min, then held for 30 min at 85°C, with maximum pressure = 41.4 kPa and (*ii*) temperature raised from 85°C to 155°C in 120 min and held for 160 min at 155°C with maximum pressure = 483 kPa.

The resulting pulp (1.52 kg dry weight; 76.3% yield, with a Klason lignin content = 22.8 g/100 g pulp) was then removed by filtration to recover the SBL (12 L, solids content = 5.68 g/100 g).

Experiment 2. Fractionation of uv-absorbing materials from SBL

Spent bisulphite liquor (450 mL, pH = 3.0) isolated from Experiment 1 was concentrated down to 116 mL at 35°C under reduced pressure. The concentrate was adjusted to pH = 2.0 with 3.48 *M* sulphuric acid (5.4 mL) and then extracted with *n*-BuOH (2 × 100 mL). The *n*-BuOH solubles were backwashed with water (2 × 50 mL) which was then added to the aqueous solubles. The *n*-BuOH solubles were then evaporated down to dryness to yield extract I (0.766 g, ϵ_{280} = 9.4 L cm^{-1} g^{-1}) in Table 1.

The aqueous phase was further treated as follows. (*i*) 3.48 *M* sulphuric acid (5.4 mL) added and the system then extracted with *n*-BuOH (200 mL) containing dicyclohexylamine (10 mL). (*ii*) The resulting aqueous phase was reacidified and extracted as described in (*i*) and then further extracted with *n*-BuOH (1 × 100 mL). Steps (*i*) and (*ii*) were then repeated with the aqueous phase (3×).

The *n*-BuOH solubles from the dicyclohexylamine extractions were combined and reduced in volume by azeotroping with water to about 50 mL (35°C, reduced pressure), and then dissolved in chloroform–methanol (50 mL, 1:1 v/v). These solubles were rapidly chromatographed on silica gel (200 g, 70–230 mesh) by eluting the column with chloroform–methanol (800 mL, 1:1 v/v). Removal of the solvents afforded the yellowish-white foam, Extract II (29.9 g).

The aqueous solubles remaining, following the *n*-BuOH/dicyclohexylamine extractions, were adjusted to pH = 7.0 (with 1.0 *M* sodium hydroxide), then extracted with diethyl ether, concentrated under reduced pressure, and freeze-dried to give the white solid, Extract IV (18.8 g) in Table 1.

TABLE 1. Relative distribution of uv-absorbing materials following extraction as shown in Fig. 3

Sample	% uv absorbance*
Crude HY-SBL	100
Extract I	8.10
Extract III	73.00
Extract IV	15.00
%Recovery	96.10

*λ = 280 nm.

Experiment 3. Release of uv-absorbing material complexed with dicyclohexylamine

Extract II (100 mg) from Experiment 2 was dissolved in chloroform–methanol (30 mL, 2:1 v/v) and then extracted with 0.1 *M* sodium hydroxide (3 × 10 mL). The sodium hydroxide solubles were combined and backwashed with diethyl ether (2 × 25 mL) and then neutralized with 1.0 *M* sulphuric acid to give Extract III in Table 1. (N.B. for GPC studies, extract II was extracted with 0.1 *M* lithium hydroxide.)

Experiment 4. Dialysis of aqueous solubles (Extract IV)

The freeze-dried material (18.6 g) from Experiment 2 (Extract IV) was dissolved in water (180 mL), placed in an Amicon ultrafiltration unit (Model TCF 10) containing a membrane (De Danske Sukkerfabrikker FS60PP, nominal molecular weight cut-off of 30 000) and dialysed as follows: (*i*) water, 200 mL; (*ii*) 50 m*M* citric acid/disodium hydrogen phosphate buffer, pH = 3.0, 250 mL; and (*iii*) water, 500 mL.

The solution was then reduced in volume (to ca. 50 mL), removed from the apparatus, adjusted to pH = 7.0 with 0.1 *M* sodium hydrox-

TABLE 2. Effect of acid sulphite treatment on HYB pulp

Exp. 5	Reaction time at maximum temperature (h)	Pulp yield (% wt. of bisulphite pulp)	κ	Sulphur content of pulp (% wt.)
i	3	47.0	42.0	0.51
ii	6	41.0	15.6	0.23
iii	9	38.8	9.9	0.17

Can. J. Chem. Downloaded from www.nrcresearchpress.com by 210.87.254.5 on 09/06/12
For personal use only.

TABLE 3. Properties of polydisperse, non-dialysable lignosulphonates released from HYB pulp

Exp. 6	Weight of concentrate (g)	Uv absorption (at λ = 280 nm* and as % of SSL obtained)	ϵ_{280} (L cm^{-1} g^{-1})
i	2.16	78.4	12.4
ii	2.17	73.4	14.1
iii	2.22	70.6	13.8

*Corrected for excess SO_2 in liquor.

ide (4.08 mL), and freeze-dried to give a white solid (1.55 g, ϵ_{280} = 4.6 L cm^{-1} g^{-1}) which contained 74.3% of the original uv absorbance in Extract IV.

Experiment 5. Resulphonation of HYB pulp

(*i*) Moist bisulphite pulp (30 g, moisture content 61.1%) from Experiment 1 was taken and placed in pH = 2.0 acid sulphite solution (200 mL, 1% Na^+, 6% SO_2) in a stainless steel bomb (250 mL). The temperature was then raised to 130°C in 45 min, held at this temperature for 3 h, and then cooled rapidly. The pulp was then filtered and washed copiously with distilled H_2O to remove any solubles.

This experiment was repeated as described above except for the time of reaction. The results are given in Table 2.

Experiment 6. Dialysis of SSL from resulphonation of a bisulphite pulp

The SSL sample from Experiment 5 (*i*) was dialysed (see Experiment 4 for apparatus used) as follows: (*a*) 385 mL were concentrated to 100 mL at pH = 2.0 and then (*b*) dialysed with water (1000 mL). The concentrate was removed and adjusted to pH = 7.0 with 0.1 *M* sodium hydroxide (10.5 mL) and freeze-dried. This procedure was also adopted for the SSL samples from Experiments 5 (*ii*) and (*iii*). The results are given in Table 3.

Results and discussion

As can be seen from Fig. 1, an HPLC technique, which is designed primarily for protein separations, provided a considerable improvement in the resolution of the components present in a sample of crude, high yield spent bisulphite liquor (HY-SBL) obtained from the pulping of black spruce (*Picea mariana*) when compared to standard gel permeation chromatography.

During the HPLC separation, specific fractions were collected every 15 s and then re-analysed under the same operating conditions. Selected ones are shown in Fig. 2. Fractions obtained during the elution of A (Fig. 1*b*) showed narrow single peaks as evidenced by the representative fraction A_2 (Fig. 2*a*). However, these fractions displayed only polydisperse behaviour since no discernible resolution into individual components occurred. All subsequent fractions collected, however, showed single peaks (for example, E, shown in Fig. 2*b*). In cases where an overlap of components occurred at the point of collection, multiple peaks indicative of mixtures were clearly evident. This is shown in Fig. 2*c* by a fraction that contained both C and D components. Note also that if the 50 individual chromatograms obtained for the re-analysis were combined, an exact facsimile to the chromatogram in Fig. 1*b* would be realised.

We also found that the paucidisperse material (i.e., components B to J in Fig. 1*b*) could be removed from the crude SBL by dialysis using an ultrafiltration membrane with a nominal molecular weight cut-off of 30 000. This suggests that the components of interest have a lower molecular weight than this cut-off value.

It is important to note that the HPLC separation described above may not be due simply to size separation since the columns used possess some ionic and reverse phase characteristics.[1] Thus, if the buffer solution was replaced by water, ionic repulsion would occur resulting in material being eluted at the void (i.e., exclusion) volume, V_0. Buffer concentrations and pH affect the separation and elution volume. For the present work, we chose the conditions given in the Experimental section which are judged to be optimum.

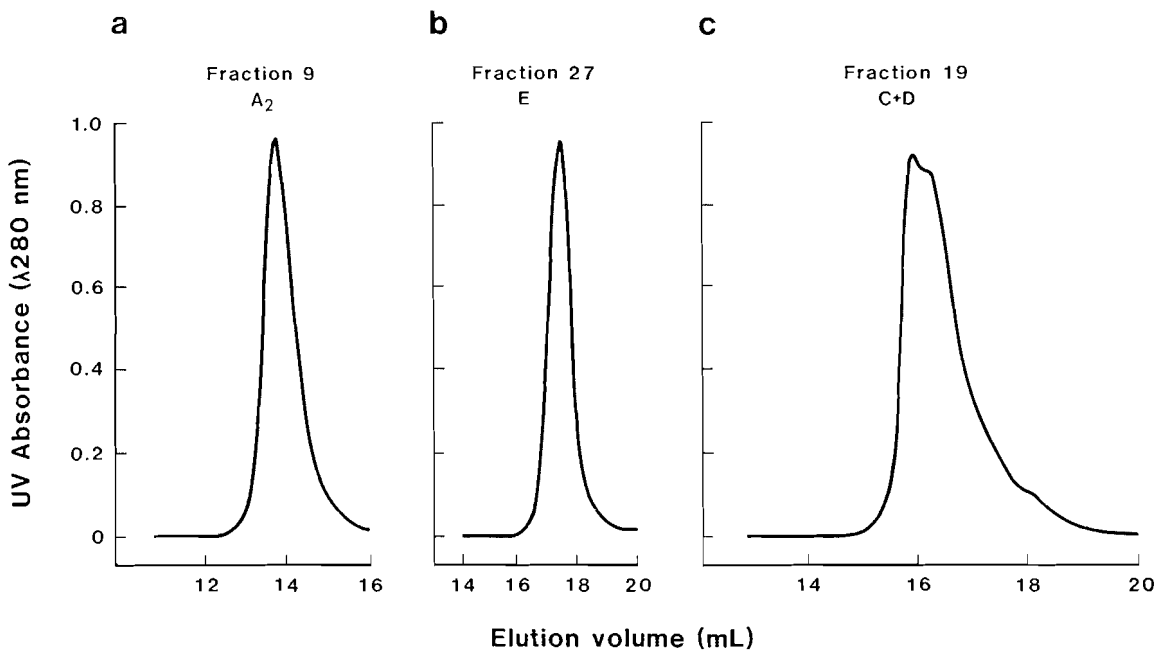

FIG. 2. Selected chromatograms of HPLC fractionated HY-SBL from spruce wood.

[1]A. H. Heckendorf. Private communication.

Can. J. Chem. Downloaded from www.nrcresearchpress.com by 210.87.254.5 on 09/06/12
For personal use only.

Can. J. Chem. Downloaded from www.nrcresearchpress.com by 210.87.254.5 on 09/06/12
For personal use only.

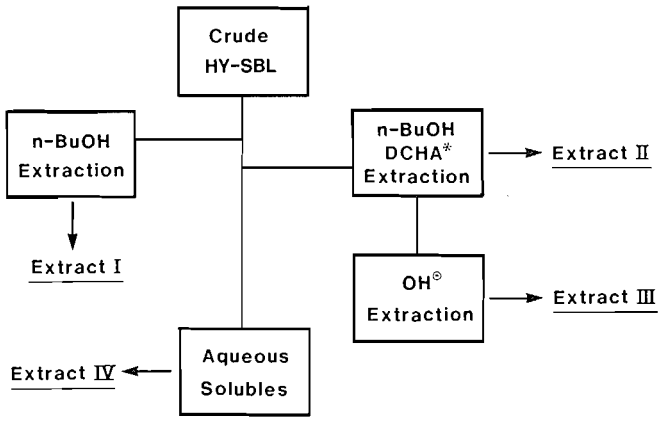

FIG. 3. Extractive fractionation of HY-SBL.
*DCHA = dicyclohexylamine.

Separations of the type shown in Fig. 1 were amenable only to sub-milligram quantities. We undertook, therefore, a bulk fractionation in order to remove both the high and the very low molecular weight material and, thus, to enrich the preparation with the discrete components shown in Fig. 1*b*. The procedure used is shown in Fig. 3 and the proportion of uv-absorbing substances in the various fractions is given in Table 1. About 8% of the uv-absorbing substances were removed (Extract I, Fig. 3) by the initial extraction with *n*-butanol (*n*-BuOH) and they probably consisted mostly of monomeric lignosulphonates (9). The lignosulphonic acids in the aqueous fraction were then complexed with dicyclohexylamine and the complex extracted with *n*-BuOH (10). As can be seen from Table 1, this fraction (Extract III) contained most of the uv-absorbing materials (ca. 75%). Treatment of this complex with sodium hydroxide (see Experimental section) released the lignosulphonates into the aqueous phase and the amine was subsequently removed by extraction with diethyl ether. After pH adjustment, Extract III was analysed by HPLC and GPC (see Fig. 4). It is immediately obvious that on comparison with the original crude SBL (see Fig. 1), considerable simplification of the chromatogram has occurred. Fractions A and K were no longer present.

Following the extraction procedure as described, the residual aqueous solution (Extract IV, Fig. 3) was found to contain mainly higher molecular weight material as evidenced by GPC and HPLC (see Fig. 5). Note that more suitable HPLC columns were used for this molecular size range. If the paucidisperse fractions were removed by dialysis (see Experimental section), the non-dialysable moiety was found to consist almost entirely of polydisperse material solubilised during delignification (Fig. 5*c*). This material has a low extinction coefficient (ϵ_{280} = 4.6 L cm^{-1} g^{-1}); this difference is probably due to the presence of non-dialysable polysaccharides (11).

It was also of interest to establish whether any additional paucidisperse material could be released by recooking the previously cooked fibres in acid sulphite liquor over different time periods (see Experiments 5, 6). About 75% of the material isolated from the low-yield spent sulphite liquor (LY-SSL) after recooking was polydisperse (see Table 3). However, the paucidisperse components removed by dialysis again showed some resolution by HPLC of the type shown in Figs. 1*b* and 4*b*.

It is quite evident that the HPLC method has given a greatly improved fractionation when compared to conventional Sephadex GPC. We believe this fractionation to be genuine since (*i*) the pattern persists before and after complexing with dicyclohexylamine and (*ii*) the components responsible for the peaks are isolable and reproducible upon further fractionation. It is our opinion that if the chromatograms of all the lignosulphonate extracts obtained by the bisulphite and sulphite treatment as described are taken into account, then approximately 50% of the lignin in spruce wood after sulphonation is isolable in paucidisperse form. It is interesting to note that this finding was anticipated by work published in 1964 (11). Lignosulphonates formed at various stages of delignification (0–95% removal) were isolated, almost immediately upon dissolution from spruce wood, by means of a continuous flow acid sulphite process. About 35% of the lignin sulphonates made soluble were removable by dialysis through a cellophane membrane. Resulphonation of high molecular weight non-dialysable lignosulphonates, whilst causing a net decrease in molecular weight, did not provide any appreciable quantities of dialysable material. This behaviour is in accord with our present recooking experiments.

The results of our present work support the view (11) that there are at least two broad classes of lignosulphonic acids produced on sulphite pulping of spruce wood, as depicted in Table 4. Type I lignosulphonates consist of dialysable material

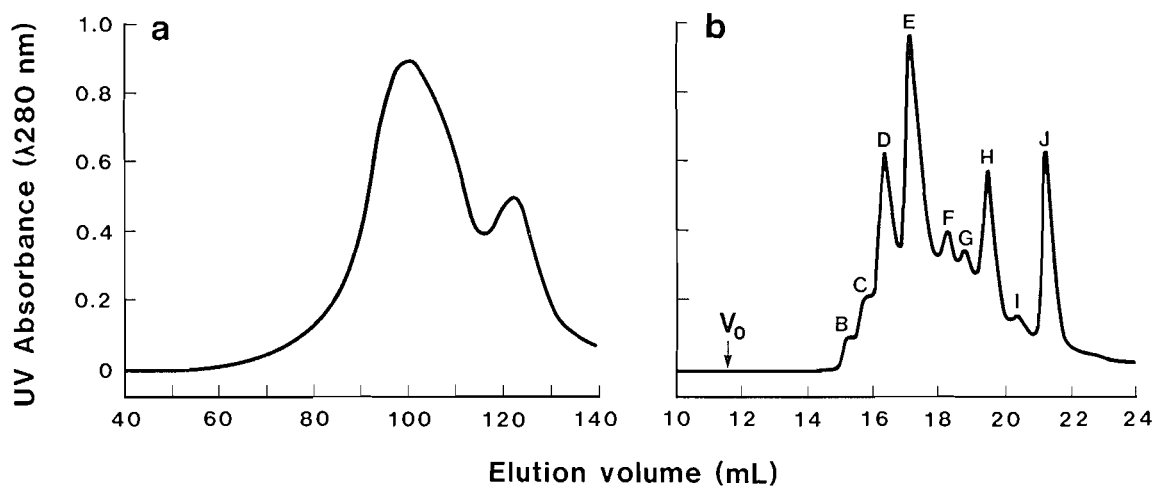

FIG. 4. Chromatograms of uv-absorbing material obtained by hydroxide treatment of lignosulphonate–DCHA complex. (*a*) GPC and (*b*) HPLC (see Fig. 1 for chromatographic conditions).

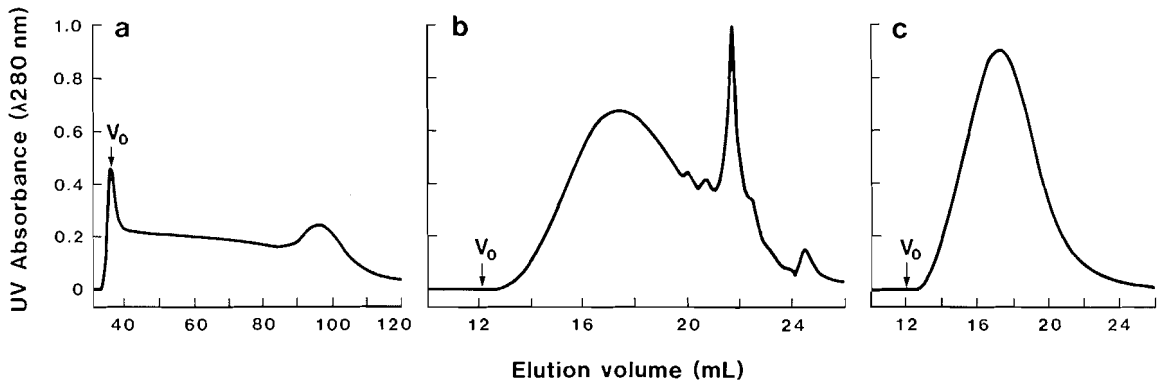

FIG. 5. Chromatograms of uv-absorbing residuals in aqueous solution following extraction with *n*-BuOH/DCHA. (*a*) GPC, (*b*) HPLC, and (*c*) non-dialysable components from (*b*). Chromatographic conditions are as for Fig. 1 except that for (*b*) and (*c*) columns used were Waters I-250 and I-125 in series.

TABLE 4. Polydispersity of lignosulphonates present in spent sulphite liquors from spruce wood

Lignosulphonic acid	Molecular size differences	Polydispersity	Percentage in HY-SBL*	Percentage in LY-SSL†
Type I	Dialysable	Paucidisperse	90	25
Type II	Non-dialysable	Widely polydisperse	10	75

*% Lignin removed = 36%.
†Remaining lignin removed on recooking = 64%.

whose average molecular weight is presumably higher than that of a simple sulphonated coniferyl alcohol derivative. Type II lignosulphonate is widely polydisperse, non-dialysable, and has a high average molecular weight, as would be expected from earlier studies (11).

The parallel between our Type I lignosulphonates and the hemilignin of Forss and Fremer (3) is apparent.

Many questions remain and are currently being addressed. For example: (*1*) Are the Type I lignosulphonates composed of isolable, individual molecular entities? If so, what are the detailed chemical structures of these components? (*2*) Is the random three-dimensional infinite polymeric network model for lignin (12–18) compatible with the observable paucidispersity of the Type I lignosulphonates? (*3*) Are Type I or Type II lignosulphonates associated with any particular morphological region in the wood? (*4*) Are Type II lignosulphonates produced by polymerisation of the protolignin during the sulphonation? This possibility cannot be entirely eliminated since it has been shown that SBL from spruce wood can be induced, by further thermal treatment, to undergo polymerisation to yield higher molecular weight material (19). (*5*) Can we produce a higher proportion of Type I material by altering the conditions of delignification?

More efficient use of the soluble lignins from high yield pulping processes may be facilitated by finding the answers to such questions.

1. (*a*) J. R. PARRISH. J. Chem. Soc. C, 1145 (1967); (*b*) J. R. PARRISH. Tetrahedron Lett. **11**, 555 (1964).
2. (*a*) V. F. FELICETTA, D. GLENNIE, and J. L. MCCARTHY. TAPPI, **50**(4), 170 (1967); (*b*) M. G. ANDRUS, D. GLENNIE, C. LUDWIG, J. L. MCCARTHY, and S. W. SCHUBERT. TAPPI, **50**(4), 186 (1967) and references therein.
3. K. FORSS and K. E. FREMER. Pap. Puu. (**8**), 443 (1965).
4. P. R. GUPTA and J. L. MCCARTHY. Macromolecules, **1**(6), 495 (1968).
5. P. R. GUPTA and J. L. MCCARTHY. Macromolecules, **1**(6), 236 (1968).
6. J. J. COLLINS, K. FORSS, W. G. GLASSER, J. S. GRATZL, and J. L. MCCARTHY. TAPPI, **55**(9), 1329 (1972).
7. J. J. COLLINS, B. F. HRUTFIORD, L. N. JOHANSON, K. FORSS, W. G. GLASSER, J. S. GRATZL, and J. L. MCCARTHY. Environmental Protection Agency Report No. EPA-660/2-74-069. June 1974.
8. J. J. COLLINS, K. FORSS, W. G. GLASSER, J. S. GRATZL, and J. L. MCCARTHY. Macromolecules, **8**(5), 565 (1975).
9. J. L. MCCARTHY and S. W. SCHUBERT. TAPPI, **50**(4), 202 (1967).
10. J. BOTTGER, T. KRAUSE, and J. SCHURZ. Papier, **7**, 305 (1975).
11. D. A. I. GORING and W. Q. YEAN. Pulp Pap. Can. **65**, T127 (1964).
12. E. NOKIHARA, M. J. TUTTLE, V. F. FELICETTA, and J. L. MCCARTHY. J. Am. Chem. Soc. **79**, 4495 (1957).
13. D. A. I. GORING, A. R. PROCTER, and W. Q. YEAN. Pulp Pap. Can. **68**, T445 (1967).
14. D. A. I. GORING and A. SZABO. TAPPI, **51**(10), 440 (1968).
15. H. I. BOLKER and H. S. BRENNER. Science, **170**, 173 (1970).
16. (*a*) D. C. JOHNSON and J. F. YAN. J. Appl. Polym. Sci. **26**, 1623 (1981); (*b*) J. F. YAN. Macromolecules, **14**, 1438 (1981).
17. D. A. I. GORING. Polymer properties of lignin and lignin derivatives from lignins. *Edited by* K. V. Sarkanen and C. H. Ludwig. J. Wiley and Sons Ltd., New York. 1971. pp. 695–768.
18. D. A. I. GORING. Am. Chem. Soc. Symp. Ser. **48**, 273 (1977).
19. B. DIX and E. ROFFAEL. Holzforschung, **35**(4), 189 (1981).

Can. J. Chem. Downloaded from www.nrcresearchpress.com by 210.87.254.5 on 09/06/12
For personal use only.

The iodo-Tamoxifens: molecular structures and syntheses of estrogens for external imaging of carcinoma

DUNCAN H. HUNTER,[1] NICHOLAS C. PAYNE,[1] ASADUR RAHMAN, JOHN F. RICHARDSON, and YOLANDA ZEA PONCE
Department of Chemistry, University of Western Ontario, London, Ont., Canada N6A 5B7

Received July 26, 1982

DUNCAN H. HUNTER, NICHOLAS C. PAYNE, ASADUR RAHMAN, JOHN F. RICHARDSON, and YOLANDA ZEA PONCE. Can. J. Chem. **61**, 421 (1983).

The *E*- and *Z*-isomers of an iodo-Tamoxifen **1** (1-(*p*-(β-dimethylaminoethoxy)phenyl)-2-(*p*-iodophenyl)-1-phenyl-1-butenes) have been prepared from the corresponding *E*- and *Z*-amino-Tamoxifens **2** (2-(*p*-aminophenyl)-1-(*p*-(β-dimethylaminoethoxy)phenyl)-1-phenyl-1-butenes) and the molecular structures have been determined from three dimensional X-ray data. Crystals of *E*-**1** are triclinic, space group $P\bar{1}$, with $Z = 2$ in a cell of dimensions $a = 10.714(2)$, $b = 14.125(3)$, $c = 8.240(2)$ Å, $\alpha = 95.78(1)$, $\beta = 92.91(1)$, and $\gamma = 71.41(1)°$; those of *Z*-**1** are monoclinic, space group $P2_1/n$, with $Z = 4$ and cell dimensions $a = 12.675(2)$, $b = 19.553(3)$, $c = 9.483(1)$ Å, and $\beta = 92.22(1)°$. Intensity data collected on an automated four circle diffractometer were used for full-matrix least-squares refinement on *F*, which converged for *E*-**1** at $R = 0.054$, 2736 observations, and for *Z*-**1** at $R = 0.042$, 3644 observations. The solution of these structures determines the configuration of these isomers as well as the respective amino precursors and allows an unambiguous assignment of the proton nmr spectra of **1**, **2** and the Tamoxifens.

DUNCAN H. HUNTER, NICHOLAS C. PAYNE, ASADUR RAHMAN, JOHN F. RICHARDSON et YOLANDA ZEA PONCE. Can. J. Chem. **61**, 421 (1983).

On a préparé les isomères *E* et *Z* des iodo-Tamoxifènes (**1**), (*p*-(β-diméthylaminoéthoxy)phényl)-1 (*p*-iodophényl)-2 phényl-1 butènes-1, à partir des amino-Tamoxifènes *E* et *Z* correspondants (**2**), (*p*-aminophényl)-2 (*p*-(β-diméthylaminoéthoxy)phényl)-1 phényl-1 butènes-1 et on a déterminé les structures moléculaires à partir des données tridimensionnelles fournies par les rayons-X. Les cristaux du composé **1**-(*E*) sont tricliniques et appartiennent au groupe d'espace $P\bar{1}$ avec $Z = 2$ et des dimensions de maille de $a = 10{,}714(2)$, $b = 14{,}125(3)$, $c = 8{,}249(2)$ Å, $\alpha = 95{,}78(1)$, $\beta = 92{,}91(1)$ et $\gamma = 71{,}41(1)°$. Les cristaux du composé **1**(*Z*) sont monocliniques et appartiennent au groupe d'espace $P2_1/n$ avec $a = 12{,}675(2)$, $b = 19{,}553(3)$, $c = 9{,}483(1)$ Å, $\beta = 92{,}22(1)°$, $Z = 4$. On a recueilli les données d'intensité à l'aide d'un diffractomètre automatique à quatre cycles et on les a affinées par la méthode des moindres carrés (matrice entière) sur *F* jusqu'à des valeurs conventionnelles de $R = 0{,}054$ pour 2736 observations dans le cas du composé **1**-(*E*) et de $R = 0{,}042$ pour 3644 observations dans le cas du composé **1**-(*Z*). La solution de ces structures détermine la configuration de ces isomères aussi bien que celle de leurs précurseurs respectifs permet d'interpréter sans ambiguité les spectres de rmn du ^1H des composés **1** et **2** et des Tamoxifènes.

[Traduit par le journal]

A forthcoming article (1) describes the preparation of the *E* and *Z* isomers of the amino-Tamoxifens **2** which are intended primarily as precursors for radiolabelled estrogens or anti-estrogens for external imaging of receptor positive carcinoma by radiology techniques. The iodo-derivatives (*E*- and *Z*-**1**) were chosen for our initial study since it was felt that the iodine atom, although large, would not seriously alter the affinity of the molecule for estrogen receptors. There are also several isotopes of iodine available which can serve a variety of purposes: iodine-127 for characterization, iodine-131 and 123 for external imaging, and iodine-125 for tissue counting and, in the extreme, for site-selective radiotherapy. We were encouraged in the use of iodine isotopes by the report (2) of the preparation of aromatic iodo compounds from aromatic diazonium salts and Na 131-I at carrier-free concentrations, albeit in modest yields (6–10%).

The iodo-Tamoxifens also provided good quality crystalline samples for structure determination by the X-ray diffraction technique. The reported (3) differences in endocrine activity of the *cis* and *trans* isomers of Tamoxifen itself made the assignment of geometry to the isomers of iodo-Tamoxifen of greater importance. Because the molecular structure of *cis*-Tamoxifen has been determined (4), it would be possible to compare its geometry with the iodo-Tamoxifens. Since the conversions of the amino-Tamoxifens to the iodo-Tamoxifens were expected to be stereospecific, the geometries of the amino-Tamoxifens could also be assigned. Finally, a study of this series of geometric isomers would allow an extension of earlier proton nuclear magnetic resonance assignments (5, 6).

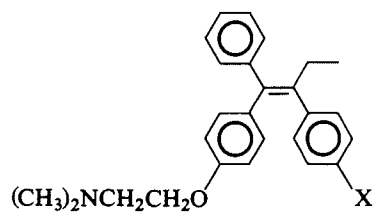

X = I, *Z*-**1**
X = NH_2, *Z*-**2**
X = H, *Z*-Tamoxifen

Results and discussion

As described in the Experimental section, under the usual diazonium ion reaction conditions either *E*-**2** or *Z*-**2** could be converted to the corresponding iodo compounds *E*-**1** or *Z*-**1**, respectively, in about 40% yields. Although these two latter compounds had fortuitously identical melting points and chromatographic behaviour, their nmr spectra were sufficiently dif-

[1]To whom all correspondence should be addressed.

Can. J. Chem. Downloaded from www.nrcresearchpress.com by 178.218.224.3 on 09/06/12
For personal use only.

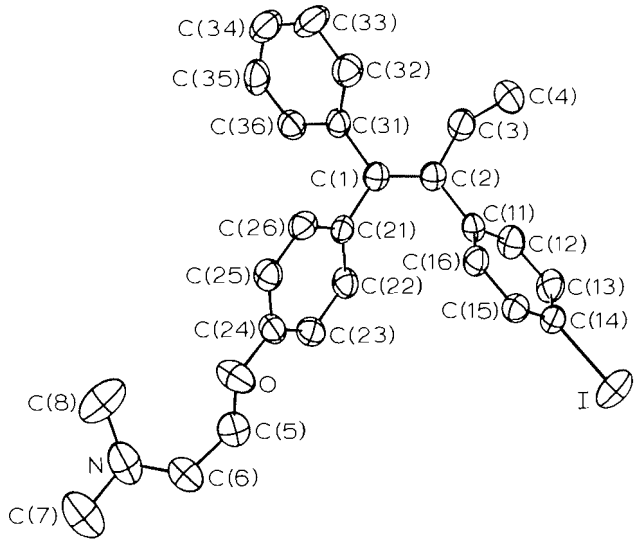

FIG. 1. A perspective view of *Z*-**1** showing the atom numbering scheme used for both isomers. Thermal ellipsoids are drawn at the 50% probability level.

ferent to indicate that one of the isomers of **2** gave one geometrical isomer of **1** and the other isomer of **2** gave the other isomer of **1**. It is assumed in these stereospecific conversions that *E*-**2** yields *E*-**1** and *Z*-**2** yields *Z*-**1**. Thus if the configuration of *E*-**1** and *Z*-**1** can be assigned to the appropriate compounds by X-ray crystallography, then the configurations for the isomers of **2** can be deduced.

It proved possible to obtain satisfactory crystals of each isomer of **1** and, as described in the Experimental section, molecular structures were determined for each, as shown in Fig. 1. It is on this basis that the isomers have been numbered in this and the forthcoming article.

Two single crystal X-ray structure analyses have shown that both structures consist of discrete molecular units; there are no unusual van der Waal's short contacts, with the shortest I—I distances being 4.411(1) Å in *E*-**1** and 4.87(2) Å in *Z*-**1**. The closest intermolecular distance of approach is 2.17 Å between H2C(7) and H2C(23) (equivalent position $1 - x, -y, -1 - z$) for *E*-**1** and 2.45 Å between atoms HlC(3) and HlC(15) at $1/2 + x, 1/2 - y, 1/2 + z$) for *Z*-**1**. Selected intramolecular dimensions for the compounds are presented in Table 1.[2] A perspective view of *Z*-**1**, showing the atom labeling scheme used for both structures, is presented in Fig. 1. Stereoviews of the molecules are given in Fig. 2.

The conformations of the molecules are indicative of major intramolecular interactions between non-bonded atoms. In the absence of such interactions the molecule would be expected to be planar as a result of π-electron delocalization. However, in each structure the phenyl rings are inclined with respect to the plane of the olefinic C atoms. The dihedral angles for the *p*-iodophenyl, *p*-(β-dimethylaminoethoxy)phenyl, and unsubstituted phenyl rings are 57, 59, and 49°, respectively for *E*-**1** and 45, 51, and 63° for *Z*-**1**. These angles compare favourably with angles of 46, 50, and 60°, and 51, 51, and 54° reported for

TABLE 1. Selected bond distances and angles

	Length (Å)	
Bond	*E*-**1**	*Z*-**1**
C(14)—I	2.104(5)	2.096(3)
C(1)—C(2)	1.342(5)	1.340(3)
C(1)—C(21)	1.484(5)	1.496(4)
C(1)—C(31)	1.495(5)	1.495(4)
C(2)—C(11)	1.485(5)	1.495(4)
C(2)—C(3)	1.516(5)	1.519(4)
C(3)—C(4)	1.516(6)	1.520(4)
C(24)—O	1.370(5)	1.378(4)
O—C(5)	1.426(6)	1.404(4)
C(5)—C(6)	1.545(7)	1.513(4)
N—C(6)	1.413(7)	1.432(4)
N—C(7)	1.430(7)	1.460(4)
N—C(8)	1.429(8)	1.416(4)
	Angle (deg)	
Bonds	*E*-**1**	*Z*-**1**
C(15)—C(14)—I	120.9(4)	119.6(2)
C(13)—C(14)—I	118.8(4)	119.8(2)
C(21)—C(1)—C(31)	114.3(4)	112.7(2)
C(21)—C(1)—C(2)	122.9(4)	125.3(3)
C(31)—C(1)—C(2)	122.8(4)	122.0(3)
C(1)—C(2)—C(11)	122.2(4)	123.3(3)
C(1)—C(2)—C(3)	123.3(4)	122.6(3)
C(11)—C(2)—C(3)	114.5(4)	114.1(2)
C(2)—C(3)—C(4)	114.6(4)	113.7(3)
C(25)—C(24)—O	115.7(5)	114.9(3)
C(23)—C(24)—O	124.9(5)	125.3(3)
C(24)—O—C(5)	118.3(4)	118.5(3)
O—C(5)—C(6)	107.6(5)	108.3(3)
C(5)—C(6)—N	112.4(5)	115.0(3)
C(6)—N—C(7)	111.3(5)	109.7(3)
C(6)—N—C(8)	110.8(6)	112.8(3)
C(7)—N—C(8)	110.9(6)	110.4(3)

the two conformers of *cis*-Tamoxifen (4). In each Tamoxifen structure the phenyl rings are tilted in the same direction with respect to the plane of the double bond. Other structural features also provide evidence of the strains imposed upon the molecule. For example, dihedral angles of 11.1 and 5.4° between the planes defined by C(1), C(21) and C(31), and C(2), C(3) and C(11) are observed for *E*-**1** and *Z*-**1**, respectively. These angles are comparable to the values of 3.4 and 6.9° reported for the two forms of *trans*-stilbene (7), and that of 8.4° in tetraphenylethylene (8). Furthermore, an inspection of the bond angles about C(1) and C(2) indicates a significant divergence from the expected angles of 120°. Similar variations in such bond angles have been observed for other substituted ethylenes (4, 7, 8).

There is good agreement between chemically related bond distances and bond angles in the two geometrical isomers. Thus the C—I bond distances of 2.104(5) and 2.097(3) Å for the two isomers are equal within experimental error, and comparable to the range of values (2.06–2.10 Å) reported for hexaiodobenzene (9) and *p*-iodotoluene (10). The C(1)—C(2) bond lengths of 1.342(5) and 1.340(3) Å are also equivalent, and are comparable to those reported for other compounds (4, 7, 8).

The conformational similarity observed in the solid state between Tamoxifen and the iodo-Tamoxifens suggests that

[2]Other bond distances and angles, calculated hydrogen atom parameters, anisotropic thermal parameters, and observed and calculated structure amplitudes for *E*-**1** and *Z*-**1** are available, at a nominal charge, from the Depository of Unpublished Data, CISTI, National Research Council of Canada, Ottawa, Ont., Canada K1A 0S2.

Can. J. Chem. Downloaded from www.nrcresearchpress.com by 178.218.224.3 on 09/06/12
For personal use only.

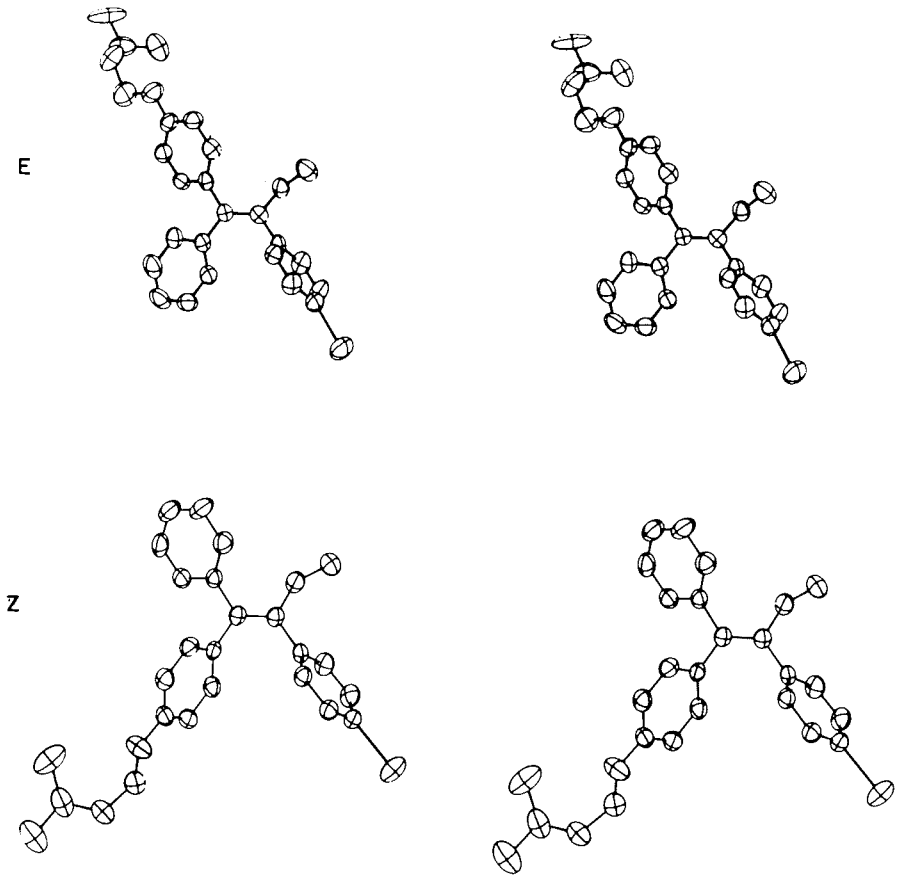

FIG. 2. A stereoview of *E*-**1** and of *Z*-**1**.

TABLE 2. Proton nmr chemical shifts for *E* and *Z* isomers of triarylbutenes

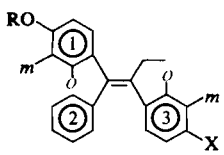

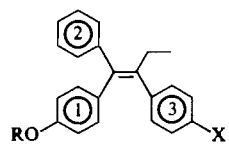

		Ar-1			Ar-3		Ar-1			Ar-3	
R	X	*o*	*m*	Ar-2	*o*	*m*	*o*	*m*	Ar-2	*o*	*m*
$Me_2NCH_2CH_2$[a]	NH_2	7.14	6.88	6.9–7.1	6.88	6.49	6.80	6.58	7.2–7.35	6.91	6.50
$Me_2NCH_2CH_2$[a]	I	7.13	6.88	6.8–7.1	6.85	7.47	6.75	6.59	7.2–7.35	6.87	7.49
$Me_2NCH_2CH_2$[b,c]	H	7.11	6.83	6.88	7.07		6.67	6.46	7.21	7.09	
CH_3[c]	H	7.12	6.79	6.86	7.06		6.70	6.49	7.22	7.08	

[a]In ppm relative to TMS in $CDCl_3$.
[b]This work.
[c]Reference 5.

even in solution the molecules should be able to adopt similar shapes. To the extent that steric demands are important in the estrogen receptors, the iodo-Tamoxifens would seem to be able to mimic the Tamoxifens.

With the molecular structures of three pairs of triarylbutenes (Tamoxifen, amino-Tamoxifen, and iodo-Tamoxifen) firmly established, it was possible to extend and support proton nmr assignments made earlier for Tamoxifen (5, 6). A comparison of the proton nmr spectra of the amino and iodo-Tamoxifens shows only slight differences in the methyl or methylene hydrogens between compounds or isomers. However, there seem to be systematic chemical shift differences in the multiplet (analyzed as an AB) due to the hydrogens on the aromatic ring bearing the β-dimethylaminoethoxy group (ring 1 of Table 2). In the *E*-isomers these signals appear about 0.3–0.4 ppm higher than in the *Z*-isomers. Conversely, the multiplet due to the aromatic hydrogens of the monosubstituted ring (ring 2 of Table 2) appears centered near 7.3 ppm for the *Z*-isomers and near 7.0 ppm for *E*-isomers of **1** and **2**. On this basis the two phenyl signals of Tamoxifen can be assigned as in Table 2 with more confidence. As suggested earlier this shift difference is presumably due to a shielding effect of the aromatic ring on C-2

Can. J. Chem. Downloaded from www.nrcresearchpress.com by 178.218.224.3 on 09/06/12
For personal use only.

TABLE 3. Crystal data

Parameter	Value	
	E-**1**	*Z*-**1**
Molecular formula	$C_{26}H_{28}INO$	$C_{26}H_{28}INO$
fw	497.42	497.42
Space group	$P\bar{1}$	$P2_1/n$
Number and 2θ range of centered reflections	27, 20° < 2θ < 25°	28, 25° < 2θ < 30°
a, Å	10.714(2)	12.675(2)
b, Å	14.125(3)	19.553(3)
c, Å	8.240(2)	9.483(1)
α, deg	95.78(1)	
β, deg	92.91(1)	92.22(1)
γ, deg	71.41(1)	
Cell volume, Å^3	1175.7	2348.4
Medium for density measurement (flotation)	CCl_4/C_6H_{12}	CH_3CH_2I/C_6H_{12}
Density (obsd.), g cm^{-3}	1.42(1)	1.42(1)
Density (calcd.), g cm^{-3}	1.41	1.41
Z	2	4
μ for MoKα, cm^{-1}	12.68	12.68

TABLE 4. Experimental conditions associated with data collection

Parameter	Value	
	E-**1**	*Z*-**1**
Radiation	MoKα, graphite monochromatized	MoKα, graphite monochromatized
Wavelength, Å	0.71073	0.71073
Temperature, °C	20	22
Approximate crystal dimensions, cm	0.027×.017×0.008	0.061×0.058×0.039
Mean ω scan width at half-height, deg	0.125	0.125
Scan range and speed	1.1° corrected for dispersion, at 1° min^{-1}	1.5° corrected for dispersion, at 2° min^{-1}
Data collected	$-h\pm k\pm l$, for 0° < 2θ < 45°	$\pm h\,k\,l$, for 0° < 2θ < 50°
Background count time (stationary crystal, stationary counter at limits of scan)	Initially 10 s, increased to 20 s for 2θ > 35°	Initially 10 s, increased to 20 s for 2θ > 45°
Standards (recorded every 200 reflections)	002, $\bar{3}00$, 040, $01\bar{2}$, $00\bar{2}$	$\bar{2}00$, 020, 200, 004, 022, $\bar{2}02$

of the butene chain and is a consequence of its non-coplanarity with the double bond as seen in the X-ray crystal structures.

Carbon-13 nmr spectra for *E*- and *Z*-**2** showed only slight differences (±1 ppm) and the uv spectra for both isomers were very similar.

Experimental section

Synthesis

Preparation of E-*1 and* Z-*1*

To a solution of 1.15 g (3 mmol) of the previously prepared (1) isomer of **2** of mp 123−124°C in 20 mL of 5 *M* hydrochloric acid at 5°C was added slowly 0.3 g (4.3 mmol) of sodium nitrite in 10 mL of H_2O. After stirring for 10 min, 0.3 g of urea was added to destroy excess sodium nitrite. After stirring an additional 15 min or until bubbling had ceased, a solution of 5 g (30 mmol) of potassium iodide was added. The temperature was then allowed to rise to ambient and the reaction was stirred for 3 h and then heated on the steam bath for a short time.

After cooling, sodium bisulfite was added to destroy any iodine present. The solution was made basic and extracted with methylene chloride. The organic layer was washed with water, dried, and evaporated to yield 0.95 g of crude material which nmr and tlc showed to be primarily *E*-**1**.

The crude reaction product was purified by column chromatography (alumina − 1% methanol in ether) and yielded 0.52 g (35%) of *E*-**1** of mp 109−110°C (from hexanes).

Its nmr spectrum ($CDCl_3$) showed a triplet (3H, 0.93 ppm), a singlet (6H, 2.25 ppm), a quartet (2H, 2.47 ppm), a triplet (2H, 2.73 ppm), a triplet (2H, 4.07 ppm), aromatic multiplets (11H, 6.8−7.3 ppm), and a doublet (2H, 7.47 ppm). *Anal.* calcd. for $C_{26}H_{28}INO$: C 62.79, H 5.67, I 25.51, N 2.82; found: C 62.83, H 5.77, I 25.28, N 2.91. Exact mass determination: calcd. for $C_{26}H_{28}INO$: *m/e* 497.122; found *m/e* 497.121.

Similarly the isomer of **2** of mp 119−120°C gave a 38% yield of *Z*-**1** of mp 109−110°C (from hexanes). Nmr($CDCl_3$) showed a triplet (3H, 0.90 ppm), a singlet (6H, 2.30 ppm), a quartet (2H, 2.42 ppm), a triplet (2H, 2.64 ppm), a triplet (2H, 3.97 ppm), and aromatic multiplets (6H, 6.5−6.9 ppm; 5H broad singlet, 7.3 ppm; 2H doublet, 7.50 ppm). *Anal.* calcd. for $C_{26}H_{28}INO$: C 62.79, H 5.67, I 25.51, N 2.82; found: C 62.89, H 5.93, I 25.15, N 3.03. Exact mass determination: calcd. for $C_{26}H_{28}INO$: *m/e* 497.122; found *m/e* 497.122.

Structure determination

Clear, colourless, prismatic crystals of *E*-**1** were obtained by recrystallization from a hexane solution. A preliminary photographic examination, employing Weissenberg and precession techniques,

Can. J. Chem. Downloaded from www.nrcresearchpress.com by 178.218.224.3 on 09/06/12
For personal use only.

TABLE 5. Atomic positional parameters ($\times 10^4$) and thermal parameters ($\times 10^3$)

	E-**1**				*Z*-**1**			
Atom	*x*	*y*	*z*	*U*(eq)[b]	*x*	*y*	*z*	*U*(eq)
I	871.6(5)[a]	10330.5(3)	2386.4(6)	92.1(4)	−1808.3(2)	364.3(1)[a]	343.9(3)	83.9(2)
O	2954(4)	1094(2)	−2080(4)	80(3)	3325(2)	1354(1)	−4844(2)	61(2)
N	4597(5)	−1186(3)	−3440(6)	85(5)	4786(2)	585(2)	−6898(3)	69(2)
C(1)	2395(4)	5218(3)	−886(5)	41(4)	2720(2)	2609(1)	435(3)	35(2)
C(2)	2870(4)	5614(3)	460(5)	44(4)	1995(2)	2455(1)	1377(3)	37(2)
C(3)	3874(4)	4990(3)	1612(6)	54(4)	1971(2)	2795(2)	2816(3)	52(2)
C(4)	3411(5)	5079(4)	3345(6)	76(5)	993(3)	3228(2)	3019(4)	75(3)
C(5)	3252(6)	571(4)	−3656(7)	101(6)	3495(3)	649(2)	−4998(4)	72(3)
C(6)	3296(6)	−524(5)	−3535(8)	104(6)	3708(3)	507(2)	−6530(4)	75(3)
C(7)	4612(7)	−2202(4)	−3439(9)	137(8)	4915(3)	350(2)	−8343(4)	95(3)
C(8)	5280(9)	−902(6)	−2037(11)	188(11)	5155(4)	1265(3)	−6736(5)	141(5)
C(11)	2443(5)	6711(3)	939(5)	44(4)	1136(2)	1943(1)	1106(3)	35(2)
C(12)	1115(5)	7234(3)	1130(5)	51(4)	846(2)	1492(2)	2146(3)	48(2)
C(13)	674(5)	8253(4)	1564(6)	60(4)	13(3)	1044(2)	1942(3)	52(2)
C(14)	1569(6)	8768(3)	1819(6)	61(4)	−534(2)	1037(1)	669(4)	43(2)
C(15)	2896(5)	8268(4)	1663(6)	70(5)	−272(2)	1477(2)	−387(3)	41(2)
C(16)	3316(5)	7247(4)	1257(6)	61(4)	548(2)	1926(1)	−159(3)	38(2)
C(21)	2607(4)	4127(3)	−1221(6)	43(4)	2852(2)	2250(1)	−939(3)	35(2)
C(22)	3109(4)	3599(3)	−2680(5)	49(4)	2912(2)	1542(2)	−1049(3)	42(2)
C(23)	3253(5)	2593(4)	−3020(6)	57(4)	3077(2)	1222(1)	−2320(3)	44(2)
C(24)	2860(5)	2089(3)	−1887(7)	56(4)	3182(2)	1609(2)	−3510(3)	41(2)
C(25)	2349(5)	2595(4)	−444(6)	58(4)	3130(2)	2314(2)	−3429(3)	42(2)
C(26)	2230(5)	3589(4)	−112(6)	57(4)	2976(2)	2625(1)	−2166(3)	39(2)
C(31)	1575(5)	5843(3)	−2152(5)	45(4)	3518(2)	3163(2)	694(3)	37(2)
C(32)	1949(5)	6590(4)	−2760(6)	57(4)	3239(2)	3842(2)	832(3)	51(2)
C(33)	1197(6)	7153(4)	−3949(6)	66(5)	3998(3)	4342(2)	1052(4)	62(2)
C(34)	57(6)	6989(4)	−4548(6)	72(5)	5044(3)	4174(2)	1129(4)	61(2)
C(35)	−313(5)	6248(4)	−3981(7)	70(5)	5340(2)	3508(2)	971(3)	57(2)
C(36)	442(5)	5668(3)	−2797(6)	54(4)	4584(2)	3006(2)	744(3)	46(2)

[a]Estimated standard deviations in this and other tables are given in parentheses, and correspond to the least significant digit.
[b]$U(\text{eq}) = (1/3)\ \sum_i \sum_j a_i^* a_j^* \mathbf{a}_i \mathbf{a}_j$.

showed the crystals possess triclinic symmetry. The space group $P\bar{1}$ (C_i^1, No. 2) (11) was chosen, and this choice was later confirmed by the successful refinement of the structure. The crystal data are summarized in Table 3.

The crystal chosen for data collection was mounted on a Picker FACS-1 computer-controlled (12) diffractometer with [100] offset approximately 17° from coincidence with the diffractometer ϕ axis. Five standard reflections were regularly monitored during data collection. These, together with an examination of crystal mosaicity at the beginning and the end of data collection, showed no significant decomposition had occurred. Coincidence losses in counting were minimized for strong reflections by using Cu foil attenuators. Details of the parameters associated with data collection are given in Table 4.

After data collection was complete the crystal was measured for an absorption correction. Seven faces were identified as $(\bar{1}00)$, $(21\bar{1})$, (321), and the forms {010} and {012}. The recorded intensities were corrected for monochromator polarization, background, Lorentz and polarization effects, and a standard deviation $\sigma(I)$ was assigned to each intensity (I), such that $\sigma(I) = [C + \frac{1}{4}(t_c/t_b)^2(b_l + b_h) + (pI)^2]^{1/2}$, where C = total counts measured in time t_c, b_l and b_h are background counts each measured in time t_b,[3] p was chosen as 0.04. A total of 3309 reflections was measured; 2387 unique data with $I > 3\sigma(I)$ were used in the solution and preliminary refinement of the structure. The data were corrected for absorption effects using the analytical method (13). Transmission coefficients varied from 0.782 to 0.900.

Clear, pale yellow, prismatic crystals of *Z*-**1** were obtained by recrystallization from petroleum ether (bp 60−80°C) solutions. Preliminary photography showed the crystals belong to the monoclinic system. The systematic absences identified, $h + l$ odd for $h0l$ and k odd for $0k0$, uniquely define the space group as $P2_1/n$ (alternate setting of $P2_1/c$, $C_{2_h}^5$, No. 14 (11)); equivalent positions $\pm(x,y,z$ and $1/2 + x, 1/2 - y, 1/2 + z)$. Crystal data are given in Table 3.

The crystal selected for data collection was mounted with [100] offset approximately 35° from coincidence with the spindle axis. The monitoring of six standard reflections revealed a steady decrease in intensity, the total decrease being about 10% over the period of data collection. A correction for this decay was applied. The intensity of the nth reflection, observed with a value I, was adjusted to I_n, where $I_n = I/(1.0 - n(2.034 \times 10^{-5}))$. The experimental conditions associated with data collection are given in Table 4.

The crystal was measured following data collection, and ten faces were identified as (110), $(1\bar{1}0)$, $(1\bar{1}1)$, (212), and the forms $\{010\}$ and $\{11\bar{1}\}$. Two fractured faces were assigned the indices $(20\bar{1})$ and $(\bar{1}2\bar{1})$. The recorded intensities were processed as before and p was chosen as 0.03. The data were corrected for absorption effects using the Gaussian method with a 8 × 14 × 6 grid (14). Transmission coefficients varied from 0.561 to 0.666. Of the 4538 reflections collected, 3184 unique observations with $I > 3\sigma(I)$ were used in the solution and preliminary refinement of the structure.

Solution and refinement of the structures

E-**1**: The I atom was located from a three-dimensional Patterson synthesis. Structure factor and difference Fourier synthesis calcu-

[3]Computing was performed on the DEC PDP-10 and the CDC Cyber 73/14 at the University of Western Ontario. Among the programs used were: cell refinement and orientation matrix, PICKTT, based on Hamilton's MODE 1; Fourier syntheses, Zalkin's FORDAP; least-squares refinement, WOCLS, a version of Ibers' NUCLS; absorption correction, AGNOST, by Cahen and Ibers; Johnson's ORTEP for illustrations; and ORFFE, Busing, Martin, and Levy's function and error program.

Can. J. Chem. Downloaded from www.nrcresearchpress.com by 178.218.224.3 on 09/06/12
For personal use only.

lations revealed the positions of the remaining 28 nonhydrogen atoms. Refinement of atomic parameters was carried out by full-matrix least-squares techniques on F, minimizing the function $\sum w(|F_o| - |F_c|)^2$ where the weight w is given by $4F_o^2/\sigma^2(F_o^2)$. Scattering factors for neutral nonhydrogen atoms were taken from Volume IV of ref. 11, while those for H were from Stewart *et al.* (15). The anomalous dispersion contribution to the scattering factor was included for the I atom and was taken from Cromer and Liberman (16).

The 28 hydrogen atoms were readily located from difference Fourier maps with electron density ranging from 0.3(1) to 0.5(1) e $Å^{-3}$. These were included in idealized positions (sp^2 or sp^3 hybridization at C, C—H 0.95 and 1.00 Å, respectively) but not refined. For the final cycles positional and anisotropic thermal parameters were refined for all nonhydrogen atoms, and the idealized H atom positions were recalculated after each cycle. The model converged (2736 unique data for which $I > \sigma(I)$, 262 variables) with agreement factors $R_1 = \sum||F_o| - |F_c||/\sum|F_o| = 0.054$ and $R_2 = (\sum w(|F_o| - |F_c|)^2/\sum wF_o^2)^{1/2} = 0.028$.

In the final cycle no parameter shift exceeded 0.06 of its estimated standard deviation. A statistical analysis of R_2 in terms of $|F_o|$, indices, $\lambda^{-1}\sin\theta$, and the diffractometer setting angles χ and ϕ showed no unusual trends. The standard deviation on an observation of unit weight is 2.33 electrons. The highest peak in a difference Fourier synthesis is of electron density 0.58(4) e $Å^{-3}$ at fractional coordinates (0.122, 0.011, 0.358) and is of no chemical significance. No evidence was found for secondary extinction. Final atomic positional parameters for nonhydrogen atoms are presented in Table 5. H atom parameters and structure amplitudes listed as $10F_o$ and $10F_c$ in electrons have been deposited.[2]

Z-**1**: The structure was solved by the heavy atom method, and all 29 nonhydrogen atoms located from a series of difference Fourier syntheses and least-squares refinements. The 28 H atoms were located with electron density varying from 0.3(1) to 0.7(1) e $Å^{-3}$, and their idealized contributions included in the calculations of F_c. The refinement of 262 variables with 3644 unique observations ($I > \sigma(I)$) converged at $R_1 = 0.042$ and $R_2 = 0.026$.

The largest shift in the final cycle was 0.02 esd. A statistical analysis of the structure factors showed no abnormal trends. Secondary extinction effects could be ignored. The error in an observation of unit weight is 3.62 electrons. The highest peak in a difference Fourier synthesis is of electron density 0.13(3) e $Å^{-3}$ at fractional coordinates (−0.196, 0.029, 0.012), and is of no chemical significance. Final positional parameters for the nonhydrogen atoms are given in Table 5. H atom parameters and a list of observed and calculated structure amplitudes (× 10 in electrons) have been deposited.[2]

Acknowledgments

The authors are grateful for financial support from the Natural Sciences and Engineering Research Council of Canada, the Academic Development Fund of the University of Western Ontario, and the Ontario Cancer Treatment and Research Foundation.

1. A. A. DRIEDGER, B. REID, D. H. HUNTER, E. LEE CHAN, and Y. ZEA PONCE. To be published.
2. G.-J. MEYER, K. ROSSLER, and G. STOCKLIN. J. Am. Chem. Soc. **101**, 3121 (1979).
3. M. J. K. HARPER and A. L. WALPOLE. Nature, **212**, 87 (1966).
4. B. T. KILBOURN, R. H. B. MAIS, and P. G. OWSTON. Chem. Commun. 291 (1968).
5. G. R. BEDFORD and D. N. RICHARDSON. Nature, **212**, 733 (1966).
6. D. J. COLLINS, J. J. HOBBS, and C. W. EMMENS. J. Med. Chem. **14**, 952 (1971).
7. A. HOEKSTRA, P. MEERSTENS, and A. VOS. Acta Crystallogr. B **31**, 2813 (1975).
8. A. HOEKSTRA and A. VOS. Acta Crystallogr. B**31**, 1722 (1975).
9. R. J. STEER, S. F. WATKINS, and P. WOODWARD. J. Chem. Soc. C, 403 (1970).
10. C. T. AHM, S. SOLED, and G. B. CARPENTER. Acta Crystallogr. B**28**, 2152 (1972).
11. International tables for X-ray crystallography. Vol. 1. Kynoch Press, Birmingham, England. 1969.
12. P. G. LENHERT. J. Appl. Crystallogr. **8**, 568 (1975).
13. J. DE MEULENAER and H. TOMPA. Acta Crystallogr. **19**, 1014 (1965).
14. D. CAHEN and J. A. IBERS. J. Appl. Crystallogr. **5**, 298 (1972).
15. R. F. STEWART, E. R. DAVIDSON, and W. T. SIMPSON. J. Chem. Phys. **42**, 3175 (1965).
16. D. T. CROMER and D. LIBERMAN. J. Chem. Phys. **53**, 1891 (1970).

Can. J. Chem. Downloaded from www.nrcresearchpress.com by 178.218.224.3 on 09/06/12
For personal use only.

Conformation of azaphosphorinane ring. Crystal structures of 2,2,6,6-tetramethyl-4,4-diphenyl-1,4-azaphosphorinanium perchlorate and 2,2,6,6-tetramethyl-4-oxo-4-phenyl-1,4-azaphosphorinan-1-oxyl (stable nitroxy radical)

MIROSLAW CYGLER[1]
Department of Biochemistry, University of Alberta, Edmonton, Alta., Canada T6G 2H7
AND
JANUSZ SKOLIMOWSKI
Institute of Chemistry, University of Łódź, Narutowicza 68, Łódź, Poland

Received June 2, 1982

MIROSLAW CYGLER and JANUSZ SKOLIMOWSKI. Can. J. Chem. **61**, 427 (1983).

Crystal structures of 2,2,6,6-tetramethyl-4,4-diphenyl-1,4-azaphosphorinanium perchlorate (**I**) and 2,2,6,6-tetramethyl-4-oxo-4-phenyl-1,4-azaphosphorinan-1-oxyl (**II**) were determined. Compound **I** crystallizes in the monoclinic space group $C2/c$ with unit cell dimensions a = 18.2967(7), b = 10.9413(6), c = 20.8714(13) Å, β = 90.79(1)° (at 115 K), and **II** crystallizes in the orthorhombic space group $Pn2_1a$ with a = 8.076(1), b = 10.139(1), c = 17.894(1) Å. Intensity data were measured on a diffractometer at 115 K for **I** and at the room temperature for **II**. The structures were solved by a combination of heavy-atom and direct methods and refined to R = 0.036 (3968 reflections) for **I** and 0.039 (1451 reflections) for **II**.

The azaphosphorinane ring adopts a chair conformation in both molecules, being flattened in the P part in **I** and in the N part in **II**. In molecule **I** the equatorial phenyl group is nearly parallel to the approximate plane of symmetry of the molecule, and the axial phenyl group is perpendicular to that plane. In molecule **II** the P=O bond is axial and the phenyl group is equatorial. The CN(O)C group is not planar. The N—O bond makes an angle of 18.0(3)° with the CNC plane. The CNC angle of 129.3(3)° is larger than that found in nitroxypiperidine analogues.

MIROSLAW CYGLER et JANUSZ SKOLIMOWSKI. Can. J. Chem. **61**, 427 (1983).

On a déterminé les structures cristallines du perchlorate de tétraméthyl-2,2,6,6 diphényl-4,4 azaphosphorinanium-1,4 (**I**) et du tétraméthyl-2,2,6,6 oxo-4 phényl-4 azaphosphorinane-1,4 oxyl-1 (**II**). Le composé **I** cristallise dans le groupe d'espace monoclinique $C2/c$ avec des dimensions de maille de: a = 18,2967(7), b = 10,9413(6), c = 20,8714(13) Å, β = 90,79(1)° (à 115 K) et le composé **II** cristallise dans le groupe d'espace orthorhombique $Pn2_1a$ avec a = 8,076(1), b = 10,139(1), c = 17,894(1) Å. On a relevé les données d'intensité à l'aide d'un diffractomètre à 115 K pour le composé **I** et à la température ambiante pour le composé **II**. On a résolu les structures par une combinaison d'atomes lourds et de méthodes directes et on les a affinées jusqu'à des valeurs de R = 0,036 (pour 3968 réflexions) dans le cas du composé **I** et de R = 0,039 (1451 réflexions) dans le cas du composé **II**.

Le cycle azaphosphorinane adopte une conformation chaise dans les deux molécules et il est applati dans la région de l'atome de phosphore dans le cas du composé **I** et dans la région de l'atome d'azote dans le cas du composé **II**. Dans la molecule **I**, le groupe phényle équatorial est quasi parallèle au plan approximatif de symétrie de la molécule et le groupe phényle axial est perpendiculaire à ce plan. Dans la molécule **II**, le lien P=O est axial et le groupe phényle est équatorial. Le groupe CN(O)C n'est pas plan. La liaison N—O fait un angle de 18,0(3)° avec le plan CNC. L'angle CNC de 129,3(3)° est plus grand que celui trouvé dans les analogues de la nitroxypipéridine.

[Traduit par le journal]

Introduction

Compounds containing heterocyclic rings with phosphorus have been widely studied recently. Much interest has been focused on 1,3,2-dioxaphosphorinanes and 1,3,2-azaoxaphosphorinanes as well as other 6-membered ring systems containing, in addition to P, other heteroatoms such as sulfur or nitrogen (1). X-ray diffraction studies of these compounds have shown that in the solid state the heterocyclic ring adopts, in most cases, a chair conformation, usually flattened at the P end. Non-chair conformations are rarely observed in the solid state. It has been suggested that the twist conformation observed in some 1,3,2-dithiaphosphorinanes (e.g. *cis* and *trans* isomers of 2-phenyl-2-oxo-5-*tert*-butyl-1,3,2-dithiaphosphorinane (2) and 2-*tert*-butyl-2-oxo-5,5-dimethyl-1,3,2-dithiaphosphorinane (3)) is due to the lowering of the chair-twist energy difference by the introduction of sulfur atoms to the ring. Incorporation of bulky substituents may also lead to non-chair conformations as is the case in *cis*-2-*tert*-butylamino-2-seleno-4,4,6-trimethyl-1,3,2-dioxaphosphorinane where the twist conformation is adopted in the solid state to avoid pronounced 1,3 *syn*–axial interactions existing in both chair forms (4).

We have pursued the synthesis of 1,4-azaphosphorinane derivatives with bulky substituents and have also succeeded in the preparation of stable nitroxy radicals incorporated in such systems (5). To the best of our knowledge, there is only one example of the crystal structure of a 1,4-azaphosphorinane derivative reported in the literature (1-methyl-4-phenyl-1,4-azaphosphorinan-4-sulfide (6)). There is no steric strain in that molecule, and the ring adopts the usual chair form. Nitroxy radicals incorporated in six-membered rings (piperidine analogues) cause a distortion of the ring, but the chair conformation is still the most stable, even if severe 2,4,6 axial interactions are present (7).

The X-ray analysis of 2,2,6,6-tetramethyl-4,4-diphenyl-1,4-azaphosphorinanium perchlorate (**I**) and 2,2,6,6-tetramethyl-

[1]On leave from Department of Crystallography, University of Łódź, Nowotki 18, Łódź, Poland.

Can. J. Chem. Downloaded from www.nrcresearchpress.com by 210.87.254.6 on 09/06/12
For personal use only.

TABLE 1. Crystal data

Parameter	Value		
	I		II
Formula	$C_{20}H_{27}NP^{+}\cdot ClO_4^{-}$		$C_{14}H_{21}NO_2P$
fw	411.86		266.30
Space group	Monoclinic, $C2/c$		Orthorhombic, $Pn2_1a$ (C_{2v}^9)
Temperature	299 K	115 K	299 K
a	18.460(1) Å	18.2967(7) Å	8.076(1) Å
b	11.011(1) Å	10.9413(6) Å	10.139(1) Å
c	21.196(2) Å	20.8714(13) Å	17.894(1) Å
β	91.93(1)°	90.79(1)°	
V	4305.9 Å^3	4177.8 Å^3	1465.2 Å^3
Z	8		4
d_x	1.271 Mg m^{-3}	1.310 Mg m^{-3}	1.207 Mg m^{-3}
Radiation	Monochromatized MoK$_\alpha$		Nb filtered MoK$_\alpha$
μr	0.08		0.1
Scan	θ/2θ		θ/2θ
Crystal dimensions	0.37 × 0.28 × 0.25 mm		0.55 × 0.29 × 0.25 mm
$2\theta_{max}$	55°		55°
No. of control reflections	3		2
Total no. of measured reflections	4830		1749
No. of reflections with $I > 2\sigma(I)$	3968		1451
Weights	From counting statistics		$w^{-1} = 1 + (F_o - 11)^2/81$
R	0.036		0.039
R_w	0.031		0.048
Max shift/esd in last l.s. cycle	0.12		0.48

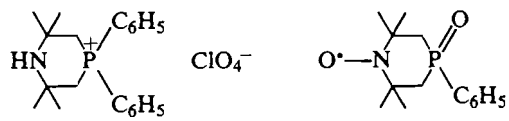

I II

4-oxo-4-phenyl-1,4-azaphosphorinan-1-oxyl (**II**) was undertaken to establish the conformation of the azaphosphorinane ring in the presence of 2,4,6 axial interactions, and to determine the influence of the nitroxy group on the ring shape.

Experimental

X-ray analysis of ***I***

Suitable crystals were obtained from a mixture of methanol and water by slow evaporation. Systematic absences on Weissenberg photographs indicated Cc or $C2/c$ as possible space groups. The presence of a perchlorate anion in the structure, often reported as being disordered, prompted us to collect X-ray data at a temperature of 115 K. Cell constants were calculated from the setting angles of 26 reflections (room temperature) and 48 reflections (low temperature), centered automatically on a Picker diffractometer. Crystal data and pertinent details of data collection are shown in Table 1. No absorption correction was applied.

E-statistics pointed toward the centrosymmetric space group $C2/c$. Direct methods (MULTAN (8)) applied in that space group gave a reasonable model. Successful refinement confirmed the space group choice. All H atoms were located on a difference map and were included in the refinement with isotropic temperature factors. The extinction parameter (9)[2] was also refined; it converged to $g = 0.457$. The NRCC PDP8-E system of programs (10) was used for data collection and structure determination. Final atomic parameters are given in Table 2.[3]

X-ray analysis of ***II***

Suitable crystals were obtained from a mixture of *n*-hexane and chloroform. Systematic absences on Weissenberg and precession photographs indicated that the possible space groups were $Pnma$ and $Pn2_1a$. Data were collected on a Picker diffractometer at room temperature. Table 1 presents the crystal data and the procedure of data collection. No absorption correction was applied.

E-statistics strongly favoured the non-centrosymmetric space group $Pn2_1a$. Attempts to solve the structure with direct methods (MULTAN) in that space group and later in $Pnma$ were unsuccessful. The position of the P atom was then determined from the Patterson map. The appearane of peaks on the Harker section $u1/2w$ but neither on $1/2vw$ nor $uv1/2$ was yet another indication in favour of space group $Pn2_1a$. Further attempts to solve the structure were performed in that space group. The position of the P atom (y coordinate set arbitrarily to 0.5) was used to calculate phases for reflections with $E > 1.7$ and $|F_c| > 0.4\,|F_o|$. These phases were input to FASTAN and were kept constant during phase refinement. The resulting E-map was centrosymmetric (as one should expect); a seven atom fragment from one enantiomorph was recognizable. The next cycle of tangent refinement, based on phases calculated from that fragment, led to the recognition of an additional five atoms. The Fourier map calculated at this point revealed all non-hydrogen atoms ($R = 0.19$). The model had not $^y m$ symmetry as would be necessary for $Pnma$ space group with $Z = 4$. Successful refinement confirmed the choice of the space group. A difference map allowed us to locate the positions of all H atoms. Their positional parameters were included in the refinement.

Scattering amplitudes for neutral atoms were taken from International tables for X-ray crystallography (11). All calculations, except direct methods, were performed with NRC crystallographic programs (12). Final atomic parameters are given in Table 3.[3]

Results and discussion

Crystal structure of ***I***

A view of the molecule with the numbering scheme is shown in Fig. 1, and bond lengths, valence and torsion angles in Table 4. The azaphosphorinane ring adopts a chair conformation in the solid state. The axial phenyl group is nearly perpendicular

[2] Expression for extinction correction used was $F_c^{corr} = |F_c|\,(1 + g|F_c|^2 Lp_2/p_1)^{-1/2}$ where L = Lorentz factor, $p_n = (1 + \cos^{2n} 2\theta)$.

[3] Tables of observed and calculated structure factors and of temperature factors are available, at a nominal charge, from the Depository of Unpublished Data, CISTI, National Research Council of Canada, Ottawa, Ont., Canada K1A 0S2.

Can. J. Chem. Downloaded from www.nrcresearchpress.com by 210.87.254.6 on 09/06/12
For personal use only.

Can. J. Chem. Downloaded from www.nrcresearchpress.com by 210.87.254.6 on 09/06/12
For personal use only.

TABLE 2. Final atomic parameters and B_{eq} for 2,2,6,6-tetramethyl-4,4-diphenyl-1,4-azaphosphorinanium perchlorate. E.s.d's refer to the last digit printed

Atom	*X*	*Y*	*Z*	B_{eq}*
Cl(1)	0.162785(25)	0.42527(4)	0.372611(22)	1.682(18)
O(1)	0.21003(10)	0.52870(15)	0.37723(9)	4.50(9)
O(2)	0.12047(8)	0.43105(16)	0.31479(6)	3.38(8)
O(3)	0.11438(8)	0.42392(16)	0.42611(6)	3.13(7)
O(4)	0.20618(8)	0.31634(14)	0.37312(8)	3.53(8)
N(1)	0.17634(8)	0.02742(13)	0.37156(7)	1.37(6)
C(2)	0.21451(10)	0.00053(17)	0.31102(9)	1.40(7)
C(201)	0.16719(10)	0.05850(19)	0.25822(9)	2.01(8)
C(202)	0.22008(11)	−0.13656(18)	0.29783(9)	1.86(8)
C(3)	0.29127(9)	0.06073(16)	0.30731(8)	1.27(7)
P(1)	0.34751(3)	0.04807(4)	0.37789(2)	1.163(17)
C(5)	0.28573(9)	0.07878(16)	0.44191(8)	1.33(7)
C(6)	0.21153(9)	0.01060(17)	0.43506(8)	1.39(7)
C(601)	0.15994(10)	0.06983(19)	0.48348(9)	1.96(8)
C(602)	0.21986(10)	−0.12397(18)	0.45307(9)	1.84(8)
C(11)	0.41597(9)	0.16534(16)	0.37384(8)	1.30(7)
C(12)	0.39475(10)	0.28708(17)	0.37069(9)	1.64(8)
C(13)	0.44703(11)	0.37761(17)	0.36630(9)	1.92(8)
C(14)	0.52089(11)	0.34668(18)	0.36373(9)	1.98(9)
C(15)	0.54178(10)	0.22576(19)	0.36614(10)	2.10(9)
C(16)	0.49004(10)	0.13424(17)	0.37113(9)	1.70(8)
C(21)	0.39456(9)	−0.09468(16)	0.38747(8)	1.23(7)
C(22)	0.41802(10)	−0.13040(17)	0.44866(9)	1.70(8)
C(23)	0.46204(11)	−0.23239(18)	0.45587(9)	2.06(9)
C(24)	0.48329(11)	−0.29801(17)	0.40261(10)	1.99(8)
C(25)	0.45981(11)	−0.26357(18)	0.34246(9)	2.10(9)
C(26)	0.41590(10)	−0.16126(17)	0.33424(9)	1.71(8)
H(1)	0.1637(9)	0.1070(15)	0.3691(7)	1.3(4)
H(31)	0.3155(9)	0.0306(15)	0.2717(8)	1.7(4)
H(32)	0.2854(9)	0.1477(15)	0.3028(7)	1.2(4)
H(51)	0.3116(9)	0.0601(16)	0.4842(8)	1.8(4)
H(52)	0.2772(9)	0.1663(15)	0.4391(7)	1.1(4)
H(211)	0.1870(10)	0.0479(16)	0.2160(8)	2.5(5)
H(212)	0.1210(10)	0.0192(16)	0.2574(8)	2.3(4)
H(213)	0.1611(10)	0.1485(16)	0.2662(8)	2.0(4)
H(221)	0.2360(10)	−0.1502(16)	0.2539(9)	2.4(5)
H(222)	0.1704(10)	−0.1749(17)	0.2979(8)	2.7(5)
H(223)	0.2508(9)	−0.1827(15)	0.3277(8)	1.5(4)
H(611)	0.1507(9)	0.1552(16)	0.4728(8)	1.7(4)
H(612)	0.1133(10)	0.0262(17)	0.4824(8)	2.4(5)
H(613)	0.1835(10)	0.0659(16)	0.5284(8)	2.1(4)
H(621)	0.2356(10)	−0.1289(15)	0.4966(8)	1.6(4)
H(622)	0.1733(10)	−0.1690(17)	0.4462(8)	2.3(4)
H(623)	0.2565(10)	−0.1724(16)	0.4268(8)	2.1(4)
H(12)	0.3452(10)	0.3091(17)	0.3703(8)	2.8(5)
H(13)	0.4326(9)	0.4632(16)	0.3639(8)	1.8(4)
H(14)	0.5558(10)	0.4072(17)	0.3624(8)	2.5(5)
H(15)	0.5901(10)	0.2026(17)	0.3650(8)	2.7(5)
H(16)	0.5048(9)	0.0533(16)	0.3724(8)	1.9(4)
H(22)	0.4065(10)	−0.0820(16)	0.4852(8)	2.1(4)
H(23)	0.4794(10)	−0.2523(17)	0.4982(8)	2.4(5)
H(24)	0.5131(10)	−0.3662(16)	0.4073(8)	2.0(4)
H(25)	0.4746(11)	−0.3099(17)	0.3045(8)	3.1(5)
H(26)	0.4017(9)	−0.1364(15)	0.2917(8)	1.7(4)

* B_{eq} is the arithmetic mean of the principal axes of the thermal ellipsoid.

to the pseudo-mirror plane of the ring, being rotated 85.8° around the C(21)—P bond, while the equatorial phenyl group is nearly parallel to that plane (rotated by 4.9° around C(11)—P). It has been found from X-ray studies that the phenyl group attached axially to a trivalent phosphorus in the phosphorinane ring displays similar orientation (13, 14). Molecular mechanics calculations performed for 1-phenyl-4-phosphorinanone (15) indicated that another orientation of an axial phenyl group is energetically unlikely because of the interactions with axial ring hydrogens. The calculated energy

TABLE 3. Final atomic parameters and B_{eq} for 2,2,6,6-tetramethyl-4-oxo-4-phenyl-1,4-azaphosphorinan-1-oxyl. E.s.d's refer to the last digit printed

Atom	X	Y	Z	B_{eq}*
P(4)	0.28248(10)	0.50000	0.86421(4)	2.70(3)
O(41)	0.3955(4)	0.4227(3)	0.8160(1)	4.2(1)
O(1)	0.0403(3)	0.1731(3)	0.9767(1)	3.5(1)
N(1)	0.0923(3)	0.2846(3)	0.9512(1)	2.7(1)
C(2)	0.2512(4)	0.3308(4)	0.9872(2)	3.0(1)
C(3)	0.2979(4)	0.4720(3)	0.9631(2)	2.9(1)
C(5)	0.0654(4)	0.4654(3)	0.8552(2)	2.9(1)
C(6)	0.0155(4)	0.3259(3)	0.8783(2)	2.8(1)
C(201)	0.2204(6)	0.3330(5)	1.0714(2)	5.0(1)
C(202)	0.3879(5)	0.2327(4)	0.9667(3)	4.7(1)
C(601)	−0.1725(5)	0.3232(5)	0.8903(3)	4.7(1)
C(602)	0.0638(6)	0.2257(4)	0.8187(2)	4.0(1)
C(11)	0.3102(4)	0.6763(3)	0.8501(2)	2.8(1)
C(12)	0.2297(4)	0.7706(3)	0.8936(2)	3.1(1)
C(13)	0.2587(5)	0.9033(4)	0.8806(2)	3.8(1)
C(14)	0.3639(5)	0.9423(4)	0.8240(2)	4.0(1)
C(15)	0.4418(6)	0.8495(4)	0.7816(2)	4.7(1)
C(16)	0.4151(5)	0.7174(4)	0.7939(2)	4.2(1)
H(31)	0.230(4)	0.539(3)	0.986(2)	2.9
H(32)	0.398(5)	0.482(4)	0.985(2)	2.9
H(51)	0.007(4)	0.526(4)	0.884(2)	2.9
H(52)	0.036(5)	0.475(5)	0.803(2)	2.9
H(211)	0.114(7)	0.390(5)	1.077(3)	5.0
H(212)	0.202(6)	0.230(6)	1.092(3)	5.0
H(213)	0.319(7)	0.363(6)	1.091(3)	5.0
H(221)	0.413(6)	0.233(6)	0.909(2)	4.7
H(222)	0.487(6)	0.258(5)	0.993(3)	4.7
H(223)	0.359(7)	0.137(5)	0.982(3)	4.7
H(611)	−0.218(7)	0.225(7)	0.901(3)	4.7
H(612)	−0.210(6)	0.384(6)	0.936(3)	4.7
H(613)	−0.218(7)	0.357(6)	0.847(3)	4.7
H(621)	0.168(5)	0.224(4)	0.809(2)	4.0
H(622)	0.022(6)	0.244(5)	0.773(3)	4.0
H(623)	0.013(6)	0.135(4)	0.836(2)	4.0
H(121)	0.148(6)	0.741(5)	0.930(2)	3.0
H(131)	0.209(7)	0.962(6)	0.913(3)	3.8
H(141)	0.389(5)	1.028(5)	0.818(2)	4.5
H(151)	0.509(7)	0.863(7)	0.747(4)	4.7
H(161)	0.481(5)	0.661(5)	0.772(2)	4.0

*B_{eq} is the arithmetic mean of the principal axes of the thermal ellipsoid. Isotropic temperature factors for H atoms were made equal to B_{eq} of the atoms to which they are attached, and were not refined.

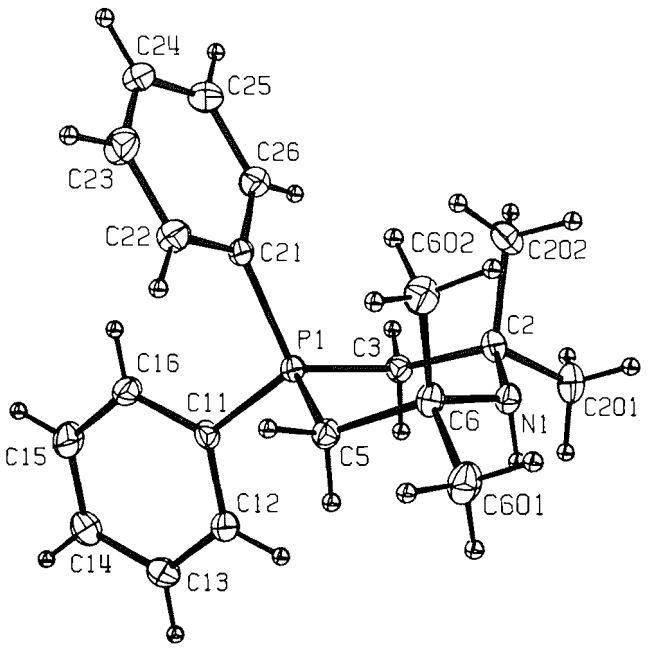

FIG. 1. View of the 2,2,6,6-tetramethyl-4,4-diphenyl-1,4-azaphosphorinanium molecule, **I**. 50% thermal ellipsoids are shown for non-hydrogen atoms.

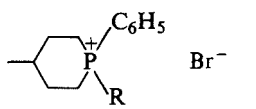

III *a*, R = C_6H_5
b, R = CH_2—C_6H_5

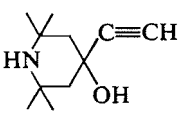

IV

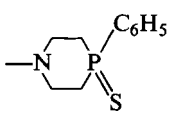

V

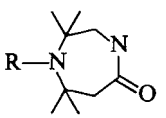

VI *a*, R = H
b, R = O

of a conformation with an equatorial phenyl group parallel to the pseudo-mirror plane of the phosphorinane ring was the same as that with a phenyl group perpendicular to that plane. Both these conformations were indeed found in the solid state in 1-phenyl-4-phosphorinanon-1-oxide, where two crystallographically independent molecules exhibited equatorial phenyl groups rotated 17.8 and 77.1° from the pseudo-mirror plane of the phosphorinane ring (16). These calculations predicted, however, the equatorial position as being slightly more favorable (0.4 kcal/mol) than the axial one, contrary to X-ray and nmr findings (1*b*, 13). Arrangements of phenyl substituents similar to that in **I** have also been found in **III***a* (17).

Comparison to other similar structures shows that the steric interactions of axial substituents on the ring are relaxed to some extent by ring flattening. The mean ring torsion angle of 48.0° is very close to the value of 47.2° found in **IV** (18) where similar steric interactions exist, but is 9.7° smaller than in **III***a* and 7.8° smaller than in **III***b* (17). The ring is more flattened in the P end, a rather typical effect for a phosphorinane moiety (Table II in ref. 19). All P—C bond lengths are equal within the experimental error, with the mean value 1.793(2) Å. The CNC angle of 122.4(1)° is 11° larger than the corresponding angle in **V** (6) and 3.1° larger than in **IV** (18). A very similar value (123.1(3)°) was found, however, in a seven-membered analogue **VI***a* (20). The wide range of observed CNC angles may indicate a relatively low bending potential around the N atom as compared to C.

Comparison of the geometry of molecule **I** with that of **III***a* shows changes which may be attributed to more severe steric interactions in the former. While the endocyclic CPC angle is equal in both molecules within experimental error, the exocyclic CPC angles indicate that the axial phenyl group in **I** has moved more toward the outside of the ring, slightly pushing the equatorial phenyl group toward the center of the ring (C_{ph}^{ax}—P—C_{ring} is 4.2° larger, C_{ph}^{ax}—P—C_{ph}^{eq} is 1.3° smaller, and C_{ph}^{eq}—P—C_{ring} is 3.5° smaller than in **III***a*). This is accompanied by an increase in endocyclic PCC angles in **I** by 4.9° on average.

The C_{meth}^{ax} . . . C_{meth}^{ax} distance of 3.243(3) Å is very similar to that found in 2,2,6,6-tetramethylpiperidines (3.214–3.383 Å,

Can. J. Chem. Downloaded from www.nrcresearchpress.com by 210.87.254.6 on 09/06/12
For personal use only.

TABLE 4. Bond distances (Å), valence angles (deg) and selected torsion angles (deg) for 2,2,6,6-tetramethyl-4,4-diphenyl-1,4-azaphosphorinanium perchlorate (**I**) and 2,2,6,6-tetramethyl-4-oxo-4-phenyl-1,4-azaphosphorinan-1-oxyl (**II**)

(*a*) Bond

Bond	Length I	Length II	Bond	Length I	Length II	Bond	Length, I
N(1)—O(1)	—	1.289(4)	P(1)—C(21)	1.793(2)	—	C(21)—C(22)	1.397(3)
N(1)—C(2)	1.482(3)	1.510(4)	C(6)—C(5)	1.554(3)	1.528(5)	C(21)—C(26)	1.389(3)
N(1)—C(6)	1.477(3)	1.503(4)	C(6)—C(601)	1.536(3)	1.533(5)	C(22)—C(23)	1.383(3)
C(2)—C(3)	1.554(3)	1.543(5)	C(6)—C(602)	1.527(3)	1.525(5)	C(23)—C(24)	1.384(3)
C(2)—C(201)	1.530(3)	1.527(5)	C(11)—C(12)	1.389(3)	1.394(5)	C(24)—C(25)	1.374(3)
C(2)—C(202)	1.529(3)	1.530(6)	C(11)—C(16)	1.399(3)	1.380(5)	C(25)—C(26)	1.387(3)
P(1)—C(3)	1.790(2)	1.796(3)	C(12)—C(13)	1.381(3)	1.386(5)	Cl(1)—O(1)	1.426(2)
P(1)—C(5)	1.794(2)	1.795(4)	C(13)—C(14)	1.395(3)	1.381(6)	Cl(1)—O(2)	1.426(2)
P(1)—O(11)	—	1.480(3)	C(14)—C(15)	1.378(3)	1.362(6)	Cl(1)—O(3)	1.435(2)
P(1)—C(11)	1.796(2)	1.819(3)	C(15)—C(16)	1.383(3)	1.375(6)	Cl(1)—O(4)	1.432(2)

(*b*) Angles

Bonds	Angle I	Angle II	Bonds	Angle I	Angle II	Bonds	Angle, I
O(1)—N(1)—C(2)	—	113.5(3)	C(21)—P(1)—C(5)	112.7(1)	—	P(1)—C(21)—C(22)	119.1(2)
O(1)—N(1)—C(6)	—	114.6(3)	C(21)—P(1)—C(11)	107.1(1)	—	P(1)—C(21)—C(26)	120.5(2)
C(2)—N(1)—C(6)	122.4(2)	129.3(3)	P(1)—C(5)—C(6)	113.6(1)	114.5(2)	C(22)—C(21)—C(26)	119.9(2)
N(1)—C(2)—C(3)	113.3(2)	112.1(3)	N(1)—C(6)—C(5)	113.1(2)	112.6(3)	C(21)—C(22)—C(23)	119.7(2)
N(1)—C(2)—C(201)	105.3(2)	106.7(3)	N(1)—C(6)—C(601)	105.9(2)	106.4(3)	C(22)—C(23)—C(24)	120.1(2)
N(1)—C(2)—C(202)	112.4(2)	108.0(3)	N(1)—C(6)—C(602)	112.5(2)	108.4(3)	C(23)—C(24)—C(25)	120.3(2)
C(3)—C(2)—C(201)	106.9(2)	107.6(3)	C(5)—C(6)—C(601)	106.3(2)	108.4(3)	C(24)—C(25)—C(26)	120.5(2)
C(3)—C(2)—C(202)	110.1(2)	111.1(3)	C(5)—C(6)—C(602)	110.9(2)	111.1(3)	C(21)—C(26)—C(25)	119.5(2)
C(201)—C(2)—C(202)	108.4(2)	111.3(4)	C(601)—C(6)—C(602)	107.8(2)	109.8(3)	O(1)—Cl(1)—O(2)	110.1(1)
C(2)—C(3)—P(1)	115.8(1)	113.9(2)	P(1)—C(11)—C(12)	119.5(2)	122.6(3)	O(1)—Cl(1)—O(3)	109.6(1)
C(3)—P(1)—C(5)	103.7(1)	97.2(2)	P(1)—C(11)—C(16)	120.3(2)	118.3(3)	O(1)—Cl(1)—O(4)	108.9(1)
C(3)—P(1)—C(11)	107.4(1)	106.5(2)	C(12)—C(11)—C(16)	120.1(2)	119.1(3)	O(2)—Cl(1)—O(3)	109.0(1)
C(5)—P(1)—C(11)	110.4(1)	107.5(2)	C(11)—C(12)—C(13)	119.8(2)	119.6(3)	O(2)—Cl(1)—O(4)	109.7(1)
O(11)—P(1)—C(3)	—	116.6(2)	C(12)—C(13)—C(14)	120.1(2)	120.3(4)	O(3)—Cl(1)—O(4)	109.5(1)
O(11)—P(1)—C(5)	—	116.5(2)	C(13)—C(14)—C(15)	120.0(2)	119.7(4)		
O(11)—P(1)—C(11)	—	111.3(2)	C(14)—C(15)—C(16)	120.5(2)	120.8(4)		
C(21)—P(1)—C(3)	115.4(1)	—	C(11)—C(16)—C(15)	119.4(2)	120.5(4)		

(*c*) Torsion angles

Bonds	Angle I	Angle II	Bonds	Angle I	Angle II
C(6)—N(1)—C(2)—C(3)	−50.1(4)	26.9(6)	C(3)—P(1)—C(5)—C(6)	45.4(4)	−60.4(6)
N(1)—C(2)—C(3)—P(1)	44.8(4)	−46.6(6)	P(1)—C(5)—C(6)—N(1)	−51.0(4)	45.8(6)
C(2)—C(3)—P(1)—C(5)	−42.9(4)	60.6(6)	C(5)—C(6)—N(1)—C(2)	53.9(4)	−26.5(6)

Table 2 in ref. 21) or in **VI***a* (3.270 Å (20)).

The H atom attached to N(1) is in close contact with O(4) of the perchlorate anion. The corresponding geometry is N . . . O = 3.208(4), H . . . O = 2.42(3) Å, and the angle N—H . . . O = 146(1)°. This weak hydrogen bond may be responsible for stabilizing the H atom in an axial position.

The perchlorate anion is tetrahedral, with bond distances and valence angles in the range 1.426(2)–1.435(2) Å and 108.9(1)–110.1(1)° respectively. The anion, although not disordered, exhibits a large amplitude of thermal motion having temperature factors with twice the magnitude of those of the azaphosphorinane moiety.

Crystal structure of ***II***

A view of the molecule with the numbering scheme is shown in Fig. 2, and bond lengths, valence and torsion angles are given in Table 4. Like **I**, this molecule also exists in a chair conformation in the solid state. The phenyl group at the P assumes an equatorial position, being nearly parallel to the pseudo-mirror plane of the ring (rotated 6.1°), while the P=O bond is axial. The same axial/equatorial preferences have also been found in **VII***a* and **VII***b* (16) and in *trans*-**VII***c* (22). In

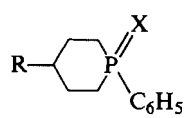

VII *a*, X = O; R = O
b, X = S; R = O
c, X = O; R = $(CH_3)_3$

Can. J. Chem. Downloaded from www.nrcresearchpress.com by 210.87.254.6 on 09/06/12
For personal use only.

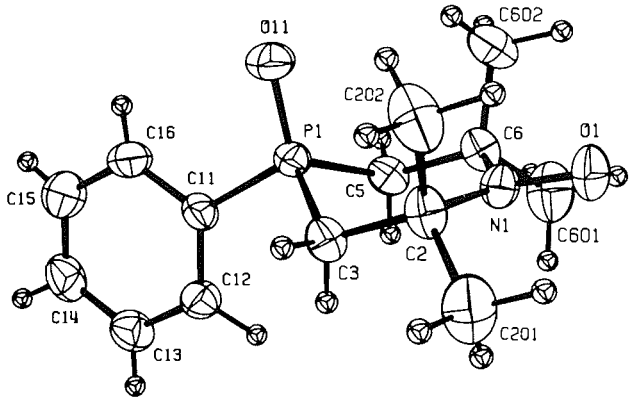

FIG. 2. View of the 2,2,6,6-tetramethyl-4-oxo-4-phenyl-1,4-phosphorinan-1-oxyl molecule, **II**. 50% thermal ellipsoids are shown for non-hydrogen atoms.

the latter case, however, the conformational preference was biased by the presence of the *tert*-butyl group, and in its *cis* isomer the phenyl group was assigned to an axial position on the basis of the nmr spectra.

Interestingly, in **V** the P=S bond assumes an equatorial position, and the phenyl group is axial (6). From the structural information available for 2-*R*-2-oxo-1,3,2-dioxaphosphorinanes, it was concluded that the P=O bond prefers an equatorial position rather than an axial one (23) and an explanation based on the interactions of lone pairs on the 1,3 oxygen atoms with an adjacent group on the P was proposed (24). An equatorial arrangement of P=O and P=S bond has also been found in the crystal structures of 1-phenyl-4,4-dimethyl-1,3,2-dithiaphosphorinan-1-oxide and -1-sulfide (3).

The conformation of the azaphosphorinane ring in **II** is influenced by the presence of the nitroxy group and differs significantly from **I** and **V**. The N part of the ring is flattened, having mean torsion angles about N—C bonds of only 26.7(6)°. The corresponding angles in **I** and **V** are 52.0 and 68.9°, respectively. The carbon analogue of **II** with the N—O group replaced by C=O, **VII***a*, does not show flattening around the carbonyl group (τ = 55.3°). Such a flattening, although to a smaller extent, was observed in piperidine nitroxides. Torsion angles around N—C bonds in these molecules vary between 30.1° (2,2,6,6-tetramethylpiperidin-4-ol-1-oxyl (25)), and 38.3° (4,7-oxido-7-methyl-7-hydroxymethyl-2,2,6,6-tetramethylpiperidin-1-oxyl (26)), with an average of ≃ 35°. In the only example of a nitroxy radical incorporated in the seven-membered ring, **VII***b* (20), the flattening is similar to that in **II** (τ_{CNCC} = 29.6°).

The flattening of the N part of the azaphosphorinane ring in **II** is correlated with puckering of the P part. The torsion angles about P—C bonds are 16° larger than in **I**.

The P—C bond lengths of 1.797(4) Å in the heterocyclic ring are in good agreement with those found in **I** and with values reported for other phosphorinane rings, while P—C_{phenyl} = 1.819(3) Å is slightly longer than the average value (≃1.800 Å) found in similar compounds. It may be noted that a similar bond length was reported for **V** (1.818(2) Å).

The nitroxy group geometry does not differ significantly (except for the CNC angle) from that found in other cyclic nitroxy derivatives. The N—O distance of 1.289(4) Å falls well within the range of observed values (see, for example, ref. 26). The CN(O)C group is not planar. The NO bond forms an angle of 18.0° with the CNC plane. The CNC angle (129.5°) is significantly (≃4°) larger than in piperidine analogues (26). A similar value was observed in the seven-membered analogue **VI***b* (20).

The comparison of the P part of the ring in **II** with analogous moieties in **VII***a* and **VII***c* shows a decrease of the endocyclic CPC angle by ≃3.3°, accompanied by a movement of the P=O bond toward the equatorial phenyl group. The latter effect is evident from the increase of the O=P—C_{ring} angle (116.5° in **II** vs. 113.2° in **VII***a* and 114.9° in **VII***c*) and the decrease of the O=P—C_{ph} angle (111.3° in **II** vs. 112.2° in the two others).

We have pointed out above that the CNC angles in **I** and **II** have values close to those found in the seven-membered ring analogues containing the same N parts, **VI***a* and **VI***b*, respectively. There are also similarities in the geometries of other corresponding fragments in these molecules, such as C(2) . . . C(6), C(3) . . . C(5), and C^{ax} . . . C^{ax} distances. One could conclude that the N part of the rings in **I** and **II** differs from that of their piperidine analogues because of the replacement of a C atom by an atom having a larger covalent radius, rather than by any particular properties of phosphorus.

Acknowledgments

The authors are grateful to Dr. E. Gabe and Dr. Y. Le Page for their aid in the data collection and for helpful discussions.

1. (*a*) D. E. C. CORBRIDGE. The structural chemistry of phosphorus. Elsevier, Amsterdam. 1974; (*b*) B. E. MARYANOFF, R. O. HUTCHINS, and C. A. MARYANOFF. *In* Topics in stereochemistry. Vol. 11. *Edited by* N. L. Allinger and E. L. Eliel. 1979. pp. 187–327; (*c*) L. D. QUIN. The heterocyclic chemistry of phosphorus. Systems based on the phosphorus–carbon bond. John Wiley and Sons, New York. 1981.
2. R. D. HUTCHINS, B. E. MARYANOFF, M. Y. CASTILLA, K. D. HARGRAVE, and A. T. MCPHAIL. J. Am. Chem. Soc. **101**, 1600 (1979).
3. B. E. MARYANOFF, A. T. MCPHAIL, and R. O. HUTCHINS. J. Am. Chem. Soc. **103**, 4432 (1981).
4. R. KINAS, W. J. STEC, and C. KRÜGER. Phosphorus Sulfur, **4**, 295 (1978).
5. J. SKOLIMOWSKI, R. SKOWRONSKI, and M. SIMALTY. Tetrahedron Lett. **50**, 4833 (1973).
6. B. M. GATEHOUSE and B. K. MISKIN. Acta Crystallogr. **330**, 2112 (1974).
7. M. CYGLER. Acta Crystallogr. B**35**, 195 (1979).
8. P. MAIN, L. LESSINGER, M. M. WOOLFSON, G. GERMAIN, and J. P. DECLERCQ. MULTAN78. A system of computer programs for the automatic solution of crystal structures from X-ray diffraction data. Universities of York, England and Louvain, Belgium. 1978.
9. A. C. LARSON. *In* Crystallographic computing. *Edited by* F. R. Ahmed. Munksgaard, Copenhagen. 1970. pp. 291–294.
10. A. C. LARSON and E. J. GABE. Computing in crystallography. *Edited by* H. Schenk, R. Olthof-Hazekamp, H. van Koningsfeld, and G. C. Bassi. Delft University Press. 1978. pp. 81–89.
11. International tables for X-ray crystallography. Vol. IV. Birmingham: Kynoch Press. 1974.
12. F. R. AHMED, S. R. HALL, M. E. PIPPY, and C. P. HUBER. J. Appl. Crystallogr. **6**, 309 (1973).
13. A. T. MCPHAIL, J. J. BREEN, and L. D. QUIN. J. Am. Chem. Soc. **93**, 2754 (1971).
14. A. T. MCPHAIL, J. J. BREEN, J. H. SOMERS, J. C. H. STEELE, JR., and L. D. QUIN. Chem. Commun. 1020 (1971).
15. N. L. ALLINGER and H. VAN VOITHENBERG. Tetrahedron, **34**, 627 (1978).
16. S. D. VENKATARAMU, K. D. BERLIN, S. E. EALICK, J. R. BAKER,

Can. J. Chem. Downloaded from www.nrcresearchpress.com by 210.87.254.6 on 09/06/12
For personal use only.

S. NICHOLAS, and D. VAN DER HELM. Phosphorus Sulfur, **7**, 133 (1979).
17. J. C. GALLUCCI and R. R. HOLMES. J. Am. Chem. Soc. **102**, 4379 (1980).
18. M. CYGLER, M. J. GRABOWSKI, J. SKOLIMOWSKI, and R. SKOWROŃSKI. Acta Crystallogr. B**34**, 2327 (1978).
19. L. D. QUIN, A. T. MCPHAIL, S. O. LEE, and K. D. ONAN. Tetrahedron Lett. **38**, 3473 (1974).
20. A. GRAND and P. REY. Acta Crystallogr. B**35**, 2149 (1979).
21. M. CYGLER, T. SKARŻYNSKI, J. SKOLIMOWSKI, and A. THOZET. Acta Crystallogr. B**36**, 2481 (1980).
22. G. D. MACDONELL, K. D. BERLIN, J. R. BAKER, S. E. EALICK, and D. VAN DER HELM. J. Am. Chem. Soc. **100**, 4535 (1978).
23. R. W. WARRENT, C. N. CAUGHLAN, J. H. HARGIS, C. K. YEE, and W. G. BENTRUDE. J. Org. Chem. **43**, 4266 (1978).
24. R. F. HUDSON and J. G. VERKADE. Tetrahedron Lett. **37**, 3231 (1975).
25. L. J. BERLINER. Acta Crystallogr. B**26**, 1198 (1970).
26. M. CYGLER. Can. J. Chem. **60**, 2392 (1982).

Can. J. Chem. Downloaded from www.nrcresearchpress.com by 210.87.254.6 on 09/06/12
For personal use only.

Synthèses et epimérisation de déoxy-spiro C-1 sucres

GEORGES REMY, LOUIS COTTIER ET GÉRARD DESCOTES
Laboratoire de Chimie Organique II, Université Lyon I, ERA 689 du C.N.R.S., 69622 Villeurbanne, France

Reçu le 12 juillet 1982

GEORGES REMY, LOUIS COTTIER et GÉRARD DESCOTES. Can. J. Chem. **61**, 434 (1983).

Les (oxo-3)-butyl-β-D-glucopyranosides de type déoxy-2, didéoxy-2,3 synthétisés à partir du tri-*O*-acétyl-D-glucal sont photolysés en hydroxyspirocétals selon un processus de type Norrish II non stéréosélectif. Leur réactivité est comparée à celle des dérivés α correspondants. L'épimérisation acidc des produits de cyclisation conduit préférentiellement aux spiro C-1 sucres de configuration α en accord avec les effets stéréoélectroniques des spirocétals.

GEORGES REMY, LOUIS COTTIER, and GÉRARD DESCOTES. Can. J. Chem. **61**, 434 (1983).

2-Deoxy and 2,3-dideoxy-3-oxo-butyl-β-D-glycopyranosides were synthesized starting from tri-*O*-acetyl-D-glucal. These β compounds undergo Norrish II type photocyclization giving the corresponding hydroxyspiroketals without stereoselectivity but with greater reactivity than the α derivatives. Acidic epimerization of these spiro C-1 sugars leads to the α anomers in accord with known stereoelectronic effects.

Can. J. Chem. Downloaded from www.nrcresearchpress.com by 210.87.254.42 on 09/06/12
For personal use only.

L'étude de la photocarbocyclisation des (oxo-3)-butylglycopyranosides a précédemment montré que la formation de spiro C-1 sucres était stéréospécifique (β-*gluco*) ou stéréosélective (α et β-*manno*) avec une réaction facilitée si l'hydrogène anomérique se situe initialement en position axiale (1−3). De même, les α-didéoxy-2,3-(oxo-3)butylglycosides subissant des photocyclisations difficiles (2), nous avons entrepris la synthèse des anomères β correspondants et étudié leur comportement photochimique pour le comparer à celui des anomères α.

Résultats

*Synthèse des déoxy-2 et didéoxy-2,3-β-D-glucopyranosides **4** et **5***

L'addition d'acétate mercurique sur le tri-*O*-acétyl-D-glucal **1** en présence d'hydroxy-1 butanone-3 permet d'obtenir selon le procédé décrit par Inglis *et al.* (4) et amélioré par Baer et Hanna (5) le composé **2** brut qui peut être soit traité par l'iodure de sodium pour donner **3**, soit photolysé en déoxy-2 glycoside **4**. Les rendements en **3** et **4** à partir de **1** sont respectivement de 25% et 16%. L'hydrogénation catalytique de **3** permet enfin de préparer **5** avec un rendement de 80% (Schéma 1).

Les structures des composés **3**, **4** et **5** sont déduites des spectres de rmn ^{1}H (tableau 1) par analogie des déplacements chimiques et constantes de couplages des protons du cycle et des protons anomériques H-1 avec les données de la littérature (5). Ainsi pour **3**, les déplacements chimiques de H-1, H-2 et H-3, (5,10 et 5,85 ppm) sont en accord avec ceux de l'éthylglycoside correspondant (5). De plus, la position de l'insaturation en 2−3 est justifiée par le processus rétro Diels−Alder de fragmentation en spectrométrie de masse (m/e = 198) caractéristique de cette structure (5). La configuration initiale β de **5** (δH-1, dd, 4, 60, $J_{1,2a}$ = 10 Hz, $J_{1,2e}$ = 4,5 Hz) permet de justifier la configuration β de **3** et la *trans*-addition de la réaction de synthèse à partir de **1**. De même, le composé **4** présente des déplacements et constantes de couplage analogues à ceux de **5** correspondant à une conformation chaise régulière pour le cycle.

*Photolyse de **3**, **4** et **5** et épimérisation des produits de photocyclisation **6**, **7** et **8***

L'irradiation en solution benzénique des composés **3**, **4** et **5** permet d'obtenir les mélanges de diastéréoisomères de spiro C-1 sucres correspondants (Schéma 1).

Comparativement aux anomères α précédemment étudiés (2) la photolyse de **3** et **5** est plus rapide et donne de meilleurs rendements en produits de photocyclisation. La séparation des quatre mélanges a été partiellement menée à bien pour **7** et **8** et non effectuée pour **6**. En effet, par chromatographie sur colonne de silice, on peut isoler les couples de diastéréoisomères se différenciant au niveau du carbone carbinolique (*cis*: A + B et *trans*: C + D) dont les structures sont établies par rmn. L'action des acides sur les mélanges permet d'aboutir aux spiro C-1 sucres thermodynamiquement les plus stables. Ainsi **7** (A + B) ou **7** (C + D) conduisent par traitement à l'acide paratoluène sulfonique avec des rendements voisins (70%) aux seuls composés **7**A et **7**C. Ces derniers composés stables en milieu acide sont de configuration α. De même, les spiro C-1 sucres insaturés **8** obtenus par photolyse de **3** donnent après traitement acide, les dérivés **8**A et **8**C avec un plus faible rendement du fait de leur fragilité (Rdt = 40%).

Ces épimérisations résultent de l'ouverture de l'un des cycles du système spirocétalique (6, 7). Pour confirmer ce processus sur un composé isolé pur précédemment (2, 8), un essai de traitement acide a été effectué sur le spiro [méthyl-3′-tétrahydrofurannol-3′]-1-2′ tétra-*O*-acétyl-2,3,4,6-β-D-glucopyranoside *trans* **9** qui a été transformé en un seul dérivé α *cis* **10** (Rdt = 70%) (Schéma 2).

Structures des spiro C-1 sucres

L'identification des spiro C-1 sucres résulte d'analyses rmn ^{1}H et ^{13}C sur les isomères **7**A,B,D isolés qui ont été appliquées aux dérivés **6** et **8**.

L'isomérie *cis-trans* localisée sur le cycle tétrahydrofuranique permet de préciser la configuration du carbone carbinolique qui est déduite des différences de déplacements chimiques Δδ en rmn ^{1}H et ^{13}C des carbones 3′ et 3″ (tableaux 1, 2, 3) précédemment établies dans d'autres séries (3, 9). Ainsi, les différences Δδ(**7**A − **7**D et **7**A − **7**C) exprimées en ppm (Δδ H-3″ = 0,20 et 0,13; Δδ C-1 = −3,0 et −3,2; Δδ C-3″ = +1,92 et 2,58) sont en accord avec une isomérie *cis* pour **7**A et *trans* pour **7**C et **7**D.

Les configurations α ou β au niveau du carbone anomère sont confirmées en rmn ^{1}H par les déplacements chimiques des protons H-3a et H-3e. Si la différence Δδ H-3a − H-3e est

Can. J. Chem. Downloaded from www.nrcresearchpress.com by 210.87.254.42 on 09/06/12
For personal use only.

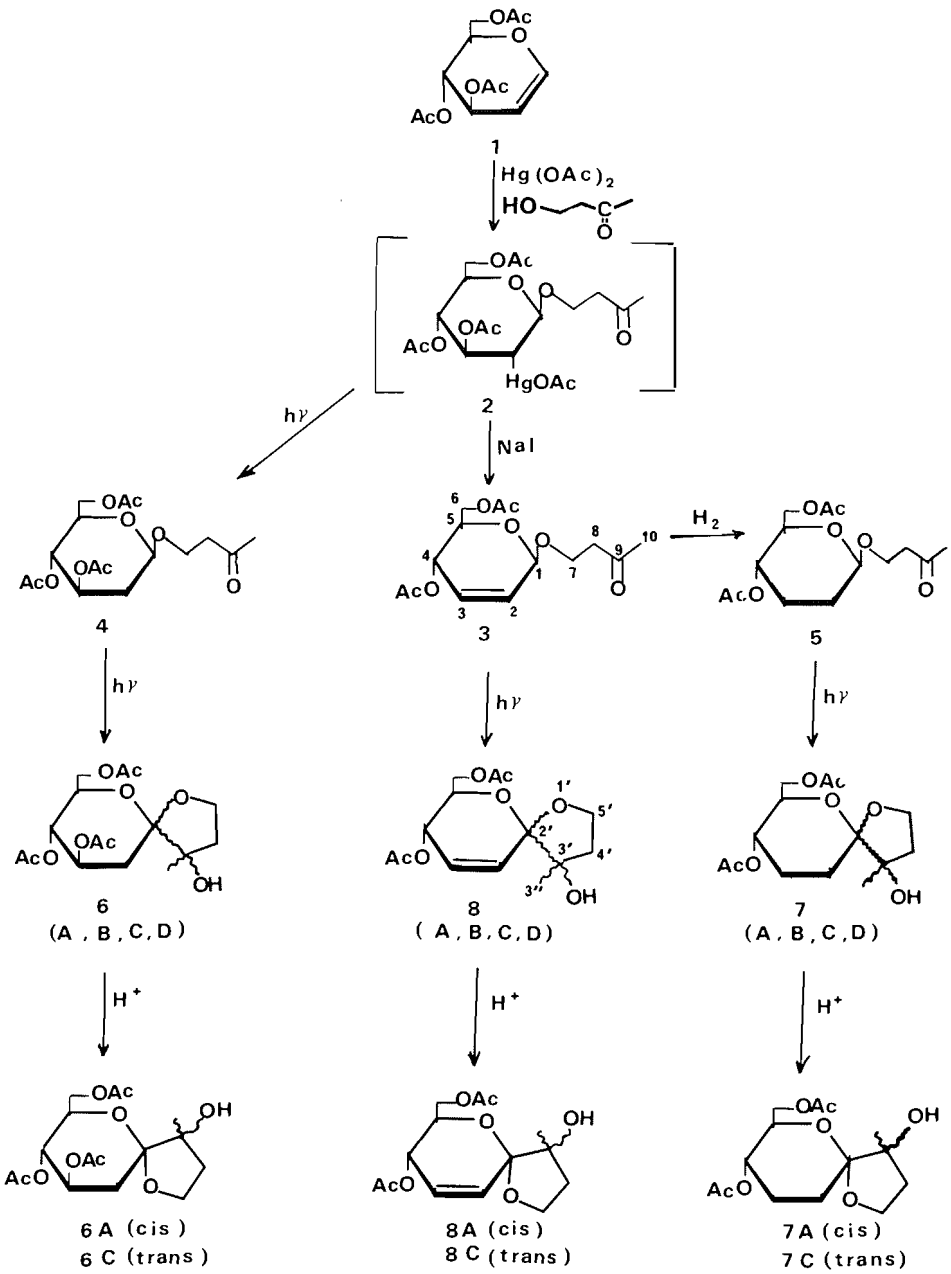

SCHÉMA 1. Synthèse et épimérisation des déoxy spiro C-1 sucres.

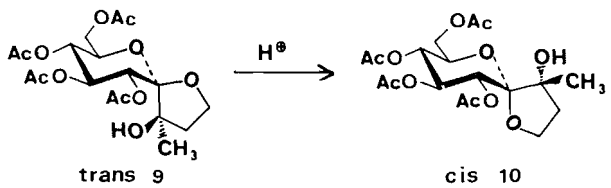

SCHÉMA 2

positive, la liaison furannique C—O est axiale (α) et provoque le déblindage de H-3a. Si cette même différence est négative, la liaison furannique C—O est équatoriale (β). Ainsi, les différences Δδ de 0,22, 0,11 et −0,22 observées respectivement pour **7**A, **7**B et **7**D confirment les configurations α de **7**A et **7**C et β de **7**D. Cette attribution est confirmée par rmn ^{13}C en comparant les déplacements chimiques des carbones C-5 des spiro C-1 sucres et du produit de départ **5**. En effet, les anomères α (**7**A et **7**C) ont un déplacement chimique pour C-5 (69,2 et 69,8 ppm) voisin de l'anomère α de **5** précédemment préparé (2) (68,6 ppm), alors que l'anomère β **7**D subit un effet γ d'environ 4 ppm (73,2 ppm).

Enfin, la conformation du cycle pyranosique correspond à une chaise qui confère aux protons du cycle des constantes de

TABLEAU 1. Déplacements chimiques (δ ppm, $CDCl_3$) des composés **8** (60 MHz), **3** (80 MHz), **5**, **10** (100 MHz) et **4**, **6**, **7** (250 MHz)

Composé	H-1	H-2a	H-2e	H-3a	H-3e	H-4	H-5	H-6	H-6′	H-8 ou H-4′	O ‖ —C—CH_3	H-10 ou H-3″
3	5,10 s (5,13)[a]		5,85 s (5,94)			5,50 d (5,21)	4,25 (4,02)	à m	3,50	2,65 t	2,20 à 3s	1,50
4	4,79 dd	3,28 dd	3,08 dd	5,08 ddd		4,89 dd	4,14 ddd	3,95 dd	3,38 dd	2,80 t	2,12 à 3s	1,90
5	4,60 dd	2,00 à m			1,70	4,75 m	4,30	à m	3,40	2,70 t	2,30 à 3s	1,90
7A				2,14 dd	1,92 dd	4,65 ddd	4,05 ddd	4,23 ddd	4,13 ddd			1,22 s
7C				2,03 dd	1,95 dd	4,13 ddd	4,05 ddd	3,68 ddd	3,58 ddd			1,35 s
8A		6,20	à m		5,90	5,05 d	4,30	à m	3,70	2,10 à 2s	2,05	1,35 s
8C		6,10	à m		5,90	5,20 d	4,30	à m	3,75	2,05 à 2s	2,0	1,25 s
6A		3,15 dd	3,06 dd		5,08 ddd	4,59 t	4,05 ddd	4,23 dd	4,13 dd			1,13 s
6B		3,05 dd	2,98 dd		5,02 ddd	4,79 dd	3,71 ddd	3,43 dd	3,27 dd			1,20 s
10		5,45 d		5,75 t		5,25 t	4,20 à m	3,50		2,00 à m	1,40	1,20 s

[a]Valeur de l'éthylglycoside correspondant (5).

TABLEAU 2. Constantes de couplages en Hz

Composé	$J_{1,2a}$	$J_{1,2e}$	$J_{2a,2e}$	$J_{2a,3a}$	$J_{2e,3a}$	$J_{2a,3e}$	$J_{2e,3e}$	$J_{3a,3e}$	$J_{3a,4}$	$J_{3e,4}$	$J_{4,5}$	$J_{5,6}$	$J_{5,6'}$	$J_{6,6'}$
3											5			
4	9,9	3,8	−11,25	9,2	6,2				10,25		10,55	2,7	5,8	−13,2
5	10	4,5									9			
7A				11,15	4,2	3,6	2,5	12,8	10,35	4,9	10,2	5,7	2,7	−12,7
7C				11,05	3,8	3,2	2,1	−12,5	10,2	5,5	10,5	5,5	2,6	−13,0
7D				7,5	5,1	4,2	1,2	−13,0	7,2	2,2	5,8	5,1	2,8	−12,7
8A									6					
8C									9					
9			−10,8	10,4	5,1				9,85		9,85	2,9	5,6	−13,0
10			−12,0	10,6	5,8				10,10		10,85	3,01	5,7	−12,7
12				9					9		9			

couplage $J_{2,3}$, $J_{3,4}$ et $J_{4,5}$ voisines de 10 Hz pour **7**A et **7**C et de 7 Hz pour **7**D qui doit présenter une certaine déformation moléculaire.

Si ces méthodes de détermination structurales utilisées pour **7** ont pu être appliquées aux dérivés **6**, les configurations des spiro C-1 sucres insaturés **8** ne peuvent être établies directement par rmn ^1H. Par contre, en rmn ^{13}C, on utilise également les différences de déplacement chimique des C-1 et C-5 pour **8**A et **8**C comparées à ceux des produits de départ **3** (5) pour lever le doute (tableau 3).

Discussion des résultats

Les données du tableau 4 montrent que les anomères β en série déoxyglucosidique sont plus réactifs que les anomères α précédemment étudiés (2). Cependant, les différences de réactivité sont plus faibles qu'en série *gluco* (2) ou *manno*. De telles différences de réactivité ont été récemment observées dans la réduction radicalaire de dérivés *O*-thiocarbonylés par les hydrures d'étain: en effet, la présence d'atome d'oxygène en β du carbone radicalaire semble favorable à sa stabilité (10). De la même façon, la présence d'un groupe acétate en 2 en position axiale ou équatoriale favorise le processus de type Norrish d'arrachement d'hydrogène anomérique.

La stéréosélectivité de la réaction de photocarbocyclisation, comme dans le cas des anomères α (2) est faible ou nulle. Cependant, un défaut de stéréosélectivité peut être compensé par une épimérisation acide qui facilite la formation de spiro C-1 sucres de configuration α. La stabilisation particulière de ces anomères résulte des effets anomères et exoanomères favorables à de telles structures, en accord avec les précédentes observations de Deslongchamps *et al.* (7) sur l'équilibre des spiroacétals.

L'influence de la conformation moléculaire devrait pouvoir être mieux cernée par l'étude en cours de la photocyclisation de systèmes présentant un équilibre conformationnel C1 ⇄ 1C comme pour les arabinosides.

Can. J. Chem. Downloaded from www.nrcresearchpress.com by 210.87.254.42 on 09/06/12
For personal use only.

TABLEAU 3. Déplacements chimiques des carbones dans $CDCl_3$ attribués par irradiation sélective des carbones (sauf pour **10**)

Composé	C-1	C-2	C-3	C-4	C-5	C-6	C-5′ ou C-7	C-4′ ou C-8	C-3′ ou C-9	C-3″ ou C-10
4	96,1	34,0	68,4	67,0	67,1	61,5	61,5	42,0	205,3	29,5
7A	103,2	25,0	21,7	67,6	69,2	63,7	64,1	38,3	80,7	22,7
7C	106,4	25,4	21,0	68,9	69,8	63,2	64,2	38,1	78,9	20,1
7D	106,2	25,4	21,5	68,2	73,2	63,8	64,3	37,3	80,4	20,8
8A	107,2	126,1	132,1	69,5	65,1	62,9	65,0	38,6	79,7	22,5
8C	109,2	125,9	132,0	69,0	66,2	63,2	65,3	37,9	81,3	20,9
6A	102,9	31,8	68,7	69,7	68,4	61,7	63,5	38,0	77,1	22,5
6C	107,0	31,9	70,0	70,7	69,0	62,7	64,5	38,0	80,8	20,2
10	103,6	68,0	73,0	68,0	68,6	61,7			79,0	21,7

Partie expérimentale

Synthèse des (oxo-3)-butyl glycosides

Les points de fusion non corrigés ont été déterminés sur un appareil Buchi. Les spectres rmn ^1H ont été tracés à température ambiante avec un spectromètre Varian A. 60 ou XL. 100, un Bruker WP 80 CW ou Cameca 250 et les spectres de rmn ^{13}C avec un Bruker WP 60 fonctionnant à 15,08 MHz par transformée de Fourrier. Les séparations chromatographiques ont été réalisées en faisant passer 0,3 à 3 g de produit brut sur 50 g à 150 g de silice (Merck 0,040−0,060 mm) contenue dans une colonne de 50 cm (ϕ 3,5 cm).

*Synthèse de l'(oxo-3)-butyl-di-*O*-acétyl-4,6-didéoxy-2,3-β-D-*érythro *hexéno-2 pyranoside* ***3***

Dix grammes (0,037 mol) du composé **1** ont été dissous dans 32,56 g (0,37 mol) d'hydroxy-1-butanone-3. Le mélange est agité sous 5 mm de mercure avec 12,3 g (0,037 mol) d'acétate mercurique. Après 2 h d'agitation, le mélange est filtré puis lavé 3 fois à l'eau, séché sur sulfate de sodium. Le mélange brut ainsi obtenu est mis en réaction avec de l'iodure de sodium (6 g) dans 200 mL d'éthanol 75%. Après 30 min d'agitation le tiers du solvant est évaporé sous vide et le résidu est extrait 7 fois à l'éther. Ces extraits sont réunis puis lavés à l'eau contenant du thiosulfate de sodium et enfin une fois à l'eau. On sèche sur sulfate de sodium. Après filtration et évaporation du solvant, le résidu est chromatographié sur colonne de silice (éther/hexane 70:30) donnant 2,8 g (0,92 mol) du composé **3** (rendement: 25%); liquide incolore; $[\alpha]_D^{23}$ +128° (*c* 1,0, $CHCl_3$). *Anal.* calc. pour $C_{14}H_{20}O_7$: C 55,89, H 6,71; trouvé: C 55,70, H 6,80.

*Synthèse de l'(oxo-3)-butyl-di-*O*-acétyl-4,6-didéoxy-2,3-β-D-*erythro *hexopyranoside* ***5***

On a hydrogéné 568 mg ($1,9 \times 10^{-3}$ mol) du composé **3** en présence de palladium sur charbon dans 20 mL d'éthanol absolu. Après filtration et chromatographie sur colonne du produit brut (éther/hexane 70:30) 487 mg ($1,61 \times 10^{-3}$ mol) du composé **5** ont été obtenus (rendement 80%); liquide incolore; $[\alpha]_D^{20}$ +144° (*c* 0,25, $CHCl_3$). *Anal.* calc. pour $C_{14}H_{22}O_7$: C 55,62, H 7,34; trouvé: C 55,80, H 7,28.

*Synthèse de l'(oxo-3)-butyl-tri-*O*-acétyl-3,4,6-déoxy-2-β-D-*gluco *hexopyranoside* ***4***

Un gramme du composé **1** (3,7 mmol) a été condensé avec l'hydroxy-1 butanone-3. Le produit brut qui en résulte a été dissous dans 40 mL de benzène (les conditions opératoires restent identiques à celles des (oxo-3)-butyl glycosides lors de la carbocyclisation) et irradié dans un tube de quartz. La réaction s'accompagne d'un dépôt de mercure; une filtration de la solution benzénique s'avère nécessaire par période de 4 h pour laisser passer la lumière. Après 20 h d'irradiation, la solution est filtrée puis le solvant est évaporé. Le résidu, chromatographié sur colonne de silice (acétate d'éthyle/hexane 7:3) donne 213 mg (0,06 mol) du composé **4** (rendement 16%); composé amorphe; $[\alpha]_D^{20}$ +57° (*c* 1,0, $CHCl_3$). *Anal.* calc. pour $C_{16}H_{24}O_9$: C 53,33, H 6,71; trouvé: C 53,60, H 6,90.

Photolyse et épimérisation des (oxo-3)-butyl glycosides

La photolyse a été réalisée dans les conditions opératoires déjà décrites (2). La lampe est munie d'un filtre Vycor. Après photolyse le solvant est évaporé puis le résidu est chromatographié sur colonne de silice.

TABLEAU 4. Caractéristiques de la photolyse des oxo-3-butyl glycosides

Composés	Temps d'irradiation (h)	Taux de conversion (%)	Rendement global (%)
3β	6	100	43
3α	10	80	29
5β	30	80	40
5α	48	90	33

Glycoside ***4***: 916 mg du composé **4** dissous dans 50 mL de benzène ont été irradiés pendant 60 h. Le produit brut obtenu après évaporation est traité à température ambiante avec 380 mg d'acide paratoluène sulfonique. Après 4 h d'agitation, le milieu réactionnel est neutralisé avec $NaHCO_3$ dissous dans l'eau. Après séchage, filtration et évaporation du solvant, le résidu est chromatographié sur colonne de silice (dichloro-1,2 éthane/acétone 85:15) pour conduire aux spiro [méthyl-3′-tétrahydrofuranol-3′] 1-2′tri-*O*-acétyl-3,4,6-α-D-*arabino* hexopyranoside **6A** *cis* (34 mg, 10^{-4} mol) et **6C** *trans* (46 mg, $0,13 \times 10^{-3}$ mol) et 182 mg ($0,55 \times 10^{-3}$ mol) de composé **4** qui n'ont pas été photolysés (rendement 10%).

Composé ***6A***: liquide jaune; $[\alpha]_D^{23}$ +84° (*c* 1,0, $CHCl_3$). *Anal.* calc. pour $C_{16}H_{24}O_9$: C 53,33, H 6,71; trouvé: C 53,60, H 6,80.

Composé ***6C***: liquide jaune; $[\alpha]_D^{23}$ +125° (*c* 1,0 $CHCL_3$). *Anal.* calc. pour $C_{16}H_{24}O_9$: C 53,33, H 6,71; trouvé: C 52,90, H 6,50.

Glycoside ***5***: 388 mg ($1,3 \times 10^{-3}$ mol) du composé **5** dissous dans 25 mL de benzène ont été irradiés pendant 60 h. Après évaporation du solvant et chromatographie sur colonne de silice (dichlorométhane/acétone 85:15) pour conduire à 63 mg (0,16 mmol) de composé **7** A + B *cis* et 92 mg (0,23 mmol) de composé **7** C + D (poids total 155 mg; rendement 40%). Epimérisation: 300 mg (10^{-3} mol) du mélange **7** A + B ont été traités par 184 mg (10^{-3} mol) d'acide paratoluènesulfonique, comme le composé **4**. Après séparation sur colonne de silice (dichloro-1,2 éthane/acétone 85:15), 211 mg ($0,7 \times 10^{-3}$ mol) du spiro [méthyl-3′ tétrahydrofuranol-3′]1-2′-di-*O*-acétyl-4,6-didéoxy-2,3-α-D-*erythro* hexopyranoside *trans* **7C** ont été isolés (rendement 70%). Solide blanc, *F* 74−76°C; $[\alpha]_D^{23}$ +105° (*c* 1,0, $CHCl_3$). *Anal.* calc. pour $C_{14}H_{22}O_7$: C 55,62, H 7,34; trouvé C 55,61, H 7,41.

Trois cent milligrammes du mélange **7** C + D ont été traités avec l'acide paratoluène sulfonique dans les mêmes conditions que le composé **4** et donnent 215 mg ($0,7 \times 10^{-3}$ mol) de spiro [méthyl-3′-tétrahydrofuranol-3′] 1-2′-di-*O*-acétyl-4,6-didéoxy-2,3-α-D-*erythro* hexopyranoside *cis* **7A** (rendement 70%); solide blanc; *F* 68°C; $[\alpha]_D^{24}$ +67,2° (*c* 1,0, $CHCl_3$). *Anal.* calc. pour $C_{14}H_{22}O_7$: C 55,62, H 7,34; trouvé: C 55,79, H 7,37.

Glycoside ***3***: 366 mg ($1,22 \times 10^{-3}$ mol) du composé **8** ont été dissous dans 26 mL de benzène et irradiés pendant 25 h. Après évaporation du solvant et chromatographie sur colonne de silice

Can. J. Chem. Downloaded from www.nrcresearchpress.com by 210.87.254.42 on 09/06/12
For personal use only.

(dichlorométhane/acétone 85:15), 90 mg du mélange **8** A + B *cis* et 93 mg de **8** C + D *trans* ont été isolés. Poids total 183 mg (0,61 mmol, rendement 43%). Epimérisation: 300 mg (10^{-3} mol) de chaque série *cis* et *trans* ont été traités en présence d'acide paratoluène sulfonique dans du dichlorométhane pour donner respectivement 123 mg de spiro [méthyl-3′-tétrahydrofuranol-3′] 1-2′-di-*O*-acétyl-4,6-didéoxy-2,3-α-D-*erythro* hexeno-2-pyranoside *trans* **8**C et 120 mg de *cis* **8**A. *Anal.* calc. pour $C_{14}H_{20}O_7$: C 55,99, H 6,71; trouvé: C 55,74, H 6,95.

Epimérisation du composé ***9*** *(2, 8)*: 150 mg (0,36 mmol) du composé **9** ont été traités avec 66 mg (0,36 mmol) d'acide paratoluène sulfonique. Après neutralisation et chromatographie sur colonne de silice (acétate d'éthyle/hexane 70:30), 105 mg (0,25 mmol) du composé **10** ont été isolés (rendement 70%); solide blanc (éther); *F* 112°C; $[\alpha]_D^{23}$ +55° (*c* 1,0, $CHCl_3$). *Anal.* calc. pour $C_{18}H_{26}O_{11}$: C 51,67, H 6,26; trouvé: C 51,90, H 6,30.

Remerciement

Les spectres rmn ^1H (250 MHz) et ^{13}C ont été faits par F. Metras et M. F. Grenier-Loustalot de l'Université de Pau et des Pays de l'Adour, Avenue Philippon, 64000 Pau, France, que nous remercions bien vivement.

1. G. REMY, L. COTTIER et G. DESCOTES. Tetrahedron Lett. 1847 (1979).
2. G. REMY, L. COTTIER et G. DESCOTES. Can. J. Chem. **58**, 2660 (1980).
3. G. REMY, L. COTTIER et G. DESCOTES. J. Carbohydr. Chem. **1**, 37 (1982).
4. G. R. INGLIS, J. P. SCHWARZ et MC LAREN. J. Chem. Soc. 1014 (1962).
5. H. H. BAER et Z. S. HANNA. Can. J. Chem. **59**, 889 (1981).
6. G. R. PETIT et W. J. BOWYER. J. Org. Chem. **25**, 84 (1960).
7. P. DESLONGCHAMPS, D. D. ROWAN, N. POTHIER, T. SAUVE et J. K. SAUNDERS. Can. J. Chem. **59**, 1105 (1981).
8. G. REMY, L. COTTIER, G. DESCOTES, R. FAURE, H. LOISELEUR et G. THOMAS-DAVID. Acta Crystallogr. Sect. B, **36**, 873 (1980).
9. (*a*) L. COTTIER, G. DESCOTES, M. F. GRENIER et F. METRAS. Tetrahedron, **37**, 2515 (1981); (*b*) L. COTTIER et G. DESCOTES. J. Heterocycl. Chem. 1271 (1977).
10. D. H. R. BARTON, W. HARTWIG et W. B. MOTHERWELL. J. Chem. Soc. Chem. Commun. 447 (1982).

Can. J. Chem. Downloaded from www.nrcresearchpress.com by 210.87.254.42 on 09/06/12
For personal use only.

Changing regioselectivity patterns in metal hydride reductions of unsymmetrically substituted cyclic anhydrides

MARGARET M. KAYSER[1]
Département de chimie, Université de Moncton, Moncton, N.B., Canada E1A 3E9

AND

JUDITH SALVADOR AND PETER MORAND
Ottawa–Carleton Institute for Research and Graduate Studies in Chemistry, University of Ottawa Campus, Ottawa, Ont., Canada K1N 9B4

Received September 9, 1982

MARGARET M. KAYSER, JUDITH SALVADOR, and PETER MORAND. Can. J. Chem. **61**, 439 (1983).

A study of L- and K-selectride reductions of unsymmetrical cyclic anhydrides attached to six-membered rings and to bridged six-membered systems sheds a new light on the effect of the conformation of the substrate molecule on the regioselectivity of metal hydride reductions. Thus, in addition to intrinsic reactivity of the carbonyl group, the antiperiplanar effect, and steric congestion, the conformation of the parent molecule should be considered in predicting regioselectivity of nucleophilic additions to cyclic anhydrides.

MARGARET M. KAYSER, JUDITH SALVADOR et PETER MORAND. Can. J. Chem. **61**, 439 (1983).

Une étude des réductions, par les sélectrides de type L et K, des anhydrides cycliques non symétriques attachés à des cycles à 6 chaînons et à des systèmes cycliques pontés à six chaînons fournit des précisions nouvelles sur l'effet de la conformation de la molécule de substrat sur la régiosélectivité des réductions par les hydrures métalliques. Ainsi, en plus de la réactivité intrinsèque du groupe carbonyle, de l'effet anti-périplanaire et de l'encombrement stérique, on doit considérer la conformation de la molécule de départ lorsqu'on prévoit la régiosélectivité des additions nucléophiles sur les anhydrides cycliques.
[Traduit par le journal]

The *gem*-disubstituted succinic anhydrides **1**, **2**, and **3** react with simple metal hydrides ($NaBH_4$ and $LiAlH_4$) to give the corresponding lactones **1***a*, **2***a*, and **3***a*, reduced selectively at the more highly substituted carbonyl group (1, 2). Similar patterns of regioselectivity are observed for $NaBH_4$ and $LiAlH_4$ reductions of anhydrides **4** and **5**, which yield respectively the lactones **4***a* (3) and **5***a* (1) as products.

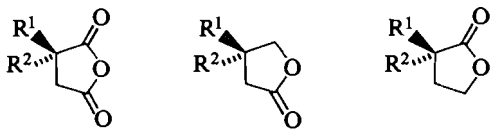

1	$R^1 = R^2 =$ Me	**1***a*	**1***b*
2	$R^1 = R^2 =$ Ph	**2***a*	**2***b*
3	$R^1 =$ Me $R^2 =$ Et	**3***a*	**3***b*

Recently (4) we have reported that reversal of selectivity (i.e. formation of lactones reduced at the less substituted carbonyl function) can be achieved when compounds **1**, **2**, and **3**, are reduced with K- or L-selectrides. We expected a similar reversal of regioselectivity in selectride reductions of anhydrides **4** and **5**, but to our dismay the only products observed were the lactones **4***a* and **5***a*. On the other hand, the bridged anhydride **6** was reduced with selectrides similarly as with $NaBH_4$ or $LiAlH_4$ exclusively at the less substituted carbonyl group, to the lactone **6***b* (Table 1).

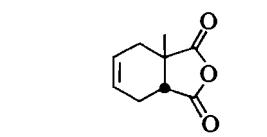

4

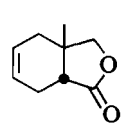

4*a*

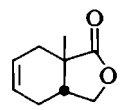

4*b*

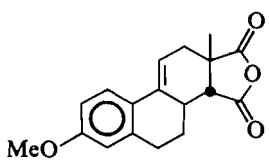

5

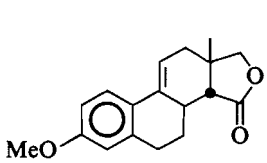

5*a*

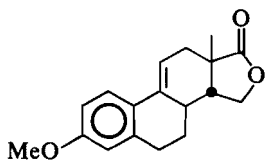

5*b*

These results, disappointing as far as synthetic applications are concerned, are nonetheless interesting from the mechanistic viewpoint. Why are the anhydrides **4** and **5** reduced always at

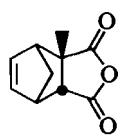

6

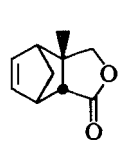

6*a*

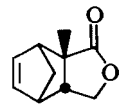

6*b*

[1]Author to whom correspondence should be addressed.

Can. J. Chem. Downloaded from www.nrcresearchpress.com by 210.87.254.105 on 09/06/12
For personal use only.

TABLE 1. Reductions of unsymmetrically substituted cyclic anhydrides

Anhydride	Method	Ratio of lactone *a*	Ratio of lactone *b*	% Yield of *isolated* lactonic product
4	$NaBH_4/LiAlH_4$	100	—	80
	selectride	100	—	50
5	$NaBH_4/LiAlH_4$	100	—	80–90
	selectride	100	—	62
6	$NaBH_4/LiAlH_4$	—	100	84–86
	selectride	—	100	50–60

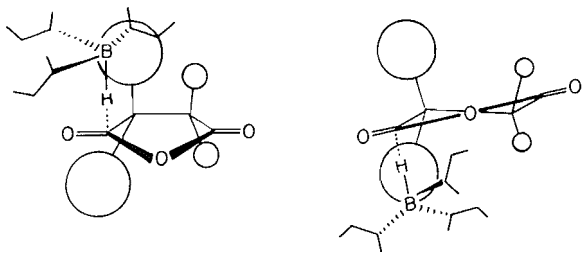

FIG. 1. Due to the size and the shape of the reagent molecule the approach to the more hindered carbonyl function is particularly unfavourable regardless of the conformation of the anhydride ring.

the more substituted carbonyl group, even with highly hindered selectrides, while compound **6** is reduced at the less hindered carbonyl group under comparable conditions?

We have suggested previously (5) that the following three factors control the regioselectivity of metal hydride reductions: (a) the intrinsic reactivity of the carbonyl group; (b) the antiperiplanar effect; (c) steric hindrance. The regioselectivity of selectride reductions of compounds **1**, **2**, and **3** may be rationalized in terms of these effects in the following manner. Due to the high steric demand of the reagent,[2] steric congestion (c) becomes the dominant factor overriding the influences of the effects (a) and (b). The reagent's approach to the more hindered carbonyl function is difficult regardless of the conformation, plannar or twisted, of the anhydride ring (Fig. 1). Thus the reaction occurs selectively at the less substituted carbonyl group.

At first glance one might expect the same type of interaction in the selectride reduction of the anhydrides **4** and **5**. However, it appears that the approach of the reagent is restricted in a different fashion. The six-membered carbocyclic ring assumes preferentially a chair-like configuration, and in the process the attached anhydride ring is distorted from a planar to a twisted configuration suitable for the antiperiplanar attack at the C—CH_3 bond (Fig. 2). In effect, while the attack on the "top" face of the anhydride ring is hindered by the methyl substituent, the "bottom" face is slightly more open. As a result, the nucleophilic attack should occur preferentially on the "bottom" face of the molecule. Moreover, as the two electronic effects promote reduction of the carbonyl group adjacent to the methyl substituent, since (a) the more highly substituted carbonyl function should be intrinsically more reactive toward nucleophilic attack (6), and (b) the conformation of the molecule permits attack antiperiplanar to the C—CH_3 bond (7), we

[2]The selectride reagent resembles in shape a large and rigid umbrella of which H is a handle.

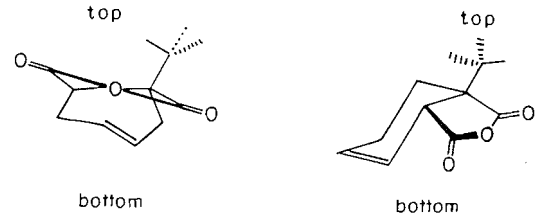

FIG. 2. The anhydride ring attached to the six membered cyclic system is distorted from planarity. Attack by the nucleophile from the "top" side is disfavoured by the presence of methyl substituent. The preferred attack: antiperiplanar to the C—CH_3 bond from the "bottom" side explains the regioselectivity observed in these reductions.

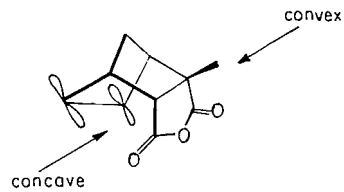

FIG. 3. Nucleophilic addition to the carbonyl group takes place from the more open convex side. The approach to the concave face is prevented by the π electrons of the double bond.

might expect hydride transfer occurring at this site (i.e. from the "bottom" side of the molecule at the carbonyl group adjacent to the methyl group).

The above considerations explain the regioselectivity observed in the reduction of anhydrides **4** and **5** by selectride reagents as well as by simple metal hydrides. The situation is different in the case of the bridged anhydride **6**. Here, the geometry of the six-carbon ring is fixed in the boat conformation by the methylene bridge. The anhydride attached to such a system is rigidly planar. It has been shown that in analogous bridged systems the nucleophile adds only from the "convex" side of the molecule (8). Thus as the attack from the "concave" side is prevented by the π electrons of the double bond, hydride must be transferred to the "convex" face of the molecule (Fig. 3).

In this case the simple metal hydrides, as well as the selectrides, can add more easily to the carbonyl function adjacent to the hydrogen atom than to the carbonyl group neighbouring the methyl substituent. Thus the reaction occurs regioselectively at the less hindered carbonyl function.

In conclusion, these examples confirm the previously proposed hypothesis stating that at least three different factors are implicated in the control of regioselectivity of metal hydride addition to the carbonyl group. The conformation of the molecule and the steric constraints associated with it, the intrinsic reactivities of two carbonyl functions, and the possibility of the antiperiplanar attack are all intimately involved. The observed selectivity is the net result of the interplay between these effects.

Experimental

The preparation of the anhydrides (**1** to **6**) has been described previously (1, 3).

Analyses of the reduction products were carried out on the crude reaction mixtures by gas–liquid chromatography and/or ^1H nmr. The lactonic product yields reported in Table 1 are the isolated yields. The modest quantities of lactones obtained reflect the difficulties encoun-

Can. J. Chem. Downloaded from www.nrcresearchpress.com by 210.87.254.105 on 09/06/12
For personal use only.

tered in isolation and purification procedures, chiefly due to the high solubility of lactones in the aqueous phase.

Melting points were determined on a Thomas Hoover capillary melting point apparatus and are uncorrected. Infrared spectra were obtained on a Beckman IR-20 spectrophotometer and ^{1}H nmr spectra in $CDCl_3$ or DMSO with TMS as internal standard on a Varian AA-100 or EM 360 A instrument. Tetrahydrofuran was refluxed under nitrogen with potassium and benzophenone until the solution became purple, then was distilled into an oven-dried flask containing the anhydride to be reduced.

General reduction procedure

The anhydride (0.005 mol) was placed in a three-neck oven-dried flask into which 50 mL of THF was subsequently distilled. The flask was fitted with an inlet post for syringes, gas inlet and outlet tubes, and a magnetic stirrer. The solution swept with a slow stream of nitrogen was cooled to −70°C in a Dry Ice − acetone bath. K- or L-selectride (1.0 *M* solution in THF, 11 mL) was injected slowly into the reaction flask. The temperature of the reaction mixture was allowed to rise to 0°C over a period of 30 to 90 min, NaOH (4 *N* solution, 2 mL) and 30% H_2O (3 mL) were added cautiously. After stirring for 15 to 20 min sodium bisulfite was added to destroy the excess peroxide. The reaction mixture was acidified to pH 2 with 6 *N* HCl and was stirred overnight. The layers were separated and the acidic aqueous layer saturated with NaCl and extracted with ether and with methylene chloride. The extraction was a crucial step due to the lactones' solubility in water. In some cases a liquid−liquid extraction of the aqueous layer with ether was carried out for 24 h. The combined organic layers were dried, the solvent reduced in volume, and the product analyzed using a Varian Vista 6000 gas chromatograph with an ionization detector using a 6 ft 3% PC 3210 column.

Lactone identification

Individual lactones were separated by chromatography on silica gel:

β,β-Dimethyl-γ-butyrolactone (1) **1***a*, ν_{max}: 1775 cm^{-1} (lactone C=O); δ: 1.20 (s, 6H, $2CH_3$), 2.34 (s, 2H, CH_2—C=O), 3.98 (s, 2H, CH_2—O).

α,α-Dimethyl-γ-butyrolactone (1) **1***b*, ν_{max}: 1770 cm^{-1} (lactone C=O); δ: 1.28 (s, 6H, $2CH_3$), 2.12 (t, 2H, CH_2—C=O), 4.26 (t, 2H, CH_2—O).

β,β-Diphenyl-γ-butyrolactone (1) **2***a*, mp 108−109°C (lit (9) mp 109−110°C); ν_{max}: 1780 cm^{-1} (lactone C=O); δ: 3.28 (s, 2H), 4.90 (s, 2H), 7.36 (m, 10H).

α,α-Diphenyl-γ-butyrolactone (1) **2***b*, mp 77−79°C; ν_{max}: 1780 cm^{-1} (lactone C=O); δ: 2.9 (t, 2H), 4.2 (t, 2H), 7.3 (s, 10H).

β-Ethyl, β-methyl-γ-butyrolactone **3***a*, ν_{max}: 1780 cm^{-1} (lactone CO); δ: 1.1 (m, 6H), 1.5 (q, 2H), 2.3 (s, 2H), 3.95 (s, 2H).

α-Ethyl, α-methyl-γ-butyrolactone **3***b*, ν_{max}: 1780 cm^{-1} (lactone CO); δ: 1.1 (m, 6H), 1.5 (q, 2H), 2.1 (m, 2H), 4.2 (t, 2H).

cis-1-Methylcyclohex-4-ene-1,2-discarboxylic acid anhydride **4***a* (3), ν_{max}: 1770 cm^{-1} (lactone CO): δ: 1.3 (s, 3H, CH_3), 2.3 (m, 6H), 3.95 (q, 2H, CH_2—O). 5.65 (m, 2H).

Steroidal lactone **5***a* (1), mp 174−176°C; ν_{max}: 1765 cm^{-1} (lactone CO); δ: 1.18 (s, 3H, CH_3), 3.80 (s, 3H, OCH_3), 4.00 (q, 2H, CH_2—O).

exo-2-Methylnorborn-5-ene-*endo*-(3-methyl-2-carbo-3a) lactone **6***b* (1), mp 137−139°C; ν_{max}: 1765 cm^{-1} (lactone CO); δ: 1.52 (s, 3H, CH_3), 4.02 (m, 2H, CH_2—O), 6.33 (m, 2H).

Acknowledgement

Financial support from the Natural Sciences and Engineering Research Council of Canada is gratefully acknowledged.

1. M. M. KAYSER and P. MORAND. Can. J. Chem. **56**, 1524 (1978).
2. D. M. BAILEY and R. E. JOHNSON. J. Org. Chem. **35**, 3575 (1970).
3. J. J. BLOOMFIELD and S. L. LEE. J. Org. Chem. **32**, 3919 (1967).
4. P. MORAND, J. SALVADOR, and M. M. KAYSER. J. Chem. Soc. Chem. Commun. 458 (1982).
5. M. M. KAYSER and G. WIPFF. Can. J. Chem. **60**, 1192 (1982).
6. M. M. KAYSER and O. EISENSTEIN. Can. J. Chem. **59**, 2457 (1981).
7. J. HUET, Y. MARONI-BARNAND, NGUYEN TRONG ANH, and J. SEYDEN-PENNE. Tetrahedron Lett. 159 (1976); NGUYEN TRONG ANH and O. EISENSTEIN. Tetrahedron Lett. 155 (1976).
8. W. L. DILLING and R. A. PLEPYS. J. Org. Chem. **35**, 2971 (1970).
9. F. SALMON-LEGAGNEUR. C. R. Acad. Sci. **227**, 437 (1948).

Can. J. Chem. Downloaded from www.nrcresearchpress.com by 210.87.254.105 on 09/06/12
For personal use only.

Methylenecyclohexenes: inversion barriers from the far-infrared spectra

TRACY L. SMITHSON, NAN IBRAHIM, AND HAL WIESER[1]
Department of Chemistry, University of Calgary, Calgary, Alta., Canada T2N 1N4

Received August 2, 1982

TRACY L. SMITHSON, NAN IBRAHIM, and HAL WIESER. Can. J. Chem. **61**, 442 (1983).

The far-infrared spectra of 3-methylenecyclohexene, 4-methylenecyclohexene, and 1-methyl-3-methylenecyclohexene in the region of 80–400 cm^{-1} are reported and interpreted mainly with a view to the two lowest out-of-plane deformations of the cyclohexene ring. Typical C-type band sequences are observed and interpreted in terms of ring inversion modes. Barriers to inversion are determined by means of a one-dimensional Hamiltonian with a quadratic-quartic potential function. Possible ground state geometries and forms of the inversion coordinates are discussed and compared to those thought to occur in the analogous cyclohexenones.

TRACY L. SMITHSON, NAN IBRAHIM et HAL WIESER. Can. J. Chem. **61**, 442 (1983).

On rapporte les spectres infrarouges du méthylène-3 cyclohexène, du méthylène-4 cyclohexène et du méthyl-1 méthylène-3 cyclohexène dans la région allant de 80 à 400 cm^{-1} et on les interprète principalement en fonction des deux déformations hors plan les plus faibles du cycle du cyclohexène. On a observé des suites de bandes de type-C typiques et on les a interprétées en fonction des modes d'inversion du cycle. On a déterminé les barrières à la rotation au moyen d'un Hamiltonien unidimensionnel avec une fonction de potentiel quadratique-quartique. On discute des géométries de l'état fondamental possible et des formes des coordonnées d'inversion et on les compare avec celles qu'on croit trouver dans les cyclohexanones analogues.
[Traduit par le journal]

Can. J. Chem. Downloaded from www.nrcresearchpress.com by 210.87.254.5 on 09/06/12
For personal use only.

Introduction

Recent far-infrared studies of cyclohexenones (1) showed that the position of the carbonyl group in relation to the double bond significantly affects the geometry of the cyclohexene ring, the barrier to planarity for the planar configuration, and the dynamic path followed by the ring inversion. It was of interest to us to pursue the underlying thought also for methylenecyclohexenes, molecules that, while similar, differ in important respects.

3-Methylenecyclohexene (3MCH)

4-Methylenecyclohexene (4MCH)

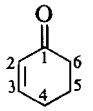

2-Cyclohexene-1-one (2CHO)

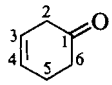

3-Cyclohexene-1-one (3CHO)

In the following we report the far-infrared spectra of 3-methylenecyclohexene and 4-methylenecyclohexene. In addition we investigated the same region of the infrared spectrum for 1-methyl-3-methylenecyclohexene (1M3MCH) with the hope of probing the effect of methyl substitution on the inversion barrier. No far-infrared or microwave spectra or electron diffraction studies have been reported previously for these compounds.

Experimental

Synthesis of the compounds

Although all three compounds have been made previously (2), our synthetic routes differed substantially from the earlier reported methods and are therefore described briefly below.

(i) 3-Methylenecyclohexene

3-Bromocyclohexene (3) was first reacted with triphenylposphine in acetonitrile to give cyclohex-3-en-1-yltriphenylphosphonium bromide (4) (96% yield, mp 220.2°C, lit. (4) mp 222–224°C). 3MCH was then prepared via the Wittig reaction (5) by adding excess paraformaldehyde to a solution of cyclohex-3-en-1-triphenylphosphine ylid, made from the bromide (43 g) and n-butyllithium (7 g) in ether (100 mL) (38% yield, bp 100–105°C, lit. (2*a*) bp 100–110°C). Final purification was achieved by preparative gc; nmr (60 MHz, $CDCl_3$): 6.30–5.55 (multiplet, 2H, vinyl), 4.70 (broad singlet, 2H, *exo*-CH_2), 2.50–1.40 (multiplet, 6H, C4 to C6 protons).

(ii) 1-Methyl-3-methylenecyclohexene

1M3MCH was made via the Wittig reaction (5) from 3-methylcyclohex-2-en-1-one (purchased from Aldrich) and methylenetriphenylphosphine ylid. The latter was prepared from triphenylmethylphosphonium bromide (29 g) (5) and n-butyllithium (55 mL of 1.6 *M* solution in hexane) in ether (200 mL). The overall yield after distillation was 42%, bp 25–28°C/12 Torr (lit. (2*b*) bp 135–136°C); nmr (60 MHz, $CDCl_3$): 5.94 (broad singlet, 1H, vinyl), 4.63 (broad singlet, 2H, *exo*-CH_2), 2.43–1.75 (multiplet, 6H, C4 to C6 protons), 1.80 (singlet, 3H, methyl).

(iii) 4-Methylenecyclohexene

The precursor 1-bromomethyl-3-cyclohexene was first synthesized by reaction of the alcohol and PBr_3 (6) in low yield (28%) and containing several other addition products. With the preferred procedure 3-cyclohexen-1-methyltosylate was refluxed with LiBr in acetone (7) giving the desired bromide in 74% yield (bp 72°C/12 Torr, lit. (6) bp 100–120°C/35 Torr). Dehydrobromination of 1-bromomethyl-3-cyclohexene was affected by reaction with DBU. The crude liquid product (30% yield) was purified by redistillation (bp 100–104°C, lit. (2*c*) bp 104–106°C); nmr (60 MHz, $CDCl_3$): 5.65 (broad singlet, 2H, vinyl), 4.72 (broad singlet, 2H, *exo*-CH_2), 2.75 (broad singlet, 2H, allylic), 2.25 (muliplet, 4H, allylic) (2*c*).

The spectra

All spectra were obtained with a Nicolet Series 8000 Interferometer, equipped with a 60 m matched variable path gas cell manu-

[1]Author to whom all correspondence should be addressed.

Can. J. Chem. Downloaded from www.nrcresearchpress.com by 210.87.254.5 on 09/06/12
For personal use only.

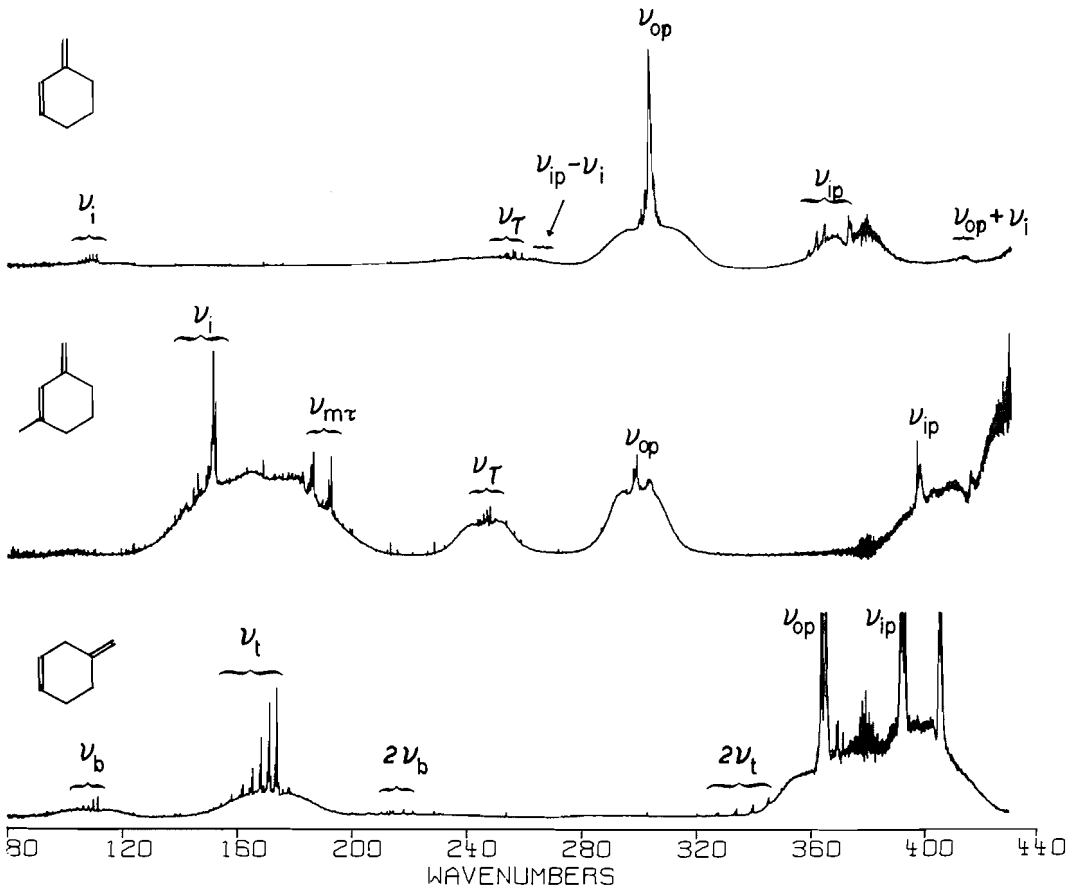

FIG. 1. Survey spectra of 3-methylenecyclohexene, 1-methyl-3-methylenecyclohexene, and 4-methylenecyclohexene.

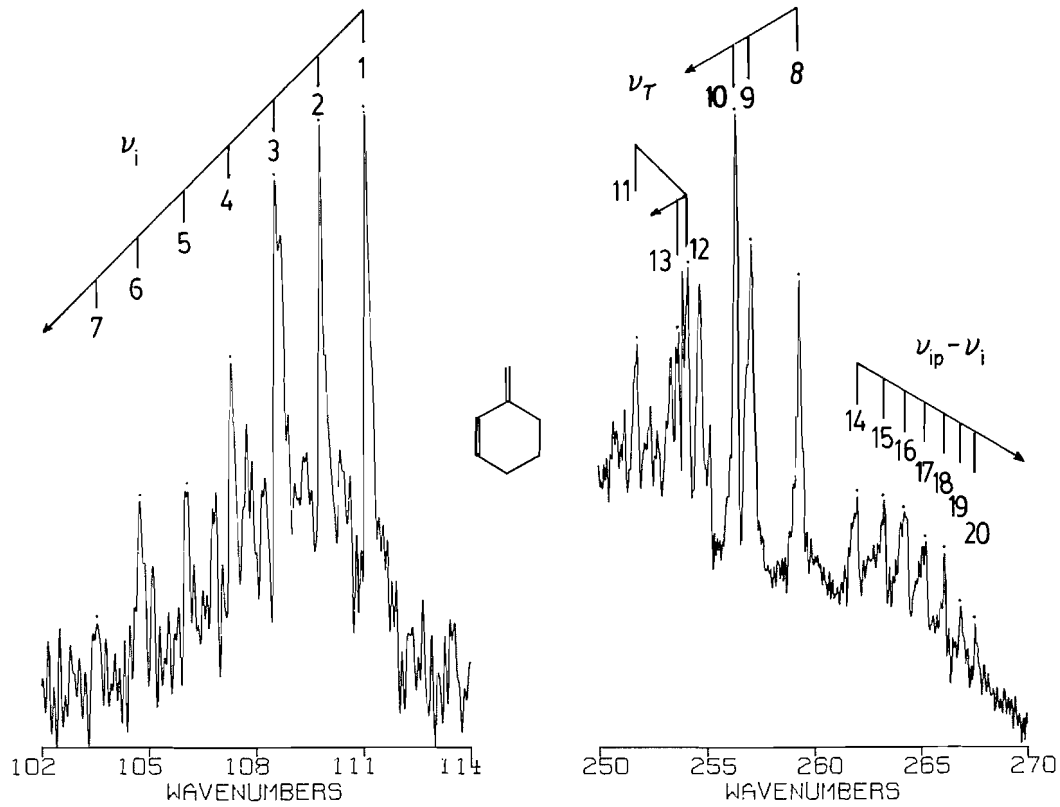

FIG. 2. Expansions of ν_i, ν_τ, and $\nu_{ip} - \nu_i$ sequences of 3-methylenecyclohexene. Same absorbance scale for both fields. Numbered bands correspond to peak positions listed in Table 1 (for ν_i) and transitions summarized in Fig. 4.

TABLE 1. Inversion transitions and parameters of 3-methylenecyclohexenes

Transition[a]		3MCH						1M3MCH		
		ν_i[b]		ν_{op}[c]		ν_{ip}[d]		ν_i[b]		
$\nu_u \leftarrow \nu_l$		No.	Obs (cm^{-1})	Δ[e]	Obs (cm^{-1})	Δ[e]	Obs (cm^{-1})	Δ[e]	No.	Obs (cm^{-1})	Δ[e]
3,2	1,0	1	111.13	0.09	111.76	0.05	111.11	0.14	34	152.74	−0.29
5,4	3,2	2	109.86	0.00	110.38	−0.07	109.54	−0.12	35	150.12	0.33
7,6	5,4	3	108.60	−0.04	109.13	−0.01	108.30	−0.01	36	146.47	0.14
9,8	7,6	4	107.32	−0.07	107.82	0.03	106.94	0.04	37	142.42	−0.18
11,10	9,8	5	106.06	−0.05			105.23	0.21			
13,12	11,10	6	104.77	0.00			104.08	0.16			
15,14	13,12	7	103.44	0.07							
Fitting parameters:[f]											
Std. dev. of obs (cm^{-1})			0.07		0.06		0.16			0.35	
$(V_2/m\gamma)$ (cm^{-1})			−31.457(31)		−31.886(42)		−31.494(79)			−76.147(380)	
$(V_4/(m\gamma)^2)$ (cm^{-1})			0.11764(116)		0.12790(272)		0.13069(348)			0.94202(4054)	
Barrier (cm^{-1})[g]			2110±24		1987±36		1897±40			1539±85	

[a]Quantum numbers of the upper (u) and lower (l) inversion levels in the respective states. Each level is doubly degenerate as reflected by the labelling.

[b]In the ground state of all other modes. The peak numbers (No.) correspond to the observed peak positions marked in Fig. 2 for 3MCH and Fig. 6 for 1M3MCH.

[c]Derived from sequences observed in the spectrum in Fig. 5 and summarized in the energy level diagram in Fig. 4c.

[d]Derived from sequences observed in the spectrum in Figs. 2 and 3 and summarized in the energy level diagram in Fig. 4b.

[e](Observed − calculated) (cm^{-1}).

[f]Evaluated with a potential function $V(q) = (V_2/m\gamma)q^2 + (V_4/m^2\gamma^2)q^4$, q the dimensionless coordinate (15). Fixed parameters: m = 100.0 u; $\gamma = 4\pi^2 c\nu/h$, ν = 100.0 cm^{-1} for 3MCH, ν = 80.00 cm^{-1} for 1M3MCH; 150 harmonic oscillator basis functions.

[g]Uncertainties reflect the estimated standard deviations for the potential constants.

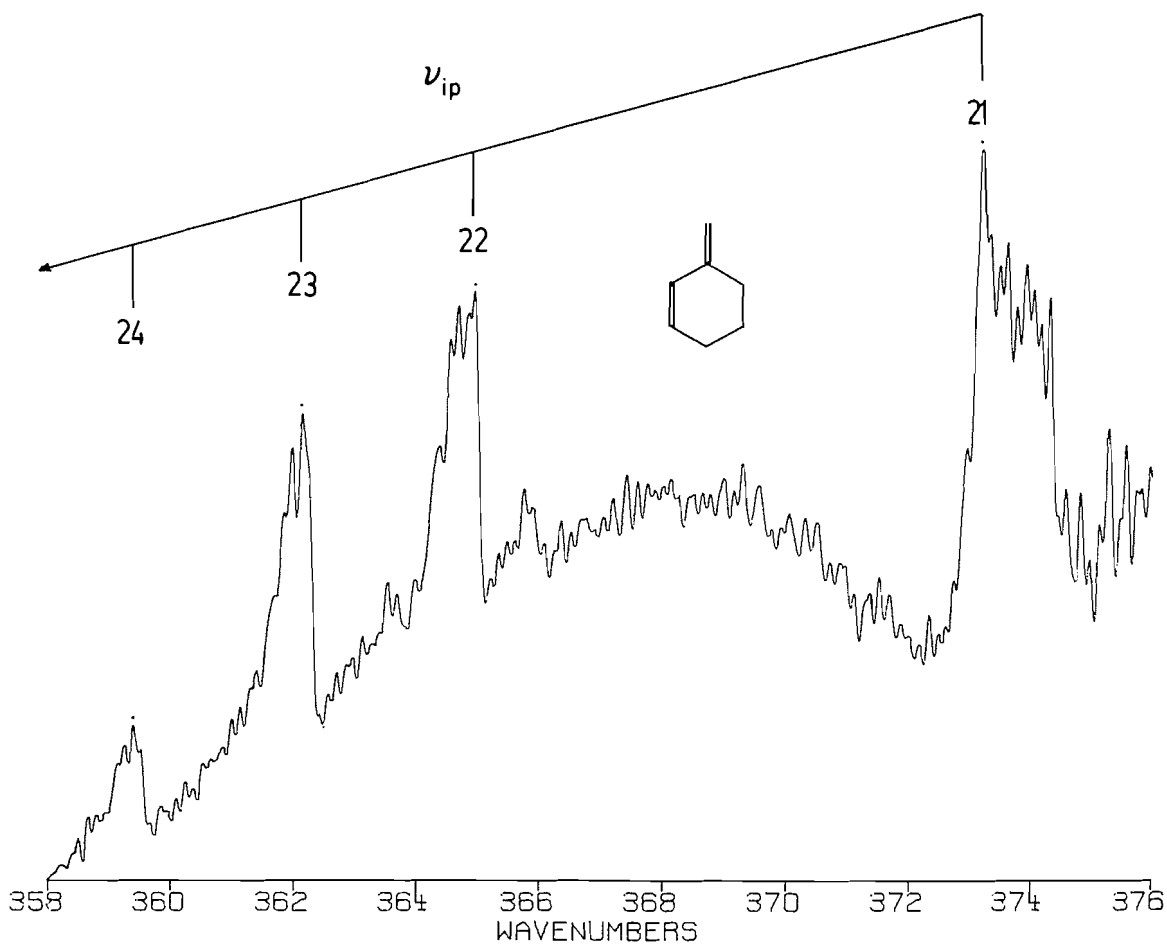

FIG. 3. Expansion of ν_{ip} sequence of 3-methylenecyclohexene. Numbered bands correspond to transitions summarized in Fig. 4a.

Can. J. Chem. Downloaded from www.nrcresearchpress.com by 210.87.254.5 on 09/06/12
For personal use only.

Can. J. Chem. Downloaded from www.nrcresearchpress.com by 210.87.254.5 on 09/06/12
For personal use only.

factured by the same company. A liquid helium cooled bolometer operating at 4.2 K with the appropriate cut-on filter was used as detector. The beamsplitter was a 6 μm Mylar and the resolution was set at 0.12 cm^{-1} with boxcar apodization. The spectra were run with saturated or reduced vapour pressures and 45 m path. On the average, 200–500 scans were accumulated to achieve optimum signal-to-noise ratios. The reported positions of the sharp absorptions are believed to be accurate to at least 0.02 cm^{-1}.

Molecular geometries and the inversion mode

In this work we are concerned primarily with the out-of-plane deformations of the cyclohexene ring. In the absence of any structure determination by microwave or electron diffraction we need to make some reasonable guesses about the ground state geometries and the probable forms of the three vibrational modes.

In all likelihood the structure of 3MCH will resemble that of 2CHO, namely, all atoms except C5 should lie in one plane (8). If a double minimum vibration is observed, therefore, we can logically assign it to an inversion of the C5 atom through that plane (ν_i), as was done for 2CHO. One reasonable choice for the second mode is a torsion about the C2—C3 (in 3MCH) bond, ν_τ. It would be restricted by the double bond character resulting from the conjugation of the two C=C groups. Indeed, there is some indirect evidence in 2CHO suggesting that the inversion of C5 is accompanied by a torsion about that bond (C1—C2 in that case) (1). We note that this same torsion is the double minimum vibration in 1,3-cyclohexadiene (9). Its barrier to planarity of 1099 cm^{-1} compares to that in 2CHO of 3640 cm^{-1} and is lower at least partially as a result of the fewer methylene hydrogen interactions. The torsion in 2CHO can be assigned to the broad Raman feature reported near 250 cm^{-1} (10) corresponding to a weak sequence of A-type Q branches spreading from 244 to 248 cm^{-1}.[2] The third out-of-plane deformation undoubtedly resembles a torsion about the endocyclic double bond. Invariably that mode is observed at higher wavenumbers (about 300–400 cm^{-1}) in other cyclohexene-type molecules and does not appear to couple significantly with the lower modes (11). It is therefore not of direct interest in our deliberations and we shall not discuss it any further.

For 4MCH (and 3CHO) we can visualize at lease two possible ground state conformations. One of these, the twisted (half-chair) form, obviously resembles that of cyclohexene in its lowest state. The second is a "bent" (boat) form which, we note, can be reached from the planar conformation by either folding the ring about the C3—C6 axis, or by rotating the two

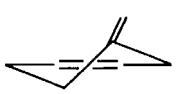

Twisted

Bent

planes containing the two double bonds against one another with C3 serving as the fulcrum. The two routes differ in the extent by which the exocyclic double bond is displaced out of the plane containing the endocyclic double bond. The true pathway likely is some combination attempting to minimize all interactions and is not easily determined from the infrared spectra, certainly not of only one isotopic species. We expect the energies of the two vibrations, namely the twist, ν_t, and the bend, ν_b, to be similar to those observed for other cyclohexene-type molecules where the latter always occurs at lower wavenumbers (11). For 3CHO we have therefore ascribed the "bend" to a sequence of Q branches starting at 77.23 cm^{-1} (1). It is this mode which is subject to a double minimum potential function, suggesting that the ground state of 3CHO is the "bent" conformation. The twist in 3CHO appears to give rise to a broad, nearly featureless absorption around 155 cm^{-1}.[2] Initially we might expect 4MCH to behave similarly to the ketone. The CCC angle of the carbonyl group is nearly the same as the corresponding angle in the vinyl group (12), and both groups apparently prefer a conformation where the C—H bonds on the adjacent C atoms are eclipsed with the π bond. We might look for a difference between the two compounds as a result of the different torsional barriers (cf. barrier to methyl torsion of 272 cm^{-1} (0.777 kcal mol^{-1}) in acetone (13) vs. 773 cm^{-1} (2.21 kcal mol^{-1}) in 2-methylpropene (14)).

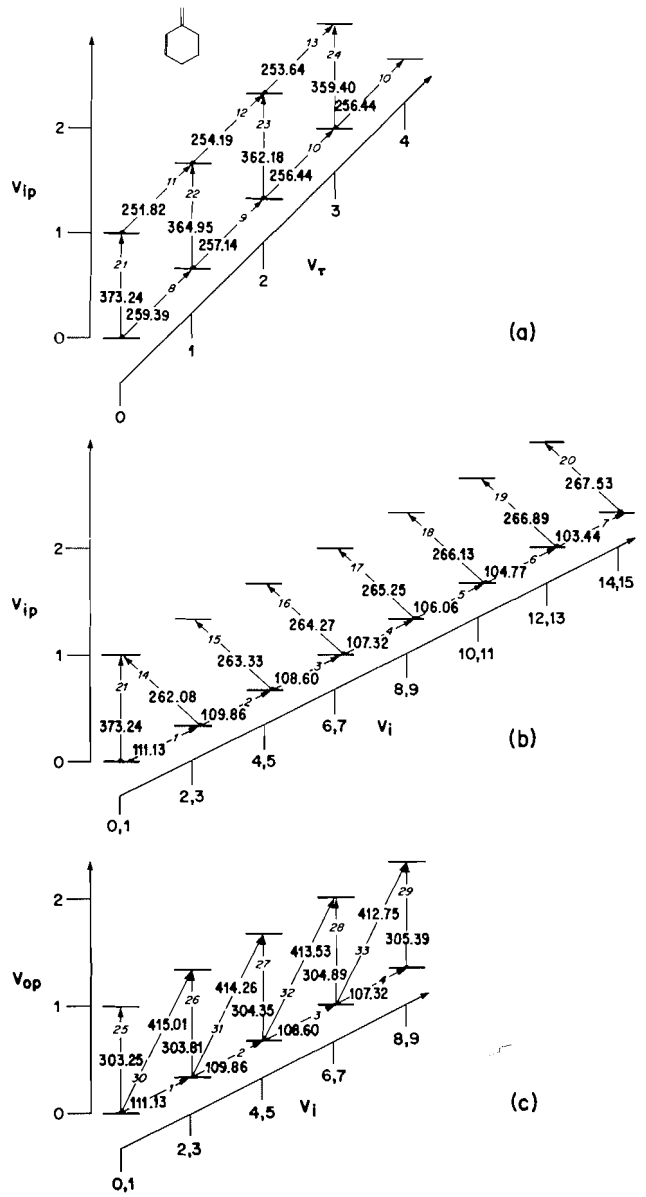

FIG. 4. Energy level diagrams for selected combination sequences of 3-methylenecyclohexene. Numbered transitions correspond to observed absorption bands displayed in Figs. 2, 3, and 5.

[2]T. L. Smithson and H. Wieser, unpublished results.

Can. J. Chem. Downloaded from www.nrcresearchpress.com by 210.87.254.5 on 09/06/12
For personal use only.

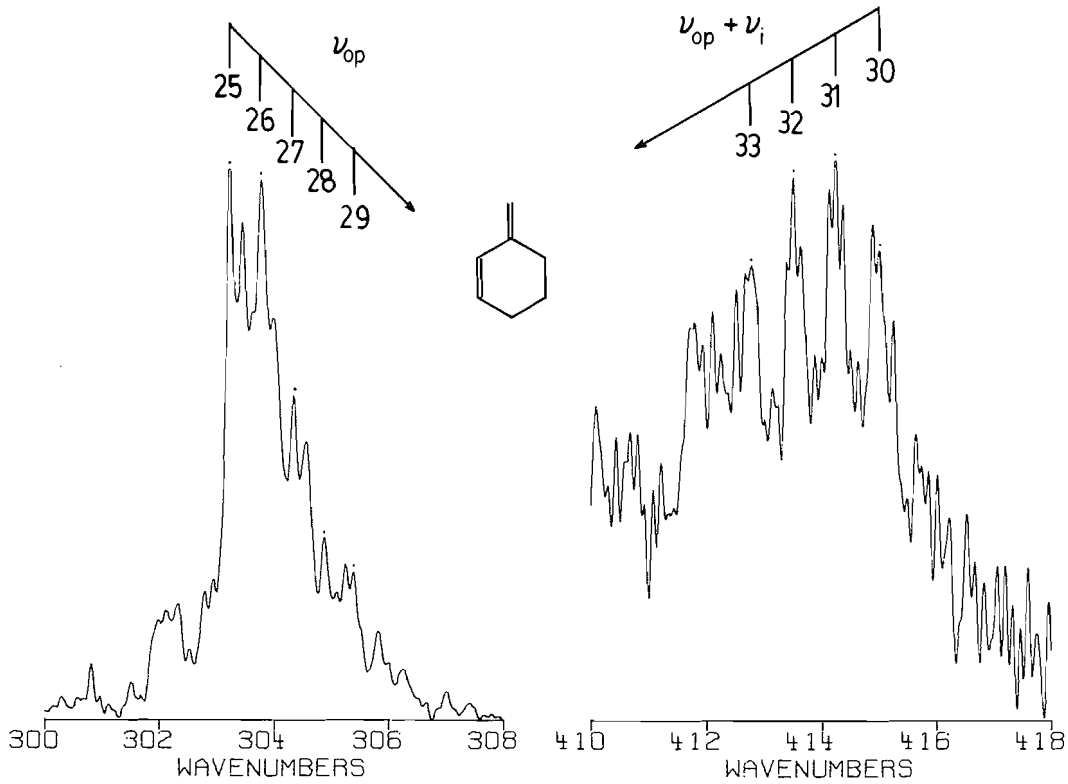

FIG. 5. Expansions of ν_{op} and $\nu_{op} + \nu_i$ sequences of 3-methylenecyclohexene. Absorbance scale of right field much expanded (cf. top spectrum in Fig. 1.) Numbered bands correspond to transitions summarized in Fig. 4c.

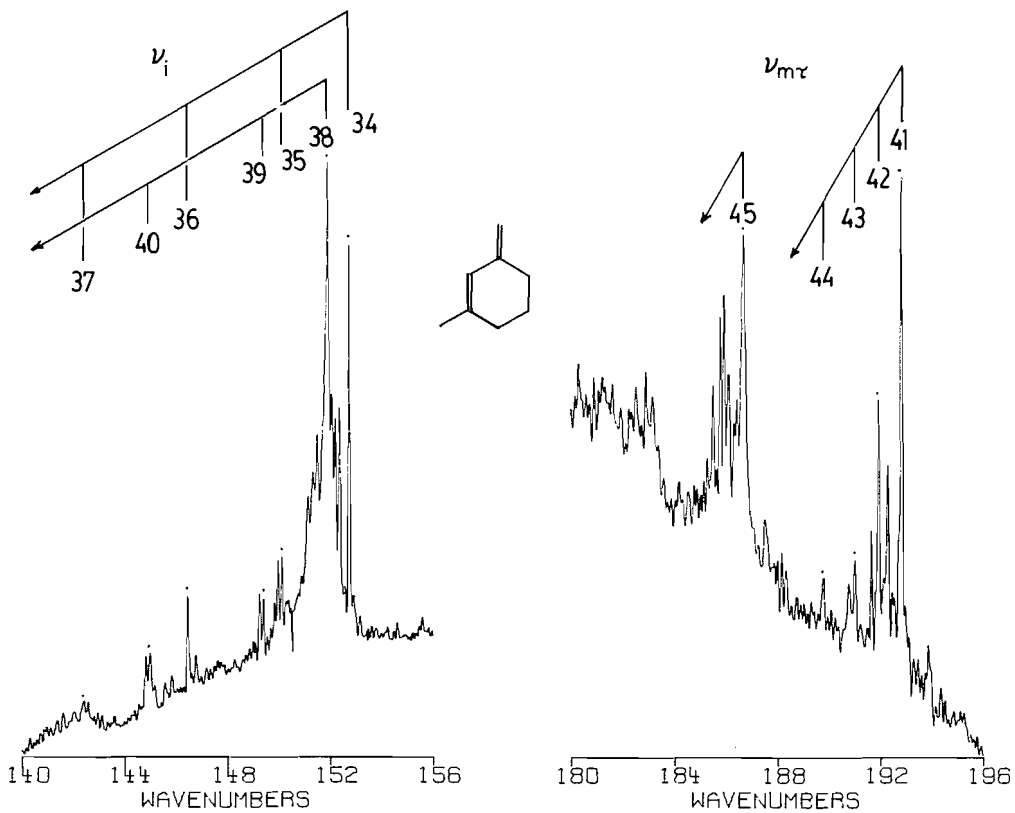

FIG. 6. Expansion of ν_i and $\nu_{m\tau}$ sequences of 1-methyl-3-methylenecyclohexene. Absorbance scale of right field expanded (cf. middle spectrum in Fig. 1). Numbered bands correspond to peak positions listed in Table 1 (for ν_i) and transitions summarized in Fig. 7.

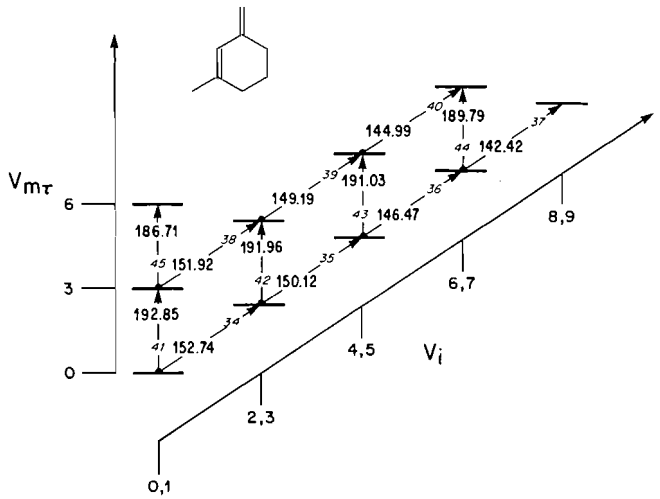

FIG. 7. Energy level diagram for ν_i and $\nu_{m\tau}$ combination sequences of 1-methyl-3-methylenecyclohexene. Numbered transitions correspond to observed absorption bands displayed in Fig. 6.

Results

3-Methylenecyclohexene

The survey spectrum of 3MCH in the region of 80–440 cm^{-1} is displayed in the top field of Fig. 1. The two out-of-plane deformations, ν_i and ν_τ, are clearly seen as weak Q branch sequences. They are replotted on an expanded scale in Fig. 2. The inversion mode ν_i forms a descending series, starting at 111.13 cm^{-1}, characteristic of a double minimum vibration subject to a relatively high barrier. We fitted the transitions with a one-dimensional Hamiltonian containing a quadratic-quartic potential function, using a computer program described elsewhere (15). The transitions and the fitting parameters are listed in Table 1.

The torsion mode ν_τ also exhibits several Q branches which evidently must arise from some kind of combination transitions. Such combinations, however, do not appear to take place with ν_i in the first instance. Rather, they can be correlated with the fundamental at 373 cm^{-1} and its sequence of combination bands displayed to lower wavenumbers (Fig. 3), as shown in the energy level diagram drawn in Fig. 4a. The fundamental of ν_τ is thereby placed at 259.39 cm^{-1} (see right field of Fig. 2). We believe that the 373 cm^{-1} fundamental can be assigned to the in-plane deformation of the exocyclic vinyl group, labelled ν_{ip} in the figures. The additional fine structure on that absorption and on its hot bands with ν_i probably is due to other combinations, but explicit assignments are very difficult. For example, one such difference band sequence based on ν_i may be observed near 265 cm^{-1} (see right field of Fig. 2 and energy level diagram in Fig. 4b), but a lack of corroborative transitions precludes a more definitive assignment. A combination sequence with ν_i is seen also on the 303 cm^{-1} fundamental which we believe is due to the out-of-plane deformation of the ex-

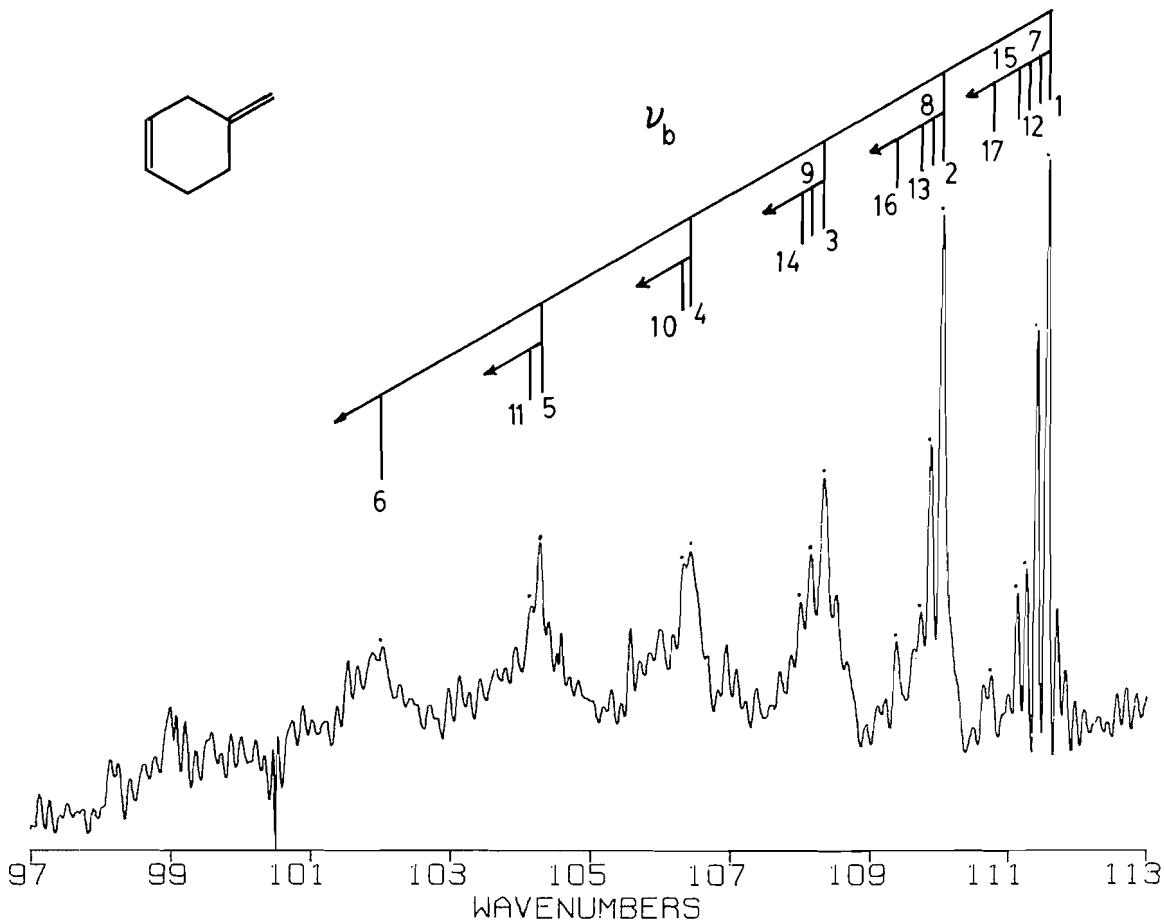

FIG. 8. Expansion of ν_b/ν_t combination sequences of 4-methylenecyclohexene. Numbered bands correspond to peak positions listed in Table 2 and Table 3 (ν_b only), and transitions summarized in Fig. 11.

Can. J. Chem. Downloaded from www.nrcresearchpress.com by 210.87.254.5 on 09/06/12
For personal use only.

Can. J. Chem. Downloaded from www.nrcresearchpress.com by 210.87.254.5 on 09/06/12
For personal use only.

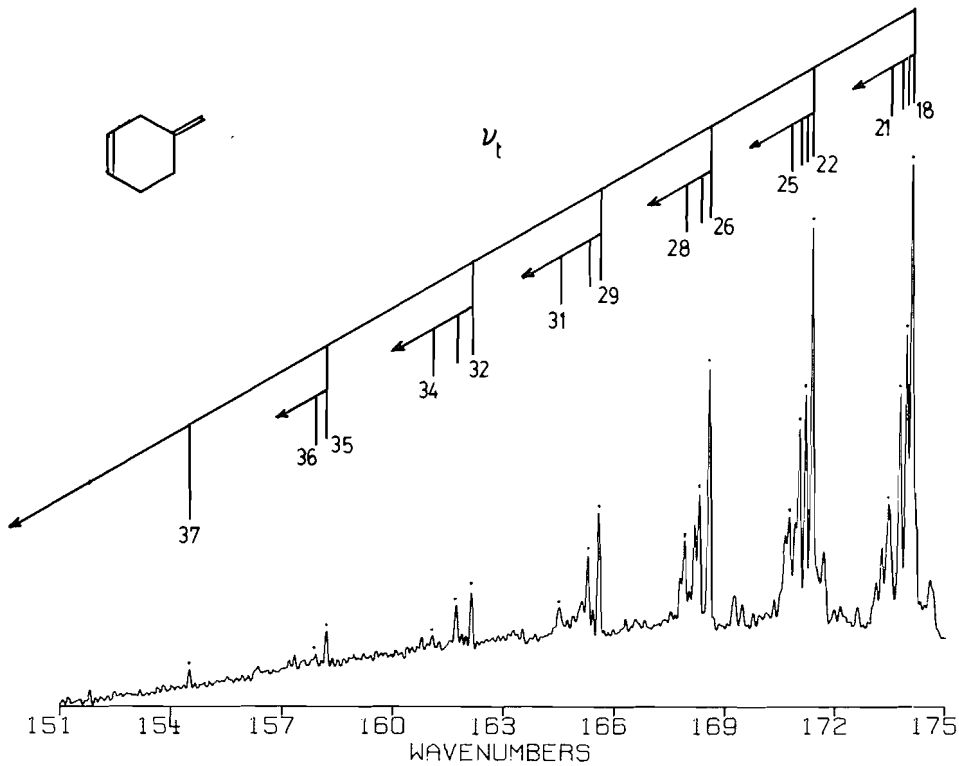

FIG. 9. Expansion of ν_b/ν_t combination sequences of 4-methylenecyclohexene. Numbered bands correspond to peak positions listed in Table 2 and 4 (ν_t only), and transitions summarized in Fig. 11.

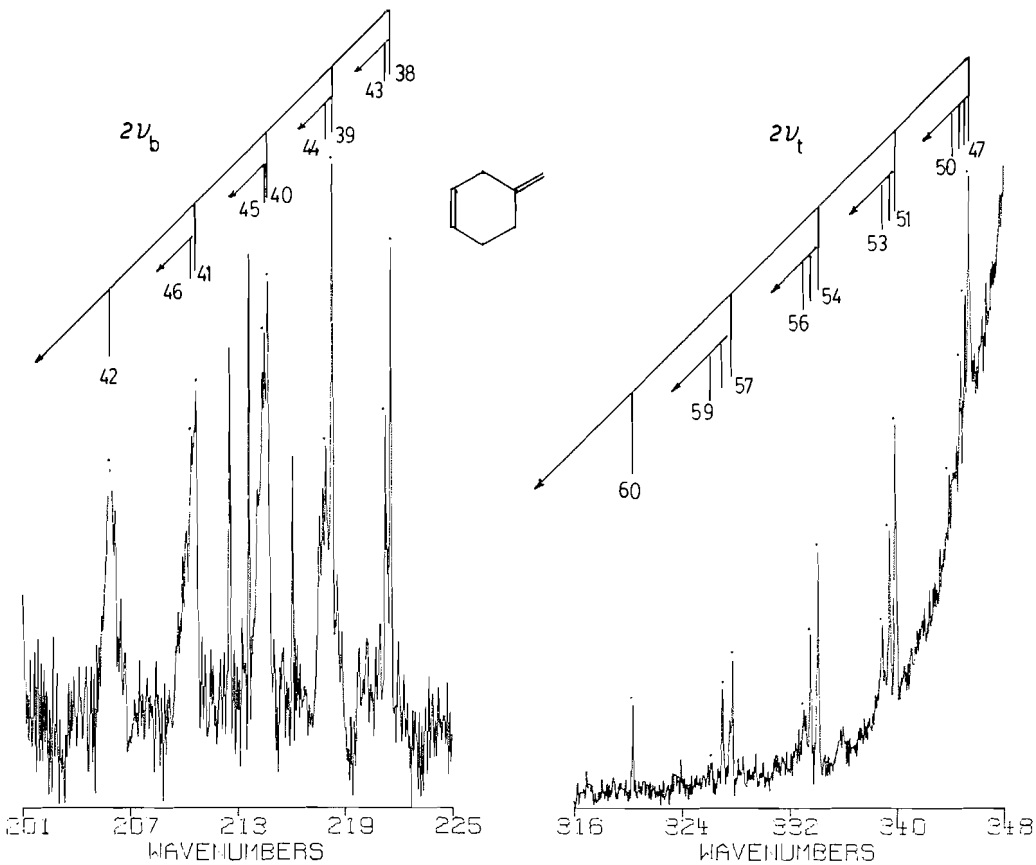

FIG. 10. Expansion of $2\nu_b$ and $2\nu_t$ sequences of 4-methylenecyclohexene. Numbered bands correspond to peak positions listed in Table 2, and transitions summarized in Fig. 11.

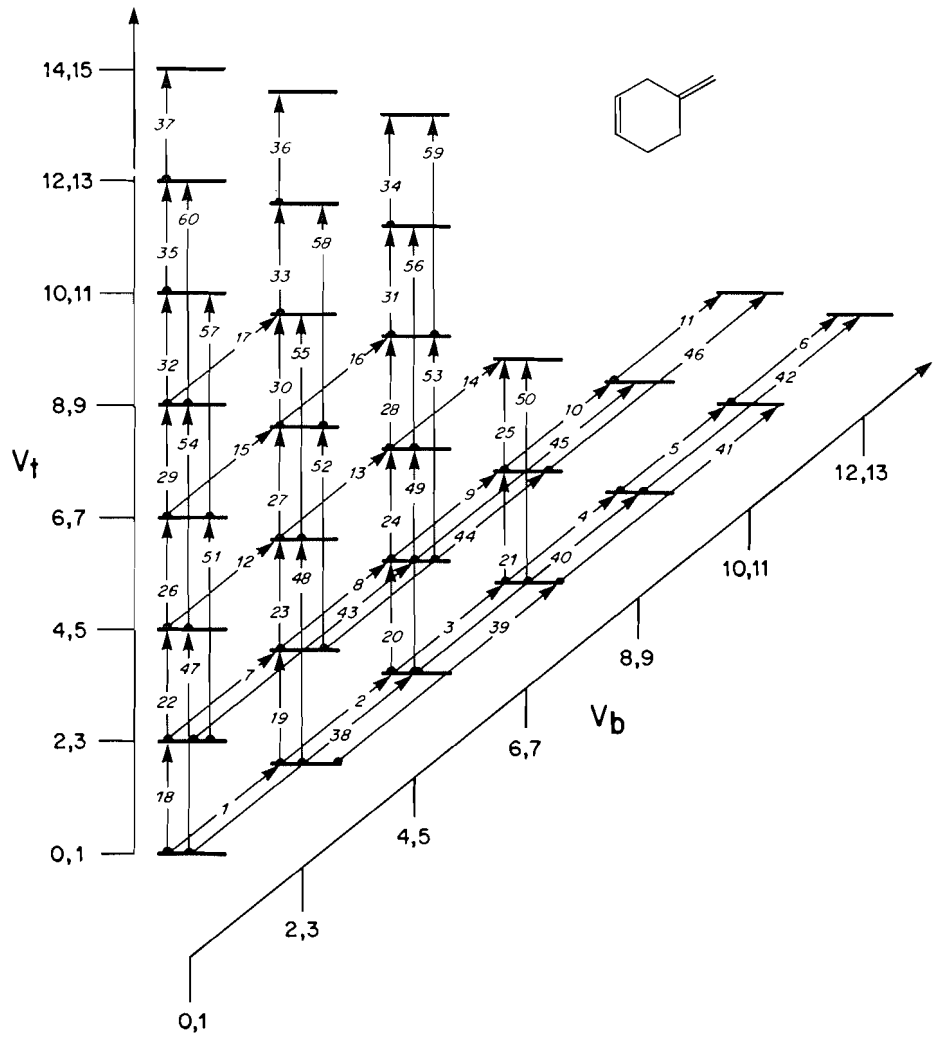

FIG. 11. Energy level diagram for ν_b/ν_t combination sequences of 4-methylenecyclohexene. Numbered transitions correspond to peak positions listed in Table 2 and observed absorption bands displayed in Figs. 8 to 10.

ocyclic vinyl group, ν_{op}, with its corresponding sum band series near 415 cm^{-1} (see Figs. 4c and 5).

1-Methyl-3-methylenecyclohexene

The survey spectrum of 1M3MCH is pictured in the center field of Fig. 1. The clearly separated ν_i sequence of 3MCH at 111 cm^{-1} is replaced by a complex C-type band near 152 cm^{-1}. Some of the structure of that band can be related unambiguously with the methyl torsion absorption ($\nu_{m\tau}$) near 190 cm^{-1} (see Figs. 6 and 7), placing the ν_i and $\nu_{m\tau}$ fundamentals at 152.74 and 192.85 cm^{-1} and revealing the ground state sequence of ν_i. This sequence is again fitted with the quadratic-quartic potential function; the results are listed in Table 1. The barrier to methyl torsion is estimated to be 900 cm^{-1} using the first two transitions (see Fig. 7) with a V_3 potential energy term in a conventional program (16) for that purpose and an optimized F number of 5.4576 cm^{-1} (standard deviation of observation of 6.0 cm^{-1}). The fundamental ν_τ has shifted to slightly lower wavenumbers upon methyl substitution, namely 248.42 cm^{-1} (see Fig. 1). Although this absorption shows a distinct Q branch sequence, its members cannot be correlated with any other vibrations in this region. Possibilities of such an interaction include the inversion mode, or the in-plane deformation of the exocyclic vinyl group as in 3MCH. There are lines among the ν_i and $\nu_{m\tau}$ bands that were left unassigned which may be inversion and/or methyl torsion transitions in the excited states of ν_τ.

4-Methylenecyclohexene

Changing the relative position of the two double bonds evidently affects the appearance of the spectrum dramatically (see lower field of Fig. 1). The distinct Q branch sequences near 111 and 174 cm^{-1} are assigned to the bend (ν_b) and the twist (ν_t) modes of the cyclohexene ring. Both exhibit pronounced substructure (see Figs. 8 and 9) which can be identified unambiguously with the help of the first overtone transitions starting at 222 and 345 cm^{-1} (shown in Fig. 10). The assignment is summarized in the energy level diagram depicted in Fig. 11 and the peak positions are listed in Table 2. Both modes in their ground and several excited states are amenable to solution with the one-dimensional Hamiltonian with a quadratic-quartic potential function, as shown in Tables 3 and 4.

Discussion and conclusions

We have analyzed the inversion absorptions for all three compounds with a one-dimensional Hamiltonian that includes a quadratic-quartic potential function and a constant reduced mass in the kinetic energy. Although the out-of-plane defor-

Can. J. Chem. Downloaded from www.nrcresearchpress.com by 210.87.254.5 on 09/06/12
For personal use only.

Can. J. Chem. Downloaded from www.nrcresearchpress.com by 210.87.254.5 on 09/06/12
For personal use only.

TABLE 2. Bend (ν_b) and twist (ν_t) transitions of 4-methylenecyclohexene

Peak[a] No.	Transitions[b] $(\nu_t\nu_b)_u \leftarrow (\nu_t\nu_b)_l$				Position (cm^{-1})	Peak[a] No.	Transition[b] $(\nu_t\nu_b)_u \leftarrow (\nu_t\nu_b)_l$				Position (cm^{-1})
1	1,0	3,2	1,0	1,0	111.56	31	9,8	5,4	7,6	5,4	164.14
2		5,4		3,2	110.05	32	11,10	1,0	9,8	1,0	162.15
3		7,6		5,4	108.36	33		3,2		3,2	161.75
4		9,8		7,6	106.45	34		5,4		5,4	161.08
5		11,10		9,8	104.30	35	13,12	1,0	11,10	1,0	158.22
6		13,12		11,10	101.90	36		3,2		3,2	157.35
7	3,2	3,2	3,2	1,0	111.41	37	15,14	1,0	13,12	1,0	154.52
8		5,4		3,2	109.89	38	1,0	5,4	1,0	1,0	221.57
9		7,6		5,4	108.16	39		7,6		3,2	218.31
10		9,8		7,6	106.35	40		9,8		5,4	214.68
11		11,10		9,8	104.17	41		11,10		7,6	210.70
12	5,4	3,2	5,4	1,0	111.27	42		13,12		9,8	205.91
13		5,4		3,2	109.75	43	3,2	5,4	3,2	1,0	221.27
14		7,6		5,4	107.88	44		7,6		3,2	217.94
15	7,6	3,2	7,6	1,0	111.14	45		9,8		5,4	214.53
16		5,4		3,2	109.40	46		11,10		7,6	210.46
17	9,8	3,2	9,8	1,0	110.74	47	5,4	1,0	1,0	1,0	345.40
18	3,2	1,0	1,0	1,0	174.07	48		3,2		3,2	345.12
19		3,2		3,2	173.92	49		5,4		5,4	344.76
20		5,4		5,4	173.76	50		7,6		7,6	344.24
21		7,6		7,6	173.45	51	7,6	1,0	3,2	1,0	339.93
22	5,4	1,0	3,2	1,0	171.36	52		3,2		3,2	339.48
23		3,2		3,2	171.19	53		5,4		5,4	338.94
24		5,4		5,4	171.03	54	9,8	1,0	5,4	1,0	334.16
25		7,6		7,6	170.75	55		3,2		3,2	333.60
26	7,6	1,0	5,4	1,0	168.58	56		5,4		5,4	333.08
27		3,2		3,2	168.30	57	11,10	1,0	7,6	1,0	327.77
28		5,4		5,4	167.90	58		3,2		3,2	327.04
29	9,8	1,0	7,6	1,0	165.60	59		5,4		5,4	326.20
30		3,2		3,2	165.30	60	13,12	1,0	9,8	1,0	320.40

[a]Peak numbers correspond to the numbers in the spectra (Figs. 8 to 10) and the energy level diagram (Fig. 11).

[b]Quantum numbers of the upper (u) and lower (l) levels in each of the twist (t) and bend (b) states. Each level is degenerate as reflected by the labelling.

TABLE 3. Bend transitions and parameters of 4-methylenecyclohexene

Transition[a]		$\nu_t = 1,0$[b]			$\nu_t = 3,2$[c]			$\nu_t = 5,4$[c]		
$\nu_u \leftarrow \nu_l$		No.	Obs (cm^{-1})	Δ[d]	No.	Obs (cm^{-1})	Δ[d]	No.	Obs (cm^{-1})	Δ[d]
3,2	1,0	1	111.56	−0.21	7	111.41	−0.11	12	111.27	−0.05
5,4	3,2	2	110.05	0.02	8	109.89	0.04	13	109.75	0.09
7,6	5,4	3	108.36	0.16	9	108.16	0.08	14	107.88	−0.04
9,8	7,6	4	106.45	0.17	10	106.35	0.11			
11,10	9,8	5	104.30	0.05	11	104.17	−0.12			
13,12	11,10	6	101.90	−0.18						
Fitting parameters:[e]										
Std. dev. of obs (cm^{-1})			0.18			0.13			0.11	
$(V_2/m\gamma)$ (cm^{-1})			−32.178(78)			−32.002(69)			−31.873(88)	
$(V_4/(m\gamma)^2)$ (cm^{-1})			0.17535(378)			0.16832(356)			0.16557(727)	
Barrier (cm^{-1})[f]			1476±24			1521±25			1534±56	

[a]As in Table 1.

[b]In the ground state of all other modes. The peak numbers (No.) correspond to the observed peak positions marked in Fig. 8 and listed in Table 2.

[c]In excited states of the twist mode. The peak numbers (No.) correspond to the observed peak positions marked in Fig. 8 and listed in Table 2.

[d](Observed − calculated) (cm^{-1}).

[e]As in footnote *f* in Table 1, except ν = 100.0 cm^{-1}, 150 basis functions for ν_t = 1,0 and 100 for 3,2 and 5,4.

[f]As footnote *g* in Table 1.

mation modes in principle could be coupled with one another or with other vibrations, the one-dimensional treatment appears to have been successful in all the cases, as judged by the standard deviations for the calculated transitions (see Tables 1, 3, and 4). It is reasonable to assume, therefore, that these deformations are relatively independent. The potential con-

TABLE 4. Twist transitions and parameters of 4-methylenecyclohexene

Transition[a]		$\nu_b = 1,0^b$			$\nu_b = 3,2^c$			$\nu_b = 5,4^c$		
$\nu_u \leftarrow \nu_l$		No.	Obs (cm^{-1})	Δ^d	No.	Obs (cm^{-1})	Δ^d	No.	Obs (cm^{-1})	Δ^d
3,2	1,0	18	174.07	−0.21	19	173.92	−0.26	20	173.76	−0.09
5,4	3,2	22	171.36	−0.08	23	171.19	−0.07	24	171.03	0.14
7,6	5,4	26	168.58	0.12	27	168.30	0.12	28	167.90	0.14
9,8	7,6	29	165.60	0.28	30	165.30	0.37	31	164.14	−0.32
11,10	9,8	32	162.15	0.17	33	161.76	0.28	34	161.09	0.14
13,12	11,10	35	158.22	−0.20	36	157.35	−0.43			
15,14	13,12	37	154.52	−0.08						
Fitting parameters:[e]										
Std. dev. of obs (cm^{-1})			0.21			0.35			0.24	
$(V_2/m\gamma)$ (cm^{-1})			−78.324(139)			−78.310(255)			−78.050(201)	
$(V_4/(m\gamma)^2)$ (cm^{-1})			0.69237(782)			0.71166(1691)			0.71842(1601)	
Barrier (cm^{-1})[f]			2215±17			2154±36			2120±36	

[a]As in Table 1.
[b]In the ground state of all other modes. The peak positions (No.) correspond to the observed peak positions marked in Fig. 9 and listed in Table 2.
[c]In excited states of the bend mode. The peak positions (No.) correspond to the observed peak positions marked in Fig. 9 and listed in Table 2.
[d]As in Table 3.
[e]As in Table 3, except 100 basis functions throughout.
[f]As in Table 3.

TABLE 5. Comparison of out-of-plane ring deformations in methylenecyclohexenes and cyclohexenones

	Position (cm^{-1})					
Designation	3MCH	2CHO	1M3MCH	3M2CHO	4MCH	3CHO
ν_i/ν_b	111.13	99.62	152.74	96.82	111.56	77.23
ν_τ/ν_t	259.39	248.32[a]	248.42	245.86[a]	174.07	~155
Inversion barriers:						
in cm^{-1}	2110	3642	1539	4567	2215/1476	463
in kcal mol^{-1}	6.03	10.4	4.40	13.1	6.33/4.22	1.32

[a]The apparent most prominent member of a series of Q branches.

stants, given in the tables in terms of the dimensionless coordinates, are to be viewed as effective constants, particularly for the inversions in the excited states of another mode. Although the method used here is not able to provide any explicit information about the dynamic form of the vibrations, other than comfirming double minimum situations, we believe it does yield reasonable estimates of barriers to inversion for the ground state conformations. Considering that we are dealing with high barriers that are determined from a relatively small number of the lowest transitions, a certain error due to extrapolation to the top of the well is also unavoidable. The uncertainties on these barriers quoted in the tables reflect the estimated standard deviations of the potential constants. A more realistic estimate of these uncertainties may be about ±10%.

In Table 5 the positions of the two lowest out-of-plane ring deformations of the methylenecyclohexenes are compared to those of the corresponding ketones. We find that the spectrum of 3MCH is similar to that of 2CHO, the fundamental of ν_i being shifted slightly to higher wavenumber and the separation between successive inversion transitions being somewhat greater (e.g., difference of 1.27 cm^{-1} between the first two transitions in 3MCH vs. 0.57 cm^{-1} in 2CHO). The intensity of ν_i is much reduced, while that of ν_τ is comparable. The latter mode again does not appear to couple with ν_i to any great extent. These observations confirm the presumption that the structure, and the form of the inversion mode, of 3MCH are quite similar to those of the ketone. The barrier to inversion, however, is considerably lower in 3MCH. This drop in barrier height is consistent with the reduced degree of conjugation of the endocyclic double bond with the vinyl group as compared to the more polar carbonyl group. The intervening single bond is thereby again implicated in the inversion mode, supporting the earlier suggestion that the inversion of C5 through the plane is facilitated to some extent by a torsion about that bond.

Methyl substitution in 3MCH appears to affect the position of the ν_i fundamental significantly as compared to the parent compound and to the corresponding ketones, whereas ν_τ remains virtually unchanged. There is clear evidence of ν_i interacting with the methyl torsion. There also are indications of ν_τ coupling with one other or possibly more vibrations, but no definitive assignments of sum or difference bands are possible. While we can pick out one sequence of ν_i, seemingly the ground state sequence, and fit it with a quadratic-quartic potential function, we cannot be assured that this is the only way of describing the vibration. This interpretation, however, which suggests a ground state conformation and a form of the inversion mode resembling that of the parent compound, is at least consistent with the notion that methyl substitution on C1

Can. J. Chem. Downloaded from www.nrcresearchpress.com by 210.87.254.5 on 09/06/12
For personal use only.

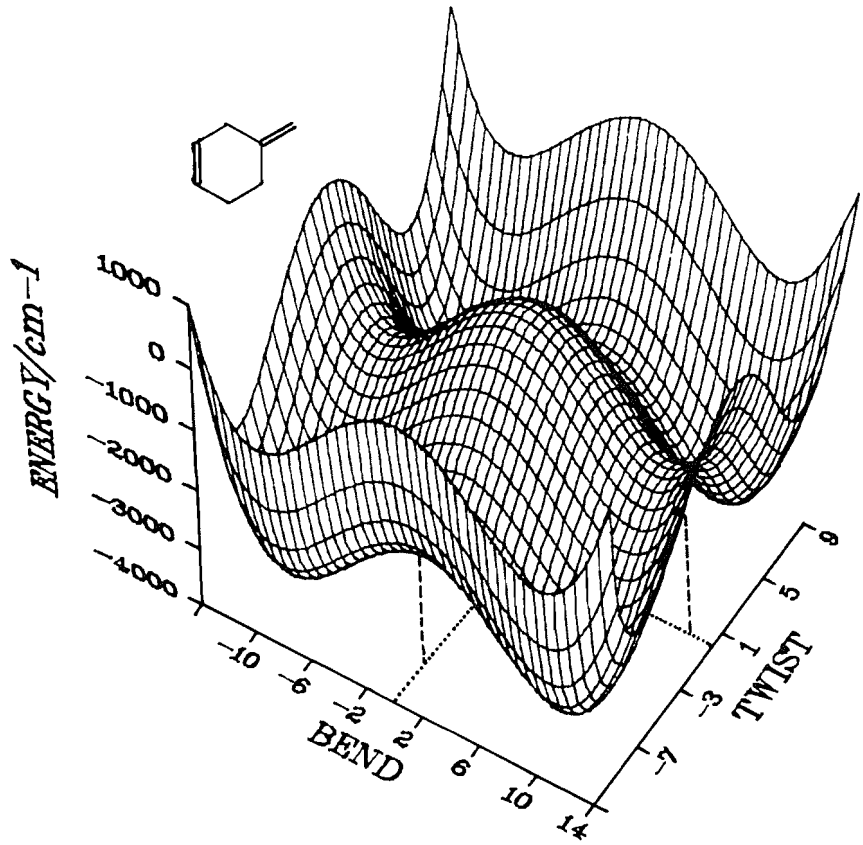

FIG. 12. Bend–twist potential energy surface in the ground state of all other modes for 4-methylenecyclohexene, using the potential function constants quoted in Tables 3 and 4.

in 3MCH diminishes the degree of conjugation. If a torsion about the C2—C3 bond accompanies the inversion of C5, the decreased conjugation indeed would lead to a lowering of the barrier to inversion. In the ketone, on the other hand, the methyl group stabilizes the conjugation thereby increasing the double bond character of the single bond (C1—C2 in that case) and hence raising the inversion barrier.

The picture emerging for 4MCH is substantially different from either the conjugated methylenecyclohexene or, surprisingly, also from the corresponding ketone, 3CHO. The fit of the one-dimensional double minimum potential for both ν_b and ν_t suggests two independent vibrations. If this interpretation is correct, 4MCH to our knowledge would constitute the first example of the type of a molecule referred to as Case 5 for five-membered rings described by Harris *et al.* (17), where the interaction term in the potential function between two out-of-plane deformation modes approaches zero and the two double minimum vibrations are completely independent. To test this hypothesis further we attempted to determine the best fitting two-dimensional potential surface described by a function of the form

$$V(x_1,x_2) = V_{21}x_1^2 + V_{22}x_2^2 + V_{41}x_1^4 + V_{42}x_2^4 + V_{mix} \times x_1^2x_2^2$$

in the appropriate Hamiltonian, using a computer program outlined elsewhere (18). When the potential constants for the two modes in their ground state are entered and constrained, V_{mix} is allowed to vary, and all excited state information is used, a very small mixing term of 0.00222(69) cm^{-1} is calculated with the effect that the fit of all transitions is being averaged. When average quadratic and quartic constants for both modes are first adjusted to produce an average fit, constraining V_{mix} to zero at the same time and using all transitions, and then these average constants are held fixed while floating V_{mix}, the calculations always attempt to drive the mixing term to zero. The fit to all observed transitions produced in this way is the same as with the first procedure. Finally, if all constants are allowed to vary simultaneously, convergence cannot be achieved and the calculation is ill-determined. These results support the interpretation of the spectrum in terms of two independent double minimum modes.

Additional evidence, in our view, is provided by the appearance of the spectrum itself. The sequence of ν_b and ν_t as well as that of their first overtones are quite regular. Members of a series in a sequence of excited states of the second mode differ very little. These observations contrast the experience made with other cyclohexene-type molecules where the sequences frequently reverse their direction and the bend and twist modes are known to interact extensively (see for example ref. 11).

The resulting potential surface is pictured in Fig. 12. The lowest energy state is 3691 cm^{-1} below the central barrier (also the barrier to planarity) and corresponds to a conformation that is somewhere between the two forms designated above as bent and twisted. The molecule may interconvert from one of the four equivalent "bent–twist" minima to another via the twisted conformation 1476 cm^{-1} above the minimum, or via the bent conformer 2215 cm^{-1} above the minimum. It must be remembered that the designation of the conformations as "bent" or "twisted" may not describe the actual situations properly since neither the infrared spectra nor the calculations referred to

Can. J. Chem. Downloaded from www.nrcresearchpress.com by 210.87.254.5 on 09/06/12
For personal use only.

Can. J. Chem. Downloaded from www.nrcresearchpress.com by 210.87.254.5 on 09/06/12
For personal use only.

above are capable of yielding any explicit information about the molecular geometry.

In summary, we note that the methylenecyclohexenes and their related ketones have provided interesting new insights into the dynamics of the out-of-plane deformations of cyclohexene-type molecules. When the double bonds are conjugated, the form of the inversion vibration appears to differ considerably from those observed previously for other related compounds. The trends in the inversion barriers follow accepted chemical concepts. When the double bonds are isolated, new and different situations arise and one can observe a trend of behaviour. Cyclohexene itself (19, 20) and oxygen substituted analogues (11, 21), being in a twisted ground state conformation, exhibit the characteristic sequences of transitions for the bend and twist vibrations. The latter is a true double minimum mode, while the former, at least in the ground state of the twist, is an anharmonic vibration constrained in the relatively deep well of the twist. The bend transitions, although they form a descending sequence, do not represent a double minimum situation; rather, the lowering in wavenumbers of consecutive members reflects the anharmonicity in the twist minimum. The molecule can interconvert between the equivalent twisted forms via a bent conformation without going through the much higher energy planar geometry, though there still seems to be some question whether the bent form constitutes a saddle point or a local minimum (21, 22). In 4MCH we find a molecule which has four equivalent conformations that are neither "twisted" nor "bent", but some intermediate. The two vibrations are independent of one another, each subject to its own double minimum potential function and displaying the characteristic descending series of transitions. Interconversion between the equivalent forms of the ground state geometry can take place via either the twisted or bent conformations which form saddle points on the potential surface. The barrier to planarity, we note, is of similar magnitude as in other cyclohexene-type molecules (e.g., 3,6-dihydropyran and 1,3-dioxene (11)). Finally, 3CHO appears to adopt a "bent" ground state geometry with a low barrier to inversion through the planar conformation. The bend vibration shows the series of absorptions typical for such a double minimum potential. The twist vibration may or may not be anharmonic, but in any event does not appear to dominate the other out-of-plane deformation.

Acknowledgements

On this occasion we would like to express our sincere gratitude to the Natural Sciences and Engineering Research Council of Canada (NSERCC) for the award in 1980 of a Major Equipment Grant which allowed us to purchase our interferometer and without which none of the work currently in progress would be possible. T.L.S. also acknowledges with thanks the award of an NSERCC Postgraduate Scholarship. This research was supported partly through a normal Operating grant from NSERCC and recently also through a generous Special Project grant from the Alberta Environment Research Trust (both to H.W.). We wish to thank A. Dunham and R. A. Kydd of this Department for permission to use their internal rotor/pseudorotation program.

1. H. WIESER, T. L. SMITHSON, and P. J. KRUEGER. J. Mol. Spectrosc. In press.
2. (*a*) Y. IMANISHI, S. KANAGAWA, and T. HIGASHIMURA. Makromol. Chem. **175**, 1761 (1917); (*b*) E. A. BRAUDE, B. F. GOFTON, G. LOWE, and E. S. WAIGHT. J. Chem. Soc. 4054 (1956); (*c*) H. BABAD, W. FLEMON, and J. B. WOOD. J. Org. Chem. **32**, 2871 (1967).
3. D. R. HOWTON. J. Am. Chem. Soc. **69**, 2060 (1947).
4. J. M. MCINTOSH and R. S. STEEVENSZ. Can. J. Chem. **55**, 2442 (1977).
5. G. WITTIG and U. SCHOELLKOPF. Org. Synth. **40**, 66 (1960).
6. J. KLEIN. Israel J. Chem. **1**, 385 (1963).
7. K. B. WIBERG and B. R. LOWRY. J. Am. Chem. Soc. **85**, 3188 (1963).
8. S. A. MANLEY and J. K. TYLER. Chem. Commun. 382 (1970).
9. L. A. CARREIRA, R. O. CARTER, and J. R. DURIG. J. Chem. Phys. **59**, 812 (1973).
10. L. A. CARREIRA, T. G. TOWNS, and T. B. MALLOY, JR. J. Chem. Phys. **70**, 2273 (1979).
11. E. A. DIXON, G. S. S. KING, T. L. SMITHSON, and H. WIESER. J. Mol. Struct. **71**, 97 (1981).
12. I. TOKUE, T. FUKUYAMA, and K. KUCHITSU. J. Mol. Struct. **23**, 33 (1974).
13. R. NELSON and L. PIERCE. J. Mol. Spectrosc. **18**, 344 (1965).
14. V. W. LAURIE. J. Chem. Phys. **34**, 1516 (1961).
15. J. A. DUCKETT, T. L. SMITHSON, and H. WIESER. J. Mol. Spectrosc. **78**, 407 (1979).
16. J. D. LEWIS, T. B. MALLOY, JR., T. H. CHAO, and J. LAANE. J. Mol. Struct. **12**, 427 (1972).
17. D. O. HARRIS, G. G. ENGERHOLM, C. A. TOLMAN, A. C. LUNTZ, R. A. KELLER, H. KIM, and W. D. GWINN. J. Chem. Phys. **50**, 2438 (1969).
18. T. L. SMITHSON, J. A. DUCKETT, and H. WIESER. J. Am. Chem. Soc. Submitted.
19. J. R. DURIG, R. O. CARTER, and L. A. CARREIRA. J. Chem. Phys. **60**, 3098 (1974).
20. T. L. SMITHSON and H. WIESER. J. Chem. Phys. **72**, 2340 (1980).
21. R. C. LORD, T. C. ROUNDS, and T. UEDA. J. Chem. Phys. **57**, 2572 (1972).
22. R. BUCOURT. *In* Topics in stereochemistry. Vol. 11. *Edited by* E. L. Eliel and N. L. Allinger. John Wiley and Sons, New York. 1974. pp. 183–187.

Synthesis of ethyl 1,2-dihydro-3*H*-pyrrolo[1,2-*a*]pyrrole-1-carboxylate by an intramolecular carbenoid reaction[1]

EDVIGE GALEAZZI, ANGEL GUZMÁN, ARACELI PINEDO, ADOLFO SALDAÑA, AND DIANA TORRE
Syntex, S.A. División de Investigación, Apartado Postal 10-820, México 10, D.F., México

AND

JOSEPH M. MUCHOWSKI[2]
Syntex Research, Institute of Organic Chemistry, Palo Alto, CA 94304, U.S.A.

Received June 9, 1982

EDVIGE GALEAZZI, ANGEL GUZMÁN, ARACELI PINEDO, ADOLFO SALDÂNA, DIANA TORRE, and JOSEPH M. MUCHOWSKI. Can. J. Chem. **61**, 454 (1983).

Cupric ion (or copper) or boron trifluoride promoted decomposition of ethyl 2-diazo-4-(pyrrol-1-yl)butanoate **6** produced mixtures of the title compound **7** and *cis* and *trans* ethyl 4-(pyrrol-1-yl)buten-2-oates **9** and **10**. The formation of **7** by these processes represents the first reported instances of the intramolecular attack of an α-oxocarbenoid or a Lewis acid complexed α-diazoalkylcarboalkoxy function on the pyrrole nucleus.

EDVIGE GALEAZZI, ANGEL GUZMÁN, ARACELI PINEDO, ADOLFO SALDÂNA, DIANA TORRE et JOSEPH M. MUCHOWSKI. Can. J. Chem. **61**, 454 (1983).

La décomposition du diazo-2(pyrrolyl-1)-4 butanoate d'éthyle **6**, initiée par l'ion cuivrique (ou le cuivre) ou par le trifluorure de bore, conduit à un mélange de **7**, le composé mentionné dans le titre, et des (pyrrolyl-1)-4 butène-2 oates d'éthyle *cis* et *trans* (**9** et **10**). La formation du composé **7** selon ce procédé représente le premier exemple d'une attaque intramoléculaire d'une fonction α-oxocarbénoide ou d'une fonction α-diazoalkylcarboalkoxy complexée avec un acide de Lewis sur le noyau pyrrole.
[Traduit par le journal]

Can. J. Chem. Downloaded from www.nrcresearchpress.com by 210.87.254.40 on 09/06/12
For personal use only.

The copper catalysed reaction of α-diazo esters with pyrroles has been known for five decades (1) and continues to be the subject of mechanistic and synthetic studies (2). It is, in fact, still one of the most reliable methods for the synthesis of pyrrole-2-acetic acid esters (3). The intramolecular version of this reaction has, to our knowledge, never been reported in the chemical literature. This paper describes the utilization of such a process for the synthesis of ethyl 1,2-dihydro-3*H*-pyrrolo-[1,2-*a*]pyrrole-1-carboxylate **7**.

The α-daizo ester **6**, required for this study, was synthesized by means of a four-step sequence from 1-(2-hydroxyethyl)-pyrrole **1**.[3] Thus, the methanesulfonate **2**, derived from **1**, was converted into the iodide **3**, and this compound, upon reaction with the sodium salt of diethyl formamidomalonate, gave the expected alkylation product **4**. Selective hydrolysis of the formamido moiety in **4** was effected with hot, dilute, aqueous hydrobromic acid, and the α-amino malonate **5**, thus obtained, was converted directly into the α-diazo ester **6** with isopentyl nitrite (29% yield from **3**).

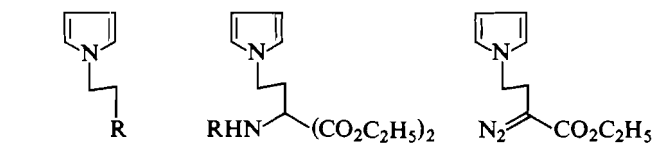

1 R = OH
2 R = OSO_2CH_3
3 R = I

4 R = COH
5 R = H

6

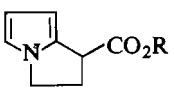

7 R = C_2H_5
8 R = H

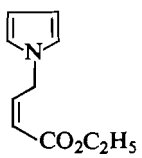

9

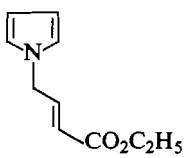

10

The accessibility of the α-diazo ester permitted an investigation of the potential utility of this compound as a source of 1,2-dihydro-3*H*-pyrrolo[1,2-*a*]pyrrole-1-carboxylic acid derivatives. Thus, curpic tetrafluoroborate catalysed decomposition of the diazo compound, in boiling hexane, gave a 70:17:13 mixture (see Table 1) of the desired bicyclic ester **7** and the *cis* and *trans* olefinic esters **9** and **10** in about 14% yield. The bicyclic ester was positively identified by saponification and conversion into the dicyclohexylammonium salt (4) of the carboxylic acid **8**, while the identity of the olefinic esters was established by means of their ir (strong CH out of plane bending band at 980 cm^{-1} for **10**) and nmr (J_{cis} = 12.0 Hz for **9** and J_{trans} = 15.7 Hz for **10**) spectroscopic properties (also see experimental section). The ratio of the bicyclic ester to the olefinic ester depended both on the amount and the nature of the promoter. In general, the combined product yields were the highest when equimolar amounts of the diazo compound and the copper reagent were used, but in no case did this yield exceed 35%. Hydrated copper(II) acetylacetonate was unique in that it gave the greatest proportion of the cyclized product and that no *cis* olefinic ester was formed.

The results described above demonstrate that intramolecular

[1]Contribution No. 613 from the Syntex Institute of Organic Chemistry.

[2]Author to whom all correspondence should be addressed.

[3]This compound was prepared, in 70% yield, by the acetic acid promoted reaction of ethanolamine with 2,5-dimethoxytetrahydrofuran (4). This synthesis is much more efficient than the previously reported one (5).

TABLE 1. Decomposition of ethyl 2-diazo-4-(pyrrol-1-yl)butanoate **6**

Promoter	Mol% promoter	Solvent	Temperature	Time (h)	% **7**, **9** + **10**[a]	Ratio **7**:**9**:**10**[a]
$Cu(BF_4)_2$[b]	10	i-Octane	Reflux	3.5	14.4	70:17:13
$Cu(BF_4)_2$	100	Hexane	Reflux	2.5	34.8	21:28:51
Cu SO_4, anh.	10	i-Octane	Reflux	6	17.8	62:16:22
Cu SO_4, anh.	100	Hexane	Reflux	3	26.6	46:30:24
Cu $SO_4 \cdot 5H_2O$	10	i-Octane	Reflux	2	14.6	61:20:19
Cu $SO_4 \cdot 5H_2O$	100	Hexane	Reflux	2	32.3	55:14:31
Cu (AcAc)$\cdot H_2O$	10	i-Octane	Reflux	1	16.2	86:0:14
Cu (AcAc)$\cdot H_2O$	100	Hexane	Reflux	2	10.8	81:0:19
Cu bronze	10	i-Octane	Reflux	24	20.7	49:28:23
TsOH:H_2O	100	Benzene	Reflux	1	8.7	0:53:47
BF_3:Et_2O	100	Dichloromethane	−20	0.25	10.6	29:48:23
			Room temp.	0.75		
BF_3:Et_2O	100	Dichloromethane	−50	2	29.8	29:49:22
			Room temp.	1		

[a]Average of two determinations.
[b]Commercial solid (Alfa) was pulverized and then dried under high vaccum, first over potassium hydroxide pellets (24 h), then over phosphorous pentoxide (24 h).

carbenoid reactions with pyrroles are indeed possible, but that, at least in the present case, preparatively useful yields of the bicyclic product are not obtained. Presumably the entropy factor, which is expected to make attack of the putative carbenoid on the pyrrole α-carbon atom more favourable, is more than offset by other effects, such as strain, and the propensity to undergo a hydrogen shift to produce olefinic products (6)[4] analogous to that observed for the carbenoids derived from α-alkyl-α-diazoketones (7).

p-Toluenesulfonic acid catalysed decomposition of **6** produced only the olefins **9** and **10**. In contrast, some cyclization did take place when the diazo ester was decomposed, at low temperature, with boron trifluoride etherate in dichloromethane solution. This reaction, which presumably is similar to the intramolecular alkylation of aromatic systems by α-diazoketones (8), deserves to be investigated further.

Experimental

The melting points were determined in a Mel-Temp melting point apparatus and are not corrected. The infrared spectra were measured with a Perkin–Elmer Model 237 grating infrared spectrophotometer. The ultraviolet spectra were recorded on a Perkin–Elmer Model 402 ultraviolet visible spectrometer. The nmr spectra were obtained with a Varian T-60 spectrometer. The chemical shifts are expressed in ppm (δ) from internal tetramethylsilane. The low and high resolution mass spectra were measured with Varian MAT CH-7 and 311A spectrometers, respectively. The gas–liquid chromatographic analyses were made with a Hewlett–Packard Model 5750 Research chromatograph (6 ft, 10% Sil. rubber S.E.30, 120°C, N_2 flame ionization).

1-(2-Methanesulfonyloxyethyl)pyrrole **2**

Triethylamine (27.9 g, 276 mmol) was added to a stirred solution of 1-(2-hydroxyethyl)pyrrole[3] (25.0 g, 225 mmol) in anhydrous dichloromethane (100 mL) cooled to −8°C. A solution of methanesulfonyl chloride (20.9 g, 270 mmol) in dichloromethane (50 mL) was added dropwise at the above temperature over a 0.75 hour period. The mixture was then mixed with 10% sodium bicarbonate solution, the organic phase was separated, washed with water and with saturated sodium chloride solution. The dichloromethane solution was dried over sodium sulfate and evaporated *in vacuo*. The residual oil (42.2 g) was sufficiently pure for use in the next step. It crystallized on standing and on recrystallization from methanol it had mp 42–42.5°C, uv (MeOH): 220 (4370) nm; ir ($CHCl_3$): 1356, 1167 cm^{-1}; nmr ($CDCl_3$) δ: 2.70 (s, 3H), 4.00–4.56 (m, 4H), 6.13 (m, 2H), 6.55 (m, 2H). *Anal.* calcd. for $C_7H_{11}NO_3S$: C 44.42, H 5.86, N 7.40; found C 44.65, H 5.91, N 7.38.

1-(2-Iodoethyl)pyrrole **3**

A solution of the methanesulfonate (25.0 g, 132 mmol) in anhydrous acetonitrile (400 mL) containing dry sodium iodide (98.4 g, 655 mmol) was heated at reflux temperature for 1.5 hours. The solution was cooled, the solvent was removed *in vacuo*, and water was added to the residue. The product was extracted into dichloromethane, the extract was dried over sodium sulfate and evaporated *in vacuo*. The residual oil (27.4 g, 94%) was sufficiently pure to be used in the next step. For analysis, a small portion of the crude iodide was subjected to column chromatography on silica gel using hexane–dichloromethane (1 : 1) as the eluting solvent; uv (MeOH): 225 (5890), 260 sh (794) nm; nmr ($CDCl_3$) δ: 3.16–3.53 (m, 2H), 4.03–4.40 (m, 2H), 6.13 (m, 2H), 6.61 (m, 2H). *Anal.* calcd. for C_6H_8IN: C 32.60, H 3.64, N 6.33; found: C 32.79, H 3.59, N 6.16.

Ethyl 2-formamido-2-ethoxycarbonyl-4-(pyrrol-1-yl)butanoate **4**

Sodium hydride in mineral oil (50%, 5.25 g, 109 mmol) was washed with hexane and then suspended in dry dimethylformamide (100 mL). Diethyl formamidomalonate (22.0 g, 109 mmol) was added to the magnetically stirred suspension and after 0.67 hours 1-(2-iodoethyl)pyrrole (20.0 g, 90 mmol) dissolved in dimethylformamide (20 mL) was added and the solution was then heated at reflux temperature for 5 hours. The cooled solution was poured into 10% hydrochloric acid solution and the product was extracted into toluene. The extract was dried over sodium sulfate and evaporated *in vacuo*. The residue was subjected to column chromatography on silica gel (50 g/g of crude product) and the desired material was eluted with hexane – ethyl acetate (89:11). The solid thus obtained (17.0 g, 64%) on crystallization from acetone–hexane had mp 88–89°C; uv (MeOH): 222 (5500) nm; ir ($CHCl_3$): 3415, 1745, 1697 cm^{-1}; nmr ($CDCl_3$) δ: 1.29 (t, 6H, J = 7.0 Hz), 2.93 (t, 2H, J = 6.7 Hz), 3.97 (t, 2H, J = 6.7 Hz), 4.30 (q, 4H, J = 7.0 Hz), 6.17 (m, 2H), 6.56 (m, 2H), 7.08 (m, 1H, exchanged with D_2O), 8.22 (s, 1H). *Anal.* calcd. for $C_{14}H_{20}N_2O_5$: C 56.74, H 6.80, N 9.45; found: C 56.78, H 6.78, N 9.49.

Ethyl 2-amino-2-ethoxycarbonyl-4-(pyrrol-1-yl)butanoate **5**

A mixture of the above formamide (5.00 g, 16.9 mmol) and 47% hydrobromic acid (14.9 g, 86.5 mmol) in water (150 mL) was stirred at reflux temperature for 0.75 hours. The solution was cooled to 5°C and made alkaline by the cautious addition of concentrated ammonium hydroxide solution. The product was extracted into ethyl acetate, the extract was washed with water, dried over sodium sulfate, and evap-

[4]We thank Dr. B. E. Maryanoff, McNeil Laboratories, for pointing this out and for providing us with relevant references.

Can. J. Chem. Downloaded from www.nrcresearchpress.com by 210.87.254.40 on 09/06/12
For personal use only.

orated *in vacuo* to give an oil (2.94 g, 65%); uv (MeOH): 222 (4170), 303 (2460) nm; ir ($CHCl_3$): 3405, 3340, 1739 cm^{-1}; nmr ($CDCl_3$) δ: 1.29 (t, 6H, J = 6.5 Hz), 2.02 (m, 2H, W_H = 6 Hz, exchanged with D_2O), 2.39 (t, 2H, J = 7.2 Hz), 4.05 (t, 2H, J = 7.2 Hz), 4.23 (q, 4H, J = 6.5 Hz), 6.15 (m, 2H), 6.58, (m, 2H). This compound was converted into the neutral oxalate salt in ethanol for analysis. After crystallization from acetone it had mp 76–78°C. *Anal.* calcd. for $C_{28}H_{40}N_4O_8$:$C_2H_2O_4$: C 53.66, H 6.76, N 8.95; found: C 53.60, H 6.59, H 8.59.

Ethyl 2-diazo-4-(pyrrol-1-yl)butanoate ***6***

A solution of the above amine (5.60 g, 20.9 mmol) in chloroform (50 mL) containing isopentyl nitrite (15.3 g, 130 mmol) was stirred at room temperature for 1 hour and then poured into dilute sodium bicarbonate solution. The organic phase was separated, combined with a chloroform extract of the aqueous phase, and then it was dried over sodium sulfate. The solvent was removed *in vacuo* and the residue was subjected to column chromatography on silica gel (50 g/g crude mixture). The pure diazo compound was eluted with hexane–dichloromethane (95:5) to give an oil (2.95 g, 69%) which was distilled *in vacuo* for analysis, bp 89–92°C/0.15 Torr; uv (MeOH): 218 (8320), 262 (10 000) nm; ir ($CHCl_3$): 2065, 1685 cm^{-1}; nmr ($CDCl_3$) δ: 1.28 (t, 3H, J = 7.3 Hz), 2.69 (t, 2H, J = 6.4 Hz), 4.06 (t, 2H, J = 6.4 Hz), 4.25 (q, 2H, J = 7.3 Hz), 6.19 (m, 2H), 6.66 (m, 2H); mass spectrum m/e (relative intensity): 179(30), 150(32), 134(20), 106(100), 80(45), 53(25). *Anal.* calcd. for $C_{10}H_{13}N_3O_2$: C 57.95, H 6.32; found: C 58.03, H 6.11.

Decomposition of the diazo compound ***6****. Formation of ethyl 1,2-dihydro-3*H*-pyrrolo[1,2-*a*]pyrrole-1-carboxylate* ***7****, and* cis *and* trans *ethyl 4-(pyrrol-1-yl)buten-2-oates* ***9*** *and* ***10***

The promoter was added to a solution of the diazo compound in the desired solvent (200 mL/g diazo compound; see Table 1) and the reaction was carried out at the temperature specified. When the diazo compound was no longer present the mixture was filtered through Celite and the filtrate was evaporated *in vacuo*. The residue could be subjected to quantitative analysis by gas–liquid partition chromatography, or separation by preparative tlc (even for gram quantities) using dichloromethane–hexane (3:2). The least and most polar compounds by tlc were **9** and **10**, respectively. A large amount of very polar material remained at the origin.

The bicyclic ester **7** was an oil; uv (MeOH): 222 (5250) nm; ir ($CHCl_3$): 1725 cm^{-1}; nmr ($CDCl_3$) δ: 1.27 (t, J = 7.2 Hz, CH_3), 2.53–2.97 (m, 2-CH_2), 3.80–4.17 (m, 1-CH and 3-CH_2), 4.25 (q, J = 7.2 Hz, OCH_2), 5.97 (m, H-6), 6.38 (m, H-7), 6.60 (m, H-5); ms (*Exact Mass*, high resolution mass spectrum) calcd. for $C_{10}H_{13}NO_2$: 179.0946; found: 179.0942.

The *cis* ester **9** also was an oil; ir ($CHCl_3$): 1717, 1645 cm^{-1}; nmr ($CDCl_3$) δ: 1.30 (t, J = 7.1 Hz, CH_3), 4.17 (q, J = 7.1 Hz, OCH_2), 5.07 (dd, J = 2.0, 6.2 Hz, NCH_2), 5.82 (dt, J = 2.0, 12.0 Hz, α-CH(olefinic)), 6.14 (m, H-3,4(pyrrole)), 6.28 (dt, J = 6.2, 12.0 Hz, β-CH(olefinic)), 6.65 (m, H-2,5(pyrrole)); ms (*Exact Mass*, high resolution mass spectrum) calcd. for $C_{10}H_{13}NO_2$: 179.0946; found: 179.0944.

The *trans* ester **10** was also an oil; ir ($CHCl_3$): 1723, 1670, 980 cm^{-1}; nmr ($CDCl_3$) δ: 1.26 (t, J = 6.9 Hz, CH_3), 4.21 (q, J = 6.9 Hz, OCH_2), 4.62 (dd, J = 1.7, 5.0 Hz, NCH_2), 5.67 (dt, J = 1.7, 15.7 Hz, α-CH(olefinic)), 6.18 (m, H-3,4(pyrrole)), 6.63 (m, H-2,5(pyrrole)), 7.02 (dt, J = 5.0, 15.7 Hz, β-CH(olefinic)); ms (*Exact mass*, high resolution mass spectrum) calcd. for $C_{10}H_{13}NO_2$: 179.0946; found: 179.0942.

*1,2-Dihydro-3*H*-pyrrolo[1,2-*a*]pyrrole-1-carboxylic acid* ***8***

A solution of the ester **7** (1.00 g, 5.59 mmol) in methanol (15 mL) and water (15 mL) containing sodium hydroxide (0.44 g, 11 mmol) was stirred at room temperature for 18 h. The methanol was removed *in vacuo*, water was added to the residue, and the solution was extracted with dichloromethane. The aqueous phase was cooled to 0°C and made acidic with concentrated hydrochloric acid. The product was extracted with ethyl acetate, the extract was washed with water and dried over sodium sulfate. The solvent was removed *in vacuo* and the residual oil was taken up in dichloromethane (20 mL). Dicyclohexylamine (1.3 mL) was added and after 0.5 hour the solvent was removed *in vacuo*. The residual solid was crystallized from dichloromethane–hexane giving material (1.52 g, 82%) with mp 152–153°C, identical in all respects to an authentic speciment of this salt (4).

1. C. D. NENITZESCU and E. SOLOMONICA. Chem. Ber. **64**, 1924 (1931).
2. B. E. MARYANOFF. J. Heterocycl. Chem., **14**, 177 (1977); German Patent No. 27 37 946 (1976); Chem. Abstr. **88**, 190 585 g (1978); B. E. MARYANOFF. J. Org. Chem. **44**, 4410 (1979); **47**, 3000 (1982).
3. A. GOSSAUER. Die chemie der pyrrole. Springer Verlag, Berlin. 1974. pp. 126–127; R. A. JONES and G. P. BEAN. The chemistry of pyrroles. Academic Press, London. 1977. pp. 269–270.
4. H. CARPIO, E. GALEAZZI, R. GREENHOUSE, A. GUZMÁN, E. VELARDE, Y. ANTONIO, F. FRANCO, A. LEON, V. PÉREZ, R. SALAS, D. VALDES, J. ACKRELL, D. CHO, P. GALLEGRA, O. HALPERN, R. KOEHLER, M. L. MADDOX, J. M. MUCHOWSKI, A. PRINCE, D. TEGG, T. C. THURBER, A. R. VAN HORN, and D. WREN. Can. J. Chem. **60**, 2295 (1982).
5. F. F. BLICKE and E. S. BLAKE. J. Am. Chem. Soc. **53**, 1015 (1931).
6. N. TAKAMURA, J. MIZOGUCHI, and S. YAMADA. Chem. Pharm. Bull. **23**, 299 (1975); M. B. SOHN, M. JONES, M. E. HENDRICK, R. R. RANDO, and W. VON E. DOERING. Tetrahedron Lett. 53, (1972).
7. D. J. CRAM and M. CORDON. J. Am. Chem. Soc. **77**, 4090 (1955); V. FRANZEN. Justus Liebigs Ann. Chem. **602**, 199 (1957).
8. A. B. SMITH and R. K. DIETER. Tetrahedron, **37**, 2407 (1981).

Can. J. Chem. Downloaded from www.nrcresearchpress.com by 210.87.254.40 on 09/06/12
For personal use only.

Effect of the partial pressures of oxygen and water vapour on the dispersity of α-Cr_2O_3 obtained by thermal decomposition of hydrated chromium(III) oxide

DIMITAR G. KLISSURSKI AND VLADIMIR N. BLUSKOV

Institute of General and Inorganic Chemistry, Bulgarian Academy of Sciences, 1040 Sofia, Bulgaria

Received August 24, 1981[1]

DIMITAR G. KLISSURSKI and VLADIMIR N. BLUSKOV. Can. J. Chem. **61**, 457 (1983).

The effect of water vapour and oxygen partial pressure on the thermal decomposition of hydrated chromium(III) oxide has been studied. A decrease in the water vapour partial pressure from 20 to 1×10^{-3} mm Hg has been found to produce a sharp increase in the specific surface area of the decomposition product (α-Cr_2O_3). Decomposition in an argon atmosphere leads to highly dispersed α-Cr_2O_3 even at relatively high temperatures (400–500°C).

DIMITAR G. KLISSURSKI et VLADIMIR N. BLUSKOV. Can. J. Chem. **61**, 457 (1983).

On a étudié l'influence de la vapeur d'eau et de la pression partielle d'oxygène sur la décomposition thermique de l'oxyde de chrome(III) hydraté. On a trouvé qu'une diminution de la pression partielle de la vapeur d'eau de 20 à 1×10^{-3} mm de Hg produit une augmentation nette de la surface spécifique du produit de décomposition (α-Cr_2O_3). La décomposition sous atmosphère d'argon conduit à du α-Cr_2O_3 hautement dispersé même à des températures relativement élevées (400–500°C).
[Traduit par le journal]

Can. J. Chem. Downloaded from www.nrcresearchpress.com by 210.87.254.6 on 09/06/12
For personal use only.

Introduction

The preparation of highly dispersed α-Cr_2O_3 is of considerable interest since this compound is a component of many oxide-type catalysts. Hydrated chromium oxides are mostly used as initial compounds.

The thermal decomposition of hydrated chromium oxides has been the subject of many investigations (1–12). Some of them have established a measurable effect of the partial pressure of oxygen on the mechanism of decomposition.

The present paper contains results of a study dedicated to the effect of the partial pressure of oxygen and water vapour on the thermal decomposition of α-$Cr_2O_3 \cdot nH_2O$ and on the dispersity and specific surface area of the α-Cr_2O_3 obtained.

Experimental

The initial xerogel of the highly dispersed α-$Cr_2O_3 \cdot nH_2O$ was obtained by a method described by Brauer (13) using precipitation from solutions of $Cr(NO_3)_3 \cdot 9H_2O$ and NH_4OH (25%) at a final pH = 7–8. The thermal decomposition was carried out in a flow of pure argon, oxygen, or air at different partial pressures of the water vapour ranging from 1×10^{-3} to 17.5 mm Hg. The samples were preliminarily dried for 15 h at 50°C.

The sintering of the initial α-$Cr_2O_3 \cdot nH_2O$ and of the obtained α-Cr_2O_3 was investigated in an argon flow at a water vapour partial pressure of 17.5 mm Hg.

The solid products of thermal decomposition were subject to thermal analysis, ir spectroscopy, and X-ray phase analysis. The specific surface areas of the samples were determined by the BET method using low-temperature nitrogen adsorption.

Results and discussion

The water content in the initial samples dried at 50°C as established by thermal analysis was 32.3%.

Figure 1 shows the effect of the water vapour partial pressure on the specific surface area of α-Cr_2O_3. The changes of this parameter for samples obtained by thermal treatment (3 h) in air at different water vapour partial pressures, in argon and oxygen flows, are shown.

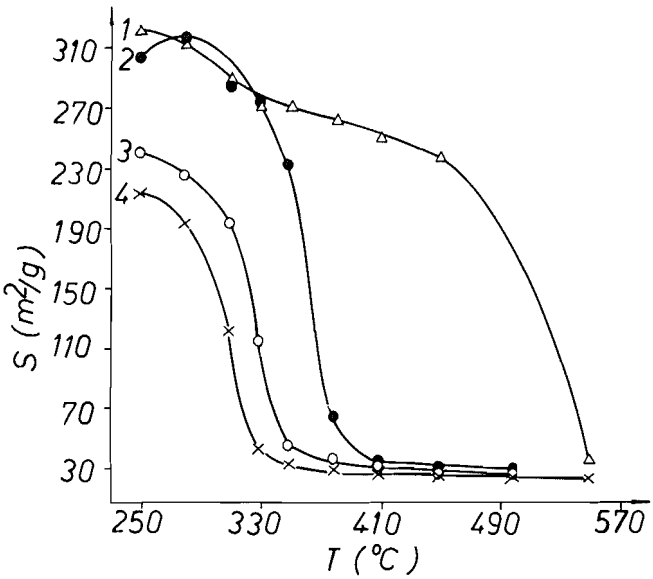

FIG. 1. Change of the specific surface areas of chromium oxides obtained: in an argon flow (curve *1*); in a "dry" air flow (curve *2*); in a "humid" air flow (curve *3*); in an oxygen flow (curve *4*).

Two temperature ranges are characteristic of the decomposition in both "humid" air (P_{H_2O} = 17.5 mm Hg) and "dry" air ($P_{H_2O} = 1 \times 10^{-3}$ mm Hg). The first interval comprises temperatures up to 330°C for "humid" air and 350°C for dry air, and is characterized by a relatively smooth decrease of the specific surface area with increasing temperature of thermal decomposition. A pronounced tendency to decrease in the specific surface areas of the α-Cr_2O_3 samples obtained in "humid" air compared to the specific surface area of samples obtained in "dry" air is observed mainly in this temperature range.

The second temperature range of decomposition is characterized by two main features: a sharp decrease in the specific surface areas and the absence of a noticeable effect of the water vapour partial pressure on the dispersity of the α-Cr_2O_3 obtained.

[1]Revision received October 5, 1982.

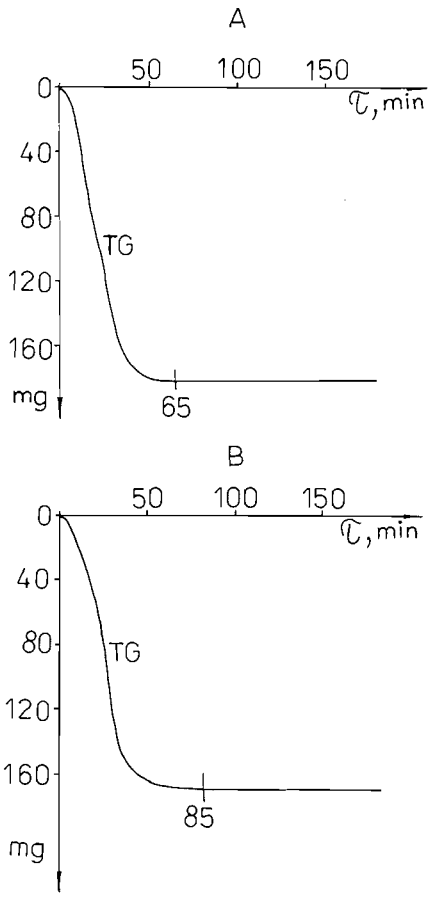

FIG. 2. TG curves obtained: *A*, in a "dry" air flow; *B*, in a "humid" air flow.

The more pronounced decrease of the specific surface areas of the samples obtained in "humid" air, which is observed mainly during the first stage of thermal decomposition, can be considered as a result of three parallel processes: (*a*) The increase of the water vapour partial pressure in the reaction space can lead to a certain decrease in the rate of thermal decomposition of the initial xerogel. (*b*) The highly dispersed α-Cr_2O_3 can be sintered according to an adsorption–desorption mechanism with the participation of water vapour (15). (*c*) The water vapour can accelerate the processes of initial crystallization and recrystallization of the α-Cr_2O_3 obtained. They proceed spontaneously with a very high rate at the second stage.

The increase in the partial pressure of the reaction product obtained during thermal decomposition may inhibit the decomposition of the initial compound. In "humid" air the initial α-$Cr_2O_3 \cdot nH_2O$ should decompose more slowly due to inhibited diffusion of the water vapour. The intensity of the diffusion flow, I, which affects the decomposition rate is defined (14) by the expression:

$$I = K(P_{Bm} - P_{H_2O})/P_{Bm}$$

where K is the rate constant, P_{H_2O}, the water vapour partial pressure, and P_{Bm}, the equilibrium dissociation pressure of the water vapour for the dehydration process

$$Cr_2O_3 \cdot 4H_2O \rightleftharpoons \alpha\text{-}Cr_2O_3 + 4H_2O_{(vapour)}$$

If the highly dispersed α-$Cr_2O_3 \cdot nH_2O$ decomposes for a longer

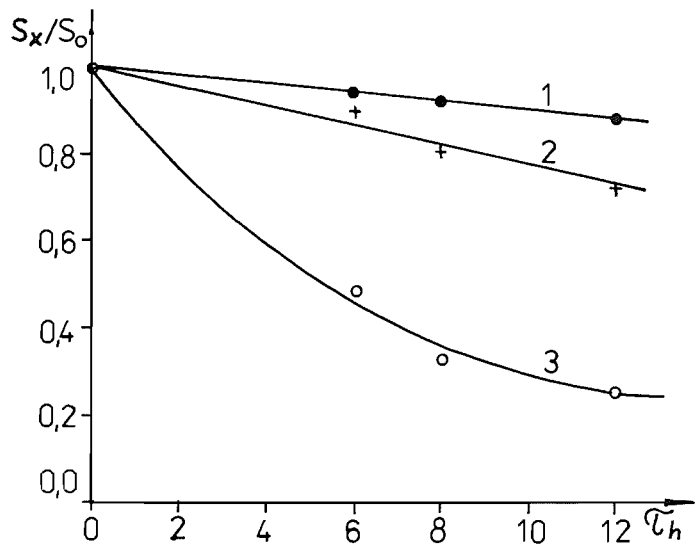

FIG. 3. Effect of sintering on the relative change in the specific surface area S_x/S_0, where S_x denotes the specific surface areas of samples sintered for different times, and S_0 is the specific surface area of the initial sample. Curve *1* presents the sintering of α-Cr_2O_3 in "dry" argon at 450°C; curve *2* corresponds to the sintering of α-Cr_2O_3 in "humid" argon at 450°C; and curve *3* shows the sintering of α-$Cr_2O_3 \cdot nH_2O$ in "humid" argon at 200°C.

time due to the increase of the water vapour partial pressure, this may accelerate the sintering.

Figure 2 shows the TG curve of the thermal decomposition of α-$Cr_2O_3 \cdot nH_2O$ in the presence of water vapour (curve *B*) and in dry air (curve *A*). Evidently, the retardation of decomposition under our conditions is insignificant. However, even when the water vapour partial pressure has no effect on the xerogel decomposition kinetics, it can measurably affect the kinetics of sintering.

Separate studies on the sintering of the initial xerogel and that of the high-dispersity α-Cr_2O_3 showed the effect of the water vapour on the sintering of xerogel to be more pronounced (Fig. 3). Because of the relatively large free surface of α-Cr_2O_3 its sintering proceeds most probably by the adsorption–desorption cycle mechanism (anion-exchange mechanism) proposed by Anderson *et al.* (15). This mechanism gives a mode of transport for a surface O^{2-} ion, which favours the sintering. It is accepted that during the desorption of a H_2O molecule it can remove an oxygen ion from the oxide surface. At the same time, O^{2-} from the initially chemisorbed water molecule remains in an adjacent position on the surface. After repeated adsorption and desorption, the surface mobility of the oxygen anions increases and the larger crystallites begin to grow at the expense of the smaller ones. The small change in the S_x/S_0 ratio is in agreement with the sintering mechanism assumed (16).

A study by thermal analysis, ir spectroscopy, and X-ray phase analysis showed that the α-Cr_2O_3 obtained crystallized only to a negligible extent within the first temperature range of decomposition. A surface structure of $HCrO_2$ was revealed by ir spectroscopy. The ir spectra showed bands at 955 and 1625 cm^{-1} which are characteristic of $HCrO_2$ (Fig. 4) (see ref. 6). The disappearance of this structure along with intensive crystallization and recrystallization were observed within the second temperature range of decomposition. The exothermal peak on the DTA curves which corresponds to the recrystallization

Can. J. Chem. Downloaded from www.nrcresearchpress.com by 210.87.254.6 on 09/06/12
For personal use only.

Can. J. Chem. Downloaded from www.nrcresearchpress.com by 210.87.254.6 on 09/06/12
For personal use only.

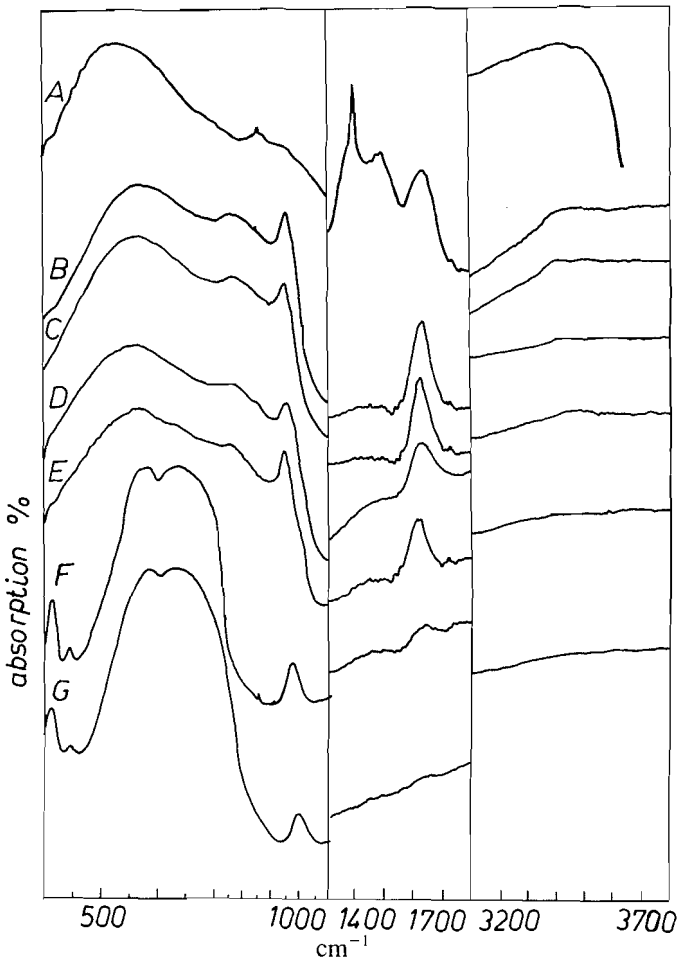

FIG. 4. Infrared spectra of: *A*, the initial xerogel; *B*, *D*, and *F*: the gel heated at 250, 330, and 350°C, respectively, in "humid" air; and *C*, *E*, and *G*: the gel heated at 250, 350, and 380°C, respectively, in dry air.

of α-Cr_2O_3 was observed at 380°C during decomposition in "humid" air and at 400°C when decomposition proceeded in "dry" air.

In addition to the water vapour, the oxygen partial pressure also substantially influenced the dispersity of the α-Cr_2O_3 obtained. Figure 1 (curves *1* and *4*) shows the results of a comparative investigation on the thermal decomposition of α-$Cr_2O_3 \cdot nH_2O$ in an oxygen flow and in a flow of pure argon. Obviously, the α-Cr_2O_3 samples obtained under argon have large specific surface areas. In this case the maximum of the exothermal peak which corresponds to the recrystallization processes is observed only at 550°C. This temperature is considerably higher than the temperature of intensive recrystallization in "dry" and "humid" air (Fig. 5). On the contrary, with increasing oxygen partial pressure (Fig. 1, curve *4*), the specific surface area of α-Cr_2O_3 decreases. The acceleration of recrystallization is in agreement with the results and interpretation of Fenerthy and Sing (1). These authors showed that CrO_3 appears during recrystallization in an oxygen atmosphere, and subsequently decomposes, forming α-Cr_2O_3. Thus centers of intensive recrystallization are created. The results of the present study unambiguously show that the dispersity of α-Cr_2O_3 obtained by thermal decomposition of $Cr_2O_3 \cdot nH_2O$ can be controlled over a large range by changing the gas phase

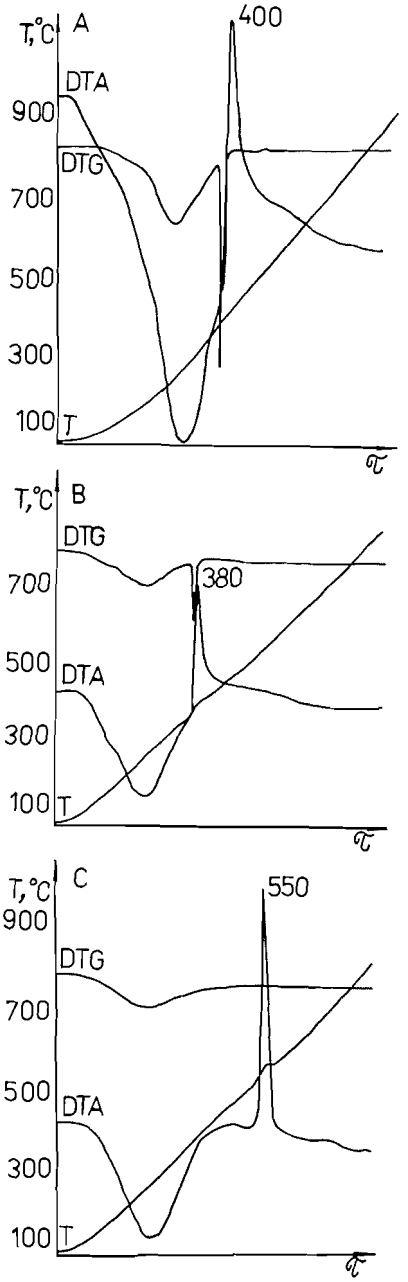

FIG. 5. DTA curves of α-$Cr_2O_3 \cdot nH_2O$, heated: *A*, in "dry" air; *B*, in "humid" air; *C*, under argon.

composition in the reaction space. This possibility is of considerable practical importance.

1. J. FENERTY and K. S. W. SING. Proc. Eur. Symp. Therm. Anal. 1st, 304 (1976).
2. M. A. ALARIO-FRANKO, J. FENERTY, and K. S. W. SING. *In* Reactivity of solids. Proc. 6th Intern. Symp. on Reactivity of Solids. Chapman and Hall, London. 1972. p. 327.
3. J. D. CARRUTHERS and K. S. W. SING. Chem. Ind. 1919 (1967).
4. F. S. BAKER, K. S. W. SING, and J. FENERTY. Chem. Ind. 718 (1970).
5. J. D. CARRUTHERS, K. S. W. SING, and J. FENERTY. Nature, **213**, 66 (1967).
6. P. RATNASAMY and A. J. LEONARD. J. Phys. Chem. **76**, 1838 (1972).
7. R. SH. MIKHAIL and S. A. SELIM. J. Appl. Chem. Biotechnol. **24**, 557 (1974).

8. R. GIOVANOLLI and W. STADELMANN. Therm. Acta, **7**, 41 (1973).
9. R. E. PROYNOVA-MEHANDJIEVA and D. R. MEHANDJIEV. Compt. Rend. Acad. Bulg. Sci. **29**, 1787 (1976).
10. M. NATARAJAN and E. A. SECCO. Phys. Stat. Sol. A**30**, R169 (1975).
11. A. ZECHINA, S. COLLUCCIA, E. GUGLIELMINOTTI, and G. GHIOTTI. J. Phys. Chem. **75**, 2774 (1971).
12. R. S. DYKE, S. B. BUTT, and C. L. HALLER. J. Catal. **25**, 378 (1972).
13. G. BRAUER (*Editor*). Handbuch der Prepar. Anorg. Chem. Ferdinand Enke Verlag, Stuttgart. 1954. p. 751.
14. A. W. SEARCY and D. BERUTO. J. Phys. Chem. **82**, 163 (1978).
15. B. J. ANDERSON and P. L. MORGAN. Trans. Faraday. Soc. **60**, 930 (1964).
16. T. ITO, M. FUITA, M. WATANABA, and T. TOKUDA. Bull. Chem. Soc. Jpn. **54**, 2412 (1981).

Can. J. Chem. Downloaded from www.nrcresearchpress.com by 210.87.254.6 on 09/06/12
For personal use only.

A highly stereoselective intramolecular aldol condensation. Part II. Synthesis of D,L-hamamelose from 2,2′-*O*-methylene-bis-D-glycerose

WALTER A. SZAREK AND B. MARIO PINTO

Carbohydrate Research Institute and Department of Chemistry, Queen's University, Kingston, Ont., Canada K7L 3N6

AND

T. BRUCE GRINDLEY

Department of Chemistry, Dalhousie University, Halifax, N.S., Canada B3H 4J3

Received February 25, 1982[1]

WALTER A. SZAREK, B. MARIO PINTO, and T. BRUCE GRINDLEY. Can. J. Chem. **61**, 461 (1983).

D,L-Hamamelose (2-*C*-hydroxymethyl-D,L-ribose) has been synthesized from 2,2′-*O*-methylene-bis-D-glycerose by application of the sequential reactions aldol condensation, mercaptolysis, and demercaptalation. The structures of the intermediate thioglycosides of D,L-hamamelose have been established by use of ^{1}Hmr and ^{13}Cmr spectroscopy. The exact composition of the equilibrium mixture of D,L-hamamelose in aqueous solution has also been established by the concomitant use of ^{1}Hmr and ^{13}Cmr spectroscopy. D-Hamamelose has been obtained from the D,L-mixture by preferential crystallization.

WALTER A. SZAREK, B. MARIO PINTO et T. BRUCE GRINDLEY. Can. J. Chem. **61**, 461 (1983).

On a synthétisé le D,L-hamamélose (*C*-hydroxyméthyl-2 D,L-ribose) à partir du *O*-méthylène-2,2′ bis-D-glycérose en faisant appel à une condensation aldolique, suivie d'une mercaptolyse et d'une élimination du mercaptan. On a établi les structures des thioglycosides intermédiaires du D,L-hamamélose en utilisant la spectroscopie de la rmn du ^{1}H et du ^{13}C. On a également établi la composition exacte du mélange à l'équilibre de D,L-hamamélose en solution aqueuse en utilisant en même temps la spectroscopie de la rmn du ^{1}H et du ^{13}C. On a obtenu le D-hamamélose par cristallisation préférentielle d'un mélange D,L.

[Traduit par le journal]

Introduction

The major product derived from the intramolecular aldol condensation of 2,2′-*O*-methylene-bis-D-glycerose (**1**), namely 2-*C*-hydroxymethyl-2,4-*O*-methylene-D,L-ribose (**2**) (1), is of interest since it represents a simple derivative of the naturally occurring branched chain sugar, hamamelose (2-*C*-hydroxymethyl-D-ribose) (**3**). Several syntheses of D-hamamelose or its derivatives have appeared in the literature (2–5). However, only two of these approaches (4, 5) gave stereospecific syntheses of the desired compounds; the other two approaches afforded mixtures of D-hamamelose and its C-2 epimer, D-epihamamelose. Accordingly, the conversion of 2,2′-*O*-methylene-bis-D-glycerose (**1**) into D,L-hamamelose was undertaken. This transformation would also constitute a chemical structure proof of the stereochemistry of the products derived from the intramolecular aldol condensation of **1**. It was anticipated that treatment of the products of the aldol condensation (1) with ethanethiol would result in the formation of the diethyl dithioacetals, as illustrated in Scheme 1. Prolonged reaction times would then be expected to give rise to the thioglycosides resulting from cleavage of the methylene acetal and subsequent displacement of an ethylthio group by one of the hydroxyl groups, as shown in Scheme 2. Since the thioglycosides can be readily converted into the free sugar, the mercaptolysis of the products of the aldol condensation was investigated as a means of converting 2,2′-*O*-methylene-bis-D-glycerose (**1**) into D,L-hamamelose.

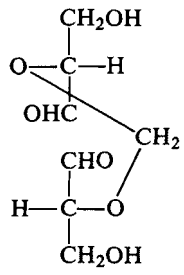

1

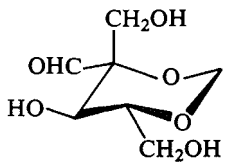

2

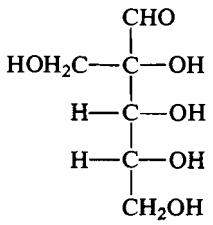

3

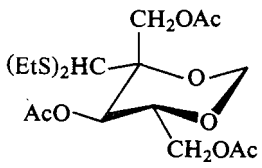

7

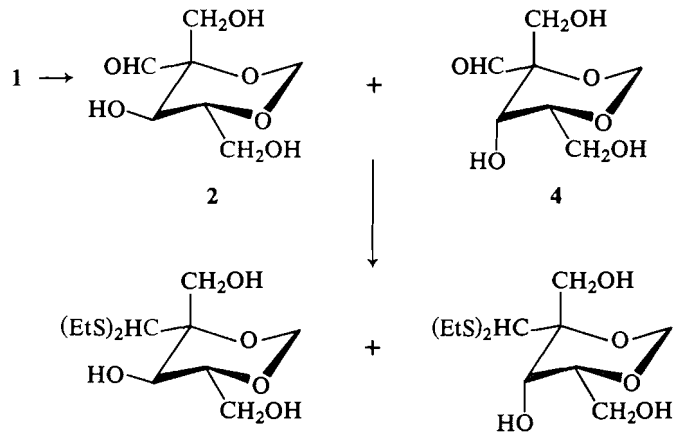

SCHEME 1

[1]Revision received October 14, 1982.

Can. J. Chem. Downloaded from www.nrcresearchpress.com by 210.87.254.6 on 09/06/12
For personal use only.

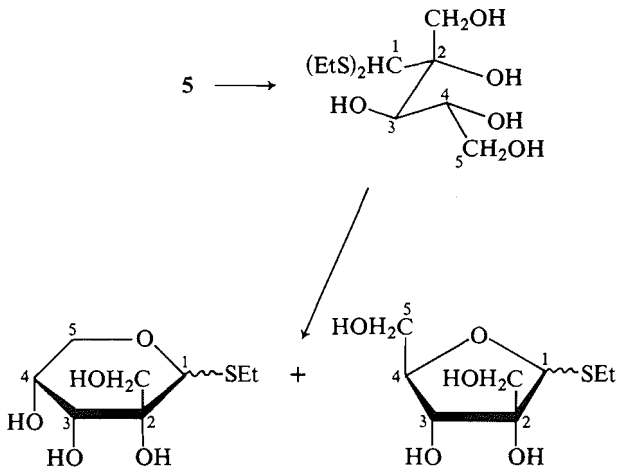

SCHEME 2

Results and discussion

Treatment of the aldol-condensation product mixture (1) with ethanethiol and hydrochloric acid for 2 h, followed by acetylation of the resulting mixture, afforded, after recrystallization, white needles which were identified as being 2-*C*-acetoxymethyl-3,5-di-*O*-acetyl-2,4-*O*-methylene-D,L-ribose diethyl dithioacetal (**7**). In contrast, treatment of the aldol-condensation product mixture with ethanethiol and hydrochloric acid for 63 h, followed by acetylation, afforded a multicomponent mixture. Fractionation of the mixture by means of high performance liquid chromatography yielded six different components. In order to facilitate further discussion, these compounds are numbered as **8**–**13**, in order of increasing polarity. Examination of the ^{1}Hmr spectra of these derivatives indicated that they were indeed thioglycosides. However, **8**, **9**, and **10** each contained four acetate groups whereas **11**, **12**, and **13** each contained only three acetate groups. It is likely that the tertiary hydroxyl group in the latter set of compounds remains unacetylated under the conditions employed (6). Deacetylation of either **8** or **11** afforded the same compound, labelled as **14**. Similarly, deacetylation of either **9** or **13** afforded **15**. Deacetylation of **10** and **12** gave separate compounds which are labelled as **16** and **17**, respectively. The structures of the four thioglycosides **14**–**17** were deduced by examination of their mass spectra, ^{1}Hmr spectra, and ^{13}Cmr spectra, as described in the following section.

Examination of the ^{13}Cmr spectral data for **14**–**17** (see Table 1) indicates that the C-4 signals in the spectra of **14** and **15** appear at δ 83.5 and δ 85.8, respectively, whereas the corresponding signals in the spectra of **16** and **17** appear at δ 69.9 and δ 70.3, respectively. It is well established (cf. refs. 7 and 8*d*) that the C-4 signals in the spectra of methyl glycopentofuranosides appear in the range δ 79 – δ 85 whereas the corresponding signals in the spectra of methyl glycopentopyranosides appear at δ 66 – δ 70. On this basis, compounds **14** and **15** can be assigned pentofuranoside structures and **16** and **17** can be assigned pentopyranoside structures. This assignment is further corroborated by the chemical-shift data for C-1 in the various compounds; the C-1 signals in the furanosides resonate at lower field than those in the pyranosides. Closer examination of the data indicates that the chemical shift of C-1 in both the furanosides has virtually the same value. This result suggests that both **14** and **15** have the same configuration at the anomeric centre since anomers of pentofuranosides generally display significant chemical-shift differences in C-1 signals. Moreover, the shielding effect of a 1,2-*cis* interaction between ethylthio and hydroxyl groups is expected to be different from that resulting from a 1,2-*cis* interaction between ethylthio and hydroxymethyl groups; if **14** and **15** were indeed anomers, then this situation would prevail and would be manifested in a chemical-shift difference between C-1 signals in the spectra of the two compounds. For example, a chemical-shift difference of 3.2 ppm for the C-1 signals in the spectra of ethyl 2-*C*-hydroxymethyl-α- and β-D-xylofuranoside, and a chemical-shift difference of 4.8 ppm for the C-1 signals in the spectra of ethyl 2-*C*-hydroxymethyl-α- and β-D-arabinofuranoside have been reported (3). Compounds **14** and **15** must, therefore, be epimeric at C-3. Since **15** was only present in low quantity, it must have resulted from the diethyl dithioacetal **6** that was, in turn, derived from the minor component of the aldol-condensation reaction (1). Hence, compound **14** is assigned the *ribo* configuration and compound **15** is assigned the *xylo* configuration. On the basis of the available data, it is not possible to assign the configuration at the anomeric centre in these two compounds. However, on the basis of an additional experiment (see later), both compounds have been assigned the stereochemistry in which the ethylthio group at C-1 and the hydroxyl group at C-2 bear a *syn* relationship to one another.

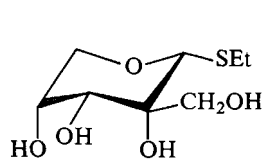

16

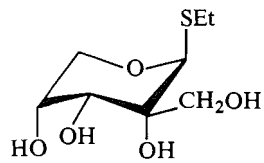

17

The assignment of stereochemistry in the pentopyranosides **16** and **17** was also performed on the basis of the ^{13}Cmr spectral data. The only major difference observed in the chemical-shift data for the two compounds is that for the C-5 carbons. Thus, C-5 in **17** is shielded by 4.7 ppm relative to C-5 in **16**; the result strongly suggests the operation of γ-*gauche* effect in the case of **17**. In this case, it is likely that **16** and **17** differ in configuration only at the anomeric centre since epimers at C-3 would also have resulted in a substantial chemical-shift difference between the C-3 signals for the two compounds; the presence of an axial hydroxyl group at C-3 would be predicted to shield both C-5 and C-1 by virtue of the γ-*gauche* effect. Compound **16** is, therefore, assigned a structure in which the ethylthio group adopts an equatorial orientation and compound **17** is assigned a structure in which the ethylthio group adopts an axial orientation. The assignment may be further substantiated by examination of the relative magnitudes of the one-bond coupling constants between C-1 and H-1 in the gated-decoupled spectra of **16** and **17**. In the case of pyranoid sugars it has been well established (8) that $^1J_{^{13}C_1-H_1}$ for the anomer in which H-1 is equatorial is greater (~10 Hz) than that for the anomer in which H-1 is axial. The difference may be a consequence of $n_O \rightarrow \sigma^*_{C-H}$ hyperconjugation in the latter case (9). The values of $^1J_{^{13}C_1-H_1}$ in **16** and **17** (153 Hz and 161 Hz, respectively) are consistent with expectations based on the above criterion. Therefore, compound **16** is identified as being ethyl 2-*C*-hydroxymethyl-1-thio-α-D- and α-L-ribopyranoside and compound **17** is identified as being ethyl 2-*C*-hydroxymethyl-1-thio-β-D- and α-L-ribopyranoside.

Can. J. Chem. Downloaded from www.nrcresearchpress.com by 210.87.254.6 on 09/06/12
For personal use only.

TABLE 1. Carbon-13 chemical-shift data[a] for 2-*C*-(hydroxymethyl)pentose derivatives

Compound[b]	Carbon								
	1	2	2′	3	4	5	SCH_2CH_3	SCH_2CH_3	$COCH_3$
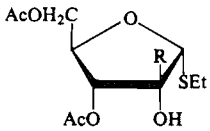 **11** R = CH_2OAc	90.7	78.7	66.1	72.6	78.2	63.0	15.2	25.3	20.6
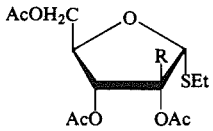 **8** R = CH_2OAc	89.4	84.1	62.8*	71.6	79.1	62.0*	14.8	25.4	20.6
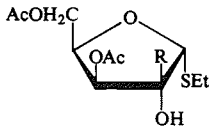 **13** R = CH_2OAc	89.8	80.0	65.8[c]	68.7[c]	74.0	63.0	14.9	26.0	20.6
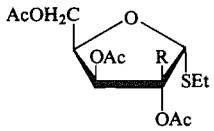 **9** R = CH_2OAc	88.1	85.9	63.7*	67.8	74.0	62.4*	14.8	25.4	20.6
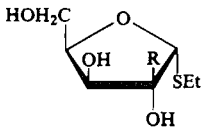 **15** R = CH_2OH	92.3	83.6	64.8*	74.5	85.8	65.6*	16.7	27.9	—
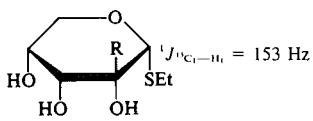 **16** R = CH_2OH	89.8	78.8	63.7	71.2*	69.6*	71.5[d]	17.1	27.7	—
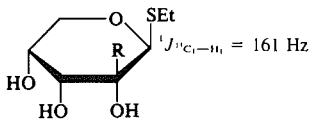 **17** R = CH_2OH	88.2	78.6	65.7	70.3	70.3	66.8[d]	16.6	27.7	—
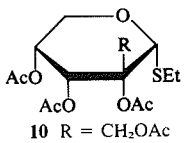 **10** R = CH_2OAc	88.7	73.5	63.5	68.3	68.3	66.1	15.3	25.8	20.7
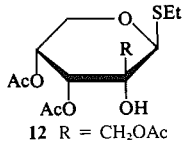 **12** R = CH_2OAc	87.1	74.0	65.4	67.9*	68.5*	61.8	14.7	25.3	20.7
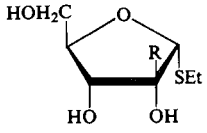 **14** R = CH_2OH	92.0	82.1	64.5*	72.5	83.5	63.2*	17.3	27.4	—

Can. J. Chem. Downloaded from www.nrcresearchpress.com by 210.87.254.6 on 09/06/12
For personal use only.

TABLE 1 *(Concluded)*

Compound[b]	Carbon 1	2	2′	3	4	5	SCH_2CH_3	SCH_2CH_3	$COCH_3$
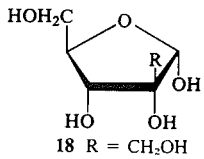 **18** R = CH_2OH	99.7	80.3	[c]	[c]	83.2	[c]	—	—	—
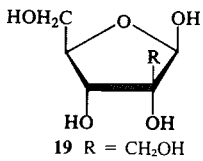 **19** R = CH_2OH	103.3	83.7	[c]	[c]	84.5	[c]	—	—	—

[a] The spectra of compounds **8–13** were measured in chloroform-*d*; chemical shifts are given in ppm downfield from internal TMS. The spectra of compounds **14–21** and **26** were measured in deuterium oxide with internal acetone as reference; chemical shifts are given with respect to the chemical shift of acetone which was taken as being 32.8 ppm.

[b] Owing to overlap of signals, only the signals for C-1 were assigned in the spectra of compounds **20**, **21**, and **26**. C-1 in **20** resonated at 97.2 ppm; C-1 in **21** resonated at 96.7 ppm; C-1 in **26** resonated at 94.7 ppm.

[c] Assignment is tentative owing to the presence of an impurity.

[d] In the gated-decoupled spectrum, these peaks appeared as triplets which showed further long-range coupling.

[e] Extensive overlap of signals did not permit unambiguous assignment of these resonances.

*Assignments may be interchanged.

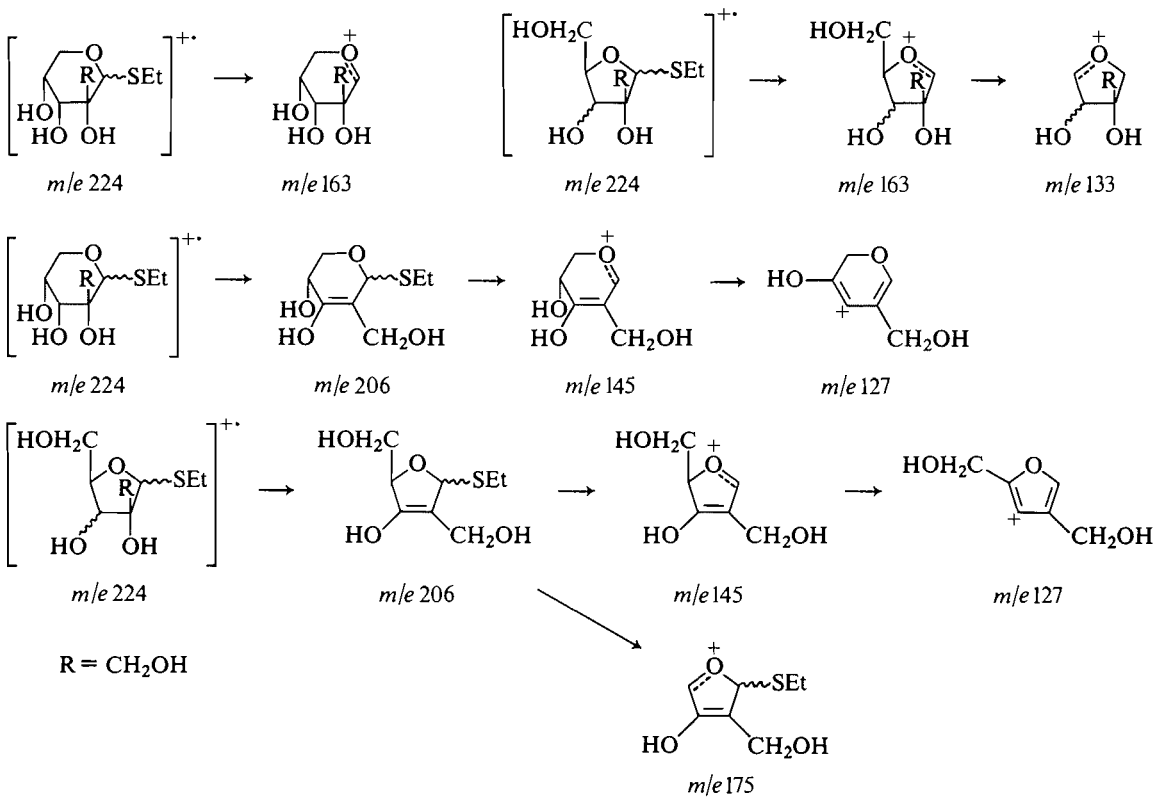

SCHEME 3

The mass-spectral data for compounds **14–17** are also consistent with the assignment of furanoid structures to **14** and **15** and of pyranoid structures to **16** and **17**. Two fragmentation modes are observed for all four compounds; the first involves loss of the ethylthio group to give an oxonium ion (*m/e* 163) and the second involves the loss of water as the initial fragmentation step to give an ion transition at *m/e* 206. The characteristic feature of the spectra of the furanosides **14** and **15** is the presence of ion transitions at *m/e* 175 and *m/e* 133; these peaks are attributed to the loss of the hydroxymethyl group at C-4 from ions having *m/e* values of 206 and 163, respectively. The peaks at *m/e* 175 and *m/e* 133 are absent in the spectra of the pyranosides **16** and **17**. The proposed fragmentation modes to account for the main ion transitions are summarized in Scheme 3.

The structures of compounds **11–17**, deduced on the basis

Can. J. Chem. Downloaded from www.nrcresearchpress.com by 210.87.254.6 on 09/06/12
For personal use only.

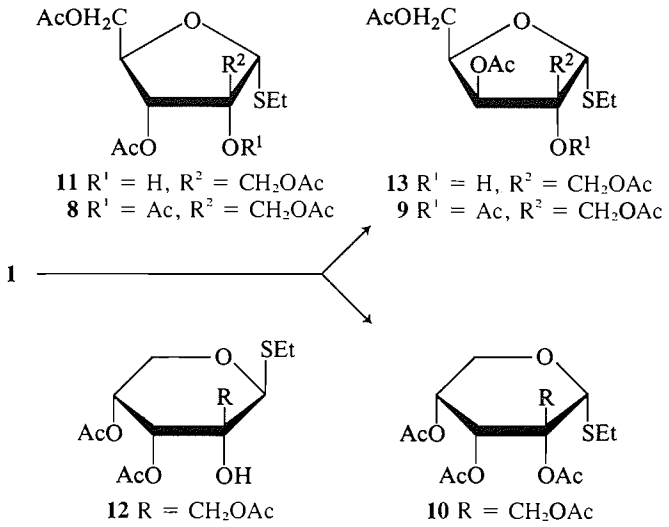

SCHEME 4

of the evidence presented in the preceding sections, are shown in Schemes 4 and 5. The ^{13}Cmr data for these compounds are presented in Table 1.

Treatment of a mixture of the thioglycosides **14** and **16** with mercuric chloride and cadmium carbonate in water (see Scheme 5) afforded, after ion-exchange chromatography, a syrup whose ^{1}Hmr spectrum in deuterium oxide was identical to that of an authentic sample[2] of D-hamamelose. The syrup had an optical rotation of $-1.4°$ in water at equilibrium. Since the reported values for the rotations of D- and L-hamamelose are $-7.0°$ (2) and $+7.3°$ (6), respectively, the syrup obtained in the above experiment must consist of a mixture of D- and L-isomers. This result is not surprising in view of the expected formation of D,L-pairs of isomers in the aldol-condensation reaction which preceded the mercaptolysis reaction (1). The sugar was further characterized by formation of the crystalline *p*-tolylsulfonylhydrazone (2, 6). Interestingly, upon seeding of the syrupy product with an authentic sample of D-hamamelose, preferential crystallization of only the D-isomer ensued, as evidenced by the optical rotation of the crystals ($[\alpha]_D^{33}$ (after 0.5 h) $-7.2°$ (*c* 0.56, H_2O)). The sample was identical in all respects with the authentic sample of D-hamamelose.

Several reports (2–6) have appeared in the literature on the synthesis of D- or L-hamamelose. However, the exact composition of the equilibrium mixture in aqueous solution has not yet been determined. Accordingly, the ^{1}Hmr and ^{13}Cmr spectroscopic investigation of the equilibrium proportions of the α- and β-furanoses and pyranoses in aqueous solution was undertaken.

The ^{1}Hmr spectrum (at 220 MHz and at 301 K) of hamamelose in deuterium oxide indicated the presence of four singlets at δ 4.79, 5.13, 5.21, and 5.28 which were attributed to the anomeric hydrogens in the two pyranoses and the two furanoses. Measurement of the spectrum under conditions of partial relaxation resulted in suppression of the residual water peak and permitted the integration of these signals; the relative intensities of the four signals at δ 4.79, 5.13, 5.21, and 5.28 were found to be 1.7:1:2.4:3, respectively. The ^{13}Cmr spectrum of hamamelose also indicated the presence of four signals attributable to the anomeric carbons in the two pyranoses and

[2]The authors are grateful to Dr. Pak-Tsun Ho for a gift of synthetic D-hamamelose.

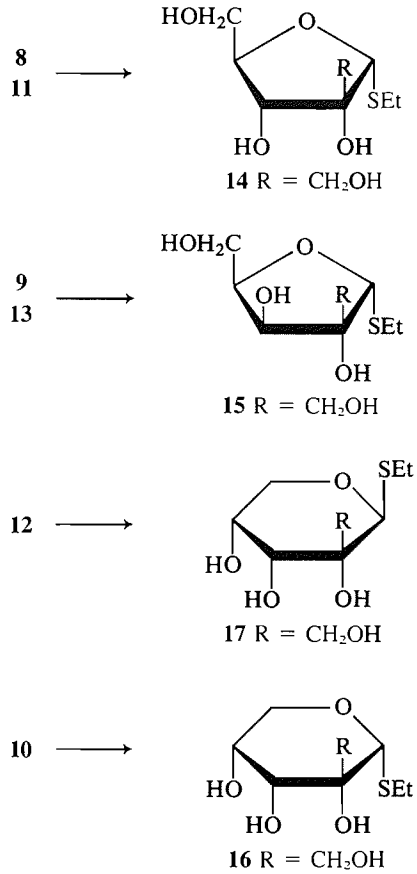

SCHEME 5

the two furanoses (see Table 1). The signals at δ 103.3 and δ 99.7 were assigned to the C-1 signals in the furanoses and those at δ 97.2 and δ 96.7 were attributed to the pyranoses. The differentiation of the signals for the two furanose anomers can also be made on the basis of the ^{13}Cmr chemical-shift data. Several ^{13}Cmr studies of ketohexofuranoses have appeared in the literature which suggest that a 1,2-*cis* interaction between two hydroxyl substituents in a furanoid ring results in greater shielding of the carbon atoms to which they are attached than a 1,2-*cis* interaction between a hydroxyl substituent and a hydroxymethyl substituent in the corresponding anomer (10), that

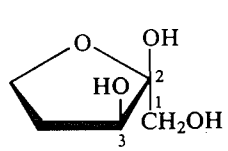

22

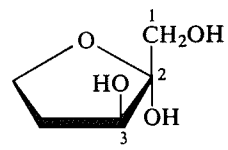

23

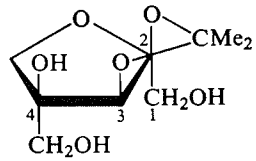

24

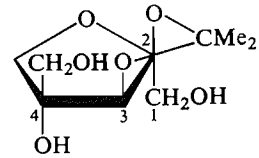

25

is, C-2 and C-3 in **22** are shielded relative to C-2 and C-3 in **23**. This "*cis* effect" has also been noted in certain derivatives of L-dendroketose (11). Thus, C-3 and C-4 in **24** were shielded by 5.2 ppm and 3.0 ppm, respectively, relative to the correspond-

Can. J. Chem. Downloaded from www.nrcresearchpress.com by 210.87.254.6 on 09/06/12
For personal use only.

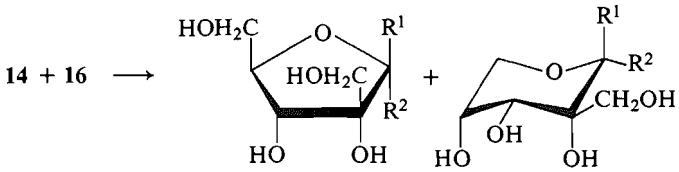

18 R¹ = H, R² = OH **20** R¹ = H, R² = OH
19 R¹ = OH, R² = H **21** R¹ = OH, R² = H

SCHEME 6

ing carbons in **25**. On the basis of these results, the signal at δ 103.3 in the ^{13}Cmr spectrum of hamamelose is assigned to C-1 in **19** and that at δ 99.7 is assigned to C-1 in **18** (see Scheme 6). In agreement with expectations, the C-2 signal in the spectrum of **18** is also shifted upfield relative to the C-2 signal in the spectrum of **19** (see Table 1).

The assignment of the signals at δ 97.2 and δ 96.7 in the spectrum of hamamelose to C-1 in **20** and **21** (see Scheme 6) should, in theory, be possible by examination of the differences in the magnitudes of the $^{1}J_{^{13}C_1-H_1}$ coupling constants, as described previously. However, the small chemical-shift difference between signals and the presence of two-bond and three-bond couplings complicated the situation since distinct doublets were not observed for the C-1 signals in the gated-decoupled spectrum. Nonetheless, the assignment can be made by careful examination of the spectra. Two situations can arise.

^{1}H-Decoupled spectrum

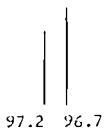

Gated-decoupled spectrum; situation A

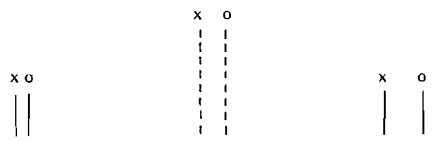

o peaks owing to **21**
× peaks owing to **20**

Gated-decoupled spectrum; situation B

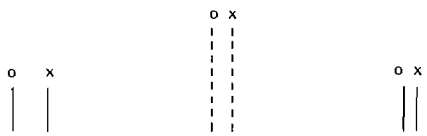

o peaks owing to **21**
× peaks owing to **20**

SCHEME 7

If the peak at δ 96.7 ppm is attributed to C-1 in **21**, then situation A in Scheme 7 will prevail since $^{1}J_{^{13}C_1-H_1}$ in **21** is expected to be larger than that in **20** (8). If, however, the peak at δ 96.7 ppm is attributed to C-1 in **20**, then situation B will prevail. Close examination of the gated-decoupled spectrum of hamamelose shows the presence of multiplets for each of the halves of the doublets for the C-1 signals of **20** and **21**. The low-field multiplet has a width at half-height of about 18 Hz whereas the high-field multiplet has a width at half-height of about 9 Hz. Since the spectrum resembles that expected for situation B in Scheme 7, the signal at δ 96.7 ppm is attributed to C-1 in **20** and that at δ 97.2 ppm is attributed to C-1 in **21**. In summary, the signals at δ 103.3, 99.7, 97.2, and 96.7 ppm in the spectrum of D-hamamelose are assigned to the anomeric carbons in the β-furanose, α-furanose, β-pyranose, and α-pyranose species, respectively.

In order to estimate the proportion of each species present at equilibrium in deuterium oxide, the ^{13}Cmr spectrum of a D-hamamelose solution (0.6 *M*) was recorded in deuterium oxide at 302 K under conditions[3] such that integrated intensities are a reliable measure of the concentration of the individual isomers present in solution. The relative intensities of the relevant ^{13}Cmr peaks were measured by means of a planimeter. The relative intensities of the peaks at δ 103.3, 99.7, 97.2, and 96.7 were 2.1:3.0:1.6:1, respectively. Therefore, D-hamamelose exists in deuterium oxide at 302 K as an equilibrium mixture of the α-furanose, β-furanose, β-pyranose, and α-pyranose isomers which are present in the ratio of 39:28:20:13 (see Table 2). The calculated ratios compare favorably with those (38:29:21:12) obtained by integration of the H-1 signals in the ^{1}Hmr spectrum of D-hamamelose in deuterium oxide at 296 K. This coincidence of values can thus be employed to assign the H-1 signals to the particular isomers of hamamelose. On this basis the singlets at δ 5.28, 5.21, 5.13, and 4.79 in the ^{1}Hmr spectrum of D-hamamelose are assigned to H-1 of the α-furanose, β-furanose, α-pyranose, and β-pyranose isomers, respectively (see Table 2).

One last point remains to be clarified, namely the question of the stereochemistry at the anomeric centre of the furanose thioglycoside **14**. Since this question is difficult to answer when only one anomer is available for investigation, an attempt was made to generate the alternate anomer of **14**. Treatment of a mixture of D,L-hamamelose with ethanethiol and hydrochloric acid for 80 h afforded a mixture of the four isomers of hamamelose as well as three thioglycosides (see Scheme 8), as judged by examination of the ^{13}Cmr spectrum of the mixture. The peaks attributable to C-1 of the thioglycosides appeared at δ 89.8, 92.0, and 94.7. The peak at δ 89.8 was assigned to C-1 of **16**, and that at δ 92.0 was assigned to C-1 of **14**. The peak at δ 94.7 did not correspond to C-1 of any of the three thioglycosides previously synthesized. This signal was, thus, assigned to C-1 of the alternate anomer of **14**, namely ethyl 2-*C*-hydroxymethyl-1-thio-β-D- and α-L-ribofuranoside (**26**). The shielding of C-1 in **14** relative to that in **26** is expected on

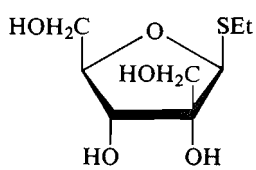

26

the basis of the "*cis* effect", as discussed previously. Compound **14**, one of the products of the original mercaptolysis

[3]The ^{13}Cmr spectra were measured on a Varian CFT-20 spectrometer using 66° pulses and 2.6 s pulse intervals. For a discussion of intensity measurements on sugars by ^{13}Cmr spectroscopy, see ref. 12.

Can. J. Chem. Downloaded from www.nrcresearchpress.com by 210.87.254.6 on 09/06/12
For personal use only.

TABLE 2. Composition of D-hamamelose in aqueous solution

Isomer	Chemical shift[a] of C-1 signal (ppm)	Chemical shift[b] of H-1 signal (ppm)	Percentage composition from ^{13}Cmr data[c]	Percentage composition from ^{1}Hmr data[d]
α-Furanose **18**	99.7	5.28	39	38
β-Furanose **19**	103.3	5.21	28	29
α-Pyranose **20**	96.7	5.13	13	12
β-Pyranose **21**	97.2	4.79	20	21

[a]From ^{13}Cmr spectrum recorded at 20.0 MHz in deuterium oxide at 302 K; chemical shifts were measured relative to that of internal acetone (δ 32.8).
[b]From ^{1}Hmr spectrum recorded at 220 MHz in deuterium oxide at 296 K; chemical shifts were measured relative to that of internal acetone (δ 2.23).
[c]Estimated from relative intensities of ^{13}Cmr signals for C-1, measured by means of a planimeter.
[d]Estimated from relative intensities of ^{1}Hmr signals for H-1 by direct integration.

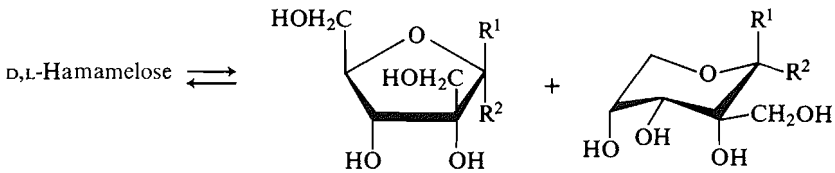

14 R^1 = H, R^2 = SEt
26 R^1 = SEt, R^2 = H

16 R^1 = SEt, R^2 = H
17 R^1 = H, R^2 = SEt

SCHEME 8

reaction, is, therefore, identified as being ethyl 2-*C*-hydroxymethyl-1-thio-α-D- and β-L-ribofuranoside. On the basis of arguments presented previously, compound **15**, the minor product of the original mercaptolysis reaction is also assigned the α-D- or β-L-configuration. Interestingly, when the nmr sample was let stand at ambient temperature for 30 h and the ^{13}Cmr spectrum was recorded again, the spectrum indicated the presence of three signals attributable to C-1 of thioglycosides at δ 92.0, 89.8, and 88.1. The absence of the peak owing to C-1 of **26** (δ 94.7) and the appearance of the peak attributable to C-1 of **17** (δ 88.1) suggest that the sample had equilibrated since the recording of the first ^{13}Cmr spectrum. The deuterium oxide solution was found to have a pD value of 4. Apparently, the ratio of thioglycosides obtained in the thioglycosidation reaction differs from that obtained in the mercaptolysis reaction. Preparative thin-layer chromatography of the mixture obtained from the thioglycosidation reaction afforded a mixture of the thioglycosides **14**, **16**, **17**, as indicated by ^{1}Hmr and ^{13}Cmr spectroscopy; in the case of the ^{13}Cmr spectrum, all of the signals for each of these compounds could be assigned.

Experimental

Melting points were determined with a Fisher–Johns apparatus and are uncorrected. Mass spectra were recorded on a CEC21-104 mass spectrometer under electron-impact conditions at 70 eV ionizing voltage. Proton magnetic resonance (^{1}Hmr) spectra were recorded on Bruker HX-60 or Varian HR-220 spectrometers; spectra were recorded at 60 MHz, unless otherwise stated. Carbon-13 magnetic resonance (^{13}Cmr) spectra were recorded on a Bruker HX-60 spectrometer equipped with a FT60M Fourier transform accessory at 15.09 MHz or a Varian CFT-20 spectrometer at 20.0 MHz. Spectra were measured in chloroform-*d* with tetramethylsilane (TMS) as internal standard, unless otherwise stated. Chemical shifts are given in ppm downfield from TMS. Spectra recorded in deuterium oxide solution were measured with respect to internal acetone whose chemical shift was taken as being 2.225 ppm relative to TMS for the ^{1}Hmr spectra and 32.78 ppm relative to TMS for the ^{13}Cmr spectra. Optical rotations were determined on a Perkin–Elmer 141 polarimeter.

Analytical thin-layer chromatography (tlc) was performed on precoated glass plates with Merck silica gel 60F-254 as the adsorbent (layer thickness 0.25 mm). The developed plates were air-dried and exposed to uv light and/or sprayed with a solution of cerium sulfate (1%) and molybdic acid (1.5%) in 10% aqueous sulfuric acid, and heated at 150°C. Preparative thin-layer chromatography was performed on precoated glass plates with Merck silica gel 60F-254 as the adsorbent (layer thickness 2 mm). Column chromatography was performed on Brinkman silica gel (70–235 mesh, E. Merck). High performance liquid chromatography was performed on a Waters Associates Prep LC/ System 500. The chromatographic solvents (v/v) employed in this work are as follows: (*A*) benzene – ethyl acetate, 1:1; (*B*) ethyl acetate – ethanol, 20:1; (*C*) 10:1; (*D*) *n*-propanol – ethyl acetate – water, 3:1:1; (*E*) toluene – ethyl acetate, 6:1.

Solvents were evaporated under reduced pressure and below 40°C.

2-C-Acetoxymethyl-3,5-di-O-acetyl-2,4-O-methylene-D,L-ribose diethyl dithioacetal (7)

The aldol-condensation product mixture (16 g), obtained from 2,2′-*O*-methylene-bis-D-glycerose (**1**) by treatment with 0.1 *N* sodium hydroxide for 7 h (1), was treated with concentrated hydrochloric acid (24 mL) and ethanethiol (24 mL) at 0°C for 1 h and then at room temperature for 1 h. The solution was poured with stirring into dry lead carbonate. Water was added and the solids were removed by filtration. The solids were thoroughly washed with water, and the combined filtrate and washings were concentrated to afford a syrup. The syrupy residue was acetylated with acetic anhydride (30 mL) and pyridine (50 mL) in the usual manner. The mixture was poured into ice-water, upon which a solid deposited. The solid was collected by filtration (15.4 g). Recrystallization from ethanol afforded a small amount of white crystals which were identified as being one of the products derived from the Cannizzaro reaction of **4** (1), namely 2-*C*-acetoxymethyl-1,3,5-tri-*O*-acetyl-2,4-*O*-methylene-D,L-*threo*-pentitol (**27**) (0.64 g), mp 144–146°C (lit. (13) mp 147–148°C for the L-isomer). The mother liquor afforded white needles which were identified as being the title compound **7**, mp 112–113°C, $[\alpha]_D^{24}$ −25.7° (*c* 1.2, chloroform); ^{1}Hmr data ($CDCl_3/C_6D_6$ (7:5)) δ: 1.11 (3H, t, SCH_2CH_3), 1.75, 1.78, 1.80 (three 3H s's, 3 OAc's), 2.66

Can. J. Chem. Downloaded from www.nrcresearchpress.com by 210.87.254.6 on 09/06/12
For personal use only.

Can. J. Chem. Downloaded from www.nrcresearchpress.com by 210.87.254.6 on 09/06/12
For personal use only.

(2H, q, SCH_2CH_3), 3.67 (1H, m, H-4), 3.98 (1H, s, H-1), 4.12 (2H, m, H-5, H-5′), 4.55 (1H, d, J = 12.8 Hz, H-2′), 4.75 (2H, AB, J = 7 Hz, O—CH_2—O), 4.96 (1H, d, J = 12.8 Hz, H-2″), 5.97 (1H, d, J = 10.2 Hz, H-3). *Anal.* calcd. for $C_{17}H_{28}O_8S_2$: C 48.2, H 6.6, S 15.1; found: C 48.0, H 6.5, S 15.0.

Mercaptolysis of 2-C-hydroxymethyl-2,4-O-methylene-D,L-ribose (2) and 2-C-hydroxymethyl-2,4-O-methylene-D,L-xylose (4)

The aldol-condensation product mixture (4.32 g), obtained by treatment of 2,2′-*O*-methylene-bis-D-glycerose (**1**) with 0.05 *N* sodium hydroxide for 3.5 h, was dissolved in concentrated hydrochloric acid (9.4 mL), and ethanethiol (9.4 mL) was added with stirring. The mixture was stirred at room temperature for 63 h and was then poured into solid lead carbonate (60 g). Water (50 mL) was added and the slurry was filtered. The solids were washed with an additional amount of water (200 mL). The filtrate and washings were concentrated to afford a syrupy solid, which was treated with pyridine (30 mL) and acetic anhydride (20 mL) at room temperature for 12 h. Sodium hydrogen carbonate solution (250 mL) was added and the mixture was stirred for several hours. The mixture was extraced with methylene chloride (4 × 75 mL). The extracts were dried over anhydrous magnesium sulfate, and concentrated to give a syrup. Thin-layer chromatography (solvent *A*) indicated the presence of a multicomponent mixture. The mixture was chromatographed using high performance liquid chromatography using solvent E as eluant to yield six different components as syrups. The component having an R_f value of 0.69 was identified as being ethyl 2-*C*-acetoxymethyl-1,3,5-tri-*O*-acetyl-1-thio-α-D- and β-L-ribofuranoside (**8**) (0.3 g); ^{1}Hmr data ($CDCl_3$) δ: 1.29 (3H, t, SCH_2CH_3),2.05, 2.10 (two 6H s's, 4 OAc's), 2.65 (2H, q, SCH_2CH_3), 4.15–4.35 (2H, m's), 4.60, 4.84 (2H, AB q, J = 12 Hz), 5.20 (2H, m), 5.62 (1H, s, H-1). The component having an R_f value of 0.64 was not obtained pure but was contaminated with compound **8** (combined yield 0.21 g). It was identified as being ethyl 2-*C*-acetoxymethyl-2,3,5-tri-*O*-acetyl-1-thio-α-D- and β-L-xylofuranoside (**9**); ^{1}Hmr data ($CDCl_3$) δ: 1.26 (3H, t, SCH_2CH_3), 2.07, 2.10, 2.12 (s's, 4 OAc's), 2.60 (2H, q, SCH_2CH_3), 4.0–4.4 (2H, m's), 4.50, 4.75 (2H, AB q, J = 12 Hz), 5.40 (2H, m), 5.51 (1H, s, H-1). The component having an R_f value of 0.59 was identified as being ethyl 2-*C*-acetoxymethyl-2,3,4-tri-*O*-acetyl-1-thio-α-D- and β-L-ribopyranoside (**10**) (0.231 g); ^{1}Hmr data ($CDCl_3$) δ: 1.31 (3H, t, SCH_2CH_3), 2.09, 2.10 (s's, 4 OAc's), 2.72 (2H, q, SCH_2CH_3), 3.9–4.5 (4H, m's), 4.78 (1H, s, H-1), 5.19 (2H, m). The component having an R_f value of 0.55 was identified as being ethyl 2-*C*-acetoxymethyl-3,5-di-*O*-acetyl-1-thio-α-D- and β-L-ribofuranoside (**11**) (0.45 g); ^{1}Hmr data ($CDCl_3$) δ: 1.31 (3H, t, SCH_2CH_3), 2.09, 2.12, 2.15 (s's, 4 OAc's), 2.69 (2H, q, SCH_2CH_3), 4.0–4.4 (5H, m's), 4.63–5.0 (2H, m), 5.34 (1H, s, H-1). A mixture of compounds **11** and **10** was also obtained (1.09 g). The component having an R_f value of 0.49 was identified as being ethyl 2-*C*-acetoxymethyl-3,4-di-*O*-acetyl-1-thio-β-D- and α-L-ribopyranoside (**12**) (0.355 g); ^{1}Hmr data ($CDCl_3$) δ: 1.30 (3H, t, SCH_2CH_3), 2.08, 2.10, 2.14 (s's, 3 OAc's), 2.64 (2H, q, SCH_2CH_3), 3.4–4.55 (5H, m's), 5.03–5.3 (3H, m's, includes H-1). A mixture of compounds **11** and **12** was also obtained (0.14 g). The component having an R_f value of 0.42 was identified as being a mixture of ethyl 2-*C*-acetoxymethyl-3,5-di-*O*-acetyl-1-thio-α-D- and β-L-xylofuranoside (**13**) and an unidentified compound that was present in low quantity (0.37 g); ^{1}Hmr data ($CDCl_3$) δ: 1.30 (3H, t, SCH_2CH_3), 2.04, 2.10, 2.14 (s's, 3 OAc's), 2.60 (2H, q, SCH_2CH_3), 4.0–4.5 (m's), 5.07 (1H, s, H-1), 5.1–5.35 (m).

Base-catalyzed solvolysis of compound 11

The triacetate **11** (0.45 g) was dissolved in chloroform (2 mL) and methanol (5 mL) and the solution was cooled to 0°C. Sodium methoxide (0.4 mL, 1.1 *N* in methanol) was added and the mixture was stored at 0°C for 12 h. Thin-layer chromatography (solvent *A*) indicated the disappearance of starting material and the appearance of a component at the baseline. The mixture was neutralized with moist Amberlite IR-120 (H^+). The resin was removed by filtration and washed with ethanol. The filtrate and washings were concentrated to yield a syrup (0.28 g) which solidified on standing. Recrystallization from chloroform afforded an amorphous solid which was identified as being ethyl 2-*C*-hydroxymethyl-1-thio-α-D- and β-L-ribofuransoside (**14**), mp 65–67°C; ^{1}Hmr data (D_2O with $(CH_3)_2CO$) δ: 1.28 (3H, t, SCH_2CH_3), 2.71 (2H, q, SCH_2CH_3), 3.59–4.04 (6H, m's), 5.36 (1H, s, H-1); M calcd. for $C_8H_{16}O_5S$: 224; found: m/e 224 (M^+). Ethyl 2-*C*-benzoyloxymethyl-3,5-di-*O*-benzoyl-1-thio-α-D- and β-L-ribofuranoside were prepared by treatment of compound **14** with benzoyl chloride and pyridine, in the usual manner. The sample was recrystallized from chloroform – petroleum ether (bp 60–80°C), mp 136–137°C. *Anal.* calcd. for $C_{29}H_{28}O_8S$: C 64.9, H 5.3, S 6.0; found: C 65.2, H 5.4, S 5.9.

Base-catalyzed solvolysis of compounds 8, 9, 10, 12, and 13

Each of the fractions obtained from the liquid chromatographic separation was subjected to the solvolysis conditions, as described for the solvolysis of compound **11**.

Base-catalyzed solvolysis of the tetraacetate **8** afforded compound **14** (0.19 g). The fraction containing **8** and **9** afforded a mixture of **14** and ethyl 2-*C*-hydroxymethyl-1-thio-α-D- and β-L-xylofuranoside (**15**) (0.13 g). Solvolysis of the fraction containing **13** afforded a syrup which was shown by tlc (solvent *B*) to consist of a component having an R_f value of 0.24 and a component at the origin. The component having an R_f value of 0.24 was obtained as a syrup by preparative thin-layer chromatography using solvent *B* as eluant, and was identified as being compound **15** (0.07 g); ^{1}Hmr data (D_2O with $(CH_3)_2CO$) δ: 1.25 (3H, t, SCH_2CH_3), 2.74 (2H, q, SCH_2CH_3), 3.64–4.24 (6H, m), 5.18 (1H, s, H-1). M calcd. for $C_8H_{16}O_5S$: 224; found: m/e 224 (M^+). Treatment of compound **10** under the solvolysis conditions afforded a syrup which was identified as being ethyl 2-*C*-hydroxymethyl-1-thio-α-D- and β-L-ribopyranoside (**16**) (0.16 g); ^{1}Hmr data (D_2O with $(CH_3)_2CO$, 340 K) δ: 1.28 (3H, t, SCH_2CH_3), 2.74 (2H, q, SCH_2CH_3), 3.44–4.14 (6H, m's), 4.79 (1H, s, H-1). M calcd. for $C_8H_{16}O_5S$: 224; found: m/e 224 (M^+). Solvolysis of the fraction containing **10** and **11** afforded a mixture of **14** and **16** (0.53 g). Base-catalyzed solvolysis of compound **12** afforded a solid (0.22 g) which was recrystallized from chloroform, and was identified as being ethyl 2-*C*-hydroxymethyl-1-thio-β-D- and α-L-ribopyranoside (**17**), mp 84–85°C; ^{1}Hmr data (D_2O with $(CH_3)_2CO$) δ: 1.27 (3H, t, SCH_2CH_3), 2.66 (2H, q, SCH_2CH_3), 3.44–4.24 (6H, m's), 5.11 (1H, s, H-1). M calcd. for $C_8H_{16}O_5S$: 224; found: m/e 224 (M^+). *Anal.* calcd. for $C_8H_{16}O_5S$: C 42.8, H 7.2, S 14.3; found: C 42.9, H 7.2, S 14.2.

2-C-Hydroxymethyl-D,L-ribose (D,L-hamamelose) (18), (19), (20), and (21)

To a solution of the thioglycosides **14** and **16** (0.532 g) in water (30 mL) was added mercuric chloride (0.90 g) and cadmium carbonate (0.50 g) and the suspension was stirred for 60 h at room temperature. The mixture was filtered through Celite and the filter cake was washed with water. The filtrate and washings were concentrated, and the syrupy residue was triturated with a small volume of ethanol. The remaining solid was filtered, and the filtrate was concentrated to a syrup which was deionized by passing it through a column of Amberlite IR-120 (H^+) and then through a column of Amberlite IR-45 (OH^-). Concentration of the resulting aqueous solution afforded a syrup (0.42 g). Thin-layer chromatography (solvent *D*) indicated the presence of a homogeneous spot having an R_f value of 0.55. The sample was identified as being 2-*C*-hydroxymethyl-D,L-ribose (**18**–**21**), $[\alpha]_D^{33}$ (after 0.5 h) −1.4° (*c* 4.18, H_2O) (lit. (2, 6) $[\alpha]_D$ +7.3° (equil. *c* 2.2, H_2O) for the L-isomer and −7.0° for the D-isomer); ^{1}Hmr data (220 MHz, D_2O with $(CH_3)_2CO$, 301 K) δ: 3.52–4.4 (m's), 4.79, 5.13, 5.21, 5.28 (four s's, H-1's). The ^{1}Hmr spectrum was identical to that of an authentic sample of D-hamamelose. The sugar (0.05 g) in methanol was heated at reflux temperature with *p*-tolylsulfonylhydrazine (0.05 g) for 1 h. Upon cooling of the reaction mixture, white crystals separated which, when recrystallized from ethanol, had mp 155–157°C (lit. (2, 6) mp 155–156°C). The syrupy sugar was seeded with a crystal of D-hamamelose. After two weeks at 0°C, a portion of the sample crystallized. The syrupy residue was

triturated with cold methanol and the crystals were collected. The crystals were identified as being 2-*C*-hydroxymethyl-D-ribose, mp 110–111°C (lit. (2) mp 110–111°C); $[\alpha]_D^{33}$ (after 0.5 h) −7.2° (*c* 0.56, H_2O) (lit. (2) $[\alpha]_D$ −7.0°).

Reaction of D,L-hamamelose with ethanethiol

D,L-Hamamelose (0.092 g) was treated with concentrated hydrochloric acid (1 mL) and ethanethiol (1 mL) at room temperature for 80 h. The mixture was poured onto solid lead carbonate. The slurry was filtered through Celite and the residue was washed with water and 95% ethanol. The filtrate and washings were concentrated to afford a syrup which was taken up in ethanol. The remaining solid was removed by filtration, and the filtrate was concentrated to afford a syrup (0.095 g). The ^{13}Cmr spectrum of the syrup in D_2O solution indicated the presence of all four isomers of hamamelose (**18**–**21**), as indicated by the four C-1 signals, as well as three C-1 signals attributable to thioglycosides. The latter peaks appeared at δ 89.8, 92.0 (major), and 94.7. The peak at δ 89.8 was assigned to C-1 of compound **17** and that at δ 92.0 was assigned to C-1 of **14**. The peak at δ 94.7 did not correspond to the C-1 signal of any of the three thioglycosides previously synthesized. This peak was, therefore, assigned to C-1 of ethyl 2-*C*-hydroxymethyl-1-thio-β-D- and α-L-ribofuranoside (**26**). The original D_2O solution of the syrup was let stand at ambient temperature for 30 h, and the ^{13}Cmr spectrum was recorded again. The spectrum now indicated the presence of three C-1 signals attributable to thioglycosides at δ 92.0, 89.8, and 88.1. The absence of the peak owing to C-1 of **26** (δ 94.7) and the appearance of the peak attributable to C-1 of **17** (δ 88.1) suggested that the sample had equilibrated since the recording of the first ^{13}Cmr spectrum. The D_2O solution was found to have a pD value of 4. Preparative thin-layer chromatography of the sample using solvent *C* as eluant gave the mixture of thioglycosides **14**, **16**, and **17**, as indicated by ^{1}Hmr and ^{13}Cmr spectroscopy.

Acknowledgements

The authors are grateful to NSERC Canada for financial assistance in the form of grants (to T.B.G. and W.A.S.) and a scholarship (to B.M.P.). They also wish to Thank Dr. A. A. Grey of the Canadian 220 MHz NMR Centre for his assistance and cooperation in the measurement of ^{1}Hmr spectra at 220 MHz.

1. W. A. SZAREK, B. M. PINTO, A. H. HAINES, and T. B. GRINDLEY. Can. J. Chem. **60**, 390 (1982).
2. W. G. OVEREND and N. R. WILLIAMS. J. Chem. Soc. 3466 (1965).
3. J.-C. DEPEZAY and A. DURÉAULT. Tetrahedron Lett. 2869 (1978).
4. P.-T. HO. Tetrahedron Lett. 1623 (1978).
5. H. PAULSEN, V. SINNWELL, and P. STADLER. Chem. Ber. **103**, 1978 (1972).
6. J. S. BURTON, W. G. OVEREND, and N. R. WILLIAMS. J. Chem. Soc. 3433 (1965).
7. R. G. S. RITCHIE, N. CYR, B. KORSCH, H. J. KOCH, and A. S. PERLIN. Can. J. Chem. **53**, 1424 (1975).
8. (*a*) A. S. PERLIN and B. CASU. Tetrahedron Lett. 2921 (1969); (*b*) K. BOCK, I. LUNDT, and C. PEDERSEN. Tetrahedron Lett. 1037 (1973); (*c*) K. BOCK and C. PEDERSEN. J. Chem. Soc. Perkin Trans. 2, 293 (1974); (*d*) K. BOCK and C. PEDERSEN. Acta Chem. Scand. Ser. B, **29**, 258 (1975); (*e*) N. J. CUSSANS and T. N. HUCKERBY. Tetrahedron, **31**, 2719 (1975); (*f*) F. R. TARAVEL and P. J. A. VOTTERO. Tetrahedron Lett. 2341 (1975).
9. J. AUGÉ and S. DAVID. Nouv. J. Chem. **1**, 57 (1977); S. DAVID. *In* Anomeric effect: origin and consequences. ACS Symposium Series, **87**. *Edited by* W. A. Szarek and D. Horton. American Chemical Society, Washington, DC. 1979. Chapt. 1.
10. L. QUE, JR. and G. R. GRAY. Biochemistry, **13**, 146 (1974); S. J. ANGYAL and G. S. BETHEL. Aust. J. Chem. **29**, 1249 (1976); S. J. ANGYAL, G. S. BETHEL, D. E. COWLEY, and V. A. PICKLES. Aust. J. Chem. **29**, 1239 (1976).
11. W. A. SZAREK, G. W. SCHNARR, H. C. JARRELL, and J. K. N. JONES. Carbohydr. Res. **53**, 101 (1977).
12. D. J. WILBUR, C. WILLIAMS, and A. J. ALLERHAND. J. Am. Chem. Soc. **99**, 5450 (1977).
13. S. J. ANGYAL and K. JAMES. Carbohydr. Res. **15**, 91 (1970).

Can. J. Chem. Downloaded from www.nrcresearchpress.com by 210.87.254.6 on 09/06/12
For personal use only.

Sedum alkaloids. V. Sedacrine, the major alkaloid of *Sedum acre*, and related bases

BRIGITTE COLAU AND CLAUDE HOOTELÉ[1]

Service de Chimie Organique, Faculté des Sciences, Université Libre de Bruxelles, B-1050 Bruxelles, Belgium

Received May 18, 1982[2]

BRIGITTE COLAU and CLAUDE HOOTELÉ. Can. J. Chem. **61**, 470 (1983).

Sedacrine, the major alkaloid of *Sedum acre*, is assigned structure **5** on the basis of spectroscopic and chemical evidence. Two minor bases, sedinone **6** and dihydrosedinine **7**, are described. Sedacrine **5**, sedinone **6**, dihydrosedinine **7**, and sedinine **3** are correlated. The absolute configurations of these alkaloids and that of sedacryptine **2** are established.

BRIGITTE COLAU et CLAUDE HOOTELÉ. Can. J. Chem. **61**, 470 (1983).

La sédacrine **5** est l'alcaloïde majeur de *Sedum acre*; sa structure est établie sur la base de ses propriétés spectrales et chimiques. Deux bases mineures, la sédinone **6** et la dihydrosédinine **7** sont décrites. La sédacrine **5**, la sédinone **6**, la dihydrosédinine **7** et la sédinine **3** de configuration absolue connue, ont été corrélées. La configuration absolue de la sédacryptine **2** est également établie.

Can. J. Chem. Downloaded from www.nrcresearchpress.com by 210.87.254.5 on 09/06/12
For personal use only.

A variety of 2- and 2,6-disubstituted piperidine alkaloids were isolated some years ago from *Sedum acre* (1–3). Some additional bases, whose structures were tentatively inferred from their fragmentation patterns, were also detected in the same species (4, 5). Recently, we described two new Sedum alkaloids, sederine **1** (6, 14) and sedacryptine **2** (7), and we assigned sedinine the modified structure **3** (8). In this communication we report the isolation and structure determination of three alkaloids: sedacrine **5**, sedinone **6**, and dihydrosedinine **7**.

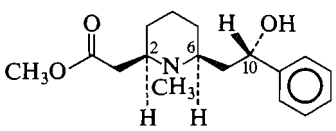

1

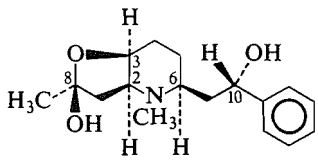

2

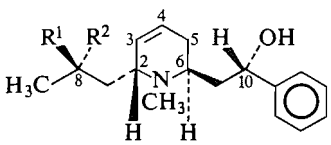

3 R^1 = OH, R^2 = H
4 R^1 = H, R^2 = OH
5 R^1, R^2 = O

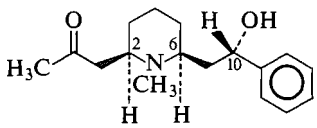

6

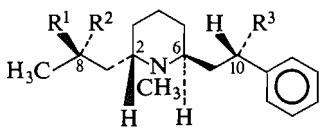

7 R^1 = R^3 = OH, R^2 = H
8 R^1, R^2 = O, R^3 = OH
11 R^1 = OH, R^2 = R^3 = H

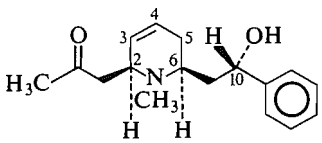

9

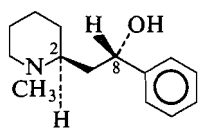

10

The crude alkaloids (0.05%) were obtained by treatment of fresh plants of *Sedum acre* with 2% aqueous hydrochloric acid and were separated mostly by countercurrent distribution and by fractional crystallization. In addition to known compounds, **5**, **6**, and **7** were isolated in the pure state.

Sedacrine 5

Sedacrine[3] (oil; $[\alpha]_D^{20}$ −130° (*c* 1.1, EtOH), $C_{17}H_{23}NO_2$ by high resolution mass spectrometry) was characterized as its perchlorate (mp 168–169°C). The free base is thermolabile and does not survive a prolonged heating in solution: although sedacrine is the major alkaloid of *Sedum acre* (0.01% from the fresh plant), it was absent in the extracts obtained by treatment of the plant material with refluxing methanol. Structure **5** is assigned to sedacrine on the base of chemical and spectroscopic evidence. The ir spectrum of **5** (CCl_4) showed the presence of a ketone carbonyl group (1720 cm^{-1}) and an intramolecularly bonded OH (broad band at 3200 cm^{-1} unaffected by dilution). The ^{1}Hmr spectrum of sedacrine established the presence of a N—CH_3 group (3H, s, 2.3 ppm), a —CH_2COCH_3 chain (3H, s, 2.1 ppm; 2H, m, 2.7 ppm; these signals disappeared after deuterium exchange in alkaline D_2O), a —CH_2-CHOH-C_6H_5 chain (1H, dd, J = 10 and 3 Hz, 4.9 ppm; 1H, broad signal, 6 ppm; 5H, m, 7.3 ppm), two protons on carbon atoms adjacent to the nitrogen (2H, 2m, 3.3 and 3.6 ppm), and two vinylic protons (2H, m, 5.3 to 5.9 ppm). The position of the double bond in **5** was established by double irradiation experiments: irradiation of the proton appearing at 3.6 ppm showed that it was coupled with the methylenic protons adjacent to the carbonyl group and with the vinylic protons. The double bond is therefore between C-3 and C-4 and not between C-4 and C-5.

The fragmentation pattern of **5** is characteristic of a 2,6-disubstituted *N*-methylpiperidine derivative (10); the major fragment ions were observed at m/z 216, 152, and 94; their compositions were ascertained by high resolution measurements.

[1]Research Associate of the National Fund for Scientific Research (Belgium) and author to whom correspondence may be addressed.

[2]Revision received August 12, 1982.

[3]The name sedacrine was coined by A. Nordal (11) for a Sedum base (oil, $C_{17}H_{23}NO_2$?, $[\alpha]_D^{15}$ −51.77° (*c* 2.4, EtOH 96%), insufficiently characterized and of questionable homogeneity. We propose therefore to retain the name sedacrine for compound **5** of the present communication.

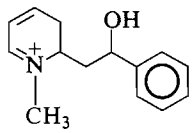

m/z 216

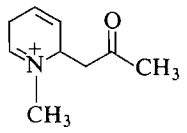

m/z 152

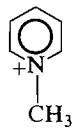

m/z 94

Reduction of the carbonyl group of **5** by lithium tri-*tert*-butoxyaluminum hydride yielded a 4:1 mixture (by ^{1}Hmr) of two epimeric alcohols. The major compound appeared identical (mp, mixture mp, [α], ^{1}Hmr) with sedinine **3** (8), implying that sedacrine and sedinine have the same relative and absolute configuration. The minor compound is therefore 8-episedinine **4**. When sedacrine was treated with α-phenylbutyric anhydride in pyridine (9), laevorotatory α-phenylbutyric acid was formed. This result establishes the absolute configuration of sedacrine as depicted in **5** (2*R*, 6*S*, 10*S*) and provides a confirmation of the absolute configuration deduced previously for sedinine **3** by application of Horeau's method to 10-deoxydihydrosedinine **11** (8).

Being a β-aminoketone, sedacrine **5** epimerizes at C-2 (retro-Michael reaction followed by recyclisation) in a variety of conditions. In methanol, at room temperature, sedacrine **5** equilibrated with 2-episedacrine **9** to give a 4:1 mixture (by ^{1}Hmr) in favor of the 2,6-*trans* compound **5**. Pure 2-episedacrine **9** could be isolated from the equilibrium mixture. The same 4:1 mixture of sedacrine **5** and 2-episedacrine **9** was obtained from **5** or from **9** in chloroform; in this case the reaction is slower than in methanol. On the other hand, sedacrine hydrochloride does not epimerize in water or in methanol at room temperature.

Sedinone 6

Sedinone was first isolated and characterized by B. Franck (1) who tentatively suggested (2) that this base had structure **6** (without stereochemical implications). Our results confirm this hypothesis and establish the relative and absolute configuration of sedinone as depicted in **6**.

The empirical formula $C_{17}H_{25}NO_2$ proposed (2) for sedinone was confirmed by high resolution mass spectrometry. The fragmentation pattern is similar to that of sedacrine **5**, the fragment ions appearing 2 units higher on the spectrum of **6** (*m/z* 218, 154, and 96). The presence of a N—CH_3 group and of the side chains —CH_2COCH_3 and —CH_2-CHOH-C_6H_5 was evident from the examination of the ^{1}Hmr spectrum. Sedinone must therefore be either identical or diastereoisomeric with dihydrosedacrine **8**.

Catalytic hydrogenation of sedacrine hydrochloride yielded dihydrosedacrine hydrochloride **8**·HCl whose ^{1}Hmr properties are different from those of sedinone hydrochloride. However, the free base **8** epimerized in methanol at room temperature to give a 1:1 mixture (by ^{1}Hmr) of **8** and **6**. Fractional crystallization of the mixture of the corresponding hydrochlorides led to the isolation of pure 2-epidihydrosedacrine hydrochloride, identical with sedinone hydrochloride (mp, mixture mp, [α]). Sedinone is therefore correctly represented by **6** (2*R*,6*S*,10*S*).

Dihydrosedinine 7

Dihydrosedinine $C_{17}H_{27}NO_2$ (by high resolution mass spectrometry) is a new minor base from *Sedum acre*. The structural attribution rests on the interpretation of the spectral properties of the base and was confirmed by direct comparison of the hydrochloride (mp, mixture mp, ir, [α]) with a sample prepared from sedinine **3** (2). The absolute configuration of dihydrosedinine is therefore as depicted in **7** (2*S*,6*S*,8*R*,10*S*). Dihydrosedinine **7** is diastereoisomeric with a base isolated from *Lobelia inflata* (12).

Absolute configuration of sedacryptine 2

The structure and relative configuration of sedacryptine **2** have previously been determined by X-ray analysis (7).

Treatment of **2** with α-phenylbutyric anhydride in pyridine led to the esterification of the hydroxyl group at C-10 (^{1}Hmr) and to the formation of laevorotatory α-phenylbutyric acid. The absolute configuration of sedacryptine is therefore (2*S*,6*S*,8*S*,10*S*) as depicted in **2**.

It is worthy of note that all the 2,6-disubstituted piperidine alkaloids isolated so far from *Sedum acre* (i.e. sederine **1**, sedacryptine **2**, sedinine **3**, sedacrine **5**, sedinone **6**, and dihydrosedinine **7**) have a common stereochemical feature: the absolute configuration at C-6 and C-10 is the same through all this series and is identical with that of the corresponding carbon atoms (C-2 and C-8) of (−)-sedamine **10** (13).

Isolation and structure determination of other Sedum alkaloids are under progress in our laboratory.

Experimental

Melting points were determined on a Kofler microscope and are uncorrected. The infrared spectra were determined on a Perkin–Elmer 237 spectrometer. Nuclear magnetic resonance spectra were recorded in $CDCl_3$ (unless otherwise stated) with TMS as internal standard on a JEOL JNM-MH-100 apparatus. Mass spectral data were obtained on a Micromass 7070F spectrometer. Optical rotations were measured on a Perkin–Elmer 141 polarimeter. The countercurrent distribution were analyzed by measuring the optical density (420 nm) of the $CHCl_3$ phase of each tube after basification (NH_4OH), drying, and addition of a $CHCl_3$ solution of picric acid.

Isolation of the alkaloids of Sedum acre

Fresh whole plants (40 kg) of *Sedum acre* (collected in October near Brussels) were treated at room temperature with 2% aqueous HCl (80 L). After three days, the solution was filtered, basified with NH_4OH, and extracted with $CHCl_3$. Evaporation of the solvent at room temperature under reduced pressure yielded a brown residue (20 g) containing the crude alkaloids. This fraction was distributed between $CHCl_3$ (250 mL) and McIlvaine buffer (pH 6.4; 250 mL). Evaporation of the organic phase yielded fraction A (18 g). The aqueous phase was basified and extracted with $CHCl_3$; removal of the solvent yielded fraction B (2 g).

Sedacrine 5

Fraction A (18 g) was dissolved in 2-butanone (50 mL) and a solution of perchloric acid in acetone was added dropwise until neutralization. Upon standing, a crystalline precipitate separated. Two successive crystallizations from 2-butanone yielded sedacrine perchlorate (5 g), mp 169°C, $[\alpha]_D^{20}$ −115° (*c* 2, methanol): ir (KBr): 3420, 3080, 2900, 1710, 1490, 1360, 1300, 1100, 765, 730, and 705 cm^{-1}. The usual work-up yielded sedacrine (oil), $[\alpha]_D^{22}$ −156° (*c* 1.7, $CHCl_3$); ms: 273 ($M^{+\cdot}$, 3%; $C_{17}H_{23}NO_2$, found: 273.1723, calcd.: 273.1730), 258 (3; $C_{16}H_{20}NO_2$, found: 258.1484, calcd.: 258.1495), 230 (6; $C_{15}H_{20}NO$, found: 230.1545, calcd.: 230.1546), 216 (25; $C_{14}H_{18}NO$, found: 216.1391, calcd: 216.1389), 152 (24; $C_9H_{14}NO$, found: 152.1071, calcd.: 152.1076), 110 (19), 108 (20), 96 (36), 94 (100; C_6H_8N, found: 94.0648, calcd.: 94.0657), 79 (16), 77 (18); the ^{1}Hmr spectrum was described above.

Sedacryptine 2

Fraction B (2 g) was subjected to a countercurrent distribution ($CHCl_3$/McIlvaine buffer pH 6; 23 transfers). Tubes 15–23 (fraction

Can. J. Chem. Downloaded from www.nrcresearchpress.com by 210.87.254.5 on 09/06/12
For personal use only.

Can. J. Chem. Downloaded from www.nrcresearchpress.com by 210.87.254.5 on 09/06/12
For personal use only.

C, 1.2 g) contained sedamine, allosedamine, and dihydrosedinine (*vide infra*). Tubes 5–14 were fractionated again by countercurrent distribution in the same conditions. Tubes 7–14 gave a colourless residue (0.7 g) which was dissolved in dry ether and treated with HCl. Crystallization of the precipitate from 2-butanone afforded 137 mg of sedacryptine hydrochloride, mp 142–143°C, $[\alpha]_D^{22}$ −49° (*c* 1.6, MeOH); ir (KBr): 3500, 3220, 3170, 2930, 2880, 2620, 2560, 1450, 1430, 1240, 1130, 1090, 1060, 1010, 960, 910, 770, and 700 cm^{-1}. The usual work-up yielded sedacryptine, mp 130–131°C (from cyclohexane), $[\alpha]_D^{22}$ −14° (*c* 1.5, $CHCl_3$); ^{1}Hmr; δ: 7.5–7.2 (5H, phenyl), 4.85 (dd, *J* = 10.5 and 2.5 Hz, 1H, C10-H), 4.05 (m, 1H, C3-H), 2.65 (m, 1H, C2-H?), 2.2 (s, N—CH_3), 1.4 (s, C8-CH_3); ms: 291 ($M^{+\cdot}$, 3%), 273 (2), 234 (3), 230 (6), 170 (100), 152 (29), 128 (3), 126 (5), 112 (46), 110 (9), 105 (5), 100 (9), 95 (26), 94 (19), 84 (11), 82 (6).

Sedinone **6**

After concentration, the mother-liquors from the sedacryptine hydrochloride crystallization afforded another crystalline residue. Three successive crystallizations from 2-butanone yielded colorless needles (95 mg) of sedinone hydrochloride, mp 176–178°C (dec.), $[\alpha]_D^{22}$ −77° (*c* 1.1, MeOH) (lit. (1) mp 175°C, $[\alpha]_D^{20}$ −79.4° (*c* 1, MeOH); ^{1}Hmr (D_2O); δ: 2.87 (s, N^+CH_3), 2.4 (s, CO—CH_3); ^{1}Hmr of the free base, δ: 7.4–7.2 (5H, phenyl), 4.9 (dd, *J*= 10 and 3 Hz, 1H, C10-H), 3.5–3.1 (2H, C2-H and C6-H), 2.5 (m, 2H, C7-2H), 2.25 (s, 3H, N—CH_3), 2.1 (s, 3H, CO—CH_3); ms: 275 ($M^{+\cdot}$, 8%, $C_{17}H_{25}NO_2$, found: 275.1891, calcd.: 275.1887), 218 (27; $C_{14}H_{20}NO$, found: 218.1545, calcd: 218.1546), 154 (100, $C_9H_{16}NO$, found: 154.1233, calcd.: 154.1233), 96 (83).

Dihydrosedinine **7**

Fraction C (1.2 g) was subjected to two successive countercurrent distributions ($CHCl_3$/McIlvaine buffer pH 7.1; 23 transfers). HCl was added to the residue (51 mg) from tubes 7–14, dissolved in ether. Crystallization from 2-butanone of the precipitate afforded dihydrosedinine hydrochloride, mp 165°C, $[\alpha]_D^{22}$ −64° (*c* 0.4, MeOH) (lit. (2) mp 168°C, $[\alpha]_D^{20}$ −67.1° (*c* 1.4, MeOH)); ^{1}Hmr of the free base, δ: 7.4–7.1 (5H, phenyl), 4.7 (dd, *J* = 9.5 and 4 Hz, 1H, C10-H), 3.85 m, 1H, C8-H), 3.1 (m, 2H, C2-H and C6-H), 2.3 (s, 3H, N—CH_3), 1.15 (d, *J* = 6 Hz, C8-CH_3); ms: 277 ($M^{+\cdot}$, 9%; $C_{17}H_{27}NO_2$, found: 277.2047, calcd.: 277.2043), 262 (2), 218 (41; $C_{14}H_{20}NO$, found: 218.1545, calcd.: 218.1546), 156 (100; $C_9H_{18}NO$, found: 156.1390, calcd.: 156.1389), 98 (42), 96 (24).

Epimerization of sedacrine

Sedacrine **5** (190 mg) was dissolved in MeOH (4 mL) and the solution was left at room temperature for one day. After evaporation of the solvent, the mixture (**5**/**9** ratio of 4:1 by ^{1}Hmr) was dissolved in 2-butanone and a solution of perchloric acid in acetone was added until neutralization. Sedacrine perchlorate (220 mg) was eliminated by repeated fractional crystallizations. The mother-liquors were evaporated to dryness and the free bases were liberated. Crystallization from cyclohexane afforded 2-episedacrine **9** (6 mg), mp 91–93°C, $[\alpha]_D^{22}$ −71° (*c* 3.3, $CHCl_3$); ir (KBr): 3100, 3020, 1715, 1450, 1435, 1355, 1325, 1140, 1050, 750, 695, and 680 cm^{-1}; ^{1}Hmr, δ: 7.4–7.2 (5H, phenyl), 5.75 (m, 1H, C4-H), 5.4 (m, 1H, C3-H), 4.9 (dd, *J* = 10 and 3 Hz, 1H, C10-H), 4.1 (m, 1H, C2-H), 3.4 (m, C6-H), 2.6 (m, 2H, C7-2H), 2.25 and 2.2 (2s, 6H, N—CH_3 and CO—CH_3); ms: 273 ($M^{+\cdot}$, 5%), 258 (3), 230 (7), 216 (48), 152 (41), 110 (39), 108 (39), 96 (72), 94 (100), 79 (48), 77 (40).

*Reduction of sedacrine with lithium tri-*tert*-butoxyaluminum hydride*

Sedacrine perchlorate (1.2 g) in THF (10 mL) was allowed to react at room temperature with lithium tri-*tert*-butoxyaluminum hydride (2 g). After 15 min, ethyl acetate was added and the mixture was evaporated to dryness. The residue was dissolved in water, basified with NH_4OH, and extracted with $CHCl_3$ to give a 4:1 mixture (by ^{1}Hmr) of sedinine **3** and 8-episedinine **4**. Fractional crystallization from 2-butanone of the mixture of the hydrochlorides (prepared by the usual work-up) yielded sedinine hydrochloride (694 mg), mp 170–172°C, $[\alpha]_D^{22}$ −145° (*c* 0.4, MeOH); the free base (mp 119–120.5°C without depression with an authentic sample, $[\alpha]_D^{22}$ −98° (*c* 0.44, MeOH) is identical with sedinine. The mother-liquors were evaporated to dryness and the residue dissolved in water, basified with NH_4OH, and extracted with $CHCl_3$. Two crystallizations from petroleum ether yielded 8-episedinine **4**, mp 120–121.5°C, $[\alpha]_D^{22}$ −102° (*c* 0.45, MeOH) (the epimeric alcohols **3** and **4** have very similar properties but the mixture melting point was strongly depressed (106–120°C); ir (KBr): 3340, 3020, 2920, 2790, 1450, 1130, 1080, 1070, 1060, 880, 760, 740, and 700 cm^{-1}; ^{1}Hmr, δ: 7.4–7.2 (5H, phenyl), 5.6 (2m, 2H, C3-H and C4-H), 4.9 (dd, *J* = 10.5 and 2.6 Hz, 1H, C10-H), 4.05 (m, 1H, C8-H), 3.3 (m, 2H, C2-H and C6-H), 2.35 (s, 3H, N—CH_3), 1.2 (d, *J* = 6 Hz, 3H, C8-CH_3); ms: 275 ($M^{+\cdot}$, 7%), 260 (5), 216 (100), 154 (77), 96 (54), 94 (65). Reduction of sedacrine perchlorate by $LiAlH_4$ afforded a 3:7 mixture of **3** and **4** in THF at room temperature and a 1:1 mixture of **3** and **4** in refluxing THF.

Catalytic hydrogenation of sedacrine

Sedacrine hydrochloride (55 mg) was dissolved in MeOH (2 mL) and hydrogenated over Pt at room temperature under 4 atmospheres for 10 min. Filtration and evaporation of the solvent yielded dihydrosedacrine hydrochloride, ^{1}Hmr (D_2O), δ: 2.8 (s, N^+CH_3), 2.2 (s, $COCH_3$).

Epimerization of dihydrosedacrine

Dihydrosedacrine was liberated from its hydrochloride and dissolved in methanol. After 5 hours at room temperature a 1:1 mixture of dihydrosedacrine **8** and sedinone **6** was obtained. Fractional crystallization from 2-butanone of the mixture of the corresponding hydrochlorides yielded sedinone hydrochloride, mp 175–179°C (dec.; mixture mp without depression), $[\alpha]_D^{22}$ −80° (*c* 0.5, MeOH).

Absolute configuration of sedacryptine and sedacrine by Horeau's method

A solution of α-phenylbutyric anhydride (0.04 mmol) in pyridine (0.5 mL) was added to the alkaloid (0.02 mmol); the mixture was allowed to stand for 15 h at room temperature. A little water was added and after 30 min the mixture was basified with NH_4OH and extracted twice with $CHCl_3$. The aqueous phase was acidified and extracted three times with $CHCl_3$. After evaporation of the solvent, the rotation of α-phenylbutyric acid was measured at the D line in benzene.

Alkaloid	Sign of the acid	Optical yield
Sedacryptine **2**	(−)	29%
Sedacrine **5**	(−)	26%

1. B. Franck. Ber. **91**, 2803 (1958), and references cited.
2. B. Franck. Ber. **92**, 1001 (1959).
3. B. Franck. Ber. **93**, 2360 (1960).
4. L. P. S. Francis and G. W. Francis. Planta Med. **32**, 268 (1977).
5. J. H. Kooy. Pharm. Weekbl. **112**, 59 (1977).
6. C. Hootelé, J. P. Etienne, and B. Colau. Bull. Soc. Chim. Belg. **88**, 111 (1979).
7. C. Hootelé, B. Colau, F. Halin, J. P. Declercq, G. Germain, and M. Van Meerssche. Tetrahedron Lett. 5061 (1980).
8. C. Hootelé, B. Colau, F. Halin, J. P. Declercq, G. Germain, and M. Van Meerssche. Tetrahedron Lett. 5063 (1980).
9. A. Horeau. *In* Stereochemistry. Fundamentals and methods. Vol. 3. *Edited by* H. B. Kagan. Georg Thierne, Stuttgart. 1977.
10. M. Spiteller-Friedmann and G. Spiteller. Monatsh. Chem. **96**, 104 (1965).
11. A. Nordal. A pharmacognostical study of sedum acre L. Johan Grundt Tanum Forlag, Oslo. 1946.
13. C. Schöpf, T. Kauffmann, P. Berth, W. Bundschuh, G. Dummer, H. Fett, G. Habermehl, E. Wieters, and W. Wüst. Ann. **608**, 88 (1957).
13. C. Schöpf, G. Dummer, W. Wüst, and R. Rausch. Ann. **626**, 134 (1959).
14. C. Piccinni-Leopardi, G. Germain, M. Van Meerssche, B. Colau, and C. Hootelé. Bull. Soc. Chim. Belg. In press.

The partial molar volumes of aqueous metal cations: their prediction and relation to volumes of activation for water exchange

THOMAS W. SWADDLE AND MARK K. S. MAK
Department of Chemistry, The University of Calgary, Calgary, Alta., Canada T2N 1N4

Received August 19, 1982

THOMAS W. SWADDLE and MARK K. S. MAK. Can. J. Chem. **61**, 473 (1983).

Partial molar volumes $\bar{V}^0$ of the Fe^{2+}, Ni^{2+}, Fe^{3+}, Cr^{3+}, Rh^{3+}, and $M(NH_3)_5OH_2^{3+}$ (M = Cr, Co, Rh, Ir) aqueous ions have been obtained by extrapolation from density measurements at 298.15 K on the perchlorate salt solutions containing added $HClO_4$ where necessary to suppress hydrolysis or oxidation. The values for these high-spin aqua-ions and others in the literature can be represented satisfactorily for ionic charges z = 1 through 4 by

$$\bar{V}^0_{abs} = 2.523 \times 10^{-6}(r + 238.7)^3 - 18.07n_c - 417.5z^2/(r + 238.7)$$

where $\bar{V}^0_{abs}$ is the absolute partial molar volume in $cm^3\ mol^{-1}$ of $M^{z+}(aq)$ relative to $\bar{V}^0_{abs} = -5.4\ cm^3\ mol^{-1}$ for $H^+(aq)$, and r is the Shannon radius in pm of M^{z+} with coordination number n_c. Volumes of activation ΔV_{ex}* for water exchange correlate inversely with $\bar{V}^0$ within the series $M^{2+}(aq)$ and $M(NH_3)_5OH_2^{3+}(aq)$ at least, allowing predictions of ΔV_{ex}* to be made from $\bar{V}^0$ or the above equation. The physical origin of these correlations is considered.

THOMAS W. SWADDLE et MARK K. S. MAK. Can. J. Chem. **61**, 473 (1983).

On a obtenu les volumes molaires partiels $\bar{V}^0$ des ions aqueux de Fe^{2+}, Ni^{2+}, Fe^{3+}, Cr^{3+}, Rh^{3+} et $M(NH_3)_5OH_2^{3+}$ (M = Cr, Co, Rh, Ir) par extrapolation à partir des mesures de densité à 298,15 K des solutions de perchlorate contenant du $HClO_4$ ajouté là où c'est nécessaire pour supprimer l'hydrolyse ou l'oxydation. On peut représenter les valeurs de ces ions aqueux à haut spin et les autres valeurs répertoriées dans la littérature pour des charges ioniques de z = 1 jusqu'à 4 par l'équation:

$$\bar{V}^0_{abs} = 2{,}523 \times 10^{-6}(r + 238{,}7)^3 - 18{,}07n_c - 417{,}5z^2/(r + 238{,}7)$$

où $\bar{V}^0_{abs}$ est le volume molaire partiel absolu en $cm^3\ mol^{-1}$ de $M^{z+}(aq)$ par rapport à $\bar{V}^0_{abs} = -5{,}4\ cm^3\ mol^{-1}$ pour $H^+(aq)$ et r est le rayon de Shannon en pm de M^{2+} avec un nombre de coordination de n_c. Il existe une relation inverse entre les volumes d'activation, ΔV_{ex}*, pour l'échange d'eau et $\bar{V}^0$ au moins dans les séries $M^{2+}(aq)$ et $M(NH_3)_5OH_2^{3+}(aq)$; on peut donc ainsi prédire ΔV_{ex}* à partir de $\bar{V}^0$, ou à partir de l'équation ci-dessus. On considère l'origine physique de ces corrélations.

[Traduit par le journal]

Our interest in the precision measurement of volume properties of aqueous metal ions stems from the observation (1, 2) that volumes of activation ΔV_{ex}* for the exchange of coordinated water on $M^{2+}(aq)$, $M(NH_3)_5OH_2^{3+}(aq)$, and possibly $M^{3+}(aq)$ seem to correlate inversely with the apparent molar volumes ϕ_v or partial molal volumes at infinite dilution $\bar{V}^0$ of the respective aqueous ions within each of these series. If this observation has any general validity, the transition states volumes must be much less sensitive to the nature of M than are either ΔV_{ex}* or $\bar{V}^0$, i.e., the transition states must resemble each other relatively closely within a series despite some differences in reaction mechanism which ΔV_{ex}* is thought to reveal (1). Furthermore, the correlations themselves would permit prediction of unknown ΔV_{ex}* values from known $\bar{V}^0$ data (or vice-versa). Finally, if a physically meaningful model is available for the prediction of $\bar{V}^0$, we have the prospect of predicting ΔV_{ex}*, and so arguably the mechanistic predisposition of a metal aqua-ion, from basic principles and quantities.

The establishment and subsequent application of such correlation and models, however, require values of $\bar{V}^0$ that are accurate to within 2 $cm^3\ mol^{-1}$ or better. Good modern data are available for aqueous Mn^{2+}, Co^{2+}, and Ni^{2+} (3–7), but for $Fe^{2+}(aq)$ there exist only older $\bar{V}^0$ values which range from −17.7 to −26.4 $cm^3\ mol^{-1}$ (8–10) (relative to $\bar{V}^0 = 0$ for $H^+(aq)$), possibly because of the rapidity of aerial oxidation of $Fe^{2+}(aq)$ in the absence of added acid (11). For $Fe^{3+}(aq)$, the $\bar{V}^0$ value cited in Millero's comprehensive review (10) can be traced back to density data of precision no better than 1 part in 10^4, which implies uncertainties in the derived molar volume of at least ±2 $cm^3\ mol^{-1}$ at 0.05 mol L^{-1}; solution densities reproducible to about 2 parts in 10^6 are now routinely measurable. In any case, addition of substantial amounts of acid is necessary to suppress hydrolysis and polymerization of iron(III) ($pK_a \sim 2$).

[1] $Fe^{3+}(aq) + H_2O \rightleftharpoons H^+ + FeOH^{2+}(aq) \rightleftharpoons$ polymers

Suppression of hydrolysis is also important for $Rh^{3+}(aq)$, ($pK_a \sim 3$), for which no $\bar{V}^0$ data have been reported, but less so for $Cr^{3+}(aq)$ ($pK_a \sim 4.5$), although a high-acidity redetermination of the $\bar{V}^0$ value of Hepler *et al.* (12) for $Cr^{3+}(aq)$ is desirable as a reference point for the other $\bar{V}^0$ data obtained from density measurements on mixed electrolyte solutions. Apparent molar volumes ϕ_v of aqueous $[M(NH_3)_5OH_2](ClO_4)_3$ at concentrations of ~0.01 mol kg^{-1} have been reported for M = Cr, Co, Rh, and Ir (13, 14), but extrapolation to infinite dilution should be attempted. We have therefore determined the ϕ_v values as a function of concentration for aqueous iron(II), iron(III), chromium(III), and rhodium(III) perchlorates in the presence of controlled amounts of perchloric acid, using nickel(II) perchlorate (3, 4) as a check on our procedures. Values of ϕ_v have also been obtained for various concentrations of $[M(NH_3)_5OH_2](ClO_4)_3$, but without added acid, since hydrolysis is unimportant for these complexes ($pK_a \sim 6$) and, in any event, the volume change accompanying simple hydrolysis is very small (15–17).

Can. J. Chem. Downloaded from www.nrcresearchpress.com by 210.87.254.6 on 09/06/12
For personal use only.

Can. J. Chem. Downloaded from www.nrcresearchpress.com by 210.87.254.6 on 09/06/12
For personal use only.

Experimental

Preparation of materials

Distilled water was passed through Barnstead deionizer and organic removal cartridges before use.

Nickel(II) and iron(II) perchlorates were made by dissolving the metals (>99.9% pure) in a slight excess of 70% $MClO_4$, warming as necessary, and evaporating to produce the solid hydrates, which were then recrystallized from dilute (<0.1 mol L^{-1}) $HClO_4$. Oxygen was excluded in all operations involving iron(II). The products contained no detectable chloride, but comparison of their H^+-ion-exchange equivalents (14) with direct metal-ion analyses (by EDTA/Zn^{2+} back-titration for Ni^{2+}, and dichromate titration for Fe^{2+}) showed that some 0.7% $HClO_4$ was typically present.

Chromium(III) perchlorate was made by reducing CrO_3 with H_2O_2 in aqueous $HClO_4$, and the recovered solid hydrate was recrystallized from 0.1 mol L^{-1} $HClO_4$. The ultraviolet spectrum of this product showed the chromium to be present exclusively as $Cr(H_2O)_6^{3+}$, free of hydrolytic polymers (18), but comparison of the chromium content (19) with the H^+-ion-exchange equivalent again showed that some 0.7% $HClO_4$ was present in the hydrate. Similarly, an iron(III) perchlorate hydrate sample from Fluka AG, of otherwise acceptable purity (17), was shown by two independent methods (reduction to Fe^{2+} followed by dichromate titration, and direct EDTA titration, versus H^+-ion-exchange) to contain 1.640% $HClO_4$ (cf. Hunt and Taube (20)).

Hexaaquarhodium(III) perchlorate was prepared by the method of Ayres and Forrester (21) and was free of $HClO_4$, according to elemental analysis and its H^+-ion-exchange equivalent.

Aquapentaammineiridium(III) perchlorate was made by base hydrolysis of $[Ir(NH_3)_5Cl]Cl_2$ (Spex HiPure) followed by precipitation with 70% $HClO_4$ and two recrystallizations from hot water. Its visible–uv spectrum was in excellent agreement with that previously reported (22). Aquapentaamminechromium(III), -cobalt(III), and -rhodium(III) perchlorates were made as described elsewhere (14, 23). In all cases, the purity of these anhydrous aquapentaammines was confirmed by H^+-ion-exchange titrations (14).

Density measurements

Solution samples of $[M(NH_3)_5OH_2](ClO_4)_3$ were prepared individually by weight. The available concentration range was limited by problems of solubility and density measurement precision. The other perchlorate salts were freely soluble but somewhat hygroscopic; their solutions were also made up by weight, individually for the higher concentrations or by dilution of stock solutions below 0.04 mol kg^{-1}, but were analyzed definitively for metal salt and (by H^+-ion-exchange) $HClO_4$ content in every case. Iron(II) perchlorate solutions were kept oxygen-free; oxidation was undetectable below 0.04 mol kg^{-1} iron(II) and negligible at the higher concentrations, after completion of the density measurements.

The density measurements were made on degassed solutions with a Sodev 02-D vibrating tube flow densimeter thermostated at 298.16 K with a constancy of ±0.001 K. The reference fluids were pure water (density d^0 = 0.997048 g cm^{-3} (24)) and dry nitrogen gas at atmospheric pressure (87 kPa).

Results

For solutions of a metal perchlorate (component 2) alone in water (component 1), the usual expression

$$[2]\quad \phi_v = [\{(1 + m_2M_2)/d\} - 1/d^0]/m_2$$

may be used to calculate the apparent molar volume ϕ_v of component 2 (formula mass M_2) at molal concentration m_2 mol kg^{-1} from the densities d and d^0 g cm^{-3} of the solution and pure water respectively (10). Equation [2] sufficed for the studies of $[M(NH_3)_5OH_2](ClO_4)_3$, but for all the other salts examined in this work a third component, perchloric acid, was also present and had to be allowed for in deriving $\phi_{v(2)}$ for component 2. The total volume V of a solution can be expressed in terms of the partial molal volumes $\bar{V}_j$ of the jth components as

$$[3]\quad V = n_1\bar{V}_1 + n_2\bar{V}_2 + n_3\bar{V}_3$$

when n_j moles of the jth component are present. For component 2, we have

$$[4]\quad \begin{aligned}\phi_{v(2)} &= (V - n_1V_1^0 - n_3\bar{V}_3)/n_2 \\ &= \{[(n_1M_1 + n_2M_2 + n_3M_3)/d] - n_1V_1^0 - n_3\bar{V}_3\}/n_2 \\ &= \{[(1 + m_2M_2 + m_3M_3)/d] - (1/d^0) - m_3\bar{V}_3\}/m_2\end{aligned}$$

The concentration dependence of $\phi_{v(3)}$ for $HClO_4$(aq) happens to be negligible over the range of ionic strengths I used here (25), so we have

$$[5]\quad \bar{V}_3 = \phi_{v(3)} + I(\partial\phi_{v(3)}/\partial I) \approx \phi_{v(3)}$$

Our measured value of $\phi_{v(3)}$ = 43.9 ± 0.2 cm^3 mol^{-1} at ~0.1 mol kg^{-1} was used for $\bar{V}_3$ in eq. [4] rather than the slightly larger literature value (25), so as to cancel possible calibration errors. Values of $\phi_{v(2)}$, hereinafter called simply ϕ_v, are listed in Table 1, together with the corresponding uncertainties $\delta\phi_v$ which were calculated by summing pessimistic estimates of possible errors in m_2, m_3, and d. These uncertainties are greater for $M(ClO_4)_2$ and $M(ClO_4)_3$ than for the ammines because the concentrations of the former solutes and of the $HClO_4$ present had to be determined titrimetrically using standardized reagents, whereas the ammine solutions were made up directly without perchloric acid from dry solid salts of established composition. The titrimetric concentrations did, however, agree with m_2 estimates based on the weights of solid hydrated salt taken, to well within the calculated error limits. The density measurements (±2 to 3 parts per million) were minor sources of error.

The question of the most appropriate way of representing the concentration dependence of ϕ_v so as to derive realistic values of the infinite-dilution value ϕ_v^0, which equals the sum of the (*additive*) infinite-dilution partial molar volumes of the aqueous ions of component 2, has been widely discussed (3, 10, 26–28). The simple Masson equation

$$[6]\quad \phi_v = \phi_v^0 + S_vc^{1/2}$$

where S_v is an empirical constant and c is the concentration of component 2 in mol L^{-1}, is now recognized to be inadequate for purposes of extrapolation to infinite dilution (10, 28).[1] Millero (10, 28) suggests the use of the Redlich–Meyer (29) equation

$$[7]\quad \phi_v = \phi_v^0 + kw^{3/2}c^{1/2} + b_vc$$

for extrapolation to infinite dilution; here, k is the Debye–Hückel slope (= 1.868 at 25°C), w is the "valence factor" (= $0.5\Sigma\nu_iz_i^2$, where z_i and ν_i are the charge and molar number of ions of the ith kind formed by component 2), and b_v is an empirical parameter which may, however, exhibit some dependence on c or I. For the system considered here, a means of handling ϕ_v data for mixed electrolyte solutions was needed. We have therefore fitted our data to the equation

$$[8]\quad \phi_v = \phi_v^0 + kwI^{1/2}/(1 + I^{1/2}) + B_vc$$

in which B_v, the only adjustable parameter, turned out to be

[1]We have chosen to convert concentrations to the molar (mol L^{-1}) scale for use with eqs. [6]–[9], in accordance with the Debye–Hückel theory.

TABLE 1. Apparent molar volumes of some transition metal perchlorates in aqueous solution at 298.15 K

Salt	[Salt] /mol kg^{-1}	[$HClO_4$] /mol kg^{-1}	d /g cm^{-3}	ϕ_v /mol cm^{-3}	$\delta\phi_v$[a] /mol cm^{-3}
$Ni(ClO_4)_2$	0.00498	—	0.998150	58.6	1.2
	0.00992	—	0.999106	60.8	
	0.02205	—	1.001501	60.1	
	0.03486	—	1.004023	60.0	
	0.04618	—	1.006243	60.0	
	0.05990	—	1.008923	60.1	
	0.03481	0.1008	1.009510	60.5	
	0.06032	0.1004	1.014451	60.5	
$Fe(ClO_4)_2$	0.00524	0.00105	0.998090	66.6	1.2
	0.01027	0.00117	0.999034	67.2	
	0.02006	0.00139	1.000876	67.2	
	0.03035	0.00163	1.002806	67.3	
	0.04021	0.00185	1.004649	67.4	
	0.05027	0.00208	1.006492	68.2	
	0.07558	0.00267	1.011208	68.1	
	0.09906	0.00320	1.015500	68.7	
	0.1267	0.00384	1.020619	68.5	
	0.1518	0.00442	1.025190	68.7	
$Cr(ClO_4)_3$	0.01001	0.1017	1.005275	97.8	1.5
	0.02012	0.1026	1.007793	100.6	
	0.03015	0.1029	1.010291	100.3	
	0.04026	0.1035	1.012836	99.6	
	0.05045	0.1041	1.015406	99.1	
	0.07567	0.1054	1.021592	100.3	
	0.1013	0.1066	1.027873	100.6	
	0.1264	0.1076	1.033956	101.0	
	0.1518	0.1086	1.040096	101.0	
$Fe(ClO_4)_3$	0.00494	0.1025	1.004069	98.3	1.2
	0.01974	0.1035	1.007853	99.0	
	0.02965	0.1045	1.010328	101.5	
	0.03961	0.1054	1.012906	100.3	
	0.04947	0.1058	1.015367	100.7	
	0.07931	0.1087	1.022930	100.7	
	0.09952	0.1104	1.027989	100.9	
	0.12493	0.1129	1.034338	101.1	
	0.15050	0.1151	1.040406	103.0	
$Rh(ClO_4)_3$	0.00511	0.1023	1.004376	90.7	2.0
	0.01016	0.1009	1.005827	92.9	
	0.02054	0.1020	1.009048	93.1	
	0.03092	0.1024	1.012216	93.5	
	0.04118	0.1022	1.015290	94.2	
	0.05094	0.1021	1.018323	92.4	
	0.06458	0.1032	1.022357	94.8	
	0.10028	0.1064	1.033198	95.0	
$[Co(NH_3)_5OH_2](ClO_4)_3$	0.01007	—	0.999608	205.5	0.5
	0.01899	—	1.001855	206.1	
	0.02729	—	1.003952	205.9	
	0.04715	—	1.008898	206.6	
$[Rh(NH_3)_5OH_2](ClO_4)_3$	0.00949	—	0.999814	212.2	0.7
	0.01028	—	1.000055	211.0	
	0.01656	—	1.001859	212.6	
	0.02192	—	1.003416	212.3	
	0.04338	—	1.009576	212.8	
$[Ir(NH_3)_5OH_2](ClO_4)_3$	0.00841	—	1.000252	211.6	1.0
	0.01073	—	1.001142	210.9	
	0.01672	—	1.003401	211.9	
	0.02493	—	1.006519	211.4	
$[Cr(NH_3)_5OH_2](ClO_4)_3$	0.01007	—	0.999432	216.3	0.6
	0.01763	—	1.001235	215.0	
	0.02574	—	1.003132	215.7	
	0.04187	—	1.006875	216.0	

[a]Total cumulative estimated uncertainty in ϕ_v.

Can. J. Chem. Downloaded from www.nrcresearchpress.com by 210.87.254.6 on 09/06/12
For personal use only.

TABLE 2. Volume properties of some aqueous transition metal perchlorates and cations at 298.15 K according to eq. [8]

M^{n+} in $M(ClO_4)_n$	ϕ_v^0 (= $\bar{V}^0_{salt}$)[a] /cm^3 mol^{-1}	B_v /L mol^{-1}	$\phi_v^{0.02}$[b] /cm^3 mol^{-1}	$\bar{V}^0_{conv}(M^{n+}aq)$[c] /cm^3 mol^{-1}
Ni^{2+}	59.0±0.4	−8	60.3	−29.2±1.2
Fe^{2+}	66.1±0.1	+3	67.6	−22.1±1.2
Cr^{3+}	95.7±0.5	−2	98.5	−36.7±1.5
Fe^{3+}	95.9±0.5	+5	98.9	−36.5±1.2
Rh^{3+}	88.8±0.6	+12	91.9	−43.5±2.0
$Co(NH_3)_5OH_2^{3+}$	203.5±0.3	−18	206.0	71.1±0.5
$Rh(NH_3)_5OH_2^{3+}$	209.8±0.5	−17	212.3	77.4±0.7
$Ir(NH_3)_5OH_2^{3+}$	209.8±0.7	−56	211.6	77.4±1.0
$Cr(NH_3)_5OH_2^{3+}$	213.8±0.9	−44	215.8	81.5±0.6

[a]Uncertainties here are standard deviations of fit to eq. [8].
[b]Value of ϕ_v calculated for reference concentration c = 0.02 mol L^{-1} (no added acid, assumed no hydrolysis).
[c]Relative to $\bar{V}^0_{conv}(H^+_{aq})$ = 0.0, assuming $\bar{V}^0(HClO_4)$ = 44.12 cm^3 mol^{-1} (25). Uncertainties are total errors as in Table 1.

TABLE 3. Partial molar volumes and ionic radii of divalent transition metal ions in water at infinite dilution at 298.15 K

	Value								
Parameter	Ca^{2+}	Mn^{2+}	Fe^{2+}	Co^{2+}	Ni^{2+}	Cu^{2+}	Zn^{2+}	Cd^{2+}	Reference
$\bar{V}^0_{conv}$[a]	−17.8	−17.6		−25.8	−29.5	−25.5	−26.6	−14.2	3
	−17.4	−17.4		−25.4	−28.4	−25.1	−24.7	−14.4	4
		−17.1		−25.6	−28.5	−25.0	−25.0	−14.2	4[b]
	−19.6			−25.5	−28.8	−25.1		−14.2	5
	−18.6	−17.3		−24.6	−28.3	−24.4	−24.4		6
			−22.1		−29.2				This work
$\bar{V}^0_{abs}$[c]	−29.2	−28.2	−32.9	−36.2	−39.6	−35.8	−36.0	−25.1	
r[d]	100.0	83.0	78.0	74.5	69.0	73.0	74.0	95.0	31

[a]Conventional partial molar volumes (/cm^3 mol^{-1}) relative to $\bar{V}^0_{conv}(H^+)$ = 0.
[b]Recalculated in ref. 3.
[c]"Absolute" partial molar volumes (/cm^3 mol^{-1}) relative to $\bar{V}^0_{abs}(H^+)$ = −5.4 cm^3 mol^{-1} (10), from averages of preceding $\bar{V}^0_{conv}$ values.
[d]Radii of unhydrated M^{2+} ions (/pm).

much less important than the b_v of eq. [7], i.e., any dependence of B_v on I can be neglected for our purposes. Equation [8] is an adaptation of that proposed by Millero (27) on the basis of the specific interaction model for mixed electrolyte solutions, and incorporates Güntelberg's assumption (30) that $\mathring{a}$ is about 310 pm. Equations [7] and [8] both reduce to the Debye–Hückel limiting law at low concentrations, as they should, whereas eq. [6] does not and is therefore invalid.

Values of ϕ_v^0 and B_v, computed using kw = 5.604 and 11.208 for 2:1 and 3:1 electrolytes respectively, are given in Table 2. By way of comparison, the Redlich–Meyer treatment (eq. [7]) of the data for $[M(NH_3)_5OH_2](ClO_4)_3$ gave ϕ_v^0 = 203.3, 209.6, 209.7, and 213.7 cm^3 mol^{-1} with b_v = −59, −58, −102, and −85 L mol^{-1} for M = Co, Rh, Ir, and Cr respectively. Conversely, reduction of the data of Hepler *et al.* (4–6) for aqueous M^{2+} and M^{3+} salts by eq. [8] gave ϕ_v^0 values which were slightly but not significantly larger than the results obtained by these authors by use of eq. [7] (e.g., for $Cr(NO_3)_3$(aq), ϕ_v^0 = 45.9 cm^3 mol^{-1} with B_v = −9.7 cm^3 L mol^{-2} according to eq. [8], cf. ϕ_v^0 = 45.4 cm^3 mol^{-1} and b_v = −41.1 cm^3 kg mol^{-2} with eq. [7] on the molal scale (12)). Finally, for $Ni(ClO_4)_2$ (aq), values of $[\phi_v - kwI^{1/2}(1 + I)^{1/2}]$ agreed satisfactorily at a given c for $[HClO_4]$ = 0.002 and 0.10 mol kg^{-1}.

Table 3 shows that our conventional partial molar volume $\bar{V}^0_{conv}$ for Ni^{2+}(aq) falls within the range of modern values, confirming that our measurements and use of eq. [8] are compatible with the best recent work. We therefore consider our data on Fe^{2+}(aq) to supersede the widely-ranging $\bar{V}^0$ values implied by earlier measurements on $FeCl_2$, $FeBr_2$, and $FeSO_4$ (8–10).

The ϕ_v value for $Fe(ClO_4)_3$ seems to be the first reported for this salt, and the extrapolated $\bar{V}^0_{conv}$ for Fe^{3+}(aq) is in only fair agreement with that obtained from imprecise data on $Fe(NO_3)_3$ (−43.7 cm^3 mol^{-1}) (9, 10). Since we have taken pains to suppress hydrolysis and have allowed for residual acid present in the solid salt, we feel our value of −36.5 ± 1.2 cm^3 mol^{-1} is the more reliable. With $Cr(ClO_4)_3$, we calculate $\bar{V}^0_{conv}$ = −36.7 ± 1.5 cm^3 mol^{-1}, which is in better agreement with the old estimate derived from $CrCl_3$ (−39.5 cm^3 mol^{-1}) (9, 10) than with the more precisely-measured value of Hepler *et al.* (12) (−41.1 ± 1.2 cm^3 mol^{-1}, recalculated via eq. [8] for consistency). The $Cr(NO_3)_3$ solutions used by Hepler *et al.* (12) contained significant quantities of nitric acid (up to about 0.03 mol L^{-1}), however, and it is not clear how the contributions of HNO_3 to the densities were taken into account. We believe our $\bar{V}^0_{conv}$ for Cr^{3+}(aq) to be realistic, but the contrast with the value of −47 cm^3 mol^{-1}, derived by Hepler *et al.* from

Can. J. Chem. Downloaded from www.nrcresearchpress.com by 210.87.254.6 on 09/06/12
For personal use only.

Can. J. Chem. Downloaded from www.nrcresearchpress.com by 210.87.254.6 on 09/06/12
For personal use only.

data by Lumme (12) for $Cr(ClO_4)_3$, is disquieting. No data on Rh^{3+}(aq) salts could be found in the literature; the present value is somewhat less precise than those for Cr^{3+}(aq) and Fe^{3+}(aq) because of the limited amount of $[Rh(H_2O)_6](ClO_4)_3$ available, but it is clear that $\bar{V}^0_{conv}$ for Rh^{3+}(aq) is some 7 cm^3 mol^{-1} more negative than $\bar{V}^0_{conv}$ for Cr^{3+}(aq) and Fe^{3+}(aq).

Apparent molar volumes for $[M(NH_3)_5OH_2](ClO_4)_3$ could not be measured over a wide concentration range because of solubility limitations, and consequently the ϕ_v values in Table 1 appear to be almost independent of concentration within the experimental uncertainty, much as do the ϕ_v data for $M(ClO_4)_2$ and $M(ClO_4)_3$ over the range 0.01–0.04 mol kg^{-1}. This is evidently due to the fortuitous near-cancellation of the second and third terms in eqs. [7] and [8] over this concentration range. That ϕ_v should indeed decrease markedly below this range as infinite dilution is approached is illustrated by recent densimetric studies of salts of large cations (including some N-base complexes) in aqueous solution at high dilution (32, 33). Interpolated values of ϕ_v for the midrange (and typical experimental) concentration of $[M(NH_3)_5OH_2](ClO_4)_3$ of 0.02 mol L^{-1}, listed in Table 2, are perhaps more closely representative of the actual experimental data than are ϕ_v^0, and agree well with the published ϕ_v values (13, 14) in this concentration regime.

Discussion

Theoretical interpretation of absolute molar volumes of M^{2+}(aq)

The data of Table 3 make it clear, for the first time, that $\bar{V}^0$ for M^{2+}(aq) varies monotonically from M = Mn through Fe and Co to Ni, and that some correlation with the crystallographic radii r of M^{2+} exists (except for M = Ca). Numerous theories have been proposed (see, e.g., refs. 3, 9, 10, 28, 34–39) to rationalize $\bar{V}^0$ for M^{z+}(aq) in terms of r, variously defined, but we propose a further one in which the existence of a first coordination sphere of n_c water ligands is explicitly acknowledged, and solvent from the second coordination sphere outwards (i.e., from the distance of closest approach of the solvent to the $M(H_2O)_{n_c}^{z+}$ unit) is treated as a continuous dielectric under electrostriction according to the Drude–Nernst equation. The effective volume V_c of the $M(H_2O)_{n_c}^{z+}$ unit must be estimated; crystallographic experience (31) indicates that this is best expressed in terms of an effective radius $(r + \Delta r)$ which allows arbitrarily for the contribution of packing voids to V_c and for the general lack of direct knowledge of the distance of closest approach of electrostricted solvent.

$$[9] \quad V_c = 4\pi N(r + \Delta r)^3/3$$

The assignment of n_c waters to the unit of volume V_c reduces the volume of the solution system by n_c times the molar volume of liquid water (18.068 cm^3 mol^{-1} at 298.15 K and 0.1 MPa). This turns out to be a major factor in $\bar{V}^0$, leading to strongly negative values at high n_c. Finally, the Drude–Nernst electrostrictive term (10) may be taken to operate at effective radius of $(r + \Delta r)$, and for r in pm we have

$$[10] \quad \bar{V}^0_{abs} = 2.523 \times 10^{-6}(r + \Delta r)^3 - 18.07n_c - 417.5z^2/(r + \Delta r)$$

where $\bar{V}^0_{abs}$ is the partial molar volume of M^{z+}(aq) on the absolute scale, with $\bar{V}^0_{abs} = -5.4$ cm^3 mol^{-1} for H^+(aq) (10). The data of Table 3 (less Cd^{2+} and Ca^{2+}), together with our $\bar{V}^0_{abs}$ values of −52.9 and −52.7 cm^3 mol^{-1} for Cr^{3+}(aq) and Fe^{3+}(aq), fit eq. [10] well with $\Delta r = 239.0 \pm 0.5$ pm when n_c is set to 6.0; there is ample evidence from nmr, EXAFS, X-ray diffraction, visible spectroscopy, and isotopic dilution that this assignment of n_c is justified, at least for the transition metal ions listed. If all the $\bar{V}^0$ data presented in Fig. 1 are fitted, with the adoption of the coordination numbers indicated, $\Delta r = 238.4 \pm 0.7$ pm. Since we consider the first data set to be more reliable on average than the second (which consists of the first set plus further values from Millero's 1972 compilation (10)), a value of $\Delta r = 238.7$ pm has been adopted in calculating the $\bar{V}^0_{abs}$ values presented in Fig. 1, in which the straight line represents perfect agreement between calculated and experimental $\bar{V}^0_{abs}$.

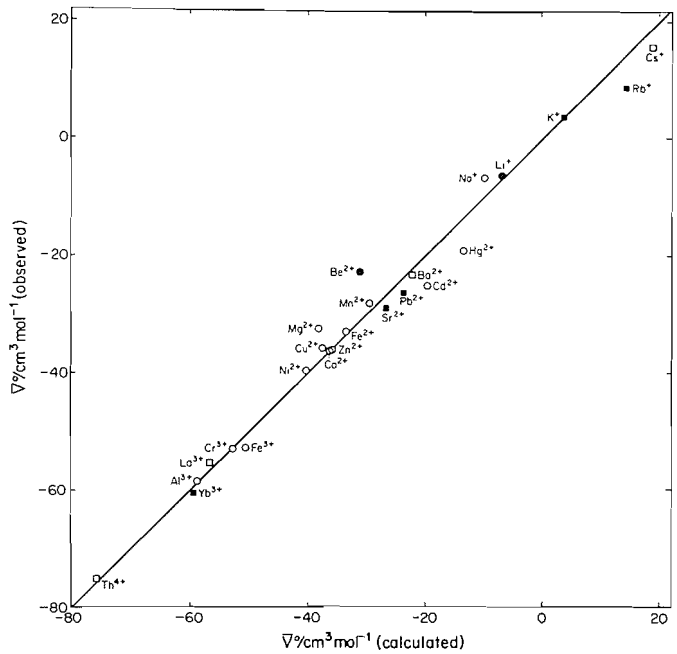

FIG. 1. Calculated and observed absolute partial molar volumes of aqueous metal ions at 298.15 K and infinite dilution, relative to $\bar{V}^0_{abs}(H^+) = -5.4$ cm^3 mol^{-1}, according to eq. [10]. Primary coordination numbers n_c are taken to be 4 (filled circles), 6 (open circles), 8 (filled squares), or 9 (open squares). Experimental $\bar{V}^0_{abs}$ values are taken from Tables 2 and 3 or from Millero's compilation (10).

This approach has an antecedent in Akitt's model of 1971 (36), but there are important differences. Akitt set Δr equal to the diameter of a water molecule, or 276 pm, whereas much closer approach of electrostricted water is possible in interligand space (e.g., along a threefold axis of octahedral $M(H_2O)_6^{z+}$), and allowance for void-space contributions needs to be made in estimating V_c. The difference between his and our Δr values is important, as a 1 pm change in $(r + \Delta r)$ results typically in about 1 cm^3 mol^{-1} change in $\bar{V}^0_{abs}$. For the same reasons, it is important to use r values appropriate to the coordination number n_c; we used Shannon's critical compilation (31) in which n_c is specified for each ionic radius given. The Shannon radii are often given only to the nearest pm, and are subject to the usual uncertainties that beset division of internuclear distances into ionic contributions, so that eq. [10] cannot be expected to predict $\bar{V}^0_{abs}$ values to better than ±1 cm^3 mol^{-1}. As noted above, however, experimental $\bar{V}^0$ data for M^{z+}(aq) are themselves often subject to uncertainties of ±2 cm^3 mol^{-1}, while the assumption of an absolute partial molar volume of −5.4 cm^3 mol^{-1} for H^+(aq) (10) is open to

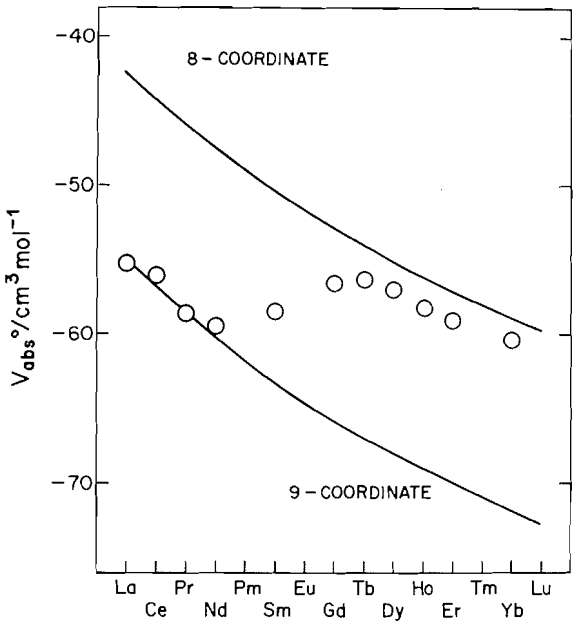

FIG. 2. Comparison of the experimental absolute partial molar volumes of Spedding *et al.* (42) for aqueous lanthanoids(III) with the predictions of eq. [10], assuming (upper curve) $n_c = 8$ and (lower curve) $n_c = 9$.

question. All in all, eq. [10] accounts for the widely-ranging experimental $\bar{V}^0$ data as well as can be expected, and we are therefore confident that the model on which it is based is a realistic representation of all simple $M^{z+}(aq)$ ions for $z = 1$ through 4.

Primary coordination numbers

The single adjustable parameter Δr in eq. [10] can be determined as accurately as necessary with measured $\bar{V}^0$ values for ions of well-established primary coordination number n_c in solution. Then, because the term 18.07 n_c (as well as the dependence of r upon n_c) makes the calculation of $\bar{V}^0_{abs}$ very sensitive to n_c, known $\bar{V}^0$ data can provide realistic n_c values so long as the appropriate crystallographic radii are available (31). In almost every case tested, we found that the $\bar{V}^0$ values corresponded to $n_c = 4$, 6, 8, or 9, as would be anticipated on geometrical grounds. For example, for $Na^+(aq)$, we calculate $\bar{V}^0_{abs} = 23.7$, 6.5, −9.9, −17.9, and −31.2 $cm^3\ mol^{-1}$ for coordination numbers 4, 5, 6, 7, and 8 respectively; the observed value of −6.6 $cm^3\ mol^{-1}$ is consistent with $n_c = 6$, in agreement with a recent X-ray diffraction study (40). Similarly, for $Sr^{2+}(aq)$, $\bar{V}^0_{abs}$ is predicted to be 1.4, −13.7, −26.7, −39.6, and −52.4 $cm^3\ mol^{-1}$ for 6-, 7-, 8-, 9-, and 10-coordination respectively; the observed value of −29.0 supports the X-ray result of $n_c = 8$ (41). Only for $Ca^{2+}(aq)$ did n_c appear to be 7, for which $\bar{V}^0_{abs}$ (calculated) is −28.0 $cm^3\ mol^{-1}$; significantly, two X-ray research groups (41, 42) have independently concluded that n_c is between 6 and 8 for $Ca^{2+}(aq)$, and probably both $Ca(H_2O)_6^{2+}$ and $Ca(H_2O)_8^{2+}$ are present simultaneously, giving a time-average n_c near 7. If water is taken to be a hard sphere of radius 138 pm, the transition from 6- to 8-coordination (octahedral to simple cubic) becomes possible when the radius of M in $M(H_2O)_6^{z+}$ is 101 pm or more; for Ca^{2+} in octahedral environments, $r = 100$ pm, and higher for higher n_c (31).

For the aqueous lanthanoid(III) ions, Spedding, Pikal, and Ayres (43) suggested that the partial molar volumes reflected a progressive changeover from predominant 9-coordination for $La^{3+}(aq)$ to 8-coordination for $Tb^{3+}(aq)$ and the higher lanthanoids(III). In Fig. 2, we display the $\bar{V}^0_{abs}$ values of Spedding *et al.* together with curves representing the smoothed theoretical $\bar{V}^0_{abs}$ data calculated with eq. [10] using Shannon's radii (31) for the appropriate coordination numbers. The separation of the two curves is about 13 $cm^3\ mol^{-1}$, so that the coincidences of $\bar{V}^0_{abs}$ of $La^{3+}(aq)-Nd^{3+}(aq)$ with the lower curve and of $Tb^{3+}(aq)-Yb^{3+}(aq)$ with the upper, within the accuracy of $\bar{V}^0$ measurements and of eq. [10], combine with recent X-ray diffraction results (44) to provide strong support for the theory of Spedding *et al.* (43).

Interestingly, $H^+(aq)$ ($r \sim 0$) fits eq. [10] reasonably well with $n_c = 2$ (giving $\bar{V}^0_{abs} = -3.6$ $cm^3\ mol^{-1}$, cf. −5.4 assumed), suggesting that its central unit consists of two water molecules joined by a short linear H-bond, much as in the structure reported (45) for the discrete ion $H_{13}O_6^+$.

Contribution of electrostriction

The average value of r for the ions covered by Fig. 1 is ~80 pm, so $(r + \Delta r)$ is typically ~320 pm and the classical electrostriction (Drude–Nernst) component of $\bar{V}^0_{abs}$ is $-1.30z^2$ $cm^3\ mol^{-1}$, which amounts to only −1.3, −5.2, −11.7, and −20.8 cm^3 mol for $Z = 1$, 2, 3, and 4 respectively. Departures of r from this average value contribute only minor discrepancies to the calculated $\bar{V}^0_{abs}$ in terms of $cm^3\ mol^{-1}$, and so eq. [10] may be approximated as follows with only minor loss of accuracy (Δr having been slightly adjusted).

$$[11]\quad \bar{V}^0_{abs} = 2.523 \times 10^{-6}(238.5 + r)^3 - 18.07n_c - 1.305z^2$$

The second term generally far outweighs the third, that is, actual complexation by solvent, rather than coulombic electrostriction, is the primary factor that leads to negative $\bar{V}^0_{abs}$ values for many metal ions in solution.

The Güntelberg approximation (30), in which the effective radii of aqueous cations is set to about 310 pm in the extended Debye–Hückel equation, may be seen to succeed for the same reason as eq. [11], viz., that water may be treated as a continuous dielectric beyond the distance of closest-approach to the complex $M(H_2O)_{n_c}^{z+}$ which has an effective radius within a few percent of 310–320 pm, electrostatic interactions being rather insensitive to the exact value of this large radius.

Hydrolysis of metal ions

The volumes V_c of the unit $M(H_2O)_{n_c}^{z+}$ and its conjugate base $M(H_2O)_{(n_c-1)}OH^{(z-1)+}$ should be virtually identical. According to eq. [11], then, the volume change ΔV_a for the reaction

$$[12]\quad M(H_2O)_{n_c}^{z+} \rightleftharpoons M(H_2O)_{(n_c-1)}OH^{(z-1)+} + H^+$$

should be

$$[13]\quad \Delta V_a = -5.4 + 1.305[z^2 - (z-1)^2] = 2.6z - 6.7$$

For $z = 3$, ΔV_a is therefore expected to be close to +1 $cm^3\ mol^{-1}$, which is precisely what is observed for $Fe^{3+}(aq)$ (17). Similar near-zero ΔV_a values have been found for the hydrolyses of other $M(H_2O)_{n_c}^{3+}$ and $M(NH_3)_5OH_2^{3+}$ ions (15–17), and the conflict with our original naive expectations of $\Delta V_a \sim +25$ $cm^3\ mol^{-1}$ (15) is now resolved.

Failures of eq. [10]

Poor predictions of $\bar{V}^0_{abs}$ can be anticipated where r is deviant or subject to substantial uncertainty, e.g., for Be^{2+}, for which n_c is almost certainly 4 but the Shannon radius (27 pm) is

Can. J. Chem. Downloaded from www.nrcresearchpress.com by 210.87.254.6 on 09/06/12
For personal use only.

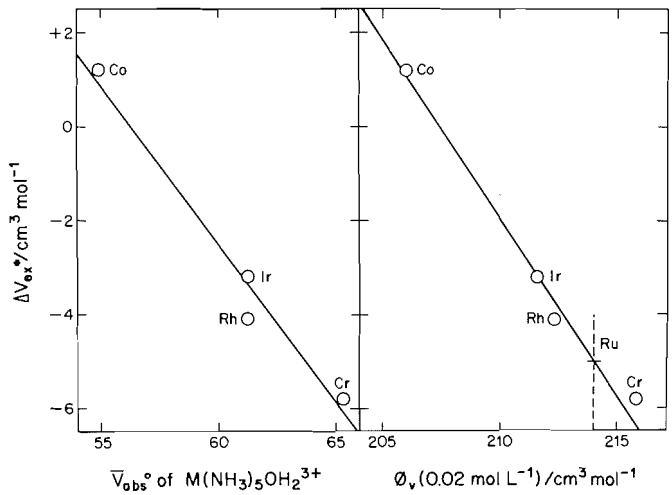

FIG. 3. Correlations of the volumes of activation ΔV_{ex}^* for water exchange on aqueous $[M(NH_3)_5OH_2](ClO_4)_3$ with (left) the absolute partial molar volumes of $M(NH_3)_5OH_2^{3+}(aq)$ and (right) the apparent molar volumes ϕ_v for the perchlorate salts (M = Co, Rh, Ir, Cr) (2).

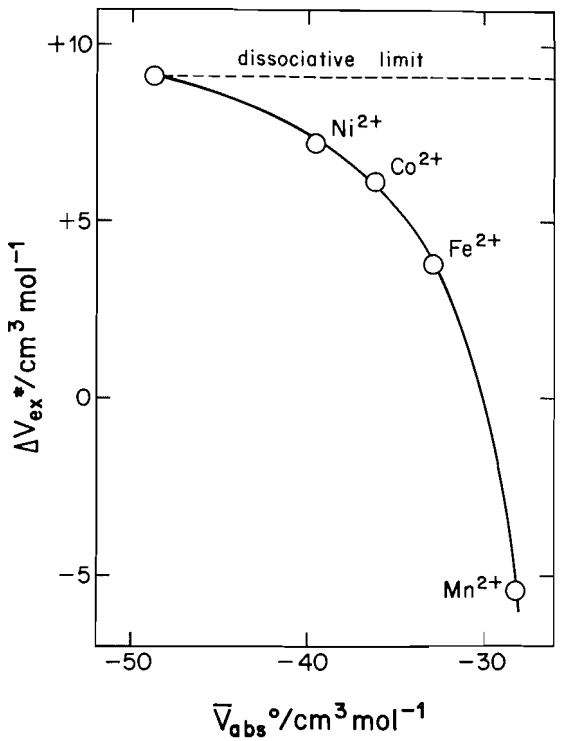

FIG. 4. Correlation of the volumes of activation ΔV_{ex}^* for water exchange on aqueous M^{2+} (M = Mn, Fe, Co, and Ni (47), and the hypothetical M^{2+} of radius 57.2 pm representing closest-packing of six water ligands) with the absolute partial molar volumes of $M^{2+}(aq)$. $\bar{V}^0_{abs}$ values from Table 3, except for the hypothetical $M^{2+}(aq)$ (from eq. [10]).

smaller than the cavity in a closest-packed tetrahedron of waters of 138 pm radius (31 pm). It would appear, however, that eqs. [10] and [11], as they stand, are simply inapplicable to *low-spin* transition metal ions. This can be anticipated from our data on $M(NH_3)_5OH_2^{3+}(aq)$; $\bar{V}^0_{abs}$ = 54.6, 60.9, 60.9, and 65.0 cm^3 mol^{-1} for M = Co, Rh, Ir, and Cr, but the corresponding ionic radii are 54.5, 66.5, 68, and 61.5 pm (31), the first three referring to spin-paired (t_{2g}^6) ions. Not surprisingly, $\bar{V}^0_{abs}$ for $Rh^{3+}(aq)$ is calculated to be −49.0 cm^3 mol^{-1} from eq. [10], whereas the measured value is −59.7 cm^3 mol^{-1}. Thus, solvated spin-paired ions are even more compact than their measured crystallographic ionic radii would suggest. More $\bar{V}^0$ data are required here.

Correlations of $\bar{V}^0$ *with* ΔV_{ex}^*

Our early observations (1) suggested that ΔV_{ex}^* correlated roughly linearly with $\bar{V}^0$ (or ϕ_v at a suitable reference concentration) with slope near −1. Figure 3 shows that this is a fair statement for the $M(NH_3)_5OH_2^{3+}$ water exchanges, although the slope is more accurately −0.71 or −0.74, depending on whether one correlates ΔV_{ex}^* with $\bar{V}^0$ or, perhaps more realistically, with ϕ_v for $c \sim 0.02$ mol L^{-1}, the mid-range of concentration in most experiments. The latter correlation permits prediction of ΔV_{ex}^* for $Ru(NH_3)_5OH_2^{3+}$ of −5 cm^3 mol^{-1}, on the basis of ϕ_v(0.02 mol L^{-1}) = 214.0 cm^3 mol^{-1}, calculated for the perchlorate salt from the data of Fairhurst and Swaddle (46). Direct measurement of this ΔV_{ex}^* is difficult (46), but will be attempted again.

For aqua exchange on $M^{2+}(aq)$, ΔV_{ex}^* is indeed inversely correlated with $\bar{V}^0$, but the correlation now seems not to be linear (Fig. 4). Nevertheless, we can use the correlation to predict ΔV_{ex}^* = +6 and −8 cm^3 mol^{-1} for M = Zn^{2+} and Cd^{2+}, from the data of Table 3. For $Cu^{2+}(aq)$, the Jahn–Teller distortion of the hexacoordinate ion makes the interpretation of kinetic parameters ambiguous (48), but in any case the correlation predicts ΔV_{ex}^* just less than +6 cm^3 mol^{-1}. The calcium ion probably does not belong in this correlation because of the possibility noted above that the coordination number may be more than six.

Included in Fig. 4 is a theoretical upper limit to ΔV_{ex}^*, estimated by assuming the water molecule to be a sphere of radius 138 pm. Since, in the limit of steric stability, the waters in $M(H_2O)_6^{z+}$ are closest-packed around a cavity of radius 57 pm (= r of M^{z+}) and therefore have an effective molar volume of 8.95 cm^3 mol^{-1} each (calculated for a cubic closest-packed array of spheres of radius 138 pm), the volume change for a limiting S_N1 or D-type process will be 18.07 − 8.95 = +9.1 cm^3 mol^{-1} (1, 49). This applies to an ideal, limiting-octahedral $M(H_2O)_6^{2+}$ ion which will have $\bar{V}^0_{abs}$ = −48.7 cm^3 mol^{-1} (eq. [10]) and has been entered as the top left limit to the correlation curve of Fig. 4. Real $M(H_2O)_6^{2+}(aq)$ should have ΔV_{ex}^* less than +9.1 cm^3 because (*a*) the ligands are not usually closest-packed, (*b*) the mode of activation may have a degree of associative character, and (*c*) the reduction of coordination number in the residual complex may lead to reduced M—OH_2 bond lengths (49, 50). All three factors will tend to increase in importance with increasing r; hence, ΔV_{ex}^* becomes less positive as r and therefore also $\bar{V}^0_{abs}$ (from eq. [11]) increase, for a given z and reaction type. The result is that the volumes of the transition states for solvent exchange, which we represent for convenience by ($\Delta V_{ex}^* + \bar{V}^0$), do not vary strongly as M is changed within a series; in each case, the reacting system seeks to make the best of the steric limitations primarily by adjusting factor (*b*).

Published ΔV_{ex}^* data on $M^{3+}(aq)$ are limited to the values −5.4 and −9.3 cm^3 mol^{-1} for $Fe^{3+}(aq)$ and $Cr^{3+}(aq)$, which refer to vastly different ionic strengths and temperatures (17, 51). Nevertheless, if correlations similar to those for $M^{2+}(aq)$ and $M(NH_3)_5OH_2^{3+}(aq)$ apply, we can anticipate that ΔV_{ex}^* for $Rh^{3+}(aq)$ will be 0 ± 2 cm^3 mol^{-1}, on the basis of Table 2.

Can. J. Chem. Downloaded from www.nrcresearchpress.com by 210.87.254.6 on 09/06/12
For personal use only.

Acknowledgements

We thank the Natural Sciences and Engineering Research Council Canada for financial assistance, and Dr. L. G. Hepler for discussions.

1. T. W. SWADDLE. *In* Mechanistic aspects of inorganic reactions. *Edited by* D. B. Rorabacher and J. F. Endicott. ACS Symp. Ser. **198**, 39 (1982).
2. T. W. SWADDLE. J. Chem. Soc. Chem. Commun. 832 (1982).
3. A. LO SURDO and F. J. MILLERO. J. Phys. Chem. **84**, 710 (1980).
4. J. J. SPITZER, P. P. SINGH, I. V. OLOFSSON, and L. G. HEPLER. J. Solution Chem. **7**, 623 (1978).
5. J. J. SPITZER, P.P. SINGH, K. G. MCCURDY, and L. G. HEPLER. J. Solution Chem. **7**, 81 (1978).
6. J. J. SPITZER, I. V. OLOFSSON, P. P. SINGH, and L. G. HEPLER. J. Chem. Thermodyn. **11**, 233 (1979).
7. J. J. SPITZER, I. V. OLOFSSON, P.P. SINGH, and L. G. HEPLER. Thermochim. Acta, **28**, 155 (1979).
8. K. FAJANS and O. JOHNSON. J. Am. Chem. Soc. **64**, 668 (1942).
9. A. M. COUTURE and K. J. LAIDLER. Can. J. Chem. **34**, 1209 (1956).
10. F. J. MILLERO. Water and aqueous solutions. *Edited by* R. A. Horne. Wiley-Interscience, Toronto. 1972. Chapt. 13.
11. K. GOTO, H. TAMURA, and M. NAGAYAMA. Inorg. Chem. **9**, 963 (1970).
12. J. J. SPITZER, I. V. OLOFSSON, P. P. SINGH, and L. G. HEPLER. Can. J. Chem. **57**, 2798 (1979).
13. U. SPITZER, R. VAN ELDIK, and H. KELM. Inorg. Chem. **21**, 2821 (1982).
14. M. J. SISLEY and T. W. SWADDLE. Inorg. Chem. **20**, 2799 (1981).
15. T. W. SWADDLE and P. C. KONG. Can. J. Chem. **48**, 3223 (1970).
16. D. R. STRANKS and N. VANDERHOEK. Inorg. Chem. **15**, 2645 (1976).
17. T. W. SWADDLE and A. E. MERBACH. Inorg. Chem. **20**, 4212 (1981).
18. J. E. FINHOLT, M. E. THOMPSON, and R. E. CONNICK. Inorg. Chem. **20**, 4151 (1981).
19. A. I. VOGEL. A textbook of quantitative inorganic analysis. 4th ed. J. Wiley and Sons, New York. 1961. p. 311.
20. J. P. HUNT and H. TAUBE. J. Chem. Phys. **19**, 602 (1951).
21. G. H. AYRES and J. S. FORRESTER. J. Phys. Chem. **63**, 1979 (1959).
22. H.-H. SCHMIDTKE. Inorg. Chem. **5**, 1682 (1966).
23. T. W. SWADDLE and D. R. STRANKS. J. Am. Chem. Soc. **94**, 8357 (1972).
24. G. S. KELL. J. Chem. Eng. Data, **12**, 66 (1967).
25. H. E. WIRTH and F. N. COLLIER, JR. J. Am. Chem. Soc. **72**, 5292 (1950).
26. J. V. LEYENDEKKERS. J. Chem. Soc. Faraday Trans. I, **77**, 1529 (1981).
27. F. J. MILLERO. Geochim. et Cosmochim. Acta, **41**, 215 (1977).
28. F. J. MILLERO. Chem. Rev. **71**, 147 (1971).
29. O. REDLICH and D. M. MEYER. Chem. Rev. **64**, 221 (1964).
30. E. GÜNTELBERG. Z. Phys. Chem. **123**, 199 (1926).
31. R. D. SHANNON and C. T. PREWITT. Acta Crystallogr. B**25**, 925 (1969); R. D. SHANNON. Acta Crystallogr. A**32**, 751 (1976).
32. C. HÄRTLING, T. MECKLENBURG, and W. SEIDEL. Ber. Bunsenges. Phys. Chem. **85**, 1012 (1981).
33. G. A. BOTTOMLEY and L. G. GLOSSOP. Aust. J. Chem. **34**, 699 (1981); **34**, 2487 (1981).
34. J. V. LEYENDEKKERS. J. Chem. Soc. Faraday Trans. I, **78**, 357 (1982).
35. J. W. AKITT. J. Chem. Soc. Faraday Trans. I, **76**, 2259 (1980).
36. J. W. AKITT. J. Chem. Soc. A, 2347 (1971).
37. J. E. DESNOYERS, R. E. VERRALL, and B. E. CONWAY. J. Chem. Phys. **43**, 243 (1965).
38. E. WHALLEY. J. Chem. Phys. **38**, 1400 (1963).
39. L. G. HEPLER. J. Phys. Chem. **61**, 1426 (1957).
40. R. CAMINITI, G. LISCHERI, G. PASCHINA, G. PICCALUGA, and G. PINNA. J. Chem. Phys. **72**, 4522 (1980).
41. J. N. ALBRIGHT. J. Chem. Phys. **56**, 3783 (1972).
42. G. LICHERI, G. PICCALUGA, and G. PINNA. J. Chem. Phys. **63**, 4412 (1975).
43. F. H. SPEDDING, M. J. PIKAL, and B. O. AYRES. J. Phys. Chem. **70**, 2440 (1966).
44. A. HABENSCHUSS and F. H. SPEDDING. J. Chem. Phys. **70**, 2797 (1979); **70**, 3758 (1979); **73**, 442 (1980).
45. R. A. BELL, G. G. CHRISTOPH, F. R. FRONCZEK, and R. E. MARSH. Science, **190**, 151 (1975).
46. M. T. FAIRHURST and T. W. SWADDLE. Inorg. Chem. **18**, 3241 (1979).
47. Y. DUCOMMUN, K. E. NEWMAN, and A. E. MERBACH. Inorg. Chem. **19**, 3696 (1980).
48. C. W. MERIDETH. Ph.D. Thesis. University of California, Berkeley. 1965.
49. T. W. SWADDLE. Inorg. Chem. **19**, 3203 (1980).
50. C. H. LANGFORD. Inorg. Chem. **18**, 3288 (1979).
51. D. R. STRANKS and T. W. SWADDLE. J. Am. Chem. Soc. **93**, 2783 (1971).

Can. J. Chem. Downloaded from www.nrcresearchpress.com by 210.87.254.6 on 09/06/12
For personal use only.

The crystal structure of free base cocaine, $C_{17}H_{21}NO_4$

RONALD J. HRYNCHUK,[1] RICHARD J. BARTON, AND BEVERLEY E. ROBERTSON[2]
Faculty of Science, University of Regina, Regina, Sask., Canada S4S 0A2

Received June 9, 1982[3]

RONALD J. HRYNCHUK, RICHARD J. BARTON, and BEVERLEY E. ROBERTSON. Can. J. Chem. **61**, 481 (1983).

The crystal structure of free base cocaine has been determined in order to compare the conformation with that observed in its salts, and to clarify the powder pattern of the pure compound. Crystals of (−)-cocaine are monoclinic, space group $P2_1$, a = 10.130(1), b = 9.866(2), c = 8.445(1) Å, β = 106.92(1)°, Z = 2, D_x = 1.25 g cm^{-3}. Data were collected with MoK$_\alpha$ radiation on a modified Picker diffractometer using the NRCC diffractometer control system. The structure was solved by direct methods and refined by least squares to final R and R_w of 0.065 and 0.062 ($w = 1/\sigma^2(F)$) using the 1818 independent reflections with $\sin\theta/\lambda < 0.7048$ and $|F|/\sigma(|F|) \leq 3.0$.

The free base exists in a piperidine chair conformation similar to the methiodide salt and the hydrochloride salt. However, the piperidine ring carbon−nitrogen bonds in the free base are shorter than those in the salts; 1.460(7) and 1.467(6) Å in the free base compared to 1.55(2) and 1.51(2) Å in the methiodide salt and 1.50(1) and 1.49(1) Å in the hydrochloride salt. Further, the orientations of the benzoxy group and the methoxycarbonyl group, with respect to the piperidine rings, are significantly different from that common to both salts. The calculated powder diffraction pattern of (−)-cocaine showed that several previously reported weak lines in powder diffraction data for this alkaloid should not be present.

RONALD J. HRYNCHUK, RICHARD J. BARTON et BEVERLEY E. ROBERTSON. Can. J. Chem. **61**, 481 (1983).

On a déterminé la structure du cristal de la base libre cocaine dans le but de comparer sa conformation avec celle de ses sels et dans le but de clarifier le diagramme de poudre du composé pur. Les cristaux de la (−)-cocaine sont monocliniques et appartiennent au groupe d'espace $P2_1$ avec a = 10,130(1), b = 9,866(2), c = 8,445(1) Å, β = 106,92(1)°, Z = 2, D_x = 1,25 g cm^{-3}. Faisant appel à un système de contrôle de diffractomètre de type NRCC, on a recueilli les données à l'aide d'une radiation MoK$_\alpha$ d'un diffractomètre de Picker modifié. On a résolu la structure par des méthodes directes et on l'a affinée par la méthode des moindres carrés jusqu'à des valeurs conventionnelles de R et de R_w de 0,065 et de 0,062 ($w = 1/\sigma^2(F)$) pour 1818 réflexions indépendantes avec $\sin\theta/\lambda < 0{,}7048$ et $|F|/\sigma(F) \leq 3{,}0$.

La base libre existe sous une conformation chaise de la pipéridine semblable au méthiodure et au chlorhydrate. Cependant les liaisons C—N du cycle pipéridine de la base libre sont plus courtes que celle des sels; 1,460(7) et 1,467(6) Å dans la base libre comparées à 1,55(2) et 1,51(2) Å pour le méthiodure et 1,49(1) Å pour le chlorhydrate. De plus, les orientations du groupe benzoxy et du groupe méthoxycarbonyle par rapport au cycle de la pipéridine sont significativement différentes de celles communes au deux sels. Le diagramme de diffraction de la poudre calculé pour la (−)-cocaine montre que plusieurs des lignes faibles rapportées antérieurement dans les données de diffraction de poudre pour cet alcaloide ne devraient pas être présentes.
[Traduit par le journal]

Introduction

The purpose of this work is to examine the structure of (−)-cocaine as its free base. The present stereochemical configuration of the natural product is derived from the crystal structure of its salts. Gabe and Barnes (1) have determined the crystal structure of (−)-cocaine hydrochloride. They showed that it had a bridged 1,5 piperidine chair conformation. Shen *et al.* (2) showed that cocaine methiodide also has a chair conformation, but there were differences in the orientations of the benzoxy and methoxycarbonyl substituents. These differences affected intramolecular contact distances and their electrostatic interactions. We determined the crystal structure of (−)-cocaine as its free base in order to compare it to that of these salts. The absolute configuration of (−)-cocaine is known to be (−)-2*R*-methoxycarbonyl-3*S*-benzoxytropane (3).

The identification of (−)-cocaine is important in forensic science because it is a drug of abuse. Pharmacologically, it acts as an anaesthetic or as a central nervous system stimulant (4). X-ray powder diffraction methods can be used for identifying cocaine and its salts. Powder diffraction methods cannot differentiate between the (−) and (+) enantiomers of cocaine, but it can distinguish these from (±)-cocaine as a racemic mixture (5). Powder data for (−)-cocaine (6−8), (−)-cocaine hydrochloride (6, 7, 9), and (−)-cocaine sulfate (6) have been published in various works. Some discrepancies exist in the powder data for (−)-cocaine since some lines were not consistently reported and, further, some lines were not observed in powder patterns of (−)-cocaine as measured by us. Therefore, in addition to comparing the structure of the free base to that of its salts, we determined the crystal structure of (−)-cocaine in order to clarify the powder pattern data. The calculated powder pattern of (−)-cocaine hydrochloride (9), from the crystal structure determination of this salt by Gabe and Barnes (1), shows that two lines in the powder pattern reported previously by Barnes and Sheppard (6) in 1954 and Owen *et al.* (7) in 1972, could not be assigned reflections. Canfield *et al.* (10, 11) solved the crystal structure of diacetylmorphine (heroin) in order to explain differences in the observed powder pattern of this drug with previously published data (6).

All of the above noted discrepancies are relatively weak lines and are probably due to sample impurities. Folen (12) lists powder diffraction data for many of the excipients and impurities commonly encountered in drug samples. Barnes and Sheppard (6), in their extensive compilation of powder data on eighty-three narcotics, emphasized the need for single crystal data.

[1]Present address: Royal Canadian Mounted Police, Crime Detection Laboratory, P.O. Box 1320, Edmonton, Alberta, Canada T5J 2N1.

[2]Author to whom all correspondence should be addressed.

[3]Revision received October 29, 1982.

Can. J. Chem. Downloaded from www.nrcresearchpress.com by 210.87.254.42 on 09/06/12
For personal use only.

Can. J. Chem. Downloaded from www.nrcresearchpress.com by 210.87.254.42 on 09/06/12
For personal use only.

TABLE 1. Atomic positions and thermal parameters[a] for all atoms, temperature factors ($\times 10^3$)

Atom	x	y	z	U(equiv.)
C(1)	0.5419(4)	0.1631(6)	0.7095(4)	46(2)
C(2)	0.4579(4)	0.2047(6)	0.5345(5)	44(2)
C(3)	0.3080(4)	0.1713(6)	0.5168(5)	49(2)
C(4)	0.2903(5)	0.0286(7)	0.5727(5)	55(3)
C(5)	0.3950(5)	0.0004(6)	0.7409(5)	55(3)
C(5)	0.3870(5)	0.1080(7)	0.8678(5)	70(3)
C(7)	0.4858(5)	0.2192(7)	0.8450(5)	62(3)
C(8)	0.1028(4)	0.2512(6)	0.3219(5)	56(3)
C(9)	0.0323(4)	0.2713(5)	0.1411(5)	47(2)
C(10)	0.0857(5)	0.2213(7)	0.0238(5)	68(3)
C(11)	0.0189(6)	0.2435(8)	−0.1419(6)	91(4)
C(12)	−0.0995(6)	0.3166(8)	−0.1875(8)	84(4)
C(13)	−0.1528(6)	0.3671(7)	−0.0719(9)	89(4)
C(14)	−0.0880(5)	0.3462(7)	0.0951(7)	72(3)
C(15)	0.5172(4)	0.1331(5)	0.4127(4)	43(2)
C(16)	0.7261(7)	0.1009(11)	0.3465(9)	82(4)
C(17)	0.6418(7)	−0.0439(8)	0.8543(6)	70(4)
N(1)	0.5324(3)	0.0158(5)	0.7182(4)	47(2)
O(1)	0.2257(3)	0.1933(4)	0.3470(3)	57(2)
O(2)	0.0560(3)	0.2836(6)	0.4306(4)	102(3)
O(3)	0.4616(3)	0.0531(4)	0.3097(3)	61(2)
O(4)	0.6481(3)	0.1713(4)	0.4393(3)	58(2)
H(1)	0.621(3)	0.184(3)	0.723(3)	12(8)
H(2)	0.464(4)	0.298(5)	0.517(5)	45(12)
H(3)	0.282(4)	0.234(5)	0.583(5)	57(13)
H(4)	0.193(5)	0.011(6)	0.573(5)	68(13)
H(5)	0.305(4)	−0.024(4)	0.493(5)	33(11)
H(6)	0.385(5)	−0.096(6)	0.777(6)	75(16)
H(7)	0.409(4)	0.081(5)	0.976(5)	45(11)
H(8)	0.287(5)	0.141(5)	0.861(5)	72(14)
H(9)	0.444(5)	0.314(6)	0.815(6)	70(16)
H(10)	0.556(4)	0.233(4)	0.940(5)	42(11)
H(11)	0.158(4)	0.168(5)	0.053(5)	55(13)
H(12)	0.064(5)	0.205(7)	−0.224(7)	95(18)
H(13)	−0.147(6)	0.333(7)	−0.306(8)	112(20)
H(14)	−0.232(7)	0.414(7)	−0.103(7)	113(23)
H(15)	−0.128(5)	0.381(6)	0.186(6)	92(18)
H(16)	0.733(9)	0.019(14)	0.381(11)	195(51)
H(17)	0.813(6)	0.147(6)	0.371(6)	100(20)
H(18)	0.699(6)	0.106(8)	0.237(8)	129(27)
H(19)	0.725(5)	−0.034(6)	0.836(6)	81(19)
H(20)	0.647(5)	−0.007(6)	0.961(7)	90(18)
H(21)	0.623(5)	−0.141(7)	0.861(6)	81(20)

[a]Thermal parameters are of the form:

$$\exp[-2\pi^2(U_{11}h^2a^{*2} + U_{22}k^2b^{*2} + U_{33}l^2c^{*2} + 2U_{12}hka^*b^* + 2U_{13}hla^*c^* + 2U_{23}klb^*c^*)]$$

where

$$U(\text{equiv.}) = \frac{1}{3}\sum_{\substack{i=1\\j=1}}^{3}[U_{ij}a_i^*a_j^*(\mathbf{a}_i\cdot\mathbf{a}_j)]$$

Experimental

(−)-Cocaine was recrystallized by slow evaporation from absolute ethanol as clusters of large, transparent, colorless, birefringent plates, from which a crystal of dimensions 0.7 mm × 1.0 mm × 0.2 mm was used for crystal structure determination. Symmetry and systematic absences were determined from precession and Weisenberg photographs. Lattice parameters were refined by least-squares methods and intensities were measured on a modified Picker diffractometer using the NRCC diffractometer control system (13). Crystal data are:

(−)-Cocaine, $C_{17}H_{21}NO_4$ Mol. wt. 303.35

Monoclinic, space group $P2_1$, a = 10.120(1), b = 9.866(2), c = 8.445(1) Å, β = 106.92(1)°, T = 25°C, V = 807.48 Å^3, Z = 2, D_x = 1.25 g cm^{-3}, D_m = 1.25(1) cm^{-3}, $\mu(\text{MoK}_\alpha)$ = 0.0958 cm^{-1}.

A total of 2489 reflections with $\sin\theta/\lambda < 0.7048$ were measured using graphite monochromatized MoK_α radiation (λ = 0.71069 Å). Of these reflections, 1818 were considered as observed with $|F|/\sigma(|F|) > 3.0$.[4] Corrections for absorption were not made.

[4]The standard deviation of an individual reflection is calculated from the counting statistics associated with its measurement with an additional factor derived from the extent by which the scatter of the standard reflections exceeds that predicted from their own counting statistics.

Can. J. Chem. Downloaded from www.nrcresearchpress.com by 210.87.254.42 on 09/06/12
For personal use only.

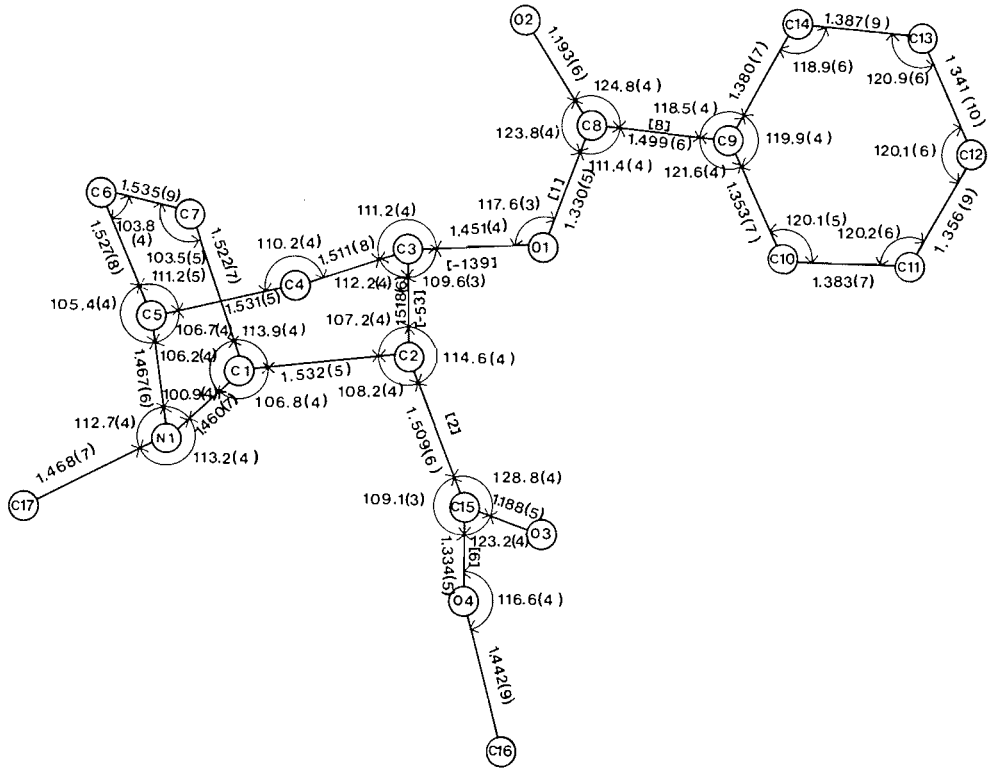

FIG. 1. Atom labelling, bond lengths, bond angles, and torsional angles for (−)-cocaine with estimated standard deviations. Numbers in square brackets are torsional angles.

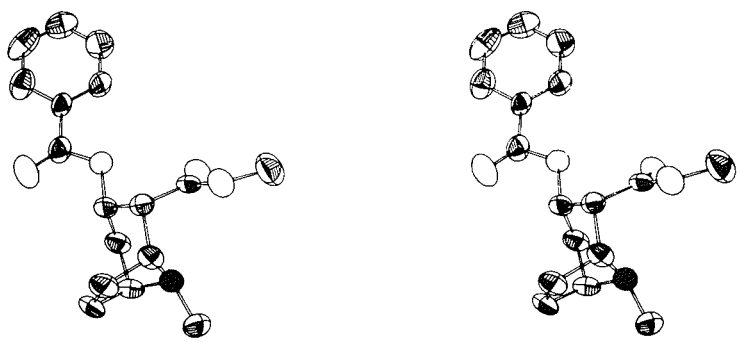

FIG. 2. Stereoscopic view of the molecule of (−)-cocaine. The nitrogen atom is black and the oxygen atoms are blank.

The crystal structure was solved by direct methods. The assignment of phases to normalized structure factors by MULTAN produced an *E*-map from which 12 of 22 nonhydrogen atoms were found. The remaining nonhydrogen atoms and some of the hydrogen atoms were located after the calculation of an electron density map. The atom positions and anisotropic temperature factors for all nonhydrogen atoms were refined by least squares. A difference map revealed all remaining hydrogen atoms. The parameters for the nonhydrogen atoms and atom positions with isotropic temperature factors for the hydrogen atoms were further refined by several cycles of least squares. It was necessary to divide these parameters into three blocks in order to accommodate the available core memory. The *x* coordinate of the nitrogen atom was held constant to fix the origin of the polar space group. This refinement converged to final agreement factors of:

$$R = \Sigma(|F_o| - |F_c|) / \Sigma|F_o| = 0.065$$

$$R_w = [\Sigma w(|F_o| - |F_c|)^2 / \Sigma w|F_o|^2]^{1/2} = 0.062 \qquad (w = 1/\sigma^2)$$

with a maximum shift/error of 0.260, and an average shift/error of 0.025 for all atoms.

All data treatment steps including structure factor calculations and preliminary least-squares refinement were carried out using the NRCC system (13). Final least-squares refinement of atom positions and temperature factors was carried out using the XRAY76 (14) system of crystallographic programs. Molecular projections were drawn using ORTEP (15).

Table 1 lists the atom positions and temperature factors for all atoms. Figure 1 shows the configuration of (−)-cocaine with atoms labelled. Bond distances and bond angles with standard deviations are indicated for nonhydrogen atoms.[5] A stereogram of the molecules is shown in Fig. 2.

Table 2 lists the calculated powder diffraction pattern, using XRAY76 (14), including the relative observed line intensities for each

[5]The structure factor table, a table of the complete atomic parameters with anisotropic thermal parameters, and a table of hydrogen atom structural parameters are available at a nominal charge from the Depository of Unpublished Data, CISTI, National Research Council of Canada, Ottawa, Ont., Canada K1A 0S2.

TABLE 2. Calculated powder pattern for (−)-cocaine. Max. θ = 30°(MoK$_\alpha$)

d	I(cal)	hkl	d	I(cal)	hkl	d	I(cal)	hkl
9.692	45	100	2.815	1	$\bar{1}03$	2.172	1	312
8.080	16	001	2.738	1	301	2.166	1	$\bar{4}22$
7.346	51	$\bar{1}01$	2.721	8	230	2.108	1	203
6.914	24	110	2.717	4	$\bar{2}31$	2.105	1	042
6.251	13	011	2.707	1	$\bar{1}13$	2.104	1	331
5.892	30	$\bar{1}11$	2.638	1	311	2.093	1	$\bar{2}33$
5.472	14	101	2.616	1	$\bar{2}13$	2.062	2	213
4.934	40	020	2.598	2	013	2.048	1	$\bar{2}42$
4.846	19	200	2.586	1	$\bar{1}32$	2.030	1	322
4.820	19	$\bar{2}01$	2.552	1	$\bar{3}22$	2.023	1	$\bar{5}01$
4.785	8	111	2.550	1	032	2.006	1	$\bar{4}31$
4.397	100	120	2.532	3	$\bar{4}01$	1.988	1	$\bar{5}02$
4.350	3	210	2.467	1	040	1.987	1	$\bar{3}41$
4.331	10	$\bar{2}11$	2.460	1	231	1.964	1	$\bar{3}33$
4.210	31	021	2.453	1	$\bar{4}11$	1.961	1	$\bar{4}23$
4.187	7	$\bar{1}02$	2.450	1	$\bar{2}32$	1.949	1	133
4.095	12	$\bar{1}21$	2.449	3	$\bar{3}03$	1.938	3	223
3.854	2	$\bar{1}12$	2.445	2	$\bar{1}23$	1.938	1	500
3.739	28	012	2.393	2	222	1.935	1	$\bar{1}24$
3.673	7	$\bar{2}02$	2.390	1	140	1.934	1	150
3.664	7	121	2.377	3	$\bar{2}23$	1.927	1	$\bar{2}24$
3.470	10	211	2.377	1	$\bar{3}13$	1.917	1	051
3.457	7	220	2.364	2	020	1.906	1	$\bar{1}51$
3.448	8	$\bar{2}21$	2.353	1	410	1.902	1	510
3.355	1	$\bar{3}01$	2.350	1	113	1.900	1	$\bar{3}42$
3.210	5	112	2.349	1	$\bar{3}31$	1.872	1	$\bar{5}21$
3.192	11	$\bar{1}22$	2.341	1	$\bar{4}12$	1.872	1	104
3.176	6	$\bar{3}11$	2.338	1	$\bar{1}41$	1.869	1	024
3.126	5	022	2.253	2	$\bar{4}21$	1.855	1	$\bar{1}43$
3.114	3	130	2.249	1	141	1.848	1	$\bar{3}24$
3.070	1	310	2.227	1	302	1.836	1	$\bar{4}04$
3.046	2	031	2.209	1	$\bar{3}32$	1.826	1	$\bar{2}51$
3.002	8	$\bar{1}31$	2.198	2	240	1.735	1	422
2.964	1	221	2.193	1	$\bar{3}23$	1.727	1	143
2.946	1	$\bar{2}22$	2.175	2	420	1.684	1	350
2.819	2	131	2.172	2	123			

reflection. A total of 107 reflections with I(cal) ≥ 1 are listed to a maximum 2θ of 30° (MoK$_\alpha$).

A single crystal of (−)-cocaine from the same sample as that used for structure determination was carefully ground to a powder. Its diffraction pattern was measured using a 114.6 mm Debye–Scherrer camera with CuK$_\alpha$ (λ = 1.5418 Å) radiation. This measured powder pattern is listed in Table 3. Line intensities from the film were visually estimated. Exposure times of up to two hours were used.

Discussion

Molecular structure

The configuration of (−)-cocaine as a free base is shown in Fig. 1 with atoms labelled and bond lengths, bond angles, and torsional angles indicated.

Like its salts, (−)-cocaine exists in a piperidine chair conformation. The angles between the planes of the ring are given in Table 4. The C(1)—N(1) and C(5)—N(1) bond lengths are 1.460(7) and 1.467(6) Å, respectively, and are shorter than those reported in the salts: 1.55(2) and 1.51(2) Å in the MeI salt, and 1.50(1) and 1.49(1) Å in the HCl salt. In the free base the C(17)—N(1) bond length is 1.468(7) Å. These shorter equivalent C—N bond lengths in the free base are comparable to the average C—N bond length of 1.475 Å expected for an unprotonated amino group (16).

The methoxycarbonyl substituent at C(2) is axial, the benzoxy substituent at C(3) is equatorial, and the methyl substituent at N(1) is also equatorial, in accordance with the known absolute configuration of (−)-cocaine (3). The orientations of these substituents relative to the bridged piperidine ring vary in the structures of the free base and its salts.

The major change in the position of the methoxycarbonyl group is shown by the C(1)—C(2)—C(15)—O(4) torsion angle. Shen *et al.* (2) observed an increase of 29° in the magnitude of this angle for the MeI salt (−46°) compared to the HCl salt (−17°) as reported by Gabe and Barnes (1). They attributed this increase to the presence of the C(18) methyl group on N(1), and its effect on the O(4)—C(1) intramolecular interaction. In the HCl salt, this O(4)—C(1) distance is only 2.63 Å compared to 2.84 Å in the MeI salt, due to the influence of the larger methyl substituent in the MeI salt. An increase in the C(1)—C(2)—C(15) bond angle was also observed: 115° in the MeI salt versus 109° in the HCl salt. In the free base, one might expect the C(1)—C(2)—C(15)—O(4) torsion angle to be less than that of the salts in order to decrease the O(4)—C(1) distance. However, this torsion angle is in fact increased in magnitude by 15° from the MeI salt to −61°. This is due to a reduction in the C(1)—C(2)—C(15) bond angle to 108.2(4)° (compared to 115(1)° and 109(1)° in the MeI and HCl salts, respectively), and a reduction in the N(1)—C(1)—C(2) bond angle to 106.8(4)° (compared to 112(1)° and 113(1)° in the MeI

Can. J. Chem. Downloaded from www.nrcresearchpress.com by 210.87.254.42 on 09/06/12
For personal use only.

TABLE 3. Measured powder patterns for (−)-cocaine and powder pattern data from literature

(−)-Cocaine[a]		Cocaine[b]		Cocaine[c]		L-cocaine[d]	
d	*I*	*d*	*I*	*d*	*I*	*d*	*I*
				+12.8	6		
9.766	40	9.72	100	9.72	55	10.3	100
8.087	20	8.08	20	8.09	25	9.04	15
		+7.72[e]	1	+7.64	2		
7.366	40	7.38	60	7.35	75	7.25	15
6.919	30	6.94	25	6.91	35		
				+6.44	2		
6.270	20	6.25	15	6.25	18		
				+6.06	2		
5.896	35	5.92	40	5.89	45	5.80	35
		+5.69	1	+5.60	2		
5.486	15	5.50	20	5.48	18	5.44	15
4.931	50	4.95	40	4.93	50	5.06	15
4.818	40	4.84	40	4.82	50	4.69	40
				+4.61	3	4.58	20
4.408	100	4.41	100	4.40	100	4.33	25
		4.33	3	4.33	4		
4.220	40	4.23	40	4.20	45		
4.105	15	4.11	15	4.10	18		
				+3.98	3	4.00	15
				3.84	5	3.92	15
3.753	30	3.75	40	3.74	40		
3.669	15	3.68	15	3.67	20		
3.458	30	3.47	40	3.46	30	3.47	25
		3.39	1	3.35	3		
3.198	30	3.20	35	3.19	25	3.20	15
3.126	10	3.13	10	3.13	10		
3.058	1	3.07	1	3.05	5	3.06	25
3.001	15	3.01	20	2.99	12	2.99	10
		2.95	1	2.95	2	2.90	15
2.824	1	2.83	5	2.82	5		
2.723	30	2.73	35	2.72	18	2.727	10
2.605	1	2.61	3	2.59	5		
2.536	1	2.55	10	2.54	6		
2.453	5	2.46	20	2.45	9		
2.395	5	2.37	10B	2.38	8		
2.363	5			2.35	4	2.315	10
		+2.30	1	+2.30	5		
2.255	1	2.26	5	2.27	6		
		2.24	1	2.25	4		
2.207	1	2.21	3				
2.176	1	2.18	10	2.17	4	2.180	10
2.109	1	2.11	5B	2.11	4	2.150	10
2.065	1	2.07	5	2.06	3		
		2.04	2	2.03	3		
1.986	1	1.99	3	1.99	4		
				1.96	3		
1.941	5	1.94	15	1.94	7		
1.905	1	1.91	5	1.91	4		
1.877	1	1.88	5	1.87	4		
1.867	1	1.85	3BB	1.85	3		
1.842	1			1.84	3		
				1.82	3		
		1.77	1				
1.742	1	1.74	5B	1.74	3		
				1.72	3		

[a]Powder pattern of (−)-cocaine sample used in this work CuK_α (λ = 1.5418) radiation; 30 min exposure at 40 kV 37 mA using a 114.6 mm Debye–Scherrer camera.
[b]CoK_α (λ = 1.790) radiation; 15 to 20 h exposure using a 114.6 mm Debye–Scherrer camera (ref. 6).
[c]CrK_α (λ = 2.291) radiation; approx. 12 h exposure using a Debye–Scherrer camera (ref. 7).
[d]CuK_α (λ = 1.5418) radiation using a diffractometer (ref. 8).
[e]+: Lines not accounted for from calculated powder pattern.

Can. J. Chem. Downloaded from www.nrcresearchpress.com by 210.87.254.42 on 09/06/12
For personal use only.

TABLE 4. Angles between planes
(a) Planes defined by atoms

Planes	Atoms
1	C(1), C(2), C(4), C(5)
2	C(2), C(3), C(4)
3	C(1), C(6), C(7), C(5)
4	C(1), N(1), C(5)
5	C(9), C(10), C(11), C(12), C(13), C(14)

(b) Angles between planes

Planes	Angles
Plane 1 and 2	45°
Plane 1 and 3	68°
Plane 1 and 4	69°
Plane 1 and 5	75°

and HCl salts, respectively). This orientation of the methoxycarbonyl group in the free base produces an O(4)—C(1) contact distance of 2.79(1) Å. Thus, even though the torsion angle in the free base is larger than in the MeI salt, the O(4)—C(1) contact distance is slightly shorter.

The major change in the position of the benzoxy group is shown by the C(2)—C(3)—O(1)—C(8) torsion angle. In the MeI and HCl salts this angle is approximately equivalent, with values of −77° and −73°, respectively. In the free base, this angle is increased to −139° through rotation about the C(3)—O(1) bond, to a position that approximately bisects the ethylene bridge on the piperidine ring (the angle between the plane of the benzene ring and the plane defined by C(1), C(2), C(4), and C(5) is 75°). This increase in torsion angle is probably due to the relative position of the methoxycarbonyl substituent at C(2), and interaction between O(1) and O(3) in these two groups, respectively. The O(3)—O(1) contact distance in the HCl salt is reported as 2.79 Å. In the free base, this is increased to 2.86 Å. Thus, in the free base, O(3) and O(1) are farther away from each other, reducing their interactions and allowing the benzoxy group to rotate to a more stable conformation. This is reflected by the bond angles about C(3) which are more equivalent in the free base than in either of the salts. The benzoxy group itself is not quite planar. The O(2)—C(8)—C(9)—C(14) torsion angle is the same in the free base and the MeI salt; i.e. +8°. This torsion angle is larger than the reported value for the HCl salt (+2°). No apparent reason for this difference is evident.

In the piperidine ring of (−)-cocaine, the ethylene bridge decreases the distance between C(2) and C(4), and C(1) and C(5) to 2.15 Å and 2.26 Å, respectively. These distances are less than those reported by Gabe and Barnes (1) (2.75 Å and 2.35 Å) because the C(1)—N(1) and C(5)—N(1) bond lengths in the free base are shorter. The piperidine ring atoms (C(1), C(2), C(4), and C(5)) are planar within 0.02°. In the free base, the C(7)—C(1)—N(1) and C(6)—C(5)—N(1) angles are larger, 106.2(4)° and 105.4(4)°, respectively, compared to 101(1)° and 102(1)° in the HCl salt and 102(1)° and 102 (1)° in the MeI salt. There is a concomitant reduction of the C(2)—C(1)—N(1) and C(4)—C(5)—N(1) bond angles in the free base.

Powder pattern

The calculated powder pattern for (−)-cocaine is listed in Table 2. A total of 107 lines with a relative $I(\text{cal}) \geq 1$ are included to a maximum 2θ of 30°. Powder patterns of (−)-cocaine, measured on the same sample used for the structure determination, and the powder patterns of (−)-cocaine, as reported in the literature, are listed in Table 3.

The calculated and measured powder patterns agree well with each other. All of the observed lines in the measured powder pattern are accounted for. The bulk of data from Barnes and Sheppard (6), and Owen *et al.* (7) also agree with the calculated powder pattern. However, each report several lines that cannot be accounted for. These lines are noted with a "+" in Table 3. Other lines reported by these authors and not observed by us, as shown in Table 3, could be accounted for from the calculated powder pattern in Table 2. These lines, however, were very weak and were not observed in the exposure times used by us. Barnes and Sheppard (6) report lines at *d* values of 7.71, 5.69, and 2.30 Å for which no reflections could be assigned. Owen *et al.* (7) report lines at *d* values of 12.8, 7.64, 6.44, 6.06, 5.60, 4.61, 3.98, and 2.30 Å for which no reflections could be assigned. No lines with these *d* values were observed in powder patterns obtained in this work, even when exposure times were lengthened. These additional lines must therefore be due to sample impurities and should not be attributed to (−)-cocaine. The data reported by Sullivan and O'Brien (8) do not agree with the other measured powder patterns, nor with the calculated patterns.

These unassigned *d* values reported above were compared to standard powder pattern data. Apart from the excipients and impurities often encountered in drugs as described by Folen (12), (−)-cocaine as a natural product occurs with other minor alkaloids of similar structure (17), such as *cis*- and *trans*-cinnamoylcocaine, methylecgonine, and benzoylecgonine. Other impurities, such as pseudococaine, can be introduced in the cocaine isolation process. However, no likely materials could be identified as the cause of these unassigned lines.

Acknowledgements

The authors thank M. Malcolm, Royal Canadian Mounted Police, Crime Detection Laboratory, Regina, Saskatchewan, for growing the crystals used in this work; K. Wolbaum, University of Regina, Regina, Saskatchewan, for his technical assistance in data collection; R. Audette, formerly with the Royal Canadian Mounted Police, Crime Detection Laboratory, Edmonton, Alberta, for his suggestion of this topic; the Royal Canadian Mounted Police, Crime Detection Laboratory, Regina, Saskatchewan, and the Natural Sciences and Engineering Research Council of Canada for financial support.

1. E. J. GABE and W. H. BARNES. Acta Crystallogr. **16**, 796 (1963).
2. M. SHEN, J. R. RUBLE, and G. HITE. Acta Crystallogr. Sect. B, **31**, 2706 (1975).
3. E. HARDEGGER and H. OTT. Helv. Chim. Acta, **38**, 312 (1955).
4. G. FODOR. The alkaloids. IX. *Edited by* R. H. F. Manske. Academic Press, New York. 1967. pp. 269–304.
5. A. C. ALLEN, D. A. COOPER, W. O. KISER, and R. C. COTTRELL. J. Forensic Sci. **26**, 12 (1981).
6. W. H. BARNES and H. M. SHEPPARD. Bull. Narc. **6**, 27 (1954).
7. J. T. R. OWEN, R. SITHIRAKS, and F. A. UNDERWOOD. J. Assoc. Off. Anal. Chem. **55**, 1171 (1972).
8. R. C. SULLIVAN and K. P. O'BRIEN. Bull. Narc. **20**, 31 (1970).
9. National Bureau of Standards, U.S. Monograph 25, Section 16. 1979. pp. 114–116.
10. D. CANFIELD, J. BARRICK, and B. C. GIESSEN. Acta Crystallogr.

Can. J. Chem. Downloaded from www.nrcresearchpress.com by 210.87.254.42 on 09/06/12
For personal use only.

Sect. B, **35**, 2806 (1979).
11. D. CANFIELD. Acta. Crystallogr. Sect. B, **37**, 1800 (1981).
12. V. A. FOLEN. J. Forensic. Sci. **20**, 348 (1975).
13. A. C. LARSON and E. J. GABE. Computing in crystallography. *Edited by* H. Shenk, R. Olthof-Hazekamp, H. van Kowiuipveld, and G. C. BASSI. Delft University Press. 1978. pp. 81–89.
14. J. M. STEWART (*Editor*). The X-ray system of crystallographic programs – X-ray 76. Tech. Rep. TR-446. Computer Science Centre, University of Maryland, College Park, MD. March, 1976.
15. C. K. JOHNSON. ORTEP Report ORNL-3794. Oak Ridge National Laboratory, TN. 1965.
16. E. BYE. Acta Chem. Scand. Ser. B, **30**, 549 (1976).
17. C. C. CLARK. Microgram XI No. 10. (Oct. 1978).

Can. J. Chem. Downloaded from www.nrcresearchpress.com by 210.87.254.42 on 09/06/12
For personal use only.

Carbon-13 chemical shifts as a probe for conformational and electronic effects in alkyl vinyl ethers

JOHN G. K. WEBB[1] AND DAVID K. YUNG
College of Pharmacy, Dalhousie University, Halifax, N.S., Canada B3H 3J5

Received August 11, 1982

JOHN G. K. WEBB and DAVID K. YUNG. Can. J. Chem. **61**, 488 (1983).

The principle of additivity of substituent chemical shifts (SCS) is applied to the carbon-13 chemical shifts of β carbons (δ_β) in a number of 1,1-disubstituted ethylenes and propenes, which includes some α-substituted alkyl vinyl ethers. An additivity relationship is observed for 34 compounds that indicates an independent polarization mechanism across the double bond for each geminal substituent. Positive deviations from additivity are observed for compounds bearing bulky substituents. The magnitude of deviations is taken as an indication of the severity of steric interactions among substituents.

Reductions in efficiency of transmission of substituent effects in ring substituted α-phenyl alkyl vinyl ethers, relative to *para*-substituted styrenes, are interpreted as the result of a variable dihedral angle between the ring and vinyl group. An explanation of the relationship between conformation and transmission of substituent effects is presented as an alternative to existing views. An angular dependence of π-polarization and resonance effects is consistent with the chemical shift data.

JOHN G. K. WEBB et DAVID K. YUNG. Can. J. Chem. **61**, 488 (1983).

On applique le principe d'additivité des déplacements chimiques du substituant (DCS) aux déplacements chimiques du carbone-13 des carbones en β (δ_β) d'une série d'éthylènes et de propènes disubstitués en position 1,1, incluant quelques éthers alkyl-vinyles substitués en position α. On a observé une relation d'additivité pour 34 composés; ceci suggère l'existence d'un mécanisme indépendant de polarisation à travers la double liaison pour chaque substituant géminé. On a observé des déviations positives par rapport à l'additivité pour des composés ayant des substituants encombrants. On considère l'ordre de grandeur des déviations comme un indice de la sévérité des interactions stériques parmi les substituants.

On interprète les diminutions de l'efficacité de la transmission des effets de substituant, dans les cycles substitués d'α-phényl alkyl vinyl éthers par rapport aux styrènes substitués en position *para*, comme étant le résultat d'un angle dièdre variable entre le cycle et le groupe vinylique. On présente une explication de la relation entre la conformation et la transmission des effets de substituant, comme une alternative aux données existantes. Une dépendance angulaire de la polarisation π et des effets de résonance est en accord avec les données de déplacements chimiques.

[Traduit par le journal]

Introduction

It has been established that the stable rotational isomer of methyl vinyl ether has a planar *s-cis* conformation (1–3). A minor component, originally thought to be the nonplanar *gauche* isomer, has been identified as having an *s-trans* conformation by infrared (4) and photoelectron spectroscopy (5). Molecular orbital studies at the *ab initio* level have confirmed these experimental findings (6–8).

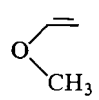

s-cis

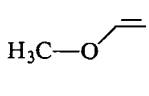

s-trans

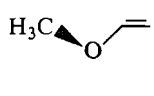

gauche

For other alkyl vinyl ethers, the nature of the alkyl group and the degree of substitution around the olefinic bond will influence conformational preferences. Accordingly, transmission of electronic effects between substituents and double bond will be affected. In our opinion these factors have not received full consideration in discussions of carbon-13 chemical shift data, particularly for α-substituted alkyl vinyl ethers (9, 10).

There has been some controversy in the literature on the mechanism of transmission of electronic effects in α-phenyl alkyl vinyl ethers. Taskinen has offered the view that the smaller ρ values observed in correlations of β-carbon chemical shifts (δ_β) versus Hammett σ constants, compared to ρ values for styrenes, are due to methoxyl induced polarization of the double bond (10). He argues that the $p-\pi$ conjugation between oxygen and the double bond results in more single bond character for the olefinic bond and a diminished response for δ_β to substituents in the phenyl ring.

Huet *et al.* have developed a different interpretation (9). These authors state that the effect of a phenyl ring on δ_β can be divided into $\beta-\pi$ and $\beta-\sigma$ effects. The first effect is considered to be diamagnetic and the second paramagnetic. They suggest that when there is a deviation of the ring from coplanarity with the double bond there is a reduction in $\beta-\pi$, whereas $\beta-\sigma$ remains unchanged. Deviations from the principle of additivity of substituent chemical shifts (SCS) are used as a foundation for this interpretation.

Our own analysis has led to a conclusion that differs essentially from Taskinen's and suggests that Huet and co-workers have inappropriately used the principle of additivity to reach a conclusion that is similar in some respects to ours. We attempt to show by means of additivity of SCS and transmission of substituent effects that nonplanarity of ring and vinyl group does account for existing carbon-13 chemical shift results in α-phenyl vinyl and propenyl ethers.

Results and discussion

Application of the principle of additivity

In applying the principle of additivity in this work, vinyl and propenyl ethers have been considered as a subgroup within a broader series of geminally substituted ethylenes, $R^1R^2C{=}CH_2$, and propenes, $R^1R^2C{=}CH(Me)$. Additivity of SCS for β-carbons in these compounds can be detected using

[1]Author to whom correspondence may be addressed.

TABLE 1. Carbon-13 chemical shift data for $R^1\ R^2\ C{=}CHR^3$

Compound	R^1	R^2	R^3	Chemical shift, δ_β [a]	ΣSCS [b]	Δ [c]	Ref.
1	(*Z*)-CO_2H	Me	Me	138.6	14.2		27
2	(*E*)-CO_2H	Me	Me	137.9	14.2		27
3	(*Z*)-CO_2Me	Me	Me	137.9	11.2	3.7	27
4	(*E*)-CO_2Me	Me	Me	136.4	11.2	3.1	27
5	Cl	CN	H	131.7	9.6		28
6	CO_2H	Me	H	126.2	3.35		27
7	CO_2Me	Me	H	125.0	0.4		27
8	COMe	Me	H	124.7	−0.15		28
9	Cl	C≡C	H	124.5	0.8		29
10	(*Z*)-Pr	Me	Me	119.2	−4.2		30
11	Me	Me	Me	118.6	−2.9		31
12	(*Z*)-Et	Me	Me	118.2	−5.4		30
13	(*E*)-*s*Bu	Me	Me	118.1	−6.25		32
14	(*Z*)-iPr	Me	Me	117.9	−7.4		32
15	(*E*)-Et	Me	Me	117.1	−5.4		30
16	(*E*)-iPr	Me	Me	116.2	−7.4		32
17	(*Z*)-iPr	Et	Me	116.0	−9.9		30
18	(*E*)-*t*Bu	Me	Me	114.8	−10.3		30
19	neoPent	Me	H	114.4	−12.9	2.5	33
20	Ph	Ph	H	114.1	−19.2	8.2	34
21	Cl	Cl	H	113.3	−11.2		35
22	Cl	Me	H	112.0	−12.45		32
23	Me	Ph	H	112.1	−16.45	3.6	24
24	iBu	Me	H	111.6	−14.3		33
25	Me	Me	H	111.3	−13.7		33
26	*t*Bu	Ph	H	111.4	−23.9	10.0	24
27	Et	Me	H	109.6	−16.2		33
28	Pr	Me	H	110.2	−15.0		33
29	nBu	Me	H	110.1	−15.5		33
30	*s*Bu	Me	H	109.8	−17.1		33
31	Et	Ph	H	109.7	−18.9	3.5	36
32	*t*Bu	*t*Bu	H	108.6	−28.6	11.6	31
33	*t*Bu	Me	H	108.3	−21.2	4.3	33
34	iPr	Me	H	108.0	−18.2		33
35	(*E*)-OMe	Ph	Me	93.9	−36.8	4.7	10
36	(*E*)-OMe	Me	Me	90.15	−34.0		17
37	(*E*)-OMe	*t*Bu	Me	89.9	−41.5	5.2	17
38	(*E*)-OMe	Et	Me	89.1	−36.5		17
39	(*E*)-OMe	iPr	Me	87.8	−38.6		17
40	OMe	Ph	H	81.65	−47.6	2.8	10
41	OEt	Me	H	81.1	−44.8		37
42	OMe	Me	H	80.4	−44.8		38
43	OMe	Et	H	79.1	−47.3		37
44	OEt	iPr	H	78.0	−49.4		37
45	OMe	iPr	H	77.6	−49.4		37
46	OEt	*t*Bu	H	77.2	−52.3	2.8	37
47	OMe	*t*Bu	H	76.9	−52.3	2.5	37

[a] Chemical shifts are in ppm relative to TMS.
[b] Individual SCS values were obtained from chemical shifts for monosubstituted ethylenes as found in the literature; see refs. 27, 29, 33, 22, and 21. For a discussion of values used for alkoxyl groups, see text.
[c] Deviations from the least-squares line for compounds not included in the correlation.

the following equation:

$$[1]\quad \delta_\beta = b(\Sigma\,\mathrm{SCS}) + \delta_0$$

The ΣSCS for disubstituted ethylenes is $(\beta(R^1) + \beta(R^2))$ and equals $(\beta(R^1) + \beta(R^2) + \alpha(\mathrm{Me}))$ for the trisubstituted compounds. The individual SCS values are derived from chemical shifts in monosubstituted ethylenes. For a perfect additivity relationship, application of eq. [1] will give a straight line of slope 1.0 and intercept equal to the chemical shift of ethylene (122.8 ppm). Chemical shifts and values for ΣSCS obtained from the literature are given in Table 1.

Some comment is required on the SCS for alkoxyl groups because of the sensitivity of these values to conformation. SCS for alkoxyl groups in vinyl ethers have negative values, which decrease in the order *s-cis* > *s-trans* ≫ *gauche*. A value of −38.0 ppm is obtained for the SCS of a methoxyl group in an *s-cis* conformation from the observed δ_β for methyl vinyl ether (85.15 ppm, this work; 85.13 (11)), and an estimated isomer

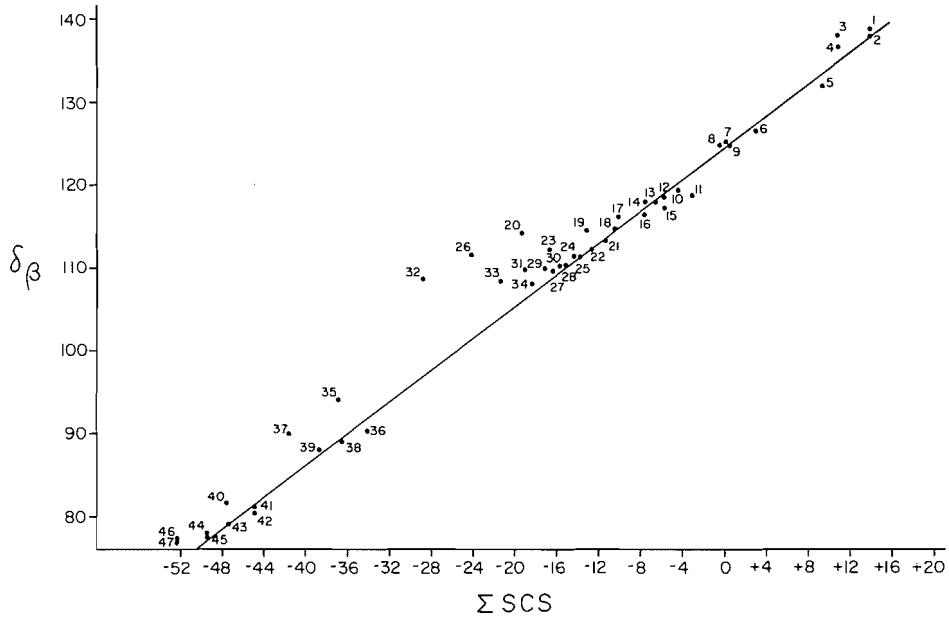

FIG. 1. Plot of δ_β vs. ΣSCS for compounds listed in Table 1.

composition of ~90% *s-cis*, with the remainder as *s-trans* (12). Estimates for the SCS of a methoxyl in an *s-trans* conformation come from two sources, δ_β in *tert*-butyl vinyl ether (SCS = −32.3 ppm) (11), and δ_β values in (*Z*)-alkyl propenyl ethers (SCS = −32.6, −32.6, and −32.4 ppm for OMe, OEt, and OiPr)[2] (13). The alkoxyl groups in these compounds are accepted as having predominantly an *s-trans* conformation (13, 14), and it has been shown by ir spectroscopy that the resonance interaction between alkoxyl and vinyl groups is independent of the size of the alkyl group (4). Both occurrences are reflected in nearly constant SCS values for these alkoxyl groups. The absence of a shielding γ-effect on δ_β for a methoxyl in an *s-trans* conformation accounts for the lower SCS value relative to a methoxyl group in an *s-cis* conformation (13–15). The chemical shift of the terminal olefinic carbon in 2-methylene-tetrahydropyran (16) provides an approximation for the SCS of a *gauche* methoxyl of −15.8 ppm. Although perhaps a rough estimate for a *gauche* methoxyl in an acyclic vinyl ether, this value does show the weak $p-\pi$ conjugation for a methoxyl group in a *gauche* conformation (16, 17).

In the α-substituted vinyl and propenyl ethers in Table 1, the α-substituent should ensure an almost complete preference for the *s-cis* conformation. Accordingly, the value of −38.0 ppm is used for β(OMe) for the methyl ethers. This same value is taken as an estimate for an *s-cis* ethoxyl, since the small difference in δ_β between methyl and ethyl vinyl ether (δ_β = 85.70 ppm (11)) likely arises from a slight increase in the *s-trans*/*s-cis* ratio for the ethyl compound, rather than from a significant difference in γ-effect between the two substituents; however, a δ-effect in ethyl vinyl ether might also contribute to the chemical shift difference.

A plot of δ_β versus ΣSCS is shown in Fig. 1. The overall trend is linear with some obvious exceptions, especially when one or both geminal substituents are large. Nonadditivity can be expressed in several ways in this type of plot. For example, a linear relationship with slope other than 1.0 but with intercept of 122.8 would suggest a constant relative enhancement or attenuation of the sensitivity of δ_β to the combined effect of the geminal substituents, depending on whether $b > 1$ or < 1. A linear relationship with slope equal to 1.0 but with intercept other than 122.8 would indicate additivity of SCS, but with each compound in the series experiencing the same constant deviation in δ_β. A combination of these two effects, as well as the observation of nonlinearity are also possible.

Our interpretation of Fig. 1 is that large positive deviations from linearity arise from steric interactions between substituents; therefore, compounds that show this effect are excluded from the calculation of regression coefficients for the least-squares line. The compounds are **2**, **19**, **20**, **23**, **26**, **31**, **32**, **33**, **35**, **37**, **40**, **46**, and **47**, and they have in common at least one bulky substituent and a deviation from the line in excess of 2 ppm. The parameters for the remaining 34 points are $b = 0.95 \pm 0.02$, $\delta_0 = 124.1$ ppm, $\bar{r} = 0.9982$. The uncertainty in the slope is expressed at the 95% confidence level (18). These values of slope and intercept indicate that additivity is nearly quantitative for this series of compounds.

The observation of additivity as shown in Fig. 1 has an important structural implication. If each substituent in the geminally disubstituted compounds exerts essentially the same effect on δ_β as in a monosubstituted ethylene, then the transmission of the effect of each substituent is independent of the presence of the other. This conclusion appears to be generally valid for combinations of geminal substituents which have different electronic properties, provided that certain steric requirements are met. For example, compounds **3**, **4**, **6–8** have a combination of electron-accepting substituents and a methyl group; compounds **10–16**, **25**, **27–30** have two alkyl groups; compounds **22**, **36–39**, **41–45** electron-donating and alkyl groups; **9** and **21** have two donors; and compound **5**, a donor and acceptor.

The effect of a substituent on δ_β in a monosubstituted ethylene is thought to arise from polarization of the double bond (19). This view is not surprising for substituents that are traditionally accepted as being π-electron donating or accepting,

[2] The chemical shift, δ_β, of *tert*-butyl propenyl ether reflects the presence of a small amount of *gauche* isomer (13).

TABLE 2. Correlations of δ_β's in α-substituted styrenes

Compound	No. of substituents, n	Slope, b	Uncertainty of slope,[a] $s_b(t)$	Correlation coefficient, $\bar{r}$	Ref.
23	10[b]	0.77	0.025	0.9992	24
26	9[b]	0.21	0.09	0.9070	24
40	6[c]	0.72	0.07	0.9973	10
35	5[d]	0.43	0.14	0.9790	10
48	5[d]	0.87	0.05	0.9993	10

[a] Product of the standard deviation of the slope, s_b, and the t distribution at the 95% confidence level for the n data points, see ref. 18.

[b] Substituents in the *para* position for **23** were: H, Me, *t*-Bu, F, Cl, OMe, NMe_2, NO_2, $SiMe_3$, and $SnMe_3$; for **26**, H, Me, *t*-Bu, F, Cl, Br, OMe, NMe_2, and NO_2.

[c] Substituents in the *para* position for **40** are: H, Me, OMe, F, Cl, and NO_2. A value of 82.06 ppm for δ_β was used for the *para* NO_2 derivative. An adjustment for solvent effect was added to the value given in ref. 9 for this compound.

[d] Substituents in the *para* position for **35** and **48** are: H, Me, OMe, F, and Cl.

TABLE 3. Comparison of deviations from additivity with twist angles of phenyl ring

Compound	Deviation from additivity[a] Δ	Twist angle, nmr method[b] θ	Twist angle, uv methods θ	Ref.
23	3.6	28.7 ± 1.7	29, 30	24
			33	25
26	10.0	62.7 ± 6.5	65, 63	24
40	2.8	31.9 ± 4.5	—	—
35	4.7	49 ± 8	—	—
48	—	21.0 ± 4.5	—	—
31	3.5	—	38	25
20	4.1[c]	—	43.5	25

[a] In ppm, as derived from Fig. 1.

[b] In degrees, as derived from slopes in Table 2; $\theta = \cos^{-1}(b^{1/2})$.

[c] One-half of the observed deviation, as each phenyl ring is considered to be twisted to the same extent; see ref. 25.

but is also confirmed for alkyl groups in a theoretical study by Libit and Hoffmann (20). It was shown that the methyl group in propene causes a net polarization of the vinyl group with the terminal carbon being more negative. Whereas there is no net transfer of electrons to the double bond, the polarization in this direction occurs through a redistribution of π-electrons. For substituents which are either donors or acceptors both charge transfer and polarization of π-electrons occur in the same direction to give more negative or positive terminal carbons, respectively. SCS values are consistent with this view, e.g., β(OMe) = −38.0 ppm, β(Ph) = −9.6 ppm, and β(Me) = −6.85 ppm. Further support is gained by linear correlations between δ_β's and π-electron densities in monosubstituted ethylenes (21) and substituted styrenes (22).

The significance of the theoretical studies, in relation to the observation of additivity for the compounds in this work, is that the π-electron redistribution brought about by charge transfer and (or) polarization mechanisms by each geminal substituent is additive as well. Thus, the presence of a strong donor like methoxyl should not so alter the character of the double bond as to inhibit an α-substituent from exercising its full polarization effect across the double bond. This is confirmed for compounds **36**, **38**, **39**, **41**–**45** where additivity is observed for δ_β. However, this conclusion does contradict Taskinen's explanation for diminished ρ values in correlations of δ_β versus σ for substituted **35** and **40** (10). He has assigned this reduction to less double bond character in the vinyl group because of $p-\pi$ conjugation between the methoxyl group and the double bond. In our opinion, the diminished ρ values and the deviation from additivity observed for **35** and **40** arise from a common source, i.e., a steric interaction wherein the phenyl ring is twisted out of the plane of the double bond.

Conformational dependence of the transmission of substituent effects

The magnitude of the deviations given for those compounds in Table 1 appears to be related to the size of the substituents, and reflects the severity of structural distortion caused by overcrowding around the double bond. Strain due to overcrowding can be released by three types of conformational change. Any or all three of the following could conceivably occur: widening of bond angles, rotation of bulky groups around single bonds adjacent to the double bond, and out-of-plane twisting deformation of the double bond. Ermer and Lifson (23) have shown that the first two mechanisms are more important except for very highly crowded olefins. Torsion around the double bond is not likely to be a factor for any of the compounds in Table 1.

Although no attempt has been made to assess the relative importance of either remaining strain-releasing mechanism, torsion around the phenyl ring – C_α bond likely provides a significant contribution to the deviations from additivity in **20**, **23**, **26**, **31**, **35**, and **40**. Additional insight into this con-

formational effect can be obtained by considering transmission of the effect of substituents in the phenyl ring on δ_β's. This can be accomplished with a linear free energy correlation and comparison of ρ-values with that of a suitable reference. Alternatively, an equivalent but more direct method is to plot δ_β values for a series of compounds versus corresponding values in the reference system, here, a series of *para*-substituted styrenes. The slope of this line is a measure of the efficiency of transmission of substituent effects and is equivalent to the ratio of ρ values obtained from δ_β vs. σ plots.

Regression coefficients are given in Table 2 for correlations of δ_β's for 1,1-disubstituted ethylenes and propenes, where one of the substituents is a substituted phenyl ring, with δ_β values of series of *para*-substituted styrenes. The slopes in Table 2 can be used to estimate the interplanar angle between phenyl and vinyl groups, if this rotation is an important factor in determining the efficiency of transmission of substituent effects. Hamer *et al.* have shown that in *para*-substituted styrenes both field (π-polarization) and resonance contributions to δ_β are primarily through-bond effects when the dihedral angle θ is $<90°$ and do vary as $\cos^2\theta$ (22, 24). Accordingly, the slopes listed in Table 2 can be taken as a measure of $\cos^2\theta$ since styrene and its *para* derivatives are considered to be planar (22, 25). Values of θ determined in this way are listed in Table 3, along with literature data for related systems and deviations from additivity, where appropriate. The values of θ for **23** and **26** are in excellent agreement with values obtained by Reynolds and co-workers (24) using uv spectroscopic methods, and provide support for the reliability of the method. It is also apparent from Table 3 that twist angles roughly parallel deviations from additivity.

Consideration of twist angles for **35**, **40**, and **48** reveals some interesting conformational features for these molecules. That

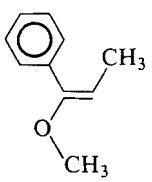

35

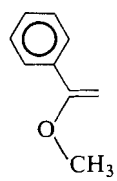

40

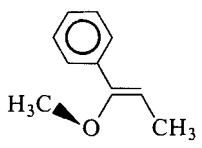

48

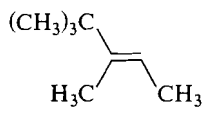

18

35 should undergo more geometrical distortion than **40** is not surprising since the *cis* methyl group in (*Z*)-1-phenylpropene causes a twist angle of ~35° for the phenyl ring (25). The extra strain introduced by an α-methoxyl group is presumably relieved by a further rotation of the phenyl ring to an angle of ~49°. It is perhaps surprising that there is apparently less strain in **48** than in **40** as indicated by a twist angle of ~21°. However, there is support for less strain with groups in this configuration from the observation of no deviation from additivity in Fig. 1 for **18**. We offer these torsional angles as an alternative explanation for the ρ values observed by Taskinen (10) for **35**, **40**, and **48**.

Unfortunately, the additivity principle cannot be applied to (*Z*)-α-substituted methyl propenyl ethers. Because the methoxyl group in these compounds is prevented from assuming an *s-cis* conformation, a mixture of molecules in *s-trans* and *gauche* conformation exists, with the proportion of *gauche* isomer increasing as the size of the α-substituent increases (17). Although it is likely that the methoxyl group in (*Z*)-α-*tert*-butyl methyl propenyl ether and in **48** adopts a predominantly *gauche* conformation (9, 10, 17), there is, to our knowledge, no reliable value available for the SCS of a *gauche* methoxyl in an uncrowded environment.

Our approach to additivity relationships differs from that of Huet *et al.* (9), who present an argument for a dihedral angular dependence of β−π, defined as a diamagnetic contribution to the observed β-effect of a phenyl group across a double bond, that is based on deviations from additivity for δ_β in **35**, **40**, **48**, and **49** (1-methoxy-1-phenyl-2-methylpropene). The main difficulty with their approach is that both **48** and **49** have a methoxyl group that is predominantly *gauche*, whereas the reference compounds from which the deviations were calculated ((*Z*)-1-methoxypropene and 1-methoxy-2-methylpropene) have methoxyl groups predominantly in the *s-trans* conformation (13, 14). The reported deviations of 17.0 and 14.8 ppm for **48** and **49** are therefore unrealistically large, because the effect of a *gauche* methoxyl on δ_β is considerably less than that of a methoxyl group in the *s-trans* conformation (16, 17). The conclusion, based on these values, that the conformation of the methoxyl group essentially determines the twist angle of the phenyl ring, and that a *gauche* methoxyl is more effective in this regard, is erroneous in our opinion.

There is also doubt concerning the interpretation of transmission of substituent effects in **40** and **49** given by Huet and coauthors. Although a reliable estimate of twist angle for **49** was not forthcoming from their data (9) because of uncertainty in the slope ($b = 0.89 \pm 0.30$, $n = 4$), we disagree with their conclusion that there is no resonance interaction between the ring and double bond, and that the large observed ρ values are due to a $\pi + \sigma$ inductive effect. We suggest that the response of δ_β in these compounds to substituents in the ring is similar to the response in α-alkyl-substituted styrenes (24). Verification of this, at least for *para*-substituted **40**, comes from a dual substituent parameter (DSP) correlation. The field (F) and resonance (R) parameters of Swain and Lupton (26) for the substituents given in Table 2 were used to find the following relationship.

$$[2]\quad \delta_\beta = 2.24\,F + 5.14\,R + 81.6,\ n = 6,\ \bar{r} = 0.9955$$

The correlation does show a sizeable resonance contribution, but with a coefficient less than the value of 7.14, which has been observed for the planar *para*-substituted styrenes (22). This observation leads to the conclusion that δ_β in substituted α-phenyl alkyl vinyl ethers reflects both π-polarization and resonance effects, and to a large extent, these effects vary as a function of dihedral angle.

Experimental

The carbon-13 nmr spectrum of methyl vinyl ether was obtained for a 20% solution in $CDCl_3$ on a Varian CFT-20 spectrometer with tetramethylsilane as internal reference.[3]

Acknowledgments

We thank Professor T. P. Forrest for reading the paper and

[3] Courtesy of Dr. D. L. Hooper, Dalhousie University, Halifax, Nova Scotia.

clarifying discussions. The financial assistance of the Medical Research Council of Canada (Grant MA-7135) is gratefully acknowledged.

1. N. L. OWEN and N. SHEPPARD. Trans. Faraday Soc. **60**, 634 (1964).
2. P. CAHILL, L. P. GOLD, and N. L. OWEN. J. Chem. Phys. **48**, 1620 (1968).
3. N. L. OWEN and H. M. SEIP. Chem. Phys. Lett. **5**, 162 (1970).
4. A. R. KATRITZKY, R. F. PINZELLI, and R. D. TOPSOM. Tetrahedron, **28**, 3441 (1972).
5. H. FRIEGE and M. KLESSINGER. J. Chem. Res. Synop. 208 (1977).
6. B. CADIOLI and U. PINCELLI. J. Chem. Soc. Faraday Trans. 2, **68**, 991 (1972).
7. I. G. JOHN and L. RADOM. J. Mol. Struct. **36**, 133 (1977).
8. F. BERNARDI, N. D. EPIOTIS, R. L. YATES, and H. B. SCHLEGEL. J. Am. Chem. Soc. **98**, 2385 (1976).
9. J. HUET, D. ZIMMERMANN, and J. REISSE. Tetrahedron, **36**, 1773 (1980).
10. E. TASKINEN. Tetrahedron, **34**, 429 (1978).
11. B. A. TROFIMOV, G. A. KALABIN, V. M. BZHESOVSKY, N. K. GUSAROVA, D. F. KUSHNAREV, and S. V. AMOSSOVA. Org. React. USSR, **11**, 367 (1974).
12. T. SCHAEFER and W. J. E. PARR. Can. J. Chem. **55**, 2835 (1977).
13. E. TASKINEN. Tetrahedron, **34**, 353 (1978).
14. J. HUET. Tetrahedron, **37**, 731 (1981).
15. J. HUET. Tetrahedron, **34**, 2473 (1978).
16. E. TASKINEN. Tetrahedron, **34**, 433 (1978).
17. E. TASKINEN. Tetrahedron, **34**, 425 (1978).
18. W. H. DAVIS and W. A. PRYOR. J. Chem. Educ. **53**, 285 (1976).
19. D. E. DORMAN, M. JAUTELAT, and J. D. ROBERTS. J. Org. Chem. **36**, 2757 (1971).
20. L. LIBIT and R. HOFFMANN. J. Am. Chem. Soc. **96**, 1370 (1974).
21. G. MIYAJIMA, K. TAKAHASHI, and K. NISHIMOTO. Org. Magn. Reson. **6**, 413 (1974).
22. G. K. HAMER, I. R. PEAT, and W. F. REYNOLDS. Can. J. Chem. **51**, 897 (1973).
23. O. ERMER and S. LIFSON. Tetrahedron, **30**, 2425 (1974).
24. G. K. HAMER, I. R. PEAT, and W. F. REYNOLDS. Can. J. Chem. **51**, 915 (1973).
25. H. SUZUKI. Electronic absorption spectra and geometry of organic molecules. Academic Press, New York. 1967. Chapt. 13.
26. C. G. SWAIN and E. C. LUPTON. J. Am. Chem. Soc. **90**, 4328 (1968).
27. J. B. STOTHERS. Carbon-13 nmr spectroscopy. Academic Press, New York. 1972. Chapt. 5.
28. L. F. JOHNSON and W. C. JANKOWSKI. Carbon-13 nmr spectra. Wiley–Interscience, New York. 1972.
29. J. KOWALESKI, M. GRANBERG, F. KARLSSON, and R. VESTIN. J. Magn. Reson. **21**, 331 (1976).
30. P. A. COUPERUS, A. D. H. CLAGUE, and J. P. C. M. VAN-DONGEN. Org. Magn. Reson. **8**, 426 (1976).
31. G. J. ABRUSCATO, P. D. ELLIS, and T. T. TIDWELL. J. Chem. Soc. Chem. Commun. 988 (1972).
32. J. W. DE HAAN and L. J. M. VAN DE VEN. Org. Magn. Reson. **5**, 147 (1973).
33. J. W. DE HAAN, L. J. M. VAN DE VEN, A. R. N. WILSON, A. E. VAN DER HOUT-LODDER, C. ALTONA, and D. H. FABER. Org. Magn. Reson. **8**, 477 (1976).
34. T. W. PROULX and W. B. SMITH. J. Magn. Reson. **23**, 477 (1976).
35. G. MIYAJIMA and K. TAKAHASHI. J. Phys. Chem. **75**, 331 (1971).
36. K. S. DHAMI and J. B. STOTHERS. Can. J. Chem. **43**, 510 (1965).
37. M. P. STROBEL, C. G. ANDRIEU, D. PAQUER, M. VAZEUX, and C. C. PHAM. Nouv. J. Chim. **4**, 101 (1980).
38. A. C. ROJAS and J. K. CRANDALL. J. Org. Chem. **40**, 2225 (1975).

Infrared and Raman spectra and X-ray diffraction studies of solid lead(II) carbonates[1]

MURRAY H. BROOKER

Chemistry Department, Memorial University of Newfoundland, St. John's, Nfld., Canada A1B 3X7

AND

S. SUNDER, PETER TAYLOR, AND VINCENT J. LOPATA

Atomic Energy of Canada Limited, Whiteshell Nuclear Research Establishment, Pinawa, Man., Canada, R0E 1L0

Received August 30, 1982

MURRAY H. BROOKER, S. SUNDER, PETER TAYLOR, and VINCENT J. LOPATA. Can. J. Chem. **61**, 494 (1983).

Four basic lead carbonates were prepared and identified by X-ray powder diffractometry. These were hydrocerussite ($Pb_3(OH)_2(CO_3)_2$), plumbonacrite ($Pb_{10}O(OH)_6(CO_3)_6$), and the two adducts $MOH \cdot 2PbCO_3$ (M = Na, K). New diffraction data are presented for the latter two compounds; they both have primitive hexagonal lattices with two formula units per unit cell. The unit cell dimensions of the sodium and potassium compounds are $a = 5.273 \pm 0.002$ Å, $c = 13.448 \pm 0.005$ Å and $a = 5.348 \pm 0.002$ Å, $c = 13.990 \pm 0.005$ Å, respectively. Six possible space groups are discussed.

Raman and infrared spectra are reported for all four compounds, and compared with those of cerussite ($PbCO_3$); assignment of the spectral features is discussed. Vibrational spectra of the two MOH adducts indicate that they are isostructural, and that the structure contains a well-defined lead sub-lattice, consistent with the X-ray data. The spectra of hydrocerussite and plumbonacrite indicate that lead is present as oxygen-bridged polymeric moieties in these solids. The carbonate ions occupy two and three independent sites in hydrocerussite and plumbonacrite, respectively.

MURRAY H. BROOKER, S. SUNDER, PETER TAYLOR et VINCENT J. LOPATA. Can. J. Chem. **61**, 494 (1983).

On a préparé quatre carbonates alcalins de plomb et on les a identifiés par la diffraction des rayons-X. Ce sont: l'hydrocérussite ($Pb_3(OH)_2(CO_3)_2$), le plumbonacrite ($Pb_{10}O(OH)_6(CO_3)_6$) et les deux adduits $MOH \cdot 2PbCO_3$ (M = Na, K). On présente des nouvelles données de diffraction pour les deux derniers composés; les deux ont des réseaux hexagonaux primitifs avec deux molécules par maille élémentaire. Les dimensions respectives de la maille pour les composés de sodium et de potassium sont: $a = 5{,}273 \pm 0{,}002$ Å, $c = 13{,}448 \pm 0{,}005$ Å et $a = 5{,}348 \pm 0{,}002$ Å, $c = 13{,}990 \pm 0{,}005$ Å. On discute des six groupes spaciaux possibles.

On rapporte les spectres infrarouges et Raman des quatre composés et on les compare avec ceux de la cérussite ($PbCO_3$); on discute de l'attribution des caractéristiques spectrales. Les spectres de vibration des deux adduits MOH indiquent qu'ils sont isostructuraux et que la structure contient un sous-réseau de plomb bien défini qui est en accord avec les données de rayons-X. Les spectres de l'hydrocérussite et du plumbonacrite indiquent que le plomb est présent dans ces solides sous la forme d'unités polymérisées ayant l'oxygène en position de pont. Les ions carbonates occupent respectivement deux et trois sites indépendants dans l'hydrocérussite et dans le plumbonacrite.

[Traduit par le journal]

I. Introduction

We are investigating the efficacy of heavy-metal oxides for removing low concentrations of $^{14}CO_2$ formed in the heavy-water of CANDU[2] nuclear reactors (1). A review of the chemistry of different lead carbonates indicated that, while the structure and spectra of cerussite ($PbCO_3$) have been studied in detail, the information available about the other carbonates of lead is incomplete, or contradictory (2–18). Apparently, there have been no reports on the Raman spectra of any lead carbonate except cerussite (2, 11, 15). We report here the infrared and Raman spectra of hydrocerussite ($Pb_3(OH)_2(CO_3)_2$), plumbonacrite ($Pb_{10}O(OH)_6(CO_3)_6$), and two complex compounds of lead carbonate, probably $NaOH \cdot 2PbCO_3$ and $KOH \cdot 2PbCO_3$, here called Na – Phase I and K – Phase I, respectively. In addition, we report powder X-ray diffraction data for the latter two phases. Spectra of cerussite ($PbCO_3$) were also recorded for comparison.

II. Experimental

(a) Preparation of lead carbonates

Cerussite was prepared by passing CO_2 through a stirred suspension of PbO in 10^{-2} mol dm^{-3} acetic acid. Hydrocerussite was prepared by the reaction of cerussite with a KOH solution in which the pH was maintained at 11 with an automatic titrator. Plumbonacrite was made by refluxing hydrocerussite in a 0.1 mol dm^{-3} solution of K_2CO_3, with the pH adjusted to 13. These preparations are described in more detail elsewhere.[3]

(b) Preparation and chemical characterization of "Na-Phase I" and "K-Phase I"

We first observed Na-Phase I as a product of reactions between cerussite or hydrocerussite with 0.1 mol dm^{-3} Na_2CO_3 solutions, around pH = 11. It was conveniently prepared as a pure phase in gram quantities by shaking a suspension of cerussite or hydrocerussite (~1 g) in Na_2CO_3 solution (0.1 mol dm^{-3}, 50–100 cm^3) in a screw-topped plastic bottle for 1–2 days at room temperature. The purity of the solid product, isolated by filtration, was readily established by X-ray diffractometry (see Table 1). The potassium analogue, K-Phase I, was not formed in analogous reactions with K_2CO_3 replacing Na_2CO_3. However, we did observe it in reactions between the various lead carbonates and more concentrated solutions of K_2CO_3, indicating that K-Phase I is somewhat more soluble than Na-Phase I. It was conveniently prepared by refluxing cerussite or hydrocerussite at ≃100°C in K_2CO_3 solution (5 mol dm^{-3}, 100 cm^3) for 1–2 days, then isolating the solid product by filtration. Care is needed in washing, to remove excess K_2CO_3 without inducing partial decomposition of the product.

[1]AECL No. 7657.

[2]*CAN*ada *D*euterium *U*ranium, Canada's natural-uranium fuelled, heavy-water moderated and cooled reactor.

[3]P. Taylor and V. J. Lopata. To be published.

Can. J. Chem. Downloaded from www.nrcresearchpress.com by 210.87.254.6 on 09/06/12
For personal use only.

TABLE 1. X-ray powder diffraction data for the phases $MOH \cdot 2PbCO_3$

	M = Na			M = K		
h k l	d_{obsd}	d_{calcd}[a]	I/I_0[c]	d_{obsd}	d_{calcd}[b]	I/I_0[c]
0 0 2	6.727	6.723	~20†	6.992	6.995	~20†
1 0 0	4.568	4.566	29	4.631	4.631	25
1 0 1	4.322	4.324	46	4.396	4.396	23
1 0 2	3.777	3.777	7	3.864	3.861	3
0 0 4	3.364	3.362	~20†	3.499	3.497	~10†
1 0 3	3.200	3.199	100	3.288	3.286	100
1 1 0	2.636	2.636	50	2.673	2.674	35
1 1 2	2.455	2.454	9	2.498	2.497	5
1 0 5	2.318	2.317	9	2.396	2.395	7
2 0 0	2.284	2.283	10	2.315	2.315	10
2 0 1	2.251	2.251	15	2.285	2.284	9
0 0 6	~2.24sh	2.241	~15†	2.332[d]	2.332	~15†
2 0 2	2.163	2.162	2	2.198	2.198	1
1 1 4	2.075	2.075	5	2.124	2.124	3
2 0 3	2.034	2.034	35	2.075	2.074	37
1 0 6	2.013	2.012	9	~2.08sh[d]	2.083	~7
2 0 4	1.8891	1.8887	2	~1.930	1.9307	1
1 0 7	1.7711	1.7707	2	1.8349	1.8350	2
2 0 5	1.7413	1.7405	1	1.7845	1.7838	2
2 1 0	1.7257	1.7259	5	~1.75sh	1.7503	5
2 1 1	~1.71sh	1.7119	<6	1.7367	1.7368	2
1 1 6	1.7074	1.7075	21	1.7573[d]	1.7573	23
2 1 2	1.6718	1.6717	1	1.6979	1.6980	1
2 1 3	1.6106	1.6106	17	1.6384	1.6387	17
2 0 6	1.5995	1.5994	4	~1.64sh[d]	1.6430	4
1 0 8	1.5770	1.5774	1	~1.635sh?	1.6360	<4
2 1 4	1.5349	1.5354	1	1.5652	1.5652	1
3 0 0	1.5223	1.5221	5	1.5434	1.5436	5
3 0 2	1.4844	1.4845	1	~1.509sh	1.5074	1
2 0 7	1.4698	1.4699	2	1.5128[d]	1.5129	2
2 1 5	1.4527	1.4525	3	1.4842	1.4839	2
1 0 9	1.4196	1.4200	6	1.4733	1.4736	7
1 1 8	~1.415sh	1.4173	<3	1.4632	1.4635	1
3 0 4	1.3861	1.3866	1	1.4120	1.4122	1
2 1 6	1.3673	1.3674	3	1.3994	1.3998	3

[a]Hexagonal, a = 5.2727 Å, c = 13.447 Å.
[b]Hexagonal, a = 5.3473 Å, c = 13.990 Å.
[c]Relative diffractometer peak heights; estimated error ±2 for $I/I_0 \leq 20$; ±5 for $I/I_0 > 20$, except for basal planes, 00*l*(†), which showed slight preferred orientation.
[d]The list for M = K does not strictly follow descending order of d, to facilitate comparison between the phases.

These two solids were analyzed for K, Na, and Pb by atomic absorption spectrophotometry (AAS) of material dissolved in dilute nitric acid, and for volatile components by thermogravimetry. The alkali data are in good agreement with the formulation $MOH \cdot 2PbCO_3$ (calcd. Na 4.0, K 6.6; obsd. Na 4.7, K 6.5). The lead analyses were relatively imprecise, due to the limitations of AAS, but the estimate of ≃70 wt.% is consistent with calculations (Na phase 72.1, K phase 70.2). Thermogravimetric measurements at a heating rate of 10°C min^{-1} showed a weight loss, after initial moisture loss, in good agreement with the calculated ($H_2O + CO_2$) contents (Na phase calcd. 13.1, obsd. 13.0, 13.0; K phase calcd. 12.7, obsd. 11.9, 12.2). In a nitrogen atmosphere the weight loss occurred in a single step at 260–370°C for each salt. In a carbon dioxide atmosphere the weight loss occurred in at least two stages, over the temperature ranges 330–510°C (Na salt) and 330–570°C (K salt). No further weight losses were observed to 600°C, the maximum temperatures of the runs. On the basis of these analytical measurements, and the similarity between our infrared spectrum for Na-Phase I and that previously reported (12) for "$3PbCO_3 \cdot Pb(OH)_2 \cdot Na_2CO_3$" ($NaOH \cdot 2PbCO_3$), we tentatively assign the formulation $MOH \cdot 2PbCO_3$ to these phases.

(c) X-ray powder diffraction (XRD) data

X-ray diffractograms were obtained from lightly packed powder samples, using a Philips PW-1150 powder diffractometer, CuK_α radiation and a diffracted-beam monochromator. Diffractograms were recorded on a strip-chart recorder for $10° \leq 2\theta \leq 140°$. Peak positions in the range $10° \leq 2\theta \leq 70°$ were determined by recording half-second integrated counts at a 2θ scan rate of 1 deg min^{-1}.

(d) Vibrational spectra

Infrared spectra were recorded on two different spectrophotometers, Perkin-Elmer models PE457 and PE225. Agreement between the two sets of spectra was excellent. Polycrystalline samples were dispersed in KBr pellets and no evidence of ion exchange was apparent. Spectra were recorded as percentage transmission between 200 and 4000 cm^{-1}.

Raman spectra were recorded using a Coderg PHO Raman spectrometer, as previously described (19). Spectra were excited using the 488.0 or 568.2 nm lines of a Control 52b Ar/Kr laser. Plasma lines from the laser were removed by narrow band-pass interference filters. Radiation power at the sample was about 200 mW at 488.0 nm, and

Can. J. Chem. Downloaded from www.nrcresearchpress.com by 210.87.254.6 on 09/06/12
For personal use only.

Can. J. Chem. Downloaded from www.nrcresearchpress.com by 210.87.254.6 on 09/06/12
For personal use only.

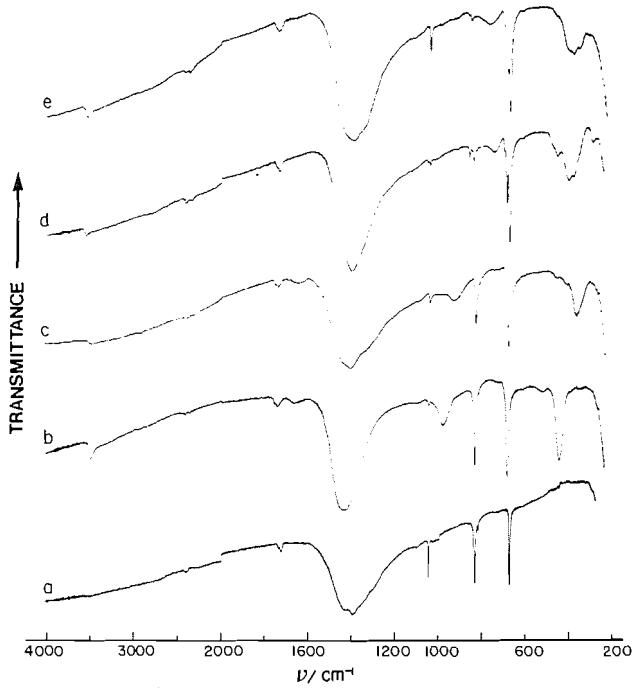

FIG. 1. Infrared spectra of (*a*) cerussite, (*b*) Na-Phase I, (*c*) K-Phase I, (*d*) plumbonacrite, and (*e*) hydrocerussite; resolution ~1 cm^{-1} below 2000 cm^{-1} and ~2 cm^{-1} above 2000 cm^{-1}.

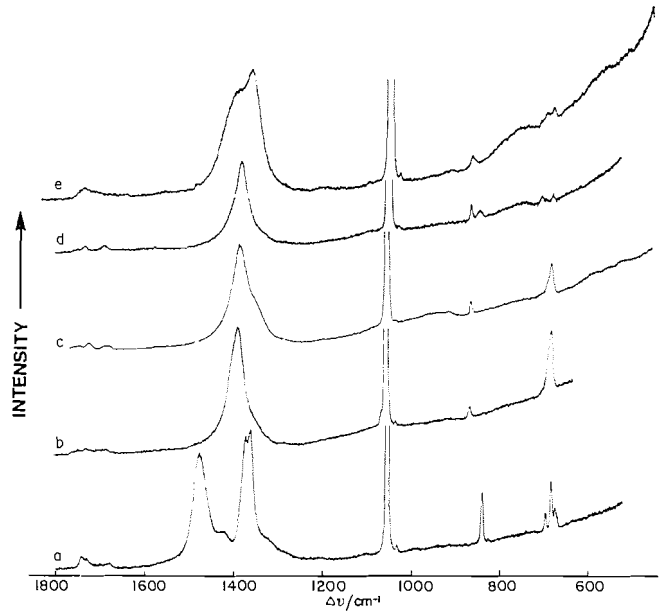

FIG. 2. Raman spectra of (*a*) cerussite, (*b*) Na-Phase I, (*c*) K-Phase I, (*d*) plumbonacrite, and (*e*) hydrocerussite as polycrystalline solids for the regions 600–1800 cm^{-1}. Spectral band pass ~2 cm^{-1}, excitation = 488.0 nm.

100 mW at 568.2 nm. Excess laser power from the blue line caused the sample to take on a yellow colouration with a concomitant loss of signal. The frequency scale was calibrated using plasma lines emitted by the laser. A 90° scattering geometry was used for recording the Raman spectra. Spectra were recorded between 20 and 4000 cm^{-1}. At a later stage of this work, a SPEX 1403 Raman spectrometer became available and all the Raman spectra were recorded again, using the new spectrometer. Agreement between the spectra obtained from the two spectrometers was excellent. Samples were polycrystalline powders, contained in Pyrex capillary tubes.

III. Results and discussion

(a) X-ray diffraction

Diffraction data for cerussite, and peak positions for hydrocerussite and plumbonacrite, were in good agreement with literature reports (9, 14, 20). As previously noted by Olby (9), preferred orientation caused some variation in the relative intensities observed for the latter two phases, especially plumbonacrite. As stated earlier, a full structure determination has only been reported for cerussite (14). Information about hydrocerussite and plumbonacrite is limited to two partial structure analyses based on electron diffraction data (21, 22). These reports predated Olby's resolution of the distinction between hydrocerussite and plumbonacrite (9). Phases described in these papers as hydrocerussite and "$PbCO_3 \cdot PbO \cdot 2H_2O$" appear now to be plumbonacrite and hydrocerussite, respectively (9).

The diffraction pattern for Na-Phase I bears little resemblance to that tabulated for "$3PbCO_3 \cdot Pb(OH)_2 \cdot Na_2CO_3$" ($NaOH \cdot 2PbCO_3$) by Bulakhova *et al.* (12), but the infrared spectrum that we obtained (Fig. 1) is very similar to that which they presented. We note that their XRD data for cerussite and hydrocerussite are also at variance with other reported data (9, 20), and with our work. Their XRD tabulation thus appears to be in error.

The diffraction patterns for Na-Phase I and K-Phase I were both indexed on the basis of primitive hexagonal unit cells, with $a = 5.273 \pm 0.002$ Å, $c = 13.448 \pm 0.005$ Å and $a = 5.348 \pm 0.002$ Å, $c = 13.990 \pm 0.005$ Å, respectively. Observed and calculated *d*-spacings of all features with $2\theta < 70°$ (CuK_α radiation) are listed in Table 1. Discrepancies between observed and calculated 2θ values were all less than 0.03°. Inspection of diffraction patterns up to $2\theta = 140°$ did not reveal any features that could not be indexed. Assuming the formula $MOH \cdot 2PbCO_3$ and $Z = 2$, calculated specific grav-

TABLE 2. Comparison of crystallographic volumes of adducts of the type "MOH·X" with their component compounds

Adduct	Sum of crystallographic volumes of components[a,b]	Crystallographic volume of adduct[b]	Percentage reduction
$NaOH \cdot 2PbCO_3$	166.5	161.88	2.8
$KOH \cdot 2PbCO_3$	178.4	173.21	2.9
$NaOH \cdot Na_3PO_4$[c]	132.6	128.6	3.0

[a]Unit cell data obtained from JCPDS Powder Diffraction File; low-temperature forms of MOH used.
[b]Per formula unit, Å^3.
[c]Reference 23.

Can. J. Chem. Downloaded from www.nrcresearchpress.com by 210.87.254.6 on 09/06/12
For personal use only.

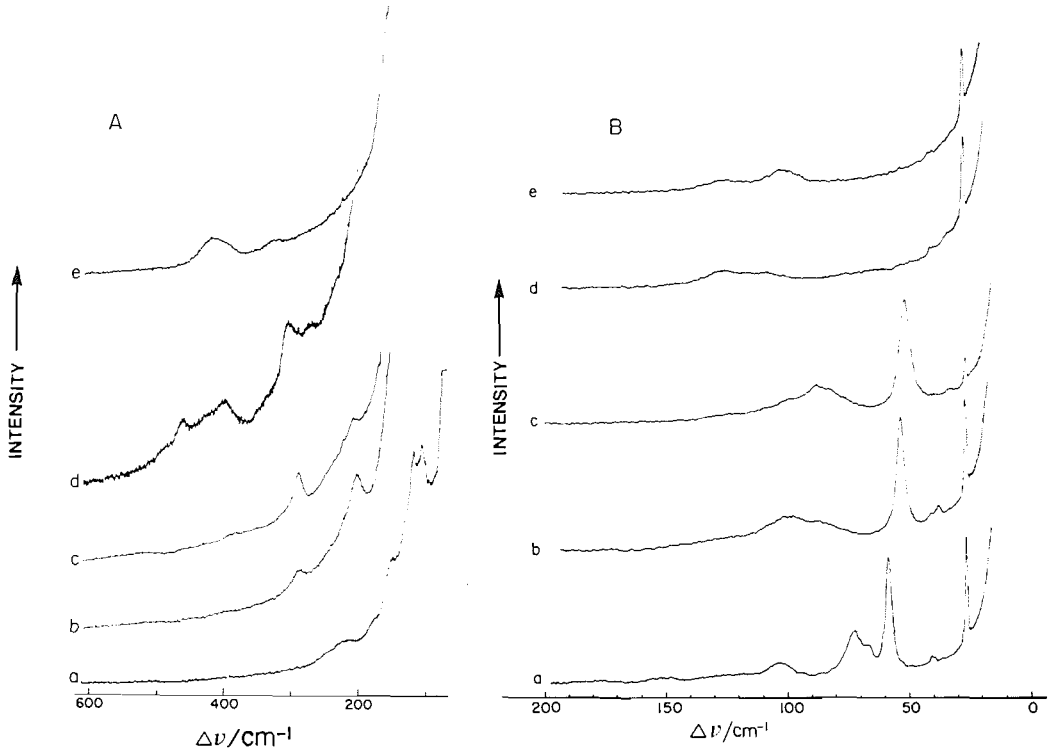

FIG. 3. Raman spectra of (*a*) cerussite, (*b*) Na-Phase I, (*c*) K-Phase I, (*d*) plumbonacrite, and (*e*) hydrocerussite as polycrystalline solids. Spectral band pass ~2 cm^{-1}. Figure 3A is for the 600−200 cm^{-1} region using 488.0 nm excitation and Fig. 3B is for the 200−20 cm^{-1} region using 568.2 nm excitation. Peaks at ~26, 38, and 41 cm^{-1} are due to plasma lines.

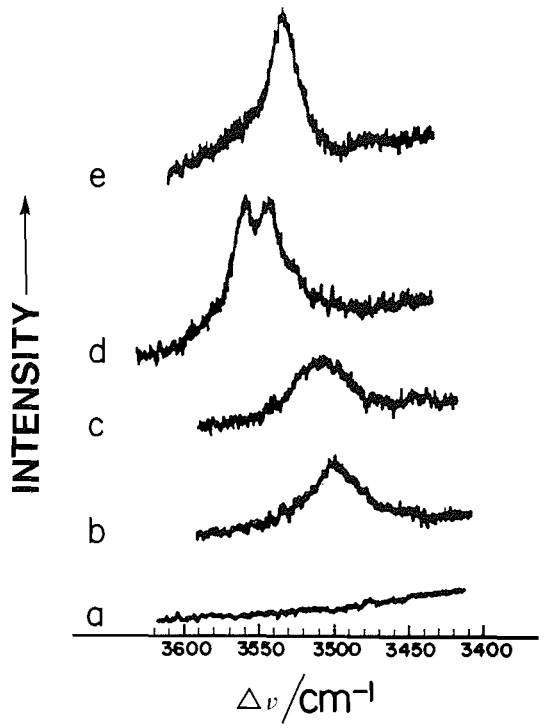

FIG. 4. Raman spectra of (*a*) cerussite, (*b*) Na-Phase I, (*c*) K-Phase I, (*d*) plumbonacrite, and (*e*) hydrocerussite as polycrystalline solids for the OH stretching region, using 568.2 nm excitation and spectral band pass ~2 cm^{-1}.

ities of the sodium and potassium salts are 5.89 and 5.66. The somewhat lower density of the potassium salt is consistent with reported density measurements for most pairs of salts NaX/KX (23). The former number is somewhat higher than the experimental value of 5.50 reported by Bulakhova *et al.* (12). Comparison of crystallographic volumes with the sum of known crystallographic volumes of $2PbCO_3$ + MOH (Table 2) shows a volume reduction of about 3% associated with reaction [1] below.

[1] $2PbCO_3(s) + MOH(s) \rightarrow MOH \cdot 2PbCO_3(s)$

A similar observation was previously reported for the adduct $Na_3PO_4 \cdot NaOH$ (24).

The similar relative intensities of features in the two diffraction patterns confirm that these phases are isostructural. Inspection of the observed reflections listed in Table 1 shows that the unit cells are primitive hexagonal. The only apparent systematic absences involve reflections with $h - k = 3n$ and $l = 2n + 1$. Since the diffraction intensities are dominated by the contribution from lead atoms, possible lead atom positions can be deduced. The observed systematic absences are consistent with the lead atoms occupying special positions *c* and *d*, or *f*, in one of the space groups $P6_3/m(C_{6h}^2)$, $P6_322(D_6^6)$, $P\bar{6}2c(D_{3h}^4)$, or $P6_3/mmc(D_{6h}^6)$, or possibly two pairs of special positions of type "*b*" in space group $P6_3(C_6^6)$ or $P6_3mc(C_{6v}^4)$ (the notation follows ref. 25). The first of these three possible allocations of special positions would result in a hexagonal lead sub-lattice with a lead atom spacing of $a/\sqrt{3}$ within the hexagonal layers, and an inter-layer spacing of $c/2$. Spectroscopic evidence for such a sub-lattice is discussed below. More detailed discussion of structure is not possible without single-crystal diffraction data.

Can. J. Chem. Downloaded from www.nrcresearchpress.com by 210.87.254.6 on 09/06/12
For personal use only.

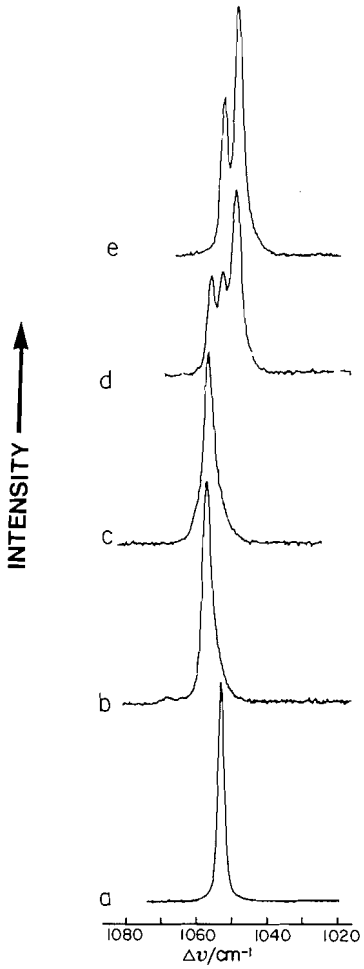

FIG. 5. High-resolution Raman spectra for (*a*) cerussite, (*b*) Na-Phase I, (*c*) K-Phase I, (*d*) plumbonacrite, and (*e*) hydrocerussite as polycrystalline solids for the ν_1 region, using 488.0 nm excitation and spectral band pass ~1 cm^{-1}.

(b) Vibrational spectra

Infrared spectra of cerussite, Na-Phase I, K-Phase I, plumbonacrite, and hydrocerussite are shown in Fig. 1. The Raman spectra are shown in Figs. 2 to 5. Figure 2 shows the Raman spectra for the region between 1800 and 600 cm^{-1} and encompasses all the fundamental internal vibrations of the carbonate ion (26, 27). Figure 3 shows the spectra below 600 cm^{-1}, down to 20 cm^{-1}, while Fig. 4 displays the spectra for the hydroxyl stretching region. Figure 5 shows the ν_1 mode band on an expanded frequency scale, recorded at higher resolution. As expected, this is by far the strongest band in the Raman spectra of the carbonates (2, 13, 15, 26–29). Frequency values for the spectral features shown in Figs. 1 to 5 are listed in Tables 3 to 5: Table 3 for cerussite, Table 4 for Na-Phase I and K-Phase I, and Table 5 for hydrocerussite and plumbonacrite. The frequency accuracy is estimated to be ±1 cm^{-1} for sharp features and ±0.2 cm^{-1} for peaks in the ν_1 region. These tables also contain qualitative relative intensities of the observed spectral features (the intensities are relative within the same compound). The Raman spectra shown in Figs. 2 to 5 were recorded under different vertical expansions for a clearer presentation and are uncorrected for the spectral response of the spectrometer.

The assignment of the bands arising from the fundamental internal vibrations of the carbonate ion is well established (2, 13, 15, 26–29) and does not require any further detailed discussion. Here we have followed Herzberg's nomenclature and numbering system (26) for the different carbonate vibrations. Although the assignment of the bands due to fundamental vibrations is straightforward, the same cannot be said for the other weaker features seen in the spectra of the carbonate minerals. White (15) has reviewed the six different assignments given in the literature for the weak feature seen about 15–20 cm^{-1} below the band assigned to the ν_2 fundamental in the infrared spectra of the carbonates. We agree with the suggestion of Sterzel *et al.* (30, 31) and Brooker and Bates (28) that this feature is due to the presence of the $^{13}CO_3^{2-}$ species in about 1% abundance in the carbonate minerals. Sterzel *et al.* have studied ^{13}C-enriched aragonite and their data support the assignment suggested in Tables 3 to 5 for this weak feature. We have collected the data for this feature in the five lead carbonates studied here in Table 6, and an average difference of about 18 cm^{-1} between the bands assigned to the ν_2 mode of $^{12}CO_3^{2-}$ and $^{13}CO_3^{2-}$ is consistent with the work of Sterzel *et al.* Similarly, there is a weak feature about 22 cm^{-1} below the strongest

TABLE 3. Vibrational spectra of cerussite

Raman[a] ($\Delta\nu$/cm^{-1}) Couture[a]	Raman[a] ($\Delta\nu$/cm^{-1}) This work	Infrared[a] (ν/cm^{-1})	Assignment[b]
58	57.4 s		[d]
	65.2 m, sh		
73	71.4 ms		
90.5	92 vw, br		Lattice modes[c]
103	102 mw		
119	123 vw		
145, 147.2	148 vw, br		
168	173 vw		
217, 227	225 w		
233, 244	245 w		
	674 w	678 s	
683	682 m		ν_4
	695 w	700 vw	
	824 vw	824 w	$\nu_2(^{13}CO_3^{2-})$
838	838 m	838 s	ν_2
	1031 vw		$\nu_1(C^{18}O^{16}O_2^{2-})$
1054	1053.5 vs	1052 ms	ν_1
	1320 sh		
1363	1364 s		
1373	1374 s		ν_3
	1425 sh	1400 vs, br	
1478	1477 s	1435 vs, br	
	1678 vw		
	1700 vw, br		$2\nu_2$
	1728 vw		
	1741 w		
		1729 w	$\nu_1 + \nu_4$
		1740 vw	

[a]m, s, w, v, sh, and br stand for medium, strong, weak, very, shoulder, and broad, respectively.

[b]Assignment of carbonate vibrations follows Herzberg's numbering system (25).

[c]See ref. 2 for the assignment of lattice modes.

[d]Lead sub-lattice vibrations.

TABLE 4. Vibrational spectra of lead carbonate – alkali metal hydroxide complex[a]

$2PbCO_3 \cdot NaOH$				$2PbCO_3 \cdot KOH$				
Raman ($\Delta\nu$/cm^{-1})		Infrared (ν/cm^{-1})		Raman ($\Delta\nu$/cm^{-1})		Infrared (ν/cm^{-1})		Assignment
37	w			33	w			
51.7	vs			50.0	vs			[b]
86	w, br			86	w, br			
98	w, br			98	vw, br			Lattice modes
125	vw							
202	m			206	mw, br			
285	m, br			289	m, br			
		360	vw					
		455	s	385	vw	379	s	ν_{Pb-O} + M^+ ion
						430	w	motion
		530	w, br			470	vw	
681	ms			682	m			ν_4
695	sh	693	s	693	sh	689	s	
		825	w			822	w	$\nu_2(^{13}CO_3^{2-})$
868	w	843	s	865	w	840	ms	ν_2
		988	m, br	940	vw	942	m, br	δ_{PbOH}
1036	vw			1036	vw			$\nu_1(C^{18}O^{16}O_2^{2-})$
1052	w, sh	1053	w	1052	w, sh			
1057.2	vs			1056.8	vs	1050	w	ν_1
1068.4	w							
~1350	w, sh			~1350	w, sh			
1392	s			1386	s	1413	vs, br	ν_3
		1435	vs, br			1430	vs, br	
1695	vw			1685	w			
1730	vw			1725	w			$2\nu_2$
1750	vw			1750	w			
		1743	w			1744	w	$\nu_1 + \nu_4$
		1758	vw			1756	w	
3500	vw	3495	w	3512	vw	3495	w	ν_{OH}

[a]See footnotes *a* and *b* under Table 3.
[b]Pb–Pb sub-lattice vibrations.

band (ν_1) in the Raman spectra of the carbonates (see Table 6). We believe that this weak feature is due to the presence of $C^{18}O^{16}O_2^{2-}$ moieties in the carbonates. Support for this suggestion comes from ^{18}O isotopic substitution studies on nitrates (32–34). Nitrate and carbonate ions have similar planar structures with symmetry D_{3h}. The ν_1 mode in $N^{16}O_3^-$ occurs at 1049 cm^{-1} while the same mode in $N^{18}O^{16}O_2^-$ occurs at 1028 cm^{-1}. This difference of 21 cm^{-1} compares favourably with the data for the ν_1 mode of carbonates collected in Table 6 and is consistent with the relative intensity measurements.

The assignments of the PbOH deformation vibrations given in Tables 4 and 5 follow the suggestion of Bulakhova *et al.* (12) and Nakamoto (27), but are only tentative without data for isotopically substituted material. The assignment of PbO stretching vibration to bands seen between 300–500 cm^{-1} in Tables 4 and 5 is in general agreement with the literature (35–37). Obviously, this region of the spectra may also contain contributions from the "combination modes" and "overtones" involving lattice vibrations. The present data are insufficient to identify in detail the origin of the different bands seen in this spectral region. The possible presence of polynuclear hydroxolead(II) cations in the basic lead carbonate structures is discussed briefly below.

The only previous report on the lattice mode of any carbonate of lead is the classic study of Couture (2), who reported single-crystal Raman spectra for cerussite. Her data are included in Table 3 for comparison purposes. Our spectra indicate a few minor additional weaker features (see Table 3) observable with the laser excitation and better instrumentation now available. The detailed symmetry assignment of the lattice modes will be discussed elsewhere in a new single-crystal study of cerussite.[4] The assignment of the OH-stretching region requires no comments.

Assignments in the 1600–1800 cm^{-1} region do require a comment. Normally, for nitrates and carbonates one observes that $2\nu_2$ is strongly Raman active only, while $\nu_1 + \nu_4$ is observed only in the infrared region (19, 28). Our assignments reflect this generality even though the regions overlap for some compounds. The multiplet structure observed in ν_2 and $2\nu_2$ of cerussite has been shown to be due to correlation field effects similar to those reported for KNO_3 (19, 34). Oriented single-crystal studies of cerussite have shown that there are two infrared peaks at 838 and 871 cm^{-1}, due to the B_{1u} and B_{2u}

[4]M. H. Brooker, unpublished work.

Can. J. Chem. Downloaded from www.nrcresearchpress.com by 210.87.254.6 on 09/06/12
For personal use only.

Can. J. Chem. Downloaded from www.nrcresearchpress.com by 210.87.254.6 on 09/06/12
For personal use only.

TABLE 5. Vibrational spectra of two basic lead carbonates[a]

Hydrocerussite		Plumbonacrite		
Raman ($\Delta\nu$/cm^{-1})	Infrared (ν/cm^{-1})	Raman ($\Delta\nu$/cm^{-1})	Infrared (ν/cm^{-1})	Assignment
49.5 vw				
		60 vw		
74 vw		72 vw		
106 w, br		105 w, br		Lattice modes
126 w, br		125 w, br		
		245 vw		
		273 w, br		
325 w		305 m	303 w	
	366 mw			
	392 m	400 m	392 mw	
415 m	~405 sh	425 w, br	416 m	ν_{PbO}
	471 vw	462 m	466 mw	
		490 w, br		
681 w	683 s	681 w	685 s	
695 w	693 m	697 w, sh	697 m	ν_4
705 w, sh	706 sh	707 w	706 w	
770 w, br	775 br	750 w, br	755 w, br	δ_{PbOH}
	837 br		834 vw	$\nu_2(^{13}CO_3^{2-})$
		848 w	846 w	
	857 w		856 vw	ν_2
865 w	869 vw	867 w	866 w	
	930 vw, br		930 vw, br	δ_{PbOH}
1028 w		1030 w		$\nu_1(C^{18}O^{16}O_2^{2-})$
			1046 vw	
	1045 m	1049.3 vvs	1049 vw	ν_1
1048.9 vvs		1053.1 s	1053 vw	
1052.6 vs	1053 vw	1056.3 vs	1057 vw	
1363 s	1350 sh			ν_3
1395 sh	1400 s	1385 s	1400 vs	
1645 vw		1690 vw		
1735 w		1732 w		$2\nu_2$
		1751 w		
	1738 w		1736 w	
			1748 vw, sh	$\nu_1 + \nu_4$
3533 w	3530 w	3541 w	3542 w	ν_{OH}
		3556 w	3560 w	

[a]See footnotes *a* and *b* under Table 3.

TABLE 6. Satellite bands arising from isotopic moieties[a]

	ν_1 bands[b]			ν_2 bands[c]		
Compounds	Main	Satellite	$\Delta\nu$	Main	Satellite	$\Delta\nu$
Cerussite	1053.5	1031	22.5	838	824	14
Na-Phase I	1057.2	1036	21.2	843	825	18
K-Phase I	1056.8	1036	20.8	840	822	18
Plumbonacrite	1052.9[d]	1030	22.9	856[e]	834	22
Hydrocerussite	1051.7[d]	1028	23.7	857	837	20
Average difference			22±2			18±4

[a]All frequency values are in units of cm^{-1}.
[b]Raman data, isotopic moiety is ($C^{18}O^{16}O_2^{2-}$).
[c]Infrared data, isotopic moiety is ($^{13}CO_3^{2-}$).
[d]Mean of Raman bands.
[e]Mean of infrared bands.

Can. J. Chem. Downloaded from www.nrcresearchpress.com by 210.87.254.6 on 09/06/12
For personal use only.

factor-group components,[4] respectively. The overtone region is complicated because the $k = 0$ selection rules are modified for overtones.

(c) Spectra-structure correlations

Cerussite has a structure analogous to aragonite and a factor-group analysis of the systems with aragonite structure (space group Pmcn, D_{2h}^{16} with four MCO_3 formula units per unit cell) has been discussed by many workers (2, 13, 15, 29). As the spectra of cerussite have been discussed earlier, we concern ourselves here mainly with the other four carbonates. The ν_1 mode is relatively weaker in the infrared spectra of the other four carbonates, particularly in Na-Phase I, K-Phase I, and plumbonacrite, compared with the spectra of cerussite (see Fig. 1). This suggests that the reduction in site symmetry of the carbonate ion is less in these compounds than in cerussite, as the ν_1 mode is infrared inactive for species with D_{3h} symmetry (27, 38). This conclusion is also supported by the Raman spectra of these compounds, the ν_2 mode being more intense in cerussite than in the other carbonates of lead (see Fig. 2). The spectra of Na-Phase I and K-Phase I are very similar, supporting the conclusion drawn from X-ray diffraction data that these salts are isostructural.

The ν_1 band in the Raman spectra showed no splitting for cerussite, although factor-group analysis predicts two bands (15). Similar behaviour is shown by aragonite (29). The ν_1 mode in Na-Phase I and K-Phase I shows only one apparent band in each Raman spectrum (see Fig. 5), but the bands are clearly asymmetric and broader than that of cerussite. This indicates the presence of at least two unresolved features, which suggests that in these compounds the carbonate ions are either on two nonequivalent sites, or the factor-group splitting is slightly greater than in cerussite. The ν_1 mode in the Raman spectra of hydrocerussite and plumbonacrite shows well-resolved bands (see Fig. 5). The results for cerussite, Na-Phase I, and K-Phase I, as well as aragonite (2, 15, 29), indicate that the factor-group splitting of the ν_1 mode in the carbonates is very small. The splitting seen in the ν_1 band of hydrocerussite and plumbonacrite must therefore be due to the presence of carbonate moieties on nonequivalent sites, or different "orbits" (39) in the unit cell. With the above assumption, one has to conclude that carbonate ions are present on at least three different sites in plumbonacrite and on at least two different sites in hydrocerussite. Furthermore, in hydrocerussite one type of carbonate site has twice the occupancy of the second type, as the two peaks in the ν_1 band of hydrocerussite have relative intensities in the raio of ~2:1. Because a unit cell of hydrocerussite contains six carbonate ions (9), there must be four of one type and two of the other. The presence of carbonates on more than one nonequivalent site in hydrocerussite and plumbonacrite is also suggested by the splittings seen for their ν_2 mode, both in their infrared and Raman spectra (see Figs. 1 and 2).

The very strong peak at 57.4 cm^{-1} in the Raman spectrum of cerussite can be assigned to a motion of the lead sub-lattice that forms a pseudohexagonal planar array. The high intensity of this band compared to that of the CO_3^{2-} rotatory band at about 100 cm^{-1} would be due to the high polarizability of Pb^{2+}. The presence of strong bands at 51.7 cm^{-1} and 50.0 cm^{-1} for Na-Phase I and K-Phase I, respectively, suggests that they also have a structure with a well-defined lead sub-lattice, similar to that of cerussite. This is consistent with the tentative conclusions drawn from the diffraction data, as discussed above.

The Raman spectrum of plumbonacrite shows two well-resolved peaks for the OH stretching band (see Fig. 4), which suggests that the OH species occupy two kinds of sites in this compound, if one assumes that the splitting is not due to factor-group splitting. Support for this assumption is provided by the absence of any splitting in the corresponding band of the other lead carbonates.

It is possible that hydrocerussite and plumbonacrite contain polymeric hydroxolead(II) cations. For example, $Pb_6O(OH)_6^{4+}$ is known to occur in the solid state as a perchlorate salt (40, 41), and probably also in aqueous solution (42). Features in the Pb—O stretching region of the Raman and infrared spectra of plumbonacrite resemble those reported for a solid later shown to contain the $Pb_6O(OH)_6^{4+}$ cation (35, 40, 43). It is possible, therefore, that plumbonacrite has the structural formula $[Pb_6O(OH)_6^{4+}][Pb^{2+}]_4[CO_3^{2-}]_6$.

1. M. S. MOZES. Evaluation of solid sorbents for the control of $^{14}CO_2$, Ontario Hydro Report #80-505-K. 1980.
2. L. COUTURE. Annales de Chimie et Physique Tomp, 1947. pp. 5–94.
3. G. KATZ and R. LEFKER. Anal. Chem. **29**, 1894 (1957).
4. C. K. HUANG and P. F. KERR. Am. Mineral. **45**, 311 (1960).
5. J. H. SCHUTTE and K. BUIJS. Nature, **192**, 351 (1961).
6. R. A. SCHROEDER, C. E. WEIR, and E. R. LIPPINCOTT. J. Res. Natl. Bur. Std. *A*. Physics and Chemistry, **66**A, 407 (1962).
7. D. A. GRISAFE and W. B. WHITE. Am. Mineral. **49**, 1184 (1964).
8. S. D. ROSS and J. GOLDSMITH. Spectrochim. Acta, **20**, 781 (1964).
9. J. K. OLBY. J. Inorg. Nucl. Chem. **28**, 2507 (1966).
10. V. N. ANDREEVA and T. F. LIMAR. Russ. J. Inorg. Chem. **15**, 1077 (1970).
11. W. P. GRIFFITHS. J. Chem. Soc. A (London), 286 (1970).
12. V. I. BULAKHOVA, E. YA BEN'YASH, M. M. SHOKAREV, and F. I. VERSHININA. Russ. J. Inorg. Chem. **17**, 11 (1972).
13. S. D. ROSS. Inorganic infrared and Raman spectra. McGraw-Hill Book Co., London. 1972. pp. 141–160.
14. K. SAUL. Z. Krist. **139**, 215 (1974).
15. W. B. WHITE. *In* The infrared spectra of minerals. *Edited by* V. C. Farmer. Mineralogical Society, London. 1974. pp. 227–234.
16. S. SARIG and F. KAHANA. Thermochim. Acta, **14**, 263 (1976).
17. M. C. BALL and M. J. CASSON. J. Inorg. Nucl. Chem. **39**, 1949 (1977).
18. J. YAMAGUCHI, Y. SAWADA, O. SAKURAI, K. UEMATSU, N. MIZUTANI, and M. KATO. Thermochim. Acta, **37**, 79 (1980).
19. M. H. BROOKER. Can. J. Chem. **55**, 1242 (1977).
20. H. E. SWANSON and R. K. FUYAT. Standard X-ray diffraction powder patterns, Natl. Bur. Std. Circ. 539 Vol. II, p. 56 (1953).
21. J. M. COWLEY. Acta Cryst. **9**, 391 (1956).
22. A. A. VORONOVA and B. K. VAINSHTEIN. Sov. Phys. — Crystallog. **9**, 154 (1964).
23. THOMAS P. WHALEY. *In* Comprehensive inorganic chemistry. Vol. 1. *Edited by* J. C. Bailar, H. J. Emeléus, R. Nyholm, and A. F. Trotman-Dickenson. Pergamon Press, Oxford. 1973. Chapt. 8.
24. P. TAYLOR, P. R. TREMAINE, and M. G. BAILEY. Inorg. Chem. **18**, 2947 (1979).
25. N. F. M. HENRY and K. LONSDALE (*Editors*). International tables for X-ray crystallography. Vol. I. Kynoch Press, Birmingham. 1965.
26. G. HERZBERG. Molecular spectra and molecular structure. II. Infrared and Raman spectra of polyatomic molecules. D. Van Nostrand Co., Inc., New York. 1962. pp. 177–179.
27. K. NAKAMOTO. Infrared and Raman spectra of inorganic and coordinate compounds. John Wiley and Sons, New York. 1978.

28. M. H. BROOKER and J. B. BATES. J. Chem. Phys. **54**, 4788 (1971).
29. R. FRECH, E. C. WANG, and J. B. BATES. Spectrochim. Acta, **36**A, 915 (1980).
30. W. STERZEL and E. CHORINSKY. Spectrochim. Acta, **24**A, 353 (1968).
31. W. STERZEL, E. J. ZEHNDER, and K. J. MÜLLER. Ber. Bunsenges Phys. Chem. **81**, 696 (1977).
32. M. ANBAR, M. HALMANN, and S. PINCHAS. J. Chem. Soc. 1242 (1960).
33. S. PINCHAS and I. LAULICHT. Infrared spectra of labelled compounds. Academic Press, London. 1971. p. 252.
34. M. H. BROOKER. J. Solid State Chem. **28**, 29 (1979).
35. V. A. MARONI and T. G. SPIRO. Inorg. Chem. **7**, 188 (1968).
36. P. RAMAMURTHY, E. A. SECCO, and M. BADRI. Can. J. Chem. **48**, 2617 (1970).
37. P. TSAI and R. P. COONEY. J. Chem. Soc. Dalton Trans. **16**, 1631 (1976).
38. J. A. GOLDSMITH and S. D. ROSS. Spectrochim. Acta, **22**, 1069 (1961).
39. R. KOPELMAN. J. Chem. Phys. **47**, 2631 (1967).
40. T. G. SPIRO, D. H. TEMPLETON, and A. ZALKIN. Inorg. Chem. **8**, 856 (1969).
41. A. OLIN and R. SÖDERQUIST. K. Tek. Hoegsk. Handl. 517 (1972).
42. S. ISHIGURO and H. OHTAKI. Bull. Chem. Soc. Jpn. **54**, 335 (1981).
43. V. A. MARONI and T. G. SPIRO. J. Am. Chem. Soc. **89**, 45 (1967).

Can. J. Chem. Downloaded from www.nrcresearchpress.com by 210.87.254.6 on 09/06/12
For personal use only.

Heats of vaporization of some monosubstituted cyclopropane, cyclobutane, and cyclopentane derivatives. Some observations on the enthalpies of isodesmic ring opening reactions of cyclobutane derivatives

RICHARD FUCHS and JOHN H. HALLMAN

Department of Chemistry, University of Houston, Houston, TX 77004, U.S.A.

Received June 11, 1982

RICHARD FUCHS and JOHN H. HALLMAN. Can. J. Chem. **61**, 503 (1983).

The following heats of vaporization at 25°C (ΔH_v^0) have been measured by vaporization calorimetry: cyclopropyl methyl ketone (39.41 ± 0.09 kJ mol^{-1}), methyl cyclopropanecarboxylate (41.27 ± 0.06 kJ mol^{-1}), cyclobutyl cyanide (44.34 ± 0.20 kJ mol^{-1}), methyl cyclobutanecarboxylate (44.72 ± 0.09 kJ mol^{-1}), ethylcyclobutane (31.24 ± 0.03 kJ mol^{-1}), and cyclopentyl cyanide (48.12 ± 0.09 kJ mol^{-1}). Values of ΔH_v^0 of the last four compounds have been combined with liquid state heats of formation to give new values of the gaseous state heats of formation (ΔH_f(g)).

When cyclobutyl cyanide, ethylcyclobutane, and cyclobutylamine are involved in hypothetical isodesmic reactions with ethane to give propane and isopropyl derivatives, the enthalpies of reaction are −102.1 ± 1.7 kJ mol^{-1} (−24.4 ± 0.4 kcal/mol), 8.3 kJ mol^{-1} (2.0 kcal/mol) less exothermic than the value for cyclobutane. Possible origins of this difference are discussed.

RICHARD FUCHS et JOHN H. HALLMAN. Can. J. Chem. **61**, 503 (1983).

Faisant appel à la calorimétrie de vaporisation, on a mesuré les chaleurs de vaporisation des composés suivants à 25°C (ΔH_v^0); la méthylcyclopropylcétone (39,41 ± 0,09 kJ mol^{-1}), le cyclopropanecarboxylate de méthyle (41,27 ± 0,06 kJ mol^{-1}), le cyanure de cyclobutyle (44,34 ± 0,20 kJ mol^{-1}), le cyclobutanecarboxylate de méthyle (44,72 ± 0,09 kJ mol^{-1}), l'éthylcyclobutane (31,24 ± 0,03 kJ mol^{-1}) et le cyanure de cyclopentyle (48,12 ± 0,09 kJ mol^{-1}). On a combiné les valeurs de ΔH_v^0) des quatre derniers composés avec les chaleurs de formation de l'état liquide pour obtenir les nouvelles valeurs des chaleurs de formation de l'état gazeux (ΔH_f(g)).

Quand le cyanure de cyclobutyle, l'éthylcyclobutane et la cyclobutylamine sont impliqués dans des réactions isodesmiques hypothétiques avec l'éthane pour donner des dérivés du propane et de l'isopropyle, les enthalpies de réactions sont −102,1 ± 1,7 kJ mol^{-1} (−24,4 ± 0,4 kcal/mol), moins exothermiques que les valeurs pour le cyclobutane par 8,3 kJ mol^{-1} (2,0 kcal/mol). On discute des origines possibles de cette différence.

[Traduit par le journal]

The cyclopropane ring has long been described as having "double bond character". Various types of addition reactions, and evidence of conjugation with adjacent unsaturated groups have been observed or calculated (1−5). The cyclobutane ring is somewhat less distorted and strained, and undergoes relatively few ring-opening reactions, with considerable difficulty. Nevertheless, the four-membered ring does have properties characteristic of strained rings (6), and calculations at the STO-3G level (5) suggest that appreciable stabilization should result from the introduction of substituents such as cyano (19 kJ mol^{-1}) and methyl (6 kJ mol^{-1}). The calculations indicate somewhat smaller stabilization of cyclobutanes than the similarly substituted cyclopropanes.

Experimentally, stabilization can be assessed from enthalpies of isodesmic reactions of substituted vs. unsubstituted cyclobutanes, which are calculated from the gaseous state heats of formation (ΔH_f^0(g)) of the reactants and products (4, 5):

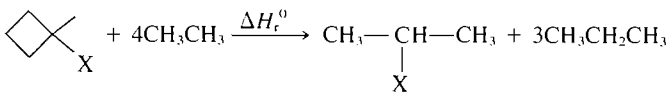

where X = H, CN, Et, and NH_2, and $\Delta H_r^0 = \sum \Delta H_f^0$(g) (products) − $\sum \Delta H_f^0$(g) (reactants). In this "group separation method" (5) each —CH_2— and —CHX— of the cyclobutane derivative is transferred to the simplest open-chain (and unstrained) compound having the same group. The reaction is exothermic due to relief of ring strain, and $-\Delta H_r^0$ is the strain energy. ΔH_r^0 should be the same where X = H and all other nonconjugating substituents, but ΔH_r should be less exothermic when a stabilizing interaction of X and the ring occurs. Stabilization or destabilization may be influenced not only by the ring-substituent bond character, but also by variation in antibonding character (strain) within the ring (5).

A few experimental thermochemical data on cyclobutane derivatives have been available (7−9) (Table 1). Based on these, the calculated values of ΔH_r^0 are: cyclobutane, −110.4 ± 1.5 kJ mol^{-1}; cyclobutyl cyanide, −96.1 ± 1.8 kJ mol^{-1}; ethylcyclobutane, −105.0 ± 1.7 kJ mol^{-1}; and cyclobutylamine, −102.5 ± 1.5 kJ mol^{-1}. ΔH_f^0(g) for methyl cyclobutanecarboxylate has been reported, but not for the isodesmic reaction product, methyl isobutyrate. Relative to cyclobutane, cyclobutyl cyanide appears to be stabilized by 14.3 kJ mol^{-1}, ethylcyclobutane, by 5.4 kJ mol^{-1}, and cyclobutylamine, by 7.9 kJ mol^{-1}, in acceptable agreement with calculated values (5).

We have reservations concerning these conclusions for two reasons. First, it has recently been demonstrated (4) that no appreciable thermochemical stabilization results from the introduction of cyano, methyl, and amino substituents onto the cyclopropyl ring, which is a more favorable system for ring-substituent interactions. We are also concerned with the sizable uncertainties in the heat of vaporization measurements on which ΔH_f^0(g) values depend (ΔH_f^0(g) = ΔH_f^0(l) + ΔH_v^0), particularly data from a source (8) containing several ΔH_v values in substantial disagreement with other measurements (4, 7).

It is the objective of the present study to provide ΔH_f^0(g)

Can. J. Chem. Downloaded from www.nrcresearchpress.com by 210.87.254.42 on 09/06/12
For personal use only.

TABLE 1. Heats of vaporization and formation (kJ mol^{-1})

Compound	ΔH_v^0 This study	ΔH_v^0 Lit.	ΔH_f^0(l)	ΔH_f^0(g)
Cyclopropyl methyl ketone	39.41±0.09			
Methyl cyclopropanecarboxylate	41.27±0.06			
Cyclobutyl cyanide	44.34±0.20	40.0±0.4[a]	103.0±1.1[a]	147.3±1.1[c]
Methyl cyclobutanecarboxylate	44.72±0.09	39.7±0.4[a]	−395.0±1.3[a]	−350.3±1.3[c]
Ethylcyclobutane	31.24±0.03	32.6±0.8[d]	−58.9±0.7[b]	−27.7±0.7[c]
Cyclopentyl cyanide	48.12±0.09	41.1±0.4[a]	0.7±2.8[a]	48.8±2.8[c]
		43.4±0.2[e]		
Cyclobutylamine				41.2±0.7[b]
Cyclobutane				28.4±0.5[b]

[a]Reference 8.
[b]Reference 7.
[c]Based on ΔH_v^0 of this study.
[d]Reference 9.
[e]Reference 10.

data of improved accuracy, so that a critical assessment of cyclobutane-substituent thermochemical stabilization can be made.

Experimental

Ethylcyclobutane (99.92%) was an API Standard Reference Material, and was used as received. Methyl cyclobutanecarboxylate was synthesized by refluxing cyclobutanecarboxylic acid with an excess of methanol in the presence of sulfuric acid as catalyst. The ester was isolated, dried, and fractionally distilled. A purity of 99.9% was established by gas chromatography, using a Shimadzu Mini 2 gc with a glass-lined system, a 30 m × 0.25 mm id SE-30 silica capillary column, and a Hewlett-Packard 3390A integrator. Cyclobutyl cyanide was obtained from Columbia Organic Chemicals Co., and the other compounds were Fluka products. Each was fractionally distilled and examined by gc. The purities were: cyclopropyl methyl ketone, 99.96%; methyl cyclopropanecarboxylate, 99.87%; cyclobutyl cyanide, 99.95%; and cyclopentyl cyanide, 99.96%.

Heats of vaporization were determined at 25.0°C by evaporating 3−11 100 μL samples of each substance in a vaporization calorimeter (4) under reduced pressure (2−200 mm Hg (0.27−27 kPa) depending on the sample volatility), and with a nitrogen flow of 0.4−2.0 mL/min. The evaporations were complete in 13−23 min. Samples over 4A molecular sieve in Mininert bottles were transferred by syringe and introduced directly into the calorimeter. Details of the calorimeter design and operation, and comparison of the results with literature values have been reported previously (4). ΔH_v^0 of *n*-hexane was measured as a model for ethylcylobutane. The new value is 31.54 ± 0.18 kJ mol^{-1}; the previously reported value (7) is 31.55 ± 0.04 kJ mol^{-1}.

Results and discussion

Heats of vaporization and gaseous state heats of formation

The standard heats of vaporization and gaseous state heats of formation at 25.0°C of cyclopropyl methyl ketone, methyl cyclopropanecarboxylate, cyclobutyl cyanide, methyl cyclobutanecarboxylate, ethylcyclobutane, and cyclopentyl cyanide are listed in Table 1. The indicated uncertainties are twice the standard deviations.

The first published values of ΔH_v^0 of cyclopropyl cyanide, cyclobutyl cyanide, cyclopentyl cyanide, and cyclohexyl cyanide (8) were 39.8 ± 0.4, 40.0 ± 0.4, 41.1 ± 0.4, and 43.6 ± 0.4 kJ mol^{-1}, respectively. The methylene increments in ΔH_v^0 are far smaller than are normally observed. The last two compounds were reexamined by Konicek (10), and higher values of 43.4 ± 0.2 kJ mol^{-1} and 51.9 ± 0.3 kJ mol^{-1} were obtained. This represents an extraordinarily large increment. Methylene increments in typical homologous series are usually 2.5−4 kJ mol^{-1} for the few lowest members of the series, increasing to ~5 kJ mol^{-1} in the higher members. We believe that the best values of ΔH_v^0 for the cyclic cyanides are 41.94 ± 0.11 (4), 44.34 ± 0.20, 48.12 ± 0.09, and 51.9 ± 0.3 kJ mol^{-1} (10).

Isodesmic reactions of cyclobutane derivatives

The following are isodesmic reactions of cyclobutane, cyclobutyl cyanide, ethylcyclobutane, and cyclobutylamine:

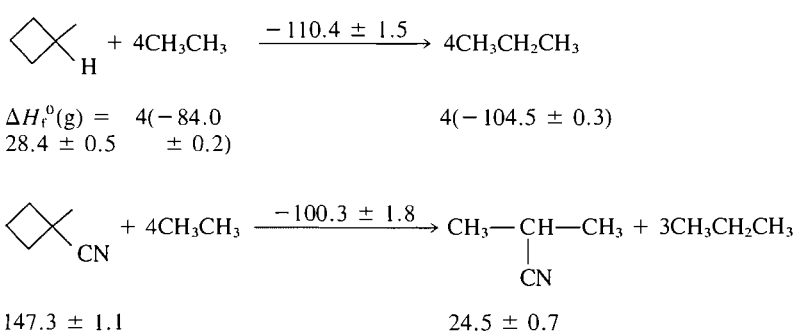

Can. J. Chem. Downloaded from www.nrcresearchpress.com by 210.87.254.42 on 09/06/12
For personal use only.

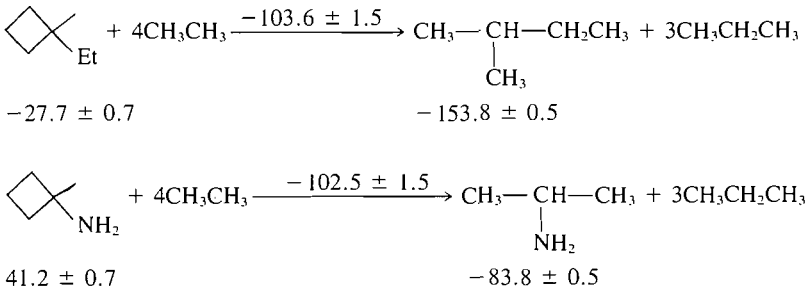

The mean value of ΔH_r^0 for the three substituted derivatives is -102.1 kJ mol^{-1}, and no individual value differs from the mean by more than the experimental uncertainty. There is, therefore, no basis for stating that these three substituents are exerting appreciably different effects. This is not to say that the —CN group, for example, has the same interactions with the cyclobutane ring as does the ethyl group, but rather that the overall thermochemical effect of various stabilizing and destabilizing interactions by the two substituents are the same. On the other hand, the substituted cyclobutanes appear to be rather uniformly stabilized by about 8.3 kJ mol^{-1} (2.0 kcal/mol) relative to cyclobutane. This is surprising, since recent data indicate no thermochemical stabilization of substituted cyclopropanes (4).

It is difficult to accept the idea that substituents stabilize cyclobutane, but not cyclopropane, particularly because the effects of three quite different substituents on cyclobutane are so uniform. One can imagine several possible explanations: (*A*) cyclobutane interacts with substituents more favorably (energetically) than does cyclopropane, for quite unrecognized reasons. (*B*) values of ΔH_f^0(g) for the substituted cyclopropanes are substantially incorrect, and are really less exothermic. These compounds would then be stabilized relative to cyclopropane. (*C*) ΔH_f^0(g) of cyclopropane is incorrect, and should be >10 kJ mol^{-1} more endothermic. The substituted cyclopropanes would be uniformly stabilized. (*D*) ΔH_f^0(g) of the substituted cyclobutanes are really all ~8 kJ mol^{-1} more endothermic than the values reported above, and none is stabilized. (*E*) the published value of ΔH_f^0(g) for cyclobutane is incorrect and should be 8.3 kJ mol^{-1} less endothermic. The substituted cyclobutanes (and cyclopropanes) would all be nonstabilized. Of these possibilities (*C*) and (*E*) seem most likely, each depending on only one incorrect value of ΔH_f^0(g). (*C*) requires that three diverse substituents have the same thermochemical effect on cyclopropane, and a uniform effect on cyclobutane. We feel that (*E*) is the most likely explanation, but it should be emphasized that we have no independent reasons to doubt the published value of ΔH_f^0(g) for cyclobutane (11–14).

Acknowledgements

Acknowledgement is made to the donors of the Petroleum Research Fund, administered by the American Chemical Society, for partial support of this research, and to The Robert A. Welch Foundation (Grant E-136) for additional support.

1. M. CHARTON. *In* Chemistry of alkenes. *Edited by* J. Zabicky. Wiley Interscience, New York, NY. 1970.
2. D. G. GARRATT, A. MODRO, K. OYAMA, G. H. SCHMID, T. T.TIDWELL, and K. YATES. J. Am. Chem. Soc. **96**, 5295 (1974).
3. F. H. ALLEN. Acta Crystallogr. B**36**, 81 (1980).
4. R. FUCHS, J. H. HALLMAN, and M. O. PERLMAN. Can. J. Chem. **60**, 1832 (1982).
5. J. D. DILL, A. GREENBERG, and J. F. LIEBMAN. J. Am. Chem. Soc. **101**, 6814 (1979).
6. A. GREENBERG and J. F. LIEBMAN. Strained organic molecules. Academic Press, New York, NY. 1978.
7. J. B. PEDLEY and J. RYLANCE. Sussex-N.P.L Computer analysed thermochemical data: organic and organometallic compounds. University of Sussex, Brighton, England. 1977.
8. H. K. HALL, JR. and J. H. BALDT. J. Am. Chem. Soc. **93**, 140 (1971).
9. W. D. GOOD, R. T. MOORE, A. G. OSBORN, and D. R. DOUSLIN. J. Chem. Thermodyn. **6**, 303 (1974).
10. J. KONICEK. Acta Chem. Scand. **27**, 1496 (1973).
11. J. COOPS and S. KAARSEMAKER. Rec. Trav. Chim. **69**, 1364 (1950).
12. S. KAARSEMAKER and J. COOPS. Rec. Trav. Chim. **71**, 261 (1952).
13. G. W. RATHJENS and W. D. GWINN. J. Am. Chem. Soc. **75**, 5629 (1953).
14. G. W. RATHJENS, N. K. FREEMAN, W. D. GWINN, and K. S. PITZER. J. Am. Chem. Soc. **75**, 5634 (1953).

Can. J. Chem. Downloaded from www.nrcresearchpress.com by 210.87.254.42 on 09/06/12
For personal use only.

The composition of the carbohydrates in the middle lamella and secondary wall of tracheids from black spruce wood

P. WHITING AND D. A. I. GORING

Pulp and Paper Research Institute of Canada and Department of Chemistry, McGill University, Montreal, P.Q., Canada H3A 2A7

Received July 22, 1982

P. WHITING and D. A. I. GORING. Can. J. Chem. **61**, 506 (1983).

Carbohydrate analyses were performed on fractions of tissue from the middle lamella and secondary wall of black spruce tracheids. The concentrations of glucose and mannose were found to be smaller in the middle lamella than in the secondary wall while the concentrations of galactose, arabinose, and xylose were slightly larger in the middle lamella than in the secondary wall. The results obtained are compared with data available in the literature for other softwood species.

P. WHITING et D. A. I. GORING. Can. J. Chem. **61**, 506 (1983).

Nous avons effectué des analyses d'hydrates de carbone sur des fractions de tissu de la lamelle médiane et la paroi secondaire de trachéides d'épinette noire. On a trouvé que les concentrations de glucose et de mannose étaient plus faibles dans la lamelle médiane que dans la paroi secondaire tandis que les concentrations de galactose, d'arabinose et de xylose étaient légèrement plus fortes dans la lamelle médiane que dans la paroi secondaire. Les résultats obtenus sont comparés aux données trouvées dans la littérature pour d'autres espèces de résineux.

Can. J. Chem. Downloaded from www.nrcresearchpress.com by 210.87.254.40 on 09/06/12
For personal use only.

Introduction

Little research has been published on the composition of the carbohydrates in the various morphological regions of the tracheids in coniferous woods. Most of the recent work in this area has dealt with the primary walls (1) and cambial tissue (2, 3) of hardwoods.

In 1961, Meier (4) measured the carbohydrate composition in the cell wall of conifer tracheids by analysis of fractions obtained through microdissection. Fibres of different degrees of maturation were microscopically distinguished and isolated. Meier found that the relative amounts of glucose and mannose were lower in the hydrolysates from the compound middle lamella than in those from the secondary wall. Galactose and arabinose showed the reverse trend. Burke *et al.* (5) measured the sugar content of the polysaccharides in the primary walls of suspension-cultured Douglas fir cells and found very little mannose and relatively high concentrations of galactose and arabinose. More recently, Hardell and Westermark (6) have developed a method for peeling layers of the cell wall from single fibres. Samples as small as 20 ng were analyzed for their carbohydrate contents. Only small differences in the relative amounts of monosaccharides were found in the various cell layers of spruce tracheids. Most notably, the authors did not find a large reduction in the relative amounts of glucose and mannose in the compound middle lamella, as was noted by Meier (4).

Recent work in our laboratory has made possible the separation of centigram quantities of tissue from the middle lamella and secondary wall of black spruce tracheids (7). In the present paper, the analyses of the carbohydrate portions of these tissue fractions are described. Results are compared with those of previous workers.

Experimental

Five samples of black spruce (*Picea mariana* (Mill.) B.S.P.) tissue of varying lignin contents were isolated according to the method of Whiting *et al.* (7). The lignin contents were measured using the acetyl bromide method described previously (7). The secondary wall tissue sample contained 22% lignin and the whole wood sample contained 27% lignin. Three samples of middle lamella tissue were prepared, ML-1, ML-2, and ML-3, with lignin contents of 39%, 50%, and 60%, respectively.

TABLE 1. Lignin and monosaccharide contents of tissue fractions expressed as grams component per gram of tissue

Component	SW*	WW†	ML-1‡	ML-2‡	ML-3‡
Lignin	0.22	0.27	0.39	0.50	0.60
Glucose	0.55	0.47	0.36	0.23	0.14
Mannose	0.15	0.16	0.10	0.09	0.05
Xylose	0.07	0.07	0.07	0.08	0.07
Galactose	0.03	0.04	0.04	0.06	0.07
Arabinose	0.02	0.02	0.04	0.05	0.05

*SW: secondary wall tissue.
†WW: whole wood flour.
‡ML: middle lamella tissue.

The polysaccharides in the tissue samples were hydrolyzed by means of a modified version of the method of Fengel and Wegener (8). Five milligrams of dry tissue were weighed accurately into a 12 × 100 mm test tube and 1.6 mL of trifluoroacetic acid was added to each sample. The tube was covered with Parafilm and allowed to stand for 48 h at room temperature. The Parafilm was removed and 0.4 mL of H_2O was added. The contents were then frozen using dry ice and acetone, and the tube was sealed under vacuum. The sealed tubes were brought to room temperature and then heated in a 100°C oven for 2 h. After cooling, the tubes were opened and dried over NaOH in a vacuum desiccator at room temperature. After drying, 1 mL of water was added and the evaporation and drying were repeated. A final cycle of water addition, evaporation, and drying was then performed on the sample. A known amount of myo-inositol was added as an internal standard.

The dried samples were dissolved in 0.8 mL of silylation-grade dimethylsulfoxide and derivatized to trimethylsilyl esters with 0.8 mL "Tri-Sil Concentrate" (Pierce Chemical Co.). The derivatized monosaccharides were separated by gas chromatography using a J & W 30 m fused silica capillary column (0.253 mm i.d.) coated with SE-30. The gas chromatograph was temperature-programmed as follows: 160°C to 220°C at 1.5°C per min; 220°C for 2 min.

The quantity of a particular monosaccharide in each tissue fraction was obtained by comparing the total area of the appropriate peaks in the chromatogram with the peak area of the internal standard.

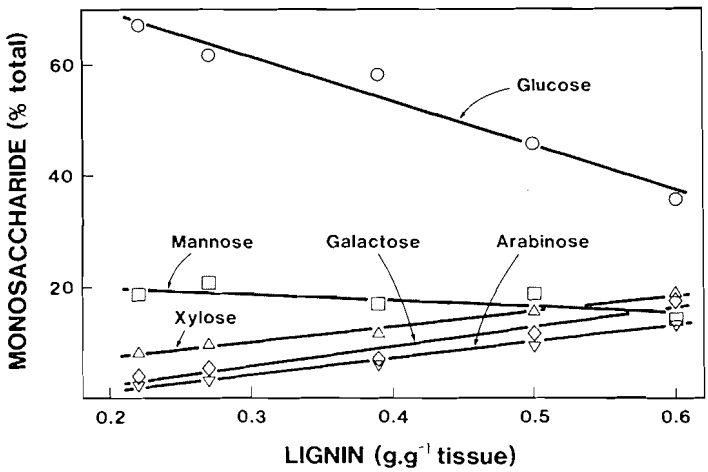

FIG. 1. Monosaccharide expressed as percent total monosaccharide vs. the lignin content for the various tissue fractions studied. The straight lines are least squares with an average correlation coefficient of 0.94.

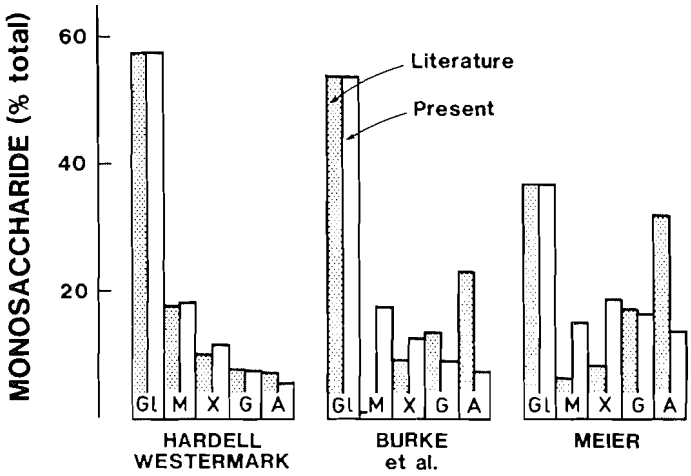

FIG. 2. Comparison of literature with present data for the distribution of monosaccharides. The present distributions were obtained from Fig. 1 by normalizing to a glucose content equal to that given in the literature. Gl, M, X, G, and A mean glucose, mannose, xylose, galactose, and arabinose respectively.

Each tissue fraction was analyzed at least three times, and the results expressed as grams of monosaccharide per gram of tissue. The reproducibility in measurement was about ±4%.

Results and discussion

The monosaccharide content of each of the tissue fractions is shown in Table 1. The monosaccharide contents, converted to percentage of the total monosaccharides, are plotted against lignin contents in Fig. 1. Note that the linear trends obtained do not represent the distribution of components across the cell wall. They arise because each tissue fraction is a mixture of secondary wall, primary wall, and middle lamella in varying proportions.

Figure 1 indicates that the contents of glucose and mannose are lower in the middle lamella than in the secondary wall, while the contents of xylose, galactose, and arabinose increase in the fractions rich in middle lamella tissue. These results are qualitatively in agreement with the trends reported by Meier (4) and Burke *et al.* (5).

We may now attempt a more quantitative comparison of the results of the present work with the data in the literature. Fractions as nearly representative of the compound middle lamella as possible were chosen. The literature data used are those of Hardell and Westermark for the M+P layer in white spruce (6), Burke *et al.* for suspension-cultured Douglas fir (5), and Meier for the M+P layer in white spruce (4). The percentage of total sugar in the hydrolysate as glucose was used to locate the tissue fraction on the line for glucose in Fig. 1. The percentage of the four other sugars corresponding to the glucose percentage was then read off. Thus we obtained the monosaccharide distribution as given by the present data corresponding to the glucose content of the plant tissues analyzed by the other workers. A comparison of these distributions with the distributions given by the other workers is shown in Fig. 2. Note that Burke *et al.*'s data for Douglas fir were recalculated on basis that the content of the five monosaccharides added together equals 100% (5).

The comparisons shown in Fig. 2 are revealing. The agreement with the data of Hardell and Westermark (6) is excellent. This is not the case with the data of Burke *et al.* (5) and Meier (4). Not only is the agreement bad but the errors are in the same directions for the two sets of comparisons, i.e., our results are high for mannose and xylose and low for galactose and arabinose in both cases. Similar trends were found when we compared our data with the results by Côté *et al.* (9) for the M+P layer in the normal wood of balsam fir.

In speculating on the origins of these discrepancies, perhaps we should note the physiological similarity of the preparations of Burke *et al.* (5), Meier (4), and Côté *et al.* (9). Meier obtained his M+P fraction by separation of the layers of cells nearest to the cambial layer (4, 10). So did Côté *et al.* (9). Burke *et al.* studied tissue-cultured primary walls (5). In all these cases a "nascent" primary wall material was used. In contrast, Hardell and Westermark fractionated single tracheids teased from lignified wood (6). In the present work, the fractions obtained were also from lignified wood (7).

Does the carbohydrate composition of the compound middle lamella change as the secondary wall grows and the cell lignifies and dies? Hardell and Westermark have posed a similar question (6). The comparisons shown in Fig. 2 suggest that it does. However, this suggestion is made with caution because of the different origins of the tissue fractions used and also because of possible differences in the species compared.

Acknowledgements

The authors wish to thank Dr. J. M. MacLeod for assistance with the gas chromatographic analyses, Mr. M. G. Paice for assistance with the hydrolysis procedure, and Dr. T. E. Timell for his excellent advice in the interpretation of the data.

1. A. DARVILL, M. MCNEIL, P. ALBERSHEIM, and D. P. DEHMER. The Biochemistry of Plants, **1**, 91 (1980).
2. G. O. ASPINALL, J. A. MOLLOY, and J. W. T. CRAIG. Can. J. Biochem. **47**, 1063 (1969).
3. B. W. SIMSON and T. E. TIMELL. Cellulose Chem. Technol. **12**, 39 (1978).
4. H. MEIER. J. Polymer Sci. **51**, 11 (1961).
5. D. BURKE, P. KAUFMAN, M. MCNEIL, and P. ALBERSHEIM. Plant Physiol. **54**, 109 (1974).
6. H.-L. HARDELL and U. WESTERMARK. The carbohydrate composition of the outer cell walls of spruce fibres. International

Can. J. Chem. Downloaded from www.nrcresearchpress.com by 210.87.254.40 on 09/06/12
For personal use only.

Symposium on Wood and Pulping Chemistry, Stockholm. Vol. 1, 1: 32 (1981).
7. P. WHITING, B. D. FAVIS, F. G. T. ST-GERMAIN, and D. A. I. GORING. J. Wood Chem. Technol. **1**, 29 (1981).
8. D. FENGEL and G. WEGENER. Hydrolysis of cellulose: mechanisms of enzymatic and acid catalysis. *Edited by* R. Brown and L. Jurasek. Advances in Chemistry Series. American Chemical Society, **181**, 145 (1979).
9. W. A. CÔTÉ, N. P. KUTSCHA, B. W. SIMON, and T. E. TIMELL. Tappi, **51**, 33 (1968).
10. H. MEIER and K. C. B. WILKIE. Holzforschung, **13**, 177 (1959).

Can. J. Chem. Downloaded from www.nrcresearchpress.com by 210.87.254.40 on 09/06/12
For personal use only.

Synthetic approaches to haplophytine. 1. Synthesis of 1-methoxy- and 1-hydroxy-6-phenyl-6-(2-pivaloylamidophenyl)non-8-ene-4,5-dione and 1-methyl-3-phenyl-3-(2-pivaloylamidophenyl)-2-pyrrolidinone

PETER YATES AND DAVID AARON SCHWARTZ

Lash Miller Chemical Laboratories, University of Toronto, Toronto, Ont., Canada M5S 1A1

Received August 24, 1982

PETER YATES and DAVID AARON SCHWARTZ. Can. J. Chem. **61**, 509 (1983).

An analysis of the structures of the alkaloid haplophytine and its dihydrobromide which is formed with rearrangement, shows that they are both derived from a 7-(2-amino-3-hydroxyphenyl)-7-aryl-9-(methylamino)-5,6-dioxononanoic acid moiety (**3**). Approaches to the synthesis of compounds related to **3** are described. The dianion **13** of phenyl(2-pivaloylamidophenyl)methane, that of methyl 2-phenyl-2-(2-pivaloylamidophenyl)acetate, and the trianion **37** of 2-phenyl-2-(2-pivaloylamidophenyl)acetic acid undergo C-alkylation and C-acylation with nucleophiles. Acylation of **13** with methyl 2,2,5-trimethoxypentanoate followed by hydrolysis gives 6-methoxy-1-phenyl-1-(2-pivaloylamidophenyl)-2,3-hexanedione. This with allyl bromide and sodium carbonate gives the O-allyl derivative, which on thermolysis is converted to its C-allyl isomer, 1-methoxy-6-phenyl-6-(2-pivaloylamidophenyl)non-8-ene-4,5-dione. The corresponding 1-hydroxy compound was prepared analogously via acylation of **13** with methyl tetrahydro-2-methoxyfuran-2-carboxylate. C-allylation of the trianion **37** gives 2-phenyl-2-(2-pivaloylamidophenyl)pent-4-enoic acid, whose methyl ester on ozonolysis followed by treatment with methylamine hydrochloride and sodium cyanoborohydride gives 1-methyl-3-phenyl-3-(2-pivaloylamidophenyl)-2-pyrrolidinone, a potential advanced intermediate for the synthesis of compounds related to **3**.

PETER YATES et DAVID AARON SCHWARTZ. Can. J. Chem. **61**, 509 (1983).

Une analyse des structures de l'alcaloide haplophytine et de son dérivé provenant d'une addition de deux moles d'acide bromhydrique qui se fait avec une transposition révèle que les deux composés proviennent de la même unité, soit l'acide (amino-2 hydroxy-3 phényl)-7 aryl-7 (méthylamino)-9 dioxo-5,6 nonanoique (**3**). On décrit des voies d'accès à des composés reliés à l'acide **3**. Le dianion **13** du phényl(pivaloylamido-2 phényl)méthane, celui du phényl-2 (pivaloylamido-2 phényl)-2 acétate de méthyle et le trianion **37** de l'acide phényl-2 (pivaloylamido-2 phényl)-2 acétique subissent une C-alkylation et une C-acylation avec les nucléophiles. L'acylation du composé **13** avec le triméthoxy-2,2,5 pentanoate de méthyle, suivie d'une hydrolyse, donne la méthoxy-6 phényl-1 (pivaloylamido-2 phényl)-1 hexanedione-2,3. Cette dernière, en présence du bromure d'allyle et du carbonate de sodium, donne le dérivé O-allyle qui, par thermolyse, se transforme en son isomère C-allyle, la méthoxy-1 phényl-6 (pivaloylamido-2 phényl)-6 nonène-8 dione-4,5. D'une façon analogue, on a préparé le composé hydroxy-1 correspondant via l'acylation du composé **13** avec le méthoxy-2 tétrahydrofuranne carboxylate de méthyle. Une C-allylation du trianion **37** conduit à l'acide phényl-2 (pivaloylamido-2 phényl)-2 penthène-2 oique dont l'ester méthylique, par ozonolyse suivie de la réaction avec le chlorhydrate de la méthylamine et le cyanoborohydrure de sodium, donne la méthyl-1 phényl-3 (pivaloylamido-2 phényl)-3 pyrrolidinone-2, un intermédiaire potentiel avancé en vue de la synthèse des composés apparentés au composé **3**.

[Traduit par le journal]

The structure of the alkaloid haplophytine incorporates the moiety **1**, where Ar is the aromatic ring of a lactonic aspidosperma alkaloid residue (1). On formation of the dihydrobromide of haplophytine the moiety **1** is converted to the moiety **2**. On treatment of the salt under mildly basic conditions, haplophytine is regenerated, i.e., the rearrangement of **1** to **2** is reversed. This reversible rearrangement reflects the fact that **1** and **2** are both condensed versions of system **3**. In order to examine transformations of type **1** ⇌ **3** ⇌ **2** further and to lay the groundwork for the synthesis of haplophytine, we have undertaken synthetic studies directed towards **4** (or an equivalent), a closely related model of **3**.

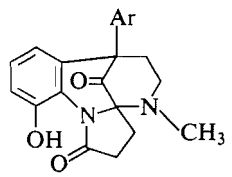

1

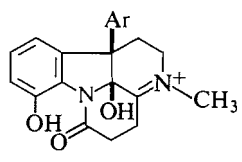

2

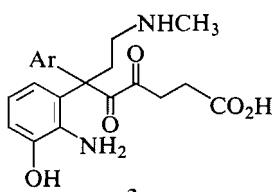

3

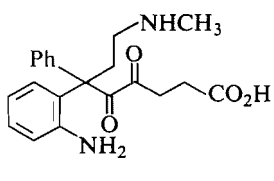

4

Our synthetic strategy (Scheme 1) entailed the use of an *o*-aminodiphenylmethane equivalent (**5**), which on substitution at the benzylic carbon with an α-oxoglutaryl equivalent would give an intermediate **6**, which on allylation at the benzylic carbon would give **7**. Oxidative cleavage of the double bond to the aldehyde followed by reductive methylamination or reductive amination and N-methylation would give **4**. Preliminary studies were conducted with *o*-nitrodiphenylmethane (**8**) as an equivalent of *o*-aminodiphenylmethane (**5**),[1] but substitution reactions at the benzylic carbon were found to occur only in low yield or not at all. We then turned our attention to the use

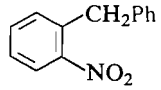

8

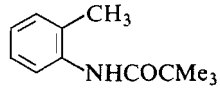

9

[1]Cf. the use of the anion of *o*-nitrotoluene as a nucleophile (2).

Can. J. Chem. Downloaded from www.nrcresearchpress.com by 210.87.254.42 on 09/06/12
For personal use only.

TABLE 1. ^{13}C nuclear magnetic resonance chemical shifts (δ, ppm) of *o*-pivaloylamidodiphenylmethyl derivatives[a]

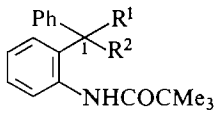

12 $R^1 = R^2 = H$
32 $R^1 = CO_2H$, $R^2 = H$
33 $R^1 = CO_2CH_3$, $R^2 = H$
38 $R^1 = CO_2H$, $R^2 = CH_2CH{=}CH_2$
21 $R^1 = COC(OCH_3)_2CH_2CH_2CH_2OCH_3$, $R^2 = H$
22 $R^1 = COCOCH_2CH_2CH_2OCH_3$, $R^2 = H$
24 $R^1 = COCOCH_2CH_2CH_2OCH_3$, $R^2 = CH_2CH{=}CH_2$

26 $R^1 =$ 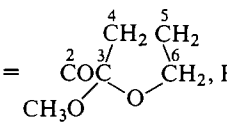 $R^2 = H$

40 $R^1,R^2 =$ 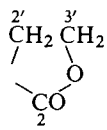

45 $R^1,R^2 =$ 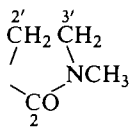

Position	Compound[b]									
	12	**32**	**33**	**38**	**21**	**22**	**24**	**26**[c]	**40**	**45**
C-1	38.5	55.5	55.8	58.8	54.7	51.3	60.8	55.0, 55.2	56.5	57.9
2	—	177.9*	174.6	177.6*	208.3	199.2*	200.4*	207.4, 207.8	179.2	176.1*
3	—	—	—	—	105.0	196.5*	200.1*	109.7, 110.0	—	—
4	—	—	—	—	29.6	33.5	35.5	33.1	—	—
5	—	—	—	—	23.1	24.0	22.6	24.4, 24.5	—	—
6	—	—	—	—	71.8	71.4	71.2	69.4, 69.6	—	—
2′	—	—	—	43.7	—	—	42.3	—	39.0	37.4
3′	—	—	—	133.3	—	—	132.6	—	66.2	47.2
4′	—	—	—	118.8	—	—	119.6	—	—	—
CONH	176.4	176.9*	176.6	177.3*	176.7	177.2	176.6	176.8	176.6	176.5*
$(CH_3)_3C$	39.4	39.3	39.4	39.2	39.4	39.5	39.5	39.4	39.2	39.3
$(CH_3)_3C$	27.3	27.0	27.2	26.8	27.2	27.3	26.8	27.2	27.1	27.3
CH_3O	—	—	52.8	—	58.3[d]	58.3	58.4	50.5	—	[e]

[a]In $CDCl_3$ solution: the assignments are in accord with the multiplicities in single frequency off-resonance decoupled spectra; assignments for a given compound marked with asterisks are interchangeable; aromatic carbon signals are not included.
[b]See below for compound structure and numbering.
[c]Mixture of diastereomers.
[d]C-6 OMe; C-3 OMe: δ 49.7, 49.8 ppm.
[e]N—Me: δ 30.9 ppm.

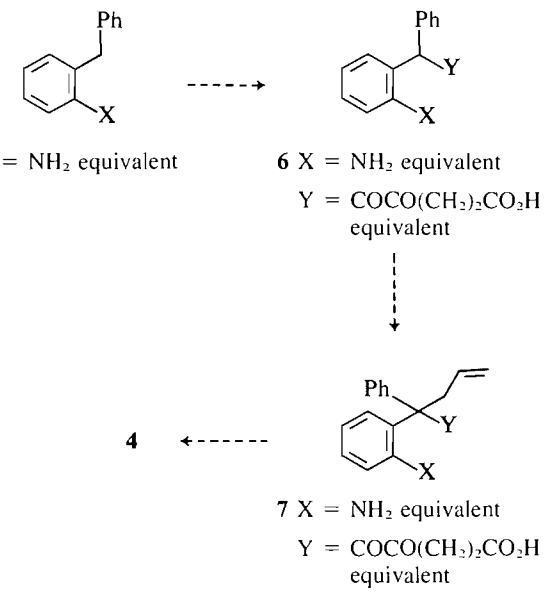

SCHEME 1

of a pivaloylamido group ($NHCOCMe_3$) as an NH_2 equivalent, based on the report of Fuhrer and Gschwend (3) that *N*-pivaloyl-*o*-toluidine (**9**) can be converted to a dianion that reacts with various electrophiles exclusively at the benzylic carbon; subsequent to this report, others have utilized pivalamides as protected amines (4). We report now on the synthesis of two compounds of type **7** by the route shown in Scheme 1 with the use of the pivalamido group as the NH_2 equivalent. It was not found possible to convert these to compounds of type **4**; attempts to surmount this hurdle are also described.

Reduction of *o*-aminobenzophenone (**10**) with sodium and ethanol (5) gave *o*-aminodiphenylmethane (**11**), which was converted to its pivaloylamide (**12**)[2] with pivaloyl chloride. Compound **12** was converted to its yellow-orange dianion **13** by treatment with two equivalents of *n*-butyllithium/TMEDA or of lithium diisopropylamide in tetrahydrofuran at −20°C. The formation of this dianion was verified by reaction with benzaldehyde to give in 98% yield a 1:1 mixture of the diastereomeric products **14** arising by exclusive attack at carbon (Scheme 2). These isomers had similar spectra, but the formation of a 1:1 mixture was apparent from the presence in the ^1H nmr spectrum of the product of two singlets of equal intensity at δ 1.05 and 1.10 ppm, assigned to the *tert*-butyl protons; they were separated and individually characterized, but individual structural assignments were not made.

We next sought to utilize the dianion **13** to introduce a latent α-oxoglutaryl residue at the benzylic carbon of **12**. The dithiane **15** was prepared from ethyl 1,3-dithiane-2-carboxylate and 3-bromo-1-methoxypropane by the general procedure of Eliel and Hartmann (6) and treated with the dianion **13**. However,

[2]The ^{13}C nmr chemical shifts for **12** and related *o*-pivaloylamidodiphenylmethyl derivatives are compared in Table 1.

Can. J. Chem. Downloaded from www.nrcresearchpress.com by 210.87.254.42 on 09/06/12
For personal use only.

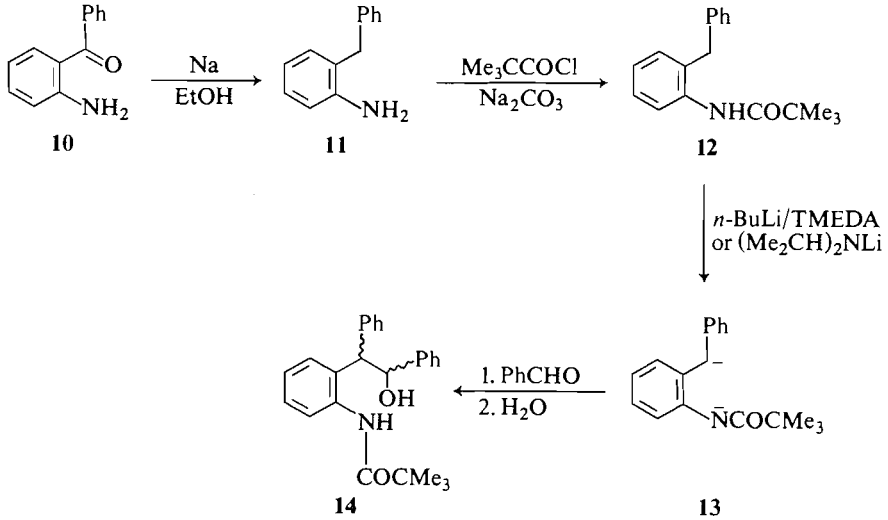

SCHEME 2

the desired acylation product **16** was not formed; instead a product was formed whose ^1H and ^{13}C nmr spectra showed it retained a carboethoxy group. This product is assigned structure **17** on the basis of the spectroscopic data (see Experimental) and is considered to arise by the route shown in Scheme 3. The unusual course of the reaction can be attributed to steric inhibition of attack by **13** on the carboethoxy group of **15** and facilitation of displacement at sulfur because of stabilization of the resulting anionic centre in **18** by that group.

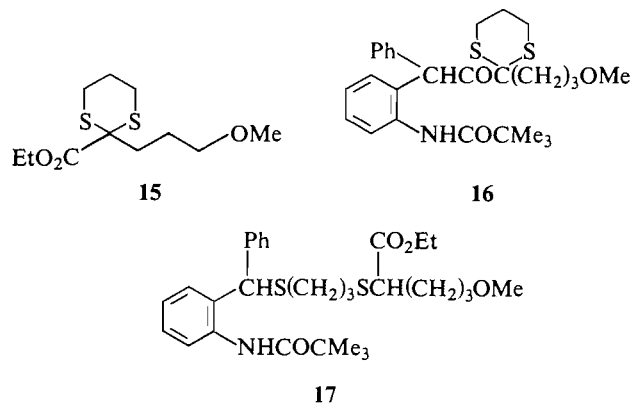

In order to circumvent this problem we turned to the use of a different latent α-oxoglutaryl residue and prepared the ketal **19** by the route shown in Scheme 4, which is analogous in part to the route used by Öhler and Schmidt (7) for the preparation of the triethoxy analogue of **20**. It was considered that use of the ketal **19** rather than the thioketal **15** would be advantageous in that there would be less steric hindrance to attack at the ester group and less propensity for anionic displacement on oxygen than on sulfur. In fact, treatment of the dianion **13** with the ketal **19** gave a product in good yield that is considered to be the desired ketone **21**, based on its elemental composition and spectra. Two features of these spectra merit comment. First, in the ir spectrum the carbonyl-stretching band occurs at 5.78 μm, which is at shorter wavelength than normal for simple acylic ketones (5.84 μm); this shift is attributed to dipole–dipole interaction of the carbonyl and C—OMe bonds (cf. the carbonyl-stretching band of 3,3-dimethoxy-2-butanone: 5.78 μm (8)). Second, in both the ^1H and ^{13}C nmr spectra

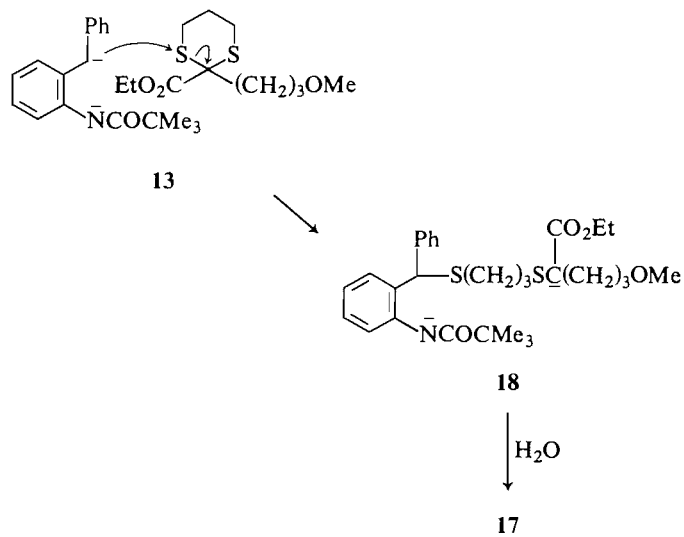

SCHEME 3

of **21** the signals of the ketal methoxy groups are distinct, due to chemical nonequivalence engendered by the benzylic chiral centre.

It was next desired to introduce an allyl group at the benzylic carbon of **21**. However, attempts to do this via dianion formation followed by treatment with allyl bromide or chloride were fruitless. One contributing factor to this failure may be that severe steric interaction in the dianion inhibits its formation. We therefore hydrolyzed the ketal **21** to the yellow α-diketone **22** with 90% formic acid (9). It was anticipated that alkylation of **22** would be more readily achieved than that of **21** because of the greater acidity of the benzylic hydrogen atom, and indeed this proved to be the case. Treatment of **22** with allyl bromide and sodium carbonate in aqueous acetone gave a product whose ^1H and ^{13}C nmr spectra showed that the allyl group had been incorporated. However, these spectra and the ir spectrum of the product showed that O-allylation rather than C-allylation had occurred and that it was a 3:1 mixture of the geometrical isomers **23** rather than the desired product **24**. It was nevertheless possible to obtain the latter by heating the O-allyl isomer mixture **23** at 90°C in toluene when Claisen

Can. J. Chem. Downloaded from www.nrcresearchpress.com by 210.87.254.42 on 09/06/12
For personal use only.

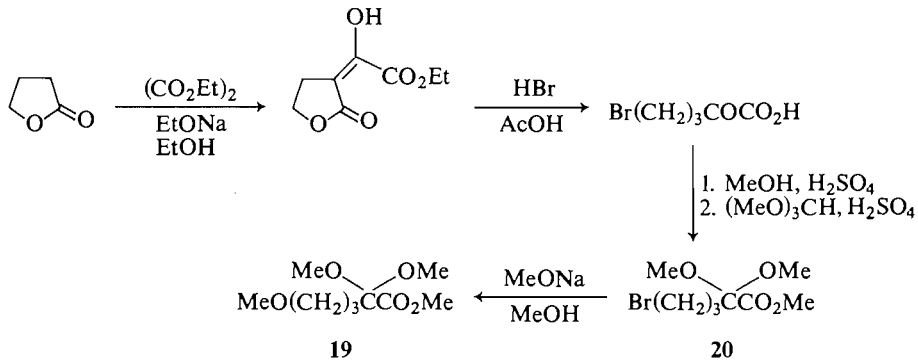

SCHEME 4

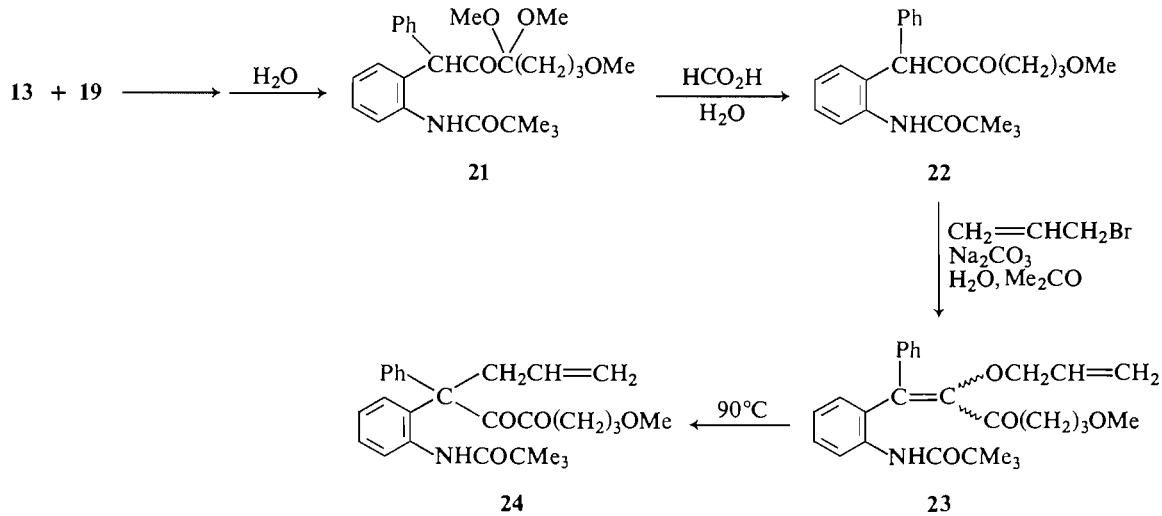

SCHEME 5

rearrangement occurred to give the α-diketone **24** (Scheme 5).[3]

Our synthetic strategy called for the eventual conversion of the methoxymethyl group of **24** to a carboxylic acid function (*vide supra*). Because we anticipated that this might call for reaction conditions that would be inimical to the other functional groups present in the molecule, we undertook the synthesis of the hydroxymethyl analogue of **24**, by a route similar to that of Scheme 5. The dianion **13** was acylated with the ester **25** (11) to give the desired ketone **26** as a 1:1 mixture of diastereomers. Hydrolysis of **26** was not straightforward: treatment with 90% formic acid gave three products **27**–**29** in turn (Scheme 6). The structural assignments are based largely on their ^{1}H nmr spectra. The hemiacetal **27** was isolated as a mixture of diastereomers and its spectrum showed two *tert*-butyl proton singlets at δ 1.10 and 1.20 ppm and two benzylic proton signals at δ 5.84 and 5.88 ppm. In the spectrum of the α-diketone **28** there is a single *tert*-butyl signal at δ 1.20 ppm and a single benzylic proton signal at δ 6.14 ppm; the downfield shift of the latter relative to the benzylic proton signals of **27** parallels the relationship of these signals in the spectra of the keto ketal **21** and the α-diketone **22**. The hemiketal **29** was also isolated as a mixture of diastereomers and its spectrum showed two *tert*-butyl proton singlets at δ 1.36 and 1.40 ppm and two benzylic proton singlets at δ 5.00 and 5.05 ppm; the upfield shift of the latter relative to the benzylic proton signals of **27** reflects the circumstance that these protons no longer have an α relationship to a ketonic group.

Although products **27**–**29** were not obtained entirely free of one another, this was not a handicap since it was found that both **27** and **28** could be converted to the allyl enol ether **30** under similar conditions to those used for the O-allylation of **22** (Scheme 5). Thus the hydrolysis of **26** was allowed to proceed for 10 minutes only, when **27** was formed as the major product accompanied by **28**, but not **29**, as a minor product, and the resulting mixture of **27** and **28** was subjected to O-allylation to give **30** in good yield. Heating of **30** in toluene at 90°C as before brought about rearrangement to the C-allyl product **31**, the desired hydroxymethyl analogue of **24**.

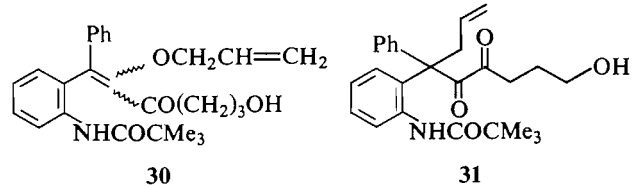

The next stage in our projected synthetic sequence was the oxidative cleavage of the ethylenic double bond in **24** or **31** followed by reductive amination. Unfortunately it was not found possible to effect this oxidation without concomitant oxidation of the α-diketone function and attempts to protect the

[3]Dauben *et al.* have recently utilized a similar reaction sequence for the C-allylation of diosphenols (10).

Can. J. Chem. Downloaded from www.nrcresearchpress.com by 210.87.254.42 on 09/06/12
For personal use only.

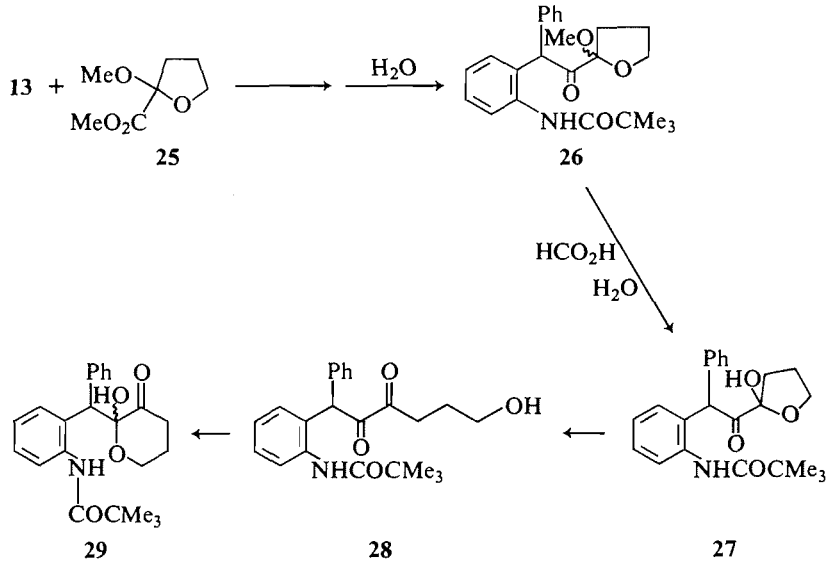

SCHEME 6

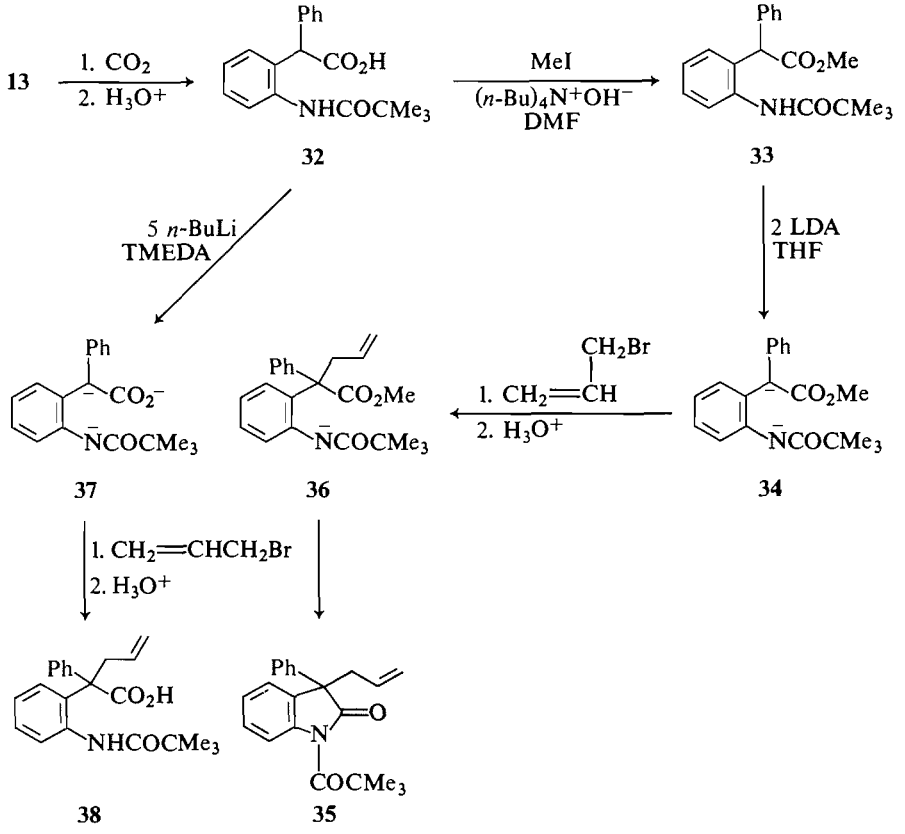

SCHEME 7

latter as a mono- or diketal failed because of the instability of **24** and **31** under acidic conditions.

We attempted to circumvent this problem by introducing the allyl substituent before elaboration of the α-diketonic residue so that its oxidative cleavage might be effected without complication. The acid **32** was prepared by carboxylation of the dianion **13** and was converted to its methyl ester **33**. An attempt to C-allylate this by treatment of its dianion **34** with allyl bromide gave the oxindole **35**. This was readily identified by comparison of its spectra with those of 3-allyl-3-phenyloxindole, which we had prepared in the course of other work. It was clear that the desired C-allylation of **33** was occurring but was accompanied by elimination of methoxide ion from the intermediate monoanion **36**. The recourse was clear, viz., reduction of the propensity of the carbonyl residue in **36** to undergo nucleophilic attack. This was achieved by the use of trianion **37** of the acid **32**, formed by treatment with five equivalents of *n*-butyllithium/TMEDA, which on reaction with allyl bromide followed by aqueous work-up gave **38** (Scheme 7).

The acid **38** was subjected to ozonolysis in aqueous meth-

Can. J. Chem. Downloaded from www.nrcresearchpress.com by 210.87.254.42 on 09/06/12
For personal use only.

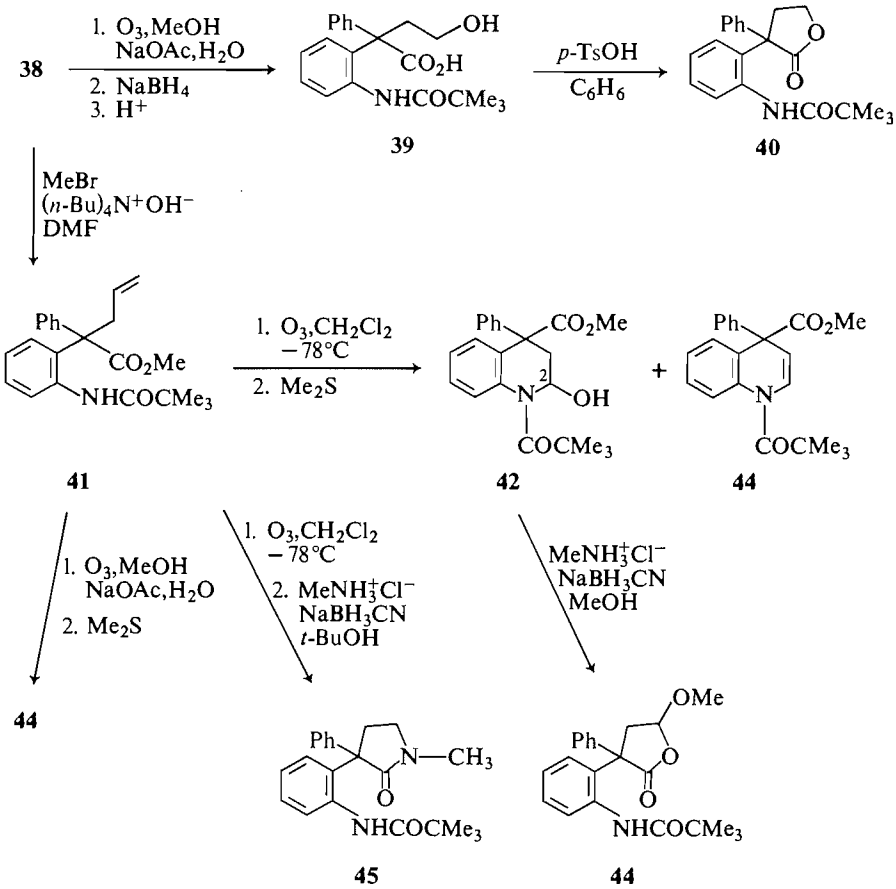

SCHEME 8

anolic solution containing sodium acetate (12) followed by reductive cleavage of the resulting ozonide with sodium borohydride to give the hydroxy acid **39**, which was lactonized with *p*-toluenesulfonic acid in benzene to **40** (Scheme 8). Attempts to reduce this with diisobutylaluminum hydride to the corresponding lactol were unsuccessful. We therefore undertook to introduce the N-methylamino function by ozonolysis of **41**, the methyl ester of **38**, to the corresponding aldehyde followed by reductive amination with methylamine. Reductive work-up of the ozonide from **41** with dimethyl sulfide gave a mixture of the hemiaminal **42**,[4] derived by attack of the amide nitrogen on the aldehyde, and a small amount of its dehydration product **43**. Treatment of **42** with methylamine hydrochloride and sodium cyanoborohydride by the method of Borch *et al.* (13) gave a mixture of diastereomeric methoxy lactones **44**, rather than the desired lactam **45**; substantiation of this structural assignment was gained from the fact that ozonolysis of **41** in aqueous methanol containing sodium acetate followed by treatment with dimethyl sulfide gave an identical product. The lactam **45** was obtained from **41** by the procedure of Martin *et al.* (14), in which the ozonide is subjected directly to reductive amination conditions with an amine and sodium cyanoborohydride in *tert*-butyl alcohol (Scheme 8). Compound **45** contains latently the 2-(methylamino)ethyl grouping of **4** and has the potential for elaboration to **4** or an equivalent, based on the methodology developed in the present work. However, the yield of its formation from **41** is low, and it will be necessary to improve this yield for it to serve as a viable intermediate.

[4]The ^{1}H nmr spectrum of **42** shows that it is a single diastereomer and that the C-2 proton is pseudoequatorial. Its ir spectrum shows that the hydroxyl proton is strongly hydrogen-bonded to the amide carbonyl group. It is tentatively assigned the configuration with the phenyl group *trans* to the hydroxyl group and pseudoequatorial.

Experimental

Melting points are uncorrected. Unless otherwise specified, the ir spectra were recorded for $CHCl_3$ solutions and the ^{1}H and ^{13}C nmr spectra for $CDCl_3$ solutions. Mass spectra were recorded at 70 eV and peak positions (*m/e*) are followed by relative abundances in parentheses. Preparative thin layer chromatography was carried out on 20 × 20 × 1-mm or 20 × 20 × 2-mm Merck silica gel "60 PF_{254}" plates with uv visualization; the bands were extracted with MeOH, the residues obtained after filtration and evaporation were slurried with $CHCl_3$, and the solutions were filtered and evaporated to give the products. Solutions in organic solvents were dried over anhydrous $MgSO_4$ and evaporated by means of a rotary evaporator at water aspirator pressure.

2-Aminodiphenylmethane (11)

This compound was prepared from *o*-aminobenzophenone (**10**) by reduction with sodium in ethanol in 90% yield according to the method of Hewett *et al.* (5); bp 110–120°C/0.05 Torr (lit. (15) bp 171–172°C/12 Torr); ir λ_{max}: 2.98 (m), 6.30 μm; ^{1}H nmr δ: 3.3 (br s, 2H; D_2O exchangeable), 3.80 (s, 2H), 6.4–7.4 (m, 9H).

Phenyl(2-pivaloylamidophenyl)methane (12)

A solution of amine **11** (20.0 g, 0.11 mol) in dichloromethane (70 mL) was added to a solution of sodium carbonate (10 g) in water (100 mL). To the stirred heterogeneous mixture, cooled in an ice water bath, was added dropwise a solution of pivaloyl chloride (14.5 g, 0.12 mol) in dichloromethane (30 mL). After the addition the ice bath was removed and the reaction mixture was stirred at room

Can. J. Chem. Downloaded from www.nrcresearchpress.com by 210.87.254.42 on 09/06/12
For personal use only.

Can. J. Chem. Downloaded from www.nrcresearchpress.com by 210.87.254.42 on 09/06/12
For personal use only.

temperature for 3 h. The phases were separated and the aqueous phase was extracted with dichloromethane (30 mL). The combined organic solutions were dried and concentrated to yield an oil which crystallized on standing. Recrystallization from hexanes yielded **12** (23.3 g, 80%) as white needles, mp 78–80.5°C; ir λ_{max}: 2.94 (w), 5.95 μm; ^{1}H nmr δ: 1.10 (s, 9H), 4.00 (s, 2H), 7.0–7.5 (m, 9H), 8.0 (m, 1H); ^{13}C nmr δ: 27.3 (q), 38.5 (t), 39.4 (s), 123.6, 124.8, 126.8, 127.6, 127.6, 128.2, 128.9, 130.6, 131.0, 136.3, 138.8, 176.4 (s); *m/e*: 267 (51), 210 (100). *Anal.* calcd. for $C_{18}H_{21}NO$: C 80.86, H 7.92, N 5.24; found: C 80.85, H 7.85, N 5.29.

*Formation of the dianion **13** of **12***[5]

Method A (n-BuLi)

A solution of amide **12** (1.00 g, 3.75 mmol), THF (5 mL), and tetramethylethylenediamine (TMEDA; 1.12 mL, 7.49 mmol) was cooled to -20°C (Dry Ice/CCl_4) and 1.95 *M* *n*-BuLi in *n*-hexane (3.84 mL, 7.49 mmol) was added dropwise with stirring. Formation of the dianion **13** was indicated by the immediate appearance of a yellow-orange color on addition of the second equivalent of base. Stirring at −20°C was continued for 10 min.

Method B (LDA)

A 2.05 *M* solution of *n*-BuLi in *n*-hexane (0.402 mL; 0.824 mmol) was added dropwise to a solution of diisopropylamine (0.124 mL, 0.824 mmol) in THF (5 mL) at −20°C. After 15 min a solution of amide **12** (0.100 g, 0.374 mmol) in THF (1.5 mL) was added dropwise with stirring at −20°C. The solution immediately became yellow-orange in color.

*Standard work-up procedure of reaction mixtures from **13***[6]

Saturated aqueous ammonium chloride was added to the reaction mixture and the heterogeneous solution was extracted twice with ether. The combined ethereal extracts were washed with saturated aqueous ammonium chloride. The combined aqueous solutions were back-extracted with ether. The combined ethereal extracts were dried and concentrated to yield the reaction product.

*1,2-Diphenyl-2-(pivaloylamidophenyl)ethanol (**14**)*[5]

To a stirred solution of dianion **13**, formed by Method A from amide **12** (1.00 g, 3.75 mmol), TMEDA (1.13 mL, 7.50 mmol), and 2.20 *M* *n*-BuLi in *n*-hexane (3.40 mL, 7.50 mmol), in THF (10 mL) at −30°C was added benzaldehyde (0.400 mL, 3.77 mmol). The reaction mixture was stirred at −30°C for 30 min and at room temperature for 1 h. The standard work-up procedure yielded 1.38 g (98%) of crude **14** as a mixture of diastereomers, mp 155–160°C.

The mixture was chromatographed on silica gel with $CHCl_3$ – ethyl acetate (1:1) as eluant to give the individual diastereomers. Diastereomer 1 (R_f 0.51), mp 170–171°C; ir λ_{max}: 2.80 (w), 2.95 (m), 5.99 μm; ^{1}H nmr δ: 1.05 (s, 9H), 3.0 (br s, 1H; D_2O exchangeable), 4.30 (d, *J* = 8 Hz, 1H), 5.40 (d, *J* = 8 Hz, 1H), 7.0–8.0 (m, 15H); *m/e*: 373 (<1), 210 (100). *Anal.* calcd. for $C_{25}H_{27}NO_2$: C 80.39, H 7.29, N 3.75; found: C 80.69, H 7.28, N 3.74. Diastereomer 2 (R_f 0.35), mp 189.5–190°C; ir λ_{max}: 2.80 (w), 2.95 (m), 5.99 μm; ^{1}H nmr δ: 1.10 (s, 9H), 3.0 (br s, 1H; D_2O exchangeable), 4.40 (d, *J* = 8 Hz, 1H), 5.40 (d, *J* = 9 Hz, 1H), 6.9–7.2 (m, 13H), 7.50 (m, 1H), 7.95 (br s, 1H); *m/e*: 373 (1), 210 (100). *Anal.* calcd. for $C_{25}H_{27}NO_2$: C 80.39, H 7.29, N 3.75; found: C 80.52, H 7.31, N 3.69.

Ethyl 1,3-dithiane-2-carboxylate

This compound was synthesized from ethyl diethoxyacetate (16), 1,3-propanedithiol, and boron trifluoride etherate in chloroform according to the procedure of Eliel and Hartmann (6); bp 90–94°C/0.25 Torr (lit. (6) bp 75–77°C/0.2 Torr).

*Ethyl 2-(3-methoxypropyl)-1,3-dithiane-2-carboxylate (**15**)*[5]

The general procedure of Eliel and Hartmann (6) was followed. Sodium hydride (50% dispersion in oil; 1.12 g, 24.3 mmol), washed with benzene (2 × 20 mL), was covered with benzene (30 mL). A solution of 3-bromo-1-methoxypropane (3.30 g, 21.2 mmol) and ethyl 1,3-dithiane-2-carboxylate (4.10 g, 21.2 mmol) in dimethylformamide (10 mL) was added dropwise to the stirred suspension of sodium hydride in benzene at 0°C over 1 h. The reaction mixture was allowed to warm to room temperature and stirred overnight. The deep red mixture was poured into water (50 mL). The phases were separated and the aqueous phase was extracted with benzene (30 mL). The combined organic solutions were dried and evaporated to yield **15** (4.69 g, 85%) as a colorless oil; ir λ_{max}: 5.80 μm; ^{1}H nmr δ: 1.35 (t, *J* = 7 Hz, 3H), 1.5–3.2 (m, 10H), 3.35 (s, 3H), 3.50 (t, *J* = 6 Hz, 2H), 4.25 (q, *J* = 7 Hz, 2H); ^{13}C nmr δ: 14.2 (q), 24.6 (t), 24.8 (t), 27.8 (t), 35.5 (t), 52.1 (s), 58.3 (q), 61.6 (t), 72.3 (t), 170.7 (s); *m/e*: 264 (15), 191 (100). *Accurate Mass* calcd. for $C_{11}H_{20}O_3S_2$: 264.0853; found: 264.0843.

*Addition of ester **15** to dianion **13**. Formation of **17***

To a stirred solution of dianion **13**, formed by Method A from amide **12** (0.150 g, 0.56 mmol), TMEDA (0.17 mL, 1.12 mmol), and 2.30 *M* *n*-BuLi in *n*-hexane (0.50, 1.15 mmol), in THF (5 mL) at −20°C was added dropwise a solution of ester **15** (0.140 g, 0.56 mL) in THF (1 mL). The reaction mixture was stirred at −20°C for 1 h and at room temperature for 15 min. The standard work-up procedure yielded an oil. The oil was placed in a molecular still and heated at 120°C (oil bath)/0.025 Torr to remove starting material. The pot residue consisted of crude **17** as an oil; ir λ_{max}: 3.00 (w), 5.74, 5.90 μm; ^{1}H nmr δ: 1.70 (s, 9H), 1.25 (t, *J* = 7 Hz, 3H), 1.5–2.0 (m, 6H), 2.5–2.9 (m, 5H), 3.20–3.50 (m, 2H), 3.25 (s, 3H), 4.20 (q, *J* = 7 Hz, 2H), 5.33 (s, 1H), 7.0–8.0 (m, 8H), 7.95 (br d, *J* = 7 Hz, 1H), 8.20 (br s, 1H); ^{13}C nmr δ: 14.2 (q), 27.4 (q), 39.5 (s), 46.6 (d), 51.9 (d), 58.5 (q), 61.4 (t), 72.0 (t), 136.5 (s), 138.3 (s), 172.5 (s), 176.5 (s); *m/e*: 531 (<1), 265 (100), 266 (80).

α-Ethoxalyl-γ-butyrolactone

This compound was prepared in 78% yield by the method of Plieninger (17) from γ-butyrolactone, diethyl oxalate, and sodium ethoxide in ethanol under nitrogen.

5-Bromo-2-oxopentanoic acid

This compound was prepared in 86% yield from α-ethoxalyl-γ-butyrolactone and hydrobromic acid in acetic acid by the method of Öhler and Schmidt (7); bp 100°C/0.05 Torr (lit. (7) bp 115°C/0.01 Torr).

Methyl 5-bromo-2-oxopentanoate

A solution of 5-bromo-2-oxopentanoic acid (28.13 g, 0.144 mol), methanol (160 mL), and concentrated sulfuric acid (2 mL) was stirred overnight at room temperature. The solvent methanol was removed, the residue was dissolved in ether (200 mL), and the solution was washed with saturated aqueous sodium bicarbonate (50 mL). The ethereal solution was dried and concentrated to yield methyl 5-bromo-2-oxopentanoate (26.17 g, 87%) as a colorless oil. The product was used without further purification; ir λ_{max}: 5.77 μm; ^{1}H nmr δ: 2.20 (m, 2H), 3.05 (t, *J* = 6.5 Hz, 2H), 3.50 (t, *J* = 6.5 Hz, 2H), 3.82 (s, 3H).

*Methyl 5-bromo-2,2-dimethoxypentanoate (**20**)*

Methyl 5-bromo-2-oxopentanoate (10.0 g, 47.8 mmol), trimethyl orthoformate (10.20 g, 96.2 mmol), methanol (15 mL), and concentrated sulfuric acid (2 drops) were stirred under nitrogen for 48 h at room temperature. Sodium bicarbonate (2 g) was added and the mixture was stirred for 0.5 h, filtered, and concentrated. The colorless liquid residue was distilled to yield ketal ester **20** (9.95 g, 75%), bp 78–83°C/0.025 Torr; ir λ_{max}: 5.72 μm; ^{1}H nmr δ: 1.5–2.2 (m, 4H), 3.20 (s, 6H), 3.37 (t, *J* = 6 Hz, 2H), 3.80 (s, 3H).

*Methyl 2,2,5-trimethoxypentanoate (**19**)*

Sodium (1.07 g, 0.046 g-atom) was added to methanol (50 mL). Following reaction of the sodium and cooling of the solution to room temperature, ester **20** (8.75 g, 34.3 mmol) was added. The solution was stirred at room temperature for 72 h. The methanol was removed,

[5]These experiments were conducted under rigorously anhydrous conditions under a positive pressure of nitrogen.

[6]This procedure is referred to in later experiments as the standard work-up procedure.

Can. J. Chem. Downloaded from www.nrcresearchpress.com by 210.87.254.42 on 09/06/12
For personal use only.

the residue was dissolved in dichloromethane (30 mL), and the solution was washed with water (15 mL). The organic solution was dried and concentrated to yield **19** (6.15 g, 87%), bp 68–70°C/0.01 Torr; ir λ_{max}: 5.74 μm; ^{1}H nmr δ: 1.2–2.2 (m, 4H), 3.22 (s, 6H), 3.24 (s, 3H), 3.35 (t, J = 6.5 Hz, 2H), 3.60 (s, 3H); ^{13}C nmr δ: 23.2 (t), 30.0 (t), 49.1 (q), 51.6 (q), 57.8 (q), 71.4 (t), 102.1 (s), 168.9 (s); *m/e*: 175 (M−OCH_3; 9), 148 (100). *Anal.* calcd. for $C_9H_{18}O_5$: C 52.41, H 8.80; found: C 52.26, H 8.77.

3,3,6-Trimethoxy-1-phenyl-1-(2-pivaloylamidophenyl)-2-hexanone (21)[5]

A slution of ketal ester **19** (4.20 g, 20.6 mmol) was added dropwise over 5 min to a stirred solution of dianion **13**, formed by method A from amide **12** (5.00 g, 18.0 mmol), TMEDA (5.64 mL, 36 mmol), and 1.90 *M* *n*-BuLi in *n*-hexane (19.7 mL, 36 mmol) at −30°C. The reaction mixture was stirred at −30°C for 30 min and at room temperature for 16 h during which time a precipitate formed. The standard work-up procedure yielded 8.5 g of an oil, which was shown by ^{1}H nmr spectroscopic analysis to be a mixture of starting amide and ketone **21**. Preparative scale medium-pressure liquid chromatography with hexane − ethyl acetate (4:1) as eluant yielded starting amide **12** (1.20 g) and ketone **21** (5.95 g, 73%; 93% based on recovered starting material) as a pale yellow oil; ir λ_{max}: 3.05 (w), 5.78, 5.94 μm; ^{1}H nmr δ: 1.10 (s, 9H), 1.2–2.2 (m, 4H), 3.14 (s, 3H), 3.25 (s, 3H), 3.35 (s, 3H), 3.20 (m, 2H), 6.00 (s, 1H), 7.0–8.5 (m, 8H), 7.95 (m, 1H), 8.35 (br s, 1H); ^{13}C nmr δ: 23.1 (d), 27.2 (q), 29.6 (d), 39.4 (s), 49.7 (q), 49.8 (q), 54.7 (d), 58.3 (q), 105.0 (s), 124.7, 125.3, 126.9, 127.0, 128.0, 128.5, 132.4, 137.2, 137.5, 176.7 (s), 208.3 (s); *m/e*: 410 (M − OCH_3; <1), 147 (100). *Accurate Mass* calcd. for $C_{25}H_{32}NO_4$ (M − OCH_3): 410.2331; found: 410.2329.

6-Methoxy-1-phenyl-1-(2-pivaloylamidophenyl)-2,3-hexanedione (22)

Ketal ketone **21** (1.00 g, 2.26 mmol) and 90% formic acid (10 mL) were stirred under nitrogen for 1 h at room temperature during which time the solution became bright yellow. Water (25 mL) was added and the solution was extracted with dichloromethane (2 × 30 mL). The combined organic extracts were dried and concentrated to an oil. The product was crystallized from hexane–benzene as long yellow needles. The yield of **22** in two crops was 600 mg (67%), mp 68–70°C; ir λ_{max}: 2.94 (w), 5.83, 5.96 μm; ^{1}H nmr δ: 1.20 (s, 9H), 1.90 (m, 2H), 2.80 (m, 2H), 3.20 (s, 3H), 3.35 (t, J = 6Hz, 2H), 6.20 (s, 1H), 7.0–8.0 (m, 10H); ^{13}C nmr δ: 24.0 (t), 27.3 (q), 33.5 (t), 39.5 (s), 51.3 (t), 58.3 (q), 71.4 (t), 125.5, 127.5, 128.1, 128.7, 128.8, 129.9, 131.6, 136.2, 136.6, 177.2 (s), 196.5 (s), 199.2 (s); *m/e*: 396 (M + 1; 6), 210 (100). *Accurate Mass* calcd. for $C_{24}H_{29}NO_4$: 395.2096; found: 395.2098.

2-Allyloxy-6-methoxy-1-phenyl-1-(2-pivaloylamidophenyl)hex-1-en-3-one (23)

A mixture of diketone **22** (1.15 g, 2.91 mmol), sodium carbonate (0.295 g, 2.89 mmol), acetone (28 mL), water (12 mL), and allyl bromide (0.50 mL, 5.78 mmol) was stirred under nitrogen at room temperature for 4 h. The acetone was removed under reduced pressure and the residue was extracted with dichloromethane (2 × 20 mL). The combined organic extracts were dried and concentrated to yield **23** (1.10 g; purity >90% by ^{1}H nmr analysis) as a 3:1 mixture of *cis*/*trans* isomers; ^{1}H nmr δ: 1.17, 1.25 (2 s, 9H), 1.80 (m, 2H), 2.40 (m, 2H), 3.1-3.4 (m, 5H), 4.20 (d, J = 5 Hz, 2H), 5.0–6.0 (m, 3H), 7.0–7.6 (m, 8H), 7.9–8.3 (m, 2H); ^{13}C nmr δ: 71.4 (t), 176.9 (s), 201.7 (s).

1-Methoxy-6-phenyl-6-(2-pivaloylamidophenyl)non-8-ene-4,5-dione (24)

A. Preliminary investigation

A ^{1}H nmr tube was charged with a solution of the enol ethers **23** (60 mg) in toluene-d_8 (1 mL). The tube was immersed in an oil bath at 90°C. At various intervals (~2 h) ^{1}H nmr spectra were taken and the progress of the reaction was followed by the diminution of the intensity of the *tert*-butyl peaks at δ 1.0 and 1.2 and the concomitant growth of the butyl peak at δ 0.95. The reaction was complete in ~24 h.

B. Preparative method

A solution of the enol ethers **23** (3.00 g) and toluene (30 mL) under nitrogen was immersed in a 90°C oil bath and heated for 24 h. The solvent was removed yielding 3.00 g of an oil. Purification by medium-pressure liquid chromatography with hexanes − ethyl acetate (4:1) as eluant yielded **24** (1.50 g, 45% from diketone **22**) as a yellow oil; ir λ_{max}: 2.96, 5.85, 5.96 μm; ^{1}H nmr δ: 0.95 (s, 9H), 1.4–3.2 (m, 8H), 3.22 (s, 3H), 4.7–5.7 (m, 3H), 6.9–8.0 (m, 10H); ^{13}C nmr δ: 22.6 (t), 26.8 (q), 35.5 (t), 39.5 (s), 42.3 (t), 53.8 (q), 60.8 (s), 71.2 (t), 119.3, 125.4, 125.9, 127.5, 127.9, 128.3, 128.6, 129.1, 129.3, 132.6, 136.9, 138.3, 176.6 (s), 200.1 (s), 200.4 (s); *m/e*: 435 (<1), 101 (100). *Accurate Mass* calcd. for $C_{27}H_{33}NO_4$: 435.2409; found: 435.2409.

Methyl tetrahydro-2-methoxyfuran-2-carboxylate (25)

A solution of 5,6-dihydro-2*H*-pyran-2-one (11) (0.750 g, 6.57 mmol), methanol (15 mL), and concentrated sulfuric acid (3 drops) was boiled under reflux for 17 h. The reaction mixture was cooled to room temperature and neutralized with solid sodium bicarbonate. Excess sodium bicarbonate was removed by filtration and the filtrate was concentrated to yield methoxy ester **25** (925 mg, 88%), bp 23–25°C/0.05 Torr; ir λ_{max}: 5.70 μm; ^{1}H nmr δ: 1.9–2.2 (m, 4H), 3.35 (s, 3H), 3.80 (s, 3H), 4.0 (m, 2H); ^{13}C nmr δ: 23.3 (t), 35.8 (t), 50.1 (q), 51.6 (q), 68.4 (t), 105.5 (s), 169.2 (s); *m/e*: 139 (15), 59 (100).

1-(2-(2-Methoxy)tetrahydrofuranyl)-2-phenyl-2-(2-pivaloylamidophenyl)ethanone (26)[5]

A solution of ester **25** in THF (5 mL) was added dropwise to a stirred solution of dianion **13**, formed by method A from amide **12** (4.84 g, 18.1 mol), TMEDA (5.47 mL, 36.2 mmol), and 2.15 *M* *n*-BuLi in *n*-hexane (16.86 mL, 36.2 mmol), in THF (40 mL) at −30°C. The reaction mixture was stirred at −30°C for 1 h and at room temperature for 2.5 h. The standard work-up procedure yielded 8.0 g of an oil. Preparative medium-pressure liquid chromatography with hexane − ethyl acetate (4:1) as eluant yielded amide **12** (1.0 g) and the diastereomeric ketones **26** (4.30 g, 62%; 76% based on recovered starting material), which crystallized on standing. Ketone **26** was recrystallized from hexanes, mp 88–89.5°C; ir λ_{max}: 2.99 (w), 5.80, 5.95; ^{1}H nmr δ: 1.00, 1.05 (2s, 9H), 1.6–2.2 (m, 4H), 3.00, 3.15 (2s, 3H), 3.8–4.2 (m, 2H), 5.82 (s, 1H), 6.8–8.0 (m, 9H), 8.40 (br s, 1H); ^{13}C nmr δ: 24.4 (t), 24.5 (t), 27.2 (q), 33.1 (t), 39.4 (s), 50.5 (q), 55.1 (d), 55.2 (d), 69.4 (t), 69.6 (t), 109.7 (s), 110.0 (s), 124.6, 125.2, 125.4, 126.8, 127.1, 127.9, 128.1, 128.4, 128.6, 131.9, 132.8, 137.3, 137.6, 176.8 (s), 207.4 (s), 207.8 (s); *m/e*: 395 (5), 101 (100). *Anal.* calcd. for $C_{24}H_{29}NO_4$: C 72.84, H 7.39, N 3.54; found: C 72.84, H 7.38, N 3.52.

1-(2-(2-Hydroxy)tetrahydrofuranyl)-2-phenyl-2-(2-pivaloylamidophenyl)ethanone (27)

Aqueous formic acid (90%; 18.5 mL) was added to **26** (2.39 g, 6.04 mmol) and the mixture became homogeneous and was stirred at room temperature for 15 min. The reaction mixture was poured into water (50 mL) and extracted with dichloromethane (2 × 50 mL). The combined organic extracts were washed with saturated aqueous sodium bicarbonate (25 mL), dried, and evaporated to yield crude **27** (2.20 g, 95%); ir_{max}: 2.95 (m), 5.80, 5.96 μm; ^{1}H nmr δ: 1.04 and 1.12 (2 s, 9H), 2.0 (m, 5H), 4.05 (m, 2H), 5.74 and 5.78 (2 s, 1H), 6.9–7.9 (m, 9H), 8.1 (br s, 1H); *m/e*: 363 (M − H_2O; <1), 210 (100). *Accurate Mass* calcd. for $C_{23}H_{25}NO_3$ (M − H_2O): 363.1834; found: 363.1829. This product was used without further purification.

6-Hydroxy-1-phenyl-1-(2-pivaloylamidophenyl)-2,3-hexanedione (28) and tetrahydro-2-hydroxy-2-(phenyl(2-pivaloylamidophenyl)methyl)-3-oxopyran (29)

Aqueous formic acid (90%; 1 mL) was added to **26** (0.075, 0.197 mmol) and the mixture became homogeneous and was stirred at room temperature for 4 h. Water (10 mL) was added and the mixture

Can. J. Chem. Downloaded from www.nrcresearchpress.com by 210.87.254.42 on 09/06/12
For personal use only.

was extracted with dichloromethane (2 × 15 mL). The combined organic extracts were washed with saturated aqueous sodium bicarbonate, dried, and concentrated to yield 180 mg of an oil. Preparative thin-layer chromatography with hexanes – ethyl acetate (7:3) as eluant gave two major bands. Band 1 (R_f 0.24–0.44) gave **28** (36 mg, 50%) as a yellow oil; ir λ_{max}: 2.95 (m), 5.80, 5.95 μm; ^{1}H nmr δ: 1.17 (s, ~9H), 1.7–2.2 (m, 3H), 2.75–3.0 (m, 2H), 4.08 (t, J = 6 Hz, 2H), 6.08 (s, 1H), 7.0–8.0 (m, ~10H); *m/e*: 363 (M – H_2O; <1), 210 (100). *Accurate Mass* calcd. for $C_{23}H_{25}NO_3$ (M – H_2O): 363.1834; found: 363.1850. Band 2 (R_f 0.45–0.64) gave **29** (16 mg, 25%) as a colorless oil; ir λ_{max}: 3.00 (m), 5.74, 5.95 μm; ^{1}H nmr δ: 1.24 and 1.26 (2s, 9H), 2.0 (m, ~5H), 4.15 (m, ~2H), 4.82 and 4.98 (2s, 1H), 7.0–8.0 (m, ~10H); *m/e*: 363 (M – H_2O; 100). *Accurate Mass* calcd. for $C_{23}H_{25}NO_3$ (M – H_2O): 363.1834; found: 363.1831.

2-Allyloxy-6-hydroxy-1-phenyl-1-(2-pivaloylamidophenyl)hex-1-en-3-one (30)

Diketone **28** (1.50 g, 3.94 mmol), acetone (50 mL), water (12.5 mL), allyl bromide (0.700 mL, 8.09 mmol), and sodium carbonate (0.420 g, 3.96 mmol) were combined and the mixture was stirred under nitrogen at room temperature for 18 h. Following removal of acetone the residue was treated with brine (15 mL) and extracted with dichloromethane (2 × 20 mL). The combined organic extracts were dried and concentrated to give **30** (1.50 g, 90%) as a pale yellow oil; ir λ_{max}: 2.95 (w), 5.78, 5.95 μm; ^{1}H nmr δ: 1.05 and 1.12 (2 s, 9H), 1.5–2.5 (m, ~5H), 3.45 (t, J = 7 Hz, 2H), 4.2 (m, 2H), 5.0–6.0 (m, 3H), 6.9–8.2 (m, ~10H).

1-Hydroxy-6-phenyl-6-(2-pivaloylamidophenyl)non-8-ene-4,5-dione (31)

A solution of enol ethers **30** (1.00 g) and toluene (10 mL) under nitrogen was immersed in a 90°C oil bath and heated for 24 h. The solvent was removed yielding 1.00 g of an oil. Purification by medium-pressure liquid chromatography with hexanes – ethyl acetate (4:1) as eluant yielded **31** (0.50 g, 45% from ketone **27**) as a yellow oil; ir λ_{max}: 2.87 (m), 5.80, 5.95 μm; ^{1}H nmr δ: 0.95 (s, 9H), 1.5–3.8 (m, 9H), 4.7–5.7 (m, 3H), 6.8–7.8 (m, ~10H); *m/e*: 403 (M – H_2O; 13), 267 (100). *Acurate Mass* calcd. for $C_{26}H_{29}NO_3$ (M – H_2O): 403.2147; found: 403.2149.

2-Phenyl-2-(2-pivaloylamidophenyl)acetic acid (32)[5]

A solution of dianion **13** was formed by method A from amide **12** (7.00 g, 26.2 mmol), TMEDA (8.50 mL, 56.4 mmol), and 1.97 *M* *n*-BuLi in *n*-hexane (26.6 mL, 52.4 mmol), in THF (60 mL) at −30°C. Carbon dioxide was bubbled through the stirred solution until the color was quenched. Stirring at −30°C was continued for 10 min and at room temperature for 10 min. Ether (50 mL) was added and the solution was extracted with aqueous 5% sodium hydroxide (2 × 50 mL). The combined aqueous extracts were acidified at 0°C with concentrated hydrochloric acid and extracted with dichloromethane (2 × 50 mL). The combined organic extracts were dried and concentrated to yield 8.00 g of a viscous oil. Crystallization from hexane–benzene yielded **32** (6.58 g, 80%) as a white solid, mp 139.5–141.5°C; ir λ_{max}: 3.0–4.0, 5.85, 6.0 μm; ^{1}H nmr δ: 0.98 (s, 9H), 5.15 (s, 1H), 7.0–7.4 (m, 8H), 7.8 (m, 1H), 8.5 (br s, 1H), 10.7 (br s, 1H; D_2O exchangeable); ^{13}C nmr δ: 27.1 (q), 39.3 (s), 55.5 (d), 125.8, 126.5, 127.4, 127.7, 128.7, 129.5, 131.6, 136.3, 176.9 (s), 177.7 (s); *m/e*: 311 (4), 209 (100). *Anal.* calcd. for $C_{19}H_{21}NO_3$: C 73.29, H 6.80, N 4.50; found: C 73.36, H 6.84, N 4.34.

Methyl 2-phenyl-2-(2-pivaloylamidophenyl)acetate (33)

The general procedure of Wegenknecht *et al.* (18) was used. Benzene (25 mL), acid **32** (0.970 g, 3.12 mmol), and 0.4 *M* tetra-*n*-butylammonium hydroxide in water (8.00 mL, 3.20 mmol) were combined and the mixture was boiled under reflux under nitrogen in a flask equipped with a Dean–Stark head and condenser. After complete azeotropic removal of the water the benzene solution was concentrated to yield a colorless oil. The oil was dissolved in dimethylformamide (15 mL) and excess methyl iodide (2 mL) was added to the stirred solution. The reaction mixture was stirred overnight at room temperature. Ether (20 mL) was added and the solution was washed with water (2 × 20 mL), saturated aqueous ammonium chloride (20 mL), water (20 mL), saturated aqueous sodium bicarbonate (15 mL), and brine (20 mL). The organic solution was dried and concentrated to yield an oil, which was passed through a plug of Florisil (15 g) with hexane – ethyl acetate (7:3) as eluant. Concentration of the eluate gave ester **33** (0.900 g, 88%) as a colorless oil. Crystallization from hexane–benzene provided an analytical sample, mp 71–73°C; ir λ_{max}: 2.89 (w), 5.78, 5.97 μm; ^{1}H nmr δ: 1.00 (s, 9H), 3.80 (s, 3H), 5.15 (s, 1H), 7.0–7.5 (m, 8H), 7.97 (br d, J = 7 Hz, 1H), 8.4 (br s, 1H); ^{13}C nmr δ: 27.2 (q), 39.4 (s), 52.8 (q), 55.8 (d), 125.0, 127.5, 128.2, 128.8, 131.6, 136.4, 137.1, 174.6 (s), 176.6 (s); *m/e*: 325 (15), 209 (100). *Anal.* calcd. for $C_{20}H_{23}NO_3$: C 73.82, H 7.12, N 4.30; found: C 73.66, H 7.03, N 4.07.

2-Phenyl-2-(2-pivaloylamidophenyl)pent-4-enoic acid (38)[5]

To a stirred solution of acid **32** (4.49 g, 14.4 mmol) and TMEDA (10.80 mL, 71.7 mmol) in THF (70 mL) cooled to −30°C was added dropwise 2.15 *M* *n*-BuLi in *n*-hexane (34.00 mL, 73.1 mmol). The solution became dark brown in color and stirring was continued at −30°C for 45 min. Allyl bromide (4 mL, 22.5 mmol) was added dropwise at −30°C, when the solution became light yellow in color. Stirring was continued at −30°C for 1 h and at 0°C for 4 h during which time a copious white precipitate was produced. Water (100 mL) was added and the solution was washed with ether (2 × 35 mL). The aqueous solution was acidified at 0°C with concentrated hydrochloric acid and extracted with dichloromethane (2 × 50 mL). The combined organic extracts were dried and concentrated to yield crude **38** (4.80 g, 95%) as a colorless oil. The product was crystallized from hexane–benzene, mp 139–140°C; ir$_{max}$: 3.0–4.0, 5.90, 6.00 μm; ^{1}H nmr δ: 0.92 (s, 9H), 3.10 (br t, J = 6 Hz, 2H), 4.6–5.4 (m, 3H), 7.0–8.0 (m, 9H), 8.4 (br s, 1H), 10.35 (br s, 1H; D_2O exchangeable); ^{13}C nmr δ: 26.8 (q), 39.2 (s), 43.7 (t), 58.8 (s), 118.8, 125.2, 126.9, 127.2, 127.9, 128.2, 128.6, 131.8, 133.3, 136.8, 140.5, 177.3 (s), 177.6 (s); *m/e*: 351 (50), 208 (100). *Anal.* calcd. for $C_{22}H_{25}NO_3$: C 75.19, H 7.17, N 3.99; found: C 75.15, H 7.44, N 4.03.

α-Phenyl-α-(2-pivaloylamidophenyl)-γ-butyrolactone (40)

Ozonized oxygen was bubbled through a solution of **38** (3.40 g, 10.0 mmol) and sodium acetate (1.55 g, 11.4 mmol), methanol (50 mL), and water (2.5 mL) cooled to −78°C. After the appearance of a persistent blue color the excess ozone was displaced with oxygen followed by nitrogen. Sodium borohydride (1.54 g, 4.05 mmol) was added at −70°C and the solution was stirred and allowed to warm to room temperature. On warming, the evolution of a gas was apparent. The solvent was removed and water (25 mL) was added to the residue. The aqueous solution was acidified with concentrated hydrochloric acid and extracted with ether (3 × 20 mL). The combined ethereal extracts were dried and concentrated to yield **39** (3.00 g) as a fluffy white solid. The solid was dissolved in benzene, a few crystals of *p*-toluenesulfonic acid were added, and the mixture was stirred at room temperature for 6 h. The benzene solution was washed with water (15 mL), dried, and concentrated to yield crude **40** (2.80 g, 83%) as a white solid. Recrystallization from hexane–benzene provided an analytical sample, mp 145–145.5°C; ir λ_{max}: 3.00 (w), 5.70, 5.96 μm; ^{1}H nmr δ: 0.95 (s, 9H), 2.2–3.4 (m, 2H), 4.40 (dd, J = 8, 6 Hz, 2H), 6.8–8.0 (m, 10H); ^{13}C nmr δ: 27.1 (q), 38.9 (s), 39.2 (t), 56.5 (s), 66.2 (t), 124.8, 126.6, 126.9, 127.7, 127.9, 128.8, 129.0, 137.5, 140.5, 176.6 (s), 179.2 (s); *m/e*: 337 (100). *Anal.* calcd. for $C_{21}H_{23}NO_2$: C 74.75, H 6.87, N 4.15; found: C 74.52, H 6.80, N 4.05.

Methyl 2-phenyl-2-(2-pivaloylamidophenyl)pent-4-enoate (41)

The esterification of acid **38** was accomplished in a manner similar to that used for methyl ester **33**. Compound **41** was obtained in 86% yield as a viscous, colorless oil; ir λ_{max}: 2.96 (w), 5.80, 5.95 μm; ^{1}H nmr δ: 0.93 (s, 9H), 3.15 (m, 2H), 3.65 (s, 3H), 4.7–5.6 (m, 3H), 7.0–7.7 (m, 8H), 7.9–8.1 (m, 2H); *m/e*: 365 (41), 208 (100). *Accurate Mass* calcd. for $C_{23}H_{27}NO_3$: 365.1990; found: 365.2001.

Can. J. Chem. Downloaded from www.nrcresearchpress.com by 210.87.254.42 on 09/06/12
For personal use only.

*Methyl 1,2,3,4-tetrahydro-2-hydroxy-4-phenyl-1-pivaloyl-4-quinolinecarboxylate (**42**) and methyl 1,4-dihydro-4-phenyl-1-pivaloyl-4-quinolinecarboxylate (**43**)*

Ozonized oxygen was bubbled through a solution of **41** (450 mg, 1.23 mmol) in dichloromethane (25 mL) cooled to −78°C. After the appearance of a persistent blue color the excess ozone was displaced by oxygen followed by nitrogen. Dimethyl sulfide (1.5 mL) was added and the solution was allowed to warm to room temperature and to stand for 24 h. It was washed with water (3 × 10 mL), dried, and concentrated to yield 450 mg of a colorless oil. Dissolution of the oil in hexane − ethyl acetate (4:1) led to precipitation of **42** as a white solid (130 mg), mp 120−122°C; ir λ_{max}: 2.80 (w), 5.76, 6.12 μm; ^{1}H nmr δ: 1.20 (s, 9H), 2.02 (dd, J = 13, 7 Hz, 1H), 3.28 (dd, J = 13, 7 Hz, 1H), 3.72 (s, 3H), 4.20 (d, J = 3 Hz, 1H; D_2O exchangeable), 5.83 (td, J = 7, 3 Hz, 1H), 6.6−7.5 (m, 9H); *m/e*: 367 (3), 206 (100). *Accurate Mass* calcd. for $C_{22}H_{25}NO_4$: 367.1784; found: 367.1792.

The residue (270 mg) from the mother liquor was separated by preparative thin-layer chromatography (silica gel) with hexane − ethyl acetate (4:1) as eluant into two major bands. Band 1 (R_f 0.3−0.53) yielded a colorless oil (100 mg), whose ^{1}H nmr spectrum indicated the presence of at least three components. On standing for a week this oil crystallized and was shown by ^{1}H nmr analysis to be mainly **42**. Band 2 (R_f 0.54−0.68) yielded **43** (43 mg) as a colorless oil; ir λ_{max}: 5.74, 5.93 (m), 6.01 (m) μm; ^{1}H nmr δ: 1.30 (s, 9H), 3.78 (s, 3H), 5.78 (d, J = 7 Hz, 1H), 6.9−7.5 (m, 9H), 7.84 (m, 1H); *m/e*: 349 (2), 206 (100). *Accurate Mass* calcd. for $C_{22}H_{23}NO_3$: 349.1678; found: 349.1688.

*γ-Methoxy-α-phenyl-α-(2-pivaloylamidophenyl)-γ-butyrolactone (**44**)*

*A. From **42***

Methylamine hydrochloride (12 mg) was added to a solution of hemiaminal **42** (35 mg, 0.095 mmol) and sodium cyanoborohydride (7 mg, 11.1 mmol) in dry methanol (2 mL) over 3 Å molecular sieves. The reaction mixture was allowed to stand overnight at room temperature. The methanolic solution was decanted and the molecular sieves were treated with methanol (2 × 5 mL). The combined methanolic solutions were concentrated and the residue was treated with 0.5 *N* hydrochloric acid (5 mL) and extracted with dichloromethane (2 × 5 mL). The combined organic extracts were dried and concentrated to yield a crude mixture of diastereomeric lactones **44** (30 mg, 85%) as a colorless oil; ir λ_{max}: 2.96 (w), 5.68, 5.95 μm; ^{1}H nmr δ: 0.88 and 0.94 (2 s, 9H), 2.4−3.4 (m, 2H), 3.54 and 3.60 (2 s, 3H), 5.5 (m, 1H), 7.0−8.0 (m, 9H), 8.3 (br s, 1H); *m/e*: 367 (39), 306 (100). *Accurate Mass* calcd. for $C_{22}H_{25}NO_4$: 367.1783; found: 367.1771.

*B. From **41***

The general procedure of Wender and Lechleiter (12) was followed. Ozonized oxygen was bubbled through a solution of **41** (95 mg, 0.26 mmol) and sodium acetate (0.04 mg) in water (0.25 mL) and methanol (5 mL) at −78°C. After the appearance of a persistent blue color the excess ozone was displaced by oxygen followed by nitrogen. Dimethyl sulfide (1 mL) was added and the solution was allowed to warm to room temperature and stand for 5 h. The solvent was removed *in vacuo*. Ether (20 mL) was added and the solution was washed with brine (2 × 10 mL). The ethereal solution was dried and concentrated to yield **44** (80 mg, 83%) as a colorless oil; its ^{1}H nmr spectrum was identical to that of the product from **42**.

*1-Methyl-3-phenyl-3-(2-pivaloylamidophenyl)-2-pyrrolidinone (**45**)*

The general procedure of Martin *et al.* (14) was followed. Ozonized oxygen was passed through a solution of olefin **41** (0.153 g, 0.42 mmol) in dichloromethane (5 mL) at −78°C. After the appearance of a persistent blue color the excess ozone was displaced by oxygen followed by nitrogen.The reaction mixture was allowed to warm to room temperature and the solvent was removed. The residue was dissolved in dry *tert*-butyl alcohol and the solution was treated with sodium cyanoborohydride (0.42 mmol) and stirred for 20 min. Methylamine hydrochloride (0.106 g, 0.84 mmol) was added and the reaction mixture was stirred for 35 h at room temperature. Hydrochloric acid (1 *N*; 10 mL) was added and *tert*-butyl alcohol was removed. Water (10 mL) was added to the residue and the aqueous solution was extracted with dichloromethane (2 × 15 mL). The aqueous solution was basified with powdered KOH and extracted with dichloromethane (2 × 10 mL). The combined organic extracts were dried and concentrated to give **45** (40 mg, 20%) as an oil; ir λ_{max}: 3.00, 5.97 μm; ^{1}H nmr δ: 0.87 (s, 9H), 2.05−2.60 (m, 2H), 2.95 (s, 3H), 3.4−3.7 (m, 2H), 6.9−7.6 (m, 8H), 7.85 (m, 1H), 9.8 (br s, 1H); ^{13}C nmr δ: 27.3, 30.8, 37.4, 39.3, 47.2, 57.9, 124.2, 126.1, 126.6, 126.7, 127.4, 128.3, 128.6, 129.8, 138.2, 146.8, 176.1, 176.5; *m/e*: 350 (35), 293 (100). *Accurate Mass* calcd. for $C_{22}H_{26}N_2O_2$: 350.1994; found: 350.2003.

Acknowledgement

We thank the Natural Sciences and Engineering Research Council of Canada for support of this work.

1. P. YATES, F. N. MACLACHLAN, I. D. RAE, M. ROSENBERGER, A. G. SZABO, C. R. WILLIS, M. P. CAVA, M. BEHFOROUZ, M. V. LAKSHMIKANTHAM, and W. ZEIGER. J. Am. Chem. Soc. **95**, 7842 (1973); P.-T. CHENG, S. C. NYBURG, F. N. MACLACHLAN, and P. YATES. Can. J. Chem. **54**, 726 (1976).
2. R. J. SUNDBERG. The chemistry of indoles. Academic Press, New York. 1970. pp. 176−177; J. BAKKE. Acta Chem. Scand. **21**, 1967 (1967); S. M. KUPCHAN, V. KAMESWAREN, and J. W. A. FINDLAY. J. Org. Chem. **38**, 405 (1973); E. E. GARCIA and R. I. FRYER. J. Heterocycl. Chem. **11**, 219 (1974).
3. W. FUHRER and H. W. GSCHWEND. J. Org. Chem. **44**, 1133 (1979).
4. J.-J. LOHMAN, D. SEEBACH, M. A. SYFRIG, and M. YOSHIFUJI. Angew. Chem. Int. Ed. Engl. **20**, 128 (1981); P. A. WENDER and A. N. WHITE. Tetrahedron Lett. **22**, 1475 (1981).
5. C. L. HEWETT, L. J. LERMIT, H. T. OPENSHAW, A. R. TODD, A. H. WILLIAMS, and F. N. WOODWARD. J. Chem. Soc. 292 (1948).
6. E. L. ELIEL and A. A. HARTMANN. J. Org. Chem. **37**, 505 (1972).
7. E. ÖHLER and U. SCHMIDT. Chem. Ber. **108**, 2907 (1975).
8. L. BRODSKY and W. C. AGOSTA. J. Org. Chem. **39**, 2928 (1974).
9. A. GORGUES and H. NORMANT. C. R. Acad. Sci. Paris, Ser. C, **265**, 1130 (1967).
10. W. G. DAUBEN, A. A. PONARAS, and A. CHOLLET. J. Org. Chem. **45**, 4413 (1980).
11. J. H. HOARE. Ph.D. Thesis, University of Toronto, 1981.
12. P. A. WENDER and J. C. LECHLEITER. J. Am. Chem. Soc. **102**, 6340 (1980).
13. R. F. BORCH, M. D. BERNSTEIN, and H. D. DURST. J. Am. Chem. Soc. **93**, 2897 (1971).
14. S. F. MARTIN and T. A. PUCKETTE. Tetrahedron Lett. 4229 (1978); S. F. MARTIN, T. A. PUCKETTE, and J. A. COLAPRET. J. Org. Chem. **44**, 3391 (1979).
15. A. R. LEPLEY, R. H. BECKER, and A. G. GUIMANINI. J. Org. Chem. **36**, 1222 (1971).
16. R. B. MOFFETT. Org. Synth. Coll. Vol. **4**, 427 (1963).
17. H. PLIENINGER. Chem. Ber. **83**, 271 (1950).
18. J. H. WAGENKNECHT, M. M. BAIZER, and J. L. CHRUMA. Synth. Commun. **2**, 215 (1972).

Synthesis of piperazine-2,5-diones related to bicyclomycin: 3-acetoxy-1,4-dibenzyl-3-[1-(2-methoxyethyl)- and 1-(2-hydroxyethyl)ethenyl]piperazine-2,5-dione. 1. Route via acyclic intermediates[1]

PETER YATES AND JOHN HAROLD HOARE
Lash Miller Chemical Laboratories, University of Toronto, Toronto, Ont., Canada M5S 1A1

Received September 10, 1982

PETER YATES and JOHN HAROLD HOARE. Can. J. Chem. **61**, 519 (1983).

3-Acetoxy-1,4-dibenzyl-3-[1-(2-methoxyethyl)ethenyl]piperazine-2,5-dione (**32**) and its 2-hydroxyethyl analogue (**46**), which possess several of the structural features of the antibiotic bicyclomycin, have been synthesized by a route involving construction of the piperazine-2,5-dione ring at a late stage in the reaction sequence. Treatment of ethyl 3-(2-methoxyethyl)-3-methylglycidate with acetic anhydride and sulfuric acid gives ethyl 2-acetoxy-3-(2-methoxyethyl)-3-butenoate (**10**), which is converted to the corresponding carboxylic acid by ethanolysis, hydrolysis, and reacetylation. This, on conversion to its acid chloride and reaction with *N,N'*-dibenzylglycinamide, gives 2-acetoxy-*N*-benzyl-*N*-(2-benzylamino-2-oxoethyl)-3-(2methoxyethyl)-3-butenamide (**21**). Compound **21**, on hydrolysis and oxidation, gives the corresponding 2-oxo compound, which on treatment with magnesium isopropylcyclohexylamide followed by acetylation yields **32**. Demethylation of **21** with alkylthiotrimethylsilanes gives the corresponding 2-hydroxyethyl compound, whose tetrahydropyranyl ether on subjection to the above reaction sequence gives the 2-(tetrahydropyran-2-yloxy)ethyl analogue of **32**. This, on hydrolysis, gives a 3:1 mixture of compound **46** and a spiro compound formed by displacement of the acetoxyl group by the hydroxyl oxygen atom of **46**.

PETER YATES et JOHN HAROLD HOARE. Can. J. Chem. **61**, 519 (1983).

On a synthétisé l'acétoxy-3 dibenzyl-1,4 [(méthoxy-2 éthyl)-1 éthenyl]-3 pipérazinedione-2,5 (**32**) et son analogue hydroxy-2 éthyle (**46**) qui possède plusieurs caractéristiques structurales de l'antibiotique bicyclomycine. On a réalisé cette synthèse selon une méthode qui fait intervenir l'élaboration du cycle pipérazinedione-2,5 lors de la dernière étape d'une série de réactions. Le (méthoxy-2 éthyl)-3 méthyl-3 glycidate d'éthyle réagit avec l'anhydride acétique et l'acide sulfurique en donnant l'acétoxy-2 (méthoxy-2 éthyl)-3 butène-3 oate d'éthyle (**10**) que l'on transforme en acide carboxylique par une éthanolyse, suivie d'une hydrolyse et d'une réacétylation. L'acide transformé en son chlorure, réagit avec la *N,N'*-dibenzylglycinamide en donnant l'acétoxy-2 *N*-benzyl *N*-(benzylamino-2 oxo-2 éthyl)(méthoxy-2 éthyl)-3 butène-3 amide (**21**). Le composé **21**, par hydrolyse suivie d'une oxydation, donne le composé oxo correspondant qui, par une réaction avec l'isopropylcyclohexylamide de magnésium suivie d'une acétylation, conduit au dérivé **32**. La déméthylation du composé **21**, par les alkylthiotriméthylsilanes, donne le composé hydroxy-2 éthyle correspondant dont l'éther tétrahydropyrannyle, soumis à la même série de réactions décrite plus haut, conduit à l'analogue (tétrahydropyrannyl)-2 oxy)-2 éthyle du composé **32**. Ce dernier soumis à une hydrolyse donne un mélange 3:1 du composé **46** et d'un composé spiro formé par déplacement du groupe acétoxyle par l'atome d'oxygène du groupe hydroxyle du composé **46**.

[Traduit par le journal]

Bicyclomycin, an antibiotic produced by *Streptomyces sapporoensis* and *S. aizuensis* (2), is a member of the large class of naturally occurring piperazine-2,5-diones with the unusual structure **1** (3, 4). It has been found to be active against Gram-negative bacteria and does not cause cross resistance to the usual antibiotics; it has also been found to stimulate the growth of chickens and swine (5). There have been several recent synthetic approaches to bicyclomycin of considerable interest (4, 6–10). We have undertaken the synthesis of the 3-acetoxypiperazine-2,5-dione derivative **2** (Bz = benzyl), which we anticipated might serve as a structural prototype for closure to the bicyclic ring system of bicyclomycin. Although

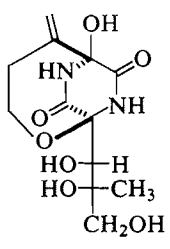

1

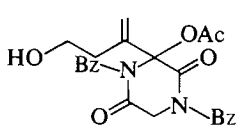

2

2 lacks the trihydroxyisobutyl side chain of **1**, the work of Nakatsuka *et al.* (7) gives promise that this can be introduced at a later stage.

Two general types of synthetic strategy were envisioned for the construction of **2**: (*i*) *route via acyclic intermediates*: construction of an intermediate of type **3**, reaction of this with *N,N'*-dibenzylglycinamide (**4**) to form a diamide **5**, and closure

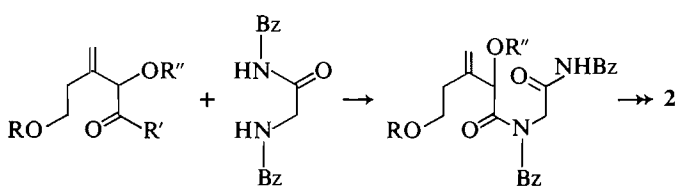

3 **4** **5**

SCHEME 1

to the piperazine-2,5-dione ring at a late stage in the synthetic sequence (Scheme 1), and (*ii*) *route via cyclic intermediates*: construction of the piperazine-2,5-dione ring at an early stage of the synthesis in the form of a 3-alkylidene derivative of type **6**, conversion to an epoxide of type **7**, and manipulation of this to introduce the desired functionality (Scheme 2). We report here on the successful application of the first approach.

[1]For a preliminary account of part of this work, see ref. 1.

Can. J. Chem. Downloaded from www.nrcresearchpress.com by 210.87.254.40 on 09/06/12
For personal use only.

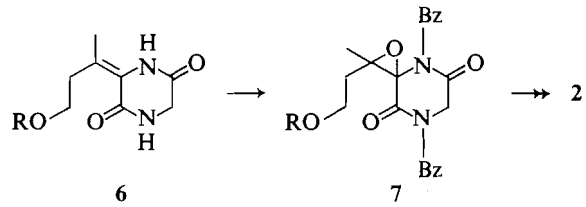

SCHEME 2

We commenced our preparation of compounds of type **3** with the synthesis of ethyl 2-hydroxy-3-(2-methoxyethyl)-3-butanoate (**13**) by the route shown in Scheme 3, based on an earlier synthesis of 2-hydroxy-3-methyl-3-butenoate by Vogel and Schinz (11). 4-Methoxy-2-butanone (**8**), prepared by addition of methanol to methyl vinyl ketone (12), was subjected to a Darzens reaction with ethyl chloroacetate and sodium ethoxide by the general procedure of Burness (13) to give the glycidic ester **9** as a mixture of *E* and *Z* isomers.[2] Treatment of **9** with acetic anhydride and sulfuric acid gave a mixture of the acetates **10**, **11**, and **12** from which the monoacetates **10** and **11** could readily be separated by distillation. The ^{1}H nmr spectrum of the mixture of monoacetates showed that very little of the acetate **15** was formed in the epoxide ring opening reaction; we attribute the regioselectivity of this reaction to the participation of the methoxyl group in the removal of a proton from the *C*-methyl group via a six-membered transition state (cf. **16**). Although it was possible in the ethyl 3,3-dimethylglycidate series (11) to convert the diacetate corresponding to **12** to the monoacetate corresponding to **10** by pyrolysis, this was not found to be possible in the case of the diacetate **12**. The mixture of monoacetates **10** and **11** was ethanolized with ethanolic hydrogen chloride giving a mixture of the unsaturated hydroxy ester **13** and the keto ester **14**, from which the latter could be removed by Girard's reagent T to give the desired compound **13**.

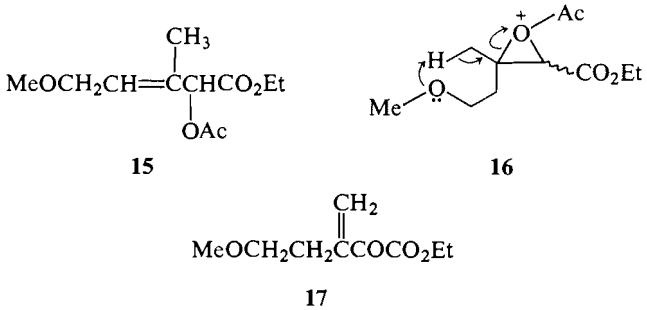

Although the secondary alcohol group of **13** would have at some stage to be oxidized to a ketonic group for the formation of **2**, we decided to convert **13** first to an amide, as indicated in Scheme 1. This was because we anticipated that oxidation of **13** to **17** might lead to complications in forming the amide bond both because of Michael-type addition to the α,β-unsaturated ketone system and the previously observed formation of pyrrolidones in reactions of pyruvic esters with amines (15). The hydroxy ester **13** was hydrolyzed with aqueous sodium hydroxide at room temperature to the hydroxy acid **18**, which was acetylated to give the acetoxy acid **19**, which was in turn converted to its acid chloride **20**. This was added to two equivalents of *N*,*N*′-dibenzylglycinamide (**4**), prepared by treatment

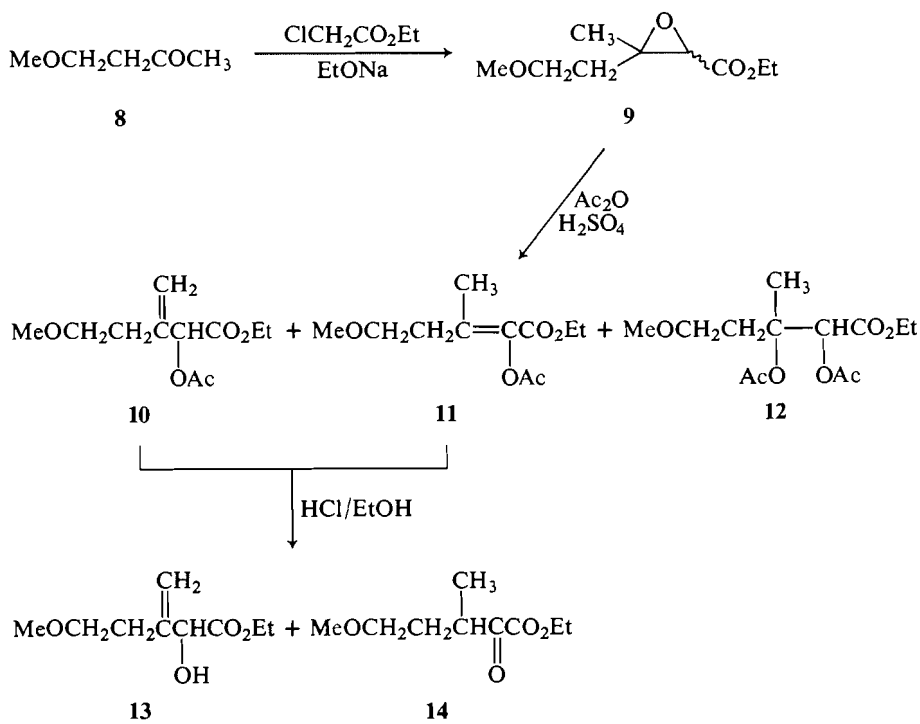

SCHEME 3

[2]In preliminary work we carried out model studies with ethyl 3,3-dimethylglycidate. This was initially prepared by the Darzens reaction of acetone with ethyl chloroacetate and potassium *tert*-butoxide (14); however, we found that under these conditions a mixture of the ethyl and *tert*-butyl esters of the glycidic acid was formed. This problem was avoided by the use of sodium ethoxide.

Can. J. Chem. Downloaded from www.nrcresearchpress.com by 210.87.254.40 on 09/06/12
For personal use only.

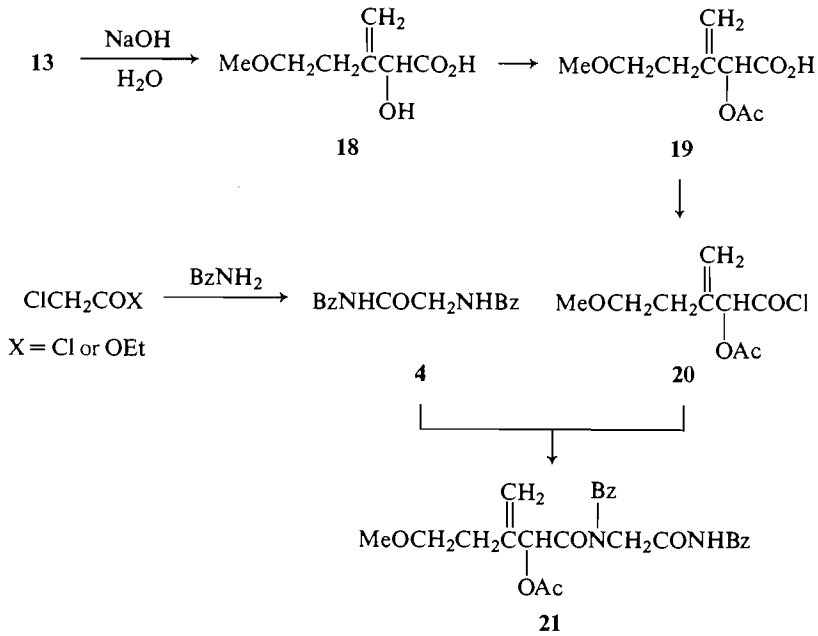

SCHEME 4

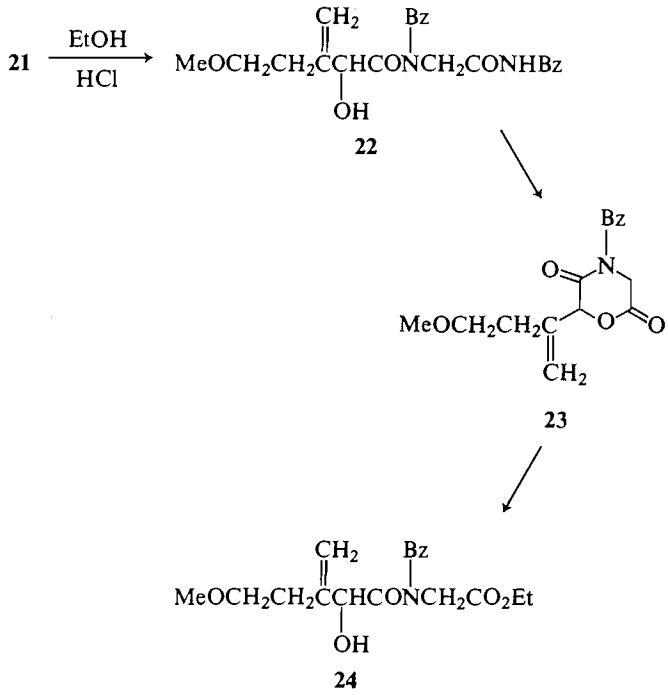

SCHEME 5

of benzylamine with chloroacetyl chloride or ethyl chloroacetate (16), giving the desired diamide **21** and the hydrochloride salt of **4** (Scheme 4). Rotational isomerism about one of the amide carbon–nitrogen bonds in **21** led to doubling of some of the signals in its ^{1}H nmr spectrum: the acetyl protons gave rise to two singlets at δ 2.17 and 2.23 ppm and the acetoxy methine proton to two singlets at δ 5.53 and 5.82 ppm.[3] Such effects of rotational isomerism together with effects due to the diastereotopic nature of the benzylic proton served to complicate the ^{1}H nmr spectra of many of the compounds related to **21** prepared in the present work.

It was now necessary to remove the acetyl group so that oxidation of the secondary alcohol to a ketonic group could be effected. An initial attempt to remove the acetyl group by treatment of **21** with ethanolic hydrogen chloride gave the ester **24**. This unusually facile amide cleavage is considered to involve the initial formation of the desired alcohol **22**, which by intramolecular displacement of benzylamine is converted to the lactone **23**, which in turn is ethanolyzed to **24** (Scheme 5). This complication was avoided by hydrolysis of **21** under basic conditions; reaction with sodium hydroxide in ethanol gave the alcohol **22** (Scheme 6). This was then oxidized with activated manganese dioxide to the ketone **25** whose formation was readily detected by ^{1}H nmr spectroscopy, in that its vinylic proton signals (δ 6.12 and 6.30 ppm) were shifted appreciably downfield relative to those of **21** (δ 5.17 ppm) and its precursors as a result of conjugation of the ethylenic double bond and the ketonic group.

The stage was now set for the closure of **25** to the corresponding piperazine-2,5-dione. It has previously been observed that oxo diamides such as **26** close spontaneously to piperazine-2,5-dione of type **27** and that the more entropically disfavored closure of the dioxo diamide **28** to the piperazinedione **29** could be effected by acid catalysis (17). However, attempts to bring about the closure of **25** at room or elevated

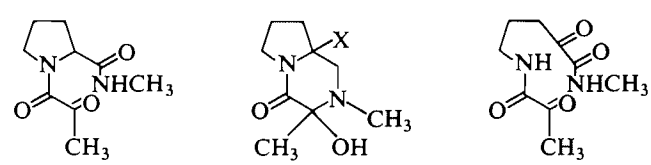

temperatures or under a variety of acidic conditions were unsuccessful. Treatment of **25** in benzene with lithium, sodium, or potassium hydride gave homogeneous reaction mixtures which gave only polymeric material on work-up. Success was

[3]Although each amide group may give rise to rotational isomers, it seems probable that the effects on the signals referred to originate from isomerism at the internal amide group.

Can. J. Chem. Downloaded from www.nrcresearchpress.com by 210.87.254.40 on 09/06/12
For personal use only.

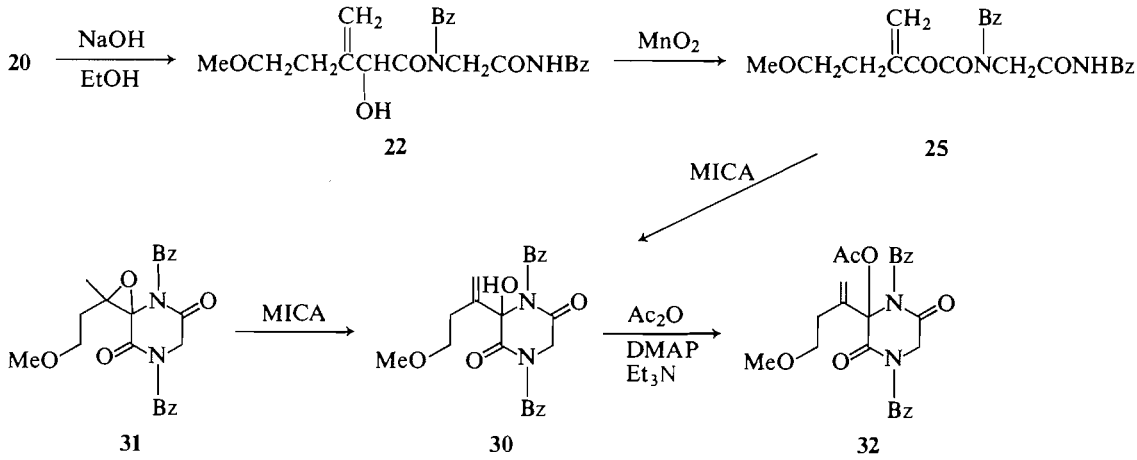

SCHEME 6

finally achieved by the use of magnesium isopropylcyclohexylamide (MICA), a reagent introduced by Corey *et al.* (18) for the conversion of epoxides to allylic alcohols, whose use for the present purpose was suggested to us by its successful application in the conversion of the epoxide **31** to **30** in our work on the synthesis of the latter via cyclic intermediates (19).

Since we had observed that the piperazine-2,5-dione **30** reverted in part to the acyclic precursor **25** on chromatography on silica (19), we decided to acetylate the hydroxyl group in order to prevent ring opening. Treatment with acetyl chloride gave a product that is considered to be the chloride **33** since it showed neither hydroxyl nor acetoxyl bands in its ir spectrum; attempted crystallization of **33** from aqueous acetone gave a mixture of **25** and **30**. Successful acetylation of **30** was accomplished with acetic anhydride and pyridine, or better with acetic anhydride, 4-(dimethylamino)pyridine (DMAP) and triethylamine (20), to give **32** (Scheme 6). Although the ir spectrum of **32** shows a normal acetoxyl band at 5.76 μm, the acetoxyl protons give rise to an abnormally high field signal in the ^{1}H nmr spectrum of **32** at δ 1.30 ppm. This is considered

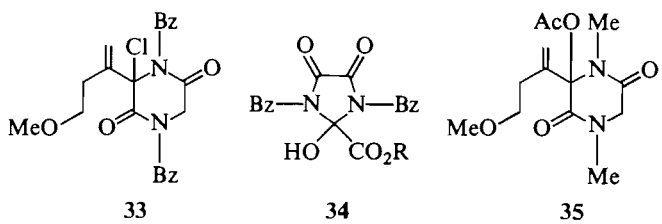

to be due to shielding resulting from "folding over" of a benzyl group; such an effect has been observed before in the spectra of some 3-benzylpiperazine-2,5-diones (21) and we have observed an analogous effect in the case of the alkoxyl protons of a series of *N,N'*-dibenzyl-4,5-dioxoimidazoline-2-carboxylic acid esters (**34**) (22). In order to confirm that the very unusual position of the acetoxyl signal of **32** was due to shielding by a benzyl group (and not to a structural misassignment!), we synthesized **35**, the *N,N*-dimethyl analogue of **32**, by a route entirely analogous to that used for the synthesis of **32**. The ^{1}H nmr spectrum of **35** showed a normal acetoxyl proton signal at δ 2.15 ppm, confirming that the abnormal position of this signal in the spectrum of **32** is due to the presence of the benzyl groups. The ^{1}H nmr spectra of **35** and its precursors were simpler than those of **32** and its precursors because of the

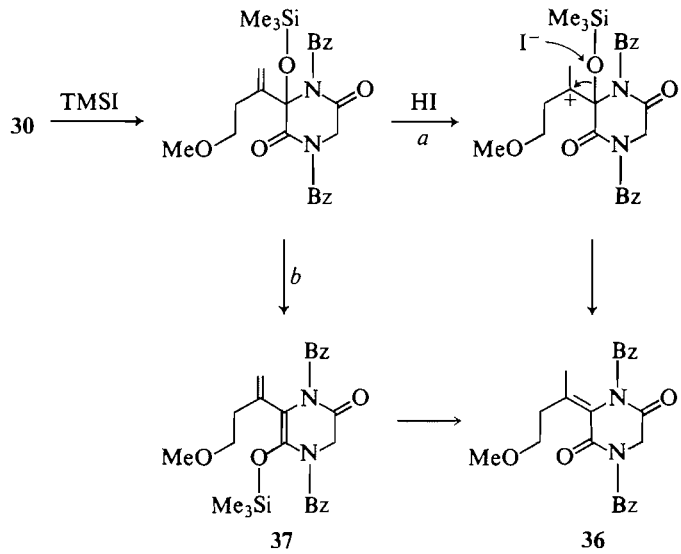

SCHEME 7

absence of diastereotopic benzylic methylene proton signals, and served further to corroborate the structural assignments.

The eventual synthesis of the bicyclic system of bicyclomycin (**1**) will require bond formation between the oxygen atom of the methoxyl group in **32** and C-6 of the piperazinedione ring. Such bond formation would be expected to occur more readily if the oxygen atom were part of a hydroxyl rather than a methoxyl group. We therefore undertook the synthesis of the hydroxy analogue of **32**.

We initially attempted to prepare this from **32** by treatment with trimethylsilyl iodide (TMSI) (23). This gave none of the desired product. Since we suspected that the lability of the acetoxyl group of **32** was responsible (cf. the formation of **33** from **30** and acetyl chloride), we investigated the reaction of **30** with two equivalents of TMSI in an attempt both to silylate the hydroxyl group and cleave the methyl ether. Surprisingly, the product obtained was the (*E*)-alkylidenepiperazinedione **36** (19). One possible mechanism for this reaction is depicted by path *a* in Scheme 7. A related reaction has been reported in which TMSI reduces α-hydroxy ketones to the corresponding ketones (24); a mechanism analogous to one proposed for this reaction (path *b* in Scheme 7) would lead to **37**, which could be converted to **36** upon acidic work-up.

Can. J. Chem. Downloaded from www.nrcresearchpress.com by 210.87.254.40 on 09/06/12
For personal use only.

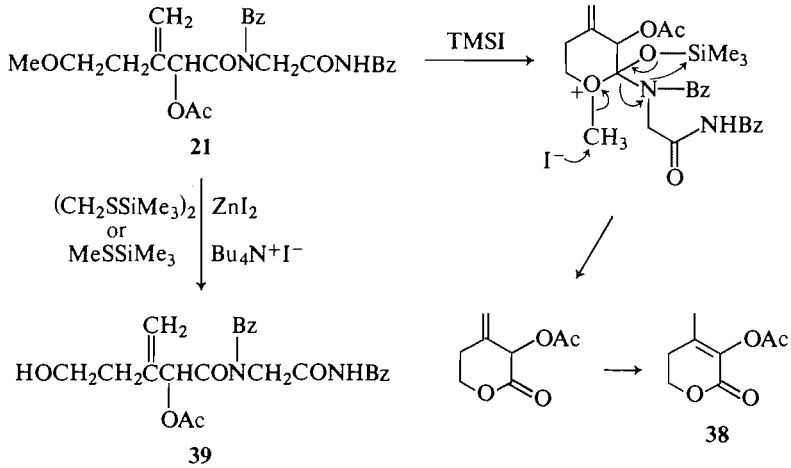

SCHEME 8

In view of these difficulties we decided to remove the *O*-methyl group at an earlier stage in the synthetic sequence. Treatment of **21** with TMSI or with TMSI generated *in situ* from trimethylsilyl chloride and sodium iodide (25) gave the *O*-acetyl derivative of 5,6-dihydro-3-hydroxy-4-methyl-2*H*-pyran-2-one (26), which could arise by the route shown in Scheme 8. Hydriodic acid generated *in situ* from *p*-toluenesulfonic acid and sodium iodide (27) failed to react with **21**. Treatment of **21** with aluminum trichloride and ethanethiol (28) gave sulfur-containing products in which the acetoxyl group had been lost. We finally investigated the use of the procedures recently introduced by Hanessian and Guindon for the cleavage of methyl ethers with thiotrimethylsilanes, zinc iodide, and tetrabutylammonium iodide (29). Compound **21** was resistant to phenylthiotrimethylsilane but was demethylated, albeit in low yield, by the use of the more reactive 1,2-ethanedithiobis(trimethylsilane) or methylthiotrimethylsilane to give the desired alcohol **39** (Scheme 8). Its formation was indicated by the appearance of a band at 2.95 μm in the ir spectrum of **39** and the absence of a methoxyl proton signal in its ^{1}H nmr spectrum.

The alcohol **39** was converted to its tetrahydropyranyl derivative **40** by reaction with 2-(*tert*-butoxy)tetrahydropyran and hydrochloric acid in methylene chloride (30),[4] which was converted to the piperazine-2,5-dione **44** via the intermediates **42** and **43** by the same sequence of reactions that had been used in the conversion of the methyl ether **20** to the piperazine-2,5-dione **30**. Attempted acetylation of **44** suffered from extensive ring opening. However, it was found that the magnesium alk-

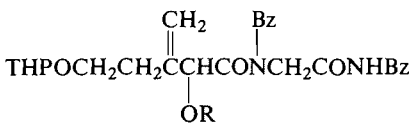

40, R = Ac
42, R = H

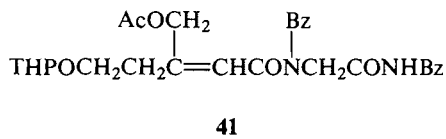

41

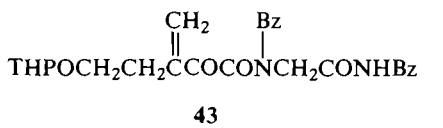

43

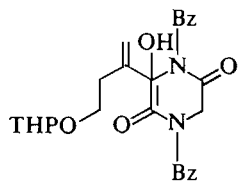

44

oxide formed as an intermediate in the cyclization of **43** to **44** with MICA could be acetylated directly with acetic anhydride to give the acetoxypiperazinedione **45**. The tetrahydropyranyl group of **45** was removed with acetic acid in aqueous tetrahydrofuran by the general procedure of Grieco *et al.* (31) to give a 3:1 mixture of the target compound **46** and the spiro compound **47** (Scheme 9), which were separated by chromatography. The ir spectrum of **46** showed a hydroxyl-stretching band at 2.90 μm and its ^{1}H nmr spectrum showed the absence of the multiplet at δ 1.6 ppm characteristic of the tetrahydropyranyl group. The spiro compound **47** showed only amide bands at 5.97 μm in the carbonyl-stretching region of its ir spectrum; in its ^{1}H nmr spectrum the vicinal methylene protons no longer gave rise to simple triplet signals as they did in the spectrum of **46** but gave rise to complex multiplets as a result of ring formation.

The acid-catalyzed conversion of **46** to **47** finds precedent in the chemistry of bicyclomycin (1) itself, which has been found (4) to undergo acid-catalyzed rearrangement to the diastereomeric spiro compounds **48** and **49** (Scheme 10).

Experimental

Melting points were determined on a Fisher–Johns apparatus and are uncorrected. Unless otherwise specified, the ir spectra were recorded for $CHCl_3$ solutions and the ^{1}H and ^{13}C nmr spectra for $CDCl_3$ solutions. Mass spectra were recorded at 70 eV and peak positions (m/e) are followed by relative abundances in parentheses. Chromatographic separations were carried out by liquid column chromatography except where otherwise indicated. All R_f values were

[4]A minor product formed in this reaction is considered to be **41**, formed by allylic rearrangement.

Can. J. Chem. Downloaded from www.nrcresearchpress.com by 210.87.254.40 on 09/06/12
For personal use only.

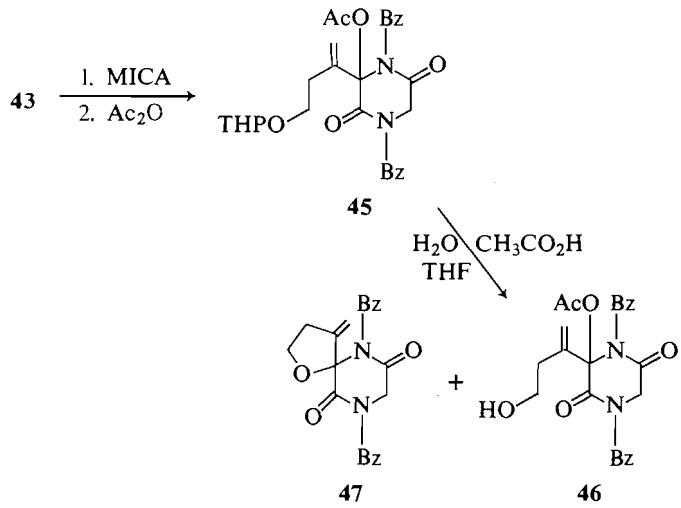

SCHEME 9

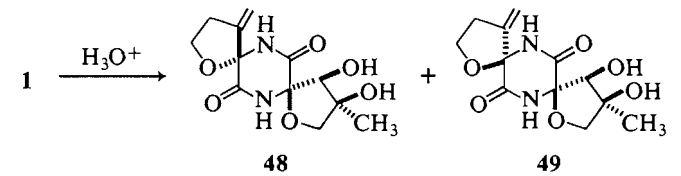

SCHEME 10

Can. J. Chem. Downloaded from www.nrcresearchpress.com by 210.87.254.40 on 09/06/12
For personal use only.

determined on analytical thin-layer chromatographic silica gel plates. Preparative thin-layer chromatography was carried out on 20 × 20 × 1-mm or 20 × 20 × 2-mm silica gel plates containing a fluorescent indicator. The bands were extracted with methanol and the residue obtained after filtration and evaporation was triturated with chloroform or dichloromethane; filtration and evaporation yielded the product; iodine or uv visualization was employed. Apparatus for the experiments that were carried out under nitrogen was flame dried immediately prior to use under a dry nitrogen flow. All organic extracts were dried over anhydrous $MgSO_4$ and evaporated by means of a rotary evaporator at water aspirator pressure.

Ethyl 3,3-dimethylglycidate

When a Darzens reaction was performed on acetone and ethyl chloroacetate with potassium *tert*-butoxide as base (14) a 1:1 mixture of ethyl and *tert*-butyl glycidates was obtained.

The procedure of Burness (13) was therefore used. Sodium ethoxide was prepared from sodium (3.61 g, 0.157 mol) and ethanol; removal of the ethanol *in vacuo* gave a solid (22.30 g) which was found to contain ~48% by weight sodium ethoxide by titration with potassium hydrogen phthalate. This solid was added portionwise with mechanical stirring to acetone (9.10 g, 0.157 mol), ethyl chloroacetate (28.85 g, 0.235 mol), and ether (125 mL) cooled to −10°C in an ice–salt bath under nitrogen. The temperature was kept below −5°C during addition of base. The mixture was then stirred in the ice–salt bath for 2 h; the ice–salt bath was removed and stirring was continued overnight at room temperature. A solution of acetic acid (2 mL) in water (48 mL) was added and the ether layer was separated. The aqueous layer was washed with ether (3 × 25 mL). The combined ether phases were dried, filtered, concentrated, and distilled at 88°C (20 Torr) to give 14.9 g (66%) of ethyl 3,3-dimethylglycidate; ir λ_{max}: 5.77 μm; ^{1}H nmr δ: 4.17 (q, J = 7 Hz, 2H), 3.25 (s, 1H), 1.38 (s, 3H), 1.35 (s, 3H), 1.27 (t, J = 7 Hz, 3H).

Reaction of ethyl 3,3-dimethylglycidate with acetic acid anhydride. Formation of ethyl 2-acetoxy-3-methyl-3-butenoate, ethyl 2-acetoxy-3-methyl-2-butenoate, and ethyl 2,3-diacetoxy-3-methylbutanoate

The procedure of Vogel and Schinz (11) was followed. Ethyl 3,3-dimethylglycidate (14.32 g, 99.5 mmol) was stirred at room temperature in freshly distilled acetic anhydride (13.4 mL). Concentrated H_2SO_4 (0.5 mL) was added with stirring and the mixture became hot. The solution was cooled on ice and after 10 min another 0.25 mL of concentrated H_2SO_4 was added. The mixture was stirred for 1 h at room temperature and 30 min at 100°C. The cooled mixture was dissolved in ether (50 mL) and the solution was washed with water (10 mL) and aqueous 10% $NaHCO_3$ (10 mL). The ether phase was dried, filtered, and concentrated. The residue was fractionally distilled. Ethyl 2-acetoxy-3-methyl-2-butenoate and ethyl 2-acetoxy-3-methyl-3-butenoate distilled at 90–95°C (10 Torr) and the diacetate, ethyl 2,3-diacetoxy-3-methylbutanoate, distilled at 98–103°C (10 Torr). The diacetate (ir λ_{max}: 5.76 μm; ^{1}H nmr δ: 5.40 (s), 4.33 (q, J = 7 Hz), 1.82 (s), 1.98 (s), 1.58 (s), 1.53 (s), 1.27 (t, J = 7 Hz)) was converted into the monoacetate mixture by pyrolysis with a Bunsen burner flame. The combined monoacetate mixture was redistilled at 95°C (10 Torr) to give ~10 g (59%) of ethyl 2-acetoxy-3-methyl-2-butenoate and ethyl 2-acetoxy-3-methyl-3-butenoate; ir λ_{max}: 5.75 μm; ^{1}H nmr δ: 5.32 (s), 5.0–5.2 (m), 4.17 (q, J = 7 Hz), 2.10 (s), 1.78 (s), 1.25 (t, J = 7 Hz).

Ethyl 2-hydroxy-3-methyl-3-butenoate

A solution of the mixture of ethyl 2-acetoxy-3-methyl-2-butenoate and ethyl 2-acetoxy-3-methyl-3-butenoate (7.11 g) in 4% HCl in ethanol (14 mL) was boiled under reflux for 1.5 h. After cooling, solid $NaHCO_3$ was added to neutralize the solution which was then filtered, concentrated, and distilled at 71–74°C (12 Torr) to give a quantitative yield of the ethanolyzed material. This mixture (4.56 g), methanol (20 mL), acetic acid (2.1 mL), and Girard reagent T (2.0 g) were boiled under reflux for 0.5 h. The cooled solution was dissolved in methylene chloride (50 mL) and the solution was washed with water (10 mL). The aqueous phase was washed several times with methylene chloride. The combined methylene chloride phases were dried, filtered, and concentrated. The residue was distilled at 68–69°C (10 Torr) to give ethyl 2-hydroxy-3-methyl-3-butenoate (3.53 g, 70%); ir λ_{max}: 2.98, 5.78 μm; ^{1}H nmr δ: 4.8–5.1 (m, 2H), 4.48 (s, 1H), 4.18 (q, J = 7 Hz, 2H), 3.28 (s, 1H), 1.73 (m, 3H)0, 1.27 (t, J = 7 Hz, 3H).

Ethyl 3-(2-methoxyethyl)-3-methylglycidate (9)

4-Methoxy-2-butanone (**8**) was prepared in 60% yield by addition of methanol to methyl vinyl ketone (12).

Ketone **8** (50.7 g, 0.497 mol) was subjected to a Darzens reaction with ethyl chloroacetate (97.3 g, 0.794 mol) and sodium ethoxide (48% by weight NaOEt; 70.7 g, 0.499 mol) in ether (425 mL) in analogous fashion to the preparation of ethyl 3,3-dimethylglycidate. Ethyl 3-(2-methoxyethyl)-3-methylglycidate (**9**) was obtained as a mixture of *cis* and *trans* isomers, bp 93–98°C (0.35 Torr), in 78% yield; ir λ_{max}: 5.62, 8.95 μm; ^{1}H nmr δ: 4.20 (q, J = 7 Hz, 2H), 3.72 and 3.33 (2 s, 1H), 3.45 (t, J = 6 Hz, 2H), 3.28 and 3.25 (2 s, 3H), 1.90 and 1.87 (2 t, J = 6 Hz, 2H), 1.42 and 1.37 (2 s, 3H), 1.28 (t, J = 7 Hz, 3H); m/e: 188 (0.2), 173 (2), 157 (5), 115 (45), 45 (100). *Anal.* calcd. for $C_9H_{16}O_4$: C 57.43, H 8.57; found: C 57.01, H 8.47.

Ethyl 2-hydroxy-3-(2-methoxyethyl)-3-butenoate (13)

Ethyl 3-(2-methoxyethyl)-3-methylglycidate (**9**) (43.54 g, 0.231 mol) was treated with acetic anhydride (34 mL) by an analogous procedure to that used for the opening of the epoxide ring of ethyl 3,3-dimethylglycidate except that only 15 drops of concentrated H_2SO_4 were used and the mixture was heated on a steam bath for ~8 h. The work-up was the same as before.

Ethyl *cis*- and *trans*-2-acetoxy-5-methoxy-3-methyl-2-pentenoate (**11**) and ethyl 2-acetoxy-3-(2-methoxyethyl)-3-butenoate (**10**) were fractionally distilled at 66–68°C (0.01 Torr) in 45% yield from ethyl 2,3-diacetoxy-5-methoxy-3-methylpentanoate (**12**), which could not be distilled without decomposition. Pyrolysis of the diacetate **12** resulted in decomposition with loss of methanol.

A solution of monoacetate mixture **10** and **11** (32.60 g, 0.142 mol) in 4% HCl in ethanol was boiled under reflux for 1.5 h and worked up in analogous fashion to the work-up of ethyl 2-hydroxy-3-methyl-3-butenoate. A quantitative yield of crude ethanolyzed mixture was

Can. J. Chem. Downloaded from www.nrcresearchpress.com by 210.87.254.40 on 09/06/12
For personal use only.

obtained. A solution of this mixture (30.75 g, 0.163 mol) and Girard's reagent T (20.0 g, 0.119 mol) in methanol (115 mL) and acetic acid (13 mL) was boiled under reflux for 0.5 h and worked up as before. The residue was distilled at 55–65°C (0.005 Torr) to give **13** in 65% yield; ir λ_{max}: 2.90, 5.76 μm; ^{1}H nmr δ: 5.13 (s, 1H), 4.98 (m, 1H), 4.62 (br s, 1H), 4.25 (q, J = 7 Hz, 2H), 3.82 (br s, 1H), 3.46 (t, J = 6 Hz, 2H), 3.37 (s, 3H), 2.33 (t, J = 6 Hz, 2H), 1.28 (t, J = 7 Hz, 3H); *m/e*: 189 (2), 188 (0.3), 171 (3), 156 (11), 115 (27), 83 (100). *Accurate Mass* calcd. for $C_9H_{16}O_4$: 188.1049; found: 188.1057.

*2-Acetoxy-3-(2-methoxyethyl)-3-butenoyl chloride (**20**)*

Ethyl 2-hydroxy-3-(2-methoxyethyl)-3-butenoate (**13**) (35.45 g, 0.188 mol) in aqueous 25% NaOH (125 mL) was stirred for 4 days at room temperature. The basic solution assumed a dark red-brown color during this time. It was then cooled in an ice bath and acidified with concentrated hydrochloric acid. The light yellow aqueous solution was saturated with sodium chloride and the resulting solution was extracted several times with methylene chloride. The combined methylene chloride phases were dried, filtered, and concentrated giving a quantitative yield of crude 2-hydroxy-3-(2-methoxyethyl)-3-butenoic acid (**18**) as a viscous yellow syrup; ir λ_{max}: 3–4, 5.64, 5.81 μm; ^{1}H nmr δ: 7.67 (bs, 2H), 5.23 (s, 1H), 5.07 (br s, 1H), 4.60 (s, 1H), 3.52 (t, J = 7 Hz, 2H), 3.32 (s, 3H), 2.35 (t, J = 6 Hz, 2H).

Compound **18** (10.0 g, 62 mmol) was dissolved in methylene chloride (50 mL) and acetyl chloride (7.35 mL, 104 mmol) was added. The mixture was stirred at room temperature for 12 h and concentrated. The residue was dissolved in saturated aqueous $NaHCO_3$ with stirring. This solution was acidified with 3 *N* hydrochloric acid and extracted several times with methylene chloride. The combined methylene chloride phases were dried, filtered, and concentrated giving 10.1 g (80%) of 2-acetoxy-3-(2-methoxyethyl)-3-butenoic acid (**19**) as a viscous syrup; ir λ_{max}: 5.79 μm; ^{1}H nmr δ: 10.32 (s, 1H), 5.40 (s, 1H), 5.31 (s, 1H), 5.15 (br s, 1H), 3.57 (t, J = 6 Hz, 2H), 3.32 (s, 3H), 2.43 (t, J = 6 Hz, 2H), 2.13 (s, 3H).

A solution of **19** (456 mg, 2.40 mmol) and oxalyl chloride (1.42 mL, 16.5 mmol) in methylene chloride (5 mL) was stirred at room temperature for 12 h. The reaction mixture was concentrated under high vacuum and the residue was distilled at 54°C (0.015 Torr) giving 2-acetoxy-3-(2-methoxyethyl)-3-butenoyl chloride (**20**) (318 mg, 60%) as a clear, colorless liquid; ir λ_{max}: 5.60, 5.74 μm; ^{1}H nmr δ: 5.55 (s, 1H), 5.38 (s, 1H), 5.30 (m, 1H), 3.57 (t, J = 6 Hz, 2H), 3.35 (s, 3H), 2.45 (t, J = 6 Hz, 2H), 2.20 (s, 3H).

*2-Acetoxy-N-benzyl-N-(2-benzylamino-2-oxoethyl)-3-(2-methoxyethyl)-3-butenamide (**21**)*

Acid chloride **20** (2.38 g, 10.8 mmol) in methylene chloride (50 mL) was stirred at room temperature while *N*,*N*′-dibenzylglycinamide (**4**) (16) (5.47 g, 21.5 mmol) in methylene chloride (10 mL) was added dropwise. After addition was complete, the mixture was stirred for 20 min. The *N*,*N*′-dibenzylglycinamide hydrochloride that had formed was filtered. The filtrate was washed with aqueous 10% $NaHCO_3$ (10 mL), aqueous 6 *N* hydrochloric acid (10 mL), and water (20 mL). The methylene chloride solution was dried, filtered, and concentrated to give a quantitative yield of 2-acetoxy-*N*-benzyl-*N*-(2-benzylamino-2-oxoethyl)-3-(2-methoxyethyl)-3-butenamide (**21**) as a pale yellow gum which resisted crystallization; ir λ_{max}: 2.99, 5.69, 5.95 μm; ^{1}H nmr δ: 7.17 (m, 11H), 5.82 (s, 0.5H), 5.53 (s, 0.5H), 5.0–5.3 (m, 2H), 3.7–4.8 (m, 6H), 3.42 (t, J = 6 Hz, 2H), 3.15 (s, 3H), 2.37 (t, J = 6 Hz, 2H), 2.33 (s, 1.5H), 2.17 (s, 1.5H); ^{13}C nmr δ: 171.4 (s), 171.0 (s), 168.9 (s), 168.0 (s), 167.4 (s), 139.6 (s), 139.5 (s), 138.2 (s), 136.0 (s), 135.3 (s), 127.2–128.9 (d), 119.2 (t), 119.1 (s), 74.6 (d), 71.3 (t), 71.2 (t), 58.5 (q), 52.1 (t), 50.3 (t), 49.4 (t), 43.4 (t), 43.3 (t), 32.9 (t), 20.6 (q); *m/e*: 438 (2), 379 (12), 91 (100). *Accurate Mass* calcd. for $C_{25}H_{30}N_2O_5$: 438.2155; found: 438.2215.

*N-Benzyl-N-(2-benzylamino-2-oxoethyl)-2-hydroxy-3-(2-methoxyethyl)-3-butenamide (**22**)*

A solution of compound **21** (1.796 g, 4.10 mmol) and NaOH (170 mg, 4.25 mmol) in ethanol (20 mL) was stirred for 8 h at room temperature. The ethanol solution was concentrated and the residue was dissolved in methylene chloride (20 mL). The solution was washed with water (5 mL), dried, filtered, and concentrated, giving a quantitative yield of **22** as a clear yellow gum; ir λ_{max}: 3, 5.95, 6.04 μm; ^{1}H nmr δ: 7.13 (m, 11H), 4.8–5.2 (m, 2H), 3.6–4.8 (m, 8H), 3.40 (t, J = 6 Hz, 2H), 3.17 (s, 3H), 2.30 (t, J = 6 Hz, 2H); *m/e*: 396 (1), 379 (2), 288 (4), 257 (6), 106 (31), 91 (100). *Accurate Mass* calcd. for $C_{23}H_{27}N_2O_3$ (M − OH): 379.2022; found: 379.2048.

*N-Benzyl-N-(2-benzylamino-2-oxoethyl)-3-(2-methoxyethyl)-2-oxo-3-butenamide (**25**)*

Compound **22** (4.37 g, 11.0 mmol) and activated manganese dioxide (32) (25 g) in methylene chloride or chloroform (170 mL) was stirred at room temperature for 14 h. The mixture was filtered through Celite and the solid was washed with hot chloroform (3 × 50 mL). The combined filtrates were concentrated leaving a quantitative yield of **25** as a pale yellow gum; ir λ_{max}: 2.98, 5.96, 6.09 μm; ^{1}H nmr δ: 7.17 (m, 11H), 6.30 (s, 1H), 6.12 (s, 1H), 3.6–4.7 (m, 6H), 3.42 (t, J = 6 Hz, 2H), 3.17 (s, 3H), 2.53 (t, J = 6 Hz, 2H); ^{13}C nmr δ: 193.6 (s), 193.4 (s), 168.2 (s), 167.4 (s), 167.1 (s), 142.6 (s), 142.2 (s), 138.0 (t), 137.8 (t), 135.4 (s), 134.6 (s), 134.2 (s), 128.9–126.7 (d), 70.7 (t), 58.4 (q), 52.5 (t), 46.5 (t), 43.4 (t), 29.5 (t); *m/e*: 394 (6), 349 (1), 303 (3), 281 (8), 253 (21), 246 (6), 91 (100). *Accurate Mass* calcd. for $C_{23}H_{26}N_2O_4$: 394.1893; found: 394.1909.

*Cyclization of **25**. Formation of 1,4-dibenzyl-3-hydroxy-3-[1-(2-methoxyethyl)ethenyl]piperazine-2,5-dione (**30**)*

A solution of magnesium isopropylcyclohexylamide (MICA) (18) in dry tetrahydrofuran (15 mL) was prepared from magnesium turnings (35 mg, 1.4 mmol), methyl bromide, and isopropylcyclohexylamine (0.5 mL, 3 mmol). Compound **25** (353 mg, 0.894 mmol) in dry tetrahydrofuran (4 mL) was syringed slowly dropwise into the stirred MICA solution at room temperature over a period of 2.5–3 h. The mixture was stirred for 18 h at room temperature and then cooled in an ice bath. Aqueous 2 *M* KH_2PO_4 (5 mL) was added to the cooled mixture. The acidified mixture was washed with methylene chloride (3 × 15 mL). The combined methylene chloride extracts were washed with water (10 mL), dried, filtered, and concentrated giving crude piperazine-2,5-dione **30** as a pale yellow gum (350 mg); ir λ_{max}: 2.98, 6.02 μm; ^{1}H nmr δ: 7.23 (m, 10H), 5.07 (m, 3H), 4.0–5.0 (m, 6H), 3.43 (t, J = 6 Hz, 2H), 3.30 (s, 3H), 2.33 (m, 2H).

Attempted crystallization of this product from combinations of chloroform, ether, ethyl acetate, and hexanes or cyclohexane was unsuccessful. Attempted crystallization from acetone–water resulted in its reversion to **25**.[5]

*3-Acetoxy-1,4-dibenzyl-3-[1-(2-methoxyethyl)ethenyl]piperazine-2,5-dione (**32**)*

Compound **30** (678 mg, 1.72 mmol) was treated with 4-dimethylaminopyridine (9 mg), acetic anhydride (2 mL), and triethylamine (2 mL) for 4 h at room temperature. The mixture was concentrated *in vacuo* and the residue was dissolved in methylene chloride (15 mL). The solution was washed with 3 *M* hydrochloric acid (5 mL) and water (5 mL), dried, filtered, and concentrated. The residue was chomatographed on silica with 20% ethyl acetate – chloroform as eluent. The product (R_f = 0.6) was eluted and the fraction concentrated to give the acetylated product **32** (359 mg, 48%) as a pale yellow gum which resisted crystallization; ir λ_{max}: 5.76, 5.98 μm; ^{1}H nmr δ: 7.20 (s, 5H), 7.15 (s, 5H), 5.60 (s, 1H), 5.40 (s, 1H), 3.7–5.3 (m, 6H), 3.50 (t, J = 6 Hz, 2H), 3.30 (s, 3H), 2.28 (t, J = 6 Hz, 2H), 1.30 (s, 3H); *m/e*: 436 (6), 393 (3), 378 (30), 113 (29), 91 (100). *Accurate Mass* calcd. for $C_{25}H_{28}N_2O_5$: 436.1998; found: 436.1995.

*3-Acetoxy-3-[1-(2-methoxyethyl)ethenyl]-1,4-dimethylpiperazine-2,5-dione (**35**)*

The following reaction sequence was carried out in analogous fash-

[5]Although neither **30** nor its precursors could be obtained in crystalline form, its spectra corresponded with those of **30** obtained by treatment of **31** with MICA; **31** and several of its precursors have been obtained in crystalline form and characterized by combustion elemental analysis (19).

Can. J. Chem. Downloaded from www.nrcresearchpress.com by 210.87.254.40 on 09/06/12
For personal use only.

ion to the preparation of compound **32** and its precursors.

Acid chloride **19** (1.14 g, 5.17 mmol) in methylene chloride (50 mL) was treated with *N*,*N'*-dimethylglycinamide (33) (1.08 g, 10.6 mmol) in methylene chloride (5 mL) to give 2-acetoxy-3-(2-methoxyethyl)-*N*-methyl-*N*-(2-methylamino-2-oxoethyl)-3-butenamide as a yellow gum (1.32 g, 89%); ir λ_{max}: 2.95, 5.71, 5.93 μm; ^{1}H nmr δ: 7.03 (br s, 0.3H), 6.57 (br s, 0.7H), 5.63 (s, 0.7H), 5.47 (s, 0.3H), 5.27 (m, 2H), 4.12 (s, 1H), 3.92 (s, 1H), 3.53 (t, J = 6 Hz, 2H), 3.33 (s, 3H), 3.11 (s, 2H), 2.98 (s, 1H), 2.80 (s, 2H), 2.73 (s, 1H), 2.43 (t, J = 6 Hz, 2H), 2.17 (s, 3H).

A solution of this product (1.03 g, 3.60 mmol) and sodium hydroxide (174 mg, 4.35 mmol) in ethanol (20 mL) was stirred for 10 h at room temperature to give 2-hydroxy-3-(2-methoxyethyl)-*N*-methyl-*N*-(2-methylamino-2-oxoethyl)-3-butenamide as a water-soluble yellow gum; ir λ_{max}: 3.02, 6.05 μm; ^{1}H nmr δ: 6.28 (br s, 1H), 5.12 (m, 2H), 4.73 (bs, 1H), 3.8–4.5 (m, 3H), 3.48 (t, J = 6 Hz, 2H), 3.28 (s, 3H), 3.00 (s, 3H), 2.74 (d, J = 4 Hz, 3H), 2.30 (t, J = 6 Hz, 2H).

This alcohol (571 mg, 2.34 mmol) and activated manganese dioxide (4.5 g) in methylene chloride (30 mL) were stirred at room temperature for 11 h to give 3-(2-methoxyethyl)-*N*-methyl-*N*-(2-methylamino-2-oxoethyl)-2-oxo-3-butenamide as a pale yellow gum (435 mg, 77%); ir λ_{max}: 3.01, 5.98, 6.02 μm; ^{1}H nmr δ: 6.90 (br s, 1H), 6.30 (m, 2H), 4.05 (m, 2H), 3.50 (t, J = 6 Hz, 2H), 3.30 (s, 3H), 3.00 and 2.93 (2 s, 3H), 2.77 (d, J = 4 Hz, 3H), 2.62 (t, J = Hz, 2H).

A solution of this product (435 mg, 1.80 mmol) in tetrahydrofuran (2 mL) was syringed into a solution of MICA prepared from magnesium turnings (63 mg, 2.6 mmol), methyl bromide, and isopropylcyclohexylamine (0.5 mL), in dry tetrahydrofuran (12 mL). The mixture was stirred overnight at room temperature and treated with 3 *M* hydrochloric acid (5 mL) to give 3-hydroxy-3-[1-(2-methoxyethyl)ethenyl]-1,4-dimethylpiperazine-2,5-dione as a pale yellow gum (403 mg, 93%), which was ether insoluble and resisted crystallization; ir λ_{max}: 6.04 μm; ^{1}H nmr δ: 5.23 (br s, 1H), 5.17 (m, 2H), 3.97 (m, 2H), 3.47 (t, J = 6 Hz, 2H), 3.30 (s, 3H), 2.98 (s, 3H), 2.90 (s, 3H), 2.27 (t, J = 6 Hz, 2H).

The hydroxy piperazinedione (40.3 mg, 1.66 mmol) was acetylated in a solution of acetic anhydride (2 mL), triethylamine (2 mL), and a few crystals of 4-dimethylaminopyridine. The mixture was stirred for 18 h at room temperature to give a gummy residue which was chromatographed on silica with 10% methanol – ethyl acetate as eluent. The product (R_f = 0.5), 3-acetoxy-3-[1-(2-methoxyethyl)ethenyl]-1,4-dimethylpiperazine-2,5-dione (**35**), was a pale yellow gum (311 mg, 66%), which resisted crystallization in a variety of solvents; ir λ_{max}: 5.79, 6.01 μm; ^{1}H nmr δ: 5.57 (s, 1H), 5.27 (m, 1H), 4.03 (s, 2H), 3.48 (t, J = 6 Hz, 2H), 3.32 (s, 3H), 2.92 (s, 3H), 2.75 (s, 3H), 2.27 (t, J = 6 Hz, 2H), 2.15 (s, 3H); *m/e*: 284 (12), 225 (100), 192 (19), 180 (14). *Accurate Mass* calcd. for $C_{13}H_{20}N_2O_5$: 284.1372; found: 284.1346.

*Reaction of **30** with trimethylsilyl iodide. Formation of (E)-1,4-dibenzyl-3-(4-methoxy-2-butylidene)piperazine-2,5-dione (**36**)*

Piperazine-2,5-dione **30** (91 mg, 0.21 mmol) was dissolved in $CHCl_3$ in an nmr tube and trimethylsilyl iodide (TMSI) (66 μL, 0.46 mmol) was added. The solution turned dark red-brown on addition of the TMSI. The reaction was followed by ^{1}H nmr spectroscopy for 19 h at room temperature. The contents of the nmr tube were dissolved in methylene chloride (15 mL) and the solution was washed with saturated aqueous Na_2SO_3 (5 mL), 3 *N* hydrochloric acid (5 mL), aqueous 10% $NaHCO_3$, and water (5 mL). The methylene chloride solution was dried, filtered, and concentrated. The residue was chromatographed on a 1-mm preparative silica gel plate with 20% ethyl acetate – chloroform as eluent. The band (R_f = 0.3) was eluted with methanol–chloroform, and the fraction concentrated, giving a gum (64 mg) whose ^{1}H nmr spectrum was identical with that of (*E*)-1,4-dibenzyl-3-(4-methoxybut-2-ylidene)piperazine-2,5-dione (**36**) (19).

*Reaction of **20** with trimethylsilyl iodide. Formation of 3-acetoxy-5,6-dihydro-4-methyl-2H-pyran-2-one (**38**)*

(*i*) Compound **20** (100 mg, 0.229 mol), TMSI (65 μL, 0.48 mmol), and $NaHCO_3$ (100 mg, 1.19 mmol) in methylene chloride (2 mL) were stirred for 18 h at room temperature. The mixture was washed with saturated aqueous Na_2SO_3 (1 mL), 3 *N* hydrochloric acid (1 mL), aqueous 10% $NaHCO_3$ (1 mL), and water (1 mL), dried, filtered, and concentrated. The residue was chromatographed on a 1-mm preparative silica gel plate with 20% ethyl acetate – chloroform as eluent. The strongly fluorescent band (R_f = 0.46) was eluted with methanol–chloroform giving **38** (26) (30 mg, 77%) as a yellow oil; ir λ_{max}: 5.65, 7.78 μm; ^{1}H nmr δ: 5.20 (t, J = 6 Hz, 2H), 2.53 (t, J = 6 Hz, 2H), 2.25 (s, 3H), 1.88 (s, 3H).

Compound **20** gave the same product on treatment with one equivalent of TMSI.

(*ii*) Reaction of **20** (114 mg, 0.260 mmol) with sodium iodide (83 mg, 0.55 mmol) and trimethylsilyl chloride (66 μL, 0.52 mmol) in acetonitrile (2 mL) for 10 h at room temperature gave a mixture of **38** and unconsumed **20** after work-up as in (*i*).

(*iii*) Reaction of **20** (152 mg, 0.347 mmol) with zinc iodide (761 mg, 2.39 mmol) and TMSI (0.35 mL, 2.46 mmol) in methylene chloride (2 mL) for 5 min at room temperature gave a mixture of **38** and unconsumed **20** after work-up as in (*i*).

*2-Acetoxy-*N*-benzyl-3-(2-hydroxyethyl)-*N*-(2-benzylamino-2-oxoethyl)-3-butenamide (**39**)*

The general procedure of Hanessian and Guindon (29) for the cleavage of methyl ethers with thiotrimethylsilanes in the presence of tetrabutylammonium iodide and zinc iodide was employed.

(*i*) A solution of **21** (185 mg, 0.422 mmol), zinc iodide (purified by washing with carbon tetrachloride; 0.65 g, 2.0 mmol), tetra-*n*-butylammonium iodide (0.47 g, 1.3 mmol), and phenylthiotrimethylsilane (34) (0.72 g, 4.0 mmol) in 1,2-dichloroethane (8 mL) was heated with stirring at 73–75°C for 20 h. Work-up with aqueous 10% $NaHCO_3$ returned only **21**.

(*ii*) A solution of **21** (125 mg, 0.285 mmol), zinc iodide (273 mg, 0.855 mmol), tetra-*n*-butylammonium iodide (167 mg, 0.428 mmol), and 1,2-ethanedithiobis(trimethylsilane) (34) (407 mg, 1.71 mmol) in 1,2-dichloroethane (5 mL) was heated with stirring at 80°C for 13 h. The mixture was cooled, washed with aqueous 10% $NaHCO_3$, dried, filtered, and concentrated. The residue was loaded on a silica gel plug with chloroform. After removal of sulfur-containing compounds by elution with chloroform, the product was eluted with ethyl acetate. Concentration of the ethyl acetate solution gave a 35% yield of **39**.

(*iii*) A similar reaction of **21** with a 2:5:1.5:1 molar ratio of 1,2-ethanedithiobis(trimethylsilane), zinc iodide, tetrabutylammonium iodide, and **21** for 3 h at 75°C gave dihydropyrone **38** and unconsumed **21** after work-up with aqueous 10% $NaHCO_3$.

(*iv*) A solution of **21** (8.27 g, 18.9 mmol), zinc iodide (15.84 g, 49.65 mmol), methylthiotrimethylsilane (12.44 g, 103 mmol), and tetra-*n*-butylammonium iodide (1.22 g, 3.30 mmol) in 1,2-dichloroethane (155 mL) was heated at 80°C for 1.5 h. During this time the solution became yellow. The solution was cooled, washed with 3 *N* hydrochloric acid (50 mL), dried, filtered, and concentrated. The residue was dissolved in chloroform and ether was added slowly to precipitate tetra-*n*-butylammonium iodide as white crystals. The solution was filtered and concentrated and the residue was chromatographed on silica with ethyl acetate as eluent. The first materials eluted were sulfur-containing compounds; **39** was then eluted (R_f = 0.4) and obtained as a viscous yellow gum which assumed a dark green color after being pumped on under high vacuum overnight (3.02 g, 38%); ir λ_{max}: 2.93, 5.74, 5.96 μm; ^{1}H nmr δ: 7.22 (m, 11H), 5.72 and 5.48 (2 s, 1H), 2.8–4.8 (m, 11H), 2.83 (t, J = 6 Hz, 2H), 2.07, 1.95 (s, 3H). Its spectra indicated that this was a cleaner product than that obtained by procedure (*ii*).

*2-Acetoxy-*N*-benzyl-*N*-(2-benzylamino-2-oxoethyl)-3-[2-(tetrahydropyran-2-yloxy)ethyl]-3-butenamide (**40**) and 3-acetoxymethyl-*N*-benzyl-*N*-(2-benzylamino-2-oxoethyl)-5-(tetrahydropyran-2-yloxy)-2-pentenamide (**41**)*

A mixture of crude **39** (3.02 g, 7.11 mmol) and tetrahydropyran-2-yl *tert*-butyl ether (15 mL) in methylene chloride (5 mL) and three drops of concentrated hydrochloric acid was stirred for 18 h at room temperature. Solid $NaHCO_3$ and $MgSO_4$ were added and the mixture

Can. J. Chem. Downloaded from www.nrcresearchpress.com by 210.87.254.40 on 09/06/12
For personal use only.

was filtered after stirring for a few min. The filtrate was concentrated under high vacuum and the residue was chromatographed on silica with 1 : 1 ethyl acetate – cyclohexane as eluent. A fraction (R_f = 0.4) was eluted after elution of residual tetrahydropyran-2-yl *tert*-butyl ether which was found to contain two components whose R_f values were very similar in a variety of solvent systems. It was re-chromatographed twice on silica with an increasing proportion of ethyl acetate (20%, 40%, 60%) in the ethyl acetate – cyclohexane eluent. The minor component (211 mg, 6%) with a slightly higher R_f was obtained as an orange gum and is considered to be **41**; ir λ_{max}: 5.75, 6.03 μm; ^{1}H nmr δ: 7.30 (m, 11H), 6.15, 5.38 (m, 1H), 3.2–5.4 (m, 13H), 2.50 (t, J = 6 Hz, 2H), 2.03, 1.95 (s, 3H), 1.13–1.80 (m, 6H); *m/e*: 449, 423, 394, 364, 255 (29), 253 (19), 91 (100).

Compound **40** was eluted last as a yellow gum (2.80 g, 77%), ir λ_{max}: 2.98, 5.71, 5.92 μm; ^{1}H nmr δ: 7.28 (m, 11H), 5.80 (s, 0.7H), 5.18 (s, 0.3H), 5.0–5.4 (m, 2H), 3.1–4.8 (m, 11H), 2.42 (t, J = 6 Hz, 2H), 2.10 (s, 1H), 2.03 (s, 2H), 1.0–1.8 (m, 6H); *m/e*: 423 (6), 364 (10), 120 (20), 106 (31), 91 (100). *Accurate Mass* calcd. for $C_{24}H_{27}N_2O_5$ (M − C_5H_9O): 423.1920; found: 423.1927.

N-*Benzyl*-N-*(2-benzylamino-2-oxoethyl)-2-hydroxy-3-[2-(tetrahydropyran-2-yloxy)ethyl]-3-butenamide (42)*

Compound **40** (2.53 g, 4.99 mmol) and sodium hydroxide (203 mg, 5.10 mmol) in absolute ethanol (50 mL) were stirred for 8 h at room temperature. An analogous work-up to that used in the preparation of **24** gave a quantitative yield of **42** as a viscous yellow gum; ir λ_{max}: 2.91, 5.98, 6.05 μm; ^{1}H nmr δ: 7.17 (m, 11H), 3.1–5.2 (m, 15H), 2.37 (m, 2H), 1.13–1.80 (m, 6H).

N-*Benzyl*-N-*(2-benzylamino-2-oxoethyl)-2-oxo-3-[2-(tetrahydropyran-2-yloxy)ethyl]-3-butenamide (43)*

Compound **42** (2.33 g, 4.99 mmol) was oxidized with activated manganese dioxide (15 g) in chloroform (150 mL) for 18 h at room temperature and worked up as in the case of **25** to give a quantitative yield of **43** as a pale yellow gum; ir λ_{max}: 2.97, 5.96, 6.08 μm; ^{1}H nmr δ: 7.27 (m, 10H), 6.73 (br s, 1H), 6.42 (m, 2H), 3.1–4.8 (m, 11H), 2.60 (t, J = 6 Hz, 2H), 1.1–1.8 (m, 6H); *m/e*: 380 (2), 363 (18), 272 (13), 181 (23), 91 (100). *Accurate Mass* calcd. for $C_{22}H_{24}N_2O_4$ (M − C_5H_8O): 380.1736; found: 380.1714.

3-Acetoxy-1,4-dibenzyl-3-[1-(2-(tetrahydropyran-2-yloxy)ethyl)-ethenyl]piperazine-2,5-dione (45)

A solution of MICA was prepared from magnesium (86 mg, 3.6 mmol), methyl bromide, and isopropylcyclohexylamine (0.6 mL) in dry tetrahydrofuran (60 mL) as in the previous cases. Compound **43** (1.274 g, 2.741 mmol) in dry tetrahydrofuran (10 mL) was syringed dropwise into the MICA solution at room temperature under nitrogen over a period of 3 h. The mixture was stirred for 15 h at room temperature during which time it turned cloudy. Acetic anhydride (0.80 mL, 8.5 mmol) was syringed into the reaction flask and the mixture was stirred for an additional 5 h at room temperature. The solution was poured into water (20 mL) and the aqueous solution was extracted with chloroform (4 × 25 mL). The combined chloroform extracts were dried, filtered, concentrated, and pumped on for 1 h under high vacuum. The residue was chromatographed on silica with 60% ethyl acetate – cyclohexane as eluent. Compound **45** was eluted first (R_f = 0.57), the next fraction (R_f = 0.43) was acetylated isopropylcyclohexylamine, and the final fraction (R_f = 0.36) contained uncharacterized polymeric products. Compound **45** was obtained as a pale yellow gum (878 mg, 63%); ir λ_{max}: 5.76, 5.99 μm; ^{1}H nmr δ: 7.27 (s, 5H), 7.23 (s, 5H), 5.70 (s, 1H), 5.47 (s, 1H), 3.3–5.4 (m, 11H), 2.33 (t, J = 6 Hz, 2H), 1.4–1.8 (m, 6H), 1.33 (s, 3H); *m/e*: 506 (1), 422 (7), 363 (11), 271 (8), 106 (24), 91 (93), 84 (100). *Accurate Mass* calcd. for $C_{29}H_{34}N_2O_6$: 506.2417; found: 506.2411.

3-Acetoxy-1,4-dibenzyl-3-(3-hydroxy-1-methylenepropyl)piperazine-2,5-dione (46) and 6,9-dibenzyl-4-methyleneoxa-6,9-diazaspiro-[4.5]decane-7,10-dione (47)

A solution of **45** (878 mg, 1.73 mmol) in acetic acid (15 mL), water (6 mL), and tetrahydrofuran (3 mL) was stirred for ~15 h at room temperature. The solvent was removed *in vacuo* and the residue was chromatographed on silica with 60% ethyl acetate – cyclohexane as eluent. The initial fraction (R_f = 0.57) returned unconsumed **45** (25 mg). The second fraction (R_f = 0.45) gave **47** (153 mg, 21%), which was crystallized from ethanol–water, mp 93–95°C; ir λ_{max}: 5.97 μm; ^{1}H nmr δ: 7.25 (m, 10H), 5.25 (m, 1H), 4.95 (m, 1H), 3.9–4.8 (m, 8H), 2.87 (m, 2H); *m/e*: 362 (15), 271 (12), 229 (9), 124 (11), 91 (100). *Accurate Mass* calcd. for $C_{22}H_{22}N_2O_3$: 362.1630; found: 362.1643.

The final fraction (R_f = 0.27) gave **46** as a colorless gum (425 mg, 58%); ir λ_{max}: 2.90, 5.70, 5.95 μm; ^{1}H nmr δ: 7.28 (s, 5H), 7.23 (s, 5H), 5.67 (s, 1H), 5.47 (s, 1H), 3.6–5.4 (m, 8H), 2.93 (br s, 1H), 2.33 (t, J = 6 Hz, 2H), 1.30 (s, 3H); *m/e*: 363 (3), 272 (3), 230 (2), 91 (22), 83 (100). *Accurate Mass* calcd. for $C_{22}H_{23}N_2O_3$ (M − $C_2H_3O_2$): 363.1709; found: 363.1704.

Acknowledgement

We thank the Natural Sciences and Engineering Research Council of Canada for support of this work.

1. J. H. HOARE and P. YATES. J. Chem. Soc. Chem. Commun. 1126 (1981).
2. T. MIYOSHI, N. MIYAIRI, H. AOKI, M. KOHASKA, H. SAKAI, and H. IMANAKA. J. Anitibiot. **25**, 569 (1972); S. MIYAMURA, N. OGASAWARA, H. OTSUKA, S. NIWAYAMA, H. TANAKA, T. TAKE, T. UCHIYAMA, H. OCHIAI, K. ABE, K. KOIZUMI, K. ASAO, K. MATSUKI, and T. HOSHINO. J. Antibiot. **25**, 610 (1972); S. MIYAMURA, N. OGASAWARA, H. OTSUKA, S. NIWAYAMA, H. TANAKA, T. TAKE, T. UCHIYAMA, and H. OCHIAI. J. Antibiot. **26**, 479 (1973).
3. T. KAMIYA, S. MAENO, M. HASHIMOTO, and Y. MINE. J. Antibiot. **25**, 576 (1972); Y. TOKUMA, S. KODA, T. MIYOSHI, and Y. MORIMOTO. Bull. Chem. Soc. Jpn. **47**, 18 (1974).
4. H. MAAG, J. F. BLOUNT, D. L. COFFEN, T. V. STEPPE, and F. WONG. J. Am. Chem. Soc. **100**, 6786 (1978); H. MAAG, J. F. BLOUNT, and T. V. STEPPE. Second Chemical Congress of the North American Continent, Aug. 25–29, 1980. Abstract No. 347.
5. M. NISHIDA, Y. MINE, T. MATSUBARA, S. GOTO, and S. KUWAHARA. J. Antibiot. **25**, 582 (1972); K. MINE and T. OSHIMA. Ger. Patent No. 2,839,730; Chem. Abstr. **90**, P202673r (1979).
6. L. V. DUNKERTON and R. M. AHMED. Tetrahedron Lett. **21**, 1803 (1980).
7. S. NAKATSUKA, K. YOSHIDA, and T. GOTO. Tetrahedron Lett. **22**, 2009, 4973 (1981).
8. R. M. WILLIAMS. Tetrahedron Lett. **22**, 2341 (1981).
9. C. SHIN, Y. SATO, and J. YOSHIMURA. Tetrahedron Lett. **22**, 2401 (1981).
10. T. FUKUYAMA, B. D. ROBINS, and R. A. SACHLEBEN. Tetrahedron Lett. **22**, 4155 (1981).
11. E. VOGEL and H. SCHINZ. Helv. Chim. Acta, **33**, 116 (1950).
12. D. E. BURKE, J. M. COOK, and P. W. LE QUESNE. J. Am. Chem. Soc. **95**, 546 (1973).
13. D. M. BURNESS. Org. Synth. Coll. Vol. **4**, 649 (1963).
14. A. J. SPEZIALE and H. W. FRAZIER. J. Org. Chem. **26**, 3176 (1961).
15. P. M. POJER and I. D. RAE. Aust. J. Chem. **23**, 413 (1970).
16. A. J. SPEZIALE and E. G. JAWORSKI. J. Org. Chem. **25**, 728 (1960).
17. U. SCHMIDT, A. PERCO, and E. ÖHLER. Chem. Ber. **107**, 2816 (1974); E. ÖHLER and U. SCHMIDT. Chem. Ber. **108**, 2907 (1975).
18. E. J. COREY, A. MARFAT, J. R. FALCK, and J. O. ALBRIGHT. J. Am. Chem. Soc. **102**, 1433 (1980).
19. P. YATES and J. H. HOARE. Can. J. Chem. In press.

20. W. STEGLICH and G. HÖFLE. Angew. Chem. Int. Ed. Engl. **8**, 981 (1969).
21. K. D. KOPPLE and D. H. MARR. J. Am. Chem. Soc. **89**, 6193 (1967).
22. J. H. HOARE and P. YATES. Heterocycles, **15**, 281 (1981).
23. M. E. JUNG and M. A. LYSTER. J. Org. Chem. **42**, 3761 (1977).
24. T.-L. HO. Synth. Commun. **9**, 665 (1979).
25. G. A. OLAH, S. C. NARANG, B. G. B. GUPTA, and R. MALHOTRA. J. Org. Chem. **44**, 1247 (1979).
26. L. LALOI, N. BÉNZÉTH, and H. GAULT. C.R. Acad. Sci. Paris, **255** 2117 (1962); L. LALOI, N. NOËL, and H. GAULT. Fr. Patent No. 1,329,011; Chem. Abstr. **59**, P12647 (1963).
27. C. A. SMITH and J. B. GRUTZNER. J. Org. Chem. **41**, 367 (1976).
28. M. NODE, K. NISHIDE, K. FUJI, and E. FUJITA. J. Org. Chem. **45**, 4275 (1980).
29. S. HANESSIAN and Y. GUINDON. Tetrahedron Lett. **21**, 2305 (1980).
30. J. S. COWIE, P. D. LANDOR, and S. R. LANDOR. J. Chem. Soc. Perkin Trans. **1**, 720 (1973).
31. P. A. GRIECO, C. S. POGONOWSKI, S. D. BURKE, M. NISHIZAWA, M. MIYASHITA, Y. MASAKI, C-L. J. WANG, and G. MAJETICH. J. Am. Chem. Soc. **99**, 4111 (1977).
32. J. ATTENBURROW, A. F. B. CAMERON, J. H. CHAPMAN, R. M. EVANS, B. A. HEMS, A. B. A. JANSEN, and T. WALKER. J. Chem. Soc. 1094 (1952).
33. J. VOLHARD. Justus Liebigs Ann. Chem. **123**, 261 (1862).
34. R. S. GLASS. J. Organometal. Chem. **61**, 83 (1973).

Can. J. Chem. Downloaded from www.nrcresearchpress.com by 210.87.254.40 on 09/06/12
For personal use only.

Structure–activity studies of β-carbolines. 1. Molecular structure and conformation of *cis*-3-carboxylic acid-1,2,3,4-tetrahydroharmane dihydrate

PENELOPE W. CODDING
Department of Chemistry, University of Calgary, Calgary, Alta., Canada T2N 1N4

Received August 16, 1982

PENELOPE W. CODDING. Can. J. Chem. **61**, 529 (1983).

The crystal structure of *cis*-3-carboxylic acid-1,2,3,4-tetrahydroharmane dihydrate, $C_{13}H_{13}N_2O_2 \cdot 2H_2O$, a putative ligand of the benzodiazepine receptor is reported. The space group is $P2_1/c$ with a = 14.850(4), b = 6.560(3), c = 14.746(4) Å and β = 117.411(8)°, Z = 4. The molecule crystallizes as a zwitterion with the unsaturated ring in a half-chair conformation. Hydrogen bonding to the water molecules included in the lattice determines the molecular packing arrangement.

PENELOPE W. CODDING. Can. J. Chem. **61**, 529 (1983).

On rapporte la structure du cristal de l'acide tétrahydro-1,2,3,4 harmane carboxylique-3 dihydrate *cis*, $C_{13}H_{13}N_2O_2 \cdot 2H_2O$, un ligand putatif du récepteur benzodiazépine. Le groupe d'espace est du type $P2_1/c$ avec a = 14,850(4), b = 6,560(3), c = 14,746(4) Å et β = 117,411(8)°, Z = 4. La molécule cristallise sous forme de zwiterrions avec une conformation demi-chaise du cycle insaturé. Les liaisons hydrogènes des molécules d'eau incluses dans le réseau déterminent l'arrangement de l'aggrégat moléculaire.

[Traduit par le journal]

Can. J. Chem. Downloaded from www.nrcresearchpress.com by 210.87.254.6 on 09/06/12
For personal use only.

Introduction

Historically, harmala alkaloids have been used therapeutically for their hypotensive activity; however, recent interest has focussed on other neurological effects. Within the last 5 years workers have found harmane (1-methyl-β-carboline, **1**), tetrahydro-β-carboline, and β-carboline-3-carboxylate derivatives in brain tissue and in urine (1, 2). The physiological function of the β-carboline compounds has been intensively studied. One proposal is that a β-carboline compound is the endogenous ligand of the benzodiazepine receptor in parallel with the endorphins and the opiate receptor (3). Harmane and other β-carbolines exhibit high-affinity competitive inhibition of a class of benzodiazepine receptors; but the specific endogenous β-carboline has not, as yet, been identified (2).

Further, Müller *et al.* (4) have demonstrated with in vitro testing that harmane and similar drugs interact with a number of neurotransmitter systems in addition to the benzodiazepine

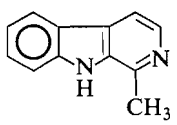

1

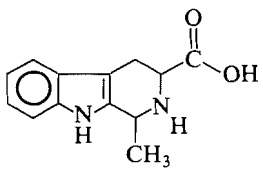

2

receptor; these include opiate, cholinergic, muscarinic, serotonin, and dopamine receptors. Minor changes in the β-carboline structure lead to substantially different affinities for these receptors. Such data, coupled with the in vivo presence of these drugs, suggest that β-carbolines may act as neurotransmitters or neuromodulators themselves.

As part of a study of the neurobiology of β-carbolines, determination of the crystal structure of 3-carboxylic acid-1,2,3,4-tetrahydroharmane (hereafter THHCA, **2**) was undertaken to obtain topochemical information on the precursor of the ester derivatives found in vivo. Conformational analysis via ^{13}C nmr of other 1,3-disubstituted unsaturated β-carbolines (5) predicted that for this compound the *cis* diastereomer with the 1,3 hydrogen atoms in axial positions would predominate.

Experimental

A racemic, commerical sample (Sigma Chemical Co., St. Louis, Missouri, U.S.A.) of the title compound was recrystallized from a water/methanol/ethanol mixture by slow evaporation. A colorless needle-shaped crystal was used for data collection on an Enraf Nonius CAD4F diffractometer. The crystal data are in Table 1. After alignment of the crystal, 25 reflections were found and indexed using the automatic searching, centering, and indexing routines of the instrument. The cell was identified as monoclinic; this lattice assignment was confirmed and the space group was determined by the examination of the intensities from a data collection ($2° < \theta \leq 10°$) over the entire sphere of reflection. Systematic absences of (0k0), $k = 2n + 1$ and ($h0l$), $l = 2n + 1$ and the symmetry of the intensities identified the space group as $P2_1/c$. Data were collected at room temperature using an $\omega/2\theta$ scan of a speed varied (for ω) between 0.8° and 6.7°/min to obtain $I > 2.5\sigma(I)$ within a measurement time of 120 s. The scan width was calculated as given in Table 1 and 2/3 of the scan time, at the center of the scan, was taken as peak (P) and 1/6 of the time at each side was taken as background (B_1 and B_2). Then $I = [P - 2(B_1 + B_2)]Q$, where Q is the scan rate and the standard deviation of the intensity is $\sigma(I) = [P + 4(B_1 + B_2)]^{1/2}Q$. Lorentz and polarization corrections were applied and E values were calculated by applying a K curve.

The structure was solved using the direct methods program PHASE from the XRAY76 system (6). All nonhydrogen atoms of THHCA were identified in the E-map which was calculated from the predicted phases. Least-squares refinement using isotropic temperature factors produced an R value of 0.30 and a difference Fourier synthesis revealed the positions of the oxygen atoms of two water molecules. After inclusion of the oxygen atoms and further isotropic refinement to R = 0.10, a difference Fourier synthesis indicated the positions of all hydrogen atoms. The zwitterionic nature of the molecule was evident at this point. Hydrogen atoms were assigned isotropic thermal parameters that were 20% larger than the atom to which they were bonded and were included in the model; however, only their positional

Can. J. Chem. Downloaded from www.nrcresearchpress.com by 210.87.254.6 on 09/06/12
For personal use only.

TABLE 1. Crystal data

Formula	$C_{13}H_{13}N_2O_2 \cdot 2H_2O$
FW	265.29
Space group	$P2_1/c$
a (Å)	14.850(4)
b (Å)	6.560(3)
c (Å)	14.746(4)
β (°)	117.411(8)
V (Å^3)	1275.3(7)
Z	4
ρ_o(g cm^{-3})	1.38
ρ_c(g cm^{-3})	1.38
Crystal dimensions (mm)	0.2 × 0.2 × 0.25
Radiation	MoKα (0.71069 Å) graphite monochromator
θ_{max} (°)	26.5
Scan range	$\Delta\omega = 1.5(0.54 + 0.347 \tan\theta)$
Unique reflections	2649
No. included in refinement ($F_c > F_o$ for unobserved reflections)	1962
$R = (\Sigma\|\|F_o\| - \|F_c\|\|/\Sigma\|F_o\|)$	0.055
μ(cm^{-1})	1.11

TABLE 2. Atomic coordinates (× 10^4) and $U_{equivalent}$ (× 10^3) for the nonhydrogen atoms in *cis*-3-carboxylic acid-1,2,3,4-tetrahydroharmane. $U_{equivalent}$ is $\frac{1}{3}$ the sum of the trace of the diagonalized U_{ij} matrix

Atom	x/a (Å)	y/b (Å)	z/c (Å)	U_{eq}
C1	3046(3)	5915(7)	2313(4)	24
C3	3125(3)	2686(7)	1428(3)	23
C4	2090(4)	1902(7)	1250(4)	27
C5	−364(4)	2313(8)	764(4)	34
C6	−1295(4)	2924(11)	679(4)	44
C7	−1411(4)	4816(10)	1048(4)	39
C8	−608(4)	6167(9)	1501(4)	35
C10	1951(3)	5333(8)	1920(4)	26
C11	1512(3)	3566(7)	1447(4)	24
C12	458(4)	3648(8)	1217(3)	28
C13	323(4)	5567(8)	1578(4)	28
C14	3514(4)	6985(8)	3338(4)	31
C31	3824(3)	940(7)	1466(4)	21
N2	3604(3)	3924(6)	2396(3)	24
N9	1241(3)	6595(7)	1997(3)	32
O1	3570(3)	2871(6)	−891(3)	44
O2	4211(3)	−3934(6)	598(3)	46
O31	4517(2)	416(6)	2314(3)	36
O32	3616(3)	147(6)	618(3)	37

parameters were refined. Refinement was blocked so that anisotropic least-squares refinement of the atomic parameters of all the nonhydrogen atoms was alternated with refinement of the atomic coordinates of the hydrogen atoms. The least-squares analysis converged with a maximum shift/error of 0.017 and an R value of 0.055 using unit weights. Atomic coordinates[1] are given in Table 2 with the atoms labeled as shown in Fig. 1. Bond distances are shown in Fig. 1 and bond angles are given in Table 3.

All computations were done using the XRAY76 system programs (6) on a Honeywell computer using the Multics operating system. Scattering factors are those of Cromer and Mann (7).

[1]The anisotropic thermal parameters, hydrogen atom parameters, and the observed and final calculated structure amplitudes are available at a nominal charge from the Depository of Unpublished Data, CISTI, National Research Council of Canada, Ottawa, Ont., Canada K1A 0S2.

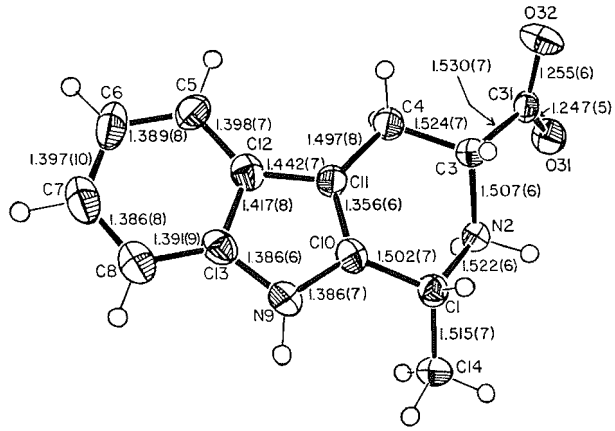

FIG. 1. Molecular structure, atomic labeling, and interatomic distances for *cis*-3-carboxylic acid-1,2,3,4-tetrahydroharmane as drawn with the computer program ORTEP(6). Probability ellipsoids were drawn at the 50% level and hydrogen atoms were assigned a spheroid of radius 0.1 Å.

Results and discussion

Figure 1 shows the structure and the interatomic distances for the zwitterion of THHCA. The two water molecules which are hydrogen-bonded to the carboxylate group are shown in Fig. 2 which shows the conformation of the molecule. The 6-membered heterocyclic ring is in a half-chair conformation with C3 0.317 Å above and N2 0.461 Å below the least-squares plane of the other four atoms (σ (plane) = 0.006 Å). Both the 1-methyl and the 3-carboxylic acid substituents are equatorial, thereby minimizing steric repulsion. This conformation can be expected to predominate in the active molecules since similar substitution patterns are observed in those β-carbolines.

In this determination THHCA is found as a zwitterion with a positive charge on N2 and the negative charge distributed over the two oxygen atoms of the carboxylate group. Although those β-carbolines with 3-substituents thus far isolated have been esters rather than acids, the evidence from ^{13}C nmr is that the half-chair conformation as observed here is determined by

TABLE 3. Bond angles (in °) for the nonhydrogen atoms in *cis*-3-carboxylic acid-1,2,3,4-tetrahydroharmane. The estimated standard deviation in the last digit is in parentheses

Angles	(°)
N2—C1—C10	105.4(4)
N2—C1—C14	109.5(3)
C10—C1—C14	114.8(5)
N2—C3—C31	110.6(3)
N2—C3—C4	110.1(4)
C4—C3—C31	111.6(4)
C3—C4—C11	110.0(4)
C6—C5—C12	118.5(5)
C5—C6—C7	121.2(5)
C6—C7—C8	121.5(6)
C7—C8—C13	117.4(6)
C1—C10—C11	126.5(5)
C1—C10—N9	123.1(4)
N9—C10—C11	110.4(4)
C4—C11—C10	122.7(4)
C4—C11—C12	129.7(4)
C10—C11—C12	107.6(5)
C5—C12—C11	134.7(5)
C5—C12—C13	119.5(5)
C11—C12—C13	105.7(4)
C8—C13—N9	129.4(5)
C8—C13—C12	121.9(5)
N9—C13—C12	108.7(5)
C1—N2—C3	112.6(3)
C10—N9—C13	107.6(4)
C3—C31—O31	118.4(4)
C3—C31—O32	114.9(4)
O31—C31—O32	126.6(5)

the bulk of the substituents rather than by the charge. It remains important that the molecule assumes an ionic form in hydrophilic solvents as this may be a key to the transport and activity of the drug. Indeed, a recent report (8) ascribes the inactivity of THHCA at BZD receptors to a negatively charged carboxylate group; however, the zwitterionic form may be what was present in these tests. Zwitterionic THHCA was obtained from the free base simply by recrystallization at a nominal pH of 7. The zwitterion is confirmed by the equal C31-to-oxygen atom distances (C31—O31 1.247(5) Å and C31—O32 1.235(6) Å) and the identification of two hydrogen atoms within bonding distance of N2 (N2—H2A 0.92(5) Å and N2—H2B 1.00(5) Å).

Since the zwitterion is formed at physiological pH and appears to be the stable form of THHCA it is useful to study the hydrogen bonds formed by this moiety as they may well reflect potential THHCA–receptor interactions. The pattern of hydrogen bond formation is shown in Fig. 2 and the dimensions of these bonds are given in Table 4. Each potential donor or acceptor of the THHCA moiety is utilized; thus THHCA could bind quite strongly to a receptor site.

The carboxyl oxygen atoms each form two hydrogen bonds, O32 bonds to each of the two water molecules of the asymmetric unit as shown in Fig. 2 and O32 bonds to the protonated nitrogen atom N2 at $(1 - x, y - \frac{1}{2}, \frac{1}{2} - z)$ and to the other

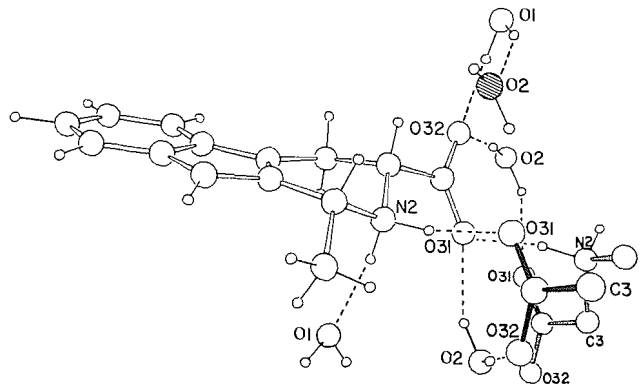

FIG. 2. Hydrogen bonding scheme for THHCA; the hydrogen bonds are dashed lines. The molecular fragment with black bonds is at $(1 - x, \frac{1}{2} + y, \frac{1}{2} - z)$; the fragment with striped bonds is at $(1 - x, y - \frac{1}{2}, \frac{1}{2} - z)$. The shaded water molecule 1 is at $(x, \frac{1}{2} - y, \frac{1}{2} + z)$, the hatched water molecule 2 is at $(x, y + 1, z)$, the water molecule 2 with dark bonds is at $(1 - x, \frac{1}{2} + y, \frac{1}{2} - z)$. Plotting done by ORTEP(6) with arbitrary spheres of radius 0.3 Å for all but H atoms (0.1 Å).

TABLE 4. Hydrogen bond dimensions for THHCA

Atoms X···H—Y	X···H (in Å)	H—Y (in Å)	X···H—Y (in °)
O32···H1(O1)—O1	1.88(6)	0.96(6)	171(5)
O32···H1(O2)—O2	1.85(6)	0.98(6)	172(6)
O31···H2B—N2	1.83(5)	0.99(5)	164(4)
O31···H2(O2)—O2	1.96(5)	0.89(4)	156(6)
O1···H2A—N2	1.91(5)	0.91(5)	169(5)
O2···H2(O1)—O1	2.11(6)	0.84(5)	148(7)

hydrogen atom of water molecule 2 at $(1 - x, \frac{1}{2} + y, \frac{1}{2} - z)$. Due to the equatorial position of the carboxylic acid moiety, an intramolecular hydrogen bond between that group and the protonated nitrogen atom is not possible. Thus N2 donates a hydrogen atom to water molecule 1 at $(x, \frac{1}{2} - y, \frac{1}{2} + z)$ and to O31 of the molecule at $(1 - x, \frac{1}{2} + y, z - \frac{1}{2})$. Facile hydrogen bond formation appears to determine the packing in these crystals; there are no other significant intermolecular contacts.

THHCA appears to be composed of a hydrophobic moiety, the indole group, and a hydrophilic moiety which participates in the hydrogen bonding. The indole group is planar (σ = 0.010 Å) and forms an angle of 58.9° to the plane of the carboxylate group. The torsion angle positioning the carboxylate group appears to be dependent on hydrogen bond formation rather than any steric effects. All the bond distances and angles found in THHCA are typical for structures of this type and confirm the ionic nature of the molecule.

It appears that maximal utilization of hydrogen bond donors and acceptors is a strong stabilizing effect in these molecules and is probably important in receptor binding. Work is in progress on several esters of the β-carbolines to further our understanding of the topochemistry of these drugs.

Acknowledgements

This research was supported by an Establishment Grant and Scholarship from the Alberta Heritage Foundation for Medical Research. The author wishes to thank Dr. K. A. Kerr for use of the diffractometer.

Can. J. Chem. Downloaded from www.nrcresearchpress.com by 210.87.254.6 on 09/06/12
For personal use only.

1. N. S. BUCKHOLTZ. Life Sci. **27**, 893 (1980), and references cited therein.
2. C. BRAESTRUP, M. NIELSEN, and C. E. OLSEN. Proc. Natl. Acad. Sci. U.S.A. **77**, 2288 (1980).
3. P. SKOLNICK and S. M. PAUL. Annu. Rep. Med. Chem. **16**, 21 (1981).
4. W. E. MÜLLER, K. J. FEHSKE, H. O. BORKE, U. WOLLERT, C. NANZAND, and H. ROMMELSPACHER. Pharmacol. Biochem. Behav. **14**, 693 (1981).
5. F. UNGEMACH, D. SOERENS, R. WEBER, M. DIPIERRO, O. CAMPOS, P. MOKRY, J. M. COOK, and J. V. SILVERTON. J. Am. Chem. Soc. **102**, 6976 (1980).
6. J. M. STEWART. The X-ray system of crystallographic programs. Computer Science Center, University of Maryland, College Park, MD. 1976.
7. D. T. CROMER and J. B. MANN. Acta Crystallogr. Sect. A, **24**, 321 (1968).
8. M. CAIN, R. W. WEBER, F. GUZMAN, J. M. COOK, S. A. BARKER, K. C. RICE, J. N. CRAWLEY, S. M. PAUL, and P. SKOLNICK. J. Med. Chem. **25**, 1081 (1982).

Can. J. Chem. Downloaded from www.nrcresearchpress.com by 210.87.254.6 on 09/06/12
For personal use only.

Arylation de glycals catalysée par les sels de palladium: nouvelle synthèse de *C*-glycosides

STANISLAS CZERNECKI ET VERONIQUE DECHAVANNE

Laboratoire de Cinétique et Mécanismes de Réactions Organiques, CNRS ER 84, Université Pierre et Marie Curie, 4, Place Jussieu, Paris, France

Reçu le 29 juillet 1982

STANISLAS CZERNECKI et VERONIQUE DECHAVANNE. Can. J. Chem. **61**, 533 (1983).

L'arylation des glycals peracétylés catalysée par les sels de palladium constitue une nouvelle synthèse de *C*-glycosides. Cette réaction est appliquée à plusieurs aromatiques, incluant des dérivés fluorés et nitrés. La régiosélectivité de la réaction au niveau de l'aromatique est expliquée par la formation d'un arylpalladium directement à partir de l'aromatique et du sel. Un mécanisme en deux étapes, impliquant une *syn*-addition de l'arylpalladium sur la double liaison du glycal, suivie d'une *syn*-élimination est proposé et discuté.

STANISLAS CZERNECKI and VERONIQUE DECHAVANNE. Can. J. Chem. **61**, 533 (1983).

The arylation of peracetylated glycals catalyzed by palladium salts provides a new synthesis of *C*-glycosides. The title reaction is applied to several aromatic compounds, including fluoro and nitro derivatives. The regioselectivity of the reaction with respect to the aromatic nucleus is explained by the formation of an arylpalladium directly from the aromatic compound and the salt. A two-step mechanism, involving *syn*-addition of the arylpalladium to the glycal double bond, followed by a *syn*-elimination is proposed and discussed.

Can. J. Chem. Downloaded from www.nrcresearchpress.com by 210.87.254.5 on 09/06/12
For personal use only.

Introduction

Notre intérêt pour l'activation sélective des glucides éthyléniques (1) nous a amené à considérer que l'arylation des oléfines catalysée par des sels de palladium pouvait présenter des potentialités intéressantes dans le domaine des glucides. Cette réaction, qui représente un exemple des nombreuses applications du palladium en chimie organique (2), est globalement la substitution d'un hydrogène de l'oléfine par un groupement aromatique. Nous avons montré récemment (3) que son application à des glycals peracétylés pouvait constituer une nouvelle synthèse de *C*-glycosides car l'arylation se fait sur le carbone C1 du dérivé glucidique. Nous reportons dans cet article l'ensemble de nos résultats concernant cette réaction aussi bien du point de vue synthétique que mécanistique.

L'arylation des oléfines simples catalysée par le palladium peut être réalisée en faisant réagir un excès de celle-ci sur un iodure d'aryle (4*a*), un organomercurique aromatique (4*b*) ou l'aromatique lui-même (4*c*). Cette réaction a été l'objet de nombreuses études, aussi bien dans le but d'en améliorer les possibilités synthétiques (2) que d'en définir le mécanisme (5). Bien que celui-ci ne soit pas complètement élucidé, un processus en deux étapes est généralement admis (2*a*, *b*) pour les deux premières méthodes; d'abord une *syn*-addition, sur la double liaison, d'un arylpalladium (ArPdX) formé *in situ* à partir des réactifs, ensuite une *syn*-élimination de HPdX qui se décompose en HX et palladium métallique. Dans le cas de l'arylation avec l'aromatique, un mécanisme différent faisant intervenir des intermédiaires à liaisons π a été également envisagé (4*c*). En fait, l'existence d'un arylpalladium n'a pas été clairement établie dans ce cas, car cette réaction a été surtout appliquée à des oléfines simples qui ne permettent pas d'étudier les implications stéréochimiques de l'intervention d'un arylpalladium.

En revanche, les exemples d'arylation d'éther d'énols catalysée par les sels de palladium sont rares; à notre connaissance, il n'y a eu que quatre tentatives de phénylation de tels composés de cette manière (6), en dehors de la notre. Les plus anciennes (6*a*, *b*), réalisées sur des éthers d'énols simples, ont conduit à des mélanges complexes avec des rendements faibles. Plus récemment, il a été montré que la phénylation du 3,4-dihydro-4*H*-pyranne à l'aide de l'iodobenzène (6*c*) conduisait au 2-phényl-3,4-dihydro-2*H*-pyranne avec un rendement acceptable. Des expériences réalisées sur des éthers de vinyle et d'alkyle (6*c*, *d*) ont révélé que la réaction était sensible à l'encombrement de la double liaison. Enfin, un travail récent (7*a*) a montré que l'alkylation et la phénylation de dérivés du dihydrofuranne et du dihydropyranne étaient également réalisables par action de carbanions sur les complexes π-allyliques du palladium de ces dérivés.

L'utilisation du palladium dans le domaine des glucides est très récente. Arai et Daves, Jr. (8) ont étudié la possibilité d'obtenir des *C*-nucléosides par action du 1,3-diméthyl-2,4-pyrimidinedione-5-yl-palladium, préparé par échange à partir de l'organomercurique correspondant, sur des glycals peracétylés. Ils ont montré que la réaction était régiospécifique, mais qu'elle conduisait essentiellement au produit résultant de l'ouverture du cycle pyrannique. D'autre part, Baer et Hanna (9) ont étudié de façon détaillée l'alkylation et l'amination de complexes π-allyliques du palladium dérivés d'alkyl hex-2-énopyranosides. Enfin, la méthoxypalladation de glycals peracétylés a été réalisée avec de bons rendements (7*b*).

Les principaux substrats que nous avons utilisés pour évaluer l'utilité de l'arylation des oléfines dans le domaine des glucides sont les 3,4,6-tri-*O*-acétyl-1,5-anhydro-2-désoxy-D-*arabino*-hex-1-énitol (tri-*O*-acétyl-D-glucal) **1** et son isomère de configuration D-*lyxo* (tri-*O*-acétyl-D-galactal) **2** qui sont faciles d'accès.[1] En ce qui concerne les aromatiques, outre le benzène, nous avons utilisé l'anisole, le *m*-méthoxyanisole, le *p*-méthoxyanisole, le *p*-nitroanisole et le *p*-fluoroanisole.

Résultats et discussion

Aspect synthétique

En faisant réagir le glycal **2** avec un excès de composé

[1]Le 3,4,6-tri-*O*-acétyl-D-glucal est commercial (Aldrich) et le 3,4,6-tri-*O*-acétyl-D-galactal a été préparé selon la référence 10.

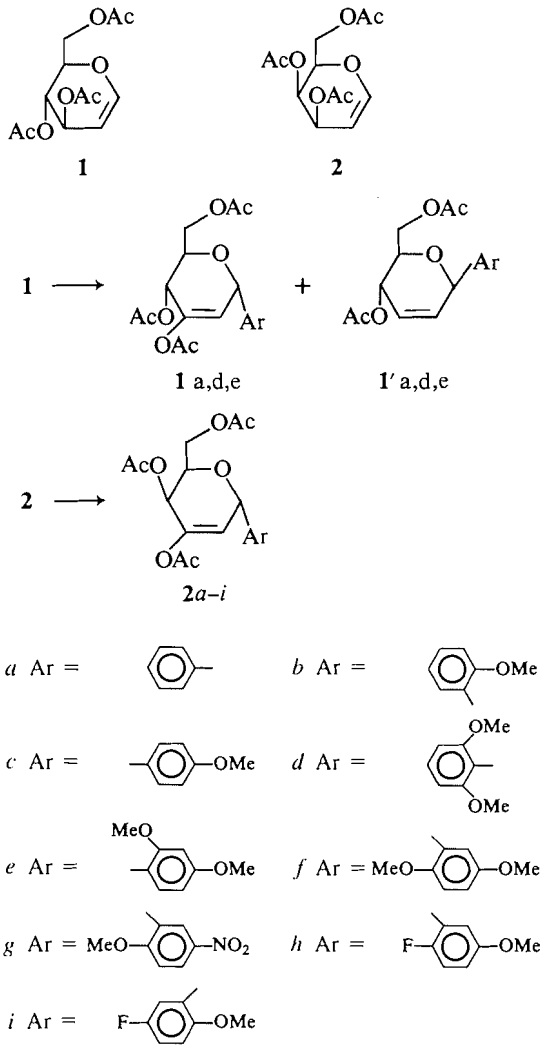

aromatique en présence d'une quantité stoechiométrique d'acétate de palladium, en solution dans l'acide acétique, on observe rapidement la formation d'un précipité noir de palladium métallique et la chromatographie sur couche mince indique la disparition du produit de départ. Après traitement (voir partie expérimentale), les composés de couplage **2***n*[2] sont isolés par recristallisation ou chromatographie sur colonne avec des rendements de 41 à 67% selon l'aromatique utilisé (Tableau 1). Le *C*-glycoside formé est accompagné de sous-produits car, dans le système étudié, plusieurs réactions parasites sont possibles. En particulier, l'isomérisation d'acétate allylique par les sels de palladium a déjà été décrite (11), et, avec les glycals peracétylés, elle conduit à des mélanges complexes, comme l'isomérisation par l'étherate de trifluorure de bore étudiée par Ferrier et Prasad (12). Nous avons vérifié qu'elle était relativement lente dans les conditions utilisées et, de plus, dans quelques cas où la transformation du glycal **1** était incomplète, nous avons pu récupérer du sucre éthylénique de départ inchangé.

Du milieu réactionnel, nous avons pu également isoler des composés plus polaires de masse molaire élevée correspondant à la dimérisation du produit de départ, réaction qui est également catalysée par les sels de palladium (13). Ces composés ont été caractérisés par spectroscopie de masse et rmn. L'importance de ces deux réactions concurrentes a été diminuée en utilisant un grand excès d'aromatique et des temps de réaction aussi courts que possible (1,5 ou 2 h à 120°C).

La troisième réaction parasite possible, la dimérisation de l'aromatique, n'est pas un inconvénient majeur, car les dimères obtenus sont aisément séparés des produits de couplage, mais elle consomme inutilement du sel de palladium. En fait, le meilleur catalyseur pour cette réaction est le chlorure de palladium (14) et avec l'acétate que nous avons utilisé, les composés biphénylés sont peu importants.

Des essais comparatifs avec d'autres sels ou en présence de triphénylphosphine (essais n° 9, 10 et 11) ont donné des rendements plus faibles ou nécessité des temps de chauffage prolongés.

Dans un premier temps, nous avons utilisé une quantité stoechiométrique de sel de palladium, car le palladium métallique qui précipite est récupéré de façon presque quantitative dans la plupart des cas (voir partie expérimentale) et peut être réoxydé en acétate avec de bons rendements (15). Nous avons montré qu'il était possible d'utiliser une quantité catalytique de sel et de réoxyder *in situ* le palladium avec de l'acétate de cuivre (essais n° 5 et 8). Toutefois, dans ces conditions, la réaction est plus lente et le rendement en *C*-glycoside diminue légèrement au profit de l'isomérisation et de la dimérisation.

Enfin, lorsque les positions de substitution sur le noyau aromatique n'étaient pas équivalentes, nous avons isolé et caractérisé les isomères correspondants (essais n° 9 et 14), sauf dans le cas de l'anisole pour lequel les produits substitués en *ortho* ou en *para* du groupe méthoxyle n'ont pas été séparés (essai n° 6) et le *p*-nitroanisole où un seul composé est formé en *ortho* du méthoxy (essai n° 13).

La réaction entre le tri-*O*-acétyl-D-glucal **1** et divers aromatiques (essais n° 1, 2, 7 et 8) conduit également à des triacétates de *C*-2-désoxyglyc-2-énosides **1***n* avec des rendements comparables. Mais dans ce cas, nous avons pu également isoler et caractériser des diacétates **1′***n*[3] qui ne possèdent pas de groupement ester d'énol sur le carbone C3.

Aspect structural

La formule des composés résultant de l'arylation a été confirmée par analyse élémentaire et leur structure déterminée par des méthodes spectroscopiques.

Les spectres d'absorption infra-rouge et ultraviolette confirment l'existence des différentes fonctions. En particulier, dans le spectre ir, on observe la bande caractéristique de la fonction ester d'énol à 1775 cm^{-1}. Les spectres uv montrent que la glycosylation de l'aromatique ne modifie pas sensiblement son absorption, ce qui confirme que la double liaison n'est pas conjuguée avec le noyau.

La spectroscopie de masse confirme la formule brute, mais surtout, nous a permis d'établir la régiosélectivité de la réaction. En effet, l'existence d'un pic intense (20−30%) correspondant à l'ion $(Ar—C{\equiv}O)^+$ dans le spectre de masse de tous les composés de couplage confirme que l'aromatique s'est bien fixé sur le carbone C1 du dérivé glucidique. Un tel type de fragmentation a été également observé pour des dérivés du dihydropyranne possédant une ramification en position 2 (6*c*). Il est à noter que la fragmentation rétrodiénique, caractéristique (9, 16, 17) des hexopyranosides correspondants a été observée, mais les pics résultants sont peu intenses.

[2]Le chiffre rappelle le glycal de départ et la lettre désigne l'aromatique.

[3]Le chiffre rappelle le glycal de départ, la lettre désigne l'aromatique et le prime signifie que le composé est 2,3-didésoxy.

Can. J. Chem. Downloaded from www.nrcresearchpress.com by 210.87.254.5 on 09/06/12
For personal use only.

TABLE 1. Résultats de l'arylation des glycals **1** et **2**

Aromatique	Essai n°	Glycal	Sel de palladium[a]	θ (°C)	*t*(h)	Rdt	Composé, T_f (°C), (% isolé)	Site d'arylation[b] 2	3	4
	1	**1**	—	80	8	64	**1***a*, huile, (54) − **1**′*a*, huile (10)		—	
	2	**1**	—	120	2	61	**1***a*, (59) − **1**′*a*, (2)		—	
	3	**2**	—	80	8	46	**2***a*, 126−126,5, (46)		—	
	4	**2**	—	120	2	51	**2***a*, (51)		—	
	5	**2**	Catalytique[c]	120	13	30	**2***a*, (30)		—	
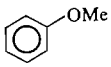	6	**2**	—	120	2	41	**2***b* + **2***c* non séparés, (41)	47	—	53[d]
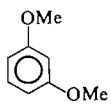	7	**1**	—	120	1,5	57	**1**′*d*, huile, (8) − **1**′*e*, huile, (4) **1**′*d*, huile, (20) − **1***e*, 88−89, (25)	40	—	60[e]
	8	**1**	Catalytique[c]	90	10	36	**1***d* + **1***e* (36)	38	—	62[e]
	9	**2**	—	120	1,5	67	**2***d*, 90−91, (23) − **2***e*, 103−104, (29)	42	—	58
	10	**2**	$Pd(acac)_2$ 1 equiv.	120	1,5	27	**2***d*, (9) − **2***e*, (18)	33	—	67
	11	**2**	+2 $P\phi_3$	120	13	49	**2***d*, (13,5) − **2***e*, (35,5)	27	—	73
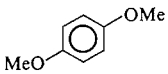	12	**2**	—	120	2	43	**2***f*, 113−114, (43)	100	—	—
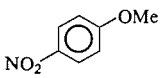	13	**2**	—	120	2	25	**2***g*, 144−145, (25)	100	—	—
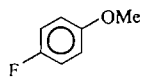	14	**2**	—	120	5	59	**2***h*, 95−96, (31) − **2***i*, 102−103 (28)	47	53	3 —

[a]$Pd(OAc)_2$ en quantité stoechiométrique sauf indication contraire.
[b]Position du reste glucidique sur l'aromatique.
[c]0,2 Équivalent de $Pd(OAc)_2$ et 1,6 équivalent de $Cu(OAc)_2 \cdot H_2O$.
[d]Proportions déterminées par rmn ^1H.
[e]Pourcentages déterminés par clhp analytique.

Les données de rmn ^1H concernant les composés résultant de l'arylation de ces glycals sont réunies dans le tableau 2. Les signaux correspondants aux protons aromatiques permettent de fixer sans ambiguité la position de la partie glycosidique sur l'aromatique sauf dans le cas du *p*-fluoroanisole pour lequel nous avons eu recours à la rmn ^{13}C. C'est la valeur de la constante de couplage entre le carbone aromatique lié à la partie glucidique et le fluor qui permet de trancher. Pour **2***g*, on observe un couplage J = 16,5 Hz pour ce signal (δ = 124,8) qui correspond à la position *ortho* par rapport au fluor. Pour **2***i*, le couplage plus faible (J = 6,1 Hz, δ = 126,9) montre que le glucide est en *méta* du fluor. Ces valeurs, quoique légèrement plus faibles, sont en accord avec celles observées par Weigert et Roberts dans le fluorobenzène (18).

Dans la série de composés **2***n* dérivés du tri-*O*-acétyl-D-galactal **2**, la faible valeur de la constante de couplage $J_{4,5}$ = 1,5 Hz est compatible avec les données de la littérature concernant des 2,3-didésoxy-*C*-glyc-2-énosides (19, 20) et correspond à une configuration *thréo* pour les carbones C4 et C5 à condition que le *C*-glycoside insaturé adopte la conformation demi-chaise $^0H_5$. Le couplage $^3J_{1,2}$ se faisant à travers, un carbone hybridé sp^2, il nous a paru hasardeux de déduire de cette seule donnée la configuration du carbone anomère. En effet, comme le soulignent Baer et Hanna (9), la relation proposée par Garbisch (20) n'est pas d'un grand secours dans le domaine des énopyranosides. Finalement, la structure du 3,4,6-tri-*O*-acétyl-2-désoxy-α-D-*thréo*-hex-2-énopyrasosylbenzène **2***a* a été déterminée par diffraction des rayons X;[4] elle montre que le glycoside possède bien la conformation demi-chaise $^0H_5$ et que le noyau phényle est en position quasi-axiale, c'est-à-dire que le carbone anomère possède la configuration α. Tous les membres de cette série étant fortement lévogyres, nous en concluons qu'ils possèdent tous la même configuration et que la nature de l'aglycone affecte peu la valeur du pouvoir rotatoire.

Dans la série de composés **1***n* dérivés du tri-*O*-acétyl-D-glucal **1** la valeur de la constante de couplage $J_{4,5}$ = 4 Hz montre que l'équilibre conformationnel de ces composés est, cette fois, en faveur de la conformation demi-chaise $^5H_0$. Dans cette conformation, le groupement acétoxy porté sur le C4 se trouve en position quasi axiale, ce qui est un facteur de stabilisation, comme l'ont montré Ferrier et Sankey (21), car les répulsions stériques et électriques avec le groupement acétoxy

[4]Cette structure, déterminée au Laboratoire de Chimie Structurale Biomoléculaire (Université Paris-Nord) dirigé par le Prof. H. Gillier-Pandraud fera l'objet d'une publication ultérieure.

Can. J. Chem. Downloaded from www.nrcresearchpress.com by 210.87.254.5 on 09/06/12
For personal use only.

TABLE 2. Données de rmn ^{1}H des *C*-glycosides

Composé	H-1	H-2	H-3	H-4	H-5	H-6,6′	$OCOCH_3$	OCH_3	H aromatiques
1*a*[a]	5,47 m $J_{1,2}$ = 2,5	5,92 d	—	5,47 m $J_{4,5}$ = 4	4,05−4,5 m		2,09 s (3H) 2,12 s (3H) 2,15 s (3H)	—	7,3−7,6 m (5H)
1′*a*[a]	5,34 s. él.	5,99 d. él. $J_{2,3}$ = 9	6,18 m $J_{3,4}$ = 1,5	5,32 m $J_{4,5}$ = 7,5	3,86 m $J_{5,6a}$ = 6	4,12dd[b] 4,26dd	2,08 s (3H) 2,10 s (3H)	—	7,27−7,45 m (5H)
1*d*	5,4 d $J_{1,2}$ = 3,5	5,9 d	—	5,48 d $J_{4,5}$ = 5	4−4,25 m		2,10 s (6H) 2,15 s (3H)	3,82 s (6H)	6,3−6,7 m (3 H)
1*e*	5,8 s	5,8 s	—	5.46 d $J_{4,5}$ = 4	4,1−4,5 m		2,08 s (3H) 2,12 s (3H) 2,14 s (3H)	3,8 s (3H) 3,84 s (3H)	6,4−6,6 m (2H) 7,42 d (^3J = 9) (1H)
2*a*[a]	5,54 d $J_{1,2}$ = 3,9	6,07 d	—	5,44 d $J_{4,5}$ = 1,5	4−4,25 m		1,96 s (3H) 2,14 s (3H) 2,18 s (3H)	—	7,3−7,5 m (5H)
2*d*	5,5 d $J_{1,2}$ = 3,5	6,05 d	—	5,45 s. él.	4−4,3 m		2,0 s (3H) 2,1 s (3H) 2,14 s (3H)	3,8 s (6H)	6,4−6,7 m (3H)
2*e*	5,86 s	5,86 s	—	5,44 s. él.	4−4,2 m		1,92 s (3H) 2,1 s (3H) 2,16 s (3H)	3,77 s (3H) 3,83 s (3H)	6,4−6,5 m (2H) 7,3 d (^3J = 8) (1H)
2*f*	5,9 s	5,9 s	—	5,47 s. él.	4,1−4,3 m		1,96 s (3H) 2,1 s (3H) 2,13 s (3H)	3,8 s (3H) 3,83 s (3H)	6,8−7,1 (3H)
2*g*	5,9 d $J_{1,2}$ = 3,5	6,15 d	—	5,5 s. él.	4,2−4,4 m		2,1 s (3H) 2,15 s (3H)	4,03 s (3H)	7,05 d (^3J = 9) (1H) 8,2−8,6 m (2H)
2*h*	5,9 d $J_{1,2}$ = 3,5	6 d	—	5,5 d $J_{4,5}$ = 1,5	4,1−4,3 m		2,0 s (3H) 2,18 s (6H)	3,83 s (3H)	6,8−7,2 m (3H)
2*i*	5,9 d $J_{1,2}$ = 3,5	6,03 d	—	5,5 d $J_{4,5}$ = 1,5	4,1−4,4 m		2,0 s (3H) 2,13 s (3H) 2,18 s (3H)	3,88 s (3H)	6,8−7,4 m (3H)

[a]Spectre à 250 MHz.
[b]$J_{5,6}$ = 3; $J_{6,6}$ = 12.

du C3 sont alors minimisées.[5] Dans cette conformation, le groupement volumineux CH_2OAc se trouve en position axiale, mais, du fait de la présence d'une double liaison entre C2 et C3, ceci n'entraîne pas de fortes interactions 1−3 déstabilisantes (21). Enfin, le carbone C1 n'étant pas lié à un hétéroatome, il n'y a pas d'effet anomère pouvant influencer profondément l'équilibre conformationnel. Les *C*-glycosides suivant généralement la règle de Hudson (22), nous avons attribué la configuration α à la liaison anomérique des composés **1***n*, car ils sont davantage dextrogyres que leurs homologues **1′***n*, dont le carbone anomère possède la configuration β (*vide infra*). Mais des déviations à cette règle ayant été observées par plusieurs auteurs aussi bien pour des alkyl 2,3-didesoxy-hex-2-énopyranosides (9, 23) que pour un couple de *C*-glycosides (24), cette configuration α des composés **1***n* a été vérifiée par rmn ^{1}H après transformation de la fonction ester d'énol en oxime (3).

En ce qui concerne les composés **1′***n*, nous avons analysé en détail le spectre rmn ^{1}H (250 MHz) du 4,6-di-*O*-acétyl-2,3-didésoxy-β-D-*érythro*-hex-2-énopyranosyl benzène **1′***a*. Une telle analyse n'a pas été possible pour les composés similaires **1′***e* et **1′***d* obtenus lors de l'arylation du tri-*O*-acétyl-D-glucal **1** avec le *m*-méthoxyanisole car ceux-ci, isolés sous forme d'huile, étaient souillés de trace de produit résultant de l'isomérisation du glycal de départ. Les protons oléfiniques résonnent vers 6 ppm sous forme d'un quartet AB ($J_{2,3}$ = 9 Hz) dont chaque signal est dédoublé par de faibles couplages vicinaux ou allyliques. Il est à noter que, comme dans les glycosides correspondants (9, 25), c'est H2 qui résonne au champ le plus fort. La constante de couplage $J_{4,5}$ = 7,5 Hz est en accord avec la valeur donnée par Ferrier pour des acétates analogues (21) et montre clairement que la configuration des C4 et C5 est *érythro* et que la conformation favorisée est demi-chaise $^0H_5$. Comme dans le cas des composés **1***n* et **2***n*, la configuration de la liaison anomérique de **1′***a* n'a pu être déterminée à l'aide de la constante de couplage $^3J_{1,2}$ qui est d'ailleurs très faible. C'est en nous fondant sur la valeur du pouvoir rotatoire que nous attribuons la configuration β au composé **1′***a*. En effet, celui-ci est faiblement dextrogyre (+3°) alors qu'un *C*-glycoside analogue, le 4′-(4,6-di-*O*-acétyl-2,3-didésoxy-α-D-*érythro*-hex-2-énopyranosyl) anisole préparé

[5]A titre de comparaison, on remarquera que la conformation $^0H_5$, adoptée pour les composés **2***n* correspond bien à une position quasi axiale de l'acétate allylique du C4.

Can. J. Chem. Downloaded from www.nrcresearchpress.com by 210.87.254.5 on 09/06/12
For personal use only.

Can. J. Chem. Downloaded from www.nrcresearchpress.com by 210.87.254.5 on 09/06/12
For personal use only.

d'une autre manière par Grinkiewicz et Zamojski (26) est fortement dextrogyre (+250°). En toute rigueur, l'aromatique n'est pas le même dans ces deux composés, mais nous avons montré dans la série dérivée du tri-*O*-acétyl-D-galactal **2** que la nature de l'aromatique influençait peu le pouvoir rotatoire.

Aspect mécanistique

En ce qui concerne le mécanisme de cette réaction, la principale question posée était de savoir si, comme pour les autres méthodes d'arylation, un arylpalladium à liaison σ était impliqué dans la réaction étudiée avec les conséquences stéréochimiques habituelles de l'intervention d'un composé de ce type (voir introduction).

Considérons d'abord la régiosélectivité de la réaction au niveau de l'aromatique. Nos résultats sont conformes à ceux obtenus par Fujiwara *et al.* (27) lors de l'arylation du styrène avec divers aromatiques et montrent que la réaction suit l'effet *ortho–para* directeur du méthoxy et *méta* orienteur du groupe nitro. Dans le cas de l'halogène (fluoro), on observe un fort pourcentage de réaction en *ortho* de celui-ci comme dans la mercuration d'aromatiques (28). Toutefois, nous ne pensons pas que la réaction soit une substitution électrophile où le rôle du palladium serait de polariser la double liaison du glycal sous forme d'un complexe π allylique cationique qui se substituerait ensuite à un hydrogène de l'aromatique. En effet, dans ce cas, le composé de couplage ne devrait pas posséder d'acétate en C3. De plus, nous n'avons pas observé de différences dramatiques de vitesse pour les aromatiques diversement substitués comme on pourrait s'y attendre dans le cas d'une substitution électrophile. Enfin, nous avons obtenu un fort pourcentage de réaction en position 2 du noyau avec l'anisole (47%) et le *m*-méthoxyanisole (40%) (tableau 1). Or, la glycosylation par substitution électrophile de l'anisole par le tri-*O*-acétyl-D-glucal **1** et le tri-*O*-acétyl-D-galactal **2** ne se fait pas en *ortho* du méthoxy (26) et celle du *m*-méthoxyanisole par des trichloroacétimidates de glycosyle en présence d'acide de Lewis ne se fait pas entre les deux groupes méthoxy (29).

L'ensemble de ces observations nous incite fortement à penser que la première étape de cette réaction est la formation d'un arylpalladium, directement à partir de l'aromatique et du sel de palladium (30). Dans le cas du *m*-méthoxyanisole, nous pensons qu'une coordination intramoléculaire de l'atome métallique favorise la palladation sur ce site. En effet, ce fort pourcentage se retrouve pour les deux glycals étudiés et reflète donc bien le site de palladation de l'aromatique. De plus, ce pourcentage décroît lorsque le palladium est fortement coordiné par d'autres ligands (acétyl-acétonate et triphényl phosphine), la coordination intramoléculaire devenant moins efficace (essais n° 10 et 11). Enfin, un tel type de coordination a été envisagée pour des organométalliques aromatiques (31) et pour des arylpalladium contenant des fonctions azotées (2*a*). Inversement, il a été montré que l'arylation catalysée par le palladium ne se fait pas entre les deux méthyles du *m*-xylène (32) pour lequel une telle coordination intramoléculaire n'est pas possible.

En ce qui concerne la régiosélectivité de l'addition de l'arylpalladium sur la double liaison du glycal, le produit principal que nous avons isolé résulte de la fixation de l'aromatique sur le carbone C1 ce qui est en accord avec les résultats de l'arylation d'éther cyclique avec un arylpalladium (6*c*, *d*) et ceux que Arai et Daves, Jr. ont obtenus lors de la préparation de *C*-nucléosides par réaction d'organopalladium sur des glycals (8).

En définitive, il nous semble raisonnable de penser que l'arylpalladium formé rapidement dans une première étape,

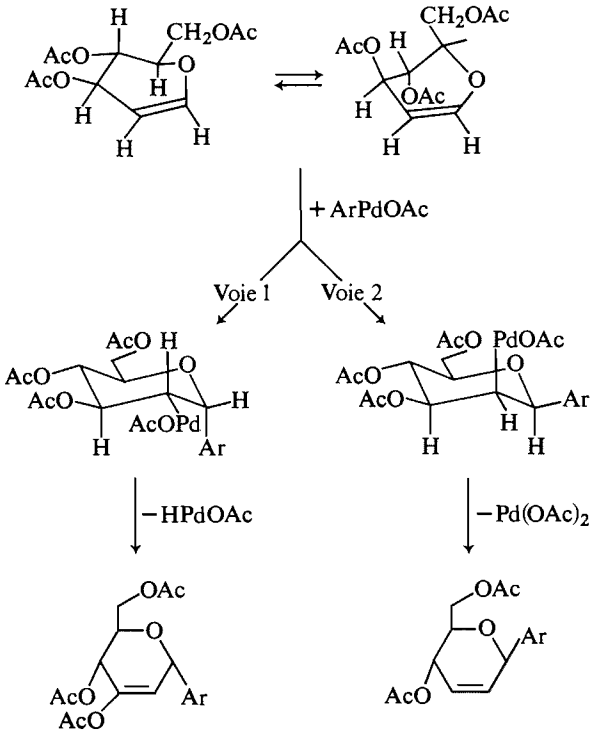

SCHÉMA 1

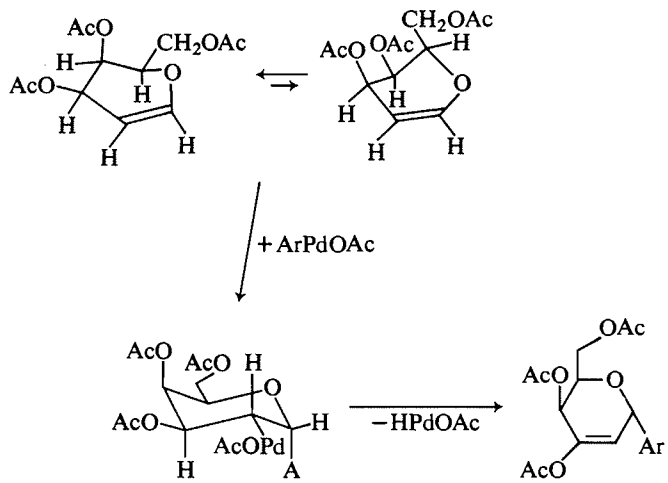

SCHÉMA 2

réagit ensuite comme à l'accoutumée sur la double liaison; *syn*-addition avec formation d'un alkylpalladium puis, dans une seconde étape, perte de XPdOAc dirigée par des facteurs stériques, le groupe X issu du glucide devant être dans une position qui permette une *syn*-élimination. Avec cela en tête, nous proposons d'expliquer les différences observées avec le tri-*O*-acétyl-D-glucal **1** et le tri-*O*-acétyl-D-galactal **2** de la façon suivante (Schémas 1 et 2).

Les conformations de ces glycals en solution ont été déterminées par rmn ^{1}H (33, 34). L'examen des modèles correspondants montre que pour le tri-*O*-acétyl-D-glucal **1** l'encombrement stérique des diastéréofaces de la double liaison est très similaire et la *syn*-addition de ArPdOAc est possible des deux côtés conduisant à deux alkylpalladium. L'un, par *syn*-élimination de HPdOAc conduit au produit principal (voie 1), tandis que le second, par *syn*-élimination de $Pd(OAc)_2$ (voie 2),

Can. J. Chem. Downloaded from www.nrcresearchpress.com by 210.87.254.5 on 09/06/12
For personal use only.

conduit à l'autre produit d'arylation. La réaction se faisant d'ailleurs vraisemblablement sur le conformère où la double liaison est la plus accessible (conformation $^4H_5$) (schéma 1).

Dans le cas du tri-*O*-acétyl-D-galactal **2**, la situation est toute autre, car l'encombrement stérique de chaque diastéréoface de la double liaison est cette fois très différent et même dans la conformation $^4H_5$ où la double liaison est la plus accessible, la présence du groupe acétate en position axiale sur C4 favorise la fixation de ArPdOAc conduisant à l'anomère α dans lequel la *syn*-élimination de HPdOAc est possible et conduit à un seul composé possédant la fonction ester d'énol (schéma 2).

Cette différence de comportement des glycals **1** et **2** n'est pas particulière à la réaction étudiée ici, mais apparaît dans d'autres réactions d'addition sur la double liaison; par exemple dans la méthoxy-mercuration (35) où le tri-*O*-acétyl-D-glucal **1** conduit à un mélange de deux organomercuriques, tandis qu'à partir du tri-*O*-acétyl-D-galactal **2**, il ne s'en forme qu'un seul. Quant à la perte de $Pd(OAc)_2$, elle a été observée par Heck (6*a*) lors de l'arylation d'acétate ou d'éther vinyliques par un mercurique aromatique en présence d'un sel de palladium. Cependant, il faut signaler qu'à partir du tri-*O*-acétyl-D-glucal, Arai et Daves, Jr. (8) ont reporté un comportement différent d'un alkylpalladium analogue de celui formé par la voie 1 (schéma 1). Ces auteurs évoquent une *anti*-élimination d'un alkoxyde pour expliquer l'ouverture du cycle pyrannique de l'unité glucidique conduisant au produit majoritaire qu'ils ont isolé et caractérisé.

Conclusion

L'arylation des glycals peracétylés par un aromatique en présence d'acétate de palladium constitue une nouvelle synthèse de *C*-glycosides. Elle présente l'avantage de transformer, en une seule étape, des dérivés faciles d'accès en composés hautement fonctionnalisés qui possèdent une fonction ester d'énol en C3, ce qui en fait des précurseurs de 2-désoxy-*C*-glycosides. La régiosélectivité de la réaction au niveau de l'aromatique peut s'expliquer par la formation d'un arylpalladium directement à partir de l'aromatique et du sel. Un mécanisme en deux étapes, impliquant la *syn*-addition de l'arylpalladium sur la double liaison du glycal suivie d'une *syn*-élimination rend bien compte de la stéréochimie des composés obtenus.

Partie expérimentale

Les points de fusion ont été déterminés en tube capillaire sur un appareil de Hoover et ne sont pas corrigés. Les pouvoirs rotatoires ont été mesurés en solution chloroformique dans une cuve de 1 dm de longueur sur un appareil Perkin–Elmer 141. Les spectres d'absorption infra-rouge (ir) ont été enregistrés sur un appareil Unicam SP3-300. Les spectres d'absorption ultraviolette (uv) de solutions dans l'éthanol 95% ont été enregistrés sur un spectromètre Beckman DK 2A. Les spectres de rmn ont été enregistrés sur des appareils Varian ou Brucker pour le proton et sur un appareil JEOL PS 100 pour le carbone. Les solvants utilisés ont été CCl_4, $CDCl_3$ et C_6D_6. Les déplacements chimiques (δ) sont exprimés en ppm en prenant le tétraméthylsilane comme référence interne. Les constantes de couplage sont exprimées en Hz. Les microanalyses ont été effectuées par le service de Microanalyse de l'Université P. et Marie Curie.

Les chromatographies sur couche mince (ccm) ont été réalisées sur des plaques prêtes à l'emploi (Alufolien, gel de silice 60 F-254 Merck de 0,2 mm d'épaisseur). La révélation des plaques était assurée, soit par observation à l'aide d'une lampe uv, soit par vaporisation d'une solution 6 *N* d'acide sulfurique suivie de chauffage à 100°C, soit en combinant les deux techniques. Les éluants utilisés étaients des mélanges d'éther éthylique distillé sur anhydride phosphorique et d'éther de pétrole (Eb: 45–55°C); éluant A: éther éthylique – éther de pétrole, 2:1, v/v; éluant B: éther éthylique – éther de pétrole, 80:20, v/v; éluant C: éther éthylique – éther de pétrole, 20:80, v/v.

Les chromatographies sur colonne ont été réalisées sur gel de silice 40 (70–230 mesh ASTM, Merck) avec l'éluant A. Les fractions étaient recueillies à l'aide d'un collecteur ISCO modèle 348 équipé d'un détecteur uv ISCO UA-5. Les chromatographies sur colonne sous pression (15 bars) ont été réalisées avec l'éluant B sur gel de silice H 60 (5–40 μm) à l'aide d'un appareil Chromatospac 100 (Jobin–Yvon) muni d'un détecteur réfractométrique. Les chromatographies liquides haute performance (clhp) ont été réalisées sur une colonne de silice (μ Porasil, l = 30 cm, Waters) à l'aide d'un appareil Constametric II équipé d'un détecteur uv à longueur d'onde variable. Pour chaque famille de composés, celle-ci correspondait au maximum d'absorption uv préalablement déterminé pour chaque chromophore, ce qui permettait le calcul des proportions des différents composés directement à partir des surfaces des pics enregistrés. L'élution était faite avec un mélange THF–heptane, 20:80, v/v (Gold Label, Aldrich) (débit 0,8 mL/min).

L'acide acétique (Rectapur, Prolabo), les composés aromatiques (Aldrich) et l'acétate de palladium (Ventron) ont été utilisés sans purification préalable.

Procédé général d'arylation

Dans un ballon muni d'un réfrigérant ascendant et protégé de l'humidité extérieure, 3 mmol de glycal sont dissoutes dans 24 mL d'acide acétique et 500 mmol de composé aromatique (ArH). On ajoute ensuite 3 mmol d'acétate de palladium. Le ballon est plongé dans un bain d'huile de silicone maintenu à température constante. On observe l'apparition rapide d'un miroir de palladium métallique sur les parois du ballon. L'avancement de la réaction est suivi par ccm (éluant A). Lorsque la réaction est terminée, on filtre le mélange réactionnel sur papier afin de récupérer le palladium métallique qui peut être ultérieurement réoxydé en acétate (15). L'acide acétique et l'aromatique sont successivement éliminés à l'aide d'un évaporateur rotatif équipé d'une trompe à eau, puis d'une pompe à palette (0,1 Torr). Le mélange brut est redissout dans 50 mL de THF et 10 mL d'eau. Après refroidissement à 0°C, on ajoute, en agitant, 100 mg de KBH_4 afin de réduire les traces de sels de palladium qui colorent la solution. Après 30 min, un nouveau précipité de palladium est obtenu et la solution est complètement décolorée. Après filtration et évaporation du THF, on extrait avec 100 mL de chloroforme. La solution chloroformique est lavée à l'eau jusqu'à pH neutre. Après séchage sur $MgSO_4$, filtration et évaporation du solvant sous pression réduite, on obtient le mélange brut. La composition de celui-ci est déterminée par clhp analytique. Dans certains cas, le produit principal cristallise directement et peut être isolé par recristallisation dans l'éthanol 95%. Les eaux-mères de recristallisation sont ensuite analysées par chromatographie sur colonne de silice. Dans les autres cas, c'est le mélange brut qui est chromatographié.

Lorsque l'arylation a été réalisée avec des quantités catalytiques de sel de palladium, le palladium métallique a été réoxydé à l'aide du monohydrate de l'acétate cuivrique. Par exemple, pour la réaction utilisant 20% d'acétate de palladium (0.6 mmol), on ajoute 4,8 mmol (959 mg) de $Cu(OAc)_2 \cdot H_2O$, au mélange réactionnel. Le traitement est également légèrement modifié. Après filtration et évaporation de l'acide acétique, le brut est dissout dans 100 mL d'éther éthylique, lavé à l'eau (3 × 20 mL), décoloré par agitation à 0°C avec 10 mL d'eau contenant 100 mg de KBH_4. La phase organique est à nouveau lavée à l'eau jusqu'à pH neutre. Après séchage sur $MgSO_4$ et filtration, le solvant et l'aromatique sont évaporés sous pression réduite à une température inférieure à 60°C. Le mélange brut obtenu est analysé comme ci-dessus.

Arylation du tri-O-acétyl-D-glucal ***1*** *avec le benzène*

L'arylation de 3 mmol de glycal **1** en présence de 3 mmol d'acétate de palladium est terminée en 8 h à 80°C comme le montre la ccm réalisée avec l'éluant C (3 élutions). La filtration permet de récupérer 240 mg de Pd (75%). La chromatographie sous pression a permis d'isoler successivement les composés suivants.

Can. J. Chem. Downloaded from www.nrcresearchpress.com by 210.87.254.5 on 09/06/12
For personal use only.

4,6-Di-O-*acétyl-2,3-didésoxy*-β-D-érythro-*hex-2-énopyranosylbenzène* ***1'a***: 87 mg (10%); huile; R_f 0,59 (éluant A); $[\alpha]_D^{20}$ +3,3° (*c* 1,34, $CHCl_3$); ir (film): 1735 (ester), 1690(C=C), 730 (alcène *cis*); uv ϵ_{257} = 553; spectre de masse: 290 (ϵ) 105 (100%) (Ar—C≡O)$^+$; *Anal.* calc. pour $C_{16}H_{18}O_5$ (290,3): C 66,19, H 6,25; trouvée: C 66,16, H 6,17.

3,4,6-Tri-O-*acétyl-2-désoxy*-α-D-érythro-*hex-2-énopyranosylbenzène* ***1a***: 565 mg (54%); huile; R_f 0,50 (éluant A); $[\alpha]_D^{20}$ +69° (*c* 1,7, $CHCl_3$); ir (film): 1755 (ester d'énol), 1740 (ester), 1690 (C=C); uv ϵ_{257} = 291; spectre de masse: 348 (ϵ) 105 (68%) (Ar—C≡O)$^+$; *Anal.* calc. pour $C_{18}H_{20}O_7$ (348,4): C 62,06, H 5,79; trouvée: C 61,82, H 5,62.

Arylation du tri-O-*acétyl*-D-*glucal* ***1*** *avec le* m-*méthoxyanisole*

Réalisée sur 3 mmol de glycal **1** en présence de 3 mmol d'acétate de palladium, la réaction est terminée en 1 h 30 à 120°C. Par filtration, on récupère 214 mg (67%) de palladium. Par chromatographie sous pression, on isole les produits suivants.

3'-Methoxy-2'-(4,6-di-O-*acétyl-2,3-didésoxy*-β-D-érythro-*hex-2-énopyranosyl) anisole* ***1'd***: 84 mg (8%); huile; R_f 0,6 (éluant A); $[\alpha]_D^{20}$ +57° (*c* 0,76, $CHCl_3$); spectre de masse: 350 (ϵ) (pic moléculaire) 165 (Ar—C≡O)$^+$.

5'-Méthoxy-2'-(4,6-di-O-*acétyl-2,3-didésoxy*-β-D-érythro-*hex-2-énopyranosyl) anisole* ***1'e***: 40 mg (4%); huile; R_f 0,5 (éluant A). Ce produit a été décelé par ccm et clhp analytique. On lui attribue cette structure d'après son temps de rétention par comparaison avec ceux des produits de couplage **1***d* et **1***e*.

3'-Méthoxy-2'-(3,4,6-tri-O-*acétyl-2-désoxy*-α-D-érythro-*hex-2-énopyranosyl) anisole* ***1d***: 245 mg (20%); huile; R_f 0,42 (éluant A); $[\alpha]_D^{20}$ +75° (*c* 1,03, $CHCl_3$); ir: 1775 (ester d'énol), 1740 (ester), 1690 (C=C); spectre de masse: 408 (ϵ), 165 (50%) (ArC≡O)$^+$.

5'-Méthoxy-2'-(3,4,6-tri-O-*acétyl-2-désoxy*-α-D-érythro-*hex-2-énopyranosyl) anisole* ***1e***: 305 mg (25%); *F* = 88 − 89°C; R_f 0,38 (éluant A); $[\alpha]_D^{20}$ +58° (*c* 1,8, $CHCl_3$); ir: 1775 (ester d'énol), 1740 (ester), 1690 (C=C); uv ϵ_{277} = 2727, ϵ_{282} = 2475; spectre de masse: 408 (12%), 165 (45%) (Ar—C≡O)$^+$; *Anal.* calc. pour $C_{20}H_{24}O_9$ (408,4): C 58,87, H 5,93; trouvée: C 58,68, H 6,15.

Nous avons également isolé un composé plus polaire (R_f 0,25, éluant A) dont le spectre de masse présente, entre autres, un pic moléculaire de *m/e* = 542. Ce composé résulte de la réaction du tri-*O*-acétyl-D-glucal **1** sur lui-même, qui conduit à un diène selon la réaction décrite par Volger (13).

La réaction a été aussi effectuée de façon catalytique, elle donne un rendement total de 36% correspondant aux produits **1***d* et **1***e*.

Arylation du tri-O-*acétyl*-D-*galactal* ***2*** *avec le benzène*

Réalisé sur 3 mmol de glycal **2** en présence de 3 mmol de $Pd(OAc)_2$, elles est terminée en 2 h à 120°C. Par filtration, on récupère 288 mg (90%) de palladium. Par cristallisation et chromatographie, on isole le 3,4,6-tri-*O*-acétyl-2-désoxy-α-D-*thréo*-hex-2-énopyranosylbenzène ***2a***: 532 mg (51%); *F* = 126−126,5°C (éthanol 95%); R_f 0,56 (éluant A); $[\alpha]_D^{20}$ −195° (*c* 1,63, $CHCl_3$); ir (KBr): 1775 (ester d'énol), 1750 (ester); uv ϵ_{257} = 291; spectre de masse: 348 (ϵ), 105 (60%) (Ar—C≡O)$^+$; *Anal.* calc. pour $C_{18}H_{20}O_7$ (348,34): C 62,06, H 5,79; trouvée: C 62,08, H 5,74.

La réaction a été également réalisée sur 3 mmol de glycal **2** en présence d'une quantité catalytique (0,6 mmol, 135 mg) d'acétate de palladium et d'acétate de cuivre monohydrate (4,8 mmol, 958 mg) dans les mêmes conditions de concentrations à 120°C. La réaction est terminée en 13 h. Par cristallisation du brut dans le méthanol et chromatographie sous pression des eaux-mères, on isole le produit de couplage **2***a* (310 mg) avec un rendement de 30%. Lors de cette manipulation, on a pu isoler aussi un produit isomère du produit de départ, l'acétate de 4,6-di-*O*-acétyl-2,3-didésoxy-D-hex-2-énopyranosyle: 103 mg (12,6%); spectre de masse: 272 (ϵ) (pic moléculaire). Son R_f dans l'éluant A est de 0,36 alors que pour le tri-*O*-acétyl-D-galactal **2** il est de 0,51.

Arylation du tri-O-*acétyl*-D-*galactal* ***2*** *avec l'anisole*

La réaction a été réalisée sur 3 mmol de glycal **2** en présence de 3 mmol d'acétate de palladium, la réaction est terminée en 2 h à 120°C. La filtration permet de récupérer 221 mg (70%) de palladium.

Le 2'-(3,4,6-tri-*O*-acétyl-2-désoxy-α-D-*thréo*-hex-2-énopyranosyl) anisole ***2b*** et le 4'-(3,4,6-tri-*O*-acétyl-2-désoxy-α-D-*thréo*-hex-2-énopyranosyl) anisole ***2c*** formés respectivement par fixation du glucide en *ortho* ou en *para* du groupe méthoxy de l'aromatique n'ont pas pu être séparés par chromatographie préparative sous pression. Le mélange recueilli (465 mg) correspond à un rendement d'arylation de 41%; *Anal.* calc. pour $C_{19}H_{22}O_8$ (378,38): C 60,37, H 5,87; trouvée: C 60,51, H 6,03. Les proportions des deux composés ont été estimées à partir des signaux des hydrogènes des groupes méthoxy qui possèdent des δ différents en rmn ^{1}H (3,98 ppm pour **2***b* et 3,87 ppm pour **2***c*). Elles correspondent à 47% de composé *ortho* **2***b* et 53% de composé *para* **2***c*.

Arylation du tri-O-*acétyl*-D-*galactal* ***2*** *avec le* m-*méthoxyanisole*

Réalisée sur 3 mmol de glycal **2** en présence de 3 mmol d'acétate de palladium, la réaction est terminée en 1 h 30 à 120°C. On récupère 211 mg (66%) de palladium. Par chromatographie, on isole les deux composés suivants.

3'-Méthoxy-2'-(3,4,6-tri-O-*acétyl-2-désoxy*-α-D-thréo-*hex-2-énopyranosyl) anisole* ***2d***: 281 mg (23%); *F* = 90−91°C (éther−pentane); R_f 0,47 (éluant A); $[\alpha]_D^{20}$ −179° (*c* 0,8, $CHCl_3$); ir (KBr): 1740 (ester), 1690 (C=C); uv ϵ_{278} = 2156; spectre de masse: 408 (14%), 165 (24%) (Ar—C≡O)$^+$; *Anal.* calc. pour $C_{20}H_{24}O_9$ (408,4): C 58,87, H 5,93; trouvée: C 58,56, H 6,13.

5'-Méthoxy-2'-(3,4,6-tri-O-*acétyl-2-désoxy*-α-D-thréo-*hex-2-énopyranosyl) anisole* ***2e***: 355 mg (29%); *F* = 103−104°C (éther−pentane); R_f 0,40 (éluant A); $[\alpha]_D^{20}$ −159° (*c* 0,88, $CHCl_3$); ir (KBr): 1740 (ester), 1690 (C=C); uv ϵ_{282} = 2475, ϵ_{278} = 2727; spectre de masse: 408 (11%), 165 (26%) (Ar—C≡O)$^+$; *Anal.* calc. pour $C_{20}H_{24}O_9$ (408,4): C 58,87, H 5,93; trouvée: C 57,87, H 7,23.

Arylation du tri-O-*acétyl*-D-*galactal* ***2*** *avec le* p-*méthoxyanisole*

L'arylation de 3 mmol de **2** en présence de 3 mmol d'acétate de palladium est terminée en 1 h 30 à 120°C. La filtration permet de récupérer 224 mg (70%) de palladium. Par cristallisation et chromatographie, on isole le 4'-méthoxy-2'-(3,4,6-tri-*O*-acétyl-2-désoxy-α-D-*thréo*-hex-2-énopyranosyl) anisole ***2f***: 516 mg (43%); *F* = 113−114°C (éthanol 95%); R_f 0,34 (éluant A); $[\alpha]_D^{20}$ −213° (*c* 1,06, $CHCl_3$); ir (KBr): 1775 (ester d'énol), 1755 (ester); uv ϵ_{293} = 5028; spectre de masse: 408 (ϵ), 165 (47%) (Ar—C≡O)$^+$; *Anal.* calc. pour $C_{20}H_{24}O_9$ (408,4): C 58,87, H 5,93; trouvée: C 58,89, H 5,85.

Arylation du tri-O-*acétyl*-D-*galactal* ***2*** *avec le* p-*nitroanisole*

Réalisée sur 3 mmol de **2** en présence de 3 mmol de $Pd(OAc)_2$, elle est terminée en 2 h à 120°C. On récupère 300 mg (94%) de palladium par filtration. Par chromatographie sous pression, on isole le 4'-nitro-2'-(3,4,6-tri-*O*-acétyl-2-désoxy-α-D-*thréo*-hex-2-énopyranosyl) anisole ***2g***: 320 mg (25%); *F* = 144−145°C (éthanol absolu); R_f 0,22 (éluant A); $[\alpha]_D^{20}$ −162° (*c* 0,5, $CHCl_3$); ir (KBr): 1775 (ester d'énol), 1755 (ester), 1510, 1335 et 1370 (C—NO_2 aromatique), uv ϵ_{305} = 11 203; spectre de masse: 423 (ϵ), 180 (30%) (Ar—C≡O)$^+$; *Anal.* calc. pour $C_{19}H_{21}O_{10}N$ (423,4): C 53,95, H 5,00, N 3,31; trouvée: C 54,07, H 5,02, N 3,38.

Arylation du tri-O-*acétyl*-D-*galactal* ***2*** *avec le* p-*fluoroanisole*

Réalisée sur 3 mmol de **2** en présence de 3 mmol de $Pd(OAc)_2$, elle est terminée en 4 h à 120°C. Par filtration, on récupère 310 mg (98%) de palladium. La chromatographie sous pression permet d'isoler les deux composés suivants.

4'-Fluoro-3'-(3,4,6-tri-O-*acétyl-2-désoxy*-α-D-thréo-*hex-2-énopyranosyl) anisole* ***2h***: 392 mg (31%); *F* = 95−96°C (éther−pentane); R_f 0,51 (éluant A); $[\alpha]_D^{20}$ −204° (*c* 1,09, $CHCl_3$); ir (KBr): 1775 (ester d'énol), 1750 (ester); uv $\epsilon_{282.5}$ = 3736; rmn ^{13}C ($CDCl_3$): 124,8 d (J_{C-C-F} = 16,5 Hz) C'3, 155,4 d (J_{C-F} = 242,6 Hz) C'4; spectre de masse: 396 (ϵ), 153 (18%) (Ar—C≡O)$^+$; *Anal.* calc. pour $C_{19}H_{21}O_8F$ (396,4): C 57,62, H 5,35; trouvée: C 57,48, H 5,45.

4'-Fluoro-2'-(3,4,6-tri-O-*acétyl-2-désoxy*-α-D-thréo-*hex-2-énopyranosyl) anisole* ***2i***: 324 mg (28%); *F* = 102−103°C (éthanol

95%); R_f 0,43 (éluant A); $[\alpha]_D^{20}$ −182° (*c* 1,03, $CHCl_3$); ir (KBr): 1775 (ester d'énol), 1750 (ester); uv ϵ_{282} = 4180; rmn ^{13}C ($CDCl_3$): 126,9 d ($J_{C-C-C-F}$ = 6,1 Hz) C′2, 156,6 d (J_{C-F} = 241,5 Hz) C′4; *Anal.* calc. pour $C_{19}H_{21}O_8F$ (396,4): C 57,62, H 5,35; trouvée: C 57,44, H 5,24.

Remerciements

Nous remercions J. Mercier et O. Convert qui ont réalisé, respectivement, les spectres de masse et de rmn au Centre de Spectrochimie de l'Université P. et M. Curie. Nous remercions également la Direction Générale à la Recherche Scientifique pour son support financier.

1. S. CZERNECKI, C. GEORGOULIS et C. PROVELENGHIOU. Tetrahedron Lett. (*a*) 2623 (1975); (*b*) 4841 (1979).
2. (*a*) B. M. TROST. Tetrahedron, **33**, 2615 (1977); (*b*) R. F. HECK. Acc. Chem. Res. **12**, 146 (1979); (*c*) J. TSUJI. Organic Synthesis with palladium compounds. Springer-Verlag, New-York. 1980.
3. S. CZERNECKI et F. GRUY. Tetrahedron Lett. 437 (1981).
4. (*a*) T. MIZOROKI, K. MORI et A. OZAKI. Bull. Chem. Soc. Jpn. **44**, 581 (1971); (*b*) R. F. HECK. J. Am. Chem. Soc. **90**, 5518 (1968); (*c*) I. MORITANI et Y. FUJIWARA. Synthesis, 524 (1973) et références citées.
5. P. M. HENRY et G. A. WARD. J. Am. Chem. Soc. **94**, 673 (1972).
6. (*a*) R. F. HECK. J. Am. Chem. Soc. **90**, 5535 (1968); (*b*) S. DANNO, I. MORITANI et Y. FUJIWARA. Tetrahedron, 4819 (1969); (*c*) I. ARAI et G. D. DAVES, JR. J. Org. Chem. **44**, 21 (1979); (*d*) A. HALLBERG, L. WESTFELD et B. HOLM. J. Org. Chem. **46**, 5414 (1981).
7. (*a*) L. V. DUNKERTON et A. J. SERINO. J. Org. Chem. **47**, 2812 (1982); (*b*) L. V. DUNKERTON, K. T. BRADY et F. MOHAMED. Tetrahedron Lett. 599 (1982).
8. I. ARAI et G. D. DAVES, JR. J. Am. Chem. Soc. **100**, 287 (1978).
9. H. H. BAER et Z. S. HANNA. Can. J. Chem. **59**, 889 (1981).
10. F. SHAFIZADEH. Methods Carbohydr. Chem. **2**, 405 (1963).
11. (*a*) P. M. HENRY. J. Am. Chem. Soc. **94**, 5200 (1972); (*b*) L. E. OVERMAN et F. M. KNOLL. Tetrahedron Lett. 321 (1979); (*c*) P. A. GRIECO, P. A. TUTHILL et H. L. SLAM. J. Org. Chem. **46**, 5005 (1981).
12. R. J. FERRIER et R. PRASAD. J. Chem. Soc. C, 581 (1969).
13. H. C. VOLGER. Recl. Trav. Chim. Pays-Bas, **86**, 677 (1967).
14. (*a*) R. VAN HELDEN et G. VERBERG. Recl. Trav. Chim. Pays-Bas, **34**, 1263 (1965); (*b*) J. M. DAVIDSON et C. TRIGGS. J. Chem. Soc. A, 1324 (1965); (*c*) M. O. UNGER et R. A. FOUTY. J. Org. Chem. **34**, 18 (1969).
15. T. A. STEPHENSON, S. M. MOREHOUSE, A. R. POWELL, J. P. HEFFER et G. WILKINSON. J. Chem. Soc. 3632 (1965).
16. A. ROSENTHAL. Carbohydr. Res. **8**, 61 (1968).
17. G. DESCOTES, P. BOULLANGER, TACHI-DUNG et J. C. MARTIN. Carbohydr. Res. **71**, 305 (1979).
18. F. J. WEIGERT et J. D. ROBERTS. J. Am. Chem. Soc. **91**, 4940 (1969).
19. G. GRYNKIEWICZ, W. PRIEBE et A. ZAMOJSKI. Carbohydr. Res. **68**, 33 (1979).
20. E. W. GARBISCH, JR. J. Am. Chem. Soc. **86**, 5561 (1964).
21. R. J. FERRIER et G. H. SANKEY. J. Chem. Soc. C, 2345 (1966).
22. (*a*) S. HANESSIAN et A. G. PERNET. Can. J. Chem. **52**, 1266 (1974); (*b*) Adv. Carbohydr. Chem. Biochem. **33**, 111 (1976); (*c*) D. L. WALKER, B. FRASER-REID et J. K. SAUNDERS. J. Chem. Soc. Chem. Commun. 319 (1974); (*d*) B. FRASER-REID, R. D. DAWE et D. B. TULSHIAN. Can. J. Chem. **57**, 1746 (1979) et références citées; (*e*) J. R. POUGNY, M. A. M. NASSR et P. SINAŸ. J. Chem. Soc. Chem. Commun. 375 (1981).
23. (*a*) R. U. LEMIEUX, K. A. WATANABE et A. A. PAVIA. Can. J. Chem. **47**, 4413 (1969); (*b*) B. FRASER-REID, B. J. CARTHY, N. L. HOLDER et M. YUNKER. Can. J. Chem. **49**, 3038 (1971).
24. R. D. DAWE et B. FRASER-REID. J. Chem. Soc. Chem. Commun. 1180 (1981).
25. R. V. LEMIEUX, K. A. WATANABE et A. A. PAVIA. Can. J. Chem. **47**, 9413 (1969).
26. G. GRINKIEWICZ et A. ZAMOJSKI. Z. Naturforsch. Teil B, **35**, 1024 (1980).
27. Y. FUJIWARA, I. MORITANI, R. ASANO, H. TANAKA et S. TERANISHI. Tetrahedron, **25**, 4815 (1969).
28. H. C. BROWN et G. GOLDMAN. J. Am. Chem. Soc. 1650 (1962).
29. R. R. SCHMIDT et M. HOFFMAN. Tetrahedron Lett. 409 (1982).
30. L. M. STOCK, K. TSE, L. J. VORVICK et S. A. WALSTRUM. J. Org. Chem. **46**, 1759 (1981).
31. S. CABIDDU, A. MACCIONI, P. P. PIRAS et A. PLUMITALLO. Gazz. Chim. Ital. **111**, 123 (1981).
32. T. ITAHARA. J. Chem. Soc. Chem. Commun. 859 (1981).
33. A. A. CHALMERS et R. H. HALL. J. Chem. Soc. Perkin Trans. 2, 728 (1974).
34. M. RICO et J. SANTORO. Org. Magn. Reson. 49 (1976).
35. K. TAKIURA et S. HONDA. Carbohydr. Res. **21**, 379 (1972).

Can. J. Chem. Downloaded from www.nrcresearchpress.com by 210.87.254.5 on 09/06/12
For personal use only.

Crystal and molecular structure of hexadecamethylcyclooctasiloxane, $[(CH_3)_2SiO]_8$

NORMAN L. PADDOCK, STEVEN J. RETTIG, AND JAMES TROTTER

Department of Chemistry, University of British Columbia, 2036 Main Mall, Vancouver, B.C., Canada V6T 1Y6

Received September 21, 1982

NORMAN L. PADDOCK, STEVEN J. RETTIG, and JAMES TROTTER. Can. J. Chem. **61**, 541 (1983).

Crystals of hexadecamethylcyclooctasiloxane are tetragonal, a = 13.9442(5), c = 8.5573(4) Å, Z = 2, space group $P4/nnc$. The structure was solved by direct methods and was refined by full-matrix least-squares procedures to a final R of 0.034 and R_w = 0.042 for 730 reflections with $I \geq 3\sigma(I)$. The molecular structure closely resembles that of $[(CH_3)_2PN]_8$. Its comparatively rigid conformation, in which the silicon atoms form a crown, is dependent on the efficient use of van der Waals interactions between two sets of four methyl groups. Important molecular dimensions (bond lengths corrected for libration) are: Si—O = 1.629(1) and 1.635(1), Si—C = 1.862(2) and 1.848(3) Å, O—Si—O = 108.99(6), Si—O—Si = 157.8(1) and 148.8(2)°.

NORMAN L. PADDOCK, STEVEN J. RETTIG et JAMES TROTTER. Can. J. Chem. **61**, 541 (1983).

Les cristaux de l'hexadécaméthylcyclooctasiloxane sont tétragonaux, a = 13.9442(5), c = 8.5573(4) Å, Z = 2, groupe d'espace $P4/nnc$. On a résolu la structure par les méthodes directes et on l'a affinée par la méthode des moindres carrés (matrice complète) jusqu'à une valeur finale de R de 0.034 et R_w de 0.042 pour 730 réflexions avec $I \geq 3\sigma(I)$. La structure moléculaire se ressemble presquement à cela de $[(CH_3)_2PN]_8$, sa conformation comparativement rigide, dans laquelle les atomes de silicium forment une couronne, étant dépendante de l'usage efficient des interactions van der Waals entre les deux ensembles de quatre groupes méthyles. Les dimensions moléculaires importantes (longeurs de liaisons corrigées pour les librations) sont: Si—O = 1.629(1) et 1.635(1), Si—C = 1.862(2) et 1.848(3) Å, O—Si—O = 108.99(6) et Si—O—Si = 157.8(1) et 148.8(2)°.

Introduction

The cyclic dimethylsiloxanes $[(CH_3)_2SiO]_n$ are isoelectronic with the cyclic dimethylphosphazenes $[(CH_3)_2PN]_n$, and there is at least a limited structural correspondence between the two series. The trimeric molecules could indeed hardly be different; the early determination of the structure of $[(CH_3)_2SiO]_3$ (1) has been repeated at −165°C (2), and the Si_3O_3 ring, like the P_3N_3 ring in $[(CH_3)_2PN]_3$ (3), found to deviate from planarity. Eight-membered rings are more conformationally versatile, but the same structures occur in both series. In the solid at low temperatures, $[(CH_3)_2SiO]_4$ has the chair conformation, with symmetry C_i (4), which changes to S_4 above −16.3°C (5, 6). The symmetry is not lowered in the liquid phase (7), the crown conformation (C_{4v}) (5, 6, 8) being specifically excluded by the Raman depolarization values (9). The corresponding phosphazene has S_4 symmetry in the crystal (10), and a metastable crystalline polymorph has been found,[1] in which the molecule has crystallographically imposed C_i symmetry and is presumably chair-shaped. No detail is known of the structures of the cyclic siloxanes $[(CH_3)_2SiO]_{5-7}$, though the central 12-membered ring in 2,2,4,4,14,14,16,16-octaphenyl-8,8,10,10,19,19,21,21-octamethyldispiro[5,5,5,5]decasiloxane is chair-shaped (11), like the P_6N_6 ring in $[(CH_3)_2PN]_6$ (12).

A comparison of the crystal structures of the dimethylphosphazenes up to $[(CH_3)_2PN]_8$ (12–14) shows the increasingly frequent occurrence of the sterically favorable GG and GT local conformations at P, and suggests that stable structures are determined by steric interactions. The comparability of the two series is apparently lost at $[(CH_3)_2SiO]_8$, because, if the molecular symmetry were S_4, as deduced from a partial structure determination (15), the molecule would contain GG′ fragments of high energy. We have therefore redetermined the crystal structure of $[(CH_3)_2SiO]_8$, both to check this point, and to allow a detailed comparison with the structure of $[(CH_3)_2PN]_8$.

[1]Tetragonal, a = 15.953, c = 7.645 Å (H. P. Calhoun, personal communication). Cf. a = 15.705, c = 6.425 Å for the stable form (10).

TABLE 1. Final positional (fractional × 10^5, H × 10^4) and isotropic thermal parameters ($U \times 10^3$ Å^2) with estimated standard deviations in parentheses

Atom	x	y	z	U_{eq}/U_{iso}
Si	1691(4)	15241(3)	15535(5)	40
O(1)*	3916(14)	25000	25000	59
O(2)*	6255(21)	6255	25000	62
C(1)	−11397(18)	13299(21)	14189(39)	66
C(2)	7034(27)	16033(22)	−3959(30)	66
H(1a)	−1369(19)	1193(21)	2453(43)	90(9)
H(1b)	−1423(23)	1846(21)	939(37)	93(9)
H(1c)	−1182(26)	783(24)	1239(38)	94(11)
H(2a)	1278(25)	1664(19)	−229(41)	81(10)
H(2b)	470(22)	2110(23)	−927(38)	97(10)
H(2c)	665(19)	1011(25)	−750(33)	88(10)

*Multiplicity 0.50.

Experimental

Crystals of hexadecamethylcyclooctasiloxane were provided by Professor J. Dale. The crystal was mounted in a general orientation and had dimensions of ca. 0.17 × 0.34 × 0.50 mm. Unit-cell parameters were refined by least-squares on 2 sin θ/λ values for 25 reflections (2θ = 30–50°) measured on a diffractometer with Mo-Kα_1 radiation (λ = 0.70930 Å). Crystal data (at 22°C) are:

$C_{16}H_{48}O_8Si_8$ fw = 593.25

Tetragonal, a = 13.9442(5), c = 8.5573(4) Å, V = 1663.9(1) Å^3, Z = 2, ρ_c = 1.184 g cm^{-3}, $F(000)$ = 640, μ(Mo-Kα) = 3.08 cm^{-1}. Absent reflections: $hk0$, $h + k$ odd, $0kl$, $k + l$ odd and hhl, l odd, space group $P4/nnc$ (D_{4h}^4, No. 126). Lattice constants agree with those reported earlier (15) but the space group reported previously ($P\bar{4}2_1c$) is not consistent with the observed systematic absences.

Intensities were measured with graphite-monochromated Mo-Kα

Can. J. Chem. Downloaded from www.nrcresearchpress.com by 210.87.254.5 on 09/06/12
For personal use only.

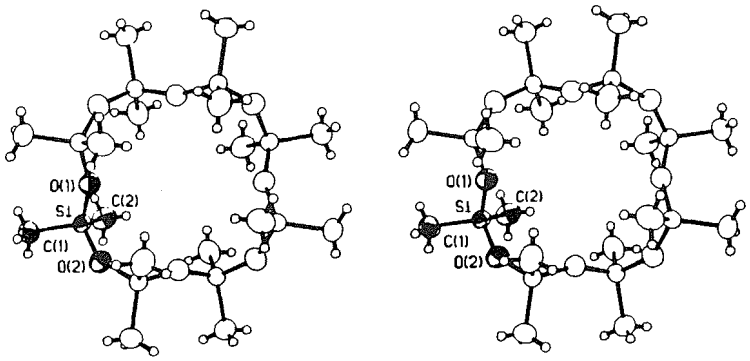

FIG. 1. Stereoscopic view of hexadecamethylcyclooctasiloxane, 50% probability thermal ellipsoids shown for the non-hydrogen atoms. Hydrogen atoms have been assigned artificially small thermal parameters for the sake of clarity.

TABLE 3. Bond lengths (Å) with estimated standard deviations in parentheses

	Length			Length	
Bond	Uncorr.	Corr.	Bond	Uncorr.	Corr.
Si —O(1)	1.6137(6)	1.629	C(1)—H(1b)	0.92(3)	
Si —O(2)	1.6221(12)	1.635	C(1)—H(1c)	0.78(3)	
Si —C(1)	1.849(2)	1.862	C(2)—H(2a)	0.82(3)	
Si —C(2)	1.830(3)	1.848	C(2)—H(2b)	0.90(3)	
C(1)—H(1a)	0.96(4)		C(2)—H(2c)	0.88(3)	

TABLE 4. Bond angles (deg) with estimated standard deviations in parentheses

Bonds	Angle (deg)	Bonds	Angle (deg)
O(1)—Si —O(2)	108.99(6)	Si —C(1)—H(1c)	103(3)
O(1)—Si —C(1)	110.16(12)	H(1a)—C(1)—H(1b)	115(3)
O(1)—Si —C(2)	109.17(11)	H(1a)—C(1)—H(1c)	88(3)
O(2)—Si —C(1)	107.77(13)	H(1b)—C(1)—H(1c)	130(3)
O(2)—Si —C(2)	110.00(12)	Si —C(2)—H(2a)	104(2)
C(1)—Si —C(2)	110.7(2)	Si —C(2)—H(2b)	111(2)
Si —O(1)—Si′	157.83(14)	Si —C(2)—H(2c)	103(2)
Si —O(2)—Si″	148.81(15)	H(2a)—C(2)—H(2b)	111(3)
Si —C(1)—H(1a)	107(2)	H(2a)—C(2)—H(2c)	103(3)
Si —C(1)—H(1b)	110(2)	H(2b)—C(2)—H(2c)	123(3)

*Here and elsewhere in this report primed and double-primed atoms are related to those in Table 1 by the symmetry operations $x, 1/2 - y, 1/2 - z$ and $1/2 - y, 1/2 - x, 1/2 - z$ respectively.

radiation ($\lambda = 0.71073$ Å) on an Enraf-Nonius CAD4-F diffractometer. An $\omega-2\theta$ scan at 1.44–10.06° min^{-1} over a range of (0.65 + 0.35 tan θ) degrees in ω (extended by 25% on both sides for background measurement) was employed. Data were measured to $2\theta = 60°$. The intensities of three check reflections, measured every 3600 s throughout the data collection, decreased uniformly by 15%, the data being corrected for isotropic decay. After data reduction, an absorption correction was applied using the Gaussian integration method (16, 17). Transmission factors ranged from 0.880 to 0.924 for 80 integration points. Of the 1211 independent reflections measured, 730 (60.3%) had intensities greater than $3\sigma(I)$ above background where $\sigma^2(I) = S + 2B + (0.04(S - B))^2$ with S = scan count and B = normalized background count.

The structure was solved by direct methods, the coordinates of the ring atoms being determined from an E-map and those of the carbon atoms from a subsequent difference map. After full-matrix least-squares refinement of the non-hydrogen atoms with anisotropic thermal parameters to $R = 0.062$, all six hydrogen atoms were positioned from a difference map and were refined with isotropic thermal parameters in subsequent least-squares cycles. The scattering factors of ref. 18 were used for non-hydrogen atoms and those of ref. 19 for hydrogen atoms. Anomalous scattering factors from ref. 20 were used for the Si atoms. The weighting scheme, $w = 1/\sigma^2(F)$ where $\sigma^2(F)$ is derived from the previously defined $\sigma^2(I)$ gave uniform average values of $w(|F_o| - |F_c|)^2$ over ranges of both $|F_o|$ and $\sin\theta/\lambda$ and was employed in the final stages of refinement. Convergence was reached at $R = 0.034$ and $R_w = 0.042$ for 730 reflections with $I \geq 3\sigma(I)$. For all 1211 reflections $R = 0.069$. The function minimized was $\Sigma w(|F_o| - |F_c|)^2$, $R = \Sigma||F_o| - |F_c||/\Sigma|F_o|$ and $R_w = (\Sigma w(|F_o| - |F_c|)^2/\Sigma w|F_o|^2)^{1/2}$.

On the final cycle of refinement the mean and maximum parameter shifts corresponded to 0.002 and 0.03σ respectively. The mean error in an observation of unit weight was 1.757. A final difference map showed no unusual features. The final positional and thermal parameters appear in Tables 1 and 2 respectively.[2] Measured and calculated structure factors have been placed in the Depository of Unpublished Data.[2]

The ellipsoids of thermal motion for the non-hydrogen atoms are

[2]The structure factor table and Table 2 (anisotropic thermal parameters) are available, at a nominal charge, from the Depository of Unpublished Data, CISTI, National Research Council of Canada, Ottawa, Ont., Canada K1A 0S2.

Can. J. Chem. Downloaded from www.nrcresearchpress.com by 210.87.254.5 on 09/06/12
For personal use only.

TABLE 5. Torsion angles (deg) with estimated standard deviations in parentheses

Atoms	Value (deg)
O(2)—Si—O(1)—Si′	−119.35(11)
C(1)—Si—O(1)—Si′	−1.31(10)
C(2)—Si—O(1)—Si′	120.48(12)
O(1)—Si—O(2)—Si″	−44.9(2)
C(1)—Si—O(2)—Si″	−164.5(2)
C(2)—Si—O(2)—Si″	74.7(2)
O(1)—Si—C(1)—H(1a)	−68(2)
O(1)—Si—C(1)—H(1b)	58(2)
O(1)—Si—C(1)—H(1c)	−160(3)
O(2)—Si—C(1)—H(1a)	51(2)
O(2)—Si—C(1)—H(1b)	177(2)
O(2)—Si—C(1)—H(1c)	−41(3)
C(2)—Si—C(1)—H(1a)	171(2)
C(2)—Si—C(1)—H(1b)	−63(2)
C(2)—Si—C(1)—H(1c)	79(3)
O(1)—Si—C(2)—H(2a)	61(2)
O(1)—Si—C(2)—H(2b)	−59(2)
O(1)—Si—C(2)—H(2c)	168(2)
O(2)—Si—C(2)—H(2a)	−59(2)
O(2)—Si—C(2)—H(2b)	−178(2)
O(2)—Si—C(2)—H(2c)	48(2)
C(1)—Si—C(2)—H(2a)	−178(2)
C(1)—Si—C(2)—H(2b)	63(2)
C(1)—Si—C(2)—H(2c)	−71(2)

shown in Fig. 1. The thermal motion has been analysed in terms of the rigid-body modes of translation, libration, and screw motion (21). The rms standard error in the temperature factors σU_{ij} (derived from the least-squares analysis) is 0.0011 Å^2. Analysis of the SiO_2C_2 unit gave rms ΔU_{ij} = 0.0009 Å^2 and physically reasonable rigid-body parameters. The appropriate bond distances have been corrected for libration (21, 22), using shape parameters q^2 of 0.08 for all atoms involved. Corrected bond lengths appear in Table 3 along with the uncorrected values; corrected bond angles do not differ by more than 1σ from the uncorrected values given in Table 4. Torsion angles are listed in Table 5.

Results and discussion

The cell dimensions obtained here are identical within experimental error to those obtained by Frevel and Hunter (15), but the space group is different. It is indeed not impossible that there should be two closely related polymorphic forms, but, in any case, the diffraction symmetry of the crystals we have examined is unambiguous, with the required molecular symmetry D_4 (Fig. 1). O(1) is in position 8(i), O(2) in 8(h), and other atoms in 16(k) (origin is taken at the centre, $\bar{1}$). The oxygen atoms thus lie on twofold axes and are all coplanar, with the Si atoms displaced alternately above and below the plane by 0.8099(4) Å. The lengths of the Si—O bonds to O(1) are slightly less (1.629(1) Å) than to O(2) (1.635(1) Å), the greater length being associated with the smaller angle, as expected if the inequality is a result of differences in σ-hybridization. The ring angle at silicon (109.0(1)°) and the C—Si—C angle (110.7(2)°) are unremarkable, and though the lengths of the Si—C bonds are significantly different (Si—C(1)(eq) = 1.862(2) Å, Si—C(2)(ax) = 1.843(3) Å), their mean value, 1.855(2) Å, is typical. The ring angles at O(1) and O(2) are 157.8(1) and 148.8(2)°, respectively.

The molecular conformation of $[(CH_3)_2SiO]_8$ is strikingly similar to that of $[(CH_3)_2PN]_8$ (14). Their molecular dimensions are similar, and both have a direct fourfold axis. Comparison

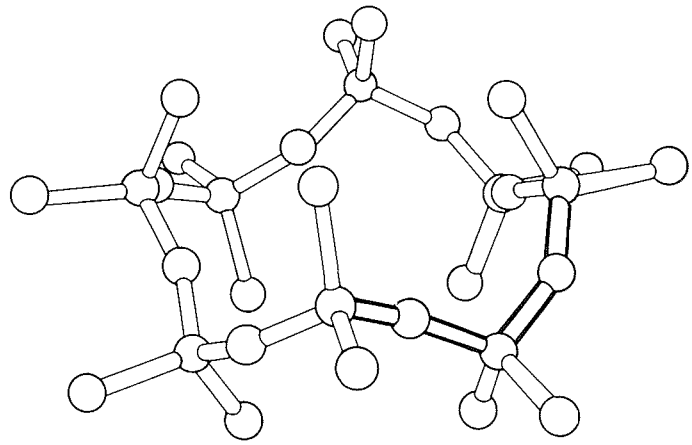

FIG. 2. General view of hexadecamethylcyclooctasiloxane showing the local conformations at silicon (heavy lines).

of the ring torsion angles shows that the local conformations are nevertheless different in the two molecules. In $[(CH_3)_2PN]_8$, GG and GT conformations alternate.[3] In $[(CH_3)_2SiO]_8$, the local conformation at silicon (shown more clearly in Fig. 2) is close to CT, the angle between the Si′—Si—Si″ and O(1)—Si—O(2) planes being 13.1° (ideally 0°). The conformational difference from $[(CH_3)_2PN]_8$ is less than might appear, because the distinctions between GG, GT, and CT disappear as the angle at O (or N) approaches 180°, and the siloxane angles are especially large (mean 153.3°). Model calculations nevertheless show that the highly polar bonds likely in the siloxanes would favor the CT conformation. The general shape of the molecules seems to be governed by the intramolecular contacts between the axial methyl groups; 3.96 Å in $[(CH_3)_2SiO]_8$, 3.82, 4.01 (mean 3.92 Å) in $[(CH_3)_2PN]_8$. These distances are attained by the slight twisting of the CT local conformation noted above, in turn made possible by a low barrier to rotation about the Si—O bond, at most a few hundred cal mol^{-1} (23). The small temperature factors (Table 2) show that the molecule is much more rigid than, for instance, $[(CH_3)_2SiO]_3$ (2), but less so than the sterically hindered $[(t\text{-}C_4H_9)_2SiO]_3$ (24). The particular conformation found (Fig. 2) clearly allows efficient use of the Van der Waals interactions at the top and the bottom of the molecule, and the consequent comparative rigidity, unusual for dimethylsiloxanes, is in agreement with the high entropy of fusion of $[(CH_3)_2SiO]_8$ (25), and with the comparatively sharp and simple spectrum of the solid (7). The methyl groups do not rotate freely about the Si—C axes.

More generally, the flexibility of the dimethylsiloxanes in the liquid and vapor phases (5, 7, 9, 25, 26), and (apart from $[(CH_3)_2SiO]_8$) their likely conformational inhomogeneity in the solid (25) results primarily from the high polarity of the Si—O bond (27), which increases the angle at oxygen, thereby increasing its deformability and decreasing the rotational barrier. This can happen in two ways. The lone pairs on oxygen may be partially delocalized into the *d*-orbitals of silicon, so becoming stereochemically ineffective. Alternatively, *d*-orbitals may not be used. If the Si—O—Si angle then approaches 180°, the unshared electrons eventually occupy orthogonal *p*-orbitals at oxygen, their density distribution being cylindrically symmetrical about the Si—O bond, and the torsional barrier

[3]Terminology of Mizushima (34).

Can. J. Chem. Downloaded from www.nrcresearchpress.com by 210.87.254.5 on 09/06/12
For personal use only.

then vanishes.

The O—Si—O angle is close to the regular tetrahedral angle, suggesting, by comparison with the phosphazene series, and in agreement with *ab initio* calculations (27), that the *d*-orbital interaction is small and the polar effect dominant. A similar conclusion was reached earlier for Si—N interactions, $X\alpha$ calculations (28) showing that polar interactions were more important than π-bonding in ensuring the skeletal planarity of $N(SiH_3)_3$.

If the torsional barrier about the Si—O bond is small, the molecular conformation of individual dimethylsiloxanes will be controlled principally by the interaction of the exocyclic groups. In making comparisons with organic structures (25, 29), it is then perhaps more appropriate to compare siloxanes $[(CH_3)_2SiO]_n$ with the cycloalkanes $(CH_2)_n$ rather than $(CH_2)_{2n}$. The conformations of cyclooctane and its derivatives have been frequently investigated by spectroscopic and X-ray methods; the boat–chair conformation is usually found. In the vapor, a large number of conformations occur (30); the crown form, specifically, being only slightly less stable, both by experiment (31) and calculation (32), than the boat–chair. In the absence of torsional barriers, the crown conformation would be expected (33), and this is indeed the arrangement found for the Si atoms in $[(CH_3)_2SiO]_8$.[4] It is not yet known whether the neglect of the torsional barrier about the Si—O bond can be helpful in the qualitative interpretation of related structures.

Acknowledgments

We thank Professor J. Dale for providing us with the crystals, the Natural Sciences and Engineering Research Council of Canada for financial support, and the University of British Columbia Computing Centre for assistance.

1. G. PEYRONEL. Atti Accad. Naz. Lincei. Rend. **16**, 231 (1954).
2. R. P. HERNANDEZ. Acta Crystallogr. Sect. A, **34**, S406 (1978).
3. R. T. OAKLEY, N. L. PADDOCK, S. J. RETTIG, and J. TROTTER. Can. J. Chem. **55**, 4206 (1977).
4. H. STEINFINK, B. POST, and I. FANKUCHEN. Acta Crystallogr. **8**, 420 (1955).
5. A. N. LAZAREV. Vibrational spectra and structure of silicates. Consultants Bureau, New York and London. 1972. pp. 270–278.
6. A. N. LAZAREV and T. F. TENISHEVA. Izv. Akad. Nauk SSSR, Ser. Khim. 1168 (1964).
7. T. ALVIK and J. DALE. Acta Chem. Scand. **25**, 2142 (1971).
8. H. KRIEGSMANN. Z. Anorg. Allg. Chem. **298**, 232 (1959); H. JANCKE, G. ENGELHARDT, R. RADEGLIA, and H. KRIEGSMANN. Spectrochim. Acta Sect. A, **25**, 85 (1969).
9. G. FOGARASI, H. HACKER, V. HOFFMANN, and S. DOBOS. Spectrochim. Acta Sect. A, **30**, 629 (1974).
10. M. W. DOUGILL. J. Chem. Soc. 5471 (1961).
11. V. E. SHKLOVER, N. G. BOKII, YU. T. STRUCHKOV, K. A. ANDRIANOV, and A. B. ZACHERNYUK. J. Struct. Chem. **15**, 755 (1974).
12. R. T. OAKLEY, N. L. PADDOCK, S. J. RETTIG, and J. TROTTER. Can. J. Chem. **55**, 3118 (1977).
13. K. D. GALLICANO, R. T. OAKLEY, N. L. PADDOCK, S. J. RETTIG, and J. TROTTER. Can. J. Chem. **55**, 304 (1977).
14. R. T. OAKLEY, N. L. PADDOCK, S. J. RETTIG, and J. TROTTER. Can. J. Chem. **55**, 2530 (1977).
15. L. K. FREVEL and M. J. HUNTER. J. Am. Chem. Soc. **67**, 2275 (1945).
16. P. COPPENS, L. LEISEROWITZ, and D. RABINOVICH. Acta Crystallogr. **18**, 1035 (1965).
17. W. R. BUSING and H. A. LEVY. Acta Crystallogr. **22**, 457 (1967).
18. D. T. CROMER and J. B. MANN. Acta Crystallogr. Sect. A, **24**, 321 (1968).
19. R. F. STEWART, E. R. DAVIDSON, and W. T. SIMPSON. J. Chem. Phys. **42**, 3175 (1965).
20. D. T. CROMER and D. LIBERMAN. J. Chem. Phys. **53**, 1891 (1970).
21. V. SCHOMAKER and K. N. TRUEBLOOD. Acta Crystallogr. Sect. B, **24**, 63 (1968).
22. D. W. J. CRUICKSHANK. Acta Crystallogr. **9**, 747 (1956); **9**, 754 (1956); **14**, 896 (1961).
23. D. W. SCOTT, J. F. MESSERLEY, S. S. TODD, G. B. GUTHRIE, I. A. HOSSENLOPP, R. T. MOORE, A. OSBORN, W. T. BERG, and J. P. MCCULLOUGH. J. Phys. Chem. **65**, 1320 (1961).
24. W. CLEGG. Acta Crystallogr. Sect. B, **38**, 1648 (1982).
25. T. ALVIK and J. DALE. Acta Chem. Scand. **25**, 2131 (1971).
26. H. OBERHAMMER, W. ZEIL, and G. FOGARASI. J. Mol. Struct. **18**, 309 (1973).
27. H. OBERHAMMER and J. E. BOGGS. J. Am. Chem. Soc. **102**, 7241 (1980).
28. L. NOODLEMAN and N. L. PADDOCK. Inorg. Chem. **18**, 354 (1979).
29. J. DALE. Angew. Chem. Int. Edit. Engl. **5**, 1000 (1966).
30. A. ALMENINGEN, O. BASTIANSEN, A. HAALAND, and H. M. SEIP. Angew. Chem. Int. Edit. Engl. **4**, 819 (1965).
31. F. A. L. ANET and V. J. BASUS. J. Am. Chem. Soc. **95**, 4424 (1973).
32. K. B. WIBERG. J. Am. Chem. Soc. **87**, 1070 (1965); J. B. HENDRICKSON. J. Am. Chem. Soc. **89**, 7036 (1967); M. BIXON and S. LIFSON. Tetrahedron, **23**, 769 (1967); N. L. ALLINGER, J. P. HIRSCH, M. MILLER, J. J. TYMINSKI, and F. A. VAN CATLEDGE. J. Am. Chem. Soc. **90**, 1199 (1968).
33. A. I. KITIAGORODSKY. Molecular crystals and molecules. Academic Press, New York and London. 1973. p. 403.
34. S. MIZUSHIMA. Structure of molecules and internal rotation. Academic Press, New York. 1954.
35. J. DALE. Acta Chem. Scand. **27**, 1115 (1973).

[4]Calculation of the non-bonded interactions in a series of conformations of $[(CH_3)_2SiO]_8$ (the oxygen atoms being assumed to make no contribution) showed the order of increasing energy to be crown < chair < chair–boat < tub ≪ saddle, the differences being principally in the Me—Me interactions. If interactions with the formal lone pairs on oxygen were important, skeletal fragments of the zigzag type, as calculated for cyclohexadecane (35) would be expected.

Can. J. Chem. Downloaded from www.nrcresearchpress.com by 210.87.254.5 on 09/06/12
For personal use only.

The chlorination of dihydroconiferyl alcohol

A. BRUCE MCKAGUE
B. C. Research, 3650 Wesbrook Mall, Vancouver, B. C., Canada V6S 2L2
STEVEN J. RETTIG AND JAMES TROTTER
Department of Chemistry, University of British Columbia, 2036 Main Mall, Vancouver, B. C., Canada V6T 1Y6
AND
GEORGE R. DOUGLAS AND EARLE R. NESTMANN
Mutagenesis Section, Environmental and Occupational Toxicology Division, Department of National Health and Welfare, Ottawa, Ont., Canada K1A 0L2

Received October 7, 1982

A. BRUCE MCKAGUE, STEVEN J. RETTIG, JAMES TROTTER, GEORGE R. DOUGLAS, and EARLE R. NESTMANN. Can. J. Chem. **61**, 545 (1983).

Aqueous chlorination of dihydroconiferyl alcohol, a phenol present in pulping liquors, gave a mixture of three products. The two major products, which formed an inseparable mixture, yielded the crystalline epoxides **1** and **8** when reacted with diazomethane. The epoxide **1** had previously been obtained by reacting one of the components isolated from mutagenic fractions of chlorination-stage effluent from a bleached kraft pulp mill with diazomethane. The results indicate dihydroconiferyl alcohol retained with pulp is chlorinated in the bleach plant to give a mixture of the spirocyclohexenediones **5** and **6**. Crystals of **8** are orthorhombic, a = 24.3048(15), b = 12.5403(9), c = 7.8653(6) Å, Z = 8, space group *Pbca*. The structure was solved by direct methods and was refined by full-matrix least-squares procedures to R = 0.029 and R_w = 0.035 for 1308 reflections with $I \geq 3\sigma(I)$. The structure analysis shows that **8** has the same relative stereochemistry as that reported earlier for **1**, but exists as a different conformer in the solid state.

A. BRUCE MCKAGUE, STEVEN J. RETTIG, JAMES TROTTER, GEORGE R. DOUGLAS et EARLE R. NESTMANN. Can. J. Chem. **61**, 545 (1983).

La chloration aqueuse de l'alcool dihydroconiféryle, un phénol que l'on trouve dans les liquides provenant de la fabrication de la pâte à papier, conduit à un mélange de trois produits. On ne peut par séparer les deux produits principaux mais ils réagissent avec le diazométhane pour donner deux époxydes cristallins (**1** et **8**). On a préparé antérieurement l'époxyde **1** en faisant réagir du diazométhane avec un des composés isolés des fractions mutagéniques rejeté à l'étape de la chloration dans une usine de pâte Kraft blanchie. Les résultats indiquent que l'alcool dihydroconiféryle retenu avec la pâte est chloré dans l'usine de blanchissage et donne un mélange des spirocyclohexènediones (**5** et **6**). Les cristaux du composé **8** sont orthorhombiques et appartiennent au groupe d'espace *Pbca* avec a = 24,3048(15), b = 12,5403(9), c = 7,8653(6) Å, Z = 8. On a résolu la structure par des méthodes directes et on l'a affinée par la méthode des moindres carrés (matrice entière) jusqu'à des valeurs de R = 0,029 et de R_w = 0,035 pour 1308 réflexions avec $I \geq 3\sigma(I)$. L'analyse de la structure révèle que le composé **8** a la même stéréochimie relative que celle rapportée antérieurement pour le composé **1**; toutefois sa conformation a l'état solide est différent.

[Traduit par le journal]

Introduction

Recently we reported the structure determination of the trichlorocyclohexenone **1** (1). Since the compound was obtained by reacting one of the constituents of bleached kraft chlorination-stage effluent with diazomethane, the corresponding cyclohexenedione **2** was suggested as the parent compound present in the effluent.

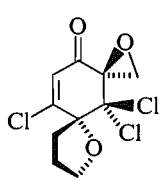

1

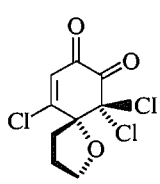

2

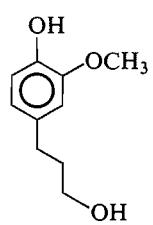

3

Analysis of the basic structural features of **2** revealed that dihydroconiferyl alcohol, **3**, a phenol present in black liquor (2, 3) and unbleached whitewater (4), contained the necessary carbon skeleton and functionality to serve as a precursor of **2**. The guaiacyl nucleus is a known source of *o*-quinones which are produced during bleaching of pulp (5, 6). Cyclization of hydroxypropyl side chains on *para*-substituted cyclohexenones to form spirotetrahydrofuranylcyclohexenones has been achieved by displacement of a leaving group at the cyclization point (7). This paper describes the remarkable transformation of dihydroconiferyl alcohol upon chlorination.

Experimental

Melting points were taken on a Kofler Micro Hot Stage and are uncorrected. Infrared (ir) spectra were recorded on a Perkin Elmer Model 727 Spectrophotometer; ultraviolet (uv) spectra on a Beckman DB-GT Spectrophotometer. Proton magnetic resonance (^{1}H nmr) spectra were recorded in deuteriochloroform using a Varian XL-100 spectrometer. Chemical shifts are given in δ units with tetramethylsilane as the internal standard. A Varian MAT CH 4B mass spectrometer was used to obtain low resolution mass spectra; an AEI MS 12 for high resolution spectra. Microanalytical services were provided by Canadian Microanalytical Service Ltd., 5704 University Blvd., Vancouver, B. C.

Liquid chromatography (lc) was performed on a Hewlett Packard Model 1084B High Performance Liquid Chromatograph equipped

Can. J. Chem. Downloaded from www.nrcresearchpress.com by 210.87.254.6 on 09/06/12
For personal use only.

Can. J. Chem. Downloaded from www.nrcresearchpress.com by 210.87.254.6 on 09/06/12
For personal use only.

with a 20 μL valve injector and variable wavelength ultraviolet detector set at 254 nm. Reverse phase partition chromatography was done on a 4.6 × 20 cm RP-8 column, 5 μm particle size, using isocratic elution with acetonitrile:water, 70:30 and a flow of 0.75 mL/min. Precoated aluminum silica gel plates containing fluorescent indicator (254 nm) were used for thin-layer chromatography (tlc).

Chlorination of dihydroconiferyl alcohol

Chlorine was gently bubbled through a stirred solution of dihydroconiferyl alcohol (500 mg, 2.75 mmol) in water (250 mL) at 50°C for 20 min. After cooling to room temperature, the yellow solution was extracted with ether. The combined extracts were washed with water, dried over anhydrous magnesium sulfate, and evaporated to give a yellow oil (700 mg). The product was purified by preparative tlc using hexane:ethyl acetate 2:1 as the developing solvent. Isolation of the major less polar band gave a mixture of 1-oxa-6,10,10-trichlorospiro[4.5]dec-6-en-8,9-dione, **5**, and 1-oxa-6,7,10,10-tetrachlorospiro[4.5]dec-6-en-8,9-dione, **6** (Scheme 1) as a clear colorless oil (295 mg); ir (film): 1710 cm^{-1}; uv (ethanol) λ_{max}: 247 nm; ^1H nmr δ: 2.2 and 4.3 (complex multiplets), 6.3 (s). A more polar, minor product was also isolated but has not been investigated.

1,6-Dioxa-4,4,10-trichlorodispiro[2.1.4.3]dodec-10-en-12-one, 7, and 1,6-dioxa-4,4,10,11-tetrachlorodispiro[2.1.4.3]dodec-10-en-12-one, 8

Diazomethane, generated from *N*-nitrosomethylurea, was bubbled through a solution of a mixture of the two diones obtained above (200 mg) in ether:methanol 9:1 (10 mL) for 1.5 h. After evaporation of the solvent the product was fractionated by preparative tlc on silica gel (benzene:ethyl acetate 95:5). Isolation of the two major uv-absorbing bands gave products which were obtained crystalline by titration with cold hexane. Recrystallization of the more polar product from ether–hexane gave colorless prisms of the trichlorodispirocyclohexenone **7**; mp 88–89°C; ir (Nujol): 1695, 1605 cm^{-1}; uv (ethanol) λ_{max}: 244 nm (ε 11 400); ^1H nmr δ: 2.3 (m, 2H), 2.8 (m, 2H), 3.15 (diffuse m, 1H), 3.45 (doublet, 1H, J = 6 Hz), 4.25 (m, 2H), 6.5 (s, 1H); ms *m/e* (% relative intensity): 284 (1.6), 282 (1.7) M^+, 136 (100). *Anal.* calcd. for $C_{10}H_9Cl_3O_3$: C 42.56, H 3.22, Cl 37.21; found: C 42.82, H 2.98, Cl 37.43. This epoxide was identical to the epoxide **1** whose structure was previously determined by X-ray crystallography (1).

Recrystallization of the less polar diazomethane product from ether–hexane gave colorless prisms of the tetrachlorodispirocyclohexenone **8**; mp 109–110°C; ir (Nujol): 1705, 1570 cm^{-1}; uv (ethanol) λ_{max}: 262 nm (ε 9,900); ^1H nmr δ: 2.3 (m, 2H), 2.8 (m, 2H), 3.15 (diffuse m, 1H), 3.5 (doublet, 1H, J = 6 Hz), 4.25 (m, 2H); ms *m/e* (% relative intensity): 320 (0.7), 318 (1.2), 316 (1.1) M^+, 281 (100), 145 (100). Exact mass calculated for $C_{10}H_8Cl_4O_3$: 315.9228; found: 315.9214.

X-ray crystallographic analysis of the tetrachlorodispirocyclohexenone 8

A crystal bounded by the five faces (followed by their distances in mm from a common origin): ±(−2 1 1), 0.069, (−2 1 −2), 0.088, (3 1 1), 0.113, and (−1 −2 0), 0.131 was mounted in a general orientation. Unit-cell parameters were refined by least-squares on 2 sin θ/λ values for 25 reflections measured on a diffractometer with Mo-Kα$_1$ radiation (λ = 0.70930 Å). Crystal data at 22°C are:

$C_{10}H_8Cl_4O_3$ fw = 317.98

Orthorhombic, a = 24.3048(15), b = 12.5403(9), c = 7.8653(6) Å, V = 2397.2(3) Å^3, Z = 8, ρ_c = 1.762 g cm^{-3}, $F(000)$ = 1280, μ(Mo-Kα) = 9.83 cm^{-1}. Absent reflections: 0kl, k odd; $h0l$, l odd; and $hk0$, h odd; uniquely indicate the space group $Pbca$ (D_{2h}^{15}, No. 61).

Intensities were measured with graphite-monochromatized Mo-Kα radiation (λ = 0.71073 Å) on an Enraf-Nonius CAD4-F diffractometer. An ω–2θ scan at 0.96–10.06° min^{-1} over a range of (0.65 + 0.35 tan θ) degrees in ω (extended by 25% on both sides for background measurement) was employed. Data were measured to 2θ = 55°. The intensities of three check reflections, measured every 3600 s throughout the data collection, remained constant to within 3%. After data reduction,[1] an absorption correction was applied using the analytical method (8, 9). Transmission factors ranged from 0.795 to 0.895. Of the 2732 independent reflections measured, 1308 (47.9%) had intensities greater than 3σ(I) above background where $\sigma^2(I) = S + 2B + (0.04(S - B))^2$ with S = scan count and B = normalized background count.

TABLE 1. Final positional (fractional × 10^5, H × 10^4) and isotropic thermal parameters (U × 10^3 Å^2) with estimated standard deviations in parentheses

Atom	x	y	z	U_{eq}/U_{iso}
Cl(1)	96190(3)	59763(7)	25250(12)	47
Cl(2)	87878(4)	51232(7)	2885(10)	43
Cl(3)	78816(4)	22731(8)	30254(14)	64
Cl(4)	75890(3)	45698(9)	43586(14)	58
O(1)	83883(9)	61693(17)	34220(27)	37
O(2)	97877(10)	36882(20)	35079(31)	51
O(3)	90393(13)	21032(21)	21502(50)	93
C(1)	83856(21)	68026(34)	49581(54)	59
C(2)	88209(23)	63886(36)	60475(63)	62
C(3)	88902(16)	52467(29)	55615(44)	37
C(4)	86491(12)	51836(24)	37398(38)	29
C(5)	90931(12)	50005(23)	23684(37)	30
C(6)	93282(12)	38837(23)	24168(42)	32
C(7)	98666(16)	36247(39)	16947(59)	50
C(8)	89060(14)	30073(28)	24950(49)	45
C(9)	83533(13)	32871(25)	30605(41)	37
C(10)	82358(12)	42763(25)	36161(39)	33
H(1a)	8014(18)	6664(35)	5545(59)	95(16)
H(1b)	8363(13)	7474(30)	4706(41)	42(10)
H(2a)	9149(23)	6798(45)	5626(72)	145(24)
H(2b)	8758(13)	6469(28)	7151(46)	40(10)
H(3a)	9231(16)	5054(26)	5568(45)	49(11)
H(3b)	8711(15)	4800(31)	6240(52)	60(13)
H(7a)	10065(15)	4120(33)	1261(49)	55(13)
H(7b)	9884(15)	2937(33)	1197(51)	59(12)

The structure was solved by direct methods, the coordinates of all non-hydrogen atoms being determined from an E-map. After full-matrix least-squares refinement of the non-hydrogen atoms with anisotropic thermal parameters to R = 0.045, all eight hydrogen atoms were located on a difference map and were refined with isotropic thermal parameters in subsequent cycles of refinement. The scattering factors of ref. 10 were used for non-hydrogen atoms and those of ref. 11 for hydrogen atoms. Anomalous scattering factors from ref. 12 were used for the Cl atoms. The weighting scheme, $w = 1/\sigma^2(F)$ where $\sigma^2(F)$ is derived from the previously defined $\sigma^2(I)$ gave uniform average values of $w(|F_o| - |F_c|)^2$ over ranges of both $|F_o|$ and sin θ/λ and was employed in the final stages of refinement. Convergence was reached at R = 0.029 and R_w = 0.035 for 1308 reflections with $I \geq 3\sigma(I)$. For all 2732 reflections R = 0.112. The function minimized was $\Sigma w(|F_o| - |F_c|)^2$, $R = \Sigma||F_o| - |F_c||/\Sigma|F_o|$ and $R_w = (\Sigma w(|F_o| - |F_c|)^2/\Sigma w|F_o|^2)^{1/2}$.

On the final cycle of refinement the mean and maximum parameter shifts corresponded to 0.06 and 0.70σ respectively. The mean error in an observation of unit weight was 1.508. A final difference map showed maximum fluctuations of −0.42 to +0.35 e Å^{-3} in the vicinity of the chlorine atoms. The final positional and thermal parameters

[1]The computer programs used include locally written programs for data processing and locally modified versions of the following: MULTAN 80, multisolution program by P. Main, M. M. Woolfson, L. Lessinger, G. Germain, and J. P. Declerq; ORFLS, full-matrix least-squares, and ORFFE, function and errors, by W. R. Busing, K. O. Martin, and H. A. Levy; FORDAP, Patterson and Fourier syntheses, by A. Zalkin; ORTEP II, illustrations, by C. K. Johnson.

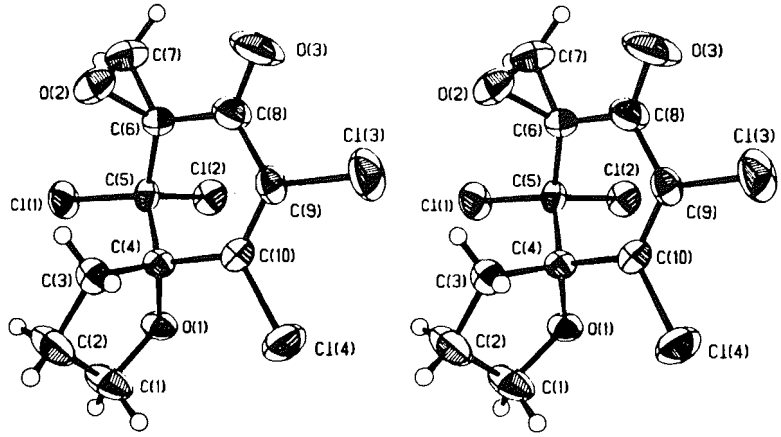

FIG. 1. Stereoscopic view of the 1,6-dioxa-4,4,10,11-tetrachlorodispiro[2.1.4.3]dodec-10-en-12-one molecule (crystallographic atom numbering), 50% thermal ellipsoids are shown for the non-hydrogen atoms.

TABLE 3. Bond lengths (Å) with estimated standard deviations in parentheses

	Length			Length	
Bond	Uncorr.	Corr.	Bond	Uncorr.	Corr.
Cl(1)—C(5)	1.774(3)	1.780	C(2)—C(3)	1.492(5)	1.495
Cl(2)—C(5)	1.803(3)	1.810	C(3)—C(4)	1.550(4)	1.556
Cl(3)—C(9)	1.712(3)	1.718	C(4)—C(5)	1.543(4)	1.549
Cl(4)—C(10)	1.717(3)	1.723	C(4)—C(10)	1.521(4)	1.526
O(1)—C(1)	1.446(4)	1.450	C(5)—C(6)	1.513(4)	1.518
O(1)—C(4)	1.412(3)	1.416	C(6)—C(7)	1.463(5)	1.467
O(2)—C(6)	1.430(4)	1.435	C(6)—C(8)	1.505(4)	1.510
O(2)—C(7)	1.441(5)	1.444	C(8)—C(9)	1.458(5)	1.461
O(3)—C(8)	1.210(4)	1.216	C(9)—C(10)	1.346(4)	1.350
C(1)—C(2)	1.457(6)	1.462			

TABLE 4. Bond angles (deg) with estimated standard deviations in parentheses

Bonds	Angle (deg)	Bonds	Angle (deg)
C(1)—O(1)—C(4)	109.6(2)	O(2)—C(6)—C(5)	118.0(3)
C(6)—O(2)—C(7)	61.3(2)	O(2)—C(6)—C(7)	59.8(2)
O(1)—C(1)—C(2)	107.0(3)	O(2)—C(6)—C(8)	112.5(3)
C(1)—C(2)—C(3)	105.9(3)	C(5)—C(6)—C(7)	122.2(3)
C(2)—C(3)—C(4)	104.1(3)	C(5)—C(6)—C(8)	114.8(2)
O(1)—C(4)—C(3)	106.8(3)	C(7)—C(6)—C(8)	117.6(3)
O(1)—C(4)—C(5)	108.7(2)	O(2)—C(7)—C(6)	59.0(2)
O(1)—C(4)—C(10)	110.3(2)	O(3)—C(8)—C(6)	119.5(3)
C(3)—C(4)—C(5)	112.9(3)	O(3)—C(8)—C(9)	122.7(3)
C(3)—C(4)—C(10)	110.3(3)	C(6)—C(8)—C(9)	117.7(3)
C(5)—C(4)—C(10)	107.8(2)	Cl(3)—C(9)—C(8)	115.7(2)
Cl(1)—C(5)—Cl(2)	107.50(15)	Cl(3)—C(9)—C(10)	123.2(2)
Cl(1)—C(5)—C(4)	110.7(2)	C(8)—C(9)—C(10)	121.1(3)
Cl(1)—C(5)—C(6)	111.4(2)	Cl(4)—C(10)—C(4)	115.0(2)
Cl(2)—C(5)—C(4)	109.5(2)	Cl(4)—C(10)—C(9)	120.2(2)
Cl(2)—C(5)—C(6)	104.9(2)	C(4)—C(10)—C(9)	124.8(3)
C(4)—C(5)—C(6)	112.6(2)		

appear in Tables 1 and 2[2] respectively. The largest parameter shift was associated with the x coordinate of H(2a). Measured and calculated structure factors have been placed in the Depository of Unpublished Data.[2]

The ellipsoids of thermal motion for the non-hydrogen atoms are shown in Fig. 1. The thermal motion has been analysed in terms of the rigid-body modes of translation, libration, and screw motion (13). The rms standard error in the temperature factors σU_{ij} (derived from the least-squares analysis) is 0.0017 Å^2. Analysis of all non-hydrogen atoms except the carbonyl oxygen atom gave rms ΔU_{ij} = 0.0044 Å^2 and physically reasonable results. The appropriate bond distances have been corrected for libration (13, 14), using shape parameters q^2 of 0.08 for all atoms involved. Corrected bond lengths appear in

[2]The structure factor table, Table 2 (anisotropic thermal parameters) and other material mentioned in the text are available, at a nominal charge, from the Depository of Unpublished Data, CISTI, National Research Council of Canada, Ottawa, Canada K1A 0S2.

Can. J. Chem. Downloaded from www.nrcresearchpress.com by 210.87.254.6 on 09/06/12
For personal use only.

TABLE 5. Intra-annular torsion angles (deg) with standard deviations in parentheses

Atoms	Torsion angle (deg)
C(4)—O(1)—C(1)—C(2)	21.2(5)
O(1)—C(1)—C(2)—C(3)	−26.7(6)
C(1)—C(2)—C(3)—C(4)	21.8(5)
C(2)—C(3)—C(4)—O(1)	−9.4(4)
C(1)—O(1)—C(4)—C(3)	−6.9(4)
C(10)—C(4)—C(5)—C(6)	−50.5(3)
C(4)—C(5)—C(6)—C(8)	48.3(4)
C(5)—C(6)—C(8)—C(9)	−19.4(5)
C(6)—C(8)—C(9)—C(10)	−4.9(5)
C(8)—C(9)—C(10)—C(4)	0.8(5)
C(5)—C(4)—C(10)—C(9)	28.6(4)

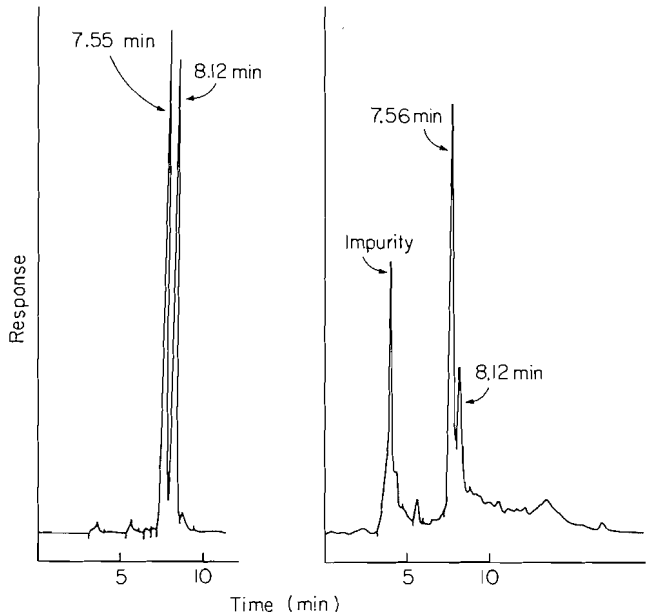

FIG. 2. Liquid chromatograms of the major product from the chlorination of dihydroconiferyl alcohol (left) and material isolated from chlorination-stage effluent (right).

Table 3 along with the uncorrected values; corrected bond angles do not differ by more than 1σ from the uncorrected values given in Table 4. Intra-annular torsion angles defining the conformations of five- and six-membered rings are listed in Table 5. Bond lengths and angles involving hydrogen and a complete listing of torsion angles (Tables 6–8) are included as supplementary material.

Results and discussion

Three products were obtained from the aqueous chlorination of dihydroconiferyl alcohol **3**. The two major products, obtained in a yield of 59% (by weight) after preparative thin-layer chromatography (tlc), could not be separated and remained non-crystalline. Liquid chromatography (lc, Fig. 2) indicated nearly equal amounts of the two components were present. The third product, obtained in 18% yield (by weight) was more polar and has not been investigated at this stage.

The mixture of the two major products contained carbonyl absorption at 1710 cm^{-1} in the ir spectrum. Complex multiplets were present at δ 2.2 and 4.3 in the ^1H nmr spectrum and an olefinic hydrogen appeared as a singlet at δ 6.3. Ultraviolet absorption was present at 247 nm. Spectral features of the mixture were very similar to the material isolated from chlorination-stage effluent during the previous study (1). In addition, the mixture had the same Rf and color reaction with 2,4-dinitrophenylhydrazine on tlc as the isolated material and the retention times were identical by lc (Fig. 2). The only difference between the product from the chlorination of dihydroconiferyl alcohol and the material isolated from chlorination-stage effluent, apart from the presence of an impurity in the isolated material (Fig. 2), was the ratio of the two components. Whereas nearly equal amounts of each component were present in the chlorination product, the isolated material contained approximately a 4:1 ratio of the same components. Since separation and complete characterization of the two major products from the chlorination of dihydroconiferyl alcohol was not possible, further characterization was done on the diazomethane reaction products as was done with the material isolated from chlorination-stage effluent (1).

Nearly equal amounts of two compounds were obtained by reaction of the two major dihydroconiferyl alcohol chlorination products with diazomethane. The two compounds were readily separable by the tlc and the more polar of these was identical to the previously described epoxide **1**. The less polar diazomethane product had carbonyl absorption at 1705 cm^{-1} and olefinic absorption at 1570 cm^{-1} in the ir spectrum. The absorption frequencies of the carbonyl and olefinic groups were shifted 10 cm^{-1} higher and 35 cm^{-1} lower, respectively, relative to the corresponding frequencies in **1**. No olefinic hydrogens were present in the ^1H nmr spectrum and the absorption maximum in the uv spectrum appeared at 262 nm, 18 nm higher than the absorption maximum of **1**. These spectral features, coupled with a molecular formula of $C_{10}H_8Cl_4O_3$ from mass spectrometry, suggested the second diazomethane reaction product was a tetrachlorocyclohexenone epoxide derived from **6**. A complete structure determination by X-ray crystallography, described in the following section of this paper, showed that the compound was **8**. By analogy with the work described previously (1), the two major products from the chlorination of dihydroconiferyl alcohol are the cyclohexenediones **5** and **6**.

A mechanism to account for formation of the cyclohexenediones is shown in Scheme 1. Demethylation of guaiacols is known to occur rapidly with aqueous chlorine (5, 15) to give the chlorinated catechols found in chlorination-stage effluent. Formation of the spirotetrahydrofuran ring could occur by displacement of chloride from a dienone-type intermediate such as **4**. A similar cyclization has recently been reported in the synthesis of theaspirone (7). Conversion of ketones to epoxides is known to be efficient when chlorine substituents are present in the α-position (16).

Crystals of **8** consist of discrete molecules (Fig. 1). The relative stereochemistry at the chiral centres (C(4) and C(6)) is the same in **1** (1) and **8**, i.e. *RR* (or *SS*, the materials being racemic), with the furan and epoxy oxygens *trans*. However, the two molecules exist in different conformational forms in the solid state, **1** having O(furan) pseudo-axial and O(epoxy) pseudo-equatorial, with these orientations reversed in **8** (Fig. 1); conformational inversion of Fig. 1[3] produces a geometry (which is not found in the solid state) which is identical with that of **1** (mirror image of Fig. 1 in ref. 1), apart from the

[3]The enantiomer of **8** in Fig. 1 has intentionally been shown with opposite chiralities at C(4) and C(6) relative to those of **1** (1) in order to compare conformations of the cyclohexenone rings.

Can. J. Chem. Downloaded from www.nrcresearchpress.com by 210.87.254.6 on 09/06/12
For personal use only.

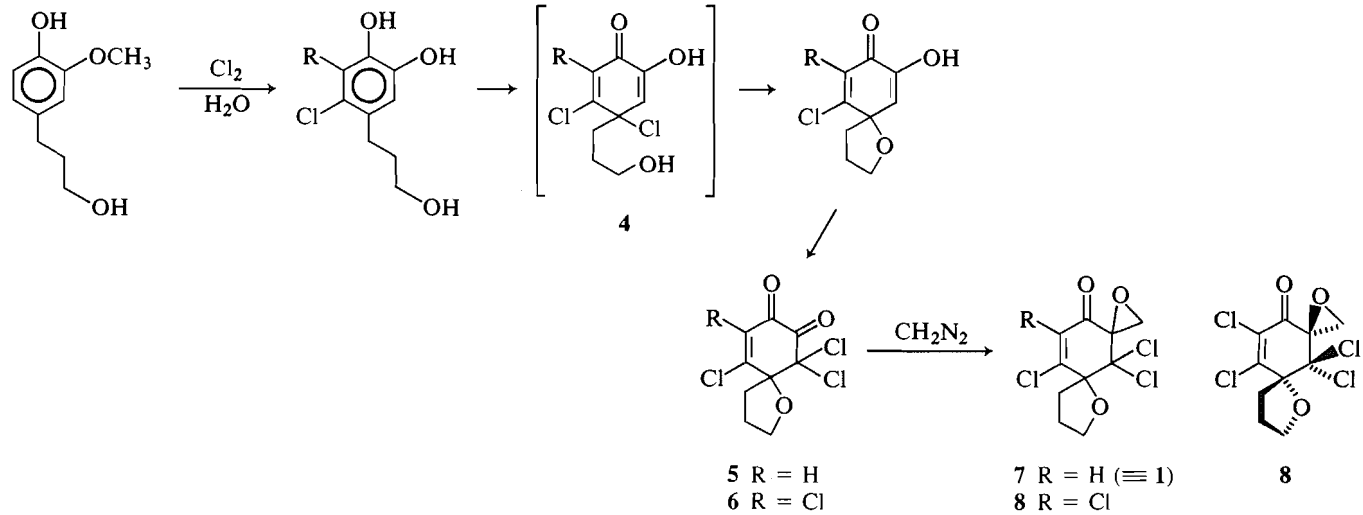

SCHEME 1

additional Cl substituent in **8**.

The geometry of the oxirane ring (area 0.909 Å^2) is normal (17, 18), although the O(2)—C(6) bond in **8** (1.435(4) Å) is 0.015(4) Å longer than that in **1** (1.420(2) Å). This difference, as well as a 0.015(4) Å shortening of the C(4)—C(5) bond (1.549(4) versus 1.564(2) Å in **1**), is believed to result from the conformational inversion of the central ring. The additional chlorine substituent at C(9) induces a significant lengthening of the C(9)=C(10) double bond (from 1.334(3) in **1** to 1.350(4) Å), consistent with the ir results discussed above. The C(1)—C(2) and C(2)—C(3) bond distances in the oxolane ring are anomalously short, probably a result of minor disordering of atoms C(1) and C(2). Other bond lengths in **8** are equal within experimental error to those in **1**. The sp^2 hybridized carbon atoms (C(8), C(9), and C(10)) are all slightly but significantly displaced from the planes of their substituents (by 0.018(4), 0.015(3), and 0.025(3) Å respectively).

Acknowledgements

This work was funded by a contract from the Department of National Health and Welfare. X-ray crystallographic analysis was made possible by financial support from the Natural Sciences and Engineering Research Council of Canada, Xerox Corporation, and the University of British Columbia Computing Centre. Mass and nmr spectra were also provided courtesy of the Chemistry Department, University of British Columbia.

1. A. B. McKAGUE, S. J. RETTIG, J. TROTTER, and G. R. DOUGLAS. Can. J. Chem. **59**, 3372 (1981).
2. T. ENKVIST, J. TURUNEN, and T. ASHORN. Tappi, **45**, 128 (1962).
3. L. LÖWENDAHL, G. PETERSSON, and O. SAMUELSON. Svensk Papperstidn. **81**, 392 (1978).
4. A. B. McKAGUE. J. Chromatogr. **208**, 287 (1981).
5. K. V. SARKANEN and C. H. LUDWIG. Lignins, occurrence, formation, structure and reactions. Wiley–Interscience, New York. 1971.
6. A. J. NONNI and C. W. DENCE. Svensk Papperstidn. **84**, R17 (1981).
7. W. M. B. KÖNST and J. TH. M. F. MAESSEN. Syn. Commun. **10**, 905 (1980).
8. P. COPPENS, L. LEISEROWITZ, and D. RABINOVICH. Acta Crystallogr. **18**, 1035 (1965).
9. J. DE MEULENAER and H. TOMPA. Acta Crystallogr. **19**, 1014 (1965).
10. D. T. CROMER and J. B. MANN. Acta Crystallogr. Sect. A, **24**, 321 (1968).
11. R. F. STEWART, E. R. DAVIDSON, and W. T. SIMPSON. J. Chem. Phys. **42**, 3175 (1965).
12. D. T. CROMER and D. LIBERMAN. J. Chem. Phys. **53**, 1891 (1970).
13. V. SCHOMAKER and K. N. TRUEBLOOD. Acta Crystallogr. Sect. B, **24**, 63 (1968).
14. D. W. J. CRUICKSHANK. Acta Crystallogr. **9**, 747 (1956); **9**, 754 (1956); **14**, 896 (1961).
15. J. M. GESS and C. W. DENCE. Tappi, **54**, 1114 (1971).
16. C. D. GUTSCHE. Organic reactions. Vol. 8. *Edited by* R. Adams. John Wiley and Sons, Inc., New York. 1954. p. 364.
17. C. FOCES-FOCES, F. H. CANO, and S. GARCIA-BLANCO. Acta Crystallogr. Sect. B, **33**, 3521 (1977).
18. M. L. MARTINEZ, F. H. CANO, and S. GARCIA-BLANCO. Acta Crystallogr. Sect. B, **33**, 3913 (1977).

Can. J. Chem. Downloaded from www.nrcresearchpress.com by 210.87.254.6 on 09/06/12
For personal use only.

Calculation of vertical ionization potentials of hydrogen peroxide by perturbation corrections to Koopmans' theorem

TSUTOMU MINATO[1] AND DELANO P. CHONG

Department of Chemistry, University of British Columbia, 2036 Main Mall, Vancouver, B.C., Canada V6T 1Y6

Received September 10, 1982

TSUTOMU MINATO and DELANO P. CHONG. Can. J. Chem. **61**, 550 (1983).

Vertical ionization potentials (VIP's) of hydrogen peroxide are calculated by perturbation corrections to Koopmans' theorem and its conformation is investigated on the basis of the calculated VIP's. The calculated VIP's compare well with the observed values. The analysis based on the VIP's gives a reasonable conformation, although the energy-optimizing procedure cannot reproduce the skew conformation. The lone pair − lone pair interactions are also discussed.

TSUTOMU MINATO et DELANO P. CHONG. Can. J. Chem. **61**, 550 (1983).

On a calculé les potentiels d'ionisation verticale (PIV) du peroxyde d'hydrogène par des corrections de perturbation du théorême de Koopman et on a étudié sa conformation à partir des PIV calculés. Les PIV calculés se comparent bien aux valeurs observées. L'analyse, fondée sur les PIV, donne une conformation raisonnable bien que le procédé d'optimisation d'énergie ne peut reproduire la conformation du squelette. On discute également des interactions doublet libre − doublet libre.

[Traduit par le journal]

Can. J. Chem. Downloaded from www.nrcresearchpress.com by 210.87.254.5 on 09/06/12
For personal use only.

I. Introduction

Recently, the conformation of organic molecules has been discussed by means of photoelectron (PE) spectroscopy if there are orbital interactions which depend on a dihedral angle (1). For example, the study on hydrazines has given a clear understanding for the lone pair − lone pair interaction as a function of a dihedral angle (2) and this understanding is used to determine the conformation of hydrazines. The lone pair − lone pair interaction in hydrogen peroxide has been studied (3). Unlike hydrazines, the situation of hydrogen peroxide is complicated by two lone pairs of each oxygen atom.

In the last few years, corrections to Koopmans' theorem (KT) have been computed with ordinary third-order Rayleigh−Schrödinger perturbation theory (RSPT) and it is shown that RSPT is capable of giving vertical ionization potentials (VIP's) corresponding to valence MO's with an average error of 0.5 eV for a double-ζ basis set (4). This accuracy is sufficient to investigate the relationship between the VIP's and the dihedral angle of hydrogen peroxide. While hydrogen peroxide is the simplest member in the family of peroxides which represents an important class of compounds, most calculations on its VIP's have been carried out within KT. The present calculations are, therefore, carried out by RSPT in order to have a basis for understanding of the experimental PE spectrum of hydrogen peroxide. Furthermore, the relationship between the VIP's and the dihedral angle is discussed and the lone pair − lone pair interactions are investigated.

II. Calculations and results

The SCF calculations are carried out with the GAUSS 76 program and the basis set is the standard 4-31G valence-double-ζ set internal to the program (5). The estimation of VIP's by RSPT has been given elsewhere (4). The truncation criterion $T = 2.6$ is used in the present calculation. Figure 1 shows the experimental geometry of hydrogen peroxide (6).

The numerical results for the VIP's at $\theta = 111.5°$, the observed value, are summarized in Table 1 together with other calculations (3, 7). In Table 1, $\Delta E(3)$ represents the difference in perturbation energies truncated after the third order. $\Delta(E^{GA})$

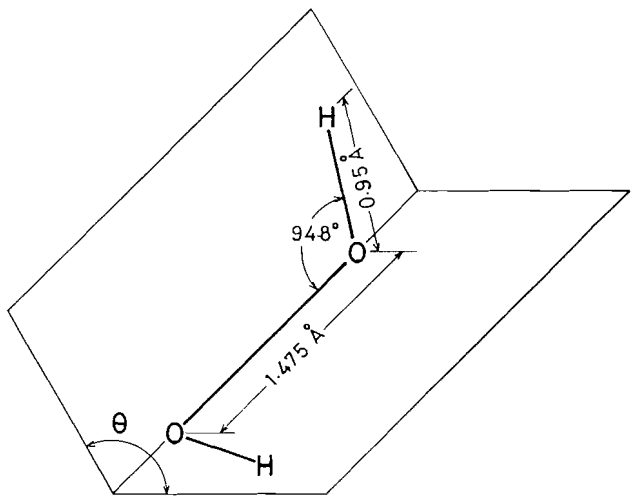

FIG. 1. The geometry of hydrogen peroxide. The dihedral angle, θ, is observed to be 111.5°.

TABLE 1. The VIP's for hydrogen peroxide (in eV)

	4*b*	5*a*	4*a*	3*b*	3*a*
Obs.[a]	11.69	12.69	15.33	17.40	17.40
Obs.[b]	11.51	12.56	15.26	17.35	17.35
KT(CNDO)[a]	12.83	13.41	14.81	18.97	18.03
KT(*ab initio*)[c]	10.88	11.34	13.48	16.60	16.27
KT(*ab initio*)[d]	13.27	13.71	15.95	18.59	18.72
KT(4-31G)	13.50	14.25	16.27	19.40[e]	19.18[e]
$\Delta E(3)$	11.36	12.49	15.10	17.29[e]	17.58[e]
$\Delta(E^{GA})$	11.15	12.34	14.98	17.08[e]	17.46[e]
Δ[SCF]	11.77	12.85			

[a] Reference 3*a*.
[b] Reference 3*c*.
[c] Reference 7*a*.
[d] Reference 7*b*.
[e] Likely breakdown of Koopmans' ordering.

[1] Present address: c/o Dr. S. Yamabe, Department of Chemistry, Nara University of Education, Takabatake-cho, Nara 630, Japan.

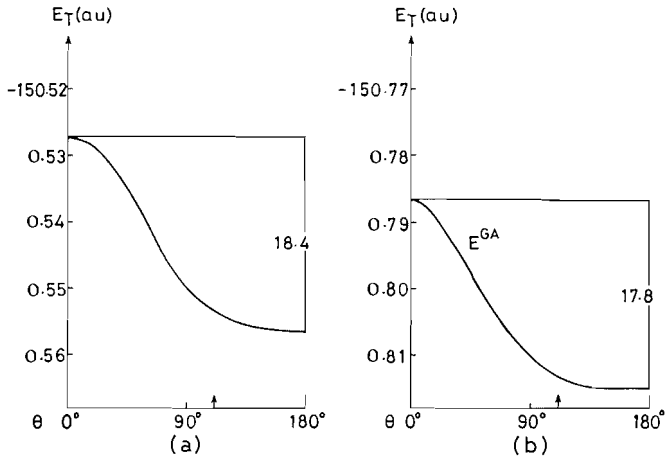

FIG. 2. The potential energy profile along the dihedral angle (θ). The arrows in this figure denote the observed dihedral angle. The energy change is in kcal/mol. (*a*) E_T calculated by the SCF method. (*b*) E_T calculated by E^{GA}.

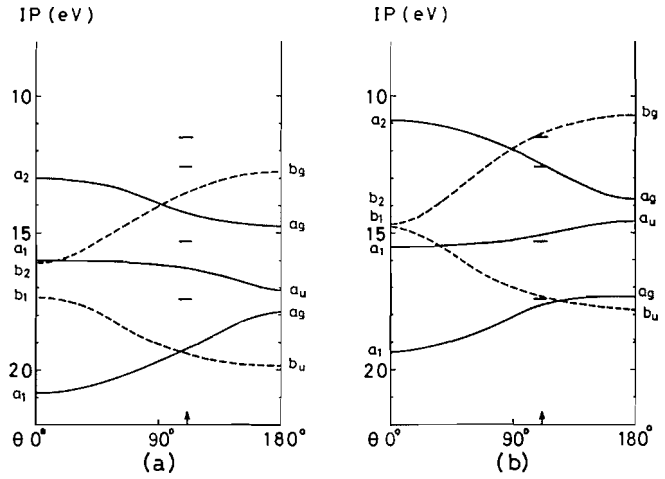

FIG. 3. The relationship between the VIP's and the dihedral angle. The arrows in this figure denote the observed dihedral angle. The bold lines stand for the PE bands. (*a*) The VIP's estimated by KT. (*b*) The VIP's estimated by $\Delta E(3)$.

is the difference between E^{GA}'s of the parent molecule and its cationic state, and E^{GA} is calculated by a geometrical approximation. The difference in scaled energy-expectation values ($\Delta\mathscr{E}$) is meaningful only for the lowest cationic state of each symmetry. Unlike other molecules, the VIP's for H_2O_2 estimated by $\Delta E(3)$ are closer to the observed values than those estimated by $\Delta(E^{GA})$. The $\Delta\mathscr{E}$ approximation also gives good values for the lowest cationic state in each symmetry. It should be noted that the assignment of the bands in the observed PE spectrum is based on the present calculation. However, the overlapping bands at ~17.4 eV cannot be unambiguously assigned on the basis of the present calculation because of the small basis set. There is a likely breakdown of Koopmans' ordering of $(3a)^{-1}$ and $(3b)^{-1}$ states.

It is interesting to check whether the energy-optimizing procedure reproduces the skew conformation of H_2O_2 or not, because calculations with a small basis set sometimes fail to reproduce the conformation of H_2O_2 (7). Therefore, the total energy of H_2O_2 (E_T) is calculated at a given θ at fixed bond lengths. Figure 2 shows E_T's by the SCF calculation and the geometrical approximation. Both calculations show that the dihedral-angle optimized geometry is a *trans*-form, although H_2O_2 is nonplanar in the ground state. In other words, such a simple procedure with a 4-31G basis set cannot reproduce the conformation of H_2O_2 .

The VIP's are calculated at a given θ by KT and $\Delta E(3)$. The results are depicted in Fig. 3. The VIP's estimated by KT are too high to be compared with the observed values as Fig. 3(*a*) shows. When the observed values are moved down in the figure by ~2 eV, the good correspondence is obtained at θ = ~110°. This θ value is in line with the observed dihedral angle, θ = 111.5° (6). On the other hand, the VIP's estimated by $\Delta E(3)$ show the good correspondence to the observed values at θ = ~110° without any movement of the observed values. Thus, the analysis based on the VIP's is more useful for investigating the conformation of H_2O_2 than the energy-optimizing procedure when the calculation is carried out with a small basis set.

III. Discussion

The lone pair − lone pair interactions are investigated in terms of localized MO's (LMO's) (8) in order to obtain the correspondence of the interactions to the PE bands. Since canonical MO's spread over a molecule, it is difficult to understand a chemical bond and a lone pair by them. On the other hand, the LMO's represent a chemical bond and a lone pair well. Therefore, the LMO's of H_2O_2 are determined and the canonical MO's are represented as linear combinations of the LMO's.

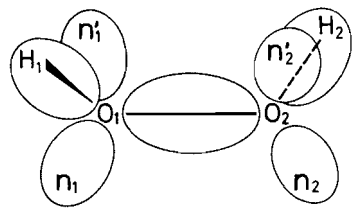

FIG. 4. Schematic presentation of the valence LMO's.

Figure 4 gives a schematic presentation of the valence LMO's. Two O—H bond orbitals and four lone pair orbitals are obtained together with the O—O bond. It is found that H_2O_2 has the eclipsed conformation for the O—H bonds and the lone pairs.

Table 2 summarizes the coefficients of the LMO's when the canonical MO's are represented as linear combinations of the LMO's. The first band ($(4b)^{-1}$) is assigned to the out-of-phase interactions between the lone pairs, and the main component is the interaction between the eclipsed lone pairs. The second band ($(5a)^{-1}$) corresponds to the in-phase interaction between the staggered lone pairs. The third band ($(4a)^{-1}$) is the ionization of an electron from the O—O bond with the in-phase interaction between the eclipsed lone pairs. The overlapping bands at 17.4 eV correspond to the interaction between the O—H bonds and that between the lone pairs.

The orbital interactions ascertain the assignment of the PE bands. Since the binding energy of an electron in the lone pairs is lower than that in the chemical bonds (the O—O and O—H bonds), the first two bands are assigned to the ionization from the lone pairs. Furthermore, the out-of-phase interaction between the eclipsed lone pairs destabilizes the orbital energy, whereas the in-phase interaction between the staggered lone pairs makes the energy level slightly low. Thus, the ionizations

Can. J. Chem. Downloaded from www.nrcresearchpress.com by 210.87.254.5 on 09/06/12
For personal use only.

TABLE 2. The coefficients of the LMO's in the canonical MO's[a]

MO	n_1	n_1'	O_1H_1	O_1O_2	n_2	n_2'	O_2H_2	Orbital character
$4b$	0.60	−0.34	−0.18	0.0	−0.60	0.34	0.18	n^e_-, n^s_-
$5a$	−0.04	0.62	−0.22	−0.36	−0.04	0.62	−0.22	n^s_+, O_1—O_2
$4a$	−0.51	0.11	−0.13	0.65	−0.51	0.11	−0.13	O_1—O_2, n^e_+
$3b$	0.17	0.53	−0.44	0.0	−0.17	−0.53	0.44	n^s_-, O—H$_-$
$3a$	0.39	−0.03	−0.51	0.42	0.39	−0.03	−0.51	O—H$_+$, O_1—O_2, n^e_+

[a]n^e_- and n^e_+ denote the out-of-phase interaction and the in-phase interaction between the eclipsed lone pairs, respectively. n^s_+ and n^s_- mean the interactions between the staggered lone pairs. O—H$_+$ and O—H$_-$ stand for the interactions between the O—H bonds.

from the lone pairs are ordered as mentioned in the previous section. The third band corresponds to the ionization from the O—O bond, because the O—O bond is more unstable (lower binding energy) than the O—H bonds. As for the overlapping bands, the ordering by KT is different from that by RSPT. The orbital interaction supports the latter ordering, because the $(3b)^{-1}$ band corresponds to the out-of-phase interactions between the O—H bonds and between the lone pairs. Furthermore, the $(3a)^{-1}$ band corresponds to the in-phase interaction between the O—H bonds and that between the eclipsed lone pairs, and the latter interaction stabilizes the $3a$ orbital well.

IV. Concluding remarks

In this study, the calculation of the VIP's of H_2O_2 based on the RSPT corrections to KT is presented, and the relationship between the VIP's and the dihedral angle of H_2O_2 is discussed. Since the present calculation is carried out with a limited basis set (4-31G), the overlapping bands at 17.4 eV cannot be unambiguously assigned. In spite of this limitation, some important results emerge. The energy-optimizing procedure with this basis set cannot reproduce the observed conformation of H_2O_2. However, a reasonable conformation is obtained by the investigation of the relationship between the VIP's and the dihedral angle. Furthermore, the orbital interactions are shown to support the assignment of the PE bands by RSPT.

Acknowledgement

The authors are grateful to the Natural Sciences and Engineering Research Council of Canada for financial support.

1. M. KLESSINGER and P. RADEMACHER. Angew. Chem. Int. Ed. Engl. **18**, 826 (1979).
2. (*a*) P. RADEMACHER. Angew. Chem. Int. Ed. Engl. **12**, 408 (1973); (*b*) P. RADEMACHER. Chem. Ber. **108**, 1548 (1975); (*c*) K. OSAFUNE, S. KATSUMATA, and K. KIMURA. Chem. Phys. Lett. **19**, 369 (1973).
3. (*a*) K. OSAFUNE and K. KIMURA. Chem. Phys. Lett. **25**, 47 (1974); (*b*) C. BATICH and W. ADAM. Tetrahedron Lett. 1467 (1974); (*c*) R. S. BROWN. Can. J. Chem. **53**, 3439 (1975).
4. D. P. CHONG, F. G. HERRING, and D. MCWILLIAMS. J. Chem. Phys. **61**, 78 (1974); **61**, 958 (1974).
5. W. J. HEHRE, W. A. LATHAN, R. DITCHFIELD, M. D. NEWTON, and J. A. POPLE. Nat. Resource Comput. Chem. Software Cat., Vol. 1, GAUSS 76 (1980).
6. R. H. HUNT, R. A. LEACOCK, C. W. PETERS, and K. T. HECHT. J. Chem. Phys. **42**, 1931 (1965).
7. (*a*) U. KALDOR and I. SHAVITT. J. Chem. Phys. **44**, 1823 (1966); (*b*) W. H. FINK and L. C. ALLEN. J. Chem. Phys, **46**, 2261 (1967).
8. C. EDMISTON and K. RUEDENBERG. Rev. Mod. Phys. **35**, 457 (1963).

Can. J. Chem. Downloaded from www.nrcresearchpress.com by 210.87.254.5 on 09/06/12
For personal use only.

Electron trapping in alcohol clusters in γ-irradiated alcohol-2,2,4-trimethylpentane-2,2-dimethylbutane glasses at 77 K

TOYOAKI KIMURA, KAZUHIRO YASUDA, SHIGEKI FUKUDA, AND KENJI FUEKI

Department of Synthetic Chemistry, Faculty of Engineering, Nagoya University, Chikusa-ku, Nagoya 464, Japan

Received September 17, 1982

TOYOAKI KIMURA, KAZUHIRO YASUDA, SHIGEKI FUKUDA, and KENJI FUEKI. Can. J. Chem. **61**, 553 (1983).

An optical absorption study has been made on electrons (e^-_{alc}) trapped in alcohol clusters in γ-irradiated 1-propanol (PrOH) − 2,2,4-trimethylpentane (TMP) − 2,2-dimethylbutane (DMB), 1-butanol (BuOH) − TMP − DMB, and 1-pentanol (PnOH) − TMP − DMB mixture glasses at 77 K. Hitherto electron transfer from the hydrocarbon region into alcohol clusters has been known to be a major process for e^-_{alc} formation in γ-irradiated alcohol−hydrocarbon glasses. However, in the present systems of PrOH−TMP−DMB, BuOH−TMP−DMB, and PnOH−TMP−DMB, this type of electron transfer was not observed and the e^-_{alc} formation was found to result only from the direct radiolysis of alcohols. In the alcohol concentration range lower than 0.2 electron fraction the yields of e^-_{alc} are less than those expected from the direct radiolysis of alcohols. The average number of alcohol molecules in a cluster in these systems is estimated to be four in the lower alcohol concentration range studied. The position of the absorption maxima for e^-_{alc} in these systems is constant within experimental uncertainties independent of alchohol concentration, which is consistent with the results of a semicontinuum model calculation.

TOYOAKI KIMURA, KAZUHIRO YASUDA, SHIGEKI FUKUDA et KENJI FUEKI. Can. J. Chem. **61**, 553 (1983).

Opérant à 77 K, on a fait une étude d'absorption optique des électrons (e^-_{alc}) piégés dans des agrégats d'alcools dans des verres irradiés aux rayons γ et formés soit de propanol-1 (PrOH)-triméthyl-2,2,4 pentane (TMP) − diméthyl-2,2 butane (DMB), soit de butanol-1 (BuOH) − TMP − DMB ou de pentanol-1 (PnOH) − TMP − DMB. On croyait savoir jusqu'à maintenant que le transfert d'électrons de la section hydrocarbonée des agrégats d'alcool était un processus important dans la formation de e^-_{alc} dans des verres d'alcool−hydrocarbure irradiés aux rayons γ. Toutefois dans les systèmes de PrOH−TMP−DMB, BuOH−TMP−DMB et PnOH−TMP−DMB étudiés ici, on n'a pas observé ce type de transfert d'électrons et on a trouvé que la formation de e^-_{alc} provient uniquement de la radiolyse directe des alcools. Pour une concentration en alcool inférieure à 0,2 fraction d'électron, les rendements en e^-_{alc} sont inférieures à ceux attendus pour une radiolyse directe des alcools. Dans ces systèmes, on évalue que pour la limite inférieure des concentrations étudiées le nombre myen de molécules d'alcool dans un agrégat est égal à quatre. Dans le domaine des incertitudes expérimentales indépendantes de la concentration d'alcool la position du maximum d'adsorption de e^-_{alc} dans ces systèmes est constante. Ceci est en accord avec les résultats obtenus en faisant un calcul en utilisant un modèle semi-continu.

[Traduit par le journal]

Introduction

Solvated or trapped electrons in alcohol−hydrocarbon mixtures have been widely investigated (1−15) and it is well known that two optical absorption bands are observed in the visible and ir regions, which are ascribed to electrons trapped in alcohol aggregates (16−21) and those trapped in a hydrocarbon matrix, respectively. In a previous study we have investigated the mechanism of electron trapping by alcohol clusters and explained this in terms of quasifree electron scavenging by alcohol clusters or electron transfer from unrelaxed hydrocarbon traps into alcohol clusters (22). In this work we have investigated trapped electrons in γ-irradiated alcohol−TMP−DMB mixture glasses at 77 K in order to obtain further information on this problem.

Neat TMP or DMB freezes at 77 K into the crystalline state. However, we have found that a mixture of TMP and DMB makes a clear glass at 77 K and that trapped electrons are not observed at all in this mixture glass when γ-irradiated at 77 K (23). The absence of trapped electrons in a γ-irradiated TMP−DMB mixed glass seems to indicate that electrons are not stably localized in this glass. In view of this it is interesting to examine how electrons can be localized in alcohol clusters in this mixed glass. There is an advantage to using the TMP−DMB mixture as a hydrocarbon component in alcohol−hydrocarbon glasses. In this glass the optical absorption spectrum of e^-_{alc} in the visible region does not overlap the high energy tail of the spectrum of trapped electrons in hydrocarbons. This makes it possible to determine directly the yield of e^-_{alc} in alcohol−TMP−DMB mixture systems.

We have used PrOH, BuOH, and PnOH as alcohols and added these alcohols to a mixture of TMP and DMB. The ratio of TMP to DMB was 1:1 in volume at room temperature.

Experimental

Hayashi Pure Chemical PrOH and BuOH (guaranteed reagent) and Nakarai Chemicals PnOH were purified by refluxing over sodium borohydride. Nakarai Chemicals DMB (guaranteed reagent) and Kishida Chemical TMP (spectro-grade) were purified using molecular sieves 13 X. Samples were degassed on a vacuum line and sealed into optical cells made of Supracil quartz. γ-Irradiation was made with ^{60}Co γ-rays. Optical absorption spectra were measured on a Hitachi Model 323 spectrophotometer. When the alcohol concentration was low, an optical cell of 10 mm optical path length was used and the dose was 2.5×10^5 rad, whereas for samples of high alcohol concentrations the optical path length was 1 or 2 mm and the dose was 0.8×10^5 rad. With these variations in the dose and the optical path length, the normalized values of observed optical densities for trapped electrons cover four orders of magnitude. The γ-irradiation and optical absorption measurement were made at 77 K.

Results and discussion

The mixture of TMP and DMB gives a clear and crackfree glass at 77 K. Since trapped electrons are not formed in this TMP−DMB glass (23), only the low energy tail of e^-_{alc} spectrum is observed in the ir region in alcohol−TMP−DMB sys-

Can. J. Chem. Downloaded from www.nrcresearchpress.com by 210.87.254.6 on 09/06/12
For personal use only.

Can. J. Chem. Downloaded from www.nrcresearchpress.com by 210.87.254.6 on 09/06/12
For personal use only.

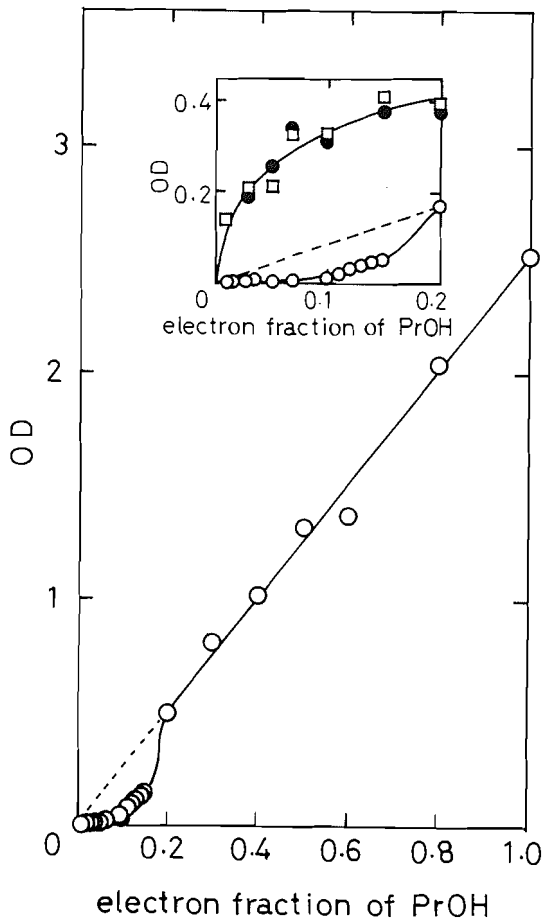

FIG. 1. Optical densities of e^-_{alc} at λ_{max} in PrOH–TMP–DMB systems at 77 K vs. electron fraction of PrOH. The dose is normalized to 0.8×10^5 rad and the optical path length to 10 mm. Inset: optical densities of e^-_{alc} at λ_{max} in PrOH–hydrocarbon systems at 77 K vs. electron fraction of PrOH. The dose is normalized to 1.1×10^5 rad and the optical path length to 3 mm. ○: PrOH–TMP–DMB (this work); ●: PrOH–MCH (the data are taken from ref. 22); □: PrOH–2MP (the data are taken from ref. 22).

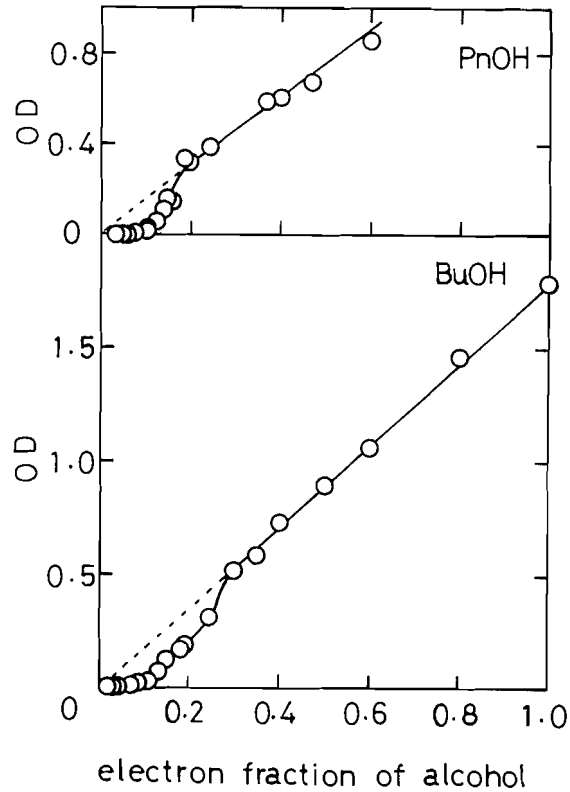

FIG. 2. Optical densities of e^-_{alc} at λ_{max} in PnOH–TMP–DMB (top) and BuOH–TMP–DMB (bottom) systems at 77 K vs. electron fraction of alcohol.

tems at 77 K. The position, λ_{max}, of the absorption maximum of e^-_{alc} is unchanged within the experimental uncertainty independent of the alcohol concentration for the PrOH–TMP–DMP, BuOH–TMP–DMB, and PnOH–TMP–DMB systems (540, 580, and 600 nm, respectively). Therefore, assuming that the molar extinction coefficient is constant, independent of the alcohol concentration (6), the relative yields of e^-_{alc} in alcohol–TMP–DMB systems can be represented by the optical densities of e^-_{alc} at λ_{max} normalized to the optical path length of 10 mm and the dose of 0.8×10^5 rad.

1. Yields of trapped electrons in alcohol clusters

Optical densities of e^-_{alc} in PrOH–TMP–DMB systems are shown as a function of electron fraction (e.f.) of PrOH in Fig. 1. It can be seen in Fig. 1 that the experimental data fit the straight line, which is drawn between the origin and the point for neat PrOH (e.f. = 1), over the PrOH concentration range from 0.2 to 1.0 e.f. and that the data points deviate downwards considerably from the straight line at PrOH concentrations less than 0.2 e.f. This contrasts remarkably with the previous results (22) for PrOH – methylcyclohexane (MCH) and PrOH – 2-methylpentane (2MP) systems, which are shown in the inset of Fig. 1 together with the present results for PrOH–TMP–DMB systems. Optical densities in the inset of Fig. 1 are normalized to the dose of 1.1×10^5 rad and the optical path length of 3 mm. The dashed line in the inset of Fig. 1 is drawn so that it extrapolates to the observed optical density of e^-_t in neat PrOH glass. All other experimental data on the yields of e^-_{alc} in alcohol–hydrocarbon glasses so far reported are similar to those in PrOH–MCH and PrOH–2MP glasses shown in the inset of Fig. 1; yields of e^-_{alc} are higher than those expected from the linear dependence on the e.f. of alcohol, implying electron transfer from the hydrocarbon region into alcohol clusters.

Optical densities of e^-_{alc} in BuOH–TMP–DMB and PnOH–TMP–DMB systems are shown as a function of e.f. of alcohol added in Fig. 2. In higher alcohol concentration range of PrOH–TMP–DMB, BuOH–TMP–DMB, and PnOH–TMP–DMB systems, the yield of e^-_{alc} is linearly dependent on the e.f. of each alcohol in the concentration range from 0.2 ~ 0.3 to 1.0 e.f. This fact indicates that the overall electron transfer from the hydrocarbon region into alcohol clusters does not seem to occur in these systems. The reason for the absence of electron transfer from the hydrocarbon region into alcohol clusters in PrOH–TMP–DMB, BuOH–TMP–DMB, and PnOH–TMP–DMB systems may be accounted for by the difference of the properties of a TMP–DMB matrix from other hydrocarbon matrices such as MCH or 2MP. Hitherto, trapped electrons have been studied in hydrocarbon glasses such as 3MP, 2MP, and MCH, in which electron mobilities are low and V_0 values are high; electrons are localized (we denote these as type I hydrocarbons). On the other hand, it is well known that electron mobilities are high and V_0 values are low in liquid methane and neopentane, in which electrons are not localized (we denote these as type II hydrocarbons). However, the type II hydrocarbons themselves do not make glasses at 77 K. The

Can. J. Chem. Downloaded from www.nrcresearchpress.com by 210.87.254.6 on 09/06/12
For personal use only.

electron mobilities and V_0 values in TMP and DMB lie between those in the type I hydrocarbons and those in the type II hydrocarbons (24–33). Therefore, we are tempted to say that the absence of electron transfer from the TMP–DMB region into alcohol clusters implies that electrons are not localized in TMP–DMB glasses. If we accept that electron transfer from unrelaxed hydrocarbon traps into alcohol clusters is the most plausible mechanism for e^-_{alc} formation in alcohol–hydrocarbon glasses at 77 K, the absence of electron transfer from the TMP–DMB region into alcohol clusters appears to indicate the absence of unrelaxed trapped electrons in the TMP–DMB region. A pulse radiolysis study is necessary to determine whether unrelaxed trapped electrons exist in TMP–DMB glasses at 77 K.

Free ion yields in TMP and DMB are higher than those in 2MP and MCH (27, 34, 35). Thus it appears that quasifree electron scavenging by alcohol clusters (4) is not the mechanism of e^-_{alc} formation in alcohol–hydrocarbon systems. The fact that the yield of e^-_{alc} is only that from direct γ-radiolysis of the added alcohols indicates that quasifree electrons generated in the TMP–DMB region are not scavenged in alcohol clusters. However, a quasifree electron scavenging mechanism cannot necessarily be excluded for e^-_{alc} formation in alcohol – type I hydrocarbon systems, because there is the possibility that the efficiency of electron scavenging by alcohol clusters is significantly lower in TMP–DMB glasses at 77 K. We have found that electron scavenging efficiencies are lower for some scavengers in TMP–DMB glasses than in type I hydrocarbon glasses at 77 K.[1]

It is interesting to compare the present results with those of Brandon and Firestone (6). According to their results by pulse radiolysis at room temperature, yields of e^-_{alc} in ethanol–neopentane and ethanol–DMB solutions are similar to those in ethanol–3MP solutions at ethanol concentrations greater than 20 mol%. This implies that the mechanism of e^-_{alc} formation in ethanol–neopentane and ethanol–DMB solutions at room temperature is different from that in alcohol–TMP–DMB glasses at 77 K. Previously we have shown that irphotobleaching of electrons trapped in the hydrocarbon matrix in PrOH – type I hydrocarbon glasses causes e^-_{alc} to be formed when the viscosity of the matrix is low (such as 3MP), but not when it is high (such as MCH) (22). Therefore, it appears that the viscosity of the matrix plays an important role for e^-_{alc} formation in alcohol–hydrocarbon systems. It has been shown that matrix viscosity affects electron scavenging in hydrocarbon glasses at 77 K (36).

2. *Number of alcohol molecules in an alcohol cluster in the lower alcohol concentration range*

In PrOH–TMP–DMB, BuOH–TMP–DMB, and PnOH–TMP–DMB systems, the yield of e^-_{alc} is considerably lower than those expected from the contribution of direct radiolysis of added alcohols when alcohol concentrations are lower than 0.2 e.f. as shown in Figs. 1 and 2. For the systems containing <0.2 e.f. alcohols, the concentration of alcohol clusters and the cluster size (the number of alcohol molecules in a cluster) would decrease with decreasing alcohol concentration. When alcohol concentrations are higher than 0.1 *M*, it has been reported that alcohol tetramers are predominant at room temperature (16–19). Thus, in our present case, it can be expected that average cluster size is four. This can be supported by the following treatment. When alcohol monomers exist together with alcohol clusters which are predominantly *n*-mers, we have the equilibrium

$$[1]\quad nA \overset{K_n}{\rightleftarrows} A_n$$

where A and A_n are alcohol monomer and *n*-mer, respectively and K_n is the equilibrium constant. Then the concentration of alcohol *n*-mers can be written as

$$[2]\quad [A_n] = K_n[A]^n$$

Equations [1] and [2] do not necessarily mean that the production of A_4 is by four A molecules coming together simultaneously but they simply provide the relation between the concentration of A_4 and A. Even if there exist a series of equilibria between A_n and A_{n-1} (n = 2, 3, and 4), it can be shown that eq. [2] holds for the overall equilibrium between A_4 and A. Assuming that the yield of e^-_{alc} is proportional to the concentration of alcohol clusters at low alcohol concentrations, the yield of e^-_{alc} is proportional to the *n*th power of the concentration of alcohol monomers which is approximated by the concentration of alcohol added. In Fig. 3, optical densities of e^-_{alc} over the lower alcohol concentration range are plotted against the fourth power of alcohol concentration. In each case of Fig. 3, the yield of e^-_{alc} is linearly dependent on the fourth power of alcohol concentration, implying the average cluster size is four in PrOH–TMP–DMB, BuOH–TMP–DMB, and PnOH–TMP–DMB glasses at 77 K.

Studies on alcohol–hydrocarbon solutions at room temperature have revealed that primary alcohols exist as monomers when the mole fraction of the alcohol is less than 0.001 for

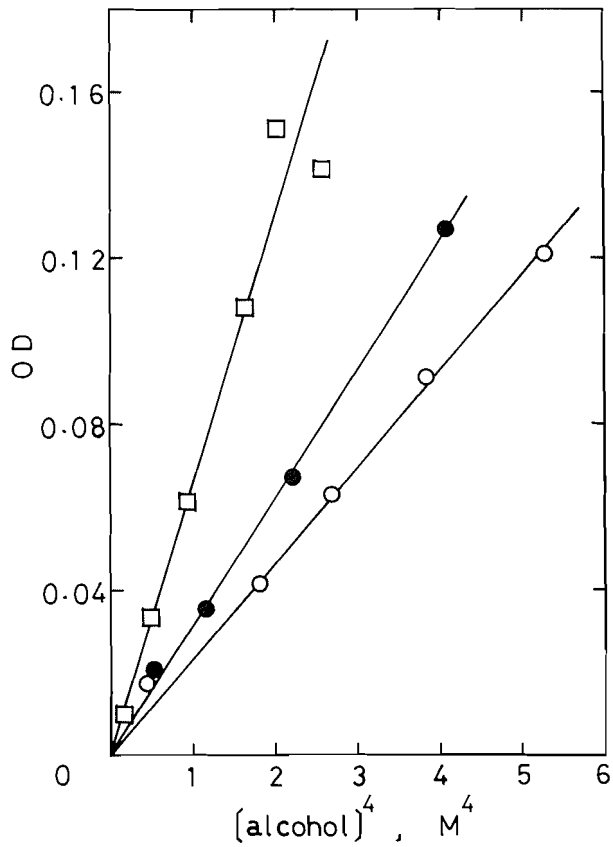

FIG. 3. Optical densities of e^-_{alc} at λ_{max} in PrOH–TMP–DMB (○), BuOH–TMP–DMB (●), and PnOH–TMP–DMB (□) systems at 77 K vs. [alcohol]⁴.

[1] T. Kimura, T. Yoshida, and K. Fueki, unpublished results.

primary alcohol − *n*-hexane (or cyclohexane) solutions (10). The value of mole fraction = 0.001 in this case corresponds to $8 \sim 9 \times 10^{-3}$ *M*. Brown *et al.* (20) and Baxendale and Sharpe (8) have shown that e^-_{alc} exist in dimer clusters over the alcohol concentration range <0.1 *M*. As has been described above, tetramers are predominant at alcohol concentration range >0.1 *M*. In our present case, the lowest alcohol concentrations studied are 0.1, 0.1, and 0.2 *M* for PrOH, BuOH, PnOH, respectively. Therefore our result that the average cluster is formed by four alcohol molecules in the present systems is consistent with those reported above (16−19). In the particular case of methanol−hydrocarbon solutions, the average alcohol cluster has been reported to be pentamer (11) and hexamer (8) even though the methanol concentration is lower than 0.1 *M*. We have also tried to investigate methanol−TMP−DMB and ethanol−TMP−DMB systems but unfortunately neither methanol nor ethanol is soluble in TMP−DMB at 77 K.

It is interesting to note that the slope of the straight line in Fig. 3 increases with increasing number of carbon atoms in an alcohol molecule. The ratio of the magnitude of the slope for PrOH−TMP−DMB, BuOH−TMP−DMB, and PnOH−TMP−DMB is 1:1.3:2.8. Taking the molar extinction coefficients of e^-_t in PrOH, BuOH, and PnOH into consideration (1.3, 0.71, and 1.25×10^4 M^{-1} cm^{-1}, respectively (37)), the ratio of electron scavenging efficiencies by PrOH, BuOH, and PnOH clusters turns out to be 1:2.5:2.9. This ratio is related to the equilibrium constant, K_n, in eq. [2], and the cross section of reaction between an electron and an alcohol cluster.

3. *Optical absorption spectrum of* e^-_{alc}

It is known that the extent of aggregation of alcohol molecules in a cluster increases with increasing alcohol concentration in a hydrocarbon matrix. Thus, it is expected that the number of alcohol layers which surround e^-_{alc} would increase with increasing alcohol concentration. In view of this, it is significant to examine how the optical absorption spectrum of e^-_{alc} is related to the number of alcohol layers. We have calculated energy levels of e^-_{alc} in a PrOH cluster with *l* PrOH layers ($l = 1 \sim 10$) in PrOH−TMP−DMB systems. The calculation was carried out within the framework of a semicontinuum model (38). The details of the present calculational procedure should be referred to ref. 38. Only the outline of calculation is given here. We have assumed that an excess electron is surrounded by the first solvation layer which consists of *N* PrOH molecules ($N = 4$ or 6). Alcohol molecules orient their dipoles symmetrically toward the electron located at the center of the cavity. Ths first solvation layer is surrounded by the second, third, ····, and *l*th layer of PrOH. We have assumed also that the excess electron interacts with the first solvation layer by a short-range interaction and beyond the first solvation layer by a long-range interaction. The total energy of the excess electron in the *i*th state is given by eq. [3],

$$[3] \quad E_t(i) = E_k(i) + E^s_e(i) + E^s_m(i) + E^l_e(i) + E^l_m(i) + E_q(i) + E_v$$

where E_k is the kinetic energy of the excess electron; E^s_e and E^s_m are the short-range electronic and medium rearrangement energies, respectively; E^l_e and E^l_m are the long-range electronic and medium rearrangement energies, respectively; E_q is the short-range repulsive interaction energy between the excess electron and the medium electrons; E_v is the energy required to form a cavity in the medium. Hydrogenic wavefunctions are used in this calculation.

TABLE 1. The calculated wavelengths, $\lambda_{1s\rightarrow 2p}$, corresponding to the $1s\rightarrow 2p$ transition energies of e^-_{alc} in PrOH−TMP−DMB systems at 77 K

Number of solvation layers (*l*)	Number of molecules in the first solvation layer (*N*)	$\lambda_{1s\rightarrow 2p}$, nm
1	4	428
	6	592
2	4	429
	6	606
3	4	435
	6	609
4	4	437
	6	609
5∼10	4	437
	6	609

The $1s\rightarrow 2p$ transition energies are calculated by eq. [4] for e^-_{alc} in a PrOH cluster.

$$[4] \quad h\nu_{1s\rightarrow 2p} = E_t(2p) - E_t(1s)$$

The corresponding wavelengths are given by $\lambda_{1s\rightarrow 2p} = c/\nu_{1s\rightarrow 2p}$. The results of calculation are shown in Table 1. It should be noted that $\lambda_{1s\rightarrow 2p}$ is nearly constant for $l = 1 \sim 10$. The observed position of absorption maxima, λ_{max}, of e^-_{alc} spectra in PrOH−TMP−DMB systems is constant within experimental uncertainties (520−540 nm). Thus, the calculated results agree, at least semiquantitatively, with the experimental results. Values of λ_{max} are also constant for BuOH−TMP−DMB and PnOH−TMP−DMB systems. The constancy of $\lambda_{1s\rightarrow 2p}$ can be accounted for by the strong short-range interaction due to the permanent dipoles of alcohol molecules in the first solvation layer. It is interesting to compare the present results with that for e^-_t in 3MHx−TMP−DMB glasses at 77 K (23), where the calculated and experimental results show that λ_{max} increases with decreasing 3MHx concentration. In this case the short-range interaction is not so strong as those in alcohol−TMP−DMB systems because the 3MHx molecule has no permanent dipole.

Acknowledgement

This work was partially supported by the Nagoya University Computation Center.

1. L. SHIELDS. J. Phys. Chem. **69**, 3186 (1965).
2. A. EKSTROM and J. E. WILLARD. J. Phys. Chem. **72**, 4599 (1968).
3. T. SAWAI and W. H. HAMILL. J. Phys. Chem. **73**, 3452 (1969).
4. G. R. FREEMAN. J. Phys. Chem. **76**, 944 (1972).
5. J. H. BAXENDALE and E. J. RASBURN. J. Chem. Soc. Faraday Trans. I, **70**, 705 (1974).
6. J. R. BRANDON and R. F. FIRESTONE. J. Phys. Chem. **78**, 792 (1974).
7. T. ITO, N. UJIKAWA, and K. FUEKI. J. Phys. Chem. **79**, 2479 (1975).
8. J. H. BAXENDALE and P. H. G. SHARPE. Chem. Phys. Lett. **41**, 440 (1976).
9. J. MAYER, J. KROH, and E. WOJCIECHOWSKA. Nukleonika, **31** 267 (1976).
10. G. A. KENNEY-WALLACE and C. D. JONAH. Chem. Phys. Lett. **47**, 362 (1977); J. Phys. Chem. **86**, 2572 (1982).
11. T. E. GANGWER, A. O. ALLEN, and R. A. HOLROYD. J. Phys.

Can. J. Chem. Downloaded from www.nrcresearchpress.com by 210.87.254.6 on 09/06/12
For personal use only.

Chem. **81**, 1469 (1977).
12. J. MAYER, J. L. GEBICKI, and J. KROH. Radiochem. Radioanal. Lett. **36**, 299 (1978).
13. J. MAYER, J. L. GEBICKI, and J. KROH. Radiat. Phys. Chem. **11**, 101 (1978).
14. J. MAYER, J. L. GEBICKI, and J. KROH. Radiat. Phys. Chem. **16**, 335 (1980).
15. M. OGASAWARA, K. SHIMIZU, H. YOSHIDA, J. MAYER, J. L. GEBICKI, and J. KROH. Radiat. Phys. Chem. **17**, 339 (1981).
16. B. D. ANDERSON, J. H. RYTTING, S. LINDENBAUM, and T. HIGUCHI. J. Phys. Chem. **79**, 2340 (1975).
17. R. AVEYARD, B. J. BRISCOE, and J. CHAPMAN. J. Chem. Soc. Faraday Trans. I, **69**, 1772 (1973).
18. T. S. S. R. MURTY. Can. J. Chem. **48**, 184 (1970).
19. A. N. FLETCHER. J. Phys. Chem. **76**, 2562 (1972).
20. B. J. BROWN, N. T. BAKER, and D. F. SANGSTER. Aust. J. Chem. **26**, 2089 (1973); **27**, 2529 (1974).
21. W. M. BARTCZAK. Ber. Bunsenges. Phys. Chem. **83**, 987 (1979).
22. M. ITO, T. KIMURA, and K. FUEKI. Can. J. Chem. **59**, 2803 (1981).
23. T. KIMURA, N. OGAWA, AND K. FUEKI. Bull. Chem. Soc. Jpn. **54**, 3854 (1981).
24. J.-P. DODLET and G. R. FREEMAN. Can. J. Chem. **50**, 2667 (1972).
25. R. A. HOLROYD and R. L. RUSSELL. J. Phys. Chem. **78**, 2128 (1974).
26. R. M. MINDAY, L. D. SCHMIDT, and H. T. DAVIS. J. Phys. Chem. **76**, 442 (1972).
27. J.-P. DODLET, K. SHINSAKA, and G. R. FREEMAN. Can. J. Chem. **54**, 744 (1976).
28. G. BAKALE and W. F. SCHMIDT. Chem. Phys. Lett. **22**, 146 (1970).
29. W. F. SCHMIDT and A. O. ALLEN. J. Chem. Phys. **52**, 4788 (1970).
30. A. O. ALLEN, T. E. GANGWER, and R. A. HOLROYD. J. Phys. Chem. **79**, 25 (1975).
31. G. BAKALE and W. F. SCHMIDT. Z. Naturforsch. **30**a, 568 (1975).
32. A. O. ALLEN and R. A. HOLROYD. J. Phys. Chem. **78**, 796 (1974).
33. R. A. HOLROYD. J. Chem. Phys. **57**, 3007 (1972).
34. W. F. SCHMIDT and A. O. ALLEN. J. Chem. Phys. **52**, 2345 (1970).
35. J. H. BAXENDALE, C. BELL, and P. WARDMAN. J. Chem. Soc. Faraday. Trans. I, **69**, 776 (1973).
36. T. KIMURA, K. FUEKI, and Z. KURI. Bull. Chem. Soc. Jpn. **46**, 2650 (1971).
37. L. KEVAN. Advances in radiation chemistry. Vol. 4. *Edited by* M. Burton and J. L. Magee. Wiley-Interscience, New York. 1974. p. 246.
38. K. FUEKI, P. A. NARAYANA, AND L. Kevan. J. Chem. Phys. **64**, 4571 (1976).

Can. J. Chem. Downloaded from www.nrcresearchpress.com by 210.87.254.6 on 09/06/12
For personal use only.

^{23}Na nuclear magnetic resonance linewidth studies of sodium tetraethylaluminate: complexes with hexamethylphosphoramide in benzene

JAMES HAROLD MEDLEY, EDDIE STEVEN MOOBERRY, AND MARION CLYDE DAY[1]
Department of Chemistry, Louisiana State University, Baton Rouge, LA 70803, U.S.A.

Received August 12, 1982

JAMES HAROLD MEDLEY, EDDIE STEVEN MOOBERRY, and MARION CLYDE DAY. Can. J. Chem. **61**, 558 (1983).

The linewidth of the ^{23}Na resonance in sodium tetraethylaluminate in benzene has been measured as a function of the ratio of [donor]:[Na^+] using the strong complexing agent hexamethylphosphoramide. In this system changes in the sodium linewidth arise primarily from changes in the nuclear quadrupole relaxation at the sodium nucleus which in turn arise from changes in the electric field gradient. As the ratio of hexamethylphosphoramide to sodium ion is increased up to 3:1 the ^{23}Na linewidth progressively decreases due to an increase in cation–anion distance in the ion pair. After a ratio of 4:1 is reached, essentially no linewidth change is noted, indicating a stable solvation number of 4 for hexamethylphosphoramide. The results of this study indicate that this is a new and promising approach to the determination of solvation numbers of the sodium ion.

JAMES HAROLD MEDLEY, EDDIE STEVEN MOOBERRY et MARION CLYDE DAY. Can. J. Chem. **61**, 558 (1983).

On a mesuré la largeur des raies de la résonance du ^{23}Na du tétraéthylaluminate de sodium dans le benzène en fonction du rapport [donneur]:[Na^+] en utilisant un puissant agent complexant: l'hexaméthylphosphoramide. Dans ce système, les variations de la largeur des raies du sodium proviennent principalement des variations de la relaxation quadrupolaire nucléaire au niveau du noyau du sodium qui a leur tour proviennent des variations du gradient de champ électrique. Quand le rapport de l'hexaméthylphosphoramide sur l'ion sodium augmente jusqu'à 3:1, la largeur des raies du ^{23}Na diminue progressivement à cause d'une augmentation de la distance cation–anion de la paire d'ions. Lorsqu'on atteint un rapport de 4:1, on n'observe plus de variation de la largeur des raies ce qui indique un nombre de solvatation stable de 4 pour l'hexaméthylphosphoramide. Les résultats de cette étude indiquent que c'est une approche nouvelle et prometteuse pour la détermination des nombres de solvatation de l'ion sodium.

[Traduit par le journal]

Introduction

With the commercial availability of high resolution multinuclear nmr spectrometers, there has been a corresponding upsurge in the interest in nmr spectroscopy of the less commonly observed nucleii (1–4). Of particular interest here is the study of the solvation of the sodium ion by means of ^{23}Na nmr (5–10), a system that is of considerable interest biologically as well as in terms of fundamental solvation theory.

Because of its spin of 3/2, the relaxation time of the ^{23}Na nucleus is dominated by the coupling of the nuclear quadrupole moment with the time-dependent electric field gradient. Presently there is no single unambiguous theory for the origin of the fluctuating electric field gradient at the nucleus that covers the full range of ion–ion and ion–solvent interactions encountered by the sodium ion in solution (11–14). Rather there are two fundamentally different theoretical models. The electrostatic approaches formulated by Valiev (11) and by Hertz (12) describe a static electric field gradient in terms of the action of point charges and electric dipoles on the central nucleus with a time dependence arising from either the lifetime of a vacancy in the first solvation sphere of the central ion (11) or the over all lifetime of the solvated state (12). The electrostatic model has met with some success in predicting the relaxation times of alkali metal and halide ions in dilute aqueous solutions (15, 16). The other model, formulated by Deverell (13), takes into account the shielding effect of the outer shell electrons on the central nucleus and is based on distortions of the inner shell *s* and *p* orbitals resulting from short range repulsive forces. The repulsive forces are postulated to arise from the interaction of another ion or solvent molecule at a distance less than the minimum of attractive potential during random collisions. These distortions can induce a fluctuating electric field gradient at the nucleus. An important result of the Deverell model arises from the contribution of the overlap integral to both the electric field gradient and the paramagnetic shielding constant which are reflected in the quadrupole relaxation time and the chemical shift respectively. Such a correlation between the ^{23}Na relaxation time and the chemical shift has been observed for a number of systems. For example, one may compare the results of a study on the solvent dependence of relaxation time of the sodium ion (17, 18) with the paper by Ehrlich, Roach, and Popov (19) on the solvent dependence of the ^{23}Na chemical shift in the limit of infinite dilution.

Recently, Delville *et al.* (14) have introduced a significant modification of the Deverell approach involving the interpretation of the correlation time, τ_c. They have made a simplifying assumption of long-lived solvation complexes, thereby identifying τ_c with the overall reorientational correlation time of the solvated complex. This approach was based on an earlier study by Kintzinger and Lehn (20). For many mixed solvent systems where there is a significant degree of preferential solvation, this approach can be very useful in the analysis of the relaxation times.

Both the Hertz–Valiev model and the Deverell model have been used with some success in describing the relaxation rates of alkali metal ions in solution. However, the selection of the solvent system seems to determine the choice of the appropriate model. The Hertz–Valiev model has been proven to be reasonably successful for dilute aqueous solutions whereas the Deverell model seems to be more appropriate in solutions of lower dielectric constant. In such solvents the extent of ion pairing may become more significant in determining the relaxation rate. Detellier *et al.* have used the Deverell approach in interpreting the ^{23}Na nmr data obtained in a study of solutions of

[1]To whom all correspondence should be addressed.

Can. J. Chem. Downloaded from www.nrcresearchpress.com by 210.87.254.6 on 09/06/12
For personal use only.

Can. J. Chem. Downloaded from www.nrcresearchpress.com by 210.87.254.6 on 09/06/12
For personal use only.

sodium perchlorate in mixed solvents consisting of THF and various unidentate and bidentate amines (6, 9, 10, 14). However, in mixed solvent systems where the two components have similar solvating abilities, a major complication in the interpretation of spectroscopic data can arise from competition for coordination sites by the two solvents. Additionally, in a chemically exchanging system the correlation time may be strongly dependent on the exchange rate (8).

A more desirable system is one in which the competition between the bulk solvent and the second solvent for coordination sites on the cation is minimal. Essentially the only known sodium salts which permit this type of system are the sodium tetraalkylaluminate salts. The solubility of these salts in hydrocarbon solvents such as cyclohexane or benzene, permits a system of the type:

$$NaAl(alkyl)_4 - \text{inert solvent} - \text{donor}$$

We have specifically selected the system:

$$NaAlEt_4 - \text{benzene} - \text{HMPA}^2$$

The usefulness of the sodium tetraalkylaluminate salts in other studies of ion–ion and ion–solvent interactions has been well documented (21).

In this study we have measured changes in the ^{23}Na nmr linewidth at one-half height as a function of the mole ratio HMPA:Na^+ in benzene solutions. The effect of the bulk solution viscosity on the linewidth is examined in light of the Debye–Stokes–Einstein expression for the rotational correlation time of a particle in solution. The results of this study (*a*) support the identification of the nmr correlation time with the rotational correlation time of a solvated species; (*b*) support the hypothesis that the solvation of the sodium ion by HMPA in benzene solution occurs via the formation of a series of stable solvated complexes of successive stoichiometries; and (*c*) indicate that this method offers a new and promising approach to the determination of solvation numbers of the sodium ion.

Experimental procedures

Sodium tetraethylaluminate was prepared by a previously reported synthesis (22). Benzene was allowed to reflux for 24 h over calcium hydride prior to distillation under a nitrogen atmosphere onto sodium wire. HMPA was refluxed for 48 h over calcium hydride at approximately 0.5 Torr prior to distillation. Deuterated benzene obtained as 99+ atom% from Aldrich Chemical Company was checked for water content by observing the reactivity with sodium tetraethylaluminate and subsequently used without further purification.

The solutions were prepared in an argon atmosphere dry box by the appropriate addition by weight of HMPA to the salt followed by dilution with benzene. Approximately 10% deuterated benzene was added for the purpose of locking on the deuterium resonance in the spectrometer. The nmr samples were prepared in 10 mm tubes in the dry box. Because of the reactivity of the salt, all spectra were recorded within one day of preparation.

Sodium-23 nmr spectra were recorded on a Bruker WP 200 FT nmr spectrometer operated at 52.94 MHz and 4.7 Tesla. The spectrometer is equipped with a broad-band tunable probehead and a PTS variable frequency source. Because of the large linewidth of the ^{23}Na resonance of some of the solutions, the spectra were acquired with a spectral window of 50 kHz with 2K memory for a digital resolution of 50 Hz/pt. Elimination of the broad sodium signal from the glass nmr tubes was accomplished by using a delay of 100 μs before the acquisition. This was determined to have no appreciable effect on the observed linewidths. Approximately 10 000 scans were required for an adequate signal-to-noise ratio. The accurately determined 90 degree pulse width was used for each acquisition. Linewidth determinations had estimated errors of ±10%.

Viscosity measurements were made using specially modified Canon-Fenske viscometers. Both arms of the viscometer were open to a nitrogen line with an oil bubbler at the nitrogen exit. The temperature was maintained to within ±0.05° with a Sargent-Welch Thermonitor constant temperature bath filled with dry mineral oil. The viscometer constants were determined with Dow-Corning Viscosity Standard silicone oil. The densities of the solutions were measured with calibrated pycnometers.

It should be noted that an unusual property of this system is the separation into two liquid phases. Since the upper phase has been observed to contain only excess benzene, spectra were recorded for the lower phase only. An unfortunate consequence of this two phase behavior is the inability to maintain a constant salt concentration over the entire range of solutions. In this particular study, the concentration ranges from 2.3 *M* for the 1:1 HMPA:$NaAlEt_4$ solution to 0.2 *M* for the 6:1 solution.

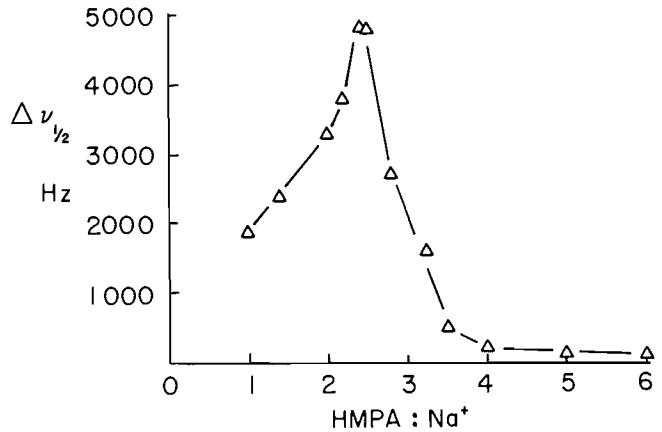

FIG. 1. Linewidth of the ^{23}Na resonance as a function of the HMPA:Na^+ ratio. Temperature 303 K.

Discussion

In Fig. 1, the dependence of the ^{23}Na nmr linewidths at one-half height is shown as a function of the HMPA:$NaAl(C_2H_5)_4$ mole ratio. Here it is noted that the linewidths show a rapid increase up to an HMPA:salt ratio of 2.5 followed by a rapid decrease. Further, it can be seen from Fig. 2 that the ^{23}Na linewidth is related closely to the solution viscosity with a maximum in the linewidth occurring where a corresponding maximum in viscosity is observed. The viscosity maximum occurring at a ratio of 2.5 implies a viscosity dependence of the linewidth. It is an accepted practice (5, 6, 14) to express the ^{23}Na linewidth as the linewidth reduced to unit viscosity. This is based on a prior assumption of a theoretical dependence of the linewidth on the viscosity. One such approach was developed by Kintzinger and Lehn (20) in a study of sodium cryptands. They used Abragam's equation for the relaxation time of a quadrupolar nucleus (23) (eq. [1]) and determined the correlation time by means of the Debye–Stokes–Einstein equation for the rotational correlation time of a particle in solution (eq. [2]).

$$[1]\quad \frac{1}{T_1} = \frac{1}{T_2} = \frac{3}{40}\frac{2I+3}{I^2(2I-1)}\left(1+\frac{\sigma^2}{3}\right)\left(\frac{e^2Qq_{zz}}{\hbar}\right)^2\tau_c$$

[2] HMPA ≡ hexamethylphosphoramide.

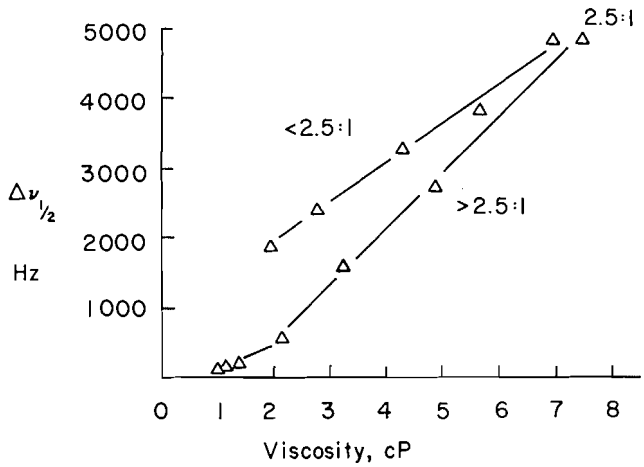

FIG. 2. Linewidth of the ^{23}Na resonance as a function of viscosity.

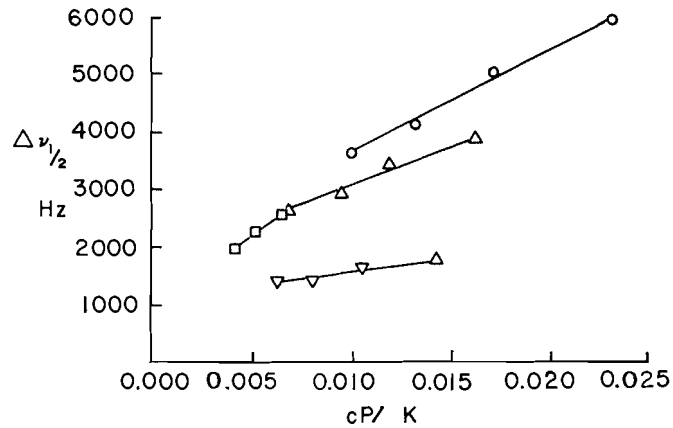

FIG. 3. Linewidths as a function of η/T for different HMPA:Na^+ ratios; curve symbols for various [HMPA]:[Na^+] are: □, 1.0:1; △, 2.0:1; ○, 2.4:1; and ▽, 3.0:1.

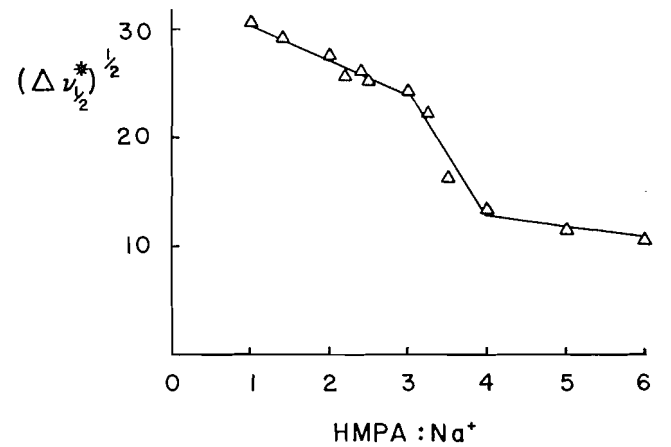

FIG. 4. Square root of the reduced linewidth ($\Delta\nu_{1/2}/\eta$) vs. the HMPA:Na^+ ratio. Temperature 303 K.

where σ = asymmetry parameter and $(e^2Qq_{zz}/\hbar) = \chi$, the quadrupole coupling constant.

$$[2] \quad \tau_c = \frac{4\pi\eta a^3}{3kT}$$

where η = viscosity and a = Stokes radius.

By a separate determination of the correlation time using the ^{13}C spin label method, they were able to show that τ_c for the complex may be described by eq. [2] provided that a correction is made for the relationship between the bulk viscosity and the microscopic viscosity. Delville *et al.* (14) have expanded this approach to include all cases where the sodium ion may be thought to exist in a stable solvation complex.

In the $NaAlEt_4$–benzene–HMPA system the correlation time for the quadrupole relaxation rate may be related to either the reorientational correlation time of a long-lived solvation complex or to a chemical exchange equilibrium such as:

$$[3] \quad [Na^+ \cdot n\text{HMPA} \cdot AlEt_4^-] + \text{HMPA} \rightleftharpoons [Na^+ \cdot (n+1)\text{HMPA} \cdot AlEt_4^-]$$

(n = 1, 2, 3). Such an equilibrium has been observed with $NaAlBu_4$ in THF (24). However, THF (Gutmann donor number = 20.0) is a much poorer donor than HMPA (donor number = 38.8). It has been shown by ^1H nmr, that in this system the equilibrium lies sufficiently far to the complexed side that a 4:1 ratio of HMPA:Na^+ consists of only solvent separated ion pairs (25). Thus it would seem probable that up to a ratio of HMPA:Na^+ of 4, there is effectively no uncomplexed HMPA in solution.

The substitution of eq. [2] into eq. [1] would imply a linear dependence of the linewidth on the η/T quotient in a nonexchanging system. Such a family of curves is shown in Fig. 3 for several different HMPA:Na^+ ratios. Here we see the expected linear behavior thereby supporting the Kintzinger–Lehn approach (20). The validity of this approach derives from the existence of stable solvated complexes.

Identification of τ_c with the rotational correlation time via eq. [2] implies that the quadrupole coupling constant, χ, should be proportional to the square root of the linewidth reduced to unit viscosity at constant temperature. A plot of the square root of the reduced linewidth versus the mole ratio HMPA:Na^+ is shown in Fig. 4. The linear decrease in the curve up to a value of 3:1 HMPA:Na^+ may be related to a linear decrease in the electric field gradient. Such a decrease can be rationalized by an increase in the cation–anion distance in the ion pair species caused by the steric influence of the bulky HMPA molecules. This decrease may be compared with the reported decrease in χ with increased complexation in the systems investigated by Delville *et al.* (14). If the linear decrease in χ is due entirely to a decrease in the electric field gradient at the nucleus by successive displacement of the anion, such linearity is expected. An additivity in the chemical shift of the ^{23}Na for successive complexes was reported by Delville *et al.* (14). Covington and Newman (26) have also predicted that additive chemical shifts should be expected for successive complexation. Under the Deverell model an additivity in the chemical shifts implies directly a linearity in χ.

The rapid decrease in the curve between 3:1 and 4:1 HMPA:Na^+ must be related to the change from contact ion pairs to solvent separated ion pairs. Above the 4:1 ratio there is very little change in the curve indicating that the solvation sphere of the sodium ion is complete at 4:1. Based on this evidence and the linear dependence of the linewidth on the viscosity temperature quotient we have therefore concluded that the solvation of the sodium ion in this system occurs via a stepwise association forming a series of solvated contact ion pairs of stoichiometries:

Can. J. Chem. Downloaded from www.nrcresearchpress.com by 210.87.254.6 on 09/06/12
For personal use only.

$(Na^+ \cdot 1HMPA|AlEt_4^-)$, $(Na^+ \cdot 2HMPA|AlEt_4^-)$, and $(Na^+ \cdot 3HMPA|AlEt_4^-)$

The previously reported (25) formation of solvent separated ion pairs at a ratio of HMPA:Na^+ of 4:1 combined with the results of this study indicate very strongly that the solvation number of the sodium ion in HMPA is four. This value does not agree with the value of three obtained by Martir *et al.* (27) and by Darensbourg *et al.* (28). However, the value of four based on our earlier study is now becoming accepted (29).

It must be noted that we have depended entirely on the measured ^{23}Na linewidth for data and not on the chemical shifts. The extremely broad resonances obtained for certain ratios (up to 5000 Hz) precludes any accurate determination of changes in the ^{23}Na chemical shift since the normal range of ^{23}Na chemical shifts is only 30 ppm (less than 2000 Hz at 52.9 MHz) (3). Covington and Newman (26) have reported the absence of any observable signal in the similar system $NaB(C_6H_5)_4$–nitromethane–HMPA in solutions where the concentration of HMPA is relatively low. This is undoubtedly caused by the extremely broad resonances such as what we observe here.

Acknowledgements

We wish to express our appreciation to the National Science Foundation for its support thru NSF grant CHE-8004473 and to the Ethyl Corporation for the aluminum alkyls.

1. B. MANN and R. K. HARRIS (*Editors*). NMR and the periodic table. Academic Press, New York. 1978.
2. F. W. WEHRLI. Nuclear magnetic resonance of the less common quadrupolar nucleii. *In* Annual Reports on NMR Spectroscopy. Vol. 9. *Edited by* E. F. Mooney and G. A. Webb. Academic Press, London. 1979. p 125.
3. C. BREVARD and P. GRANGER. Handbook on high resolution multinuclear NMR. John Wiley and Sons, New York. 1981.
4. A. I. POPOV. Pure Appl. Chem. **51**, 101 (1979).
5. P. LASZLO. Angewandt Chem. Int. Ed. Eng. **17**, 254 (1978).
6. C. DETELLIER and P. LASZLO. Helv. Chim. Acta, **59**, 1346 (1976).
7. H. GUSTAVSON, G. SIEGEL, B. LINDMAN, and L. FRANSSON. FEBS Lett. **86**, 127 (1978).
8. H. GUSTAVSON, B. LINDMAN, and T. BULL. J. Am. Chem. Soc. **100**, 4655 (1978).
9. C. DETELLIER AND P. LASZLO. Bull. Soc. Chim. Belg. **84**, 1087 (1975).
10. C. DETELLIER, A. GERSTMANS, and P. LASZLO. Inorg. Nucl. Chem. Lett. **15**, 93 (1979).
11. K. A. VALIEV. Sov. Phys. JETP, **11**, 883 (1961).
12. H. G. HERTZ. Ber. Bunsenges. Phys. Chem. **77**, 688 (1973).
13. C. DEVERELL. *In* Progress in nuclear magnetic resonance. Vol. 4. *Edited by* J. W. Emsley, J. Feeney, and L. H. Sutcliffe. Pergamon Press, London. 1969. Chapt. 4.
14. A. DELVILLE, C. DETELLIER, A. GERSTMANS, and P. LASZLO. J. Magn. Reson. **42**, 14 (1981).
15. H. G. HERTZ. Ber. Bunsenges. Phys. Chem. **65**, 20 (1961).
16. H. G. HERTZ, M. HOLZ, R. KLUTE, G. STALIDIS, and V. VERSCHMOLD. Ber. Bunsenges. Phys. Chem. **78**, 24 (1974).
17. A. I. MISHUSTIN and Y. M. KESSLER. J. Soln. Chem. **4**, 779 (1975).
18. Y. M. KESSLER, A. I. MISHUSTIN, and A. I. PODKOVYRIN. J. Soln. Chem. **6**, 114 (1977).
19. R. H. EHRLICH, E. ROACH, and A. I. POPOV. J. Am. Chem. Soc. **92**, 4989 (1970).
20. J. P. KINTZINGER and J. M. LEHN. J. Am. Chem. Soc. **96**, 3313 (1974).
21. M. C. DAY. Pure Appl. Chem. **49**, 75 (1977).
22. F. W. FREY, JR., P. KOBETZ, G. C. ROBINSON, and T. O. SISTRUCK. J. Org. Chem. **26**, 2950 (1961).
23. A. ABRAGAM. Principles of nuclear magnetism. Clarendon Press, Oxford. 1961. Chapt. 8.
24. C. N. HAMMONDS, T. D. WESTMORELAND, and M. C. DAY. J. Phys. Chem. **73**, 4374 (1969).
25. N. AHMAD and M. C. DAY. J. Am. Chem. Soc. **99**, 941 (1977).
26. A. K. COVINGTON and K. E. NEWMAN. Pure Appl. Chem. **51**, 2041 (1979).
27. W. MARTIR, A. E. ALLEGRIA, and G. R. STEVENSON. J. Am. Chem. Soc. **98**, 7955 (1976).
28. M. Y. DARENSBOURG, D. J. DARENSBOURG, D. BURNS, and D. A. DREW. J. Am. Chem. Soc. **98**, 3127 (1976).
29. M. Y. DARENSBOURG, P. JIMINEZ, J. R. SACKETT, J. M. HANCKEL, and R. L. KUMP. J. Am. Chem. Soc. **104**, 1521 (1982).

Can. J. Chem. Downloaded from www.nrcresearchpress.com by 210.87.254.6 on 09/06/12
For personal use only.

A practical synthesis of an anthracyclinone synthon

CHIU-MING WONG, HING-YAT LAM,[1] AND WASIMUL HAQUE
Department of Chemistry, University of Manitoba, Winnipeg, Man., Canada R3T 2N2

AND

AI-QIAO MI AND GUI-SHU YANG
Chengdu Institute of Organic Chemistry, Chinese Academy of Sciences, Chengdu, People's Republic of China

Received August 6, 1982

CHIU-MING WONG, HING-YAT LAM, WASIMUL HAQUE, AI-QIAO MI, and GUI-SHU YANG. Can. J. Chem. **61**, 562 (1983).

The important intermediate 2-acetyl-5,8-dimethoxytetralin (**8**) in the syntheses of anthracycline antitumor drugs is easily prepared in high yield on a large scale. Conversion of 2,4-pentanedione to 3-(2,5-dimethoxybenzyl)-hex-5-en-2-one (**9**) was carried out in a three-step, one-pot process by C-alkylating it with 2,5-dimethoxybenzyl bromide, then allyl bromide followed by a retro-Claisen condensation. Conversion of **9** to the tetralin (**8**) was done first by ozonolysis to the aldehyde (**10**) followed by cyclization and reduction of the latter by trimethylsilane in trifluoracetic acid – acetone.

CHIU-MING WONG, HING-YAT LAM, WASIMUL HAQUE, AI-QIAO MI et GUI-SHU YANG. Can. J. Chem. **61**, 562 (1983).

On a préparé, avec de bons rendements et sur une grande échelle, l'acétyl-2 diméthoxy-5,8 tétraline (**8**), un intermédiaire important lors de la synthèse des médicaments antituméraux du type anthracycline. On réalise la tranformation de la pentanedione-2,4 en (diméthoxy-2,5 benzyl)-3 hexène-5 one-2 (**9**) en trois étapes effectuées dans un même récipient en faisant une C-alkylation avec le bromure de diméthoxy-2,5 benzyle, puis une autre avec le bromure d'allyle, le tout suivi d'une condensation du type rétro-Claisen. On a réalisé la transformation du composé **9** en la tétraline (**8**) d'abord à l'aide d'une ozonolyse qui conduit à l'aldéhyde (**10**) puis par une cyclization et une réduction de cette dernière à l'aide du triméthylsilane dans un mélange d'acide trifluoroacétique et d'acétone.

[Traduit par le journal]

Introduction

The anthracycline antibiotics are a group of molecules, members of which, such as adriamycin (**1**), daunomycin (**2**) and carminomycin-1 (**3**) are recognized as some of the most potent and clinically useful antitumor drugs (1). Despite the wide clinical application of these three compounds and their simple derivatives, commonly regarded as the first-generation anthracycline antitumor drugs, their cumulative dose-related cardiotoxicity (2) severely restricts their usefulness, especially as maintenance therapeutic agents. During the past decade this has triggered a surge of intensive research activity for better analogues. Derivatives both of synthetic and natural origin, such as 4-demethoxydaunomycin (**4**) (3), 11-deoxydaunomycin (**5**) (4), 4-demethoxy-11-deoxydaunomycin (**6**) (5), and 4-demethoxy-4′-deoxyadriamycin (**7**) (6) show great potential as substitutes for the first-generation anthracycline drugs. The preferred synthetic process for these anthracycline molecules is the classical approach developed earlier in our laboratory and slightly modified by the Farmitalia group using 2-acetyl-5,8-dimethoxytetralin (**8**)[2] or its simple derivatives as intermediates. A number of such processes were reported (5–7). However, our early synthesis of the tetralin (**8**) is difficult to handle on a large scale and other processes reported later were also found to be unsatisfactory for large-scale production. We would like to report a process which greatly simplifies the preparation of this tetralin on a large scale.

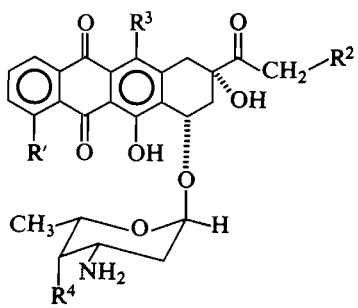

1 $R^1 = OCH_3$, $R^2 = R^3 = R^4 = OH$
2 $R^1 = OCH_3$, $R^2 = H$, $R^3 = R^4 = OH$
3 $R^1 = R^3 = R^4 = OH$, $R^2 = H$
4 $R^1 = R^2 = H$, $R^3 = R^4 = OH$
5 $R^1 = OCH_3$, $R^2 = H$, $R^3 = H$, $R^4 = OH$
6 $R^1 = R^2 = R^3 = H$, $R^4 = OH$
7 $R^1 = R^4 = H$, $R^2 = R^3 = OH$

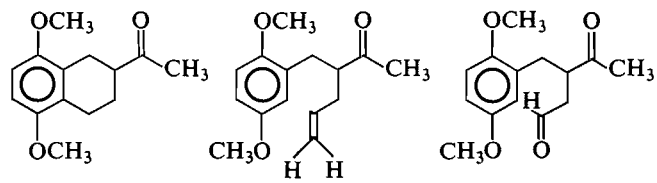

8 **9** **10**

Results and discussion

The intermediate 3-(2,5-dimethoxybenzyl)-hex-5-en-2-one (**9**) was prepared via a three-step process without isolation by alkylating 2,4-pentanedione with 2,5-dimethoxybenzyl bromide and then with allyl bromide in acetone solution in the

[1]American Leukemia Society Fellow, School of Medicine, University of Manitoba.

[2]More appropriate according to the "Definitive Rules for the Nomenclature of Organic Chemistry" than 1,4-dimethoxy-6-acetyltetralin used in our early publications.

Can. J. Chem. Downloaded from www.nrcresearchpress.com by 210.87.254.42 on 09/06/12
For personal use only.

Can. J. Chem. Downloaded from www.nrcresearchpress.com by 210.87.254.42 on 09/06/12
For personal use only.

presence of excess potassium carbonate, followed by evaporating the acetone and a retro-Claisen condensation in basic methanolic solution. The crude product so obtained was purified by distillation under reduced pressure. The olefinic bond of (**9**) was then cleaved by ozonolysis giving the aldehyde (**10**) in excellent yield. Large scale preparation of 2,5-dimethoxybenzyl bromide was carried out by irradiating, with a Hanovia medium pressure mercury lamp, an anhydrous carbon tetrachloride solution of 2,5-dimethoxytoluene and *N*-bromosuccinimide under a stream of dry nitrogen. Ring bromination becomes the major reaction if moisture or high concentration of bromine is present. Two lamps were required for larger scale preparation.

The tetralin (**8**) was formed in over 85% yield by dissolving the aldehyde (**10**) in trifluoroacetic acid followed by reduction with trimethylsilane in the presence of excess acetone.

Conversion of the tetralin (**8**) or its simple derivative to daunomycin (2), 4-demethoxydaunomycin (3), 11-deoxydaunomycin (4), 4-demethoxy-11-deoxydaunomycin (5), and other anthracyclines have been reported. This facile and economical process greatly simplified the large-scale preparation of many important anthracyclinones.

Experimental

Infrared spectra were recorded on a Perkin–Elmer 710 infrared spectrometer. Nuclear magnetic resonance spectra were recorded on a Varian A-56/60A or a Bruker WH-90 spectrometer, using $CDCl_3$ as solvent and tetramethylsilane as internal standard unless otherwise specified. Mass spectra were recorded on a Finnigan 1015 and high resolution mass spectra were recorded on a A.E.I. MS-50 mass spectrometer. Melting points were measured on a Fisher–Johns apparatus and were not corrected.

*Preparation of 3-(2,5-dimethoxybenzyl)-hex-5-en-2-one (**9**)*

To a five-liter three-necked flask equipped with a mechanical stirrer, mercury seal, dropping funnel, and condenser was added finely ground anhydrous potassium carbonate (420 g), acetone (3 L), 2,4-pentanedione (100 g), and 2,5-dimethoxybenzyl bromide (260 g). This was heated under reflux for a period of 30 h with vigorous stirring. Allyl bromide (150 mL) was then added through the dropping funnel and reflux was continued for an additional 24 h. The acetone solution was cooled in an ice bath, filtered, and the filtrate was evaporated under reduced pressure to give a syrupy residue. To the residue was added an aqueous methanolic sodium hydroxide solution (2.5 L) (water 1 L, methanol 1.5 L, sodium hydroxide 150 g) and the solution was heated for 10 h in an oil bath kept at 70°C, concentrated by distilling off part of the methanol under reduced pressure, diluted with water (1 L), and extracted with chloroform (3 × 800 mL). The combined chloroform extracts, after washing with water and drying over anhydrous magnesium sulfate, were evaporated to give the crude product (**9**) (187 g) which was purified by distillation, (152 g) (130–140°C/3 Torr). The distilled product shows ir (cm^{-1}): 1700 (CO), 1640 (C=C), 1595 (aromatic); nmr (δ): 6.67 (broad s, 5H, aromatic), 5.75 (m, 1H, —C*H*=CH_2), 4.95 (m, 2H, —CH=C*H*$_2$), 3.70 (s, 3H, —OCH_3), 3.64 (s, 3H, —OCH_3), 1.95 (2, 3H, —$COCH_3$); mass spectrum *m/z:* 248, 207, 149, 121; *Exact Mass* (high resolution mass spectrum, 100%) calcd. for $C_{15}H_{20}O_3$: 248.1407; found: 248.1404.

*Preparation of 3-(2,5-dimethoxybenzyl)-1,4-dioxopentane (**10**)*

Ozone from two ozone generators (12 000 V, 60 mA transformers) was introduced through two gas dispersion tubes into a two-liter flask containing methylene chloride (1 L) and the hexenone (**9**) (90 g), while keeping the solution at −20°C until thin-layer chromatography showed the complete disappearance of the starting material (~4 h). Nitrogen was passed through the solution instead of ozone during the development of the thin-layer plate. Trimethyl phosphite (60 mL) was added to the solution which was then heated under reflux for a period of 16 h. The solution was then cooled, washed with water, dried over anhydrous magnesium sulfate, and evaporated under reduced pressure to give a colorless oily residue (90 g) which crystallized from ether after cooling in a Dry-Ice bath; mp 44–45°C; ir (cm^{-1}): 2750 (aldehyde C—H), 1730 (aldehyde C=O), 1710 (ketone); nmr (δ): 9.38 (s, 1H, —C*H*O), 6.60–6.82 (m, 3H, aromatic), 3.80 (s, 3H, —OCH_3), 3.75 (s, 3H, s, —OCH_3), 2.19 (s, 3H, s, —$COCH_3$); mass spectrum, *m/z*: 250, 175, 150; *Exact Mass* (100%), calcd. for $C_{14}H_{18}O_4$: 250.1200; found: 250.1204.

*Preparation of 2-acetyl-5,8-dimethoxytetralin (**8**)*

Trifluoroacetic acid (500 mL) was cooled in an ice–salt bath to −7°C. To the acid was added the aldehyde (**10**) (50 g) in portions within one minute with vigorous stirring which was continued for a period of 15 min, while maintaining the same temperature (−5 to −7°C). Acetone (150 mL) was added followed by trimethylsilane (21 g) and stirring was continued for an additional 10 min. Most of the excess acetone and trifluoracetic acid were then removed under reduced pressure and the residue was dissolved in chloroform (700 mL) and the solution washed with water, 5% sodium bicarbonate solution, dried over anhydrous magnesium sulfate, and evaporated under reduced pressure to give an oily residue (46 g) which was crystallized from methanol; mp 101–102°C. The total crystalline product (38 g) is identical in every respect and showed no melting point depression with the sample previously reported from our laboratory.

Acknowledgements

Financial support from NSERC and Farmitalia Carlo Erba of Italy are greatly appreciated. The authors also wish to thank both referees for valuable suggestions and comments.

1. (*a*) F. ARCAMONE. Medicinal chemistry. Vol. 17. Academic Press, New York. 1981. pp. 25–40; (*b*) F. ARCAMONE. Lloydia, **40**, 45 (1977); (*c*) G. F. GAUSE, M. G. BRAZHNIKOVA, and V. A. SHORIN. Cancer Chemother. Rep. Part 1, **58**, 255 (1974).
2. (*a*) M. R. BRISTOW, M. E. BILLINGHAM, J. W. MASON, and T. R. DANIELS. Cancer Treat. Rep. **62**, 873 (1978); (*b*) E. A. LEFRAK, J. PITHA, and S. ROSENHEIM, Cancer Chemother. Rep. **6**, 203 (1975).
3. F. ARCAMONE. Medicinal chemistry. Vol. 17. Academic Press, New York. 1981. pp. 259–274,
4. F. ARCAMONE, G. CASSINELLI, F. DIMATTEO, S. FORENZA, M. C. RIPAMONTI, G. RIVOLA, A. VIGEVANI, T. MCCABE, and J. CLARDY. J. Am. Chem. Soc. **102**, 1462 (1980).
5. K. TATSUTA and T. TAKEUCHI. J. Antibiot. **33**, 1581 (1980).
6. F. ARCAMONE, G. FRANCHI, A. CASAZZA, and S. PENCO. Farmitalia Carlo Erba S. P. A. Belg. BE. 888, 784 (Cl. C07D), 28 Aug. 1981, Appl. 2047, 13 May, 1981.
7. (*a*) C. M. WONG, D. POPIEN, R. SCHWENK, and J. TE RAA. Can. J. Chem. **49**, 2712 (1971); (*b*) C. M. WONG, R. SCHWENK, D. POPIEN, and T. L. HO. Can. J. Chem. **51**, 466 (1973); (*c*) F. ARCAMONE, L. BERNARDI, B. PATTELLI, P. GIARDINO, A. DIMARCO, A. M. CASAZZA, C. SORANZO, and G. PRATESI. Experientia, **34**, 1255 (1978); (*d*) F. ARCAMONE, L. BERNARDI, B. PATELLI, and A. DIMARCO. Ger. Patent 2,601,785 (July 29, 1976); (*e*) A. S. KENDE, D. P. CURRAN, Y. TSAY, and J. E. MILLS, Tetrahedron Lett. 3537 (1977); (*f*) T. H. SMITH, A. N. FUJIWARA, W. W. LEE, H. Y. WU, and D. HENRY, J. Org. Chem. **42**, 3653 (1977); (*g*) J. S. SWENTON, P. W. RAYNOLDS, and M. J. MANNING. Tetrahedron Lett. 2383 (1977); (*h*) S. TERASHIMA, W. JEW, and K. KOGA. Tetrahedron Lett. 4937 (1978); (*i*) J. R. WISEMAN, N. I. FRENCH, R. K. HALLMARK, and K. G. CHIONG. Tetrahedron Lett. 3765 (1978); (*j*) A. V. RAMA RAO, V. H. DESHPANDE, and N. LAXMA REDY. Tetrahedron Lett. 2661 (1980); (*k*) J. B. BLADE AND P. HODGE. J. Chem. Soc. Chem. Commun. 85 (1979); (*l*) A. V. RAMA RAO, A. R.

MEHENDALE, and K. B. REDDY. Tetrahedron Lett. 2415 (1982); (*m*) M. J. BROADHURST, C. H. HASSALL, and G. J. THOMAS. J. Chem. Soc. Chem. Commun. 158 (1982); (*n*) F. ARCAMONE, P. LOMBARDI, D. GANDOLFI, AND S. PELNERO. Chem. Ind. (London) 810 (1981).

8. F. ARCAMONE. Medicinal chemistry. Vol. 17. Academic Press, New York. 1981. pp. 86–88.

Can. J. Chem. Downloaded from www.nrcresearchpress.com by 210.87.254.42 on 09/06/12
For personal use only.

Stereospecific vicinal oxyamination of *N*-substituted 1,2,3,6-tetrahydropyridines and 1,2-dihydropyridines by *N*-chloro-*N*-metallocarbamates

SUSHIL K. DUBEY AND EDWARD E. KNAUS[1]

Faculty of Pharmacy and Pharmaceutical Sciences, University of Alberta, Edmonton, Alta., Canada T6G 2N8

Received July 14, 1982

SUSHIL K. DUBEY and EDWARD E. KNAUS. Can. J. Chem. **61**, 565 (1983).

The vicinal oxyamination of 1-substituted 1,2,3,6-tetrahydropyridines (**2**) affords a mixture of the regioisomeric *cis*-hydroxycarbamates **3** and **4**. The *tert*-butoxycarbonylamino and hydroxyl substituents for **3** and **4** assume the equatorial and axial orientations respectively, irrespective of the substituent position. Acid hydrolysis of **3***a* and **4***a* affords the *cis*-aminoalcohols **5** and **6**. The regiospecific oxyamination of 1-methyoxycarbonyl-1,2-dihydropyridine occurs at the 5,6-olefenic bond to yield the hydroxycarbamates **15** and **16**. Reduction of **15** or **16** with palladium on charcoal affords the same vicinal hydroxy and methoxycarbamates **17** to **20** which may arise via the aziridine intermediate **21**.

SUSHIL K. DUBEY et EDWARD E. KNAUS. Can. J. Chem. **61**, 565 (1983).

L'oxyamination vicinale des tétrahydro-1,2,3,6 pyridines (**2**) substituées en position 1 donne un mélange d'hydroxycarbamates *cis* régioisomères **3** et **4**. Les substituants *tert*-butoxycarbonylamino et hydroxyle des composés **3** et **4** sont respectivement en positions équatorial et axiale indépendamment de la position du substituant. L'hydrolyse acide des composés **3***a* et **4***a* conduit aux aminoalcools *cis* **5** et **6**. L'oxyamination régiospécifique de la méthoxycarbonyl-1 dihydro-1,2 pyridine a lieu au niveau de la liaison oléfinique en positions 5,6 en donnant les hydroxycarbamates **15** et **16**. La réduction des composés **15** et **16** par le palladium sur du charbon fournit les mêmes hydroxy et méthoxycarbamates vicinaux **17** à **20** qui peuvent être obtenus via un intermédiaire aziridine **21**.

[Traduit par le journal]

The stereospecific vicinal oxyamination reaction of olefins developed by Sharpless and co-workers is a useful procedure for the synthesis of *cis*-β-aminoalcohol derivatives. One of these procedures employs a stoichiometric quantity of a (*tert*-alkylimido)-osmium reagent (**1***a*) (1). The other procedures, which require a catalytic quantity of osmium tetroxide, use Chloramine-T for the *in situ* generation of **1***b* (2) and *N*-chloro-*N*-metallocarbamates for the *in situ* generation of **1***c* (3).

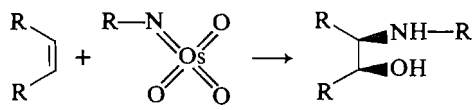

1*a* R = *tert*-Alkyl
b R = Ts
c R = Alkyl(arylalkyl)OCO

In earlier studies, we reported that reduced pyridyl nitrogen heterocycles offer potential for the development of new agents (4) with significant analgesic, hyperglycemic, antiinflammatory, and antimicrobial activities (5). It was therefore of interest to investigate the reaction of reduced pyridines with **1***c* as a method to effect the *cis* addition of hydroxyl (OH) and carbamate (*t*-BuOCONH) moieties across an olefenic bond. Heterocyclic *cis*-β-aminoalcohols are attractive medicinal intermediates for use (6) in the design of pharmacologically active nitrogen heterocycles. We now describe the vicinal oxyamination of *N*-substituted 1,2,3,6-tetrahydropyridines (**2**) and 1,2-dihydropyridines (**14**) using the powerful *N*-chloro-*N*-argento(mercury)carbamate-based oxyamination reagent **1***c*.

The oxyamination of 1-benzoyl-1,2,3,6-tetrahydropyridine (**2***a*) afforded a 1:1 mixture of the regioisomers *cis*-1-benzoyl-3-hydroxy-4-*tert*-butoxycarbonylaminopiperidine (**3***a*) and *cis*-1-benzoyl-3-*tert*-butoxycarbonylamino-4-hydroxypiperidine (**4***a*) in 18 and 63% yield, using Procedures A and B respectively (Scheme 1). Similar reactions employing 1-benzenesulfonyl- (**2***b*), 1-*tert*-butoxycarbonyl- (**2***c*), 1-methoxycarbonyl- (**2***d*), and 1-acetyl- (**2***e*) 1,2,3,6-tetrahydropyridines also yielded a mixture of regioisomers **3** and **4** (Table 1). We found that the *t*-BuOCONClNa + $AgNO_3$ (1:2) carbamate-based oxyamination system (Procedure B) was superior to the *t*-BuOCONClNa + $Hg(NO_3)_2$ + Et_4NOAc (1.5:0.75:1) system (Procedure A) since it provided higher yields of **3** and **4**, required shorter reaction times, and gave rise to a cleaner reaction mixture from which the products could be isolated more easily. The lower yield of **3** and **4** and the failure of **2***b* to react, using Procedure A, may be due to the competitive formation of an organomercury complex (**3***b*). *N*-Benzyl-1,2,3,6-tetrahydropyridine (**2***f*) did not react using either procedure. This is most likely due to some type of complexation with the free electron pair on nitrogen at the 1-position of **2***f*. On the other hand, oxyamination of 1-cyano-1,2,3,6-tetrahydropyridine (**11**) gave 1-aminocarbonyl-1,2,3,6-tetrahydropyridine (**13**) in 16.2 and 20% yield, using Procedures A and B respectively. The most likely intermediate in the oxidation of **11** to **13** is **12** since **11** does not react with osmium tetroxide. Furthermore, **11** did not react with *t*-BuOCOClNa and $AgNO_3$ (Procedure B) when OsO_4 was not present in the reaction mixture. The lone electron pair on the tetrahydropyridine nitrogen of **11** appears to play a significant role in the oxidation of **11** to **13** since the cyano group of acetonitrile[2] and 3-cyanopyridine (Procedure B) does not react under similar conditions.

The *tert*-butoxycarbonyl moiety of **3** and **4** was easily removed, affording the desired *cis*-β-aminoalcohols **5** and **6**. Treatment of **3***a* and **4***a* with 30% hydrogen bromide in acetic acid yielded **5** (76%) and **6** (81%) respectively. Reaction of **5** with thiophosgene and phosgene gave the respective bicyclic

[1]Author to whom correspondence may be addressed.

[2]Acetonitrile is employed as solvent in the oxyamination reactions using Procedures A and B.

Can. J. Chem. Downloaded from www.nrcresearchpress.com by 210.87.254.6 on 09/06/12
For personal use only.

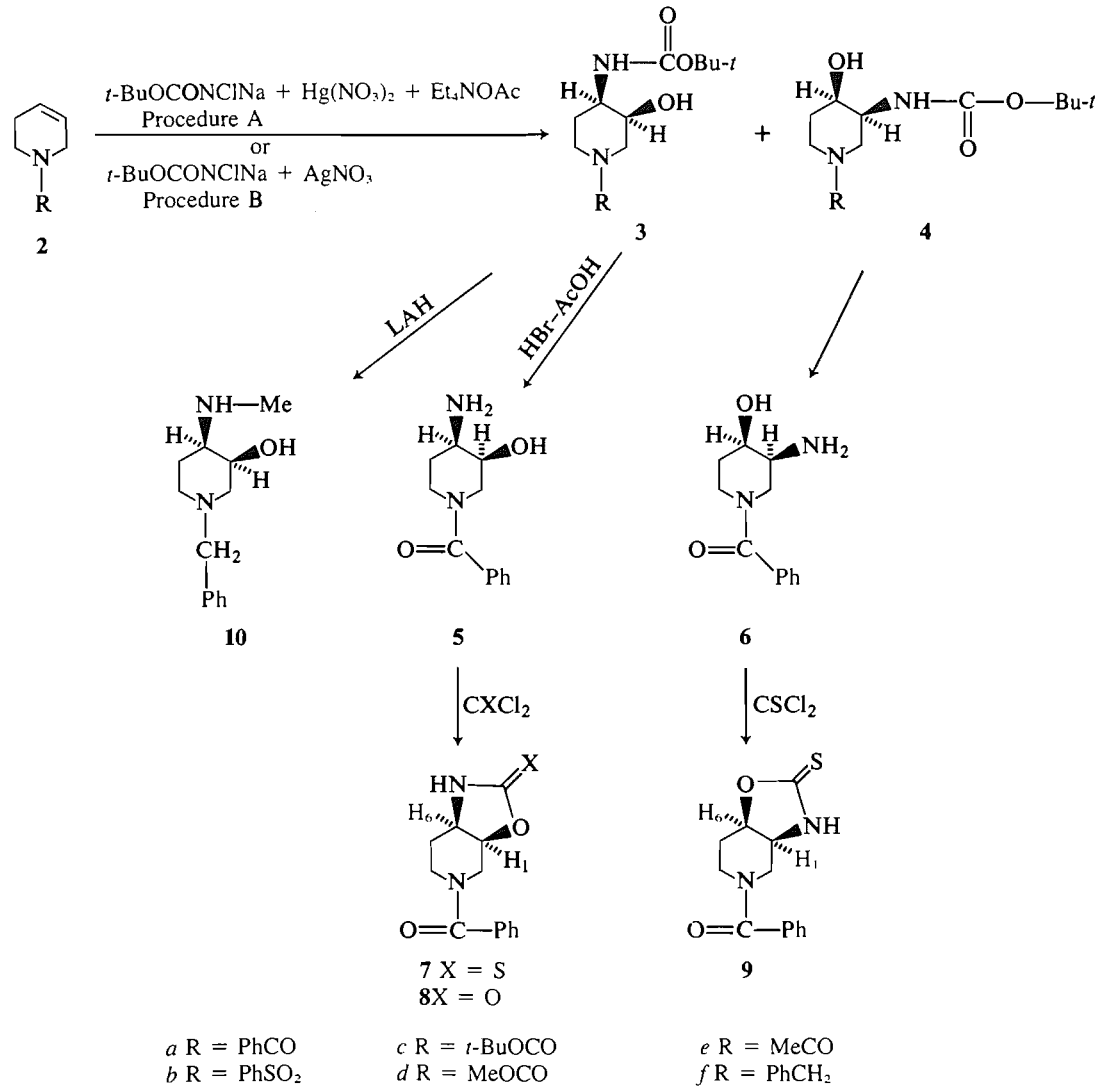

SCHEME 1

products 3-benzoyl-9-oxa-3,7-diazabicyclo[4.3.0]nonan-8-thione (**7**, 12.7%) and the 8-one analogue **8** (34.7%). A similar thiophosgene cyclization of **6** gave rise to **9** (13.3%). The *tert*-butoxycarbonylamino group was readily converted to a methylamino group since reduction of **3***a* using lithium aluminum hydride afforded the *cis*-β-methylaminoalcohol (**10**) in quantitative yield.

The assignment of the regiochemistry and stereochemistry for the two regioisomers **3** and **4** formed in the vicinal oxyamination of **2** was based largely on ^{1}H nmr and mass spectral studies. Proton resonance assignments rest largely on decoupling experiments. The question whether the vicinal oxyamination reaction affords products **3** and **4** in which the hydroxyl and carbamate substituents are *cis* to each other was solved by measurement of the coupling constants or width at half-height (W_H) of the protons at C-3 and C-4 in their ^{1}H nmr spectra. The ^{1}H nmr spectra of **3** and **4***a*,*c*–*e* were poorly resolved at room temperature. The poor resolution observed, even at 200 MHz, may be due to strong hydrogen-bonding (4*i*) and/or to the presence of rotational conformers which differ in configuration at the carbonyl-to-nitrogen (amide) bond of the piperidine ring nitrogen (4*g*, 7). The spectra of **3***a* and **4***a* are well resolved at 120°C which should be sufficient to disrupt hydrogen bonding and/or induce coalescence of the rotamers. In contrast, the spectra of **3***b* and **4***b*, in which hindered internal rotation abut NSO_2Ph is not possible, exhibited well-resolved spectra at room temperature.

Extensive decoupling experiments were performed for **3***a*, **4***a*, **3***b*, and **4***b* to establish the stereochemistry of the substituents at C-3 and C-4, whereas selected double resonance studies were carried out for the remaining products **3** and **4**, as required, to assign the position of the hydroxyl and *tert*-butoxycarbonylamino substituents. The N*H*CO_2-*t*-Bu and OH groups exhibit absorptions in the 4.5 to 6.5 δ range. The hydroxyl group appears at higher field and displays a coupling constant of 4 to 5 Hz while the carbamoyl proton absorbs at lower field and generally appears as a broad multiplet or doublet (J = 7 to 8 Hz) (Table 1).

Irradiation at the resonance frequency for the NH proton at C-4 of **3***a* led to the identification of the signal due to the C-4H appearing at 3.6 δ. Specifically, irradiation at the frequency of the C-4H identified the signals due to the protons at C-3 and C-5. Irradiation of the signal at 3.72 δ due to the C-3 proton identified the methylene protons at C-2 which were assigned the axial and equatorial positions based on the magnitude of their coupling to the H-3 proton. The axial proton at C-2 appears as a doublet (J = 13 Hz) of doublets (J = 2 Hz) with the large coupling due to geminal coupling of the C-2 protons.

Can. J. Chem. Downloaded from www.nrcresearchpress.com by 210.87.254.6 on 09/06/12
For personal use only.

TABLE 1. Physical and spectral data of *cis*-1-substituted-3-hydroxy-4-*tert*-butoxycarbonylaminopiperidines (**3**) and *cis*-1-substituted-3-*tert*-butoxycarbonylamino-4-hydroxypiperidines (**4**)

Compound	R	% Yield, procedure A:B	Melting point, °C	Reaction time (h), procedure A:B	Ratio **3**/**4**	Nuclear magnetic resonance (Me_2SO-d_6), δ	Formula[a]
3*a*[b]	PhCO		169			7.4 (m, 5H, Ph), 5.84 (distorted d, J = 7 Hz, 1H, NH[d]), 4.57 (d, J = 4 Hz, 1H, OH), 3.9–4.07 (m, 1H, H_{6eq}), 3.76–3.9 (m, 1H, H_{2eq}), 3.68–3.76 (m, 1H, H_{3eq}), 3.52–3.68 (m, 1H, H_{4ax}), 3.17 (d, $J_{2ax-2eq}$ = 13 Hz of d, $J_{2ax-3eq}$ = 2 Hz, 1H, H_{2ax}), 2.98 (d, $J_{6ax-6eq}$ = 14 Hz of d, $J_{5ax-6eq}$ = 11 Hz of d, $J_{5eq-6ax}$ = 3.5 Hz, 1H, H_{6ax}), 1.48–1.86 (m, 2H, H_5), 1.42 (s, 9H, *t*-Bu)	$C_{17}H_{24}N_2O_4$
		18:63		72:24	1:1[c]		
4*a*[b]	PhCO		155			7.39 (m, 5H, Ph), 5.72–5.84 (d, J = 7 Hz, NH[d]), 4.58–4.66 (d, J = 4 Hz, 1H, OH), 3.84–3.96 (m, 1H, H_{4eq}), 3.62–3.77 (m, 1H, H_{2eq}), 3.28–3.62 (m, 3H, H_6, H_{3ax}), 3.22 (d, $J_{2ax-2eq}$ = 12 Hz of d, $J_{2ax-3ax}$ = 9 Hz, 1H, H_{2ax}), 1.61–1.72 (m, 2H, H_5), 1.36 (s, 9H, *t*-Bu)	$C_{17}H_{24}N_2O_4$
3*b*[c]	$PhSO_2$		194			7.59–7.8 (m, 5H, Ph), 6.4 (J = 7.2 Hz, 1H, NH[d]), 5.2 (d, J = 4.5 Hz, 1H, OH), 3.68–3.78 (m, 1H, H_{3eq}), 3.24–3.48 (m, 3H, H_{4ax}, H_{2eq}, H_{6eq}), 2.63 (d, $J_{2ax-2eq}$ = 12 Hz of d, $J_{2ax-3eq}$ = 2 Hz, 1H, H_{2ax}), 2.48 (d, $J_{6ax-6eq}$ = 12 Hz of d, $J_{5eq-6ax}$ = 3.5 Hz, 1H, H_{6ax}), 1.64–1.86 (m, 1H, H_{5ax}), 1.46–1.64 (m, 1H, H_{5eq}), 1.38 (s, 9H, *t*-Bu)	$C_{16}H_{24}N_2O_5S$
		0:50		72:96	1:2.5[c]		
4*b*[c]	$PhSO_2$		Viscous oil			7.5–7.9 (m, 5H, Ph), 6.35 (d, J = 8 Hz, 1H, NH[d]), 4.8 (d, J = 3.5 Hz, 1H, OH), 3.64–3.8 (m, 1H, H_{4eq}), 3.42–3.64 (m, 1H, H_{3ax}), 3.12–3.42 (m, 2H, H_{2eq}, H_{6eq}), 2.3–2.64 (m, 2H, H_{2ax}, H_{6ax}), 1.6–1.8 (m, 2H, H_5), 1.41 (s, 9H, *t*-Bu)	$C_{16}H_{24}N_2O_5S$
3*c*[f]	*t*-BuOCO		145			6.05 (m, 1H, NH[d]), 4.6 (d, J = 4.5 Hz, 1H, OH), 3.68–3.84 (m, 2H, H_{2eq}, H_{6eq}), 3.6–3.66 (m, 1H, H_{3eq}), 3.4–3.54 (m, 1H, H_{4ax}), 2.96 (d, $J_{2ax-3eq}$ = 12 Hz of d, $J_{2ax-3eq}$ = 1.5 Hz, 1H, H_{2ax}), 2.76–2.9 (m, 1H, H_{6ax}), 1.58–1.7 (m, 2H, H_5), 1.4 (s, 18H, *t*-Bu)	$C_{15}H_{28}N_2O_5$
		22:29		72:30	1:1[e]		
4*c*[f]	*t*-BuOCO		116			5.84–6.1 (m, 1H, NH[d]), 4.71 (d, J = 4.5 Hz, 1H, OH), 3.64–3.88 (m, 1H, H_{4eq}), 3.3–3.6 (m, 3H, H_{2eq}, H_{3ax}, H_{6eq}), 3.0–3.24 (m, 2H, H_{2ax}, H_{6ax}), 1.48–1.68 (m, 2H, H_5), 1.42 (s, 18H, *t*-Bu)	$C_{15}H_{28}N_2O_5$
3*d*[f]	MeOCO		139			5.98–6.26 (m, 1H, NH[d]), 4.69 (d, J = 4.5 Hz, 1H, OH), 3.72–3.9 (m, 2H, H_{2eq}, H_{6eq}), 3.6–3.72 (m, 1H, H_{3eq}), 3.58 (s, 3H, OMe), 3.4–3.56 (m, 1H, H_{4ax}), 3.0 (d, $J_{2ax-2eq}$ = 14 Hz, of d, $J_{2ax-3eq}$ = 2Hz, 1H, H_{2ax}), 2.79–2.94 (m, 1H, H_{6ax}), 1.42–1.76 (m, 2H, H_5), 1.4 (s, 9H, *t*-Bu)	$C_{12}H_{22}N_2O_5$
		18:54		72:30	1:1[g]		
4*d*[f]	MeOCO		Viscous oil			5.9–6.2 (m, 1H, NH[d]), 4.76 (d, J = 4 Hz, 1H, OH), 3.7–3.88 (m, 1H, H_{4eq}), 3.26–3.69 (m, 6H, H_{2eq}, H_{3ax}, H_{6eq}, OMe), 3.05–3.26 (m, 2H, H_{2ax}, H_{6ax}), 1.32–1.74 (m, 11H, H_5, *t*-Bu)	$C_{12}H_{22}N_2O_5$
3*e*[h]	MeCO		131			5.7–5.92 (m, 1H, NH[d]), 4.4–4.7 (m, 1H, OH), 2.54–4.32 (m, 6H, H_{2ax}, H_{2eq}, H_{3eq}, H_{4ax}, H_{6ax}, H_{6eq}), 1.98 (s, 3H, COMe), 1.3–1.76 (m, 11H, H_5, *t*-Bu)	$C_{12}H_{22}N_2O_4$
		10:46		72:30	1:1[i]		
4*e*[h]	MeCO		188			5.73–5.9 (m, 1H, NH[d]), 4.5–4.68 (m, 1H, OH), 3.76–3.9 (m, 1H, H_{4eq}), 2.84–3.6 (m, 5H, H_2, H_{3ax}, H_6), 1.96 (s, 3H, COMe), 1.49–1.74 (m, 2H, H_5), 1.4 (s, 9H, *t*-Bu)	$C_{12}H_{22}N_2O_4$

[a]All compounds gave analyses for C, H, and N within ± 0.4% of theoretical values.
[b]The nmr spectrum was determined at 120°C.
[c]Products **3** and **4** were separated by silica gel column chromatography.
[d]Exchange with deuterium oxide.
[e]The nmr spectrum was determined at 25°C.
[f]The nmr spectrum was determined at 60°C.
[g]On standing **3***d* cyrstallizes from the reaction mixture. Washing with hexane–ether removes the soluble **4***d*.
[h]The nmr spectrum was determined at 110°C.
[i]Separated by fractional recrystallization from benzene–hexane.

Irradiation at the resonance frequency of the C-3 proton resulted in the collapse of the small coupling (J = 2 Hz) for the C-2_{ax} proton. This small coupling constant of 2 Hz for J_{2ax-3} can only be explained if the proton at C-3 is equatorial and the C-3 hydroxyl substituent is axial. The width at half-height (W_H) for the resonance of the C-4H is large compared to that for the C-3H indicating that the C-4H must be axial (8). These assignments are consistent with the observation that irradiation of the frequency due to the C-4NH results in simplification of the C-4H to a multiplet exhibiting coupling constants of 10.5, 4, and 3 Hz. The large coupling constant of 10.5 Hz is possible if the C-4H is axial, which would be consistent with the large $J_{4ax-5ax}$ and smaller $J_{4ax-5eq}$ and $J_{4ax-3eq}$ coupling constants observed. Thus, the C-4 *tert*-butoxycarbonylamino group must be equatorial with the C-3 and C-4 substituents in a *cis*-configuration.

The ^{1}H nmr spectrum of **4***a* exhibited a doublet (J = 12 Hz) of doublets (J = 9 Hz) for the C-2_{ax} proton with the large 12 Hz coupling due to geminal coupling of the C-2 methylene protons. The 9 Hz coupling is characteristic of a $J_{2ax-3ax}$ interaction indicating that the C-3H must be axial and the carbamate substituent is equatorial. The width at half-height (W_H = 10.5

Can. J. Chem. Downloaded from www.nrcresearchpress.com by 210.87.254.6 on 09/06/12
For personal use only.

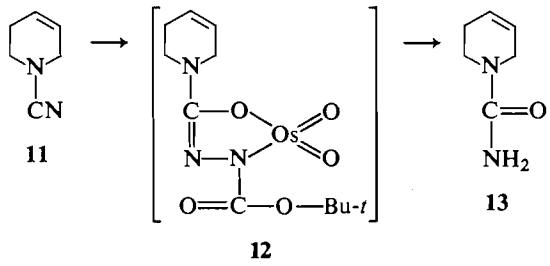

SCHEME 2

Hz) for the resonance due to the C-4H suggests it is equatorial (8). Irradiation of the resonance due to the C-4 hydroxyl proton resulted in the simplification of the absorption for the C-4H to a multiplet showing three nearly equivalent coupling constants of about 4 Hz at 3.84 to 3.96 δ. These observed couplings also indicate the C-4H is equatorial, in which case one would expect $J_{4eq-5ax}$, $J_{4eq-5eq}$, and $J_{3ax-4eq}$ coupling constants of about 4 Hz, thereby establishing the configuration of the C-4 hydroxyl substituent as axial.

The results of these ^{1}H nmr studies indicate that the vicinal oxyamination reaction of *N*-substituted -1,2,3,6-tetrahydropyridines (**2**) affords *cis*-aminoalcohol derivatives **3** and **4** in which the *tert*-butoxycarbonylamino and hydroxyl substituents assume the equatorial and axial orientations respectively, irrespective of the substituent position.

The regioisomers **3** and **4** are readily distinguished using mass spectrometry. For example, the 3-hydroxy isomers **3** exhibit a low abundance $M^+ - 18$ peak due to the loss of water, a very prominent $M^+ - 75$ ion which corresponds to the bicyclic structure illustrated in Scheme 3, and usually a less abundant $M^+ - 117$ ion due to loss of a *t*-BuOCONH$_2$ fragment. On the other hand, the 4-hydroxy isomers **4** do not exhibit a $M^+ - 18$ ion but they do display a very prominent $M^+ - 117$ ion relative to $M^+ - 74$ and $M^+ - 75$ peaks. The difference in the fragmentation pathways for **3** and **4** suggests 1,3-interactions are important. The regiochemistry of the isomers **3** and **4** can therefore be readily assigned using mass spectrometry (see Table 2).

The oxyamination reaction of 1-substituted 1,2-dihydropyridines was also examined. Thus, reaction of 1-methoxycarbonyl-1,2-dihydropyridine (**14**) with *N*-chloro-*N*-sodio-*tert*-butylcarbamate and silver nitrate afforded a mixture of the two regioisomers **15** and **16** (50%) in a ratio of 1:1. A similar reaction employing mercuric nitrate and tetraethylammonium acetate (Procedure A) in place of silver nitrate (Procedure B) gave a very complex reaction mixture from which **15** and **16** could not be readily isolated. The oxyamination reaction of 1-methyl-1,2-dihydropyridine using Procedures A and B also afforded a complex mixture of products, whereas no reaction occurred with 1-methanesulfonyl-1,2-dihydropyridine and 1-ethoxycarbonyl-1,4-dihydropyridine.

The identification of the two regioisomers **15** and **16** was based primarily on ^{1}H nmr and ir spectral data. The ^{1}H nmr spectra of **15** and **16** clearly indicated that addition occurred at the 5,6- rather than the 3,4-olefenic bond of **14**. The small $J_{2,3}$ coupling constant of 3 Hz suggests the C-2 hydroxyl and C-3 *tert*-butoxycarbonylamino substituents of **15** are in the *cis*-configuration which is consistent with the known mechanism of this reaction (1–3). The dihedral angle between a C-3 pseudoequatorial or pseudoaxial hydrogen and the C-4H is very similar, thereby precluding assignment of the stereochemistry

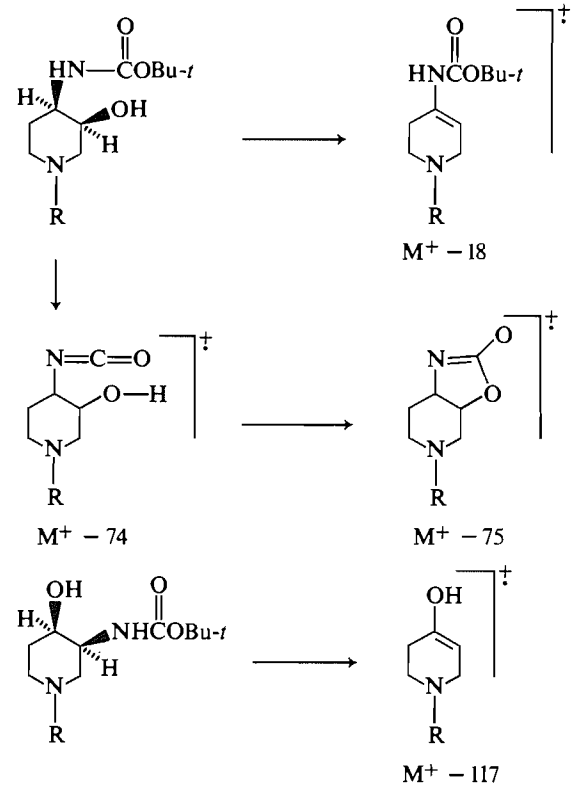

SCHEME 3

of the C-3H based on the magnitude of the coupling constant for $J_{3,4}$. The ^{1}H nmr spectrum of **16** was very complex, even at 100°C, due to strong hydrogen-bonding effects and/or the presence of two rotational conformers which differ in configuration at the carbonyl-to-nitrogen (carbamate) bond of the tetrahydropyridine ring nitrogen (4*g*, 7).

The 4,5-olefenic bond of the 1,2,3,6-tetrahydropyridines **15** and **16** was hydrogenated using palladium on charcoal and hydrogen gas. It was expected the stereochemistry of the C-3 substituents could then be assigned from the magnitude of the $J_{3,4}$ values. Reduction of **15** in this way afforded **17** (19.5%), **18** (9.7%), **19** (24.5%), and **20** (29.9%). The mechanism for the formation of **17**–**20** is not known. One plausible explanation is attack by methoxyl (**17** and **18**) and hydroxyl (**19** and **20**) species upon an aziridine intermediate such as **21** (6). It is not known why the hydroxy species is incorporated solely into

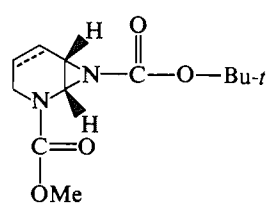

21

the C-3 position and the methoxyl species only into the C-2 position. The hydroxycarbamates **15** and **16** are stable in the presence of 10% palladium on charcoal in methanol at 25°C. A similar reduction of **16** gave **17** (14.1%), **18** (14.1%), **19** (40.6%), and **20** (4%).

The stereochemistry of the C-2 and C-3 substituents in which the C-3H is axial can be assigned the *cis*-configuration based on the small $J_{2,3}$ values for **17** and **19**, which are 2.8 and 5 Hz

Can. J. Chem. Downloaded from www.nrcresearchpress.com by 210.87.254.6 on 09/06/12
For personal use only.

TABLE 2. Some mass spectral data for **3** and **4**

Compound	m/e Measured[a]	m/e Calcd.	Relative intensity	Fragment
3*a*	320.1730	320.1763	0.27	$C_{17}H_{24}N_2O_4$ (M^+)
	302.1625	302.1630	5.9	$C_{17}H_{22}N_2O_3$ ($M^+ - H_2O$)
	247.1068	247.1083	12.5	$C_{13}H_{15}N_2O_3$ ($M^+ - t\text{-}C_4H_9O$)
	246.0999	246.1005	28.2	$C_{13}H_{14}N_2O_3$ ($M^+ - t\text{-}C_4H_9OH$)
	245.0926	245.0927	27.1	$C_{13}H_{13}N_2O_3$ ($M^+ - C_4H_{11}O$)
	203.944	203.9446	6.9	$C_{12}H_{13}NO_2$ ($M^+ - t\text{-}C_4H_9OCONH_2$)
4*a*	321[b]	321	41.0	$C_{17}H_{25}N_2O_4$ ($M + 1$)$^+$
	247.1080	247.1083	7.19	$C_{13}H_{15}N_2O_3$ ($M^+ - t\text{-}C_4H_9O$)
	246.0987	246.1005	1.8	$C_{13}H_{14}N_2O_3$ ($M^+ - t\text{-}C_4H_9OH$)
	245.0923	245.0927	4.1	$C_{13}H_{13}N_2O_3$ ($M^+ - C_4H_{11}O$)
	203.0941	203.0946	100.0	$C_{12}H_{13}NO_2$ ($M^+ - t\text{-}C_4H_9OCONH_2$)
3*b*	357[b]	357	26.4	$C_{16}H_{25}N_2O_5S$ ($M + 1$)$^+$
	283.0726	283.0753	12.5	$C_{12}H_{15}N_2O_4S$ ($M^+ - t\text{-}C_4H_9O$)
	282.0649	282.0674	9.4	$C_{12}H_{14}N_2O_4S$ ($M^+ - t\text{-}C_4H_9OH$)
	281.0596	281.0596	33.1	$C_{12}H_{13}N_2O_4S$ ($M^+ - C_4H_{11}O$)
4*b*	357[b]	357	30.4	$C_{16}H_{24}N_2O_5S$ ($M + 1$)$^+$
	283.0738	283.0753	4.8	$C_{12}H_{15}N_2O_4S$ ($M^+ - t\text{-}C_4H_9O$)
	281.0590	281.0596	8.3	$C_{12}H_{13}N_2O_4S$ ($M^+ - C_4H_{11}O$)
	239.0630	239.0616	32.7	$C_{11}H_{13}NO_3S$ ($M^+ - t\text{-}C_4H_9OCONH_2$)
3*c*	317*b*	317	18.3	$C_{15}H_{29}N_2O_5$ ($M + 1$)$^+$
	219.1894	219.1893	0.3	$C_{15}H_{26}N_2O_4$ ($M^+ - H_2O$)
	242.1243	242.1267	3.0	$C_{11}H_{18}N_2O_4$ ($M^+ - C_4H_9OH$)
	241.1190	241.1192	11.9	$C_{11}H_{17}N_2O_4$ ($M^+ - C_4H_{11}O$)
4*c*	316.1990	316.1999	0.5	$C_{15}H_{28}N_2O_5$ (M^+)
	243.1342	243.1345	0.7	$C_{11}H_{19}N_2O_4$ ($M^+ - C_4H_9O$)
	199.1209	199.1209	17.7	$C_{10}H_{17}NO_3$ ($M^+ - C_4H_9OCONH_2$)
3*d*	275[b]	275	100.0	$C_{12}H_{23}N_2O_5$ ($M + 1$)$^+$
	256.1408	256.1423	0.4	$C_{12}H_{20}N_2O_4$ ($M^+ - 18$)
	200.0791	200.0797	58.2	$C_8H_{12}N_2O_4$ ($M^+ - C_4H_9O$)
	199.0718	199.0718	66.6	$C_8H_{11}N_2O_4$ ($M^+ - C_4H_9OH$)
	157.0735	157.0739	12.6	$C_7H_{11}NO_3$ ($M^+ - C_4H_9OCONH_2$)
4*d*	274.1525	274.1529	0.8	$C_{12}H_{22}N_2O_5$ (M^+)
	201.0861	201.0875	10.7	$C_8H_{13}N_2O_4$ ($M^+ - C_4H_9O$)
	200.0788	200.0797	20.6	$C_8H_{12}N_2O_4$ ($M^+ - C_4H_9OH$)
	199.0717	199.0718	32.7	$C_8H_{11}N_2O_4$ ($M^+ - C_4H_{11}O$)
	157.0743	157.0739	99.8	$C_7H_{11}NO_3$ ($M^+ - C_4H_9OCONH_2$)
3*e*	259.[b]	259	83.5	$C_{12}H_{23}N_2O_4$ ($M + 1$)$^+$
	240.1469	240.1474	2.1	$C_{12}H_{20}N_2O_3$ ($M^+ - H_2O$)
	185.0916	185.0926	26.8	$C_8H_{13}N_2O_3$ ($M^+ - C_4H_9O$)
	184.0845	184.0847	64.2	$C_8H_{12}N_2O_3$ ($M^+ - C_4H_9OH$)
	183.0769	183.0769	37.1	$C_8H_{11}N_2O_3$ ($M^+ - C_4H_{11}O$)
	141.0763	141.0790	67.0	$C_7H_{11}NO_2$ ($M^+ - C_4H_9OCONH_2$)
4*e*	258.1577	258.1580	0.4	$C_{12}H_{22}N_2O_4$ (M^+)
	185.0924	185.0926	6.8	$C_8H_{13}N_2O_3$ ($M^+ - C_4H_9O$)
	184.0839	184.0847	2.2	$C_8H_{12}N_2O_3$ ($M^+ - C_4H_9OH$)
	183.0768	183.0769	3.4	$C_8H_{11}N_2O_3$ ($M^+ - C_4H_{11}O$)
	141.0765	141.0790	100	$C_7H_{11}NO_2$ ($M^+ - C_4H_9OCONH_2$)

[a]High resolution electron impact (70 ev) spectra unless otherwise indicated.
[b]Chemical ionization (NH_3) mass spectra.

respectively. This indicates that the C-2H of **17** and **19** must be equatorial and the respective methoxy and *tert*-butoxycarbonylamino substituents would therefore be axial. On the other hand, when the C-3H is equatorial, as for **18** and **20**, it is not possible to assign the stereochemistry of the C-2 substituents since $J_{2,3ae}$ is similar to $J_{2,3ee}$. The chemical shift values (δ) observed for the H_2 protons of **17** (5.24), **18** (5.14), **19** (5.7), and **20** (5.61) would suggest that the C-2H of **18** and **20** are also equatorial. This assignment would be consistent with the fact that a 2-methyl or 2-(3-pyridyl) substituent on a 1-benzoylpiperidine ring system exists in the axial orientation (10,11).

Experimental

Melting points were determined with a Büchi capillary apparatus and are uncorrected. Infrared spectra (potassium bromide unless otherwise noted) were taken on a Unicam SP 1000 spectrometer. Nuclear magnetic resonance spectra were determined for solutions in deuterochloroform or deuterodimethylsulfoxide with a Bruker WH-200, WH-400, or Varian EM 360A spectrometer. Double resonance studies were used to confirm assignments. Mass spectra were measured on a AEI MS-50 mass spectrometer. Preparative high pressure liquid chromatography was performed using a Water's Prep LC/System 500A using Prep Pak-500 Silica cartridges. The *N*-substituted -1,2,3,6-tetrahydropyridines **2** were prepared using standard procedures for acylation or alkylation of 1,2,3,6-tetrahydropyridine. 1-Methoxy-

Can. J. Chem. Downloaded from www.nrcresearchpress.com by 210.87.254.6 on 09/06/12
For personal use only.

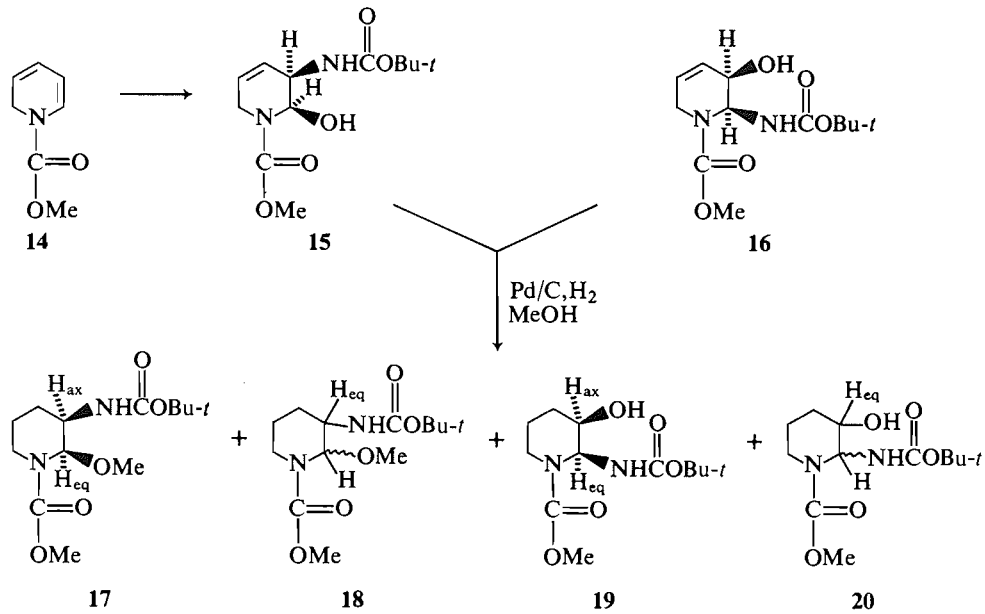

SCHEME 4

carbonyl-1,2-dihydropyridine was prepared according to the procedure of Fowler (9).

cis-*1-Substituted-3-hydroxy-4*-tert-*butoxycarbonylaminopiperidines (3) and* cis-*1-substituted-3*-tert-*butoxycarbonylamino-4-hydroxypiperidines (4)*

Procedure A

In a one-necked flask (250 mL), a mixture of *N*-chloro-*N*-sodio-*tert*-butylcarbamate (3*b*) (7.5 mmol) and mercuric nitrate (3.75 mmol) in acetonitrile (100 mL) was stirred for 15 min. To this suspension water (22 mmol), *N*-substituted-1,2,3,6-tetrahydropyridine (**2**, 5 mmol), and a solution of osmium tetroxide (0.05 mmol) in *tert*-butyl alcohol (2*b*) was added. The mixture was stirred at 25°C for 5–10 min after which tetraethylammonium acetate (5 mmol) was added. The reaction was allowed to proceed until the 1,2,3,6-tetrahydropyridine **2** was consumed (see Table 1 for times). When the reaction was completed, a saturated solution of sodium chloride was added to precipitate the remaining metallic ion.[3] The solution was filtered and extracted with chloroform (3 × 50 mL). The combined organic extracts were washed with a saturated solution of sodium chloride, dried (Na_2SO_4), and the solvent removed *in vacuo* to yield the crude hydroxycarbamates **3** and **4**. Regioisomers **3** and **4** were separated by silica gel column chromatography or fractional crystallization as indicated in Table 1.

Procedure B

A mixture of *N*-chloro-*N*-sodio-*tert*-butylcarbamate (3*b*) (7.5 mmol) and silver nitrate (15 mmol) in acetonitrile (100 mL) was allowed to stir for 15 min at 25°C. Water (22 mmol), *N*-substituted 1,2,3,6-tetrahydropyridine (**2**, 5 mmol), and a solution of osmium tetroxide (0.05 mmol) in *tert*-butyl alcohol (2*b*) were added to this suspension. The reaction was allowed to proceed with stirring at 25°C until all the olefin was consumed as indicated by tlc. The isolation procedure was identical to that of Procedure A.

cis-*1-Benzoyl-3-hydroxy-4-aminopiperidine (5)*

A solution of 30% HBr in acetic acid (5 mL) was added to a solution of **3***a* (1.6 g, 5 mmol) in methanol (10 mL) at 0°C with stirring. The reaction was allowed to proceed at 25°C for an additional 20 min. The solvent was removed *in vacuo* and the residue basified to pH 10, using aqueous sodium hydroxide prior to extraction with ether (20 mL) and then chloroform (3 × 50 mL). The combined organic extracts were dried (Na_2SO_4) and the solvent removed *in vacuo* to yield **5** as an oil which solidified on standing at room temperature after several days, yield 0.84 g (76%); mp 130–131°C; ir: 3380, 3300, 3100–3180 (OH and NH_2), 1620–1635 (CO); nmr ($CDCl_3$) δ: 7.48 (m, 5H, Ph), 2.8–5.0 (m, 6H, H_2, H_6, H_3, H_4), 2.28 (br s, 3H, NH_2, OH, exchange with deuterium oxide), 1.4–2.0 (m, 2H, H_5). *Exact Mass* calcd. for $C_{12}H_{16}N_2O_2$: 220.1212; found (high-resolution ms): 220.1210.

cis-*1-Benzoyl-3-amino-4-hydroxypiperidine (6)*

Hydrolysis of **4***a*, using the procedure outlined for the preparation of **5**, afforded **6**: yield (81%); mp 120–122°C; ir: 3360, 3300, 3140–3220 (OH, NH_2), 1635 (CO); nmr ($CDCl_3$) δ: 7.42 (m, 5H, Ph), 2.76–4.24 (m, 6H, H_2, H_6, H_3, H_4), 2.15 (br s, 3H, NH_2, OH, exchanges with deuterium oxide), 1.6–2.0 (m, 2H, H_5). *Exact Mass* calcd. for $C_{12}H_{16}N_2O_2$: 220.1212; found (high resolution ms): 220.1210.

3-Benzoyl-9-oxa-3,7-diazabicyclo[4.3.0]nonan-8-thione (7)

A solution of thiophosgene (0.228 mL, 3 mmol) in dry tetrahydrofuran (5 mL) was added dropwise to a solution of **5** (0.66 g, 3 mmol) and triethylamine (0.9 mL, 6 mmol) in dry tetrahydrofuran (30 mL) at −65°C with stirring over a 20 min period. The reaction was allowed to proceed for 30 min prior to warming to 25°C. Triethylamine hydrochloride was removed by filtration, the filtrate was concentrated *in vacuo*, and the residue was washed with water. Chromatography on a 0.5 cm × 9.0 cm silica gel column with chloroform as eluant afforded **7**, yield (0.1 g, 12.7%); mp 203°C; ir: 3360 (NH), 1630 (CO); nmr ($CDCl_3$ + DMSO-d_6) δ: 7.46 (m, 5H, Ph), 4.82–5.38 (m, 1H, H_1), 4.2–4.62 (m, 1H, H_6), 3.32–4.08 (m, 4H, H_2, H_4), 3.1 (br s, 1H, NH, exchanges with deuterium oxide), 1.76–2.32 (m, 2H, H_5). *Exact Mass* calcd. for $C_{13}H_{14}N_2O_2{}^{32}S$: 262.0776; found (high resolution ms): 262.0773.

3-Benzoyl-9-oxa-3,7-diazabicyclo[4.3.0]nonan-8-one (8)

Reaction of **5** with phosgene using the procedure outlined for the preparation of **7**, afforded **8**, yield (34.7%); mp 145–146°C; ir: 3280 (NH), 1750–1760 (OCO), 1625 (COPh); nmr ($CDCl_3$) δ: 7.4 (m, 5H, Ph), 6.85 (s, 1H, NH, exchanges with deuterium oxide), 4.55–5.05 (m, 1H, H_1), 3.24–4.38 (m, 5H, H_6, H_2, H_4), 1.62–2.18 (m, 2H, H_5). *Exact Mass* calcd. for $C_{13}H_{14}N_2O_3$: 246.1005; found (high resolution ms): 246.1004.

3-Benzoyl-7-oxa-3,9-diazabicyclo[4.3.0]nonan-8-thione (9)

Reaction of **6** with thiophosgene, using the procedure outlined for

[3]The sodium bisulfite treatment to reduce and remove the small amount of osmium that may be bound to the organic products was omitted since this resulted in a more complex reaction mixture.

Can. J. Chem. Downloaded from www.nrcresearchpress.com by 210.87.254.6 on 09/06/12
For personal use only.

Can. J. Chem. Downloaded from www.nrcresearchpress.com by 210.87.254.6 on 09/06/12
For personal use only.

the preparation of **7**, gave **9**, yield (13.3%); mp 210–211°C; ir: 3360 (NH), 1630 (COPh); nmr ($CDCl_3$ + DMSO-d_6) δ: 7.45 (m, 5H, Ph), 4.97–5.38 (m, 1H, H_6), 4.0–4.54 (m, 1H, H_1), 3.2–3.9 (m, 4H, H_2, H_4), 2.84 (br s, 1H, NH, exchanges with deuterium oxide), 1.9–2.4 (m, 2H, H_5). *Exact Mass* calcd. for $C_{13}H_{14}N_2O_2{}^{32}S$: 262.0776; found (high resolution ms): 262.0775.

cis-*1-Benzoyl-3-hydroxy-4-methylaminopiperidine (10)*

Lithium aluminum hydride (0.3 g, 8 mmol) was added slowly to a solution of **3***a* (0.64 g, 2 mmol) in dry tetrahydrofuran (25 mL) with stirring at 0°C. The reaction mixture was allowed to reflux for 24 h. After cooling, a solution of 10% aqueous sodium hydroxide was added to destroy the lithium aluminum hydride, the mixture was filtered, and the solvent was removed *in vacuo* to give a viscous oil. Purification of the reaction mixture by elution from a 1 cm × 20 cm silica gel column using chloroform–methanol (9:1 v/v) as eluant gave **10** as a viscous oil, yield (0.32 g, 72.7%); nmr ($CDCl_3$) δ: 7.37 (m, 5H, Ph), 3.78–4.1 (m, 1H, H_3), 3.56 (s, 2H, CH_2Ph), 2.0–3.24 (m, 7H, H_2, H_4, H_6, OH, NH), 1.52–2.0 (m, 2H, H_5). *Exact Mass* calcd. for $C_{13}H_{20}N_2O$: 220.1576; found (high resolution ms): 220.1574.

1-Aminocarbonyl-1,2,3,6-tetrahydropyridine (13)

The oxyamination of **11** (5 mmol) as outlined in Procedure A afforded a solid which was purified by elution from a silica gel column using a gradient of hexane–chloroform to afford **13**, yield (16.2%); mp 121–122°C; ir: 3400, 3220 (NH_2), 1660 (CO); nmr ($CDCl_3$) δ: 5.83 (m, 2H, H_4, H_5), 4.7 (br s, 2H, NH_2, exchanges with deuterium oxide), 3.95 (m, 2H, H_6), 3.56 (t, $J_{2,3}$ = 6 Hz, 2H, H_2), 2.25 (m, 2H, H_5). *Exact Mass* calcd. for $C_6H_{10}N_2O$: 126.0794; found (high resolution ms): 126.0795. This product was identical (ir, nmr) to an authentic sample prepared from the reaction of 1-chlorocarbonyl-1,2,3,6-tetrahydropyridine with ammonia.

Oxyamination of **11** using Procedure B afforded **13** (20%).

cis-*1-Methoxycarbonyl-2-hydroxy-3*-tert-*butoxycarbonylamino-1,2,3,6-tetrahydropyridine (15) and* cis-*1-methoxycarbonyl-2*-tert-*butoxycarbonylamino-3-hydroxy-1,2,3,6-tetrahydropyridine (16)*

A mixture of *N*-chloro-*N*-sodio-*tert*-butylcarbamate (7.8 g, 45 mmol) and silver nitrate (15 g, 90 mmol) in acetonitrile (200 mL) was allowed to stir for 15 min at 25°C. Water (132 mmol), 1-methoxycarbonyl-1,2-dihydropyridine (9) (4.17 g, 30 mmol), and a solution of osmium tetroxide (0.3 mmol) in *tert*-butylalcohol was added to this suspension. The reaction was allowed to proceed with stirring at 25°C for 24 h. The mixture of **15** and **16** obtained, following the isolation procedure described in Procedure A, was separated by preparative hplc using hexane–ether (1:4 v/v) at a flow rate of 250 mL/min. Removal of the solvent from the 1000–1500 mL fractions gave **15** (1.85 g, 22.7%), mp 119–120°C; ir: 3340–3360 (OH, NH), 1720 (NHCO), 1680 (NCO_2Me); nmr (Me_2SO-d_6, 50°C) δ: 6.26–6.44 (m, 1H, NH), 5.84 (d, J = 5 Hz, 1H, OH), 5.68–5.8 (d, $J_{4,5}$ = 10 Hz of d, $J_{3,4}$ = 3 Hz of d, $J_{4,6ax}$ = 3 Hz of d, $J_{4,6eq}$ = 3 Hz, 1H, H_4), 5.6–5.68 (m, $J_{2,3}$ = 3 Hz, 1H, H_2), 5.36–5.48 (d, $J_{4,5}$ = 10 Hz of d, $J_{5,6ax}$ = 1.5 Hz of d, $J_{5,6eq}$ = 1.5 Hz, 1H, H_5), 4.03–4.16 (m, 1H, H_3), 3.86–4.03 (d, J_{gem} = 18 Hz of d, $J_{4,6eq}$ = 3 Hz of d, $J_{3,6eq}$ = 3 Hz, 1H, H_{6eq}), 3.66 (s, 3H, CO_2Me), 3.44–3.68 (m, 1H, H_{6ax}), 1.4 (s, 9H, *t*-Bu). *Exact Mass* calcd. for $C_8H_{11}N_2O_5$ (M^+ − 57): 215.0668; found (high resolution ms): 215.0655; CI (NH_3) for $C_{12}H_{20}N_2O_5$: M + 1, 273 and 2 M + 1, 545. Collection of the 1500–1750 mL fraction yielded a mixture of **15** and **16** (0.4 g, 4.9%), whereas the 1750–2750 mL eluate afforded **16** (1.82 g, 22.4%) as a viscous oil; ir: 3420–3460 (OH), 3350–3380 (NH); nmr (Me_2SO-d_6, 100°C) δ: 5.4–6.3 (m, 4H, NH, H_2, H_4, H_5), 5.04 (d, J = 6 Hz, 0.5H, H-bonded OH), 4.24 (m, 0.5H, OH), 3.34–4.08 (6H, H_3, H_6, OMe), 1.4 (s, 9H, *t*-Bu). *Exact Mass* calcd. for $C_{12}H_{20}N_2O_5$: 272.1372; found (high resolution ms): 272.1363.

cis-*1-Methoxycarbonyl-2-methoxy-3*-tert-*butoxycarbonylaminopiperidine (17)*, *1-methoxycarbonyl-2-methoxy-3*-tert-*butoxycarbonylaminopiperidine (18)*, cis-*1-methoxycarbonyl-2*-tert-*butoxycarbonylamino-3-hydroxypiperidine (19)*, *and 1-methoxycarbonyl-2*-tert-*butoxycarbonylamino-3-hydroxypiperidine (20)*

Hydrogenation of **15** (0.6 g, 2.2 mmol) in 200 mL methanol using 100 mg 10% palladium on charcoal and hydrogen gas at 25 psi for 7 h at 25°C, followed by filtration and removal of the solvent *in vacuo*, afforded a mixture of **17–20**. Purification on a 1 cm × 30 cm silica gel column using chloroform as eluant gave initially a mixture of **17** and **18** (0.185 g, 29.2%) in a ratio of 2:1, calculated from the integrals for the C-2H of **17** and **18** at 5.24 and 5.14 δ respectively. Fractional crystallization of this mixture from hexane–ether (1:9 v/v) gave pure samples of **17** and **18** which showed the following spectral data.

Compound **17**, ir: 3360 (NH), 1720 (NHCO), 1695–1705 (NCO_2Me); nmr (Me_2SO-d_6, 70°C) δ: 6.18–6.38 (m, 1H, NH), 5.24 (d, $J_{2eq-3ax}$ = 2.8 Hz, 1H, H_{2eq}), 3.66–3.82 (d, $J_{6eq-6ax}$ = 12.5 Hz of d, $J_{2,3}$ = 3 Hz, 1H, H_{6eq}), 3.66 (s, 3H, CO_2Me), 3.26–3.48 (m, 1H, H_{3ax}), 3.2 (s, 3H, OMe), 2.66–2.90 (m, 1H, H_{6ax}), 1.34–1.86 (m, 13H, H_4, H_5, *t*-Bu); *Exact Mass* calcd. for $C_{13}H_{24}N_2O_5$: 288.1685; found (high resolution ms): 288.1679.

Compound **18**, mp 110–111°C; ir: 3340 (NH), 1720 (NHCO), 1680–1690 (NCO_2Me); nmr δ: 6.70–6.96 (br s, 1H, NH), 5.14 (d, $J_{2,3}$ = 1.5 Hz, 1H, H_2), 3.70–3.82 (d, $J_{6eq-6ax}$ = 12.5 Hz of d, $J_{5,6}$ = 3 Hz, 1H, H_{6eq}), 3.50–3.67 (m, 1H, H_{3eq}), 3.63 (s, 3H, CO_2Me), 3.18 (s, 3H, OMe), 2.8 (ddd, 1H, H_{6ax}), 1.64–1.88 (m, 2H, H_4), 1.2–1.5 (m, 11H, H_5, *t*-Bu). *Exact Mass* calcd. for $C_{13}H_{24}N_2O_5$: 288.1685; found (high resolution ms): 288.1685.

Further elution with chloroform gave **20** (0.18 g, 29.9%), mp 160°C; ir: 3360, 3460 (OH, NH), 1715 (NHCO), 1685–1700 (NCO_2Me); nmr (Me_2SO-d_6, 50°C) δ: 7.24 (d, J = 7.5 Hz, 1H, NH), 6.8–6.9 (br s, 1H, OH), 5.52–5.7 (m, 1H, H_2), 3.78 (m, 4H, H_{6eq}, CO_2Me), 3.38–3.48 (m, 1H, H_{3eq}), 2.91 (sextet, 1H, H_{6ax}), 1.16–2.08 (m, 13H, H_4, H_5, *t*-Bu). *Exact Mass* calcd. for $C_{12}H_{20}N_2O_4$ (M^+ − 18): 256.1423; found (high resolution ms): 256.1427; CI (NH_3): M + 1, 275.

Continued elution with chloroform gave **19** (0.148 g, 24.5%), mp 161–163°C; ir: 3460 (OH), 3340 (NH), 1720 (NHCO), 1685–1700 (NCO_2Me); nmr (Me_2SO-d_6, 50°C) δ: 6.74 (d, J = 8 Hz, 1H, NH), 5.7 (d, $J_{2,NH}$ = 8 Hz of d, $J_{2eq,3ax}$ = 5 Hz, 1H, H_{2eq}), 4.86 (d, J = 5 Hz, 1H, OH), 3.64–3.7 (m, 1H, H_{6eq}), 3.6 (s, 3H, CO_2Me), 3.48 (sextet, $J_{3,4ax}$ = 10 Hz, $J_{3,4eq}$ = 5 Hz, $J_{2,3}$ = 5 Hz, $J_{3,OH}$ = 5 Hz, 1H, H_{3ax}), 2.81 (ddd, 1H, H_{6ax}), 1.2–1.8 (m, 13H, H_4, H_5, *t*-Bu). *Exact Mass* calcd. for $C_{12}H_{22}N_2O_5$: 274.1529; found (high resolution ms): 274.1526.

Hydrogenation of **16** (0.5 g, 1.84 mmol), as outlined for **15** above, afforded a mixture of **17** and **18** (0.15 g, 28.3%) in a ratio of 1:1, **20** (0.021 g, 4%), and **19** (0.215 g, 40.6%).

Acknowledgement

We are grateful to the Natural Sciences and Engineering Research Council of Canada (Grant No. A0531) for financial support of this work.

1. (*a*) K. B. SHARPLESS, D. W. PATRICK, L. K. TRUESDALE, and S. A. BILLER. J. Am. Chem. Soc. **97**, 2305 (1975); (*b*) D. W. PATRICK, L. K. TRUESDALE, S. A. BILLER, and K. B. SHARPLESS. J. Org. Chem. **43**, 2628 (1978); (*c*) S. G. HENTGES and K. B. SHARPLESS. J. Org. Chem. **45**, 2257 (1980).
2. (*a*) K. B. SHARPLESS, A. O. CHONG, and K. OSHIMA. J. Org. Chem. **41**, 177 (1976); (*b*) E. HERRANZ and K. B. SHARPLESS. J. Org. Chem. **43**, 2544 (1978).
3. (*a*) E. HERRANZ, S. A. BILLER, and K. B. SHARPLESS. J. Am. Chem. Soc. **100**, 3596 (1978); (*b*) E. HERRANZ and K. B. SHARP-

LESS. J. Org. Chem. **45**, 2710 (1980).
4. (*a*) E. E. KNAUS, F. M. PASUTTO, C. S. GIAM, and E. A. SWINYARD. J. Heterocycl. Chem. **13**, 481 (1976); (*b*) E. E. KNAUS and K. REDDA. J. Heterocycl. Chem. **13**, 1237 (1976); (*c*) E. E. KNAUS and K. REDDA. Can. J. Chem. **55**, 1788 (1977); (*d*) T. A. ONDRUS, E. E. KNAUS, and C. S. GIAM. Can. J. Chem. **56**, 1026 (1978); (*e*) F. M. PASUTTO and E. E. KNAUS. Can. J. Chem. **57**, 2371 (1979); (*f*) T. A. ONDRUS, E. E. KNAUS, and C. S. GIAM. Can. J. Chem. **57**, 2342 (1979); (*g*) E. E. KNAUS, K. AVASTHI, and C. S. GIAM. Can. J. Chem. **58**, 2447 (1980); (*h*) K. AVASTHI and E. E. KNAUS. J. Heterocycl. Chem. **18**, 375 (1981); (*i*) K. AVASTHI and E. E. KNAUS. Can. J. Pharm. Sci. **16**, 52 (1981).
5. (*a*) E. E. KNAUS, K. REDDA, and F. W. WANDELMAIER. U. S. Patent No. 4 088 653, May 9, 1978; (*b*) K. REDDA, L. A. CORLETO, and E. E. KNAUS. Can. J. Chem. **57**, 2981 (1979); (*c*) T. A. ONDRUS and E. E. KNAUS. Can. J. Pharm. Sci. **14**, 55 (1979); (*d*) K. REDDA, L. A. CORLETO, and E. E. KNAUS. J. Med. Chem. **22**, 1079 (1979); (*e*) B. K. WARREN and E. E. KNAUS. J. Med. Chem. **24**, 462 (1981); (*f*) J. M. YEUNG, L. A. CORLETO, and E. E. KNAUS. J. Med. Chem. **25**, 191 (1982).
6. J. E. BACKVALL, K. OSHIMA, R. E. PALERMO, and K. B. SHARPLESS. J. Org. Chem. **44**, 1953 (1979).
7. (*a*) W. A. SZAREK, S. WOLFE, and J. K. N. JONES. Tetrahedron Lett. 2743 (1964); (*b*) G. YAMAMOTO and M. RABAN. J. Org. Chem. **41**, 3788 (1976).
8. L. M. JACKMAN and S. STERNHELL. Nuclear magnetic resonance spectroscopy in organic chemistry. 2nd ed. Pergamon Press, Toronto, Ont. 1969. p. 288.
9. F. W. FOWLER. J. Org. Chem. **37**, 1321 (1972).
10. E. WENKERT, J. S. BINDRA, C. J. CHANG, D. W. COCHRAN, and F. M. SCHELL. Acc. Chem. Res. **7**, 46 (1974).
11. F. JOHNSON. Chem. Rev. **68**, 375 1968).

Can. J. Chem. Downloaded from www.nrcresearchpress.com by 210.87.254.6 on 09/06/12
For personal use only.

Synthesis of (±)-epiisopodophyllotoxin

MARGARET B. GLINSKI AND TONY DURST

Ottawa–Carleton Institute for Graduate Studies and Research in Chemistry, University of Ottawa, Ottawa, Ont., Canada K1N 9B4

Received July 23, 1982

MARGARET B. GLINSKI and TONY DURST. Can. J. Chem. **61**, 573 (1983).

The synthesis of (±)-epiisopodophyllotoxin commencing with 6-bromopiperonal dimethyl acetal is described. The carbon skeleton of isoepipodophyllotoxin was assembled via a Diels–Alder reaction between the hydroxyquinodimethane generated photochemically from 6-(3′,4′,5′-trimethoxybenzyl)-piperonal, obtained from the bromoacetal above, and dimethyl fumarate. This Diels–Alder adduct was converted in five steps into the title compound. The overall yield for the seven steps was 15%.

MARGARET B. GLINSKI et TONY DURST. Can. J. Chem. **61**, 573 (1983).

On décrit une synthèse de la (±) épiisopodophyllotoxine faisant appel à l'acétal diméthylique du bromo-6 pipéronal comme produit de départ. On a édifié le squelette carboné de la isoépipodophyllotoxine en utilisant une réaction de Diels–Alder entre le fumarate de diméthyle et l'hydroxyquinodiméthane produit photochimiquement à partir du (triméthoxy-3′,4′,5′ benzyl)-6 pipéronal provenant du bromoacétal. L'adduit de Diels–Alder permet d'obtenir le composé mentionné dans le titre. Le rendement global des 7 étapes est de 15%.

[Traduit par le journal]

Can. J. Chem. Downloaded from www.nrcresearchpress.com by 210.87.254.105 on 09/06/12
For personal use only.

Introduction

Podophyllotoxin **1**, a naturally occurring lignan lactone isolated from *Podophyllum peltatum* is of considerable interest due to its cytotoxic activity (for a recent review, see ref. 1). Indeed, two glycosylated derivatives of **1**, Etoposide, **2** (VP-16), and Teniposide, **3** (VM-26), are in clinical use as agents against small cell lung and bladder cancers (2).

As part of a program concerning the synthesis of podophyllotoxin derivatives, we have completed the synthesis of (±)-epiisopodophyllotoxin **4**.[1] This compound still contains the highly strained *trans*-fused lactone of podophyllotoxin which is considered important for biological activity (3), but has a *trans* relationship between the 1-aryl substituent and the lactone carbonyl group, compared to the *cis* arrangement of these substituents in podophyllotoxin. (±)-Epiisopodophyllotoxin has previously been synthesized by Gensler and Johnson (4) in low overall yield commencing with 3,4,5-trimethoxybenzene and piperonylic acid.

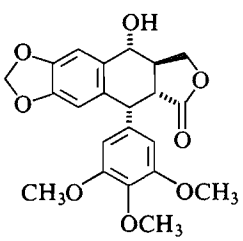

1

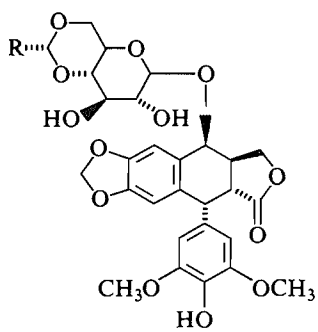

2 R = CH_3

3 R =

[1]In the nomenclature for these compounds, "iso" and "epi" refer to inversion of configuration at positions 1 and 4, relative to naturally occurring podophyllotoxin.

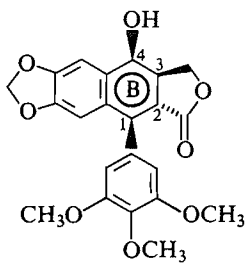

4

Discussion and results

The carbon skeleton of **4** was generated via a Diels–Alder reaction between the dienol **5** obtained by photoenolization of 6-(3′,4′,5′-trimethoxybenzyl)-piperonal, **6**, and dimethyl fumarate. Sammes and co-workers (5) have shown that in general, *ortho*-substituted benzaldehydes undergo isomerization to *o*-quinodimethanes when irradiated in solvents such as benzene, acetone, or THF with a medium-pressure Hg lamp, and that these intermediates can be trapped with a variety of dienophiles including dimethyl acetylene dicarboxylate and maleic anhydride (6).

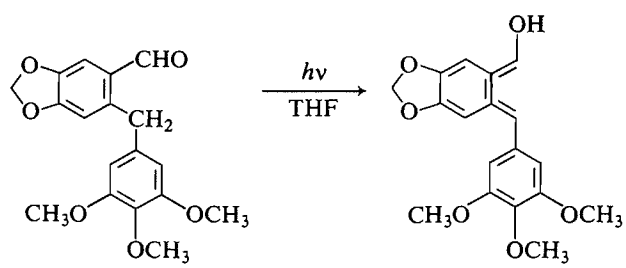

6 **5**

A synthesis of **6** had previously been reported by Sammes and co-workers (6) via a six-step sequence with an overall yield of 17%, utilizing 6-bromopiperonal ethylene ketal and 3,4,5-trimethoxybenzaldehyde as starting materials. We have found it possible to prepare **6** in 84% yield from 6-bromopiperonal dimethyl acetal, by treatment with *n*-BuLi, *n*-$Bu_3P \cdot CuI$, and

Can. J. Chem. Downloaded from www.nrcresearchpress.com by 210.87.254.105 on 09/06/12
For personal use only.

3,4,5-trimethoxybenzyl bromide. The use of n-$Bu_3P \cdot CuI$ was crucial for the coupling reaction; no coupling was observed in the absence of the above reagent or when it was replaced by $MgBr_2$, CuI, or $FeCl_3$.

Irradiation of **6** in THF in the presence of dimethyl fumarate afforded the diester **9**, mp 198°C, as the only isolable adduct in 47% yield. The structure was assigned as **7**, based on analogy with earlier work (5) which had shown that the Diels–Alder reaction of dienols such as **5** with dimethyl fumarate or maleic anhydride gave adducts in which the hydroxyl group and the *"ortho"* carbonyl substituent were *cis* to each other. This was corroborated by the proton nmr spectrum of **7** (see Experimental section) and those of the derivatives **10**, **11**, and **4** (see Scheme 2).

The ester group *ortho* to the hydroxyl function in **7** was selectively reduced upon reaction with 3 equiv. of $LiHBEt_3$ in THF at −78°C, followed by warming to 25°C to furnish the crystalline diol **8**, mp 155°C, in 70% yield.

Direct saponification of **8** to the acid **9** was not possible without considerable decomposition. Consequently the diol was protected as the acetonide **10** (90%), prior to carrying out the basic ester hydrolysis (83%). Subsequent deprotection furnished **9**, mp 230–234°C (dec.) in 65% overall yield from **8**. Lactonization of **9** to (±)-epiisopodophyllotoxin, mp 258–260°C (lit. (4) mp 255°C (dec.)), was accomplished using DCC as the activating agent, Scheme 2. The sequence from **7** to **4** was based on a similar series of reactions developed by Kuhn and co-workers (7) and by Rajapaksa and Rodrigo (8) for the conversion of **11** to podophyllotoxin **1**.

The stereochemical assignments for **4** and the intermediates **7**–**10** were readily confirmed by the observed coupling constants in the B-ring (structure **4**) in these intermediates. In particular, in the acetonide **10**, the 3.0 Hz coupling between H_3 and H_4 is clearly consistent with an axial–equatorial arrangement between H_3 and H_4, while the large 11.6 Hz J for H_1 (δ = 4.06) requires a diaxial relationship between H_1 and H_2.

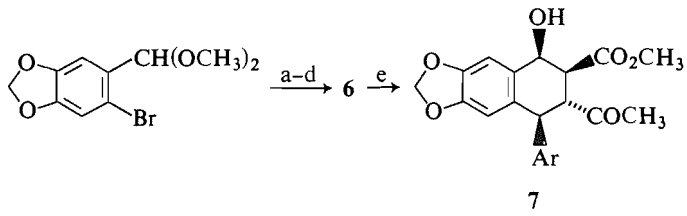

7

Reagents: (a) n-BuLi/THF, −78°C; (b) n-$Bu_3P \cdot CuI$; (c) 3,4,5-tri-methoxybenzyl bromide; (d) H^+/H_2O; (e) $h\nu$/THF/dimethyl fumarate.

SCHEME 1

H_3 in **11** appears as a triplet, J = 11.6 Hz, thus necessitating two axial–axial relationships. In (±)-epiisopodophyllotoxin, **4**, $J_{H_1H_2}$ and $J_{H_3H_4}$ are 11.0 Hz, and 3.0 Hz, respectively, while the same two coupling constants in podophyllotoxin are 4.4 and 9.1 Hz.

Experimental

General comments

Nuclear magnetic resonance spectra were taken on Varian HA-100, T-60, and FT-80 spectrometers in $CDCl_3$ solution with TMS as internal standard. Infrared spectra were obtained in $CHCl_3$ solution using a Perkin–Elmer 470 spectrophotometer. Melting points, Gallenkamp apparatus, are uncorrected.

6-(3',4',5'-Trimethoxybenzyl)-piperonal (6)

To a solution of 278 mg (1 mmol) of 6-bromopiperonal dimethyl acetal (8) in 1 mL of dry THF at −78°C under N_2 was added 0.42 mL of n-BuLi (2.4 M in hexanes). The solution was stirred for 10 min and then treated with 196 mg (0.5 mmol) of n-$Bu_3P \cdot CuI$ dissolved in 0.5 mL of THF. After a further 10 min at −78°C, 130 mg (0.5 mmol) of 3,4,5-trimethoxybenzaldehyde, dissolved in a small volume of THF, was added. The reaction mixture was kept at −78°C for 1 h and then at room temperature for a further 18 h before quenching with a

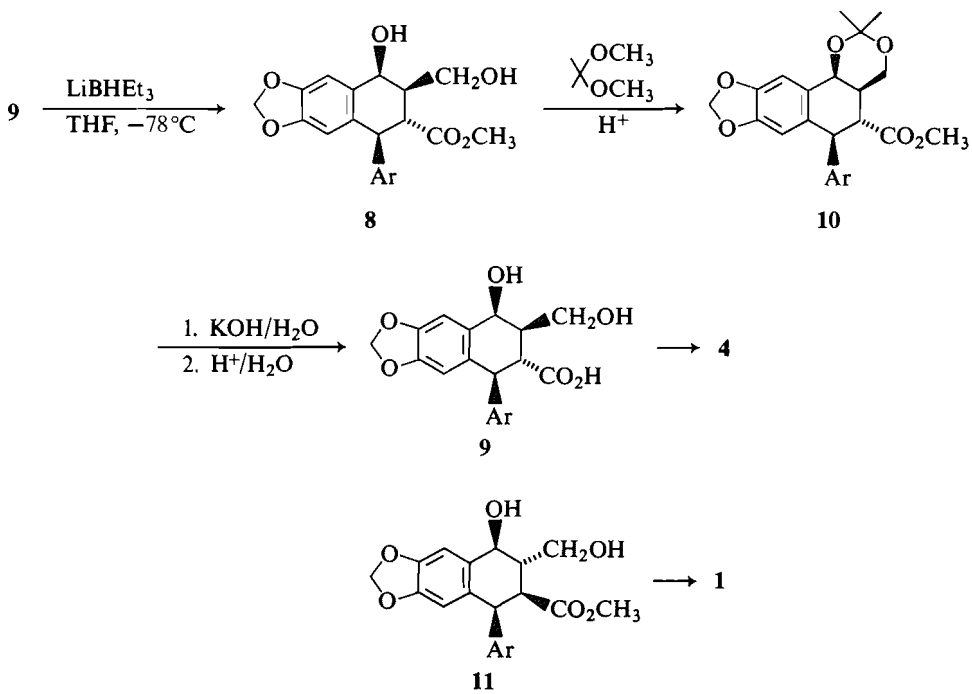

SCHEME 2

saturated NH_4Cl solution. A typical work-up followed by column chromatography on silica gel (3:1 hexanes – ethyl acetate) afforded 148 mg of a colorless oil which was identified by nmr as the dimethyl acetal of the desired aldehyde; ^1H nmr: 3.27 (3, 3H), 3.80 (3, 9H), 3.93 (s, 2H), 5.88 (s, 2H), 5.90 (s, 1H), 6.35 (s, 2H), 6.45 (s, 1H), and 7.07 (s, 1H).

The oil was dissolved in 10 mL of methanol and 1 mL of 5% HCl was added. The title aldehyde began to crystallize from the solution within a short time. The product was filtered and recrystallized from ether–hexanes to yield 140 mg (84%, overall) of 6-(3′,4′,5′-trimethoxybenzyl)-piperonal as fine colorless needles, mp 123°C (lit. (6) mp 124–125°C); ir: 1690 cm^{-1}; ^1H nmr: 3.84 (s, 6H), 3.86 (s, 3H), 4.34 (3, 2H), 6.08 (s, 2H), 6.38 (s, 2H), 6.72 (s, 1H), 7.36 (s, 1H), 9.93 (s, 1H); ^{13}C nmr: 189.6, 153.4, 152.6, 147.1, 140.4, 136.7, 135.9, 128.6, 111.0, 109.0, 105.7, 102.1, 60.9, 56.1, 37.7.

Photolysis of ***6*** *in the presence of dimethyl fumarate*

A solution of **6** (660 mg, 2.0 mmol) and 288 mg (2.0 mmol) of dimethylfumarate in 100 mL of dry THF was irradiated for 18 h in a quartz apparatus with a long uv lamp at room temperature under a nitrogen atmosphere. The solvent was evaporated and the crude solid was recrystallized from $CHCl_3$–ether to furnish 450 mg (47%) of **7**, mp 198°C, as colorless plates; ir: 3300–3500 (br), 1720 (s), 1590 (s) cm^{-1}; ^1H nmr: 2.27 (OH), 3.19 (dd, J = 12, 3 Hz, 1H), 3.42 (dd, J = 12, 10.5 Hz, 1H), 3.50 (s, 3H), 3.75 (s, 3H), 3.79 (s, 6H), 3.85 (s, 3H), 4.02 (d, J = 10, 1H), 5.07 (d, J = 3 Hz, 1H), 5.89 (s, 2H), 6.47 (s, 1H), 6.54 (s, 2H), 6.77 (s, 1H); ^{13}C nmr: 174.9, 172.8, 153.3, 153.0, 143.2, 146.6, 138.3, 131.7, 108.9, 108.6, 106.0, 101.22, 68.0, 60.9, 56.2, 52.3, 51.8, 48.7, 45.6. *Anal.* calcd. for $C_{24}H_{26}O_{10}$: C 60.75, H 5.53; found: C 61.13, H 5.71.

Reduction of diester 7

Diester **7** (474 mg, 1 mmol) was dissolved in 10 mL of dry THF and cooled to −78°C under a nitrogen atmosphere. $LiBEt_3H$ (3.0 mmol) was added by syringe and the solution was allowed to warm for an hour to room temperature and then stirred for an additional 18 h. The reaction mixture was quenched with 1% HCl and then worked up in the usual manner to yield a yellowish solid which was recrystallized from ether–hexanes to afford 312 mg (70%) of the diol **8** as colorless needles, mp 155°C; ir: 3300–3500 (br), 1725 (s), 1600 (s) cm^{-1}; ^1H nmr: 2.45 (m, 1H), 3.00 (t, J = 11 Hz, 1H), 3.52 (s, 3H), 3.79 (3, 6H), 3.84 (s, 3H), 3.80 (OH, 2H), 4.0–4.3 (m, 3H), 5.01 (d, J = 3 Hz, 1H), 5.89 (s, 2H), 6.26 (s, 1H), 6.30 (s, 2H), 6.83 (s, 1H). *Anal.* calcd. for $C_{23}H_{26}O_9$: C 61.87, H 5.87; found: C 61.63, H 5.55.

Ketalization of diol 8

The diol **10** (340 mg, 0.76 mmol) and TsOH (10 mg) were dissolved in 2,2-dimethoxypropane (5 mL). The solution was kept at room temperature for 3 h, diluted with 25 mL of CH_2Cl_2, and washed with 25 mL of 10% $NaHCO_3$. The organic extracts were dried and the solvent evaporated. Recrystallization of the crude product from ether–hexanes afforded 330 mg (90%) of the acetonide **9** as colorless needles, mp 181–182°C; ir: 1720 (s), 1590 (m) cm^{-1}; ^1H nmr: 1.47 (s, 3H), 1.63 (s, 3H), 2.03 (m, 1H), 3.40 (t, J = 11.6 Hz, 1H), 3.43 (s, 3H), 3.65 (dd, J = 12.0, 2.0 Hz, 1H), 3.75 (s, 6H), 3.80 (s, 3H), 4.06 (d, J = 11.6 Hz, 1H), 4.18 (dd, J = 12.0, 3.5 Hz, 1H), 4.83 (d, J = 3.0 Hz, 1H), 5.87 (d, J = 1.4 Hz, 1H), 5.91 (d, J = 1.4 Hz, 1H), 6.23 (s, 1H), 6.30 (s, 2H), 6.67 (s, 1H). *Anal.* calcd. for $C_{26}H_{30}O_9$: C 64.18, H 6.22; found: C 64.12, H 5.96.

Diolcarboxylic acid ***9***

The acetonide **10** (50 mg) was saponified by heating for 4 h in a 1:1 mixture of 1% aqueous KOH and dioxane. Ether was added to the cooled mixture and the aqueous phase was separated and acidified. The acid was extracted from the aqueous phase by extracting 3 times with 10 mL of CH_2Cl_2. The extracts were dried and evaporated, yielding 40 mg (83%) of the intermediate ketal acid as a colorless powder, mp 181–183°C; ir: 2500–3500 (br), 1700 (s), 1590 (s) cm^{-1}; ^1H nmr: 1.46 (s, 3H), 1.63 (s, 3H), 2.01 (m, 1H), 3.48 (t, J = 11.6 Hz, 1H), 3.69 (dd, J = 12.0, 2.0 Hz, 1H), 3.80 (s, 6H), 3.85 (s, 3H), 4.01 (d, J = 11.6 Hz, 1H), 4.09 (dd, J = 12.0, 3.5 Hz, 1H), 4.81 (d, J = 3 Hz, 1H), 5.86 (d, J = 1.4 Hz, 1H), 5.88 (d, J = 1.4 Hz, 1H), 6.24 (s, 1H), 6.35 (s, 2H), 6.71 (s, 1H), 11.20 (br, COOH); *Mol. Wt.* calcd.: 472.4; found: 472. *Anal.* calcd. for $C_{25}H_{28}O_9$: C 63.55, H 5.97; found: C 63.20, H 6.17.

The above acetonide (130 mg) was converted to **9** by stirring at room temperature for 24 h with a mixture of 12 mL of 1:1 of 1% HCl and dioxane. Usual work-up afforded, after recrystallization from acetone–ether, 100 mg of **9** as small colorless needles, mp 230–234°C; ir: 2500–3500 (br), 1710 (s), 1590 (s) cm^{-1}; nmr: 2.47 (m, 1H), 3.08 (t, J = 11.0 Hz, 1H), 3.79 (s, 6H), 3.84 (s, 3H), 3.95 (br, 3 × OH), 4.00–4.27 (m, 3H), 5.07 (d, J = 3.0 Hz, 1H), 5.85 (s, 2H), 6.26 (s, 1H), 6.30 (s, 2H), 6.82 (s, 1H). *Anal.* calcd. for $C_{22}H_{24}O_9$: C 61.10, H 5.60; found: C 61.28, H 5.69.

(±)-Epiisopodophyllotoxin, ***4***

Acid **9** (50 mg, 0.12 mmol) and DCC (30 mg, 0.12 mmol) were dissolved in 4 mL of dry THF. The solution was kept at room temperature for 3 h, treated with 0.2 mL of H_2O and 0.1 mL of glacial acetic acid, and left for an additional 30 min. The solvents were then evaporated and the residue triturated with 5 mL of CH_2Cl_2. The CH_2Cl_2 soluble fraction was purified on preparative tlc (ether) and afforded 37 mg (75%) of **4** as a colorless powder, mp 258–260°C ($CHCl_3$/ether) (lit. (4) mp 255°C); ir: 3350–3550 (br), 1775 (s) cm^{-1}; nmr: 2.03 (OH), 2.68 (m, 1H), 3.29 (dd, J = 14.0, 11.2 Hz, 1H), 4.11 (m, 1H), 3.82 (s, 6H), 3.85 (s, 3H), 4.03 (d, J = 10 Hz, 1H), 4.46 (m, 1H), 4.94 (d, J = 3.0 Hz, 1H), 5.93 (s, 2H), 6.39 (s, 1H), 6.44 (s, 2H), 6.78 (s, 1H). *Anal.* calcd. for $C_{22}H_{22}O_8$: C 63.76, H 5.35; found: C 63.89, H 5.41.

Acknowledgement

The continued financial support of NSERC in the form of an operating grant to T.D. and a postgraduate scholarship to M.G.B. is gratefully acknowledged.

1. I. JARDINE. Med. Chem. **16**, 319 (1980).
2. P. A. RADICE, P. A. BUNN, and O. C. IHDE. Cancer Treat. Rep. **63**, 1231 (1979).
3. C. F. BREWER, J. D. LOIKE, S. B. HOROWITZ, H. STERNLICHT, and W. J. GENSLER. J. Med. Chem. **22**, 215 (1979).
4. W. J. GENSLER and F. JOHNSON. J. Am. Chem. Soc. **85**, 3670 (1963).
5. (*a*) S. M. MELLOWS and P. G. SAMMES. J. Chem. Soc. Chem. Commun. 21 (1971); (*b*) P. G. SAMMES. Tetrahedron, **32**, 405 (1976).
6. B. J. ARNOLD, S. M. MELLOWS, and P. G. SAMMES. J. Chem. Soc. Perkin Trans. **1**, 1266 (1973).
7. J. RENZ, M. KUHN, and A. VON WARTBURG. Justus Liebigs Ann. Chem. **681**, 207 (1965).
8. D. RAJAPASKA and R. RODRIGO. J. Am. Chem. Soc. **103**, 6208 (1981).

Can. J. Chem. Downloaded from www.nrcresearchpress.com by 210.87.254.105 on 09/06/12
For personal use only.

The effect of stereochemistry on $^1J_{C-H}$ at the sp^2 carbons of oxime, hydrazone, and imine derivatives of aldehydes

ROBERT R. FRASER AND MONIQUE BRESSE

Ottawa–Carleton Institute for Research and Graduate Studies in Chemistry, University of Ottawa, Ottawa, Ont., Canada K1N 9B4

Received September 7, 1982

ROBERT R. FRASER and MONIQUE BRESSE. Can. J. Chem. **61**, 576 (1983).

A comparison of the magnitudes of $^1J_{C-H}$ at the aldehydic carbon of both the *syn* and *anti* isomers of aldehyde derivatives (oximes, hydrazones, and imines) has shown a consistently greater value, by about 20 Hz, for the *syn* isomer. Regardless of its origin, this stereochemical correlation should prove useful in providing configurational assignments.

ROBERT R. FRASER et MONIQUE BRESSE. Can. J. Chem. **61**, 576 (1983).

On a effectué une comparaison des ordres de grandeur des $^1J_{C-H}$ au niveau du carbone aldéhydique des isomères *syn* et *anti* des dérivés d'aldéhyde (oximes, hydrazones et imines); cette valeur est systématiquement plus grande d'environ 20 Hz pour l'isomère *syn*. Sans tenir compte de son origine, cette corrélation stéréochimique devrait s'avérer utile pour faire des attributions de configuration.

[Traduit par le journal]

Can. J. Chem. Downloaded from www.nrcresearchpress.com by 210.87.254.6 on 09/06/12
For personal use only.

Introduction

One of the most widely studied of all nmr parameters is $^1J_{C-H}$, the coupling constant between a carbon atom and a hydrogen atom directly bonded to it. A recent review (1), which summarizes both the experimental and the theoretical contributions to the field, identifies a number of structural features which affect ^1J, but only one of these, the hybridization of the carbon atom, appears to be the dominant factor.

There have been many studies involving a correlation between the stereochemistry of a pair of diastereomers and the magnitude of $^1J_{C-H}$. An axial H at C-1 of carbohydrates or at C-2 in simple tetrahydropyrans generally exhibits a $^1J_{C-H}$ which is 8 to 10 Hz smaller than that for an equatorial C—H (2, 3). In piperidine derivatives, $^1J_{C-H}$ for a proton α to nitrogen and *trans* to the lone pair on nitrogen (i.e., axial) is 6 to 10 Hz smaller than when *gauche* (equatorial) (4). Similar lone pair effects have been noted in trimethylene sulfites (5) and 1,3-dioxanes (6). The effect can be rationalized on the same basis as the anomeric effect. Thus, as shown in Scheme 1, the axial conformer of 2-chlorotetrahydropyran possesses a resonance structure involving an $n-\sigma^*$ interaction between an unshared pair of electrons at oxygen and the axial C—Cl bond. This should produce an increase in the "*s*-character" of the equatorial C—H bond and hence a larger $^1J_{C-H}$. The analogous $n-\sigma^*$ interaction involving an axial C—H in the equatorial conformer should be much less important. In the absence of a substituent at C-2 this $n-\sigma^*$ interaction with an axial C—H will contribute more *p*-character to the axial C—H bond, thereby accounting for the smaller $^1J_{C-H}$ for axial hydrogens α to a lone pair.

In both aziridines (7) and oxaziridines (8) a C—H bond *trans* to the lone pair shows a 6–10 Hz smaller value for $^1J_{C-H}$ than when *cis* to it for similarly expressed reasons.

The influence of lone-pair orientation on $^1J_{C-H}$ when the carbon involved has sp^2 hybridization has received considerable theoretical attention. For oximes, the *syn* (*Z*) isomer has been calculated to have the larger $^1J_{C-H}$. Three independent theoretical treatments have estimated the difference to be from 10 to 60 Hz (9–11). A few calculations were also reported for

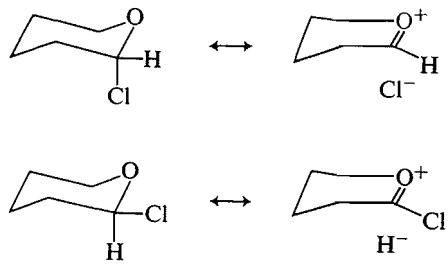

SCHEME 1

acetaldehyde hydrazone and two imines of acetaldehyde. The results of all the theoretical calculations are presented in Table 1. In contrast to the theoretical interest, only two pairs of *syn–anti* isomers, those of acetaldoxime and isobutyraldoxime have been determined and the experimental values for $^1J_{C-H}$ in these compounds are also reported in Table 1. The best agreement with these values, in both absolute magnitude and *syn–anti* differences, is provided by the calculations of Pople's group (9).

In view of the lack of any experimental data on imines and hydrazones, coupled with current developments in the synthesis of *syn* aldimines (13) and hydrazones (14), we have prepared two pairs of *syn* and *anti* hydrazones and four diastereomeric pairs of imines in order to measure $^1J_{C-H}$ in each compound. We have also examined the isomeric propionaldoximes for comparison with earlier results. The results should provide data to indicate possible stereochemical effects on $^1J_{C-H}$ as well as for comparison with the theoretical predictions.

Results

We have synthesized each *syn* aldimine and hydrazone by the reaction sequence presented in Scheme 2. As has been shown for a wide range of carbonyl derivatives, including oximes and their ethers, hydrazones, and imines (14), the products of lithiation (for a recent review, see ref. 15) and of their subsequent alkylation (13–15) both possess the *syn* config-

Can. J. Chem. Downloaded from www.nrcresearchpress.com by 210.87.254.6 on 09/06/12
For personal use only.

TABLE 1. Calculated values for $^1J_{C-H}$ in $R_2C{=}N{-}X$

Compound		$^1J_{syn}$	$^1J_{anti}$	Reference
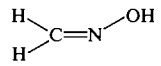		186	167	9
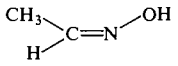	and *anti*	141	131	10
		183	122	11
		182	160	9
		(177)[a]	(163)	7
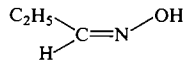	and *anti*	178	157	9
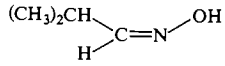	and *anti*	(174)[a]	(162)	12
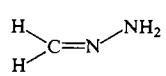		185	176	9
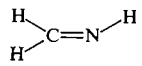		183	146	11
		181	167	9
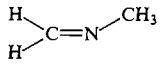		176	176	9

[a] The values appearing in brackets are values measured experimentally.

uration at the central C—N bond.[1] There is, however, a significant difference in oximes and their ethers in that they are configurationally stable at room temperature. Hydrazones and imines, on the other hand, slowly invert at nitrogen, the rate being dependent upon their structure and the medium. Half-lives of a few minutes to a few hours are normal (16). For both aldimines (13, 17) and aldehyde hydrazones (14) the equilibrium, once attained, gives exclusively the *anti* isomer. For our purpose of measuring the ^{13}C spectra of the initial *syn* alkylation product, it was necessary to retard the inversion process by measuring each spectrum below ambient temperature. A sufficiently low temperature was utilized to allow accumulation of ^{13}C transients over a four-hour period without significant inversion taking place. In this way, fully coupled spectra were obtained having signal-to-noise ratios sufficient to allow the measurement of $^1J_{C-H}$ to a precision of ±2 Hz in most cases. In those cases where the precision exceeded ±2 its value is given in Table 2. The fully-coupled spectra of the *anti* isomers were accumulated overnight, thereby yielding values for ^1J of slightly better precision. For two of the *anti* isomers the spectra were also obtained at low temperatures. In each of these instances, ^1J did not change with the change in temperature. The results of all the measurements of ^1J are presented in Table 2.

There is a clear correlation between the magnitude of ^1J and the configuration at the sp^2 nitrogen atom. For all *syn–anti*

[1]The first *ab initio* calculations (18) suggested a repulsive interaction between the lone pair on nitrogen and the electron density at the α carbon to be responsible for destabilization of the *anti* isomer. Recent, more refined calculations suggest a considerably more complex rationale is required (19).

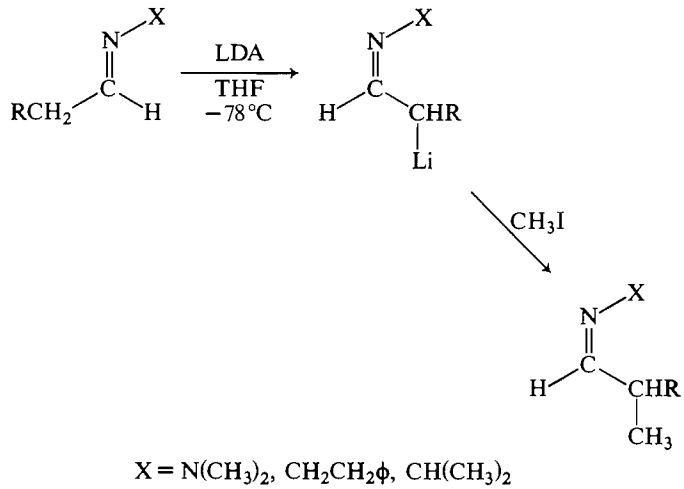

X = $N(CH_3)_2$, $CH_2CH_2\phi$, $CH(CH_3)_2$

SCHEME 2

TABLE 2. Values for $^1J_{C-H}$ in carbonyl derivatives[a]

Compound	$^1J_{syn}$ (Hz)	$^1J_{anti}$ (Hz)
(a) Oxime		
$CH_3CH_2CH{=}N \sim OH$	173	160
(b) Hydrazones		
$CH_3CH_2CH{=}N{\sim}N(CH_3)_2$	174(−20)[b]	155
$(CH_3)_2CHCH{=}N{\sim}N(CH_3)_2$	170(−20)	154
(c) Imines		
$CH_3CH_2CH{=}N{-}(CH_2)_2\phi$	170(−35)	153
$(CH_3)_2CHCH{=}N{-}(CH_2)_2\phi$	171(−30) [±3][c]	154
$(CH_3)_3CCH{=}N{\sim}(CH_2)_2\phi$		155(−18) 155
$CH_3CH_2CH{=}N{-}CH(CH_3)_2$	170(−20) [±4][c]	151(−25) 152.5
$(CH_3)_2CH{-}CH{=}NCH(CH_3)_2$	170(−50)	152
$(CH_3)_3CCH{=}N{-}CH(CH_3)_2$		150

[a] Unless specified by the figure in brackets, the temperature is 25°C.
[b] Temperature at which spectrum was measured appears in brackets.
[c] Square brackets indicate the precision, if it exceeds ±2 Hz.

pairs $^1J_{syn}$ is greater than $^1J_{anti}$ or, expressed in an alternate way, a C—H bond *trans* to the lone pair on nitrogen exhibits the smaller $^1J_{C-H}$. This of course parallels the correlations between $^1J_{C-H}$ and the lone pair orientation at nitrogen in three-membered rings and in various oxygen and nitrogen heterocycles. Whether it is more appropriate to attribute the smaller ^1J to a greater $n-\sigma^*$ interaction when the lone pair is *trans* to the C—H bond in imines and hydrazones or to differences in the N—C—H bond angle[2] is primarily a question of semantics since the two factors are related.

One clear indication of the results in Table 2 is the constancy of $^1J_{syn}$ (170–174 Hz), $^1J_{anti}$ (150–155 Hz), and Δ^1J (12–13 Hz for oximes, 16–19 Hz for hydrazones, and 17–19 Hz for imines). ^1J also appears to be insensitive to the location of the substituent and to whether the substituent is primary or secondary. These results are in contrast to the predictions of Maciel *et al.* (9) whose calculation suggested a decrease in Δ^1J in the

[2]Bond angle effects on ^1J cycloalkanes have long been recognized and are still a subject of current interest (21).

series oximes > hydrazones > imines. The same prediction of the effects of substituents at nitrogen was also made earlier in a qualitative sense by Gil and Teixeira-Dias (20). Obviously, the coupling constants do not show the anticipated sensitivity to the electronegativity of a β-substituent.

The large and constant difference between $^1J_{syn}$ and $^1J_{anti}$ provides the chemist with a useful complement to the existing methods for the determination of configuration in carbonyl derivatives. For example, the *syn–anti* differential shifts normally seen for protons (12) and ^{13}C nuclei (22, 23) would not be reliably applied to sterically congested systems such as the two imines of pivalaldehyde whose ^1J values are given in Table 2. These two imines were obtained as the sole products from lithiation and methylation of the analogous isobutyraldimines. The values for ^1J of 150 and 155, for the *N*-isopropyl and *N*-(2)-phenethyl derivatives respectively, are a strong indication of the *anti* configuration for both, as is the fact that neither one shows a tendency to isomerize. This proof of configuration is obtained very simply and directly compared to the classical alternative of having to synthesize the same imine from a highly inaccessible class of compounds, the tertiary carboxaldehydes.

Experimental

All ^{13}C nmr spectra were recorded using a Varian FT-80 spectrometer operating at a frequency of 20 MHz. All coupling constants were obtained from fully coupled spectra by measuring the separation of the centers of the two multiplets for the sp^2 carbon atom. The chemical shifts of those carbons which were unobscured by background absorption could be readily assigned by analogy with previous data on aldehyde derivatives (21) and are presented below. For all nmr measurements, 1 *M* solutions in tetrahydrofuran were used and the chemical shifts are reported using the solvent signal at δ 69.00 as reference.

Propionaldoxime was prepared from the reaction of 5 g of hydroxylamine hydrochloride in 40 mL of 4% sodium hydroxide with 2.5 mL of propionaldehyde at 40°C for fifteen minutes. Extraction of the reaction mixture with ether and drying of the extracts gave a mixture of the two propionaldoximes in a *syn/anti* ratio of 40:60; ^{13}C nmr δ_{syn}: 19.6 (Cα), 151.8 (C=N); δ_{anti}: 24.5 (Cα), 153.0 (C=N).

The *anti* hydrazones were prepared by the method described by Corey and Enders (24). The two *syn* hydrazones were prepared by lithiation and alkylation of acetaldehyde and propionaldehyde hydrazones as reported earlier (14) and in each case the crude product in tetrahydrofuran solution was transferred to an nmr tube under an argon atmosphere, then capped and wrapped with Parafilm prior to the accumulation of transients at low temperature. *anti*-Propionaldehyde *N*,*N*-dimethylhydrazone gave ^{13}C signals at δ 27.8 (Cα), 138.7 (C=N); the *syn* isomer gave one visible signal at δ 161.9 (C=N). The *anti* form of isobutyraldehyde *N*,*N*-dimethylhydrazone gave ^{13}C signals at δ 33.2 (Cα), 143.0 (C=N); the *syn* isomer gave a signal at δ 167.9 (C=N).

The *anti* imines have been prepared by the reaction of the requisite aldehyde and amine at 0°C in pentane (except for the isopropyl imine of acetaldehyde whose low boiling point required the use of toluene as solvent). After one hour the pentane solution was decanted from the water which had formed and was dried over potassium carbonate. The filtered solution was then distilled to yield the imine. From the ^{13}C spectra, the chemical shifts for the sp^2 carbon (C=N) and the sp^3 (N—C) carbon of both isomers were obtained and are summarized below. Propionaldehyde *N*-isopropylimine, *anti* isomer, δ: 162.6 (C=N), 62.9 (N—C); *syn* isomer, δ: 163.4 (C=N), 52.1 (N—C). Isobutyraldehyde *N*-isopropylimine, *anti* isomer, δ: 166.0 (C=N), 63.5 (N—C); *syn* isomer, δ: 169.5 (C=N), 51.5 (N—C). Pivalaldehyde *N*-isopropylimine, *anti* isomer, δ: 168.7 (C=N), 61.4 (N—C). Propionaldehyde 2-phenethylimine, *anti* isomer, δ: 165.9 (C=N), 64.5 (N—C); *syn* isomer, δ: 170.8 (C=N), 54.3 (N—C). Isobutyraldehyde 2-phenethylimine, *anti* isomer, δ: 169.9 (C=N), 64.3 (N—C); *syn* isomer, δ: 174.0 (C=N), 53.9 (N—C). Pivalaldehyde 2-phenethylimine, *anti* isomer, δ: 172.4 (C=N), 64.1 (N—C).

Acknowledgements

The authors wish to thank the Natural Sciences and Engineering Research Council of Canada for financial support. The technical assistance of Mr. Raj Capoor in running the ^{13}C spectra is greatly appreciated.

1. P. E. HANSEN. Prog. Nucl. Magn. Reson. Spectrose. **15**, 181 (1981).
2. J. AUGÉ and S. DAVID. Nouv. J. Chem. **1**, 57 (1976).
3. A. S. PERLIN. Pure Appl. Chem. **50**, 1401 (1978).
4. Y. TAKEUCHI, P. J. CHIVERS, and T. A. CRABB. J. Chem. Soc. Chem. Commun. 210 (1974); see also G. VAN BINST and D. TOURWE. Tetrahedron Lett. 257 (1974).
5. P. ALBRIKTSEN. Acta Chem. Scand. **27**, 3889 (1973).
6. K. BOCK and L. WIEBE. Acta Chem. Scand. **27**, 2676 (1973).
7. T. YONEZAWA and I. MORISHIMA. J. Mol. Spectrosc. **27**, 210 (1968).
8. W. B. JENNINGS, D. R. BOYD, C. G. WATSON, E. D. BECKER, R. B. BRADLEY, and D. M. JERINA. J. Am. Chem. Soc. **94**, 8501 (1972).
9. G. E. MACIEL, J. W. MCIVER JR., N. S. OSTLUND, and J. A. POPLE. J. Am. Chem. Soc. **92**, 1 (1970).
10. T. YONEZAWA, I. MORISHIMA, K. FUKUTA, and Y. OHMORI. J. Mol. Spectrosc. **31**, 341 (1969).
11. M. S. GOPINATHAN and P. T. NARASIMHAN. Mol. Phys. **22**, 473 (1971).
12. G. J. KARABATSOS, R. A. TALLER, and F. M. VANE. J. Am. Chem. Soc. **85**, 2327 (1963).
13. R. R. FRASER and J. BANVILLE. J. Chem. Soc. Chem. Commun. 47 (1979).
14. K. G. DAVENPORT, H. EICHENAUER, D. ENDERS, M. NEWCOMB, AND D. E. BERGBREITER. J. Am. Chem. Soc. **101**, 5654 (1979); see also K. G. DAVENPORT, M. NEWCOMB and D. E. BERGBREITER. J. Org. Chem. **46**, 3143 (1981).
15. R. R. FRASER. The *syn* effect and the use of enolate equivalents in synthesis. *In* Comprehensive carbanion chemistry. *Edited by* T. Durst and E. Buncel. Elsevier/North Holland. 1982.
16. R. R. FRASER and N. CHUAQUI-OFFERMANNS. Can. J. Chem. **59**, 3007 (1981).
17. J. HINE and C. Y. YEH. J. Am. Chem. Soc. **89**, 2669 (1967).
18. K. N. HOUK, R. W. STROZIER, N. G. RONDAN, R. R. FRASER, and N. CHUAQUI-OFFERMANNS. J. Am. Chem. Soc. **102**, 1426 (1980).
19. R. W. STROZIER. Ph.D. thesis, Univ. of Pittsburgh.
20. V. M. S. GIL AND J. J. C. TEIXEIRA-DIAS. Mol. Phys. **15**, 47 (1968).
21. M. W. BAUM, A. GUENZI, C. A. JOHNSON, and K. MISLOW. Tetrahedron Lett. 31 (1982).
22. R. R. FRASER, J. BANVILLE, F. AKIYAMA, and N. CHUAQUI-OFFERMANNS. Can. J. Chem. **59**, 705 (1981).
23. G. E. HAWKES, K. HERWIG, and J. D. ROBERTS. J. Org. Chem. **39**, 1017 (1974).
24. E. J. COREY and D. ENDERS. Chem. Ber. **111**, 1337 (1978).

Can. J. Chem. Downloaded from www.nrcresearchpress.com by 210.87.254.6 on 09/06/12
For personal use only.

Structure and magnetism in a hydroxy bridged binuclear copper(II) system with a "tunable" binuclear centre

LAURENCE K. THOMPSON
Department of Chemistry, Memorial University of Newfoundland, St. John's, Nfld., Canada A1B 3X7

Received September 24, 1982

LAURENCE K. THOMPSON. Can. J. Chem. **61**, 579 (1983).

The molecular structure of $[Cu_2(PAP)(OH)(IO_3)_3].4H_2O$ (PAP = 1,4-di(2′-pyridyl)aminophthalazine) has been determined by single crystal X-ray diffraction. $[Cu_2(PAP)(OH)(IO_3)_3].4H_2O$ belongs to the space group $P2_1/c$ with a = 7.266(1), b = 15.269(1), c = 25.870(1) Å, β = 96.40(1)°, V = 2852.2 Å^3, Z = 4. The copper coordination geometry lies between a square pyramid and a trigonal bipyramid and the two copper(II) centres are bridged by three groups: N_2 (phthalazine), hydroxide, and bidentate iodate, in a structure which is analogous to that reported for $[Cu_2(PAP)(OH)Cl_3].1.5H_2O$. Replacing the chlorine bridge by iodate has the effect of forcing the two metal centres further apart, thus creating a larger Cu—O—Cu bridge angle. This increase in oxygen bridge angle (101° to 114°) is also reflected in the enhanced antiferromagnetic exchange ($-2J(Cl)$ = 201 cm^{-1}, $-2J(IO_3)$ = 335 cm^{-1}). Other groups of varying size (e.g. Br, NO_3, SO_4) can act as bridges between the two copper centres in systems of this sort with the resultant variation in copper–copper separation and oxygen bridge angle.

LAURENCE K. THOMPSON. Can. J. Chem. **61**, 579 (1983).

On a déterminé la structure moléculaire du $[Cu_2(PAP)(OH)(IO_3)_3].4H_2O$ (PAP = di-(pyridil-2′)amino-1,4 phtalazine) par diffraction de rayons-X sur un monocristal. Le composé $[Cu_2(PAP)(OH)(IO_3)_3].4H_2O$ appartient au groupe d'espace $P2_1/c$ avec a = 7,266(1), b = 15,269(1), c = 25,870(1) Å, β = 96,40(1)°, V = 2852,2 Å^3, Z = 4. La géométrie de coordination du cuivre se situe entre une pyramide à base carrée et une bipyramide trigonale et les deux centres de Cu(II) sont en position de pont entre trois groupes; le N_2 (phtalazine), l'hydroxyde et l'iodate bidentate dans une structure qui est semblable à celle rapportée par le $[Cu_2(PAP)(OH)Cl_3].1,5H_2O$. Le remplacement du chlore en position de pont par un iodate a pour effet d'obliger les deux centres métalliques à s'éloigner l'un de l'autre créant ainsi un angle de pont Cu—O—Cu plus grand. Cette augmentation de l'angle du pont oxygène (101° à 114°) se réflète également dans l'augmentation de l'échange antiferromagnétique ($-2J(Cl)$ = 201 cm^{-1}, $-2J(IO_3)$ = 335 cm^{-1}). D'autres groupes de dimensions variables (par exemple: Br, NO_3, SO_4) peuvent agir comme pont entre les deux centres cuivre des systèmes de ce type avec comme conséquence une variation de la séparation cuivre–cuivre, et de l'angle du pont oxygène.

[Traduit par le journal]

Introduction

Binuclear copper(II) complexes involving antiferromagnetic exchange between metal centres are potential models for binuclear copper protein centres which take part in biological reactions involving molecular oxygen, such as oxygen transport (1) and oxygen activation (2–4). Magnetic measurements on protein extracts indicate strong antiferromagnetic exchange between the copper(II) centres in Rhus vernicifera laccase (5) ($-2J > 1000$ cm^{-1}) and in oxyhemocyanin (Megathura crenulata; $-2J > 1250$ cm^{-1}) (5, 6). Strong antiferromagnetic exchange is observed in binuclear copper(II) systems involving single hydroxy bridges (7–9) and exchange increases with increasing bridge angle (7). In systems of this sort the copper(II) centres are assumed to be superexchange coupled via the hydroxy bridge. An oxygen bridge, from, e.g., tyrosine or even a hydroxide group itself, has been suggested as the superexchange medium for both oxyhemocyanin (9, 10) and enzymes containing Type III copper centres (8) and other donor groups around the copper centres are thought to include histidine (8, 11–13). Metal–metal separations in oxyhemocyanins are reported to be in excess of 3.50 Å (3.55 Å (12) and 3.67 Å (13)) according to EXAFS studies.

Complexes of the type $[Cu_2(PAP)(OH)X_3]$ (X = Cl, Br, IO_3), $[Cu_2(PAP)(RCOO)_3]$ (Fig. 1, PAP = 1,4-di(2′-pyridyl)-aminophthalazine) have been reported (14) and X-ray structural studies on $[Cu_2(PAP)(OH)Cl_3].1.5H_2O$ indicate a triple bridge between the metal centres, including chloride and hydroxide bridges in addition to the phthalazine N—N bridge (14–16) (Fig. 2). Two independent molecules exist in the structure with Cu–Cu separations of 3.001(2) and 2.972(2) Å and Cu—O—Cu bridge angles of 101.8(2) and 100.1(2)° respectively. Moderate antiferromagnetic exchange is observed for this system $-2J = 201$ cm^{-1}. This complex has been shown to exhibit catecholase activity (17) and also appears to catalyze the oxidation of ascorbic acid (18).

In this report the full structural details of the complex $[Cu_2(PAP)(OH)(IO_3)_3].4H_2O$ are presented and the effect of altering the size of the non-hydroxy bridge group (Cl, Br, IO_3) on the dimensions of the binuclear unit, especially the Cu—O(H)—Cu bridge angle, and the magnitude of the magnetic exchange between the metal centres is examined.

Experimental

Deep turquoise-blue crystals of $[Cu_2(PAP)(OH)(IO_3)_3].4H_2O$ were obtained according to the procedure previously described (14). Satisfactory elemental analyses were obtained for this compound. Magnetic susceptibility data were collected for $[Cu_2(PAP)(OH)X_3].1.5H_2O$ (X = Cl, Br) as a function of temperature (4.2–109 K) using a PAR 150A, VSM, courtesy of Professor J. Reedijk, State University Leiden, Leiden, Netherlands. The data were corrected for underlying diamagnetism (19) and temperature-independent paramagnetism ($N_\alpha = 60 \times 10^{-6}$ egsu/mol Cu). X-ray structural data have been provided by Dr. A. W. Hanson, National Research Council (Atlantic Research Laboratory).

X-ray crystallographic analysis for $[Cu_2(PAP)(OH)(IO_3)_3].4H_2O$

Crystal data (at 22°C) are:

$C_{18}H_{23}N_6O_{14}I_3Cu_2$ fw = 1055.22

Monoclinic, $P2_1/c$, a = 7.266(1), b = 15.269(1), c = 25.870(1) Å,

Can. J. Chem. Downloaded from www.nrcresearchpress.com by 210.87.254.6 on 09/06/12
For personal use only.

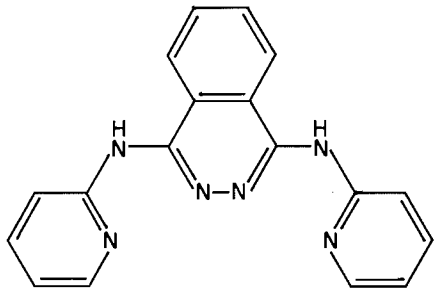

FIG. 1. PAP(1,4-di(2′-pyridyl)aminophthalazine).

$\beta = 96.40(1)°$, $V = 2852.2$ Å^3, $Z = 4$ (MoKα, $\lambda\alpha_1 = 0.7093$ Å); $\mu = 4.9$ mm^{-1}, $D_x = 2.457$ g cm^{-3}.

The crystals were deep blue, and of compact habit. The specimen used for all measurements was a solid bounded by faces {001}, {011}, and {100}, of extreme dimensions 0.13 and 0.24 mm. The relative intensities of the independent reflections with $2\theta < 55°$ were measured with a Picker four-circle diffractometer, using MoKα radiation (graphite monochromator). The $\theta-2\theta$ scan method was used, and individual reflection profiles were analysed as described by Grant and Gabe (20). The standard deviations of the measured intensities were evaluated from counting statistics, and those for which $I_{net} < 2\sigma(I_{net})$ were considered to be unobserved and were omitted from the analysis. The observed reflections numbered 5185, of a possible 6599. Absorption corrections (ranging from 1.67 to 2.48) were applied.

The structure was solved by direct methods (MULTAN) (21). The Cu and I positions were apparent in the first E-map, and a Fourier synthesis, phased on the contributions of these atoms, revealed the positions of the remaining non-H atoms of the PAP and iodate groups. Refinement was by block-diagonal least-squares, minimizing $\Sigma\omega\Delta F^2$, where $\omega^{-1} = \sigma^2(F_o) + 0.001F_o^2$. When the refinement converged a difference Fourier synthesis revealed five residual peaks at about the right distance (2.6 to 3.0 Å) from the iodate O atoms, and from each other, to be attributed to water molecules. Two of these peaks were smaller than the rest, and as only four water molecules were believed to be present, a disordered structure was postulated. The three largest peaks were assumed to be O atoms with full occupancy, and the remaining two to be O atoms with an occupancy ratio of 0.5. The H atoms of the PAP groups were assigned reasonable starting positions, and the hydroxyl H atom located in a ΔF synthesis. The H atoms of the water molecules were not located. Refinement converged at $R = 0.028$ (observed reflections only; including unobserved $R = 0.046$; $R_\omega = 0.044$). Although the refinement is satisfactory, and the disordered water structure is physically reasonable, it must be emphasized that the distribution of occupancy ratios has been assumed quite arbitrarily. However, any attempt to refine the occupancy ratios would require equally arbitrary assumptions concerning the thermal motion. The computer program system is specified in ref. 22. The atomic scattering factors were taken from ref. 23. The final fractional coordinates and thermal parameters appear in Tables 1 and 2[1] respectively. Observed and calculated structure factors (Table 3) have been placed in the Depository of Unpublished Data.[1]

Results and discussion

Infrared data have suggested that a variety of anions, other than hydroxide, can be introduced as bridge groups between the metal centres in binuclear copper complexes of pyridylphthalazine ligands, and preliminary X-ray studies have shown the presence of a nitrate bridge and a sulphate bridge in

[1]Tables 2 and 3 are available, at a nominal charge, from the Depository of Unpublished Data, CISTI, National Research Council of Canada, Ottawa, Ont., Canada K1A 0S2.

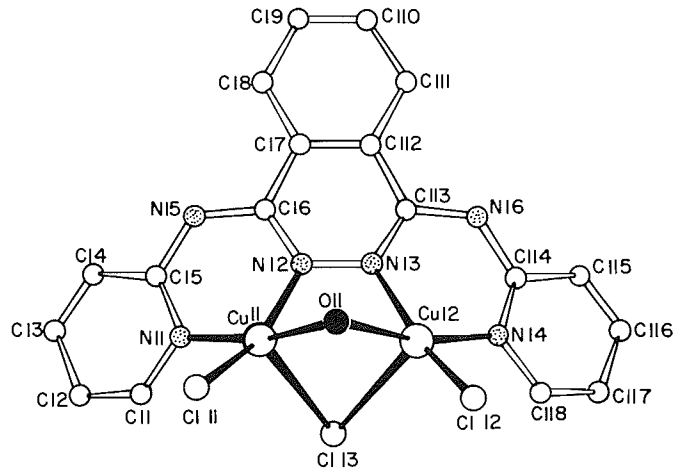

FIG. 2. Molecular structure and labelling scheme for $[Cu_2(PAP)(OH)Cl_3].1.5H_2O$.

the related systems $[Cu_2(PAP4Me)(OH)(H_2O)_2(NO_3)_2]NO_3$ (PAP4Me = 1,4-di(4′-methyl-2′-pyridyl)aminophthalazine) (24, 25) and $[Cu_2(PAP)(OH)Cl(SO_4)].2H_2O$ (25). A bromide bridge is also found in the complex $[Cu_2(PAP)(OH)Br_3].1.5H_2O$ (25). As the size of the anionic bridge group is varied (X = Cl, Br, IO_3, NO_3, SO_4 etc.) the metal–metal separation and hydroxy bridge angle change accordingly (tuning).

Structure description of μ-[1,4-di(2′-pyridyl)aminophthalazine-N^1,N^3,N^4,N^6]-μ-iodato-diiodato-μ-hydroxodicopper(II) tetrahydrate

The molecular structure of $[Cu_2(PAP)(OH)(IO_3)_3].4H_2O$ is shown in Fig. 3 and consists of a pair of copper(II) centres bound simultaneously to the tetradentate phthalazine ligand and bridged by three groups: the phthalazine N_2, a hydroxide, and a bidentate iodate. Selected intramolecular bond distances and angles are given in Table 4. The copper coordination sphere, CuN_2O_3, has a five-coordinate structure intermediate between a trigonal bipyramid (hydroxide group axial) and a square pyramid (apical ligand from the bridging iodate) and can be described as a distortion of either. A distorted square pyramidal description is preferred, however, because it better describes the copper coordination geometry in the related compounds $[Cu_2(PAP)(OH)Cl_3].1.5H_2O$ (16), $[Cu_2(PAP)(OH)Cl(SO_4)].2H_2O$ (25), and $[Cu_2(PAP)(OH)Br_3].1.5H_2O$ (25) (Cl, SO_4, Br, respectively, at the apical sites). In one further example, $[Cu_2(PAP4Me)(OH)(H_2O)_2(NO_3)_2]NO_3$ (24, 25), a six-coordinate geometry occurs at each copper centre, which can be seen as the result of a sixth ligand being added to a basic square pyramidal structure. A bidentate chelating nitrate group is bound at one copper centre while two water molecules occur at the other.

Copper–nitrogen bond lengths are close to 2 Å and are similar to those found in the complex $[Cu_2(PAP)(OH)Cl_3].1.5H_2O$ (16), as are bond lengths in the ligand framework itself. The bond lengths of the two copper centres to the oxygen bridge atom are somewhat smaller (2.4% on average) than those in the chloro complex, and since the copper–copper separation is larger (3.165 Å) the Cu—O—Cu bridge angle increases accordingly. The ligand has a non-planar configuration in which the pyridine rings are canted with respect to the phthalazine group. The average dihedral angle between the

Can. J. Chem. Downloaded from www.nrcresearchpress.com by 210.87.254.6 on 09/06/12
For personal use only.

TABLE 1. Final fractional coordinates for the atoms of $[Cu_2(PAP)(OH)(IO_3)_3].4H_2O$

Atom	X	Y	Z
Cu(1)	0.86123(9)	−0.02304(4)	0.17893(2)
Cu(2)	0.86441(9)	0.18397(4)	0.18519(2)
I(1)	0.94655(4)	−0.06586(2)	0.05710(1)
I(2)	0.47033(4)	0.08902(2)	0.10704(1)
I(3)	0.97052(5)	0.21724(2)	0.06924(1)
O(1)	0.9706 (5)	0.0817 (2)	0.1593 (1)
O(2)	0.9856 (5)	−0.0955 (2)	0.1259 (1)
O(3)	1.0715 (5)	−0.1546 (3)	0.0316 (1)
O(4)	1.1122 (6)	0.0208 (3)	0.0523 (2)
O(5)	0.6178 (5)	−0.0054 (2)	0.1210 (1)
O(6)	0.6344 (5)	0.1770 (2)	0.1208 (2)
O(7)	0.3520 (6)	0.0922 (3)	0.1638 (2)
O(8)	0.9890 (5)	0.2600 (2)	0.1362 (1)
O(9)	1.2092 (6)	0.2327 (3)	0.0588 (2)
O(10)	0.8592 (7)	0.3088 (3)	0.0373 (2)
N(1)	0.7582 (6)	−0.1322 (3)	0.2038 (2)
N(2)	0.8623 (6)	−0.1041 (3)	0.2925 (2)
N(3)	0.8486 (6)	0.0309 (3)	0.2510 (2)
N(4)	0.8481 (6)	0.1218 (3)	0.2531 (2)
N(5)	0.8590 (7)	0.2515 (3)	0.3009 (2)
N(6)	0.7567 (6)	0.2894 (3)	0.2141 (2)
C(1)	0.6740 (8)	−0.1872 (3)	0.1672 (2)
C(2)	0.6110 (9)	−0.2694 (4)	0.1798 (2)
C(3)	0.6317 (8)	−0.2954 (3)	0.2311 (2)
C(4)	0.7124 (8)	−0.2392 (3)	0.2690 (2)
C(5)	0.7757 (7)	−0.1581 (3)	0.2535 (2)
C(6)	0.8812 (7)	−0.0153 (3)	0.2941 (2)
C(7)	0.9459 (8)	0.0246 (3)	0.3430 (2)
C(8)	1.0115 (9)	−0.0230 (4)	0.3879 (2)
C(9)	1.0720(10)	0.0190 (4)	0.4333 (2)
C(10)	1.0692 (9)	0.1101 (4)	0.4358 (2)
C(11)	1.0096 (8)	0.1587 (4)	0.3927 (2)
C(12)	0.9456 (7)	0.1166 (3)	0.3456 (2)
C(13)	0.8813 (7)	0.1623 (3)	0.2980 (2)
C(14)	0.7736 (7)	0.3100 (3)	0.2644 (2)
C(15)	0.7103 (8)	0.3888 (4)	0.2828 (2)
C(16)	0.6283 (9)	0.4477 (4)	0.2477 (2)
C(17)	0.6083 (9)	0.4273 (3)	0.1949 (2)
C(18)	0.6738 (8)	0.3474 (3)	0.1801 (2)
W(1)	0.3340 (7)	0.3007 (3)	0.4620 (2)
W(2)	0.5962 (8)	0.0797 (3)	0.0033 (2)
W(3)	0.4776(10)	0.3698 (4)	0.0512 (3)
W(4A)	0.6339(14)	0.2142 (9)	0.4318 (5)
W(4B)	0.5616(20)	0.0474(11)	0.4208(11)
HO(1)	0.067 (9)	0.087 (4)	0.159 (3)
HN(2)	0.897 (7)	−0.137 (3)	0.319 (2)
HN(5)	0.906 (8)	0.270 (4)	0.327 (2)
HC(1)	0.662 (7)	−0.168 (3)	0.128 (2)
HC(2)	0.588 (8)	−0.296 (4)	0.153 (2)
HC(3)	0.607 (8)	−0.350 (4)	0.241 (2)
HC(4)	0.740 (8)	−0.246 (4)	0.312 (2)
HC(8)	1.019 (7)	−0.087 (3)	0.383 (2)
HC(9)	1.103 (11)	−0.012 (5)	0.456 (3)
HC(10)	1.103 (8)	0.140 (4)	0.464 (2)
HC(11)	1.026 (10)	0.228 (5)	0.399 (3)
HC(15)	0.726 (7)	0.395 (3)	0.313 (2)
HC(16)	0.596 (7)	0.497 (3)	0.256 (2)
HC(17)	0.625 (14)	0.479 (7)	0.168 (4)
HC(18)	0.700 (9)	0.331 (4)	0.141 (3)

average plane of a pyridine ring and the mean plane of the phthalazine moiety is 25° whereas for the complex $[Cu_2(PAP)(OH)Cl_3].1.5H_2O$ it is 29° (15).

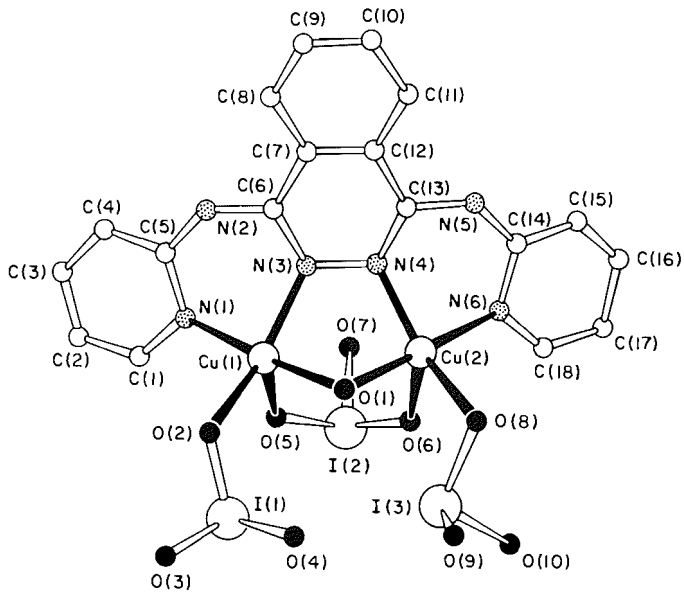

FIG. 3. Molecular structure and labelling scheme for $[Cu_2(PAP)(OH)(IO_3)_3].4H_2O$.

The structure of the iodate complex is also of special interest because of the role of the iodate groups. Examples of inorganic compounds involving ionic, monodentate, bidentate, and even tridentate iodate have been reported (26–29) where the polyfunctional nature of the iodate often involves loosely bound layers and chains of metal centres. However, examples of coordination complexes involving nitrogen donor ligands and bound iodate appear to be lacking and the structure of $[Cu_2(PAP)(OH)(IO_3)_3].4H_2O$ may be the first example of such a system involving iodates with mixed functionality. As is typical of iodates three oxygen atoms are bound to the iodine in a trigonal pyramidal arrangement with I—O bond lengths in the range 1.773–1.842 Å while more distant contacts (I—O 2.764–3.464 Å) complete coordination spheres of six or seven oxygen atoms around each iodine.

An X-ray structural study of the complex $[Cu_2(PAP)(OH)Br_3].1.5H_2O$ has shown this system to be isomorphous with $[Cu_2(PAP)(OH)Cl_3].1.5H_2O$ (Fig. 2, Br replaced by Cl). Bond lengths and angles not involving Br are effectively identical to those found for the chloro derivative (25). Some relevant structural data for this system are given in Table 5.

Magnetism and structure

Magnetic susceptibility data for $[Cu_2(PAP)(OH)Br_3].1.5H_2O$ are shown as a function of temperature in Fig. 4 with a best fit line which was calculated using the Van Vleck equation (30) for an exchange coupled pair of copper(II) ions (eq. [1]):

$$[1]\quad \chi_m = \frac{N\beta^2 g^2}{3kT}\left[1 + \frac{1}{3}\exp(-2J/kT)\right]^{-1} + N_\alpha$$

where $2J$ is the singlet–triplet splitting or exchange integral. The parameters giving the best fit for this compound are $\langle g \rangle = 2.10$ and $2J = -186$ cm^{-1}, which were obtained by minimizing the function

$$E = \Sigma\,[(\chi_{obs} - \chi_{calc})T]^2$$

A sharp rise in the susceptibility is observed below 10 K, which can be attributed to the presence of monomer impurity. How-

Can. J. Chem. Downloaded from www.nrcresearchpress.com by 210.87.254.6 on 09/06/12
For personal use only.

Can. J. Chem. Downloaded from www.nrcresearchpress.com by 210.87.254.6 on 09/06/12
For personal use only.

TABLE 4. Selected interatomic distances and angles in $[Cu_2(PAP)(OH)(IO_3)_3].4H_2O$

Atoms	Distance (Å)	Atoms	Angle (deg)
Cu(1)—Cu(2)	3.165(1)	N(1)—Cu(1)—O(1)	176.2(2)
Cu(1)—N(1)	1.965(4)	N(1)—Cu(1)—N(3)	89.2(2)
Cu(1)—N(3)	2.050(4)	N(3)—Cu(1)—O(1)	88.1(2)
Cu(1)—O(1)	1.882(3)	N(3)—Cu(1)—O(5)	117.1(2)
Cu(1)—O(5)	2.204(4)	N(3)—Cu(1)—O(2)	153.4(2)
Cu(1)—O(2)	2.049(3)	O(2)—Cu(1)—O(5)	89.5(2)
Cu(2)—N(4)	2.012(4)	O(1)—Cu(1)—O(2)	92.8(2)
Cu(2)—N(6)	1.973(4)	O(1)—Cu(1)—O(5)	92.5(2)
Cu(2)—O(8)	2.007(3)	O(2)—Cu(1)—N(1)	88.4(2)
Cu(2)—O(6)	2.227(4)	O(5)—Cu(1)—N(1)	91.1(2)
Cu(2)—O(1)	1.897(3)	Cu(1)—N(3)—N(4)	116.0(3)
C(1)—N(1)	1.359(7)	Cu(1)—O(1)—Cu(2)	113.8(2)
C(5)—N(2)	1.397(7)	N(3)—N(4)—Cu(2)	115.9(3)
N(2)—C(6)	1.363(6)	N(6)—Cu(2)—O(1)	178.4(2)
C(6)—N(3)	1.318(6)	N(4)—Cu(2)—N(6)	89.4(2)
N(3)—N(4)	1.389(6)	N(4)—Cu(2)—O(1)	89.2(2)
N(4)—C(13)	1.314(6)	N(4)—Cu(2)—O(6)	121.2(2)
C(13)—N(5)	1.375(6)	N(4)—Cu(2)—O(8)	154.0(2)
N(5)—C(14)	1.394(7)	O(6)—Cu(2)—O(8)	84.8(1)
C(14)—N(6)	1.331(7)	O(1)—Cu(2)—O(6)	89.9(2)
N(6)—C(18)	1.343(7)	O(1)—Cu(2)—O(8)	91.4(2)
I(1)—O(2)	1.828(4)	O(6)—Cu(2)—N(6)	91.5(2)
I(1)—O(3)	1.797(4)	O(8)—Cu(2)—N(6)	89.6(2)
I(1)—O(4)	1.802(4)		
I(1)...O(1)	3.464(4)		
I(1)...O(4)	2.898(4)		
I(1)...O(5)	3.188(4)		
I(1)...W(1)	2.886(5)		
I(2)—O(5)	1.809(4)		
I(2)—O(6)	1.805(4)		
I(2)—O(7)	1.783(4)		
I(2)...O(4)	3.008(4)		
I(2)...O(9)	3.074(5)		
I(2)...W(2)	2.932(5)		
I(3)—O(8)	1.842(3)		
I(3)—O(9)	1.800(4)		
I(3)—O(10)	1.773(4)		
I(3)...O(1)	3.116(4)		
I(3)...O(3)	2.764(4)		
I(3)...O(4)	3.218(4)		
I(3)...O(6)	2.975(4)		

ever, considering the magnitude of the exchange, the correction due to this paramagnetic species is considered to be small and so has not been included. Magnetic exchange data for the chloro- and iodato-complexes are calculated similarly and listed in Table 5, which includes relevant structural data for the binuclear centres in these systems. Other preliminary structural data for the systems $[Cu_2(PAP)(OH)Cl(SO_4)].2H_2O$ and $[Cu_2(PAP4Me)(OH)(H_2O)_2(NO_3)_2]NO_3$ are also included for comparison (24, 25). These complexes have bidentate sulphate and nitrate bridges, respectively, between the copper centres, in addition to the N_2 (phthalazine) and hydroxy bridges. The oxygen bridge angles in these systems (Table 5) are slightly larger than that observed for the iodate complex and although exchange integrals have not yet been measured the lower room temperature magnetic moments indicate enhanced exchange. It is evident that as the metal–metal separation is increased, together with the Cu—O—Cu angle, the spin exchange between the two copper(II) centres is enhanced. Dimensions at the binuclear centres in the chloro- and bromo-complexes are very similar and the presence of the larger bromine bridge between the two copper(II) centres appears to have had little effect on the metal–metal separation and the oxygen bridge angle. Rather, the bromine bridge has been accommodated with somewhat longer metal–halogen bonds and a smaller bridge angle than in the chloro-complex. The exchange integrals for these two complexes are comparable reflecting the general similarity in the dimensions at the binuclear centres.

Recent reports of binuclear copper complexes involving just single hydroxy bridges have included nitrogen-containing ligands with much more flexibility than the pyridylphthalazines, and which do not have binucleating fragments, like the diazine nitrogen pair, situated together (8, 9). Oxygen bridge angles, metal–metal separations and hence exchange integrals are somewhat larger in these systems. In one case for an oxygen bridge angle of 143.7° and a Cu–Cu separation of 3.642 Å an exchange integral $-2J \simeq 1000\ cm^{-1}$ was observed (9). Exchange integrals of this magnitude approach those observed in real protein systems (5, 6).

The PAP and PAP4Me binuclear copper complexes involving Cl, Br, IO_3, NO_3, and SO_4 bridges have metal–metal separations of <3.25 Å and Cu—O—Cu bridge angles of <116°. Clearly with these ligands, even with large bridge groups inserted between the copper centres, the metal–metal separation and oxygen bridge angle cannot be increased to levels at which protein-like exchange is likely to exist. However, in the case of binuclear copper complexes of the ligands PAP6Me and PAP46DiMe (methyl groups at the 6-position and 4,6-positions of the pyridine rings respectively), for which room temperature magnetic moments of <0.9 BM have been observed (24, 31) it is possible that larger metal–metal separations and oxygen bridge angles exist. No structural or variable temperature susceptibility data are yet available on these systems.

The copper centres in the PAP(R) (R = H, 4Me) complexes are part of six-membered chelate rings and a comparison of the dimensions of the binuclear centres in these systems with those in comparable systems involving five-membered chelate rings reveals that for such systems larger metal–metal separations exist and in one case a larger oxygen bridge angle is found. In

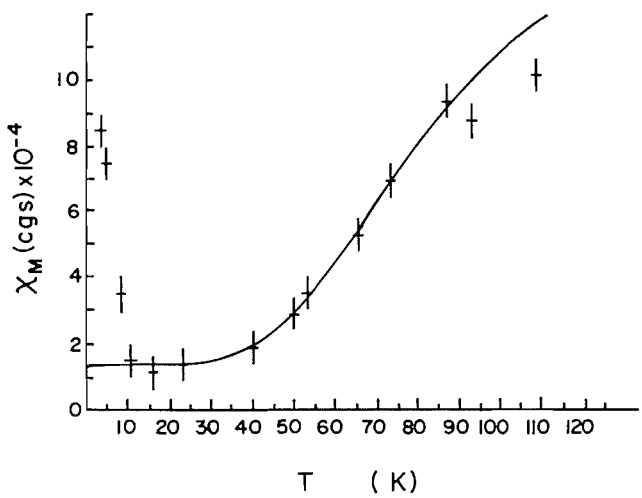

FIG. 4. Magnetic susceptibility data (†) for $[Cu_2(PAP)(OH)Br_3].1.5H_2O$. The solid line was calculated from eq. [1] with $g = 2.10$, $2J = -186\ cm^{-1}$, and $N_\alpha = 120 \times 10^{-6}$ cgsu.

TABLE 5. Magnetic and key structural parameters for $[Cu_2(PAP)(OH)X_3].yH_2O$ (X = Cl, Br, y = 1.5; X = IO_3, y = 4) and related systems

	Cu—O—Cu (deg)	Cu - - -Cu (Å)	$\langle g \rangle$	$-2J$ (cm^{-1})	μ (BM) (RT)
$[Cu_2(PAP)(OH)Cl_3].1.5H_2O$	101.8(2), 100.1(2)	3.001(2), 2.972(2)	2.28	201	1.60
$[Cu_2(PAP)(OH)Br_3].1.5H_2O$	102.9(3), 101.3(3)	3.010(2), 2.986(3)	2.10	186	1.66
$[Cu_2(PAP)(OH)(IO_3)_3].4H_2O$	113.8(2)	3.165(1)	1.95	335	1.34*
$[Cu_2(PAP)(OH)Cl(SO_4)].2H_2O$	115.6(2)	3.211(1)	—	—	1.01
$[Cu_2(PAP4Me)(OH)(H_2O)_2(NO_3)_2]NO_3$	115.3(2)	3.138(1)	—	—	1.12

*Magnetic data from ref. 14.

the complex $[Ni_2(dhph)_2(H_2O)_4]Cl_4.2H_2O$ (dhph = 1,4-dihydrazinophthalazine) a metal–metal separation of 3.791 Å is found (32) while the complex $[Cu_2LCl_3(OH)(H_2O)]$ (L = 3,6-bis-(2′-pyridyl)pyridazine) has a metal–metal separation of 3.376 Å and a Cu—O—Cu bridge angle of 126.5° (no exchange data are quoted for this system) (33).

Diazine systems are, therefore, capable of forming binuclear complexes with metal–metal separations approaching those found in protein systems. It seems likely that tetradentate phthalazine and pyridazine ligands, with biomimetic nitrogen donor substituents, capable of forming five-membered chelate rings could produce binuclear copper complexes with dimensions and exchange characteristics typical of oxyhemocyanin and the Type III copper centres. We are currently involved in a programme of synthesis of copper complexes of such systems involving histidine-like substituents and their structural and magnetic characterization.

Acknowledgments

We thank the Natural Sciences and Engineering Research Council of Canada for financial support for this study and Dr. A. W. Hanson (National Research Council, Atlantic Research Laboratory) for X-ray structural results.

1. R. LONTIE and L. VANQUICKENBORNE. *In* Metal ions in biological systems. Vol. 3. *Edited by* H. Sigel. Marcel-Dekker, New York. 1974. pp. 183–200.
2. J. A. FEE. Struct. Bond, **23**, 1 (1975).
3. W. H. VANNESTE and A. ZUBERBÜHLER. *In* Molecular mechanisms of oxygen activation. *Edited by* O. Hayaishi. Academic Press, New York. 1974, and references therein.
4. E. OCHIAI. Bioinorganic chemistry, an introduction. Allyn and Bacon Inc., Boston. 1977, and references therein.
5. D. M. DOOLEY, R. A. SCOTT, J. ELLINGHAUS, E. I. SOLOMON, and H. B. GRAY. Proc. Natl. Acad. Sci. U.S.A. **75**, 3019 (1978).
6. E. I. SOLOMON, D. M. DOLLEY, R. H. WANG, H. B. GRAY, M. CERDONIO, F. MOGNO, and G. L. ROMANI. J. Am. Chem. Soc. **98**, 1029 (1976).
7. M. S. HADDAD and D. N. HENDRICKSON. Inorg. Chim. Acta, **28**, L121 (1978).
8. P. L. BURK, J. A. OSBORN, M-T. YOUINOU, Y. ANGUS, R. LOUIS, and R. WEISS. J. Am. Chem. Soc. **103**, 1273 (1981).
9. P. K. COUGHLIN and S. J. LIPPARD. J. Am. Chem. Soc. **103**, 3228 (1981).
10. A. R. AMUNDSEN, J. WHELAN, and B. BOSNICH. J. Am. Chem. Soc. **99**, 6730 (1977).
11. S. SUZUKI, J. KINO, M. KIMURA, W. MORI, and A. NAKAHARA. Inorg. Chim. Acta, **66**, 41 (1982).
12. M. S. CO, R. A. SCOTT, and K. O. HODGSON. J. Am. Chem. Soc. **103**, 984 (1981).
13. J. M. BROWN, L. POWERS, B. KINCAID, J. A. LARRABEE, and T. G. SPIRO. J. Am. Chem. Soc. **102**, 4210 (1980).
14. L. K. THOMPSON, V. T. CHACKO, J. A. ELVIDGE, A. B. P. LEVER, and R. V. PARISH. Can. J. Chem. **47**, 4141 (1969).
15. J. C. DEWAN and L. K. THOMPSON. Can. J. Chem. **60**, 121 (1982).
16. G. MARONGIU and E. C. LINGAFELTER. Acta Crystallogr. B**38**, 620 (1982).
17. A. B. P. LEVER, B. S. RAMASWAMY, and S. R. PICKENS. Inorg. Chim. Acta, **46**, L59 (1980).
18. L. K. THOMPSON. Unpublished results.
19. E. KÖNIG. Magnetic properties of transition metal complexes. Springer-Verlag, Berlin. 1966.
20. D. F. GRANT and E. J. GABE. J. Appl. Crystallogr. 11, 114 (1978).
21. G. GERMAIN, P. MAIN, and M. M. WOOLFSON. Acta Crystallogr. A**27**, 368 (1971).
22. A. C. LARSON and E. J. GABE. Computing in crystallography. Delft University Press, Delft, Holland. 1978.
23. International tables for X-ray crystallography. Vol IV. Kynoch Press, Birmingham, England. 1974. p. 99.
24. D. V. BAUTISTA, J. C. DEWAN, and L. K. THOMPSON. Can. J. Chem. **60**, 2583 (1982).
25. A. W. HANSON. Private communication.
26. H. BACH and H. KÜPPERS. Acta Crystallogr. B**34**, 263 (1978).
27. V. S. ZLOCZYSTI, H. HART, and R. FRYDRYCH. Acta Crystallogr. B**32**, 753 (1976).
28. R. LIMINGA, S. R. BOOLES, S. GHOSE, and C. WAN. Acta Crystallogr. B**34**, 2398 (1978).
29. S. GHOSE, C. WAN, and O. WITTKE. Acta Crystallogr. B**34**, 84 (1978).
30. J. H. VAN VLECK. The theory of electric and magnetic susceptibilities. Oxford University Press, London. 1932. Chapt. IX.
31. G. BULLOCK, F. W. HARTSTOCK, and L. K. THOMPSON. Can. J. Chem. **61**, 57 (1983).
32. J. E. ANDREW and A. B. BLAKE. J. Chem. Soc A, 1408 (1969).
33. M. GHEDINI, G. DE MUNNO, G. DENTI, A. M. MANOTTI LANFREDI, and A. TIRIPICCHIO. Inorg. Chim. Acta, **57**, 87 (1982).

Can. J. Chem. Downloaded from www.nrcresearchpress.com by 210.87.254.6 on 09/06/12
For personal use only.

Préparation et oxydation anodique d'acides β-cétaliques. Application à la synthèse de γ-bisdioxolannes symétriques et des γ-dicétones dérivées

JACQUES EINHORN

Institut Curie, Service de Chimie, section de Biologie, 26, rue d'Ulm, 75231 Paris Cedex 05, France

ET

JEAN-LOUIS SOULIER, CATHY BACQUET ET DANIEL LELANDAIS[1]

Laboratoire de Chimie Organique Structurale, Bâtiment F, 4 Place Jussieu, 75230 Paris Cedex 05, France

Reçu le 3 août 1982

JACQUES EINHORN, JEAN-LOUIS SOULIER, CATHY BACQUET et DANIEL LELANDAIS. Can. J. Chem. **61**, 584 (1983).

L'oxydation anodique d'acides carboxyliques porteurs en β de la fonction acide d'un groupement dioxolanne conduit avec de bons rendements aux γ-bisdioxolannes symétriques. L'hydrolyse de ces composés fournit aisément les γ-dicétones correspondantes. La méthode de préparation des acides de départ est décrite.

JACQUES EINHORN, JEAN-LOUIS SOULIER, CATHY BACQUET, and DANIEL LELANDAIS. Can. J. Chem. **61**, 584 (1983).

Anodic oxidation of carboxylic acids with β-dioxolane substituents leads to good yields of symmetrical γ-bisdioxolanes. Hydrolysis of these compounds easily provides the corresponding γ-diketones. The synthesis of the starting acids is described.
[Journal translation]

L'oxydation anodique de carboxylates β-cétonique (type A) en milieu hydroorganique nous avait conduit à des γ-dicétones symétriques (1) par dimérisation du radical intermédiaire selon le schéma 1.

Cependant cette réaction n'est pas univoque, et à côté de la γ-dicétone, une cétone saturée $R^1COR^2R^3H$ se forme, issue de la capture par le radical d'un hydrogène du milieu.

Nous montrons que cette difficulté peut être levée dans certains cas, lorsque les β-cétocarboxylates sont remplacés par leurs dioxolannes. Nous avons alors obtenu, avec des rendements élevés des γ-bisdioxolannes qui conduisent facilement aux γ-dicétones.

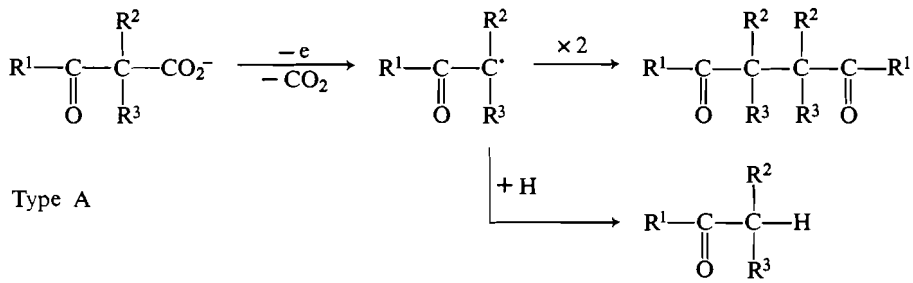

SCHÉMA 1

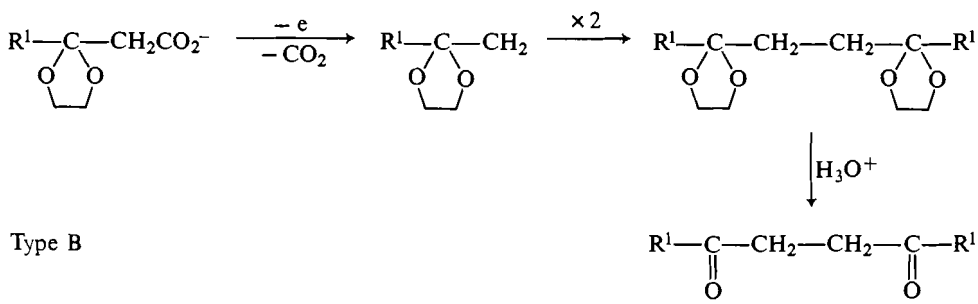

SCHÉMA 2

Comme nous le verrons préalablement, l'obtention de ces composés a nécessité d'une part l'étude générale du comportement électrochimique des carboxylates β-cétaliques, d'autre part la mise au point d'une synthèse des acides correspondants.

[1]Auteur à qui adresser toute correspondance.

I. Comportement électrochimique des carboxylates β-cétaliques. Recherche des conditions conduisant à la dimérisation

L'électrolyse des carboxylates β-cétaliques (type B), dans les conditions qui avaient mené à la dimérisation dans le cas de carboxylates β-cétoniques (type A), s'effectue avec un rendement en courant anormalement faible (inférieur à 5%) et la

Can. J. Chem. Downloaded from www.nrcresearchpress.com by 210.87.254.105 on 09/06/12
For personal use only.

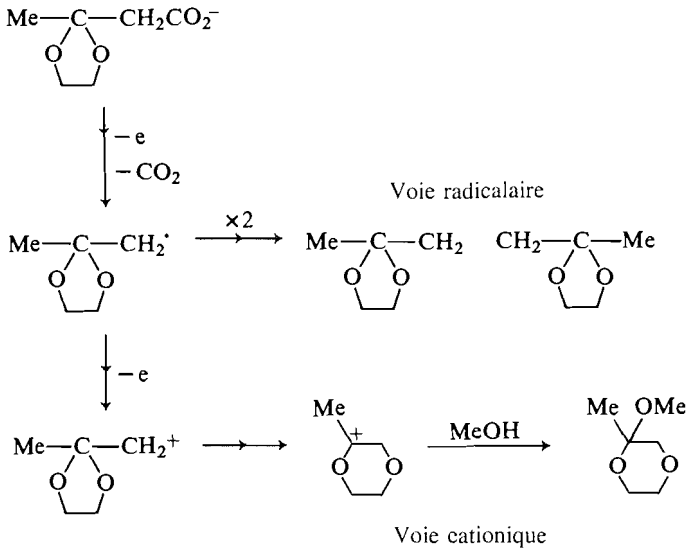

SCHÉMA 3

plus grande partie du carboxylate de départ est retrouvée en fin de réaction. Il en est de même si l'électrolyse est conduite en milieu acide (90% d'acide β-cétalique et 10% du carboxylate correspondant), pourtant connu pour favoriser la formation du radical (2).

Une explication à ce phénomène peut être proposée: dans les conditions de travail utilisées, le potentiel imposé supérieur à 2,2 V ne suffit pas à bloquer l'oxydation de l'eau, comme c'est généralement le cas dans la réaction de Kolbe classique (3). Au contraire l'oxydation de l'eau se poursuit parallèlement à celle des ions carboxylates (type B) ce qui affaiblit beaucoup le rendement en courant. Il est probable que les ions carboxylates β-cétaliques soient solvatés par l'eau au niveau des atomes d'oxygène du groupement dioxolanne et contribuent eux-mêmes au transport de l'eau au voisinage de l'électrode. L'utilisation du milieu aqueux ou hydroorganique étant donc exclu, notre intérêt s'est porté sur les solvants organiques en particulier le méthanol réputé (2) favorable à la dimérisation.

En fait l'électrolyse du carboxylate B en solution dans le méthanol sur électrode de platine (condition favorisant là aussi le radical) fournit, avec un rendement médiocre, un mélange de deux produits en quantité équivalente: le bisdioxolanne issu de la voie radicalaire et le méthoxy-2 méthyl-2 dioxanne-1,4 issu d'une oxydation ultérieure du radical en carbocation selon le schéma 3. (L'étude de la voie cationique a été décrite par ailleurs (4).)

Finalement le dimère ne peut être obtenu qu'en travaillant sur platine, dans le méthanol anhydre et en milieu acide c'est à dire en utilisant au départ un mélange de 90% d'acide β-cétalique et 10% du sel de potassium correspondant. La réalisation de toutes ces conditions imposait une dernière difficulté; en effet l'obtention des acides β-cétaliques n'était pas évidente à priori, vue la sensibilité relative du groupement dioxolanne en milieu acide.

II. Préparation d'acides β-cétaliques

Nous avons dû mettre au point une méthode facile d'accès à ces composés jusqu'alors peu ou mal connus puisque seuls deux d'entre-eux sont cités dans la littérature.

L'un (5) a été obtenu avec un rendement médiocre à partir de l'acide pentyne-3 oïque, l'autre (6) n'a pas été isolé. Afin

TABLEAU 1. Préparation des acides β-cétaliques

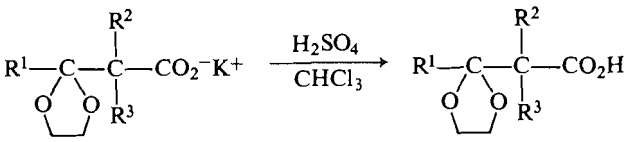

No	R^1	R^2	R^3	Rendement
6	CH_3	H	H	95
7	C_2H_5	H	H	97
8	$(CH_3)_2CH$	H	H	99
9	$(CH_3)_3C$	H	H	98
10	$CH_3(CH_2)_4$	H	H	98
11	Cyclohexyle	H	H	99
12	CH_3	CH_3	H	95
13	CH_3	CH_3	CH_3	95

d'éviter au maximum la dégradation ultérieure de l'acide β-cétalique nous l'avons relargué et extrait du milieu réactionnel aqueux au fur et à mesure de sa formation. Ainsi l'hydrolyse par une solution d'acide sulfurique 12 *N*, à froid, des carboxylates β-cétaliques en solution dans un mélange eau–chloroforme (1:1) saturé en chlorure de sodium fournit les acides correspondants avec d'excellents rendements (Tableau 1).

III. Synthèse des γ-bisdioxolannes

L'électrolyse des acides β-cétaliques a pu être effectuée avec le maximum de conditions favorables à l'orientation vers la voie radicalaire: pH acide, méthanol, anode de platine, forte densité de courant (voir partie expérimentale). Les rendements en dimère sont consignés dans le tableau suivant (Tableau 2).

Lorsque les γ-bisdioxolannes cristallisent au fur et à mesure de leur formation (R^1 = tertiobutyl, cyclohexyl), en se déposant sur l'anode ils diminuent considérablement la densité du courant qui doit être de l'ordre de 0,25 A/cm^2 pour favoriser la réaction radicalaire (2). Le rendement en bisdioxolanne est alors médiocre. Pour pallier cet inconvénient nous avons ajouté au milieu réactionnel du benzène anhydre, qui en solubilisant le γ-bisdioxolanne formé permet de mener à bien l'électrolyse.

Par ailleurs, le tableau montre que les dimères symétriques sont obtenus avec d'excellents rendements dans tous les cas où R^2 et R^3 sont des atomes d'hydrogène. Dans le cas où R^2 est un groupement méthyle, la réaction conduit, avec un faible rendement global, à un mélange de produits contenant 4% de bisdioxolanne issu de la voie radicalaire. Les autres produits formés, dont le principal est un méthoxy-2 dioxanne-1,4, sont tous issus de la voie cationique (4), voir schéma 1. Dans le cas où R^2 et R^3 sont des groupements méthyle, aucun produit d'origine radicalaire n'a pu être mis en évidence; seul le produit d'origine cationique est isolé.

Il faut donc noter la différence remarquable de comportement électrochimique entre les carboxylates β-cétoniques et les carboxylates β-cétaliques.

Dans le cas des carboxylates β-cétoniques la voie radicalaire est fortement favorisée; en effet il faut deux substitutions en α de la fonction cétonique par des groupement alkyles (inducteurs donneurs de façon plus générale) pour abaisser suffisamment le potentiel d'ionisation du radical formé intermédiairement et permettre une oxydation ultérieure en carbocation (1, 7). Le cas des carboxylates β-cétaliques est inverse:

Can. J. Chem. Downloaded from www.nrcresearchpress.com by 210.87.254.105 on 09/06/12
For personal use only.

TABLEAU 2. Dimérisation d'acides β-cétaliques

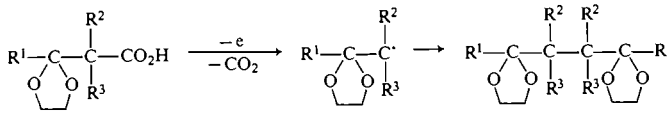

No	R^1	R^2	R^3	Rendements
14	CH_3	H	H	95
15	C_2H_5	H	H	96
16	$(CH_3)_2CH$	H	H	65
17	$(CH_3)_3C$	H	H	74 (26)[a]
18	$CH_3(CH_2)_4$	H	H	85
19	Cyclohexyle	H	H	63 (31)
20	CH_3	CH_3	H	4
	CH_3	CH_3	CH_3	0

[a]Les chiffres entre parenthèses indiquent les rendements obtenus sans addition de benzène.

c'est la voie cationique qui est favorisée (4) et la voie radicalaire ne peut devenir importante que si le carbone en α de la fonction cétalique n'est pas substitué. Enfin, quelque soit la structure du carboxylate (β-cétonique ou β-cétalique), il faut toujours mener la réaction de Kolbe dans les conditions expérimentales les plus favorables à la voie choisie:

cationique: milieu aqueux basique, anode en graphite
radicalaire: milieu méthanolique acid, anode en platine

IV. Obtention de γ-dicétones symétriques

Par hydrolyse acide des bisdioxolannes obtenus précédemment il est possible de passer aux γ-dicétones avec de bons rendements. Les résultats sont résumés dans le tableau 3.

Dans la plupart des cas, le rendement global en γ-dicétone à partir des esters de départ, est supérieur aux rendements observés au laboratoire pour la dimérisation directe des carboxylates β-cétoniques.

Nous avons constaté par ailleurs qu'un contrôle rigoureux des conditions opératoires lors de l'hydrolyse des γ-bisdioxolannes permet d'isoler le monodioxolanne:

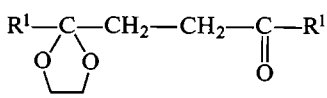

Cette réaction est à l'étude au laboratoire.

Enfin grâce aux bons rendements obtenus dans la dimérisation, il est possible d'effectuer des dimérisations mixtes par couplage entre deux radicaux différents. Les résultats obtenus feront l'objet d'une publication ultérieure.

Partie expérimentale

Les spectres rmn ont été effectués sur un appareil E.M. 360 en solution dans le tétrachlorure de carbone ou le deutérochloroforme (référence interne hexaméthyldisiloxane).

Préparation des esters β-cétoniques et des dioxolannes

1. Mode opératoire, général

Les esters substitués en α de la fonction cétonique ont été préparés par alcoylation de l'acétyl acétate d'éthyle selon Cournot (10). Tous les autres esters ont été préparés selon la méthode de Viscontini (11) suivie d'une méthanolyse (12). Les dioxolannes correspondants sont obtenus selon Salmi (13). Les dioxolannes substitués en α du groupement dioxolanne ont déjà été décrits dans la littérature (14, 15).

TABLEAU 3. Hydrolyse des bisdioxolannes en γ-dicétones

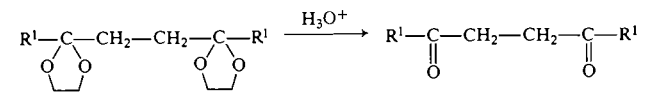

R	Rendement	Ref
CH_3	95	
C_2H_5	82	8
$(CH_3)_2CH$	82	8
$(CH_3)_3C$	69	8
$CH_3(CH_2)_4$	85	9
Cyclohexyle	81	8

2. Produits isolés

Dioxolanne de l'oxo-3 pentanoate de méthyle, ***1***

Rendement 60%; Eb_2 69°C; rmn ($CDCl_3$): 3,96 (s, 4H), 3,65 (s, 2H), 2,63 (s, 3H), 1,76 (q, 2H), 0,9 (t, 3H) ppm. *Anal.* calc. pour $C_8H_{14}O_4$: C 55,16, H 8,10; trouvée: C 54,93, H 8,17.

Dioxolanne du méthyl-4 oxo-3 pentanoate de méthyle, ***2***

Rendement 42%; Eb_{12} 96°C; rmn ($CDCl_3$): 3,93 (s, 4H), 3,66 (s, 3H), 2,63 (s, 2H), 2 (m, 1H), 0,9 (d, 6H) ppm. *Anal.* calc. pour $C_9H_{16}O_4$: C 57,43, H 8,57; trouvée: C 57,38, H 8,68.

Dioxolanne du diméthyl-4,4 oxo-3 pentanoate de méthyle, ***3***

Rendement 34%; $Eb_{0.5}$ 79°C; rmn ($CDCl_3$): 4 (m, 4H), 3,63 (s, 3H), 2,73 (s, 2H), 0,9 (s, 9H) ppm. *Anal.* calc. pour $C_{10}H_{18}O_4$: C 59,38, H 8,97; trouvée: C 59,47, H 9.

Dioxolanne de l'oxo-3 octanoate de méthyle, ***4***

Rendement 70%; $Eb_{0.1}$ 82°C; rmn (CCl_4): 3,9 (s, 4H), 3,6 (s, 3H), 2,46 (s, 2H), 1,96 à 0,56 (m, 11H) ppm. *Anal.* calc. pour $C_{11}H_{20}O_4$: C 61,09, H 9,32; trouvée: C 60,89, H 9,40.

Dioxolanne du β-oxo cyclohexane propionate de méthyle, ***5***

Rendement 48%; $Eb_{0.5}$ 112°C; rmn ($CDCl_3$): 3,96 (s, 4H), 3,7 (s, 3H), 2,66 (s, 2H), 2 à 0,83 (m, 11H) ppm. *Anal.* calc. pour $C_{12}H_{20}O_4$: C 63,13, H 8,83; trouvée: C 63,05, H 9,05.

Saponification des esters β-cétaliques (mode opératoire général)

Une solution de 0,11 mol de potasse dans 40 mL d'eau est ajoutée à température ambiante à 0,1 mol de dioxolanne. Une agitation magnétique est maintenue jusqu'à ce que le milieu soit homogène. Deux extractions à l'éther sont effectuées pour éliminer toute trace d'ester n'ayant pas réagi. Dans le cas des esters substitués en α du groupement dioxolanne il est nécessaire de porter à reflux le mélange réactionnel pour que la saponification soit complète. La solution aqueuse est évaporée à sec.

Synthèse des acides β-cétaliques

1. Mode opératoire général

Un mélange contenant une mol de carboxylate β-cétalique séché, 100 mL d'eau distillée, 200 mL de chloroforme est saturé en chlorure de sodium puis refroidi à 0°C. L'acidification est réalisée à cette température par de l'acide sulfurique 12 *N* jusqu'à pH = 1. Le sulfate de potassium formé et le chlorure de sodium sont filtrés, le filtrat extrait par 2 L de chloroforme. Après séchage sur sulfate de magnésium et évaporation du chloroforme à 25°C, l'acide cristallise, le plus souvent spontanément. Le produit peut être conservé plusieurs mois à 0°C.

2. Produits isolés

Acide (méthyl-2 dioxolanne-1,3 yl-2)-2 acétique, ***6***

Rendement 95%; F 27°C; rmn (CCl_4): 11,6 (s, 1H), 3,9 (s, 4H), 2,6 (s, 2H), 1,45 (s, 3H) ppm. *Anal.* calc. pour $C_6H_{10}O_4$: C 49,31, H 6,90; trouvée: C 49,25, H 6,87.

Acide (éthyl-2 dioxolanne-1,3 yl-2)-2 acétique (16), ***7***

Rendement 97%; F 24°C; rmn (CCl_4): 11 (s, 1H), 3,9 (s, 4H), 2,56 (s, 2H), 1,8 (q, 2H), 0,8 (t, 3H) ppm.

Acide (isopropyl-2 dioxolanne-1,3 yl-2)-2 acétique, ***8***

Rendement 99%; F 48°C; rmn (CCl_4): 10,86 (s, 1H), 4 à 3,66 (m,

Can. J. Chem. Downloaded from www.nrcresearchpress.com by 210.87.254.105 on 09/06/12
For personal use only.

Can. J. Chem. Downloaded from www.nrcresearchpress.com by 210.87.254.105 on 09/06/12
For personal use only.

4H), 2,56 (s, 2H), 2,3 à 1,8 (m, 1H) ppm. *Anal.* calc. pour $C_8H_{14}O_4$: C 55,16, H 8,10; trouvée: C 55,34, H 8,29.

Acide (tertiobutyl-2 dioxolanne-1,3 yl-2)-2 acétique, ***9***

Rendement 98%; F 64°C; rmn (CCl_4): 11,46 (s, 1H), 4,1 à 3,8 (m, 4H), 2,66 (s, 2H), 0,93 (s, 9H) ppm. *Anal.* calc. pour $C_9H_{16}O_4$: C 57,43, H 8,57; trouvée: C 57,39, H 8,61.

Acide (pentyl-2 dioxolanne-1,3 yl-2)-2 acétique, ***10***

Rendement 98%; $Eb_{0.05}$ 106°C; rmn (CCl_4): 11,4 (s, 1H), 3,9 (s, 4H), 2,5 (s, 2H), 1,96 à 0,63 (m, 11H) ppm. *Anal.* calc. pour $C_{10}H_{18}O_4$: C 59,38, H 8,97; trouvée: C 59,62, H 9.

Acide (cyclohexyl-2 dioxolanne-1,3 yl-2)-2 acétique, ***11***

Rendement 99%; $Eb_{0.05}$ 110°C; rmn (CCl_4): 11,13 (s, 1H), 4,1 à 3,7 (m, 4H), 2,56 (s, 2H), 2,16 à 0,83 (m, 11H) ppm. *Anal.* calc. pour $C_{11}H_{18}O_4$: C 61,66, H 8,47; trouvée: C 61,45, H 8,47.

Acide méthyl-2 (méthyl-2 dioxolanne-1,3 yl-2)-2 acétique, ***12***

Rendement 95%; F 10°C; rmn (CCl_4): 11,7 (s, 1H), 3,9 (s, 4H), 2,65 (q, 1H), 1,35 (s, 3H), 1,15 (d, 3H) ppm. *Anal.* calc. pour $C_7H_{12}O_4$: 52,49, H 7,55; trouvée: C 52,57, H 7,48.

Acide diméthyl-2,2 (méthyl-2 dioxolanne-1,3 yl-2)-2 acétique, ***13***

Rendement 95%; F 36°C; rmn (CCl_4): 9,7 (s, 1H), 3,9 (s, 4H), 1,35 (s, 3H), 1,20 (s, 6H) ppm. *Anal.* calc. pour $C_8H_{14}O_4$: C 55,16, H 8,10; trouvée: C 55,09, H 8,14.

Obtention des bisdioxolannes

1. Condition d'électrolyse: mode opératoire général

L'appareil utilisé est un potentiostat Tacussel modèle PRT 40-5X permettant d'imposer un potentiel fixe à l'anode. Les mesures coulométriques ont été faites à l'aide d'un intégrateur Tacussel type IG5-LN monté un série sur le circuit. L'intensité du courant est vérifiée par un ampèremètre monté sur le circuit de la cathode. La cellule d'électrolyse est constituée par une cuve de verre entourée d'une jaquette permettant de maintenir une circulation d'eau de refroidissement. L'anode est une lame de platine de 9 cm^2 et la cathode une lame de platine de 3 cm^2.

Dans la cellule non divisée une solution de 0,1 mol d'acide et de 0,01 mol de potasse dans 100 mL de méthanol sec est introduite. L'électrolyse est effectuée sous agitation magnétique et la tension imposée est toujours supérieure à 2,2 volts par rapport à l'électrode de référence au calomel. L'électrolyse est arrêtée quand le pH de la solution devient neutre à légèrement basique, ce qui correspond à 0,3 faradays environ. Dans le cas où le dimère précipite en cours d'électrolyse, du benzène sec est ajouté pour solubiliser le produit formé. Le mélange réactionnel est évaporé, lavé deux fois par 50 mL d'eau, extrait trois fois par 50 mL de chloroforme puis séché sur sulfate sodium. Le chloroforme est évaporé à 25°C. Les bisdioxolannes sont recristallisés dans l'éther de pétrole ou distillés sous vide.

2. Produits isolés

Bis (méthyl-2 dioxolanne-1,3 yl-2)-1,2 éthane (17), ***14***

Rendement 95%; F 58°C; rmn (CCl_4): 3,8 (s, 4H), 1,5 (s, 2H), 1,2 (s, 3H) ppm.

Bis (éthyl-2 dioxolanne-1,3 yl-2)-1,2 éthane, ***15***

Rendement 96%; $Eb_{0.01}$ 112°C; rmn (CCl_4): 3,8 (s, 4H), 1,5 (q, 2H), 0,8 (t, 3H) ppm. *Anal.* calc. pour $C_{12}H_{22}O_4$: C 62,48, H 9,63; trouvée: C 62,68, H 9,72.

Bis (isopropyl-2 dioxolanne-1,3 yl-2)-1,2 éthane, ***16***

Rendement 65%; F 60°C; rmn (CCl_4): 3,8 (s, 4H), 1,43 (s, 2H), 2,06 à 1,33 (m, 1H), 0,83 (d, 6H) ppm. *Anal.* calc. pour $C_{14}H_{26}O_4$: C 65,08, H 10,14; trouvée: C 65,24, H 10,01.

Bis (tertiobutyl-2 dioxolanne-1,3 yl-2)-1,2 éthane, ***17***

Rendement 74%; F 154°C; rmn (CCl_4): 4,16 à 3,8 (m, 4H), 2,66 (s, 2H), 0,9 (s, 9H) ppm. *Anal.* calc. pour $C_{16}H_{30}O_4$: C 67,09, H 10,56; trouvée: C 67,18, H 10,64.

Bis (pentyl-2 dioxolanne-1,3 yl-2)-1,2 éthane, ***18***

Rendement 85%; $Eb_{0.05}$ 65°C; rmn (CCl_4): 3,93 (s, 4H), 1,63 (s, 2H), 1,56 à 0,6 (m, 11H) ppm. *Anal.* calc. pour $C_{18}H_{34}O_4$: C 68,75, H 10,90; trouvée: C 68,39, H 10,89.

Bis (cyclohexyl-2 dioxolanne-1,3 yl-2)-1,2 éthane, ***19***

Rendement 63%; F 102°C; rmn (CCl_4): 3,8 (s, 4H), 1,4 (s, 2H), 2 à 0,7 (m, 11H) ppm. *Anal.* calc. pour $C_{20}H_{34}O_4$: C 70,94, H 10,13; trouvée: C 70,89, H 9,98.

Bis (méthyl-2 dioxolanne-1,3 yl-2)-2,3 butane, ***20***

Rendement 4%; F 31°C; rmn (CCl_4): 3,8 (s, 8H), 2,2 à 1,7 (m, 2H), 1,15 (s, 6H), 0.9 (m, 6H) ppm. *Anal.* calc. pour $C_{12}H_{22}O_4$: C 62,48, H 9,63; trouvée: C 62,46, H 9,70.

Obtention des γ-dicétones

1. Mode opératoire général

A une solution de 0,05 mol de bis dioxolanne dans 40 mL de dioxanne, sont ajoutés 50 mL d'une solution à 10% d'acide sulfurique. Le mélange est agité pendant trois heures à température ambiante, puis 50 mL d'une solution molaire de soude sont additionnés. Après trois extractions au chloroforme, séchage sur sulfate de magnésium et évaporation des solvants, le résidu est distillé (voir Tableau 3).

1. M. CHKIR, D. LELANDAIS et C. BACQUET. Can. J. Chem. **59**, 945 (1981).
2. M. H. BAIZER. Organic electrochemistry. M. Dekker, New York. 1973 p. 476.
3. J. H. P. UTLEY. Annu. Rep. **65**, 231 (1968).
4. D. LELANDAIS, C. BACQUET et J. EINHORN. Tetrahedron, **37**, 3131 (1981).
5. E. JONES, G. WHITHAM et M. WHITING. J. Chem. Soc. 3201 (1954).
6. P. R.VAGELOS et A. WALBERTS. Anal. Biochem. **1**, 8 (1960).
7. D. LELANDAIS et M. CHKIR. C.R. Acad. Sci. Ser. C, **281**, 721 (1975).
8. W. SUDWEEKS et S. BROADBENT. J. Org. Chem. **40**, 1131 (1975).
9. H. STETTER et H. J. BENDER. Chem. Ber. **4**, 1226 (1981).
10. A. COURNOT. Bull. Soc. Chim. Fr. **35**, 98 (1906).
11. M. VISCONTINI et N. MECKING. Helv. Chem. Acta. **35**, 2280 (1952).
12. H. HUNSDIECKER. Ber. B, **75**, 447 (1942).
13. E. J. SALMI. Chem. Ber. B, **71**, 1803 (1938).
14. R. JACQUIER, C. PETRUS, F. PETRUS et I. VERDUCCI. Bull. Soc. Chim. Fr. 1978 (1970).
15. H. BAGANG et S. RABE. Chem. Ber. **98**, 3652 (1965).
16. E. JONES, C. WHITHAM et M. WHITING. J. Chem. Soc. 3207, (1954).
17. F. CHASTRETTE, M. MASSAMBAY et M. CHASTRETTE. Bull. Soc. Chim. Fr. 601 (1974).

Comment: The H_3O^+ ion in aqueous sulfuric acid

PAUL A. GIGUÈRE
Département de Chimie, Université Laval, Québec (Qué.), Canada G1K 7P4

Received October 20, 1982

(Ref. Can. J. Chem. **59**, 2591 (1981))

In a recent paper Cox *et al.* (1) have reported their principal factor analysis of the Raman spectra of aqueous sulfuric acid solutions. One of their conclusions is that two water molecules, rather than one, are required for the first ionization of H_2SO_4. As a result, the only ionic species apparent in the more concentrated solutions are ion pairs of HSO_4^- and $H_3O^+ \cdot H_2O$ (*or $H_5O_2^+$ if this entity has a real existence*). Now, there are enough data in the literature to rule out off-hand the latter hypothesis. In a paper published twenty-five years ago in this journal (2), but not quoted by Cox *et al.*, we reported the first infrared absorption spectra of two concentrated solutions of sulfuric acid: one of composition near the trihydrate, the other, near the monohydrate. The first one showed very clearly the bending band of H_3O^+, ν_4, at about 1740 cm^{-1}, beside the ν_2 water band at 1645 cm^{-1}. In the second one, the two bands had merged, giving a broad maximum ca. 1710 cm^{-1}. A further, more extensive study of these spectra has confirmed the above interpretation (3), showing, in addition, that the characteristic band of HSO_4^- at 1050 cm^{-1} reaches maximum intensity at the dihydrate composition, when that of H_2SO_4 at 967 cm^{-1} has practically disappeared. If the cation were the improbable $H_5O_2^+$, then that solution would be a pure liquid electrolyte, analogous to a fused salt, a most unlikely situation.

What distinguishes the genuine $H_5O_2^+$ ion from a complex like $H_3O^+ \cdot H_2O$, is the very short O···O distance (<2.45 Å) with the excess proton located halfway; that is, in a single-minimum potential well. It has been identified by diffraction methods only in the crystalline dihydrates (or higher hydrates) of some mineral acids (4). Not all of them, however. A case in point is precisely the dihydrate of sulfuric acid, which has been found by three-dimensional, single-crystal analysis (5) to consist exclusively of SO_4^{2-} and H_3O^+ ions. Since the $H_5O_2^+$ ion does not exist in that solid, where it could be stabilized by the crystal field, then *a fortiori* it does not exist in the liquid acid.

In contrast, the H_3O^+ ion, a much more widespread species, has been ascertained, in particular by neutron diffraction, not only in solid acid hydrates, but also in concentrated solutions of hydrochloric acid (6). There is no reason why the cation in aqueous sulfuric acid should be different. Incidentally, in these solutions where fast proton transfer is so predominant, the very short-lived water molecule cannot be viewed as preferably solvating the cation, as implied by the $H_3O^+ \cdot H_2O$ formula (1), rather than the HSO_4^- anion. Likewise, the latter cannot be qualified as "free", even within quotation marks, in these thoroughly hydrogen-bonded solvent systems. A better description would be solvent-separated vs. contact ion pairs.

R. A. Cox has communicated his full agreement with the above conclusions.

1. R. A. COX, Ü. L. HALDNA, K. L. IDLER, and K. YATES. Can. J. Chem. **59**, 2591 (1981).
2. M. FALK and P. A. GIGUÈRE. Can. J. Chem. **35**, 1195 (1957).
3. P. A. GIGUÈRE and R. SAVOIE. Can. J. Chem. **38**, 2467 (1960).
4. J. O. LUNDGREN and I. OLOVSSON. *In* The hydrogen bond. Vol. II. *Edited by* F. Schuster, G. Zundel, and C. Sandorfy. North-Holland Publishing Co., Amsterdam. 1976. p. 473.
5. I. TAESLER and I. OLOVSSON. J. Chem. Phys. **51**, 4213 (1969).
6. R. TRIOLO and A. H. NARTEN. J. Chem. Phys. **63**, 3624 (1975).

Can. J. Chem. Downloaded from www.nrcresearchpress.com by 210.87.254.6 on 09/06/12
For personal use only.

An MNDO study of sulfenium ions

JACK LEON GINSBURG[1]
Department of Chemistry, Saint Mary's University, Halifax, N.S., Canada B3H 3C3

AND

RICHARD FRANCIS LANGLER
Department of Chemistry, Florida Institute of Technology, Melbourne, FL 32901, U.S.A.

Received August 24, 1982

JACK LEON GINSBURG and RICHARD FRANCIS LANGLER. Can. J. Chem. **61**, 589 (1983).

An MNDO study has been carried out on a variety of substituted sulfenium ions and sulfides. Relative stabilities in the gas phase have been calculated for several pairs of regioisomeric sulfenium ions. It is shown that sulfenium ions are stabilized by π-donors and that the substituent electronegativity is not an important factor. The potential implications of this result for the mechanism by which chlorosulfonium cations are converted into sulfenium ions in solution is discussed. Substituent effects on the energetics of sulfenium ion formation from sulfides have been obtained. It is shown that these effects also are related to the substituent's π-donating ability. A frontier-orbital analysis of selected sulfenium ions has been done and is discussed.

JACK LEON GINSBURG et RICHARD FRANCIS LANGLER. Can. J. Chem. **61**, 589 (1983).

On a réalisé une étude de MNDO sur une série d'ions sulfénium substitués et de sulfure. On a calculé les stabilités relatives en phase gazeuse de plusieurs paires d'ions sulfénium régioisomères. On montre que les donneurs π stabilisent ces ions sulfénium et que l'électronégativité du substituant n'est pas un facteur important. On discute des implications potentielles de ce résultat sur le mécanisme par lequel on transforme les cations chlorosulfonium en ions sulfénium en solution. On a évalué l'effet des substituants sur les niveaux d'énergie impliqués lors de la formation d'ions sulfénium à partir de sulfures. On montre que ces effets sont également reliés à la capacité de donneur π du substituant. On a effectué une analyse d'orbitale frontière de certains ions sulfénium choisis et on en discute.

[Traduit par le journal]

Can. J. Chem. Downloaded from www.nrcresearchpress.com by 210.87.254.5 on 09/06/12
For personal use only.

Introduction

As part of our continuing program to study the chlorination reactions of organosulfur compounds, we have reported an examination of sulfide chlorinations conducted in aprotic media (1). The chlorination of asymmetric sulfides may give rise to a pair of regioisomeric α-chlorosulfides as shown in reaction [1].

[1] $R_1CH_2SCH_2R_2 + ClX \rightarrow R_1CH_2SCHClR_2 + R_1CHClSCH_2R_2 + HX$

The presently accepted mechanism for these reactions (*vide* Scheme 1) is due to Wilson and Huang (2) and proceeds through the intermediacy of a sulfenium ion (**A**, Scheme 1).

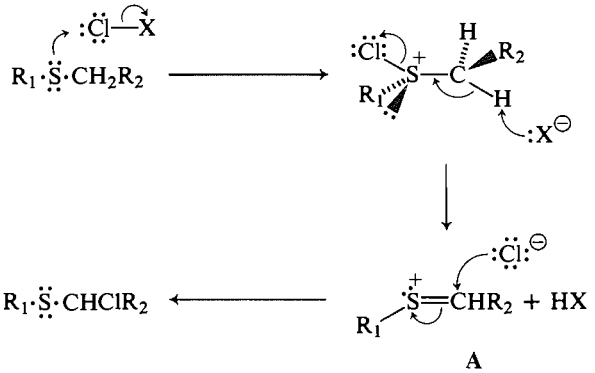

SCHEME 1

Following Hammond's postulate,[2] we have decided to undertake a theoretical study of sulfenium ions, in the hope that we could shed some light on the nature of substituents which control regiochemistry in the E2 step of the mechanism (shown in Scheme 1) for sulfide chlorinations. Our initial objectives were (*i*) to see if the regioisomeric sulfenium ion with the lower calculated gas phase ΔH_f was the one formed preferentially in solution, (*ii*) to establish whether substituent effects for calculated regioisomeric sulfenium ions would correlate with substituent electronegativity values,[3] and (*iii*) given the absence of solvent effects on regioselectivity in these reactions, to determine whether MO computations would indicate the need for a more complex array of mechanisms to account for the outcome of sulfide chlorinations. We note that the outcome of our study may also have relevance to synthetic reactions involving sulfenium ions. In that area, sulfenium ions are known as thionium ions and are advanced as "supercarbonyl" equivalents (4).

We have chosen to examine the set of sulfenium ions **1***a* → **1***y*, as defined under structure **1**.

Method

All computations were done using the MNDO (Modified Neglect of Differential Overlap) semiempirical method (5–7). Geometries were

[1]To whom all correspondence should be addressed.

[2]"If two states, as for example, a transition state and an unstable intermediate, occur consecutively during a reaction process and have nearly the same energy content, their interconversion will involve only a small reorganization of molecular structure" (3).

[3]Regiochemical outcomes of sulfide chlorinations have been shown to correlate with the substituent electronegativity difference of the groups present in the sulfide substrate (1).

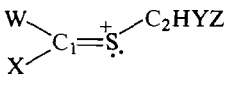

1

1*a*	W = Cl	X = H	Y = H	Z = H
1*b*	W = H	X = H	Y = Cl	Z = H
1*c*	W = OH	X = H	Y = H	Z = H
1*d*	W = H	X = H	Y = OH	Z = H
1*e*	W = SH	X = H	Y = H	Z = H
1*f*	W = H	X = H	Y = SH	Z = H
1*g*	W = F	X = H	Y = H	Z = H
1*h*	W = H	X = H	Y = F	Z = H
1*i*	W = CN	X = H	Y = H	Z = H
1*j*	W = H	X = H	Y = CN	Z = H
1*k*	W = H	X = $CO_2C_2H_5$	Y = H	Z = H
1*l*	W = H	X = H	Y = $CO_2C_2H_5$	Z = H
1*m*	W = H	X = CF_3	Y = H	Z = H
1*n*	W = H	X = H	Y = CF_3	Z = H
1*o*	W = H	X = Ph	Y = H	Z = H
1*p*	W = H	X = H	Y = Ph	Z = H
1*q*	W = H	X = CH_3	Y = H	Z = H
1*r*	W = H	X = H	Y = CH_3	Z = H
1*s*	W = H	X = H	Y = H	Z = H
1*t*	W = CH_3	X = CH_3	Y = H	Z = H
1*u*	W = H	X = H	Y = CH_3	Z = CH_3
1*v*	W = Cl	X = Cl	Y = H	Z = H
1*w*	W = H	X = H	Y = Cl	Z = Cl
1*x*	W = H	X = Ph	Y = Cl	Z = H
1*y*	W = Cl	X = H	Y = Ph	Z = H

fully optimized[4] using the Davidon–Fletcher–Powell algorithm (8, 9). A program written by Walter Thiel and modified by the National Resource for Computation in Chemistry was used (10). For species for which the occurrence of *cis-trans* isomers is possible, computations were done for both isomers.

The MNDO method has been found to give better results than the MINDO/3 method for, among other properties, heats of formation and molecular geometries (6, 7, 11). It is arguable that, for relative energies, MNDO results are comparable to minimal basis set *ab initio* results (12).

Since its formulation the MNDO method has been used in numerous investigations, including studies involving substituent effects (e.g. refs. 13–16).

Results and discussion

The sulfenium ion geometries will not be discussed in detail but it is important to note that, in all cases studied, the WXC_1SC_2 framework (structure **1**) is planar or nearly so. Hence analysis in terms of a WC_1S or XC_1S π system is valid.

Relative regioisomeric stabilities

Table 1 presents the calculated relative gas phase stabilities, $\Delta\Delta H_f$, of some regioisomeric sulfenium ion pairs. $\Delta\Delta H_f$ is a measure of the stabilizing ability of a substituent relative to that of H (in the case of **1***x* and **1***y*, C_6H_5 relative to Cl). It is noteworthy that $\Delta\Delta H_f$'s do not correlate with substituent electronegativity differences, contrary to the expectation of Ahern *et al.* (1). In fact, the highly electronegative CF_3 group is destabilizing relative to H.

Tables 2 through 4 present results pertinent to the analysis of factors which are important in determining the relative regioisomeric stabilities. Results for the unsubstituted sulfenium

[4]For species containing phenyl substituents, the phenyl rings were constrained to be planar, with equal C—H bond lengths and 120° HCC and CCC bond angles.

TABLE 1. Calculated relative stabilities of regioisomeric sulfenium ions and sulfenium ions implicated by experiment

Sulfenium ion	ΔH_f (kcal/mol)	$\Delta\Delta H_f$ (kcal/mol)	Sulfenium ion intermediate implicated by calculations	Sulfenium ion intermediate implicated by experiment*
1*a*	203	−4	**1***a*	**1***a*
1*b*	207			
1*c*	137	−20	**1***c*	—
1*d*	157			
1*e*	199	−13	**1***e*	—
1*f*	212			
1*g*	159	−11	**1***g*	—
1*h*	170			
1*i*	245	−4	**1***i*	**1***i*
1*j*	249			
1*k*	125	−3	**1***k*	**1***k*
1*l*	128			
1*m*	79	+3	**1***n*	—
1*n*	76			
1*o*	207	−20	**1***o*	**1***o*
1*p*	227			
1*q*	192	−8	**1***q*	**1***q*
1*r*	200			
1*s*	207	—	—	—
1*t*	182	−12	**1***t*	**1***t*
1*u*	194			
1*v*	203	−7	**1***v*	**1***v*
1*w*	210			
1*x*	204	−18	**1***x*	**1***y*
1*y*	222			

*Experimental results summarized in ref. 1.

Can. J. Chem. Downloaded from www.nrcresearchpress.com by 210.87.254.5 on 09/06/12
For personal use only.

TABLE 2. Pertinent sulfenium ion (structure **1**) π-bond orders*

Ion	π-Bond orders		
	C_1S	C_1W	C_1X
1*a*	0.79	0.43	—
1*b*	0.85	—	—
1*c*	0.63	0.65	—
1*d*	0.86	—	—
1*e*	0.70	0.62	—
1*f*	0.86	—	—
1*g*	0.73	0.51	—
1*h*	0.86	—	—
1*i*	0.82	0.30	—
1*j*	0.86	—	—
1*k*	0.86	—	0.11
1*l*	0.86	—	—
1*m*	0.90	—	0.08
1*n*	0.84	—	—
1*o*	0.60	—	0.61
1*p*	0.87	—	—
1*q*	0.80	—	0.26
1*r*	0.86	—	—
1*s*	0.86	—	—
1*t*	0.76	0.23	0.24
1*u*	0.87	—	—
1*v*	0.75	0.39	0.40
1*w*	0.85	—	—
1*x*	0.56	—	0.63
1*y*	0.82	0.40	—

*For species for which *cis–trans* isomers are possible, the lower energy isomer is presented.

TABLE 3. Electron donation into the C_1S^+ moiety*

Ion	π and σ electron donation		
	W	X	CHYZ
1*a*	0.13π, 0.02σ	0.15σ	0.25σ
1*b*	0.14σ	0.15σ	0.22σ
1*c*	0.31π, −0.16σ	0.16σ	0.24σ
1*d*	0.12σ	0.13σ	0.41σ
1*e*	0.29π, 0.09σ	0.15σ	0.22σ
1*f*	0.13σ	0.14σ	0.28σ
1*g*	0.18π, −0.23σ	0.18σ	0.27σ
1*h*	0.15σ	0.12σ	0.33σ
1*i*	0.08π, −0.09σ	0.16σ	0.24σ
1*j*	0.15σ	0.13σ	0.22σ
1*k*	0.14σ	0.11σ	0.24σ
1*l*	0.15σ	0.13σ	0.19σ
1*m*	0.16σ	0.12σ	0.28σ
1*n*	0.14σ	0.14σ	0.16σ
1*o*	0.10σ	0.38π, 0.03σ	0.21σ
1*p*	0.12σ	0.13σ	0.37σ
1*q*	0.12σ	0.08π, 0.14σ	0.24σ
1*r*	0.12σ	0.14σ	0.28σ
1*s*	0.13σ	0.14σ	0.24σ
1*t*	0.06π, 0.16σ	0.06π, 0.14σ	0.23σ
1*u*	0.14σ	0.12σ	0.28σ
1*v*	0.11π, 0.03σ	0.12π, 0.05σ	0.26σ
1*w*	0.13σ	0.15σ	0.21σ
1*x*	0.11σ	0.39π, 0.04σ	0.16σ
1*y*	0.11π, −0.02σ	0.16σ	0.37σ

*For species for which *cis–trans* isomers are possible, the lower energy isomer is presented.

ion, **1***s*, are presented to facilitate the analysis. Table 2 shows that, except for the $CO_2C_2H_5$ substituted pair, for which there is virtually no difference in C_1S π bond orders, the more stable regioisomer has the lower C_1S π bond order. The extent of C_1S π bond weakening can be seen by comparing the bond orders to that of the unsubstituted sulfenium ion, **1***s*. Note that the destabilizing CF_3 group causes an increase in the C_1S π bond order when substituted at C_1 with respect to that of the unsubstituted sulfenium ion. These results indicate that substituent participation in the sulfenium ion π system is an important stabilizing factor.

Calculated C_1S π bond length differences, although quite small, reinforce this observation. In each case, the more stable regioisomer has the greater C_1S bond length. Differences range from 0.06 Å for the C_6H_5 or OH substituted pairs to 0.01 Å for the CF_3, Cl, or $CO_2C_2H_5$ substituted pairs. Also, the C_1S bond length of the less stable regioisomer of each pair is within 0.01 Å of that, 1.59 Å, of the unsubstituted sulfenium ion.

Tables 3 and 4 give the results of population analyses of the sulfenium ions studied. Table 3 essentially gives differences between the population analysis of the given sulfenium ion and the population analysis of the isolated components of the sulfenium ion. With the exception of $CO_2C_2H_5$, each stabilizing substituent is a π-donor with respect to the C_1S^+ moiety. The relative degree of stabilization is independent of whether or not the substituent is a good σ-donor or indeed of whether it is a σ-donor or σ-acceptor. There is a rough correlation between $\Delta\Delta H_f$'s and π-donor abilities, but SH would be expected to be a better stabilizer and CH_3 a worse stabilizer based on their π-donor abilities.

Table 4 gives details of the population analyses of the π systems. In the unsubstituted sulfenium ion, **1***s*, C_1 (structure **1**) has a population of 0.5 π electrons and S has a population of 1.5 π electrons. As expected, sulfenium ions having substituents only at C_2 (structure **1**) do not have a π electron distribution significantly different from that of the unsubstituted sulfenium ion. Different π-donor groups substituted at C_1 affect the relative π electron distribution to different extents. The substituent stabilizing abilities correlate with increases in π electron population at S better than with total increases in π electron populations at C_1 and S. For example, OH donates 0.31 π electron to the C_1S^+ moiety, and SH donates 0.29 π electron. OH increases the π electron population at S by 0.21 electron, and SH increases it by 0.13 electron. $\Delta\Delta H_f$ for OH as a substituent is −20 kcal/mol and $\Delta\Delta H_f$ for SH is −13 kcal/mol. The destabilizing CF_3 group, which is neither a π-donor or acceptor, induces a shift in the π electron distribution such that the population at S is 0.08 π electron smaller than it is in the unsubstituted sulfenium ion.

To summarize the preceding results, no correlation between substituent electronegativity values and relative regioisomeric stabilities has been found. Instead it has been found that sulfenium ions are stabilized by substituents which are π-donors with respect to the C_1S^+ moiety. Relative regioisomeric stabilities are roughly correlated with the extent of substituent π electron donation into the C_1S^+ moiety and well correlated with

Can. J. Chem. Downloaded from www.nrcresearchpress.com by 210.87.254.5 on 09/06/12
For personal use only.

Can. J. Chem. Downloaded from www.nrcresearchpress.com by 210.87.254.5 on 09/06/12
For personal use only.

TABLE 4. Sulfenium ion (structure **1**) π-electron populations*

Ion	π-electron population			
	C_1	S	W	X
1*a*	0.59	1.54	1.87	—
1*b*	0.48	1.52	—	—
1*c*	0.60	1.71	1.69	—
1*d*	0.50	1.50	—	—
1*e*	0.66	1.63	1.71	—
1*f*	0.49	1.51	—	—
1*g*	0.57	1.61	1.82	—
1*h*	0.50	1.50	—	—
1*i*	0.56	1.51	1.93	—
1*j*	0.50	1.50	—	—
1*k*	0.53	1.49	—	—
1*l*	0.51	1.50	—	—
1*m*	0.60	1.42	—	—
1*n*	0.47	1.53	—	—
1*o*	0.64	1.73	—	5.62
1*p*	0.53	1.48	—	—
1*q*	0.52	1.56	—	1.92
1*r*	0.52	1.49	—	—
1*s*	0.50	1.51	—	—
1*t*	0.53	1.59	1.94	1.94
1*u*	0.52	1.49	—	—
1*v*	0.65	1.58	1.89	1.88
1*w*	0.49	1.51	—	—
1*x*	0.63	1.75	—	5.61
1*y*	0.61	1.51	1.89	—

*For species for which *cis*–*trans* isomers are possible, the lower energy isomer is presented.

the amount of π electron population increase at S. Of the substituents studied which do not participate in the π system one, $CO_2C_2H_5$, is weakly stabilizing, and the other, CF_3, is weakly destabilizing.

Mechanistic implications

Table 1 presents a comparison of $\Delta\Delta H_f$ values for pairs of regioisomeric sulfenium ions aong with the sulfenium ion structures implicated by experiment as the actual reaction intermediates.[5] Qualitatively, the theoretical results are in accord with experiment — viz. all experimentally tested substituents are better directing groups than hydrogen. Quantitatively, the trends are somewhat disturbing, i.e. (*i*) the $\Delta\Delta H_f$ (−4 kcal/mol) for the chlorosulfenium ions **1***a*, **1***b* in conjunction with $\Delta\Delta H_f$ (−8 kcal/mol) for the methylsulfenium ions **1***q*, **1***r* suggests that methyl is a better directing group than chlorine, whereas experimentally chlorine is a much better directing group than methyl (1), (*ii*) the direct comparison of chlorine and phenyl in sulfenium ions **1***x*, **1***y* clearly indicates that phenyl is a much better directing group than chlorine, whereas experimentally the opposite is true (1), and (*iii*) the established semiquantitative correlation between ΔX_p and regiochemistry in asymmetric sulfide chlorinations (1, 17) indicates that the regioisomeric sulfenium ion **1***m* should be formed exclusively, whereas the $\Delta\Delta H_f$ value (+4 kcal/mol) indicates that **1***n* should predominate.[6]

In order to integrate the observed directing abilities of the substituents with the calculated parameters, we would like to make the following mechanistic proposals.[7] For sulfides which bear substituents with low electronegativities, such as hydrogen, methyl, and phenyl, the mechanism for the elimination step should be a relatively central E2 elimination as pictured in Scheme 1. Indeed Scheme 1 represents Wilson's conclusion about the chlorination of benzyl methyl sulfide. Substituent directing abilities would then originate with their π electron releasing abilities as indicated by our computations. For sulfides bearing more electronegative substituents such as cyano, chloro, and fluoro, the mechanism would shift towards an $E1_{cb}$-like pathway, with regioselectivity being determined by the substituent's ability to facilitate CH bond breaking. In this transition state, the substituents would be utilizing inductive abilities which are independent of the presence of a carbon *p* orbital with the appropriate orientation for a resonance interaction. This shift in mechanism would tend to make the electronegative substituents better directing groups than methyl or phenyl. In as much as the shift towards as $E1_{cb}$-like mechanism involves an earlier transition state, it makes the transition state-sulfenium ion analogy inapplicable. The possibility that sulfides with strongly electron-withdrawing groups react via the intermediacy of an ylide has been discredited (1).

These mechanistic implications will be investigated using both semiempirical and, where necessary, *ab initio* methods.

Energetics of sulfenium ion formation

Although the $\Delta\Delta H_f$ values (listed in Table 1) for regioisomeric sulfenium ion pairs are most appropriate for a theoretical treatment of chlorination reactions of sulfides, we felt that a more generally useful assessment of substituent effects on the energetics of sulfenium ion formation would be obtained by a comparison of the ΔH_r value for the reaction shown in reaction [2] with the ΔH_r value for the reaction shown in reaction [3].

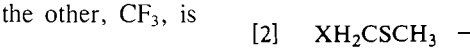

[2] $XH_2CSCH_3 \longrightarrow XHC{=}\overset{\oplus}{S}CH_3 + \overset{\ominus}{H}$

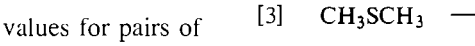

[3] $CH_3SCH_3 \longrightarrow H_2C{=}\overset{\oplus}{S}CH_3 + \overset{\ominus}{H}$

As expected, the substituents are ordered by the computations in a way which reflects their π-donating abilities. Thus, $\Delta\Delta H_r$, $\Delta H_r[2] - \Delta H_r[3]$, is −28 kcal/mol and −26 kcal/mol for the strong π-donors X = C_6H_5 and X = OH respectively while, for X = CF_3, $\Delta\Delta H_r$ = +15 kcal/mol. Other values of $\Delta\Delta H_r$ range from −15 kcal/mol for X = SH to +4 kcal/mol for X = CN. These results will have obvious relevance for reactions which furnish sulfenium ions reversibly or for irreversible reactions which produce sulfenium ions via a late transition state.

Frontier-orbital analysis

As part of our study of sulfenium ions, we have calculated population numbers for selected sulfenium ion LUMO's,

[5]Experimental results have been presented which indicate that regioiosomeric sulfenium ions are not interconvertible under the usual reaction conditions (1).

[6]We hope to pursue the chlorination of selected 2,2,2-trifluoroethyl sulfides shortly.

[7]It should be noted that (*i*) there are no known cases of sulfide chlorinations for which a change in solvent has induced a significant change in regiochemistry despite the fact that solvents used range in polarity from pentane (1) to aqueous acetic acid (18) and (*ii*) evidence has been presented indicating that sulfenium ion formation is irreversible (1).

TABLE 5. Population numbers of sulfenium ion lumo's*

Sulfenium ion	Atom†	Population number	Atom†	Population number
1*a*	C_1	0.71	S	0.22
1*c*	C_1	0.70	O(ω)	0.15
			S	0.14
1*e*	C_1	0.67	S	0.18
			S(ω)	0.14
1*g*	C_1	0.72	S	0.19
1*i*	C_1	0.65	S	0.23
1*k*	C_1	0.72	S	0.25
1*m*	C_1	0.69	S	0.29
1*o*	C_1	0.50	S	0.11
			Ph (*ortho* carbon)	0.13
			Ph (*para* carbon)	0.13
1*q*	C_1	0.73	S	0.22
1*s*‡	C_1	0.75	S	0.25
1*t*	C_1	0.71	S	0.20
1*v*	C_1	0.67	S	0.21
1*x*	C_1	0.49	S	0.10
			Ph (*ortho* carbon)	0.13
			Ph (*para* carbon)	0.14

*Only the larger population numbers are included for each sulfenium ion.
†Structure **1** defines the location for W, X, Y, and Z.
‡The results for **1***s* are typical for all sulfenium ions **1** in which X = W = H.

which are presented in Table 5. These population numbers indicate the preferred site for nucleophilic attack in accord with Frontier-Orbital arguments (19). As expected, C_1 (structure **1**), is the preferred electrophilic site in all sulfenium ions studied. The secondary choice for nucleophilic attack in most sulfenium ions is the sulfur atom, which would give rise to an ylide. Sulfur would be expected to become the preferred electrophilic site in systems for which nucleophilic attack at carbon is subject to severe steric hindrance. Interestingly, no sulfenium ion studied develops significant electrophilicity at C_2 (structure **1**), despite the fact that nucleophilic attack there would furnish a ground state thiocarbonyl compound and a disubstituted methane. Finally, we note that sulfenium ions bearing strong π-donors on C_1 tend to develop secondary electrophilic sites in the π-donor rather than on the sulfur atom (i.e. **1***c*, **1***e*, **1***o*, and **1***x*).

Conclusions

1. Sulfenium ions are stabilized by π-donors.
2. There is no correlation between substituent electronegativities and relative regioisomeric sulfenium ion stabilities.
3. The observed directing abilities of the substituents with respect to chlorinations can be reconciled with the calculated relative regioisomeric stabilities if sulfides which have substituents with low electronegativities follow an E2 mechanism and sulfides which have substituents with high electronegativities follow an $E1_{cb}$-like mechanism.
4. C_1 (structure **1**) is the preferred site for nucleophilic attack in the sulfenium ions studied. S is the secondary site in most cases, but sulfenium ions bearing strong π-donors tend to develop secondary sites on the π-donor. No sulfenium ion studied develops significant electrophilicity at C_2 (structure **1**).

Acknowledgements

One of the authors (J.L.G.) wishes to acknowledge the financial support of the Natural Sciences and Engineering Research Council of Canada. We wish to thank the staffs of the Computer Centers at Saint Mary's University and the Florida Institute of Technology for technical assistance and Dalhousie University and the Florida Institute of Technology for use of their computing facilities.

1. T. P. AHERN, D. G. KAY, and R. F. LANGLER. Can. J. Chem. **56**, 2422 (1978).
2. G. E. WILSON, JR. and M. G. HUANG. J. Org. Chem. **35**, 3002 (1970).
3. A. STREITWIESER, JR. and D. H. HEATHCOCK. Introduction to organic chemistry. 2nd ed. MacMillan, New York. 1981. p. 115.
4. B. M. TROST, M. VAULTIER, and M. L. SANTIAGO. J. Am. Chem. Soc. **102**, 7029 (1980).
5. M. J. S. DEWAR and WALTER THIEL. J. Am. Chem. Soc. **99**, 4899 (1977).
6. M. J. S. DEWAR and WALTER THIEL. J. Am. Chem. Soc. **99**, 4907 (1977).
7. M. J. S. DEWAR, M. L. MCKEE, and H. S. REPZA. J. Am. Chem. Soc. **100**, 3607 (1978).
8. R. FLETCHER and M. J. D. POWELL. Comp. J. **6**, 163 (1963).
9. W. C. DAVIDON. Comp. J. **10**, 406 (1968).
10. W. THIEL/NRCC. QCPE **11**, 379 (1979).
11. M. J. S. DEWAR and H. S. REPZA. J. Am. Chem. Soc. **100**, 58 (1978).
12. M. J. S. DEWAR and G. P. FORD. J. Am. Chem. Soc. **101**, 5558 (1979).
13. G. P. FORD and J. D. SCRIBNER. J. Am. Chem. Soc. **103**, 4281 (1981).
14. J. MIREK and A. SIGULA. THEOCHEM, **3**, 85 (1981).
15. V. BARONE, P. CRISTINZIANO, F. LELJ, and N. RUSSO. THEOCHEM, **3**, 239 (1982).
16. A. F. CUTHBERTSON and C. GLIDEWELL. THEOCHEM, **4**, 71 (1982).
17. W. R. HARDSTAFF and R. F. LANGLER. *In* Sulfur in organic and inorganic chemistry. Vol. 4. *Edited by* A. Senning. M. Dekker, Inc., New York. 1982.
18. R. F. LANGLER, Z. A. MARINI, and E. S. SPALDING. Can. J. Chem. **57**, 3193 (1979).
19. I. FLEMING. Frontier orbitals and organic chemical reactions. Wiley, London. 1976.

Can. J. Chem. Downloaded from www.nrcresearchpress.com by 210.87.254.5 on 09/06/12
For personal use only.

I. Order–disorder transitions and solid state reaction kinetics in Na_2SO_4–K_2SO_4 system

FOR ERRATA SEE
V. 62 #6 1984 P. 1227

M. SUNITHA KUMARI AND ETALO A. SECCO[1]

Chemistry Department, St. Francis Xavier University, Antigonish, N.S., Canada B2G 1C0

Received September 3, 1982

M. SUNITHA KUMARI and ETALO A. SECCO. Can. J. Chem. **61**, 594 (1983).

The physicochemical aspects of the order–disorder phase transitions occurring in the Na_2SO_4–K_2SO_4 system were investigated by thermal analyses, infrared absorption, and X-ray diffraction methods.

Kinetic and structural studies on the compounds $KNaSO_4$ and $K_3Na(SO_4)_2$ are reported in more detail.

M. SUNITHA KUMARI et ETALO A. SECCO. Can. J. Chem. **61**, 594 (1983).

Faisant appel à l'analyse thermique, a l'absorption infrarouge et à la diffraction de rayons-X, on a étudié les aspects physicochimiques des transitions de phase ordre–désordre se produisant dans le système Na_2SO_4–K_2SO_4.

On rapporte d'une façon plus détaillée les études de structure et de cinétique effectuées sur le $KNaSO_4$ et le $K_3Na(SO_4)_2$.

[Traduit par le journal]

Introduction

Our study on phase transitions in Na_2SO_4 (1) has revealed a number of interesting effects such as the dependence of the enthalpy of transition, the dependence of the transition temperature, and the dependence of the transition kinetics on the presence of K_2SO_4. Since Na_2SO_4 and K_2SO_4 are isostructural, orthorhombic at room temperature, our earlier work on phase transitions in K_2SO_4 (2) could be extended to embrace the complete Na_2SO_4–K_2SO_4 composition range.

The early papers of Nacken (3) and Janecke (4) recorded the Na_2SO_4–K_2SO_4 phase diagram showing the existence of solid–solid phase transitions over the whole range of composition. These early phase diagrams, however, leave a number of questions unanswered, e.g. the existence of compounds, the nature of the phase transitions, etc. Although the compounds $KNaSO_4$ and $K_3Na(SO_4)_2$ have been known for some time, it was only recently that Okada *et al.* (5) have determined both structures to be trigonal at room temperature.

This paper reports the results of a study on the condensed phase transitions in the Na_2SO_4–K_2SO_4 system and the kinetics of the solid state reactions between Na_2SO_4 and K_2SO_4 leading to the formation of $KNaSO_4$ and $K_3Na(SO_4)_2$ using thermal analyses, DSC, infrared spectroscopy, and X-ray diffractometry techniques.

Experimental

Anhydrous Na_2SO_4 was from two sources, Fisher Certified Stock and Alfa Products ultrapure grade. Anhydrous K_2SO_4 was Alfa Products ultrapure grade. There was no discernible difference in the measured physicochemical and thermal properties of the Na_2SO_4–K_2SO_4 samples using Na_2SO_4 from both sources.

Fused Na_2SO_4–K_2SO_4 samples were prepared by fusing the requisite composition mixture, previously well ground manually in a mortar and pestle, of the respective sulfates in a Pt crucible.

X-ray diffraction patterns were obtained using a Norelco diffractometer with CuK_α radiation. Diffraction patterns at elevated temperatures were recorded with a Model X-86-N high temperature accessory (Materials Research Corp.) attached to the Norelco unit (6). The infrared spectra were recorded on a Perkin-Elmer Model 180 spectrophotometer equipped with a high temperature cell, maximum 375°C, using the standard KBr disc technique.

DTA traces were obtained on a duPont 990 Thermal Analyzer in a flowing N_2 (ultrapure) atmosphere using ignited Al_2O_3 as reference material. The precision of a melting temperature measurement was ±5°C whereas the transition temperature measurement was better than ±2°C. The enthalpies of transformation were evaluated with the DSC accessory to the 990 DTA module using the heats of fusion or transition for In, Sn, Zn, AgI, CsCl, K_2SO_4 as references; samples were encapsulated in Al containers — identical results, within experimental error were obtained using Au containers.

In the solid state kinetics measurements each sample of Na_2SO_4–K_2SO_4 mixture of constant mass was ground manually to a uniform consistency; the sample was maintained at the set temperature in the DTA cell in the isothermal mode for the required time interval. The fraction of reaction of $KNaSO_4$ or $K_3Na(SO_4)_2$, α, was evaluated by comparing the DSC enthalpic peak areas in the heat mode of the individual transitions in the reacted sample relative to the peak areas of the transitions in the pure state of their respective compounds. A small constant contribution of the second compound was always present; this contribution was subtracted to obtain the net result. Attempts to cross-check the DSC kinetic data with X-ray diffraction data was not possible due to the lack of reproducibility of the characteristic X-ray peak heights originating with a low degree of crystallinity

Results and discussion

Phase diagram

The transition temperatures recorded on DTA traces are plotted versus composition in Fig. 1 (Fig. 1(*a*) represents the solid–liquid phase diagram and Fig. 1(*b*) represents the solid–solid phase diagram along with hysteresis effects) the two plots are in general agreement with Nacken's report (3). Figure 2 gives the enthalpy change, ΔH_t and entropy change, ΔS_t dependence on composition for the solid–solid phase transitions.

The solid–liquid diagram resembles a minimum type solid solution normally expected for isostructural binary systems with the noteworthy absence of the liquidus curve in the 50–100% Na_2SO_4 region. A theoretical analysis of the minimum type solid solution has been done by Reisman (7) using computer-derived models. These models incorporate the ΔH of fusion for both components and involve dimer–monomer transformation or dissociation of one component on melting. The minimum is displaced markedly toward the lower melting component when the higher melting component is assumed to

[1]To whom all correspondence should be addressed.

Can. J. Chem. Downloaded from www.nrcresearchpress.com by 210.87.254.40 on 09/06/12
For personal use only.

Can. J. Chem. Downloaded from www.nrcresearchpress.com by 210.87.254.40 on 09/06/12
For personal use only.

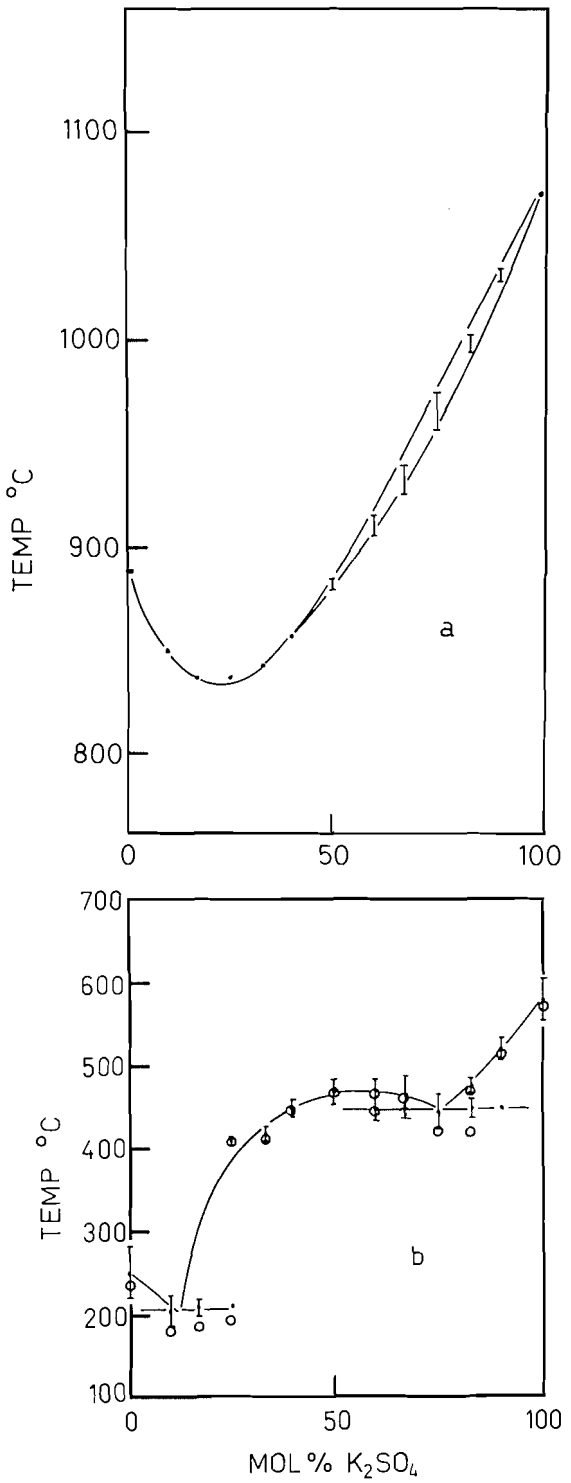

FIG. 1. (*a*) Solid–liquid phase diagram Na_2SO_4–K_2SO_4 system; vertical bars indicate endotherm width. (*b*) Solid–solid phase diagram Na_2SO_4–K_2SO_4 system; ●, area of endotherm, $\sim\Delta H_t$; ○, cool mode exotherm.

undergo dissociation and vice versa. The minimum at 75% Na_2SO_4 in Fig. 1(*a*) supports K_2SO_4 dissociation on melting according to the above model.

The solid state phase diagram, Fig. 1(*b*), resembles the solid solution behavior usually encountered in substitutional alloys, e.g. Cu–Au. The substitutional solid solution can incorporate a high degree of order with respect to occupancy of preferred

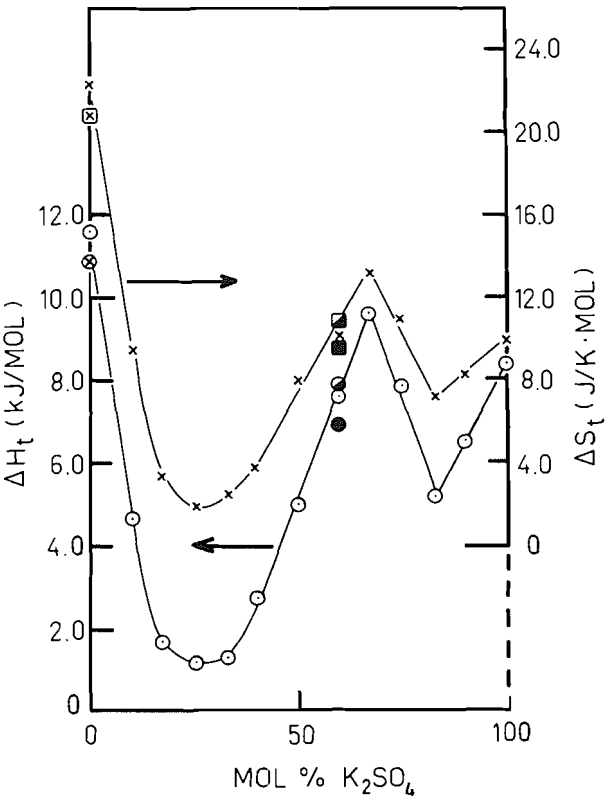

FIG. 2. Plots of enthalpy and entropy changes for solid–solid phase transitions in Na_2SO_4–K_2SO_4 system. ☒, ⊗, Eysel's value (1); ■, ●, physical mixture; ◪, ◑, after 15 days storage.

TABLE 1. X-ray diffraction data

	$K_3Na(SO_4)_2$			$KNaSO_4$		
	25°C		500°C	25°C		500°C
hkl	d^a (Å)	d_{obs} (Å)	d_{obs} (Å)	d^b (Å)	d_{obs} (Å)	d_{obs} (Å)
100	4.98	4.95	4.95	4.94	4.89	
101	4.10	4.11	4.22	4.67	4.60	4.20
002	3.69	3.71	4.07	4.10	4.05	
102	2.97	2.98	3.16	3.69	3.60	3.18
110	2.85	2.87	2.87	2.95	2.90	
003	2.46	2.48	2.50	2.84	2.83	2.83
200				2.65	2.62	
				2.45	2.44	

[a] ASTM File No. 6-0429.
[b] ASTM File No. 1-0978.

lattice sites by the ionic species resulting in solid compounds; such structures are also referred to as superlattices or superstructures. Okada *et al.* (5) have identified the specific lattice positions of the Na, K, and SO_4 ions in $KNaSO_4$ and $K_3Na(SO_4)_2$ compound structures. At the transition temperature the ordered arrangement of the ions becomes less ordered and the compound is said to undergo an order–disorder transformation. X-ray diffraction data above the phase transition temperature, Table 1, show the basic structure of $K_3Na(SO_4)_2$ to remain effectively the same whereas the unit cell dimensions in the lattice increase along the *c*-axis. The diffraction pattern for $KNaSO_4$ above the transition temperature, however, shows

TABLE 2. Infrared absorption frequencies (cm^{-1})

Frequency					
Free SO_4^{2-} (8)	$K_3Na(SO_4)_2$	$KNaSO_4$	Na_2SO_4	90:10 Na_2SO_4:K_2SO_4	Assignment
ν_1, 981(A_1)	990	995	990	995	Symmetric stretching
ν_2, 451(E)	445	448		448	Symmetric bending
ν_3, 1104 (F_2)	1180 1110	1175 1110	1105	1175 1110	Asymmetric stretching
ν_4, 613 (F_2)	610	615	618	628 608	Asymmetric bending
$2\nu_3$	2170	2180	2170	2180	Combination
$\nu_1+\nu_3$	2070	2090	2100	2100	

only three clearly identifiable peaks indicating that the structure is altered drastically.

From Fig. 1(*b*) the existence of $K_3Na(SO_4)_2$ may be questioned since its composition coincides with the minimum which appears as an eutectoid suggesting a mixture of $KNaSO_4$ and K_2SO_4. However, our X-ray patterns show no evidence of K_2SO_4 lines in 60:40, 67:33, and 75:25 mole ratios for K_2SO_4:Na_2SO_4 at 20°C or 500°C. Furthermore, the trend of ΔH_t and ΔS_t values in Fig. 2 is consistent with the interpretation of mixing for $KNaSO_4$ and $K_3Na(SO_4)_2$.

The infrared spectra at room temperature reveal the absorption frequencies for $KNaSO_4$ and $K_3Na(SO_4)_2$ given in Table 2. The fundamental frequencies for the SO_4 species of T_d symmetry have been reported (8) at 981 cm^{-1} (A_1), 451 cm^{-1} (E), 1104 cm^{-1} (F_2), and 613 cm^{-1} (F_2). Of these four fundamentals only the F_2 modes are ir-active in the free ion state but in the crystal state the selection rules are relaxed (9). The detailed infrared spectra, transmission and reflectance, of $KNaSO_4$ and $K_3Na(SO_4)_2$ single crystals along with their factor group analyses are to be reported elsewhere.

Our infrared data may have a bearing on the recent studies of the high temperature phase transition of Na_2SO_4 reported recently by El-Kabbany *et al.* (10). The samples of Na_2SO_4 were incorporated in a KBr matrix using the disc technique. Their infrared data show a high correlation with our spectral data for prolonged heating of Na_2SO_4 in KBr matrix and also Na_2SO_4–K_2SO_4 fused mixtures. Milne (11) showed that the infrared spectra of M_2SO_4 (M = Li, Na, K, Cs) measured in nine alkali metal halide discs change due to ion exchange and solid solution formation. It is expected that the ion exchange reaction would be accelerated at the high temperature.

The infrared spectra of $KNaSO_4$ and $K_3Na_2(SO_4)_2$ recorded at 375°C, 75–100°C below the transition temperatures, the limit of our high temperature attachment, showed no discernible difference relative to their room temperature spectra. The infrared spectra of 83% Na_2SO_4, showing all the absorption frequencies at room temperature common to $KNaSO_4$ and $K_3Na(SO_4)_2$, displayed no change in its characteristic absorption frequencies, above its transition temperature, 250°C. This latter result suggests that the phase transition involves a relative displacement of Na and K on lattice sites with no change in their interaction with SO_4 species, that is, no alteration of SO_4 symmetry in the solid. Assuming the order–disorder phase transition occurring in 83% Na_2SO_4 to parallel the phase transition in KNa_2SO_4 or $K_3Na(SO_4)_2$, it might be concluded that the order–disorder transition is effected mainly by cation reorientation.

The higher values of ΔH_t and ΔS_t for the $67K_2SO_4$:$33Na_2SO_4$ and $60K_2SO_4$:$40Na_2SO_4$ compositions, Fig. 2, relative to those values for $KNaSO_4$ and $K_3Na(SO_4)_2$ suggest the existence of compounds but X-ray diffraction patterns and infrared spectra do not support this suggestion. The ΔH_t and ΔS_t values for 60:40 and 67:33 are also higher than those values calculated and determined for respective physical mixtures of $KNaSO_4$ and $K_3Na(SO_4)_2$. The 67:33 composition sample, representing 1:1 mole ratio of $KNaSO_4$ and $K_3Na(SO_4)_2$, exhibited only one thermal peak (DTA and DSC) 24 h after fusion, Fig. 3, but resolved itself into the two peaks characteristic of $KNaSO_4$ and $K_3Na(SO_4)_2$ after 15 days storage in a desiccator yielding still higher ΔH_t and ΔS_t values; the two characteristic peaks remained unchanged after 100 days. The additional contribution to ΔH_t and ΔS_t is attributed to mixing or relative increased disorder of the two compounds in the lattice network, i.e. $\Delta S_t = \Delta S_{mix} + \Sigma\Delta S_i$ where ΔS_{mix} is the extra contribution and $\Sigma\Delta S_i$ represents the contribution from the proportionate compounds. Such an interpretation analogous to extra relaxation energy associated with order–disorder model of ion exchange in crystals developed by Barrer and his group (12) leads to ΔS_{mix} = 0.91 J/mol K for the metastable single peak and ΔS_{mix} = 1.54 J/mol K for the stable two peak state in 60:40 sample and ΔS_{mix} = 2.84 J/mol K for the 67:33 composition.

Solid state kinetics

(*i*) Reaction between Na_2SO_4 and K_2SO_4

The best fit between the experimental results and the fifteen known kinetic equations, over the temperature range 529–585°C for reaction fraction α up to 0.80, was obtained for the special case of the treatment given by Avrami (13). The relationship was cast into a second-order rate expression by Honig *et al.* (14) which at sufficiently large t takes the form

$$[1] \quad (1 - \alpha)^{-1} = 1 + \sigma G N_g t$$

where $(1 - \alpha)$ represents the fraction unreacted, σ is the shape factor, G is the lineal growth rate of the new phase, N_g is the initial density of germ nuclei, and t is the time. Equation [1] is also recognized as the integrated form of the second-order rate law, where integration of

$$d\alpha/dt = k(1 - \alpha)^2$$

yields

Can. J. Chem. Downloaded from www.nrcresearchpress.com by 210.87.254.40 on 09/06/12
For personal use only.

Can. J. Chem. Downloaded from www.nrcresearchpress.com by 210.87.254.40 on 09/06/12
For personal use only.

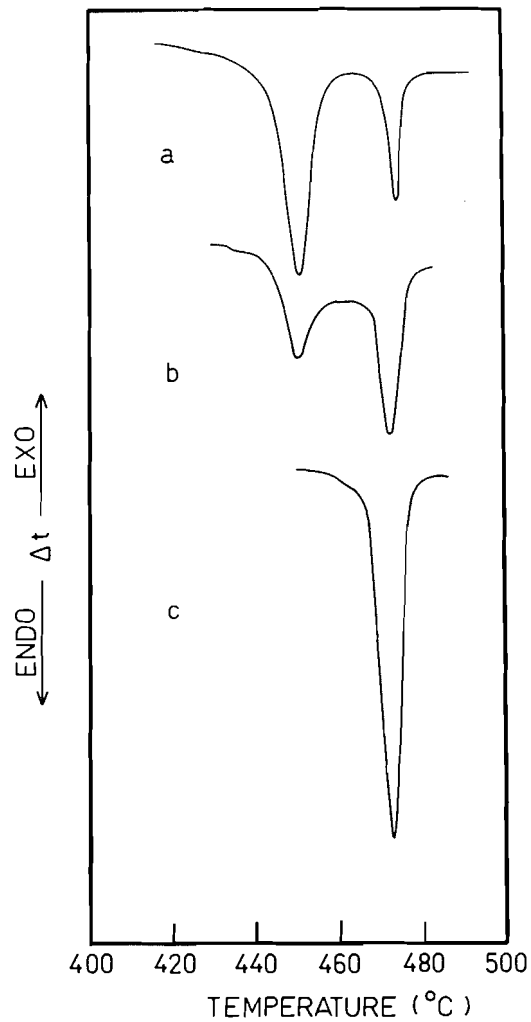

FIG. 3. DSC traces of $67K_2SO_4:33Na_2SO_4$ mole ratio; (*c*) 24 h after fusion, (*b*) after 15 days storage; (*a*) physical mixture.

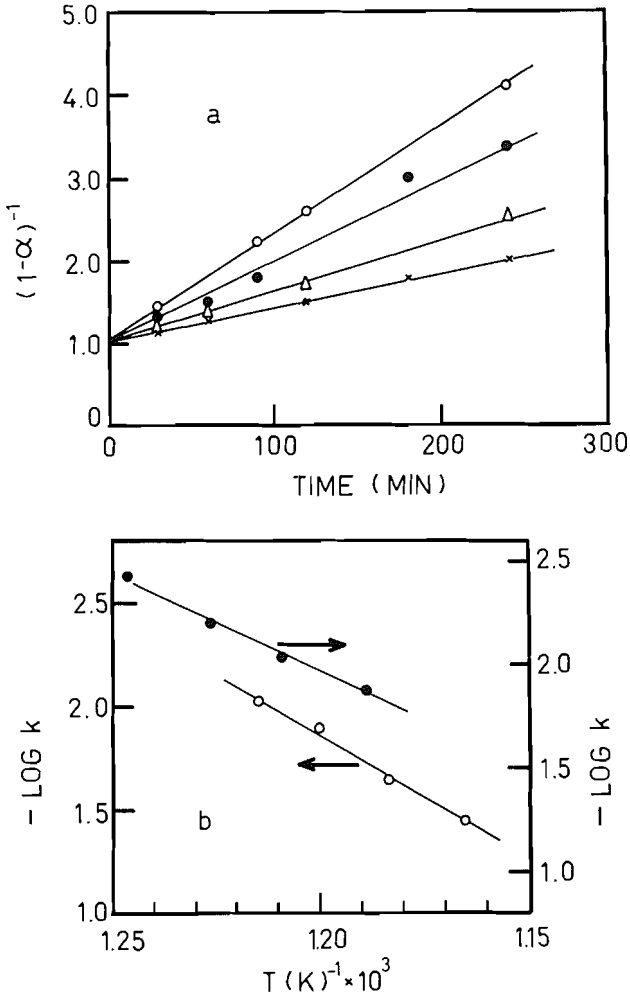

FIG. 4. (*a*) Plot of $(1 - \alpha)^{-1}$ versus time, second order rate law. $KNaSO_4$: ● 550°C, ○ 560°C; $K_3Na(SO_4)_2$: × 529°C, △ 542°C. (*b*) Plot of log k versus T^{-1}. ● $K_3Na(SO_4)_2$; ○ $KNaSO_4$.

$$[2] \quad (1 - \alpha)^{-1} = 1 + kt$$

Plots of $(1 - \alpha)^{-1}$ versus time yield straight lines, typical plots for both compounds are given in Fig 4(*a*), whose slopes equal the composite quantity σGN_g taken to be the formal rate constant k, along with an intercept of unity. The slopes of the standard Arrhenius plots of log k versus $1/T$ K, Fig. 4(*b*), yield activation energy values of 232 ± 20 and 165 ± 15 kJ for $KNaSO_4$ and $K_3Na(SO_4)_2$, respectively.

The Avrami–Honig model was found applicable to the single reactant case (15) where σ and N_g are considered to be effectively constant and the rate constant dependence on temperature was visualized to originate with the term G in the composite rate constant. The second-order rate behavior involving two reactants in solid state reactions is not common and the mechanism for such a reaction rate must incorporate relatively mobile species. The reaction mechanism envisaged for this case is where Na^+ and K^+ are the effective reacting species in a sublattice of SO_4^{2-} units and the fundamental reaction step, to a first approximation, is the ordering of Na^+ and K^+ on crystallographically preferential lattice sites to yield the two compounds. This latter model could be classified as a type of quasi-homogeneous solid state ionic reaction where a simple first-order dependence on the two principal reactants results in the overall second-order rate. The proposed model requires the cations to be highly mobile relative to the reaction rate constants at the temperatures studied. This requirement is satisfied according to the high ionic conductivity data reported in the following article.

(*ii*) Phase transition reaction

The solid–solid phase transition in $KNaSO_4$ and in $K_3Na(SO_4)_2$ exhibit properties characteristic of a first-order transition.

From DSC heating traces for various heating rates, linear plots of log Δt vs. $1/T$ K, where Δt is the peak height at a specific temperature T (16), and log ϕ/T_p^2 vs. $1/T$ K, where T_p is the peak temperature for the specific heating rate ϕ (17) can be used to obtain the activation energy values, E_a, for the phase transition. Highly consistent linear plots of the above relationships gave (*i*) E_a values of 500 ± 80 kJ/mol for recycled stored samples of $K_3Na(SO_4)_2$ and (*ii*) E_a values of 1000 ± 150 kJ/mol for freshly prepared individual samples of $K_3Na(SO_4)_2$ and $KNaSO_4$. These high E_a values are consistent with activation energy values reported for phase transitions in K_2SO_4 (18), ZnS (15), and anthranilic acid (19). The lower E_a value for the recycled samples relative to the freshly prepared individual samples suggest a different activated state.

Acknowledgment

The authors are indebted to the Natural Sciences and Engineering Research Council of Canada for financial support.

1. R. MacL. Murray and E. A. Secco. Can. J. Chem. **56**, 2616 (1978).
2. M. Natarajan and E. A. Secco. Can. J. Chem. **53**, 1542 (1975).
3. R. Nacken. News Jahrb. Mineral. Geol. **24**, 55 (1907).
4. E. Janecke. Z. Physik. Chem. **64**, 346 (1908).
5. K. Okada and J. Ossaka. Acta Crystallogr. B**36**, 919 (1980).
6. E. A. Secco. Can. J. Chem. **42**, 2143 (1964).
7. A. Reisman. Phase equilibria. Academic Press, New York. 1970. Chapts. 29, 30.
8. M. Hass and G. B. B. M. Sutherland. Proc. R. Soc. London Ser. A, **236**, 427 (1956).
9. K. Nakamoto. Infrared spectra of inorganic and coordination compounds. John Wiley and Sons, Inc., New York. 1973.
10. F. El-Kabbany, Y. Badr, and M. Tosson. Phys. Stat. Sol. (a) **63**, 699 (1981).
11. J. W. Milne. Spectrochim. Acta, **32**A(6), 1347 (1976).
12. R. M. Barrer and J. Klinowski. Geochim. Cosmochim. Acta, **43**, 755 (1979) and references therein.
13. M. Avrami. J. Chem. Phys. **8**, 212 (1940).
14. A. W. Czanderna, J. M. Honig, and C. N. R. Rao. Trans. Faraday Soc. **54**, 1069 (1958).
15. T. Bansagi, E. A. Secco, O. K. Srivastava, and R. R. Martin. Can. J. Chem. **46**, 2881 (1968).
16. G. O. Piloyan, I. D. Ryabchikov, and O. S. Novikova. Nature, **212**, 1229 (1966).
17. W. W. Wendlandt. J. Chem. Educ. **38**, 571 (1961); H. E. Kissinger. Anal. Chem. **29**, 1702 (1957).
18. F. A. I. El-Kabbany. Phys. Stat. Sol. (a) **58**, 373 (1980).
19. K. Rajeshwar and E. A. Secco. Can. J. Chem. **54**, 2509 (1976).

Can. J. Chem. Downloaded from www.nrcresearchpress.com by 210.87.254.40 on 09/06/12
For personal use only.

II. Electrical conductivity and phase transition studies on pure and doped $(Cd^{2+}, Gd^{3+})KNaSO_4$ and $K_3Na(SO_4)_2$

M. SUNITHA KUMARI AND ETALO A. SECCO[1]

Chemistry Department, St. Francis Xavier University, Antigonish, N.S., Canada B2G 1C0

Received September 3, 1982

M. SUNITHA KUMARI and ETALO A. SECCO. Can. J. Chem. **61**, 599 (1983).

Electrical conductivity measurements on pure and doped $KNaSO_4$ and $K_3Na(SO_4)_2$ reveal high ionic conductivity values in the high temperature phase. High conductivity values ascribed to Na^+ resemble a superionic or fast-ion conductor.

M. SUNITHA KUMARI et ETALO A. SECCO. Can. J. Chem. **61**, 599 (1983).

Les mesures de conductivité électrique du $KNaSO_4$ et du $K_3Na(SO_4)_2$ à l'état pur et à l'état dopé révèlent de fortes valeurs de conductivité ionique dans la phase à haute température. Les fortes valeurs de conductivité attribuées à l'ion Na^+ se rapprochent de celles d'un conducteur superionique ou d'un conducteur de type ion rapide.

[Traduit par le journal]

Introduction

The results of our study on the kinetics of the solid state reaction betwen Na_2SO_4 and K_2SO_4 (1) forming the compounds $KNaSO_4$ and $K_3Na(SO_4)_2$ were interpreted in terms of a model assuming highly mobile Na^+ and K^+ species. The reaction kinetic data suggest diffusion coefficients in the range $10^{-6}-10^{-7}$ cm^2 s^{-1} and ionic conductivity of $\sim 10^{-2}$ (ohm cm)$^{-1}$ for the temperature region studied, that is, ~400°C below the melting temperature. Electrical conductivity measurements on $KNaSO_4$ and $K_3Na(SO_4)_2$ would provide critical data bearing on the proposed model of highly mobile cations.

Solids exhibiting ionic conductivities comparable to those of melts or liquids are referred to as superionic conductors (SIC's) or solid electrolytes. These fast-ion conductors have attracted considerable attention because of (*i*) their promise in applications in high-energy-density-batteries and (*ii*) their unusual transport behavior. Also $(Na,K)_2SO_4$ compositions have been suggested as potential electrolytes in applications for SO_2 detectors (2–4). The prospect that electrical conductivity measurements on pure and doped $KNaSO_4$ and $K_3Na(SO_4)_2$ might be rewarding from the fundamental as well as the practical aspect is the basis for this study.

Experimental

The pure $KNaSO_4$ and $K_3Na(SO_4)_2$ compounds used were from the earlier study (1). The doped compounds (Cd^{2+}, Gd^{3+}) were prepared by fusing the requisite dopant composition previously ground manually in a mortar and pestle, in a covered Pt crucible. The $CdSO_4$ was Fisher Certified grade and $Gd_2(SO_4)_3$ was Alfa Ventron Corp of stated purity 99.9%.

Electrical conductivity measurements were made on compressed specimen in a stainless steel conductivity cell. The experimental procedure for these measurements as described earlier (5), maintained the sample by a spring-loaded support between stainless steel leads using two polished Pt discs as electrodes. The two surfaces of the sample were touched with graphite (Dag # 154 Acheson) to ensure proper contact. The conductivity was measured under reduced pressure ($\sim 10^{-3}$ Torr) at 1 kHz as a function of temperature using a GR 1608-A impedance bridge; the heating rate was 60 deg h^{-1}. Conductivity measurements at 0.1 and 10 kHz revealed indistinguishable σ values up to 600°C for $K_3Na(SO_4)_2$. Temperature was monitored by using standardized chromel–alumel thermocouples with a Keithley digital multimeter.

[1] To whom all correspondence should be addressed.

The compressed polycrystalline sample was 1 mm thick and ~30 mm^2 in surface area approximating a square — it was the crack-free portion recovered from the compressed disc. Our failure to obtain clean compressed discs with $KNaSO_4$ and $K_3Na(SO_4)_2$ is consistent with Garrett's observation (6) that single crystals grown by the Czochralski method shattered on cooling. The pressure- or temperature-promoted order–disorder phase transformation in these compounds is most likely responsible for the disintegrating behavior of the disc or single crystal.

Results and discussion

The temperature dependence of the ionic conductivity is given by the Arrhenius-type expression

$$\sigma = (ne^2\lambda^2\nu/kT) \exp(-\Delta G/kT)$$

which reduces to

$$\sigma = (\sigma_0/T) \exp(-Q_c/kT)$$

where σ_0 represents the composite constant $(ne^2\lambda^2\nu/k)$, n, the number of ions per unit volume, e, the ionic charge, λ, the distance between two jumps positions, ν, the jump frequency, k, the Boltzmann constant, and Q_c is the activation energy for ionic motion, assuming the conductivity to be effectively ionic with negligible electronic or hole contribution.

Plots of log (σT) vs. $1/T$ K for pure and doped $KNaSO_4$ and pure and doped $K_3Na(SO_4)_2$ are presented in Figs. 1 and 2, respectively. Similar plots are given for untreated stock Na_2SO_4, 90:10 mol% Na_2SO_4:K_2SO_4, 33:67 mol% Na_2SO_4:K_2SO_4 along with pure $KNaSO_4$ in Fig. 3 for comparison purposes. $K_3Na(SO_4)_2$ samples doped with 6 mol% $CdSO_4$ and 2 mol% $Gd_2(SO_4)_3$, not shown in Fig. 2, exhibited the same $\sigma-T$ behavior as the 4 mol% $CdSO_4$ doped sample. $KNaSO_4$ doped with 6 mol% $CdSO_4$, not shown in Fig. 1, gave the same $\sigma-T$ behavior as the 4 mol% doped sample. Similar $\sigma-T$ behavior for 6 mol% and 4 mol% $CdSO_4$ in either $K_3Na(SO_4)_2$ or $KNaSO_4$ suggests a saturation point of Cd^{2+} in the lattice. The cooling $\sigma-T$ curve of each Cd^{2+} doped $KNaSO_4$ sample, typified by 2 mol% in Fig. 1, showed an anti-hysteresis in contrast to hysteresis observed for all $K_3Na(SO_4)_2$ samples. The temperature independence and anti-hysteresis of greater than 4 mol% Cd^{2+} concentrations are consistent with vacancy-cation cluster formation as proposed for anion conductors (7). The plots show the expected order–disorder phase transition and hysteresis effects consis-

Can. J. Chem. Downloaded from www.nrcresearchpress.com by 210.87.254.42 on 09/06/12
For personal use only.

Can. J. Chem. Downloaded from www.nrcresearchpress.com by 210.87.254.42 on 09/06/12
For personal use only.

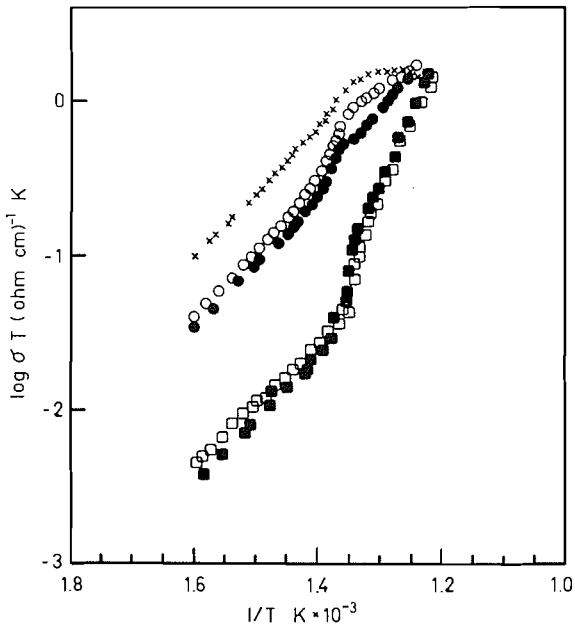

FIG. 1. log σT versus $1/T$ plots for $KNaSO_4$, pure and doped; ■, □, pure $KNaSO_4$, cool and heat modes, respectively; ●, ○, 2 mol% Cd^{2+} in $KNaSO_4$, cool and heat modes respectively; × 4 mol% Cd^{2+} in $KNaSO_4$, heat mode.

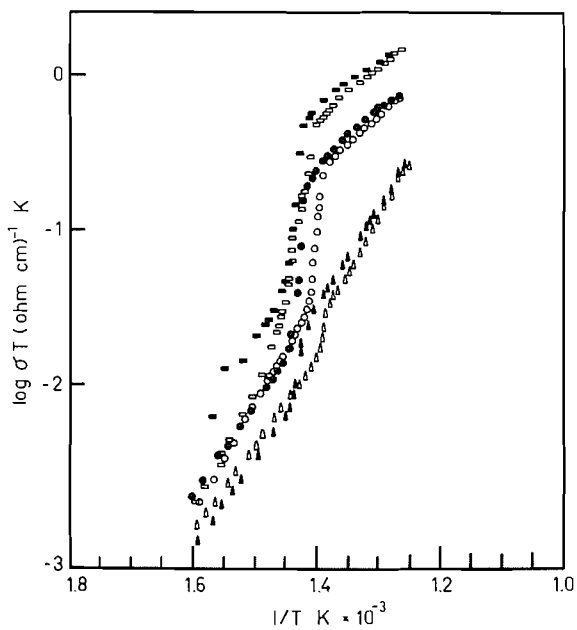

FIG. 2. log σT versus $1/T$ plots for $K_3Na(SO_4)_2$, pure and doped; ▲, △, pure $K_3Na(SO_4)_2$, cool and heat modes, respectively; ●, ○, 2 mol% Cd^{2+} in $K_3Na(SO_4)_2$, cool and heat modes, respectively; ■, □, 4 mol% Cd^{2+} in $K_3Na(SO_4)_2$, cool and heat modes, respectively.

tent with the DTA traces recorded in part I of this work (1).

The conductivity data presented in Figs. 1, 2, and 3 along with the conductivity data reported for K_2SO_4 (8) lead us to conclude that the major contributing species is the Na^+ ion. Cd^{2+} and Gd^{3+} were chosen as the dopants with the expectation that each would preferentially replace Na^+ in the lattice, $r_{Gd^{3+}} = r_{Cd^{2+}} = r_{Na^+} = 100 \pm 2$ pm, and not K^+ since $r_{K^+} = 133$ pm. The presence of Cd^{2+} or Gd^{3+} on Na^+ sites in the lattice would generate Na^+ vacancies in accordance with the electroneutrality

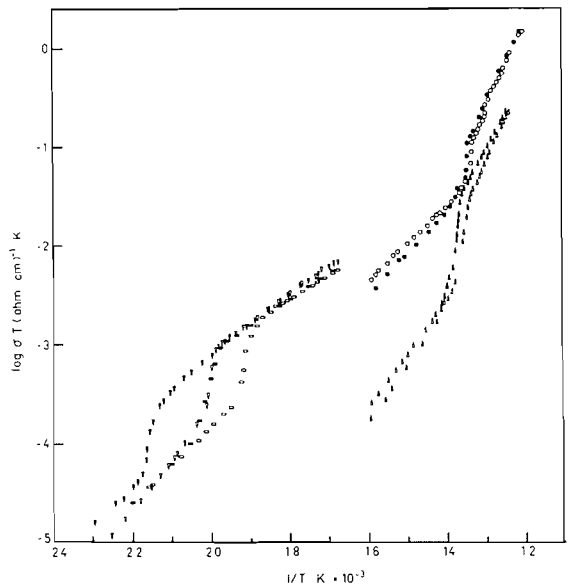

FIG. 3. log σT versus $1/T$ plots for Na_2SO_4 and $(NaK)SO_4$ compositions; ■, □, pure Na_2SO_4, cool and heat modes, respectively; ▼, ▽, 90:10 mol% Na_2SO_4:K_2SO_4, cool and heat modes, respectively; ●, ○, pure $KNaSO_4$, cool and heat modes, respectively; ▲, △, 33:67 mol% Na_2SO_4:K_2SO_4, cool and heat modes, respectively.

requirement — the agreement between 4 mol% Cd^{2+} and 2 mol% Gd^{3+} conductivity suggests equal vacancy concentration. Vacancies would permit greater facility of Na^+-ion mobility and therefore enhance the ionic conductivity consistent with the $\sigma-T$ data shown in Figs. 1 and 2. The activation energy values for ionic conductivity are tabulated in Table 1. The constant Q_c value, 78 ± 3 kJ/mol, for Na_2SO_4 and all $KNaSO_4$ samples in the pre-transition region suggests a common ionic conductivity mechanism; the Q_c values for $K_3Na(SO_4)_2$ compositions show an increasing trend. The constant Q_c value, 71 kJ/mol, for doped $K_3Na(SO_4)_2$ is in contrast with the temperature independence of 4 mol% Cd^{2+} in $KNaSO_4$ in the post-transition region.

The activation energy values for the ionic conductivity Q_c in the temperature region 800–850 K for $KNaSO_4$ and $K_3Na(SO_4)_2$ are 183 ± 18 and 135 ± 15 kJ/mol, respectively. These Q_c values are in acceptable agreement, considering limits of experimental procedures with the activation energy values E_a for the solid state reaction between Na_2SO_4 and K_2SO_4, in the same temperature range, leading to the formation of $KNaSO_4$ and $K_3Na(SO_4)_2$ (1). The agreement between Q_c and E_a values lends strong support for the proposed reaction model of highly mobile cations. Furthermore, the Q_c values for the phase transition reaction were determined to be 610 ± 100 and 700 ± 100 kJ/mol for $KNaSO_4$ and $K_3Na(SO_4)_2$, respectively; these values are within the range of the E_a values determined from DSC heating plots reported earlier (1).

The $\sigma-T$ data reported in this study show that selectively doped simple compounds such as $KNaSO_4$ and $K_3Na(SO_4)_2$ exhibit very high Na^+ ion conductivity in the high temperature phase analogous to the system of compounds $Na_3Zr_2Si_2PO_{12}$ referred to as NASICON (Na superionic conductor) (9). The proposed model of highly mobile Na^+ in a fixed sublattice of SO_4^{2-} in $(K, Na)_2SO_4$ compounds parallels the accepted model of highly mobile Ag^+ in a fixed network of I^- in Ag I compounds (10). This correlation suggests that other mixed alkali

TABLE 1. Ionic conductivity activation energy values, Q_c, of compounds

Composition	Temperature region[a]	Q_c (kJ/mol)		
		Na_2SO_4	$KNaSO_4$	$K_3Na(SO_4)_2$
Pure	A	78	76.5	111.5
	B	400	610	700
	C	55	183	134
2 mol% Cd^{2+}	A	—	81.5	135
	B	—	191	750
	C	—	50	72
4 mol% Cd^{2+}	A	—	78.5	149
	B	—	0	470
	C	—	0	71

[a] A, pre-transition; B, transition; C, post-transition.

or monovalent metallic sulfates combined with pure or doped Na_2SO_4, or also Na_2XO_4, might yield similar high conductivity values in the high temperature phase.[2]

[2] After completion of this manuscript we chanced upon the recent work by Hofer *et al.* (11) which reports parallel and consistent results in this subject area, and reports on sulfate-based solid electrolytes in ref. 12.

Acknowledgement

The authors are indebted to the Natural Sciences and Engineering Research Council of Canada for financial support.

1. M. S. KUMARI and E. A. SECCO. Can. J. Chem. **61**, 594 (1983).
2. F. J. SALZANO and L. NEWMAN. J. Electrochem. Soc. **119**, 1273 (1972).
3. M. GAUTHIER, A. CHAMBERLAND, A. BELANGER, and M. POIRIER. J. Electrochem. Soc. **124**, 1584 (1977) and references therein.
4. K. J. JACOB and D. B. RAO. J. Electrochem. Soc. **126**, 1842 (1979).
5. M. NATARAJAN and E. A. SECCO. Can. J. Chem. **52**, 712 (1974).
6. J. D. GARRETT. Private communication.
7. H. SCHMALZRIED. Z. Phys. Chem. **105**, 47 (1977).
8. M. NATARAJAN and E. A. SECCO. Can. J. Chem. **53**, 1542 (1975).
9. J. B. GOODENOUGH, H. Y.-P. HONG, and J. A. KAFALAS. Mater. Res. Bull. **11**, 203 (1976).
10. K. FUNKE. Prog. Solid State Chem. **11**, 345 (1976).
11. H. H. HOFER, W. EYSEL, and U. V. ALPEN. J. Solid State Chem. **36**, 365 (1981).
12. P. VASHISHTA, J. N. MUNDY, and G. K. SHENOY (*Editors*). Fast ion transport in solids. Elsevier North-Holland Inc., New York. 1979.

Can. J. Chem. Downloaded from www.nrcresearchpress.com by 210.87.254.42 on 09/06/12
For personal use only.

Additivity methods for estimating heats of vaporization of organic compounds

J. PETER GUTHRIE[1] AND KATHLEEN F. TAYLOR

Department of Chemistry, University of Western Ontario, London, Ont., Canada N6A 5B7

Received July 27, 1982

J. PETER GUTHRIE and KATHLEEN F. TAYLOR. Can. J. Chem. **61**, 602 (1983).

Additivity methods for heats of vaporization of organic liquids have been developed using both bond and group additivity parameters. For the bond level parameters, 429 compounds could be fitted using 36 parameters, with a weighted standard deviation of 0.32 kcal/mol, and only 23 deviations of more than 1 kcal/mol. For the group level parameters, 388 compounds could be fitted using 57 parameters, with a weighted standard deviation of 0.19 kcal/mol, and only 7 deviations of more than 1 kcal/mol. The problem of correlation among parameters is discussed and the significant terms in the correlation matrix are given. The new parameters are compared to previous parameterization schemes.

J. PETER GUTHRIE et KATHLEEN F. TAYLOR. Can. J. Chem. **61**, 602 (1983).

Faisant appel aux paramètres d'additivité de liaison et de groupe, on a mis au point des méthodes d'additivité pour évaluer les chaleurs de vaporisation des liquides organiques. Dans le cas des paramètres de liaison, on peut adapter 429 composés à 36 paramètres avec une déviation standard pondérée de 0,32 kcal/mol et avec seulement 23 déviations supérieures à 1 kcal/mol. Dans le cas des paramètres de groupe, on peut adapter 388 composés à 57 paramètres avec une déviation standard pondérée de 0,19 kcal/mol et avec seulement 7 déviations supérieures à 1 kcal/mol. On discute du problème de corrélation entre les paramètres. On a comparé les nouveaux paramètres avec les paramètres antérieurs.

[Traduit par le journal]

Can. J. Chem. Downloaded from www.nrcresearchpress.com by 210.87.254.5 on 09/06/12
For personal use only.

Introduction

We have made use of thermochemical determinations of heats of formation of organic compounds in calculating the free energies of formation of these compounds. From free energies of formation of suitable analogs it has been shown to be possible to determine the free energies of formation of unobservable intermediates. As part of this process we have had to obtain heats of vaporization and vapor pressures at 25°C, often from meager experimental data. In order to make it easier to perform these calculations we have looked for ways to make more reliable estimates either from the molecular structure or from such experimental data as may exist.

We wish to report methods based on bond and group additivity for heats of vaporization. Benson (1, 2) has shown the immense utility of additivity methods. In general, in the series of approximations: atom, bond, and group additivity, the higher approximations give better agreement with experiment, but require many more parameters. In a practical sense it is important to determine for each property the lowest level at which useful precision is obtained, so that the maximum number of compounds can be covered by a limited set of parameters, even though one will always use the highest level of approximation for which all of the parameters are available. For entropies and heat capacities atomic additivity leads to useful precision, but for enthalpies at least bond additivity is normally necessary, and group additivity is definitely preferred.

There has been recent interest in additivity relationships for heats of vaporization (3–19). We have endeavored to base the present parameterization exclusively on experimental heats of vaporization, using the more reliable calorimetric values which are now becoming available.

There are, of course, limitations to the use of additivity methods which, if ignored, can lead to misleading estimates. All such methods are only interpolation procedures, and can only be used for compounds which are very similar to those upon which the additivity scheme is based. Since compounds which are chemically interesting often have unusual chemical features, estimation of thermodynamic quantities for such compounds generally involves extrapolation and consequently errors in the thermodynamic quantities, which are larger than for the original parameter fitting. Caution and a due regard for error and propagation of error are in order.

Results

Table S1[2] gives the compounds which we used, the experimental heats of vaporization, and the values calculated at the bond and group additivity levels. Data were gathered from the literature, starting with the compilation of Cox and Pilcher (9), which not only gives heat of vaporization data, but indicates the origin of each value and gives an estimate of the precision of the value. We have tried to gather all available data from the recent literature. The compilation of Pedley and Rylance (20) was very helpful in this regard, although it does not give information about the origin of heat of vaporization values, so that one must check the original papers. Carboxylic acids pose a problem because the acids are partially but not completely dimerized in the gas phase, so that the measured heat of vaporization is a composite quantity (21, 22); we have chosen to use heats of vaporization corresponding to conversion of liquid to monomeric vapor, even though this means that fewer compounds can be included and these values have larger error limits. Our interest is in methods for estimation of thermochemical quantities, which normally means monomeric substances in the gas phase. Compounds which were unique representatives of a parameter were, as far as possible, not included in the final least-squares calculations. This was more of a problem in the group level calculations. For the bond level calculations, the only calorimetric heat of vaporization which

[1]E. W. R. Steacie Fellow, 1980–1982.

[2]Copies of the Supplementary Material may be obtained, at a nominal charge, from the Depository of Unpublished Data, CISTI, National Research Council of Canada, Ottawa, Ont., Canada K1A 0S2.

Can. J. Chem. Downloaded from www.nrcresearchpress.com by 210.87.254.5 on 09/06/12
For personal use only.

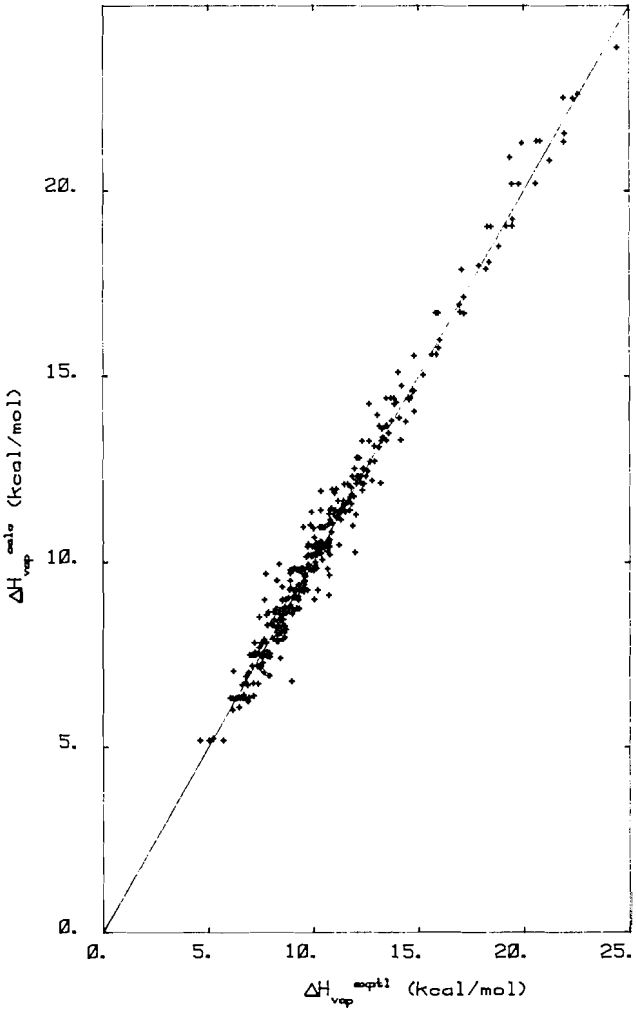

FIG. 1. Calculated vs. experimental values for heats of vaporization using the bond level paramaters; data from Table S1.

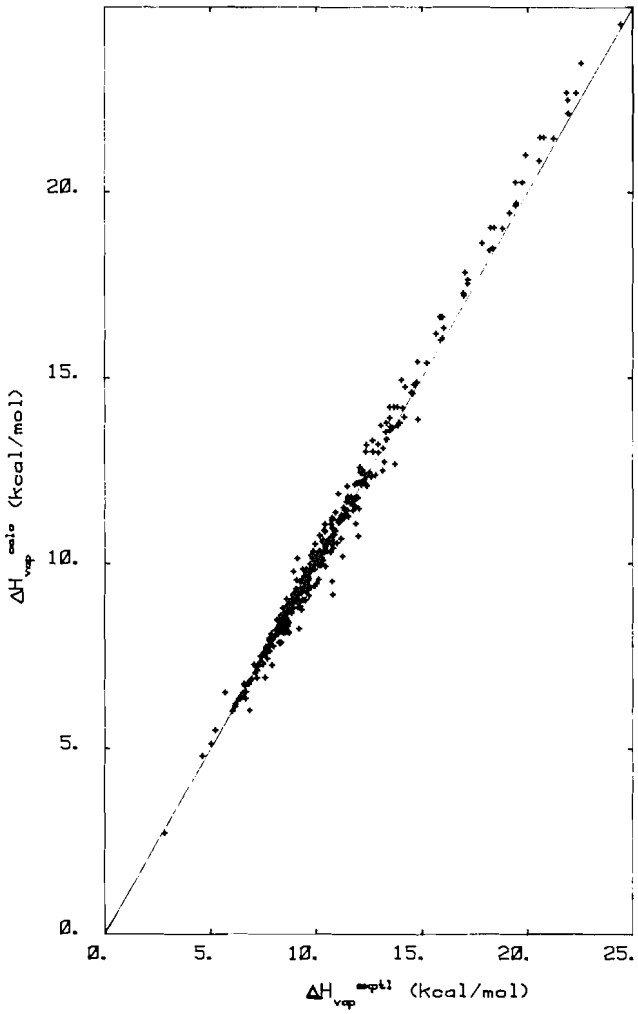

FIG. 2. Calculated vs. experimental values for heats of vaporization using the group level parameters; data from Table S1.

was not included was that for nitrobenzene (9), since this compound has a unique bond. Numerous compounds were left out of the group level calculations, as indicated in Table S1. Figures 1 and 2 show the quality of the agreement which was obtained.

Table 1 gives the bond level parameters which were evaluated by least-squares fitting. Table 2 gives the group level parameters which were evaluated by least squares. For both bond and group parameters we have followed Hine's notation (23) rather than Benson's (2). In both tables we have included the significant (absolute value greater than 0.5) elements of the correlation matrix. This matrix is quite sparse, and is symmetrical, so we have been able to present the relevant parts of it quite consisely; elements appear only once at the lower numbered parameter. A non-zero element in the correlation matrix means that the corresponding parameters are not independent and that there could be major changes in the two parameters with little change in the overall fit, if the changes were properly related. Thus for those parameters for which there is a significant element in the correlation matrix, the present values must be considered provisional, and may change when further data are added to the set. The present set of parameters is self consistent, even if the absolute values of some parameters are not yet well defined. It should be noted that there are sizeable uncertainties in some of the parameters, as reported by the least-squares program. In some cases these reflect the problem of covariance. Clearly any calculations using these ill-defined parameters will be subject to greater uncertainty. It has unfortunately not been common for either the statistical uncertainties in the parameters or the correlation matrix to be reported in similar parameterizations of thermochemical data. We believe that it is important to give this information, in order that anyone planning to use the parameters can assess the probable reliability of calculations based upon them.

It should be noted that the overall fit, as shown in Figs. 1 and 2, and as measured by the weighted standard deviation, is quite good: for the bond level parameters, the weighted standard deviation is 0.32 kcal/mol; for the group level parameters, it is 0.19 kcal/mol. For the bond level parameters, 23 compounds out of 429 showed deviations of calculated from observed of more than 1 kcal/mol; only one showed a deviation of more than 2 kcal/mol. For the group level parameters, 7 compounds out of 388 showed deviations of more than 1 kcal/mol, the largest being 1.6 kcal/mol. We feel that this quality of fit means that for compounds for which the parameters are presently well defined, either of these estimation procedures will give good estimates. It should be stressed that such methods are necessarily interpolation procedures, estimating unknown values on the basis of known values for related compounds; as the estimation becomes more an extrapolation, the accuracy must

TABLE 1. Bond level parameters for estimating heats of vaporization

No.	Bond	Parameter	Error	Correlation[a]
1	C—H	0.43	0.01	2, −0.99; 10, −0.8; 18, −0.7; 24, −0.5
2	C—C	0.31	0.04	10, 0.8; 18, 0.7; 24, 0.5
3	Cd—H	0.74	0.11	4, −0.7
4	Cd—C	0.50	0.12	
5	Quat[b]	−1.12	0.08	
6	5-Ring[c]	0.89	0.14	
7	C—C_B	0.49	0.77	8, −0.99; 9, 0.99; 12, −0.9; 17, 0.9; 20, 0.9; 23, −0.96; 27, 0.5; 29, −0.9; 33, 0.99; 34, 0.9
8	C_B—C_B	0.72	0.77	9, −0.999; 12, 0.9; 17, −0.9; 20, −0.9; 23, 0.97; 27, −0.5; 29, 0.9; 33, −0.99; 34, −0.9
9	C_B—H	0.60	0.77	12, −0.95; 17, 0.9; 20, 0.9; 23, −0.97; 27, 0.5; 29, −0.96; 33, 0.99; 34, 0.9
10	C—O	0.90	0.03	18, 0.5
11	O—H	4.21	0.14	13, −0.6
12	C_B—O	1.87	0.42	17, −0.8; 20, −0.8; 23, 0.9; 27, −0.5; 29, 0.9; 33, −0.9; 34, −0.8
13	H-bond[d]	2.44	0.24	
14	C—CO	2.08	0.08	15, −0.7
15	O—CO	1.93	0.10	16, −0.9
16	CO—H	2.66	0.10	
17	C_B—CO	1.86	0.81	20, 0.9; 23, −0.8; 27, 0.5; 29, −0.9; 33, 0.9; 34, 0.9
18	C—N	0.36	0.06	19, −0.6
19	N—H	1.60	0.05	
20	C_B—N	2.83	0.81	23, −0.9; 27, 0.5; 29, −0.9; 33, 0.9; 34, 0.9
21	C—CN	5.66	0.10	
22	C_d—CN	6.12	0.48	
23	C_B—N_B	1.73	0.40	27, −0.5; 29, 0.9; 33, −0.96; 34, −0.9
24	C—S	1.89	0.08	26, −0.5
25	S—CO	1.54	0.74	
26	S—H	2.01	0.13	
27	C_B—S	2.31	1.40	29, −0.5; 33, 0.5; 34, 0.5
28	S—S	2.15	1.47	
29	C_B—S_B	1.83	0.41	33, −0.9; 34, −0.8
30	C—Br	3.99	0.14	35, −0.5
31	C—Cl	2.70	0.04	
32	C_d—Cl	2.42	0.07	
33	C_B—F	0.75	0.77	34, 0.9
34	C_B—Cl	2.31	0.84	
35	C—F	−0.34	0.13	
36	C—I	4.86	0.36	

[a]Number of correlated parameter (column 1), correlation coefficient.
[b]Quaternary center: four non-hydrogen groups on a central carbon.
[c]Five membered ring, either all carbon or heterocyclic, saturated or with one double bond.
[d]Intermolecular hydrogen bond; not counted for an OH which can form a 5 or 6 membered ring intramolecular hydrogen bond, etc.

be expected to fall.

In these calculations it was necessary to add two points to the set of data in order to force a satisfactory parameterization. At the bond level, the parameters involving aromatic rings are not well defined, because of extensive correlation. To get the program to converge at all it was necessary to include a point for naphthalene, based on the observed heat of sublimation (24) and the heat of fusion (25). With this compound included it was possible to get convergence, but the correlation problem is still severe, and it is obvious that the parameter values will change as more data become available. These problems are a consequence of treating benzene rings as composed of C_B⋯C_B bonds, each being a one-and-a-half bond (23), rather than as hexavalent atoms (1). By so doing, we can easily include nitrogen and sulfur heterocycles at the price of correlation problems, which might have been avoided had we followed Benson and Buss (1). It seemed important to be able to include as many compounds as possible; the problem of correlation should be temporary, since it should disappear with additional data.

At the group level, we observed that there was a strong correlation between $[CH_3(X)]$ and $[CH_2(C)_2]$ which had the effect of generating parameters which did not fit the set of *n*-alkanes very well, although the overall fit was satisfactory. When ΔH_{vap} for the *n*-alkanes is plotted as a function of the number of carbon atoms, a good straight line is obtained. The

Can. J. Chem. Downloaded from www.nrcresearchpress.com by 210.87.254.5 on 09/06/12
For personal use only.

TABLE 2. Bond level parameters for estimating heats of vaporization

No.	Group	Parameter	Error	Correlation[a]
1	$CH_3(X)$	1.36	0.01	2, −0.6
2	$CH_2(C)_2$	1.21	0.01	
3	$CH(C)_3$	0.73	0.03	
4	$C(C)_4$	0.08	0.08	
5	$CH_2(C)(C_d)$	1.34	0.28	8, −0.7; 42, −0.5
6	$CH(C)_2(C_d)$	1.14	1.05	
7	$C(C)_3(C_d)$	−0.29	0.71	
8	C_dH_2	1.00	0.36	38, −0.7; 10, −0.5
9	$C_dH(C)$	1.23	0.27	10, −0.7; 38, −0.7; 39, −0.5
10	$C_d(C)_2$	1.16	0.28	38, 0.5
11	C_BH	1.34	0.02	12, −0.7; 13, −0.5; 37, −0.5; 43, −0.5; 52, −0.5
12	$C_B(C)$	1.11	0.05	
13	$CH_2(C_B)(C)$	0.79	0.18	
14	$CH(C)_2(C_B)$	0.24	0.24	
15	$C(C)_3(C_B)$	−0.57	2.19	
16	OH(C)	7.43	0.51	20, −0.5; 22, −0.96
17	$O(C)_2$	2.00	0.08	18, −0.9
18	$CH_2(C)(O)$	0.84	0.05	
19	$CH(C)_2(O)$	0.00	0.15	
20	$C(C)_3(O)$	−0.37	0.27	22, 0.5
21	$CH_2(O)_2$	0.14	0.69	
22	1° or 2° OH	0.39	0.53	
23	Intramol H-bond	−2.46	0.18	
24	$CO(C)_2$	4.79	0.15	25, −0.5
25	$CH_2(C)(CO)$	0.37	0.13	
26	$CH(C)_2(CO)$	−0.18	0.20	
27	CO(C)(O)	4.45	0.44	28, −0.99; 31, 0.99
28	O(CO)(C)	0.64	0.44	31, −0.99
29	$C(C)_3(CO)$	−1.01	0.18	
30	OH(CO)	6.33	2.43	
31	HCO(X)	4.78	0.44	
32	$CH_2(C)(N)$	0.43	0.13	33, −0.9; 34, 0.9; 35, −0.97; 36, −0.95; 37, 0.6
33	$NH_2(C)$	4.33	0.15	34, −0.9; 35, 0.9; 36, 0.9; 37, −0.6
34	$CH(C)_2(N)$	−0.44	0.19	35, −0.9; 36, −0.9; 37, 0.5
35	$NH(C)_2$	3.71	0.25	36, 0.9; 37, −0.5
36	$N(C)_3$	2.88	0.40	37, −0.5
37	$C_B(N)$	2.29	0.25	
38	$CH_2CN(C_d)$	7.24	0.65	
39	C_dHCN	6.72	0.52	
40	$CH_2CN(C)$	7.09	0.10	
41	$CHCN(C_2)$	6.08	0.10	
42	$C_dCN(C)$	6.05	0.96	
43	$N_B(C_B)_2$	2.83	0.18	
44	$CH_2(C)(S)$	1.34	0.12	46, 0.7; 47, 0.6; 48, −0.8; 49, −0.8
45	CO(C)(S)	5.29	0.51	
46	$CH(C)_2(S)$	0.74	0.20	47, 0.6; 48, −0.8; 49, −0.7
47	$C(C)_3(S)$	−0.56	0.22	48, −0.7; 49, −0.7
48	SH(C)	3.82	0.16	49, 0.7
49	$S(C)_2$	3.66	0.19	
50	$C_B(S)$	1.09	1.11	
51	S(C)(S)	2.69	0.50	
52	C_BCl	2.91	0.25	
53	$CH_2Br(C)$	5.22	0.11	
54	$CHBr(C)_2$	4.40	0.24	
55	$CH_2Cl(C)$	4.19	0.05	
56	$CHCl_2(C)$	5.44	0.14	
57	C_BF	1.46	0.06	

[a]Number of correlated parameter, correlation coefficient.

line corresponding to the initial parameters did not fit these points well; the slope was too large, leading to deviations for the longer alkanes. In order to force a good fit to the alkanes we inserted a "value" for ethane which was calculated by extrapolation of the best line through the *n*-alkane data. This value was assigned an error of 0.001 to give it a high statistical

Can. J. Chem. Downloaded from www.nrcresearchpress.com by 210.87.254.5 on 09/06/12
For personal use only.

Can. J. Chem. Downloaded from www.nrcresearchpress.com by 210.87.254.5 on 09/06/12
For personal use only.

weight. This is really a way of assigning a value to the parameter $[CH_3(X)]$ and led to the results in Tables 2 and S1 and Fig. 2.

Ducros *et al.* (18, 19) have recently reported a group level scheme for heats of vaporization. Their results differ somewhat from ours because they used non-calorimetric as well as calorimetric data and also parameterized rather differently. We have restricted our data base to calorimetric values.[3] Although vapor pressure measurements can lead to accurate heats of vaporization, they have frequently led to values in error by more than the quoted uncertainty. Morawetz has stated (26): "It is quite evident that many vapor pressure measurements, from which most vaporization enthalpies given in the literature are derived, must be rather inaccurate. It is also obvious that uncertainties attached to vaporization enthalpies obtained in this way are often far too optimistic." Furthermore, it seems quite hazardous to base a parameterization, even in part, upon heats of vaporization estimated by empirical rules, even though such rules are often very useful, and seem quite reliable within restricted classes of compound. We have endeavored to delete all non-calorimetric values from our database. In many cases our parameters are very similar to those of Ducros *et al.*, but there are frequent differences. The important lesson is that, because of the problem of parameter correlation, one cannot compare or mix parameters from different fittings without careful consideration of the nature of the data bases used, the parameterization schemes employed, and whether the parameters being compared are relatively independent of other parameters or show tight covariance.

Other, more limited, parameterizations have been reported by Stein (17) and Cramer (16). Stein used only alkanes, and his scheme contains a constant term, RT, included on theoretical grounds. His values are $[CH_3(X)] = 1.14$, and $[CH_2(C)_2] = 1.17$. Since the constant term amounts to 0.593 kcal/mol, these values are in effect very similar in effective fit to the data to our values, at least for the lower alkanes. This can be shown by writing the corresponding equation for heat of vaporization as a function of number of carbons for the *n*-alkanes:

$$[1] \quad \Delta H_{vap} = 2.87 + 1.17\,(n - 2)$$

$$[2] \quad \Delta H_{vap} = 2.72 + 1.21\,(n - 2)$$

Equation [1] represents Stein's parameters, and eq. [2] represents ours. The difference is quite small except for very large n. Cramer has reported a much more ambitious scheme showing that numerous experimental properties of liquids related in some way to intermolecular interactions can be related to a set of two major and three minor intrinsic molecular parameters which are themselves additive constitutive properties depending on structure. ΔH_{vap} was included in the set, although this was by no means a central feature of the paper. From his data we may calculate the corresponding group parameters (his approach can be converted to a group contributions scheme, although this is not the way the correlations are presented): $[CH_3(X)] = 2.206$, and $[CH_2(C)_2] = 0.771$, with a constant term of 0.55 kcal/mol. This appears to be a quite different result from that found in the other treatments, including ours, but in fact the calculated values come out quite similar for hydrocarbons of the size included in Cramer's database, methane to pentane. Furthermore he appears to have used heats of vaporization at the normal boiling point, rather than at 25°C, so that exact comparison is not possible. Where there is intrinsic correlation of the parameters, data spanning a wide range of n are needed to establish both parameters rather than just a correlated pair of values. His values lead to eq. [3].

$$[3] \quad \Delta H_{vap} = 4.46 + 0.77\,(n - 2)$$

There have been reports of group additivity methods for vapor pressures (60, 61) which in principle could lead to heats of vaporization. These methods appear to lead to good estimates of vapor pressures within the, so far, limited range of compounds which have been examined. Jensen *et al.* (60) have not directly considered heats of vaporization. Macknick and Prausnitz (61) showed that heats of vaporization at the normal boiling point, calculated by differentiation of the equation generated by their group equivalents scheme for heavy hydrocarbons, gave an average error of ±5.4%.

There do not appear to have been any previous attempts to determine bond level parameters for H_{vap}. Since the fit is not much worse than with group level parameters, and there is a marked reduction in the number of parameters required to fit a larger number of compounds, we feel that the bond level approach will be useful to chemists carrying out thermochemical calculations. Nevertheless, it remains true that it is preferable to use group level calculations whenever the necessary parameters are known.

[3]Strictly the data of Fuchs and Peacock (27, 30, 33, 46) are not purely calorimetric values since a combined gas chromatographic – calorimetric method was used. Since this semi-calorimetric method has been carefully calibrated by comparison with true calorimetric values (30, 33, 46), we felt it was justifiable to include these data.

1. S. W. BENSON and J. H. BUSS. J. Chem. Phys. **29**, 546 (1958).
2. S. W. BENSON. Thermochemical kinetics. 2nd ed. Wiley, New York. 1976.
3. H. WIENER. J. Chem. Phys. **15**, 419 (1947); J. Am. Chem. Soc. **69**, 17, 2636 (1947).
4. H. WIENER. J. Phys. Chem. **52**, 766 (1948); **52**, 1082 (1948).
5. J. R. PLATT. J. Chem. Phys. **15**, 419 (1947).
6. J. R. PLATT. J. Phys. Chem. **56**, 328 (1952).
7. J. B. GREENSHIELDS and F. D. ROSSINI. J. Phys. Chem. **62**, 271 (1958).
8. K. J. LAIDLER. Can. J. Chem. **34**, 626 (1956).
9. J. D. COX and G. PILCHER. Thermochemistry of organic and organometallic compounds. Academic Press, London. 1970.
10. E. G. LOVERING and K. J. LAIDLER. Can. J. Chem. **38**, 2367 (1960).
11. E. G. LOVERING and O. M. NOR. Can. J. Chem. **40**, 199 (1962).
12. L. H. THOMAS. J. Chem. Soc. 2132 (1959).
13. E. MORAWETZ. J. Chem. Thermodyn. **4**, 139 (1972).
14. M. MANSSON, P. SELLERS, G. STRIDH, and S. SUNNER. J. Chem. Thermodyn. **9**, 91 (1977).
15. V. MAJER, V. SVOBODA, S. HALA, and J. PICK. Collect. Czech. Chem. Commun. **44**, 637 (1979).
16. R. D. CRAMER III. J. Am. Chem. Soc. **102**, 1849 (1980).
17. S. E. STEIN. J. Chem. Soc. Faraday Trans. 1, **77**, 1457 (1981).
18. M. DUCROS, J. F. GRUSON, and H. SANNIER. Thermochim. Acta, **36**, 39 (1980).
19. M. DUCROS, J. F. GRUSON, H. SANNIER, and I. VELASCO. Thermochim. Acta, **44**, 131 (1981).
20. J. B. PEDLEY and J. RYLANCE. Sussex-NPL computer analyzed thermochemical data: organic and organometallic compounds. University of Sussex, Brighton, England. 1977.
21. J. KONICEK and I. WADSO. Acta Chem. Scand. **24**, 2612 (1970).
22. C. H. D. CALIS-VAN GINKEL, G. H. M. CALIS, C. W. M. TIMMERMANS, C. G. DE KRUIF, and H. A. J. OONK. J. Chem. Thermodyn. **10**, 1083 (1978).

23. J. HINE and P. K. MOOKERJEE. J. Org. Chem. **40**, 292 (1975).
24. E. MORAWETZ. J. Chem. Thermodyn. **4**, 461 (1972).
25. J. P. MCCULLOGH, H. L. FINKE, J. F. MESSERLY, S. S. TODD, T. C. KINCHELOE, and G. WADDINGTON. J. Phys. Chem. **61**, 1105 (1957).
26. E. MORAWETZ. J. Chem. Thermodyn. **4**, 455 (1972).
27. R. FUCHS and L. A. PEACOCK. Can. J. Chem. **57**, 2302 (1979).
28. I. WADSO. Acta Chem. Scand. **20**, 536 (1966).
29. I. A. HESSENOPP and D. W. SCOTT. J. Chem. Thermodyn. **13**, 415 (1981).
30. L. A. PEACOCK and R. FUCHS. J. Am. Chem. Soc. **99**, 5524 (1977).
31. M. MANSSON, P. SELLERS, G. STRIDH, and S. SUNNER. J. Chem. Thermodyn. **9**, 91 (1977).
32. V. MAJER, V. SVOBODA, S. HALA, and J. PICK. Collect. Czech. Chem. Commun. **44**, 637 (1979).
33. R. FUCHS and L. A. PEACOCK. Can. J. Chem. **56**, 2493 (1978).
34. V. SVOBODA, V. CHARVATOVA, V. MAJER, and J. PICK. Collect. Czech. Chem. Commun. **46**, 2984 (1981).
35. I. A. HOSSENLOPP and D. W. SCOTT. J. Chem. Thermodyn. **13**, 423 (1981).
36. I. WADSO. Acta Chem. Scand. **20**, 544 (1966).
37. M. MANSSON. J. Chem. Thermodyn. **1**, 141 (1969).
38. K. KUSANO and I. WADSO. Acta Chem. Scand. **24**, 2037 (1970).
39. K. KUSANO and I. WADSO. Acta Chem. Scand. **25**, 219 (1971).
40. K. KUSANO and I. WADSO. Bull. Chem. Soc. Jpn. **44**, 1705 (1971).
41. E. M. ARNETT and D. OANCEA. J. Chem. Educ. **52**, 269 (1975).
42. C. SVENSSON. J. Chem. Thermodyn. **11**, 593 (1979).
43. V. MAJER, Z. WAGNER, V. SVOBODA, and V. CADEK. J. Chem. Thermodyn. **12**, 387 (1980).
44. I. A. HOSSENLOPP and D. W. SCOTT. J. Chem. Thermodyn. **13**, 405 (1981).
45. S. SUNNER, C. SVENSSON, and A. S. ZELEPUGA. J. Chem. Thermodyn. **11**, 491 (1979).
46. R. FUCHS and L. A. PEACOCK. Can. J. Chem. **58**, 2796 (1980).
47. J. CIHLAR, V. HYNEK, V. SVOBODA, and R. HOLUB. Collect. Czech. Chem. Commun. **41**, 1 (1976).
48. V. SVOBODA, F. VESELY, R. HOLUB, and J. PICK. Collect. Czech. Chem. Commun. **42**, 943 (1977).
49. P. SELLERS. J. Chem. Thermodyn. **9**, 139 (1977).
50. G. GEISELER, K. QUITZSCH, H.-P. HOFMANN, and R. PFESTORF. Z. Phys. Chem. (Leipzig), **252**, 170 (1972).
51. M. MANSSON. J. Chem. Thermodyn. **4**, 865 (1972).
52. I. WADSO. Acta Chem. Scand. **23**, 2061 (1969).
53. V. MAJER, V. SVOBODA, J. KOUBEK, and J. PICK. Collect. Czech. Chem. Commun. **44**, 3521 (1979).
54. L. PETROS, V. MAJER, J. KOUBEK, V. SVOBODA, and J. PICK. Collect. Czech. Chem. Commun. **44**, 3533 (1979).
55. P. B. HOWARD and I. WADSO. Acta Chem. Scand. **24**, 145 (1970).
56. J. KONICEK. Acta Chem. Scand. **27**, 1496 (1973).
57. V. SVOBODA, V. MAJER, F. VESELY, and J. PICK. Collect. Czech. Chem. Commun. **42**, 1755 (1977).
58. V. MAJER, L. SVAB, and V. SVOBODA. J. Chem. Thermodyn. **12**, 47 (1980).
59. V. MAJER, V. SVOBODA, A. POSTA, and J. PICK. Collect. Czech. Chem. Commun. **46**, 817 (1981).
60. T. JENSEN, A. FREDENSLUND, and P. RASMUSSEN. Ind. Eng. Chem. Fundam. **20**, 239 (1981).
61. A. B. MACKNICK and J. M. PRAUSNITZ. Ind. Eng. Chem. Fundam. **18**, 348 (1979).

Can. J. Chem. Downloaded from www.nrcresearchpress.com by 210.87.254.5 on 09/06/12
For personal use only.

Polarized Raman spectra of an oriented single crystal of barium nitrite monohydrate

O. P. LAMBA, H. D. BIST, AND Y. S. JAIN[1]

Department of Physics, Indian Institute of Technology, Kanpur 208016, India

Received August 10, 1982

O. P. LAMBA, H. D. BIST, and Y. S. JAIN. Can. J. Chem. **61**, 608 (1983).

The symmetries of the observed Raman lines in the 4000–30 cm^{-1} region in different orientations of a single crystal of $Ba(NO_2)_2 \cdot H_2O$ have been determined and the spectra have been analysed in terms of the phonons originating from the internal modes of the NO_2^- and H_2O groups and the external lattice modes. The longitudinal-optical and transverse-optical (LO–TO) splittings arising from the Coulomb forces in the crystal are reported for the first time.

O. P. LAMBA, H. D. BIST et Y. S. JAIN. Can. J. Chem. **61**, 608 (1983).

On a déterminé les symétries des raies de Raman observées dans la région de 4000–30 cm^{-1}, pour les différentes orientations d'un cristal unique de $Ba(NO_2)_2 \cdot H_2O$ et on a analysé les spectres en fonction des phonons provenant des modes internes des groupes NO_2^- et H_2O et des modes de réseau externe. On rapporte pour la première fois les déplacements longitudinal-optique et transverse-optique (LO–TO) provenant des forces de Coulomb dans le cristal.

[Traduit par le journal]

1. Introduction

$M(NO_2)_2 \cdot H_2O$ (M = Ba, Sr, Ca, and Mg) form a simple series of hydrated nitrites. Out of these, only $Ba(NO_2)_2 \cdot H_2O$ (BNM) forms stable and well developed crystals, for which recent X-ray reinvestigations (1) have established the correct polar space group C_6^2 (or C_6^3). The solid has been studied extensively by several physical methods (2–8). Special interest has developed in this recently due to its use as pyroelectric infrared radiation detector (9). Infrared and Raman spectra of polycrystalline samples of BNM have recently been published (10–12). The only report on polarized Raman spectra of single crystals (13) utilized a conventional mercury source.

The present Raman investigation was performed using laser excitation in order to obtain unambiguous symmetry assignments of the internal and lattice phonons originating from the optically active motions of the NO_2^-, H_2O, and Ba^{2+} units in the crystal.

2. Experimental

Single crystals were grown by slow evaporation of aqueous solution of BNM prepared by a method reported earlier (12). The axes of the well developed hexagonal prisms elongated along ⟨001⟩ axis (polar Z-axis) were determined from the knowledge of crystal morphology.

The crystals of BNM show maximum transmission and minimum optical rotatory power near 500 nm (5). The 514.5-nm emission line of the Ar^+ ion laser (Spectra-Physics 165-09) was used to excite the Raman scattering from a small crystal (ca. 3 × 2 × 2 mm). The scattered radiation observed at right angles was dispersed in a Spex 1403 double monochromator equipped with a cooled photomultiplier C 31034 tube and a Spex digital photon counting system DPC-2. The spectral slit widths employed were ~1 cm^{-1} – 3 cm^{-1}.

3. Crystal structure and phonon symmetry

The hexamolecular unit cell of BNM crystal belongs to the C_6^2 space group (1). The stoichiometric sheets (consisting of Ba^{2+}, two types of NO_2^- ions, and H_2O molecules, and running normal to the polar axis of the crystal) are interlinked through hydrogen bonds. All these Ba^{2+}, two symmetrically independent NO_2^- ions, and the H_2O molecules occupy the sites of C_1 symmetry in the unit cell. The correlation of the different symmetry species of the free NO_2^- or H_2O groups with the site and the factor groups is shown in Table 1.

TABLE 1. Correlation diagram for the free, site and unit cell symmetry of NO_2^- and H_2O groups in the $Ba(NO_2)_2 \cdot H_2O$ crystal

Free state C_{2v}	Site C_1	Crystal[a] C_6
A_1 (ν_1, ν_2, T_Z)		A (R, ir)
A_2 (R_Z)	A	B (inactive)
B_1 (T_X, R_Y)		E_1 (R, ir)
B_2 (ν_3, T_Y, R_X)		E_2 (R)

[a]In parentheses are shown the activity of the particular symmetry species.

Under the unit cell approximation, the dynamics of BNM crystal can be described in terms of 180 phonon branches including 3 acoustical ones. A factor group analysis of the normal modes at the centre of Brillouin zone ($K = 0$) yields the following symmetry reduction:

$$\Gamma_{180} = 30A(\text{R, ir}) + 30B(\text{inactive}) + 30E_1(\text{R, ir}) + 30E_2(\text{R})$$

The complete optical Raman spectrum is therefore expected to comprise $29A + 29E_1 + 30E_2$ modes. The symmetry species and the number of phonon branches arising from the different modes of H_2O, NO_2^-, and Ba^{2+} groups are presented in Table 2. The vibrational modes are classified approximately into the internal and the external modes.

The Raman tensors for crystals with C_6-hexagonal symmetry are given by Loudon (14). These tensors indicate that the A phonons are polarized parallel to the Z-axis, while the E_1 phonons are polarized in the XY plane. Further, the A and E_1 modes being simultaneously infrared and Raman-active are expected to split into a longitudinal-optical (LO) and a transverse-optical (TO) branch (vide infra, Section 4*F*).

4. Results and discussion

A. Phonon frequencies

Four spectra were recorded for XX, YX, YZ, and ZZ polarizations to define the vibrations of the BNM crystal at room

[1]Permanent address: Department of Physics, North-Eastern Hill University, Shillong-793003, India.

Can. J. Chem. Downloaded from www.nrcresearchpress.com by 210.87.254.6 on 09/06/12
For personal use only.

TABLE 2. Symmetry classification of phonons in the $Ba(NO_2)_2 \cdot H_2O$ crystal

Modes[a]	Species A	B	E_1	E_2	N^b
(*i*) Internal modes:					
a. $H_2O(C_{2v})$					
$\nu_1^W(A_1)$	1	1	1	1	6
$\nu_2^W(A_1)$	1	1	1	1	6
$\nu_3^W(B_2)$	1	1	1	1	6
Total:	3	3	3	3	18
b. $NO_2^-(C_{2v})$					
$\nu_1^N(A_1)$	2	2	2	2	12
$\nu_2^N(A_1)$	2	2	2	2	12
$\nu_3^N(B_2)$	2	2	2	2	12
Total:	6	6	6	6	36[c]
(*ii*) External modes:					
a. Librations of H_2O					
Rocking: $R^W(B_2)$	1	1	1	1	6
Wagging: $W^W(B_1)$	1	1	1	1	6
Twisting: $T^W(A_2)$	1	1	1	1	6
Total:	3	3	3	3	18
b. Librations of NO_2^-					
Rocking: $R^N(B_2)$	2	2	2	2	12
Wagging: $W^N(B_1)$	2	2	2	2	12
Twisting: $T^N(A_2)$	2	2	2	2	12
Total:	6	6	6	6	36
c. Optical translations of Ba^{2+}, NO_2^-, and H_2O	11	12	11	12	69
Acoustical translations	1		1		3
Grand total:	30	30	30	30	180

[a]Superscripts W and N refer to the modes of H_2O and NO_2^- groups.
[b]Total number of phonon branches originating from the modes of respective molecular units.
[c]Internal modes contributed by two symmetrically independent NO_2^- ions in the unit cell.

Can. J. Chem. Downloaded from www.nrcresearchpress.com by 210.87.254.6 on 09/06/12
For personal use only.

temperature. Figure 1 depicts mainly the internal mode regions of the H_2O and NO_2^- groups, while Fig. 2 covers the low frequency region. No bands were observed in the multiphonon 1700–3200 cm^{-1} region and the bending mode of H_2O appeared very faintly in the *YX* spectrum only at ~1650 cm^{-1}. Peak frequencies of the Raman active phonons for the observed bands in different spectra are given in Table 3 along with our assignments in column 5. The infrared frequencies measured from the powdered sample (12) are also included in the last column to facilitate comparison. The accuracy for the Raman bands is ±2 cm^{-1} generally, but may be ±5 cm^{-1} in the OH-stretching region.

B. Internal modes of H_2O molecule

The stretching region 3200–3600 cm^{-1} of water molecule in BNM (cf Fig. 1) shows only two modes at 3502 (*YX*, *XX*, and *ZZ* spectra) and around 3360 cm^{-1} (*ZZ* and *YX* spectra), the former being strong in the *YX* spectrum and the latter in the *ZZ* spectrum. This intensity change would go against treating the two bands as ν_3 and ν_1 of water. The large frequency difference 142 cm^{-1} would also suggest that the two bands are due to two independent groups of OH oscillators, with different polarizability derivatives. Wood reports (11) that there is no significant difference in ir absorption for the stretching modes for radiation polarized parallel and normal to *Z*-axis, and he concludes that the two modes have dipole moment changes neither parallel nor perpendicular to the molecular C_2 axis. The polarizability derivatives could still be different for the two OH oscillators.

The six crystallographically equivalent H_2O molecules occupying C_1 sites in BNM lattice are highly distorted. Hence, in group theory, each mode of H_2O is expected to split into three Raman and two ir-active components under the point group C_6 (cf. Table 1). The absence of such splitting in the Raman spectra, as also in the ir spectra (12) even at low temperature, leads us to conclude that the intra- and inter-molecular interactions are extremely weak.

C. Librational modes of H_2O molecules

In our polarized Raman spectra of the single crystal or of the powder, these modes appear as extremely weak and diffuse bands, and therefore no additional information could be drawn regarding their librational dynamics. However, these modes appearing strong in infrared have been characterized on the basis of well known criteria (12).

D. Internal modes of NO_2^- ion

As can be seen from Tables 1 and 2, the internal modes of NO_2^- ion are expected to show multiple structure because there are two non-equivalent NO_2^- ions in the unit cell. The spectra (cf. Fig. 1) show only two bands corresponding to each of the ν_2 and ν_3 modes, which are obviously due to site splitting. The totally symmetric mode ν_1 shows a single band, which has a

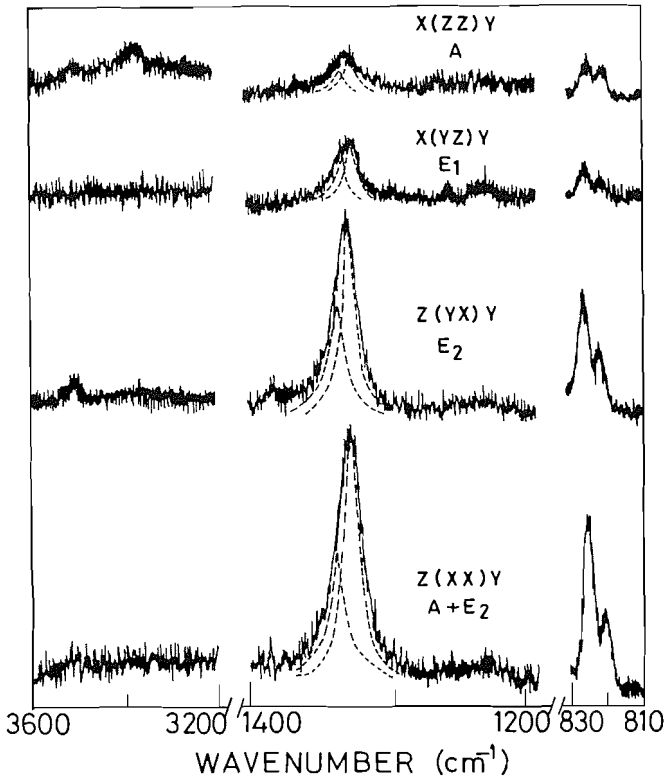

FIG. 1. Polarized Raman spectra of a $Ba(NO_2)_2 \cdot H_2O$ single crystal. For 3200–3600 cm^{-1} region: scan time 1 cm^{-1}/s, slits 300 MIC and laser power at sample ~100 mW. For 810–1400 cm^{-1} region, the respective values are 0.1 cm^{-1}/s, 200 MIC, and ~120 mW. Full scale is 2 K and integrated time 0.5 s for both the regions.

distinct asymmetry, so that a graphical resolution is used to deduce the two components. These modes are assigned and their polarization states are as indicated in columns 1–4 of Table 3. It is noted that the vibrations of NO_2^- ions have their polarizations more or less in both the principal directions of the hexagonal crystal. This is in agreement with Wood's conclusion for ir spectra (11).

The weak modes appearing around 1376 cm^{-1} in this region can be attributed to the multiphonon transition $\nu_2(NO_2^-$ ion) + H_2O libration at 559 cm^{-1} (cf. Table 3, column 6). The possibility that these bands could arise from the possible presence of NO_3^- ion as an impurity was ruled out since the totally symmetric vibration of the NO_3^- ion around 1050 cm^{-1} was non-traceable in the Raman spectra.

E. Low-lying lattice phonons

The $K = 0$ lattice phonons of Ba^{2+}, H_2O, and NO_2^- units in BNM expected below 500 cm^{-1} in the Raman spectrum can be associated with $17A + 17E_1 + 18E_2$ phonons excluding three acoustical $A + E_1$ phonons and $3A + 3E_1 + 3E_2$ modes corresponding to H_2O librations which are not observed in the Raman spectra of the single crystal (cf. Table 2). The observed spectra show that most of the bands occur in all the polarizations (cf. Table 3), which indicates an appreciable mixing of the rotational and translational modes.

In order to assign the modes of NO_2^- we note that: (*i*) the translatory and libratory modes of NO_2^- ion are expected below ~200 cm^{-1} (15) and (*ii*) NO_2^- librations, like those of H_2O, are expected to be weak in the Raman and moderately strong in the infrared spectra. The assignments of the NO_2^- and H_2O groups given in Table 3 are on these criteria. However, further distinction between translations and librations of NO_2^- is not possible due to an appreciable mixing and the reduced site symmetry C_1 (Table 1).

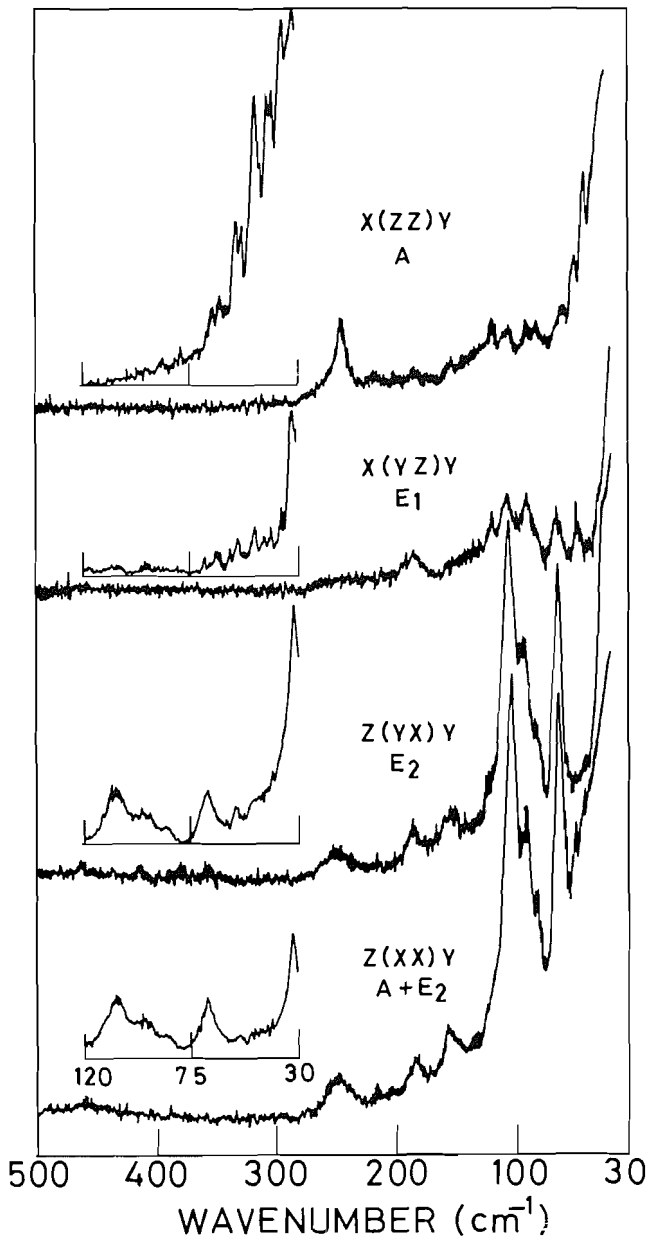

FIG. 2. Polarized Raman spectra of a $Ba(NO_2)_2 \cdot H_2O$ single crystal below 500 cm^{-1}. For 30–500 cm^{-1} region: scan time 0.2 cm^{-1}/s, slits 200 MIC, laser power at sample ~130 mW and full scale 2 K. For inset spectra (30–120 cm^{-1} region), the respective values are 0.2 cm^{-1}/s, 100 MIC, ~150 mW, and 10 K. Integrated time for both the regions are the same as in Fig. 1.

The strong Raman bands near Raleigh wing around 100 cm^{-1} or below this obviously belong to the translations of Ba^{2+} units in view of the large mass of the cation. It is noted that the bands in this region, mainly due to monoatomic units, are observed with almost similar intensities in both the Raman and infrared spectra.

F. LO and TO phonons

As mentioned earlier, the polar phonons comprising A and E_1 representations of point group C_6 are expected to show

Can. J. Chem. Downloaded from www.nrcresearchpress.com by 210.87.254.6 on 09/06/12
For personal use only.

TABLE 3. Observed frequencies[a] (cm^{-1}) of Raman active phonons and their polarizations in a $Ba(NO_2)_2 \cdot H_2O$ single crystal

$A+E_2$ $Z(XX)Y$	E_2 $Z(YX)Y$	E_1 $X(YZ)Y$	A $X(ZZ)Y$	Assignments[b]	Infrared powder[c]
1. Internal modes					
(*i*) H_2O molecule					
3502 vw	3502 w			$\nu_{OH(1)}^{W}$	3502 m
	3360 vw		3360 w	$\nu_{OH(2)}^{W}$	3360 s
	~1650 vw			ν_2^{W}	1651 m
(*ii*) NO_2^- ion					
	1382 vw		1376 vw 1366 vw	ν_2^{N} + Wag^{W}	
1328 s	1328 s	1327 w	1328 w	ν_1^{N}	1328 m
1336 sh	1336 sh	1334 sh	1336 sh		~1345 sh
1260 vw	1260 ?	1260 w		ν_3^{N}	1260 vs
1237 w	1234 vw	1235 w			1240 vs
826 m	826 m	824 w	825 w	ν_2^{N}	825 m
820 w	821 w	820 w	819 w		820 m
2. External modes					
(*i*) H_2O librations					
				$Twist^{W}$	692 m
(Extremely broad and diffuse bands)				Wag^{W}	559 s
				$Rock^{W}$	452 s
(*ii*) Other lattice modes					
460 vw	460 vw				?
	414 vw				410 w
	382 vw			t^{W}	385 w
	?				372 m
	355 vw				354 w
247 w	246 w		244 m		248 m
218 vw			216 w		219 s
203 vw			203 w		208 wsh
184 w	186 w	186 m		l^{N} and t^{N}	187 wsh
152 w			152 m		153 m
138 w			136 w		133 m
	120* vw	121 w	120 m		117 m
107 s	109 s	109 w	108 w		106 s
97 vw	95* vw	93 w	94 w		95 w
87 vw	85* vw	85 w	86 w		86 w
65 m	65 m	67 (LO)	66 (LO)		65 m
		64 (TO)	63 (TO)		
47 vw		48 m	47 m	t^{B}	48 m
53 vw		55 (LO)	55 (LO)		53 m
		53 (TO)	52 (TO)		
		43 (LO)	42 (LO)		41 m
		40 (TO)	40 (TO)		
		37 (LO)	36 (LO)		
33 w	33 w	32 (TO)	32 (TO)		32 w

[a]Measured from the spectra recorded in the geometries indicated under heads of columns 1–4; uncertain band positions have been question marked (?); bands arising due to spillover of strong bands in other polarizations have been starred (*).

[b]Superscripts W, N, and B refer to the modes of H_2O, NO_2^-, and Ba^{2+} units, respectively, l and t stand for librations and translations of these units.

[c]The bands above 410 cm^{-1} are recorded on P.E.-580 spectrophotometer (ref. 12), and below this are recorded on Polytech-30 instrument at Indian Institute of Technology, Madras, India.

LO–TO splittings. Our spectra of these species do not provide any indication of such splittings on the bands assigned to H_2O or NO_2^-. However, in the low frequency region near the Raleigh wing (cf. insets of *ZZ* and *YZ* spectra in Fig. 2) 8 bands of good intensity are observed, which can be arranged into four pairs, each one arising from LO and TO components of the theoretically allowed phonon branches of A and E_1 species. As expected, the lower frequency component (TO) of each pair has higher intensity than the corresponding LO phonon.

Acknowledgements

We are grateful to Professor D. P. Khandelwal for helpful discussions and to Department of Science and Technology, New Delhi, for financial assistance.

1. S. C. ABRAHAMS, J. L. BERNSTEIN, and R. LIMINGA. J. Chem. Phys. **72**, 5857 (1980).
2. J. IOH, R. KUSAKA, and R. KIRIYAMA. Mem. Inst. Sci. Ind. Res. Osaka Univ. **14**, 2 (1957).

Can. J. Chem. Downloaded from www.nrcresearchpress.com by 210.87.254.6 on 09/06/12
For personal use only.

3. V. V. GLADKII and I. S. ZHELUDEV. Sov. Phys. Crystallogr. **10**, 50 (1965); **12**, 788 (1968).
4. T. OJA, R. A. MARINO, and P. J. BRAY. Phys. Lett. **28**A, 16 (1968).
5. V. I. BURKOV, V. A. KIZEL, Z. B. PEREKALINA, N. L. KOZLOVA, and G. S. SEMIN. Sov. Phys. Crystallogr. **18**, 196 (1973).
6. S. HAUSSÜHL. Acta Crystallogr. **34**A, 547 (1978).
7. R. LIMINGA, S. C. ABRAHAMS, and J. L. BERNSTEIN. J. Appl. Crystallogr. **13**, 516 (1980).
8. P. K. GALLAGHER, S. C. ABRAHAMS, D. L. WOOD, F. SCHREY, and R. LIMINGA. J. Chem. Phys. **75**, 1903 (1981).
9. S. A. HAMID. Phy. Stat. Solid. A, **53**, K75 (1979).
10. G. BRINK and M. FALK. Spectrochim. Acta, **27**A, 1811 (1971).
11. D. L. WOOD. J. Chem. Phys. **75**, 4809 (1981).
12. O. P. LAMBA and H. D. BIST. J. Phys. Chem. Solids. In press.
13. A. TRAMER and J. P. MATHIEU. Compt. Rend. **249**, 392 (1959).
14. R. LOUDON. Adv. Phys. **13**, 423 (1964).
15. Y. SATO. J. Phys. Soc. Jpn. **20**, 275 (1965).

Can. J. Chem. Downloaded from www.nrcresearchpress.com by 210.87.254.6 on 09/06/12
For personal use only.

Nuclear analogs of β-lactam antibiotics. XVI. Aldol condensations of N-protected 4-tritylthio-2-azetidinones

ALAIN MARTEL,[1] JEAN COLLERETTE, JACQUES BANVILLE,[2] JEAN-PAUL DARIS, PHILIPPE LAPOINTE, BERNARD BELLEAU,[3] AND MARCEL MÉNARD

Les Laboratoires Bristol du Canada, 100, boul. de l'Industrie, Candiac (Qué.) Canada J5R 1J1

Received September 1, 1982

ALAIN MARTEL, JEAN COLLERETTE, JACQUES BANVILLE, JEAN-PAUL DARIS, PHILIPPE LAPOINTE, BERNARD BELLEAU, and MARCEL MÉNARD. Can. J. Chem. **61**, 613 (1983).

The reaction of acetaldehyde with enolates of N-protected 4-tritylthio-2-azetidinones **4***b* and **4***c* was studied. While the lithium enolate of *N*-methoxymethylazetidinone **4***b* gave only *trans S** 3-(1′-hydroxyethyl)azetidinone **8** the corresponding tetrabutylammonium enolate gave a mixture of *trans R** and *trans S** azetidinones **8** and **9**. The metal enolate of *N*-(*tert*-butyldimethylsilyl)-4-tritylthio-2-azetidinone **4***c* gave all four possible isomers.

ALAIN MARTEL, JEAN COLLERETTE, JACQUES BANVILLE, JEAN-PAUL DARIS, PHILIPPE LAPOINTE, BERNARD BELLEAU et MARCEL MÉNARD. Can. J. Chem. **61**, 613 (1983).

On a étudié la réaction de l'acétaldéhyde avec les énolates des tritylthio-4 azétidinones protégées au niveau de l'azote (**4***b* et **4***c*). Alors que l'énolate lithié de la *N*-méthoxyméthylazétidinone (**4***b*) donne uniquement la *S** (hydroxy-1 éthyl)-3 azétidinone *trans* (**8**) l'énolate correspondant du tétrabutylammonium donne un mélange des azétidinones *R** *trans* et *S** *trans* (**8** et **9**). L'énolate métallique de la *N*-(*tert*-butyldiméthylsilyl) tritylthio-4 azétidinone-2 (**4***c*) donne les 4 isomères possibles.
[Traduit par le journal]

Thienamycin (**1**) (1) and the structurally related olivanic acids (**2**) (2) are characterized, unlike classical β-lactam antibiotics, by a 6-(1′-hydroxyethyl) side chain. Although their configurations at positions 1′ and 6 are inverted, both display remarkable antibacterial properties. Their discovery has generated intensive synthetic work directed towards stereospecific incorporation of such 6-side chains not only to the carbapenem nucleus but also to the related penems (**3**) (3–5). In paper XV (6*a*) of this series we described our own effort at converting preformed 6-unsubstituted penems (**5**) to 6-(1′-hydroxyethyl)

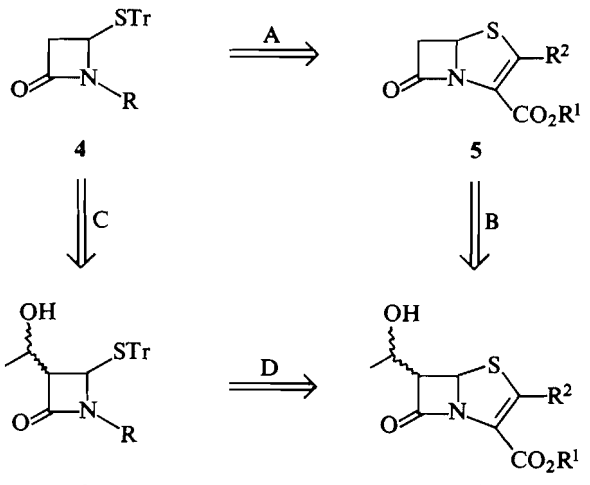

a R = H; *b* R = CH_2OCH_3; *c* R = $Si(CH_3)_2tC_4H_9$

SCHEME 1

and other 6-substituted penems (**7**, **3**): metallation of **5** followed by aldol condensation to acetaldehyde (Scheme 1B) was found to afford a single "unnatural" diastereomeric (1′*R**, 5*R**, 6*R**) 6-hydroxyethylpenem ruling out the use of preformed penems for the preparation of "natural" isomers of **7**.

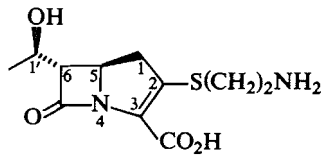

(1′*R*, 5*R*, 6*S*)

1

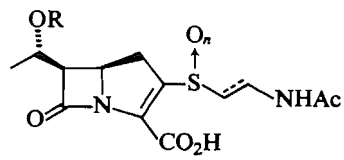

(1′*S*, 5*R*, 6*R*)

2 *n* = 0,1
R = H, SO_3H

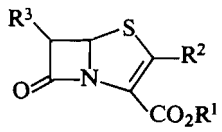

3

To overcome this problem and at the same time retain the versatile methodology developed for the preparation of 6-unsubstituted penems (Scheme 1A) (6*b*) we required an easy conversion of the key intermediate **4** to properly 6-substituted intermediates like **6** which would allow extension of Scheme 1A to Scheme 1D. This paper describes transformation of **4**, via aldol condensation, to all four possible isomers of **6**. Subsequent papers will report stereospecific conversions of **4** to "natural" **6** where the nitrogen protecting group actually consists of the Woodward phosphoranylidene acetic ester residue required to complete the annulation of the thiazole ring.

N—C-3 Dimetallation of azetidinone **4***a* and aldol reaction with acetaldehyde, in a manner similar to that described by Durst *et al.* (7) for 4-alkylazetidinones, would have provided the shortest method for the introduction of the 3-hydroxyethyl substituent. Possibly because of the different nature of the 4-substituent, azetidinone **4***a* proved to be completely unstable, even at −78°C, to dimetallation conditions. On the other hand, properly N-1 protected **4** were found to give stable monometallated enolates that underwent aldol condensation to

[1]Author to whom correspondence may be addressed.

[2]Holder of a National Research Council of Canada Industrial Postdoctoral Fellowship, 1979–1980.

[3]McGill University.

Can. J. Chem. Downloaded from www.nrcresearchpress.com by 210.87.254.42 on 09/06/12
For personal use only.

TABLE 1. Stereochemical composition of the aldol condensations

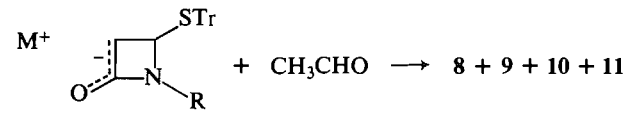

Expt. no.	Starting material	R	M^+	Solvent[a]	Yield, %	8	9	% *trans*	10	11	% *cis*
1	**4***b*	CH_2OCH_3	Li	THF	80	100	0	100	0	0	0
2	**4***b*	CH_2OCH_3	Bu_4N	THF	33[d]	52	48	100	0	0	0
3	**4***c*	Si+	Li	THF	92	39	32	71	12	17	29
4	**4***c*	Si+	Li	Ether[b]	90	38.2	30.5	68.7	18.4	12.9	31.3
5	**4***c*	Si+	Li	Ether[c]	90	44	24.6	68.6	18	13.4	31.4
6	**4***c*	Si+	MgBr	Ether	95	30.1	19.7	49.8	31	19.2	50.2
—	**17**[e]	Si+	Li	THF	92	37	46	83	14	2	16

[a]Reaction to −78°C except for Expt. 5; reaction time 10 min except for Expts. 4 and 5.
[b]Reaction quenched (HCl) after 1 min.
[c]Reaction mixture allowed to warm to 20°C and stirred 2 h.
[d]62% **4***b* recovered unchanged.
[e]Reference 14.

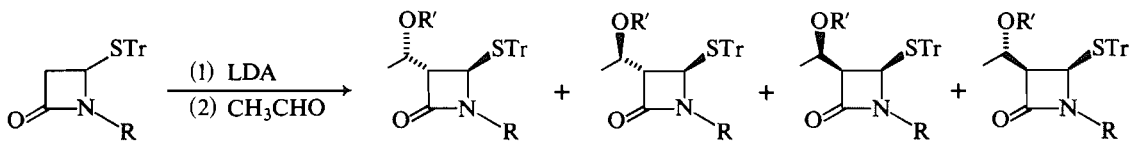

a R = R′ = H; *b* R = CH_2OCH_3, R′ = H; *c* R = $Si(CH_3)_2tC_4H_9$, R′ = H;

d R = $Si(CH_3)_2tC_4H_9$, R′ = CO_2PNB

SCHEME 2

acetaldehyde in high yields. Two types of protecting group were selected: a sterically small group, with potential metal chelating properties, the methoxymethyl group, and a sterically demanding, chemically inert, N-substituent, the *tert*-butyldimethylsilyl group.

Methoxymethylation of **4***a* was carried out by quenching the nitrogen anion (NaH, THF, MeOH) with bromomethyl methyl ether and afforded crystalline **4***b* in 91% yield. Silylation of **4***a* with *tert*-butyldimethylsilyl chloride in DMF in the presence of triethylamine provided crystalline **4***c* in 89% yield.

The protected azetidinones, **4***b* and **4***c*, were conveniently metallated in an appropriate solvent (Table 1) at −78°C by addition of a slight excess (1.1 equiv.) of preformed LDA (8). Aldol condensation to acetaldehyde was effected under what are assumed to be conditions of kinetic control (−78°C, 10 min) (9*a*). Metal interchange, when required, was achieved by adding an equivalent of anhydrous magnesium bromide (10), zinc chloride (10), or tetrabutylammonium fluoride (11) to the lithium enolate prior to addition of acetaldehyde. Reaction products were separated and purified by hplc. The stereochemical composition of the aldol products under a variety of conditions is summarized in Table 1.

Stereochemical assignments were determined from ^{1}Hmr coupling constants correlation as listed in Table 2.[4] The *cis*−*trans* relationships were readily established on the basis that for 2-azetidinones $J_{3-4}cis > J_{3-4}trans$ (12). It followed that isomers **10***c* and **11***c* with J_{3-4} = 4.5 and 4.6 Hz possessed a *cis* arrangement and **8***b*, **9***b*, **8***c*, and **9***c*, with J_{3-4} = 0.9−2.5 Hz, a *trans* geometry. Configurations at position 1′ were assigned from the observation first made by House *et al.* (10), and corroborated by others in the β-lactam area (4, 5, 13, 14) that, for aldol condensation products, J_{ab} is larger

[4]All compounds described in this paper are racemic mixtures. Structural formulae and stereochemical designations refer to the enantiomer related to natural products, thienamycin and olivanic acid.

Can. J. Chem. Downloaded from www.nrcresearchpress.com by 210.87.254.42 on 09/06/12
For personal use only.

TABLE 2. ^{1}H nuclear magnetic resonance spectra[a]

Compound	H-1′	$J_{1'-3}$	H-3	J_{3-4}	H-4	CH_3	$J_{1'-2'}$	Arom.	Others
8*b*	2.83	4.6	3.06 (dd)	2.0	4.42 (d)	1.12 (d)	6.3	7.1–7.5	4.37 (ABq, 2H), 3.17 (s, 3H), 1.35 (bs, 1H)
8*c*	2.85 (dq)	2.7	3.02 (dd)	1.8	4.32 (d)	1.02 (d)	6.0	7.1–7.6	0.95 (s, 9H), 0.25 (s, 6H)
8*d*	3.72 (dq)	1.8	3.10 (bt)	1.8	4.08 (d)	1.20 (d)	6.5	7.1–7.6 8.2 (d)	5.1 (s, 2H), 1.0 (s, 9H) 0.28 (s, 3H), 0.31 (s, 3H)
9*b*	3.65	5.5	3.3 (dd)	2.5	4.28 (d)	1.05 (d)	6.5	6.9–7.5	4.2 (2H), 3.15 (s, 3H), 1.55 (bs, 1H)
9*c*	3.15–3.55 (m)	3.7	3.32	0.9	4.02			7.2–7.6	0.87 (m, 12H), 0.12 (s, 3H), 0.10 (s, 3H)
9*d*	4.5 (b sextet)	6.0	3.58 (dd)	1.5	3.97 (d)	1.1	6.0	7.1–7.5 8.17 (d)	5.1 (s, 2H), 0.7 (s, 9H), 0.2 (s, 6H)
10*c*	2.39 (dq)	0.9	3.02 (dd)	4.5	4.70 (d)	1.0 (d)	6.5	7.2–7.5	0.97 (s, 9H), 0.36 (s, 3H), 0.34 (s, 3H)
10*d*	3.52 (dq)	0.5	2.95 (dd)	4.5	4.74 (d)	1.1	6.5	7.1–7.6 8.16 (d)	5.30 (ABq, 2H), 1.07 (s, 9H), 0.37 (s, 6H)
11*c*	3.78 (dq)	8.2	3.10 (dd)	4.6	4.30 (d)	1.22 (d)	6.3	6.8–8.0	0.95 (s, 9H), 0.22 (s, 3H), 0.17 (s, 3H)
11*d*	4.53 (b sextet)	5.8	3.32 (dd)	4.8	4.31 (d)	1.44 (d)	6.0	7.1–7.5 8.15 (d)	4.95 (ABq, 2H), 0.95 (s, 9H), 0.22 (s, 3H), 0.20 (s, 3H)

[a]Recorded at 80 MHz in $CDCl_3$ using tetramethylsilane as internal standard. Chemical shifts are in δ (ppm) and coupling constants in Hz.

for the *threo* (*trans R**, *cis S**) than for the *erythro* (*trans S**, *cis R**) isomer. Accordingly the *trans* compounds **9***b*, **9***c*, and **9***d*[5] with $J_{1'-3}$ = 5.5, 3.7, and 6.0 Hz were assigned a *R** configuration and the corresponding **8***b*, **8***c*, and **8***d*, with smaller $H_{1'}-H_3$ coupling constants (4.6, 2.7, and 2.0 Hz), a *S** arrangement. The *cis* isomers **11***c* and **11***d* with $J_{1'-3}$ = 8.2 and 5.6 Hz were given the *S**, and **10***c* and **10***d*, with 0.9 and 0.5 Hz, the *R** configuration.

It has been shown by Dubois *et al.* (15), Heathcock and co-workers (9), House *et al.* (10), and Evans *et al.* (16) that aldol stereoselection is governed by a pericyclic process involving the incoming aldehyde, the enolate anion, and the metal countercation. In this hypothesis the stereochemical control of the reaction is effected by the various steric nonbonded interactions in the pseudocyclic transition state. The capacity of the metal cation to accommodate ligands and the polarity of the solvent were also shown to exert an influence on the formation of the cyclic intermediate. Scheme 3 depicts such intermediates for the products of Table 1.

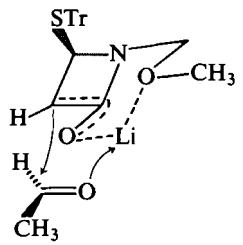

16

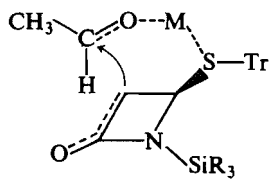

18

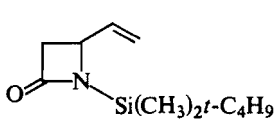

17

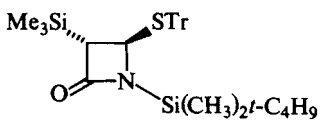

19

[5]Reaction conditions will appear in a future publication.

In the absence of sterically demanding substitution on the nitrogen atom of the azetidinone (Expts. 1 and 2, Table 1) the bulky tritylthio group at 4β directed hydroxylation exclusively to the less hindered α-face of the molecule; no *cis*-aldols were detected in the reaction mixture. The surprisingly high stereochemical control observed with the lithium enolate of **4***b* (Expt. 1), giving exclusively the *S** configuration at position 1′, likely resulted from a combination of two concurrent effects: because of the pseudo 1,3-diaxial interaction with the C-4α-proton in transition state **13**, the methyl group of the incoming aldehyde should end up principally in the equatorial position (**12**) giving the *trans S** **8***b* as the major isomer; internal lithium chelation in the enolate, **16**, prior to addition of acetaldehyde, according to an hypothesis advanced by Meyers and Reider (17) to explain the abnormal behavior of alkoxyalkyl esters in the aldol condensation, should also strongly favor exclusive formation of intermediate **12**. This high stereoselectivity was lost under conditions that do not favor formation of stable metal chelates (Expt. 2): condensation of the ammonium enolate of **4***b* to acetaldehyde was found to be much slower, giving only 33% of a 1:1 mixture of the two *trans* aldols **8***b* and **9***b* after 15 min. This clearly shows that metal chelation provides not only stereochemical control but also reduces the energy barrier to the condensation products.

In the presence of a sterically important substituent on the nitrogen atom (Expt. 3) *trans*/*cis* stereoselectivity was greatly reduced. On the one hand, one could reason that steric interference between the bulky groups at positions 1 and 4 of azetidinone **4***c* would increase the relative population of the α-face N-substituent with the consequence that the C-4α proton is no longer the only important interaction-maker at the α-face. As a result transition states **14** and **15** are not destabilized, relative to **12** and **13**, to the same extent and the proportion of *cis* product is increased accordingly (*trans*/*cis* = 7:3). On the other hand, azetidinone **17** (14), with a smaller size substituent at position 4, was reported to give a *trans*/*cis* ratio of 83:16, which indicates that the presence of a sulfur atom at position 4 of azetidinone **4***c* is partly responsible for the lowered *trans*/*cis*

Can. J. Chem. Downloaded from www.nrcresearchpress.com by 210.87.254.42 on 09/06/12
For personal use only.

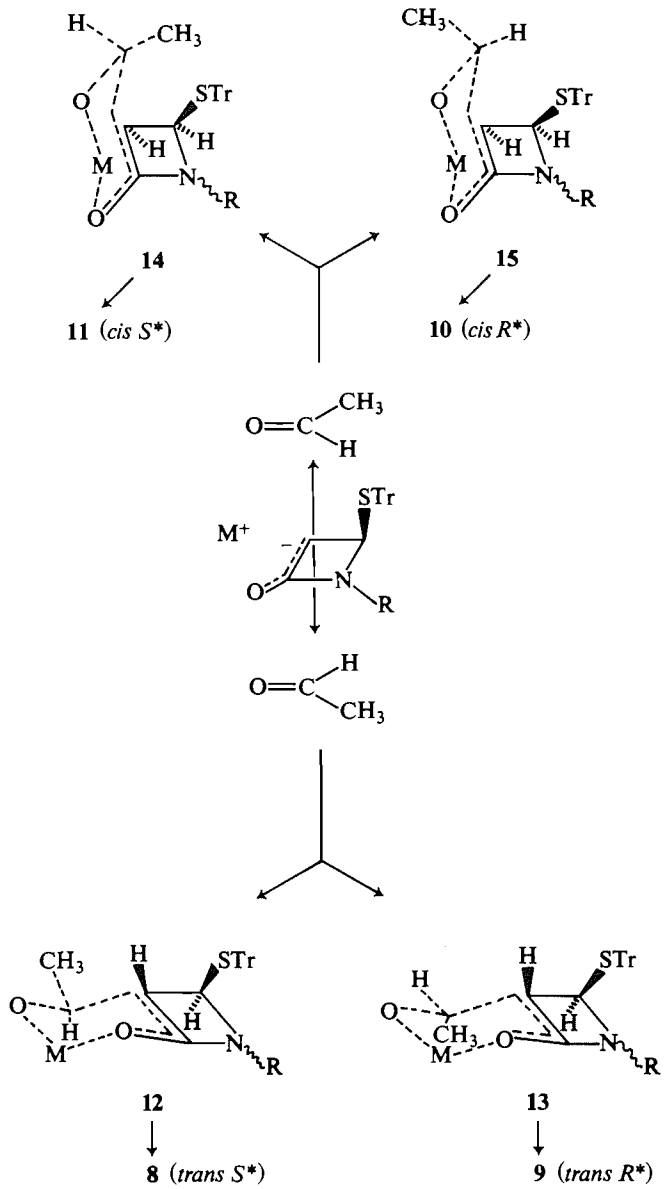

SCHEME 3

ratio observed with **4***c*. Possibly, under conditions of kinetic control, chelation to sulfur (18), as depicted in **18**, would facilitate β-face approach and favor transition to **14** and **15**. This effect was not noted with **4***b* because of the greater propensity of oxygen to chelate with metals. In such a hypothesis enhancement of the chelating properties of the cationic center would strengthen chelation to sulfur and increase the proportion of attack to the more hindered β-face; indeed replacing lithium by the divalent magnesium (19) gave a *trans*/*cis* ratio approaching unity (Expts. 4 and 6).

Little change in the *trans*/*cis* ratio was observed when THF was replaced by a less polar solvent (Expts. 3 and 4) or when the condensation was carried under conditions likely to permit thermodynamic equilibration (Expt. 5). It is interesting to note that the highly abnormal *cis R**/*cis S** < 1 ratio in THF (Expt. 3) changed, in ether (Expt. 4), to a ratio that is more in line with nonbonded interactions in **14** and **15**.

Attempts to disrupt the organized transition state from **4***c* were unsuccessful. Use of the highly dissociating solvent HMPT (9*b*) led to the discovery of a mild deprotection reaction for N-silyl protected azetidinones:[5] solution of **4***c* in HMPT (or DMF), in the presence of a nucleophile (diisopropylamine from LDA, NaN_3,...) at low temperature afforded a quantitative yield of **4***a*. Attempts to generate the ammonium enolate with tetrabutylammonium fluoride also resulted in protecting group removal (the corresponding bromide and iodide were completely insoluble in THF at −78°C and did not bring any change in the *trans*/*cis* ratio). The ammonium enolate could have possibly been obtained by treatment of the O-trimethylsilyl enol ether of **4***c* with an equivalent of tetrabutylammonium fluoride; treatment of the lithium enolate of **4***c* with trimethylsilyl chloride not unexpectedly (20, 21) afforded only the C-silylation product **19**.[6]

In summary, the stereochemistry of aldol condensation products of 4-tritylthioazetidinones with acetaldehyde varied according to the type and size of the nitrogen protecting group, with minimal effect from solvent or reaction conditions. The strength of the chelation of the metal cation, not only with the enolized carbonyl group itself but also with other electronegative groups, on the azetidinone was found to be an important factor in the stereochemical control of the reaction. The four possible isomers of **6** were obtained but neither the methoxymethyl nor the *tert*-butyldimethylsilyl protecting groups provided the "natural" isomers of **6** as major products. Stereoselective conversion of **4** to "natural" **6** will make the object of a forthcoming publication.

Experimental

Melting points were determined on a Gallenkamp melting point apparatus and are not corrected. The infrared spectra were recorded on a Perkin−Elmer 267 grating infrared spectrophotometer.

The ^1H nuclear magnetic resonance data were taken with either a Varian EM-360A (60 MHz) or a Varian CFT-20 (80 MHz) nmr spectrometer using tetramethylsilane as an internal standard. The analyses were performed by Micro-Tech Laboratories, Skokie, Illinois and Daessle Microanalysis, Montréal, Que.

Tetrahydrofuran was freshly distilled from $LiAlH_4$. Anhydrous ether (Mallinckrodt) and *n*-butyllithium in hexane (Aldrich) were used as supplied. Commercial CH_3CHO was distilled prior to use. Diisopropylamine was distilled from CaH_2 and stored over NaOH.

1-Methoxymethyl-4-tritylthio-2-azetidinone (4b)

A solution of 4-tritylthio-2-azetidinone (**4***a*) (1.38 g, 4.0 mmol) in THF (10 mL) was added to a well stirred suspension of sodium hydride (300 mg of commercial 50% oil dispersion, 4.1 mmol, washed with pentane) in THF (10 mL) maintained at −15°C (ice−methanol bath). Methanol (15 drops) was added and the mixture was stirred at −15°C for 0.5 h. Bromomethyl methyl ether (0.58 g, 4.6 mmol) was added, the mixture was stirred for 2 h, diluted with ether, washed with water and brine, dried ($MgSO_4$), and concentrated to leave an oil (1.72 g). Crystallization from pentane gave the title compound **4***b* as a white solid (1.41 g, 3.64 mmol, yield: 91%), mp 72−76°C; ir (CH_2Cl_2) ν_{max}: 1765 (β-lactam C=O) cm^{-1}; ^1Hmr ($CDCl_3$) δ: 7.4−7.2 (15H, m, aromatic H), 4.6−4.37 (H-4), 4.43 (2H, center of ABq, CH_2), 3.25 (3H, s, CH_3), 2.93 (1H, dd, J = 15.4, J = 4.1, H-3), 2.68 (1H, dd, J = 15.4, J = 3.4, H-3). *Anal.* calcd. for $C_{24}H_{23}NO_2S$: C 74.00, H 5.95, N 3.59, S 8.23; found: C 73.97, H 6.02, N 3.74, S 8.20.

*1-(*tert*-Butyldimethylsilyl)-4-tritylthio-2-azetidinone (4c)*

Triethylamine (1.62 mL, 11.6 mmol) was added dropwise in 5 min to a cooled (ice bath) solution of 4-tritylthio-2-azetidinone (**4***a*) (3.50 g, 10.1 mmol) and *tert*-butyldimethylsilyl chloride (1.68 g,

[6]Use of **19** as starting material for new C-3 substituted azetidinones will make the object of a subsequent paper.

Can. J. Chem. Downloaded from www.nrcresearchpress.com by 210.87.254.42 on 09/06/12
For personal use only.

TABLE 3. Analytical data for **8***c*, **9***c*, **10***c*, **11***c*

Compound	Melting point, 0°C	Infrared ($CHCl_3$) ν_{max}, cm^{-1} OH	C=O	*Anal.* for $C_{30}H_{37}NO_2SSi$ Calcd.	Found
8*c*	134–136	3580 (w) 3560–3200 (m)	1735 (s)	C 71.52 H 7.40 N 2.78 S 6.36	71.30 7.41 2.55 6.30
9*c*	158–159	3560 (m) 3500–3300 (w)	1745 (s)	C Idem H Idem N Idem S Idem	71.50 7.51 2.60 6.46
10*c*	171–172	3540–3300 (m)	1745 (s)	C Idem H Idem N Idem S Idem	71.27 7.43 2.51 6.31
11*c*	152–153	3550 (m) 3500–3300 (w)	1735 (s)	C Idem H Idem N Idem S Idem	71.28 7.41 2.48 6.19

12.7 mmol) in DMF (35 mL). The reaction mixture was stirred at room temperature for 18 h, diluted with water (250 mL) and ether (200 mL), the organic phase washed with water (3 × 50 mL), dried, and concentrated to leave an oil (4.33 g). Crystallization from pentane gave the title compound **4***c* as a white solid (4.1 g, 8.9 mmol, yield: 89%), mp 113–114°C; ir (CH_2Cl_2) ν_{max}: 1735 (β-laetam C=O) cm^{-1}; ^{1}Hmr ($CDCl_3$) δ: 7.8–7.2 (15H, m, aromatic H), 4.2 (1H, dd, J = 4, J = 2, H-4), 2.63 (1H, dd, J = 16, J = 4, H-3), 2.13 (1H, dd, J = 16, J = 2, H-3), 1.0 (9H, s, *t*-Bu), 0.35 (6H, s, CH_3). *Anal.* calcd. for $C_{28}H_{33}NOSSi$: C 73.15, H 7.24, N 3.05, S 6.97; found: C 73.27, H 7.32, N 2.97, S 6.94.

trans S* *3-(1'-hydroxyethyl)-1-methoxymethyl-4-tritylthio-2-azetidinone* (*8*b)

A solution of lithium diisopropylamide was prepared in THF (5 mL) at low temperature (Dry Ice – acetone bath) from *n*-butyllithium (1.0 mL, 1.6 *M* in hexane, 1.6 mmol) and diisopropylamine (0.25 mL, 1.84 mmol). After 30 min a solution of 1-methoxymethyl-4-tritylthio-2-azetidinone (**4***b*) (421 mg, 1.42 mmol) in THF (6 mL) was added dropwise and the solution was stirred for 15 min. Acetaldehyde (3 mL) ws added dropwise followed, after 20 min, by water (30 mL). The mixture was acidified to pH 3 with 2% aqueous HCl and extracted with ethyl acetate (5 × 20 mL). The combined organic phases were washed with brine, dried, and concentrated to leave an oil which crystallized upon trituration with ether (440 mg, 1.01 mmol, yield: 80%) mp 188.5–189°C; ir (CH_2Cl_2) ν_{max}: 3610 (m, OH), 1755 (s, β-lactam C=O) cm^{-1}. *Anal.* calcd. for $C_{26}H_{27}NO_3S$: C 72.02, H 6.28, N 3.23, S 7.39; found: C 71.94, H 6.02, N 3.21, S 7.40.

trans S* *and* R* *3-(1'-hydroxyethyl)-1-methoxymethyl-4-tritylthio-2-azetidinones* (*8*b *and* *9*b)

A solution of lithium diisopropylamide (0.482 mmol) was prepared at −78°C (Dry Ice – acetone bath) in dry ether (3 mL) from *n*-butyllithium (0.101 mL, 2.52 *M* in hexane, 0.482 mmol) and diisopropylamine (0.067 mL, 0.482 mmol). After 20 min, a solution of azetidinone **4***b* (0.171 g, 0.439 mmol) in a mixture of dry ether (1 mL) and THF (1 mL) was added dropwise and the resulting clear solution was stirred at −78°C for 15 min. A solution of tetrabutylammonium fluoride (0.96 mL of a 0.5 *M* solution in THF, 0.48 mmol) was then added. A precipitate was formed with the generation of a slight pink colour. After 5 min at −78°C, the reaction mixture was quenched with acetaldehyde (0.2 mL, excess), and the stirring continued for 15 more min. A saturated solution of NH_4Cl was added and the mixture was extracted with ethyl acetate (2 × 25 mL). The combined organic phases were washed with brine and dried ($MgSO_4$) and concentrated to leave an oil (228 mg). This was chromatographed on silica gel (10 g), using a mixture of benzene and ethyl acetate (6:4) to give back substrate (**4***b*) (106 mg, 62% recovery) and a mixture of two isomeric alcohols which were separated by chromatography on thick layer plates (same solvent system). The alcohol with high R_f (33 mg, 0.076 mmol, yield: 17%) was identical to **8***b*, mp 188.5–189.5°C. The alcohol with low R_f (30 mg, 0.069 mmol, yield: 16%) was obtained as an oil which crystallized with difficulty (hexane), mp 94–95°C; ir (CH_2Cl_2) ν_{max}: 3600 (m, OH), 1760 β-lactam C=O) cm^{-1}. *Anal.* calcd. for $C_{26}H_{27}NO_3S$: C 72.02, H 6.28, N 3.23, S 7.39; found: C 71.77, H 6.36, N 3.15, S 7.43.

trans S* *and* R* *and* cis R* *and* S* *1-(*tert*-*butyldimethylsilyl)-3-(1'-hydroxyethyl)-4-tritylthio-2-azetidinone* (*8*c, *9*c, *10*c, *11*c)

1. *In THF*

To a solution of diisopropylamine (15.0 mL, 10.8 g, 0.107 mmol) in THF (450 mL) maintained at −78°C was added dropwise *n*-butyllithium (42.0 mL, 2.22 *M* in hexane, 0.093 mmol). The mixture was stirred for 30 min and a solution of **4***c* (30.0 g, 65.4 mmol) in THF (250 mL) was added slowly. After 15 min stirring, acetaldehyde (35 mL, excess) was added in one portion. The reaction mixture was allowed to react 15 more min, poured on saturated aqueous NH_4Cl solution (1 L), and acidified to pH 2 with 10% aqueous HCl. The aqueous phase was extracted with ethyl acetate (3 × 500 mL). The organic phases were combined, washed with brine (1 × 500 mL), dried (Na_2SO_4), and concentrated to leave an oil which was found to consist of a mixture of 4 isomers with respective R_f on silica gel MO6F (benzene/ether, 3:1): **8***c*, 0.4; **9***c*, 0.3; **10***c*, 0.5; **11***c*, 0.22. The isomeric ratio was determined on a Waters Associates Prepak-500-Silica column (see Table 1). The same reaction was repeated on **4***c* (294 g, 0.640 mol). Crystallization of the oily residue in petroleum ether 30–60°C after work-up gave a mixture of isomers **8***c* and **9***c* as a white solid. The mother liquor was found to contain mainly isomers **10***c* and **11***c*. All four isomers were then separated by hplc to give title compounds (296.8 g, 0.589 mol) in 92% combined yield.

2. *In ether*

n-Butyllithium (15.6 mL, 1.6 *M* in hexane, 25 mmol) was added dropwise to a solution of diisopropylamine (4.0 mL, 28 mmol) in ether (150 mL) maintained at −78°C (Dry Ice – acetone bath). After 0.5 h a solution of **4***c* (9.2 g, 20 mmol) in ether (100 mL) was added dropwise; after 15 min acetaldehyde (30 mL) was added in one portion. After 1 min an aliquot (10 mL) was quenched with saturated aqueous NH_4Cl and worked up according to the above procedure (see Table 1 for the isomeric ratio). Another aliquot (10 mL) was allowed to warm up to 20°C, stirred for a 2 h period, worked up, and the isomeric ratio determined by hplc (see Table 1).

Can. J. Chem. Downloaded from www.nrcresearchpress.com by 210.87.254.42 on 09/06/12
For personal use only.

Can. J. Chem. Downloaded from www.nrcresearchpress.com by 210.87.254.42 on 09/06/12
For personal use only.

3. *With the magnesium enolate*

A solution of LDA prepared at −20°C (Dry Ice − CCl_4) from *n*-butyllithium (0.22 mL, 2.52 *M* in hexane, 0.55 mmol) and diisopropylamine (0.077 mL, 0.055 mmol) in THF (3 mL) was stirred for 15 min and cooled at −78°C. It was treated with 1-(*tert*-butyldimethylsilyl)-4-tritylthio-2-azetidinone (230 mg, 0.50 mmol). After 15 min stirring at −78°C the solution was treated dropwise with a solution of $MgBr_2$ in ether (0.224 mL, 2.45 *M*, 0.55 mmol). A precipitate was formed and the mixture was warmed in a CCl_4 − Dry Ice bath for 1 min to solubilize the solid. The clear solution was cooled again (Dry Ice − acetone bath) and acetaldehyde (0.2 mL) was added in one portion. The mixture was stirred for 15 min and worked up as above (see Table 1 for the proportion of isomers).

trans-*1-(*tert-*Butyldimethylsilyl)-3-trimethylsilyl-4-tritylthio-2-azetidinone (**19**)*

A solution of lithium diisopropylamide (25.6 mmol) was prepared at −78°C in THF (120 mL) from diisopropylamine (3.58 mL, 25.6 mmol) and *n*-butyllithium (10.1 mL, 2.52 *M* in hexane, 25.6 mmol). After 30 min at −78°C, a solution of 1-(*tert*-butyldimethylsilyl)-3-tritylthio-2-azetidinone (11.2 g, 24.4 mmol) in THF (25 mL) was added dropwise, followed after 10 min by a solution of trimethylsilyl chloride (2.78 g, 25.6 mmol) in THF (5 mL) containing a few drops (2−3) of triethylamine. After 10 min at −78°C, the clear mixture was poured onto a solution of saturated ammonium chloride (200 mL) and extracted with ethyl acetate (3 × 100 mL). The combined organic extracts were washed with brine, dried ($MgSO_4$), and concentrated to leave a white solid which was recrystallized from a mixture dichloromethane−hexanes to give white cubes (11.7 g, 22.0 mmol, yield: 90%), mp 157−158°C; ir (KBr disk) ν_{max}: 1742 (s, β-lactam C=O), 840 (C—Si) cm^{-1}; ^{1}Hmr ($CDCl_3$) δ: 7.9−7.3 (m, 15H, aromatics), 3.84 (d, 1H, *J* = 1.7, H-4), 3.21 (d, 1H, *J* = 1.7, H-3), 0.88 (s, 9H, *t*-Bu), 0.04 and −0.06 (2s, 2 × 3H, $Si(CH_3)_2$), −0.20 (s, 9H, $Si(CH_3)_3$). *Anal.* calcd. for $C_{31}H_{41}NOSSi_2$: C 70.00, H 7.77, N 2.63, S 6.03; found: C 70.25, H 7.91, N 2.65, S 6.10.

Acknowledgements

We would like to thank Drs. Y. Ueda and E. Ruediger for helpful discussions during the preparation of this manuscript. We also thank Messrs. G. Lacasse and P. Rivest for 80 MHz ^{1}Hmr spectra during the course of this work.

1. G. Albers-Schönberg, B. H. Arison, O. D. Hensens, J. D. Hirshfield, K. Hoogsteen, E. A. Kaczka, R. E. Rhodes, J. S. Kahan, F. M. Kahan, R. W. Ratcliffe, E. Walton, L. J. Ruswinkle, R. B. Morin, and B. G. Christensen. J. Am. Chem. Soc. **100**, 6491 (1978).
2. (*a*) A. G. Brown, D. F. Corbett, A. J. Eglington, and T. T. Howarth. Chem. Commun. 523 (1977); (*b*) D. F. Corbett, A. J. Eglinton, and T. T. Howarth. Chem. Commun. 954 (1977); (*c*) A. G. Brown, D. F. Corbett, A. J. Eglington, and T. T. Howarth. J. Antiobiot. **32**, 961 (1979).
3. R. D. G. Cooper. *In* Topics in antibiotics chemistry. Vol. 3, *Edited by* P. G. Sammes. Ellis Horwood Ltd., Chichester. 1980. p. 101.
4. H. R. Pfaendler, J. Gosteli, and R. B. Woodward. J. Am. Chem. Soc. **102**, 2039 (1980).
5. (*a*) V. M. Girijavallabhan, A. K. Ganguly, S. W. McCombie, P. Pinto, and R. Rizvi. Tetrahedron Lett. 3485 (1981); (*b*) S. W. McCombie, A. K. Ganguly, V. M. Girijavallabhan, P. D. Jeffrey, S. Lin, and P. Pinto. Tetrahedron Lett. 3489 (1981); (*c*) A. Yoshida, T. Hayashi, N. Takeda, S. Oida, and I. Ohki. Chem. Pharm. Bull. **29**, 2899 (1981); (*d*) T. Hayashi, A. Yoshida, N. Takeda, S. Oida, S. Sugawara, and E. Ohki. Chem. Pharm. Bull. **29**, 3158 (1981).
6. (*a*) Y. Ueda, A. Martel, J. P. Daris, B. Belleau, and M. Ménard. Can. J. Chem. **60**, 904 (1982); (*b*) A. Martel, P. Dextrase, J. P. Daris, R. Saintonge, P. Lapointe, T. T. Conway, I. Monkovic, G. Kavadias, Y. Ueda, P. Elie, S. Patil, G. Caron, J. L. Douglas, M. Ménard, and B. Belleau. Can. J. Chem. **60**, 942 (1982).
7. T. Durst, R. Van Den Elgen, and R. Legault. Can. J. Chem. **52**, 3206 (1974).
8. T. Durst and M. J. LeBelle. Can. J. Chem. **50**, 3196 (1972).
9. (*a*) W. A. Kleschick, C. T. Buse, and C. H. Heathcock. J. Am. Chem. Soc. **99**, 247 (1977); (*b*) C. H. Heathcock, C. T. Buse, W. A. Kleschick, M. C. Pirrung, J. E. Sohn, and J. Lampe. J. Org. Chem. **45**, 1066 (1980).
10. H. O. House, D. S. Crumrine, A. Y. Teranishi, and H. D. Olmstead. J. Am. Chem. Soc. **95**, 3310 (1973).
11. (*a*) I. Kuwajima and E. Nakamura. J. Am. Chem. Soc. **97**, 3257 (1975); (*b*) R. Noyori, K. Yokoyama, J. Sakata, I. Kuwajima, E. Nakamura, and M. Shimizu. J. Am. Chem. Soc. **99**, 1265 (1977).
12. P. V. Demarco and R. Nagarajan. Cephalosporins and penicillins: chemistry and biology. *Edited by* E. H. Flynn. Academic Press, New York. 1972. pp. 330−340.
13. F. DiNinno, T. R. Beattie,and B. G. Christensen. J. Org. Chem. **42**, 2960 (1977).
14. F. A. Bouffard and B. G. Christensen. J. Org. Chem. **46**, 2208 (1981).
15. (*a*) J. E. Dubois and M. Dubois. Tetrahedron Lett. 4215 (1967); (*b*) J. E. Dubois and P. Fellmann. C.R. Acad. Sci. Ser. C., **274**, 1307 (1972); (*c*) J. E. Dubois and P. Fellmann. Tetrahedron Lett. 1225 (1975); (*d*) P. Fellmann and J. E. Dubois. Tetrahedron, **34**, 1349 (1978).
16. D. A. Evans, E. Vogel, and J. V. Nelson. J. Am. Chem. Soc. **101**, 6120 (1979).
17. A. I. Meyers and P. J. Reider. J. Am. Chem. Soc. **101**, 2501 (1979).
18. J. A. Aimetti and M. S. Kellogg. Tetrahedron Lett. 3805 (1979).
19. F. A. Cotton and G. Wilkinson. Advanced inorganic chemistry. 4th ed. Interscience, New York. 1980. Chapts. 4 and 8.
20. K. Kühlein and H. Jensen. Justus Liebigs Ann. Chem. 369 (1974).
21. S. Kano, T. Ebata, K. Funaki, and S. Shibuya. Synthesis, 746 (1978).

Carbonyl ylides and carbenes from thermolysis of oxadiazolines. Substituent effects on intramolecular and intermolecular reactions of carbonyl ylides

MICHEL BÉKHAZI AND JOHN WARKENTIN[1,2]

Department of Chemistry, McMaster University, Hamilton, Ont., Canada L8S 4M1

Received June 23, 1982

MICHEL BÉKHAZI and JOHN WARKENTIN. Can. J. Chem. **61**, 619 (1983).

Thermolysis of a 2-methoxy-Δ^3-1,3,4-oxadiazoline involves loss of N_2 with formation of a carbonyl ylide. The fate of the carbonyl ylide depends on its environment and on the other substituents present. Thus, the ylides from 2-methoxy-2,5,5-trimethyl-Δ^3-1,3,4-oxadiazoline (**1**) and from 2-methoxy-2-(4-methoxyphenyl)-5,5-dimethyl-Δ^3-1,3,4-oxadiazoline (**2**) are trapped very efficiently by methanol. However, the ylide from **1** is trapped much less efficiently than that from **2** by dimethylacetylene dicarboxylate, *cis*-1,2-dichloroethylene, or norbornadiene. A major competitive process in the case of **1** is fragmentation of the ylide to carbonyl compounds and carbenes, the latter being trapped by alkenes to form cyclopropanes. An intramolecular 1,4-H transfer is also competitive under some conditions. The ylide from **2** does not appear to fragment, nor does it undergo the 1,4-H transfer, but it cyclizes efficiently to the oxirane in the absence of trapping agents.

Preliminary estimates of rate constants for cyclization of the ylide from **2** to form the oxirane ($k_{cycl}^{31°C} = 1.3 \times 10^6\ s^{-1}$) and for its additions to norbornadiene and to dimethylacetylene dicarboxylate ($1 \times 10^5\ M^{-1}\ s^{-1}$ and $1 \times 10^9\ M^{-1}\ s^{-1}$, respectively) are reported. If it is assumed that the ylide from **1** would add to dimethylacetylene dicarboxylate with a similar rate constant, then the yield for that process can be used to place a lower limit of $10^{10}\ s^{-1}$ on the rate constant for fragmentation of that ylide at 31°C.

MICHEL BÉKHAZI et JOHN WARKENTIN. Can. J. Chem. **61**, 619 (1983).

La thermolyse de la méthoxy-2 Δ^3-oxadiazoline-1,3,4 fait intervenir une perte de N_2 avec formation d'un ylure de carbonyle. Le sort de l'ylure de carbonyle dépend de son environnement et des autres substituants présents. Ainsi, à l'aide du méthanol, on peut piéger très efficacement les ylures provenant de la méthoxy-2 triméthyl-2,5,5 Δ^3-oxadiazoline-1,3,4 (**1**) et de la méthoxy-2 (méthoxy-4 phényl)-2 diméthyl-5,5 Δ^3-oxadiazoline-1,3,4 (**2**). Cependant on piège moins efficacement l'ylure issu du composé **1** que celui provenant du composé **2** lorsqu'on utilise comme piège les composés suivants: l'acétylènedicarboxylate de diméthyle, le dichloro-1,2 éthylène-*cis* ou le norbonène. Un processus compétitif important dans le cas du composé **1** est la fragmentation de l'ylure de carbonyle en composés carbonylés et en carbènes; ces derniers, piégés par les alcènes, conduisent aux cyclopropanes. Dans certaines conditions, un transfert intramoléculaire-1,4 d'hydrogène entre également en compétition. L'ylure provenant du composé **2** ne semble ni se fragmenter ni subir de transfert-1,4 d'hydrogène; toutefois, en l'absence de pièges, il se cyclise d'une manière efficace pour former un oxiranne.

On rapporte les évaluations préliminaires des constantes de vitesse de cyclisation de l'ylure provenant du composé **2** pour donner l'oxiranne ($k_{cycl}^{31°C} = 1,3 \times 10^6\ s^{-1}$ et pour ses additions sur le norbornadiène et sur l'acétylène dicarboxylate de diméthyle ($1 \times 10^5\ M^{-1}\ s^{-1}$ et $1 \times 10^9\ M^{-1}\ s^{-1}$ respectivement). On pense que l'ylure provenant du composé **1** peut s'additionner sur l'acétylènedicarboxylate de diméthyle avec une constante de vitesse identique; le rendement de ce processus peut alors être utilisé pour définir une limite inférieure de $10^{10}\ s^{-1}$ pour la constante de vitesse de fragmentation de cet ylure à 31°C.

[Traduit par le journal]

Introduction

The formation of carbonyl ylides from photochemical or thermal decomposition of Δ^3-1,3,4-oxadiazolines is now well established, eq. [1] (1–5). Although some of the chemistry of

[1] 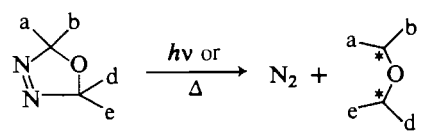

carbonyl ylides has been elucidated, including some intermolecular reactions (eqs. [2] and [3]) (1–4) and some intramolecular reactions (eqs. [4]–[6], refs. 2, 3, 6–11), very little is known about the relationships between substituents and the preferred reaction pathway.

[2] 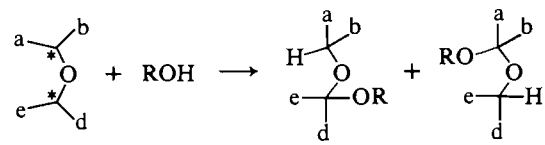

[3] 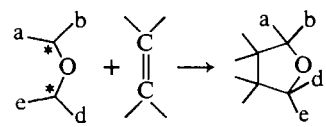

[4] 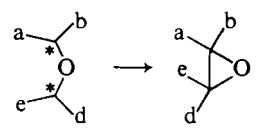

[5] 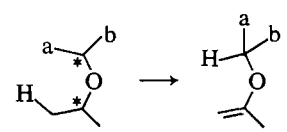

[1] Author to whom correspondence should be addressed.

[2] For a preliminary account of part of this work, see ref. 2.

Can. J. Chem. Downloaded from www.nrcresearchpress.com by 210.87.254.40 on 09/06/12
For personal use only.

Can. J. Chem. Downloaded from www.nrcresearchpress.com by 210.87.254.40 on 09/06/12
For personal use only.

[6] 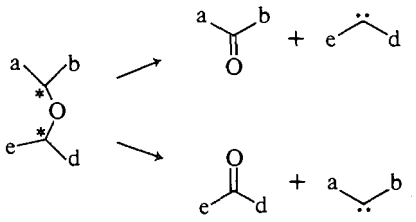

We wish to report a comparison of the fates of the alkoxy-substituted carbonyl ylides derived from **1** and **2**. These have the potential to react, not only in accordance with eqs. [2]–[5], which are available to most carbonyl ylides, but also in accordance with eq. [6]. Fragmentation (eq. [6]) appears to require, at one reactive site of the ylide, a substituent, such as amino or alkoxy, capable of conjugative donation of electron density (2, 12).

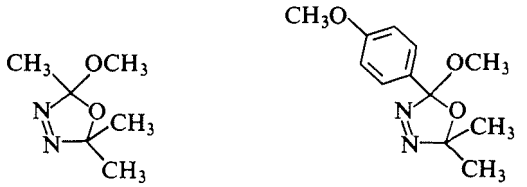

1 **2**

Results and discussion

Oxadiazolines **1** and **2** were prepared by oxidation of appropriate acylhydrazones of acetone with lead tetraacetate in methanol, eq. [7].

[7] $(CH_3)_2C{=}NNHCOR + Pb(OAc)_4 \xrightarrow{CH_3OH}$ 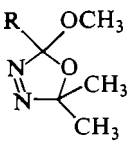

1, R = CH_3
2, R = p-$C_6H_4OCH_3$

*Thermolysis of **1** in methanol-d_4 and in methanol*

Decomposition of **1** in CD_3OD was monitored by ^1H nmr spectroscopy. The reaction was first order with $k^{79.5°C}_{CD_3OD} = 5.3 \times 10^{-6}$ s^{-1} and afforded a mixture of **3** and **4**, eq. [8], in the ratio **3**/**4** ≃ 3:7 (2).

[8] 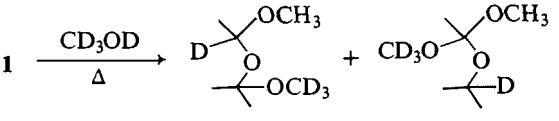

3 **4**

Acetone and methylacetate were not obtained and partial fragmentation of the ylide intermediate is therefore ruled out. Thermolysis of **1** in methanol, followed by addition of dilute aqueous HCl, resulted in partial hydrolysis of the products of thermolysis. Acetone, 1,1-dimethoxyethane, methyl acetate, and 2-propanol were found but 2-methoxypropane was not detected. This result is compatible with formation of ^1H analogues of **3** and **4** and it also rules out the intermediacy of 2-propylidene (dimethylcarbene) which would be expected to attack methanol by "insertion" into the OH bond (13–20), eq. [9].

[9] $(CH_3)_2C{:} + CH_3OH \longrightarrow (CH_3)_2CHOCH_3$

Analogous results were obtained when **2** was decomposed in methanol-d_4 at 79.5°C. The absence of acetone, methyl p-methoxybenzoate, and oxirane indicated that trapping of the carbonyl ylide intermediate was complete.

Thermolysis of **1** and **2** was also carried out in neat alkenes and in dimethylacetylene dicarboxylate (**5**) in order to compare the efficiencies of trapping of the corresponding ylides. The ylide from **2** was trapped quantitatively in the neat dipolarophile **5** at 79.5°C (eq. [10]) with formation of the dihydrofuran derivative **6**.

[10] 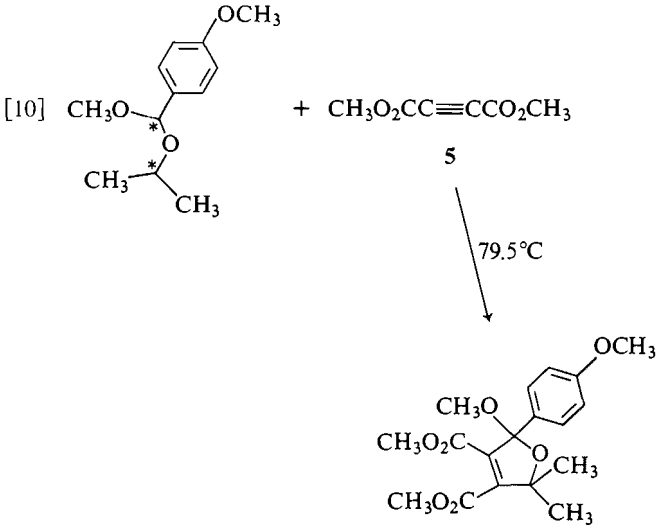

5 **6**

When neat norbornadiene was employed as a dipolarophile nearly half of the ylide derived from **2** was intercepted to form **7**, although the major product was the oxirane **8** formed by cyclization of the ylide, eq. [11].

[11] 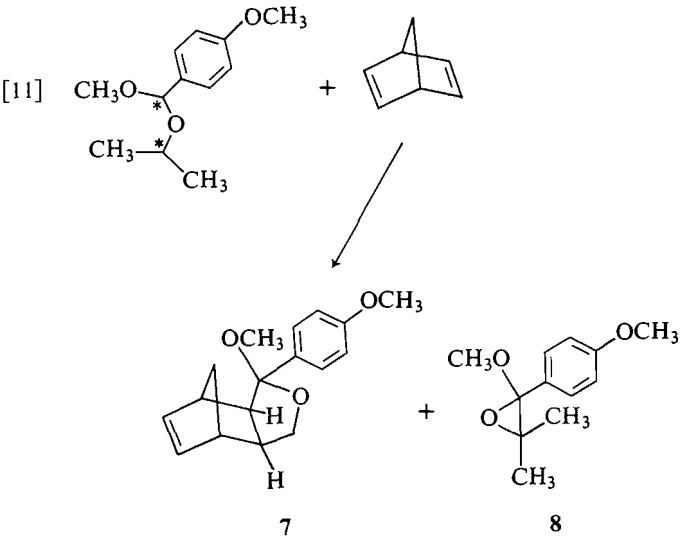

7 **8**

Can. J. Chem. Downloaded from www.nrcresearchpress.com by 210.87.254.40 on 09/06/12
For personal use only.

Estimates of the rate constants for the cycloadditions, and for ring closure to oxirane, were made as follows. The oxadiazoline **2** was subjected to laser flash photolysis[3] in benzene and the decay of the ylide intermediate was followed by monitoring the uv absorption after the flash. Decay followed 1st order kinetics with $k_{benzene}^{31°C} = 1.3 \times 10^6\ s^{-1}$. Since thermolysis of **2** in benzene at 79.5°C leads to oxirane in high yield, the measured rate constant must be that for cyclization. An estimate of the second order rate constant for trapping the ylide by norbornadiene at 31°C could then be made by assuming that the ratio **7**/**8** = 4:5 is independent of temperature in the range from 79.5°C to 31°C and by using 9.4 *M* for the concentration of neat diene.[4] This rough procedure gave $k_{diene}^{31°C} \simeq 1.1 \times 10^5\ M^{-1}\ s^{-1}$. Direct measurement of the rate constant for trapping of the same ylide by **5** in acetonitrile using laser flash spectroscopy[3] gave $k_5^{31°C} = 1.0 \times 10^9\ M^{-1}\ s^{-1}$. It follows that **5** is an excellent trap for ylides; at a concentration as low as $1.2 \times 10^{-3}\ M$ it would capture 50% of that ylide and permit 50% to excape by cyclization to oxirane, provided that the rate constants are not highly solvent dependent. Norbornadiene, which is a very reactive olefin, is about 4 orders of magnitude slower than **5** in this role.

Despite the high reactivity of **5**, complete trapping of the ylide derived from **1** could not be achieved with this dipolarophile. In neat **5**, only about 27% of the ylide generated from **1** was trapped as the cycloadduct **9** at 79.5°C (eq. [12]). The remaining ylide was partitioned among the intramolecular processes described in eqs. [4]–[6]. Those reactions must

[12] 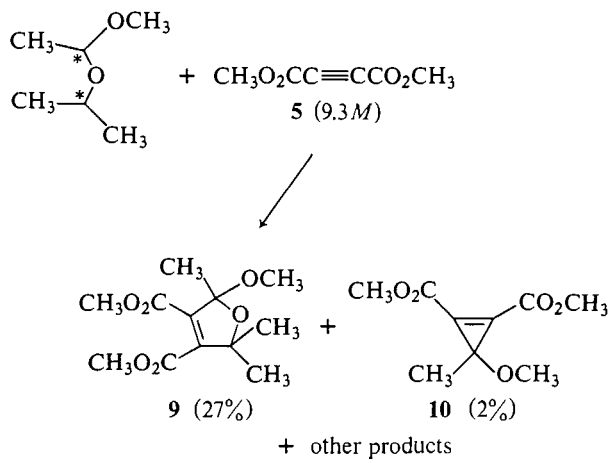

therefore be extremely fast. If cycloaddition of the ylide (eq. [12]) has a rate constant $\geq 10^9\ M^{-1}\ s^{-1}$ at 79.5°C,[5] then the yield (27%, eq. [12]) implies that the competing unimolecular processes have rate constants of the order of $10^{10}\ s^{-1}$ at 79.5°C.[6] Therefore trapping of an alkoxy trialkyl carbonyl ylide, like that from **1**, is not expected to be efficient unless the trapping agent is a very reactive species, such as **5** or triplet oxygen, present in high concentration.

Neat norbornadiene, for example, did not intercept the ylide derived from **1**, nor did tetramethylethylene or 2-methoxypropene. *cis*-1,2-Dichloroethylene (neat) proved effective in trapping about 20% of the ylide from **1**, indicating that its reactivity rivals that of **5**. These results are in qualitative accord with previously reported effects of dipolarophile substituents on the rates of 1,3-cycloadditions (22, 23). Electron-withdrawing substituents enhance an alkene's reactivity toward a dipole of the HOMO type (22, 23).

The products of ylide trapping by *cis*-1,2-dichloroethylene are shown in eq. [13]. Assignment of gross structure is based on their mass spectra and on their ^{1}H nmr spectra (Experimental section). The isomer with a two-proton singlet at δ4.30 was

[13] 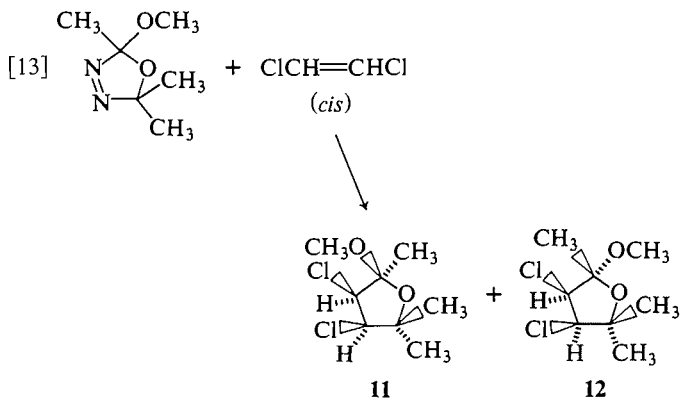

assigned structure **11**, in which the chemical shifts of the two methine hydrogens are coincidentally identical. The isomer with an AB quartet at δ4.33 and δ4.75 was assigned structure **12** because the different magnetic environments of the methine hydrogens are reasonably attributed to the *cis* methoxy group. A small coupling constant (4.9 Hz) between those hydrogens, together with evidence for the concerted character of 1,3-cycloadditions (24), was used to assign *cis*-dichloro stereochemistry to **12**. The same *cis*-stereochemistry was assigned to **11**, partly on the basis of mechanism (24) and partly on the basis of the magnetic equivalence of the methine hydrogens. If those were in a *trans* relationship, one would have to be *cis* to the methoxy group, making magnetic equivalence less likely.

An interesting conclusion can be drawn from the above estimates of rate constants for the unimolecular reactions of the ylide derived from **1**. Even if that ylide had 100% diradical character it should not be capable of atom abstraction, during its lifetime, from many substrates which are susceptible to attack by radicals. For example, abstraction of Cl from CCl_4, which has a second order rate constant of the order of $10^6\ M^{-1}\ s^{-1}$ at 80°C,[7] is probably too slow by several orders of magnitude in neat CCl_4 (ca. 10 *M*) to compete effectively with fragmentation and 1,4-H transfer.

The products formed on thermolysis of **1** in CCl_4 at 79.5°C are shown in Scheme 1, which also depicts the possible origins. Although some of the routes are speculative at this time, they are based largely on precedents such as radical pair formation

[3] We are grateful to Dr. J. C. Scaiano for running these preliminary experiments for us. A description of the apparatus can be found in ref. 21.

[4] $4(1.3 \times 10^6)[ylide] = 5\ k_{diene}[ylide] \times 9.3$ leads to $k_{diene}^{31°C} = 1.1 \times 10^5\ M^{-1}\ s^{-1}$. The assumption that the first and second order rate constants have the same temperature coefficient should not lead to serious error for a 50° change.

[5] The rate constant for trapping of the ylide from **2** with **5** is $10^9\ M^{-1}\ s^{-1}$ at 31°C (see above). That for trapping of the ylide from **1** with **5** should be at least as large at 79.5°C.

[6] $k_{unimol} \simeq \dfrac{10^9 \times 9.3 \times 73}{27} = 2.5 \times 10^{10}\ s^{-1}$.

[7] The rate constant for abstraction of Cl from CCl_4 by cyclohexyl radical is $5.5 \times 10^5\ M^{-1}\ s^{-1}$ at 80°C (25) and it should represent an upper limit for the rate constant for abstraction by the ylide from **1**, which has "tertiary" radical sites.

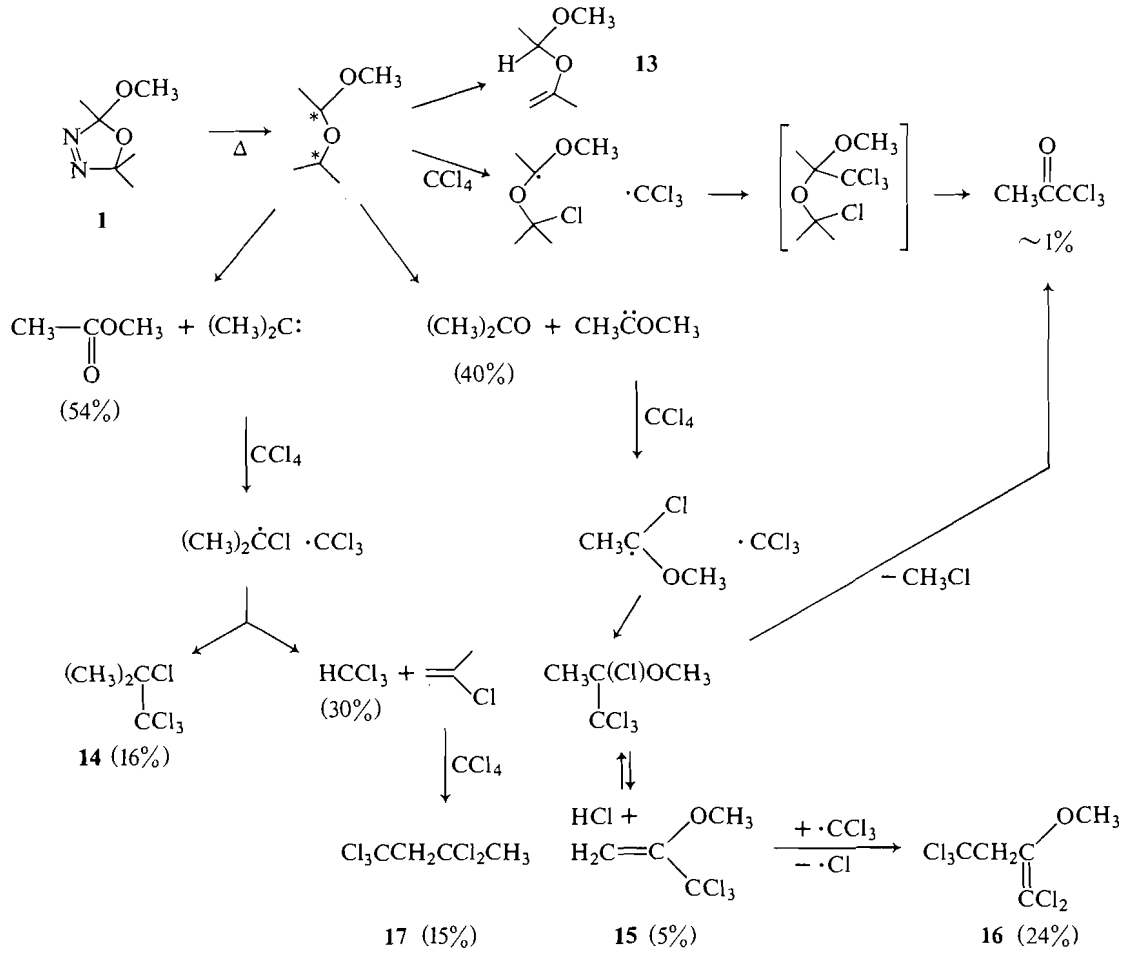

SCHEME 1

from reaction of singlet carbenes with CCl_4 (26, 27) or with hydrocarbons (28), radical pair disproportionation, ionization of α-halo ethers, and radical chain addition of CCl_4 to olefins. An exception is 1,1,1-trichloroacetone which may have arisen via unprecedented Cl-abstraction by the carbonyl ylide. That process should be slow on the time scale by which the ylide lives, as argued above, and the yield (ca. 1%) is in line with expectation.[8] Products **16** and **17**, which remained to be identified at the time of publication of our preliminary communication (2), look very much like materials derived from radical reactions of CCl_4 with alkene precursors and the route to **17** accounts nicely, in part, for the chloroform that is observed.

Additional evidence (other than that provided in Scheme 1) for the intermediacy of carbenes came from attempts to trap the ylide from **1** with alkenes. Tetramethylethylene and 2-methoxypropene failed to intercept any ylide from **1**, but gave, instead, the cyclopropanes of eq. [14] and [15]. Decomposition

[14] **1** + $(CH_3)_2C{=}C(CH_3)_2$ →

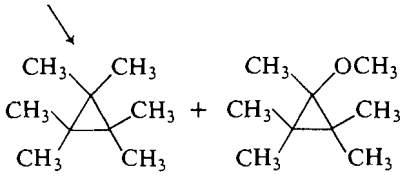

[15] **1** + $CH_2{=}C(OCH_3)CH_3$ →

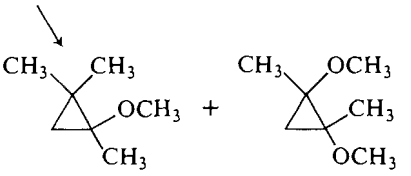

of **1** in neat **5** gave, in addition to the cycloadduct from ylide trapping, a trace of a compound tentatively identified as 1,2-dicarbomethoxy-3-methoxy-3-methylcyclopropene (**10**), eq. [12]; ^1H nmr δ: 1.30 (s, 3H), 3.71 (s, 3H), 3.86 (s, 6H); ms *m/z* (fragment, %): 185 ($C_8H_9O_5$, 16), 169 ($C_8H_9O_4$, 24), 111 ($C_5H_3O_3$, 100), 83 ($C_4H_3O_2$, 12), 59 ($C_2H_3O_2$, 80). These observations tend to support the postulate of Scheme 1, that free carbenes are involved, although alternative explanations may be possible.

A complete explanation of the substituent effects on intra- and intermolecular reactions of carbonyl ylides is not possible at this time. Electronic effects on thermodynamic stabilities of the different conformations of carbonyl ylides are known (qualitatively) from theory (12) and some thermodynamic barriers to fragmentation have also been estimated (12). Steric effects on the various pathways open to a carbonyl ylide are largely unknown. Further work in this area is in progress.

Experimental

Synthesis of oxadiazoline 1

To an ice-cold solution of lead tetraacetate (44.3 g, 0.10 mol) in dry

[8] An alternative mechanism, in which 1,1,1-trichloroacetone comes from an α-halo ether, is indicated in Scheme 1.

Can. J. Chem. Downloaded from www.nrcresearchpress.com by 210.87.254.40 on 09/06/12
For personal use only.

Can. J. Chem. Downloaded from www.nrcresearchpress.com by 210.87.254.40 on 09/06/12
For personal use only.

methanol (300 mL) was added acetone-*N*-acetylhydrazone (11.4 g, 0.10 mol), with stirring. When the yellow colour of the solution was discharged, potassium hydroxide (pellets, 10 g) was added and the resulting solution was stirred at ice temperature for 2 hours. After the solution had been concentrated with a rotary evaporator, water was added and the aqueous solution was extracted with CH_2Cl_2. The organic layer was then washed with water and dried over $CaCl_2$ before the solvent was evaporated. The residue was distilled from a bulb at ambient temperature to a receiver in liquid nitrogen, at 10^{-2} Torr, after prior freeze–pump–thaw degassing. Nitrogen was bubbled through the distillate to remove a trace of dichloromethane and the residual liquid was redistilled to afford pure 2-methoxy-2,5,5-trimethyl-Δ^3-1,3,4-oxadiazoline (**1**) 8.5 g, 60%); ^{1}H nmr δ: 1.43 (s, 3H), 1.55 (s, 6H), 3.06 (s, 3H); ^{13}C nmr δ: 23.4, 24.0, 25.1, 50.4 (OCH_3), 119.9 (C-5), 133.7 (C-2); ms (CI/NH_3) *m/z*: 162 (M^+). *Anal.* calcd. for $C_6H_{12}N_2O_2$: C 49.98, H 8.39, N 19.43; found: C 50.28, H 8.39, N 19.32.

Synthesis of oxadiazoline 2

A procedure analogous to the one described above for **1** was used to oxidize acetone-*N*-(4-methoxybenzoyl)hydrazone. The crude product left after the dichloromethane had been removed under reduced pressure was chromatographed on basic alumina in a water-cooled column using 5% ether in hexane. The first fraction to elute from the column was 2-methoxy-2-(4-methoxyphenyl)-5,5-dimethyl-Δ^3-1,3,4-oxadiazoline, **2** (59% yield); ^{1}H nmr δ: 1.40 (s, 3H), 1.56 (s, 3H), 3.06 (s, 3H), 3.67 (s, 3H), 6.73 (d, 2H, J = 9.5 Hz), 7.43 (d, 2H, J = 9.5 Hz); ^{13}C nmr (−20°C) δ: 24.06, 24.50, 50.74, 55.28, 113.69, 121.81 (C-5), 127.81, 128.24, 133.22 (C-2), 160.24.

Thermolysis of 1 and 2

In a typical experiment, the oxadiazoline (20 mg) dissolved in about 0.5 mL of freshly distilled solvent, containing CH_2Cl_2 as internal standard, was sealed into an nmr tube after three freeze–pump–thaw cycles at 10^{-2} Torr. The sealed tube was then heated in an oil bath at 79.5°C. For kinetics, the tube was withdrawn from time to time and several integrals of reactant and product signals were recorded along with the integral for internal standard. Such sealed samples were also used to estimate yields of the major products by ^{1}H nmr.

Bulb-to-bulb distillation of the mixture of products was generally employed to separate solvent and volatile products from nonvolatile products. The volatile and nonvolatile fractions were then examined by nmr, gc, and gc/ms to identify the various components. Samples for nmr were collected from a gc column (10 ft × 1/4 in.) packed with OV-17 (10%) unless otherwise indicated.

Thermolysis of 2 in 5

A solution of **2** (23.6 mg, 1.0×10^{-4} mol), in freshly-distilled **5**, was heated for 7 h at 79.5°C. Bulb-to-bulb distillation separated most of the unreacted **5** from the adduct **6**. Column chromatography on basic alumina with 20% ether in CCl_4 for elution was used to purify **6**; ^{1}H nmr ($CDCl_3$) δ: 1.66 (s, 3H), 1.68 (s, 3H), 3.32 (s, 3H), 3.71 (s, 3H), 3.80 (s, 3H), 3.82 (s, 3H), 6.89 (d, 2H, J = 9.0 Hz), 7.41 (d, 2H, J = 9.0 Hz); ^{13}C nmr δ: 26.95, 50.96, 52.16, 55.08, 87.10 (C-5), 111.28 (C-2), 113.40, 128.23, 130.72, 138.62, 142.49, 159.88, 162.73, 163.09; ms *m/z* (fragment, %): 319 ($C_{17}H_{19}O_6$, 100), 260 ($C_{15}H_{16}O_4$, 25), 245 ($C_{14}H_{13}O_4$, 18), 135 ($C_8H_7O_2$, 42), 107 (C_7H_7O, 12), 77 (C_6H_5, 5).

Oxirane 8

A major product from the thermolysis of **2** in norbornadiene, tetramethylethylene, tetrachloroethylene, and ethyl vinyl ether was an oil identified as **8**; ^{1}H nmr δ: 1.02 (s, 3H), 1.54 (s, 3H), 3.21 (s, 3H), 3.84 (s, 3H), 6.93 (d, 2H, J = 9.0 Hz), 7.37 (d, 2H, J = 9.0 Hz); ^{13}C nmr δ: 20.05, 20.30, 52.50, 55.35, 67.33, 100.05, 113.81, 129.52, 131.86, 160.14; ms *m/z* (fragment, %): 208 ($C_{12}H_{16}O_3$, 6), 193 ($C_{11}H_{13}O_3$, 4), 177 ($C_{11}H_{13}O_2$, 2), 151 ($C_9H_{11}O_2$, 100), 135 ($C_8H_7O_2$, 56), 107 (C_7H_7O, 4), 77 (C_6H_5, 9).

Norbornadiene adduct 7

Bulb-to-bulb distillation removed most of the excess norbornadiene from the products, **7** and **8**. Those products were separated by tlc on silica plates (2 mm thick) using 5% ether in CCl_4. The first band contained oxirane **8** and the second consisted of **7**; ^{1}H nmr δ: 0.95–1.02 (m, 1H), 1.38 (s, 3H), 1.51 (s, 3H), 1.80–2.88 (m, 5H), 2.91 (s, 3H), 3.82 (s, 3H), 6.08 (s, broad, 2H), 6.78 (d, 2H, J = 9.0 Hz), 7.36 (d, 2H, J = 9.0 Hz); ^{13}C nmr δ: 23.93, 31.60, 42.63, 43.51, 44.17, 48.70, 55.13, 60.10, 82.02, 109.43, 113.15, 128.57, 131.86, 139.24, 159.05; ms *m/z* (fragment, %): 269 ($C_{18}H_{21}O_2$, 35), 203 ($C_{13}H_{15}O_2$, 100), 135 ($C_8H_7O_2$, 72), 107 ($C_7H_7O_3$, 8), 77 (C_6H_5, 20).

Dihydrofuran derivative 9

Adduct **9** was identified from its ^{1}H and ^{13}C nmr spectra and from its mass spectrum; ^{1}H nmr δ: 1.48 (s, 6H), 1.64 (s, 3H), 3.27 (s, 3H), 3.83 (s, 6H); ^{13}C nmr δ: 26.02, 26.60, 51.24, 53.80, 83.12, 109.39, 133.64, 141.24, 161.06, 162.88; ms *m/z* (fragment, %): 243 ($C_{11}H_{15}O_6$, 18), 227 ($C_{11}H_{15}O_5$, 18), 169 ($C_8H_9O_4$, 100), 157 ($C_7H_9O_4$, 70), 111 ($C_5H_3O_3$, 38), 109 ($C_6H_5O_2$, 7).

Cyclopropene, 10

The adduct **10**, derived from reaction of 1-methoxyethylidene with dimethylacetylene dicarboxylate, was separated from other components of the mixture of products by gc; ^{1}H nmr δ: 1.30 (s, 3H), 3.71 (s, 3H), 3.86 (s, 6H); ms *m/z* (fragment, %): 185 ($C_8H_9O_5$, 16), 169 ($C_8H_9O_4$, 24), 111 ($C_5H_3O_3$, 100), 83 ($C_4H_3O_2$, 12), 59 ($C_2H_3O_2$, 80).

Tetrahydrofuran derivatives, 11 and 12

These products were separated from excess *cis*-1,2-dichloroethylene by bulb-to-bulb distillation at 10^{-2} Torr. They were separated from one another by gc at 120°C with a 10 ft × 0.25 in. column packed with OV-17 (10%); ^{1}H nmr of **12**, δ: 1.39 (s, 3H), 1.42 (s, 3H), 1.54 (s, 3H), 3.30 (s, 3H), 4.33 (d, 1H, J = 4.9 Hz), 4.75 (d, 1H, J = 4.9 Hz); ms *m/z* (fragment, %): 197, 199 ($C_7H_{11}O_2Cl_2$; 10, 6)), 181, 183 ($C_7H_{11}OCl_2$; 40, 28), 161, 163 ($C_7H_{10}O_2Cl$; 36, 13), 145, 147 ($C_7H_{10}ClO$; 32, 10), 119, 121 (C_5H_8ClO; 100, 35), 103, 105 (C_4H_4ClO; 78, 24), 67 (C_4H_3O; 39); ^{1}H nmr of **11**, δ: 1.38 (s, 3H), 1.46 (s, 3H), 1.50 (s, 3H), 3.31 (s, 3H), 4.30 (s, 2H); ms, identical to that of **12**.

1,1,1,2-Tetrachloro-2-methylpropane (14)

The residue left after bulb-to-bulb distillation of the volatiles obtained upon thermolysis of **1** in CCl_4 was chromatographed at 100°C in a column (10 ft × 0.25 in.) packed with DEGS (10%). Product **14** was collected as a white solid which sublimed at 180°C (lit. (29) mp 178.6–179.6°C); ^{1}H nmr δ: 2.0 (s,); ms *m/z* (fragment): 159, 161, 163 ($C_4H_6Cl_3$), 123, 125 ($C_3H_5Cl_2$).

3,3,3-Trichloro-2-methoxypropene (15)

The separation described above afforded **15** as an oil; ^{1}H nmr δ: 4.00 (s, 3H), 4.52 (d, 1H, J = 4.0 Hz), 5.50 (d, 1H, J = 4.0 Hz); ms *m/z* (fragment): 174, 176, 178 ($C_4H_5OCl_3$), 117, 119, 121 (CCl_3), 57 (C_3H_5O).

1-Methoxy-1,2,2-trimethylcyclopropane (18)

This compound was isolated by gc from the products of thermolysis of **1** in 2-methoxypropene; ^{1}H nmr of **18**, δ: 0.13 (d, 1H, J = 4.9 Hz), 0.49 (d, 1H, J = 4.9 Hz), 1.07 (s, 3H), 1.18 (s, 3H), 1.36 (s, 3H), 3.27 (s, 3H); ms *m/z* (fragment, %): 114 ($C_7H_{14}O$, 3), 99 ($C_6H_{11}O$, 100), 83 (C_6H_{11}, 4), 67 (C_5H_7, 24).

trans-*1,2-Dimethyl-1,2-dimethoxycyclopropane (20)*

The products of thermolysis of **1** in 2-methoxypropene included this compound which was isolated by gc; ^{1}H nmr δ: 0.54 (s, 2H), 1.43 (s, 6H), 3.27 (s, 6H); ms *m/z* (fragment, %): 130 ($C_7H_{14}O_2$, 1), 115 ($C_6H_{11}O_2$, 100), 99 ($C_6H_{11}O$, 22), 83 (C_5H_7O, 10), 67 (C_5H_7, 13), 51 (C_4H_3, 4).

Hexamethylcyclopropane and methoxypentamethylcyclopropane

These compounds were isolated by gc from the products of thermolysis of **1** in tetramethylethylene. Hexamethylcyclopropane: ^{1}H nmr δ: 0.96 (s) (lit. (30) 0.94 (s)); ms *m/z* (fragment, %): 126 (C_9H_{18}, 15), 111 (C_8H_{15}, 100), 69 (C_6H_9, 29). 1-Methoxy-1,2,2,3,3-pentamethyl-

cyclopropane: ^{1}H nmr δ: 1.09 (s, 6H), 1.21 (s, 6H), 1.41 (s, 3H), 3.23 (s, 3H); ms *m/z* (fragment, %): 142 ($C_9H_{18}O$, 2), 127 ($C_8H_{15}O$, 100), 111 (C_8H_{15}, 13), 95 (C_7H_{11}, 23), 69 (C_6H_9, 7).

Acknowledgement

Financial support of this research by the Natural Sciences and Engineering Research Council of Canada is gratefully acknowledged.

1. M. BÉKHAZI and J. WARKENTIN. J. Org. Chem. **47**, 4870 (1982).
2. M. BÉKHAZI and J. WARKENTIN. J. Am. Chem. Soc. **103**, 2473 (1981).
3. N. SHIMIZU and P. D. BARTLETT. J. Am. Chem. Soc. **100**, 4260 (1978).
4. R. W. HOFFMANN and H. L. LUTHARDT. Chem. Ber. **101**, 3861 (1968).
5. P. RAJAGOPALAN and B. G. ADVANI. Tetrahedron Lett. 2689 (1967).
6. E. WEITZ and A. SCHEFFER. Chem. Ber. **54**, 2327 (1921).
7. E. F. ULLMAN and J. E. MILKS. J. Am. Chem. Soc. **84**, 1315 (1962).
8. E. F. ULLMAN. J. Am. Chem. Soc. **85**, 3529 (1963).
9. E. F. ULLMAN and J. E. MILKS. J. Am. Chem. Soc. **86**, 3814 (1964).
10. D. R. ARNOLD and L. A. KARNISCHKY. J. Am. Chem. Soc. **92**, 1404 (1970).
11. D. SEYFERTH and W. E. SMITH. J. Organometal. Chem. **26**, C55 (1971).
12. K. N. HOUK, N. G. RONDAN, C. SANTIAGO, C. J. GALLO, R. GANDOUR, and G. W. GRIFFIN. J. Am. Chem. Soc. **102**, 1504 (1980).
13. D. BETHELL, A. R. NEWALL, and D. J. WHITTAKER. J. Chem. Soc. B, 23 (1971).
14. U. G. KANG and H. SCHECHTER. J. Am. Chem. Soc. **100**, 651 (1978).
15. R. V. HOFFMANN and H. SCHECHTER. J. Am. Chem. Soc. **100**, 7934 (1978).
16. H. TOMIOKA, G. W. GRIFFIN, and K. NISHIYAMA. J. Am. Chem. Soc. **101**, 6009 (1979).
17. A. PADWA, T. J. BLACKLOCK, R. LOZA, and R. POLNIASZEK. J. Org. Chem. **45**, 2181 (1980).
18. H. TOMIOKA, H. OKUNO, and Y. IZAWA. J. Chem. Soc. Perkin Trans. 2, 1636 (1980).
19. H. TOMIOKA, H. OKUNO and Y. IZAWA. J. Org. Chem. **45**, 5278 (1980).
20. W. KIRMSE, K. LOOSEN, and H. D. SLUMA. J. Am. Chem. Soc. **103**, 5935 (1981).
21. J. C. SCAIANO. J. Am. Chem. Soc. **102**, 7747 (1980).
22. K. N. HOUK. Acc. Chem. Res. **8**, 361 (1975).
23. K. N. HOUK and L. L. MUNCHAUSEN. J. Am. Chem. Soc. **98**, 937 (1976).
24. R. HUISGEN. J. Org. Chem. **33**, 2291 (1967).
25. M. G. KATZ, A. HOROWITZ, and L. A. RAJBENBACH. Int. J. Chem. Kinet. **7**, 183 (1975).
26. H. D. ROTH. J. Am. Chem. Soc. **93**, 1527 (1971).
27. H. D. ROTH. Acc. Chem. Res. **10**, 85 (1977).
28. P. C. WONG, D. GRILLER, and J. C. SCAIANO. J. Am. Chem. Soc. **81**, 5934 (1981).
29. A. O. ROGERS and R. E. NELSON. J. Am. Chem. Soc. **58**, 1028 (1936).
30. H. U. HOSTETTLER. Tetrahedron Lett. 1941 (1965).

Can. J. Chem. Downloaded from www.nrcresearchpress.com by 210.87.254.40 on 09/06/12
For personal use only.

Transfer thermodynamics of *p*-nitroaniline in aqueous solutions of some ionic and non-ionic cosolvents and the structuredness of the solvents

JAYATI DATTA[1] AND KIRON K. KUNDU[2]

Physical Chemistry Laboratories, Jadavpur University, Calcutta - 700 032, India

Received June 30, 1982

JAYATI DATTA and KIRON K. KUNDU. Can. J. Chem. **61**, 625 (1983).

Standard free energies (ΔG_t^0) and entropies (ΔS_t^0) of transfer of *p*-nitroaniline (*p*NA) from water to aqueous mixtures of some ionic and non-ionic cosolvents like KBr, urea (U), propylene glycol (PG), glycerol (GL), dioxane (D), and 1,2-dimethoxyethane (DME) have been determined from solubility measurements at different temperatures. The observed ΔG_t^0–composition profile in KBr solution appears to result from the well known salting-out effect of the salt and those in aqueous poly-ols and ethers are the result of the combined effects of dispersion and "acid–base" type interactions but that in aqueous urea solutions is governed by the "salting-out" type interaction by the predominant zwitterionic form of urea. The observed $T\Delta S_t^0$–composition profiles as well as those obtained after correcting for the "cavity-effect", as estimated tentatively by the scaled particle theory (SPT), were examined in the light of Kundu *et al.*'s semi-quantitative theory proposed earlier. The latter profiles suggest that unlike isopropyl alcohol (IPA), the poly-ols and ethers as well as KBr and urea induce structure breaking of three dimensional (3D) water structure right from the initial compositions. Moreover, the observed "roller-coaster" type behaviour of the profile in aqueous urea is indicative of the effect of urea–water aggregation around 4–10 *m* urea. Also, the observed graded reduction of structure-promoting effect of IPA in PG and GL cosolvent systems confirms that structuring and destructuring ability of a cosolvent depends on the ratio of hydrophobicity to hydrophilicity of the cosolvent.

JAYATI DATTA et KIRON K. KUNDU. Can. J. Chem. **61**, 625 (1983).

A partir des mesures de solubilité à différentes températures, on a déterminé les énergies libres et les entropies de l'état normal (ΔG_t^0) et (ΔS_t^0) de transfert de la *p*-nitroaniline (*p*NA) de l'eau aux mélanges aqueux de quelques cosolvants ioniques et non ioniques tel le HBr, l'urée (U), le propylèneglycol (PG), le glycérol (GL), le dioxanne (D) et le diméthoxy-1,2 éthane (DME). Le profil de composition vs. ΔG_t^0 observé dans une solution de KBr semble provenir de l'effet de relargage bien connu du sel et celui observé dans les polyols et dans les éthers aqueux est le résultat des effets combinés de dispersion et des interactions du type "acide base"; toutefois celui observé pour les solutions aqueuses d'urée est gouverné par une interaction de type relargage provoquée par la forme zwittérionique prédominante de l'urée. On a examiné les profils de composition vs. $T\Delta S_t^0$ observés ainsi que ceux obtenus après corrections pour "l'effet de cavité" tels qu'évalués par la théorie de la particule à l'échelle (TPE) à la lumière de la théorie semiquantitative proposée antérieurement par Kundu *et al.* Les derniers profils suggèrent que contrairement à l'alcool isopropylique (AIP), les polyols et les éthers ainsi que le KBr et l'urée induisent une rupture de la structure tridimensionnelle (3D) de l'eau directement à partir des compositions initiales. De plus, le comportement de type "montagnes russes" du profil dans l'urée en solution aqueuse est une indication de l'effet d'agrégation urée–eau entre 4–10 *m* d'urée. La réduction graduelle observée de l'effet d'activation de la structure de l'AIP dans les systèmes de cosolvant de PG et de GL confirme également que la capacité de structurer et de déstructurer d'un cosolvant dépend du rapport de l'hydrophobicité/hydrophillicité du cosolvant.

[Traduit par le journal]

Introduction

It is now well recognised that transfer enthalpies and entropies of electrolytes and non-electrolytes often provide useful information regarding the relative structuredness of solvents. In fact, transfer enthalpies, ΔH_t^0, and entropies, ΔS_t^0, of various solutes have been found (1–5) to pass through maxima at certain critical compositions of aqueous aliphatic mono-ols, which are believed to stem from enhancement and subsequent breakdown of three dimensional (3D) tetrahedral structure of water (4) in the solvents. In a series of papers (6), we have examined the observed characteristic maxima of ΔS_t^0 of hydrogen halides (HX) in aqueous mono-ols in the light of "four-step transfer process" (7) and demonstrated from a semi-quantitative theory (6) that ΔS_t^0 (HX) might serve as a structural probe. But in view of the fact that electrostatic effect accompanying the transfer of HX is likely to confuse the issue, we have also extended these studies with some suitable non-electrolytes like benzoic acid (HBz) (8) and *p*-nitroaniline (*p*NA) (9) as probes. In fact, by adopting a logical model of these amphiphilic solutes and introducing appropriate modifications of the "four-step transfer process", we have demonstrated (8, 9) that ΔS_t^0 of these non-electrolytes as well might serve as suitable structural probes. Very recently (10), however, when we applied ΔS_t^0 of HBz as a structural probe in various aqueous ionic and non-ionic cosolvents like LiCl, KBr, D, acetonitrile (ACN), PG, and GL, it appeared that the conclusions derived for these non-ionic cosolvents are at variance not only with those obtained from earlier studies but also with that expected from structural and electronic consideration. But when ΔS_t^0's were corrected for the "cavity-effect" ΔS_t^0(cav), as estimated by use of the scaled particle theory (SPT) (11, 12), and the resultant "interaction effect" (12) ΔS_t^0(int) when examined in the light of our theory, impart the expected structural conclusions regarding these cosolvent systems. It has been therefore concluded that "cavity effect" significantly contributes to the observed ΔS_t^0 at least in the case of large-sized non-electrolytes like HBz, and that the rest ΔS_t^0(int) being appertained more to the theory, gives a better reflection of the

[1]Nee Sinha, holder of a Senior Research Fellowship of the Council of Scientific and Industrial Research, New Delhi.

[2]To whom all correspondence should be addressed.

Can. J. Chem. Downloaded from www.nrcresearchpress.com by 210.87.254.42 on 09/06/12
For personal use only.

TABLE 1. Coefficients a, b, and c of eq. [2] and free energies (ΔG_t^0) and entropies (ΔS_t^0) of transfer of p-nitroaniline from water to aqueous mixtures of different ionic and non-ionic cosolvents at 25°C

FOR ERRATA SEE V61 #6 1983 P. 1291

	Wt% of organic cosolvent or molality (m) of electrolyte	Mol% of cosolvent	a/kJ mol^{-1}	b/kJ mol^{-1} K^{-1}	c/kJ mol^{-1} K^{-1}	ΔG_t^0/kJ mol^{-1}	ΔS_t^0/J mol^{-1} K^{-1}	$T\Delta S_t^0$/kJ mol^{-1}
H_2O[a]	0	0	41.17	−0.2501	0.02756	0	0	0
IPA[a]	10	3.23	54.35	−0.3704	0.04039	−0.87	34	10
	20	6.98	92.14	−1.1170	0.14797	−2.94	60	18
	30	11.39	−3.74	0.8274	−0.13851	−5.76	35	10
	50	23.08	−85.47	2.4614	−0.37879	−8.49	10	3
PG	10	2.56	−70.24	2.3477	−0.36296	−0.49	19	5
	30	9.21	−60.99	2.2787	−0.35736	−2.70	52	15
	50	19.15	93.71	−1.2555	0.17031	−5.40	54	16
	70	35.59	77.86	−0.1254	0.00279	−8.81	48	14
GL	10	2.11	−242.27	6.1887	−0.93530	0.35	11	3
	30	7.66	−276.39	4.6898	−0.71179	−1.26	16	5
	50	16.22	−236.52	5.9528	−0.89883	−3.32	13	4
	70	31.11	−240.98	5.9654	−0.89900	−5.12	16	5
D	10	2.22	−43.60	1.6699	−0.26049	−1.86	10	3
	30	8.06	185.92	−3.5242	−0.51309	−7.25	24	7
	50	16.98	81.18	−1.3523	0.19111	−11.95	11	3
DME	10	2.17	115.93	−1.8673	0.26630	−2.06	19	6
	30	7.89	165.34	−2.9967	0.43301	−6.67	33	10
	50	16.66	151.43	−2.7347	0.39290	11.23	42	12
Urea	11.52	3.76	14.91	0.2755	−0.04995	1.12	−6	−1.8
	20.31	7.11	19.66	0.1677	−0.03442	2.01	−2	−0.6
	29.64	11.22	28.94	−0.0738	0.00199	2.73	−4	−1.2
	36.83	14.89	31.04	−0.1685	0.01700	3.26	−9	−2.7
KBr	0.5	0.89	−68.09	2.2077	−0.33942	0.07	−14	−4
solution	1	1.77	−115.48	3.2613	−0.49644	0.36	−16	−5
	2	3.48	6.17	0.4348	−0.07218	0.83	−16	−5
	3	5.13	30.32	−0.1330	−0.13181	1.24	−18	−5
	4	6.72	26.08	−0.0458	0.00031	1.61	−23	−7

[a]The a, b, c values were obtained from the reported values of the coefficients of equation used in ref. 9.

solvent structural features relative to that in water. In view of this, it seems highly imperative to check if this contention is true in the case of pNA as well.

We therefore report here the parallel studies with pNA as a probe in aqueous solutions of various ionic and non-ionic cosolvents like KBr, U, D, DME, PG, and GL. As in the case of HBz, the choice of KBr rests on the fact that being a hydrophilic electrolyte, it is a well known "electrophilic" structure breaker (13) of 3D water structures, the behaviour of $\Delta S_t^0(p\text{NA})$ will be reverse to that in aqueous mono-ols, which are well known 3D water structure makers at initial compositions. And this will then offer an extra confidence to the applicability of $\Delta S_t^0(p\text{NA})$ as a structural probe. Again, it is well known that since structuredness of urea–water solutions is a "hot topic" (refs. 14, 15 and relevant cross references therein and in ref. 16) from the point of biochemical interests. So it has been extensively studied from various angles including $\Delta S_t^0(\text{HX})$ (16a), relative entropies of ionization of water, $\delta(\Delta S_{ion}^0)$ (16b) and $\Delta S_t^0(\text{HBz})$ (8). It should be of particular interest to check if the structural information derived from the present study tallies with those derived from our previous studies in particular. Aqueous solutions of others like D and DME and poly-ols like PG and GL are similar. The latter two cosolvent systems are particularly relevant since the results of these two solvents with graded increase of hydrophilic group from mono-ol IPA to di-ol PG and thence to tri-ol GL are likely to substantiate the earlier (10, 17, 18) contention that an increase in hydrophilicity or H-bonding sites of cosolvents decreases the stabilization of 3D structures of water.

As in our previous papers (8–11), we have evaluated the transfer free energies (ΔG_t^0) and entropies (ΔS_t^0) of pNA from water to the aqueous mixtures of the above-noted ionic and non-ionic cosolvents from the measured solubilities of pNA at seven equidistant temperatures ranging from 5 to 35°C.

Experimental

The quality and methods of purification of the solvents D (18), DME (18), PG (19), and GL (19) have been described. Urea (BDH, AR) was used (16) without further purification, as before. KBr (Merck, GR) was used after drying *in vacuo*. Water used was triply distilled. pNA (Reidel) was used after recrystallizing twice from 75% ethanol and then drying *in vacuo*, as before (9).

The method adopted for the measurement of solubility of pNA in different solutions was essentially similar to that described earlier (9). The saturated solutions were diluted with water as required. Absorbance values of these solutions were determined as 380 nm by use a Perkin Elmer (Model 200) spectrophotometer. As before (9), the molar extinction coefficient of pNA in the diluted solutions was taken to be that in pure water, viz. 1.28×10^4, as the diluted solutions are practically aqueous bereft of the effect of the cosolvents present. Saturation at a given temperature was attained in all the solvents within 7–10 days. The maximum uncertainties in the measured solubilities are about ±1%.

Can. J. Chem. Downloaded from www.nrcresearchpress.com by 210.87.254.42 on 09/06/12
For personal use only.

Can. J. Chem. Downloaded from www.nrcresearchpress.com by 210.87.254.42 on 09/06/12
For personal use only.

Results

The observed molar solubilities (S) of pNA at different temperatures in different solvents as well as in pure water are given elsewhere.[3] Notably, except in 50 wt.% D and DME mixtures, solubilities of pNA in most other solvents lie below 0.1 m. So, as in previous cases (8–10), assuming the effect of activity coefficient factor to be negligibly small, the free energies of solutions (ΔG_s^0) of pNA at different temperatures were calculated on molar scale using the relation

$$[1] \quad \Delta G_s^0 = -RT \ln S$$

These were then fitted by the method of least squares to an equation of the form

$$[2] \quad \Delta G_s^0 = a + bT + cT \ln T$$

where T is the absolute temperature. The values of the coefficients a, b, and c are presented in Table 1. These reproduce the experimental data to within ±0.02 kJ. The free energies (ΔG_t^0) and entropies (ΔS_t^0) of transfer of pNA from the standard state in water to that in the solvent at 25°C were calculated on mole fraction scale using relations [3] and [4], respectively.

$$[3] \quad \Delta G_t^0 = {}_s\Delta G_s^0(p\text{NA}) - {}_w\Delta G_s^0(p\text{NA}) = -RT \ln S_s/S_w - RT \ln M_s\rho_w/M_w\rho_s = (a_s - a_w) + (b_s - b_w)T + (c_s - c_w)T \ln T - RT \ln M_s\rho_w/M_w\rho_s$$

$$[4] \quad \Delta S_t^0 = (b_w - b_s) + (c_w - c_s) + (c_w - c_s) \ln T + R \ln M_s\rho_w/M_w\rho_s + RT\left[\frac{d \ln \rho_w}{dT} - \frac{d \ln \rho_s}{dT}\right]$$

where T = 298.15 K, M, ρ, and d ln ρ/dT terms are appropriate molar mass, density, and temperature coefficients of $\log_e$ (density) of the solvents, respectively, and the subscript s refers to the solvent mixtures and w to water. The required densities of the solvents were taken from the literature given in Table 2 and those for d ln ρ/dT at 298.15 K were obtained from the slopes of the plots of ln ρ vs. T at that temperature. ΔG_t^0 and ΔS_t^0 values are presented in Table 1. The maximum uncertainties in these quantities as calculated by Please's method (20) are ±0.03 kJ mol^{-1} and ±2 J K^{-1} mol^{-1}, respectively.

Discussion

Transfer free energies

Figure 1 shows the variations of ΔG_t^0 of pNA with mol% of cosolvents including that for IPA + water system taken from our previous paper (9) for the sake of comparison. While the profiles for aqueous solutions of KBr as well as urea become increasingly positive, those for other aquo-organic mixtures become increasingly negative and at any composition the relative order of $|-\Delta G_t^0|$ is D > DME ≫ IPA > PG > GL.

The observed increased destabilization of pNA with increased proportion of ionic cosolvent KBr though conforms with the expected well known salting-out effect (21) that in urea–water mixtures seems to be somewhat intriguing. Now, as indicated in our previous paper (9), the most important contributor of pNA is the zwitterionic form:

And, since the "acid–base" interactions (22) through $=\overset{+}{N}H_2$ and $=NO_2^-$ charge centres of pNA and the "acid–base" centres of cosolvent molecules or their aquo-complexes (22) are likely to be nullified, the overall stabilization of pNA should be guided chiefly by dispersion interactions through the aromatic nucleus. The observed order of $|-\Delta G_t^0|$ of pNA viz. IPA > PG > GL also confirms this, as the hydrophobicity of these cosolvents dictating dispersion interactions also decreases in the same order.

Evidently, the observed order of stabilization of pNA in aqueous aprotic and protic cosolvents, viz. D + water > IPA + water, seemingly suggests that the effect of dispersion interaction of D and DME exceeds that of protic cosolvents like IPA, PG, and GL, as is expected from the larger polarisability and hydrophobicity of the aprotic cosolvents compared to that of the protic cosolvents. Moreover, while the hydrophobicity of DME molecule with $2CH_3$-groups is likely to be more than that of D, the flexibility of CH_3-induced negatively charged ethereal O-centres makes DME molecules more hydrophilic than D (18) and thus compensates the hydrophobic effect to a large extent. It seems that the lesser acidity of DME + water mixtures dictates their relative position.

But, as indicated in our previous papers (8, 16), in urea–water mixtures the predominant zwitterionic form of urea molecule probably makes the solvents increasingly more basic as well as more acidic compared to water. The observed increasingly negative values of $\Delta G_t^0(H^+)$ (16*b*, 23) and $\Delta G_t^0(OH^-)$ (16*b*) based on tetraphenylarsonium tetraphenylboride (Ph_4AsPh_4B) reference electrolyte assumption (24) also confirm the same. Consequently, the acid–base type interactions of pNA through $=\overset{+}{N}_2$ and $=NO_2^-$ charge centres would have caused increased stabilization of pNA. Again, recent studies have shown that although urea is an organic molecule, but possibly because of the effect or predominant zwitterionic form it shows little tendency to undergo such dispersion interaction with aromatic nucleus (8), e.g. its ability to stabilize the large Ph_4As^+ is insignificant compared to dimethyl sulphoxide or alcohols (23), and benzoic acid (8) is only slightly more stabilized in urea + water mixtures than in pure water, despite the fact that stabilization of —COOH group is more in urea + water mixtures than in water. Evidently, increased destabilization of pNA in aqueous urea solutions is an involved problem. Possibly, the predominant zwitterionic form of urea molecules capable of engaging three water molecules through 3 H-bond centres (25, 26) exerts a "salting-out" type effect on pNA molecule as ions do in salt solutions. Apparently, the same is true for HBz (8) in aqueous urea solutions. But the effect of stabilization of —COOH group by more basic aqueous urea possibly overcomes the "salting-out" type effect of zwitterionic form of urea and makes ΔG_t^0(HBz) values slightly negative, as observed (8).

Transfer entropies

Figure 2 shows the observed $T\Delta S_t^0$ composition profiles of pNA for the aqueous mixtures of these ionic and non-ionic cosolvents along with that of IPA (9). Notably, as in the case of HBz (10), the profile of pNA for the salt solutions moves increasingly downward with a hump around 2 to 6 mol% KBr, while that for the urea solutions exhibits a "roller-coaster" type behaviour — with a broad minimum around 3–4 mol% U followed by a maximum around 8 to 10 mol% U. But the

[3]A complete set of the data referred to above is available, at a nominal charge, from the Depository of Unpublished Data, CISTI, National Research Council of Canada, Ottawa, Ont., Canada K1A 0S2.

TABLE 2. Values of free energy [$\bar{G}$(cav)], enthalpy [$\bar{H}$(cav)], and entropy [$\bar{S}$(cav)] of cavity formation, ΔS_t^0(cav), ΔS_t^0(int), and the required solvent parameter α ($cm^3\ K^{-1}\ mol^{-1}$) in aqueous mixtures of different ionic and non-ionic solutes at 25°C

Wt% of organic cosolvent or molality (m) of electrolyte	$\alpha \times 10^6$	$\bar{G}$(cav)/ kJ mol^{-1}	$\bar{H}$(cav)/ kJ mol^{-1}	$\bar{S}$(cav)/ J $mol^{-1}\ K^{-1}$	ΔS_t^0(cav)/ J $mol^{-1}\ K^{-1}$	ΔS_t^0(int)/ J $mol^{-1}\ K^{-1}$	$T\Delta S_t^0$(int)/ kJ mol^{-1}
			IPA–water mixtures[a] "IPA = 0.457 nm"[b]				
0	223[c]	83.3	9.7	−247	0	0	0
10	246	79.0	10.3	−230	17	17	5
20	461	75.1	18.9	−188	58	2	1
30	753	70.2	29.2	−137	109	−74	−2
50	880	60.4	30.1	−101	146	−135	−40
			PG–water mixtures[d] "PG = 0.461 nm"[e]				
10	358	79.7	15.2	−216	30	−11	−3
30	597	72.8	24.0	−164	83	−31	−9
50	688	65.2	25.8	−131	115	−61	−18
70	526	56.1	17.7	−129	118	−70	−21
			GL–water mixtures[f] "GL = 0.498 nm"[g]				
10	345	82.0	15.3	−223	23	−12	−4
30	398	79.2	18.4	−204	43	−27	−8
50	497	75.5	23.9	−173	74	−61	−18
70	478	70.8	23.8	−158	89	−73	−22
			D–water mixtures[h] "D = 0.480 nm"[i]				
10	394	79.4	16.6	−211	36	−26	−8
30	689	71.3	26.9	−149	98	−74	−22
50	779	62.2	27.5	−116	130	−119	−35
			DME–water mixtures[j] "DME = 0.69 nm"[k]				
10	518	94.9	31.6	−212	34	−15	−5
30	691	128.6	93.8	−117	130	−97	−29
50	689	232.8	390.3	−525	772	−730	−218
			Urea–water mixtures[l] "Urea = 0.441 nm"[m]				
11.52	531	85.1	25.1	−201	46	−52	−15
20.31	435	86.4	21.9	−216	31	−33	−10
29.64	390	88.1	21.2	−224	22	−26	−8
36.83	361	89.5	21.1	−229	17	−27	−8
			KBr solutions[n] "K^+ = 0.266 nm"; "Br^- = 0.390 nm"[o]				
0.5	246	82.8	10.7	−242	5	−19	−6
1	249	84.2	11.2	−245	2	−18	−5
2	357	85.6	16.8	−231	16	−32	−10
3	391	86.6	18.8	−227	19	−35	−10
4	412	88.3	20.6	−227	20	−43	−13

[a] The required density data at different temperatures for computing α (obtained from the slope at 25°C of the density vs. temperature plot) and V at each solvent composition, were taken from ref. 45.
[b] Calculated by Farrell's method, from the partial molar volume reported in ref. 46.
[c] Reference 35.
[d] Relevant data for α and V were obtained from ref. 37.
[e] Partial molal volume data being obtained from ref. 38.
[f] Relevant data for α and V were obtained from ref. 39.
[g] Calculated from partial molar volume reported in ref. 36.
[h] Relevant data for α and V were taken from ref. 40.
[i] Calculated from partial molar volume reported in ref. 41.
[j] Relevant density data obtained from refs. 35, 36.
[k] Reported in ref. 42.
[l] Relevant density data obtained from ref. 7c.
[m] Reported in ref. 12.
[n] Relevant density data obtained from ref. 43.
[o] Reference 44.

Can. J. Chem. Downloaded from www.nrcresearchpress.com by 210.87.254.42 on 09/06/12
For personal use only.

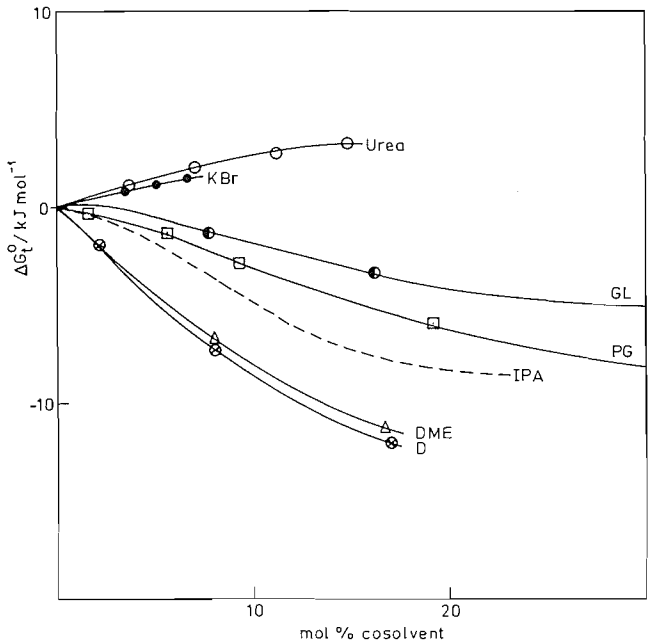

FIG. 1. Variation of ΔG_t^0 of *p*NA with composition in aqueous mixtures of different ionic and non-ionic cosolvents at 25°C.

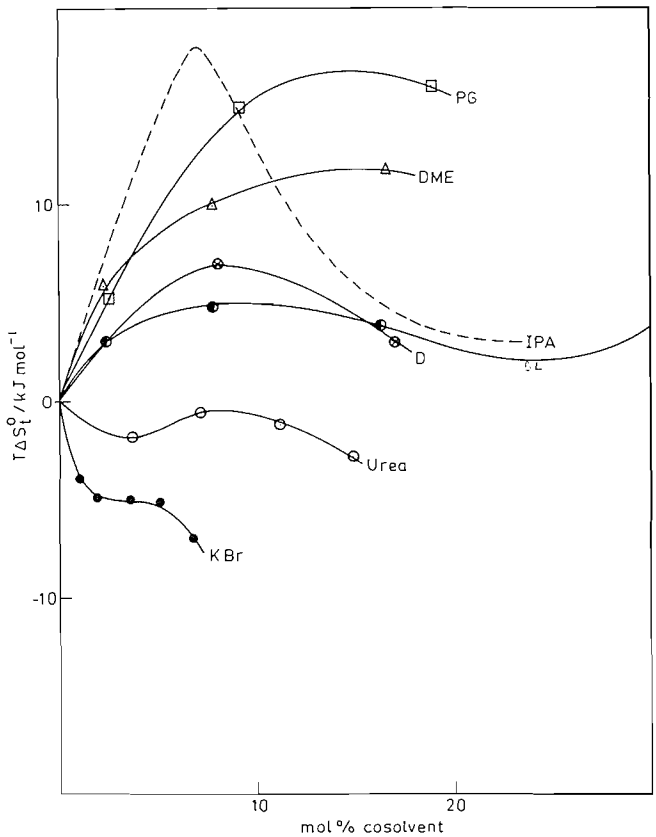

FIG. 2. Variation of $T\Delta S_t^0$ of *p*NA with composition in aqueous mixtures of different ionic and non-ionic cosolvents at 25°C.

profiles for other organic cosolvent systems pass through the characteristic maxima, though fairly broad ones as compared to those for mono-ols, as have been observed in the case of HBz.

If the dictates of the semi-quantitative theory proposed in the previous paper (9) referred to earlier be taken as a guide, then the observed sharply downward trend of $T\Delta S_t^0$–composition profile in KBr solutions is as expected the result of 3D structure-breaking propensity of the salt. Also, the observed hump in the profile is possibly the effect of superimposition of the electrophilic structural order induced by hydration of K^+ and the observed downward trend thereafter is possibly the effect of packing imbalance caused by the shortage of interstitial spaces with the increased proportion of the cosolvent, as is true in other cases. Notably, exactly similar behaviour has also been observed in the case of HBz. Similarly, the initial downward trend of the profile in aqueous urea solutions is indicative of the effect of structure-breaking propensity of urea. This is also in accord with our earlier contention (9, 16*b*) that urea molecules, being sterically debarred from entering the tetrahedral structure of water, occupy interstitial spaces forming a regular solution (27) and thus induce the breakdown of 3D structures of water. The observed broad maximum around 8 to 10 mol% urea is again indicative of the introduction of some structural order in the solvent possibly by the formation of urea–water aggregates (8, 16*b*, 28, 29). The downward trend thereafter is possibly the effect of "packing imbalance", as usual.

On the other hand, according to the tenets of the said theory the observed maxima in $T\Delta S_t^0$–composition profiles for the other aquo-organic cosolvents appear to suggest that, like IPA, all these cosolvents viz. D, DME, PG, and GL promote the 3D structures of water at initial compositions and break down the same at higher compositions due to "packing imbalance". Moreover, the relative behaviour of the profiles in aqueous PG and GL systems compared to that in IPA system is more or less similar to that observed in the case of HBz in these solvent systems and of HX in aqueous ethylene glycol (EG) and GL solvent systems (19). This seemingly confirms our earlier contention that the "structure-promoting" ability of hydrophobic —CH_3 groups in IPA is somewhat reduced due to "specific site hydration effect" (19, 30) when these are successively replaced by partially hydrophilic —CH_2OH groups, as in PG and GL.

However, contrary to the conclusions noted above, various studies (see the appropriate references given in refs. 18, 31) including our recently observed $T\Delta S_t^0$(HX) (18) or transfer entropies of ionization of water $T\delta(\Delta S^0)$ and $T\Delta S_t^0(H_2O)$ derived thereof (31), in D + water and DME + water mixtures have indicated that unlike IPA, D and DME induce 3D structure breaking right from the initial compositions. Moreover, the relative positions of these profiles in D + water and DME + water mixtures are also at variance with those for ΔY_t(HX) $[\equiv \Delta S_t^0(H^+) + \Delta S_{t,ch}^0(X^-)]$ where $\Delta S_{t,ch}^0$ is the non-Born or chemical contribution (18), and also with the expected relative structure-breaking effect of these cosolvents, which is larger in DME than D. These observations substantiate our earlier contention derived from HBz (10) as a probe that there is a missing point in our semi-quantitative treatment for the larger-sized amphiphilic solutes like HBz (8) or *p*NA (9).

In fact, as indicated by various authors (12, 32, 33) including us (10), ΔS_t^0 is effectively composed of two parts: one part ΔS_t^0(cav) is associated with the creation of a cavity of suitable size to accommodate the solute and the other part ΔS_t^0(int) is associated with the interactions of the solvent molecules surrounding the cavity among themselves as well as the solute, both relative to that in water, i.e.

$$[5] \quad \Delta S_t^0 = \Delta S_t^0(\text{cav}) + \Delta S_t^0(\text{int})$$

So, as contended by us earlier (10), the missing point in our

Can. J. Chem. Downloaded from www.nrcresearchpress.com by 210.87.254.42 on 09/06/12
For personal use only.

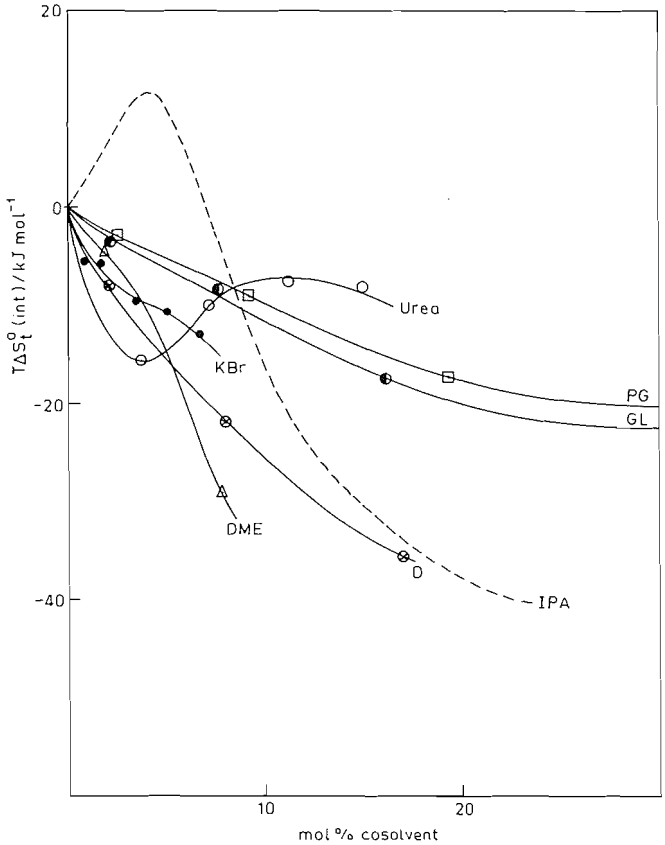

FIG. 3. Variation of $T\Delta S_t^0$(int) of *p*NA with composition in different ionic and non-ionic cosolvents at 25°C.

theory is that these amphiphilic solutes, being somewhat larger in size, at least compared to HX etc., the entropy changes due to cavity formation might significantly contribute to the observed ΔS_t^0 values.

Following a similar procedure as in HBz (10), we have tentatively computed the molar free energy $\bar{G}$(cav), enthalpy $\bar{H}$(cav), and entropy $\bar{S}$(cav) of formation of a cavity of diameter of equivalent hard sphere of *p*NA molecule[4] in water and the aqueous cosolvents including IPA, using Desrosiers' SPT relations (12). The hard sphere diameter of water has been taken as 0.276 nm (32*b*) and those for other cosolvent molecules/ions have been either taken from literature (see Table 2) or computed by Farrell's method (35). The required values of α, the coefficients of thermal expansion of the solvents, were obtained from literature or from the slopes at 25°C of the plots of $-$ log (density) versus temperature in the solvents (see Table 2). The essential parameters so computed: $\bar{G}$(cav), $\bar{H}$(cav), $\bar{S}$(cav), and ΔS_t^0 [$\equiv_s \bar{S}$(cav) $-$ $_w\bar{S}$(cav)] for different solvent systems are presented in Table 2. Significantly enough, ΔS_t^0(int) values as obtained by subtracting the ΔS_t^0(cav) values from the corresponding experimentally observed ΔS_t^0 values, show an exactly similar pattern as has been observed in the case of HBz. Thus, as could be seen from Fig. 3, while $T\Delta S_t^0$(int)–composition profile for IPA–water system still retains the "characteristic maxima", those for all the organic cosolvent systems take downward trends right from the initial composition. The corresponding profile for KBr solution takes more downward trend than that of $T\Delta S_t^0$–composition profile. Thus it confirms that it is the $T\Delta S_t^0$(int)–composition profiles rather than the $T\Delta S_t^0$–composition profiles which are in accord with the dictates of our earlier theory and that it is ΔS_t^0(int) which should really stand for the overall entropy changes involved in the "four-step transfer process" (9, 13) at least for larger sized solutes.

Thus, as contended in the case of HBz, if the characteristic maxima of ΔS_t^0(int)–composition profile of IPA + water mixture be taken to stem from the 3D structure-promoting propensity of IPA, and the downward trend right from the initial composition in salt solution like KBr be taken as the result of 3D structure-breaking effect of the salt, then the observed downward trends of the corresponding profiles in other aquo-organic solvents can be taken as the reflection of the structure-breaking propensities of the organic cosolvents. Strikingly enough, the relative positions of these profiles in D + water and DME + water mixtures get reversed and hence suggest that DME is a more effective structure breaker than D, as is expected from intrinsic and structural features of the cosolvent molecules. The observed initial inverse behaviour of these profiles, however, is possibly the Born-type electrostatic effect on the zwitterionic form of *p*NA, for at this region dielectric constant effects of DME + water mixtures are inverse that of D + water mixtures (18).

Similarly, the pronounced roller-coaster behaviour of ΔS_t^0(int) profiles in urea–water mixtures also substantiates the earlier contention that urea is an effective 3D water structure breaker right from the initial composition but induces some structural order due to the possible formation of urea–water aggregates around 4–10 mol% U, as indicated earlier.

Again, the relative positions of the ΔS_t^0(int) profiles in aqueous mixtures of IPA, PG, and GL systems are also indicative of the fact that the structuring effect of 2 CH_3— groups in IPA is so much reduced by the successive replacement of —CH_3 groups by partially hydrophilic —CH_2OH groups that while PG is a moderate structure breaker, GL is a fairly strong one. This is also expected from the "specific-site" hydration effect of the increasing —OH groups of the latter cosolvents (19).

Thus the results of the present studies fully support the earlier contention that structuring and destructuring ability of a cosolvent depends upon the effective ratio of hydrophobicity to hydrophilicity of the cosolvents. Increase of hydrophobic sites shifts the equilibrium $(H_2O)_{bulky} \leftrightarrow (H_2O)_{dense}$ towards left and increase of hydrophilicity towards right.

Acknowledgements

Thanks are due to the University Grants Commission, Government of India and to the Council of Scientific and Industrial Research, Government of India for awarding research fellowships to J. Datta.

[4]The diameter of the equivalent hard sphere of *p*NA molecule was taken to be 0.72 nm as has been tentatively estimated from the structural geometry of the molecule taking the appropriate bond lengths and bond angles etc. from Pauling's monograph (34). Notably, the diameter of the solute is not that sensitive a parameter as the diameters of cosolvent molecules (11, 12, 35) are.

1. S. RAJENDER and R. LUMRY. Biopolymers, **9**, 1125 (1970).
2. (*a*) E. M. ARNETT, W. G. BENTRUDE, J. J. BURKE, and P. M. C. DUGGLEBY. J. Am. Chem. Soc. **87**, 1541 (1965); (*b*) E. M. ARNETT. *In* Physico-chemical processes in mixed solvents. *Edited by* F. Franks. Heinemann, London. 1967. p. 105.
3. (*a*) A. BEN NAIM. J. Phys. Chem. **71**, 4002 (1967); A. BEN NAIM and S. BALL. Trans. Faraday Soc. **60**, 1736 (1964); (*b*) A. BEN

Can. J. Chem. Downloaded from www.nrcresearchpress.com by 210.87.254.42 on 09/06/12
For personal use only.

NAIM. *In* Water and aqueous solutions. *Edited by* R. A. Horne. Wiley-Interscience, New York, NY. 1972. p. 6425.
4. F. FRANKS and D. G. IVES. Q. Rev. Chem. Soc. **20**, 1 (1966).
5. (*a*) J. JUILLARD. J. Chem. Soc. Faraday Trans. I, **78**, 37 (1982); **78**, 43 (1982); (*b*) Y. POINTUD and J. JUILLARD. J. Chem. Soc. Faraday Trans. I, **73**, 1907 (1977).
6. (*a*) K. BOSE, A. K. DAS, and K. K. KUNDU. J. Chem. Soc. Faraday Trans. I, **71**, 1838 (1975); (*b*) K. DAS, K. BOSE, and K. K. KUNDU. J. Chem. Soc. Faraday Trans. I, **73**, 655 (1977); (*c*) K. BOSE, K. DAS, A. K. DAS, and K. K. KUNDU. J. Chem. Soc. Faraday Trans. I, **74**, 1051 (1978).
7. (*a*) K. K. KUNDU. Ind. J. Chem. **10**, 303 (1972); (*b*) K. K. KUNDU, D. JANA, and M. N. DAS. Electrochim. Acta, **18**, 95 (1973).
8. K. DAS, A. K. DAS, K. BOSE, and K. K. KUNDU. J. Phys. Chem. **82**, 1242 (1978).
9. K. BOSE and K. K. KUNDU. Can. J. Chem. **55**, 3961 (1977).
10. J. DATTA and K. K. KUNDU. J. Phys. Chem. **86**, 4055 (1982).
11. R. A. PIEROTTI. J. Phys. Chem. **69**, 281 (1965); Chem. Rev. **76**, 717 (1976).
12. N. DESROSIERS and J. E. DESNOYERS. Can. J. Chem. **54**, 3800 (1976).
13. M. KAMINSKI. Discuss. Faraday Soc. **24**, 171 (1957).
14. J. E. DESNOYERS and C. R. JOLICOEUR. *In* Modern aspects of electrochemistry. No. 5. *Edited by* B. E. Conway and J. O'M Bockris. Plenum Press, New York. 1967. p. 1.
15. (*a*) P. R. PHILLIP, J. E. DESNOYERS, and A. HADE. Can. J. Chem. **51**, 187 (1973); (*b*) P. R. PHILLIP, G. PERRON, and J. E. DESNOYERS. Can. J. Chem. **52**, 1709 (1974); (*c*) N. DESROSIERS, G. PERRON, J. G. MATHIESON, B. E. CONWAY, and J. E. DESNOYERS. J. Soln. Chem. **3**, 789 (1974).
16. (*a*) K. K. KUNDU and K. MAZUMDAR. J. Chem. Soc. Faraday Trans. I, **69**, 806 (1973); **71**, 1422 (1975); (*b*) A. K. DAS and K. K. KUNDU. J. Phys. Chem. **79**, 2604 (1975).
17. R. K. MOHANTY, T. S. SARMA, S. SUBRAMANIAN, and J. C. AHLUWALIA. Trans. Faraday Soc. **67**, 305 (1971).
18. J. DATTA and K. K. KUNDU. Can. J. Chem. **59**, 3149 (1981).
19. I. N. BASUMULLICK and K. K. KUNDU. Can. J. Chem. **57**, 961 (1979).
20. N. W. PLEASE. Biochem. J. **56**, 196 (1954).
21. (*a*) F. LONG and W. MCDEVIT. J. Am. Chem. Soc. **74**, 1090 (1952); (*b*) V. F. SERGEEVA. Russ. Chem. Rev. **34**, 309 (1965).
22. (*a*) D. FEAKINS. *In* Physico-chemical processes in mixed aqueous solvents. *Edited by* F. Franks. Heinemann, London. 1967. p. 71. (*b*) D. FEAKINS. *In* Hydrogen bonded solvent systems. *Edited by* A. K. Covington and P. Jones. Taylor and Francis, London. 1968. p. 235.
23. K. DAS and K. K. KUNDU. J. Soln. Chem. **8**, 189 (1979).
24. B. G. COX, G. R. HEDWIG, A. J. PARKER, and D. W. WATTS. Aust. J. Chem. **27**, 477 (1974); A. J. PARKER. Electrochim. Acta, **21**, 671 (1976).
25. P. MUKHERJEE and A. RAY. J. Phys. Chem. **67**, 190 (1963).
26. E. G. FINER, F. FRANKS, and M. J. TAIT. J. Am. Chem. Soc. **94**, 4424 (1972).
27. H. S. FRANK and F. FRANKS. J. Chem. Phys. **48**, 4796 (1966).
28. W. P. JENCKS. Catalysis in chemistry and enzymology. McGraw Hill, New York, NY. 1969. p. 332.
29. J. C. MACDONALD, J. SERPHILLIPS, and J. J. GUERRERA. J. Phys. Chem. **77**, 370 (1973).
30. M. J. TAIT, A. SUGGETT, F. FRANKS, S. ABLETT, and R. A. QUICKENDEN. J. Soln. Chem. **2**, 131 (1972).
31. J. DATTA and K. K. KUNDU. Can. J. Chem. **59**, 3141 (1981).
32. (*a*) C. TREINER. Can. J. Chem. **55**, 682 (1977); (*b*) C. TREINER, P. TZIAS, and M. CHEMLA. J. Chem. Soc. Faraday Trans. I, **72**, 2007 (1977).
33. M. H. ABRAHAM and A. NASEHZADEH. Can. J. Chem. **57**, 2004 (1979).
34. L. PAULING. The nature of the chemical bond. 3rd ed. Oxford and IBH Publishing Co., Calcutta. 1960.
35. J. T. EDWARD and P. G. FARRELL. Can. J. Chem. **53**, 2965 (1975).
36. R. N. ROY, E. E. SWENSSON, G. LACROSS, JR., and C. W. KREUGER. *In* Advance Chemical Series 155. *Edited by* W. E. Furter. 1976.
37. G. CURME and F. THORNSTONE. Glycols. Reinhold, New York. 1952.
38. K. NAKANISHI, N. KATO, and N. MARUYAMA. J. Phys. Chem. **71**, 814 (1982).
39. I. N. BASU MALLICK AND K. K. KUNDU. Can. J. Chem. **57**, 961 (1982).
40. F. HAVORKS, R. A. SCHAFER, and D. DREISBACH. J. Am. Chem. Soc. **58**, 2264 (1936).
41. F. FRANKS, M. A. J. QUICKENDEN, D. S. REID, and B. WATSON. Trans. Faraday. Soc. **66**, 582 (1970).
42. V. VITI, P. L. INDOVINA, F. PODO, L. RADICS, and G. NEMETHY. Mol. Phys. **27**(2), 541 (1974).
43. G. P. BAUXTER and C. C. WALLACE. J. Am. Chem. Soc. **38**, 70 (1916).
44. H. S. HARNED and B. B. OWEN. Physical chemistry of electrolytic solutions. 3rd ed. Reinhold, New York. 1958. p. 164.
45. K. DAS, K. BOSE, A. DAS, and K. K. KUNDU. J. Electrochim. Acta, **23**, 159 (1978).
46. M. E. FRIEDMAN and H. A. SCHERAGA. J. Phys. Chem. **69**, 3795 (1965).

Can. J. Chem. Downloaded from www.nrcresearchpress.com by 210.87.254.42 on 09/06/12
For personal use only.

COMMUNICATIONS

Coupling of allylic pivalates with lithium and magnesium organocopper reagents. Reversal of regiochemistry

HSING-JANG LIU AND LI-KANG HO

Department of Chemistry, University of Alberta, Edmonton, Alta., Canada T6G 2G2

Received October 21, 1982

HSING-JANG LIU and LI-KANG HO. Can. J. Chem. **61**, 632 (1983).

Allylic pivalates undergo efficient coupling with both lithium diorganocuprates and RMgX–CuI (2:1) complexes resulting in the predominant formation of the "S_N2"-type and the "S_N2'"-type products respectively.

HSING-JANG LIU et LI-KANG HO. Can. J. Chem. **61**, 632 (1983).

On décrit des réactions efficaces de couplage de pivalates allyliques à des diorganocuprates de lithium ainsi qu'à des complexes RMgX–CuI (2:1) qui conduisent à la formation prédominante de produits de type "S_N2" et "S_N2'" respectivement.

[Traduit par le journal]

Can. J. Chem. Downloaded from www.nrcresearchpress.com by 210.87.254.40 on 09/06/12
For personal use only.

During the course of our recent studies on the synthetic application of thiol esters (1), it was observed that conjugated enones possessing the general structure **1** reacted readily with lithium dimethylcuprate leading directly to compounds of type **2**. Further investigation revealed that the unusual replacement of the ketone carbonyl with a *gem*-dimethyl group occurred via the lactone intermediate **3** which was shown by independent experiments to couple with lithium dimethylcuprate with remarkable efficiency in spite of the steric congestion at the site of reaction. Extrapolation of these results suggested that allylic pivalates might possess interesting properties in coupling with organocuprates.[1] We wish to report here a study of such coupling with organocuprates.

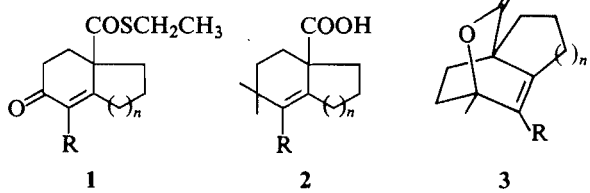

1 **2** **3**

R = H or CH_3; n = 1 or 2

In accordance with our expectations, allylic pivalates were found to react smoothly with lithium diorganocuprates as well as with RMgX–CuI (2:1) complexes under mild conditions, giving rise to coupling products in high yields. In a typical experiment involving lithium diorganocuprate, a solution of alkyllithium (6 mmol) was added with stirring to a suspension of freshly recrystallized (3) cuprous iodide (3.6 mmol) in ether (20 mL) at 0°C under an argon atmosphere. After 10 min, the mixture was chilled to −40°C and a solution of the allylic pivalate (1 mmol) in ether (5 mL) was introduced. The reaction was monitored by tlc. Upon completion (1–4 h), the reaction mixture was acidified with 1 *N* aqueous hydrochloric acid and extracted with ether. Work-up of the extracts in the usual manner gave the crude product which was purified by column chromatography on silica gel and/or by Kugelrohr distillation. With the magnesium cuprates, the reactions were carried out in a similar fashion except that a molar ratio of 6:3:1 was used for alkylmagnesium halide (in place of alkyllithium), cuprous iodide,[2] and the reactant and the reaction temperature was maintained at 0°C throughout. Several reactions attempted at −40°C failed.

Table 1 summarizes the results obtained. The allylic pivalates examined included both the primary and the secondary ones with the double bond substituted in various patterns.[3] In principle, an allylic pivalate could couple with a diorganocuprate in two different ways, involving either the α-carbon bearing the pivaloxy group to give the "S_N2"-type product or the γ-carbon with simultaneous migration of the double bond to give the "S_N2'"-type product. Experimental results showed that the coupling proceeded with a high degree of regioselectivity with both the lithium and the magnesium-containing reagents. More interestingly, a complementary mode of selectivity was displayed by these two types of reagents. With lithium diorganocuprates, the general mode is the displacement at the α-carbon as indicated by the predominant formation of the "S_N2"-type product in all the reactions studied except one (Entry 9) in which the double bond of the allylic pivalate

[1]In an isolated case (cf. ref. 2, Table 1), allyl pivalate **i** was shown to couple with lithium dimethylcuprate giving triene ester **ii** as the major product.

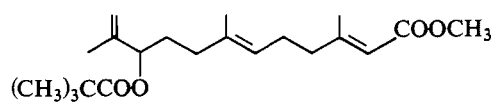

i

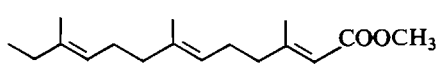

ii

[2]The reactions were less effective when smaller amounts of cuprous iodide were used.

[3]These pivalates were readily prepared from the corresponding alcohols by esterification with pivaloyl chloride (1.5 equiv.) and pyridine (1.2 equiv.) in ether at room temperature. We have also attempted to examine the 3° allylic pivalates but have not been able to make these substrates effectively due to their instability; numerous attempts to esterify 3-methyl-4-cholesten-3-ol and *trans*-2-methyl-3-decen-2-ol resulted consistently in the formation of the dehydration products in major quantities.

Can. J. Chem. Downloaded from www.nrcresearchpress.com by 210.87.254.40 on 09/06/12
For personal use only.

TABLE 1. Coupling of allylic pivalates with lithium and magnesium organocopper reagents

Entry	Allylic pivalate R = $COC(CH_3)_3$	Reagents	Time[b] (h)	Product(s) (ratio[c])		% Yield
1	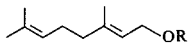	*n*-BuLi/CuI	2	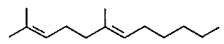		100
2		*n*-BuMgBr/CuI	1	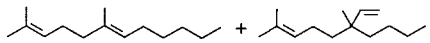	(1:3)	95
3	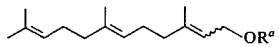	EtLi/CuI	2	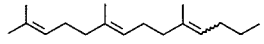 [a]		95
4		EtMgBr/CuI	1.5	[f]	(1:4)	100
5		*n*-BuLi/CuI	2	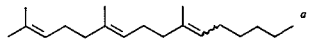 [a]		100
6		*n*-BuMgBr/CuI	1	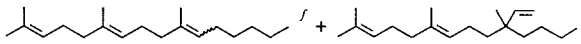 [f]	(1:6)	99
7		MeLi/CuI	2[e]	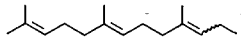 [a]		90
8		MeMgI/CuI	8.5[d]	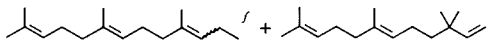 [f]	(1:6)	65
9	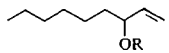	*n*-BuLi/CuI	1	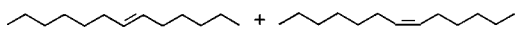	(6:1)	92
10		*n*-BuMgBr/CuI	1	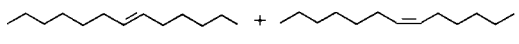	(2:1)	92
11	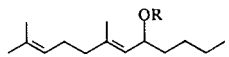	MeLi/CuI	4	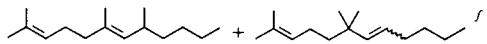 [f]	(7:1)	62
12		MeMgI/CuI	3	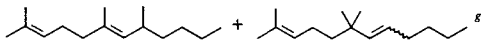 [g]	(1:6)	97
13	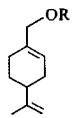	*n*-BuLi/CuI	2	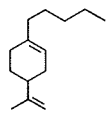		92
14		*n*-BuMgBr/CuI	1	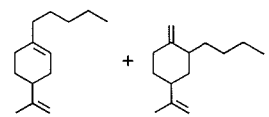	(1:11)	73
15	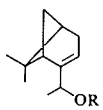	*n*-BuLi/CuI	2	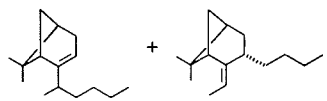	(2.2:1)	81
16		*n*-BuMgBr/CuI	1.5	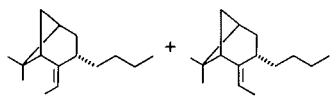	(1.5:1)	86

[a] $E:Z \simeq 2.5:1$.
[b] Unless otherwise stated, reactions were carried out according to the general procedures described in the text.
[c] This reaction was performed at −20°C.
[d] This reaction was performed at room temperature.
[e] The ratios of products were determined by nmr (^1H and ^{13}C) and/or gc analyses.
[f] The ratio of the two geometric isomers could not be determined with reasonable accuracy.
[g] $E:Z \simeq 15:1$.

system is terminal.[4] With the magnesium organocopper reagents, the major product obtained without any exception was found to be that resulting from γ-attack. It is also noteworthy that the double bond geometry remained intact whenever the reaction proceeded via α-substitution (Entries 1, 2, 11, and 12).

The ability of allylic pivalates to undergo efficient coupling with both the lithium and the magnesium organocopper reagents with reversal of regiochemistry promises to have broad synthetic utility. Other allylic esters[5] so far explored often show inconsistent and thus rather unpredictable regioselectivity when subjected to coupling with lithium organocopper reagents and in general do not couple effectively with magnesium organocopper reagents. This is further substantiated by the following experiments. Farnesyl acetate was treated with ethylmagnesium bromide – cuprous iodide (2:1) complex under the same conditions used for the corresponding pivalate (Entry 4). Upon completion of the reaction (1 h), 3-ethyl-3,7,11-trimethyl-1,6,10-dodecatriene and 2,6,10-trimethyl-2,6,10-tetradecatriene were isolated in 4:3 ratio and in 27% total yield. Similarly, treatment of farnesyl acetate with *n*-BuMgBr – CuI (2:1) complex gave a total of 43% yield of two coupling products, 2,6,10-trimethyl-2,6,10-hexadecatriene and 2,6,10-trimethyl-10-vinyl-2,6-tetradecadiene in a ratio of 4:3. These results are considerably inferior to those obtained for farnesyl pivalate (Entries 4 and 6) in terms of yield and regioselectivity.

[4]This finding is in agreement with a previous observation cited in footnote 1.

[5]For a recent review on coupling reactions of allylic esters, see ref. 4.

Acknowledgments

We are grateful to the Natural Sciences and Engineering Research Council of Canada and the University of Alberta for financial support.

1. H. J. Liu, L. K. Ho, and H. K. Lai. Can. J. Chem. **59**, 1685 (1981).
2. R. J. Anderson, C. A. Henrick, J. B. Siddall, and R. Zurflüh. J. Am. Chem. Soc. **94**, 5379 (1972).
3. G. B. Kauffman and L. A. Teter. Inorg. Synth. **7**, 9 (1963).
4. R. M. Magid. Tetrahedron, **36**, 1901 (1980).

Can. J. Chem. Downloaded from www.nrcresearchpress.com by 210.87.254.40 on 09/06/12
For personal use only.

Total synthesis of the C-3 – C-17 segment of boromycin[1]

Stephen Hanessian, Daniel Delorme,[2] Peter C. Tyler, Gilles Demailly, and Yves Chapleur

Department of Chemistry, University of Montreal, Montreal, P.Q., Canada H3C 3V1

Received November 30, 1982

Stephen Hanessian, Daniel Delorme, Peter C. Tyler, Gilles Demailly, and Yves Chapleur. Can. J. Chem. **61**, 634 (1983).

The C-3 – C-17 segment of boromycin having five asymmetric centers was synthesized from D-arabinose and D-glucose as chiral precursors. Constitutional and stereochemical identity was established by comparison of the synthetic product with a sample obtained from the degradation of the antibiotic.

Stephen Hanessian, Daniel Delorme, Peter C. Tyler, Gilles Demailly et Yves Chapleur. Can. J. Chem. **61**, 634 (1983).

Le segment C-3 – C-17 de la boromycine comprenant cinq centres asymmétriques a été synthétisé à partir du D-arabinose et du D-glucose comme précurseurs chiraux. L'identité constitutionnelle et la stéréochimie du produit synthétique a été vérifiée par comparaison avec un échantillon obtenu à partir de l'antibiotique même.

In a previous publication from this laboratory (1), we described the total synthesis and stereochemical identity of the $C_{18}H_{32}O_5$ lactone degradation product **1** from boromycin (2, 3) (Scheme 1). This entity corresponds to the C-3′ – C-17′ (upper) segment of the antibiotic and constitutes an important advanced intermediate in a program directed at the total synthesis of boromycin (for another approach, see ref. 4). The conceptual basis and overall synthetic strategy of our approach is outlined in Scheme 1 where it is clear that logical bond-breaking sequences lead to the lactones **1** and **2**, which in turn can be related to three chiral precursors. The acyclic fragment can be envisaged to arise from 2-deoxy-D-*erythro*-pentose.

We now wish to report on the total synthesis of the C-3 – C-17 (lower) segment of boromycin, namely, lactone **2** in enantiomerically pure form, based on a strategy that recognizes *carbohydrate-type symmetry* in this challenging target (5).

The starting pentose derivative **3** (oil, $[\alpha]_D$ −7.8°; *m/e* 280, MH^+)[3] (Scheme 2) can be obtained in high yield from the readily available D-arabinose utilizing the useful procedure of Wong and Gray (6). Adjustment of functionality by sequential *O*-protection and desulfonylation gave intermediate **4**, $[\alpha]_D$

[1]Portions of this work were communicated at the IVth International Conference on Organic Synthesis (IUPAC), Tokyo, Japan, Aug. 22–27, 1982 (Plenary lecture); see ref. 1.

[2]NSERCC predoctoral fellow.

[3]New compounds had spectroscopic (^{1}H nmr 400 and 90 MHz) and mass spectral characteristics that were in accord with their structure. Optical rotations were measured in chloroform. The nmr data and other physical characteristics have been submitted as supplementary material and are available on request, at a nominal charge, from the Depository of Unpublished Data, CISTI, National Research Council of Canada, Ottawa, Ont., Canada K1A 0S2.

system is terminal.[4] With the magnesium organocopper reagents, the major product obtained without any exception was found to be that resulting from γ-attack. It is also noteworthy that the double bond geometry remained intact whenever the reaction proceeded via α-substitution (Entries 1, 2, 11, and 12).

The ability of allylic pivalates to undergo efficient coupling with both the lithium and the magnesium organocopper reagents with reversal of regiochemistry promises to have broad synthetic utility. Other allylic esters[5] so far explored often show inconsistent and thus rather unpredictable regioselectivity when subjected to coupling with lithium organocopper reagents and in general do not couple effectively with magnesium organocopper reagents. This is further substantiated by the following experiments. Farnesyl acetate was treated with ethylmagnesium bromide – cuprous iodide (2:1) complex under the same conditions used for the corresponding pivalate (Entry 4). Upon completion of the reaction (1 h), 3-ethyl-3,7,11-trimethyl-1,6,10-dodecatriene and 2,6,10-trimethyl-2,6,10-tetradecatriene were isolated in 4:3 ratio and in 27% total yield. Similarly, treatment of farnesyl acetate with *n*-BuMgBr – CuI (2:1) complex gave a total of 43% yield of two coupling products, 2,6,10-trimethyl-2,6,10-hexadecatriene and 2,6,10-trimethyl-10-vinyl-2,6-tetradecadiene in a ratio of 4:3. These results are considerably inferior to those obtained for farnesyl pivalate (Entries 4 and 6) in terms of yield and regioselectivity.

[4]This finding is in agreement with a previous observation cited in footnote 1.

[5]For a recent review on coupling reactions of allylic esters, see ref. 4.

Acknowledgments

We are grateful to the Natural Sciences and Engineering Research Council of Canada and the University of Alberta for financial support.

1. H. J. Liu, L. K. Ho, and H. K. Lai. Can. J. Chem. **59**, 1685 (1981).
2. R. J. Anderson, C. A. Henrick, J. B. Siddall, and R. Zurflüh. J. Am. Chem. Soc. **94**, 5379 (1972).
3. G. B. Kauffman and L. A. Teter. Inorg. Synth. **7**, 9 (1963).
4. R. M. Magid. Tetrahedron, **36**, 1901 (1980).

Can. J. Chem. Downloaded from www.nrcresearchpress.com by 210.87.254.5 on 09/06/12
For personal use only.

Total synthesis of the C-3 – C-17 segment of boromycin[1]

Stephen Hanessian, Daniel Delorme,[2] Peter C. Tyler, Gilles Demailly, and Yves Chapleur
Department of Chemistry, University of Montreal, Montreal, P.Q., Canada H3C 3V1

Received November 30, 1982

Stephen Hanessian, Daniel Delorme, Peter C. Tyler, Gilles Demailly, and Yves Chapleur. Can. J. Chem. **61**, 634 (1983).

The C-3 – C-17 segment of boromycin having five asymmetric centers was synthesized from D-arabinose and D-glucose as chiral precursors. Constitutional and stereochemical identity was established by comparison of the synthetic product with a sample obtained from the degradation of the antibiotic.

Stephen Hanessian, Daniel Delorme, Peter C. Tyler, Gilles Demailly et Yves Chapleur. Can. J. Chem. **61**, 634 (1983).

Le segment C-3 – C-17 de la boromycine comprenant cinq centres asymmétriques a été synthétisé à partir du D-arabinose et du D-glucose comme précurseurs chiraux. L'identité constitutionnelle et la stéréochimie du produit synthétique a été vérifiée par comparaison avec un échantillon obtenu à partir de l'antibiotique même.

In a previous publication from this laboratory (1), we described the total synthesis and stereochemical identity of the $C_{18}H_{32}O_5$ lactone degradation product **1** from boromycin (2, 3) (Scheme 1). This entity corresponds to the C-3′ – C-17′ (upper) segment of the antibiotic and constitutes an important advanced intermediate in a program directed at the total synthesis of boromycin (for another approach, see ref. 4). The conceptual basis and overall synthetic strategy of our approach is outlined in Scheme 1 where it is clear that logical bond-breaking sequences lead to the lactones **1** and **2**, which in turn can be related to three chiral precursors. The acyclic fragment can be envisaged to arise from 2-deoxy-D-*erythro*-pentose.

We now wish to report on the total synthesis of the C-3 – C-17 (lower) segment of boromycin, namely, lactone **2** in enantiomerically pure form, based on a strategy that recognizes *carbohydrate-type symmetry* in this challenging target (5).

The starting pentose derivative **3** (oil, $[\alpha]_D$ −7.8°; *m/e* 280, MH^+)[3] (Scheme 2) can be obtained in high yield from the readily available D-arabinose utilizing the useful procedure of Wong and Gray (6). Adjustment of functionality by sequential *O*-protection and desulfonylation gave intermediate **4**, $[\alpha]_D$

[1]Portions of this work were communicated at the IVth International Conference on Organic Synthesis (IUPAC), Tokyo, Japan, Aug. 22–27, 1982 (Plenary lecture); see ref. 1.

[2]NSERCC predoctoral fellow.

[3]New compounds had spectroscopic (^{1}H nmr 400 and 90 MHz) and mass spectral characteristics that were in accord with their structure. Optical rotations were measured in chloroform. The nmr data and other physical characteristics have been submitted as supplementary material and are available on request, at a nominal charge, from the Depository of Unpublished Data, CISTI, National Research Council of Canada, Ottawa, Ont., Canada K1A 0S2.

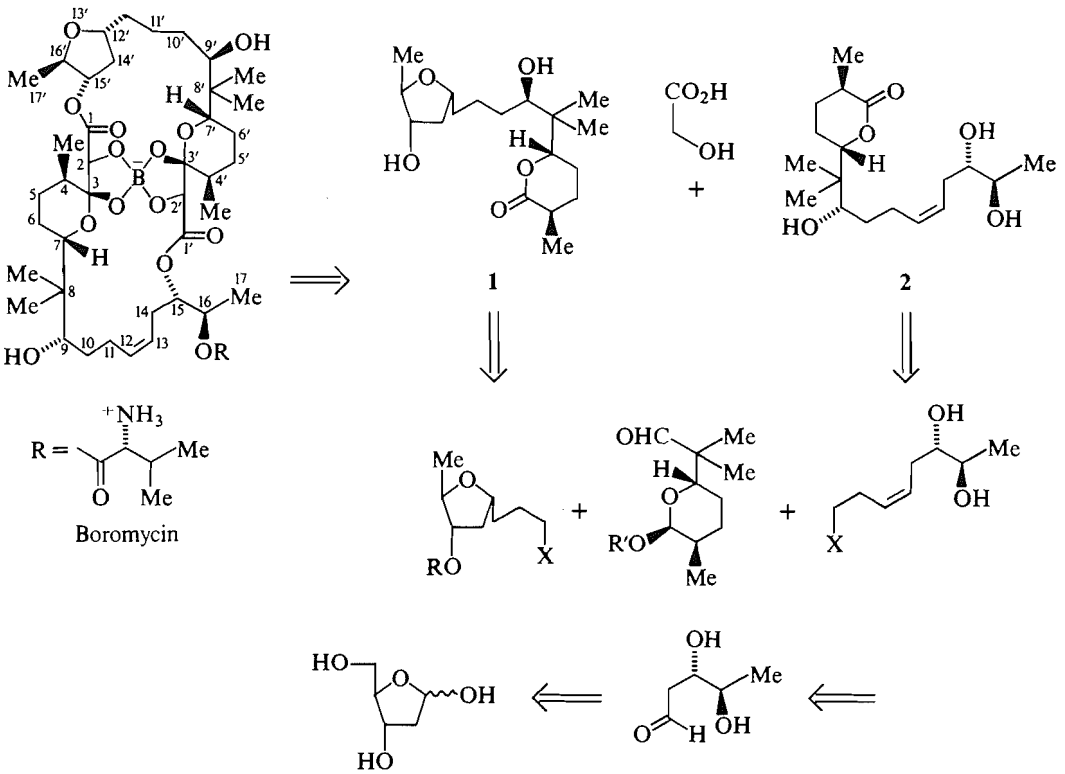

SCHEME 1

$-21.5°$; CI ms, m/e 507, MH^+, in which the hydroxyl groups of the diol are suitably protected. Brominolysis of **4** proved extremely efficient (7) and led to the aldehyde **5**, $[\alpha]_D$ $-32.8°$; CI ms, m/e 401, MH^+, which was subjected to a three-carbon extension reaction using Wittig methodology (8) under conditions that favor the formation of the desired *Z*-olefin (9) to give **6**, $[\alpha]_D$ $-15.6°$; CI ms, m/e 536, MH^+. Indeed, detailed spectroscopic analysis of the product revealed only traces of the isomeric *E*-product. Having access to the aldehyde component, which corresponds to the C-3 – C-9 tetrahydropyran portion of boromycin (1) and is a common intermediate for the elaboration of the lactones **1** and **2**, we were now faced with a choice of C—C bond-forming reaction to secure the C-9 – C-10 junction in the target. Among several options available to us, we chose the sulfone route which proved to be highly efficient. Thus, treatment of **6** with the aldehyde **7** (1) afforded a mixture of diastereoisomeric β-hydroxy sulfones **8** in very high yield. Reductive desulfonylation (10) was easily achieved on the corresponding β-keto sulfone derivative to give **9**, $[\alpha]_D$ $+25.5°$; CI ms, m/e 636, $MH^+ - OMe$; 594, $MH^+ - Me_3CO$, etc., which was reduced with sodium borohydride to a 1:1 mixture of syrupy epimeric alcohols **10**, $[\alpha]_D$ $+11.2°$, and **11**, $[\alpha]_D$ $+26.4°$. These proved to be easily separable by flash column chromatography and the undesired component could be recycled with high overall efficiency by an oxidation (Collins) – reduction sequence.

Having thus completed the total synthesis of an intermediate that corresponds to the C-3 – C-17 segment of boromycin, it was deemed necessary to secure unambiguous evidence for its constitutional and stereochemical identity by correlation with a degradation product of the antibiotic. Thus, in one series of reactions, **10** was converted into the *O*-triacetyl derivative **12**, $[\alpha]_D$ $+17.9°$, by an uneventful sequence of reactions and in good overall yield.[4] In another series of reactions, a sample of desvaline boromycin (1, 3) was subjected to controlled cleavage,[5] and the resulting lactones **1** and **2** were isolated by chromatography. Acetylation (Ac_2O, pyr.) of **2** gave material identical in all respects ($[\alpha]_D$, ms, 400 MHz nmr, and 2-D nmr) with the synthetic sample **12**. High resolution nmr spectroscopy, in particular, proved to be invaluable and led to interesting observations. Thus, it is noteworthy that the chemical shift of the geminal methyl groups in **12** was found at 0.95 ppm as a single peak while in the epimeric **9**(*R*) derivative, prepared independently from **11**, the methyl groups were found to be nonequivalent, with signals at 1.00 and 0.88 ppm. An anticipated difference in the magnitudes of optical rotation (compare, $[\alpha]_D$ $+32.7°$ for the C-9 epimer) also denotes a different orientation about the C-9 – C-10 bond.

We were now ready to transform **10** into the corresponding *O*-protected lactone and the initial judicious choice of protecting groups proved rewarding. Thus, it was possible to selectively hydrolyze the *tert*-butyl glycoside in **10** and to achieve conversion to the syrupy lactone **13**, $[\alpha]_D$ $-10.8°$, in high overall yield. Incorporation of a glycolic acid unit in this lactone, and in its C-3′ – C-17′ counterpart (1), should provide subtargets in forms suitable for esterification and macrolactonization en route to boromycin. These challenging objectives are presently under active study.

[4]The following steps were involved: (a) Bu_4NF, THF; (b) Ac_2O, pyr.; (c) aqueous AcOH; (d) pyridinium chlorochromate, CH_2Cl_2; (e) aqueous HCl, THF; (f) Ac_2O, pyr. Overall yield 50%.

[5]The cleavage was done as follows: (a) Ac_2O, DMAP, CH_2Cl_2; (b) aqueous HCl, THF; (c) H_5IO_6, THF; (d) aqueous LiOH, THF; (e) aqueous HCl, THF; (f) Ac_2O, pyr. DMAP. Overall yield 60% of lactones **1** and **2** (1:1 ratio by weight).

Can. J. Chem. Downloaded from www.nrcresearchpress.com by 210.87.254.5 on 09/06/12
For personal use only.

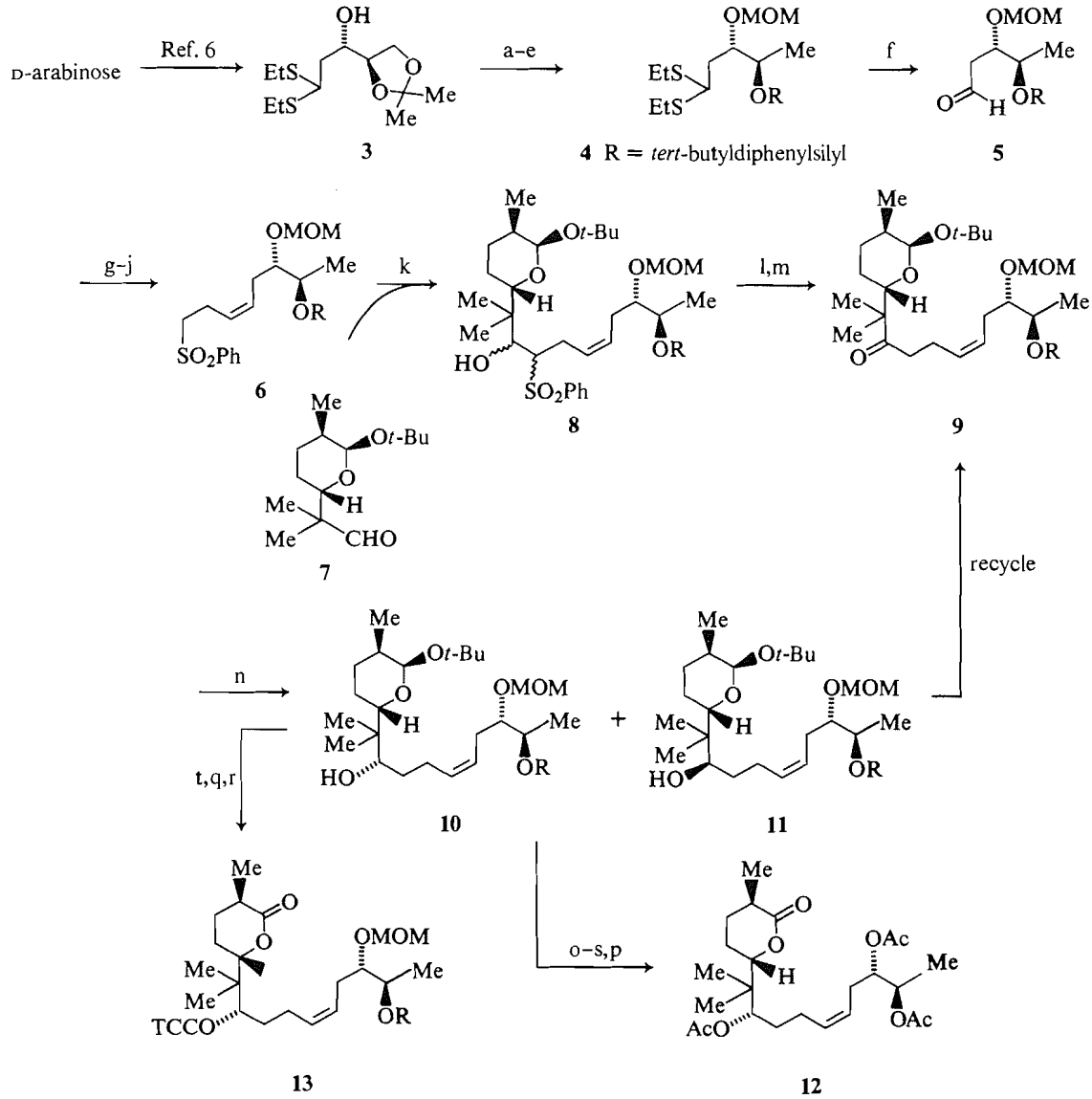

SCHEME 2. (a) $MeOCH_2Cl$, NaH, DMF, 0°C, 97%; (b) 80% aqueous AcOH, 55°C, quant; (c) TsCl, pyr., CH_2Cl_2, 0°C → r.t., 75%; (d) $Li(Et)_3BH$, THF, 0°C, 65%; (e) *tert*-butyldiphenylsilyl chloride, imidazole, DMF, r.t., 76%; (f) Br_2, aqueous $NaHCO_3$, ether, 5°C, 83%; (g) Ph_3P⁄⁄⁄⁄OTHP, THF/40% HMPA, 75%; (h) 2.5% HCl, MeOH(anhyd), 0°C → r.t., 97%; (i) PhSSPh, Bu_3P, CH_2Cl_2, r.t., 87%; (j) $KHSO_5$, aqueous MeOH, 0°C → r.t., 97%; (k) **6** and **7**, THF/10% HMPA, −78°C; add LDA, 95%; (l) Collins, 94%; (m) Al(Hg), 10% aqueous THF, r.t., 91%; (n) $NaBH_4$ aqueous EtOH, r.t., 88%; (o) Bu_4NF, THF, r.t., 83%; (p) Ac_2O, pyr., ~quant; (q) aqueous AcOH, THF, 55°C; (r) pyridinium chlorochromate, NaOAc, CH_2Cl_2, 87%, 2 steps; (s) aqueous 6 *M* HCl, ~quant; (t) trichloroethoxycarbonyl chloride, pyr., 97%.

Can. J. Chem. Downloaded from www.nrcresearchpress.com by 210.87.254.5 on 09/06/12
For personal use only.

Acknowledgements

We wish to thank the Natural Sciences and Engineering Research Council of Canada, and le Ministère de l'éducation du Québec for financial support, and the CNRS (France) for fellowships to G. D. and Y. C. We express our gratitude to Professor V. Prelog and Ciba-Geigy, Basel for a sample of boromycin. High resolution and 2-D nmr spectra were recorded by Dr. P. M. Tan and mass spectra by Mr. M. Evans of this department. We thanks Yves Dufresne for his assistance as a summer undergraduate research student.

1. S. HANESSIAN, P. C. TYLER, G. DEMAILLY, and Y. CHAPLEUR. J. Am. Chem. Soc. **103**, 6243 (1981); see also, S. HANESSIAN, D. DELORME, P. C. TYLER, G. DEMAILLY, and Y. CHAPLEUR. Pure Appl. Chem. In press; Abstr. Papers 27th Natl. Org. Symp. Nashville, Tenn., June 21–25, 1981, p. 67.
2. R. HUTTER, W. KELLER-SCHIERLEIN, F. KRUSEL, V. PRELOG, G. C. RODGERS, JR., P. SUTER, G. VOGEL, W. VOSER, and H. ZAHNER. Helv. Chim. Acta, **50**, 1533 (1967).
3. J. D. DUNITZ, D. M. HAWLEY, D. MIKLOS, D. N. J. WHITE, Y. BERLIN, R. MARUSIC, and V. PRELOG. Helv. Chim. Acta, **54**, 1790 (1971); W. MARSH, J. D. DUNITZ, and D. N. J. WHITE. Helv. Chim. Acta, **57**, 10 (1974).
4. J. D. WHITE. Abstr. Papers 179th Natl. Meeting of the American Chemical Society, Houston, Texas, March 24–28, 1979, ORG. 48; M. A. AVERY, J. D. WHITE, and B. H. ARISON. Tetrahedron Lett. **22**, 3132 (1981).
5. S. HANESSIAN. Acc. Chem. Res. **12**, 59 (1979).
6. M. Y. H. WONG and G. R. GRAY. J. Am. Chem. Soc. **100**, 3548 (1978).
7. S. HANESSIAN and R. FRENETTE. Tetrahedron Lett. 3391 (1979);

J. DEFAYE. Bull. Soc. Chim. Fr. 2686 (1964).
8. S. R. SCHOW and T. C. MCMORRIS. J. Org. Chem. **44**, 3760 (1979).
9. P. E. SONNET. J. Org. Chem. **39**, 3793 (1974).
10. B. M. TROST and D. P. CURRAN. Tetrahedron Lett. **22**, 1287 (1981).

An exceptional 5-*endo*–*trig* reversal; a convergent synthesis of daunomycinone

B. A. KEAY
Department of Chemistry, University of Waterloo, Waterloo, Ont., Canada N2L 3G1
AND
R. RODRIGO[1]
Department of Chemistry, Wilfrid Laurier University, Waterloo, Ont., Canada N2L 3C5

Received November 30, 1982

B. A. KEAY and R. RODRIGO. Can. J. Chem. **61**, 637 (1983).

A convergent AB + CD route to daunomycinone (**1**) is described. The AB segment is synthesized from the Diels–Alder adduct (**3**) of an isobenzofuran and methyl vinyl ketone by means of an unusual 5-*endo*–*trig* cleavage (**3** → **4**). The CD half (**9**) is combined with the AB by the Kraus annelation technique to provide a 9-deoxy daunomycinone derivative (**12***a*) which is subsequently oxygenated.

B. A. KEAY et R. RODRIGO. Can. J. Chem. **61**, 637 (1983).

Voici la description d'un tracé convergent AB + CD vers le daunomycinone (**1**). Le segment AB est synthétisé à partir de l'adduct Diels–Alder d'un isobenzofuranne et méthyl vinyl cétone à l'aide d'un clivage inhabituel 5-*endo*–*trig* (**3** → **4**). La portion CD (**9**) est combinée à AB par la technique d'annellation Kraus afin de fournir un dérivé 9-déoxy daunomycinone (**12***a*) qui est par la suite oxigéné.

[Traduit par le journal]

The glycoside daunomycine, an anthraquinone antibiotic of the anthracycline group, was isolated from *Streptomyces* species in 1963. The deluge of synthetic activity that followed the clinical trial and application of some of these antibiotics in cancer chemotherapy continues unabated and needs no recounting (for a comprehensive review, see ref. 1). Problems in anthracyclinone synthesis have been capably defined (2) and elegantly solved (3), particularly with respect to the aglycone daunomycinone **1**. In this report we offer a synthesis of **1** incorporating regiocontrolled AB + CD convergence and a new, efficient construction of the AB segment.

Our method features the "isobenzofuran – Diels–Alder" techniques developed (4) in this laboratory for a one-step construction of the requisite carbon skeleton. Thus the known lactol **2**, easily prepared from 2,3-dicyanohydroquinone (5) or 2,5-dimethoxybenzyl alcohol,[2] reacts smoothly with methyl vinyl ketone under mild acid catalysis to provide the bridged Diels–Alder adduct **3** in 90% yield. This molecule contains all the desired carbon and oxygen atoms, barring the 9-hydroxyl group, of the AB half of daunomycinone. The 7-hydroxyl group of the molecule, frequently a "difficult" function introduced later in many previous syntheses, develops from the oxygen atom of the isobenzofuran intermediate, the bridging oxygen atom of **3**. It is realized by an unusual 5-*endo*–*trig* reversal, formally a retro-Michael reaction, triggered by treatment of **3** with methanolic methoxide ion. The reaction is a remarkably smooth process (90% of **4**) yielding no other recognizable products, for a supposedly disfavoured pathway (7). We are investigating its mechanism but so far have failed to obtain any firm data to support an alternative rationalization. Sodium amalgam reduction of the enone (95%) and protection of the benzyl alcohol as a *tert*-butyl dimethylsilyl ether (90%) were unexceptional steps which provided **5**, our AB synthon lacking only the C-9 tertiary hydroxyl group of **1**. The addition–cyclization technique developed by Kraus and Sugimoto (8) for anthraquinone synthesis offered the best hope for regiocontrolled production of daunomycinone from **5**, but in subsequent applications of the Kraus method yields were reported (9) to be only moderate when acidic hydrogen atoms or carbonyl functions were present in the enone component. In accordance with these considerations, **5** was reduced with DIBAL-H (90%) and subjected to anodic oxidation (10). The resulting benzoquinone ketal **6** produced in 90% yield was hydrolysed with a pH 5 acetate buffer to provide a 4:1 mixture[3] of monoketals **7***a* and **7***b* (total 86%) which were separated by flash chromatography but are more conveniently carried through as a mixture for separation at a more opportune stage later on. The mixture was silylated (90%) to provide **8***a* and **8***b*, and was now ready for the Kraus annelation.

The cyanophthalide **9**, our CD segment, was easily prepared in three steps from *m*-anisaldehyde. The latter was converted into its dimethyl acetal, regiospecifically deprotonated (11), and quenched with carbon dioxide. Treatment of the resulting

[1]Author to whom correspondence may be addressed.

[2]2,5-Dimethoxybenzyl alcohol was converted to its vinyl ether and lithiated (6). The lithiated species was reacted with dimethyl formamide and hydrolyzed to the lactol **2**.

[3]This was a disappointing result in view of the >95% regioselectivity obtained previously in the hydrolysis of a similar bis-ketal (Swenton and co-workers (9)).

Can. J. Chem. Downloaded from www.nrcresearchpress.com by 210.87.254.5 on 09/06/12
For personal use only.

J. DEFAYE. Bull. Soc. Chim. Fr. 2686 (1964).
8. S. R. SCHOW and T. C. MCMORRIS. J. Org. Chem. **44**, 3760 (1979).
9. P. E. SONNET. J. Org. Chem. **39**, 3793 (1974).
10. B. M. TROST and D. P. CURRAN. Tetrahedron Lett. **22**, 1287 (1981).

An exceptional 5-*endo*–*trig* reversal; a convergent synthesis of daunomycinone

B. A. KEAY
Department of Chemistry, University of Waterloo, Waterloo, Ont., Canada N2L 3G1
AND
R. RODRIGO[1]
Department of Chemistry, Wilfrid Laurier University, Waterloo, Ont., Canada N2L 3C5

Received November 30, 1982

B. A. KEAY and R. RODRIGO. Can. J. Chem. **61**, 637 (1983).

A convergent AB + CD route to daunomycinone (**1**) is described. The AB segment is synthesized from the Diels–Alder adduct (**3**) of an isobenzofuran and methyl vinyl ketone by means of an unusual 5-*endo*–*trig* cleavage (**3** → **4**). The CD half (**9**) is combined with the AB by the Kraus annelation technique to provide a 9-deoxy daunomycinone derivative (**12***a*) which is subsequently oxygenated.

B. A. KEAY et R. RODRIGO. Can. J. Chem. **61**, 637 (1983).

Voici la description d'un tracé convergent AB + CD vers le daunomycinone (**1**). Le segment AB est synthétisé à partir de l'adduct Diels–Alder d'un isobenzofuranne et méthyl vinyl cétone à l'aide d'un clivage inhabituel 5-*endo*–*trig* (**3** → **4**). La portion CD (**9**) est combinée à AB par la technique d'annellation Kraus afin de fournir un dérivé 9-déoxy daunomycinone (**12***a*) qui est par la suite oxigéné.

[Traduit par le journal]

The glycoside daunomycine, an anthraquinone antibiotic of the anthracycline group, was isolated from *Streptomyces* species in 1963. The deluge of synthetic activity that followed the clinical trial and application of some of these antibiotics in cancer chemotherapy continues unabated and needs no recounting (for a comprehensive review, see ref. 1). Problems in anthracyclinone synthesis have been capably defined (2) and elegantly solved (3), particularly with respect to the aglycone daunomycinone **1**. In this report we offer a synthesis of **1** incorporating regiocontrolled AB + CD convergence and a new, efficient construction of the AB segment.

Our method features the "isobenzofuran – Diels–Alder" techniques developed (4) in this laboratory for a one-step construction of the requisite carbon skeleton. Thus the known lactol **2**, easily prepared from 2,3-dicyanohydroquinone (5) or 2,5-dimethoxybenzyl alcohol,[2] reacts smoothly with methyl vinyl ketone under mild acid catalysis to provide the bridged Diels–Alder adduct **3** in 90% yield. This molecule contains all the desired carbon and oxygen atoms, barring the 9-hydroxyl group, of the AB half of daunomycinone. The 7-hydroxyl group of the molecule, frequently a "difficult" function introduced later in many previous syntheses, develops from the oxygen atom of the isobenzofuran intermediate, the bridging oxygen atom of **3**. It is realized by an unusual 5-*endo*–*trig* reversal, formally a retro-Michael reaction, triggered by treatment of **3** with methanolic methoxide ion. The reaction is a remarkably smooth process (90% of **4**) yielding no other recognizable products, for a supposedly disfavoured pathway (7). We are investigating its mechanism but so far have failed to obtain any firm data to support an alternative rationalization. Sodium amalgam reduction of the enone (95%) and protection of the benzyl alcohol as a *tert*-butyl dimethylsilyl ether (90%) were unexceptional steps which provided **5**, our AB synthon lacking only the C-9 tertiary hydroxyl group of **1**. The addition–cyclization technique developed by Kraus and Sugimoto (8) for anthraquinone synthesis offered the best hope for regiocontrolled production of daunomycinone from **5**, but in subsequent applications of the Kraus method yields were reported (9) to be only moderate when acidic hydrogen atoms or carbonyl functions were present in the enone component. In accordance with these considerations, **5** was reduced with DIBAL-H (90%) and subjected to anodic oxidation (10). The resulting benzoquinone ketal **6** produced in 90% yield was hydrolysed with a pH 5 acetate buffer to provide a 4:1 mixture[3] of monoketals **7***a* and **7***b* (total 86%) which were separated by flash chromatography but are more conveniently carried through as a mixture for separation at a more opportune stage later on. The mixture was silylated (90%) to provide **8***a* and **8***b*, and was now ready for the Kraus annelation.

The cyanophthalide **9**, our CD segment, was easily prepared in three steps from *m*-anisaldehyde. The latter was converted into its dimethyl acetal, regiospecifically deprotonated (11), and quenched with carbon dioxide. Treatment of the resulting

[1]Author to whom correspondence may be addressed.

[2]2,5-Dimethoxybenzyl alcohol was converted to its vinyl ether and lithiated (6). The lithiated species was reacted with dimethyl formamide and hydrolyzed to the lactol **2**.

[3]This was a disappointing result in view of the >95% regioselectivity obtained previously in the hydrolysis of a similar bis-ketal (Swenton and co-workers (9)).

Can. J. Chem. Downloaded from www.nrcresearchpress.com by 210.87.254.6 on 09/06/12
For personal use only.

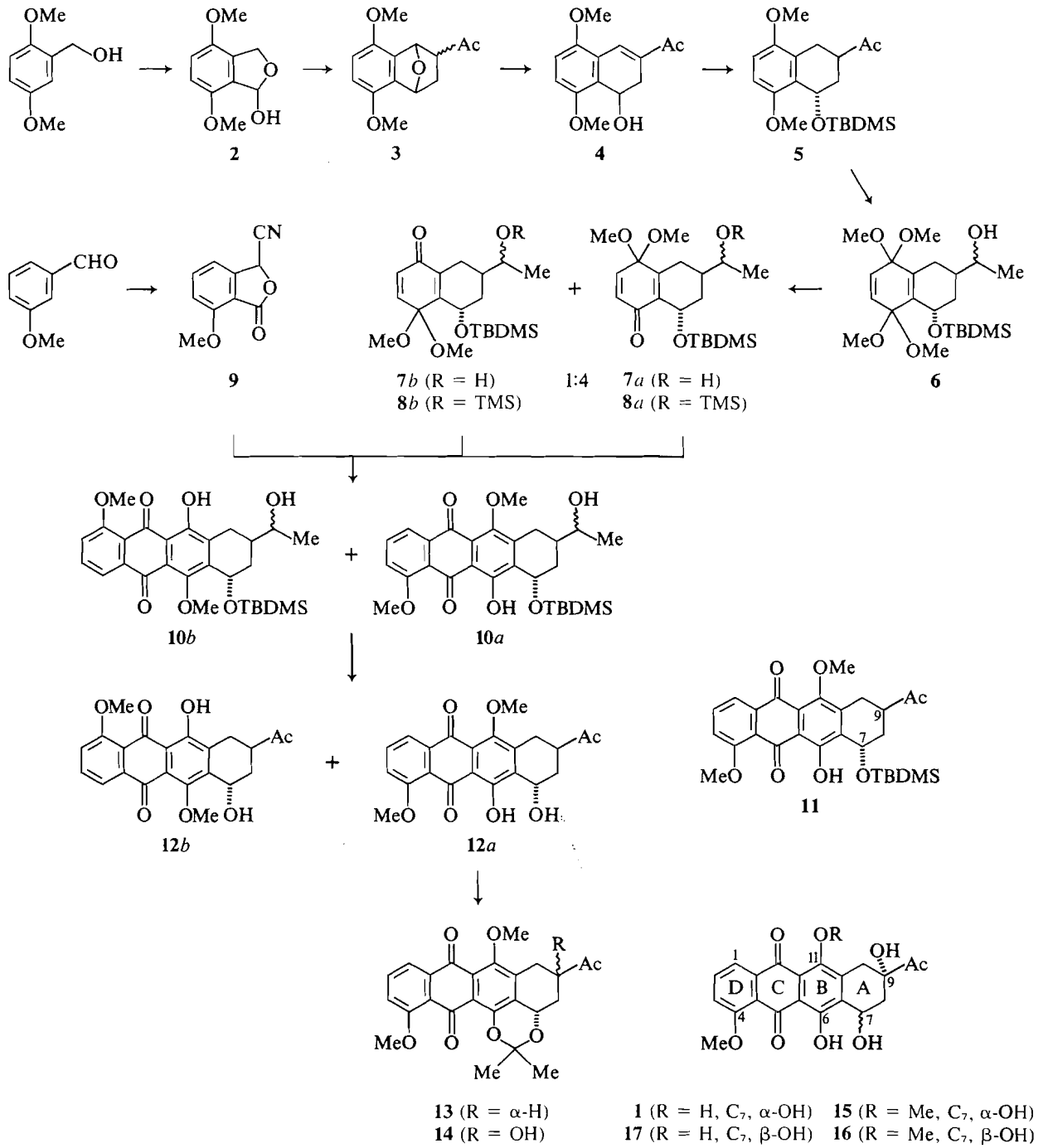

SCHEME 1. The synthesis of daunomycinone (**1**).

lactol with potassium cyanide and acetic acid provided the cyanohydrin which cyclized to **9** upon crystallization. Deprotonation of **9** with LDA/HMPA, followed by treatment with the monoketal mixture (**8***a* + **8***b*) and work-up with 20% aqueous acetic acid, provided an excellent yield (87%) of anthraquinones **10***a* + **10***b*. Reoxidation of the free alcohol proceeded efficiently (85%, **11**) with PDC in DMF and this was followed by removal (93%) of the silyl protecting group with acid. Therefore the entire AB + CD attachment sequence (**5** → **12***a* + *b*) proceeded in an excellent overall yield of 40% (seven steps). The slight structural differences that exist between regioisomers **12***a* and **12***b* can now be profitably exploited. In particular the *peri*-dihydroxy system at C-6,C-7 in **12***a* was converted to an acetonide (**13**, 80%) by 2-methoxy propene/*p*-toluene sulfonic acid treatment of the mixture in dry methylene chloride; **12***b*, which cannot form such an acetonide, is then easily separated from **12***a* by chromatography.

The ^{1}H nmr spectra of **5** (80 MHz), **11**, and **13** (400 MHz) were examined with and without H-7 decoupling to establish the C-7,C-9 relative configurations shown for these intermediates. All *J* values for protons at C-8, C-9, and C-10 in **11** and **13** were measured and the results in **11** found to be virtually identical with published values[4] for 9-deoxydaunomycinone. Oxygenation of the acetonide **13** was accomplished re-

[4]Reference 1, p. 179.

Can. J. Chem. Downloaded from www.nrcresearchpress.com by 210.87.254.6 on 09/06/12
For personal use only.

producibly in 85% yield by a modified Gardner procedure (12) to produce a 2:3 diastereomeric mixture of 9-hydroxy ketones **14**, and followed by brief acid hydrolysis to remove the protecting isopropylidene group. Column chromatography provided the individual diols **15** and **16** in the same ratio. Ring A coupling constants measured from the 400 MHz spectra of **15** and **16** correlate well with those reported (13) for isodaunomycinone and isoepidaunomycinone respectively. Boron trichloride demethylation at −78°C was selective for the C-11 methoxyl group in both cases and subsequent work-up with aqueous bicarbonate provided daunomycinone **1** (from **15**) and epidaunomycinone **17** (from **16**). Again, a 400 MHz spectrum of our synthetic product had all chemical shifts and coupling constants identical with those published (14) for daunomycinone. Since epidaunomycinone **17** has been previously isomerized (15) to daunomycinone, this concludes our synthesis[5] in fourteen steps and ca. 14% yield from **2**.

Acknowledgements

We thank the Natural Sciences and Engineering Research Council of Canada for financial support. The 400 MHz spectra were obtained at the South-Western Ontario NMR Centre funded by a major installation grant from NSERC Canada.

1. F. ARCAMONE. Doxorubicin anticancer antibiotics. *In* Medicinal chemistry. Vol. 17. Academic Press, New York. 1981.
2. T. R. KELLY. Ann. Rep. Med. Chem. **14**, 288 (1979).
3. T. R. KELLY, J. VAYA, and L. ANANTHASUBRAMANIAM. J. Am. KIMBALL, D. R. WALT, and F. JOHNSON. J. Am. Chem. Soc. **103**, 1561 (1981); J. P. GESSON and M. MONDON. Chem. Commun. 421 (1982); M. J. BROADHURST, C. H. HASSAL, and G. J. THOMAS. Chem. Commun. 158 (1982); J. Chem. Soc. Perkin Trans. 1, 2227 (1982); 2239 (1982); 2249 (1982); Y. TAMURA, A. WADA, M. SASHO, K. FUKUNAGA, H. MAEDA, and Y. KITA. J. Org. Chem. **47**, 4376 (1982); H. SEKIZAKI, M. JUNG, J. M. MCNAMARA, and Y. KISHI. J. Am. Chem. Soc. **104**, 7372 (1982).
4. B. A. KEAY, D. K. W. LEE, and R. RODRIGO. Tetrahedron Lett. 3363 (1980); B. A. KEAY and R. RODRIGO. J. Am. Chem. Soc. **104**, 4725 (1982), and ref. 6 therein; B. A. KEAY and R. RODRIGO. Can. J. Chem. In press.
5. C. D. PERCHONOCK and B. LOEV. Prostaglandins, **15**, 623 (1978).
6. R. C. RONALD, J. M. LANSINGER, T. S. LILLIE, and C. J. WHEELER. J. Org. Chem. **47**, 2541 (1982).
7. J. E. BALDWIN and L. I. KRUSE. Chem. Commun. 233 (1977); J. E. BALDWIN, J. CUTTING, W. DUPONT, L. KRUSE, L. SILBERMAN, and R. C. THOMAS. Chem. Commun. 736 (1976).
8. G. A. KRAUS and H. SUGIMOTO. Tetrahedron Lett. 2263 (1978).
9. T. LI and Y. L. WU. J. Am. Chem. Soc. **103**, 7007 (1981); M. G. DOLSON, B. L. CHENARD, and J. S. SWENTON. J. Am. Chem. Soc. **103**, 5263 (1981).
10. D. R. HENTON, R. L. MCCREERY, and J. S. SWENTON. J. Org. Chem. **45**, 369 (1980).
11. H. P. PLAUMAN, B. A. KEAY, and R. RODRIGO. Tetrahedron Lett. 4921 (1979).
12. J. N. GARDNER, F. E. CARLON, and D. GNOJ. J. Org. Chem. **33**, 3294 (1968).
13. K. KROHN and K. TOLKIEHN. Chem. Ber. **112**, 3453 (1979).
14. T. H. SMITH, A. N. FUJIWARA, W. W. LEE, H. Y. WU, and D. W. HENRY. J. Org. Chem. **42**, 3653 (1977).
15. A. S. KENDE, Y. TSAY, and J. E. MILLS. J. Am. Chem. Soc. **98**, 1967 (1976).

[5]Full details will be published later. All new compounds provided analytical and/or spectroscopic data entirely consistent with their structures.

FOR ERRATA SEE
V. 61 #6 1983 P. 1291

Can. J. Chem. Downloaded from www.nrcresearchpress.com by 210.87.254.6 on 09/06/12
For personal use only.

ADDITIONS AND CORRECTIONS/AJOUTS ET CORRECTIONS

Vol. 59, 1981

Oliver E. Edwards, John Dixon, John W. Elder, Ralph J. Kolt, and Maurice Lesage. Protonated cyclopropanes in α-aminoketone deamination.

Page 2103, line 16. The statement "Collins . . . did not extend the conception to their other example" is erroneous. In J. Am. Chem. Soc. **89**, p. 1658, l. 16 it is clearly stated that both tosylates **2** and **14** hydrolyse through the same intermediates.

Page 2104. The use of the terms *exo*- and *endo*-cations implies that the ions remain sterically unique by virtue of neighboring group or counter ion involvement.

Pages 2105, 2106. The term "participation" is used loosely for rate determining nitrogen loss to a classical cation followed very rapidly by sigma bond involvement.

We thank Prof. C. J. Collins for critical comments.

Vol. 60, 1982

Patrick M. Henry, Nita A. Lewis, and Henry Taube. Some observations on the Pd(II)-catalysed ferrocenylation of acrylonitrile.

Page 1143. The ^{1}H nmr spectrum of 3,3-diethoxypropanenitrile was interpreted as resulting from the presence of two different diastereomers in solution. This is unnecessary since the chemical shift nonequivalence of the geminal protons follows from their being diastereotopic. The CH_2 signals should therefore appear as the AB part of the ABX_3 system, which would be compatible with the reported spectrum.

We are grateful to Drs. E. L. Eliel and R. K. Norris for bringing this matter to our attention.

$^{45}Sc(\alpha,\alpha n)^{44}Sc^{m+g}$: a monitor reaction for alpha particle induced reactions[1]

PHILIP A. BEELEY,[2] JUDITH AARONSON, KONSTANTINOS KOKKAS, AND JAMES J. HOGAN

Department of Chemistry, McGill University, Montreal, P.Q., Canada H3A 2K6

Received August 9, 1982

This paper is dedicated to Professor Leo Yaffe on the occasion of his 65th birthday

PHILIP A. BEELEY, JUDITH AARONSON, KONSTANTINOS KOKKAS, and JAMES J. HOGAN. Can. J. Chem. **61**, 641 (1983).

The excitation function for the $^{45}Sc(\alpha,\alpha n)^{44}Sc^{m+g}$ reactions have been measured at beam energies from 20 to 90 MeV. These provide a beam monitor for alpha particle induced reaction studies. The excitation functions and isomer ratios are discussed with particular reference to an apparent error in the decay scheme of $^{44}Sc^{m}$.

PHILIP A. BEELEY, JUDITH AARONSON, KONSTANTINOS KOKKAS et JAMES J. HOGAN. Can. J. Chem. **61**, 641 (1983).

On a mesuré la fonction d'excitation des réactions $^{45}Sc(\alpha,\alpha n)^{44}Sc^{m+g}$ avec des énergies de faisceau de 20 à 90 MeV. Ces réactions fournissent un contrôle de faisceau pour les études des réactions induites par les particules α. On discute des fonctions d'excitation et des rapports d'isomères en faisant référence particulièrement à une erreur apparente dans le schéma de désintégration du $^{44}Sc^{m}$.

[Traduit par le journal]

Can. J. Chem. Downloaded from www.nrcresearchpress.com by 210.87.254.105 on 09/06/12
For personal use only.

Introduction

In the past several years, there has been considerable interest in the study of alpha particle induced reactions, much of it generated by the wide variety of mechanisms thought to be responsible for the experimental results. These include inelastic scatter of the alpha from the nucleus exciting low lying collective states (1), pickup reactions (2), binary fragmentation of the incident particle (3), dissolution of the alpha particle into four nucleons in the nuclear field (4), and interaction of the alpha with individual nucleons initiating an intranuclear cascade (5). During the latter, the alpha may undergo multiple scatters or break up into four nucleons (6).

Activation experiments to measure excitation functions of alpha particle induced reaction products have been hampered by the lack of a convenient means of monitoring the intensity of the incident alpha beam. This is particularly the case for experiments carried out in the internal beam of a cyclotron, or from stacked foil experiments in which Faraday cup measurements may be impractical.

The commonly used beam monitor at energies above 65–70 MeV is the $^{27}Al(\alpha,4p3n)^{24}Na$ reaction studied by Probst *et al.* (7). The excitation function for this reaction reaches a plateau at 65–70 MeV where the cross section is about 40 mb, then decreases very slowly to about 30 mb at $E_\alpha > 150$ MeV. The reaction is quite clean, producing no other activities with a lifetime between 10 min (^{27}Mg) and 21 h (^{28}Mg).

Unfortunately, this reaction can not be used as a monitor below about 60 MeV, and no other reaction of α on ^{27}Al provides a reasonable alternative, either because of short lifetimes (^{27}Mg, ^{28}Al, ^{29}Al), low cross section (^{28}Mg), low count rate (^{22}Na), or steeply varying excitation function (^{29}Al).

Therefore it was decided to examine the possible alpha induced reactions, "find" a more convenient monitor, and measure its excitation function. The requirements of a good monitor are many; usually one or more must be sacrificed for practical reasons. We sought: (a). a readily available monoisotopic target; (b). a reaction of low threshold energy and moderately large cross section, which is relatively energy insensitive; (c). a product with an easily measureable gamma ray of reasonable half life; (d). minimum production of other activities, and in particular, minimum production of other gamma rays which might interfere with other measurements in activation experiments. This rather stringent set of requirements is met by the reaction $^{45}Sc(\alpha,\alpha n)^{44}Sc^{m,g}$.

Scandium is easily obtainable in high purity as the trioxide powder, Sc_2O_3, or as the pure metallic foil. The excitation function for the metastable and ground states is found to be 100 ± 30 mb and 70 ± 20 mb, respectively, from about 25–30 MeV to 100 MeV and presumably well beyond. The half lives of ≃58 h for the metastable and ≃4 h for the ground state provide a convenient decay period whether for a long irradiation or a short. Moreover each decays through a single intense transition with no other transition occurring with a branch greater than 1%.

The most appealing aspect of this reaction as a monitor, however, is in the dearth of gamma rays produced from other activities at energies up to 1400 keV making it easy to incorporate the Sc_2O_3 powder monitor right into the target mixture of an activation experiment. In Table 1, all nuclides expected to be present ten minutes after irradiation, and all gamma rays more than 10% abundant, are listed. A spectrum measured twelve hours after the end of a one hour irradiation (Fig. 1) is discussed below.

The purpose of this work, then, is to measure the excitation function of the $^{45}Sc(\alpha,\alpha n)^{44}Sc^{m,g}$ reaction for use as an internal beam monitor in alpha particle irradiations. We have used as the primary monitor various reactions measured by Probst *et al.* (7), carrying out two sets of experiments, one at low energies using the 6 min ^{29}Al, the other at high energies using ^{24}Na. The lower portion of Table 1 shows the characteristics of the activities produced in reactions on aluminum.

These experiments, using relatively thick targets and an internal monitor, are also compared with measurements of Chen and Miller (8) of the same reaction at low energies ($E_\alpha < 40$

[1]This work is dedicated to Leo Yaffe. It is particularly appropriate in that he and his colleagues R. B. Moore, D. A. Newton, and S. Sarkar are the authors of the beam monitor study for proton induced reactions used for many years at the McGill University synchrocyclotron.

[2]Present address: Carbohydrate Research Institute, Queen's University, Kingston, Ontario.

TABLE 1. Nuclides with half-life between 1 s and 100 days formed in this work

Nuclide	Half life	Gamma rays, keV	Branch, >10%	Comment
^{48}V	15.98 days	983.5	100.0	Low σ, (α,*n*)
		1312.1	97.5	
^{47}V	31.3 min	None		
^{45}Ti	3.08 h	None		
^{47}Sc	3.35 days	159.4	68.5	
^{46}Sc	83.8 days	889.3	100.0	Low count rate
		1120.5	100.0	Low count rate
^{44}Sc^{m}	58.6 h	271.2	86.6	IT to ground
		1157.0	99.9	From ground
^{44}Sc^{g}	3.93 h	1157.0	99.9	
^{43}Sc	3.89 h	372.9	22.0	
^{44}K	22.1 min	1157.0	58.0	Low σ, (α,4*pn*)
^{43}K	22.3 h	372.9	87.8	
		397.0	11.5	
		593.6	11.1	
		617.8	80.0	
^{42}K	12.36 h	1524.6	18.8	
^{41}Ar	1.83 h	1293.6	99.2	Gas
^{29}Al	6.56 min	1273.2	89.1	
^{28}Mg	20.9 h	400.6	36.0	Low σ, (α,3*p*)
		941.7	36.0	
		1342.2	52.1	
^{27}Mg	9.46 min	843.8	73.0	Low σ, (α,3*pn*)
		1014.4	27.1	
^{24}Na	15.02 h	1368.5	100.0	
		2754.1	100.0	

MeV) measured with thin targets in an external beam using a Faraday cup to monitor the beam intensity.

Experimental

Targets

Targets were intimate mixtures of high purity powdered Al and 99.999% Sc_2O_3. Two sets of targets were prepared according to whether the low cross section, short half-life, ^{29}Al was to be used as primary monitor, or the higher cross section, long lived ^{24}Na. It is noteworthy that the measurements of Probst *et al.* (7) on 9.46 min ^{27}Mg were rejected as a monitor in this work out of concern for the (unknown) sensitivity of this reaction cross section to the ^{27}Al(*n*,*p*)^{27}Mg reaction. The analogous ^{27}Al(*n*,α)^{24}Na reaction has been shown to be of minimal concern at energies above 50–60 MeV (9).

The target mixtures, usually about 20 mg, were contained in 1 mm inside diameter, 1-mil (0.025 mm), high purity Al tubing, rolled flat to minimize the target thickness. The specific target arrangements were identical to those used in previous reaction studies undertaken in the McGill Radiochemistry Laboratory (10).

Irradiations

All irradiations were carried out in the internal beam of the McGill University Synchrocyclotron at a radius corresponding to the desired beam energy[3] for periods ranging from 5 s to 5 min. Typically beam currents were about 700 namps.

Counting

After irradiation, the targets were disassembled and the powder was analyzed for gamma ray activity. Samples were counted on a 100 cm^3 activated volume Ge(Li) crystal used in conjunction with 4000 channel pulse height analysis. Typically, the activity was followed for about two weeks or about five half-lives of the longest lived species of interest (58 h ^{44}Sc^{m}).

[3]P. A. Beeley and R. B. Moore, private communication.

Data analysis

The beam energies reported are the nominal beam energies corrected for degradation in passing through the outer aluminum tubing and in the target itself. The stopping power tables and equations of Williamson and Boujot (11) were used to calculate the beam energy entering and leaving the target mixture and an exponential average was determined to be the mean, and therefore reported, beam energy for each experiment. It is estimated that this average energy is known to ±2 MeV while the total variation in energy striking a target may be as great as ±5 MeV. It is for this reason that an excitation function which is relatively insensitive to beam energy is critical for a monitor reaction, and suggests the initial sharp increase from threshold of the excitation functions should not be used in future studies as a monitor.

The gamma ray spectra, about 40 from each of the experiments, were analyzed by hand to evaluate the peak heights of interest. The decay curves generated were followed for a minimum of five half-lives for the longest lived species, and for 8–10 half-lives for short lived ^{29}Al. The decay curves were fit by a weighted least-squares procedure which accounts for both the statistical uncertainty in each data point and the scatter of the data points about the curve.

The efficiency curve for the Ge(Li) detector was taken from analysis of a mixed gamma ray source available from the Atomic Energy Research Establishment, Harwell, England, sold commercially by Amersham Corp., of Oakville, Ont. It consists of nine radionuclides having eleven principal gamma rays evenly spaced between 88 and 1836 keV.

Because some questions will arise in the Discussion, it is worth stating clearly the assumptions made in the decay scheme of ^{44}Sc. The metastable state, ^{44}Sc^{m}, was assumed (12) to undergo isomeric transition to the ground state 98.6% of the time, emitting 866 gamma rays per 1000 decays; the remaining 12.0% goes into conversion electrons. The isomer also decays to excited levels of ^{44}Ti 1.4% of the time, feeding the 1157.0 keV gamma ray transition to the extent of 13.7 gamma rays per 1000 decays. The ground state, ^{44}Sc^{g}, is assumed to populate the same 1157.0 keV level in 99.89% of all decays. With assumed half-lives of 2.44 days and 3.90 hours, respectively, this leaves as the working equation for the decay of the 1157.0 keV line

Can. J. Chem. Downloaded from www.nrcresearchpress.com by 210.87.254.105 on 09/06/12
For personal use only.

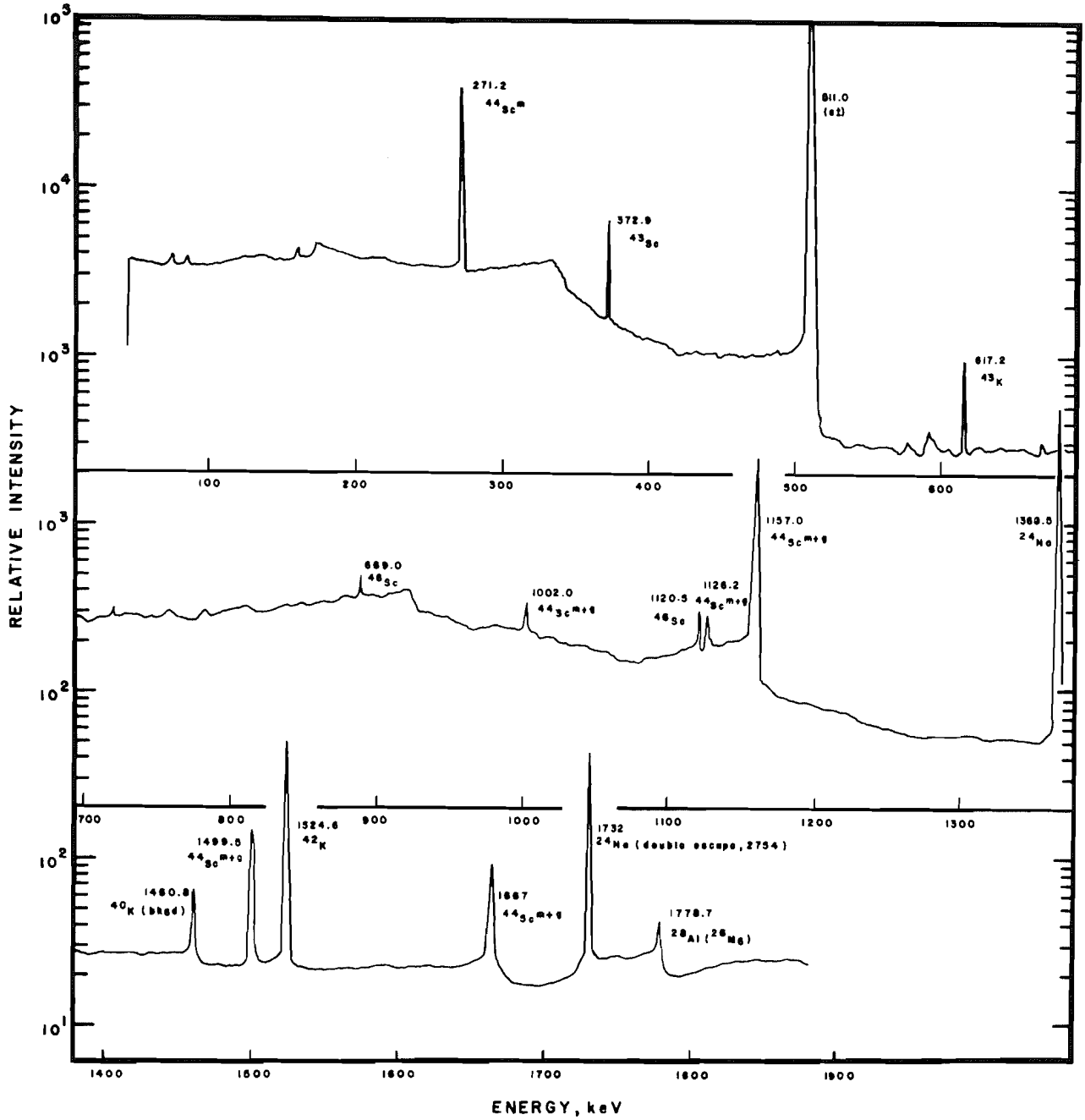

FIG. 1. The gamma ray spectrum measured in one hour twelve hours after the end of a 75 MeV irradiation of the target mixture. At energies above 1000 keV, the spectrum has been artifically smoothed.

$$A(t) = 1.069A_m^0 e^{-\lambda_m t} + (0.9989A_g^0 - 1.0556A_m^0)e^{-\lambda_g t}$$

where the subscripts m and g refer to the metastable and ground states.

The cross sections for the isomers of ^{44}Sc were finally determined by comparison to production of ^{29}Al and ^{24}Na after making corrections for detector efficiency, target composition, and decay characteristics.

Results

As outlined above, two independent means of measuring the cross section for ^{44}Sc^m exist. One is by the 271.2 keV gamma ray emitted in the isomeric transition to the ground state; the other is by analysis of the growth and decay of the 1157.0 keV gamma ray populated following beta decay. When these two analyses were performed on the experimental data, a clearly discernible pattern emerged (see Table 2). Cross sections measured from the isomeric transition were consistently greater than those determined from the growth and decay. The discrepancy is not great. The ratio of the two values is 1.075 ± 0.029 with individual experiments ranging from 1.043 to 1.101. Since the statistical error associated with each analysis is 3–5%, any single experiment has the two values just within the experimental uncertainty. However, that all nine sets of data have a similar discrepancy is felt to be beyond the statistical limits. We return to discuss this point below.

The two sets of results for ^{44}Sc^m are therefore presented in Table 2 along with the cross sections for production of ^{44}Sc^g, the isomer ratios, and the total cross sections for the ^{45}Sc$(\alpha,\alpha n)^{44}$Sc reaction. The latter two columns are calculated using the average of the two sets of ^{44}Sc^m data. In Fig. 2, the

Can. J. Chem. Downloaded from www.nrcresearchpress.com by 210.87.254.105 on 09/06/12
For personal use only.

TABLE 2. Cross sections in mb for production of isomers of $^{44}Sc^{m+g}$

E, MeV	$^{44}Sc^{m}$(271.2)	$^{44}Sc^{m}$(1157.0)	$^{44}Sc^{g}$	m(6+)/g(2+)	$^{44}Sc^{m+g}$
19.3	10.3 ± 0.3	9.7 ± 0.3	6.2 ± 0.3	1.61 ± 0.10	16.2 ± 0.4
27.1	90.2 ± 3.7	85.0 ± 3.7	50.5 ± 1.6	1.73 ± 0.09	138.1 ± 4.0
32.0	137.0 ± 3.1	125.7 ± 3.2	80.9 ± 1.7	1.62 ± 0.05	212.2 ± 3.6
39.7	90.5 ± 3.5	82.3 ± 3.7	69.9 ± 3.1	1.29 ± 0.08	156.3 ± 4.8
43.3	84.8 ± 2.5	81.2 ± 2.5	74.2 ± 1.9	1.12 ± 0.04	157.2 ± 3.1
51.2	109.0 ± 5.2	98.8 ± 5.4	75.2 ± 4.6	1.38 ± 0.11	179.1 ± 7.1
62.0	115.4 ± 4.4	106.6 ± 4.4	72.8 ± 2.8	1.52 ± 0.08	183.8 ± 5.2
71.1	129.5 ± 3.3	121.5 ± 3.4	77.7 ± 2.0	1.62 ± 0.06	203.2 ± 4.0
83.2	121.0 ± 3.0	115.4 ± 3.1	80.6 ± 1.7	1.50 ± 0.05	198.8 ± 3.5

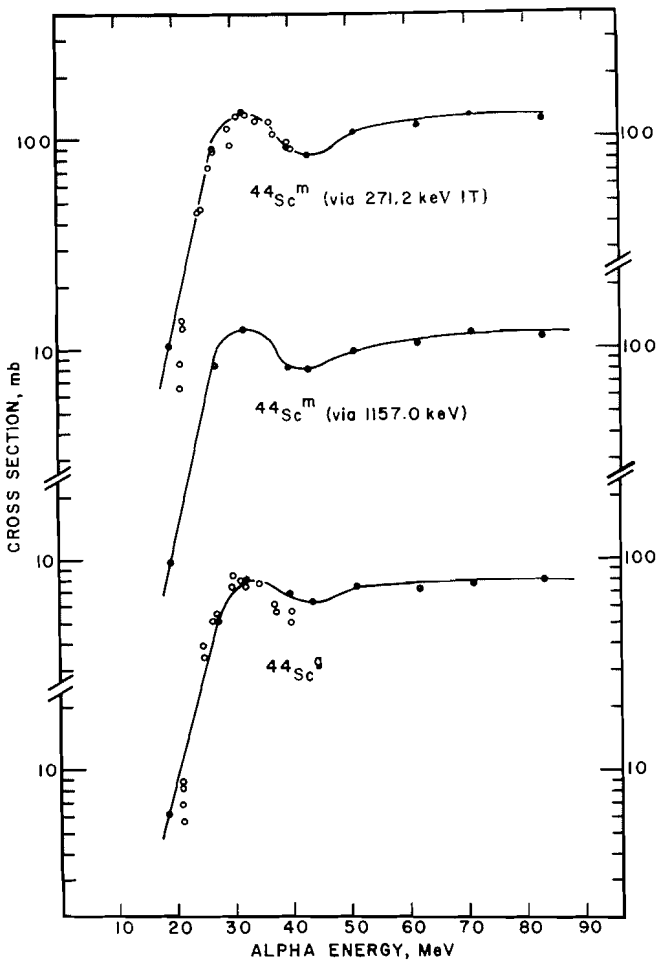

FIG. 2. The experimental excitation functions for the $^{45}Sc(\alpha,\alpha n)^{44}Sc^{m,g}$ reactions. The top two graphs represent the production of $^{44}Sc^{m}$ as determined by measurements of the isomeric transition, and growth and decay, respectively. Closed circles are data measured in this work. Open circles are taken from ref. 8.

experimental excitation functions are plotted along with data measured earlier at low energies by Chen and Miller (8).

Discussion

The gamma ray spectrum

The gamma ray spectrum recorded in a one-hour count taken twelve hours following the end of a 75 MeV irradiation is shown in Fig. 1. For monitor purposes, the scandium reaction provides an extremely clean spectrum, suitably for use as an internal monitor in activation experiments. Ignoring the ^{24}Na peak, which would not be present if a scandium monitor were being used, there are only two peaks of consequence at energies up to 1400 keV. These are the ^{43}Sc and ^{43}K peaks at 372.9 and 617.2 keV. The peaks of interest, 271.2 and 1157.0 keV, are clearly defined with integrated areas several hundred times greater than background. If analysis of the monitor is deferred for several days or a week, often a convenience in activation experiments, the two remaining interfering peaks are greatly reduced while the peaks of interest remain (due to reduced background) factors of more than one hundred above background.

The cross section of $^{44}Sc^{m}$

As stated above, the two cross sections measured for the production of $^{44}Sc^{m}$ differ by a factor of about 7% depending upon whether they are measured by the 271.2 keV isomeric transition or the 1157.0 keV gamma ray which follows beta decay. In most work, it would suffice to average the two values, either explicitly noting the discrepancy, or including it in the estimate of uncertainty in the data. This was not considered acceptable given the fundamental prupose of this work, to evaluate a monitor excitation function for alpha particle induced reaction studies. Inevitably the usefulness of this work arises from other studies which will be done, and which will evaluate the $^{44}Sc^{m}$ production cross section by one or the other of the two methods. Since it is felt the discrepancy is real, reproducible in nine experiments, both sets of data are reported in Table 2 and shown in Fig. 2.

There are only three likely sources for such a discrepancy: the relative half-lives of the isomer and the ground state, the detector efficiency calibration curve, or the assumed decay schemes.

The half-lives are very well characterized; the "best" values have changed by not more than 1–2% over the quarter century since the isotope was first studied (13). Errors of 10% in the relative half-lives would be needed to produce a 7% error.

The efficiency calibration curve was generated using the mixed gamma ray reference standard produced at the Atomic Energy Research Establishment, Harwell, England. One of the activities, ^{203}Hg, has a line at 279 keV (very near the 271.2 keV isomeric transition); a second, ^{60}Co, has a line at 1173.2 keV, quite close to the transition at 1157.0. These standard sources have an overall uncertainty of ±2.5% and ±1.5%, respectively. Points defining the efficiency curve fit very well along a straight line on a log E – log efficiency plot. A 7% error would be clearly discernible. The efficiency curves are not felt to be the source of the discrepancy.

The decay scheme of ^{44}Sc was taken from the Table of Isotopes (12), wherein the gamma ray intensities have been

Can. J. Chem. Downloaded from www.nrcresearchpress.com by 210.87.254.105 on 09/06/12
For personal use only.

Can. J. Chem. Downloaded from www.nrcresearchpress.com by 210.87.254.105 on 09/06/12
For personal use only.

adopted from the work of Coleman and Meyer (14). The conversion coefficient for the 271.2 keV isomeric transition, measured by Blue and Bleuler (13), is assumed in both the Table of Isotopes and the nuclear data compilation of Endt and Smith (15) to be 0.139, approximately a factor of 2 greater than the value necessary to produce agreement between the measured values. Because that work was performed nearly thirty years ago with NaI detectors and a vintage magnetic spectrograph, it is tempting to suggest this as the source of the discrepancy. However, the remarkable accuracy of gamma ray energies, half-lives, and branching ratios reported in ref. 13 make such an assumption unjustifiable. Blue and Bleuler also suggested the spin of the isomer to be 6+. This was confirmed in the course of atomic hyperfine splitting experiments by Harris and McCullen (16) which were used to determine the nuclear moments of ^{44}Sc.

A theoretical value of the conversion coefficient may be calculated from the formulation of Segrè (17) for an $E4$ transition (6+ $\rightarrow$ 2+) of 271.2 keV. The calculated value of 0.117 is not in unreasonable agreement with experiment (13).

A final possible source of the discrepancy is the branching ratio to the 1157.0 keV level in the daughter ^{44}Ti. However the observed beta transition is normal allowed ($\Delta I = 0, \Delta\pi =$ no) while a transition to the ground state is 2nd forbidden (2, no) and it is very unlikely that any reasonable decay ocurs to the ground state.

Thus, while it is felt that the discrepancy between the two measurements is real, there is no obvious source of the error. As stated above, because of the nature of this work we have reported both values, such that an experimenter may use the one appropriate to his own measurements.

The excitation function for the ^{45}Sc(α,αn)^{44}Sc reaction

The final excitation functions are shown in Fig. 2. The agreement at low incident energies with the earlier work of Chen and Miller (8) is excellent. This is particularly noteworthy because the earlier work was performed with thin targets; the observed agreement serves as a check on the accuracy of the energy determination for the thick targets used in this work (stopping powers calculated from ref. 11). Only in the measurements of the production cross section for the ground state at the highest energies utilized by Chen and Miller is there a discrepancy of about 20%. It should be noted that Chen and Miller evaluated the cross section of ^{44}Sc^{m} using the 271.2 keV isomeric transition; for this reason their data is plotted on the upper graph of Fig. 2. Like ours, they would lie about 7% higher than the middle curve of Fig. 2 for the ^{44}Sc^{m} measured by growth and decay of the 1157.0 keV line.

The last two columns of Table 2 list the isomer ratios and total reaction cross sections for production of ^{44}Sc. In each case, the average of the two ^{44}Sc^{m} measurements has been used in the calculation.

The first peak represents the contribution to the overall reaction of events in which an alpha particle is emitted. The second long plateau arises from reactions in which two protons and three neutrons are emitted as has been previously discussed (6). The isomer ratio shows a dip at energies of 40–50 MeV very similar to that observed and discussed in earlier work performed in this laboratory on similar proton induced reactions (18). The initial small increase reflects the increasing angular momentum deposition in compound nuclear reactions. The dip occurs during a mechanistic change from compound nucleus reactions to those in which pre-equilibrium cascade processes involving emission of an alpha predominate. Finally, when the emission of individual nucleons from a compound nucleus again becomes the primary mechanism, the isomer ratio once more increases. If studies were carried out at still higher energies, it is expected that the isomer ratio would again decrease as pre-equilibrium emission became the dominant mechanism. It is possible that this decrease is just noticeable in this work at the highest energy data point.

Summary

We have presented in this work the excitation function of the ^{45}Sc(α,α*n*)^{44}Sc reaction at incident energies from 20–90 MeV. It is hoped that this work will provide a beam monitor for alpha particle induced reaction studies, analogous to that work performed by Leo Yaffé and colleagues (19) used for many years in proton induced reactions.

Acknowledgment

This work was made possible by a grant from the Natural Sciences and Engineering Research Council of Canada.

1. C. MAYER-BORICKE. Nukleonika, **22**, 1131 (1977).
2. G. CHEVENERT, N. S. CHANT, I. HALPERN, G. GLASHAUSSER, and D. L. HENDRIE. Phys. Rev. Lett. **27**, 434 (1971).
3. J. R. WU, C. C. CHANG, H. D. HOLMGREN, and R. W. KOONTZ. Phys. Rev. C, **20**, 1284 (1979).
4. E. GADIOLI and E. GADIOLI-ERBA. Z. Phys. A, **299**, 1 (1981).
5. A. MIGNEREY, M. BLANN, and W. SCOBEL. Nucl. Phys. A, **273**, 125 (1976).
6. J. J. HOGAN, E. GADIOLI, E. GADIOLI-ERBA, and B. V. JACAK. Proc. 3rd Int. Conf. Nucl. React. Mech. Varenna, Italia, June, 1982.
7. H. J. PROBST, S. M. QAIM, and R. WEINREICH. Int. J. Appl. Radiat. Isot. **27**, 431 (1976).
8. K. CHEN and J. M. MILLER. Phys. Rev. B, **134**, 1269 (1964).
9. J. B. CUMMING. Ann. Rev. Nucl. Sci. **13**, 261 (1963).
10. J. S. FOSTER, J. W. HILBORN, and L. YAFFE. Can. J. Phys. **36**, 555 (1958).
11. C. WILLIAMSON and J. P. BOUJET. Rep. CEA 2189, CENS. Saclay, France, 1962.
12. C. M. LEDERER and V. S. SHIRLEY. Table of Isotopes. 7th ed. Wiley, New York. 1977.
13. J. W. BLUE and E. BLEULER. Phys. Rev. **100**, 1324 (1955).
14. G. COLEMAN and R. A. MEYER. Phys. Rev. C, **13**, 847 (1976).
15. P. M. ENDT and P. B. SMITH. Nucl. Phys. A, **310**, 657 (1978).
16. D. L. HARRIS and J. D. MCCULLEN. Phys. Rev. **132**, 310 (1963).
17. E. SEGRÈ. Nuclei and particles. 2nd ed. Benjamin, London. 1977.
18. J. J. HOGAN. J. Inorg. Nucl. Chem. **35**, 705 (1973).
19. D. A. NEWTON, S. SARKAR, L. YAFFE, and R. B. MOORE. J. Inorg. Nucl. Chem. **35**, 361 (1973).

Fission probability in the ^{232}Th(p,p′$x$nf) reaction at low energy

CHIEN CHUNG[1]
Department of Chemistry, University of Maryland, College Park, MD 20742, U.S.A.
JAMES J. HOGAN
Department of Chemistry, McGill University, Montreal, P.Q., Canada H3A 2K6
AND
HANS H. MÜLLER
Institute of Physics, University of Zurich, Zurich, Switzerland

Received September 4, 1982

This paper is dedicated to Professor Leo Yaffe on the occasion of his 65th birthday

CHIEN CHUNG, JAMES J. HOGAN, and HANS H. MÜLLER. Can. J. Chem. **61**, 646 (1983).

In our recent works, a model was developed to calculate many of the features of ^{232}Th(p,X) reactions with incident proton energies to 100 MeV. The model reproduced many properties such as spallation excitation functions, total fission cross sections, the symmetric/asymmetric mass ratio, and fission charge dispersion data. In this work, the model approach is extended to consider the fission probability in ^{232}Th(p,p′$x$nf) fission channels. A comparison of the results calculated from the model to the experimental data shows very good agreement, and again justifies the approach of the model.

CHIEN CHUNG, JAMES J. HOGAN et HANS H. MÜLLER. Can. J. Chem. **61**, 646 (1983).

Dans notre récent travail, nous avons mis au point un modèle pour calculer plusieurs des caractéristiques des réactions du ^{232}Th(p,X) avec des protons incidents d'énergie allant jusqu'à 100 MeV. Le modèle reproduit plusieurs propriétés, telles les fonctions d'excitation de fission, les sections droites de fission totale, le rapport de masse symétrique/asymétrique et les données de dispersion de charge de fission. Dans ce travail, nous avons développé l'approche du modèle dans le but de considérer la probabilité de fission dans les canaux de fission du ^{232}Th(p,p′$x$nf). Une comparaison des résultats calculés à partir du modèle aux données expérimentales montre un très bon accord et justifie encore l'approche du modèle.
[Traduit par le journal]

Introduction

In our recent papers (1–3), a modified version of the Pre-Equilibrium/Exciton Model with fission option, developed by Gadioli and co-workers (4), was applied to the ^{232}Th(p,X) reaction with incident proton energies to 100 MeV. Many features, such as spallation excitation functions, total fission cross sections, the symmetric/asymmetric fission ratio, and fission charge dispersion data were successfully reproduced. More recently (5), the same model calculation was applied to the ^{238}U(p,X) reaction system on which much more experimental data are available. Again, most, if not all, experimental data including the properties mentioned above as well as the post-fission neutron multiplicity were well reproduced. All together, these works comprise a rather comprehensive study of heavy target reaction/fission with excitation energies to 100 MeV.

In this model, the fission probability, P_f, defined as the probability that a nucleus ^{A}Z of given excitation energy fissions, was assumed to be energy dependent. The form of the energy dependence could not be directly tested; however, the excellent agreement between our calculations and 27 excitation functions of spallation products and 133 fission charge dispersion data points suggested our treatment of P_f was valid. This assumption contradicts earlier treatments of P_f as being independent of excitation energy.

In a comprehensive review of 69 fission/spallation reaction cross sections in the 1950's, Vandenbosch and Huizenga (6) concluded that for nuclei with $Z \geq 90$, excited up to 23 MeV, the fission probability which is deduced from such data is independent of excitation energy. With more data available, Hyde (7) later arrived at a similar conclusion for nuclei excited to 40 MeV. It should be pointed out that their conclusions were derived from many simplifying assumptions such as averaging the fissioning mass from different targets and projectiles at different excitation energies, implicitly indicating that the fission probability was independent of, or weakly dependent on, the excitation energy to 40 MeV. Without comparison to a directly measured P_f, the question of the form of the excitation energy dependence or even whether such a dependence exists could not be verified.

A recent experimental contribution of Eder *et al.* (8) measured the P_f of the ^{232}Th(p,p′$x$nf) reaction at E_p = 52.5 MeV, providing for the first time a direct insight into the fission probability of fissioning isotopes with Z of 90 and excited to about 40 MeV. Measurement of the emitted proton energy in coincidence with fission fragments allowed extraction of the excitation energy of the fissioning nucleus. In this work, we have tested our model calculation, using the same energy dependent fissionability and without modification of any parameters, to reproduce the P_f data in this ^{232}Th(p,p′$x$nf) reaction. In the following sections, we provide an interpretation of the experimental data and a brief description of the calculation, followed by discussions of the comparison of the theoretical predictions with the data.

Data and calculation

A. *The fission probability data*

Eder *et al.* (8) irradiated the natural thorium target with

[1]Present address: Department of Physics, Brookhaven National Laboratory, Upton, L.I., New York 11973, U.S.A.

Can. J. Chem. Downloaded from www.nrcresearchpress.com by 210.87.254.40 on 09/06/12
For personal use only.

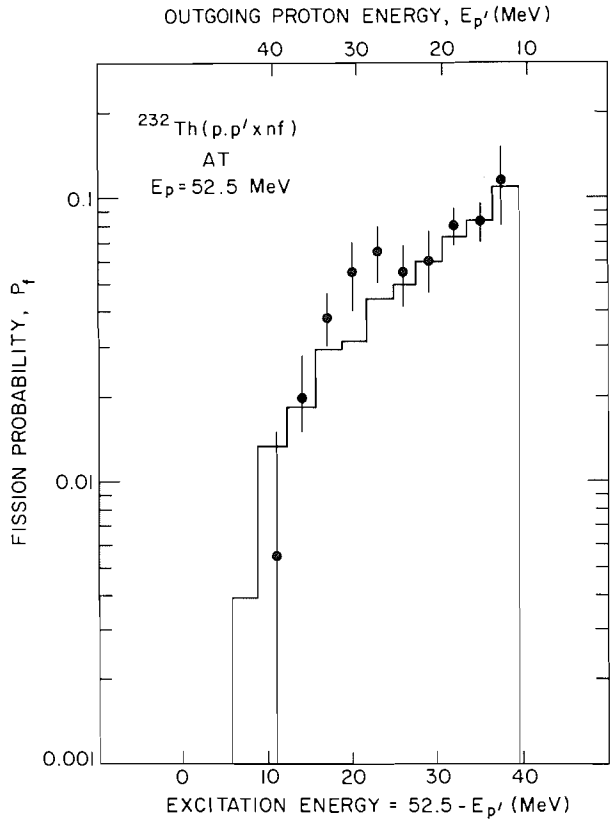

FIG. 1. The fission probability, P_f, of the ^{232}Th(p,p'$x$nf) reaction at 52.5 MeV. The data points and uncertainties are taken from ref. 8; the histogram is the calculated results of the Pre-Equilibrium/Exciton Model performed in this work.

incident protons of 52.5 MeV. With coincidence circuitry, they used an $E - \Delta E$ telescope to measure the outgoing proton kinetic energy, $E_{p'}$, and a Si-surface barrier detector to record the coincident fission fragment. The singles spectrum of proton energies (without coincidence) was also measured to account for all (p,p'X) reactions including the coincident (p,p'$x$nf) fissioning channels. The fission probability, P_f, of the ^{232}Th(p,p'$x$nf) reaction system was then derived from both the singles and coincident spectra. The data for P_f, as a function of proton energy is reproduced in Fig. 1, taken from ref. 8.

With 52.5 MeV incident protons, multi-chance fission, (p,p'$x$nf) with $x = 0-4$, is energetically possible, corresponding to the fissioning isotopes $^{232-228}$Th. Thus each data point represents a mixed P_f from different fissioning nuclides with various excitation energies, weighted according to each fission channel's population. The term *excitation energy* in Fig. 1, taken from the original caption in ref. 8, should be interpreted as the fissioning excitation energy only for the contributions from first chance fission, (p,p'f), and as residual energy for other (p,p'$x$nf) fissioning channels in which some neutrons may have been emitted before fission.

B. The Exciton Model calculation with fission option

The model calculation is essentially identical to that presented and discussed in our recent studies of ^{232}Th(p,X) reactions (1, 3). A modified version of the Pre-Equilibrium/Exciton Model with fission option (1, 4) is used. In the pre-equilibrium stage, α particles as well as nucleons may be emitted and multi-particle emission is allowed. After equilibrium is reached, excited nuclei are allowed to de-excite either by evaporation of neutrons, protons, α particles, or by fissioning. The fission probability, P_f, defined as $\Gamma_f/(\Gamma_f + \Gamma_n + \Gamma_p + \Gamma_\alpha)$ where Γ_f, Γ_n, Γ_p, and Γ_α are the fission, neutron, proton, and α emission widths, respectively, is evaluated at the moment of scission. The energy-dependent widths are calculated exactly as in eqs. [1]–[3] in ref. 1. Fission barriers were evaluated by Gadioli *et al.* (9), while particle binding energies are taken from those compiled by Wapstra and Gove (10), and the pairing energies are those of Nemirovski and Adamchuk (11). The ratio of the level density parameter in the distorted fissioning nucleus to that in the ground state, $a_f/a_{n'} = 1.05$, is the same as that employed in our earlier works (1, 3, 5).

The calculation follows, on an event by event basis, the evolution of the de-excitation of the p + ^{232}Th system. When one and only one proton is emitted and fission follows, i.e., an event of ^{232}Th(p,p'$x$nf) occurs, the following data are stored: the kinetic energy of the outgoing proton, $E_{p'}$, the identity of the fissioning nucleus, ^AZ, as well as its fissioning energy, and the fission probability, P_f. To simulate the experimental conditions, the P_f evaluated from various (p,p'$x$nf) events are further grouped into twelve bins of emitted proton energy. The final fission probability for the system is calculated for each bin weighting by the population in that energy bin.

Discussion

In this work, 40 000 cascades were followed; of these, there were 281 (p,p'$x$nf) events recorded. As a function of the emitted proton energy, the calculated values of the fission probability, P_f, are shown in the histogram of Fig. 1. A good agreement exists between the experimental values and the theory at all energies; the statistical error in the calculation is about 15%.

For residual energies less than 17.5 MeV, the only open fission channel corresponds to (p,p'f) events. Therefore, the data points in this region reflect the probability of fission of ^{232}Th. The experimental data clearly indicate the energy dependence of P_f, and the theory reproduces the variation very well. If the fissionability, P_f, were independent of excitation energy the measured values of P_f would reflect only the spectrum of pre-equilibrium proton energies. This is known (12) to be rather flat at these incident energies.

With increasing residual energy, the Th fission reaction becomes more complex in that more than a single fission channel is open. The experimental value of P_f then reflects not only the energy dependence of the fissionability but also the relative population and energy spectrum of different fissioning nuclei. In the region of "excitation energy" above 27.5 MeV, all fission channels, (p,p'$x$nf), $x = 1-4$, become energetically possible. Again the data are reproduced very well in this region. The good agreement suggests that the Exciton Model is reproducing the energy distributions of each residual nucleus which may undergo fission as well as giving an indication of the energy dependence of the fissionability.

In the intermediate energy region, which the calculation slightly underestimates, the statistical uncertainty in the histogram is approximately 20%. While this does not entirely account for the underestimate, it suggests that a small error in either a neutron binding energy or a fission barrier for a single nucleus could easily compensate for the difference. In either case, the good agreement at both low and high energies underscores the basic validity of the approach taken. In the model calculation, however, no account is taken of angular momentum effects. It is less likely that angular momentum effects seriously alter the results of proton-induced reactions which

Can. J. Chem. Downloaded from www.nrcresearchpress.com by 210.87.254.40 on 09/06/12
For personal use only.

involve only a small angular momentum transfer, although these effects might be expected to play a major role in fission induced by moderate energy α's or heavy ions (13).

In conclusion, an excitation energy dependent P_f calculation coupled with the Pre-Equilibrium/Exciton Model approach has been applied to the ^{232}Th(p,p′$x$nf) reaction. A comparison of the results calculated from the model to the experimental data (8) shows very good agreement. Strong evidence from those data indicates that the fission probability is explicitly energy dependent. The good agreement between the theoretical predictions and the measured P_f, particularly in the low energy region, further justifies the form of the energy dependence used in this, and earlier (1, 3, 5) work.

Acknowledgments

This work was made possible by grants from the Natural Sciences and Engineering Research Council of Canada. We wish to thank Professor Ettore Gadioli of the National Institute of Nuclear Physics, University of Milan, Italy, for many helpful discussions. We further acknowledge the kind cooperation of Professor William Walters of the University of Maryland.

1. J. J. HOGAN, E. GADIOLI, E. GADIOLI-ERBA, and C. CHUNG. Phys. Rev. C**20**, 1831 (1979).
2. C. CHUNG and J. J. HOGAN. Proc. Int. Conf. Nucl. Phys. Berkeley, CA. Report LBL-11118. 1980. p. 296.
3. C. CHUNG and J. J. HOGAN. Phys. Rev. C**24**, 180 (1981).
4. E. GADIOLI, E. GADIOLI-ERBA, and J. J. HOGAN. Phys. Rev. C**16**, 1404 (1977).
5. C. CHUNG and J. J. HOGAN. Phys. Rev. C**25**, 899 (1982).
6. R. VANDENBOSCH and J. R. HUIZENGA. Proc. 2nd UN Conf. Peaceful Uses of Atomic Energy. Vol. 15, Paper P/688. Geneva. 1958.
7. E. K. HYDE. Nuclear properties of the heavy elements. Vol. III. Fission phenomena. Prentice Hall, NJ. 1964. p. 328.
8. G. EDER, H. JASICEK, R. PRASAD, P. RIEHS, H.H. MULLER, W. REICHART, P. SCHOBER, S. STEINER, B. STROHMAIER, and M. UHL. Acta Phys. Austriaca, **52**, 125 (1980).
9. E. GADIOLI, E. GADIOLI-ERBA, and A. MORONI. Z. Phys. A**288**, 39 (1978).
10. A. H. WAPSTRA and N. B. GOVE. Nucl. Data, A**9**, 268 (1971).
11. P. E. NEMIROVSKI and YU. V. ADAMCHUCK. Nucl. Phys. **39**, 551 (1962).
12. F. E. BERTRAND and R. W. PEELLE. Phys. Rev. C**8**, 1045 (1973).
13. H. DELAGRANGE, A. FLEURY, and J. M. ALEXANDER. Phys. Rev. C**17**, 1706 (1978).

Can. J. Chem. Downloaded from www.nrcresearchpress.com by 210.87.254.40 on 09/06/12
For personal use only.

Yields of products in the spontaneous fission of ^{252}Cf by direct γ-ray spectroscopy

L. TOPPARE, H. N. ERTEN, AND N. K. ARAS
Department of Chemistry, Middle East Technical University, Ankara, Turkey

Received July 15, 1982

This paper is dedicated to Professor Leo Yaffe on the occasion of his 65th birthday

L. TOPPARE, H. N. ERTEN, and N. K. ARAS. Can. J. Chem. **61**, 649 (1983).

Yields of products both in the light and heavy sides in the spontaneous fission of ^{252}Cf were measured by direct γ-ray spectroscopy technique. By suitably choosing collection, cooling, and counting times, it was possible to observe products with half-lives between 1 min and 1 h. A definite fine structure, as observed in the case of thermal neutron fission of ^{235}U and ^{239}Pu, was not observed. A graphical method was utilized to obtain the number of neutrons as a function of fragment mass using cumulative chain yields.

L. TOPPARE, H. N. ERTEN et N. K. ARAS. Can. J. Chem. **61**, 649 (1983).

Faisant appel à la technique de spectroscopie de rayons gamma, on a mesuré les rendements en produits légers et en produits lourds provenant de la fission spontanée du ^{252}Cf. En choisissant convenablement la collection, le refroidissement et les temps de dénombrement, il est possible d'observer des produits dont le temps de demi-vie se situe entre une minute et une heure. On n'a pas observé une structure fine définie, telle qu'observée dans le cas de la fission par neutron thermique de ^{235}U et du ^{239}Pu. On a utilisé une méthode graphique pour obtenir le nombre de neutrons en fonction de la masse du fragment utilisant les rendements de chaîne cumulatifs.

[Traduit par le journal]

Can. J. Chem. Downloaded from www.nrcresearchpress.com by 210.87.254.5 on 09/06/12
For personal use only.

Introduction

In most low energy fission, when the chain yields are plotted as a function of mass number A, a double-humped mass distribution curve is obtained. In the thermal neutron fission of ^{235}U, in the region of the heavy peak, irregularities from smooth behavior were observed (1). These were explained by the influence of shell structure. These shell effects occur also in the spontaneous fission of ^{242}Cm but no such effects are reported for the spontaneous fission of ^{252}Cf (2–4).

With the advent of Ge(Li) detectors, several properties of fission products such as yields, ranges, etc., have been studied by direct γ-ray spectroscopy (5, 6). The high resolving power and the possibility of observing a large number of isotopes in one spectrum are the main advantages of this technique. Another advantage is that this method enables one to study short-lived products without losing time in chemical separations. Measuring fission yields by observing direct γ-ray spectra with semiconductor detectors was utilized by several groups (5, 7, 8). The aim of this work was to study yields of fission products in the spontaneous fission of ^{252}Cf especially those of short half-lives by this technique. By suitably choosing collection times of products, cooling and counting times, it was possible to observe products with half-lives between 1 min and 1 h. Previous yield determinations were restricted to products with half-lives of several hours or longer and were done mainly by radiochemical methods (2–4, 9).

Experimental

A 1 μg ^{252}Cf source electroplated on a nickel backing which was obtained from the Radiochemical Center, Amersham, was used. Fission products were collected using aluminium catcher foils. The thickness of the ^{252}Cf source was much less than the ranges of the fission fragments and the collection efficiencies of the isotopes studied were assumed to be the same. The collection time was systematically varied from a few minutes to several minutes. Three sets of experiments were done. The first set was designed to determine yields of products with half-lives of a few minutes. Five minutes of collection, 30 s of cooling, and 200 s of counting times were found to be suitable in these experiments. In the second set of experiments, collection times of 30 min, cooling time of 5 min, and counting times of 800 s were employed. The last set of experiments was designed to study products with half-lives close to 1 h. Collection times of 1 h and cooling and counting times of 15 min and 67 min, respectively, were used. The γ-ray spectra arising from the products were observed with a 30 cm^3 Ge(Li) detector coupled to a 4096 channel analyzer.

TABLE 1. Radioactive decay characteristics of fission products studied in this work*

Isotope	Half-life	γ-Ray energy (keV)	Absolute intensity (%)
^{101}Mo	14.6 m	590.9	20
^{104}Tc	18 m	358.0	89
^{106}Tc	36 s	270.1	85
^{109}Rh	90.1 s	326.5	62
^{116g}Ag	2.68 m	513.5	84
^{131}Sb	23 m	642.1	23
^{135}I	6.7 h	526.6	7.2
^{136m}I	46 s	381.6	98
^{137}Xe	3.83 m	455.5	33
^{138g}Cs	32.2 m	409.0	4.1
^{141}Ba	18.3 m	276.9	22.3
^{144}La	39.8 s	397.4	98
^{146}Ce	13.9 m	218.2	18
^{149}Nd	1.73 h	211.3	27.3
^{151}Nd	12.4 m	117.1	59.6

*From refs. 10, 11.

Calculations

The cumulative yields were determined by using a method based on comparison with a reference nuclide. ^{139}Xe, ^{141}Ba, and in some cases, ^{108}Ru and ^{134}Te were used as reference isotopes. Calculations were sometimes done by using more than one γ ray belonging to the decay of a single species as well as using more than one reference species. The γ-ray peak areas were corrected for absolute line intensities, conversion electrons, and efficiency of the detector. Table 1 gives the decay characteristics of the species suitable for the study as well as γ-ray energies and their absolute intensities (10, 11). The decay of γ lines selected for yield determinations was followed for over

TABLE 2. Fission yields (in %) from the spontaneous fission of ^{252}Cf

Isotope	Cumulative yield (This work)	Chain yield (This work)	Literature values	
			Ref. 13	Ref. 4
^{101}Mo	3.23±0.40	3.23±0.40	—	3.7±0.1
^{104}Te	5.50±0.40	5.51±0.42	—	—
^{106}Te	5.51±0.20	5.62±0.52	5.75±0.58	5.8±0.3
^{109}Rh	5.18±0.20	5.20±0.52	5.60±0.56	—
^{116g}Ag	1.60±0.20	1.63±0.22	—	—
^{131}Sb	1.20±0.20	1.80±0.30	1.64±0.16	1.8±0.1
^{135}I	4.80±0.10	5.34±0.11	3.86±0.39	4.9±0.4
^{136m}I	0.60±0.10*	—	—	—
^{137}Xe	4.60±0.20	4.85±0.20	—	5.2±0.2
^{138}Cs	5.61±0.10	5.63±0.11	—	—
^{141}Ba	6.00±0.20	6.08±0.20	6.08±0.61	5.8±0.4
^{144}La	5.40±0.20	5.59±0.20	—	5.7±0.2
^{146}Ce	3.82±0.10	3.89±0.10	—	—
^{149}Nd	2.42±0.10	2.42±0.10	2.81±0.28	—
^{151}Nd	1.72±0.10	1.77±0.11	1.60±0.16	—

*Independent yield.

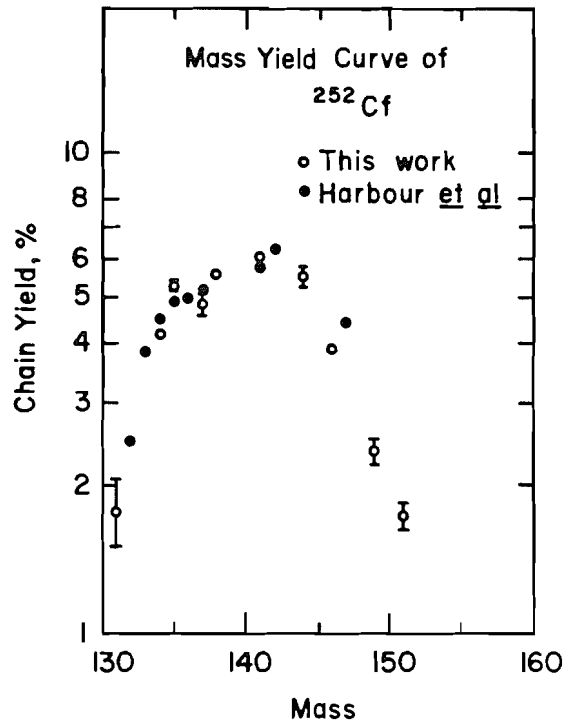

FIG. 1. Mass-yield curve for heavy products from the spontaneous fission of ^{252}Cf. A = 134 yield is taken from ref. 14.

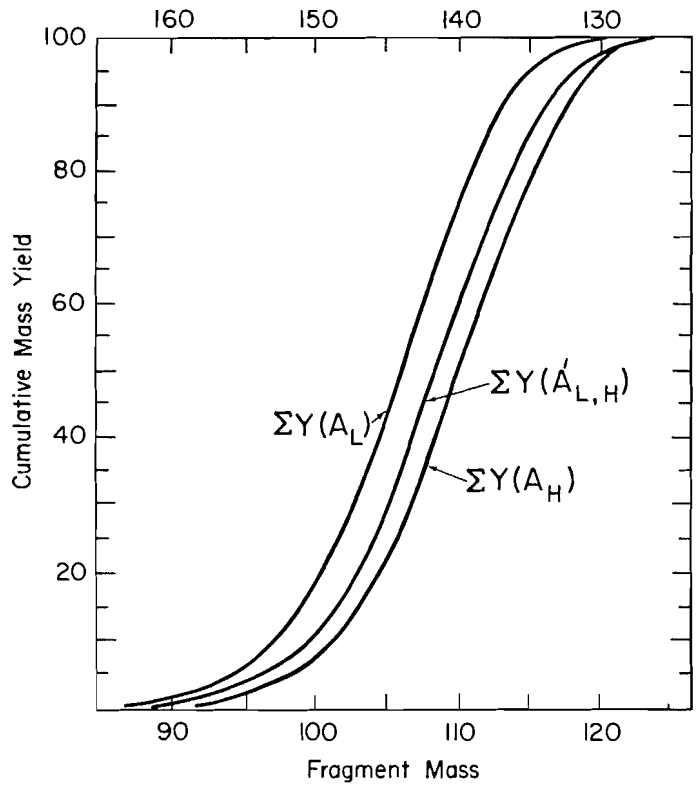

FIG. 2. The cumulative chain yields of light and heavy fission products, ($\Sigma Y(A_L)$, $\Sigma Y(A_H)$), plotted against mass number. Middle curve shows the cumulative chain yields, $\Sigma Y(A'_{L,H})$, before neutron emission from the work of Walsh and Boldeman (17).

four half-lives and only those lines with correct half-lives were used.

If the half-life of a precursor in a chain is very short compared to that of the product of interest and the collection time, the decay chain may be considered to begin at that product. In such cases single growth and decay equations could be used. Those products with appreciable contributions from precursors were dealt with by using Batemann equations.

Results and discussion

Mass chains found to be suitable for study by this technique were 101, 104, 106, 109, 116, 131, 135, 137, 138, 141, 144, 146, 149, and 151. The cumulative fission yield values found in this work are given in Table 2. Chain yields were obtained from these values by estimating fractional cumulative yields (12). In most cases the corrections amounted to less than 10%. A comparison with radiochemical results (4, 13) is also given in Table 2. The errors shown are those arising from counting statistics. As seen in Fig. 1, an asymmetric mass distribution is observed with no convincing evidence of fine structure, in

Can. J. Chem. Downloaded from www.nrcresearchpress.com by 210.87.254.5 on 09/06/12
For personal use only.

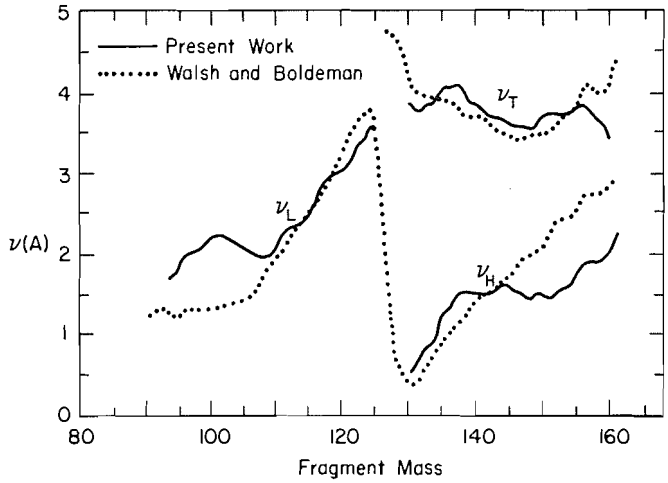

FIG. 3. The variation of number of neutrons as a function of mass number.

agreement with previous literature work (2, 3, 12, 13).

The chain yield values available in the literature and the values obtained in this work enabled us to obtain weighted average chain yields for mass chains 85 through 165. After normalization of the light and heavy peaks to 100% each, average mass values were determined for the two peaks as: $\bar{A}_L = 106.1$ and $\bar{A}_H = 141.8$. The average number of neutrons emitted promptly was obtained from the relation

$$\bar{\nu} = A_f - (\bar{A}_L + \bar{A}_H), \text{ as } \bar{\nu} = 4.1$$

This value is in fair agreement with those reported in the literature (8, 15).

A graphical method first used by Terrell (16) was utilized to obtain the number of neutrons as a function of fragment mass using cumulative chain yields. The cumulative mass yields of light and heavy fission products were plotted versus mass number as shown in Fig. 2. The middle curve shows the pre-neutron emission cumulative chain yields versus fragment mass number taken from the work of Walsh and Boldeman (17). By extrapolating this line horizontally towards the light and heavy sides, neutron number emitted by light and heavy fragment masses were obtained. The results are shown in Fig. 3. The results are in good agreement with those reported in the literature (8, 15, 17, 18) except at very heavy and very light fragments. Also note that the values of ν_A calculated for very light and heavy fragments are known to be unreliable because mass dispersion hinders accurate measurement of fragment yields that are very small.

1. H. G. THODE and R. L. GRAHAM. Can. J. Res. **25A**, 1 (1974).
2. L. E. GLENDENIN and E. P. STEINBERG. J. Inorg. Nucl. Chem. **1**, 45 (1955).
3. W. E. NERVIK. Phys. Rev. **119**, 1685 (1960).
4. R. M. HARBOUR, M. EICHOR, and D. E. TROUTNER. Radiochem. Acta, **15**, 146 (1971).
5. G. E. GORDON, J. W. HARVEY, and H. NAKAHARA. Nucleonics, **24**, No. 12, 62 (1966).
6. G. YENER, O. BIRGÜL, and N. K. ARAS. Nucl. Phys. A**307**, 173 (1978).
7. J. BLACHOT, L. C. CARRAZ, P. CAVALLINI, E. MONNAND, and F. SCHUSLER. J. Radioanal. Chem. **7**, 309 (1971).
8. J. BLACHOT, P. CAVALLINI, A. FERRIEU, and R. LOUIS. J. Radioanal. Chem. **26**, 107 (1975).
9. H. GÖKTÜRK, O. BIRGÜL, H. N. ERTEN, and N. K. ARAS. J. Inorg. Nucl. Chem. **37**, 2247 (1975).
10. H. G. BÖRNER, W. F. DAVIDSON, J. ALMEDIA, J. BLACHOT, J. A. PINSTON, and P. H. M. VAN ASSCHE. Nucl. Inst. Meth. **164**, 579 (1979).
11. C. M. LEDERER and V. S. SHIRLEY (*Editors*). Table of isotopes. 7th ed. John Wiley, New York. 1978.
12. H. N. ERTEN and N. K. ARAS. J. Inorg. Nucl. Chem. **41**, 149 (1979).
13. K. F. FLYNN, J. E. GINDLER, and L. E. GLENDENIN. J. Inorg. Nucl. Chem. **37**, 881 (1975).
14. H. N. ERTEN, O. BIRGÜL, and N. K. ARAS. J. Inorg. Nucl. Chem. **40**, 183 (1978).
15. J. P. UNIK, J. E. GINDLER, L. E. GLENDENIN, K. F. FLYNN, A. GORSKI, and R. K. SJOBLOM. Proc. Symp. on Phys. Chem. Fission, IAEA-SM-174/209. 1964.
16. J. TERRELL. Phys. Rev. **127**, 880 (1962).
17. R. L. WALSH and J. W. BOLDEMAN. Nucl. Phys. A**276**, 189 (1977).
18. M. KILDIR and N. K. ARAS. Phys. Rev. C**25**, 365 (1982).

Can. J. Chem. Downloaded from www.nrcresearchpress.com by 210.87.254.5 on 09/06/12
For personal use only.

Catalytic transfer hydrogenation of benzylic and styryl compounds with palladium/carbon and 2-propanol. Selective removal of *O*-benzyl groups from carbohydrate derivatives

VANGA S. RAO AND ARTHUR S. PERLIN

Department of Chemistry, McGill University, Montreal, P.Q., Canada H3C 3G1

Received August 11, 1982

This paper is dedicated to Professor Leo Yaffe on the occasion of his 65th birthday

VANGA S. RAO and ARTHUR S. PERLIN. Can. J. Chem. **61**, 652 (1983).

2-Propanol is shown to be an effective hydrogen donor, in the presence of palladium/carbon, for catalytic transfer hydrogenation reactions of benzylic and styryl compounds, e.g., for the quantitative conversion of cinnamyl alcohol into 3-phenylpropanol. In the reduction of derivatives of cinnamic acid, decarboxylation also occurs. During the latter reaction, the phenyl group appears to function as an anchoring group for the palladium atom, because derivatives of phenylpropanoic acid are decarboxylated more readily than are those of phenylacetic acid. In hydrogenolysis reactions, aryl alcohols undergo disporportionation whereas benzyl ethers, represented by *O*-benzyl and related derivatives of carbohydrates, are smoothly cleaved. Although 2-propanol is less reactive as a hydrogen donor than formic acid, it exhibits greater selectivity, as illustrated by relative rates of hydrogenolysis of *O*-benzyl and *O*-benzylidene substituents. The use of alumina-supported palladium is more effective than palladium/carbon for promoting stepwise removal of *O*-benzyl substituents, as shown by the preparation of methyl 2-*O*-benzyl- and -3-*O*-benzyl-α-D-glucopyranoside from the 2,3-di-*O*-benzyl derivative. A possible relationship between the orientation of *O*-benzyl groups and the chemical shift differences between the diastereotopic benzylic protons is described.

VANGA S. RAO et ARTHUR S. PERLIN. Can. J. Chem. **61**, 652 (1983).

On montre que le propanol-2 est un donneur efficace d'hydrogène en présence de palladium/charbon lors de réactions d'hydrogénation par transfert catalytique, des composés benzyliques et styryles; par exemple, pour la transformation quantitative de l'alcool cinnamique en phényl-3 propanol. Il se produit également une décarboxylation lors de la réduction de l'acide cinnamique. Lors de cette dernière réaction, la fixation de l'atome de palladium semble se faire sur le groupe phényl puisque les dérivés de l'acide phénylpropanoique sont décarboxylés plus facilement que ceux de l'acide phénylacétique. Dans les réactions d'hydrogénolyse, l'alcool arylique subit une dismutation alors que les éthers benzyliques comme les dérivés *O*-benzyle ou apparentés des carbohydrates se clivent de façon douce. En dépit du fait que le propanol-2 est moins actif que l'acide formique en tant que donneur d'hydrogène, il présente une plus grande sélectivité qui est démontrée par les vitesses relatives d'hydrogénolyse des substituants *O*-benzyle et *O*-benzylidène. Le palladium déposé sur de l'aluminium est plus efficace que le palladium/charbon pour promouvoir l'élimination par étapes des substituants *O*-benzyle; cette propriété est illustrée par la préparation des *O*-benzyl-2 et *O*-benzyl-3 α-D-glucopyrannosides de méthyle à partir du dérivé de-*O*-benzyl-2,3. On décrit une relation possible entre l'orientation des groupes *O*-benzyle et les différences de déplacement chimique entre les protons benzyliques diastéréotopiques.

[Traduit par le journal]

Introduction

Transfer hydrogenation reactions catalysed by palladium on carbon (Pd/C) have been reported recently for a number of aryl ethers, aryl alcohols, and styryl derivatives (1). Disproportionation and isomerization reactions were among those observed, and also it was shown (2) that benzyl ethers, notably *O*-benzyl protecting groups of carbohydrate derivatives, were very effectively hydrogenolysed when formic acid was the hydrogen donor. Many other compounds may be utilized as hydrogen donors (3), providing that their oxidation potential is low enough to permit hydrogen transfer under mild conditions. However, as the effectiveness of a donor compound and the characteristics of the reaction it promotes can vary widely, an examination of possible donors is always warranted. 1-Phenylethanol is a recently-found example (1) of a compound that functions well in this capacity. Other secondary alcohols, not necessarily aromatic, also may be suitable. Indeed, 2-propanol has been employed as a hydrogen donor with Raney nickel (4) and $HIrCl_2(Me_2SO)_3$ (5) catalysts. The objective of the present study was to examine the potential of 2-propanol for use with Pd/C catalyst, an additional stimulus being its good solvent properties and its ease of removal from reaction products.

Results and discussion

Reduction of styryl derivatives

Among compounds that have been hydrogenated with 2-propanol and Raney nickel catalyst (4*b*) is *trans*-stilbene (**1**). Bibenzyl (**3**) was obtained as the product in only 40% yield, and a prolonged reaction period led to the formation of 1-cyclohexyl-2-phenylethane. By contrast, bibenzyl (**3**) was isolated in quantitative yield when either *trans*-(**1**) or *cis*-(**2**) stilbene was heated under reflux for 24 h in 2-propanol, in the presence of Pd/C catalyst (Table 1). Similarly, cinnamyl alcohol (**4**) was converted completely into 3-phenylpropanol under the same conditions.

Clearly, then, 2-propanol can serve as an effective hydrogen donor in transfer hydrogenations catalysed by Pd/C. However, other reactions may be promoted as well, depending on the nature of the compounds involved (see Table 1).

An unusual type of example was encountered with *cis*-(**5**) or *trans*-(**6**) 4′-hydroxycinnamic acid and *trans*-3′-methoxy-4′-hydroxycinnamic acid (**7**). That is, when heated under reflux in 2-propanol containing the suspended catalyst, **5**, or **6** and **7** gave 4-ethylphenol (**8**) and 2-methoxy-4-ethylphenol (**9**), respectively, in quantitative yield. It is possible that reduction of the double bond occurred first, by analogy with the reactions of

Can. J. Chem. Downloaded from www.nrcresearchpress.com by 210.87.254.40 on 09/06/12
For personal use only.

TABLE 1. Reactions of benzylic and styryl compounds on Pd/C catalyst

Compound	Product(s)[a]	Mass spectrum[b] (m/z)
PhCH=CHPh (**1**, *trans*; **2**, *cis*)	$PhCH_2CH_2Ph$[c] (**3**)	182(M, 85.8); 91($PhCH_2$, 100)
$PhCH=CHCH_2OH$ (**4**)	$PhCH_2CH_2CH_2OH$[c]	136(M, 46.9); 118(M − H_2O, 82.7); 117(M − H_3O, 87.3); 105($PhCH_2CH_2$, 44); 91($PhCH_2$, 100)
4′-$HOC_6H_4CH=CHCOOH$ (**5**, *cis*; **6**, *trans*)	4′−$HOC_6H_4CH_2CH_3$[c] (**8**)	122(M, 72.9); 107(M − CH_3, 62.1)
3′-CH_3O-4′-$HOC_6H_3CH=CHCOOH$ (**7**, *trans*)	3′-CH_3O-4′-$HOC_6H_3CH_2CH_3$[d] (**9**)	152(M, 90); 137(M − CH_3, 100); 122(137 − CH_3, 44.3)
3′-CH_3O-4′-$HOC_6H_3CH=CHCOOH$ (**7**, *trans*)	3′-CH_3O-4′-$HOC_6H_3CH=CH_2$[e]	150(M, 100); 135(M − CH_3, 84.7)
4′-$HOC_6H_4CH_2CH_2COOH$ (**10**)	4′-$HOC_6H_4CH_2CH_3$[c] (**8**)	122(M, 67); 107(M − CH_3, 100)
4′-$DOC_6H_4CH_2CH_2COOD$ (**10** − d_2)	4′-$HOC_6H_4CH_2CH_3$[f] (**8**)	122(M, 33)
	4′-$HOC_6H_4CH_2CH_2D$ (**8**-*d*)	123(M, 20.8)
Ph_2CHOH (**14**)	Ph_2CH_2[c] (**15**)	168(M, 98.7); 91($PhCH_2$, 66.9)
	Ph_2CO[c] (**16**)	182(M, 41.4); 105(PhCO, 65)
3′-CH_3O-4′-$CH_3OC_6H_3CH_2COOH$ (**11**)	3′-CH_3O-4′-$CH_3OC_6H_3CH_3$[g]	152(M, 100); 137(M − CH_3, 62.7)

[a]The yield was ≥95%, unless otherwise specified in the text (also see Experimental).
[b]Only ions pertinent for structural identification are listed (relative intensities).
[c]The ^1H nmr spectrum was indistinguishable from that presented in ref. 11.
[d]^1H nmr data ($CDCl_3$), δ: 6.95–6.52 (3H, m, Ph), 5.23 (1H, br. s, D_2O-exchangeable, OH), 3.87 (3H, s, OCH_3), 2.57 (2H, q, CH_2; J = 7 Hz), 1.22 (3H, t, CH_3; J = 7 Hz).
[e]^1H nmr data ($CDCl_3$), δ: 7.0–6.7 (3H, m, Ph), 6.6 (1H, dd, CH; J_{cis} = 11 Hz, J_{trans} = 17 Hz), 5.52 (1H, dd, CH_2; $J_{gem} \cong$ 1.5 Hz, J_{trans} = 17 Hz), 5.07 (1H, dd, CH_2; $J_{gem} \cong$ 1.5 Hz, J_{cis} = 11 Hz), 3.87 (3H, s, OCH_3).
[f]Isolated as a 65:35 mixture of undeuterated and monodeuterated compound (estimated by mass spectroscopy (M/M + 1)); reaction conditions were not rigorously anhydrous.
[g]^1H nmr data ($CDCl_3$), δ: 3.85 (6H, s, OCH_3), 2.3 (3H, s, CH_3).

1, **2**, and **4**, and that decarboxylation then followed. Favoring this sequence of events is the fact that the hypothetical reduction product, 3-(4′-hydroxyphenyl)-propanoic acid (**10**), was smoothly decarboxylated in 2-propanol, yielding 4-ethylphenol (**8**). Nevertheless, it was found that Pd/C can promote direct decarboxylation of an α,β-unsaturated acid at an elevated temperature. Hence compound **7**, in refluxing 1,4-dioxane (bp 101°C) for 48 h, was converted into 3-methoxy-4-hydroxystyrene (~65% yield), although at room temperature (in methanol), *trans*-4′-hydroxycinnamic acid (**6**) has been shown (1) to be stable. By comparison, the propanoic acid derivative (**10**) was fully decarboxylated under reflux in 1,4-dioxane in 48 h, and 50% decarboxylated in methanol at reflux temperature. Consequently, as products **8** and **9** were formed quantitatively in 2-propanol (bp 83°C), it is likely that the decarboxylation processes involved mainly the alkanoic acids, rather than **5**, **6**, and **7** directly.

Derivatives of phenylacetic acid, i.e., 3,4-dimethoxy-(**11**) and 4-nitro-(**12**)[1] phenylacetic acid, were decarboxylated only to the extent of ~50% in 48 h over 10% Pd/C in 2-propanol. Nonaromatic acids were even less reactive. Thus, 1,2:3,4-di-*O*-isopropylidene-D-galacturonic acid remained essentially unaffected in the presence of 10% Pd/C or 5% $Pd/CaCO_3$ in either refluxing 2-propanol or 1,4-dioxane, and stearic acid was recovered unchanged after heating under reflux with 10% Pd/C in 1,4-dioxane.

It appears, therefore, that the presence of a phenyl moiety in the substrate is necessary to effect complete, or partial, decarboxylation, possibly because it serves as an anchoring group for the palladium atom in the transition state. The notable difference in reactivity between the phenylpropanoic acid and

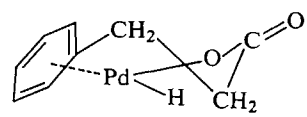

13

phenylacetic acid derivatives also suggests that with the former the palladium atom is readily held near the centre of electron density of the phenyl ring in the transition state (e.g., **13**), whereas an equally stable disposition of the atom seems less feasible with the two-carbon chain of the acetic acid derivatives. Similarly, the fact that **7** undergoes only partial decarboxylation suggests a relatively weak interaction due to unfavorable geometry as compared with **13**. Consistent with the latter possibility, it is worth noting that when the hydroxyl groups of 3-(4′-hydroxyphenyl)-propanoic acid (**10**) were deuterated by exchange with deuterium oxide, and decarboxylation with Pd/C in 1,4-dioxane then carried out, the product was the expected 2-deutero-1-(4′-hydroxyphenyl)-ethane.

Hydrogenolysis of aryl alcohols

Previously (1), it was shown that diphenylmethanol (**14**) is hydrogenolysed to diphenylmethane (**15**) by Pd/C in combination with formic acid whereas, when the hydrogen donor was omitted, a mixture of **15** and benzophenone (**16**) was produced. This disproportionation reaction has now been observed as well in attempting to use 2-propanol as the donor, in that **14** yielded a 1:1 mixture of **15** and **16**. Apparently then, diphenyl-

[1]Although the nitro group may be expected to undergo reduction, there was no suggestion from the ^1H nmr spectrum of the material recovered that the aryl moiety had been modified.

Can. J. Chem. Downloaded from www.nrcresearchpress.com by 210.87.254.40 on 09/06/12
For personal use only.

TABLE 2. ^{1}H nuclear magnetic resonance data for methyl *O*-benzyl-D-glucopyranosides[a]

Compound	2-OCH_2Ph (J_{gem})	Δ^b	3-OCH_2Ph (J_{gem})	Δ^b	Compound	2-OCH_2Ph (J_{gem})	Δ^b	3-OCH_2Ph (J_{gem})	Δ^b
Methyl 2-*O*-benzyl-α-D-glucopyranoside (**25**)	4.72, 4.65 (12.0)	0.07	—	—	Methyl 2-*O*-benzyl-β-D-glucopyranoside (**28**)	4.92, 4.65 (11.5)	0.27	—	—
-3,4,6-triacetate	4.69, 4.63 (12.4)	0.06	—	—	-3,4,6-triacetate	4.77, 4.53 (12.0)	0.24	—	—
Methyl 3-*O*-benzyl-α-D-glucopyranoside (**24**)	—	—	5.04, 4.77 (11.6)	0.27	Methyl 3-*O*-benzyl-β-D-glucopyranoside (**27**)	—	—	5.00, 4.73 (11.5)	0.27
-2,4,6-triacetate	—	—	4.66, 4.56 (11.6)	0.10	2,4,6-triacetate	—	—	4.61	0.00
Methyl 2,3-di-*O*-benzyl-α-D-glucopyranoside (**17**)	4.79,[c] 4.69 (12.0)	0.10	5.05,[c] 4.73 (11.6)	0.32	Methyl 2,3-di-*O*-benzyl-β-D-glucopyranoside (**26**)	4.93,[c,d] 4.70[c] (11.5)	0.23	4.97,[c,d] 4.67[c] (11.5)	0.30
-4,6-diacetate	4.79,[c] 4.66 (12.0)	0.13	4.89,[c] 4.65 (11.8)	0.24	-4,6-diacetate	4.83,[c] 4.61 (11.6)	0.22	4.90,[c] 4.70	0.20
					Methyl 2,3,4-tri-*O*-benzyl-β-D-glucopyranoside	4.92 and 4.82	(11.0)[d]		Δ=0.10
						4.90 and 4.71	(11.0)[d]		Δ=0.19
						4.86 and 4.64	(10.7)[d]		Δ=0.22
					-6-acetate	4.94 and 4.81	(10.9)[d]		Δ=0.13
						4.90 and 4.72	(11.0)[d]		Δ=0.18
						4.85 and 4.56	(10.8)[d]		Δ=0.29

[a] Chemical shifts (δ) and spacings (Hz).
[b] Difference in chemical shifts of AB pair.
[c] Assignments may be reversed.
[d] The AB pair was identified by applying a weak rf at the frequency of one of the A or B transitions, and observing the submultiplet pattern of the transitions having an energy level in common with the perturbed transition (see ref. 8).

methanol itself was a more effective hydrogen donor in the formation of **15** than was 2-propanol (although much less effective than formic acid), thereby accounting for a disproportionation (oxidation–reduction) process. The resistance of benzophenone (**16**), accumulated in the reaction mixture, towards reduction by the external hydrogen donor was checked in a separate experiment, in which benzophenone itself was recovered unchanged. This was not unexpected, as carbonyl groups are generally not susceptible to transfer hydrogenation unless a Lewis acid promoter is present (e.g., $FeCl_3$ (3*a*)), or the carbonyl group is part of a potential aromatic system, as in quinones or decalones (3*b*). Also excluded by these experiments was the possibility that disproportionation occurred, rather than complete hydrogenolysis to **15**, because of inactivation of the catalyst or of an inadequate proportion of it.

Selective removal of O-*benzyl substituents of carbohydrate derivatives*

The foregoing results, showing that 2-propanol can serve as an effective hydrogen donor, stimulated a comparison of its use with that of formic acid (2) in the hydrogenolysis of *O*-benzyl and related substituents of carbohydrate derivatives. In general, the reactions promoted by 2-propanol in the presence of Pd/C catalyst proved to be considerably slower than with formic acid, and also showed a remarkably high degree of selectivity.

The use of a 48 h period of reflux in 2-propanol containing a suspension of 10% Pd/C permitted quantitative removal of the two *O*-benzyl groups from methyl 2,3-di-*O*-benzyl-α-D-glucopyranoside (**17**), and of the *O*-trityl group from methyl 6-*O*-trityl-β-D-glucopyranoside (**18**). By contrast, only about 24 h was needed for these hydrogenolysis reactions when formic acid was the hydrogen donor (2). Nevertheless, 2-propanol was found to exhibit much higher selectivity than formic acid in some instances. With methyl 2,3-di-*O*-benzyl-4,6-*O*-benzylidene-α-D-glucopyranoside (**19**), only the *O*-benzyl groups were removed in 48 h, to give methyl 4,6-*O*-benzylidene-α-D-glucopyranoside (**20**) exclusively. This selectivity is analogous to that found (6) in the hydrogenolysis of **19** with palladium hydroxide in the presence of cyclohexene, although the latter reaction was more rapid. In the presence of formic acid (2) only methyl α-D-glucopyranoside was obtained. The latter was formed from **19** in 2-propanol only by extending the reaction period to 144 h. However, the *O*-benzylidene group was far more labile when it was the sole type of hydrogenolyzable function present. Thus, in separate experiments, acetal **20** and its β-anomer (**21**) yielded methyl α- and β-D-glucopyranoside, respectively, in 48 h.

Another instance of the relatively high selectivity of 2-propanol was found in the fact that although the *O*-trityl group of **18** was easily removed, that of the corresponding 2,3,4-tri-*O*-acetyl derivative (**22**) was virtually unaffected, in contrast to its lability in the presence of formic acid (2). Although competitive inhibition (7) by the *O*-acetyl groups was a possible factor, another possibility was steric hindrance of the

Can. J. Chem. Downloaded from www.nrcresearchpress.com by 210.87.254.40 on 09/06/12
For personal use only.

Can. J. Chem. Downloaded from www.nrcresearchpress.com by 210.87.254.40 on 09/06/12
For personal use only.

trityl C—O bond to adequate exposure on the catalytic surface. Thus, neither the *O*-trityl nor *O*-benzyl substituents of methyl 2,3,4-tri-*O*-benzyl-6-*O*-trityl-β-D-glucopyranoside (**23**) were appreciably susceptible to hydrogenolysis in 48 h under reflux in 2-propanol containing 10% Pd/C. The marked sensitivity to structural variations of 2-propanol, as compared with formic acid, was seen also in its failure to cleanly promote removal of the *O*-benzyl groups of reducing derivatives 2,3,4,6-tetra-*O*-benzyl-D-glucopyranose and 2,3,5-tri-*O*-benzyl-D-arabinofuranose. Although these compounds were converted into D-glucose and D-arabinose, respectively, in the presence of formic acid (2), the products of their reactions with 2-propanol were complex and appeared (nmr evidence) to have incorporated 2-propyl groups.

Partial selectivity in the removal of carbohydrate O-benzyl groups

Chemical shifts of benzylic protons

In addition to variations in reaction characteristics offered by a change in the hydrogen donor employed, other differences are also to be expected when the catalyst adsorbant is altered. An example of this is afforded in the *O*-debenzylation of methyl 2,3-di-*O*-benzyl-α-D-glucopyranoside (**17**). The use of palladium (5%) on alumina in 2-propanol led to the formation of substantial quantities of two intermediate products (R_f 0.37 and 0.26, in 1:1 ethyl acetate–acetone) as well as methyl α-D-glucopyranoside, whereas the latter was essentially the sole product of the Pd/C mediated reaction. Isolated chromatographically, the intermediate products were identified as methyl 3-*O*-benzyl-α-D-glucopyranoside (**24**; R_f 0.37) and methyl 2-*O*-benzyl-α-D-glucopyranoside (**25**; R_f 0.26). In an analogous manner, methyl 2,3-di-*O*-benzyl-β-D-glucopyranoside (**26**) afforded the corresponding 3-*O*-benzyl (**27**; R_f 0.40) and 2-*O*-benzyl (**28**; R_f 0.33) glucosides. It is noteworthy that in both series the 2-*O*-benzyl derivative (**25** and **28**) was substantially more polar, perhaps ascribable to more effective cooperative binding to the chromatographic adsorbant by the 3,4,6-trihydroxy sequence in these isomers, as compared with the more dispersed 2,4,6-sequence.

Products **24**, **25**, **27**, and **28** were identified by comparing their ^{1}H nmr spectra with those of the corresponding *O*-acetylated compounds; i.e., the downfield shifts induced on esterification readily gave the positions of the free hydroxyl groups present.

A noteworthy feature of these spectra is the magnitude of chemical shift differences between diastereotopic benzylic protons, because it appears to indicate a specific dependency on the position of a given *O*-benzyl substituent. For example, the two benzylic protons of 3-*O*-benzyl derivative **24** differ in chemical shift by 0.27 ppm (Table 2) whereas those of the 2-*O*-benzyl derivative (**25**) differ by only 0.07 ppm. Models

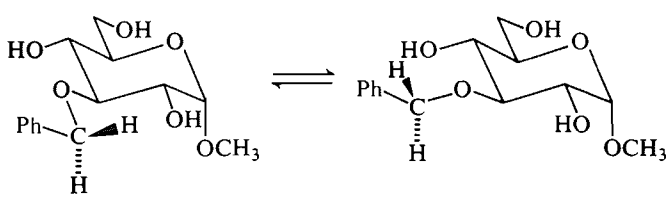

29 **30**

suggest that the 3-*O*-benzyl group may adopt such energetically favorable orientations as represented by **29** and **30**. In these arrangements, presumably, one of the benzylic protons is exposed to overall stronger deshielding than the other by an adjacent oxygen atom (as illustrated), i.e., by O-2 or O-4, respectively,[2] leading to the substantial differences observed in their chemical shifts. Analogous considerations for the 2-*O*-benzyl group of **25** suggest that a chemical shift difference of a similar order (0.27 ppm) might be expected if the group tends to be oriented as in **31**, although not as in **32**, where neither of the protons would be exposed to the deshielding

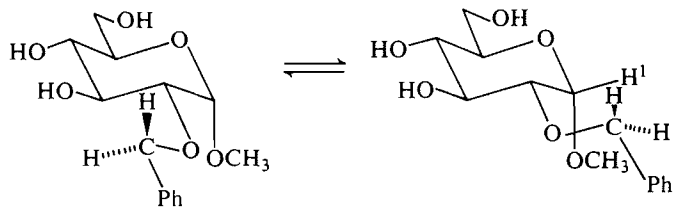

31 **32**

influence of a nearby oxygen atom. Possibly, therefore, **32** is the major contributor to the time-averaged orientation of the 2-*O*-benzyl group because of the small difference observed (0.07 ppm, Table 2).

Data for the β-anomers reinforce these proposals. Orientations possible for the 3-*O*-benzyl group of **27** are expected to be closely analogous to those in **24** (i.e., **29** and **30**) and, as can be seen (Table 2), the same difference in chemical shift (0.27 ppm) is found for both anomers. By contrast, the magnetic environment of the 2-*O*-benzyl group of **28** differs from that of its α-anomer (**25**) by being in close proximity to either O-1 (as in **32**, in which H^1 and OCH_3 have been interchanged) or O-3 (as in **31**), thereby allowing for disparate shielding of the two benzylic protons. Indeed, the chemical shift difference (0.27 ppm) is much larger for **28** than for **25**, in accord with expectation.

Additional support for these proposals concerning orientations favored by *O*-benzyl substituents comes from the effects of acetylation on the chemical shifts. That is, the replacement of OH by $OCOCH_3$, which should be associated with a change in magnetic anisotropy, had a marked effect on the chemical shift difference (Table 2) only in those instances when differential shielding by adjacent oxygen atoms has been invoked. Hence, when the 3-*O*-benzyl group is sandwiched between two neighboring *O*-acetyl groups, the difference is reduced from 0.27 ppm for **24** to 0.10 ppm, and for **27** to zero. There was little change, however, upon acetylation of 2-*O*-benzyl derivative **25**, and only a minor decrease (from 0.27 to 0.24 ppm) for its β-anomer (**28**), O-1 of which was unaltered by esterification. It is also worth noting that the chemical shift differences observed (Table 2) for the anomeric 2,3-di-*O*-benzyl glucosides (**17** and **26**) and their 4,6-di-*O*-acetyl derivatives, correspond closely to those found with their mono-*O*-benzyl analogs, and these differences appear to be largely maintained in the presence of a third *O*-benzyl group, at C-4, as in methyl 2,3,4-tri-*O*-benzyl-β-D-glucopyranoside (Table 2).

[2]The shielding influence of these oxygen atoms may differ, depending on the rotamer populations of OH-2 and OH-4. Although these populations are not known, the possibility that one rotamer is strongly favored (not necessarily the same one for all secondary OH groups) has been shown (9) for OH-2 of α-D-glucopyranose. Hence, OH groups may help to determine the orientation of an adjacent *O*-benzyl group, and vice versa.

Can. J. Chem. Downloaded from www.nrcresearchpress.com by 210.87.254.40 on 09/06/12
For personal use only.

Experimental

Solutions were evaporated below 40°C under diminished pressure. Eastman Chromagram sheets of silica gel with fluorescent indicator were used for thin-layer chromatography. Preparative thin-layer chromatography plates of ~2 mm thickness were made with Merck silica gel GF_{254} (Type 60) containing 13% calcium sulfate as binder. The ^1H nmr spectra of compounds listed in Table 1 were recorded with a Varian T-60 spectrometer. Spectra at 400 MHz (Bruker WH-400) were obtained for compounds **26**–**28**, the diacetates of **17** and **26**, and methyl 2,3,4-tri-*O*-benzyl-β-D-glucopyranoside, with the aid of homonuclear decoupling. Spectra of the other carbohydrate derivatives were recorded with a Varian XL-200 spectrometer. Chemical shifts (δ) are reported with reference to tetramethylsilane. Mass spectra were obtained with an LKB 9000 spectrometer at an ion source voltage of 70 eV.

Palladium (5% and 10%) on activated carbon, palladium (5%) on alumina, and compounds **1**, **2**, **4**, **5**, **6**, **7**, **10**, **11**, **12**, **14**, **16**, and stearic acid were obtained from Aldrich Chemical Co. Inc., and 2,3,4,6-tetra-*O*-benzyl-D-glucose and 2,3,5-tri-*O*-benzyl-D-arabinose from Pfanstiehl Laboratories (Waukegan, IL). Compounds **17**–**21**, **22**, **26**, and di-*O*-isopropylidene-D-galacturonic acid were available from earlier work.

Hydrogenolysis of aryl alcohols and reduction of styryl derivatives

A solution of the aryl alcohol or styryl derivative (0.2 g) in 10 mL of 2-propanol (warmed when the compound was not soluble at room temperature) was added to a stirred suspension of 10% palladium on carbon (1 g) in refluxing 2-propanol (10 mL), protected from moisture with Drierite. After 48 h, the catalyst was filtered off and washed with 2-propanol, and the combined filtrate and washings were evaporated. The residue was vacuum dried briefly when the product was not expected to be highly volatile. In all reactions except those of **11** and **12**, tlc indicated that the starting compound was converted quantitatively into a single product (two products from **14**); nmr and mass spectroscopy confirmed that the product was invariably of high purity. Yields of product recovered: from **1** or **2** (0.2 g, 98%, mp 52°C); from **4** (0.2 g, 98%); from **5** or **6** (~0.14 g, 93%, mp 42–45°C); from **7** (0.15 g of **9**, 96%); from **11** (~50% interconversion, estimated by nmr); from **12** (~50% interconversion, estimated by nmr). The product was identified by comparison of its mass spectrum and/or ^1H nmr spectrum with that of an authentic sample.

Removal of O-*benzyl*, O-*benzylidene*, *or* O-*trityl groups of carbohydrate derivatives*

A solution of the carbohydrate derivative (0.2 g) in 2-propanol (10 mL) (warmed when the compound was not soluble at room temperature) was added to a stirred suspension of 10% palladium on carbon (1 g) in refluxing 2-propanol[3] (10 mL), protected from moisture by Drierite. When, as shown by periodic tlc examination, the starting material had disappeared, the catalyst was filtered off, washed successively with 2-propanol and water, and the filtrate and washings were combined and evaporated. The vacuum dried residue, dissolved in a suitable solvent, was characterized by comparing its ^1H nmr spectrum with that of the known compound.

*Selective removal of the 2,3-*O*-benzyl groups of* ***19***

Following the general procedure described above, a solution of methyl 2,3-di-*O*-benzyl-4,6-*O*-benzylidene-α-D-glucopyranoside (**19**) (0.2 g) in 10 mL of warm 2-propanol was added to a slurry of 10% palladium on carbon (1 g) in refluxing 2-propanol (10 mL). After 6 h, tlc (eluant: EtOAC) indicated the presence of 3 components (R_f 0.70 (**19**), 0.65 (trace), and 0.13), whereas at 48 h, **19** had disappeared and only the product of R_f 0.13 remained. The ^1H nmr spectrum of the latter in $CDCl_3$, following exchange with D_2O, was indistinguishable from that of methyl 4,6-*O*-benzylidene-α-D-glucopyranoside (**20**).

Removal of individual O-*benzyl groups from* ***17*** *and* ***26***

In a representative experiment, a solution of methyl 2,3-di-*O*-benzyl-α-D-glucopyranoside (**17**) (0.2 g) in 2-propanol (10 mL) was added to a stirred suspension of 5% palladium on alumina (2 g) in refluxing 2-propanol (15 mL), protected from moisture. After 3 h, tlc (1:1 acetone/EtOAC) showed three spots having R_f values of 0.49 (**17**), 0.37, and 0.26, the latter two being relatively faint. At 26 h, at which time all three spots were of about equal intensity, the catalyst was filtered off, washed with 2-propanol, and the combined filtrate and washings were evaporated.[4] The individual components of the residue were separated by preparative thin-layer chromatography on silica plates (~2 mm) using the above solvent mixture as eluant, and were isolated from the silica by washing successively with chloroform, acetone, and methanol, followed by evaporation of the combined washings. The compounds having R_f 0.37 and 0.26 (~0.03 g each) were identified as methyl 3-*O*-benzyl (**24**) and methyl 2-*O*-benzyl-α-D-glucopyranoside (**25**), respectively, by comparing their ^1H nmr spectra with those of the corresponding triacetates (prepared with pyridine and acetic anhydride). The ^1H nmr data for **24**: δ: 3.46 (OCH_3), 3.66 (H-2), 4.78 (H-1, $J_{1,2}$ = 3.6); for its 2,4,6-triacetate: δ: 1.88, 2.01, 2.04 (3 × $COCH_3$), 3.35 (OCH_3), 3.82 (H-5, $J_{5,6}$ = 4.8, $J_{5,6'}$ = 2.4), 3.93 (H-3, $J_{3,4}$ = 9.6), 4.03 (H-6′), 4.16 (H-6, $J_{6,6'}$ = 12.4), 4.84 (H-2, $J_{2,3}$ = 9.6), 4.91 (H-1, $J_{1,2}$ = 3.6), 5.03 (H-4, $J_{4,5}$ = 9.6). The ^1H nmr data for **25**: δ: 3.33 (OCH_3), 3.36 (H-2, $J_{2,3}$ = 9.4), 3.91 (H-3, $J_{3,4}$ = 9.4), 4.60 (H-1, $J_{1,2}$ = 3.6); for its 3,4,6-triacetate: δ: 2.01, 2.03, 2.09 (3 × $COCH_3$), 3.42 (OCH_3), 3.60 (H-2, $J_{2,3}$ = 9.6), 3.98 (H-5, $J_{5,6}$ = 4.4, $J_{5,6'}$ = 2.0), 4.07 (H-6′), 4.30 (H-6, $J_{6,6'}$ = 12.4), 4.70 (H-1, $J_{1,2}$ = 3.6), 5.00 (H-4, $J_{4,5}$ = 9.6), 5.48 (H-3, $J_{3,4}$ = 9.6). The ^1H nmr data for **17**: δ: 3.40 (OCH_3), 3.51 (H-2, $J_{2,3}$ = 9.4), 3.82 (H-3, $J_{3,4}$ = 9.4), 4.63 (H-1, $J_{1,2}$ = 3.6); for its 4,6-diacetate: δ: 1.91, 2.06 (2 × $COCH_3$), 3.39 (OCH_3), 3.59 (H-2, $J_{2,3}$ = 9.5), 3.84 (H-5, $J_{5,6}$ = 5.0, $J_{5,6'}$ = 2.2), 3.92 (H-3, $J_{3,4}$ = 9.5), 4.00 (H-6′), 4.21 (H-6, $J_{6,6'}$ = 12.3), 4.59 (H-1, $J_{1,2}$ = 3.7), 4.99 (H-4, $J_{4,5}$ = 10.2). The data for the benzylic protons of these compounds are given in Table 2.

Following the same procedure with methyl 2,3-di-*O*-benzyl-β-D-glucopyranoside (**26**), three components having R_f 0.53 (**26**), 0.40, and 0.33 were separated by preparative thin-layer chromatography. The latter two were identified as methyl 3-*O*-benzyl- (**27**) (~20% yield) and methyl 2-*O*-benzyl-β-D-glucopyranoside (**28**) (~20% yield), respectively, by comparing their ^1H nmr spectra with those of the derived triacetates. The ^1H nmr data for **27**: δ: 3.37 (H-5, $J_{5,6}$ = 3.6, $J_{5,6'}$ = 4.9), 3.50 (H-2, $J_{2,3}$ = 9.1), 3.56 (OCH_3), 3.79 (H-6′), 3.90 (H-6, $J_{6,6'}$ = 11.8), 4.24 (H-1, $J_{1,2}$ = 7.7); for its 2,4,6-triacetate: δ: 1.96, 2.01, 2.08 (3 × OCH_3), 3.49 (OCH_3), 3.60 (H-5, $J_{5,6}$ = 4.8, $J_{5,6'}$ = 2.4), 3.70 (H-3, $J_{3,4}$ = 9.2), 4.13 (H-6′), 4.24 (H-6, $J_{6,6'}$ = 12.0), 4.35 (H-1, $J_{1,2}$ = 7.6), 5.06 (H-2, $J_{2,3}$ = 9.2), 5.15 (H-4, $J_{4,5}$ = 9.2). The ^1H nmr data for **28**: δ: 3.20 (H-2, $J_{2,3}$ = 9.1), 3.34 (H-5, $J_{5,6}$ = 3.3, $J_{5,6'}$ = 4.7), ~3.5 (H-3, H-4), 3.56 (OCH_3), 3.81 (H-6′), 3.89 (H-6, $J_{6,6'}$ = 11.8), 4.34 (H-1, $J_{1,2}$ = 8.0); for its 3,4,6-triacetate: δ: 1.84, 1.93, 2.01 (3 × $COCH_3$), 3.34 (H-2, $J_{2,3}$ = 9.2), 3.52 (OCH_3), 3.59 (H-5, $J_{5,6}$ = 4.8, $J_{5,6'}$ = 2.4), 4.04 (H-6′), 4.22 (H-6, $J_{6,6'}$ = 12.0), 4.35 (H-1, $J_{1,2}$ = 7.6), 4.91 (H-4, $J_{4,5}$ = 9.2), 5.09 (H-3, $J_{3,4}$ = 9.2). The ^1H nmr data for **26**: δ: 3.34 (H-5, $J_{5,6}$ = 3.6, $J_{5,6'}$ = 5.0), 3.39 (H-2, $J_{2,3}$ = 9.1), 3.46 (H-3, $J_{3,4}$ = 9.1), 3.56 (H-4, $J_{4,5}$ = 9.1), 3.58 (OCH_3), 3.77 (H-6′), 3.88 (H-6 $J_{6,6'}$ = 11.8), 4.37 (H-1, $J_{1,2}$ = 7.7); for its 4,6-diacetate: δ: 1.92, 2.07 (2 × $COCH_3$), 3.49 (H-2, $J_{2,3}$ = 9.1), 3.56 (H-5, $J_{5,6}$ = 4.9, $J_{5,6'}$ = 2.4), 3.58 (OCH_3), 3.60 (H-3, $J_{3,4}$ = 9.1), 4.08 (H-6′), 4.24 (H-6, $J_{6,6'}$ = 12.2), 4.34 (H-1, $J_{1,2}$ = 7.8), 5.04 (H-4, $J_{4,5}$ = 10.0). The

[3]2-Propanol was added when necessary to make up for volume loss due to evaporation, especially when the reaction time was very long.

[4]Methyl α-D-glucopyranoside, the major product (40%), was conveniently separated from the three more mobile products, because it was largely adsorbed on the catalyst (less strongly on Pd/C), from which it was eluted subsequently by washing with water.

data for the benzylic protons of these compounds are given in Table 2.

*Methyl 2,3,4-tri-*O*-benzyl-6-*O*-trityl-β-D-glucopyranoside (**23**) and methyl 2,3,4-tri-*O*-benzyl-β-D-glucopyranoside*

Compound **23** was prepared from methyl 6-*O*-trityl-β-D-glucopyranoside (**18**) by benzylation with benzyl bromide and sodium hydride in the presence of tetrabutylammonium iodide in dry tetrahydrofuran according to the procedure described (10) for some related compounds. The ^{1}H nmr data for **23**: δ: 3.27 (H-6′), 3.43 (H-5, $J_{5,6}$ = 2.0, $J_{5,6'}$ = 3.6), 3.57 (H-2), 3.62 (H-6, $J_{6,6'}$ = 10.0), 3.64 (H-3, $J_{3,4}$ = 9.2), 3.69 (OCH_3), 3.87 (H-4, $J_{4,5}$ = 9.2), 4.40 (H-1, $J_{1,2}$ = 7.6), 4.39 and 4.72 (OCH_2, J_{gem} = 10.0), 4.83 and 4.92 (OCH_2, J_{gem} = 11.0), 4.79 and 5.01 (OCH_2, J_{gem} = 11.0), 6.8–7.6 (Ph).

Methyl 2,3,4-tri-*O*-benzyl-β-D-glucopyranoside was obtained as a syrup from **23**, by hydrolysis in 70% acetic acid at 100°C for 1 h. The ^{1}H nmr data: δ: 3.39 (H-5, $J_{5,6}$ = 2.7, $J_{5,6'}$ = 4.6), 3.39 (H-2, $J_{2,3}$ = 9.0), 3.56 (OCH_3), 3.57 (H-4, $J_{4,5}$ = 9.5), 3.67 (H-3, $J_{3,4}$ = 9.5), 3.71 (H-6′), 3.87 (H-6, $J_{6,6'}$ = 12.0), 4.35 (H-1, $J_{1,2}$ = 7.8). The data for the benzylic protons, as well as for those of the 6-acetate, are given in Table 2.

Acknowledgments

The authors express their gratitude to the Natural Sciences and Engineering Research Council of Canada for generous support, to J. Finkenbine for mass spectra, and to P. V. M. Tan for 400 MHz ^{1}H nmr spectra.

1. V. S. RAO and A. S. PERLIN. J. Org. Chem. **47**, 367 (1982).
2. V. S. RAO and A. S. PERLIN. Carbohydr. Res. **83**, 175 (1980).
3. (*a*) G. BRIEGER and T. -H. FU. J. Chem. Soc. Chem. Commun. 757 (1976); G. BRIEGER, T. J. NESTRICK, and T. -H. FU. J. Org. Chem. **44**, 1876 (1979); (*b*) G. BRIEGER and T. J. NESTRICK. Chem. Rev. **74**, 567 (1974).
4. (*a*) E. C. KLEIDERER and E. C. KORNFIELD. J. Org. Chem. **13**, 455 (1948); (*b*) M. J. ANDREWS and C. N. PILLAI. Indian J. Chem. Sect. B, **16**, 465 (1978).
5. (*a*) M. GULLOTTI, R. UGO, and S. COLONA. J. Chem. Soc. C, 2652 (1971); (*b*) J. TROCHA-GRIMSHAW and H. B. HENBEST. Chem. Commun. 544 (1967).
6. S. HANESSIAN, T. J. LIAK, and B. VANASSE. Synthesis, 396 (1981).
7. (*a*) K. KINDLER and W. PESCHKE. Justus Liebigs Ann. Chem. **501**, 191 (1933); (*b*) E. A. BRAUDE, R. P. LINSTEAD, and K. R. H. WOOLDRIDGE. J. Chem. Soc. 3586 (1954).
8. R. FREEMAN and W. A. ANDERSON. J. Chem. Phys. **37**, 2053 (1962).
9. A. S. PERLIN. *In* Isotopes in organic chemistry. Vol. 3. *Edited by* C. C. Lee and E. Buncel. Elsevier, Amsterdam. 1977. p. 217.
10. S. CZERNECKI, C. GEORGOULIS, and C. PROVELENGHIOU. Tetrahedron Lett. 3535 (1976).
11. C. J. POUCHERT and J. R. CAMPBELL (*Editors*). The Aldrich library of nmr spectra. Aldrich Chemical Co., Milwaukee, WI. 1980.

Can. J. Chem. Downloaded from www.nrcresearchpress.com by 210.87.254.40 on 09/06/12
For personal use only.

The cleavage of aryl-metal bonds by elemental fluorine: synthesis of aryl-fluorides[1]

MICHAEL J. ADAM, JOFFRE M. BERRY,[2] LAURANCE D. HALL,[3] BRIAN D. PATE, AND THOMAS J. RUTH
TRIUMF and Faculty of Pharmaceutical Sciences, University of British Columbia, Vancouver, B.C., Canada, V6T 2A3

Received August 12, 1982

This paper is dedicated to Professor Leo Yaffe on the occasion of his 65th birthday

MICHAEL J. ADAM, JOFFRE M. BERRY, LAURANCE D. HALL, BRIAN D. PATE, and THOMAS J. RUTH. Can. J. Chem. **61**, 658 (1983).

The reaction of elemental fluorine with phenyl derivatives of tin, lead, germanium, silicon, mercury, and thallium has been studied with the aim of developing a general method for labelling aromatic compounds with radioactive ^{18}F. Rapid synthesis of fluorobenzene was achieved in varying chemical yields up to 70%, depending largely upon the metal substrate used, with aryl–tin compounds giving the highest yields. Radiochemical yields are also given for the synthesis of ^{18}F-fluorobenzene from the cleavage of aryl–tin bonds with ^{18}F-F_2.

MICHAEL J. ADAM, JOFFRE M. BERRY, LAURANCE D. HALL, BRIAN D. PATE et THOMAS J. RUTH. Can. J. Chem. **61**, 658 (1983).

On a étudié la réaction du fluor élémentaire avec les dérivés phénylés de l'étain, du plomb, du germanium, du silicium, du mercure et du thalium, en mettant au point une méthode générale de marquage des composés aromatiques avec le ^{18}F radioactif. On a réalisé une synthèse rapide du fluorobenzène avec des rendements chimiques allant jusqu'à 70% qui varient principalement en fonction du substrat métallique utilisé; on obtient les rendements les plus élevés avec les composés aryle–étain. On donne également les rendements radiochimiques de la synthèse du ^{18}F-fluorobenzène à partir du clivage des liaisons aryl–étain par le ^{18}F-F_2.

[Traduit par le journal]

Can. J. Chem. Downloaded from www.nrcresearchpress.com by 210.87.254.40 on 09/06/12
For personal use only.

Introduction

The group IVB metals (Si, Ge, Sn, Pb) and also mercury and thallium have all been employed successfully in halogenating aromatic compounds (2) with chlorine, bromine, and iodine. There is, however, a paucity of information in the literature on the fluorination of organometallic compounds (3, 4) and also on the use of organometallic compounds, containing the metals listed above, in radiohalogen labelling (5–7). This has prompted us to investigate the utility of these metals in developing a general method for activating aromatic rings toward fluorination for the purpose of labelling with ^{18}F.

The labelling of aromatic compounds with radioactive ^{18}F ($t_{1/2}$ = 110 min), for use in positron emission tomography (PET) (8), places several stringent requirements on the chemistry. The reaction must be rapid, it must use a form of fluorine which can be labelled with ^{18}F, and must be efficient in its use of that active fluorine.

To date, no one satisfactory method exists for synthesizing ^{18}F-labelled aryl fluorides, however, several methods have been used with some success. These include the Balz Schiemann reaction (9), the triazene decomposition method (10), the nucleophilic displacement of fluorine by fluoride (11), and direct fluorination with xenon difluoride (12). Each of these methods has serious limitations and it is generally accepted that there is a need to increase the armamentarium of aromatic fluorination methods available to the radiochemist.

Aryl fluorination is an important area because of the large number of useful and potentially useful pharmaceuticals containing the phenyl moiety. Despite the difficulties of labelling with ^{18}F, a number of ^{18}F-containing aromatic drugs have already been synthesized, such as phenyl amino acids (9) and butyrophenone neuroleptic drugs (9, 13). Other ^{18}F-compounds which may be of interest include phenyl fatty acids, benzodiazepines, and also simple fluorinated aromatics that can be used as precursors of more complex systems. Even fluorobenzene labelled with ^{18}F may be a useful radiopharmaceutical, as it has the potential of being a myelin marker used to study the demyelination process associated with multiple sclerosis; iodobenzene has already been shown to be useful in this regard (14). Clearly these and other areas would be advanced by the development of rapid and efficient methods of aromatic fluorination.

Results and discussion

Simple addition of fluorine to aromatic nuclei is rare (15, 16), because the reaction is usually accompanied by unselective partial or total replacement of hydrogen (15). One method of achieving site selectivity is to metallate one carbon atom in the ring, for which there is ample precedent in the literature (2, 17, 18), forming a carbon–metal bond which is highly reactive toward an electrophilic fluorinating reagent.

For a given organic moiety, attached to the metal centre, the rate ordering for its cleavage by chlorine, bromine, and iodine is similar for all the metals used in this study (2, 19, 20). For example, aryl–metal bonds are cleaved more rapidly than those between metals and alkyl groups. This is particularly important for radiolabelling, since by selecting the other metal substituents to be alkyl groups, the activity can be conserved in the cleaved aromatic ring.

Fortunately, this same rate differential also applies to cleavage by fluorine. As shown in Table 1, only the phenyl group of $PhSn(Bu)_3$ was fluorinated, to produce fluorobenzene; no butyl fluoride could be detected. Since, for the present study,

[1]For a preliminary communication see ref. 1.

[2]British Columbia Institute of Technology, 3700 Willingdon Avenue, Burnaby, B.C., V5G 3H2.

[3]Chemistry Department, University of British Columbia, Vancouver, B.C., V6T 1W5.

TABLE 1. Reaction conditions and yields of fluorobenzene for cleavage of aryl–metal substrates by F_2

Compound	Solvent	Temp. °C	% Yield
$PhSn(nBu)_3$	$CFCl_3$	−78	70 (38 radiochemical)
	CCl_4	0	48
Ph_4Sn	$CFCl_3$	−78	15 (8 radiochemical)
	CCl_4	0	56
Ph_4Si	$CFCl_3$	−78	2.4
	CCl_4	0	7
Ph_4Ge	$CFCl_3$	−78	7
	CCl_4	0	12
Ph_4Pb	$CFCl_3$	−78	ND[a]
	CCl_4	0	48
Ph_2Hg	$CFCl_3$	0	36
	$CFCl_3$	−78	26
	CCl_4	0	26
PhHgTFA	CH_3CN	0	2.5
PhHgOAc	CH_3CN	0	5.4
PhHgCl	CH_3CN	0	3.8
$PhTl(TFA)_2$	$CFCl_3$	−78	ND
	CCl_4	0	ND
	CH_3CN	0	ND

[a]Not detected.

we were interested in measuring the effect that the various metals have on the metal–phenyl bond cleavage rate, mixed ligands were not necessary for all compounds shown in Table 1.

It was already known that within the group IVB elements the M—C bond becomes progressively more easily broken thermally and chemically (2) as one descends the group. The yields of fluorobenzene obtained from the various group IV metal compounds shown in Table 1 do seem to be in agreement with this predicted pattern with tin and lead substrates giving higher yields of fluorobenzene than the germanium or silicon substrates.

The mercury and thallium salts shown in Table 1 were included in this study because they can be prepared by mild electrophilic addition reactions (17), and it was felt that this might confer a synthetic advantage for some aryl substrates. Of the two classes of mercury compounds studied one would predict, as was observed, that the diphenyl compound would be more reactive than the phenyl mercury salts, since the salts contain highly electronegative anions.

The aryl–mercury salts were, unfortunately, insoluble in $CFCl_3$ and CCl_4, and gave no detectable amount of fluorobenzene upon fluorination. Therefore acetonitrile was used as the reaction solvent; fluorine reacts only slightly with acetonitrile.

The thallium salt failed to yield fluorobenzene in any solvent used, possibly due to the fact that it contains two electron-withdrawing substituents.[4]

The results with mercury and thallium salts are very interesting, since even though fluorine is the most reactive halogen, it fluorinates these compounds very poorly, or not at all, in contrast to the results obtained by treating these same compounds with other halogens (2, 19, 21).

[4]A referee has suggested that the observed lack of reactivity of $ArTl(OCOCF_3)_2$ compounds toward F_2 probably reflects the unusual stability of $ArTlF_2$ intermediates and, hence, their corresponding reluctance to break down to ArF + TlF.

The radiochemical yields were obtained only for the two tin compounds; these were calculated as the percentage of activity associated with the pure ^{18}F-fluorobenzene, after hplc, based on the total ^{18}F-F_2 activity obtained from the target. Radiochemical yields for the other substrates are expected to be approximately half that of the chemical yields when working at the present concentrations of carrier fluorine; 50% radiochemical yield is the maximum obtainable, since one fluorine atom of the F_2 molecule attaches to the tin centre.

The total time required for extraction of the ^{18}F-F_2 gas from the target into the reaction vessel, the reaction itself, and subsequent work-up is on the order of one hour, which is not unduly long compared with the half-life of ^{18}F (110 min.) Another attractive feature of this method is that the precursor organometallic starting materials are stable, and can be stored indefinitely prior to fluorination with ^{18}F-F_2.

Experimental

Tetraphenyltin, diphenylmercury, tetraphenyllead, phenylmercury acetate, and phenylmercury chloride were purchased from Alfa Products, Danvers, MA, and tetraphenylgermanium and tetraphenylsilane were purchased from PCR Research Chemicals Inc., Gainesville, FL. Phenylthallium bis-trifluoroacetate (21), phenylmercury trifluoroacetate (21, 22), and phenyltributyltin (23) were prepared from existing literature methods. Freon-11 ($CFCl_3$) was purchased from Matheson, Edmonton, Alberta, and distilled and stored over 4 Å molecular sieves. Acetonitrile was purchased from BDH Chemicals, Vancouver, British Columbia, and was distilled from calcium hydride and stored over 4 Å molecular sieves. Fluorine (1% in Ne) was purchased from Matheson, Whitby, Ontario, and the amount used assayed by bubbling through potassium iodide and titrating with thiosulfate as described elsewhere (24, 25).

Gas chromatography was performed with a Hewlett–Packard 5840A, equipped with an FID detector using a 6 ft × 1/8 in. stainless steel column packed with 10% SP-1000 on 80–100 mesh Supelcoport (Supelco-Inc., Bellefonte, PA) at 70°C and a nitrogen carrier flow-rate of 12 mL/min. All chemical yields were determined by gc using the internal standard method with toluene as the internal standard. The hplc was performed with a Waters system (Waters Associates, Inc., Milford, MA) using a C-18 Radial-Pak column with an ethanol–water (60:40) eluant and uv detection at 254 mm. The ^1H nmr measurements were performed on a 270 MHz spectrometer and ^{19}F nmr spectra were obtained using a Varian XL-100 spectrometer. Radioactive samples were assayed on a Beckmann 8000 scintillation counter.

Fluorine gas must be handled with great care (26). For this reason we constructed the stainless steel manifold shown in Fig. 1, with stainless steel bellows valves (NUPRO Co., Willoughby, OH). Connections from the manifold to glassware were made with Teflon tubing (1/16 or 1/8 in. od) using Swagelok fittings (Crawford Fitting Co., Salon, OH) and Teflon ferrules. The manifold and fluorine tank are stationed inside a fume hood designed for use with radioisotopes. The gas target system will be described in detail elsewhere, and is essentially a stainless steel, gas-tight cylinder placed in the 500-MeV proton beam line at TRIUMF, and filled with a mixture of 0.1% F_2/Ne via 1/8 in. od stainless steel tubes connected to the gas manifold.

Reaction of elemental fluorine with aryl–metal substrates

The anhydrous organometallic compound (120 μmol) was dissolved or suspended in Freon-11 ($CFCl_3$), CCl_4, or acetonitrile (10 mL) and added to the reaction vessel (1 cm od × 20 cm length with cooling jacket), which had been previously dried and flushed with an inert gas. A stream of inert gas was passed through the mixture which was cooled by solid CO_2 or ice, packed around the outside of the reaction vessel. The gas flow was stopped after the mixture had cooled and then the manifold was flushed several times with dilute fluorine to passivate the system. The 50 mL ballast bulb (see Fig. 1) was then filled to 30 psig with 1% F_2 (60 μmol), sealed off, and the

Can. J. Chem. Downloaded from www.nrcresearchpress.com by 210.87.254.40 on 09/06/12
For personal use only.

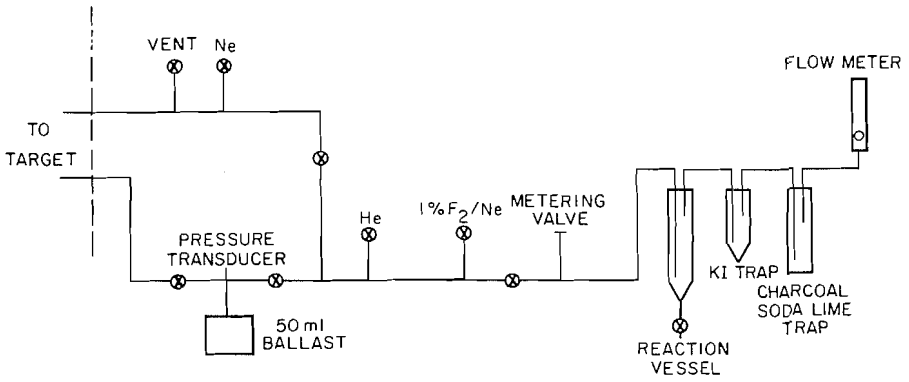

FIG. 1. Schematic of the fluorine gas handling manifold; ^{18}F-F_2 reaction system.

rest of the manifold then flushed with He. The F_2 in the ballast bulk was then allowed to vent into the reaction vessel at <50 mL/min. Any residual F_2 was flushed from the manifold with He gas and added to the reaction. A KI/H_2O trap was placed on the exhaust side of the reaction vessel to detect any F_2 that was not absorbed in the reaction.

After F_2 addition, the mixture was purged with He and then drained from the reaction vessel and distilled. The distillate, now free from starting material and metal fluorides, was analyzed by hplc and gc. In reactions that used CCl_4 as the solvent, ^1H nmr can be used to analyze the products in the distillate directly. The only product detected showed an identical resonance pattern to that of an authentic sample of fluorobenzene.

Synthesis of ^{18}F-fluorobenzene using ^{18}F-F_2

For experiments with radioactive ^{18}F-F_2 the initial non-radioactive F_2 was allowed to bleed from the 50 mL ballast bulk into the target described above, followed by Ne at 150 psig to force the fluorine bolus into the target (18). After irradiation with the proton beam, the radioactive gas was allowed to expand back through the manifold into the reaction vessel under its own pressure. Due to the increased system volume, now including that of the target and transfer lines, the flow rate used was 100 mL/min, and the total time required for extraction of the active gas was 40 min.

Acknowledgements

We thank the Mr. and Mrs. P. A. Woodward's Foundation for generous financial support.

1. M. J. ADAM, B. D. PATE, T. J. RUTH, J. M. BERRY, and L. D. HALL. J. Chem. Soc. Chem. Commun. 733 (1981).
2. G. E. COATES and K. WADE. Organometallic compounds. Methuen and Co. Ltd., London 1967.
3. E. K. S. LIU and R. J. LAGOW. J. Organomet. Chem. **145**, 167 (1978).
4. R. C. LAROCK. Tetrahedron, **38**, 1713 (1982).
5. G. W. M. VISSER, E. L. DIEMER, and F. M. KASPERSEN. J. Labelled Compd. Radiopharm. **17**, 657 (1980).
6. D. L. GILLILAND, G. P. BASMADJIAN, A. P. MARCHAND, G. H. HINKLE, A. EARLYWINE, and R. D. ICE. J. Radioanal. Chem. **65**, 107 (1981).
7. D. E. SEITZ, G. L. TONNESEN, S. HELLMAN, R. N. HANSON, and S. J. ADELSTEIN. J. Organomet. Chem. **186**, C33 (1980); G. L. TONNESEN, R. N. HANSON, and D. E. SEITZ. Int. J. Appl. Radiat. Isot. **32**, 171 (1981).
8. A. P. WOLF. Semin. Nucl. Med. **11**, 2 (1981); M. E. PHELPS. Semin. Nucl. Med. **11**, 32 (1981).
9. A. J. PALMER, J. C. CLARK, and R. W. GOULDING. *In* Radiopharmaceuticals and other compounds labelled with short-lived radionuclides. *Edited by* M. J. Welch. Pergamon Press, New York, NY. 1977. p. 57.
10. T. J. TEWSON and M. J. WELCH. J. Chem. Soc. Chem. Commun. 1149 (1979); J. S. NG, J. A. KATZENELLENBOGEN, and M. R. KILBOURN. J. Org. Chem. **46**, 2520 (1981).
11. F. CACACE, M. SPERANZA, A. P. WOLF *et al.* J. Labelled Compd. Radiopharm. **18**, 1721 (1981).
12. G. FIRNAU, R. CHIRAKAL, S. SOOD, and E. S. GARNETT. J. Labelled Compd. Radiopharm. **18**, 3 (1981).
13. T. J. TEWSON, M. E. RAICHLE, and M. J. WELCH. Brain Res. **192**, 291 (1980).
14. K. A. FREY, D. M. WIELAND, L. E. BROWN, W. L. ROGERS, and B. W. AGRANOFF. Ann. Neurol. **10**, 214 (1981).
15. M. HUDLICKY. Chemistry of organic fluorine compounds. Ellis Horwood Ltd., New York. 1976.
16. F. CACACE, P. GIACOMELLO, and A. P. WOLF. J. Am. Chem. Soc. **102**, 3511 (1980).
17. W. KITCHING. Organomet. Chem. Rev. **3**, 35 (1968).
18. A. MCKILLOP, J. S. FOWLER, M. J. ZELESKO, J. D. HUNT, E. C. TAYLOR, and G. MCGILLIVRAY. Tetrahedron Lett. 2423 (1969).
19. F. R. JENSEN and B. RICKBORN. Electrophilic substitution of organomercurials. McGraw Hill, New York. 1968.
20. A. K. SAWYER. Organotin compounds. Vol. 1. Marcel Dekker, Inc., New York. 1971.
21. A. MCKILLOP, J. D. HUNT, M. J. ZELESKO, J. S. FOWLER, E. C. TAYLOR, G. MCGILLIVRAY, and F. KIENZLE. J. Am. Chem Soc. **93**, 4841 (1971).
22. H. C. BROWN and R. A. WIRKKALA. J. Am. Chem. Soc. **87**, 1447 (1966).
23. R. K. INGHAM, S. D. ROSENBERG, and H. GILMAN. Chem Rev. **60**, 459 (1960).
24. V. CASELLA, T. IDO, A. P. WOLF, J. S. FOWLER, R. R. MACGREGOR, and T. J. RUTH. J. Nucl. Med. **21**, 750 (1980).
25. D. A. SKOOG and D. M. WEST. Fundamentals of analytical chemistry. Holt, Rhinehart and Winston, New York. 1965. pp. 485–490.
26. MATHESON GAS DATA BOOK. Matheson Co., Inc., Rutherford, NJ. 1971. pp. 211–215.

Can. J. Chem. Downloaded from www.nrcresearchpress.com by 210.87.254.40 on 09/06/12
For personal use only.

Production of ^{18}F-labelled molecular fluorine with a medical mini-cyclotron

MIRKO DIKSIC[1] AND YOJIRO TODA[2]

Medical Cyclotron Unit, Montreal Neurological Institute, McGill University, 3801 University Street, Montreal, P.Q., Canada H3A 2B4

Received August 13, 1982

This paper is dedicated to Professor Leo Yaffe on the occasion of his 65th birthday

MIRKO DIKSIC and YOJIRO TODA. Can. J. Chem. **61**, 661 (1983).

It has been demonstrated that several hundred millicuries of ^{18}F-F_2 can be produced with a small medical cyclotron using deuteron irradiation of a mixture of 0.5% fluorine in neon at an initial pressure of 405 kPa (4 atm). A high-current deuteron beam from a medical mini-cyclotron was used. Extraction efficiency for ^{18}F-molecular fluorine from the target box for the irradiation of one hour or less was 61−68%. Specific activity of extracted anhydrous molecular fluorine is about 133.2 GBq/mmol (3.6 Ci/mmol) and 216.82 GBq/mmol (5.86 Ci/mmol) after one- and two-hour irradiation, respectively. A passivation of the target box by a short irradiation of fluorine−neon mixture was demonstrated.

MIRKO DIKSIC et YOJIRO TODA. Can. J. Chem. **61**, 661 (1983).

On a démontré qu'il est possible de produire plusieurs centaines de millicuries de ^{18}F-F_2 avec un petit cyclotron médical utilisant l'irradiation au deutéron d'un mélange à 0,5% de fluor dans du néon à une pression initiale de 405 kPa (4 atm). On a utilisé un faisceau de deutéron à fort courant provenant d'un mini-cyclotron médical. L'efficacité d'extraction du fluor (^{18}F) moléculaire à partir de la boîte cible pour une irradiation durant une heure ou moins est de 61−68%. L'activité spécifique du fluor moléculaire anhydre extrait est d'environ 133,2 GBq/mmol (3,6 Ci/mmol) et de 216,82 GBq/mmol (5,86 Ci/mmol) respectivement après une et deux heures d'irradiation. On a démontré que la boîte cible est rendue passive par une courte irradiation du mélange de fluor−néon.

[Traduit par le journal]

Introduction

Several review papers have described radiopharmaceuticals labelled with ^{18}F (1−3). One reagent that has shown great promise in the synthesis of labelled radiopharmaceuticals to be used in conjunction with positron emission tomography for mapping of human organs is ^{18}F-labelled anhydrous molecular fluorine. ^{18}F has a half-life of only 110 min (4), and 1.85−3.7 GBq (50−100 mCi) of ^{18}F-labelled anhydrous fluorine is needed to start the labelling procedure and maintain enough radioactivity at the end for patient use.

The role of ^{18}F-labelled molecular fluorine in the synthesis of ^{18}F-labelled 2-deoxy-2-fluoro-D-glucose (2-FDG) has been well established (5−8).[3] 2-Deoxy-2-fluoro-D-glucose is the tracer most frequently used to measure in vivo regional cerebral glucose utilization with positron emission tomography (PET) in man (8, 9). To date the only available method for synthesis of ^{18}F-2-FDG used in PET studies involves ^{18}F-labelled molecular fluorine. Accordingly heavy demands have been put on medical cyclotrons to produce molecular fluorine.

The production of ^{18}F-labelled molecular fluorine by means of a cyclotron with a deuteron energy of 12 MeV and up has been well documented (5, 6, 10, 11). ^{18}F-fluorine has also been produced with a Tandem Van de Graff with nominal deuteron energy on the target gas of 11 MeV, but because of low beam intensity (7) the amounts produced have not reached levels needed for synthesis of ^{18}F-2-FDG used in clinical studies. Problems with the production of ^{18}F-molecular fluorine and subsequent extraction from the target derive from the chemical characteristics of fluorine, and especially of atomic fluorine. The fluorine produced in a ^{20}Ne(d, α) nuclear reaction is atomic, and very reactive. To overcome these problems the groups involved in the production of ^{18}F-2-FDG use different amounts of molecular fluorine as a carrier.

New syntheses (12−14) for 2-FDG overcome these problems and make mini-cyclotrons even more useful for the preparation of multi-portions of ^{18}F-2-FDG (12, 13) in one-hour irradiation periods. In this paper we report on the targetry used and the yields achieved in routine production of ^{18}F-labelled anhydrous molecular fluorine by means of a high-current medical mini-cyclotron.[4]

Targetry and gas handling system

Target

The target is made from a solid piece of nickel with an oval shaped opening for the gas. The shape of the target resembles the shape of the beam but is larger in size to allow for the spread of the beam which occurs when deuterons are scattered by the target gas (15). The dimensions of our target are shown in Fig. 1 with a cross section in Fig. 2. The beam hits the walls of the target about 10 cm from the entrance foil. The reason for this is a well-known beam spread which has been discussed in more detail in ref. 15. With this scatter the beam apparently becomes wider than 15 mm, which is the height of the target box. From a simple geometrical calculation we have estimated that maximal loss of the beam from this spread is about 5% and the measurements of ^{18}F production described in this paper are not able to detect this loss.

The target's two openings have to be closed with material resistant to the corrosive fluorine atmosphere inside the target box. A 10 mm thick nickel plate is used to close the target on the back (H in Fig. 1). This plate is attached to the target body

[1]Author to whom correspondence should be addressed.

[2]Permanent address: Japan Steel Works, 4 Chatsu-Machi, Muroran, Hokkaido, Japan.

[3]M. Diksic, including unpublished synthesis of ^{18}F-2-FDG.

[4]Japan Steel Works (JSW) BC-10/7 Mini-Cyclotron.

Can. J. Chem. Downloaded from www.nrcresearchpress.com by 210.87.254.5 on 09/06/12
For personal use only.

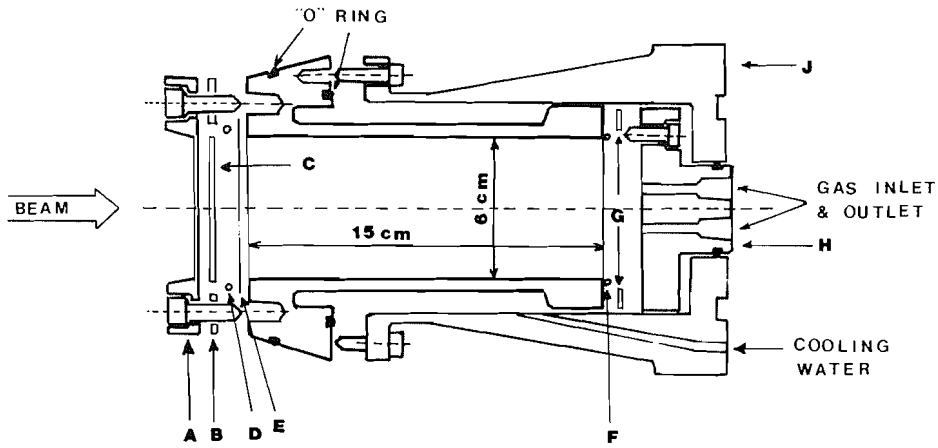

FIG. 1. Cross section of the target assembly for the production of ^{18}F-molecular fluorine (for more details see text).

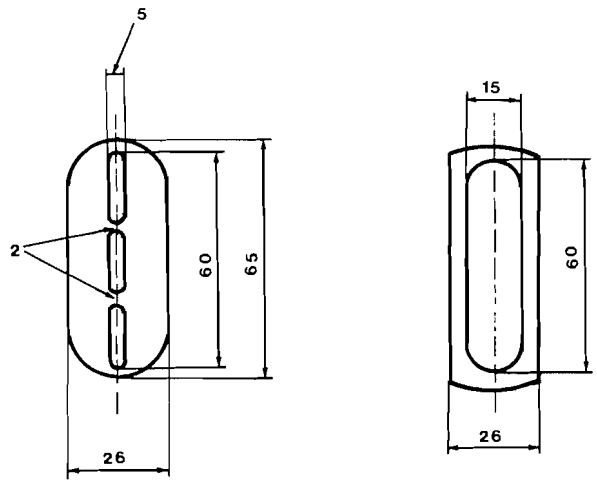

FIG. 2. Entrance foil reinforcement (C) and vertical cross section of the target chamber. All dimensions are in millimeters.

with a few bolts to ensure an even and reliable seal between the plate, metal "O" ring (F in Fig. 1), and the target body. The metal "O" ring is made from stainless steel tubing covered by a thin layer of silver. Spacers (B and G in Fig. 1) are used to prevent overtightening of the plates onto metal "O" rings (D and F in Fig. 1).

Another "O" ring (D in Fig. 1) is used on the front to obtain a seal between the entrance foil (E in Fig. 1), "O" ring, and the cover plate (A in Fig. 1). The entrance foil is sealed with a metal "O" ring attached to the target body and to the entrance plate with twelve bolts. To strengthen the entrance foil an aluminum reinforcement is placed over it (C in Figs. 1 and 2). The entrance foil is made from 20 μm thick aluminum with a 0.3 μm nickel layer on the side exposed to the gases in the target box. This foil is prepared by vacuum evaporation of nickel on aluminum foil. The entire target body is enclosed in an aluminum housing (J in Fig. 1) which is sealed to the body of the target with Buna "O" rings. Appropriate cooling of the target is very important. Deionized water at a temperature of about 20°C circulates between the aluminum housing (J in Fig. 1) and target body at the rate of 3.5 L/min. After the target box is firmly pressed into the target area there is a small space between the cyclotron exit foil and the target entrance foil. Precooled helium gas is pumped into the space to cool both foils.

Passivation

We have experimented to see if there is any need for the passivation described by the Brookhaven group (10, 16). In our first set of experiments the target was passivated by heating it in an oven to 200°C (16) with 1% fluorine in neon at a pressure of 202.7 kPa (2 atm) for two hours. After cooling, the target was evacuated and kept overnight under 202.7 kPa (2 atm) of 0.5% fluorine in neon. After this procedure the target was considered ready for ^{18}F-F_2 production. In the second set, the target was passivated by irradiating 0.5% fluorine in neon at 405 kPa (4 atm) pressure for 15 min with 50 μA. The target was then evacuated and considered ready for production of ^{18}F-labelled molecular fluorine. We observed no difference in production of ^{18}F-fluorine in the target boxes passivated by either procedure. Our observation supports that of the Brookhaven National Laboratory[5] for the target gas irradiated at a pressure of 2533 kPa (25 atm).

Fluorine transport

The fluorine transport system is built from nickel pipe, 3.16 mm (1/8 in.) od and 1.59 mm (1/16 in.) id. Pieces of the pipes are connected with Monel swageloks. The last portion of the fluorine transport pipe is made from small-diameter Teflon tubing, the end of which has been pierced several times with a needle. The holes ensure good contact of ^{18}F-fluorine gas with the reaction solution, e.g. solution of sodium acetate in acetic acid. The valves[6] used are made from Monel with metal gaskets. Whenever the transport system is not being used for production of ^{18}F it is filled with target gas and kept under 152 kPa (1.5 atm) pressure. Before the system is used again, gas is pumped out and a new gas mixture is introduced for irradiation.

Results and discussion

The target used in our work was irradiated with deuterons of a nominal current of about 50 μA and an energy on the target gas of about 6.2 MeV. The energy loss was calculated by using range and stopping power data from ref. 17 and taking the energy of the deflected internal beam as 7.1 MeV. The energy of the deflected beam was determined by measuring spectra of elastically and inelastically scattered particles on ^{12}C and ^{197}Au. These measurements were made by JSW before the cyclotron

[5]A. P. Wolf, private communication, 1982.

[6]Nupro Company, 4800 E. 345th St., Willoughby, Ohio.

Can. J. Chem. Downloaded from www.nrcresearchpress.com by 210.87.254.5 on 09/06/12
For personal use only.

Can. J. Chem. Downloaded from www.nrcresearchpress.com by 210.87.254.5 on 09/06/12
For personal use only.

was delivered to us. They quote the energy of deuterons as 7.10 ± 0.03 MeV. The target box is electrically isolated and the current integrated during irradiation. The target system has a nominal volume of 135 mL. The beam that actually strikes the target foil reinforcement is about 56 μA. About 6 μA of current is lost on the aluminum reinforcement used to strengthen the entrance foil, as well as in the scatter on the reinforcement. The intensity loss on the reinforcement was also measured by JSW before the cyclotron was shipped to us.

We have used 1% fluorine in research purity neon,[7] diluted in the target box to 0.5% fluorine with research purity neon. Measurement of the actual amount of fluorine contained in our target system before irradiation revealed that it contains 115 ± 5 μmol of molecular fluorine when a pressure of 405 kPa is used. The gases are passed through a HF trap obtained from Matheson. The trap is regenerated every time the fluorine cylinder is changed. The target is irradiated at a pressure of 405 kPa (4 atm) measured with the beam off. The pressure rises to 516.8 kPa (5.1 atm) under irradiating conditions. At the pressure of 405 kPa, the energy loss, as calculated from the range data (17), is more than that needed to degrade the deuteron energy below the threshold for the $^{20}Ne(d,\alpha)$ reaction.

After entering the target, the beam is spread as a result of a scatter. The scattered beam has fewer target atoms between the wall and the place of scatter and accordingly less chance that projectiles will interact with the target nucleus and produce ^{18}F before hitting the wall. Energy loss also resulted from the scatter. Both these factors would reduce the yield of ^{18}F. In our work we made a practical evaluation of these factors on the yield of ^{18}F.

By visual examination we can see that the beam is hitting the walls of the target box about 10 cm from the entrance foil. There is also some indication that the beam is hitting the back plate of the target. In this case, the energy of deuterons hitting the back plate is insufficient to induce $^{20}Ne(d,\alpha)$ reaction and would not contribute to the loss of ^{18}F, at least not to any significant level. We reached that conclusion by irradiating the gas mixture at an initial pressure of 304 (3 atm) and 405 kPa (4 atm) (with beam on, the pressure rises to 4.1 and 5.1 atm, respectively). We have not noticed any significant difference in the yield of ^{18}F-fluorine by irradiating the target gas at an initial pressure of 304 or 405 kPa (3 or 4 atm). If the energy of the beam reaching the back plate were high enough to induce a $^{20}Ne(d,\alpha)$ reaction, then we should notice a decrease in the yield of ^{18}F when the target pressure is reduced. The lower density would increase the energy of deuterons hitting the back plate of the target box and, with that, the yield of fluorine-18 would be reduced.

At the beginning of our work we used a 10 cm long target. The yield of ^{18}F was significantly lower than that obtained with the 15 cm long target presently used (see Table 1). Since the yield of ^{18}F was significantly lower in the shorter target, we have concluded that the energy of deuterons hitting the back plate was high enough to induce a $^{20}Ne(d,\alpha)$ nuclear reaction. The inside surfaces of both targets are well polished to reduce loss of ^{18}F (5, 6, 10, 15, 16) through chemical reaction between atomic fluorine and the surface of the target box. For eight months the target has been in routine use for the production of ^{18}F-labelled molecular fluorine without major problems.

TABLE 1. The yield of molecular fluorine extracted from target box*

Irradiation time	Yield: 10 cm long target (mCi)	Yield: 15 cm long target (mCi)
4 h	300	470 (46)†
2 h	214	330 (49)
1 h	—	250 (61)
30 min	—	150 (67)
20 min	—	105 (68)
15 min	40	80 (68)

*Standard deviation for the yields is 12%.
†Extraction yield in per cent is calculated by taking saturation yield of 1.3 Ci. Before averaging, yields were normalized to 50 μA beam current.

Taking the calculated yield as 100% we are able to extract above 60% of radioactivity from the 15 cm long target box after irradiation times equal to or less than one hour (Table 1). Calculated yields are obtained by integrating the experimental excitation function taken from ref. 18 and the stopping power for deuterons from ref. 17. The thick target calculated saturation activity for 6.2 MeV deuterons is 1.3 Ci. This agrees well with results given in ref. 10. The equation used for the integration has been described elsewhere (19). Since no one else uses the target box at the same pressure we do, it is not possible to compare our extraction yield directly with that of other groups.

Our results for the production of ^{18}F-fluorine are given in Table 1. As expected, a 15 cm long target gives better yields, because in a 10 cm target, the beam does not deposit all effective energy in the target gas. It was observed earlier that the thermal heating reduces the gas density in the beam strike and, along with that, the ^{18}F yield (10, 15). The effective density of the gas is reduced, and as a result the energy of the deuterons in a 10 cm long target box is not deposited into the target gas, as discussed earlier (15). A target 15 cm long maintained at a pressure of 4 atm (beam off), is sufficiently long to reduce the beam energy to a level below that needed to induce a $^{20}Ne(d,\alpha)$ reaction. As observed earlier (15), more fluorine radioactivity is extracted from the target when the irradiation time is shorter.

On average, the target foil is pin-holed after six hours of irradiation and has to be changed. This is certainly not satisfactory and we hope to replace the window with a more durable one. We have experimented with Havar and with nickle-plated Havar foils, as suggested by Dr. Wieland.[8]

Specific activity

Specific activity was determined by first measuring the amount of ^{18}F-fluorine extracted from the target. These measurements were done by reducing ^{18}F-fluorine with potassium iodide and determining the released iodine gravimetrically by precipitating it as AgI (after extracting it with $CHCl_3$) (20), or volumetrically by titrating it with 0.05 *N* sodium thiosulfite. First, the following reaction occurs: $F_2 + 2I^- \rightarrow I_2 + 2F^-$. When iodine is titrated with thiosulfate, the following reaction occurs: $I_2 + 2S_2O_3^{2-} \rightarrow 2I^- + S_4O_6^{2-}$ (21). Radioactivity of ^{18}F-fluoride produced after reduction with I^- was measured in an isotope calibrator. At present we extract from the target after one-hour irradiation about 70 μmol of molecular fluorine (fluorine carrier) as determined by the methods above. After one

[7]Matheson of Canada.

[8]B. W. Wieland, private communication, September, 1982.

hour of irradiation the specific activity of fluorine is 133.2 GBq/mmol (3.6 Ci/mmol) expressed at the EOB. Shorter irradiation times produce lower specific activity fluorine and, with that, lower specific activity final product.

Conclusion

A medical mini-cyclotron with a deflected deuteron energy (before exiting through the exit foil) of 7.10 ± 0.03 MeV and beam intensity on the target gas of about 50 μA can produce, on the average, 12.21 GBq (330 mCi) (EOB) of ^{18}F-labelled molecular fluorine in a two-hour irradiation. This represents the radioactivity extracted from the target box as molecular fluorine available for radiochemical synthesis in our high level radiochemistry laboratory. The activity is sufficient to prepare enough ^{18}F-2-FDG for three PET studies of glucose metabolism in patients when the new high-yield syntheses (12, 13) of ^{18}F-2-FDG is used. After this new high-yield synthesis and a two-hour irradiation, the radioactivity of ^{18}F-2-FDG produced and available for patient use one hour after EOB is about 1.85 GBq (50 mCi). In a more modest operation, a one-hour irradiation should be sufficient to produce enough ^{18}F-F_2 and FDG for two patient studies. We also came to the conclusion that it is sufficient to passivate the target simply by irradiating the target gas in it for 15–20 min.

Our results demonstrate for the first time that good recovery of molecular fluorine can be achieved from a low pressure target irradiated with a high current beam, thereby proving the value of a small medical cyclotron in PET research.

Warning: We would remind our fellow scientists that fluorine is a highly toxic and reactive gas. It should be handled cautiously by trained personnel only.[9]

Acknowledgements

This work was supported in part by the Medical Research Council of Canada, the National Cancer Institute of Canada, the Cone Memorial Research Fund of the Montreal Neurological Institute, and a Killam Fellowship to one of us (M.D.). Our thanks go to Drs. W. Feindel and L. Yamamoto for their continuous encouragement and interest in this work. M.D. expresses special thanks to Professor Leo Yaffe, Department of Chemistry, McGill University, for his interest in this project and permission to use his counting equipment. We also thank the operator of our medical cyclotron, Stephen Irwin, for his dedicated work and Dean Jolly, who helped us in one stage of this project. Our thanks are extended to Dr. V. Lees for editing this manuscript.

[9]More details are given in Matheson Bulletin No. TB-115.

1. J. S. FOWLER. Positron-emitting nuclides and their synthetic incorporation in radiopharmaceuticals. *In* The chemistry of radiopharmaceuticals. *Edited by* N. D. Heindel, H. D. Burns, T. Honda, and L. W. Brady. Masson Publishing USA, Inc., New York. 1977. p. 109, and references therein.
2. G. D. ROBINSON. Prospects for ^{18}F radiopharmaceuticals. *In* Radiopharmaceuticals. *Edited by* G. Subramanian, B. A. Rhodes, J. F. Cooper, and V. J. Sodd. N.Y. Society of Nuclear Medicine. 1975. p. 141, and references therein.
3. A. J. PALMER, J. C. CLARK, and R. W. GOULDING. Int. J. Appl. Radiat. Isot. **28**, 53 (1977).
4. C. M. LEDERER and V. S. SHIRLEY (*Editors*). Table of isotopes. 7th ed. John Wiley and Sons, New York. 1978.
5. T. IDO, C.-N. WAN, V. CASELLA, J. S. FOWLER, A. P. WOLF, M. REIVICH, and D. E. KUHL. J. Labelled Compd. Radiopharm. **14**, 175 (1978).
6. J. R. BARRIO, N. S. MACDONALD, G. D. ROBINSON, JR., A. NAJAFI, J. S. COOK, and D. E. KUHL. J. Nucl. Med. **22**, 372 (1981).
7. W. J. SHAUGHNESSY, S. J. GATLEY, R. D. HICHWA, L. M. LIEBERMAN, and R. J. NICKLES. Int. J. Appl. Radiat. Isotopes, **32**, 23 (1981).
8. M. REIVICH, D. KUHL, A. WOLF, J. GREENBERG, M. PHELPS, T. IDO, V. CASELLA, E. HOFFMAN, A. ALVAI, and L. SOKOLOFF. Circ. Res. **44**, 127 (1979).
9. M. E. PHELPS, J. C. MAZZIOTTA, and S.-C. HUANG. J. Cereb. Blood Flow and Metab. **2**, 113 (1982), and references therein.
10. V. CASELLA, T. IDO, A. P. WOLF, J. S. FOWLER, R. R. MACGREGOR, and T. J. RUTH. J. Nucl. Med. **21**, 750 (1980).
11. G. T. BIDA, R.L. EHRENHAUFER, A. P. WOLF, J. S. FOWLER, R. R. MACGREGOR, and T. J. RUTH. J. Nucl. Med. **21**, 758 (1980).
12. M. DIKSIC and D. JOLLY. Int. J. Appl. Radiat. Isotopes. In press.
13. C.-Y. SHIUE, P. A. SALVADORI, A. P. WOLF, J. S. FOWLER, and R. R. MACGREGOR. J. Nucl. Med. **23**, 899 (1982).
14. M. J. ADAM. J. Chem. Soc. Chem. Commun. 730 (1982).
15. B. W. WIELAND, D. J. SCHLYER, T. J. RUTH, and A. P. WOLF. J. Labelled Compd. Radiopharm. **18**, 27 (1981).
16. R. M. LAMBRECHT, R. NEIRINCKX, and A. P. WOLF. Int. J. Appl. Radiat. Isot. **29**, 175 (1978).
17. C. W. WILLIAMSON, J.-P. BOUJOF, and J. PICARD. Centre d'Etudes Nucléaires de Saclay, Report CEA-R 3042 (1966).
18. T. NOZAKI, M. IWAMOTO, and T. IDO. Int. J. Appl. Radiat. Isot. **25**, 303 (1974).
19. M. DIKSIC, J.-L. GALINIER, H. MARSHALL, and L. YAFFE. Int. J. Appl. Radiat. Isot. **28**, 885 (1977).
20. M. DIKSIC, L. YAFFE, and D. G. SARANTITES. Phys. Rev. C, **10**C, 1172 (1980).
21. G. D. CHRISTIAN. Analytical chemistry. 3rd ed. J. Wiley and Sons, New York. 1980. p. 269.

Can. J. Chem. Downloaded from www.nrcresearchpress.com by 210.87.254.5 on 09/06/12
For personal use only.

Nuclear charge distribution in fission: fractional cumulative yields of isotopes of krypton and xenon in $^{249}Cf(n_{th},f)$ and $^{250}Cf(sp.f)$[1]

H.-H. MEIXLER,[2] K. WOLFSBERG,[3] AND H. O. DENSCHLAG[4]

Institut für Kernchemie, Universität Mainz, D-6500 Mainz, Germany

Received August 23, 1982

This paper is dedicated to Professor Leo Yaffe on the occasion of his 65th birthday

H.-H. MEIXLER, K. WOLFSBERG, AND H. O. DENSCHLAG. Can. J. Chem. **61**, 665 (1983).

The fractional cumulative yields (%) of the following rare gas isotopes were determined radiochemically in the thermal neutron induced fission of ^{249}Cf and in the spontaneous fission of ^{250}Cf and the following results were obtained for the two processes, respectively: ^{89}Kr: 77.6 ± 1.5, —; ^{91}Kr: $31.0^{+3.1}_{-1.7}$, $34.8^{+4.3}_{-3.2}$; ^{92}Kr: 9.5 ± 1.3, $9.9^{+4.2}_{-2.1}$; ^{139}Xe: 32.0 ± 3.5, 23.6 ± 6.0; ^{140}Xe: 12.5 ± 2.0, 14.7 ± 7.0; ^{141}Xe: 4.0 ± 0.3, $9.1^{+10.4}_{-6.7}$; ^{142}Xe: 0.9 ± 0.1, ≤3.61, and ^{143}Xe: 0.22 ± 0.08, —. The results are discussed with respect to the systematics of nuclear charge distribution in fission.

H.-H. MEIXLER, K. WOLFSBERG et H. O. DENSCHLAG. Can. J. Chem. **61**, 665 (1983).

On a déterminé par radiochimie les rendements cumulatifs fractionnaires (%) des gaz rares mentionnés ci-dessous lors de la fission du ^{249}Cf induite par les neutrons thermiques et lors de la fission spontanée du ^{250}Cf. On a obtenu les résultats suivants pour les deux processus: ^{89}Kr: 77,6 ± 1,5, —; ^{91}Kr: $31,0^{+3,1}_{-1,7}$, $34,8^{+4,3}_{-3,2}$; ^{92}Kr: 9,5 ± 1,3, $9,9^{+4,2}_{-2,1}$; ^{139}Xe: 32,0 ± 3,5, 23,6 ± 6,0; ^{140}Xe: 12,5 ± 2,0, 14,7 ± 7,0; ^{141}Xe: 4,0 ± 0,3, $9,1^{+10,4}_{-6,7}$; ^{142}Xe: 0,9 ± 0,1, ≤3,61 et ^{143}Xe: 0,22 ± 0,08, —. On discute les résultats en fonction de la systématique de la distribution de la charge nucléaire lors de la fission.

[Traduit par le journal]

Introduction

The knowledge of independent yields in the fission of ^{250}Cf was very limited at the beginning of the present work, and it was felt that a larger and more representative data basis was important for the purpose of testing and further developing yield systematics. Measurements of both, the thermal neutron induced fission of ^{249}Cf and the spontaneous fission of ^{250}Cf, allow one to consider the effect of excitation energy of the compound nucleus, a parameter that has been studied extensively at higher energies and other fissioning systems by Yaffe and co-workers (1).

We have used the "emanation method" to measure the fractional cumulative yields of various xenon and krypton isotopes in the thermal neutron induced fission of ^{249}Cf and in the spontaneous fission of ^{250}Cf. This method has been developed by Wahl (2) and was applied very successfully to the study of various fission reactions (2–6).

The principle of the emanation technique consists of the stopping of fragments from a thin fission source in a metal stearate layer. Among the fission products only the inert gases (Kr and Xe) are able to diffuse through the stearate into an adjacent volume, where they subsequently decay into longer-lived descendants. Thus during irradiation (or exposure to a spontaneously fissioning source), a continuous (on-line) separation is taking place between descendants produced via inert gas precursors escaping the stearate and those that are formed directly and remain within the stearate. The ratio of the activity of a descendant outside the stearate to the total thus gives directly the fractional cumulative yield of the inert gas precursor.

Experimental

The basic set-up used for the study of the thermal neutron induced fission of ^{249}Cf is shown in Fig. 1. It was made of plexiglass to avoid high (n,γ)-activities for convenient handling of the container after irradiation. The target consisted of 10 μg of ^{249}Cf electrodeposited on a platinum disc. In part of the experiments (^{143}Xe), a target of 10 μg of ^{249}Cf deposited on a steel cylinder was used (Fig. 1, alternative target holder *b*).

Before irradiation the targets were covered with sufficient magnesium stearate to stop all fission fragments. The container was lined with filter paper (Whatman No. 1) and evacuated using a hypodermic needle inserted through a serum bottle stopper. The irradiation was carried out at room temperature in the thermal column of the Mainz TRIGA Reactor for times of 30 min (A = 141, 142), 1 h (A = 91, 92, 139), and 6 h (A = 89, 140, 143) in a neutron flux of 3×10^{10} n/(cm^2 s). After the irradiation and a waiting time sufficient for the rare gas to decay, the container was checked for tightness again, vented, and dismantled.

For the experiments with ^{250}Cf, a set up of nearly identical design made of brass was used. The serum bottle stopper was replaced by a needle valve. The target was 1.2 μg of ^{250}Cf electrodeposited on a platinum disc. The preparation of the container (introduction of magnesium stearate, lining, and evacuation) was as described above for ^{249}Cf. The exposure time to the spontaneously fissioning ^{250}Cf source was 2 h (A = 141, 142), 15 h (A = 139, 140), and 20 h (A = 91, 92). The times were longer than they were for ^{249}Cf in order to improve counting statistics and to minimize errors due to the time required for mounting and dismantling the container. The uncertainty due to the latter problem was included in the errors given.

In both fission reactions the descendants to be counted ($^{89,91,92}Sr$, $^{139-142}Ba$, ^{143}Ce) were isolated chemically from the two fractions (magnesium stearate and paper liner) after complete decay of all precursors. For this purpose, paper and stearate were dissolved separately after the addition of the respective carriers (Sr, Ba, Ce) using mixtures of nitric acid and perchloric acid (2).

[1]In part from a doctoral thesis (H.-H. M.).

[2]Present address: Lederindustrie-BG, Lorzinstr. 2, D-65 Mainz 31, Germany.

[3]Visiting scientist, permanent address: Los Alamos National Laboratory, Los Alamos, NM 87545, U.S.A.

[4]To whom all correspondence should be addressed.

Can. J. Chem. Downloaded from www.nrcresearchpress.com by 210.87.254.42 on 09/06/12
For personal use only.

Can. J. Chem. Downloaded from www.nrcresearchpress.com by 210.87.254.42 on 09/06/12
For personal use only.

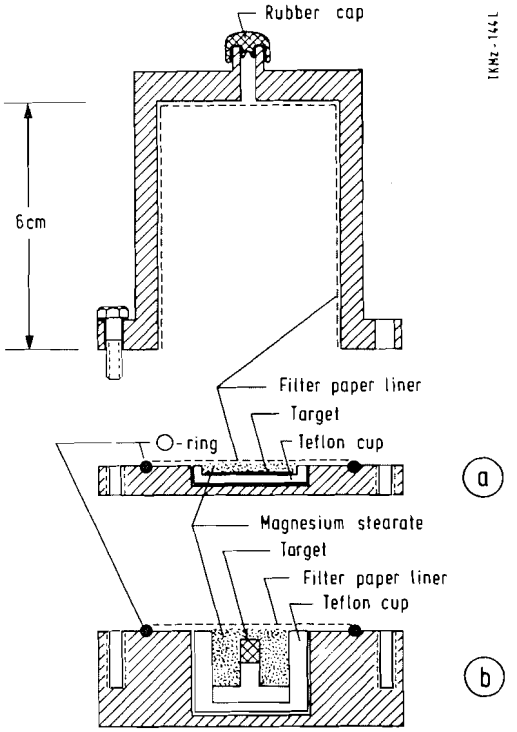

FIG. 1. Cross-sectional view of cylindrical irradiation container with target holders for (*a*) planar targets and (*b*) cylindrical targets.

The separation of barium and strontium (7, 8) was based on the precipitation of the nitrates from cold concentrated nitric acid, a scavenging precipitation of $Fe(OH)_3$ and the precipitation of barium as chromate. Strontium was isolated from the filtrate of the barium chromate precipitate. After a second addition of barium carrier, precipitation of barium chromate and filtration, strontium carbonate was precipitated, centrifuged, and redissolved in HCl. After a scavenging precipitation of $Y(OH)_3$, $SrCO_3$ was reprecipitated.

The chemical separation of cerium (A = 143) was limited to the precipitation of cerium oxalate from the initial fission product solution after a delay time of 1 day because of the selectivity of the γ-ray measurement.

The precipitates of barium chromate, strontium carbonate, and cerium oxalate were filtered on Millipore filters, dried, weighed, and mounted for counting.

For the measurements, the decay of the characteristic γ-rays was followed simultaneously in both fractions using two similar, calibrated Ge(Li) detectors. In the case of mass-89 chain the decay of ^{89}Sr was followed using a low background, anticoincidence β proportional counter.

The fractional cumulative yields (YFC) were calculated according to

$$[1]\quad \mathrm{YFC} = \frac{A_G}{A_G + A_S} \cdot V_k \cdot Y_D$$

where A_G and A_S represent the initial activities, corrected for chemical yield, of the inert gas and stearate fractions, respectively. The correction factor V_k accounts for the small gas volume between the stearate grains; it was 1.012 for the planar target configuration and 1.016 for the cylindrical target. The symbol Y_D represents the fractional cumulative yield of the descendent counted; it amounted to 0.71 ± 0.02 for ^{142}Ba (8) in $^{249}Cf(n_{th},f)$. The value of Y_D, unknown for ^{142}Ba in $^{250}Cf(sp.f)$, was set equal to unity in order to include the full uncertainty into the upper limit obtained for YFC(^{142}Xe). In all other cases it was estimated to be nearly unity on the grounds of the systematics to be discussed later.

The general method outlined above was tested using the neutron induced fission of ^{235}U, and the following results comparable to the corresponding published values (in parentheses) were obtained.

^{139}Xe: YFC = 0.81 ± 0.04 (0.82 ± 0.02 (2))

^{140}Xe: YFC = 0.58 ± 0.01 (0.596 ± 0.01 (2))

TABLE 1. Fractional cumulative yields (%) in the thermal neutron induced fission of ^{249}Cf and in the spontaneous fission of ^{250}Cf

Isotope	$^{249}Cf(n_{th},f)$	$^{250}Cf(sp.f)$
^{89}Kr	77.6±1.5	
^{91}Kr	$32.0^{+3.1}_{-1.7}$	$34.8^{+4.3}_{-3.2}$
^{92}Kr	9.5±1.3	$9.9^{+4.2}_{-2.1}$
^{139}Xe	32.0±3.5	23.6±6.0
^{140}Xe	12.5±2.0	14.7±7.0
^{141}Xe	4.0±0.3	$9.1^{+10.4}_{-6.7}$
^{142}Xe	0.9±0.1	≤3.6
^{143}Xe	0.22±0.08	

Results

The fractional yields obtained in this work are given in Table 1. The errors indicated include systematic errors. In the case of the spontaneous fission of ^{250}Cf they are, however, mainly due to the poor counting statistics obtained because of the rather weak ^{250}Cf source.

Discussion

The fission yields measured in the present work and values found in the literature will be discussed in the framework of the systematics of nuclear charge distribution in the asymmetric region of nuclear fission developed by Wahl and co-workers (3, 9, 10).

The fractional independent yields (YFI) of the isobars with atomic number Z along a β-decay chain are described by the bell-shaped "Gaussian" distributions characterized by their maximum (Z_p) and width (standard deviation, σ) values and modulated by even–odd factors (EOF). Instead of Z_p, ΔZ is frequently given, which is the deviation of Z_p from Z_{UCD}, a value calculated assuming unchanged charge density of compound nucleus and fragments, i.e. fission products prior to prompt neutron emission. The value of ΔZ represents polarization of the nuclear charge in the compound nucleus at scission. The mathematical basis of the systematics model is given in the following equations.

$$[2]\quad \mathrm{YFI}(Z) = F^{-1}\mathrm{EOF}^{a(Z)}\int_{Z-0.5}^{Z+0.5} P(Z)\,\mathrm{d}Z$$

where $a(Z) = +1$ for even Z nuclides and -1 for odd Z nuclides, and

$$[3]\quad P(Z) = \frac{1}{\sqrt{2\pi\sigma^2}} \exp\left[\frac{-(Z - Z_p)^2}{2\sigma^2}\right]$$

where

$$Z_p = Z_{UCD} + \Delta Z = (A + \nu_A)\cdot\frac{Z_F}{A_F} + \Delta Z$$

A, mass number of fission products; ν_A, average number of prompt neutrons emitted by fragments to form mass A; Z_F and A_F atomic and mass numbers of fissioning nucleus (Z_F = 98 and A_F = 250); and F is a normalization factor assuring that the sum of all fractional independent yields within one chain re-

TABLE 2. Compilation of yields for the thermal neutron induced fission of ^{249}Cf used in the present analysis and number (ν_A) of prompt neutrons emitted (derived from the mass yields in ref. 22 as described in ref. 10); generally, cumulative yields are given; nuclides whose independent yields are stated are marked *; fractional yields derived from absolute yields are in parentheses; calculated fractional yields were obtained from the model using the parameters listed in Table 3 (model F)

Nuclide	Absolute yield (%)	Chain yield ref. 22 (%)	Fractional yield (%)	ν_A	Calculated fractional yield (%)	Reference
^{82}Br*	0.0015±0.00012	0.016±0.005	(9±3)	1.27	8.8±2.0	11
^{89}Kr	—	—	77.6±1.5	1.27	70.9±4.4	[d]
^{91}Kr	—	—	32 ±3	1.27	26.8±4.2	[d]
^{92}Kr	—	—	9.5±1.3	1.27	9.9±2.1	[d]
^{94}Sr	0.67±0.08	1.13±0.12	(59 ±9)	1.27	76.0±3.9	12
^{96}Nb*	0.0044±0.0006	1.75±0.40	(0.25±0.07)	1.27	0.36±0.23	13
^{103}Mo	—	—	87 ±20	2.12	90.4±2.1	12
^{106}Tc	5.20±0.39	5.56±0.45	(94 ±10)	2.57	80.5±3.4	12
^{109}Ru	—	—	71 ±14	2.80	75.4±3.9	12
^{112}Pd	—	—	94.6±1.3	3.12	96.5±1.1	12
^{112}Ag*	—	—	3.5±0.8	3.12	3.5±1.1	14
^{129}Sb	1.21±0.06	1.51±0.12	(80 ±8)	0.99	82.4±3.1	15
^{129}Sb	1.23±0.05	1.51±0.12	(81 ±7)	0.99	82.4±3.1	11
^{131}Sb	1.78±0.19	2.66±0.21	(67 ±9)	0.89	42.1±5.6	12
^{132}Sb[b]	1.06±0.10	3.91±0.63	(27 ±5)	1.01	23.0±3.8	12
^{132}Te	—	—	76 ±2	1.01	80.5±3.4	16
^{132}Te	—	—	82 ±5	1.01	80.5±3.4	12
^{133}Te[b]	2.91±0.28	4.83±0.19	(60 ±6)	1.21	60.7±5.4	12
^{134}Te	—	—	29 ±6	1.30	32.2±4.7	16
^{134}Te[a]	—	—	39 ±3	1.30	32.2±4.7	12
^{134}Te	1.59±0.13	4.78±0.53	(33 ±5)	1.30	32.2±4.7	12
^{134}Te	2.32±0.19	4.78±0.53	(49 ±7)	1.30	32.2±4.7	15
^{134}I*	3.30±0.60	4.78±0.53	(69 ±15)	1.30	53.8±6.0	15
^{135}I	3.3 ±0.2	5.68±0.23	(58 ±4)	1.39	63.9±5.1	13
^{135}I	4.05±0.16	5.68±0.23	(71 ±4)	1.39	63.9±5.1	15
^{135}Xe*	1.91±0.14	5.68±0.23	(34 ±3)	1.39	34.3±4.9	15
^{135}Xe*	—	—	36 ±3	1.39	34.3±4.9	17
^{136}I[b]	1.51±0.44	5.61±1.29	(27 ±10)	1.53	37.8±5.2	12
^{136}Cs*	0.32±0.06	61 ±1.29	(5.7±1.7)	1.53	7.2±1.7	18
^{136}Cs*	0.34±0.02	61 ±1.29	(6.1±1.4)	1.53	7.2±1.7	13
^{136}Cs*	0.42±0.01	5.61±1.29	(7.5±1.7)	1.53	7.2±1.7	11
^{136}Cs*	0.47±0.02	5.61±1.29	(8.5±1.2)	1.53	7.2±1.7	12
^{137}Xe	4.29±0.62	5.66±0.34	(76 ±12)	1.66	77.1±3.9	12
^{138}Xe	2.47±0.21	5.98±0.36	(41 ±4)	1.78	57.9±5.6	12
^{138}Xe[a,c]	—	—	46 ±7	1.78	57.9±5.6	12
^{138}Cs*[a]	—	—	36 ±3	1.78	36.6±5.1	19
^{139}Xe	—	—	32 ±3.5	1.92	28.7±4.4	[d]
^{139}Ba*	—	—	14 ±3	1.92	15.8±2.9	8
^{140}Xe	—	—	12.5±2	2.04	12.5±2.5	[d]
^{140}Cs	2.15±0.17	5.37±0.32	(40 ±4)	2.04	59.2±5.5	12
^{140}La*	—	—	3.5±0.1	2.04	2.4±0.8	20
^{141}Xe	—	—	4.0±0.3	2.15	3.2±1.0	[d]
^{142}Xe	—	—	0.9±0.1	2.22	0.7±0.4	[d]
^{142}La*	—	—	29 ±2	2.22	20.8±3.5	8
^{143}Xe	—	—	0.22±0.08	2.30	0.1±0.1	[d]
^{150}Pm*	0.019±0.002	1.72±0.40	(1.1 ±0.3)	2.87	2.5±0.9	21

[a]Corrected for fractional yield of last chain member.
[b]Sum of isomers.
[c]Fraction of 2.9 min ^{138m}Cs that decays by β^--decay has been neglected.
[d]This work.

mains equal to unity after the modulation by the even–odd factors. F is given by

$$[4]\quad F = \sum_{Z'=Z-6}^{Z'=Z+6} \mathrm{EOF}^{a(Z')} \int_{Z'-0.5}^{Z'+0.5} P(Z')\,\mathrm{d}Z'$$

Correspondingly, for fractional *cumulative* yields (YFC), eq. [2] may be written as

$$[5]\quad \mathrm{YFC} = F^{-1} \sum_{Z'=Z-6}^{Z'=Z} \mathrm{EOF}^{a(Z')} \int_{Z'-0.5}^{Z'+0.5} P(Z')\,\mathrm{d}Z'$$

The three parameters used for the description of charge distribution (ΔZ, σ, EOF) may, in principle, be obtained for each mass chain by fitting the equation given above to the experimental yields. However, these three open parameters require at

Can. J. Chem. Downloaded from www.nrcresearchpress.com by 210.87.254.42 on 09/06/12
For personal use only.

TABLE 3. Parameters obtained in the fit of the yields in $^{249}Cf(n_{th},f)$ and, for comparison, values for $^{252}Cf(sp.f)$ and $^{235}U(n_{th},f)$ from ref. 10

Fission reaction	Model[a]	ΔZ^{140}	σ	EOZ	EON	S	FIT
$^{249}Cf(n_{th},f)$	P	0.36±0.03	0.63±0.02	1.10±0.05	0.94±0.04	0.025±0.002	1.4
$^{249}Cf(n_{th},f)$	F	0.35±0.02	0.64±0.02	1.07±0.05	1.05±0.04	0.025±0.002	1.4
$^{252}Cf(sp.f)$	P	0.46±0.03	0.59±0.02	0.97±0.04	1.00±0.04	0.001±0.003	1.10
$^{235}U(n_{th},f)$	P	0.46±0.01	0.53±0.01	1.25±0.02	1.08±0.02	0.008±0.001	0.84

[a]Fit model as defined following eq. [6] (F = fragment fit; P = product fit).

least four known yields per mass chain. Because sufficient number of yields are generally not available for individual chains in $^{249}Cf(n_{th},f)$, the global fit method developed by Wahl (10) and verified for the well known fission reactions of $^{235}U(n_{th},f)$, $^{233}U(n_{th},f)$, $^{239}Pu(n_{th},f)$, and $^{252}Cf(sp.f)$ was chosen. In this approach, simple relations are used for the mass dependence of the three parameters (σ, EOF, and ΔZ), thus allowing the increase of the number of input yields in the fit of all mass chains in the asymmetric region.

The relations assumed are: (*1*) The width parameter σ is constant, i.e. independent of A. (*2*) The even–odd factor EOF is composed of an even–odd factor for protons (EOZ) and an even–odd factor for neutrons (EON) that are both independent of A.

$$[6]\quad EOF = EOZ^{a(Z)}EON^{b(N)}$$

$a(Z)$ is set +1 for fission products with even proton numbers (Z) and −1 for those with odd Z. $b(N)$ is defined accordingly for even and odd neutron numbers. However, taking into account the prompt neutron emission, two variants were used. The first one is identical to the one given by Wahl (10) and is based on the neutron number in fission *products* (after neutron emission). The second one is based on the neutron number (N') in fission *fragments*[5] (before neutron emission). The two variants will be differentiated in the following discussion by the terms "product fit" and "fragment fit". (*3*) ΔZ is at most linearly dependent on the mass split (heavy fragment mass $A'_h = A_h + \nu_A$).

$$[7]\quad \Delta Z(A'_h) = \Delta Z^{140} + S(A'_h - 140)$$

where ΔZ^{140} is the charge polarization at fission fragment mass $A' = A + \nu_A = 140$, and S is the slope of the $\Delta Z(A'_h)$ line with respect to A'_h.

The complementarity of heavy and light (primary) fragments entails $\Delta Z(A'_h) = -\Delta Z(A_F - A'_h)$, i.e., ΔZ values of complementary fragments are equal but of opposite sign.

Consequently, the charge distribution in the asymmetric region may be described by the following five parameters: (*i*) ΔZ^{140}, charge polarization at mass $A'_h = 140$; (*ii*) S, variation of charge polarization with mass (slope of ΔZ-line); (*iii*) σ, width of "Gaussian" charge distribution curve; (*iv*) EOZ, even–odd pairing effect for protons; and (*v*) EON, even–odd pairing effect for neutrons.

Table 2 shows the fission yields and ν_A values used in the present analysis of the reaction $^{249}Cf(n_{th},f)$. Absolute fission yields are given when they are sufficiently different from chain yields to allow the calculation of fractional yields.

The yields (absolute or fractional) are given as they were obtained in the respective experiments. For the conversion of absolute yields to fractional yields, the current compilation of chain yields of Meek and Rider (22) was used. The numbers (ν_A) of prompt neutrons emitted were calculated by Wahl using also this compilation of chain yields (22) according to ref. 10 and kindly supplied to us.

In the case of the spontaneous fission of ^{250}Cf no other values of fractional yields are known to us. This reaction will be discussed later.

Equation [3] or [5] above has been fitted to the experimental fractional independent and cumulative yield data, respectively (Table 2), using the computer code LSP (23), a modification of the general least-squares program ORGLS (24).[6] The fit was carried out for the two alternative definitions of EON based on product or fragment neutron numbers as given by eq. [6]. In addition to the experimental error of the yield values, a "model error" $\sigma_{mod} = 0.1(YFI)^{2/3}$, as defined in ref. 10, was included in the analysis, and the larger one of both, σ_{exp} or σ_{mod}, was chosen as error of the input yields.

The resulting two sets of values for the five parameters above are listed in Table 3. A diagnostic number (FIT) that indicates the goodness of fit defined as in ref. 10 is also given in the table.

$$[8]\quad FIT = \left[\frac{1}{n}\sum\frac{(\text{observed} - \text{calculated})^2}{\text{error}}\right]^{1/2} = \left(\frac{\chi^2}{n}\right)^{1/2}$$

n being the number of observations minus the number of parameters varied. For large values of n, FIT = 1 would indicate agreement between data (within their error limits) and model. The values of FIT given in Table 3 indicate that the model is basically applicable to the neutron induced fission of ^{249}Cf. The last column of Table 2 gives values of fractional yields calculated on the basis of the model using the parameters given in Table 3 (fragment fit F). Of the 46 values listed 38 show agreement within the error margins with the corresponding experimental values. This is also considered to indicate reasonable agreement between model and experiment.

In addition to the results concerning the neutron induced fission of ^{249}Cf, Table 3 gives values for the thermal neutron induced fission of ^{235}U and the spontaneous fission of ^{252}Cf that were obtained in an identical calculation by Wahl (10).

The errors of the parameters given in Table 3 are essentially the statistical errors of the fit and do not include systematic errors. Possible systematic errors have been tested for the reaction $^{249}Cf(n_{th},f)$ by carrying out fits with the following vari-

[5]In this second variant, due to correction for prompt neutron emission applied to experimental fission product masses, the fragment neutron numbers are generally non-integer. In the present analysis, N' = even ± 0.5 was considered even and N' = odd ± 0.5 was considered odd.

[6]LSP is a program adapted to the Mainz HB-66/80 from a program kindly supplied to us by A. C. Wahl.

Can. J. Chem. Downloaded from www.nrcresearchpress.com by 210.87.254.42 on 09/06/12
For personal use only.

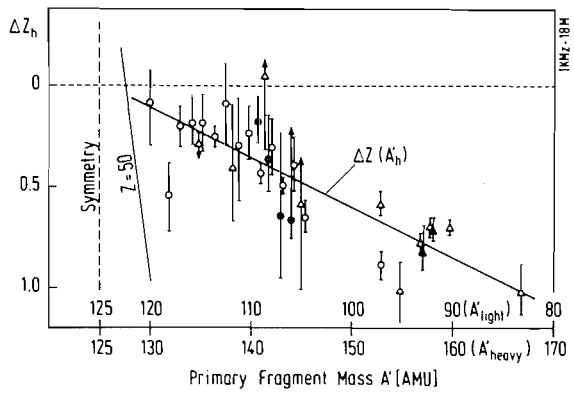

FIG. 2. Plot of ΔZ versus primary fragment mass. The line $\Delta Z(A'_h)$ (eq. [3]) was obtained in the fit. Data points were calculated from the experimental yields using $\sigma = 0.64$, EOZ = 1.07, EON = 1.05 (see Table 3). Triangles: light fragments. Circles: heavy fragments. Open symbols: $^{249}Cf(n_{th},f)$. Full symbols: $^{250}Cf(sp.f)$. Error bars are experimental errors only.

ations of the input values: (*a*) the number of yields included in the fit has been varied; (*b*) the errors associated to the yields have been varied by inclusion or exclusion of the "model errors" discussed above; (*c*) alternative sets of ν_A-values derived from the thermal neutron induced fission of ^{235}U and from the spontaneous fission of ^{252}Cf were used.

The conclusion of these tests was that possible systematic errors are covered when twice the error margins given in Table 3 are assumed.

In the following discussion, the two sets of five parameters of the charge distribution in $^{249}Cf(n_{th},f)$ will be discussed briefly and will be compared to the well known cases of $^{252}Cf(sp.f)$ and $^{235}U(n_{th},f)$ also listed in Table 3.

The first point concerns a comparison of the two fits of $^{249}Cf(n_{th},f)$ based on the even–odd factors of either fragments or products. The reason for these two mathematical approaches is the uncertainty on the origin of a possible even–odd factor for neutrons. In principle, it could be due to two reasons: (*a*) a preferential population of even neutron fission products in prompt neutron emission and (*b*) a survival of paired neutron configurations at scission.

The two cases should be reflected in the model by setting the criterion for even neutron configurations in either fission *products* (model: P in Table 3) or in fission *fragments* (model: F in Table 3).

A comparison of the EON values resulting from the two fits clearly speaks in favor of a survival of paired neutron configurations at scission. The value of EON < 1 in fission *products* that indicates a predominance of *uneven* neutron numbers is due to the emission of predominantly *uneven* neutron numbers ($\nu_A \approx 1$ or 3; Table 2) from predominantly *even* neutron *fragments*. To demonstrate this effect, the fission yield data of ^{249}Cf were divided in two groups: (*1*) with $\nu_A \approx$ even and (*2*) with $\nu_A \approx$ odd, and a product-fit was carried out for each group with the following results:

(1) ν_A even ± 0.5, EON = 1.08 ± 0.11

(2) ν_A odd ± 0.5, EON = 0.87 ± 0.05

Consequently, the fit values based on *fragment* masses are believed to be more reliable and the following discussion will be based on these values. Nevertheless, a certain influence of pairing on the prompt neutron emission cannot be excluded. EON is certainly the parameter with the largest systematical uncertainties. Fortunately, as it turns out from a comparison of the two fit modes for ^{249}Cf (F and P in Table 3), the results on ΔZ, σ, EOZ, and S are almost not affected by the uncertainty of EON.

When comparing the results for $^{249}Cf(n_{th},f)$ with those obtained for $^{235}U(n_{th},f)$ and $^{252}Cf(sp.f)$ (10) some significant differences are found (Table 3). The value of ΔZ^{140} is definitely smaller than the corresponding values for ^{235}U and ^{252}Cf. The value of S, on the other hand, is larger than the corresponding values for ^{235}U and ^{252}Cf and indicates a fairly pronounced slope of the ΔZ line with increasing mass asymmetry of the fission fragments for ^{249}Cf. The ΔZ line resulting from the fit and the ΔZ values derived from the single experimental yield values are shown in Fig. 2.

Our findings are in general agreement with the following two previously made observations: (1) Troutner and co-workers observed that, in the mass range A = 134 to 140, the value of ΔZ_h for $^{249}Cf(n_{th},f)$ is 0.2 (19) or 0.3 to 0.4 (20) charge units smaller than for $^{235}U(n_{th},f)$; (2) Gäggeler and von Gunten (13) found a larger value of ΔZ_h for very asymmetric fission modes in $^{249}Cf(n_{th},f)$. Whereas these earlier statements are based on the assumption of a value of $\sigma = 0.56$ derived from $^{235}U(n_{th},f)$ and no even–odd pairing effect (EOZ = EON = 1) (13) or an even–odd pairing effect identical to the one in $^{235}U(n_{th},f)$ (19, 20), the present analysis is based on experimental values of these constants resulting in the same fit.

The value of σ for $^{249}Cf(n_{th},f)$ is significantly larger than the value found for the fission of ^{235}U (Table 3). This result is in qualitative agreement with other evidence for larger σ-values in $^{249}Cf(n_{th},f)$. Monzyk and Troutner (8) indicate σ-values of 0.68 ± 0.03 and σ = 0.71 ± 0.04 in chains 140 and 142, respectively. Dickens and McConnell (12) observed mean values of σ = 0.67 and σ = 0.58 for heavy and light fragments, respectively. Quantitatively, the values in ref. 8, applying to single chains, are even larger than the average values found in this work. The results of ref. 12 rely on a constant value of $\Delta Z(A'_h)$. This assumption is not in agreement with the results of this work (Fig. 2). The present analysis is based on a more comprehensive experimental information including the results given in refs. 8 and 12 and takes into account the mass dependence of $\Delta Z(A'_h)$ as well as the pairing effects. The values of σ given in Table 3 for $^{249}Cf(n_{th},f)$ are therefore believed to be quantitatively more reliable.

It appears from Table 3 that the σ value of $^{252}Cf(sp.f)$ lies between those of ^{235}U and ^{249}Cf. The situation may be rationalized by the effects of the mass of the fissioning systems and of the excitation energy at scission (spontaneous versus neutron induced fission).

Concerning the rather difficult question of the even–odd factors EOZ and EON, the results obtained in the present work are somewhat preliminary. The evidence is clearly for less pairing than in the fission of ^{235}U, but to our surprise we find indication of survival of some proton pairing which was not found in the fission of ^{252}Cf. The difficulties concerning the evaluation of EON due to prompt neutron emission have been discussed above.

For the spontaneous fission of ^{250}Cf, no fractional yields except those determined in the present work are known to us. Consequently no reliable analysis of the type discussed above for $^{249}Cf(n_{th},f)$ could be made. Since the values of the yields determined in both reactions $^{249}Cf(n_{th},f)$ and $^{250}Cf(sp.f)$ are quite similar (Table 1), the analysis is limited to a simple

Can. J. Chem. Downloaded from www.nrcresearchpress.com by 210.87.254.42 on 09/06/12
For personal use only.

comparison of the ΔZ-values calculated from the experimental yields using the parameters $\sigma = 0.64$, EOZ = 1.07, and EON = 1.05 (Table 3) and the ν_A(Cf) values (Table 2) corresponding to the masses of interest, renormalized to a $\nu_{tot} = 3.53$ (13). The resulting values are shown in Fig. 2 (full symbols). No significant difference is found between the two reactions. One may thus conclude that the difference in excitation energy between induced and spontaneous fission of ^{250}Cf seems to be expressed mainly in the number of neutrons emitted.

Acknowledgements

We are grateful to Professor A. C. Wahl for the permission to use his fit program, for his help in adapting it to the HB-66/80 computer at this university, and for providing the prompt neutron data used in this work.

We would like to thank the Transplutonium Production Program of the USDOE for providing the materials used in the experiments. One of us (K.W.) gratefully acknowledges financial support by GSI (Darmstadt) during his stay at this institute.

1. J. L. GALINIER and L. YAFFE. J. Inorg. Nucl. Chem. **39**, 1497 (1977); M. DIKŠIĆ, J. L. GALINIER, H. MARSHAL, and L. YAFFE. J. Inorg. Nucl. Chem. **41**, 795 (1979).
2. A. C. WAHL. J. Inorg. Nucl. Chem. **6**, 263 (1958).
3. A. C. WAHL, R. L. FERGUSON, D. R. NETHAWAY, D. E. TROUTNER, and K. WOLFSBERG. Phys. Rev. **126**, 1112 (1962).
4. K. WOLFSBERG. Phys. Rev. **137**, B929 (1965); J. Inorg. Nucl. Chem. **33**, 587 (1971).
5. K. WOLFSBERG and G. P. FORD. Phys. Rev. C**3**, 1333 (1971).
6. K. WOLFSBERG. J. Inorg. Nucl. Chem. **37**, 1125 (1975).
7. L. E. GLENDENIN. *In* Radiochemical studies: the fission products. *Edited by* C. D. Coryell and N. Sugarman. McGraw-Hill Book Company, Inc., New York. 1951. Book 3. p. 1460.
8. M. A. MONZYK and D. E. TROUTNER. Phys. Rev. C**20**, 212 (1979).
9. A. C. WAHL, A. E. NORRIS, R. A. ROUSE, and J. C. WILLIAMS. *In* Physics and chemistry of fission. IAEA, Vienna. 1969. p. 813.
10. A. C. WAHL. J. Radioanal. Chem. **55**, 111 (1980).
11. B. V. KURCHATOV, L. N. MOROZOV, V. I. NOVGORODTSEVA, V. A. PCHELIN, L. V. CHISTYAKOV, and V. M. SHUBKO. Yad. Fiz. **14**, 943 (1971).
12. J. K. DICKENS and J. W. MCCONNELL. Phys. Rev. C**24**, 192 (1981).
13. H. GÄGGELER and H. R. VON GUNTEN. Phys. Rev. C**17**, 172 (1978).
14. D. E. TROUTNER and R. M. HARBOUR. J. Inorg. Nucl. Chem. **35**, 11 (1973).
15. J. E. GINDLER, L. E. GLENDENIN, and D. J. HENDERSON. J. Inorg. Nucl. Chem. **43**, 1743 (1981).
16. D. E. TROUTNER and R. M. HARBOUR. Phys. Rev. C**4**, 505 (1971).
17. R. M. HARBOUR, D. E. TROUTNER, and K. W. MCMURDO. Phys. Rev. C**10**, 769 (1974).
18. K. F. FLYNN and H. R. VON GUNTEN. Helv. Chim. Acta, **52**, 2216 (1969).
19. M. EICHOR and D. E. TROUTNER. J. Inorg. Nucl. Chem. **36**, 3880 (1974).
20. D. E. TROUTNER and R. M. HARBOUR. J. Inorg. Nucl. Chem. **34**, 801 (1972).
21. H. GÄGGELER, H. R. VON GUNTEN, and H. S. PRUYS. J. Inorg. Nucl. Chem. **38**, 205 (1976).
22. B. F. RIDER. Compilation of fission product yields. Valleeitos Nuclear Center. 1981. Report NEDO-12154-3C ENDF 322.
23. H.-H. MEIXLER. Program Library Institut für Kernchemie, Universität Mainz.
24. C. A. BUSING and H. A. LEVY. Oak Ridge National Laboratory Report No. ORNL-TM-271. 1962.

Can. J. Chem. Downloaded from www.nrcresearchpress.com by 210.87.254.42 on 09/06/12
For personal use only.

Muonium atoms in liquid and solid neopentane

B. W. NG, J. M. STADLBAUER, Y. C. JEAN,[1] AND D. C. WALKER

Chemistry Department and TRIUMF,[2] University of British Columbia, Vancouver, B.C., Canada V6T 1Y6

Received August 23, 1982

This paper is dedicated to Professor Leo Yaffe on the occasion of his 65th birthday

B. W. NG, J. M. STADLBAUER, Y. C. JEAN, and D. C. WALKER. Can. J. Chem. **61**, 671 (1983).

Relatively long-lived muonium atoms have been observed in neopentane (dimethylpropane). The yields of all muon states are found to be essentially the same in liquid and solid neopentane and the same as those in water. These results have bearings on three matters of current interest in muonium chemistry: the origin of the "background" spin relaxation; the formation mechanism; and the change in yields at the liquid–solid phase transition. These data were obtained by the μSR technique (muon spin rotation) at the TRIUMF accelerator.

B. W. NG, J. M. STADLBAUER, Y. C. JEAN et D. C. WALKER. Can. J. Chem. **61**, 671 (1983).

On a observé dans le néopentane (diméthyl propane) des atomes de muonium dont le temps de vie est relativement long. On a trouvé que les rendements de tous les états muon sont essentiellement les mêmes dans le néopentane et également les mêmes que ceux de l'eau. Ces résultats portent sur trois sujets d'intérêt courant dans la chimie du muonium; les fondements de la relaxation de spin, le mécanisme de formation et les variations du rendement à la transition de phase liquide solide. On a obtenu ces données par la technique du RSμ (rotation de spin du muon) dans l'accélérateur TRIUMF.

[Traduit par le journal]

Introduction

Muonium is the short-lived neutral atom (chemical symbol Mu) formed as the bound state of a positive muon with an electron. It has been established as a light isotope of hydrogen, and is particularly useful because it can be observed by nuclear physics counting techniques with great sensitivity and on short reaction timescales (1, 2). Most of the liquid phase studies have involved Mu in water, although it has been detected with reduced lifetime in alcohols (3) and saturated hydrocarbons (4). Its mechanism of formation is not yet settled, nor is it clear why there is always an apparent "background" decay to the Mu signals — though a physical explanation based on the magnetic field has recently been offered (5).

In order to help resolve these problems we have studied purified neopentane in both condensed phases. This compound is of particular interest for three reasons. First, all of its hydrogen atoms are present in methyl groups, so Mu could be long-lived and thus easier to study than in hydrocarbons containing methylene hydrogens. Second, neopentane is known to have an unusually large free ion yield in radiolysis, despite its low dielectric constant. This is attributable to the enormous mobility of quasifree electrons in this medium due to the molecules' being almost spherical (6). Thus, if the spur model of muonium formation (7) is valid, the muonium yield in neopentane should differ markedly from both water and hexane. Third, neopentane has a convenient melting point and a simple solid structure. Therefore it is a suitable medium in which to study the effect of phase transitions on the muon yields.

Experimental

μSR facilities at the TRIUMF accelerator in Vancouver were used in this study. The technique is described in detail elsewhere (1, 2) and the apparatus used is sketched in Fig. 1. A high energy positive muon strikes the sample under study, stops in it, associates chemically with it, then decays to a positron in 2.2 μs on average. The time between the muon's arrival and its decay (when observed by a positron detector) gives one point in a lifetime histogram. The sample is held in a transverse magnetic field, so that the spin of the muon (initially polarized) precesses with a Larmor frequency determined by the chemical state of the muon. As the positron is emitted preferentially along the muon's spin direction, the lifetime histogram has the precession frequency superposed on it. Two types of muon state are readily observable — that of the free muonium atom, and muons in diamagnetic environments (collectively grouped under D). The yields in these two states (A_M and A_D), plus the decay constant of Mu (λ), are obtained by computer-fitting the amplitudes in the time-histogram to eq. [1],

$$[1]\quad N(t) = N_0 \exp(-t/\tau_\mu)\{1 + A_D \cos(\omega_D t + \phi_D) + A_M \exp(-\lambda t) \cos(\omega_M t - \phi_M)\} + B_g$$

where $N(t)$ is the signal amplitude at time t, ω_M and ω_D are the precession frequencies of Mu and diamagnetic muons, with ϕ_M and ϕ_D their initial phase angles, τ_μ is the muon lifetime, N_0 a normalization factor, and B_g the background count rate. The yields are normalized to fractions of the incident muons (P) by use of $P_M = 2A_M/A_0$ and $P_D = A_D/A_0$, where A_0 is the diamagnetic amplitude under identical conditions in a medium, such as CCl_4 or Al, in which all muons are known to form diamagnetic states. The 2 appears in P_M because only that half of the total Mu ensemble with parallel muon and electron spins is observable in μSR. (In the antiparallel atom the muon spin is depolarized by rapid hyperfine oscillations.)

P_M, P_D, and λ are the three parameters of interest obtained from the histograms modulated by the muon spin rotation. In these experiments there is no added solute so λ corresponds to the observed background decay constant in the pure solvent (λ_0). This could correspond to chemical reactions with the solvent, or with residual impurities, or it could be a physical or experimental artifact.

Neopentane was provided for us by Professor Ito, having been carefully purified by shaking with H_2SO_4, washing, drying, and distilling. The sample was deoxygenated by freeze–pump–thaw cycles and vacuum-sealed in a 100 mL round-bottomed glass flask. About 10^7 events were collected on each of three positron counters for the sample held at four temperatures between 209 and 295 K (melting

[1]Permanent address: Physics Department, University of Missouri-Kansas City, Kansas City, MO 64110, U.S.A.

[2]TRIUMF stands for Tri University Meson Facility on the campus of the University of British Columbia, Vancouver, B.C., Canada.

Can. J. Chem. Downloaded from www.nrcresearchpress.com by 210.87.254.40 on 09/06/12
For personal use only.

Can. J. Chem. Downloaded from www.nrcresearchpress.com by 210.87.254.40 on 09/06/12
For personal use only.

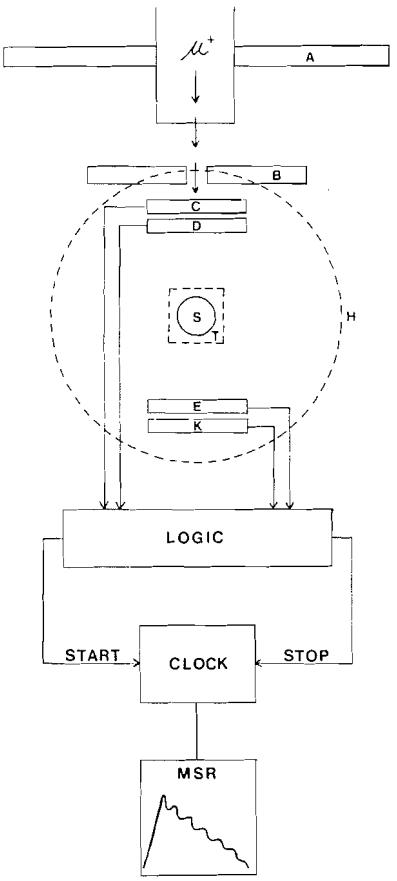

FIG. 1. Sketch of the apparatus used for a typical μSR measurement, showing only one set of positron counters. A is lead shielding; B a lead collimator; C and D are the muon "start" counters; S is the sample sealed in glass bulb after deoxygenation; T is a styrofoam cryostat controlled by flowing cold gas at a controlled rate through it; H are the magnetic field coils giving a field out of the paper so that the longitudinally polarized muon precesses in the plane of the paper; E and K are the positron "stop" counters. The start signal is registered by C, D, $\overline{E}$ and the stop by $\overline{B}$, E, K.

point 253 K). Temperature control was achieved in a closed styrofoam container through which cold helium gas was passed at a variable rate. The temperature was determined by a thermocouple in contact with the cell wall, and was monitored continuously throughout a μSR experiment.

Results and discussion

Figure 2 shows typical μSR histograms for neopentane: in (*a*) only the high frequency Mu precession can be observed, in (*b*) only the low frequency diamagnetic muon signals are discernible. The lines represent the computer fits to eq. [1] by a χ^2-minimization procedure (1, 2). Best values were obtained from the fits for three independent histograms, and the average values of P_M, P_D, and λ_0 are reported in Table 1 for four temperatures. P_L is the "missing fraction" equal to $1 - P_M - P_D$, the fraction of muons which are not observed. In unsaturated compounds some of this fraction appears as muonium radicals, but this is not expected in neopentane.

These results are of interest in three respects. First, they provide a measure of the yields in a hydrocarbon which has some physical properties intermediate between linear hydrocarbons and weakly polar alcohols and ethers — particularly with regard to the radiation chemical free ion yields (9). Neo-

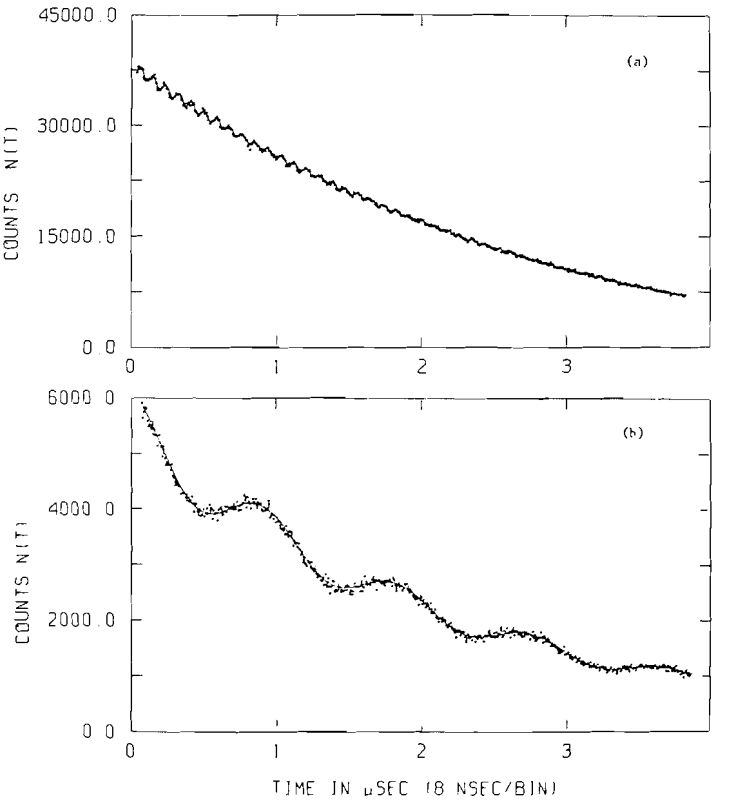

FIG. 2. μSR histograms (dots) and computer fits (lines) for liquid neopentane at 295 K: (*a*) showing the muonium precession with 8 G transverse magnetic field; (*b*) showing the diamagnetic muon precession at 80 G.

pentane provides a medium — attributed to the sphericity and non-polarizability of its molecules (6) — in which quasifree electrons are exceptionally mobile (see Table 2). In finding that the probability of muonium formation is essentially the same as that in water on the one hand, with its large free ion yield, and *n*-hexane on other, with its minute free ion yield, leads us again (4) to the conclusion that the spur model (7) of muonium formation does not account for the yields in different liquids. This is underscored by the comparison provided in Table 2, where the muon yields are seen to be essentially the same for solvents ranging from *c*-hexane to water, despite a complete change in the polarity, solvating power, and spur electron survival probabilities. Instead, one inclines to the view that Mu formation depends on the probability of hot Mu* emerging from the epithermal stages of the track without having undergone a hot atom abstraction or substitution reaction. Perhaps the probability of such hot atom reactions occurring relative to thermalization is very similar for saturated molecules composed of fully hydrogenated C and O atoms.

The second major interest in these results lies in the fact that the yields barely change at the liquid–solid phase transition or with temperature over the range studied. Certainly there is no marked break at the melting point. This is in sharp contrast to water (7) and the condensed noble gases Ar, Kr, and Xe (10), with the Ar result being given in Table 3. Whether this is peculiar to neopentane or common to hydrocarbons remains to be seen. In these other media there was a complete absence of a missing fraction in the solid phase, with P_M increasing markedly as the material was solidified (see Table 3).

Third, the λ_0 value found for neopentane approximately

TABLE 1. Values of λ_0, P_M, P_D, and P_L in neopentane in liquid and solid phases

Phase	T/K	$\lambda_0/10^6$ s^{-1}	P_M	P_D	P_L[a]
Liquid	295±3	0.26±0.03	0.18±0.02	0.55±0.02	0.27±0.03
Liquid	259±2	0.30±0.07	0.14±0.02	0.60±0.02	0.26±0.03
Solid	238±2	0.17±0.06	0.14±0.01	0.59±0.02	0.27±0.03
Solid	209±2	0.33±0.13	0.19±0.02	0.61±0.02	0.20±0.04

[a] $P_L = 1 - P_M - P_D$.

TABLE 2. Physical properties affecting electron escape from spurs, and P_M, P_D, and P_L values obtained for four pure liquids at 295 K

Liquid	G_{ei}/G_t[a]	μ[b]	ϵ[c]	V_0[d]	P_M	P_D	P_L	Reference
Neopentane	0.97	70	1.8	−0.39	0.18	0.55	0.27	This work
c-Hexane	0.99	0.4	1.8	+0.01	0.20	0.69	0.11	4
Methanol	0.62	0.0006	33	NA	0.23	0.62	0.15	3, 4
Water	0.38	0.002	78	NA	0.20	0.62	0.18	3, 4

[a] Fraction of total radiation-produced electrons (G_t = 4.5) which do not escape intraspur neutralization to become free ions.
[b] Mobility in cm^2 V^{-1} s^{-1} (ref. 8).
[c] Static dielectric constant.
[d] Conduction band energies of electrons in the liquid at 295 K.

TABLE 3. The effect of phase (and temperature) on the various muon yields in neopentane, water, and argon

Medium	Phase	T/K	P_M	P_D	P_L	Reference
Neopentane	Liquid	295	0.18	0.55	0.27	This work
Neopentane	Solid	209	0.19	0.61	0.20	This work
Water	Liquid	295	0.20	0.62	0.18	7
Water	Solid	272	0.52	0.48	0	7
Argon	Liquid	85	0.48	0.02	0.50	10
Argon	Solid	77	0.91	0.008	0.08	10

equals the smallest values found for any system at TRIUMF (4, 11–13) or at Schweizerisches Institut fur Nuclearforschung, Villigen (near Zurich, Switzerland) (3, 14). The implication is, therefore, that this "background" decay rate of Mu is not a genuine chemical process but is an experimental or physical artifact. This has recently been emphasized by the fact that Nagamine *et al.* (5), using a pulsed muon beam with 50 ms between pulses, have obtained much smaller values of λ_0 — down to 0.05×10^6 s^{-1}. Indeed, Miyake *et al.* (15) have just found small λ_0 values in neopentane and tetramethylsilane. The most probable explanation for the difference is suggested (5) to arise from a beating of the two-frequency precession of muonium and field inhomogeneities, even at ~8 G. This seems to be correct because by fitting the relaxation in ultrapure water over long lifetimes (8 μs gate) to a multifrequency equation rather than to [1], there was a significant reduction in the apparent value of λ_0 (16). Our net conclusion is that Mu does not react with neopentane at a measurable rate: therefore, that the abstraction reaction [2]

[2] $\mathrm{Mu} + \mathrm{C(CH_3)_4} \rightarrow \mathrm{MuH} + \mathrm{C(CH_3)_3\dot{C}H_2}$

has a bimolecular rate constant, $k_M < \lambda_0/[\text{neat liquid}]$, i.e. $k_M < 3 \times 10^4\ M^{-1}$ s^{-1}.

Summary

Neopentane (dimethyl propane) has proved to be most interesting in all three aspects of this study. (*i*) On the question of changes at the liquid–solid transition, this is the first compound to show no significant change in muon yields. Previously a marked change was found for both highly-polar, strongly hydrogen-bonded molecules such as water whose structure changes markedly on freezing, and for the avidly non-polar, barely polarizable heavy noble-gas molecules. This absence of a significant change at the melting point of neopentane is found to occur regardless of whether the solid was glassy or polycrystalline. (*ii*) The fact that neopentane has provided the longest-lived muonium hitherto — equal to that of water — tends to corroborate this slowest of rates as a physical artifact rather than a chemical reaction. The result therefore also implies — providing the *n*-hexane and *c*-hexane samples (4) were equally free of reactive impurities — that reaction of Mu with —CH_2— groups is observable whereas that with —CH_3 groups is not. (*iii*) The muon yields are in accord with previous overall conclusions (4): namely, that diamagnetic muon yields are not connected to radiolysis free-ion yields, nor muonium yields with geminate-ion yields of radiolysis. It apparently makes no difference what the electron escape probability is, one gets the same muon yields for all saturated hydrogenated compounds. Such findings seem to be at variance with the expectations of a spur model.

Acknowledgements

We are particularly indebted to Professor Yasuo Ito and Mr. Y. Miyake for kindly providing the purified neopentane,

Can. J. Chem. Downloaded from www.nrcresearchpress.com by 210.87.254.40 on 09/06/12
For personal use only.

for helpful discussions, and for sending their results. The continued financial support of NSERC of Canada is greatly appreciated.

1. J. H. BREWER and K. M. CROWE. Ann. Rev. Nucl. Part. Sci. **28**, 239 (1978).
2. D. G. FLEMING, D. M. GARNER, L. C. VAZ, D. C. WALKER, J. H. BREWER, and K. M. CROWE. Adv. Chem. Ser. **175**, 279 (1979).
3. P. W. PERCIVAL, E. RODUNER, and H. FISCHER. Chem. Phys. **32**, 353 (1978).
4. Y. ITO, B. W. NG, Y. C. JEAN, and D. C. WALKER. Can. J. Chem. **58**, 2395 (1980).
5. K. NAGAMINE, K. NISHIYAMA, J. IMAZATO, H. NAKAYAMA, M. YOSHIDA, Y. SAKAI, H. SATO, and T. TOMINAGA. Chem. Phys. Lett. **87**, 186 (1982).
6. J-P. DODELET and G. R. FREEMAN. Can. J. Chem. **50**, 2667 (1970).
7. P. W. PERCIVAL, E. RODUNER, and H. FISCHER. Adv. Chem. Ser. No. **175**, 335 (1979).
8. A. O. ALLEN. NSRDS-NBS, 57. 1976.
9. A. O. ALLEN. NSRDS-NBS, 58 (1976).
10. R. F. KIEFL, J. B. WARREN, G. M. MARSHALL, and C. J. ORAM. J. Chem. Phys. **74**, 308 (1981).
11. Y. C. JEAN, J. H. BREWER, D. G. FLEMING, D. M. GARNER, R. J. MIKULA, L. C. VAZ, and D. C. WALKER. Chem. Phys. Lett. **57**, 293 (1978).
12. B. W. NG, Y. C. JEAN, Y. ITO, T. SUZUKI, J. H. BREWER, D. G. FLEMING, AND D. C. WALKER. J. Phys. Chem. **85**, 454 (1981).
13. B. W. NG. M.Sc. thesis, University of British Columbia. 1980.
14. P. W. PERCIVAL, E. RODUNER, H. FISCHER, M. CAMANI, F. N. GYGAX, and A. SCHENCK. Chem. Phys. Lett. **47**, 11 (1977).
15. Y. ITO, Y. MIYAKE, Y. TABATA, K. NISHIYAMA, and K. NAGAMINE. Private communication.
16. B. W. NG *et al.* Unpublished data.

Can. J. Chem. Downloaded from www.nrcresearchpress.com by 210.87.254.40 on 09/06/12
For personal use only.

A possible resurrection of the *ab initio* maximum overlap (MOM) method[1]

M. A. WHITEHEAD AND G. D. ZEISS[2]

Department of Chemistry, McGill University, 801 Sherbrooke St. W., Montreal, P.Q., Canada H3A 2K6

Received August 27, 1982

This paper is dedicated to Professor Leo Yaffe on the occasion of his 65th birthday

M. A. WHITEHEAD and G. D. ZEISS. Can. J. Chem. **61**, 675 (1983).

A constrained variational theory is applied to the *ab initio* maximum overlap (MOM) method. The results for N_2, HF, CO, and LiH, in which MOM wavefunctions satisfy constraints based on RHF, experimental or theoretical values, are discussed. The numerical results show that constraining the MOM wavefunctions with one or more constraints corrects the worst deficiencies in accuracy in the wavefunctions.

M. A. WHITEHEAD et G. D. ZEISS. Can. J. Chem. **61**, 675 (1983).

On a appliqué une théorie variationnelle contrainte à la méthode *ab initio* de recouvrement maximum (MOM). On discute des résultats obtenus pour N_2, HF, CO et LiH en utilisant des fonctions d'onde MOM qui satisfont des contraintes basées sur les valeurs RHF expérimentales ou théoriques. Les résultats numériques révèlent que cette contrainte des fonctions d'onde MOM par une plusieurs contraintes corrige, au niveau de l'exactitude, les pires déficiences des fonctions d'onde.

[Traduit par le journal]

Can. J. Chem. Downloaded from www.nrcresearchpress.com by 210.87.254.6 on 09/06/12
For personal use only.

Introduction

The maximum overlap of atomic orbitals on neighboring atoms as a measure of bond strength (1–3), with the concept of hybridization (4, 5) has provided a simple, useful model of the chemical bond (6). Maximum overlap has been used to determine nonequivalent hybrid orbitals in hydrocarbon molecules (7, 8) and to provide qualitative understanding of trends in experimental measurements on these molecules (9, 10).

However, in the face of extended basis set multiconfigurational calculations and the arrival of the multiple-scattering X_α method, the maximum overlap method, MOM, has died out (11–14).

In this paper the authors hope to show how the MOM theory may be resurrected to give good service in the future by ensuring that the MOM wavefunctions can be made as accurate as Hartree Fock wavefunctions, or better, without the need to iterate, thus providing fast accurate results to aid chemical interpretation (14, 16).

Of the procedures for maximum overlap (7, 8, 15–22), that of Lykos and Schmeising (20) was most suitable for the present study, because their MOM wavefunctions can be directly compared with RHF (21, 22) and NDDO[3] wavefunctions. Secondly, the secant-parameterization method used in the constrained RHF calculations (21) is easily adapted to this version of the MOM method. Thirdly, the MOM method of Lykos and Schmeising is similar to other approximate molecular orbital methods, and therefore the results from constrained MOM calculations are relevant to other methods: Lykos and Schmeising (20) and others (23, 24) have shown the close correspondence between the maximum overlap and simple Hückel methods (25, 26). Several semi-empirical approximate RHF methods, among them the CNDO (27–29) and extended Hückel (30) methods, rely on the Wolfsberg–Helmholz (31) approximation, in which interatomic off-diagonal elements of the Fock matrix are assumed to be proportional to the corresponding overlap matrix elements. In the context of the π-electron approximation, Ruedenberg (32) showed that there is a close connection between the validity of the "zero differential overlap" approximation and the extent to which the maximum overlap molecular orbitals approximate the true eigenvectors of the Fock matrix.

The maximum overlap method of Lykos and Schmeising (20) differs from the traditional approach in which the bond overlap between two localized atomic orbitals is maximized (15). The MOM wavefunction determined according to the procedure of Lykos and Schmeising (20) is invariant with respect to unitary transformations of the occupied MO's. Therefore the concept of localized (33) or hybridized atomic orbitals loses some significance; these concepts have their own fundamental problems anyway (33).

This maximum overlap method (20) posseses certain advantages (34) over other approximate molecular orbital methods. Because no parameters are required, the maximum overlap method is an *ab initio* procedure, and a MOM wavefunction is invariant to the same types of transformations as an RHF wavefunction (35), unlike neglect-of-differential-overlap wavefunctions (27).

Free variational MOM wavefunctions are compared with RHF and NDDO wavefunctions elsewhere (21, 22). One-electron property expectation values calculated with MOM wavefunctions are usually poorer than NDDO or RHF expectation values. MOM values of energy-related properties such as T and r_A^{-1} are small because MOM underestimates the charge density in the inner shell region. Both NDDO and MOM wavefunctions suffer from *excessive s–p promotion*. MOM, like the NDDO method, is unreliable in reproducing the quantitative and qualitative characteristics of interatomic charge transfer.

The disadvantages of MOM have been discussed (20, 31): it does not distinguish between basis functions according to energy considerations, which leads to severe distortion in MOM wavefunctions. Thus for CO, free variational MOM wavefunctions give equal $2p\pi_C$ and $2p\pi_O$ populations, and in the absence of constraints, there is no interatomic transfer of π

[1]This paper is dedicated to Leo Yaffe, a fine scientist, a stimulating colleague, good opponent, and sincere friend.

[2]Present address: 2610 West 10th Ave., Vancouver, B.C. V6K 2J7.

[3]G. D. Zeiss and M. A Whitehead, to be published.

Can. J. Chem. Downloaded from www.nrcresearchpress.com by 210.87.254.6 on 09/06/12
For personal use only.

electron density. For LiH, the wavefunction obtained using MOM is unrealistic; the basis set is not strictly minimal (36) and the lithium 1*s* orbital is considered bonding. A test of the constrained variational method is how effective suitable chosen constraints are in correcting inherent deficiencies in MOM.

The constrained MOM equations

The constrained maximum overlap equations are derived in a manner similar to that used to obtain the constrained RHF equations (27, 37). A single configuration wavefunction is used, and the total molecular overlap Γ, defined (20) by

$$[1] \quad \Gamma = 2 \sum_{\nu}^{n} \sum_{i}^{m} |\langle \chi_i | \phi_\nu \rangle|^2$$

$$[2] \quad = 2 \sum_{\nu}^{n} \sum_{i,j}^{m} c_{i\nu} c_{j\nu} [\mathbf{S}^2]_{ij}$$

where

$$[3] \quad \phi_\nu = \sum_{i}^{m} \chi_i c_{i\nu}$$

where χ_i are known one-electron functions, and $\mathbf{S}^2$ is the square of the overlap matrix, [3] is maximized subject to the usual orthonormality restrictions on the molecular orbitals ϕ_ν, and to the imposed constraint conditions (21) [4],

$$[4] \quad 2 \sum_{\nu}^{n} \sum_{ij}^{m} \langle \chi_i | M_q - \mu_q / 2n | \chi_j \rangle c_{i\nu} c_{j\nu} = 0 \qquad q = 1 \ldots\ldots s$$

where M_q is the property operator of the qth property and μ_q is its known expectation value (37) which constrains the Hamiltonian. By analogy with the constrained RHF equations (21) the constrained maximum overlap equations are written in the form (37)

$$[5] \quad \sum_{j}^{m} G'_{ij} c_{j\nu} = \sum_{j}^{m} S_{ij} c_{j\nu} d'_\nu$$

The "fictitious" total overlap operator matrix G'_{ij} is given by

$$[6] \quad G'_{ij} = [\mathbf{S}^2]_{ij} + \sum_{q}^{s} \lambda_q \langle \chi_i | M_q - \mu_q / 2n | \chi_j \rangle$$

The s Lagrange multipliers λ_q are chosen so that the s constraint equations [4] are satisfied. The d'_ν are the roots of the secular equation

$$[7] \quad |G'_{ij} - d'_\nu S_{ij}| = 0$$

The occupied molecular orbitals are the n eigenvectors of G'_{ij} corresponding to the n largest eigenvalues d'_ν.

If no constraint other than orthonormality is imposed on the wavefunction, then the solutions of [5] are free variational maximum overlap orbitals which are equivalent (20) to the canonically orthogonal orbitals defined by Löwdin (38). Thus, the coefficients determining the free variational maximum overlap molecular orbitals are given by

$$[8] \quad c_{i\nu} = U_{i\nu} d_\nu^{-1/2}$$

where $U_{i\nu}$, $i = 1, m$, is an eigenvector of the overlap matrix S_{ij} and d_ν is the corresponding eigenvalue.

The calculations were performed using the secant-parameterization procedure (21) which was easily adapted to the constrained MOM method; *computation times were very short* because there were *no self-consistency requirements*. As an example, details of a calculation on CO in which the wavefunction is constrained to reproduce the RHF value for the dipole moment are given in Table 1. Although the free variational MOM value of the dipole moment is poor, the constraint procedure converges rapidly to the constrained dipole moment value.

TABLE 1. CO. Determination of a singly constrained MOM wavefunction using the secant-parameterization procedure (21). The wavefunction is constrained to give the RHF expectation value of the dipole moment x_n. The value of the Lagrange multiplier, the remaining error in x_n, and the total overlap are given for each step. Slater exponents were used (37)

Iteration	$\lambda^{(i)}$	$\Delta^{(i)}$	Γ
0	0.0	−1.91881	16.6280
1	0.09350	−0.16642	16.5494
2	0.10230	−0.02639	16.5357
3	0.10396	−0.00054	16.5330
4	0.10399	2×10^{-6}	16.5329

Constrained MOM calculations using constraints based on RHF expectation values

Several singly and multiply constrained maximum overlap wavefunctions were determined for four diatomic molecules; N_2, HF, CO, and LiH. Each wavefunction was constrained to reproduce one or more property expectation values calculated with an RHF wavefunction and the same basis set. The resulting constrained maximum overlap wavefunctions are compared with RHF wavefunctions using the same criteria employed previously (19, 39). Constraining a maximum overlap wavefunction may decrease the total molecular energy, and the energy lowering is useful for assessing the effectiveness of constraints.

The maximum overlap calculations used the same STO-4G basis functions with Slater exponents that were employed in the NDDO (23, 40) calculations.

N_2

Most constraints improve property expectation values, Table 2, and lower the Standard Deviation in Reduced Errors, which assesses the overall quality of a wavefunction (39) and energies, Table 3. With the exception of the $[E_N^c]$ constrained wavefunction, constrained wavefunctions improve values of T and r_N^{-1} which indicates improvement in the inner shell regions near the nuclei. Because $-\theta_n^c$, r_n^2, $-q_N^c$, and $T + V_{nc}$ are sensitive to $s-p$ promotion and because constraints decrease $s-p$ promotion they are improved. The $2s$ and $2p\sigma$ gross populations, Table 4, computed with these constrained wavefunctions agree with the RHF values, as do the calculated property expectation values and energies.

The constrained MOM is economical for determining nonvariational wavefunctions: two constraint conditions determine a nonvariational minimum basis set wavefunction for N_2 (to within a unitary transformation). Four complete cycles were required for convergence. The property expectation values and the energy calculated with the $[r_N^{-1}, -\theta_n^c]$ constrained wavefunction reproduce the RHF results.

HF[4]

In most cases single constraints cause lower energies and SDRE (40) values, Table 6, and improve property expectation

[4]Tables 5 through 17 are available, at a nominal charge, from the Depository of Unpublished Data, CISTI, National Research Council of Canada, Ottawa, Ont., Canada K1A 0S2.

Can. J. Chem. Downloaded from www.nrcresearchpress.com by 210.87.254.6 on 09/06/12
For personal use only.

TABLE 2. N_2. One-electron property expectation values computed with free variational and constrained (RHF constraints) MOM wavefunctions. Slater exponents were used. The properties are defined in refs. 21 and 37; atomic units for all properties

Constraints	T	r_N^{-1}	$-\theta_n^e$	r_n^2	E_N	$-q_N^e$	$T+V_{ne}$
None	107.20	21.453	17.927	37.967	1.3240	2.5744	−193.14
T	108.24	21.533	17.918	37.969	1.1264	2.5612	−193.22
[a] r_N^{-1}	108.56	21.555	17.903	37.966	1.0577	2.5490	−193.21
[b] $-\theta_n^e$	108.17	21.550	16.865	37.328	1.3179	1.8904	−193.54
[c] E_N	107.34	21.464	17.927	37.967	1.2999	2.5737	−193.16
[d] $-q_N^e$	107.97	21.537	16.872	37.333	1.3673	1.8920	−193.51
[e] $T+V_{ne}$	108.47	21.572	16.895	37.349	1.2309	1.9074	−193.54
$r_N^{-1}, -\theta_n^e$	108.25	21.556	16.865	37.327	1.2978	1.8912	−193.54

T = Electronic kinetic energy.
[a]Diamagnetic contribution to the diamagnetic shielding at the nucleus.
[b]Electronic component of the molecular quadrupole moment, ea_0^2.
[c]Electronic component of the Hellman–Feynman electric field strength at the nculeus, ea_0^{-2}.
[d]Electronic component of the electric field gradient at the nucleus, ea_0^{-3}.
[e]One electron contribution to the total energy, e^2/a_0.

TABLE 3. N_2. Reduced errors, percentages of properties improved, molecular energies, and SDRE (40) values for free variational and constrained (RHF constraints) MOM wavefunctions. Percentile ranks according to the SDRE (40) and energy criteria are given in parentheses.

Constraints	SDRE	Energy[a]	Properties Improved (%)	Reduced errors (×100) T	r_N^{-1}	$-\theta_n^e$	r_n^2	E_N	$-q_N^e$	$T+V_{ne}$	E
None	1.431(87)	−131.7940(75)	0	−174	−161	112	132	18	124	136	134
T	1.135(50)	−131.8077(50)	59	−0	−36	111	132	−135	121	108	123
r_N^{-1}	1.283(62)	−131.7835(87)	79	53	−0	110	131	−188	119	111	142
$-\theta_n^e$	0.090(12)	−131.9656(12)	100	−11	−8	0	0	14	−0	1	0
E_N	1.337(75)	−131.8026(62)	59	−151	−144	112	132	0	124	130	127
$-q_N^e$	0.346(37)	−131.9591(37)	79	−45	−33	0	1	52	0	9	5
$T+V_{ne}$	0.318(25)	−131.9594(25)	83	38	25	3	4	−53	2	−0	5
$r_N^{-1}, -\theta_n^e$	0.010(0)	−131.9660(0)	100	1	0	0	0	−1	0	−0	0

[a]Hartrees = 27.2107 eV = 4.35942×10^{-11} erg.

TABLE 4. N_2. Gross atomic orbital populations computed for constrained (RHF constraints) (21) MOM wavefunctions. Slater exponents were used (37)

Wavefunction	$1s$	$2s$	$2p\sigma$
Free variational RHF	2.002	1.738	1.260
Free variational MOM	2.008	1.397	1.595
Constrained MOM T	1.998	1.416	1.586
Constrained MOM r_N^{-1}	1.993	1.428	1.579
Constrained MOM $-\theta_n^e$	2.003	1.737	1.260
Constrained MOM E_N^e	2.007	1.399	1.594
Constrained MOM $-q_N$	2.005	1.732	1.262
Constrained MOM $T+V_{ne}$	1.999	1.734	1.267

values, Table 5. The calculated T, r_F^{-1}, and E_F^e are in better agreement with the RHF values suggesting improved charge density distribution in the fluorine inner shell region.

The gross orbital populations, Table 7, show that most constraints reduce the gross population of the hydrogen $1s$ orbital and increase the fluorine $2s$ population. However, with one exception, constraints significantly lower the $2p\sigma_F$ populations. In MOM, $2p\sigma$ orbitals usually contribute more to the total overlap than $2s$ orbitals, and therefore $2p\sigma$ populations are less altered by perturbations. In the RHF, and to a lesser extent the NDDO method, a $2s$ electron is more tightly bound than a $2p\sigma$ electron, and $2s$ populations are not significantly changed by most single constraints. The $[-q_F^e]$ constraint modifies the $2p\sigma_F$ population and the value is in good agreement with the RHF value. The hydrogen $1s$ population is poor, however.

Double constraints based on one of the properties $-q_F^e$, $T + V_{ne}$, $-\theta_n^e$, or r_n^2, which are sensitive to s–p promotion, and a property such as r_H^{-1}, $-q_H^e$, or x_n, which are sensitive to the apportionment of charge density between the fluorine and hydrogen atoms, lead to wavefunctions close to the RHF wavefunction, even in the fluorine inner shell region.

CO

In almost all cases, constraints lower energies and SDRE (40) values, Table 9, and improve most property expectation values, Table 8, compared to the free variational results. The gross orbital populations, Table 10, indicate that single constraints mainly alter the distribution of π charge density between the carbon and oxygen atoms. The $[r_O^{-1}]$, $[x_n]$, $[r_n^2]$, and $[T + V_{ne}]$ constrained MOM wavefunctions give gross $2p\pi$ populations in good agreement with the RHF values. The only constraints which significantly alter the $2p\sigma$ populations are $[-\theta_n^e]$, $[r_n^2]$, $[T + V_{ne}]$, and $[-q_O^e]$. The $2p\sigma_C$ populations obtained with the $[-\theta_n^e]$ and $[r_n^2]$ constrained wavefunctions agree well with the RHF values. The $[r_n^2]$ constraint is particularly effective, reducing the charge density in the diffuse car-

Can. J. Chem. Downloaded from www.nrcresearchpress.com by 210.87.254.6 on 09/06/12
For personal use only.

bon antibinding region, and improving the π charge distribution. The most effective multiple constraints use x_n or r_O^{-1}, which are sensitive to the distribution of π charge, $-\theta_n^e$ or $T + V_{ne}$, which are sensitive to $s-p$ hybridization in the carbon nonbonding orbital, or $-q_O^e$, which is sensitive to $s-p$ promotion at the oxygen atom. The $[x_n, -\theta_n^e, -q_O^e]$ constrained wavefunctions give $2p\sigma$ and $2p\pi$ populations at both the carbon and oxygen atoms in good agreement with the RHF values.

LiH

The MOM wavefunction for LiH is very poor, because the basis set is not strictly minimal. With the exception of the $[E_{Li}^e]$ and $[F]$ constraints, single constraints dramatically improve property expectation values, Table 11, and lower energies and SDRE values, Table 12. The $[T + V_{ne}]$ constrained wavefunction gives an energy which is only 0.003 hartrees above the RHF value. Most single constraints greatly increase lithium $1s$ populations, Table 13, improve values of T and r_{Li}^{-1}, and reduced $2s$ and $2p\sigma$ populations. The $[T]$, $[r_{Li}^{-1}]$, $[r_n^2]$, $[-q_H^e]$, $[-V_{ne}]$, and $[T + V_{ne}]$ constraints most improve the lithium $1s$ and $2s$ populations. The $[r_H^{-1}]$, $[x_n]$, $[r_n^2]$, $[-V_{ne}]$, and $[T + V_{ne}]$ constraints increase the charge density near the proton and the resulting hydrogen $1s$ populations agree well with the RHF value. The gross populations, property expectation values, and energy calculated with the $[-\theta_n^e, r_n^2]$ constrained wavefunction are in excellent agreement with the RHF values.

Constrained MOM calculations on CO and LiH using constraints based on experimental and theoretical expectation values

Constrained MOM calculations were performed on CO and LiH using constraints based on experimental and theoretical expectation values. CO and LiH were chosen because the MOM wavefunctions for both molecules suffer from severe defects due to inadequacies of MOM. For CO, MOM predicts equal populations for the $2p\pi_C$ and $2p\pi_O$ orbitals. For LiH, MOM gives a completely unreasonable wavefunction mainly because the basis set is not minimal.

CO

With a few exceptions, single constraints improve all property expectation values, Table 14, and lower energies and SDRE values, Table 15. Some of the singly constrained wavefunctions give energies lower than the value calculated with the free variational NDDO wavefunction.[2] As above, $[r_O^{-1}]$, $[x_n]$, $[r_n^2]$, and $[T + V_{ne}]$ give the greatest improvement, mainly due to a more realistic distribution of π charge density in the molecule (37).

Multiple constraints do not significantly improve the energies, or SDRE values, compared to the corresponding singly constrained wavefunctions, because many expectation values calculated with singly constrained wavefunctions are comparable in accuracy with the RHF values, and therefore little further improvement due to additional constraints can be expected.

LiH

For LiH, constraints invariably improve the MOM wavefunction, Table 16 and 17. The most effective constraints, $[T]$, $[r_{Li}^{-1}]$, $[r_n^2]$, $[-V_{ne}]$, and $[T + V_{ne}]$, in the calculations involving RHF constraints, were also found to be the most effective constraints in the present calculations. Note that the energy calculated with the $[T + V_{ne}]$ constrained wavefunction is very close to the RHF value. In several cases multiple constraints result in lower energies, but not lower SDRE values, compared to the corresponding singly constrained wavefunctions.

Conclusion

The constrained MOM calculations based on RHF constraints have been used to compare the effects of different constraints on MOM wavefunctions. Constraints based on r_n^2 and $T + V_{ne}$ were found to be particularly effective in improving MOM wavefunctions. Helmann–Feynman constraints led to poor results. As in the NDDO calculations,[2] single constraints mainly alter the interatomic charge transfer. A significant difference between the NDDO and MOM calculations is that $2p\sigma$ populations are less affected by constraints than $2s$ populations in the MOM calculations. This is because $2p\sigma$ orbitals make a greater contribution to the total overlap than $2s$ orbitals.

MOM suffers from several defects which can cause MOM wavefunctions to be unrealistic, as for CO and LiH. For both molecules single constraints based on *experimental* or *theoretical expectation values* are able to correct the worst deficiencies of the wavefunctions. Calaculated property expectation values and energies are dramatically improved. As in the NDDO calculations, multiple constraints based on experimental or theoretical expectation values were not found to be effective.

Thus by constraining an MOM wavefunction with r_n^2 *or* $T + V_{ne}$, a wavefunction comparable to the RHF wavefunction in SDRE or Energy overall character may perhaps be achieved without iteration, either in the MOM or energy calculation stage. With experimental constraints, the wavefunctions of the MOM method may be made as good overall as the RHF wavefunction, or even "better", if agreement with experiment is the criterion of goodness.

Similar comments may apply to the Hückel (25, 26) and Extended Hückel (30) methods. Consequently, the worst deficiencies of the MOM, Hückel, and Extended Hückel methods, which are so simple in application, can perhaps be removed by constraining. This would ensure that the wavefunctions and thus the atomic, bond, and molecular charges etc. would be chemically significant and theoretically justified.

The present constrained variational maximum overlap method may offer a new future to these well-tried and accepted methods in organic and inorganic chemistry.

Acknowledgement

This research was supported by the National Research Council of Canada.

1. L. PAULING. J. Am. Chem. Soc. **53**, 3225 (1931).
2. J. C. SLATER. Phys. Rev. **37**, 481 (1931).
3. R. S. MULLIKEN. Phys. Rev. **41**, 67 (1932).
4. L. PAULING. Proc. Natl. Acad. Sci. USA. **14**, 359 (1928).
5. L. PAULING. J. Am. Chem. Soc. **53**, 1367 (1931).
6. C. A. COULSON. Valence, 2nd ed. Oxford University Press. 1965.
7. M. RANDIĆ and Z. MAKSIĆ. Theor. Chim. Acta, **3**, 59 (1965).
8. L. KLASINC, Z. MAKSIĆ, and M. RANDIĆ. J. Chem. Soc. 755 (1966).
9. M. RANDIĆ and Z. B. MAKSIĆ. Chem. Rev. **72**, 43 (1972).
10. M. RANDIĆ. Int. J. Quantum Chem. **8**, 643 (1974).
11. S. BISKUPIC and P. PELIKAN. Chem. Zvesti. Ceskosl. **30**, 319 (1976); R. BOCA, P. PELIKAN, and L. VALKO. J. Mol. Struct. **1**, 161 (1978).

12. F. WEINHOLD and T. K. BRUNCK. J. Am. Chem. Soc. **98**, 3745 (1976).
13. R. JANOSCHEK. Z. Naturforsch. A, **32**, 1188 (1977); Z. B. MAKSIC, K. KOVACEVIC, and M. VAMPOLA. Z. Naturforsch A, **36**, 1196 (1981).
14. KING-MO SUN and WAI-KEE LI. Croat. Chem. Acta, **49**, 75 (1977).
15. J. N. MURRELL. J. Chem. Phys. 32, 767 (1960).
16. A. GOLEBIEWSKI. Trans. Faraday Soc. **57**, 1849 (1961).
17. A. GOLEBIEWSKI. Acta Phys. Polon. **23**, 243 (1963).
18. A. GOLEBIEWSKI. Acta Phys. Polon. A, **37**, 319 (1970).
19. T. L. GILBERT and P. G. LYKOS. J. Chem. Phys. **34**, 2199 (1961).
20. P. G. LYKOS and H. N. SCHMEISING. J. Chem. Phys. **35**, 288 (1961); G. DEL RE. Theor. Chim. Acta, **1**, 188 (1963); R. REIN, S. ADAMS, S. NIR, and T. J. SWISSLER. Chem. Phys. Lett. **21**, 483 (1973).
21. G. D. ZEISS and M. A. WHITEHEAD. Can. J. Chem. **61**, 128 (1983).
22. G. D. ZEISS and M. A. WHITEHEAD. Int. J. Quantum Chem. In press.
23. B. H. CHIRGWIN and C. A. COULSON. Proc. R. Soc. A, **201**, 196 (1950).
24. R. MANNE. Int. J. Quantum Chem. **2**, 69 (1968).
25. E. HÜCKEL. Z. Physik, **70**, 204 (1931).
26. G. W. WHELAND. J. Am. Chem. Soc. **64**, 900 (1942).
27. J. A. POPLE, D. P. SANTRY, and G. A. SEGAL. J. Chem. Phys. **43**, S129 (1965); J. A. POPLE and G. A. SEGAL. J. Chem. Phys. **43**, S136 (1965); J. Chem. Phys. **44**, 3289 (1966).
28. R. J. BOYD and M. A. WHITEHEAD. J. Chem. Soc. Dalton Trans. 73 (1972); 78 (1972); 81 (1972).
29. M. TAKASUKA. Spectrosc. Lett. **14**, 695 (1981).
30. R. HOFFMAN. J. Chem. Phys. **39**, 1397 (1963).
31. M. WOLFSBERG and L. HELMHOLZ. J. Chem. Phys. **20**, 837 (1952).
32. K. RUEDENBERG. J. Chem. Phys. **34**, 1861 (1961).
33. T. S. TSENG and M. A. WHITEHEAD. J. Chem. Soc. Faraday Trans. 2. In press; J. Comput. Chem. **3**, 552 (1982).
34. R. J. BARTLETT and Y. OHRN. Theor. Chim. Acta, **21**, 215 (1971).
35. C. C. J. ROOTHAAN. Rev. Mod. Phys. **23**, 69 (1951).
36. R. S. MULLIKEN. Rev. Mod. Phys. **32**, 232 (1960).
37. G. D. ZEISS. Ph.D. Thesis, McGill University, 1976. Chapt. IV.
38. P.-O. LOWDIN. Phil. Mag. Suppl. **5**, 1 (1956).
39. G. D. ZEISS and M. A. WHITEHEAD. J. Comput. Chem. Submitted.
40. G. D. ZEISS and M. A. WHITEHEAD. J. Comput. Chem. In press.

Can. J. Chem. Downloaded from www.nrcresearchpress.com by 210.87.254.6 on 09/06/12
For personal use only.

Dynamic mechanical studies of partially ionized and neutralized Nafion polymers

THEIN KYU,[1] MITSUAKI HASHIYAMA,[2] AND ADI EISENBERG
Department of Chemistry, McGill University, Montreal, P.Q., Canada H3A 2K6

Received August 31, 1982

This paper is dedicated to Professor Leo Yaffe on the occasion of his 65th birthday

THEIN KYU, MITSUAKI HASHIYAMA, and ADI EISENBERG. Can. J. Chem. **61**, 680 (1983).

The dynamic mechanical properties of Nafion precursor were determined as a function of the degree of conversion to the sodium ionomer, and those of the acid as a function of the degree of conversion to the cesium salt. A run was also made on the barium neutralized material, as well as on a remolded sample of a partly converted precursor. The precursor shows four dispersions which (in order of decreasing temperature) are identified with the glass transition, motions of the ether side chains, CF_2 groups in the backbone, and pendant SO_2F groups. Four relaxation regions are also seen in the ionomer, which are identified with the glass transition of the ionic regions and of the matrix, as well as with motions of the ether side chains and the backbone CF_2 groups. While the polymers in the acid and the salt forms are compatible, as seen by the gradual movement of the ionic glass transition peak to higher temperatures with increasing degree of neutralization, the salt and the precursor are not compatible. In the barium salt, the ionic glass transition peak occurs at a temperature close to the melting point of the crystalline regions, and most likely contains a contribution from that process also.

THEIN KYU, MITSUAKI HASHIYAMA et ADI EISENBERG. Can. J. Chem. **61**, 680 (1983).

On a déterminé les propriétés mécaniques du précurseur du Nafion en fonction du degré de transformation en l'ionomère du sodium et de celles de l'acide en fonction du degré de sa transformation en sel de césium. On a également fait une détermination sur des composés neutres de baryum aussi bien que sur un échantillon modifié d'un précurseur partiellement transformé. Le précurseur montre quatre dispersions (dans l'ordre d'une diminution de température) que l'on a identifiées avec la transition du verre, et avec les mouvements de la fonction éther des chaînes latérales, des groupes CF_2 du squelette et des groupes SO_2F. On a également vu dans l'ionomère quatre régions de relaxation que l'on a identifiées avec la transition du verre des régions ioniques et de la matrice aussi bien qu'avec les movements de la fonction éther des chaînes latérales et des groupes CF_2 du squelette. Alors que les polymères sous forme d'acide et de sel sont compatibles, comme on l'a vu d'après le mouvement graduel du pic de transition ionique du verre à des températures plus élevées avec une augmentation du degré de neutralisation ionique, le sel et le précurseur ne sont pas compatibles. Dans le cas du sel de baryum le pic de transition ionique du verre apparaît à une température voisine du point de fusion des régions cristallines, et comporte vraisemblablement une contribution de ces régions.

[Traduit par le journal]

I. Introduction

The dynamic mechanical properties of the Nafion polymers, which are ionic (1), are dramatically different from those of the precursor (2, 3), which is nonionic. As might be expected, the changes depend on the nature and the concentration of the ionic species which is introduced. The precursor is an inert hydrophobic polymer containing the fluorocarbon backbone with perfluorinated ether side chains terminated by an $—SO_2F$ group, which is converted to an $—SO_3H$ group or its salt in Nafion (4, 5).

The structure and properties of the Nafions have been explored extensively by various techniques (5); it has been concluded that the Nafions are phase-separated (1, 6–9) and can be represented by a three phase model with hydrophobic amorphous and crystalline regions and hydrophilic ionic domains (6). Where water is introduced into the Nafions, it is accommodated in the ionic regions (8–15). The unique structure of the Nafions gives them unusual properties such as high water permeability (16), permselectivity with regard to ion transport (17–21), and many other features (5) which are absent in the precursor. It is therefore not surprising that many properties of the Nafions differ profoundly from those of the precursor before ionization.

The results of a previous study (2) of the mechanical and dielectric properties of the precursor are summarized below to demonstrate the dramatic changes which occur on ionization. Four relaxation peaks (labelled α_P, β_P, γ_P, and δ_P in descending order of temperature) were evident over the temperature range from −195°C to ca. 125°C. These peaks were identified with the glass transition of the fluorocarbon matrix, the relaxation of the ether side chains, the local short range motions of the $—CF_2—$ backbone, and the rotation of the $—SO_2F$ groups, respectively. In the original publication (2), the peaks were named α, β', β'', and γ, the β' and β'' peaks coalescing into a broad skewed peak over the frequency range studied. With this revised nomenclature, the γ relaxations in the precursor and in the Nafions now reflect the same mechanism, as will be indicated below.

For Nafion acid, three relaxation peaks termed α, β, and γ in descending order of temperature were observed over the temperature range from −160°C to ca. 150°C (1). Upon neutralization with various alkali salts, the peak temperatures of the α and β regions shifted upward by over 100°C in both cases, while that of the γ peak remained essentially the same. Early evidence revealed that the β peak was strongly affected by the presence of water, but that there was little or no influence of water on the α peak in Nafion acid. The γ peak position was not affected at the low levels of water content investigated

[1]Present address: Polymer Research Institute, University of Massachusetts, Amherst, MA 01003, U.S.A.

[2]Present address: Toyo Rubber Company Ltd., Ibaraki-shi, Osaka, Japan.

Can. J. Chem. Downloaded from www.nrcresearchpress.com by 210.87.254.42 on 09/06/12
For personal use only.

Can. J. Chem. Downloaded from www.nrcresearchpress.com by 210.87.254.42 on 09/06/12
For personal use only.

in both the acid and its salts. These α, β, and γ peaks were first assigned to the glass transition of the fluorocarbon matrix, the relaxation of the ionic domains, and the short range molecular motion of the $—CF_2—$ backbone, respectively. The δ peak, which was identified with the rotational motion of the $—SO_2F$ group in the precursor, was not detected in the dielectric and torsional pendulum studies of Nafion acid.

Since the rheological properties of the precursor differ greatly from those of the Nafion salts, there is no doubt that these properties must depend on the extent of ionization. It should therefore be of interest to follow the changes in the mechanical properties of the precursor in the course of conversion to the Nafion salts by preparing samples ionized to varying extents; the results of such a study are presented in the first part of this article. Also, the Nafion acid shows a substantially different relaxation behavior from that of its salts, the properties of which are therefore also expected to depend on the degree of neutralization. The effect of the degree of neutralization of Nafion acid on the mechanical relaxation behavior is explored in the second part of this work. Finally, a comparison is made between the barium and cesium salt of highly neutralized Nafion to confirm the proposed reinterpretation of the α and β peaks in that material.

II. Experimental

A. Materials

1. Preparation of partially ionized Nafion-Na

The precursor material with an equivalent weight of 1200 used in the present study is similar to that employed previously (2). The precursor film proved too thin to be tested directly on the torsional pendulum; accordingly several sheets of the material were melt pressed in a heated laboratory press at 250°C for five minutes and then cooled to ambient temperature. The final sample was 50 mm long, 6 mm wide, and 1 mm thick. Samples were annealed at 130°C for 6 hours in a vacuum oven and then weighed. Partially ionized samples were prepared by immersing the precursor samples in a 10% NaOH solution at ca. 75°C for varying periods of time. The samples thus prepared were dried at 130°C for 6 hours and reweighed. The conversion was calculated from the weight difference of the ionized Nafions and the precursor samples.

As shown in Fig. 1, the conversion of $—SO_2F$ to $—SO_3Na$ is slow initially, reaching ca. 80% after 8 hours and then gradually levelling off at ca. 90% after 24 h. This behavior is in line with the fact that the precursor is a hydrophobic material in which NaOH diffusion must be extremely slow, with the conversion taking place initially at the surface of the sample. Once the outermost layer is converted to the Nafion salt, the rate of water diffusion appears to be greatly enhanced, allowing the conversion of the inner layers into ionic Nafion material. The conversion is therefore expected to occur layer by layer producing a heterogeneous material with a "sandwich" structure, which is a composite of the Nafion salt (outer layers) and the precursor (inner layer). To ascertain whether Nafion is compatible with its precursor, an additional sample with approximately 56% Nafion-Na was prepared by immersing the precursor in a 10% NaOH solution at 75°C for about 6 hours, and remolding at 280°C in a laboratory hot press for about 20 min. If the Nafion salt and the precursor were compatible, this procedure would permit interdiffusion and blending of the two phases. A comparison of the relaxation behaviour of the original and remolded samples would then show whether or not the Nafion-Na and the precursor are compatible (22).

2. Preparation of partially neutralized Nafion-Cs

The starting material used in this study was Nafion acid (Nafion-H) of equivalent weight 1155 in the form of sheets with thickness ca. 1.3 mm, which were cut into strips 6 mm wide and 30 mm long. These samples were dried at 160°C under vacuum for 24 h and weighed. The acid samples were first boiled in distilled water to ensure extensive swelling, and then immersed in 0.1 *N* CsOH solution for differing time periods, which gave varying degrees of neutralization. The samples were again immersed in boiling water for about 24 h in order to achieve a homogeneous distribution of the cations present in the specimens; they were dried again at 160°C and reweighed. The samples prepared in this way were calculated to be ca. 39%, 50%, 76%, and 90% neutralized. In contrast to the partially ionized Nafion-Na samples prepared from the precursor, the diffusion coefficient of the Cs^+H in both Nafion acid and its salts is high (23), resulting in a final sample containing a homogeneous distribution of cations.

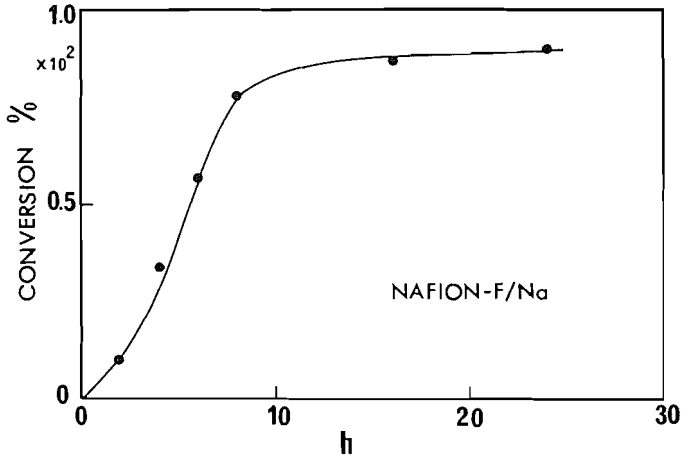

FIG. 1. Conversion of the precursor into partially-ionized Nafion-Na in 10% NaOH solution at ca. 75°C, as a function of time.

3. Preparation of the barium salt of Nafion-H

The divalent Ba salt of Nafion was prepared in a similar manner to the Nafion-Cs samples by immersing Nafion-H in a $BaCl_2$ solution. The degree of neutralization of the Ba salt was determined to be ca. 77%.

B. Experimental procedures

Dynamic mechanical studies were performed on a torsional pendulum which has been described previously (24). The samples were 30–60 mm long, 1.0–1.3 mm thick, and 6 mm wide. The temperature ranges of the experiments were −195°C to 250°C for the partially ionized Nafion-Na samples, −160°C to 250°C for the partially neutralized Nafion-Cs salts, and −160°C to 310°C for the Nafion-Ba sample. The frequencies were ca. 1 Hz at low temperatures, gradually decreasing with increasing temperature to ca. 0.1 Hz.

Since the Nafions are very sensitive to water, all of the samples were dried at 140–160°C under vacuum for 6–24 h to remove absorbed water. The samples were stored under vacuum in a desiccator until the torsional pendulum tests were carried out. Sample clamping in the apparatus was usually accomplished within 5 minutes. All experiments were then conducted in a helium gas environment at low temperatures and under vacuum at high temperatures.

III. Results

1. Partially ionized Nafion-Na

Figure 2 shows the storage and loss shear moduli G' and G'', and the loss tangent tan δ_G of the precursor obtained on the torsional pendulum over the temperature range from −195°C to 130°C at ca. 1 Hz. Although data were acquired at ca. 2.5°C intervals, alternate experimental points only were plotted (at 5°C intervals) for the sake of clarity. Above 130°C, measurements were no longer possible due to experimental limitations resulting from the softness of the sample. The relaxation behavior of the precursor is consistent with previous results from dielectric and vibrating reed studies (2), in which

Can. J. Chem. Downloaded from www.nrcresearchpress.com by 210.87.254.42 on 09/06/12
For personal use only.

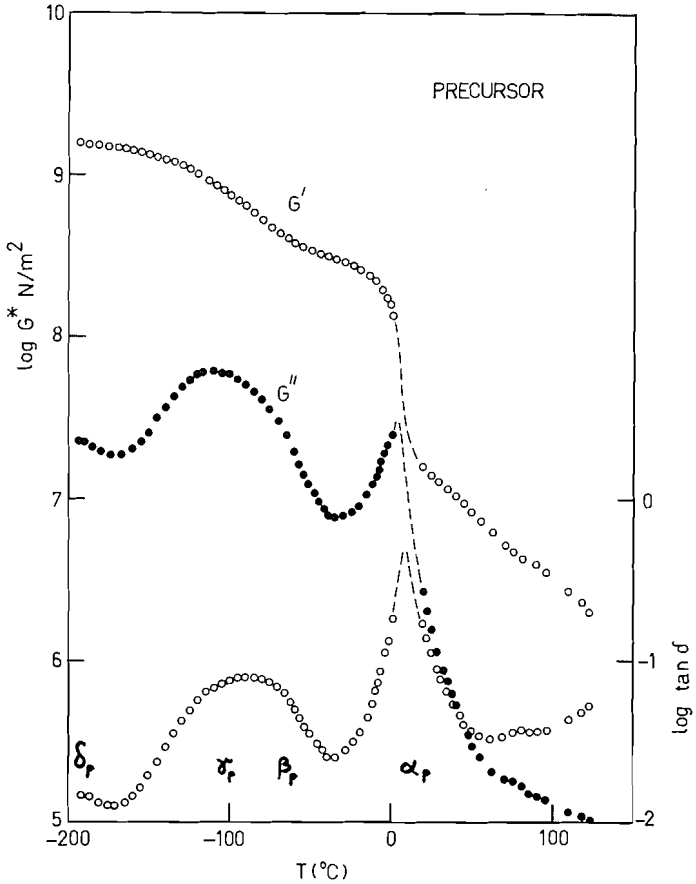

FIG. 2. Variation of G', G'', and tan δ_G with temperature for the precursor from torsional pendulum studies at ca. 1 Hz.

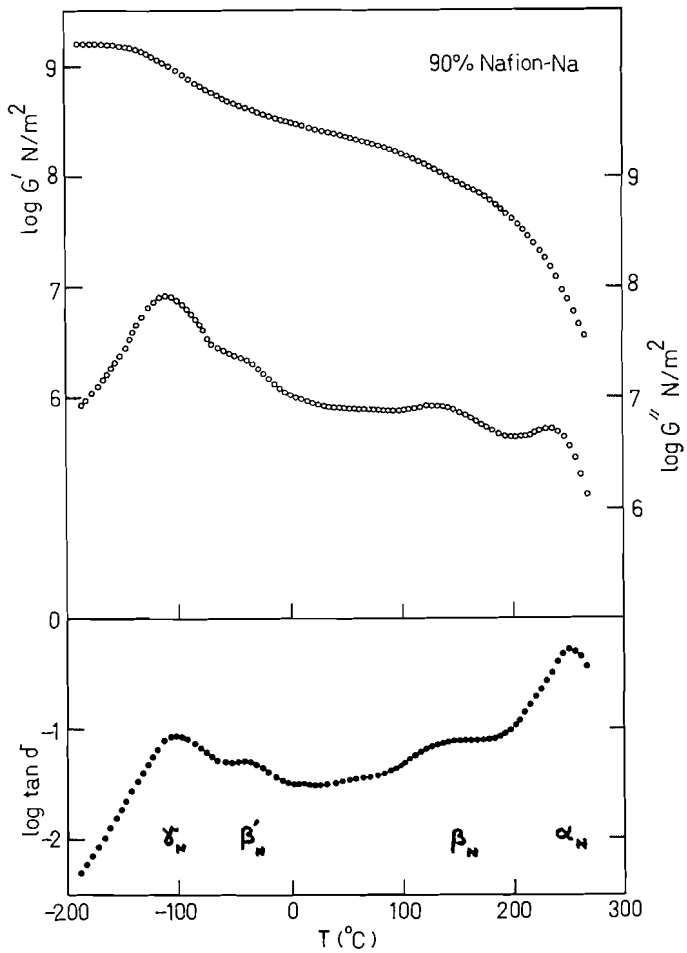

FIG. 3. Variation of G', G'', and tan δ_G with temperature for 90% conversion Nafion-Na from torsional pendulum studies at ca. 1 Hz.

four relaxation regions were seen, one of these manifesting itself as a skewed composite peak (see below). These peaks are labelled, in this paper, α_P, β_P, γ_P, and δ_P, in descending order of temperature. In the previous study (2) they were labelled α, β', β'', and γ; however, the molecular mechanism responsible for the β'' peak in the precursor corresponds to that of the γ peak in the Nafions and in polytetrafluoroethylene (PTFE). Therefore, in order to avoid confusion, the β'' peak has been relabelled as the γ_P peak and the γ peak from the original work was necessarily relabelled as a δ_P peak.

The onset of the δ_P peak is clearly observed in Fig. 2 at ca. -170 to -190°C. Another peak occurs at ca. -100°C in both the G'' and the tan δ_G curves; both of these peaks are broad and skewed, as was previously observed (2). These skewed peaks are considered to be the sum of two overlapping peaks – the β_P and the γ_P relaxations. The highest temperature α_P dispersion is seen at ca. 10°C; the drastic drop in G' and the sharpness of the tan δ_G peak are characteristic of typical glass transition behavior of a neutral amorphous polymer.

Figure 3 shows the relaxation behaviour of the Nafion-Na sample of highest degree of ionization (90%), G', G'', and tan δ_G having been plotted with respect to temperature. Four distinct relaxation regions are evident, the peaks being labelled α_N, β_N, β'_N, and γ_N in order of decreasing temperature. The curves are very similar to those of the previous study (1) with the exception of the β'_N peak which appears at ca. -30°C in the Nafions with the highest degree of ionization; this peak was not as distinct in the mechanical spectrum of the dry samples tested previously as it is in the present study.

The lowest temperature δ_P peak, which was detected as a tail in the spectrum of the precursor, has disappeared both in the G'' and the tan δ_G curves of the highly ionized Nafion-Na samples. Also, this δ peak was not observed in the dielectric studies of the Nafion acid (1), strongly indicating that the peak may be a unique feature of the precursor which is not encountered in the ion-containing Nafion materials. In the previous study, this relaxation was identified with the motion of —SO_2F groups.

In the γ region, G' decreases markedly with temperature, with the corresponding G'' and tan δ_G plots indicating a peak centred around -100°C. The γ peak is more symmetrical and slightly higher in intensity than that of the precursor, supporting the earlier suggestion that the peak which appears at ca. -100°C in the precursor could result from the overlapping of the β_P and γ_P dispersions. In addition, a minor β'_N peak, which is not present as a separate peak in the precursor, is evident at ca. -30°C in the highly ionized Nafion-Na samples.

The highest temperature relaxation (α_N) occurs at ca. 240°C; it is the peak of greatest intensity in tan δ_G curve, with the β_N peak appearing as a shoulder at ca. 140°C. This behavior is identical to that observed previously. The initial assignment of the relaxation mechanisms of these two peaks must be re-evaluated, however; this aspect will be discussed in a later section of this paper.

Figure 4 shows a comparison of the relaxation behaviors of the nonionized precursor and the partially ionized Nafion-Na specimens with varying degrees of conversion (10%, 34%,

Can. J. Chem. Downloaded from www.nrcresearchpress.com by 210.87.254.42 on 09/06/12
For personal use only.

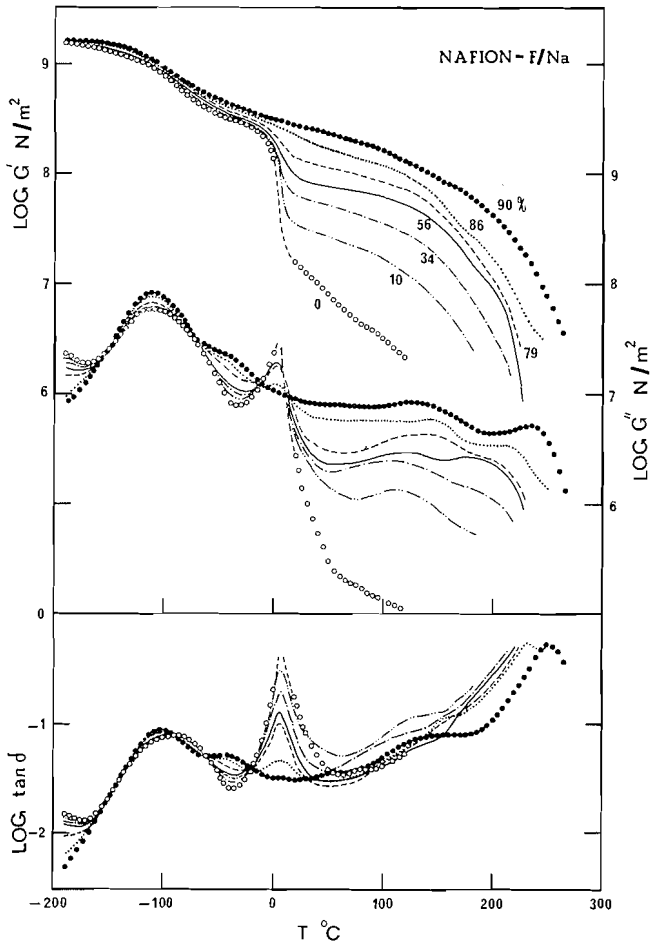

FIG. 4. Variation of G', G'', and tan δ_G with temperature for the percursor and partially ionized Nafion-Na samples at ca. 1 Hz.

56%, 79%, 86%, and 90%). The experimental points for the samples with intermediate extents of conversion have been omitted for the sake of clarity.

At the lowest temperatures achieved, i.e. in the δ region, samples with low degrees of conversion reveal the δ relaxation process as a tail in both the G'' and tan δ_G curves. The intensity of the δ peak decreases with increasing degree of conversion, eventually disappearing in the two highest (86% and 90%) conversion samples. Thus, it is clearly seen that the δ process exists only in the precursor.

At about −100°C, the G'' and tan δ_G curves for the low conversion samples show a skewed peak similar to that observed in the precursor where it was interpreted as being due to overlapping of the β_P and γ_P dispersions. The symmetry and intensity of this peak both increase with increasing conversion, however. Concurrently, a minor β'_N peak gradually appears at ca. −30°C, as a shoulder on the lower temperature γ peak. This would suggest that the overlapping β_P and γ_P relaxation processes in the precursor are split into two separate β'_N and γ_N dispersions, with increasing degree of ionization of the Nafion salt. It should be emphasized that the occurrence of the β'_N peak is prominent only in the Nafion materials of a high level of conversion.

In the glass transition region of the precursor, the α_P relaxation is very clearly defined, with sharp peaks observable in both the G'' and tan δ_G curves along with a dramatic drop-off in the G' plot. The intensity of this α_P peak decreases systematically with increasing degree of conversion, almost disappearing in the highest conversion Nafion-Na sample. The storage modulus G' correspondingly increases with increasing degree of conversion, with values for the highest (90%) conversion sample being over an order of magnitude higher than those of the precursor for temperatures greater than about 0°C.

As the temperature increases further, the G' and G'' curves of the precursor decrease monotonously with no additional peaks seen in the tan δ_G curve. The 10% conversion sample does show a peak (labelled β) in the G'' curve at ca. 130°C; as the degree of conversion increases, another high temperature peak, designated α, is evident in the G'' curves. This α peak is not seen in the tan δ_G curves for the low conversion samples due to an experimental limitation resulting from the softness of the samples. In the G'' plots, both the α and β peak positions shift to higher temperatures with increasing degree of conversion while the magnitudes of G' and G'' increase dramatically. The tendency for the β peak to move to higher temperatures with increasing conversion, accompanied by a slight depression of the G'' peak height, is reflected also in the tan δ_G curves. In the α region, the tan δ_G curves also move to higher temperature with increasing conversion; a clear peak is only evident in the highest conversion samples due to experimental limitations.

The decreasing intensity of the α_P peak (the glass transition of the precursor) accompanied by the increase in that of the α_N and β_N peaks (which will be identified below as the glass transitions of the ionic domains and the polymer matrix, respectively) in Nafion-Na with increasing conversion is reminiscent of typical relaxation phenomena observed in immiscible polymer blends. This behavior is further explored in Fig. 5 in which the torsional pendulum results for the original 56% conversion sample and a remolded specimen are compared. The γ region is almost identical in both cases. In the α_P region, the tan δ_G peaks for both systems are comparable. At elevated temperatures, however, the intensity of the β_N peak in the G'' and tan δ_G curves of the remolded sample is somewhat greater than that of the original Nafion, while the opposite behavior is observed for the α peak. The peak positions of both α and β peaks remain the same, however. This latter observation suggests that the precursor and the Nafion salt are probably incompatible.

2. *Partially neutralized Nafion-H/Cs*

Figure 6 shows torsional pendulum results for Nafion-H and Nafion-Cs samples with various degrees of neutralization (39%, 50%, 79%, and 90%). The Nafion acid (0% neutralization) reveals three distinct peaks in the tan δ_G versus temperature curve, which are termed α, β, and γ in descending order of temperature.

In the γ region, the position of the tan δ_G peak is not affected substantially by changes in the degree of neutralization: its magnitude does increase slightly with increasing degree of neutralization, however. A minor dispersion, analogous to the β'_N peak of the highly ionized Nafion-Na, is seen as a shoulder at ca. −20°C in the case of the 90% neutralized Nafion-Cs.

A broad β peak occurs in the 0−100°C temperature interval for the partially neutralized Nafion-Cs samples. With the exception of the 39% neutralized sample, the position of the tan δ_G peak in the β region shows a tendency to shift to higher temperature with increasing Cs^+ content. The height of the β peak, however, decreases gradually as the degree of neutralization increases. The decrease in G' in this region, while not pronounced, is still discernible.

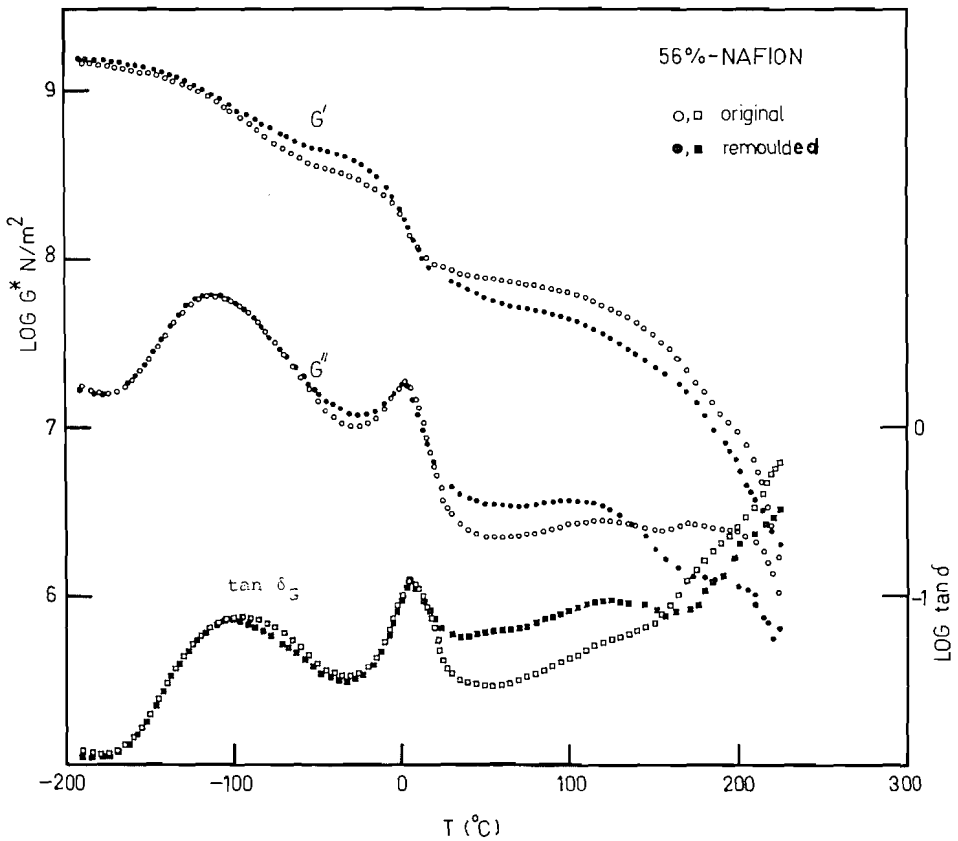

FIG. 5. Comparison of G', G'', and tan δ_G for original and remolded Nafion-Na of 56% conversion.

In the α region, G' drops drastically and a systematic movement of the falling portion of the G' curve to higher temperatures with increasing neutralization is very clear. The corresponding tan δ_G peak (the α peak) migrates to higher temperatures, accompanied by a slight increase in the peak height.

3. The barium salt of Nafion

Figure 7 shows the variation of G', G'', and tan δ_G with temperature for a Nafion-Ba sample. The γ relaxation appears at about the same temperature and has a comparable intensity to that of the monovalent ionic salts of Nafion. The β dispersion, which overlaps with the lower temperature γ peak, appears at ca. -20°C corresponding to the β'_N peak of the highly ionized Nafion-Na (Fig. 3) and the highly neutralized Nafion-Cs (Fig. 6) materials. However, the peak intensity is much greater here than in the monovalent salts.

As the temperature is increased, a very small shoulder is seen at ca. 210 in the G'' and tan δ_G curves. The G' curve, which is very flat up to about 200°C, begins to drop off fairly quickly at higher temperatures, with a peak seen at ca. 270°C in the G'' curve; this peak is not evident in the tan δ_G curve. This dispersion coincides to some extent with the crystal melting temperature of the monovalent salts, as revealed by differential scanning calorimetry (9, 25) and wide-angle X-ray diffraction studies (9, 26). There are probably contributions to this peak from both crystal melting and glass transition processes.

IV. Discussion

1. The precursor and partially ionized Nafion-Na

The low temperature δ_P relaxation of the precursor, previously observed in dielectric and vibrating reed studies, was detected as an increase in the energy dissipation over the temperature range from -170 to -190°C in the present torsional pendulum experiments. It had not been observed in the previous torsional pendulum study, since that work covered a temperature range of only -150 to 25°C. The gradual disappearance of the δ peak with increasing degree of neutralization confirms that the relaxation mechanism involved must be unique to the percursor; it is likely associated with the motion of $-SO_2F$ groups, as has been previously suggested.

The peak present in the spectrum of the precursor at ca. -100°C is broad and skewed, which was considered to be due to the overlapping of the γ_N and β_N peaks. Dielectric and mechanical studies suggest that the relaxation mechanisms responsible for these two peaks involve local $-CF_2-$ backbone motions and ether side chain motions, respectively. For low degrees of conversion from the precursor to the Nafions, the shape and temperature position of this peak are retained. However, materials with higher degrees of conversion yield more symmetrical peaks in the temperature region centred about -100°C, with an additional minor peak (β'_N) appearing at ca. -30°C in the case of the two highest conversion samples. This latter relaxation is not present as a separate dispersion in the precursor. Since the height and symmetry of this minor peak increase with increasing conversion, it is reasonable that the overlapping γ_P and β_P peaks of the precursor are split into two separate peaks with the introduction of a large number of ionic groups into the polymer. Since the β_P peak has been associated with the ether side chain motion, the β'_N process of Nafion may be related to a type of ether side chain motion which is influenced by ionic forces originating with the phase separated ionic domains.

In an earlier study of the Nafions by Yeo and Eisenberg (1) this β' peak was not seen to the extent observed here in the dry

Can. J. Chem. Downloaded from www.nrcresearchpress.com by 210.87.254.42 on 09/06/12
For personal use only.

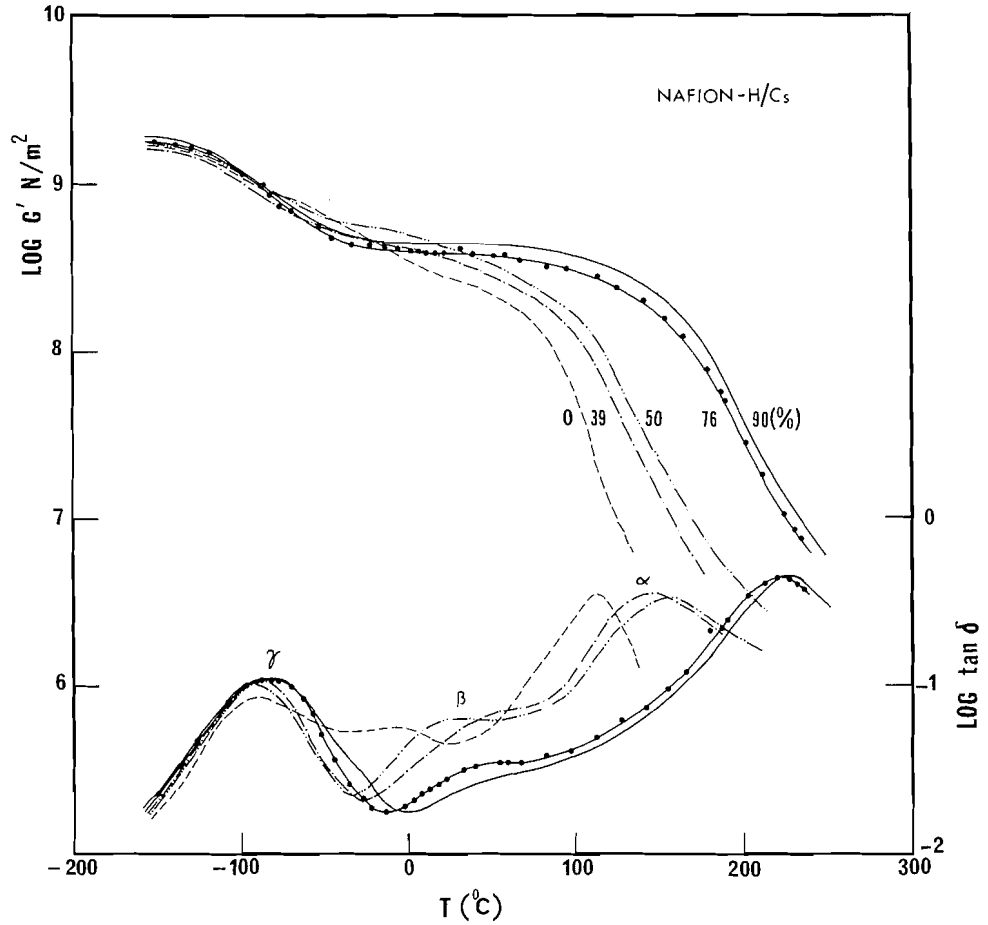

FIG. 6. Variation of G' and tan δ_G with temperature for Nafion-Cs with varying degrees of neutralization at ca. 1 Hz.

monovalent salts. Instead, a similar β peak was found in about the same temperature region in hydrated Nafions, this peak migrating to lower temperatures with increasing water content and eventually merging with the γ peak. It is tempting to suggest that the β′ peak may be related to the water-plasticized β peak observed in the previous Nafion-H samples. If this were the case, however, the position of the β′ peak should depend on the moisture content. Since samples with a low degree of conversion contain fewer ionic sites than those with higher conversions, there should be less residual water in the former materials. Hence the peak would be expected at a higher temperature for a specimen with a lower degree of conversion. Since the β peak appears to move to higher temperatures with increasing conversion, it is probably not related to the previously observed water-plasticized β peak in Nafion-H.

The identification of the γ peak is relatively straightforward; its temperature position in both the precursor and the Nafions is close to that observed for the relaxation in PTFE (27). The activation energy of the process as determined in dielectric studies is also comparable to that observed in PTFE. Thus, the γ relaxation in Nafion may have the same origin as the relaxation in PTFE where it is attributed to local —CF_2— backbone motions.

In the glass transition or α_P region of the precursor, which occurs at ca. 0°C, the intensity of the G'' and tan δ_G peaks decreases with increasing degree of ionization, the peak temperature remaining constant. At higher temperatures still, two peaks (denoted β and α, in ascending order of temperature) appear in the G'' curves of the partially ionized Nafion-Na samples, both peaks shifting to higher temperatures with increasing degree of ionization. These motions reflect the strong ionic interactions within the polymer. Certainly the α_P peak of the precursor is associated with the glass transition of the precursor matrix, while the β_N and α_N peaks of the Nafions could be associated with the glass transitions of the matrix and the ionic domains of the ion-containing phase separated system. This assignment of the α_P peak of the precursor to the T_g of the nonionized matrix is generally accepted, while that of the α_N and β_N relaxations is somewhat speculative, and will be discussed more fully in a subsequent section.

There is considerable similarity between the relaxation behavior of the original and remolded 56% conversion Nafion-Na samples; the temperature positions of the glass transition (or α_P relaxation) of the precursor and those of the glass transitions of the matrix and ionic domains of the Nafion salt (the β_N and α_N dispersions respectively) remain the same. This would suggest that the two systems are independent of each other.

2. *Partially neutralized Nafions*

The γ peak in the partially neutralized Nafion-Cs samples occurs at ca. −90°C, regardless of the degree of neutralization of the specimens, which is consistent with the results of the previous study as well as with those of the partially ionized Nafion-Na materials. The relaxation mechanism is likely the same as that occurring in PTFE or the precursor, where the peak has been assigned to local —CF_2— backbone motions. In contrast to its effect on the α and β peaks, the influence of the degree of neutralization on the temperature position of the γ

Can. J. Chem. Downloaded from www.nrcresearchpress.com by 210.87.254.42 on 09/06/12
For personal use only.

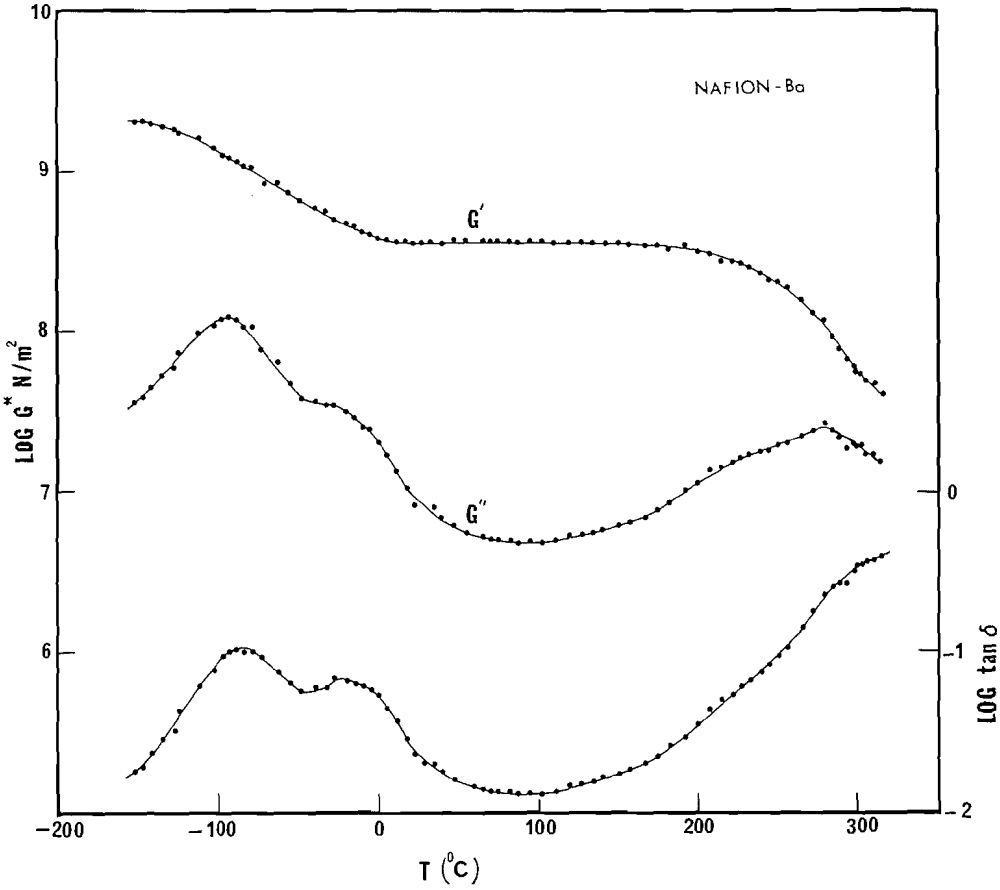

FIG. 7. Variation of G', G'', and tan δ_G with temperature for Nafion-Ba at ca. 1 Hz.

peak appears to be extremely small. A very small dispersion, corresponding to the β'_N minor peak of highly ionized Nafion-Na, occurs at about the same temperature in the case of highly neutalized Nafion-Cs. The relaxation mechanism here is probably the same as that of the β'_N peak.

Except for the 39% neutralization sample, the position of the β peak shifts to higher temperatures with increasing degree of neutralization, while the peak intensity decreases markedly. This behavior is quite common in the hydrocarbon based ionomers which generally show two tan δ peaks in the glass transition region (28, 29), the lower temperature peak showing a gradual movement to higher temperatures with increasing ion content, accompanied by a slight decrease in intensity. This peak is identified with the T_g of the matrix. In the present case, this behavior is explainable on the basis that increased neutralization enhances the strength of the ionic interactions in the material, which in turn reduces the mobility of the fluorocarbon matrix, thereby increasing the peak temperature while depressing the relaxation intensity. If this β relaxation represented the T_g of the ionic region, one would not expect such a decrease in the relaxation strength with increasing degree of neutralization.

The tan δ_G peak position for the α relaxation, which corresponds to a pronounced drop-off in G', moves dramatically to higher temperatures with increasing degree of neutralization, accompanied by a slight increase in the peak height. This feature is common to other ionomer systems in which the higher temperature peak shifts markedly to higher temperatures with increasing ion content. This higher temperature peak may be identified with the T_g of the ionic region.

The qualitative similarity of the tan δ_G behaviour of the Nafions to that of many other ionomers suggests that the initial assignments of the relaxation mechanisms of the α and β peaks to the glass transitions of the non-ionic phase and the highly polar ionic phase respectively should be reevaluated. The original assignments regarding these peaks were based on preliminary results which suggested that the α peak showed little or no sensitivity to moisture content, with the β peak undergoing a dramatic change with water content. This finding does not agree with the results of recent underwater stress relaxation studies (25) in which movement of the primary transition (α relaxation) is clearly observed.

The water sensitivities of both the α and β peaks are not surprising in view of the fact that the sizes of the phase-separated regions are very small. The two phases are expected to be in intimate contact with each other as a result of their small size (5). Therefore, any change in one of the phases would be expected to have a strong effect on the other phase. With the matrix and the ionic regions in such close proximity, water molecules can be accommodated very close to the fluorocarbon backbone, and would thus have the ability to interact with or plasticize the matrix, if only by creating a "soft" surface near the fluorocarbon regions. Since a majority of the ether side chains are expected to be anchored in the ionic regions through their polar end groups, the mobility of the backbone chains may be controlled, to some extent, by these side chains. Plasticization by water of the ionic domains would thus influence not only the molecular motions within the ionic domains, but also motions of the fluorocarbon backbone chains, implying that a water sensitivity for both the α and β peaks is reasonable.

Can. J. Chem. Downloaded from www.nrcresearchpress.com by 210.87.254.42 on 09/06/12
For personal use only.

Thus the α and β peaks may logically be reassigned to the glass transitions of the ionic and nonionic phases respectively.

Further support for this assignment of the α peak may be found in the torsional pendulum results for the divalent Nafion-Ba salt, where the primary relaxation temperature (indicated by a rapid falling-off in G' and a peak in G'') is at a much higher temperature than the corresponding relaxations of the monovalent ionic systems.

The α dispersion possibly contains contributions from the crystal melting process since its temperature position corresponds to the crystal melting temperature found in DSC (9, 25) and WAXD (9, 26) studies of the monovalent salts. It is also likely, however, that the glass transition temperature of the material has been raised to such a high level that the peak would be due to two mechanisms, i.e. crystal melting and the T_g of the ionic region. The assignment of the α region of the Nafions to the matrix T_g is most unlikely; it is difficult to conceive that the matrix T_g would be higher than the crystal melting temperature. Hence it seems reasonable to assign the α peak to the glass transition of the ionic regions while attributing the β peak to the glass transition of the Nafion matrix.

In summary, four relaxation regions are observed in dynamic mechanical studies of the precursors. The highest temperature relaxation, labelled α_P, is due to the glass transition of the material; the β_P relaxation is seen next, and is tentatively assigned to ether side chain motions. Very close to it appears the γ_P relaxation due to CF_2 backbone motions, which is mechanistically identical with the γ peak found in pure PTFE. Finally, the δ_P peak is associated with motions of the SO_2F groups. In the ionomers, the α_N peak is due to glass transition of the dry ionic regions (with possible contributions from crystal melting in the divalent salts), while the β_N peak is associated with the glass transition of the matrix. The β'_N region, in parallel with β_P, is assigned to the ether side chains, while the γ peak, again in parallel with γ_P, is due to backbone CF_2 motions. The assignments of α_N and β_N as due to the glass transitions of the ionic regions and of the matrix, respectively, reverse the previous assignment and are supported by results obtained on a barium neutralized material.

Acknowledgements

It is a pleasure to thank Dr. John Williams for his valuable assistance in the preparation of the manuscript. We are indebted to the DuPont Company and the Olin Chemicals Group for samples and to the Olin Chemicals Group and the U.S. Army Research Office for their financial support of this work.

1. S. C. YEO and A. EISENBERG. J. Appl. Polym. Sci. **21**, 875 (1977).
2. I. M. HODGE and A. EISENBERG. Macromolecules, **11**, 289 (1978).
3. N. G. BOYLE, V. J. MCBRIERTY, and A. EISENBERG. Macromolecules. **16**, 80 (1983).
4. W. G. F. GROT, E. G. MUNN, and P. N. WALMSLEY. 131st Meeting of the Electrochemical Society, Houston, Texas. 1972.
5. A. EISENBERG and H. L. YEAGER (*Editors*). Perfluorinated ionomer membranes. A.C.S Symposium Series, #180 Feb. 1982.
6. R. DUPLESSIX, M. ESCOUBES, B. RODMACQ, F. VOLINO, E. ROCHE, A. EISENBERG, and M. PINERI. Water in polymers. A.C.S. Symposium Series #127. *Edited by* S. P. Rowland. 1980. pp. 469 and 478.
7. B. RODMACQ and M. PINERI. Rev. Phys. Appl. **15**, 1179 (1980).
8. E. J. ROCHE, M. PINERI, R. DUPLESSIX, and A. M. LEVELUT. J. Polym. Sci. Polym. Phys. Ed. **19**, 1 (1981).
9. T. D. GIERKE, G. E. MUNN, and F. C. WILSON. J. Polym. Sci. Polym. Phys. Ed. **19**, 1667 (1981).
10. R. A. KOMOROSKI and K. A. MAURITZ. J. Am. Chem. Soc. **100**, 7487 (1978).
11. S. R. LOWRY and K. A. MAURITZ. J. Am. Chem. Soc. **102**, 4665 (1980).
12. R. A. KOMOROSKI and K. A. MAURITZ. Perfluorinated ionomer membranes. *Edited by* A. Eisenberg and H. L. Yeager. A.C.S. Symposium Series #180. A.C.S. Washington, DC. 1982. Chapt. 7.
13. M. FALK. Can. J. Chem. **58**, 1495 (1980).
14. M. FALK. Perfluorinated ionomer membranes. *Edited by* A. Eisenberg and H. L. Yeager. A.C.S. Symposium Series #180. A.C.S. Washington, DC. 1982. Chapt. 8.
15. C. HEITNER-WIRGUIN, E. R. BAUMINGER, A. LEVY, F. LABENSKY DE KANTER, and S. OFER. Polymer, **21**, 1327 (1980).
16. T. TAKAMATSU, M. HASHIYAMA, and A. EISENBERG. J. Appl. Polym. Sci. **24**, 2199 (1979).
17. S. F. BURKHARDT. 152nd Meeting of the Electrochemical Society, Atlanta, Georgia. 1977.
18. R. S. YEO and J. MCBREEN. J. Electrochem. Soc. **126**, 1682 (1979).
19. H. L. YEAGER and B. KIPLING. J. Phys. Chem. **83**, 1836 (1979).
20. H. L. YEAGER, B. KIPLING, and R. S. DOTSON. J. Electrochem. Soc. **127**, 303 (1980).
21. M. SUHARA and Y. ODA. *In* Proceedings of the Electrochemical Society, Symposium on Ion Exchange. Vol. 81–82. *Edited by* R. S. Yeo and R. P. Buck. 1981. pp. 290–302.
22. SORJA KRAUSE. Polymer–polymer compatibility. *In* Polymer blends. Vol. 1. *Edited by* D. R. Paul and S. Newman. Academic Press, New York. 1978. Chapt. 2. pp. 15–113.
23. H. L. YEAGER. *In* Perfluorinated ionomer membranes. *Edited by* A. Eisenberg and H. L. Yeager. A.C.S Symposium Series #180, A.C.S. Washington, DC. 1982. Chapt. 4.
24. B. CAYROL. Segmental mobility in poly-*p*-phenylene ethers and related materials. Doctoral Thesis, McGill University. March 1972.
25. T. KYU and A. EISENBERG. J. Polym. Sci. In press.
26. M. FUJIMURA, T. HASHIMOTO, and H. KAWAI. Macromolecules, **14**, 1309 (1981).
27. N. G. MCCRUM. J. Polym. Sci. **34**, 355 (1959).
28. A. EISENBERG and M. KING. Ion-containing polymers. Academic Press, New York. 1977.
29. M. RIGDAHL and A. EISENBERG. J. Polym. Sci. Polym. Phys. Ed. **19**, 164 (1981).

Can. J. Chem. Downloaded from www.nrcresearchpress.com by 210.87.254.42 on 09/06/12
For personal use only.

Chemistry of enol silyl ethers. A general synthesis of 3-hydroxyhomophthalates and a biomimetic synthesis of sclerin[1]

P. BROWNBRIDGE, T. H CHAN,[2] M. A. BROOK, AND G. J. KANG
Department of Chemistry, McGill University, Montreal, P.Q., Canada H3A 2K6

Received August 31, 1982

This paper is dedicated to Professor Leo Yaffe on the occasion of his 65th birthday

P. BROWNBRIDGE, T. H CHAN, M. A. BROOK, and G. J. KANG. Can. J. Chem. **61**, 688 (1983).

A general synthesis of 3-hydroxyhomophthalates is developed and applied to the synthesis of sclerin (**24**), a compound possessing plant-growth activity; the critical step in the synthesis of **24** can be considered as the controlled condensation of a di-β-carbonyl unit with a tri-β-carbonyl unit.

P. BROWNBRIDGE, T. H CHAN, M. A. BROOK et G. J. KANG. Can. J. Chem. **61**, 688 (1983).

On a développé une synthèse générale des hydroxy-3 homophtalates et on l'a appliquée à la synthèse de la sclérine (**24**), un composé possédant une activité dans la croissance des plantes; on peut considérer que l'étape clé dans la synthèse de **24** est la condensation contrôlée d'une unité β-dicarbonylée sur une unité β-tricarbonylée.

[Traduit par le journal]

There are no well-established methods for the synthesis of benzenoid compounds from acyclic precursors. The syntheses of polysubstituted aromatic natural products in general rely on the stepwise introduction of substituents on some simpler aromatic precursors based on conventional aromatic chemistry.

It is well recognized though, in nature, that condensation of poly-β-carbonyl compounds is a major pathway for the biogenesis of aromatic natural produts (3, 4). Efforts to mimic this reaction in the laboratory have met, however, with limited success, mainly because of the difficulty of controlling the specificity of the direction of condensation (4). Such control is particularly critical when the poly-β-carbonyl precursor is composed of mixed acetate and propionate units.

Recently, we have introduced (2) the use of 1,3-bis-(trimethylsiloxy)-1-methoxybuta-1,3-diene (**1**) as the dianion equivalent of methyl acetoacetate (**2**) (5). Two factors induced us to examine the reactions of **1** in rather extensive detail

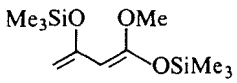

1

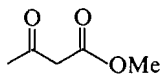

2

(1, 2, 6). The first is that enol silyl ethers are known to complement enolate anions in their chemical reactivities. A case in point is that, whereas enolates can be alkylated by primary or secondary halides, enol silyl ethers are alkylated by tertiary halides (7). It is also known that enol silyl ethers can condense with various carbonyl compounds or their functional equivalents under Lewis acid conditions (8) in contrast to the basic conditions inherent in enolate anion chemistry. The second factor is that the acetoacetate unit is one of the fundamental building blocks in the biogenesis of natural products (3, 4). It thus seemed possible that **1** can be quite useful in the synthesis of natural products, especially aromatic compounds derived from the condensation of acetoacetate and other poly-β-carbonyls.

[1]Part 12 of the series. For Part 11, see ref. 1. For preliminary accounts of this work, see ref. 2.

[2]Author to whom correspondence should be addressed.

Results and discussion

Reaction of electrophiles with 1,3-bis(trimethylsiloxy)-1-methoxybuta-1,3-diene (**1**)

In our original preparation of **1**, methyl 3-trimethylsiloxybut-2-enoate (**3**) was first deprotonated with LDA in THF/TMEDA followed by quenching with trimethylchlorosilane. The removal of TMEDA from the products proves to be tedious since it requires long periods of time under high vacuum and is

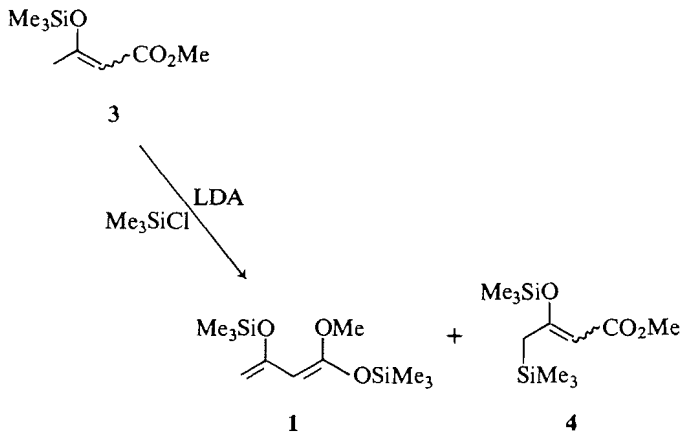

1 **4**

accompanied by some decomposition of **1**. We have now modified the procedure and eliminated the use of TMEDA. Furthermore, we have found that the reaction temperature has an effect on the product distribution. In the temperature range of −42° to −78°C, with or without TMEDA, the product is mainly **1** (93−95%), whereas at higher temperatures, the C-silylated isomer **4** is obtained as well. The rearrangement of **1** to **4** is fairly rapid at high temperature (9), for example, during gc conditions, but is sufficiently slow at ambient temperature so that **1** can be kept in the freezer for at least two weeks without obvious isomerization. Judging from its nmr spectrum, **1** exists entirely as one geometrical isomer, tentatively assigned as the *E*-isomer (2). However, in the gc analysis of **1**, two peaks, in addition to the peak for **4**, are invariably observed in a ratio of about 1:3. From gc−ms, the two have the same molecular ion and are believed to be the *E*- and *Z*-isomers of **1**.

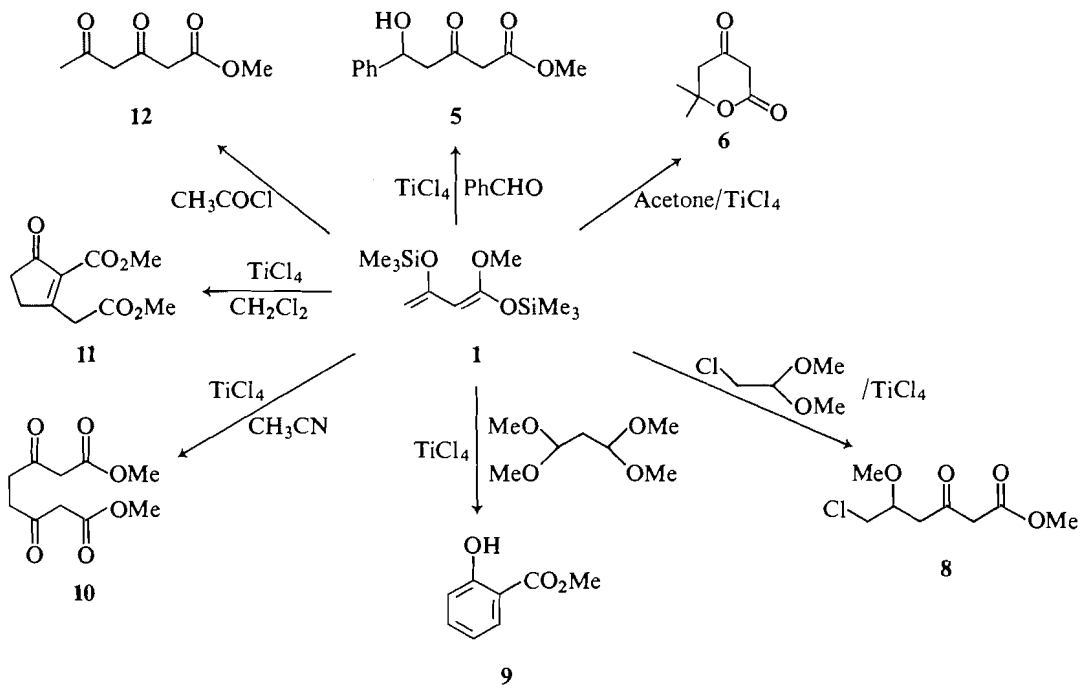

SCHEME 1

Reactions of **1** with a number of carbon electrophiles have been examined (Scheme 1). Benzaldehyde reacted with **1** in the presence of titanium tetrachloride to give the adduct **5** in good yield (72%). Similarly, reaction of **1** with acetone and titanium tetrachloride gave the lactone **6** which exists as a mixture of keto–enol tautomers. It is clear that **1**, though having two nucleophilic sites at C-2 and C-4, reacts with electrophiles preferentially at C-4 (γ-attack).[3] While these reactions are not formally different from the reactions of the acetoacetate dianion with the same carbonyl compounds (5), the fact that reactions of **1** are conducted under acid-catalyzed conditions offers new opportunities. Acetals can be used as functional equivalents of carbonyl compounds in the condensation reaction. Thus chloroacetaldehyde dimethyl acetal (**7**) condenses with **1** in the presence of titanium tetrachloride to give the adduct **8**. When malonaldehyde bis(dimethylacetal) is used as the electrophile, methyl salicylate (**9**) is obtained in 48% yield. In the formation of **9**, a second condensation must have occurred at C-2 of **1** and the other acetal function followed by the elimination of the methoxy moiety and aromatization. We have explored this method of cyclo-aromatization and the results have been reported elsewhere (see also below) (11, 12).

Because imines have been reported to condense with enol silyl ethers under $TiCl_4$ conditions (13), we became interested in the possibility of using nitriles as the carbon electrophiles. When **1** was dissolved in acetonitrile in the presence of $TiCl_4$, no condensation product was observed. Instead, the compound dimethyl 3,5-dioxooctanedioate (**10**) was obtained in 77% yield. The compound **10** is clearly derived from the dimerization of **1**. Dimerization of ketene silyl acetal by $TiCl_4$ has previously been observed (14*a*) and has recently been exploited by us as a method of cyclopropane synthesis (14*b*). The formation of **10** can also account for another observation, viz., when **1** was mixed with $TiCl_4$ in methylene chloride as the solvent, the cyclopentenone **11** was obtained as the major product. In the less donating solvent CH_2Cl_2, $TiCl_4$ is sufficiently acidic to effect the cyclization of **10** to **11**. Indeed, this is one of the routes by which methyl *cis*-jasmonate has been synthesized (15).

Reaction of **1** with acetyl chloride occurred readily even in the absence of titanium tetrachloride to give a complicated mixture of compounds. When the reaction was conducted in ether at −78°C, the tri-β-carbonyl compound **12** was isolated in ~30% yield. When **1** was reacted with acetyl chloride *and* titanium tetrachloride, an aromatic compound **13** was isolated in 32% yield (11). It is clear that **13** is derived from two molecules of **1** and one acetyl group. It also seemed to us that this condensation may offer a simple and general synthesis of 3-hydroxyhomophthalate esters. To explore this, we sought to understand the factors which control the reaction, as well as to improve the yield.

A general synthesis of 3-hydroxyhomophthalates

The cycloaromatization reaction proposed by us (11, 12) involves the condensation of two 3-carbon units, one with two nucleophilic sites and the other containing two electrophilic sites, as in eq. (1). Compound **1** and similar bisenol silyl ethers

[1] 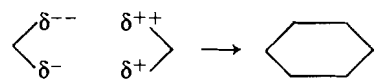

constitute the 3-carbon fragments with two nucleophilic sites, with C-4 being more reactive (δ^{--}) than C-2 (δ^{-}). Various equivalents of β-dicarbonyl compounds constitute the 3-carbon electrophilic components. The regiochemistry of the reaction is controlled by the differential reactivities of these sites. In our previous publication, we have established that, within the same component, the order of reactivity of the electrophilic sites is ketone > acetal or monothioacetal. For β-oxy-α,β-unsaturated ketones, the conjugate position is more electrophilic towards **1** than the carbonyl position. We have now established the

[3]Preference for γ-regioselectivity appears to be common for 1-siloxydienes; see ref. 10.

relative reactivities of other carbonyl functional groups or equivalents in their reactions with **1** under $TiCl_4$ conditions.

In a competitive reaction of **1** with an equal mixture of benzaldehyde and 4-trimethylsiloxy-3-penten-2-one (**14**), under $TiCl_4$ activation, a 10:1 mixture of **5** and **15** was obtained. On the other hand, the reaction of **1** with an equal mixture of acetone and **14** under identical conditions gave a ~1:1 mixture of **6** and **15**.

There is, however, no condensation of **1** with ester carbonyls or with the conjugate position β-oxy-α,β-unsaturated esters. For example, **1** did not condense with **3** to give any aromatic compound. These experiments establish therefore qualitatively the following order: aldehyde > conjugated position of β-oxy-α,β-unsaturated ketone ~ isolated ketone > carbonyl position of β-oxy-α,β-unsaturated ketone > acetal or monothioacetal > conjugate position of β-oxy-α,β-unsaturated ester or ester carbonyl.

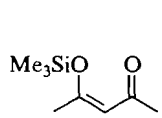

14

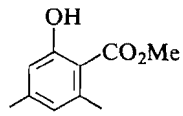

15

To return to the formation of **12** from the reaction of **1** with $AcCl/TiCl_4$, the first step in the reaction is to form an initial tri-β-carbonyl adduct. While the adduct has most likely the structure **16**, one cannot entirely eliminate from consideration the possibilities **17** or **18**. The tri-β-carbonyl compound reacts then with another molecule of **1** according to eq. [1] to give the aromatic compound **13**. From the order of reactivities discussed above, **17** would have given us the wrong regiochemistry for **13** and is thus excluded. Either **16** or **18** can account for the formation of **13** with the correct regiochemistry.

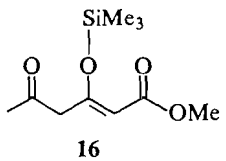

16

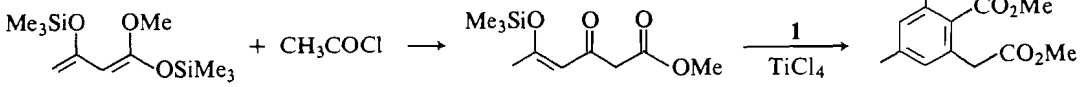

1 **18** **13**

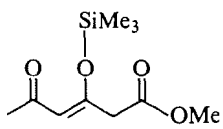

17

To resolve the two possibilities, we modified the acetylating agent. In place of acetyl chloride, trimethyl orthoacetate was used. The reaction proceeded extremely well and gave a much improved yield of **13** (65% isolated). In this case, the corresponding tri-β-carbonyl adduct would be **19**, **20**, or **21**. Structure **20**, on subsequent cycloaromatization with **1**, would have given the wrong regioisomer. Structure **21**, which has to be derived from **20** by the elimination of MeOH, is considered unlikely under the reaction conditions from our previous experience with β-keto acetals (11, 12). Structure **19**, the equivalent of **16**, can then account for the formation of **13**, provided that the β-oxy-α-β-unsaturated ester group, though unreactive towards **1** in an intermolecular fashion, may well participate in an intramolecular step in the cycloaromatization reaction.

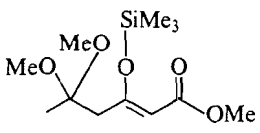

19

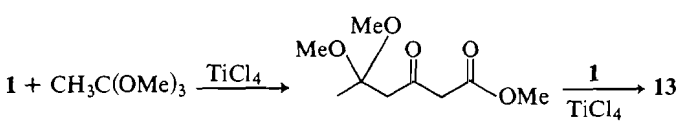

20

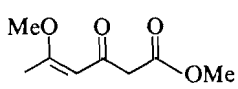

21

Anhydrides can be used equally as well as the acylation agent in the formation of 3-hydroxyhomophthalate esters. This provides a general synthesis of dimethyl 5-substituted-3-hydroxyhomophthalates (**22**) (Table 1). With isobutyric anhydride, the product contained a substantial amount of methyl 6-methyl-3,5-dioxoheptanoate (**23**, 31%) even though two mole equivalents of **1** were used. We presume that, in this case, the cycloaromatization reaction is slow owing to the steric effect of the isopropyl group. γ-Butyrolactone can, though less effectively, serve as the acylating agent to give compound **22** (R = HO $(CH_2)_3$-).

A biomimetic synthesis of sclerin

Sclerin (**24**), a metabolite isolated from *Sclerotinia* fungi, possesses interesting plant growth activity (16). Its biosynthesis has been investigated extensively by labelling experiments (17–19); essentially, it can be considered as the condensation product of a penta-β-carbonyl precursor. A few chemical syntheses of sclerin have previously been reported (20–22), based on conventional aromatic chemistry, often with the inherent problem of regioselection in electrophilic aromatic substitution and giving low overall yields. We have

TABLE 1. Products of the reaction of **1** with various electrophiles in the presence of $TiCl_4$

Electrophile	Product **22**	% Yield	Melting point (°C)
$HC(OMe)_3$	R = H	68	53–55
$MeC(OMe)_3$	R = Me	65	82–83
$(MeCO)_2O$	R = Me	69	
$(PhCO)_2O$	R = Ph	72	109–110
$(Pr^iCO)_2O$	R = i-Pr[a]	42	165–166.5
	23	31	Oil
γ-Butyrolactone	$R=HO(CH_2)_3$-	13	Oil

[a]Isolated as the benzylic monoacid.

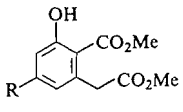

22

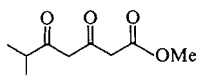

23

now applied the cycloaromatization reaction which has the construction of the hexasubstituted benzene ring as the critical step (Scheme 2) to the synthesis of sclerin.

1,3-Bis(trimethylsiloxy)-1-methoxy-penta-1,3-diene (**25**) was prepared from 3-trimethylsiloxy-pent-2-enoate in a manner similar to the preparation of **1**. From its nmr spectrum, **25** appears to exist mainly as one geometric isomer, probably the *E,E* isomer. Compound **25** condenses with benzaldehyde/$TiCl_4$ to give the aldol adduct **26** indicating again that in **25**, C-4 is the more reactive nucleophilic site.

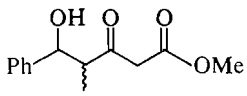

26

Condensation of **25** (2 mole equivalents) with trimethyl orthoacetate in the presence of titanium tetrachloride (2 mole equivalents) gave in 53% yield the aromatic compound **27** as colourless prisms, mp 85–85.5°C. The structure of **27** is evident from its ^1H nmr spectrum ($CDCl_3$) which showed three aromatic methyl peaks (δ 2.17, 2.21, and 2.25), two ester methyl peaks (δ 3.68 and 3.87), methylene hydrogens at δ 3.91, and a phenolic OH at δ 11.04. Its ir (3150 br, 1735, 1663, and 1599 cm^{-1}) in $CHCl_3$ and mass (M^+, *m/e* 266, 83%; *m/e* 234 ($M - MeOH)^+$, 100%) spectra are also consistent with its structure. Methylation of **27** with 2 mole equivalents of LDA and 1 mole equivalent of methyl iodide gave in 80% yield dimethyl sclerinate (**28**), mp 113–114°C (lit. (24) mp 113–116°C). The conversion of **28** into **24** was readily accomplished by using sodium hydroxide followed by acid.

In a recent review article (4), the hope was expressed that the aesthetically pleasing route of biogenetic-type synthesis can, in selected cases, provide commercially attractive routes to natural products of economic importance. In the present synthesis of sclerin, by using enol silyl ethers as the nucleophiles, carbonyl equivalents as the electrophiles, and titanium tetrachloride as the activating agent, a controlled condensation of a dicarbonyl unit with a tri-carbonyl unit in the construction of **27** is demonstrated. It is recognized that the condensation is of the abnormal type, giving a homophthalic acid structure, whereas many phenolic natural products have the resorcinol skeleton derived from a more common type of head-to-tail condensation. Our next task, to show the versatility of the proposed

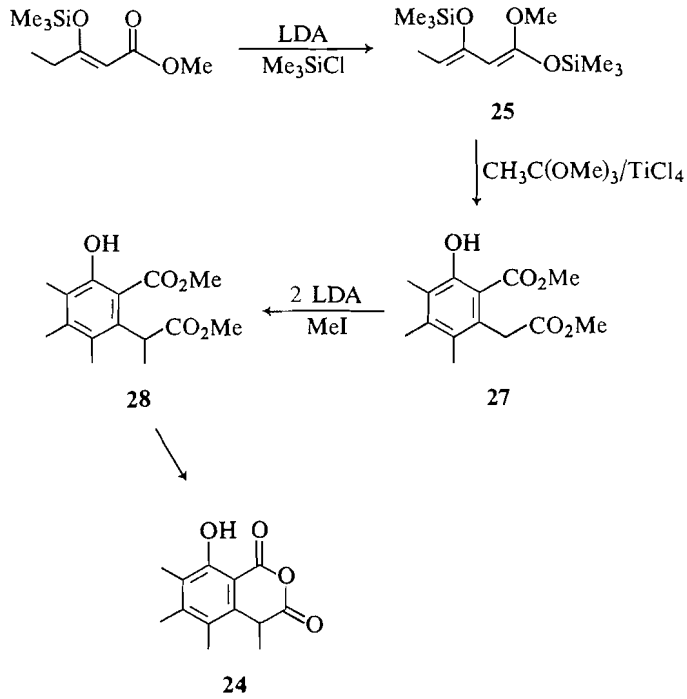

SCHEME 2

cycloaromatization for the synthesis of phenolic natural products, must therefore aim in that direction (1).

Experimental

General

Melting and boiling points are uncorrected. Infrared spectra were obtained from films on NaCl plates for liquids and from solutions in 0.1 mm NaCl cells for solids, using a Perkin–Elmer 297 spectrophotometer. The ^1H nmr spectra were recorded on Varian T-60 and T-60A instruments, with Me_4Si as internal standard. Mass spectra were obtained on a Hewlett–Packard 5984A or an LKB 9000 machine operating at 70 eV. Column chromatography was performed on silica gel 60 (Merck). Et_3N, $i\text{-}Pr_2NH$, and TMEDA were dried by distillation from CaH_2; hexane, CCl_4, and benzene from P_2O_5; CH_2Cl_2 from P_2O_5 and then from CaH_2. THF was distilled under nitrogen from sodium–benzophenone directly into the reaction vessel. Microanalyses were performed by Guelph Chemical Laboratories Ltd.

1,3-Bis(trimethylsiloxy)-1-methoxybuta-1,3-diene (**1**) was prepared according to reported procedure (11) with slight modification. To a solution of 1.0 mL diisopropylamine (7.1 mmol) in 25 mL of dry THF under argon, 5.0 mL of 1.5 *M* n-butyllithium in hexane was added after cooling to 0°C and the reaction mixture was cooled to −78°C. A quantity of 1.1 g of methyl 3-trimethylsiloxybut-2-enoate (5.9 mmol) was added and the solution stirred for 2 min. Then the reaction was quenched with 1.2 mL trimethylchlorosilane (9.5 mmol). The solvent was removed under reduced pressure after a further 10 min and the residue was washed and filtered with cold dry hexane. The hexane was removed from the filtrate *in vacuo* to yield **1** in 93% yield. When the above preparation was carrried out at room temperature, the product was found to be a mixture of **1** and **4** (~3:1) (9). The ratio of **1** to **4** was changed to about 10:1 when the reaction temperature was lowered to 0°C, and essentially pure **1** was obtained if the reaction temperature was below −23°C. Compound **1** can be kept in a stoppered container for up to 2 weeks in the freezer without obvious decomposition but is slowly hydrolysed to **3** when exposed to air.

1,3-Bis(trimethylsiloxy)-1-methoxypenta-1,3-diene (**25**) was prepared according to literature procedure (12).

Reaction of 1 with benzaldehyde

To a well-stirred mixture of **1** (1.04 g, 4 mmol) and benzaldehyde

(0.43 g, 4 mmol) in 4 mL CH_2Cl_2 under nitrogen at −78°C, titanium tetrachloride (0.45 mL, 4 mmol) was added. After 3 h, the dark red mixture was added to aqueous $NaHCO_3$ and extracted with ether. The extract was dried ($MgSO_4$) and evaporated to give an oil which was column chromatographed (eluant $CHCl_3$) to give *methyl 5-hydroxy-3-oxo-5-phenylpentanoate* (**5**, 0.64 g, 72%) as a colorless oil with spectroscopic data similar to those reported (5).

Reaction of 1 with acetone

The reaction was performed as above except that ethyl acetate was used for extraction. The product, 6,6-dimethyltetrahydropyran-2,4-dione (**6**, 76%), was colorless plates, mp 131−132°C (from CH_2Cl_2); ir ($CHCl_3$): 3350 br, 1727 cm^{-1}; ^1H nmr shows an approximately 2:3 mixture of diketo and enol forms (1:1 $CDCl_3$ − $(CD_3)_2CO$), δ: 1.48 (enol) and 1.52 (keto) (each s, 6H, Me_2C), 2.52 (enol) and 2.73 (keto) (each s, 2H, 5-CH_2), 3.43 (s, $COCH_2CO$), 5.18 (s, $HOC{=}CHCO$), 6.3 (br s, enol OH); ms *m/z*: 142 (M^+, 15%), 127 (41), 85 (90), 84 (100), 56 (72). *Anal.* calcd. for $C_7H_{10}O_3$: C 59.14, H 7.09; found C 59.05, H 7.37.

Reaction of 1 with chloroacetaldehyde dimethyl acetal

The reaction was performed as for above. The crude product was purified by column chromatography (eluant CH_2Cl_2) to give methyl 6-chloro-5-methoxy-3-oxohexanoate (**8**, 35%) as a colorless oil. Infrared (film): 1745, 1719 cm $^{-1}$; ^1H nmr ($CDCl_3$), δ: 2.87 (d, 2H, J = 6 Hz, $CHCH_2Cl$), 3.41 (s, 3H, OMe), 3.51 (s, 2H, CH_2CO_2Me), 3.66 (d, 2H, J = 4 Hz, $CHCH_2CO$), 3.76 (s, 3H, CO_2Me), 3.8−4.2 (m, 1H, $MeOCH$); EI−ms *m/z*: 177 (M − OMe, 1%), 159 (M − CH_2Cl, 22), 101 (53), 93 (72), 85 (64), 69 (100), 59 (68); Cl−ms (isobutane): 211 ($^{37}Cl - MH^+$, 3%), 209 ($^{35}Cl - MH^+$, 12), 177 (100).

Reaction of 1 with malonaldehyde bis(dimethylacetal)

A solution of **1** (1.30 g, 5 mmol) in CH_2Cl_2 (15 mL) was added dropwise to a mixture of 1,1,3,3-tetramethoxypropane (0.82 g, 5 mmol) and $TiCl_4$ (0.55 mL, 5 mmol) in dry CH_2Cl_2 (20 mL) at −78°C under nitrogen. After 3 h, the mixture was allowed to warm to 0°C, added to aqueous $NaHCO_3$, and extracted with ether. The extracts were dried ($MgSO_4$) and evaporated to give an oil (0.73 g). Column chromatography eluted with CH_2Cl_2 gave a colorless oil; which was identified to be methyl salicylate (**9**) from its spectra and characteristic wintergreen odour (0.36 g, 48%).

Dimerization reactions of 1

To a solution of **1** (1.56 g, 6 mmol) in dry CH_2Cl_2 (5 mL) under nitrogen at −78°C was added $TiCl_4$ (0.70 mL, 6.3 mmol). The dark red mixture was allowed to warm to 0°C and stirred overnight. It was added to aqueous $NaHCO_3$ (the aqueous phase was dark blue due to Ti^{3+}; the mixture was stirred vigorously until air oxidation removed the blue colour) and extracted with ether, the aqueous layer being retained. The ether extracts were dried ($MgSO_4$) and evaporated to give only methyl acetoacetate (0.21 g). The aqueous phase was acidified (HCl) and extracted with ethyl acetate. These extracts were dried (Na_2SO_4) and evaporated to give a brownish solid (0.40 g). Recrystallization from cyclohexane gave methyl (2-methoxycarbonyl-3-oxocyclopent-1-enyl)acetate (**11**) (17), colorless plates, mp 75−76°C, 0.33 g (52%); ^1H nmr ($CDCl_3$), δ: 2.4−3.0 (m, 4H, CH_2CH_2), 3.75 and 3.84 (each 3H, s, CO_3Me), 3.89 (s, 2H, CH_2CO_2Me); ms *m/z*: 212 (M^+, 20%), 180 (96), 149 (100), 148 (56). When the reaction was performed as above but with acetonitrile as solvent, the ether extract gave dimethyl 3,5-dioxooctanedioate (17) (**10**, 77% yield after column chromatography eluted with CH_2Cl_2) as a colorless oil. Infrared (film): 1747, 1718 cm^{-1}; ^1H nmr ($CDCl_3$), δ: 2.81 (s, 4H, $COCH_2CH_2CO$), 3.46 (s, 4H, $COCH_2CO_2Me$), 3.68 (s, 6H, CO_2Me); ms *m/z*: 230 (M^+, 13%), 212 (4), 157 (32), 129 (100), 115 (14), 101 (42), 97 (42), 55 (56). No cyclopentenone **11** was formed in this case.

Reaction of 1 with acetyl chloride

A mixture of **1** (1.04 g, 4 mmol) and acetyl chloride (0.23 mL) was stirred in dry Et_2O (3 mL) at −78°C under nitrogen for 4 h. The mixture was poured into dilute HCl and extracted with ether. Drying ($MgSO_4$) and evaporation of the extracts gave a colorless oil (0.48 g) which was an approximately 1:2 mixture of the product and methyl acetoacetate by nmr. This oil was pumped under high vacuum until no more weight loss occurred, to give methyl 3,5-dioxohexanoate (**12**), a colorless oil (0.21 g, 30%) with spectroscopic data similar to those reported (5).

Reaction of 1 with trimethyl orthoformate

A solution of **1** (5.2 g, 20 mmol) in CH_2Cl_2 (10 mL) was added to a mixture of trimethyl orthoformate (1.06 g, 10 mmol) and $TiCl_4$ (2.2 mL, 20 mmol) in CH_2Cl_2 (15 mL) at −78°C under nitrogen. After 3 h, the mixture was allowed to warm to room temperature and stirring continued overnight. It was then added to aqueous $NaHCO_3$ and extracted with CH_2Cl_2. The extracts were dried (Na_2SO_4), evaporated, and the residue purified by column chromatography eluted with CH_2Cl_2 to give methyl (3-hydroxy-2-methoxycarbonylphenyl)acetate (**22***a*, R = H, 1.53 g, 68%) as colorless needles, mp 53−55°C (from pentane) (lit. (23) mp 55−57°C).

Reaction of 1 with trimethyl orthoacetate

When the reaction was performed as above (2:1:2, $TiCl_4$/$MeC(OMe)_3$/**1**), methyl (3-hydroxy-2-methoxycarbonyl-5-methylphenyl)acetate (**13**) (11) was produced in 65% yield as colorless needles, mp 82−83°C.

Reaction of 1 with acetic anhydride

Titanium tetrachloride (1.0 mL) was added to a well-stirred mixture of **1** (2.39 g, 9.2 mmol) and acetic anhydride (0.46 g, 4.6 mmol) in CH_2Cl_2 (10 mL) at −78°C under nitrogen. This dark red solution was stirred for 2 h at −78°C, then overnight at room temperature. It was added to aqueous $NaHCO_3$ and extracted with ether. The extracts were dried, evaporated, and the resulting solid recrystallized from methanol to give methyl (3-hydroxy-2-methoxycarbonyl-5-methylphenyl)-acetate (**13**, 0.75 g, 69%) (11).

Reaction of 1 with benzoic anhydride

Reaction of **1**, benzoic anhydride, and $TiCl_4$ as described above gave methyl 5-hydroxy-4-methoxycarbonyl-(1,1′-biphenyl)-3-acetate (**22**, R = Ph) as colorless prisms, mp 109−110°C (from CCl_4−cyclohexane), in 72% yield: ir ($CHCl_3$): 3400 br, 1739, 1670, 1621 cm^{-1}; ^1H nmr ($CDCl_3$), δ: 3.65 (s, 3H, CH_2CO_2Me), 3.83 (s, 3H, $ArCo_2Me$), 3.89 (s, 2H, CH_2CO_2Me), 6.90 (d, 1H, J = 2 Hz, Ar), 7.14 (d, 1H, J = 2 Hz, Ar), 7.2−7.6 (m, 5H, Ph), 11.3 (br s, 1H, OH); ms *m/z*: 300 (M^+, 88%), 268 (97), 240 (100), 236 (50), 225 (92). *Anal.* calcd. for $C_{17}H_{16}O_5$: C 67.99, H 5.37; found: C 68.08, H 5.46.

Reaction of 1 with isobutyric anhydride

The reaction was carried out under the above conditions to give an approximately 3:2 mixture of methyl [3-hydroxy-2-methoxycarbonyl-5-(1-methylethyl)phenyl]acetate (**22**, R = i-Pr) and methyl 3,5-dioxo-6-methylheptanoate (**23**) which could not be separated by column chromatography. The mixture was dissolved in 5% aqueous NaOH and extracted with ether. The aqueous layer was treated with aqueous NH_4Cl until neutral (pH 8) and extracted again with ether. The ether extract on drying ($MgSO_4$) and evaporation gave a colorless oil (0.29 g, 31%) which was **23**. It had ir (film): 3420 br, 1743 1661, 1618 cm^{-1}; ^1H nmr ($CDCl_3$), δ: 1.14 (d, 6H, J = 7 Hz, Me_2CH), 2.1−2.7 (m, 1H, Me_2CH), 3.21 (S, 2H, CH_2CO_2Me), 3.69 (S, 3H, CO_2Me), 5.51 (S, 1H, HO—C=CH—CO), 13.3 (br s, 1H, enol OH); ms *m/z*: 186 (M^+, 9%), 143 (83), 101 (100). The aqueous layer from the above was acidified (HCl) and further extracted with ether. Drying ($MgSO_4$) and evaporation of these organic extracts gave a colorless solid which was recrystallized from CCl_4. It was [3-hydroxy-2-methoxy-carbonyl-5-(1-methylethyl)phenyl]acetic acid (42% yield), mp 165−166.5°C; ir ($CHCl_3$): 3100 br, 1713, 1669, 1622 cm^{-1}; ^1H nmr ($CDCl_3$), δ: 1.24 (d, 6H, J = 7 Hz. Me_2CH), 2.85 (septet, 1H, J = 7 Hz, Me_2CH), 3.89 (s, 5H, $ArCO_2Me$ and CH_2CO_2H), 6.57 (d, 1H, J = 2 Hz, Ar), 6.82 (d, 1H, J = 2 Hz, Ar), 11.2 (br s, 2H, OH); ms *m/z*: 252 M^+, 56%), 220 (66), 202 (75), 192 (100). *Anal.* calcd. for $C_{13}H_{16}O_5$: C 61.90 H 6.39; for $C_{13}H_{16}O_5 \cdot \frac{1}{2}H_2O$: C 59.79, H 6.51; found: C 60.19, H 6.16.

*Reaction of **1** with γ-butyrolactone*

The reaction was carried out as above and the product on work-up was purified by column chromatography (eluant ether). A considerable quantity of dimethyl 3,5-dioxooctanedioate (**10**) was isolated. In addition, methyl [3-hydroxy-5-(3-hydroxypropyl)-2-methoxy carbonylphenyl]acetate (**22**, R = $HO(CH_2)_2$-) was obtained as a colorless oil (13%). It had ir ($CHCl_3$): 3440 br, 1737, 1669, 1622 cm^{-1}; ^1H nmr ($CDCl_3$), δ: 1.6−2.1 (m, 2H, $CH_2CH_2CH_2$), 2.3 (br s, 1H, CH_2OH), 2.5−2.8 (m, 2H, $ArCH_2CH_2$), 3.63 (t, 2H, J = 6.5 Hz, CH_2CH_2OH), 3.68 (s, 3H, CH_2CO_2Me), 3.27 (s, 5H, $ArCO_2Me$ and $ArCH_2CO_2Me$), 6.55 (d, 1H, J = 2 Hz, Ar), 6.78 (d, 1H, J = 2 Hz, Ar), 11.19 (s, 1H, ArOH); ms m/z: 282 (M^+, 30%), 250 (32), 222 (36), 206 (100), 184 (94).

*Reaction of **25** with benzaldehyde*

To a well-stirred mixture of **25** (1.79 g, 6.5 mmol) and benzaldehyde (0.69 g, 6.5 mmol) in dry CH_2Cl_2 (5 mL) under nitrogen at −78°C, was added $TiCl_4$ (0.72 mL, 6.5 mmol). After 3 h, the mixture was warmed to 0°C, poured into aqueous $NaHCO_3$, and extracted with ether. The extracts were dried ($MgSO_4$) and evaporated to give a yellow oil (1.60 g), which was a 3:1 mixture of diastereoisomers of the aldol condensation product by nmr. Column chromatography eluted with CH_2Cl_2 gave a partial separation of these diastereoisomers, but also caused partial cyclization of the major isomer to the lactone. (4*R*(*S*), 5*S*(*R*))-Methyl 5-hydroxy-4-methyl-3-oxo-5-phenylpentanoate (**26**, the original minor diastereoisomer, 0.35 g, 22%) was a colorless oil, R_f 0.61, ir (film): 3420 br, 1751, 1719 cm^{-1}; ^1H nmr ($CDCl_3$), δ: 1.97 (d, 3H, J = 6.5 Hz, $MeCH$), 3.18 (s, 2H, $COCH_2$), 3.2−3.6 (m, 1H, $MeCHCH$), 3.59 (s, 3H, CO_2Me), 5.07 (d, 1H, J = 8.5 Hz, $PhCHCH$), 7.28 (s, 5H, Ph); ms m/z: 236 (M^+, 23%), 215 (50), 125 (100). (4R(*S*), 5*R*(*S*))-Methyl 5-hydroxy-4-methyl-3-oxo-5-phenylpentanoate (0.37 g, 23%) was a colorless oil, R_f 0.60, ^1H nmr ($CDCl_3$), δ: 0.88 (d, 3H, J = 7 Hz, $MeOH$), 3.2−3.6 (m, 1H, $MeCHCH$), 3.65 (s, 2H, $COCH_2$), 3.73 (s, 3H, CO_2Me), 4.94 (d, 1H, J = 10.5 Hz, $PhCHOH$), 7.30 (s, 5H, Ph); the ir and mass spectra were similar to the above. (5*R*(*S*), 6*R*(*S*))-2,4-Dioxo-5-methyl-6-phenyltetrahydro-(2*H*)pyran (0.37 g, 27%) was colorless needles, mp 161−162°C (from CCl_4), R_f 0.2, ir ($CHCl_3$): 1766, 1731 cm^{-1}; ^1H nmr ($CDCl_3$), δ: 1.00 (d, 3H, J = 7 Hz, $MeOH$), 2.4−3.0 (m, 1H, $MeCHCH$), 3.58 and 3.65 (ABq, 2H, J_{AB} = 19 Hz, $COCH_2$), 5.25 (d, 1H, J = 10 Hz, $PhCHCH$), 7.37 (s, 5H, Ph); ms m/z: 204 (M^+, 14%), 98 (100). *Anal.* calcd. for $C_{12}H_{12}O_3$: C 70.57, H 5.92; for $C_{12}H_{12}O_3 \cdot \frac{1}{4}H_2O$: C 69.08, H 5.99; found: C 69.05, 69.15, H 5.77, 5.95.

*Methyl(3-hydroxy-2-methoxycarbonyl-4,5,6-trimethylphenyl)acetate (**27**)*

A solution of **25** (3.3 g, 12 mmol) in CH_2Cl_2 (6 mL) was added to a mixture of trimethyl orthoacetate (0.72 g, 6 mmol) and $TiCl_4$ (1.3 mL, 12 mmol) in CH_2Cl_2 (6 mL) under nitrogen at −78°C. Stirring was continued for 2 h at −78°C, then overnight at room temperature. The mixture was added to aqueous $NaHCl_3$ and extracted with ether. The extracts were dried ($MgSO_4$) and evaporated, and the remaining oil purified by column chromatography (CH_2Cl_2) to give the *homophthalate derivative* **27** (0.84 g, 53%) as colorless prisms, mp 85−85.5°C (from methanol); ir ($CHCl_3$): 3100 br, 1734, 1663, 1599 cm^{-1}; ^1H nmr ($CDCl_3$), δ: 2.17, 2.21 and 2.25 (each s, 3H, $MeAr$), 3.68 (s, 3H, CH_2CO_2Me), 3.87 (s, 3H, $ArCO_2Me$), 3.91 (s, 2H, CH_2CO_2Me), 11.04 (s, 1H, OH): ms m/z: 266 (M^+, 83%), 234 (100), 206 (86), 202 (77), 191 (87), 174 (85). *Anal.* calcd. for $C_{14}H_{18}O_5$: C 63.14, H 6.81; found: C 63.01, H 6.76.

*Methyl 1-(3-hydroxy-2-methoxycarbonyl-4,5,6-trimethylphenyl)propionate (**28**)*

n-Butyllithium (1.3 mL of a 1.6 *M* solution in hexane) was added to diisopropylamine (0.3 mL, 2.2 mmol) in dry THF (5 mL) under nitrogen at 0°C. The solution was cooled to −78°C and a solution of **27** (0.25 g, 0.94 mmol) in dry THF (10 mL) added dropwise. The yellow anion was stirred for 2 h, then a solution of iodomethane (0.14 g) in dry HMPA (1 mL) was added. The anion was decolorized at once. After 1 h, aqueous NH_4Cl and $Na_2S_2O_3$ were added, the mixture allowed to come to room temperature and extracted with ether. The extracts were dried ($MgSO_4$) and evaporated (finally under high vacuum). The residue was recrystallized from cyclohexane to give dimethyl sclerinate (0.21 g, 80%), colorless prisms, mp 113−114°C (lit. (24) mp 113−116°C), ^1H nmr ($CDCl_3$), δ: 1.50 (d, 3H, J = 7 Hz, $MeCHCO$), 2.17, 2.20 and 2.23 (each s, 3H, $MeAr$), 3.5 g (s, 3H, $CHCO_2Me$), 3.80 (s, 3H, $ArCO_2Me$), 4.20 (q, 1H, J = 7 Hz, $MeCHCO$), 10.70 (s, 1H, OH); ms m/z: 280 (M^+, 54%), 248 (48), 220 (66), 205 (100).

*Sclerin (**24**)*

The above ester **28** (0.20 g) and NaOH (0.10 g) were heated under reflux in aqueous ethanol (5 mL) for 0.5 h. The mixture was cooled, acidified (dilute HCl), and extracted with ethyl acetate. The extracts were dried ($MgSO_4$), evaporated, and the residue recrystallized from CCl_4 to give sclerin, mp 119−121°C, (lit (24) mp 123°C), nmr and ir similar to those reported.

1. T. H. CHAN and T. CHALY. Tetrahedron Lett., **23**, 2935 (1982).
2. T. H. CHAN and P. BROWNBRIDGE. J. Chem. Soc. Chem. Commun. 20 (1981); 578 (1979).
3. J. H. RICHARDS and J. B. HENDRICKSON. The biosynthesis of steroids, terpenes and acetogenins. Benjamin, New York. 1964.
4. T. M. HARRIS and C. M. HARRIS. Tetrahedron, **33**, 2159 (1977).
5. S. N. HUCKIN and L. WEILER. J. Am. Chem. Soc. **96**, 1082 (1974); Can. J. Chem. **52**, 5157 (1974).
6. P. BROWNBRIDGE and T. H. CHAN. Tetrahedron Lett. 4437 (1979).
7. (*a*) T. H. CHAN, I. PATERSON, and J. PINSONAULT. Tetrahedron Lett. 4183 (1977); (*b*) M. T. REETZ. Angew. Chem. Int. Ed. Engl. **21**, 96 (1982).
8. T. MUKAIYAMA, K. BANNO, and V. NAIASAKE. J. Am. Chem. Soc. **96**, 7503 (1974); T. MUKAIYAMA. Angew. Chem. Int. Ed. Engl. **16**, 817 (1977).
9. G. ANDERSON, D. W. CAMERON, G. I. FEUTRILL, and R. W. READ. Tetrahedron Lett. **22**, 4347 (1981); P. R. BROOK, B. DEVADAS, and P. G. SAMMES. J. Chem. Res. (S), 134 (1982).
10. I. FLEMING and T. V. LEE. Tetrahedron Lett. 705 (1981); S. DANISHEFSKY, M. PRISBYLLA, and B. LIPISKO. Tetrahedron Lett. 805 (1980).
11. T. H. CHAN and P. BROWNBRIDGE. J. Am. Chem. Soc. **102**, 3534 (1980).
12. T. H. CHAN and P. BROWNBRIDGE. Tetrahedron, **31**, Suppl. 1, 387 (1981).
13. I. OJIMA, S. INABA, and K. YOSHIDA. Tetrahedron Lett. 3643 (1977).
14. (*a*) S. INABA and I. OJIMA. Tetrahedron Lett. 2009 (1977); (*b*) T. H. CHAN and I. H. M. WALLACE. Tetrahedron Lett. **23**, 799 (1982).
15. F. JOHNSON, K. G. PAUL, and D. FAVARE. Ger. Patent No. 2, 508, 295; Chem. Abstr. **84**, 59 (1976); **84**, 783 (1976).
16. Y. SATOMURA and A. SATO. Agric. Biol. Chem. **29**, 337 (1965).
17. R. E. COX and J. S. E. HOLKER. J. Chem. Soc. Perkin Trans. **1**, 2077 (1976).
18. M. YAMAZAKI, Y. MAEBAYASHI, and T. TOKOROYAMA. Tetrahedron Lett. 498 (1977).
19. M. J. GARSON and J. STAUNTON. J. Chem. Soc. Chem. Commun. 158 (1978); J. Chem. Soc. Perkin Trans. 1, 2584 (1981).
20. T. TOKOROYAMA, S. MAEDA, T. NISHIKAWA, and T. KUBOTA. Tetrahedron, **25**, 1047 (1969).
21. T. TOKOROYAMA, T. NISHIKAWA, K. ANDO, M. NOMURA, and T. KUBOTA, Nippon Kagaku Kaishi, 136 (1974).
22. M. MATSUI, Y. SUGIMURA, K. YAMASHITA, M. MORI, and T. OGAWA. Agric. Biol. Chem. **32**, 492 (1968).
23. K. NITTA, C. KAKARE, I. YAMAMOTO, and Y. YAMAMOTO. Agric. Biol. Chem. **27**, 813 (1963).
24. T. TOKOROYAMA, T. KAMIKAWA, and T. KUBOTA. Tetrahedron, **24**, 2345 (1968).

Precise Q_β measurements for $A = 91$ to 93 mass chains

R. IAFIGLIOLA, M. CHATTERJEE,[1] H. DAUTET, AND J. K. P. LEE
Foster Radiation Laboratory, McGill University, Montreal, P.Q., Canada H3A 2B2

Received August 31, 1982

This paper is dedicated to Professor Leo Yaffe on the occasion of his 65th birthday

R. IAFIGLIOLA, M. CHATTERJEE, H. DAUTET, and J. K. P. LEE. Can. J. Chem. **61**, 694 (1983).

The Q_β values of $^{91-93}$Rb, $^{91-93}$Sr, and $^{92-93}$Y were measured using mass-separated Rb sources obtained from an on-line isotope separator. A $\Delta E-E$ detector telescope consisting of a 300 μm × 300 mm^2 Si ΔE- and a 15 mm × 500 mm^2 Ge(HP) E detector was used. Results are in general agreement with recently published values but some discrepancies are indicated.

R. IAFIGLIOLA, M. CHATTERJEE, H. DAUTET et J. K. P. LEE. Can. J. Chem. **61**, 694 (1983).

On a mesuré les valeurs Q_β du $^{91-93}$Rb, du $^{91-93}$Sr et du $^{92-93}$Y, en utilisant des sources de Rb à masse séparée obtenues à l'aide d'un séparateur d'isotope à un canal. On a utilisé un téléscope détecteur de $\Delta E-E$ consistant en un détecteur de ΔE- de 300 μm × 300 mm^2 Si et un détecteur de E de 15 mm × 500 mm^2 Ge(HP). Les résultats s'accordent en général avec les valeurs récemment publiées, mais on indique quelques divergences.

[Traduit par le journal]

1. Introduction

The measurement of Q_β values for successive β decays along a mass chain is an effective method to deduce atomic masses, and for nuclei far off the β stability valley this is the most versatile and commonly applicable method. In general, two types of detector systems have been used: plastic scintillators and thick Ge(HP) detectors. The plastic scintillation detectors are capable of handling high counting rates, and, therefore, often the data have better statistics. Also, the detector response function for electrons and positrons is simpler, and thereby facilitates the analysis process. On the other hand, the Ge(HP) detector has a built-in energy calibration and is capable of yielding better energy resolution and stability. Under suitable conditions, precise Q_β values can be obtained.

The β spectra of neutron-rich Rb isotopes and their daughters have been studied using both plastic scintillator (1, 2) and Ge(HP) detectors (3, 4) and in some cases, Q_β values with only a few keV uncertainties have been reported (3). However, closer examination of these reported values indicates that there still exist some discrepancies among various groups. We have measured the β-decay energies of $^{91-93}$Rb and their daughter products using a $\Delta E-E$ telescope consisting of solid state detectors. The Q_β values were deduced and the uncertainties due to various contributing factors were examined.

2. Experimental methods

The Rb isotopes were produced by the fission of ^{238}U induced by 100 MeV protons at the McGill synchrocyclotron facility. These fission products were isotopically separated by the McGill on-line mass separator (5, 6) using a Ta foil as ionization surface and then focussed onto a thin aluminium foil located in a low background area, about 8 m away from the target chamber. The detector telescope consisted of a 300 mm^2 × 300 μm thick Si ΔE detector and a 500 mm^2 × 15 mm thick Ge(HP) E detector. A 10 mm thick brass collimator with a 200 mm^2 circular opening was placed in front of the telescope. A fast coincidence between signals from the two detectors opened a linear gate to allow the summed linear pulses from the detectors to be processed by an ADC. The relative energy matching was adjusted using a ^{207}Bi source and the absolute energy calibration was obtained from the E detector response to standard γ-ray sources. Pulser pulses were fed to the preamplifiers to check the electronic stability and to measure the possible pile-up effects.

A typical experimental run proceeded as follows: the Rb source was collected; both the cyclotron and the ion beams were then switched off; and, after an appropriate pause time, the β spectrum was accumulated for a certain time. The cycle was repeated until the desired statistics were reached. For most of the isotopes, different counting rates were used with different source-to-detector distances. In some cases, a Ge(Li) detector was used for β−γ coincidence gating.

The β spectra were analyzed using a multi-branch analysis program. Basically, the analysis consisted of two procedures. First, a search for the β end-point energy was made using the highest energy branch, through a least-square fit method. Then, a multi-branch analysis over a wide energy range was carried out, yielding a distribution of β intensities, feeding various higher excited energy states (or regions). Although, this analysis procedure does not usually allow precise determination of β end-point energies of branches leading to excited states, it does provide a check on the consistency of reported β feeding branches. Under favourable conditions such as a strong isolated feeding branch to one particular level, precise β end-point energy can be deduced. The detector response function used was based on a Monte-Carlo calculation (7), and then adjusted to fit the β spectra of ^{32}P and ^{88}Rb. The resultant fit to the ^{88}Rb spectrum is demonstrated in Figs. 1 and 2. In Fig. 1, a Kurie plot of the highest energy portion of the spectrum is shown. The known shape was incorporated and a Q_β value of 5310 ± 10 keV was obtained. Figure 2 shows a fit down to the 1 MeV region using known branching ratios. The good overall fit indicates the validity of the analysis procedure. For higher electron energies, an extrapolated response function was used and a good fit to the ^{92}Rb data over a wide energy range (6−8 MeV) was obtained.

The uncertainties associated with the measurements are the combined contributions from several sources: energy calibration, β response function, limited energy range where a fit can be made and effects from background pile-up and summing effects. In principle, the energy calibration should contribute little towards the uncertainties. However, there is always a limitation due to the lack of convenient standard high energy γ-rays, the available accumulation time, and the stability of the system. In our case, it is also compounded by the summing of ΔE and E pulses. We estimated this contribution to be 1.5 keV for each MeV of electron energy. To test the dependence of the β end-point energy and the goodness-of-fit on the response function, we have analysed these spectra using slightly different response functions (typically changing the parameters by ~10%). In general, they yield a poorer overall fit (higher χ^2 values) but do not

[1]Present address: Saha Institute of Nuclear Physics, Calcutta, India.

Can. J. Chem. Downloaded from www.nrcresearchpress.com by 210.87.254.105 on 09/06/12
For personal use only.

Can. J. Chem. Downloaded from www.nrcresearchpress.com by 210.87.254.105 on 09/06/12
For personal use only.

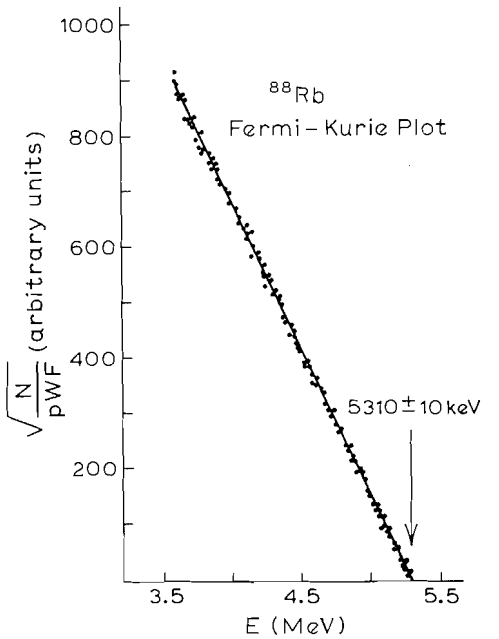

FIG. 1. The Fermi–Kurie plot for the high energy region of the ^{88}Rb β spectrum. The fit extends over an energy range of approximately 1.8 MeV.

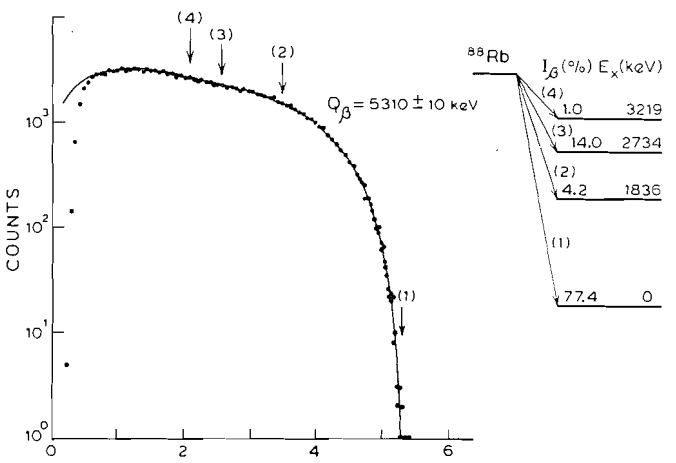

FIG. 2. The ^{88}Rb data and fit obtained by using a multi-branch fitting program. The fit includes the four highest intensity β branches and extends over an energy region of 1.3 to 5.3 MeV.

appreciably alter the β end-point energies. We estimate that this contribution is about 5–10 keV towards the total uncertainty. The effect of the limited energy range for fitting is dependent on the decay characteristics of the isotope being studied. Usually the fitting covers the region from E_{max} until the next important branch occurs, and if this is ~500 keV or more, reliable E_{max} can be extracted. The actual uncertainty, however, is dependent on the relative magnitude of the background to the high energy branch. To achieve high precision it is important that the spectrum be free from background, pile-up and β–γ summing effects. In our actual experimental runs, we have attempted to minimize the interference from these undesirable effects: the ΔE–E coincidence requirement eliminates the γ-ray events; the source-to-detector distance is large (typically ~10 cm) to minimize β–γ summing effect; the counting rate was kept low (≤500 cps) to minimize pile-up; and a low background was achieved by proper ion beam alignment and the switching-off of both cyclotron and ion beams during accumulation. We estimate that these contributed about 5–25 keV towards the quoted uncertainties. Besides these contributions, there are still some other sources of uncertainties such as counting statistics, but they are comparatively small for all the spectra studied here.

It should be noted that in the literature, some β end-point energies were reported with a few keV uncertainties. Since the details of the actual breakdown of the sources of these uncertainties was not presented, it is not possible to make direct comparisons.

3. Experimental results and discussions

The experimental β end-point energies and the deduced Q_β values are tabulated in Table 1, together with some of the recently reported values. The adopted values in the 1977 mass table (8) were also included for comparison. The E_{max} values shown correspond to the end-point energies of the highest energy branches. Among the results from groups using Ge(HP) detectors, generally good agreement in E_{max} is obtained except for ^{93}Rb, where our value is 45 to 50 keV lower, just outside the error bars quoted. Based on these results and using the adopted mass excesses (8) of ^{91}Y, and ^{92,93}Zr, the mass excesses of the isotopes studied were deduced. They are shown in the table together with the results from the direct mass measurements (9).

For ^{91}Rb decay, the E_{max} values obtained from different Ge(HP) measurements are consistent. Rehfield (4) has assigned the high energy branch to feed the 93 keV state in ^{91}Sr while Decker *et al.* (3) have suggested a feeding to the ground state and thus the discrepancy in the Q_β values listed. In the present work, the analysis is not sufficiently sensitive to distinguish this difference and we have accepted the assignment of Decker *et al.* (3).

For ^{92}Sr decay, the coincidence requirement for ΔE and E pulses was bypassed. A ΔE pulse alone opened the linear gate for the summed ΔE and E pulses to be processed by the ADC. The spectrum had a high energy component resulting in a relatively high overall uncertainty for the low energy branch.

In the ^{93}Sr decay β spectrum, the highest energy branch has an E_{max} of 4110 ± 20 keV. The multi-branch analysis yields a β feeding distribution as shown in Fig. 3, consistent with the reported β transition intensities to the excited states of ^{93}Y in the proposed decay schemes (10, 11) of ^{93}Sr. Also, the E_{max} of the β spectrum obtained in coincidence with the 888 keV γ-ray yielded a Q_β value of 4140 ± 50 keV, in agreement with the singles data. The present work therefore yields a β feeding branch of 4.5% from ^{93}Sr to the ground state of ^{93}Y. This conclusion is in contradiction to the proposed ^{93}Sr decay schemes (10, 11), in which the absence of this β branch was used to support a J^π assignment of $7/2^+$ for ^{93}Sr ground state. Therefore, our present conclusion, if adopted, would require the change of the spin-parity assignments for levels in ^{93}Sr and ^{93}Y. This direct ground state feeding was also suggested by Stippler *et al.* (12).

4. Conclusion

We have used a ΔE–E telescope of solid state detectors to study the β spectra from separated $^{91-93}$Rb sources and their daughters. The emphasis was placed on obtaining consistent and clean spectra, with minimal interference from both background and γ-rays, such that β end-point energies could be determined reliably using fits over extended energy regions. Multi-branch analysis was adopted to check consistency with currently existing decay schemes. Results are in general agreement with recently reported values. For the ^{93}Sr decay, our

Can. J. Chem. Downloaded from www.nrcresearchpress.com by 210.87.254.105 on 09/06/12
For personal use only.

TABLE 1. Experimental E_{max} and Q_β values and deduced mass excesses

Isotope	E_{max} (keV)	Q_β (keV) This work	Q_β (keV) Others	Mass excess (keV) This work	Mass excess (keV) Ref. 9
^{88}Rb	5310±10	5310±10	5318 ± 4 (3) 5310 ± 10 (4) 5309 ± 11 (8)*		
^{91}Rb	5850±20	5850±20	5857 ± 8 (3) 5950 ± 20 (4) 5760 ± 40 (1) 5700 ± 40 (8)*	−77791±25	−77800±35
^{91}Sr	2709±15	2709±15	2704.5± 3 (3) 2684 ± 4 (8)*	−83641±15	
^{92}Rb	8080±30	8080±30	8111 ± 15 (3) 8080 ± 15 (4) 7980 ±100 (12) 8080 ±160 (1) 7770 ±200 (8)*	−74826±40	−74840±40
^{92}Sr	536±20	1920±20	1930 ± 30 (8)*	−82906±25	
^{92}Y	3630±15	3630±15	3634 ± 16 (8)*	−84826±15	
^{93}Rb	7440±30	7440±30	7485 ± 15 (3) 7490 ± 15 (4) 7405 ±100 (12) 7360 ± 70 (8)*	−72685±40	−72755±65
^{93}Sr	4110±20	4110±20	4130 ±100 (10) 4150 ± 70 (8)*	−80125±25	
^{93}Y	2880±15	2880±15	2890 ± 20 (8)*	−84235±15	

*Compiled value from 1977 mass table.

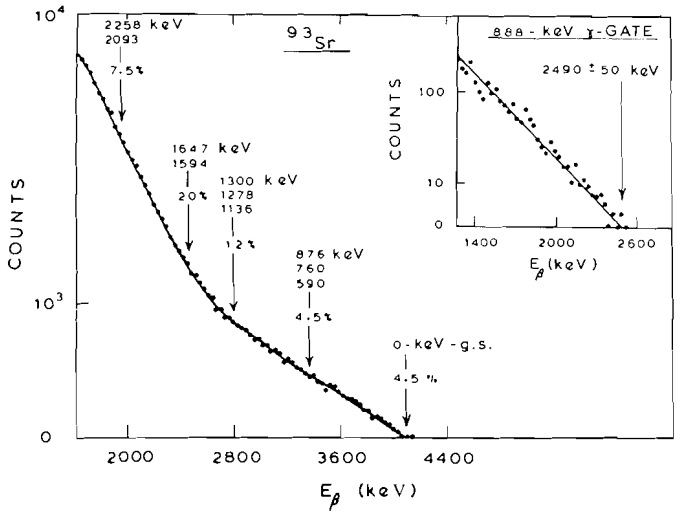

FIG. 3. The β spectrum from ^{93}Sr decay and the multi-branch fit using β branches shown. The insert shows the β spectrum obtained in coincidence with the 888 keV γ-ray, which depopulates the 1647 keV level of ^{93}Y.

result suggests a beta branch feeding directly to the ground state of ^{93}Y and if so, a major revision of spin-parity assignment for levels in ^{93}Sr and ^{93}Y will be required.

Acknowledgement

This work was supported by the Natural Sciences and Engineering Research Council of Canada.

1. F. K. WOHN and W. L. TALBERT, JR. Phys. Rev. C**18**, 2328 (1978).
2. U. KEYSER, H. BERG, F. MUNNICH, B. PAHLMANN, R. DECKER, and B. PFEIFFER. Atomic masses and fundamental constants. Vol. 6. *Edited by* J. A. Nolen, Jr. and W. Benenson. Plenum Press. 1980. p. 443.
3. R. DECKER, K. D. WUNSCH, H. WOLLNIK, E. KOGLIN, G. SIEGERT, and G. JUNG. Z. Phys. A**294**, 35 (1980).
4. D. M. REHFIELD. Ph.D. Thesis, McGill University. 1977.
5. J. K. P. LEE, G. PILAR, B. L. TRACEY, and L. YAFFE. J. Inorg. Nucl. Chem. **37**, 2035 (1975).
6. L. NIKKINEN, B. P. PATHAK, L. LESSARD, and J. K. P. LEE. Nucl. Inst. Meth. **175**, 425 (1980).
7. B. J. VARLEY, J. E. KITCHING, W. LEO, J. MISKIN, R. B. MOORE, K. D. WUNSCH, R. DECKER, H. WOLLNIK, and G. SIEGERT. Nucl. Inst. Meth. **190**, 543 (1981).
8. A. H. WAPSTRA and K. BOS. Atom. Data Nuclear Data Tables, **19**, 175 (1977).
9. M. EPHERRE, G. AUDI, C. THIBAULT, R. KLAPISCH, G. HUBER, F. TOUCHARD, and H. WOLLNIK. Phys. Rev. C**19**, 1504 (1979).
10. E. ACHTERBERG, F. C. IGLESIAS, A. E. JECH, J. A. MORAGUES, D. OTERO, M. L. PEREZ, A. N. PROTO, J. J. ROSSI, and W. SCHEUER. Phys. Rev. C**10**, 2526 (1974).
11. C. J. BISCHOF and W. L. TALBERT, JR. Phys. Rev. C**15**, 1047 (1977).
12. R. STIPPLER, F. MUNNICH, H. SCHRADER, J. P. BOCQUET, M. ASGHAR, G. SIEGERT, R. DECKER, B. PFEIFFER, H. WOLLNIK, E. MONNAND, and F. SCHUSSLER. Z. Phys. A**284**, 95 (1978).

Momentum transfer in the fragmentation of copper by 400-GeV protons

JAMES B. CUMMING

Chemistry Department, Brookhaven National Laboratory, Upton, NY 11973, U.S.A.

Received August 31, 1982

This paper is dedicated to Professor Leo Yaffe on the occasion of his 65th birthday

JAMES B. CUMMING. Can. J. Chem. **61**, 697 (1983).

Mean momenta transferred to products of the fragmentation of copper by 400-GeV protons have been determined by the thick-target thick-catcher technique. Comparison with data for incident protons and heavy ions indicates that the limiting fragmentation region has been reached and supports a simple relationship between momentum and energy transfers in peripheral reactions which had been proposed previously.

JAMES B. CUMMING. Can. J. Chem. **61**, 697 (1983).

Faisant appel à la technique de la cible épaisse et du récepteur épais, on a déterminé les moments moyens transferrés aux produits résultant de la fragmentation du cuivre par les protons à 400 GeV. La comparaison avec les données relatives aux protons incidents et aux ions lourds indique qu'on atteint la région de fragmentation limite et cette comparaison vient appuyer une relation simple entre le moment et les transferts d'énergie dans les réactions périphériques qui a été proposée antérieurement.

[Traduit par le journal]

Can. J. Chem. Downloaded from www.nrcresearchpress.com by 210.87.254.6 on 09/06/12
For personal use only.

Introduction

Studies of the interactions of high-energy projectiles with complex nuclear targets lead to an overall picture of great complexity (1, 2). Attempts to understand such reactions frequently start with the assumption of a two-step mechanism. For reactions induced by nucleons (3), and more recently, also for heavy-ion-induced reactions (4), this is embodied in cascade plus evaporation (and/or fission) calculations. A two-step mechanism also underlies the various forms of the abrasion–ablation picture of heavy-ion reactions (5). There is considerable evidence that such a model is not appropriate for central collisions with heavy target elements such as gold and uranium. The violent processes that are associated with a high multiplicity of emitted particles and lead to products a hundred or more masses removed from the target are not well understood (6). In particular, unusual fragment angular distributions (7, 8) and evidence (9–11) that the time scale for the production of light- to medium-mass fragments is comparable to the time of the initial interactions appear to pose serious problems for any two-step model.

On the other hand, some simplifications appear if one focuses on the less violent encounters which can be classified under the generic term of target fragmentation. A target fragment is a major remnant of that portion of a target nucleus which appears to have been the spectator to the region of projectile–target interaction or overlap (fireball in one model (12)). Linear momentum transfer between a projectile and a target fragment is expected to be low. For heavy-ion projectiles, an equivalent process in the moving system results in projectile fragments which have nearly the beam velocity. Many observations of target or projectile fragmentation appear consistent with two hypotheses originally associated with peripheral hadron–hadron reactions at high energies (see ref. 13 for a review). The hypothesis of *limiting fragmentation* predicts that both cross sections and energy spectra of fragments should become independent of bombarding energy at sufficiently high energies. The second, *factorization*, asserts that these fragment properties can be written as a product of target and projectile factors. For example, in the case of cross sections, the target fragment mass-yield curve would depend on the type of projectile only via the total cross section as a scaling factor.

The present paper deals with the fragmentation of copper targets where some 70% of the total reaction cross section leads to products consistent with the above hypotheses (14). In previous work (15), a simple model was proposed which related the momentum transferred to a target fragment to the excitation deposited in the initial or abrasion step of these reactions. It was predicted that momentum transfers associated with a given product should approach a limit as bombarding energy increases (consistent with limiting fragmentation) and that this limit was determined by the energetics of the particular reaction selected. In the analysis of the available data (15–17), the validity of the model and the actual positions of the asymptotes depended strongly on data from a single experiment with 28-GeV protons (16). Reported below are new results obtained at 400-GeV which show the existence of asymptotic limits to momentum transfer in a model-independent way and confirm, as well, the predictions of the model based on data for lower energy projectiles.

Experimental

The present experiment was an outgrowth of work at the Fermi National Accelerator Laboratory (FNAL) intended to supply precise absolute cross sections for beam monitoring and diagnostic purposes (18). With recoil catchers in some target stacks, recoil properties could be determined simultaneously with the desired cross sections. The techniques were identical to those reported previously (15, 16). Three thick-target thick-catcher stacks were irradiated in vacuum with 400-GeV protons in the enclosure 99 area of the neutrino hall at FNAL. The first two stacks consisted of a 47 mg/cm^2 Cu foil with 17 mg/cm^2 Mylar catcher foils on the upstream and downstream sides. An additional Mylar on the upstream side served as a blank, and the four foils were vacuum encapsulated between pieces of 11 mg/cm^2 heat sealable Mylar. After irradiations with 10^{15} protons, the stacks were sent to BNL where circular samples, 8.2 cm^2 in area, were punched out. Approximately 99% of the total activity was contained in the punched areas. γ-Ray spectra were recorded for the various samples at a 1-cm distance from a Ge(Li) detector over a period of ~50 days. Full-energy peak intensities were resolved from the spectra

and their decay curves analyzed by various computer programs. In a third irradiation, performed approximately one year after the first two, catcher foils of 7 mg/cm^2 were used to reduce ^{7}Be production which appeared to interfere with the determination of several products. Although the third target was exposed to only 4×10^{14} protons, the simultaneous use of three Ge(Li) detectors and a reduced sample-to-detector distance resulted in some improvement in nominal statistical accuracy of this experiment in comparison with the first two. Also, at the time of the third irradiation, the samples from the first two were combined and assayed to obtain the only results for ^{22}Na and also improved data for the long-lived nuclides, ^{54}Mn and ^{57}Co.

Results

On examination of the extensive data base, 15 nuclides which could be assayed with ≈5% or better precision were selected for further attention. Extending from ^{58}Co to ^{22}Na, these species provide a representative sample of fragments ranging from those having mass numbers near that of the target to species involving the loss of ~40 nucleons. Corrections were applied for the production of ^{22}Na and ^{24}Na from impurities in the catcher foils. In the worst case these amounted to 5% of the activity observed in the back catcher.

Ten of the 15 selected nuclides could be assayed by two or more γ-rays, thus providing checks on the spectral resolution procedures. Also, in the third irradiation, internal consistency between data from three detectors could be examined for all species. Two basic quantities were obtained for each nuclide, γ-ray, detector, and irradiation. These are *FW* and *BW*, where *F* is the fraction of the total activity produced in the target observed in the front catcher, *B* the fraction in the back catcher, and *W* is the target thickness (mg/cm^2). *FW* and *BW* represent the effective mean range of a particular recoil projected in the forward and backward direction, respectively. Where multiple determinations for a species were available in a given run these were averaged initially for the separate runs with statistical weights from the spectral and decay curve resolutions. Data for each nuclide were then averaged for the three runs. In this step, additional 2% errors were folded in to account for possible systematic effects in the individual irradiations. Whenever an average was calculated, checks were made for internal consistency. If these were not satisfactory, errors were increased appropriately.

Mean values of *FW* and *BW* obtained from this analysis are plotted in Fig. 1 as a function of $\Delta A = 63.5 - A_f$, where A_f is the fragment mass number. A typical (average) error on a value of *FW* or *BW* is ±2.5%, comparable to the size of the points. Individual errors range from 1.3% for favorable cases to 5.4% for a few poorly determined species. The straight lines having unit slope in Fig. 1 (a log–log plot) are intended to show the general trends: both *FW* and *BW* are approximately proportional to ΔA and the ratio F/B is not strongly dependent on ΔA.

One of the more striking deviations from smooth trends in Fig. 1 appears for ^{51}Cr at $\Delta A = 12.5$. Values of *FW* and *BW*, particularly the latter, seem low. Chromium-51 was assayed via the 320-keV γ-ray which is present only to the extent of 9.8% of the decays. It was thought that the intense Compton continuum of the 478-keV γ-ray of ^{7}Be interfered with the analysis of the low intensity 320-keV line in the catcher foils, and indeed, values of *FW* and *BW* from the third irradiation, in which the relative amount of ^{7}Be was reduced by a factor of 2.4, were 5 and 8% higher, respectively, than the average results from the first two experiments.

Included in Fig. 1 for comparison with the present results at 400 GeV are data for six nuclides obtained at a bombarding energy of 28 GeV (16). There is a tendency for the lower energy points to fall slightly above those measured at 400 GeV. The mean difference, 3.7%, is not large considering the experimental errors, and it is clear there are no major changes associated with a 14-fold increase in bombarding energy for a wide range of products. The asymptotic region appears to have been nearly reached at the lower energy as we shall see in the more detailed analysis which follows.

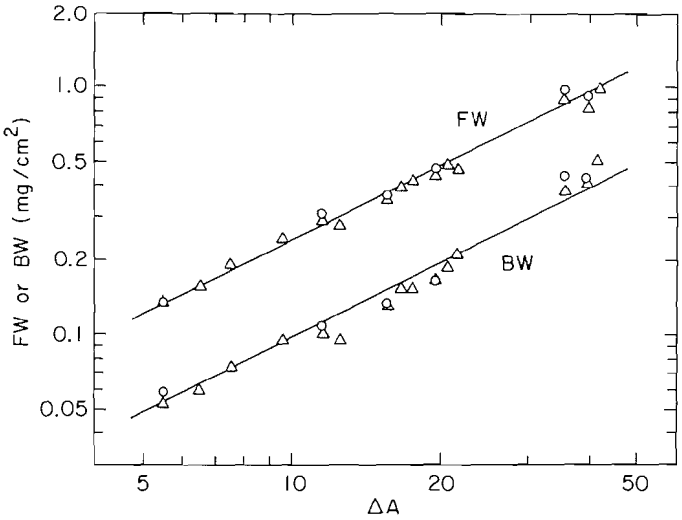

FIG. 1. Dependence of experimentally determined mean ranges projected in the forward and backward directions (*FW* and *BW*) on the mass number difference between the target and fragment ($\Delta A = 63.5 - A_f$). Open triangles show the present results, circles show those obtained at 28 GeV, ref. 16. The straight lines with unit slope indicate general trends.

Analysis and discussion

To examine the results of the present experiment in more detail, it was assumed that the two-step model could be applied to transform the measured values of *FW* and *BW* into mean values for the apparent velocity of the moving source ($\beta_\parallel$ which is $v_\parallel$ in units of *c*) after the initial abrasion interaction and then an additional component of velocity, *V*, due to the second or ablation step of the reaction. The same nonlinear, iterative least-squares procedure incorporating polynominal fits to tabulated range-energy curves (19, 20) was used for this transformation as had been applied in the analysis of the lower-energy results (15). Because we have only two measured quantities, *FW* and *BW*, we can at best derive results for only two parameters $\beta_\parallel$ and *V*.[1]

Focusing first on $\beta_\parallel$, it had been concluded (15) that the measured values at 28 GeV were near their asymptotic limits in the spirit of limiting fragmentation. Analysis in terms of a simple model (to be discussed below) for momentum transfer in peripheral fragmentation reactions predicted that only a 3.3% further decrease should be observed. We compare in Table 1 the values of $\beta_\parallel$ derived from the present experiment with those reported at 28 GeV reduced by this percentage. For the six isotopes in common to the two experiments, agreement between the experimental values at 400 GeV and those pre-

[1]The values derived for $\beta_\parallel$ and *V* are relatively insensitive to additional parameters such as an anisotropic distribution of *V* or a perpendicular component of the first step velocity, see ref. 15.

Can. J. Chem. Downloaded from www.nrcresearchpress.com by 210.87.254.6 on 09/06/12
For personal use only.

TABLE 1. Comparison of moving source velocities derived from the present experiment with those predicted from data at 28 GeV

Isotope	Source velocity, $10^3\ \beta_\parallel$	
	Observed	Predicted[a]
^{24}Na	5.45±0.17	5.49±0.38
^{28}Mg	5.41±0.29	5.20±0.35
^{44}Sc	3.38±0.07	3.33±0.07
^{48}V	2.71±0.07	2.70±0.06
^{52}Mn	2.36±0.05	2.34±0.07
^{58}Co	1.25±0.03	1.14±0.07

[a] Values from ref. 15 reduced by 3.3% as suggested by a simple model, see text.

dicted by the model is well within the errors and is strong evidence that the asymptotic limit has now been reached.

A broader picture of the target fragmentation process is given in Fig. 2 where values of V and $\beta_\parallel$ for three representative fragments, ^{24}Na, ^{48}Sc, and ^{58}Co, are plotted as a function of projectile rapidity, Y. Rapidity is a convenient velocity-related variable ($Y = \tanh^{-1}\beta$) which, when small, is nearly equal to β. In this figure the right-most points (at $Y = 6.76$) are from the present work and those at $Y = 4.13$ are the previous results at 28 GeV. At lower rapidities, data for incident ^{4}He and ^{12}C ions are also included. In addition to work from this laboratory, results for ^{24}Na obtained by Crespo *et al.* (17) are also included. A striking feature which has been commented upon previously (15) is the lack of a strong dependence of recoil properties on the projectile type when comparisons are made at the same velocity. Also significant is the fact that the initial abrasion interaction (characterized by $\beta_\parallel$) is much more dependent on projectile rapidity than is the second or ablation step (characterized by V). The arbitrary smooth curves in the upper panel of Fig. 2 suggest the new data on V are a continuation of a slightly decreasing trend. It has been pointed out (15) that the numerical values of V are consistent with those expected from a random-walk addition of small kicks due to the emission of nucleons or small aggregates of nucleons in the ablation step. Some change in the mix of emitted nucleons and α particles as the projectile energy decreases, particularly increased α emission as a more energy-efficient path to fragments, could account for part of the rise in V. However, a more prosaic reason may be problems in the determination of V and $\beta_\parallel$ from the experimental FW and BW values. Assumptions necessary for this transformation become less justified as the F/B ratio becomes large, and this is the case at low rapidity.

We return now to an examination of the dependence of source velocity, $\beta_\parallel$, on Y. The curves in the lower panel of Fig. 2 are least-squares fits to the function,

$$[1]\quad \beta_\parallel = \beta_\parallel^\infty\,(1 + k\sqrt{1-\beta^2})/\beta$$

where $\beta_\parallel^\infty$ is the asymptotic limiting value for a given product and k is a parameter dependent on details assumed for the initial interaction. From the derivation of eq. [1], it follows that $\beta_\parallel^\infty$ can be equated to $\Delta E_T/m_T$, where m_T is the mass of the fragment precursor, i.e., prior to mass loss in the ablation step, and ΔE_T is the prefragment excitation energy. The curves in Fig. 2 are for k held at unity. Although results for only three nuclides are shown in this figure, the fitting procedure simultaneously included data for ^{28}Mg, ^{44}Sc, and ^{52}Mn. In the case of a fit with six independent values of $\beta_\parallel^\infty$, the root-mean-square deviation

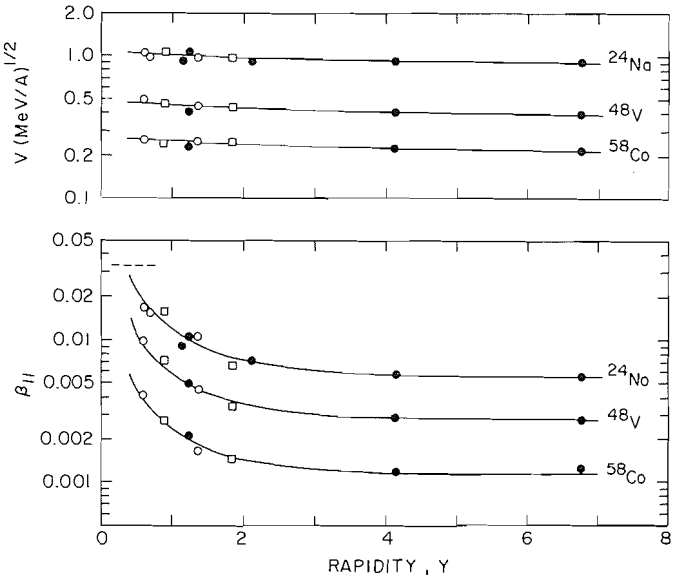

FIG. 2. Dependence of V (upper panel) and $\beta_\parallel$ (lower panel) on projectile rapidity. Filled circles are data for incident protons from the present work (at $Y = 6.76$) and from refs. 15, 16, 17. Open circles are for incident alpha particles from refs. 16, 17. Open squares are results for ^{12}C ions, refs. 15, 16.

of 42 points from the smooth curves was 8.3%. Including k as an additional parameter gave a value of $k = 1.03 \pm 0.10$ with no significant improvement in the quality of the fit. Because the term $\sqrt{1-\beta^2}$ in eq. [1] is only 2×10^{-3} at 400 GeV, the asymptotic limits determined by the new data are nearly independent of k and hence also independent of details of the various possible models.

The $k = 1$ form of eq. [1] may be recognized as being identical to an exact equation derived by Turkevich (quoted by ref. 21), from the assumption that the initial interaction consisted of a single elastic collision between a projectile and a target nucleon in which the latter remained trapped by the nucleus. It was difficult to understand why such a simple model could successfully fit data for reactions which appeared to involve more complex interactions (22). However, recent work (23, 24) has shown that eq. [1] with $k = 1$ can be derived as an approximation from a less restrictive single collision or multiple independent collision model involving small momentum and energy transfers in each step. While such approximations appear to be valid for the fragmentation of light- to medium-mass nuclei such as copper, serious problems appear for more complex (and presumably less peripheral) reactions in heavier targets. For example, for ^{128}Ba production from uranium by high-energy protons, Pandian and Porile (25) have reported a value of $k = 27$ and a $\beta_\parallel^\infty$ value corresponding to an excitation of only 67 MeV, much too low to be reasonable for the loss of 110 nucleons in a deep spallation process. As noted in the Introduction, a breakdown of the underlying two-step assumption occurs for still more complex reactions.

The present experiment has emphasized the high-energy asymptotic region (at energies of many GeV/nucleon) where momentum transfers reach lower limits dictated by the energetic requirements for a particular reaction. Of equal or perhaps greater interest are upper limits to linear momentum transfers which may occur at low energies. Figure 2 indicates a rapid increase of $\beta_\parallel$ for a wide range of products as Y decreases. However, at some point these curves will intersect rising curves

Can. J. Chem. Downloaded from www.nrcresearchpress.com by 210.87.254.6 on 09/06/12
For personal use only.

determined by the projectile's momentum. Maxima in the vicinity of such intersections would signal a transition in reaction mechanism from low- to high-energy processes, i.e., from complete fusion and/or deep inelastic collisions which are efficient in transferring momentum, to the rather inefficient peripheral fragmentation mechanism. Galin *et al.* (26) have recently studied the interaction of 30- to 84-MeV/nucleon ^{12}C ions (Y = 0.24 to 0.42) with Ni, Au, and U targets. They concluded that the maximum momentum transfer associated with the average processes detected with their counter systems was limited to 2 GeV/c. For a copper target, this corresponds to the $\beta_{\parallel} = 0.034$ shown as a dashed line in Fig. 2. Such a limit is not unreasonable given the general trends of Fig. 2, but the radiochemical results do tend to suggest that the limit for a specific product will depend on that product and hence the range of excitation energies which was selected. Extensions of studies of the fragmentation of copper targets into this lower energy region are now in progress to explore this in more detail.

Acknowledgments

On the special occasion of this commemorative issue of the Canadian Journal of Chemistry, I would like to extend warmest personal greetings to Professor Leo Yaffe and acknowledge his significant contributions toward the understanding of high-energy nuclear reactions. The hospitality and cooperation of the FNAL staff during the present work are greatly appreciated. Particular thanks are due Dr. S. I. Baker for arranging the irradiations and air shipments. This work was performed at Brookhaven National Laboratory under contract with the U.S. Department of Energy and supported by its Office of High Energy and Nuclear Physics.

1. J. HUDIS. *In* Nuclear chemistry. Vol. I. *Edited by* L. Yaffe. Academic Press, New York. 1968. p. 169.
2. A. S. GOLDHABER and H. H. HECKMAN. Ann. Rev. Nucl. Part. Sci. **28**, 161 (1978).
3. H. W. BERTINI, A. H. CULKOWSKI, O. W. HERMANN, N. B. GOVE, and M. P. GUTHRIE. Phys. Rev. C**17**, 1382 (1978).
4. Y. YARIV and Z. FRAENKEL. Phys. Rev. C**20**, 2227 (1979).
5. J. D. BOWMAN, W. J. SWIATECKI, and C. F. TSANG. Lawrence Berkeley Laboratory Report No. LBL-2908, 1973.
6. A. I. WARWICK, A. BADEN, H. H. GUTBROD, M. R. MAIER, J. PÉTER, H. G. RITTER, H. STELZER, H. H. WIEMAN, F. WEIK, M. FREEDMAN, D. J. HENDERSON, S. B. KAUFMAN, E. P. STEINBERG, and B. D. WILKINS. Phys. Rev. Lett. **48**, 1719 (1982).
7. L. P. REMSBERG and D. G. PERRY. Phys. Rev. Lett. **35**, 361 (1975).
8. N. T. PORILE, D. R. FORTNEY, S. PANDIAN, R. A. JOHNS, T. KAISER, K. WIELGOZ, T. S. K. CHANG, N. SUGARMAN, J. A. URBON, D. J. HENDERSON, S. B. KAUFMAN, and E. P. STEINBERG. Phys. Rev. Lett. **43**, 918 (1979).
9. J. B. CUMMING, R. J. CROSS, J. HUDIS, and A. M. POSKANZER. Phys. Rev. **134**, B167 (1964).
10. A. M. POSKANZER, G. W. BUTLER, and E. K. HYDE. Phys. Rev. C**3**, 882 (1971).
11. D. R. FORTNEY and N. T. PORILE. Phys. Rev. C**22**, 670 (1980).
12. G. D. WESTFALL, J. GOSSET, P. J. JOHANSEN, A. M. POSKANZER, W. G. MEYER, H. H. GUTBROD, A. SANDOVAL, and R. STOCK. Phys. Rev. Lett. **37**, 1202 (1976).
13. H. BØGGILD and T. FERBEL. Ann. Rev. Nucl. Sci. **24**, 451 (1974).
14. J. B. CUMMING, P. E. HAUSTEIN, T. J. RUTH, and G. J. VIRTES. Phys. Rev. C**17**, 1632 (1978).
15. J. B. CUMMING, P. E. HAUSTEIN, and H.-C. HSEUH. Phys. Rev. C**24**, 2162 (1981).
16. J. B. CUMMING, P. E. HAUSTEIN, and H.-C. HSEUH. Phys. Rev. C**18**, 1372 (1978).
17. V. P. CRESPO, J. M. ALEXANDER, and E. K. HYDE. Phys. Rev. **131**, 1765 (1963).
18. S. I. BAKER, C. R. KERNS, S. PORDES, J. B. CUMMING, A. SOUKAS, V. AGORITSAS, and G. R. STEVENSON. Unpublished results.
19. L. C. NORTHCLIFFE and R. F. SCHILLING. Nucl. Data, A**7**, 233 (1970).
20. L. WINSBERG. At. Data Nucl. Data Tables, **20**, 389 (1977).
21. N. T. PORILE and N. SUGARMAN. Phys. Rev. **107**, 1410 (1957).
22. A. M. POSKANZER, J. B. CUMMING, and R. WOLFGANG. Phys. Rev. **129**, 374 (1963).
23. J. B. CUMMING. Phys. Rev. Lett. **44**, 17 (1980).
24. A. ABUL-MAGD, J. HÜFNER, and B. SCHURMANN. Phys. Lett. **60**B, 327 (1976).
25. S. PANDIAN and N. PORILE. Phys. Rev. C**23**, 427 (1981).
26. J. GALIN, H. OESCHLER, S. SONG, B. BORDERIE, M. F. RIVET, I. FOREST, R. BIMBOT, D. GARDÈS, B. GATTY, H. GUILLEMOT, M. LEFORT, B. TAMAIN, and X. TARRAGO. Phys. Rev. Lett. **48**, 1787 (1982).

Can. J. Chem. Downloaded from www.nrcresearchpress.com by 210.87.254.6 on 09/06/12
For personal use only.

Heavy target fragment yields in the interaction of 28 GeV protons with ^{238}U

B. V. JACAK,[1] W. LOVELAND,[2] D. J. MORRISSEY,[1] P. L. MCGAUGHEY, and G. T. SEABORG
Nuclear Science Division, Lawrence Berkeley Laboratory, University of California, Berkeley, CA 94720, U.S.A.

Received August 31, 1982

This paper is dedicated to Professor Leo Yaffe on the occasion of his 65th birthday

B. V. JACAK, W. LOVELAND, D. J. MORRISSEY, P. L. MCGAUGHEY, and G. T. SEABORG. Can. J. Chem. **61**, 701 (1983).

The yields of target fragments from the interaction of 28 GeV protons with ^{238}U have been measured, with special attention being given to those fragments with $160 \leq A \leq 200$. From the measured fragment yields, isobaric production cross sections were calculated. Significant yields ($\sigma(A) \sim 1-10$ mb) of heavy target fragments ($160 \leq A \leq 210$) were found. These fragments are believed to be the non-fissioning survivors from the population of highly excited residual nuclei produced in the initial p-nucleus collision. A pedagogical calculation of the fission − particle emission competition shows how the initial highly excited heavy nuclei could evaporate ~20−50 particles while surviving fission competition.

B. V. JACAK, W. LOVELAND, D. J. MORRISSEY, P. L. MCGAUGHEY et G. T. SEABORG. Can. J. Chem. **61**, 701 (1983).

On a mesuré les rendements en fragments de cibles provenant de l'interaction de protons à 28 GeV avec ^{238}U, en portant une attention spéciale aux fragments avec $160 \leq A \leq 200$. On a calculé les sections droites de production isobare à partir de la mesure de ces rendements de fragment. On a observé des rendements importants ($\sigma(A) \sim 1-10$ mb) en fragments de cibles lourds ($160 \leq A \leq 210$). On croit que ces fragments sont les survivants qui n'ont pas subi de fission et qui faisaient partie de la population de noyaux résiduels fortement excités produits lors de la collision initiale p-noyau. Un calcul pédagogique de la compétition entre l'émission des particules et la fission montre comment le noyau lourd fortement excité initialement peut disperser ~20−50 particules tout en survivant à la compétition de fission.

[Traduit par le journal]

Introduction

Five years ago, Loveland *et al.* (1) reported that in the interaction of 25 GeV ^{12}C with ^{238}U, one observed in addition to the expected fission fragments, large yields of heavy target fragments with $160 \leq A \leq 200$.[3] Subsequently, McGaughey *et al.* (2) reported observing the production of these fragments in the interaction of 8 GeV ^{20}Ne with ^{238}U although the magnitude of their yields was less. These observations were significant for a number of reasons. First, since such products had not been observed in the interaction of relativistic protons with ^{238}U (see ref. 3 for a summary of these data), it appeared that these reaction products were produced by a mechanism unique to nucleus−U collisions as compared to nucleon−U collisions. A study of these products might then offer the possibility of studying unique aspects of nucleus−nucleus collisions. Second, the question arose as to how such products could be formed. If they were spallation products, that meant that ~60 *A* units were removed from the target during the initial reaction and the subsequent deexcitation of the target fragment. Naively one might have expected the heavy nucleus to fission rather than allow such an extended evaporation process to occur.

Because of the importance of the issues raised by the observation of large heavy fragment yields in relativistic nucleus−U collisions, we thought it to be prudent to carefully re-examine the pattern of target fragment yields in relativistic p−U collisions to see if any evidence could be found for heavy target fragment survivors of the primary projectile−target encounter. Accordingly we report in this paper the observation of such fragments, produced in significant quantities, in the interaction of 28 GeV p with ^{238}U. We use a pedagogical model of fission − particle emission competition to show how these heavy target fragments could be formed from the highly excited products of the initial p−U collision.

Experimental

A natural uranium foil of thickness 33.5 mg/cm^2 surrounded by mylar catcher foils of thickness 35.5 mg/cm^2 was irradiated for 63 min in an external beam of 28 GeV protons from the Alternating Gradient Synchrotron at Brookhaven National Laboratory with an average particle intensity of 7.8×10^{13} protons/min. The intensity of the beam striking the target was determined by measuring the yields of ^{22}Na and ^{24}Na in a 12.72 mg/cm^2 Al foil irradiated simultaneously with the U foil. The following monitor production cross sections (4) were used: $\sigma(^{24}Na) = 8.0 \pm 0.3$ mb; $\sigma(^{22}Na) = 9.8 \pm 1.0$ mb.

Following a one day delay for shipment of the irradiated foils to the Lawrence Berkeley Laboratory, analysis of the radioactivities of the target fragments began. The irradiated U foil and the mylar catcher foils were cut approximately in half; the target was counted before and after the cutting process, allowing an exact determination of the relative fractions. One half of the target and its associated mylar catcher foils were subjected to direct γ-ray spectroscopy, while a chemical group separation procedure was applied to the other 33.5 mg/cm^2 U foil half without its catcher foils. In the former case, all of the target fragments should have been stopped in the U foil-catcher assembly (5−15); in the latter case, attention was focused on the yields of the heavy ($160 \leq A \leq 210$) fragments and based upon prior experiments on the ranges of n-deficient heavy rare-earth nuclides (12), only a negligible fraction of the total yield of these products should escape from the U foil. (For the yields of the As and Sb isotopes measured by radiochemical techniques and direct foil counting, no discernible difference between the two measurement techniques was noted.) The chemical procedure used was that developed by Kratz and co-workers (16) with minor modifications. It is based on the volatility and ion exchange behavior of the bromide complexes of the elements. Chem-

[1]Present address: National Superconducting Cyclotron Laboratory, Michigan State University, East Lansing, MI 48824, U.S.A.

[2]Present address: Department of Chemistry, Oregon State University, Corvallis, OR 97331, U.S.A.

[3]The heavy fragment yields reported in ref. 1 are now known to be overestimates due to difficulties in integrating the charge dispersions to give isobaric yields.

Can. J. Chem. Downloaded from www.nrcresearchpress.com by 210.87.254.5 on 09/06/12
For personal use only.

Can. J. Chem. Downloaded from www.nrcresearchpress.com by 210.87.254.5 on 09/06/12
For personal use only.

TABLE 1. Target fragment yields in the interaction of 28 GeV p + ^{238}U

Nuclide	Measured production cross section (mb)	Previous results (mb)	Calculated independent yield (mb)	Isobaric yield (mb)
^{71}As	3.4 ±0.2	1.2[a]	3.4 ±0.3	19.3±1.9
^{72}As	4.7 ±0.3[j]	4[a]	4.5 ±0.5	18.4±1.8
^{74}As	6.9 ±0.3[j]	6.2[a]	6.9 ±0.7	18.2±1.8
^{76}As	6.2 ±0.4[j]	8.0 ±2.0[b]	6.2 ±0.6	22.0±2.2
^{84}Rb	8.5 ±0.05	6.9 ±0.3[c]	8.5 ±0.8	21.4±2.1
^{86}Y	3.7 ±0.4		3.2 ±0.3	24.8±2.6
^{87}Y	7.2 ±0.08		6.1 ±0.6	25.4±2.5
^{87M}Y	9.0 ±0.8		7.5 ±0.7	31.3±3.1
^{88}Zr	4.6 ±0.2		4.2 ±0.7	39.8±4.0
^{89}Zr	4.4 ±0.2		3.7 ±0.4	18.1±1.8
^{90}Nb	2.7 ±0.2		2.4 ±0.2	28.8±2.9
^{91}Sr	8.7 ±0.5	(14.3 ±0.4[d])		
^{92M}Nb	0.24±0.08		0.24±0.08	14.2±1.4
^{93M}Mo	0.82±0.34		0.82±0.34	20.9±2.1
^{95}Zr	13.5 ±0.4		12.8 ±1.3	23.9±2.4
^{95}Nb	7.7 ±0.8		7.7 ±0.8	20.9±2.1
^{95}Tc	3.2 ±0.07		2.9 ±0.3	9.7±1.0
^{96}Nb	5.4 ±0.5		5.4 ±0.5	83.9±8.4
^{96}Tc	2.18±0.06		2.2 ±0.2	—
^{97}Zr	11.8 ±1.2		11.8 ±1.2	—
^{99}Mo	17.0 ±0.4		11.5 ±1.1	32.9±3.3
^{100}Rh	2.3 ±0.5		2.2 ±0.5	43.6±9.2
^{101M}Rh	4.0 ±0.5		4.0 ±0.5	—
^{105}Ru	10.4 ±0.2		8.3 ±0.8	37.3±3.7
^{105}Rh	20.7 ±1.4		12.3 ±1.2	32.2±3.2
^{106M}Ag	2.1 ±0.2		2.1 ±0.2	—
^{111}In	5.0 ±0.1	5.0 ±0.5[e]	4.2 ±0.4	22.9±2.3
^{118M}Sb	2.0 ±0.1[j]		2.0 ±0.2	—
^{119M}Te	2.1 ±0.7[j]		2.1 ±0.7	—
^{120}Sb	3.4 ±0.1[j]		3.4 ±0.3	—
^{121}Te	4.4 ±0.4		3.4 ±0.3	4.4±0.4[k]
^{122}Sb	5.7 ±0.3[j]		5.6 ±0.6	22.0±2.2[l]
^{123}I	6.9 ±0.04	(9.5 ±0.3[f])	6.0 ±0.6	6.9±0.7[k]
^{124}Sb	5.6 ±0.3[j]		5.6 ±0.6	23.1±2.3[l]
^{124}I	2.2 ±0.1	(3.0 ±0.1[f])	2.2 ±0.2	5.5±0.5[k]
^{125}Xe	6.3 ±2.3	6.4 ±1[b]	6.0 ±2.2	6.6±2.4[k]
^{126}Sb	3.7 ±0.2[j]		3.7 ±0.4	21.7±2.2[k]
^{127}Sb	7.2 ±0.4[j]		2.6 ±0.3	19.8±2.0[k]
^{127}Cs	7.7 ±0.6		7.6 ±0.8	8.7±0.9[l]
^{128}Sb	2.7 ±0.1[j]		1.9 ±0.2	20.8±2.1[k]
^{128}Ba	2.6 ±0.09	(6.5 ±0.5[d]) 6.0 ±0.3[g]	2.6 ±0.3	10.7±1.1[l]
^{129}Cs	8.3 ±2.4	(9.5 ±0.2[f])	1.8 ±0.5	7.8±2.3[l]
^{132}La	13.1 ±0.07		10.8 ±1.1	11.9±1.2[k]
^{141}Ce	6.2 ±0.3		3.5 ±0.3	14.1±1.4[l]
^{143}Ce	4.3 ±0.2	6.8 ±0.5[i] 7.1 ±0.9[h]	2.7 ±0.3	15.2±1.5[l]
^{145}Eu	4.7 ±0.08	4.0 ±0.4[i] 5.9 ±0.8[h]	1.8 ±0.2	4.8±0.5
^{147}Gd	3.8 ±2.2	3.1 ±0.3[i] 4.7 ±0.5[h]	2.4 ±1.4	3.9±2.3
^{149}Gd	5.0 ±0.7	6.5 ±1.0[h] 4.5 ±0.5[i]	0.94±0.12	5.4±0.7
^{151}Tb	8.9 ±5.7	3.4 ±0.2[h]	3.5 ±2.3	9.0±5.8
^{152}Tb	3.1 ±0.04		0.54±0.05	3.0±0.3
^{160}Er	2.7 ±0.8		2.7 ±0.8	2.7±0.8
^{166}Yb	6.2 ±0.3	4.9 ±0.5[h]	6.2 ±0.6	6.9±0.7
^{171}Lu	3.2 ±0.1	0.034±0.041[h]	1.1 ±0.1	3.7±0.4
^{173}Hf	5.2 ±0.4		2.6 ±0.3	5.1±0.5
^{182}Os	4.1 ±0.3		4.0 ±0.4	13.2±1.3
^{185}Ir	2.9 ±0.5[j]		2.8 ±0.5	9.4±1.7
^{186}Ir	2.4 ±0.9[j]		2.3 ±0.9	4.3±1.6
^{188}Ir	6.6 ±2.2[j]		4.6 ±1.6	7.2±2.5
^{190}Ir	1.1 ±0.1[j]		1.1 ±0.1	5.4±0.6
^{191}Pt	10.3 ±1.9		7.0 ±1.3	11.0±2.1
^{192}Ir	0.18±0.07[j]		0.18±0.07	10.5±3.9
^{195M}Hg	1.2 ±0.2		1.2 ±0.2	—
^{201}Pb	2.6 ±0.2		2.6 ±0.3	3.4±0.3
^{203}Pb	3.1 ±0.2		1.9 ±0.2	2.9±0.3
^{203}Bi	0.71±0.37[j]		0.71±0.37	2.0±1.1
^{204}Bi	2.9 ±0.4[j]		2.9 ±0.4	3.8±0.5
^{205}Bi	3.5 ±0.4[j]		3.3 ±0.4	3.7±0.4
^{207}Po	3.0 ±0.5		2.9 ±0.5	3.9±0.7
^{232}Pa	3.6 ±0.3		3.6 ±0.4	5.2±0.5
^{233}Pa	9.8 ±0.5		9.2 ±0.9	10.2±1.0
^{234}Pa	3.2 ±0.9		3.2 ±0.9	4.3±1.2

[a]Reference 35.
[b]Reference 36.
[c]Reference 37.
[d]Reference 38 (11.5 GeV p).
[e]Reference 39.
[f]Reference 40 (11.5 GeV p).
[g]Reference 41.
[h]Reference 3.
[i]Reference 42.
[j]Yields from chemically separated fraction.
[k]Isobaric yield from n-poor portion of charge distribution.
[l]Isobaric yield from n-rich portion of charge distribution.

Can. J. Chem. Downloaded from www.nrcresearchpress.com by 210.87.254.5 on 09/06/12
For personal use only.

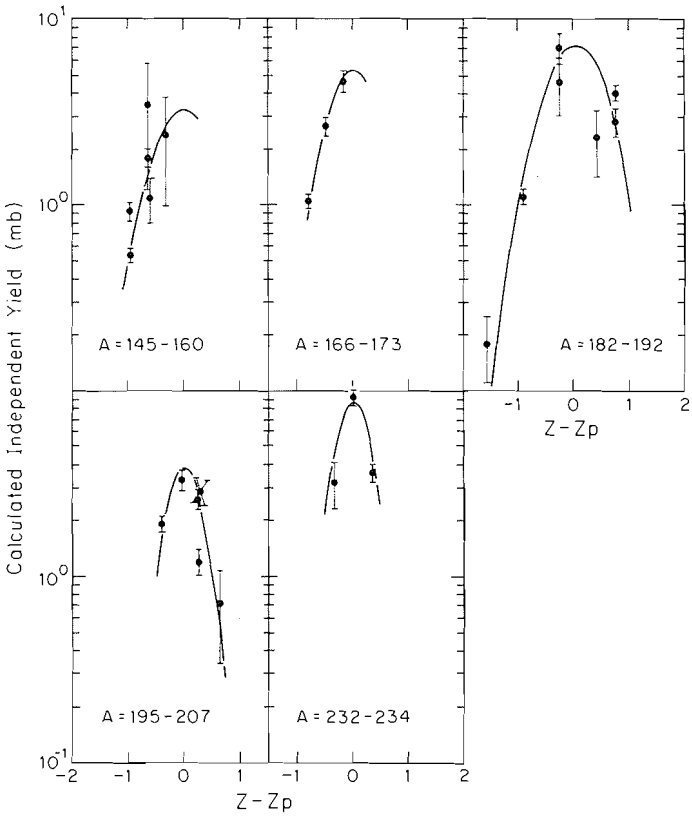

FIG. 1. The charge dispersion curves obtained in this work for the heaviest target fragments are shown as a function of the mass region of the products. The parameters that describe the center and width of the individual curves are given in Table 2.

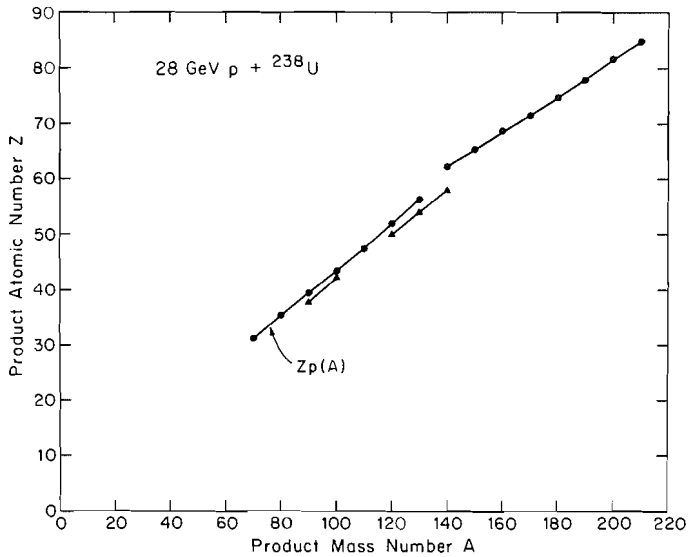

FIG. 2. The values of the most probable primary fragment charge, Z_p, as determined by fitting the data in Figs. 1 and 3 are shown as a function of product mass number. For $84 \leq A \leq 96$ and $118 \leq A \leq 143$, the Z_p corresponding to both the n-rich and n-deficient components of the charge distribution are shown.

ical yields of various elements were calculated by comparison of the separated radioactivities with those in the unseparated foil or where available, by the yield of various tracers employed in the chemistry.

The assay of the target fragment radioactivities and the calculation of measured nuclidic production cross sections from them was done using standard techniques that have been described previously (17).

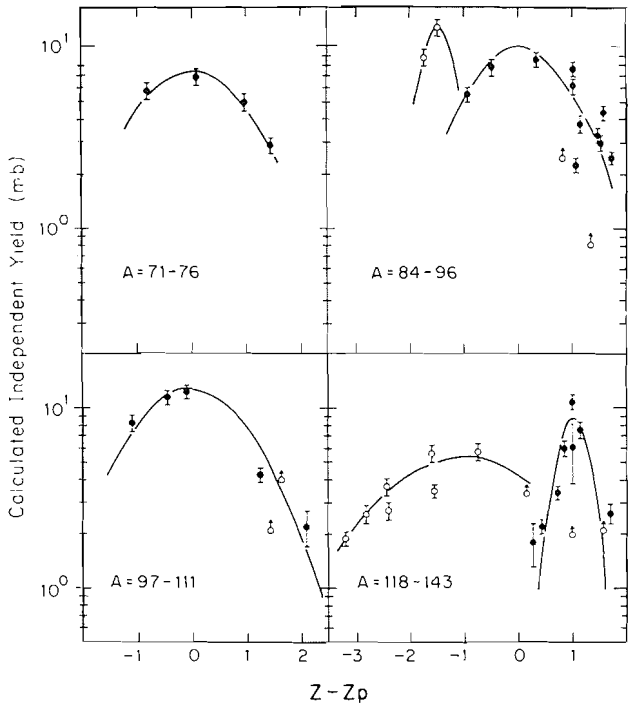

FIG. 3. The charge dispersion curves obtained in this work for the intermediate mass fragments are shown as a function of the mass region of the products.

The results of these measurements for the interaction of 28 GeV protons with ^{238}U are summarized in Table 1. Also tabulated in Table 1 for comparison with the present data are other measurements of the target fragment yields in the interaction of ^{238}U with protons of energy 11.5–29 GeV. (At proton energies above 10 GeV, the target fragment yields are known to be essentially independent of proton energy (8, 18).)

No corrections were made for reactions induced by secondary particles because we have no experimental measurement of the magnitude of the effect for our bombardment. Based upon the known systematics of such corrections (3), we would expect this correction to be very small, given the thickness of our target, for the neutron-deficient nuclides on which this paper focuses and to be 10% for the neutron-rich nuclei.

The measured cumulative-yield production cross sections (which include contributions from nuclei produced by radioactive decay) were corrected for this decay feeding by an iterative fitting of Gaussian distributions to the measured data in a manner described previously (19). These are shown in Table 1 as "calculated independent yield". In making this correction, one assumes Gaussian charge dispersions; i.e., the independent yield cross sections can be represented by a histogram that lies along a Gaussian curve, at constant mass number. This is written as:

$$[1]\quad \sigma(Z,A) = \sigma(A)\left\{[2\pi s_z^2(A)]^{-1/2}\exp\left[\frac{[Z - Z_p(A)]^2}{-2s_z^2(A)}\right]\right\}$$

with the three parameters: $\sigma(A)$ the total isobaric yield, $s_z(A)$ the Gaussian width parameter, and $Z_p(A)$ the most probable Z value for that isobar. By assuming that $\sigma(A)$ varies smoothly and slowly as a function of mass number A and is roughly constant within a small A range, one can iteratively fit the measured data, determining $Z_p(A)$ and $s_z(A)$ for limited mass regions. The results of this procedure are shown in Figs. 1, 2, and 3, with the values of $s_z(A)$ and $Z_p(A)$ being tabulated in Table 2. The values of $s_z(A)$ are believed to be known to 0.1Z units while the values of $Z_p(A)$ are believed to be known to $0.3s_z(A)$. In the mass regions (84–96, 97–111, and 118–143) where fission is an important contributor to the product yields, the charge dispersions are either very broad or double-humped, a fact previously noted (3). The

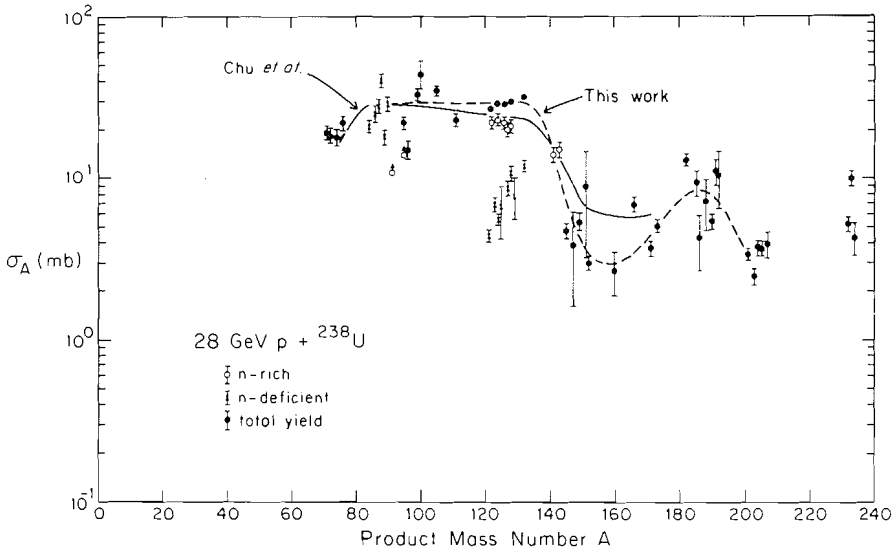

FIG. 4. The target fragment mass distribution, $\sigma(A)$ obtained in this work for the interaction of 28 GeV protons with U is shown along with the previous radiochemical data (3). Closed circles represent the total isobaric yield while the open circles and crosses represent the isobaric yield of the n-rich and n-deficient species at a given A value. The dashed line is to guide the eye through the data of this work.

TABLE 2. Charge dispersion parameters[a]

Mass number range	s_z	$Z_p(A) = a + bA$	
		a	b
71–76	1.00	−0.380	0.450
84–96 neutron-rich	0.300	−1.69	0.439
84–96 neutron-deficient	0.900	−2.600	0.410
97–111	1.00	−1.00	0.439
118–143 neutron-rich	1.50	0.750	0.410
118–143 neutron-deficient	0.300	0.380	0.429
145–160	0.500	15.8	0.330
166–173	0.500	15.35	0.330
182–192	0.500	15.2	0.330
195–207	0.300	15.4	0.330
232–234	0.300	7.80	0.368

[a] $s_z(A)$ was taken to be roughly independent of A over a small A range and $Z_p(A)$ was represented by a linear function of A over the same range.

isobaric or mass yield for each data point was calculated (19) and the resulting fragment mass distribution is shown in Fig. 4 and Table 1 along with the previously published work of Chu *et al.* (3).

Results and discussion

Heavy fragment yields

The primary focus of this paper is on the yields of the heavy ($160 \leq A \leq 210$) fragments produced by the interaction of 28 GeV p with ^{238}U. However, since the yields of many of these fragments were measured by off-line γ-ray spectroscopy of chemically separated fractions in which the chemical yields were determined by comparisons with the radionuclide activities in the unseparated foils, the accuracy of the heavy fragment measurements is directly related to the accuracy of all the radionuclide activity measurements. In Fig. 5, we compare the measured cumulative yield radionuclide production cross sections from this work with values determined previously for this or similar reactions (data from Table 1). The average ratio of the cross sections measured in this work to those determined previously is 1.10, indicating overall general agreement between this work and previous work. There is, however, a

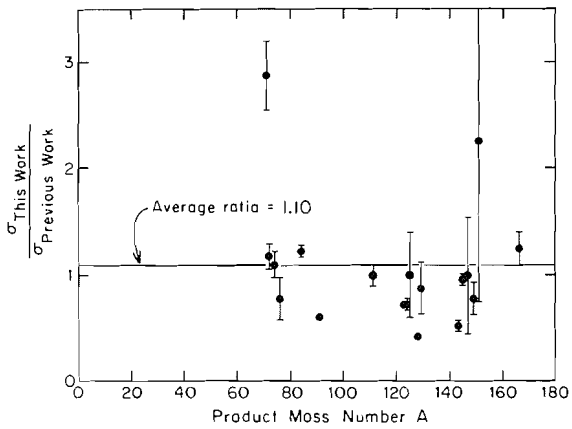

FIG. 5. The ratio of the measured nuclidic production cross sections in this work to those measured previously (see Table 1).

certain scatter to the ratios perhaps due to the fact that the values reported herein were the results of a single measurement rather than the combination of many measurements as frequently reported in the past.

The measured cumulative-yield radionuclide production cross sections for species with $173 \leq A \leq 207$ range, in general, from 1 to 10 mb, indicating without a doubt that these fragments are produced in significant yields in the interaction of 28 GeV p with ^{238}U. The charge dispersions for the species with $182 \leq A \leq 207$ are moderately well-defined (Fig. 1) and thus the isobaric yields derived from them (Fig. 4) of 5–10 mb for these fragments appear to be reasonably well established (they do significantly exceed the measured radionuclide production cross sections because of the correction for unobserved members of the mass chains). The production of these heavy fragments is, therefore, a process with a total cross section of ~250 mb. In any case, the yields of these fragments are significantly higher than would be expected for fission fragments based upon the shapes of the single fragment mass spectra (3, 13, 14), which show a pattern of sharply decreasing yields from $A = 120$ to $A = 170$ (where the isobaric yields are ~5 mb).

Given the existence of significant yields of fragments with

Can. J. Chem. Downloaded from www.nrcresearchpress.com by 210.87.254.5 on 09/06/12
For personal use only.

Can. J. Chem. Downloaded from www.nrcresearchpress.com by 210.87.254.5 on 09/06/12
For personal use only.

$160 \leq A \leq 210$, the question arises as to the mechanism for their formation. High energy proton induced reactions have generally been described in the framework of a two-step model in which the reaction proceeds via a first step of a fast intranuclear cascade as the incident proton interacts with the target nucleons followed by a slower second step in which the target residue of the first step deexcites by emission of nucleons or light nuclei or fission. Conventional intranuclear cascade calculations (20–22) of the first step of the reaction have been restricted to projectile energies of ~1000 MeV/u where only single isobar or pion production is considered. Other calculational models for the first step of the reaction, such as the abrasion–ablation (23) or firestreak models (24, 25), which do work properly at projectile energies above 1000 MeV/u are not appropriate for proton-induced reactions. (In the firestreak model the incident proton is divided into collinear tubes leading to the stopping of pieces of the proton in the target, an unrealistic situation, while the abrasion–ablation model is generally thought (24) to treat the excitation energy given to the target residue in an overly simplistic and erroneous manner.) Thus we do not have a realistic calculational model for treating the first step of the reaction between a 28 GeV proton and a ^{238}U nucleus.

Nonetheless we have attempted to pursue the question of the origin of the heavy ($160 \leq A \leq 210$) fragments in a didactic manner. We have assumed an initial distribution of target fragment mass, charge, and excitation energy as might be appropriate for the first, fast stage of the p–U collision and then attempted to compute the final product distribution after deexcitation of these primary residues. In doing so, we can show the types of events that could lead to products in the $160 \leq A \leq 210$ region. Figure 6 shows the shape of the assumed fragment distribution from the 28 GeV p + ^{238}U reaction after the first, fast step of the reaction. (This distribution is predicted by the firestreak model (25) for the 28 GeV p + ^{238}U reaction; a very similar distribution is predicted by the VEGAS intranuclear cascade code (20) for the interaction of 1 GeV protons with ^{238}U.) The charge distributions associated with the A and E^* distributions of Fig. 6 are generally centered about the valley of β-stability.

The deexcitation of the members of this initial fragment distribution was calculated using the EVA3 code of McGaughey and Morrissey (26). EVA3 is a modification of the original stepwise Monte Carlo treatment (27–29) of the deexcitation of nuclei by particle emission and fission known as the DFF code. The original DFF code was modified to include a more realistic treatment of fission competition. The excitation energy (E^*) dependence of Γ_f/Γ_n is given by (30)

$$[2]\quad \Gamma_f/\Gamma_n = \frac{4A^{2/3}a_f(E^* - B_n)}{[K_0 a_n 2a_f^{1/2}(E^* - E_f)^{1/2} - 1]} \times \exp\left[2a_n^{1/2}(E^* - B_n) - 2a_f^{1/2}(E^* - E_f)^{1/2}\right]$$

where Γ_f and Γ_n are the fission and neutron emission widths, respectively, A the mass number of the nucleus with excitation energy E^*, neutron binding energy B_n, fission barrier height E_f, and K_0 is the rms value of the projection of the angular momentum on the nuclear axis of symmetry. The values of the level density parameters at the fission saddle point a_f, and the equilibrium deformation a_n, were chosen in a manner discussed later. The fission barrier heights are calculated using the simple approximate formula of Cohen and Swiatecki (31)

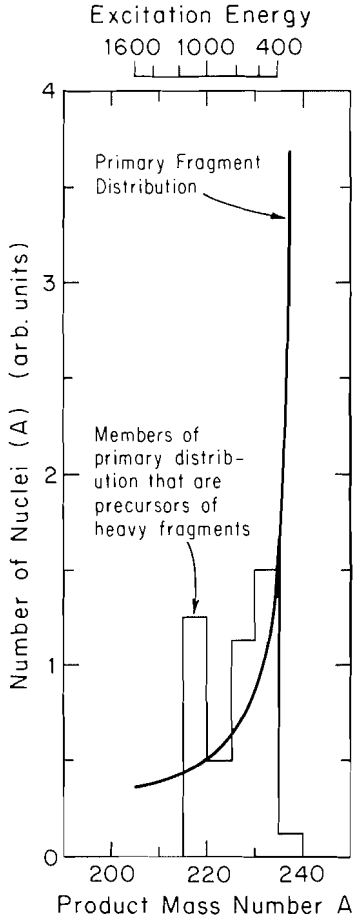

FIG. 6. The shape of the initial primary fragment distribution as a function of product mass number after the fast step of the reaction of 28 GeV p + ^{238}U. Also shown are those members of the initial distribution which deexcited to produce final fragments with $160 \leq A \leq 210$.

$$[3]\quad \begin{aligned} E_f &= 0.38\,(0.75 - x)E_s^0 && \text{for } 1/3 \leq x \leq 2/3 \\ E_f &= 0.83\,(1 - x)^3 E_s^0 && \text{for } 2/3 \leq x \leq 1 \end{aligned}$$

where the fissionability parameter, x, is given by

$$[4]\quad x = \frac{Z^2}{50.88A\left(1 - 1.7826\left(\frac{A - 2Z}{A}\right)^2\right)}$$

and $E_s^0 = 17.80A^{2/3}$. The variations of the widths of the fission mass distributions as a function of the Z, A, and E^* of the fissioning system are calculated using the formalism of Nix (32).

Several thousand deexcitation chains were followed to determine which members of the initial fragment distributions, if any, survive to form fragments with final mass numbers of $160 \leq A \leq 210$. The fraction of the initial population that survives to form heavy fragments is a very sensitive function of the level density parameters a_f and a_n. In Fig. 7 we show the results of two calculations of the final fragment distributions (starting with the initial fragment distribution of Fig. 6) made with two separate assumptions about a_f/a_n, i.e., $a_f/a_n = 1.0$ and $a_f/a_n = 1.1$. (Both of these choices for a_f/a_n are reasonable for the nuclei and excitation energies encountered (30).) The yields of the heavy fragments change dramatically with this small variation in a_f/a_n, as is illustrated in Fig. 7 and was also

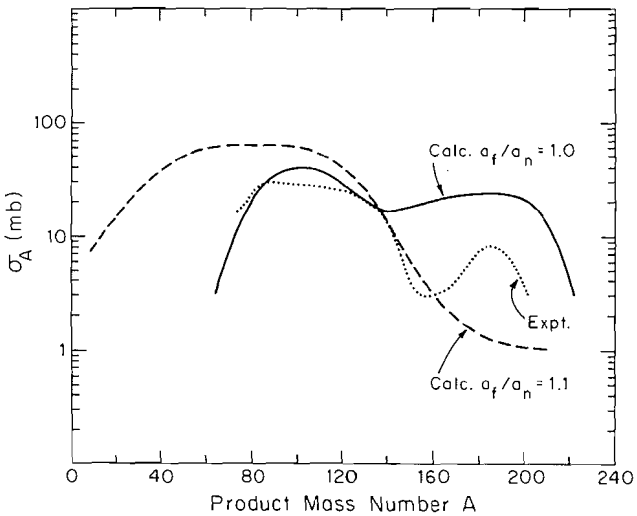

FIG. 7. The effect of two different values of a_f/a_n upon the calculated final fragment distribution is shown.

observed by Wilkins, Steinberg, and Kaufman (33). To study exactly which initial fragments survive fission decay to become heavy fragments, we arbitrarily fixed a_f/a_n using the formula

$$[5] \quad a_f = \left[1 + \frac{0.1}{\log_{10}(E^* - E_f)}\right] a_n$$

Using eq. [5] to fix the a_f/a_n ratio in our model, we then studied the outcome of ~3000 deexcitation chains to see which members of the initial fragment population survived to become heavy fragments and how they "escaped" fission. In Fig. 6 we show those members of the initial fragment population that survived to form fragments with $160 \leq A \leq 210$. As one can see from examining Fig. 6, these survivors are fairly evenly distributed in mass number from 215 to 235. Because the initial distribution falls steeply with decreasing mass number, the lower mass initial fragments from the fast first stage of the reaction must have a greater probability of surviving to become heavy fragments despite their high excitation energy. This is, of course, due to the steeply decreasing fissionability of nuclei within the Ra–Th–U region with decreasing Z and A. Due to this, the yield of heavy fragments should increase in reactions with heavy targets where a larger fraction of the initial fragment distribution has lower Z and A. Thus greater heavy fragment yields are expected in the reaction of high energy protons with ^{232}Th or in the reaction of relativistic heavy ions (which remove more mass from the target than protons) with ^{238}U.

Deexcitation chains that lead to heavy fragments generally start, especially for primary fragments of high Z and A, with copious charged particle emission (to escape the region of high fissionability) followed by long chains of successive neutron emission (as the nuclei are very n-rich due to the charged particle emission). The average deexcitation chain leading from the primary to the final heavy fragment distribution removes 53 nucleons and approximately 770 MeV of excitation energy. The average number of particles emitted is 34, with the relative abundances: n-66%, p-9%, d-9%, t-9%, ^{3}He-1%, and ^{4}He-6%. The relative numbers of particles emitted are approximately what one would expect (27) for any heavy nucleus excited to 700 MeV. One might conclude that events producing fragments with $160 \leq A \leq 210$ contain an unusually large fraction of the "deeper" spallation events from the fast initial stage of the reaction, and of these events the ones leading to heavy fragment survivors consist of those which happen to begin their deexcitation by emitting several charged particles rather than fissioning.

Fission fragment yields

The most important new data reported in this paper are the yields of the heavy fragments from the interaction of 28 GeV protons with ^{238}U. However, as remarked upon earlier, we did measure the yields of the fission fragments simultaneously with the heavy fragments and the two measurements are connected in a variety of ways. Figure 4 shows the isobaric yields of all the fragments (from the 28 GeV p + ^{238}U reaction) measured in this work along with a summary (3) of previous radiochemical measurements for this reaction. For the fragments with $70 \leq A \leq 140$, there is general agreement between the previous work and the isobaric yields from the current work (especially considering that the data reported herein are the result of a single measurement). The fragment yield distribution in this A region appears to have a plateau-like structure unlike the more sharply peaked fragment distribution seen (13, 34) in the reaction of 11.5 GeV protons with ^{238}U. Some fragments with $A < 70$ were observed as well, however the quality of the data was not as high as for the heavier fragments, so these data are not included.

In the fragment mass region $140 \leq A \leq 160$, there is general agreement between the *measured* cumulative yield cross sections of this work and previous work (Table 1, Fig. 5) but disagreement exists as to the isobaric yields that should be deduced from the measured data. The charge dispersions fitted to the data in this work are not well-defined because of the lack of measurements of *very* neutron-deficient and any possible neutron-rich species. In previous work (3), the charge distribution for $A = 147$ was found to be double humped with significant neutron-deficient and neutron-rich components. The neutron-rich nuclides seen by Chu *et al.* (3) were not seen in this work and thus we have no evidence for a broad double-humped charge dispersion in this work. Therefore we conclude that any discrepancies between the isobaric yields measured in this work and previous work are more apparent than real. These discrepancies serve as a warning about the difficulty of deducing fragment isobaric yields in a complex reaction without an extensive set of primary measured radionuclide yields.

Conclusion

The principal things we have learned from this study are:

(1) Heavy fragments ($160 \leq A \leq 210$) are produced with significant yields in the interaction of 28 GeV protons with ^{238}U.

(2) These heavy fragments could result from primary fragments that have emitted large numbers of charged particles early in their deexcitation and could represent the "deeper" spallation portions of the primary fragment distribution.

(3) We would expect larger production cross sections of heavy residues for proton induced reactions with lighter targets such as ^{232}Th or ^{208}Pb, or for heavy-ion induced reactions with ^{238}U.

Acknowledgements

We wish to thank Marilyn Rodder for her help in performing the chemical separations and Dr. J. B. Cumming for arranging the AGS irradiation and the shipment of the sample to LBL.

This work was supported by the Director, Office of Energy

Can. J. Chem. Downloaded from www.nrcresearchpress.com by 210.87.254.5 on 09/06/12
For personal use only.

Research, Division of Nuclear Physics of the Office of High Energy and Nuclear Physics of the U.S. Department of Energy under Contract DE-AC03-76SF00098.

1. W. LOVELAND, R. J. OTTO, D. J. MORRISSEY, and G. T. SEABORG. Phys. Rev. Lett. **39**, 320 (1977).
2. P. L. MCGAUGHEY, D. J. MORRISSEY, W. LOVELAND, and G. T. SEABORG. Lawrence Berkeley Laboratory Report No. LBL-9711. 1980. p. 92.
3. Y. Y. CHU, E. M. FRANZ, G. FRIEDLANDER, and P. J. KAROL. Phys. Rev. C**4**, 2202 (1971).
4. J. B. CUMMING, G. FRIEDLANDER, J. HUDIS, and A. M. POSKANZER. Phys. Rev. **127**, 950 (1962); J. B. CUMMING. Private communication.
5. R. BRANDT. Radiochim. Acta, **16**, 148 (1972).
6. S. K. CHANG and N. SUGARMAN. Phys. Rev. C**8**, 775 (1973).
7. K. BEG and N. T. PORILE. Phys. Rev. C**3**, 1631 (1971).
8. O. SCHEIDEMANN and N. T. PORILE. Phys. Rev. C**14**, 1534 (1976).
9. J. A. PANONTIN and N. T. PORILE. J. Inorg. Nucl. Chem. **3**, 1775 (1970).
10. M. LAGARDE-SIMONOFF and G. N. SIMONOFF. Phys. Rev. C**20**, 1498 (1979).
11. Y. W. YU and N. T. PORILE. Phys. Rev. C**7**, 1597 (1973).
12. J. B. CUMMING and K. BACHMANN. Phys. Rev. C**6**, 1362 (1972).
13. B. D. WILKINS, E. P. STEINBERG, and S. B. KAUFMAN. Phys. Rev. C**19**, 856 (1979).
14. L. P. REMSBERG, F. PLASIL, J. B. CUMMING, and M. L. PERLMAN. Phys. Rev. **187**, 1597 (1969).
15. Y. W. YU, N. T. PORILE, R. WARASILA, and O. A. SCHAEFFER. Phys. Rev. C**8**, 1091 (1973).
16. J. V. KRATZ, J. O. LILJENZIN, and G. T. SEABORG. Inorg. Nucl. Chem. Lett. **10**, 951 (1974).
17. D. J. MORRISSEY, D. LEE, R. J. OTTO, and G. T. SEABORG. Nucl. Inst. Meth. **158**, 499 (1979).
18. P. M. STARZYK and N. SUGARMAN. Phys. Rev. C**8**, 1448 (1973).
19. D. J. MORRISSEY, W. LOVELAND, M. DE SAINT-SIMON, and G. T. SEABORG. Phys. Rev. C**21**, 1783 (1980).
20. K. CHEN, Z. FRAENKEL, G. FRIEDLANDER, J. R. GROVER, J. M. MILLER, and Y. SHIMAMOTO. Phys. Rev. **166**, 949 (1969).
21. G. D. HARP. Phys. Rev. C**10**, 2387 (1974).
22. H. W. BERTINI, A. H. CULKOWSKI, O. W. HERMANN, N. B. GOVE, and M. P. GUTHRIE. Phys. Rev. C**17**, 1382 (1978).
23. J. D. BOWMAN, W. J. SWIATECKI, and C. F. TSANG. Lawrence Berkeley Laboratory Report No. LBL-2908, 1973; D. J. MORRISSEY, W. R. MARSH, R. J. OTTO, W. LOVELAND, and G. T. SEABORG. Phys. Rev. C**18**, 1267 (1978).
24. W. D. MYERS. Nucl. Phys. A**296**, 117 (1978); J. GOSSETT, J. I. KAPUSTA, and G. D. WESTFALL. Phys. Rev. C**18**, 844 (1978).
25. P. L. MCGAUGHEY, D. J. MORRISSEY, and G. T. SEABORG. Lawrence Berkeley Laboratory Report No. LBL-11588, 1981. p. 159.
26. P. L. MCGAUGHEY and D. J. MORRISSEY. Private communication.
27. I. DOSTROVSKY, P. RABINOWITZ, and R. BIVINS. Phys. Rev. **111**, 1659 (1958).
28. I. DOSTROVSKY, Z. FRAENKEL, and P. RABINOWITZ. Proc. 2nd UN Int'l Conf. Peaceful Uses of At. Energy **15**, 301 (1958).
29. I. DOSTROVSKY, Z. FRAENKEL, and G. FRIEDLANDER. Phys. Rev. **116**, 683 (1959).
30. R. VANDENBOSCH and J. R. HUIZENGA. Nuclear fission. Academic, New York. 1973. p. 233.
31. S. COHEN and W. J. SWIATECKI. Ann. Phys. NY, **22**, 406 (1963).
32. J. R. NIX. Nucl. Phys. A**130**, 241 (1969).
33. B. D. WILKINS, E. P. STEINBERG, and S. B. KAUFMAN. Phys. Rev. C**19**, 856 (1979).
34. Y. W. YU. Phys. Rev. C**22**, 933 (1980).
35. G. FRIEDLANDER. Physics and chemistry of fission. Vol. II. 1965. p. 265.
36. J. HUDIS, T. KIRSTEN, R. W. STOENNER, and O. A. SCHAEFFER. Phys. Rev. C**1**, 2019 (1970).
37. E. M. FRANZ and G. FRIEDLANDER. Phys. Rev. C**4**, 1671 (1971).
38. K. BEG and N. T. PORILE. Phys. Rev. C**10**, 167 (1974).
39. N. T. PORILE. Phys. Rev. **148**, 1235 (1966).
40. Y. W. YU and N. T. PORILE. Phys. Rev. C**10**, 167 (1974).
41. Y. Y. CHU, E. M. FRANZ, and G. FRIEDLANDER. Nucl. Phys. B**40**, 428 (1972).
42. K. BACHMANN. J. Inorg. Nucl. Chem. **32**, 1 (1970).

Can. J. Chem. Downloaded from www.nrcresearchpress.com by 210.87.254.5 on 09/06/12
For personal use only.

Some new amide complexes of thorium tetrachloride and *N*-thiocyanate

KENNETH W. BAGNALL, XING-FU LI, PO-JUNG PAO, AND ABDUL-GHANY MOHAMMAD AL-DAHER
Chemistry Department, University of Manchester, Manchester M13 9PL, England

Received August 31, 1982

This paper is dedicated to Professor Leo Yaffe on the occasion of his 65th birthday

KENNETH W. BAGNALL, XING-FU LI, PO-JUNG PAO, and ABDUL-GHANY MOHAMMAD AL-DAHER. Can. J. Chem. **61**, 708 (1983).

The amide complexes $[ThCl_4L_3]$, where L = $CH_3CON(CH_3)_2$ (dma), $C_2H_5CON(CH_3)_2$ (dmpa), $C_2H_5CON(C_2H_5)_2$ (depa), or $(CH_3)_3CCON(CH_3)_2$ (dmpva), $[Th(NCS)_4L_4]$, where L = dmpa, depa, dmiba ($(CH_3)_2CHCON(CH_3)_2$), or dmpva, and $[Th(NCS)_4(dmpva)_3]$ have been prepared and their ir spectra reported. The observations are discussed in terms of the steric crowding about the thorium atom using a cone-packing model.

KENNETH W. BAGNALL, XING-FU LI, PO-JUNG PAO et ABDUL-GHANY MOHAMMAD AL-DAHER. Can. J. Chem. **61**, 708 (1983).

On a préparé des complexes d'amide des types $[ThCl_4L_3]$ où L = $CH_3CON(CH_3)_2$ (dma), $C_2H_5CON(CH_3)_2$ (dmpa), $C_2H_5CON(C_2H_5)_2$ où $(CH_3)CCON(CH_3)_2$ (dmpva), $[Th(NCS)_4L_4]$ où L = dmpa, depa, dmba $(CH_3)_2$), dmpva et $[Th(NCS)_4(dmpva)_3]$ et on rapporte leurs spectres ir. On discute des observations en termes d'encombrement stérique autour de l'atome de thorium en utilisant un modèle d'entassement dans un cone.

[Traduit par le journal]

Introduction

N,*N*-Dialkylamide complexes of thorium tetrachloride, $[ThCl_4L_x]$, where $x = 2$ (L = $(CH_3)_3CCON(CH_3)_2$, dmpva (1)), 3 (L = dmiba (1)), or 4 (L = $HCON(CH_3)_2$, dmf (2) or $CH_3CON(CH_3)_2$, dma (3)) have been recorded, whereas uranium tetrachloride forms bis complexes with the bulkier ligands dmiba, dmpva (1), $C_2H_5CON(CH_3)_2$ (dmpa), and $C_2H_5CON(C_2H_5)_2$ (depa) (4), as well as compounds of composition $UCl_4.2.5L$ (L = dmf (5), dma (6), dmpa, and depa (4)). An x-ray crystal structure determination has shown that $UCl_4.2.5$depa is ionic, $[UCl_3(depa)_4]^+[UCl_5(depa)]^-$, and that the coordination geometry about the 7-coordinate uranium atom in the complex cation is pentagonal bipyramidal (4). In the corresponding complexes of the *N*-thiocyanate, $[U(NCS)_4L_x]$ ($x = 4$, L = dma (7), dmpa or dmiba (8), and $x = 3$, L = dmiba and dmpva (acetone solvate) (8)), the coordination geometry in $[U(NCS)_4(dmiba)_3]$ has also been shown to be pentagonal bipyramidal (8). In contrast to uranium, the only recorded amide complex of thorium thiocyanate appears to be $[Th(NCS)_4(dma)_4]$ (3). It was therefore of interest to attempt the synthesis of complexes formed by thorium tetrachloride and tetrathiocyanate with a series of amides of increasing bulk and to correlate the results in terms of the cone angle approach which we described briefly in a recent paper (9).

Experimental

The handling of air- and moisture-sensitive products and the drying of solvents was carried out as described previously (10). $ThCl_4$ (11), $[ThCl_4(dma)_4]$ (3), and the amides used as ligands (1) were prepared by published methods. Hydrated Cs_2ThCl_6 was prepared from aqueous HCl (17) and dehydrated by heating with thionyl chloride under reflux.

Physical measurements

Infrared spectra were recorded over the range 4000–625 cm^{-1} (NaCl plates) using a Perkin Elmer 257 or Pye Unicam SP3-200 instrument, and for the range 4000–200 cm^{-1} (CsI plates) a Perkin Elmer 225 spectrometer was used. The samples were mounted as Nujol mulls or recorded in dichloromethane solution, using the solvent as the standard. ^{1}H-nmr spectra were recorded for CD_2Cl_2 or d^8-thf solutions using a 60 MHz Perkin Elmer 12B and a 220 MHz PE R34 spectrometer. X-Ray powder photographs of finely divided samples were obtained using a Debye Scherrer 19 cm camera with CuKα radiation (λ = 1.54178 Å).

Analyses

Elemental analyses (C, H, N, Cl, S, Th) were carried out by Mr. M. Hart and staff of the microanalysis laboratory of the Chemistry Department. The chemical analyses are summarized in Table 1.

Preparation of the complexes

(1) $[ThCl_4L_3]$ (L = dmpa, depa, and dmpva)

(*i*) $ThCl_4$ (0.5015 g, 1.345 mmol) was dissolved in thf (30 cm^3); the solution was centrifuged after stirring (10 min) and any insoluble material was discarded. A large excess of dmpa (1 g, 10 mmol) was added and, after stirring for 8 h, the solution was vacuum evaporated to 5 cm^3. A mixture of *n*-pentane and toluene (10 cm^3, 2:1 v/v) was then added to precipitate the white product. The precipitate was washed with the above mixed solvent (2×5 cm^3), then with *n*-pentane (5 cm^3) and vacuum dried. Yield, 40%. $[ThCl_4(depa)_3]$ was prepared in exactly the same way (yield, 40%), whereas for $[ThCl_4(dmpva)_3]$ the thf solution of $ThCl_4$ was vacuum evaporated to dryness before the addition of dmpva (yield, 70%). $[ThCl_4(dmpa)_3]$, $[ThCl_4(dmpva)_3]$, and the known complexes $[ThCl_4(dmiba)_3]$ and $[ThCl_4(dma)_4]$ were also prepared by stirring Cs_2ThCl_6 (1 g, 1.4 mmol) with a large excess of ligand (3 g) overnight. The filtrate was diluted with dichloromethane (~5 cm^3), filtered, and the filtrate was evaporated to small volume (~2 cm^3) and the complexes were then precipitated by the addition of *n*-pentane. Yields, ca. 30%. Alternatively, the reaction of the amide with Cs_2ThCl_6 was carried out using a mixture of acetone and the ligand in the same way; after stirring for 3 days the resulting solution was treated as before. Yields, ca. 30%.

(2) $[ThCl_4(dma)_3]$

$[ThCl_4(dma)_4]$ (1 g, 1.39 mmol) was dissolved in thf (10 cm^3) and stirred (20 min). Addition of a mixture of *n*-pentane and toluene (10 cm^3, 2:1 v/v) precipitated a white solid which was redissolved in thf (10 cm^3) and reprecipitated as above (two cycles). The final product was washed with *n*-pentane (5 cm^3) and vacuum dried. Yield, 40%.

(3) $[Th(NCS)_4L_4$ (L = dmpa, depa, and dmiba)

Can. J. Chem. Downloaded from www.nrcresearchpress.com by 210.87.254.105 on 09/06/12
For personal use only.

TABLE 1. Chemical analyses (%)*

Complex	Th	C	H	N	S	Cl
$[ThCl_4(dma)_3]$	37.1	21.9	4.2	6.4	—	21.2
	(36.5)	(22.7)	(4.3)	(6.6)	—	(22.3)
$[ThCl_4(dmpa)_3]$	34.3	26.6	4.8	6.0	—	19.5
	(34.3)	(26.6)	(4.9)	(6.2)	—	(20.9)
$[ThCl_4(depa)_3]$	30.6	33.1	6.0	5.6	—	18.3
	(30.5)	(33.1)	(6.0)	(5.5)	—	(18.6)
$[ThCl_4(dmpva)_3]$	29.7	33.0	6.0	5.5	—	18.0
	(30.5)	(33.1)	(6.0)	(5.5)	—	(18.6)
$[Th(NCS)_3(dmpa)_4]$†	26.5	33.0	5.1	12.9	14.1	—
	(26.7)	(33.2)	(5.1)	(12.9)	(14.8)	—
$[Th(NCS)_4(depa)_4]$†	22.9	39.2	6.4	11.3	12.7	—
	(23.7)	(39.2)	(6.2)	(11.4)	(13.1)	—
$[Th(NCS)_4(dmiba)_4]$†	25.4	37.0	6.0	11.4	12.9	—
	(25.1)	(36.4)	(5.7)	(12.1)	(13.9)	—
$[Th(NCS)_4(dmpva)_4]$	24.9	37.9	5.9	11.5	13.7	—
	(24.5)	(36.7)	(6.3)	(11.8)	(13.5)	—
$[Th(NCS)_4(dmpva)_3]$	26.9	35.3	5.3	10.7	14.8	—
	(27.2)	(35.2)	(5.3)	(11.5)	(15.1)	—

*Calculated analytical figures in parentheses.

†Well crystalline specimens of these thiocyanate compounds gave low thorium analyses, probably because of free solvent trapped in the crystal lattice.

(*i*) Solid KNCS (0.4883 g, 5.0246 mmol) was added to a suspension of $[ThCl_4(dmpa)_3]$ (0.8505 g, 1.2557 mmol) in thf (30 cm^3). After stirring for 2 h, dmpa (~0.5 g, 5 mmol) was added, and the mixture was stirred for 24 h. The mixture was then centrifuged and the supernatant liquid was vacuum evaporated to dryness. The solid so obtained was washed with a mixture of *n*-pentane and toluene (3 × 5 cm^3, 2:1 v/v), then dissolved in dichloromethane. After centrifugation the supernatant liquid was vacuum evaporated to dryness and finally vacuum dried for 8 h. Yield, 40%.

(*ii*) Solid KNCS (0.3225 g, 3.3185 mmol) was added to a solution of $ThCl_4$ (0.3103 g, 0.830 mmol) in thf (30 cm^3). After stirring for 2 h, dmpa (1 g, 10 mmol) was added, after which the procedure described in (*i*) was followed. Yield, 40%.

$[Th(NCS)_4(depa)_4]$ and $[Th(NCS)_4(dmiba)_4]$ were prepared in the same way as $[Th(NCS)_4(dmpa)_4]$ and were obtained in similar yield. The depa complex was also prepared from Cs_2ThCl_6; KNCS (0.55 g, 5.2 mmol) was added to Cs_2ThCl_6 (1 g, 1.4 mmol) in acetone (20 cm^3). After stirring for 2 h, an excess (2 g, 15.5 mmol) of depa was added and the mixture was stirred for 24 h. The filtrate was evaporated to dryness, the residue was washed with a mixture of *n*-pentane and toluene and dissolved in dichloromethane as in (*i*), and the final solution was evaporated to small volume. Colourless crystals of the complex separated from this solution on addition of the *n*-pentane–toluene mixture (2:1 v/v). These were washed with *n*-pentane and vacuum dried for 5 h. Yield, 25%.

(4) Attempted preparation of $[Th(NCS)_4(dmiba)_3]$

$[U(NCS)_4(dmiba)_3]$ is obtained (8) by adding a mixture of *n*-pentane and toluene (2:1 v/v) to a solution of $[U(NCS)_4(dmiba)_4]$ in dichloromethane until a cloudiness develops, followed by dropwise addition of dichloromethane to clear the solution; on standing the product crystallises out in poor yield. The same procedure left $[Th(NCS)_4(dmiba)_4]$ unaffected.

(5) $[Th(NCS)_4(dmpva)_4]$ and $[Th(NCS)_4(dmpva)_3]$

$[Th(NCS)_4(dmpva)_4]$ was prepared in the same way as the dmpa complex (method (*ii*) above); during the evaporation of the thf solution to 5 cm^3 volume, a yellowish-white solid separated which had the approximate composition $Th(NCS)_4.5dmpva$. However, on completing the dichloromethane/*n*-pentane cycle described for method 3 (*ii*) white $[Th(NCS)_4(dmpva)_4]$ was obtained. Yield, 40%. When this product was dissolved in toluene, in which it is only slightly soluble, and the solution was evaporated to small volume, then treated with *n*-pentane, the white tris complex, $[Th(NCS)_4(dmpva)_3]$, precipitated. Yield, 30%.

Results and discussion

Thorium tetrachloride complexes

As mentioned in the introduction, the stoichiometries of the three known amide complexes of thorium tetrachloride, $[ThCl_4L_x]$, are 1:4 (L = dma (3)), 1:3 (L = dmiba (1)), and 1:2 (L = dmpva (1)) which suggests that the stoichiometry of the complex formed depends on the bulk of the amide ligand. Calculation of the values of the total cone angle factors,[1] Σc.a.f., for these compounds, following the procedure outlined in ref. 9, indicated that the thorium environment in $[ThCl_4(dma)_4]$ was overcrowded (Σc.a.f. ~ 0.92), whereas in $[ThCl_4(dmiba)_3]$ the value of Σc.a.f. was 0.82, in the stable region, and for $[ThCl_4(dmpva)_2]$ Σc.a.f. was calculated to be only 0.72, indicating a marked degree of undercrowding. These calculations suggested that amide complexes of composition $[ThCl_4L_3]$ should be the most stable with respect to the loss or gain of a molecule of ligand in the $ThCl_4$/amide systems.

In considering the equilibria:

$$[ThCl_4L_2] + L \rightleftharpoons [ThCl_4L_3]$$
$$K_3 = [ThCl_4L_3]/[ThCl_4L_2][L]$$

and

$$[ThCl_4L_3] + L \rightleftharpoons [ThCl_4L_4]$$
$$K_4 = [ThCl_4L_4]/[ThCl_4L_3][L]$$

[1]Two terms are used to describe steric effects. Firstly, the cone angle factor (c.a.f.), which is the solid angle of the cone comprising the metal center at the apex and the primary co-ordinating atom or the complete ligand, divided by 4π. Secondly, there is the fan angle which describes the crowding in the plane; this is the angle subtended by the primary co-ordinating atom (f.a.) or the whole ligand (f.a.s.) in the various symmetry planes. For further discussion, see ref. 9.

Can. J. Chem. Downloaded from www.nrcresearchpress.com by 210.87.254.105 on 09/06/12
For personal use only.

TABLE 2. Infrared spectra, cm^{-1}

Complex	Nujol mull		thf solution		CH_2Cl_2 solution	
	ν_{CO}	$\Delta\nu_{CO}$	ν_{CO}	$\Delta\nu_{CO}$	ν_{CO}	$\Delta\nu_{CO}$
$[ThCl_4(dma)_3]$	1600	50	1600	50	1590	60
			1650(vw)	0		
$[ThCl_4(dmpa)_3]$	1600	50	1600	50	1590	60
			1650	0		
$[ThCl_4(depa)_3]$	1580	70	1570	80	1570	80
	1610	40	1650	0	1630	20
$[ThCl_4(dmiba)_3]$	1585	65	1590	60	1590	60
			1650	0	1640	10
$ThCl_4.2.5dmiba$	1590	60	1590	60	—	
			1650(vw)	0		
$[ThCl_4(dmpva)_3]$	1560(b)	70	1555	75	—	
			1630	0	—	
$[Th(NCS)_4(dmpa)_4]$	1590	60	1575	75	1590	60
			1650	0		
$[Th(NCS)_4(depa)_4]$	1580	70	1585	65	1575	75
			1650	0		
$[Th(NCS)_4(dmiba)_4]$	1580	70	1590	60	1590	60
			1650	0	1630(vw)	20
$[Th(NCS)_4(dmpva)_4]$	1565	65	1570*	60	1565	65
			1635*	−5		
$[Th(NCS)_4(dmpva)_3]$	1560	70	1565	65	1570	60
			1630	0		

*Toluene solution, 1560 cm^{-1} ($\Delta\nu$, 70 cm^{-1}) and 1610 cm^{-1} ($\Delta\nu$, 20 cm^{-1}). b = broad; vw = very weak.

one can see that the actual number of ligands bonded to the thorium atom will depend on both the ligand concentration in the preparative medium and the complexation constant, K_3 or K_4. Consequently, in order to cover a given system completely, the preparative conditions must be designed to cover not only the normal 2- to 3-fold excess of the stoichiometric requirement of the ligand in the solvent system used, but also the two extreme concentrations, [L] = 0 (solvent only) and the pure ligand. The first condition is simply established by repeatedly washing the complexes which have been isolated by the normal procedure with the solvent, or by repeated recrystallisation if the complexes have a reasonable solubility in the selected solvent, discarding the solution of the ligand released by dissociation, and the second condition is achieved by treating the solid tetrahalide with the pure ligand.

The first procedure, when applied to the known complex $[ThCl_4(dma)_4]$, led to the isolation of $[ThCl_4(dma)_3]$, whereas the second procedure yielded $[ThCl_4(dmpva)_3]$. In the cases of dmpa and depa, the tris complexes yielded products of composition close to $ThCl_4.2.8dmpa$ and $ThCl_4.2.75depa$ when repeatedly washed with thf, and the known (1) $[ThCl_4(dmiba)_3]$ under similar treatment yielded a product of composition close to $ThCl_4.2.5dmiba$, which may be analogous to the known complexes $UCl_4.2.5L$ (L = dmf (5), dma (6), dmpa and depa (4)). However, its X-ray powder photograph is virtually identical to that of $[ThCl_4(dmiba)_3]$. Similar treatment of $[ThCl_4(dmpva)_3]$ yielded the known $[ThCl_4(dmpva)_2]$, although the analysis of the product at an intermediate stage was close to that to be expected for $ThCl_4.2.5dmpva$.

The four new tris amide complexes are white solids, almost insoluble in thf, except for $[ThCl_4(dmpva)_3]$, which has an appreciable solubility, and all are insoluble in acetone and in hydrocarbons, but are soluble in dichloromethane.

In their ir spectra (Table 2), the frequency of ν_{CO} for the amide ligand is decreased by 50 to 80 cm^{-1}, indicating that the amides are bonded to the metal via the carbonyl oxygen atom. In the spectra recorded for dilute solutions of the complexes in thf there is evidently some dissociation, as shown by the weak to very weak free ligand feature at 1650 cm^{-1} in all of them, but this is less marked for the complexes in dichloromethane, in which only the ir spectra of $[ThCl_4(depa)_3]$ and $[ThCl_4(dmpva)_3]$ exhibit additional features for which $\Delta\nu_{CO}$ is only 20 and 10 cm^{-1} respectively, suggesting weakly bonded ligand and, possibly, rapid exchange between bonded and non-bonded ligand.

The ^1H-nmr spectra (Table 3) of the tris complexes, $[ThCl_4L_3]$, were recorded in CD_2Cl_2 (L = dmpa, dmiba) and in d^8-thf (L = dmpva) using TMS as standard. The small induced shifts, $\Delta\delta$, are consistent with slight deshielding of the ligand protons consequent upon electron donation from the carbonyl oxygen atoms of the ligand, and there is no appreciable difference between the spectra recorded at room (27°C) and low (−50°C) temperatures for the dmpa and dmiba complexes. In the case of $[ThCl_4(dmpva)_3]$, the room temperature spectrum shows only two resonances, whereas at −60°C the spectrum indicates that the exchange between bonded and free ligand is slow on the nmr time scale and that the barrier to rotation of the nitrogen methyl groups is increased, leading to the appearance of three main resonances for the (N)—CH_3 groups, which are a combination of the four possible resonances, and two resonances for the (C)—CH_3 groups.

Thorium thiocyanate complexes

The calculated total cone angle factor, Σc.a.f., for the tris amide complexes, $[Th(NCS)_4L_3]$, is only 0.71, indicating that such complexes are unlikely to be isolable unless the groups R

Can. J. Chem. Downloaded from www.nrcresearchpress.com by 210.87.254.105 on 09/06/12
For personal use only.

TABLE 3. ^{1}H-nmr spectra, δ ppm (27°C)*

	(C)—CH_3	—CH_2—CH	(N)—CH_3
dmpa	1.00(t)	2.22(quart)	2.82, 2.92(s)
$[ThCl_4(dmpa)_3]$	1.33(t)	2.71(quart)	3.21, 3.29(s)
Δδ, ppm	0.33	0.49	0.38
dmiba	1.05(d)	2.79(quint)	2.86, 3.00(s)
$[ThCl_4(dmiba)_3]$	1.34(d)	2.99(quint)	3.22, 3.36(s)
Δδ, ppm	0.29	0.20	0.36
dmpva	1.22(s)	—	2.97(s)
$[ThCl_4(dmpva)_3]$	1.38(s)	—	3.16(s)
Δδ, ppm	0.16	—	0.19
dmpva(−60°C)	1.22(s)	—	3.16, 2.84(s)
$[ThCl_4(dmpva)_3]$(−60°C)	1.48, 1.22(d)	—	(3.40, 3.37), 3.21, 2.90(s)
Δδ, ppm	0.24, 0	—	—

*s = singlet; d = doublet; t = triplet; quart = quartet; quint = quintet.

and/or R′ in the amide $RCON(R')_2$ are bulky, as has been found in the analogous uranium(IV) system, in which tris complexes, $[U(NCS)_4L_3]$ have been isolated only for L = dmiba and dmpva (acetone solvate) (8). The tetrakis amide complexes, $[Th(NCS)_4L_4]$ (L = dmpa, depa, dmiba, and dmpva), were prepared by treating the corresponding chloride complex, Cs_2ThCl_6(depa only), or thorium tetrachloride, with potassium thiocyanate and an excess of the ligand in thf and attempts were made to degrade the dmiba and dmpva compounds to the tris complexes.This was unsuccessful in the case of dmiba complex, but $[Th(NCS)_4(dmpva)_3]$ was obtained by dissolving $[Th(NCS)_4(dmpva)_4]$ in toluene, evaporating to small volume and then precipitating the product by addition of *n*-pentane.

Some features of the ir spectra of these complexes (Nujol mulls and solutions in thf or dichloromethane) are given in Table 2. The shifts in ν_{CO} on complexation are similar in magnitude to those observed for the corresponding chloride complexes and, like the latter, there is evidence for some dissociation of the ligand from the spectra of $[Th(NCS)_4L_4]$ in thf solution for all four ligands, and only for L = dmiba and dmpva in dichloromethane solution. The frequencies of the stretching vibrations ν_{CN} and ν_{CS} of the linear NCS ion are 2040−2045 cm^{-1} and ~740 cm^{-1} respectively for mulls, whereas ν_{CN} for solutions in thf and dichloromethane is 2010 and 2020 cm^{-1} respectively. These values are consistent with N-bonded thiocyanate groups (12−16).

Acknowledgements

The authors are indebted to Mr. M. A. Hart for the microanalyses (C, H, N, S, Cl, Th), to the Governments of the People's Republic of China (to X.-f. Li and P.-j Pao) and of Iraq (to A. G. M. Al-D.) for support.

1. K. W. BAGNALL, J. G. H. DU PREEZ, J. BAJOREK, L. BONNER, H. COOPER, and G. SEGAL. J. Chem. Soc. Dalton Trans. 2682 (1973).
2. T. MOELLER and D. S. SMITH. U.S. Report AFOSR-TN-58-559, 1958.
3. K. W. BAGNALL, D. BROWN, P. J. JONES, and P. S. ROBINSON. J. Chem. Soc. 2531 (1964).
4. K. W. BAGNALL, R. L. BEDDOES, O. S. MILLS, and X.-F. LI. J. Chem. Soc. Dalton Trans. 1361 (1982).
5. P. GANS and B. C. SMITH. J. Chem. Soc. 4177 (1964).
6. K. W. BAGNALL, A. M. DEANE, T. L. MARKIN, P. S. ROBINSON, and M. A. A. STEWART. J. Chem. Soc. 1611 (1961).
7. K. W. BAGNALL, D. BROWN, and R. COLTON. J. Chem. Soc. 2527 (1964).
8. K. W. BAGNALL, X.-F. LI, G. BOMBIERI, and F. BENETOLLO. J. Chem. Soc. Dalton Trans. 19 (1982).
9. K. W. BAGNALL and X.-F. LI. J. Chem. Soc. Dalton Trans. 1365 (1982).
10. K. W. BAGNALL, J. EDWARDS, J. G. H. DU PREEZ, and R. F. WARREN. J. Chem. Soc. Dalton Trans. 140 (1975).
11. K. W. BAGNALL, D. BROWN, P. J. JONES, and J. G. H. DU PREEZ. J. Chem. Soc. A, 737 (1966).
12. A. SABATINI and I. BERTINI. Inorg. Chem. **4**, 1665 (1965); 5, 1025 (1966).
13. S. FRONAEUS and R. LARSSON. Acta Chem. Scand. **16**, 1447 (1962).
14. S. PECILE. Inorg. Chem. **5**, 210 (1966).
15. J. LEWIS, R. S. NYHOLM, and P. W. SMITH. J. Chem. Soc. 4590 (1961).
16. A. TURCO and C. PECILE. Nature (London), **191**, 66 (1961).
17. J. R. FERRARO. J. Inorg. Nucl. Chem. **4**, 283 (1957).

Can. J. Chem. Downloaded from www.nrcresearchpress.com by 210.87.254.105 on 09/06/12
For personal use only.

The synthesis of 11*R*- and 11*S*-HETE and of 11-*R*,*S*-HPETE methyl esters

GEORGE JUST AND CORINNE LUTHE
Department of Chemistry, McGill University, Montreal, P.Q., Canada H3A 2K6

AND

MINH TAN PHAN VIET
Laboratoire Régional de R.M.N., Département de Chimie, Université de Montréal, Montréal (Qué.), Canada H3C 3V1

Received August 31, 1982

This paper is dedicated to Professor Leo Yaffe on the occasion of his 65th birthday

GEORGE JUST, CORINNE LUTHE, and MINH TAN PHAN VIET. Can. J. Chem. **61**, 712 (1983).

Methyl 11*R*- and 11*S*-hydroxyeicosa-5*Z*,8*Z*,12*E*,14*Z*-tetraenoate (**17***R*, **17***S*) (11-HETE) and the corresponding 11-hydroperoxide **19** (11-HPETE) have been prepared from readily available starting materials. The yields were approximately 25% for 11*R*,*S*-HETE, and 5% each for 11*R*- and 11*S*-HETE.

Extensive 400 MHz ^{1}H nmr studies of **17** (nOe difference, 2D *J*-resolved) were undertaken to confirm the structure. Some conformational properties are discussed.

GEORGE JUST, CORINNE LUTHE et MIN TAN PHAN VIET. Can. J. Chem. **61**, 712 (1983).

On a préparé les hydroxy-11*R* et 11*S* eicosatétraène-5*Z*,8*Z*,12*E*,14*Z* oate de méthyle (**17***R*,**17***S*) (H-11ETE) ainsi que l'hydroperoxyde-11 (**19**) (HP-11ETE) à partir de produits de départ facilement accessibles. Les rendements sont approximativement de 25% pour les H-11*R*,*S*ETE et de 5% chacun pour les H-11*R* et H-11*S* ETE.

On a fait appel à une étude poussée par rmn du ^{1}H à 400 MHz du composé **17** (différence de eOn, 2D résolu pour *J*) pour confirmer la structure. On discute de quelques propriétés conformationnelles.

[Traduit par le journal]

The total synthesis of enantiomerically pure 11-HETE has only recently been described (1–3). We wish to report full details of an expeditious synthesis of 11*R*- and 11*S*-HETE **17**, and of the corresponding 11-HPETE **19**.

Condensation of the ethoxyethylidene ether of glycidol (**8**) with the lithium anion of the methoxypropylidene ether of propargyl alcohol (**7**) gave adduct **2**, which was acetylated to provide **3**. Mild acid hydrolysis of **3**, followed by mesylation of the resulting alcohol **4**, gave **5** which provided iodide **6** upon treatment with sodium iodide.

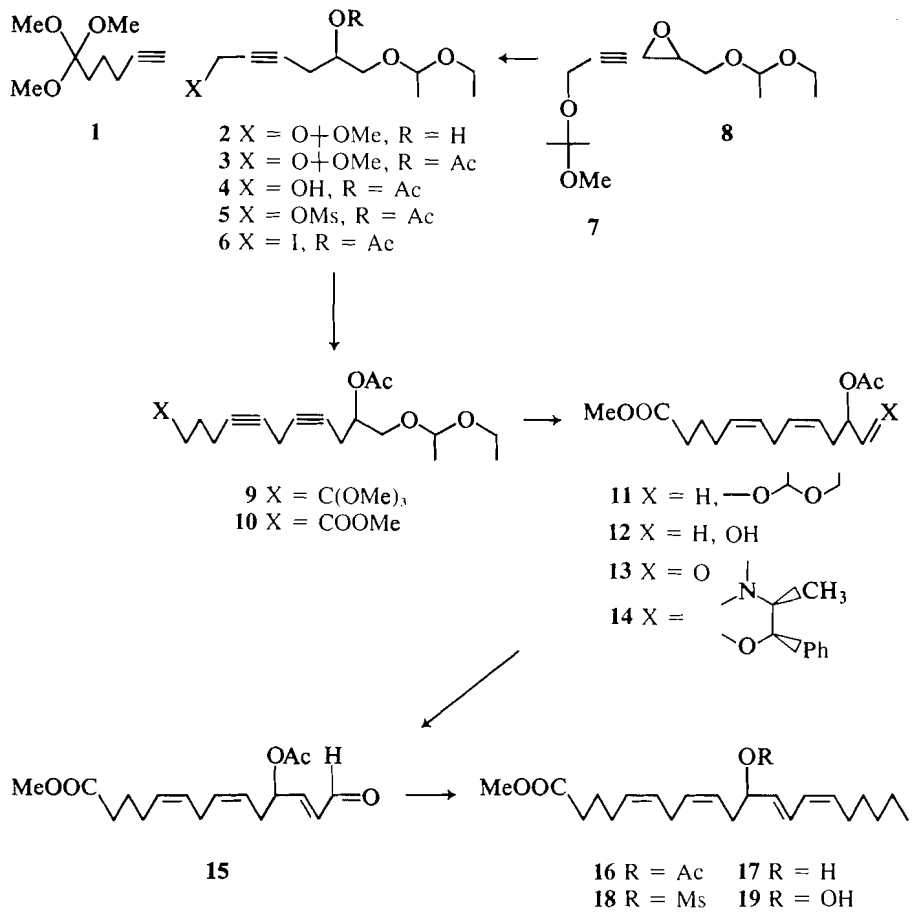

Can. J. Chem. Downloaded from www.nrcresearchpress.com by 210.87.254.5 on 09/06/12
For personal use only.

Can. J. Chem. Downloaded from www.nrcresearchpress.com by 210.87.254.5 on 09/06/12
For personal use only.

Reaction of **6** with an anionic species generated from acetylenic orthoester **1** (2) by addition of one equivalent of butyllithium and one equivalent of cuprous iodide at −78°C gave orthoester **9** in what appeared to be a quantitative yield. This reaction requires some comment since approximately 30% of **9** was formed at −30°C within a few minutes, the balance of the reaction requiring a day at room temperature. The use of less CuI gave variable yields of **9**. Some hydrolysis of the acetate function was noted so that the reaction product was routinely reacetylated. Since tlc of the product showed two spots due to hydrolysis of orthoester **9** to ester **10**, probably in part on the tlc plate but perhaps during work-up, the product was submitted to very mild acid hydrolysis at this stage to give ester **10**.

Catalytic hydrogenation with Brown's nickel boride catalyst (4), followed by acid hydrolysis, gave alcohol **12**. Up to this point, all steps had proceeded seemingly in quantitative yield, as established by tlc and nmr, and no purification beyond extractions was necessary. Nevertheless, since the next few steps all involved sensitive compounds (**13**, **14**, and **15**) which were prone to decomposition upon standing, **12** was submitted to flash chromatography to remove very minor impurities which had accumulated over the 9-step sequence. The fact that the overall yield for the sequence was only ~50% was probably due to the relative volatility of the various intermediates. Certainly, chromatography at intermediate stages did not in any way enhance either yields or purity of alcohol **12**.

Although the simultaneous hydrolysis of the orthoester and ethoxyethylidene functions in **9** could be performed, it was noted that, in contrast to diolefins **11** and **12**, diacetylenes of type **9** or **10** were very fragile molecules which at times decomposed upon mere standing, or on exposure to silica gel.

Oxidation of **12** with dimethyl sulfoxide – oxalyl chloride using the recently described method of Swern and co-workers (5) gave aldehyde *R,S*-**13**. Treatment of *R,S*-**13** with *l*-ephedrine and 10 mol% pyridinium tosylate gave a mixture of diastereomeric ephedrine derivatives **14**, which were separated by flash chromatography.

The major isomers having the highest and second highest R_f-values had the 11*R* and 11*S* configurations, respectively (3). The minor isomers (~10% each) were not isolated, although, on larger runs, this could have easily been done. Hydrolysis of **14***R* and **14***S* gave **13***R* and **13***S*, each in approximately 20% yield, based on alcohol **12**.

Subsequent elaboration of the 12*E*,14*Z* diene systems follows that described for the *tert*-butyldimethylsilyl ether (2) corresponding to acetate **13** (3), and involves reaction of **13** with formylmethylenetriphenylphosphorane (6), followed by transformation of the *E*-α,β-unsaturated aldehyde **15** with triphenylhexylphosphonium bromide to give **16**. Treatment of tetraene acetate **16** thus obtained with methanolic sodium methoxide gave 11-HETE **17**, contaminated with 10–15% of its 14*E*-isomer, which was readily removed by flash chromatography.

When the same sequence was repeated with resolved aldehydes **13***R* and **13***S*, 11*R*-**17**, $[\alpha_D^{21}]$ 11.2° (10.97° (1)) and 11*S*-**17**, $[\alpha_D^{21}]$ −11.3° (CH_2Cl_2) were obtained.

Conversion to 11-HPETE **19** was accomplished in the following manner (7): **17** was transformed to mesylate **18** at −65°C by means of methanesulfonyl chloride/NEt_3. Addition of 90% hydrogen peroxide in ether gave hydroperoxide **19** in approximately 70% yield, contaminated with what appeared to be 30% of various isomers of 15-HPETE. Purification by hplc gave 11-HPETE **19** in 10–30% yield. Its 400 MHz ^{1}H nmr spectrum was virtually indistinguishable from that of **17**, except for the 11-proton, which appeared at 4.5 ppm, 0.3 ppm downfield from that of **17**. Its structure was confirmed by reduction of **19** (70% purity) with methanolic stannous chloride. Flash chromatography gave as major product **17**, identified by gc–ms of its trimethylsilyl ether. Its ^{1}H nmr was virtually identical to that of **17** described by Corey and Kang (1).

An extensive 400 MHz ^{1}H nmr study of **17** was undertaken to establish if the molecule has a conformational preference. This goal could not be achieved. However, a complete assignment was made as described in the following. The proton signals are sufficiently dispersed so that coupling connectivities between protons could be established by use of 1D homodecoupling experiments. Chemical shifts and coupling constants (except for $^3J_{18-19}$) were measured accurately from the 1D spectrum and 2D *J*-resolved spectra and are given in Table 1. The signals of protons H6, H8, H9, and H15 overlap (Fig. 1a); however, the separated signal for each proton could be observed from the nOe difference spectra (8). For example, when H14 was irradiated, the signal of H15 was enhanced while H6, H8, and H9 were not affected; the difference spectra washed out the signals of these latter protons, and only the signal of H15 is observed (Fig. 1b). Due to the spin echo nature of *J*-resolved 2D spectroscopy and the large applied resolution enhancement factor, the small coupling constants and the small differences in coupling constants can be observed and measured. The cross section plots (Fig. 1c) of the *J*-resolved 2D spectrum show well-resolved signals for all but the H8 and H9 olefinic protons. Because of the second order effect, the two latter protons produced the complex pattern depicted in the contour plot (Fig. 1d). The coupling constants $^3J_{5-6}$, $^3J_{8-9}$, $^3J_{12-13}$, and J_{14-15} are fully consistent with the configurations of the double bonds depicted in Fig. 1 (9).

For conformationally labile molecules, nOe data do not present evidence to infer a conformational preference.[1] However, the nOe results when H13 and H14 were irradiated (nOe between H12 and H14, negligible nOe between H13 and H14) indicate that the protons H13 and H14 are *anti*, in perfect agreement with the value $^3J_{13-14}$ (9). The large nOe between H13 and H16 may suggest that the less sterically crowded conformation (C14—C15 bond *anti* to C16—C17 bond) is preferred. Positive and negative nOe were observed when protons H10 were saturated (see Table 2). Where dipole–dipole interaction is the dominant relaxation mechanism, alternating sign nOe is to be expected (10) in a series of neighboring protons. In fact, at least in one conformation, the protons H10b—H10a—H9—H8 are contiguous; for example when H10a was irradiated, the signal of proton H9 increased (positive effect) but the signal of proton H8 decreased (negative effect). The remaining nOe results may be satisfactorily interpreted in terms of the described structure.

Experimental[2]

Methoxyisopropylidene propargyl alcohol (7)

To a solution of propargyl alcohol (8.4 g, 150 mmol) in dry CH_2Cl_2 (400 mL) at 5°C under N_2 were added methoxypropene (11.9 g, 165 mmol) and pyridinium tosylate (3.77 g, 15 mmol). The reaction mixture was stirred at 5°C for 3.5 h; the product was then extracted with CH_2Cl_2 (2 × 500 mL); the CH_2Cl_2 extracts were washed with aqueous $NaHCO_3$ (4 × 50 mL), water (2 × 50 mL), and dried over $MgSO_4$.

[1]The nOe data confirm the assignment and are given in Table 2.

[2]For general procedures, see ref. 11.

TABLE 1. ^{1}H chemical shifts and coupling constants of **17**

Proton	δ(ppm)	J(Hz)
H2	2.197	H2–H3 = 7.3
H3	1.693	H3–H4 = 7.3
H4	2.067	H4–H5 = 7.3; H4–H6 = 1.3
H5	5.383	H5–H6 = 10.7; H5–H7 = 1.5
H6	5.509	H6–H7 = 7.2
H7	2.869	H7–H8 = 7.0; H7–H9≤1.0
H8	5.61	H8–H9 = 10.8; H8–H10a≤1.0; H8–H10b≤1.0
H9	5.58	H9–H10a = 7.1; H9–H10b = 6.5
H10a	2.463	H10a–H11 = 6.9; H10a–H10b = −14.0
H10b	2.377	H10b–H11 = 5.8
H11	4.195	H11–H12 = 6.0; H11–H13 = 1.4; H11–OH = 4.2
H12	5.781	H12–H13 = 15.2; H12–H14≤1.0
H13	6.801	H13–H14 = 11.1; H13–H15 = 1.1
H14	6.202	H14–H15 = 10.3; H14–H16≃1.3
H15	5.536	H15–H16 = 7.6
H16	2.259	H16–H17 = 7.4
H17	1.421	H17–H18 = 7.5
H18,H19	1.30	H19–H20 = 6.9
H20	0.969	
OCH_3	3.455	
OH	var	

The solvent was removed at atmospheric pressure and the product recovered by vacuum distillation (65°C, 43 Torr) in 70% yield; ^{1}H nmr (CCl_4) δ: 1.26 (s, 6H, $2CH_3$), 2.17 (t, 1H, $J \sim 2$ Hz, H—C≡C), 3.07 (s, 3H, OCH_3), 3.92 (d, 2H, $J \sim 2$ Hz, CH_2).

Ethoxyethylidene glycidol (8)

To a solution of glycidol (8.8 g, 120 mmol) in dry CH_2Cl_2 (400 mL) at 5°C under N_2 were added ethyl vinyl ether (17.3 g, 240 mmol) and pyridinium tosylate (3 g, 12 mmol). After half an hour the reaction mixture was warmed to room temperature and was stirred at 22°C for 3 h. Extraction with CH_2Cl_2 (2 × 500 mL) and washing of the CH_2Cl_2 extracts with aqueous $NaHCO_3$ (4 × 50 mL) and water (2 × 50 mL) gave, after drying over $MgSO_4$ and distillation, **8**, bp 75°C/20 Torr; ^{1}H nmr ($CDCl_3$) δ: 1.25 (t, 3H, $J = 7$ Hz, CH_2CH_3), 1.30 (d, 3H, $J \sim 5$ Hz, $CHCH_3$), 2.47–4.33 (m, 7H), 4.70 (q, 1H, $J \sim 6$ Hz, $CHCH_3$).

Acetylenic alcohol 2

To protected propargyl alcohol **7** (7.7 g, 60 mmol) in dry THF (60 mL) at 5°C under N_2 was added first *n*-butyllithium (55 mmol) and then glycidol derivative **8** (7.3 g, 50 mmol) and dry HMPA (3 mL). The reaction mixture was brought to room temperature and was then stirred at 65°C for ~2.5 h. The solvents were removed at reduced pressure and the residue extracted with ether (2 × 300 mL); the ether extracts were washed with phosphate buffer (pH 4.5, 2 × 50 mL), water (3 × 50 mL), and dried over $MgSO_4$. Evaporation of the solvent yielded fairly pure **2** as an oil which was used as such without further purification; ^{1}H nmr ($CDCl_3$) δ: 1.20 (t, 3H, $J \sim 7$ Hz, CH_2CH_3), 1.32 (d, 3H, $J \sim 5$ Hz, $CHCH_3$), 1.35 (s, 6H, $2CH_3$), ~2.3–4.3 (m, 10H), 3.20 (s, 3H, OCH_3), 4.57–4.90 (m, 1H, OCHOEt); ms (*m/e*, 16 eV): 259 ($M^+ - CH_3$), 201 ($M^+ - CH_3CHOCH_2CH_3$), 171 ($M^+ - CH_2OCHCH_3OCH_2CH_3$), 141 ($Me_2(MeO)COCH_2C{\equiv}CCH_2^+$), 133 ($M^+ - 141$), 103 ($M^+ - 171$), 73 ($CH_3CHOCH_2CH_3^+$).

Acetate 3

To crude alcohol **2** (2.,7 g, 10 mmol) in anhydrous ether (50 mL) were added 4-dimethylaminopyridine (122 mg, 1 mmol) and acetic anhydride (1.9 mL, 20 mmol). The reaction mixture was stirred at room temperature for 1 h and was then extracted with ether (2 × 350 mL); the ether extracts were washed with aqueous $NaHCO_3$ (2 × 50 mL), water (3 × 50 mL), and dried over $MgSO_4$. Evaporation of the solvent, followed by azeotroping the excess acetic acid and acetic anhydride with toluene, yielded acetate **3**, which was used without further purification in the next step; ^{1}H nmr (CCl_4) δ: 1.05 (t, 3H, $J \sim 7$ Hz, CH_2CH_3), 1.18 (d, 3H, $J \sim 5$ Hz, $CHCH_3$), 1.18 (s, 6H, $2CH_3$), 1.90 (s, 3H, $COCH_3$), ~2.3–2.6 (m, 2H), 3.02 (s, 3H, OCH_3), ~3.1–5.0 (m, 8H); ms (*m/e*, 16 eV): 301 ($M^+ - CH_3$), 73 ($CH_3CHOCH_2CH_3^+$).

Propargylic alcohol 4

To acetate **3** (790 mg, 2.5 mmol) in methanol (20 mL) was added PPTS (25 mg); the reaction mixture was stirred at 5°C for ~1 h, and was then extracted with ether (2 × 350 mL); the ether extracts were washed with aqueous $NaHCO_3$. Evaporation of the solvent gave alcohol **4** as an oil, which was used as such for the following reaction; ^{1}H nmr ($CDCl_3$) δ: 1.18 (t, 3H, $J \sim 7$ Hz, CH_2CH_3), 1.28 (d, 3H, $J \sim 5$ Hz, $CHCH_3$), 2.07 (s, 3H, $COCH_3$), ~2.4–2.7 (m, 2H), ~3.1–5.2 (m, 9H); ms (*m/e*, 16 eV): 244 (M^+), 229 ($M^+ - CH_3$), 73 ($CH_3CHOCH_2CH_3^+$).

Mesylate 5

To alcohol **4** (454 mg, 1.86 mmol) in dry CH_2Cl_2 (10 mL) at 5°C, under N_2, were added triethylamine (1.3 mL, 9.3 mmol) and methanesulfonyl chloride (0.58 mL, 7.4 mmol). The reaction was over immediately (tlc); the reaction mixture was extracted with ether (2 × 175 mL); the ether extracts were washed with cold dilute aqueous HCl (2 × 30 mL), $NaHCO_3$ (3 × 30 mL), water (3 × 30 mL), and dried over $MgSO_4$. Mesylate **5**, thus obtained, was used without further purification for conversion into the corresponding iodide; ^{1}H nmr (CCl_4) δ: 1.05 (t, 3H, $J \sim 7$ Hz, CH_2CH_3), 1.08 (d, 3H, $J \sim 5$ Hz, $CHCH_3$), 1.92 (s, 3H, $COCH_3$), ~2.3–2.6 (m, 2H), 2.95 (s, 3H, SO_2CH_3), ~3.0–3.7 (m, 4H), ~4.4–5.0 (m, 4H).

Iodide 6

To mesylate **5** (592 mg, 1.84 mmol) in acetone (10 mL) was added sodium iodide (1.1 g, 7.3 mmol); the reaction mixture was stirred for 1 h at room temperature and was then extracted with ether (2 × 200 mL); the ether extracts were washed with aqueous $NaHCO_3$ (1 × 100 mL, 1 × 50 mL), water (3 × 50 mL), and dried over $MgSO_4$. Iodide **6**, thus obtained, was used without further purification. On several occasions, evaporation of the ether resulted in decomposition of the iodide. This problem was remedied by use of CH_2Cl_2 as extraction solvent; ^{1}H nmr (CCl_4) δ: 1.10 (t, 3H, $J \sim 7$ Hz, CH_2CH_3), 1.18 (d, 3H, $J \sim 5$ Hz, $CHCH_3$), 1.95 (s, 3H, $COCH_3$), ~2.3–2.6 (m, 2H), ~3.2–3.7 (m, 6H), ~4.4–5.0 (m, 2H); ms (*m/e*, 16 eV): 339 ($M^+ - CH_3$), 265 ($M^+ - (OCHCH_3OCH_2CH_3)$).

Can. J. Chem. Downloaded from www.nrcresearchpress.com by 210.87.254.5 on 09/06/12
For personal use only.

Can. J. Chem. Downloaded from www.nrcresearchpress.com by 210.87.254.5 on 09/06/12
For personal use only.

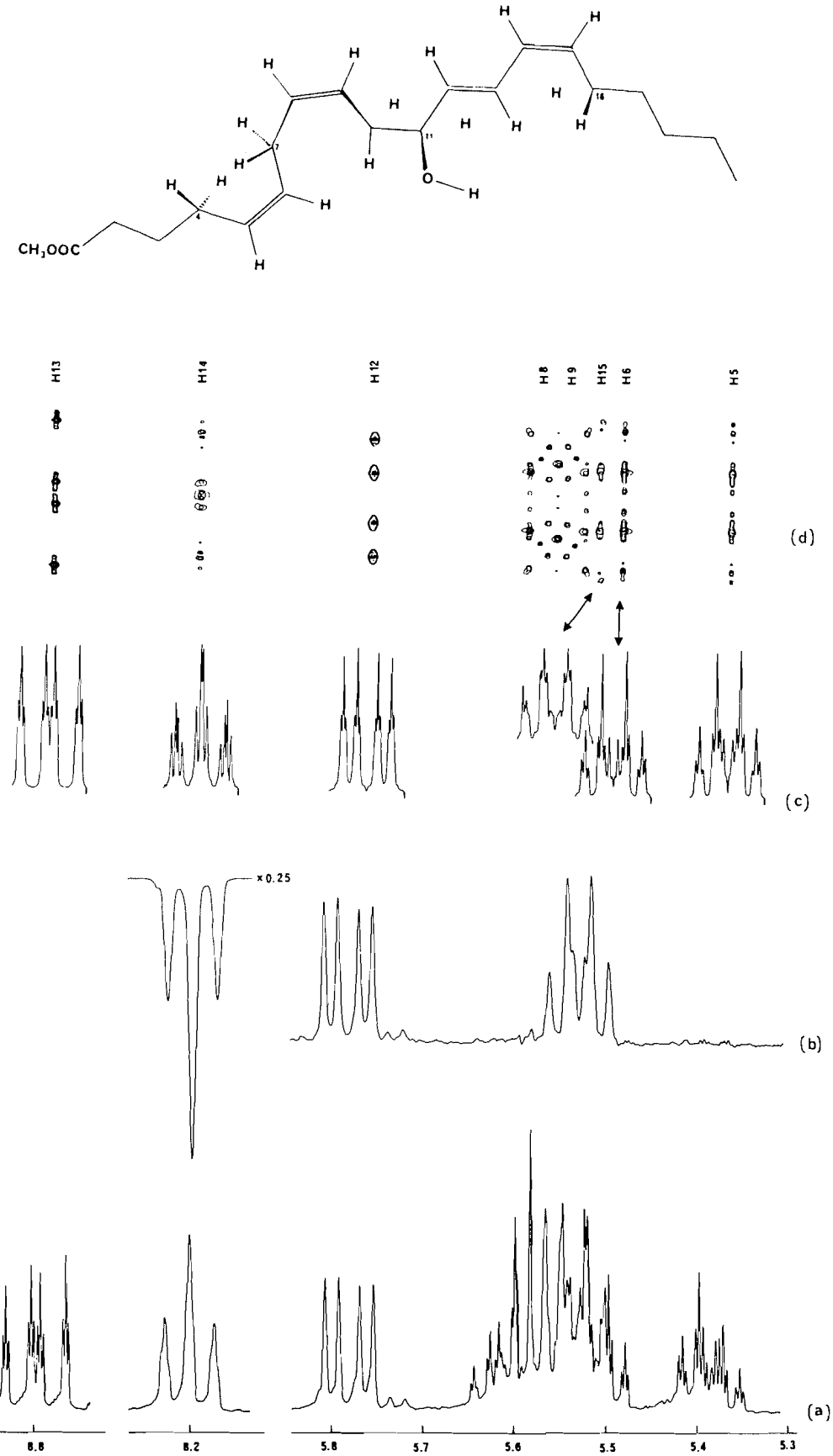

FIG. 1. Structure and examples of 400 HMz ^{1}H partial spectra of **17**; (a) 1D spectrum; (b) nOe difference spectrum; (c) cross section plots of the *J*-resolved ^{1}H 2D spectrum; (d) contour plots of the *J*-resolved ^{1}H 2D spectrum.

TABLE 2. Nuclear Overhauser effects in **17**

Irradiated proton	Observed proton	% Area change[a]
H7	H4	5
	H6	4
	H8	4
	H10a	≤1
	H10b	≤1
H10a[b]	H8	~−2
	H9	~4
	H11	4
	H12	2.5
	H13	1.5
H10b[b]	H8	~5
	H9	~1
	H11	4
	H12	4
	H13	3
	H14	−1.5
H11	H9	~3
	H10a	~2
	H10b	~2
	H12	4
	H13	7.5
	OH	5.5
H13	H11	9
	H12	<1
	H14	<1
	H16	7
	OH	4
H14	H12	18
	H13	<1
	H15	20

[a]Positive value indicates an increase, negative value a decrease.
[b]Subsaturation decoupling level was used.

Ester ***10***

To acetylenic orthoester **1** (146 mg, 0.85 mmol) and CuI (161 mg, 0.85 mmol) in dry THF (1.5 mL) at −78°C under an argon atmosphere, was added dropwise *n*-butyllithium (0.51 mL, 0.81 mmol); after 15 min iodide **6** (250 mg, 0.71 mmol) in THF (1 mL) was added. The reaction mixture was brough to room temperature over a 0.5 h period, stirred at room temperature for 22 h, and added to aqueous pH 4 buffer (~20 mL); the product was extracted with ether (2 × 150 mL), the ether extracts were washed with H_2O (4 × 20 mL) and dried over $MgSO_4$. Evaporation of the solvents at reduced pressure, followed by a standard reacetylation, gave orthoester acetate **9** in about 85% yield.

Orthoester **9** was generally contaminated with some of its hydrolysis product, ester **10**, as could be seen by the ^1H nmr spectrum: 3.12 (s, OCH_3), 3.55 (s, CO_2CH_3).

To crude orthoester **9** (300 mg, 0.75 mmol) in MeOH/H_2O (4:0.1 mL) at 5°C was added PPTS (9 mg, 5%); after 4 h stirring at 5°C the reaction mixture was extracted with ether (2 × 170 mL), the ether extracts were washed with aqueous $NaHCO_3$ (3 × 40 mL), H_2O (3 × 30 mL), dried over $MgSO_4$, and evaporated under reduced pressure to afford ester **10** as an oil in quantitative yield; ^1H nmr (CCl_4) δ: 1.07 (t, 3H, J ~ 7 Hz, CH_2CH_3), 1.15 (d, 3H, J ~ 5 Hz, $CHCH_3$), ~1.5–2.6 (m, 8H), 1.90 (s, 3H, $COCH_3$), ~2.8–3.0 (m, 2H), ~3.0–5.0 (m, 6H), 3.50 (s, 3H, CO_2CH_3); ms (m/e, 70 eV): 263 (M^+ − $OCHCH_3OCH_2CH_3$), 203 (263 − AcOH).

Diolefin ***11***

To nickel acetate (0.5 g, 2 mmol) in a 2-necked flask equipped with a septum, was added 3 mL of 95% ethanol. The flask was connected to the hydrogenation apparatus and was flushed with hydrogen. The catalyst was produced by injecting 4 mL of a 0.5 *M* solution of sodium borohydride in 95% ethanol to the rapidly stirred solution of nickel acetate. The reaction vessel was reflushed with hydrogen and ethylene diamine (0.2 mL) was added. Hydrogenation was then initiated by introducing diacetylenic ester **10** (176 mg, 0.5 mmol) in ~1 mL ethanol via the septum. Hydrogen uptake was quantitative within an hour and then virtually ceased. The reaction mixture was filtered through Celite, the ethanol was removed under reduced pressure, and the residue extracted with ether (2 × 150 mL); the ether extracts were washed with H_2O (4 × 30 mL), dried over $MgSO_4$, and evaporated *in vacuo* to give di-olefinic ester **11** as an oil in 90% yield; ^1H nmr (CCl_4) δ: 1.28 (t, 3H, J ~ 7 Hz, CH_2CH_3), 1.35 (d, 3H, J ~ 5 Hz, $CHCH_3$), ~1.3–4.2 (m, 14H), 2.10 (s, 3H, $COCH_3$), 3.71 (s, 3H, CO_2CH_3), ~4.5–5.2 (m, 2H), ~5.3–5.7 (m, 4H, 2 CH=CH); ms (m/e, 70 eV): 311 (M^+ − OEt), 267 (M^+ − $OCHCH_3OCH_2CH_3$).

*Methyl 11-acetoxy-12-hydroxydodeca-5Z,8Z-dienoate (**12**)*

To acetal **11** (580 mg, 1.63 mmol) in MeOH (7 mL) was added PPTS (20 mg, 0.08 mmol); the reaction mixture was stirred at 35°C for 2 h and was then extracted with ether (2 × 160 mL); the ether extracts were washed with H_2O (1 × 70 mL, 5 × 30 mL) and dried over $MgSO_4$. Evaporation of the solvent, followed by flash chromatography (petroleum ether – ethyl acetate 5:4), gave pure alcohol **12**; ^1H nmr (CCl_4) δ: ~0.9–3.5 (m, 13H), 1.83 (s, 3H, $COCH_3$), 3.42 (s, 3H, CO_2CH_3), ~4.3–4.7 (m, 1H), ~4.9–5.4 (m, 4H, 2 CH=CH); ms (m/e, 70 eV): 224 (M^+ − AcOH), 206 (M^+ − AcOH − H_2O).

Aldehyde ***13***

To a solution of oxalyl chloride (74 mg, 0.58 mmol) in dry methylene chloride (3 mL) at ~55°C, under argon, was added dimethylsulfoxide (91 mg, 1.16 mmol, in 0.75 mL CH_2Cl_2); after 2 min, alcohol **12** (150 mg, 0.53 mmol) in 1 mL CH_2Cl_2 was added. Stirring at −55°C was continued for an additional 15 min and triethylamine (267 mg, 2.64 mmol) added. After 5 min the reaction was warmed to room temperature, water was added, and the mixture was extracted with ether (2 × 150 mL); the ether extracts were washed with water (4 × 25 mL), dried over $MgSO_4$, and evaporated to give aldehyde **13** as an oil. It was used as such in the subsequent resolution with ephedrine or Wittig reaction with formylmethylenetriphenylphosphane; ^1H nmr (CCl_4) δ: ~1.2–3.0 (m, 10H), 2.20 (s, 3H, $COCH_3$), 3.67 (s, 3H, CO_2CH_3), 5.00 (t, J ~ 6 Hz, 1H), ~5.2–5.7 (m, 4H, 2 CH=CH), 9.57 (s, 1H, CHO); ms (m/e, 70 eV): 282 (M^+), 222 (M^+ − AcOH).

l-*Ephedrine derivative* ***14*** *of aldehyde* ***13***

A solution of aldehyde **13** (230 mg, 0.82 mmol), *l*-ephedrine (269 mg, 1.63 mmol), and PPTS (20 mg, 10 mol%) in dry methylene chloride (4 mL) was stirred under N_2 at 40°C for 3 h and at room temperature for 5 h to effect a complete conversion of **13** to **14**. The CH_2Cl_2 was evaporated to yield the two desired ephedrine derivatives **14***R* and **14***S* which were separated by slash chromatography (petroleum ether – ethyl acetate 10:2, 20% yield of each); ^1H nmr ($CDCl_3$) δ of **14***S* (lower R_f): 0.53 (d, 3H, J = 7 Hz, CH_3), ~1.1–3.0 (m, 10H), 1.90 (s, 3H, $COCH_3$), 2.30 (s, 3H, NCH_3), 3.47 (s, 3H, CO_2CH_3), 3.85 (d, 1H, J = 4 Hz), ~4.7–5.4 (m, 7H), 7.13 (s, 5H, C_6H_5); of **14***R* (higher R_f): 0.57 (d, 3H, J = 7 Hz), ~1.1–3.0 (m, 10H), 2.03 (s, 3H $COCH_3$), 2.20 (s, 3H, NCH_3), 3.50 (s, 3H, CO_2CH_3), 3.75 (d, 1H, J = 2 Hz), ~4.7–5.5 (m, 7H), ~7.0–7.4 (m, 5H, C_6H_5); ms (m/e, 70 eV): 429 (M^+), 398 (M^+ − OCH_3), 176 (cyclic—NMeCHMeCHPhOCH—$^+$).

*Aldehydes 14*R *and 14*S

To ephedrine derivative **14***R* (125 mg, 0.29 mmol) in MeOH (5 mL) was added 1 mL aqueous 0.5 *N* HCl. The solution was stirred at 33°C for ~4 h and was then extracted with ether (2 × 150 mL); the ether extracts were washed with dilute aqueous HCl (1 × 50 mL, 1 × 20 mL), water (4 × 20 mL), and dried over $MgSO_4$. Evaporation of the solvent gave crude aldehyde **13***R* in ~90% yield; it was used without further purification in the subsequent Wittig reaction. An identical procedure was used to produce **13***S*.

Can. J. Chem. Downloaded from www.nrcresearchpress.com by 210.87.254.5 on 09/06/12
For personal use only.

Can. J. Chem. Downloaded from www.nrcresearchpress.com by 210.87.254.5 on 09/06/12
For personal use only.

Methyl 11-acetoxy-14-oxo-tetradeca-5Z,8Z,12E-trienoate (15)

The aldehyde **13** (85 mg, 0.30 mmol) in dry DMF (2 mL) under Ar was added formylmethylenetriphenylphosphorane (100 mg, 0.33 mmol). The reaction mixture was stirred at 42°C for 4 h and was then extracted with ether (2 × 150 mL). The ether extracts were washed with water (4 × 20 mL) and dried over $MgSO_4$; evaporation of the solvent followed by flash chromatography (petroleum ether – ethyl acetate 12:3) gave α,β-unsaturated aldehyde **15** as an oil in ~50% yield; ^{1}H nmr (CCl_4) δ: ~1.4–2.9 (m, 10H), 2.00 (s, 3H, $COCH_3$), 3.53 (s, 3H, CO_2CH_3), ~5.0–5.7 (m, 4H, CH=CH), 6.0 (ABXY octet, 1H, C13, $J_{13,12}$ = 16, $J_{13,14}$ = 7, $J_{13,11}$ = 1 Hz), 6.60 (ABXq, 1H, C12, $J_{12,13}$ = 16, $J_{12,11}$ = 4 Hz), 9.43 (d, 1H J = 7 Hz, CHO); ms (m/e, 70 eV): 248 (M^+ – AcOH).

Methyl 11-acetoxyeicosa-5Z,8Z,12E,14Z(E)-tetraenoate (16)

To *n*-hexyltriphenylphosphonium bromide (107 mg, 0.25 mmol) in dry THF (3 mL) at room temperature under an argon atmosphere and was added *n*-butyllithium (0.18 mmol); after 15 min, the reaction mixture was cooled to −78°C, and aldehyde **15** (46 mg, 0.15 mmol) in THF (1 mL) was added dropwise via syringe. The reaction was over immediately; it was warmed up rapidly by immersion into a 20°C water bath, poured into pH 4 buffer (50 mL), and extracted with ether (2 × 150 mL). The ether extracts were washed with water (4 × 30 mL), dried over $MgSO_4$, and evaporated to give acetate **16** contaminated with some of its 14*E* isomer.

Methyl 11-hydroxyeicosa-5Z,8Z,12E,14Z-tetraenoate (17)

Crude acetate **16** (49 mg, 0.13 mmol) in dry methanol (4 mL) containing a catalytic amount of sodium methoxide was stirred at room temperature for 0.5 h, and was then neutralized with strong acidic resin (AM-120 H^+). Removal of the resin, followed by evaporation of the methanol, gave alcohol **17** contaminated with its 14*E* isomer. The latter was removed by flash chromatography (petroleum ether – ethyl acetate 9:2); me (m/e, 70 eV): trimethylsilylether: 406 (M^+), 283 (M^+ – CH=CHCH=CH$(CH_2)_4CH_3$), 225 ($(Me)_3SiOCHCH$=CHCH=CH$(CH_2)_4CH_3$).

Methyl 11-hydroperoxyeicosa-5Z,8Z,12E,14Z-tetraenoate (19)

To alcohol **17** (10 mg, 0.030 mmol) in dry CH_2Cl_2 (1.6 mL) under an argon atmosphere at −65°C was added triethylamine (0.017 mL, 0.12 mmol), the methanesulfonyl chloride (0.0035 mL, 0.045 mmol). After 0.5 h, 90% hydrogen peroxide (0.04 mL, 1.6 mmol) was added in 0.5 mL ether at −81°C. After 15 min, water was added and the reaction mixture extracted with ether–pentane (2:1) (60 mL); the ether–pentane extracts were washed with cold water (10 × 10 mL), dried over $MgSO_4$, and evaporated to yield hydroperoxide **19** contaminated with ~30% of its 15-hydroperoxy isomers (^{1}H nmr evidence only).

Purification by hplc was carried out using a straight-phase column (Altex Ultra-Sil), and petroleum ether – ethyl acetate as solvent system. The hydroperoxide mixture decomposed on the column, giving first a less polar material, then **19**, followed (shoulder) by other hydroperoxides (15-HPETE's). Only 10–30% of **19** could be isolated.

The crude mixture of HPETE's (1 mg, 70% **19**, 30% others by 400 MHz ^{1}H nmr) was reduced with $SnCl_2$ (12 mg) in 0.5 mL methanol for 2 min at room temperature. Extraction with ether–pentante 1:1, and washing with pH 4 buffer and water gave, after drying, a mixture. Separation by hplc, using the same column and petroleum ether – ethyl acetate (10:1) gave, as the major product, **17**.

Experimental section for ^{1}H nmr of 17

The solution of **17** (~10^{-2} *M*) was made up in C_6D_6, and degassed through 5 cycles of freeze–pump–thaw. The ^{1}H spectra were obtained on the Brüker WH-400 located at the "Laboratoire Régional de RMN" at the Université de Montréal. The 1D FID were accumulated with 16K data points and zero-filled before being Fourier transformed to obtain a digital resolution better than 0.1 Hz. The steady-state nOe difference spectra were obtained by subtraction of FID or transformed spectra; transients were collected after preirradiation (10–12 s) at selective frequencies and recycled to average the drift effect. For the protons H10a and H10b, subsaturation power levels were used to achieve partial selectivity; for other protons, complete saturation power levels were used. The T_1 of the protons obtained by nonselective inversion recovery were in the range of 0.8 to 2 s.

The 2D *J* spectra were obtained with the automated Brüker program. Because of the memory storage limit, the window of f_2 dimension only covers the downfield part of the spectra (1100 Hz), the frequency offset was carefully chosen to avoid the foldover problem. The digital resolution is 0.268 Hz after zero-filling in both f_1 and f_2. A Gaussian resolution enhancement function is applied in both t_1 and t_2 directions before doing the Fourier transform.

The coupling constants are calculated directly by first order analysis for the well-dispersed proton signals and from the simulated spectra using the standard PANIC program from the Brüker software package.

Acknowledgements

We wish to thank the Natural Sciences and Engineering Research Council of Canada for financial support, and Dr. O. Mamer, of the Biomedical Mass Spectrometry Unit, McGill University, for an excellent mass spectrometry service.

1. E. J. COREY and J. KANG. J. Am. Chem. Soc. **103**, 4618 (1981).
2. G. JUST and C. LUTHE. Tetrahedron Lett. 1331 (1982).
3. G. JUST, C. LUTHE, and P. POTVIN. Tetrahedron Lett. 2285 (1982).
4. C. A. BROWN and V. K. AHUJA. J. Chem. Soc. Chem. Commun. 553 (1973).
5. A. J. MANCUSO, S. L. HUANG, and D. SWERN. J. Org. Chem. **43**, 2490 (1978).
6. S. TRIPETT and D. M. WALKER. J. Chem. Soc. 1266 (1961).
7. E. J. COREY, J. O. ALBRIGHT, A. E. BARTON, and S. HASHIMOTO. J. Am. Chem. Soc. **102**, 1435 (1980).
8. L. D. HALL and J. K. M. SANDERS. J. Am. Chem. Soc. **102**, 5703 (1980).
9. L. M. JACKMAN and S. STERNHELL. Applications of nuclear magnetic resonance spectroscopy in organic chemistry. Pergamon Press, New York. 1969.
10. R. A. BELL and J. K. SAUNDERS. Can. J. Chem. **46**, 3421 (1968).
11. G. JUST and C. LUTHE. Can. J. Chem. **58**, 2286 (1980).

The mechanisms of the physicochemical reactions in diorite used in the construction of ancient royal Egyptian statues

JOANNA MCFARLANE,[1] KRISTINE M. WILSON-YANG, SIDNEY JOSEPH,[2] CARLA FREY,[2] AND GEORGE BURNS
Lash Miller Chemical Laboratory, University of Toronto, Toronto, Ont., Canada M5S 1A1

Received September 1, 1982

This paper is dedicated to Professor Leo Yaffe on the occasion of his 65th birthday

JOANNA MCFARLANE, KRISTINE M. WILSON-YANG, SIDNEY JOSEPH, CARLA FREY, and GEORGE BURNS. Can. J. Chem. **61**, 718 (1983).

During the heights of ancient Egyptian civilization, statues of deities and pharaohs were often constructed of hard and colourful igneous rocks, such as granite and diorite. Most of these statues remain in an excellent state of preservation. However, others have unexpectedly fragmented, in some cases only a few years after having been excavated in near-perfect condition. In the present work it is shown that two interrelated physicochemical processes contribute to this degradation: (1) the infiltration of saline H_2O and (2) subsequent alteration of the constituent minerals. Conclusions were reached on the basis of neutron activation and atomic absorption analyses of rock samples from two sites in Upper Egypt and leached soluble salts therefrom. These samples were identified as quartz diorites on the basis of petrographic and X-ray spectroscopic examination. The chemical significance of the geological nature of the stone is discussed. Possible precautions to be observed in the field are presented.

JOANNA MCFARLANE, KRISTINE M. WILSON-YANG, SIDNEY JOSEPH, CARLA FREY et GEORGE BURNS. Can. J. Chem. **61**, 718 (1983).

Lors de la grande époque de la civilisation egyptienne, on a souvent construit les statues des déesses et des phaarons avec des roches ignées dures et colorées, tel le granite et la diorite. La plupart de ces statues sont encore en excellent état. Cependant dans quelques cas, d'autres qui étaient dans un état presque parfait lorsqu'elles ont été découvertes se sont fragmentées subitement quelques années après leur excavation. Dans ce travail, on montre que deux processus physicochimiques interreliés contribuent à cette dégradation: (1) l'infiltration d'eau salée et (2) l'altération subséquente des constituants minéraux. Nos conclusions se fondent sur des analyses par activation neutronique et par absorption atomique de deux échantillons de roches provenant de deux endroits de la Haute Egypte; on avait débarassé ces échantillons des sels solubles qu'ils contenaient. Les échantillons sont identifiés comme étant des quartz-diorites en se basant sur l'examen pétrographique et spectroscopique aux rayons-X. On discute de la signification chimique de la nature géologique de la pierre. On suggère quelques précautions à observer dans ce domaine.

[Traduit par le journal]

Introduction

Ancient Egyptians, especially in times of prosperity, honoured their deities and pharaohs with statues and chapels made of strong igneous rock (1). Many beautiful dioritic monuments have been excavated in Giza, near Cairo, as well as in Deir el-Bahri and Karnak, in Upper Egypt. These works of art are representative of the best ancient Egyptian stone craftsmanship and most were discovered in almost perfect condition. A statue of Thutmose[3] III, an 18th dynasty pharaoh (1490–1436 B.C.), unearthed in the Deir el-Bahri complex, dominated by the funerary temple of Queen Hatshepsut, even partly retained its original decorative pigments. Such pigments are rarely retained on dioritic monuments. Unfortunately, a few years after having been exposed to the atmosphere, this statue developed deep cracks. Its condition had so greatly deteriorated in the past fifteen years that it was necessary to encase it in concrete on site to prevent it from completely crumbling under its own weight.

Many other statues of igneous rock have deteriorated in a similar manner, such as a torso of Queen Hatshepsut, now in the Louvre, several dioritic figures, now in the Boston Museum of Fine Art (2), as well as some statues in the National Museum, Cairo. On the other hand, dioritic statues of the goddess Sekhmet, presently in the Louvre, are in nearly perfect condition, as are the statues of Khufu and Menkure which were discovered in Giza.

Little systematic investigation has been done to elucidate the processes which have destroyed statues of diorite. It was suggested (2) that the damage was caused by intense heating and presumably rapid cooling with water. Although the constituent minerals of igneous rocks do have different coefficients of thermal expansion (1, 3),[4] it is unlikely that this phenomenon would have contributed to the sudden degradation of the statues as the rock from which they were sculpted had survived temperature fluctuations over geological time. This theory also fails to explain the pattern of cracking and the apparent lack of carbonaceous material on the surfaces.

A more probable cause of this type of degradation is the infiltration of soluble salts into the rock pores and crystallization of the salts therein. This is a well-known phenomenon and has been seen frequently in modern stone (1). In addition, the geological literature (11–18) provides some insight into the degradative interaction of water and the minerals found in some igneous rocks. The development of possible structural weaknesses would be critical in the extended existence of dioritic monuments.

It was decided therefore to explore these possibilities with

[1]Holder of an NSERC Undergraduate Summer Research Award, 1982, at the University of Toronto.

[2]University of Toronto undergraduate scholars.

[3]J. H. Breasted's, rather than A. Gardiner's, spelling is used throughout.

[4]Scientific staff, Deir el-Bahri, private communication.

the aim of providing a reasonable and archaeometrically useful explanation of this deterioration.

Removal of fragments of diorite from ancient Egyptian statues is very ill-advised, since these works of art are clearly irreplaceable. However, we were fortunate to receive permission from the President of the Egyptian Antiquities Organization and its Permanent Committee to collect samples of archaeometric, but not archaeological or Egyptological, value in Karnak and the Deir el-Bahri area. Two specimens were collected, one from the Deir el-Bahri temple complex and one from the Karnak temples. The first was found near the pyramid in the Mentuhotep I Temple. It is most likely that it originated from a wall from the Thutmose III Temple, immediately adjacent, which had collapsed.[5] Upon close inspection, this sample appeared to be identical in composition and condition to the aforementioned statue of this pharaoh, found near the centre of the Thutmose III Temple. The second sample was found near the dioritic doorway of Queen Hathepsut's chapel from which it had fallen. The chapel is adjacent to and immediately north of the Main Sanctuary of the Karnak temples.

It was decided first to classify the rock samples petrographically using multielement X-ray fluorescence and thin-section analyses. The samples were then subjected to a regimen of washing to investigate the presence of soluble salts. The resulting solutions and washed and unwashed samples were then analyzed by atomic absorption and nuclear activation analyses.

Experimental

Samples

The Deir el-Bahri specimen consisted of two subsamples, DG-1 and DG-2, 10 and 57 g in mass respectively. The Karnak sample KG-1 had a mass of 7 g. All samples were stored in sealed polyethylene bags and manipulated with tweezers to avoid salt contamination.

X-ray fluorescence

Sample preparation

Two 400 mg samples of DG-1, chipped from opposite sides of the fragment, were ground with a mortar and pestle to an approximately 200 mesh powder. Two grams of Spectroflux*105 (Johnson Matthey Chemicals) and 10 mg NH_4NO_3 were added to each powdered sample, and intimately mixed. The mixture was fused in a Pt/Au crucible over a Bunsen burner for 15 min and subsequently moulded into a disc 30 mm in diameter and 2 mm thick.

Instrumental procedure

A Philips X-ray spectrograph with a W target and a LiF scintillation detector (Chemistry Department, University of Toronto) operated at a voltage of 28 kV and a current of 24 mA, was used to determine qualitatively the presence of elements heavier than Sc. To extend the quantitative determination to lighter elements a Siemens sequential X-ray spectrometer (Geology Department, University of Toronto), interfaced with a PDP11 microcomputer operated with a Cr target at a voltage of 45 kV and a current of 44 mA, was employed. The following elements were detected: Mg using an ADP[6] crystal; Al, Si, and P using a PET[7] crystal; and Fe, Ca, Ti, K, and Mn using LiF.

Thin section analysis

Sample preparation and instrumental procedure

Fragments, each about 0.7 cm in diameter, of DG-1, DG-2, and KG-1, were placed on a 5 mm thick by 2.5 cm in diameter disk made of 1 drop of hardener/4 mL resin SW (Metaserv Metset). They were then immersed in a 1 drop hardener/5 mL resin mixture, and placed under a light vacuum for 10 min. This allows some impregnation of the samples to avoid losses on cutting. The samples were then sectioned, using anhydrous ethanol as a coolant, and mounted on microscope slides. The minerals in the samples were identified using a Leitz Orthoplan petrographic microscope (Geology Department, University of Toronto).

Atomic absorption and neutron activation analyses

Sample preparation

Three 800-mg subsamples of DG-1 were prepared for analyses of soluble ions present in the rock matrix using the following method. A preliminary wash involved the immersion of each fragment in deionized water for 20 s which was then diluted in a volumetric flask. Each fragment was then stirred in 25 mL of deionized H_2O for 24 h using a magnetic stirrer. The resulting heavy wash solution was filtered, using Whatman #1 filter paper, and diluted in a volumetric flask. Both the preliminary and heavy wash solutions were then analyzed by atomic absorption spectrometry.

Three 1-mL aliquots of one of these pairs of solutions were analyzed by neutron activation analysis, along with a second set of wash solutions. This set was prepared following the method previously described, except the preliminary washes were performed by rinsing the fragments with six small aliquots of deionized H_2O, with a total volume of less than 25 mL.

Six 800-mg fragments were removed from each of the DG-1, DG-2, and KG-1 samples. Half of these fragments underwent preliminary washes. They were immersed and swirled gently three times each in 10 mL of deionized H_2O for 10 s. All the samples were then subjected to heavy washes using the method described earlier. Neutron activation analyses were performed on these solutions, on filter papers used in the preparation of the heavy washed, on one unwashed sample of DG-1, and on blanks of deionized H_2O, deionized H_2O passed through a filter paper, and the filter papers used in the preparation of the blanks. For a subsequent atomic absorption analysis, the wash solutions were further diluted and modified to contain 2% by volume HCl, 214 ppm Sr, and 857 ppm Cs.

Instrumental procedure of atomic absorption analysis

A Techtron Model AA-4 atomic absorption spectrophotometer (Chemistry Department, University of Toronto) was used with Varian Na and Ca, Hanau Original K hollow cathode lamps and an air/acetylene flame. Calibration curves were prepared with standard solutions of 0.5, 1.0, 4.0, and 8.0 ppm Na; 1.0, 4.0, 8.0, 16.0, and 20.0 ppm K; and 1.0, 5.0, 10.0, and 20.0 ppm Ca; and with standard solutions of Na/Ca/K respectively, with concentrations in ppm of 500/4.99/1.67, 1.00/0.998/0.334, 0.500/0.499/0.167, and 0.0500/0.0499/0.0167, prepared to mimic the unknown composition. In addition each standard was 214 ppm in Sr and 857 ppm Cs.

Instrumental procedure of neutron activation analysis

Irradiation of the samples was done in the University of Toronto SLOWPOKE Reactor. Gamma-ray collection and analysis was done using one of the two Ge(Li) detectors coupled with a Canberra 8180 multichannel analyzer.

The wash samples were irradiated in 1-mL vials for 5 min at a neutron flux of 1.0×10^{12} neutrons/cm^2 s. A one minute decay time before gamma counting was necessary for the transfer of the liquid to unirradiated vials for the five minute count. The mass of liquid transferred was determined separately. The concentrations of the elements were calculated with respect to 5.1 ppm Al, 1620 ppm Mg, 960 ppm Ca, 40.8 ppm Na, and 63.2 ppm Cl standard solutions.

The filter paper samples, as well as the unwashed rock sample, were irradiated for one minute at a neutron flux of 1.0×10^{11} neutrons/cm^2 s. After a decay period of 18 min the gamma activity of the samples was counted for 5 min. The concentrations of the elements were determined with respect to standards of 101 ppm Al, 1608 ppm Mg, 19 200 ppm Na, and 25 000 ppm Cl.

Results

(i) *X-ray fluorescence analysis*

The X-ray fluorescence study using the Philips spectrograph

[5]Private communication from Mme. J. Lipinska, Head of the Polish Mission at Deir el-Bahri.

[6]Ammonium dihydrogen phosphate ($NH_4H_2PO_4$).

[7]Pentaerythritol [$C(CH_2OH)_4$].

TABLE 1. Elemental composition by X-ray fluorescence (Siemens spectrometer)

Element[a]	Weight (%±0.1%)
O	42.8
Si	23.1
Fe	12.0
Al	6.6
Ca	4.6
Mg	2.3
Ti	2.0
K	1.9
P	1.1
Mn	0.2
Total	96.6

[a]DG-1, two subsamples.

qualitatively indicated the presence of La, Fe, and Ti (La is a major constituent of Spectroflux*105). The fairly high abundance of Fe and Ti in the fused sample was verified by the quantitative results from the Siemens spectrometer. These elemental concentrations are listed in Table 1 and were identical for both DG-1 samples studied. The fusion process lowered the sensitivity of the technique because of dilution by Spectroflux*105. The spectra of the lighter elements were especially affected because their fluorescent X-rays were absorbed by the diluent (4). Nonetheless, this effect was counterbalanced by the high concentrations of these elements. The concentrations of the elements sum to 96.6±0.1%. The balance is probably due to the presence of unanalyzed Na and trace elements.

(ii) *Thin section analysis*

The thin sections revealed that the rocks under investigation were quartz diorites, as there was 10 to 15% quartz in the KG-1 sample and 30% quartz present in the Deir el-Bahri rocks. The plagioclase, a sodium–calcium alumino-silicate, of the Deir el-Bahri rocks had been altered to clay minerals to a greater extent than the Karnak plagioclase, which also contained some muscovite. More biotite, but less apatite, was observed in the KG-1 thin section than in those of DG-1 and DG-2. Large crystals of magnetite and 1 grain of calcite were seen in all the samples. The KG-1 rocks also contained hematite, and very small amounts of feldspar and zircon. Approximately 10% hornblende was noticed in the Deir el-Bahri rocks.

(iii) *Atomic absorption analysis*

During the preliminary washes of the sample preparation, many of the fragments broke apart. After overnight stirring, the samples had completely disintegrated. They formed a slurry at the bottom of a suspension of what was suspected to be fine alumino-silicates. The Na, Ca, and K calibration curves were linear well within the range of the diluted wash water samples. The enhancement of the K signal due to the presence of other alkali metals in the rock matrix was simulated in the K standard solutions by the addition of an amount of Na, approximately equivalent to the concentrations found in the sample solutions in the first analysis, and by the preparation of one standard solution to contain both Na and K, in the second. In addition, CsCl was added to the wash solutions to suppress the ionization of K and $SrCl_2$ was added to reduce the formation of Ca oxides in the flame in the second set of analyses[8] (5). Results and calibration curves were statistically analyzed via ref. 19.

The results of the geological samples, of the wash water, and of the filter paper by atomic absorption and neutron activation analyses are listed in Table 2.

(iv) *Neutron activation analysis*

The following elements were observed to be present in the rocks by neutron activation analysis: Mg, Al, Ca, Na, Cl, Mn, V, and Ti, but for only the first five were concentrations determined. I and Br were searched for in the wash waters but no conclusive evidence was obtained for their presence. The standard solutions of Na, Mg, Ca, Cl, and Al were of much greater concentration than the sample wash solutions. They provided good counting statistics with spectral peaks of a few thousand counts above the background. The peak was considered to be statistically significant if the standard deviation, determined as the square root of the gross peak plus background counts, was less than 30% (4). Otherwise, only a detection limit was reported, as indicated by the approximate values of the weight percentages of Mg from the wash water analyses in Table 2.

Al was found in the deionized water blanks. This was probably desorbed from the walls of the polyethylene vials, and was subtracted from the concentration found in the preliminary wash solutions. Measurable concentrations of Na, Al, and Cl were found in the filtered deionized water blanks; these were subtracted from their concentrations in the overnight wash solutions. The filter paper blanks contained significant amount of Na, Al and Ca; the concentrations of these elements were subtracted from the washed rock residue. The Na present in the blanks of the filtered deionized water and the filter papers was most likely from the manual handling of the filter papers. This contamination is suspected to have occurred before the papers were used in these experiments, as special care was taken to avoid direct contact between the paper and the hands of the analyst. Repetitive analyses of the blanks and standard solutions were performed to ensure the reproducibility of these results.

Ratios of the weight percentages of Na/Ca, Na/Cl, Al/Ca, Al/Cl, and Ca/Cl were calculated for the species remaining in the samples after washing, and the elements leached from the rocks during this process, to determine whether the dissolved salts were part of the diorite matrix itself. These ratios are presented in Table 3.

Discussion

The results of the X-ray fluorescence analysis of DG-1 (Table 1) indicate a low silicate and a high ferro-magnetic mineral content characteristic of a diorite[9] (6). The notable Ti concentration characteristic of Egyptian rocks was present in the geological material on the filter papers (7). As the elemental concentrations of the two sampling sites on opposite sides of the fragment were identical, it was felt that the rock was petrographically homogeneous.

The thin sections allowed the samples from both excavation sites to be further classified as quartz diorites. The differences in the mineralogy of these rocks indicated that they may have originated from different quarries, although some of these variations could have been due to the inhomogeneity of the rocks.

It was found that the surface contamination of the rocks, in the form of dust and dirt adsorbed through burial and sub-

[8]K. M. Wilson-Yang, unpublished, 1979.

[9]C. Traunecker of the centre franco-égyptien d'études des temples de Karnak, private communication (1979).

TABLE 2. Mean concentrations of elements in the rock fragments as weight percent

	Na	K	Ca	Cl	Al	Mg
AA[a]						
DG-1	0.06±0.01	0.02±0.01	0.05±0.00			
DG-1	0.02±0.01	0.03±0.02	0.02±0.01			
DG-2	0.05±0.01	0.03±0.01	0.03±0.01			
KG-1	0.05±0.03	0.06±0.02	0.04±0.01			
NAA[b]						
DG-1	0.05±0.01		0.01±0.00	0.04±0.00		
DG-1	0.03±0.01		0.05±0.02	0.01±0.01	0.15±0.04	≦0.013
DG-2	0.04±0.03		0.08±0.05	0.01±0.01	0.1 ±0.1	≦0.013
KG-1	0.05±0.01		0.09±0.05	0.05±0.02	0.10±0.06	≦0.014
NAA[c]						
DG-1	2.0±0.1		4.5±0.6	0.03±0.01	4.2±0.2	2.4±0.2
DG-2	2.2±0.2		4.6±0.6	0.03±0.01	4.6±0.4	2.4±0.3
KG-1	2.5±0.3		4.3±0.3	0.03±0.01	4.9±0.4	2.2±0.1
NAA[d]						
DG-1	2		5		6	

[a]Atomic absorption; wash waters.
[b]Neutron activation; wash waters.
[c]Neutron activation; washed rock.
[d]Neutron activation; unwashed rock.

TABLE 3. Ratios of average concentrations[a]

	Cl/Ca	Al/Cl	Na/Cl	Na/Ca	Na/Al	Al/Ca
With wash water elemental concentrations						
DG-1	0.1	20	4	0.6	0.2	3
DG-2	0.2	8	3	0.5	0.4	1
KG-1	0.6	2	1	0.6	0.5	1
With washed rock elemental concentrations						
DG-1	0.007	100	67	0.44	0.48	0.93
DG-2	0.007	140	67	0.48	0.48	1.0
KG-1	0.007	200	80	0.58	0.51	1.1

[a]From neutron activation analyses.

sequent handling, was not significant. Samples chipped from both the exposed surfaces and the interiors of the rocks showed no notable differences in the concentrations of the elements leached from the different fragments in the preliminary washes. Variations in the masses of dissolved elements indicated the rock had not been homogeneously degraded, not unexpected in a coarse-grained igneous rock.

The Na and Ca concentration, determined by the two different analytical techniques, corroborated each other. The Na results were reproducible between analytical techniques. Those of Ca were less so; however, the observed deviations were found to be statistically insignificant at the 95% confidence level, except for those observed in the results from the Karnak sample. The atomic absorption results have an inherently better precision than those obtained from the neutron activation analysis; the latter technique was employed near its detection limit in many of the samples. However, the precision of both methods was limited primarily by the inhomogeneity of the samples. Inhomogeneity was the probable explanation for the high chloride ion concentration in one of the DG-1 fragments.

The Mg concentrations in the wash waters were only approximated, as the small Mg peak in the gamma-ray spectrum was quite often not statistically significant with respect to the high background count in the same energy region. K was not searched for in the neutron activation analysis, as the 0.017 weight percent observed previously in the atomic absorption study would not have been detectable under the conditions of analysis used.

It was determined that the elemental concentrations of Na, Ca, Cl, Al, and Mg in the washed rocks were very similar among the samples from different sites, as were the rocks' external macroscopic characteristics. In addition, no provenance differences were apparent in the concentrations of the elements leached from the rocks, except in the case of chloride ion. The concentrations of leachable chloride ion in the samples were different, being 0.002 ± 0.001 molal for DG-1, 0.004 ± 0.002 molal for DG-2, and 0.014 ± 0.006 molal for KG-1. The Na/Cl mole ratios were also dissimilar, being respectively 6.5, 5, and 1.6.

In all samples, there were significant differences in concentration ratios as compared to chloride ion, between those calculated from the leachable ions and the nonleachable ones. These are reported in Table 3. The Na/Ca, Na/Al, and Al/Ca ratios did not vary much between those determined from the concentrations of leachable elements and those calculated from the insoluble ones. So, only the chloride ion was proportionately more concentrated in the wash waters than in the geological material left on the filter paper.

This excess of chloride ions washed from the rock samples suggests that chloride salts (8) had been deposited within the

rock matrices. This evidence suggested that degradation of the quartz diorite was due to NaCl and, to a lesser extent, KCl and $CaCl_2$. Sulphates and carbonates, which were not studied in this work, could have participated in this degradation process (9). The Na/Cl mole ratios were greater than unity, indicating an excess of Na which could have been either present in the rock as a salt other than NaCl, or leached from the diorite itself.

The soil of Egypt is known to be saline (8). This suggests that rocks and statues buried for thousands of years will eventually become salinized through salt-transporting ground water or through rare rains percolating through the earth. Since the construction of the first dam on the Nile, and the High Dam near Aswan (1965), irrigation has greatly increased the salt content of soil and monuments at Karnak (10). This increase is not seen at Deir el-Bahri, which is situated in the hills on the West Bank of the Nile. That the Karnak samples were more extensively salinized than the ones from Deir el-Bahri was evident from the greater amount of chloride ion washed from the KG-1 rocks than from the DG-1 and DG-2 rocks. This result is in complete agreement with our recent computational studies of salinization in the Karnak area (10).

Upon excavation of the quartz diorite, the absorbed water gradually evaporated and the salts present crystallized. Pressures on the micropores of the rock, due to the crystallization of the salts, would have likely caused its deterioration. Under natural conditions the NaCl crystal can exert 605 atm on the surrounding minerals, which is enough to crack most rocks (1). The presence of Na, Ca, and K cations in the wash waters provided evidence that the degradation of the quartz diorite samples was at least in part due to the salinization process. Other examples of a similar degradation due to salinization have been observed in granite (11), and in sandy limestone in the Saudi Arabian desert (3).

The existence of salinization does not preclude the presence of other deterioration mechanisms. The rate and extent of degradation of a rock depends also on the weathering of individual minerals within its matrix. Granite has been observed to crumble when water reacts with the biotite in the rock (12). The degradation of plagioclase in diorite may proceed by one or more mechanisms, including the leaching of cations from the silica lattice by hydrogen ion activity on its surface (13, 14), or to depths greater than one or two unit cells (15). The sequence of minerals formed in plagioclase alteration has been studied by transmission electron microscopy (16). The leaching of silica, which in turn renders the rock more porous, is another suspected mechanism of igneous rock weathering (17). Mechanical degradation of rocks was suggested to occur upon their excavation (18). In addition, it is highly probably that microfractures caused by crystallization of soluble salts during burial, i.e. in dry periods between rains, accelerates the destruction of the mineral structure. Fresh surfaces for potential attack by water would be created.

That the quartz diorite in our samples is slightly leached by water, with which it was saturated for thousands of years, was indicated by the similarity between the weight percent ratios of Na/Ca, Na/Al, and Al/Ca in the wash waters and those of the unleached elements in the rock (Table 3). The presence of the fine alumino-siliceous suspension in the wash waters, confirmed in the neutron activation analysis by the high Al concentrations, was an indication of the degree to which the rocks had decomposed. The most conclusive evidence for such a mechanism, however, came from a study of thin sections of the rock, where the alteration products of clay minerals and muscovite were clearly visible in the plagioclase. This weathering process was more extensive in the quartz diorite from Deir el-Bahri than in that from Karnak.

The actual extent to which the quartz diorite was leached was not great, as no significant difference was noted in the elemental concentrations of Na in the washed and unwashed rock samples. But as the concentrations of leached elements were so much lower than those in the rock, their contribution to the elemental concentrations as a whole in the quartz diorite would have been negligible.

In our quartz diorite samples, ground water weathered the plagioclase, and perhaps biotite and other minerals. The clay minerals formed at the site of the weathering and the microcracks in the rock became saturated with water while it was buried, weakening its structure by enlarging these imperfections. Upon excavation and the evaporation of this absorbed water, these plate-like minerals became more compact. This caused strain and distortion of the rock matrix, which eventually contributed to its cracking.

Conclusions

These experimental results strongly suggest that the quartz diorite degradation seen in Egyptian antiquities occurs via two interrelated mechanisms. Cracks in the rock result from the crystallization of salts absorbed into its matrix. Salt-induced dislocations will accelerate weathering during burial and swelling and contraction of subsequent mineral alteration products will contribute to crumbling upon unearthing. The relative importance of these mechanisms has been shown to vary according to the precise mineralogy of the rock and the nature of the soil in which the monument is buried.

Careful observation of burial environments could save many dioritic artifacts from rapid degradation. In the case of obviously damp soils, the objects should be immediately protected from evaporation. Storage, whether in a field warehouse or permanently in a museum, must be in an appropriately humid, isothermal environment. Artifacts which already demonstrate cracking and crumbling require careful encasement in a suitable, safe restraining medium in the field. Consolidation and other conservation treatments must as always only be performed after thoroughly testing all procedures, recalling the often friable nature of these unique treasures.

Acknowledgements

We appreciate greatly the permission granted to us by the Egyptian Antiquities Organization to collect some samples from sites of archaeometric importance. We give special thanks to Drs. Shahata Adam and Ali el Khouli for their efforts on behalf of our endeavours in Egypt. Our field work was greatly facilitated by Mr. Mohammed el Saghir, Chief Inspector of Antiquities at Luxor, Mr. Sayed Abdel Hamid, Chief Inspector at Karnak, Mr. S. G. Bishay of the Research and Conservation Centre, Cairo, and by Mr. Yehia M. Eid, then Inspector of the West Bank, Luxor.

We wish to thank the centre franco-égyptien d'études des temples de Karnak for its interest in our research and especially C. Traunecker for his stimulating discussions. We appreciate the assistance of the American Research Centre in Egypt, Cairo. Our collaboration with the Egypto-Polish Archaeological Expedition, Deir el-Bahri, especially with the Head, Mme. J. Lipinska, is gratefully acknowledged. The initial insight into some of the archaeometric problems in Upper Egypt

was provided to us by Dr. Hismat Messiha and the late Dr. Zaki Iskander.

We wish to thank Mr. T. C. Billard and Mr. K. Nielson of the Chemistry Department at the University of Toronto for their advice on some chemical aspects of our work. We thank Dr. R. Hancock at the SLOWPOKE Reactor, and Drs. M. Gorton, C. Cermignani, and J. M. Allen of the Geology Department for their guidance and enthusiastic advice which they provided in a significant part of our instrumental study.

One of us (J.M.) would like to thank Dr. L. Yaffe for her initiation into the exciting field of Archaeometry.

This work was supported by the Natural Sciences and Engineering Research Council of Canada and by the University of Toronto.

1. E. M. WINKLER. Stone: properties, durability in man's environment. 2nd ed. Springer-Verlag, New York. 1975.
2. W. K. SIMPSON. MFA Bulletin, **77**, 36 (1979).
3. R. W. CHAPMAN. Am. J. Sci., **280**, 116 (1980).
4. E. P. BERTIN. Principles and practice of X-ray spectrometric analysis. Plenum Press, New York. 1970.
5. R. K. HANSEN and R. H. HALL. Anal. Chem. Acta, **92**, 307 (1977).
6. R. F. MUELLER and S. K. SAXENA. Chemical petrology. Springer-Verlag, New York. 1970. p. 50.
7. R. SAID. The geology of Egypt. Elsevier Publishing Co., New York. 1962. p. 259.
8. K. L. GAURI. The ARCE Newsletter, **114**, 35 (1981).
9. C. TRAUNECKER. Kêmi, **20**, 213 (1970).
10. T. C. BILLARD and GEORGE BURNS. Nature, **285**(5767), 654 (1980).
11. W. C. BRADLEY, J. T. HUTTON, and C. R. TWIDALE. J. Geol. **87**, 121 (1979).
12. J. VAN TASSEL and W. H. GRANT. J. Geol. **88**, 360 (1980).
13. G. P. ROGERS and H. D. HOLLAND. Geology, **7**, 278 (1979).
14. R. A. BERNER and G. R. HOLDREN, JR. Geology, **5**, 369 (1977).
15. R. A. NIXON. Geology, **7**, 221 (1979).
16. R. PAGE and H. R. WENK. Geology, **7**, 393 (1979).
17. E. M. WINKLER. J. Geol. **87**, 119 (1979).
18. E. M. DURRANCE. Geol. Mag. **106**, 496 (1969).
19. H. H. KU (*Editor*). Precision measurement and calibration. NBS Special Publication 300, **1**, 225-5-20, 213-5-10 (1979).

Analyses of construction materials by neutron-capture prompt γ-ray activation analysis

D. L. ANDERSON AND G. E. GORDON
Department of Chemistry, University of Maryland, College Park, MD 20742, U.S.A.

AND

E. A. LEPEL
Pacific Northwest Laboratory, Richland, WA 99352, U.S.A.

Received September 2, 1982

This paper is dedicated to Professor Leo Yaffe on the occasion of his 65th birthday

D. L. ANDERSON, G. E. GORDON, and E. A. LEPEL. Can. J. Chem. **61**, 724 (1983).

Neutron-capture prompt γ-ray activation analysis (PGAA) was used to measure concentrations of up to 18 elements in cement, sand, aggregate, and concretes and up to 9 elements in several types of steel. All major elements except oxygen are measurable in both types of samples. The observed elements, especially Ca and B, in concrete and its constituents allow one to determine the amount of cement used in the concrete, but additional elements would be needed to distinguish sand and aggregate.

D. L. ANDERSON, G. E. GORDON et E. A. LEPEL. Can. J. Chem. **61**, 724 (1983).

On a utilisé l'analyse de la capture électronique rapide par activation aux rayons γ (ARAG) pour mesurer les concentrations de 18 éléments du ciment, du sable, du gravier et du béton et de 9 éléments contenus dans différents types d'aciers. On peut mesurer tous les éléments principaux, à l'exception de l'oxygène, dans les deux types d'échantillons. D'après les concentrations d'éléments observés, spécialement le Ca et le B dans le béton et ses constituants, on peut déterminer la quantité de ciment utilisé dans le béton; toutefois il faut des éléments additionnels pour établir une distinction entre le sable et le gravier.
[Traduit par le journal]

Can. J. Chem. Downloaded from www.nrcresearchpress.com by 210.87.254.105 on 09/06/12
For personal use only.

Introduction

Previous studies of neutron-capture prompt γ-ray activation analysis (PGAA) with the use of neutron beams from nuclear reactors have demonstrated the technique's ability to measure concentrations of most major and minor elements and the trace elements B, Cd, Nd, Sm, and Gd in crustal materials such as soil, rocks, coal, and fly ash (1, 2). The uses of PGAA could be greatly expanded if portable systems based on isotope neutron sources (e.g., ^{252}Cf) or 14-MeV generators could be developed. Transportable sources could, for example, be used in geological exploration, for real time analysis of raw material or process streams in industry or to monitor the quality of materials at large construction sites. As both neutrons and high energy prompt γ-rays have long ranges in materials, PGAA has great advantages over essentially all other real time analytical methods, e.g., X-ray fluorescence, for the analysis of bulky, inhomogeneous materials because the other methods use signals of limited range that sample only surface materials, which may not be representative of the bulk material. In one of the first efforts to develop a working system, Reynolds *et al.* (3) developed a prototype ^{252}Cf-based system for analysis of coal for ash and sulfur content, which is now being tested in a coal-fired power plant. Vartsky *et al.* (4) have developed and are using a portable system based on a ^{238}Pu–Be neutron source for *in vivo* determination of Cd concentration in human kidneys and livers. It is being used to screen workers in industrial jobs that subject them to high exposure to Cd.

In general, beams of neutrons from reactors are easier to use than the neutrons from an isotopic source because the latter usually have lower fluxes which vary with distance from the source, as does the thermalization of the energy spectrum. Furthermore, to maximize sensitivity, one generally needs to use a large sample volume, which makes the effective geometry for γ-ray detection a complex function of neutron flux and thermalization. For these reasons, fundamental studies of potential applications of portable systems can be done more easily with neutron beams from reactors. Results of these studies will indicate the maximum number of elements that are likely to be observed with portable systems, and the best accuracy, sensitivity, and limits of detectability achievable. These results would allow a decision to be made as to whether or not it would be worthwhile to attempt development of a portable system for the intended application.

As noted, some potential applications of portable PGAA are in the construction industry, e.g., for quality control in plants that manufacture construction materials such as cement and steel or at construction sites, where contractors or inspectors might wish to monitor the quality of steel beams or concrete prior to or after installation. In order to determine the possible applicability of portable PGAA to these problems, we have used reactor-based PGAA to analyze samples of concrete and its ingredients as well as several types of steel.

Experiment

Cement, sand, aggregate, and concrete were obtained from construction sites of the Washington Public Power Supply System (WPPSS). The sand and aggregates (rock with a size range of 0.6–1.2 cm) used in the WPPSS concrete were obtained from along the Columbia River. The concrete samples were from test borings of shielding concrete intended for use at the WPPS power reactors. Samples for PGAA were prepared by forming ~1-g pellets of concrete, cement, and pulverized aggregate in a high pressure press and sealing them in Mylar bags. Sand would not form pellets and was placed loose in the Mylar bags. The steel samples were also formed into rather loose pellets to yield a geometrical configuration for which

TABLE 1. Photopeaks used for analysis of construction materials

Element	γ-Energy (keV) and source nuclide	
	Concretes and ingredients	Steel samples
H	2223.3 (^{2}H)	—
B	477.6 (^{7}Li)	477.6 (^{7}Li)
Na	472.3, 869.1, 874.4 (^{24}Na)	—
Mg	585.1 (^{25}Mg)	—
Al	1778.9 (^{28}Si)	—
Si	1273.3, 2092.8, 3539.2 (^{29}Si)	—
S	840.4 (^{33}S)	—
Cl	516.9, 786.3 + 788.4 (doublet) 1164.7 (^{36}Cl)	—
K	770.5 (^{40}K)	—
Ca	1942.7 (^{41}Ca)	—
Ti	341.7, 1381.5 (^{49}Ti)	341.7, 1381.5 (^{49}Ti)
V	1433.9 (^{52}Cr)	1433.9 (^{52}Cr)
Cr	—	749.0 (^{51}Cr); 834.9, 1784.8 (^{54}Cr)
Mn	212.0 (^{56}Mn); 847.0 (^{56}Fe)	847.0 (^{56}Fe)
Fe	352.3, 692.0 (^{57}Fe)	352.3, 692.0, 1725.2 (^{57}Fe)
Co	—	447.6, 555.8 (^{60}Co)
Ni	—	464.9, 878.1 (^{59}Ni)
Mo	—	719.6, 778.2 (^{96}Mo)
Cd	558.3 (^{114}Cd)	—
Nd	696.5 (^{144}Nd)	—
Sm	334.0, 439.4 (^{150}Sm)	—
Gd	181.9, 944.2, 962.1, 977.1 (^{158}Gd)	—

neutron self-shielding corrections could be calculated. The steel pellets had masses of 1.5 to 3 g.

The Mylar bags containing the samples were suspended in the center of Plexiglas sample holders with nylon fishing line to minimize the mass of material in the neutron beam. The sample holders were placed at a 45-degree angle with respect to the beam and to the axis of the Ge(Li) detector collimation system which is perpendicular to the beam. As described elsewhere (1, 5), the PGAA system uses a vertical beam on the top of the National Bureau of Standards (NBS) reactor. The neutron beam has a flux of about 2×10^{8} n/cm^{2}-s over a 3-cm diameter and a Cd (Cu) ratio of about 55. Samples were irradiated for up to 2 h and the spectra were obtained with a Ge(Li) detector of about 24% efficiency (relative to a 7.6- × 7.6-cm NaI crystal) surrounded by a large split-annulus NaI crystal that could be operated as an anti-Compton shield or pair detector. Spectra were stored and interpreted using a Tennecomp TP-5000 multichannel analyzer system based on a Digital Equipment Corp. PDP 11/34 minicomputer.

Typical spectra observed with the PGAA are given elsewhere (1, 5), as well as lists of the γ-rays used for the assay of the various elements. Concentrations of observed elements were determined by relating the areas of up to 5 peaks for each element to those of standards of the pure elements or simple compounds of them, with corrections for any flux changes based on the count rate observed with a Cr standard before or after irradiations of samples and other standards. In order to monitor the performance of the PGAA system, samples of standards for crustal materials were analyzed along with the samples: International Atomic Energy Agency standard soil, IAEA Soil 5, and the U.S. Geological Survey (USGS) standard rock, BHVO-1 (Hawaiian Basalt). In the case of the steels, the NBS Standard Reference Material SRM 1155 Steel was used as the standard for V, Mn, Fe, Co, Ni, and Mo. We used separate standards for Ti and B, whose concentrations are not certified in SRM 1155. To monitor the performance of PGAA for these samples, we also analyzed SRM 123C Steel. Table 1 presents the photopeak energies (and source nuclide) used for analysis in these samples. Note that delayed γ's were used for Al, V, and Mn, and that B is measured via the 477.6 keV γ-ray of ^{7}Li resulting from the ^{10}B(n,α) reaction.

Results

Results of analyses of the soil and rock standards are listed in Table 2. The errors expressed represent the combined procedural and statistical uncertainties in the case where a single photopeak was used. Where more than one photopeak was analyzed, the error represents the standard deviation of the results obtained from these combined with the procedural error. There is agreement within limits of error for all certified values in IAEA Soil 5. This is reasonable agreement with the information values with the major exceptions of B, Gd, and Si. Our value for B is surely the more accurate as our PGAA results for B in many standards have been quite reliable (1). Similarly, PGAA results for Gd are normally very accurate and the information value for Gd is surely much too high, as Sm and Gd concentrations are found to be almost equal in most crustal materials. We suspect that the Si information value is too high. Note that with PGAA, we observe all major and minor elements that are normally measured by geochemists except phosphorus (whose concentration is usually much less than 1%). As the concentration of oxygen is not usually measured, geochemists traditionally account for it by expressing concentrations of the elements in terms of their common oxides (e.g., Al_2O_3, Na_2O, etc.). We use the same method on PGAA data for crustal samples and are usually able to account for 96 to 100% of the sample mass (1). The major ambiguity of this approach for PGAA data is that we cannot distinguish between FeO and Fe_2O_3, which are both determined in wet chemical analyses. In soil, we feel it is safe to assume that the Fe is present as Fe_2O_3. Applying this method to both sets of data, we account for 98% of the soil mass with PGAA, whereas the IAEA data yield 104%, probably because of too high a Si value. Note that in summing the concentrations from PGAA, we are missing small contributions of mainly C and P_2O_5.

Can. J. Chem. Downloaded from www.nrcresearchpress.com by 210.87.254.105 on 09/06/12
For personal use only.

TABLE 2. PGAA analyses of soil and rock standards (one sample each)

	Concentration (% unless noted)			
	IAEA Soil 5		USGS BHVO-1	
Element	This work	Certified value[a]	This work	Gladney/Goode[b]
H	0.53±0.01	—	—	0.019 (1)[c]
B (μg/g)	85.7±0.4	(63)	3.6±0.3	2.3 (1)[c]
Na	1.92±0.04	1.92±0.11	1.69±0.06	1.64±0.06 (8)
Mg	1.8±0.4	(1.5)	4.2±0.4	4.30±0.12 (8)
Al	8.15±0.16	8.19±0.28	7.3±0.3	7.30±0.12 (8)
Si	27.3±0.3	(33)	22.7±0.6	23.3±0.4 (7)
S	0.18±0.04	—	—	0.01 (1)
Cl (μg/g)	315±12	—	80±30	92±4 (4)
K	1.86±0.01	1.86±0.15	0.42±0.02	0.46±0.07 (12)
Ca	2.54±0.07	(2.2)	8.12±0.12	8.18±0.12 (7)
Ti	0.52±0.01	(0.47)	1.63±0.03	1.60±0.05 (7)
V (μg/g)	160±60	(151)	350±50	314±12 (5)
Mn (μg/g)	900±100	852±37	1200±50	1270±40 (8)
Fe	4.41±0.19	4.45±0.19	8.28±0.11[d]	8.49±0.18 (10)[d]
Cd (ng/g)	1300±130	(1500)	200±100	120 (1)[c]
Nd (μg/g)	24±13	29.9±1.6	33±17	24±6 (6)
Sm (μg/g)	5.02±0.09	5.42±0.39	5.97±0.05	6.1±0.7 (7)
Gd (μg/g)	4.22±0.04	(35)	5.6±0.4	7±2 (7)
Total (as oxides)	97.9±1.0	104	97.5±1.6	99.7±0.9

[a] International Atomic Energy Agency Information Sheet Soil-5. Values in parentheses are information values, not certified.
[b] Gladney and Goode (6). Number of values in compilation is given in parentheses.
[c] Only value is from this laboratory (M. P. Failey thesis, 1979).
[d] Oxide calculated using observed fraction Fe as FeO, 78.7%, Gladney and Goode (6).

TABLE 3. PGAA analyses of concretes and ingredients (one sample each)

	Concentration (% unless noted)					
	WPPSS samples					Rancho Seco concrete
Element	Sand	Cement	Aggregate	Concrete #1	Concrete #2	
H	0.28±0.01	0.088±0.014	0.15±0.01	0.61±0.01	0.61±0.01	0.60±0.01
B (μg/g)	8.0±0.4	66.1±0.3	5.7±0.2	15.4±0.3	15.1±0.1	25.9±0.1
Na	2.35±0.04	0.33±0.08	2.16±0.10	1.68±0.05	1.56±0.09	1.35±0.08
Mg	2.3±0.5	1.7±0.4	2.2±0.3	1.7±0.3	1.3±0.1	2.2±0.4
Al	7.43±0.13	2.00±0.01	6.71±0.08	5.25±0.10	5.18±0.05	5.85±0.19
Si	29.5±1.0	10.2±0.2	26.2±0.5	22.9±0.1	23.5±0.4	25.5±0.6
S	—	1.02±0.01	—	0.22±0.04	0.15±0.01	0.16±0.02
Cl (μg/g)	50±10	—	72±7	50±20	67±5	56±15
K	1.31±0.03	0.53±0.02	1.15±0.02	1.06±0.02	0.92±0.01	0.83±0.02
Ca	5.48±0.13	43.1±0.3	4.8±0.1	11.6±0.1	12.76±0.05	11.1±0.2
Ti	1.30±0.01	0.111±0.002	1.06±0.01	0.75±0.01	0.74±0.01	0.343±0.004
V (μg/g)	390±60	—	430±70	500±60	360±20	400±80
Mn (μg/g)	1210±60	1000±100	1160±40	1030±70	800±10	810±50
Fe	8.01±0.14	2.13±0.02	6.96±0.05	5.02±0.10	4.97±0.04	3.61±0.10
Cd (ng/g)	—	—	—	—	200±40	350±110
Nd (μg/g)	—	—	24±13	—	14±5	33±12
Sm (μg/g)	6.85±0.04	1.96±0.02	5.65±0.05	4.47±0.01	4.14±0.02	3.25±0.02
Gd (μg/g)	6.45±0.10	1.51±0.11	5.65±0.12	4.17±0.05	3.89±0.06	3.02±0.17
Total (as oxides)	109.6±2.3	96.9±0.9	96.7±1.2	96.1±0.8	97.8±0.9	99.4±1.5

Concentrations are not certified in USGS standard rocks. Instead, compilations of data from various laboratories are used to establish accepted values. Except for the B value based on an earlier observation from our laboratory, the agreement of the present results with the data compiled by Gladney and Goode (6) is excellent.

Results of PGAA of the cement, sand, aggregate, and concretes are listed in Table 3. With PGAA we are able to determine concentrations of 20 to 23 elements in these types of samples. Except for the WPPSS sand (for which we suspect a weighting error), the summations of oxides are between 96 and 100%.

Can. J. Chem. Downloaded from www.nrcresearchpress.com by 210.87.254.105 on 09/06/12
For personal use only.

TABLE 4. Resolution of concrete composition into contributions from constituents

Element	Concentration (% unless noted)			
	Avg. of WPPSS concretes	Combinations (4% H_2O, 20% cement in all)		
		38% sand 38% aggregate	0% sand 76% aggregate	76% sand 0% aggregate
H	0.61±0.01	0.60	0.56	0.64
B (μg/g)	15.2±0.2	18.2	17.5	18.8
Na	1.64±0.05	1.7	1.7	1.7
Mg	1.4±0.2	2.0	2.0	1.9
Al	5.20±0.05	5.8	5.5	6.0
Si	23.1±0.2	22.2	22.0	22.5
K	0.98±0.06	1.0	0.98	1.0
Ca	12.4±0.3	12.3	12.2	12.4
Ti	0.74±0.01	0.88	0.82	0.93
Mn (μg/g)	850±100	1060	1080	1040
Sm (μg/g)	4.3±0.2	4.9	4.7	5.1
Gd (μg/g)	4.0±0.2	4.7	4.6	4.8

TABLE 5. PGAA analyses of steel samples (one sample each)

Element	Concentration (% unless noted)				
	Low-carbon	Stainless		NBS SRM 123C	
	SA 302	SA 316	SA 304	This work (2 samples)	Certificate
B (μg/g)	1.0±0.3	5.0±0.4	3.2±0.2	2.35±0.05	—
Ti (μg/g)	160±60	—	—	60±10	—
V (μg/g)	110±50	740±150	670±100	350±20	—
Cr	≤0.12	17.3±0.2	19.2±0.2	17.7±0.3	17.4
Mn	1.4±0.2	1.3±0.2	1.76±0.10	1.69±0.03	1.7
Fe	96.6±1.1	65.5±0.6	69.3±1.2	67.2±0.1	67.2
Co	≤0.12	0.14±0.01	0.112±0.008	0.110±0.001	0.12
Ni	≤0.05	13.1±0.15	9.68±0.13	11.35±0.03	11.3
Mo	0.45±0.03	2.05±0.02	—	0.23±0.01	0.22
Total	98.6±1.2	99.2±0.7	100.1±1.2	98.3±0.3	97.9

A major question in the studies of these materials is that of finding if one can determine the amounts of cement, sand, aggregate, and water present in the concrete on the basis of elements measurable with PGAA. We have made this test by normalizing the sand concentrations to 100% and then attempting to find a linear combination of the constituents that will sum to the average composition of the two WPPS concretes, with the results summarized in Table 4 for elements measured in all but water, which we assume is pure.

As shown in Table 4, we can make quite a reasonable fit to the composition of concrete with a mix of 4% H_2O, 20% cement, 38% sand, and 38% aggregate. There is little uncertainty in the 20% figure for cement, as the concentrations of many elements are quite different in cement from sand and aggregate: B, Na, Al, Si, Ca, Ti, Sm, and Gd. The water content is fixed rather firmly by the residual H after that from the other components is included. However, concentrations of the elements determined by PGAA are so similar in sand and aggregate that we cannot determine their relative contributions to the concrete. This point is emphasized in Table 4, where we show the range of concentrations obtained for sand contributions at the extremes of 0 and 76%. Unfortunately, differences in predicted concentrations in the concrete are so small that we cannot determine the sand/aggregate ratio. The compositions of the sand and aggregate are very similar, probably because the sand formed from the aggregates in the same source region (along the Columbia River) by physical processes (erosion, freezing, and thawing) that caused little chemical modification. In general, one would expect sands to be somewhat different in composition from the aggregates used in concrete. The samples are being subjected to INAA at Pacific Northwest Laboratories in order to determine if there are greater differences for some trace elements that are not observable by PGAA.

In Table 5 are shown the results of the steel analyses. The agreement of our results with the certified values for SRM 123C is extremely good. For the steels we have simply summed the observed concentrations and find that we account for 98 to 100% of the sample masses. We see that PGAA provides very good analyses of steels that pick up nearly all elements whose concentrations determine the physical properties of the steels. The major exception to this is carbon, whose concentration has a strong effect on the properties of steel. We observe carbon with PGAA in materials that contain considerable amounts of it, e.g., coals, biological samples, but the sensitivity for carbon is too low to observe it in these steels.

Discussion

We have shown that, with irradiations less than 2 h, PGAA provides reliable analyses of concrete and its constituents for up to 18 elements and steels for 9 elements, which account for 98

Can. J. Chem. Downloaded from www.nrcresearchpress.com by 210.87.254.105 on 09/06/12
For personal use only.

to 100% of the masses of the steel samples. The elements observable would allow one to determine the water and cement contents of concrete, but the compositions of the particular sand and aggregate used in this study were so similar that we could determine only the sums of their contributions, but not their relative amounts. In general, there would probably be more difference between their compositions, so one could probably distinguish between them. The PGAA method can be used to observe nearly all elements that determine the properties of steel, the major exception being carbon. In general, the fluxes of neutrons available from portable sources will be lower than those of the neutron beam; however, the effective masses of samples observable could be up to several kg in a field or plant operation, giving the possibility for similar analyses in few-minute periods.

Acknowledgements

We thank the staff of the NBS reactor for their excellent help and cooperation during this work. The University of Maryland portion of the work was supported in part by the U.S. Department of Energy under Contract No. DE-AS05-76ER-05173. The PNL portion of the work was supported by the Nuclear Regulatory Commission under Related Services Agreement with U.S. Department of Energy under Contract DE-AC06-76RLO-1830.

1. M. P. FAILEY, D. L. ANDERSON, W. H. ZOLLER, G. E. GORDON, and R. M. LINDSTROM. Anal. Chem. **51**, 2209 (1979).
2. C. C. GRAHAM, M. D. GLASCOCK, J. J. CARNI, J. R. VOGT, and J. G. SPAULDING. Anal. Chem. **564**, 1623 (1982).
3. G. REYNOLDS, E. ELIAS, T. GOZANI, T. MAUNG, and V. ORPHAN. Nuclear assay of coal. Vol. 1. Coal composition by prompt neutron activation analysis — basic experiments. Electric Power Research Institute Report EPRI FP-989, Jan. 1979.
4. D. VARTSKY, K. J. ELLIS, N. S. CHEN, and S. H. COHN. Phys. Med. Biol. **22**, 1085 (1977).
5. D. L. ANDERSON, M. P. FAILEY, W. H. ZOLLER, W. B. WALTERS, G. E. GORDON, and R. M. LINDSTROM. J. Radioanal. Chem. **63**, 97 (1981).
6. E. S. GLADNEY and W. E. GOODE. Geostandards Newslett. **5**, 31 (1981).

Can. J. Chem. Downloaded from www.nrcresearchpress.com by 210.87.254.105 on 09/06/12
For personal use only.

The irradiation of alkyl siloxanes in the adsorbed state. Part 3. The irradiation chemistry of hexamethyldisiloxane adsorbed onto silica

K-S. MAENG,[1] G. R. BROWN, G. J. TRUDEL,[2] AND L. E. ST-PIERRE
Department of Chemistry, McGill University, Montreal, P.Q., Canada H3A 2K6

Received September 15, 1982

This paper is dedicated to Professor Leo Yaffe on the occasion of his 65th birthday

K-S. MAENG, G. R. BROWN, G. J. TRUDEL, and L. E. ST-PIERRE. Can. J. Chem. **61**, 729 (1983).

Enhanced production of hydrogen, methane, and ethane from the γ-irradiation of hexamethyldisiloxane (MM) adsorbed onto silica compared to that from liquid MM results from energy transfer from the solid to the adsorbed layer. Chemical reactions with the surface are shown by deuterated products from the irradiation of MM on a deuterated silica and from extensive chemical cross-linking to the surface. These reactions predominate in the first monolayer of coverage.

K-S. MAENG, G. R. BROWN, G. J. TRUDEL et L. E. ST-PIERRE. Can. J. Chem. **61**, 729 (1983).

La production accrue d'hydrogène, de méthane et d'éthane observée lors de l'irradiation aux rayons-γ de l'hexaméthyldisiloxane (MM) adsorbé sur de la silice par comparaison avec les résultats obtenus avec du MM liquide provient d'un transfert d'énergie du solide à la couche adsorbée. On met en évidence des réactions chimiques avec la surface grâce à la formation de produits deutériés lors de l'irradiation du MM adsorbé sur de la silice deutériée et à partir d'une réticulation chimique importante de la surface. Ces réactions prédominent dans la première monocouche de matière.

[Traduit par le journal]

Can. J. Chem. Downloaded from www.nrcresearchpress.com by 210.87.254.40 on 09/06/12
For personal use only.

The use of γ-irradiation to effect chemical cross-linking for the production of rubbers is well-known. Since solid filler materials are used to enhance the properties of the final rubber, the effect of their presence on the irradiation chemistry is of special interest in our preparation of "ideal" elastomers.

Studies of the decomposition by γ-radiation of organic and inorganic materials adsorbed on chemically inert mineral supports have shown that excitation energy delivered to the solid from the radiation can migrate to the surface and become available for decomposition of the adsorbate. This has been evidenced by the enhancement of radiolysis products in the presence of a solid substance. For instance, Rabe *et al.* (1, 2) have reported a twentyfold increase in nitrogen yield for the irradiation of azoethane adsorbed on MgO as compared to the yield from liquid azoethane. Large increases have also been reported in the total gas yields from irradiation of isopropyl benzene at low coverages on silica gel (3) and of N_2O adsorbed onto silica (4).

Chahal and St. Pierre (5) have shown conclusively that chemical reaction occurs between a siloxane and silica when the system is exposed to γ-radiation. Chemical reaction with the surface has also been demonstrated by the fact that 85% of the methane produced by the irradiation of CD_3I in the presence of silica is CD_3H (6).

The present study compares the radiolysis behaviour of pure hexamethyldisiloxane (MM), described previously (7), with that when it is adsorbed onto silica. Through this comparison a number of phenomena, including the energy transfer in the siloxane–silica system, can be defined quantitatively.

Experimental

The materials, irradiation methods, and some of the analytical methods used have been described previously (7, 8). Experimental methods specifically involved with the adsorbed species are described below:

Preparation of the samples

Silica (~2 g, Cabosil M-5, 200 m^2/g) was placed into a 50 mL flask and degassed at room temperature by pumping until the pressure remained unchanged at 10^{-6} Torr for 2–3 h. Previously deaerated MM was transferred into the flask in the amount required for the desired degree of surface coverage, as determined by calculations (9) based on previous studies in this laboratory (10). Hexagonal packing with a cross-sectional area of 78 $Å^2$ was assumed for the adsorbed MM molecules. The flask was sealed, under vacuum, and allowed to equilibrate overnight before irradiation.

Analysis of irradiation products

After irradiation the sample flask was reattached to the vacuum system using a side arm with a "break-seal". The flask was cooled to Dry Ice temperature and the gaseous products were collected and analyzed as described previously (7, 8). The "liquid" products were then distilled from the sample flask, at room temperature, to a trap cooled to liquid nitrogen temperature. These products were analyzed by vpc.

Measurement of chemisorption

After product removal, the samples described above were washed ~30 times with 10 mL aliquots of benzene to remove physisorbed material. After they had been heated at 150° for 24 h in a vacuum oven the samples were pressed into a disc for infrared analysis. From the intensity of the absorption band at 2960 cm^{-1} (due to methyl groups) compared to that prior to irradiation and the data from C—H analysis the nature and amount of material chemically attached to the surface could be obtained.

Deuterated silica

Some deuterated silica was prepared, by exchange with D_2O, to determine whether production of gaseous products involved reactions with the surface. This exchange was accomplished by adding D_2O, under vacuum, to the silica and repeatedly heating to 100°C and cooling to liquid nitrogen temperature. After the water had been removed, this procedure was repeated with another aliquot of D_2O. The extent of deuteration was determined by ir, from the relative intensities of the absorption bands at 3750 and 2760 cm^{-1}, due to OH and OD groups, respectively, on the silica surface.

Results and discussion

Uniform coverage of the surface by the physisorbed MM was

[1]Present address: Chungnam National University, Daejon, Korea.
[2]Present address: Concordia University, Montreal, Canada.

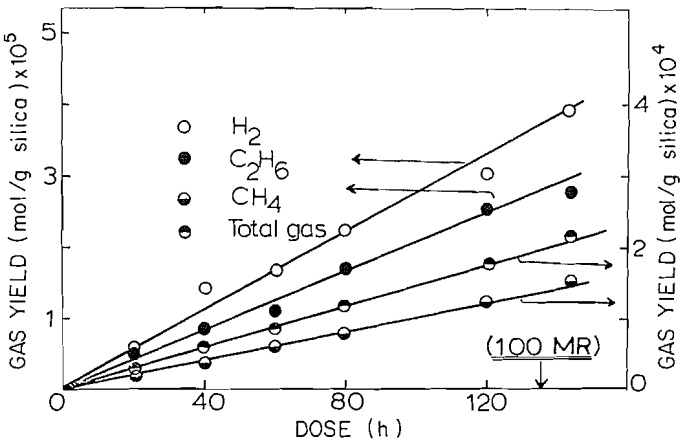

FIG. 1. The effect of radiation dose on gas yields from one monolayer of MM on silica (dose rate = 0.74 Mrad/h).

TABLE 1. *G* values for gas yields from pure MM and from MM on the silica at one monolayer coverage

Gas	Pure MM	Monolayer MM on silica
H_2	0.65	5.34
CH_4	2.22	18.4
C_2H_6	0.35	3.98
Total	3.22	27.7

assumed in the treatment of results. Calculation of the radiation dose received was on the basis of the adsorbed organic layer only. However, when discussing energy transfer, the energy absorbed by the inorganic fraction is considered.

1. *Effect of dose*

A. *Gas products from one monolayer*

The gaseous products of the irradiation of a monolayer of MM adsorbed onto silica are the same three, H_2, CH_4, and C_2H_6, produced by irradiation of pure liquid MM (7). The yields increase linearly with increasing dose up to 106 MR (Fig. 1). The *G* values, calculated from the slopes, along with the *G* values for production from pure MM are in Table 1. The yields of H_2 and of CH_4 are approximately 9 times greater than the yields from pure MM while the C_2H_6 yield is ~11 times greater.

Since MM adsorbed on to silica does not yield gases in the absence of irradiation, even after very long contact times, transfer of considerable radiation energy from the silica to MM is apparent.

B. *Liquid products from one monolayer*

At monolayer coverage of MM on silica the number of liquid products is greatly diminished compared to those from irradiation of pure MM. Only —SiOSiCH$_2$CH$_3$[3] and octamethyltrisiloxane (MDM), are produced. The yields increase nonlinearly with increasing dose (Fig. 2) and the *G* values (Fig. 3) are not much different than those for pure MM (1.1 and 0.5, respectively (11)).

C. *Radiation induced chemisorption*

It is evident from Fig. 2 that the total yield of the two liquid

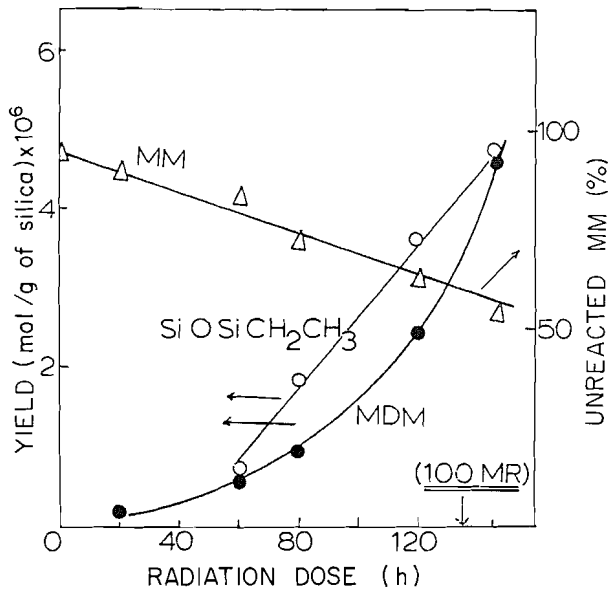

FIG. 2. The variation in the amount of unreacted MM and of the yields of liquid products from the irradiation of one monolayer of MM on silica with dose (dose rate = 0.74 Mrad/h).

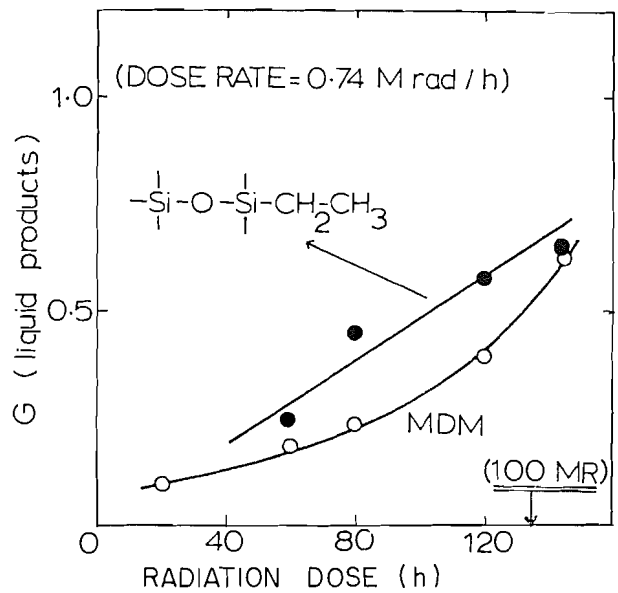

FIG. 3. The dependence on dose of the *G* values for liquid products from the irradiation of one monolayer of MM on silica.

products, at 100 MR, accounts for only 4.5% of the MM reacted (47%). This suggests that much of the MM, or its fragments, reacts in another manner. Accordingly, ir analysis of the washed and devolatilized silica from the irradiation was undertaken, as described in the Experimental section, to determine the degree of chemisorption or "cross-linking to the surface".

The *G* value and yields of MM chemisorbed as function of dose for one monolayer of physisorbed MM are illustrated in Fig. 4. A correction was made for the minute amount of chemisorption (6.5% of total material adsorbed after 10 days) that occurs in the absence of irradiation. Furthermore, in calculating the percentage MM chemisorbed from the amount of carbon present on the silica, the chemisorbed species was assumed to have the same carbon content as MM, specifically 44.4%. This is probably higher than the actual value, since the

[3]This "short" notation is used in this paper. The valence of all Si atoms is satisfied by the required number of methyl groups, thus —Si—O—Si—CH$_2$—CH$_3$ refers to (CH$_3$)$_3$Si—O—Si(CH$_3$)$_2$—CH$_2$CH$_3$.

Can. J. Chem. Downloaded from www.nrcresearchpress.com by 210.87.254.40 on 09/06/12
For personal use only.

TABLE 2. Deuterated gas yields from γ-radiolysis of one monolayer of MM on a deuterated silica surface

	Hydrogen			Methane			Ethane			
Product	H_2	HD	D_2	CH_4	CH_3D	CH_2D_2	C_2H_6	C_2H_5D	$C_2H_4D_2$	$C_2H_3D_3$
%	17.1	52.4	30.5	56.1	40.2	3.7	84.6	7.7	5.1	2.6
G (value)	4.55	13.91	8.04	5.94	4.26	0.39	1.35	0.12	0.08	0.04

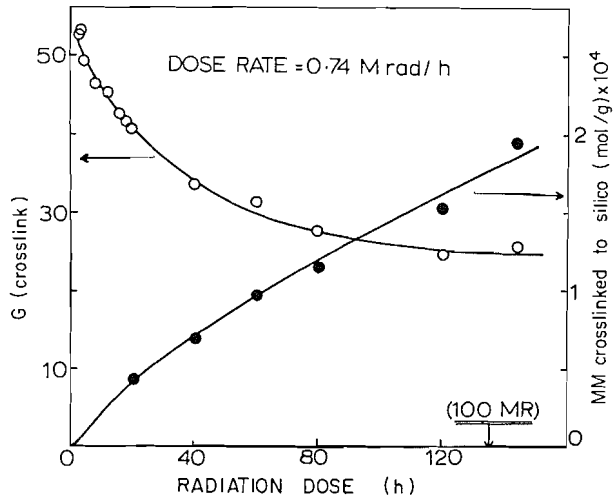

FIG. 4. The effect of radiation dose on the extent of cross-links to the silica surface during irradiation of one monolayer of MM on silica.

fragmentation patterns of pure MM indicate that the irradiation product undergoing chemisorption is probably one lacking a methyl group (40.8% carbon) or lacking a hydrogen atom (44.7% carbon) (12). The amount of MM chemisorbed on the surface increases with increasing dose but the G value for cross-linking to silica decreases with increased dose. This decrease is of course related to the diminishing concentration of unreacted MM with increased time or dose. The maximum coverage shown in Fig. 4 represents a chemical attachment of an MM fragment every ≈200 Å^2 of the silica surface. Based on an area of 78 Å^2 per MM the extent of surface coverage, θ, is ≈0.4.

D. *Chemical reactions at the interface*

That the silica surface is directly involved in the irradiation chemistry is also evident from the mass spectrometric analysis of the gaseous samples obtained from irradiating MM physisorbed on a silica surface which had been treated with deuterium oxide. Approximately 50% of the methane was produced as CH_3D, while 85% of the ethane was C_2H_6 with the remainder being composed of C_2H_5D, $C_2H_4D_2$, $C_2H_3D_3$ (Table 2).

2. *Effect of surface coverage*

For the study of product yields at surface coverages other than a monolayer, samples were prepared by admitting to a known quantity of silica sufficient MM to effect a calculated coverage assuming that all the MM was physisorbed. In the calculations the total MM present was used in calculating the energy absorbed in the organic phase.

A. *Gas products*

The effect of coverage on the yields and on the G values for the gaseous products is presented in Figs. 5 and 6. The G values for H_2 and CH_4 undergo a rapid and continuous decrease with increasing coverage suggesting that they are formed, at least in

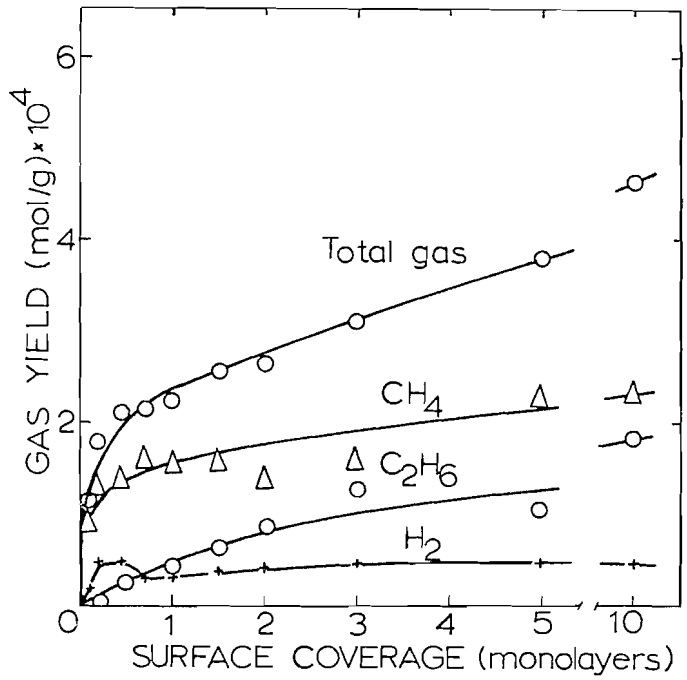

FIG. 5. The dependence on surface coverage of gas yields from the irradiation of MM on silica (dose = 106 Mrad).

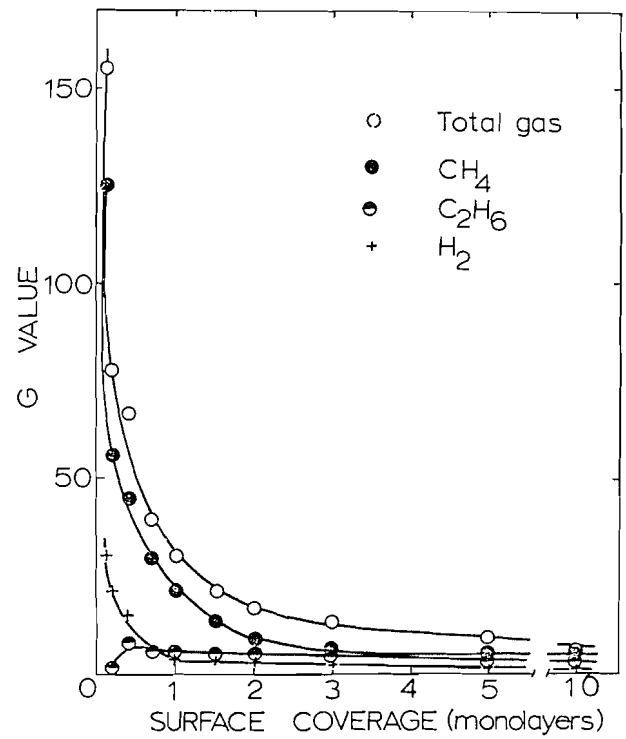

FIG. 6. The dependence on surface coverage of the G values for the gaseous products from the irradiation of MM on silica (dose = 106 Mrad).

Can. J. Chem. Downloaded from www.nrcresearchpress.com by 210.87.254.40 on 09/06/12
For personal use only.

Can. J. Chem. Downloaded from www.nrcresearchpress.com by 210.87.254.40 on 09/06/12
For personal use only.

part, by a reaction between the silica and the first layer of MM. This is the region where energy transfer to the MM can be expected to take place. The asymptotic approach of the curves to the abscissa shows that the maximum enhancement is realized below one monolayer. At greater coverage the yields approach those for MM in its liquid state.

On the other hand, ethane yields increase up to one monolayer coverage followed by a slight but continuous decrease thereafter. This suggests that although ethane formation is associated with the transferred energy it is not directly dependent on the presence of the silica as appears to be the case for H_2 and CH_4. This suggestion gains credence from the fact that at very low coverage ethane is not formed. This suggests that it is formed by the reaction of CH_3 fragments formed near the silica surface. At very low coverages these fragments react exclusively with the surface to form CH_4 resulting in the very high $G(CH_4)$. As the coverage increases a bimolecular reaction involving a methyl fragment and probably a parent MM molecule becomes more prominent.

From gas yields it is obvious that the highest percentage of energy transfer is realized at coverages well below a monolayer.

B. *Liquid products*

Liquid products were formed in detectable amounts only at one monlayer and above. At one monolayer the liquid products, shown in Fig. 2, were —Si—O—Si—CH_2CH_3 and MDM, with trace amounts of such cyclics as octamethylcyclotetrasiloxane (D_4) and decamethylcyclopentasiloxane (D_5).

At ten monolayer coverage, nine products were found (Table 3). Of the products formed, only the methyl addition product, —Si—O—Si—CH_2CH_3, is present in a yield approximating that from the liquid state. MDM, on the other hand, which is a product from a demethylated fragment, exhibits a tenfold increase over the yield from pure MM. Reference to Fig. 3 shows that the G value for this MDM increases with dose, suggesting that it is formed from reaction products of the initial irradiation event. These products may react either with the surface or with a MM molecule. As the dose increases the surface becomes less available because of the chemisorption and reaction with MM increases.

The fragmentation behaviour of MM (12) suggests the predominant ion fragment is —Si—O—Si^+. This ion can then undertake an electrophilic attack on an unreacted MM molecule yielding MDM.

$$—Si—O—Si^+ + —Si—O—Si— \rightarrow —Si—O—Si—O—Si— + —Si^+$$

Attack by the product ion Me_3Si^+ on MM will, however, result in an exchange with no new product formed. This can be assumed to continue until neutralization or reaction with the surface occurs. The presence of the silica and the energy transfer from that species enhances the yield of the initial ion and thus the yield of MDM. At higher coverages the competition of the MM with the surface for reaction with the initial ion is enhanced, with the resulting increased yields.

The sharply diminished yields in all other liquid products compared to those from pure MM, with the lowest yields being at low coverages, may be explained on the basis of competition at the surface. It seems surprising, however, that even at 10 monolayers the yield of dimer is only ~1/6 that from pure MM.

TABLE 3. Liquid products at ten monolayers of MM on silica[a] (dose = 106 MR)

Products	Moles ($\times 10^6$)	G values ($\times 10^2$) Ten monolayers MM	Pure MM
—$SiCH_3$	0.922	0.618	3.0
—SiOSi—H	2.34	1.56	12
—SiOSi—Et	44.7	30	34
MDM	358	240	21
D_4	9.03	6.04	—
MD_2M	0.653	0.438	60
—SiOSiSiOSi—	4.51	3.02	17
D_5	1.54	1.03	—
—$SiOSiCH_2SiOSi$—	3.82	2.56	116

[a]MM (unreacted): 41.7%.

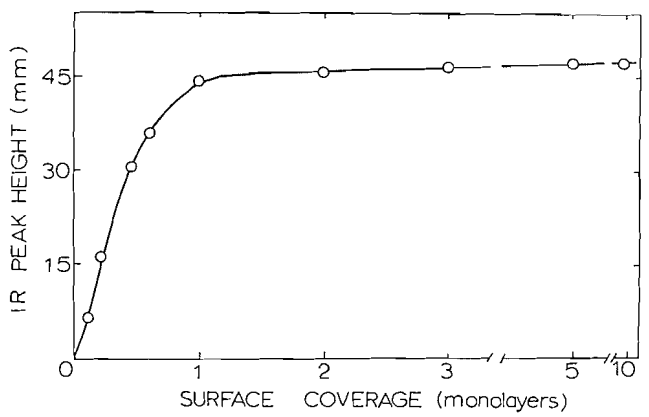

FIG. 7. The effect of MM coverage on the infrared absorption at 2960 cm^{-1} due to material cross-linked to the surface (dose = 106 Mrad).

C. *Chemisorption (fixed dose = 106 MR)*

Figure 7 gives the effect of coverage on the extent of chemisorption that occurs at a dose of 106 MR. These results, obtained by ir analysis of irradiated samples that had been treated as described previously, indicate that the major portion of the silica–MM reaction is between the primary layer of adsorbed MM and the silica.

At a coverage of 0.4 monolayer adsorbed, a maximum is obtained in the fraction of available MM that attaches to the silica (Fig. 8) after irradiation with 106 MR. This suggests that the process of energy transfer occurs only at specific sites on the adsorbent surface and that these are expended at a coverage in excess of 0.4 monolayer. The nature or origin of such centres is a matter of conjecture but will be discussed in a later publication.

It seems reasonable to assume that $G_{(\text{total gas observed})} - G_{(\text{total gas for liquid MM})} = G_{(\text{cross-links to silica})}$. At ten monolayer coverage the G value for total gas is 6.06 (Fig. 6) as compared to 3.22 for pure MM (11). On this basis $G_{(\text{cross-links to silica})}$ is equal to 2.84, which is an excellent agreement with the value of 2.79 obtained directly (Fig. 9). However, the G values for total liquid products at ten-layer coverage and for liquid MM are identical, i.e. 2.8. For pure siloxanes (MM) it is normally found that $G_{(\text{total gas})}$, $= G_{(\text{liquid product})}$ (13). That this is not so for adsorbed MM may be associated with the excess yield of MDM referred to previously. The G value of 2.79 for cross-linking to the surface is in good agreement with the G values found for cross-linking in other siloxane–siloxane systems, e.g.,

Can. J. Chem. Downloaded from www.nrcresearchpress.com by 210.87.254.40 on 09/06/12
For personal use only.

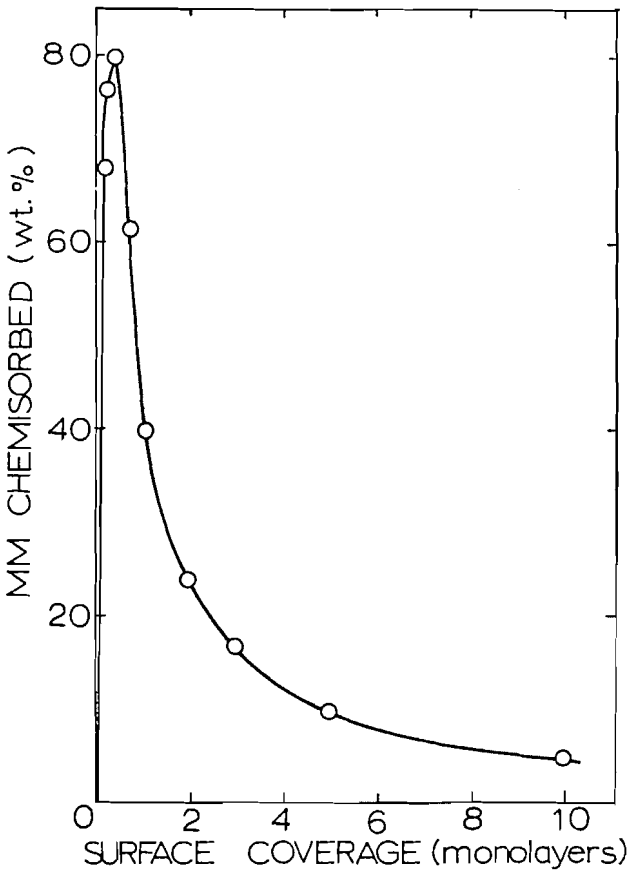

FIG. 8. Percent of initial MM chemically absorbed to silica due to irradiation as a function of surface coverage (dose= 106 Mrad).

2.5 ± 0.3 by Barnes *et al.* (14), 3.0 by Miller (15), and a value of 2.5 ± 0.4 found by St. Pierre *et al.* (13), and would undoubtedly reduce to that value at still higher coverages.

Summary and conclusions

This study of the irradiation chemistry of hexamethyldisiloxane adsorbed onto silica shows some product yields to be markedly enhanced by the presence of the silica while other products have sharply diminished yields. Control of the surface composition has allowed the determination of the interphase reactions occurring, while changes in extent of surface coverage have shown the enhancement to occur predominantly at the surface of the particle. Chemisorption to the surface of the silica is a major result of the irradiation of physisorbed MM. The effects of various parameters on the products and on the interaction between the MM and silica is interpreted on the basis of an energy transfer mechanism. Details of this mechanism will be described in a future publication.

These results will also be used to rationalize the structure and behaviour of elastomeric composites.

Acknowledgements

The authors wish to acknowledge the financial support of NSERC and FCAC for this work.

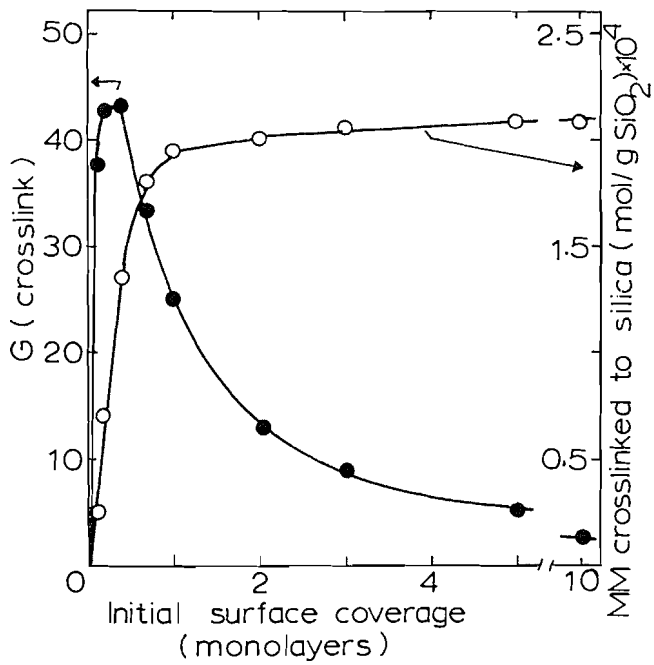

FIG. 9. The effect of extent of surface coverage on the extent of cross-links to the silica surface during irradiation by a 106 Mrad dose.

In submitting this paper to the "Leo Yaffe Issue" of the Canadian Journal of Chemistry, we give witness to our esteem and affection for an excellent scientist and a good friend. Leo has been to all of us truly "A man for all seasons".

1. J. G. RABE, B. RABE, and A. O. ALLEN. J. Am. Chem. Soc. **86**, 3887 (1964).
2. J. G. RABE, B. RABE, and A. O. ALLEN. J. Phys. Chem. **70**, 1098 (1966).
3. E. A. ROJO and R. R. HENTZ. J. Phys. Chem. **70**, 2919 (1966); G. G. MEISELS, W. H. HAMILL, and R. R. WILLIAMS, JR. J. Phys. Chem. **61**, 1456 (1957).
4. N. H. SAGERT and R. W. ROBINSON. Can. J. Chem. **46**, 2075 (1968).
5. R. S. CHAHAL and L. E. ST-PIERRE. Can. J. Chem. **47**, 2311 (1969).
6. N. H. SAGERT, J.A. REID, and R. W. ROBINSON. Can. J. Chem. **48**, 17 (1970).
7. K-S. MAENG, G. J. TRUDEL, and L. E. ST-PIERRE. Polymer (Korea), **6**, 98 (1982).
8. K-S. MAENG, G. J. TRUDEL, and L. E. ST-PIERRE. Polymer (Korea), **6**, 107 (1982).
9. D. A. YOUNG and A. D. CROWELL. Physical adsorption of gases. Butterworth, London. 1962 p. 226.
10. H. BRENDER. Thesis, McGill University, Montreal, 1971.
11. H. A. DEWHURST and L. E. ST-PIERRE. J. Phys. Chem., **64**, 1063 (1960).
12. V. YU. ORLOV. J. Gen. Chem. USSR, **37**, 2188 (1967).
13. L. E. ST-PIERRE, H. A. DEWHURST, and A. M. BUECHE. J. Poly. Sci. **36**, 105 (1959).
14. W. BARNES, H. W. DEWHURST, R. W. KILB, and L. E. ST-PIERRE. J. Poly. Sci. **36**, 525 (1959).
15. A. A. MILLER. J. Am. Chem. Soc. **82**, 3519 (1960).

Platinum group elements in seawater. I. Palladium

H. V. WEISS
Radiation Physics, Naval Ocean Systems Center, San Diego, CA 92152, U.S.A.
AND
JAMES FRESCO
Department of Chemistry, McGill University, Montreal, P.Q., Canada H3A 2K6

Received September 16, 1982

This paper is dedicated to Professor Leo Yaffe on the occasion of his 65th birthday

H. V. WEISS and JAMES FRESCO. Can. J. Chem. **61**, 734 (1983).

Palladium was coprecipitated quantitatively from seawater with an added bismuth carrier precipitated as a sulfide. The ^{109}Pd formed upon neutron irradiation of the isolated material was measured by γ-ray spectrometry following radiochemical purification. By this procedure the concentration of palladium in Pacific coastal water was measured as $2.2 \pm 1.2 \times 10^{-10}$ g per L.

H. V. WEISS et JAMES FRESCO. Can. J. Chem. **61**, 734 (1983).

On a fait coprécipiter quantitativement le palladium de l'eau de mer avec un support de type bismuth ajouté sous forme de sulfure. Faisant appel à la spectrométrie de rayons γ, on a mesuré le ^{109}Pd formé par irradiation neutronique du produit isolé après une purification radiochimique. Le procédé a permis de mesurer la concentration en palladium de l'eau côtière du Pacifique. Elle est de $2,2 \pm 1,2 \times 10^{-10}$ g par L.

[Traduit par le journal]

Introduction

Reports of the concentration of platinum group elements in the oceans are non-existent. On the basis of recent work it was concluded that the concentration of palladium was less than 4 ng/kg (1). Minute oceanic quantities combined with insufficiently sensitive analytical procedures have undoubtedly contributed to the neglect of this family of elements. The recent development of a kilolitre seawater sampling system (2) has stimulated our interest in oceanic species such as the platinum group that have heretofore eluded detection. Since the crustal abundance of palladium is considerably greater than that of the other platinum group elements, its search was favored as an entree to the subject.

The procedure involved separation of palladium with added bismuth carrier subsequently precipitated as a sulfide from volumes of seawater in the range 660–1680 L. The solids were collected on filter membranes, dissolved therefrom, and then activated with neutrons. After radiochemical purification the radiations from ^{109}Pd were measured by γ-ray spectrometry, a value from which the concentration of palladium in a sample was derived.

This report describes the results of such measurements with Pacific Ocean waters off the coast of California.

Experimental

Chemicals

Palladium carrier solution (9.63 mg/mL) and stock palladium standard solution (122 μg/mL) were prepared by dissolving 99.999% pure palladium in aqua regia and diluting with de-ionized water.

Bismuth carrier solution (4 mg/mL) was prepared by dissolution of 100.0% pure bismuth metal in dilute nitric acid.

Holdback carrier solutions used in radiochemical purification steps were 10 mg/mL of the ion of interest.

Other chemicals used were analytical reagent grade.

Isolation of palladium from seawater

Preliminary experiments with palladium radiotracer in 1 L volumes of seawater indicated that when seawater containing 10 or 20 mL/L of hydrochloric acid and 0.5 mg/L of bismuth is treated with hydrogen sulfide gas, the palladium is quantitatively recovered with the solid phase to the extent of 98.5 ± 4.2% and 94.7 ± 2.8% at the respective hydrochloric acid concentrations.

Separation of particulates from seawater

The separation of solids from seawater was achieved by forcing the fluid through a Hi Vol-60 filtration apparatus (Nuclepore Corporation, Pleasanton, California 94566) at 50 psi with a pump of fiberglass construction powered by a 7 Hp motor. An in-line flow sensor coupled to a batch controller affords measurement of accumulated volume.

The Hi Vol-60 consists of a stainless steel housing which is provided with plastic plates and screens that support up to 60 Nuclepore membrane filters each of which is 293 mm in diameter. With this apparatus certain solids in 3000 L of seawater have been separated in less than 15 min (2).

Samples and sample treatment

Seawater samples were obtained from a Naval Ocean Systems Center facility at the southern end of Pt. Loma, California whose main purpose was to provide large volumes of fresh seawater to tanks that supported marine life. The design was such that water flowed through a 24 in. diameter concrete pipe to a concrete-lined sump whose bottom was 25 ft below sea level. The sea-ward open end of the pipe was situated 760 ft from the shore line, 5 ft above the sediment and at mean-tide, 10 ft from the water surface. From the sump, a pump of stainless-steel construction transports the water to the shore-based tanks through 2 in. diameter polyvinyl chloride (PVC) tubing. Access to this water was available for this study through a shunt controlled with a PVC valve.

From the shunt water was collected in a 40 000 L fiberglass tank on two occasions (27 April and 8 July 1982). Upon accumulation of an appropriate volume, the seawater was immediately filtered through the Hi Vol-60 system fitted with membranes of 0.45 μm porosity. The filtrate was collected in a 3 400 L polyethylene-lined dolphin-holding tank. During this process concentrated hydrochloric acid was siphoned into the sample to give a final concentration of 10 mL/L. Mixing was assisted by the introduction of a stream of compressed air bubbles conducted through a manifold of submerged fritted glass discs. When

Can. J. Chem. Downloaded from www.nrcresearchpress.com by 210.87.254.42 on 09/06/12
For personal use only.

Can. J. Chem. Downloaded from www.nrcresearchpress.com by 210.87.254.42 on 09/06/12
For personal use only.

mixing was judged to be complete, the requisite quantity of bismuth carrier was introduced into the sample and homogeneity was attained through further mixing. The compressed air stream was then exchanged with a stream of hydrogen sulfide gas to precipitate bismuth sulfide. The precipitate was collected on either 30 or 60 Nuclepore membranes, depending upon the sample volume to be processed. Sample volumes ranged from 660–1680 L. The filtrate from the bismuth sulfide scavenged seawater was collected in another polyethylene dolphin-holding tank, to ultimately provide data on a blank. The volume of water used for the blank was 1400 L.

From 250–500 L fresh water was pumped through the Hi Vol filtration system from another holding tank containing water to remove residual sea salts.

The Hi Vol system was disassembled and the sulfide was dissolved from the surface of the filters by soaking each successively in a basin of freshly prepared aqua regia. The filters were then successively rinsed in another basin of distilled water.

The aqua regia and wash solution were combined and resulted in a volume of 3–3.5 L which was evaporated to a volume of 10 mL. About 25 mL of nitric acid were added and again the volume was reduced. This treatment was twice repeated. The final solution was transferred with concentrated nitric acid washings to two 14-mL polyethylene vials. A known weight of iron wire was affixed to each vial to serve as a flux monitor.

Blanks

The filtrate from bismuth sulfide scavenged seawater, after addition of bismuth carrier and hydrochloric acid equivalent to the quantities added initially, was processed in the manner described for samples.

A reagent blank consisted of 8 L of concentrated hydrochloric acid and 400 mg of bismuth carrier. This mixture, after evaporation to a volume of 10 mL, was prepared for irradiation by repeated nitric acid additions and evaporations, such that essentially all BiOCl was solubilized.

Irradiation and post-irradiation procedure

Samples, blanks, and standards (1.22 μg Pd) were irradiated for 2 h in the lazy susan compartment of the TRIGA nuclear reactor at the University of California, Irvine. The thermal neutron flux was 1.7×10^{12} neutrons cm^{-2} s^{-1}. After irradiation the solutions were transferred from their vials with hot nitric acid. One mL volumes of palladium, sodium, and copper carriers were added to the sample and blank solutions and successive evaporations to near dryness were performed with added nitric and hydrochloric acids.

Following dilution with 50 mL 0.4 *M* nitric acid the solutions were filtered to remove small amounts of BiOCl. A 4 mL volume of 1% dimethylglyoxime was added to each solution and after precipitation of the palladium dimethylglyoximate, the chelate was filtered and washed with 0.4 *M* nitric acid in a sintered glass crucible. The chelate was dissolved in hot concentrated nitric acid and evaporated to dryness.

After dissolution in 0.4 *M* nitric acid and addition of fresh sodium and copper carriers, the precipitation and destruction of the chelate was repeated twice more. The final residue was dissolved in 50 mL 1 *M* hydrochloric acid and hydrogen sulfide gas was bubbled through the solution for about 30 s. The palladium sulfide formed was filtered onto a 1-cm membrane filter, mounted on a 1-cm aluminum planchet, and covered with a thin Mylar film.

The irradiated palladium standards, after addition of palladium carrier, were reduced in volume to remove excess nitric acid and were then precipitated directly as the sulfide and mounted for measurement as described above.

Measurements

The 88 keV photopeak of palladium-109 was counted with a 38-cm^3 Ge (Li) detector linked to a 4096-channel pulse height analyzer. These data were transferred to a computer which provided the net counting rate for this nuclide. The decay of the photopeak was followed through several half-lives.

Flux monitors

The iron wire flux monitors were γ-ray counted with a NaI (Tl) well-type detector coupled to a scaler. ^{109}Pd counting rates were normalized for variations in flux.

TABLE 1. The concentration of palladium in a reagent and seawater blank and in seawater collected on two different dates corrected for the seawater blank

	Volume (L)	Pd concentration ($g/L \times 10^{-10}$)
Blanks		
Reagent	(800)*	0.79
Seawater	1400	0.98
Seawater		
27 April 1982	660	3.47
	990	0.52
	1680	2.37
8 July 1982	890	2.32

*The bismuth carrier and hydrochloric acid which comprised the reagent blank were in amounts equivalent to that added to an 800 L sample.

Palladium carrier recoveries

Sample, blank, and standard palladium sulfide precipitates and 0.5 mL volumes of palladium carrier comparators were transferred to 1.4 mL polyethylene vials after complete ^{109}Pd decay. The vials were irradiated sequentially for 1 min in the pneumatic tube assembly of the TRIGA nuclear reactor at full-power level. The initial ^{109}Pd activity measurements were corrected for chemical yield according to the palladium carrier counting rates.

Results and discussion

The carrier yield for samples and blanks ranged from 40–75% and the yield for the standards was about 97%. Further, with the irradiation schedule used about 700 counts min^{-1} μg^{-1} palladium are acquired in the photopeak area at the end of irradiation. Initial counting period of an irradiated sample was usually 15–30 min in duration and occurred about 6 h after the end of irradiation, a time at which less than 30% of the activity had undergone decay. Thus even for samples of the least activity, the counting error was of the order of 10%.

During the course of radiochemical purification γ-ray spectra were acquired. The major contaminants were ^{24}Na, ^{198}Au, and a 0.51 Mev photopeak which was probably attributable to the copper contaminant in the hydrochloric acid used to acidify the seawater samples. Repeated dimethylglyoxime precipitations were required to eliminate the tentatively identified ^{64}Cu, the other contaminants having been essentially decontaminated with the first purification step.

The decay of samples and blanks was consistent with the half-life of ^{109}Pd (13.5 h).

The concentration of palladium in blanks and seawater samples collected on two different dates appear in Table 1. The quantity of palladium in the reagent blank was 0.79×10^{-10}g/L-equiv. The relative contribution of hydrochloric acid and bismuth salt to this value was not established. The bismuth sulfide scavenged seawater blank (0.98×10^{-10} g/L) was only slightly greater than the reagent blank. This result indicates that manipulations involved in sample treatment from the time of collection up to preparation for irradiation are essentially noncontaminating.

The palladium concentration in four seawater samples, after subtraction of the seawater blank, averaged $2.17 \pm 1.22 \times 10^{-10}$ g/L. The magnitude of the standard deviation is attri-

butable to an inordinately low value of 0.52×10^{-10} g/L for the 990-L sample. The basis for this discrepancy is not understood. During the course of this study adsorption of activated palladium on the surface of the irradiation vials was encountered; however, this source of error was obviated by rinsing the vials with hot nitric acid which effects quantitative desorption. Other explanations such as non-quantitative bismuth sulfide precipitation or collection are considered remote.

The average palladium value is within the range reported for the concentration of a number of the rare earth elements, indium and scandium (3). These appear to be the least concentrated of the non-radioactive elements in seawater. Although factors such as seawater speciation which is principally carbonate for rare earths, hydroxide for indium and scandium (4), and probably chloride for palladium make a comparison uncertain, it appears that only in the case of palladium is a low crustal abundance, 0.01 gt^{-1} (5), accompanied by a low seawater concentration.

Acknowledgement

We thank John Ruffoni, a San Diego State University student, for his assistance in the operation of the large volume sampler to separate bismuth sulfide from seawater.

1. K. J. R. ROSMAN, J. R. DE LAETER, and A. CHEGWIDDEN. Talanta, **29**, 279 (1982).
2. H. V. WEISS. Application for letters patent. Isolation from seawater of radionuclides. U. S. Navy Case No. 64531, 10 June 1982.
3. P. L. BREWER. Chemical oceanography. *Edited by* J. P. Riley and G. Skinner. Vol. 1. 2nd ed. Academic Press, New York, NY. 1975. pp. 417–420.
4. D. R. TURNER, M. WHITFIELD, and A. G. DICKSON. Geochim. Cosmochim. Acta, **45**, 855 (1981).
5. J-C. ALLÈGRE and G. MICHAUD. Introduction to geochemistry. Reidel Publishing Co., Boston, MA. 1974. p. 10.

Can. J. Chem. Downloaded from www.nrcresearchpress.com by 210.87.254.42 on 09/06/12
For personal use only.

Barriers to rotation of the cyclopentadienyl ligand: spin-lattice relaxation time measurements and atom–atom potential calculations on cyclopentadienyl manganese and rhenium tricarbonyl and vanadium tetracarbonyl complexes

D. F. R. GILSON,[1] G. GOMEZ, I. S. BUTLER,[1] AND P. J. FITZPATRICK

Department of Chemistry, McGill University, 801 Sherbrooke Street West, Montreal, P.Q., Canada H3A 2K6

Received September 17, 1982

This paper is dedicated to Professor Leo Yaffe on the occasion of his 65th birthday

D. F. R. GILSON, G. GOMEZ, I. S. BUTLER, and P. J. FITZPATRICK. Can. J. Chem. **61**, 737 (1983).

The barriers to cyclopentadienyl ring rotation in the solid phase have been measured by spin-lattice relaxation time methods for the organometallic complexes $CpMn(CO)_3$ (7.24 kJ mol^{-1}), $CpRe(CO)_3$ (7.15 kJ mol^{-1}), and $CpV(CO)_4$ (7.07 kJ mol^{-1}), where Cp = η^5-C_5H_5. Nonbonded atom–atom potential calculations of the barriers in these complexes and in $BzCr(CO)_3$ (Bz = η^6-C_6H_6) show that the molecular conformation of the Mn and Re compounds is determined by crystal packing forces and that concerted ring motions are possible for the cyclopentadienyl complexes, but not for the benzene chromium tricarbonyl.

D. F. R. GILSON, G. GOMEZ, I. S. BUTLER et P. J. FITZPATRICK. Can. J. Chem. **61**, 737 (1983).

Faisant appel aux méthodes de temps de relaxation spin-réseau, on a mesuré les barrières à la rotation du cycle du cyclopentadiényle en phase solide des complexes organométalliques $CpMn(CO)_3$ (7,24 kJ mol^{-1}), $CpRe(CO)_3$ (7,15 kJ mol^{-1}) et $CpV(CO)_4$ (7,07 kJ mol^{-1}) où Cp = η^5-C_5H_5. Des calculs de barrières de potentiel entre atome et atome non liés, dans ces complexes et dans le $BzCr(CO)_3$ (Bz = η^6-C_6H_6) montrent que la conformation moléculaire des composés du Mn et du Re est déterminée par les forces d'entassement du cristal et que les mouvements concertés de cycle sont possibles pour les complexes du cyclopentadiényle, mais non pour le benzène chrome tricarbonyle.

[Traduit par le journal]

Introduction

There has been a revival of interest in recent years in the long-standing controversy over the possible bonding modes of the cyclopentadienyl ligand in organometallic π-complexes (1, 2). In most cases the carbon–carbon bond lengths within the cyclopentadienyl ring appear to be equal, but occasionally distortions of the ring geometry are reported and interpreted in terms of contributions from "allyl-ene" or diene structures having C_{2v} symmetry arising from preferential interaction of one of the two degenerate Cp ring π-orbitals with the metal *d* orbitals (3–8). Perhaps the most convincing evidence to date has been presented for complexes containing penta-methyl or penta-chloro substituted cyclopentadienyl ligands where the librational motion of the ring is damped compared with that of the unsubstituted ligands (3, 4, 6). For unsubstituted cyclopentadienyl rings, recent X-ray studies on the rhenium (7) and manganese (8) tricarbonyl complexes, including a low temperature study[2] on the latter, have clearly shown the presence of bond length variations.

Confirmation of such bonding patterns for the cyclopentadienyl ligand via X-ray crystallography requires precise structural studies which include appropriate rigid body librational analyses and corrections to the observed bond distances for thermal effects. Despite the obvious connection between cyclopentadienyl ring motion and these librational effects there has been relatively little attention paid to the dynamics of ring rotation in the solid state. Nuclear magnetic resonance line-width and second moment studies generally do not exhibit line broadening transitions down to 77 K, the lowest temperature easily accessible in such experiments, and thus the barrier to the ring rotation must be less than 12 kJ mol^{-1} (9). Spin-lattice relaxation time measurements have been more profitable and rotational barriers have been reported for Cp_2Fe (10, 11), Cp_2Ru (10, 11), Cp_2TiCl_2, (10), Cp_2MoCl_2 (12), $CpTiCl_3$, $Cp_2Mo_2(CO)_6$, and Cp_2TiS_5 (13). In addition, several less orthodox techniques have been applied. The ^{13}C chemical shift anisotropy in several cyclopentadienyl complexes is averaged by ring rotation at 77 K so that the barriers could not be determined (14), but for the heavily substituted decamethylferrocene, $(\eta^5\text{-}C_5Me_5)_2Fe$, the motion is limited at low temperature permitting the measurement of a barrier of 13.5 kJ mol^{-1} (15). Bennet *et al.* (16) have analysed the X-ray data from several organometallic complexes and derived barrier heights assuming a form for the potential function. Eisenberg *et al.* (17) have employed mechanical spectroscopy to study reorientational behaviour of some cyclopentadienyl platinum complexes dissolved in a polystyrene matrix.

The theoretical studies of molecular conformation and rotational barriers in transition metal complexes have been reviewed by Albright (18). Low barriers are predicted to occur for η^4-cyclobutadienyl – ML_3, η^5-cyclopentadienyl – ML_3, and η^7-cycloheptatrienyl – ML_3 complexes. Such calculations refer, of course, to the electronic contribution to the internal barrier and in the solid phase this will be augmented by intermolecular contributions and the molecular conformation will be affected by crystal packing forces.

Fyfe and co-workers (11) have applied nonbonded, atom–atom potential calculations to ferrocene, ruthenocene, and bis(benzene)chromium(0) complexes and, although their calculations for ferrocene were based upon the wrong crystal structure (19, 20), they demonstrated that this technique can provide useful information on the origin and magnitudes of the various contributions to the rotational barriers. In view of the interest in the structure and conformation of transition metal complexes, we have undertaken spin-lattice relaxation time measurements on cyclopentadienyl complexes of manganese

[1]Authors to whom correspondence may be addressed.

[2]P. J. Fitzpatrick, Y. Le Page, and I. S. Butler. Unpublished results.

Can. J. Chem. Downloaded from www.nrcresearchpress.com by 210.87.254.5 on 09/06/12
For personal use only.

Can. J. Chem. Downloaded from www.nrcresearchpress.com by 210.87.254.5 on 09/06/12
For personal use only.

and rhenium tricarbonyl, for which precise crystal structures are available (7, 8), and the vanadium tetracarbonyl analogue, together with nonbonded atom–atom potential calculations on these compounds and on (η^6-benzene)tricarbonylchromium(0) for which an experimental determination of the barrier to rotation has been reported (21).

Experimental

Tricarbonyl (η^5-2,4-cyclopentadien-1-yl)manganese(I) was a generous gift from Ethyl Corporation. The analogous rhenium complex was prepared by a modification (7) of the procedure reported by Green and Wilkinson (22). Tetracarbonyl(η^5-2,4-cyclopentadien-1-yl)-vanadium(I) was purchased from Strem Chemical Co. and recrystallized from CH_2Cl_2, then sublimed *in vacuo* (10 Torr/40°C). Spin-lattice relaxation times were measured at 33 MHz using a Spin-Lock CPS2 pulsed nmr spectrometer. A 180° – τ – 90° pulse sequence was used and the free induction decays captured on a Biomation 805 transient recorder and then plotted on a strip-chart recorder. The sample temperature was controlled by a flow of cooled nitrogen gas and measured (±1 K) using a copper/constantan thermocouple and digital thermometer.

Atom–atom potential energy calculations were performed using programs written in these laboratories.

Results and discussion

Spin-lattice relaxation time measurements

The experimental T_1 versus reciprocal temperature plots are shown in Fig. 1 for $CpMn(CO)_3$, $CpRe(CO)_3$, and $CpV(CO)_4$. The solid curves were obtained by nonlinear least-squares fits of the data to equation [1]

$$[1]\quad \frac{1}{T_1} = \frac{2}{3}C\left\{\frac{\tau}{1+\omega^2\tau^2} + \frac{4\tau}{1+4\omega^2\tau^2}\right\}$$

where C is a constant related to the change in second moment of the resonance line, ω is the resonance frequency, and $\tau = \tau_0 \exp(E/RT)$ is a correlation time for the motion. This expression exhibits a minimum in T_1 when $\omega\tau = 0.62$. Such minima were observed for $CpMn(CO)_3$, 0.08 s at 105 K, and $CpRe(CO)_3$, 0.10 s at 99 K, but not for the vanadium tetracarbonyl compound at the lowest temperature studied (92 K) and therefore the "high" temperature limit of eq. [1], $\omega\tau \ll 1$, was used;

$$[2]\quad \frac{1}{T_1} = \frac{10}{3}C\tau$$

The T_1 plot for the rhenium complex showed a slight discontinuity in the region 150 to 170 K. This was possibly due to the presence of some diethyl ether which could not be removed during purification.

The results are listed in Table 1 and it can be seen that the barriers to rotation are approximately the same for the three cyclopentadienyl complexes: $CpMn(CO)_3$, 7.24 ± 0.20 kJ mol^{-1}; $CpRe(CO)_3$, 7.15 ± 0.40 kJ mol^{-1}; and $CpV(CO)_4$, 7.07 ± 0.16 kJ mol^{-1}. This result is not too surprising for the manganese and rhenium compounds since these are isostructural (7, 8) with similar packing densities. A comparison with the barrier for $CpV(CO)_4$ cannot be made at this time since the published crystal structure may not be correct (see discussion below).

Also included in the table are values of the barriers to rotation for other cyclopentadienyl complexes that have been measured by spin-lattice relaxation time methods. In the case of Cp_2MoCl_2 and Cp_2TiS_5 there are different barriers for different

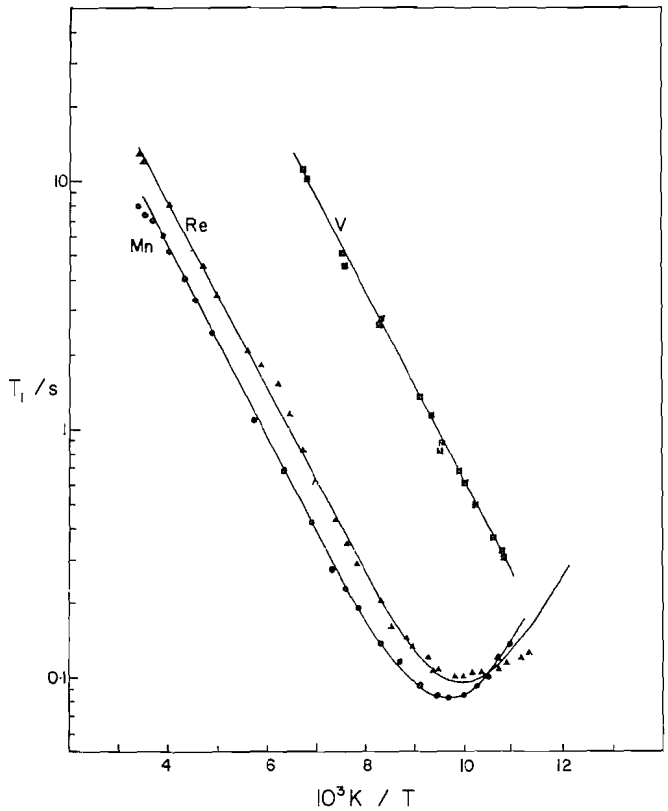

FIG. 1. Spin lattice relaxation time versus reciprocal temperature for $CpMn(CO)_3$, $CpRe(CO)_3$ and $CpV(CO)_4$.

rings which arise from either crystallographic or chemical inequivalence (12, 13). For molecules with "cylindrical" symmetry, i.e, the molecular symmetry axis and the five-fold axis of the ring coincide, the barriers all lie in the range 7–9 kJ mol^{-1}.[3] In X-ray structure determinations such low barriers will result in large anisotropic thermal parameters and thus complicate any attempts to determine small deviations in ring bond lengths. Studies at low temperature are, obviously, advisable for molecules of this type.

Atom–atom potential energy calculations

The energy of interaction between molecules in a solid is assumed to be an additive function of the individual interatomic terms and to depend only on the distance between the atoms. Thus by summing over all interactions within a given cut-off distance the lattice energy can be computed. If this is done as a function of the angle of rotation of a given molecule or group then the dependence of lattice energy on the angle gives the potential barrier for rotation. The "probe" molecule rotates within a rigid lattice, which may overestimate the barrier to rotation (see later discussion).

Various expressions have been used to describe the potential, in particular, the Buckingham (exp-6) and Lennard–Jones (12-6) functions, eqs. [3] and [4] respectively;

$$[3]\quad V(r) = Ar^{-6} + B\exp(-Cr)$$

$$[4]\quad V(r) = 4\epsilon[(\sigma/r)^6 - (\sigma/r)^{12}]$$

where A, B, and C or ϵ and σ are parameters characteristic of a given atom pair and are derived by fitting to experimental

[3]Ruthenocene is a particular exception.

TABLE 1. Barriers to rotation for cyclopentadienyl transition metal π complexes determined by spin lattice relaxation time measurements

	C rad $s^{-2}\times10^{9}$	τ_0 $s\times10^{-13}$	$C\tau_0$ rad $s^{-1}\times10^{-4}$	E kJ mol^{-1}	Ref.
$CpMn(CO)_3$	2.70	6.45	—	7.24	Present work
$CpRe(CO)_3$	2.25	5.43	—	7.15	Present work
$CpV(CO)_4$	—	—	3.15	7.07	Present work
$CpTiCl_3$	1.4	0.25	—	8.8	13
Cp_2Fe	3.32	6.16	—	8.33	11
Cp_2Ru	4.22	2.10	—	18.91	11
$Cp_2Mo_2(CO)_6$	1.77	8.20	—	13.60	13
Cp_2MoCl_2	0.64	0.063	—	12.76	12
	1.20	0.404	—	8.64	
	—	—	807.0	1.47	
Cp_2TiCl_2	—	—	—	2.09	10
Cp_2TiS_5	0.61	12.6	—	9.0	13
	—	—	58.0	7.7	

TABLE 2. Nonbonded atom–atom potential function constants

Set[a]	Atoms	A kJ mol^{-1}	B kJ $mol^{-1}\times10^{-4}$	C $Å^{-1}$
I	C—C	1761	29.96	3.68
	H—H	121	2.05	4.29
	O—O	1085	32.51	4.18
II	C—C	1880	29.92	3.60
	H—H	168	1.20	3.74
	O—O	1085	32.51	4.18
III	C—C	2254	31.22	3.60
	H—H	72.8	0.713	3.74
	O—O	1085	32.51	4.18

[a]Sets IV–VI use eq. [5] for interactions involving oxygen.

TABLE 3. Lennard–Jones potential constants for interactions involving metal atoms

Atoms	ϵ kJ mol^{-1}	σ Å
C—M	3.65	3.49
C—H	2.63	3.02
C—O	6.41	3.52
M—M	10.04	3.60

data such as molecular or crystal structures, heats of sublimation, lattice energies, elastic constants, etc. It is assumed that each set of parameters is transferable from one system to another and that appropriate combining rules apply for heteroatomic interactions

$$A_{ij} = (A_{ii} + A_{jj})^{1/2} \; ; \; B_{ij} = (B_{ii} + B_{jj})^{1/2}$$

$$C_{ij} = (C_{ii} + C_{ij})/2$$

and, similarly,

$$\epsilon_{ij} = (\epsilon_{ii}\cdot\epsilon_{jj})^{1/2} \; ; \; \sigma_{ij} = (\sigma_{ii} + \sigma_{jj})/2$$

A large number of different parameter sets have appeared in the literature and Mirsky has reviewed the published data and proposed a set of recommended values (23). Not all the available parameters are suitable since the method of initial parametrization can impose constraints. For instance the choice of C—H distance of ca. 0.95 Å, typically found in an X-ray structure determination, is obviously not appropriate for use in cases where the constants were based on a bond length of 1.08 Å. While the parameters for carbon and hydrogen are fairly well defined, this is not true for oxygen. We have, therefore, arbitrarily chosen empirically derived functions for oxygen together with some of the more commonly used parameter sets since the primary aim of this study was not to determine new parameters but rather to explore the utility of the atom–atom potential method for examining the nature of the barriers.

The potential parameters are given in Table 2. Set I used the general values recommended by Mirsky (23), and sets II and III employed those given by Williams (24, 25) for C···C, H···H, and C···H interactions, based upon his calculations on hydrocarbons, coupled with the oxygen potential constants from Mirsky's review via the combining rules mentioned above. Set II includes the constants suggested by Boyd and Fyfe (26) as the most useful. Lastly, the carbon and hydrogen potentials of sets I–III were combined with parameters for oxygen derived from the empirical equation [5], suggested by Gavezotti and Simonetta (27), to give sets IV–VI.

$$[5] \quad V(r) = 30000 \exp(-13r/d_0) - 0.14\,(d_0/r)^6$$

where d_0 is the sum of the van der Walls radii of the two atoms involved in the potential. A Lennard–Jones potential was used for all interactions involving the metal atoms where the values of ϵ and σ were determined by calculating the lattice energies of several metal carbonyl complexes and comparing these with experimental enthalpies of sublimation. Since the effect upon the calculated barrier height of terms involving metal atom interactions was found to be very small, no further attempt was made to optimize these parameters and the same functions were used for all metals, Table 3.

The manganese and rhenium complexes have the same crystal structure, space group $P2_1/n$, with four molecules per unit cell which are all related by symmetry, and thus the calculations needed to be performed only for one molecule. To

Can. J. Chem. Downloaded from www.nrcresearchpress.com by 210.87.254.5 on 09/06/12
For personal use only.

Can. J. Chem. Downloaded from www.nrcresearchpress.com by 210.87.254.5 on 09/06/12
For personal use only.

TABLE 4. Calculated barriers[a] to rotation of the Cp ring (kJ mol^{-1})

Parameter set	$CpMn(CO)_3$	$CpRe(CO)_3$
I	11.3	13.0
II	17.6	20.0
III	11.7	13.4
IV	8.8	9.6
V	13.4	14.2
VI	7.9	9.2
Experimental	7.24	7.15

[a]Intramolecular contribution = 0; electronic contribution = 0. The barrier for the $M(CO)_3$ moiety was calculated to be a minimum of 50 kJ mol^{-1} and therefore this group was considered to be rigidly fixed in the lattice.

simplify the computation, idealized symmetric ring coordinates were used rather than the crystallographically determined atomic positions. A cut-off distance of 8 Å was used to save computation time.

The results of the calculations for the manganese and rhenium complexes are given in Table 4. The rather surprising result for the vanadium tetracarbonyl complex was that no significant barrier to rotation occurs. The crystal structure of this compound was reported by Wilford *et al.* (28) to be orthorhombic with four molecules per unit cell, each required to have mirror symmetry. The position of the carbon atoms of the ring was best described by a disorder among two equally preferred orientations rotated by 36° with respect to each other. The existence of the mirror plane would, in fact, lead to a zero barrier height. The electronic barrier in a $CpML_4$ system is expected to be extremely small (29), and therefore it seems likely that the disorder in the crystal has led to an incorrect structure. It is possible that our T_1 measurements were made on a different crystal form or that a phase transition occurs in this compound. In any event a re-examination of the crystal structure of cyclopentadienylvanadium tetracarbonyl appears to be worthwhile.

For the tricarbonyl complexes there is no intramolecular barrier arising from nonbonded interactions and the total potential is entirely intermolecular in origin. From Table 3 it can be seen that parameter sets IV and VI gave barrier heights closest to the experimental values in both cases. The potential functions suggested by Mirsky gave poor agreement, which is somewhat disappointing as these are intended to be the most consistent set and transferable from one system to another.

The major contributions arise from C—H and O—H interactions which together comprise over 80% of the total in all cases. It appears that the parameters used for oxygen and the Williams parameters used in sets II and V are too attractive, although it must be emphasized that it is the rotational barriers that are being compared and not the total lattice energy. The parameters cited by Mirsky for oxygen may not be suitable for carbonyl groups in organometallic complexes of this type. The choice of the Simonetta function has, however, led to quite good agreement. In Fig. 2 the data for $CpMn(CO)_3$, obtained with set IV, are used to illustrate the use of these calculations to derive information on the origin of the barrier. The figure shows the breakdown of the potential into contributions from ring–ring and ring–carbonyl interactions. A significant contribution, about 40–45%, arises from ring–ring terms (the same conclusion can be drawn from all the parameter sets). In calculating the angular dependence of the lattice energy the "probe" molecule or group is rotated in an otherwise rigid

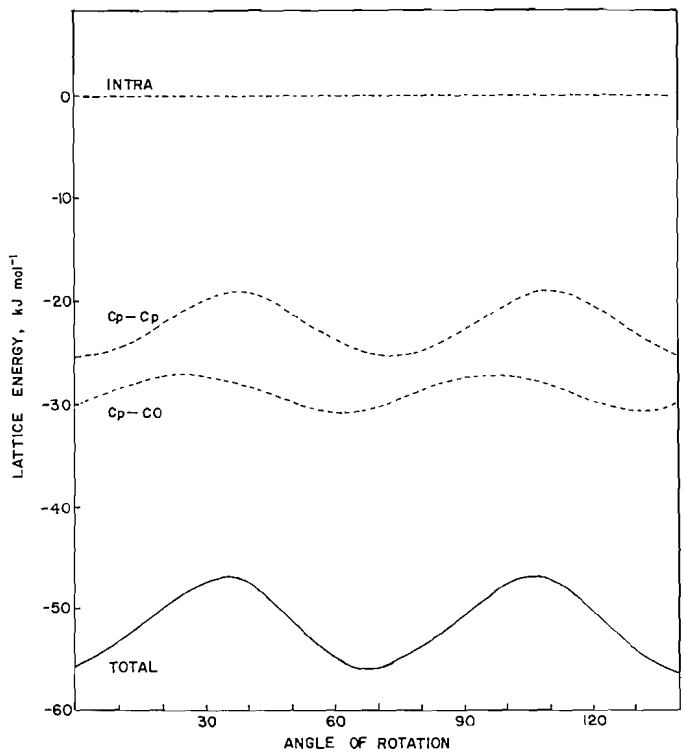

FIG. 2. Angular dependence of the calculated lattice energy for $CpMn(CO)_3$ using parameter set IV.

lattice. This procedure does not take into account the possibility of any cooperative or correlated motion of the reorienting species. An examination of the different contributions shows, however, that ring–ring interactions are very important and therefore close agreement between calculated and experimental barrier heights might not be expected in such cases. In their study of the application of the atom–atom potential method to rotational barriers and lattice energies in planar aromatic hydrocarbons Fyfe and co-workers (30) concluded that the justification for the neglect of concerted motions lies simply in the fact that agreement is obtained between calculation and experiment. This point will be discussed later in more detail.

The actual minimum in the calculated potential for both the manganese and the rhenium complexes does not occur at exactly 0° but is shifted slightly, i.e., the input coordinates are not, apparently, the equilibrium position. Part of the discrepancy may be due to the fact that the input coordinates were modified to an ideal symmetric structure but the separate contributions from ring–ring and ring–carbonyl sources do not themselves have minima at zero angle of rotation. Since there is no internal barrier the molecular conformation depends entirely upon the crystal packing forces and a balance is achieved by rotations of the two halves of the molecule in opposite directions. This is very sensitive to the form of the potential functions and the input coordinates.

The $BzCr(CO)_3$ molecule (Bz = η^6-C_6H_6) seemed to us to be an excellent choice for further testing the atom–atom potential method. The conformation in the crystal is staggered, with the possibility that there is some localization of the bonding in the aromatic ring such that the C—C bonds *trans* to the carbonyl groups are slightly shorter (31). Albright *et al.* (32) have calculated that an electronic barrier to rotation of about 1.3 kJ mol^{-1} exists for the delocalized structure and 81 kJ mol^{-1} if the

TABLE 5. Calculated barriers to rotation of the benzene ring (kJ mol^{-1})

Parameter set	Intra	Inter	Electronic[a]	Total
I	0.9	21.0	1.3	23.2
II	1.1	29.7	1.3	32.1
III	1.0	21.9	1.3	24.2
IV	0.9	14.5	1.3	16.7
V	1.1	17.3	1.3	19.7
VI	1.0	13.7	1.3	16.0
Experimental[b]				17.6

[a]Reference 32.
[b]Reference 21.

bonding is completely localized. The activation energy for benzene ring rotation in the solid phase has been measured by Delisle *et al.* (21), using spin lattice relaxation times, to be 17.6 kJ mol^{-1}. Thus this complex provides a system in which the same atom types occur as in the cyclopentadienyl compounds but where the experimental barrier is much larger and includes an internal component with an electronic contribution.

The lattice energies were calculated using the same parameter sets with the crystal structure data of Rees and Coppens (31). The results are given in Table 5. When the total barrier is considered, i.e., the calculated electronic contribution is included, the best agreement with experiment is again found for parameter sets IV and VI. Fig. 3 shows the angular dependence for the total nonbonded atom–atom potential divided into intra- and intermolecular contributions and also into ring–ring and ring–carbonyl dependences. The ring–ring contribution shows almost no angular dependence and thus there is probably no correlated rotation in this complex. The intramolecular barrier is about 1 kJ mol^{-1} which, when added to the calculated electronic value of 1.3 kJ mol^{-1}, is in good agreement with the value of 2.1 kJ mol^{-1} derived from the electron diffraction study (33). The calculated potential shows no shift in the potential from the input coordinates.

The agreement between the experimental and calculated barrier heights for the cyclopentadienyl complexes, where no internal barrier occurs and there is a strong possibility of concerted motion of the rings, and for the benzene ring rotation, where there is a moderate internal barrier and no strong ring–ring interaction, seems to indicate that the neglect of cooperative motions may be justified. However, this conclusion is based only on the agreement for the barrier heights and not for the total lattice energies. The constants in the atom–atom potential functions are derived by fitting to physical properties of materials at or close to equilibrium lattice positions and are more sensitive to the shape of the potential function near its minimum. Rotation of the probe molecule leads to close contact distances with neighbouring molecules and a sensitivity to the repulsive part of the potential. This effect could be overcome if cooperative motions can occur. It is to be expected in such cases that the calculated barrier will be larger than the experimentally determined value. This is what is observed in the present study using parameter sets IV and VI. Alternatively, a potential function with a less steep repulsive term might be more suitable for calculations of barrier heights but would not give acceptable total lattice energies.

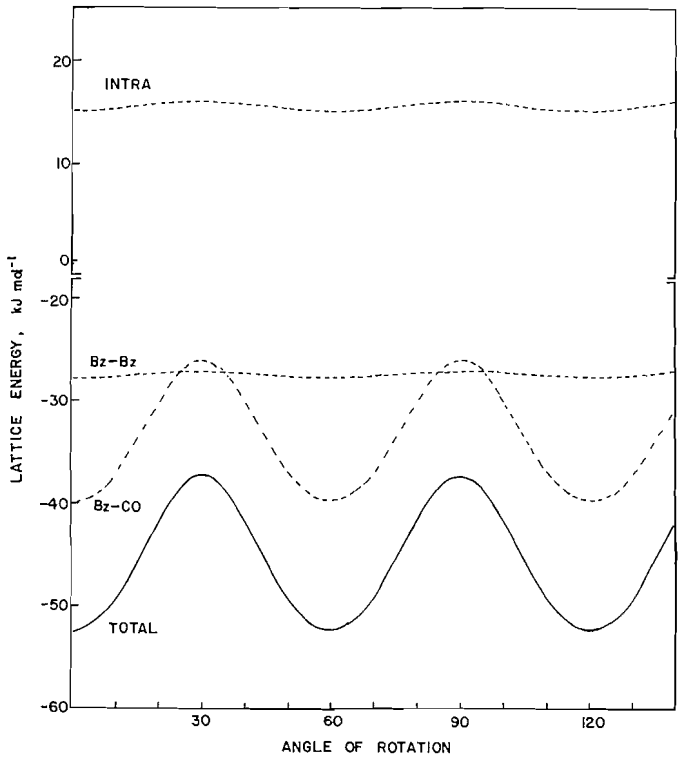

FIG. 3. Angular dependence of the calculated lattice energy for $BzCr(CO)_3$ using parameter set IV.

Acknowledgements

This work was supported by grants from the Natural Sciences and Engineering Research Council of Canada. P.J.F. acknowledges a McGill University Graduate Research Fellowship. The authors are grateful to Dr. Alan Shaver for discussions.

1. M. J. BENNETT, M. R. CHURCHILL, M. GERLOCH, and R. MASON. Nature, **201**, 1318 (1964).
2. P. J. WHEATLEY. Perspect. Struct. Chem. **1**, 23 (1967).
3. V. W. DAY, B. R. STULTS, K. J. REIMER, and A. SHAVER. J. Am. Chem. Soc. **96**, 1227 (1974).
4. V. W. DAY, K. J. REIMER, and A. SHAVER. J. Chem. Soc. Chem. Commun. 404 (1975).
5. A. MITSCHLER, B. REES, and M. S. LEHMANN. J. Am. Chem. Soc. **100**, 3390 (1978).
6. L. R. BYERS and L. F. DAHL. Inorg. Chem. **19**, 277 (1980), and references therein.
7. P. J. FITZPATRICK, Y. LE PAGE, J. SEDMAN, and I. S. BUTLER. Inorg. Chem. **20**, 2852 (1981).
8. P. J. FITZPATRICK, Y. LE PAGE, and I. S. BUTLER. Acta Crystallogr. Sect. B, **37**, 1052 (1981).
9. S. E. ANDERSON. J. Organomet. Chem. **71**, 263 (1974), and references therein.
10. C. H. HOLM and J. A. IBERS. J. Chem. Phys. **30**, 885 (1959).
11. A. J. CAMPBELL, C. A. FYFE, D. HAROLD-SMITH, and K. R. JEFFREY. Mol. Cryst. Liq. Cryst. **36**, 1 (1976).
12. I. S. BUTLER, P. J. FITZPATRICK, D. F. R. GILSON, G. GOMEZ, and A. SHAVER. Mol. Cryst. Liq. Cryst. **71**, 213 (1981).
13. D. F. R. GILSON and G. GOMEZ. J. Organomet. Chem. To be published.
14. D. E. WEMMER and A. PINES. J. Am. Chem. Soc. **103**, 34 (1981).
15. D. W. WEMMER, D. J. RUBEN, and A. PINES. J. Am. Chem. Soc. **103**, 28 (1981).
16. M. J. BENNET, W. L. HUTCHEON, and B. M. FOXMAN. Acta Crystallogr. Sect. A, **31**, 488 (1975).

Can. J. Chem. Downloaded from www.nrcresearchpress.com by 210.87.254.5 on 09/06/12
For personal use only.

17. A. EISENBERG, A. SHAVER, and T. TSUTSUI. J. Am. Chem. Soc. **102**, 1416 (1980).
18. T. A. ALBRIGHT. Acc. Chem. Res. **15**, 149 (1982).
19. P. SEILER and J. D. DUNITZ. Acta Crystallogr. Sect. B, **35**, 1068 (1979); **35**, 2020 (1979).
20. F. TAKUSEGAWA and T. F. KOETZLE. Acta Crystallogr. Sect. B, **35**, 1074 (1979).
21. P. DELISLE, G. ALLEGRA, E. R. MOGNASCHI, and A. CHIERICO. J. Chem. Soc. Faraday Trans. 2, **71**, 207 (1975).
22. M. L. H. GREEN and G. WILKINSON. J. Chem. Soc. 4314 (1958).
23. K. MIRSKY. *In* Computing in crystallography. Delft University Press. 1978.
24. D. E. WILLIAMS. Acta Crystallogr. Sect. A, **30**, 71 (1974).
25. D. E. WILLIAMS. Trans. Am. Crystallogr. Assoc. **6**, 21 (1970).
26. R. K. BOYD and C. A. FYFE. J. Phys. Chem. Solids, **39**, 693 (1970).
27. A. GAVEZOTTI and M. SIMONETTA. Acta Crystallogr. Sect. A, **31**, 645 (1975).
28. J. B. WILFORD, A. WHITLA, and H. M. POWELL. J. Organomet. Chem. **8**, 495 (1967).
29. T. A. ALBRIGHT, R. HOFFMANN, Y. TSE, and T. D'OTTAVIO. J. Am. Chem. Soc. **101**, 3812 (1979).
30. R. K. BOYD, C. A. FYFE, and D. A. WRIGHT. J. Phys. Chem. Solids, **35**, 1355 (1974).
31. B. REES and P. COPPENS. Acta Crystallogr. Sect. B, **29**, 2516 (1973).
32. T. A. ALBRIGHT, P. HOFMAN, and R. HOFFMANN. J. Am. Chem. Soc. **99**, 7546 (1977).
33. N. S. CHIU, L. SHAFER, and R. SEIP. J. Organomet. Chem. **101**, 331 (1975).

Can. J. Chem. Downloaded from www.nrcresearchpress.com by 210.87.254.5 on 09/06/12
For personal use only.

Adducts of triphenyllead isothiocyanate and selenocyanate with some O- and N-donor ligands

RYSZARD WOJTOWSKI, IVOR WHARF, AND MARIO ONYSZCHUK[1]
Department of Chemistry, McGill University, Montreal, P.Q., Canada H3A 2K6

Received September 22, 1982

This paper is dedicated to Professor Leo Yaffe on the occasion of his 65th birthday

RYSZARD WOJTOWSKI, IVOR WHARF, and MARIO ONYSZCHUK. Can. J. Chem. **61**, 743 (1983).

The preparation and properties of triphenyllead selenocyanate have been reinvestigated. Infrared spectra show that the solid is polymeric with strong Pb—Se and weak Pb—N bonds; in benzene or CH_2Cl_2 solutions ν(CN) values are consistent with the $Ph_3PbSeCN$ bonding mode. The first 1 : 1 adducts of triphenyllead selenocyanate with hexamethylphosphoramide (HMPA), pyridine-*N*-oxide (pyO), 4-picoline-*N*-oxide (4-picO), and triphenylphosphine oxide (TPPO) have been prepared; infrared data show that $Ph_3PbSeCN \cdot L$ (L = pyO, 4-picO, TPPO) are selenocyanates, but the HMPA adduct is an isoselenocyanate. The adducts dissociate in benzene and ν(CN) frequencies show that both N-bonded and Se-bonded adduct isomers are present. In contrast, the adducts $Ph_3PbNCS \cdot L$ (L = HMPA, pyO, 4-picO, TPPO) are N-bonded in the solid state and in benzene solution where they are undissociated. Amine adducts, $Ph_3PbNCS \cdot L$ (L = pyridine, β-picoline, γ-picoline, pyrrolidine (pyrrol), piperidine (pipy), cyclohexylamine ($CyNH_2$)) and $Ph_3PbNCS \cdot 2L$ (L = morpholine (morph)), as well as $Ph_3PbNCSe \cdot$ pipy and 2 $Ph_3PbNCSe \cdot 3L$ (L = pyrrol or morph) have been prepared, but these are less stable than adducts with O-donor ligands. Infrared data suggest that amine adducts of Ph_3PbNCS have N-bonded and/or ionic thiocyanate groups while all $Ph_3PbSeCN$—amine adducts contain the selenocyanate ion.

RYSZARD WOJTOWSKI, IVOR WHARF et MARIO ONYSZCHUK. Can. J. Chem. **61**, 743 (1983).

On a étudié de nouveau la préparation et les propriétés de sélénocyanate triphénylé de plomb. Les spectres infrarouges montrent que le solide est un polymère avec de fortes liaisons Pb—Se et de faibles liaisons Pb—N; dans des solutions de benzène ou de CH_2Cl_2, les valeurs de ν(CN) sont en accord avec le mode de liaison du $Ph_3PbSeCN$. On a préparé les premiers adduits 1 : 1 de sélénocyanate triphénylé de plomb avec l'hexaméthylphosphoramide (HMPA), la *N*-oxyde de pyridine (pyO), la *N*-oxyde de picoline-4 (picO-4) et l'oxyde de triphénylphosphine (TPPO); les données infrarouges révèlent que les $Ph_3PbSeCN \cdot L$ (L = pyO, picO-4, TPPO) sont des sélénocyanates, mais que l'adduit du HMPA est un isosélénocyanate. Les adduits se dissocient dans le benzène et les fréquences ν(CN) montrent que les isomères d'adduits liés par l'azote et liés par le Se sont présents. Par contre, les adduits $Ph_3PbNCS \cdot L$ (L = HMPA, pyO, picO-4, TPPO) sont liés par l'azote à l'état solide et en solution dans le benzène où ils ne sont pas dissociés. On a préparé les adduits d'amine, $Ph_3PbNCS \cdot L$ (L = pyridine, β-picoline, γ-picoline, pyrrollidine (pyrrol), pipéridine (pipy), cyclohexylamine ($CyNH_2$) et le $Ph_3PbNCS \cdot 2L$ (L = morpholine (morph)) ainsi que le $Ph_3PbNCSe \cdot$ pipy et le $2Ph_3PbNCSe \cdot 3L$ (L = pyrrol ou morph) mais ils sont moins stables que les adduits avec les ligands donneurs d'oxygène. Les données infrarouges suggèrent que les adduits d'amine du Ph_3PbNCS ont des groupes thiocyanates liés par l'azote et/ou une façon ionique tandis que tous les adduits du $Ph_3PbSeCN$—amine contiennent l'ion sélénocyanate.

[Traduit par le journal]

Introduction

While several reports of adducts of triphenyltin chalcocyanates with O- and N-donor ligands have appeared (1–4), as well as of diphenyltin isothiocyanate adducts (4–6), much less is known about adducts of phenyllead chalcocyanates. Following the report ten years ago of some anionic complexes, e.g. $Ph_3Pb(NCS)_2^-$ and $Ph_2Pb(NCS)_4^{2-}$ (7, 8), we began a study of adduct formation by phenyllead chalcocyanates, first reporting adducts of diphenyllead isothiocyanate (9) and then adducts of triphenyllead isocyanate (10). This series is now continued with consideration of adduct formation by triphenyllead isothiocyanate and selenocyanate, using NCX group frequencies, particularly ν(CN) and ν(CX), as criteria of bonding mode of the NCX group in both solid state and solution species.

Although triphenyllead isothiocyanate is well known, the selenocyanate analogue has been only partially characterized (11). We now report a more detailed study of this compound together with a convenient synthesis from the readily available starting material, triphenyllead acetate.

[1]Author to whom correspondence should be addressed.

Experimental

All solvents and liquid ligands were stored over molecular sieves, while solid ligands were used as received. Potassium selenocyanate (Aldrich) was used as quickly as possible after being received, while triphenyllead acetate (Alfa) was recrystallized from acetonitrile before use. Triphenyllead isothiocyanate was prepared previously (12). Microanalyses for C, H, and N were done by Guelph Chemical Laboratories Ltd., Guelph, Ontario, while molecular weights were determined by Spang Microanalytical Laboratory, Eagle Harbor, Michigan. Infrared spectra were recorded on a Nicolet-7199 interferometer fitted with a KBr beam splitter. Samples were studied as Nujol mulls or as solutions in 0.1 mm sodium chloride cells. Values of ν(CN) absorbances were obtained by direct integration of the absorbance spectra. The nmr (^{31}P) spectra were obtained as described elsewhere (13).

Preparations

Triphenyllead selenocyanate

Triphenyllead acetate (25.0 g) and potassium selenocyanate (10.0 g) were stirred in refluxing methanol (1.0 L) for 2.5 h. The turbid solution was filtered and left overnight in a refrigerator. The white crystals formed were filtered, washed with water, and air-dried. Further product was obtained by adding water (1 L) to the filtrate and letting the mixture stand for several hours; yield, 90%, mp 192°C

Can. J. Chem. Downloaded from www.nrcresearchpress.com by 210.87.254.42 on 09/06/12
For personal use only.

Can. J. Chem. Downloaded from www.nrcresearchpress.com by 210.87.254.42 on 09/06/12
For personal use only.

(dec.). *Anal.* calcd. for $(C_6H_5)_3PbSeCN$: C 42.0, H 2.8, N 2.6%; found: C 41.2, H 2.7, N 2.7.

Adducts of triphenyllead selenocyanate

Method A

Triphenyllead selenocyanate (I) was dissolved in a hot toluene solution of the solid ligand. On cooling the clear solution (filtered if necessary) overnight at room temperature (or in the refrigerator) the crystalline *adduct* formed.

Prepared in this manner were *$Ph_3PbSeCN \cdot TPPO$*, from I (1.0 g), TPPO (1.0 g) in toluene (8 mL); yield, 56%, mp 130°C. *Anal.* calcd. for $C_{37}H_{30}NOPPbSe$: C 54.1, H 3.7, N 1.7%; found: C 53.6, H 3.7, N 1.8; *$Ph_3PbSeCN \cdot pyO$*, from I (2.5 g), pyO (2.0 g) in toluene (70 mL); yield, 43%, mp 93°C. *Anal.* calcd. for $C_{24}H_{20}N_2OPbSe$: C 45.1, H 3.2, N 4.4%; found: C 45.3, H 3.1, N 4.5; and *$Ph_3PbSeCN \cdot 4\text{-}picO$*, from I (1.0 g), 4-picO (0.5 g) in toluene (50 mL); yield, 66%, mp 102°C. *Anal.* calcd. for $C_{25}H_{22}N_2OPbSe$: C 46.0, H 3.4, N 4.3%; found: C 46.0, H 3.4, N 4.3.

Method B

Triphenyllead selenocyanate (I) was dissolved in the hot liquid ligand. The crystalline *adduct* formed on allowing the clear mixture to stand overnight at room temperature (or in the refrigerator).

Prepared in this manner were *$Ph_3PbNCSe \cdot pipy$*, from I (1.0 g) in piperidine (6.0 mL); yield, 82%, dec. 100°C. *Anal.* calcd. for $C_{24}H_{26}N_2PbSe$: C 45.9, H 4.2, N 4.5%; found: C 46.1, H 4.3, N 4.7; *$2Ph_3PbNCSe \cdot 3morph$*, from I (1.0 g) in morpholine (6.0 mL); yield, 86%, dec. 105°C. *Anal.* calcd. for $C_{50}H_{57}N_5O_3Pb_2Se_2$: C 44.5, H 4.3, N 5.2%; found: C 44.3, H 4.4, N 5.3; and *$2Ph_3PbNCSe \cdot 3pyrrol$*, from I (2.0 g) in pyrrolidine (2 g); yield, 70%, dec. 77°C. *Anal.* calcd. for $C_{50}H_{57}N_5Pb_2Se_2$: C 46.1, H 4.4, N 5.4%; found: C 46.3, H 4.6, N 5.6.

Triphenyllead isoselenocyanate – hexamethylphosphoramide (1:1)

Adding pentane (10 mL) slowly to a stirred solution of I (2.0 g) in HMPA (8 mL) at room temperatures gave the crystalline adduct; yield, 90%, mp 92°C. *Anal.* calcd. for $C_{25}H_{33}N_4OPPbSe$: C 41.6, H 4.6, N 7.8%; found: C 41.7, H 4.8, N 8.0.

Adducts of triphenyllead isothiocyanate

These were obtained using Method A given above. Reactions of triphenyllead isothiocyanate (II) with amines often gave oils which could only be crystallized with some difficulty.

Prepared in this manner were *$Ph_3PbNCS \cdot TPPO$*, from II (1.65 g), TPPO (2.8 g) in toluene (50 mL); yield, 45%, mp 147–8°C (dec.). *Anal.* calcd. for $C_{37}H_{30}NOPPbS$: C 57.4, H 3.9, N 1.8%; found: C 57.9, H 4.0, N 1.7; *$Ph_3PbNCS \cdot pyO$*, from II (1.65 g), pyO (2.0 g) in toluene (50 mL); yield, 75%, mp 125–126°C. *Anal.* calcd. for $C_{24}H_{20}N_2OPbS$: C 48.7, H 3.4, N 4.7%; found: C 48.7, H 3.4, N 4.8; *$Ph_3PbNCS \cdot 4\text{-}picO$*, from II (1.65 g), 4-picO (2.0 g) in toluene (50 mL); yield, 80%, mp 109°C. *Anal.* calcd. for $C_{25}H_{22}N_2OPbS$: C 49.6, H 3.8, N 4.6%; found: C 49.5, H 3.7, N 4.5; *$Ph_3PbNCS \cdot py$*, from II (1.65 g), py (2.4 g) in toluene (30 mL); yield, 52%, dec. 180°C. *Anal.* calcd. for $C_{24}H_{20}N_2PbS$: C 50.1, H 3.5, N 4.9%; found: C 49.8, H 3.5, N 4.8; *$Ph_3PbNCS \cdot \beta\text{-}pic$*, from II (1.65 g), β-pic (6.4 g) in toluene (100 mL); yield, 70%, dec. 122°C. *Anal.* calcd. for $C_{25}H_{22}N_2PbS$: C 50.9, H 3.8, N 4.8%; found: C 51.0, H 3.7, N 4.7; *$Ph_3PbNCS \cdot \gamma\text{-}pic$*, from II (1.65 g), γ-pic (4.8 g) in toluene (50 mL); yield, 80%, dec. 123°C. *Anal.* calcd. for $C_{25}H_{22}N_2PbS$: C 50.9, H 3.8, N 4.8%; found: C 50.9, H 3.7, N 4.8. *$Ph_3PbNCS \cdot CyNH_2$*, from II (3.3 g), cyclohexylamine ($CyNH_2$) (10.0 g) in toluene (75 mL); yield, 75%, dec. 115°C. *Anal.* calcd. for $C_{25}H_{28}N_2PbS$: C 50.2, H 4.7, N 4.6; *$Ph_3PbNCS \cdot 2morph$*, from II (1.65 g), morpholine (27 g) in toluene (75 mL); yield, 85%, dec. 100°C. *Anal.* calcd. for $C_{27}H_{33}N_3O_2PbS$: C 48.3, H 5.0, N 6.3%; found: C 48.1, H 4.7, N 6.3; and *$Ph_3PbNCS \cdot pyrrol$*, from II (3.3 g), pyrrolidine (1.7 g) in toluene (50 mL); yield, 95%, dec. 133°C. *Anal.* calcd. for $C_{23}H_{24}N_2PbS$: C 48.7, H 4.3, N 4.9%; found: C 48.9, H 4.3, N 4.7.

Triphenyllead isothiocyanate – piperidine (1:1)

Triphenyllead isothiocyanate (1.65 g) was stirred with a refluxing toluene (100 mL) solution of piperidine (4.25 g) for 30 min. The mixture was then stirred at room temperature for 48 h, during which time the oil first formed changed to the crystalline *adduct*; yield, 97%, dec. 140°C. *Anal.* calcd. for $C_{24}H_{26}N_2PbS$: C 49.6, H 4.5, N 4.8%; found: C 49.4, H 4.4, N 4.8.

All adducts were filtered, washed with a little pentane or ether, and dried in vacuum at room temperature.

TABLE 1. Correlation of selenocyanate bonding type with selenocyanate vibrational frequencies (cm^{-1})

Bonding type	ν(CN)	ν(CSe)	δ(NCSe)
$NCSe^-$	2070[a]	558	424, 416
M—NCSe	2090–2050[b] br	650–600	460–410
M—SeCN	2130–2070[c] sp	550–520	410–370
M—NCSe—M	2150–2100	640–550	410–390

NOTE: Integral molar absorptivity ranges (solution spectra) are:
[a] $A_{CN} = (2-3) \times 10^4\ M^{-1}\ cm^{-2}\ (NCSe)^{-1}$
[b] $A_{CN} = (5-12) \times 10^4\ M^{-1}\ cm^{-2}\ (NCSe)^{-1}$
[c] $A_{CN} = (0.5-1.5) \times 10^4\ M^{-1}\ cm^{-2}\ (NCSe)^{-1}$

Results and discussion

The infrared spectra (1700–400 cm^{-1}) of all compounds showed the absorptions expected for the "Ph_3Pb" moiety as well as, for the adducts, ligand peaks including those shifted by ligand coordination to the lead atom. Of particular interest are frequencies for the NCS and NCSe group vibrations as these indicate the mode of coordination. Since the vibrational criteria for NCS bonding types were reproduced earlier (9), the similar criteria (14) for determining NCSe bonding type are now given in Table 1 for use in the discussion below. The ν(CN) ranges overlap considerably implying this criterion should be used with great caution. However, like ν(CS), ν(CSe) appears to provide a better distinction between M—NCSe and M—SeCN bonding modes. In addition, the ν(CSe) absorption is more easily observed since it is of weak to medium intensity and it often occurs in a region relatively free of other absorptions. The deformation modes, δ(NCSe), are less useful since they are weak, overlap with phenyl group bands, and sometimes occur beyond the spectral range (400 cm^{-1}), although the very weak overtones can be observed.

(i) Ph_3PbNCS and $Ph_3PbSeCN$

Infrared data (Table 2) show, using the criteria (14), that triphenyllead isothiocyanate uses bridging thiocyanate groups to form a polymeric structure analogous to those found for crystalline Ph_3SnNCS (15) and Ph_3PbNCO (16), as previously suggested by Bertazzi *et al.* (7) on the basis of ν(CN) alone. All spectra have the expected weak lower frequency $\nu(^{13}CN)$ peak while a $Ph_3Pb^{15}NCS$ sample gave not only the required lower ν(CN) values but also a decrease in ν(CS), indicating the mixing of these two vibrations.

As reported earlier (11), triphenyllead selenocyanate is a white air-stable solid, but it decomposes at a lower temperature than its thiocyanate analogue. The infrared data (Table 3), especially ν(CSe), show the material to have bridging selenocyanate groups giving a polymeric structure, unlike the earlier assumption (11) of lead–selenium bonding only, based on the ν(CN) value alone. Triphenyllead selenocyanate is slightly soluble in benzene and the sharp ν(CN) band (Fig. 1(a)) shifts *upwards* on solution indicating that the lead–selenium bond is retained when the Pb—NCSe—Pb bridge is broken. Tri-

TABLE 2. Thiocyanate group frequencies (cm^{-1}) (ir data) for Ph_3PbNCS and adducts with O-donor ligands

Compound	Solid state			Benzene solution[a]	
	ν(CN)	ν(CS)	δ(NCS)	ν(CN)	$A_{CN}(M^{-1}\ cm^{-2}\ (NCS)^{-1})$
Ph_3PbNCS	2098[b] vs 2058 w	760 vw	440 sh 457 w	—	—
$Ph_3Pb^{15}NCS$	2064 vs 2020 w	752 vw	462 w	—	—
$Ph_3PbNCS \cdot HMPA$	2057[c] vs 2010 w	797[c] vw	495[c] vw	2036[d]	$10 \pm 1 \times 10^4$[d]
$Ph_3PbNCS \cdot pyO$	2039 vs	798 vw	487 w	2076 w, br, sh 2032 vs	$9 \pm 1 \times 10^4$
$Ph_3PbNCS \cdot 4\text{-picO}$	2045 vs 2003 w	801 vw	[e]	2036	$12.5 \pm 1 \times 10^4$
$Ph_3PbNCS \cdot TPPO$	2053 vs	807 vw	[e]	2066 s 2042 vs	—

[a]Concentration 0.005–0.01 *M*.
[b]Literature (7), ν(CN) 2092 vs, 2050 sh.
[c]Reference 11.
[d]Previous values (11): ν(CN), 2042 cm^{-1}; $A_{CN} = 12 \times 10^4\ M^{-1}\ cm^{-2}\ (NCS)^{-1}$.
[e]Obscured by ligand bands.

TABLE 3. Selenocyanate group frequencies (cm^{-1}) (ir data) for $Ph_3PbSeCN$ and adducts with O-donor ligands

Compound	Solid state			ν(CN) solution spectra in	
	ν(CN)	ν(CSe)	2δ(NCSe)	C_6H_6[c]	CH_2Cl_2[c]
$Ph_3PbSeCN$	2107 vs 2063 w	566 w–m	759 vw 798 vw	2139[d] sp	2136[f] sp
$Ph_3PbNCSe \cdot HMPA$	2053 vs, br 2010 w	609 w–m	837[a] vw	2139 s, sp 2123 s, sp 2037 vs, br	2136 w, sp 2114 m, sp 2056 vs
$Ph_3PbSeCN \cdot pyO$	2106 s, sp 2061 vw	[b]	787 vw	2138 vs, sp 2125 m, sp ~2031 m, br	2136 s, sp 2120 vs, sp 2054 m
$Ph_3PbSeCN \cdot 4\text{-picO}$	2105 s, sp 2061 vw	547 vw	775 vw 796 vw	2138 m, sp 2123 vs, sp 2038 m, br	2135 w–m, sp 2117 vs, sp 2055 s
$Ph_3PbSeCN \cdot TPPO$	2119 s, sp 2055 w	[b]	[b]	2139 vs, sp 2125 m, sp 2037 m, br	2136 s, sp 2117 vs, sp 2054 s

[a]δ(NCSe), 418 cm^{-1} (w).
[b]Obscured by ligand bands.
[c]Concentrations 0.005–0.01 *M*.
[d]Saturated solution (<0.003 *M*).
[e]Concentrations 0.01–0.05 *M*; qualitative intensities given for 0.030–0.035 *M* solutions.
[f]Concentrations 0.006–0.012 *M*; $A_{CN} = 0.5 \times 10^4\ M^{-1}\ cm^{-2}\ (NCSe)^{-1}$.

phenyllead selenocyanate is more soluble in dichloromethane and the ir spectrum of this solution (Fig. 2(a)) again has only a single sharp peak whose molar absorptivity indicates a Pb—SeCN structure in solution.

Triphenyllead isothiocyanate with its negligible solubility in noncoordinating solvents and higher decomposition temperature is even more strongly bridging than Ph_3PbNCO (10, 16) with both having Pb—N as the stronger bond. However, $Ph_3PbSeCN$, soluble in noncoordinating solvents, has weaker SeCN bridging with Pb—Se as the stronger bond, in contradiction to Norbury's observation (14) that thiocyanate and selenocyanate groups generally show similar strong bridging properties. This is the case with the analogous tin compounds where $Ph_3SnNCSe$ with ν(CN) at 2110 cm^{-1} (vs br) and ν(CSe) at 594 cm^{-1} (wm) (17) is clearly an isoselenocyanate similar to Ph_3SnNCS (15), with strong NCSe bridges.

(ii) Adducts with O-donor ligands

Triphenyllead isothiocyanate formed adducts with only the stronger O-donor ligands used here (HMPA, 4-picO, pyO, and TPPO). Although toluene solutions of dimethylsulphoxide (DMSO), *N,N*-dimethylformamide (DMF), *N,N*-dimethylacetamide (DMA), or trimethylphosphate (TMP) dissolve the thiocyanate indicating adduct formation, all attempts to isolate a solid adduct always produced unreacted Ph_3PbNCS. This contrasts with the formation of Ph_3PbNCO adducts with these

Can. J. Chem. Downloaded from www.nrcresearchpress.com by 210.87.254.42 on 09/06/12
For personal use only.

Can. J. Chem. Downloaded from www.nrcresearchpress.com by 210.87.254.42 on 09/06/12
For personal use only.

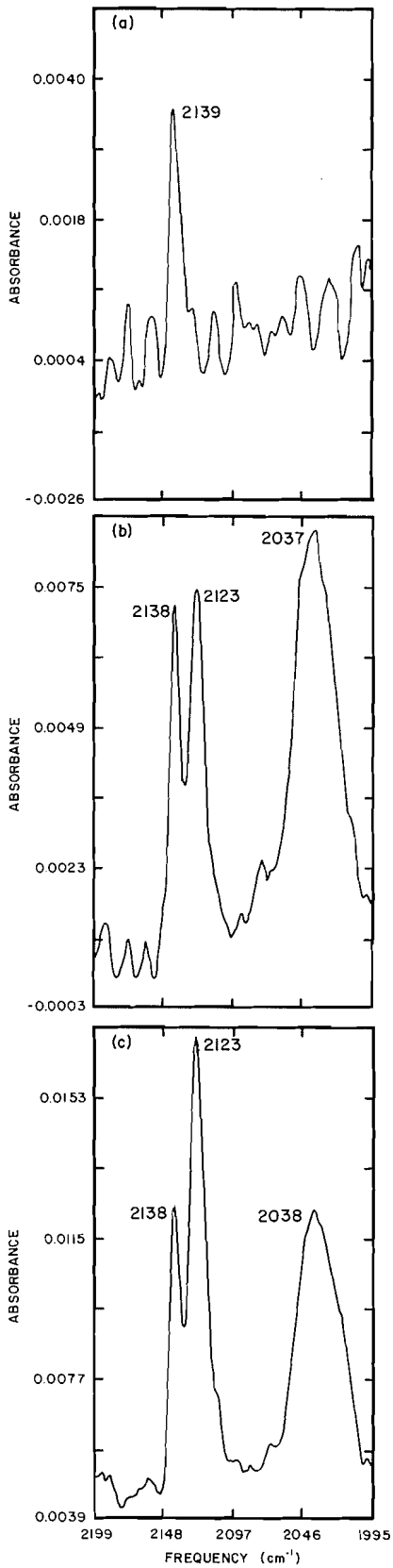

FIG. 1. Infrared spectra in the ν(CN) region of: (a) $Ph_3PbSeCN$ in C_6H_6 (saturated), (b) $Ph_3PbNCSe \cdot HMPA$ in C_6H_6 (0.008 *M*), (c) $Ph_3PbSeCN \cdot 4\text{-picO}$ in C_6H_6 (0.010 *M*).

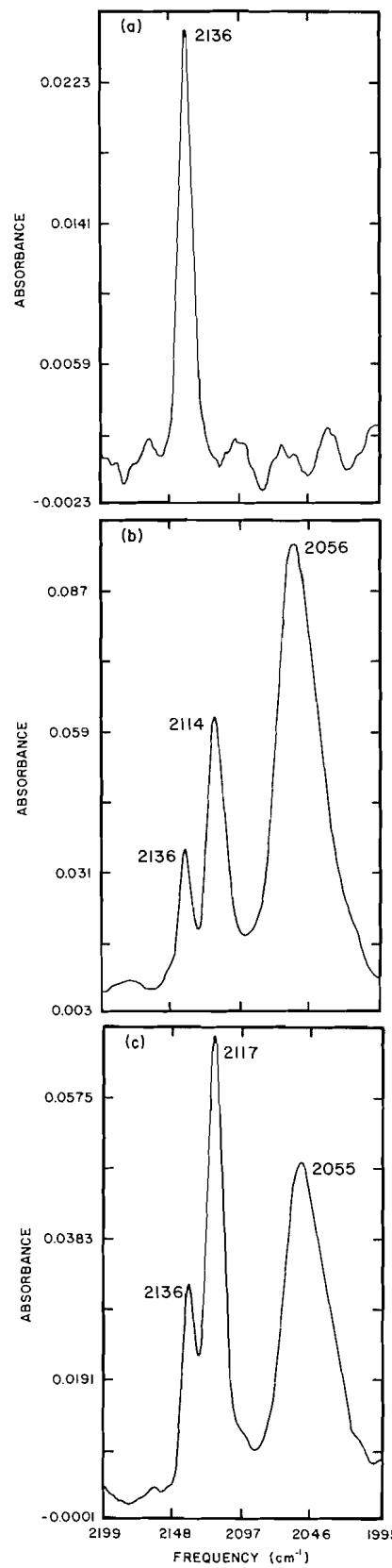

FIG. 2. Infrared spectra in the ν(CN) region of: (a) $Ph_3PbSeCN$ in CH_2Cl_2 (0.012 *M*), (b) $Ph_3PbNCSe \cdot HMPA$ in CH_2Cl_2 (0.035 *M*), (c) $Ph_3PbSeCN \cdot 4\text{-picO}$ in CH_2Cl_2 (0.033 *M*).

ligands, and could imply that Ph_3PbNCS is a weaker Lewis acid. Since, however, molecular weight measurements (10) show $Ph_3PbNCS \cdot HMPA$ to be undissociated when compared with its isocyanate analogue, the apparent inability of

Can. J. Chem. Downloaded from www.nrcresearchpress.com by 210.87.254.42 on 09/06/12
For personal use only.

Ph_3PbNCS to form adducts must be due to its much lower solubility caused by its more strongly bridged structure as discussed earlier. As expected, no adducts were obtained with weaker ligands like tetrahydrofuran, acetone, urea, etc.

The adducts of Ph_3PbNCS with O-donor ligands reported here are white air-stable solids with sharp melting points, which are soluble in nonpolar solvents like benzene and dichloromethane but are insoluble in pentane. Thiocyanate group vibrational data (Table 2) show all adducts have only N-bonded thiocyanate in the solid state, as is also the case for most of the adducts in benzene solution. However, the TPPO adduct is anomalous by having two ν(CN) absorptions in benzene solution, and further study is required for this more complex system.

Triphenyllead selenocyanate also formed adducts with only the stronger O-donor ligands (HMPA, 4-picO, pyO, and TPPO) used here, and no adduct with DMSO or DMF could be isolated. This is probably a reflection of the weaker acceptor power of $Ph_3PbSeCN$ since this is itself soluble in the preparative solvents used here. Molecular weight data (benzene, 0.01 *M*; 37°C), found (calcd.) for $Ph_3PbSeCN \cdot$4-picO, 471 (653), and $Ph_3PbNCSe \cdot$HMPA, 435 (723), show adducts are dissociated in benzene solution, the value for the HMPA suggesting the acceptor strengths of $Ph_3PbSeCN$ and Ph_3PbCl are similar. A detailed comparison cannot be made since $Ph_3PbNCSe \cdot$HMPA isomerizes in benzene solution (*vide infra*). All adducts are white stable solids with sharp melting points somewhat below those for the thiocyanate adducts.

Adducts of $Ph_3PbSeCN$ with 4-picO, pyO, and TPPO show a sharpening of the ν(CN) band and a decrease in the value of ν(CSe) compared with the Lewis acid (Table 3), consistent with a terminal Se-bonded selenocyanate, showing that the weaker lead–nitrogen bond in $Ph_3PbSeCN$ is broken by these ligands. In contrast, the HMPA adduct has ν(CSe) shifted to higher frequency and the ν(CN) band broadened and shifted to lower frequency, showing this compound to be an *iso*selenocyanate like the O-donor adducts of $Ph_3SnNCSe$ (3, 17). This structural change caused by an apparently minor variation in ligand implies similar bond strengths for the alternate Pb—NCSe and Pb—SeCN bonding modes and raises the possibility of isomers. This was confirmed by the benzene solution spectra of the adducts (Table 3) where ν(CN) absorptions at 2139 (sp), ~2125 (sp), and ~2035 (br) cm^{-1} may be assigned to $Ph_3PbSeCN$, L—(Ph_3)Pb—SeCN, and L—(Ph_3)Pb—NCSe species, respectively. While linkage isomerism for selenocyanate complexes is known in transition metal complexes (18), to our knowledge this is the first example observed involving coordination to a main group (d^{10}) element. That the effect due to change in ligand from HMPA to 4-picO is of molecular rather than crystal lattice origin is evident by comparing the relative intensities of the ν(CN) absorptions for the two isomers in the benzene solution spectra of the two adducts (Fig. 1). Spectra of dichloromethane solutions of the adducts (Table 3, Fig. 2) show two sharp peaks which may be assigned to $Ph_3PbSeCN$ and L(Ph_3)PbSeCN as before. However, the shift to higher frequency (~20 cm^{-1}) of the third band is large when compared with the smaller solvent shifts (<10 cm^{-1}) of the ν(CN) band of $Ph_3PAuNCS$ observed for a wide range of solvents (19), and the 2055 cm^{-1} peak may be due to the selenocyanate ion. The complexity of the system is shown by the ^{31}P nmr spectrum of $Ph_3PbNCSe \cdot$HMPA in $CDCl_3/CH_2Cl_2$ at 190 K, with chemical shifts positive downfield from 85% H_3PO_4 external reference. As well as free HMPA (δ_P = 26.5 ppm), three peaks are observed at: δ_P = 24.64 ppm, $^2J_{Pb-P}$ = 132 Hz; δ_P = 24.3 ppm, $^2J_{Pb-P}$ = 135 Hz; δ_P = 23.4 ppm, $^2J_{Pb-P}$ = 92 Hz; with their intensities decreasing in the same order. These four peaks imply that a process besides dissociation and isomerization, perhaps ionization, occurs in this system.

(iii) Adducts with N-donor ligands

Reactions with amines proved disappointing for Ph_3PbNCS and $Ph_3PbSeCN$ as found earlier for $Ph_2Pb(NCS)_2$ (9) and Ph_3PbNCO (10), and not all adducts obtained had the expected (1:1) stoichiometry. Triphenyllead isothiocyanate formed 1:1 adducts with pyridine and β- and γ-picolines, but not with α-picoline, even when Ph_3PbNCS was mixed with the neat ligand. Similarly, no adducts of Ph_3SnNCS (4) or $Ph_3SnNCSe$ (3) with α-picoline have been reported. While this may be due to steric hindrance by the α-methyl group, calorimetric titration studies (20) of the reactions of pyridine, α-picoline, and γ-picoline with several organotin halides have shown the steric effect is due to an entropy factor rather than a change in the enthalpy of metal–ligand bond formation. Unlike its tin analogue, triphenyllead selenocyanate does not form adducts with pyridine, β-, or γ-picoline, perhaps due to its weaker acceptor power.

Adduct formation with aliphatic amines proved elusive. Only the use of neat morpholine, pyrrolidine, or piperidine gave adducts with triphenyllead selenocyanate, while a cyclohexylamine adduct formed only with Ph_3PbNCS. Other ligands tried were aniline, diethylamine, triethylamine, quinoline, and 2,2′-bipyridine.

The N-donor ligand adducts reported here are white solids except those with pyrrolidine, which are yellow, and $Ph_3PbNCS \cdot CyNH_2$, which is light brown. All lose ligand slowly when heated and the decomposition temperatures were obtained using sealed tubes. All adducts except $Ph_3PbNCS \cdot$pipy dissolved in benzene or toluene containing some excess ligand.

Infrared data for the amine adducts of Ph_3PbNCS (Table 4) and $Ph_3PbSeCN$ (Table 5) show that all except $Ph_3PbNCS \cdot$pyrrol decompose to some extent when mulled, consistent with the general instability of these adducts. Values of ν(CN), ν(CS), and δ(NCS) for the triphenyllead isothiocyanate adducts with pyridines and pyrrolidine are consistent with N-bonded thiocyanate, as in the O-donor ligand adducts. However, for the morpholine adduct, the lower sharp ν(CN) peak together with the ν(CS) and δ(NCS) values indicates the presence of ionic thiocyanate, the compound probably having an ionic structure such as $Ph_3Pb(morph)_2^+(NCS)^-$. For $Ph_3PbNCS \cdot L$ (L = pipy or $CyNH_2$), the two ν(CN) peaks are consistent with the presence of both N-bonded and ionic thiocyanate groups, although the splitting could be a crystal lattice effect. However, the same two ν(CN) absorptions occur in the benzene solution spectrum of $Ph_3PbNCS \cdot$TPPO noted earlier where this cannot be the case. All three $Ph_3PbSeCN$–amine adducts had a lower frequency, sharp ν(CN) absorption, but no increase in ν(CSe) when compared with the parent Lewis acid. This behaviour suggests $(NCSe)^-$ is present, implying an ionic formulation as well for these adducts. Crystal structure determinations are clearly necessary to test the ionic formulae proposed above.

The amine ligands used here have donor strengths, based on their Gutmann donor number (DN) values (21), greater than the O-donor ligands which form stable adducts with Ph_3PbNCS and $Ph_3PbSeCN$. However, the DN value is an enthalpic mea-

TABLE 4. Thiocyanate group frequencies (cm^{-1}) (ir data, Nujol mull) for amine adducts of Ph_3PbNCS

Compound	ν(CN)		ν(CS)	δ(NCS)
$Ph_3PbNCS \cdot py$	2093[a] w–m,	2045 vs 1997 w	800 vw	476 vw 481
$Ph_3PbNCS \cdot \beta$-pic	2093[a] w,	2047 vs 2001 vw	805 w	469 w 475 vw
$Ph_3PbNCS \cdot \gamma$-pic	2094[a] w,	2057 vs 2009 vw	794 vw	473 w 476 sh
$Ph_3PbNCS \cdot$ pyrrol	2060 vs, br	2016 w	790 vw	470 w 474 w
$Ph_3PbNCS \cdot$ pipy	2090[a] m,	2068 m 2054 s	781 vw	—
$Ph_3PbNCS \cdot CyNH_2$	2088[a] sh,	2065 s 2047 vs	—	—
$Ph_3PbNCS \cdot 2$ morph	2090[a] m,	2065 s, sp	754 w	496 w

[a]ν(CN) for Ph_3PbNCS.

TABLE 5. Selenocyanate group frequencies (cm^{-1}) (ir data, Nujol mull) for amine adducts of $Ph_3PbSeCN$

Compound	ν(CN)		ν(CSe)	δ(NCSe) [2δ(NCSe)]
$Ph_3PbSeCN \cdot$ pipy	2107[a] w–m,	2067 vs, sp 2021 vw	544 vw	418 w [831 vw]
2 $Ph_3PbSeCN \cdot 3$ pyrrol	2103[a] w,	2062 vs, sp 2018 vw	573 w	416 w
2 $Ph_3PbSeCN \cdot 3$ morph	2106[a] s–m,	2062 s, sp 2020 w	522 w 571 w	415 w

[a]ν(CN) for $Ph_3PbSeCN$.

sure of donor power and neglects entropy factors which may be more important for amines where the donor atom is embedded in the bulk of the molecule. Thus for attachment of the amine to an aryltin or -lead moiety, while a strong M—N bond might be readily formed, weak steric hindrance could hinder free rotation of the bound amine in solution or constrain the possible arrangements of the bound ligand in the solid state causing an adverse entropy change on adduct formation, and thus accounting for the generally weak nature of the amine adducts formed by Ph_3PbNCO (10), Ph_3PbNCS, and $Ph_2Pb(NCS)_2$ (9). In contrast, the O-donor ligands used here have donor atoms which protrude from the bulk of the molecule causing less steric hindrance for adducts of these ligands. This hypothesis is supported by the results of calorimetric studies by Graddon of the reaction $R_2SnCl_2 + L \rightarrow R_2SnCl_2 \cdot L$ in benzene; e.g. for R = Ph, when L = pyO (22), $\Delta H = -39$ kJ/mol, $K = \infty$ (25°C), and when L = py (20), $\Delta H = -48$ kJ/mol, $K = 80$ (25°C), showing pyridine to be the better donor on an enthalpic basis but entropy effects cause the pyridine adduct to be less stable than that with pyridine-*N*-oxide.

(iv) Factors affecting the mode of chalcocyanate coordination to the triphenyllead moiety

Chalcocyanates (NCX^-; X = O, S, Se, or Te) are all potentially ambidentate ligands and the choice of donor atom (N or X) to complex with a given metal ion has been generally rationalized by Pearson's "hard and soft acid – base principle" as discussed in detail by Norbury (14). A study of the equilibrium, $Ph_3Pb^+(solv) + X^-(solv) \rightleftarrows Ph_3PbX(solv)$ in methanol (23), showed lead in the Ph_3Pb^+ ion to have borderline soft acid character. Thus selenium, being even "softer" than sulphur, will show a greater tendency to bind to lead, in this case sufficient to overcome the intrinsically greater donor ability of the nitrogen atom.

The occurrence of linkage isomers of $Ph_3PbSeCN$ adducts with O-donor ligands may be taken as an example of symbiosis. Coordination of a "hard" O-donor ligand to Ph_3Pb will stabilize the L—Pb—NCSe structure relative to the L—Pb—SeCN isomer, and the possible Pb—N or Pb—Se bonds now become more equivalent in energy which is the condition required for linkage isomerism to occur when, as is the case with main group metal complexes, kinetic control cannot be the cause.

Acknowledgements

We are very grateful for the financial support of le Gouvernement du Québec, Ministère de l'Education, and of the Natural Sciences and Engineering Research Council of Canada.

1. T. N. SRIVASTAVA and P. C. KAMBOJ. Indian J. Chem. A. **19**, 167 (1980).

Can. J. Chem. Downloaded from www.nrcresearchpress.com by 210.87.254.42 on 09/06/12
For personal use only.

2. T. N. SRIVASTAVA and P. C. KAMBOJ. J. Indian Chem. Soc. **56**, 857 (1979).
3. T. N. SRIVASTAVA, P. C. SRIVASTAVA, and S. K. SRIVASTAVA. Indian J. Chem. A, **20**, 443 (1981).
4. J. H. HOLLOWAY, G. P. MCQUILLAN, and D. S. ROSS. J. Chem. Soc. (A) 1935 (1971).
5. T. N. SRIVASTAVA and M. P. AGARWAL. J. Inorg. Nucl. Chem. **32**, 3416 (1970).
6. F. P. MULLINS and C. CURRAN. Can. J. Chem. **53**, 3200 (1975).
7. N. BERTAZZI, G. ALONZO, A. SILVESTRI, and G. CONSIGLIO. J. Organometal. Chem. **37**, 281 (1972).
8. N. BERTAZZI, G. ALONZO, G. C. STOCCO, and L. PELLERITO. J. Organometal. Chem. **80**, 225 (1974).
9. R. MAKHIJA and M. ONYSZCHUK. J. Organometal. Chem. **135**, 261 (1977).
10. J. S. ASPLER, R. WOJTOWSKI, I. WHARF, R. MAKHIJA, and M. ONYSZCHUK. J. Organometal. Chem. **205**, 53 (1981).
11. E. E. AYNSLEY, N. N. GREENWOOD, G. HUNTER, and M. J. SPRAGUE. J. Chem. Soc. (A) 1344 (1966).
12. I. WHARF, M. ONYSZCHUK, J. M. MILLER, and T. R. B. JONES. J. Organometal. Chem. **190**, 417 (1980).
13. I. WHARF, M. ONYSZCHUK, D. M. TALLETT, and J. M. MILLER. Can. J. Spectrosc. **24**, 123 (1979).
14. A. H. NORBURY. Adv. Inorg. Chem. Radiochem. **17**, 254 (1975).
15. A. M. DOMINGOS and G. M. SHELDRICK. J. Organometal. Chem. **67**, 257 (1974).
16. T. N. TARKHOVA, E. V. CHUPRUNOV, L. E. NIKOLAEVA, M. A. SIMONOV, and N. V. BELOV. Sov. Phys.-Crystallogr. **23**, 281 (1978).
17. I. WHARF and M. ONYSZCHUK. To be published.
18. R. J. BALAHURA and N. A. LEWIS. Coord. Chem. Rev. **20**, 109 (1976).
19. J.B. MELPOLDER and J. L. BURMEISTER. Inorg. Chim. Acta, **49**, 115 (1981).
20. Y. FARHANGI and D. P. GRADDON. J. Organometal. Chem. **87**, 67 (1975).
21. V. GUTMANN and R. SCHMID. Coord. Chem. Rev. **12**, 263 (1974).
22. D. P. GRADDON and B. A. RANA. J. Organometal. Chem. **136**, 19 (1977).
23. S. STAFFORD, H.-J. HAUPT, and F. HUBER. Inorg. Chim. Acta, **11**, 207 (1974).

Can. J. Chem. Downloaded from www.nrcresearchpress.com by 210.87.254.42 on 09/06/12
For personal use only.

Nuclear mean free paths and transparency at intermediate energies[1]

PAUL J. KAROL

Department of Chemistry, Carnegie–Mellon University, Pittsburgh, PA 15213, U.S.A.

Received September 1, 1982

This paper is dedicated to Professor Leo Yaffe on the occasion of his 65th birthday

PAUL J. KAROL. Can. J. Chem. **61**, 750 (1983).

The soft-spheres model of nuclear reaction cross sections incorporating tapered density distributions is used to evaluate nucleon mean free paths and transparencies at intermediate energies. Comparison with similar calculations employing uniform density distributions shows the latter to give misleading results that nevertheless have been used in recent years as evidence that the physics of the nucleon–nucleon interaction within nuclei is incompletely understood.

PAUL J. KAROL. Can. J. Chem. **61**, 750 (1983).

On a utilisé le modèle de sphères mous des sections droites d'une réaction nucléaire incorporant les distributions de densité non uniforme pour évaluer les trajectoires moyennes libres du nucléon et les transparences à des énergies intermédiaires. La comparaison avec des calculs analogues utilisant les distributions de densité uniforme montrent que ces derniers donnent des résultats erronés que l'on a néanmoins utilisés récemment comme la preuve d'une compréhension incomplète de la physique de l'interaction nucléon–nucléon à l'intérieur du noyau.

[Traduit par le journal]

1. Introduction

Transparency of a nucleus toward an incident projectile has always served as a convenient term for explaining the difference between geometric cross sections and total reaction cross sections. When target nuclei and projectiles have well-defined boundaries, i.e. sharp edges, nuclear transparency can be precisely quantified as has been done by Fernbach *et al.* (1) and Bradt and Peters (2). In a recent report, DeVries and Peng (3) analyzed total reaction cross sections for ^{12}C, ^{16}O, and ^{40}Ca towards medium energy protons, deuterons, and α particles. From a semiclassical formula [2], they derived nuclear transparency values for each experimental case. DeVries and Peng concluded (*i*) that composite-projectile collisions are more transparent than proton collisions with the same nucleus, (*ii*) that such an observation is at variance with conventional experience, and (*iii*) that, therefore, the implications have theoretical significance.

In what will prove to be a related situation, attention has been drawn recently to what has been termed (4) "a serious problem that past theoretical calculations have appeared to yield a mean free path of roughly 3 fermis for nucleons of energy 50–150 MeV whereas the experimental value in this energy range is approximately 5 fermis".

The following report will address both the issue of nuclear transparency and the mean free path of intermediate energy nucleons in complex nuclei.

2. Total reaction cross sections

At and above intermediate energies, where Coulomb effects are negligible, theoretical total reaction cross sections σ_R may be reduced to a calculation of $T(r)$, the probability that at impact parameter r, the projectile will pass through the target without interaction. Then

$$[1] \quad \sigma_R = 2\pi \int [1 - T(r)] r dr$$

$T(r)$ is calculated assuming straight-line trajectory using free two-body nucleon–nucleon collision cross sections σ. At and above intermediate energies, Pauli blocking modifications to σ become relatively minor and will be neglected to keep our discussion simpler. For a single particle point projectile and a uniform density (ρ) target nucleus of radius $R = R_0 A^{1/3}$

$$[2] \quad \sigma_R = \pi R^2 [1 - \{1 - (1 + 2KR)e^{-2KR}\}/2K^2R^2] = \pi R^2 [1 - T]$$

where the attenuation coefficient $K = \sigma\rho$ is the reciprocal of the projectile's mean free path λ. For zero mean free path, the opaque nucleus result $\sigma_R = \pi R^2$ is obtained. The term on the right within the square brackets of [2] is identified with nuclear transparency. Furthermore, for two colliding uniform density composite nuclei, the zero mean free path limit, or *hard-sphere* model gives

$$\sigma_R = \pi R_0^2 (A_P^{1/3} + A_T^{1/3})^2$$

This expression has been phenomenologically modified (2) with limited success to allow for transparency by introducing a corrective overlap parameter b in the form

$$[3] \quad \sigma_R = \pi R_0^2 (A_P^{1/3} + A_T^{1/3} - b)^2$$

implying that

$$T \sim 2b/(A_P^{1/3} + A_T^{1/3})$$

Hudis (5) has pointed out that transparencies calculated according to uniform hard-sphere density distributions are "probably lower limits since the transparency is very dependent on the assumed nuclear density distribution and the use of diffuse nuclear boundary will almost certainly yield higher values". In fact, the assumption or application of a sharp density distribution to either the calculation of nuclear transparency or the estimation of particle mean free paths from experimental total reaction cross sections is misleading as will be shown.

[1]This work was performed under the auspices of the U.S. Department of Energy Division of Nuclear Physics Office of High-Energy Physics and Nuclear Physics.

Can. J. Chem. Downloaded from www.nrcresearchpress.com by 210.87.254.40 on 09/06/12
For personal use only.

TABLE 1. Comparison of σ_R from the semiclassical soft spheres model with the Glauber Model at 1.05 GeV/A

Projectile + target	σ_R Soft spheres (6)	σ_R Glauber model (9)
p + a	104 mb	108 mb
p + ^{12}C	279	267
p + ^{16}O	338	340
p + ^{40}Ar	647	637
p + ^{208}Pb	1837	1815
a + ^{12}C	550	560
a + ^{16}O	670	680
a + ^{208}Pb	2600	2580
^{40}Ar + ^{208}Pb	4850	4810

Total reaction cross sections for single projectile and composite projectile interactions with target nuclei that incorporate realistically tapered density distributions can be evaluated using the author's *soft-spheres* model (6). In this semiclassical model, which contains no free parameters, $T(r)$ is calculated using Gaussian density distributions for both projectile (P) and target (T). The distributions are normalized to the "true" density profiles at the nuclear surface. One obtains

$$[4] \quad \ln T(r) = \chi \exp\left[-r^2/(a_T^2 + a_P^2)\right]$$

where

$$\chi = \frac{\pi^2 \sigma(E) \rho_T(0) \rho_P(0) a_T^3 a_P^3}{(a_T^2 + a_P^2)}$$

in which

$$a = (2/3)^{1/2} R_{rms} \qquad A \leq 40$$
$$= [(4ct + t^2)/4 \ln 5] \qquad A > 40$$

and

$$\rho(0) = A/(a\pi^{1/2})^3 \qquad A \leq 40$$
$$= \tfrac{1}{2}\rho_0 \exp (c/a)^2 \qquad A > 40$$

where c, t, and ρ_0 are the radial, skin thickness, and central density parameters of the Fermi distribution and R_{rms} is the root mean square radius, all determined from electron scattering data (7). $\sigma(E)$ is the energy-dependent two-body elementary collision cross section (see ref. 6 for complete details). The soft-spheres model using [1] and [4] gives

$$[5] \quad \sigma_R = \pi(a_T^2 + a_P^2)[E_1(\chi) + \ln \chi + \gamma]$$

where E_1 is the exponential integral and γ is Euler's constant (8). At somewhat lower energies, the Coulomb barrier, projectile deBroglie wavelength, and Pauli blocking corrections can be included. That the soft-spheres equation is accurate can be seen by a comparison with recent Glauber model calculations (9) in Table 1 and experiments in Table 2 for a variety of projectile–target systems. In Fig. 1 the soft-spheres calculated results are compared to some experimental σ_R's compiled by DeVries and Peng (10).

3. Transparency

Any attempt to use a diffusely tapered density distribution to calculate nuclear transparency is frustrated by the lack of a defined outer nuclear limit. That is, the transparency approaches 100% because of peripheral contributions where ρ approaches zero asymptotically. One way of illustrating this, which also suggests a scheme for circumventing the problem, is by using a sharp cutoff.

TABLE 2. Comparison of σ_R from the soft spheres model with experiment

Projectile–target (energy GeV/A)	σ_R Experiment*	σ_R Soft spheres
p–Be (0.53)	195.4±6.2	198.4
p–B (0.53)	213±6	217
p–C (0.53)	233±5	231
p–O (0.53)	290±15	291
p–Al (0.53)	433.2±7.7	428
p–Fe (0.53)	712±13	732
p–Cu (0.53)	788±17	793
p–Ge (0.53)	877±18	862
p–Sn (0.53)	1201±23	1203
p–Pb (0.53)	1781±46	1739
p–C (0.87)	260±14	264
p–C (2.1)	270±14	266
p–a (0.87)	120±6	105
p–a (2.1)	111±6	106
p–d (2.1)	60±16	72.5
d–d (2.1)	134±8	141
d–a (0.87)	198±10	216
d–a (2.1)	203±8	218
a–a (0.87)	262±18	268
a–a (2.1)	276±14	269
a–C (0.87)	527±20	547
a–C (2.1)	535±19	549
C–C (0.87)	939±50	951
C–C (2.1)	888±44	954

*The 530 MeV proton data from ref. 19, the others from unpublished data of J. A. Jaros, LBL-3849 (1975).

Letting σ_R' represent the total reaction cross section of a projectile on a target whose densities have been abruptly truncated at impact distance R, we have

$$[6] \quad \sigma_R' = 2\pi \int_0^R [1 - T(r)] r dr$$
$$= \pi R^2 \left[1 - (2/R^2) \int_0^R T(r) r dr\right]$$

Comparison of [6] with [2] allows us to identify a nuclear transparency, T_R, corresponding to truncation at distance R from the target center:

$$[7] \quad T_R = (2/R^2) \int_0^R T(r) r dr$$

Using $T(r)$ from [4] one may obtain

$$[8] \quad T_R = (a_T^2 + a_P^2)[E_1(\chi_R) - E_1(\chi)]/R^2$$

where χ_R is given by

$$\chi_R = \chi \exp\left[-R^2/(a_T^2 + a_P^2)\right]$$

The sharp cutoff nuclear transparency has been calculated according to [8], as a function of cutoff distance, for the several systems considered by DeVries and Peng. The results of these calculations are plotted in Fig. 2. These demonstrate that, as the sharp cutoff is extended to larger and larger impact parameters, the value assigned to "nuclear transparency" approaches unity.

It is unreasonable, of course, to extend the truncation indefinitely because eventually one reaches impact parameters that contribute negligibly to the total reaction cross section. One can adopt this realization as a means for selecting a reasonable

Can. J. Chem. Downloaded from www.nrcresearchpress.com by 210.87.254.40 on 09/06/12
For personal use only.

Can. J. Chem. Downloaded from www.nrcresearchpress.com by 210.87.254.40 on 09/06/12
For personal use only.

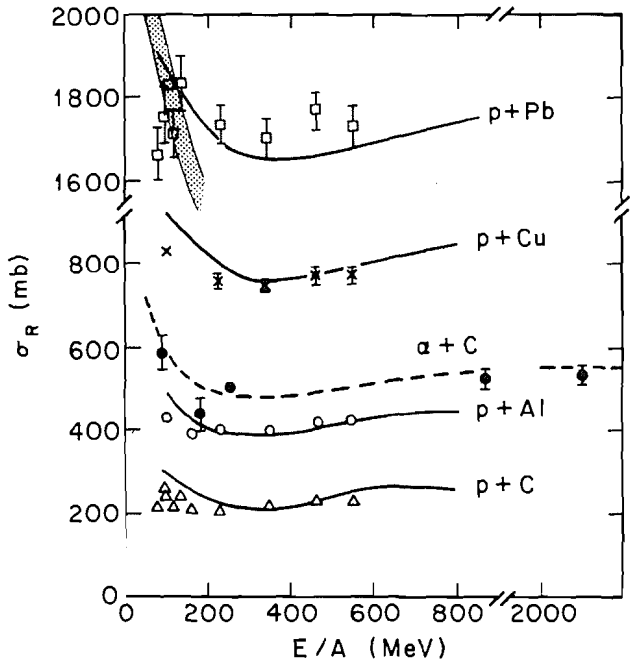

FIG. 1. Comparison of medium energy total reaction cross sections: smooth curves, calculated by the soft spheres model (6); experimental data, compiled by DeVries and Peng (3); shaded region from optical model analysis of Nadasen *et al.* (13).

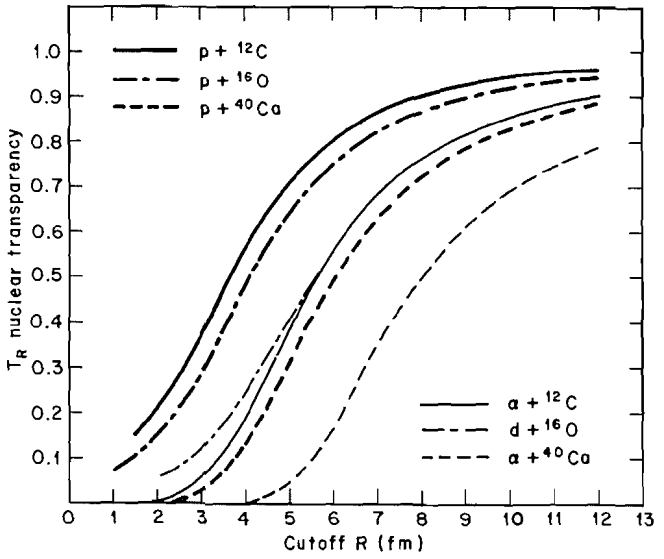

FIG. 2. Nuclear transparencies at E = 300 MeV/A calculated according to [8] for diffuse nuclei as a function of truncation radius R.

cutoff radius. Shown in Fig. 3 is the 300 MeV "fractional" reaction cross section for p + ^{12}C calculated from [8] as a function of the cutoff R. An appropriate *cutoff radius* R_c may be defined by summing the projectile and target radii at which each of the densities falls to 10% of the central values. At $R = R_c$, greater than 90% of the total reaction cross section is accounted for by truncating the overlap between projectile and target density distribution tails. The results of such a procedure are tabulated in Table 3 for the cases examined by DeVries and Peng. Our results demonstrate that the trend in transparency is *not* contrary to conventional expectations.

Chen *et al.* (11), employing step density distributions in

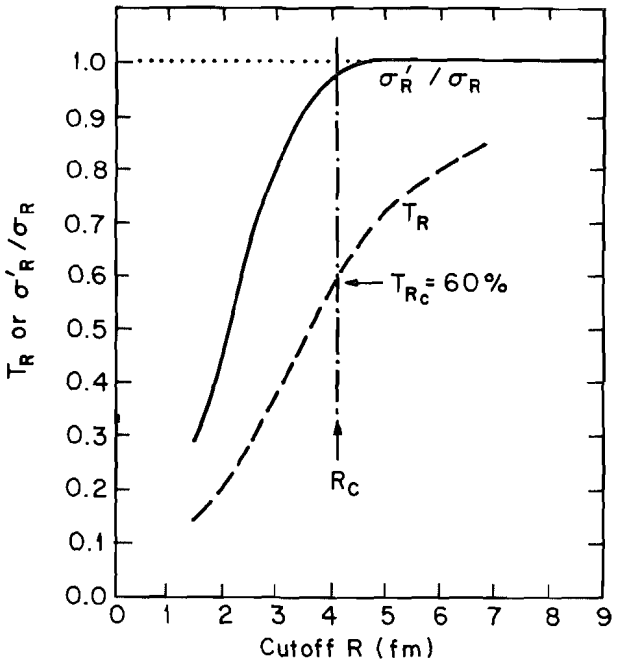

FIG. 3. Determination of sharp cutoff radius and resulting transparency for p + ^{12}C at 300 MeV.

TABLE 3. Extrapolated nuclear transparencies at 300 MeV/A

System	R_c (fm)	T_{R_c} (%) Tapered density (this work)	T (%) Uniform density (ref. 3)
p + ^{12}C	4.05	60	36
p + ^{16}O	4.40	57	32
p + ^{40}Ca	4.82	29	32
a + ^{12}C	5.08	42	52
d + ^{16}O	6.10	59	59
a + ^{40}Ca	5.84	16	44

intranuclear cascade (INC) calculations for 375 MeV protons on ^{75}As and ^{209}Bi, showed that the "transparency" increased from 13% to 48% and 9% to 37% respectively in going from a square (uniform) distribution to a diffuse-skinned step function that approximated the electron-scattering results. INC calculations are in qualitative agreement with the transparency arguments developed in this work. The truncation method embodied in [8] gives 40% and 29% for the ^{75}As and ^{209}Bi proton transparencies respectively at 375 MeV using R_c as outlined above.

From the above description, it should be clear that use of uniform density distributions can indeed be misleading. Equivalent errors arise when discussions of the mean free path of nucleons in complex nuclei are undertaken. The remainder of the report will address this issue.

4. Nucleon mean free path

In recent years, a number of publications have called attention to the apparent discrepancy between the mean free path of nucleons derived from scattering experiments and that which arises from the impulse approximation. Schiffer (12) and Nadasen *et al.* (13) have considered proton scattering as analyzed through the optical model. Total reaction cross sections derived from the complex optical potential parameters are em-

TABLE 4. Proton total reaction cross sections at 90 MeV

Target	σ_R Using $\lambda = 4.5$ fm	σ_R Using $\lambda = 1/\sigma\rho$	σ_R Experimental
^{12}C	127	288	245
^{27}Al	249	495	430
^{90}Zr	766	1130	1077
^{208}Pb	1384	1845	1831

ployed in [2] to estimate attenuation coefficients K and subsequently λ. As a consequence of using the (inappropriate) uniform density formula, $\lambda = 5.3$ fm is obtained at 150–180 MeV. On the other hand, using $\rho = 0.16$ nucleons/fm^3, $\sigma_{pp} = 2.4$ fm^2, and $\sigma_{pn} = 4.2$ fm^2, one expects $\lambda \sim 2.5$ fm. The discrepancy arises in the misleading application of the sharp density distribution. A tapered density distribution, using the (density-dependent) $1/\lambda = \sigma\rho(r)$ expression, does a reasonable job of reproducing total reaction cross sections derived from optical model analysis of scattering data, being ~15% too large, at the worst, in this energy region as seen in Fig. 1. Moreover, using the soft-spheres model, one may calculate the values for the nucleon–nucleon cross section σ needed to fit the range of σ_R's obtained by Nadasen *et al.* (13) in their optical model analyses and shown as the shaded region in Fig. 1 for ^{208}Pb. Mean free paths are derived from these using $\rho = 0.16$ nucleons/fm^3 and yield $\lambda = 2.9 \pm 0.7$ fm. That value is in distinct contrast to the much larger mean free path obtained using a uniform density nucleus and cited above. Interestingly, Negele and Yazaki (4) use the parameters of ref. 13 to derive a local optical model result $\lambda_L \sim 3$ fm and a non-local result $\lambda_{NL} \sim 4$ fm at 150–200 MeV and conclude that much of the long-mean-free-path discrepancy is resolved in favor of the experimentally determined (sic) $\lambda \sim 5$ fm by proper treatment of non-locality.

Another way of illustrating the discordance associated with long mean free path is to examine the total reaction cross section *predicted* by longer λ. Redish and Schneider (14) claim that with various target nuclei, λ for 90 MeV protons is 4.5 fm. This can be countered in a relatively straightforward manner. With $\lambda = 4.5$ fm, the implication is that the effective nucleon–nucleon collision cross section within the nucleus is 14 mb. Using this value in the soft-spheres model, total reaction cross sections for several nuclei are calculated and listed in Table 4 along with σ_R calculated with "normal" λ and experimental data (15). Long mean free paths are inconsistent with measured σ_R's. At lower energies, Ginocchio and Blann (16) showed that INC calculations for protons on ^{89}Y and ^{54}Fe give poor results when proposed long mean free paths are utilized. However, the validity of semiclassical kinematics is questionable here. Furthermore, Hogan *et al.* (17) pointed out that Ginocchio and Blann, in neglecting refraction and reflection of the intranuclear proton, underestimate σ_R owing to the nonlinear transport through the target. Recalculation by Hogan *et al.* removes much of the discrepancy.

The 5–30% disagreement between σ_R's (and consequently λ's) derived from optical model fits to scattering and those of either attenuation measurements or theoretical calculations involving diffuse nuclear surfaces seems to imply incomplete knowledge about the more complex interactions and pathways in projectile–target interactions, not necessarily reflecting problems with the nucleon–nucleon two-body collisions. Recently, Ray (18) used second order KMT formalism including Pauli, short-range dynamical, and center-of-mass correlation to compute σ_R. Very good agreement was obtained above 400 MeV, but an overestimation by 15–25% at lower energies was regarded as an indication that multiple scattering calculations are inadequate below 400 MeV.

5. Conclusions

The total reaction cross section, perhaps the most basic nuclear reaction observable (4), is calculated semiclassically at intermediate energies by propagation of the projectile through the nuclear environment up to and including the point of first intranuclear particle–particle collision. Whether or not the physics of subsequent propagation, cascading, or other (collective or non-collective) interactions is understood through single or multiple collision pictures is essentially irrelevant following that initial interaction. Consequently, a naive statement about σ_R is that its interpretation entails the fewest theoretical assumptions. An analogous claim can be made for direct experimental measurements of total reaction cross sections, i.e. attenuation measurements. Values for σ_R derived from optical model analysis of elastic scattering are inherently more model dependent. There is no disagreement between experiment and theory concerning the validity of employing mean free paths derived from the impulse approximation nor in the trends of nuclear transparencies that have included proper consideration of the diffuse nuclear surface. Deceptively large λ's and "misbehaving" transparencies are illusions brought about by application of the uniform nuclear density distribution to the interpretation of experimental results.

1. S. FERNBACH, R. SERBER, and T. B. TAYLOR. Phys. Rev. **75**, 1352 (1949).
2. H. L. BRADT and B. PETERS. Phys. Rev. **77**, 54 (1950).
3. R. M. DEVRIES and J. C. PENG. Phys. Rev. Lett. **43**, 1373 (1979).
4. J. W. NEGELE and K. YAZAKI. Phys. Rev. Lett. **47**, 71 (1981).
5. J. HUDIS. High energy nuclear reactions. Vol. 1. *Edited by* L. Yaffe. John Wiley, New York. 1967.
6. P. J. KAROL. Phys. Rev. C, **11**, 1203 (1975).
7. C. W. DEJAGER, H. DEVRIES, and C. DEVRIES. Atomic data and nuclear data tables. **14**, 479 (1974).
8. M. ABRAMOWITZ and I. A. STEGUN. Handbook of mathematical functions. Dover, NY. 1968.
9. S. BARSHAY, C. B. DOVER, and J. P. VARY. Phys. Rev. C, **11**, 360 (1975).
10. R. M. DEVRIES and J. C. PENG. Phys. Rev. C, **22**, 1055 (1980).
11. K. CHEN, Z. FRAENKEL, G. FRIEDLANDER, J. R. GROVER, J. M. MILLER, and Y. SHIMAMOTO. Phys. Rev. **166**, 949 (1968).
12. J. P. SCHIFFER. Nucl. Phys. A, **335**, 339 (1980).
13. A. NADASEN, P. SCHWANDT, P. P. SINGH, W. W. JACOBS, A. D. BACHER, P. T. DEBEVEC, M. D. KAITCHUCH, and J. T. MEEK. Phys. Rev. C, **23**, 1023 (1981).
14. F. REDISH and D. M. SCHNEIDER. Phys. Lett. B, **100**, 101 (1981).
15. P. KIRBY and W. T. LINK. Can. J. Phys. **44**, 1847 (1966).
16. J. GINOCCHIO and M. BLANN. Phys. Lett. B, **68**, 405 (1977).
17. J. J. HOGAN, K. I. BURNS, E. GADIOLI, E. GADIOLI ERBA, and G. TAGLIAFERRI. Lett. Nuov. Cim. **23**, 89 (1978).
18. L. RAY. Phys. Rev. C, **20**, 1857 (1979).
19. P. U. RENBERG, D. F. MEASDAY, M. PEPIN, P. SCHWALLER, B. FAVIER, and C. RICHARD-SERRE. Nucl. Phys. A, **183**, 81 (1972).

Can. J. Chem. Downloaded from www.nrcresearchpress.com by 210.87.254.40 on 09/06/12
For personal use only.

Identification of 26-minute Zr-84[1]

SEIICHI SHIBATA[2] AND PAUL J. KAROL

Department of Chemistry, Carnegie–Mellon University, Pittsburgh, PA 15213, U.S.A.

Received September 1, 1982

This paper is dedicated to Professor Leo Yaffe on the occasion of his 65th birthday

SEIICHI SHIBATA and PAUL J. KAROL. Can. J. Chem. **61**, 754 (1983).

An unknown γ-ray of energy 112.5 keV was found in zirconium fractions chemically extracted from isotopically enriched molybdenum targets bombarded with 500 and 800 MeV protons. All evidence suggests that the γ-ray is identifiable with the decay of ^{84}Zr to ^{84}Y. A half-life of 25.7 ± 0.5 min was obtained for ^{84}Zr, which is considerably longer than previously reported half-lives. The absolute abundance of the 112.5 keV γ-ray was also determined. Relative production cross sections for ^{84}Zr were calculated using these results and were consistent with the values interpolated from isotopic distribution curves for spallation reactions.

SEIICHI SHIBATA et PAUL J. KAROL. Can. J. Chem. **61**, 754 (1983).

On a trouvé un rayon γ inconnu ayant une énergie de 112,5 keV dans les fractions de zirconium extraites chimiquement des cibles de molybdène enrichies isotopiquement et bombardées avec des protons de 500 et de 800 MeV. Toutes les preuves suggèrent que le rayon γ peut être identifié avec la désintégration du ^{84}Zr en ^{84}Y. On a obtenu une demi-vie de 25,7 ± 0,5 minute pour le ^{84}Zr. Ce temps est de beaucoup supérieur à ceux rapportés antérieurement. On a aussi déterminé l'abondance absolue du rayon γ de 112,5 keV. A partir de ces résultats, on a calculé les sections droites de production relative du ^{84}Zr et les valeurs calculées sont en accord avec celles obtenues par interpolation à partir des courbes de distribution isotopique des réactions où des particules sont éjectées artificiellement du noyau.

[Traduit par le journal]

Can. J. Chem. Downloaded from www.nrcresearchpress.com by 210.87.254.6 on 09/06/12
For personal use only.

In spallation reaction studies by proton activation of enriched isotopic molybdenum targets at intermediate energies, an unassignable gamma-ray of energy 112.5 keV was found. This γ-ray was always observed in zirconium fractions isolated radiochemically from the targets under investigation. Also in the zirconium fractions, γ-rays emitted from neutron-deficient daughter yttrium nuclides were observed. Growth of the 112.5 keV γ-ray activity was not observed in any zirconium fraction.

The half-life of the 112.5 keV γ-ray emission was analyzed by the CLSQ decay curve analysis program (1). The results of these analyses are indicated in Table 1. A half-life of 25.7 min was obtained.

According to the literature (2), there is no appropriate isotope which has a half-life of 26 min. However, in 1971, Doron and Blann (3) had reported the observation of a 112.5 keV γ-ray which decayed with the half-life of 26 min. They used heavy-ion reactions in order to produce nuclides far from the line of β-stability and some γ-rays were unidentifiable, the 112.5 keV among them. Doron and Blann concluded that the 112.5 keV gamma was emitted from either ^{84}Y^{m} or ^{84}Zr based on cross bombardment techniques in combination with compound nucleus evaporation calculations. However, they were unable to obtain further information because growth of the daughter nuclide was not observed in their data analysis.

Following our irradiations of (ammonium molybdate) targets, the chemical separations of yttrium and zirconium from each other and from other elements was performed in every sample. A 6 *M* HNO_3 solution of the target, containing milligram amounts of carriers for niobium, zirconium, and yttrium was extracted with 0.5 *M* TTA in xylene which removed yttrium. Hydrophobic phase separation filter paper was used to speed the separations. The organic phase was diluted with xylene to give 0.05 *M* TTA. Zirconium was extracted using concentrated HCl containing a small amount of hydrogen peroxide to suppress the co-extraction of niobium. Zirconium hydroxide was coprecipitated with base in the aqueous phase following addition of iron(III) carrier. Time from end of bombardment to end of separation was routinely less than ten minutes. In measuring the gamma spectra of the zirconium samples, radiochemical purity was verified by the absence of independent yttrium activities.

TABLE 1. Half-life of ^{84}Zr from measurements of the 112.5 keV γ transition

Target	E_p (MeV)	Half-life (min)
^{92}Mo	800	26.1±1.6
^{92}Mo	800	24.2±0.9
^{96}Mo	800	29.3±2.3
^{92}Mo	800	27.8±1.2
^{100}Mo	800	23.4±2.1
^{92}Mo	800	25.8±1.0
^{92}Mo	500	26.4±2.6
Weighted mean		25.7±0.5

The 112.5 keV γ-ray was never observed in an yttrium fraction. Therefore, it was assumed that ^{84}Zr emitted the 112.5 keV γ-ray despite substantial disparity with the published half-lives of ^{84}Zr; 16 min (4) and 5 min (5). The latter did not report γ-ray emissions from ^{84}Zr. During the course of our determinations, yet another report on ^{84}Zr appeared, this one declaring the half-life to be 3.7 min (6). For analysis via daughter measurement, counting rates of γ-rays emitted from ^{84}Y were assayed. The result for the 1040 keV γ-ray whose abundance is 56.8% (2), is shown in Fig. 1. ^{84}Y also emits 793 keV (98%)

[1]This work was performed under the auspices of the U.S. Department of Energy Division of Nuclear Physics Office of High-Energy Physics and Nuclear Physics.

[2]Permanent address: Institute for Nuclear Study, University of Tokyo, Tokyo, Japan.

Can. J. Chem. Downloaded from www.nrcresearchpress.com by 210.87.254.6 on 09/06/12
For personal use only.

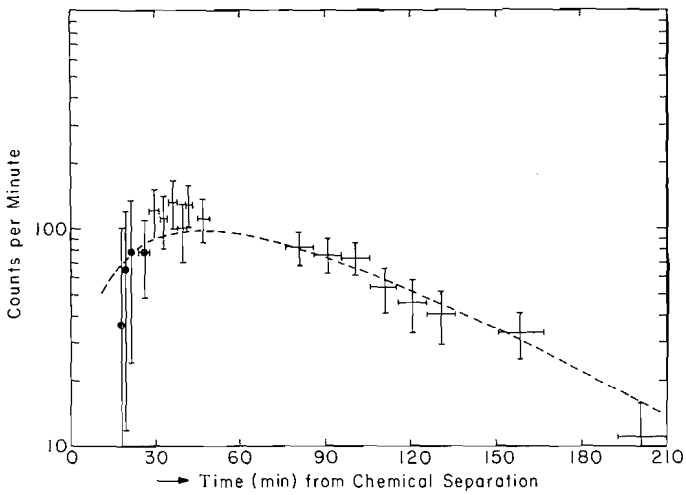

FIG. 1. Counting rate of 1040 keV γ-ray emitted from ^{84}Y in a zirconium fraction plotted as a function of time. Target = ^{92}Mo and E_p = 800 MeV. Dotted curve corresponds to the predicted counting rate of the 1040 keV γ-ray produced from decay of ^{84}Zr.

TABLE 2. Absolute abundance of the 112.5 keV γ-ray

Target	E_p (MeV)	Abundance
^{92}Mo	800	0.978±0.081
^{92}Mo	800	1.060±0.091
^{92}Mo	800	0.966±0.071
^{96}Mo	800	0.917±0.209
^{100}Mo	800	0.828±0.231
Weighted mean		0.984±0.044

and 974 keV (77.5%) γ-rays, but these were interfered with by γ-rays from 1.6-hour ^{84}Zr, also present in the zirconium samples and in greater yield.

The absolute abundance of the 112.5 keV γ-ray was calculated using the standard parent–daughter growth and decay equations (7) and the counting data of 112.5 keV and 1040 keV γ-rays. The results are indicated in Table 2. The calculated growth–decay curve of ^{84}Y produced from the 26-min decay of initially pure ^{84}Zr is compared with the data in Fig. 1 on an absolute basis and is seen to reproduce the data. In the heavy-ion reaction study of Doron and Blann (3), it is likely that the growth of ^{84}Y was not found due to the relatively high yield of ^{84}Y independently produced by the reaction and because chemical separation of yttrium from zirconium was not performed.

The relative production cross sections for ^{84}Zr from intermediate energy proton bombardment of several medium mass targets were calculated using the abundance of 98.4% and the half-life of 25.7 min, each determined in this work. One example is shown in Fig. 2. The production cross section for ^{84}Zr is consistent with the smooth isotopic distribution curve. Similarly good fits were also obtained for samples from other targets not shown, confirming the accuracy of the identification.

If ^{84}Zr were to decay to the reported 4.6-second ^{84}Y^{m} (8), growth of the daughter nuclide's 1040 keV gamma should not be observed and only a 793 keV γ-ray with a half-life of 26 min would have been seen because ^{84}Y^{m} does not decay by isomeric transition to ^{84}Y^{g}. This alternative is inconsistent with the experimental results described above. Therefore, identification of the 112.5 keV γ-ray as being emitted from ^{84}Zr with the half-life of 26 min seems well substantiated. The simple decay scheme proposed for ^{84}Zr → ^{84}Y is shown in Fig. 3.

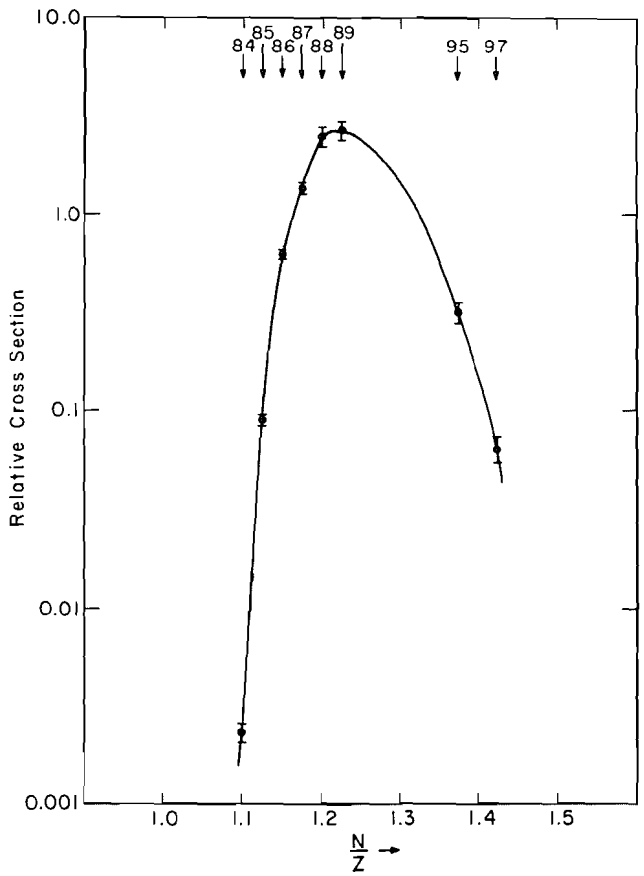

FIG. 2. Isotopic distribution curve for Zr including ^{84}Zr. Target = ^{100}Mo and E_p = 800 MeV.

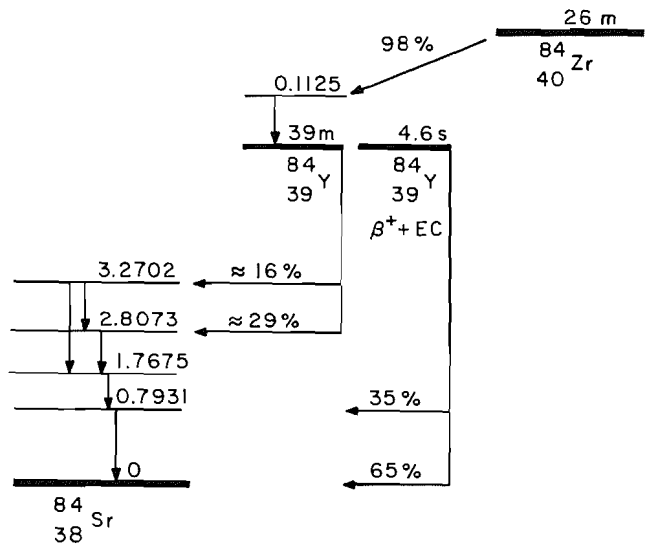

FIG. 3. Proposed decay scheme for ^{84}Zr.

Acknowledgement

The authors wish to acknowledge the cooperation and hospitality of Dr. B. J. Dropesky and the staff of the Clinton P. Anderson Los Alamos Meson Physics Facility during the investigations.

NOTE ADDED: While this manuscript was in preparation a preprint was received from P. Haustein (Brookhaven National Laboratory) which reports use of the helium-jet recoil transfer technique and the Ni-58(Si-58, $2p$) reaction in identification of 28-minute Zr-84 and relative abundances of gamma-rays.

1. J. B. CUMMING. Application of computers to nuclear- and radiochemistry. *Edited by* G. D. O'Kelley. NAS-NS 3107. National Academy of Sciences, Washington, DC. 1963. p. 25.
2. C. M. LEDERER and V. S. SHIRLEY. Table of istopes. 7th ed. Wiley, New York. 1978.
3. T. A. DORON and M. BLANN. Nucl. Phys. A, **161**, 12 (1971).
4. N. G. ZAITSEVA, V. V. KUZNETSOV, M. YA. KUZNETSOVA, MA HO IK, G. MUSIOL, H. SHU-JUN, C. MO-LUNG, and V. G. CHUMIN. Yad. Fiz. **1**, 385 (1965); trans. Sov. J. Nucl. Phys. **1**, 273 (1965).
5. Y. W. YU and A. A. CARETTO, JR. J. Inorg. Nucl. Chem. **33**, 3223 (1971).
6. S. DELLA NEGRA, C. DUPRUN, H. GAUVIN, J. P. HUSSON, D. JACQUET, and Y. LEBEYEC. Proc. Fourth Int. Conf. on Nuclei Far from Stability. Helsingor, Denmark. CERN-81-09. 1981. p. 157.
7. G. FRIEDLANDER, J. W. KENNEDY, E. S. MACIAS, and J. M. MILLER. Nuclear and radiochemistry. 3rd ed. Wiley, New York. 1981.
8. R. IAFIGLIOLA and J. K. P. LEE. Phys. Rev. C, **13**, 2075 (1975).

Can. J. Chem. Downloaded from www.nrcresearchpress.com by 210.87.254.6 on 09/06/12
For personal use only.

The synthesis of bridged biphenyl and naphthyl compounds by the photolytic and thermal extrusion of SO_2[1]

DAVID N. HARPP[2] AND DENNIS F. MULLINS
Department of Chemistry, McGill University, Montreal, P.Q., Canada H3A 2K6

Received September 9, 1982

This paper is dedicated to Professor Leo Yaffe on the occasion of his 65th birthday

DAVID N. HARPP and DENNIS F. MULLINS. Can. J. Chem. **61**, 757 (1983).

The photolytic and flash vacuum thermolytic behavior of several SO_2-containing cyclic compounds was studied. The expulsion of SO_2 by flash vacuum thermolysis afforded the corresponding bridged compounds in high yield.

DAVID N. HARPP et DENNIS F. MULLINS. Can. J. Chem. **61**, 757 (1983).

On a étudié le comportement photolytique et le comportement thermolytique sous vide éclair de plusieurs composés cycliques contenant du SO_2. L'expulsion du SO_2 par thermolyse sous vide éclair fournit avec un fort rendement les composés pontés correspondants.

[Traduit par le journal]

Can. J. Chem. Downloaded from www.nrcresearchpress.com by 210.87.254.105 on 09/06/12
For personal use only.

The use of thermolytic (2) and photolytic (3) means to induce expulsion of sulfur dioxide from cyclic molecules as a method for the formation of new carbon–carbon bonds has been employed for many years. Perhaps the area of greatest interest for the past decade has involved sulfone pyrolyses for the preparation of cyclophanes (4).

A standard method for the synthesis of the required sulfone-containing molecule involves the reaction of a dibromide **1** with sodium sulfide **2** to yield a cyclic sulfide **3**. Oxidation of

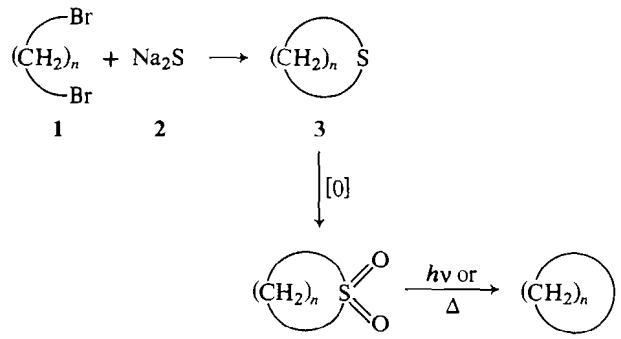

1 **2** **3** **4** **5**

sulfide **3** provides the cyclic sulfone **4** (5). Thermolytic or photolytic extrusion of SO_2 from **4** and concomitant ring closure results in the formation of **5** with a new carbon–carbon bond. Our interest in such molecules was, in part, stimulated by our development of the chemistry of certain sulfur-transfer reagents (6) which permit easy access to the requisite sulfur-containing precursors (7). These molecules encompass the three types of bonding arrangements for one sulfur and two oxygen atoms, sulfoxylate esters **6**, sulfinate esters **7**, and sulfones **8**. Only the sulfone is obtained by oxidation of a sulfide.

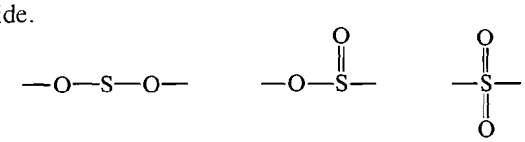

6 **7** **8**

[1]Organosulfur Chemistry, Part 43. For Part 42, see ref. 1.
[2]Author to whom all correspondence should be addressed.

The reaction of bis-benzimidazolyl sulfide **9** with 2,2′-bis-(hydroxymethyl)biphenyl **10** inserts the sulfur between the oxygens to form the cyclic sulfoxylate ester **11** which is sometimes isolable, often depending on the α-substituents (6, 7). This cyclic sulfoxylate thermally rearranges to the thermodynamically more stable cyclic sulfinate ester **12** and eventually to the stable sulfone **13**. Utilizing this approach, a series of cyclic sulfoxylate esters, sulfinate esters, and sulfones were prepared and their thermolytic and photochemical behavior studied.

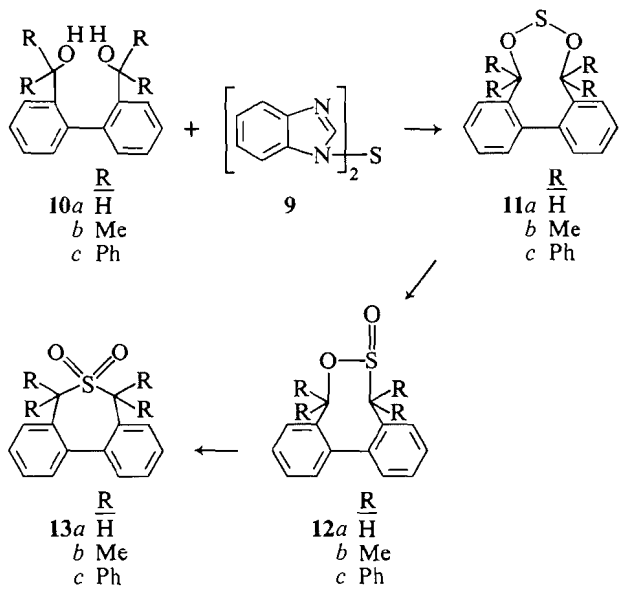

10*a* R = H
b R = Me
c R = Ph

9

11*a* R = H
b R = Me
c R = Ph

13*a* R = H
b R = Me
c R = Ph

12*a* R = H
b R = Me
c R = Ph

Flash vacuum thermolysis (FVT) of sulfinate ester **12***a* through a quartz tube heated to 700°C at a pressure of 0.05 Torr afforded a 90% isolated yield of 9,10-dihydrophenanthrene **14** containing less than 1% phenanthrene **15**.

In contrast, Durst *et al.* (3*c*) found that the photolysis of ester **12***a* in degassed methanol at 254 nm gave 9,10-dihydrophenanthrene **14** and phenanthrene **15** in a ratio of 9:1. We performed this photolysis in several other solvents but could not lower the phenanthrene percentage below 10%.

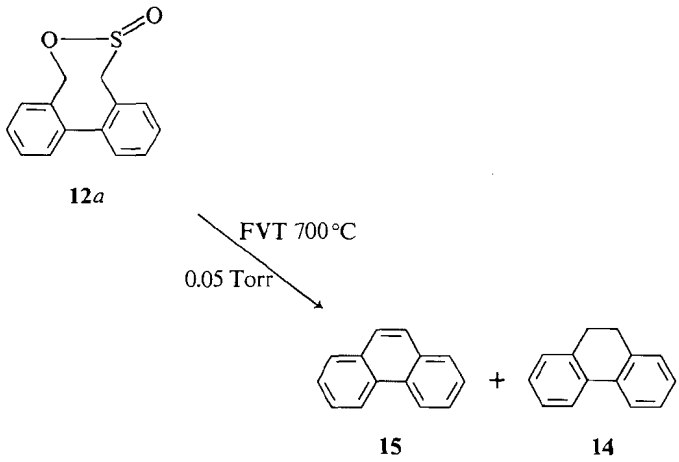

The thermolysis of sulfone **13***b* at 600°C and 0.05 Torr provided a 90% yield of a mixture of 80% 9,9,10,10-tetramethyl-9,10-dihydrophenanthrene **16** and 20% 2-(2-isopropenyl)-2′-(-2-isopropyl)biphenyl **17**; compound **16** is the first example of a 9,9,10,10-tetraalkyl substituted 9,10-dihydrophenanthrene. A possible intermediate formed by the thermal

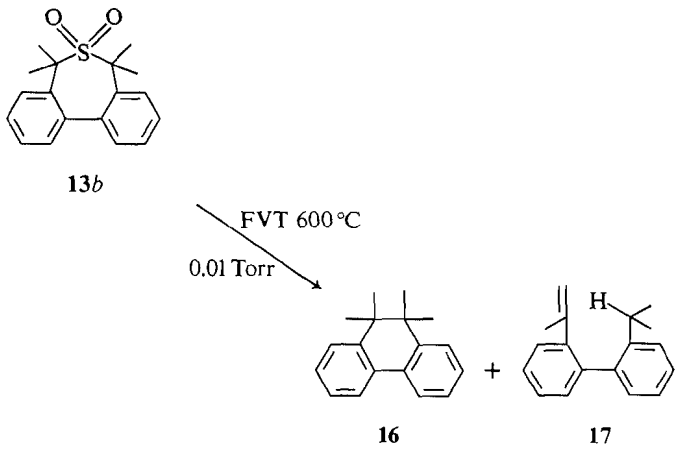

expulsion of SO_2 from **13***b* might be **18**. Electrocyclic ring closure would afford **16**, while a convenient rationalization for the formation of **17** could involve a thermally-allowed antarafacial 1,7-sigmatropic hydrogen shift from **18**.

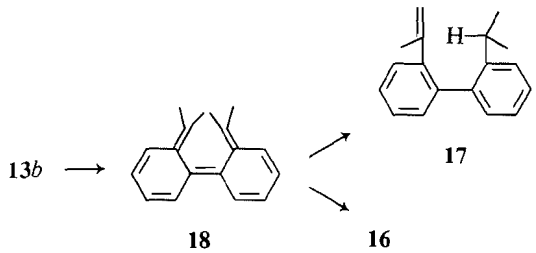

A literature analogy for this pathway is found in the work of McCullough and co-workers (8), in the photolytic conversion of **19** to **20** and **21**. They observed the short-lived transient **22** during the flash photolysis of **19**. They also proposed that the hydrogen transfer from **22** to **21** proceeds by way of a photochemically-allowed antarafacial 1,5-sigmatropic shift.

The solution photolysis at 254 nm of sulfone **13***b* yields the

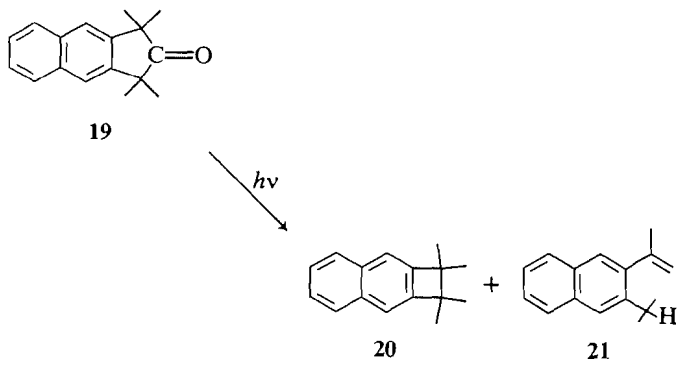

same two products, **16** and **17**. However, in this case the hydrogen transfer product **17** predominates in a ratio of 3:1. Performing this photolysis in different solvents and at different

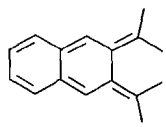

wavelengths did not significantly change this distribution. Carrying out the thermolysis of sulfone **13***b* at a higher temperature, however, alters the ratio. At 850°C, 9,10-dimethylphenanthrene **23** was formed in 60% yield. This derivative

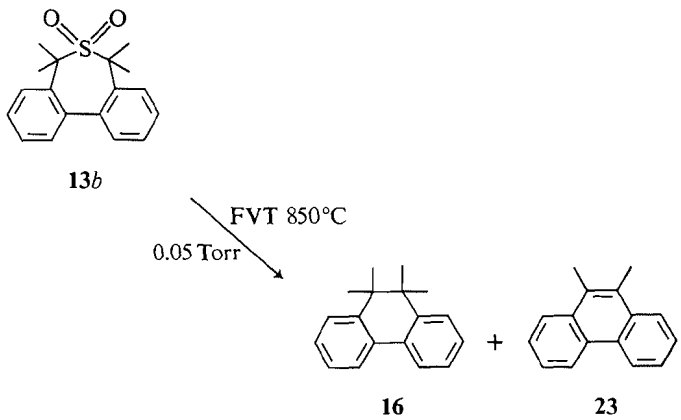

likely results from the tetramethyl compound **16**. Flash vacuum thermolysis of **16** at 850°C afforded 67% **23** and recovery of starting material **16** (16%) although we have no information as to the disposition of the 2 lost methyl groups.

The cyclic ester **24** produced a quantitative yield of pure acenapthene **25** when subjected to FVT conditions at 500°C and 0.05 Torr. Photolysis in benzene using 360 nm light give the same results.

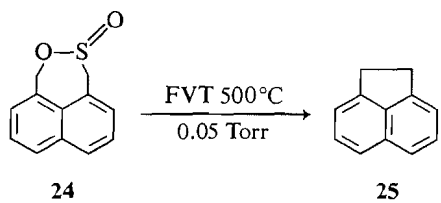

Can. J. Chem. Downloaded from www.nrcresearchpress.com by 210.87.254.105 on 09/06/12
For personal use only.

TABLE 1. Mass spectral behaviour of selected substrates

Compound	M − SO_2	M − SO	M − SO_2 − R	M − SO − R
	m/e (intensity)			
12*a* R = H	180(100)			
13*b* R = Me	236(32)		221(100)	
24 R = H	154(81)			
11*c* R = Ph		500(50)		423(100)
26 R = Ph		474(20)		397(100)
30	206(3) 207(21)			

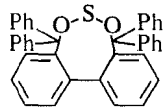

11*c*

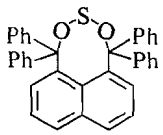

26

FVT and solution photolysis of the two tetraphenyl sulfoxylates **11***c* and **26** did not yield any identifiable products.

A study of the mass spectra of these SO_2-containing compounds gave some indication as to why the two tetraphenyl sulfoxylates **11***c* and **26** do not lose SO_2 cleanly when subjected to FVT or solution photolysis. The three compounds **12***a*, **13***b*, and **24** which undergo clean SO_2 expulsion and subsequent ring closure show significant peaks corresponding to the loss of SO_2 (see Table 1). The two tetraphenyl sulfoxylates **11***c* and **26** do not show mass spectral fragments corresponding to the loss of SO_2, but rather the loss of SO. The results might suggest that

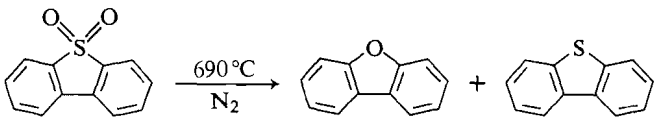

27 **28** **29**

the FVT of these two sulfoxylates would yield cyclic ethers in a manner similar to the thermolysis of dibenzothiophene-5,5-dioxide **27**, which yields dibenzofuran **28** and dibenzothiophene **29** in a ratio of 6:1 (9). However, no such cyclic ethers were observed in the product mixtures.

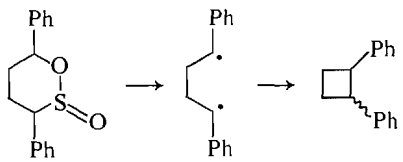

30 **31** **32**

The mass spectrum of the six-membered cyclic sulfinate ester **30** shows a strong molecular ion at *m/e* 272 (70%) and a peak for the loss of SO_2 minus 1H (*m/e* 207, 45%). Based on our previous results, the expected thermolytic pathway would be the loss of SO_2 to form intermediate **31** which could ring close to form the cyclobutane **32**.

Kopecky and Soler (10) have performed FVT studies on a similar system, 3,6-diphenyl-3,4,5,6-tetrahydropyridazine **33**. Thermolysis of *cis*-**33** at 205°C in a sealed tube yielded styrene

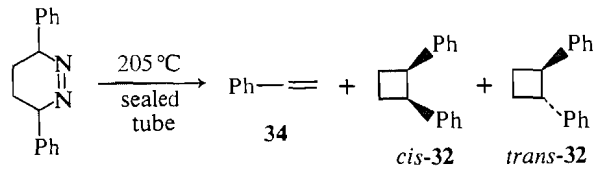

33 **34** *cis*-**32** *trans*-**32**

34 (67%), *cis*-1,2-diphenylcyclobutane *cis*-**32** (21%), *trans*-1,2-diphenylcyclobutane *trans*-**20** (12%), plus a trace of 1-phenyltetralin **35**. The FVT of **30** at 450°C did not yield any diphenylcyclobutane. The crude thermolysate contained three products which were separated by preparative gas chromato-

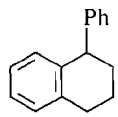

35

graphy and identified as 1,1-diphenylethylene **36** (19%), 1,1-diphenyl-1,3-butadiene **37** (21%), and 1-phenyl-3,4-dihydronaphthalene **38** (38%).

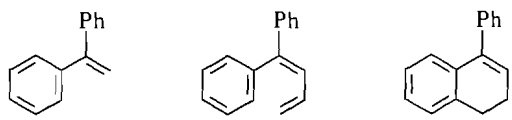

36 **37** **38**

The formation of these products can be rationalized by initial formation of the postulated diradical **31***a* by the loss of SO_2; ring closure of the diradical resonance contributor **31***b* would form the unstable intermediate **39** which upon aromatization

Can. J. Chem. Downloaded from www.nrcresearchpress.com by 210.87.254.105 on 09/06/12
For personal use only.

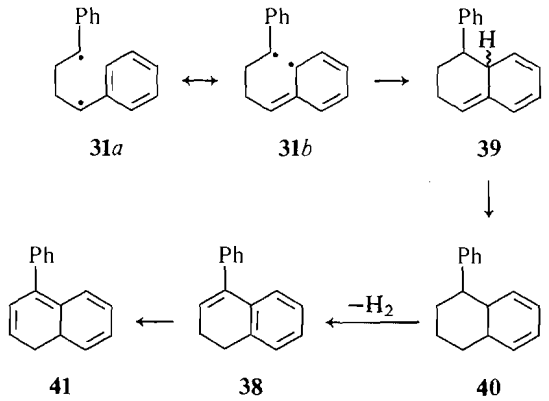

gives 1-phenyl-1,2,3,4-tetrahydronaphthalene **40**. Loss of H_2 from **40** would result in the observed product **38**. A 1,5-sigmatropic shift in **38** would produce 1-phenyl-4,10-dihydronaphthalene **41** which upon electrocyclic ring opening would form the observed 1,1-diphenyl-1,3-butadiene **37**. The reverse reaction, that is the thermal ring closure of **37** to **38**, has been observed by Weber and co-workers, with the 1,5-sigmatropic shift being demonstrated by deuterium labelling (11). The formation of α-phenylstyrene **36** may result from **40** as Trahanovsky and Swenson postulate for the thermolysis of tetralin **42**, that a retro-Diels–Alder produces benzocyclobutene **43** which rearranges to styrene **44**. A small amount of 1,2-dihydronaphthalene **45** is also produced (12).

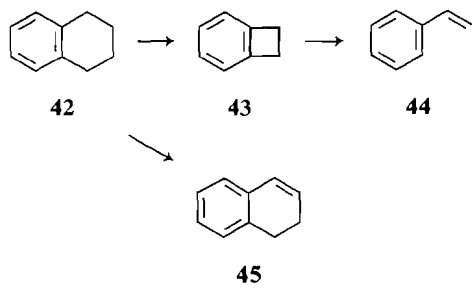

It must be emphasized that the above reactions are occurring under high vacuum and temperature and "normal" reaction pathways may not be applicable.

Experimental

Chemical reagents were obtained from commercial sources and used without purification, unless otherwise noted. Melting points were obtained in open capillaries on a Gallenkamp block apparatus and, along with boiling points, are uncorrected.

Solvents specified as dry were treated in the following manner: tetrahydrofuran, freshly distilled from the blue sodium ketyl of benzophenone; benzene, distillation of 20% of volume, retaining the residue. Anhydrous diethyl ether was used as obtained from a freshly opened can obtained from Mallinckrodt Canada Ltd. Purified solvents were stored over 4 Å molecular sieves under an atmosphere of dry nitrogen.

Infrared spectra were recorded with a Perkin–Elmer Model 257 or 297 grating spectrophotometer, calibrated with the 1602 cm^{-1} line of polystyrene. The ^1H nmr spectra were recorded on a Varian Associates T-60, T-60A, or XL-200 spectrometer in $CDCl_3$ solution, unless otherwise specified. The ^{13}C nmr spectra were recorded on a Bruker WH90 spectrometer operating at 22.63 MHz. The nmr data are reported in δ units (ppm) relative to internal tetramethylsilane (TMS) using the abbreviations: s, singlet; d, doublet; t, triplet; q, quartet; m, multiplet; b, broad. The ^1H nmr spectra were recorded at 60 MHz unless otherwise specified and ^{13}C nmr spectra were recorded at 22.63 MHz. Mass spectra were obtained using an LKB 9000 mass spectrometer at 70 eV using a direct insertion probe. Gas-chromatographic mass spectral analyses were obtained using a Hewlett–Packard 5984A system equipped with a 2 m × 3 mm od glass column of 6% OV-101 on Chromosorb W High Performance (100/120 mesh). Mass spectral data are reported as fragment identification *m/e* $M^{+\cdot} - X(\%)$.

Gas-chromatographic analyses were performed on a Hewlett–Packard Model 5751A or 5734A research chromatograph using the following 2 m × 3 mm od stainless steel columns: 10% S.E.-30 Ultraphase on Chromosorb W (A/W-DMCS, 80/100 mesh), 5% OV-101 on Chromosorb W (A/W-DMCS, 80/100 mesh). Preparative gas-chromatographic separations were performed on a Varian Associates Autoprep 700 or Hewlett–Packard 5751A chromatograph equipped with a 2 m × 6 mm od aluminum colum packed with 15% S.E.-30 on Chromosorb W (A/W-DMCS, 60/80 mesh). Thin-layer chromatography (tlc) was performed on E. Merck silica gel 60PF-254 (E. Merck) spread on 20 cm × 20 cm plates to a thickness of 2 mm using the specified solvent systems.

Photolyses were done using a Rayonet Reactor with 254, 300, and 360 nm tubes, using quartz or Pyrex sample tubes. Flash vacuum thermolyses were performed using an all-quartz apparatus with the hot zone heated by an electrical resistance furnace. The cold probe was cooled by Dry Ice – acetone at −78°C.

Ultraviolet absorptions were obtained on a Pye–Unicam spectrophotometer in the designated solvents.

Elemental analyses were carried out by Galbraith Laboratories, Knoxville, Tenn. or by Guelph Microanalytical Services, Guelph, Ont.

*Thermolysis of 5H,8H-dibenzo[d,f][1,2]oxathiocin-1-oxide (**12**a)*

Cyclic sulfinate ester **12***a* (0.1 g, 0.41 mmol) was thermolyzed with a sublimation temperature of 150°C through a hot zone of 700°C at a pressure of 0.05 Torr. The yellow solid which collected on the cold probe (−78°C) was washed off with chloroform and chromatographed by preparative tlc (silica gel, toluene). This afforded 9,10-dihydrophenanthrene **14** (0.065 g, 90%) identified by comparison of the ^1H nmr and gc with an authentic sample.

*Photolysis of 5H,8H-dibenz[d,f][1,2]oxathiocin-1-oxide (**12**a)*

Photolysis of **12***a* (0.1 g, 0.41 mmol) in 15 mL of degassed methanol for 18 h through quartz at 254 nm yielded a mixture of 9,10-dihydrophenanthrene **14** and phenanthrene **15** (9:1) as analyzed by gc (S.E.-30).

*Thermolysis of 2H,7H-2,2,7,7-tetramethyldibenz[a,e]thiepine (**13**b)*

Thermolysis of cyclic sulfone **13***b* (0.1 g, 0.33 mmol) with a sublimation oven temperature of 210°C through a hot zone of 520°C at 0.01 Torr yielded a yellow solid on the cold probe which when chromatographed on preparative tlc (silica gel, hexanes) was separated into two fractions; A: 2-(2-isopropenyl)-2′-(2-isopropyl)biphenyl **17** (0.01 g, 12%); ^1H nmr δ: 7.6–7.2 (m, 8H), 6.1–5.9 (d, 2H), 2.9 (q, 1H, J = 8 Hz), 1.65 (s, 3H), 1.1 (d, 3H, J = 8 Hz), 1.05 (d, 3H, J = 8 Hz); ms $M^{+\cdot}$: 236 (0.1), $M-15$, 221 (2), $M-54$, 182 (63), 105 (100), 77 (60), 50 (30). B: 9,9,10,10-tetramethyl-9,10-dihydrophenanthrene **16** (0.63 g, 80%); ^1H nmr δ: 8.1–7.3 (m, 8H), 1.8–1.0 (bs, 12H); ms $M^{+\cdot}$: 236 (40), $M-15$, 221 (100), $M-30$, 206 (51), $M-58$, 178 (20), 165 (18). *Anal.* calcd.: C 91.30, H 8.71; found: C 91.47, H 8.53.

*Photolysis of **13**b*

Photolysis of cyclic sulfone **13***b* (0.1 g, 0.33 mmol) in 8 mL methanol and 2 mL methylene chloride through quartz at 254 nm for five hours yielded 9,9,10,10-tetramethyl-9,10-dihydrophenanthrene

Can. J. Chem. Downloaded from www.nrcresearchpress.com by 210.87.254.105 on 09/06/12
For personal use only.

16 (25%) and 2-(2-isopropenyl)-2′-(2-isopropyl)biophenyl **17** (74%) by gc. Photolysis in ether at 254 nm and in methylene chloride at 350 nm with benzophenone as sensitizer yielded similar product ratios.

Thermolysis of ***13****b at 850°C*

Thermolysis of **13***b* (0.1 g, 0.33 mmol) 850°C/0.05 Torr yielded three compounds by gc analysis (S.E.-30); 2-(2-isopropenyl)-2′-(2-isopropyl)biphenyl **17** (2%), 9,9,10,10-tetramethyl-9,10-dihydrophenanthrene **16** (24%), and 9,10-dimethylphenanthrene **23** (60%); mp 135–138°C (lit. (13) mp 138–139°C; ^{1}H nmr δ: 8.4–7.0 (m, 8H), 2.5 (s, 6H); ms $M^{+\cdot}$: 206 (89), M − 15, 191 (100).

*Thermolysis of 9,9,10,10-tetramethyl-9,10-dihydrophenanthrene (****16****)*

Thermolysis of **16** (0.1 g, 0.42 mmol) at 850°C/0.05 Torr yielded a mixture of **16** (26%) and **23** (64%) by gc analysis (S.E.-30).

*Thermolysis of 3*H*-naphtho[*d,e*][1,2]oxathiepin-1-oxide (****24****)*

Thermolysis of **24** (0.1 g, 0.46 mmol) 500°C/0.05 Torr with a sublimation oven temperature of 100°C yielded pure acenaphthene **25** (0.06 g, 91%) by gc and nmr comparison with an authentic sample.

Photolysis of ***24***

Photolysis of **24** (0.1 g, 0.46 mmol) in 12 mL degassed benzene at 350 nm through Pyrex for 18 h yielded acenaphthene **25** (80%) pure by gc.

*Thermolysis of 3,6-diphenyl-1,2-oxathiane-1-oxide (****30****)*

Thermolysis of **30** (0.1 g, 0.37 mmol) at 450°C/0.05 Torr with a sublimation oven temperature of 150°C yielded three compounds which were separated by preparative gc (2 m × 6 mm od 15% S.E.-30). They were 1,1-diphenyl ethylene **36** (0.014 g, 20%); ^{1}H nmr δ: 7.35 (s, 10H), 5.45 (s, 2H); ms $M^{+\cdot}$: 180 (100), M − 1, 179 (74), M − 2, 178 (72), M − 15, 165 (70); 1,1-diphenyl-1,3-butadiene **37** (0.016 g, 21%); ^{1}H nmr δ: 7.4–7.2 (m, 10H), 6.8 (d, 1H, J = 11 Hz), 6.5 (m, 1H), 5.3 (d, 1H, J = 17 Hz), 5.1 (d, 1H, J = 11 Hz); ms $M^{+\cdot}$ + 1, 207 (100), M + 2, 208 (59), 102 (61); 1-phenyl-3,4-dihydronaphthalene **38** (0.029 g, 38%); ^{1}H nmr δ: 7.4–7.1 (m, 9H), 5.1 (t, 1H, J = 6 Hz), 2.8 (t, 2H, J = 8 Hz), 2.4 (m, 2H); ms $M^{+\cdot}$: 206 (100), M − 15, 191 (60), 205 (30), 91 (40), identified by comparison of ^{1}H nmr and mass spectral data with published spectra for these compounds.

Acknowledgements

We thank the Natural Sciences and Engineering Research Council of Canada and the Department of Education of Quebec for financial support of this work. We are particularly grateful to Dr. D. J. H. Smith for valuable discussions on the FVT technique.

1. D. N. Harpp, H. A. Kader, and R. A. Smith. Sulfur Lett. **1**, 59 (1982).
2. (*a*) R. F. Brown. Pyrolytic methods in organic chemistry. Academic Press, New York and London. 1980; (*b*) F. Vögtle and L. Rossa. Angew. Chem. Int. Ed. Engl. **18**, 515 (1979); G. Seybold. Angew. Chem. Int. Ed. Engl. **16**, 365 (1977).
3. (*a*) M. P. Cava, R. H. Schlessinger, and J. P. van Meter. J. Am. Chem. Soc. **86**, 3173 (1964); (*b*) R. S. Givens, R. J. Olsen, and P. L. Wylies. J. Org. Chem. **44**, 1608 (1979); (*c*) T. Durst, J. C. Chuang, N. K. Sharma, and D. J. H. Smith. Can. J. Chem. **56**, 512 (1978).
4. D. J. Cram and J. M. Cram. Acc. Chem. Res. **4**, 204 (1971).
5. D. H. Hunter and J. B. Stothers. Can. J. Chem. **51**, 2884 (1973).
6. D. N. Harpp, K. Steliou, and T. H. Chan. J. Am. Chem. Soc. **100**, 1222 (1978).
7. K. Steliou. The chemistry of azole sulfides. Ph.D. Thesis, McGill University (1978).
8. K. Kamal de Fonseka, J. J. McCullough, and A. J. Yarwood. J. Am. Chem. Soc. **101**, 3277 (1979).
9. E. K. Fields and S. Meyerson. J. Am. Chem. Soc. **88**, 2836 (1966).
10. K. R. Kopecky and J. Soler. Can. J. Chem. **52**, 2111 (1974).
11. P. B. Valkovich, J. L. Conger, F. A. Castiello, T. D. Brodie, and W. P. Weber. J. Am. Chem. Soc. **97**, 901 (1975).
12. W. S. Trahanovsky and K. E. Swenson. J. Org. Chem. **46**, 2984 (1981).
13. T. Nishio, M. Yoshioka, H. Aoyama, and N. Sugiyama. Bull. Chem. Soc. Jpn. **46**, 2253 (1973); G. W. Griffen and A. Manmade. J. Org. Chem. **37**, 2589 (1972).

Can. J. Chem. Downloaded from www.nrcresearchpress.com by 210.87.254.105 on 09/06/12
For personal use only.

Mass spectra of some substituted methylcyclosiloxanes

E. PELLETIER AND J. F. HARROD
Chemistry Department, McGill University, 801 Sherbrooke Street West, Montreal, P.Q., Canada H3A 2K6

Received September 15, 1982

This paper is dedicated to Professor Leo Yaffe on the occasion of his 65th birthday

E. PELLETIER and J. F. HARROD. Can. J. Chem. **61**, 762 (1983).

The mass spectra of the substituted methylcyclosiloxanes $+Si(CH_3)(X)O+_n$, where X = H (n = 4, 5 and 6), X = C_6H_5 (n = 3 and 4), X = Br (n = 3 and 4), X = $Co(CO)_4$ (n = 4 and 5) have been measured. The compounds X = H fragment by the same kinds of substituent loss and ring contraction mechanisms as previously reported for the compounds X = CH_3 but also by the loss of methylhydrogensilanone. The compounds X = Ph fragment by loss of benzene from an intramolecularly bridging benzenonium ion, formed from $[M - CH_3]^{+\cdot}$ and by losses of the phenylmethylsilanone fragments. The compounds X = Br only undergo substituent loss without ring fragmentation. The compounds X = $Co(CO)_4$ show stepwise loss of all CO groups from $[M]^{+\cdot}$, $[M - Co(CO)_4]^+$, and $[M]^{++}$.

E. PELLETIER et J. F. HARROD. Can. J. Chem. **61**, 762 (1983).

On a mesuré les spectres de masse des méthylcyclosiloxanes substitués $+Si(CH_3)(X)O+_n$ ou X = H (n = 4, 5 et 6), X = C_6H_5 (n = 3 et 4), X = Br (n = 3 et 4), X = $Co(CO)_4$ (n = 4 et 5). Les composés X = H se fragmentent selon les mêmes mécanismes de perte de substituant et de contraction de cycle rapportés antérieurement pour les composés du type X = CH_3, mais ils se fragmentent également en perdant de la méthylhydrogensilanone. Les composés X = Ph se fragmentent en perdant du benzène à partir de l'ion benzenonium, en position de pont intramoléculaire, formé à partir de $[M - CH_3]^{+\cdot}$ et en perdant des fragments de phénylméthylsilanone. Les composés du type X = Br subissent uniquement une perte de substituant sans fragmentation du cycle. Les composés du type X = $Co(CO)_4$ perdent par étapes tous les groupes CO à partir de $[M]^{+\cdot}$, de $[M - Co(CO)_4]^+$ et de $[M]^{++}$.

[Traduit par le journal]

Can. J. Chem. Downloaded from www.nrcresearchpress.com by 210.87.254.40 on 09/06/12
For personal use only.

Introduction

In the course of a current project we have used, or newly synthesized, a variety of methylcyclosiloxanes of the general formula **1**. The mass spectra of these compounds have been routinely measured as a part of their structural characterization.

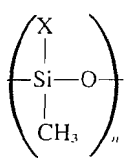

Substituent X	Abbreviation
CH_3	D_n
C_6H_5	D_n^{Ph}
Br	D_n^{Br}
$Co(CO)_4$	D_n^{Co}
H	D_n^H

1

A number of interesting features which have emerged from these studies are presented in the present paper.

The literature on the mass spectrometry of cyclosiloxanes is limited to the detailed study of the fully methylated compounds (1, 2). A useful review of the mass spectrometry of organosilicon compounds has been published by Coutant and Robinson (3).

Results

The methylhydrogencyclosiloxanes

In each spectrum of D_n^H (n = 4, 5, 6) the heaviest ions are $[M - 1]^+$ and $[M - 15]^+$ and the relative intensities of these ions diminish with increasing ring size (Fig. 1). The absence of $[M]^{+\cdot}$ is a common feature of methylsiloxane fragmentation due to the facile loss of $CH_3^{\cdot}$ from the parent ions (1, 2). Another evident feature of the spectrum is the high intensity of the peaks m/e 73, 59, and 45 in D_5^H and D_6^H compared to D_4^H.

The spectra of D_n^H are considerably richer in lines than those of D_n. For example, the spectrum of D_5^H (Fig. 1) shows eleven peaks of relative intensity >10 per cent, whilst D_5 shows only three major peaks at $[M - 15]^+$, $[M - 103]^+$, and m/e 73 (1–3). The two groupings of lines at $[M - 47]^+$, $[M - 61]^+$, and $[M - 75]^+$, and at $[M - 107]^+$, $[M - 121]^+$, and $[M - 135]^+$, consistently present in D_n^H, are separated by a characteristic mass increment of 60 amu. Exact mass measurements on D_5^H show this increment to be in fact due to two processes: loss of SiO_2 and also of $(CH_3)HSiO$ (Table 1). The separation between the lines of these two groups, as well as those between the light ions at m/e 73, 59, and 45, all correspond to a mass increment of 14 amu. Contrary to the case of D_n, no evidence for significant currents of doubly charged ions was observed, except in D_6^H where m/e 179 can be attributed to $[M - 2]^{++}$.

The methylphenyl- and the methylbromocyclosiloxanes

The mass spectra of D_n^{Ph} (n = 3 and 4) are given in Fig. 2. Both compounds show the molecular ion at low intensity on the oscillograms. The major peaks in both spectra occur at $[M - 15]^+$ and $[M - 93]^+$. It is clear that the distribution of peaks in these two compounds is quite different from that in D_n and D_n^H and reflects a very different fragmentation mechanism.

The spectra of D_3^{Br} and D_4^{Br} are notable for their simplicity (Fig. 3). In neither case is $[M]^+$ observed, and the strongest peaks are due to $[M - CH_4]^{+\cdot}$ and $[M - HBr]^{+\cdot}$. Apart from these peaks, the only others with relative abundance >10 per cent are those at m/e 128 and 129 (D_3^{Br}) and at m/e 197, 198, and 199 (D_4^{Br}) attributed to doubly charged $[M - 2Br]^{++}$. As expected, HBr^+ (m/e 80, 82) and Br^+ (m/e 79, 81) are present in both spectra.

Can. J. Chem. Downloaded from www.nrcresearchpress.com by 210.87.254.40 on 09/06/12
For personal use only.

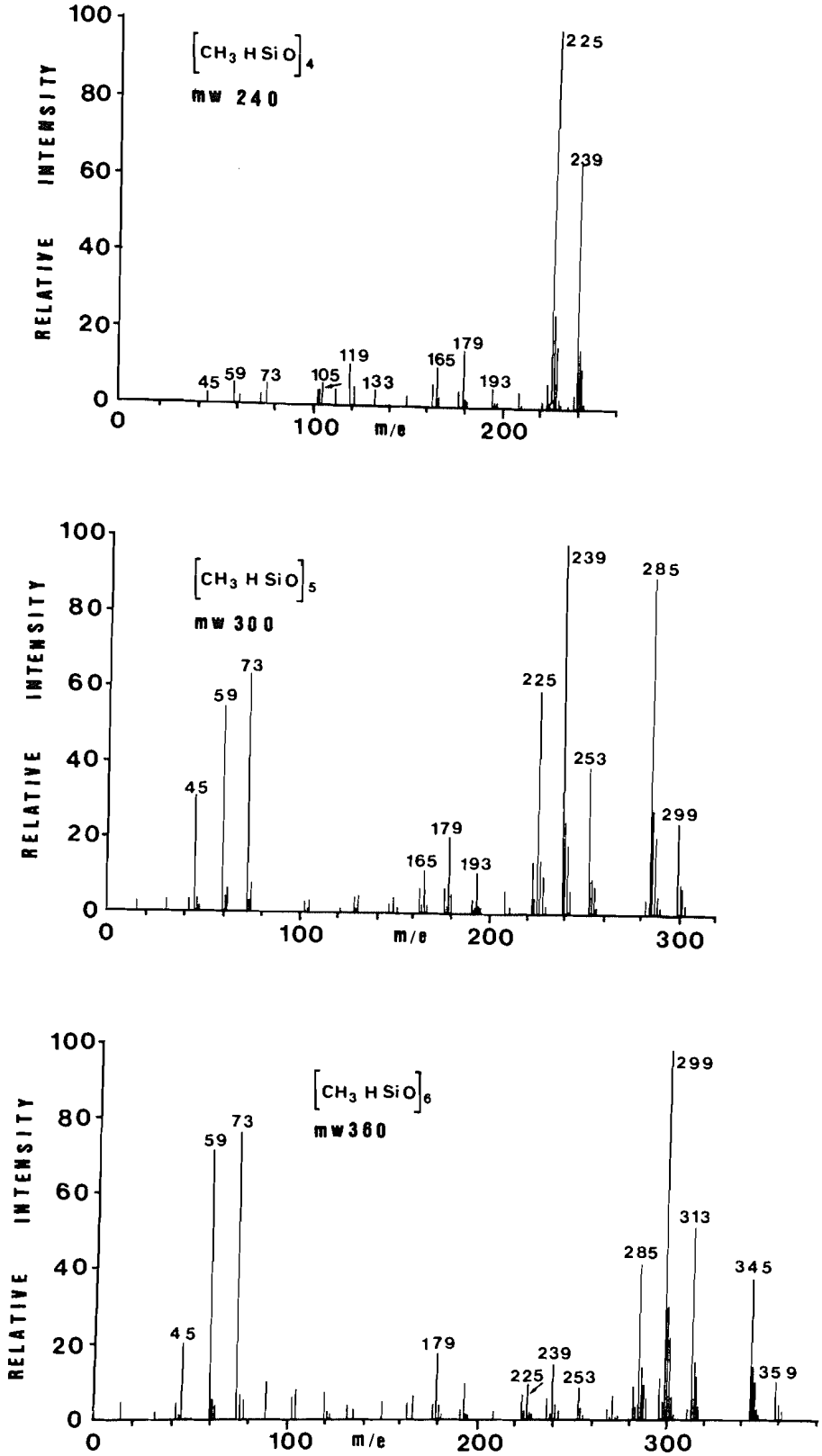

FIG. 1. Mass spectra of methylhydrogencyclosiloxanes, D_n^H (n = 4, 5, 6).

The tetracarbonylcobaltmethylcyclosiloxane

The expanded spectra of D_4^{Co} and D_5^{Co} are shown in Figs. 4 and 5. The presence of geminate series of lines is highlighted. The first series (noted a_1, a_2, a_3...), beginning at the highest mass, corresponds to the stepwise loss of all CO ligands from $[M]^{+\bullet}$. The second series (noted b_1, b_2, b_3...), beginning at $[M - 171]^+$, corresponds to stepwise loss of all CO ligands from $[M - Co(CO)_4]^+$. Also, quite important in terms of total ion current are the series of CO dissociations from doubly charged ions, evidenced by the large number of peaks separated

Can. J. Chem. Downloaded from www.nrcresearchpress.com by 210.87.254.40 on 09/06/12
For personal use only.

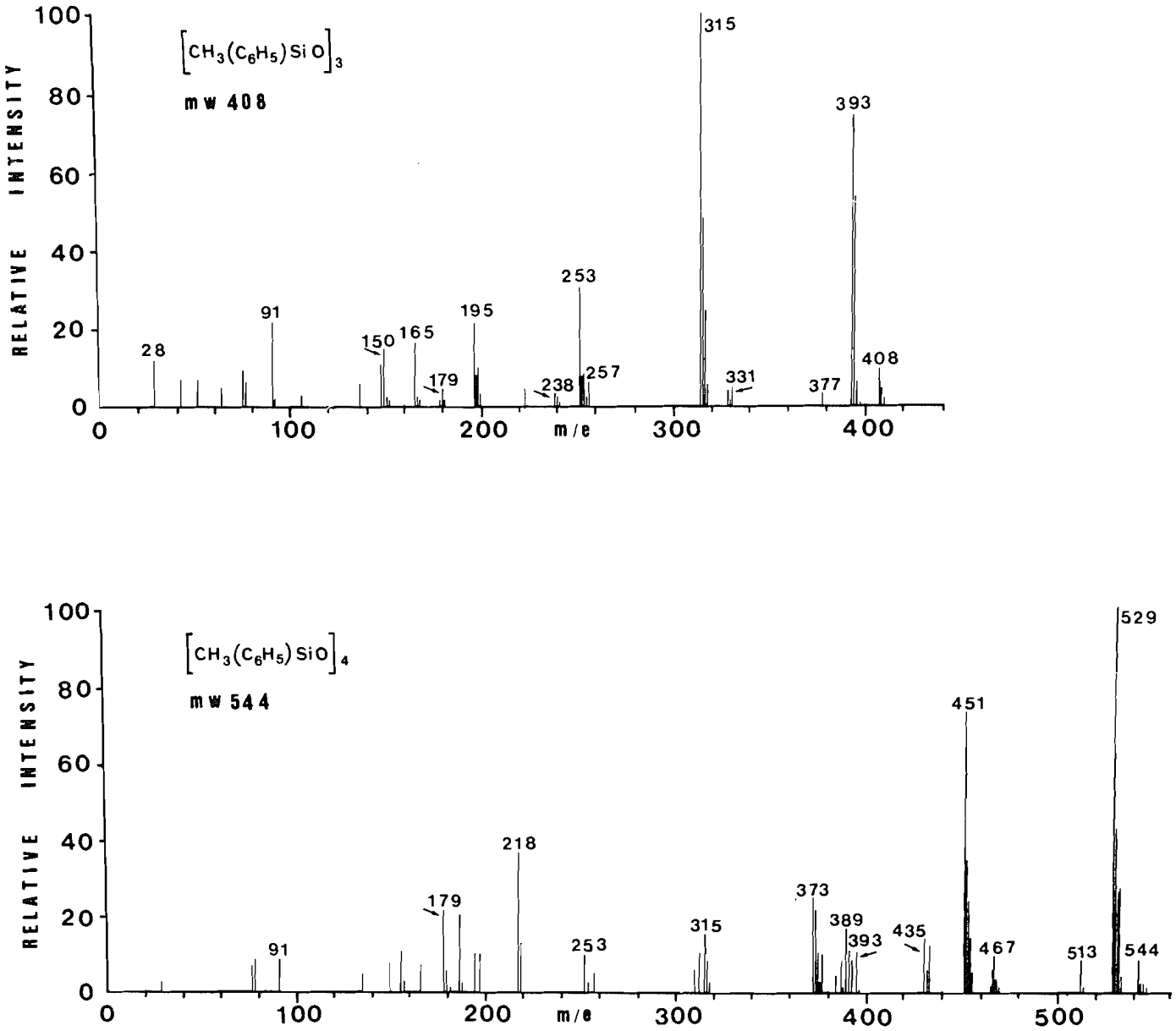

FIG. 2. Mass spectra of methylphenylcyclosiloxanes, D_n^{Ph} (n = 3 and 4).

TABLE 1. (a) Some ions in spectra of D_n^H series

Metastable ions	Observed	Calculated
in D_4^H	142	$(179)^2/225 = 142.4$
D_5^H	201	$(239)^2/285 = 200.4$
D_6^H	259	$(299)^2/345 = 259.1$

(b) High resolution mass measurements on D_5^H:

Ions$^+$	m/e	Observed	Calculated
$[M - 47]^+$	253	252.988	252.984 ($C_4H_{13}Si_4O_5$)
$[M - 61]^+$	239	238.965	238.968 ($C_3H_{11}Si_4O_5$)
$[M - 75]^+$	225	224.951	224.953 ($C_2H_9Si_4O_5$)
$[M - 107]^+$	193	192.958	192.981 ($C_3H_9Si_3O_4$)
$[M - 121]^+$	179	178.999	179.002 ($C_3H_{11}Si_3O_3$)
		178.964	178.965 ($C_2H_7Si_3O_4$)
$[M - 135]^+$	165	164.984	164.986 ($C_2H_9Si_3O_3$)
		164.947	164.949 ($C_1H_5Si_3O_4$)

by 14 amu in the m/e 200 to 500 region of the spectrum of D_5^{Co} (Fig. 5).

Discussion

The methylhydrogencyclosiloxanes

Previous studies of mixed methylhydrogensiloxane systems have shown that fragmentation by either methyl or by hydrogen loss occurs with similar ease. Thus, the cyclopentasiloxane $\text{-(-Si(CH}_3)_2\text{—O-)}_4\text{-(-Si(CH}_3)\text{H—O-)-}$ fragments by loss of both $Si(CH_3)_4$ and $HSi(CH_3)_3$ (2). In the fragmentation of $H(CH_3)_2Si\text{—O-(-Si(CH}_3)_2\text{—O-)-}_2Si(CH_3)_3$ the dominant process, following initial $CH_3^{\cdot}$ loss, is loss of $HSi(CH_3)_3$ to produce $[M - 89]^+$ (3). Either hydrogen or methyl migration could give rise to these products, but the data do not allow a distinction to be made. Thus, it would not be unreasonable to assume that the fragmentation of D_n^H occurs by the same mechanism as previously proposed (1, 2) for D_n ($n \geq 5$), but with both CH_3 and H undergoing dissociation and migration. The key step in this mechanism is a ring contraction in the ion

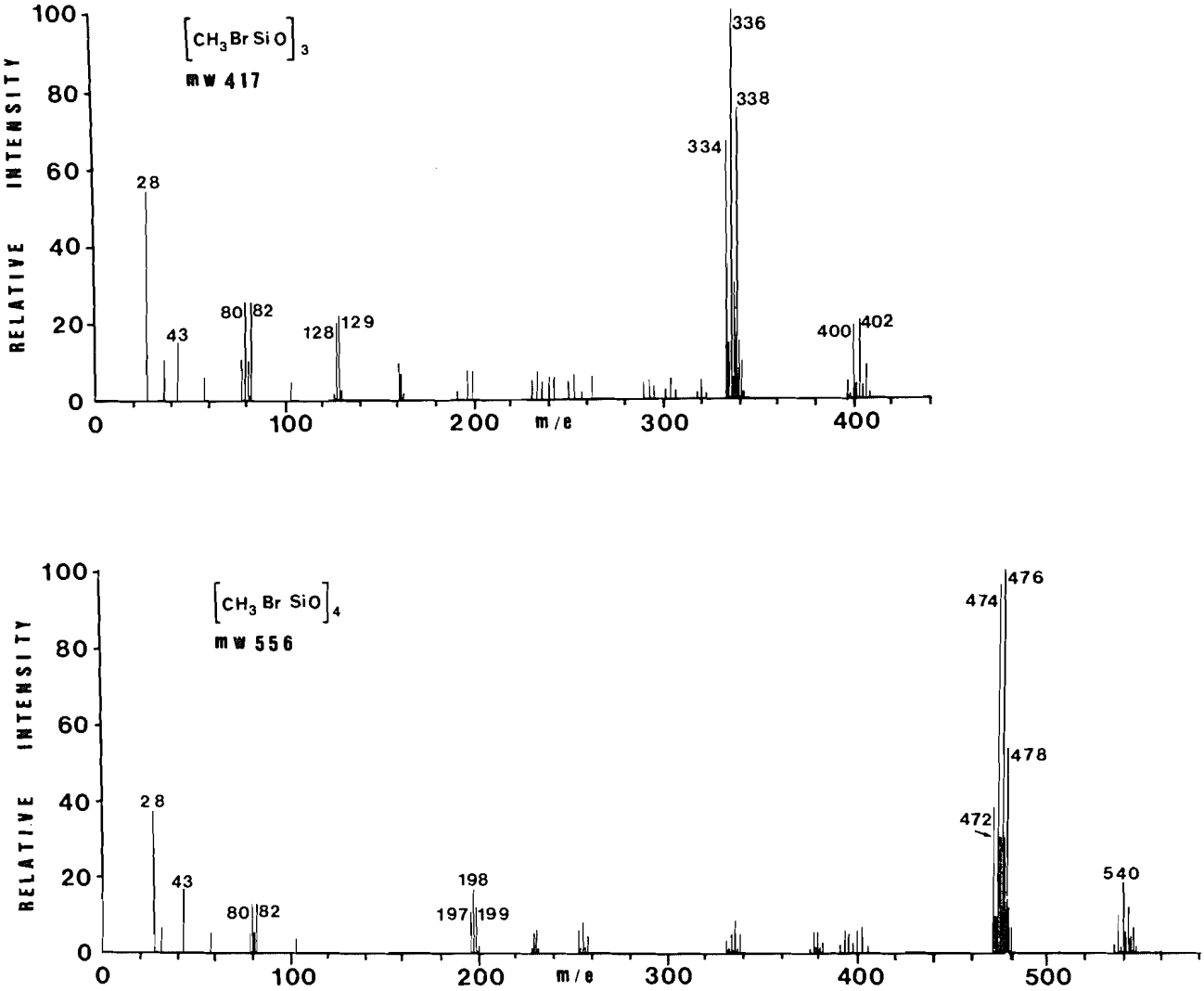

FIG. 3. Mass spectra of methylbromocyclosiloxanes, D_n^{Br} (n = 3 and 4).

following initial loss of $CH_3^{\bullet}$. A similar scheme for D_n^H, where it is assumed that either $CH_3^{\bullet}$ or $H^{\bullet}$ can be lost to form the initial cation fragment, and either CH_3 or H can participate in the subsequent migration accompanying ring contraction, is shown in Scheme 1. The contracted rings $[M - 1]^+$ and $[M - 15]^+$ lead to the formation of the series $[M - 47]^+$, $[M - 61]^+$, and $[M - 75]^+$ by loss of the appropriate neutral silanes, $H_{3-n}Si(CH_3)_n$, as exemplified for $[M - 15]^+$ in Scheme 2. The nature of ions proposed in Scheme 2 is supported by peak matching for D_5^H (Table 1). Metastable ions corresponding to fragmentation $[M - 15]^+ \rightarrow [M - 61]^+ + H_3SiCH_3$ are observed in all spectra of D_n^H. The second grouping of three peaks, $[M - 107]^+$, $[M - 121]^+$, and $[M - 135]^+$, is generated by loss of SiO_2 or $(CH_3)HSiO$ from the first group. Scheme 3 highlights the presence of two ions $[M - 121]^+$ which come from $[M - 61]^+$, both completely resolved in high resolution spectrum of D_5^H (Table 1).

The methylphenylcyclosiloxanes

Since D_5^{Ph} has not been isolated, our measurements were restricted to the n = 3 and 4 compounds. The observed spectra conform quite well to a mechanism recently proposed for the fragmentation of aryl substituted linear siloxanes (4). The most interesting feature of this mechanism, shown in Scheme 4, involves the formation of an intramolecularly bridging benzenonium ion from $[M - 15]^+$, followed by either loss of benzene or, to a much lesser degree, methane (4). A second aspect of the mechanism is the elimination of the elements by phenylmethylsilanone from the $[M - 15]^+$, and for D_4^{Ph} the $[M - 93]^+$ ion. These hypotheses account for most of the important observed heavier ions in D_n^{Ph}.

The rather intense $[M - 155]^+$, m/e 253, and $[M - 213]^+$, m/e 195, for D_3^{Ph} (much weaker in D_4^{Ph}) suggest a relatively important initial fragmentation by loss of $C_6H_5^{\bullet}$, with the resulting ion undergoing losses of either benzene or the elements of phenylmethylsilanone, analogous to the reactions of $[M - CH_3]^+$. The loss of CH_3 from $[M - C_6H_5]^+$ could also make a substantial contribution to $[M - 92]^+$, in addition to that made by loss of $C_6H_5^{\bullet}$ from $[M - CH_3]^+$.

The absence of peaks at $[M - 202]^+$ and $[M - 150]^+$ indicates that ring contractions of the $[M - CH_3]^+$ ion by loss of $[Si(CH_3)_2(C_6H_5)]^+$ and $[Si(CH_3)(C_6H_5)_2]^+$, such as occur with D_n and D_n^H, do not occur with D_n^{Ph}.

No ring contraction, either by transannular migration or by loss of silanone fragments, was observed with D_n^{Br}. The major ions in both spectra, $[M - CH_4]^{+\bullet}$ and $[M - HBr]^{+\bullet}$, are

Can. J. Chem. Downloaded from www.nrcresearchpress.com by 210.87.254.40 on 09/06/12
For personal use only.

Can. J. Chem. Downloaded from www.nrcresearchpress.com by 210.87.254.40 on 09/06/12
For personal use only.

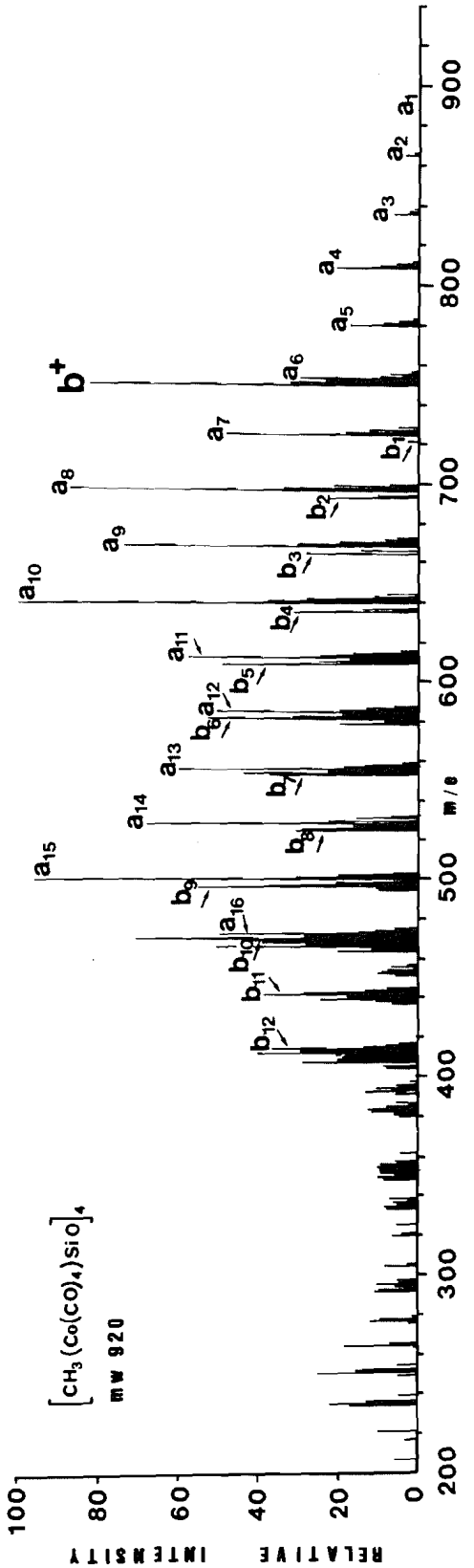

FIG. 4. Mass spectrum of tetracarbonylcobaltmethylcyclotetrasiloxane, D_4^{Co}. Peak noted b^+ stands for ion $[M - 171]^+$ m/e 749.

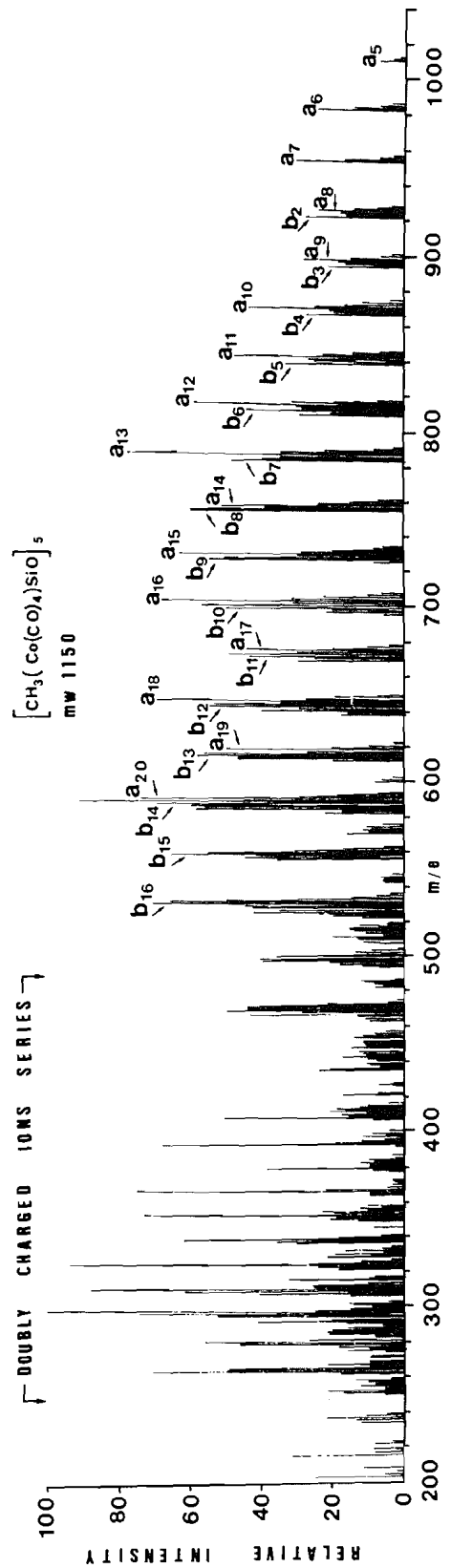

FIG. 5. Mass spectrum of tetracarbonylcobaltmethylcyclopentasiloxane, D_5^{Co}.

Can. J. Chem. Downloaded from www.nrcresearchpress.com by 210.87.254.40 on 09/06/12
For personal use only.

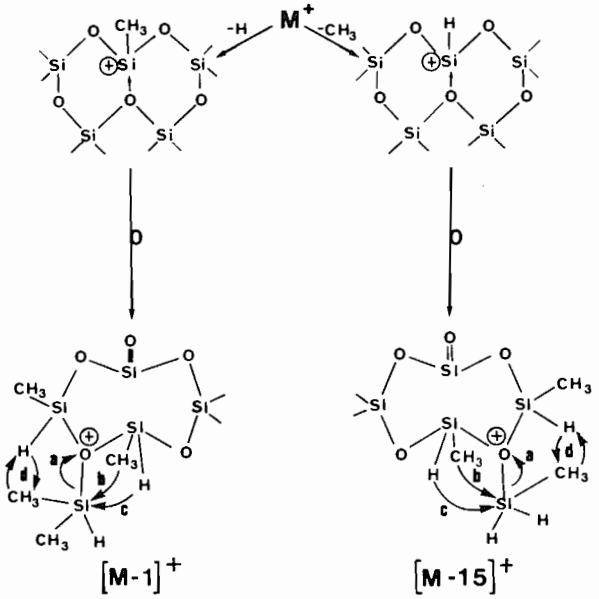

SCHEME 1. Transannular migration and ring contraction of D_n^H.

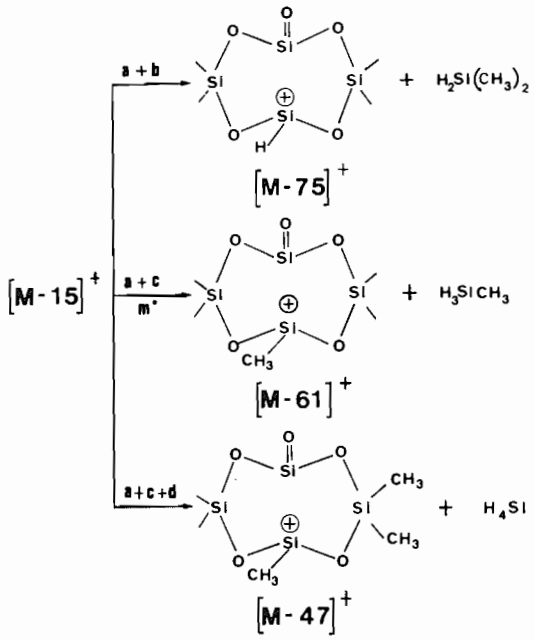

SCHEME 2. Fragmentation of ion $[M - 15]^+$.

formed by the abstraction either by a CH_3 group or a bromine atom of a hydrogen atom from an adjacent or a transannular methyl group. This mechanism is favoured because of the spatial disposition of substituents on the siloxane rings.

The loss of fragments to form doubly charged ions is particularly evident in D_n and D_n^{Br} ($n = 3$ and 4) compared to D_n^{Ph} and D_n^H. Apparently the absence of alternative facile fragmentation pathways is responsible for such behaviour in these cases.

The tetracarbonylcobaltmethylcyclosiloxanes

Metal carbonyls and their derivatives undergo stepwise loss of CO ligands under mass spectrometry conditions (5). It is usual for such compounds to show a stepwise loss of all CO groups to produce the base metal ion, or the metal ion plus

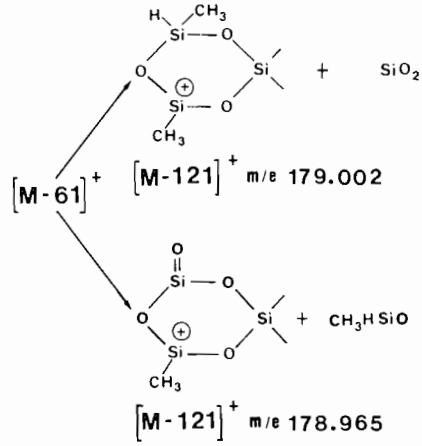

SCHEME 3. Fragmentation of ion $[M - 61]^+$.

original substituents other than CO. The low ionization potentials of transition metal atoms also result in the common appearance of multiply-charged ions in carbonyl mass spectra. To our knowledge, one of the heaviest clusters for which a complete mass spectrometric analysis has been reported is $Ru_6C(CO)_{17}$. This compound shows a stepwise loss of seventeen CO groups from both the singly and doubly charged ions (6).

The mass spectra of several simple silylcobalttetracarbonyls have been reported and they show the typical stepwise loss of CO (7). The spectra of the compounds reported in the present study have a number of novel features. The most striking aspect of the spectra is the fact that one can observe the stepwise loss of such a large number of CO groups. Since D_n^H rings of $n > 5$ are fairly easily obtainable by chromatographic separation of a CH_3SiHCl_2 hydrolysate, and since there is no reason to believe that they cannot be converted to the appropriate D_n^{Co} analogues, one could envisage molecules with many more than the reported twenty CO ligands for D_5^{Co}. The relatively high volatility of these compounds, together with their high molecular weight, suggests that they may have some value as mass markers.

Unlike the fragmentation of carbonyl clusters, where breakup of the metal cluster does not usually occur under mass spectrometer operating conditions, the D_n^{Co} compounds do show loss of metal fragments. Thus, the most obvious feature of the spectra is the presence of the two series corresponding to stepwise loss of $4n$CO molecules from $[M]^{+\cdot}$. A more careful scrutiny of the spectra also shows the presence of a series corresponding to stepwise loss of $4n$CO molecules from $[M]^{++}$ (Fig. 5).

Although $[M - 15]^+$ was detected at low abundance for both $n = 4$ and 5, no CO loss series was detected for this ion.

In conclusion, it is evident that the carbonyl fragmentation occurs with such ease that none of the fragmentation processes that occur in other cyclosiloxanes, even the loss of CH_3, are significantly activated in the D_n^{Co} compounds.

Experimental

Synthesis of substituted cyclosiloxanes

The compounds D_n^{Ph} and D_n^H were prepared according to published procedures (8, 9).

The compounds D_n^{Br} were prepared by reaction of D_n^{Ph} with Br_2 at low temperature. The compounds D_n^{Co} were prepared by reactions of D_n^H with $Co_2(CO)_8$, following a modification of published procedures (10). The compound D_3^{Co} could not be prepared due to the great

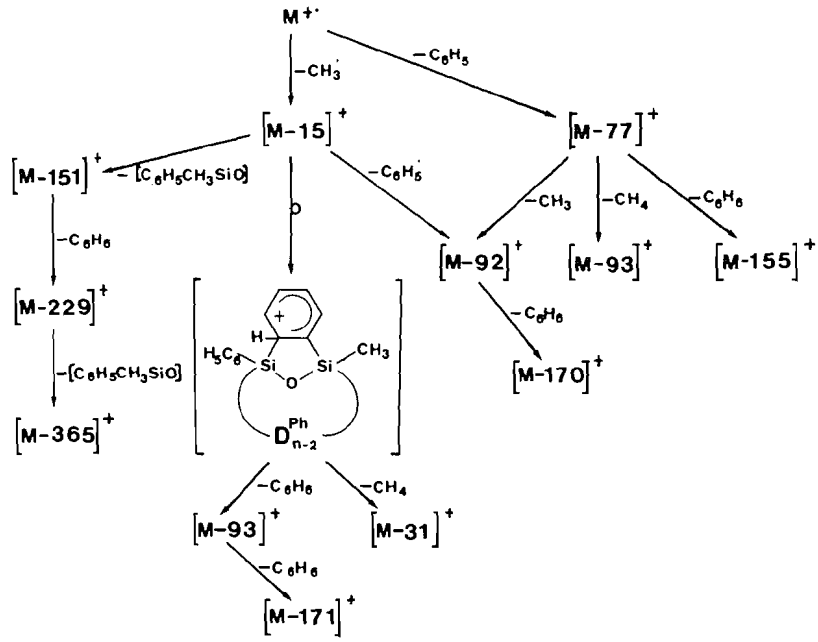

SCHEME 4. Fragmentation pattern of methylphenylcyclosiloxanes.

instability of D_3^H. An alternative synthesis by reaction of D_3^{Br} with $Co(CO)_4^-$ was unsuccessful.

Measurement of mass spectra

The low resolution spectra of D_n^H and D_n^{Co} were measured on an LKB (model 9000) instrument (electron energy 70 eV, source temperature 270°C). D_4^H was introduced directly as a pure compound at an inlet temperature of 100°C. The spectra of D_5^H and D_6^H were obtained following separation of a CH_3SiCl_2H hydrolysate, stripped of D_4^H, on a two-metre glass column of 6 per cent OV-101 at a temperature of 135°C. Samples of D_4^{Co} and D_5^{Co} were introduced directly at probe temperatures of 46 and 50°C respectively.

The low resolution spectra of D_n^{Ph} and D_n^{Br} were measured on a DuPont 21-492B instrument (electron energy 70 eV, source temperature 250°C). D_3^{Ph} and D_4^{Ph} were introduced directly at probe temperatures of 55 and 80°C respectively. Both D_n^{Br} compounds were sufficiently volatile to be introduced directly at ambient temperature.

The high resolution measurements have been performed on a AEI MP902 spectrometer (at 70 eV ionizing energy and source temperature 250°C) at Laboratoire de spectrometrie de masse, Université de Montréal, Québec.

Acknowledgements

The authors thank the Natural Sciences and Engineering Research Council of Canada and the Fonds FCAC de Québec for financial support of this work and for scholarships to E. P.

1. W. J. A. VAN DEN HEUVEL, J. L. SMITH, R. A. FIRESTONE, and J. L. BECK. Anal. Lett. **5**, 285 (1972).
2. G. R. PICKERING, C. S. OLLIFF, and K. J. RUTT. Org. Mass Spectrom. **10**, 1035 (1975).
3. J. E. COUTANT and R. J. ROBINSON. *In* Analysis of silicones. *Edited by* A. L. Smith. J. Wiley and Sons, New York. 1974. Chapt. 12. pp. 338–375.
4. R. E. SWAIM, W. P. WEBER, H. G. BOETTEGER, M. EVANS, and F. M. BUCKHOFF. Org. Mass Spectrom. **15**, 304 (1980).
5. M. R. LITZOW and T. R. SPALDING. *In* Mass spectrometry of inorganic and organometallic compounds. *Edited by* M. F. Lappert. Elsevier Scientific, Amsterdam. 1973.
6. B. F. G. JOHNSON, R. D. JOHNSTON, and J. LEWIS. (*a*) J. Chem. Soc. (A), 2865 (1968); (*b*) J. Chem. Soc. Dalton Trans. 2606 (1975).
7. F. E. SAALFELD, M. V. MCDOWELL, A. G. MACDIARMID, and R. E. HIGHSMITH. Int. J. Mass Spectrom. Ion Phys. **9**, 197 (1972), and references therein.
8. R. O. SAUER, W. J. SCHEIBER, and S. D. BREWER. J. Am. Chem. Soc. **68**, 962 (1946).
9. R. N. LEWIS. J. Am. Chem. Soc. **70**, 1115 (1948).
10. J. F. HARROD and A. J. CHALK. J. Am. Chem. Soc. **89**, 1133 (1965).

Can. J. Chem. Downloaded from www.nrcresearchpress.com by 210.87.254.40 on 09/06/12
For personal use only.

Archaeological ceramic differentiation using trace element patterns

BRYAN E. SNOW,[1] JOHN M. D'AURIA,[2] AND RICHARD SHUTLER, JR.[1]
Simon Fraser University, Burnaby, B.C., Canada V5A 1S6

AND

JOHN G. PAYNE
Vancouver Petrographics Ltd., Fort Langley, B.C., Canada V0X 1J0

Received September 21, 1982

This paper is dedicated to Professor Leo Yaffe on the occasion of his 65th birthday

BRYAN E. SNOW, JOHN M. D'AURIA, RICHARD SHUTLER, JR., and JOHN G. PAYNE. Can. J. Chem. **61**, 769 (1983).

Ceramic sherds of "primitive" manufacture from an archaeological site on Fuga Moro Island, Philippines, were analyzed for trace element contents using energy dispersive X-ray fluorescence (EDXRF) to ascertain the probability of obtaining differentiation between stylistic classes (wares) and technological types within the ware. Following analysis and differentiation of these samples, using standard archaeologic and petrographic techniques, the initial focus of the study was to isolate surface factors which could distort or otherwise affect the final elemental characterizations. Once these factors were identified and eliminated, a simple procedure was then developed employing trivariate analysis of specific observed elements that unambiguously segregated the studied sherds, both according to ware and technological type within each ware. The key elements for ware differentiation were Zn, Br, and Sr while type differentiation was achieved using Ca, Ti, Mn, and Rb.

BRYAN E. SNOW, JOHN M. D'AURIA, RICHARD SHUTLER, JR. et JOHN G. PAYNE. Can. J. Chem. **61**, 769 (1983).

On a déterminé la teneur en oligoéléments des fragments de céramique de construction "primitive" provenant d'un site archéologique de l'île de Fuga Moro, Phillipines. On a utilisé la flourescence de rayons-X d'énergie dispersante (FRXED) pour essayer d'établir une distinction entre les classes élégantes (porcelaines) et les types technologiques à l'intérieur de la porcelaine. A la suite de l'analyse et de la différenciation de ces échantillons à partir des techniques archéologiques et pétrographiques normales, le but initial de l'étude est d'isoler les facteurs de surface qui peuvent déformer ou affecter d'une façon ou d'une autre les caractérisations élémentaires finales. Une fois ces facteurs identifiés et éliminés, on a mis au point une méthode simple qui fait appel à l'analyse à "trois variables" des éléments observés spécifiquement que l'on peut isoler sans aucun doute des fragments étudiés selon la porcelaine et le type technologique dans chaque porcelaine. Les éléments principaux qui permettent de différencier les porcelaines sont: le Zn, le Br et le Sr tandis que l'on différencie le type de porcelaine à l'aide du Ca, du Ti, du Mn et du Rb.

[Traduit par le journal]

Introduction

Perhaps the single, most fundamental problem confronting all archaeologists is the classification of observed phenomena. Nowhere is this more demanding than in the study of ancient ceramics. Due to their abundance, ceramics have come to play a major role in archaeological constructs of past peoples and ordinations of cultural developments. They are extensively utilized in both the Old and New World as time markers and cultural diagnostics. By and large, however, archaeologists have responded to the difficulties of ceramic classification in a nonrigorous manner. They have developed a priori, broad generalized classificatory units[3] which rely upon a few selective characteristics or "attributes" to denote membership. In most ceramic classifications, the attributes traditionally employed are stylistic in nature and usually concentrate upon aspects of decoration or surface treatment.

Armed with such classificatory schemes, archaeologists have been invading, in growing numbers and with some success, the realm of the physical sciences. They have been concerned with questions of provenance (i.e., identifying the source(s) of ceramic manufacturing) or characterization (i.e., isolating distinctive chemical patterning). The response of the physical sciences has been laudable. Working independently or jointly with the archaeologists, physical scientists have employed a variety of techniques for multi trace element analysis in an attempt to address these problems (*1–14*). The results have provided some interesting and highly significant information for the study of archaeological ceramics. There is one important fact, however, that characterizes all of this research. The physical scientist is dependent upon the archaeologist for the initial classification of the ceramics and, in all likelihood, the actual selection of the sherd samples to be analyzed. Since all archaeological classifications are essentially interpretations of observed variability, this presents a very basic problem. If the archaeologist has employed a traditional approach, he has formed his classificatory units by visual inspection of a few obvious stylistic attributes. The resultant units are broad and generalized in nature and, if he has merely sorted his ceramics in accordance with pre-existing stylistic typologies, may be completely nonanalytical. Classificatory units obtained in this manner may conceal significant variability in technological or nonstylistic attributes; i.e., variability which may be linked to trace element patterning.

Given the generalizing tendencies of many archaeological classifications, the success enjoyed by the researchers cited above seems nothing short of incredible until one considers the cultural context of the analyzed ceramics. All of these studies deal with ceramics from highly advanced Old World cultures where the production of pottery had reached a high level of standardization, both in clay source utilization and technological process. In such contexts, the most variable attributes at the intra-assemblage level are indeed stylistic and are there-

[1]Department of Archaeology.

[2]Department of Chemistry; author to whom correspondence should be addressed.

[3]For example, "types", "wares", "varieties", "sub-types", "classes", etc.

Can. J. Chem. Downloaded from www.nrcresearchpress.com by 210.87.254.105 on 09/06/12
For personal use only.

Can. J. Chem. Downloaded from www.nrcresearchpress.com by 210.87.254.105 on 09/06/12
For personal use only.

fore easily and accurately depicted by traditional classifications.

In so-called "primitive" pre-wheel (i.e., potter's wheel) societies, there exists no such sophisticated standardization. Usually, each adult female within a given settlement was responsible for the family's pottery production, so variability becomes markedly intensified. It is within these contexts that stylistic classifications most effectively mask technological variability and may create difficulties for the physical scientist attempting multi trace element analysis.

Perhaps the single, most ambitious multi trace element analysis of "primitive" ceramics was undertaken by Leo Yaffe and his co-workers at McGill University (15). This research examined Ontario Iroquois and St. Lawrence Iroquois pottery. One of its stated objectives was to investigate associations between chemical groups and traditional classificatory units (15). Since Iroquoian ceramic classification is wholly dependent upon stylistic attributes and is extremely generalizing in nature (16), their findings in this regard may have direct relevance to the points just raised. Interestingly, the research could not find any significant correlation between the traditional classificatory units employed by the archaeologists and the analytically determined chemical groups of the physical scientists (15).

Our intent in this report is to examine the relationship of intra-assemblage technological variability to multi trace element patterning in a primitive ceramic context. Specifically, are there chemical patterns present which are dependent upon technological rather than stylistic factors? Further, can such patterns differentiate between different stylistic classes and between different technological groups? We have employed nondestructive, energy dispersive X-ray fluorescence (EDXRF) to address this question. Our study sample is derived from two, distinct, stylistic classes of red slipped[4] earthenware recovered from the 1978 excavation[5] of a small beach ridge site ($78M_1$-Site 2) on Fuga Moro Island, Philippines. We offer the resultant data primarily as an aid to physical scientists who are interested in the chemical analysis of "primitive" ceramics. Furthermore, the results suggest that archaeologists may be oversimplifying the complexity of "primitive" ceramics when they opt for stylistic classifications and, as a result, are overlooking important avenues of research.

Archaeology

Fuga Moro is 1 kilometre east of the mountainous northeastern peninsula of Luzon, along the San Vincente Strait (Fig. 1). It is approximately 1 kilometre in diameter and, during low tide, is connected by a reef along its northernly margin to the larger island of Paluai. As is commonly the case upon many sites in the region, no dateable organic material was recovered during the excavations. The discovery, however, of several Chinese porcelain sherds indicates that the site was being occupied sometime during the 14th to early 16th Centuries A.D. (17).

The two stylistic classes utilized in this study jointly total 679 sherds or approximately 80% of the analyzable ceramics recovered from the site. They are designated herein as Wares A and B, respectively. They exhibit stylistic variability in terms of surface treatment and slip appearance. For the samples studied here the thickness of the slip was less than about 50 microns. Their respective sherd incidences and distinguishing stylistic attributes are briefly summarized in Table 1.

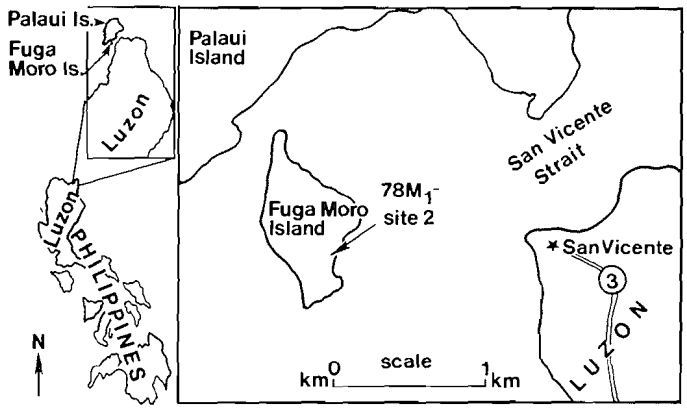

FIG. 1. Geographic position of Fuga Moro Island, Philippines and site location ($78M_1$-Site 2).

The archaeological analysis of these ceramics had been technologically oriented and had provided a detailed understanding of the patterned variability present within each ware. This permitted the segregation of internal "technological types" within each ware which exhibited variability in one or more of the following aspects: (1) apparent paste texture, (2) nonplastic size, (3) plastic state, (4) paste colour, (5) construction, and (6) secondary forming.[6] Wares A and B each had four internal technological types. Each type was numerically labelled according to the ware designation (i.e., Type A1, A2, A3, A4; Type B1, B2, B3, B4). It was noted that the technological types of Ware A were specifically associated with different vessel forms. Type A1 consisted of only jar sherds, Type A2 of only bowl sherds, Type A3 of only lid sherds, and Type A4 of only stove sherds. The technological types of Ware B were composed solely of jar sherds. The respective sherd incidences and technological attributes of each type are summarized in Table 2.

The final step in the archaeological analysis was to mineralogically identify the nonplastics. Sherds were randomly selected from each technological type within the wares, were thin sectioned, and then analyzed petrographically.[7] Two major mineralogical groups were discovered which directly correlated with Wares A and B. In other words, the wares were stylistically *and* petrographically distinct (see Table 3).

All sherds of Ware A, *regardless of technological type*, exhibited unzoned plagioclase, abundant quartz, and dacite. Andesite was extremely rare and volcanic glass absent. Types A1 and A2 comprised a distinct subgroup containing abundant diorite–epidote, clinopyroxene, and lesser green hornblende, while Types A3 and A4 represented a second subgroup characterized by very abundant quartz, higher biotite content, and only red-brown hornblende. (Type A4 also contained large amounts of rice husks and straw.)

All sherds of Ware B, *regardless of technological type*, exhibited abundant porphyritic andesite, often associated with volcanic glass particles. Dacite was of low frequency and

[4]A slip is a fluid suspension of clay applied to a ceramic surface in order to alter surface colour and texture or to render vessels less permeable; typically it is quite thin (~ microns).

[5]Excavation conducted by Dr. Richard Shutler as a joint project with the Philippine National Museum, under the permit granted by the Philippine Center for Advanced Studies.

[6]For a definition of these terms, consult refs. 18 and 19.

[7]For a description of petrographic techniques, consult ref. 18.

TABLE 1. Distinguishing stylistic attributes of wares

Ware designation	*n*	Surface finish	Surface texture	Surface lustre	Slip appearance
A	547	Burnished	Smooth	Low	Watery, dark red, uncrazed
B	132	Smoothed	Slightly grainy	Matte	Earthy, weak red, uncrazed

TABLE 2. Technological attributes of types

Type	*n*	Paste texture	Nonplastic size range*	Plastic alteration	Paste colour	Construction	Secondary forming
A1	495	Medium	Fine–medium	Sintered	Uniform, clear, rarely zoned	Modeled	Opposed paddling & scraping (smooth paddle)
A2	30	Medium	Fine–medium	Sintered	Uniform, clear, rarely zoned	Coiled	Scraping (unpaddled)
A3	16	Medium	V. fine – fine	Rarely Sintered	Uniform, clear	Molded	Scraping (unpaddled)
A4	6	Medium	V. fine – v. coarse	Exterior vitrified	Nonuniform exterior highly oxidized	Coiled	Unopposed paddling & scraping (smooth paddle)
B1	54	Dense	Fine–medium	Well sintered	Uniform, clear, rarely zoned	Modeled	Opposed paddling; no scraping (grooved paddle)
B2	35	Medium	Medium–coarse	Sintered	Nonuniform, strongly zoned	Modeled	Opposed paddling; no scraping (smooth paddle)
B3	29	Open–medium	Medium–coarse	Sintered	Nonuniform, strongly zoned	Modeled	Opposed paddling; no scraping (grooved paddle)
B4	14	Medium	V. fine – fine	Sintered	Uniform, brown	Modeled	Opposed paddling; no scraping (smooth paddle)

*Nonplastic size expressed according to the Wentworth scale (20).

quartz, diorite, and epidote were rare or absent. Types B1 and B2 comprised a single subgroup which exhibited lower andesite counts and both red-brown and green hornblende. Type B3 was slightly different and exhibited high andesite counts and only red-brown hornblende. Type B4 was similar to B1 and B2 but displayed high frequencies of clinopyroxene and actinolite.

In summary, therefore, the archaeological analysis had resulted in the separation of two major stylistic groups which were designated Wares A and B. Within each ware, analysis also revealed four technological subdivisions which were termed Types A1–A4 and B1–B4. Subsequent petrographic analysis indicated the nonplastic components of the respective wares were radically distinct. Some evidence of nonplastic variability among the technological types of each ware was also noted. The results of the petrographic study substantially strengthened the archaeological classification and suggested the likelihood that the wares had been manufactured in different locales. The point is stressed that the archaeological classification was completed prior to both the petrographic and subsequent trace element analyses.

Experimental

EDXRF was selected for this study because it is nondestructive and rapid and does not require extensive sample pretreatment. Sherds were analyzed in the intact or pristine state for several reasons. Firstly, a technique could not be devised that achieved complete separation of the plastic (i.e., the clay) from the nonplastic (i.e., mineral and organic inclusions) fraction. The abundance of soft, weathered particles such as plagioclase and andesite within the pastes meant that any attempt to disaggregate the sherds would powder these inclusions and contaminate the plastic anyway. Secondly, if separation of the two fractions could be accomplished, its merits would be questionable. Since primitive potters intentionally modified the characteristics of clay bodies by adding or removing nonplastics, presumably for technological or functional reasons, pertinent behavioural data of archaeological interest could be lost.

It has become common practice to remove by mechanical means the surfaces of ceramic samples prior to trace element analysis in order to analyze the "bulk" composition of the paste. While this may expedite the analytical process and remove the threat of surface contamination, it can also result in the loss of important archaeological data. For instance, all sherds of both Ware A and B are slipped on one or both surfaces. The slips are an integral aspect of the sample; indeed, they are an integral aspect of most Philippine ceramics. They represent a potential source of chemical variability that should be considered in any context in which they occur. Furthermore, when dealing with unslipped pottery, there are numerous techniques and processes which may be employed in contour refinement or surface finish which differentially cause technologically related alterations in the paste structure of the vessel walls and surfaces and could conceivably result in distinctive chemical patterning.

Even if these archaeological concerns are not appreciated, the relative merit of "bulk" over "surface" analysis has been addressed previously and no systematic differences vis-a-vis group segregation were found to exist (8). This suggests that the entire question may be more a debate of technique and preference than a question of scientific

Can. J. Chem. Downloaded from www.nrcresearchpress.com by 210.87.254.105 on 09/06/12
For personal use only.

Can. J. Chem. Downloaded from www.nrcresearchpress.com by 210.87.254.105 on 09/06/12
For personal use only.

TABLE 3. Distribution of nonplastic particles in wares A and B*

Section No.	Type	No. of fragments	Plag.§	Hblde. rb.	Hblde. gr.	Act.	Cpx.	Dior. & QDi.	Epi.	Qtz.	Bio.	Dac. cgr.	Dac. fgr.	And.	Volc. Gl.	Opq.	Hem.	Qtzt.	Mmic.	Other
5	A1	371	26.7	0.3	7.5	—	12.7	1.6	13.2	15.6	1.3	4.6	5.7	1.9	—	4.8	3.8	0.3	—	
7	A1	530	21.2	0.2	5.7	—	11.0	13.4	8.3	12.1	0.4	3.0	3.4	0.9	—	12.0	4.7	0.7	2.8	
36	A1	245	19.6	—	6.9	—	4.9	18.8	6.9	16.7	—	10.3	1.6	1.2	—	3.3	2.4	—	3.1	
37	A2	630	23.1	0.2	6.0	—	9.9	9.1	7.6	19.7	—	5.7	1.6	1.1	—	8.2	3.5	1.1	3.2	
2	A3	400	45.6	10.6	—	1.6	0.8	—	0.3	22.8	2.7	2.9	5.8	2.3	—	2.7	2.0	—	—	
11(ext)	A4	205	31.7	10.2	—	0.5	0.4	0.5	5.3	29.3	2.4	4.8	6.3	1.0	—	4.4	4.4	—	—	Rice husks†
11(int)	A4	238	36.2	13.9	—	0.5	—	0.5	8.8	26.8	2.4	6.4	12.5	0.9	—	2.4	1.0	—	—	Rice husks
17	B1	455	53.3	(26.1)‡		—	0.3	—	—	—	—	1.1	4.2	9.8	1.0	2.6	1.5	—	—	
21	B1	561	49.9	4.8	15.2	—	0.3	—	0.2	2.0	—	—	2.7	14.8	5.9	1.2	3.0	—	—	
27	B2	422	42.2	(15.1)		—	—	0.2	—	0.5	1.9	—	0.4	29.2	3.3	3.3	1.9	0.2	1.7	
20	B3	582	37.3	16.7	—	—	0.3	0.4	—	—	0.9	—	1.0	38.2	3.3	1.5	—	—	0.2	Carb. (0.2)
22	B3	335	36.7	9.9	—	0.5	—	—	—	1.1	1.1	—	1.4	43.0	1.8	2.1	1.8	—	—	
19	B4	534	23.4	(13.7)		10.6	29.5	—	—	—	0.4	—	—	13.6	—	8.4	—	0.4	—	

*In this table, the entries given in the nonplastic columns represent values in approximate volume percent.
†Rice husks not included in row totals.
‡Values in brackets indicate hornblende is gradational between red-brown and green.
§*Nonplastic Abbreviations:* Plag, plagioclase; Hblde., hornblende; rb., red-brown; gr., green; Act., actinolite; Cpx., clinopyroxene; Dior., diorite; QDi., quartz diorite, granodiorite; Epi., epidote; Qtz., quartz; Bio., biotite; Dac., dacite; cgr., coarser grained; fgr., finer grained (cherty); And., andesite; Volc. Gl., volcanic glass; Opq., opaques; Hem., hematite (all translucent red and brown oxides); Qtzt., quartzite; Mmic., metamorphic aggregates; Carb., carbonate.

import and that the real concern should be to identify the types of contaminants or alterations which exist within the sample prior to analysis. Because of these considerations, mechanical stripping of the sample surfaces was rejected in this study. Sherds were analyzed instead along their intact surfaces *after* considerable effort was expended to isolate and exclude surface effects which produced distortion in the chemical patterns.

Sample treatment

The only initial treatment given to the sample was a vigorous scrubbing of all sherd surfaces in warm water. When necessary, small portions were broken off the corner of each sherd to permit containment within the sample cup. This produced no loss of sample integrity since the fragments were simply glued back onto the parent sherds after analysis was complete. In all cases, however, the samples could be considered infinitely thick for purposes of X-ray absorption effects. Since absolute concentrations were not determined, interelemental effects were ignored.

Apparatus

Relative determinations of the trace element concentrations in the pottery samples were made by photon-excited, secondary target, energy dispersive X-ray fluorescence analysis. A complete description of this system (Kevex Corp.) is presented elsewhere (21, 22). An Au anode X-ray tube was the primary radiation source while a Mo secondary target/filter system was used in all analyses. The selection of Mo was predicated by the fact that a reasonable number of trace elements in the samples were excited by the Mo (K_α and K_β) radiation. Each sample was analyzed for four minutes with the X-ray tube voltage at 40 keV and current at 20 mA.

The emitted elemental X-rays were detected integrally using a Si(Li) X-ray spectrometer and the spectra accumulated in 512 channel groups with a Nuclear Data, Model 812, data acquisition system. Typical X-ray spectra from the slipped exterior surface of Types A1 and B1 sherds are presented in Fig. 2. In general, X-rays were observed for elements K, Ca, Ti, Mn, Fe, Cu, Zn, As, Br, Rb, Sr, Y, and Pb, in addition to the coherent (Rayleigh) and incoherent (Compton) scattering peaks (see Fig. 2). The intensity of the lines for K and Cu was sufficiently low that they were not useful in further consideration. While the intensity of the lines for As and Pb was sufficiently high to warrant inclusion in this study, they exhibited such wide scale variability that they were not used in any subsequent interpretations.

Spectral analyses and data presentation

Due to the difficulty in obtaining quantitative concentrations for nonhomogeneous, intact sherds and the desire not to disaggregate the archaeological sample, absolute concentrations were not determined. Indeed, recent studies by Saleh *et al.* (14) indicate the importance of interelemental correlations as opposed to individual elemental concentrations in the characterization of ceramic samples. Thus, each photopeak of interest from these infinitely thick samples was simply integrated and normalized to that of the Compton scattering peak. This procedure makes the analysis independent of sample shape and of variations in the incident radiation. The relative errors quoted are due primarily to the statistics accumulated in individual peaks.

Results will be presented graphically on triangular axes plots with these normalized data from groups of three elements expressed as percentages of their combined totals. We opted for this procedure rather than a calculated metric procedure because it provided a quick and visually obvious means for revealing patterns of elemental correlations in large bodies of data, that is understandable to both physical scientists and archaeologists.

Results and discussion

Reproducibility

The reproducibility of the system and the method of data analysis was determined by making ten nonconsecutive analyses of a single arbitrary sherd (Type B2, slipped exterior surface) in different positions. The mean of the observed nor-

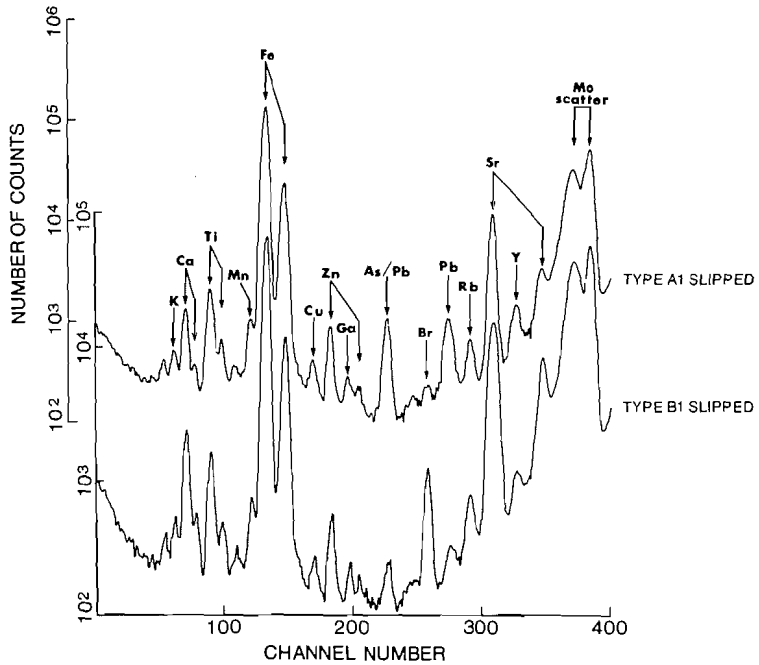

FIG. 2. Typical X-ray spectra from slipped surfaces of a Type A1 and B1 sherd with elements of interest labelled.

TABLE 4. Summary of statistics of reproducibility study

Element*	Normalized photopeak areas† Mean ($\times 10^{-2}$)	S.D. (%)
Ca	4.0	4.5
Ti	7.3	5.6
Mn	1.0	17
Fe	333	3.6
Zn	2.0	11.0
As/Pb (L_α)	1.2	18
Br	1.9	8.4
Pb (L_β)	1.5	13.2
Rb	1.0	23
Sr	44.2	3.0
Y	3.3	11.4

*Unless indicated, here and in subsequent tables, these are for observed K_α peaks.

†Normalized to observed Compton scattering peak.

TABLE 5. Surface effects: slipped surface

Element	Normalized mean peak areas ($\times 10^{-2}$)* I†	II‡	III§
Ca	4.4(27)	4.8(15)	5.2
Ti	7.4(16)	6.2(11)	5.9
Mn	1.7(32)	1.7(46)	2.9
Fe	535(11)	465(12)	414
Zn	3.4(32)	3.2(39)	1.9
As/Pb (L_α)	2.2(85)	1.1(102)	0.54
Br	0.29(65)	0.43(27)	0.32
Pb (L_β)	2.5(71)	1.5(87)	0.61
Rb	1.6(24)	1.5(22)	1.7
Sr	36.8(15)	36.4(11)	35.2
Y	3.4(21)	3.7(18)	3.5

*Mean peak areas normalized to the Compton intensity; standard deviation (%) in brackets.

†Type A1/exterior; clean, unworn; 23 samples.

‡Type A1/exterior; carbon stained, unworn; 13 samples.

§Type A1/exterior; clean, waterworn; 1 sample.

malized photopeak areas and the standard deviations are presented in Table 4. While the observed variations were, in general, quite small, a better appreciation of the relative variation in the context of the type of data treatment utilized later can be observed when the normalized peak areas are displayed graphically as percentages on triangular axes. For instance, Fig. 3(a) presents the Ca–Ti–Mn areas, expressed as percentages of their combined totals per location. The *maximum* range along both the Ca and Ti axes is 4.2%, while that along the Mn axis is 3.9%. In other words, such presentations indicate that the observed relative values for these three elements from a single sherd in different positions are, as expected, quite similar.

Surface effects

Of considerable interest was the determination of whether or not *surface state* affected the EDXRF analysis. There were two major factors to consider in this regard. Firstly, some sherds were waterworn. This could conceivably affect surface readings, particularly those of slipped surfaces since the slips were thin and easily eroded. Secondly, many of the sherds exhibited carbon staining or actual carbon encrustations, along one or both surfaces, which had built up during either firing or usage. This too could affect surface readings. To examine first how surface state affected the analysis of slipped exterior surfaces, we randomly selected 37 sherds from Type A1. Twenty-three of these had clean, unworn slipped surfaces free of carbon, 13 had unworn slipped surfaces stained by carbon in degrees varying from slight to intense, and one sherd had a clean slipped surface which was badly waterworn. The normalized data for these samples, labelled I, II, and III, respectively, are summarized in Table 5. Inspection of these data revealed that the mean values were generally similar for each group; however, there were seemingly some small scale variations. Both the carbon stained sherds and the single waterworn specimen ex-

Can. J. Chem. Downloaded from www.nrcresearchpress.com by 210.87.254.105 on 09/06/12
For personal use only.

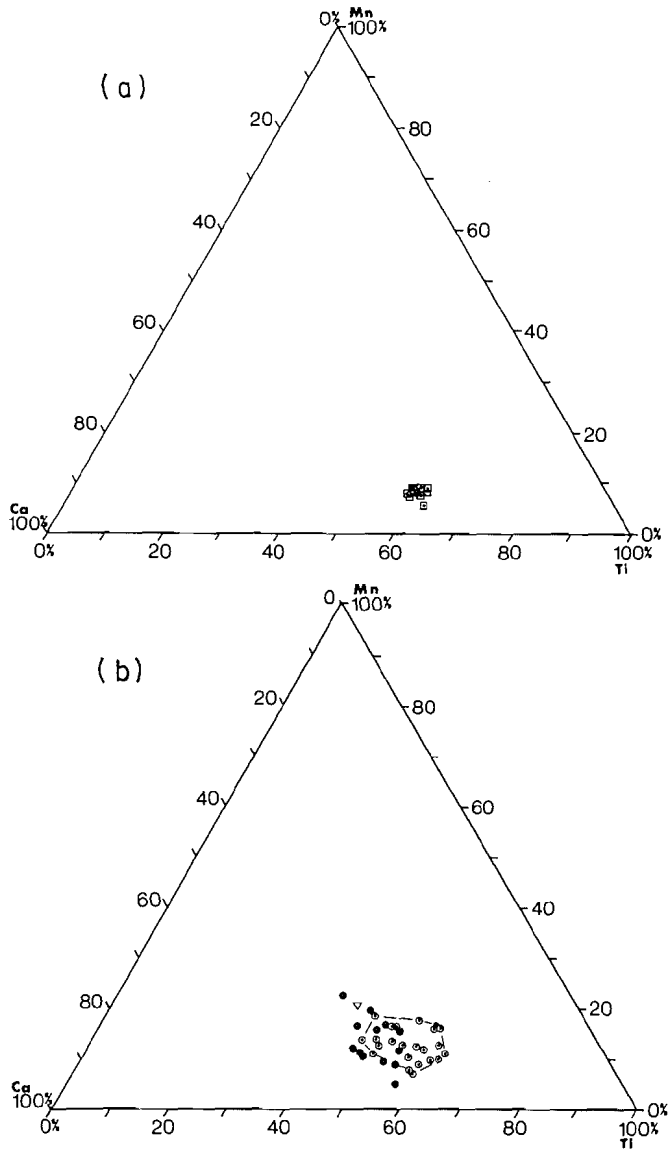

FIG. 3. (a) Triangular plot of the observed individual X-ray intensities from Ca, Ti, and Mn, expressed as percentages of their combined sum, for ten nonconsecutive runs along the slipped exterior surface of a Type B2 sherd in different orientations. (b) Similar representation as for (a) for Ca, Ti, and Mn along the slipped exterior surfaces of 37 Type A1 sherds comparing carbon stained (●), waterworn (▽), and clean (⊙) specimens. Broken line drawn for convenience only.

hibited slightly higher Ca and slightly lower Ti and Fe relative concentrations. Furthermore, while the Mn levels of the clean group and the carbon stained group were virtually identical, the latter exhibited a higher standard deviation. When these data are presented on a Ca–Ti–Mn triangular plot (Fig. 3(b)) the carbon stained sherds and the single waterworn specimen tended to distort the distribution observed for clean sherds. We decided, therefore, to exclude all carbon stained and/or waterworn sherds from studies of slipped surfaces as these would have interefered with further discrimination of the technological types within each ware.

Along the unslipped interior surfaces, carbon deposition was even more common and more frequently intense. A cursory analysis of interior, carbon stained surfaces of all types indicatd similar broadening in correlations of the elements mentioned above. Accordingly, carbon stained sherds were also excluded from the analysis of unslipped surfaces.

TABLE 6. Water wearing effects: unslipped surfaces

Element	Normalized mean peak areas ($\times 10^{-2}$)* III†	IV‡
Ca	4.7(18)	5.4(11)
Ti	3.7(14)	4.1(23)
Mn	1.1(42)	1.3(17)
Fe	228(23)	220(20)
Zn	1.7(50)	1.7(12)
As/Pb (L_α)	1.1(35)	1.0(34)
Br	1.2(25)	1.1(60)
Pb (L_β)	0.71(50)	0.64(62)
Rb	1.7(25)	1.8(19)
Sr	88.7(9)	83.2(8)
Y	1.2(26)	1.8(18)

*Mean peak areas normalized to the Compton intensity; standard deviation (%) in brackets.
†Type B3/exterior; unworn; 5 samples.
‡Type B3/interior; waterworn; 6 samples.

The effects of water wearing upon unslipped interior surfaces, free of surface carbon, required further specific study. To do this, we selected 11 sherds from Type B3, a type frequently displaying waterworn specimens. Five of the sherds had clean, unslipped surfaces unaltered by water wearing, while 6 had clean, unslipped surfaces altered by water wearing in degrees varying from slight to intense. The normalized data for these two groups (labelled III and IV) are summarized in Table 6. Inspection of these data indicated only slight differences between the two groups. When the peak areas were expressed on a Ca–Ti–Mn triangular plot, both groups formed a single discrete cluster (Fig. 4(a)). Accordingly, the exclusion of waterworn sherds from the analysis of unslipped surfaces could not be justified.

In the above discussion of surface state, it will be noted that a distinction has been drawn between slipped and unslipped surfaces. This distinction is what we termed *surface aspect*. The aspect of a surface is obviously significant and the separation of the two aspects is usually easily maintained; however, care must be taken when dealing with the interior surfaces of jar sherds. Here, the slip is often applied to the interior of the rim and may drip downward depositing slip traces along the body. To examine the variability induced by this phenomenon, 27 Type A1 sherds were analyzed along the interior surface. (These specimens were derived from the same sample of A1 sherds previously employed to study surface effects. Ten of the original 37 were excluded because of interior carbon staining.) Eleven of these lacked slip traces, while 16 exhibited slip traces. The normalized data for the two groups (labelled V and VI) are summarized in Table 7. Upon casual inspection, the mean values did not seem radically different but the standard deviations associated with the slip traces group were considerably higher. When the peak areas were expressed on a Ca–Mn–Y triangular plot, the greater variability of the slip traces group was obvious (Fig. 4(b)). We interpreted these results as indicating that careful segregation of surface aspect was imperative at all times.

In summary, therefore, these initial studies indicated the following.

(1) The range in elemental variability within a single intact sherd was small and well within reproducible limits. The data

Can. J. Chem. Downloaded from www.nrcresearchpress.com by 210.87.254.105 on 09/06/12
For personal use only.

Can. J. Chem. Downloaded from www.nrcresearchpress.com by 210.87.254.105 on 09/06/12
For personal use only.

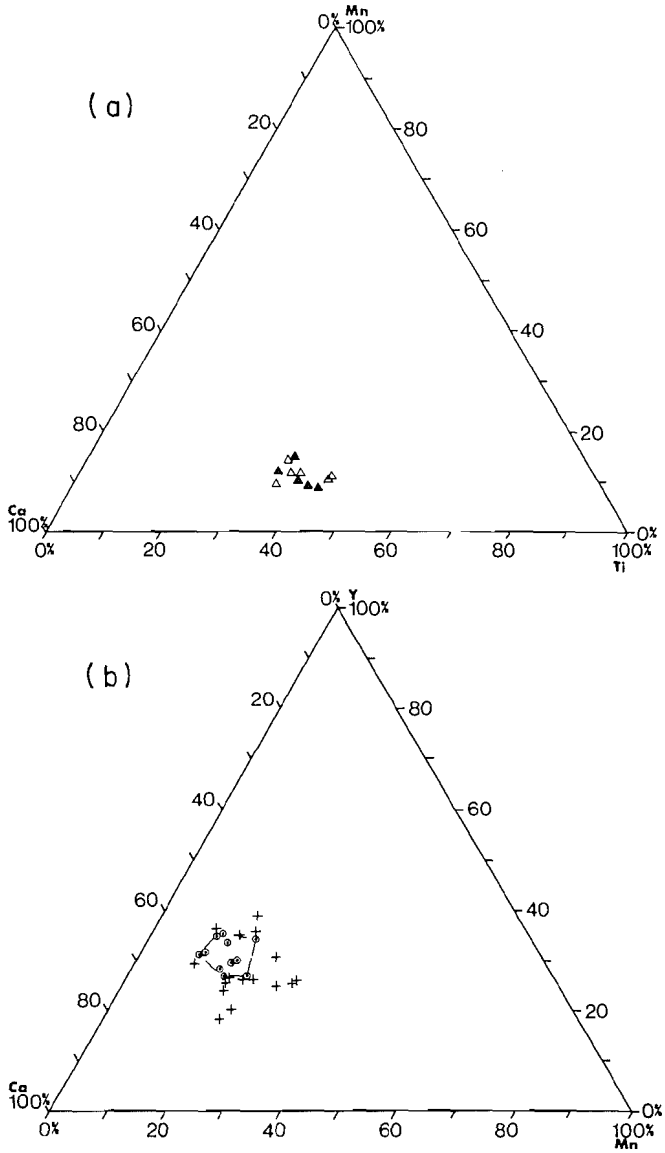

FIG. 4. (a) Similar representation as for Fig. 3(a) for Ca, Ti, and Mn along the unslipped interior surfaces of 11 Type B3 sherds comparing unworn (▲) and waterworn (△) specimens. (b) Similar representation as for Fig. 3(a) for Ca, Ti, and Y along the interior surfaces of 27 Type A1 sherds illustrating the greater variability of specimens with slip traces (+) as compared to those without slip traces (⊙). Broken line drawn for convenience only.

could be graphically expressed upon triangular axes resulting in discrete clustering.

(2) Surface state affected the EDXRF analysis. Carbon stained or encrusted sherds had to be excluded from the study of both slipped and unslipped surfaces. Waterworn sherds had to be excluded from the study of slipped surfaces but not from the study of unslipped surfaces.

(3) Surface aspect had to be carefully controlled. Slipped surfaces or even those exhibiting slip traces could not be directly compared to unslipped surfaces.

Ware differentiation/slipped surface

Fifty sherds of Ware A and 31 sherds of Ware B were selected for analysis along the slipped surface. Samples were randomly chosen from the remaining sherds of each type after exclusion of all carbon stained and waterworn specimens. In the cases of Type A4 and Types B2–B4, the number of sherds studied represented *all* of the analyzable specimens remaining after exclusion of carbon stained and waterworn sherds. The normalized data for the respective technological types per ware (i.e., A2–A4, B1–B4) are summarized in Table 8 (Col. I of Table 5 presents data for Type A1).

TABLE 7. Surface aspect

Element	Normalized mean peak areas ($\times 10^{-2}$)* V†	VI‡
Ca	6.2(12)	6.0(14)
Ti	7.5(13)	7.2(23)
Mn	1.7(25)	2.3(33)
Fe	497(10)	505(18)
Zn	5.5(31)	3.9(45)
As/Pb (L_α)	2.9(82)	2.7(171)
Br	0.39(42)	0.45(62)
Pb (L_β)	2.9(76)	3.0(150)
Rb	1.5(17)	1.6(25)
Sr	37.5(9)	37.9(19)
Y	3.5(12)	3.2(29)

*Mean peak areas normalized to the Compton intensity; standard deviation (%) in brackets.
†Type A1/interior; slip traces absent; 11 samples.
‡Type A1/interior; slip traces present; 16 samples.

These data indicated significant elemental variability between each ware. Visual inspection revealed that the relative levels of Zn, Br, and Sr exhibited the clearest differences. When these data are expressed as percentages of their combined totals (using a scaling factor of 0.1 for Sr for convenience in the graphical presentation) and displayed graphically on a triangular plot (Fig. 5(a)), two well separated clusters are obtained. Clearly, these two different wares can be differentiated simply using these three elemental levels.

The differences in Br content between the two wares is interesting and merits further comment. The depositional environment is identical for each ware inasmuch as they were found in direct association in the same deposits. As such, the possibility is extremely remote that the differential in Br could have been induced by some post-burial phenomenon. Pearlman and Asaro (6) have suggested that Br is extremely variable, at least, in the context of ceramics from a single Nile Valley site. Perhaps these observations do not apply for other contexts such as Northern Luzon. This requires additional research. The above authors also noted that Br might be sensitive to firing conditions, noting that 90% of the Br disappeared after firing a sample of Nile Valley clay at a temperature of 800°C in an electrical furnace. Since earthenwares may be frequently fired below this temperature and are subject to uneven firing conditions, particularly if open firing is practiced, it is possible that Br could often be retained in such circumstances. It may be, therefore, that the differences in Br between the two wares indicate radically different firing conditions but, although this is a very attractive speculation from the archaeological viewpoint, it, too, requires additional research. The intent in this study is to indicate that the Br content is patterned in direct accordance to the previously defined archaeological wares. In short, there is a significant difference in this element, in addition to Zn and Sr, between the two wares that cannot be discarded a priori simply because previous research in another context has found it extremely variable and less useful in discrimination.

TABLE 8. Ware differentiation: slipped surfaces

Elements	Normalized mean peak areas ($\times 10^{-2}$)*						
	A2 (12)†	A3 (13)†	A4 (2)†	B1 (15)†	B2 (6)†	B3 (5)†	B4 (5)†
Ca	5.7(17)	4.8(15)	4.1(17)	5.7(14)	4.7(17)	4.9(10)	5.9(18)
Ti	7.9(18)	5.0(11)	4.1(17)	4.1(13)	7.7(34)	3.6(8)	6.3(19)
Mn	2.9(18)	2.4(21)	4.6(10)	.97(48)	1.5(48)	0.93(38)	4.4(28)
Fe	530(15)	383(10)	539(3)	221(14)	415(28)	227(9)	463(16)
Zn	3.4(17)	3.1(39)	3.2(1.3)	1.4(40)	1.9(33)	1.6(27)	2.2(18)
As/Pb (L_α)	1.5(62)	1.4(93)	0.89(38)	0.56(92)	0.86(42)	1.0(50)	1.2(37)
Br	0.27(54)	0.25(67)	0.52(32)	1.9(51)	1.4(43)	1.4(36)	1.7(43)
Pb (L_β)	1.8(52)	1.5(87)	1.3(19)	0.47(104)	1.2(18)	0.93(64)	1.3(51)
Rb	1.6(18)	1.7(30)	2.4(9)	1.4(18)	1.6(63)	2.2(18)	1.2(25)
Sr	41.4(14)	38.0(22)	30.3(8)	88.5(10)	46.0(7)	81.4(6)	66.2(19)
Y	3.0(22)	2.9(28)	4.3(6)	1.7(22)	3.2(17)	1.5(34)	1.8(36)

*Mean peak areas normalized to the Compton intensity; standard deviations (%) in brackets.
†Number of samples per type.

TABLE 9. Ware differentiation: unslipped surfaces

Elements	Normalized mean peak areas ($\times 10^{-2}$)*				
	A1 (11)†	B1 (9)†	B2 (9)†	B3 (11)†	B4 (2)†
Ca	6.2(12)	5.6(16)	4.0(14)	5.1(15)	6.0(12)
Ti	7.5(13)	4.0(12)	6.9(18)	3.9(20)	6.2(3)
Mn	1.7(25)	1.0(48)	1.1(17)	1.2(29)	4.0(20)
Fe	497(10)	213(20)	324(20)	223(20)	469(15)
Zn	5.5(31)	1.2(75)	1.9(31)	1.7(32)	1.9(35)
As/Pb (L_α)	2.9(82)	0.52(54)	1.3(44)	1.1(33)	1.4(12)
Br	0.39(42)	1.6(47)	1.2(36)	1.1(44)	2.1(52)
Pb (L_β)	2.9(76)	0.49(55)	1.4(59)	0.67(54)	1.0(10)
Rb	1.5(17)	1.3(22)	1.3(33)	1.8(21)	1.6(15)
Sr	37.5(9)	88.9(7)	47.6(17)	85.7(9)	64.6(29)
Y	3.5(12)	1.4(51)	2.6(22)	1.6(28)	2.1(11)

*Mean peak areas normalized to the Compton intensity; standard deviations (%) in brackets.
†Number of samples per type.

Ware differentiation/unslipped surface

Eleven sherds of Type A1 and 31 sherds of Ware B were selected for analysis along the unslipped surface. Types A2, A3, and A4 were exluded due to surface aspect; i.e., these were slipped on both surfaces. Samples were randomly chosen after exclusion of all carbon stained specimens. In the cases of Types B1, B2, and B4, the number of sherds studies represented *all* of the analyzable specimens remaining after exclusion of carbon stained sherds. The normalized data for Type A1 and Types B1–B4 are summarized in Table 9.

As before, when the peak areas for Zn, Br, and Sr were expressed on a triangular plot, two clusters are obtained (Fig. 5(b)). These clusters were more widely separated than those obtained for the slipped surface although it should be emphasized that the number of sherds representing Ware A was much reduced. Even so, these results indicate that ware differentiation for the unslipped surface was also achieved.

Type differentiation

(a) *Types A1–A4 (slipped surface)*

From the data presented in Table 8, A3 was immediately distinguishable by its relatively low Fe content. A4 was also distinctive due to its high Mn, Rb, and Y levels. Both of these types also exhibited reduced Ti. A1 and A2 seemed the most similar; however, A2 exhibited higher Ca and Mn levels.

When the peak areas for Ca, Ti, and Mn were expressed on triangular axes, A1, A3, and A4 formed discrete, separated clusters. A2 formed a cluster between A1 and A3 and exhibited partial linkage with A1 (Fig. 6). Although there was some overlap between A1 and A2 clusters, the data presented in Fig. 6 clearly indicated that each technological type displayed an individual pattern of interelemental correlations for Ca, Ti, and Mn.

(b) *Types B1–B4 (slipped surface)*

From the data presented in Table 8, significant variation among the four technological types was evident. B1 and B3 seemed most similar, exhibiting low Ti and Fe with very high Sr levels. Alternatively, B2 and B4 displayed much greater Ti and Fe and much lower Sr contents.

There were, however, differences in other elements between each of the above pairs. In the case of B1 and B3, higher Rb was evident in the latter. In the case of B2 and B4, the former was characterized by low Ca and high Y, while the latter was characterized by high Ca and Mn.

When the peak areas for Ca, Ti, and Mn were expressed on a triangular plot, Types B2 and B4 formed separated clusters. A third cluster was formed by the combined B1 and B3 sherds (Fig. 7(a)). Only when Rb was considered, for example, on a

Can. J. Chem. Downloaded from www.nrcresearchpress.com by 210.87.254.105 on 09/06/12
For personal use only.

Can. J. Chem. Downloaded from www.nrcresearchpress.com by 210.87.254.105 on 09/06/12
For personal use only.

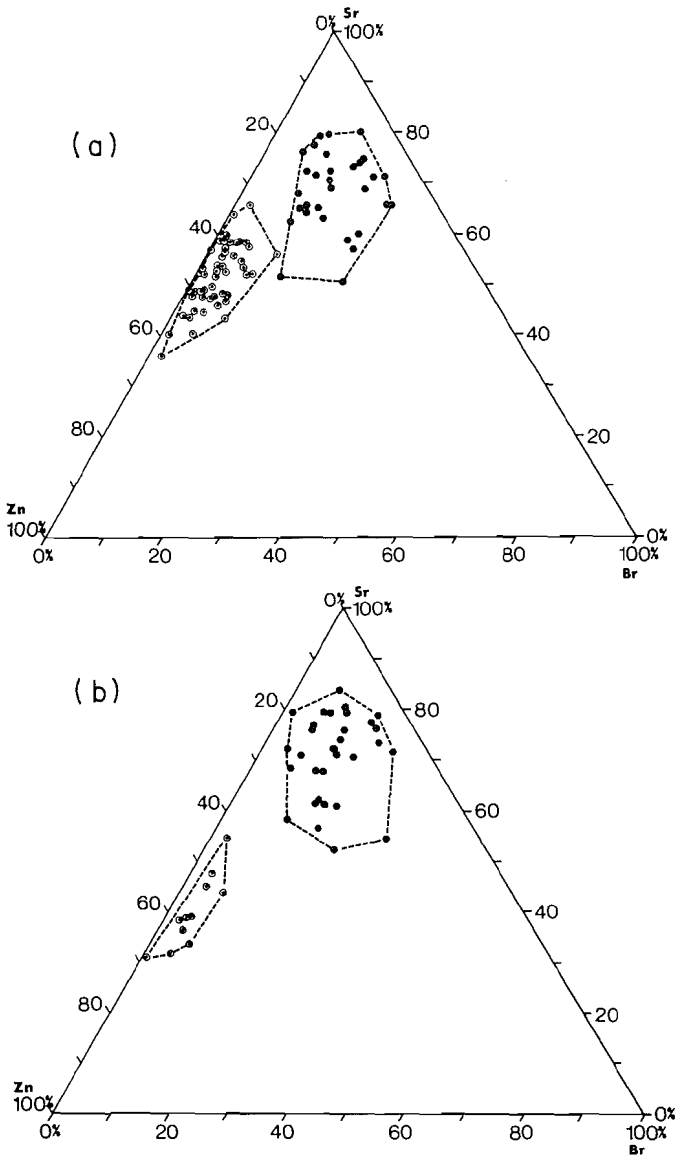

FIG. 5. (a) Similar representation as Fig. 3(a) for Zn, Br, and Sr along the slipped aspect of 60 Ware A (⊙) and 31 Ware B (●) sherds (Sr scaled by a factor of 0.1). Broken lines drawn for convenience only. (b) Similar representation as Fig. 3(a) for Zn, Br, and Sr along the unslipped aspect of 11 Ware A (⊙) and 31 Ware B (●) sherds (Sr scaled by a factor of 0.1). Broken line drawn for convenience only.

Ca–Mn–Rb plot was a distinction visible between B1 and B3 (e.g., Fig. 7(b)). As a result, we were once more left with the conclusion that each technological type displayed an individual pattern of interelemental correlations.

(c) *Types B1–B4 (unslipped surface)*

From the data presented in Table 9, B1 and B3 remained similar in their mutual expression of low Ti and Fe associated with high Sr. B3 still exhibited a slightly higher Rb content but seemingly not to the degree noted along the slipped surface. B2 and B4 continued to exhibit much higher Ti and Fe and much lower Sr, although the amount of Fe in B2 was considerably reduced from that of the slipped surface. B2 remained characterized by low Ca and high Y, while B4 still displayed particularly high Ca and Mn.

When the peak areas for Ca, Ti, and Mn were expressed on triangular axes, B2 and B4 again formed separated clusters.

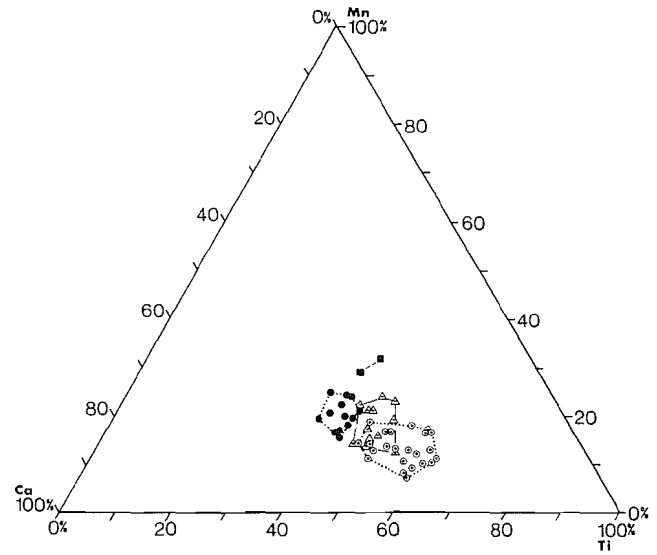

FIG. 6. Similar representation as Fig. 3(a) for Ca, Ti, and Mn for slipped aspect of 23 Type A1 (⊙), 12 Type A2 (△), 13 Type A3 (●), and 2 Type A4 (■) sherds. Broken lines drawn for convenience only.

The cluster for B2 had become much more discrete, even though the number of sherds studied had been increased. B1 and B3 formed a third cluster but the distribution of B3 had also become more discrete (Fig. 8(a)). Differences in Rb were still in evidence for B1 and B3 on a Ca–Mn–Rb plot (Fig. 8(b)). Once again, it was concluded that each technological type exhibited an individual pattern of interelemental correlations.

Conclusion

The primary objective of this report was to examine the relationship of intra-assemblage variability to multi trace element patterning in a primitive ceramic context. The results indicate that it was indeed possible to isolate an interelemental correlation which differentiated the stylistic classes (i.e., Wares A and B). Further, it was also possible to isolate interelemental correlations which reflected chemical differences among each of the four technological types per ware. It should be pointed out that these differentiations were demonstrated using only trivariate correlations, avoiding the need for the use of sophisticated multivariate statistical analyses of the data. The latter approach, however, could lead to a greater, more definitive discrimination, particularly when studying a large, more diverse set of samples.

It is obvious that the ware discrimination would have been evident without any prior archaeological segregation of the samples. In other words, the total sample could have been treated as a single unit, analyzed by EDXRF, and the "archaeologically correct" ware differentiation would have been obvious. It is, however, a debatable point whether or not all of the technological types per ware would have been so readily perceived. Most certainly some, e.g. A3, B2, and B4, would have been easily identified and segregated. Regardless of the latter, however, the importance of understanding and appreciating technological variability within stylistic classes when conducting multi trace element analysis should now be evident.

Another interesting aspect of the results is that surface effects can be recognized and eliminated through careful study, thereby avoiding the necessity of mechanical surface stripping and

Can. J. Chem. Downloaded from www.nrcresearchpress.com by 210.87.254.105 on 09/06/12
For personal use only.

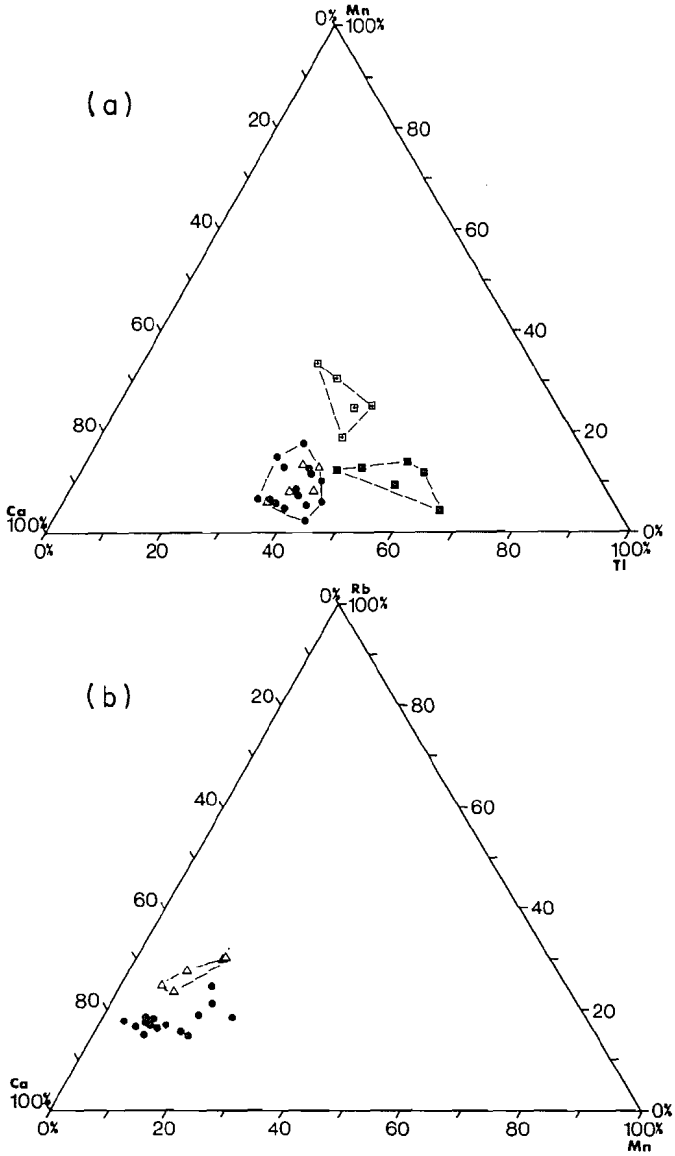

FIG. 7. (a) Similar representation as Fig. 3(a) for Ca, Ti, and Mn for slipped aspect of 15 Type B1 (●), 6 Type B2 (■), 5 Type B3 (△), and 5 Type B4 (⊡) sherds. Broken lines drawn for convenience only. (b) Similar representation as Fig. 3(a) for Ca, Mn, and Rb for slipped aspect of 15 Type B1 (●) and 5 Type B3 (△) sherds. Broken line drawn for convenience only.

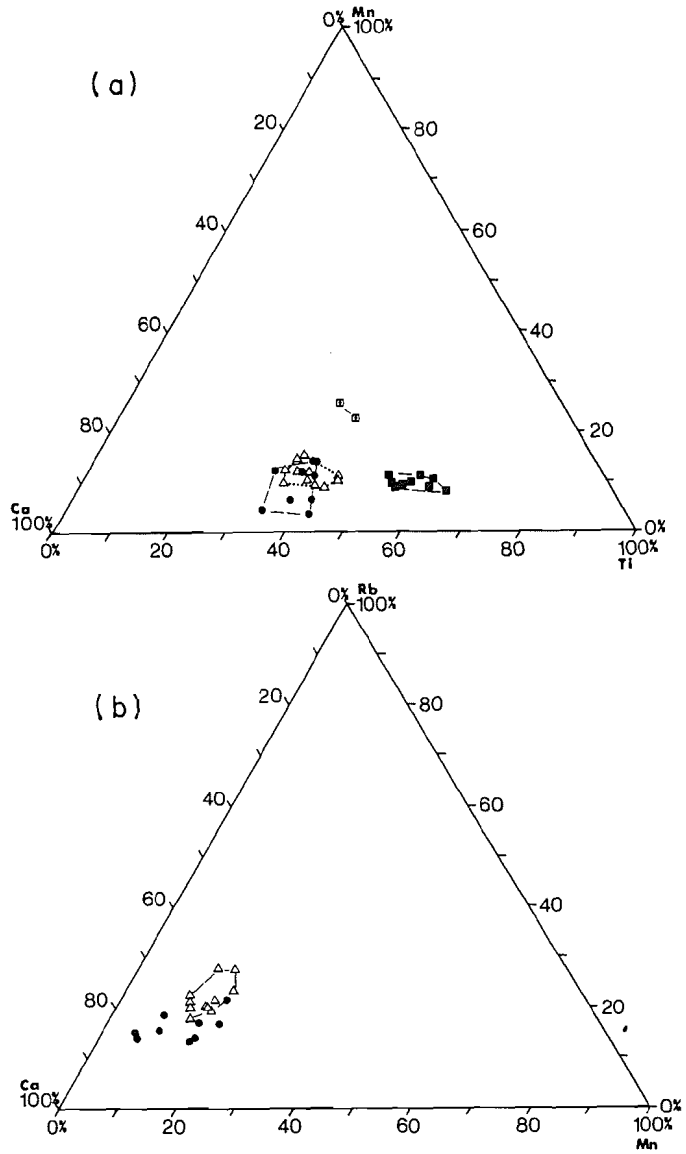

FIG. 8. (a) Similar representation as for Fig. 3(a) for Ca, Ti, and Mn for unslipped aspect of 9 Type B1 (●), 9 Type B2 (■), 11 Type B3 (△), and 2 Type B4 (⊡) sherds. Broken lines drawn for convenience only. (b) Similar representation as for Fig. 3(a) for Ca, Mn, and Rb for unslipped aspect of 9 Type B1 (●) and 11 Type B3 (△) sherds. Broken line drawn for convenience only.

the resultant omission of potentially significant clay bodies such as slips from the analysis. In a related point, the whole question of mechanical surface stripping needs critical review in terms of its validity in earthenware contexts. Unlike high temperature ceramics such as porcelains and stonewares, earthenwares are frequently permeable since they are composed of a network of pores and voids which readily permit penetration of "foreign" substances deep within the walls of the vessel. If such substances are not recognized and accounted for at the surface, the "bulk" analysis of earthenware sherds could be seriously questioned. In other words, contaminants on the surface may indicate contaminants within the paste and no amount of surface stripping will avoid the problem.

The use of normalized elemental yields rather than absolute elemental concentrations in this study will undoubtedly draw criticisms. It should be emphasized, however, that the data presentation strongly relies upon interelemental correlations expressed upon triangular plots. These plots have long been recognized as useful tools by geologists and we believe they have a similar usefulness in the presentation of multi trace element data. Both absolute and relative data can be graphically shown on such plots as a series of trivariate correlations. Such correlations may be better able to resolve trace element patterning than treating each element as an independent variable.

From an archaeological perspective, these results open many avenues of research. Firstly, they suggest that ceramic stylistic groups may be directly determined by EDXRF analysis. Secondly, they demonstrate the significance of technological variability. Most importantly, however, they suggest that a study in which archaeological, petrographic, and compositional data are combined can lead to a broader appreciation of the factors governing ceramic variability. If this is the case, there is a very

real possibility that archaeologists may be able to view ceramic variability in terms of human behaviour and manufacturing processes rather than as a series of static, stylistic configurations in space and time.

1. H. W. CATLING, A. E. BLIN-STOYLE, and E. E. RICHARDS. Archaeometry, **4**, 31 (1961).
2. H. W. CATLING. Archaeometry, **6**, 1 (1963).
3. H. W. CATLING and M. MILLETT. Archaeometry, **8**, 3 (1965).
4. H. W. CATLING and A. MILLETT. Archaeometry, **11**, 3 (1969).
5. A. MILLETT and H. W. CATLING. Archaeometry, **9**, 92 (1966).
6. I. PERLMAN AND F. ASARO. Archaeometry, **11**, 21 (1969).
7. A. B. POOLE and L. R. FINCH. Archaeometry, **14**, 79 (1972).
8. E. T. HALL, F. SCHWEIZER, and P. A. TOLLER. Archaeometry **15**, 53 (1973).
9. A. BIEBER, D. W. BROOKS, G. HARBOTTLE, and E. V. SAYRE. Archaeometry, **18**, 59 (1977).
10. W. B. STERN and J. P. DESCOEUDRES. Archaeometry, **19**, 73 (1977).
11. O. BIRGUL, M. DIKSIC, and L. YAFFE. J. Radioanal. Chem. **39**, 45 (1977).
12. O. BIRGUL, M. DIKSIC, and L. YAFFE. Archaeometry, **21**, 203 (1979).
13. J. L. JORON, M. TREUIL, and H. JAFFREZIC. J. Radioanal. Chem. **39**, 63 (1977).
14. N. SALEH, L. CARLSSON, A. B. HALLAK, and C. BENNET. Nucl. Instrum. Methods, **181**, 527 (1981).
15. B. G. TRIGGER, L. YAFFE, M. DIKSIC, J. L. GALINIER, H. MARSHALL, and J. F. PENDERGAST. Can. J. Arch. **4**, 119 (1980).
16. R. S. MACNEISH. Iroquois pottery types. Bulletin 124, National Museum of Canada, Ottawa. 1952.
17. F. L. JOCANO. Philippine prehistory. Philippine Center for Advanced Studies, Diliman, Quezon City. 1975.
18. A. O. SHEPARD. Ceramics for the archaeologists. Publication 609, Carnegie Inst. of Wash., Wash., DC. 1971.
19. O. S. RYE. Pottery technology. Manuals on Archaeology 4, Taraxacum, Wash. 1981.
20. C. K. WENTWORTH. Science, **77**. 633 (1933).
21. I. G. STUMP, J. CARRUTHERS, J. M. D'AURIA, D. A. APPLEGARTH, and A. G. F. DAVIDSON. Clin. Biochem. **10**, 234 (1977).
22. D. E. NELSON, J. M. D'AURIA, and R. B. BENNETT. Archaeometry, **17**, 85 (1975).

Can. J. Chem. Downloaded from www.nrcresearchpress.com by 210.87.254.105 on 09/06/12
For personal use only.

The decay of 56-s ^{148}Ce to levels of odd–odd ^{148}Pr

N. K. ARAS,[1] C. CHUNG, S. FALLER, C. A. STONE, AND W. B. WALTERS
Department of Chemistry, University of Maryland, College Park, MD 20742, U.S.A.

AND

R. L. GILL, M. SHMID,[2] AND R. E. CHRIEN
Physics Department, Brookhaven National Laboratory, Upton, NY 11973, U.S.A.

Received September 8, 1982

This paper is dedicated to Professor Leo Yaffe on the occasion of his 65th birthday

N. K. ARAS, C. CHUNG, S. FALLER, C. A. STONE, W. B. WALTERS, R. L. GILL, M. SHMID, and R. E. CHRIEN. Can. J. Chem. **61**, 780 (1983).

The decay of ^{148}Ce to levels of ^{148}Pr has been studied using mass-separated sources. A half-life of 56 ± 1 s has been measured for the decay of ^{148}Ce. A level scheme containing 40 γ rays and 15 excited levels is proposed for ^{148}Pr. Strongly β-fed 1^+ levels have been identified at 390 and 520 keV that are similar in position to 1^+ levels observed in isotonic ^{146}La and isotopic ^{146}Pr.

N. K. ARAS, C. CHUNG, S. FALLER, C. A. STONE, W. B. WALTERS, R. L. GILL, M. SHMID et R. E. CHRIEN. Can. J. Chem. **61**, 780 (1983).

On a étudié la désintégration du ^{148}Ce en divers niveaux de ^{148}Pr en utilisant des sources de masses séparées. On a établi que la demi-vie de la désintégration du ^{148}Ce est de 56 ± 1 s. On propose un diagramme de niveau contenant 40 rayons γ et 15 niveaux excités pour le ^{148}Pr. A 390 et à 520 keV, on a identifié des niveaux 1^+ qui sont fortement favorisés par les particules β; ces niveaux sont semblables du point de vue de la position, au niveau 1^+ observé pour le ^{146}La isotonique et le ^{146}Pr isotopique.

[Traduit par le journal]

Can. J. Chem. Downloaded from www.nrcresearchpress.com by 210.87.254.42 on 09/06/12
For personal use only.

Introduction

In a series of studies of the chemical separation and radioactive decay of neutron-rich Ce fission products (1–3), the half-lives of ^{147}Ce and ^{148}Ce were reported to be 56 and 48 s, respectively. Some difficulty was encountered, however, in assigning the observed γ rays to the correct nuclide and establishing an accurate level scheme for both ^{147}Pr and ^{148}Pr. Subsequent studies (4, 5) of the decay of ^{148}Pr have differed with respect to the ground state spin of ^{148}Pr and on the presence of isomerism in ^{148}Pr. γ-Ray intensity measurements in the $A = 148$ chain on mass separated sources have been reported recently that support the presence of two isomers in ^{148}Pr (6). In this paper, we report a study of the decay of ^{148}Ce isolated from ^{235}U fission products by the on-line mass separator TRISTAN. Forty γ rays are established in a level scheme containing 15 levels, and evidence is presented to support the proposed (5) 1^- ground state for ^{148}Pr.

Experimental procedures

The mass 148 nuclides were produced from fission in an integrated target-ion source assembly of the on-line mass separator TRISTAN located at the High Flux Beam Reactor at Brookhaven National Laboratory. The operation of the TRISTAN facility and the data collection system have been described in several recent publications (7–9) and references therein. For these experiments a high-temperature Re surface-ionization source (9) containing a graphite cloth impregnated by 5 g of 93% enriched ^{235}U was used. The flux of neutrons at the target was 1.5×10^{10} n cm^{-2} s^{-1}. The power input to the ion source ranged up to 2000 W corresponding to a maximum temperature of 2000°C.

The ion beam from the mass separator is deposited on aluminized mylar tape that can be moved from the deposit point (parent port) to secondary positions (daughter ports) at several fixed distances from the parent port. The objectives of these experiments included study of the decay of 0.6-s ^{148}Ba and the 2-min ^{148}Pr isomers, as well as a study of the decay of ^{148}Ce. To accommodate all of these objectives, the activity was accumulated at the parent port for 512 s where the growth of the activities was observed and γ–γ coincidences were measured. The activity was then moved to a daughter port 60 cm away where the decay of the various activities was followed by accumulating sixteen sequential 8192-channel spectra for 32-s time intervals each. During the 2-s transport time most of the 0.6-s ^{148}Ba activity was lost and activity from 1.0-s ^{148}La was observed only in the first of the sixteen spectra.

Three Ge detectors were employed in this study, a 5-cm^3 planar detector with a full-width-at-half-maximum (FWHM) of 480 eV at 121 keV and a low-energy cut-off below 3 keV, a cylindrical 75-cm^3 n-type Ge detector with <1.8 keV FWHM at 1.33 MeV and a low-energy cut-off of 10 keV, and a cylindrical 80-cm^3 p-type Ge detector with <1.8 keV FWHM at 1.33 MeV. The 5-cm^3 planar detector and the p-type cylindrical detectors were used to measure singles and coincidence spectra at the parent port and the n-type detector was used at the daughter port to measure the time-dependent singles spectra.

The energy values for several of the more intense γ rays in the $A = 148$ chain were determined in the high precision measurements of fission product γ-ray energies by Börner *et al.* (10) using a curved crystal spectrometer. We used the intense γ rays at 158.468 ± 0.005 and 301.702 ± 0.016 keV from ^{148}La and ^{148}Pr decay, respectively, for an internal calibration of all three detectors.

In a separate shorter experiment, the 5-cm^3 planar detector was moved to the daughter port to obtain a spectrum free from the γ rays of 0.6-s ^{148}Ba and 1.0-s ^{148}La. For this measurement, activity was collected at the parent port for 72 s and then moved to an intermediate shielded position for 10 s to allow the Ba and La to decay. The activity was then moved to the daughter port where it was counted for 72 s.

The β feeding to the low-spin isomer of ^{148}Pr was studied in a separate experiment in which the $A = 148$ chain was brought to equi-

[1]Permanent address: Department of Chemistry, Middle East Technical University, Ankara, Turkey.

[2]Present address: 11 Pinsker Street, Rehovot, Israel.

librium at the parent port using a low-temperature Ta surface ionization ion source. A spectrum of the full chain at equilibrium was taken from which the ratio of the intensity 105-keV γ ray in ^{148}Ce decay to the intensity of the 158-keV γ ray in ^{148}La decay could be used to compute the absolute intensity of the 105-keV γ ray from the known (11) decay scheme of ^{148}La to ^{148}Ce. The calculation requires the assumptions that no Ce is independently extracted (9), that there is no significant ground state branching (11) in the decay of ^{148}La to ^{148}Ce, and that there is little E2 mixing in the intense low-energy transitions that feed the ground state (12). The 105-keV γ ray is a clean peak with no known interferences from the decay of ^{148}Ba, ^{148}La, or ^{148}Pr.

Experimental results

In Fig. 1 is shown a portion of the γ-ray spectrum between 90 and 300 keV taken at the parent port during the 512-s collection period with the 5-cm^3 planar detector. In Table 1 are listed the energies, intensities, transition assignments, and major coincidences of the γ rays that are attributed to the decay of ^{148}Ce. These γ rays were identified by their half-lives in the time-dependent spectra, and/or by their presence in coincidence gates set on intense γ rays clearly associated with ^{148}Ce decay.

The energy values that we determine using the internal calibration are in agreement with those found by Börner *et al.* (10). Our best values are for intense γ rays below 200 keV that gave sizeable peaks in the high gain spectrum taken with the 5-cm^3 planar detector. Considerably larger uncertainties are associated with weak γ rays whose energy values were determined in the large detectors because of the high Compton background of the other chain members in the singles spectra or small peak areas in the coincidence spectra.

It is possible that Börner *et al.* (10) may have some assignments of close-lying doublets inverted. They assigned a 120.941 ± 0.003 keV γ ray to ^{148}Ce decay and a 121.169 ± 0.003 keV γ ray to ^{146}Ba decay. Our value of 121.21 ± 0.01 indicates that these assignments should probably be inverted. They also assign γ rays at 117.336, 190.839, 233.844, and 247.086 keV to ^{148}Ce decay that are beyond the uncertainties for their measurements and our measurements for γ rays at 116.92, 191.6, 233.7, and 247.52, respectively. As these are relatively weak γ rays in ^{148}Ce decay, the γ rays observed by Börner *et al.* (10) may be placed in other fission product nuclides or may be part of unresolved doublets or multiplets. In a more complex situation, the 247-keV γ ray that we observe is a part of a doublet with a 246.66 ± 0.06-keV γ ray from ^{148}Ba decay and the γ ray listed by Börner *et al.* (10) is a part of a doublet with a 246.736 ± 0.015-keV that is assigned to ^{132}Sn decay.

A half-life value of 56 ± 1 s was determined from the weighted average for the most intense γ rays whose decay curves are shown in Fig. 2. This value is identical to the half-life attributed to ^{147}Ce decay from the earlier chemical studies (3) and from recent studies of mass separated sources (14). In Fig. 3 is shown a small section of the sum of all 16 singles spectra taken at the daughter port showing the intense 301-keV γ ray from ^{148}Pr decay, the 324-keV γ ray from ^{148}Ce decay and the complete absence of any activity at 314.7 keV which is the most intense γ ray in the decay of 13-min ^{147}Pr (14). Thus we can be certain that the 56 ± 1 s half-life we measure for ^{148}Ce is not influenced by the presence of any mass 147 contamination.

The decay scheme

The proposed decay scheme of ^{148}Ce is shown in Fig. 4. This

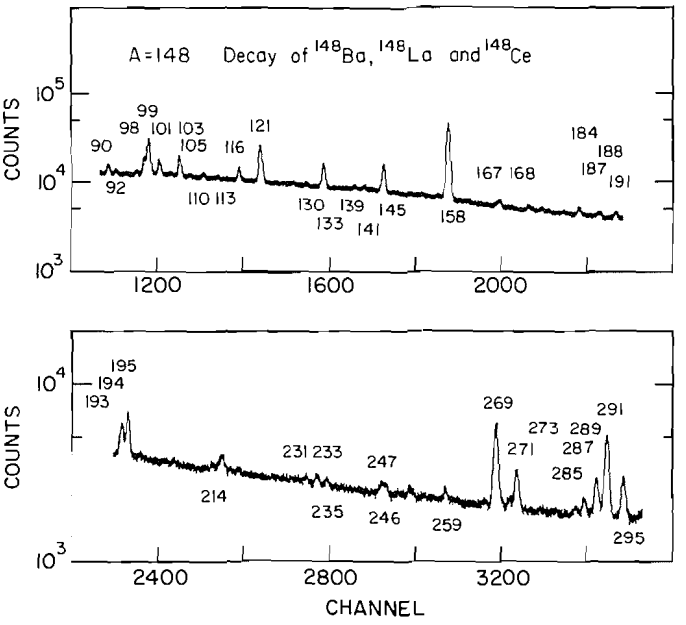

FIG. 1. γ-Ray spectrum taken at the parent port with the 5-cm^3 planar detector showing the region between 90 and 298 keV. The γ-ray energies listed above the spectrum are for ^{148}Ce γ rays and the energies below the spectrum are from ^{148}Ba or ^{148}La decay or background.

decay scheme has been constructed from the coincidence results some of which are tabulated qualitatively in Table 1. The components of the multiplet between 98 and 101 keV and 192 and 196 keV were easily resolved in the coincidence spectra with the exception of the doublet at 98 keV. As the 98 keV peak is observed in its own gate as well as in the 191- and 325-keV gates, a doublet at 98 keV must be postulated. The 101-keV gate was also important as it showed the 191- and 184-keV γ rays and the 98- and 105-keV γ rays as well as the strong 289-keV γ ray.

From the decay scheme we can immediately note that γ rays at 90, 98, 99, 105, and 121 must have conversion coefficients greater than ~0.5 to carry the γ-ray intensity feeding into the 98-, 99-, 105-, 121-, and 196-keV levels to ground. For example, the 121-keV level is fed by γ rays with intensities of at least 1127 (neglecting additional conversion electron feeding). As the intensity of the 121-keV γ ray is only 790, the total conversion coefficient, α_T, must be larger than 0.4. For a 100 keV γ ray, the E1, M1, and E2 α_T values (13) are 0.25, 1.33, and 2.14, respectively. We can thus conclude that the six levels below 200 keV have the same parity and are connected by M1, E2, or M1/E2 mixed transitions.

The strong β feeding of the levels at 390 and 520 keV marks these levels as 0^+ or 1^+ levels. The systematic trends of the odd–odd Pr levels are shown in Fig. 5. These trends and the current (14) spin and parity assignments for ^{147}Ce and ^{147}Pr both indicate negative parity for the low-lying levels of ^{148}Pr. We have thus computed the β-branching and log *ft* values from γ-ray imbalances deduced from the differences between γ-ray and conversion-electron intensities feeding out of and into each level. The conversion-electron intensities have been computed by assuming E1 multipolarity for the transitions out of levels above 380 keV, M1 multipolarity for the γ rays out of the levels below 380 keV, and E2 multipolarity for the 98.0-keV transition to ground that will be described later. The predominance

Can. J. Chem. Downloaded from www.nrcresearchpress.com by 210.87.254.42 on 09/06/12
For personal use only.

TABLE 1. Energies, intensities, placements, and coincidences of γ rays following the β^- decay of ^{148}Ce to levels of ^{148}Pr

γ-ray energy (keV)					Placement[c]		Coincidences[f]				
Börner *et al.*[a]	Present work	I_γ	α_T(M1)	I_{tot}[b]	From	To	98	99	105	121	196
	74.5(5)[d]	8(4)[d]	3.3	34	196	121				W	
	90.89(3)	123(7)	1.8	340	196	105			S		
98.166(3)	98.0(1)	93(5)	2.3(E2)	310	98	G.S.	S				
	98.0(1)	77(5)	1.4	190	196	98	S				
	98.99(3)	742(40)	1.4	1780	99	G.S.					
101.029(4)	101.04(3)	215(11)	0.24(E1)	270	390	289	S		S		
	103.2(1)	15(15)	0.24(E1)	19	390	287		S			
105.200(30)	105.20(3)	314(15)	1.2	690	105	G.S.					
117.336(7)[e]	116.92(3)	225(12)	0.18(E1)	270	390	273			W		
121.169(3)	121.21(3)	790(38)	0.77	1400	121	G.S.					
	167.8(2)	66(7)	0.27(E1)	70	520	352					
	168.52(4)	20(3)	0.27	25	273	105			M		
	184.53(4)	99(5)	0.22	120	289	105			S		
	187.9(2)	90(5)	0.04(E1)	94	520	332					
	188.5(3)	69(7)	0.20	83	287	99		S			
190.839(6)[e]	191.6(1)	99(6)	0.19	120	289	98	S				
	193.8(2)	20(4)	0.04(E1)	21	468	273			W		
	194.69(5)	240(3)	0.04(E1)	250	390	196			S		S
195.977(14)	195.96(4)	390(20)	0.18	460	196	G.S.					
	231.6(2)	20(4)	0.12	22	352	121				S	
233.844(13)[e]	233.71(5)	60(6)	0.03(E1)	62	520	287					
247.086(25)[e]	247.52(9)	56(6)	0.088	61	352	105			M		
269.519(45)	269.49(5)	1018(51)	0.017(E1)	1035	390	121				S	
	271.5(2)	40(6)	0.017(E1)	41	468	196	S		W		S
	273.77(5)	326(16)	0.072	350	273	G.S.					
	285.5(1)	48(5)	0.015(E1)	50	390	105			S		
	287.17(10)	110(10)	0.064	117	287	G.S.					
	289.64(6)	340(20)	0.062	360	289	G.S.					
291.724(17)	291.67(3)	≡1000(50)[g]	0.014(E1)	1010	390	99		S			
	324.85(5)	453(20)	0.01(E1)	457	520	196	S		S	W	S
	332.7(1)	90(9)	0.045	94	332	G.S.					
	346.3(2)	35(4)	0.01(E1)	35	468	121				S	
	352.4(2)	106(12)	0.04	110	352	G.S.					
	369.09(12)	97(13)		97	468	99		S			
	375.0(2)	41(9)		42	765	390					
	390.79(16)	79(14)		79	390	G.S.					
	399.43(19)	46(12)		46	520	121				S	
421.778(62)	421.68(5)	218(11)		218	520	99		S			
	478.17(12)	80(12)		80	765	287		W			
	521.2(2)	41(9)		41	626	105			W		

[a]These data are taken from the curved crystal studies of gross fission product γ-ray decay by Börner *et al.* (10).

[b]The total intensities were computed by assuming pure M1 multipolarity except where noted. Conversion coefficients were interpolated from the data of Rosel *et al.* (13).

[c]As elsewhere in this paper γ rays and level energies in keV are referred to without the decimal and digits beyond the decimal except for the 98.99-keV γ ray which is referred to as 99.

[d]The parentheses contain the uncertainties of the last digits of the numbers to which they are attached.

[e]These γ rays observed by Börner *et al.* (10) may not be the same as we observe in this work.

[f]Qualitative indication of coincidence strength: S = strong, M = medium, W = weak.

[g]Absolute γ-ray intensities per 100 decays may be computed by multiplying the relative intensities by 0.0167.

of M1 transitions in the odd–odd $N = 83$ isotones has been discussed extensively by Macphail and Summers-Gill (12) as a part of their study of ^{144}Pm levels. A Q_β value of 2050 keV has been taken from the studies of Stippler *et al.* (17). A ground state β branch of (4 ± 5)% has been determined from the ratio of γ-ray peaks at 105 and 158 keV in the experiment with the Ta ion source. Because of the uncertainties associated with the possibility of significant E2 mixing in the low-energy γ rays and unobserved weak transitions from higher-lying levels obscured by the other mass 148 activities, β branches with less than 2% intensity have not been shown in Fig. 4 and an upper limit of 9% is shown for the ground state β branch.

Spin and parity assignments

The 390-keV 0^+ or 1^+ level feeds eight of the nine levels below 300 keV that appear to have negative parity. If the 390-keV level were to be a 0^+ level, all eight of these levels would have 1^- spin and parity, as a 0^+ to 0^- γ transition is not possible and a 0^+ to 2^- M2 transition would be highly hindered. As the systematic trends indicate the possibility of both 0^- and 2^- levels near the ground state, the 0^+ assignment for the 390-keV level is quite unlikely. A similar but weaker argument can be made for the level at 520 keV. The 99-, 121-, 196-, 289-, and 352-keV levels show significant γ-ray intensity imbalance that we attribute to β feeding, and are limited to spin

Can. J. Chem. Downloaded from www.nrcresearchpress.com by 210.87.254.42 on 09/06/12
For personal use only.

Can. J. Chem. Downloaded from www.nrcresearchpress.com by 210.87.254.42 on 09/06/12
For personal use only.

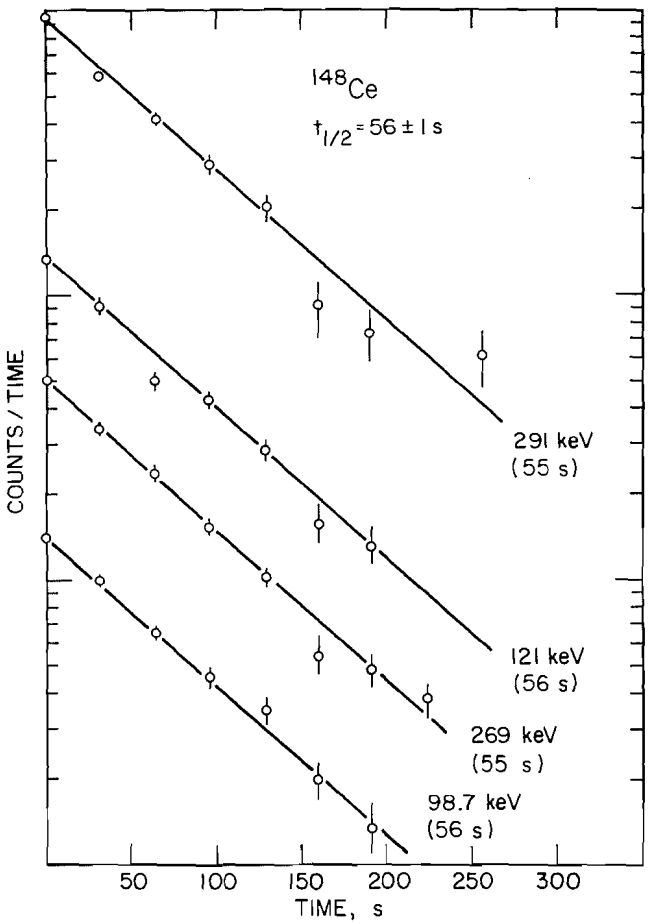

FIG. 2. Decay curves for four intense ^{148}Cc γ rays. The 98.7-keV peak is a combination of the peaks at 98 and 99 keV.

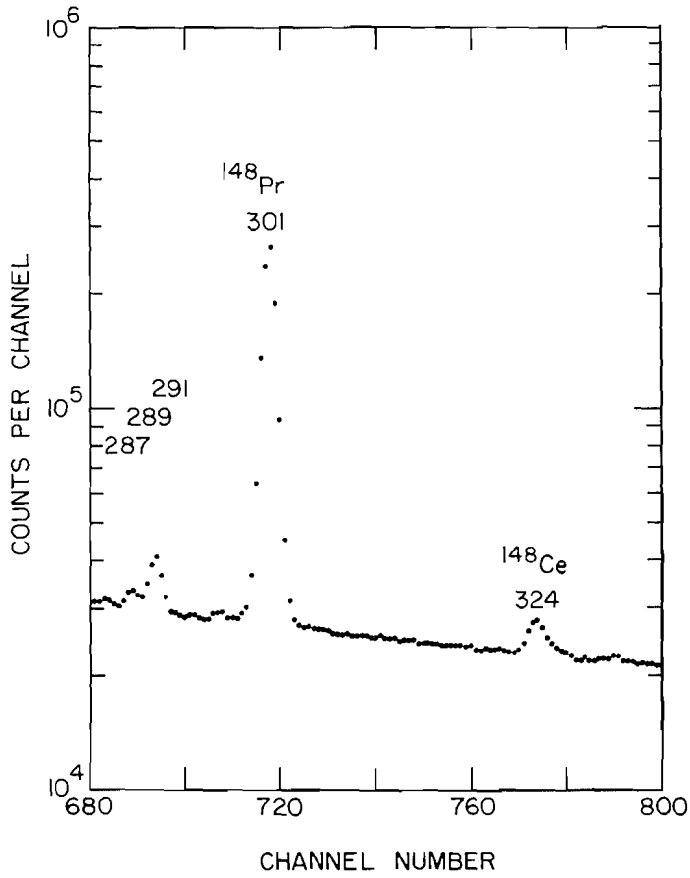

FIG. 3. γ-Ray spectrum taken at the daughter port with the n-type Ge detector of sources collected for 512 s and counted for 512 s showing the γ rays between 300 and 325 keV.

and parity of 0^- or 1^-.

The 98-keV level is the only level below 300 keV that could be a 3^- level as it is the only level below 300 keV that is not fed by the 1^+ level at 390 keV. The gates on the 184- and 191-keV γ rays are shown in Fig. 6. These two γ rays have equal intensities and depopulate the 289-keV level. As the total intensity out of this level is 600 units, gates on these γ rays should each show 99/600 of the 215 intensity units of the 101-keV γ ray that feeds into the 289-keV level. Thus, the 101-keV peak in these spectra should be approximately equal and represent γ rays with 36 units of intensity. The 98- and 105-keV γ rays should reflect the 99 intensity units of the gating γ ray but be reduced by the fraction of the transition that undergoes electron conversion. For the 105-keV transition for which a theoretical M1 or α_T of 1.17 may be calculated, the γ intensity should be 45.6. Thus, the calculated ratio of the peak intensities for the 101- and 105-keV γ rays in the 184-keV gate should be 0.78 ± 0.03 which compares with the observed ratio of those intensities of 0.85 ± 0.07.

It may be seen that the 98-keV peak in the 191-keV gate is smaller than the 101-keV peak. As the detector efficiency varies little from 98 to 105 keV, either the conversion coefficient is higher or another transition depopulates this level. If we use the observed ratio of peak intensities of 0.76 ± 0.06 for the 98- and 101-keV peaks to compute an α_T for the 98-keV transition, a value of 2.6 ± 0.3 is obtained. As the α_T for a 98-keV E2 transition is 2.31, the 98-keV transition to the ground state can be assigned E2 multipolarity.

Discussion

The studies by Ikeda *et al.* (5) that indicated the presence of isomerism in ^{148}Pr suggested $1^{\pm}$ for the spin and parity of the low-spin ^{148}Pr isomer and $4^{\pm}$ for the high spin isomer. Our data could accommodate 0^-, 1^-, or 2^- for the spin and parity of the low-spin isomer. The strong β feeding to the 2^+ level in ^{148}Nd reported by Taylor and Singh (4) and by Ikeda *et al.* (5) rules out the 0^- possibility. As the 98-keV level is fed by the levels at 196 and 289 keV whose spins and parities are limited to 0^- or 1^- by the β feeding from 0^+ ^{148}Ce, an upper limit of 3^- for the spin and parity of the 98-keV level can be established. In view of the E2 character of the 98-keV transition to the ground state, 1^- is the favored choice for the ground state spin and parity of ^{148}Pr, although 2^- cannot be totally excluded. The single-particle half-lives for the 100-keV M2, E3, and M3 transitions are 10 μs, 1 s, and 60 s, respectively. These half-lives indicate that a 4^- 2-min isomer must be below 100 MeV in order to show the sizeable β branching observed by Ikeda *et al.* (5) or that any isomer with a 2-min half-life lying above the (3^-) level at 98 keV would require spin of ≥ 6.

We have searched for evidence of any γ-branching from low-lying levels into any such isomer. In the decay of ^{144}Ba, ~15% of the decay cascades through a single strong E2 transition from a 2^- level into a possible 4^- level at 16 keV (8). We have not observed any low-energy γ rays in the coincidence spectra gated on γ rays that feed the levels at 98, 99, 105, 121, 196, 273, 289, or 332 keV.

The systematic level structure of the low-lying levels of the

Can. J. Chem. Downloaded from www.nrcresearchpress.com by 210.87.254.42 on 09/06/12
For personal use only.

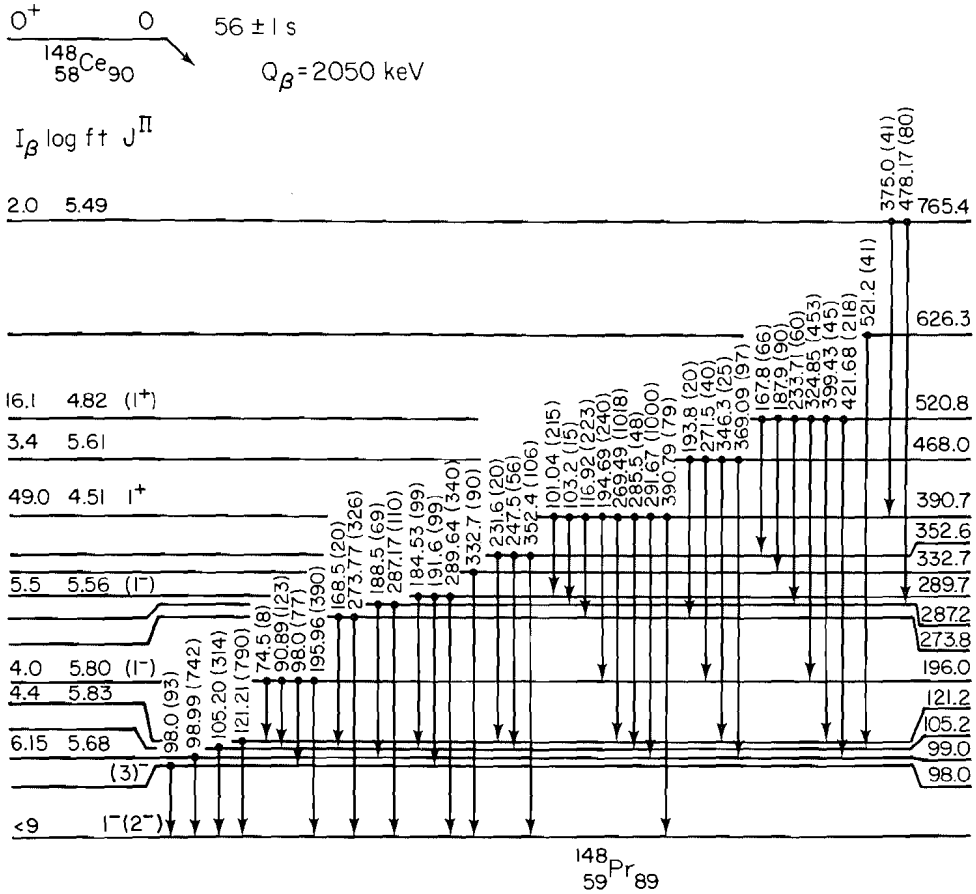

FIG. 4. Decay scheme of ^{148}Ce to levels of ^{148}Pr.

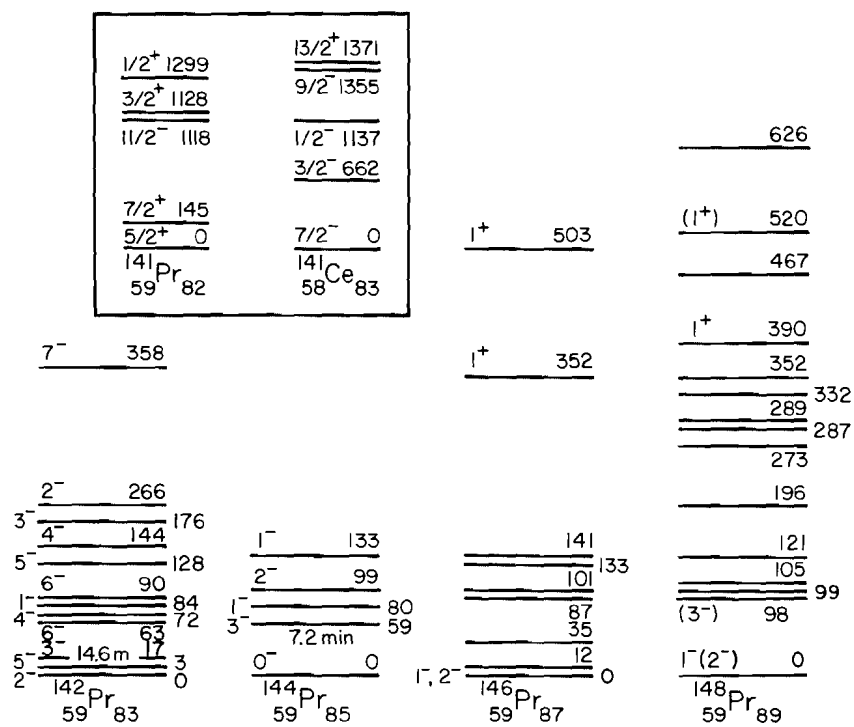

FIG. 5. Low-lying levels of odd–odd ^{142}Pr, ^{144}Pr, ^{146}Pr, and ^{148}Pr along with the single particle levels in ^{141}Pr and ^{141}Ce. The data are taken from refs. 15 and 16.

odd–odd Pr nuclides is consistent with the single particle structures shown in the inset in Fig. 5. The odd proton in $g_{7/2}$ or $d_{5/2}$ positive parity orbitals and the odd neutron in $f_{7/2}$ or $p_{3/2}$ negative parity orbitals combine to give low-lying negative parity

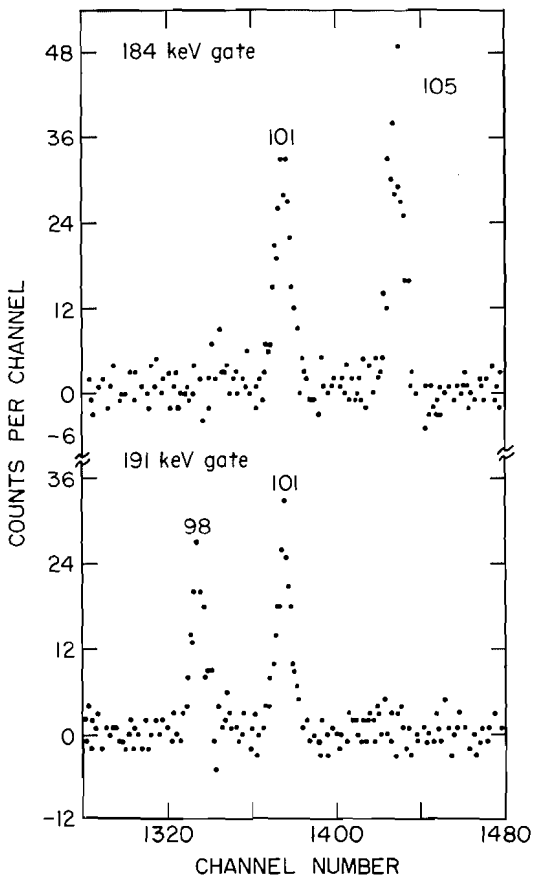

FIG. 6. Portions of the coincidence spectra gated on the 184- and 191-keV γ rays.

multiplets. The presence of low-lying 1^+ states in both ^{146}Pr and ^{148}Pr is not easily attributed to single-particle proton and neutron configurations. Only one such configuration, the $\pi_{h11/2}\nu_{h9/2}$ combination is possible and it should lie at higher energy. More likely is a configuration involving the $f_{7/2}$ or $p_{3/2}$ neutron, the $h_{11/2}$ proton and core excitation. As low-lying negative parity states with spins ranging from 3/2 to 15/2 are known (18) below 600 keV in $^{149}_{61}Pm_{88}$ these states could couple with the odd neutron in a negative parity orbital to give rise to low-lying positive parity states.

In summary, our study of the decay of ^{148}Ce to levels of ^{148}Pr has accounted for the earlier difficulties in assigning γ rays to ^{147}Ce and ^{148}Ce decay. We have shown that ^{148}Ce has a 56 ± 1 s half-life that is undistinguishable from the 55 ± 1 s half-life determined (14) for ^{147}Ce. Moreover, important γ rays near 90, 117, 198, 269, and 284 keV are found in mass-separated sources of both nuclides. The observed low-lying level structure is seen to be analogous to the structure of ^{146}Pr. No direct observation of the high-spin isomer proposed by Ikeda *et al.* (5) has been observed, but its position must lie below 100 keV if it is a 4^- isomer. The 3^- ground state proposed by Taylor and Singh (4) is ruled out by the presence of a 390-keV γ ray from the 1^+ level at 390 keV to the ground state.

Acknowledgements

The authors wish to express their appreciation for the support of this work by the U.S. Department of Energy. The non-BNL authors also wish to acknowledge the continued hospitality of the Physics Department at BNL and the interest in these studies by Dr. R. F. Casten and the members of the Neutron Nuclear Physics Group.

1. P. O. ARONSSON, G. SKARNEMARK, E. KVALE, and M. SKARESTAD. Inorg. Nucl. Chem. Lett. **10**, 753 (1974).
2. P. O. ARONSSON, G. SKARNEMARK, and M. SKARESTAD. J. Inorg. Nucl. Chem. **36**, 1689 (1974).
3. T. BJORNSTAD, E. KVALE, G. SKARNEMARK, and P.O. ARONSSON. J. Inorg. Nucl. Chem. **39**, 1929 (1977).
4. H. W. TAYLOR and B. SINGH. J. Phys. G**5**, 1445 (1979).
5. Y. IKEDA, H. YAMAMOTO, K. KAWADE, T. TAKEUCHI, T. KATOH, and T. NAGAHARA. J. Phys. Soc. Jpn. **47**, 1039 (1979).
6. G. GOWDY, R. E. CHRIEN, Y. Y. CHU, R. L. GILL, H.-I. LIOU, M. SHMID, M. L. STELTS, D. S. BRENNER, T. YEH, K. SISTEMICH, H. YAMAMOTO, C. CHUNG, and W. B. WALTERS. Bull. Am. Phys. Soc. **26**, 552 (1981).
7. R. L. GILL, M. L. STELTS, R. E. CHRIEN, V. MANZELLA, H.-I. LIOU, and S. SHOSTAK. Nucl. Inst. Meth. **186**, 243 (1981).
8. C. CHUNG, W. B. WALTERS, R. GILL, M. SHMID, R. E. CHRIEN, and D. S. BRENNER. Phys. Rev. C**26**, 1198 (1982).
9. M. SHMID, R. L. GILL, and C. CHUNG. Nucl. Inst. Meth. In press.
10. H. BÖRNER, W. F. DAVIDSON, J. ALMEIDA, J. BLACHOT, J. A. PINSTON, and P. H. M. VAN ASSCHE. Nucl. Inst. Meth. **164**, 579 (1979).
11. R. L. GILL, M. SHMID, A. WOLF, R. E. CHRIEN, Y. Y. CHU, D. S. BRENNER, K. SISTEMICH, F. K. WOHN, H. YAMAMOTO, C. CHUNG, and W. B. WALTERS. Phys. Rev. C. In press.
12. M. R. MACPHAIL and R. G. SUMMERS-GILL. Nucl. Phys. A**263**, 12 (1976).
13. F. ROSEL, H. M. FRIES, K. ALDER, and H. C. PAULI. At. Data Nucl. Data Tables, **21**, 236 (1978).
14. F. SCHUSSLER, B. PFEIFFER, H. LAWIN, E. MONNAND, J. MUNZEL, J. A. PINSTON, and K. SISTEMICH. Proc. 4th Int. Conf. on Nuclides Far from Stability, CERN, 81-09, 1981. p. 589.
15. C. M. LEDERER and V. S. SHIRLEY (*Editors*). Table of isotopes. McGraw Hill, New York. 1977.
16. H. YAMAMOTO, Y. IKEDA, K. KAWADE, T. KATOH, and T. NAGAHARA. J. Inorg. Nucl. Chem. **42**, 1539 (1980).
17. R. STIPPLER, F. MUNNICH, H. SCHRADER, K. HAWERKAMP, R. DECKER, B. PFEIFFER, H. WOLLNICK, E. MONNAND, and F. SCHUSSLER. Z. Physik A, **285**, 287 (1978).
18. E. W. SCHNEIDER, M. D. GLASCOCK, W. B. WALTERS, and R. A. MEYER. Z. Physik A**291**, 77 (1979).

Can. J. Chem. Downloaded from www.nrcresearchpress.com by 210.87.254.42 on 09/06/12
For personal use only.

Mass spectrometric determination of Rb fission yields from ^{3}He and ^{4}He induced fission of ^{238}U and ^{232}Th[1]

P. L. REEDER

Pacific Northwest Laboratory, Richland, WA 99352, U.S.A.

Received July 15, 1982

This paper is dedicated to Professor Leo Yaffe on the occasion of his 65th birthday

P. L. REEDER. Can. J. Chem. **61**, 786 (1983).

Cumulative and independent fission yields of Rb isotopes have been measured for ^{3}He and ^{4}He induced fission of ^{232}Th and ^{238}U at bombarding energies slightly above the Coulomb barriers. The on-line mass spectrometric technique provided yields for masses 89–97. Mean masses and widths of the Rb independent yield distributions were obtained and were compared to other fissioning systems with excitation energies up to 160 MeV.

P. L. REEDER. Can. J. Chem. **61**, 786 (1983).

On a mesuré les rendements en isotopes de Rb résultant de fissions cumulatives et indépendantes lors de la fission du ^{232}Th et du ^{238}U induite par ^{3}He et ^{4}He à des énergies de bombardement légèrement supérieures aux barrières de Coulomb. La technique de spectrométrie de masse à canal unique fournit des rendements pour des masses de 89 à 97. On a déterminé les masses moyennes et les largeurs des distributions de rendement indépendantes du Rb et on a comparé ces valeurs à celles obtenues avec d'autres systèmes de fission ayant des énergies d'excitation allant jusqu'à 160 MeV.

[Traduit par le journal]

Introduction

The fission of ^{238}U and ^{232}Th by moderate energy helium ions (20–60 MeV) has been studied previously by both radiochemical (1–6) and mass spectrometric techniques (7, 8), to determine cumulative and independent yields of various fission products. Cumulative yields of fission products at or near stability are used to determine the mass–yield curves whereas independent yields are used to determine charge distributions. The particular example of $^4\text{He} + {}^{232}\text{Th} \rightarrow {}^{236}\text{U}$ gives the same compound nucleus as $n_{th} + {}^{235}\text{U} \rightarrow {}^{236}\text{U}$. Hence comparisons of mass and charge distributions can be made as a function of excitation energy for this system. As the excitation energy increases symmetric fission becomes prominent, thus changing the shape of the mass–yield curve. Likewise the most probable charge (Z_p) of a given isobaric mass chain shifts toward stability. This shift is more rapid for isobaric chains in the heavy mass peak than for chains in the light mass peak (8–10). These results along with studies of neutron emission and fission energetics (11) show that the excitation energies of heavy fragments increase more rapidly than the excitation energies of light fragments as the bombarding energy increases. McHugh and Michel (8) have shown that there is no change in the width of the charge distributions up to 39 MeV excitation in ^{236}U whereas other work with proton induced fission from 20–85 MeV does show an increase in the width of the charge distribution (10, 12).

The previous studies of helium ion induced fission have measured yields of relatively long-lived or stable nuclides. In the present work we have measured fission yields for very neutron-rich Rb isotopes with half-lives as short as 0.17 s by use of "on-line" mass spectrometry. "On-line" mass spectrometry was developed for the study of short-lived isotopes of the alkali metals (13–15). Production cross sections for isotopes of Rb and Cs have been measured by this technique for U, Th, and Ta targets bombarded with protons (10, 16–18). Independent fission yields of Rb and Cs isotopes have been measured for thermal neutron fission of ^{235}U (16, 19–21) fast neutron fission of ^{238}U (22), and thermal neutron fission of ^{239}Pu (23).

The work reported here used the "on-line" technique to measure cumulative and independent yields of Rb isotopes from fission of ^{238}U and ^{232}Th by ^{3}He and ^{4}He ions at energies slightly above the Coulomb barrier. The excitation energies are thus intermediate between thermal neutron induced fission and fission with moderate energy protons. The independent yields were analyzed for the mean mass and width of the distributions to determine how these parameters vary with composition of the fissioning system and with excitation energy.

Experimental

The technique of on-line mass spectrometry involves placing a suitable target in the ion source of a mass spectrometer and bombarding the target with projectiles from an accelerator or reactor. Nuclear reaction products diffuse out of a graphite matrix and are ionized by surface ionization on a hot tantalum surface.

At Washington University, St. Louis, a small (15-cm radius, 60 degree magnetic sector) mass spectrometer was installed at the end of an external beam pipe at the 54-in sector-focused cyclotron.[2] The target consisted of ^{238}U or ^{232}Th powder (10 μm size) intimately mixed with graphite powder and pressed into a small block about 100 mg/cm^2 thick. The ratio of metal-to-graphite was 4-to-1 by weight. At 32-MeV, a ^{3}He beam intensity of 1 μA gave a typical ^{91}Rb counting rate of about 15 000 ions/s. The peak-to-valley ratio between equally-abundant adjacent masses was about 4 for Rb fission products. Although Cs fission products were seen with comparable counting rates, the resolution of this small instrument was not sufficient to give reliable yield measurements for Cs.

The maximum energy ^{3}He beam from the cyclotron was 34 MeV. However, the beam had to pass through a 0.010-mm stainless steel foil

[1]Research at Washington University supported by USAEC contract AT(11-1)-1608 and at Pacific Northwest Laboratory by DOE contract DE-AC06-76RLO.

[2]The mass spectrometer was obtained from Dr. R. Bernas, Orsay, and was originally used by Dr. R. Klapisch for on-line studies of Li isotopes (see ref. 24).

Can. J. Chem. Downloaded from www.nrcresearchpress.com by 210.87.254.40 on 09/06/12
For personal use only.

TABLE 1. Summary of diffusion studies of Rb isotopes from a uranium plus graphite target at 1600°C

Mass	Radioactive half-life (s)	Beam pulse (s)	Diffusion components: Half-times[a] (s) 1	2	3	Relative abundance 1	2	3
89	900	0.4	0.13±0.02	0.52±0.02	69±11	0.38	0.22	0.40
89	900	1.0	0.10±0.01	0.48±0.02	64±11	0.35	0.25	0.40
92	4.4	0.4	0.12±0.01	0.61±0.02	11.9±0.6	0.62	0.24	0.14
92	4.4	1.0	0.12±0.01	0.53±0.01	5.2±0.1	0.59	0.25	0.16
94	2.7	0.4	0.10±0.01	0.49±0.02	29±3	0.58	0.27	0.15
94	2.7	1.0	0.11±0.01	0.49±0.01	15±1	0.57	0.29	0.14
Adopted diffusion components			0.12	0.61		0.69	0.31	

[a] Uncorrected for radioactive half-life.

separating the cyclotron vacuum from the mass spectrometer vacuum and a 0.013-mm tantalum foil surrounding the target. These foils reduced the beam energy by about 2 MeV. Because of the thick targets, fission could occur at all energies down to the Coulomb barrier. Thus a weighted average energy was calculated based on the known excitation functions for ^{3}He and ^{4}He induced fission of ^{238}U (25–27). The excitation function for ^{3}He + ^{232}Th was not known so the weighted average energy was assumed to be the same as for ^{3}He + ^{238}U at the same bombarding energy.

A critical factor in the measurement of relative yields of different isotopes is the diffusion time of the radioactive isotopes out of the target matrix. Diffusion can be described by the sum of several exponentially decaying components. Up to five components were resolved from the diffusion curves of Chaumont (16).

Diffusion times of three different Rb isotopes were measured for 34 MeV ^{3}He on ^{238}U under the conditions of the experiments here. The accelerating voltage and magnetic field were adjusted to give the desired mass. The cyclotron beam was switched on for a short time interval (0.4 or 1.0 s). A 200 channel multiscaler was switched on simultaneously with the beam-on signal and ion pulses as a function of time were stored for 8 s. Thus the growth and disappearance of ions could be recorded using the same length of beam pulse as in the independent yield measurements described below. Cycles were repeated until sufficient numbers of counts were obtained. The disappearance curves were resolved by a least-squares computer program. Good fits were obtained with just three components. The resulting "half-times" and abundances are shown in Table 1.

The half-times of the two shortest components were corrected for the radioactive decay half-lives and were averaged to obtain the diffusion half-times of 0.12 and 0.61 s. The longest-lived component varies for different isotopes and different bombardment times. It is probably due to a combination of a constant background plus a background which changes due to beam heating. The counting rates of stable Rb and Sr isotopes increased significantly when the beam was switched on. The large abundance and long half-time for the third component at mass 89 may be due to interference from stable ^{88}Sr or decay of ^{89}Kr.

Cumulative yields

The relative cumulative yields of Rb isotopes were measured by scanning the mass spectrum rapidly while the cyclotron beam was on continuously. The mass spectrum was scanned by holding the magnetic field constant and imposing a triangular waveform to the accelerating voltage at a repetition rate of 25 cycles/s. Sweep up and sweep down mass spectra were stored separately in 100 channel segments of a multiscaler. The Rb fission product mass region was covered in two separate runs, one for masses 88–96 and the other for masses 91–99. After each run was a 15 min delay before measuring the background mass spectra. This delay allowed long-lived isotopes to diffuse out of the target. These background spectra had to be normalized to the beam-on spectra since beam heating increased the counting rate of stable isotopes. Normalizations were performed at mass 88 or mass 98 for the two separate runs. The beam-on data were corrected for background, overlap from adjacent peaks (about 5%), saturation factor, loss due to radioactive decay, and loss due to diffusion of Kr precursors.

The saturation factor corrected for those isotopes whose half-lives were an appreciable fraction of the total run time. The maximum corrections were 40% for mass 89 and 2% for mass 90 for a run with 34 MeV ^{3}He on a ^{238}U target.

The correction for radioactive decay requires knowledge of the diffusion components as described above. If there were a single diffusion component, the observed yield would be equal to the true yield times the fraction of Rb ions which diffuse before decaying.

For multiple diffusion components the relationship becomes

$$[1] \quad Y_{obs} = Y_{true} \sum_i A_i \left(\frac{t}{t + t_D^i}\right)$$

where Y_{obs} = observed yield, Y_{true} = true yield, t = radioactive half-life, t_D^i = half-time of i-th diffusion component, A_i = abundance of i-th diffusion component.

Since the longest of the three diffusion components measured here did not correspond to actual diffusion of Rb, only the two shortest diffusion components were used in calculating this correction. This correction amounted to a few percent for masses 92–94 but increased to a factor of 2.15 for mass 97 where the radioactive half-life is only 0.17 s.

In order for the yields measured in these experiments to be truly cumulative, it is necessary that there be no loss of Br and Kr precursors due to diffusion. It is possible to measure the diffusion time of Kr by observing the disappearance curves of Rb isotopes for several minutes after the accelerator beam is shut off. The Rb isotopes with short-lived Kr precursors disappear immediately, indicating that there are no Rb diffusion components with half-times greater than a few seconds. However, ^{89}Rb which has a 3.1 min ^{89}Kr precursor persists in the mass specta for several minutes after the beam is turned off. The observed half-time for ^{89}Rb is about 70 s which is a combination of the 186 s radioactive half-life of ^{89}Kr and a 112 s diffusion half-life of Kr. Similar observations were made on Cs isotopes where ^{135}Cs and ^{137}Cs were seen to persist long after the beam was shut off. (Diffusion times of about an hour were

Can. J. Chem. Downloaded from www.nrcresearchpress.com by 210.87.254.40 on 09/06/12
For personal use only.

TABLE 2. Relative cumulative yields of Rb isotopes[a,b]

Mass	Target Projectile Energy[c] (MeV)	^{235}U n Thermal[d]	^{238}U ^{3}He $25.3^{+2.7}_{-3.6}$	^{238}U ^{3}He $28.1^{+3.9}_{-6.4}$	^{238}U ^{4}He $-25.5^{+2.0}_{-4.2}$	^{232}Th ^{3}He $-28.1^{+3.9}_{-6.7}$[e]
89		0.83	1.48±0.2 (2)	0.96±0.04 (2)	0.90±0.02 (2)	0.30±0.06 (4)
90		1.00	1.00±0.05 (2)	1.00±0.04 (2)	0.96±0.03 (2)	1.00±0.03 (4)
91		0.98	0.93 (2)	0.91±0.02 (2)	1.00±0.05 (2)	0.93 (8)
92		0.83	0.77±0.01 (2)	0.71 (4)	0.82 (4)	0.74±0.02 (8)
93		0.61	0.62±0.01 (2)	0.55±0.01 (4)	0.71±0.04 (4)	0.47±0.02 (8)
94		0.29	0.35±0.01 (2)	0.28±0.01 (4)	0.32±0.03 (4)	0.31±0.01 (8)
95		0.14	0.26±0.05 (2)	0.15±0.02 (4)	0.15±0.01 (4)	0.18±0.03 (8)
96		0.030		0.047±0.007 (2)	0.08±0.04 (2)	
97		0.007		0.012±0.006 (2)		

[a] Numbers in parentheses are the number of determinations.
[b] Uncertainties are based only on the standard deviation of the mean values. Values with no uncertainty were used to normalize different runs.
[c] Weighted average energy of bombarding projectile (see text — Experimental). Energy range is from maximum energy down to Coulomb barrier.
[d] Reference 28.
[e] Average energy assumed equal to value for ^{238}U target for equal incident energy (see text — Experimental).

indicated for Xe.) If there were Kr diffusion components with half-times shorter than the observed 112 s component, the corrections for precursor loss described below would be too small. However, previous studies concerning the diffusion of Kr and Xe under similar target conditions had no evidence for any shorter-lived diffusion components (16, 21). Any longer-lived Kr diffusion component would have little effect since the Kr nuclides of interest would decay before diffusing and thus contribute to the Rb cumulative yield in the normal manner.

Although there is no information on the diffusion times of Br under the conditions used here, the half-lives are considerably shorter — the longest one of interest being 4.5 s for ^{89}Br. Also the contributions of Br isotopes to the cumulative yield of Rb isotopes are no more than 25% for mass 89 and 11% for mass 90. These estimates are based on recommended fission yields for n_{th} + ^{235}U (28). The actual contribution of Br is less for ^{3}He and ^{4}He induced fission because the independent yield distributions for these cases are shifted toward the line of stability as will be discussed below.

With the assumptions that no Br was lost by diffusion and that all the Kr diffuses with a 112 s half-time, the correction for precursor loss by diffusion is given by the expression

$$[2] \quad Y_{obs} = Y_{true}\left(\frac{(CY_{Kr})(F) + (IY_{Rb})}{(CY_{Rb})}\right)$$

where Y_{obs} = observed yield, Y_{true} = true yield, CY_{Kr} = cumulative yield of Kr, CY_{Rb} = cumulative yield of Rb, IY_{Rb} = independent yield of Rb, and F = fraction of Kr which decays before diffusing. The fraction F is estimated from the diffusion time (t_D) and half-life (t) of the Kr isotope according to the expression

$$[3] \quad F = \frac{t_D}{t + t_D}$$

To make this correction, it is necessary to know the isobaric distribution at each mass number. From the work of McHugh and Michel (8), one can estimate independent and cumulative yields for He ion induced fission at these excitation energies using the assumption of a Gaussian charge distribution curve with a constant width parameter. The correction for precursor loss by diffusion raised the mass 89 yield by about 45% and the mass 90 yield by 17% relative to the most neutron-rich isotopes.

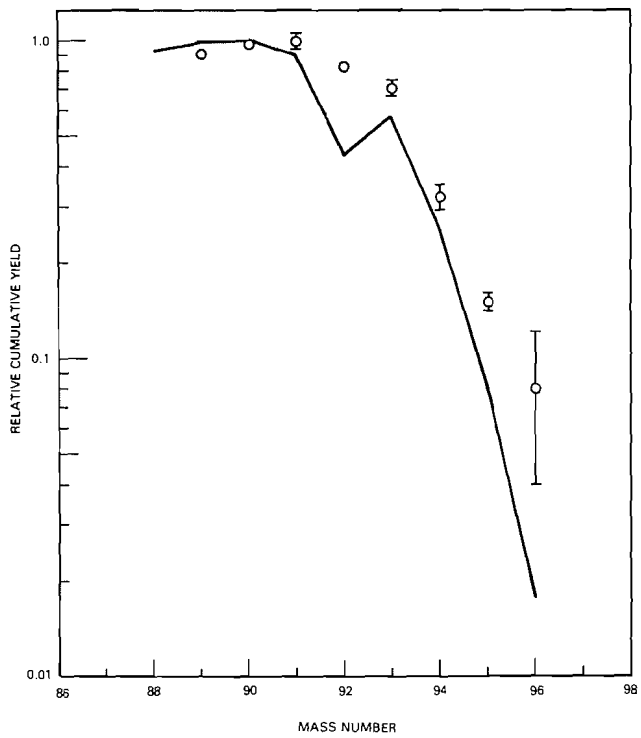

FIG. 1. Relative cumulative yields of Rb isotopes for two fissioning systems with same E^* (20 MeV) and different N/Z. ○, 25.5 MeV ^{4}He + ^{238}U (N/Z = 1.574); —, 14 MeV n + ^{239}Pu (N/Z = 1.553) (recommended yields from ref. 28).

The relative cumulative yields for mass spectra obtained with increasing and decreasing accelerating voltage were calculated separately and were considered as independent determinations. Different runs were normalized to a common isotope. The results were averaged and normalized to 1.00 for the

Can. J. Chem. Downloaded from www.nrcresearchpress.com by 210.87.254.40 on 09/06/12
For personal use only.

Can. J. Chem. Downloaded from www.nrcresearchpress.com by 210.87.254.40 on 09/06/12
For personal use only.

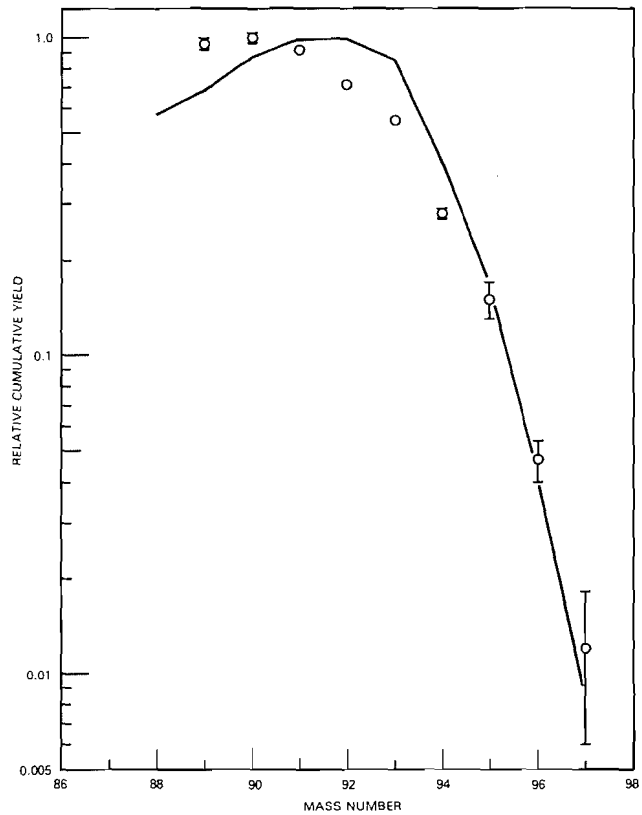

FIG. 2. Relative cumulative yields of Rb isotopes for two fissioning systems with same N/Z (1.564) and different E^*. ○, 28.1 MeV ^{3}He + ^{238}U (E^* = 37 MeV); —, fission spectrum neutrons + ^{240}Pu ($E^* \simeq 7$ MeV) (recommended yields from ref. 28).

most abundant isotope. The final results are presented in Table 2. For comparison, the recommended cumulative yields for thermal neutron fission of ^{235}U are also given (28).

In general, the distributions of relative cumulative yields for fission at moderate excitation energy are similar to those at low excitation energy. Mass 89 appears to be unusually high for 25.3 MeV ^{3}He + ^{238}U and unusually low for 28.1 MeV ^{3}He + ^{232}Th. This may be due to uncertainties in some of the correction factors which were large at this mass number. An additional complication at mass 89 was the possible interference of stable ^{88}Sr due to the relatively poor mass resolution of the mass spectrometer. The present data can be compared with cumulative yields from other fissioning systems to show changes due to composition of the compound nucleus or to excitation energy. For example, the system 25 MeV ^{4}He + ^{238}U has the same excitation energy (20 MeV) as 14 MeV n + ^{239}Pu whereas the compound nuclei are ^{242}Pu and ^{240}Pu, respectively. The Rb cumulative yields for those two systems are plotted in Fig. 1. The 14 MeV n + ^{239}Pu data are the recommended values (28). The distribution of Rb fission products is shifted toward more neutron-rich isotopes for the compound nucleus with more neutrons.

The effect of increasing the excitation energy is illustrated in Fig. 2, which shows the relative Rb cumulative yields for 28 MeV ^{3}He + ^{238}U and for fission spectrum neutron fission of ^{240}Pu (28). Both systems have the compound nucleus ^{241}Pu but the excitation energy is 37 MeV and about 7 MeV, respectively. Higher excitation energy shifts the Rb distribution to more neutron-deficient products.

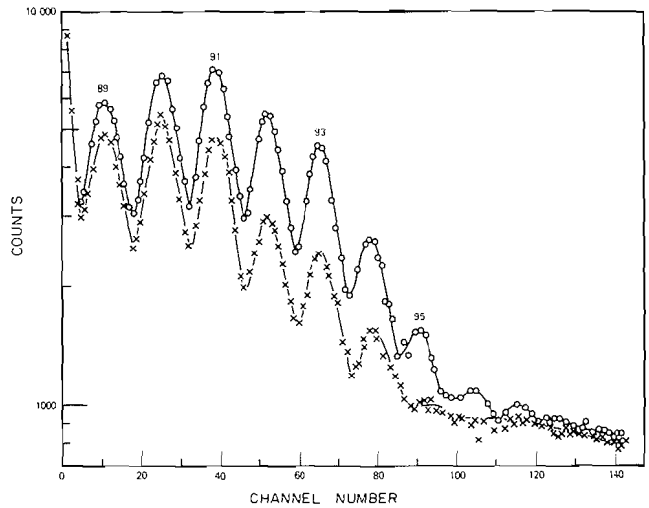

FIG. 3. Mass spectrum from Rb independent yield experiment. Upper curve = beam on. Lower curve = beam off. Beam-off spectrum normalized to beam-on spectrum below mass 89.

Independent yields

The measurement of Rb independent yields must be done in a time interval short compared to the radioactive half-lives of the Kr precursors. Thus a pulsed beam procedure was used in which mass spectra were recorded with "beam-on" for a short time interval and were separately recorded with "beam-off" for the same time interval. The system was automated such that a typical cycle started with 0.4 s of beam during which time 10 scans of the mass spectrum were recorded in the first 200 channels of the multiscaler. The beam was turned off and another 10 scans of the mass spectrum were added to the data in the first 200 channels. These 20 scans were called the "beam-on" spectrum and contained the short diffusion-time components plus background. Then 20 more scans were recorded in the second set of 200 channels and were called the "beam-off" spectrum. This cycle was repeated until sufficient statistics were obtained (up to 80 000 scans). Although equal numbers of scans were recorded in the beam-on and beam-off spectra the two spectra still had to be normalized to each other at a mass region free from fission products to account for the increased background due to beam heating during the beam pulse. The length of the beam pulse and the memory storage locations were controlled by a 4-channel pre-determined timer and mercury relays. The cyclotron beam was shut off by interrupting the Rf power at a low-power stage in the cyclotron Rf amplifier system.

A spectrum composed of two runs covering the Rb fission product region from mass 89–98 is shown in Fig. 3. The beam-off spectrum has been shifted upwards by a factor of 1.16 to account for the beam heating effect.

After normalization of the beam-off spectra to the beam-on spectra, the net counts were obtained for each mass peak. These values were then corrected for the overlap of adjacent mass peaks. As before, sweep-up field and sweep-down field were considered as independent determinations. Counts at each mass peak were calculated relative to a common mass and averaged for the several determinations. The random errors were determined from the standard deviations of the average values. The relative counts obtained in this manner were corrected by a factor which took into account the individual half-

TABLE 3. Relative independent yields of Rb isotopes[a,b]

Mass	Target / Projectile / Energy[c] (MeV) / $(N/Z)_{CN}$[f]	^{235}U / n / Thermal[d] / 1.565	^{238}U / ^{3}He / $25.3^{+2.7}_{-3.6}$ / 1.564	^{238}U / ^{3}He / $28.1^{+3.9}_{-6.4}$ / 1.564	^{238}U / ^{4}He / $25.5^{+2.0}_{-4.2}$ / 1.574	^{232}Th / ^{3}He / $28.1^{+3.0}_{-6.7}$[e] / 1.554
89		0.070	0.25±0.02 (2)	0.32±0.05 (4)		0.67±0.08 (2)
90		0.27	0.62±0.05 (2)	0.74±0.04 (4)	0.37±0.03 (2)	0.90±0.04 (2)
91		0.72	1.00 (2)	1.00 (5)	0.78±0.04 (2)	1.00 (2)
92		1.00	0.96±0.02 (2)	0.95±0.02 (6)	1.00 (2)	0.91±0.07 (4)
93		0.98	0.85±0.01 (2)	0.79±0.03 (6)	0.97±0.07 (2)	0.76±0.03 (4)
94		0.51	0.43±0.01 (2)	0.42±0.02 (6)	0.59±0.05 (2)	0.53±0.02 (4)
95		0.25	0.20±0.01 (2)	0.25±0.02 (6)	0.35±0.02 (2)	0.31±0.04 (4)
96		0.056	0.12±0.09 (2)	0.11±0.02 (2)		
97		0.014		0.076±0.009 (2)		
	$\langle A \rangle$	92.35	91.84	91.55	92.40	91.16
	$\langle N/Z \rangle_{Rb}$[g]	1.496	1.482	1.474	1.497	1.464
	Width	1.47	1.70	2.10	1.74	2.52

[a] Numbers in parentheses are the number of values used in determining average
[b] Uncertainties are based only on the standard deviation of the mean values. Values with no uncertainty were used to normalize different runs.
[c] Weighted average energy of bombarding projectile (see text).
[d] Reference 28.
[e] Average energy assumed equal to value for ^{238}U target for equal incident energy.
[f] N/Z value for compound nucleus.
[g] N/Z value for mean mass of Rb distribution.

lives of the Rb isotopes and their Kr precursors, the Rb and Kr diffusion times, and the time intervals for beam-on and beam-off. This factor is discussed in the Appendix.

The final results for the relative independent yields of the Rb isotopes are given in Table 3. Included in this table are the recommended values for thermal neutron fission of ^{235}U for comparison (28). The mean value of the isotopic distribution of Rb ($\langle A \rangle$), the N/Z value corresponding to the mean mass, and the standard deviation (width) of this distribution are also given in Table 3 for each of the fissioning systems. The determination of $\langle A \rangle$ and the width using the method of moments adopted in previous works (16, 18) is not adequate here because the mass range covered is not always symmetric about the peak yield. The mean mass and width were therefore determined from a least-squares fit of the data to a Gaussian curve. Previous work has shown that the Rb distributions for both neutron and charged particle induced fission are reasonably well fitted by Gaussian curves although this is not always true for Cs distributions (10, 17).

The shifts in Rb yields as functions of the composition of the compound nucleus and of excitation energy are clearly seen in the independent yield distributions. In Fig. 4 are shown the relative independent yields of Rb isotopes for 25 MeV ^{4}He + ^{238}U and 14 MeV n + ^{239}Pu. The mean mass of the Rb distribution is shifted upwards by 0.86 mass units for the compound nucleus ^{242}Pu relative to the compound nucleus ^{240}Pu when both are at the same excitation energy (20 MeV). The widths of the two distributions are essentially the same. In Fig. 5, the relative independent yields are shown for 28 MeV ^{3}He + ^{238}U and for fission spectrum neutron fission of ^{240}Pu. The ^{241}Pu compound nucleus with 37 MeV excitation energy gives a Rb distribution which is shifted downward by 0.95 mass units relative to ^{241}Pu at 7 MeV excitation energy. The width is broadened for fission at the higher excitation energy.

Discussion

In order to correlate the existing data on Rb independent yield distributions for fission with thermal neutrons, protons, ^{3}He, and ^{4}He, one must consider the differences in excitation energy, E^*, and the differences in the composition of the compound nucleus. A convenient parameter for the composition of the compound nucleus is the neutron-to-proton ratio, $(N/Z)_{CN}$. It would be useful to compare the experimentally measured values of mean mass and width versus one of the parameters E^* or $(N/Z)_{CN}$ independent of the other parameter.

The available data on Rb isotopic distributions are summarized in Table 4. The table includes two sets of yields from thermal neutron fission of ^{235}U which were not measured by the on-line mass spectrometric technique (29, 30). All the other experiments were done with this technique. To make comparisons on a common basis, all the previously published Rb distributions have been fitted to Gaussian curves. The mean mass and width parameters given in Table 4 are the centroid and standard deviation from the least-squares fit. For charged particle fission the parameters given in Table 4 are essentially the same as those given in the original publications even when the original parameters were determined by the method of moments.

Inspection of the widths in Table 4 shows a generally small dependence on $(N/Z)_{CN}$ and a strong dependence on excitation energy, E^*. These trends are illustrated in Fig. 6 where the widths are plotted versus the excitation energy. For thermal neutron fission of ^{235}U, the recommended value (28) is plotted with an error bar corresponding to the range of experimental values. Two of the widths from the present work do not seem to fit the general trend. For the ^{3}He + ^{238}U point at an excitation energy of 27 MeV, the enhanced width can be explained by the Gaussian curve not being a good representation of the experimental data. Omission of the mass 95–97 yields gives a

Can. J. Chem. Downloaded from www.nrcresearchpress.com by 210.87.254.40 on 09/06/12
For personal use only.

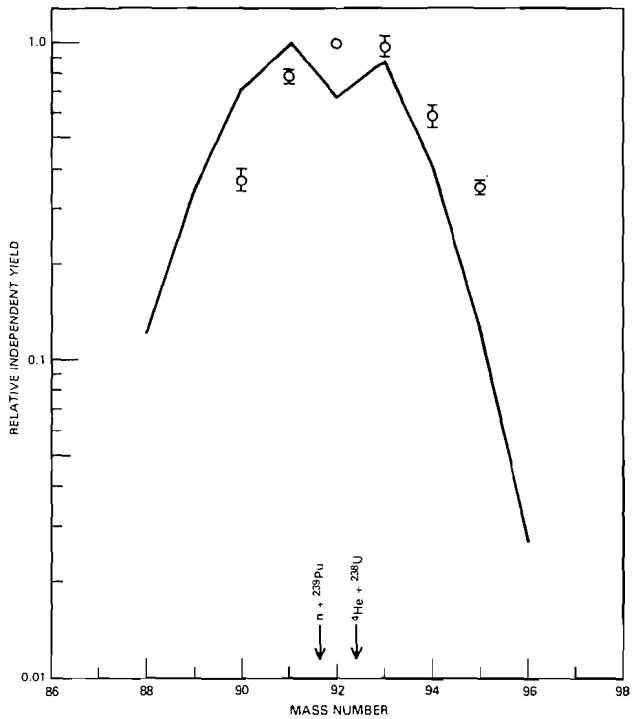

FIG. 4. Relative independent yields of Rb isotopes for two fissioning systems with same E^* (20 MeV) and different N/Z. ○, 25.5 MeV ^{4}He + ^{238}U (N/Z = 1.574); —, 14 MeV n + ^{239}Pu (N/Z = 1.553) (recommended yields from ref. 28). Arrows indicate mean masses.

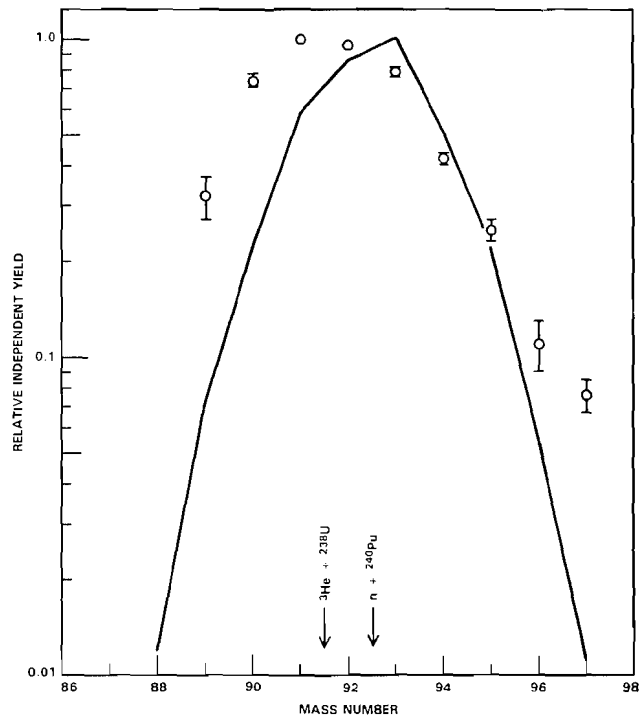

FIG. 5. Relative independent yields of Rb isotopes for two fissioning systems with same N/Z (1.564) and different E^* ○, 28.1 MeV ^{3}He + ^{238}U (E^* = 37 MeV); —. fission spectrum neutrons + ^{240}Pu ($E^* \simeq 7$ MeV) (recommended yields from ref. 28). Arrows indicate mean masses.

TABLE 4. Summary of Rb independent yield distributions for various fissioning systems up to 160 MeV excitation energy

Target	Projectile	$(N/Z)_{CN}$	E^* (MeV)	$\langle A \rangle$	$\langle N/Z \rangle_{Rb}$	$(N/Z)_{CN} - \langle N/Z \rangle_{Rb}$	Width	Reference
^{232}Th	p	1.560	33	91.43	1.471	0.089	1.63	18
			54	90.75	1.453	0.107	1.77	10
			63	90.80	1.454	0.106	1.70	18
			79	90.59	1.448	0.112	1.82	18
			101	90.41	1.444	0.116	1.94	18
			160	89.97	1.432	0.128	2.14	16
^{232}Th	^{3}He	1.554	36	91.16	1.464	0.090	2.52	[a]
^{235}U	n_{th}	1.565	6.5	92.28	1.494	0.071	1.47	16
			6.5	92.33	1.495	0.070	1.41	20
			6.5	92.71	1.506	0.059	1.31	19
			6.5	92.47	1.499	0.066	1.62	21
			6.5	92.24	1.493	0.072	1.49	29
			6.5	92.29	1.494	0.071	1.45	30
^{235}U	p	1.538	55	90.43	1.444	0.094	1.83	10
^{238}U	n	1.598	≃7	93.48	1.526	0.072	1.36	22
^{238}U	p	1.570	45	91.52	1.474	0.096	1.82	10
			55	91.41	1.471	0.099	1.84	10
			65	91.26	1.466	0.104	1.89	10
			85	91.14	1.463	0.107	2.01	17
			105	91.08	1.462	0.108	2.13	17
			161	90.49	1.446	0.124	2.28	16
^{238}U	^{3}He	1.564	34	91.84	1.482	0.082	1.70	[a]
			37	91.55	1.474	0.090	2.10	[a]
^{238}U	^{4}He	1.574	20	92.40	1.497	0.077	1.74	[a]
^{239}Pu	n	1.553	6.5	92.40	1.497	0.056	1.76	23

[a] Present work.

Can. J. Chem. Downloaded from www.nrcresearchpress.com by 210.87.254.40 on 09/06/12
For personal use only.

Can. J. Chem. Downloaded from www.nrcresearchpress.com by 210.87.254.40 on 09/06/12
For personal use only.

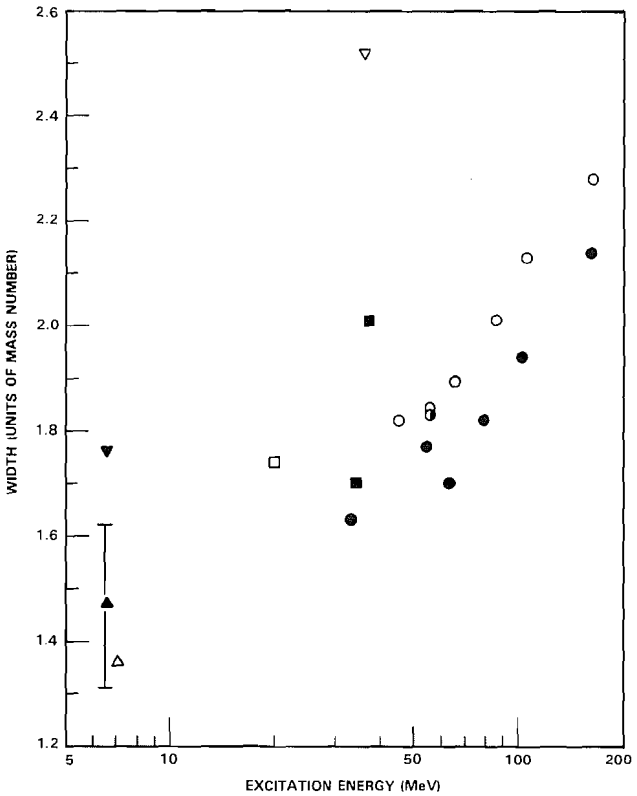

FIG. 6. Width of Rb independent yield distribution for several fissioning systems as a function of excitation energy of the compound nucleus. ●, p + ^{232}Th; ◑, p + ^{235}U; ○, p + ^{238}U; ▲, n + ^{235}U; △, n + ^{238}U; ▼, n + ^{239}Pu; ▽, ^{3}He + ^{232}Th; ■, ^{3}He + ^{238}U; □, ^{4}He + ^{238}U. Error bar indicates range of values for n_{th} + ^{235}U from different measurements.

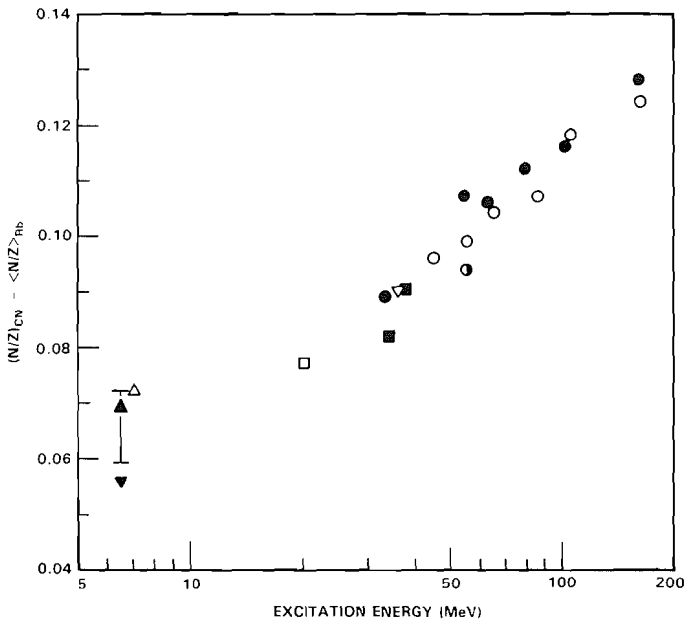

FIG. 7. The difference between $(N/Z)_{CN}$ and $\langle N/Z \rangle_{Rb}$ for several fissioning systems as a function of excitation energy of the compound nucleus. Data symbols are the same as for Fig. 6. Error bar indicates range of values for n_{th} + ^{235}U from different measurements.

better fit to the Gaussian curve and results in a smaller width in agreement with the other data. This explanation does not apply to the width of the ^{3}He + ^{232}Th distribution. In this case all the yields are well fit by the Gaussian curve. This distribution is far too wide in comparison with the other data and should be treated with suspicion unless confirmed elsewhere.

The mean masses for the distribution of independent yields of Rb isotopes shown in Table 4 depend on both the excitation energy, E^*, and the $(N/Z)_{CN}$. If one subtracts the N/Z ratio corresponding to the mean mass of the Rb distribution, $\langle N/Z \rangle_{Rb}$, from the $(N/Z)_{CN}$, the dependence on the composition of the compound nucleus is minimized. When $(N/Z)_{CN} - \langle N/Z \rangle_{Rb}$ is plotted versus E^*, the data cluster about a single curve as shown in Fig. 7. All four points from the present work are consistent with the previous work.

The shift of $\langle N/Z \rangle_{Rb}$ away from $(N/Z)_{CN}$ as excitation energy increases is due to increased neutron emission either as pre-fission neutrons, or as post-fission neutrons (10, 17, 18, 31). The relationship between $(N/Z)_{CN} - \langle N/Z \rangle_{Rb}$ and the number of neutrons emitted can be derived from the definition of the most probable charge for a model of charge distribution in fission. The commonly used model of Unchanged Charge Density (UCD) states that the neutron-to-proton ratio of the fragments is equal to that of the fissioning nucleus. The most probable charge (Z_p) for a particular fragment is thus

$$[4] \quad Z_p = A_{frag}\left(\frac{Z_{CN}}{A_{CN} - \nu_{pre}}\right)$$

where A_{frag} is the mass of the fragment, Z_{CN} is the nuclear charge of the compound nucleus, A_{CN} is the mass of the compound nucleus, and ν_{pre} is the number of pre-fission neutrons. With the additional assumptions that the number of neutrons in the fission product (N_{prod}) is equal to the number of neutrons in the fragment (N_{frag}) minus the number of post-fission neutrons (ν_{post}) for that fragment and that the charge of the fission product (Z_{prod}) is equal to the charge of the fission fragment ($Z_{prod} = Z_{frag} = Z_p$) eq. [4] can be rearranged to give

$$[5] \quad [(N/Z)_{CN} - \langle N/Z \rangle_{prod}] = \frac{\nu_{pre}}{Z_{CN}} + \frac{\nu_{post}}{Z_{prod}}$$

For the fissioning systems considered in Fig. 7, Z_{CN} varies by $\leq$3%, so variations in $(N/Z)_{CN} - \langle N/Z \rangle_{Rb}$ are due to the number of neutrons emitted. Previous work (10, 17, 18) has shown that the UCD model is not adequate and that a better model for charge distribution is the Equal Charge Displacement (ECD) model. The ECD model states that the distance of the most probable charge from the most stable charge for that mass is the same as for its complementary fragment. For the particular case of the Rb isotopes, previous work (10) showed that

$$[6] \quad Z_p^{ECD} = Z_p^{UCD} + 0.4$$

Equation [5] is then modified to

$$[7] \quad [(N/Z)_{CN} - \langle N/Z \rangle_{prod}] = \frac{\nu_{pre}}{Z_{CN}} + \frac{\nu_{post}}{Z_{prod}} + \frac{0.4}{Z_{prod}}\left(\frac{A_{CN} - \nu_{pre}}{Z_{CN}}\right)$$

The additional term is rather insensitive to changes in excitation energy, so variations in $(N/Z)_{CN} - \langle N/Z \rangle_{Rb}$ are again dominated by changes in the number of neutrons emitted.

Authors of earlier papers have used a similar analysis with additional information about pre-fission neutron emission to determine the number of post-fission neutrons from the heavy fragment as well as from the light fragment (10, 17, 18). Figure 7 and eq. [7] show that the ^{3}He and ^{4}He induced fission reac-

Can. J. Chem. Downloaded from www.nrcresearchpress.com by 210.87.254.40 on 09/06/12
For personal use only.

tions studied here are consistent with the earlier results for proton and neutron induced fission with regard to neutron emission as a function of excitation energy.

Conclusions

The cumulative and independent fission yields of Rb isotopes have been measured here for ^{3}He and ^{4}He induced fission of ^{232}Th and ^{238}U at energies slightly above the Coulomb barrier. The widths of the independent yield distributions for Rb isotopes are dominated by the effect of excitation energy rather than the N/Z of the compound nucleus.

The mean mass of the Rb independent yield distribution is a function of the composition of the fissioning system $(N/Z)_{CN}$ and the excitation energy, E^*. At a constant E^*, the N/Z of the mean mass of the Rb yield distribution is approximately equal to the $(N/Z)_{CN}$ minus a constant which is independent of $(N/Z)_{CN}$. This constant is related to the number of neutrons emitted before fission and to the number of neutrons emitted by the particular fragment after fission.

Acknowledgments

The experimental data for this work was obtained with the assistance of A. Ramamoorthy.

We are indebted to the late Rene H. Bernas who provided us with the mass spectrometer and supported us with valuable advice. We also express our gratitude to Robert Klapisch for many helpful discussions prior to and during this work. The assistance of Lazar Djordjevic with instrumentation for the mass spectrometer is greatly appreciated. Computing facilities at Washington University were supported under National Science Foundation Grant No. G-22296. We are grateful to Ray Warner and Nate Ballou for their comments on this manuscript.

1. R. VANDENBOSCH, T. D. THOMAS, S. E. VANDENBOSCH, R. A. GLASS, and G. T. SEABORG. Phys. Rev. **111**, 1358 (1958).
2. B. M. FOREMAN, W. M. GIBSON, R. A. GLASS, and G. T. SEABORG. Phys. Rev. **116**, 382 (1959).
3. L. J. COLBY, JR. and J. W. COBBLE. Phys. Rev. **121**, 1410 (1961).
4. L. J. COLBY, JR., M. L. SHOAF, and J. W. COBBLE. Phys. Rev. **121**, 1415 (1961).
5. H. G. HICKS, H. B. LEVY, W. E. NERVIK, P. C. STEVENSON, J. B. NIDAY, and J. C. ARMSTRONG, JR. Phys. Rev. **128**, 700 (1962).
6. T. C. ROGINSKI, M. E. DAVIS, and J. W. COBBLE. Phys. Rev. C**4**, 1361 (1971).
7. Y. Y. CHU. University of California Radiation Laboratory Report No. UCRL-8926, 1959.
8. J. A. MCHUGH and M. C. MICHEL. Phys. Rev. **172**, 1160 (1968).
9. D. R. NETHAWAY and H. B. LEVY. Phys. Rev. **139**, B1505 (1965).
10. B. L. TRACY, J. CHAUMONT, R. KLAPISCH, J. M. NITSCHKE, A. M. POSKANZER, E. ROECKL, and C. THIBAULT. Phys. Rev. C**5**, 222 (1972).
11. S. C. BURNETT, R. L. FERGUSON, F. PLASIL, and H. W. SCHMITT. Phys. Rev. C**3**, 2034 (1971).
12. L. YAFFE. Second Symp. on the Physics and Chemistry of Fission. IAEA, Vienna. 1969. p. 701.
13. R. KLAPISCH. Ann. Rev. Nuclear Sci. **19**, 33 (1969).
14. I. AMAREL, R. BERNAS, J. CHAUMONT, R. FOUCHER, J. JASTRZEBSKI, A. JOHNSON, R. KLAPISCH, and J. TEILLAC. Arkiv for Fysik, **36**, 77 (1967).
15. R. KLAPISCH, J. CHAUMONT, C. PHILIPPE, I. AMAREL, R. FERGEAU, M. SALOME, and R. BERNAS. Nucl. Instrum. Meth. **53**, 216 (1967).
16. J. CHAUMONT. Thesis, Faculty of Sciences at Orsay, University of Paris, 1970.
17. J. K. P. LEE, G. PILAR, B. L. TRACY, and L. YAFFE. J. Inorg. Nucl. Chem. **37**, 2035 (1975).
18. L. NIKKINEN, B. P. PATHAK, L. LESSARD, and I. S. GRANT. Phys. Rev. C**22**, 617 (1979).
19. P. L. REEDER, J. F. WRIGHT, and R. A. ANDERL. Conference on Nuclear Cross Sections and Technology, Washington, DC. March 3–5, 1975. National Bureau of Standards NBS-SP-425.
20. S. J. BALESTRINI, R. DECKER, H. WOLLNIK, K. D. WUNSCH, G. JUNG, E. KOGLIN, and G. SIEGERT. Phys. Rev. C**20**, 2244 (1979).
21. M. SHMID, Y. NIR-EL, G. ENGLER, and S. AMIEL. J. Inorg. Nucl. Chem. **43**, 867 (1981).
22. S. J. BALESTRINI and L. FORMAN. Phys. Rev. C**10**, 1872 (1974).
23. S. J. BALESTRINI and L. FORMAN. Phys. Rev. C**12**, 413 (1975).
24. R. KLAPISCH and R. BERNAS. Nucl. Instrum. Meth. **38**, 291 (1966); R. Klapisch. Thesis. Faculty of Science at Orsay, University of Paris. 1970.
25. V. E. VIOLA and T. SIKKELAND. Phys. Rev. **128**, 767 (1962).
26. K. W. MACMURDO and J. W. COBBLE. Phys. Rev. **182**, 1303 (1969).
27. E. F. MEYER, JR., W. H. BUTTON, and K. ARNOLD. J. Inorg. Nucl. Chem. **33**, 2745 (1971).
28. B. F. RIDER. Compilation of fission product yields. 1980. NEDO-12154-3(B).
29. W. LANG, H.-G. CLERC, H. WOHLFARTH, H. SCHRADER, and K.-H. SCHMIDT. Nucl. Phys. A**345**, 34 (1980).
30. R. B. STRITTMATTER and B. W. WEHRING. Int. Conf. Neutron Physics and Nuclear Data for Reactors and Other Applied Purposes, Harwell, Sept. 25–29, 1978.
31. H. UMEZAWA, S. BABA, and H. BABA. Nucl. Phys. A**160**, 65 (1970).

Appendix

The correction factor for growth, decay, and diffusion was derived as follows. For each mass peak the following equations are defined for the observed counts in the "beam-on" spectrum (α) and "beam-off" spectrum (β).

$$\alpha = N_1 + N_1^p + N_2 + N_2^p + B$$

$$\beta = N_3 + N_3^p + B$$

where N_1, N_2, and N_3 refer to the observed counts due to independent formation and diffusion of Rb, N_1^p, N_2^p, and N_3^p refer to the observed counts due to Rb produced by decay of Kr precursors. The subscripts 1, 2, and 3 refer to three time regions: 1. period with beam actually on during "beam-on" spectrum (10 scans); 2. period with beam-off during "beam-on" spectrum (10 scans); 3. period for "beam-off" spectrum (20 scans). B is the counts due to the constant background. The variable background due to beam heating was accounted for by including a third component with the two other diffusion components described in the main text.

For each of the time regions i (i = 1, 2, 3) the number of observed ions is given by

$$N_i = \epsilon n I \sigma F_i$$

$$N_i^p = \epsilon n I \sigma_p F_i^p$$

where ϵ is the overall efficiency of the mass spectrometer for ionizing and detecting a given isotope of Rb (this efficiency was assumed to be constant for all isotopes of Rb), n is the number of target atoms per cm^2, I is the intensity of the incident

beam, σ is the cross section for independent formation of Rb isotopes, σ_p is the cross section for the cumulative formation of Kr isotopes, F_i is the factor which accounts for growth, decay, and diffusion of independently formed Rb during the time interval i, and F_i^p is the factor which accounts for the growth, decay, and diffusion of Rb from decay of Kr precursors during the time interval i.

The F_i and F_i^p factors depend only on the time intervals, the radioactive half-lives of the Rb and Kr isotopes and the Rb and Kr diffusion times. The derivations of the F_i and F_i^p equations are based on standard equations for growth and decay of radioactive species. However, the radioactive decay constants are generally replaced with effective rate constants which include the effect of a particular diffusion component. The factors were calculated separately for each diffusion component, weighted by the relative abundance of each diffusion component, and then combined.

After algebraic manipulation, the expression for the relative cross section of a given Rb isotope becomes

$$\sigma_{Rel} = \frac{\alpha - \beta}{F_1 + F_2 - F_3 + (\sigma_p/\sigma)\,(F_1^p + F_2^p - F_3^p)}$$

Unfortunately σ_p/σ represents the ratio of the cumulative Kr yield to the independent Rb yield both of which are unmeasured quantities for these fissioning systems. In fact, the latter quantity is the number to be determined in this experiment. However, one can adopt the charge distribution parameters of McHugh and Michel (8) and obtain approximate values for the ratio σ_p/σ. The estimated ratios varied from 3.86 at mass 89 to 0.0147 at mass 95. The F_i^p factors were greatest at mass 91 but when combined with the cross section ratios, the greatest correction for Kr precursors occurred at mass 90 with 39% correction. At mass 92 and above, the correction was less than 7%. The correction factors F_i for growth, decay, and diffusion of independently formed Rb were less than 1% for masses up to and including ^{94}Rb for the 0.4 s beam pulse. At mass 95 the correction was 22%. One run with 2 s beam pulses had larger corrections of up to 7% at mass 94 and 42% at mass 95.

Can. J. Chem. Downloaded from www.nrcresearchpress.com by 210.87.254.40 on 09/06/12
For personal use only.

Triplet-state benzophenone-sensitized photoreduction of bis(acetylacetonato)copper(II): the generation and stability of copper(I) complexes

YUAN L. CHOW AND GONZALO E. BUONO-CORE

Department of Chemistry, Simon Fraser University, Burnaby, B.C., Canada V5A 1S6

Received May 4, 1982

This paper is dedicated to Professor Harry E. Gunning on the occasion of his 65th birthday

YUAN L. CHOW and GONZALO E. BUONO-CORE. Can. J. Chem. **61**, 795 (1983).

Triplet-state benzophenone rapidly sensitized the photoreduction of $Cu(acac)_2$ in alcohols to give polymeric Cu(acac) as black precipitates. The binary complexes of Cu(acac) of polypyridines, polysulfide, olefins, acetylenes, and carbon monoxide could be generated in solution under an inert atmosphere when a ligand was present *in situ* during photoreduction or added after an appropriate photoreduction was completed. Except Cu(acac)—$(PPh_3)_2$, the Cu(acac) complexes of various ligands are sensitive to air oxidation, but show a wide range of reactivity towards disproportionation and photolysis. In the presence of terminal acetylenes, amorphous copper(I) acetylides were isolated in good yields.

YUAN L. CHOW et GONZALO E. BUONO-CORE. Can. J. Chem. **61**, 795(1983).

La benzophénone à l'état triplet sensibilise rapidement la réduction photochimique du $Cu(acac)_2$ dans des alcools en donnant le Cu(acac) polymerisé sous la forme d'un précipité noir. Les complexes binaires de Cu(acac), de polypyridines, de polysulfure, d'oléfines, d'acétylènes et de monoxyde de carbone peuvent être produites en solution sous atmosphère inerte lorsqu'un ligand est présent "*in situ*" pendant la photoréduction ou s'il est ajouté après qu'une photoréduction appropriée soit complétée. A l'exception du Cu(acac)—$(PPh_3)_2$, les complexes du Cu(acac) de divers ligands sont sensibles à l'air, mais ils exhibent un large domaine de réactivité vis-à-vis de la dismutation de la photolyse. En présence d'acétylènes terminaux, on isole avec de bons rendements des acétylures de cuivre(I) amorphes.

[Traduit par le journal]

Can. J. Chem. Downloaded from www.nrcresearchpress.com by 210.87.254.6 on 09/06/12
For personal use only.

Introduction

We have shown (1) that bis(acetylacetonato)copper(II), $Cu(acac)_2$, is photoreduced in the presence of certain aromatic ketone sensitizers in hydrogen-donating solvents to give an amorphous black precipitate which reacts with triphenylphosphine to afford crystalline acetylacetonatobis(triphenylphosphine)copper(I), $Cu(acac)(PPh_3)_2$. In this photoreduction, alcohols were concurrently oxidized to the corresponding ketones and acetylacetone was produced in nearly quantitative yields. On prolonged irradiation, the black precipitate was transformed to copper metal. These observations have led us to conclude that in the primary step $Cu(acac)_2$ is photoreduced to a copper(I) complex, the black precipitate, which may react by a combination of disproportionation and/or photoreduction to give copper metal. $Cu(acac)_2$ and several other transition metal acetylacetonates are known to quench triplet transients generated by flash photolysis of aromatic ketones and hydrocarbons (2–5). However, the chemical consequences of the quenching has not been investigated so far, except in our recent report (1).

In order to carry out mechanistic studies of this intriguing sensitization process, it is necessary to clarify the pattern of the photoreduction of $Cu(acac)_2$ to copper(I) complexes. In this report, we describe the benzophenone-sensitized photoreduction in the presence of various ligands aiming to demonstrate the product pattern of the primary photoreduction.

Experimental

General conditions and materials

Melting points were determined on a Fisher-Johns apparatus and were uncorrected. Infrared spectra were obtained with a Perkin-Elmer 457 spectrophotometer, ultraviolet–visible spectra with a Cary 17 spectrophotometer, mass spectra and gc–ms with a Hewlett-Packard Model 5985, and nmr spectra with a Varian A56/60 or XL-100 in $CDCl_3$ solution using TMS as an internal standard. Elemental analyses were carried out by Mr. M. K. Yang on a Perkin-Elmer 240 microanalyser.

Olefins and acetylenes were redistilled and sealed under nitrogen. Other ligands were used as supplied by commercial sources. Unless specified otherwise, an immersion type photocell (Hanovia type) was used. The light source was a Hanovia 450 W or 200 W medium pressure mercury lamp. Nitrogen was scrubbed with a Fieser's solution and dried with H_2SO_4 and NaOH pellets.

Sensitized photoreduction in the absence of ligands

A solution of benzophenone and $Cu(acac)_2$ in methanol, ethanol, 2-propanol, tetrahydrofuran, or a mixture of 2-propanol and *t*-butanol (1:1) was photolyzed in an overhead irradiator (1) under nitrogen to give black precipitates. The precipitates were quickly filtered and washed with the solvent. The ir spectra in Nujol were identical and showed absorptions at 1580(s), 1550(s), 1530(s), 1190(w), 1020(m), 940(m), 785(m). Most of these peaks are shown by $Cu(acac)_2$ with different intensities. The black precipitate gave blue color immediately on exposure to air.

After 24 h, the solid showed the presence of blue particles on the surface. This solid was treated with methanol to give a solution and a solid. The solution was evaporated to give $Cu(acac)_2$. The solid was treated with acetylacetone in ethanol to give $Cu(acac)_2$ under nitrogen and was assumed to be cupric oxide.

A solution of $Cu(acac)_2$ (5.7×10^{-3} *M*) and benzophenone (7.9×10^{-2} *M*) in methanol (100 mL) showed OD of 0.36 at 620 nm (Fig. 1). The solution was irradiated as above for 3 h to give the black precipitate suspended in a clear solution: the residual OD of the clear solution at 620 nm was 0.092. One half of the suspension was left under nitrogen for 12 h to give a blue solution and copper metal; the absorption of the supernatant solution at 620 nm was 0.22. The other half of the suspension was exposed to air for 12 h to give a blue solution with OD 0.36.

Sensitized photoreduction in the presence of various ligands

2,2'-Dipyridine: Irradiation of a solution containing $Cu(acac)_2$ (300 mg, 1.15 mmol), benzophenone (400 mg), and 2,2'-dipyridine (180 mg, 1.15 mmol) in methanol (200 mL) under nitrogen rapidly developed a red color in 1/2 h. This solution was stable for 16 h under nitrogen. On exposure to air, the red color was replaced by a blue color (λ_{max}, 620 nm) with a lifetime of 60 s. To a part of the red solution triphenylphosphine in methanol was added under nitrogen. The solu-

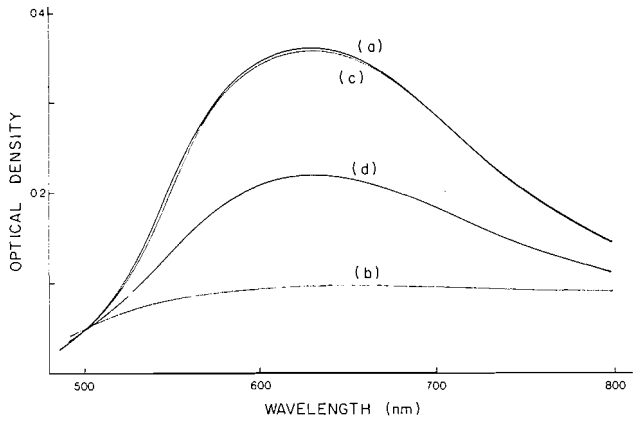

FIG. 1. The spectral changes of triplet-state benzophenone-(7.9×10^{-2} *M*) sensitized photoreduction of Cu(acac)$_2$ (5.7×10^{-3} *M*) in methanol (100 mL): (*a*) before irradiation, (*b*) the photolysate after 3 h irradiation, (*c*) the air-exposed photolysate, (*d*) the photolysate kept under nitrogen in the dark for 12 h.

tion was worked up in a similar way as described previously to afford Cu(acac)(Ph$_3$P)$_2$; mp 175–178°C; the ir spectrum was identical to that of an authentic sample (1). On prolonged photolysis of the red solution for 18 h, a small amount of copper metal was deposited.

Ethylenediamine: A solution of Cu(acac)$_2$ (100 mg, 3.8 mmol), benzophenone (138 mg), and ethylenediamine (46 mg, 7.6 mmol) in methanol (40 mL) exhibited a deep blue color. This solution was irradiated under nitrogen to afford a pale yellow solution in 1.5 h. This solution deposited a trace amount of copper metal and turned to pale blue in 45 min but discharged the color immediately on addition of triphenylphosphine and gave Cu(acac)(Ph$_3$P)$_2$: mp 176–179°C; the ir spectrum was superimposable with the previous one. The pale yellow photolysate immediately became the original deep blue within seconds after exposure to the air. Continued irradiation of the pale blue solution for another 1/2 h caused a deposit of metallic copper on the wall.

2,5-Dithiahexane: A solution of Cu(acac)$_2$ (300 mg, 1.15 mmol), 2,5-dithiahexane (141 mg, 1.15 mmol), and benzophenone (400 mg) in methanol (220 mL) was photolyzed under nitrogen to give a yellow solution in 20 min. This yellow solution remained unchanged for 16 h under nitrogen but became blue (λ_{max} 620 nm) within 30 seconds after exposure to air. A part of this solution (2 mL) and a methanol solution (2 mL, 6×10^{-3} *M*) of 2,2′-dipyridine were mixed under nitrogen to give a red solution showing λ_{max} 427. To the remainder of the photolysate, triphenylphosphine (600 mg) in methanol (30 mL) was added under nitrogen. After 10 h, the solution was worked up in a usual manner to give Cu(acac)(Ph$_3$P)$_2$ (382 mg): mp 165–170°C.

Bis-(2-methoxyethyl)ether: On irradiation of a solution containing Cu(acac)$_2$ (250 mg, 0.95 mmol), benzophenone (500 mg), and bis(2-methoxyethyl)ether (650 mg, 4.75 mmol) in methanol (50 mL) under nitrogen, metallic copper appeared on the wall in 15 min. In 26 min, the solution became colorless and a shiny copper mirror was formed.

Styrene: A solution of Cu(acac)$_2$ (500 mg, 1.92 mmol), benzophenone (1 g), and styrene (9.61 mmol) in methanol (200 mL) was photolysed under nitrogen slowly to give a pale blue solution in 8 h, but no black precipitate was formed. This solution immediately turned to blue color on exposure to air. Part of this solution was taken and reacted with triphenylphosphine in methanol under nitrogen to give Cu(acac)(Ph$_3$P)$_2$: mp 170–175°C. The remaining solution was irradiated further to deposit a trace amount of copper metal in 3 h. The photolysate was diluted with water and extracted with ether in the usual manner to give a crude oil which contained only styrene and benzophenone by gc analysis.

Norbornene: On irradiation of a methanol solution (200 mL) of Cu(acac)$_2$ (500 mg, 1.92 mmol), benzophenone (1.0 g), and norbornene (800 mg, 8.5 mmol), a reddish copper metal suspension developed in 20 min and a copper mirror was formed in 30 min. The red suspension turned to blue solution in 10–15 min on exposure to air. The pale blue solution was worked up as above to give acetylacetone, benzophenone, and norbornene and small amounts of benzhydrol and oxetanes derived from benzophenone.

Carbon monoxide: A methanol solution (5 mL) containing Cu(acac)$_2$ (5.6×10^{-3} *M*) and benzophenone (1.5×10^{-2} *M*) in a Pyrex tube was irradiated under purging of carbon monoxide for 20 min to give a colorless solution. The solution remained clear in the dark under constant carbon monoxide purging for 3 h. The clear solution deposited copper metal and turned to blue rapidly when carbon monoxide was replaced with a stream of argon. To a clear solution obtained from a similar photolysis was added triphenylphosphine (15 mg) in methanol under carbon monoxide. The solution was worked up to give Cu(acac)(Ph$_3$P)$_2$: mp 175–178°C.

To two tubes of the colorless solution obtained in a similar manner, 0.2 mL each of styrene and 1,3-pentadiene was added to each tube, respectively. The solutions remained colorless. When purging of carbon monoxide was replaced by a stream of argon, the two solutions remained clear colorless for 2 and 4 h, respectively; at these times they started to deposit copper metal and showed a pale blueish color.

Spectroscopic determination of Cu(I) complexes: A methanol solution containing known concentration of Cu(acac)$_2$, benzophenone, and a ligand (e.g. byp, phen, and DTH) in a uv cell (10 mm) was irradiated. At each 30 s interval, uv spectra were recorded to show emergence of new maxima. The molar extinction coefficients were calculated from the optical density at the stationary state.

A solution containing Cu(acac)$_2$ (1.2×10^{-2} *M*), benzophenone (6×10^{-2} *M*) in methanol – methylene chloride (1:1, 5 mL) was irradiated under carbon monoxide for 5 h to afford a colorless solution. A sample taken in an ir cell showed weak absorption at 2100 cm^{-1}. Continued irradiation of the colorless solution for 2 h caused the deposition of metallic copper.

Sensitized photoreduction in the presence of terminal acetylenes

A solution of Cu(acac)$_2$ (ca. 2 mmol), benzophenone (5 mmol), and a terminal acetylene (5 mmol) in methanol (200 mL) was irradiated under nitrogen for 2–4 h to form a yellow-colored precipitate. The precipitate was filtered and washed with methanol to afford amorphous solid of the copper(I) acetylide. The pale blue filtrate was diluted with water (200 mL) and extracted with ether (3 × 50 mL). The ether solution was washed with water, dried, and evaporated. The residue was analysed by gc (10% SE-30, 100–240°C at 10°/min) to give peaks corresponding to acetylacetone (rt 1.2 min), the acetylene, and benzophenone (rt 7.3 min, nearly quantitative recovery by internal standards).

When *t*-butylacetylene was used in the photolysis a yellow solution was obtained. The photolysate was diluted with water and extracted with ether to afford a crude product. The crude product was chromatographed on silica gel; ether elution gave copper(I) *t*-butylacetylide **3** (102 mg, 37%); mp 82°C decomp. (lit. mp 80–140°C) (6); ir (CCl_4) 2000(w) cm^{-1}; nmr (CCl_4) δ 1.83(s) ppm.

The biscuprous acetylide **4** was obtained as a dark brown solid (70% yield) and exploded when dried in desiccator; mp 140–155°C decomp.; ir (Nujol) 2120(w), 1280(s), 1020(w) cm^{-1}; nmr (pyridine) 4.07 ppm(s).

Copper(I) *n*-butylacetylide **2** was obtained as a yellow–green solid in 90% yield; mp 145–185°C decomp. (lit. mp 182°C decomp.) (7); ir (Nujol) 1927 cm^{-1}. The *n*-butylacetylide **2** (50 mg) and triphenylphosphine (92 mg) in acetonitrile (30 mL) were stirred at room temperature for 48 h. The precipitate was recrystallized from acetonitrile to afford hexynyl(triphenylphosphine)copper(I) (29 mg); mp 157°C decomp.; ir 3050, 1585, 1480, 1432, 1090, 740, and 695 cm^{-1}. *Anal.* calcd. for $C_{24}H_{24}PCu$: C 70.85, H 5.90; found: C 71.33, H 5.95.

Copper(I) phenylacetylide **1** was obtained as a yellow solid (72%); mp 230°C decomp. (lit. 230–235°C) (7); ir (Nujol) 1930(w), 1485(m), 750(s), 690(s) cm^{-1}. The acetylide **1** (50 mg) and triphenylphosphine (80 mg) were stirred in acetonitrile (10 mL) under nitrogen for 12 h. The residue was recrystallized from toluene – petroleum ether to give yellow needles of phenylethynyl(triphenylphos-

Can. J. Chem. Downloaded from www.nrcresearchpress.com by 210.87.254.6 on 09/06/12
For personal use only.

Can. J. Chem. Downloaded from www.nrcresearchpress.com by 210.87.254.6 on 09/06/12
For personal use only.

phine)copper(I) (71 mg, 55%); mp 201–203°C decomp. (lit. mp 202–204°C decomp.) (8); ir (Nujol) 2030(m), 1435(s), 750(s), and 700 cm^{-1}. *Anal.* calcd. for $C_{26}H_{20}CuP$: C 73.17, H 4.69; found: C 72.92, H 4.76.

The reaction of copper(I) acetylide with iodobenzene

A mixture of an acetylide (1–0.5 mmol) and an equivalent amount of iodobenzene (1–0.5 mmol) in dry pyridine was heated at 120°C for 8 h. The solution was diluted with water and extracted with ether. The residue was analysed by gc peak-matching method or gc–ms to show the percentage yield of phenylacetylenes. 1,6-Diphenyl-1,5-hexadiyne was recrystallized from ethanol as light yellow crystals (44%); mp 45–48°C (lit. mp 48°C) (9); nmr ($CDCl_3$) 2.70(s,4H), 7.27(m,10H); ms *m/e* 230 (m^+,15), 115(100).

Photolysis of $Cu(acac)_2$ in the presence of internal acetylenes

A solution of $Cu(acac)_2$ (500 mg), benzophenone (2.5 g), and diphenylacetylene (700 mg) in methanol (200 mL) was irradiated under nitrogen to give a white crystalline precipitate after 20 min. Filtration under nitrogen atmosphere afforded Cu(acac)(PhC≡CPh) **12** (194 mg, 29%); mp (sealed under N_2) 225°C decomp.; ir (Nujol) 1970(m), 1593(s), 1540(s), 1280(m), 1035(m), 793(m), 767(s), and 705(s) cm^{-1}; ms *m/e* 340(M^+,1.0), 179(20), 178(100), 152(16); ms by chemical ionization *m/e* 356(1.0), 180(14), 179(100), 101(70). Prolonged photolysis caused the darkening of the solution and eventual copper metal deposition. The white crystals on exposure to air turned greenish and to a dark black solid. Even working in a nitrogen glove box, **12** did not give good elemental analysis. The white crystals **12** were placed in an nmr tube and $CDCl_3$ was condensed in the tube in a vacuum line. On warming to room temperature, it turned to a brownish solution which showed signals at 2.02 and 2.30 ppm (s for CH_3) and 7.43(m) in a ratio of 6:10.

The complex **12** (50 mg) and triphenylphosphine (100 mg) in ether (10 mL) was stirred under nitrogen for 48 h. The solution was filtered to give $Cu(acac)(PPh_3)_2$ (26 mg); mp 171–176°C (1).

A similar photolysis in the presence of 3-hexyne turned the photolysate to pale blue in 20 min and then to dark brown in 35 min. At this point, copper metal started to appear. On exposure of the photolysate to air, it turned to blue solution. To the photolysate triphenylphosphine was added. After stirring for 2 h, the solution was worked up to give $Cu(acac)(PPh_3)_2$ (124 mg) (1).

Photolysis of $Cu(acac)_2$ in the presence of alkynol ***9***

A solution of $Cu(acac)_2$ (500 mg), benzophenone (1 g), and 3,5-dimethyl-1-hexyn-3-ol, **9** (500 mg), in methanol (200 mL) was irradiated under nitrogen for 4 h to give a dark yellow solution. The solution was diluted with water and was extracted with ether to give dark brown ether layer and pale blue aqueous layer. The ether solution was worked up under nitrogen purging to give a brown solid which showed ir pattern superimposable with $Cu(acac)_2$. The filtrate was analysed by gc peak matching to give benzophenone and alkynol **9** but no other peaks. In a separate photolysis, the dark yellow photolysate was stirred with triphenylphosphine under nitrogen for 5 h to give $Cu(acac)(PPh_3)_2$ (190 mg, 30%); mp 175–178°C (1).

Copper(I) acetylide of alkynol ***9***

A solution containing $CuSO_4 \cdot 5H_2O$ (5 g), concentrated ammonium hydroxide (20 mL), and water (80 mL) was treated with hydroxylamine hydrochloride (2.84 g) under nitrogen for 10 min. To this pale blue solution, alkynol **9** (2.52 g) was added to give an orange precipitate. The precipitate was dissolved in ether and was dried. The residue from the ether extracts was dried in a desiccator to give amorphous orange semi-solid (550 mg); ir (KBr) 3500–3400, 2950(s), 1470(m), 1370(s), 1260(m), 1160(s), 1080(w), 975(w), 935(m), 920(m), and 860(w) cm^{-1}. The compound **11** dissolved in methanol was warmed up to 50°C. On cooling, copper metal deposited on the bottom. The filtrate was worked up to give alkynol **9**. Compound **11** and triphenylphosphine in ether deposited a red amorphous solid; no melting below 300°C; ir (KBr) 3400, 3040, 2940, 1560, 1475, 1430, 1150, 1090, 740, and 690 cm^{-1}.

Results and discussion

Irradiation of a solution of benzophenone and $Cu(acac)_2$ in ethanol or 2-propanol rapidly deposited black precipitates which were quantitatively changed to metallic copper under prolonged irradiation. The black precipitates were formed much faster in these solvents than in methanol (1). The heterogeneous photolysate was rapidly oxidized by air to give a quantitative yield of $Cu(acac)_2$, and the air oxidation was even faster when more acetylacetone was added to the photolysate. Under nitrogen, the black precipitate in the suspension was slowly disproportionated to copper metal and $Cu(acac)_2$; the concentration of the latter was exactly one-half of the original as shown by the absorption at 620 nm (Fig. 1). The black precipitates were sparingly soluble in most solvents and in the solid state slowly changed to $Cu(acac)_2$ and an unkown solid under air in several days. Fortunately, the precipitates in the photolysate reacted readily with triphenylphosphine to afford stable $Cu(acac)(PPh_3)_2$ which was obtained previously by photolysis in methanol in the presence of triphenylphosphine. The black precipitates were also obtained in the direct photolysis of $Cu(acac)_2$ in alcohols by irradiation of the charge-transfer ligand to metal (CTTM) band at 240 nm (Corex filter), and have been assumed to be $Cu(acac)(ROH)_x$, where ROH was an alcohol (10). This formulation was obviously incorrect since all black precipitates obtained in various alcohols or tetrahydrofuran exhibited the same ir spectrum which contained neither typical ir absorption bands of alcohol ligands nor the OH absorption. Since the ir spectrum was very similar to that of $Cu(acac)_2$ except for some details, the black precipitates are more likely polymers of Cu(acac). Polymeric complexes of copper(I) derivatives are well known; some of them have been shown to have short Cu—Cu distances(2.71 Å) implying facile interactions (11).

However, the benzophenone-sensitized photolysis of $Cu(acac)_2$ in the presence of various ligands, such as 1,2-diamino derivatives, 2,5-dithiahexane (DTH), bis(2-methoxyethyl)ether (diglyme), carbon monoxide, acetylenes, and olefins (except cyclohexene), did not form the black precipitates but, instead, gave colored solutions. These solutions exhibited varied stability toward air oxidation with visual lifetimes ranging from several minutes to several seconds on exposure to air. For example, while colored solutions derived from 1,10-phenanthroline (phen), 2,2′-dipyridine (bpy), and DTH are relatively stable, those derived from ethylenediamine (en) and carbon monoxide were oxidized instantly on exposure to air. Most of these solutions react with triphenylphosphine to give $Cu(acac)(Ph_3P)_2$ indicting the presence of the copper(I) complexes. The solutions of copper(I) complexes derived from bpy, phen, and DTH were stable under nitrogen and, also toward the photolysis conditions for more than 16 h. The absorption maxima of these copper(I) complexes were determined to give the following data: for bpy λ_{max} 427 nm (ϵ, 2500) and 520 nm (shoulder), for phen λ_{max} 430 nm (ϵ, 7600) and 570 nm (ϵ, 2600), and for DTH λ_{max} 575 nm (ϵ, 1400). The absorption maxima in the former two are in close agreement with those of $Cu(bpy)_2^+$ and $Cu(phen)_2^+$ at λ_{max} 435 nm, which has been assigned to a charge transfer to ligand (CTTL) band (12, 13) according to the assumption that phen and bpy are relatively good π-acceptors and weak α-donors. The copper(I) complex of carbon monoxide was stable under continuous carbon monoxide purging but rapidly disproportionated to give copper metal and a blue solution of $Cu(acac)_2$ when carbon monoxide was displaced by nitrogen from the solution. It showed a weak

absorption at 2100 cm^{-1}. This low frequency, in comparison to 2143 cm^{-1} for CO, suggests a weak back donation of copper $3d$ electron to a CO π-antibonding orbital. Carbonyl complexes of copper(I) are rare (14, 15) due to their lability. Though these informations do not reveal the structure, these complexes probably have molecular formulae of $Cu(acac)L_x$, where $x = 1$ or 2 for the bidentate or monodentate ligands L, respectively. The reaction pattern is summarized in Scheme 1.

$$Cu(acac)_2 + R_2CHOH \xrightarrow[Ph_2CO]{} Cu(acac) + acacH + R_2CO$$

$$\text{Cu(acac)} \longrightarrow \text{Polymeric solid} \xrightarrow[acacH]{O_2} Cu(acac)_2 + H_2O$$

$$\text{Cu(acac)} \xrightarrow{L} Cu(acac)L_x \xrightarrow{L} Cu(acac)(PPh_3)_2 \quad (PPh_3)$$

$$Cu(acac)L_x + acacH \xrightarrow{O_2} Cu(acac)_2 + H_2O + xL$$

$$2Cu(acac)L_x \xrightarrow{N_2} Cu^0 + Cu(acac)_2 + xL$$

SCHEME 1

Owing to their instability toward oxygen, these copper(I) complexes could not be isolated for further investigation. However, the solutions of these copper(I) complexes exhibited a wide range of stability toward disproportionation in the dark under nitrogen and prolonged irradiation under the same photolysis conditions. While the following observations were qualitative, they provided some indication of their reactivity and stability. The solutions of copper(I) complex from phen, bpy, and DTH were stable under nitrogen and also were hardly photolabile. The phosphine complexes, Cu(acac) $(PPh_3)_2$, and probably other analogues (16–19), were most stable presumably due to extensive back bonding and could be handled under ambient conditions indefinitely. At the other extreme were the cases of the sensitized photoreduction in the presence of diglyme and norbornene in which copper metal was almost immediately formed as the blue solution started to bleach. This indicates that olefins and polyethers coordinate with Cu(acac) so weakly that their complexes are readily decomposed by disproportionation or photolysis, or by both pathways. Indeed, it is well known that olefins form labile copper(I) complexes (20–30). Similar photolysis in the presence of styrene was very slow, owing to the quenching of triplet state benzophenone by styrene. The solutions of copper(I) complexes containing carbon monoxide and en were generated rapidly by photolysis as colorless solutions. Under an inert atmosphere in the dark, these solutions started to deposit copper metal within a few hours. On continuing irradiation these solutions were photolysed to deposit copper metal in about the same time required for disproportionation. These complications prevented us from drawing a clear conclusion as to whether the copper formations were due to disproportionation or photolysis; the former cause was more probable. In all these photolyses, the black precipitates were not formed and the photolysates readily reacted with PPh_3 to give Cu(acac) $(PPh_3)_2$; these observations confirm the formation of Cu(acac) complexes.

Because of competitive quenching of triplet state benzophenone, it was not feasible to prepare copper(I) complex of a conjugated olefin by this photoreduction. However, a photolysate of the Cu(acac) complex of carbon monoxide reacted with styrene or 1,3-pentadiene to give solutions containing the corresponding Cu(acac) complexes under carbon monoxide. As the resulted solutions did not disproportionate for a long time under argon, it was concluded that the Cu(acac) complexes of these olefins had been formed.

Similar photolysis of $Cu(acac)_2$ and benzophenone in the presence of terminal acetylenes in methanol proceeded rapdily to give the corresponding acetylides **1**–**4** (Table 1) as colored solids or solutions. Bisacetylide **4** derived from 1,5-hexadiyne is *explosive when dry*. From the photolysates, benzophenone was recovered quantitatively and acetylacetone and unreacted acetylenes were detected by gc. Though it is known that a $Cu^{2+}-Cu^{+}$ salt mixture is a good catalytic system for the coupling of terminal acetylenes (24), such products were not detected by gc analysis. These acetylides were identified by reacting with iodobenzene in pyridine (6, 7) to give the corresponding phenylacetylenes **5**–**8** (see Table 1). In addition, acetylides **1** and **2** reacted with triphenylphosphine to give crystalline complexes $[(PhC{\equiv}C)Cu(PPh_3)]$ and $[C_4H_9C{\equiv}CCu(PPh_3)]$ (8). The latter was formed only in the presence of a large excess of triphenylphosphine and was not prepared previously.

$$Cu(acac)_2 + RC{\equiv}CH \xrightarrow[Ph_2CO]{h\nu} CuC{\equiv}CR + 2acacH$$

$$CuC{\equiv}CR + C_6H_5I \xrightarrow[Pyridine]{} PhC{\equiv}CR + (CuI)$$

Similar photolysis of $Cu(acac)_2$ and benzophenone in the presence of 3,5-dimethyl-1-hexyn-3-ol (**9**) gave a dark yellow solution which was quantitatively oxidized in air to a blue solution of $Cu(acac)_2$. The same dark yellow solution was also obtained when photolytically generated black precipitate was reacted with alkynol **9**. This complex reacted with triphenylphosphine to give Cu(acac)$(PPh_3)_2$, indicating that the Cu(acac) complex of the alkynol **10** was formed. The copper(I) acetylide derived from alkynol **9**, $[(CH_3)_2CHCH_2C(CH_3)(OH)C{\equiv}CCu]$ **11**, was stable to air oxidation and exhibited an ir absorption at 2000 cm^{-1}. The photolysate was worked up by ether extraction to give alkynol **9**, benzophenone, and $Cu(acac)_2$. The unstable complex **10** must contain acetylacetonate and alkynol **9** as ligands. The latter, conceivably, contributes both α-hydroxy and acetylenic groups as two coordination sites as shown in the proposed structure. Analogy to such a complex can be found in platinum–alkynol complexes (25). The sensitized photolysis of $Cu(acac)_2$ in the presence of 2-butyn-1,4-diol gave similar results; as the complex decomposed much faster under various conditions, it was not investigated further.

A similar photolysis in the presence of diphenylacetylene gave Cu(acac)$(C_6H_5CCC_6H_5)$ **12**, as colorless needles showing an ir absorption at 1975 cm^{-1}. Dissolution of the complex **12** in methanol, chloroform, or other organic solvents quickly decomposed it to give a brown solution; the solution in $CDCl_3$, however, displayed the signal for the methyl protons of acetylacetone at 2.02 and 2.30 ppm and that for phenyl protons at 7.43 ppm in a 6:10 ratio. The complex **12** also readily reacted with triphenylphosphine to give Cu(acac)$(PPh_3)_2$ and slowly decomposed on storage either under nitrogen or oxygen. In the presence of 3-hexyne, similar photolysis apparently gave $[Cu(acac)(EtC{\equiv}CEt)]$ **13** which showed a similar pattern of behavior as above. Further studies of this complex were not carried out owing to its instability.

The limited data on structure shown indicate that **12** has the

Can. J. Chem. Downloaded from www.nrcresearchpress.com by 210.87.254.6 on 09/06/12
For personal use only.

TABLE 1. Copper(I) acetylides and phenylacetylenes

Acetylides		% Yield	Melting point (°C)	Infrared (cm^{-1})‡	Phenylacetylenes*	
C_6H_5—C≡CCu	**1**	72	230°C decomp.	1930	$C_6H_5C{\equiv}CC_6H_5$	**5**
$CH_3(CH_2)_3$—C≡CCu	**2**	90	145–185°C decomp.	1927	$CH_3(CH_2)_3C{\equiv}CC_6H_5$	**6**
$(CH_3)_3C$—C≡CCu†	**3**	37	82°C decomp.	2000	$(CH_3)_3CC{\equiv}CC_6H_5$	**7**
$(CH_2$—C≡CCu$)_2$	**4**	67	140–155°C decomp.	2120	$(CH_2C{\equiv}CC_6H_5)_2$	**8**

*The product obtained from the acetylides reaction with iodobenzene.
†This acetylide was obtained as a soluble compound; others precipitated directly from photolysates.
‡The carbon–carbon stretching bond for acetylides in which 2120 cm^{-1} for **4** is weak.

molecular formula Cu(acac)(PhCCPh) and that the carbon–carbon triple bond is probably coordinated in the side-on mode (26–28) in view of the ir absorption at 1975 cm^{-1} and ease of

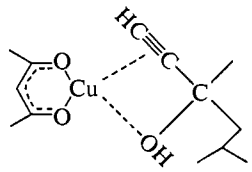

10

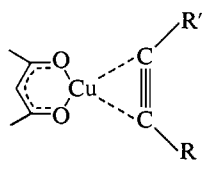

12

the displacement of the diphenylacetylenic moiety by triphenylphosphine. Assuming that complex **12** has a monomeric constitution, the acetylene should act as a bidentate ligand by donating four electrons (26) to the copper(I) center. The number of known mononuclear metal complexes which contain coordinated acetylene remains few in spite of extensive studies on acetylene coordination complexes with various transition metals (29–34). Such mononuclear complexes are generally regarded as intermediates in the catalytic process of acetylene oligomerization on account of the activated triple bond (31–34). Although the isolation of acetylene complexes of copper(I) tetrachloroaluminate have been reported (35, 36), the details are not available. In view of well established X-ray structures of nickel (37), palladium (32, 38), platinum (33, 39), and tungsten (26) complexes of acetylenes, the structure as shown is suggested as the copper(I) complex of diphenylacetylene. Such a structure is explained by an in-plane σ-bond and perpendicular π-orbital overlap between the metal and acetylenic linkage (26–28).

Purely from the consideration of pK_a values of acetylene (pK_a 25) and acetylacetone (pK_a 9), a bimolecular displacement on Cu(acac) does not seem to be a reasonable mechanism for the formation of copper(I) acetylides from terminal acetylenes. It is simplest to assume that all acetylenes reacted with Cu(acac) to form coordinate complexes similar to that shown in structure **12**. For terminal acetylenes, the $C_{(sp)}H$ bond becomes polarized because of electron donation to the metal center. A similar proposal has been made to account for carbonium ion-like reactivity of acetylene carbons in platinum complexes (33). The acetylides are most likely formed from intramolecular displacement, and precipitated as polymers.

$$\text{Cu(acac)(RC}{\equiv}\text{CH)} \rightarrow \text{Cu(acac)(RC}{\equiv}\text{C}^-) + \text{H}^+$$
$$\rightarrow \text{CuC}{\equiv}\text{CR} + \text{acacH}$$

While adequate information could not be obtained to assign structures to each copper(I) complex owing to failure in isolation, the lack of the formation of polymeric Cu(acac) as well as the formation of Cu(acac)$(PPh_3)_2$ on reacting with triphenylphosphine indicates that the benzophenone-sensitized photoreduction of Cu(acac)$_2$ generates Cu(acac) which can coordinate with various types of ligands to form a variety of copper(I) complexes. By analogy with copper(I) acetylides (8) and halides (40), the insolubility, non-crystallinity, and ready disproportionation in solid states of the black precipitates may suggest that they are polymers of Cu(acac) with indeterminate compositions and structures. Polymeric copper(I) complexes are not uncommon (40) and generally utilize heteroatoms for bridging of copper(I) centers as shown by X-ray analysis. While the reactivities of these copper(I) complexes show a wide range of variations, their reactions toward oxidation, substitution, photolysis, and/or disproportionation vary considerably with changes in ligands. Presumably, these reactivities are related to the strength of the copper–ligand bonds and depend on the extent of the back donation of electrons through π-overlap of the bonds. It is noteworthy that under the photolysis conditions, the oxetenes, or their derivatives, corresponding to the addition of triplet state benzophenone to these acetylenes (41) are not detected. This is not surprising since we have demonstrated that Cu(acac)$_2$ quenches triplet-state benzophenone efficiently with $k_q = (3.6–6.8) \times 10^9\ M^{-1}\ s^{-1}$ (42): the reaction of the latter with acetylenes is obviously unimportant at the concentration ratio of Cu(acac)$_2$ to acetylenes used in the photolysis.

It is well known that certain copper(II) complexes are readily reduced by phosphines (16–19) and electrolysis (43). In spite of the difficulty encountered in the isolation of the copper(I) complexes, the present sensitized photoreduction demonstrates an advantageous route to prepare certain copper(I) complexes that are difficult to prepare by conventional reduction methods. First, since the reducing species is generated by photoexcitation and at any given time its concentration is low, the rate and extent of the reduction can be regulated easily to avoid over-reduction. Secondly, the reducing power is related to *excited state reduction potential*, e.g., the sum of the reduction potential and the triplet state energy of a ketone (42). It is, in theory, possible to choose a matching sensitizer to effect the reduction of a specific step without affecting others. Thirdly, the system offers certain manoeuverability in ligand interchange reactions, in particular, if ligands, such as styrene and 1,3-pentadienes, react with triplet-state sensitizers and cannot be added in the photolysis. For example, the Cu(acac) complex of carbon monoxide can be made easily by the sensitized photoreduction and a desired ligand then added to give the corresponding Cu(acac) complexes.

Acknowledgement

The authors are indebted to the Natural Sciences and Engineering Council of Canada, Ottawa, for financial support of the research project.

Can. J. Chem. Downloaded from www.nrcresearchpress.com by 210.87.254.6 on 09/06/12
For personal use only.

1. G. BUONO-CORE, K. IWAI, Y. L. CHOW, T. KOYANAGI, A. KAJI, and J. HAYAMI. Can. J. Chem. **57**, 8 (1979).
2. A. J. FRY, R. S. H. LIU, and G. S. HAMMOND. J. Am. Chem. Soc. **88**, 4781 (1961).
3. F. WILKINSON and A. FARMILO. J. Chem. Soc. Faraday Trans. II, 604 (1976).
4. G. PORTER and M. R. WRIGHT. Discuss. Faraday Soc. **27**, 18 (1959).
5. J. A. BELL and H. LINSCHITZ. J. Am. Chem. Soc. **85**, 528 (1963).
6. H. O. HOUSE and M. J. UMEN. J. Org. Chem. **38**, 3893 (1973).
7. C. E. CASTRO, E. J. GANGHAM, and D. C. OWSLEY. J. Org. Chem. **31**, 4071 (1966).
8. G. E. COATES and C. PARKIN. J. Inorg. Nucl. Chem. **22**, 59 (1961).
9. F. BOHLMAN and E. BRESINSKY. Ber. **100**, 1209 (1967).
10. H. D. GAFNEY and R. L. LINTVEDT. J. Am. Chem. Soc. **93**, 1623 (1971).
11. F. A. COTTON and G. WILKINSON. Advanced inorganic chemistry. 3rd ed. John Wiley and Sons, Inc., New York. 1972. p. 907.
12. R. J. P. WILLIAMS. J. Chem. Soc. 137 (1955).
13. G. FERRAUDI and S. MURALIDHARAN. Coord. Chem. Rev. **36**, 45 (1981).
14. M. PASQUALI, C. FLORIANI, and A. G. MANFREDOTTI. J. Chem. Soc. Chem. Commun. 921 (1978); M. PASQUALI, G. MALINI, C. FLORIANI, and A. G. MANFREDOTTI. J. Chem. Soc. Chem. Commun. 937 (1979).
15. T. TSUDA, H. HABU, S. HORIGUCHI, and T. SAEGUSA. J. Am. Chem. Soc. **96**, 5930 (1974).
16. R. A. ZELONKA and M. C. BAIRD. Can. J. Chem. **50**, 1269 (1972).
17. F. H. JARDINE, L. RULE, and A. G. VOHRA. J. Chem. Soc. A, 238 (1970).
18. W. A. ANDERSON, A. J. CARTY, G. J. PALENIK, and G. SCHREIBER. Can. J. Chem. **49**, 761 (1971).
19. D. GIBSON, B. F. G. JOHNSON, and J. LEWIS. J. Chem. Soc. A, 367 (1970).
20. D. A. EDWARDS and R. RICHARDS. J. Organomet. Chem. **86**, 407 (1975).
21. M. B. DINES. Inorg. Chem. **11**, 2949 (1972).
22. P. F. RODESILER and E. L. AMMA. J. Chem. Soc. Chem. Commun. 599 (1974).
23. H. L. HAIGHT, J. R. DOYLE, N. C. BAENZIGER, and G. F. RICHARDS. Inorg. Chem. **2**, 1301 (1963).
24. T. H. RUTLEDGE. Acetylenic compounds. Reinhold Book Co., New York. 1969. p. 245.
25. J. CHATT, R. G. GUY, and L. A. GUY. Nature, **184**, 562 (1959).
26. B. C. WARD and J. L. TEMPLETON. J. Am. Chem. Soc. **102**, 1532 (1980); R. B. KING. Inorg. Chem. **7**, 1044 (1968).
27. J. CHATT and L. A. DUNCANSON. J. Chem. Soc. 2939 (1953).
28. M. J. S. DEWAR. Bull. Soc. Chim. Fr. **18**, 79 (1951).
29. W. HUBEL. *In* Organic synthesis via metal carbonyls. Vol. 1. *Edited by* I. Wendler and P. Pins. Wiley-Interscience, New York. 1968. p. 273.
30. R. S. DICKSON and P. J. FRASER. Adv. Organomet. Chem. **12**, 323 (1974).
31. S. OTSUKA and A. NAKAMURA. Adv. Organomet. Chem. **14**, 245 (1976).
32. P. M. MAITLIS. Pure Appl. Chem. **33**, 489 (1973).
33. M. H. CHISHOLM and H. C. CLARK. Acc. Chem. Res. **6**, 202 (1973).
34. F. G. A. STONE. Acc. Chem. Res. **14**, 318 (1981).
35. F. L. CARTER and E. W. HUGHES. Acta Crystallogr. **10**, 801 (1957).
36. G. A. CHUKHADZHYAN, G. A. GEVORKYAN, and V. P. KUKOLEV. Russ. J. Org. Chem. **46**, 905 (1976).
37. P. W. JOLLY and G. WILKE. The organic chemistry of nickel. Vol. 1. Academic Press, New York. 1974. p. 244.
38. R. S. DICKSON and J. A. IBERS. J. Organomet. Chem. **36**, 191 (1972).
39. J. CHATT, R. G. GUY, and L. A. DUNCANSON. J. Chem. Soc. 827 (1961).
40. E. N. BAKER and P. M. GARRICK. J. Chem. Soc. Dalton, 416 (1978).
41. H. POLMAN, A. MOSTERD, and H. J. T. BOS. Rec. Trav. Chim. **92**, 845 (1973).
42. Y. L. CHOW, G. E. BUONO-CORE, B. MARCINIAK, and C. BEDDARD. Can. J. Chem. **61**, 801 (1983).

Can. J. Chem. Downloaded from www.nrcresearchpress.com by 210.87.254.6 on 09/06/12
For personal use only.

Mechanistic studies of aromatic ketone-sensitized photoreduction of bis(acetylacetonato)copper(II)

YUAN L. CHOW, GONZALO E. BUONO-CORE, BRONISLAW MARCINIAK, AND CAROL BEDDARD
Department of Chemistry, Simon Fraser University, Burnaby, B.C., Canada V5A 1S6

Received April 28, 1982

This paper is dedicated to Professor Harry E. Gunning on the occasion of his 65th birthday

YUAN L. CHOW, GONZALO E. BUONO-CORE, BRONISLAW MARCINIAK, and CAROL BEDDARD. Can. J. Chem. **61**, 801 (1983).

Bis(acetylacetonato)copper(II), $Cu(acac)_2$, quenches triplet excited states of ketones and polynuclear aromatic hydrocarbons efficiently, but only aromatic ketones with high triplet energy successfully sensitize photoreduction of $Cu(acac)_2$ in alcohols under nitrogen to give derivatives of acetylacetonatocopper(I), Cu(acac). For the triplet state benzophenone-sensitized photoreduction of $Cu(acac)_2$, the quantum yields of photoreduction (Φ_C) and those of benzophenone disappearance (Φ_B) were determined in methanol with various concentrations of $Cu(acac)_2$. The values of the quenching rate constant, k_q, determined from these two types of monitors on the basis of the proposed mechanism were in good agreement ($6.89 \sim 7.35 \times 10^9\ M^{-1}\ s^{-1}$). This value was higher, by a factor of about two, than that obtained from the monitor of the benzophenone triplet decay rates generated by flash photolysis in the presence of $Cu(acac)_2$. The quenching rate constants of various aromatic ketone and hydrocarbon triplet states by $Cu(acac)_2$ were determined by flash photolysis to be in the order of the diffusion rate constant and the quantum yields of these photoreductions were found to be far from unity. Paramagnetic quenching, with contributions of electron exchange and charge transfer, was proposed as a possible quenching mechanism. For a series of aromatic ketone sensitizers with higher triplet energy, this mechanism was used to rationalize the observed high quenching rate constants in contrast to the low quantum yields of photoreduction.

YUAN L. CHOW, GONZALO E. BUONO-CORE, BRONISLAW MARCINIAK et CAROL BEDDARD. Can. J. Chem. **61**, 801 (1983).

Le bis(acétylacétonato)cuivre(II) $Cu(acac)_2$ inhibe efficacement les états excités triplets des cétones et des hydrocarbures aromatiques polynucléaires mais seules les cétones aromatiques avec un triplet à haute énergie sensibilisent avec succès la photoréduction du $Cu(acac)_2$ dans les alcools sous atmosphère d'azote en donnant des dérivés d'acétylacétonato-cuivre(I), Cu(acac). On a déterminé, dans le méthanol et pour diverses concentrations en $Cu(acac)_2$, les rendements quantiques de photoréduction (Φ_C) et ceux de la disparition de la benzophénone (Φ_B) lors de la réduction du $Cu(acac)_2$ photosensibilisée par la benzophénone à l'état triplet. Les valeurs de la constante d'inhibition, k_q, déterminées à partir de ces deux types de contrôle sur la base du mécanisme proposé s'accordent bien ($6{,}89 \sim 7{,}35 \times 10^9\ M^{-1}\ s^{-1}$). Cette valeur est plus élevée d'un facteur d'environ de deux que celle obtenue à partir du contrôle de vitesse de désintégration du triplet de la benzophénone produite par la photolyse flash en présence du $Cu(acac)_2$. On a déterminé les constantes de vitesse d'inhibition de plusieurs cétones aromatiques et des états triplets des hydrocarbures par le $Cu(acac)_2$; elles sont de l'ordre de la constante de vitesse de diffusion et on a trouvé que les rendements quantiques de ces photoréductions sont loin d'être unitaires. On propose comme mécanisme possible d'inhibition, une inhibition paramagnétique avec des contributions d'échange d'électron et de transfert de charge. Dans le cas d'une série de sensibilisateurs de cétone aromatique avec un triplet à grande énergie, on a utilisé ce mécanisme pour rationaliser les fortes constantes d'inhibition observées par contraste avec les faibles rendements quantiques de la photoréduction.

[Traduit par le journal]

Introduction

We have shown (1) that bis(acetylacetonato)copper(II), $Cu(acac)_2$, can undergo ketone-sensitized photoreduction to form copper(I) complexes in hydrogen-donating solvents such as alcohols and tetrahydrofuran. Transition metal ions and complexes of β-diketonates are known to be efficient quenchers of the triplet state of a number of organic sensitizers (2–6). Porter and Wright (4) have defined this process as paramagnetic quenching. This explanation has been widely adapted to describe the interaction of excited states with radicals, such as nitric oxide (7), nitroxides (7–15), oxygen (16, 17), and paramagnetic metal ions and complexes (2–6). Investigations aiming to clarify the mechanism of the quenching process generally utilize simpler stable radicals as quenchers (7–13) which enhance deactivation of electronically excited molecules. The paramagnetic quenching of triplet state sensitizers by metal ions and complexes is generally investigated by flash excitation (2–5); however, the fate of the quenchers has not attracted any serious studies. Spin-allowed catalyzed intersystem crossing (4, 7, 9, 10, 18, 19) has been proposed to account for such quenching without physical changes in quenchers. While energy transfer has been ruled out for this quenching process (2, 4), at least one group favors this mechanism (3, 8). We are intrigued by the fact that, in spite of efficient quenching, certain ketones (e.g., benzophenone, anthrone, xanthone, etc.) sensitize the $Cu(acac)_2$ reduction efficiently, while fluorenone and *p*-methoxyacetophenone are totally inefficient as sensitizers (1).

On the basis of qualitative observations (1), we have described the general reaction pattern and have suggested that the sensitized photoreduction occurs by electron transfer from $Cu(acac)_2$ to the triplet excited states of ketones but probably not by energy transfer. The main reasons for this conclusion are the failure to correlate the triplet energy levels of these ketones with the occurrence of the sensitized photoreduction. We have since recognized that a monolithic mechanism cannot explain the whole range of quenching reactions and the overall mechanism may involve a complex sequence of charge transfer, electron exchange, and hydrogen abstraction. We have concentrated our efforts on unravelling the kinetics and mechanism of triplet state benzophenone-sensitized $Cu(acac)_2$ photoreductions. The results are described in this report.

Can. J. Chem. Downloaded from www.nrcresearchpress.com by 210.87.254.40 on 09/06/12
For personal use only.

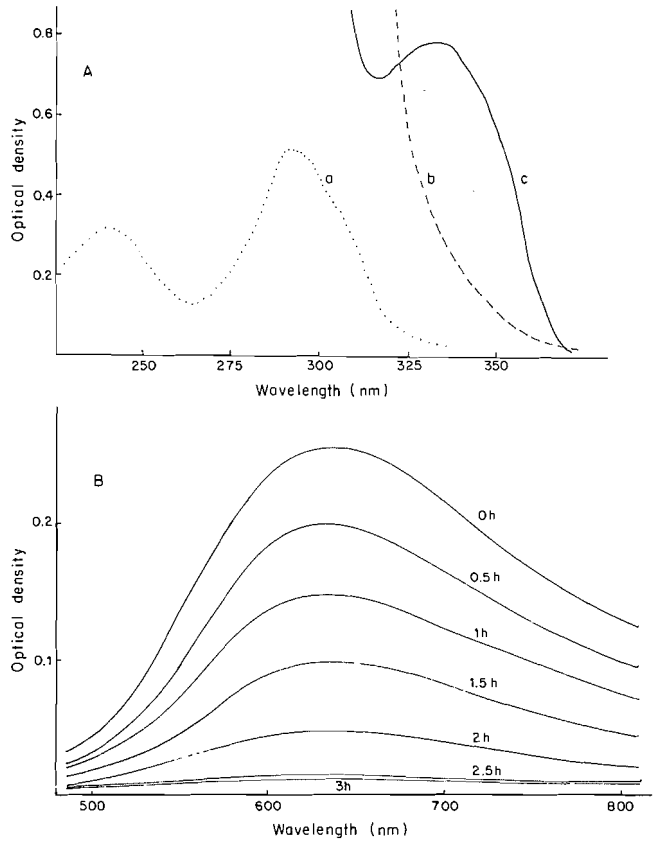

FIG. 1. (*A*) The absorption spectra in methanol: (*a*) $Cu(acac)_2$, 2×10^{-5} *M*; (*b*) $Cu(acac)_2$, 5×10^{-4} *M*; and (*c*) benzophenone, 5×10^{-3} *M*. (*B*) Photolysis of a methanol (200 mL) solution containing $Cu(acac)_2$, 5.75×10^{-3} *M*; benzophenone, 6.60×10^{-3} *M*; and triphenylphosphine, 1.15×10^{-2} *M* monitored at 500–800 nm.

TABLE 1. Average quantum yields of $Cu(acac)_2$ disappearance sensitized by benzophenone in methanol and other alcohols[a,b]

$[Cu(acac)_2] \times 10^3$ *M*	% conversion	Φ_C
0.6	16.6	0.09
0.8	15.3	0.11
1.0	20.8	0.14
2.0	18.2	0.17
4.0	14.2	0.18
6.0	12.4	0.23
8.0	12.4	0.23
10.0	10.8	0.25
2.0	—	0.40[c]
2.0	—	0.52[d]

[a]The solutions (5 mL) were irradiated for 5–20 min to cause percentage decomposition of $Cu(acac)_2$ as indicated. For each reaction about three readings were taken to give the average quantum yields.

[b]Except for the last two sets of data, the concentrations of benzophenone and triphenylphosphine were 0.4 *M* and 0.01 *M*. For the last two sets the corresponding concentrations were 0.1 *M* and 4×10^{-3} *M* respectively.

[c]The quantum yield was measured in ethanol.

[d]The quantum yield was measured in isopropanol.

Results

Quantum yield determinations

We have found that, among the Cu(acac) complexes obtained in benzophenone-sensitized photoreduction, only $Cu(acac)(Ph_3P)_2$ was not oxidized by air and was thermally and photolytically stable under the photolysis conditions. Taking advantage of the stability, as well as the low reactivity of triphenylphosphine relative to $Cu(acac)_2$ with the triplet state benzophenone (20) (*vide infra*), the reaction was run in the presence of triphenylphosphine so that the photolysate could be analyzed spectroscopically at 620 nm for $Cu(acac)_2$ and/or by gas and liquid chromatography. The analytical data provided the quantum yield of benzophenone disappearance (Φ_B) and that of $Cu(acac)_2$ disappearance (Φ_C).

TABLE 2. The quantum yields of the benzophenone (5×10^{-2} *M*) disappearance by $Cu(acac)_2$ quenching in the presence of triphenylphosphine (1×10^{-2} *M*) in methanol[a]

Concentration $Cu(acac)_2$ ($\times 10^3$ *M*)	Φ_B[b]	Φ_B^0/Φ_B
10	0.110	9.91
6	0.144	7.71
4	0.201	5.52
2	0.418	2.66
1	0.418	2.66
0.8	0.729	1.52
0.5	1.07	1.04
0.0	1.11[c]	1.00

[a]The solutions (5 mL) were irradiated for 15 min to cause <12% of the benzophenone decomposition.

[b]Averaged values from two sets of experiments.

[c]The quantum yield, in the absence of $Cu(acac)_2$ but in the presence of triphenylphosphine (10^{-2} *M*), was taken as Φ_B^0.

Quantum yields were measured in methanol solutions containing proper concentrations of materials (Fig. 1) on the merry-go-round apparatus, using a benzophenone–benzhydrol actinometer (21). The quantum yield of disappearance of $Cu(acac)_2$, Φ_C, in methanol in the presence of triphenylphosphine and benzophenone was determined at various concentrations of $Cu(acac)_2$ by following the decrease in the 620 nm absorption (Fig. 1). The quantum yield, Φ_C, increased steadily in the $Cu(acac)_2$ concentration range of 10^{-3}–10^{-2} *M* and reached nearly the limiting value of 0.25 at 10^{-2} *M* (Table 1). At this concentration, the photoreduction of benzophenone was drastically reduced, as could be seen later in the quantum yields of benzophenone disappearance, Φ_B (Table 2). In preparative scale experiments, where concentrations of $Cu(acac)_2$ were higher than 10^{-2} *M*, the formation of the benzopinacol and the loss of benzophenone were not observed. The quantum yields of $Cu(acac)_2$ disappearance, Φ_C, under comparable conditions in methanol, ethanol, and 2-propanol were found to increase in the same order (Table 1), indicating higher quantum yields in better hydrogen-donating solvents.

In order to evaluate the nature of quenching processes, the quantum yields of the $Cu(acac)_2$ disappearance by various sensitizers were determined under comparable conditions and the reduction half-wave potential (E_{A/A^-}) of sensitizers was measured by cyclic voltammetry. These data are summarized in Table 3. In these experiments, the sensitizer concentrations were adjusted so that >98% of the incident light was absorbed by the sensitizers in every case except biacetyl. In the last case, only 68% of the light was absorbed by biacetyl and its quantum yields were normalized to the 100% absorption. For the purpose of maintaining the same conditions to compare the efficiency of quenchings, the concentration of $Cu(acac)_2$ was set at 2×10^{-3} *M*. While this did not give the limiting quantum yields for each sensitizer, it did provide the comparison of the overall reduction efficiency of sensitizers.

Unfortunately, the quantum yields Φ_C in the absence of

Can. J. Chem. Downloaded from www.nrcresearchpress.com by 210.87.254.40 on 09/06/12
For personal use only.

TABLE 3. The quenching rate constants of triplet sensitizers by $Cu(acac)_2$ and quantum yields of $Cu(acac)_2$ disappearance in methanol[a]

No.	Sensitizer	Quenching rate constant[b] $k_q \times 10^{-9}\ M^{-1}\ s^{-1}$	E_T (kcal/mol)[c]	E_{A/A^-} (eV)[d]	$-E_T - E_{A/A^-}$ (kcal/mol)	Φ_C
1	Anthrone	−(435)[g]	72.0	−0.81	−53.4	0.29
2	Benzophenone	3.6(535)	69.1	−1.36	−37.8	0.19
3	Xanthone	5.6(610)	74.2	−1.17	−47.3	0.16
4	Benzil	0.95(480)	53.7	−1.20	−26.1	0.067
5	Acetophenone	—	74.1	−1.54	−38.7	0.057
6	Biacetyl	—	54.9	−0.80	−37.5	0.023
7	2-Acetonaphthone	1.86(430)	59.3	−1.44	−26.4	0.013
8	Fluorenone	~0.99(420)[h]	53.3	−0.79	−35.1	0.00
9	Propiophenone	7.61(365)	74.6	−1.56[f]	−38.7	—
10	*p*-Methoxyacetophenone	5.35(390)	71.7	−1.70[f]	−32.6	0.00
11	Duroquinone	3.76(430)	53.0	−0.84[e]	−33.7	—
12	Anthracene	1.24(425)	42.0	−1.92[e]	+ 2.2	0.00
13	Phenanthrene	2.17(483)	62.2	−2.44[e]	− 6.1	0.00
14	Pyrene	1.91(520)	48.0	−2.09[e]	+ 0.1	0.00

[a]For the quantum yield measurements, 5 mL of solution was irradiated for 15 min with an accompanying actinometric determination. The concentration of $Cu(acac)_2$ was $2 \times 10^{-3}\ M$, of triphenylphosphine $4 \times 10^{-3}\ M$, and those of the sensitizers 0.1 *M*.

[b]Flash photolysis was carried out in MeOH solution in the presence of $Cu(acac)_2$ at several concentrations, and the triplet signal decays were monitored at the wavelength given in the parentheses.

[c]The energy of the lowest triplet state quoted from ref. 22.

[d]The reduction half-wave potential in eV determined by cyclic voltammetry. These can be converted to the unit in kcal/mol by a factor of 23.01.

[e]The reduction potential values are quoted from ref. 23.

[f]The two reduction potentials are quoted from Wagner (24). We are grateful to Professor Wagner for the data and other suggestions.

[g]The correlation of k_{obs} with the concentrations of $Cu(acac)_2$ was poor.

[h]The transient signal was weak, and only an approximate value was obtained.

triphenylphosphine could not be accurately determined because of the formation of black precipitates and their easy air oxidation to regenerate $Cu(acac)_2$. As it was desirable to know Φ_C unencumbered by the presence of triphenylphosphine, the quenching experiments were run without triphenylphosphine, and the photolysates were quickly filtered from the black precipitate for uv determinations. This method did not afford reproducible Φ_C values and provided only approximate data. However, it was noted that, for anthrone, benzophenone, xanthone, acetophenone, and biacetyl sensitizations, the Φ_C values obtained by this method were in the same decreasing order and the same order of magnitude shown in Table 3.

Studies by flash photolysis

In view of the drastic quenching of the photoreaction of triplet state benzophenone, as shown by the lack of the formation of benzopinacol in the preparative studies, as opposed to the low quantum yields of the photoreduction of $Cu(acac)_2$ (see Table 1), it was necessary to measure the quenching rate constants of sensitizer triplet states by $Cu(acac)_2$ under comparable conditions. Taking advantage of the fact that most triplet state absorption spectra are well known by the flash excitation technique, the rate constants of these reactions could be determined directly without being encumbered by the follow-up reactions. Thanks to Scaiano, who made his nitrogen laser-pulsed flash photolysis apparatus (337.1 nm, 8 ns, 3 mJ) (25) available to us, we measured the lifetimes of the triplet state decay of these sensitizers in the absence ($\tau_0 = 1/k_0$) and in the presence ($\tau_{expt} = 1/k_{expt}$) of the various concentrations of $Cu(acac)_2$ ranging from 10^{-3} to $10^{-5}\ M$. The concentrations of sensitizers were about $10^{-4}\ M$ and the kinetics of the triplet state decays were monitored at the wavelength indicated (Table 3). In each case, the decay of the triplet signals was analyzed by fitting of the corresponding time profiles from which the pseudo-first-order decay patterns were ascertained and their rate constants, k_{expt}, determined. The quenching rate constants, k_q, were determined from the Stern−Volmer plots according to eq. [1] where [A] is the concentration of $Cu(acac)_2$.

$$[1] \quad k_{expt} = k_0 + k_q[A]$$

In Fig. 2, log k_q was plotted against the lowest triplet state energies (E_T) and also against $-(E_T + E_{A/A^-})$, the free energy available in the electron transfer process for sensitizers, according to Weller's empirical relation (26−28).

Analysis of Fig. 2*a* and 2*b* by a non-linear least-square data analysis (a program written by K. E. Newman of this Department) showed the correlations were poor in both but slightly better in the latter case. The correlation coefficients were improved if the point due to benzil was omitted. Unusually low quenching rate constants of the benzil triplet have been noted previously (2), and the transient spectra in the presence of $Cu(acac)_2$ showed signals other than the triplet signal. The poor correlation of the plots failed to support either an energy transfer or a simple electron transfer mechanism. However, the general trends hinted that subtle relations might exist between k_q and E_T, as well as E_{A/A^-}. It was visually noted that moderately good correlation could be made with those points arising from aromatic ketones, i.e., excluding the points due to aromatic hydrocarbons and benzil. Characteristically, the variation of k_q was only within an order of magnitude in spite of large variations in E_T or $-E_T - E_{A/A^-}$; that is, the imaginary slopes were about 0.2 per eV. The resistance of diamagnetic Cu(I) complexes of triphenylphosphine, 2,2′-dipyridine, and 1,10-phenanthroline toward the photoreduction was confirmed (1). The diamagnetic acetylacetonates of magnesium(II) could not be photoreduced under similar benzophenone sensitization conditions, nor was the rate of benzophenone photoreduction affected. It was reported that diamagnetic $Cu(CN)_2^-$, Zn^{2+}, and Ga^{3+} ions failed to quench triplet state naphthalene. As the

Can. J. Chem. Downloaded from www.nrcresearchpress.com by 210.87.254.40 on 09/06/12
For personal use only.

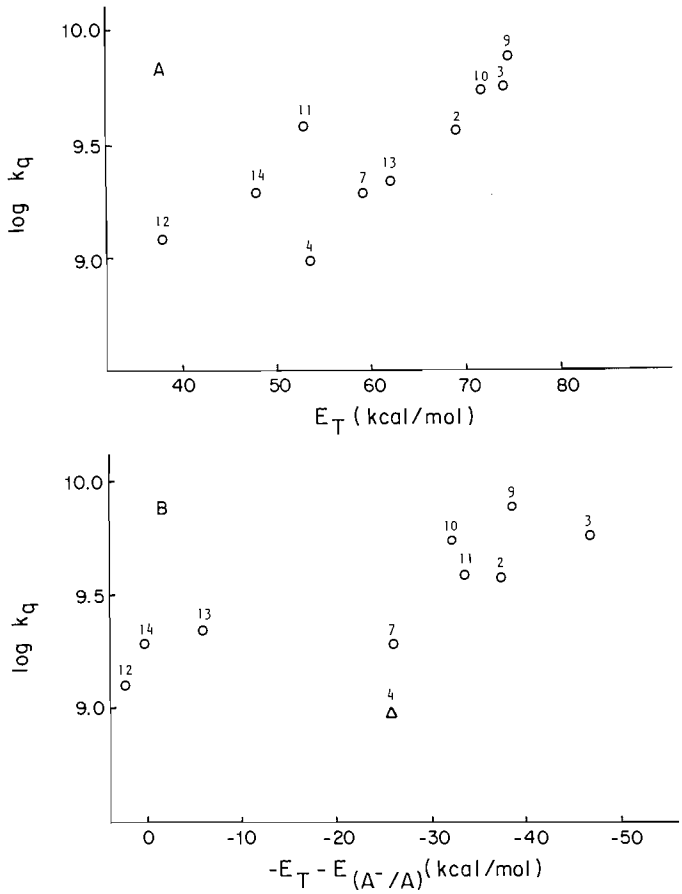

FIG. 2. The correlation of log k_q with (*a*) the lowest triplet state energy E_T and (*b*) $-E_T - E_{A/A^-}$.

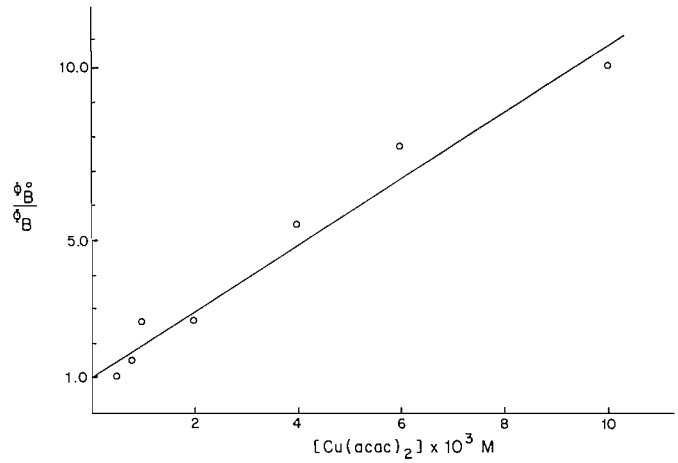

FIG. 3. The Stern–Volmer plot of benzophenone disappearance against the concentrations of $Cu(acac)_2$.

copper(II) state is paramagnetic and $Cu(acac)_2$ in methanol shows distinct esr signals, $Cu(acac)_2$ must quench triplet state sensitizers by paramagnetic interaction as proposed previously (4, 7, 18, 19).

Kinetic analysis

The results presented so far have led us to assume that the interaction of the sensitizer triplet state with $Cu(acac)_2$, which is referred to as a complex for the moment, must be partitioned into a successful reduction yielding Cu(acac), benzophenone, acetylacetone, and the $\cdot CH_2OH$ radical on one hand, and an unsuccessful reduction on the other. On the basis of this assumption, a mechanism as represented by reactions [2]–[7] was proposed for the kinetic analysis of the sensitized reduction of $Cu(acac)_2$. The unsuccessful reaction is shown in reaction [7] in which the complex reverts to benzophenone and $Cu(acac)_2$. The successful reaction as in reaction [6] involves an irreversible hydrogen abstraction from methanol, the rate constant k_p of which contains the term of fixed concentration of methanol and [C] is the concentration of the complex.

$$[2] \quad Ph_2CO \xrightarrow[I]{h\nu} Ph_2CO(\text{singlet})$$

$$Ph_2CO(\text{singlet}) \xrightarrow{\alpha} Ph_2CO(\text{triplet}) \qquad \alpha I$$

$$[3a] \quad {}^*Ph_2CO + CH_3OH \rightarrow Ph_2\dot{C}OH + \dot{C}H_2OH \qquad k_m[B^*][MeOH]$$

$$[3b] \quad {}^*Ph_2CO + Ph_3P \rightarrow \text{Products} \qquad k_n[B^*][PPh_3]$$

$$[4] \quad {}^*Ph_2CO \rightarrow Ph_2CO + \Delta + h\nu \qquad k_d[B^*]$$

$$[5] \quad {}^*Ph_2CO + Cu(acac)_2 \rightarrow [\text{Complex}] \qquad k_q[B^*][A]$$

$$[6] \quad [\text{Complex}] + CH_3OH \rightarrow acacH + \dot{C}H_2OH + Ph_2CO + Cu(acac) \qquad k_p[C]$$

$$[7] \quad [\text{Complex}] \rightarrow Cu(acac)_2 + Ph_2CO \qquad k_b[C]$$

On the basis of this mechanistic assumption, the following equations are derived where α is the fraction of the intersystem crossing ($\alpha = 1$ for benzophenone) (29) and [A] is the concentration of $Cu(acac)_2$.

$$[8] \quad \frac{\Phi_B^0}{\Phi_B} = 1 + k_q\tau[A]$$

where $\tau = 1/(k_d + k_m[MeOH] + k_n[Ph_3P])$

$$[9] \quad \frac{1}{\Phi_C} = \frac{1}{\alpha\beta} + \frac{1}{\alpha\beta k_q\tau[A]}$$

where $\beta = k_p/(k_p + k_b)$.

The efficiency of quenching of triplet state benzophenone by $Cu(acac)_2$ was elaborated by measuring the quantum yields of benzophenone disappearance, Φ_B, in the presence of varying concentrations of $Cu(acac)_2$ as shown in Table 2. A Stern–Volmer plot of Φ_B^0/Φ_B against $Cu(acac)_2$ concentration according to eq. [8] gave a straight line (correlation coefficient = 0.9854, see Fig. 3) with a slope of $k_q\tau = 9.65 \times 10^2\ M^{-1}$.

The quantum yields of $Cu(acac)_2$ disappearance, Φ_C, obtained in methanol (Table 1), were used to plot $1/\Phi_C$ vs. $1/[A]$, according to eq. [9] as shown in Fig. 4. This correlation gave a straight line with a correlation coefficient 0.9793 from which the slope ($= 1/\beta\tau k_q$) 3.91×10^{-3} and intercept ($= 1/\beta$) 3.86 were obtained. The term $k_q\tau$ was calculated to be $9.87 \times 10^2\ M^{-1}$ in excellent agreement with that obtained from the Stern–Volmer plot, i.e., the monitoring of benzophenone disappearance. The intercept of 3.86 also shows that the limiting Φ_C in the benzophenone-sensitized $Cu(acac)_2$ decomposition is ca. 0.25 and k_b/k_p is calculated to be ca. 2.9.

The lifetime τ in eqs. [8] and [9] contained a component due to the quenching of triplet state benzophenone by triphenylphosphine. As the presence of triphenylphosphine is an experimental imperative, it was necessary to evaluate the contribution of this quenching process to the lifetime τ. Although the bimolecular rate constant of the quenching of triplet state benzophenone by triphenylphosphine was determined to be $4 \times 10^8\ M^{-1}\ s^{-1}$ in benzene (20), it is desirable to determine the

Can. J. Chem. Downloaded from www.nrcresearchpress.com by 210.87.254.40 on 09/06/12
For personal use only.

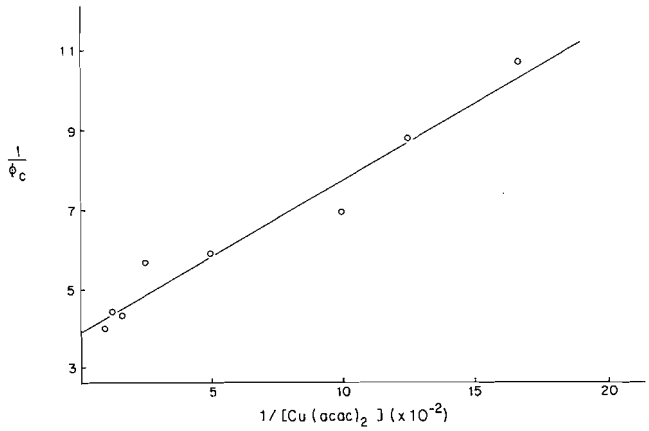

FIG. 4. The plots of reciprocals of the quantum yield of $Cu(acac)_2$ disappearance against reciprocals of $Cu(acac)_2$ concentrations in methanol.

quenching rate constant in methanol since, in a separate study, we found that this quenching induced some reactions involving methanol. For this purpose, the benzophenone photoreduction in methanol was run in various concentrations of triphenylphosphine and the quantum yields of benzophenone disappearance, Φ_n, were determined. The Stern–Volmer plot gave a slope of 92.93 M^{-1} (correlation coefficient 0.9917), according to eq. [10], where τ^0 is the decay lifetime of triplet state benzophenone in methanol.

$$[10] \quad \Phi^0/\Phi_n = 1 + k_n\tau^0[PPh_3]$$

It is obvious in these static quenching experiments that the absolute values of k_n and k_q can be calculated if the accurate value of τ^0, or $1/(k_d + k_m[CH_3OH])$, is known. If we adapt the decay rate constant of triplet state benzophenone in methanol, as measured by flash photolysis (30), as the starting point, $k_d + k_m[CH_3OH]$ is 3.8×10^6 s^{-1} and, therefore, τ^0 is 2.6×10^{-7} s, from which the following quenching rate constants are obtained.

$$k_n = (3.5 \pm 0.4) \times 10^8\ M^{-1}\ s^{-1}$$
$$k_q = (6.89 \pm 1.0) \times 10^9\ M^{-1}\ s^{-1}$$
(from Φ_B monitor, Fig. 3)

or

$$k_q = (7.35 \pm 1.4) \times 10^9\ M^{-1}\ s^{-1}$$
(from Φ_C monitor, Fig. 4)

Discussion

For a photochemical reaction as complex as the present one, the proposed mechanism as shown in reactions [2]–[7] is probably just the essential steps to visualize the sensitization and redox processes. Since the kinetic analysis based on the monitor of benzophenone disappearance Φ_B (Fig. 3) and of $Cu(acac)_2$ disappearance Φ_C (Fig. 4) gives reasonably good straight lines and their $k_q\tau$ values are in excellent accord, this mechanistic scheme provides a basis for the discussion. An immediate question is the higher values of k_q determined by the static quenching experiments by a factor of about 2 than that determined by flash photolysis (Table 3). Remembering that computation of the former static quenching rate constants k_q (and also k_n) depends on the size of the lifetime of triplet state benzophenone τ^0 in methanol, the discrepancy may not be real and may even be acceptable in view of the diversity of techniques. In addition, the higher k_q values may be attributed to the presence of triphenylphosphine in the static experiments. Since the absorption spectrum >400 nm of $Cu(acac)_2$ in the presence of up to 0.05 M triphenylphosphine is not changed at all, there is no new complex species present in the solution. As this solution is photostable, there is no direct interaction between excited state $Cu(acac)_2$ and triphenylphosphine. However, it is not inconceivable that triphenylphosphine participates during the course of the interaction of triplet state benzophenone with $Cu(acac)_2$ in some way facilitating the quenching processes; e.g., a participation in substitution reactions with the proposed complex (*vide infra*) is quite conceivable.

The proposed mechanism contains two contentious steps that require discussion, namely, the nature of the quenching process and the decay pattern of the complex. We shall discuss the latter first. The kinetic analysis leads us to conclude that the limiting quantum yield Φ_C, obtained in the benzophenone-sensitized photoreduction of $Cu(acac)_2$, arises from the partition of the complex between successful photoreduction (reaction [6]) and unsuccessful one (reaction [7]); i.e., k_b/k_p is determined to be 2.9 from Fig. 4. This conclusion is supported, firstly, by the observation that the quantum yields Φ_C at the same concentration of $Cu(acac)_2$ increase in better hydrogen-donating solvents as shown in Table 1; e.g., increasingly higher Φ_C in MeOH < EtOH < 2-PrOH. Secondly, as shown in Table 3, the relatively invariable k_q values of quenching as opposed to the wide variation of Φ_C requires that the efficient quenching process must be modified by a partition scheme to account for product patterns.

For the nature of the quenching process, while the data of Table 3 and the plots of Fig. 2 do not support a single mechanism either by energy transfer or electron transfer for the whole range of quenching studied, at least they indicate that log k_q of aromatic ketone triplets (except benzil) is related to $-E_T - E_{A/A^-}$. The invariance of k_q of duroquinone and benzophenone with respect to the E_T difference may be cited as an example, among others, which is contrary to an energy transfer. This is not a viable mechanism since the majority of these sensitizers (Table 3) have insufficient triplet energy levels to cause electronic transition of the $Cu(acac)_2$ CTTM band at 240 nm, the electronic transition which results in photodecomposition by direct photolysis (1). The advocate of energy transfer also suggested that only when the metal complex ligand field state can accept electronic energy with appreciable rates, such energy transfer may occur (3).

A pathway based on the reduction of $Cu(acac)_2$ by the ketyl radical $Ph_2\dot{C}OH$ formed in reaction [3*a*] merits consideration since it is known that xanthone, benzophenone, and acetophenone can be photoreduced while fluorenone and *p*-methoxyacetophenone do not undergo photoreduction in alcohols (31–33).[1] Indeed, this mechanism has been invoked to explain the photolytic dehydrogenation of cyclohexane in the presence of benzophenone and copper(II) pivalate (33). On the following grounds, we believe this mechanism cannot be operating. First of all, since triplet state benzophenone is almost totally quenched at $Cu(acac)_2$ concentrations above 10^{-2} M and the limiting quantum yield of copper(I) complexes at these concentrations is far below unity ($\Phi_C = 0.25$), one would still obtain photoreduction products of benzophenone, e.g., benzopinacol, if reaction [3*a*] is the sole quenching pathway. As the benzophenone photoreduction is virtually reduced to insignificant amounts above 10^{-2} M $Cu(acac)_2$, it contradicts the hy-

[1]We are grateful to Dr. Scaiano for a copy of the preprint.

Can. J. Chem. Downloaded from www.nrcresearchpress.com by 210.87.254.40 on 09/06/12
For personal use only.

Can. J. Chem. Downloaded from www.nrcresearchpress.com by 210.87.254.40 on 09/06/12
For personal use only.

drogen abstraction mechanism. Secondly, the quenching rate constant (k_m) for reaction [3*a*], that is, the bimolecular rate constant for the hydrogen abstraction by triplet state benzophenone, cannot be higher than $1.5 \times 10^5\ M^{-1}\ s^{-1}$ as judged from the lifetime in methanol (30). Considering $k_q = 3.6 \times 10^9\ M^{-1}\ s^{-1}$ for reaction [5], as determined by monitoring the triplet state decay in flash photolysis, hydrogen abstraction of triplet state benzophenone from methanol will not be competitive unless the $Cu(acac)_2$ concentration is 10^{-2} or lower. It will be most unlikely that two mechanisms are operating in the sensitized photoreduction of $Cu(acac)_2$ depending on the concentrations of quenchers.

The mechanistic interpretation of the quenching of triplet sensitizers by paramagnetic metal ions and complexes is complicated by solvent effects and electrostatic effects of the partners. The theory of paramagnetic quenching has evolved along the idea of "catalyzed intersystem crossing", developed by Porter and co-workers (7, 10, 18, 19). On the basis of nitric oxide quenching of aromatic hydrocarbon triplet states (7), Porter's group has proposed that paramagnetic quenching involves contributions from electron exchange (9, 10) mixed with charge transfer (7, 18) within a collision complex. While the extent of the contributions of charge transfer depends on solvent polarity, redox potentials and triplet state energy levels, this contribution tends to be more important in the higher triplet energy region of sensitizers. The quenching rate constants are also higher in this region (7).

As a group, aromatic ketones (except benzil) show similar photochemical and sensitization behavior. The moderately good correlations of log k_q vs. $-E_T - E_{A/A^-}$ as well as log k_q vs. E_T for the aromatic ketones with higher triplet energy shown in Fig. 2 suggest that the dual quenching mechanism discussed above can be operating for these sensitizers. In analogy to the proposal made by Porter's group (34), a complex from excited state ketones and $Cu(acac)_2$ in polar solvent, such as methanol, should have a high dipole moment which would lower the energy level of the charge transfer state. Thus, reasonably stabilized ketyl radical anions might be formed under the conditions unless a methoxyl group at the *para* position destabilizes the formation (see Table 3, No. 10). $Cu(acac)_2$ exhibits two irreversible oxidation waves by cyclic voltametry in acetonitrile at +1.47 and 1.72 eV. Certainly, at the first oxidation potential, most triplet excited ketones have enough reduction energy to complete the charge transfer interaction. Therefore, the complex proposed in reaction [5] may be elaborated as **1** or **2**. Direct electron transfer from triplet state benzophenone to $Cu(acac)_2$ is deemed unlikely for energetic reasons (35), and supported by the failure of triplet state *p*-methoxyacetophenone to sensitize the photoreduction. The transient $Cu(acac)_2^{\ddagger}$ species should have the copper(III) state as in **3** but may rapidly transfer to Cu(II)–ligand radical species as in **4** by analogy with general intramolecular redox behavior of copper(III) complexes (36, 37). We assume a loose association of $Cu(acac)^+$ with the acetylacetonyl radical as in **2** as the intermediate from which the latter reacts irreversibly by hydrogen abstraction from methanol (or solvents) as in reaction [6]. The back transfer of an electron from the benzophenone ketyl radical anion to $Cu(acac)^+$ completes the successful reduction process. At this stage, all the reactants become neutral species and no significant electrostatic attraction can be encountered. The overall reaction consists of an indirect electron migration from the ligand to the copper center using triplet state benzophenone as an energy pump.

$$*Ph_2CO + Cu(acac)_2 \rightarrow \underset{\mathbf{1}}{[Ph_2CO^{\cdot-} \ldots Cu(acac)_2^{+\cdot}]} \rightarrow$$

$$\underset{\mathbf{2}}{[Ph_2CO^{\cdot-} \ldots Cu(acac)^+ \ldots acac^{\cdot}]} \rightarrow Ph_2CO + Cu(acac) + acac^{\cdot}$$

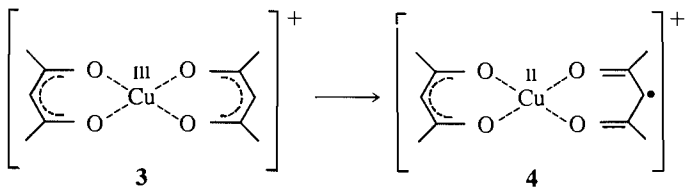

3 **4**

From the quantum yield dependence of the photoreduction on alcohols, it is most appropriate to view reactions [6] and [7] as competing processes in which a higher degree of the charge transfer contribution and a better hydrogen-donating alcohol leads to higher quantum yields in the sensitized photoreduction. In this context, the failure of triplet state aromatic hydrocarbons to sensitize the photoreduction may be interpreted as a rapid reverse charge transfer (reaction [7]), which may be regarded as the spin-allowed intersystem crossing (7, 10).

While the proposed mechanistic model is in reasonable agreement with the observations and kinetic analysis, it needs more refinements and supporting evidence. The presence of the acetylacetonyl radical during the photoreduction has been gained by trapping of the radical by simple olefins as the addition products and by 2-nitroso-2-methylpropane as the stable nitroxide radical (38). In the presence of 5 mol% of *p*-dinitrobenzene, a good electron scavenger (39, 40), the benzophenone-sensitized photoreduction of $Cu(acac)_2$ is inhibited for 5–6 h while the uninhibited photoreduction completed the reaction in only 3 h: both *p*-nitrobenzene and benzophenone are recovered (41). Control experiments show that *p*-dinitrobenzene is completely decomposed by a benzophenone-sensitized photoreaction, probably by the energy transfer process, and that *p*-dinitrobenzene is extremely inefficient to sensitize $Cu(acac)_2$ photodecompositions. While the quenching mechanism by *p*-dinitrobenzene has not been determined, the quenching certainly indicates that some kind of electron transfer is involved in the sensitized photoreduction.

In conclusion, this report demonstrates that the triplet state of various sensitizers are quenched by $Cu(acac)_2$, and also by other paramagnetic transition metal β-diketonate complexes as well (2), very efficiently by paramagnetic quenching but only aromatic ketone sensitizers with relatively high triplet energy successfully sensitize the $Cu(acac)_2$ photoreduction via a charge transfer intermediate in the presence of hydrogen-donating solvents. The efficiency of the sensitized photoreduction depends on the degree of charge transfer contribution of the collision complexes and the hydrogen abstraction of the acetylacetonyl radical. Energy transfer from triplet state aromatic ketones to $Cu(acac)_2$ is probably slow, at least by an order of magnitude, in spite of the fact that the latter has a low energy level.

Experimental

General conditions and materials

Ultraviolet and visible spectra were obtained with a Cary 17 spectrophotometer. A Hewlett-Packard Model 5985 spectrometer was used to perform gc coupled with mass spectrometry. The hplc machine was constructed with a LDC Model 711 solvent delivery system, a

Can. J. Chem. Downloaded from www.nrcresearchpress.com by 210.87.254.40 on 09/06/12
For personal use only.

Rheodyne Model 7120 syringe loading sample injector, a Partisil PXS 10/25 Whatman analytical column, and LDC Model 1203 UV monitor (254 nm). Commercially available sensitizers were purified by distillation or recrystallization–sublimation. Other conditions are the same as those described in the previous papers (1).

Apparatus

For large scale preparations, an immersion type photocell or an overhead irradiation set-up, as described previously (1), were used. Quantum yield determinations were carried out in small phototubes in a "merry-go-round". The Pyrex phototubes of ca. 5 mL capacity (1.2 cm diameter × 10 cm length) were equipped with a gas inlet and outlet which had a mercury seal. The light source was a Hanovia 450-W (679A36) or 200-W (654A36) medium pressure lamp, placed in a Pyrex water cooling jacket.

Cyclic voltammetry

The half-wave reduction potentials ($E_{1/2}$) were determined in acetonitrile by cyclic voltammetry using a three-electrode cell with a P.A.R. Electrochemistry System Model 170 (Princeton Applied Research Corp., Princeton, NJ). The working electrode was a platinum microdisc and the counter electrode was a platinum wire. A silver wire electrode was used as a reference electrode which was shown to be 100 mV more positive to a sce in water and 0.1 *M* tetraethylammonium chloride (TEAC) as supporting electrolyte. The half-wave potential of $Cu(acac)_2$ was determined in acetonitrile in the presence of tetraethylammonium perchlorate with reference to sce. The measured data were subtracted by 0.1 eV to afford E_{A/A^-} given in Table 3.

Quantum yield determination

Generally, stock solutions of $Cu(acac)_2$, triphenylphosphine, and sensitizers were prepared. Aliquots of each solution were pipetted into a volumetric flask (10 mL) to prepare solutions for irradiation with the required concentrations. For actinometry, benzene solutions 0.05 *M* in benzophenone and 0.1 *M* in benzhydrol were used. The remaining benzophenone was determined by following the changes in the optical density at 333 nm and/or by hplc analysis. A quantum yield of 0.74 was assumed for the secondary actinometry (21). The solutions (4 or 5 mL) in phototubes were deaerated with purified nitrogen and irradiated for a prescribed length of time (generally 5–20 min) to cause <20% conversion. The photolysates were analyzed immediately for decreases of $Cu(acac)_2$ by determining the absorbance at 620 nm. After that, hplc analyses of photolysates were carried out using 2% isopropanol in hexane solvent to afford the quantum yields of benzophenone disappearance. For each series of measurements, two to four tubes of solutions were irradiated for 5, 10, 15, or 20 min, and the solutions were analyzed. The quantum yields were calculated and the average values were obtained.

For sensitized photoreduction, the concentrations of various sensitizers were adjusted to absorb more than 98% of incident light, except biacetyl. In this case, biacetyl absorbs only 68% of the incident light, calculated at 330 nm. The quantum yields were corrected to compensate for the partial absorption of light. For the benzophenone-sensitized photoreduction, the proportion of the incident light absorbed by benzophenone was calculated using the absorbance at 330 nm. The decrease of benzophenone and $Cu(acac)_2$ was corrected to represent the total incident light. From these data, the quantum yields of benzophenone and $Cu(acac)_2$ disappearance were calculated and tabulated in Tables 1 and 2.

For determinations of the quantum yields of $Cu(acac)_2$ without added triphenylphosphine, phototubes containing the solutions (5 mL) of $Cu(acac)_2$ and benzophenone were irradiated in the usual manner. The solutions were filtered through a sintered glass filter quickly. The uv spectra of the solution were taken immediately. The quantum yields of a single series varied as much as ±10%. The order of the Φ values was the same as shown in Table 3.

For the determination of the quenching rate constant of the triplet state benzophenone by triphenylphosphine, solutions of benzophenone (0.05 *M*) in methanol containing triphenylphosphine (0.0025–0.035 *M*) were irradiated for 55 min to cause 8 ~ 35% conversion. For each concentration, the average of two readings was taken. Two series of experiments were run to give the averaged $k_q\tau$.

Flash photolysis

For flash photolysis, methanol (Aldrich, Gold Label) was used as received. The solutions of sensitizers (ca. 10^{-2}–10^{-3} *M*) and $Cu(acac)_2$ (10^{-3}–10^{-4} *M*) were placed in Suprasil quartz cells of 3 mm optical path and deaerated with oxygen-free argon. The samples were excited with the pulses from a Molectron UV-400 nitrogen laser. The flash apparatus, interfaced to a PDP 11/55 computer, as described previously (25), was used. The Stern–Volmer plots and quenching rate constants for each series were carried out by the same computer.

Acknowledgements

Support of this research by the Natural Sciences and Engineering Research Council of Canada, Ottawa, is gratefully acknowledged. The authors thank Mr. Peter Hoang for assistance in cyclic voltammetry and Dr. J. C. Scaiano for the use of the flash photolysis apparatus.

1. G. E. Buono-Core, K. Iwai, Y. L. Chow, T. Koyanagi, A. Kaji, and J. Hayami. Can. J. Chem. **57**, 8 (1979); Y. L. Chow and G. E. Buono-Core. Can. J. Chem. **61**, 795 (1983).
2. A. J. Fry, R. S. H. Liu, and G. S. Hammond. J. Am. Chem. Soc. **88**, 4781 (1966); G. S. Hammond and R. P. Foss. J. Phys. Chem. **68**, 3739 (1964); R. P. Foss, D. O. Cowan, and G. S. Hammond. J. Phys. Chem. **68**, 3747 (1964).
3. F. Wilkinson and A. Farmilo. J. Chem. Soc. Faraday II, 604 (1976).
4. G. Porter and M. R. Wright. Discuss. Faraday Soc. **27**, 18 (1959).
5. J. A. Bell and H. Linschitz. J. Am. Chem. Soc. **85**, 528 (1963); H. Linschitz and L. Pekkarinen. J. Am. Chem. Soc. **82**, 2411 (1960).
6. J. C. W. Chien and W. P. Conner. J. Am. Chem. Soc. **90**, 1001 (1968); A. Heller and E. Wasserman. J. Phys. Chem. **42**, 949 (1965).
7. O. L. J. Gijzeman, F. Kaufman, and G. Porter. J. Chem. Soc. Faraday II, **69**, 727 (1973).
8. A. R. Watkins. Chem. Phys. Lett. **29**, 526 (1974); **70**, 262 (1980).
9. V. A. Kuzmin and A. S. Tatikolov. Chem. Phys. Lett. **53**, 606 (1978).
10. R. E. Schwerzel and R. A. Caldwell. J. Am. Chem. Soc. **95**, 1382 (1973).
11. G. Porter and M. W. Windsor. Proc. R. Soc. Ser. A, **245**, 238 (1958).
12. S. Kusuhara and R. Hardwick. J. Chem. Phys. **41**, 2386 (1964).
13. S. Seigel and H. S. Judeikis. J. Chem. Phys. **48**, 1613 (1968).
14. P. de Mayo. Acc. Chem. Res. **4**, 41 (1971).
15. A. K. Hoffman, A. M. Feldman, E. Gelblum, and W. G. Hodgson. J. Am. Chem. Soc. **86**, 639 (1964).
16. K. Gollnick. Adv. Photochem. **6**, 1 (1968).
17. R. Wayne. Adv. Photochem. **7**, 311 (1969).
18. J. N. Murrell. Mol. Phys. **3**, 319 (1960).
19. G. J. Hoytink. Discuss. Faraday Soc. **45**, 14 (1968); G. J. Hoytink. Acc. Chem. Res. **2**, 114 (1969).
20. R. S. Davidson and P. F. Lambeth. Chem. Commun. 1098 (1969); J. B. Guttenplan and S. G. Cohen. J. Am. Chem. Soc. **94**, 4040 (1972); S. G. Cohen and N. M. Stein. J. Am. Chem. Soc. **93**, 6542 (1971); J. C. Scaiano. J. Photochem. **2**, 71 (1973).
21. G. S. Hammond and P. A. Leermakers. J. Phys. Chem. **66**, 1148 (1962).
22. S. L. Murov. Handbook of photochemistry. Marcel Dekker, Inc., New York, NY. 1973. p. 5; D. O. Cowan and

R. L. DRISKO. Elements of organic photochemistry. Pullman Press, New York, NY. 1976. p. 224.
23. C. K. MANN and K. K. BARNES. Electrochemical reactions in non-aqueous solutions. M. Dekker, New York, NY. 1974; L. MEITES and P. ZUMAN. Electrochemical data. Part 1. Vol. A. John Wiley, New York, NY. 1974.
24. P. J. WAGNER. Private communications.
25. P. K. DAS, M. V. ENCINAS, R. D. SMALL, JR., and J. C. SCAIANO. J. Am. Chem. Soc. **101**, 6965 (1979); R. D. SMALL, JR. and J. C. SCAIANO. J. Phys. Chem. **82**, 2662 (1978).
26. D. REHM and A. WELLER. Ber. Bunsenges. **73**, 834 (1969).
27. J. B. GUTTENPLAN and S. G. COHEN. Tetrahedron Lett. 2163 (1972).
28. C. R. BOCK, T. J. MEYER, and D. G. WHITTEN. J. Am. Chem. Soc. **97**, 2909 (1975); V. BALZANI, F. BALLETTA, and F. SCANDOLA. J. Am. Chem. Soc. **97**, 102 (1980).
29. W. M. MOORE, G. S. HAMMOND, and R. P. FOSS. J. Am. Chem. Soc. **83**, 2789 (1961); G. S. HAMMOND, W. P. BAKKER, and W. M. MOORE. J. Am. Chem. Soc. **83**, 2795 (1961).
30. M. R. TOPP. Chem. Phys. Lett. **32**, 144 (1975).
31. J. C. SCAIANO. J. Am. Chem. Soc. **102**, 19 (1980).
32. G. A. DAVIS, P. A. CARAPELLUCCI, K. SZOC, and J. D. GRESSER. J. Am. Chem. Soc. **91**, 2264 (1969).
33. G. H. JONES, D. W. EDWARDS, and D. PARR. J. Chem. Soc. Chem. Commun. 969 (1976).
34. L.K. PETTERSON, G. PORTER, and M. R. TOPP. Chem. Phys. Lett. **7**, 612 (1979); O. L. J. GIJZEMAN, F. KAUFMAN, and G. PORTER. J. Chem. Soc. Faraday II, **69**, 708 (1973).
35. P. K. DAS. Tetrahedron Lett. 1307 (1981).
36. J. LATI and D. MEYERSTEIN. J. Chem. Soc. Dalton, 334 (1978).
37. G. FERRAUDI. Inorg. Chem. **17**, 7141 (1978).
38. Y. L. CHOW and G. E. BUONO-CORE. J. Am. Chem. Soc. **104**, 3770 (1982).
39. R. C. KERBER, G. W. URRY, and N. KORNBLUM. J. Am. Chem. Soc. **87**, 4520 (1965); N. KORNBLUM and S. D. BOYD. J. Am. Chem. Soc. **92**, 5783 (1970).
40. J. F. BUNNETT. Acc. Chem. Res. **11**, 413 (1978); R. G. SCAMEHORN and J. F. BUNNETT. J. Org. Chem. **42**, 1449 (1977).
41. G. E. BUONO-CORE. Unpublished results.

Can. J. Chem. Downloaded from www.nrcresearchpress.com by 210.87.254.40 on 09/06/12
For personal use only.

Infrared absorption and resonance Raman scattering of photochromic triphenylformazans

J. W. LEWIS and C. SANDORFY

Département de chimie, Université de Montréal, Montréal (Qué.), Canada H3C 3V1

Received June 7, 1982

This paper is dedicated to Professor Harry E. Gunning on the occasion of his 65th birthday

J. W. LEWIS and C. SANDORFY. Can. J. Chem. **61**, 809 (1983).

The infrared and resonance Raman spectra of the two long-lived forms of triphenylformazan and several of its derivatives have been examined. The spectra of unsymmetrically ^{15}N-labelled derivatives suggest that two tautomers exist for each of the two forms. This observation is confirmed by the spectra of 1-(*p*-halophenyl)-3,5-diphenylformazans. The spectra of the non-chelate forms of these latter compounds demonstrate that the position of the tautomeric equilibrium is influenced by the electron-attracting ability of the *para*-halo-substituent. A comparison of the resonance Raman spectra of the two forms leads to the conclusion that excited state proton transfer is the initial photoevent in the photochromism of the triphenylformazans.

J. W. LEWIS et C. SANDORFY. Can. J. Chem. **61**, 809 (1983).

Les spectres infrarouges et Raman de résonance des deux formes de longue durée de vie du triphénylformazane et quelques uns de ses dérivés ont été examinés. Les spectres des dérivés asymétriquement marqués par ^{15}N montrent qu'il existe deux tautomères pour chacune des deux formes. Cette observation est confirmée par les spectres du 1-(*p*-halophényl)-3,5-diphénylformazane. Les spectres des formes non-chélatées de ces derniers composés montrent que la position de l'équilibre tautomérique est influencée par le pouvoir attracteur d'électron de l'halogène substitué en position *para*. La comparaison des spectres Raman de résonance des deux formes nous amène à conclure que le transfert d'un proton à l'état électroniquement excité est l'étape photochimique initiale de la transformation photochromique des triphénylformazanes.

Introduction

1,3,5-Triphenylformazan and some of its derivatives are characterized by rather unusual ground state as well as excited state properties. The unusual ground state properties afford comparative studies of tautomeric pair structures. The excited state properties of these compounds offer excellent opportunities for investigations of proton transfer, photochromism, and photo-induced isomerization. The electronic absorption spectrum of the triphenylformazan species that is eventually generated by means of a photo-initiated first event is characterized by an absorption band at higher energy than that of the initial molecular species. Most photochromic compounds, on the other hand, exhibit new absorption bands at lower energy upon irradiation.

The photochromic properties of triphenylformazan have been studied on four occasions. Kuhn and co-workers (1, 2), on the basis of ultraviolet–visible absorption measurements, proposed a cyclic scheme involving three photochemical and three thermochemical reactions to account for their results (Scheme 1, left). More recently Langbein (3) and Grummt and Langbein (4), on the basis of flash photolytic investigations, proposed the modified scheme (Scheme 1, right). Despite the obvious differences between the two schemes, both clearly suggest that under continuous irradiation a photostationary state involving **D** and **C** should be achieved.

The work of Otting and Neugebauer (5) appears to be the

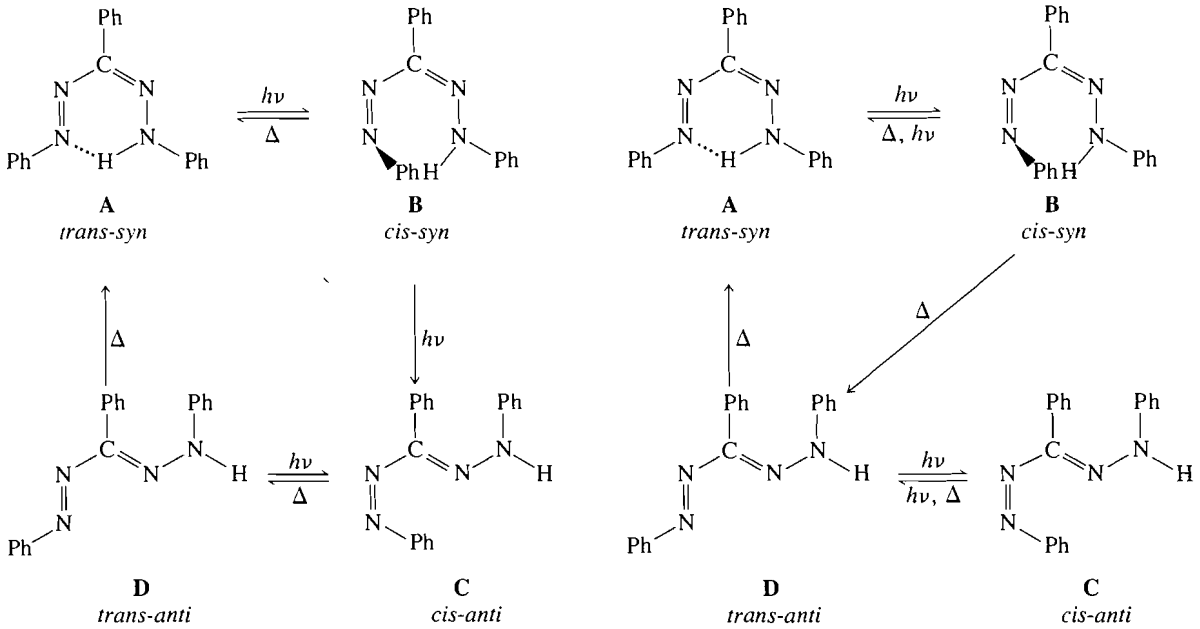

SCHEME 1

Can. J. Chem. Downloaded from www.nrcresearchpress.com by 210.87.254.40 on 09/06/12
For personal use only.

Can. J. Chem. Downloaded from www.nrcresearchpress.com by 210.87.254.40 on 09/06/12
For personal use only.

only infrared spectroscopic investigation of both the chelate and non-chelate forms of triphenylformazan. These authors, by means of partial ^{15}N-labelling, assigned several infrared absorption bands of isomers **A** and **D** and retained for them the structures proposed by Kuhn and co-workers. Other authors (6–10) also studied the infrared absorptions of isomer **A** of triphenylformazan, several derivatives of triphenylformazan, and several metal complexes of these derivatives. In spite of these several studies, there still appear to exist ambiguities in the infrared band assignments.

Fischer and co-workers (11), in a nuclear magnetic resonance study of ^{15}N-proton coupling in unsymmetrically substituted triphenylformazan derivatives, demonstrated that the two structures which might be drawn for isomer **A** are not resonance hybrids but tautomeric pairs. It was further shown that the position of the tautomeric equilibrium is a function of the substituents present on the phenyl groups at N_1 and N_5.

The present investigation, involving infrared absorption (IR) and resonance Raman (RR) scattering, is designed to probe the photochromic transformation, to provide a more complete assignment of the vibrational bands of the chelate and non-chelate forms of triphenylformazans, to further explore the tautomeric-pair structures of these forms, to investigate the possibility of excited state proton transfer, and to furnish a more intimate description of the vibrational bands associated with the chromophores. In this latter aspect, RR spectroscopy is a most powerful tool since only a few of the many possible vibrations are selectively enhanced.

The photochromic triphenylformazans are well suited to RR investigation since broad band or relaxed fluorescence is not a problem for either the chelate or non-chelate forms of the compounds, resonance with the lowest energy electronic transition of both forms is easily attained with an argon-ion laser, and the long lifetime of the non-chelate forms permits the independent study of both forms. In addition, both species are not subject to photochemical degradation so long as the exciting wavelengths are limited to the visible region of the spectrum. In order that the above goals might be achieved, IR absorption and RR scattering data for the chelate and non-chelate forms of several triphenylformazans are presented and discussed in some detail. The triphenylformazans investigated in this study include 1,3,5-triphenylformazan (TPF), (1-^{15}N)TPF, (1,2-^{15}N)TPF, (2,4-^{15}N)TPF, and (1,2,4,5-^{15}N)TPF, as well as the 1-(*p*-chlorophenyl)-, 1-(*p*-bromophenyl)-, and 1-(*p*-iodophenyl)-3,5-diphenylformazans (1-(*p*-XP)-3,5-DPF) and 1-(*p*-bromophenyl)-2-^{15}N-3,5-diphenylformazan.

Experimental

The TPF used in this study was prepared by reducing triphenyltetrazolium chloride with dextrose in basic solution and by means of the procedure of Neugebauer and Küchler (12). (2,4-^{15}N)TPF was prepared by means of the literature method (5). The remaining ^{15}N-labelled derivatives were prepared by means of suitable modifications of these procedures. Aniline-^{15}N and sodium nitrite-^{15}N, both of 95% isotopic purity, were products of Merck, Sharp and Dohme, Ltd., Montreal. The remaining derivatives were also prepared by means of suitable modifications of the above procedures.

The ultraviolet–visible and IR absorption spectra were recorded by means of a Cary 17 spectrometer and a Perkin-Elmer 621 spectrometer, respectively. The RR spectra were recorded by means of a Spex Ramalog-6 spectrometer which was equipped with a Coherent Radiation Innova 90-5 argon-ion laser.

The presented RR spectrum of the chelate form of each of the derivatives was recorded from a 25 mL solution of the derivative in carbon tetrachloride. This solution was circulated through a 0.8 mm glass capillary by means of a peristaltic pump. The short lifetime of the non-chelate form in carbon tetrachloride solution insures that a substantial buildup of this form will not occur; however, each of the spectra contains contributions from a few percent of the non-chelate form.

The RR spectra of the non-chelate forms of these compounds were recorded by means of the rotating cell technique (13, 14). In the laser beam the small quantity of the chelate form in the rotating cell is rapidly converted to the non-chelate form; hence, an essentially pure spectrum of this form was obtained without resorting to computer subtraction techniques.

In pure, dry benzene and dichloromethane the lifetimes of the non-chelate forms of these compounds are sufficient for the recording of the IR spectra by means of standard techniques. Thus, the spectrum of the chelate form was recorded, the solution within the IR cell was irradiated for approximately 15 min, and then the spectrum of the corresponding non-chelate form was recorded.

The irradiation source was an Oriel Model 7340 equipped with a 200 W medium pressure mercury arc. The source output was filtered by 12 cm of water to remove the IR portion of the spectrum and by a cut-off filter, Corning 3387, to remove the ultraviolet–visible portion of the spectrum below about 475 nm.

Results and discussion

The solution spectra of TPF and the ^{15}N-labelled derivatives, recorded before and after irradiation, are reproduced in Figs. 1 and 2. A comparison of the spectra of the chelate and non-chelate forms would seem to imply that the C=N stretching bands occur at higher frequencies in the spectra of the non-chelate forms. The shifts of these bands to higher frequencies, upon irradiation, were explained (5) in terms of the rupture of the hydrogen bond and the loss of the resonance stabilization of the six-membered chelate ring.

The C=N stretching bands located near 1510 cm^{-1} in the unirradiated solution spectra are complicated by the fact that they are overlapping with phenyl group bands. It is thus difficult to precisely locate these bands in terms of wavenumbers. Upon irradiation and the resultant opening of the chelate ring, the C=N stretching bands shift to higher energy as expected and appear as well-defined bands. The 1500 cm^{-1} phenyl group bands are now also easily distinguished. Note that (see Scheme 2) two discernable C=N stretching bands are expected only in the case of (1,2-^{15}N)TPF. While it is not possible to fully characterize these two bands in the unirradiated solution spectrum, the irradiated solution spectrum exhibits two bands, at 1565 and 1551 cm^{-1}, which are attributable to the C=^{14}N and C=^{15}N stretching modes, respectively. These data are not consistent with a possible assignment of these bands as ^{14}N—H and ^{15}N—H deformation modes, since, if this were true, two bands would also be expected in the spectrum of (1-^{15}N)TPF.

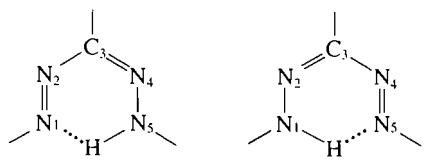

SCHEME 2

The RR spectra of the chelate forms and the corresponding spectra of the non-chelate forms of the triphenylformazans are given in Figs. 3 and 4, respectively. In order to facilitate the direct comparison of the two forms, the spectra of the chelate

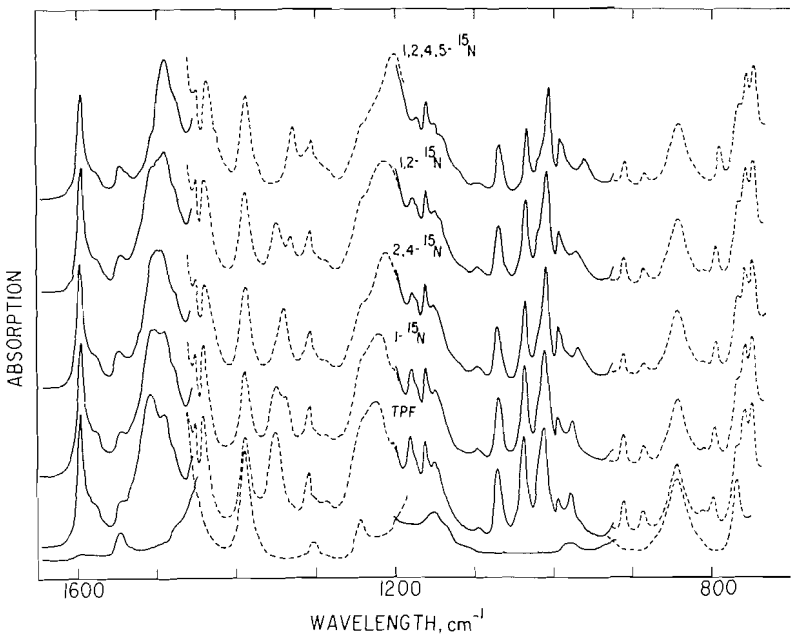

FIG. 1. Infrared absorption spectra of triphenylformazan derivatives in solution. Chelate forms. The solutions are approximately 0.2 *M*. Solvent absorptions are indicated by the lowermost traces. --- Dichloromethane solution; —benzene solution.

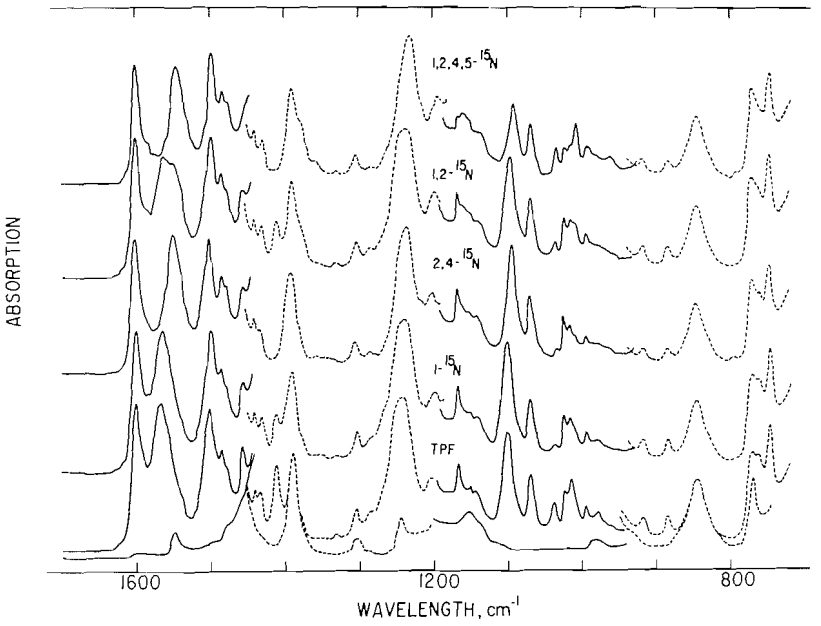

FIG. 2. Infrared absorption spectra of triphenylformazan derivatives in solution. Non-chelate forms. The experimental conditions are identical to those given for Fig. 1, except that the solutions were irradiated for approximately 15 min.

and non-chelate forms of TPF are reproduced in Fig. 5. For reference purposes the ultraviolet–visible absorption spectra of the two forms of TPF are also shown in Fig. 6.

The RR spectral results for TPF should be compared with those of *trans*-azobenzene (15–27). Raman bands of *trans*-azobenzene have been observed (15) at 1589 (phenyl), 1489 (phenyl), 1472 (phenyl), 1442 (νN=N), 1313 (phenyl), 1183 ("Azo-Schlange" (Snake vibration)?), and 1146 cm^{-1} (νC—N). In general it can be seen that the RR spectra of TPF and its derivatives are very similar to that of *trans*-azobenzene. This is especially true for the non-chelate forms of TPF derivatives since these are, in reality, *trans*-azoaromatics. Except for the absence or weakness of TPF bands corresponding to the 1489 and 1472 cm^{-1} phenyl bands of *trans*-azobenzene, there is a one-to-one correspondence for the other bands. In addition, the spectra of the TPF derivatives contain a few bands not reported in the RR spectra of *trans*-azobenzene. (Bands equivalent to the 1277 and 1212 cm^{-1} Raman bands of TPF may also exist for *trans*-azobenzene. See, for example, the IR spectroscopic study of Kübler and co-workers (26) and the Raman study of Brandmüller and co-workers (16).) It is then of interest to analyze a few of the more important bands in the spectra of the chelate forms of the TPF derivatives and to compare these results with those of the non-chelate forms and with those of *trans*-azobenzene.

A medium intensity band appears in the 1600 cm^{-1} region of

Can. J. Chem. Downloaded from www.nrcresearchpress.com by 210.87.254.40 on 09/06/12
For personal use only.

Can. J. Chem. Downloaded from www.nrcresearchpress.com by 210.87.254.40 on 09/06/12
For personal use only.

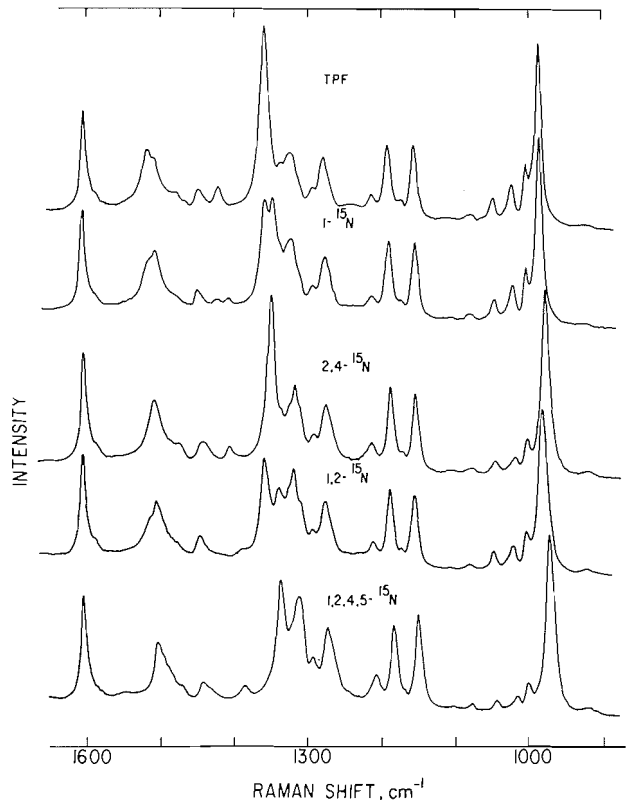

FIG. 3. Resonance Raman spectra of triphenylformazan derivatives in solution. Chelate forms. The solutions are approximately 7×10^{-4} *M* TPF in CCl_4. Experimental conditions: scan rate 1 cm^{-1} s^{-1}, integration time 1 s, 10 K counts full scale, slits 400 μ, laser power 90-110 mW at sample and excitation wavelength 488.0 nm.

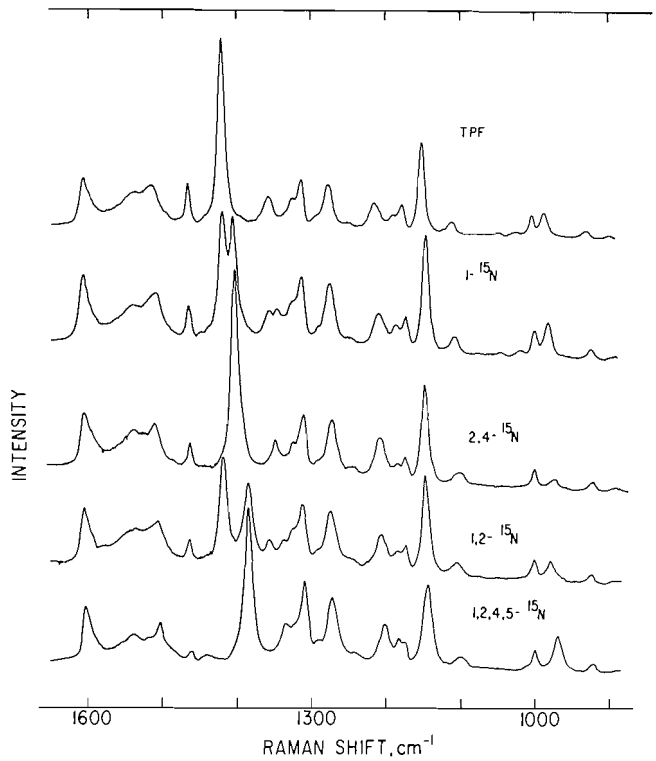

FIG. 4. Resonance Raman spectra of triphenylformazan derivatives in solution. Non-chelate forms. The experimental conditions are identical to those listed for Fig. 3, except that the sample was contained in a rotating cell.

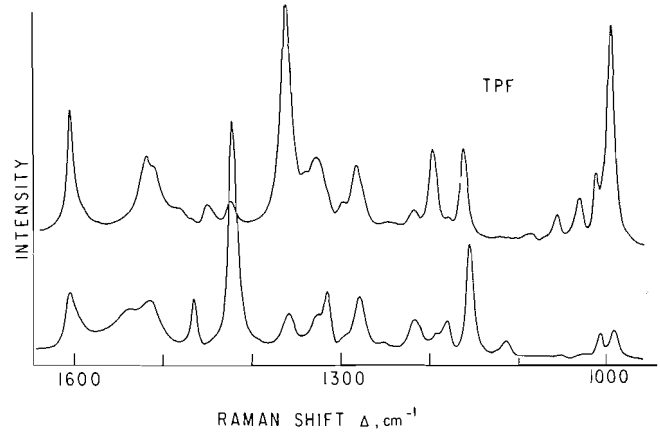

FIG. 5. Resonance Raman spectra of triphenylformazan in solution. Top spectrum: chelate form. Bottom spectrum: non-chelate form. The experimental conditions are identical to those listed for Fig. 3.

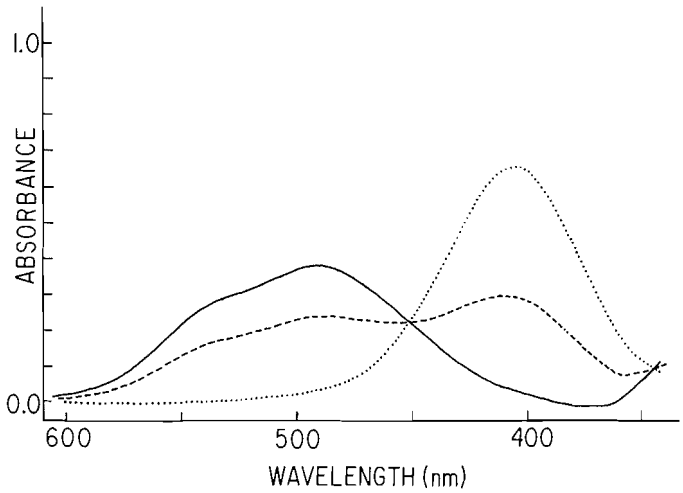

FIG. 6. Electronic absorption spectra of triphenylformazan chelate and non-chelate forms. 2.38×10^{-4} *M* TPF benzene, 0.1 cm cell.

all the spectra shown in Fig. 4. This 1604 cm^{-1} band exhibits no sensitivity to ^{15}N-labelling but does show sensitivity to substitution on the phenyl groups (see below). For these reasons the 1604 cm^{-1} band is most probably attributable to a vibration of the phenyl groups and is not, therefore, attributable to the stretching vibration of the C=N group as previously postulated (9).

The relative intensity of the 1604 cm^{-1} band decreases in the spectra of the non-chelate forms. The chelate form of TPF is probably approximately planar; hence, the 1604 cm^{-1} RR band contains contributions from all three phenyl groups. On the other hand, it is doubtful that the non-chelate form of TPF could be planar and a decrease in the intensity of the 1604 cm^{-1} RR band is therefore expected. A similar decrease in intensity was not observed in the IR spectra shown in Figs. 1 and 2. The origin of this band is undoubtedly similar to that of the 1589 cm^{-1} band of *trans*-azobenzene reported by Hacker (15).

The bands that occur in the 1360−1335 cm^{-1} region of the spectra of the chelate forms exhibit the largest (up to 20 cm^{-1}) isotope shifts of all the spectral bands and are attributed to the N=N stretching vibration. Brandmüller and co-workers (16) observed a 10 cm^{-1} decrease in the N=N stretching frequency of *trans*-azobenzene upon replacing one nitrogen atom with

Can. J. Chem. Downloaded from www.nrcresearchpress.com by 210.87.254.40 on 09/06/12
For personal use only.

nitrogen-15 and the present spectra of (1-^{15}N)TPF indicate an 11 cm^{-1} and a 14 cm^{-1} shift for the chelate and non-chelate forms, respectively. The larger isotope shifts observed in the spectra of TPF derivatives indicate that these N=N motions are purer than is that of *trans*-azobenzene.

The low value, 1357 cm^{-1}, of the N=N stretching energy of TPF is probably due to the intramolecular hydrogen bond and to some chelate ring resonance, although it is believed that the former has the largest effect. The N=N stretching band of the non-chelate form of TPF is located at 1418 cm^{-1} or 61 cm^{-1} to higher energy than that of the chelate form. This stretching energy may be slightly perturbed since, as indicated above, the N=N stretching motion of the non-chelate forms may couple with a higher energy phenyl group vibration. The intensity of the phenyl group band is largest for the unlabelled TPF and it decreases with increasing ^{15}N-substitution. The 1418 cm^{-1} N=N stretching band of the non-chelate form of TPF should therefore be compared with the 1442 cm^{-1} N=N stretching band of *trans*-azobenzene (15, 16).

It was previously implied that two distinguishable N=N stretching bands were possible for (1-^{15}N)TPF and (1,2-^{15}N)TPF. These bands are weak in the IR spectra and most of the corresponding bands of the non-chelate forms are obscured by solvent absorption. These bands are, however, among the strongest bands in the RR spectra. There can thus be no question concerning the origins of these pairs of bands in the spectra of both the chelate and non-chelate forms. The pairs of bands in the spectra of (1-^{15}N)TPF must arise from the ^{14}N=^{14}N and ^{14}N=^{15}N stretching motions and those in the spectra of (1,2-^{15}N)TPF must arise from the ^{14}N=^{14}N and ^{15}N=^{15}N stretching motions. Thus, two tautomers or labelled isomers (5, 11) must exist for these compounds in both forms.

It should also be noted that the N=N stretching motions of the chelate forms may couple with a lower energy motion. The intensities and isotope shifts of these particular N=N stretching bands therefore may not reflect their true values.

The weak bands in the 1360−1335 cm^{-1} region of the spectra of the non-chelate forms represent the N=N stretching bands of a small fraction of the unconverted chelate forms. Compare, for example, the spectra reproduced in Fig. 5.

One or two very weak bands are also observed in the 1420−1380 cm^{-1} region of the spectra of the chelate forms. These bands are due to small quantities of the non-chelate forms that are produced at the laser focal point in the solutions. The origins of these bands were established by varying the peristaltic pump speed. A decrease in pump speed results in an increase in the intensity of this band. (Also, see Fig. 5 for a direct comparison of the spectra of the two forms.)

The second most intense RR band in the spectrum of the chelate form of TPF is located at 984 cm^{-1}. The equivalent bands in the spectra of the ^{15}N-labelled analogues shift to lower energy as the number of ^{15}N-atoms increases. It will also be noticed that the position of this band is also sensitive to the location of the ^{15}N-atoms in the formazan ring. For example, (2,4-^{15}N)TPF exhibits a band at 975 cm^{-1} while the corresponding band of (1,2-^{15}N)TPF is found at 979 cm^{-1}.

Otting and Neugebauer (5) attributed a weak band near 980 cm^{-1} in the IR spectrum of TPF to the breathing mode of a six-membered unsaturated ring. The present RR data confirm this assignment since the band position is a function of both the number and location of ^{15}N-atoms in the formazan ring, the band disappears upon the irradiation of the solution (i.e., the formation of the non-chelate form) and shifts to 960 cm^{-1} in the spectrum which is recorded from a TPF solution in methanol-d_1 where the ring hydrogen is replaced by deuterium.

The combination of the IR and RR spectra of TPF and four of the ^{15}N-labelled isomers permits a more complete assignment of the observed bands. Fortunately, some of the most important bands, such as those due to the C=N and N=N stretching modes as well as the chelate ring breathing mode, appear very prominently in one type of spectrum or the other, but not in both types. The combination of IR and RR spectra thus avoids ambiguities in band assignments which might result if only one type of spectrum were examined.

The RR spectra also quite clearly demonstrate that, upon irradiation, the chelate ring opens. These spectra show that conjugation between the N=N group and the C=N group is essentially lost when the chelate ring opens and, thus, that the non-chelate form of TPF must have a considerably distorted geometry. This information concerning a distorted geometry is uniquely contained in the RR spectra.

Finally, the IR and RR spectra demonstrate that two C=N and two N=N stretching bands are observable in the spectra of selectively ^{15}N-labelled derivatives. The isotope shifts observed in these spectra are comparable to those observed in the spectra of model compounds which are not capable of chelate formation. These facts lead to the conclusion that the two forms of unsymmetrically ^{15}N-labelled TPF derivatives exist in solution as an equilibrium mixture of two tautomers.

In the previous paragraphs the major IR absorption and RR scattering bands of TPF were identified and it was shown that two distinguishable tautomers exist for both the chelate and non-chelate forms of suitably ^{15}N-labelled triphenylformazans. In each case where spectroscopically distinguishable tautomers were possible both were confirmed by means of their RR and IR spectra. As intuitively expected, however, the two tautomers were found to be present in nearly equal proportions. We now wish to consider examples for which equal proportions of the tautomers are not expected.

The compounds to be examined here may be represented by Scheme 3 where *p*-X represents a halogen (chlorine, bromine,

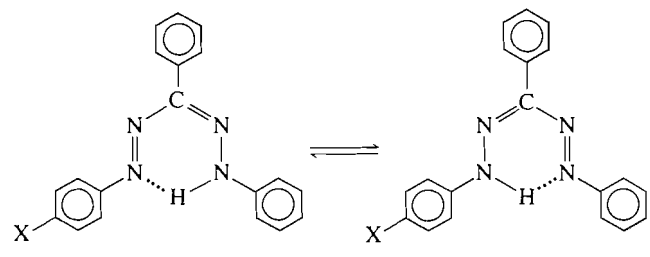

a b

SCHEME 3

or iodine). In all these cases the two tautomers are expected in unequal proportions. The proportions of each tautomer in a solution should be a function of the electron-donating ability of the 1-(*p*-X-phenyl) group as pointed out by Fischer and coworkers (11). Despite the fact that the halogens are electron-attracting substituents, it is assumed that the 1-(*p*-X-phenyl) group remains an electron donor, but it is a less effective one.

The RR spectra of the chelate forms of the *p*-halophenyl derivatives shown in Fig. 7 are remarkably similar to that of the parent, TPF. Two regions of these spectra deserve further comment. These are the regions near 1600 cm^{-1} and near 1350 cm^{-1}. The 1600 cm^{-1} region contains the phenyl group

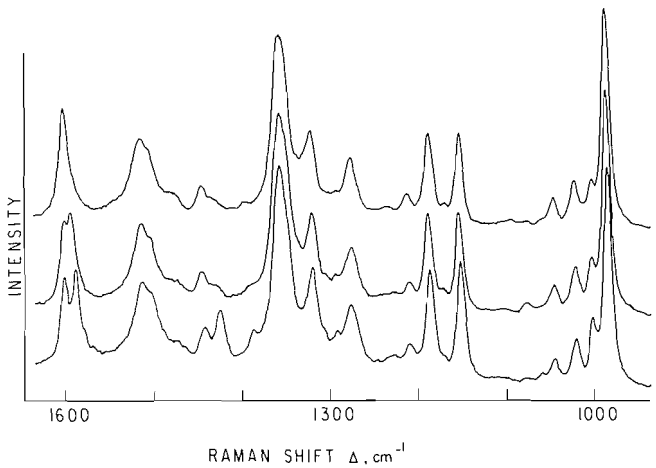

FIG. 7. Resonance Raman spectra of triphenylformazan derivatives in solution. Chelate forms. Top to bottom: 1-(*p*-chlorophenyl)-, 1-(*p*-bromophenyl)-, 1-(*p*-iodophenyl)-3,5-diphenylformazan. The experimental conditions are identical to those listed for Fig. 3.

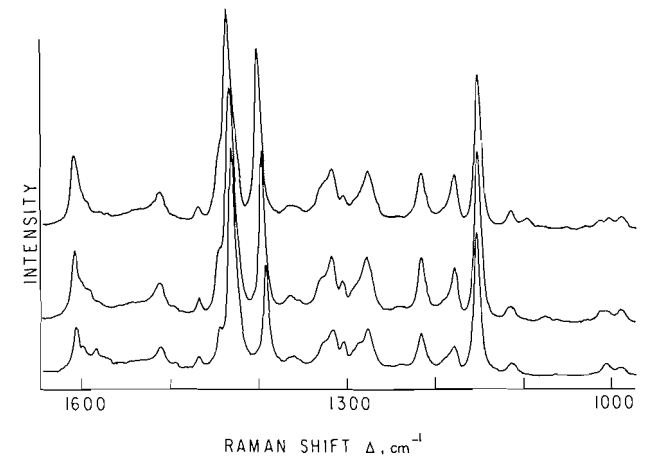

FIG. 8. Resonance Raman spectra of triphenylformazan derivatives in solution. Non-chelate forms. Top to bottom: 1-(*p*-chlorophenyl)-, 1-(*p*-bromophenyl)-, 1-(*p*-iodophenyl)-3,5-diphenylformazan. The experimental conditions are identical to those listed for Fig. 3.

vibrations (28) and it is observed that a distinction may be made between the band of the *p*-halophenyl group and that of the phenyl group. The band of the *p*-halophenyl group occurs at lower energy than that of the phenyl group and decreases in energy as the atomic number of the halogen increases; i.e., the band is found at 1604 cm^{-1} for the chlorophenyl group, 1595 cm^{-1} for the bromophenyl group, and 1589 cm^{-1} for the iodophenyl group. The region near 1350 cm^{-1} contains the N=N double bond stretching band as was previously shown. These particular bands in the spectra of the chelate forms appear to be composed of two overlapping bands and it is probable that these correspond to the N=N double bond stretching of the two tautomers shown in Scheme 3. The differences between the N=N stretching energies of the two tautomers are not sufficient for the resolution of the two bands, but with better electron-withdrawing substituents resolution of the two bands should be possible.

The RR spectra of the non-chelate forms of the *p*-halophenyl derivatives reproduced in Fig. 8 are, however, somewhat different from that of the parent, TPF. First, it will be noticed that the lower energy phenyl group bands, each assigned as a vibration of that phenyl group substituted with a halogen, have essentially disappeared from the spectra. Second, and more importantly, two bands are now observed in the region expected to contain the N=N stretching bands. These pairs of bands occur at 1433 and 1399 cm^{-1}, 1431 and 1395 cm^{-1}, and 1429 and 1390 cm^{-1}, respectively, for the series *p*-chlorophenyl, *p*-bromophenyl, and *p*-iodophenyl. It is observed that the intensities of the lower energy components of these pairs of bands and the energies of both components decrease in the same series order. The interpretation of these pairs of bands in terms of mechanical coupling or Fermi resonance is ruled out since the shift of both bands in the same direction cannot occur in either case. The existence of both *cis*- and *trans*-isomers is also eliminated as a possible explanation since two bands are observed only in cases involving unsymmetrical substitutions.

These results are interpreted to imply that two tautomers exist for both the chelate and non-chelate forms of these molecules and that the relative proportions of a tautomer in solution is a function of the electron-attracting ability of the *para*-substituent on the phenyl group at the 1-position.

In order to assign a particular component of these pairs of N=N stretching bands to a particular tautomer, it is necessary to resort to chemical intuition and to model compound data found in the literature. If, as shown in Scheme 3, the two chelate tautomers are considered as unsymmetrical *trans*-azoaromatics then it should be concluded that "tautomer **a**" with the N=N bond located nearer the *p*-halophenyl group would exhibit the higher energy N=N stretching band. For example, it has been shown (29) that the energies of the N=N stretching bands of a series of *trans*-azoaromatics range from 1463 cm^{-1} for the electron-attracting *p*-nitrophenyl group to 1391 cm^{-1} for the electron-donating *p*-dimethylaminophenyl group. These data are, of course, relevant to non-cyclic azo-derivatives in which the resonance stabilization of a chelate ring cannot tend to equalize the vibrational energies. It is contended, however, that the general trend is applicable to the chelate forms of the triphenylformazans although the differences between the vibrational energies of the tautomers are expected to be smaller and the related two bands of the chelate forms are not resolved. (Compare the asymmetrical shape of the 1357 cm^{-1} bands in Fig. 7 and the symmetrical shape of the corresponding band of TPF in Fig. 3.)

These arguments are particularly applicable to the non-chelate forms of the triphenylformazans illustrated below. These isomers are true unsymmetrical *trans*-azoaromatics; hence, the N=N stretching bands of the two isomers should be well separated and this is certainly observed in the spectra. It is thus concluded that the higher energy, more intense components of the pairs of bands, see Fig. 8, may be attributed to the N=N stretching modes of those tautomers with the N=N bonds nearer the *p*-halophenyl group (isomer **c** shown in Scheme 4).

The question now arises as to which of the chelate tautomers should be the preferred one. Intuitively, one would select tautomer **b** of Scheme 3. It is not possible to determine the identity of the preferred tautomer solely on the basis of the RR spectra of the chelate forms of the *p*-halophenyl derivatives. The relevant N=N stretching bands are broadened when compared to the corresponding band of TPF and are suggestive of two overlapping bands; but, little else can be derived from these observations. Fortunately, the RR spectra of 1-(*p*-bromophenyl)-2-^{15}N-3,5-diphenylformazan shown in Fig. 9 do

Can. J. Chem. Downloaded from www.nrcresearchpress.com by 210.87.254.40 on 09/06/12
For personal use only.

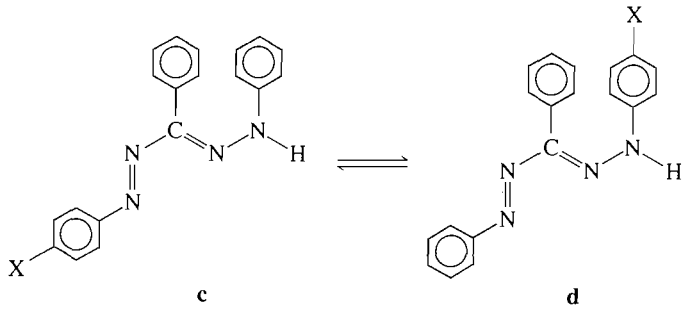

c d

SCHEME 4

confirm the proposal made above. The spectrum of the chelate form of this derivative clearly exhibits two bands, at 1359 and 1347 cm^{-1}, which are attributable to the N=N stretching modes of the two tautomers. The lower energy, less intense band is due without question to the $^{14}N=^{15}N$ stretching mode. The corresponding single band of the unlabelled derivative is located at 1357 cm^{-1}. (It should be noted that while the two bands of (1-^{15}N)TPF, Fig. 3, are of equal intensity, the higher energy band of the brominated compound is much more intense.) It should be carefully noted that the $^{14}N=^{15}N$ stretching mode is uniquely possible for that tautomer of 1-(*p*-bromophenyl)-2-^{15}N-3,5-diphenylformazan with the N=N bond adjacent to the *p*-bromophenyl group. *This particular spectrum therefore unequivocally demonstrates that the preferred tautomers of the chelate forms of the* p-*halophenyl derivatives are those with the N=N bond adjacent to the phenyl group; that is to say tautomer* ***b*** *in Scheme 3*. This spectrum, in comparison with other ^{15}N-labelled derivatives, also shows that the energies of the N=N stretching modes of the **a** and **b** tautomers of the *p*-halophenyl derivatives are very nearly equal. For example, energy differences, $(\nu_{(^{15}N=^{15}N)} - \nu_{(^{14}N=^{15}N)})$, of 12 and 11 cm^{-1}, respectively, are observed in the spectra of 1-(*p*-BrP)-2-^{15}N-3,5-DPF and (1-^{15}N)TPF. Thus, for the chelate forms of these molecules the *p*-halo substituent has only a small effect on the N=N stretching mode.

The fact that tautomer **b**, in Scheme 3, of the *p*-halophenyl derivatives is preferentially populated with respect to tautomer **a** is firmly established by these RR experiments. In contrast, the interpretation of the spectra of the non-chelate forms of these compounds leads to the conclusion that tautomer **c**, in Scheme 4, is preferentially populated. *It is therefore necessary to propose that excited state proton transfer must occur. Tautomer* ***c*** *cannot otherwise be formed from tautomer* ***b***.

On the basis of the present experimental data it is postulated that excited state proton transfer occurs as the primary photoevent in the photochromic transformation of triphenylformazans. This proposal also requires that changes be made in the mechanism of the transformation.

As pointed out by Grummt and Langbein (4), if the formation of **C** (Scheme 1) results from two single photon reactions as implicated by the scheme of Kuhn and co-workers (1, 2), then there must exist a range in which the absorbance of **D** that is formed in a single flash exhibits a quadratic dependence on the intensity of the flash (30). Grummt and Langbein found no such dependence and, hence, ruled out the formation of **D** by means of two consecutive single photon reactions. On the other hand, the schemes proposed by both these groups of researchers appear to indicate that **D**⇆**C** photostationary state would be achieved under continuous irradiation.

Under the conditions of the present RR experiments on the non-chelate forms of the triphenylformazans, this photostationary state should certainly be attained. The RR spectra of these non-chelate forms should, therefore, contain contributions from both the *trans-anti* and *cis-anti* isomers. The N=N stretching energies of *trans* and *cis* isomers should be separated by approximately 70 cm^{-1}. For example, the N=N stretching band of *trans*-azobenzene is located at 1442 cm^{-1} (15, 16) in the Raman spectrum and that of *cis*-azobenzene is located at 1511 cm^{-1} (26) in the IR spectrum. All the Raman spectra of the non-chelate form of triphenylformazans exhibit a weak band near 1465 cm^{-1}; but, the band undergoes only a small isotope shift as a result of secondary effects. An assignment of this band as being due to the *cis*-N=N stretching mode is therefore highly questionable. It is concluded that the present Raman data offer no confirmation of the presence of isomer **C** as shown in Scheme 1.

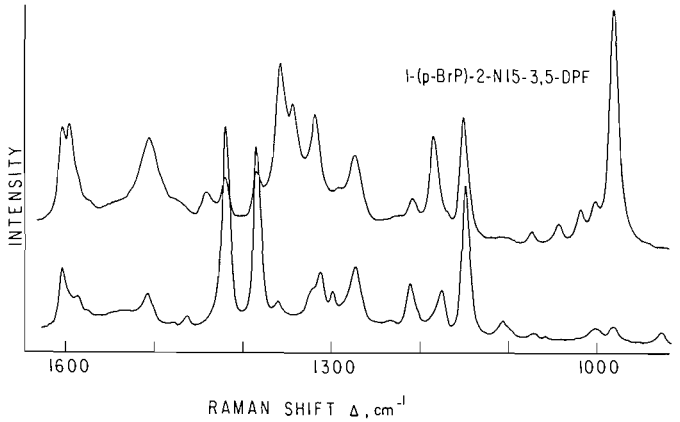

FIG. 9. Resonance Raman spectra of triphenylformazan derivatives in solution. Top: chelate form. Bottom: non-chelate form of 1-(*p*-bromophenyl)-2-^{15}N-3,5-diphenylformazan. The experimental conditions are identical to those listed for Figs. 3 and 4.

Conclusions

The combination of the IR and RR spectra of the two forms of triphenylformazans provides a wealth of information related to the photochromism of these compounds. The IR and RR spectra of unsymmetrically ^{15}N-labelled derivatives clearly demonstrate the presence of two tautomers of the chelate and non-chelate forms. The IR spectrum of the non-chelate form of (1,2-^{15}N)TPF exhibits two C=N stretching bands and the RR spectra of both forms of (1-^{15}N)TPF and (1,2-^{15}N)TPF exhibit two N=N stretching bands. The RR spectra of these derivatives also demonstrate that the N=N stretching mode may couple with either a higher or lower energy mode. The amount of coupling depends on the nearness of the N=N stretching energy to either 1470 or 1325 cm^{-1}. The RR spectra of azoaromatics with N=N stretches in either of these regions should, therefore, be approached with some caution.

The RR spectra of the 1-(*p*-halophenyl)-3,5-diphenylformazans confirm that two tautomers exist for each of the two forms. The spectra of the non-chelate forms of these derivatives show that the position of the tautomeric equilibrium is influenced by the *p*-halo substituent. The combination of ^{15}N-labelling and phenyl substitutions, as evidenced in the RR spectra, lead to the conclusion that excited state proton transfer is the primary photoevent in the photochromism of these compounds.

These RR results cast some doubt on the previously proposed

Can. J. Chem. Downloaded from www.nrcresearchpress.com by 210.87.254.40 on 09/06/12
For personal use only.

mechanisms. Both the previously proposed mechanisms suggest a **D**⇌**C** photostationary state and the present RR investigations give no evidence for isomer **C**, the *cis-anti* isomer. The lifetime of the **C** isomer is given as 90 s (2); hence, under continuous laser irradiation a sufficient amount for detection by RR spectroscopy should be present at a photostationary state.

In view of the facts that excited state proton transfer occurs as a primary photoevent and that the *cis-anti* isomer is not observed in the RR spectra, the present study confirms only the **A** and **D** isomers of triphenylformazan. Further study is needed to establish the presence or absence of the **B** and **C** isomers.

Acknowledgements

Financial assistance from the Natural Sciences and Engineering Research Council of Canada, the Ministère de l'Education du Québec, and the Canada Council through the grant of the Killam Memorial Scholarship to C.S. is gratefully acknowledged.

1. I. HAUSSER, D. JERCHEL, and R. KUHN. Chem. Ber. **82**, 195 (1949).
2. R. KUHN and H. M. WEITZ. Chem. Ber. **86**, 1189 (1953).
3. H. LANGBEIN. J. Prakt. Chem. **321**, 655 (1979).
4. U.-W. GRUMMT and H. LANGBEIN. J. Photochem. **15**, 329 (1981).
5. W. OTTING and F. A. NEUGEBAUER. Chem. Ber. **102**, 2520 (1969).
6. P. R. JOHNSON and D.A. THORNTON. Spectrosc. Lett. **7**, 293 (1974).
7. G. ARNOLD and C. SCHIELE. Spectrochim. Acta, **25**A, 685 (1969).
8. G. ARNOLD and C. SCHIELE. Spectrochim. Acta, **25**A, 697 (1969).
9. B. BACCAR, R. MATHIS, A. SECCHES, J. BARRANS, and F. MATHIS. J. Mol. Struct. **7**, 369 (1971).
10. M. J. W. LEFÈVRE, J. B. SOUSA, and R. L. WERNER. Aust. J. Chem. **9**, 151 (1956).
11. P. B. FISCHER, B. L. KAUL, and H. ZOLLINGER. Helv. Chim. Acta, **51**, 1449 (1968).
12. F. A. NEUGEBAUER and B. KÜCHLER. Liebigs. Ann. Chem. **706**, 104 (1967).
13. W. KIEFER and H. J. BERNSTEIN. Appl. Spectrosc. **25**, 501 (1971).
14. W. KIEFER and H. J. BERNSTEIN. Appl. Spectrosc. **25**, 609 (1971).
15. H. HACKER. Spectrochim. Acta, **21**, 1989 (1965).
16. J. BRANDMÜLLER, H. HACKER, and H. W. SCHRÖTTER. Chem. Ber. **99**, 765 (1966).
17. A. GRUGER, N. LECALVÉ, and P. DIZABO. J. Chim. Phys. **69**, 291 (1972).
18. K. MACHIDA, B. K. KIM, Y. SAITO, K. IRAGASHI, and T. UNO. Bull. Chem. Soc. Jpn. **47**, 78 (1974).
19. Y. SAITO, B. K. KIM, K. MACHIDA, and T. UNO. Bull. Chem. Soc. Jpn. **42**, 2111 (1974).
20. T. UNO, H. LEE, Y. SAITO, and K. MACHIDA. Spectrochim. Acta, **32**A, 1319 (1976).
21. T. UNO, B. K. KIM, Y. SAITO, and K. MACHIDA. Spectrochim. Acta, **32**A, 1179 (1976).
22. P. J. TROTTER. Appl. Spectrosc. **31**, 30 (1977).
23. K. KUMAR and P. R. CAREY. Can. J. Chem. **55**, 1444 (1977).
24. J.-C. MERLIN. Thèse Université des Sciences et Techniques de Lille, 1979. p. 32.
25. J. L. LORRIAUX, J.-C. MERLIN, A. DUPAIX, and E. W. THOMAS. J. Raman Spectrosc. **8**, 81 (1979).
26. R. KÜBLER, W. LÜTTKE, and S. WECKHERLIN. Z. Elektrochem. **64**, 650 (1960).
27. S. KOIDE, Y. UDAGAWA, N. MIKAMI, K. KAYA, and M. ITO. Bull. Chem. Soc. Jpn. **45**, 3542 (1972).
28. G. HERZBERG. Infrared and Raman spectra. van Nostrand Company, New York. 1945. p. 364.
29. N. B. COLTHUP, L. H. DALY, and S. E. WIBERLEY. Introduction to infrared and Raman spectroscopy. 2nd ed. Academic Press, Inc., New York. 1975. p. 331.
30. U. LACHISH, A. SHAFFERMAN, and G. STEIN. J. Chem. Phys. **64**, 4205 (1976).

Can. J. Chem. Downloaded from www.nrcresearchpress.com by 210.87.254.40 on 09/06/12
For personal use only.

New photoresists for deep ultraviolet (<300 nm) exposure

E. A. CHANDROSS, E. REICHMANIS, C. W. WILKINS, JR., AND R. L. HARTLESS
Bell Laboratories, 600 Mountain Ave., Murray Hill, NJ 07974, U.S.A.

Received June 21, 1982

This paper is dedicated to Professor Harry E. Gunning on the occasion of his 65th birthday

E. A. CHANDROSS, E. REICHMANIS, C. W. WILKINS, JR., and R. L. HARTLESS. Can. J. Chem. **61**, 817 (1983).

The increasing density of devices in large scale integrated circuits has created a need for lithographic techniques that have higher resolution (≈1 μm) than can be achieved with conventional (≈400 nm) optical technology. By operating in the deep uv (200−300 nm) region of the spectrum, one can reduce diffraction effects and increase resolution. Because of the high optical density of conventional photoresists in this wavelength range, new materials are needed. This paper presents an overview of new positive resists that we have developed. These include methacrylate polymers that undergo photochemical chain scission and two-component (photosensitive solution inhibitor − alkali soluble matrix resin) systems.

E. A. CHANDROSS, E. REICHMANIS, C. W. WILKINS, JR. et R. L. HARTLESS. Can. J. Chem. **61**, 817 (1983).

L'augmentation de densité des appareils des circuits intégrés à l'échelle industrielle à créé le besoin de recourrir à des techniques lithographiques ayant une résolution supérieure (≈1 μm) à celle que l'on peut atteindre avec la technologie optique conventionnelle (≈400 nm). En opérant dans la région de l'uv lointain (200−300 nm), on peut réduire l'effet de diffraction et augmenter la résolution. À cause de la forte densité optique des photorésistances conventionnelles dans ce domaine de longueur d'onde, on a besoin de nouveaux matériaux. Cette publication présente un survol des nouvelles résistances positives que nous avons mises au point. Elles comprennent les polymères du type méthacrylate qui subissent une scission photochimique de leur chaîne et de systèmes à deux composés (un inhibiteur en solution photosensitive et une résine soluble dans les alcalis). [Traduit par le journal]

Introduction

The manufacture of integrated circuits involves the crucial step of defining mask patterns on a silicon substrate. After intermediate steps, it allows one to add additional elements (dopants) to the silicon which alter its properties, or to fabricate structures such as metal "wires" that are essential for the device. Virtually all circuit production uses a photosensitive thin organic film as the image forming medium. It is exposed by projection or contact printing, processes analogous to the well-known technology of conventional photography. The resist must withstand subsequent chemical processing steps, such as hydrofluoric acid etching of silicon dioxide, and it is also desirable that it be attacked relatively slowly in the fluorocarbon plasma etching processes now coming into use.

Photoresists were originally developed for the manufacture of printing plates and printed wiring boards. This is a well-established technology, going back over a century. A good deal of chemistry and ingenuity has characterized the art of photolithography, and the reader is referred to two books (1, 2) for historical background.

A photoresist film is one whose solubility in an appropriate developer is changed substantially by exposure to actinic radiation. There are two types of resists, positive and negative (Fig. 1). The former become more soluble upon exposure; the latter show opposite behavior. Conventional resists are generally sensitive to light in the 365−436 nm region of the spectrum. These wavelengths imply the use of a mercury arc lamp, the brightest conventional source. As technology has developed, the use of shorter wavelength radiation, such as X-rays and electrons, has been studied. The former is still in development; the latter is used extensively in the manufacture of the masks for optical printing. The reason for going to shorter wavelengths is the search for higher resolution which is needed as device features get ever smaller. At present the state of the art 64 kilobit memory chips require features as small as 2−3 μm.

Optical lithography is a well-established technology, and it is of interest to see how far it can be pushed in the search for higher resolution. There are many aspects to the question of the resolution that can be obtained in a resist film. Much depends

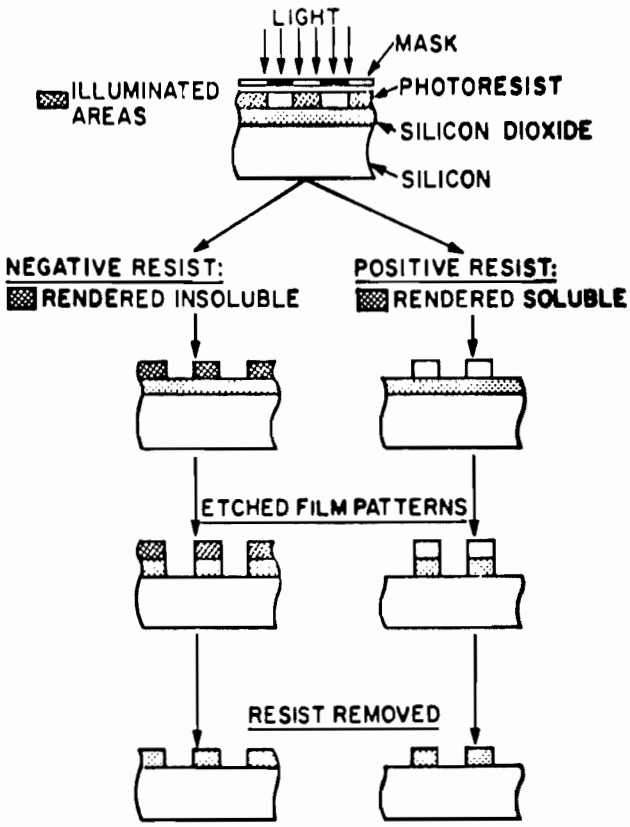

FIG. 1. Pictorial view of the operation of positive and negative resists.

Can. J. Chem. Downloaded from www.nrcresearchpress.com by 210.87.254.40 on 09/06/12
For personal use only.

on the properties of the polymer materials and their response to the developers as well as the subsequent processing conditions. Present interest centers about the 1 μm element size. As we approach the wavelength of the light used to form the resist image (≈0.4 μm), it is clear that diffraction effects should increase in importance. This has led to a strong interest in exploring the use of 200−300 nm light to minimize diffraction. Printing equipment for this region of the spectrum is expected to be available in the near future. This paper presents an overview of the routes we have explored for deep uv resist technology.

Resist design

General considerations

The first decision to be made is which wavelength region should be used for resist exposure. We believe that the high pressure mercury arc lamp that is currently used will continue to be the best exposure source for the near future. This implies that resist response should be optimized for the 230−280 nm region. The choice represents a compromise between exposure at the shortest possible wavelength and a reasonable exposure time for a 12.7 cm diameter silicon wafer, allowing for the relatively low Hg lamp output at $\lambda < 300$ nm.

An important consideration is the match between the exposure source output spectrum and the absorption spectrum of the photoresist film which is usually 0.5−1 μm thick. It is important to have relatively uniform exposure throughout the thickness of the film in order to obtain vertical walls in the resist image. This suggests a low optical density, and we prefer to keep the optical density of the film below 0.3 for the range of significant source output. Conventional materials are nearly opaque (OD >1) for $\lambda < 300$ nm, and it is impossible to obtain uniform exposure through the film thickness unless the film is very thin. This is the reason that new photoresists are needed.

Sensitivity is generally defined as the amount of incident exposure light, in J cm^{-2}, that is required to give a satisfactory image after development. This does not take into account the match between the output and absorption spectra mentioned above. We prefer to measure sensitivity at a particular wavelength. The practical measure of sensitivity is simply the time it takes to make a resist image with a given exposure tool.

Resist contrast is defined in a manner similar to that of conventional photography. One plots the amount of resist film thickness remaining after development versus the log of the exposure dose. This usually gives a curve which is fairly linear as the thickness approaches zero. Contrast (γ) is defined as the slope in this region. The higher γ is, the more the resist behaves as if it has a threshold exposure for development. This behavior is desirable because it indicates less sensitivity to stray light and/or diffracted light. High contrast is desirable for high resolution imaging.

Conventional materials require exposures of 50−200 mJ cm^{-2}. For positive resists, it is unlikely that sensitivities significantly better than 50 mJ cm^{-2} can be achieved. It should be noted that sensitivity is fundamentally measured in photons cm^{-2} and one will necessarily have to have more J cm^{-2} to have the same photon flux as the wavelength is decreased. Thus, deep uv lithography will require more light (joules), in a region of decreasing lamp output, to cause the same photochemical effect that would be observed with existing materials at conventional wavelengths.

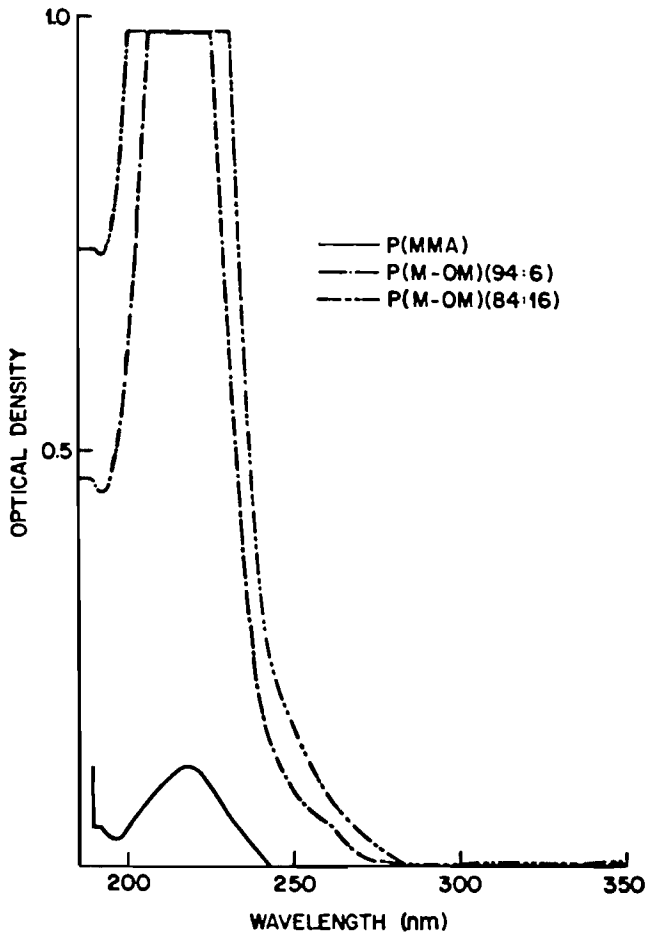

FIG. 2. Absorption spectra of PMMA and P (M−OM) films, nominally 1 μm thick. The mole ratios of the copolymers are given in parentheses.

Resist mechanisms

Negative resists are polymers having reactive groups that undergo photochemical crosslinking reactions either with themselves (e.g., cinnamate dimerization) or with a photosensitive small molecule (e.g., ethylenic polymer groups with bisazido compounds). In general, negative resists exhibit a greater tendency to swell during development than positive resists. The absorption of developer solvent plasticizes the film and limits the resolution that can be obtained to ~2 μm in ~1 μm thick films. For this reason we chose to design new positive resists for use in the deep uv region.

There are two general mechanisms that are used in positive resist chemistry. One involves the degradation of a polymer to material of significantly lower molecular weight. This is essentially opposite to the change induced in a negative resist. If the molecular weight distribution is shifted sufficiently, one can then dissolve the irradiated regions. Poly(methyl methacrylate), PMMA, is the best known example of this group (3). It is capable of extremely high resolution, using deep uv light, e-beam, X-ray, or ion beam exposure, but it is too insensitive to be practical. The low optical sensitivity is not surprising. PMMA has only pivalate ester chromophores, and they absorb weakly at 220 nm (Fig. 2). The combination of weak absorption and poor lamp output does not bode well for a reasonable exposure time. Sensitization is not possible because there is no low-lying excited state of the ester chromophore.

Can. J. Chem. Downloaded from www.nrcresearchpress.com by 210.87.254.40 on 09/06/12
For personal use only.

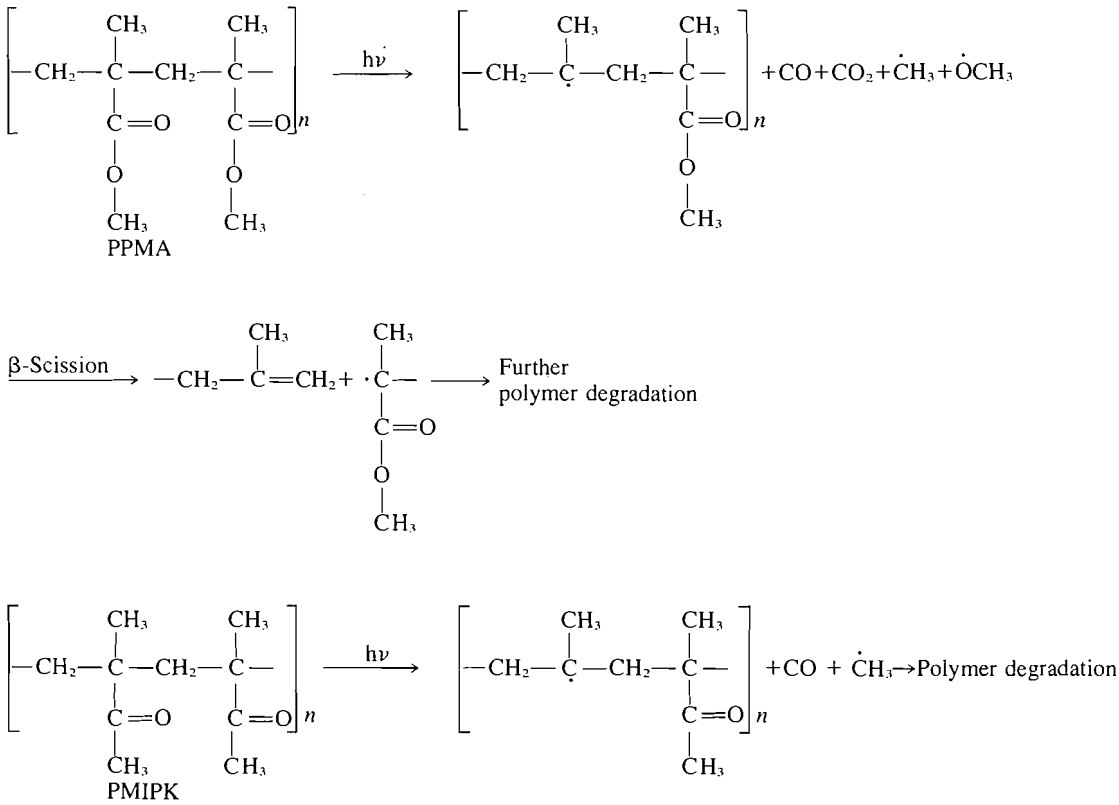

FIG. 3. The mechanism proposed for the photodegradation of PMMA and the poly(vinyl ketone)s.

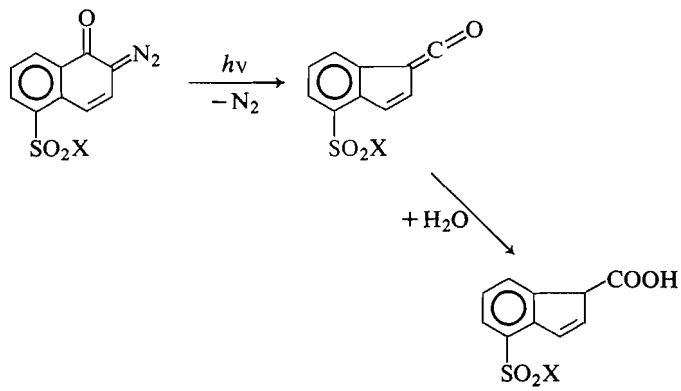

FIG. 4. The photochemical conversion of a naphthoquinone diazide to an alkali-soluble carboxylic acid, as in conventional positive photoresist. X is usually an aryloxy group.

The mechanism of PMMA photodegradation is thought to involve radical formation followed by β-cleavage of the polymer backbone (Fig. 3). The same process can occur in poly(vinyl alkyl ketone)s which have also been used as resists. Because of their weak absorption of light (carbonyl chromophore, $\lambda \approx 280$ nm, $\epsilon \approx 25$), sensitizers are required.

The second type of positive resist has been used extensively for some time. It is a two-component system that operates via an ingenious mechanism.[1] The major component is a Novolak resin (phenol-formaldehyde) that is soluble in aqueous alkali. The minor component is a photosensitive hydrophobic compound, a substituted naphthoquinone diazide, that is photochemically converted to an alkali-soluble indenecarboxylic acid (Fig. 4). The ability of the "solution inhibitor" to prevent developer attack is destroyed by light, and the irradiated portion of the film can be dissolved preferentially by aqueous alkali. These materials are optically dense below 300 nm, even in 0.5 μm films, and thus they cannot be used for deep uv exposure.

New PMMA resists

Our work in this area is based on the hope that it would be possible to add small amounts (>15 mol%) of photosensitive groups that would lead to backbone cleavage while maintaining the excellent filmforming and high resolution properties of PMMA itself.

A known example of this approach is the incorporation of the acyloximino ester chromophore, devised by Delzenne *et al.* (4). They noted that irradiation of solutions of copolymers of MMA and 3-methacryloyloximino-2-butanone, in the 365 nm region (weak absorbance), led to a decrease in molecular weight. This seemed to be a good starting point because the acyloximino group has a strong absorption at 220 nm whose tail extends beyond 240 nm. Photolysis in the solid state is not necessarily the same as that in solution because of the cage effect of the matrix that favors the reformation of broken bonds, but one can expect some similarity.

The absorption spectra of two of these copolymers, as well as that of the parent PMMA, are given in Fig. 2. The photodegradation envisaged for the copolymer is shown in Fig. 5. As expected, the photosensitivity observed increases with the amount of acyloximino monomer incorporated. The results are given in Table 1.

A further increase in sensitivity can be obtained by the incor-

[1]Reference 2, p. 149.

Can. J. Chem. Downloaded from www.nrcresearchpress.com by 210.87.254.40 on 09/06/12
For personal use only.

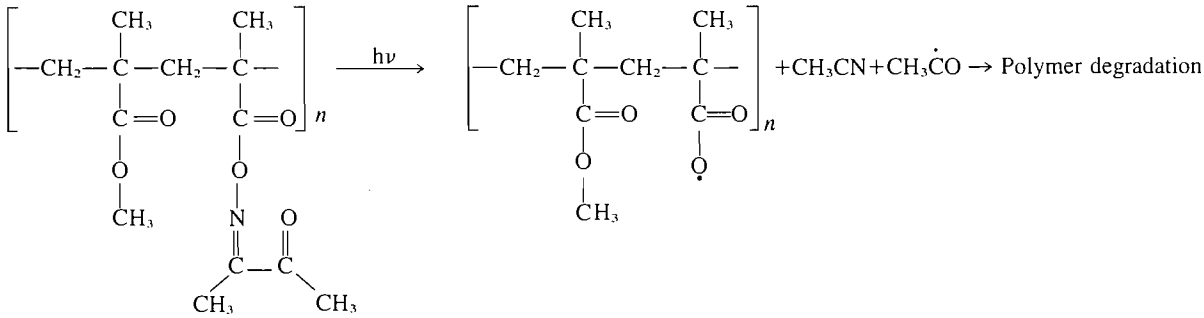

P (M−OM)

FIG. 5. The photodegradation proposed for P(M−OM).

TABLE 1. Properties of copolymers of methyl methacrylate and 3-methacryloyloximino-2-butanone

Polymer	Composition	Mol. wt. (10^{-5})	Mol. wt/ Mol. no.	Sensitivity[a] (full output 1 kW Hg−Xe lamp)
PMMA[b]	—	—	—	1
P (M−OM[c])	97:3	1.39	2.06	0.5
P (M−OM)	94:6	2.87	1.86	0.25
P (M−OM)	84:16	2.48	2.04	0.03
P (M−OM)	63:37	1.88	2.35	0.02
P (M−OM−CN[d])	69:16:15	2.78	1.98	0.012

[a]Exposure required relative to PMMA; developed with methyl isobutyl ketone.
[b]duPont, Elvacite 2010, "high molecular weight".
[c]3-Methacryloyloximino-2-butanone.
[d]Methacrylonitrile.

TABLE 2. Photosensitization of P (M−OM)

Polymer	Sensitizer (%)	E_t (Sens.) (kcal mol^{-1})	Sensitivity[a] (full output, 1kW) Xe−Hg lamp)
P (M−OM)[b]	—	—	0.25
P (M−OM)[b]	*p-tert*-Butylbenzoic acid (10)	—	0.1
P (M−OM)[b]	*N*-acetylcarbazole (10)	68.3[c]	0.08
P (M−OM)[b]	Benzophenone (10)	68.5[d]	0.25

[a]Relative exposure required, PMMA = 1, developed with methyl isobutyl ketone.
[b]P (M−OM) (94:6).
[c]Reference 11.
[d]Reference 12.

poration of methacrylonitrile (5). It is likely that this is primarily a consequence of polymer properties rather than a direct effect on the photochemical reaction. The most sensitive material was found to be a terpolymer of methyl methacrylate, the oximino methacrylate, and methacrylonitrile, in the ratio of 69:16:15. This polymer is more than 50 times as sensitive as PMMA to 240 nm light. When sensitized with *tert*-butylbenzoic acid, it requires an exposure of less than 30 mJ cm^{-2} and gives high resolution images. The limits of its use for optical printing have not yet been thoroughly explored.

In addition to the use of benzoic acids as short wavelength sensitizers, the polymers can be made sensitive to longer wavelength ($\approx$ 300 nm) light by the addition of photosensitizers such as *N*-acetylcarbazole (Table 2) (6). It appears that singlet energy transfer is involved.

Indenone is another monomer that can be incorporated into PMMA by conventional free radical copolymerization (7). Indenone is prepared by *in situ* hydrolysis of the ethylene ketal just before polymerization because it polymerizes too readily to be stored. The high reactivity of the α,β-disubstituted ethylene is attributed to the presence of the antiaromatic cyclopentadienone moiety. The amount of indenone incorporated into the copolymer is controlled by its concentration in the polymerization solution.

Absorption spectra of typical copolymers are shown in Fig. 6. It is clear that this system can be optimized for exposure in either the 280 or 250 nm region by appropriate choice of the indenone concentration. The amount actually incorporated is readily determined by optical spectroscopy.

We assume that indenone reacts as an α,β-unsaturated ketone, and the mechanism postulated for photodegradation is shown in Fig. 7. It is analogous to that accepted for PMMA and

Can. J. Chem. Downloaded from www.nrcresearchpress.com by 210.87.254.40 on 09/06/12
For personal use only.

Can. J. Chem. Downloaded from www.nrcresearchpress.com by 210.87.254.40 on 09/06/12
For personal use only.

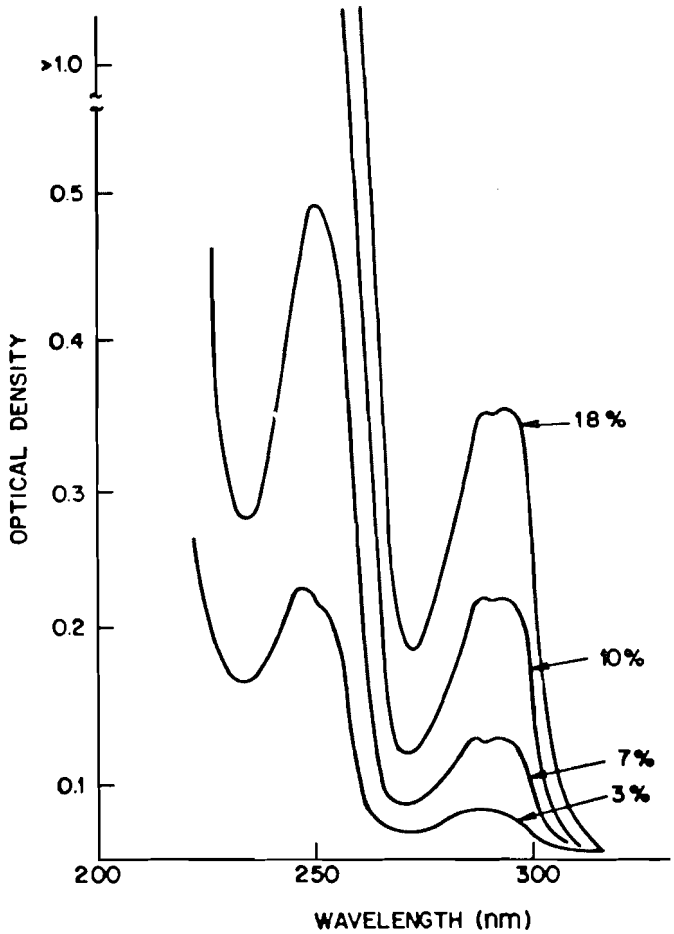

FIG. 6. Absorption spectra of films of poly(methyl methacrylate-co-indenone), ≈1 μm thick. The mol% of indenone is indicated for each curve.

assumes the normal Norrish α-cleavage of a carbonyl group. The copolymer is quite sensitive, requiring an exposure of only 0.06 J cm^{-2} at 248 nm when 3% indenone is present. Sensitivity is proportional to absorption as long as the optical density of the film is low. A complete set of results is given in Table 3. The high sensitivity is explained on the basis of the steric strain present in the cyclopentanone moiety. It is well known that the rate of α-cleavage increases in the order cyclohexanone < cyclopentanone < cyclobutanone. The analogous open chain copolymer incorporating phenyl vinyl ketone is far less sensitive (×80) than the indenone copolymer. A preliminary lithographic evaluation of poly(MMA-co-indenone) indicated that it is capable of high resolution (≈ 1 μm) and that it has a contrast similar to that of PMMA.

Solution inhibitor deep ultraviolet resist (8)

The conventional two-component resist system was described in the introduction. It contains a large fraction of phenol moieties that absorb strongly for λ < 300 nm, a region of high absorption for the quinone diazide additive as well. There is a "minimum" in the resist absorption at ≈260 nm where the optical density is ≈0.5 μm^{-1}. Thus, in order to use a system like this for exposure at λ < 300 nm, both a new matrix resin and a new photosensitive element are necessary.

The choice of a resin seemed straightforward, based on what is known about the performance of the conventional material. We require a film-forming polymer that will dissolve at a reasonable rate in aqueous alkali, serve as a host for the photosensitive solution inhibitor, and not interfere in the photochemistry of the latter. We selected copolymers of methyl methacrylate and methacrylic acid (MAA) because they offer an easy route to adjusting the alkali solubility of the matrix. They are optically transparent in the region of interest to us.

The selection of a photochemical reaction for the solution inhibitor is far less obvious. We were led to the *o*-nitrobenzyl

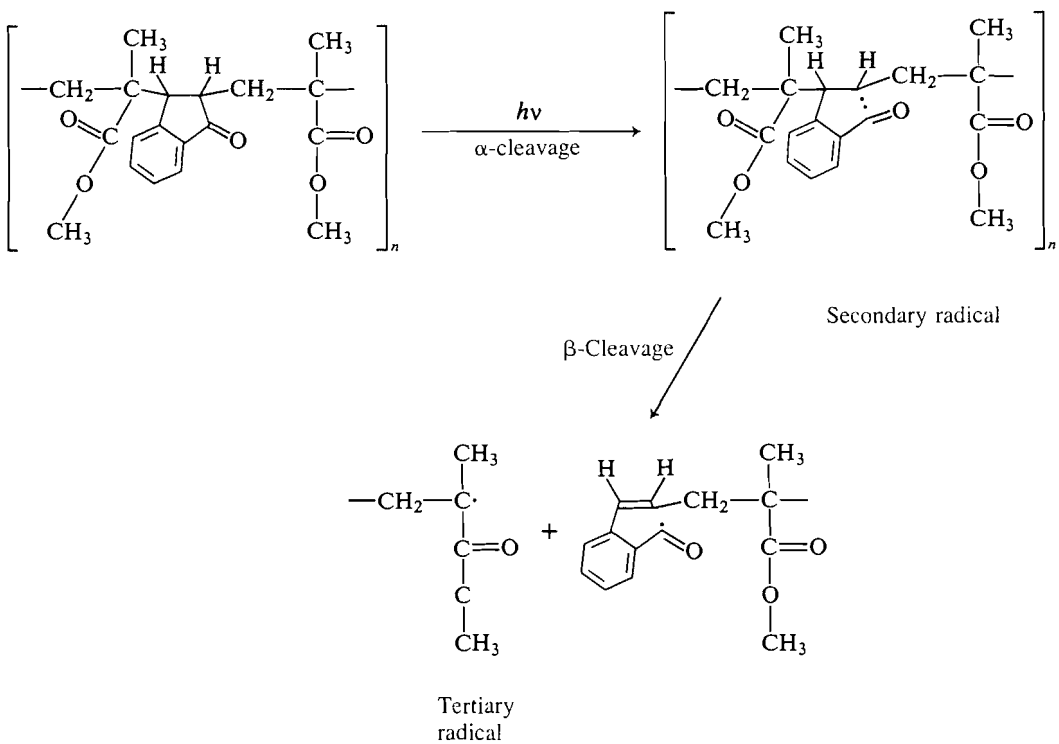

FIG. 7. The mechanism postulated for the photodegradation of poly(methyl methacrylate-co-indenone).

TABLE 3. Photosensitivity of poly(methyl methacrylate-co-indenone)[a]

Indenone content	Film OD		Exposure required (J/cm^2)	
	at 280 nm	at 248 nm	at 280 nm	at 248 nm
3%	0.3	0.22	0.6	0.06
7%	0.7	0.53	0.2	0.02–0.06
18%	0.16	1.1	0.1	0.13

[a]Developed with methyl isobutyl ketone saturated with water.

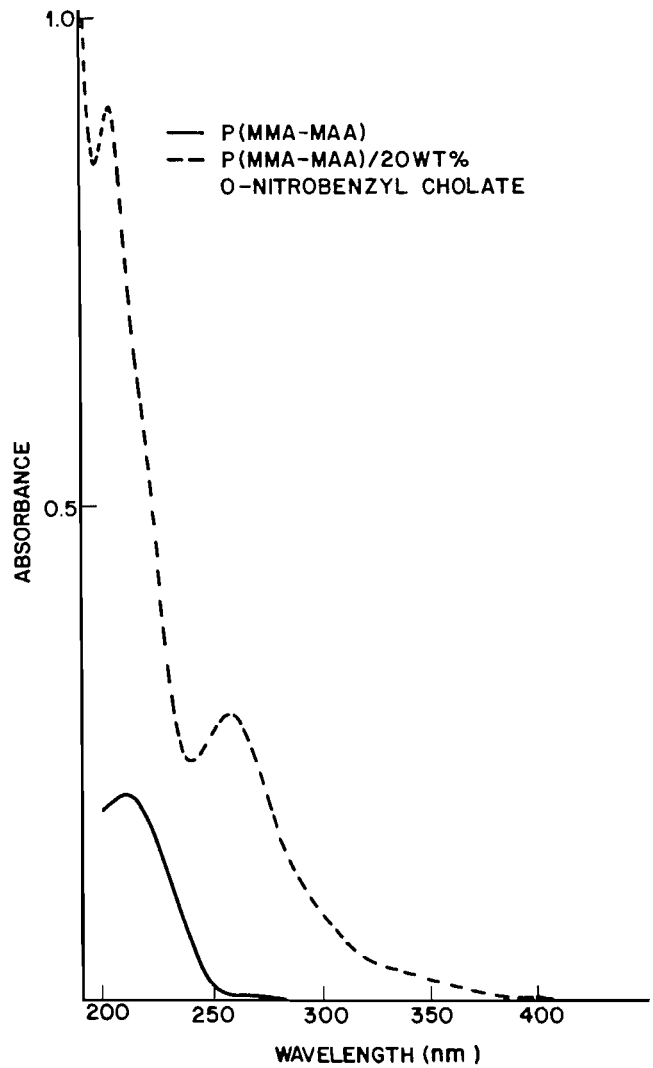

FIG. 8. Absorption spectrum of *o*-nitrobenzyl cholate in a P(MMA–MAA) film, ≈1 μm thick.

ester rearrangement for two reasons. This photochemistry is well known for the facile conversion of carboxylic acid esters to the free acids, and the absorption spectrum of the nitrobenzene chromophore seemed well suited to our purpose (Fig. 8).

The *o*-nitrobenzyl ester rearrangement functions as a photochemical switch to liberate the alkali-soluble carboxylic acid (Fig. 9). We thought it would be advantageous to choose the R group to be as large as possible so that it would occupy a substantial volume fraction of the resist film. Such a species would then function as an amplifier for the effect of the change in the small photosensitive moiety. Our first choice was cholic acid. The free acid is very soluble in aqueous alkali

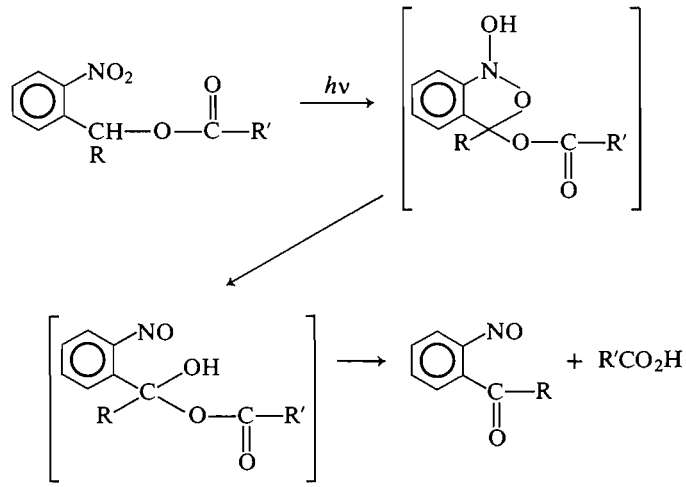

FIG. 9. Photochemical reaction of an *o*-nitrobenzyl ester to liberate the parent acid.

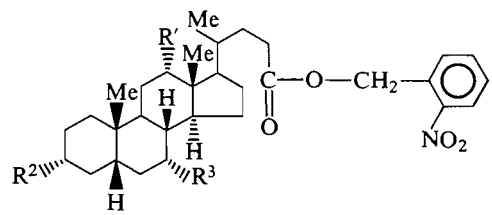

R^1_1, R^2_2, R^3_3 = OH

FIG. 10. Structure of *o*-nitrobenzyl cholate.

(≈500 g L^{-1}), while the aliphatic esters are insoluble. It is far more effective than anything else we have studied such as decanoic acid, fluorenone-3-carboxylic acid (a photosensitizer), and various phthalic acid half-esters.

ortho-Nitrobenzyl cholate (Fig. 10) was synthesized by the reaction of sodium cholate with *o*-nitrobenzyl chloride in aqueous alcohol. The poly(MMA-co-MAA) was prepared by conventional free-radical polymerization. The molecular weight and composition of the resin have an effect on the overall sensitivity; material having a ratio of 75:25 and a molecular weight of ca. 75 000 is quite satisfactory. The solution inhibitor is present at ca. 20% by weight. The developer that works best is an aqueous solution of Na_2CO_3 (10% by weight).

The resist films are spin coated conventionally from cyclopentanone solution. The absorption spectrum of a typical film is shown in Fig. 8. It is clear that this resist is well suited for exposure in the 260 nm region where the sensitivity is ≈0.2 J cm^{-2} for a typical system. Sensitivity depends on a number of factors (inhibitor concentration, baking time and temperature before exposure, developer composition, and procedure) that must be studied further to allow the choice of a practical material. We have made contact prints that demonstrate 1 μm resolution (Fig. 11).

The unexpected result that came out of our initial studies was the unusually high contrast ($\gamma > 5$) of this resist system. The analogous conventional system has a contrast of ≤2.5; the PMMA systems show $\gamma < 2$. There is no way to predict or rationalize contrast, but we can say that this system comes closer to "threshold exposure" behavior than any other organic photoresist. We believe that the clue to understanding the high contrast lies in the unusual development characteristics ob-

Can. J. Chem. Downloaded from www.nrcresearchpress.com by 210.87.254.40 on 09/06/12
For personal use only.

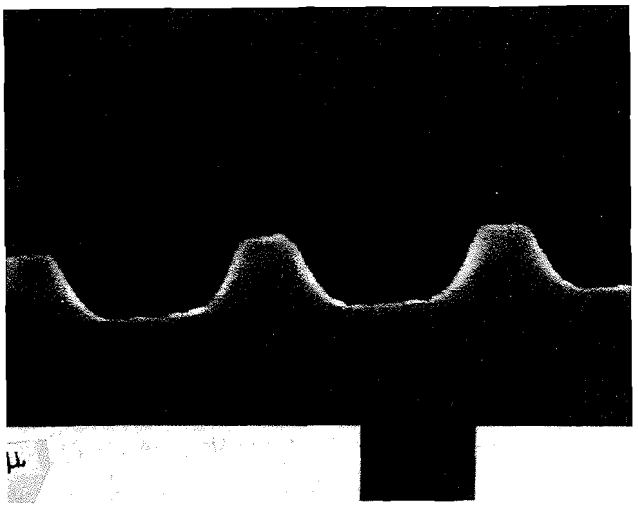

FIG. 11. 1 μm Lines and spaces contact-printed in *o*-nitrobenzyl cholate/P (MMA–MAA) photoresist. The space in the light portion of the figure at the bottom is 1 μm.

served for these films. The exposed regions are swollen but not dissolved directly by the alkaline developer. They dissolve subsequently in the water used to rinse the film. This may be a reflection of "salting out" the ionized resin polymer by the alkaline developer. The swelling does not seem to have a deleterious effect on the resolution that can be obtained. More work has been done on this system, and the reader is referred to recent presentations (9, 10).

Summary

The work described here demonstrates that one can design new resist systems for the deep ultraviolet. There is a lot of work required to optimize any resist system after its basic chemistry is shown to be promising. This investment should become more attractive as imaging equipment for this region of the spectrum becomes available. Optical lithography is a well-known, attractive technology, and we hope that it can be used to make high-density integrated circuit devices having feature sizes less than one micrometer.

1. J. KOSAR. Light sensitive systems. John Wiley and Sons, Inc., New York, NY 1965.
2. W. S. DEFOREST. Photoresist: materials and processes. McGraw–Hill Book Co., New York, NY 1975.
3. B. J. LIN. IBM. J. Res. Dev. **20**, 213 (1976).
4. G. A. DELZENNE, U. LARIDON, and H. PEETERS. Eur. Polym. J. **6**, 933 (1970).
5. E. REICHMANIS and C. W. WILINS, JR. ACS organic coatings and plastics chemistry preprints. **43**, 243 (1980).
6. E. REICHMANIS, C. W. WILKINS, JR., and E. A. CHANDROSS. J. Electrochem. Soc. **127**, 2514 (1980).
7. R. L. HARTLESS and E. A. CHANDROSS. J. Vac. Sci. Technol. **19**, 1333 (1981).
8. E. REICHMANIS, C. W. WILKINS, JR., and E. A. CHANDROSS. J. Vac. Sci. Technol. **19**, 1338 (1981).
9. E. REICHMANIS, C. W. WILKINS, JR., and E. A. CHANDROSS. 161st Meeting. The Electrochemical Society, Montreal, Canada, May 9–14, 1982. Abstract No. 268.
10. C. W. WILKINS, JR., E. REICHMANIS, and E. A. CHANDROSS. 161st Meeting. The Electrochemical Society, Montreal, Canada, May 9–14, 1982. Abstract No. 267.
11. M. ZANDER. Ber. Bunsenges. Phys. Chem. **72**, 1161 (1968).
12. J. G. CALVERT and J. N. PITTS. Photochemistry. John Wiley, New York, NY. 1966. p. 298.

Can. J. Chem. Downloaded from www.nrcresearchpress.com by 210.87.254.40 on 09/06/12
For personal use only.

Optimization of ion trapping characteristics for studies of ion photodissociation[1]

RICHARD JAMES HUGHES, RAYMOND EVANS MARCH,[2] AND ALEXANDER BALDWIN YOUNG[3]

Department of Chemistry, Trent University, Peterborough, Ont., Canada K9J 7B8

Received June 30, 1982

This paper is dedicated to Professor Harry E. Gunning on the occasion of his 65th birthday

RICHARD JAMES HUGHES, RAYMOND EVANS MARCH, and ALEXANDER BALDWIN YOUNG. Can. J. Chem. **61**, 824 (1983).

In order to characterize unambiguously photochemical energy absorption and subsequent intramolecular relaxation dissociation, collision-free conditions are required. Isolated molecule photochemistry may be studied in a quadrupole ion store (QUISTOR) under near collision-free conditions. Photodissociation of primary ions, H_2^+ and CH_4^+, has been described and we have reported on the slow multiphoton induced dissociation of protonated dimers of 2-propanol in the infrared region. Ions may be trapped in a QUISTOR in either a total storage mode wherein ions of different masses are stored simultaneously, or a mass selective mode wherein single ion species are isolated. Utilization of the QUISTOR as an ion/molecule reactor in the total ion storage mode facilitates the formation of secondary ions chosen for study, their isolation, and irradiation. Determination of the ranges of ion masses which may be stored in each mode is described. In the total storage mode, ion mass-to-charge ratios to m/e 455 have been observed. Selective storage to m/e 219 is reported, though with poor resolution. The effects of variation in trapping parameters including drive frequency and physical dimensions of the device are discussed.

RICHARD JAMES HUGHES, RAYMOND EVANS MARCH et ALEXANDER BALDWIN YOUNG. Can. J. Chem. **61**, 824 (1983).

Des conditions de collision libre sont nécessaires pour caractériser sans ambiguité l'absorption d'énergie photochimique et la relaxation et dissociation intramoléculaire subséquentes. On doit étudier la photochimie de la molécule isolée dans une réserve d'ions quadrupolaire (QUISTOR) dans des conditions de quasi collision libre. On a décrit la photodissociation des ions primaires H_2^+ et CH_4^+ et nous avons rapporté la dissociation induite par multiphoton lent des dimères protonés de propanol-2 dans la région infrarouge. Les ions peuvent être piégés dans un QUISTOR soit dans un mode d'emmagasinage total où les ions de masse différente sont emmagasinées silmultanément, soit dans un mode de sélection de masse où les ions simples sont isolés. L'utilisation du QUISTOR comme un réacteur d'ion/molécule dans le mode d'emmagasinage total facilite la formation des ions secondaires choisis pour étude, leur isolation et leur irradiation. On décrit la détermination des intervalles des masses d'ions qui peuvent être emmagasinés dans chacun des modes. On a observé, dans le mode d'emmagasinage total, des rapports masse d'ions/charge de $m/e = 455$. On rapporte un emmagasinage sélectif avec un rapport $m/e = 219$ mais avec une faible résolution. On discute des effets de la variation des paramètres de piégeage incluant la fréquence de conduite et les dimensions physiques de l'appareillage.

[Traduit par le journal]

Introduction

In a recent review of ion photodissociation by Dunbar (1), three phases of the short history of such studies were recognized. The initial studies in the 1960's were carried out in the laboratories of Dunn (2) and Dehmelt (3); the second stage began in 1970 as photodissociation became a major area of interest to ion cyclotron resonance (ICR) spectroscopy with at least six ICR laboratories active in such studies; and the third stage, beginning in 1973, saw the renewed application of mass-filter type instruments to these problems. To this historical perspective as of 1977, one may add a fourth stage of slow multiphoton induced ion dissociation studies initiated in 1978 with the work of Beauchamp and co-workers (4). Among the early studies originating from Dehmelt's laboratory were a few studies on the photodissociation of H_2^+ and CH_4^+ carried out using RF quadrupole traps (5). Recently, we reported (6) on the slow multiphoton induced dissociation of the protonated dimer of 2-propanol using a quadrupole ion store (QUISTOR). While QUISTOR work may be nearly synonymous with that of ICR (7), in that positive and negative ion storage may be effected under virtually collision-free conditions, resonance ejection may be utilized to identify precursors (8), and ion photodissociation may be induced upon irradiation in the ultraviolet, visible (5), and infrared regions (6), there are essential differences between the two techniques. The QUISTOR may be operated not only as a total ion storage device (cf. ICR), but as a mass spectrometer (9) and as a specific ion reactor (10) in which the device is operated initially in a mass selective mode with relaxation to total ion storage. Furthermore, collisional focusing of the entire ion cloud concentrated at the centre of the quadrupole field, which has been proposed earlier (11) and has been demonstrated by fluorescence observations (12), greatly facilitates ion photodissociation with a single pass of a laser beam through the centre of the device. As it is thus no longer necessary to use mesh electrodes so that the entire storage volume may be illuminated, solid electrodes with concomitant finer control of the quadrupole field may be used to effect mass selectivity of medium resolution, i.e. $M/\Delta M \approx 300$.

The ultimate objective of the present work is to determine the optimum operating conditions for the consecutive creation and storage (in the total ion storage mode) of a primary or secondary ion of choice, isolation of the chosen ion species (in the mass selective mode), followed by simultaneous irradiation of the ion and relaxation of the field (to the total ion storage mode) in order to effect trapping and subsequent mass analysis of the ionic photofragments. In practice, mode switching has been achieved (10) but the mass ranges of ions which can be manipulated thus have not been explored in detail. We report here the present level of optimization of QUISTOR characteristics with respect to the ranges of ion mass-to-charge ratios which

[1]This paper was presented at the 65th Conference of the Chemical Institute of Canada, May 30 – June 2, 1982, in Toronto, under the title Mass storage range of the QUISTOR.

[2]Adjunct Professor, Department of Chemistry, Queen's University, Kingston, Ont.

[3]Registered in the Ph.D. programme in Chemistry of Queen's University.

Can. J. Chem. Downloaded from www.nrcresearchpress.com by 210.87.254.40 on 09/06/12
For personal use only.

Can. J. Chem. Downloaded from www.nrcresearchpress.com by 210.87.254.40 on 09/06/12
For personal use only.

may be stored in the total ion storage mode and in the mass selective mode. In an accompanying publication (28) are reported the results of multiphoton dissociation in the QUISTOR of gas-phase ions derived from 2-propanol and its deuterated analogues using low-intensity infrared CO_2 laser radiation at 944 cm^{-1}.

Theory

The conventional quadruopole mass filter employs four stainless steel rods to which is applied a composite DC and RF potential $\pm\phi_0$. Mass separation is effected according to the criterion of path stability as the ions traverse the length of the rod–electrode assembly from source to detector. With the z-axis as the direction of ion travel, mass separation is achieved by applying $+\phi_0$ to rods in the $x-z$ plane and $-\phi_0$ to rods in the $y-z$ plane. For the QUISTOR, the three electrodes (one ring and two end-caps) are in the form of a hyperboloid of one sheet combined with a hyperboloid of two sheets, respectively. Due to the rotational symmetry of the QUISTOR, any point in the inner volume defined by the electrodes can be expressed in terms of a radial coordinate r and an axial coordinate z. The inner radius of the ring electrode is denoted r_0 and the distance from the centre of the trap to either end-cap electrode is denoted z_0. From the Laplace condition

$$[1] \quad \nabla^2\phi = 0$$

the relative magnitudes of r_0 and z_0 are thence determined to be

$$[2] \quad r_0^2 = 2z_0^2$$

and the entire structure is depicted schematically in Fig. 1.

The form of the potential ϕ_0 is a combination of a DC component U and a sinusoidally varying component V_0 such that

$$[3] \quad \phi_0 = U + V_0 \cos \Omega t$$

where Ω is the angular frequency ($2\pi f$) and V_0 is the amplitude of the alternating potential developed between oppositely charged electrodes. The potential at any point inside the QUISTOR is given by [4].

$$[4] \quad \phi(r, z) = (U + V_0 \cos \Omega t)\,(r^2 - 2z^2)/2r_0^2$$

The force acting upon an ion in the z-direction is given by

$$[5] \quad -eE_z = m\frac{d^2z}{dt^2}$$

which together with [4] gives

$$[6] \quad \frac{d^2z}{dt^2} - \frac{2e}{mr_0^2}(U + V_0 \cos \Omega t)z = 0$$

Expression [6] is in fact an equation of the Mathieu type for which the general form is

$$[7] \quad \frac{d^2z}{d\gamma^2} - (a_z + 2q_z \cos 2\gamma)z = 0$$

with the transformations

$$[8] \quad a_z = \frac{8eU}{mr_0^2\Omega^2}$$

$$[9] \quad q_z = \frac{4eV_0}{mr_0^2\Omega^2}$$

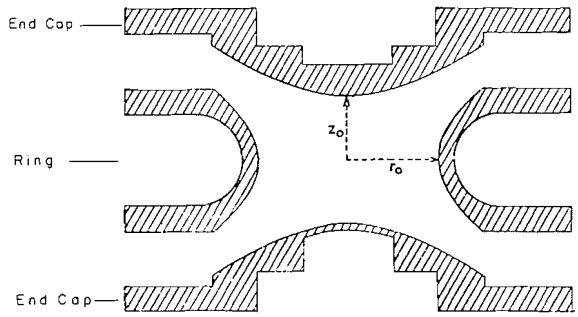

FIG. 1. Section through the hyperbolic structure of the QUISTOR showing the dimensions r_0 and z_0.

$$[10] \quad \gamma = \frac{\Omega t}{2}$$

where U is the DC voltage, V_0 is the 0–p RF voltage, m/e is the mass-to-charge ratio, r_0 is the radius of the ring electrode, and Ω is the radial frequency of the RF voltage.

An analogous treatment of the motion in the r-direction gives

$$[11] \quad \frac{d^2r}{dt^2} + \frac{e}{mr_0^2}(U + V \cos \Omega t)r = 0$$

so that

$$[12] \quad a_z = -2a_r$$

and

$$[13] \quad q_z = -2q_r$$

The detailed solution of the Mathieu equation has been presented elsewhere (13). An essential feature is that the trajectories of the ions within the device are found to be either "stable", i.e. the value of displacement periodically passes through zero, or "unstable" in which case the displacement increases towards infinity. The stability of the trajectory depends upon the numerical values of the parameters a and q and of course, for the practical purpose of trapping ions in a QUISTOR, the trajectories of the ions in the r- and z-directions must both be stable simultaneously. This leads to a "stability envelope" for the QUISTOR in a,q space, which is illustrated in Fig. 2. For any particular ion the values of a and q must be within the enclosed area if it is to have a stable trajectory. The other lines crossing the stability envelope are so-called iso-β lines corresponding to loci of a,q coordinates such that the various wave forms of the trajectories of the ions all possess the same frequencies and general character (14), although the amplitudes of the oscillations may be different. The β values are related to the dominant secular frequencies, ω_r and ω_z:

$$[14] \quad \omega_z = \frac{\beta_z\Omega}{2}$$

As the oscillation frequency is mass dependent, i.e.

$$[15] \quad \omega_z = \beta_z\frac{\Omega}{2} = \left(a_z + \frac{q_z^2}{2}\right)^{1/2}\frac{\Omega}{2}$$

and in the z-direction with $a_z = 0$

$$[16] \quad \omega_z = \left(\frac{q_z^2}{2}\right)^{1/2}\frac{\Omega}{2} = \frac{\sqrt{2}\,eV_0}{mr_0^2\Omega}$$

it is possible to effect resonance ejection of ions of specific mass-to-charge ratio (6).

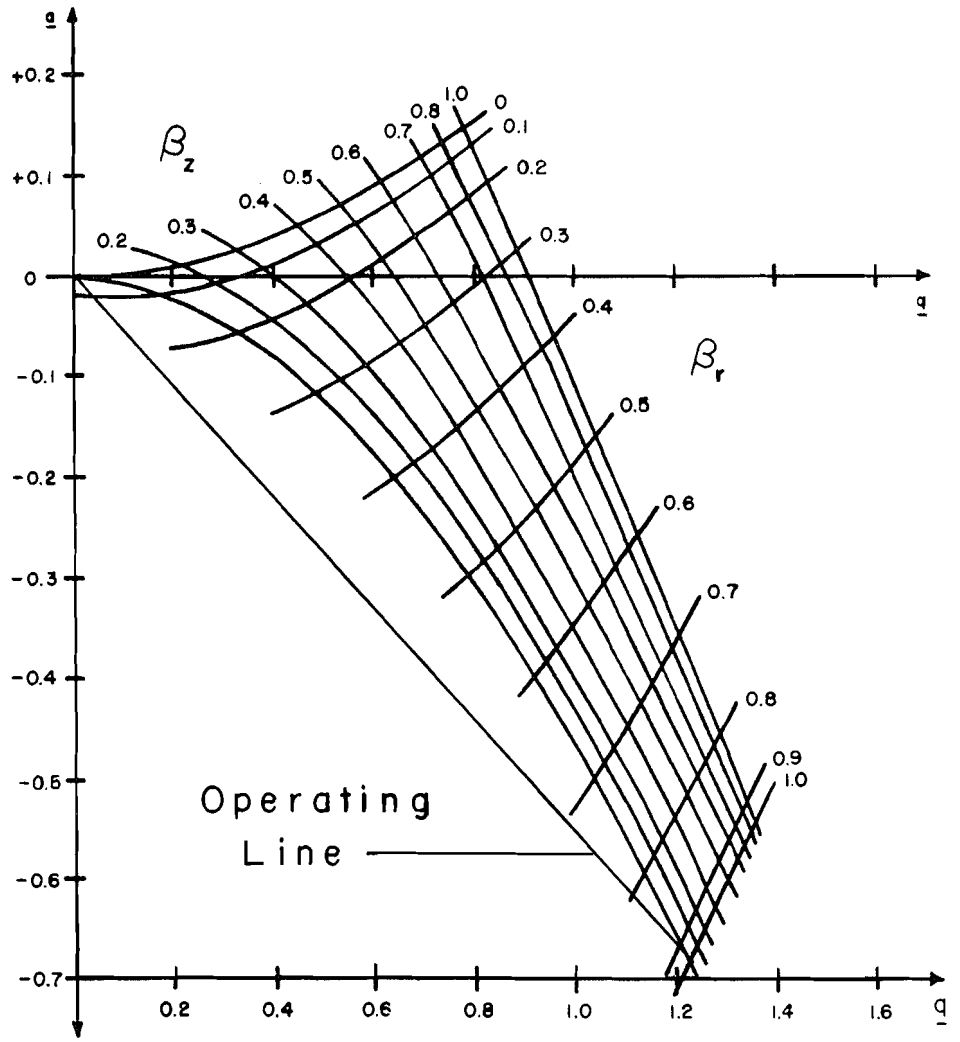

FIG. 2. Stability envelope near the origin for the QUISTOR with the operating line of constant U/V, and showing some iso-β lines.

The trapping potential, ϕ_0, may be applied in various fashions to the QUISTOR electrodes. Bonner (15) has summarized as follows the operating modes according to the application of these potentials. Mode I: Analogous to the operation of the mass filter, the combined RF and DC voltage, ϕ_0, is applied to the ring electrode and $-\phi_0$ to the end-caps. Mode II: ϕ_0 is applied to the ring and the end-caps earthed. Mode III: The DC component of ϕ_0 is applied to the end-caps and the RF component to the ring.

In this laboratory, the QUISTOR is operated exclusively in Mode II. Although Mode I has the advantage of doubling the values of a and q at a given U and V and hence doubling the effective mass range, this mode necessitates interfacing the rectangular extraction pulse, which empties the trap, with the applied RF and DC potential.

Operation of the QUISTOR along the q-axis, i.e. with zero applied DC potential ($a = 0$), corresponds to a total ion storage mode. It is expected from [9] and Fig. 2 that for a fixed value of V_0 a range of values of m/e will be stable, corresponding to q_z ($=-2q_r$) lying within the limits 0 to 0.91. It may be noted that, at a given value of V_0, ions are stored with different efficiencies so a degree of mass selectivity may result (16).

To operate the QUISTOR as a mass spectrometer, mass selective ion storage is used in which applied potentials are chosen so as to yield pairs of a,q values close to either the upper or lower apex of the stability diagram in Fig. 2, so that only ions of one m/e value are stable (and hence stored) at a time. As in the conventional quadrupole mass filter, therefore, a mass spectrum may be generated by varying U and V_0 at a constant ratio of U/V_0 such that for each mass the a,q coordinates move along the operating line shown in Fig. 2. Experimental results for a limited mass range have been reported by Dawson *et al.* (17), Harden and Wagner (18), Mastoris (19), Sheretov *et al.* (20), and more recently by Mather *et al.* (9) operating in Mode I.

The common regions in a,q space for both axial and radial stability give rise to but a single diagram, shown in Fig. 2, which is accessible experimentally. The diagram has two apices of interest, one of which lies above the q-axis and one below. For the mass filter, the stability diagram is symmetric ($a_x = -a_y$) about the q-axis and either apex may be used for mass selectivity. For the QUISTOR, the diagram is asymmetric ($a_z = -2a_r$) and although both apices may be used for mass selectivity the lower apex is preferred as it is more sharp and affords a higher possible resolution. However, when mode switching is required only the upper apex ($q_z < 0.91$) may be used, wherein relaxation of the DC component determines a point on the q-axis lying within the stability diagram. For the

Can. J. Chem. Downloaded from www.nrcresearchpress.com by 210.87.254.40 on 09/06/12
For personal use only.

Can. J. Chem. Downloaded from www.nrcresearchpress.com by 210.87.254.40 on 09/06/12
For personal use only.

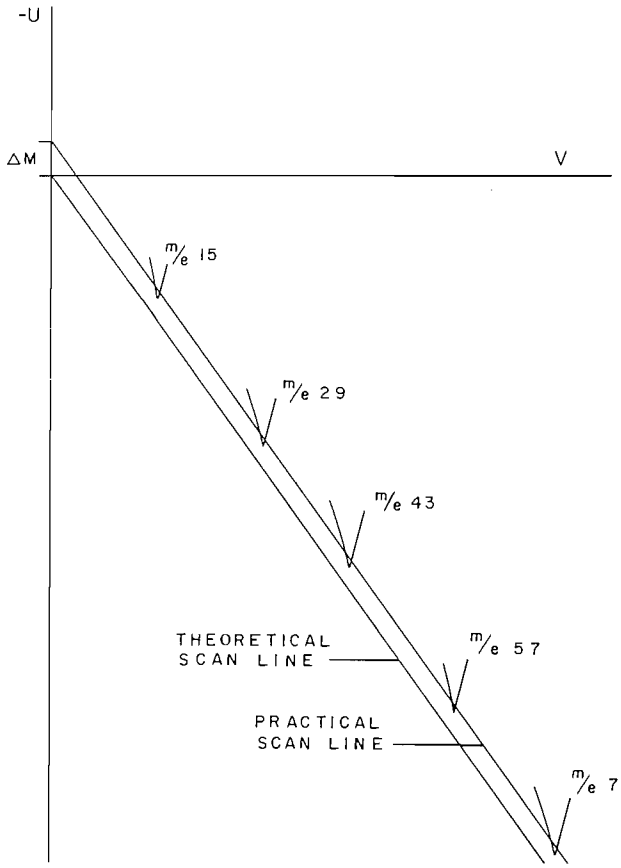

FIG. 3. Lower apices of experimental stability diagrams for five ions in U, V space. The apices are shifted by space-charge within the trap; a DC offset (ΔM) is necessary to intersect the stability diagram apex for each mass.

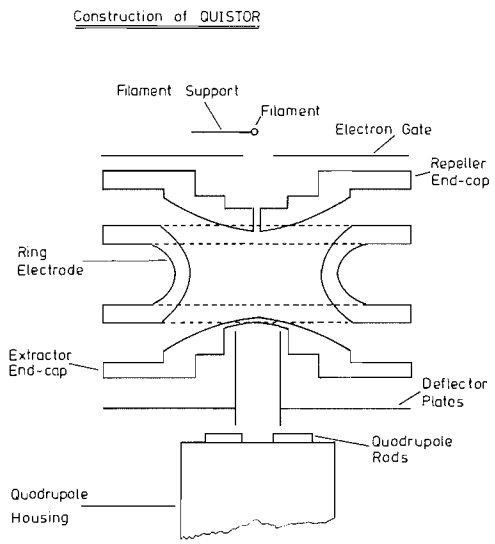

FIG. 4. A section through the QUISTOR showing the orientation with respect to the quadrupole mass filter. The QUISTOR, which is mounted on a separate flange, abuts the ion source of the mass filter. The ion source, which is not shown here, both facilitates ion transmission from QUISTOR to mass filter and provides mass calibration.

lower apex, q_z is always greater than 0.91 and relaxation of the DC component would locate a point on the q-axis lying beyond the stability diagram.

Mass selectivity in the QUISTOR may be visualized more

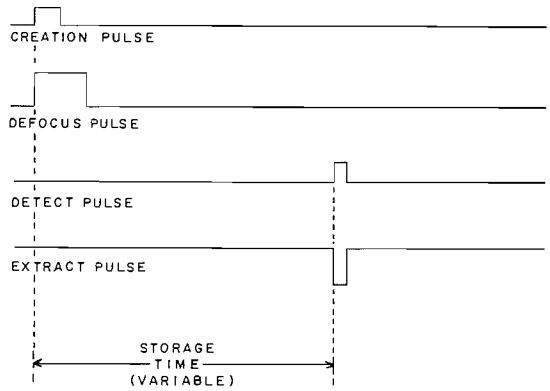

FIG. 5. DC pulse sequence for operation of the QUISTOR in the mass selective mode.

readily when the stability diagrams are plotted in terms of U and V, whereupon a stability diagram is generated for each value of m/e. In order to generate a mass spectrum, the QUISTOR is operated at a constant DC/RF ratio (and multi-pulsed fashion) such that each successive m/e value is stable within the trap as ϕ_0 is ramped, and an apex of each diagram is intersected so as to yield good peak shapes of adequate resolution. The theoretical stability diagrams are derived from consideration of a single ion in the field of the QUISTOR. In practice, may ions are stored simultaneously and the resulting space charge may induce distortion of the stability diagram (14, 21–25). The diagrams are shifted from their predicted locations, as shown in Fig. 3, so that the practical scan line does not go through the origin and does not have the predicted ratio of DC/RF of 0.28. The effect of space charge may be considered in terms of an additional DC voltage to the electrodes leading to a net change in the U coordinate in Fig. 3 and described as ΔM. Experimentally, ΔM is available as a variable parameter as is the ratio of DC/RF. It should be noted that a negative voltage for ΔM must be applied to the ring in order to compensate for the positive space charge. A DC voltage of opposite polarity is required when ΔM is applied to the end-cap electrodes.

From an examination of q_z [9], it is seen that the range of m/e values which can be stored within the useful range of q_z is inversely proportional to the physical dimensions of the QUISTOR (r_0^2) and to the drive frequency (Ω^2). Each of these parameters is examined in turn.

Experimental

The experimental arrangement is depicted in Fig. 4 wherein the QUISTOR is operated in a repetitively pulsed fashion as described elsewhere (6). A typical pulse sequence for mass-selective operation is depicted in Fig. 5. The precise separation of the QUISTOR electrodes was maintained with ruby spheres of diameter 9.5 mm countersunk into the electrodes; the spheres were obtained from the Specialty Ball Company, Rocky Hill, Connecticut, U.S.A. Electrons are produced from the heated tungsten filament which s biased at −70 V. The electron gate is held at −100 V to exclude electrons from the trap and is pulsed periodically to approximately −10 V for 50–200 μs to allow electrons into the trap which then ionize the sample molecules at a pressure of 2–4 mPa. After a predetermined storage time, positive ions are extracted through perforations in the extractor end-cap by a negative rectangular pulse of −60 V amplitude and several RF cycles duration. The ions travel between the deflector plates and then into the mass filter assembly.

In the total storage mode the deflector plates may be held at a low

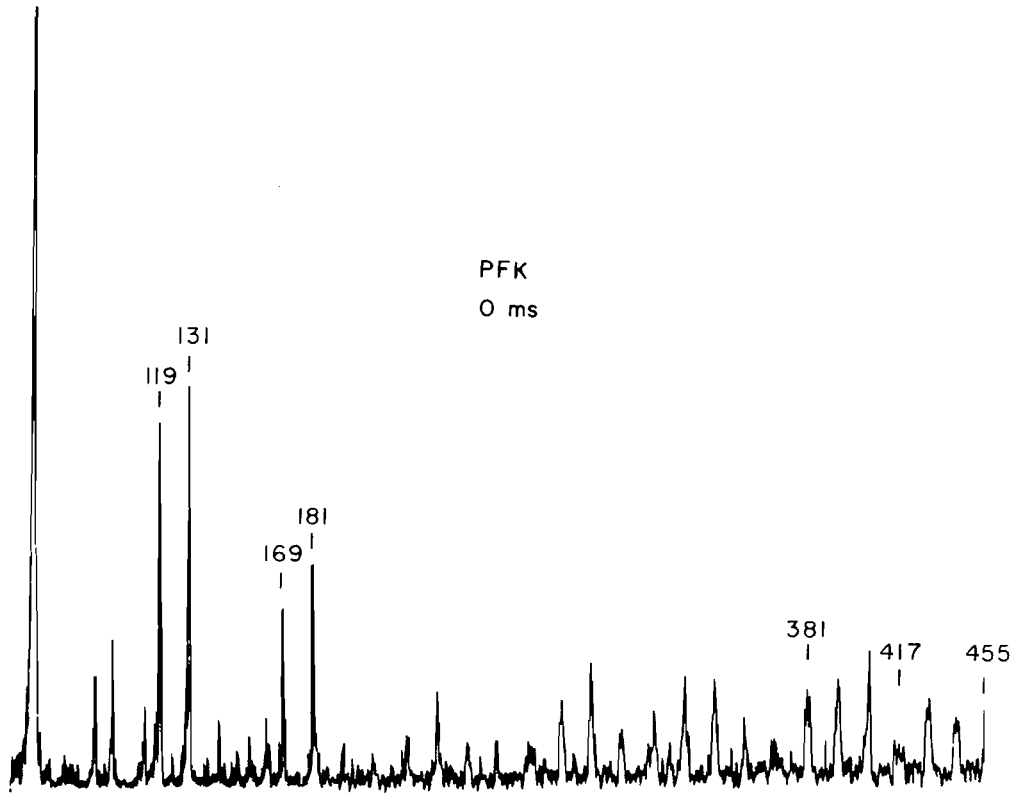

FIG. 6. QUISTOR total storage spectrum of PFK at 3 mPa pressure and 0 ms of storage. RF drive 600 V 0−p at 1.7 MHz. No applied DC (equivalent to e.i. spectrum).

positive potential (2−5 V) to focus the entire ion beam into the mass analyser. In the selective storage mode unstable ions exit the trap spontaneously during the mass sorting process, which takes several hundred microseconds, and a positive pulse (80 V) is applied to one of the deflector plates to defocus these ions and prevent them from reaching the detector. As the mass filter is not actively employed in the selective storage mode, this defocus pulse may be applied to one pair of rods to ensure that unstable ions do not reach the detector (9, 26). The trapping potential ϕ_0 is supplied to the ring electrode by an Extranuclear Laboratories Quadrupole Power Supply, Model 011-15, which was modified as proposed by Todd and co-workers (9) to enable selection of the correct U/V_0 ratios to operate at either the upper or lower apex of the QUISTOR stability envelope.

Results and discussion

Gaseous ions are trapped in the QUISTOR for periods of up to 125 ms which corresponds to the lowest pulse frequency, 8 Hz, at our disposal. Ions may be trapped in the total storage mode ($a = 0$) or mass selectively. Let us examine first the mass range of ions which may be stored simultaneously, i.e. in the total storage mode. In this mode,stored ions are ejected from the QUISTOR and analysed subsequently with a mass filter, thus determination of the range of m/e values stored simultaneously is dependent upon the mass range of the filter tandem to the QUISTOR.

Until recently the trapped ion of greatest m/e value which could be detected from the QUISTOR was $C_4F_9^+$, at m/e 219, which is one of the more abundant ions produced by electron impact of perfluorokerosene (PFK). This mass range determination was restricted by the mass range of the quadrupole mass filter (Vacuum Generator Q7B) which was nominally 200 amu.

A new quadrupole mass filter (Vacuum Generators QXK400) has been used to extend the detectable limit of the total ion storage mass range. In Figs. 6 and 7 are shown the mass spectra of ions derived from perfluorokerosene in the total ion storage mode, at 0 ms (corresponding to a normal electron impact spectrum) and after 30 ms of total ion storage, respectively. The spectrum at zero storage time can be compared with the normal mass spectrum obtained with the quadrupole mass filter as the original filament assembly of the mass filter is intact and in place, and with the calibration mass spectrum of PKF supplied by the manufacturer. Virtually all of the primary ions expected from PFK, up to m/e 455, have been observed with operation of the QUISTOR as an electron impact source. The mass spectrum obtained after 30 ms of ion storage, as shown in Fig. 7, demonstrates the ion storage capability of the QUISTOR up to m/e 455, i.e. $C_{11}F_{17}^+$, at the extreme mass limit of the QXK400. The relatively high intensities of peaks corresponding to $m/e > 380$ is extremely encouraging and indicative that the mass range of the QUISTOR in the total ion storage mode may be considerably in excess of the present observation. In this work, the QUISTOR is driven with a modified Extranuclear Laboratories 011-15 power supply and the mass filter with the QXK400 power supply. The mass range of the mass filter has been extended to approximately 800 amu when driven by the Extranuclear power supply but it is not possible to use the Extranuclear power supply to drive both the QUISTOR and the mass filter simultaneously.

Comparison of the mass spectra in Figs. 6 and 7 yields a great deal of information on the ion-chemistry of the PFK system at 2 mPa. As there is little information in the chemical literature on high molecular weight fluorocarbon ion/molecule chemistry, a brief commentary may be of interest here. $C_2F_5^+$ (m/e 119) and $C_3F_7^+$ (m/e 169) decrease rapidly in intensity

Can. J. Chem. Downloaded from www.nrcresearchpress.com by 210.87.254.40 on 09/06/12
For personal use only.

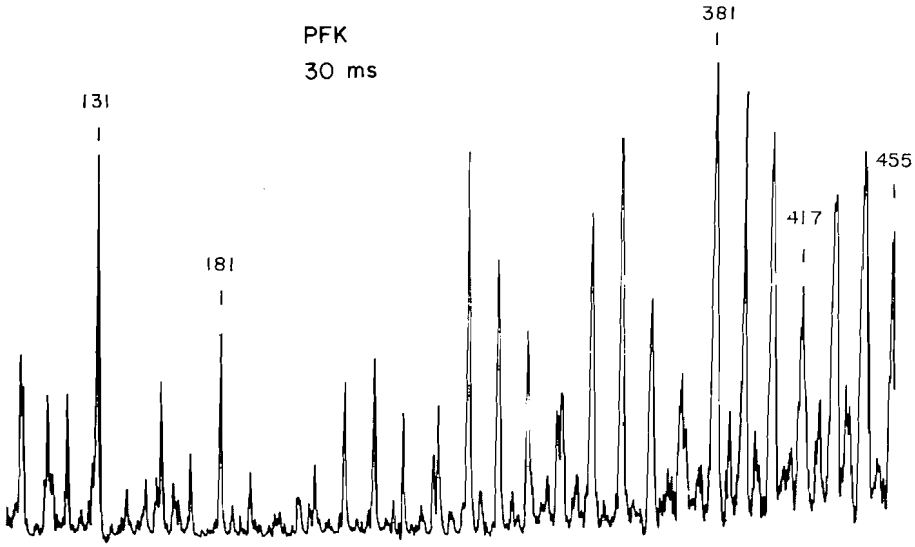

FIG. 7. Total storage spectrum of PFK after 30 ms with operating conditions as in Fig. 6.

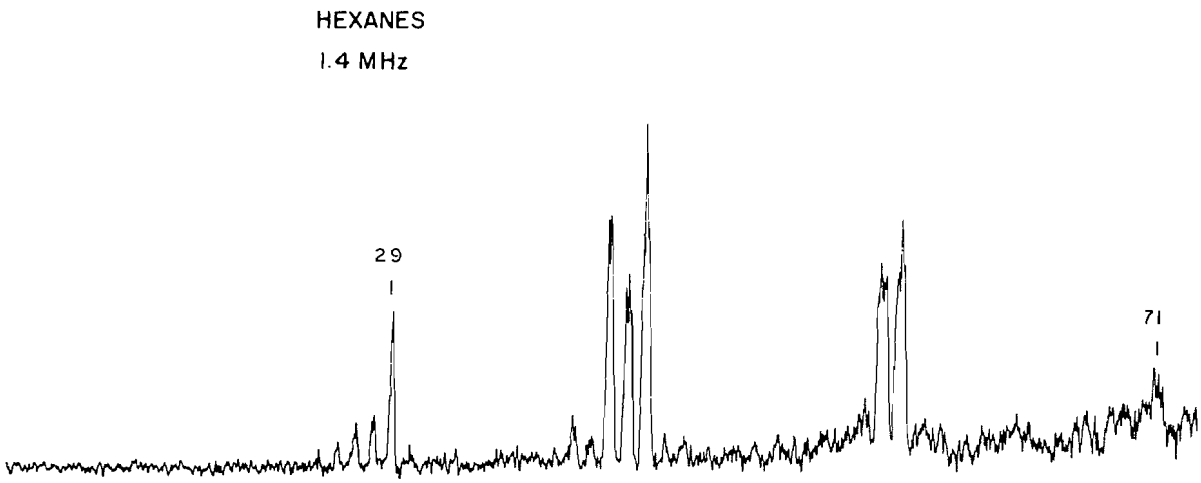

FIG. 8. Illustration of partial mass selectivity in the QUISTOR of ions derived from mixed hexane isomers. Here, the negative DC bias (ΔM) is insufficient to counteract the space-charge and the ramped DC/RF scan line fails to intersect the apices of stability diagrams for ions of low m/e ratio.

with reaction time while $C_3F_5^+$ (m/e 131) and $C_4F_7^+$ (m/e 181) increase in intensity along with $C_6F_{11}^+$ (m/e 281), $C_7F_{13}^+$ (m/e 331), $C_8F_{15}^+$ (m/e 381), and $C_9F_{17}^+$ (m/e 431). Thus there appears to be some degree of enhanced stability (or unreactivity) for ions of the type $C_nF_{2n-1}^+$. Similarly, examination of the peaks for $C_7H_{11}^+$ (m/e 293), $C_8F_{13}^+$ (m/e 343), $C_9F_{15}^+$ (m/e 393), and $C_{10}F_{17}^+$ (m/e 443) indicates a slightly diminished stability for ions of the type $C_nF_{2n-3}^+$; a further diminution in stability is observed for ions of the type $C_nF_{2n-5}^+$. In summary, the ion-chemistry as elucidated from the mass spectra in Figs. 6 and 7 shows that series of ions are formed with increasing stability such that $C_nF_{2n-1}^+ > C_nF_{2n-3}^+ > C_nF_{2n-5}^+$.

Mass selective operation of the QUISTOR has been demonstrated in the range m/e 12 (C^+) to m/e 100 ($C_7H_{16}^+$) with heptane (9), and in cylindrical devices to m/e 86 ($C_6H_{14}^+$) with hexane (26). Both the resolution of the mass spectrum, defined as $M/\Delta M$, and the intensity of each peak are extremely sensitive to the ratio of DC/RF and to the applied DC bias, ΔM. A mixture of hexane isomers was chosen for examination. The gross effects of the magnitude of ΔM and the DC/RF ratio are shown in Fig. 8; a mass spectrum extending from m/e 25–71 was obtained wherein the lower masses have not been selected. In this case the ΔM was insufficiently negative (<-0.8 V) and the DC/RF ratio too low (<0.28). The resolution at m/e 29 is ~100 and diminished to ~70 at m/e 57. In Fig. 9, ΔM is made more negative (−2 V) and the DC/RF ratio in excess of 0.30, only the ions of $m/e < 29$ are observed with good resolution though here the resolution at m/e 29 is ~150 and diminishes with m/e ratio. The diminution of resolution with m/e ratio signifies that the DC/RF is higher than ideal.

For the mass spectrum shown in Fig. 10, where ΔM was set at −0.8 V and the DC/RF ratio at 0.290, a range of masses from m/e 13–71 was selectively stored. Peaks corresponding to C_3 and C_4 ions are seen to be of much higher intensity than the remainder of the spectrum. A change in the DC/RF of 0.67% (0.290 to 0.292) produced the mass spectrum shown in Fig. 11, in which normal relative peak intensities have been restored but m/e 71 was not observed. Thus the question arises as to whether there are unique settings of ΔM and DC/RF ratio at which the potentially high resolution of which the QUISTOR ought to be capable is realizable over a range of masses. Let us examine two factors: (*i*) the magnitude of ΔM which should

Can. J. Chem. Downloaded from www.nrcresearchpress.com by 210.87.254.40 on 09/06/12
For personal use only.

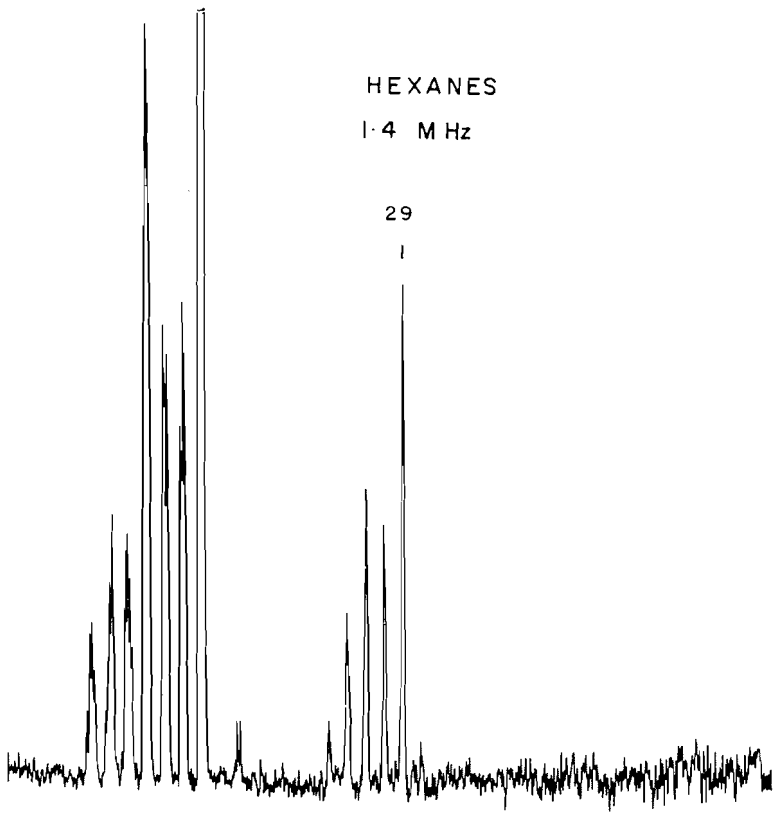

FIG. 9. As for Fig. 8, but here both the ΔM bias and the ramped DC/RF ratio are too high so that only the apices of stability diagrams for $m/e < 30$ are intersected.

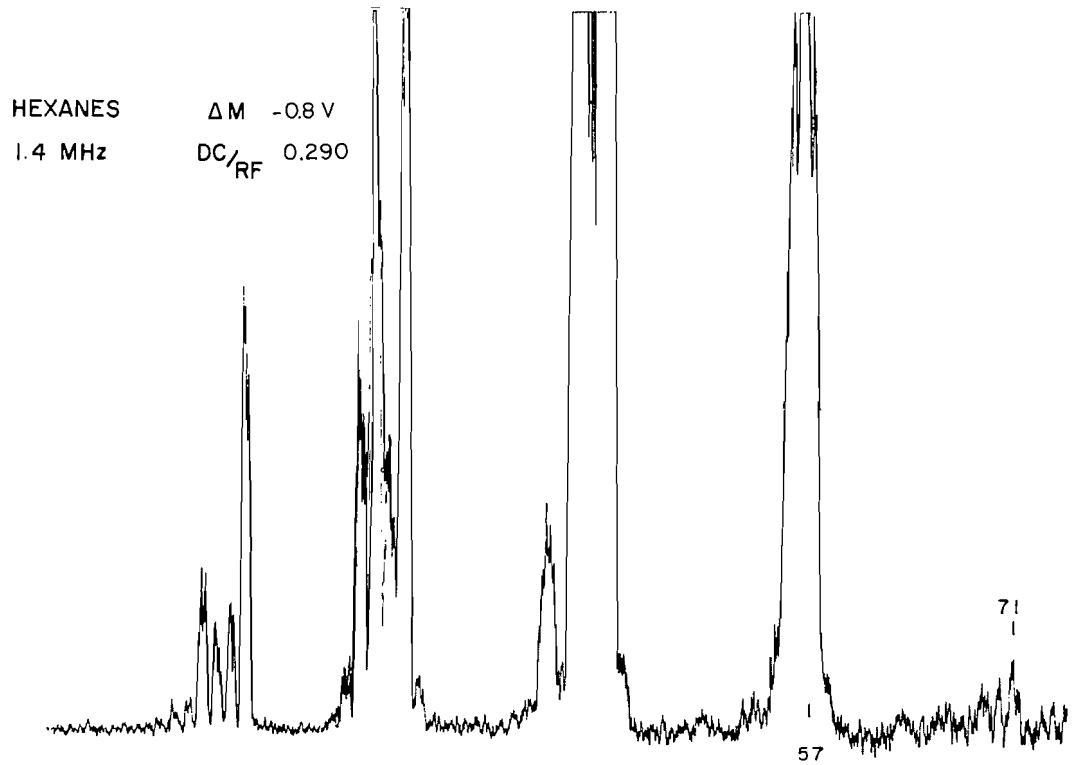

FIG. 10. Illustration of QUISTOR mass selectivity of ions derived from mixed hexane isomers over the range m/e 13−71; 2 mPa, 1.4 Mhz, $\Delta M = -0.8$ V, DC/RF = 0.290.

balance the space charge of the stored ions, and (*ii*) the degree of distortion of stability diagrams for ions of differing m/e values though of equal intensities and stored under similar conditions. Firstly, the variation in relative peak intensities in

Can. J. Chem. Downloaded from www.nrcresearchpress.com by 210.87.254.40 on 09/06/12
For personal use only.

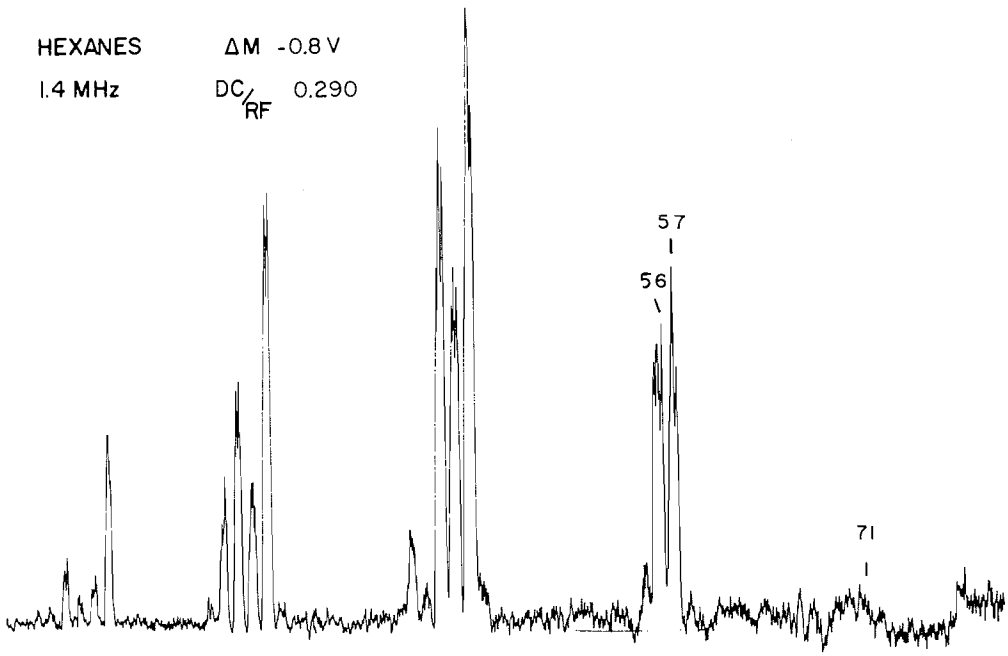

FIG. 11. As for Fig. 10 with the DC/RF ratio increased to 0.292. Resolution of the mass spectrum is considerably enhanced (cf. Fig. 10) with accompanying decrease in signal intensity.

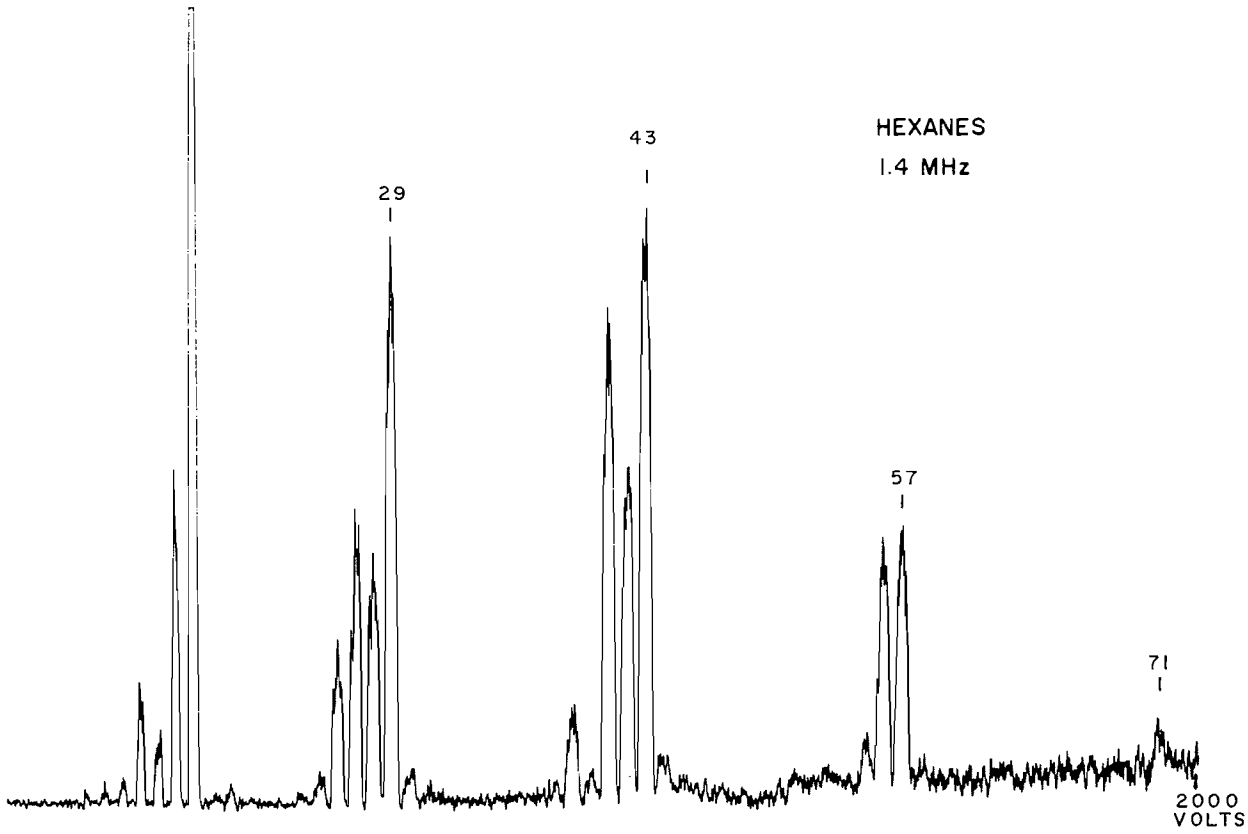

FIG. 12. Optimum mass spectum obtainable with mixed hexane isomers; 2 mPa, 1.4 MHz, $\Delta M = -1.0$ V, DC/RF = 0.293, maximum RF was 2000 V p-p, scan rate = 4 s amu^{-1}.

a normal mass spectrum would indicate that compensation for space charge should vary with m/e value. Secondly, although little experimental work (9, 26) has been carried out in this area, there is some evidence to suggest that stability diagram distortions for Ne^+ and Ar^+ are not identical under similar experimental conditions. Thus it is concluded that ultimate optimization of ΔM and DC/RF ratio would require adjustment of these parameters for each ion species. While such optimization could be achieved possibly with microprocessor control it would yield little of immediate value. Mass selective oper-

Can. J. Chem. Downloaded from www.nrcresearchpress.com by 210.87.254.40 on 09/06/12
For personal use only.

Can. J. Chem. Downloaded from www.nrcresearchpress.com by 210.87.254.40 on 09/06/12
For personal use only.

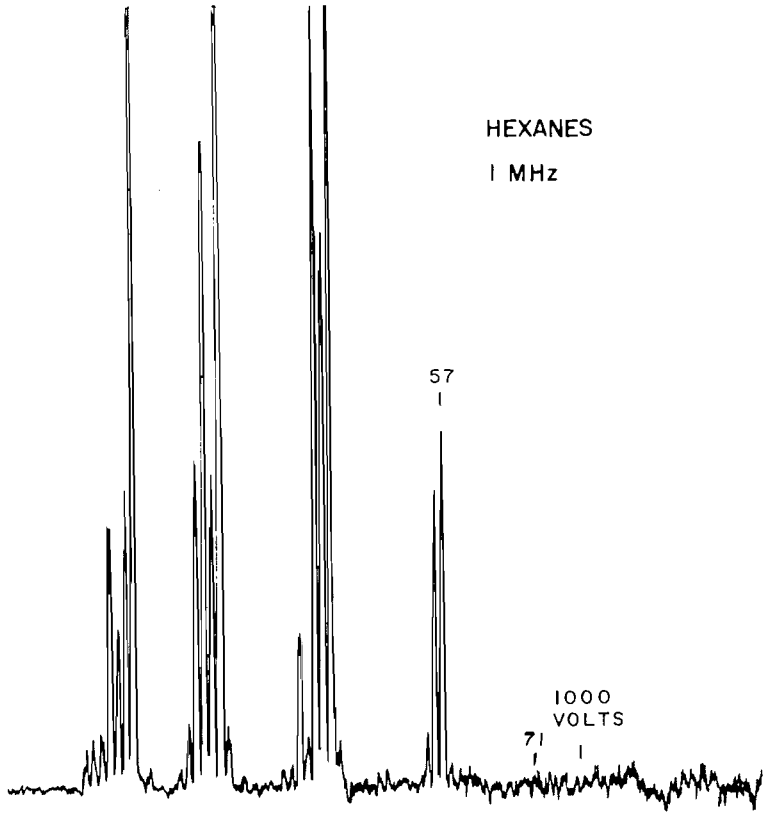

FIG. 13. As for Fig. 12. The drive frequency has been lowered to 1.0 MHz and the maximum RF was 1000 V p-p.

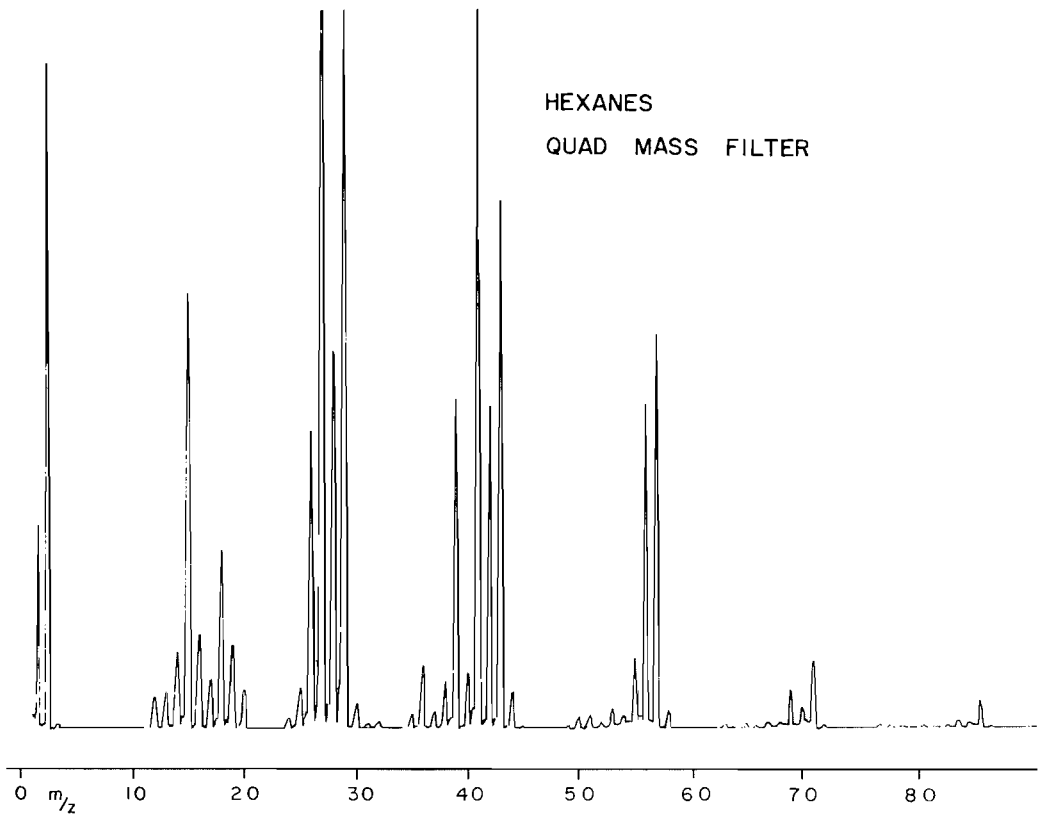

FIG. 14. Electron impact spectrum of mixed hexane isomers obtained from the VG QXK 400 quadrupole mass filter.

ation of the QUISTOR for ion photodissociation studies per se does not necessitate the generation of mass spectra. However, the optimum mass spectrum of mixed hexane isomers at a drive frequency of 1.4 MHz is shown in Fig. 12; it should be noted that m/e 71 was stored selectively with an RF voltage (0−p) of slightly less than 2000 V.

Can. J. Chem. Downloaded from www.nrcresearchpress.com by 210.87.254.40 on 09/06/12
For personal use only.

In accordance with [7] and [8], the a_z and q_z values are inversely proportional to Ω^2, therefore when the drive frequency is reduced to 1.0 MHz the effective mass range should be doubled for a given applied voltage or a given ion should be stored selectively at half the previous voltage. This dependance is shown in Fig. 13 where m/e 71 is observed, albeit faintly at slightly less than 1000 V. The relative peak intensities of the spectrum in Fig. 13 are in good agreement with the electron impact spectrum shown in Fig. 14 which was obtained with the mass filter alone. A prominent peak at m/e 18 in these spectra is due to H_2O^+. The trace of water present served as an indicator of ion/molecule reactions during the mass sorting period which could have produced H_3O^+ at m/e 19; none was observed, hence the selectivity process is rapid.

Values for a_z and q_z are also inversely proportional to r_0^2. All of the above storage spectra were obtained with a QUISTOR for which a value of 1.0×10^{-2} m was chosen for r_0, the internal radius of the ring electrode. While some studies have been carried out with smaller QUISTORS, e.g. $r_0 = 7.0 \times 10^{-3}$ m (27) with an $(m/e)_{max} = 107$ and $r_0 \simeq 3.5 \times 10^{-4}$ m (12) with which Ba^+ ions at m/e 137 were stored, and storage capabilities of quadrupole ion traps of different sizes having cylindrical symmetry have been examined cursorily (26), no systematic examination of the mass storage range dependance on r_0 has been made. A new QUISTOR has been constructed recently in this laboratory with $r_0 = 6.0 \times 10^{-3}$ m. In the total storage mode a mass spectrum of PFK has been obtained for the range m/e 69–381 under the following conditions; 2 ms storage, 2 mPa, 1.8 Mhz, 600 V 0–p. These storage conditions correspond to values for q_z of 0.73 and 0.13 for m/e 69 and m/e 381, respectively. With the small QUISTOR in the mass selective mode, ions derived from m/e 219 are observable though of poor resolution, furthermore the peaks show marked splitting. This work is in progress.

Conclusion

We conclude that the QUISTOR is viable as a photochemical reactor for photodissociation studies of gaseous ions. The ion storage capability in the total storage mode has been shown to extend to m/e 455 and possibly beyond. Though not of direct interest to photodissociation studies, the extended mass storage capability may facilitate low pressure chemical ionization studies, pursued previously for low molecular weight compounds, to molecules of interest with higher molecular weights. The demonstrated ranges for mass selectivity are encouraging for the isolation of single ion species for irradiation.

Acknowledgements

The authors acknowledge with thanks the financial support of Trent University, the Natural Sciences and Engineering Research Council of Canada (for Operating and Equipment Grants), Imperial Oil Company Limited, Air Resources Branch of the Ontario Ministry of the Environment, and Queen's University for a Graduate Student Assistantship to A.B.Y. We acknowledge also the technical assistance of G. Wynn, C. J. S. Stuart, and W. King.

1. R. C. DUNBAR. *In* Gas phase ion chemistry. Vol. II. *Edited by* M. T. Bowers. Academcic Press, New York. 1974. Chapt. 14.
2. G. H. Dunn. *In* Atomic collision processes. *Edited by* M. R. C. McDowell. North-Holland Publ., Amsterdam. 1964p. 997; Phys. Rev. **172**, 1 (1968); F. Von Busen and G. H. Dunn. Phys. Rev. A, **5**, 1726 (1972).
3. H. G. DEHMELT and K. B. JEFFERTS. Phys. Rev. **125**, 1318 (1962); H. G. DEHMELT. Adv. At. Mol. Phys. **3**, 53 (1967); **5**, 190 (1969).
4. R. L. WOODIN, D.S. BOMSE, and J. L. BEAUCHAMP. J. Am. Chem. Soc. **100**, 3248 (1978).
5. E. S. ENSBERG and K. B. JEFFERTS. Astrophys. J. **195**, L89 (1975); K. B. JEFFERTS. Phys. Rev. Lett. **20**, 39 (1968); **23**, 1476 (1969).
6. R. J. HUGHES, R. E. MARCH, and A. B. YOUNG. Int. J. Mass Spectrom. Ion Phys. **42**, 255 (1982).
7. R. C. DUNBAR. *In* Chemical reactivity and reaction paths. *Edited by* G. Klopman. Wiley–Interscience, New York. 1974. p. 339.
8. M. A. ARMITAGE, J. E. FULFORD, DUONG-NHU, R. J. HUGHES, and R. E. MARCH. Can. J. Chem. **57**, 2108 (1979).
9. R. E. MATHER, R. M. WALDREN, and J. F. J. TODD. *In* Dynamic mass spectrometry. Vol. 5. *Edited by* D. Price and J. F. J. Todd. Heyden and Son Limited, London. 1978. p. 71.
10. J. E. FULFORD and R. E. MARCH. Int. J. Mass Spectrom. Ion Phys. **26**, 155 (1978).
11. R. F. BONNER and R. E. MARCH. Int. J. Mass Spectrom. Ion Phys. **22**, 17 (1976); **25**, 411 (1977).
12. W. NEUHAUSER, M. HOHENSTRATT, P. E. TOSCHEK, and H. G. DEHMELT. Appl. Phys. **17**, 123 (1978); Phys. Rev. Lett. **41**, 223 (1978).
13. P. H. DAWSON. *In* Quadrupole mass spectrometry and its applications. *Edited by* P. H. Dawson. Elsevier,Amsterdam. (1976). Chapts. II–IV.
14. E. FISCHER. Z. Physik. **156**, 26 (1959).
15. R. F. BONNER. Int. J. Mass Spectrom. Ion Phys. **23**, 249 (1977).
16. G. LAWSON and J. F. J. TODD. Anal. Chem. **49**, 1619 (1977).
17. P. H. DAWSON, J. W. HEDMAN, and N. R. WHETTEN. Rev. Sci. Instrum. **40**, 144 (1969).
18. C. S. HARDEN and P. E. WAGNER. Edgewood Arsenal Special Publication EASP 100-93 (1971); Edgewood Arsenal Technical Report EATR 4545 (1971).
19. S. MASTORIS. UTIAS-TN-172 University of Toronto, Canada (1972).
20. É. P. SHERETOV, V. A. ZENKIN, and O. I. BOLIGATOV. Instrum. Exp. Tech. USSR. **14**, 195 (1971).
21. F. G. MAJOR and H. G. DEHMELT. Phys. Rev. **170**, 91 (1968).
22. É. P. SHERETOV, V. A. ZENKIN, and V. F. SAMODUROV. Sov. Phys. Tech. Phys. **18**, 282 (1973).
23. C. SCHWEBEL, P. A. MÖLLER, and PHAM TU MANH. Rev. Phys. Appl. **10**, 227 (1975).
24. J. F. J. TODD, R. M. WALDREN, R. E. MATHER, and G. LAWSON. Int. J. Mass. Spectrom. Ion Phys. **28**, 141 (1978).
25. J. E. FULFORD, DUONG-NHU HOA, R. J. HUGHES, R. E. MARCH, R. F. BONNER, and G. J. WONG. J. Vac. Sci. Technol. **17** (4), 829 (1980).
26. R. E. MATHER, R. M. WALDREN, J. F. J. TODD, and R. E. MARCH. Int. J. Mass Spectrom. Ion Phys. **33**, 201 (1980).
27. R. E. MATHER, G. LAWSON, J. F. J. TODD, and J. M. B. BAKKER. Int. J. Mass Spectrom. Ion Phys. **28**, 347 (1978).
28. R. J. HUGHES, R. E. MARCH, and A. B. YOUNG. Can. J. Chem. **61**, 834 (1983).

Multiphoton dissociation of ions derived from isopropanol and deuterated analogues in a QUISTOR with low power CW infrared laser radiation[1]

RICHARD JAMES HUGHES, RAYMOND EVANS MARCH,[2] AND ALEXANDER BALDWIN YOUNG[3]
Department of Chemistry, Trent University, Peterborough, Ont., Canada K9J 7B8

Received June 30, 1982

This paper is dedicated to Professor Harry E. Gunning on the occasion of his 65th birthday

RICHARD JAMES HUGHES, RAYMOND EVANS MARCH, and ALEXANDER BALDWIN YOUNG. Can. J. Chem. **61**, 834 (1983).

A versatile technique employing pulsed quadrupole ion storage mass spectrometry and a low power CW CO_2 laser for the study of slow infrared multiphoton dissociation of gaseous ions under near collision-free conditions is described. Multiphoton dissociation of gaseous ions derived from isopropanol, 2-d_1-isopropanol, isopropan-d-ol and perdeuteroisopropanol, with irradiation for up to 110 ms with intensities of ~20 W cm^{-2}, was effected. Irradiation of proton (or D^+) bound alcohol dimers showed that three dissociative reaction channels are utilized in multiphoton dissociation: the photodissociation yield for the dissociative reaction channel of lowest activation energy increases and becomes dominant with collisional and radiative relaxation of the ions. Of the three ionic photoproducts of multiphoton dissociation of proton bound alcohol dimers, only the protonated ether is found to be photodissociative under the prevailing conditions. The photochemical stability of the ion formed by loss of the elements of propene from the proton bound alcohol dimer contrasts sharply with the multiphoton dissociation of the proton bound alcohol–water mixed dimer, and serves to demonstrate the applicability of multiphoton dissociation to distinguish between gaseous ion isomers.

The large extent of dissociation observed with low laser fluence is indicative of both the rapid collisionally-induced migration of ions to the centre of the QUISTOR (and hence the laser beam) and also the predominance of multiphoton absorption over radiative and collisional deactivation processes in the time and pressure domains employed here.

RICHARD JAMES HUGHES, RAYMOND EVANS MARCH et ALEXANDER BALDWIN YOUNG. Can. J. Chem. **61**, 834 (1983).

On décrit une technique versatile qui utilise la spectrométrie de masse à emmaganisage d'ion quadrupolaire pulsé et un laser CW à CO_2 à faible puissance pour étudier la dissociation multiphoton infrarouge d'ions à l'état gazeux dans des conditions pratiquement sans collisions. On effectue la dissociation multiphoton des ions gazeux provenant de l'isopropanol, de l'isopropanol *O*-*d*, de l'isopropanol *d*-2 et du perdeutéroisopropanol avec une irradiation allant jusqu'à 110 ms et des intensités d'environ 20 W cm^{-2}. L'irradiation d'alcools dimères liés par le proton (ou D^+) a montré que trois voies de réaction dissociatives sont utilisées dans la dissociation multiphoton; le rendement de la photodissociation de la voie de réaction dissociative de plus faible énergie d'activation augmente et devient prépondérant avec la relaxation collisionnelle et radiative des ions. Des trois photoproduits ioniques de la dissociation multiphoton des alcools dimères liés par le proton, on a trouvé que seul l'éther protoné peut être photodissocié dans les conditions existantes. La stabilité photochimique de l'ion formé par suite de la perte des éléments du propène à partir de l'alcool dimère lié par le proton contraste nettement avec la dissociation multiphoton du dimère mixte alcool–eau lié par le proton et sert à démontrer la validité de la dissociation multiphoton dans la distinction des isomères d'ions gazeux.

Le fort taux de dissociation observé avec un laser de faible puissance est une indication de la migration rapide induite par collision des ions vers le centre du QUISTOR (et par conséquent la faisceau du laser) et également de la prédominance de l'absorption multiphoton sur les processus de désactivation radiative et collisionnelle dans les domaines de temps et de pression.
[Traduit par le journal]

Introduction

The characterization of intramolecular relaxation subsequent to photochemical excitation requires near collision-free conditions for study; in general, single species chemistry of a molecule or ion cannot be ascertained unambiguously unless the mean time between collisions is greater than that required for excitation and for unimolecular decomposition. Recently, methods have been developed for studying the infrared (ir) multiphoton photochemistry of gas-phase ions under near collision-free conditions, using pulse ion cyclotron resonance (ICR) spectroscopy (1, 2).

Brauman and co-workers (1) have used a pulsed CO_2 laser to study the photophysics of megawatt ir multiphoton dissociation and to probe vibrational relaxation in gas-phase ions. Beauchamp and co-workers (2) have demonstrated that, as dissociation probabilities of *isolated* molecules depend only on energy fluence and not on peak laser power (3), a relatively low power CW CO_2 laser (several watts) can effect dissociation processes in gaseous ions provided that an ion is irradiated for sufficiently long times under nearly collision-free conditions. Among the early studies of ion photodissociation originating from Dehmelt's laboratory in the 1960's (4) were a few studies on the photodissociation of H_2^+ and CH_4^+ carried out using radio-frequency quadrupole traps (5). The application of such a quadrupole ion store (QUISTOR) has been extended now to slow ir multiphoton induced dissociation of gaseous ions. Photodissociation of the protonated dimer of 2-propanol, which was reported earlier (6), was achieved by the absorption of 11 photons in the ir region. A comparison of the characteristics of the QUISTOR with those of ICR is presented in the accompanying paper (12); while the two techniques are similar, ions stored in the QUISTOR are concentrated at the centre of the quadrupole field which has both axial and radial symmetry, and ion photodissociation studies are carried out at 8–10 Hz compared to 1 Hz with ICR.

[1]Presented initially at the 65th Conference of the Chemical Institute of Canada, May 30 – June 2, 1982 in Toronto.

[2]Adjunct Professor, Department of Chemistry, Queen's University, Kingston.

[3]Registered in the Ph.D. programme in Chemistry of Queen's University.

Can. J. Chem. Downloaded from www.nrcresearchpress.com by 210.87.254.105 on 09/06/12
For personal use only.

Can. J. Chem. Downloaded from www.nrcresearchpress.com by 210.87.254.105 on 09/06/12
For personal use only.

In view of the extensive work of Bomse and Beauchamp (2*c*) on the multiphoton dissociation of proton bound alcohol dimers, isopropanol was selected for initial study in the QUISTOR and the study was extended to an examination of unimolecular reaction energetics in deuterated analogues of isopropanol. Infrared multiphoton dissociation has been employed (2*f*, *g*) in order to distinguish between structural isomers of gaseous ions, and this technique has been used here to distinguish between a protonated alcohol–water cluster ion and the ion formed by loss of alkene from a proton bound alcohol dimer.

The ion/molecule reactions of protonated aliphatic alcohols have been studied in some detail, with particular emphasis given to isopropanol using ion cyclotron double resonance (7, 8) and by the application of resonance ion ejection to quadrupole ion-storage mass spectrometry (9). Well-characterized bimolecular processes occur in the isopropanol system whereby reaction intermediates are readily prepared as stable species. Primary ions (particularly *m/z* 43) formed by electron impact react with neutral isopropanol molecules to form protonated isopropanol, $(CH_3)_2CHOH_2^+$, *m/z* 61, which reacts further with isopropanol to form the activated protonated dimer, *m/z* 121:

$$[1]\quad \underset{m/z\ 61}{(CH_3)_2CHOH_2^+} + (CH_3)_2CHOH \rightarrow \underset{m/z\ 121}{[(i\text{-}C_3H_7OH)_2H^+]^*}$$

The activated proton bound isopropanol dimer may dissociate back to reactants, or be collisionally or radiatively stabilized

$$[2]\quad [(i\text{-}C_3H_7OH)_2H^+]^* \xrightarrow[-h\nu]{M} \underset{m/z\ 121}{(i\text{-}C_3H_7OH)_2H^+}$$

where M is a neutral isopropanol molecule. Alternatively, H_2O may be eliminated to form a protonated ether

$$[3]\quad \left(\underset{m/z\ 121}{(i\text{-}C_3H_7OH)_2H^+}\right)^* \longrightarrow \underset{m/z\ 103}{(i\text{-}C_3H_7)_2OH^+} + H_2O$$

or propene may be lost

$$[4]\quad \left(\underset{m/z\ 121}{(i\text{-}C_3H_7OH)_2H^+}\right)^* \longrightarrow \underset{m/z\ 79}{(i\text{-}C_3H_7OH)H^+(OH_2)} + C_3H_6$$

In the absence of other specific data, the enthalpy change for [1] is assumed to be comparable to the measured enthalpy changes for the analogous reaction of H_3O^+, $CH_3OH_2^+$, and $(CH_3)_2OH^+$ (10). The activation energies for [3] and [4] are not known, though [3] is reported as the decomposition pathway of minimum activation energy (2*c*). Multiphoton dissociation of the proton bound dimer of isopropanol was induced in order to demonstrate the application of the QUISTOR for single ion photochemistry studies.

Experimental

Although the apparatus has been described in detail previously (6) and in the accompanying paper, some modifications have been made. The laser diffraction grating is replaced by a plane gold surfaced mirror and is thus operating at 944 cm^{-1} for all experiments. The laser power is monitored by a homemade thermocouple device mounted outside the second sodium chloride window. The output of the thermocouple is displayed on a microvoltmeter (Digitec 268) and recorded on a chart recorder (Leeds and Northrup, Speedomax W). The thermocouple output is calibrated to the laser power using a Laser Power Probe (Optical Engineering Inc.). Beam shape is monitored by burning business cards. The QUISTOR/tank/pump assembly is portable and mounted on four adjustable feet. Maximum laser intensity within the QUISTOR is achieved by adjustment of the assembly while the extent of dissociation of the protonated dimer of 2-propanol is monitored.

The time scale of the experiment, typically 100 ms, is provided by a square wave generator (Heathkit model SG18A) also driving a mechanical chopper (PAR 222), which is phase locked to the input signal. The beam is chopped such that a dark period precedes the irradiation period with the duration of each being equal. The square wave generator also triggers the creation pulse (Hewlett Packard Pulse Generator, Model 214A) which in turn triggers the extraction pulse (Hewlett Packard, Model 214B) which is advanced by ~1 ms. The creation pulse (80 V, 90 μs) is applied to an electron gate situated between the filament and the top end cap. The gate is normally held at −90 V to bar electrons from the trap. The extraction pulse (−50 V, 10 μs) triggers a scan delay generator (Ortec Brookdeal Model 9425) which provides a trigger, or detection pulse of 100 μs width, 90 μs after the extraction pulse. The detection pulse drives a Linear Gate (Ortec Brookdeal Model 9415). The QUISTOR is operated in mode II as described in the accompanying paper, the RF potential (typically 500–550 V) being supplied by an Extranuclear Laboratories Quadrupole Power Supply, Model 011-15, modified for QUISTOR storage work. Following irradiation, product ions are mass analyzed by a quadrupole mass filter (Vacuum Generators, QXK 400) either by running a complete mass spectrum or, in this work, by single monitoring. The pulse sequence is shown in Fig. 1.

In those experiments in which Quadrupole Resonance ejection was employed, the output signal of the chopper triggers a toneburst (Wavetek, Model 134) applied to the top end cap concomitant with the laser irradiation period. The toneburst of a chosen frequency resonantly ejects ions of a particular mass-to-charge ratio. The ions ejected in this work are either the protonated (or D^+) parent alcohol or the proton (or D^+) bound dimer of the alcohol.

In studies of dissociation pathways, a third pulse generator (Berkely Nucleonics Corp., Model 8010) is used. In this work, the square wave output is used to trigger the BNC pulse generator which in turn triggers the creation pulse. The extraction pulse is triggered also by the square wave output (negative slope). This mode of triggering allows the creation pulse to be advanced to any position within the 100 ms time frame of the experiment.

The ion structure experiments are performed in two ways, the first being a resonant ejection of *m/z* 121, the protonated dimer of isopropanol, with concurrent laser irradiation while monitoring the behaviour of *m/z* 79, the postulated proton bound dimer of water and isopropanol. In the second set of experiments, *m/z* 83 is synthesized *in situ* by clustering D_2O molecules and deuteronated isopropan-*d*-ol ions. At low pressures (0.7 to 1 mPa) clustering is favoured, whereas at higher pressures (5 mPa) *m/z* 82 is produced via unimolecular dissociation of *m/z* 124, the deuterated analogue of the proton bound dimer of isopropanol.

Some of the isopropanol experiments are performed using pulse sequences previously described (1). All regions labelled Laser On refer to the mechanically chopped laser previously described, whereas Continuous Laser refers to laser irradiation for the total duration of the experiment.

Isopropan-*d*-ol was purchased from Aldrich; perdeuteroisopropanol and 2-d_1-isopropanol were obtained from Merck, Sharp and Dohme. The samples were used without further purification, other than degassing by several freeze/thaw pumping cycles prior to an experiment.

Results and discussion

Bomse and Beauchamp have reported (2*c*) that at pressure $<4 \times 10^{-2}$ mPa ir multiphoton dissociation of the proton bound dimer of isopropanol, $(ROH)_2H^+$ where R is i-C_3H_7, occurs principally by

$$[5]\quad \underset{m/z\ 121}{(ROH)_2H^+} + nh\nu \longrightarrow \underset{m/z\ 103}{R_2OH^+} + H_2O$$

and that the alternate dissociation pathways

Can. J. Chem. Downloaded from www.nrcresearchpress.com by 210.87.254.105 on 09/06/12
For personal use only.

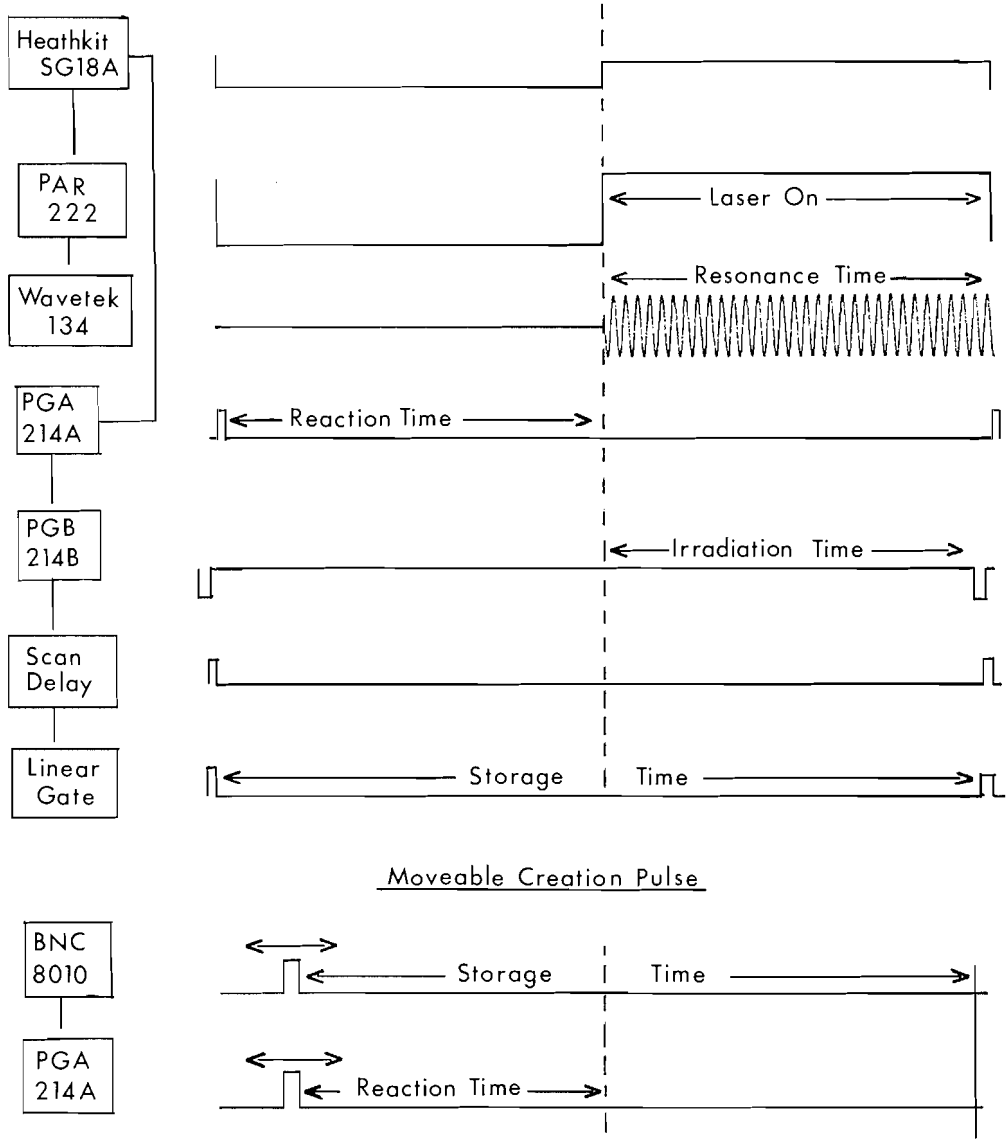

FIG. 1. Pulse sequence used in single ion monitoring with typically 100 ms of ion storage, 50 ms of laser irradiation concurrent with resonance ejection. The appended moveable creation pulse was employed in studies of multiple dissociation pathways induced by multiphoton absorption with respect to variation in internal energy of the irradiated ion.

$$[6]\quad \underset{m/z\ 121}{(ROH)_2H^+} + n'h\nu \longrightarrow \underset{m/z\ 61}{ROH_2^+} + ROH$$

where $n' = 11$, and

$$[7]\quad \underset{m/z\ 121}{(ROH)_2H^+} + n''h\nu \longrightarrow \underset{m/z\ 79}{(ROH)H^+(OH_2)} + C_3H_6$$

together account for not more than 2% of the photodissociated $(ROH)_2H^+$. In apparent contrast with these findings, multiphoton dissociation of $(ROH)_2H^+$ in the QUISTOR at a pressure of 5.3 mPa showed that all three reaction pathways [5], [6], and [7] were open. As the pressure and cycling frequency of the ICR technique are not readily obtained with the QUISTOR, a more circuitous study was carried out in order to verify the observations and to attempt a reconciliation of the conclusions.

In Fig. 2 are shown two single ion monitoring traces of the abundance of proton bound alcohol dimer, m/z 121, throughout the reaction time range 60–100 ms, at a pressure of 5.3 mPa. Resonance ejection of the precursor ion, m/z 61, was initiated at 55 ms reaction time. The upper trace, marked toneburst (m/z 61), shows that the rate of formation of proton bound dimers, m/z 121, is diminishing during the time 60–80 ms due to relatively gentle removal of precursor ion; a maximum abundance is reached at ~80 ms followed by a slow decline in abundance due mainly to ion losses by ion–ion and ion–neutral scattering processes.

The lower trace, marked chopped laser, shows the abundance of m/z 121 under the same conditions of storage but with resonance ejection of precursor after 55 ms of reaction time, concurrent with laser irradiation for up to 55 ms, at the conclusion of which the cycle is recommenced; thus the thermal (or dark) and irradiation periods were of equal duration. Irradiation was carried out with a CW CO_2 laser of 20 Wcm^{-2} at 944 cm^{-1}. The increasing reduction in abundance of m/z 121 throughout the irradiation period shows the degree of photodissociation of the proton bound dimer. The inset in the lower right hand corner of Fig. 2 is illustrative of the technique by which changes in ion abundance (diminution or enhancement) upon laser irradiation of the system is monitored at a specific reaction

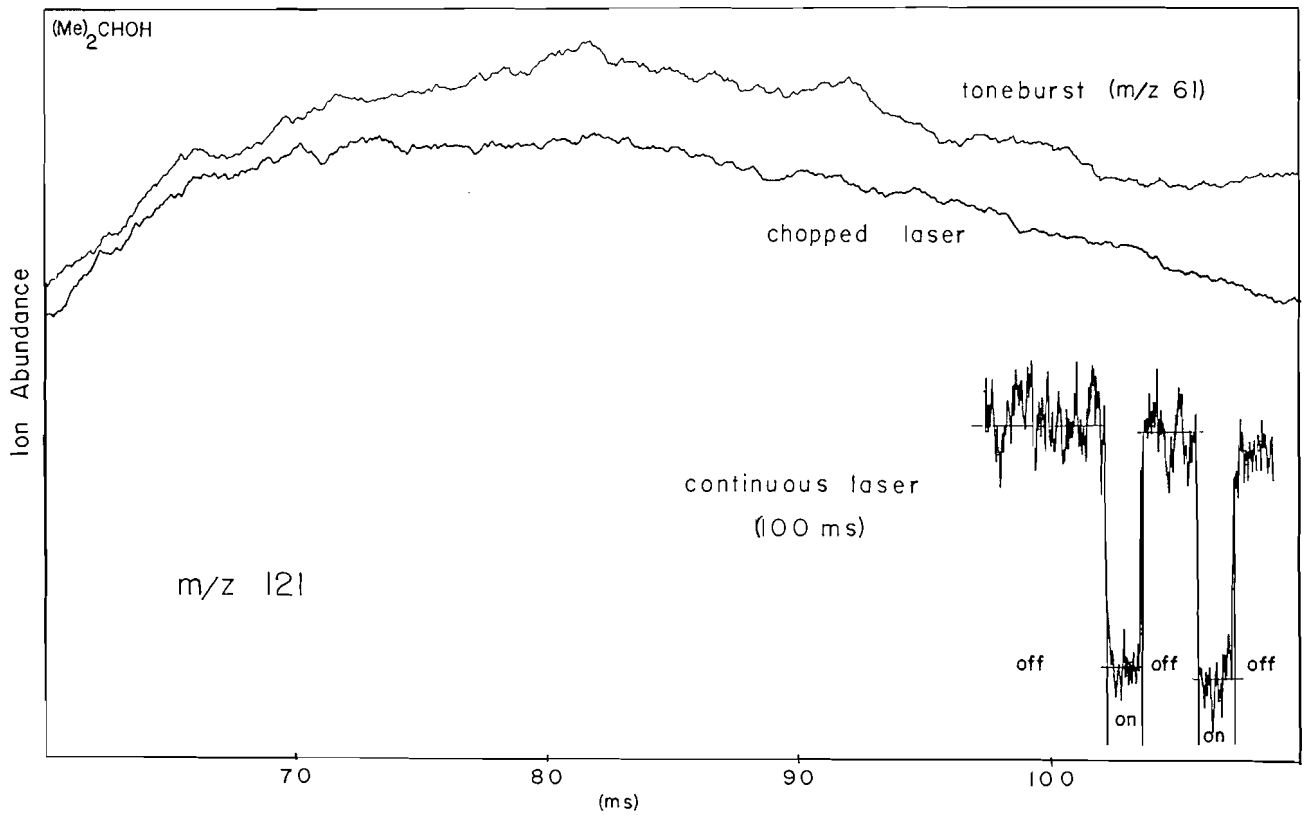

FIG. 2. Ion abundance versus storage time profiles of proton bound alcohol dimer, m/z 121, derived from ion/molecule reactions in isopropanol. Toneburst is QUISTOR resonance ejection (QRE) of m/z 61, the protonated parent alcohol precursor of m/z 121, commencing at 55 ms of storage time. Chopped laser refers to 55 ms of storage followed by 55 ms of laser irradiation with concurrent resonance ejection of m/z 61. Continuous laser refers to irradiation throughout 100 ms of storage time. CW CO_2 laser irradiation of 20 W cm^{-2} at 944 cm^{-1}. All experiments were performed at 5.3 mPa.

time; the baseline which is recorded routinely is not shown here. The observations of m/z 121 abundance shown in the inset were obtained after 100 ms of storage time. The signal intensity due to the steady state attained through the thermal reactions [1]–[4] was monitored initially and designated "off" in that the laser was not employed. During the next several ion creation, storage, reaction, and sampling cycles the laser was "on" continuously during the reaction time of 100 ms, and the ion abundance was reduced due to diminution of the steady state concentration on account of additional photochemical removal processes such as [5]–[7]. Successive thermal steady state abundances shown in the inset show a gradual decline in signal intensity; this effect is due to a diminution in pressure in the QUISTOR caused by heating of the device during continuous irradiation. The effect is more pronounced with a new small QUISTOR, $r_o = 6.0 \times 10^{-3}$ m, as described in the accompanying paper; allowance for the heating of the device was made subsequently.

As photodissociation of the proton bound dimer, m/z 121, was effected with the laser at 944 cm^{-1}, an examination was made of the possible involvement of each of reactions [5]–[7], in turn, and the results are shown in Figs. 3–5, respectively. In Fig. 3, the ion abundance of the protonated ether, m/z 103, over the same reaction time and conditions as for Fig. 2 is shown. The upper and lower traces from the single ion monitoring experiments are similar in profile; the lower trace, marked toneburst m/z 61, is remarkably similar to the corresponding trace for m/z 121 in Fig. 2. The resonance ejection of the precursor ion, m/z 61, initiated at 55 ms of storage causes a falloff in the rate of formation of m/z 103; a maximum abundance at ~90 ms is observed followed by an indication in the next 20 ms of ion loss processes. The time-delayed maximum is as anticipated in that the resonantly ejected m/z 61 ion is a precursor but once removed in that m/z 121 is the immediate precursor of m/z 103. The upper trace was obtained under the same conditions of pressure and resonance ejection of m/z 61 after 55 ms; laser irradiation was initiated after 55 ms (concurrent with resonance ejection). There is a small but significant difference in the upper and lower single ion monitoring traces showing that the abundance of m/z 103 is increased upon laser irradiation, as expected, and that reaction [5] is operative. The inset shown in Fig. 3 is similar to that of Fig. 2; though the signal is noisy the enhancement of the m/z 103 signal intensity upon irradiation is clearly evident.

In Fig. 4 are shown single ion monitoring traces of protonated isopropanol, m/z 61. The trace marked toneburst (m/z 61) illustrates the steady diminution of the m/z 61 ion signal upon gentle resonance ejection; the ions may be ejected more rapidly by increasing the peak-to-peak voltage of the radio-frequency toneburst shown in Fig. 1. The trace marked normal is that of the unperturbed thermal ion abundance showing a steady decline with time as m/z 61 is consumed through, for example, reaction [1]. The top trace shows an enhancement of m/z 61 upon laser irradiation after 60 ms of storage; the increase in m/z 61 was observed also upon continuous irradiation throughout 100 ms of storage as shown in the inset in Fig. 4. Thus reaction [6] is observed to be operative, showing that a minimum of 11 photons (not allowing for collisional deacti-

Can. J. Chem. Downloaded from www.nrcresearchpress.com by 210.87.254.105 on 09/06/12
For personal use only.

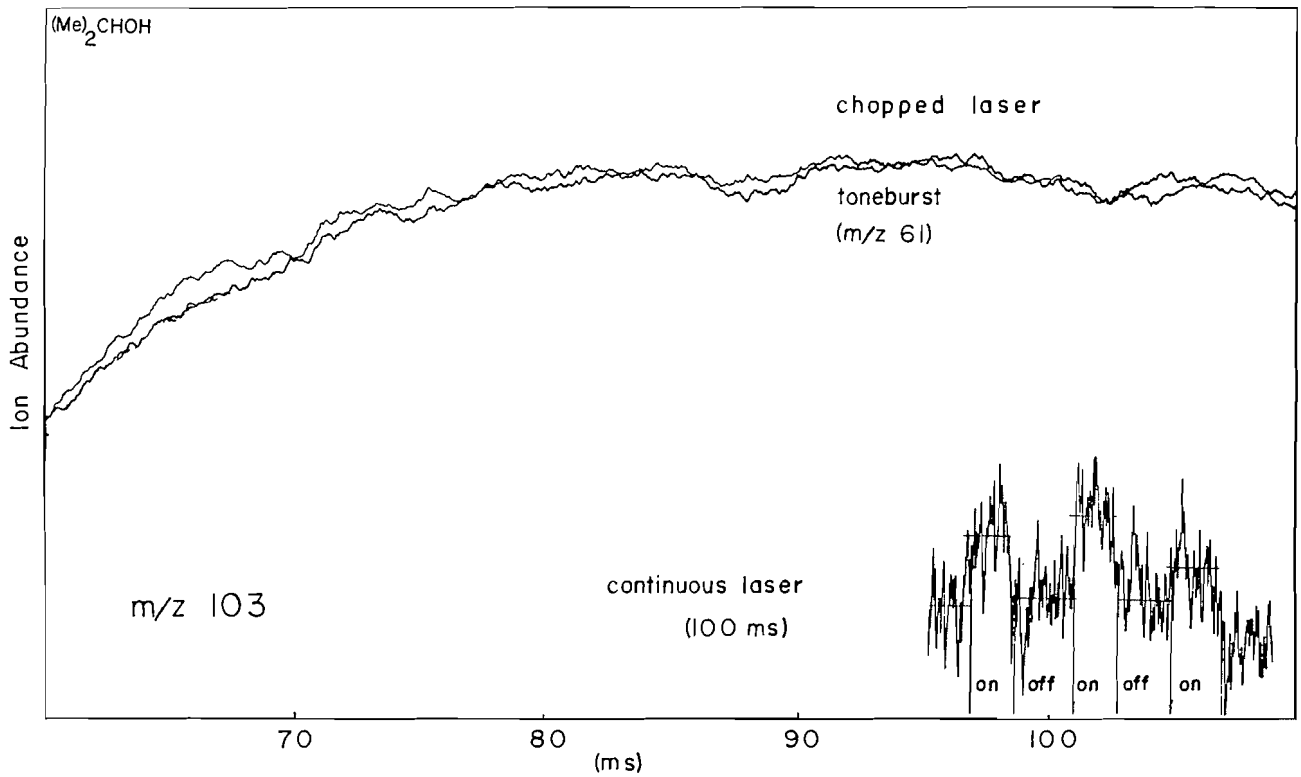

FIG. 3. Ion abundance versus storage time profile of m/z 103. Conditions as for Fig. 2.

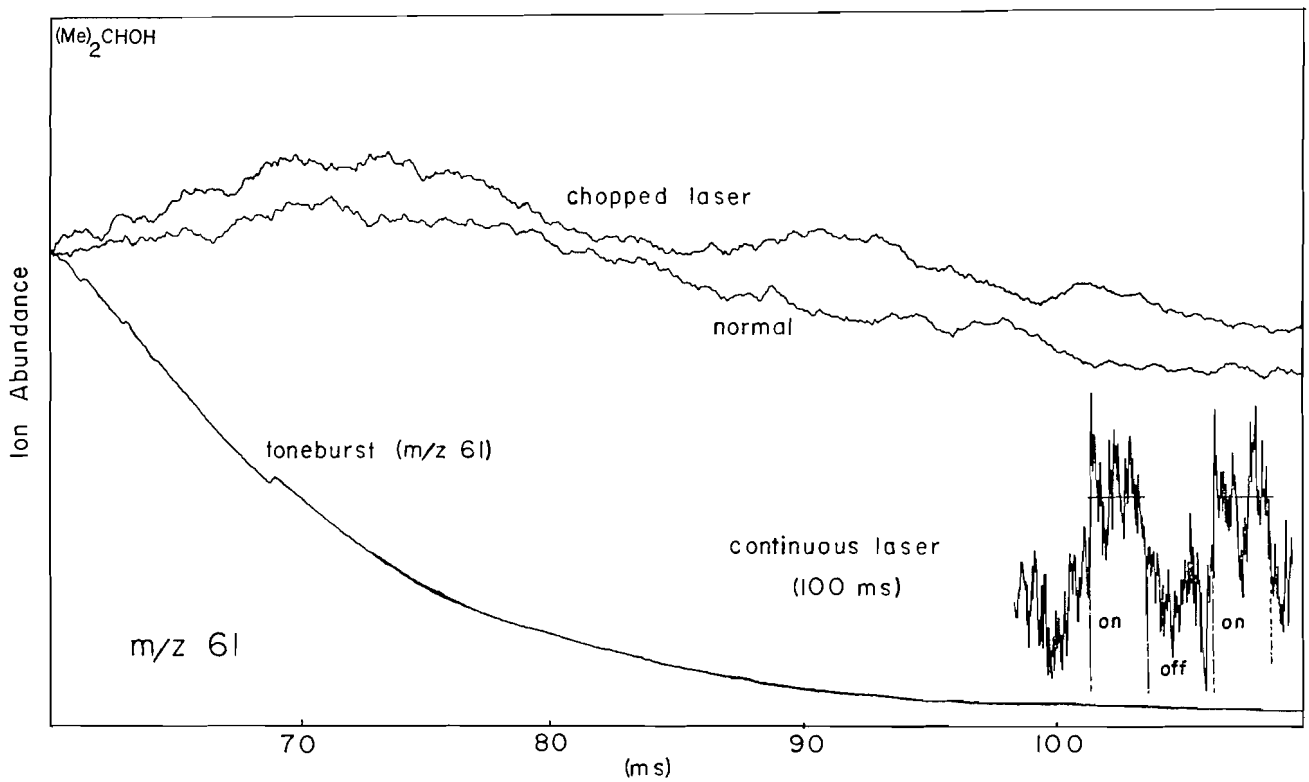

FIG. 4. Ion abundance versus storage time profile of m/z 61. The normal trace corresponds to the ion intensity from dark or thermal ion/molecule reactions. Conditions as for Fig. 2.

vation or radiative loss) have been absorbed by the proton bound alcohol dimer.

Reaction [7] was then examined. Chemically activated proton bound alcohol dimer ions formed in [1] may lose an alkene neutral (C_3H_6) as in [4] to produce the m/z 79 ion which may be tentatively identified as a proton bound mixed dimer of isopropanol and water. The lower traces each marked toneburst (m/z 61) in Fig. 5 show that the m/z 79 ion abundance profile

Can. J. Chem. Downloaded from www.nrcresearchpress.com by 210.87.254.105 on 09/06/12
For personal use only.

Can. J. Chem. Downloaded from www.nrcresearchpress.com by 210.87.254.105 on 09/06/12
For personal use only.

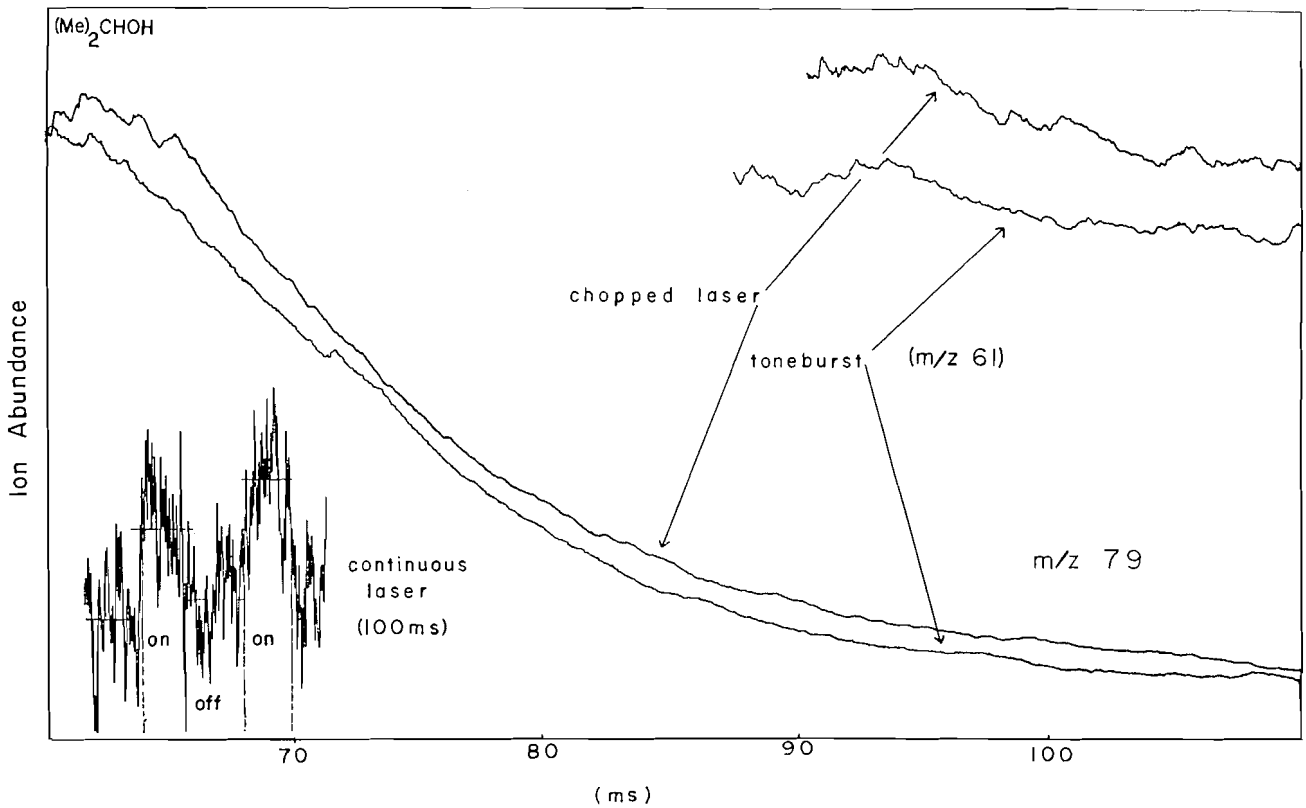

FIG. 5. Ion abundance versus storage time profiles of m/z 79. Conditions as for Fig. 2.

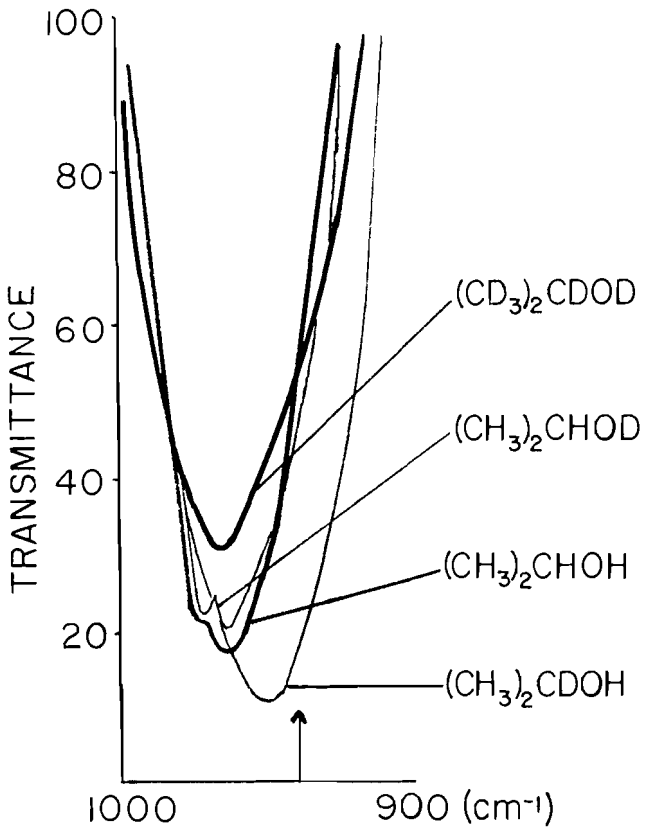

FIG. 6. Single photon infrared absorption spectrum in the range 1000 to 900 cm^{-1} for isopropanol, isopropan-d-ol, 2-d_1-isopropanol, and perdeuteroisopropanol. Vertical arrow marks laser wavelength.

matches closely that of m/z 61 marked toneburst in Fig. 4; this is as expected. The toneburst or resonance ejection of m/z 61 was initiated after 55 ms of storage. The traces in the top right hand corner of Fig. 5 are amplified by a factor of 6 to show more clearly the effect of chopped laser irradiation. The upper curves marked chopped laser show an enhancement of m/z 79 upon laser irradiation concurrent with resonance ejection of m/z 61. This effect is seen also upon continuous irradiation for 100 ms as shown in the inset in Fig. 5. Thus it appears that reaction [7] is operative, that photodissociation of the proton bound alcohol dimer under these operating conditions follows all three reaction channels described by reactions [5]–[7].

Multiphoton absorption by gaseous ions appears to occur at laser wavelengths corresponding to absorption in the single photon absorption ir spectrum. The ir absorption spectra in the vicinity of 944 cm^{-1} were obtained for isopropanol and its deuterated analogues, 2-d_1-isopropanol, isopropan-d-ol, and perdeuterated isopropanol, and are shown in Fig. 6. The spectra were obtained with a Perkin–Elmer 700 ir spectrophotometer under conditions of saturated vapour pressure of each alcohol and in a thermally equilibrated gas cell. Each of the isopropanols shows strong absorption at 944 cm^{-1}, hence each deuterated analogue was examined in turn in order to determine the relative weights for the reaction pathways corresponding to reactions [5]–[7]. The observations, obtained at 5.3 mPa, are reported in Table 1 as *changes* in ion abundance for each of the major ions, wrought initially by laser irradiation and subsequently by laser irradiation concurrent with resonance ejection of the appropriate proton (or D^+) bound alcohol dimer. The data for isopropan-d-ol are incomplete. The extent of photodissociation for each of the dimer ions formed from isopropanol, 2-d_1-isopropanol and perdeuterated isopropanol is in

TABLE 1. Isopropanol and deuterated analogues: a comparison of infrared laser induced changes in ion abundances

$(CH_3)_2CHOH$			$(CH_3)_2CDOH$			$(CD_3)_2CDOD$			$(CH_3)_2CHOD$	
m/z	ΔI^a (%)	ΔI^b (%)	m/z	ΔI^a (%)	ΔI^b (%)	m/z	ΔI^a (%)	ΔI^b (%)	m/z	ΔI^a (%)
61	32	~0	62	14	8	70	42	~0	63	+
79	28	0	80	18	0	90	11	0	82	+
103	29	(14)	105	13	(12)	118	~0	(40)	104	~0
121	(56)	(100)	123	(54)	(100)	138	(68)	(100)	124	( )

[a]Change in ion abundance from that observed after 100 ms of storage to that observed after 100 ms of storage with laser irradiation during the final 50 ms. Parentheses indicate a decrease in ion abundance.

[b]As for footnote *a* but with resonance ejection of the appropriate proton bound alcohol dimer concurrent with laser irradiation.

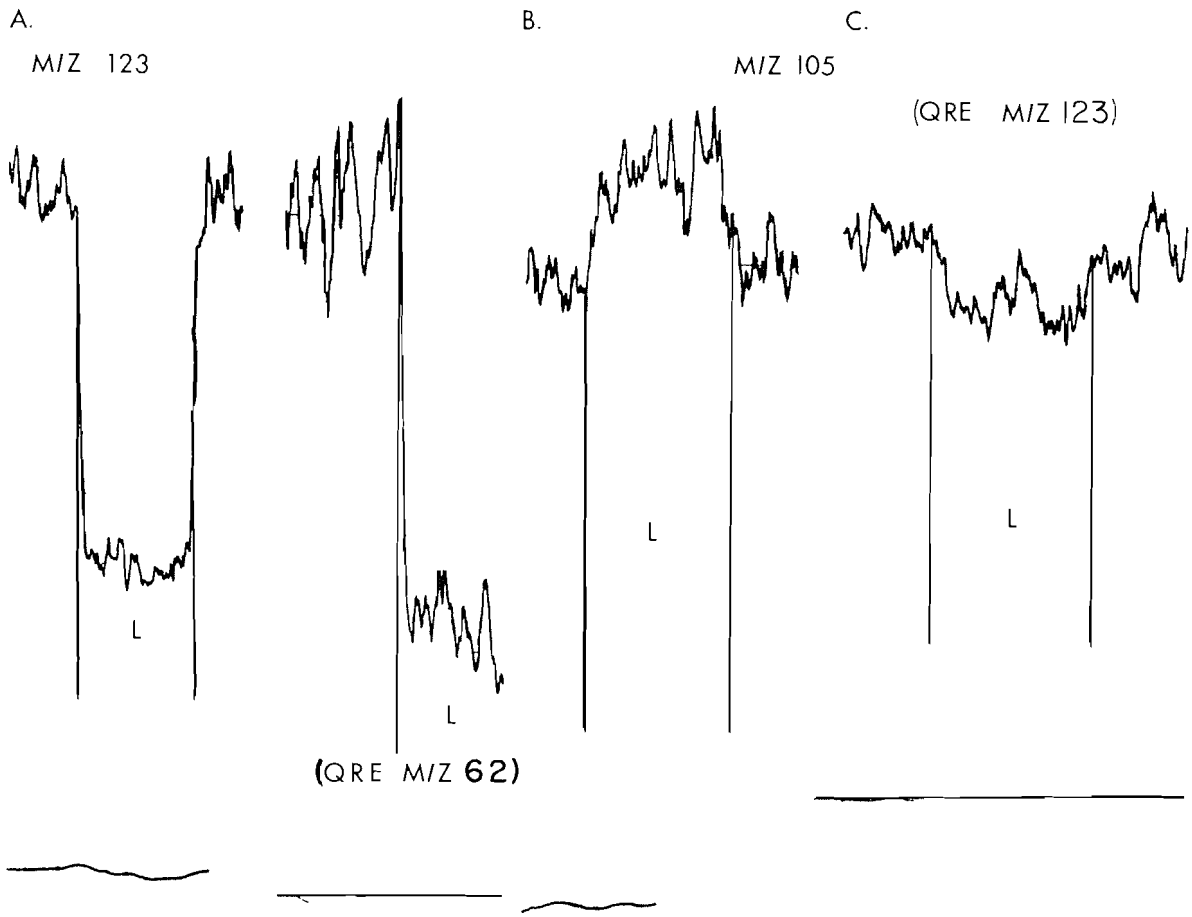

FIG. 7. Single ion monitored abundances of ions derived from 2-d_1-isopropanol, at 5.3 mPa. L refers to 50 ms of storage followed by 50 ms of CW CO_2 laser irradiation of 20 W cm^{-2} at 944 cm^{-1}. A: protonated dimer of 2-d_1-isopropanol, m/z 123, followed by irradiation concurrent with QUISTOR resonant ejection (QRE) of m/z 62; B: protonated ether, m/z 105; C: m/z 105, irradiated concurrently with resonant ejection of m/z 123. Baseline as indicated.

reverse order to that anticipated from the single photon absorption spectra shown in Fig. 6. The variation in the extent of photodissociation appears to be real in that photolysis of proton bound mixed alcohol dimers produces intermediate yields. This work will be reported in more detail when completed.

Zero change in ion abundance for m/z 118 in perdeuteroisopropanol was observed initially, and thus it appeared that [5] was not an available reaction channel in this system in contrast with isopropanol and 2-d_1-isopropanol. However, irradiation of m/z 118 in the absence of m/z 138 brought about a decrease in ion abundance as shown in Table 1. This behaviour is explained in the text following.

In all of the above experiments, it has been assumed that only photon absorption by the proton bound dimer is of importance. Photon absorption and subsequent photoexcitation of neutral molecules can be ignored as the residence time of neutrals in the laser beam is extremely short (~10 μs). Photoexcitation of protonated alcohol, m/z 61, can be ignored when m/z 61 is resonance ejected rapidly. Photoexcitation of the remaining species of importance, m/z 79 and m/z 103, was explored, together with the corresponding ions derived from the deuterated analogues.

In Fig. 7 are shown single ion monitoring traces of ions derived from 2-d_1-isopropanol. The two traces marked A are

Can. J. Chem. Downloaded from www.nrcresearchpress.com by 210.87.254.105 on 09/06/12
For personal use only.

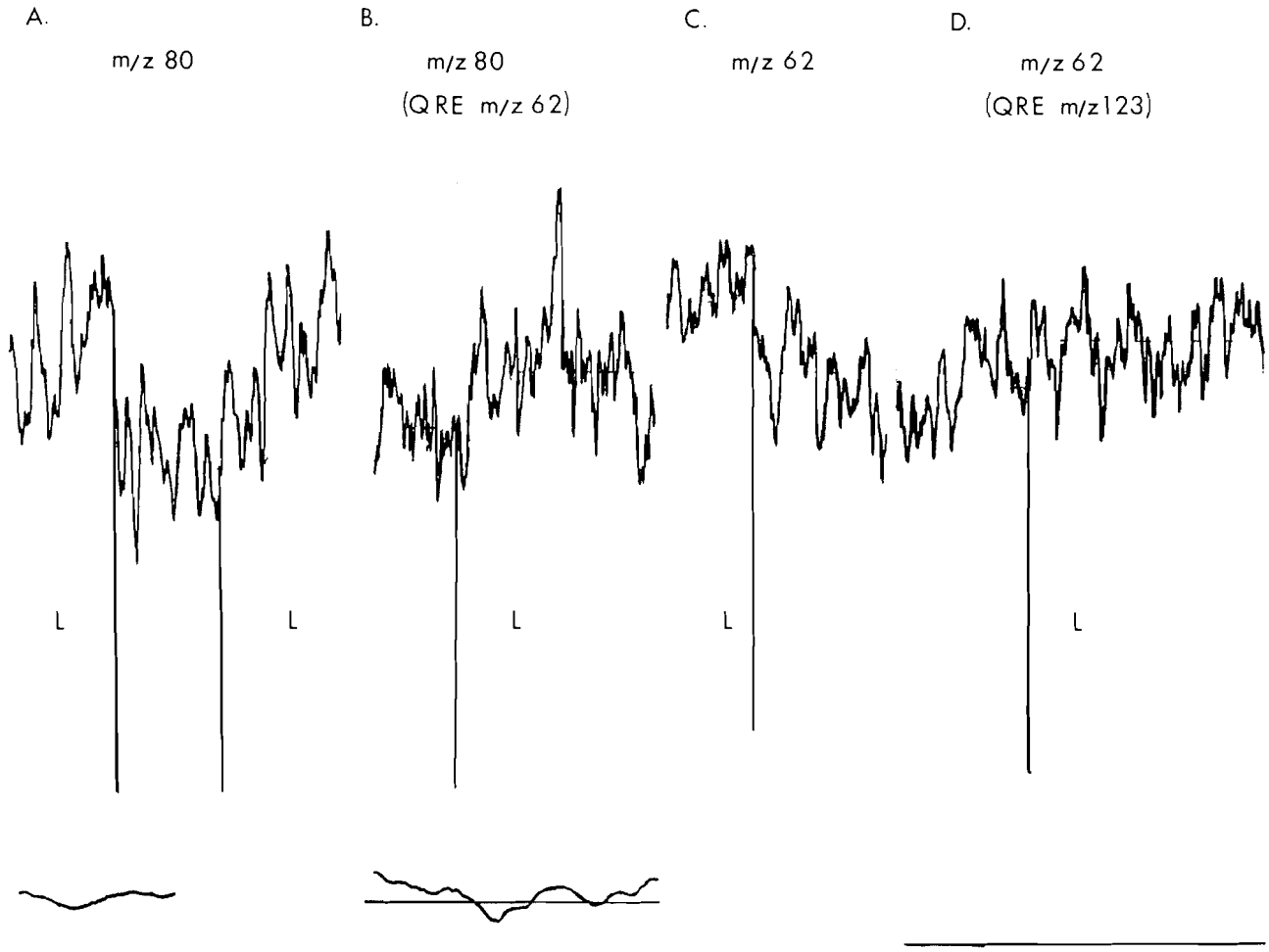

FIG. 8. Single ion monitored abundances of further ions derived from 2-d_1-isopropanol, at 5.3 mPa. A: m/z 80; B: m/z 80 with QRE of m/z 62; C: m/z 62; D: m/z 62 with concurrent QRE of m/z 123. Conditions as for Fig. 7.

for the proton bound alcohol dimer, m/z 123. It should be noted that the dimer contains two deuterium atoms, one from each alcohol molecule, and is proton, not deuterium, bound. In each case, the initial part of the trace corresponds to thermal conditions for 100 ms of storage while the parts marked L refer to 50 ms of storage followed by 50 ms of laser irradiation. In the first of the two traces marked A, some 55% dissociation of dimer, m/z 123, is observed; with resonance ejection of protonated alcohol, m/z 62, as shown in the second A trace, reactions [1] and [2] have been arrested and some 60% of dimer photodissociated. Trace B shows the anticipated increase in the protonated ether, m/z 105, with laser irradiation. Isotopic scrambling is not observed in the chemically activated proton bound dimer and reaction [5] results in the loss of H_2O rather than D_2O or HDO from m/z 123. As m/z 123 is the precursor of m/z 105, irradiation of the ion assembly in the absence of m/z 123 (wrought by resonance ejection) should not induce any change in the prevailing m/z 105 ion abundance. However, as can be seen from trace C obtained under the above conditions, a diminution in m/z 105 ion abundance is observed upon laser irradiation. Thus the increase in m/z 105 ion abundance in trace B is the net increase arising from the photoproduction [5] and the photodissociation process

$$[8]\quad \underset{m/z\ 105}{((CH_3)_2CD)_2OH^+} + n^{111}h\nu \longrightarrow \text{products}$$

Identification of the products of [8] was not possible, but this process affords an excellent example of the application of ion storage mode switching in the QUISTOR as discussed in the accompanying paper. Multiphoton dissociation of protonated diisopropyl ether has not been reported previously. However, the observation is not entirely unexpected as Beauchamp and co-workers (2*b*) have observed the ir laser photochemistry of protonated diethyl ether. They reported that the laser-induced process is

$$[9]\quad (C_2H_5)_2OH^+ + nh\nu \longrightarrow C_2H_5OH_2^+ + C_2H_4$$

rather than loss of alkane to form protonated acetaldehyde. Thus while multiphoton dissociation of m/z 105 may be anticipated, and the reaction analogous to [9] for protonated diisopropyl ether may be operative, the structure of m/z 105 remains to be verified. The m/z 105 ions observed here were formed from the alcohol dimer, and we have not examined the isomer formed by protonation of diisopropyl ether.

In Fig. 8 are shown results of examination of m/z 80 (note that the proton bound dimer apparently sheds C_3H_5D as expected) and the protonated alcohol, m/z 62. The parts of the traces marked L refer to 50 ms of storage followed by 50 ms of laser irradiation; the unmarked sections refer to 100 ms of thermal storage. The m/z 80 ion abundance, trace A, shows the expected increase in intensity with laser irradiation [7] and, similarly, an expected increase when m/z 62 is resonantly ejected. In trace C, where m/z 62 is monitored, the expected

Can. J. Chem. Downloaded from www.nrcresearchpress.com by 210.87.254.105 on 09/06/12
For personal use only.

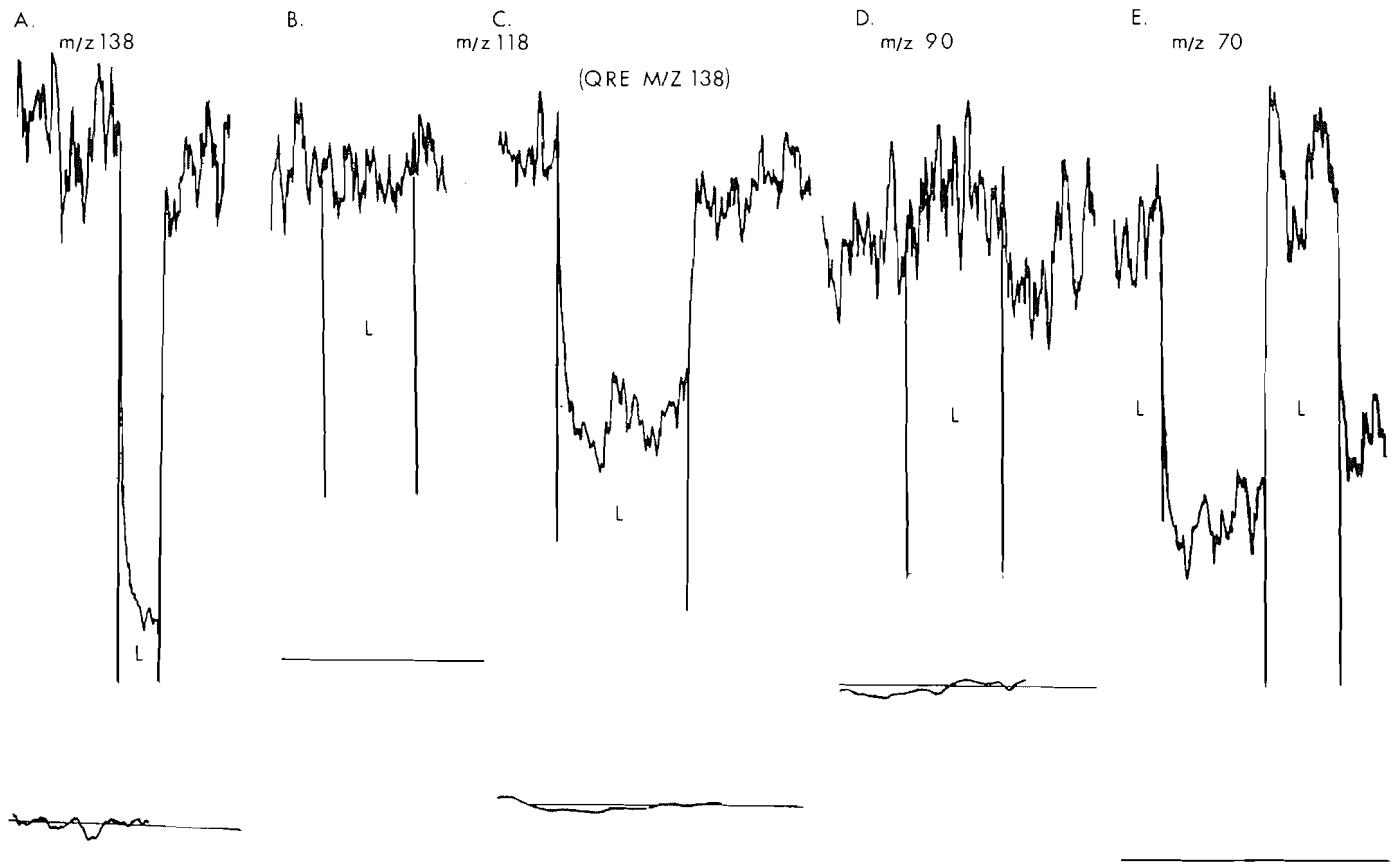

FIG. 9. Single ion monitored abundances of selected ions derived from perdeuteroisopropanol. A: m/z 138, the proton (D^+) bound perdeuterated alcohol dimer; B: m/z 118; C: m/z 118 with concurrent QRE of m/z 138; D: m/z 90; E: m/z 70. Conditions as for Fig. 7.

increase with laser irradiation is observed. Although the signal is very noisy in trace D in which m/z 62 is monitored, it appears that upon resonance ejection of m/z 123, thus removing the possibility of [6] occurring, laser irradiation induces a small signal enhancement which may be indicative that m/z 62 is a photoproduct of [8].

Of the four isopropanol analogues investigated, the proton (D^+) bound alcohol dimer most susceptible to multiphoton dissociation is that derived from perdeuteroisopropanol, m/z 138, as is shown in Table 1 and in trace A of Fig. 9 where approximately 70% of the dimer is dissociated. This evidence indicates that the majority of ions were irradiated by the narrow laser beam directed through the centre of the QUISTOR. The ion of m/z 118 (correspondng to m/z 103 protonated ether in the isopropanol system) was monitored as shown in traces B and C. In trace B, 50 ms of laser irradiation following 50 ms of thermal storage produced no obvious change in ion abundance from that observed after 100 ms of storage; lower, in trace C where the dimer, m/z 138, is ejected, laser irradiation of 50 ms duration following 50 ms of storage caused a reduction of signal intensity of approximately 42%. Thus, we conclude that the null change in trace B is due to almost exact compensation by [5] for the relatively high degree of photodissociation wrought by [8]. Traces D and E show the expected increases in ion abundance with laser radiation of m/z 90 (corresponding to m/z 79) and m/z 70 (corresponding to m/z 61), respectively.

Structure of m/z *79;* $(CH_3)_2CHOH \cdot H^+ \cdot OH_2$

The losses of the elements of C_3H_6 and H_2O by [7] and [5], respectively, from the proton bound alcohol dimer suggest that the ion formed by loss of C_3H_6, m/z 79, may have the structure of a proton bound mixed dimer of alcohol and water. In this event, m/z 79 should absorb ir photons from the laser via the alcohol moiety and, eventually, be photodissociated to regenerate protonated alcohol. Such a postulate may appear to be supported by the possibility of a reaction sequence of [5] and [9]. However, at 5.3 mPa pressure, as shown in trace A of Fig. 10, no change in ion abundance of m/z 79 was observed when irradiated in the absence of m/z 121 which was resonance ejected. Thus it is concluded that either the m/z 79 ion species is transparent to radiation at 944 cm^{-1}, which is unlikely as this would require a major change in hybridization, or the binding is much stronger than that of a proton bound alcohol—water dimer which is reported as 100 kJ mol^{-1} for $CH_3OH_2^+$—H_2O (10) and therefore of a different nature. The proton (D^+) bound mixed dimer of isopropan-*d*-ol with D_2O, m/z 83, was formed at a relatively low pressure of 0.67 mPa. Due to the considerably greater proton affinity of isopropan-*d*-ol (assumed to be equal to that of isopropanol) than that of D_2O, 816 kJ mol^{-1} cf. 690 kJ mol^{-1} (11), only a trace of the alcohol was added to D_2O, hence the partial pressure of the alcohol in the reaction chamber is not known. After 100 ms storage at 0.67 mPa, negligible proton (D^+) bound alcohol dimer was observed. While the signal intensity of m/z 83 was low and is shown in trace B of Fig. 10, the signal does appear to diminish with 50 ms of laser irradiation following 50 ms of storage compared to the signal intensity after 100 ms of storage. With the pressure restored to 5.3 mPa, the signal intensity of m/z 82 shows, in trace C of Fig. 10, a marked increase upon irradiation and

Can. J. Chem. Downloaded from www.nrcresearchpress.com by 210.87.254.105 on 09/06/12
For personal use only.

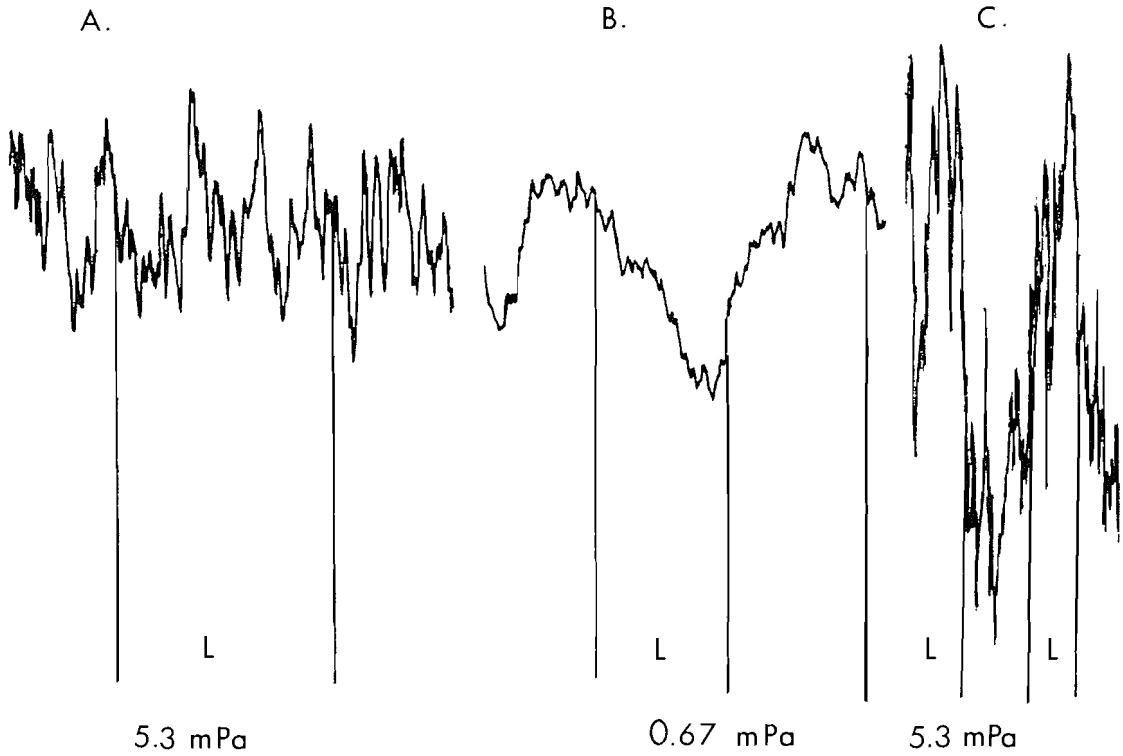

FIG. 10. Single ion monitored abundances of ions of the form $i\text{-}C_3H_7OH \cdot H^+ \cdot OH_2$. A: m/z 79 ions derived from isopropanol by [7] at 5.3 mPa with QRE of protonated dimer m/z 121; B: m/z 82 ions produced by clustering D_2O with $iso\text{-}C_3H_7OD_2^+$ at 0.67 mPa (N.B. only a minute trace of protonated dimer, m/z 124, was observed at this pressure); C: m/z 82 ion derived from $iso\text{-}C_3H_7OD$ by [7] at 5.3 mPa. Irradiation conditions as for Fig. 7.

photodissociation of the proton (D^+) bound alcohol dimer $(i\text{-}C_3H_7OD)_2D^+$ of m/z 124 which loses C_3H_6 by [7] to yield m/z 82. Thus it is concluded, principally from the results portrayed in traces A and B of Fig. 10, that the product ion of [7] differs in structure from that of a proton bound mixed dimer of alcohol and water. It is important to note that in the clustering of D_2O with $i\text{-}C_3H_7OD_2^+$, a mixed dimer of m/z 83 results, whereas alkene loss from the symmetrical dimer, $(i\text{-}C_3H_7OD)_2D^+$, results in an ion of m/z 82.

Let us consider a plausible structure for the proton bound isopropanol dimer m/z 121 and the possible mechanisms by which isomeric forms of m/z 79 may be produced. The m/z 121 ion may lose C_3H_6 in a concerted action involving 6 atoms, to yield I. Two different forms of rearrangement are then possible, the first rearrangement to yield II and IV produces an asymmetric ion of the form $R^+ \cdot H_2O \cdot H_2O$, whereas the alternative rearrangement produces the symmetric ion, III, $H_2O \cdot R^+ \cdot OH_2$. While structure III has been proposed previously (2*c*), a mechanism for its formation was not discussed.

Ion relaxation

Proton bound alcohol dimers formed initially by [1] in a chemically activated state, and observed at the expiry of a chosen trapping period, may be either radiatively stabilized under collision-free conditions or radiatively and collisionally stabilized at higher pressures. At an operating pressure of 5.3 mPa the time between ion–neutral collisions is approximately 0.38 ms, which is appreciable with respect to the normal storage and irradiation periods employed here. A crude experiment within the limitations of the equipment was attempted in which proton bound alcohol dimers were irradiated as a function of ion age, age being crudely synonymous with storage time, relaxation time, and average number of collisions

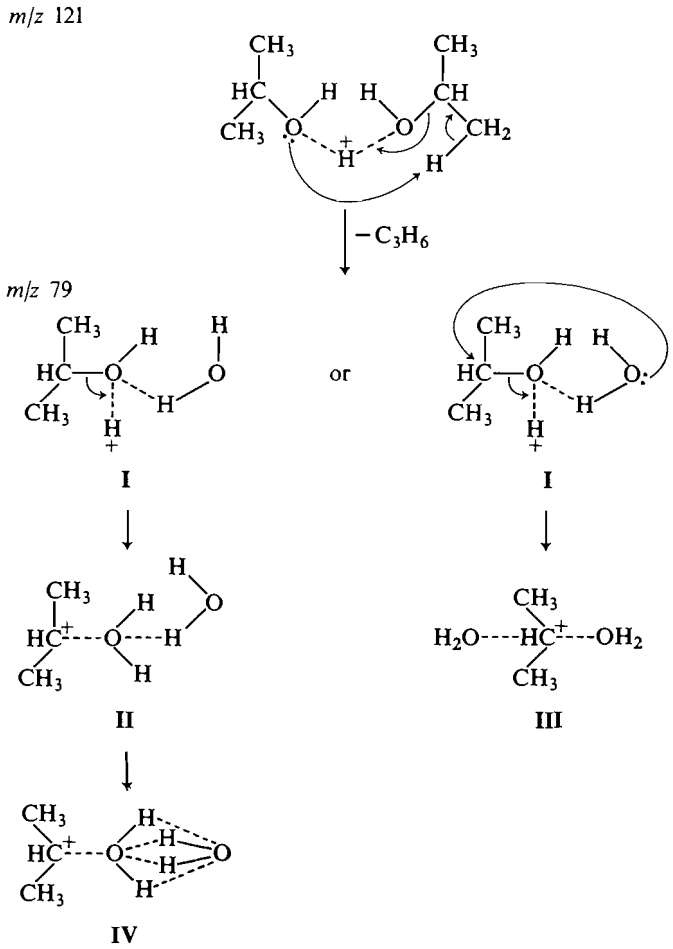

Can. J. Chem. Downloaded from www.nrcresearchpress.com by 210.87.254.105 on 09/06/12
For personal use only.

Can. J. Chem. Downloaded from www.nrcresearchpress.com by 210.87.254.105 on 09/06/12
For personal use only.

suffered by the ion. While primary ions are formed virtually instantaneously in 50 μs, the peak intensity of proton bound alcohol dimers is attained after 40–50 ms of storage leading to a distribution of ions at any given storage time. Nevertheless the distributions of ion ages will broaden with storage time from a narrow distribution initially for pure nascent ions. The distribution functions may be calculated from the ion abundance profiles with time, but this calculation has not been completed. Ideally, an irradiation period of several milliseconds should be used to probe the effect of ion relaxation on dissociation pathways but the chopping facility and the fluence of the CW CO_2 laser dictated a minimum irradiation period of 50 ms. Thus, proton bound alcohol dimers were irradiated for a constant period of 50 ms; irradiation was commenced initially after 5 ms of storage and subsequently delayed to longer storage times. Ions were mass analyzed at the conclusion of irradiation. From the results of each mass analysis, the reduction in signal intensity of the dimer ion and the changes in signal intensity of m/z 103, m/z 61, and m/z 79 due to [5]–[7], respectively, were noted. Photoinduced signal intensity changes obtained at a common amplification of detector signal indicated the degree to which each dissociative pathway was followed. In arriving at the m/z 103 signal intensity change, allowance was made for photodissociation of m/z 103 by determining the m/z signal intensity change with resonance ejection of the dimer ion. Photodissociation yields, expressed as a percentage of the total yield of photodissociation products, are plotted versus relaxation time and sampling time as shown in Fig. 11. The experiment is crude for the reasons expressed above and the scatter of the data points is appreciable, yet the observed behaviour may indicate a reconciliation of experimental findings reported here with those of Beauchamp (2*c*) which are shown as filled data points in Fig. 11. Let us assume that, on average, $(ROH)_2H^+$ requires an induction period of 35 ms of laser irradiation under the prevailing conditions of pressure and laser power in order to acquire the energy necessary, but not necessarily sufficient, for dissociation. As the time between successive collisions is 0.38 ms, the average number of collisions suffered by ions not detected (and presumed to have dissociated) at the shortest sampling time will range from 100–145 collisions, and from 210–250 collisions at the maximum sampling time. Thus the experiment encompasses a possible range of 100–250 collisions on average and a twofold range of radiative probabilities for nascent ions activated initially with some 125 kJ mol^{-1}. All those dissociative pathways [5]–[7] were observed.

At the shortest sampling (or relaxation) time the photodissociation yields of m/z 103 and m/z 61 were almost equal at approximately 50%. As sampling time was delayed, the photodissociation yield of m/z 103 increased at the expense of that for m/z 61; the yield of m/z 79 remained sensibly constant throughout at 4%. It is concluded that photoescalation of partially relaxed $[(ROH)_2H^+]^*$ may induce preferentially the reverse of [1]; the less the nascent ion is relaxed the fewer will be the number of photons required for reversal of [1]. The more relaxed the ion becomes, the greater is the dominance of [5] as a dissociation pathway. The invariance of the photodissociation yield of m/z 79 is suggested to be associated with an isomerization process. The dominance of [5] as a dissociative channel in Beauchamp's work is concluded to be due to near complete radiative relaxation during the relatively long (~1 s) storage time; the pressure region employed in ref. 2*c* corresponds to a collision frequency of 10 s^{-1}.

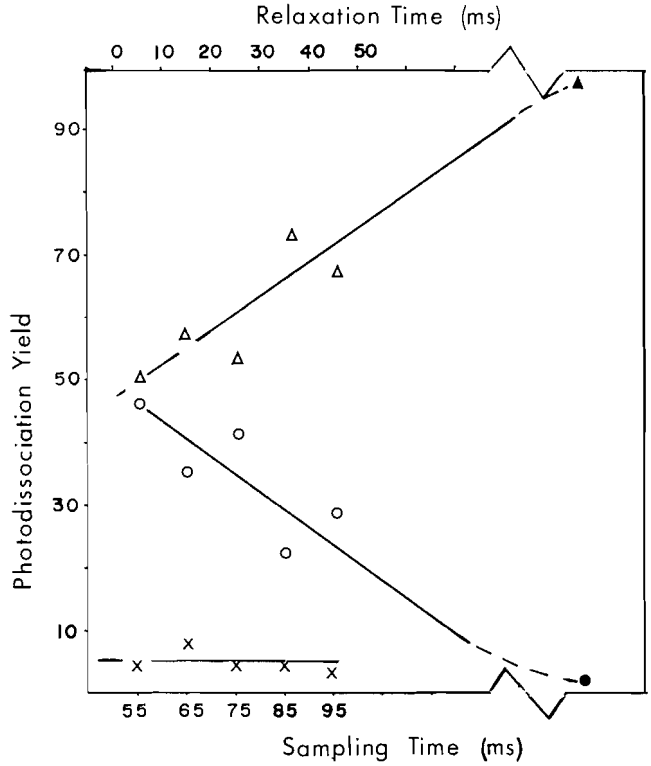

FIG. 11. Plot of photodissociation yield versus sampling time and relaxation time for the three multiphoton dissociation products of $(i\text{-}C_3H_7OH)_2H^+$. Relaxation time is defined as the period of ion storage from initiation of ion creation by electron impact to the commencement of laser irradiation. At the conclusion of 50 ms of irradiation the ions were mass analyzed. Sampling time refers to the total storage time and is equal to the relaxation time plus the irradiation time which was held constant at 50 ms. Relaxation time scale is proportional to the number of collisions suffered by each ion prior to irradiation, while sampling time is proportional to the number of collisions during the entire period of ion storage. 50 ms CW CO_2 laser irradiation of 20 W cm^{-2} at 944 cm^{-1}; pressure 5.3 mPa. △, m/z 103 product of [5]; ○, m/z 61 product of [6]; ×, m/z 79 product of [7]. △ and ○ which correspond to m/z 103 and m/z 61, respectively, were observed by Beauchamp at 4×10^{-2} mPa with a relaxation time of 500 ms and a sampling time of 950 ms.

There are several possible extensions of the present results which are either being explored in this laboratory or contemplated for study. Improved absorptivities of gaseous ions can be obtained by monitoring dissociation as a function of wavelength. Collisional and radiative relaxation of chemically activated ions may be probed by temporal variation of laser irradiation, and complemented by probing of resonance activated, i.e. selectively heated, ions. Individual ion species may be isolated in the QUISTOR and subsequently irradiated under total ion storage conditions in order to accumulate ionic photoproducts. The time scale of slow multiphoton absorption allows for radiative losses, hence ir spontaneous emission lifetimes may be studied.

Summary and conclusions

The ability to distinguish structural isomers of gaseous ions on the basis of ir absorbance is of great interest in that it would complement the capabilities of mass spectrometry. However, it is exceedingly difficult to observe ir absorption directly, due to the low densities of gaseous ions which can be assembled, e.g. the maximum number of ions which may be trapped simulta-

neously in the QUISTOR is $\sim 10^9$ ions based on the space charge. As the extent of multiphoton excitation depends on energy fluence rather than laser intensity, slow multiphoton induced dissociation can be effected in target molecules or ions irradiated under near collision-free conditions, provided that excitation rates exceed the rates for spontaneous emission. Thus slow multiphoton dissociation offers an indirect method for determining ir absorption spectra of gaseous ions and can be a source of ion structural information which previously was not obtainable. In addition, ir multiphoton excitation presents a novel method for ion fragmentation which can be employed as a further distinguishing criterion. Slow ir multiphoton dissociation of polyatomic gaseous ions constitutes a convincing demonstration of the incoherence of the process.

It is concluded that (*i*) slow multiphoton dissociation may be employed to determine the dissociation pathway of lowest activation energy provided that the photon-absorbing ions are well relaxed. (*ii*) Thermal dissociation pathways may be followed by partially relaxed or unrelaxed ions upon multiphoton absorption. (*iii*) Dissociation via the reaction channel with the lowest activation energy is always observed but not necessarily exclusively. (*iv*) Slow multiphoton dissociation may be employed to distinguish between isomers. (*v*) The ion formed by loss of H_2O from the proton bound alcohol dimer is itself photodissociative. (*vi*) While the ir absorption spectrum of gaseous ions may mimic the wavelength dependance of single photon absorption by neutrals, the order of relative absorbances by neutrals is not necessarily maintained with gaseous ions.

Can. J. Chem. Downloaded from www.nrcresearchpress.com by 210.87.254.105 on 09/06/12
For personal use only.

Acknowledgements

The authors acknowledge with thanks the financial support of Trent University, the Natural Sciences and Engineering Research Council of Canada (for operating and equipment grants), Imperial Oil Company Limited, and Queen's University for a Graduate Student Assistantship. We acknowledge also the technical assistance of G. Wynn, C. J. S. Stuart, and W. King, and the laboratory assistance of Charlotte Kohn supported by a Canadian Industries Limited Summer Studentship. We are greatly appreciative of the cooperation of Drs. C. W. Willis and D. Rayner of the National Research Council of Canada for the loan of the CO_2 laser.

1. (*a*) R.N. ROSENFELD, J.M. JASINSKI, and J. I. BRAUMAN. Chem. Phys. Lett. **71**, 400 (1980); (*b*) R.N. ROSENFELD, J.M. JASINSKI, and J. I. BRAUMAN. J. Am. Chem. Soc. **101**, 3999 (1979); (*c*) J. M. JASINSKI, R.N. ROSENFELD, F. K. MEYER, and J. I. BRAUMAN. J. Am. Chem. Soc. **104**, 652 (1982); (*d*) R. N. ROSENFELD, J. M. JASINSKI, and J. I. BRAUMAN. J. Am. Chem. Soc. **104**, 658 (1982); (*e*) J. M. JASINSKI and J. I. BRAUMAN. J. Chem. Phys. **73**, 6191 (1980).
2. (*a*) R. L. WOODIN, D. S. BOMSE, and J. L. BEAUCHAMP. J. Am. Chem. Soc. **100**, 3248 (1978); (*b*) D. S. BOMSE, R. L. WOODIN, and J. L. BEAUCHAMP. J. Am. Chem. Soc. **101**, 5503 (1979); (*c*) D. S. BOMSE and J. L. BEAUCHAMP. J. Am. Chem. Soc. **103**, 3292 (1981); (*d*) C. A. WIGHT and J. L. BEAUCHAMP. Chem. Phys. Lett. **77**, 30 (1981); (*e*) L. R. THORNE and J. L. BEAUCHAMP. J. Chem. Phys. **74**, 5100 (1981); (*f*) C. A. WIGHT and J.L. BEAUCHAMP. J. Am. Chem. Soc. **103**, 6499 (1981); (*g*) D. S. BOMSE, D. W. BERMAN, and J. L. BEAUCHAMP. J. Am. Chem. Soc. **103**, 3967 (1981).
3. J. G. BLACK, E. YABLONOVITCH, N. BLOEMBERGEN, and S. MUKAMEL. Phys. Rev. Lett. 38, 1131 (1977).
4. H. G. DEHMELT and K. B. JEFFERTS. Phys. Rev. **125**, 1318 (1962); H. G. DEHMELT. Adv. At. Mol. Phys. **3**, 53 (1967); Adv. At. Mol. Phys. **5**, 190 (1969).
5. E. S. ENSBERT and K. B. JEFFERTS. Astrophys. J. **915**, L89 (1975); K. B. JEFFERTS. Phys. Rev. Lett. **20**, 39 (1968); **23**, 1476 (1969).
6. R. J. HUGHES, R. E. MARCH, and A. B. YOUNG. Int. J. Mass Spectrom. Ion Phys. **42**, 255 (1982).
7. J. L. BEAUCHAMP and R. D. DUNBAR. J. Am. Chem. Soc. **92**, 1477 (1970).
8. T. A. LEHMAN, T. A. ELWOOD, J. T. BURSEY, M. M. BURSEY, and J. L. BEAUCHAMP. J. Am. Chem. Soc. **93**, 2108 (1971).
9. M. A. ARMITAGE, J. E. FULFORD, D. N. HOA, R. J. HUGHES, and R. E. MARCH. Can. J. Chem. **57**, 2108 (1979).
10. P. KEBARLE. Ann. Rev. Phys. Chem. **28**, 445 (1977).
11. J. L. BEAUCHAMP. *In* Interactions between ions and molecules. *Edited by* P. Ausloos. Plenum Press, New York. 1974. p. 415.
12. R. J. HUGHES, R. E. MARCH, and A. B. YOUNG. Can. J. Chem. **61**, 824 (1983).

A new ion-pair state of iodine chloride[1]

J. C. D. BRAND, U. D. DESHPANDE, A. R. HOY, AND E. J. WOODS
Department of Chemistry, University of Western Ontario, London, Ont., Canada N6A 5B7

Received July 5, 1982

This paper is dedicated to Professor Harry E. Gunning on the occasion of his 65th birthday

J. C. D. BRAND, U. D. DESHPANDE, A. R. HOY, and E. J. WOODS. Can. J. Chem. **61**, 846 (1983).

A previously-unknown ion-pair state of ICl has been identified and characterized in sequential transitions using polarization-labelling spectroscopy. This state is designated $1(^3P_1)$, indicating a state of axial electronic angular momentum $\Omega = 1$ correlating diabatically at dissociation with the states $I^+(^3P_1) + Cl^-(^1S_0)$ of the separated ions. The electronic energy and local potential constants for levels with $v = 1-7$ are (in cm^{-1}) $T_e = 45552.805(23)$, $\omega_e = 184.854(13)$, $\omega_e x_e = 0.6737(13)$, $B_e = 0.058898(42)$, and $\alpha = 2.485(93) \times 10^{-4}$, and the equilibrium bond distance is 3.231 Å.

J. C. D. BRAND, U. D. DESHPANDE, A. R. HOY et E. J. WOODS. Can. J. Chem. **61**, 846 (1983).

On a identifié un état de paire d'ions des composés ICl inconnu antérieurement et on l'a caractérisé dans des transitions séquentielles utilisant la spectroscopie de marquage par polarisation. On désigne cet état $1(^3P_1)$, indiquant un état du moment angulaire électronique axial $\Omega = 1$ corrélant diabatiquement à une dissociation avec les états $I^+(^3P_1) + Cl^-(^1S_0)$ des ions séparés. L'énergie électronique et les constantes de potentiel local des niveaux avec $v = 1-7$ sont de (en cm^{-1}) $T_e = 45552{,}805(23)$, $\omega_e = 184{,}854(13)$, $\omega_e x_e = 0{,}6737(13)$, $B_e = 0{,}058898(42)$ et $\alpha = 2{,}485(93) \times 10^{-4}$ et la distance d'équilibre de liaison est de 3,231 Å.

Introduction

With a few exceptions, the low-lying electronically-excited states of ICl are not well characterized. The transition from the ground state to the low-lying, case c $A\,^3\pi_1$ state has been analyzed extensively (1, 2), while the tangled O^+ states, B, B' are understood in principle (3) and have been the subject of comprehensive lifetime studies (4). Although constants of the $\Omega = 1$ E state have recently been determined by King *et al.* (5), no other sub-Rydberg states of the molecule are known at the present time. A critical summary of work published through 1976 is given in the monograph by Huber and Herzberg (6). It is worth noting that the band system $D-A$ in this monograph becomes $E-A$ according to the revised assignments of King and co-workers.

Polarization-sensitive laser methods offer a powerful means of studying excited states of molecules. Besides the drastic simplification compared to conventional absorption/emission spectra, these techniques also allow us to determine the electronic angular momentum of the excited state directly and unambiguously. This paper reports the identification and characterization of a previously unknown $\Omega = 1$ sub-Rydberg state of ICl lying ca. 0.8 eV higher than the E state. A search for this state was undertaken on the hypothesis that E is almost certainly the lowest-energy $\Omega = 1$ ion-pair state of ICl, correlating in a diabatic approximation with the ground states of the separated ions, $Cl^-(^1S) + I^+(^3P_2)$: since the $^3P_1$ excited state of I^+ lies about 0.9 eV higher than $^3P_2$ (7) the next-higher $\Omega = 1$ ion-pair state can be expected within roughly 1 eV of the E state. The energy and potential constants of the new state bear out this expectation; therefore we refer to the state, following the notation suggested by Tellinghuisen (8), as $1(^3P_1)$.

Experimental

The instrumentation used for polarization spectroscopy has been described elsewhere (9). In order to access the $1(^3P_1)$ state from the ground state of ICl, selected rotational transitions of the $A \leftarrow X$ system were pumped with a narrow-band laser and the $1(^3P_1) \leftarrow A$ transitions probed with a second, broadband laser. Energy and intensity (Franck–Condon) considerations then require that the pump laser be operated with R590(R6G), R610(RhB), or R640 dyes (10) as lasing media, using PTP (29100–29700 cm^{-1}) in the broadband probe. The XeCl excimer laser used to pump these dyes does not allow us to probe at frequencies higher than 29700 cm^{-1}. The signal transmitted through crossed polarizers was photographed in the 17-th order of a 3.4 m spectrograph using Kodak SA-1 emulsion, and the frequency measurements referred to an Fe/Ne hollow-cathode emission superimposed on the spectrum in the usual way. Development of the spectrum normally required $1-3 \times 10^3$ pump–probe pulse sequences, corresponding to a realtime exposure of ca. 20 μs.

The 20 cm sample cell contained ICl vapor in equilibrium with excess solid at 0°C. Commercial ICl (Eastman) was used without purification. Interference from I_2 transitions was minimal. The spectra were essentially unchanged after 10^3-10^4 pulses, thus the possible buildup of I_2 and Cl_2 during exposure has no significant effect. The cell location was chosen so that the (nominally) 8 ns pump and probe pulses arrived simultaneously at the sample.

Spectra of $I^{37}Cl$ were obtained without enrichment. Polarization-labelled spectra are sufficiently sparse that no interference occurs between transitions of the isotopes at natural abundance. $I^{35}Cl$ and $I^{37}Cl$ transitions were recorded in a ratio of about 2:1

Electronic assignment

The spectra recorded in this work were obtained using linearly-polarized pump and probe pulses, the two polarizations being oriented at 45° to one another. Typical signals recorded under these conditions are shown in Fig. 1. Each of these signals is a transition of the $1(^3P_1) \leftarrow A$ band system: selective labelling by the pump limits a band to just two transitions P(J) and R(J), where J is the rotational quantum number of the A-state level populated by the pump. It is an important diagnostic test that the Q-branch signal is weaker than P or R, irrespective of whether the transition pumped in the $A-X$ system belongs to a Q-branch or to P/R. In fact, unless J is small ($J \leq 5$), the Q-branch signals are below detection threshold and escape observation altogether. The P and R signals are accompanied by collision-induced satellites which extend over a considerable range of J when the parent signal is strong.

The intensity distribution has been derived recently in a

[1]Publication No. 286 from the Photochemistry Unit, University of Western Ontario. Work supported by the Natural Sciences and Engineering Research Council of Canada.

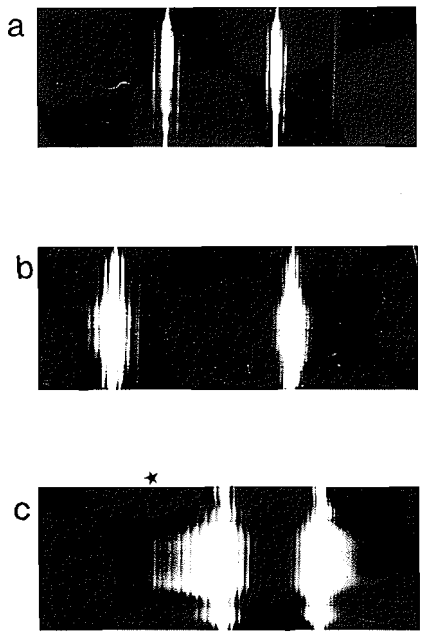

FIG. 1. Polarization spectra of the $1(^3P_1) \leftarrow A$ band system. (*a*) the Q-pumped, $v = 1-15$ band of $I^{35}Cl$: parent transitions, accompanied by weak $\Delta J = \pm 1$ collision-transfer satellites, are R30 (29418.66 cm^{-1}) and P30 (29411.58 cm^{-1}). (*b*) R-pumped 4–19 band of $I^{35}Cl$: parent transitions are R51 (29521.31 cm^{-1}) and P51 (29509.41 cm^{-1}). In this spectrum, and in (*c*) below, the saturation caused by the pump pulse is sufficiently high that the parent lines are reversed. (*c*) Q-pumped 3–17 band of $I^{35}Cl$: parents are P27 (29543.3 cm^{-1}) and R27 (29549.7 cm^{-1}). The weak feature marked * is the R-branch of another transition. Frequency increases towards the right in this diagram. The red-degradation of bands in the $1(^3P_1) \leftarrow A$ system is clearly shown by the distribution of collision satellites. These spectrograms are selected to illustrate the formation of collision satellites, and the parent transitions are broadened by overexposure.

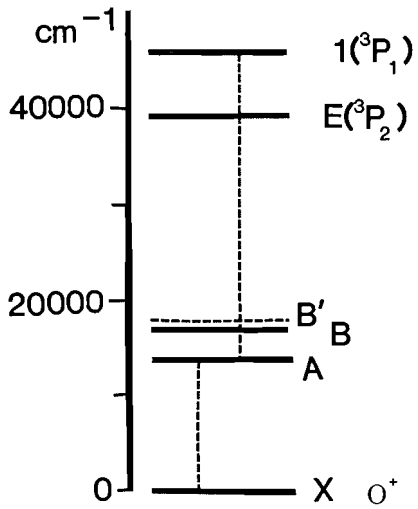

FIG. 2. Identified sub-Rydberg states of ICl. Vertical lines indicate the pump–probe sequence used in this work.

small signal approximation by Carlson *et al.* (11). In the ICl system the $A \leftarrow X$ pumped transition is $\Omega = 1 \leftarrow 0$; therefore, since the case *c* selection rules are $\Delta\Omega = 0, \pm 1$ the *final* state may have $\Omega = 0^{\pm}$, 1, or 2. When the probed transition is perpendicular, i.e., $0^- \leftarrow 1$, $0^+ \leftarrow 1$, or $2 \leftarrow 1$, the theoretical intensity distribution for all except small values of J indicates that for Q-branch pumping the Q-branch of the probed transition will be stronger than P or R in the last two cases. For the case $0^- \leftarrow 1$ the conditions are reversed, that is, pumping in a P- or R-branch will lead to a strong Q-branch, and vice versa. None of these possibilities describes the spectra in Fig. 1, where the P, R intensities far outweigh that of the Q-branch, irrespective of whether the pumped transition is P, Q, or R. (Finer details in these spectra are due to collision satellites and are discussed below.) The observed spectra correspond uniquely with a parallel, $\Omega = 1 \leftarrow 1$, transition between the intermediate and final states of the pump–probe sequence. Accordingly the final state can be identified unambiguously with a $\Omega = 1$ state. This assignment relative to that of other known sub-Rydberg states is shown schematically in Fig. 2.

TABLE 1. Combination differences (cm^{-1}) for collision satellites in the $1(^3P_1) \leftarrow A$ system; the parent transitions are pumped in Q27, 17–0 of $A \leftarrow X$

	$\Delta_2F(J) = R(J-1) - P(J+1)$			$\Delta_2F(J) = R(J-1) - P(J+1)$	
J''	Ref. 1	This paper	J	Ref. 1	This paper
32	8.550	8.553	27	7.255	7.232
31	8.295	8.291	25	6.715	6.706
30	8.037	8.036	24	6.491	6.45
29	7.767	7.758	23	6.214	6.18
28	7.501	7.465	22	5.914	5.96

[a] J refers to rotational levels of $v = 17$ in the intermediate, A state.

The abundance of collision-induced satellites at the moderate sample pressure of $\lesssim 4$ Torr was not expected. Assignments for the satellites seen in, for example, Fig. 1*c* are perfectly definite as shown by the compilation of A state combination differences in Table 1. It is worth noting in passing that analysis of the satellites enables us to assign the pumped transition without knowledge of the pump frequency. The intensity of the satellites falls off smoothly as ΔJ increases, though the rate at which intensity decreases is somewhat less on the low-frequency compared to the high-frequency side. Evidently this corresponds to a net trend to lower energy by collision transfer, as one expects intuitively. The collisions involved here are exceedingly weak, since a $\Delta J = 1$ transfer corresponds to $\Delta E \approx 2BJ \approx 3\ cm^{-1}$ at $J = 27$, which is much less than kT.

In Fig. 1*a*, the $\Delta J = 1$ satellite intensity is 10–12 times weaker than that of the parent line. If we can assume that T_1, the time-constant for J-changing collisions, and T_2, the constant for redistribution among M-sublevels of the same J, are such that $T_2 \gg T_1$ — which is supported by admittedly slender evidence from the spectrum of I_2 vapor (12) — the rate constant T_1^{-1} is calculated to be between one and two orders of magnitude greater than hard sphere. This value of T_1^{-1} is quite similar in magnitude to the rate constant for electronic self-quenching of the A state as reported some years ago by Holleman and Steinfeld (13). Although these two processes are physically distinct, it is natural to assume that the large cross-section implied in both cases is due to the field associated with the permanent electric moment. Since the selection rules for matrix elements of μ are $\Delta J = \pm 1$, $\Delta\Omega = 0$, $+ \leftrightarrow -$ we expect that the propensity rule for pure rotational transfers will be as shown in Fig. 3: this rule has been tacitly assumed in the second and fifth columns of Table 1. At present the data available do not distinguish whether the more remote satellites are populated directly or by a $\Delta J = \pm 1$ cascade.

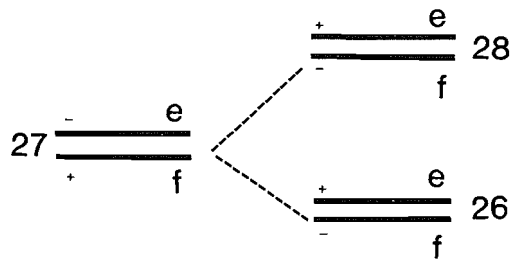

FIG. 3. Schematic representation of rotational relaxation in the A state of the $1(^3P_1) \leftarrow A \leftarrow X$ sequence. The pumped transition is identified with Q27 (see Fig. 1*c* and Table 1). $\Delta J = \pm 1$ collision transfers are assumed to obey a dipole propensity rule $\Delta\Omega = 0$, $+ \leftrightarrow -$. The Λ-type doubling is greatly exaggerated.

TABLE 2. Electronic energy and Dunham constants (in cm^{-1}) of the ion-pair states of $I^{35}Cl$

	$1(^3P_1)^a$	$E\ 1(^3P_2)^b$
$Y_{0,0}(\sim T_e)$	45552.805(23)	39107.8(16)
$Y_{1,0}(\omega_e)$	184.854(13)	168.99(52)
$Y_{2,0}(-\omega_e x_e)$	−0.6737(13)	−0.357(39)
$Y_{0,1}^e(B_e^e)$	$5.8931(29)\times10^{-2}$	$5.685(28)\times10^{-2}$
$Y_{0,1}^f(B_e^f)$	$5.8865(13)\times10^{-2}$	
$Y_{1,1}^e(-\alpha^e)$	$-2.592(46)\times10^{-4}$	$-2.21(40)\times10^{-4}$
$Y_{1,1}^f(-\alpha^f)$	$-2.378(47)\times10^{-4}$	
$Y_{0,2}^e$	$-1.35(51)\times10^{-8}$	
$Y_{0,2}^f$	$-2.59(33)\times10^{-8}$	
r_e/Å	3.231	3.289

[a] The stated uncertainty is 1σ.
[b] Reference 5.

Potential function

The electronic energy and potential constants for the $1(^3P_1)$ state were determined from an all-lines, simultaneous least-squares fit of term values for $I^{35}Cl$ and $I^{37}Cl$ using a Dunham expansion. Local constants for $I^{35}Cl$ are summarized in Table 2. In the approximation that the potential function is identical for $I^{35}Cl$ and $I^{37}Cl$, as assumed in the refinement, the isotopic relationships are,

$$[1]\quad Y_{k,l}(37) = \rho^{l+k/2}\, Y_{k,l}(35)$$

where $\rho = 0.95765$ is the ratio of reduced masses.

Constants given by King *et al.* (5) for the E state of ICl are reproduced in Table 2 for comparison. The $1(^3P_1)$ and E states are in fact very similar, at least when compared to other states of the manifold: ω_e, for example, is 384 cm^{-1} in the X state and 420–445 cm^{-1} in Rydberg states whereas the frequencies for $1(^3P_1)$ and E are not only much smaller but fall within 10% of one another. This family likeness, which extends to r_e and other constants, indicates that both are ion-pair states I^+Cl^- as originally forecast by Mulliken (14) and tentatively confirmed by King *et al.* (5). An alternative notation for E is therefore $1(^3P_2)$.

Experience with the diatomic alkali halides shows that the potential function of an ion-pair state is described quite well by the "truncated-Rittner" model of Brumer and Karplus (15),

$$[2]\quad V(r) = T_\infty + A\exp(-br) - e^2/r - [\alpha(I^+) + \alpha(Cl^-)]e^2/2r^4 - C\,(I^+Cl^-)/r^6$$

Here, r is the ion–ion distance, the α's are ion polarizabilities, C/r^6 is the London approximation (16) to the van der Waals attraction,

TABLE 3. Parameters of the Rittner potential function

Parameter	Value: Calcd.	Value: Obsd.[a]	% error
T_∞/cm^{-1}	7.963×10^{4}[b]		
A/cm^{-1}	2.942×10^{7}		
$b/Å^{-1}$	2.602		
$\alpha(Cl^-)/Å^3$	3.69[c]		
$\alpha(I^+)/Å^3$	4[d]		
$Y_{0,0}/cm^{-1}$	4.5677×10^{4}	4.5553×10^{4}	0.3
$Y_{1,0}/cm^{-1}$	184.9		0.0
$Y_{2,0}/cm^{-1}$	−0.655	−0.674	2.9
$Y_{0,1}/cm^{-1}$	5.89×10^{-2}		0.0
$Y_{1,1}/cm^{-1}$	-2.80×10^{-4}	2.49×10^{-4}	12

[a] Table 2.
[b] References 1, 7, 17.
[c] Reference 18.
[d] Assumed value.

$$[3]\quad C(I^+Cl^-) = (3/2)\,\alpha(I^+)\alpha(Cl^-)\omega(I^+)\omega(Cl^-)/[\omega(I^+) + \omega(Cl^-)]$$

and A and b are parameters in an empirical term describing the short-range interaction. For dissociation into $I^+(^3P_1) + Cl^-(^1S_0)$ the $r = \infty$ term value T_∞, relative to $T_e = 0$ for the X state, can be calculated from the ionization potential of I_{atomic} (7), the electron affinity of Cl_{atomic} (17) and the dissociation energy of the X state. The ion polarizability for Cl^- is known (18) while that for I^+ can be estimated without serious error. If the ω's in [3] are identified with ionization potentials, the only two remaining parameters to be determined from the observed potential constants are A and b. The function [2] is therefore overdetermined in that five spectroscopic constants (Table 2) are available to fix two parameters.

The procedure followed is that A and b are first determined from the conditions $(dV(r)/dr)_e = 0$ and $(d^2V(r)/dr^2)_e = 4\pi^2c^2\omega_e^2\mu$. The complete potential curve can then be calculated. At $r = r_e$ the computed $V(r_e) \equiv T_e$ is in excellent agreement with the observed values of $Y_{0,0}$ (T_e), as shown in Table 3. Likewise the anharmonic part of $Y_{1,1}$ is proportional to the third derivative $(d^3V(r)dr^3)_e$, while $Y_{2,0}$ is determined by the third and fourth derivatives; here too the agreement is satisfactory though less good than for $Y_{0,0}$. The fact that the first five derivatives, $(d^nV/dr^n)_e$ for $n = 0$ through 4, are accounted for consistently affords definite physical evidence that the state in question is highly ionic in the region where r is not greatly different from r_e. However, extrapolation to a limit in which dissociation occurs into separated ions is a diabatic approximation. As Mulliken (14) has emphasized there are Rydberg states of atomic halogens lying below the $I^+(^3P_1) + Cl^-(^1S_0)$ asymptote: therefore at large r the curve will sidestep, in order to observe the non-crossing rule, to a channel leading to two neutral atoms one of which must be in a low-lying Rydberg state.

1. E. HULTHÉN, N. JOHANSSON, and U. PILSÄTER. Ark. Fys. **14**, 31 (1958); E. HULTHÉN, N. JÄRLSÄTER, and L. KOFFMAN. Ark. Fys. **18**, 479 (1960).
2. J. A. COXON, R. M. GORDON, and M. A. WIKRAMAARATCHI. J. Mol. Spectrosc. **79**, 363 (1980).
3. M. S. CHILD. Mol. Phys. **32**, 1495 (1976).
4. C. D. OLSON and K. K. INNES. J. Chem. Phys. **64**, 2405 (1976).
5. G. W. KING, I. M. LITTLEWOOD, R. G. MCFADDEN, and J. R. ROBINS. Chem. Phys. **41**, 379 (1979).

6. K. P. HUBER and G. HERZBERG. Molecular spectra and molecular structure. Vol. IV. Van Nostrand Reinhold Co., New York. 1979.
7. C. E. MOORE. U.S. Natl. Bur. Stand. Circ. 467 (1949).
8. K. S. VISWANATHAN, A. SUR, and J. TELLINGHUISEN. J. Mol. Spectrosc. **86**, 393 (1981).
9. J. C. D. BRAND, K. J. CROSS, and N. P. ERNSTING. Chem. Phys. **59**, 405 (1981).
10. Exciton Chemical Co. Inc., Dayton, Ohio.
11. N. W. CARLSON, A. J. TAYLOR, K. M. JONES, and A. L. SCHAWLOW. Phys. Rev. **24**A, 822 (1981).
12. J. C. D. BRAND and R. J. HAYWARD. Chem. Phys. Lett. **68**, 369 (1979).
13. G. W. HOLLEMAN and J. I. STEINFELD. Chem. Phys. Lett. **12**, 431 (1971).
14. R. S. MULLIKEN. Phys. Rev. **46**, 549 (1934); J. Chem. Phys. **55**, 288 (1971).
15. P. BRUMER and M. KARPLUS. J. Chem. Phys. **58**, 3903 (1973).
16. F. LONDON. Trans. Faraday Soc. **33**, 8 (1937).
17. R. S. BERRY and C. W. REIMANN. J. Chem. Phys. **38**, 1540 (1963).
18. A. DALGARNO. Adv. Phys. **11**, 281 (1969).

Photochemistry of acetylene

H. OKABE[1]

NASA/Goddard Space Flight Center, Laboratory for Extraterrestrial Physics, Astrochemistry Branch, Greenbelt, MD 20771, U.S.A.

Received July 5, 1982

This paper is dedicated to Professor Harry E. Gunning on the occasion of his 65th birthday

H. OKABE. Can. J. Chem. **61**, 850 (1983).

Photochemical and fluorescence studies of acetylene initiated by absorption of light in the vacuum ultraviolet have been described. The photochemical primary process consists of (1) the formation of $C_2 + H_2$, (2) the production of $C_2H + H$, and (3) the formation of a metastable acetylene. The quantum yield of process (1) is about 0.1 and that of process (2) is 0.06 at 1849 Å and 0.3 at 1470 Å. The metastable acetylene either reacts with ground state acetylene to produce diacetylene or is deactivated by collisions with the walls, inert gases, or by fluorescence. A quasicontinuous emission is observed in the 4000 to 6000 Å region when acetylene is exposed to incident wavelengths below 1305 Å. This emission is ascribed to an electronically excited ethynyl radical. The rates of reaction $C_2H + H_2 \rightarrow C_2H_2 + H$ and $C_2H + RH \rightarrow C_2H_2 + R$ ($RH = CH_4$, C_2H_6, C_3H_8) have been measured. The photochemistry of acetylene in the Jovian and Titan atmospheres is briefly discussed.

H. OKABE. Can. J. Chem. **61**, 850 (1983).

On décrit les études de fluorescence et photochimiques de l'acétylène initiés par l'absorption de lumière dans l'ultraviolet sous vide. Le processus photochimique initial consiste (1) en la formation de $C_2 + H_2$, (2) en la production de $C_2H + H$ et (3) en la formation d'acétylène métastable. Le rendement quantique du premier processus est d'environ 0,1 et celui du 2e processus est de 0,06 à 1849 Å et de 0,3 à 1470 Å. L'acétylène métastable réagit soit avec l'acétylène à l'état fondemental pour produire le diacétylène ou est désactivé par suite des collisions avec les parois, les gaz inertes ou par fluorescence. On observe une émission quasi continue dans la région allant de 4000 à 6000 Å lorsqu'on expose l'acétylène à des longueurs d'ondes incidentes en dessous de 1305 Å. On attribue cette émission à un radical éthynyl excité électroniquement. On a mesuré les vitesses de réaction: $C_2H + H_2 \rightarrow C_2H_2 + H$ et $C_2H + RH \rightarrow C_2H_2 + R$ ($RH = CH_4$, C_2H_6, C_3H_8). On discute brièvement de la photochimie de l'acétylène dans les atmosphères de Jovian et de Titan.

[Traduit par le journal]

Introduction

Acetylene is one of the simplest hydrocarbons and as such it has been the subject of numerous photochemical studies in recent years (1). Major photochemical products are diacetylene, ethylene, hydrogen, and small amounts of vinylacetylene and benzene (2–4), while the Cd ($^3P_1$) sensitized reaction (5) produces benzene and vinylacetylene and the Hg ($^3P_1$) sensitized reaction (6) forms benzene, vinylacetylene, and hydrogen. On the other hand, the vacuum ultraviolet photolysis of acetylene in low temperature matrices has produced $C_2(X^1\Sigma_g^+)$ (7) and C_2H (7, 8) suggesting that the primary process may be: (1) $C_2H_2 \xrightarrow{h\nu} C_2 + H_2$; (2) $C_2H_2 \xrightarrow{h\nu} C_2H + H$. In addition to these reactions another gas phase process producing an electronically excited ethynyl radical, C_2H^*, is found (9, 10) below the incident wavelength 1305 Å.

The substantial production of metastable acetylene has also been suggested in the vacuum ultraviolet photolysis of acetylene (2, 3, 11). However, the quantum yields of these processes have not been determined. Acetylene has recently been detected in the Jovian (12) and Titan (13) atmospheres. It has been suggested (14) that acetylene plays an important role in the catalytic decomposition of hydrogen and methane in the planetary atmospheres.

Fluorescence from C_2H_2 has recently been detected in the spectral region 2500–3500 Å by light absorption near 2200 Å (15). Below 2000 Å no fluorescence arising from acetylene has been observed. This article describes some recent studies on (1) the quantum yield of the photochemical primary process of acetylene, (2) the reaction of ethynyl radical with H_2 and hydrocarbons, and discusses acetylene photochemistry in the Jovian and Titan atmospheres based on the results obtained from these studies.

Fluorescence and predissociation

The bond dissociation energy $D_0(H—C_2H)$ of 5.38 ± 0.05 eV has been determined by the author (16). This energy corresponds to the incident wavelength 2306 Å. Recently Abramson *et al.* (15) have found that even with 2207 Å excitation, 1900 cm^{-1} above the dissociation threshold, the fluorescence lifetime is of the order of 3 μs, indicating no dissociation of the excited acetylene occurs. At 2000 Å excitation, however, the fluorescence yield becomes 10^{-4} and at 1849 Å no fluorescence was seen (17). This weak predissociation is also observed in chloroacetylene fluorescence (1). The predissociation generally occurs much more rapidly above the dissociation threshold in triatomic molecules (SO_2, NO_2, CS_2) and in some four-atomic molecules (1) (formaldehyde, ammonia, thiophosgene). Fluorescence with vibrational structure has been observed by Brus (15) in the 2500–3500 Å region when acetylene in low temperature rare-gas matrices is irradiated by the ArF 1933 Å laser light.

Another quasicontinuous fluorescence has been observed by the author (9) and by Becker *et al.* (10), when acetylene is excited by incident wavelengths below 1305 Å. The fluorescence spectrum, shown in Fig. 1, lies in the 4000 to 6000 Å region with no apparent structure. Since both C_2H_2 and BrC_2H produce the similar quasicontinuum, it is most likely that this emission arises from an electronically excited C_2H (C_2H^*), and not from $C_2H_2^*$. Although the lifetime of fluorescence is 6 μs (10), similar to that excited by the incident wavelength, 2207

[1]NAS–NRC Senior Research Associate, on leave from the National Bureau of Standards, Washington, DC. 20234, U.S.A.

Can. J. Chem. Downloaded from www.nrcresearchpress.com by 210.87.254.42 on 09/06/12
For personal use only.

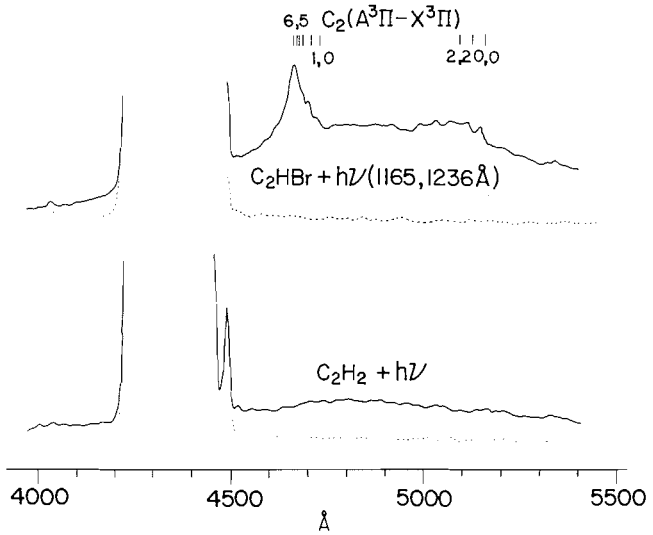

FIG. 1. The fluorescence spectrum produced from the photolysis of BrC_2H and C_2H_2 by the Kr lamp; the sample pressure is about 0.1 Torr; the resolution 10 Å; the broken lines indicate the background level; a large signal in the 4200 to 4500 Å region is due to the scattered emission lines from the lamp; from ref. 9.

Å (15), the fluorescence spectrum of the former (C_2H^*) is in the visible and quasicontinuous while the spectrum of the latter ($C_2H_2^*$) is in the ultraviolet and has vibrational structure.

From the threshold wavelength 1305 Å corresponding to $h\nu = 9.50$ eV for the production of C_2H^* from C_2H_2, in conjunction with the heat of reaction for $C_2H_2 \rightarrow C_2H + H$ (5.38 ± 0.05 eV), the author (9) obtained the electronic energy of C_2H, 4.11 ± 0.05 eV, corresponding to the incident wavelength, 3017 ± 40 Å. However, absorption or laser induced emission of C_2H has apparently not been found in this region. The long fluorescence lifetime indicates that the C_2H absorption may be too weak to detect.

Photochemical process

Primary process

Important progress has been made by Lange and Wagner (18) in understanding acetylene photochemistry. They have obtained the rate constant of the reaction

$$C_2H + C_2H_2 \rightarrow C_4H_2 + H$$

by measuring with the mass spectrometer the decay of C_2H and have obtained $k = 5 \times 10^{-11}$ cm^3 molec^{-1} s^{-1}. They have also found the product to be mainly diacetylene. Laufer and Bass (19) have also obtained the rate constant of 3×10^{-11} by measuring the rise time of C_4H_2 by absorption. Since the reaction is fast, the production of C_4H_2 by combination of C_2H may be neglected in the steady state photolysis of acetylene. Thus the quantum yield of process [1], where $C_2H_2^*$ means an initially formed singlet state,

$$[1] \quad C_2H_2 \xrightarrow{h\nu} C_2H_2^* \rightarrow C_2H + H$$

may be obtained from the quantum yield of diacetylene, $\phi_{C_4H_2}$. Amounts of diacetylene have been measured by absorption at 1642 Å, which corresponds to a strong Rydberg transition (see Fig. 2). The photolysis of acetylene has been performed at 1470 Å and 1849 Å, corresponding respectively to the transition to the Rydberg state and to the $\tilde{B}\ ^1B_u$ state ($v'_3 = 0$); see Fig. 3. The quantum yield of diacetylene at 1470 Å has been measured as a function of C_2H_2 pressure. The results are shown in Fig. 4. It can be seen that diacetylene is formed from the pressure independent process as well as the pressure dependent process. The quantum yield of the pressure independent process (direct dissociation) is 0.3. Higher yields of diacetylene at higher pressures of acetylene must arise from the reaction of a metastable acetylene, $C_2H_2^{**}$, with ground state acetylene (20).

$$[2] \quad C_2H_2^* \rightarrow C_2H_2^{**}$$
$$C_2H_2^{**} + C_2H_2 \rightarrow C_2H + C_2H_3$$
$$C_2H + C_2H_2 \rightarrow C_4H_2 + H$$

At low pressure of acetylene, $C_2H_2^{**}$ must be deactivated by wall collisions or by fluorescence.

$$C_2H_2^{**} \xrightarrow{\text{walls}} C_2H_2$$

The metastable acetylene can also be quenched by the addition of N_2 or He, resulting in the decrease of $\phi_{C_4H_2}$, as shown in Fig. 5. The quenching is not complete even by the addition of 400 times as much He or N_2 as acetylene at 1470 Å. When acetylene pressure is low (below 0.7 Torr), the addition of N_2 has no effect on the production of diacetylene since $C_2H_2^{**}$ does not contribute to the formation of diacetylene. At 1849 Å photolysis (21) $\phi_{C_4H_2}$ is also dependent on the pressure of acetylene. At the low pressure limit $\phi_{C_4H_2}$ is 0.06, 1/5 of that at 1470 Å. The results are shown in Fig. 6. The addition of N_2 or He reduces $\phi_{C_4H_2}$ to a constant value of 0.05, indicating that the quenching of $C_2H_2^{**}$ is complete above the partial pressure of 150 Torr N_2 or He (see Fig. 7). At 1849 Å, quenching of $C_2H_2^{**}$ requires less partial pressure of inert gas than at 1470 Å.

The state of metastable acetylene is not clear. Wetmore and Schaefer (22) calculate the low-lying triplet states to be *cis* $^3A_2$ (4.50 eV), *trans* ^3A_u (4.13 eV), *trans* ^3B_u (3.78 eV), and *cis* $^3B_2$ (3.43 eV). Since $C_2H_2 + C_2H_2 \rightarrow C_2H_3 + C_2H$ is endothermic by 3.91 eV, $C_2H_2^{**}$ must have energy above 3.91 eV to form C_4H_2. Hence it is probable that *cis* $^3A_2$ or *trans* ^3A_u is formed by absorption both at 1470 and 1849 Å. On the other hand, in the Hg and Cd sensitized reactions mainly *trans* ^3B_u, or *cis* $^3B_2$ may be formed, since in these reactions very little diacetylene is detected as a product (5, 6).

Another primary process is the production of molecular hydrogen

$$[3] \quad C_2H_2 \xrightarrow{h\nu} C_2H_2^* \rightarrow C_2 + H_2$$

The quantum yield of H_2 production is about 0.1 both at 1470 (20) and 1849 Å (21). The electronic state of C_2 is most likely to be $X^1\Sigma_g^+$ as indicated in the photolysis of acetylene in low temperature matrices (7). Little is known about the rate constant or products of the reaction $C_2\ X^1\Sigma_g^+$ with acetylene (23).

The sum of processes [1] and [3] is still much less than unity, indicating the substantial production of $C_2H_2^{**}$, process [2]. The quantum yield of diacetylene at 1849 Å (Fig. 6) increases to a maximum at about 10 Torr of acetylene and then decreases with further increase of acetylene, indicating the formation of another product, probably benzene, which has been detected by Tsukada and Shida (4). The reaction for benzene formation would be

Can. J. Chem. Downloaded from www.nrcresearchpress.com by 210.87.254.42 on 09/06/12
For personal use only.

Can. J. Chem. Downloaded from www.nrcresearchpress.com by 210.87.254.42 on 09/06/12
For personal use only.

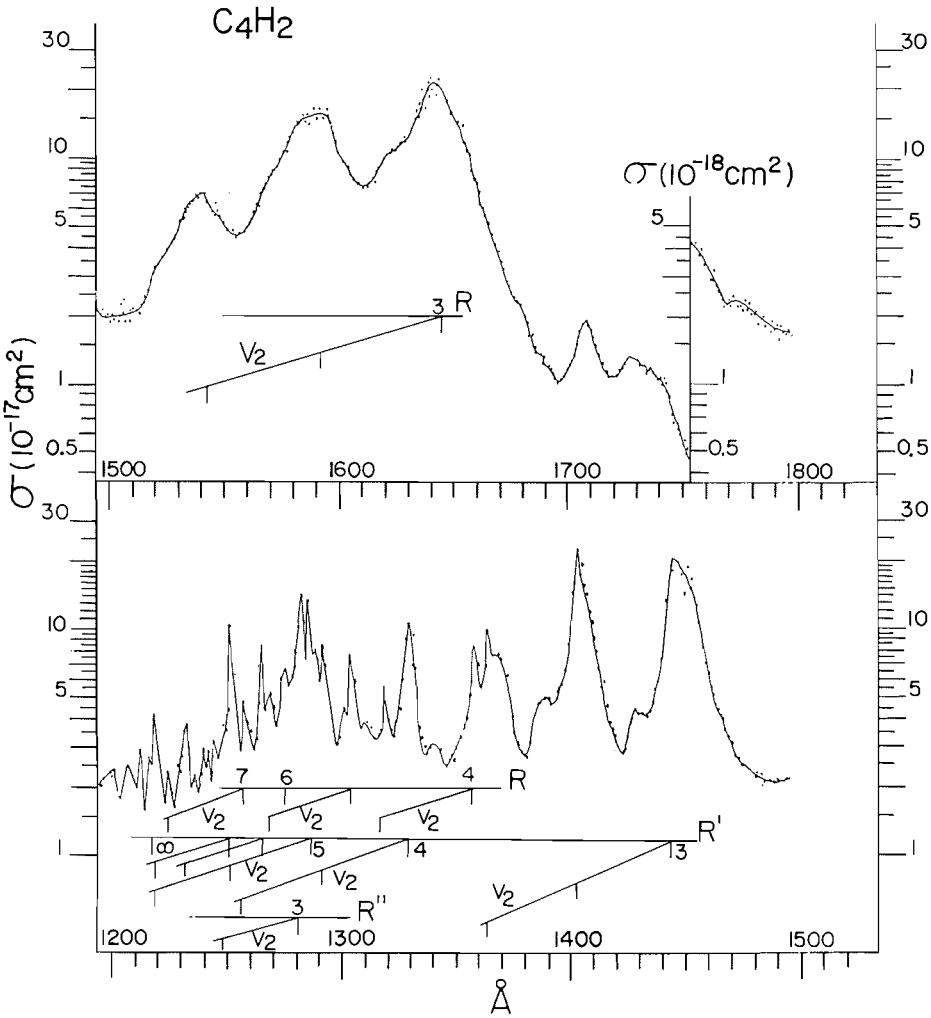

FIG. 2. Absorption cross sections of diacetylene in the 1200 to 1800 Å region. Almost all strong peaks observed belong to two Rydberg series R and R′ with associated ν_2 (C≡C) stretching vibration, leading to the ionization potential 10.18 eV at 1217 Å. Below 1300 Å a third Rydberg series R″ appears with associated ν_2 vibration. A strong peak at 1642 Å has been used for measuring the amounts of diacetylene produced (from ref. 20).

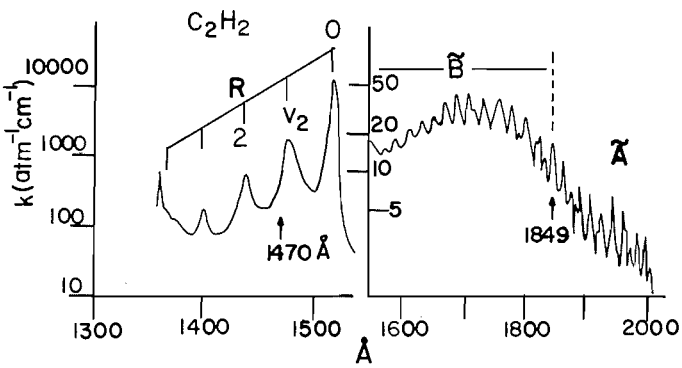

FIG. 3. Absorption coefficients, k, of acetylene in the 1400 to 2000 Å region; k is given in units of atmospheres and cm at 0°C, base e. At 1470 Å acetylene is excited to a Rydberg state, while at 1849 Å the B ^1B_u state, $\nu_3' = 0$ is formed; from ref. 28.

$$C_2H_2^{**} + 2C_2H_2 \rightarrow C_6H_6$$

Photolysis of C_2H_2–H_2, C_2H_2–hydrocarbon mixtures

Figure 8 shows $\phi_{C_4H_2}$ decreases with the addition of H_2, indicating the occurrence of the reaction (18)

[4] $C_2H + H_2 \rightarrow C_2H_2 + H$

in competition with the formation of diacetylene

[5] $C_2H + C_2H_2 \rightarrow C_4H_2 + H$

From reactions [4] and [5] we obtain

$$[6]\quad \phi^0_{C_4H_2}/\phi_{C_4H_2} = 1 + \frac{k_4(H_2)}{k_5(C_2H_2)}$$

where $\phi^0_{C_4H_2}$ is the quantum yield of diacetylene formation without H_2 and $\phi_{C_4H_2}$ is that with H_2. The plot, $\phi^0_{C_4H_2}/\phi_{C_4H_2}$ against $(H_2)/(C_2H_2)$ gives a straight line with the slope k_4/k_5, as shown in Fig. 9. The least-squares analysis of the plot gives $k_4/k_5 = 0.00775 \pm 0.00068$, that is, reaction [5] is 130 ± 11 times as fast as reaction [4]. Similar plots have been made for CH_4, C_2H_6, and C_3H_8. The results are given in Table 1. The rate constant of H abstraction by C_2H increases as $H_2 < CH_4 < C_2H_6 < C_3H_8$ and for propane the rate is one half as fast as that for acetylene.

Photochemistry of acetylene in the Jovian and Titan atmospheres

Acetylene has been detected in the Jovian atmosphere (12)

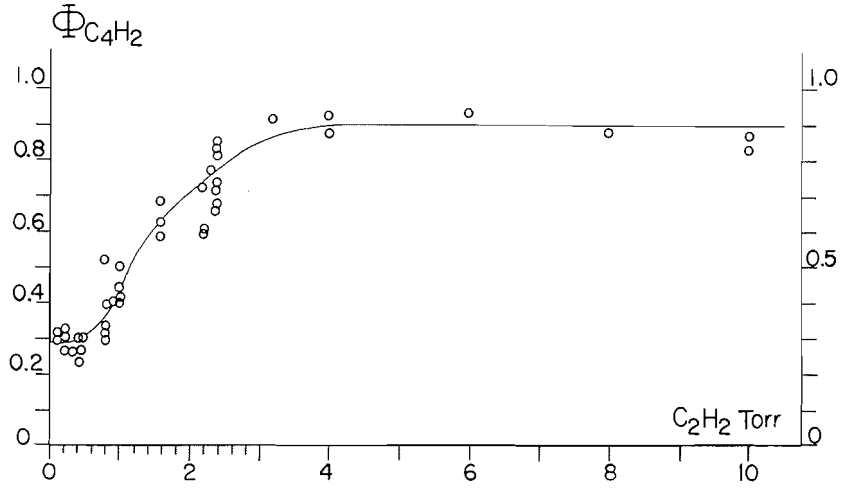

FIG. 4. The quantum yield of diacetylene formation $\phi_{C_4H_2}$ from acetylene photolysis at 1470 Å as a function of acetylene pressure; from ref. 20.

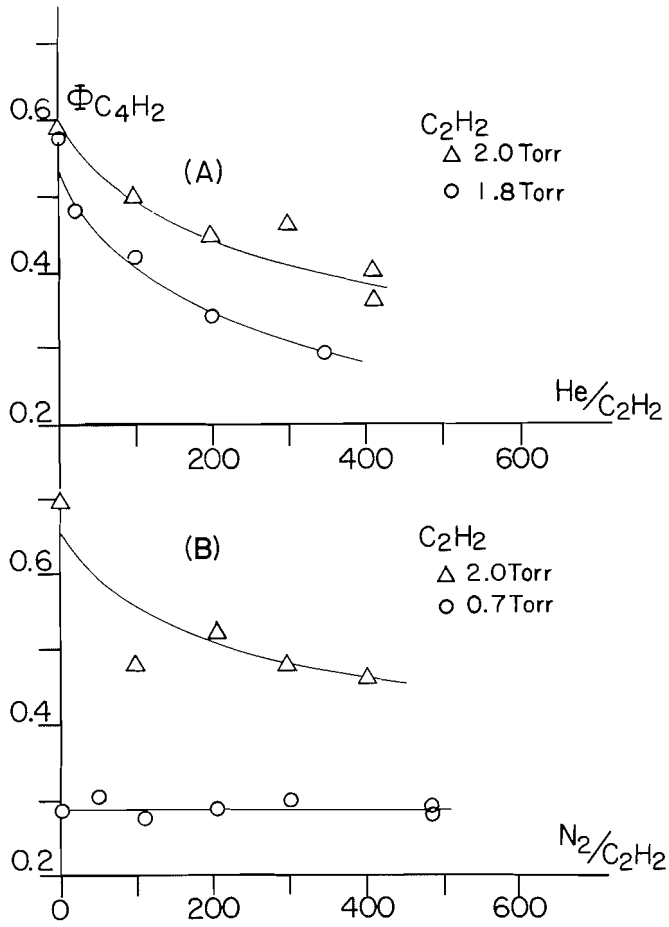

FIG. 5. The quantum yield of diacetylene formation in the 1470 Å acetylene photolysis as a function of (A) He pressure, (B) N_2 pressure; from ref. 20.

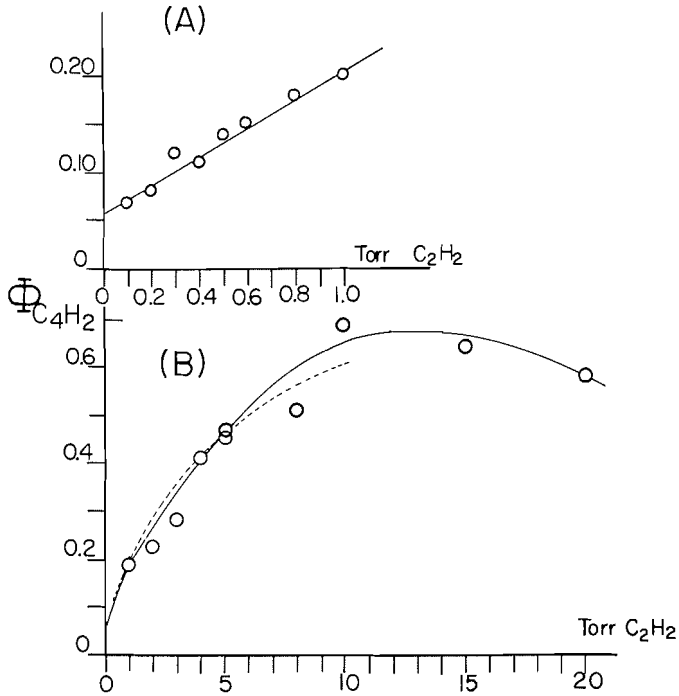

FIG. 6. The quantum yield of diacetylene as a function of acetylene pressure, λ = 1849 Å; from ref. 21.

and more recently in the Titan atmosphere (13). The reaction of C_2H produced from acetylene photolysis by absorption of solar radiation is mainly with H_2 in the Jovian atmosphere since H_2 is the most abundant species.

$$C_2H_2 \xrightarrow{h\nu} C_2H + H$$

$$C_2H + H_2 \rightarrow C_2H_2 + H$$

The two reactions correspond to the sensitized dissociation of H_2 by C_2H_2 since there is no net change in the concentration of acetylene. Acetylene absorbs solar radiation in the spectral region up to 2400 Å where the solar intensity is significantly greater than that below 1000 Å, the region of H_2 absorption. Hence the C_2H reaction plays an important role in the destruction of H_2. On the other hand, in the Titan atmosphere where methane is abundant, the production of C_2H from acetylene photolysis and the subsequent reaction with methane

$$C_2H_2 \xrightarrow{h\nu} C_2H + H$$

$$C_2H + CH_4 \rightarrow C_2H_2 + CH_3$$

is an important destruction mechanism of methane. Strobel estimates (14) that the destruction of CH_4 by the above mech-

Can. J. Chem. Downloaded from www.nrcresearchpress.com by 210.87.254.42 on 09/06/12
For personal use only.

TABLE 1. Reaction rates of C_2H with H_2 and hydrocarbons at room temperature

Reaction	Ratio	Rate constant (10^{-11} cm^3 molec^{-1} s^{-1})	
$C_2H+H_2 \rightarrow C_2H_2+H$	0.0077 ± 0.0007^a	0.023 ± 0.002^d	0.017^e
	0.0049^b	0.015^d	1.2 ± 0.3^f
$C_2H+CH_4 \rightarrow C_2H_2+CH_3$	0.032 ± 0.002^a	0.10 ± 0.006^d	0.12 ± 0.02^g
			0.48 ± 0.1^f
$C_2H+C_2H_6 \rightarrow C_2H_2+C_2H_5$	0.240 ± 0.015^c	0.72 ± 0.05^d	0.65 ± 0.04^g
$C_2H+C_3H_8 \rightarrow C_2H_2+C_3H_7$	0.469 ± 0.041^c	1.4 ± 0.1^d	—
$C_2H+C_2H_2 \rightarrow C_4H_2+H$	1	3	3.1 ± 0.2^b
			5^e

[a] From ref. 20.
[b] From ref. 19.
[c] From ref. 21.
[d] Calculated from the ratios assuming 3×10^{-11} cm^3 molec^{-1} s^{-1} for $C_2H + C_2H_2$.
[e] From ref. 18.
[f] From ref. 24.
[g] From ref. 25.

Can. J. Chem. Downloaded from www.nrcresearchpress.com by 210.87.254.42 on 09/06/12
For personal use only.

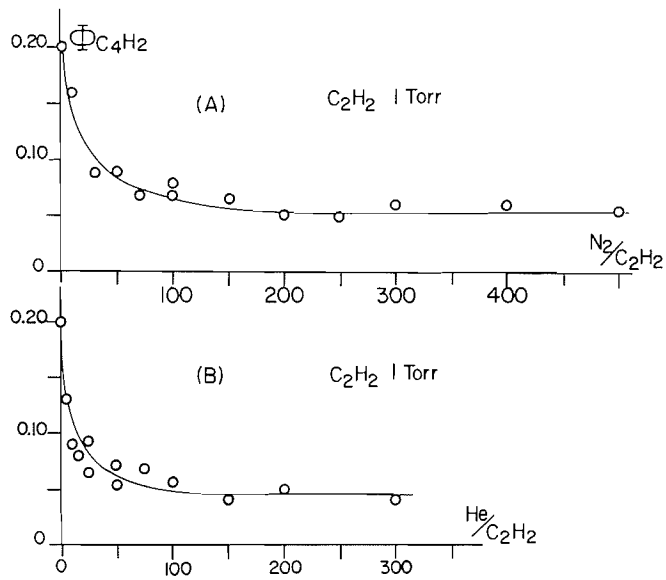

FIG. 7. The effect of the addition of N_2 and He on $\phi_{C_4H_2}$, λ = 1849 Å; from ref. 21.

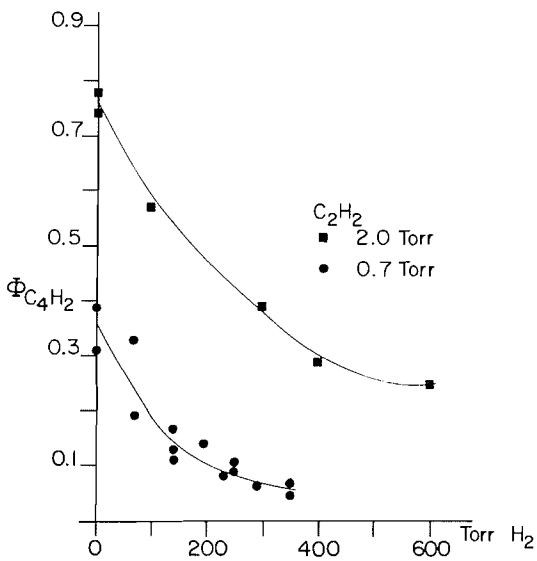

FIG. 8. The quantum yield of diacetylene formation in the 1470 Å photolysis of C_2H_2 as a function of partial pressure of H_2.

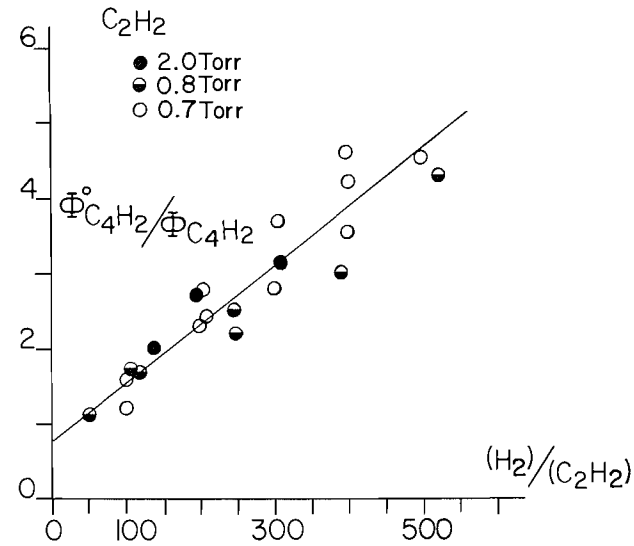

FIG. 9. The plot of the ratio of the quantum yield of diacetylene without and with H_2 as a function of $(H_2)/(C_2H_2)$. The least-squares analysis of the slope gives the rate constant ratio of 130 ± 11 for processes [5] to [4]. See text.

TABLE 2. Relative rates of reaction of C_2H with H_2 and hydrocarbons in the Titan atmosphere[a]

Molecule	Rate constant cm^3 molec^{-1} s^{-1} at 170 K[b]	Mixing ratio[c]	Relative rate
CH_4	7×10^{-13}	3×10^{-2}	1
C_3H_8	1.4×10^{-11}	2×10^{-5}	1.3×10^{-2}
C_2H_6	7.2×10^{-12}	2×10^{-5}	0.7×10^{-2}
C_2H_2	3×10^{-11}	2×10^{-6}	3×10^{-3}
H_2	4.1×10^{-15}	$\sim10^{-3}$	2×10^{-4}

[a] From ref. 21.
[b] Calculated assuming activation energies of 2.9 and 0.5 kcal mol^{-1} for H_2 and CH_4 respectively and no activation energy for other hydrocarbons, from ref. 26.
[c] From refs. 13 and 27.

anism is just as important as the photolysis of methane by solar radiation if the quantum yield for C_2H production from acetylene photolysis is 0.06 in the 1450–2000 Å region, the most effective wavelength region of solar radiation absorbed by acet-

ylene since radiation below 1450 Å is absorbed by methane. Table 2 shows the relative rates of C_2H with H_2 and hydrocarbons present in the Titan atmosphere. The main reaction route of C_2H is the destruction of CH_4 to form methyl radicals, which combine with each other to form ethane. Subsequently propane may be generated by the acetylene catalyzed dissociation of ethane. Small amounts of diacetylene found in the Titan atmosphere (13) are probably formed by $C_2H + C_2H_2$ as shown in Table 2.

It has been suggested that the photolysis of acetylene may produce $C_2X^1\Sigma_g^+$. It is known that $C_2X^1\Sigma_g^+$ reacts with H_2 and CH_4 (23). However, it is not known what products are formed from these reactions, the information needed for more detailed understanding of acetylene photochemistry of the Jovian and Titan atmospheres.

1. H. OKABE. Photochemistry of small molecules. Wiley, New York. 1978.
2. M. ZELIKOFF and L. M. ASHENBRAND. J. Chem. Phys. **24**, 1034 (1956).
3. S. TAKITA, Y. MORI, and I. TANAKA. J. Phys. Chem. **72**, 4360 (1968); **73**, 2929 (1969).
4. M. TSUKADA and S. SHIDA. Bull. Chem. Soc. Jpn. **43**, 3261 (1970).
5. S. TSUNASHIMA and S. SATO. Bull. Chem. Soc. Jpn. **41**, 2281 (1968).
6. S. SHIDA and M. TSUKADA. Bull. Chem. Soc. Jpn. **43**, 2740 (1970).
7. D. E. MILLIGAN, M. E. JACOX, and L. ABOUAF-MARGUIN. J. Chem. Phys. **46**, 4562 (1967).
8. M. JINGUJI, C. A. MCDOWELL, and P. RAGHUNATHAN. J. Chem. Phys. **61**, 1489 (1974).
9. H. OKABE. J. Chem. Phys. **62**, 2782 (1975).
10. K. H. BECKER, D. HAAKS, and M. SCHURGERS. Z. Naturforsch. Teil A, **26**, 1770 (1971).
11. L. J. STIEF, V. J. DECARLO, and R. J. MATALONI. J. Chem. Phys. **42**, 3113 (1965).
12. A. TOKUNAGA, R. F. KNACKE, and T. OWEN. Astrophys. J. **209**, 294 (1976).
13. W. C. MAGUIRE, R. A. HANEL, D. E. JENNINGS, V. G. KUNDE, and R. E. SAMUELSON. Nature, **292**, 683 (1981).
14. D. F. STROBEL. Planet Space Sci. **30**, 839 (1982).
15. E. ABRAMSON, C. KITTRELL, J. L. KINSEY, and R. W. FIELD. J. Chem. Phys. **76**, 2293 (1982); L. E. BRUS. J. Mol. Spectrosc. **75**, 245 (1979).
16. H. OKABE and V. H. DIBELER. J. Chem. Phys. **59**, 2430 (1973).
17. S. HAMAI and F. HIRAYAMA. J. Chem. Phys. **71**, 2934 (1979).
18. W. LANGE and H. Gg. WAGNER. Ber. Bunsenges. Physik. Chem. **79**, 165 (1975).
19. A. H. LAUFER and A. M. BASS. J. Phys. Chem. **83**, 310 (1979).
20. H. OKABE. J. Chem. Phys. **75**, 2772 (1981).
21. H. OKABE. J. Chem. Phys. Submitted.
22. R. W. WETMORE and H. F. SCHAEFER III. J. Chem. Phys. **69**, 1648 (1978).
23. L. PASTERNACK and J. R. MCDONALD. Chem. Phys. **43**, 173 (1979); V. M. DONNELLY and L. PASTERNACK. Chem. Phys. **39**, 427 (1979).
24. A. M. RENLUND, F. SHOKOOHI, H. REISLER, and C. WITTIG. Chem. Phys. Lett. **84**, 293 (1981).
25. A. H. LAUFER. J. Phys. Chem. **85**, 3828 (1981).
26. R. L. BROWN and A. H. LAUFER. J. Phys. Chem. **85**, 3826 (1981).
27. T. OWEN. Sci. Am. **246**, 98 (1982).
28. T. NAKAYAMA and K. WATANABE. J. Chem. Phys. **40**, 558 (1964).

Can. J. Chem. Downloaded from www.nrcresearchpress.com by 210.87.254.42 on 09/06/12
For personal use only.

Photoisomerizations of protonated 5-methylhex-3-en-2-one and 4-methylpent-2-enoic acid. Evidence for charge localization during photoisomerization

RONALD F. CHILDS,[1] TINA DICLEMENTE, EUNICE F. LUND-LUCAS, TIMOTHY J. RICHARDSON, AND CAROL V. ROGERSON

Department of Chemistry, McMaster University, Hamilton, Ont., Canada L8S 4M1

Received July 5, 1982

This paper is dedicated to Professor Harry E. Gunning on the occasion of his 65th birthday

RONALD F. CHILDS, TINA DICLEMENTE, EUNICE F. LUND-LUCAS, TIMOTHY J. RICHARDSON, and CAROL V. ROGERSON. Can. J. Chem. **61**, 856 (1983).

The photoisomerizations of protonated 5-methylhex-3-en-2-one and 4-methylpent-2-enoic acid have been examined. In each case a relatively rapid *cis/trans* isomerization about the carbon–carbon partial double bond and a slower conversion to protonated dihydrofuran **2H** or protonated lactone **5H**, respectively, were observed. The transformation of the acyclic cations to the five-membered ring cations was shown to occur by a photo-initiated, intramolecular hydride shift from the γ to β carbon atom. This shift is fully in accord with an excited state twisting/charge localization model for the excited states of these systems. Control experiments and the thermal chemistry of these ions is described.

RONALD F. CHILDS, TINA DICLEMENTE, EUNICE F. LUND-LUCAS, TIMOTHY J. RICHARDSON et CAROL V. ROGERSON. Can. J. Chem. **61**, 856 (1983).

On a étudié les isomérisations photochimiques de la méthyl-5 hexèn-3 one-2 protonée et de l'acide méthyl-4 pentanoique-2. On a observé dans chaque cas une isomérisation *cis/trans* relativement rapide autour de la double liaison partielle carbone–carbone et une transformation plus lente en dihydrofurane protoné **2H** ou en lactone protonée **5H** respectivement. On montre que la transformation des cations acycliques en cations de type cycle à cinq chainons se produit par l'intermédiaire d'un glissement d'hydrure intramoléculaire initié photochimiquement à partir de l'atome de carbone en γ vers l'atome de carbone en β. Ce glissement est en parfait accord avec un modèle de localisation de charge déformant de l'état excité pour les états excités de ces systèmes. On décrit des expériences de vérification et la chimie thermique de ces ions.

[Traduit par le journal]

Can. J. Chem. Downloaded from www.nrcresearchpress.com by 210.87.254.40 on 09/06/12
For personal use only.

Protonated α, β-unsaturated enones, enals, carboxylic acids, and imines undergo photoinduced *E/Z* isomerizations about the carbon–carbon and either carbon–oxygen or carbon–nitrogen partial double bonds (1–4). These photoisomerizations, which would appear to involve singlet states, proceed with high quantum efficiencies, e.g. eqs. [1] and [2], (3, 4).

[1] 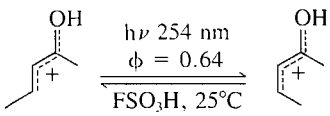

[2] 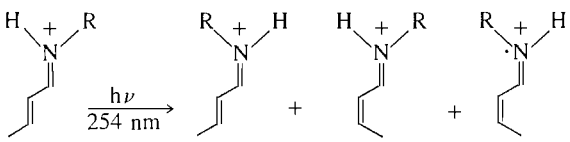

The photoisomerizations shown in eqs. [1] and [2] parallel the *E/Z* isomerizations of the protonated Schiff base derivatives of retinal involved in the chemistry of vision (5). On the basis of molecular orbital calculations, Salem and Bruckmann (6) have suggested that twisting about the C(11)—C(12) double bond of the π,π* excited singlet state of the visual pigments is accompanied by a major change in charge distribution. This involves movement of the positive charge from the nitrogen atom, where it is largely centered in the ground state, to the other end of the molecule. A comparable charge redistribution could occur during the photoisomerization shown, for example, in eq. [1]. In this case a twisted excited state in which the positive charge is largely localized on the β-carbon might be expected, eq. [3].

[3] 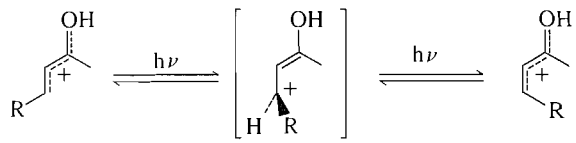

The twisted structure shown in [3] can be regarded as a secondary cation. If R were a substituent such as an isopropyl group, it is conceivable that a hydride shift from the γ to β carbon might occur. This would result in the formation of a tertiary cation which could subsequently undergo several possible dark reactions. These include bonding between the γ and β carbons to form a protonated cyclopropyl ketone, bonding of the carbon and oxygen atom with the formation of a furan derivative, or a reverse hydride shift to give the starting material. In order to examine such possibilities we have investigated the photoisomerizations of protonated 5-methylhex-3-en-2-one, **1H**, and 4-methyl-2-pentenoic acid.

Results

Protonation and thermal control experiments

The protonation of **1** and subsequent thermal isomerization to **2H** in a variety of acids has been reported by Brouwer *et al.* (7). We have found directly comparable results when using FSO_3H as the acid, eq. [4].

[4] 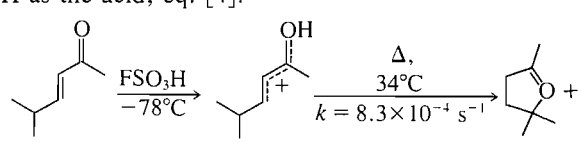

1 **1H** **2H**

[1]Author to whom correspondence should be addressed.

Can. J. Chem. Downloaded from www.nrcresearchpress.com by 210.87.254.40 on 09/06/12
For personal use only.

With FSO_3D as a solvent **1D** was observed to rearrange to **2D** with incorporation of a single deuterium at C3, eq. [5]. The selectivity of this deuterium incorporation was clearly shown in the ^1H nmr spectra of **2D**, where the signal due to the C3 proton was a broadened triplet of relative intensity one while the resonance attributed to the C4 protons was a doublet of relative intensity two. No deuterium incorporation could be detected in **1D** during the course of the isomerization and further deuterium exchange of **2D** was slow in FSO_3D at room temperature.

[5] 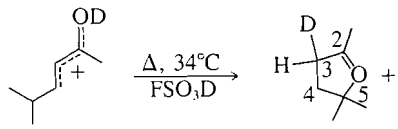

1D **2D**

The protonated cyclopropyl ketone **3H** is a potential photoproduct of **1H**. Pittman and McManus (8) have reported that **3** very rapidly rearranges to **2H** when dissolved in 90% H_2SO_4. Using FSO_3H/SO_2ClF as the acid, it was possible to protonate **3** at −78°C and observe **3H**. The ^1H nmr spectrum of **3H** (Table 1) was consistent with its assigned structure (9). At −50°C, **3H** isomerized to a mixture of **2H** and **1H** in a ratio of 1:2.4.

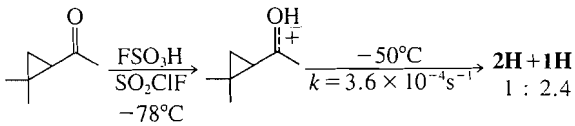

3 **3H**

The acid **4** was cleanly protonated upon dissolution in FSO_3H to give **4H**. This cation was stable at room temperature, but on heating to 60°C partially isomerized to **5H**. This latter species was identified on the basis of the similarity of its ^1H nmr spectrum to that of **2H**. Other competing reactions of **4H** occurred at 60°C which limited the yield of **5H** obtained. These other products have not been fully characterized (10). In CF_3SO_3H these competing side reactions did not occur, and **4H** was cleanly converted to **5H**.

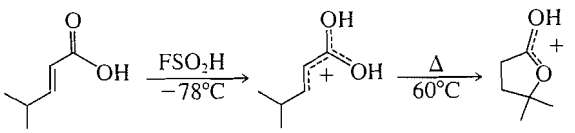

4 **4H** **5H**

Photoisomerizations of 1H and 4H

The uv spectrum of **1H** exhibited a strong absorption band with a maximum at 278 nm. Irradiation (254 nm) of a FSO_3H solution of **1H** at −70°C led to the formation of two products. The composition of the irradiated solutions was determined by low temperature ^1H nmr spectroscopy conducted directly on the irradiated solutions. The cation **2H** was identified as one of the photoproducts of **1H**. The second product formed and detected was **6H**, the *cis*-isomer of **1H**. The latter ion was readily identified by its ^1H nmr spectrum, Table 1, which displayed the characteristic coupling constant of 11 Hz between H(3) and H(4) (1). No thermal isomerizations of **1H** or **6H** occurred under the conditions used for this photoreaction. At higher temperatures, **6H** was found to isomerize thermally to **2H**, with a first order rate constant of 2.0×10^{-4} s^{-1} at +2°C ($\Delta G^{\ddagger}$ = 20.3 kcal/mol).

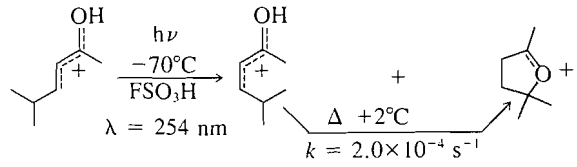

1H **6H** **2H**

The photoisomerization was followed as a function of time and the results are shown in Fig. 1.[2] As can be seen from this figure, the relative concentration of **6H** rose to a maximum after some five to six hours of irradiation and subsequently decreased to zero. The final and only product observed after 24 h irradiation was **2H**. As is usual with these photoreactions in FSO_3H, the material balance was excellent.

Careful examination of the ^1H nmr spectra obtained during the photoisomerization of **1H** failed to reveal any detectable (<10%) amounts of the protonated cyclopropyl ketone **3H**. While **3H** was shown to be thermally stable at −70°C, the temperature at which the photoreactions were carried out, it was found to photoisomerize to a mixture of **1H**, **2H**, and **6H** under the same conditions as used in the irradiation of **1H**.

The quantum yield for the conversion of **1H** to **6H** was measured using a relative method and a value of 0.37 ± 0.05 (−70°C) found. Removing the dissolved oxygen in the FSO_3H solutions by sparging with argon had no apparent effect on the photochemical efficiency of this reaction.

Irradiation of **1D** in FSO_3D at −70°C led to the formation of **6D** and eventually **2D**. Deuterium incorporation at C3 of **2D** was clearly apparent from the ^1H nmr spectrum of the resulting solution. The resonance at 3.78 ppm attributed to the C3 proton appeared as a broadened triplet of only half the intensity of the doublet at 2.39 ppm associated with the methylene group on C4.

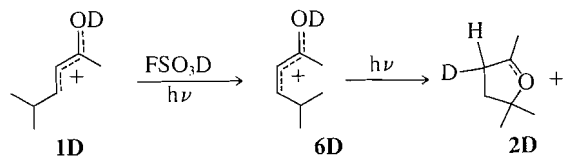

1D **6D** **2D**

The protonated carboxylic acid **4H** (λ_{max} = 240 nm) was irradiated at −70°C in FSO_3H (254 nm). The products were shown to be the *cis* isomer **7H** and protonated furan **5H** by ^1H nmr spectroscopy. As with the protonated ketone **1H**, the *cis* isomer **7H** was produced rapidly and **5H** less efficiently, Fig. 2. The *cis* isomer **7H** was shown to be thermally stable under the reaction conditions. At 0°C, **7H** isomerized to **5H**, $k=1.8\times10^{-4}$ s^{-1}; $\Delta G^{\ddagger}$ = 20.6 kcal/mol.

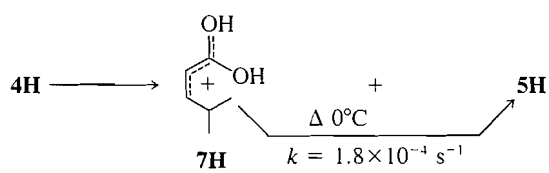

Discussion

The overall photochemical transformations of protonated ketone **1H** and acid **4H** are similar. These are relatively efficient

[2]This type of experiment assumes the lamp intensity to be constant.

TABLE 1. Proton chemical shifts of cations[a]

Compound	Chemical shift, ppm						Coupling constants, Hz			
	H1	H2	H3	H4	H5	H6	$J_{2,3}$	$J_{3,4}$	$J_{4,5}$	$J_{5,6}$
1H	2.92		6.78 d	8.52 dd	3.05 m	1.23 d		17.75	6	7
2H		(2.84)	3.78 t	2.39 t	(1.78)			8		
3H	2.70 m	(1.70,1.64)	2.70 m	(2.94)[b]		—	—	—	—	—
4H	—	6.21 d	8.17 dd	2.68 m	(1.16) d		16	7	7	—
5H			3.50 t	2.53 t	(1.77)		—	8	—	—
6H	2.94	—	6.73 d	7.64 t	—	1.18 d	—	11	11	6
7H		6.07 d	7.30 dd	3.43 m	(1.13) d	—	12	12	7	—

[a]Solvent FSO_3H; $(CH_3)_4N^+BF_4^-$ used as internal standard taken as δ 3.10; chemical shifts in brackets refer to methyl group resonances; d, doublet; t, triplet; m, multiplet.
[b]Acetyl group methyl resonance.

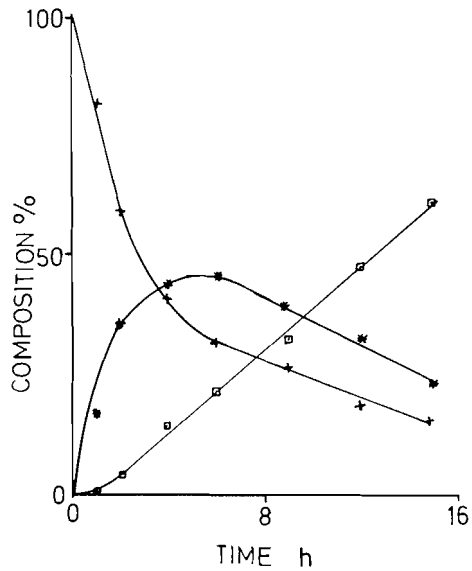

FIG. 1. Photoisomerization of **1H** as a function of irradiation time.

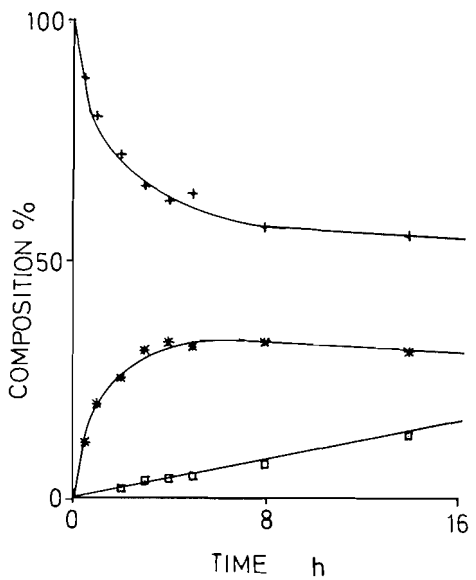

FIG. 2. Photoisomerization of **4H** as a function of irradiation time.

cis/trans isomerizations about the carbon–carbon partial double bonds and less efficient closures to the cyclic cations **2H** and **5H**, respectively. The thermal control experiments described above preclude the possibility that these reactions are thermally induced.

It has not been possible to observe emission from any of the protonated carbonyl compounds described, and there is no direct evidence for the nature of the excited state involved in these reactions. The absence of any effect of molecular oxygen on the reaction suggests that either singlet states or short lived triplet states are involved. Protonation of a carbonyl group raises the energy of n,π^* states, and π,π^* states are expected to be the lowest energy states (11).

The photochemically induced formation of these cyclic products from protonated α,β-unsaturated carbonyl compounds represents a new type of reaction characteristic of these systems. Other protonated enones studied previously have not undergone a comparable ring closure. For example, protonated pent-3-en-2-one or crotonic acid do not form cyclic cations even on prolonged irradiation. It is clear that the additional pair of methyl substituents on the cations **1H** and **4H** is important in facilitating this ring closure reaction.

The formation of protonated furan derivatives can be accounted for by a photochemically induced hydride shift from the tertiary γ-carbon to β-vinyl carbon. The tertiary cation so produced could then undergo reaction with the enol oxygen and lead eventually to the observed cyclic products.

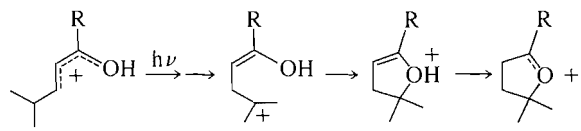

R = CH_3 or OH

Such a pathway for the production of the protonated furan should proceed equally well from both the *cis* and *trans* carbon–carbon double bond isomers. This would indeed seem to be the case with the protonated acids **4H** and **7H**, Fig. 2, where **5H** is produced at the outset of the reaction; however, it is not the result which prevails with the protonated ketones **1H** and **6H**. It is apparent from the changes in composition which occur as the duration of irradiation is increased (Fig. 1) that a lag exists in the formation of **2H**. The relative concentration of **6H** reaches a maximum and then drops in such a way that the ratio of **1H** to **6H** approaches a constant value of 2:3. These observations are consistent with a mechanistic scheme in which a photoequilibrium is established between **1H** and **6H** and a somewhat less efficient photochemical conversion of **6H** to **2H**, eq. [6]. There is ample precedent for the establishment of

Can. J. Chem. Downloaded from www.nrcresearchpress.com by 210.87.254.40 on 09/06/12
For personal use only.

a photostationary state between the *cis* and *trans* isomers of a protonated enone (1, 3), and indeed the observed quantum yield for the conversion of **1H** to **2H** is very similar to that found for protonated 3-penten-2-one at the same temperature. However, the preferential conversion of **6H** rather than **1H** to **2H** raises questions about the hydride shift sequence proposed above.

[6] $$\mathbf{1H} \underset{254\ nm}{\overset{h\nu}{\rightleftharpoons}} \mathbf{6H} \longrightarrow \mathbf{2H}$$

The photochemical conversion of the *cis* isomer **6H** to **2H** suggests this reaction could proceed by a photo-initiated hydride transfer to oxygen, eq. [7]. Such a reaction, which may be compared to the photoenolization of the *cis* isomer of the unprotonated ketone (12) and other related enones (13), would produce the oxygen protonated dienol **8H**. This species would be expected to be very short lived in FSO_3H and be converted to **2H** by protonation C3, proton loss from oxygen, and further protonation at C4 (14). If a "photoenolization" type process were operative, then deuterium incorporation at both C3 and C4 of **2H** would be expected to occur when the reaction is carried out in FSO_3D. This is not the case, and in FSO_3D irradiation of **1D** leads only to **2D** in which a single deuterium atom is incorporated at C3. This result effectively excludes the "photoenolization" type reaction sequence and demonstrates that intramolecular migration of the hydrogen from the γ to β carbon must occur during the transformation of **6D** to **2D**.

[7] 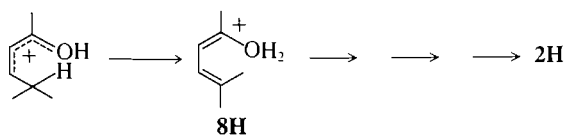

8H

The question remains as to why the photo-conversion of **6H** to **2H** is much more efficient than the comparable conversion of **1H** to **2H**. It is possible that a conformational difference exists between **1H** and **2H**. For bonding to occur between a positive centre at C5 and oxygen, it is essential that the C2—C3 bond have an *s-cis* configuration. On the basis of calculations reported for the π, π* excited state energy surfaces of acrolein (15), a substantial barrier to rotation about the C2—C3 bond of **1H** and **6H** would be expected in their singlet excited states. Thus the ground state conformation about the C2—C3 bond of **6H** and **1H** would be expected to be maintained in their excited states. Confirmation that the origin of the difference in the efficiency of conversion of **1H**, **6H** to **2H** derives from a ground state conformational effect is evident from the results obtained with the protonated acid. In this case, as has been pointed out above, the *trans* and *cis* isomers **4H** and **7H** are converted to **5H**. In these protonated acids the two oxygens on C1 remove the possibility of two conformations about the C1—C2 bond.

Definitive information on the ground state conformations of protonated enones is lacking. It is possible that **1H** prefers to exist in an *s-trans* conformation while **6H** could have a higher proportion of the *s-cis* conformer. Models indicate that **6H** is a highly congested cation in either conformation and it would seem unlikely that it is completely planar. This conclusion is supported by the anomalously high chemical shift observed for the C4 proton resonance of **6H** as compared to other comparable protonated enones and enals, indicating that the fraction of positive charge at C4 of **6H** is diminished relative to other protonated enones.

In conclusion, the results we have obtained indicate that a hydride shift from the γ to β carbon of an appropriately substituted protonated α,β-unsaturated carbonyl compound can occur on photo-excitation. The occurrence of this hydride shift is dependent on the substituents on the carbon. In the present cases two methyl groups on the γ-carbon allow this shift to occur in competition with the efficient *cis/trans* isomerizations about the carbon—carbon partial double bond. The occurrence of the hydride shift is apparent in the formation of protonated dihydrofuran derivatives, although the formation of a small amount of a protonated cyclopropyl ketone **3H** cannot be ruled out. At this stage it is not known whether the hydride shift is reversed thermally in competition with protonated dihydrofuran or protonated lactone formation. Deuterium labelled compounds are currently being prepared to investigate these possibilities. Overall we conclude that the occurrence of this hydride shift is consistent with the twisting/charge polarization model of the excited state of protonated carbonyl compounds.

Experimental

General

The ^1H nmr spectra were obtained on Varian EM-390 or Brucker WP-80 instruments. FSO_3H was distilled twice and checked by uv spectroscopy to ensure transparency in the 250 nm region before use. Samples were protonated by adding cooled FSO_3H to weighed amounts of **1** and **4** in nmr tubes cooled in Dry Ice—acetone. Solution was achieved by mixing the contents of the tubes with a thin glass rod.

Purification of 5-methyl-3-hexen-2-one, 1

Commercial samples of **1** (Aldrich Chemical Company) were found to be contaminated with 5-methyl-4-hexen-2-one (20%), and difficulty was experienced in separating the two isomers. The following procedure was adopted. A commercial sample of **1** (2 g) was dissolved in concentrated H_2SO_4 (10 mL) at 0°C and subsequently added to an excess of saturated $NaHCO_3$ solution with stirring at 0°C. The aqueous solution was extracted with CH_2Cl_2 (3 × 15 mL), the CH_2Cl_2 solution dried (K_2CO_3), and the solvent removed to give an oil. Purification by glpc using a Carbowax column gave pure **1**.

4-Methyl-2-pentenoic acid, 4

This acid was prepared from 5-methyl-3-hexen-2-one using a procedure identical to that used for the synthesis of 3-methylcrotonic acid from mesityl oxide (16). Yield 30%; ^1H nmr ($CDCl_3$) δ: 1.07 (6H, d, J = 6 Hz, CH_3), 2.43 (1H, m, C4H), 5.73 (1H d, J = 16, C2H), 7.03 (1H, d, d, J = 16 and 8 Hz, C3H).

Photoisomerizations

These were carried out using a Rayonet photoreactor (Southern New England Ultraviolet Co.) and 253.7 nm lamps. The samples, contained in 5 mm quartz nmr tubes, were cooled in a partially silvered quartz Dewar held at −70°C with a FTS Flexicool FC 2084P1 refrigeration unit. The reaction was followed by low temperature ^1H nmr spectroscopy.

Quantum yields were measured using the relative method described previously (3) with protonated 3-penten-2-one as an actinometer.

Acknowledgment

The financial support of the Natural Sciences and Engineering Research Council of Canada is gratefully acknowledged.

1. R. F. CHILDS, E. F. LUND, A. G. MARSHALL, W. J. MORRISEY, and C. V. ROGERSON. J. Am. Chem. Soc. **98**, 5924 (1976).
2. R. F. CHILDS and M. E. HAGAR. Can. J. Chem. **58**, 1788 (1980).

Can. J. Chem. Downloaded from www.nrcresearchpress.com by 210.87.254.40 on 09/06/12
For personal use only.

3. R. F. CHILDS and A. W. COCHRANE. J. Org. Chem. **46**, 1086 (1981).
4. R. F. CHILDS and B. D. DICKIE. J. Chem. Soc. Chem. Commun. 1269 (1981).
5. R. R. BIRGE. Ann. Rev. Biophys. Bioeng. **10**, 315 (1981); R. UHL and E. W. ABRAHAMSON. Chem. Rev. **81**, 291 (1981).
6. L. SALEM and P. BRUCKMAN. Nature, **258**, 526 (1975).
7. D. M. BROUWER, J. A. VAN DOORN, and A. A. KIFFEN. Recl. Trav. Chim. Pays-Bas. **94**, 198 (1975).
8. C. U. PITTMAN, JR, and S. P. MCMANUS. J. Am. Chem. Soc. **91**, 5915 (1969).
9. G. A. OLAH, P. W. WESTERMAN, and J. NASHIMURA. J. Am. Chem. Soc. **96**, 3584 (1973), C. U. PITTMAN, JR, and G. A. OLAH. J. Am. Chem. Soc. **87**, 5123 (1965).
10. G. A. OLAH and M. CALIN. J. Am. Chem. Soc. **90**, 405 (1968).
11. R. F. CHILDS. Rev. Chem. Intermed. **3**, 285 (1980).
12. N. C. YANG and M. J. JORGENSEN. Tetrahedron Lett. 1203 (1964).
13. A. DEFLANDRE, A. L'HEUREUX, A. RIOUEL, and J. LEMAIRE. Can. J. Chem. **54**, 2127 (1976); K. N. WAN and A. C. WEEDON, J. Chem. Soc. Chem. Commun. 1235 (1981).
14. K. E. HINE and R. F. CHILDS. J. Am. Chem. Soc. **95**, 3289 (1973).
15. A. DEVAQUET. J. Am. Chem. Soc. **94**, 3160 (1972); R. R. BIRGE and P. A. LEERMAKERS. J. Am. Chem. Soc. **94**, 8105 (1972); J. F. GRAF and C. P. LILLYA. Mol. Photochem. **9**, 227 (1979).
16. L. I. SMITH, W. W. PRITCHARD, and L. J. SPILLANE. Org. Synth. Collect. Vol. **3**, 302 (1947).

Can. J. Chem. Downloaded from www.nrcresearchpress.com by 210.87.254.40 on 09/06/12
For personal use only.

A kinetic study of the reactions of OH radicals with fluoroethanes. Estimates of C—H bond strengths in fluoroalkanes[1,2]

JEAN-PIERRE MARTIN[3] AND GEORGE PARASKEVOPOULOS

Division of Chemistry, National Research Council of Canada, Ottawa, Ont., Canada K1A 0R9

Received July 5, 1982

This paper is dedicated to Professor Harry E. Gunning on the occasion of his 65th birthday

JEAN-PIERRE MARTIN and GEORGE PARASKEVOPOULOS. Can. J. Chem. **61**, 861 (1983).

A kinetic study of the reactions of OH radicals with a series of fluoroethanes in the gas phase is presented. OH radicals were generated by flash photolysis of H_2O vapor in the vacuum uv ($\lambda > 165$ nm) and were monitored in absorption by time-resolved attenuation of resonance radiation at 308.15 nm [$OH(A^2\Sigma^+ \rightarrow X^2\Pi)$]. The following absolute rate constants (in units of 10^9 cm^3 mol^{-1} s^{-1} at the 95% confidence limit) were determined at 298 K: $k_{CH_2FCH_2F} = 67.7 \pm 7.2$, $k_{CH_2FCHF_2} = 11.0 \pm 1.1$, $k_{CH_3CF_3} = 1.03 \pm 0.26$, $k_{CH_2FCF_3} = 3.10 \pm 0.35$, $k_{CHF_2CF_3} = 1.50 \pm 0.17$.

From a linear correlation of the present and previously published rate constants with bond dissociation energies, the following quantities (in kcal mol^{-1} at 298 K) were estimated to be: $D(CH_3CHF—H) = 96.3 \pm 1.5$, $D(CH_2FCHF—H = 98.8 \pm 1.0$, $D(CF_3CHF—H) = 103.5 \pm 1.0$, $D(CHF_2CF_2—H) = 103.0 \pm 1.5$, and $\Delta H_f^0(CH_3\dot{C}HF) = -18.7 \pm 1.6$, $\Delta H_f^0(CF_3\dot{C}HF) = -162.7 \pm 2.3$.

JEAN-PIERRE MARTIN et GEORGE PARASKEVOPOULOS. Can. J. Chem. **61**, 861 (1983).

Nous présentons une étude par cinétique en phase gazeuse des réactions entre les radicaux hydroxyles (OH) et une série d'éthanes fluorés. Les radicaux OH sont générés par photolyse-éclair de vapeur d'eau dans l'uv lointain ($\lambda > 165$ nm) et sont détectés par absorption résolue dans le temps de radiation en résonance à 308.15 nm [$OH(A^2\Sigma^+ \rightarrow X^2\Pi)$].

Nous obtenons les constantes de vitesse absolues suivantes, en unités de 10^9 cm^3 mol^{-1} s^{-1} à 298 K: $k_{CH_2FCH_2F} = 67.7 \pm 7.2$, $k_{CH_2FCHF_2} = 11.0 \pm 1.1$, $k_{CH_3CF_3} = 1.03 \pm 0.26$, $k_{CH_2FCF_3} = 3.10 \pm 0.35$, $k_{CHF_2CF_3} = 1.50 \pm 0.17$. Les écarts-type sont exprimés à un niveau de confiance de 95%.

A partir d'une corrélation linéaire entre la constante de vitesse et l'énergie de dissociation du lien C—H, nous évaluons les quantités suivantes, en kcal mol^{-1} à 298 K, comme suit: $D(CH_3CHF—H) = 96.3 \pm 1.5$, $D(CH_2FCHF—H) = 98.8 \pm 1.0$, $D(CF_3CHF—H) = 103.5 \pm 1.0$, $D(CHF_2CF_2—H) = 103.0 \pm 1.5$, $\Delta H_f^0(CH_3\dot{C}HF) = -18.7 \pm 1.6$, $\Delta H_f^0(CF_3\dot{C}HF) = -162.7 \pm 2.3$.

Introduction

There is considerable interest in the reactions of hydroxyl radicals with hydrocarbons and halocarbons, because of the important role that these reactions play in combustion and in the chemistry of the atmosphere. As a result, rate constants for reactions of OH radicals with a variety of classes of compounds have been determined for use in numerical modeling of these processes. The data, often verified in several laboratories (1), are of sufficient accuracy that empirical relationships may now be drawn between structure and reactivity (see, for example, ref. 2). Such relationships, when established, may allow estimates of rates to be made based on bond properties, and conversely, may also help in estimating needed bond properties from kinetic measurements.

In a previous paper (3), we have reported absolute rate constants for hydrogen abstraction by OH radicals from fluorocarbons, and have presented a linear correlation between the logarithm of the room-temperature rate constants and the corresponding C—H stretching frequencies for several alkanes and fluoroalkanes. In the case of CH_3CH_2F, with non-equivalent C—H bonds, the correlation indicated that hydrogen abstraction occurred mainly from the α position of CH_3CH_2F. This was later confirmed by product analysis (4).

In the present paper, we have extended our previous work to include the fluoroethanes and have explored correlations of rate constants with stretching frequencies and with bond dissociation energies. Thus, we report absolute rate constants at 298 K for the reactions of OH with CH_2FCH_2F, CH_2FCHF_2, CH_3CF_3, CH_2FCF_3, and CHF_2CF_3 in the gas phase; these were measured using the flash photolysis – resonance absorption technique. We also present and discuss empirical correlations of the rate constants for alkanes and fluoroalkanes from this and our previous work with the average stretching frequencies $\langle\nu_{C-H}\rangle$ of equivalent C—H bonds, and with bond dissociation energies. From the latter correlation we have estimated plausible values of the bond dissociation energies of $CH_3CHF—H$, $CH_2FCHF—H$, $CF_3CHF—H$, and $CHF_2CF_2—H$, and of enthalpies of formation in the gas phase at 298 K, for the radicals $CH_3\dot{C}HF$ and $CF_3\dot{C}HF$.

Experimental

The apparatus and experimental technique have been described in detail before (5, 6), and will be mentioned here briefly. The apparatus consists of a fast flash photolysis system coupled to a spectrophotometric detection system. Hydroxyl radicals were produced by flash photolysis of small pressures of water vapour (0.2–0.8) Torr in the vacuum uv ($\lambda > 165$ nm). The flash lamp was operated at discharge energies of 60 and 150 J. The OH concentration was monitored by following the time-resolved attenuation of the OH resonance radiation ($Q_1^{(3)}$ rotational line of the (0,0) band of the $A^2\Sigma^+ \rightarrow X^2\Pi$ transition) produced by a microwave discharge in a flowing low pressure Ar/H_2O mixture, as described before (5, 6). Signal averaging was used to improve the signal-to-noise ratio. Rate measurements were made in the range $(0.5–5) \times 10^4$ s^{-1}, by using 24–100 flashes.

The reactant gases were analyzed by gc/ms using a Finnigan gas chromatograph – mass spectrometer. Quantitative determinations of the impurities were made on 5-ft columns packed with Porapak QS or Porapak N and were based on peak areas. The purity levels (and the major impurities) were as follows: CH_2FCH_2F, 98.38% (CH_2FCHF_2,

[1]NRCC No. 20651.

[2]Part IX of Rates of OH radical reactions. For part VIII, see ref. 37.

[3]NRCC Research Associate, 1980–1982. Present address: Alcan International Ltd., Jonquiere, P.Q., Canada G7S 4K8.

Can. J. Chem. Downloaded from www.nrcresearchpress.com by 210.87.254.6 on 09/06/12
For personal use only.

Can. J. Chem. Downloaded from www.nrcresearchpress.com by 210.87.254.6 on 09/06/12
For personal use only.

1.53%; a pentafluorobutane isomer, 0.09%); CH_2FCHF_2, >99.50% (CO_2, trace; CHF_2CHF_2, 0.14%; an octafluorobutane isomer, 0.18%; a heptafluoroisobutane isomer, 0.15%); CH_3CF_3, 99.6% (CO_2, 0.005%; $CFClCH_2$, 0.40%); CH_2FCF_3, >99.7% (CO_2, trace; CH_3CF_3, 0.10%; CHF_2CF_3, 0.16%; CF_2ClCF_2Cl, 0.02%; CF_2CFCl, trace; $CHClCF_2$, trace; $CHClFCF_3$, trace; CH_2ClCF_3, trace); CHF_2CF_3, 99.24% (CH_3CF_3, 0.62%; CH_3CHF_2, 0.06%; CH_2FCF_3, 0.08%). The olefin impurity (CH_2CFCl) in CH_3CF_3 was completely removed by shaking the fluorocarbon for 1/2 hour with concentrated sulfuric acid containing a few crystals of $KMnO_4$. No significant olefin impurity was present in the other fluorocarbons because there was no difference in rate constants determined before and after treatment with H_2SO_4. The reagent gases and H_2O were subjected to several freeze–pump–thaw cycles and were further degassed at 77 K before each experiment. He >99.999% pure was used directly from the cylinder.

Results

Various aspects of the experimental conditions, procedure, and treatment of the data are given in refs. 5 and 6. The effect of multiple flashes (i.e. accumulation of reaction products) on the measured rates was tested by flashing a given mixture 2, 4, 8, 16, and 32 times and comparing the resulting rates. Although no significant difference was detected, only 8 flashes per mixture were used.

The initial OH concentration estimated from the initial absorption of the resonance radiation (5, 6) was $\sim(5-8) \times 10^{-12}$ mol cm^{-3} and $(1-2) \times 10^{-11}$ mol cm^{-3} for flash energies of 60 and 150 J respectively. The experiments were carried out under pseudo-first-order conditions with [fluoroethane] $\gg$ [OH]. The pseudo-first-order rate constant, k_I, was obtained from the slopes of the linear plots of ln [OH] against time (5, 6). The values of k_I obtained for varying fluorocarbon concentrations are related to the second-order rate constant, k_{II}, by the equation $k_I = \alpha + k_{II}$[fluorocarbon]. Plots of k_I against the fluorocarbon concentration are shown in Fig. 1 for all the fluorocarbons studied. The second-order rate constants, k_{II}, were evaluated from the slopes of these plots by weighted least-squares fits of the above equation to the points with weights $w = 1/\sigma^2$, where σ is the error in k_I evaluated as described before (5, 7). The small intercepts observed in Fig. 1 cannot be ascribed to a single predominant cause; their significance has been discussed in detail in refs. 5 and 6. The measured values of k_{II} are given in Table 1.

The experiments were done at pressures of 20–600 Torr depending on the amount of fluorocarbon required to obtain the desired rate. For the faster reactions the pressure was made up with He when necessary. The measured rates were found to be independent of pressure for all the fluorocarbons studied.

Evaluation of potential systematic errors

As discussed previously (5), the overall accuracy of our measurements, based on analysis of the flash period, electronic bandwidth, system linearity, and the analog-to-digital converter resolution, is ±5%. The principal potential sources of significant systematic errors are, therefore, secondary reactions of OH radicals (*a*) with radicals formed by photolysis of the reactant by the flash, (*b*) with the radical products of the initial reaction, and (*c*) with impurities which react with OH faster than the fluorocarbon reactant. Each of these possibilities will now be examined in detail.

The fluoroethanes are completely transparent to the photolysis light (9) ($\lambda > 165$ nm) and therefore no photodecomposition with consequent radical formation takes place.

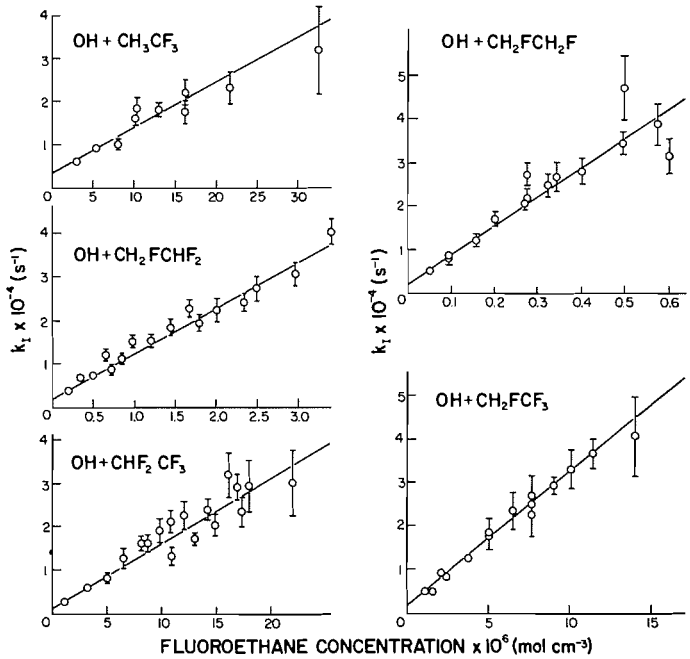

FIG. 1. Plots of pseudo-first-order rate constant, k_I, against the fluoroethane concentration.

TABLE 1. Absolute rate constants, k_{II}, for the reactions of OH radicals with fluoroethanes at 298 K

Reactant	$10^{-9} \times k_{II}$[a] (cm^3 mol^{-1} s^{-1})	Number of experiments	Reference
CH_2FCH_2F	67.7±7.2	16	This work
CH_2FCHF_2	11.0±1.1	16	This work
	29.5±3.0		10
CH_3CF_3	1.03±0.26	10	This work
	0.90±0.60		10
CH_2FCF_3	3.10±0.35	18	This work
	4.16±0.54		10
CHF_2CF_3	1.50±0.17	18	This work
	3.01±0.60		10

[a]The indicated uncertainties are: for this work the 95% confidence limits calculated from the standard deviation and Student's *t* distribution (8), for ref. 10 those stated by the authors.

The maximum effect on the measured rates of the secondary reaction of OH with the radical product of the initial reaction was estimated by numerical simulation of the system (6). Assuming that $k_{OH+radical} \approx 1 \times 10^{14}$ cm^3 mol^{-1} s^{-1} (i.e., the collision rate) it was calculated that the measured rate constants would be increased as a result of the secondary reaction by 3.5% and 7% for [OH] $\approx 1 \times 10^{-11}$ mol cm^{-3} and [OH] $\approx 2 \times 10^{-11}$ mol cm^{-3}, respectively. That secondary reactions of OH with radicals were negligible was confirmed by experiments in which the measured rates were not affected within the experimental error, when the OH concentration was changed by a factor of 4, effected by varying both the pressure of H_2O (0.2–0.8 Torr) and the flash discharge energy (60 and 150 J).

In all the fluoroethanes studied (except CH_3CF_3), the small amounts of impurities react with OH slowly enough so as not to have any significant effect on the measured rate constants at the concentrations present. In the case of CH_3CF_3 the CH_2CFCl impurity (0.4%) caused a 20-fold increase in the rate until it

Can. J. Chem. Downloaded from www.nrcresearchpress.com by 210.87.254.6 on 09/06/12
For personal use only.

was completely removed by treatment with concentrated sulfuric acid, as described in the previous section. As a precaution, we tested all the fluoroethanes studied for undetected olefinic impurities by measuring rates on samples treated with sulfuric acid. In all other cases no significant change in rate was found, indicating the absence of olefin contamination, or, in the case of CH_2FCF_3, that the traces of CF_2CFCl and $CHClCF_2$ present were too small to have any significant effect on the rate measurements.

Discussion

Comparison of rate constant values

Clyne and Holt (10) have reported rate parameters for four of the fluoroethanes studied in this work. They used the discharge flow technique with resonance fluorescence detection of OH. Their values are listed in Table 1 together with ours. With the exception of CH_3CF_3 for which the two determinations agree well, their values for CH_2FCF_3, CHF_2CF_3, and CH_2FCHF_2 are 1.4 to 2.7 times larger than ours. The obvious sources of systematic errors, discussed in the previous section, would all lead to an increase rather than a decrease of the measured rate constant. The reactions of OH with fluoroalkanes are comparatively slow and therefore the presence of even small amounts of fast reacting impurities could increase the observed rate constants. The detection in the present work of minute amounts of olefinic impurities in two fluoroethanes indicates the need for careful analysis and purification of the samples used for rate determinations. Some of the rate constants which appear too large in ref. 10 may have been affected by such impurities.

Correlation of rate constants with bond properties

Several attempts have been made to correlate rate constants for hydrogen abstraction by OH with various bond properties (2, 3, 11–13). A general expression (2) relating rate constants with temperature, molecular parameters, and bond dissociation energies (experimental or estimated), allows estimation of rate constants in many cases to within a factor of 3 but does not work well with halocarbons. Other, more specific correlations have also been examined (11–13), in which a function of the room temperature rate constant k (i.e. log k, log (k/n), log $(k/\sqrt{n})$, where n is the number of hydrogen atoms in the reacting molecule) has been correlated with the bond dissociation energy, D_{C-H}. Of these, a linear plot of log (k/n) at 300 K against D_{C-H} values for some simple saturated organics gives the better correlation (13).

We have presented, in a previous paper (3), a linear correlation between either the log $(k/\sqrt{n})$ or log k and the "isolated" stretching frequencies, ν^{is}_{C-H}, for several alkanes and fluoroalkanes (ν^{is}_{C-H} values are listed by McKean (14) and are obtained by substitution in the molecule of all hydrogens except one by deuterium). The two fluoroethanes studied in this work for which ν^{is}_{C-H} values are available, i.e., CH_3CF_3 (ν^{is}_{C-H} = 3010.0 cm^{-1} (15)), and CHF_2CF_3 (ν^{is}_{C-H} = 3000.7 cm^{-1}, measured in this laboratory on a Nicolet Model 7199 FTIR spectrometer), fit very well on the lines of both log k and log $(k/\sqrt{n})$ given in Fig. 3 of ref. 3.

Before proceeding further, it should be noted that in these correlations and those to be described below, which involve rate constants at one temperature, the assumption is made that for a homologous series of compounds the preexponential factors remain constant after correction for the number of equivalent C—H bonds, and that the difference in reactivity reflects differences in activation energies which can be correlated sometimes with bond properties. The preexponential factors (per C—H bond) reported by Greiner (16) for a series of alkanes are essentially constant. Furthermore, from the successful correlations (3, 13) involving alkanes and fluoroalkanes described above, it appears that the assumption is indeed justified for the reactions of OH with these compounds.

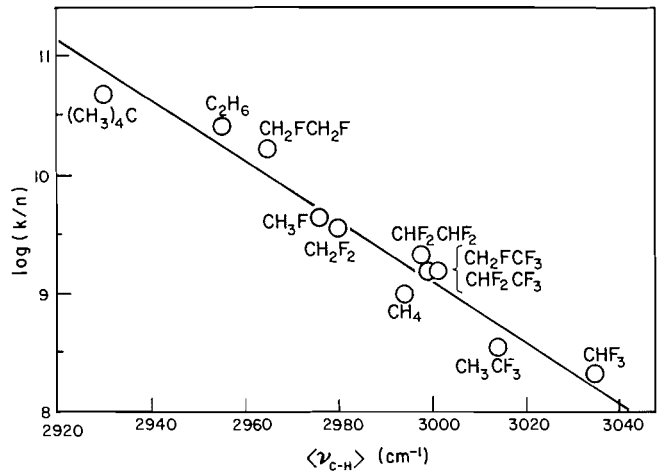

FIG. 2. Correlation of log (k/n) with the average stretching frequency $\langle\nu_{C-H}\rangle$ for selected alkanes and fluoroalkanes with equivalent C—H bonds. The straight line was obtained by least-square fits to the points except that for CHF_3 (see text): slope = $-2.56 \pm 0.25 \times 10^{-2}$, intercept = 85.8 ± 7.5.

TABLE 2. Data used in the correlation of log (k/n) with $\langle\nu_{C-H}\rangle$ in Fig. 2

Compound	log $(k/n)^a$	$\langle\nu_{C-H}\rangle^b$ (cm^{-1})	Sources of ν_{C-H}
CH_4	8.99±0.04	2994	17
C_2H_6	10.42±0.05	2955	19
$(CH_3)_4C$	10.66±0.05	2930	20
CH_3F	9.64±0.04	2976	17
CH_2F_2	9.55±0.05	2980	17
CHF_3	8.32±0.21	3035	21
CH_2FCH_2F	10.23±0.05	2965	22
CH_3CF_3	8.54±0.11	3014	23
CH_2FCF_3	9.19±0.05	2999	24
CHF_2CHF_2	9.32±0.12	2998	25
CHF_2CF_3	9.18±0.05	3000.7	This work

[a]The rate constants were obtained in this laboratory (this work, refs. 3, 5, and 18) except for that of CHF_2CHF_2 which was taken from ref. 10.

[b]The average frequencies, $\langle\nu_{C-H}\rangle$, were calculated by averaging the C—H stretching frequencies from assigned spectra given in the references; the degeneracies were used as weights and the effects of *gauche* and *trans* isomers were taken into account when applicable.

Correlation of log (k/n) with average stretching frequencies

Correlations involving "isolated" stretching frequencies, although capable of distinguishing between non-equivalent C—H bonds, have limited predictive usefulness, because such frequencies are difficult to obtain experimentally, and hence are not available for many compounds. A potentially more useful correlation, from this point of view, may be with the average stretching frequencies $\langle\nu_{C-H}\rangle$ from a set of equivalent C—H bonds. The concept was introduced by Bernstein (17) who showed that it correlates with bond lengths and with bond dissociation energies. The $\langle\nu_{C-H}\rangle$ values are obtained by aver-

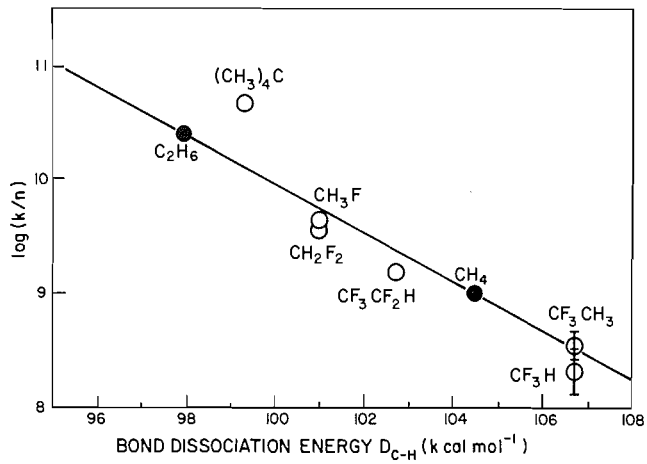

FIG. 3. Correlation of log (k/n) with the bond dissociation energy for selected alkanes and fluoroalkanes. The straight line was drawn connecting the points for CH_4 and C_2H_6 (see text).

aging (using the degeneracies as weights) the C—H stretching frequencies from assigned, gas phase, infrared, and Raman spectra of the corresponding compounds. In Fig. 2, log (k/n) is plotted against $\langle\nu_{C-H}\rangle$ for paraffins and fluoroparaffins with equivalent C—H bonds. The data used and their sources are given in Table 2. The plot is reasonably linear and allows estimates of rate constants to be made to within better than a factor of 2.

The value of ν_{C-H} for CHF_3 is known only approximately because of Fermi resonance (14, 21), the magnitude of which is uncertain (14). The value of $\nu_{C-H} = 2990\ cm^{-1}$ (14) used in our previous paper may have been too low due to too large a correction applied to ν_{C-H} (14). For this reason the point for CHF_3 was placed in Fig. 2 using the experimental value $\nu_{C-H} = 3035\ cm^{-1}$ (21) without correction. The point lies close to the straight line, but in view of the uncertainty involved, it was not used in determining the slope of the straight line in Fig. 2.

Correlation of log (k/n) with bond dissociation energies

Such a correlation is shown in Fig. 3, where log (k/n) is plotted against the bond dissociation energies, D_{C-H}, for alkanes and fluoroalkanes. The straight line in the figure was drawn connecting the points for CH_4 and C_2H_6 for which D_{C-H} values appear to be better established (26–28). The other points in the plot were placed using recommended D_{C-H} values. Although it is, perhaps, somewhat surprising that the alkanes and fluoroalkanes, which are not strictly homologous, fall on a single line in Fig. 3, the correlation seems to indicate that the fluorine atom does not substantially alter the reactivity of a C—H bond outside of its effect on D_{C-H}.

Estimates of bond dissociation energies were made using the correlation line in Fig. 3 and the experimental values of log (k/n), and are listed in Table 3 together with the recommended values in the literature. As may be seen in the table the estimated D_{C-H} values (except that for *neo*-C_5H_{12}) agree well with the literature values obtained from kinetic studies that involve different assumptions (26). The agreement supports the validity of the empirical correlation and hence the estimated bond dissociation energies of CH_3CHF—H, CH_2FCHF—H, CF_3CHF—H, and CHF_2CF_2—H for which there are no reported values. The $D(CH_3CHF—H) = 96.3$ kcal mol^{-1} was estimated using the rate constant of hydrogen abstraction from the α position of CH_3CH_2F which is 85% of the overall rate constant (3, 4).

TABLE 3. Comparison of estimated bond dissociation energies with literature values

Bond	D_{C-H} (kcal mol^{-1}) Estimated[a]	Literature value[b]	Reference
CH_3—H	—	104.5±1.0[c]	26, 27, 28
CH_3CH_2—H	—	98.0±1.0	26, 27
$(CH_3)_3CCH_2$—H	97.0±1.5	99.3±1.0	26
CH_2F—H	101.6±1.0	101.0±2.0	26, 29
CHF_2—H	102.0±1.0	101.0±2.0	26, 29
CF_3—H	107.6±1.5	106.7±1.0	30
CH_3CHF—H	96.3±1.5	—	—
CH_2FCHF—H	98.8±1.0	—	—
CF_3CH_2—H	106.7±1.5	106.7±1.1	31
CF_3CHF—H	103.5±1.0	—	—
CHF_2CF_2—H	103.0±1.5	—	—
CF_3CF_2—H	103.7±1.0	102.7±1.0	32

[a]The quoted uncertainties are approximate and are based on the 1 kcal uncertainty of D_{C-H} for CH_4 and C_2H_6.

[b]The literature values are usually recommended values based often on several determinations.

[c]The value of $D(CH_3—H)$ is based on critical reviews of the earlier data (26, 27) and on recent determinations (28).

The reported value $D(neo\text{-}C_5H_{11}—H) = 99.3$ kcal mol^{-1} (26) is significantly higher than that estimated from the correlation (97.0 kcal mol^{-1}); it is also higher than $D(C_2H_5—H) = 98.0$ kcal mol^{-1} (26, 27). On the basis of the activation energies for hydrogen abstraction from *neo*-C_5H_{12} and C_2H_6 by OH (1.68 and 2.45 kcal mol^{-1} (16), respectively) it may be expected that $D(neo\text{-}C_5H_{11}—H) < D(C_2H_5—H)$ and not the opposite. It could be that $D(C_2H_5—H)$ is substantially higher than reported (26, 27) (i.e. >99 kcal mol^{-1}); however, since the D_{C-H} value of ethane appears to be the better established (26, 27), there may be a need for reexamination of the D_{C-H} of neopentane.

The point for CHF_3 lies close to the straight line in Fig. 3. Thus, the present correlation does not support a suggestion made by Baulch and Campbell, in a recent review of gas-phase reactions of OH radicals (33), that the room temperature rate constant of OH + CHF_3 may be higher than the reported value (3) by about an order of magnitude.

From $D(CH_3CF_2—H) = 99.5 \pm 1.0$ kcal mol^{-1} reported by Pickard and Rodgers (34), it was estimated using the correlation that the rate constant for hydrogen abstraction from the α position of CH_3CHF_2 by OH is $\sim 1.23 \times 10^{10}$ cm^3 mol^{-1} s^{-1}. This corresponds to about 55–63% abstraction from the α position, based on the range of values of the total rate constant (3, 35), 2.23×10^{10} to 1.94×10^{10} cm^3 mol^{-1} s^{-1}.

Finally, from the estimated $D(CH_3CHF—H) = 96.3 \pm 1.5$ kcal mol^{-1} and $D(CF_3CHF—H) = 103.5 \pm 1.0$ kcal mol^{-1}, and the reported heats of formation in the gas phase at 298 K, $\Delta H_f^0(CH_3CH_2F) = -62.9 \pm 0.4$ kcal mol^{-1} (36), $\Delta H_f^0(CF_3CH_2F) = -214.1 \pm 2.0$ kcal mol^{-1} (36), and $\Delta H_f^0(H) = 52.1 \pm 0.001$ kcal mol^{-1} (27), we estimated the heats of formation of the radicals $\Delta H_f^0(CH_3\dot{C}HF) = -18.7 \pm 1.6$ kcal mol^{-1}, and $\Delta H_f^0(CF_3\dot{C}HF) = -162.7 \pm 2.3$ kcal mol^{-1}.

Acknowledgments

We thank M. E. Bednas for the mass-spectrometric analysis,

Can. J. Chem. Downloaded from www.nrcresearchpress.com by 210.87.254.6 on 09/06/12
For personal use only.

Dr. D. R. Strobach of E. I. du Pont de Nemours and Company for providing a sample of CH_2FCF_3, and Dr. D. L. Singleton for useful discussions.

1. R. ATKINSON, K. R. DARNALL, A. C. LLOYD, A. M. WINER, and J. N. PITTS, JR. Adv. Photochem. **11**, 375 (1979).
2. J. HEICKLEN. Int. J. Chem. Kinet. **13**, 651 (1981).
3. W. S. NIP, D. L. SINGLETON, R. OVEREND, and G. PARASKEVOPOULOS. J. Phys. Chem. **83**, 2440 (1979).
4. D. L. SINGLETON, G. PARASKEVOPOULOS, and R. S. IRWIN. J. Phys. Chem. **84**, 2339 (1980).
5. R. P. OVEREND, G. PARASKEVOPOULOS, and R. J. CVETANOVIĆ. Can. J. Chem. **53**, 3374 (1975).
6. R. OVEREND and G. PARASKEVOPOULOS. J. Phys. Chem. **82**, 1329 (1978).
7. R. J. CVETANOVIĆ, R. P. OVEREND, and G. PARASKEVOPOULOS. Proceedings of the Symposium on Chemical Kinetics Data for the Upper and Lower Atmosphere, Warrenton, Va, Sept. 15–18, 1974; Int. J. Chem. Kinet. Symp. No. 1, 249 (1975).
8. R. J. CVETANOVIĆ, D. L. SINGLETON, and G. PARASKEVOPOULOS. J. Phys. Chem. **83**, 50 (1979).
9. P. SAUVAGEAU, J. DOUCET, R. GILBERT, and C. SANDORFY. J. Chem. Phys. **61**, 391 (1974).
10. M. A. A. CLYNE and P. M. HOLT. J. Chem. Soc. Faraday Trans. 2, **75**, 582 (1979).
11. C. J. HOWARD and K. M. EVENSON. J. Chem. Phys. **64**, 197 (1976).
12. J. S. GAFFNEY and S. Z. LEVINE. Int. J. Chem. Kinet. **11**, 1197 (1979).
13. R. ATKINSON. Int. J. Chem. Kinet. **12**, 761 (1980).
14. D. C. MCKEAN. Chem. Soc. Rev. **7**, 399 (1978); D. C. MCKEAN, J. L. DUNCAN, and L. BATT. Spectrochim. Acta, **29**A, 1037 (1973).
15. D. C. MCKEAN, H. BÜRGER, and G. PAWELKE. J. Mol. Struct. **55**, 99 (1979).
16. N. R. GREINER. J. Chem. Phys. **53**, 1070 (1970).
17. H. J. BERNSTEIN. Spectrochim. Acta, **18**, 161 (1962).
18. G. PARASKEVOPOULOS and W. S. NIP. Can. J. Chem. **58**, 2146 (1980).
19. G. E. HANSEN and D. M. DENNISON. J. Chem. Phys. **20**, 313 (1952).
20. K. SHIMIZU and H. MURATA. Bull. Chem. Soc. Jpn. **30**, 487 (1957).
21. A. RUOFF, H. BÜRGER, and S. BIEDERMANN. Spectrochim. Acta, **27**A, 1359 (1971); C. C. COSTAIN. J. Mol. Spectrosc. **9**, 317 (1962).
22. P. KLABOE and J. R. NIELSEN. J. Chem. Phys. **33**, 1764 (1960).
23. H. BÜRGER, H. NIEPEL, and G. PAWELKE. Spectrochim. Acta, **36**A, 7 (1980).
24. J. R. NIELSEN and C. J. HALLEY. J. Mol. Spectrosc. **17**, 341 (1965); D. F. HARNISH and R. P. HIRSCHMANN. Appl. Spectrosc. **24**, 28 (1970).
25. P. KLABOE and J. R. NIELSEN. J. Chem. Phys. **32**, 899 (1960).
26. J. A. KERR. Chem. Rev. **66**, 465 (1966).
27. S. W. BENSON. Thermochemical kinetics. 2nd ed. Wiley, New York. 1976. pp. 289, 309.
28. M. H. BAGHAL-VAYJOOEE, A. J. COLUSSI, and S. W. BENSON. J. Am. Chem. Soc. **100**, 3214 (1978); Int. J. Chem. Kinet. **11**, 147 (1979).
29. J. A. KERR and D. M. TIMLIN. Int. J. Chem. Kinet. **3**, 427 (1971).
30. K. C. FERGUSON and E. WHITTLE. J. Chem. Soc. Faraday Trans. 1, **68**, 295 (1972) and references therein.
31. E. C. WU and A. S. RODGERS. J. Phys. Chem. **78**, 2315 (1974).
32. B. S. EVANS and E. WHITTLE. Int. J. Chem. Kinet. **13**, 59 (1981) and references therein.
33. D. L. BAULCH and I. M. CAMPBELL. *In* Gas kinetics and energy transfer. Vol. 4. *Edited by* P. G. Ashmore and R. J. Donovan. Specialist Periodical Reports, The Chemical Society, London. 1981. p. 137.
34. J. M. PICKARD and A. S. RODGERS. J. Am. Chem. Soc. **99**, 691 (1977).
35. C. J. HOWARD and K. M. EVENSON. J. Chem. Phys. **64**, 4303 (1976).
36. S. S. CHEN, A. S. RODGERS, J. CHAO, R. C. WILHOIT, and B. J. ZWOLINSKI. J. Phys. Chem. Ref. Data, **4**, 441 (1975).
37. G. PARASKEVOPOULOS, D. L. SINGLETON, and R. S. IRWIN. J. Phys. Chem. **85**, 561 (1981).

Can. J. Chem. Downloaded from www.nrcresearchpress.com by 210.87.254.6 on 09/06/12
For personal use only.

The photochemistry of phenanthrene-substituted molecules[1,2]

HOWARD E. ZIMMERMAN AND GUO-SHENG WU
The Chemistry Department, University of Wisconsin, Madison, WI 53706, U.S.A.

Received July 5, 1982

This paper is dedicated to Professor Harry E. Gunning on the occasion of his 65th birthday

HOWARD E. ZIMMERMAN and GUO-SHENG WU. Can. J. Chem. **61**, 866 (1983).

The photochemistry of 3-methyl-3-(9-phenanthryl)-1-butene was examined as part of an investigation into the effects of having two π chromophores of widely different energies participating in a di-π-methane rearrangement. We observed both direct and sensitized reactivity with quantum yields $\phi^{DIR} = 0.043$ and $\phi^{SENS} = 0.053$. The primary reaction product from both direct and sensitized photolyses was 1,1-dimethyl-2-(9-phenanthryl)cyclopropane. However, in practice this product was obtained only from sensitized irradiations where it was almost completely unreactive. The triplet reactivity is unusual in that the typical free rotor decay exhibited by triplets does not lead to inhibition of di-π-methane reactivity in this case. This point is discussed. The intersystem crossing efficiency of the phenanthryl vinyl methane reactant was obtained from the sensitization of biacetyl phosphorescence by the phenanthrene derivative at varying biacetyl concentrations. This was $\phi_{isc} = 0.86$. This result and the bracketing relationships signify that essentially all of the direct irradiation rearrangement utilizes T_1. In addition, from these experiments, $^3k_{d(tot)}$ was determined as 5.8×10^3 s^{-1}. Similarly, $^3k_r = 250$ s^{-1} which is the slowest di-π-methane rearrangement encountered thus far. The rearrangement of the cyclopropane product to form 2-methyl-4-(9-phenanthryl)-1-butene was also investigated. $^1\phi$ was determined to be 0.091 and $^3\phi$ was determined as 0.00072. Thus the interesting contrast was encountered in which the di-π-methane rearrangement proceeds from the triplet while the rearrangement of the cyclopropane product proceeds most efficiently from the singlet.

HOWARD E. ZIMMERMAN et GUO-SHENG WU. Can. J. Chem. **61**, 866 (1983).

On a étudié la photochimie du méthyl-3-(phénanthryl-9-)-3 butène-1 comme un aspect de la recherche portant sur les effets de la presénce de deux chromophores π d'énergies très différentes participant à la transposition di-π-méthane. Nous avons observé les deux réactivités directe et sensibilisée avec des rendements quantiques $\phi^{DIR} = 0{,}043$ et $\phi^{SENS} = 0{,}535$. Le diméthyl-1,1 (phénanthryl-9)-2 cyclopropane et le produit primaire de réaction à partir de la photolyse directe et de la photolyse sensibilisée. Cependant, en fait, on obtient ce produit uniquement à partir des irradiations faites en présence de photosensibilisateurs où il est presque complètement inactif. La réactivité du triplet est inhabituelle en ce sens que la désintégration par centrifiguration libre typique exhibée par les triplets ne conduit pas à une inhibition de la réactivité du di-π-méthane dans ce cas. On discute de ce point. On retrouve l'efficacité du croisement intersystème du réactif phénanthrylvinyl méthane à partir de la sensibilisation de la phosphorescence du biacétyle par le dérivé du phénanthrène à des concentrations variables de biacétyle. Cette efficacité est de $\phi_{cis} = 0{,}86$. Ce résultat et la relation d'encadrement signifient qu'essentiellement toutes le transpositions par irradiation directe utilisent T_1. De plus, on a déterminé à partir de ces expériences que $^3k_{d(tot)}$ est de $5{,}8 \times 10^3$ s^{-1}. De la même façon, on a trouvé $^3k_r = 250$ s^{-1} ce qui correspond à la plus lente transposition di-π-méthane à jamais observée. On a également étudié la transposition du produit du cyclopropane qui donne le méthyl-2 (phénanthryl-9)-4 butène-1. On a trouvé que $^1\phi$ est de 0,091 et $^3\phi$ est de 0,00072. Ainsi, on a trouvé un contraste intéressant à savoir: la transposition di-π-méthane se produit à partir du triplet tandis que la transposition du produit du cyclopropane se fait d'une manière plus efficace à partir du singulet.

[Traduit par le journal]

Introduction

In our investigations dealing with the di-π-methane rearrangement (2*c*), we encountered some unusual effects in which the presence of a low energy π chromophore led to an unusually slow-reacting excited state in the di-π-methane rearrangement (2*a*). In pursuing the generality of this phenomenon, we have utilized phenanthryl-substituted systems. A system of particular interest was 3-methyl-3-(9-phenanthryl)-1-butene **1** because of the presence of the very low energy phenanthryl moiety and also because of the similarity of this reactant to the phenyl relative we had previously (3) investigated.

Results

Synthesis of photochemical reactants and potential photoproducts

The desired di-π-methane reactant **1** was synthesized as outlined in Scheme 1. Additionally, two potential photoproducts, 1,1-dimethyl-2-(9-phenanthryl)cyclopropane **2** and 3-methyl-3-(9-phenanthryl)-1-butene **3** were prepared, and these syntheses are included in Scheme 1. Details are to be found in the experimental section.

*Exploratory photolysis of the 3-methyl phenanthryl butene **1***

It was observed that direct irradiation under preparative conditions led to an isomeric phenanthryl butene **3**. Comparison with authentic material, synthesized as outlined in Scheme 2, showed this photoproduct to be 2-methyl-4-(9-phenanthryl)-1-butene **3**. Since mechanistic reasoning suggested that it was unlikely that this conversion was a one-step, single photon process, irradiations were carried out to shorter conversions. Indeed, under these conditions a new photoproduct dominated the reaction mixture. This proved identical with the synthetically prepared 1,1-dimethyl-2-(9-phenanthryl)cyclopropane **2**. These runs are outlined in Scheme 2 and the experimental section.

In contrast, xanthone sensitized irradiation of the phenanthryl vinyl methane **1** led cleanly to the dimethyl phenanthryl cyclopropane **2** with no observable secondary conversion to 2-methyl-4-(9-phenanthryl)-1-butene **3**. Again, note

[1]This is Paper 135 of our photochemical series. For Paper 134, see ref. 1.

[2]For Papers 128–133, see refs. 2*a*–*f*, respectively.

Can. J. Chem. Downloaded from www.nrcresearchpress.com by 210.87.254.5 on 09/06/12
For personal use only.

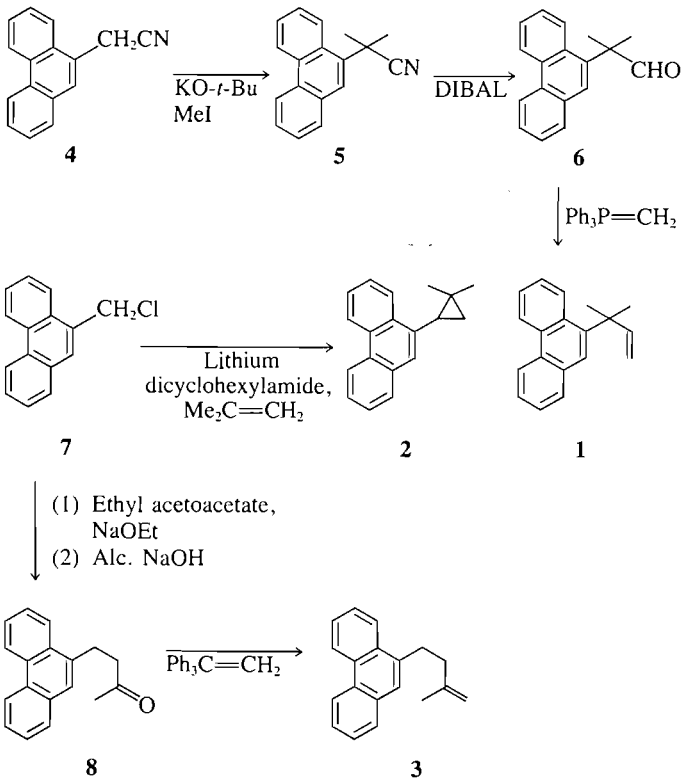

SCHEME 1. Synthesis of 3-methyl-3-(9-phenanthryl)-1-butene **1** and potential photoproducts **2** and **3**.

Scheme 2.

To confirm that direct irradiation of the dimethyl cyclopropane **2** did, indeed, give rise to the 2-methyl-4-(9-phenanthryl)-1-butene **3**, the direct photolysis of cyclopropane **2** was independently carried out and a facile conversion to **3** was observed as depicted in Scheme 2.

A further check (note the experimental section) showed that the direct irradiation of the 2-methyl butene **3** did not lead to its progenitors **1** and **2**.

Still another control was the behavior of phenanthryl cyclopropane **2** on sensitization with xanthone. Only unreacted phenanthryl cyclopropane **2** was found, thus accounting for the sensitized photolyses of phenanthryl vinyl methane **1** giving only phenanthryl cyclopropane photoproduct **2**.

A summary of the photochemical rearrangements is given in Scheme 2.

Reactivity of the vinyl phenanthryl methane 1; quantum yield, rate, and intersystem crossing measurements

Quantum yields were determined using the Black Box apparatus (4) and electronic actinometer (5) described in our earlier publications. All quantum yields were determined with extrapolation to zero conversion, a procedure which proved to be necessary for meaningful efficiencies. Similarly suitable solution filters were used. Thus it was made certain that photoproducts were not absorbing any appreciable fraction of the light. A summary of the quantum efficiencies obtained is included in Scheme 2.

Additional experimental data needed for mechanistic purposes included the intersystem crossing efficiency of the phenanthryl vinyl methane **1** and the rate of decay of its triplet. The

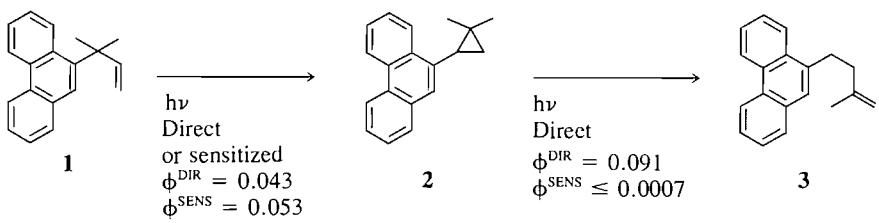

SCHEME 2. Photochemical interconversions of phenanthryl-substituted systems.

method of Wilkinson and DuBois (6) and Sandros (7) has proven useful in our previous efforts (8).

We begin with eq. [1] which gives a linear relationship between the reciprocal of biacetyl phosphorescence and the reciprocal of concentration of biacetyl. Here ϕ_P is the observed phosphorescence emission of biacetyl sensitized by hydrocarbon **1**. BI refers to biacetyl, HC refers to the hydrocarbon, ${}^3k_{d(tot)}$ is the total rate of triplet decay by all processes, τ is the triplet lifetime of the hydrocarbon of interest, k_{ET} is the rate of triplet energy transfer to biacetyl, ϕ_{isc}^{HC} is the quantum yield of intersystem crossing of the hydrocarbon, and ϕ_P^{BI} is the phosphorescence efficiency of biacetyl. It can be seen from this equation that the intercept and slope of a plot of $1/\phi_P$ versus

$$[1] \quad 1/\phi_P = 1/\phi_P^{BI}\,[1/\phi_{isc}^{HC} + {}^3k_{d(tot)}^{HC}/\phi_{isc}^{HC}k_{ET}[BI]]$$

$1/[BI]$ are given as in eqs. [2*a*] and [2*b*]. Also the ratio of slope to intercept affords the ratio of the triplet decay rate to the bimolecular rate of energy transfer; note eq. [2*c*]. Here K is an instrumental constant, and REF refers to a reference compound

$$[2a] \quad \text{Intercept} = K(1/\phi_{isc}^{HC})$$

$$[2b] \quad \text{Slope} = K({}^3k_{d(tot)}^{HC}/\phi_{isc}^{HC}k_{ET})$$

$$[2c] \quad \text{Slope/intercept} = {}^3k_{d(tot)}^{HC}/k_{ET} = k_{ET}\,\tau$$

$$[2d] \quad \text{Intercept (HC)/intercept (REF)} = \phi_{isc}^{REF}/\phi_{isc}^{HC}$$

whose intersystem crossing efficiency is known.

For this treatment, biphenyl was used as a standard of known (7, 8) intersystem crossing efficiency. Here $\phi_{isc}^{REF} = 0.81$. Use of eq. [2*d*] led to a value of $\phi_{isc}^{HC} = 0.86$ for the phenanthryl vinyl methane **1**.

Similarly, eq. [2*c*] was utilized with the assumption that the rate of energy transfer is given by the rate of diffusion. This seems valid, since the triplet energy of biacetyl T_1(BI) is 56 kcal/mol compared with 66.5 kcal/mol observed for T_1 of the phenanthryl vinyl methane **1**. It has been noted (9) that triplet transfer processes which are 10 kcal/mol or more exothermic usually are diffusion controlled. Additionally, a bimolecular rate of diffusion of 2.3×10^{10} s^{-1} was calculated from the modified Debye equation (10).[3]

[3]The form $k_{diff} = 8RT/2000\,n$ was used.

Can. J. Chem. Downloaded from www.nrcresearchpress.com by 210.87.254.5 on 09/06/12
For personal use only.

TABLE 1. Summary of quantum yields and rates

Quantum yields

Compound	Additive	Quantum yield
Phenanthryl vinyl methane **1**	None	0.043
Phenanthryl vinyl methane **1**	Xanthone	0.053
Phenanthryl cyclopropane **2**	None	0.091
Phenanthryl cyclopropane **2**	Xanthone	≤0.0007

Triplet rates

Compound	Lifetime, μs	$^3k_{d(tot)}$, s^{-1}	ϕ_{isc}	^3k_r, s^{-1}
Biphenyl	28[a]	3.5×10^4	0.81[b]	
Phenanthryl vinyl methane **1**	170	5.8×10^3	0.86	250

[a]Compare ref. 7 which gives a value of 30 μs.
[b]Value taken from ref. 7.

This led to 0.17 milliseconds for the lifetime (τ) of the phenanthryl vinyl methane triplet ^{3}**1**. This corresponds to a rate of decay of $^3k_{d(tot)}$ of 5.8×10^3 s^{-1}.

Finally, with the total rate of decay of T_1 known and with the triplet quantum yield known (i.e. $\phi^{SENS} = 0.053$), it was possible to determine the rate of triplet rearrangement of **1** by use of the relation $^3k_r = {}^3k_{d(tot)}{}^3\phi$. This afforded $^3k_r = 250$ s^{-1}.

The various rate values obtained are summarized in Table 1.

Reactivity of the phenanthryl cyclopropane 2

As noted above, in the direct irradiations of the phenanthryl vinyl methane **1**, it was found that the intermediate phenanthryl cyclopropane **2** was observable only at low conversion. Additionally, independent checks starting with cyclopropane **2** revealed the facile direct rearrangement to afford the 2-methyl phenanthryl butene **3** and also the contrasting lack of reactivity of cyclopropane **2** in sensitized irradiations as suggested by the qualitative exploratory runs described above. Note Scheme 2.

It was desired to obtain a quantitative measure of this behavior. Thus, the quantum yield in the direct irradiation of **2** was determined as 0.091. In xanthone sensitization runs, an upper limit was established as 0.0007 for the quantum yield. These results are included in Scheme 2 and Table 1.

Interpretative discussion

Gross rearrangement mechanisms

A number of aspects of the results deserve comment and interpretation. We begin with the structural details of the two rearrangements uncovered. The transformation of the phenanthryl vinyl methane **1** to the phenanthryl cyclopropane **2** is outlined in qualitative resonance terms in Scheme 3. Also, included in Scheme 3 is the mechanism suggested for the rearrangement of the phenanthryl cyclopropane (i.e. **2**) to afford the 2-methyl phenanthryl butene **3**.

Thus, excitation and intersystem crossing of the phenanthryl vinyl methane **1** affords its triplet ^{3}**1**, effectively the first reactant, as shown in Scheme 3. Application of the usual mechanism for the aryl–vinyl version of the di-π-methane rearrangement (2*c*, 11) to this system leads to the observed phenanthryl cyclopropane **2**.

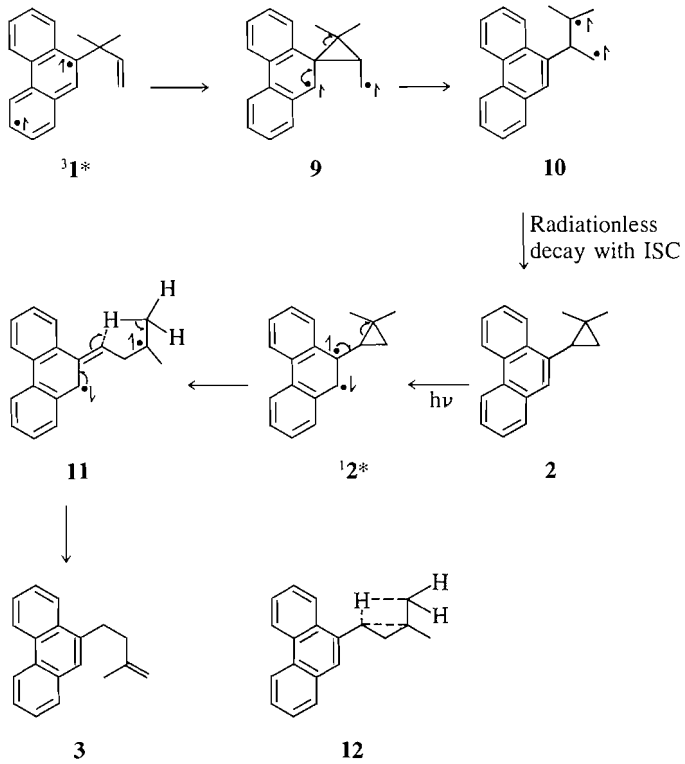

SCHEME 3. Structural aspects of the rearrangement mechanisms.

Also, Scheme 3 outlines a mechanism for conversion of the phenanthryl cyclopropane **2** to the 2-methyl phenanthryl butene **3**. This involves opening of the benzylic bond of the three-membered ring regiospecifically to afford the more stable of two *a priori* possible diradicals, that is, to form diradical **11** in which one odd-electron center is stabilized by being tertiary. The alternative three-ring opening would afford a diradical with one electron center at a primary carbon. Intramolecular hydrogen transfer via a 5-membered ring transition state leads directly to the observed 2-methyl phenanthryl butene product **3**. An alternative mechanism (12, 13) has the ring opening and hydrogen transfer steps concerted so that, as the three-membered ring is in the process of opening, hydrogen transfer begins.[4] This mechanism involves the transfer of the locus of excitation (14)[5] from the phenanthryl moiety to the four-ring, four-electron Hückel cyclic array as depicted by structure **12** in Scheme 3. With a near HOMO–LUMO degeneracy in such an array (16), excitation flow in this direction does, indeed, become exothermic and favorable. Thus the ΔP elements (14, 15) become small for that part of the system which is most diradicaloid and has a local near degeneracy. This general point is discussed further below in connection with reaction multiplicity.

Multiplicity of the rearranging excited states

Having considered the gross, skeletal nature of the reaction

[4]For a summary of some known examples of the rearrangement, see ref. 12. For evidence of concertedness, note ref. 13.

[5]Note ref. 2*e* for a general discussion. For a specific example of energy flow during excited state reaction, see ref. 15.

Can. J. Chem. Downloaded from www.nrcresearchpress.com by 210.87.254.5 on 09/06/12
For personal use only.

mechanisms, we turn to the reaction multiplicities. For the rearrangement of the phenanthryl vinyl methane **1** to afford the phenanthryl cyclopropane **2**, it is clear from the sensitization runs that the triplet when generated does react. Furthermore, the efficiency of the reaction originating with the triplet T_1 in such sensitization reactions proves to be somewhat greater (i.e. $\phi^{SENS} = 0.053$) than that in the direct irradiations ($\phi^{DIR} = 0.043$) where the initial species formed is S_1. At this point one may conclude that in the direct irradiation T_1 is a permissive species undergoing the rearrangement.

To proceed further we need to utilize the intersystem crossing efficiency ($\phi_{isc} = 0.86$) as determined (note Table 1). We use one ($2f$) of the two (1, $2f$) "bracketing relationships" which proved useful in our earlier studies. Note eq. [3]. Using

$$[3a] \quad {}^1\phi \leq \phi^{DIR} - \phi^{SENS}\,\phi_{isc}$$

$$[3b] \quad {}^1\phi \leq (0.043) - (0.053)(0.86) = 0.002$$

the experimentally observed values of the direct and sensitized irradiations and also the determined intersystem crossing efficiency, we conclude in eq. [$3b$] that the intervention of S_1 of phenanthryl vinyl methane **1** is vanishing and, therefore, that the observed photochemistry in the direct irradiations must derive from the triplet.

Contrasting with the photochemistry of the di-π-methane rearrangement of **1** is the photochemical rearrangement of the phenanthryl cyclopropane **2** to afford the 2-methyl phenanthryl butene **3**. Here it is clear that formation of the triplet of **2** by xanthone sensitization leads to no reaction, while the direct irradiation proceeds with a reasonable efficiency (i.e. $\phi^{DIR} = 0.091$). From this we can conclude that it is the singlet which successfully rearranges and that T_1 is unreactive. One likely rationale for the lack of reactivity of the triplet cyclopropane ^{3}**2** is occurrence of a reversible opening to form the triplet counterpart of diradical **11** of Scheme 3. The rearrangement of the singlet via a cyclic array such as defined by species **12** in Scheme 3 would proceed rapidly.

Such behavior would be another example of the exchange integral control of excited state reactivity by multiplicity (17). Thus, for cases with two possible routes along an excited state hypersurface, we have categorized these alternatives as "large K" and "small K" type reactions depending on the magnitude of the exchange integral and thus the singlet–triplet splitting at the critical points along the reaction coordinate. The general rule is that singlet excited states prefer small K reactions while triplets prefer large K mechanisms (17, 18).

In the present instance the singlet process is the cyclic process leading to the 2-methyl phenanthryl butene **3**. To the extent that this is a concerted process (12, 13), the result is in accord with our previous generalization that pericyclic processes tend to have small K values due to a "mismatch" of their highest bonding and lowest antibonding MO's. The triplet process is three-ring opening. Such openings tend to have large K values in analogy to the double-bond twisting case we discussed earlier. This situation is summarized in Fig. 1.

Still another point regarding three-ring opening of the phenanthryl cyclopropane **2** triplet is the analogy of this process to the common "free rotor" energy dissipation of triplets (8). In reversible three-ring opening a molecule breaks and reforms a bond which has both σ and π components, while in the standard free-rotor effect it is a purely π orbital which is reversibly broken. However the analogy is close.

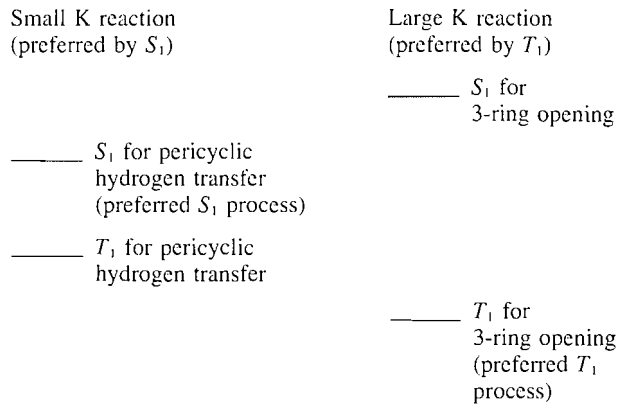

FIG. 1. Large K and small K control of reactivity of the cyclopropane **2**.

Another aspect of interest is the reaction of the phenanthryl vinyl methane **1** by way of T_1 even in the direct irradiations. This signifies that intersystem crossing of the vertical S_1 excited state is more rapid that any rearrangement of S_1. This has analogy in some of the barrelenes. For example, 2,3-naphthobarrelene rearranges, albeit by vinyl–vinyl rather than aryl-vinyl bridging, with analogous rapid intersystem crossing with T_1 being the reactive species in the di-π-methane process (19).

The rates of photochemical rearrangement and related processes

The most remarkable result encountered is the unusually slow rate of rearrangement of the phenanthryl vinyl methane triplet ^{3}**1**: $^3k_r = 250\ s^{-1}$. This is the most slowly rearranging excited state thus far encountered.

Parallel to this slow rate of rearrangement is a slow rate of decay, namely $^3k_{d(tot)} = 5.8 \times 10^3\ s^{-1}$. We note with interest that the decay rate is only slightly greater than the decay rate reported for the phenanthrene triplet itself where $^3k_{d(phen)} = 3 \times 10^3\ s^{-1}$ and τ(phen) = 333 μs (7). Thus, despite a very slow rate of decay, the quantum efficiency of the rearrangement is still reasonable. This is a particularly interesting phenomenon which extends to both singlet and triplet reactivity. Thus, although rates of decay of singlet and triplet excited states range from the present 250 s^{-1} to over $10^{12}\ s^{-1}$, quantum yields for a large variety of reactions remain in the range of 1.0–0.0001 due to the parallelisms between rates of reaction and decay. It appears that there is a fundamental reason for this parallelism. One likely rationale is that the same factors which are responsible for molecular reaction are also involved in molecular decay.

Finally, this is not the first example where particularly small rates of reaction and decay have been observed. In the photochemistry of the corresponding naphthyl vinyl methane ($2a$) the same type of behavior was encountered, except that it was the singlet which was involved. It appears that having a very low energy chromophore, as one of two which interact to rearrange, leads to a lifetime which is characteristic of that low energy chromophore and this type of behavior. Energy is available from the low energy chromophore and deliverable at the sites of bond alteration, but this delivery is slow. The overall excited state lifetime is dominated by the normal lifetime of the low energy chromophore.

Experimental

2-Methyl-2-(9-phenanthryl)propionitrile

To a solution of 10.0 g (89 mmol) of potassium *tert*-butoxide in

Can. J. Chem. Downloaded from www.nrcresearchpress.com by 210.87.254.5 on 09/06/12
For personal use only.

Can. J. Chem. Downloaded from www.nrcresearchpress.com by 210.87.254.5 on 09/06/12
For personal use only.

100 mL of anhydrous ether at −78°C was added a solution of 5.00 g (23 mmol) of 9-phenanthrylacetonitrile (20) and 19.0 g (134 mmol) of methyl iodide in 50 mL of anhydrous ether over 15 min under nitrogen. After an additional 1 hour at −78°C the mixture was stirred at room temperature for 1 hour. Addition of water, ether extraction of the organic phase, washing the organic layer successively with aqueous ammonium chloride, sodium thiosulfate, sodium chloride, and then drying over magnesium sulfate and concentrating *in vacuo*, followed by chromatography on silica gel and elution with hexane, afforded material which was recrystallized from hexane to yield 4.53 g (80%) of 2-methyl-2-(9-phenanthryl)propionitrile, mp 97–97.5°C.

The spectral data were: ir ($CHCl_3$): 3.27 (m), 3.36 (s), 3.40 (s), 3.48 (m), 4.42 (w), 4.46 (s), 5.85 (w), 6.25 (m), 6.53 (w), 6.67 (s), 6.89 (s), 7.19 (s), 7.24 (s), 7.30 (s), 7.94 (s), 8.48 (s), 8.55 (s), 10.0 (m), 10.4 (m), 10.9 (s), 11.2 (s), 13.9 (m), 15.4 (m), 16.1 (m) μ; nmr ($CDCl_3$) δ: 2.08 (s, 6H, 2 CH_3), 7.68–8.04 (m, 6H, arom), 8.68–8.96 (m, 3H, arom); ms *m/e* (245 calcd. for $C_{18}H_{15}N$): 246 (rel. abund. 5.2, M + 1), 245 (40.4, M), 230 (53.1, M − Me), 215 (9.3, M − 2Me), 205 (0.4, M − CH_2CN), 204 (11.1, M − CH_2CNH), 191 (2.7, M − C_3H_4N), 190 (1.1, M − C_3H_5N), 178 (20.3, phenanthrene), 55 (13.7, CH_3 + CH_2 + CN), 54 (0.2, C_3H_4N), 41 (26.4, MeCN), 40 (1.6, CH_2CN). *Anal.* calcd. for $C_{18}H_{15}N$: C 88.13, H 6.16; found: C 88.21, H 6.21.

2-Methyl-2-(9-phenanthryl)propionaldehyde

To 2-methyl-2-(9-phenanthryl)propionitrile (402 mg, 1.64 mmol) in 20 mL of anhydrous hexane at 0°C was added 2.0 mL (2.0 mmol) of 1 *M* diisobutylaluminum hydride in hexane, the mixture stirred for 20 min at 0°C, then 20 min at room temperature, and then refluxed for 24 h. Saturated ammonium chloride (20 mL) was added and the mixture stirred for 30 min followed by addition of 15 mL of 2% sulfuric acid and then hexane, filtration, ether extraction of the aqueous phase, washing the organic phase with brine and then water, drying, and concentrating. The residue was chromatographed on a 2 × 20 cm silica gel column. Elution with 500 mL of 5% ether in hexane followed by recrystallization from 50% aqueous ethanol afforded 213 mg (52%) of 2-methyl-2-(9-phenanthryl)propionaldehyde, mp 66–67°C, along with 83 mg of reactant.

The spectral data for the aldehyde were: ir ($CHCl_3$): 3.31 (s), 3.38 (s), 3.41 (s), 3.48 (s), 3.57 (m), 3.70 (m), 5.78 (s), 6.25 (m), 6.67 (m), 6.78 (s), 6.89 (s), 7.17 (m), 7.24 (m), 7.75 (s), 8.13 (m), 8.69 (m), 9.26 (m), 10.4 (m), 11.0 (s), 12.2 (m), 13.9 (m), 16.1 (m) μ; nmr ($CDCl_3$) δ: 1.64 (s, 6H, 2 Me), 7.64–7.98 (m, 6H, arom), 8.64–8.84 (m, 3H, arom), 9.80 (s, 1H, CHO); ms *m/e* (calcd. for $C_{18}H_{16}O$: 248.1200): 248.1199. *Anal.* calcd. for $C_{18}H_{16}O$: C 87.06, H 6.50; found: C 87.07, H 6.61.

3-Methyl-3-(9-phenanthryl)-1-butene

Ethereal methylenetriphenylphosphorane was prepared from reaction of 19.6 g (50.8 mmol) of methyltriphenylphosphonium bromide in 200 mL of anhydrous ether by addition of 40 mL (60 mmol) of 1.5 *M* n-butyllithium in hexane. After 4 h a solution of 12.4 g (50 mmol) of 2-methyl-2-(9-phenanthryl)propionaldehyde in 50 mL of anhydrous ether was added. Precipitation of triphenylphosphine oxide began immediately. After 2 hours of reflux the mixture was worked up by treatment with water, hexane extraction, washing with brine, water, drying over magnesium sulfate, concentration *in vacuo*, and chromatography on a 2.5 × 95 cm silica gel column packed with hexane. Hexane elution afforded 5.6 g of crude product which was recrystallized from 95% ethanol at low temperature to afford 4.7 g (38%) of 3-methyl-3-(9-phenanthryl)-1-butene, mp 28–29°C. In a second run 4.31 g (44%) of product was obtained from 9.84 g of reactant.

The spectral data were: ir ($CHCl_3$): 3.26 (m), 3.32 (m), 3.37 (s), 6.14 (m), 6.25 (m), 6.67 (m), 6.94 (m), 7.19 (m), 7.30 (w), 7.46 (w), 8.00 (m), 8.69 (w), 8.93 (w), 9.18 (w), 9.95 (s), 11.2 (s), 13.9 (m), 16.1 (m) μ; uv (EtOH) λ_{max}: 214 nm (log ε 4.48), 252 nm (log ε 4.75), 296 nm (log ε 4.00); nmr ($CDCl_3$) δ; 1.64 (s, 6H, 2 Me), 5.0–5.56 (m, 2H, $=CH_2$), 5.96–6.12 (m, 1H, —CH=), 7.60–7.92 (m, 6H, arom), 8.52–8.82 (m, 3H, arom); ms *m/e* (calcd. for $C_{19}H_{18}$: 246): 246 (15.9 rel. intensity, parent mass M), 231 (38.4, M − Me), 216 (47.0, M − 2 Me), 178 (100, phenanthrene). *Anal.* calcd. for $C_{19}H_{18}$: C 92.63, H 7.37; found: C 92.63, H 7.50.

4-(9-Phenanthryl)-2-butanone

To sodium ethoxide prepared from 690 mg (30 mmol) of sodium and 20 mL of absolute ethanol was added 5.2 g (40 mmol) of ethyl acetoacetate under nitrogen. This cloudy solution was then pumped into a suspension of 6.00 g (25.8 mmol) of 9-chloromethylphenanthrene (21) dissolved in 40 mL of absolute ethanol. After a 1.5 h reflux, 26 mL (80 mmol) of 3 *M* sodium hydroxide was added. This was followed by refluxing for 1.5 h more, and then stirring at room temperature for 2 h. Then 50 mL of 50% (v:v) phosphoric acid was added with stirring at room temperature for 5 h. Approximately 30 mL of ethanol was removed *in vacuo*, the residue was ether extracted, the extracts washed with bicarbonate, then water, dried over magnesium sulfate, and concentrated *in vacuo*. Silica gel chromatography gave 3.5 g (54%) of essentially pure 4-(9-phenanthryl)-2-butanone, mp 90–92°C. Recrystallization from hexane–acetone, hexane–benzene, and from 80% ethanol brought the mp to 94.5–95°C without appreciable loss.

The spectral data were: ir ($CHCl_3$): 3.26 (m), 3.38 (s), 3.43 (m), 3.50 (m), 5.76 (s), 6.67 (m), 7.25 (m), 8.47 (s), 8.55 (s), 9.57 (m), 11.2 (w), 12.3 (m), 13.7 (s) μ; nmr ($CDCl_3$) δ: 2.16 (s, 3H, Me), 2.84–3.00 (m, 2H, $CH_2C{=}O$), 3.32–3.50 (m, 2H, CH_2), 7.20–8.88 (m, 9H, arom); ms *m/e* (calcd. for $C_{18}H_{16}O$: 248): 249 (6.2, M + 1), 248 (53.2, M), 205 (40.6, M − acetyl), 191 (88.2, M − $MeCOCH_2$), 178 (19.0, phenanthrene), 71 (4.7, $MeCOCH_2CH_2$), 57 (24.9, $MeCOCH_2$), 43 (65.9, acetyl). *Anal.* calcd. for $C_{18}H_{16}O$: C 87.06, H 6.50; found: C 87.04, H 6.61.

2-Methyl-4-(9-phenanthryl)-1-butene

Methylenetriphenylphosphorane was prepared under nitrogen from 3.92 g (10.2 mmol) of methyltriphenylphosphonium bromide in 60 mL of anhydrous ether and 7.5 mL (11.1 mmol) of 1.5 *M* butyllithium in hexane. Following 4 h at room temperature, 2.48 g (10.0 mmol) of 4-(9-phenanthryl)-2-butanone in 25 mL of anhydrous benzene was added. Precipitation of triphenylphosphine oxide began at once. After overnight refluxing, water was added and the aqueous phase was hexane extracted. The extracts were washed with brine, water, dried over magnesium sulfate, concentrated *in vacuo*, and chromatographed on a 2 × 75 cm silica gel column, eluted with hexane, 1% ether, 2% ether, and 3% ether in hexane to give 1.90 g of 4-(9-phenanthryl)-1-butene which was recrystallized from hexane, benzene–hexane, and 95% ethanol to give 1.23 g (50%) of product, mp 40–40.5°C.

The spectral data were: ir ($CHCl_3$): 3.27 (s), 3.32 (w), 3.41 (s), 3.51 (w), 6.06 (s), 6.13 (w), 6.25 (w), 6.69 (m), 6.89 (s), 6.99 (m), 7.14 (w), 7.28 (w), 7.64 (w), 8.00 (m), 8.20 (m), 8.55 (w), 8.93 (w), 9.62 (m), 10.0 (m), 10.5 (m), 11.2 (s), 13.7 (s), 14.4 (m), 16.1 (m) μ; uv (EtOH) λ_{max}: 209 nm (log ε 4.60), 249 nm (log ε 4.75), 291 nm (log ε 3.90), 322 nm (log ε 3.35); nmr ($CDCl_3$) δ: 1.72 (s, 3H, Me), 2.36–2.44 (m, 2H, CH_2), 3.00–3.10 (m, 2H, CH_2), 4.76 (s, 2H, CH_2), 7.20–8.44 (m, 9H, arom); ms *m/e* (calcd. for $C_{19}H_{18}$: 246): 247 (3.8, M + 1), 246 (26.8, M), 231 (0.1, M − Me), 192 (12.8, M − $CH_2{=}CMeCH_2$ + 1), 191 (100, M − $CH_2{=}CMeCH_2$—), 178 (0.9, phenanthrene). *Anal.* calcd. for $C_{19}H_{18}$: C 92.63, H 7.37; found C 92.56, H 7.36.

1,1-Dimethyl-2-(9-phenanthryl)cyclopropane

Lithium dicyclohexylamide was prepared by slow addition of 15.3 mL (13.8 mmol) of 0.9 *M* methyllithium in ether to 2.50 g (13.8 mmol) of dicyclohexylamine in 5.0 mL of anhydrous ether and this base was transferred under nitrogen to the dropping funnel attached to a 150 mL flask. The apparatus had been carefully dried and a dry nitrogen atmosphere was initially used. The flask also was fitted with a Dry Ice condenser. With 2.50 g (11.0 mmol) of 9-chloromethylphenanthrene (21) in 5.0 mL of anhydrous ether in the flask, a gentle stream of isobutylene was passed into the flask with Dry Ice

Can. J. Chem. Downloaded from www.nrcresearchpress.com by 210.87.254.5 on 09/06/12
For personal use only.

–acetone cooling until 16 mL (165 mmol) of isobutene had been collected. A slight stream of isobutene was continued during the run. Then the lithium dicyclohexylamide solution was added with stirring at a rate to maintain gentle refluxing. This required 20 min. After an additional 20 min (longer reaction times led to lower yields) the mixture was treated with water, the solid which separated was washed with hexane, and the combined organic phase washed with 5% HCl, then with brine, water, dried over magnesium sulfate, concentrated *in vacuo*, and the residue chromatographed on a 1.5 × 70 cm silica gel column. Elution with hexane, followed by recrystallization from methanol afforded 0.734 g (27%) of 1,1-dimethyl-2-(9-phenanthryl)cyclopropane as white needles, mp 116–116.5°C.

The spectral data were: ir ($CHCl_3$): 3.27 (m), 3.32 (s), 3.36 (s), 3.40 (m), 3.48 (s), 4.16 (m), 6.25 (w), 6.54 (w), 6.90 (m), 6.99 (m), 7.19 (w), 7.35 (m), 7.64 (w), 8.20 (s), 8.62 (w), 8.94 (s), 9.26 (m), 9.52 (m), 10.5 (w), 12.8 (s), 14.8 (s), 15.7 (w) μ; uv (EtOH) λ_{max}: 210 nm (log ε 4.05), 252 nm (log ε 4.30), 300 nm (log ε 3.60); nmr ($CDCl_3$) δ: 0.72 (s, 3H, *cis*-Me), 0.8–1.0 (m, 2H, CH_2), 1.50 (s, 3H, *trans*-Me), 2.16–2.24 (m, 1H, CH), 8.64–7.48 (m, 9H, arom); ms *m/e* (calcd. for $C_{19}H_{28}$: 246): 247 (rel. abund. 21.9, M + 1), 246 (100, M), 231 (78.2, M − CH_3), 216 (29.8 M − 2Me), 204 (8.5, M − Me_2C), 203 (62.9, M − Me_2CH), 178 (13.7, phenanthrene). *Anal.* calcd for $C_{19}H_{18}$: C 92.63, H 7.37; found C 92.35, H 7.36.

General irradiation procedures

All irradiations were preceded by degassing with vanadous purified nitrogen for 1 hour and the photolyses were conducted under this atmosphere. Exploratory irradiations were carried out using a 450 W Hanovia medium pressure immersion lamp apparatus. Quantitative irradiations were performed using the Wisconsin Black Box apparatus described earlier (4). Light input was monitored with electronic actinometry (5). Potassium ferrioxalate (22) was used for calibration.

Exploratory direct photolysis of 3-methyl-3-(9-phenanthryl)-1-butene

A solution of 150 mg (0.61 mmol) of the methyl phenanthryl butene in 500 mL of *tert*-butyl alcohol was photolyzed for 2 hours through 1 mm of Corex using the preparative apparatus. Solvent removal *in vacuo* left 141 mg of material which was chromatographed on a 1.5 cm × 75 cm silica gel column. Elution with hexane and then 1% ether with 50 mL fractions gave 62 mg (41%) of starting material in fractions 4–7 and 33 mg (22%) of product in fractions 8–13. Stripping the column with 5% ether afforded 25 mg of unidentified products. The starting material was identified by nmr comparison with an authentic sample and the product was recrystallized to mp 39–40°C and proved to be identical with synthetically prepared 2-methyl-4-(9-phenanthryl)-1-butene.

In a run to shorter (1 hour) conversion, photolysis of 150 mg (0.61 mmol) afforded 97 mg of starting material, 21 mg of 2-methyl-4-(9-phenanthryl)-1-butene and 5 mg of unidentified material. The mass balance was 82% and the conversion was 14%.

Low conversion photolysis of 3-methyl-3-(9-phenanthryl)-1-butene; observation of di-π-methane product

Irradiation of 753 mg of 3-methyl-3-(9-phenanthryl)-1-butene in 500 mL of *tert*-butyl alcohol was carried out for 20 min through 1 mm of Corex, and work-up as above. Silica gel chromatography as well as thin layer chromatography proved ineffectual in separating the photoproduct. Chromatography using pentane on 1:1 silica gel – alumina and elution in 25 mL fractions gave fractions 11–13, which were recrystallized from methanol to afford 53 mg of 1,1-dimethyl-2-(9-phenanthryl)cyclopropane, mp 115–116°C, with spectral properties identical to those of authentically synthesized compound. Also, 604 mg of starting material was obtained from the early silica gel chromatography fractions and from fractions 4–8 of the alumina – silica gel chromatogram.

Direct photolysis of 1,1-dimethyl-2-(9-phenanthryl)cyclopropane

A solution of 150 mg of the cyclopropane in 500 mL of *tert*-butyl alcohol was irradiated for 2 hours through 1 mm of Corex. Chromatography on a 2.5 × 95 cm silica gel column packed with hexane but eluted with 1% ether in hexane and with 25 mL fractions gave 39 mg of reactant in fractions 3–7 after methanol recrystallization. Fractions 8–11 were recrystallized from benzene–hexane to afford 53 mg (35%) of 2-methyl-4-(9-phenanthryl)-1-butene, mp 38.5–40°C. This material proved spectrally identical with the authentic material described above.

Direct photolysis of 2-methyl-4-(9-phenanthryl)-1-butene; control run

Photolysis of 150 mg of the 2-methyl alkene for 1 hour through Corex (1 mm), followed by the usual work-up, afforded 130 mg of reactant, isolated by chromatography, and no isolable photoproducts.

Sensitized irradiation of 3-methyl-3-(9-phenanthryl)-1-butene

A solution of 87 mg (0.354 mmol) of the 3-methyl alkene together with 392 mg (2.0 mmol) of xanthone was irradiated in 250 mL of *tert*-butyl alcohol in the Black Box apparatus (4) utilizing the following filter: Cell 1, 0.2 *M* nickel sulfate hexahydrate in 10% sulfuric acid; Cell 2, 0.4 *M* cobalt sulfate in 10% sulfuric acid; Cell 3, 0.10 *M* stannous chloride dihydrate in 15% HCl. This combination gave λ_{max} for transmission at 345 nm and was opaque below 322 nm and above 385 nm; 3.29 meinsteins were absorbed. Then the photolysate was concentrated *in vacuo* and chromatographed on a 2.5 × 35 cm silica gel column. Hexane elution gave 82 mg of oil, and 10% ether gave 378 mg of xanthone. Chromatography of the oil on a 1:1 alumina–silica gel column packed and eluted with pentane with 50 mL fractions gave 59 mg of starting material by recrystallization of fractions 8–17 from 95% ethanol and 16.1 mg (18.5%) of 1,1-dimethyl-2(9-phenanthryl)cyclopropane, mp 114.5–116°C, by recrystallization of fractions 19–23 from methanol. The cyclopropane product proved identical in physical properties to authentic material described above.

Sensitized irradiation of 1,1-dimethyl-2-(9-phenanthryl)cyclopropane

A solution of 87 mg (0.354 mmol) of 1,1-dimethyl-2-(9-phenanthryl)cyclopropane and 392 mg (2.0 mmol) of xanthone in 250 mL of *tert*-butyl alcohol was irradiated in the Black Box apparatus (4) as described above using the same nickel–cobalt–stannous filter combination described previously for use with xanthone. Light output was monitored showing absorption of 3.075 meinsteins. Concentration *in vacuo* and chromatography on a 2.5 × 37 cm silica gel column gave with hexane elution 79 mg of the reactant cyclopropane, identified by its physical properties. Elution with 10% ether afforded 370 mg of xanthone. No further compounds could be observed.

Quantum yield determinations

These measurements were made on the Wisconsin Black Box apparatus (4). Direct irradiations were made using the following triple filter solution (filter A): Cell 1, 2 *M* nickelous sulfate hexahydrate in 10% sulfuric acid; Cell 2, 0.80 *M* cobalt sulphate heptahydrate in 10% sulfuric acid; Cell 3, 1.23×10^{-3} *M* bismuth chloride in 40% hydrochloric acid. This combination was opaque below 260 nm and above 300 nm. Sensitized irradiations used filter B: Cell 1, 0.50 *M* nickelous sulfate in 15% sulfuric acid; Cell 2, 2.0 *M* cobaltous sulfate in 5% sulfuric acid; Cell 3, 1.0 *M* cupric sulphate in 5% sulfuric acid. This combination had a transmission maximum at 337 nm (20%) and was opaque below 310 and above 375 nm. Electronic actinometry (5) was employed and calibration was with potassium ferrioxalate (22). Assays for reactant and products used a phenanthrene internal standard. A 4 × 240 mm hplc column packed with 5–10 μ spherical silica coated with C-18 reverse phase and 40% water in acetonitrile as the eluting solvent were employed. Ultraviolet scanning at 254 nm was used for detection. Planimetry was accomplished using a PDP-11/55 minicomputer along with a Bitpad (Summagraphics Co.) digitizer. For each quantum yield, determinations were made at several extents of conversion and a linear plot to zero conversion was made. Note Table 2 for details.

Fluorescence and phosphorescence measurements

These were made on an Aminco–Bowman spectrophotometer. Measurements were made with a series of diminishing slit openings to make certain that the results were slit independent. Wavelength inde-

TABLE 2. Quantum yield determinations for irradiation of 3-methyl-3-(9-phenanthryl)-1-butene to afford 1,1-dimethyl-2-(9-phenanthryl)-cyclopropane; dependence on conversion

Reactant, mmol	Light abs, meinstein	Product conversion %	Product conversion mmol	ϕ
Direct runs				
0.38	0.470	4.58	0.0174	0.0370
0.38	0.355	3.53	0.0134	0.0377
0.35	0.301	3.34	0.0117	0.0389
0.38	0.192	2.13	0.0081	0.0421
0.35	0.140	1.63	0.0057	0.0408
0.35	0.0823	0.99	0.00345	0.0419
0.50	0.0411	0.35	0.00175	0.0425
0.60	0.0255	0.18	0.0011	0.0432
0.50	0.0129	0.11	0.00055	0.0427
Xanthone sensitized runs				
0.28	0.306	5.14	0.0144	0.0471
0.25	0.276	4.85	0.0121	0.0439
0.26	0.144	2.65	0.0069	0.0480
0.29	0.149	2.51	0.0073	0.0490
0.30	0.0822	1.42	0.00425	0.0518
0.27	0.0319	0.61	0.00165	0.0517
0.27	0.0101	0.20	0.00053	0.0525
0.09	0.0030	0.18	0.00016	0.0533

pendence was assured by using a biphenyl standard. Degassing was accomplished with 10 freeze–thaw cycles using liquid nitrogen and 20 min pumping time per cycle. An arrangement was devised whereby the freeze–thaw operation was carried out in a separate tube and transferred to the square quartz cell at the end by inverting. The design assured no contact with grease or ground joints. This procedure avoided the common cracking of square quartz tubing on freeze–thaw. Biacetyl concentrations were varied in the range 10^{-5}–10^{-7} M with the phenanthryl vinyl methane at 2.24×10^{-3} M. Plots of biacetyl phosphorescence at 510 nm vs. $[BI]^{-1}$ were linear with biacetyl concentration low enough to preclude singlet energy transfer. The slopes and intercepts were determined at several slit settings and the results proved independent of this variable.

Acknowledgments

Support of this research by NIH Grant GM07487, the National Science Foundation, and a fellowship to G.S.W. from the People's Republic of China is gratefully acknowledged. The synthetic aspects of this research were supported by NIH while the mechanistic portions were supported by NSF.

1. H. E. ZIMMERMAN and R. A. BUNCE. J. Org. Chem. **47**, 3377 (1982).
2. (*a*) H. E. ZIMMERMAN and J. R. BLINN. Tetrahedron, **37**, 3237 (1981); (*b*) H. E. ZIMMERMAN. Tetrahedron, **37**, 753 (1981); (*c*) H. E. ZIMMERMAN. *In* Rearrangements in ground and excited states. *Edited by* P. deMayo. Academic Press, New York. 1980. Chapt. 16; (*d*) H. E. ZIMMERMAN, J. H. PENN, and C. W. CARPENTER. Proc. Natl. Acad. Sci. U.S.A. **79**, 2128 (1982); (*e*) H. E. ZIMMERMAN. Chapt. 2 *in* Top. Curr. Chem. **100**, 45 (1982); (*f*) H. E. ZIMMERMAN and D. J. KREIL. J. Org. Chem. **47**, 2060 (1982).
3. H. E. ZIMMERMAN, M. G. STEINMETZ, and C. L. KREIL. J. Am. Chem. Soc. **100**, 4146 (1978).
4. H. E. ZIMMERMAN. Mol. Photochem. **3**, 281 (1971).
5. H. E. ZIMMERMAN, T. P. CUTLER, V. R. FITZGERALD, and T. J. WEIGHT. Mol. Photochem. **8**, 379 (1977).
6. F. WILKINSON and J. T. DUBOIS. J. Chem. Phys. **39**, 377 (1963).
7. K. SANDROS. Acta Chem. Scand. **23**, 2815 (1969).
8. H. E. ZIMMERMAN, K. S. KAMM, and D. P. WERTHEMANN. J. Am. Chem. Soc. **97**, 3718 (1975).
9. H. E. ZIMMERMAN and K. G. HANCOCK. J. Am. Chem. Soc. **90**, 3749 (1968).
10. (*a*) P. DEBYE. Trans. Electrochem. Soc. **82**, 265 (1942). (*b*) A. H. ALWATTAR, M. D. LUMB, and J. B. BIRKS. *In* Organic molecular photophysics. Vol. 1. *Edited by* J. B. Birks. 1973. p. 422.
11. H. E. ZIMMERMAN, R. W. BINKLEY, R. S. GIVENS, and M. A. SHERWIN. J. Am. Chem. Soc. **89**, 3932 (1967).
12. S. S. HIXSON. *In* Organic photochemistry. Vol. 4. *Edited by* A. Padwa. Marcel Dekker, New York. 1979. pp. 208–211.
13. (*a*) P. H. MAZZOCHI and R. S. LUSTIG. J. Am. Chem. Soc. **97**, 3707 (1975). (*b*) **97**, 3714 (1975).
14. (*a*) H. E. ZIMMERMAN and M. G. STEINMETZ. J. Chem. Soc. Chem. Commun. 231 (1978); (*b*) H. E. ZIMMERMAN, W. T. GRUENBAUM, R. T. KLUN, M. G. STEINMETZ, and T. R. WELTER. J. Chem. Soc. Chem. Commun. 228 (1979).
15. H. E. ZIMMERMAN, M. G. STEINMETZ, and C. L. KREIL. J. Am. Chem. Soc. **100**, 4146 (1978).
16. (*a*) H. E. ZIMMERMAN. J. Am. Chem. Soc. **88**, 1564 (1966); (*b*) J. Am. Chem. Soc. **88**, 1566 (1966); (*c*) Acc. Chem. Res. **4**, 272 (1971); (*d*) Quantum mechanics for organic chemists. Academic Press, New York. 1975; (*e*) *In* Pericyclic reactions. Vol. 1. *Edited by* A. Marchand and R. Lehr. Academic Press, New York. 1977; (*f*) Acc. Chem. Res. **5**, 393 (1972).
17. (*a*) H. E. ZIMMERMAN, D. ARMESTO, M. G. AMEZUA, T. P. GANNETT, and R. P. JOHNSON. J. Am. Chem. Soc. **101**, 6367 (1979); (*b*) H. E. ZIMMERMAN and R. E. FACTOR. Tetrahedron, Suppl. I, **37**, 125 (1981); (*c*) H. E. ZIMMERMAN, J. H. PENN, and M. R. JOHNSON. Proc. Natl. Acad. Sci. U.S.A. **78**, 2021 (1981).
18. (*a*) H. E. ZIMMERMAN and G. A. EPLING. J. Am. Chem. Soc. **94**, 3647 (1972). (*b*) H. E. ZIMMERMAN and G. A. EPLING. J. Am. Chem. Soc. **94**, 8749 (1972).
19. H. E. ZIMMERMAN and C. O. BENDER. J. Am. Chem. Soc. **92**, 4366 (1970).
20. F. MOSETTIG and J. KAMP. J. Am. Chem. Soc. **55**, 2995 (1933).
21. G. M. BADGER, W. CARRUTHERS, J. W. COOK, and R. SCHOENTAL. J. Chem. Soc. 169 (1949).
22. C. G. HATCHARD and C. A. PARKER. Proc. R. Soc. London, Ser. A, **235**, 518 (1956).

Can. J. Chem. Downloaded from www.nrcresearchpress.com by 210.87.254.5 on 09/06/12
For personal use only.

Quantum capture and redox storage[1]

MELVIN CALVIN

Department of Chemistry and Lawrence Berkeley Laboratory, University of California, Berkeley, CA 94720, U.S.A.

Received July 5, 1982

This paper is dedicated to Professor Harry E. Gunning on the occasion of his 65th birthday

MELVIN CALVIN. Can. J. Chem. **61**, 873 (1983).

Over many years multiple investigations of the mechanism of the primary quantum conversion steps in natural photosynthesis have exposed the participation of some kind of manganese complex in the oxidation of water to molecular oxygen and the participation of a number of iron hemes in the electron transport chain between the two photosystems. It is almost certain that the participation of an iron–sulfur protein on the reduction side of the photosynthetic electron transfer scheme plays a role in the formation of reduced pyridine nucleotide through ferredoxin and in the evolution of hydrogen in plants deprived of CO_2 but having the hydrogenase present. The physical arrangement of the components is important as well, and the participation of at least one phase boundary (and probably two) in the same transport chain is likely. We have used this information to try to construct a synthetic chloroplast that would accomplish quantum conversion into stored energy in the form of intermediate oxidant and intermediate reductant. These could then be converted, respectively, into a useful oxidation product, or molecular oxygen, on the one hand, and molecular hydrogen, or a more useful reduction product, on the other.

MELVIN CALVIN. Can. J. Chem. **61**, 873 (1983).

Des recherches multiples échelonnées sur plusieurs années ont permis d'approfondir le mécanisme des étapes de la transformation quantique primaire lors de la photosynthèse naturelle et de mettre à jour la participation de certains complexes de manganèse lors de l'oxydation de l'eau en oxygène moléculaire et la participation d'un certain nombre d'hèmes de fer dans la chaîne de transfert d'électrons entre les deux systèmes photochimiques. Il est presque certain que la participation d'une protéine à base de fer-soufre du côté réduction du schéma de transfert photosynthétique d'électron joue un rôle dans la formation du nucléotide portant une pyridine réduite via la ferredoxine et dans l'évolution de l'hydrogène dans les plantes privées de CO_2 mais contenant l'hydrogénase. La disposition physique des composants est aussi importante et la participation d'au moins une phase limite (et probablement deux) dans la même chaîne de transport est probable. Nous avons utilisé cette information pour essayer de construire un chloroplaste synthétique qui pourrait accomplir cette transformation quantique en énergie de stockage sous la forme d'oxydant ou de réducteur intermédiaire. Ces derniers peuvent alors être transformés respectivement d'une part en un produit d'oxydation utile ou en oxygène moléculaire et d'autre part en hydrogène moléculaire ou en un produit de réduction plus utile.

[Traduit par le journal]

Introduction

Artificial photosynthesis is a process that mimics the principles of green plant photosynthesis with a totally synthetic device (chemical system) that will capture the quanta from the sun and store them as stable chemicals (1–3). The primary problem of catching, converting, and storing visible light into stable chemical form involves devising a system in which the short-lived energy of a sensitizer can be stored in some stable chemical form, usually by a redox reaction in which an electron is transferred from one point to another point nearby. If energy is to be stored after the electron is transferred, the system must be in a higher energy stage than it was before, that is, the immediate products of the electron transfer reaction will have a great tendency to back-react. Therefore, two problems must be solved: (*1*) We must convert the excitation of the sensitizer (chlorophyll in the green plant) in a very short time to a pair of redox molecules neighboring to each other, which must be capable of back-reacting to give energy. (*2*) We must prevent that back-reaction from occurring, while the two objects are close to each other, until we can move and store them in far greater stability. The green plant has evolved over several billion years and accomplishes these steps with a high degree of efficiency. Our problem is to generalize from what we know of green plant quantum conversion to some physical-chemical principles and to construct an entirely synthetic device that will be successful in splitting the water molecule to yield reductant and oxidant, e.g., hydrogen and oxygen.

The natural material of the green plant in which these reactions occur in the chloroplast is a series of very thin membranes (about 40 Å thick) containing molecules of various types. The membrane is unsymmetrical, suggesting that what takes place in the membrane is a result of two different quantum acts, one on either side of the membrane.

Photosensitized electron transfer across bilayer membranes

Photoelectron transfer in nature, as represented in Fig. 1, shows that two quanta are absorbed in succession, and the quantum at 680 nm removes an electron from the water molecule through a manganese complex and raises that electron to a higher energy level, which is high enough to generate molecular hydrogen. The green plant, however, uses two quanta because the charge does not go directly from the first acceptor to NADPH, but rather goes through a series of downhill electron transfers with the generation of some ATP, the general energy currency of all living organisms. A second quantum then raises that electron again, whence it passes through a sequence of electron transferring agents such as iron–sulfur proteins, eventually reducing NADP to NADPH. The combination of NADPH formed here plus the ATP formed in the first quantum act together to reduce carbon dioxide to sugars. With this two-quantum process and the asymmetrical membrane structure as a model, its seems altogether reasonable that an early step in a synthetic quantum conversion process should be

[1]This manuscript represents a summary of the plenary lecture in the Symposium in Honor of H. E. Gunning. V. Physical Photochemistry, at the meeting of the Canadian Institute of Chemistry, Toronto, Canada, May 31, 1982.

Can. J. Chem. Downloaded from www.nrcresearchpress.com by 210.87.254.5 on 09/06/12
For personal use only.

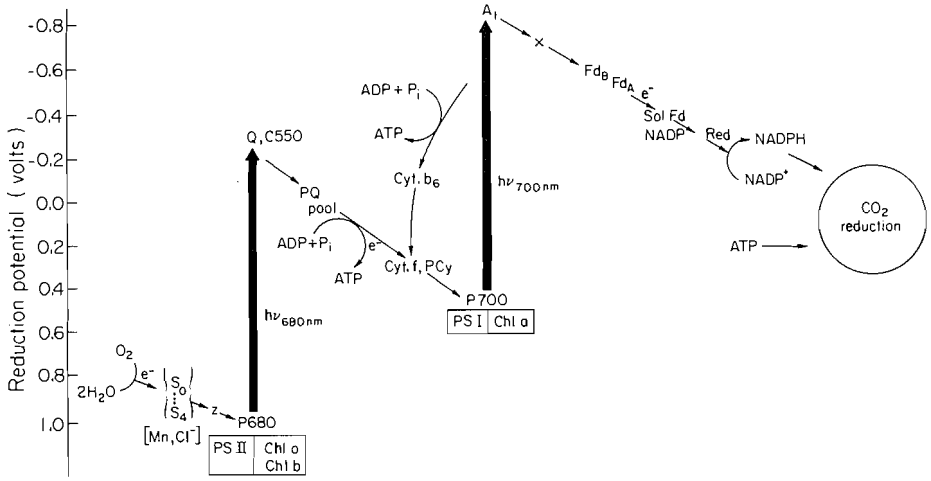

FIG. 1. Photosynthetic electron transfer scheme.

the transfer of an electron across a membrane.

It has been possible to construct a synthetic membrane with sensitizers on both sides and to demonstrate the passage of an electron from one side of the membrane to the other side (4, 5). The membrane consists of interfaces between phases, a water phase, an oil phase, and another water phase (6). Sensitizers have been placed on either side of the membrane at the interface between the water and oil phases. We have suggested as a basic physical principle that the electron must pass through the membrane. Before that happens, however, we must use the principles of photoelectron transfer across a phase boundary to stabilize the first reaction product of the quantum conversion act. The step would be the transfer of an electron from the donor to the acceptor at the phase boundary, i.e., separating the two phase boundary membranes into two separate parts. The transmission of an electron from the water phase, through the insulating membrane barrier to the other water phase, was demonstrated in vesicles using both synthetic and natural surfactant lipids (phospholipids). The synthetic lipids could be either dipolar or monopolar.

When we examined the natural system in the green plant we realized that chlorophyll, the sensitizer molecule, is actually a surfactant dyestuff. The chlorophyll has a hydrophylic head with a hydrophobic tail which is characteristic of surfactant structure. It was necessary to devise surfactant sensitizers more stable than the chlorophyll of the green plant. As one sensitizer molecule, we have used zinc porphyrin, which is more versatile and is capable of having a variety of substituent groups with both positive and negative charges, which can change the solubility function. The zinc porphyrin can also become a surfactant dyestuff by suitable adjustment of substituents. The synthetic electron acceptor, methylviologen or heptylviologen, was modeled after propylviologen sulfonate, a netural molecule, becoming a negative ion only after an electron is passed into it. When one electron is added to the heptylviologen, changing it from a dipositive to monopositive material, it becomes a free radical with a blue color which is stable by itself but not stable to oxygen. It is thus possible to monitor the color and measure the number of electrons transferred across a vesicle wall. The surfactant dyestuff on both sides of the membrane with the electron acceptor (heptylviologen) on the outside of the membrane is shown in Fig. 2. There is a donor system on the other side of the membrane which is irreversibly oxidized by Ru^{3+} to generate Ru^{2+} and oxidation products. An

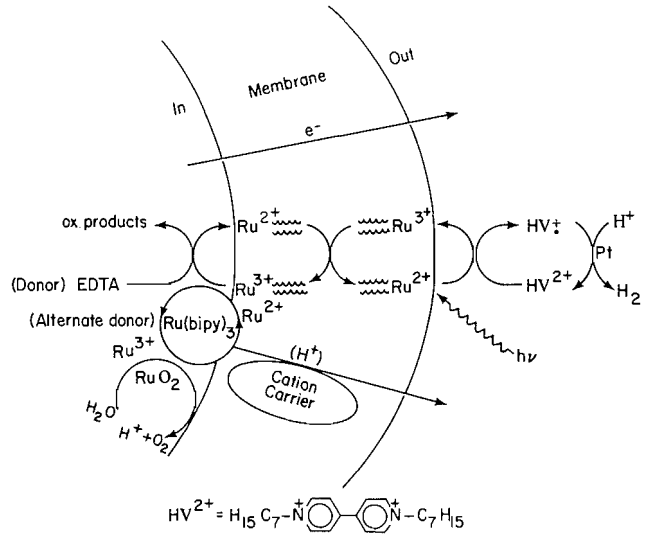

FIG. 2. Scheme for photosensitized electron transfer across a lipid vesicle wall.

alternative donor [$Ru(bipy)_3^{2+}$] has an oxidation potential (as $Ru(bipy)_3^{3+}$] high enough to produce oxygen from water, if there is a surface, such as ruthenium oxide (7), which can accumulate four positive charges. It is possible to make hydrogen on the other side of the membrane by providing a platinum surface to give the two-electron collection which is needed (2).

It is therefore possible to perform a photochemical electron transfer from the inside to the outside of the membrane, producing a reduction product on one side of the membrane and an oxidation product on the other side, which cannot back-react because the membrane prevents it. This is the basic, fundamental structure of the photosynthetic membranes in the green plant chloroplasts.

A number of experiments (8) were performed to test this idea (Fig. 3). A donor was placed on the inside of the membrane and an acceptor (methylviologen) on the outside. In the membrane (lower left), there is some surfactant acceptor present with a ruthenium surfactant sensitizer which produces a viologen radical on the outside; the reaction occurs rapidly at first and then gradually slows. The second experiment (upper) used methylviologen, without heptylviologen, and proceeded more slowly. In the third case (lower right) an electron carrier was

Can. J. Chem. Downloaded from www.nrcresearchpress.com by 210.87.254.5 on 09/06/12
For personal use only.

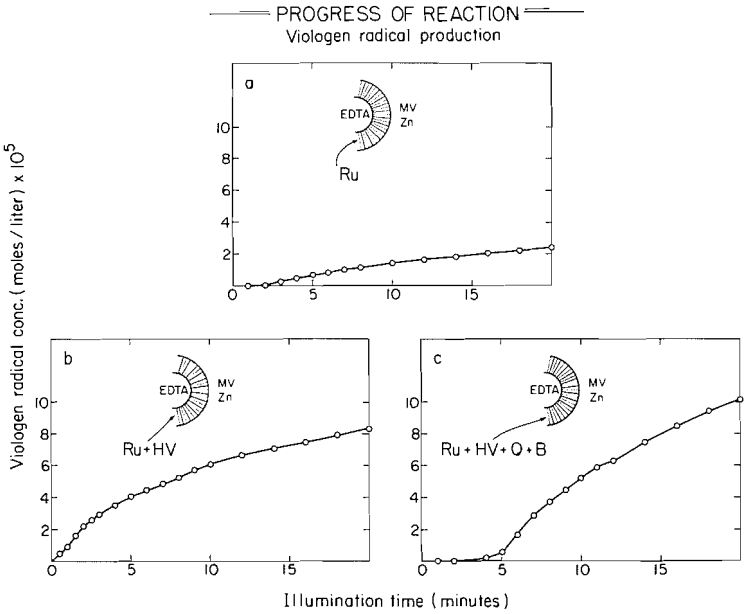

FIG. 3. Cofactors in photoelectron transfer reactions across a membrane sensitized by $Ru(bipy)_3$, EDTA as donor, MV or electron acceptor and Q *p*-benzoquinone as electron carrier, Zn^{2+} added on the outside to prevent any reaction with leaked EDTA.

added to the membrane which had little effect. This last experiment, together with the one without added carrier, did show that an electron carrier is not necessary to achieve electron transfer across a membrane.

The electron exchange between Ru^{2+} and Ru^{3+} across the membrane is an isoenergetic reaction, which is the reason electron tunneling occurs so readily. We have shown by kinetic arguments that this electron transport is the rate-limiting step in the overall reaction. If that is so, then it should be possible to accelerate electron transfer by putting the proper potential across the membrane by selectively adding ions (such as potassium and sodium) on the inside and outside of the membrane with an ionophore in the membrane, a molecule which allows only passage of potassium ions (9). By varying the concentration of ions in the membrane system the potassium ion can be made to flow through the membrane down a concentration gradient while the sodium will be unable to come back. This generates a positive charge on the outside and a negative charge on the inside of the membrane, accelerating electron transfer from the inside to the outside. This experiment can also be reversed, in which case the electron transfer is slowed down. Thus, the potential construction across the membrane helps to substantiate our hypothesis with respect to the mechanism by which the electron transfer is occurring.

Energy transfer on membrane surfaces

Recently (10) we have studied in greater detail the dynamics of the initial quenching reaction of $Ru(bipy)_3$, using the convenient ferricyanide ion in the bulk phase as the quencher (acceptor). A non-linear Stern–Volmer behavior indicated that a significant fraction of excited molecules was inaccessible to the quencher (Fig. 4). Treatment of the data by a modified Stern–Volmer plot showed that only 66% of the luminescent sensitizer molecules were accessible to the quencher (11). Presumably these were the sensitizers on the outside. When ferricyanide quencher was placed both inside and outside the vesicle, all the luminescent molecules were available for quenching and normal Stern–Volmer behavior was observed

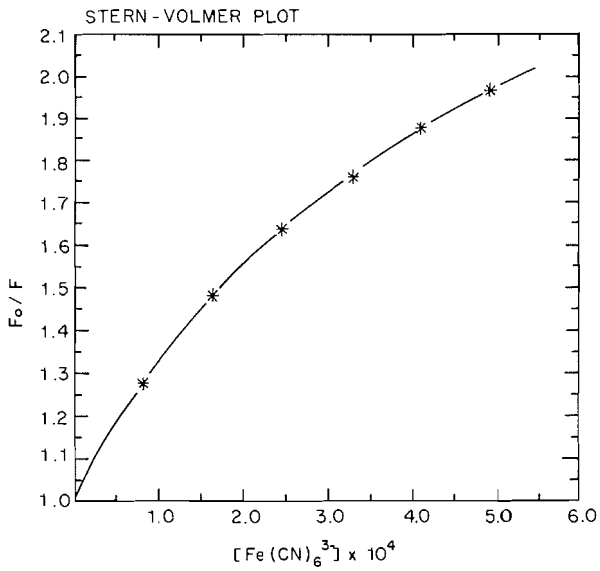

FIG. 4. Luminescence quenching of $Ru(bipy)_3^{2+}$ with quencher outside of vesicles only.

(Fig. 5). From the fraction of quenchable luminescence and the known thickness of the lipid bilayer and the assumption that the head groups of the sensitizer lie at the surfaces, the outer diameter of the vesicles could be computed to be about 350 Å.

We found that over a wide range of sensitizer concentration in the lipid the percent of quenchable luminescence remained constant at 66%, indicating that there was no energy exchange between sensitizers *across* the membrane during the excitation lifetime even when the number of transmembrane neighbors was greatly increased. On the other hand, increase in surface sensitizer concentration *did* result in larger quenching rate constants, suggesting that exciton coupling may be taking place among sensitizers on the same side of the membrane. By this mechanism, the effective surface area over which a particular excitation can interact with quencher is increased, and, therefore, in a diffusion-controlled quenching reaction, the quench-

Can. J. Chem. Downloaded from www.nrcresearchpress.com by 210.87.254.5 on 09/06/12
For personal use only.

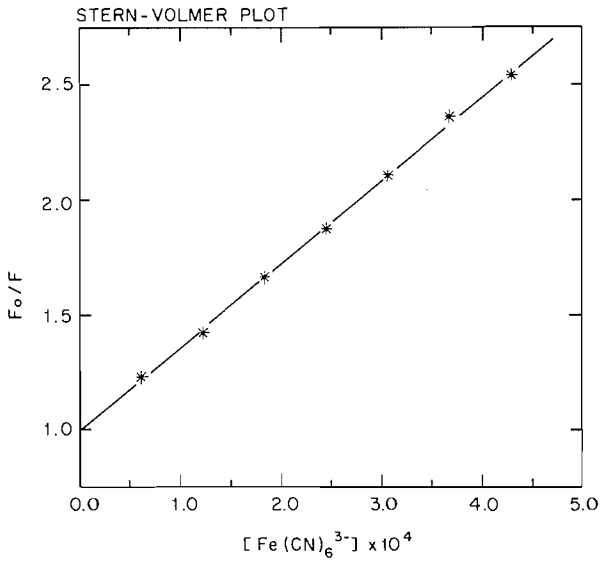

FIG. 5. Luminescence quenching of $Ru(bipy)_3^{2+}$ with quencher inside and outside of vesicles.

ing rate itself is increased.

Implications of this added excitation migration process in the overall dynamics of photosensitized electron transport are still being explored. However, our major conclusion is unchanged, namely, that the mechanism of electron transport through the vesicle wall is by charge exchange between surfactant $Ru(bipy)_3^{3+}$ and $Ru(bipy)_3^{2+}$ on opposite sides.

A method entirely independent of fluorescence was then used to check on our vesicle size determination. The vesicles were prepared in a buffer containing ^{14}C-labelled sucrose, which does not penetrate the bilayer. After gel filtration to remove the outside sucrose, the observed radioactivity of the vesicle suspension gave a measure of the total internal volume. Then from the total amount of lipid present and the known membrane thickness the average vesicle diameter could be computed to be about 500 Å, in fair agreement with the value obtained from the fraction of sensitizer that is quenchable. The two values could be made consistent by assuming either that the sensitizer head groups protrude from the lipid surfaces into the aqueous phases by about 15 Å or that the surface density of sensitizer on the inside is somewhat smaller than on the outside, perhaps because of the higher degree of curvature.

Photosensitized electron transfer in water-in-oil emulsions

It is also possible to transfer an electron across a single phase boundary in an emulsion (12) (Fig. 6). The photosensitizer used is zinc tetraphenylporphyrin sulfonate, a negatively charged material with four sulfonic acid groups, which is water soluble and will remain in a water droplet. The acceptor, methylviologen, is also water soluble. The donor, thiophenol, is in the interphase region. When this particular system is illuminated, the zinc–TPPS becomes excited, the excited state transfers an electron to the methylviologen which produces the blue color, the zinc–TPPS becomes oxidized, and the oxidized zinc–TPPS returns to the reduced form through the polar thiol group which concentrates at the water–toluene interface. When thiol is oxidized from sulfhydryl to disulfide, it moves away from the interface and is now oil soluble. Thus the separation of the oxidized product (disulfide) from the reduced product (viologen radical) is achieved by forming them in two separate phases.

The inner surface of the water droplet is surrounded by positively charged surfactants which affect the efficiency of this reaction. The positive charge attracts negatively charged zinc sensitizer but repels the positively charged electron acceptor. It is possible to use a neutral electron acceptor such as PVS, and to raise the quantum yield substantially.

Photosensitized electron transfer reactions in SiO_2 colloids

It occurred to us that it might be possible to use a surface potential to achieve separation, without having the charge go across the membrane boundary. It is possible to arrange the system in such a way that the surface potential of the interface will be the controlling factor in the efficiency of the electron transfer (13–15) if the right particles are used with the correct charge distribution and proper structure of donors/acceptors/sensitizers. We chose silica particles which are highly negatively charged to test this hypothesis, performing the experiments at pH 9 to be sure that the positive sensitizer is closely attached electrostatically to the negatively charged surface. The neutral electron acceptor, PVS, can approach either a positive or negative surface. When the sensitizer (Ru^{2+}) is illuminated and excited it can pass its electron to the neutral acceptor, creating a $PVS^{\cdot}$ radical which changes the charge on the ruthenium sensitizer from +2 to +3. The Ru^{3+} is held even more tightly to the negatively charged surface, and the electron acceptor, now negatively charged, is ejected from the field around the negative particles. Thus, the back-reaction of the two materials, which should energetically go back downhill, is prevented (Fig. 7). It is possible to regenerate the sensitizer by using a neutral donor. This reaction, using either positively charged ruthenium or zinc as sensitizer, is shown (Fig. 8) as a function of the light absorbed. The experimental data for the ruthenium (Fig. 8*a*) and for the zinc tetramethylpyridinium porphyrin (Fig. 8*b*) indicate that addition of silica particles prevents the back-reaction. A confirmation of this information was found through flash photolysis experiments which follow the first milliseconds of the reaction. The flash photolysis data show the amount of reduced methylviologen, and there is no question that the silica allows the reduction of the PVS while the negative surface prevents the reduced viologen from back-reacting with the oxidized ruthenium. The retardation of back-reaction can be modified by reducing the negative potential on the silica particles either by adding some salt or decreasing the pH; both of these changes increase the speed of the back-reaction.

We would like to move those electrons even further away from the silica particles by using another electron carrier. We have used PVS as a shuttle to reduce ferri- to ferrocyanide. The ferricyanide has three negative charges and ferrocyanide has four, and neither can approach closely the highly negative charged SiO_2 particles. It would be difficult to reduce directly ferri- to ferrocyanide because of the high potential energy of the negatively charged ferricyanide in the field of the silica particles. Therefore, the neutral PVS can be used as a shuttle because it can approach the silica particle. PVS is converted from a neutral to a negative molecule, is ejected from the negative field of the particle and reaches the ferricyanide and reduces it to ferrocyanide. The shuttle can then go back and accept another electron (Figs. 7 and 9). The same shuttle function occurs in the chloroplasts where the electron transfer chain pulls the electron further away from the initial sensitized membrane surface.

Can. J. Chem. Downloaded from www.nrcresearchpress.com by 210.87.254.5 on 09/06/12
For personal use only.

Can. J. Chem. Downloaded from www.nrcresearchpress.com by 210.87.254.5 on 09/06/12
For personal use only.

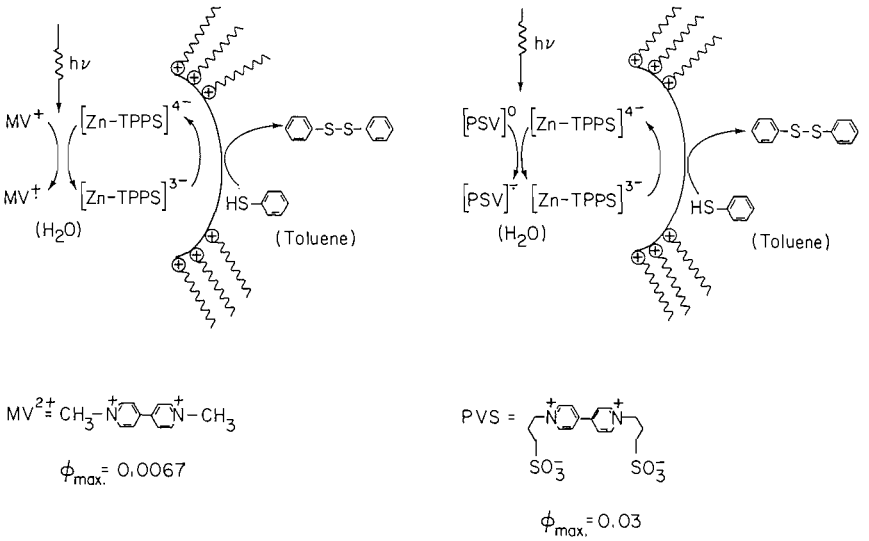

FIG. 6. Electron transfer across interface of water—oil emulsion leading to separation of redox products. Zinc tetraphenylporphyrin sulfonate is photosensitizer. Quantum yields using two acceptors, methylviologen (MV^{2+}) on the left and propylviologen sulfonate (PVS^0) on the right are compared.

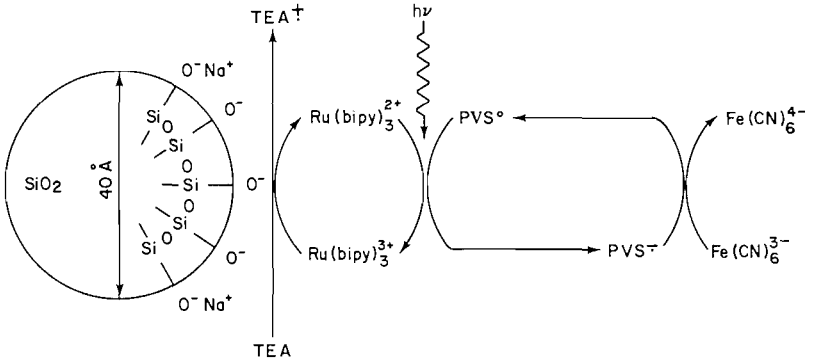

FIG. 7. Schematic function of SiO_2 particles in separating multicharged photoproducts.

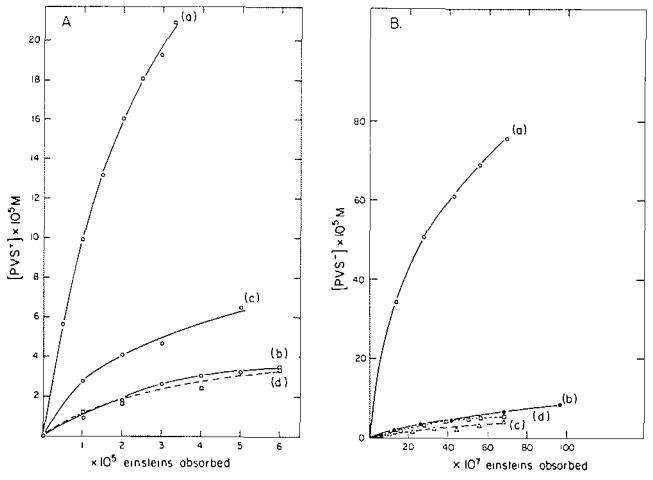

FIG. 8. Propylviologen radical, PVS^-, formation as a function of light absorbed, monitored by the increase of absorbance at $\lambda = 602$ nm ($\epsilon = 12500\ M^{-1}\ cm^{-1}$). (*A*) $Ru(bipy)_3^{2+}$ as sensitizer; (*a*) SiO_2 system; (*b*) homogeneous system; (*c*) micellar system; (*d*) NaLS micellar system with 0.1 *M* NaCl. (*B*) Zn—$TMPyP^{4+}$ and Zn—$TPPS^{4-}$ as sensitizers; (*a*) SiO_2 system with Zn—$TMPyP^{4+}$; (*b*) homogeneous system with Zn—$TMPyP^{4+}$; (*c*) SiO_2 system with Zn—$TPPS^{4-}$; (d) homogeneous system with Zn—$TPPS^{4-}$

As mentioned earlier, we can control the negative potential on the silica surface by adding salt to the environment, which reduces the negative surface potential, controlling what can approach the surface. Other surfaces, such as that of sodium laurylsulfonate micelles (Fig. 10) have surface potentials much lower than that of silica.The quantum yield, therefore, can be controlled by the negative charge of the particle upon which the reaction is occurring. Thus, PVS could be used as a shuttle between two different negatively charged particles, one of the negative particles generating hydrogen and the other generating oxygen (Fig. 11).

Device for photodecomposition of water

We have outlined two different methods for generating or building a device to separate water into its constituent parts using only synthetic materials for this purpose. We have also indicated how such a device can be constructed. We have already used vesicles which are spontaneously formed microspheres composed of phospholipids or synthetic lipids. These vesicles are 40 Å thick and the particle itself is 500 Å in diameter. It may also be possible to use synthetic membranes, which were developed for artificial kidneys or desalinization membranes, and spun in the form of hollow fibers (16). The hollow fibers are the sites for the sensitizers and the medium

Can. J. Chem. Downloaded from www.nrcresearchpress.com by 210.87.254.5 on 09/06/12
For personal use only.

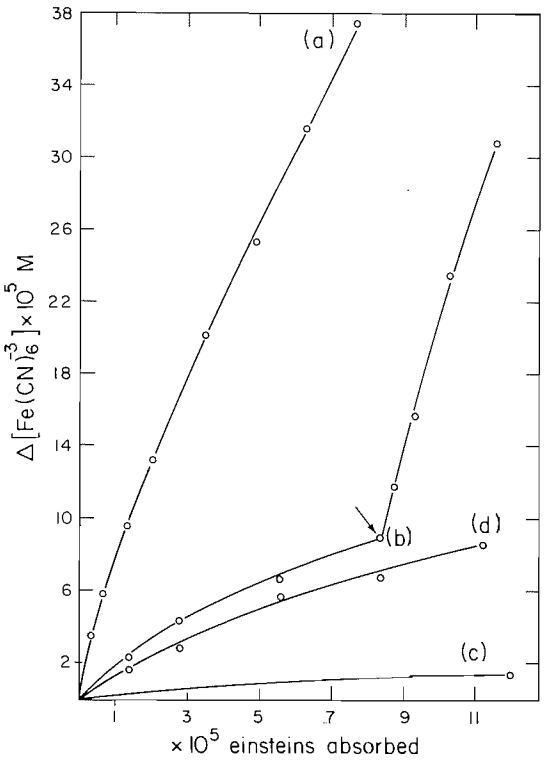

FIG. 9. Reduction of $K_3Fe(CN)_6$ as a function of light absorbed. (*a*) SiO_2 system including PVS^0 addition; (*b*) SiO_2 system. Arrow indicates time of PVS^0 addition. (*c*) homogeneous system; (*d*) NaLS micellar system.

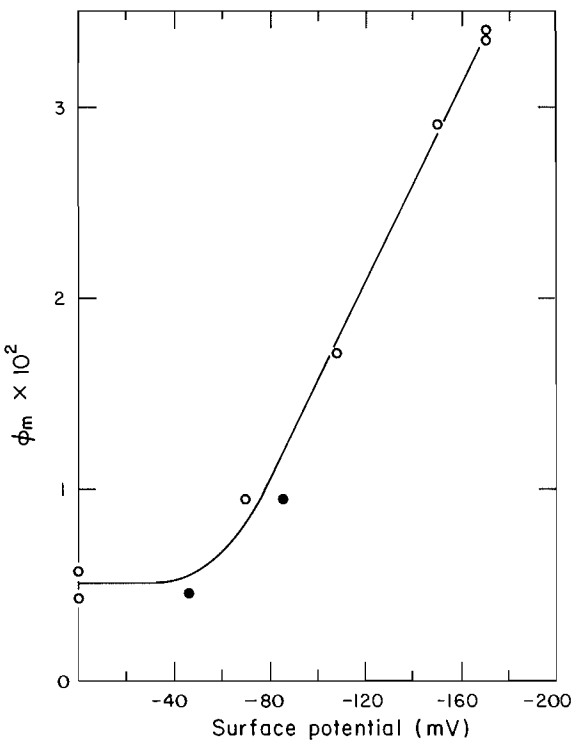

FIG. 10. Quantum yield for propylviologen, PVS^-, formation as a function of surface potential of negatively charged interfaces. (○) SiO_2 system; (●) NaLS micellar system.

through which the electrons can move. Our experiments used a hollow fiber originally synthesized for a desalinization membrane. We stained the fiber with oil-soluble porphyrin by swelling the fiber with an organic solvent (dioxane). The sensitizer (zinc tetraphenylporphyrin), when dissolved in the dioxane, penetrates the swollen fibers; the solvent is then washed out with water, leaving behind in the fiber the water-insoluble sensitizer. Therefore, it has been possible to create a stained fiber with a wall thickness of about 80 microns, containing a dyestuff which resists water. A substantial amount of sensitizer-dyestuff material is required in order to have one dyestuff molecule every 40 Å of fiber body. When an electron is removed from the outside of this hollow fiber, the hole may jump 40 Å each time to reach the other side.

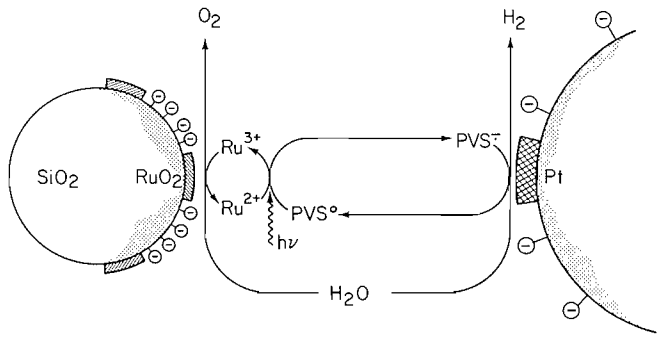

FIG. 11. Utilization of SiO_2 colloids in the photodecomposition of water.

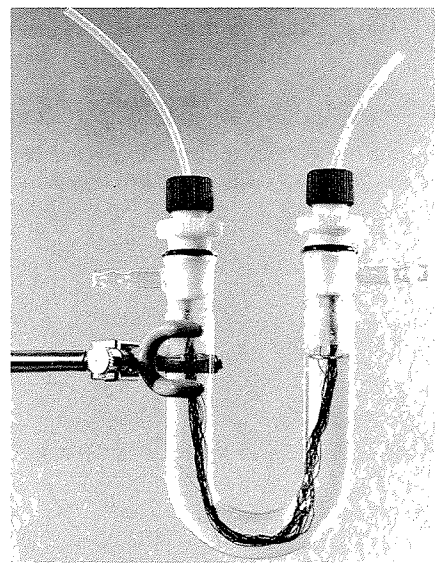

FIG. 12. Hollow fiber apparatus for photodecomposition of water.

The hollow fibers are mounted so the inside and outside can be reached separately (Fig. 12). In this prototype for the system, the inside of the hollow fibers is connected to the inside of the upper plastic tubes, and the outside is connected to the water layer which is accessible to the side-arms of the U-tubes.

With the hollow fiber (membrane) device for photoelectrochemically transferring electrons from one side to the other, it will be possible to place the catalyst for hydrogen production on one side and the catalyst for oxygen production on the other. The reactions have all been performed separately but not yet together in a single device.

Development of catalysts for artificial photosynthetic systems

Until recently, we have not used our knowledge of the natu-

Can. J. Chem. Downloaded from www.nrcresearchpress.com by 210.87.254.5 on 09/06/12
For personal use only.

ral catalysts used by the green plants for the generation of hydrogen from water and generation of oxygen as a byproduct. We have used the phase boundary idea, the surfactant sensitizer idea, the photoelectron transfer idea, and the charge migration idea, but not what we know about the function of the natural catalysts that produce the final products in the plant.

The natural catalyst for molecular hydrogen in plants turns out to be an iron–sulfur cluster of four iron atoms and four sulfur atoms hanging in a protein by mercaptide groups of the cysteine residues of the polypeptide. It is possible to construct a synthetic iron–sulfur cluster that is the catalyst for hydrogen production and this has been done electrochemically but not yet photochemically (17). However, we have recently used synthetic iron–sulfur clusters to determine their photoelectron accepting capability. If one of the synthetic iron–sulfur clusters, tetra[alkyl(aryl)mercapto-μ_4-sulfido-iron], is placed in the water solution with the ruthenium or zinc sensitizer, it quenches the fluorescence of the sensitizer either by energy transfer or by accepting an electron from the excited sensitizer. We propose that the latter mechanism is the correct one (18). We have thus indicated a hydrogen-generating system which does not require platinum as a catalyst by using the iron–sulfur clusters.

Not as much is known, however, about the oxygen-generating catalyst. Manganese is indicated, and experiments over many years have sought to determine the state of that manganese. At one time, we felt it was a binuclear manganese compound, but more recent experiments indicate that the manganese must also be in a cluster, containing at least two manganese (perhaps four, in actuality) because it is necessary to move four electrons from the water to make molecular oxygen.

With the idea that the oxygen-generating catalyst contains two manganese atoms, we synthesized the type of molecule(s) which would have the required characteristics. Our first efforts involved manganese atoms on a rigid bridge-type connection; this turned out to be unsuccessful (19, 20). We then turned our attention to constructing a flexible binuclear manganese compound in which the manganese atoms could change the distance between each other. This can be explained as follows: two manganese porphyrin molecules hooked together by a flexible chain could be in solution; two water molecules could enter, changing the distance between the manganese atoms in the porphyrin molecules, closing the hook so to speak. Then the electrons would be removed via the manganese atoms and the two oxygen atoms could be brought together to make oxygen (21).

We have synthesized a mononuclear surfactant manganese compound (22), and inserted it into a thin membrane together with a zinc porphyrin. By photoexciting the zinc compound it was possible to eject an electron from the zinc to an aqueous viologen acceptor (23). The oxidized zinc in the membrane then extracts an electron from the nearby manganese, also in the membrane, indicating that it is possible to oxidize the manganese catalyst by sensitized oxidation. This is similar to the process used to reduce the iron–sulfur clusters (catalysts) on the hydrogen evolution side. The experimental basis for this observation is shown in Fig. 13. The data indicate that the back-reaction between the reduced acceptor (viologen in the water) and photo-oxidized catalyst in the membrane is inhibited. This inhibition occurs by (*1*) organizing the manganese compound and the photosensitizer (zinc porphyrin) on one side of a membrane interface (Fig. 14), while the acceptor resides in the aqueous phase; (*2*) making the membrane interface negatively charged; and (*3*) using a zwitterionic acceptor, propylviologen sulfonate, whose reduction product is then repelled from the membrane surface. These experiments suggest that the back-reaction between the oxidized zinc sensitizer and the reduced propylviologen sulfonate acceptor is retarded by the negatively charged membrane (Fig. 14).

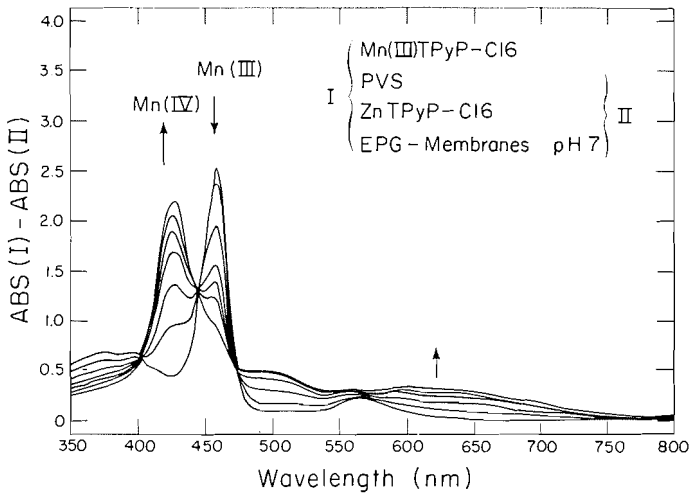

FIG. 13. Difference spectra between system I and system II after illumination.

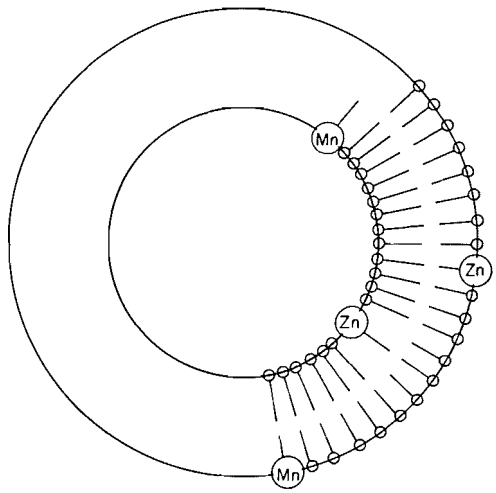

FIG. 14. Single unilamellar vesicle with diameter between 200 and 500 Å, prepared by sonication with indicated ratio between phospholipid and sensitizer of 86:3:1 with PVS added outside the vesicle. Phospholipid: MnTPyP-C16: ZnTPyP-C16 = 86:31; 10^{-3} *M* PVS outside, pH 7.

Conclusion

We can look forward to the creation of an artificial system for photosynthesis, using the principles of synthetic chloroplasts to mimic the way the green plant takes quanta to generate oxidizing power (oxygen) on one side of the membrane and reducing power (hydrogen) on the other. We have used analogues of most of the components of the natural photosynthetic system to achieve the synthetic chloroplasts: (*1*) The phase boundary concept, (*2*) the charge distribution idea, (*3*) electron transfer across the membrane via isoenergetic electron exchange (electron carriers), and (*4*) the use of two catalysts, one for the hydrogen evolution and the other for the oxygen evolution side. We have achieved, outside the green plant, all of

the parts of the natural system; it now remains to put them together into one device.

In our efforts to devise means for the photolysis of water using the light and creating hydrogen as a fuel, we have found that oxygen is generated as a byproduct. In actuality, molecular oxygen, because it is not a fuel, is not the material which is the most useful. It should be possible to use the electron transfer step sometime before molecular oxygen is formed to generate an intermediate oxidant such as a peroxide which is a more useful chemical reactant.

Therefore, it now appears that it will be possible to capture the energy of the sun for energy use (to make molecular hydrogen) and also for chemical use in the form of intermediate oxidants which are used in many chemical processes. The systems described accomplish both of the necessary requirements for a useful solar energy device: (*1*) The capture of the quantum and its conversion to some other energy form and (*2*) the storage of that energy for indefinitely long periods with the possibility of its recovery at will in some convenient form. The green plant has always performed these functions.

Acknowledgment

This work was supported by the Office of Energy Research, Office of Basic Energy Sciences, Chemical Sciences Division of the U. S. Department of Energy under Contract No. DE-AC03-76FS-00098.

1. M. CALVIN. Acc. Chem. Res. **11**, 369 (1979). Faraday Discuss. R. Soc. Chem. **70**, 383 (1980).
2. J. S. CONNOLLY (*Editor*). Photochemical conversion and storage of solar energy. Academic Press, New York. 1981.
3. J. KIWI, K. KALYANASUNDARAM, and M. GRÄTZEL. Struct. Bonding, **49**, 37 (1982).
4. W. E. FORD, J. W. OTVOS, and M. CALVIN. Nature, **274**, 507 (1978).
5. W. E. FORD, J. W. OTVOS, and M. CALVIN. Proc. Natl. Acad. Sci. USA, **76**, 3590 (1979).
6. F. SZOKA, JR. and D. PAPAHADJOPOULOS. Ann. Rev. Biophys. Bioeng. **9**, 467 (1981).
7. J. KIWI and M. GRÄTZEL. Angew. Chem. Int. Ed. Eng. **17**, 860 (1978).
8. W. E. FORD. Ph.D. thesis, University of California, Berkeley. 1980.
9. C. LAANE, W. E. FORD, J. W. OTVOS, and M. CALVIN. Proc. Natl. Acad. Sci. USA, **78**, 2017 (1981).
10. D. E. BAKER. M.S. thesis. University of California, Berkeley. 1982.
11. S. S. LEHRER. Biochemistry, **10**, 3254 (1971).
12. I. WILLNER, W. E. FORD, J. W. OTVOS, and M. CALVIN. Nature, **280**, 823 (1979).
13. I. WILLNER, J. W. OTVOS, and M. CALVIN. J. Am. Chem. Soc. **103**, 3203 (1981).
14. S. S. ATIK and J. K. THOMAS. J. Am. Chem. Soc. **103**, 3550 (1981).
15. P. A. BRUGGER, M. GRÄTZEL, T. GUARR, and G. MCLENDON. J. Phys. Chem. **86**, 944 (1982).
16. C. C. WAMSER, J. W. OTVOS, and M. CALVIN. Lawrence Berkeley Laboratory Report 12539, March 1981.
17. K. TANAKA, M. TANAKA, and T. TANAKA. Chem. Lett. Jpn. 895 (1981).
18. M.-J. JUN, R. WOHLGEMUTH, J. W. OTVOS, and M. CALVIN. To be published.
19. S. R. COOPER and M. CALVIN. J. Am. Chem. Soc. **99**, 6623 (1977).
20. S. R. COOPER and M. CALVIN. J. Am. Chem. Soc. **100**, 7248 (1978).
21. J. A. GRANT. Unpublished results.
22. Y. OKUNO, W. E. FORD, and M. CALVIN. Synthesis, **7**, 537 (1980).
23. R. WOHLGEMUTH, J. W. OTVOS, and M. CALVIN. Proc. Natl. Acad. Sci. U.S.A. **79**, 511 (1982).

Can. J. Chem. Downloaded from www.nrcresearchpress.com by 210.87.254.5 on 09/06/12
For personal use only.

Molecular models for recombination and disproportionation of radicals[1]

SIDNEY W. BENSON

Hydrocarbon Research Institute, University of Southern California, Los Angeles, CA 90007, U.S.A.

Received July 5, 1982

This paper is dedicated to Professor Harry E. Gunning on the occasion of his 65th birthday

SIDNEY W. BENSON. Can. J. Chem. **61**, 881 (1983).

The modified Gorin model of recombination as a long range interaction of weakly bound radicals, constrained only by steric forces, is rederived to give a collision impact parameter 11% larger than r_{max}, the separation at the centrifugal maximum. This larger impact parameter resolves some of the earlier difficulties with secondary and tertiary radicals. By imposing a new constraint, that the orientation of the radicals be such as to permit exchange forces to act, a new model is developed in which $k_r = 1/4\ Z_r\ \alpha$, where α represents the product of fractions of active surface areas of each radical available for bonding. Excellent agreement is obtained in estimating values of k_r.

Analysis of disproportionation is made to show that it cannot be described by the tight transition state but must also be governed by similar, long range exchange forces between the bond being attacked and the same "active surface" of the abstracting radical. Using an ad hoc radius for C$^{\cdot}\cdots$H—C equal to 4 Å it is possible to reproduce the data on alkyl radical disproportionation to within ±10%.

The model predicts a small decrease in rate of recombination with increasing temperature. This decrease is more pronounced for bulkier radicals and at higher temperatures (>900 K).

SIDNEY W. BENSON. Can. J. Chem. **61**, 881 (1983).

On a procédé à une nouvelle dérivation du modèle de recombinaison de Gorin modifé en tant qu'interaction à longue distance des radicaux faiblement liés et encombrés uniquement par des forces stériques dans le but de donner un paramètre d'impact collisionnel de 11% supérieur au r_{max}, la séparation au maximum centrifuge. Ce plus grand paramètre d'impact résoud quelques-unes des difficultés antérieures rencontrées avec les radicaux secondaires et tertiaires. En imposant une nouvelle contrainte, à savoir que l'orientation des radicaux doit être telle qu'elle permet aux forces d'échanges d'agir, on a mis au point un nouveau modèle dans lequel $k_r = 1/4\ Z_r\alpha$, où α représente le produit des fractions des surfaces actives de chaque radical disponible pour la liaison. On obtenu un excellent accord en évaluant k_r.

On a analysé la dismutation pour montrer qu'on ne peut pas la décrire par l'état de transition intime mais qu'elle doit aussi être gouvernée par des forces d'échange à longue distance semblables entre le lien attaqué et la même "surface active" du radical qui provoque l'élimination. En utilisant un rayon "ad hoc" pour C$^{\cdot}\cdots$H—C égal à 4 Å, il est possible de reproduire les données relatives à la dismutation des radicaux alkyles avec une marge d'erreur de ±10%.

Le modèle prédit une légère diminution de la vitesse de recombinaison quand la température augmente. Cette diminution est plus prononcée pour les radicaux encombrés et se manifeste à des températures plus élevées (>900 K).

[Traduit par le journal]

Introduction

Transition State Theory permits us to model chemical reactions as though we were modeling equilibria. That is, we can treat the metastable short-lived transition state complex as though it were a normal molecule. Almost two decades of testing such models against experimental data have seen the development of what are known as "tight" and "loose" transition states. The loose transition state was originally developed by Gorin (1) to describe the recombination of methyl radicals and has since been generalized to describe all radical–radical recombinations (2). The loose transition state resembles two weakly interacting radicals, with their active centers separated by $r^{\ddagger}$ about 2.6 to 3.2 times the normal bonding distance r_0. The relation employed has been derived (2) as:

$$[1] \quad r^{\ddagger}/r_0 = (6V_0/RT)^{1/6}$$

where V_0 is the potential energy of the bond being formed and T is the absolute temperature. The distances so obtained for $r^{\ddagger}$ correspond, curiously enough, to van der Waals' distances for many molecules. At $r^{\ddagger}$ the recombining centers have a potential of interaction of about $RT/2$, a very weak interaction.

At the other end of the reaction spectrum is the tight transition state which has been found to characterize well the transition states[2] for metathesis reactions between molecules and radicals, at least for those reactions whose intrinsic activation energies exceed 1–2 kcal. With metathesis we include the addition of radicals or atoms to unsaturated systems which may be looked upon as the metathesis of π-bonds as opposed to σ-bonds which characterize atom transfers. From an electron point of view both metathesis and addition reactions are 3-center, 3-electron systems:

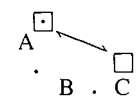

σ-Bond metathesis

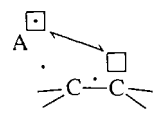

π-Bond metathesis

The bonding distances in these reactions are taken as 0.3 Å larger than normal bond lengths and stretching and bending force constants are assumed to be 1/2 their normal values so that the corresponding frequencies are about 0.7 of their normal value.

[1]This work has been supported by grants from the National Science Foundation (CHE 7826623) and the U.S. Army Research Office (DAAG 27-76-G-0195).

[2]In general it is possible to predict the *A*-factors and their temperature dependence within an uncertainty of a factor of 2 or less. The chief uncertainty arises from the uncertainty in knowing whether one is dealing with a linear or bent transition state A$\cdots$B$\cdots$C.

Can. J. Chem. Downloaded from www.nrcresearchpress.com by 210.87.254.40 on 09/06/12
For personal use only.

Can. J. Chem. Downloaded from www.nrcresearchpress.com by 210.87.254.40 on 09/06/12
For personal use only.

In the present paper we will discuss a model for radical–radical interactions which will have characteristics of both the loose and tight transition states depending on whether we are considering recombination or disproportionation, respectively. What is most striking about these reactions is that they appear to have zero activation energy for both channels, recombination and disproportionation. Highly branched radicals such as *tert*-butyl appear to deviate from this general rule, showing a small decrease in rate of recombination with increasing temperature (6). Also striking about radical–radical reactions is that the rate constants generally fall between the limits of $10^{10.5}$ to $10^{8.0}$ L/mol-s, for all radical species. In fact, a mean value of $10^{9.5\pm0.5}$ would fit 90% of all systems studied.

Recombination of radicals; collision dynamics

Despite intensive efforts extending over a 30-year period, few if any radical–radical rate constants are known to better than a factor of 2 in accuracy. While recent studies show a greater reproducibility, they still show differences of this order between different experimental techniques (3). The most extensively studied system has been methyl recombination, for which 11 separate studies since 1967 yield values for k_r centered about $10^{10.4}$ L/mol-s near 300 K. Values range from $10^{10.38}$ to $10^{10.76}$ (3).[3] Studies at higher temperatures suggest a small decrease in k_r with increasing temperatures. This is difficult to separate from the fall-off in rate with pressure at temperatures above 900 K.

Because of the fact that k_r values are near collision frequencies, it has been useful to compare k_r with collision frequencies corrected for electronic degeneracies. If we write k_r in these terms:

$$[2] \quad k_r = g_e Z_r \alpha$$

then g_e is the ratio of electronic partition functions $g^{\ddagger}/g_1g_2$ for the transition state and radicals. It is usually equal to 1/4, corresponding to the spin factors for radicals which has spin 1/2 forming a singlet recombination product. Z_r is the collision frequency using $r^{\ddagger}$ (eq. [1]) for the collision diameter, while α is the steric factor for the collision and reflects the fact that, at the given separation of active centers $r^{\ddagger}$, not all angular orientations of both radicals are possible. In simple cases it is possible to calculate α directly (2) as a product of the fractions of the solid angles available to each species in the transition state. This modified Gorin model has been called "the restricted, free rotor model" and has been derived from an oversimple model of two point particles moving under the influence of central forces (2). The equation of motion for such a system can be described by:

$$[3] \quad E_0 = \frac{1}{2}\mu(\dot{r})^2 + E_0\frac{b^2}{r^2} - 2\frac{V_0 r_0^6}{r^6} = \frac{1}{2}\mu(\dot{r}_0)^2$$

where r is the radial separation of the point particles with initial relative kinetic energy E_0, impact parameter b, normal bond length r_0, and potential energy of dissociation V_0. E_0b^2/r^2 represents the centrifugal force in the polar trajectory; μ is the reduced mass of the system. The term in V_0 assumes that the valence forces can be represented by an r^{-6} potential at large distances.

In the usual derivation one calculates the forces by differentiation of the potential energy and calculates r_{max}, the separation at which the net force is zero. This is the centrifugal maximum in the potential function where the centrifugal and bonding forces are just equal. At smaller distances the bonding forces are larger, while at longer distances the repulsive centrifugal forces are dominant.

The trajectory described by eq. [3] (which neglects shorter range repulsive forces) is a complex, but smooth, path characterized for each initial set of values of E_0 and b by a distance of closest approach r_c. If, in the course of the trajectory, $r \leq r_{max}$ and $\dot{r}_{max} \leq 0$, then, since the forces are attractive in this region, $\dot{r}$ will remain negative and the trajectory will speed in towards the origin with increasing radical velocity. Note that, since we start with separated partices, $\dot{r}_0$ is initially negative. These trajectories resemble very much those for the Langevin Model for ion–molecule encounters which, in fact, historically provided the inspiration for the model (1). For real molecules the inclusion of short range repulsive forces in eq. [3] will prevent encounters at the origin.

While r_{max} is the minimum collision diameter required for a close encounter it is not the impact parameter for collision. One can calculate the latter by imposing two conditions on the collision. We want to know, for a given E_0, what impact parameter $b^{\ddagger}$ will satisfy the condition that $r_{max} \leq r_c$. On applying this to eq. [3], we find a result very similar to eq. [1]:

$$[4] \quad b^{\ddagger} = 1.5(V_0/E_0)^{1/6}$$

If we take $\langle E_0 \rangle = RT$, then

$$[5] \quad b^{\ddagger} = 1.5(V_0/RT)^{1/6}$$

Although functionally the same as eq. [1], the coefficient is about 11% larger and hence the cross section is about 23% larger.

While functionally of the correct form, eq. [5] does not represent the result of proper averaging of $b^{\ddagger}(E)$ over a Boltzman population. This latter is given by:

$$[6] \quad \langle b^{\ddagger}(E) \rangle = \int_0^{\infty} b^{\ddagger} P(E) dE$$

and using the appropriate P(E) (9)[4] we find:

$$[7] \quad \langle b^{\ddagger}(E) \rangle = 1.52\left(\frac{V_0}{RT}\right)^{1/6}$$

a result which differs from eq. [5] by about 1.5%

A somewhat larger correction is found when we take the proper average of Z_r over a Boltzman population. Z_r is given by (9):

$$[8] \quad Z_r = \pi(b^{\ddagger})^2 c_r$$

where c_r is the relative translational velocity of the colliding pair ($\dot{r}_\theta$ in eq. [2]). Replacing $b^{\ddagger}$ by its value from eq. [4] and setting $E_0 = 1/2\mu c_r^2$, we have:

$$[9] \quad Z_r = \pi(1.5)^2\left(\frac{2V_0}{\mu}\right)^{1/3}\langle c_r \rangle^{1/3}$$

The Boltzman average is then:

$$[10] \quad \langle Z_r \rangle = 2.25\left(\frac{2V_0}{\mu}\right)^{1/3}\langle c_r \rangle^{1/3}$$

[3] All the literature to the end of 1977 will be found in Vol. II; Vol. I summarizes data on radical metathesis.

[4] It can be shown that

$$\langle C^n \rangle = \left(\frac{2RT^{n/2}}{\mu}\right)\frac{\Gamma[(n+3)/2]}{\Gamma(3/2)}$$

$$[11] \qquad = \frac{2.25}{(\mu/2)^{1/2}}(V_0)^{1/3}(RT)^{1/6}(1.02)$$

This result is 10% smaller than the result obtained by averaging c_r and $b^\ddagger$ separately and then substituting in eq. [8].

An observation on the dynamics of the encounter described by eq. [3] is appropriate. In the absence of any forces, $r_c = b^\ddagger$ is realized at $\theta = 90°$ when the particles pass each other. During this entire trajectory $r \geq b^\ddagger$. In the presence of attractive forces, r will become less than b at $\theta \doteq 90°$. We observe that $b^\ddagger = 1.11\ r^\ddagger$ marks the boundary line between close and distant encounters.

Methyl radical recombination

For CH_3 recombination, $\Delta H_r^\circ = -90.4$ kcal/mol at 300 K (4). Correcting this to 0 K and for zero point energy we find $V_0 = 96$ kcal so that $r^\ddagger$ (300 K) = 4.84 Å and $\langle b^\ddagger \rangle = 5.37$ Å. Using $g_c = 1/4$ we derive $Z_r = 2.8 \times 10^{11}$ L/mol-s and $k_r = 7.0 \times 10^{10}$. Comparing this with the experimental mean value of 2.4×10^{10} at 300 K we see that $\alpha = 0.34$, implying that 0.66 of all the possible geometric conformations of two CH_3 groups with carbon atoms 5.37 Å apart will not lead to recombination. At this separation, however, we can find that the hindered free rotor model gives no angular correction, that is, $\alpha = 1$. Using a 1.2 Å van der Waals' radius for H, we find that the methyl radicals can rotate freely at $b^\ddagger$ (C—C) = 5.37 Å. We could conclude that the potential function is incorrect and that the true $b^\ddagger$ (C—C) = 3.42 Å which would then give the observed k_r for $\alpha = 1$. This, however, is not an acceptable solution. At 3.42 Å, the methyl radicals are appreciably constrained in their orientation and α would have to be appreciably less than 1.

We should like to suggest an approximate solution to this dilemma for which again a relatively simple model may be adopted. The hindered free-rotor model is a necessary but not a sufficient condition for radical recombination. In order for recombination to occur, exchange forces must be operative between the two radicals. This in turn requires an overlap between the unoccupied electron orbitals. A conformation of two CH_3 radicals in which a H-atom lies along the line of centers, while not involving any van der Waals' repulsion at $b^\ddagger$, $b^\ddagger$ (C—C) = 5.37 Å, also does not permit orbital overlap

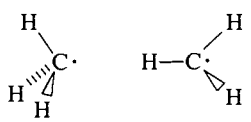

(noninteracting methyl radicals, $r = b^\ddagger$)

and thus cannot lead to the weak attraction required by the Gorin Model. Such an analysis suggests a modified model in which we draw a sphere centered on the free radical atom; for $\dot{C}H_3$ it is $\dot{C}$. The radius of this sphere is taken as $r = b^\ddagger/2$. We can now assign the surface of this sphere as active or inactive, depending on whether it is occupied by free electron density (active) or closed shell electrons (inactive). A critical collision for recombination is then considered to occur when two such spheres make contact with their active surfaces touching. In such configurations orbital overlap may occur. When these active areas are in contact, attraction is possible and recombination can take place.

If we represent by β the fraction of the "surface area" of the CH_3 radical of radius = 5.37/2 = 2.68 Å (centered at C) which is active, then $(1 - \beta)$ is the inactive fraction and $\alpha \leq \beta^2$. The inequality is used since, for radicals more complex than CH_3,

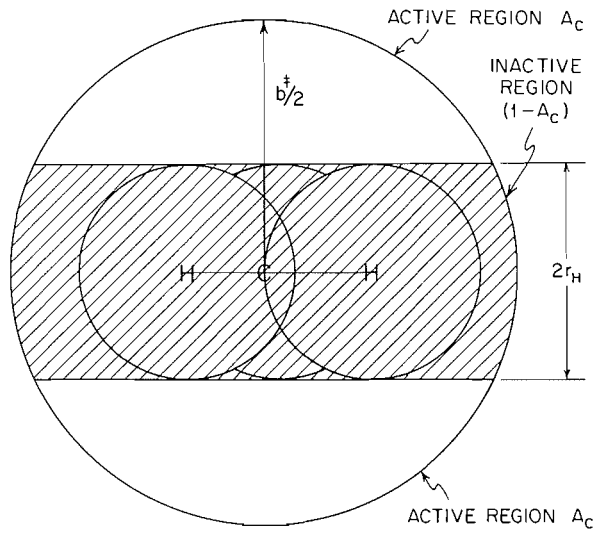

FIG. 1. Methyl radical in projection showing regions active and inactive (shaded) in recombination. r_H is the van der Waals' radius of the H atom; $b^\ddagger$ is the impact parameter for recombination. The third H atoms is behind the two shown.

nonbonded interactions between other portions of the radicals may inhibit contact between the active areas.[5] Using an experimental $\alpha = 0.34$ for CH_3 recombination, we can estimate the active area as $\beta = 0.66$ and the exluded region due to the H atoms $(1 - A) = 0.34$ of the surface area. Figure 1 shows such a sphere for $\dot{C}H_3$.

Is this physically reasonable? A simple model suggests that it is. If we take, as a model of the CH_3 radical, one which is planar so that the H-atoms form a belt around the center then we can project the area of this belt as a zone, symmetrical about the center of the sphere with a width equal to the van der Waals' radius of H of 1.2 Å. This belt subtends a zenith angle of approximately 27° about either side of the equator of this 2.68 Å sphere centered on C, and the zone would subtend 0.45 of the total surface area for $\beta = 0.55$ and $\alpha = 0.30$, in excellent agreement. If we assign to CH_3 a tetrahedral geometry and make the same calculation but assume we have two active areas, a large one with azimuth angle of 83° and a smaller one on the back of the CH_3 with azimuth angle of 44°, the total active area is 58% and $\alpha = 0.34$, not much different. Both models assume that front and back of the CH_3 radical are available for overlap and yield a recombination value differing by about 20% from the "best" observed value.

Baulch and Duxbury (5) have recently made a survey and analysis of k_r for CH_3 radicals and proposed a preferred value of log $k_r = 10.38$ in the range 250–420 K.

From an electron orbital point of view such a model corresponds to an orbital centered on carbon and occupied by a single electron. Pauli exclusion guarantees that this odd electron will be restricted to a volume in space outside the van der Waals' region occupied by the other bound electrons in the system, namely the electron-pairs in the adjacent C—H bonds. This would account for the "shadowing" effect of the neighboring bonds and the restriction of the "active" area or volume to that region in space available to the odd electron.

In Table 1 we list values for k_r taken from the literature together with calculated values of β^2 and α_{exp}. For two different

[5] This is because, at the cone angle of 80°, the axial H atoms are nearly in van der Waals' contact with each other.

Can. J. Chem. Downloaded from www.nrcresearchpress.com by 210.87.254.40 on 09/06/12
For personal use only.

TABLE 1. Restricted free rotor model with correction for electron overlap

Radicals	log k_r (exp) (L/mol-s)[a]	$r^{\ddagger}$ (Å) (calcd)	log $g_e Z_r$ (L/mol-s)[b]	α[c] (exp)	$\beta_i\beta_j$ (calcd)	β_i (calcd)
2 CH_3	10.4	5.37	10.75	0.34	0.30	0.55
2 C_2H_5	10.0	5.29	10.60	0.20	0.18	0.42
2 i-C_3H_7	9.7	5.24	10.50	0.13	0.10	0.31
2 *t*-Bu	9.1	5.19	10.45	0.028	0.029	0.17
Me – *t*-Bu[d]	10.2±0.3	5.30	11.05	0.12	0.10	0.55/0.19
2 Allyl	9.9	4.72	10.75	0.12	0.16	0.4
2 CF_3	9.7	5.44	10.55	0.15	0.14	0.38
2 CCl_3	9.6	5.34	10.30	0.12	0.07	0.27
Cl+CCl_3	9.8	6.02	10.65	0.23	0.27	0.27

[a] Experimental values from ref. 3.
[b] Calculated using $r^{\ddagger}$ (calcd) and $g_e = 1/4$. $Z_r = \pi(r^{\ddagger})^2\bar{v}/\sigma$ where $\bar{v}$ = relative velocity at 300 K and $\sigma = 2$ for identical radicals.
[c] From experimental data and eq. [2].
[d] Using dissociation rate constant of ref. 10, of a bond dissociation energy of 83.5 kcal/mol, and an estimated $\Delta S^{\circ}_{300} = -45 \pm 1.5$ eu to calculate k_r at 800 K.

radicals recombining, $\dot{R}_i$ and $\dot{R}_j$, we use the product $\beta_i\beta_j$.

tert-Butyl radical recombination

Among the lowest values observed for the rate of radical recombination is that for *t*-Bu. While some experimental values have shown an alarming spread, the most recent and direct measurements are centered about k_r (*t*-Bu) = 1×10^9 L/mol-s with an uncertainty of about a factor of 2 (3). We calculate $r^{\ddagger}$ = 5.19 Å using a value of V_0 estimated at about 77 kcal/mol. This gives $\langle Z_r \rangle = 3.6 \times 10^{10}$ L/mol-s and hence $\alpha = 0.028$ and $\beta = 0.16$. If we construct a bent model for *t*-Bu with a cone angle of 80°, about half-way between tetrahedral and a flat model, we estimate an active surface fraction β equal to 0.17. We do not include the back side of the *tert*-butyl but only the open side.[5] We also fix the geometry of the H-atoms as corresponding to three axial and six equatorial. This yields β^2 = 0.029, in excellent agreement with the experimental result. Volumes for ethyl and i-propyl may be calculated in similar fashion or else by interpolating the values of β between *tert*-butyl and methyl. Table 1 shows values estimated in this fashion. The agreement with experiment, as evidenced by the comparison of β^2 or $\beta_i\beta_j$ with α, is within the experimental uncertainty for all of these systems.

The effect of temperature on k_r is complex. Overall, the model would appear to predict an increase in k_r varying as $T^{1/6}$. This arises from an increased collision velocity going as $T^{1/2}$ and a decreased collision cross section going as $b^2 \propto T^{-1/3}$. In the range from 300 K to 600 K, over which most measurements have been made, the increase would come to a factor of $2^{1/6}$ = 1.12, too small an effect to be measured. However, as $b^{\ddagger}$ decreases, the collision radius decreases with it and the projected van der Waals' area of the bound atoms such as H in CH_3 becomes a larger part of the inactive surface. Hence β decreases and in the case of CH_3 radicals, which are simpler than most, we estimate a net decrease in recombination rate of the order of $T^{-1/6}$ or about 12% at 600 K.

For bulkier radicals such as *tert*-butyl the situation must be examined more closely. The collision radius we have calculated, of $5.19/2 \simeq 2.60$ Å at 300 K, is smaller than the largest van der Waals' dimension, which is about 3.20 Å. Thus the methyl groups project somewhat beyond the surface of our effective collision sphere and the calculated value of β^2 in Table 1 ignores this. In those conformations where these methyl boundaries touch each other there is an added van der Waals' constraint on the orientation for which a rough estimate reduces β^2 by about 8% at 300 K. At 600 K, with $b/2$ reduced by 12% to 2.32 Å, the van der Waals' repulsion is appreciably larger.

Some efforts have been made to measure CH_3 recombination in shock tubes near 1500 K. At this temperature b = 4.11 Å and $\beta^2 \leq 0.18$, a reduction of a factor of 3 in active area over that at 300 K. However, the effect on k_r is only a reduction of a factor of 2.3 because of the increase in collision rate. No firm data are available for comparison (8).

For many radicals, efforts have been made to deduce recombination rate constants from Arrhenius *A*-factors for the reverse reaction, measured at high temperatures, and the overall entropy change in the reaction. In the case of *tert*-butyl radicals, at 1000 K we deduce $b^{\ddagger}$ = 4.26 Å and there is now considerable restriction in the transition state, both on the mutual orientation of the two radicals and on their internal rotation. In parallel conformation the methyl groups on the opposing *t*-Bu radicals are only 5.3 Å apart (assuming tetrahedral geometry), yielding an effective active area of about 0.07 of the surface. The recombination rate would be reduced by a factor of about 6 compared to its value at 300 K. Data in the range 700–800 K suggest that this may be indeed the case (6).

Radical disproportionation; activation energy

Radical disproportionation is generally a very exothermic reaction with no activation energy and very large rate constants. One which has been well studied, relative to recombination, is that between C_2H_5 radicals. The ratio of rates of disproportionation to recombination, k_d/k_r is 0.14 over a very broad temperature range (3) and is also relatively insensitive to solvent or gas phase. The reaction is exothermic by 61 kcal/mol and if we adopt $k_r = 1 \times 10^{10}$ L/mol-s, then $k_d = 1.49 \times 10^9$ L/mol-s within the same accuracy with which k_r is known. Values for i-propyl and *tert*-butyl are somewhat higher, by factors of about 1.5 and 2 respectively (3). Since these are metathetical reactions, it is instructive to compare them with the known metathesis of radicals with molecules.

Most H-atom metathesis of alkyl radicals with hydrocarbons have intrinsic activation energies near 10 kcal, 90% of the known values lying within ±3 kcal of this number. They are not very sensitive to the exothermicity of the reaction except when $\Delta H \sim 0$, such as for $CH_3 + CH_4$, when they tend to reach maximum values near 14 or 15 kcal (3). Because C—H bond

Can. J. Chem. Downloaded from www.nrcresearchpress.com by 210.87.254.40 on 09/06/12
For personal use only.

strengths lie in the range 84–105 kcal/mol, the exothermicities of metatheses are in the range 0–20 kcal/mol, considerably less than that for disproportionation.

It is of interest to try to understand the reason that radical disproportionations have zero activation energy. In the usual metathesis reaction, we change from the reactants in which we have two bonding electrons in the σ-bond being attacked to the tight transition state in which we have two one-electron bonds. Thus the number of bonding electrons is constant. The extra

$$\square \leftarrow\cdot\rightarrow \boxdot$$
$$A\cdot + B{:}C \rightleftharpoons [A\cdot B\cdot C]^{\ddagger} \rightleftharpoons A{:}B + C\cdot + \text{heat}$$

electron, initially on the attacking radical in the transition state is shared between the entering and leaving groups or atoms. It has been found that if either or both of these is a strong electrophile, the activation energy is thereby decreased (7). It has been suggested that the intrinsic activation energy in these reactions arises from the repulsion between the nonbonding electron and one of the two bonding electrons with which it has a similar spin orientation, essentially a type of triplet repulsion. The situation in disproportionation shows an interesting difference. Again, using two ethyl radicals, we can picture the electron distribution as:

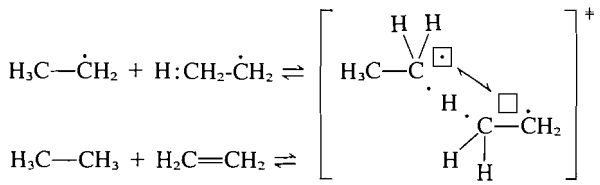

The nonbonding electron can be displaced into an empty orbital associated with the near-neighbor carbon atom as shown, or even begin to participate in the formation of the π-bond, a bonding orbital. This near-neighbor carbon is thus acting as an electrophile and converting a nonbinding electron into a bonding electron. However one interprets such a model, it seems quite reasonable that the activation energy is lowered relative to metathesis and not surprising that it is zero, considering the large exothermicity of the overall reaction.

There are not too many cases reported of disproportionation between radicals involving transfer of atoms other than H. In the few cases that are known of Cl atom transfer, the activation energies reported are either zero or not more than 0.5 kcal (3). A number of reactions are classified as metatheses which are really radical recombinations followed by dissociation. Thus the reaction $H + HO_2 \rightarrow 2OH$, while overall involving O atom transfer, is really a radical recombination.

$$H + HO_2 \rightleftharpoons (HO_2H)^* \rightarrow 2OH$$

Radical disproportionation A-*factors*

The Arrhenius *A*-factor for disproportionation reactions turn out to be anomalously large compared to normal metathesis reactions. Thus, the tight transition state used to characterize metathesis yields *A*-factors of the order of 10^7 to 10^8 per H-atom, at least a factor of 10 lower than the values observed for disproportionation. If we calculate the *A*-factor for ethyl disproportionation by the usual procedure (Table 2), we estimate a value of $10^{7.9}$ L/mol-s, about a factor of 20 lower than the observed value.

Moreover, the usual tight transition state does not give us much flexibility. With 2 one-electron bonds in the C·H·C configuration, the neighboring groups attached to the carbon atoms are at most about 2.8 Å apart (using $r(C\cdot H) = 1.4$ Å) and hence very close to van der Waals' contact. Bending the C·H·C angle by 40° would achieve this if only H atoms were attached to the carbon atoms.

An even more dramatic view of these *A*-factors is afforded by the *A*-factor for the reverse reaction. In the case of ethyl disproportionation this would be the metathesis of C_2H_6 with C_2H_4:

$$C_2H_6 + C_2H_4 \rightarrow 2C_2H_5$$

The entropy increase in this reaction is 9.4 eu so that, using $10^{9.1}$ L/mol-s as the *A* factor for the reverse reaction, we calculate $A = 10^{11.2}$ L/mol-s! If we assign the two partners a collision diameter of 5 Å, the *A*-factor would correspond to the total collision rate at 300 K!

Transition state theory is of course a more sophisticated picture of collision theory. The low *A*-factors calculated for metathesis merely reflect the steric inhibition placed on a possible collision. One can make a direct collision calculation which demonstrates this. If we require a 1.4 Å separation in the C—H bond to be formed, then we can calculate the collision rate for such an event subject to steric constraints. For $2C_2H_5$, assuming 6 abstractable H atoms (3 on each ethyl), we can calculate $k_d = 3.8 \times 10^{10}\ \beta_H\beta_C$ L/mol-s (for singlet collision). Here $\beta_H\beta_C = \alpha$, the steric requirements on the possible orientation of each partner in the collision. If we allow each partner to undergo independent rotations about a fixed (C—H) collision geometry equal to an azimuthal deflection of 30°, we can calculate $\alpha = 4.5 \times 10^{-3}$ and $k_d = 1.8 \times 10^8$ L/mol-s. This is about 2.5 times larger than the transition state model because 30° is too high a flexibility for the assigned (C—H) contact distance. If we had restricted this to 24° we would have recovered the transition state result. It is still about a factor of 10 less than the observed k_d (C_2H_5).

All of these results imply that the interaction between two ethyl radicals must occur at larger separations than we have been calculating. We gain some idea by looking at the product ($\sigma^2 = \beta_H\beta_C$). The chosen values gave us a product 10 times too small. Hence $\sigma = \beta_i$ ($i = 1, 2$) must be increased about three-fold to reproduce the data. For example, if we make $r(C—H) = \sigma = 4.3$ Å, keeping β_i fixed or increasing both appropriately, we could reproduce k_d. At distances like 4.3 Å, however, van der Waals' interactions between hydrocarbons are negligible compared to *RT* and there is no reason why this distance should be significant. Let us suppose, however, that free radicals have a net dipole moment. If they are not exactly planar we would expect a net dipole along the electron orbital. Since the C—H bond has a small dipole moment we would then expect a dipole–dipole interaction which could be represented by:

$$[12] \quad E_{d-d} = \frac{2\mu_1\mu_2\cos\gamma}{r_{12}^3}$$

where γ is the azimuth angle between the C—H bond and the electron orbital dipole. Reasonable dipole moments for these would be 0.32 D for the C—H bond and 1.5 D for the C· moment. Let us assume that these are centered in the midpoint of the C—H bond and the carbon nucleus, respectively, and both oriented along their respective bond directions. Such an interaction is now relatively long range and begins to resemble the recombination model. We can look for the distance at which this interaction is of the order of *RT* at 300 K, assuming

Can. J. Chem. Downloaded from www.nrcresearchpress.com by 210.87.254.40 on 09/06/12
For personal use only.

TABLE 2. Tight transition state calculation of A-factor for ethyl disproportionation
$2C_2H_5 \rightleftarrows [CH_3—CH_2 \cdot H \cdot CH_2—CH_2]^{\ddagger}$

Degree of freedom	Correction to $\Delta S^{\ddagger}_{300}$ (eu)[a]
Symmetry; R ln 3	2.2
External rotation, R ln 2	1.4
1 barrier $V_0 \rightarrow 0$ kcal	1.4
1 barrier $V_0 \rightarrow 0.5$ kcal	1.3
1 barrier $V_0 \rightarrow 1.5$ kcal	0.8
4 C—C—C bond decrease by 0.7 in frequency	2.8
Reaction coordinate: (C—C) stretch at 900 cm^{-1}	−0.2
	Total 9.7 eu

$\Delta S^{\ddagger} = -33.0$ eu (correct to concentration units by +8.4 eu)

$$A_{300} = \left(\frac{ekT_0}{h}\right) e^{\Delta S^{\ddagger}/R} = 10^{7.9} \text{ L/mol-s}$$

[a] $\Delta S^{\ddagger}$ for model reaction using n-C_4H_{10} to represent transition state: $\Delta S^{\ddagger}_{300} = -42.7$ eu

TABLE 3. Steric factors for radical disproportionation

Radical pair	log k_d[a] (L/mol-s)	Reduced mass (amu)	$(\beta_C/\beta_{Me})_{obs}$	$(\beta_R/\beta_{Me})_{calcd}$[b]
$CH_3 + C_2H_5$	9.15	10.0	1	1.00 (0.55)
$C_2H_5 + C_2H_5$	9.15	14.5	0.8	0.76 (0.46)
i-Pr × i-Pr	9.4	21.5	0.6	0.56 (0.31)
t-Bu × t-Bu	9.5	28.5	0.42	0.34 (0.19)

[a] Data from ref. 3 except for $CH_3 + C_2H_5$ for which $k_d/k_r = 0.04$ is known and we have estimated k_r from the geometric mean law $k_{r12} = 2(k_{r11}k_{r22})^{1/2}$.
[b] Steric factors taken from Table 1 for radical recombination. Absolute fractions for each radical are shown in parentheses (from Table 1).

that $\gamma \leq 30°$. We find (eq. [3]) that $r_{12} \leq 2.75$ Å for a C···H distance of 2.20 Å which corresponds to a C···H···C distance of about 3.9 Å. At these larger distances there is much less steric inhibition and an azimuthal angle between the two ethyls of even up to 40° can be accommodated. In fact $r^{\ddagger}$ (C·H) = 2.2 Å, together with azimuthal angles of 40°, will reproduce k_d for ethyls.

In the absence of precise information on the Ċ moment let us proceed empirically. In Table 3 are collected some experimental data on alkyl radical disproportionations. We can represent k_d in the same way in which we treated k_r:

$$[13] \quad k_d = \frac{1}{4}Z_d\alpha = \frac{1}{4}Z_d\beta_C\beta_H$$

Z_d is a "hard sphere" collision rate $= \pi\sigma_d^2\,\bar{v} = \pi\sigma_d^2 (8RT/\pi\mu)^{1/2}$ in which μ is the reduced mass of the collision and σ_d the collision diameter. For nonidentical radicals two possible reactions are possible. Z_d includes the correction for the fact that disproportionation of two identical radicals can occur from either one through an asymmetric transition state. β_C and β_H are the fractions of solid angle available to the collision pair at the carbon radical (β_C) and abstracted H respectively. Without detailed knowledge, there are three parameters in eq. [13], σ_d, β_C, and β_H. We can reduce these by making a relative comparison.

Let us assume that in the cases listed in Table 3, the same number of H atoms in each CH_3 group are available for disproportionation and that β_H is a transferable constant for a methyl group. Ethyl, i-Pr, and *tert*-butyl then have β_H factors in the simple ratio 1:2:3 reflecting the number of available methyl groups. If we further assume that the dynamical, long range interaction is the same, then σ_d is the same for all pairs. By taking ratios of k_r for the different pairs relative to methyl, correcting for reduced masses and numbers of methyls, we can deduce ratios of β_R/β_{Me} which are shown in the 4th column of Table 3. In the last column of Table 3 are shown the ratios of fractions of surface, relative to CH_3, which are active in recombination. The two columns agree to within the experimental uncertainty.

This agreement suggests that the long range forces active in disproportionation are similar to the exchange forces active in recombination. This would help explain the fact that the ratios k_d/k_r show little temperature variation. The developing C—H bond would resemble a hydrogen bond with exchange character. A simple ad hoc model may then be constructed to reproduce the value of k_d.

Let us assume that at r(C···H···C) = 4.0 Å, the critical interaction is of the order of RT and that the same fraction of active area of the carbon center that we computed for recombination is also active in disproportionation. Then we can compute from the data in Table 3 that, for the methyl group, $\beta_H = 0.067$. This corresponds to a conical section of the methyl sphere with an azimuth angle of 30°, small enough to suggest that only one of the three H atoms is active in disproportionation. If all three were active, then for each the azimuth angle would be reduced to 17°. From a chemical point of view, it would be reasonable to expect attack on axial H-atoms which are in the *trans* position to the odd electron. This would facilitate π-bond formation.

Can. J. Chem. Downloaded from www.nrcresearchpress.com by 210.87.254.40 on 09/06/12
For personal use only.

1. E. GORIN. J. Chem. Phys. **7**, 263 (1979); **7**, 642 (1979).
2. S. W. BENSON. Thermochemical kinetics. 2nd ed. John Wiley and Sons, New York. 1976.
3. J. A. KERR and S. J. MOSS. CRC handbook of bimolecular and termolecular gas reactions. Vol. II. CRC Press, Inc., Boco Raton, FL. 1981.
4. M. H. BAGHAL-VAYJOOEE, A. COLUSSI, and S. W. BENSON. J. Am. Chem. Soc. **100**, 3214 (1978); Int. J. Chem. Kinet. **11**, 147 (1979).
5. D. L. BAULCH and J. DUXBURY. Combust. Flame, **37**, 313 (1980).
6. K. Y. CHOO, P. L. BEADLE, L. W. PISKIEWICZ, and D. M. GOLDEN. Int. J. Chem. Kinet. **8**, 45 (1976).
7. Z. ALFASSI and S. W. BENSON. Int. J. Chem. Kinet. **5**, 879 (1973).
8. K. GLÄNZER, M. QUACK, and J. TROE. 16th Symp. Int. Combust. Proc. 949 (1976); J. TROE. Am. Rev. Phys. Chem. **29**, 223 (1978).
9. S. W. BENSON. The foundations of chemical kinetics. Reprint Ed. Krieger Publ. Co., Malabar, FL. 1982. p. 144.
10. J. ENGLE, A. COMBE, M. LETORT, and M. NICLAUSE. C.R. Acad. Sci. **244**, 453 (1957).

Can. J. Chem. Downloaded from www.nrcresearchpress.com by 210.87.254.40 on 09/06/12
For personal use only.

Chemically-modified electrodes in photoelectrochemical cells[1]

MARYE ANNE FOX,[2] JAMES R. HOHMAN, AND PRASHANT V. KAMAT
Department of Chemistry, University of Texas at Austin, Austin, TX 78712, U.S.A.

Received July 5, 1982

This paper is dedicated to Professor Harry E. Gunning on the occasion of his 65th birthday

MARYE ANNE FOX, JAMES R. HOHMAN, and PRASHANT V. KAMAT. Can. J. Chem. **61**, 888 (1983).

Tin oxide and titanium dioxide semiconductor electrodes have been covalently modified by the attachment of functionalized olefins and arenes through surface silanation or via a cyanuric chloride linkage. The excited state and electrochemical properties of the molecules so attached are significantly affected by the semiconductor. Photocurrent measurements and time-resolved laser coulostatic monitoring have been employed to elucidate the mechanism of charge injection on these modified surfaces.

MARYE ANNE FOX, JAMES R. HOHMAN et PRASHANT V. KAMAT. Can. J. Chem. **61**, 888 (1983).

On a modifié de façon covalente des électrodes de semi-conducteur à l'oxyde d'étain et au boroxyde de titane en y attachant des oléfines fonctionnalisées et des arènes au moyen d'une silanation de surface ou au moyen d'un lien chlorure cyanurique. L'état excité et les propriétés électrochimiques des molécules ainsi attachées sont affectés fe façon significative par le semi-conducteur. On a utilisé les mesures de photocourant et l'enregistrement coulostatique de laser résolu en fonction du temps pour élucider le mécanisme d'injection de charge sur ces surfaces modifiées.

[Traduit par le journal]

Can. J. Chem. Downloaded from www.nrcresearchpress.com by 210.87.254.5 on 09/06/12
For personal use only.

Introduction

Recently the harnessing of solar energy to catalyze kinetically inhibited processes or to drive endothermic reactions has become a widely sought goal. The most promising approaches to the solution of this problem involve photoredox reactions in which an electron is separated from an excited state donor. This electron–hole separation is inherently endothermic and a significant driving force for energy dissipative recombination exists. Only in specially designed systems can this tendency for recombination be sufficiently suppressed for net chemistry to be observed. Because the directional field which develops at an electrode–electrolyte interface can significantly assist such photoinduced electron transfers, these reactions are often accomplished in photoelectrochemical cells (1). The inherent band properties of semiconductors, together with band bending induced when such materials are placed in contact with an electrolyte, inhibit back electron transfer (2), so that electron–hole separation is most easily achievable at the surface of a semiconductor electrode.

There are two basic modes in which photoeffects can be observed at the semiconductor–electrolyte interface: band gap excitation of the semiconductor or sensitized irradiation of a dye molecule adsorbed or chemically attached to the surface of the semiconductor. The first method has been extensively investigated. Typically, band gap excitation leads to high quantum efficiencies for electron–hole separation, and the main limitation of this mode lies in the vexing dilemma imposed by requirements for both photostability and for utilization of large fractions of the incident solar light. That is, those durable semiconductor materials which can withstand extended use in photoelectrochemical cells (e.g., metal oxides) absorb efficiently only in the ultraviolet region of the spectrum and hence are incapable of capturing visible photons to initiate redox chemistry. Those materials which do absorb strongly throughout the solar spectrum (e.g., silicon, metal chalcogenides, sulfides, etc.) are not photostable under prolonged irradiation and require surface modification (as yet not well-defined) for extended use.

The second mode of inducing photoeffects in photoelectrochemical cells, sensitization, has also been limited by seemingly contradictory demands. On the one hand, efficient absorption of light by the sensitizer requires that substantial quantities of the absorptive dye be attached to the electrode surface, but if more than monolayer coverage is attained an insulating layer builds up and the vectorial component of the electrical field, which is required for the assisted electron–hole generation, is diminished dramatically.

Since surface modification is required for extended photoresponsiveness in either mode, we felt that a basic investigation of new synthetic procedures for attachment of photoresponsive molecules and of the effect of the attachment on the excited state properties of such molecules was required. We describe in this paper some of our recent efforts at studying photoredox processes at specifically tailored surfaces and how such modified semiconductors can be usefully employed in mechanistic investigations of charge generation at the photosensitive electrode–electrolyte interface.

Results and discussion

Four methods for attaching highly conjugated organic molecules to the semiconductor surface have been attempted in this study: silanation with tetrachlorosilane, e.g., eq. [1],

[1]This manuscript was presented as an invited paper at a symposium on Photochemical Devices as part of the Symposium on Pure and Applied Photochemistry at the 65th Canadian Chemical Conference and Exhibition, Toronto, June 1982.

[2]Author to whom correspondence may be addressed.

[1] 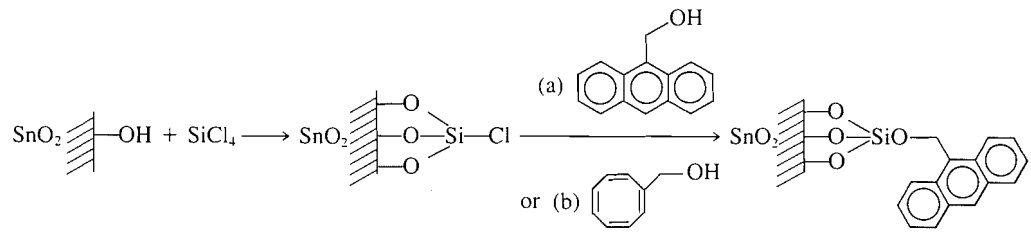

1*a*

the use of cyanuric chloride as a linking reagent, e.g., eq. [2],

[2] 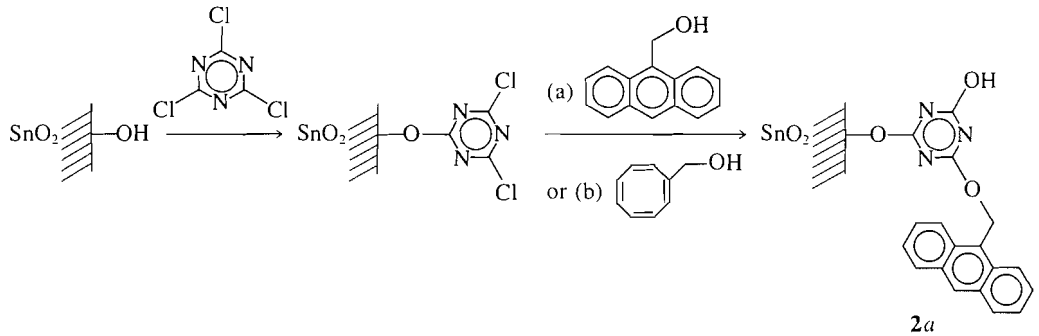

2*a*

the electropolymerization of functionalized monomers, e.g., eq. [3],

[3] 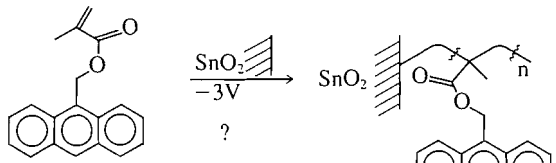

7 3

and the adsorption of preformed polymers onto a surface, e.g., eq. [4].

[4] 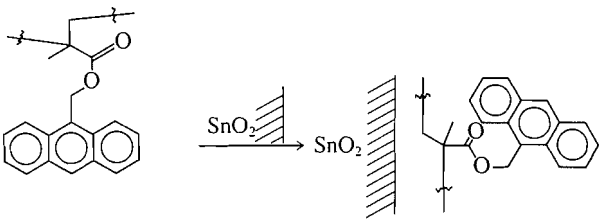

4

Reasonable monolayer surface alteration (attachment of alcohols **5** and **6**) could be achieved using either the commonly

5 6

employed liquid phase procedure (dip silanation, ref. 3) or a gas phase silanation (4), followed by liquid phase attachment of the organic substrate. The usual techniques for the use of cyanuric chloride as a linking agent also proved effective.

Electrodes **1***a*, **1***b*, **2***a*, and **2***b* prepared in this fashion showed well-resolved waves characteristic of the electroactive organic compound when the well-washed electrodes were immersed in a nonaqueous electrolyte and studied by cyclic voltammetry. Examples of typical traces so obtained are shown in Figs. 1–3. Figure 1 represents the cyclic voltammetric trace of **5** as a 10^{-3} *M* solution in acetonitrile containing 0.1 *M* tetrabutyl ammonium perchlorate (TBAP). A similar reduction wave is evident in the scans of modified electrodes **1***a* (Fig. 2) and **2***a* (Fig. 3) in contact with inert electrolyte (TBAP), although the reversibility of the couple is significantly diminished. Such reduced reversibility will undoubtedly limit the functional lifetime of such a modified surface in photogalvanic operation unless a sacrificial redox system dissolved in the electrolyte can be employed to restore the original surface coverage.

Emission spectroscopy can also be used to establish the successful modification. Figure 4 shows the fluorescence spectrum of a dilute solution of **5** in ethanol. Comparison of this spectrum with that obtained on electrode **1***a* (Fig. 5) shows nearly identical band features, although some broadening and small shifts of the emission maxima have occurred on the surface.

In contrast to these successful surface modifications, our attempted electropolymerization of aryl-substituted vinyl monomers gave poor coverage. Although both methacryloyl chloride and methyl methacrylate could be effectively polymerized by applying a −3 V potential, arylated derivative **7**, prepared by esterification of methacryloyl chloride with **5**, gave no detectable evidence of electrode coating, eq. [3]. Murray and co-workers have similarly observed that cathodic polymerization fails unless the reduction center (i.e., the arene) is conjugated with the vinyl group (5).

Our initial suspicion that the polymerization was inhibited by substantial steric interference by the peri-hydrogens in **7** in the transition state for the chain lengthening step is probably incorrect since conventional solution phase initiation of the polymerization proceeds normally. If the polymer is preformed in solution and is fractionated to obtain relatively low molecular

Can. J. Chem. Downloaded from www.nrcresearchpress.com by 210.87.254.5 on 09/06/12
For personal use only.

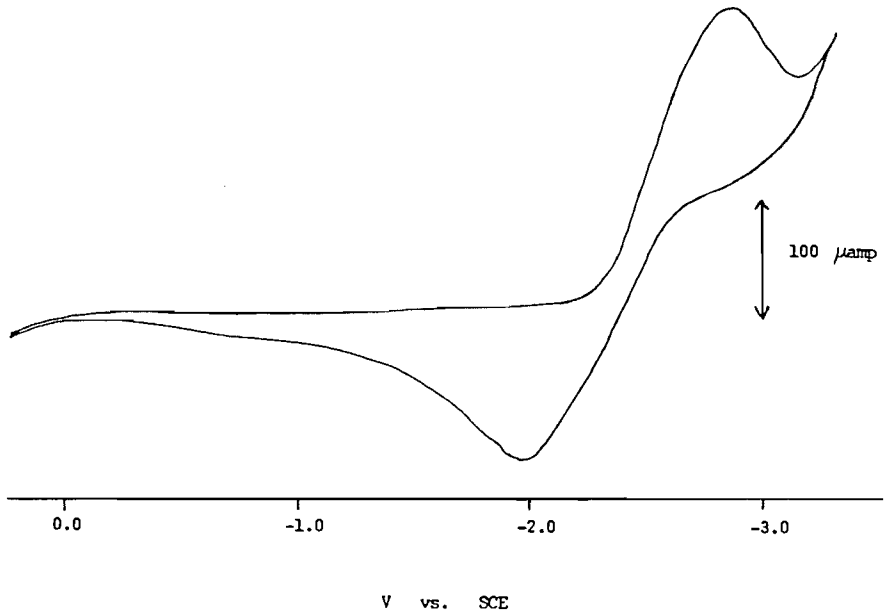

FIG. 1. Cyclic voltammogram of **5** (10^{-3} *M*) in anhydrous acetonitrile containing 0.1 *M* TBAP. SnO_2, room temperature, scan rate = 100 mV/s.

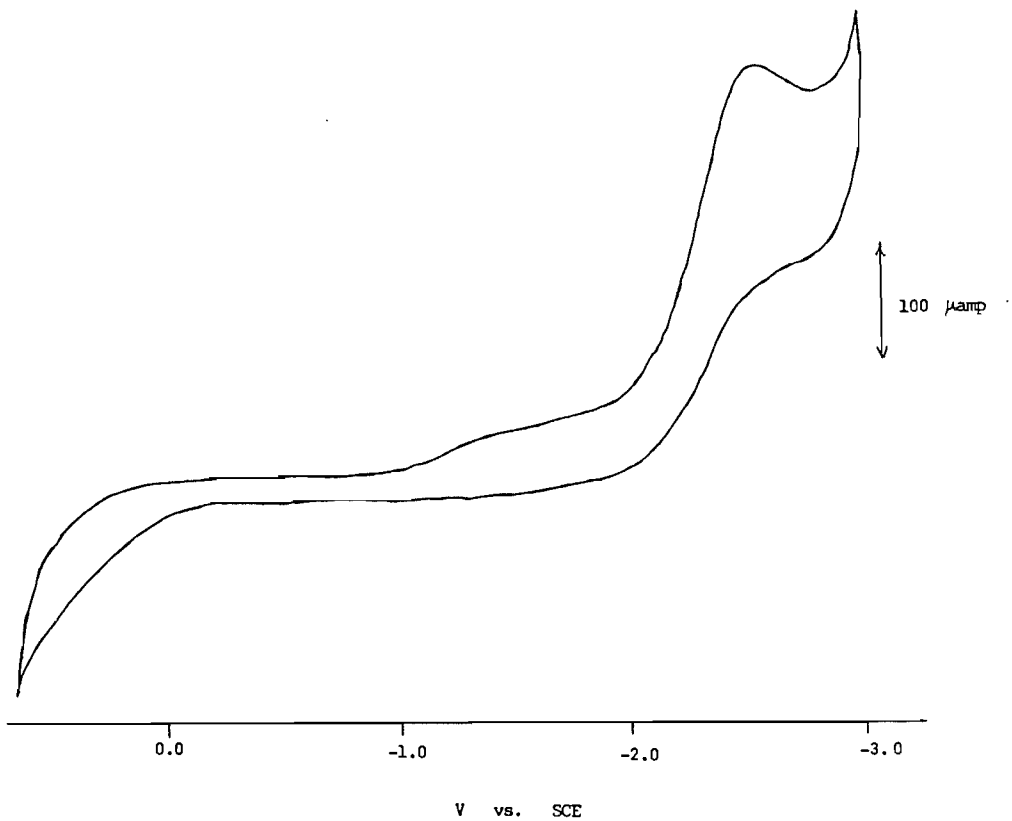

FIG. 2. Cyclic voltammogram of **1***a* in anhydrous acetonitrile containing 0.1 *M* TBAP. Room temperature, scan rate = 100 mV/s.

weight cuts, the resulting sample can be applied, as a methylene chloride solution, to the electrode. Upon solvent evaporation, the polymer adheres and characteristic waves (Fig. 6) can be observed when scanned by cyclic voltammetry as described above. Redox couples (e.g., ferrocene) added to the electrolyte can be oxidized or reduced reversibly through this polymeric coating. Unfortunately, the polymer proved to be light sensitive, with deesterification occurring upon exposure to room light either in solution or at the electrode surface.

The electrodes so obtained were studied by monitoring improvements in sensitized photocurrents produced at the modified electrode compared with those observed with reversible adsorption of the sensitizing dye. For example, previous work in our laboratory has shown that anodic photocurrent can be observed if cyclooctatetraene dianions are excited at the surface of metal oxide electrodes in a photogalvanic cell (6). The net

Can. J. Chem. Downloaded from www.nrcresearchpress.com by 210.87.254.5 on 09/06/12
For personal use only.

Can. J. Chem. Downloaded from www.nrcresearchpress.com by 210.87.254.5 on 09/06/12
For personal use only.

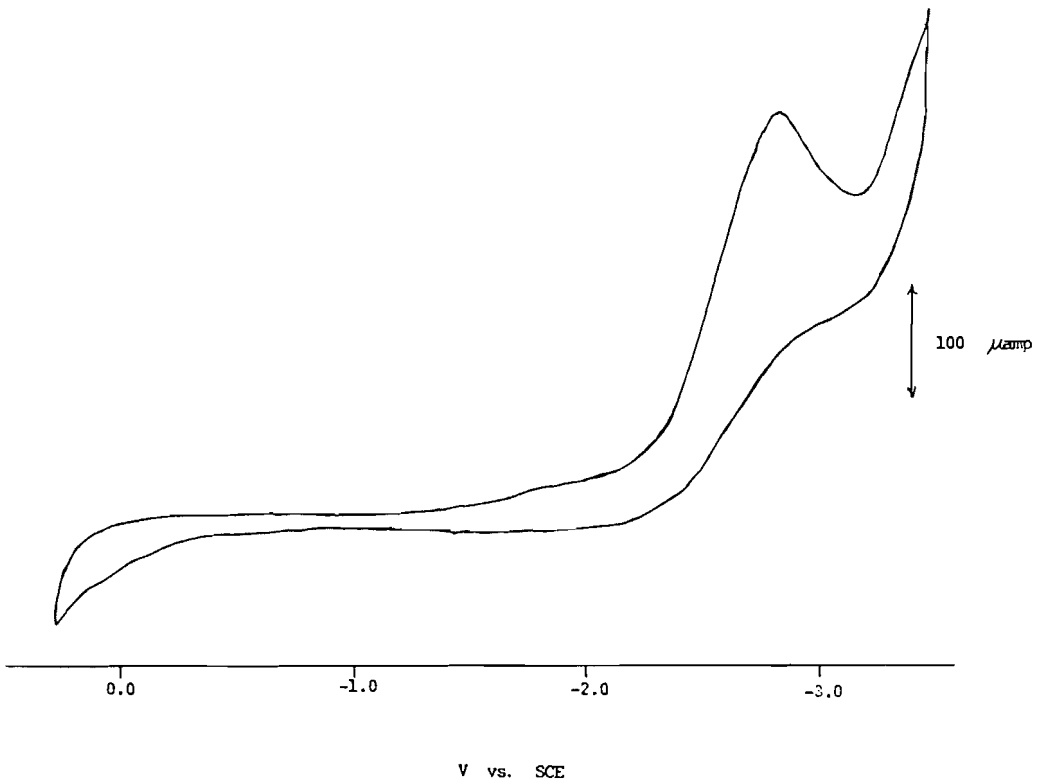

FIG. 3. Cyclic voltammogram of **2***a* in anhydrous acetonitrile containing 0.1 *M* TBAP. Room temperature, scan rate = 100 mV/s.

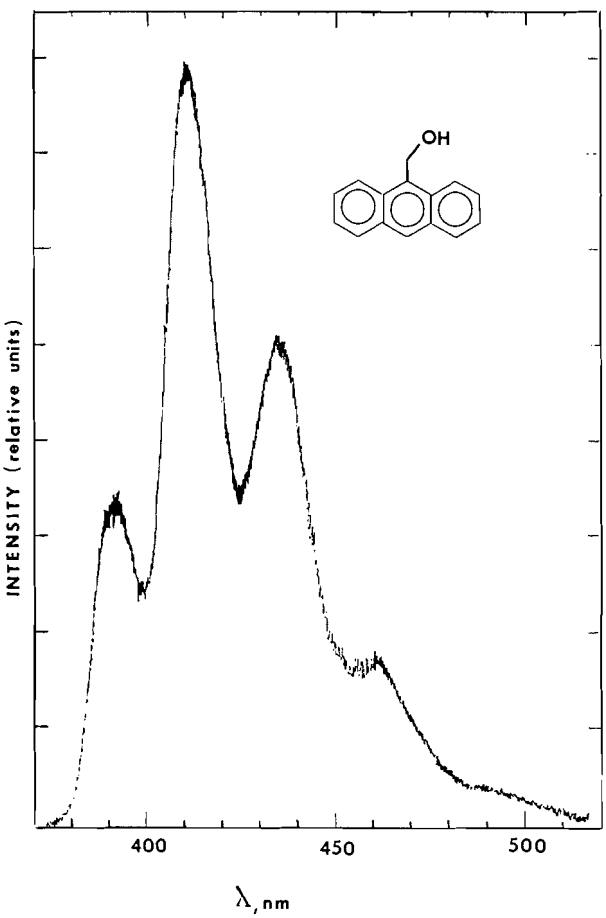

FIG. 4. Fluorescence spectrum of **5** (10^{-4} *M*) in ethanol.

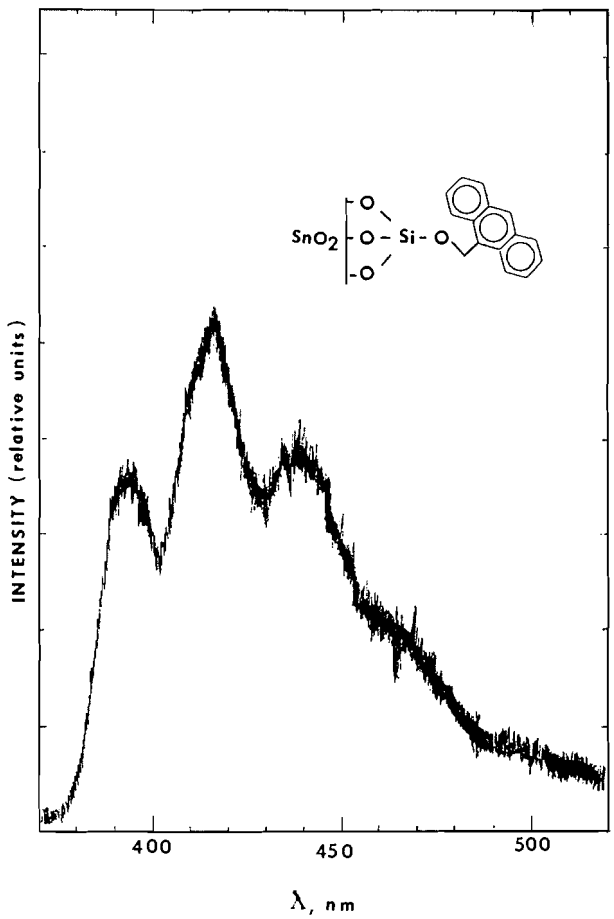

FIG. 5. Fluorescence spectrum of **1***a* (front face).

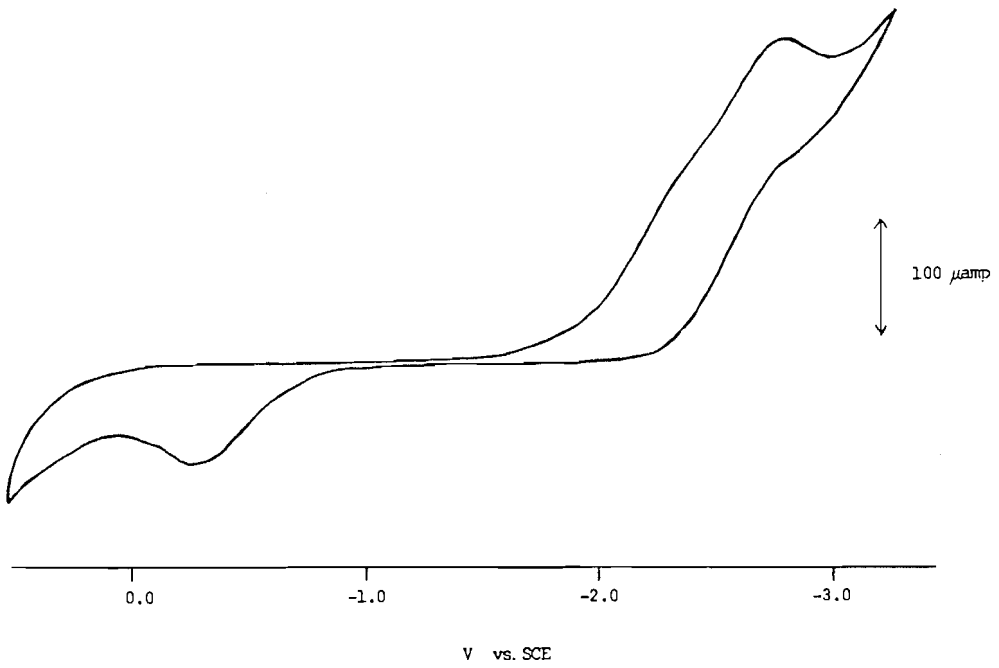

FIG. 6. Cyclic voltammogram of **4** in anhydrous acetonitrile containing 0.1 *M* TBAP. Room temperature, scan rate = 100 mV/s.

chemistry observed can be summarized as in eq. [5].

[5] 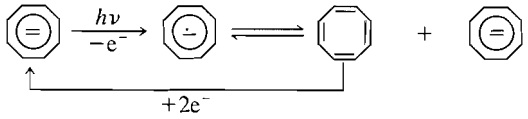

Here electron transfer from the dianion to the semiconductor is the primary photoprocess leading to the development of anodic current. Our projection that surface modification might influence the relative kinetics for energy dissipative back electron transfer vs. current producing dismutation was realized in our observation that more than order-of-magnitude enhancement (factors of 20–25-fold improvement) of sensitized photocurrents could be observed on **1***b* compared with those obtained on the native surface (7). Unfortunately, surface degradation during photogalvanic operation was more significant with **1***b* than with the native surface.

Laser-induced time resolved coulostatic measurements (8) reinforce the idea that surface modification does indeed influence the details of the kinetics of electron transfer at the surface of modified electrodes (9). Upon flash excitation of a native TiO_2 electrode in a photoelectrochemical cell, a coulostatic pulse rapidly develops (electron–hole pair formation) which ultimately decays back to its equilibrium value. We find that covalent modification of the semiconductor surface with non-electroactive molecules strongly influences the rate of this decay. Figure 7 illustrates the decay profiles for TiO_2 in native and silanized form. Clearly, the modification process itself diminishes the ability of the semiconductor to induce photoredox reactions, probably by introducing new surface states and/or recombination sites, unless the molecule attached is photo- or electroactive. Whether electroactive covalent modification will displace the surface states to positions outside the band gap or to where they are inacessible to the majority carrier (10) is at present still unknown.

Whether modification affects the intrinsic properties of the semiconductor was another question of interest. By determining the potential at which the onset of photocurrent begins (11, 12) or by characterizing the change in space-charge capacitance produced by the depletion layer at the surface of the semiconductor (13), we can define the band positions in native and in our unmodified electrodes. As in previous studies in our group (14), we find no dramatic alterations of band positions or interface energetics upon monolayer derivatization.

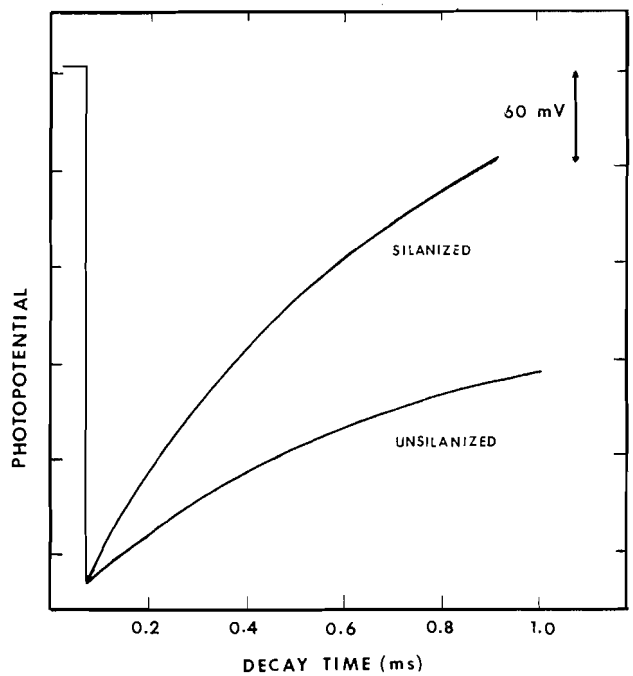

FIG. 7. Coulostatic decay profiles for native and silanized TiO_2.

Preliminary results show that the electroactive polymers described above, e.g., **4**, exert profound effects both on quantum yields for emission and on lifetime of dye molecules electrostatically adsorbed into the polymers. At least tenfold enhancement of both the fluorescence efficiency and the fluorescence lifetime are observed when highly absorptive oxocarbon dyes

Can. J. Chem. Downloaded from www.nrcresearchpress.com by 210.87.254.5 on 09/06/12
For personal use only.

Can. J. Chem. Downloaded from www.nrcresearchpress.com by 210.87.254.5 on 09/06/12
For personal use only.

are incorporated into polyvinylpyridine, a well-known electropolymerizable species, compared with normal solution phase properties. Such effects were also observed in our mechanistic investigation of sensitization (15) at modified semiconductor surfaces (16) and may be of significant importance to the general problem of expanding the photoresponsive region of stable semiconductors. Continuing effort within our research group is being directed toward the goal of systematically studying excited state properties of molecules confined within the double layer of such electrodes.

Experimental

General

Techniques for material purification, photocurrent measurements, and electrochemical analyses were identical to those previously reported (7). Experimental details relevant to the cyclic voltammograms shown in the figures are listed in the relevant captions. General techniques for electrode pretreatment and for surface modification by silanation or by employing cyanuric chloride as a linking agent have also been described elsewhere (7, 16). The fluorescence spectra reported here were obtained at room temperature in a Spex fluorometer either in the normal 90° mode (for solution phase measurements) or in the front face reflective mode (for measurements on surfaces). Laser coulostatic measurements were conducted on an apparatus nearly identical to that described by Perone *et al.* (8).

Compound 7

The acrylate monomer used in the polymerization studies was obtained by esterification of methacryloyl chloride (Aldrich) with 9-hydroxymethyl anthracene (17). To a solution of freshly distilled methacryloyl chloride (1 g, 0.01 mol) in dry tetrahydrofuran (THF) containing 100 mg pyridine was added dropwise 9-hydroxymethylanthracene (1.5 g, 0.007 mol). The resulting solution was heated under reflux for 45 min. The solvent and unreacted acid chloride were removed by distillation and the residue was recrystallized from petroleum ether.

Polymerization of **7** was attempted by applying a potential of −3 V (vs. SCE) to a SnO_2 or TiO_2 electrode immersed in a solution of **7** (0.02 *M*) in dry acetonitrile containing 0.1 *M* TBAP. After rinsing the electrode with freshly distilled solvent, the electrode was immersed in acetonitrile containing inert electrolyte. No evidence of a wave attributable to an anthracene derivative was evident.

Solution phase polymerization was accomplished, in collaboration with Professor S. E. Webber of this department, by heating a dilute solution of **7** in dry THF containing small quantities of azoisobutyronitrile. Details of the fractionation and polymer characterization will be published elsewhere. The fractionated polymer was dissolved in minimal methylene chloride and was applied to a tin oxide electrode. The solvent was allowed to evaporate and the resulting electrode was washed thoroughly with dry methylene chloride and acetonitrile. A cyclic voltammetric scan of the resulting electrode in acetonitrile containing TBAP showed a well-defined wave characteristic of an anthracene derivative.

Acknowledgements

This research was generously supported by the U.S. Department of Energy, Fundamental Interactions Branch, Division of Chemical Sciences. M.A.F. is grateful for support as an Alfred P. Sloan Research Fellow and as a Camille and Henry Dreyfus Teacher–Scholar. The flash coulostatic measurements were conducted at the Center for Fast Kinetics Research which is supported by the National Institutes of Health and by the University of Texas at Austin. The polymer characterization described here was conducted in collaboration with Professor S. E. Webber, to whom we are grateful for practical advice and encouragement.

1. A. J. BARD. Science, **207**, 139 (1980).
2. A. J. NOZIK. Ann. Rev. Phys. Chem. **29**, 189 (1978).
3. R. M. MURRAY. Acc. Chem. Res. **13**, 135 (1980).
4. I. HALLER. J. Am. Chem. Soc. **100**, 8050 (1978).
5. P. DENISEVICH, H. D. ABRUNA, C. R. LEIDNER, T. J. MEYER, and R. W. MURRAY. Inorg. Chem. **21**, 2153 (1982).
6. M. A. FOX and KABIR-UD-DIN. J. Phys. Chem. **83**, 1800 (1979).
7. J. R. HOHMAN and M. A. FOX. J. Am. Chem. Soc. **104**, 401 (1982).
8. S. P. PERONE, J. H. RICHARDSON, S. B. DEUTSCHER, J. ROSENTHAL, and J. W. ZIEMER. J. Electrochem. Soc. **127**, 2580 (1980).
9. P. V. KAMAT and M. A. FOX. J. Phys. Chem. In press.
10. A. HELLER. Am. Chem. Symp. Ser. **146**, 57 (1981).
11. K. NAKATANI and H. TSUBOMURA. Bull. Chem. Soc. Jpn. **50**, 583 (1977).
12. P. A. KOHL and A. J. BARD. J. Am. Chem. Soc. **99**, 7531 (1977).
13. H. GERISCHER. *In* Physical chemistry: an advanced treatise. Vol. IX A. *Edited by* H. EYRING, D. HENDERSON, and W. JOST. Academic Press, New York. 1970.
14. KABIR-UD-DIN, R. C. OWEN and M. A. FOX. J. Phys. Chem. **85**, 1679 (1981).
15. M. A. FOX, F. J. NOBS, and T. A. VOYNICK. J. Am. Chem. Soc. **102**, 4036 (1980).
16. M. A. FOX, F. J. NOBS, and T. A. VOYNICK. J. Am. Chem. Soc. **102**, 4029 (1980).
17. F. H. C. STEWART. Aust. J. Chem. **13**, 478 (1960).

Decay dynamics of aromatic thione triplet states in fluid solution[1]

A. SAFARZADEH-AMIRI, R. E. VERRALL, AND R. P. STEER

Department of Chemistry, University of Saskatchewan, Saskatoon, Sask., Canada S7N 0W0

Received July 5, 1982

This paper is dedicated to Professor Harry E. Gunning on the occasion of his 65th birthday

A. SAFARZADEH-AMIRI, R. E. VERRALL, and R. P. STEER. Can. J. Chem. **61**, 894 (1983).

Phosphorescence emission and excitation spectra, quantum yields, and lifetimes of several aromatic thiones have been measured in fluid solution at room temperature. Excitation to any of the excited electronic states accessible in the near-uv and visible regions of the spectrum results in population of the lowest triplet state with near unit quantum yield. Triplets of relatively inflexible thiones decay non-radiatively with rate constants of the order of 10^5 s^{-1} whereas thiones capable of higher amplitude flexion or group rotation exhibit non-radiative decay constants $\geq 10^7$ s^{-1} at infinite dilution in aprotic solvents. Self-quenching occurs at diffusion-controlled rates.

A. SAFARZADEH-AMIRI, R. E. VERRALL et R. P. STEER. Can. J. Chem. **61**, 894 (1983).

On a mesuré l'émission par phosphorescence, les spectres d'excitation, les rendements quantiques et les temps de vie de plusieurs thiones aromatiques dans une solution fluide à la température ambiante. L'excitation de n'importe quel état électronique excité, accessible dans les régions du proche uv et visible des spectres, conduit à une population du plus faible état triplet avec un rendement quantique proche de l'unité. Les triplets des thiones relativement inflexibles se désintègrent d'une manière non radioactive avec des constantes de vitesse de l'ordre de 10^5 s^{-1} tandis que les thiones qui peuvent subir une flexion de plus grande amplitude ou une rotation de groupe ont des constantes de désintégration non radioactive de $\geq 10^7$ s^{-1} à dilution infinie dans des solvants aprotiques. L'arrêt automatique se produit à des vitesses contrôlées de diffusion.

[Traduit par le journal]

Introduction

Thiocarbonyl compounds exhibit a number of photochemical and photophysical properties which are unusual compared with those of compounds containing only first and second row elements (1–3). For example, as a consequence of their relatively large S_2–S_1 electronic energy gaps, some thiones fluoresce efficiently and react chemically from excited singlet states other than S_1 (1). The tetraatomic thiocarbonyl, thiophosgene, has been shown to undergo a unique excited singlet – excited singlet energy pooling reaction in the gas phase which can populate S_2 with high efficiency (4). There is also substantial evidence of strong spin–orbit coupling in thiones which leads to unusual physical and dynamic properties of their triplet states (5–7). Thus, thiones are among the few organic molecules which phosphoresce in fluid solution at room temperature.

The $T_1 \leftarrow S_0$ absorption in aromatic thiones in fluid solution is often spectrally distinct from other electronic absorption systems and has an oscillator strength which is only about one order of magnitude smaller than that of the corresponding $S_1 \leftarrow S_0$ transition (1). Thus T_1 may be populated either by direct absorption in the $T_1 \leftarrow S_0$ system or by intersystem crossing with high efficiency subsequent to excitation within the singlet manifold. Decay of the lowest triplet is dominated by intersystem crossing to the ground state, leading to small phosphorescence quantum yields and relatively short triplet lifetimes in either matrices at low temperature or in fluid solution. In dilute aprotic fluid solvents photochemical decay processes are minor (8) whereas self-quenching dominates at higher substrate concentrations (9, 10) and very rapid oxygen quenching dominates in air-saturated solutions (11).

To date the most detailed studies of the spectroscopy and photophysics of aromatic thiones in solution have been carried out on xanthione (XT, see Fig. 1). Absorption, emission, and excitation spectra of xanthione in fluid solution, in glasses, and in a Shpolskii matrix have been reported by Huber and coworkers (5, 12–14). These spectral studies and previous ODMR experiments (6) have been interpreted as indicating that the T_1 and T_2 states of xanthione are energetically very close and that the lowest triplet is of mixed $n,\pi^*-\pi,\pi^*$ character. Burland (7, 15) has shown that the triplet state of xanthione has a very large zero field splitting parameter, D (measured in a xanthone host at $T \geq 2$ K), and this has been taken as evidence in support of a mechanism of O_2–triplet thione quenching which involves strong "intramolecular" spin–spin coupling in the encounter complex (11).

The photochemical reactions of the triplet states of numerous aliphatic and aromatic thiones have been described previously (16–19). By contrast, the spectroscopic and photophysical properties of only a few aromatic thiones have been investigated. In this paper we present the results of studies of the spectroscopy and triplet state decay dynamics of seven aromatic thiones (Fig. 1) in fluid solution and examine the effects of molecular structure on these properties.

Experimental

1. Apparatus

Emission and emission excitation spectra were taken either on a single photon counting spectrofluorimeter previously described (20) or on a laser fluorimeter described below. An Optronics Laboratory 1000 W calibrated quartz-iodine lamp was used to obtain spectral correction factors for the detection system, according to the method of Parker (21). Emission quantum yields were determined using solutions of either quinine sulfate ($\phi_f = 0.55$ in 0.1 M H_2SO_4 (22)) or tetracene ($\phi_f = 0.17$ in cyclohexane (23)) as standards. Absorption spectra were taken on a Cary 118 spectrophotometer. All measurements were performed at a room temperature of 22°C.

Phosphorescence lifetimes were measured in the early stages of the work by a time-correlated single photon counting method similar to that described by Ware *et al.* (24) except that a free-running, N_2-filled

[1]Presented, in part, to the Symposium on Pure and Applied Photochemistry 65th Annual Conference of the Chemical Institute of Canada, Toronto, Ontario, May 30 – June 2, 1982.

Can. J. Chem. Downloaded from www.nrcresearchpress.com by 210.87.254.40 on 09/06/12
For personal use only.

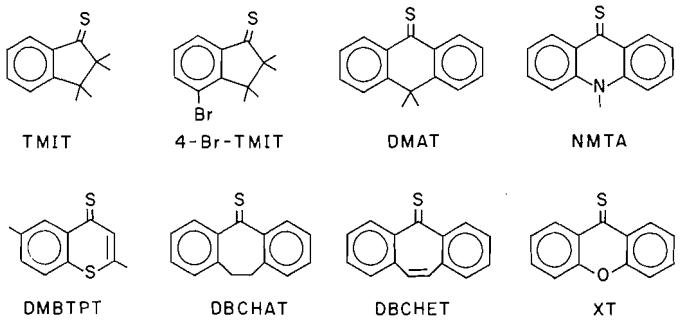

FIG. 1. Thione structures.

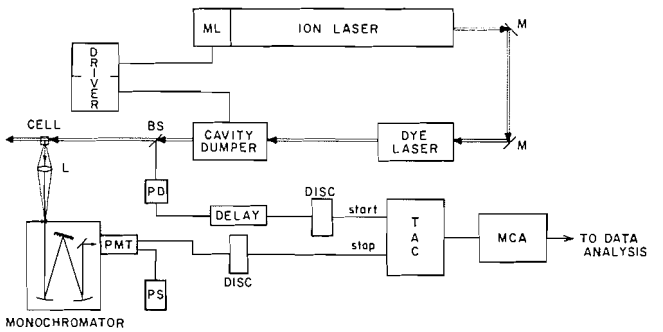

FIG. 2. Experimental apparatus. M, mirror; BS, beamsplitter; L, lens; PD, photodiode; PMT, photomultiplier tube; PS, power supply; DISC, discriminator; TAC, time to amplitude converter; MCA, multichannel analyzer; ML, mode locker (not employed in these experiments).

flash lamp was used as an excitation source. An argon-ion pumped, cavity-dumped, R6G dye laser was used for excitation later in the work, and a schematic diagram of this apparatus is shown in Fig. 2. A Spectra-Physics, Model 171, argon ion laser operating CW at 514.5 nm pumped a rhodamine 6G dye laser whose output was tuned by means of a birefringent filter. In the cavity-dumped configuration, the standard dye laser output coupler is removed, the cavity is lengthened, and pulsed output is obtained by means of an intra-cavity acousto-optic modulator. Average output powers of up to 200 mW, pulse widths of 12 ns, and pulse repetition rates between single shot and 4 MHz are obtainable with this system, which can also be used to synchronously pump the dye laser when the ion laser is mode-locked. In a typical experiment, an argon ion laser pump power of 2 W produced an average cavity-dumped output power of 2 mW at 582 nm and a repetition rate of 80 kHz. Samples were contained in a clear-sided 1 cm square quartz cell with provision for degassing, which intercepted the beam at Brewster's angle. Emission was collected with a telescope lens system, which, together with the cell, was enclosed in a light-tight box.

Start pulses were obtained by means of a beam splitter, photodiode and discriminator, and were delayed relative to stop pulses by means of appropriate lengths of coaxial cable. Emission was viewed in first order through a Jarrell-Ash, 0.75 m monochromator equipped with an 1800 l/mm holographic grating. A thermoelectrically cooled, red-sensitive RCA 31034 photomultiplier tube provided stop logic pulses, via a constant fraction discriminator, to an Ortec Model 473 biased TAC, the output of which was fed to a Northern, Model NS433, multichannel analyzer operating in the pulse height analysis mode. Deconvolution, background subtraction, and data analysis were performed on a time-shared DEC 2060 computer using standard programs. Single exponential phosphorescence decays with excellent statistical "goodness-of-fit" were obtained without exception.

2. Materials

2,2,3,3-Tetramethylindanthione (TMIT), 4-Br-2,2,3,3-tetramethylindanthione (4-Br-TMIT), 9,9-dimethylanthrathione (DMAT), 2,3,6,7-dibenzocycloheptane-1-thione (DBCHAT), and 2,3,6,7-dibenzocycloheptene-1-thione (DBCHET) were prepared from the corresponding ketones by treatment with P_2S_5 (25). 2,2,3,3-Tetramethylindanone was prepared by the method of Rothstein and Saboor (26) and was halogenated by a standard method (27) to give the 4-bromoketone. 2,6-Dimethyl-4H-1-benzthiopyran-4-thione (DMBTPT) was prepared from the corresponding ketone (28) by the method of Pederson *et al.* (29). *N*-Methylthioacridone (NMTA) was prepared as described previously (11). Solvents were purified by standard techniques and showed negligible luminescence under the conditions used to obtain emission spectra and lifetimes.

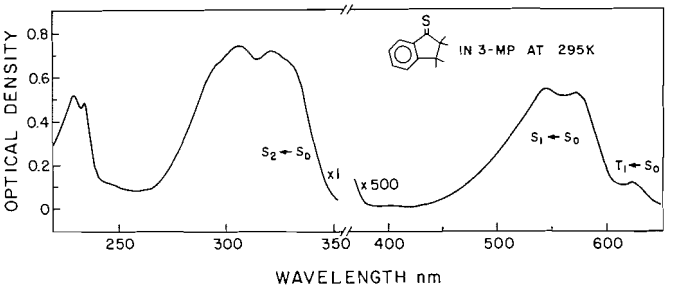

FIG. 3. Absorption spectrum of TMIT in 3-MP at 295 K.

Results

The uv-visible absorption spectrum of TMIT in 3-MP, shown in Fig. 3, is typical of many aromatic thiones in fluid solution at room temperature. The long wavelength absorption ($\lambda > 400$ nm) is due to two separate transitions both nominally of $n \rightarrow \pi^*$ character centered on the thiocarbonyl moiety. The lower energy absorption ($\epsilon_{max} = 3.8\ M^{-1}\ cm^{-1}$) is reasonably well-resolved from the higher energy absorption and is assigned (*vide infra*) as $T_1 \leftarrow S_0$ ($\tilde{a}^3A_2 \leftarrow \tilde{X}^1A_1$ in C_{2v} symmetry). The higher energy of these two long wavelength transitions has an ϵ_{max} of 20.0 $M^{-1}\ cm^{-1}$, an origin near 17240 cm^{-1} and is assigned as $S_1 \leftarrow S_0$ ($\tilde{A}^1A_2 \leftarrow \tilde{X}^1A_1$ in C_{2v}). This absorption is weakly structured in fluid solution at room temperature with distinct bands occurring 860 cm^{-1} and 2290 cm^{-1} to the blue of the 17240 cm^{-1} band. Structure in the $T_1 \leftarrow S_0$ absorption system is masked by the stronger $S_1 \leftarrow S_0$ absorption at room temperature, but structure in both systems becomes much more distinct in low temperature matrices. The first strong transition ($\lambda_{max} = 322$ nm, $\epsilon_{max} = 1.3 \times 10^4\ M^{-1}\ cm^{-1}$) lies in the near-uv and is overlapped by a second strong transition ($\lambda_{max} = 308$ nm) on the basis of its polarization spectrum. The spectral data for TMIT and the other thiones examined in this work are summarized in Table 1. Data for xanthione is provided for comparison (5, 12–14).

Excitation of all of these thiones except DBCHAT and DBCHET in either their weak visible absorption systems or their strong transitions in the near-uv–blue regions in degassed fluid solution at room temperature produces emission in the red and near infrared, assigned as $T_1 \rightarrow S_0$ phosphorescence (*vide infra*). DBCHAT and DBCHET emit too feebly for the emission to be observed at room temperature, but phosphorescence may be seen readily in a 3-MP glass at 77 K. A typical corrected spectrum, that of TMIT in degassed 3-MP at room temperature, is shown in Fig. 4. These spectra are qualitatively similar to the phosphorescence spectra of other aromatic thiones (5, 30–33). Identical phosphorescence spectra (albeit of varying intensities) were obtained by exciting in any of the weak visible or stronger near-uv absorptions. The corrected

Can. J. Chem. Downloaded from www.nrcresearchpress.com by 210.87.254.40 on 09/06/12
For personal use only.

TABLE 1. Spectral data for several aromatic thiones

	$T_1 \leftarrow S_0$		$S_1 \leftarrow S_0$			$S_2 \leftarrow S_0$	
Compound	Origin[a] (cm^{-1})	ϵ_{max} (M^{-1} cm^{-1})	Origin[b] (cm^{-1})	ϵ_{max} (M^{-1} cm^{-1})	Structure[c] (cm^{-1})	λ_{max} (nm)	ϵ_{max} (M^{-1} cm^{-1})
TMIT	15 920	3.8	17 240	20.0	860,2290	322	1.3×10^4
4-Br-TMIT	15 600	4.0	17 100	20.8	920,1920	335	0.88×10^4
DMBTPT	15 110	~10	16 000	32.2	310,750,1120 1540,2800	410	2×10^4
NMTA	14 900	7.0	15 800	16.5	~390	488	2.1×10^4
DMAT	13 640	—	15 900	135	900,1850 (Sh)	350[d]	2.7×10^4
DBCHAT	13 610	—	λ_{max} = 608 nm	268	820,1730	316	1.4×10^4
DBCHET	14 100	—	λ_{max} = 596 nm	203	—	403	0.60×10^4
XT[e]	15 143	8	16 093	20	—	423	1.6×10^4

[a]Highest energy band in phosphorescence spectrum in hydrocarbon solvents at 77 K.
[b]Lowest energy band in $S_1 \leftarrow S_0$ absorption spectrum in hydrocarbon solvents at 295 K.
[c]Position of subsequent bands relative to the "origin".
[d]Poorly resolved.
[e]From refs. 5 and 12–14.

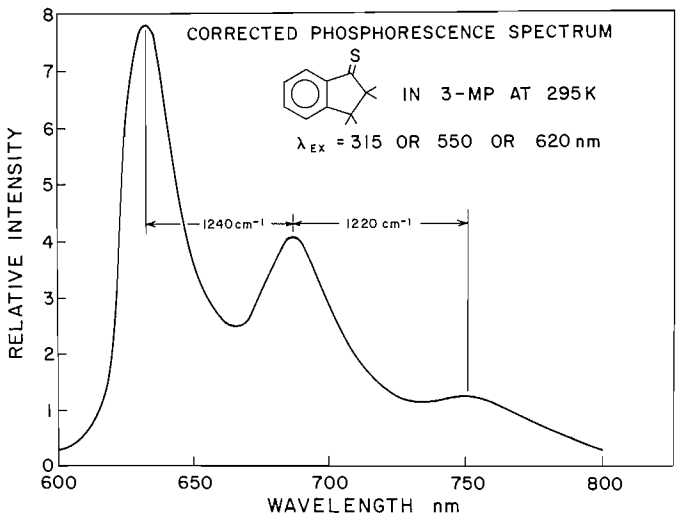

FIG. 4. Corrected phosphorescence emission spectrum of TMIT in 3-MP at 295 K.

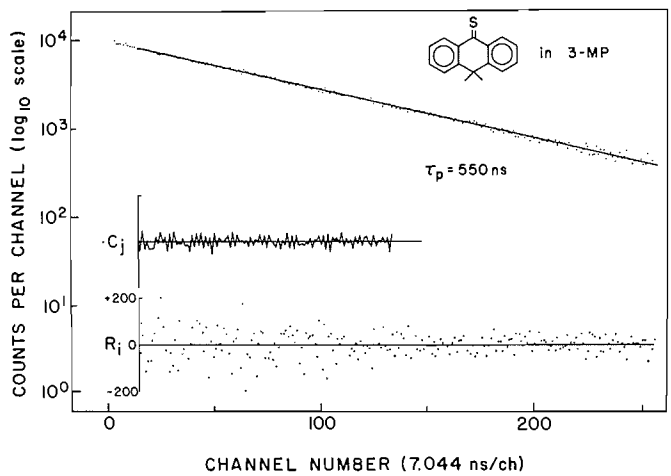

FIG. 5. Log_{10} (number of counts per channel) vs. channel number for DMAT in 3-MP at 295 K. Channel width 7.044 ns. R_i is the distribution of weighted residuals and C_j is the autocorrelation function, both plotted as a function of channel number. The solid line is computed from a single exponential decay function with phosphorescence lifetime of 550 ns.

phosphorescence excitation spectra follow the thione absorption spectra closely.

No emission identifiable as fluorescence from S_1 could be detected upon excitation either to S_1 or to higher singlets. However, excitation of most of these thiones in their strong uv–blue absorptions produced weak emission assignable as fluorescence from upper excited singlet states. The upper state decay dynamics of these thiones will be the subject of a forthcoming paper.

In fluid solution the quantum yield of phosphorescence decreases with increasing thione concentration due to self-quenching. Measurement of phosphorescence quantum yields and lifetimes as a function of thione concentration gave data which fit the Stern–Volmer relationship

$$[1] \qquad \frac{\phi_p^0}{\phi_p} = 1 + k_q \tau_p^0 [T]$$

where ϕ_p^0 and ϕ_p are the phosphorescence quantum yields at infinite and finite dilution respectively, k_q is the bimolecular self-quenching rate constant, τ_p^0 is the phosphorescence lifetime at infinite dilution, and [T] is the molar concentration of thione. Typical lifetime data, obtained with the laser excited, time-correlated single photon counting method, are presented in Fig. 5. In this figure R_i is the distribution of weighted residuals and C_j is the autocorrelation function (34). Excellent fits of the data to a single exponential decay law were observed in all cases. Values of k_q and τ_p^0 were obtained by measuring the slope and intercept, respectively, of

$$[2] \qquad \frac{1}{\tau_p} = \frac{1}{\tau_p^0} + k_q [T]$$

where τ_p is the observed phosphorescence lifetime at finite thione concentration. A typical plot, for NMTA in 3-MP at 295 K, is shown in Fig. 6. Table 2 gives values of ϕ_p^0 and τ_p^0 for the several thiones investigated in this study, together with calculated values of the rate constants for the first order radiative, k_{r,T_1}, and non-radiative, k_{nr,T_1}, decay of T_1 in 3-MP at 295 K.

The role of the solvent in determining the triplet decay rate and mechanism was investigated for NMTA and for TMIT. A linear relationship between k_q and the reciprocal of the solvent viscosity at constant temperature was observed, as illustrated for NMTA in Fig. 7. Benzene appears to be a somewhat exceptional solvent, having a value of k_q which is about 50% smaller

Can. J. Chem. Downloaded from www.nrcresearchpress.com by 210.87.254.40 on 09/06/12
For personal use only.

TABLE 2. Thione photophysical decay parameters

Compound	Solvent	ϕ_p^0	τ_p^0 (μs)	$k_{q,self}$ (M^{-1} s^{-1})	k_{r,T_1} (s^{-1})	k_{nr,T_1} (s^{-1})	k_{nr,S_1} (s^{-1})
TMIT	3-MP	2.35×10^{-2}	16.5	0.88×10^{10}	1.42×10^{3}	5.84×10^{4}	$> 2 \times 10^{9}$
4-Br-TMIT	3-MP	1.68×10^{-2}	14.7	1.06×10^{10}	1.13×10^{3}	6.65×10^{4}	$> 1 \times 10^{9}$
NMTA	3-MP	1.6×10^{-2}	2.96	1.42×10^{10}	5.4×10^{3}	3.3×10^{5}	$> 5 \times 10^{9}$
DMAT	3-MP	7.9×10^{-4}	1.52	1.03×10^{10}	5.2×10^{2}	6.6×10^{5}	$> 1 \times 10^{10}$
DMBTBT[a]	3-MP	$\sim 1 \times 10^{-2}$	—	$\sim 1 \times 10^{10}$	$\sim 5 \times 10^{3}$	—	$> 5 \times 10^{9}$
XT[b]	3-MP	$\sim 8 \times 10^{-3}$	2.70	1.7×10^{10}	$\sim 3 \times 10^{3}$	$\sim 3.7 \times 10^{5}$	$> 10^{11}$

[a]Estimated by comparison with TMIT.
[b]From refs. 5 and 12 to 14.

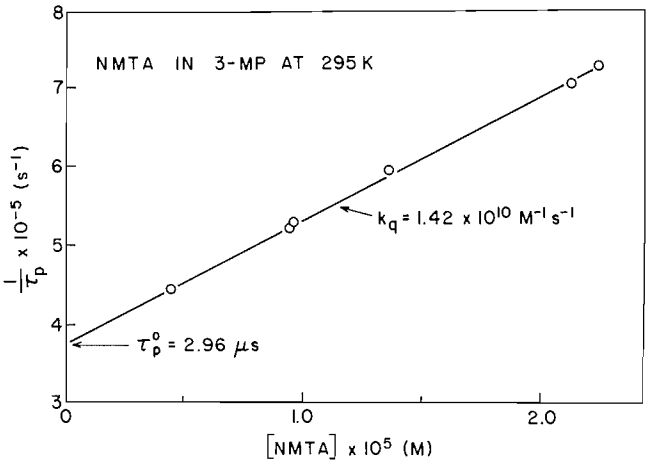

FIG. 6. Stern–Volmer plot for the self-quenching of NMTA phosphorescence.

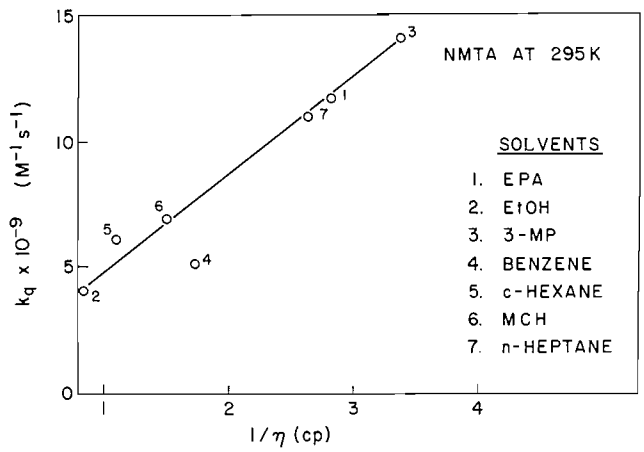

FIG. 7. k_q vs. η^{-1} for NMTA in various solvents.

than expected. There is some evidence of ground state NMTA–benzene interaction, however, because an isosbestic point at 464 nm appears in absorption spectra of NMTA in cyclohexane as a function of added benzene concentration. This point was not pursued further in this work, but may be of relevance in explaining the difference between the S_2 lifetime of xanthione in benzene (12 ps (35)) compared with 3-MP (60 ps (14)).

Phosphorescence spectra of TMIT and 4-Br-TMIT were also measured in *n*-chlorobutane and *n*-bromobutane. The spectra show loss of structure in the halobutane solvents, but are otherwise similar to spectra in 3-MP. Quantum yields of phosphorescence are nearly identical in all three solvents.

Photochemical reactions of the thiones were monitored by measuring the decrease in optical density in the strong uv–blue absorption of the thione. No evidence of significant photochemical reaction was observed when these thiones were illuminated in their weak, visible absorption systems in degassed, aprotic solvents at room temperature for thione concentrations up to 10^{-4} *M*. In oxygenated solutions the corresponding ketone is produced photochemically. NMTA is one of the most photoreactive thiones and the production of *N*-methylacridone in this system could be monitored by the growth of absorption in the spectral window near 400 nm between the thione $S_2 \leftarrow S_0$ and $S_3 \leftarrow S_0$ absorption systems. Evidence that thione triplets abstract hydrogen from hydrogen-donating solvents and addends has been obtained by Huber *et al.* (5, 8) for xanthione and by de Mayo and co-workers (18), for other thiones. Similar evidence is available from measurements of thione triplet lifetimes as a function of the nature of the solvent in the present work. Lifetimes are generally shorter in protic than aprotic solvents, whereas in aprotic solvents the product of the square of the solvent refractive index and the phosphorescence lifetime at infinite dilution is constant.

Discussion

The absorption spectra of the aromatic thiones examined in this study are similar to those of other aromatic thiones in fluid solution previously reported (5, 30, 31, 33). The longest wavelength absorption is assigned to the direct T_1 $^3(n,\pi^*) \leftarrow S_0$ transition and appears as a weak, but spectrally resolved band in TMIT, 4-Br-TMIT, NMTA, and DMBTPT as it does in xanthione (5). The oscillator strength of this transition lies between 1×10^{-5} and 3×10^{-5} for these thiones. The assignment is made on the basis of the magnitude of the oscillator strength, the overlap of this band with the highest energy band in the emission (phosphorescence) spectrum, the blue shift of this band in more polar solvents, and the decay characteristics of the (triplet) excited state produced on absorption (*vide infra*) as well as their polarization spectra (36). In the other thiones studied, the nearby $S_1 \leftarrow S_0$ transitions are substantially stronger, perhaps owing to the greater flexibilities of these molecules, and the weaker $T_1 \leftarrow S_0$ transitions are not distinct in the absorption spectra. Their approximate triplet energies can nevertheless be discerned from their phosphorescence emission and, in some cases, excitation spectra in glasses at 77 K. The relatively large oscillator strength of the $T_1 \leftarrow S_0$ transition compared, for example, with the corresponding ketones, may be ascribed in part to efficient spin–orbit coupling (37) which prevails in aromatic thiones.

The $S_1 \leftarrow S_0$ absorptions lie to slightly higher energies in the visible and have oscillator strengths about an order of magnitude larger than those of the corresponding $T_1 \leftarrow S_0$ transi-

Can. J. Chem. Downloaded from www.nrcresearchpress.com by 210.87.254.40 on 09/06/12
For personal use only.

Can. J. Chem. Downloaded from www.nrcresearchpress.com by 210.87.254.40 on 09/06/12
For personal use only.

tions (when the latter are spectrally distinct). From their intensities, energy, and behavior as a function of solvent polarity, these transitions are clearly forbidden by electric dipole selection rules and are of $n \rightarrow \pi^*$ character. Each is well-separated from the first strong electric-dipole-allowed $\pi \rightarrow \pi^*$ transition in the near-uv–blue. The approximate $S_2 - S_1$ energy gaps, calculated from energy differences between the absorption maxima of the $S_2 \leftarrow S_0$ and $S_1 \leftarrow S_0$ systems, vary from ca. 5000 cm^{-1} for NMTA to ca. 12,200 cm^{-1} for TMIT.

Emission in the red and near-infrared regions of the spectrum may be excited in any of the visible or near-uv–blue absorption systems. The emission is assigned as $T_1 \rightarrow S_0$ phosphorescence on the basis of (*i*) a comparison of the measured radiative rate constants for T_1 (Table 2) with approximate values calculated from the $T_1 \leftarrow S_0$ integrated absorption coefficient (38), (*ii*) the observation that the emission is quenched at a near diffusion-controlled rate by molecular oxygen and by anthracene whose triplet energy (42.7 kcal mol^{-1} (39)) is lower than or approximately equal to those of the thiones examined in this study, (*iii*) the spectral properties of the emission, and (*iv*) comparisons with other aromatic thiones of similar structure known to phosphoresce (5, 30, 31, 33).

The only other possible interpretation of the emission and absorption data is that the long wavelength weak absorption is part of the $S_1 \leftarrow S_0$ system and that the emission observed is $S_1 \rightarrow S_0$ fluorescence. However, all available photochemical and photophysical evidence from other systems (1) indicates that the S_1 states of aromatic, aliphatic, and aralkyl thiones in fluid solution are very short-lived and cannot be identified with emitting states having lifetimes in the microsecond range, such as those observed in this work. Only tetraatomic thiones such as H_2CS and Cl_2CS in the gas phase are known (1) to fluoresce from S_1 with high quantum yields ($\phi_f \rightarrow 1$). By contrast the lowest excited singlet states of several larger organic thiones in solution have been shown to decay very rapidly via intersystem crossing to T_1 ($\phi_{isc} \rightarrow 1$). The lifetime of xanthione S_1, for example, has previously been estimated to be $<10^{-11}$ s (13, 35).

Vibrational structure in the corrected phosphorescence spectra of all the thiones examined in the present study is poorly resolved in fluid solution at room temperatures, but does exhibit a characteristic peak-to-peak separation of ca. 1200 to 1300 cm^{-1}. This frequency has previously been ascribed to the thione ground state C—S stretching mode. However, recent work by Mahaney and Huber on xanthione in a Shpolskii matrix (14) has demonstrated that the vibrational bands observed in the room temperature spectrum undoubtedly result from the superposition of several closely spaced vibrational features, and that the features of greatest intensity are due to ring vibrations. Only gross vibrational features are observable in the room temperature spectra, and a discussion of vibrational assignments will not be pursued further here.

The corrected phosphorescence excitation spectra very closely resemble the absorption spectra throughout the visible and near-uv regions. The implication of this observation is that the emitting state is T_1 and the quantum yield of triplet formation is very nearly equal to unity, regardless of whether T_1, S_1 or higher singlets are populated initially. In dilute, degassed solutions employing aprotic solvents, there is no evidence of significant photochemical activity for any of the thiones, regardless of excitation wavelength, in agreement with a previous observation for xanthione (8) in which the quantum yield of xanthione disappearance in 3-MP at room temperature was found to be 0.005. The quantum yield of fluorescence from S_1 is too small to be measured ($\phi_f(S_1 \rightarrow S_0) < 10^{-4}$), and from S_2 is no more than 2.4% (36). The phosphorescence lifetime of a 7.13×10^{-5} *M* solution of TMIT was 1.03 μs when excited into S_1 at 582 nm and 1.04 μs when excited into T_1 at 627 nm.

These observations are all consistent with the suggestion that the quantum yield of triplet formation is 1.0 regardless of excitation wavelength. Moreover, at fixed thione concentration over both visible absorption systems the equality

$$[3] \qquad I_{p,S}/I_{p,T} = \epsilon_S L_S/\epsilon_T L_T$$

holds within an estimated experimental error of ±15%. Here $I_{p,S}/I_{p,T}$, ϵ_S/ϵ_T and L_S/L_T are the ratio of the measured phosphorescence intensity at a fixed emission wavelength excited in the $S_1 \leftarrow S_0$ absorption to that excited in the $T_1 \leftarrow S_0$ absorption, ϵ_S/ϵ_T is the ratio of the molar extinction coefficient at the wavelengths of excitation in the singlet system to that in the triplet system, and L_S/L_T is the ratio of the excitation intensity at the wavelength of excitation in the singlet system to that in the triplet system respectively. The suggestion that $\phi_{isc}(S_1 \rightarrow T_1) = 1.0$ for the aromatic thiones investigated in this study is in complete accord with the results of previous work on similar systems (1). An upper limit of 10^{-4} for the quantum yield of $S_1 \rightarrow S_0$ fluorescence may be established from the sensitivity of the emission detection system used in the present work. Using S_1 radiative lifetimes estimated from the integrated absorption coefficients (37, 38) of the $S_1 \leftarrow S_0$ transitions, lower limits of the rate constants for the non-radiative decay of S_1 (i.e. for $k_{isc}(S_1 \rightarrow T_1)$ may be obtained. These values are given in Table 2 and indicate that the S_1 lifetimes must be no longer than of nanosecond duration and may be much shorter. By comparison a rate constant of $S_1 \rightarrow T_1$ intersystem crossing in excess of 10^{11} s^{-1} has been estimated for xanthione (35) in benzene.

The S_1–T_1 energy gaps of the tetraatomic thiones, whose $S_1 \rightarrow S_0$ fluorescence quantum yields approach unity in the gas phase, are very similar to the S_1–T_1 energy gaps of the aromatic thiones studied here; ca. 1000–2000 cm^{-1}. The electronic matrix elements coupling the S_1 and T_1 states are therefore expected (40) to be similar for the two groups of compounds. The vast difference in their behavior may therefore be ascribed to the much larger density of accepting vibronic states in the triplet manifolds of the larger thiones and to the irreversible decay rate enhancing influence of the solvent.

Both the magnitude of k_q and its variation with the solvent viscosity indicate that the self-quenching process is diffusion controlled. In degassed, aprotic solvents at room temperature, quantum yields of thione disappearance are estimated to be <0.01. Thus concentration quenching is the only important intermolecular decay pathway at the thione triplet concentrations encountered in this study. A similar result has also been obtained for the self-quenching of xanthione (9) and for the quenching of triplet xanthione by other thiones (10).

It is interesting to note that, based on the data presented here, at the higher triplet concentrations obtainable on thione $S_1 \leftarrow S_0$ or $T_1 \leftarrow S_0$ excitation with pulsed-laser systems, triplet–triplet interaction could be responsible for a significant fraction of the intermolecular triplet decay processes in fluid solution. Because many of these same thiones also fluoresce from S_2 with quantum yields of the order of 1%, and have S_2–S_0 energy gaps which are almost invariably less than twice their T_1–S_0 energy gaps, these systems are well-suited for

Can. J. Chem. Downloaded from www.nrcresearchpress.com by 210.87.254.40 on 09/06/12
For personal use only.

studying the $2T_1 \rightarrow S_2 + S_0$ triplet–triplet annihilation process. This work is in progress.

The variation in k_r and k_{nr} of the triplet states with thione structure is difficult to interpret definitively on the basis of the data presently at hand. Nevertheless, a qualitative interpretation appears to be possible. Relatively rigid aromatic thiones such as xanthione, TMIT, NMTA, and DMBTPT exhibit relatively small $S_1 \leftarrow S_0$ extinction coefficients, $T_1 \leftarrow S_0$ absorption systems which are resolved from the $S_1 \leftarrow S_0$ absorptions, and triplet non-radiative decay constants of the order of 10^5 s^{-1} (sufficiently small that phosphorescence quantum yields of the order of 1% are observed in fluid solution at room temperature). On the other hand, thiones such as DBCHAT and DBCHET which are capable of higher amplitude ring bending vibrations, or which are capable of unrestricted rotations of groups α to the C=S group such as thiobenzophenone and the aralkyl thiones studied by Hui *et al.* (33) show substantially higher $S_1 \leftarrow S_0$ extinction coefficients, $T_1 \leftarrow S_0$ absorptions which are generally not resolved from the $S_1 \leftarrow S_0$ absorptions at room temperature, and exhibit triplet non-radiative decay constants which are large enough ($>10^7$ s^{-1}) to dominate totally the triplet decay process. No phosphorescence is seen from this latter group of compounds in fluid solution at room temperature, but weak phosphorescence may be observed in matrices at low temperature. These observations suggest that the interaction of the S_1 state with upper singlets via symmetry breaking ring vibrations and perhaps group rotations may be responsible for the major part of the intensity of the electric dipole forbidden $S_1 \leftarrow S_0$ absorption, and that these same vibrations and rotations may be responsible for promoting the non-radiative decay of the thione triplets. Similar observations on a limited number of aromatic thiones have been made by Serafimov *et al.* (31).

The decay parameters of triplet TMIT and 4-Br-TMIT were measured in both hydrocarbon and heavy atom-containing solvents in order to examine the influence of both internal and external heavy atom perturbations on triplet thione decay dynamics. The $T_1 \leftarrow S_0$ molar extinction coefficient at λ_{max} is slightly larger for 4-Br-TMIT than for TMIT itself, indicative of greater spin–orbit coupling in the molecule containing the heavy atom, as expected (37). However, the measured intrinsic radiative lifetime (k^{-1}_{r,T_1}) for TMIT is slightly shorter than for 4-Br-TMIT in hydrocarbon solvents, whereas the rate constant for the non-radiative decay of triplet TMIT is slightly smaller than that for 4-Br-TMIT. Aside from broadening the emission and absorption spectra, the use of heavy-atom-containing solvents had little effect on the decay dynamics. These effects are seemingly inconsistent with expectations based upon the results of similar experiments with aromatic hydrocarbons and ketones (37). Unkown at present are the extent to which the $T_1 \leftarrow S_0$ absorption system is buried under the $S_1 \leftarrow S_0$ absorption, and the location and influence of other nearby triplet states. In xanthione there is evidence (6, 7, 14) that T_2, nominally $^3(\pi,\pi^*)$, lies very close in energy to T_1, nominally $^3(n,\pi^*)$, and that T_1 therefore has a large component of $^3(\pi,\pi^*)$ character. The location of higher energy triplet states in these thiones and the spectroscopic disentangling of the $S_1 \leftarrow S_0$ and $T_1 \leftarrow S_0$ transitions are under further investigation.

Acknowledgements

The authors wish to thank the Natural Sciences and Engineering Research Council of Canada for its continuing support of this work. One of us (A. S-A.) wishes to thank the University of Saskatchewan for the award of a Postgraduate Scholarship. Technical assistance of D. Demmer and D. James with some of the laser experiments is gratefully acknowledged. The authors thank Dr. J. D. Laposa, McMaster University for a sample of tetracene and Dr. A. Maciejewski for helpful discussions.

1. R. P. STEER. Rev. Chem. Intermed. **4**, 1 (1981).
2. P. DE MAYO. Acc. Chem. Res. **9**, 52 (1976).
3. N. J. TURRO, V. RAMAMURTHY, W. CHERRY, and W. FARNETH. Chem. Rev. **78**, 125 (1978).
4. D. J. CLOUTHIER, A. R. KNIGHT, R. P. STEER, and P. A. HACKETT. J. Chem. Phys. **72**, 1560 (1980).
5. D. A. CAPITANIO, H. J. POWNALL, and J. R. HUBER. J. Photochem. **3**, 225 (1974).
6. A. H. MAKI, P. SVEJDA, and J. R. HUBER. Chem. Phys. **32**, 369 (1980).
7. D. M. BURLAND. J. Chem. Phys. **75**, 2635 (1981).
8. U. BRUHLMANN and J. R. HUBER. J. Photochem. **10**, 205 (1979).
9. U. BRUHLMANN and J. R. HUBER. Chem. Phys. Lett. **54**, 606 (1978).
10. R. RAJEE and V. RAMAMURTHY. J. Photochem. **11**, 135 (1979).
11. A. SAFARZADEH-AMIRI, D. A. CONDIRSTON, R. E. VERRALL, and R. P. STEER. Chem. Phys. Lett. **77**, 99 (1981).
12. J. R. HUBER and M. MAHANEY. Chem. Phys. Lett. **30**, 410 (1975).
13. M. MAHANEY and J. R. HUBER. Chem. Phys. **9**, 371 (1975).
14. M. MAHANEY and J. R. HUBER. J. Mol. Spectrosc. **87**, 438 (1981).
15. D. M. BURLAND. Chem. Phys. Lett. **70**, 508 (1980).
16. P. DE MAYO and H. SHIZUKA. Mol. Photochem. **5**, 339 (1973).
17. A. H. LAWRENCE and P. DE MAYO. Mol. Photochem. **5**, 361 (1973).
18. J. R. BOLTON, K. S. CHEN, A. H. LAWRENCE, and P. DE MAYO. J. Am. Chem. Soc. **97**, 1832 (1975).
19. A. H. LAWRENCE, C. C. LIAO, P. DE MAYO, and V. RAMAMURTHY. J. Am. Chem. Soc. **98**, 2220 (1976).
20. T. OKA. A. R. KNIGHT, and R. P. STEER. J. Chem. Phys. **66**, 699 (1977).
21. C. A. PARKER. Photoluminescence of solutions. Elsevier, New York. 1968.
22. W. H. MELHUISH. J. Opt. Soc. Am. **54**, 183 (1964).
23. C. D. AMATA, M. BURTON, W. P. HELMAN, P. K. LUDWIG, and S. A. RODEMEYER. J. Chem. Phys. **48**, 2374 (1968).
24. W. R. WARE. *In* Creation and detection of the excited state. Vol. IA. *Edited by* A. Lamola. Marcel Dekker, New York. 1971. p. 213.
25. F. ARNDT and L. LORENZ. Ber. **63**, 3129 (1930).
26. E. ROTHSTEIN and M. A. SABOOR. J. Chem. Soc. 425 (1943).
27. D. E. PEARSON, H. W. POPE, and W. W. HARGROVE. Org. Synth. **40**, 7 (1960).
28. H. NAKAZUMI, A. SADA, and T. KITAO. Chem. Lett. 387 (1979).
29. B. S. PEDERSON, S. SCHEIBYE, N. H. NIELSSON, and L. A. WESSON. Bull. Chem. Soc. Belg. **87**, 223 (1978).
30. D. S. L. BLACKWELL, C. C. LIAO, R. O. LAUTFY, P. DE MAYO, and S. PASZYC. Mol. Photochem. **4**, 171 (1972).
31. O. SERAFIMOV, U. BRUHLMANN, and J. R. HUBER. Ber. Bunsen-Gesellsch Phys. Chem. **79**, 202 (1975).
32. M. MAHANEY and J. R. HUBER. J. Photochem. **5**, 333 (1976).
33. M. H. HUI, P. DE MAYO, R. SUAN, and W. R. WARE. Chem. Phys. Lett. **31**, 257 (1975).
34. D. K. C. MACDONALD. Noise and fluctuations: an introduction. Wiley, New York. 1962.
35. R. W. ANDERSON, JR., R. M. HOCHSTRASSER, and H. J. POWNALL. Chem. Phys. Lett. **43**, 224 (1976).
36. A. SAFARZADEH-AMIRI, R. E. VERRALL, and R. P. STEER. Unpublished results.

37. S. P. McGLYNN, T. AZUMI, and M. KINOSHITA. Molecular spectroscopy of the triplet state. Prentice-Hall, Englewood Cliffs, NJ. 1969.
38. S. J. STRICKLER and R. A. BERG. J. Chem. Phys. **37**, 814 (1962).
39. S. L. MUROV. Handbook of photochemistry. Marcel Dekker, New York. 1973.
40. K. F. FREED. Acc. Chem. Res. **11**, 74 (1978) and references therein.

Can. J. Chem. Downloaded from www.nrcresearchpress.com by 210.87.254.40 on 09/06/12
For personal use only.

Photovoltaic properties of CdS/phthalocyanine heterojunction cells[1]

A. M. Hor and R. O. Loutfy

Xerox Research Centre of Canada, 2480 Dunwin Drive, Mississauga, Ont., Canada L5L 1J9

Received July 8, 1982

This paper is dedicated to Professor Harry E. Gunning on the occasion of his 65th birthday

A. M. Hor and R. O. Loutfy. Can. J. Chem. **61**, 901 (1983).

Photovoltaic heterojunction solar cells formed between *n*-type cadmium sulfide, CdS, and various p-type phthalocyanines (Pc) such as H_2Pc, ZnPc, MgPc, CuPc, MnPc, PbPc, and VOPc were investigated. The cells were prepared by electrodepositing thin CdS films onto conducting indium-tin oxide (ITO) followed by sequential vacuum deposition of the phthalocyanines and gold layers. Among the seven phthalocyanines studied, ZnPc and MgPc exhibited the highest photovoltaic activity. Some optimization work was done for both the ZnPc and MgPc heterojunction devices. The optimum thickness of CdS and phthalocyanines was found to be 500 and 850 Å, respectively. Under an illumination of 50 mW cm^{-2}, the photovoltaic characteristics of the ITO/CdS/ZnPc/Au cell were: V_{oc} = 0.54 volts, J_{sc} = 285 μA cm^{-2}, and η = 0.10%, while the ITO/CdS/MgPc/Au cell delivered V_{oc} = 0.46 volts, J_{sc} = 231 μA cm^{-2}, and η = 0.066%.

A. M. Hor et R. O. Loutfy. Can. J. Chem. **61**, 901 (1983).

On a étudié les cellules solaires photovoltaïques à jonction hétérogène entre le sulfure de cadmium (CdS) de type-*n* et plusieurs phtalocyanines (Pc) de type-*p*, telles H_2Pc, ZnPc, MgPc, CuPc, MnPc, PbPc et VOPc. On a préparé les cellules par dépôt électrolytique de films minces de CdS sur l'oxyde conducteur d'indium et d'étain (OIT) suivi de dépôts successifs sous vide de couches de phtalocyanines et d'or. Parmi les 7 phtalocyanines étudiées, la ZnPc et la MgPc montrent la plus forte activité photovoltaïque. On a réalisé quelques travaux d'optimisation pour les deux dispositifs d'hétérojonction: ZnPc et MgPc. On a trouvé que l'épaisseur optimum de CdS et des phtalocyanines est respectivement de 500 et de 850 Å. Sous une illumination de 50 mW/cm^2, les caractéristiques photovoltaïques de la cellule OIT/CdS/ZnPc/Au sont de: V_{oc} = 0,54 volt, J_{sc} = 285 μA cm^{-2} et η = 0,10% tandis que la cellule OIT/CdS/MgPc/Au donne V_{oc} = 0,46 volt, J_{sc} = 231 μA cm^{-2} et η = 0,066%.

[Traduit par le journal]

Introduction

Phthalocyanines (Pc) have been recognized as an important class of organic semiconductive and photoconductive materials. These substances have found applications in the fields of reprography (1–4), organic photovoltaic cells (5–7), and more recently as infrared dyes in optical storage systems (8). One of their important potential uses will be as photocatalyst and spectral sensitizer in solar energy conversion.

Ghosh *et al.* (6) had investigated photovoltaic devices made of Al/magnesium phthalocyanine (MgPc)/Ag and observed an open-circuit voltage of 0.90 V and a short-circuit current of 9.5×10^{-8} A under an unspecified light intensity. From their measurements of capacitance–voltage ($C-V$) characteristics and action spectra, they confirmed the presence of a Schottky barrier at the Al/MgPc interface. A photovoltaic efficiency of 0.01% was quoted for the cell illuminated with a monochromatic light of 690 nm.

Later, Fan and Faulkner (7) reported their results for metal-free phthalocyanine (H_2Pc) and zinc phthalocyanine (ZnPc) cells with In and Al as blocking electrodes and Au as an ohmic contact. Cells with Al electrodes exhibited a power conversion efficiency 2 to 3 orders of magnitude lower than those with In electrodes. This was attributed to the presence of an insulating Al_2O_3 layer at the Al/Pc interface. Their best cell of In/ZnPc/Au had a conversion efficiency of 0.023% at a low light intensity of 2 mW cm^{-2} though an estimated quantum efficiency of 14.2% was claimed.

Both groups used phthalocyanines purchased from commercial suppliers without further purification. Also the thickness of the Pc films in their cells, i.e. 1500 Å in ref. 6 and 3000 Å in ref. 7, were much larger than the sum of the Schottky barrier width and diffusion length of minority carriers (electrons) or excitons which were estimated to be about 300 Å and 150 Å respectively (6). Uncontrolled impurities and incompatible thickness certainly have detrimental effects on the cell performance.

Recently, Wagner and Loutfy (9) employed a novel heterojunction cell in which the barrier electrode was an electrodeposited CdS film. CdS film can transmit more than 70% of light above 500 nm and thus does not interfere with the absorption of Pc in the visible region. More important, it is a n-type semiconductor with a Fermi level E_f = ~4.0 eV which is suitable for interfacing with phthalocyanines (E_f ~ 4.6 to 4.8 eV) to produce a reasonable built-in potential of 0.7 V at their junction. From their capacitance–voltage data of various CdS/MgPc cells they found that the barrier width was not sensitive to the thickness of CdS and hence concluded that the band bending or built-in potential essentially occurred within the Pc. Interestingly, these solid state devices were found to be very stable.

The main objectives of this work are: (*i*) to evaluate the effectiveness of various Pc in CdS/Pc photovoltaic cells, and (*ii*) to optimize the cell performance for the most promising phthalocyanines.

Experimental

Materials

A series of Pc including H_2Pc, MgPc, ZnPc, vanadyl phthalocyanine (VOPc), copper phthalocyanine (CuPc), lead phthalocyanine (PbPc), and manganese phthalocyanine (MnPc) have been studied in this work. They were purchased from Eastman Kodak and they were purified by sublimation. Indium-tin-oxide (Nesatron) glass plates were obtained from Pittsburg Glass Corp. with a sheet resistance of 70 Ω/square and optical transmission >83%. All other chemicals were obtained from common commercial sources.

[1]Presented at the 65th Annual Chemical Institute of Canada Conference, May 30 – June 2, 1982.

Can. J. Chem. Downloaded from www.nrcresearchpress.com by 210.87.254.40 on 09/06/12
For personal use only.

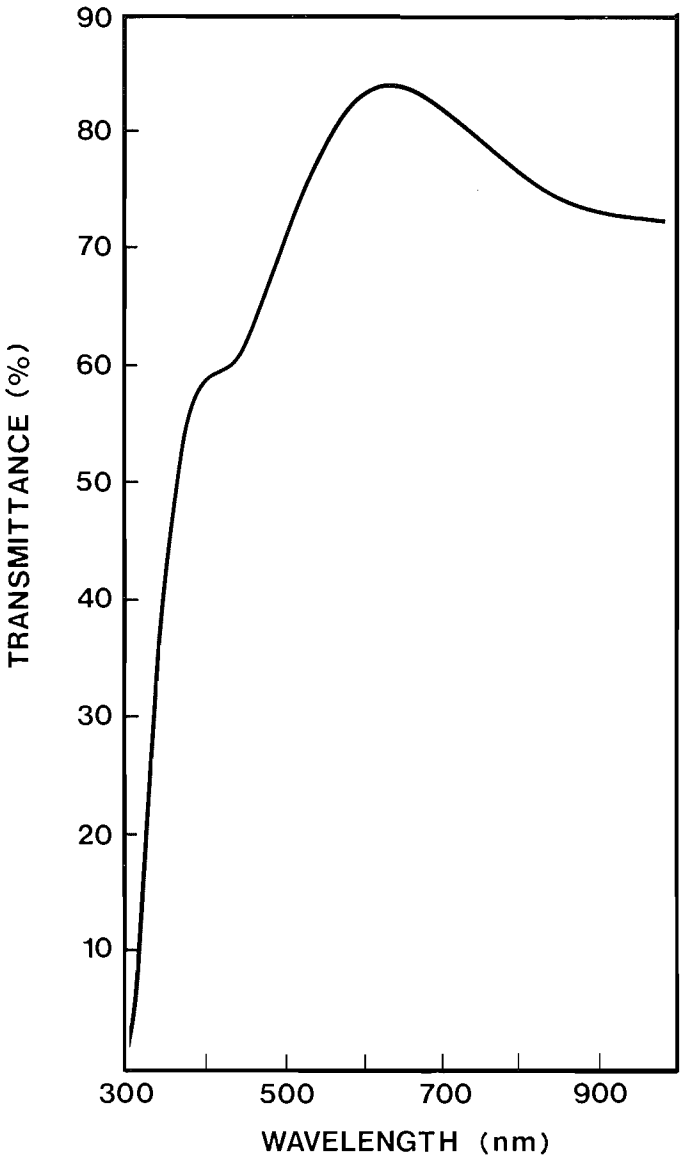

FIG. 1. Transmission spectrum of CdS (1600 Å) on Nesatron.

Device fabrication

Thin films of CdS were cathodically deposited (10) onto the Nesatron substrate from a solution of 400 mL dimethyl sulfoxide (DMSO) containing 0.6 g of sulfur and 1.0 g of cadmium chloride. The thickness of CdS films formed depended on the duration of electrodeposition. Figure 1 shows the transmission spectrum of a CdS film (1600 Å thick) deposited on the Nesatron. Above 500 nm it can transmit more than 70% of the incident light. The CdS-coated Nesatron substrates were cut into 2 in. × 2 in. square slides. A thin film of the phthalocyanine material was vacuum deposited onto the CdS-coated Nesatron. The deposition was carried out in a Balzer's vacuum coater at a base pressure of less than 10^{-6} mbar. Finally a Au electrode of 400 Å thickness was deposited onto the Pc film to complete the cells as shown in Fig. 2.

Measurements

All the measurements performed on the cells were carried out in air. The current–voltage ($J-V$) measurements were made by biasing the cells with an EG&G Polarographic Analyser Model 174A. Current and voltage readings were monitored by our data acquisition system built from a HP 9845B computer. The light source was a 1 kW Oriel Solar Simulator and light intensities were measured by a Karl Lambrecht light probe. Optical absorption spectra were recorded on a

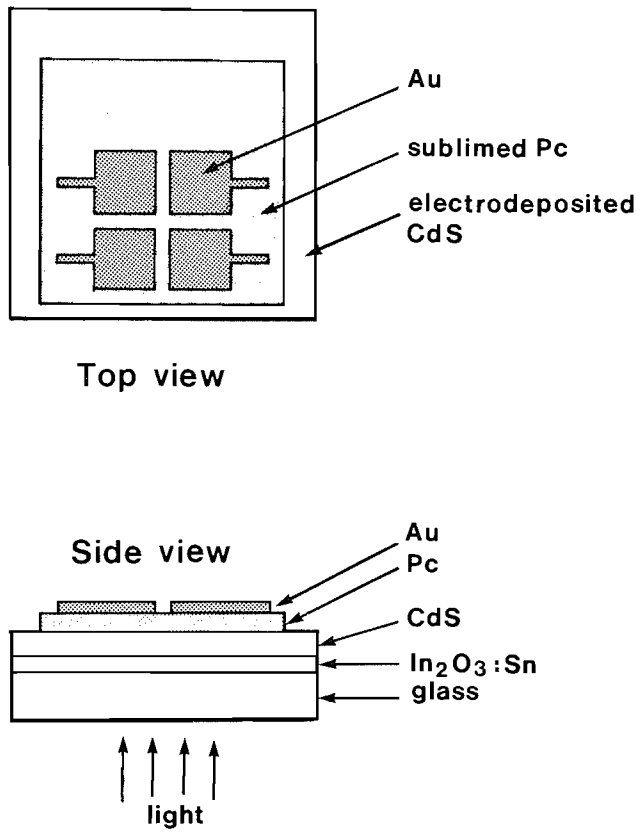

FIG. 2. Structure of a CdS/Pc heterojunction cell.

Cary 17 spectrophotometer. The light source for action spectrum measurements consisted of a 150-W Xe lamp and a $\frac{1}{4}$-m Jarrel Ash monochromator. The action spectra of the device were measured as described previously (11).

Results and discussion

1. *Dark* J–V *curve*

All Cds/Pc heterojunction cells display a rectifying behaviour in the dark. The dark $J-V$ curve of a typical CdS/MgPc cell is shown in Fig. 3. In the forward bias mode the Au electrode was polarized positive with respect to the CdS electrode.

2. *Action spectra*

In Fig. 4 the photocurrent action spectra of a typical CdS/MgPc heterojunction cell illuminated through the CdS and Au electrodes respectively are shown together with the absorption spectrum of a MgPc film deposited on a glass slide. A better agreement is seen between the optical absorption and the action spectrum obtained from illuminating the CdS electrode, verifying that the photoactive junction is situated at the interface between CdS and MgPc. Similar results were observed for other phthalocyanines.

3. *Comparison of various CdS/Pc cells*

In order to compare the performance of various cells a standardized cell structure was adopted which consisted of 1600 Å of CdS, 700 Å of Pc, and 400 Å of Au. These values were chosen on the basis of the optimal results reported in ref. 9. The cells were illuminated through the CdS electrode with simulated solar light of 50 mW cm^{-2}. Figure 5 shows the light $J-V$ curve of a CdS/MgPc device from which the characteristic photovoltaic parameters like open-circuit voltage V_{oc}, short-

Can. J. Chem. Downloaded from www.nrcresearchpress.com by 210.87.254.40 on 09/06/12
For personal use only.

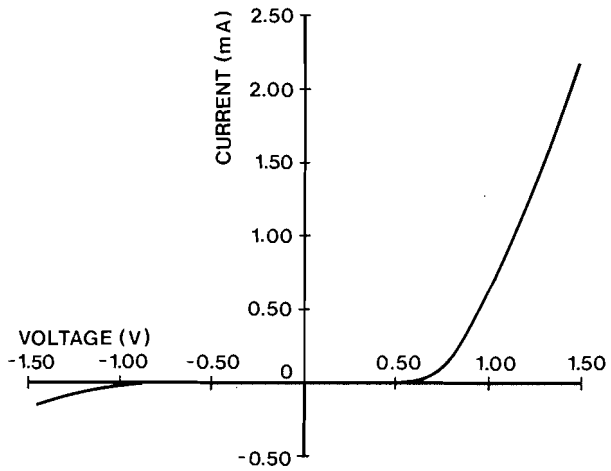

FIG. 3. Current–voltage curve of a CdS/MgPc cell in dark.

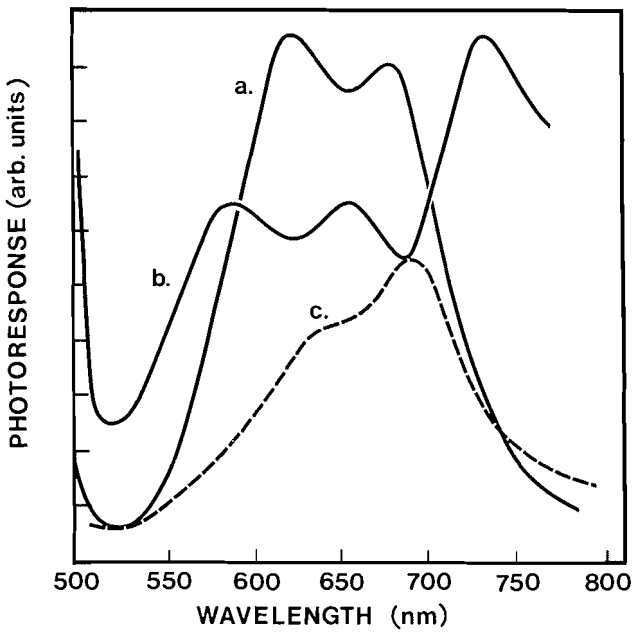

FIG. 4. Photocurrent action spectra of a CdS/MgPc cell illuminated (a) through the CdS electrode, and (b) through the Au electrode. (c) Absorption spectrum of a MgPc film.

circuit current J_{sc}, fill factor f.f., and conversion efficiency η can be evaluated. The results obtained from various cells are presented in Table 1. Among these cells MnPc hardly showed any photovoltaic activity. For all other cells the V_{oc} varied over a range from 0.41 to 0.55 V but the J_{sc} varied by a factor of ~3.5. The low fill factor usually observed in organic photovoltaic devices is attributed to the large series resistances derived from both CdS and Pc.

The magnitude of V_{oc} depends on the extent of band bending in the Pc at the CdS/Pc interface, hence on the difference in energy between their Fermi levels. Unfortunately, there are no reliable values for Fermi levels of Pc in the solid state and therefore we cannot explain, in a straightforward manner, the trend of V_{oc} observed for the Pc cells. Since Pc are p-type semiconductors with the top of the valence band located at about 5.0 eV with respect to the reference vacuum level, their Fermi levels may lie a fraction of an eV above the valence band. The exact location of the Fermi level within the band gap

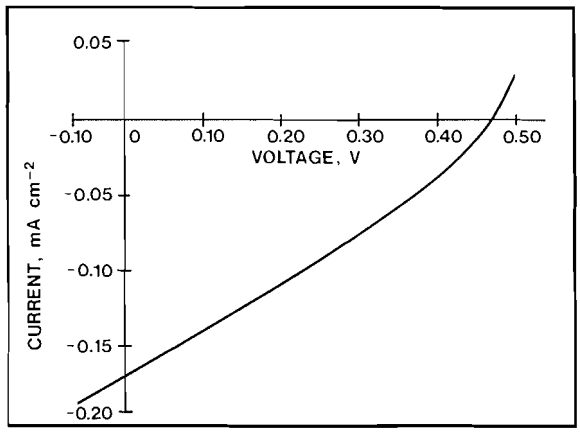

FIG. 5. Current–voltage curve of a CdS/MgPc cell under 50 mW/cm^{-2} of illumination.

of a semiconductor is known to be affected by several factors: impurity concentrations, surface states, etc. The observed V_{oc} values for all cells except MnPc suggested that their Fermi levels are at ~4.7 eV. The crystal ionization potential of MnPc has been estimated to be 4.16 eV (12) which can be considered as equivalent to the location of the top of the valence band. Obviously, interfacing MnPc with CdS would not produce any band bending in Pc and this may explain why no photovoltaic activity was observed from MnPc cells.

For these Pc cells, their photocurrents increased linearly with light intensity but the V_{oc} increased only logarithmically. This behaviour is illustrated by the data plotted in Figs. 6 and 7 for a ZnPc cell. The photocurrent J_{sc} and V_{oc} therefore can be analysed with the aid of the diode equation

$$V_{oc} = \frac{n\,kT}{q} \ln\left(\frac{J_{sc}}{J_0} + 1\right)$$

where kT = 0.025 eV at room temperature, q = electronic charge, n = diode factor, and J_0 = reverse saturation current.

The value of n was obtained from the slope of the plot of V_{oc} vs. log J_{sc}, and J_0 was then calculated from the diode equation. The values of n and J_0 are also included in Table 1. The reverse saturation current J_0 decreases as the value of n approaches one, and this appears to be consistent with the picture that a better diode would have a smaller leakage current. However, low J_0 and small n did not lead to good performance for H_2Pc, CuPc, and VOPc cells. This implies that the rectifying property at the junction, measured by the magnitude of n and J_0, is not the dominant factor in governing the performance of the photovoltaic devices studied. Probably, the carrier-generation efficiency is more important.

The photocarrier generation process in organic materials is very complex (13). The absorption of a photon creates an exciton rather than free carriers. The excitons can migrate from molecule to molecule or thermalize to form bound electron-hole pairs at impurity centers, defects, or interfaces. The electron-hole pair may terminate its life through recombination or dissociation into free carriers. The dissociation step is generally favored in the region of high electric field which happens to be near the CdS/Pc interface in our heterojunction cells. Some free carriers may be lost through trapping or recombination and only those which reach the collecting electrodes will contribute to the observed photocurrent. Our experimental data indicate that the conversion efficiencies of the CdS/Pc heterojunction cells decrease in the following order: ZnPc >

Can. J. Chem. Downloaded from www.nrcresearchpress.com by 210.87.254.40 on 09/06/12
For personal use only.

TABLE 1. Photovoltaic characteristics of CdS/Pc cells*

	H_2Pc	ZnPc	MgPc	VOPc	PbPc	CuPc	MnPc
V_{oc}, V	0.524	0.524	0.469	0.555	0.412	0.497	0.044
J_{sc}, μA cm^{-2}	94.6	188	173	97.5	108	52	20
f.f.	0.422	0.344	0.320	0.258	0.290	0.470	—
η, %	0.042	0.068	0.052	0.028	0.024	0.024	—
n	1.28	2.97	1.87	1.46	3.60	0.94	—
J_0 A cm^{-2}	7.1×10^{-14}	1.6×10^{-7}	7.8×10^{-9}	2.8×10^{-11}	2.2×10^{-6}	3.8×10^{-15}	—

*Cell configuration: Nesatron/CdS (1600 Å)/Pc (700 Å)/Au (400 Å).

TABLE 2. Optimization of MgPc cells*

MgPc, Å	700	850	1000	1000	1200	850
CdS, Å	500	500	500	1000	1000	1600
V_{oc}, V	0.485	0.462	0.437	0.425	0.416	0.469
J_{sc}, μA cm^{-2}	152	231	230	222	216	172
f.f.	0.319	0.305	0.300	—	—	0.319
η, %	0.046	0.066	0.060	—	—	0.052

*Cell configuration: Nesatron/CdS/MgPc/Au (400 Å).

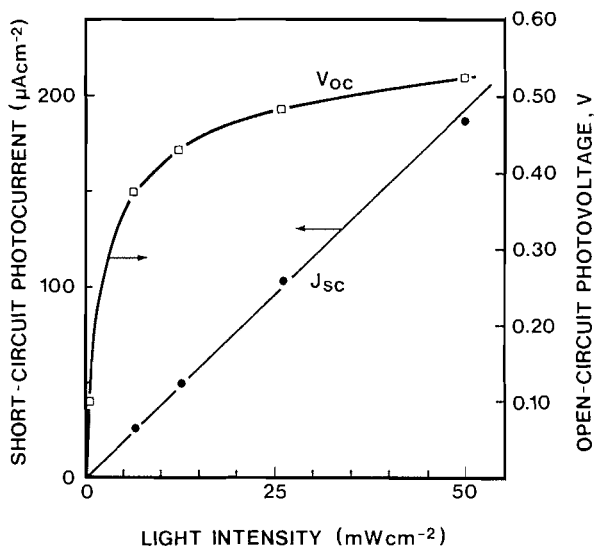

FIG. 6. Short-circuit photocurrent and open-circuit photovoltage as a function of light intensity for a CdS/ZnPc cell.

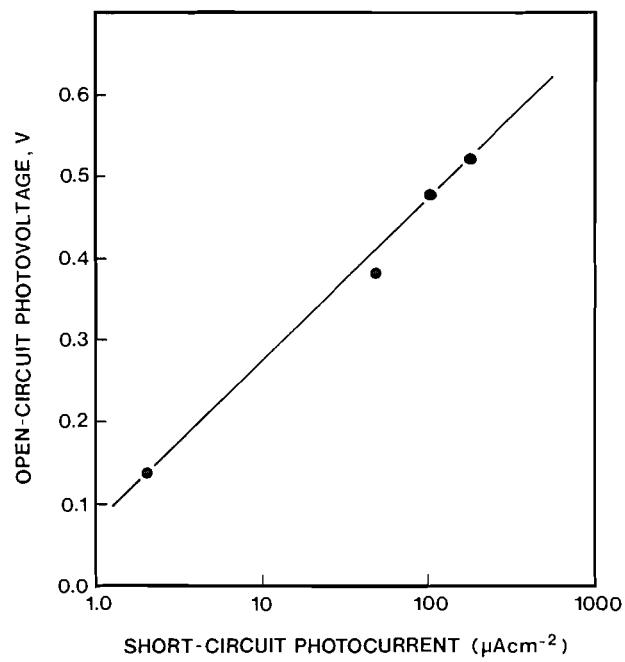

FIG. 7. Plot of open-circuit photovoltage vs. logarithm of short-circuit photocurrent for a CdS/ZnPc cell.

MgPc > H_2Pc > VOPc, PbPc, CuPc > MnPc. In view of the complex nature of various processes involved in the photocarrier generation, a simple explanation for the observed trend is very unlikely. An attempt to rationalize the conversion efficiencies of Al/Pc solar cells in terms of the oxidation potentials of Pc's was also unsuccessful (14).

According to the results listed in Table 1, we can single out ZnPc and MgPc as the most promising candidates for further investigation.

4. *Optimization of MgPc and ZnPc cells*

The optimization of MgPc and ZnPc cells was carried out by adjusting the film thickness of both CdS and Pc. For MgPc cells, the thickness of CdS was varied from 500 Å to 1600 Å and that of MgPc from 700 to 1200 Å. Table 2 summarizes the photovoltaic data obtained from a series of MgPc devices studied. Although cells with CdS thinner than 500 Å had been fabricated, serious electrical shortings did not allow any meaningful investigation. The shorting problems were most likely due to the presence of large imperfections in the very thin CdS films. The photovoltaic performance of MgPc cells remained almost constant when the CdS films ranged from 500 Å to 1000 Å and the MgPc film from 850 Å to 1200 Å. The best MgPc cell, which was fabricated with 850 Å of MgPc and 500 Å of CdS, had the following characteristics: V_{oc} = 0.462 V, J_{sc} = 231 μA cm^{-2}, η = 0.066% at an illumination of 50 mW cm^{-2}.

For the optimization of ZnPc cells, the CdS film was held constant at 500 Å while the ZnPc film was varied from 700 to 1200 Å. The results are presented in Table 3. The performance of the ZnPc cells was more sensitive to the thickness of the organic layer. The best ZnPc cell consisted of 850 Å ZnPc and 500 Å CdS and its photovoltaic characteristics were V_{oc} = 0.534 V, J_{sc} = 285 μA cm^{-2}, and η = 0.10% under the same illumination.

Can. J. Chem. Downloaded from www.nrcresearchpress.com by 210.87.254.40 on 09/06/12
For personal use only.

TABLE 3. Optimization of ZnPc cells*

ZnPc, Å	700	850	1200
CdS, Å	500	500	500
V_{oc}, V	0.506	0.534	0.522
J_{sc}, μA cm^{-2}	197	285	105
f.f.	0.350	0.350	0.365
η, %	0.070	0.10	0.040

*Cell configuration: Nesatron/CdS/ZnPc/Au (400 Å).

Thus, for both MgPc and ZnPc cells, the optimum thickness of Pc films is 850 Å. Since the width of the Schottky barrier has been determined to be ~500 Å in Pc (9), one can estimate that the diffusion length of excitons in Pc is ~350 Å which agrees reasonably well with Fan and Faulkner's value of 200 Å (7). The absorptions of light both inside and outside the barrier region contribute to the generation of photocurrent.

Conclusion

Among the seven Pc's studied in this work, ZnPc and MgPc show the greatest promise. At present, the only optimization done was related to the effect of film thickness of CdS and Pc. Future work will involve the improvement of their photoconducting characteristics which can only be gained by varying the fabrication conditions.

Acknowledgements

This work was supported in part by the National Research Council of Canada through an I.R.A.P. grant. The authors would like to thank T. Pietrobon for purifying most of the Pc used in this work and Dr. H. Wagner for many useful discussions.

1. J. W. WEIGL, J. MAMMINO, G. L. WHITAKER, R. W. RADLER, and J. F. BYRNE. Current problems in electrophotography. *Edited by* W. F. Berg and K. Hauffe. Walter de Gruyter, Berlin. 1972. p. 287.
2. R. J. KEMP. U.S. Patent No. 3,789,216 (1974).
3. F. SHIMADA, M. MATSUZAKI, and M. UEHARA. U.S. Patent No. 4,218,528 (1980).
4. S. GRAMMATICA and J. MORT. Appl. Phys. Lett. **38**, 445 (1981).
5. R. O. LOUTFY, J. H. SHARP, C. K. HSIAO, and R. HO. J. Appl. Phys. **52**, 5218 (1981).
6. A. K. GHOSH, D. L. MOREL, T. FENG, R. F. SHAW, and C. A. ROWE, JR. J. Appl. Phys. **45**, 230 (1974).
7. F. FAN and L. R. FAULKNER. J. Chem. Phys. **69**, 3341 (1978).
8. T. L. BLOOM *ET AL.* U.S. Patent Application Ser. No. 837853.
9. H. J. WAGNER and R. O. LOUTFY. J. Vac. Sci. Technol. **20**, 300 (1982).
10. A. S. BARANSKI, W. R. FAWCETT, A. C. MCDONALD, and R. M. D. NOBRIGA. J. Electrochem. Soc. **128**, 963 (1981).
11. R. O. LOUTFY and J. H. SHARP. J. Chem. Phys. **71**, 1211 (1979).
12. R. O. LOUTFY and Y. C. CHENG. J. Chem. Phys. **73**, 2902 (1980).
13. H. MEIER. Organic semiconductors. Verlag Chemie, Weinheim. 1974.
14. M. MARTIN, J. J. ANDRE, and J. SIMON. Nouv. J. Chim. **5**, 485 (1981).

Can. J. Chem. Downloaded from www.nrcresearchpress.com by 210.87.254.40 on 09/06/12
For personal use only.

Energy partitioning in some atom/radical reactions found in atmospheric pollution systems[1]

D. J. DONALDSON AND J. J. SLOAN

National Research Council of Canada, Division of Chemistry, 100 Sussex Drive, Ottawa, Ont., Canada K1A 0R6

Received July 12, 1982

This paper is dedicated to Professor Harry E. Gunning on the occasion of his 65th birthday

D. J. DONALDSON and J. J. SLOAN. Can. J. Chem. **61**, 906 (1983).

A modification of the arrested relaxation infrared chemiluminescence technique has been used to study the energy disposal in two atom–radical reactions. Vinyl and formyl radicals were generated chemically and their subsequent reactions with O atoms (in the case of vinyl) and F atoms (in the case of formyl) were followed. Product CO emission was observed in the system O/C_2H_3. Emission from both CO and HF was seen in the F/HCO system. The O/C_2H_3 reaction gives rise to substantially higher excitation in the CO product than does the F/HCO case. In each case, bound intermediates may be formed; the differences in energy diposal are discussed in terms of the possible influence of these intermediates.

D. J. DONALDSON et J. J. SLOAN. Can. J. Chem. **61**, 906 (1983).

On a utilisé une modification de la technique de chémiluminescence infrarouge de relaxation à l'arrêt pour étudier le dégagement d'énergie des deux réactions du type atome–radical. On a produit chimiquement des radicaux vinyle et formyle et on a suivi leurs réactions avec les atomes d'oxygène (dans le cas du vinyle) et avec les atomes de fluor (dans le cas du formyle). On a observé une émission de CO produit par le système O/C_2H_3. On a noté une émission à la fois de CO et de HF par le système F/HCO. La réaction du O/C_2H_3 donne lieu à une excitation nettement plus forte dans le CO produit que dans le cas du F/HCO. Il peut se former dans chaque cas des intermédiaires liés; on discute des différences de dégagement d'énergie en fonction de l'influence possible de ces intermédiaires.

[Traduit par le journal]

Introduction

The atmospheric chemical system involves many hundreds of reactions (1–5). These frequently occur in interconnected cycles, in which the products of a previous step are the reagents of a subsequent one. Since the rates of most reactions depend sensitively on the energy content of their reagents, this interdependence makes it important to understand the energy partitioning in such a system.

A great deal of work has been done on the measurement of energy partitioning in atom/molecule reactions and many excellent reviews of this subject exist (6, 7). However, a large fraction of the reactions important to atmospheric chemistry involve free radicals as either reagents or products (4) and the measurement of energy partitioning in such reactions is much more difficult. Although laser induced fluorescence techniques have made total rate measurements possible for many of these atom/radical reactions (8–10), energy partitioning measurements, which yield reaction rates as a function of internal energy of the products, can be made for only a very few radical systems (for example those involving OH).

We have constructed a machine, based on a low pressure infrared chemiluminescence apparatus, designed to measure energy partitioning in many simple atom/radical reactions which are important to the chemistry of tropospheric pollution. In previous work with this apparatus, we have reported measurements on the reactions of F atoms with OH (11), HNF (12), and C_2H_3 (13) radicals. Studies of F atom reactions with HS and NH_2 are also under way. In the following, we report our energy partitioning measurements on the reactions of O atoms with C_2H_3 radicals, and of F atoms with CHO radicals.

Experimental

The apparatus is based on a low pressure infrared chemiluminescence machine which has been described in detail previously (14). Recent modifications to the machine described in ref. 14 include the substitution of a Varian VHS 400 (8000 L/s) diffusion pump for the previous one, and the substitution of a homemade high conductance (38 cm inside diameter) cryobaffle for the one described in ref. 14. The new cryobaffle is not optically dense, but retains nearly two thirds of the pumping speed of the diffusion pump, at some expense in backstreaming.

A cross sectional sketch of the cylindrical vacuum chamber in which the reactions occur is shown in Fig. 1. A cylindrical liquid nitrogen reservoir, shown as the dotted area in the figure, is suspended from the top of the chamber. A series of copper vanes is suspended vertically from the underside of this reservoir. These are arranged in

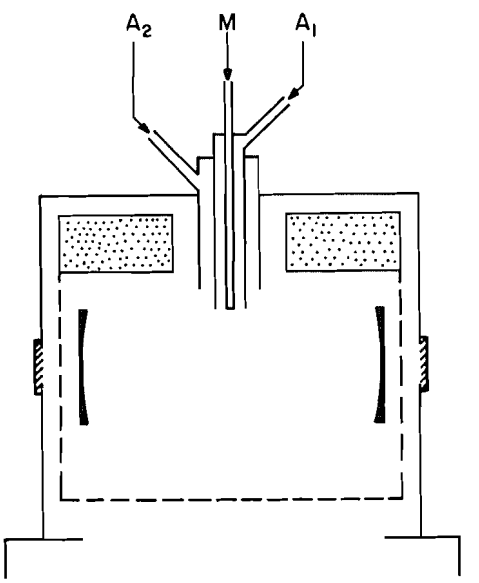

FIG. 1. Cross sectional sketch of the vacuum chamber showing three concentric reagent inlet tubes at top centre. M: vertically adjustable inlet tube for molecular reagent. A_1, A_2: atomic reagent inlets. Liquid nitrogen reservoir is dotted-in area. Curved surfaces are multipass light collection mirrors.

[1]Issued as NRCC No. 20694.

Can. J. Chem. Downloaded from www.nrcresearchpress.com by 210.87.254.40 on 09/06/12
For personal use only.

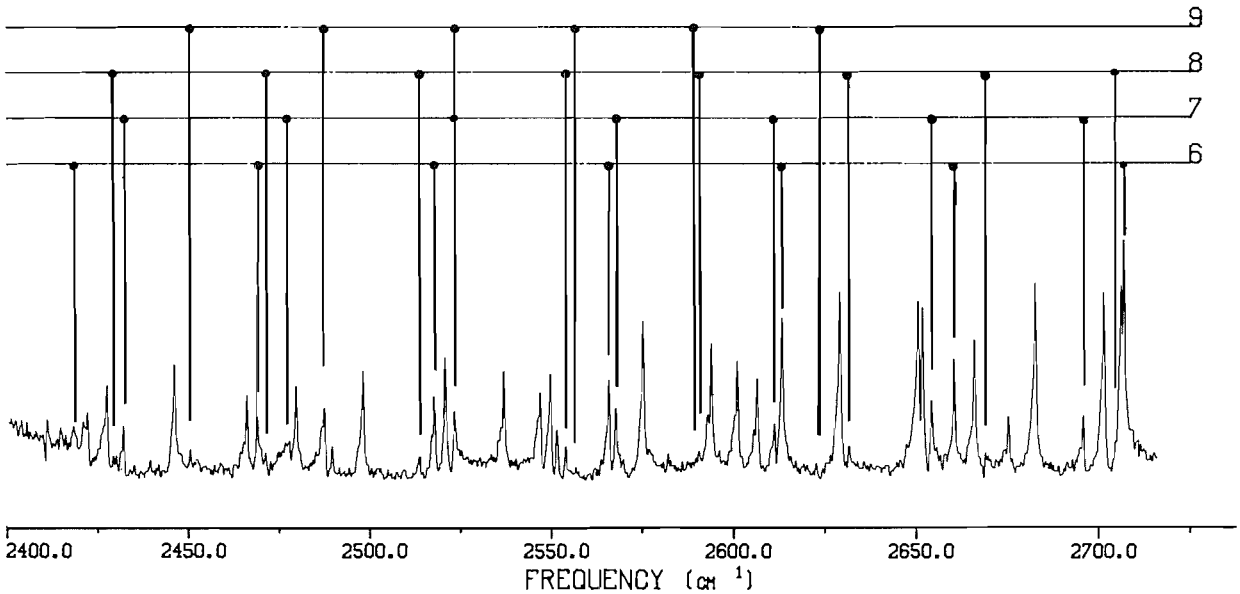

FIG. 2. A segment of the spectrum of the high-v' HF produced in reaction [1].

a radial pattern such that they effectively enclose the volume indicated by the dashed line in the figure. A reactor consisting of three concentric glass tubes is fixed to the lid of the vacuum chamber. The reactor, which is based on a previous design (15), is used to form the radical being studied in a chemical reaction between the molecular precursor M (which effuses through holes drilled radially in the wall of the central tube near its tip) and A_1, an atomic reagent. In the experiments reported here, A_1 is an F atom generated in a 2450 MHz, 100 watt microwave discharge in SF_6. For the vinyl radical studies, the molecular precursor, M, is C_2H_4, and the vinyl radicals are produced in the reaction:

$$[1]\quad F + C_2H_4 \rightarrow C_2H_3 + HF(v' \leq 2)\ \Delta H_0^0 = -29 \text{ kcal mol}^{-1}$$

Formyl radicals are produced if the precursor, M, is formaldehyde:

$$[2]\quad F + H_2CO \rightarrow HCO + HF(v' \leq 4)\ \Delta H_0^0 = -49 \text{ kcal mol}^{-1}$$

The location of the tip of the M injector, and thus the extent of these precursor reactions, can be adjusted from a position about 5 cm inside the A_1 tube to about 3 cm beneath its outlet.

Following the precursor reaction, the radicals mix with atoms A_2, which are added via the outermost of the three concentric tubes. For the $O + C_2H_3$ studies, A_2 is an oxygen atom formed in a second 2450 MHz, 100 watt discharge in O_2. In this case the following reaction occurs:

$$[3]\quad O + C_2H_3 \rightarrow CO(v' \leq 22) + CH_3\ \Delta H_0^0 = -120 \text{ kcal mol}^{-1}$$

For the formyl radical study (precursor reaction [2]), atom A_2 is a second F-atom, and the ensuing reaction is:

$$[4]\quad F + HCO \rightarrow CO(v' \leq 21) + HF(v' \leq 14)\ \Delta H_0^0 = -115 \text{ kcal mol}^{-1}$$

The indicated product vibrational states (v') in reactions [1] to [4] are the maximum levels which can be formed from the indicated exoergicities in each case. These were observed for reactions [1] and [2], but not for reactions [3] and [4], for reasons to be discussed shortly.

Results

1. *The $O + C_2H_3$ reaction*

For this system, the precursor reaction [1] has been extensively studied previously (16–18). It is known that this reaction partitions about 60% of the available energy into HF vibration and rotation. Therefore the vinyl radical receives a relatively small amount of the reaction energy. Reaction [1] has also been measured in this laboratory in connection with a study of the F + C_2H_3 reaction (19). It was shown that under the conditions of the F/C_2H_3 study, which are the same as those of the present experiments, the small amount of excitation energy partitioned into the vinyl radical by reaction [1] must be lost in collisions with the parent C_2H_4 before the former undergoes secondary processes such as reaction [3]. It is therefore assumed in the following that the C_2H_3 reagent in [3] has been thermalized to the temperature of the C_2H_4 (300 K).

The reaction of the C_2H_3 radicals with the F-atoms not consumed in reaction [1] provides a convenient means to monitor the concentration of the C_2H_3 radical in the present study. The F + C_2H_3 reaction, which was analysed in ref. 19, is about 98 kcal mol^{-1} exoergic, and thus can populate HF vibrational levels up to $v' = 11$. Its precursor (reaction [1]) is 29 kcal mol^{-1} exoergic, and can only populate HF levels up to $v' = 3$. Therefore, all emission from HF($v' \geq 3$) must come from the reaction of C_2H_3 radicals. A segment of the emission from high-v' HF recorded in the present experiments is shown in Fig. 2. For reasons discussed in ref. 19, HF($v' = 9$) was the highest level observed in the F/C_2H_3 system. However, the emission shown in Fig. 2 serves to demonstrate that the vinyl radicals were present in high concentration.

When O atoms are added to the F/C_2H_4/C_2H_3 system via the outer reactor tube (A_2 in Fig. 1), CO emission is observed. A sample of this emission appears in Fig. 3. In this figure, the band origins for the various vibrational levels CO($v' = 1$–7) are indicated. The lower trace is recorded if no F atoms are present in the system, and shows weak emission from CO($v' = 1, 2$) only. The upper trace, shown with the same vertical gain as the lower, appears when F atoms (and hence C_2H_3 radicals) are present. In this case, strong emission from all the indicated CO levels is observed. This is a lower limit to the maximum CO level produced, however, because the infrared detector used (InSb) becomes quite insensitive below about 1950 cm^{-1}.

The upper spectrum shows that highly vibrationally excited CO is produced in reaction [3]. The limit imposed by the present detector prevents the determination of the maximum excitation, and of the accurate population distribution. A HgCdTe detector which is sensitive at longer wavelengths than

Can. J. Chem. Downloaded from www.nrcresearchpress.com by 210.87.254.40 on 09/06/12
For personal use only.

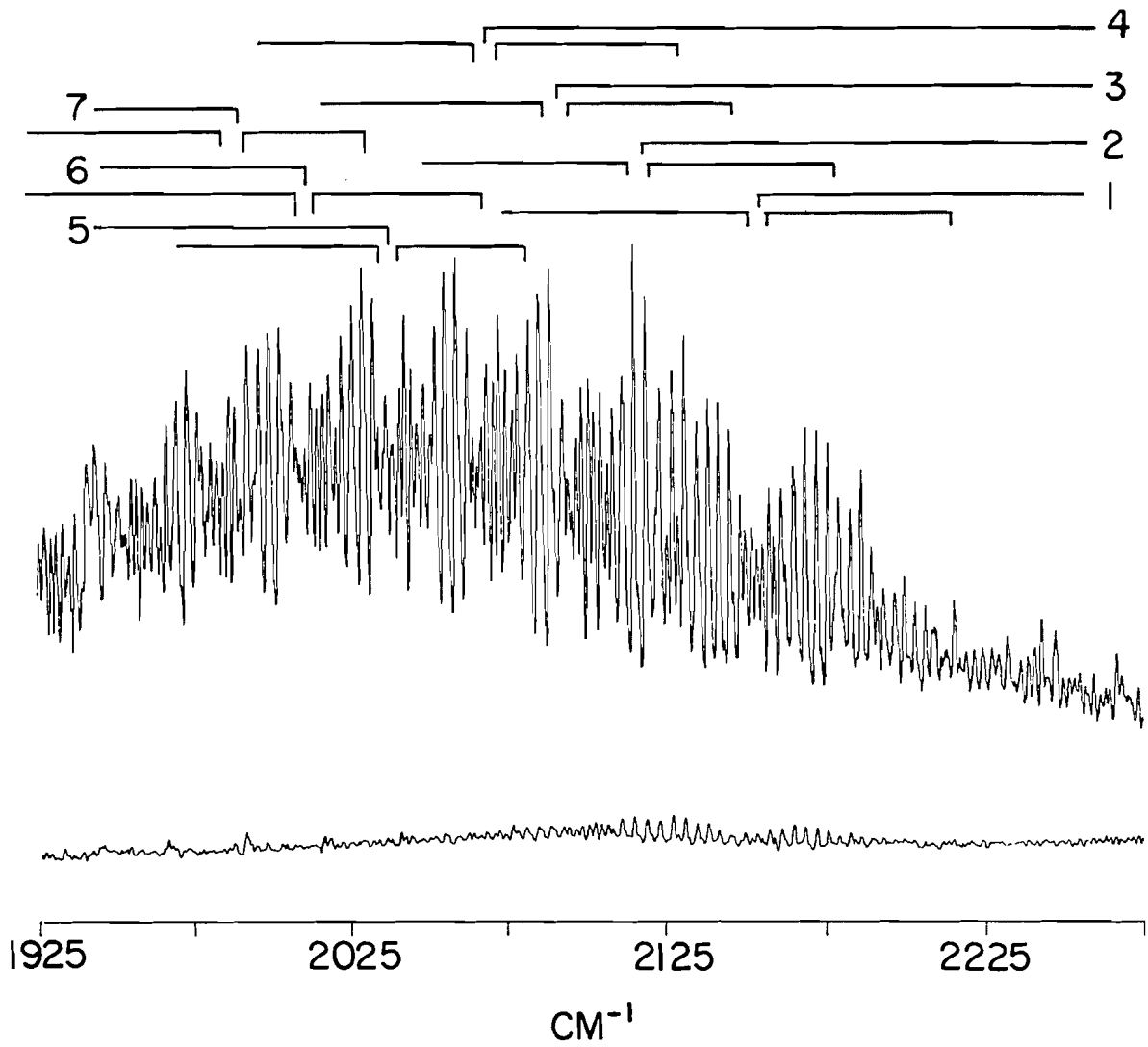

FIG. 3. CO emission from O/C_2H_3 system. Lower trace: F atom discharge off. Upper trace: F atom discharge on. Same reagent flows and vertical gain in each case.

the InSb detector will be installed to make these measurements. The emission in the lower trace originates in the O/C_2H_4 system. The latter reaction has been extensively studied (20–23), and it has been concluded that the major channel is a substitution producing hydrogen and a vinoxy radical: $O + C_2H_4 \rightarrow H + C_2H_3O$. We believe the CO signal shown in the lower trace of Fig. 3 is due to the decomposition of the vinoxy radical produced in this reaction, possibly in a collision-assisted process. Assuming room temperature reagents, the process $O + C_2H_4 \rightarrow C_2H_3O + H \rightarrow CO + CH_3 + H$ releases about 14–16 kcal mol^{-1} to the products. This is enough to create $CO(v' = 2)$, as observed in the lower trace of Fig. 3.

2. The F + HCO reaction

The precursor reaction [2] for this system has also been studied extensively (24, 25) and the HF vibrational distribution has been determined. This reaction also channels a large fraction – about 57% (25) – of its available energy into the HF product. The exoergicity of reaction [2] is 48.6 kcal mol^{-1}. This is enough to populate the product HF up to the $v' = 4, J' = 13$ level. The HF distribution measured in previous experiments (25) on this reaction peaks strongly in $v' = 3$ and shows substantial population to the maximum allowed level.

In the present experiments, this previously-observed HF distribution can be reproduced by choosing low reagent flows (SF_6: 1.0 μmol s^{-1}; H_2CO: 0.5 μmol s^{-1}) and extending the injector tip 3 cm outside the end of the A_1 tube. The resulting distribution is shown in Fig. 4 (squares). The maximum energetically allowed level for reaction [2] is indicated by an arrow.

When the reagent flows are increased (total SF_6: 2.8 μmol s^{-1}; H_2CO: 1.7 μmol s^{-1}), the injector tip is withdrawn 7 mm inside the A_1 tube, and F atom discharges are run in both tubes A_1 and A_2, the HF distribution indicated by the circles in Fig. 4 was obtained. Here, the $HF(v' \leq 4)$ which is predominantly created in the precursor reaction [2] has begun to be vibrationally deactivated. Concurrently, emission from levels $HF(v' \geq 5)$ has appeared. The latter levels can be created only in reaction [4]. The triangular points show the populations of the levels $v' \geq 5$ scaled up by a factor of 10., This shows that the latter distribution decreases rapidly with increasing vibrational excitation, in contrast to that of the $v' \leq 4$ levels.

A portion of the HF spectrum from which the upper levels (circular points) in Fig. 4 were calculated is reproduced in Fig. 5. Only transitions from levels not accessible to reaction [2] – $HF(v' \geq 5)$ – are assigned. This illustrates the signal-to-noise ratio obtained in the data for these particular experiments.

Can. J. Chem. Downloaded from www.nrcresearchpress.com by 210.87.254.40 on 09/06/12
For personal use only.

Can. J. Chem. Downloaded from www.nrcresearchpress.com by 210.87.254.40 on 09/06/12
For personal use only.

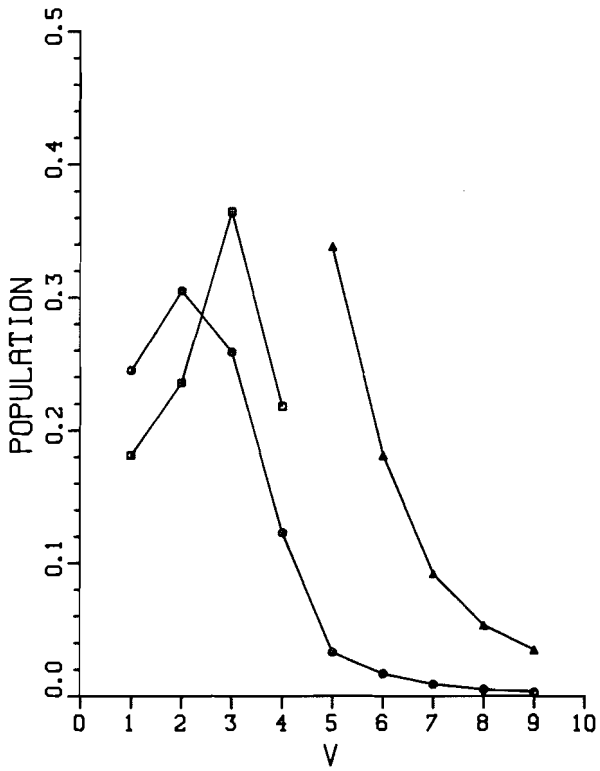

FIG. 4. HF vibrational distributions from $F/H_2CO/HCO$ system. □: Low reagent flows, injector fully extended. ○: Increased reagent flows, injector partially withdrawn. △: Vertical gain increased by 10×.

Under the conditions of increased reagent flows and double F atom discharges just described, emission was recorded from CO as well as from HF. The CO emission is shown in Fig. 6. The band origins for levels up to $v' = 4$ are indicated as before. The CO emission intensity decreases smoothly with increasing vibrational level until it blends with the noise. However, in the spectrum displayed in Fig. 6, emission from all levels up to and including $v' = 5$ could be unambiguously assigned. This CO emission intensity responds to changes in the experimental conditions (reagent flows and injector location) in the same way as that of the HF($v' \geq 5$) emission shown in Fig. 5. Additionally, the CO emission does not appear without the higher-flow conditions which gave the intense HF($v' \geq 5$) emission just described. The origin of the CO emission is therefore believed to be the same as that of the HF($v' \geq 5$), reaction [4].

Discussion

The atom/radical reactions [3] and [4] both give rise to easily-detectable CO fundamental emission. These are secondary reactions in the sense that each requires a reagent which is generated in a previous reaction in the flowing gas mixture. In order to be observable in the conditions of the present experiment (total pressure in the reaction zone about 10^{-2} Torr, total residence time of the flowing gases about 0.2 ms), these reactions must be very fast, with cross sections at least gas kinetic.

In spite of superficial similarities, however, these reactions appear to differ in some more fundamental respects. Comparison of the CO emission spectrum in Fig. 3 (from reaction [3]) with that shown in Fig. 6 (from reaction [4]) shows that the former creates much more vibrational excitation in the CO than the latter, even though the reactions have approximately the same exoergicity. (The value of ΔH_0^0 shown in eq. [3] is based on $\Delta H_{0,f}^0$ (g) of C_2H_3 = 69 kcal mol^{-1} (26). However, this may be as much as 10 kcal mol^{-1} too high (27).) A quantitative determination of the difference in the CO excitation created by these reactions cannot be made until the extent of the CO excitation in reaction [3] is known. However, it is clear from the figures that this difference is significant.

We have previously shown (19) that the measured HF distribution for the reaction $F + C_2H_3 \rightarrow HF + C_2H_2$ agrees with that predicted by a phase space calculation (28) which yields the distribution expected from the statistical decomposition of a microcanonical system consisting of the energized intermediate (vinyl fluoride) having the transition state geometry calculated

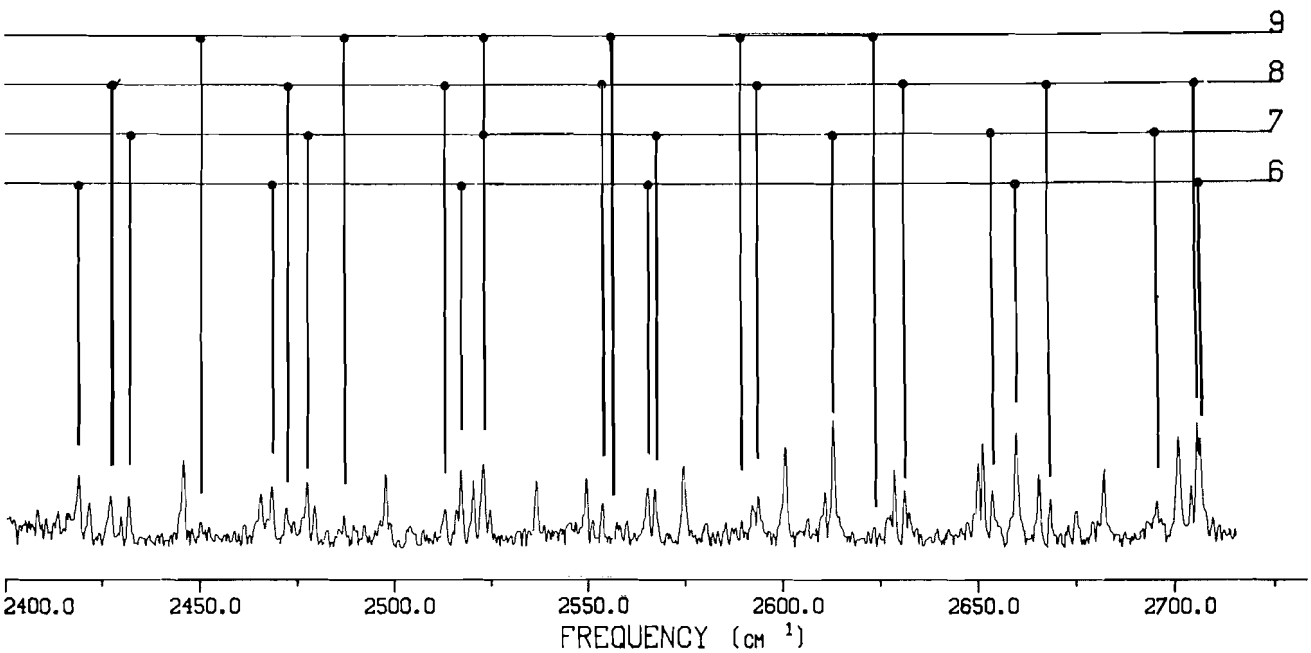

FIG. 5. High-v' HF emission from $F/H_2CO/HCO$ system. Only levels $v' > 5$ have been indicated.

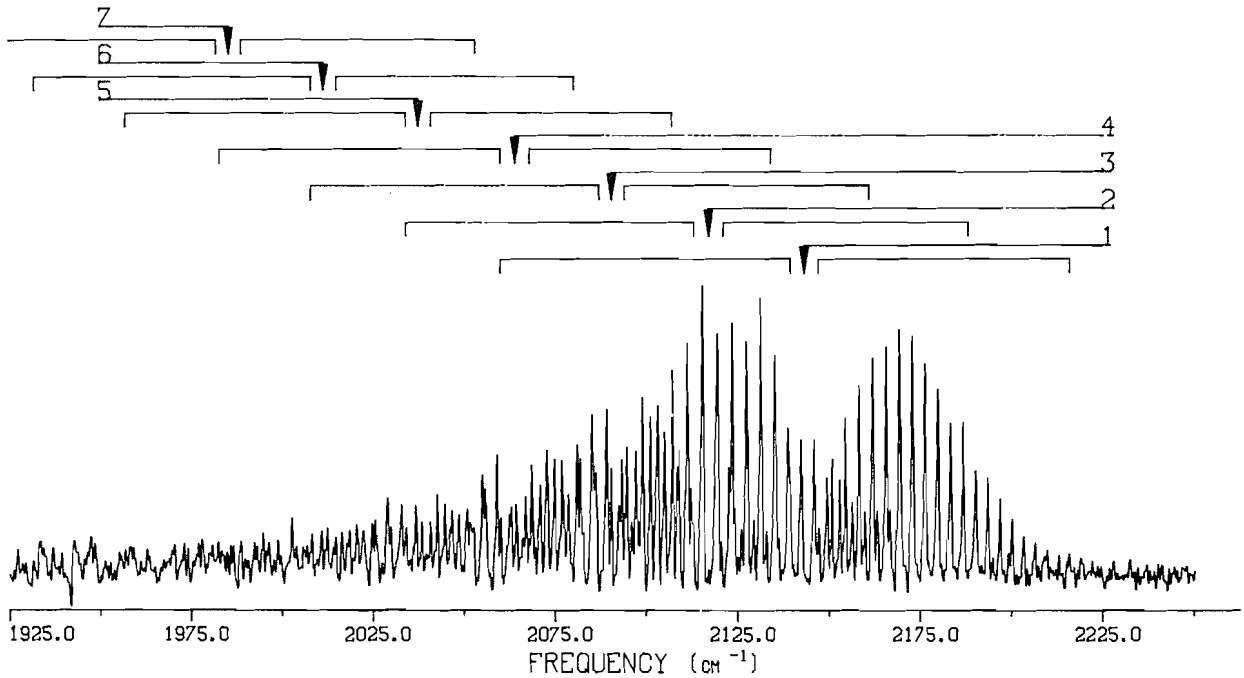

FIG. 6. CO emission from $F/H_2CO/HCO$ system. Band origin, R branch (to the left) and P branch (to the right) for transitions from the first four vibrational levels have been indicated.

in ref. 29. The F/C_2H_3 reaction resembles the F/HCO reaction in that the assumed intermediate in both cases is a strongly bound, closed shell molecule in which decomposition to products requires the unimolecular elimination of HF. A preliminary calculation has been done on the F/HCO system, and the result was found to agree roughly with high-v' distribution measured in reaction [4]. However, the quality of the experimental data is not yet high enough to permit a final conclusion to be made on this point.

The fact that the HF distributions from either of these reactions (F/C_2H_3 or F/HCO) would be found to be statistical is somewhat surprising in view of the very large exoergicity of both reactions. The total energy of the vinyl fluoride intermediate is about 100 kcal mol^{-1} above the HF + C_2H_2 products, and the HFCO is about 116 kcal mol^{-1} above separated HF + CO. In the former case, this is 20–30 kcal mol^{-1} (29) and in the latter, it is 40–50 kcal mol^{-1} (28) above the calculated minimum exit channel barrier. In view of this, it seems surprising that the potential energy well representing the intermediate, although very deep, should have any influence at all, since the RRKM lifetime of such a highly energized species would be very short indeed.

In Figs. 3 and 6 it was seen that the energy partitioned into the CO product of the O + C_2H_3 reaction was much greater than for the case of the F/HCO reaction. In the former case, the intermediate vinoxy radical is about as highly energized as the HFCO is in the latter reaction. The total energy of the O/C_2H_3 system, including that of the reagents, is about 120 kcal mol^{-1}. The minimum barrier to decomposition of the vinoxy radical to CO and CH_3 is not known, but it is likely to be much less than that of the HFCO and vinyl fluoride systems, because in the O/C_2H_3 case the intermediate is a radical which requires only a hydrogen atom migration before decomposition. If the exit channel barrier to C_2H_3O decomposition is somewhat lower than those of the other two reactions, the nonstatistical CO distribution may simply imply that the vinoxy system does not remain in the vicinity of the intermediate well in the potential energy surface as long as the F atom systems do.

Further work on these systems is under way. Accurate measurements of the CO energy distributions for reactions [3] and [4] will be made, and the extent to which these differ from completely statistical distributions will be determined. This information will also permit the complete determination of the energy partitioning in the F + HCO reaction, since it will involve direct measurement of the energy content of all products.

1. F. KAUFMAN. Annu. Rev. Phys. Chem. **30**, 411 (1979).
2. J. S. CHANG and W. H. DUEWER. Annu. Rev. Phys. Chem. **30**, 443 (1979).
3. J. W. MCGOWAN, R. H. KUMMLER, and F. R. GILMORE. Adv. Chem. Phys. **28**, Excitation and deexcitation processes relevant to the upper atmosphere. Wiley–Interscience, New York. 1975.
4. J. ALISTER KERR. *In* Frontiers of free radical chemistry. *Edited by* W. A. Pryor. Academic Press, New York. 1980.
5. R. A. COX and R. G. DERWENT. *In* Gas kinetics and energy transfer. Vol. 4. The Chemical Society, London. 1981.
6. I. W. M. SMITH. *In* Gas kinetics and energy transfer. Vol. 2. The Chemical Society, London. 1977.
7. B. E. HOLMES and D. W. SETSER. *In* Physical chemistry of fast reactions. Vol. 2. *Edited by* I. W. M. Smith. Plenum Press, New York. 1980.
8. I. MESSING, S. V. FILSETH, C. M. SADOWSKI, and TUCKER CARRINGTON. J. Chem. Phys. **74**, 384 (1981).
9. M. N. R. ASHFOLD, M. A. FULLSTONE, G. HANCOCK, and G. W. KETLEY. Chem. Phys. **55**, 245 (1981).
10. (*a*) J. E. BUTLER, J. W. FLEMING, L. P. GOSS, and M. C. LIN. Chem. Phys. **56**, 355 (1981); (*b*) H. H. NELSON, L. PASTERNACK, J. R. EYLER, and J. R. MCDONALD. Chem. Phys. **60**, 231 (1981); (*c*) D. GUTMAN, N. SANDERS, and J. E. BUTLER. J. Phys. Chem. **86**, 66 (1982).
11. J. J. SLOAN, D. G. WATSON, J. M. WILLIAMSON, and J. S. WRIGHT. J. Chem. Phys. **75**, 1190 (1981).
12. J. J. SLOAN, D. G. WATSON, and J. S. WRIGHT. Chem. Phys. **63**, 283 (1981).

Can. J. Chem. Downloaded from www.nrcresearchpress.com by 210.87.254.40 on 09/06/12
For personal use only.

13. J. J. SLOAN and D. G. WATSON. J. Chem. Phys. **74**, 744 (1981).
14. R. G. MACDONALD and J. J. SLOAN. Chem. Phys. **31**, 165 (1978).
15. B. A. BLACKWELL, J. C. POLANYI, and J. J. SLOAN. Chem. Phys. **24**, 25 (1977).
16. (*a*) J. M. PARSON and Y. T. LEE. J. Chem. Phys. **56**, 4658 (1972); (*b*) J. M. FARRAR and Y. T. LEE. J. Chem. Phys. **65**, 1414 (1976).
17. (*a*) J. G. MOEHLMANN and J. D. MCDONALD. J. Chem. Phys. **62**, 3061 (1965); (*b*) J. G. MOEHLMANN, J. T. GLEAVES, J. W. HUDGENS, and J. D. MCDONALD. J. Chem. Phys. **60**, 4790 (1974).
18. (*a*) Y. K. VASILJEV, V. B. IVANOV, E. F. MAKAROV, A. Y. RJABENKO, and V. L. TALROSE. Izv. Adak. Nauk SSSR, Ser. Khim. 215, 119 (1974); (*b*) D. J. BOGAN and D. W. SETSER. J. Chem. Phys. **64**, 586 (1976).
19. D. J. DONALDSON, D. G. WATSON, and J. J. SLOAN. Chem. Phys. **68**, 95 (1982).
20. G. INOUE and H. AKIMOTO. J. Chem. Phys. **74**, 425 (1981).
21. K. KLEINERMANNS and A. C. LUNTZ. J. Phys. Chem. **85**, 1966 (1981).
22. H. E. HUNZIKER, H. KNEPPE, and H. R. WENDT. J. Photochem. **17**, 377 (1981).
23. R. J. BUSS, R. J. BASEMAN, G. HE, and Y. T. LEE. J. Photochem. **17**, 389 (1981).
24. D. J. BOGAN, D. W. SETSER, and J. P. SUNG. J. Phys. Chem. **81**, 888 (1979).
25. R. G. MACDONALD and J. J. SLOAN. Chem. Phys. **31**, 165 (1978).
26. D. M. GOLDEN and S. W. BENSON. Chem. Rev. **69**, 125 (1969).
27. H. OKABE. Photochemistry of small molecules. Wiley–Interscience, New York. 1978.
28. K. MOROKUMA, S. KATO, and K. HIRAO. J. Chem. Phys. **72**, 6800 (1980).
29. S. KATO and K. MOROKUMA. J. Chem. Phys. **74**, 6285 (1981).

Can. J. Chem. Downloaded from www.nrcresearchpress.com by 210.87.254.40 on 09/06/12
For personal use only.

Reagent and product energy distributions for the reaction $F + OH(v) \rightarrow HF(v') + O$[1]

D. J. DONALDSON AND J. S. WRIGHT

Ottawa–Carleton Institute for Research and Graduate Studies in Chemistry, Carleton Campus, Carleton University, Ottawa, Ont., Canada K1S 5B6

AND

J. J. SLOAN

Division of Chemistry, National Research Council, 100 Sussex Drive, Ottawa, Ont., Canada K1A 0R6

Received July 8, 1982

This paper is dedicated to Professor Harry E. Gunning on the occasion of his 65th birthday

D. J. DONALDSON, J. S. WRIGHT, and J. J. SLOAN. Can. J. Chem. **61**, 912 (1983).

The hydroxyl radical is generated in various vibrational states by three reactions: $F + H_2O \rightarrow HF + OH$ ($v = 0$), $H + NO_2 \rightarrow NO + OH$ ($v \leq 3$), and $H + O_3 \rightarrow O_2 + OH$ ($v = 7-9$). The OH so produced reacts with F atoms according to $F + OH(v) \rightarrow HF(v') + O$. The vibrational populations of OH and HF are obtained by the low pressure infrared chemiluminescene technique.

D. J. DONALDSON, J. S. WRIGHT et J. J. SLOAN. Can. J. Chem. **61**, 912 (1983).

On forme le radical hydroxyde sous différents états vibrationnels au moyen de trois réactions: $F + H_2O \rightarrow HF + OH$ ($v = 0$), $H + NO_2 \rightarrow NO + OH$ ($v \leq 3$) et $H + O_3 \rightarrow O_2 + OH$ ($v = 7-9$). Le radical OH ainsi produit réagit avec les atomes de fluor selon l'équation: $F + (OH)(v) \rightarrow HF(v') + O$. On a obtenu les populations vibrationnelles du OH et de HF par la technique de chimiluminescence par infrarouge à faible pression.

[Traduit par le journal]

Introduction

Reactions of the hydroxyl radical play an important role in atmospheric photochemistry (1, 2). In the upper atmosphere OH is produced in vibrationally excited states by the reaction of hydrogen atoms with ozone. Emission from these states is considered to be the major source of the Meinel OH bands (3).

The laboratory study of reactions of vibrationally excited OH began with the work of Coltharp *et al.* (4) and Streit and Johnston (5) on $OH(v) + O_3$. Spencer and Glass (6) produced OH ($v = 1$) in high yield and studied its reactions with a variety of molecules. In a paper closely related to the present one, Blackwell *et al.* (7) prepared OH in two vibrational distributions by reaction with $H + O_3$ and $H + NO_2$, and reacted the OH (v) with atomic chlorine to produce vibrationally excited HCl. Infrared emission from the HCl was monitored and converted into product populations, using an infrared chemiluminescene technique similar to the present one.

In this paper we report the results of a low pressure ir chemiluminescence study of the reaction of F + OH, where the OH is prepared in three different pre-reactions:

[PR1] $F + H_2O \rightarrow HF + OH$ ($v = 0$), $\Delta H^\circ_O = -17.4$ kcal/mol

[PR2] $H + NO_2 \rightarrow NO + OH$ ($v = 0-3$), $\Delta H^\circ_O = -28$ kcal/mol

[PR3] $H + O_3 \rightarrow O_2 + OH$ ($v = 7-9$), $\Delta H^\circ_O = -77.1$ kcal/mol

The OH so prepared then reacts with atomic fluorine:

[R1,R2,R3] $F + OH(v) \rightarrow HF(v') + O(^3P)$, $\Delta H^\circ_O = -33.7$ kcal/mol

This reaction will be labelled [R1], [R2], [R3], according to whether the OH reagent has been prepared by reaction [PR1], [PR2], or [PR3]. In addition to [R1]–[R3], reaction [PR3] can provide enough reagent excitation to populate excited electronic states or rearrangement channels of the products, including

[R4] $F + OH \rightarrow HF + O(^1D)$, $\Delta H^\circ_O = +11.7$ kcal/mol

[R5] $F + OH \rightarrow HF + O(^1S)$, $\Delta H^\circ_O = +63$ kcal/mol

[R6] $F + OH \rightarrow OF + H$, $\Delta H^\circ_O = +48.9$ kcal/mol

In the following, the effect of OH reagent excitation on the observed HF product excitation will be presented.

Experimental

These experiments were carried out in an arrested relaxation infrared chemiluminescence apparatus which has been described previously (8). It was fitted with an adjustable reagent inlet device in which the OH reagent was produced. In experiments with H_2O and NO_2, the vessel walls were cooled with liquid nitrogen. In experiments involving ozone, the coolant was a Dry Ice/methanol slurry, in order to avoid condensing liquid ozone inside the system. Fluorine atoms were generated in a 100 W, 2450 MHz discharge in CF_4 gas (Matheson, 99.7%). Hydrogen atoms were obtained from H_2 gas in the same way. NO_2 was vacuum distilled from a cylinder and stored at −80°C until used. Ozone was generated in a manner described previously (9) and stored over silica gel at −80°C until used.

The adjustable reagent inlet which was used to generate OH for the case of reaction [PR1] was similar to that used in a previous study with this system by Sloan *et al.* (ref. 10, hereafter Paper I). Briefly, it consists of a 6 mm diameter quartz tube inside a 25 mm diameter Teflon tube. H_2O is admitted to the quartz tube which is sealed at its end, except for small holes through which the vapour escapes laterally. F atoms flow down the Teflon tube and reaction [PR1] occurs at the mixing point which can be adjusted vertically over a range of about 5 cm. The pressure in this mixing region is estimated to range from about 1 mTorr to 10 mTorr. As discussed in I, the OH from [PR1] is all formed in the $v = 0$ state. This result, which was reported in I, has been confirmed by repeated experiments. The secondary reaction [R1] also occurs within and below this mixing region.

[1]Issued as NRCC No. 20784.

Can. J. Chem. Downloaded from www.nrcresearchpress.com by 210.87.254.105 on 09/06/12
For personal use only.

Can. J. Chem. Downloaded from www.nrcresearchpress.com by 210.87.254.105 on 09/06/12
For personal use only.

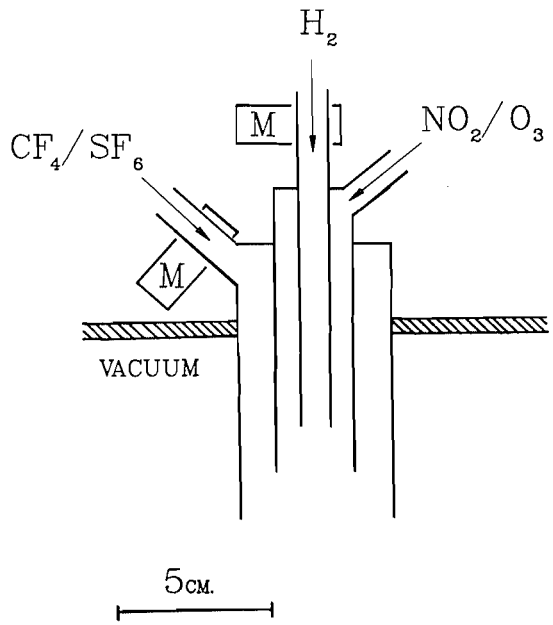

FIG. 1. Geometry of reagent inlet for NO_2 and O_3 experiments. F-atoms and H-atoms form as CF_4 and H_2 pass microwave discharges, labelled M.

The reagent inlet used in the O_3 and NO_2 experiments is shown in Fig. 1. It consists of three concentric quartz or Pyrex tubes, all of which are Teflon-coated. The H-atoms generated in the discharge flow down the inner tube and react with the NO_2 or O_3 which is admitted via the middle tube. F-atoms pass down the outer tube and encounter the OH (v) formed in reactions [PR2] and [PR3]. The F + OH (v) reaction occurs in the low-pressure region beneath the reactor inlets (the pressure rapidly drops to about 10^{-5} Torr in the centre of the vacuum chamber). For this reason the product HF from this reaction suffers virtually no vibrational energy transfer collisions.

Results

The results from the experiments using [PR1] are shown in Fig. 2 (10). The vibrational distribution of OH produced from reaction [PR1] is indicated as a single spike at $v = 0$. Because the activation energy for reaction [R1] is expected to be zero, the total energy available to products is about 34 kcal/mol (indicated as E'_{TOT}, Fig. 2). This is sufficient to populate HF ($v' \leq 3$). Reaction [PR1] also produces HF in states $v' = 0$ and 1; this cannot be separated from the contribution to these levels produced by reaction [R1]. The observed HF population in levels 0 and 1 is therefore due to reactions [PR1] and [R1], whereas for levels 2 and 3 it originates only from reaction [R1].

The result, shown in Fig. 2 and described in more detail in ref. 10, demonstrates that the reaction with ground state OH produces internally excited HF with vibrational energy up to the limit of the energy available (E'_{TOT}). However, the highest HF vibrational levels have smaller populations than the lower ones; the product excitation decreases with increasing vibrational level.

The reagent inlet configuration shown in Fig. 1 was used to explore the effect of OH vibrational excitation. For intermediate levels (up to OH ($v = 3$)), [PR2] was the source of vibrationally excited OH. The H-atoms for [PR2] were produced in a microwave discharge in H_2 (indicated as M in Fig. 1). However some undissociated molecular H_2 remains after such a discharge, and some vibrationally excited H_2 is produced in the high temperature plasma. As a result, the reaction between

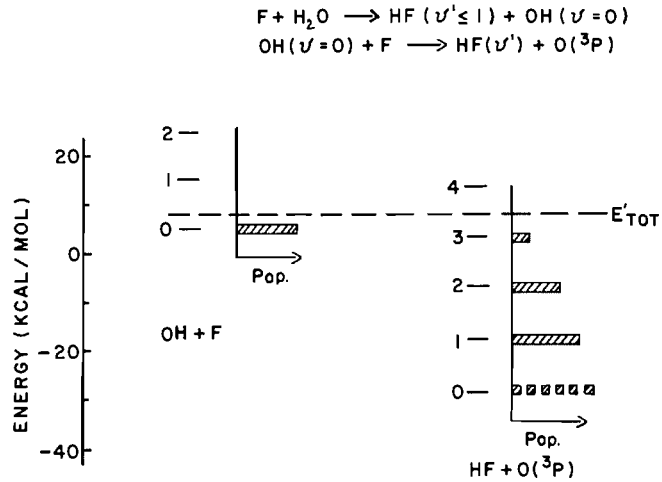

FIG. 2. Vibrational populations (hatched bars) at each quantum level for OH and HF. The population in HF ($v' = 0$) is unknown, as indicated by the dashed bar.

F-atoms and the remaining ground state H_2 produces HF with vibrational excitation up to $v' \leq 3$, while that with the vibrationally excited H_2 produces detectable amounts of HF ($v' \leq 4$). These HF emission spectra could be measured with both microwave discharges operating but with the NO_2 (and hence the OH) absent from the reactor. This provides a means whereby the HF populations produced by these interfering reactions could be determined, and subsequently subtracted from those measured with the OH reagent present.

In order to obtain the most accurate distributions for this subtraction, experiments were carried out in which CO_2 was substituted for the NO_2 in the reactor inlet. CO_2 was chosen for this purpose because it is not chemically reactive in this system, and it mimics, at least approximately, the vibrational deactivation (of HF) and the gas dynamic (e.g. momentum transfer) properties of NO_2. The HF vibrational distribution measured in the CO_2 "blank" experiment is indicated as squares in Fig. 3b. For the levels HF ($v' \leq 3$) the populations are within 5% of those produced by the F + H_2 reaction alone (11); the small difference arises from some deactivation and a small contribution fom the vibrationally excited H_2 reaction.

The small population in HF ($v' = 4$) is entirely due to the reaction with vibrationally excited H_2. Several experiments were carried out which explored the effect on the $v' = 4$ population of H_2 flow, added rare gas, differing F-atom precursors (SF_6 and CF_4), and an added HF deactivator, such as CO_2. These showed that while the vibrationally excited H_2 could not be completely eliminated, its effect, as judged by the HF ($v' = 4$) population, was reproducible for a given H_2 flow. As a result, a set of conditions was chosen which provided adequate H-atom concentrations with a known background HF population from the interfering reactions.

When NO_2 was substituted for CO_2 in the experiment,OH emission from the H + NO_2 reaction was observed. The OH distribution obtained under the flow conditions chosen for this study is shown in Fig. 3a. In this experiment, only the vibrationally excited OH could be determined, since the measurement is based on emission spectroscopy, but [PR2] also forms OH in its ground vibrational state. Under collision-free conditions the OH ($v = 0$) and OH ($v = 1$) levels are formed in approximately equal amounts by [PR2] (12). However, in the conditions of the present experiment, some deactivation of the

Can. J. Chem. Downloaded from www.nrcresearchpress.com by 210.87.254.105 on 09/06/12
For personal use only.

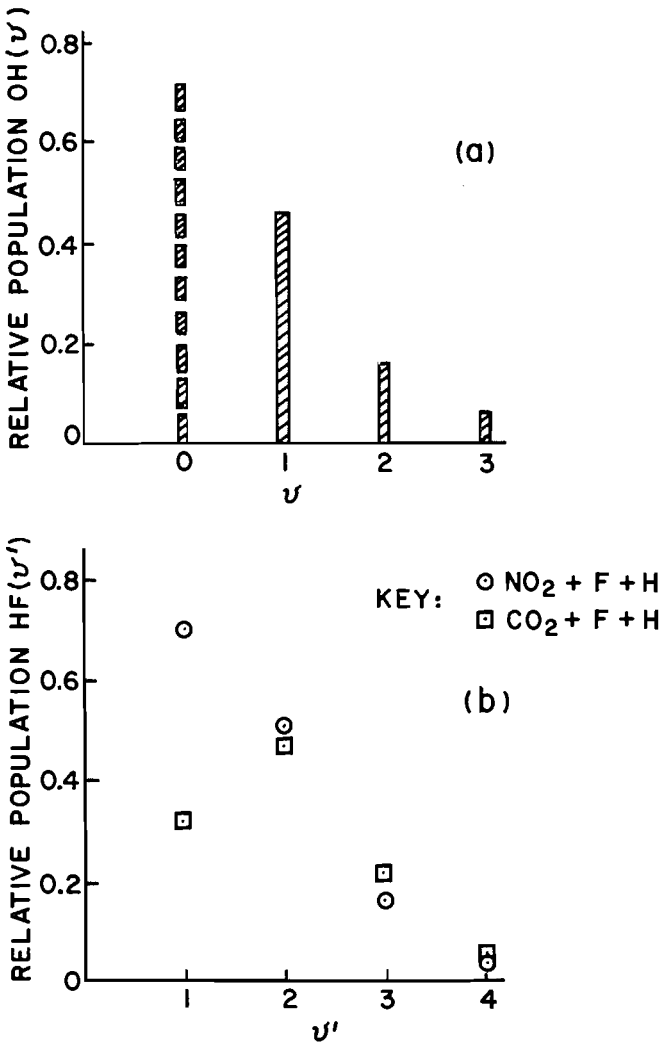

FIG. 3. (a) Vibrational populations of OH from H + NO_2 → OH (v) + NO. The dashed bar indicates an unknown, but probably large population in $v = 0$. (*b*) Vibrational populations of HF from two experiments: F + H + NO_2 (circles), F + H + CO_2 (squares).

vibrationally excited OH by NO_2 would be expected (9, 13). Rough calculations, based on the amount by which the observed OH ($v \geq 1$) distribution is collisionally deactivated (9, 12), suggest that the $v = 0$ population is between about 1 and 3 times that of the $v = 1$ level.

The effect of the OH (v) produced in [PR2] is shown by the circles in Fig. 3. In this case there is a substantial increase in the population of HF ($v' = 1$) and a small increase in that of HF ($v' = 2$) over those measured in the CO_2 "blank" experiment. The combined error in the two experiments are large, about 5%, for each vibrational level. Thus the remaining populations are, within this uncertainty, unchanged by the reaction with NO_2. Comparison of these results with those shown in Fig. 2 for the F + OH ($v = 0$) reaction shows that modest excitation of the OH (mostly to the $v = 1$ level) does not lead to any measurable increase in the product HF excitation.

Figure 4 shows the result of substantial vibrational excitation in the OH reagent. In this case the OH (v) was produced by reaction [PR3]. The same interferences from the F + H_2 reactions occurred in this case as well, and contributed to the observed HF ($v \leq 4$) populations. The HF ($v' \leq 3$) levels have been omitted from the figure for this reason. The reaction with

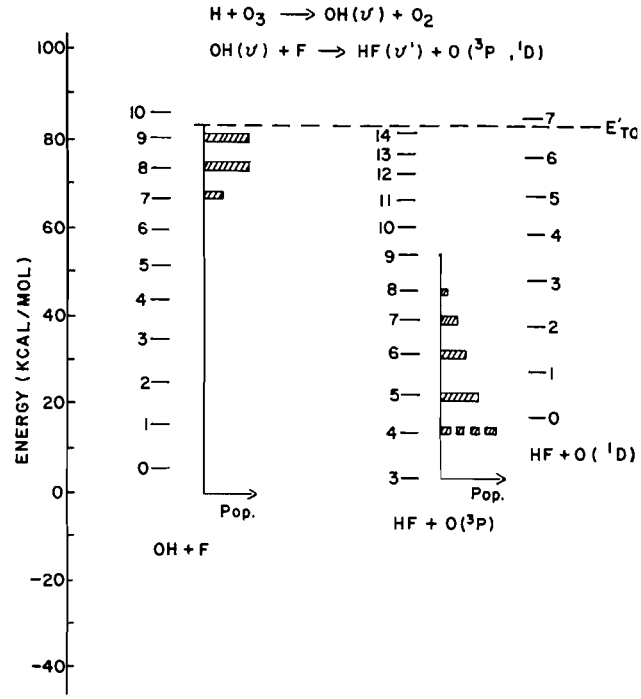

FIG. 4. Vibrational populations (hatched bars) for reagent OH ($v = 7-9$) and product HF ($v' \leq 8$). The dashed bar at HF ($v' = 4$) indicates that the levels $v' \leq 4$ may also be populated from the F + H_2 reaction. Also shown (at right) is the vibrational manifold for HF on the excited electronic surface HF + O (^1D).

vibrational excited H_2 contributes about 5% to the population of the $v' = 4$ level, which has been shown as a dashed bar to indicate this uncertainty.

It is clear from Fig. 4 that substantial (up to $v = 9$) vibrational excitation of the OH has resulted in a comparable increase in the vibrational excitation of the HF product. An increase in the maximum excitation of the OH reagent by about 50 kcal mol^{-1} (from $v = 3$ to $v = 9$) results in a nearly equal increase in the maximum observed HF product excitation (from $v' = 2$ to $v' = 8$).

Discussion

The electronic state correlation diagram, obtained for the FOH system by a combination of known thermochemistry and *ab initio* calculations reported in Paper I, is reproduced here and shown in Fig. 5.

Progress across the potential energy surface is indicated by the angle θ which changes from 90° (reagents) to 0° (products) during the course of the reaction. Inspection of Fig. 5 shows that two states, $^3\Pi$ and $^3\Sigma^-$, directly correlate ground state reactants F (^2P) + OH ($^2\Pi$) to ground state products HF ($^1\Sigma^+$) + O (^3P). However, the triplet barrier of ca. 12 kcal/mol cannot be surmounted by reaction [R1]. As discussed in I, an alternative path involving formation of the $^1A'$ HOF complex, followed by a crossing to the triplet surface in the exit channel (dashed circle) is required to explain the observed HF product formation in $v' \geq 1$. The presence of the HOF potential well and the presence of an exit channel barrier near the surface crossing would increase the lifetime of the HOF complex. As discussed in Paper I, if the complex is long-lived, the energy should be partitioned statistically among the product degrees of freedom. This is consistent with the distribution shown in Fig. 2. The results obtained with [PR2] show that modest

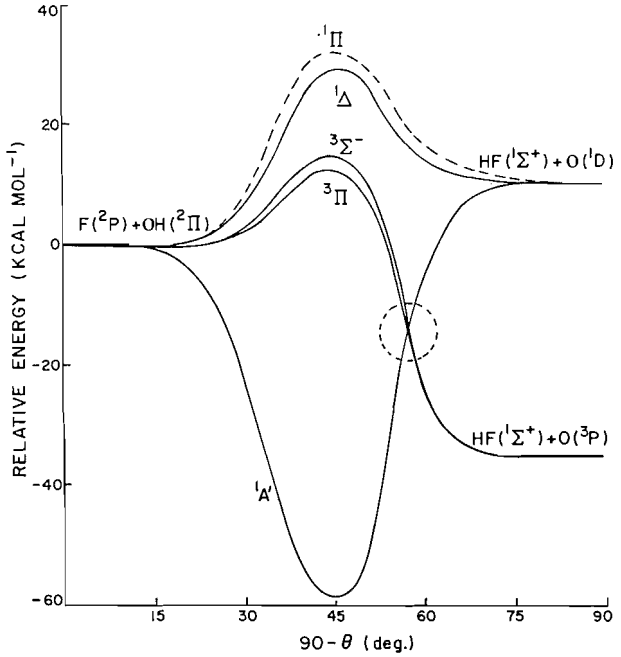

FIG. 5. Electronic state correlation diagram for the FOH system, taken from Paper 1.

vibrational excitation of the OH reagent (mostly to OH (v = 1)) does not appear to modify the dynamics of the reaction measurably. However, a substantial increase in vibrational excitation of the OH reagent causes a comparable increase in the maximum observed HF product excitation. This result is qualitatively the same as that obtained from the Cl + OH reaction reported in ref. 7. In that case, however, the reaction between the ground state reagents is virtually thermoneutral, and hence an increase in the energy of the reagent to a certain level led to an increase in the product energy to the same (absolute) level.

While the two reactions exhibit the same qualitative behaviour (increased reagent vibrational excitation leads to an increase by a comparable amount in the product vibrational excitation), the exoergicity of the FOH reaction makes a direct comparison difficult. The F + OH (v = 0) reaction, although substantially exoergic, does not efficiently partition its reaction energy into product vibration. It was suggested in ref. 10 that this may be an indication that a relatively long-lived FOH intermediate is formed. However, when the OH has substantial vibrational excitation, this excess reagent energy appears to be partitioned efficiently into product vibration. This suggests there is a difference in the efficiency with which reaction exoergicity and excess reagent energy are partitioned into product vibration. Such a difference would necessarily require non-statistical energy partitioning, and hence a change from the statistical behaviour of the reaction with OH (v = 0).

A second interpretation is possible for this observation; it is suggested by the third column of energy levels in Fig. 4. The product oxygen atom may be formed in its first electronically excited state, O (^1D), as indicated by the direct correlation shown in Fig. 5. If this occurs, only enough energy remains to excite the HF up to the v' = 6 level. If most of the reaction goes via this channel, then the large populations in levels HF ($v' \leq 6$) would imply substantial population up to the maximum thermochemically allowed limit. This, in turn would indicate a direct, non-ergodic reaction in which a large amount of the reaction exoergicity is partitioned into product vibration.

To distinguish between these two possibilities is an exceedingly difficult experimental problem; it is impossible with apparatus which is presently available. Substantial modifications to the apparatus are presently being carried out. It is hoped that these will decrease the uncertainty in the measured populations and present a clearer result in which the small differences in population predicted by the two models may be resolvable.

Concurrently, classical trajectory studies of the reactions on the various potential energy surfaces are also being carried out to better quantify the precise shapes of the distributions expected from the different possible reaction dynamics. It is hoped that these efforts will reveal the origins for the effect reported here. Presently, however, it can be concluded that the reaction with vibrationally cold OH gives low product vibrational excitation, a result which is consistent with the formation of a long-lived intermediate. In contrast to this, vibrational excitation in the reagent is channelled fairly efficiently into vibration in the product, a result which implies that the reaction with the vibrationally excited reagents is a direct process.

1. H. S. JOHNSTON. Science, **173**, 517 (1971).
2. F. S. ROWLAND and M. J. MOLINA. Rev. Geophys. Space Phys. **13**, 1 (1975).
3. A. B. MEINEL. Astrophys. J. **111**, 555 (1950).
4. R. N. COLTHARP, S. D. WORLEY, and A. E. POTTER. Appl. Opt. **10**, 1786 (1971).
5. G. E. STREIT and H. S. JOHNSTON. J. Chem. Phys. **64**, 95 (1976).
6. J. E. SPENCER and G. P. GLASS. Int. J. Chem. Kinet. **9**, 111 (1977).
7. B. A. BLACKWELL, J. C. POLANYI, and J. J. SLOAN. Chem. Phys. **24**, 25 (1977).
8. (*a*) R. G. MACDONALD and J. J. SLOAN. Chem. Phys. **31**, 165 (1978); (*b*) D. J. DONALDSON, D. G. WATSON, and J. J. SLOAN. Chem. Phys. **68**, 95 (1982).
9. J. C. POLANYI and J. J. SLOAN. Int. J. Chem. Kinet. **15**, 51 (1975).
10. J. J. SLOAN, D. G. WATSON, J. M. WILLIAMSON, and J. S. WRIGHT. J. Chem. Phys. **75**, 1190 (1981).
11. (*a*) J. C. POLANYI and K. B. WOODALL. J. Chem. Phys. **57**, 1574 (1972); (*b*) D. S. PERRY and J. C. POLANYI. Chem. Phys. **12**, 419 (1976).
12. J. A. SILVER, W. L. DIMPFL, J. H. BROPHY, and J. L. KINSEY, J. Chem. Phys. **65**, 1811 (1976).
13. M. A. NAZAR, J. C. POLANYI, W. J. SKRLAC, and J. J. SLOAN. Chem. Phys. **16**, 411 (1976).

Can. J. Chem. Downloaded from www.nrcresearchpress.com by 210.87.254.105 on 09/06/12
For personal use only.

A search for a gas-phase free-radical inversion displacement reaction at a saturated carbon atom[1]

R. A. BACK

Chemistry Division, National Research Council of Canada, 100 Sussex Drive, Ottawa, Ont., Canada K1A 0R9

Received July 12, 1982

This paper is dedicated to Professor Harry E. Gunning on the occasion of his 65th birthday

R. A. BACK. Can. J. Chem. **61**, 916 (1983).

Five thermal and photochemical reaction systems have been examined in an attempt to detect or to place upper limits on the rates of the simple inversion reaction, $CH_3 + CH_4 \rightarrow C_2H_6 + H$, and its reverse. No positive evidence was obtained for the occurrence of these reactions. An upper limit for the rate constant for the forward reaction of 0.063 M^{-1} s^{-1} at 802 K was obtained from the thermal decomposition of methane, and upper limits of 0.044 and 0.14 at 823 and 983 K respectively were estimated from the thermal decomposition of ethane. Other systems examined were the thermal decomposition of azomethane in the presence of methane, and the mercury-photosensitized decompositions of methane and ethane, which were complicated by unexpected side reactions.

R. A. BACK. Can. J. Chem. **61**, 916 (1983).

On a étudié cinq systèmes de réaction thermique et photochimique dans le but de déceler ou de situer les limites supérieures des vitesse de la réaction d'inversion simple: $CH_3 + CH_4 \rightarrow C_2H_6 + H$ et de la réaction inverse. On n'a pas obtenu la preuve formelle de l'existence de ces réactions. On a obtenu une limite supérieure pour la constante de vitesse de la réaction directe de 0,063 M^{-1} s^{-1} à 802 K à partir de la décomposition thermique du méthane et on a évalué des limites supérieures de 0,044 et de 0,14 à 823 et 983 K respectivement. On a examiné d'autres systèmes tels: la décomposition thermique de l'azométhane en présence de méthane et les décompositions photosensibilisées par le mercure, du méthane et de l'éthane. Ces décompositions se sont compliquées par la présence des réactions secondaires non prévues.

[Traduit par le journal]

Introduction

No simple free-radical displacement inversion reaction at a saturated carbon atom has apparently ever been observed. A large potential-energy barrier can be expected for such a reaction, and a knowledge of its activation energy and frequency factor is important to an understanding of the reaction dynamics, and more practically, to determine whether inversion reactions might be significant in particular reaction systems. The prototype

[1] $H + CH_4 \rightarrow CH_4 + H$

in which an H-atom approaches the carbon atom along one of the C—H axes, displacing the H-atom from the opposite side, would lead to isotopic exchange. This would be almost impossible to detect, however, in competition with the efficient methyl-radical chain reaction which leads to the same result (1). Inversion reactions of more practical interest are

[2] $CH_3 + CH_4 \rightarrow C_2H_6 + H$

and its reverse,

[3] $H + C_2H_6 \rightarrow CH_3 + CH_4$

Reaction [2] was suggested almost 50 years ago as a possible chain propagation step in the thermal decomposition of methane (2), for reasons that are no longer valid, and recent studies of this system (3) concluded that there was no evidence for its occurrence at temperatures down to 1000 K. The initial stages of the methane decomposition appear to be accounted for by the simple non-chain mechanism,

[4] $CH_4 \rightarrow CH_3 + H$

[5] $H + CH_4 \rightarrow H_2 + CH_3$

[6] $2CH_3 \rightarrow C_2H_6$

Reaction [4] is rate-controlling, and the rate $R = 2k_4[CH_4]$. If reaction [2] were important, a chain reaction would ensue, yielding $H_2 + C_2H_6$, the same products as before:

[2] $CH_3 + CH_4 \rightarrow C_2H_6 + H$

[5] $H + CH_4 \rightarrow H_2 + CH_3$

Net reaction $2CH_4 \rightarrow H_2 + C_2H_6$

It can be easily shown that the rate expression then becomes

$$R = 2k_4[CH_4] + 2k_2(k_4/k_6)^{1/2}[CH_4]^{3/2}$$

Activation energies associated with the non-chain and chain process would be E_4 and $(E_2 + \frac{1}{2}E_4 - \frac{1}{2}E_6)$ respectively. Taking $E_4 = 107.6$ (3) and $E_6 = 0$, it can be seen that if E_2 is less than 54 kcal/mol, the second term will have a lower activation energy than the first and might be expected to become important at sufficiently low temperatures. Conversely, if E_2 exceeded 54 kcal/mol the chain reaction could become important at high temperatures. It could also become important at much higher temperatures when the dissociation of ethane (the reverse of reaction [6]) becomes fast, essentially preventing the removal of methyl radicals by reaction [6] and allowing their concentrations to build up to very high values. In fact, it has been suggested that this occurs in the decomposition of methane in a shock tube at temperatures from 2000 to 2500 K (4).

In the present study, the following systems were examined in an attempt to detect reaction [2] or to place upper limits on its rate: (*1*) the thermal decomposition of methane; (*2*) the mercury-photosensitized decomposition of methane; (*3*) the thermal decomposition of azomethane in the presence of methane; (*4*) the thermal decomposition of ethane; (*5*) the mercury-photosensitized decomposition of ethane. The first

[1]NRCC No. 20639.

Can. J. Chem. Downloaded from www.nrcresearchpress.com by 210.87.254.40 on 09/06/12
For personal use only.

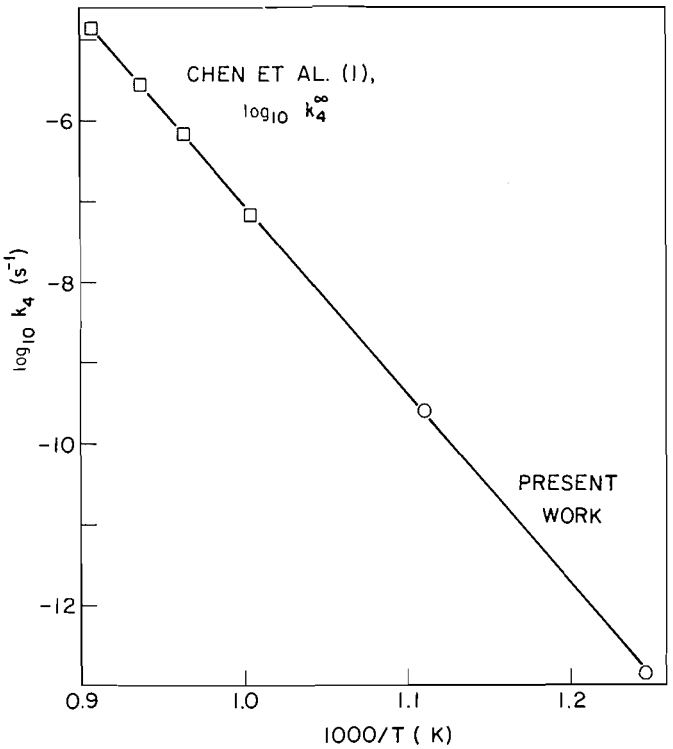

FIG. 1. Arrhenius plot of k_4, the first-order rate constant for the dissociation of methane.

three systems involve reaction [2] directly, the last two indirectly through reaction [3] to which it can be related thermochemically.

The thermal decomposition of methane

Previous studies in this laboratory (3) established that the initial stages of the decomposition from 995 to 1103 K are well accounted for by reactions [4], [5], and [6], with reaction [4] exhibiting some unimolecular pressure dependence, and no evidence for the occurrence of reaction [2]. The present experiments have extended these measurements to 899 and 802 K at pressures of about 1000 Torr where k_4 should be close to its high-pressure limit. Methods were similar to those used previously (3), with the quartz reaction vessel conditioned before each experiment by admitting air at the pyrolysis temperature for several hours to remove any carbon deposit. Without this conditioning, high and irregular rates were obtained, and it is clear that surface effects are more serious at these lower temperatures. Experiments in unconditioned sealed Pyrex vessels at pressures up to 10 atm also gave erratic results. Data from the conditioned vessel are shown in Fig. 1 together with the earlier data of Chen *et al.* (1), and it is clear that they are in close agreement with an extrapolation of k_4^∞ from the latter; i.e., there is no evidence for the occurrence of reaction [2]. Reaction times needed at 802 K to give measureable C_2H_6 were several months, and it seems impractical to extend these measurements to still lower temperature.

No ethylene was observed in any of these experiments, as would have been expected if secondary decomposition of ethane were occurring, and there is no reason to doubt that initial primary yields of ethane, and hence initial rates of reaction [4], were measured. It can be estimated that if reaction [2] had occurred to an extent 10% that of reaction [4] at our lowest temperature, we should have detected an enhanced rate of ethane formation. From this, an upper limit of $k_2 = 0.063\ M^{-1}\ s^{-1}$ can be estimated, taking a value of $k_6 = 4 \times 10^{10}\ M^{-1}\ s^{-1}$. If a frequency factor of $10^{10}\ M^{-1}\ s^{-1}$ is assumed, this corresponds to a lower limit of about 40 kcal/mol for E_2.

In their shock-tube studies Tabayashi and Bauer (4) found that values of $A_2 = 8 \times 10^{10}\ M^{-1}\ s^{-1}$ and $E_2 = 40$ kcal/mol in their reaction model gave the best fit to their data. These parameters give a value of $k_2 = 0.92\ M^{-1}\ s^{-1}$ at 802 K, about 15 times higher than our estimated upper limit.

The mercury-photosensitized decomposition of methane

This system merely substitutes a new initiation step,

[7] $Hg(^3P_1) + CH_4 \rightarrow Hg(^1S_0) + CH_3 + H$

for reaction [4] in the pyrolysis mechanism, permitting an extension of the measurements to lower temperatures at which the purely thermal reaction is too slow. Using methods similar to those used previously (5), the decomposition was studied at temperatures from 553 to 863 K, thus overlapping both the thermal decomposition studies and our earlier mercury-photosensitized experiments (5). Quantum yields of ethane at several temperatures are shown in Fig. 2 as a function of methane concentration. These data are in essential agreement with our earlier studies, with quantum yields rising with increasing pressure and temperature. If reactions [7], [5], and [6] were quantitative, the quantum yield should have been unity, independent of temperature and pressure. The observed values, and their variation, probably reflect as before an incomplete and temperature-dependent quenching of $Hg(^3P_1)$ in reaction [7], with perhaps some loss of CH_3, and thence C_2H_6, by the incomplete suppression of the combination reaction,

[8] $CH_3 + H \rightarrow CH_4$

For our present purposes, the important observations are that the quantum yield of ethane is always less than unity and shows no sharp upward trend with temperature as might be expected from the onset of a chain reaction, propagated by reaction [2], with an activation energy in the 20–50 kcal/mol range (cf. the mercury-photosensitized decomposition of ethane at high temperature (6) in which a chain decomposition is propagated by the decomposition of the ethyl radical). An activation energy of about 6 kcal/mol can be estimated from Fig. 2 at a methane concentration of $8 \times 10^{-3}\ M$, much too low for the inversion reaction. Because of uncertainties in the efficiencies of reactions [5], [6], and [7], it is impossible to calculate a meaningful upper limit for reaction [2] from this system, but there is no positive evidence for its occurrence.

The thermal decomposition of azomethane in the presence of methane

In this system again a new initiation step,

[9] $C_3NNCH_3 \rightarrow 2CH_3 + N_2$

is substituted for reaction [4] in the methane pyrolysis. In pure azomethane this is followed by the reaction

[10] $CH_3 + CH_3NNCH_3 \rightarrow CH_4 + CH_3NNCH_2$

and reaction [6]. Subsequent reactions of CH_3NNCH_2 and other radicals with azomethane lead to a short-chain reaction with a chain length of 2 or 3, yielding N_2, CH_4, C_2H_6, and some higher products (7). With methane present, this chain may be partly suppressed by the reversal of reaction [10].

Can. J. Chem. Downloaded from www.nrcresearchpress.com by 210.87.254.40 on 09/06/12
For personal use only.

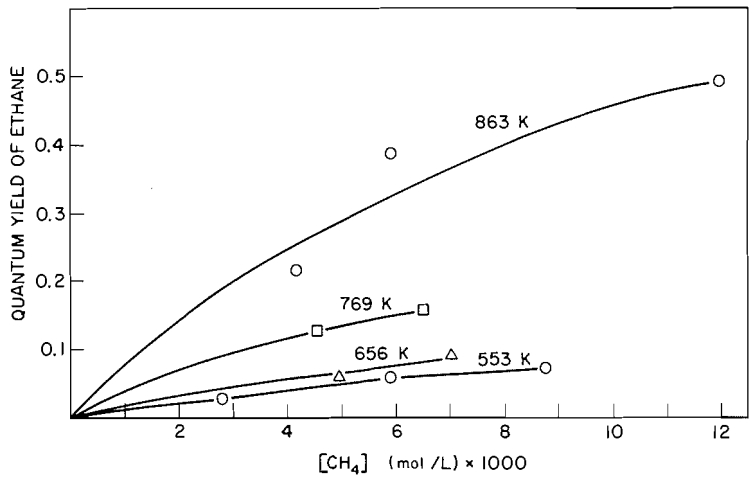

FIG. 2. Quantum yields of ethane vs. methane concentration in the mercury-photosensitized decomposition of methane.

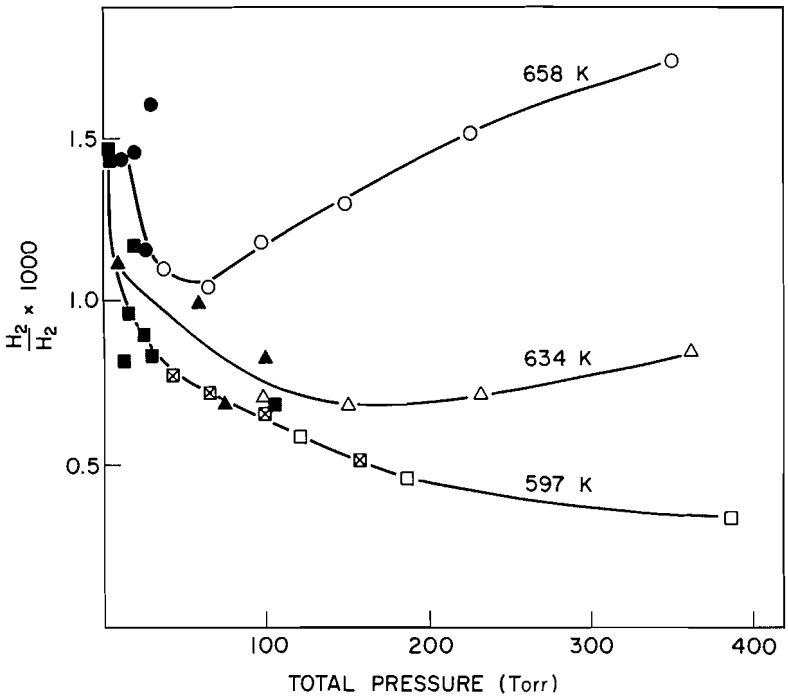

FIG. 3. Variation with pressure of the product ratio H_2/N_2 in the thermal decomposition of azomethane in the presence of CH_4 and CO_2. ●▲■ = pure azomethane; ○△□ = added CH_4; ⊠ = added CO_2. Pressures of CO_2 have been multiplied by an efficiency factor of 0.3.

If to this mechanism we now add the inversion reaction, [2], followed by reaction [5] the net result would be, as in the methane pyrolysis, a chain reaction yielding H_2 and C_2H_6. Formation of H_2 has not been reported in previous studies of the pyrolysis of azomethane alone, and its appearance on the addition of CH_4 at temperatures at which reaction [4] is negligible should be a sensitive indicator of reaction [2].

The decomposition of azomethane was studied in a static system at temperatures of 597, 634, and 658 K, both alone and in the presence of methane. Yields of N_2 and H_2 were measured by gas chromatography on a silica gel column at room temperature with argon carrier gas, which gave a good sensitivity for hydrogen on a thermal conductivity detector. Pressures of azomethane ranged from about 1 to 100 Torr and the extent of decomposition was between 10 and 50%, based on nitrogen yields.

Hydrogen, previously unreported, was found to be a very minor product in the decomposition of azomethane itself, with yields between about 0.08 and 0.16% of the N_2 at the lowest pressures employed. The H_2/N_2 ratio decreased with increasing pressure of azomethane at all three temperatures. At 597 K, the addition of CH_4 caused a further *decrease* in the ratio; at the higher temperatures, an initial decrease was followed by a slight increase in H_2/N_2 at 634 K and by a larger increase at 658 K. These results are shown in Fig. 3 where the H_2/N_2 ratio is plotted against total pressure.

The source of H_2 from the azomethane decomposition is not clear. The pressure dependence suggests collisional stabiliza-

Can. J. Chem. Downloaded from www.nrcresearchpress.com by 210.87.254.40 on 09/06/12
For personal use only.

Can. J. Chem. Downloaded from www.nrcresearchpress.com by 210.87.254.40 on 09/06/12
For personal use only.

tion of an excited intermediate, and to test this possibility experiments were done at 597 K with CO_2 added to azomethane. The results are also shown in Fig. 3; again the H_2/N_2 ratio was reduced and if an efficiency for CO_2 of 0.3 relative to CH_4 is assumed, the data coincide with those for the addition of CH_4. One possible source of H_2 is the decomposition of excited ethane formed by methyl combination,

[11] $2CH_3 \rightarrow C_2H_6^* \rightarrow H_2 + C_2H_4$

[12] $\rightarrow H + C_2H_5$

Reaction [12] requires an additional 11 kcal/mol above the combination energy, while reaction [11] probably requires rather less but would have a lower frequency factor. While for most purposes the combination of methyl radicals can be regarded as pressure-independent at the pressures and temperatures employed, the occurrence of 0.1% dissociation via reaction [11] or [12] is not impossible. Further studies are planned to test this explanation of the production of H_2 from azomethane, which must for the moment remain tentative.

The increase in the H_2/N_2 ratio on the addition of CH_4 at 658 K shows the right kinetics for production of H_2 by the inversion reaction, [2], followed by [5]. Assuming reactions [11] and [12] to be roughly independent of temperature, and reaction [2] to be negligible at 597 K, then subtracting the curve at 597 K from that at 658 K in Fig. 3 should give an approximate measure of the contribution of reaction [2] to the hydrogen yield at the higher temperature. From steady-state kinetics based on a simplified mechanism comprising reactions [2], [5], [6], and [9], it can be shown that the ratio

$$H_2/N_2 = k_2[CH_4]/k_6k_9[CH_3NNCH_3]$$

from which a value of $k_2 = 186\ M^{-1}\ s^{-1}$ may be estimated at 658 K. This is an impossibly high value, since from the methane pyrolysis we have already established an upper limit for k_2 at 802 K of 0.032 and it must be concluded that reaction [2] is not the cause of the increase in H_2/N_2 at 658 K when methane is added to azomethane. The absolute yield of H_2 is small, and some very minor secondary reactions could be responsible, but these are still enough to make measurements of k_2 in this system impossible.

The thermal decomposition of ethane

This system and the following one are chosen to provide evidence for the occurrence of reaction [3], the reverse of [2], rather than reaction [2] itself. The thermochemistry of the equilibrium is well established, with $\Delta S^0 = -8.5$ cal/mol degree, $\Delta H^0 = 15.8$ kcal/mol, and $\Delta C_p = 1.3$ cal/mol deg for reaction [2]. Reaction [3] will thus have an activation energy about 16 kcal/mol lower than reaction [2], and a higher frequency factor, and would appear to be more easily detected, with $k_3/k_2 = 4 \times 10^5$ at 1000 K.

The thermal decomposition of ethane in a static system at temperatures between 550 and 620 K follows to a good approximation the free-radical chain mechanism (8),

[13] $C_2H_6 \rightarrow 2CH_3$

[14] $CH_3 + C_2H_6 \rightarrow CH_4 + C_2H_5$

[15] $C_2H_5 \rightarrow C_2H_4 + H$

[16] $H + C_2H_6 \rightarrow H_2 + C_2H_5$

[17] $2C_2H_5 \rightarrow C_4H_{10}$ (or $C_2H_4 + C_2H_6$)

Reactions [15] and [16] constitute a chain reaction forming $H_2 + C_2H_4$, the major products of the decomposition.

If the inversion reaction,

[3] $H + C_2H_6 \rightarrow CH_3 + CH_4$

occurred, followed by reactions [14] and [15], the result would be a new chain reaction operating in parallel to the previous one, yielding $2CH_4 + C_2H_4$. The thermal decomposition of ethane has been very thoroughly studied, and we have done no new experiments on this system. Methane is a product, but it has always been attributed to reactions [13] and [14], and its yield has in fact been used to measure the rate of reaction [13]. From the data of Lin and Back (8), who measured both CH_4 and H_2, and thereby the rates of chain initiation and propagation respectively, kinetic chain lengths of 150 and 125 can be estimated at 823 and 893 K at pressures of about 300 Torr of ethane. If we estimate somewhat arbitrarily that 10% additional formation of methane by reaction [3] could have been detected, then reaction [3] could have been no more than a fraction $(0.1/(2 \times \text{chain length}))$ of the rate of the propagation step, [16], with which it is in direct competition. Rate constants for reaction [16] of 3.0×10^8 and $3.7 \times 10^8\ M^{-1}\ s^{-1}$ can be estimated from the literature (9) for temperatures of 823 and 893 K respectively, from which upper limits of $k_3 = 1.48$ and $2.01 \times 10^5\ M^{-1}\ s^{-1}$ can be calculated. Finally, from the thermodynamic relations between k_2 and k_3, upper limits for k_3 of 0.044 and 0.14 $M^{-1}\ s^{-1}$ at 823 and 893 K respectively can be estimated; these are slightly lower than the upper limits obtained from the methane decomposition, which gave a limit of 0.063 $M^{-1}\ s^{-1}$ at 802 K.

The mercury-photosensitized decomposition of ethane

As with methane, mercury photosensitization substitutes a new radical source in the ethane decomposition (6, 10),

[18] $Hg(^3P_1) + C_2H_6 \rightarrow Hg(^1S_0) + C_2H_5 + H$

replacing reaction [13]. At temperatures at which the latter is negligible, the inversion reaction, [3], followed by [14], becomes the only source of CH_4, which should therefore be a sensitive indicator of its occurrence. An interfering source of methyl radicals (and thence methane) which must be avoided is the "cracking" reaction,

[19] $H + C_2H_5 \rightarrow C_2H_6^* \rightarrow 2CH_3$

This can be minimized (10) by working at low light intensity (which gives low concentrations of H and C_2H_5) and high ethane pressure, which reduces the concentration of H by enhancing its removal in reaction [16]. Experimental methods were similar to those used in methane. Product analysis was done either by removing all the noncondensible gases through a trap at −196°C, and measuring H_2 and CH_4, or by simply analysing a small portion of the reaction mixture for CH_4 and n-C_4H_{10}, using gas chromatography in both cases.

In experiments at 298 K, as the light intensity was reduced and ethane pressure increased, the ratio CH_4/C_4H_{10} fell to values less than 0.002, showing that reaction [19] could be almost completely suppressed. The decomposition under these conditions should follow to a good approximation the simple mechanism consisting of reactions [18], [16], and [17]. If now the temperature is increased until reaction [3] begins to compete with reaction [15], the ratio of rates will be given by $R_3/R_{16} = CH_4/2C_4H_{10}$ (neglecting the disproportionation of ethyl radicals). Experiments were done at 498 and 556 K and pressures

of a few hundred Torr, and unexpectedly large yields of methane were found, with values of CH_4/C_4H_{10} about 0.6 and 1.4 respectively, much too high for the methane to be coming from reaction [3]. Measurements of the CH_4/H_2 ratio confirmed the large yields of methane. The source of this methane is not clear; production of $2CH_3$ in a temperature-dependent primary dissociation, which might have been missed in earlier studies (5, 10), is one possibility, and experiments to test this are planned. For the present purposes, the production of methane, by whatever means, frustrates for the moment the attempt to use this system to detect the inversion reaction.

Concluding remarks

We have examined five systems which showed some promise of detecting or putting upper limits on the inversion reactions, [2] and [3]. There is no positive evidence in any of these systems for the occurrence of these reactions. The lowest upper limits for their rates are derived from the thermal decompositions of methane and ethane at 802, 823, and 893 K. Attempted measurements in two of the more promising systems, the azomethane–methane decomposition and the mercury-photosensitized decomposition of ethane, failed because of the unexpected formation, from other sources, of H_2 and CH_4, respectively, the products which it was hoped would be sensitive indicators of the inversion reactions. Addition of excess H_2 to the ethane–Hg system, for example, may be a way to ensure that H-atoms are the only primary products. Finally, the reaction of H-atoms (produced by mercury photosensitization) with cyclopropane or cyclobutane in an inversion reaction analogous to reaction [3], should yield *n*-propyl or *n*-butyl radicals with an activation energy much reduced by the release of ring strain energy, and perhaps offer the best hope of observing such an inversion reaction. It is worth noting, in a symposium honoring Professor Gunning, that the mercury-photosensitized reactions in which he pioneered can still be very useful in kinetic studies of free-radical reactions.

1. C.-J. CHEN, M. H. BACK, and R. A. BACK. Can. J. Chem. **55**, 1624 (1977).
2. L. S. KASSEL. J. Am. Chem. Soc. **57**, 833 (1935).
3. C.-J. CHEN, M. H. BACK, and R. A. BACK. Can. J. Chem. **53**, 3580 (1975).
4. K. TABAYASHI and S. H. BAUER. Combust. Flame, **34**, 63 (1979).
5. R. A. BACK and D. VAN DER AUWERA. Can. J. Chem. **40**, 2339 (1962).
6. S. BYWATER and E. W. R. STEACIE. J. Chem. Phys. **19**, 319 (1951); **19**, 326 (1951).
7. Y. PAQUIN and W. FORST. Inter. J. Chem. Kinet. **5**, 691 (1973).
8. M. C. LIN and M. H. BACK. Can. J. Chem. **44**, 505 (1966).
9. T. C. CLARK and J. E. DOVE. Can. J. Chem. **51**, 2147 (1973).
10. R. A. BACK. Can. J. Chem. **37**, 1834 (1959).

Can. J. Chem. Downloaded from www.nrcresearchpress.com by 210.87.254.40 on 09/06/12
For personal use only.

Quenching of $O_2(c^1\Sigma_u^-)v = 0$ by $O(^3P)$, $O_2(a^1\Delta_g)$, and other gases

REX D. KENNER AND ELMER A. OGRYZLO

Department of Chemistry, University of British Columbia, Vancouver, B.C., Canada V8T 1W5

Received July 13, 1982

This paper is dedicated to Professor Harry E. Gunning on the occasion of his 65th birthday

REX D. KENNER and ELMER A. OGRYZLO. Can. J. Chem. **61**, 921 (1983).

Spectroscopic and kinetic results for the quenching of $O_2(c^1\Sigma_u^-)$ are presented, including the first reported laboratory observation of gas phase emission from vibrational levels greater than zero for this state. In addition, the absolute rate constants for quenching of the lowest vibrational level by $O(^3P)$, $O_2(a^1\Delta_g)$, $O_2(X^3\Sigma_g^-)$, CO_2, SF_6, HE, and Ar are given. These results are compared with the results of atmospheric modeling studies. Qualitative evidence is presented for the formation of $O_2(a^1\Delta_g)$ and $O_2(a^1\Sigma_g^+)$ in the quenching of this state.

REX D. KENNER et ELMER A. OGRYZLO. Can. J. Chem. **61**, 921 (1983).

On présente les résultats spectroscopiques et cinétiques de la rupture du $O_2(c^1\Sigma_u^-)$ en incluant les premières observations de laboratoire publiées sur l'émission en phase gazeuse à partir de niveaux vibrationnels de cet état supérieure à zéro. De plus, on donne les constantes de vitesse absolue pour le piégage du niveau vibrationnel le plus bas par $O(^3P)$, $O_2(a^1\Delta_g)$, $O_2(X^3\Sigma_g^-)$, CO_2, SF_6, He et Ar. On a comparé ces résultats avec les résultats d'études de modèles atmosphériques. On présente des preuves qualitatives de la formation de $O_2(a^1\Delta_g)$ et de $O_2(a^1\Sigma_g^+)$ lors du piégeage de cet état.

[Traduit par le journal]

Can. J. Chem. Downloaded from www.nrcresearchpress.com by 210.87.254.6 on 09/06/12
For personal use only.

Oxygen is the second most abundant element in the Earth's atmosphere and is responsible for much of the visible and ultraviolet emission from the upper atmosphere (1–5). On the dark side of the Earth the principal energy source for these emissions is the recombination of atoms generated by photodissociation during the day (6). Six bound states arising from the recombination of two ground state oxygen atoms have now been observed, both in the Earth's nightglow (1–5) and in the laboratory (7–10). While the kinetics of the lower two excited singlet states of O_2, $O_2(a^1\Delta_g)$ and $O_2(b^1\Sigma_g^+)$, are relatively well understood (11), only recently has much progress been made in understanding the three higher metastable states: $O_2(A^3\Sigma_u^+)$, $O_2(c^1\Sigma_g^-)$, and $O_2(A'^3\Delta_u)$. Note the redesignation of the $(^3\Delta_u)$ state as A' rather than C (12). Detailed spectroscopic investigations of these three u-states were first reported by Herzberg (13, 14) and the transitions between them and the ground state, $O_2(X^3\Sigma_g^-)$ are referred to as the Herzberg I, II, and III systems respectively.

Emission of the Herzberg I system was first seen in the laboratory by Broida and Gaydon (15) in oxygen afterglows. Three subsequent laboratory studies (16–18) have reported values for the composite emission rate constant, k_A, in the expression

$$I_A = k_A[O]^2[M]/[O_2]$$

A fourth study (19) reported absolute rate constants for reactions with $O(^3P)$, O_2, and Ar. Subsequent work in this laboratory has refined these rate constants as well as extending the list of quenchers investigated.[1]

The $O_2(A'^3\Delta_u)$ state is much less well understood. Transitions to this state were first observed as diffuse triplets in the high pressure absorption of molecular oxygen by Wulf (20) and Finklnburg and Steiner (21). These absorptions were subsequently seen by Herzberg (14) who, using a very long pathlength, observed fragments of two weak triple-headed bands at pressures of several atmospheres. More recently, emission from the $O_2(A')$ state has been reported in matrix isolation studies in N_2 and rare gas hosts at low temperatures (22–25). In the gas phase, two emission systems, $A' \rightarrow X$ and $A' \rightarrow a$, have been identified by Slanger (4, 10) who observed them in helium–oxygen afterglows as well as in NO-titrated afterglows. He also identified these transitions in the spectrum of the nightglow of Venus (26) and confirmed the earlier suggestion by Chamberlain (27) that some of the features of the Earth's nightglow could be explained by $A' \rightarrow a$ transitions (5).

Until the advent of exploration of the nearby planets of our solar system, little was known about the $O_2(c^1\Sigma_u^-)$ state. Herzberg (14) had analyzed six bands observed in long-path absorption and two very weak bands were observed by Degen (28) in argon–oxygen afterglows. From his rotational analysis of these emission bands and Herzberg's absorption results, Degen was able to determine the molecular constants and construct a Delandres table for the $c \rightarrow X$ transition (28).

When the Russion spacecrafts Venera 9 and 10 recorded the visible nightglow of Venus, a simple system of eleven emission bands was found (29). This sequence was first correctly identified by Lawrence *et al.* (30) as the $v' = 0$ sequence of the $c \rightarrow X$ transition. These workers were also able to reproduce the spectrum in the laboratory by adding carbon dioxide to a helium–oxygen afterglow (30). It should be noted that the Venusian atmosphere contains large amounts of carbon dioxide (31).

Later, Slanger (10) and Kenner *et al.* (32) showed that carbon dioxide was not essential for the observation of these bands. The latter authors (32) showed that with the appropriate conditions, the Herzberg II band system could be made the dominant visible emission in an argon–oxygen afterglow. They also found that several gases other than carbon dioxide, notably some chlorofluorocarbons, were effective in enhancing the Herzberg II emission relative to that of the other states of O_2. In 1953 Herzberg (14) suggested that some of the features of the Earth's nightglow could be due to emission from the $O_2(c)$ state and this has now been confirmed by Slanger (5).

Much of the current interest in the $O_2(c)$ state derives from an attempt to explain the strong emission line at 557.7 nm emitted by atomic oxygen, $O(^1S)$ in the Earth's nightglow

[1]R. D. Kenner and E. A. Ogryzlo; unpublished work.

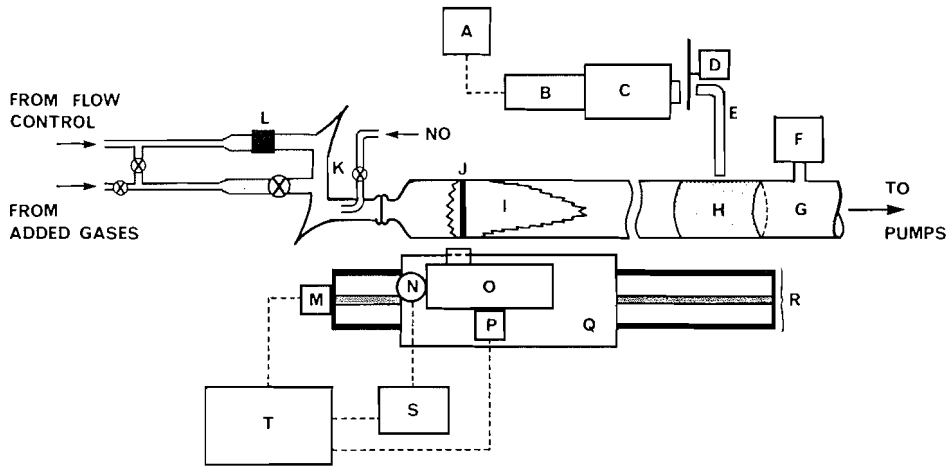

FIG. 1. Diagram of flow-discharge apparatus: A, lock-in amplifier; B, intrinsic Ge-detector; C, quarter-meter monochromator; D, light chopper; E, quartz light fiber; F, capacitance manometer; G, 38 mm id flowtube; H, aluminum reflector; I, emitting region; J, nickel screen; K, light traps; L, microwave discharge; M and P, stepping motors; N, photomultiplier; O, quarter-meter monochromator; Q, monochromator stage; R, guide rail for monochromator stage; S, photon counter; T, minicomputer.

(33). Llewellyn and co-workers (34) have proposed that energy transfer from the higher vibrational levels of $O_2(c)$ is the source of this excitation energy.

[1] $\quad O_2(c)v > 1 + O(^3P) \rightarrow O_2(X) + O(^1S)$

In addition, they have proposed (35) that O_2 quenching of this state is the source of $O_2(b)$ in the upper atmosphere. To verify these hypotheses it is necessary to have a much better understanding of the initial states formed in the atom recombination and of the rates of vibrational relaxation and quenching for the states involved.

The kinetics of the $O_2(c)$ state in the gas phase have been investigated in only one laboratory study. Kenner *et al.* (32) have shown, by comparison with the Herzberg I emission, that in an argon–oxygen afterglow the emission intensity from the lowest vibrational level of $O_2(c)$ is first order in O, second order in M and inversely proportional to O_2:

$$I_c = k_c[O][M]^2/[O_2]$$

In the present paper are reported the first measurements of the absolute rate constants for quenching of the zero vibrational level of $O_2(c^1\Sigma_u^-)$, as well as some qualitative observations about its formation following surface-catalyzed recombination of oxygen atoms.

Experimental

The method used to determine the quenching constants for $O_2(c)$ has been developed in this laboratory and was used in previous studies on $O_2(A)$ and $O(^1S)$ (36). It is based on the work of Harteck and co-workers (37–40) on surface-catalyzed emission in which a nickel surface is used to catalyze the recombination of oxygen atoms. Mannella and Harteck (39) reported the strong catalysis of the $O_2(A)$ and $O_2(b)$ emissions by this method and Kenner and Ogryzlo (36) have reported the additional observation of $O_2(A')$, $O_2(c)$, and $O(^1S)$ emissions. With the formation of the excited states on the nickel surface, the flow along the tube becomes a time axis and the rate of decay of the species under investigation can be measured as a function of the concentrations of various quenching species.

The apparatus consisted of a fairly conventional discharge flow system with a 38 mm diameter flow tube approximately 75 cm long (Fig. 1). The discharge was excited by a 2.45 GHz microwave generator through a quarter-wave cavity. The gas flows to the system were controlled by needle valves and monitored with calibrated flowmeters; pressures were measured with capacitance manometers. A 1000 L/min (STP) pumping system gave linear flow rates of about 12 m/s at the pressures used in these experiments (2–4 Torr).

The atomic oxygen concentration was determined by adding a measured amount of NO and measuring the intensity of the resulting NO_2 emission. (The light fiber used for this intensity measurement was connected to the monochromator stage in line with the monochromator entrance slit and is not shown in Fig. 1). The $O_2(a)$ concentration was determined from its emission intensity at 1.27 μm as measured with a calibrated intrinsic germanium detector. Separate experiments showed that $O_2(a)$ remained essentially constant down the flowtube under the operating conditions used in these experiments.

Argon was purified by passage through a titanium-filled furnace at 800 K; helium by passage through a liquid nitrogen-cooled trap filled with activated charcoal. Ultra high purity oxygen was used as recieved, as were all other gases (with the exception of NO, which was vacuum distilled).

Decay curves were collected using the movable monochromator and photomultiplier. The output of this photomultiplier was connected to a photon counter and interfaced with a microcomputer. The monochromator wavelength scan and the drive screw for the monochromator stage were driven by stepping motors which were also interfaced with the computer. The data were collected by determining the count rate at each of a number of fixed points along the flowtube; the results were stored on disk for later treatment using any of several programs. Experimental decay rates were determined using a regression analysis of the semilog plots of the data. The value of the intercept of this plot was also determined (the position of the nickel screen being taken as zero time) and should represent the total amount of $O_2(c)v = 0$ formed.

Results

In the matrix studies of Goodman and Brus (23), a risetime was observed for the emission from $O_2(c)v = 0$ following photoexcitation of the $v = 6$ level of $O_2(A')$. In the present system, one can observe a risetime associated with the emission from $O_2(c)v = 0$ following surface-catalyzed atom recombination. This is illustrated in Fig. 2. The apparent risetime associated with the $O_2(A)v = 0$ is an artifact of the experimental system. Clearly, the $O_2(c)v = 0$ is peaking later with a slower decay than is the $O_2(A)v = 0$. This difference can be increased by using argon instead of helium as the carrier gas, or by reducing the concentration of the quenching species.

In Fig. 3 are shown two spectra taken in an argon system and

Can. J. Chem. Downloaded from www.nrcresearchpress.com by 210.87.254.6 on 09/06/12
For personal use only.

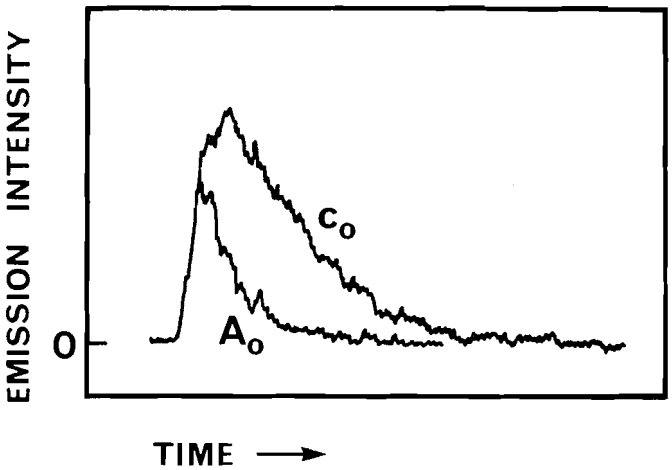

FIG. 2. Emission intensity as a function of time for two bands in the emission from surface-catalyzed recombination of O-atoms in helium. Upper curve: $O_2(c^1\Sigma_u^-)v = 0$; Lower curve: $O_2(A^3\Sigma_u^+)v = 0$

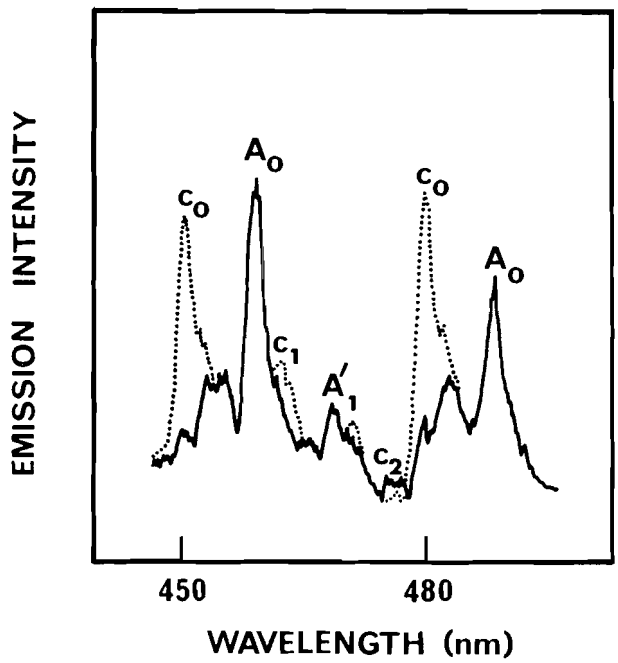

FIG. 3. Emission intensity as a function of wavelength from surface-catalyzed recombination of O-atoms in argon. Solid spectrum measured at the nickel surface. Dotted spectrum measured approximately 1.6 milliseconds downstream of the nickel and normalized to the solid curve using the A_0 peak (intensity of dotted curve approximately doubled in this normalization).

normalized by the $O_2(A)v = 0$ peaks (the intensity of the solid spectrum is divided approximately by two). The solid curve is taken at the nickel surface and shows only a small emission intensity from the $O_2(c)v = 0$. In the dotted curve, taken approximately 1.6 ms downstream of the nickel, the $O_2(c)v = 0$ bands are very prominent. In addition, close examination of the spectrum shows that the $O_2(c)v = 1$ and $v = 2$ are present and that the $v = 2$ level decays relative to $O_2(A)v = 0$ while the $v = 1$ increases. Spectra taken at even later times show emission exclusively from the zero level of $O_2(c)$, as do those of conventional O-atom recombination with added carbon dioxide (30).

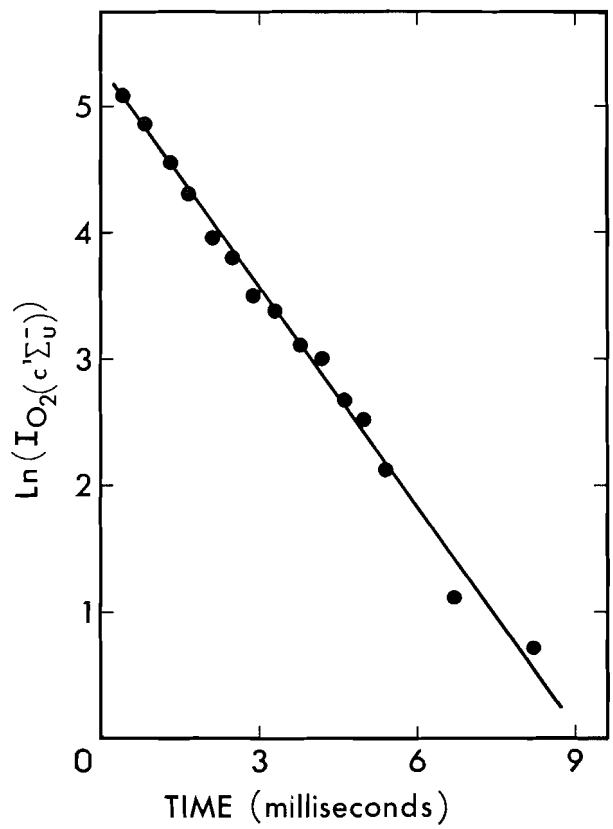

FIG. 4. Typical semilog decay curve determined using peak intensity in argon at 2.5 Torr total pressure.

The kinetic data were collected by measuring the intensity of the emission of $O_2(c)v = 0$ at fixed points along the flowtube. This was done in two ways. First, a small region of the spectrum was scanned at each point; the resulting peaks were integrated and fitted to an exponential decay. Second, only the peak intensity was measured at each point, followed by a similar fitting technique. Since the two methods gave similar results, only the second was used for most of the data reported here. A typical decay curve is shown in Fig. 4.

In the present apparatus the concentration of the oxygen atoms can be varied at constant $[O_2]$ by changing the power applied to the microwave discharge and/or by varying the flow through the discharge by use of the discharge bypass. These changes also affect the concentration of the $O_2(a)$. The range of concentrations of either of these species which could be obtained while holding the other constant was quite small, so it was decided to vary both over the full range available and use multiple regression analysis to extract the rate constants. This method still leads to larger uncertainties than one would like due to partial correlation between the two concentrations.

Working with argon as the carrier gas at 2.50 Torr, the concentrations of O and $O_2(a)$ were varied from 0.50 to 8.1 $\times$ 10^{13} and 0.40 to 1.9 $\times$ 10^{13} molecules cm^{-3} respectively. The resulting rate constants with uncertainties are:

[2] $O_2(c)v = 0 + O(^3P) \rightarrow$ quenched products

$k_2 = (5.9 \pm 0.6) \times 10^{-12}$

[3] $O_2(c)v = 0 + O_2(a) \rightarrow$ quenched products

$k_3 = (6.0 \pm 2.4) \times 10^{-12}$

Can. J. Chem. Downloaded from www.nrcresearchpress.com by 210.87.254.6 on 09/06/12
For personal use only.

TABLE 1. Rate constants for quenching of $O_2(A^3\Sigma_u^+)v = 2$ and $O_2(c'\Sigma_u)v = 0$ by various gases

Quenching species	$O_2(A^3\Sigma_u^+)v = 2^a$	$O_2(c'^1\Sigma_u^-)v = 0^b$
$O(^3P)$	$(1.29\pm0.1)\times10^{-11}$ [c,d]	$(5.9\pm0.6)\times10^{-12}$
$O_2(a^1\Delta_g)$	$(8.1\pm1.6)\times10^{-11}$	$(6.0\pm2.4)\times10^{-12}$
O_2	1.3×10^{-13}	3×10^{-14}
CO_2	7×10^{-13}	$<6\times10^{-14}$
SF_6	6×10^{-13}	2×10^{-13}
N_2O	1.8×10^{-12}	4×10^{-13}
He		6×10^{-15}
Ar	7.2×10^{-16}	6×10^{-16}

[a] R. D. Kenner and E. A. Ogryzlo, unpublished work.
[b] This paper.
[c] All units are cm^3 molecule^{-1} s^{-1}.
[d] Indicated error limits are the 1σ statistical uncertainties.

in units of cm^3 molecule^{-1} s^{-1}. The intercept is 53 ± 21 s^{-1}, which is the sum of all other quenching rates in the system. These other rates would include quenching by oxygen, argon, and walls. The values found in a previous study for $O_2(A)$ are listed for comparison in Table 1.

Similar experiments were conducted in helium at a pressure of 3.00 Torr and the total experimentally measured decay rate was found to be very much faster. This leads to larger uncertainties in the exponential fits and in the resulting rate constants. The results were

$$k_2 = (4.4 \pm 2.2) \times 10^{-12}$$

$$k_3 = (12.5 \pm 6.4) \times 10^{-12}$$

in units of cm^3 molecule^{-1} s^{-1} with an intercept of 576 ± 178 s^{-1}. These rate constants agree, within the listed uncertainties, with those determined in argon. The intercept is, however, approximately ten times larger. Given that the O_2 concentrations were similar and assuming no change in the rate of wall quenching, this implies that helium is a much better quencher of $O_2(c)v = 0$ than is argon.

With the rate constants for O and $O_2(a)$ quenching measured, that for O_2 could be determined. For these experiments, the gas flows through the discharge and the power applied to the discharge were kept approximately constant. Oxygen was then added after the discharge through the first fixed inlet. The oxygen atom concentration was monitored upstream of the nickel screen and was found to remain constant within experimental error. The oxygen atom concentration downstream of the nickel did, however, vary a little and the concentration of the $O_2(a)$ was slightly reduced by the addition of O_2.

Using the previously obtained rate constants, the experimental decay rate, k_{exp}, could be corrected for these changes and from the slope of a plot of $k_{corr} = k_{exp} - k_2[O] - k_3[O_2(a)]$ as a function of $[O_2]$ (see Fig. 5), one obtains $k_4 = 3 \times 10^{-14}$ cm^3 molecules^{-1} s^{-1} for

[4] $O_2(c)v = 0 + O_2 \rightarrow$ quenched products

The intercept on this plot is 15 s^{-1} which indicates that the combined wall and argon quenching is quite small. This is in sharp contrast with the results for $O_2(A)$ which is quenched by walls with unit efficiency (19).

The rate of quenching by three other gases was also investigated. These gases were carbon dioxide, sulfur hexafluoride, and nitrous oxide. The carbon dioxide was of particular interest since it is known that the $O_2(c)v = 0$ is enhanced by the addition of this gas in a conventional atom recombination experiment (10, 30). In this case, no quenching could be detected within experimental error and only an upper limit to the quenching rate constant could be estimated. This limit is shown in Table 1. The intercepts of the semilog plots of the decay curves were found to increase in an almost linear fashion with increasing carbon dioxide concentration, which implies an increased production of $O_2(c)v = 0$ with added carbon dioxide.

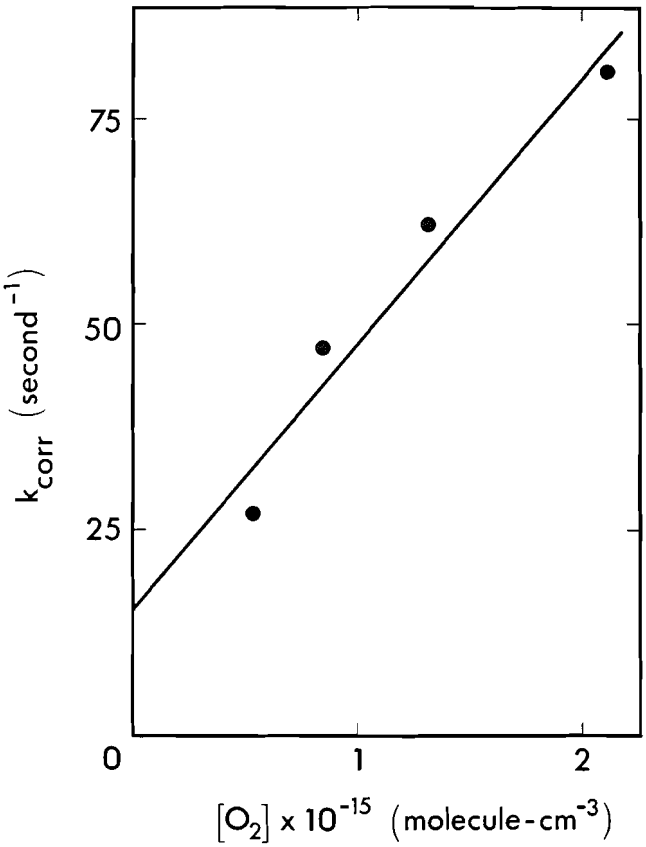

FIG. 5. A plot of k_{corr} as a function of molecular oxygen concentration $k_{corr} = (k_{exp} - k_0[O] - k_a[^1\Delta])$. The slope of the line gives $k_{O_2} = 3 \times 10^{-14}$ cm^3 molecule^{-1} s^{-1}.

Both sulfur hexafluoride and nitrous oxide were found to be good quenchers of $O_2(c)v = 0$ (see Table 1). When nitrous oxide was used as the quencher, the intercepts of the semilog decay plots were found to increase slightly with increasing N_2O concentration.

In contrast, even though sulfur hexafluoride enhances the intensity of the Herzberg II emission relative to that of the Herzberg I in argon–oxygen afterglows,[2] the intercepts of the semilog decay plots decrease with increasing SF_6 concentration.

Discussion

From the spectra of the surface-catalyzed emission, one can identify emission bands from the first six vibrational levels of $O_2(A)$, the first six levels of $O_2(A')$, but only the lowest three levels of $O_2(c)$ (19, 20, 36, 39). It should be noted that all three of these levels of $O_2(c)$ are at equal or lower energy than the

[2] R. D. Kenner, E. A. Ogryzlo, and S. Turley; unpublished work.

Can. J. Chem. Downloaded from www.nrcresearchpress.com by 210.87.254.6 on 09/06/12
For personal use only.

Can. J. Chem. Downloaded from www.nrcresearchpress.com by 210.87.254.6 on 09/06/12
For personal use only.

zero level of $O_2(A')$ (4, 28). There is no evidence in the present system to suggest that the upper levels of $O_2(c)$ are populated in the surface-catalyzed recombination.

It therefore remains possible that recombination occurs principally into the triplet manifold ($(O_2(A)$ and $O_2(A')$) followed by intersystem crossing to the $O_2(c)$ state from the lowest level of $O_2(A')$, as suggested by Kenner *et al.* (32).

A similar conclusion can be reached from the matrix isolation studies (22, 23, 25) where, in the absence of a heavy atom effect, emission is observed only from $O_2(A')v = 0$ in cases where $O_2(c)v = 2$ lies above $O_2(A')v = 0$ and only from $O_2(c)v = 0$ if $O_2(c)v = 2$ lies below $O_2(A')v = 0$. An exception to this is the work of Schoen and Broida (41) who used electron bombardment as the excitation source. It has been suggested (42) that $O_2(c)$ is formed preferentially by this method.

The detailed path of vibrational relaxation in these electronically excited states is not known so it is difficult to draw any quantitative conclusions from the observed risetimes. Qualitatively, as one would expect, the risetime is observed to increase in the presence of low quencher concentrations.

The rate constants measured in this study are summarized in Table 1, with those for $O_2(A)v = 2$ shown for comparison. Also included are estimates for quenching by argon and helium derived from the intercepts of the $O/O_2(a)$ multiple regression fit assuming no wall quenching. The error limits for these rate constants are difficult to estimate. The O-atom concentration and the $O_2(a)$ concentration were ultimately based on the absolute rate constant for the NO + O reaction and the relative spectral distribution of this emission. This rate constant has an estimated uncertainty of ±30% (43) and the relative intensity at 1.27 μm is uncertain by a factor of about two (44). Other sources of error should have been small (see, however, ref. 45). At the flow rates used here no corrections should be needed for flow parameters and the plug flow approximation should be justified (46). The uncertainties listed for the O and $O_2(a)$ quenching rate constants are the 1σ statistical uncertainties. All values given for $O_2(c)v = 0$ should be good to within ±50% and those given for $O_2(A)v = 2$ better than that.[1]

The rate constants for quenching of $O_2(c)$ have not been measured directly before. Some of them have, however, been estimated in computer modeling of the upper atmosphere. Greer *et al.* (35) have proposed

[5] $O_2(c) + O \rightarrow$ quenched products

$$k_5 = 3 \times 10^{-11} \text{ cm}^3 \text{ molecule}^{-1} \text{ s}^{-1}$$

[6] $O_2(c) + O_2 \rightarrow$ quenched products

$$k_6 = 5 \times 10^{-13} \text{ cm}^3 \text{ molecule}^{-1} \text{ s}^{-1}$$

Both of these values are larger than those found here but they refer to the Earth's upper atmosphere where $O_2(c)$ shows a high vibrational excitation with the level of maximum population being $v' = 7$ according to Slanger (5). Quenching of these upper levels, at least in the case of O, could be faster than that for the zeroth level due to additional product channels (see later discussion).

In the study by Krasnopolsky (47), he reports

$$k_5 = 2.5 \times 10^{-12} \text{ cm}^3 \text{ molecule}^{-1} \text{ s}^{-1}$$

$$k_6 = 1 \times 10^{-12} \text{ cm}^3 \text{ molecule}^{-1} \text{ s}^{-1}$$

[7] $O_2(c) + M \rightarrow$ quenched products

$$k_7 = 1 \times 10^{-15} \text{ cm}^3 \text{ molecule}^{-1} \text{ s}^{-1}, \text{ M–Ar, He}$$

These values were derived using the nightglow results from Venus and therefore pertain to $v = 0$ (30). The O quenching constant is smaller than the one reported here but the difference could be a temperature effect since the temperature of the emitting layer on Venus is about two hundred Kelvin (31), whereas the laboratory measurements were done at room temperature.

The rate constants for the quenching of $O_2(c)v = 0$ are all smaller than the corresponding values for quenching of $O_2(A)v = 2$ (see Table 1). For both states the rate constants for quenching by $O(^3P)$ and $O_2(a)$ are larger than those for any other quenchers. This difference can probably be attributed to more favorable energy transfer pathways in the case of the $O_2(A)$ state.

Greer *et al.* (35) have suggested that $O(^1S)$ is formed in the quenching of $O_2(c)v > 1$ by $O(^3P)$ (reaction [1]). However, this pathway is energetically unavailable to the zeroth vibrational level (reaction [2]). Since the formation of $O(^1S)$ in the quenching of $O_2(A)$ is an energetically accessible and spin-allowed product channel for reaction [8],

[8] $O_2(A) + O(^3P) \rightarrow$ quenched products

the difference in the values of the rate constants for reactions [2] and [8] could be due partly to the addition of the $O(^1S)$ product channel in reaction [8].

Similar arguments appear to be applicable for processes involved in quenching by $O_2(a)$. Consider the following three processes for which rate constants are now available:

[9] $O(^1S) + O_2(a) \rightarrow$ quenched products

$$k_g = 2 \times 10^{-10} \text{ cm}^3 \text{ molecule}^{-1} \text{ s}^{-1} \text{ (36, 48)}$$

[10] $O_2(A) + O_2(a) \rightarrow$ quenched products

$$k_{10} = 8 \times 10^{-11} \text{ cm}^3 \text{ molecule}^{-1} \text{ s}^{-1} \text{ (footnote 1)}$$

$O_2(c) + O_2(a) \rightarrow$ quenched products

$$k_3 = 6 \times 10^{-12} \text{ cm}^3 \text{ molecule}^{-1} \text{ s}^{-1}$$

For the first, $O_2(a)$ quenching of $O(^1S)$, Slanger and Black (49) have found that a major product channel involves energy transfer to $O_2(a)$ with $O(^1S)$ relaxing to $O(^3P)$. The $O_2(a)$ is excited in a vertical transition to one of the higher u-states in the vicinity of the dissociation limit and is in part dissociated.

In the second process, a similar energy transfer to $O_2(a)$ can take place. However, those transitions of $O_2(A)$ with sufficient energy to excite $O_2(a)$ to the higher u-states or to lead to its dissociation are not vertical transitions. These transitions will therefore have a lower probability than the corresponding reaction involving $O(^1S)$ and thus the smaller rate constant is not unexpected.

For the third process, $O_2(a)$ quenching of $O_2(c)v = 0$, the total energy is insufficient for dissociation. The extra energy required would reduce the rate constant for dissociation by at least a factor of thirty, virtually eliminating this product channel. In addition, the Franck–Condon factors for the energy pooling process would be even less favorable than those for $O_2(A)$ and a further reduction in the quenching rate constant is quite reasonable.

The failure to detect any quenching of $O_2(c)v = 0$ by carbon dioxide is consistent with the observation of strong emission from this state in the nightglow of Venus (29). The fact that the total production of $O_2(c)v = 0$ increases with increasing CO_2 concentration indicates that CO_2 is competing with some loss process of the precursor state or states of $O_2(c)v = 0$. An

analysis of the effect of carbon dioxide on the risetime for $O_2(c)v = 0$ could be important in determining the identity of these precursor states.

In conclusion, two other qualitative observations are worth noting. First, in an experiment designed to test the prediction of Greer *et al.* (35) that $O_2(b)$ is formed in the O_2 quenching of $O_2(c)$, oxygen was added through a movable inlet downstream of the nickel screen into the region of the surface-catalyzed emission. When the $O_2(b)$ was monitored as a function of distance along the flow tube, a localized rise in the $O_2(b)$ was found just downstream of the O_2 addition. This would seem to be direct confirmation of the predicted mechanism.

Secondly, it was observed that the concentration of the $O_2(a)$, measured downstream of the nickel screen, increased slightly when carbon dioxide was added. This would be the expected result if the suggestion of Llewellyn and Solheim (50) that O quenching of $O_2(c)v = 0$ leads to $O_2(a)$ is correct, since carbon dioxide increases the yield of $O_2(c)v = 0$.

Acknowledgement

This work was supported by the Air Force Office of Scientific Research, Air Force Systems Command, USAF, under Grant No. AFOSR-79-0088. The United States Government is authorized to reproduce and distribute reprints for governmental purposes notwithstanding any copyright notation hereon.

1. A. B. MEINEL. Trans. Am. Geophys. Union, **31**, 24 (1950).
2. H. P. GUSH and H. L. BUIJS. Can. J. Phys. **42**, 1037 (1964).
3. J. W. CHAMBERLAIN. Astrophys. J. **121**, 277 (1955).
4. T. G. SLANGER. Chem. Phys. Lett. **66**, 344 (1979).
5. T. G. SLANGER and D. L. HUESTIS. J. Geophys. Res. **86**, 3551 (1981).
6. S. CHAPMAN. Proc. R. Soc. London Ser. A, **132**, 353 (1931).
7. G. HERZBERG. Naturwissenchaften, **20**, 577 (1932).
8. J. W. ELLIS and H. O. KNESER. Z. Physik. **86**, 583 (1933).
9. H. D. BABCOCK and L. HERZBERG. Astrophys. J. **108**, 167 (1948).
10. T. G. SLANGER. J. Chem. Phys. **69**, 4779 (1978).
11. E. A. OGRYZLO. *In* Singlet oxygen. *Edited by* H. Wasserman. Academic Press, New York. 1979. p. 35.
12. K. P. HUBER and G. HERZBERG. Constants of diatomic molecules. Van Nostrand, Princeton, NJ. 1979.
13. G. HERZBERG. Can. J. Phys. **30**, 185 (1952).
14. G. HERZBERG. Can. J. Phys. **31**, 657 (1953).
15. H. P. BROIDA and A. G. GAYDON. Proc. R. Soc. London Ser. A, **222**, 181 (1954).
16. R. A. YOUNG and R. L. SHARPLESS. J. Chem. Phys. **39**, 1071 (1963).
17. R. A. YOUNG and G. BLACK. J. Chem. Phys. **44**, 3741 (1966).
18. R. J. MCNEAL and S. C. DURANA. J. Chem. Phys. **51**, 2955 (1969).
19. R. D. KENNER and E. A. OGRYZLO. Int. J. Chem. Kinet. **12**, 501 (1980).
20. O. R. WULF. Proc. Natl. Acad. Sci. U.S.A. **14**, 609 (1928).
21. W. FINKLNBERG and W. STEINER. Z. Physik. **79**, 69 (1932).
22. J. L. RICHARDS and P. M. JOHNSON. J. Chem. Phys. **65**, 3948 (1976).
23. J. GOODMAN and L. E. BRUS. J. Chem. Phys. **67**, 1482 (1977).
24. R. R. SMARDZEWSKI. Ber. Bunsenges. Phys. Chem. **82**, 108 (1978).
25. R. R. SMARDZEWSKI. J. Chem. Phys. **68**, 2878 (1978).
26. T. G. SLANGER and G. BLACK. Geophys. Res. Lett. **5**, 947 (1978).
27. J. W. CHAMBERLAIN. Astrophys. J. **128**, 713 (1958).
28. V. DEGEN. Can. J. Phys. **46**, 783 (1968).
29. V. A. KRASNOPOL'SKII, A. A. KRYS'KO, V. N. POGASHEV, and V. A. PARSHEV. Cosmic Res. USSR. **14**, 687 (1977).
30. G. M. LAWRENCE, C. A. BARTH, and V. ARGABRIGHT. Science, **195**, 573 (1977).
31. N. D. SZE and M. B. MCELROY. Planet. Space Sci. **23**, 763 (1975).
32. R. D. KENNER, E. A. OGRYZLO, and S. TURLEY. J. Photochem. **10**, 199 (1979).
33. D. R. BATES. Planet. Space Sci. **29**, 1061 (1981).
34. G. WITT, J. STEGMAN, B. SOLHEIM, and E. J. LLEWELLYN. Planet. Space Sci. **27**, 341 (1979).
35. R. G. H. GREER, E. J. LLEWELLYN, B. H. SOLHEIM, and G. WITT. Planet. Space Sci. **29**, 383 (1981).
36. R. D. KENNER and E. A. OGRYZLO. J. Photochem. **18**, 379 (1982).
37. R. R. REEVES, G. MANNELLA, and P. HARTECK. J. Chem. Phys. **32**, 946 (1960).
38. G. G. MANNELLA, R. R. REEVES, and P. HARTECK. J. Chem. Phys., **33**, 636 (1960).
39. G. G. MANNELLA and P. HARTECK. J. Chem. Phys. **34**, 2177 (1961).
40. P. HARTECK and R. R. REEVES, JR. Disc. Faraday Soc. **37**, 82 (1964).
41. L. J. SCHOEN and H. P. BROIDA. J. Chem. Phys. **32**, 1184 (1960).
42. B. H. SOLHEIM and E. J. LLEWELLYN. Planet. Space Sci. **27**, 473 (1979).
43. A. FONTIJN, C. B. MEYER, and H. I. SCHIFF. J. Chem. Phys. **40**, 64 (1964).
44. M. SUTOH, Y. MORIOKA, and M. NAKAMURA. J. Chem. Phys. **72**, 20 (1980).
45. T. CARRINGTON. Int. J. Chem. Kinet. **14**, 517 (1982).
46. F. KAUFMAN. Prog. React. Kinet. **1**, 3 (1960).
47. V. A. KRASNOPOLSKY. Planet. Space Sci. **29**, 925 (1981).
48. T. G. SLANGER and G. BLACK. Geophys. Res. Lett. **8**, 535 (1981).
49. T. G. SLANGER and G. BLACK. J. Chem. Phys. **75**, 2247 (1981).
50. E. J. LLEWELLYN and B. H. SOLHEIM. NATO–ASZ Proceedings, Lillehaumen, Norway. May, 1980.

Can. J. Chem. Downloaded from www.nrcresearchpress.com by 210.87.254.6 on 09/06/12
For personal use only.

The formation of ozone and peroxyacetyl nitrate (PAN) in the urban atmospheres of Alberta[1]

E. PEAKE

Kananaskis Centre for Environmental Research, The University of Calgary, Calgary, Alta., Canada T2N 1N4

AND

H. S. SANDHU

Research Management Division, Alberta Department of the Environment, Edmonton, Alta., Canada T5K 2J6

Received July 13, 1982

This paper is dedicated to Professor Harry E. Gunning on the occasion of his 65th birthday

E. PEAKE and H. S. SANDHU. Can. J. Chem. **61**, 927 (1983).

Atmospheric temperature inversions frequently trap pollutants in the urban atmospheres of Alberta leading to photochemical air pollution. Peroxyacetyl nitrate (PAN) was monitored, for the first time in Alberta, from November 1980 to August 1981 at the University of Calgary using electron capture gas chromatography. Measurements were made at one-half-hour intervals from July, 1981 to February, 1982 at a downtown location. Maximum PAN concentrations were recorded at the University and downtown sites on August 14 at 1400 h, 1981 and the values were 2.4 and 6.6 ppb, respectively. In each case the maximum PAN peak coincided with the afternoon peak in ozone concentrations, 79 ppb at the University and 59 ppb at the downtown site. Surprisingly, a high value of 2.3 ppb PAN was recorded at the University during January of 1981 giving rise to questions regarding the influence of low temperatures and solar radiation on the photochemical formation of PAN. Calculations employing a simple photochemical model for PAN and ozone formation have been carried out and comparisons made between the observed and the computed values.

E. PEAKE et H. S. SANDHU. Can. J. Chem. **61**, 927 (1983).

Les inversions de température atmosphérique piègent fréquemment les agents polluants dans les atmosphères urbains de l'Alberta conduisant ainsi à une pollution photochimique de l'air. On décelé le nitrate de peroxyacétyle (NPA) pour la première fois en Alberta du mois de novembre 1980 au miois d'août 1981 à l'université de Calgary en utilisant un chromatographe en phase gazeuse à capture électronique. On a effectué les mesures à des intervalles d'une demi-heure du mois de juillet 1981 au mois de février 1982 en un point du centre ville. On a enregistré les concentrations maximales en NPA le 14 août 1981 à 14 h tant à l'université qu'au centre ville alors que les valeurs observées étaient respectivement 2,4 et 6,6 ppb. Dans chaque cas, la concentration maximale de NPA coincide avec le pic dans les concentrations d'ozone de l'après-midi soit 79 ppb à l'université et 59 ppb au centre ville. D'une façon surprenante, le fait qu'on ait enregistré à l'université une concentration de NPA aussi élevée que 2,3 ppb durant le mois de janvier 1981 remet en question l'influence des faibles températures et de la radiation solaire sur la formation photochimique du NPA. On a effectué des calculs en utilisant un modèle photochimique simple pour la formation du NPA et de l'ozone et on a comparé les valeurs observées avec celles obtenues par le calcul.

[Traduit par le journal]

Introduction

Peroxyacetyl nitrate (PAN) and ozone are the two important secondary photochemical air pollutants found in the urban atmosphere (1–3). Of the two, PAN is the more useful indicator of photochemical reactions in polluted air as, unlike ozone, it appears to have no large natural source (2–7). Both are strong oxidants which are phytotoxic in high concentrations (8, 9), and can affect human health (3). PAN is a strong eye irritant and has been cited as a possible etiological agent in the high incidence of skin cancer observed in tropical regions as compared to temperate ones (10–12).

Previous studies of PAN have related its occurrence to primary pollutants such as nitrogen oxides and hydrocarbons (13–15). The formation of PAN in the polluted atmosphere is believed to be initiated by the photooxidation of hydrocarbons leading to aldehydes and, subsequently, peroxyacyl radicals. These radicals in turn react with nitrogen oxides to form peroxyacetyl nitrate and lesser amounts of peroxypropionyl nitrate (2, 15, 16). The concentration of PAN in the urban atmosphere is influenced not only by solar radiation but also by the magnitude of primary pollutant emissions and meteorological parameters such as temperature, mixing volumes, and ventilation rates.

Ozone measurements for Alberta cities and computer modelling of photochemical air pollution under Alberta climatic conditions have been reported previously (17–20). Although theoretical calculations are available, no field observations have been made so far of PAN concentrations in the Alberta atmosphere to validate the existing models. In general, information on PAN concentrations for other Canadian cities is lacking. To our knowledge, the only study presently underway is in Simcoe, Ontario (21).

For the past decade Alberta has undergone the highest rate of economic growth of any Canadian province. As a consequence the major cities of Calgary and Edmonton have undergone a rapid increase in population. Each is expected to double its population by the year 2000. Despite advances in pollution control technologies, increased emission of pollutants, such as nitrogen oxides and hydrocarbons from industrial and transportation sources, are to be expected. Already concentrations of nitrogen oxides in Alberta's cities are amongst the highest in Canada during winter months (18).

Another important factor in PAN and ozone formation is the

[1]Presented at the 65th Annual Conference of the Chemical Institute of Canada, Toronto, Ont., Canada, May 30 – June 2, 1982.

Can. J. Chem. Downloaded from www.nrcresearchpress.com by 210.87.254.40 on 09/06/12
For personal use only.

Can. J. Chem. Downloaded from www.nrcresearchpress.com by 210.87.254.40 on 09/06/12
For personal use only.

effect of climate. Calgary is in the northern cool temperate zone. It is located at a latitude of 51°N, an elevation of 1050 m, 650 km from the Pacific Ocean, and 100 km east of the Continental Divide created by the Rocky Mountains. Mean daily temperatures range from 10.9°C in July to −10.6°C in January. Average mixing heights are about 2100 m in summer and 360 m in the winter. Mixing heights are often much less than the average and vary greatly as Calgary is subject to temperature inversions and to chinook phenomena.

Measurements of PAN have been made in European cities situated at similar northern latitudes but PAN concentrations have not been reported for cities with the cold, dry, continental climate of Alberta. The cities of Calgary and Edmonton, separated by 300 km and with no other major city within 500 km, can be considered isolated area sources of pollutants. This provides an opportunity to study PAN formation and degradation under cold, dry, climatic conditions.

In 1980 a research program was initiated by the Alberta Department of the Environment to understand, predict, and ultimately control photochemical air pollution. The objectives of this program are: (1) to measure the present rural and urban concentrations of peroxyacetyl nitrate; (2) to establish the relationship among PAN, ozone, and major primary pollutants such as nitrogen oxides, hydrocarbons, and carbon monoxide under Alberta climatic conditions; (3) to compare PAN and ozone concentrations in Alberta with those of other regions; and (4) to identify the role of PAN in the long-range transport of air pollutants.

Experimental

Analysis of PAN in the ambient atmosphere

PAN was measured by gas chromatography at two locations in Calgary and at a single site in the Kananaskis Valley, 70 km to the west of Calgary. One Calgary sampling site was located in the city center at Alberta Environment's air quality monitoring station. The second site was at The University of Calgary, 6 km northwest of the city center.

The gas chromatograph used at the University was a Tracor model 560, and at the downtown and Kananaskis sites a Varian model 3700. Both instruments were equipped with nickel 63 electron capture detectors. The chromatographic column was a 1 m by 1.5 mm inside diameter glass column packed with 5% Carbowax 600 on Chromosorb W, High Performance, 80/100 mesh (Chromatographic Specialties). The carrier gas was nitrogen with a flow rate of 50 mL per minute. The detector temperature was 80°C and the oven and injection port temperatures were 33°C. Samples were manually introduced into the Tracor instrument using a 5 mL gas tight syringe. The Varian chromatograph was equipped with an automated gas sampling system. This system consisted of a Valco gas sampling valve with air actuator and air switch, a 5 mL Teflon sample loop, a Reciprotor pump, and a Valco digital valve sequence programmer. A Hewlett Packard model 3390 integrator was activated by the sequence programmer to report results. A 2 m by 6.4 mm Teflon tube connected the gas chromatograph to an Ace glass manifold used to introduce ambient air into Alberta Environment's air monitoring station.

Samples were taken and automatically analyzed every 30 minutes, 24 hours per day, at the downtown sampling site from July 12, 1981 to April 7, 1982. At the University, samples were taken during working hours only, generally 0700 to 1600 h Mountain Standard Time, each week day from November 19, 1980 to August 30, 1981. Preliminary sampling of PAN at the Kananaskis station began in April of 1982 and is continuing.

Synthesis of PAN and instrument calibration

Hazard

PAN and ethyl nitrite are explosive. Workers should be protected by shields, gloves, and goggles.

A series of PAN standards with concentrations of 0.1 ppb to 20 ppb PAN in dry air were generated to calibrate the gas chromatograph electron capture detectors. The generation of these standards presented a number of problems. PAN is highly reactive in the vapor form and explosive as a liquid. Great care is required during PAN synthesis and the standards, once prepared, degrade rapidly.

At least five reactions have been used to synthesize PAN (22−25) but the most convenient is the photolysis of ethyl nitrite in oxygen (25).

The first step in PAN synthesis was the preparation of ethyl nitrite:

$$C_2H_5OH + H_2SO_4 \rightarrow C_2H_5OSO_2OH + H_2O$$

$$C_2H_5OSO_2OH + NaNO_2 \rightarrow C_2H_5ONO + NaHSO_4$$

Ethyl nitrite was synthesized by the addition of 5.5 mL of cooled sulphuric acid to 5.7 mL of cooled ethanol in a 50 mL Erlenmeyer flask immersed in an ice bath. The flask was fitted with a one-hole stopper and connected with a Teflon tube to a U-shaped glass trap cooled in a Dry Ice − acetone bath. Upon addition of 6.9 g of sodium nitrite to the Erlenmeyer flask, ethyl nitrite vapor passed through the tube and was retained by the trap. Once the reaction was complete the Teflon stopcocks on the trap were closed and the trapped ethyl nitrite was stored at 0°C until used in the synthesis of PAN (note, ethyl nitrite boils at 17°C).

A simple, inexpensive system was devised for the preparation of the small quantity of PAN required in the calibration of the gas chromatographs. PAN was synthesized in a 2-L Teflon bag by the photolysis of ethyl nitrite in an oxygen atmosphere:

$$C_2H_5ONO + 2O_2 \xrightarrow{h\nu} CH_3\overset{\overset{O}{\|}}{C}OONO_2 + H_2O$$

The trap was warmed (both stopcocks open) to produce ethyl nitrite vapor, 0.25 mL of which was injected into the Teflon bag containing oxygen. The bag was irradiated with a 20 watt "mineral light" from which the filter had been removed to allow passage of all wavelengths of ultraviolet light. Injections of ethyl nitrite vapor were repeated every 15 minutes over a 3-hour period. PAN was transferred into a glass trap cooled in a Dry Ice − acetone bath by gently squeezing the bag, forcing the PAN vapor through a Teflon tube into the trap. The PAN was then transferred into an infrared gas cell by evacuating the cell and connecting it to the trap which was gently warmed to room temperature. From the infrared spectrum the concentration of PAN in the cell was calculated with an absorptivity of 13.9×10^4 ppm^{-1} m^{-1} at 8.30 micron. This band is one of the more intense in the spectrum of PAN and is free from interferences from PAN decomposition products (26).

Standards for the calibration of the gas chromatograph were made by diluting PAN vapor (0.005 to 0.5 mL) from the infrared cell into a measured volume of air in a 50-L Teflon bag (0.1 to 20 ppb). A linear response was obtained with concentrations of PAN up to 20 ppb. A detection limit of 0.03 ppb and a precision of 0.03 ppb at 1 ppb was obtained for ambient air samples with the Tracor model 560 gas chromatograph. The Varian 3700 gas chromatograph was far less sensitive to PAN than the Tracor model 560. The sensitivity of the system was also limited by the ability of the integrator to discriminate between instrument noise and the onset of a chromatographic peak. These factors combined to give a detection limit of 0.2 ppb.

Results and discussion

PAN concentrations in the Calgary atmosphere

Mean concentrations of PAN in Calgary are lower than those reported for major cities in the southern United States (Tables 1−3) (27). The overall mean concentration of PAN at the University of Calgary from 0800 to 1700 h, December 1, 1980 to August 31, 1981, was 0.22 ppb. At the downtown site, where one-half-hour samples were taken 24 hours per day from

TABLE 1. Ambient atmospheric concentrations of PAN at the University of Calgary sampling site; December 1, 1980 to August 31, 1981. All data in parts per billion (ppb)

Month	Monthly means	Mean of daily maxima (monthly)
Dec 1980	0.11 (n*= 21)	0.13 (n = 21)
Jan 1981	0.16 (n = 22)	0.33 (n = 22)
Feb 1981	0.12 (n = 20)	0.15 (n = 20)
Mar 1981	0.12 (n = 19)	0.22 (n = 19)
Apr 1981	0.20 (n = 21)	0.29 (n = 21)
May 1981	0.35 (n = 11)	0.47 (n = 11)
Jun 1981	0.26 (n = 20)	0.37 (n = 20)
Jul 1981	0.30 (n = 22)	0.53 (n = 22)
Aug 1981	0.40 (n = 22)	0.92 (n = 22)
Overall mean:	0.22 (1313 observations)	
Mean of daily maxima:	0.38 (n = 175)	
Maxima (overall):	2.4 (Aug. 14, 1981)	

*n = number of days with observations.

TABLE 2. Ambient atmospheric concentrations of PAN at the downtown Calgary sampling site; July 12, 1981 to February 28, 1982. All data in parts per billion (ppb)

Month	Monthly means	Mean of daily maxima (monthly)
Jul 1981	0.24 (n*= 11)	0.82 (n = 11)
Aug 1981	0.49 (n = 31)	2.05 (n = 31)
Sep 1981	0.23 (n = 28)	0.97 (n = 28)
Oct 1981	0.02 (n = 23)	0.28 (n = 23)
Nov 1981	0.01 (n = 30)	0.08 (n = 30)
Dec 1981	0.00 (n = 31)	0.03 (n = 31)
Jan 1982	0.08 (n = 31)	0.08 (n = 31)
Feb 1982	0.12 (n = 28)	0.44 (n = 28)
Overall mean:	0.14 (9089 observations)	
Mean of daily maxima:	0.59 (n = 213)	
Maxima (overall):	6.6 (Aug 14, 1981)	

*n = number of days with observations.

July 12, 1981 to February 28, 1982, the mean concentration of PAN was 0.14 ppb. The mean daily maxima at the University was 0.38 ppb whereas at the downtown location it was somewhat higher, 0.59 ppb. The maximum concentrations of PAN measured at the University and downtown were 2.4 and 6.6 ppb, respectively.

Most previous studies of PAN in the urban atmosphere have been carried out over shorter time periods, generally a few weeks. During the summer months in Houston, Texas, mean daytime PAN concentrations of about 1.0 ppb with a maximum of 15.6 ppb were recorded (28). For a one month period from mid-July to mid-August, 1973, Spicer (29) reported an average of 1.8 ppb PAN in St. Louis, Missouri, with daily maxima averaging 4.6 ppb and a maximum of 19 ppb. By comparison, the August 1981 mean for downtown Calgary was 0.49 ppb, the mean daily maximum was 2.1 ppb, and the maximum recorded was 6.6 ppb. Calgary's atmospheric concentrations of PAN are similar to those reported for northern European cities: Riso, Denmark; Goteborg, Sweden; Delft, Netherlands; Essen, West Germany; and Harwell, England (Table 4). They are far lower than levels measured in the Los Angeles basin where long term studies have been carried out. The yearly average at Riverside, California, for 1980 during the hours of 0800 to 2000 was 4.9 ppb, and the highest concentration recorded was 41.6 ppb (27).

At first glance it would appear that PAN concentrations, as given by the overall mean concentrations in Tables 1 and 2, were higher at the University than at the downtown sampling site, 0.22 ppb versus 0.14 ppb. However, the University data included only daytime readings when PAN concentrations are expected to be highest, whereas the downtown data were taken over a full 24-hour period. PAN concentrations were actually higher at the downtown location. For example on August 14, 1981 between the hours of 0800 and 1600 the mean PAN concentration at the downtown site was 2.0 ppb versus 0.84 ppb at the University. On 15 days during July and August, 1981, PAN was measured simultaneously at both stations. The mean concentration over these periods was 1.3 ppb at the downtown location and 0.57 ppb at the University, a 2.2-fold greater concentration at the downtown site. It was during this period that the maximum concentrations of PAN were recorded at both the University and downtown locations, 2.4 ppb and 6.6 ppb on August 14, again, more than a 2-fold greater concentration downtown. These PAN concentrations are believed to be too low to injure plants or to present a health problem to man except possibly for some highly susceptible allergic individuals (3).

Diurnal variations in PAN concentrations

The diurnal pattern of PAN concentrations in the Calgary atmosphere is illustrated in Fig. 1 for the University location, and Fig. 2 for the downtown Calgary sampling site. PAN generally starts forming between 0700 and 0800 h in the Calgary area during the summer months. The peak PAN concentration is usually achieved by 1200 or 1300 h although on occasion the afternoon peak may be delayed until as late as 1500 h. On days with comparable data, the afternoon maximum in the PAN concentrations occurred at about the same time at both the downtown and University of Calgary locations. This is in contrast to the situation at Riverside, California, where oxidants which are generated locally reach a maximum by 1000 or 1100 h but in addition a "smog front", advected from Los Angeles, produced a second maximum at about 1500 h (27). The spacing between the downtown and University of Calgary sampling sites is relatively small, only 6 km, and such a "front" effect caused by movement from the downtown area to the University may not be distinguishable.

Factors influencing PAN formation

PAN is believed formed in the urban atmosphere by those hydrocarbons which yield acetylperoxy radicals upon photooxidation. Peroxyacyl radicals react with nitrogen oxides to form peroxyacyl nitrates (2, 16). Thus a close relationship might be expected to exist between the occurrence of the primary pollutants, nitrogen oxides and hydrocarbons, with that of the secondary pollutants, ozone and PAN. Such a relationship is well known for the nitrogen oxides and ozone; nitric oxide is oxidized to nitrogen dioxide leading to the formation of ozone (3). It is not the absolute amount of nitrogen oxides which controls the abundance of ozone but rather the ratio of the nitrogen dioxide to nitric oxide. The mechanisms of PAN formation are quite different from those of ozone. PAN is the terminal product of a chain of free radical reactions whereas, with ozone, the generation process is self perpetuating.

In Calgary, the primary pollutants, nitrogen oxides, carbon monoxide, and hydrocarbons, show similar diurnal concentration patterns (Fig. 3). The maximum concentration of each

Can. J. Chem. Downloaded from www.nrcresearchpress.com by 210.87.254.40 on 09/06/12
For personal use only.

TABLE 3. Summary of ambient PAN monitoring in North America (27). All data in parts per billion (ppb)

City	Sampling period	Monthly average	Mean daily max.	Daily observation	Reference
East and Mid-West					
Simcoe, Ont.	June–Dec 1980	2	—	5.6	21
Hoboken, NJ	June–Aug 1970 (1000–1600 h)	3.7	—	9.9	16
New Brunswick, NJ	Sept 30 – Dec 8, 1978 (0800–1800 h)	2.7	—	10.5	30
Downington, PA	Aug 16 – Sept 22, 1979	1	2.2	5.0	31
Wilmington, OH	Aug 1974	—	2.0	4.1	16
St. Louis, MO	June–Aug 1973 (1000–1600 h)	6.3	—	25	16
St. Louis, MO	July 18 – Aug 16, 1973	1.8	4.6	19	29
Houston, TX	July 2–23 1976 (1000–1600 h)	1.0	—	11.5	31
Houston, TX	June 1 – Oct 31, 1977	0.6	—	15.6	28
West					
Calgary, Alta. residential	Dec 1, 1980 – Aug 31, 1981 (0800–1600 h)	0.2	0.4	2.4	This report
Calgary, Alta. downtown	July 12, 1981 – Feb 28, 1982	0.1	0.6	6.6	This report
Salt Lake City, UT	—	—	10–20	54	32
Los Angeles, CA	Sept, 1965 Oct, 1965	38 60	— —	210 —	33
Los Angeles, CA	Sept–Nov 1968 (1000–1600 h)	—	10–30	65.5	16
West Covina, CA	Aug 24 – Sept 28, 1973	8.8	22.4	46	29
Riverside, CA	Aug 1967 – Apr 1968 (0800–1800 h)	4.6	—	58	8
Riverside, CA	Jan–Dec 1980 (0800–2000 h)	4.9	25.1	41.6	27

occurs at the same time on a given day. The hydrocarbon concentrations, however, show far less variation than do the carbon monoxide and nitrogen oxides, with sufficient hydrocarbons available at all times to participate in the formation of peroxyacyl radicals.

As shown by the monthly means in Tables 1 and 2 the highest concentrations of PAN occurred in May and August. This may be explained on the basis of solar radiation intensity and duration, temperature, and pollutant concentrations (Table 5). In the winter months concentrations of primary pollutants are high but the intensity and duration of solar radiation and the atmospheric temperature are low. Conversely, during the summer, solar radiation reaches its maximum intensity and duration and temperatures are highest, but pollutant concentrations are low. During spring and autumn months the possibility exists for the simultaneous occurrence of high levels of pollutants together with high solar radiation and temperatures resulting in the generation of PAN. Thus solar radiation is

Can. J. Chem. Downloaded from www.nrcresearchpress.com by 210.87.254.40 on 09/06/12
For personal use only.

TABLE 4. Summary of world-wide measurements of ambient PAN concentrations (excluding North America) (27). All data in parts per billion (ppb)

City and country	Sampling period	Daily average	Monthly average	Daily max	Max. observation	Reference
Riso, Denmark	11 June – 23 Sept 1980	—	—	0.9	4.2	34
Goteborg, Sweden	17 June – 9 Sept 1980	—	—	0.8	3.5	34
Delft, Netherlands	June 1972 – Nov 1972	0.6	—	1.4	16	35
Delft, Netherlands	June 1973 – Oct 1973	2	—	—	ca. 20	36
Essen, W. Germany	June 1978 – Sept 1978	1	1	—	3.6	37
Harwell, England	Nov 1974 – Oct 1975	1	0.27	—	8.9	5
London, England	Aug 1974 – Oct 1975	—	—	—	16.1	5
Central Tokyo, Japan	June 13 – July 13, 1973	—	—	—	31.2	38
Suburban Tokyo, Japan	July 1 – Aug 31, 1972	—	—	—	8.2	38
Ohme, Japan	June 13 – July 6 1973	—	—	—	13.5	38
Tokyo, Japan	Sept 20 – Nov 30, 1972	—	—	ca. 5	6.7	39

Can. J. Chem. Downloaded from www.nrcresearchpress.com by 210.87.254.40 on 09/06/12
For personal use only.

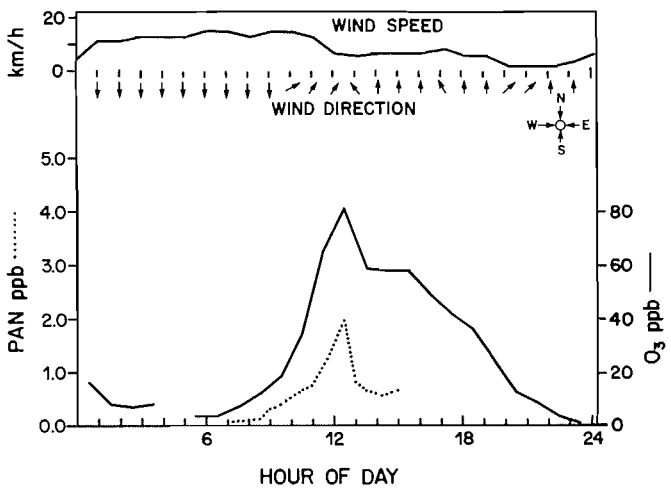

FIG. 1. Ozone and PAN concentrations and wind speed and direction at The University of Calgary, August 11, 1981.

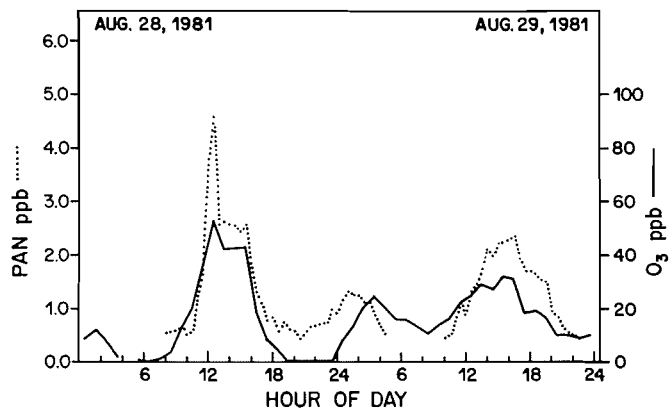

FIG. 2. Ozone and PAN concentrations in downtown Calgary, August 28 and 29, 1981.

believed to be the limiting factor in the formation of PAN during the winter months in Calgary (51°N) whereas the abundance of the primary pollutants, the precursors of PAN, is the limiting factor in the summer months. This is in contrast to the Los Angeles basin (31°N) where evidence suggests that solar radiation is not a limiting factor (41).

Temperature is one of the factors which influence the rate of PAN generation. Most PAN measurements have been made in the southern United States where temperatures are warm. Other measurements of PAN have been made mostly during the summer months in the more northerly United States and in Europe. PAN was found in Calgary, however, on several days when the temperature did not exceed 0°C. The highest PAN concentrations recorded at the University of Calgary were 2.4 ppb on August 14 and 2.3 ppb on January 27. The maximum temperature on August 14 was 27°C; on January 27 it was only +1°C. On March 7, 1982 the maximum temperature was −4°C but 1.5 ppb PAN was recorded in downtown Calgary.

These findings confirm the results of modelling studies of a

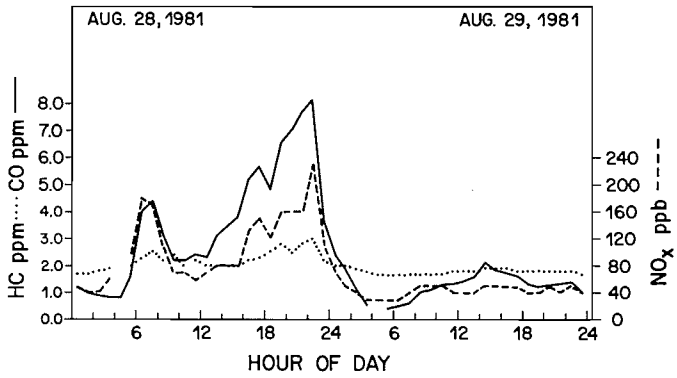

FIG. 3. Concentrations of hydrocarbons, carbon dioxide, and nitrogen oxides in downtown Calgary, August 28 and 29, 1981.

TABLE 5. Monthly mean values of total daily solar radiation on an horizontal surface at Suffield 50°16′N (40) and mean temperature (42) and mean nitrogen oxides concentration at Calgary 50°50′N, 1977 to 1981 (18)

	Solar radiation MJ/m^2/day	Temperature °C	Nitrogen oxides ppm
January	4.94	−10.9	0.13
February	8.56	−7.4	0.12
March	14.03	−4.3	0.09
April	17.87	3.3	0.06
May	21.53	9.3	0.05
June	23.52	13.2	0.04
July	25.06	16.5	0.05
August	20.60	15.2	0.06
September	14.45	10.7	0.08
October	9.29	5.7	0.10
November	5.14	−2.6	0.12
December	3.84	−7.6	0.13

TABLE 6. PAN/ozone ratios on selected days at The University of Calgary and downtown Calgary

	University	Downtown
Jan 2, 1981	38	—
Jan 27, 1981	4	—
Jul 29, 1981	35	12
Aug 6, 1981	43	17
Aug 14, 1981	33	9
Aug 25, 1981	120	31
Jan 25, 1982	—	1
Feb 15, 1982	—	7

general photochemical air pollution system carried out by Bottenheim *et al.* (19). The model showed lower rates of product formation under winter conditions due to solar altitude rather than temperature. The rate of primary formation of major radicals, HO, HO_2, and RO_2, together with their participation in several chain length reactions, are the driving forces in these systems. Primary formation of these radicals is largely unaffected by temperature. Chain lengths are dependent upon the activation energies of the reactions involved, which are generally small, thus temperature has little influence. Conversely solar attitude is expected to have a much greater effect since these radicals are produced primarily by photochemical reactions (19).

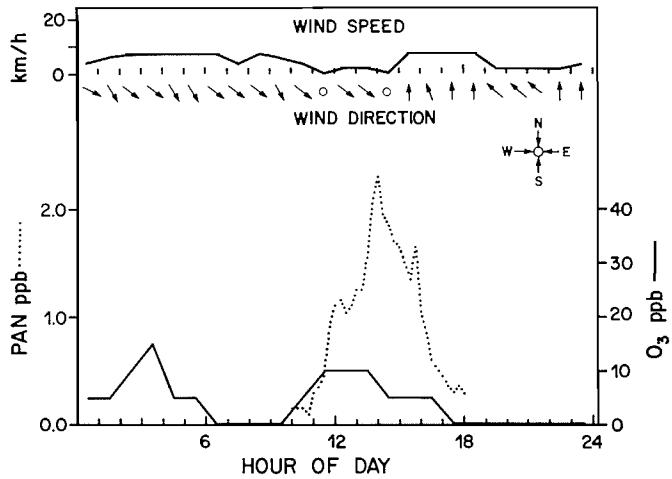

FIG. 4. Ozone and PAN concentrations and wind speed and direction at The University of Calgary, January 27, 1981.

Ozone–PAN relationships

The photochemical oxidants, PAN and ozone, are generated by related photochemical processes, each usually reaching maximum concentrations simultaneously in the early afternoon.

The peak afternoon concentration of PAN is much less than the corresponding ozone maximum. During episodes with high concentrations of photochemical smog in Los Angeles or in Japan, ozone/PAN ratios of 10 have been reported (8, 38). In Europe, ratios are commonly 50 (4, 43, 44). In downtown Calgary, ratios as low as 1 were measured (Table 6). Such low ratios occurred when the background concentration of ozone was first suppressed by nitrogen oxides followed by photochemical ozone and PAN formation. Ozone/PAN ratios at the University were generally higher than downtown. On August 14, the day of maximum PAN concentrations both downtown and at the University, the ratio was 33 at the University compared with 9 downtown. The mean ratio for fourteen days when PAN was measured both at the University and downtown was 65 at the University and 21 downtown. Overall ozone concentrations are higher at the University than downtown (means for 1981 of 18.3 ppb and 10.3 ppb respectively) reflecting the University location upwind of the major transportation sources of nitrogen oxides. Downtown Calgary ozone concentrations are suppressed by nitric oxide emissions. On days of relatively high pollution, during the winter months, low ozone/PAN ratios may result, even at the University, from suppression of ozone by nitric oxide rather than from high PAN concentrations. For example, on January 27, a ratio of 4 was measured at the University. The PAN concentration was 2.3 ppb while the ozone concentration was only 10 ppb.

Comparison of the primary pollutant concentrations, with the corresponding ozone and PAN concentrations, showed the generation of ozone and PAN after a decline in the overall concentration of nitrogen oxides which corresponded to the conversion of NO to NO_2 (Figs. 2 and 3). In some cases, however, PAN maxima occurred coincident with maximum concentrations of the primary pollutants. On January 27, 1981, high nitrogen oxide concentrations were recorded at the University, and the maximum PAN concentration of 2.3 ppb occurred simultaneously with a maximum of 410 ppb nitrogen oxides (Figs. 4 and 5), both NO and NO_2 reaching a maximum at that time.

Can. J. Chem. Downloaded from www.nrcresearchpress.com by 210.87.254.40 on 09/06/12
For personal use only.

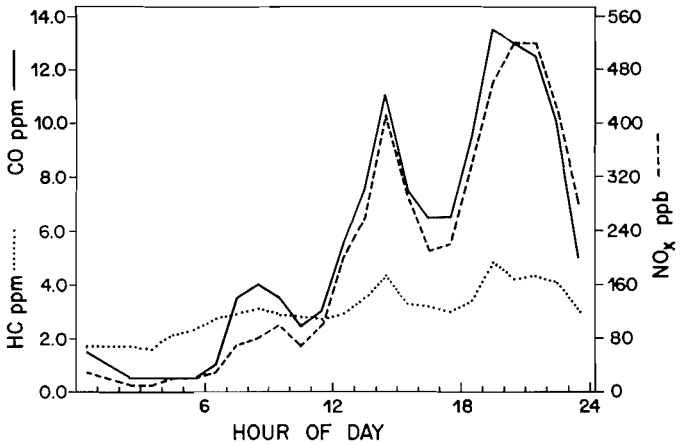

FIG. 5. Concentrations of hydrocarbons, carbon dioxide, and nitrogen oxides at The University of Calgary, January 27, 1981.

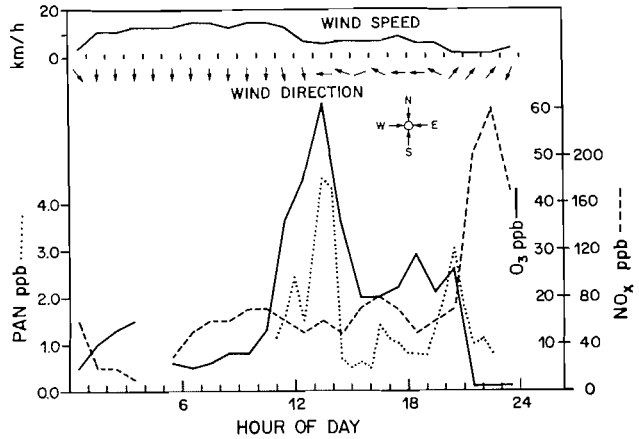

FIG. 6. Ozone, PAN, and nitrogen oxide concentrations and wind speed and direction in downtown Calgay, August 28, 1981.

Generally only one peak in the PAN concentration occurred each day, usually during the afternoon, but on occasion a second peak occurred later in the day. On August 28 a secondary PAN maximum occurred at 2400 h (Fig. 6). This would suggest either that sufficient peroxyacyl radical existed to allow the generation of PAN to proceed after dark (16) or that an air mass moved from the downtown area of the city during the afternoon and returned in the evening to produce a second PAN peak. Air moves along the river valley in Calgary in response to adiabatic heating and cooling.

Persistence and long range transport of PAN

If the two maxima in PAN concentration were the result of air mass movement, the relative concentrations of PAN, 4.5 ppb at 1130 h and 3.0 ppb at 2030 h, are of interest. As the downtown sampling site is centrally located, it is assumed that the maximum PAN concentrations occur at that location. Therefore the maximum loss of PAN by a combination of chemical reactions in the atmosphere and interaction with surfaces during the 9-hour period was about 33%. In all likelihood there would be some mixing of the air mass and dilution of the PAN, therefore the rate of PAN destruction would be less than 33%.

PAN and ozone decay rates have been measured over grass, soil, and water. Deposition velocities of PAN over grass and soil were similar, 0.21 and 0.26 cm/s, but were considerably lower over water, 0.02 cm/s (5, 45). These rates indicate that surface chemical reaction is the major mechanism of PAN removal from the atmosphere rather than gas phase reactions with other pollutants such as nitric oxide (46). Surface reactions are also believed to be responsible for the daily cycle in atmospheric ozone concentrations (47). The deposition velocity of ozone is about 3 times greater than that of PAN over grass and about 6 times greater over soil. Thus PAN is more persistent in the atmosphere than ozone. Although PAN in the Calgary atmosphere generally decreased rapidly in concentration during the late afternoon, it would sometimes persist overnight. It should be emphasized that a decline in PAN concentration may not mean that the PAN was degraded; it may simply mean that an unpolluted air mass has replaced the polluted air or that the mixing height has increased. In the Los Angeles basin, where very large polluted air masses may be expected, PAN averaged 17.7 ppb over one 18-day period with readings as high as 26 ppb at midnight (27).

On several days the maximum PAN concentrations occurred after a change in wind direction which may have signaled the breakup of the temperature inversion (Figs. 1, 4, and 6). Should the breakup of the nocturnal temperature inversion have preceded the occurrence of the PAN maximum it would support the thesis that PAN degrades primarily by contact with surfaces (43). Presumably PAN would persist above the thermal inversion whereas the PAN below the temperature inversion would be degraded. At the breakup of the inversion, air containing higher concentrations of PAN would be brought to ground level.

Calgary is located about 100 km east of the Rocky Mountains with no large city within 650 km to the west, the direction of the prevailing winds. Edmonton, the nearest major city, is 300 km to the north. Thus, Calgary is isolated from major urban sources of air pollution. To determine the quality of air approaching Calgary, monitoring of PAN and ozone was begun in April of 1982 in the Kananaskis Valley on the edge of the Rocky Mountains 70 km west of Calgary. Preliminary results periodically show the presence of PAN in concentrations up to 0.5 ppb. It seems unlikely that the observed PAN was generated locally from anthropogenic pollutants. Generation from local natural emissions may be possible (48) but long range transport is the most likely mechanism.

Recent studies in northern Sweden (56–58°N) have shown transport of PAN for about 1000 km in air masses moving mainly over the sea (29). The source of PAN in southern Scandinavia is probably Great Britain or the central continent. PAN is more stable over water than over land and the sources of pollutants in industrialized Great Britain and Europe are large. In contrast, there are no large sources of pollutants on the North American continent to the northwest of Calgary and sources to the west and southwest are small in comparison with those of Europe. If Vancouver or Seattle, the only major cities to the west, were the source, PAN or its precursors would be transported 650 km over land before reaching the Kananaskis sampling site. Deposition velocities of PAN are about 10 times greater over land than over water (45). In order for PAN to reach the Kananaskis site it must be transported at such an altitude that there is no easy contact with the ground. To the west of Calgary are five mountain ranges with peaks up to 3800 m high. On the eastern edge of the mountains, air from higher altitudes sweeps down to the plains. In this zone PAN, which may have been transported thousands of kilometers or

Can. J. Chem. Downloaded from www.nrcresearchpress.com by 210.87.254.40 on 09/06/12
For personal use only.

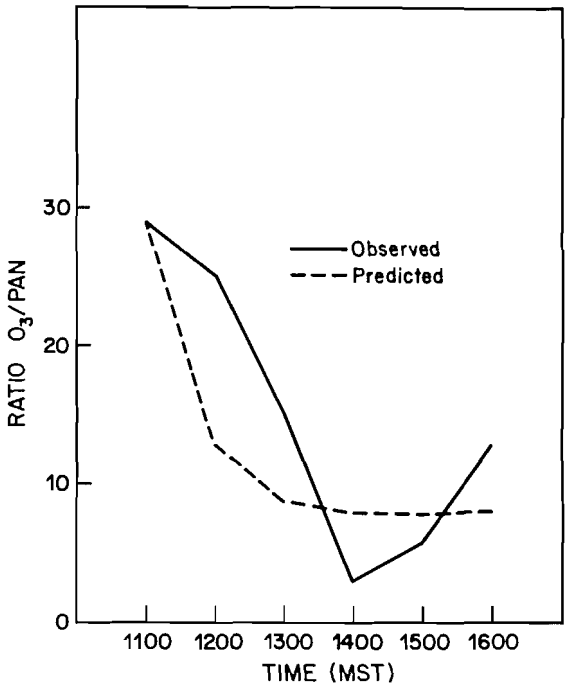

FIG. 7. Predicted ozone/PAN ratios (19) and observed ratios for downtown Calgary, August 14, 1981. Initial conditions for computation; ozone 29.0 ppb, PAN 1.0 ppb, NO 0.01 ppm, NO_2 0.08 ppm, paraffinic hydrocarbons 1.76 ppm, olefinic hydrocarbons 0.44 ppm, aromatic hydrocarbons 0.44 ppm, temperature 20.0°C, relative humidity 47%.

perhaps existed in the upper atmosphere naturally or as a result of anthropogenic pollutants, may be brought to ground level. The Kananaskis sampling site located on the eastern slopes of the Rocky Mountains is in a position to intercept and monitor this air.

Model calculations

Bottenheim *et al.* (19) studied the effect of temperature and solar altitude variation on the chemical processes which take place in a general photochemical air pollution system at 60°N latitude. Eleven photochemical and 100 dark reactions of 11 initial reactants were considered. The assumption of no atmospheric dilution of products and reactants was employed in these computations. Ambient air pollutant concentrations measured at 1100 h and appropriate photochemical rate parameters for Calgary's solar altitudes for August 14 were used in our computations. The calculated O_3/PAN ratio is displayed as a function of time in Fig. 7 along with initial pollutant concentrations, temperature, and relative humidity values.

Observed O_3/PAN values for the same day are also shown in Fig. 7. Considering the assumptions of no dilution of reactants and products in the model, the trend in the observed ratios is reasonably predicted by the computations. Further work is underway to improve the model in the light of these observations.

Acknowledgements

We express our appreciation to the Alberta Department of the Environment for their financial support and to the many members of the Department who cooperated on this project, in particular, T. J. Spackman and D. D. Bensler for providing technical information and assistance often on very short notice, M. Choukalos for his help in computing, and G. R. Peck and the staff of the Pollution Control Division for their patience and efficiency in answering our many requests for information and data. We also thank the staff of the Kananaskis Centre for Environmental Research for conducting analyses, and collecting and compiling data. We especially thank M. A. MacLean, D. R. Connery, L. Dunne, and D. Patton for their invaluable assistance and E. C. Rhodes of The University of Calgary Geography Department for supplying meteorological data. Lastly, we thank P. J. Temple and O. C. Taylor of the Statewide Air Pollution Research Center, University of California, Riverside, for providing us with an advance copy of a manuscript recently submitted for publication (27).

1. A. J. HAAGEN-SMIT. Ind. Eng. Chem. **44**, 1342 (1952).
2. E. R. STEPHENS. Adv. Environ. Sci. Technol. **1**, 119 (1969).
3. NATIONAL RESEARCH COUNCIL. Ozone and other photochemical oxidants. National Academy of Sciences, Washington, DC. (1977).
4. H. NIEBOER and J. VAN HAM. Atmos. Environ. **10**, 115 (1976).
5. S. A. PENKETT, F. J. SANDALLS, and B. M. R. JONES. VDI Ber. **270**, 47 (1977).
6. P. E. COFFEY and W. M. STASIUK. Environ. Sci. Technol. **9**, 59 (1975).
7. R. R. STICKSEL. The stratosphere as a source of surface ozone. Presented at the 68th Annual Meeting of the Air Pollution Control Association, Boston, Massachusetts, June 15–20 (1975).
8. O. C. TAYLOR. J. Air Pollut. Control Assoc. **19**, 347 (1969).
9. O. C. TAYLOR and D. C. MACLEAN. Nitrogen oxides and the peroxyacyl nitrates. *In* Recognition of air pollution injury to vegetation: a pictorial atlas. *Edited by* J. S. Jacobson and A. C. Hill. Air Pollut. Control Assoc., Pittsburgh. 1970. pp. E1–E14.
10. E. R. STEPHENS, E. F. DARLEY, O. C. TAYLOR, and W. E. SCOTT. Proc. Am. Petrol. Inst. Sect. III, **40**, 325 (1960).
11. J. B. MUDD. Peroxyacyl nitrates. *In* Responses of plants to air pollution. *Edited by* J. B. Mudd and T. T. Kozlowski. Academic Press, New York. 1975.
12. J. E. LOVESTOCK. Ambio, **6**, 131 (1977).
13. J. N. PITTS. J. Air Pollut. Control Assoc. **9**, 658 (1969).
14. K. L. DEMERJIAN, J. A. KERR, and J. G. CALVERT. Adv. Environ. Sci. Technol. **4**, 1 (1974).
15. T. A. HECHT, J. H. SEINFELD, and M. C. DODGE. Environ. Sci. Technol. **8**, 327 (1974).
16. W. A. LONNEMAN, J. J. BUFALINI, and R. L. SELLA. Environ. Sci. Technol. **10**, 374 (1976).
17. H. S. SANDHU. A study of photochemical air pollutants in the urban airsheds of Edmonton and Calgary. Alberta Department of the Environment (1975).
18. ENVIRONMENT CANADA. National Air Pollution Surveillance, Annual Summaries.
19. J. W. BOTTENHEIM, S. E. BRASLAVSKY, and O. P. STRAUSZ. Environ. Sci. Technol. **11**, 801 (1977).
20. J. W. BOTTENHEIM and O. P. STRAUSZ. Atmos. Environ. **13**, 1085 (1979).
21. R. CORKUM, W. GIESBRECHT, T. BARDSLEY, and E. CHERNIAK. Can. J. Chem. To be published.
22. B. W. GAY, R. C. NOONAN, J. J. BUFALINI, and P. L. HANST. Environ. Sci. Technol. **10**, 82 (1976).
23. T. M. KRAVETZ, S. W. MARTIN, and G. D. MENDENHALL. Environ. Sci. Technol. **14**, 1262 (1980).
24. A. J. KACMAREK, I. J. SOLOMAN, and M. LUSTIG. J. Inorg. Nucl. Chem. **40**, 574 (1978).
25. E. R. STEPHENS, F. R. BURLESON, and E. A. CARDIFF. J. Air Pollut. Control Assoc. **15**, 87 (1965).
26. P. ADAMSON, and H. GUNTHARD. Spectrochim. Acta Part A, **36**, 473 (1980).
27. P. J. TEMPLE and O. C. TAYLOR. World-wide ambient measurements of peroxyacetyl nitrate (PAN) and implications for plant injury. Atmos. Environ. In press.

Can. J. Chem. Downloaded from www.nrcresearchpress.com by 210.87.254.40 on 09/06/12
For personal use only.

28. R. T. JORGEN. Ambient peroxyacetyl nitrate (PAN) measurements in the Houston area. Rockwell International Corporation, Atomics International Division, Air Monitoring Center (1978).
29. C. A. SPICER. Fate of nitrogen oxides in the atmosphere. Battelle Columbus Laboratories and the United States Environmental Protection Agency (1974).
30. E. BRENNAN. PAN concentrations in ambient air in New Jersey. Dept. of Plant Pathology, Cook College, Rutgers, The State University, New Brunswick, NJ. 1979.
31. H. WESTBERG, K. ALLWINE, and E. ROBINSON. Measurement of light hydrocarbons and studies of oxidant transport beyond urban areas. United States Environmental Protection Agency. Office of Research and Development, Research Triangle Park, NC. 1978.
32. D. T. TINGEY and A. C. HILL. Utah Acad. Sci. Proc. **44**, 387 (1968).
33. H. MAYRSOHN and C. BROOKS. The analysis of PAN by electron capture gas chromatography. Presented at Western Regional Meeting, Am. Chem. Soc., Nov. 18, 1965.
34. T. NIELSEN, U. SAMUELSSON, P. GRENNFELT, and E. L. THOMSEN. Nature, **293**, 553 (1981).
35. R. BOS, R. GUICHERIT, and A. HOOGEVEEN. Sci. Total Environ. **7**, 159 (1977).
36. R. GUICHERIT. The occurrence of photochemical oxidants and their precursors in Western Europe. Proc. Symp. Occur. Control Photochem. Pollut. 1976.
37. P. BRUCHMAN and P. EYNCK. Schrift. Landessanst Immission Lands NW. **29**, 19 (1979).
38. S. IZUMIKAWA, N. ITO, M. FUNAZIMA, T. HIRONO, H. YOKATA, M. SOUFUKA, K. ASAKUNO, K. NAKANO, and T. OODAIRA. Ann. Rep. Tokyo Metro. Res. Inst. Environ. Prot. **1975**, 9 (1975).
39. H. FUKUDA and K. TERAKADO. Tokyo Nagyo Scikenzo Sakuko, Feb. 1974, 35 (1974).
40. J. E. HAY. A tabulation and analysis of solar radiation data for Alberta. Alberta Research Council and Alberta Environment, Information Series 79, August, 1977.
41. H. NIEBOER, W. P. CARTER, A. C. LLOYD, and J. N. PITTS. Atmos. Environ. **10**, 731 (1976).
42. ALBERTA ENVIRONMENT. Climate of Alberta. Report for 1980. Published by Alberta Environment (1981).
43. L. J. BRASSER, R. GUICHERIT, and C. HUYGEN. VDI Ber. **270**, 25 (1977).
44. S. A. PENKETT. Environ. Pollut. Manage. **8**, 8 (1978).
45. J. A. GARLAND and S. A. PENKETT. J. Air Pollut. Control Assoc. **28**, 482 (1976).
46. E. A. SCHUCK and E. R. STEPHENS. Adv. Environ. Sci. **1**, 73 (1969).
47. J. A. GARLAND and R. G. DERWENT. Q. J. R. Meteorol. Soc. **105**, 169 (1979).
48. F. W. WENT. Nature, **187**, 641 (1960).

Can. J. Chem. Downloaded from www.nrcresearchpress.com by 210.87.254.40 on 09/06/12
For personal use only.

Factors affecting product formation in the photolysis of α-spirocyclopropyl ketones

PETER YATES AND PATRICK HUGH HELFERTY[1]

Lash Miller Chemical Laboratories, University of Toronto, Toronto, Ont., Canada M5S 1A1

Received July 13, 1982

This paper is dedicated to Professor Harry E. Gunning on the occasion of his 65th birthday

PETER YATES and PATRICK HUGH HELFERTY. Can. J. Chem. **61**, 936 (1983).

Photolysis of spiro[2.5]oct-7-en-4-ones results in exclusive β-cleavage in methanol to give 2-ethenylcyclohex-2-en-1-ones and in hydrocarbon solvents to give (*E*)- and (*Z*)-2-ethylidenecyclohex-3-en-1-ones. The solvent effect is ascribed to the role of methanol in stabilizing trienol intermediates and engendering their intermolecular ketonization. Photolysis of 8-methylenespiro[2.5]octan-4-ones in methanol gives 2-ethenylcyclohex-2-en-1-ones and bicyclo[4.3.0]non-1(6)-en-2-ones; irradiation in methanol-*O-d* indicates that the former type of product is formed mainly via a trienol intermediate. Photolysis of 8-methylenespiro[2.5]octan-4-ones in benzene gives 2-ethenylcyclohex-2-en-1-ones together with (*E*)- and (*Z*)-2-ethylidene-3-methylenecyclohexan-1-ones; the latter undergo photoconversion to the former during the irradiation. 6,6-Dimethylspiro[2.4]-heptan-4-one on photolysis in methanol undergoes α-cleavage to give 4-methoxy-7,7-dimethyl-5-oxaspiro[2.5]octane as the major product, whereas under the same conditions 6,6-dimethylspiro[2.5]octan-4-one is reduced to the corresponding alcohol and 6,6,8-trimethylspiro[2.5]octan-4-one undergoes β-cleavage to give 2-ethyl-3,5,5-trimethylcyclohexan-1-one as the major primary product; this trichotomy is interpreted in terms of ring-size and steric factors.

PETER YATES et PATRICK HUGH HELFERTY. Can. J. Chem. **61**, 936 (1983).

La photolyse des spiro[2.5] octène-7 ones-4 dans le méthanol donne par suite d'un clivage exclusif en β,,les éthényl-2 cyclohexène-2 ones-1 et dans les solvants hydrocarbonés, elle conduit aux éthylidène-2 cyclohexène-3 ones-1 (*E*) et (*Z*). On attribue l'effet de solvant au rôle du méthanol dans la stabilisation des intermédiaires triénol dont il provoque la cétonisation intermoléculaire. La photolyse des méthylène-8 spiro[2.5] octanones-4 dans le méthanol conduit aux éthényl-2 cyclohexène-2 ones-1 et aux bicyclo[4.3.0] nonène-1(6) ones-2. L'irradiation dans le méthanol-*O-d* indique que le premier type de composé se forme principalement via un intermédiaire triénol. La photolyse des méthylène-8 spiro[2.5] octanones-4 dans le benzène donne les éthényl-2 cyclohexène-2 ones-1 ainsi que les éthylidène-2 méthylène-3 cyclohexanones-1 (*E*) et (*Z*). Les derniers composés subissent une conversion photochimiques pendant l'irradiation. La diméthyl-6,6 spiro[2.4] heptanone-4, par photolyse dans le méthanol, subit une clivage α en donnant comme produit principal la méthoxy-4 diméthyl-7,7 oxa-5 sprio[2.5] octane, tandis que dans les mêmes conditions la diméthyl-6,6 spiro[2.5] octanone-4 est reduit à l'alcool correspondant et la triméthyl-6,6,8 spiro[2.5] octanone-4 subit un clivage β donnant comme produit principal la éthyl-2 triméthyl-3,5,5 cyclohexanone-1. On interprète cette trichotomie en fonction de la dimension du cycle et de facteurs stériques.

[Traduit par le journal]

Cycloalkanones have been found to give a wide variety of products upon ultraviolet irradiation in solution. But the primary chemical processes leading to these products are relatively few. The most important of these reactions are α-cleavage (Norrish type 1 reaction) (1–3) and intramolecular or intermolecular hydrogen abstraction (1, 3). β-Cleavage has also been observed in the case of certain structural types. Examination of cases where β-cleavage occurs suggests that two of the structural factors that favor such cleavage are (*i*) relief of ring strain and (*ii*) stabilization of a developing biradical or zwitterion or their equivalents (3). Thus, the β-cleavage of α,β-cyclopropyl ketones (e.g. **1** (4)) and α,β-epoxy ketones (e.g., **3** (5)) can be attributed to the former factor, and that of α-sulfonyloxy ketones (e.g., **4** (5)) and cyclooct-4-en-1-one (**5**) (6) to the latter (Scheme 1).[2]

In the case of cyclopropyl ketones it has been shown that alkyl substitution on the cyclopropane ring favors β-cleavage (4, 7),[3] which is also favored if the σ* orbital of the bond undergoing cleavage can overlap efficiently with the π* orbital of the carbonyl group (1). A combination of these factors has been invoked to account for the preference for cleavage of one cyclopropyl bond rather than another (1, 3, 4). However, additional factors must also contribute to the relative yields of α- and β-cleavage products. Thus, in *tert*-butyl alcohol compound

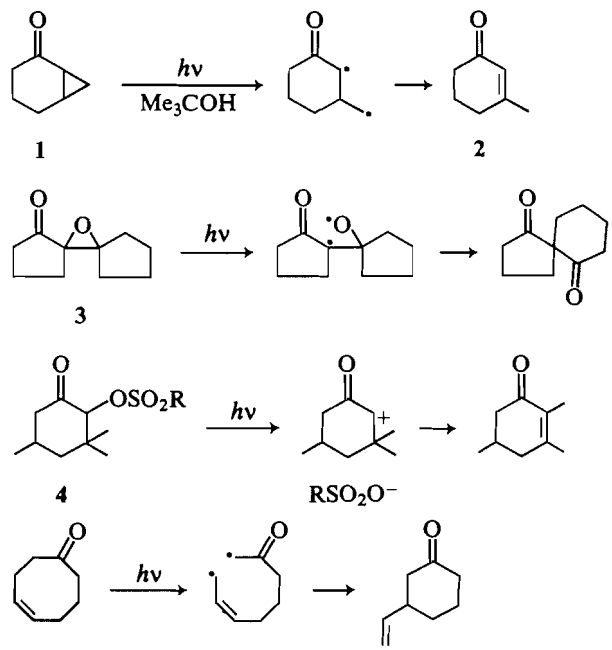

SCHEME 1

[1]Present address: Research Department, Imperial Oil Ltd., Sarnia, Ont.

[2]Although it is probable that these types of reactions often proceed via diradical or zwitterionic intermediates or their equivalents (3), it is not excluded that in some cases they are concerted (3, 6).

[3]Such substitution can also provide another pathway for β-cleavage, i.e., Norrish type 2 reaction (4, 7).

Can. J. Chem. Downloaded from www.nrcresearchpress.com by 210.87.254.6 on 09/06/12
For personal use only.

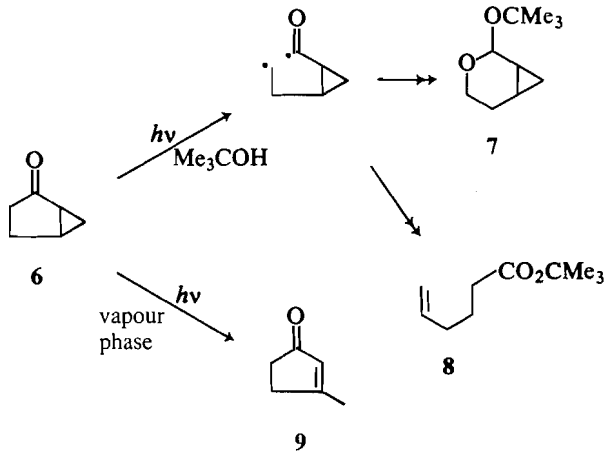

SCHEME 2

6, unlike **1**, gives the α-cleavage products **7** and **8**, although in the vapor phase it gives the β-cleavage product **9** analogous to **2** (8) (Scheme 2). Further the α-spirocyclopropyl ketones **10** and **13** on irradiation in methanol give only α-cleavage products (9, 10) (Scheme 3),[4] although it would appear that the β-cyclopropyl bonds are as favorably disposed for β-cleavage as the cyclopropyl bond in **1** that undergoes β-cleavage in *tert*-butyl alcohol.

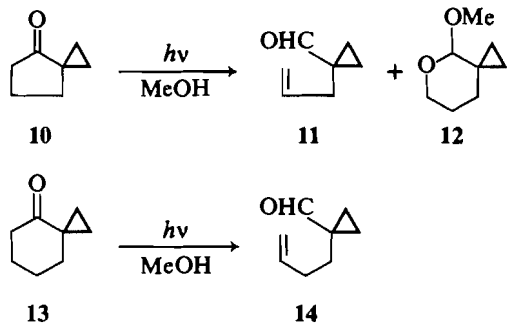

SCHEME 3

We report now on an investigation of the products formed on ultraviolet irradiation of several β,γ-unsaturated α-spirocyclopropyl ketones. It was anticipated that the presence of the ethylenic double bond would provide a second factor favoring β-cleavage (*vide supra*) and that this would be the sole primary chemical process. We also describe studies of the products formed on irradiation of three substituted derivatives of **10** and **13**, which relate to another interesting dichotomy – although both **10** and **13** upon irradiation in methanol undergo exclusive α-cleavage, **10** gives both the enal **11** and the acetal **12** as primary products, while **13** gives exclusively the enal **14**.

Photolysis of spiro[2.5]oct-7-en-4-ones

Irradiation of 6,6,8-trimethylspiro[2.5]oct-7-en-4-one (**15**) (12) in methanol through Pyrex or quartz gave 2-ethenyl-3,5,5-trimethylcyclohex-2-en-1-one (**16**) (Scheme 4). As the reaction proceeded the rate of product formation decreased (cf. ref. 5);[5] this is attributed to competitive uv absorption by the product,

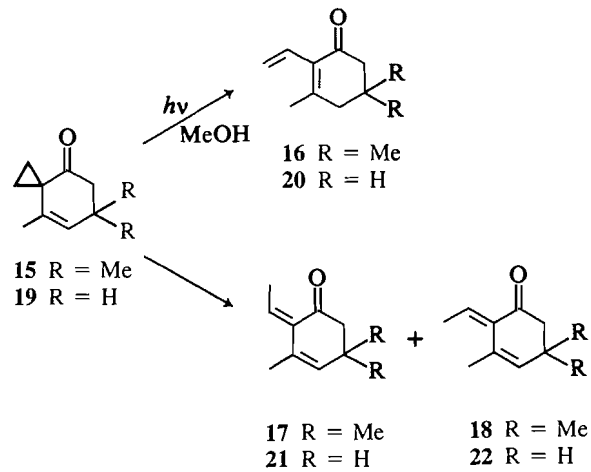

SCHEME 4

which can readily dissipate its excitation energy by *cis–trans* isomerization about the vinyl double bond without net chemical change. Irradiation of **15** in benzene or hexanes through quartz gave a 2:1 mixture of (*Z*)-(**17**) and (*E*)-2-ethylidene-3,5,5-trimethylcyclohex-3-en-1-one (**18**) together with unconsumed **15**; no **16** was observed in the product mixture. Irradiation of **17** in benzene gave a 2:1 mixture of **17** and **18**. Photolysis of **15** through quartz in a 9:1 mixture of benzene and methanol gave **16** (35%), **17** (10%), and **18** (5%) together with unconsumed **15** (47%). Irradiation of **16** in benzene and of a mixture of **17** and **18** in methanol returned starting material only, demonstrating that **16** and the ethylidene compounds do not interconvert photochemically. Photolysis of 8-methylspiro[2.5]oct-7-en-4-one (**19**) (12, 13) gives analogous results, with formation of 2-ethenyl-3-methylcyclohex-2-en-1-one (**20**) in methanol and a mixture of (*Z*)-(**21**) and (*E*)-2-ethylidene-3-methylcyclohex-3-en-1-ones in hydrocarbon solvents.

The structures of the dienones **16**–**18** and **20**–**22**, like those of the other products isolated in the present work, were assigned on the basis of spectroscopic data (see Experimental). In the cases of **16**–**18** the assignments were confirmed by comparison with samples obtained by independent synthesis from 3,5,5-trimethyl-2-(2-(4-morpholinyl)ethyl)-2-cyclohexen-1-one (**23**) (12) by the route shown in Scheme 5. Treatment of **23** with hydrogen peroxide gave amine oxide **24**,

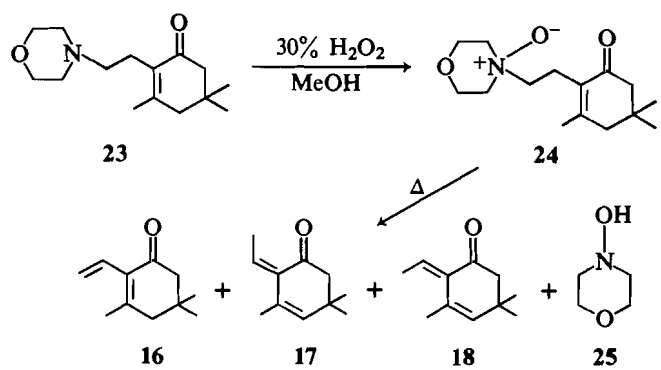

SCHEME 5

[4]Additional products are formed by subsequent reactions of **11** and **14**. In n-hexane **10** gives a trace of the β-cleavage product, 2-ethylcyclopentanone, and **13** gives **14** and the β-cleavage product, 2-ethylcyclohexanone in a ~4:1 ratio (11).

[5]Product formation on irradiation of β,γ-unsaturated α-spirocyclopropyl ketones in methanol through Pyrex generally stopped after ~30% conversion to products. Analogous irradiation through quartz stopped after ~60% conversion to products.

Can. J. Chem. Downloaded from www.nrcresearchpress.com by 210.87.254.6 on 09/06/12
For personal use only.

Can. J. Chem. Downloaded from www.nrcresearchpress.com by 210.87.254.6 on 09/06/12
For personal use only.

which on being heated at 105°C underwent Cope elimination of *N*-hydroxymorpholine (**25**) to give a 4:1 mixture of **16** and **17** and a small amount of **18** (~2%). The ethylidene compounds **17** and **18** are considered to be formed from **24** via isomerization of **16**, perhaps catalyzed by **25**.

We propose that the effect of solvent on the photochemistry of the spiro compounds **15** and **19** can be interpreted in terms of reaction pathways of the type shown for **15** in Scheme 6. Initial β-cleavage gives the biradical **26**, which is converted to the trienol **27** by a 1,4 hydrogen shift. In methanol the trienol ketonizes intermolecularly by proton transfer to and from the solvent to give **16**, the only observed product in this solvent. If trienol **27** is formed in hydrocarbon solvents proton transfer would proceed intramolecularly to give **17**, which would photoequilibrate to the observed product mixture of **17** and **18**. However, in the latter solvents formation of **27** from the biradical **26** would be less favorable than in methanol and it is considered that **17** and **18** are also formed directly from **26** via 1,2 hydrogen transfer.

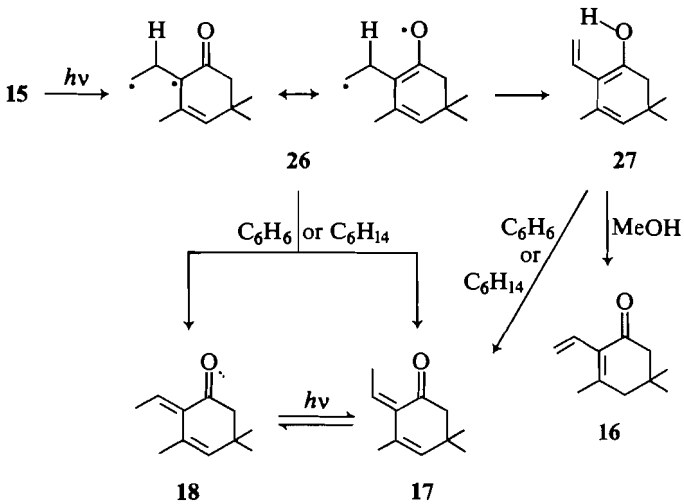

SCHEME 6

The nature of the excited state(s) leading to the reaction products was not investigated, but analogous products have been observed to be formed previously from both the $n \rightarrow \pi^*$ singlet and triplet states of α-cyclopropyl ketones (14). As anticipated (*vide supra*), the presence of the ethylenic double bond exerts a striking effect on the course of the photolyses. Photolysis of the corresponding saturated α-spiro cyclopropyl ketone **13** in methanol gives as the only primary product the enal **14**, formed via α-cleavage (9) (Scheme 3). Although analogous α-cleavage of **15** would give the biradical **28** in which enal formation would be blocked by the geminal methyl groups, in the case of **19** such cleavage would give the biradical **29** in which it would be expected that facile intramolecular hydrogen transfer would occur to give **30**. The fact that both **15** and **19** give only β-cleavage products and no α-cleavage products could be due to facilitation of the former process by a change in the excitation process resulting from the presence of the ethylenic double bond and/or by the stabilization by the latter of the transition state involved in the cleavage of the cyclopropyl ring. That the latter factor plays an important role is suggested by the allylic relationship of the ethylenic double bond to one of the developing radical centers in the transition state for the formation of biradicals of type **26** by β-cleavage.

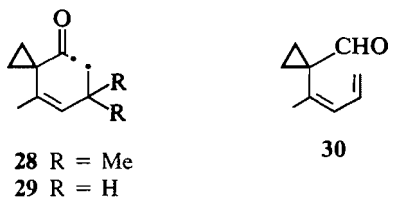

28 R = Me
29 R = H

30

Additional evidence for the involvement of the ethylenic double bond was forthcoming from a study of the photolysis of dispiro compound **31** (12). This gave products **32**–**34** analogous to those obtained from **15** and **19** (Scheme 7). Only

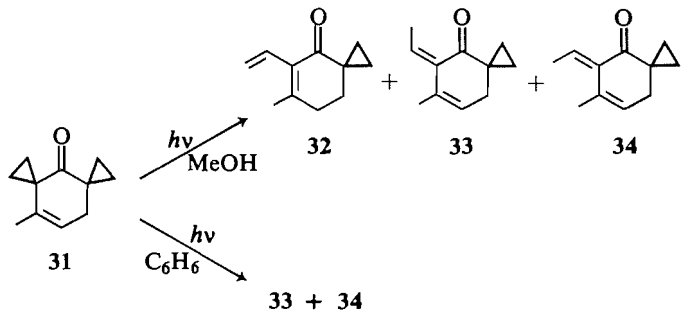

SCHEME 7

products resulting from cleavage of the cyclopropyl ring conjugated with the ethylenic double bond were detected, confirming the importance of the role of the latter in the β-cleavage reactions. An interesting difference in the case of **31** from those of **15** and **19** was the fact that its photolysis in methanol in quartz led to all three types of product **32**–**34**, whereas only a product of type **32** was obtained from **15** and **19** under these conditions. This may reflect an increase in the energy of the transition state leading from the biradical analogous to **26** to the trienol analogous to **27** (cf. Scheme 6) relative to the energy of those leading directly from the former to **33** and **34** because of reduced conjugative interaction between the carbonyl group and the remaining cyclopropyl ring. In benzene only the ethylidene compounds **33** and **34** were formed in analogy with the results for **15** and **19**.

Photolysis of 8-methylenespiro[2.5]octan-4-ones

Our initial work on the photochemistry of the 8-methylenespiro[2.5]octan-4-ones was carried out on mixtures of these compounds with the corresponding 8-methylspiro[2.5]oct-7-en-4-ones; it was later found possible to isolate pure samples of the former and examine them separately (12). Irradiation of a 4:1 mixture of *exo* and *endo* spiro ketones **35** and **15** in methanol gave a 5:3 mixture of **16** and 4,4-dimethylbicyclo[4.3.0]-non-1(6)-en-2-one (**36**) together with unconsumed **35** and **15** (Scheme 8). Compound **36** must be formed from **35** since none of it is formed on irradiation of **15**. Further, the amount of **36** formed was less than that of **35** consumed and the amount of **16** formed was greater than that of **15** consumed, demonstrating that **35** also gives rise to **16** (*vide infra*).

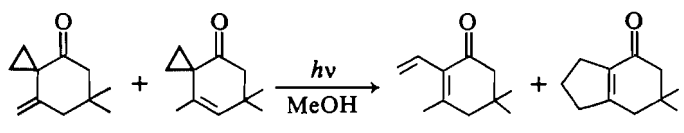

SCHEME 8

Can. J. Chem. Downloaded from www.nrcresearchpress.com by 210.87.254.6 on 09/06/12
For personal use only.

The formation of **36** on irradiation of **35** is analogous to previously reported photochemical vinylcyclopropane–cyclopentene rearrangements of unsaturated cyclopropyl carbonyl compounds (15). It also appears to have a close resemblance to the formation of the dihydrofuran **38** on irradiation of the spiro dione **37** (16) and may be formulated as occurring in analogous fashion (Scheme 9).

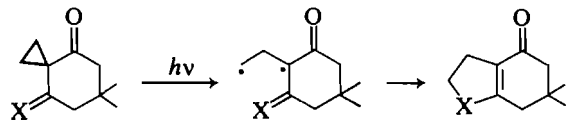

35 X = CH_2 **36** X = CH_2
37 X = O **38** X = O

SCHEME 9

In order to elucidate the mechanism of formation of **16** from **35**, the latter was irradiated in methanol-*O*-*d*. After 4 hours an 11:1 mixture of **16** and **36** together with unconsumed **35** was obtained (confirming that **16** was formed from both **35** and **15** when the mixture of the two was irradiated in methanol). ^{1}H nuclear magnetic resonance and mass spectroscopic analysis showed that the **16** formed in methanol-*O*-*d* was a 9:1 mixture of **16**-3′-*d* (**39**) and unlabelled **16**. Thus in its ^{1}H nmr spectrum the allylic methyl signal (δ 2.00) was broader than the corresponding signal in the spectrum of unlabelled **16** and the ratio of its area to that of the signal of the geminal methyl groups (δ 1.05) was 2.1:6. In its mass spectrum peaks at *m/e* 165, 109,

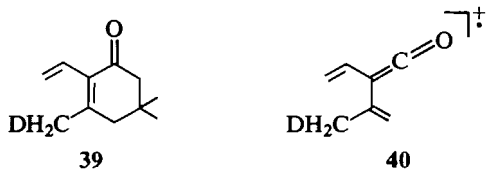

39 **40**

and 81 with relative abundances of 62, 66, and 100, respectively, replaced peaks of unlabelled **16** at *m/e* 164, 108, and 80 with relative abundances of 64, 68 and 100, respectively. The *m/e* 109 peak in the spectrum of **39** can readily be interpreted as arising from **40**, the product of a retro-Diels–Alder fragmentation of the molecular ion. Examination of the ^{1}H nmr and mass spectra of unconsumed **35** after irradiation in methanol-*O*-*d* for 4 hours and of **16** recovered after irradiation in methanol-*O*-*d* under identical conditions showed that only minor amounts (<10%) of deuterium were incorporated.

These results show that there are two mechanisms for the photoconversion of **35** to **16**. One is analogous to that postulated for the formation of **16** from **15** (route *a* in Scheme 10); ketonization of the trienol **42** in methanol-*O*-*d* would lead to the introduction of deuterium as in **39**. The other involves a 1,4-hydrogen shift to carbon rather than oxygen in the biradical **41** (route *b* in Scheme 10) and would account for the formation of unlabelled **16**.

Irradiation of a 1.1:1 mixture of the *exo* and *endo* spiro ketones **43** and **19** in methanol gave products **20** and **44** analogous to those obtained from the mixture of **35** and **15** (Scheme 11), and it could be demonstrated that **20** is formed from both **43** and **19**. Irradiation of **43** in benzene through quartz gave in addition to compounds **20** and **44** the two ethylidene compounds **45** and **46** (Scheme 11); the amounts of **45** and **46**

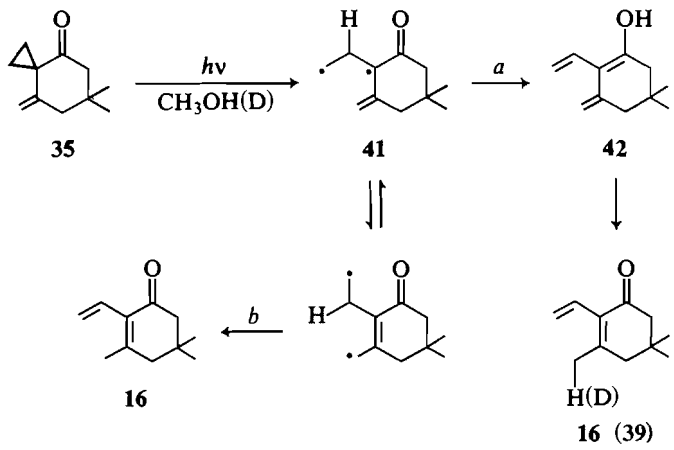

35 **41** **42**
16 **16** (39)

SCHEME 10

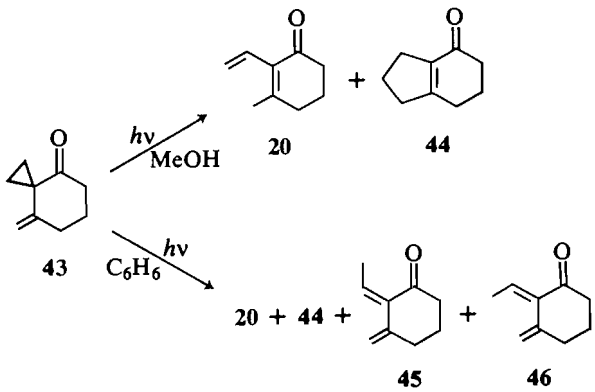

20 **44**
43
45 **46**

SCHEME 11

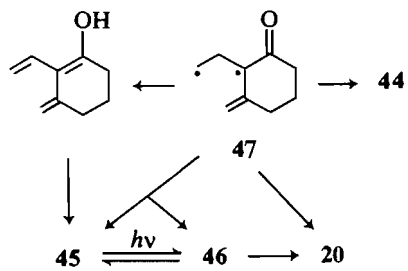

47
45 **46** **20** **44**

SCHEME 12

reached a maximum early in the photolysis and then decreased. These products are considered to be derived from the initially formed biradical **47** as outlined in Scheme 12. The formation of **45** and **46** on irradiation of **43** in benzene is analogous to the formation of ethylidene compounds on similar irradiation of **15** and **19**. The formation of **20** under these conditions finds no analogy in the cases of **15** and **19**; it is attributable to isomerization of **46** and perhaps also to direct hydrogen transfer in the biradical **47**.

A preliminary examination of the photolysis of **35** in benzene clearly indicated that it behaved in analogous fashion to **43** in this solvent. In addition to **16** and **36**, the products formed in methanol, two other products were formed whose amounts reached a maximum early in the photolysis and then decreased. These were not characterized but their gc retention times were similar to those of **45** and **46** and they are considered to be the analogous ethylidene compounds **48** and **49**.

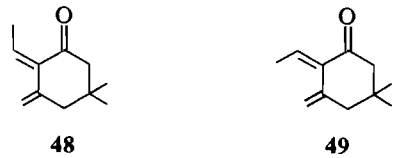

48 **49**

Preparation and photolysis of spiro[2.4]- and spiro[2.5]-alkan-4-ones

6,6-Dimethylspiro[2.4]heptan-4-one (**52**) and 6,6-dimethylspiro[2.5]octan-4-one (**55**) were prepared by the route shown in Scheme 13. Alkylation of **50** and **53** (17) with iodoethyl acetate (cf. ref. 18) followed by treatment with 48% hydrobromic acid gave **51** and **54**, respectively, which with ethanolic potassium hydroxide gave **52** and **55**, respectively.[6] 6,6,8-Trimethylspiro[2.5]octan-4-one (**56**) was prepared by hydrogenation of a mixture of **15** and **35** (12).

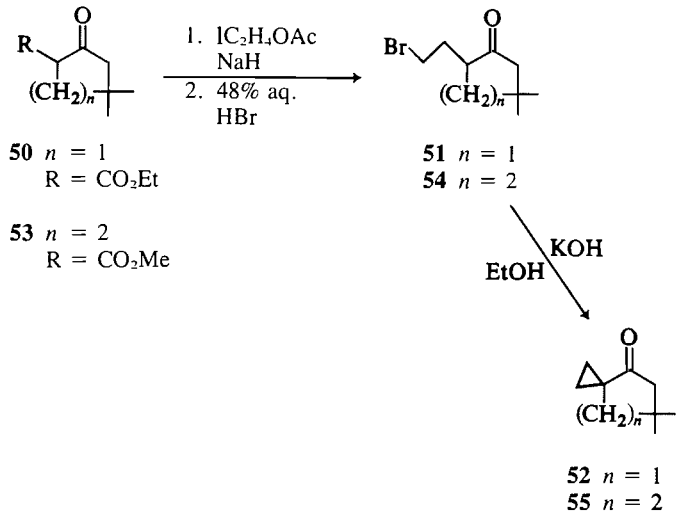

50 $n = 1$, R = CO_2Et

53 $n = 2$, R = CO_2Me

51 $n = 1$
54 $n = 2$

52 $n = 1$
55 $n = 2$

SCHEME 13

Irradiation of **52** in methanol for 8 hours gave a single major product (85%), which was identified as the cyclic acetal **57**, and 5% of unconsumed **52**. Irradiation of **55** in methanol for 13 hours also gave a single major product (72%), which was identified as the reduction product **58**; this was confirmed by its oxidation to **55**. Peaks at 5.76 μm and δ 3.60 (m) in the ir and ^1H nmr spectra, respectively, of the crude photolysate, suggested the presence of a minor amount of a methyl ester; no evidence was obtained for the presence of a cyclic acetal analogous to **57**. The major products from **52** and **55** are considered to arise by the routes shown in Scheme 14 (cf. refs. 2, 9, 10).[7]

Irradiation of **56** in methanol through Pyrex for 21 hours gave two major products and at least eight minor products. One of the former was identified as **59** and one of the minor products as **60** by comparison of their ir and ^1H nmr spectra and gc retention times with those of authentic samples. Compound **60** was prepared by ethylation of isophorone (12, 20) and compound **59** was obtained by hydrogenation of **60** (12, 21). The other major product, which was not obtained free of **59**, is assigned structure **61** and is considered to be formed by further photolysis of **59** (Scheme 15). The formation of such a ketene-derived product from the cyclohexanone **59** is expected, and indeed the gc retention time of the major product formed on photolysis of **59** in methanol was the same as that of the product from **56** and its ir and ^1H nmr corresponded to those features of the spectra of the mixture of the latter product and **59** that are attributable to **61**. Further photolysis of **60** is not a significant source of products in the photolysate from **56** since upon irradiation in methanol through Pyrex for 25 hours **60** gave, in addition to unconsumed starting material, only one product (8%), which had the same gc retention time as a minor component (<1%) of the photolysate from **56**.

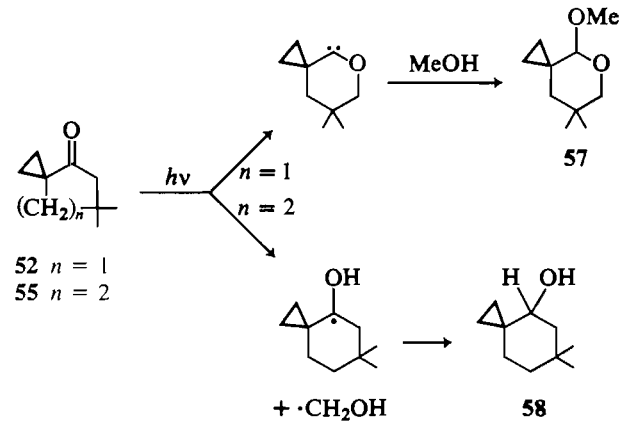

52 $n = 1$
55 $n = 2$

57 **58**

SCHEME 14

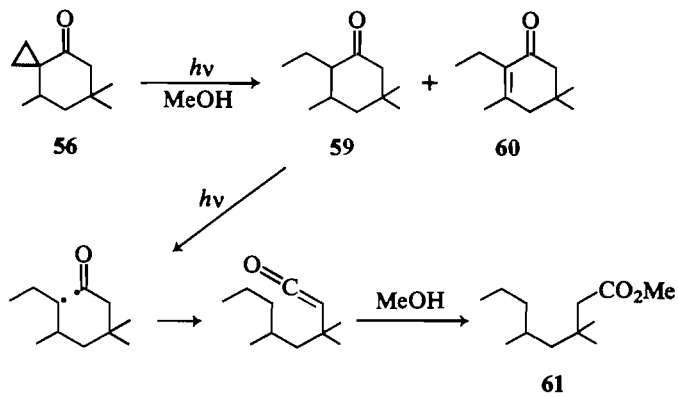

56 **59** **60** **61**

SCHEME 15

The formation of **59** from **56** may occur in two fashions (Scheme 16); by initial β-cleavage to give the biradical **62** followed by two successive intermolecular transfers of hydrogen atoms or by initial intermolecular hydrogen transfer, as proposed in the case of **55**, followed by cyclopropane ring opening and a second such transfer (cf. ref. 22). The biradical **62** also can serve as the source of **60** via several routes, two of which are indicated in Scheme 16: 1,4 intramolecular hydrogen transfer would give **60** directly, while 1,5 transfer would give the biradical **63**, which could give **60** via a 1,2 transfer (cf. ref. 4).

Discussion and summary

All of the photochemical reactions of the β,γ-unsaturated spiro α-cyclopropyl ketones investigated here can be most

[6]Attempted preparation of **52** by a route modeled on an earlier synthesis of spiro[2.4]heptan-4-one (**10**) (19) foundered on the low regioselectivity of the formation of 4,4-dimethyl-1-(trimethylsiloxy)-cyclopentene from 3,3-dimethylcyclopentanone.

[7]A referee has kindly suggested that the fact should be pointed out that reaction of a cyclic ketone to give a ring-expanded acetal via an oxacarbene intermediate (2) has been termed the Yates Rearrangement by others; we are happy to do so.

Can. J. Chem. Downloaded from www.nrcresearchpress.com by 210.87.254.6 on 09/06/12
For personal use only.

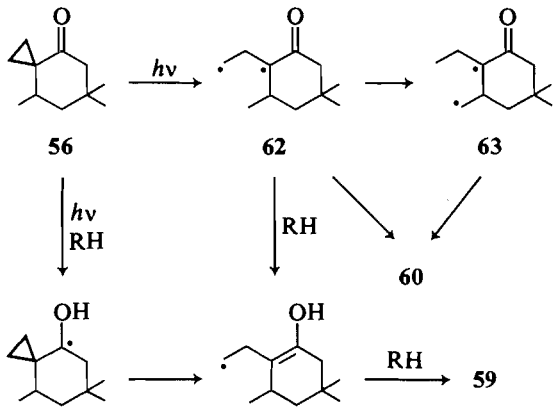

SCHEME 16

readily interpreted in terms of initial β-cleavage to give a biradical intermediate. This exclusive β-cleavage is in accord with expectation based on the view that such cleavage is favored both by release of ring strain and by conjugative stabilization of the developing biradical. Although it is well known that α-cleavage is reversible (1, 2), it seems unlikely that reversible α-cleavage is competing with β-cleavage in the present cases, since compound **19** fails to give the dienal **30** (*vide supra*). The interesting solvent effect on the nature of the products formed from the biradical intermediates can be interpreted consistently in terms of the previously proposed role of methanol in favoring the formation of trienols of type **27** from the biradicals in providing an intermolecular pathway for their subsequent ketonization to 2-ethenylcyclohex-2-en-1-ones. The fact that in the cases of the *exo* compounds **35** and **45** such products are formed in hydrocarbon solvents, in addition to 2-ethylidene compounds of type **46**, while the *endo* compounds **15** and **19** give only 2-ethylidene compounds of type **18** is readily explicable in terms of their formation by further reaction of the 2-ethylidene compounds of type **46** via a 1,5-sigmatropic shift of hydrogen (cf. **64**). Such a shift could occur either thermally in suprafacial fashion or photochemically in antarafacial fashion (23) but would be geometrically impossible in 2-ethylidene compounds of type **18**. As noted previously, 2-ethenylcyclohex-2-en-1-ones could also be formed by hydrogen transfer in biradicals of type **47** (cf. **65**), a process which again is not geometrically feasible in the biradicals formed from the *endo* compounds **15** and **19** (cf. **66**).

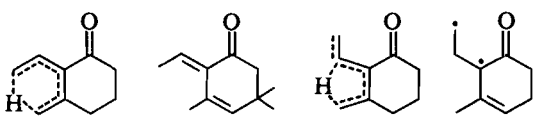

64 **18** **65** **66**

The photochemistry of the three saturated α-cyclopropyl ketones **50**, **53**, and **56** shows a remarkable trichotomy of reactivities. Compound **50** undergoes α-cleavage, **53** is reduced without cleavage, and **56** undergoes β-cleavage. The formation of the oxacarbene-derived acetal **57** as the major product from **50** is in accord both with the earlier observation that the parent spiro[2.4]heptan-4-one (**10**) gives the enal **11** together with the oxacarbene-derived product **12** (9, 10) and with the proposal that oxacarbene formation occurs *faute de mieux* (2), since the geminal substitution in **50** precludes enal formation. The failure of **53** to form an analogous product seems unlikely to be due to inhibition of α-cleavage, but reflects rather that such cleavage is reversible (*vide supra*) and that reclosure of the resulting biradical to a seven-membered cyclic oxacarbene is unfavorable entropically.[8] The fact that **56** undergoes β-cleavage but **53** does not is ascribed to the steric interaction of the 8-methyl group of **56** with the cyclopropyl ring. This interaction will be ameliorated if the cyclopropane ring undergoes cleavage and we consider this to be the driving force for such β-cleavage, a consideration that applies whichever of the two routes proposed for the formation of the major product (Scheme 16) is operative. Finally it may be noted that β-cleavage of the cyclopropane ring in α-spirocyclopropyl ketones has also been observed to be a reversible reaction (7, 24) and thus the occurrence of such reversible cleavage cannot be excluded in the cases of **50** and **53**. The fact that only **56** gives products resulting from β-cleavage could then be ascribed to retardation of reclosure resulting from the steric interaction referred to previously.

Experimental

Melting points were determined on a Fisher–Johns apparatus and are uncorrected. The ir spectra were taken in $CHCl_3$ solution and the ^1H and ^{13}C nmr spectra in $CDCl_3$ solution unless otherwise specified. The uv spectra were taken in 95% ethanol and/or hexane solution as indicated. Gas chromatographic (gc) analyses were carried out on a Varian 2700 gas chromatograph, equipped with a flame ionization detector. The temperatures of the in-column injector and detector were set at 260°C and 335°C, respectively; oven temperatures ranging from 90°C to 120°C were used. The flow rate of the carrier gas (nitrogen) was maintained at 30 mL/min. Unless otherwise indicated, a 6-ft glass column (od 1/8 in., id 2 mm) packed with 3% OV-101 on Chromosorb G(HP), 80/100 was utilized. The only other column used was a 6-ft glass column (od 1/8 in., id 2 mm) packed with 3% OV-17 on Chromosorb W(HP), 80/100. The relative intensities and retention times were determined with a Varian Chromatography Data System 111C; since in some cases there was peak overlap and the relative intensities are uncorrected for variation in the response factors, the relative product yields given are approximate only. Preparative gc separations were carried out on a Varian GC 920 gas chromatograph, equipped with a thermal conductivity detector. The temperatures of the in-column injector and detector were set at 245°C and 260°C, respectively; an oven temperature of 120°C was utilized. The flow rate of the carrier gas (nitrogen) was maintained at 40 mL/min. A 6-ft aluminum column (3/8 in. od) packed with 5% OV-101 on Chromosorb G(HP), 80/100 was utilized. Analytical thin-layer chromatography (tlc) was carried out on 70 × 20 × 0.25-mm silica gel LK6F plates from Whatman Inc. Preparative tlc was carried out on 20 × 20-cm plates coated with a 1-mm or 2-mm layer of silica gel or neutral alumina and activated at 150°C for 30 min prior to use. Column chromatography was performed on silica gel (Grace-Davison, grade 923, 100/200. Organic solutions were dried over anhydrous $MgSO_4$ and concentrated on a rotary evaporator under water aspirator pressure. Photolyses were carried out with a Hanovia 450-W medium-pressure mercury arc lamp type 679 A36 surrounded by a quartz water-cooling jacket. All photolysis solutions were flushed with a stream of dry nitrogen for 30 min immediately prior to irradiation.

Photolysis of 6,6,8-trimethylspiro[2.5]oct-7-en-4-one (15) in methanol. Formation of ethenyl compound 16

Spirooctenone **15** (12) (100 mg, 0.610 mmol) in methanol (10 mL) was irradiated through Pyrex for 23 h. Gas chromatographic analysis after 2, 6, and 23 h showed the formation of only one product to the

[8]Alternatively, as suggested by Professor Keith Yates, closure to the oxacarbene may occur, but because of the unfavorable geometry of a seven-membered cyclic oxacarbene this reaction may be readily reversible.

Can. J. Chem. Downloaded from www.nrcresearchpress.com by 210.87.254.6 on 09/06/12
For personal use only.

Can. J. Chem. Downloaded from www.nrcresearchpress.com by 210.87.254.6 on 09/06/12
For personal use only.

extent of 10, 19, and 32%, respectively, having the same retention times as **16** (*vide infra*). The ^{1}H nmr and ir spectra of the photolysate confirmed the presence of unconsumed **15** and ethenyl compound **16**.

*Photolysis of **15** in benzene. Formation of ethylidene compounds **17** and **18***

Spirooctenone **15** (109 mg, 0.665 mmol) in benzene (11 mL) was irradiated through quartz for 19 h. The gc analysis showed the presence of unconsumed **15** (82%) together with two photoproducts in a 2:1 ratio, having retention times identical to those of **17** and **18** (*vide infra*). The ^{1}H nmr and ir spectra of the photolysate confirmed the presence of unconsumed **15** and *Z*- and *E*-ethylidene compounds **17** and **18**.[9]

*Photolysis of **15** in hexanes. Formation of ethylidene compounds **17** and **18***

Spirooctenone **15** (109 mg, 0.665 mmol) in hexanes (10 mL) was irradiated through quartz for 18 h. The gc analysis showed the presence of **15** (81%) together with ethylidene compounds **17** and **18** in a 2:1 ratio. The ^{1}H nmr and ir spectra of the photolysate confirmed the presence of these compounds.

*Photolysis of **15** in 10% methanol in benzene. Formation of **16**, **17**, and **18***

Spirooctenone **15** (140 mg, 0.854 mmol) in 10% methanol in benzene (14 mL) was irradiated through quartz for 24 h. The gc analysis revealed the presence of unconsumed **15** (47%) together with ethenyl compound **16** (35%), *Z*-ethylidene compound **17** (10%), and *E*-ethylidene compound **18** (5%). The ^{1}H nmr and ir spectra of the photolysate confirmed the presence of these compounds.

*Preparation of 2-ethenyl-3,5,5-trimethylcyclohex-2-en-1-one (**16**) and (Z)-2-ethylidene-3,3,5-trimethylcyclohex-3-en-1-one (**17**) from **23***

A solution of **23** (12) (7.30 g, 29.1 mmol) in methanol (30 mL) was cooled in an ice bath and 30% aqueous hydrogen peroxide (10.0 mL, 158 mmol) was added over 30 min. The solution was allowed to warm to room temperature and was stirred for 68 h after which platinum black (prepared by warming together potassium tetrachloroplatinate, sodium acetate, and formic acid followed by centrifugation to collect the precipitate) was added. When gas evolution was complete the solution was centrifuged and the supernatant solution was removed. The catalyst was washed with methanol, the suspension was centrifuged, and the supernatant solutions were combined and concentrated in a 25-mL round-bottomed flask. The flask, fitted with a vacuum-distillation assembly, was submerged in an oil bath and the pressure was reduced (12 Torr). The oil bath was heated from 25° to 120°C at ~2°C/min and held at 120°C for 20 min during which time a colorless liquid, bp 81°–88°C (12 Torr), distilled. The oil bath was heated at ~1°C/min to 150°C and a liquid, bp 88°–97°C (12 Torr) distilled, after which the still-head temperature dropped. The viscous pot material was transferred to a molecular still and heated at 100°C (0.025 Torr) to recover unconsumed **23** (695 mg, 9.5%). The ^{1}H nmr spectrum of the combined earlier distillates (5.25 g) showed that they contained a mixture of **16**, **17**, and *N*-hydroxymorpholine (**25**). This mixture was dissolved in ether, washed with 0.1 *N* hydrochloric acid and water, dried, and concentrated to give a mixture (~4:1 by gc analysis) of 2-ethenyl-3,5,5-trimethylcyclohex-2-en-1-one (**16**) and (*Z*)-2-ethylidene-3,5,5-trimethylcyclohex-3-en-1-one (**17**) (3.31 g, 69%, 79% based on recovered **23**). This mixture (2.00 g) was chromatographed on silica gel with 20% ether in hexanes; **17** (356 mg) was eluted first, followed by a small amount of its *E* isomer **18** (22 mg). and then **16** (1.59 g). The last was molecularly distilled at 95°C (12 Torr) to give pure **16** (1.45 g); ir λ_{max}: 3.42(w), 6.02, 6.18(w) μm; uv λ_{max} (ε) (95% ethanol): 220 (8890), 259 (8460) nm; ^{1}H nmr δ: 1.05 (s, 6H), 2.00 (s, 3H), 2.27 (s, 4H), 5.2–5.6 (m, 2H), 6.1–6.7 (m, 1H); ^{1}H nmr δ (C_6D_6): 0.75 (s, 6H), 1.60 (br s, 3H), 1.73 (br s, 2H), 2.08 (s, 2H), 5.36 (dd, J = 3, 11 Hz, 1H), 5.78 (dd, J = 3, 18 Hz, 1H), 6.61 (br dd, J = 11, 18 Hz, 1H); ^{13}C nmr δ: 198.6, 154.4, 132.2, 129.9, 119.9, 51.9, 47.6, 32.6, 28.3, 22.2; *m/e*: 164 (64), 80 (100). *Anal.* calcd. for $C_{11}H_{16}O$: C 80.44, H 9.82; found: C 80.29, H 9.85.

Molecular distillation of the *Z*-ethylidene compound at 95°C (12 Torr) gave pure **17** (331 mg); ir λ_{max}: 3.49 (m), 5.94, 6.12 (w), 6.26 (m) μm; uv λ_{max} (ε) (hexanes): 221.5 (12 000), 268 (5600), 322 (128) nm; uv λ_{max} (ε) (95% ethanol): 223 (10 000), 279 (3760) nm; ^{1}H nmr δ: 1.08 (s, 6H), 1.82 (d, J = 1.2 Hz, 3H), 2.17 (dd, J = 7.5 Hz, 0.85 Hz, 3H), 2.41 (s, 2H), 5.54 (m, 1H), 6.06 (qd, J = 7.5 Hz, 0.85 Hz, 1H); ^{13}C nmr δ: 202.2 (s), 135.9 (d), 134.8 (s), 132.4 (d), 131.1 (s), 55.2 (t), 35.6 (s), 29.6 (q), 19.5 (q), 15.8 (q); *m/e*: 164 (44), 149 (100). *Anal.* calcd. for $C_{11}H_{16}O$: C 80.44, H 9.82; found: C 80.22, H 9.79.

*Photolysis of **17**. Preparation of (E)-2-ethylidene-3,5,5-trimethylcyclohex-3-en-1-one (**18**)*

Z-Ethylidene compound **17** (300 mg, 1.83 mmol) was dissolved in benzene (30 mL) and irradiated through Pyrex for 1 h. Gas chromatographic analysis after 30 min and after 1 h showed the product to be a 2:1 mixture of **17** and **18**. Evaporation of the solvent followed by preparative tlc (20% ether in hexanes) gave **17** (183 mg) and its *E* isomer **18** which was molecularly distilled at 95°C (12 Torr) to give pure (*E*)-2-ethylidene-3,5,5-trimethylcyclohex-3-en-1-one (**18**; 89 mg, 30%, 76% based on recovered **17**); ir λ_{max}: 3.41 (m), 5.92, 6.12 (m), 6.26 (m) μm; uv λ_{max} (ε) (hexanes): 224 (8640), 269 (5750), 318 (sh, 162), 330 (148), 344 (109), 354 (52) nm; uv λ_{max} (ε) (95% ethanol): 224 (8000), 277 (3790) nm; ^{1}H nmr δ: 1.08 (s, 6H), 2.03 (d, J = 7.5 Hz, 3H), 2.10 (d, J = 2 Hz, 3H), 2.36 (s, 2H), 5.62 (m, 1H), 6.75 (qd, J = 7.5 Hz, 1.9 Hz, 1H); ^{13}C nmr δ: 201.1, 139.2, 134.4, 132.6, 130.8, 52.2, 33.8, 29.3, 23.0, 15.5; *m/e*: 164 (40), 149 (100). *Anal.* calcd. for $C_{11}H_{16}O$: C 80.44, H 9.82; found: C 80.21, H 9.83.

*Irradiation of **16** in benzene*

Compound **16** (75 mg, 0.457 mmol) was dissolved in benzene (7.5 mL) and irradiated through Pyrex for 17 h. Evaporation of the solvent returned unconsumed **16** (by gc and ^{1}H nmr spectroscopic analysis). None of the ethylidene compounds **17** and **18** were present.

*Irradiation of **17** and **18** in methanol*

A 2:1 mixture of **17** and **18** (30.0 mg, 0.18 mmol) was dissolved in methanol (3.0 mL) and irradiated through Pyrex for 2.5 h. The gc analysis of the photolysate showed that it was a 1.9:1 mixture of **17** and **18** containing none of ethenyl compound **16**.

*Photolysis of 8-methylspiro[2.5]oct-7-en-4-one (**19**) in methanol. Formation of ethenyl compound **20***

Spirooctenone **19** (12) (37.3 mg, 0.274 mmol) was dissolved in methanol (3.7 mL) and irradiated through Pyrex for 6.5 h. Gas chromatographic analysis after 3.5, 5.5, and 6.5 h showed the formation of only one product to the extent of 18, 20, and 24%, respectively, having the same retention time as **20** (*vide infra*). This solution was then irradiated through quartz for 5.5 h. Gas chromatographic analysis after 2, 3.5, and 5.5 h showed that **20** was present to the extent of 44, 51, and 63%, respectively, together with unconsumed **19**. The ^{1}H nmr spectrum of the photolysate confirmed the presence of unconsumed **19** and ethenyl compound **20**.

*Photolysis of **19** in benzene. Preparation of (Z)- and (E)-2-ethylidene-3-methylcyclohex-3-en-1-one (**21** and **22**)*

Spirooctenone **19** (1.28 g, 9.41 mmol) was dissolved in benzene (125 mL) and irradiated through quartz for 6 h. The gc analysis of the crude photolysate showed the presence of unconsumed **19** (82%) together with two photoproducts (12% and 6%) having retention times different from that of **20**. The oil obtained on evaporation of the solvent was chromatographed on silica gel (100 g) with 10% ether in hexanes and the eluate was separated into five fractions. The first band eluted was shown by gc analysis to contain the major photoproduct.

[9]Individual structural assignments for **17** and **18** and other such pairs of *Z* and *E* isomers were made on the basis of a detailed analysis of their spectra, which will be discussed elsewhere.

Can. J. Chem. Downloaded from www.nrcresearchpress.com by 210.87.254.6 on 09/06/12
For personal use only.

Preparative tlc (10% ether in hexanes, 3 elutions) of the oil obtained on evaporation of the solvent, followed by molecular distillation at 75°C (12 Torr), gave (*Z*)-2-ethylidene-3-methylcyclohex-3-en-1-one (**21**; 82.2 mg, 6.4%); ir λ_{max}: 3.46 (m), 5.93, 6.09 (w), 6.27 (m) μm; uv λ_{max} (ε) (hexanes): 223 (9060), 269 (4460), 324 (sh, 90) nm; ^{1}H nmr δ: 1.82 (d, J = 2 Hz, 3H), 2.10 (d, J = 8 Hz, 3H), 2.3−2.6 (m, 4H), 5.65 (m, 1H), 5.98 (q, J = 8 Hz, 1H); ^{13}C nmr δ: 201.7, 135.3, 134.0, 131.8, 124.3, 40.4, 24.8, 19.5, 15.8; *m/e*: 136 (100), 121 (32). *Mol. Wt.* calcd. for $C_9H_{12}O$: 136.0888; found (ms): 136.0882.

The second and fourth fractions contained mixtures of **19** and **21** and of **19** and the minor photoproduct, respectively, whereas the third fraction contained only unconsumed **19**. Gas chromatographic analysis of the oil obtained on evaporation of the fifth fraction (33.0 mg) showed that it was primarily (85%) the minor photoproduct together with unconsumed **19** (15%). Preparative tlc (10% ether in hexanes, 3 elutions) of this fraction followed by molecular distillation at 80°C (12 Torr) gave (*E*)-2-ethylidene-3-methylcyclohex-3-en-1-one (**22**; 26.4 mg, 2.1%); ir λ_{max}: 3.42 (w), 5.92, 6.11 (w), 6.27 (m) μm; uv λ_{max} (ε) (hexanes): 224 (6900), 270 (4300), 316 (sh, 220), 330 (sh, 140), 342 (sh, 115) nm; ^{1}H nmr δ: 2.07 (d, J = 8 Hz) and 2.15 (m) (6H), 2.3−2.6 (m, 4H), 5.84 (m, 1H), 6.77 (qd, J = 8 Hz, 1.5 Hz, 1H); ^{13}C nmr δ: 201.6, 135.6, 133.7, 132.4, 127.8, 37.1, 22.9, 22.8, 15.4; *m/e*: 136 (100), 121 (51). *Mol. Wt.* calcd. for $C_9H_{12}O$: 136.0888; found (ms): 136.0861.

*Photolysis of **21** in benzene. Formation of **22***

Z-Ethylidene compound **21** (28.2 mg, 0.207 mmol) was dissolved in benzene (2.8 mL) and irradiated through quartz for 45 min. The gc analysis of the photolysate showed that it was a mixture of **21** (65%) and its *E* isomer **22** (35%). The ^{1}H nmr spectrum of the photolysate confirmed the presence of **21** and **22**.

*Photolysis of 8-methyldispiro[2.1.2.3]dec-8-en-4-one (**31**) in methanol. Preparation of 5-ethenyl-6-methylspiro[2.5]oct-5-en-4-one (**32**) and formation of **33** and **34***

Dispirodecenone **31** (12) (800 mg, 4.94 mmol) was dissolved in methanol (80 mL) and irradiated through quartz for 8 h. The gc analysis of the photolysate showed that it was a mixture of unconsumed **31** (44%) together with one major (45%) and two minor (6% and 4%) photoproducts. The gc retention times of the minor photoproducts were identical to those of ethylidene compounds **33** and **34**, obtained by irradiation of **31** in benzene (*vide infra*). The ^{1}H nmr spectrum of the photolysate confirmed the presence of the ethylidene compounds. Column chromatography of the photolysate on silica gel (100 g) with 3% ether in hexanes gave two fractions. The first band eluted was shown by gc analysis to contain unconsumed **31** together with **33** and **34**. Preparative tlc of the oil obtained on evaporation of the solvent from the second fraction, followed by molecular distillation at 90°C (12 Torr), gave 5-ethenyl-6-methylspiro[2.5]oct-5-en-4-one (**32**; 207 mg, 26%): ir λ_{max}: 3.43 (m), 6.04, 6.30 (w) μm; uv λ_{max} (ε) (hexanes): 254 (5630), 314 (sh, 76) nm; ^{1}H nmr δ: 0.55−0.98 (m, 2H), 0.98−1.43 (m, 2H), 1.78 (br t, J = 6.5 Hz, 2H), 2.10 (s, 3H), 2.2−2.6 (m, 2H), 5.2−5.6 (m, 2H), 6.2−6.8 (m, 1H); ^{1}H nmr δ (C_6D_6): 0.2−0.7 (m, 2H), 0.9−1.5 (m, 4H), 1.66 (d, J = 4 Hz, 3H), 1.8−2.2 (m, 2H), 5.2−5.9 (m, 2H), 6.4−7.0 (m, 1H); ^{13}C nmr δ: 197.1, 156.1, 133.6, 130.5, 119.5, 31.8, 30.2, 25.9, 22.4, 16.1; *m/e*: 162 (100). *Anal.* calcd. for $C_{11}H_{14}O$: C 81.44, H 8.70; found: C 81.18, H 8.75.

*Photolysis of **31** in benzene. Preparation of (Z)- and (E)-5-ethylidene-6-methylspiro[2.5]oct-6-en-4-one (**33** and **34**)*

Dispirodecenone **31** (275 mg, 1.70 mmol) was dissolved in benzene (28 mL) and irradiated through quartz for 8 h. The gc analysis of the photolysate showed that it was a mixture of unconsumed **31** (82%) and ethylidene compounds **33** (11%) and **34** (7%). None of the ethenyl compound **32** formed on irradiation of **31** in methanol was present. The oil obtained on evaporation of the solvent was subjected to preparative tlc (5% ether in hexanes, 3 elutions). Molecular distillation of the oil from the first band at 90°C (12 Torr) gave (*Z*)-5-ethylidene-6-methylspiro[2.5]oct-6-en-4-one (**33**; 24.2 mg, 9%); ir λ_{max}: 3.46 (m), 5.98, 6.08 (sh), 6.29 (m) μm; uv λ_{max} (ε) (hexanes): 222 (10 300), 277 (5500), 323 (sh, 180) nm; ^{1}H nmr δ: 0.48−1.08 (m, 2H), 1.08−1.47 (m, 2H), 1.88 (m, 3H), 2.17 (d, J = 8 Hz, 3H), 2.33 (m, 2H), 5.55 (m, 1H), 6.12 (q, J = 8 Hz, 1H); ^{13}C nmr δ: 201.4, 134.7, 134.3, 133.7, 123.6, 33.6, 27.1, 20.2, 19.4, 16.5; *m/e*: 162 (45), 147 (49), 134 (100). *Mol. Wt.* calcd. for $C_{11}H_{14}O$: 162.1045; found (ms): 162.1045.

The second band contained unconsumed **31**. The oil obtained from the third band was molecularly distilled at 90°C (12 Torr) to give (*E*)-5-ethylidene-6-methylspiro[2.5]-oct-6-en-4-one (**34**; 14.6 mg, 5%); ir λ_{max}: 3.44 (m), 5.96, 6.12 (w), 6.27 (m) μm; uv λ_{max} (ε) (hexanes): 220 (3020), 262 (1880), 318 (sh, 111) nm; ^{1}H nmr δ: 0.57−1.02 (m, 2H), 1.02−1.47 (m, 2H), 2.01 (d, J = 8 Hz) and 2.12 (m) (8H), 5.87 (m, 1H) and 6.67 (qd, J = 8 Hz, 1 Hz, 1H); ^{13}C nmr δ: 201.0, 136.8, 133.0, 132.1, 126.6, 32.6, 25.1, 22.6, 20.0, 15.7; *m/e*: 162 (40), 147 (100), 134 (23). *Mol. Wt.* calcd. for $C_{11}H_{14}O$: 162.1045; found (ms): 162.1042.

*Photolysis of **33** in benzene. Formation of **34***

Z-Ethylidene compound **33** (30.1 mg, 0.186 mmol) was dissolved in benzene (3.0 mL) and irradiated through quartz for 30 min. The gc analysis of the photolysate showed that it was a mixture of **33** (62%) and its *E* isomer **34** (38%). The ^{1}H nmr spectrum of the photolysate confirmed the presence of **33** and **34**.

*Photolysis of a mixture of 6,6-dimethyl-8-methylenespiro[2.5]octan-4-one (**35**) and **15** in methanol. Preparation of 4,4-dimethylbicyclo[4.3.0]non-1(6)-en-2-one (**36**) and formation of **16***

A 4:1 mixture of spiro ketones **35** and **15** (12) (5.00 g, 30.5 mmol) in methanol (500 mL) was irradiated through quartz for 23 h. The gc analysis of the photolysate showed that it contained **35** (48%), **15** (14%), **16** (24%), and **36** (14%). The photolysate was chromatographed on silica gel (500 g) with 20% ether in hexanes. Spiro ketones **35** and **15** (2.28 g, 46%) were eluted together, folowed by ethenyl compound **16** (928 mg, 19%). The third band (549 mg, 11%) contained **36**, which was shown by gc analysis to be 86% pure. This material (225 mg) was purified by preparative tlc on alumina with 30% ether in hexanes and molecularly distilled at 110°C (12 Torr) to give 4,4-dimethylbicyclo[4.3.0]non-1(6)-en-2-one (**36**; 178 mg); ir λ_{max}: 3.42 (w), 6.05, 6.10 (sh) μm; uv λ_{max} (ε) (95% ethanol): 250 (5750) nm; ^{1}H nmr δ: 1.08 (s, 6H), 1.7−2.2 (m, 2H), 2.23 (s, 4H), 2.3−2.8 (m, 4H); ^{13}C nmr δ: 197.4, 163.4, 136.4, 51.8, 41.0, 37.8, 35.1, 28.8, 28.6, 21.8; *m/e*: 164 (29), 108 (100); *Mol. Wt.* calcd. for $C_{11}H_{16}O$: 164.1201; found (ms): 164.1201.

*Photolysis of **35** in methanol-O-d. Incorporation of deuterium into **16***

Spirooctanone **35** (12) (76.6 mg, 0.467 mmol) in methanol-*O-d* (7.0 mL) was irradiated through quartz. Gas chromatographic analysis at hourly intervals showed the formation of **16** and **36**. After 4 h the solution contained 60% **35**, 21% **16**, and 19% **36**. Evaporation of the solvent followed by preparative tlc on silica gel with 20% ether in hexanes separated the mixture into three components. The first compound eluted was unconsumed **35** (33.6 mg, 44%), which was analyzed for deuterium content by ^{1}H nmr and mass spectroscopy. The ^{1}H nmr spectrum showed no evidence for significant deuterium incorporation. The parent ion peak in the mass spectrum occurred at *m/e* 164; M + 1/M was 19% (observed for unirradiated **35** M + 1/M: 14%; calcd.: 12%). The oil isolated from the middle band was molecularly distilled at 95°C (12 Torr) to give a colorless liquid (13.9 mg, 18%) having ^{1}H nmr spectra in $CDCl_3$ and C_6D_6 corresponding to those of unlabelled **16**, with the following exceptions: the peak at δ 2.00 (in $CDCl_3$) was broader and its area corresponded to 2.1 rather than 3.0 proton relative to the six-proton peak at δ 1.05; the peak at δ 1.60 (in C_6D_6) was broader and its area corresponded to 2.1 rather than 3.0 protons relative to the six-proton peak at δ 0.75. Its mass spectrum had peaks at *m/e* 166 (20), 165 (62), 164 (13), 109 (66), and 81 (100).

*Irradiation of **16** in methanol-O-d*

Ethenyl compound **16** (30.0 mg, 0.183 mmol) in methanol-*O-d* (3.0 mL) was irradiated through quartz for 4 h. Evaporation of the solvent and examination of the residue by ^{1}H nmr spectroscopy (C_6D_6)

Can. J. Chem. Downloaded from www.nrcresearchpress.com by 210.87.254.6 on 09/06/12
For personal use only.

showed that significant amounts of deuterium (>5%) had not been incorporated at any position in the starting material (peak areas were compared to that of the six-proton peak at δ 0.75). The parent ion peak in its mass spectrum occurred at *m/e* 164; M + 1/M was 26% (observed for unirradiated **16** M + 1/M: 19%; calcd.: 12%.

*Photolysis of a mixture of 8-methylenespiro[2.5]octan-4-one (**43**) and **19** in methanol. Preparation of 2-ethenyl-3-methylcyclohex-2-en-1-one (**20**) and bicyclo[4.3.0]non-1(6)-en-2-one (**44**)*

A mixture of spiro ketones **43** (52%) and **19** (48%) (12) (1.37 g, 10.1 mmol) was dissolved in methanol (137 mL) and irradiated through quartz for 8 h. The gc analysis of the photolysate showed that it was a mixture of **20** (21%) and **44** (3%), together with unconsumed **43** (41%) and **19** (35%). Evaporation of the solvent gave an oil (1.14 g) which was chromatographed on silica gel (100 g) with 20% ether in hexanes. The first band eluted (826 mg, 60%) consisted of a mixture of **43** and **19**. The oil obtained from the second band was molecularly distilled at 80°C (12 Torr) to give 2-ethenyl-3-methylcyclohex-2-en-1-one (**20**; 168 mg, 12%); ir λ_{max}: 3.43 (m), 6.04, 6.21 (m) μm; uv λ_{max} (ε) (hexanes): 222 (6120), 252.5 (5950), 325 (51) nm; ^{1}H nmr δ: 1.7−2.2 (m) and 2.07 (s) (5H), 2.2−2.6 (m, 4H), 5.3−5.7 (m, 2H), 6.1−6.8 (m, 1H); ^{1}H nmr δ (C_6D_6): 1.1−2.0 (m) and 1.63 (s) (7H), 2.17 (br t, *J* = 6 Hz, 2H), 5.37 (dd, *J* = 3 Hz, 11 Hz, 1H), 5.69 (dd, *J* = 3 Hz, 18 Hz, 1H), 6.59 (dd, *J* = 11 Hz, 18 Hz, 1H); ^{13}C nmr δ: 197.8 (s), 156.6 (s), 133.2 (s), 130.0 (d), 119.6 (t), 38.1 (t), 33.2 (t), 21.9 (q), 21.7 (t); *m/e*: 136 (100). *Mol. Wt.* calcd. for $C_9H_{12}O$: 136.0888; found (ms): 136.0895.

The mobile phase was changed to 1:1 ether−hexane and a third band was eluted. The oil obtained by evaporation of the solvent was molecularly distilled at 85°C (12 Torr) to give bicyclo[4.3.0]non-1(6)-en-2-one (**44**; 29 mg, 2%; 87% pure by gc): ir λ_{max}: 3.44 (m), 6.04, 6.12 (sh) μm (lit. (25) ir λ_{max} (neat): 6.00 μm); *m/e*: 136 (54), 108 (100). *2,4-Dinitrophenylhydrazone*: mp 248−249°C (lit. (25) 247−247.5°C).

*Irradiation of **43** in benzene*

Spiro ketone **43** (12) (132 mg, 0.971 mmol) in benzene (13 mL) was irradiated through quartz. Gas chromatographic analysis after 3 h showed the presence of unconsumed **43** (8.9 min, 57%), ethenyl compound **20** (15.7 min, 12%), and bicyclic compound **44** (23.3 min, 13%) together with two other photoproducts (**45** and **46**; 11.5 min and 12.7 min, 17%). The ^{1}H nmr spectrum of the oil obtained by evaporation of the solvent had multiplets at δ 4.87 and 5.18, and quartets at δ 6.20 (*J* = 7.5 Hz) and 6.71 (*J* = 7 Hz) in addition to peaks attributable to **43**, **20**, and **44**. The oil was redissolved in benzene (13 mL) and irradiated through quartz for 8 h (total 11 h). The gc analysis showed that, as the reaction proceeded, the proportion of **43**, **45**, and **46** decreased and that of **20** and **44** increased such that after 11 h the mixture contained 30% **43**, 25% **20**, 33% **44**, and 12% **45** and **46**. The ^{1}H nmr spectrum of the photolysate confirmed the presence of **43**, **20**, and **44**.

*Irradiation of **35** in benzene*

Spiro ketone **35** (25.0 mg, 0.152 mmol) in benzene (2.5 mL) was irradiated through Pyrex for 5 h. The gc analysis showed the presence of unconsumed **35** (9.6 min, 72%), ethenyl compound **16** (14.4 min, 6%), and bicyclic compound **36** (21.3 min, 7%) together with two other photoproducts (**48** and **49**, 10.4 min (6%) and 13.5 min (6%)). Thereafter the proportion of **48** and **49** decreased and that of **16** and **36** increased such that after 4 h gc analysis indicated that the solution contained 62% **34**, 2% **48**, 3% **49**, 16% **16**, and 16% **36**. The ^{1}H nmr spectrum of the photolysate confirmed the presence of **35**, **16**, and **36**.

*Preparation of 6,6-dimethylspiro[2.4]heptan-4-one (**52**)*

Ethyl 4,4-dimethyl-2-oxocyclopentanecarboxylate (17) (**50**; 1.40 g, 7.62 mmol) was added to toluene (distilled from calcium hydride, 30 mL) and sodium (224 mg, 9.81 mmol) and the resulting mixture was boiled under reflux. After 1 h, 2-iodoethyl acetate (2.74 g, 12.8 mmol) was added and the mixture was boiled under reflux for 10 h (18). After cooling, 0.2 *N* hydrochloric acid (10 mL) was added, the layers were separated, and the aqueous layer was extracted with toluene (3 × 10 mL). The combined organic solutions were washed with saturated aqueous sodium bicarbonate, dried, and evaporated. Unconsumed starting materials were removed by distillation (60°−110°C (12 Torr)). The residue (1.13 g) was heated with 48% hydrobromic acid (9.5 mL) on a steam bath for 2 h. The solution was neutralized with sodium bicarbonate and extracted with ether (3 × 15 mL). The combined extracts were washed with water, dried, and evaporated to give an oil (**51**, 681 mg); ir λ_{max}: 5.78 μm; ^{1}H nmr δ: 3.50 (m). This was dissolved in 30% ethanolic potassium hydroxide (7.0 mL) and the solution was boiled under reflux for 3 h. After cooling, the solution was neutralized with 0.2 *N* hydrochloric acid and extracted with ether (3 × 15 mL). The combined extracts were washed with saturated aqueous sodium chloride and dried, and the solvent was evaporated giving an oil which was molecularly distilled at 75°C (12 Torr) to give 6,6-dimethylspiro[2.4]heptan-4-one (**52**; 214 mg, 20% based on **50**); ir λ_{max}: 3.40 (m), 5.81 μm; ^{1}H nmr δ: 0.88 (m, 2H), 1.1−1.4 (m) and 1.20 (s) (8H), 1.88 (s, 2H), 2.23 (s, 2H); ^{13}C nmr δ: 219.0 (s), 53.8 (t), 46.2 (t), 35.2 (s), 29.3 (s), 28.6 (q), 17.8 (t); *m/e*: 138 (62), 123 (100). *Mol. Wt.* calcd. for $C_9H_{14}O$: 138.1045; found (ms) 138.1024.

*Preparation of 6,6-dimethylspiro[2.5]octan-4-one (**55**)*

Methyl 4,4-dimethyl-2-oxocyclohexanecarboxylate (17) (**53**: 13.1 g, 71.2 mmol) was added to toluene distilled from calcium hydride (250 mL) and sodium (1.80 g, 78.3 mmol) and the resulting mixture was boiled under reflux. After 1 h, 2-iodoethyl acetate (27.2 g, 127 mmol) was added and the mixture was boiled under reflux for 10 h (18). After cooling, 0.2 *N* hydrochloric acid (50 mL) was added, the layers were separated, and the aqueous layer was extracted with toluene (3 × 40 mL). The combined organic solutions were washed with saturated aqueous sodium bicarbonate, dried, and evaporated. Unconsumed starting materials were recovered by distillation (bp 60°−110°C (12 Torr)). The residue (6.10 g) was heated with 48% hydrobromic acid (35 mL) on a steam bath for 3 h. The acidic solution was neutralized with sodium bicarbonate and extracted with ether (4 × 30 mL). The combined extracts were washed with water, dried, and evaporated to give an oil (**54**; 5.12 g); ir λ_{max}: 5.87 μm; ^{1}H nmr δ: 3.48 (t). This oil was dissolved in 30% ethanolic potassium hydroxide (70 mL), and the solution was boiled under reflux for 3 h. After cooling, the solution was neutralized with 0.2 *N* hydrochloric acid and extracted with ether (4 × 50 mL). The combined extracts were washed with saturated aqueous sodium chloride and dried, and the solvent was evaporated to give an oil (2.26 g). Column chromatography of this material on silica gel with 2:1 hexanes and ether followed by molecular distillation at 80°C (12 Torr) gave 6,6-dimethylspiro[2.5]octan-4-one (**55**; 1.60 g, 15% based on **53**); ir λ_{max}: 3.45 (m), 5.93 μm; uv λ_{max} (ε) (hexanes): 285 (36) nm; ^{1}H nmr δ: 0.61 (m, 2H), 1.05 (s) and 1.15 (m) (8H), 1.6−1.8 (m, 4H), 2.20 (s, 2H); ^{13}C nmr δ: 211.3 (s), 53.6 (t), 37.0 (t), 33.6 (s), 30.6 (t), 28.9 (q), 27.5 (s), 17.2 (t); *m/e*: 152 (34), 96 (100). *Anal.* calcd. for $C_{10}H_{16}O$: C 78.90, H 10.59; found: C 78.78, H 10.58.

*Photolysis of 6,6-dimethylspiro[2.4]heptan-4-one (**52**). Formation of 4-methoxy-7,7-dimethyl-5-oxaspiro[2.5]octane (**57**)*

Spiroheptanone **52** (167 mg, 1.21 mmol) was dissolved in methanol (17 mL) and irradiated through Pyrex. Gas chromatographic analysis after 8 h showed the presence of unconsumed **52** (5%), a major photoproduct (85%), and a minor photoproduct (10%). Evaporation of the solvent gave an oil that was shown by ^{1}H nmr and ir spectroscopy to be primarily **57**. Preparative gc of a portion of this oil gave 4-methoxy-7,7-dimethyl-5-oxaspiro[2.5]octane (**57**); ir λ_{max}: 3.43 (m), 9.14, 9.73 μm; ^{1}H nmr δ: 0.1−0.7 (m, 4H), 0.89 (s) and 1.13 (s) and 0.7−1.3 (m) (8H), 3.14 (dd, *J* = 11 Hz, 2 Hz, 1H), 3.40 (s, 3H), 3.59 (br d, *J* = 11 Hz, 1H), 3.67 (m, 1H), 3.80 (s, 1H); *m/e*: 170 (1), 155 (7), 142 (76), 139 (15), 83 (100). *Mol. Wt.* calcd. for $C_{10}H_{18}O_2$: 170.1307; found (ms): 170.1289.

*Photolysis of 6,6-dimethylspiro[2.5]octan-4-one (**55**). Formation of 6,6-dimethylspiro[2.5]octan-4-ol (**58**)*

Spirooctanone **55** (350 mg, 2.30 mmol) in methanol (35 mL) was irradiated through Pyrex for 8 h. Gas chromatographic analysis showed the presence of unconsumed **55** (retention time 7.0 min), a major photoproduct **58** (retention time 7.2 min) (**55** + **58** = 88%),

Can. J. Chem. Downloaded from www.nrcresearchpress.com by 210.87.254.6 on 09/06/12
For personal use only.

and a minor photoproduct (6%). Several other products, each less than 3%, were also present. This oil (280 mg) was redissolved in methanol and irradiated through Pyrex for 5 h. The gc analysis and ir and ^{1}H nmr spectroscopy of the photolysate showed that <5% of **55** remained. The gc analysis showed the presence of the major photoproduct **58** (72%), a minor photoproduct (11%), and nine other minor photoproducts (1−4% each). A portion of this product was chromatographed on a 1-mm silica gel plate (20% ether in hexanes). A low R_f band was isolated and was shown by gc analysis to contain 87% of **58**; ir λ_{max}: 2.87 μm; ^{1}H nmr δ: 0.1−0.7 (m, 4H), 0.7−1.6 (m) and 0.97 (s) and 1.03 (s) (12 H), 2.37 (br s, 1H; absent after treatment with D_2O), 3.1−3.7 (m, 1H); *m/e*: 154 (11), 136 (55), 121 (100). *Mol. Wt.* calcd. for $C_{10}H_{18}O$: 154.1358; found (ms): 154.1352.

Oxidation of 58. Formation of 55

The remainder of the oil from the photolysis of **55** (*vide supra*) (150 mg) was dissolved in methylene chloride (1.0 mL) and the solution was added to a suspension of pyridinium chlorochromate (221 mg, 102 mmol) in methylene chloride (3.0 mL). The resulting mixture was stirred at room temperature under nitrogen for 2 h, after which ether (5.0 mL) was added and the supernatant solution was decanted from the black gum. The gum was washed with ether (3 × 3.0 mL) and the combined washings and supernatant solution were passed through a pad of Florisil. Evaporation of the solvent gave an oil (117 mg) that was shown by gc analysis and by ^{1}H nmr and ir spectroscopy to be **55**.

Photolysis of 6,6,8-trimethylspiro[2.5]octan-4-one (56). Formation of 2-ethyl-3,5,5-trimethylcyclohexan-1-one (59), 2-ethylisophorone (60), and methyl 3,3,5-trimethyloctanoate (61)

Spirooctanone **56** (12) (208 mg, 1.86 mmol) was dissolved in methanol (31 mL) and irradiated through Pyrex. The gc analysis after 13 h showed the presence of unconsumed **56** (retention time 11.2 min, 54%), two major products (retention times 8.6 min (**59**; 19%) and 14.7 min (**61**; 14%)), and six minor products (1−4% each). Irradiation for a further 8 h (total 21 h) gave a mixture that contained **56** (48%), **59** (18%), **61** (17%), and seven minor products (1−5% each). The gc analysis on OV-17 on which the peaks of **56** and **60** do not overlap showed the presence of a minor component (8%), the retention time of which was identical to that of 2-ethylisophorone (**60**) (12, 20). The retention times of the major products were identical to those of 2-ethyl-3,5,5-trimethylcyclohexan-1-one (**59**) (12, 21) and of methyl-3,3,5-trimethyloctanoate (**61**), the major product formed on irradiation of **59** in methanol (*vide infra*). The photolysate from the irradiation of **56** was chromatographed on a 2-mm silica gel plate (20% ether in hexanes) to give an oil (R_f 0.62) that was shown by gc analysis to contain primarily the two major photoproducts. Comparison of the ir and ^{1}H nmr spectra of this oil with those of **59** and of the major product formed on irradiation of **59** confirmed the presence of **59** and **61**. A second band (R_f 0.48) was isolated and was shown by gc analysis and by ir and ^{1}H nmr spectroscopy to be unconsumed **56**. A third band (R_f 0.38) was shown by gc analysis and by ir and ^{1}H nmr spectroscopy to be primarily 2-ethylisophorone (**60**).

Irradiation of 59. Formation of 61

Ketone **59** (12, 21) (28.8 mg, 0.171 mmol; ir λ_{max}: 5.88 μm) was dissolved in methanol (3.0 mL) and irradiated through Pyrex. The gc analysis after 3 h showed the presence of a minor amount of unconsumed **59** (retention time 8.6 min) together with one major product (retention time 14.7 min). Evaporation of the solvent gave an oil having the following spectroscopic features corresponding to those assigned to **61** in the spectra of the mixture of **61** and **59** obtained from the photolysis of **56**: ir λ_{max}: 5.77 μm; ^{1}H nmr δ: 0.7−1.5 (m), 1.02 (s), 2.18 (s), 3.62 (s). The gc retention times of all of the minor products corresponded to those of minor products formed on photolysis of **56**.

Acknowledgements

We thank the Natural Sciences and Engineering Research Council of Canada for support of this work and Messrs. Baldev Gambhir, Nick Plavac, and Leo Dugbe for technical assistance.

1. N. J. TURRO. Modern molecular photochemistry. The Benjamin/Cummings Publishing Co., Inc., Menlo Park, CA. 1978. Chapts. 10 and 13.
2. P. YATES and R. O. LOUTFY. Acc. Chem. Res. **8**, 209 (1975); P. YATES. J. Photochem. **5**, 91 (1976).
3. H. E. ZIMMERMAN. Adv. Photochem. **1**, 183 (1963); H. E. ZIMMERMAN, S. S. HIXSON, and E. F. MCBRIDE. J. Am. Chem. Soc. **92**, 2000 (1970); H. E. ZIMMERMAN and C. M. MOORE. J. Am. Chem. Soc. **92**, 2023 (1970); H. E. ZIMMERMAN and T. W. FLECHTNER. J. Am. Chem. Soc. **92**, 6931 (1970).
4. W. G. DAUBEN, L. SCHUTTE, G. W. SHAFFER, and R. B. GAGOSIAN. J. Am. Chem. Soc. **95**, 468 (1973); W. G. DAUBEN, G. W. SHAFFER, and E. J. DEVINY. J. Am. Chem. Soc. **92**, 6273 (1970); W. G. DAUBEN, L. SCHUTTE, and R. E. WOLF. J. Org. Chem. **34**, 1849 (1969).
5. H. J. WÜTCHRICH, A. SIEWINSKI, K. SCHAFFNER, and O. JEGER. Helv. Chim. Acta, **56**, 239 (1973); S. IWASAKI and K. SCHAFFNER. Helv. Chim. Acta, **51**, 557 (1968); K. SCHAFFNER and O. JEGER. Tetrahedron, **30**, 1891 (1974).
6. J. K. CRANDALL, C. F. MAYER, J. P. ARRINGTON, and R. J. WATKINS. J. Org. Chem. **39**, 248 (1974).
7. E. LEE-RUFF and P. G. KHAZANIE. Can. J. Chem. **56**, 803 (1978).
8. L. D. HESS and J. N. PITTS, JR. J. Am. Chem. Soc. **89**, 1973 (1967).
9. J. K. CRANDALL and R. J. SEIDEWAND. J. Org. Chem. **35**, 697 (1970).
10. D. R. MORTON, E. LEE-RUFF, R. M. SOUTHAM, and N. J. TURRO. J. Am. Chem. Soc. **92**, 4349 (1970).
11. A. SONODA, I. MORITANI, J. MIKI, T. TSUJI, and S. NISHIDA. Bull. Chem. Soc. Jpn. **45**, 1777 (1972).
12. P. H. HELFERTY, P. MAHLER, and P. YATES. J. Chem. Soc. Chem. Commun. 1084 (1979); P. YATES, P. H. HELFERTY, and P. MAHLER. Can. J. Chem. **61**, 78 (1983).
13. M. S. NEWMAN, V. DEVRIES, and R. DARLAK. J. Org. Chem. **31**, 2171 (1966).
14. D. G. MARSH and J. N. PITTS, JR. J. Am. Chem. Soc. **93**, 326 (1971).
15. M. J. JORGENSEN. J. Am. Chem. Soc. **91**, 6432 (1969); L. A. PAQUETTE, G. V. MEEHAN, R. P. HENZEL, and R. F. EIZEMBER. J. Org. Chem. **38**, 3250 (1973).
16. T. OKADA, K. KAMOGAWA, M. KAWANISI, and H. NOZAKI. Bull. Chem. Soc. Jpn. **43**, 2908 (1970).
17. W. F. BERKOWITZ and S. C. GRENETZ. J. Org.Chem. **41**, 10 (1976); G. SPYCKERELLE, A. C. GREINER, P. ALBRECHT, and G. OURISSON. J. Chem. Res. (M) 3801 (1977).
18. K. KUROSAWA and S. FUJISE. Nippon Kagaku Zasshi, **83**, 327 (1962); Chem. Abstr. **58**, 12504h (1963).
19. I. RYU, S. MURAI, and N. SONODA. Tetrahedron Lett. 4611 (1977).
20. H. TSUKASA and S. SAITO. Nippon Kagaku Kaishi, 1555 (1974); Chem. Abstr. **81**, 1355501g (1974).
21. H. HENECKA. Chem. Ber. **81**, 197 (1948).
22. D. G. MARSH, J. N. PITTS, JR., K. SCHAFFNER, and A. TUINMAN. J. Am. Chem. Soc. **93**, 333 (1971).
23. R. B. WOODWARD and R. HOFFMANN. The conservation of orbital symmetry. Verlag Chemie, Weinheim/Bergstr., Germany. 1970. pp. 123−124.
24. R. O. LOUTFY and P. YATES. J. Am. Chem. Soc. **101**, 4694 (1979).
25. G. L. LANGE and T.-W. HALL. J. Org. Chem. **39**, 3819 (1974).

The effect of silanes on the mercury-photosensitized decomposition of nitric oxide

T. N. BELL, G. SOTO-GARRIDO, AND A. G. SHERWOOD

Department of Chemistry, Simon Fraser University, Burnaby, B.C., Canada V5A 1S6

Received July 13, 1982

This paper is dedicated to Professor Harry E. Gunning on the occasion of his 65th birthday

T. N. BELL, G. SOTO-GARRIDO, and A. G. SHERWOOD. Can. J. Chem. **61**, 946 (1983).

The decomposition of NO, photosensitized by $Hg6^3P$ atoms, leads to N_2 and N_2O. The decomposition rate is enhanced by the silanes Me_2SiF_2 and $MeSiF_3$. A mechanism is proposed involving the formation of complexes of the silanes with electronically-excited NO.

T. N. BELL, G. SOTO-GARRIDO et A. G. SHERWOOD. Can. J. Chem. **61**, 946 (1983).

La décomposition du NO, photosensibilisée par des atomes de $Hg6^3P$, conduit au N_2 et au N_2O. Les silanes du type Me_2SiF_2 et $MeSiF_3$ augmentent la vitesse de décomposition. On propose un mécanisme qui implique la formation de complexes des silanes avec le NO excité électroniquement.

[Traduit par le journal]

Can. J. Chem. Downloaded from www.nrcresearchpress.com by 210.87.254.42 on 09/06/12
For personal use only.

Introduction

The $Hg(6^3P_1)$ photosensitized decomposition of NO has been studied by several workers (1–5) and a mechanism proposed by Strausz and Gunning involves the formation of $^4\pi NO$ molecules (designated NO*) in the quenching reaction of Hg* with NO.

[1] $Hg + h\nu \rightarrow Hg^*$

[2] $Hg^* + NO \rightarrow NO^*$

[3] $NO^* + NO \rightarrow 2NO$

[4] $NO^* + NO \rightarrow N_2O_2^*$

[5] $N_2O_2^* \rightarrow N_2 + O_2$

[6] $N_2O_2^* + NO \rightarrow N_2O + NO_2$

Our interest in adding methyl fluoro silanes was to determine if collisions with $NO(^4\pi)$ would cause C—Si bond cleavage to yield fluorosilyl radicals. No evidence of such a photosensitized reaction was found. Instead, it was found that the silanes enhanced the decomposition of NO in forming N_2 and N_2O.

Experimental

A gas-circulating, closed reaction system was used, whereby the reactants were pumped over a pool of liquid Hg, held at 50°C through a condenser kept at 25°C, then through a reaction vessel made of Suprasil. The total volume of the circulatory reaction system was 238 mL and, of this, the 1 cm path-length reaction vessel had a volume of 36.6 mL. A low pressure mercury lamp was used to generate the 2537 Å resonance line. The 1849 Å resonance line was removed with a Vycor 7910 filter.

A conventional vacuum line, containing metering, dosing, and fractionating systems, was connected to the reaction system. Analyses were carried out by gas chromatography and mass spectrometry.

Reproducibility of results was obtained by washing the detachable cell with nitric acid, followed by thorough drying between each experimental run.

Materials

Nitric oxide, obtained from Matheson Company, was distilled at low pressure through a liquid-oxygen-cooled trap. $MeSiF_3$ and Me_2SiF_2, obtained from PCR Research Chemicals, Inc., were degassed and distilled, the reagents being collected at −160°C and −130°C, respectively. SiF_4, from Matheson Company, was degassed and distilled. The purified reagent was collected at −160°C.

Results

Initial experiments were carried out to determine the quenching cross section of $MeSiF_3$ for $Hg6^3P_1$ by the chemical method (6). These results indicated a quenching cross section too small for accurate measurement but certainly lower than the value of 0.19 Å^2 reported for Me_2SiF_2 (7).

Since the quenching cross section of NO for $Hg6^3P_1$ is 24.7 Å^2 (8), quenching of NO–silane mixtures will be predominantly by NO.

Quantitative measurements of product yields were restricted to N_2 and N_2O, since the other major product, NO_2, reacts with mercury to give involatile products.

Reaction times were chosen so that the extent of decomposition of NO was generally less than 1%, although up to 3% decomposition was necessary in runs with low NO concentrations.

The mercury photosensitized decomposition of *n*-butane–N_2O mixtures was used for actinometry (6).

In all cases, the reaction of NO–silane mixtures results in no measurable consumption of silane and no products additional to those formed in the NO/Hg systems.

The effect of light intensity is shown in Table 1. Quantum yields are, within experimental error, independent of light intensity.

Experiments were carried out to determine the effect of composition of the reaction mixture on the product quantum yields. The results are given in Table 2 for $MeSiF_3$–NO mixtures and in Table 3 for Me_2SiF_2–NO mixtures. Experiments were also done with SiF_4–NO mixtures but it appeared that the presence of SiF_4 had only a small effect on the yields of N_2O and N_2.

The data in Tables 2 and 3 show that the quantum yields of N_2 and N_2O increase markedly with increasing pressures of $MeSiF_3$ and Me_2SiF_2 for a fixed pressure of NO. When the silane is kept constant and NO increased, the quantum yield of N_2O decreases in both cases while that of N_2 increases markedly for Me_2SiF_2 and slightly for $MeSiF_3$.

The magnitude of these observed effects is such that the enhanced decomposition of NO caused by the silanes is in the order $Me_2SiF_2 > MeSiF_3 \gg SiF_4$.

Discussion

The data in Tables 1, 2, and 3 indicate that the quantum yields of N_2 and N_2O are markedly increased by the presence

TABLE 1. Quantum yields as a function of light intensity

	I_{ab} (μeinstein min^{-1})	Φ_{N_2} (mol $einstein^{-1} \times 10^2$)	Φ_{N_2O} (mol $einstein^{-1} \times 10^2$)
$P_{MeSiF_3} = P_{NO} = 99.6$ Torr	11.2	1.84±0.17	1.55±0.07
	5.43	2.11±0.16	1.63±0.07
$P_{Me_2SiF_2} = 50.6$ Torr; $P_{NO} = 100.5$ Torr	11.2	4.16±0.16	3.34±0.10
	5.43	5.15±0.17	3.38±0.03

TABLE 2. Quantum yields of N_2 and N_2O in the $MeSiF_3$–NO reaction

P_{NO} (Torr)	P_{MeSiF_3} (Torr)	Φ_{N_2} (mol $einstein^{-1} \times 10^2$)	Φ_{N_2O} (mol $einstein^{-1} \times 10^2$)
98.4	0	0.077	0.22
98.4	76.3	1.12	1.35
98.4	99.1	1.36	2.00
98.4	135.8	1.58	2.92
98.4	160.2	1.45	2.97
98.4	188.5	1.95	3.05
98.4	235.4	1.85	4.03
98.4	291.0	2.05	4.72
	($I_{abs} = 13.2$ μeinstein min^{-1})		
10.4	100.2	2.40	6.91
31.4	100.2	1.65	4.57
79.8	100.2	1.80	2.14
50.5	100.2	1.80	2.82
101.0	100.2	2.13	1.64
203.0	100.2	2.02	1.09
300.3	100.2	2.09	0.93
	($I_{abs} = 11.2$ μeinstein min^{-1})		

TABLE 3. Quantum yields of N_2 and N_2O in the Me_2SiF_2–NO reaction

P_{NO} (Torr)	$P_{Me_2SiF_2}$ (Torr)	Φ_{N_2} (mol $einstein^{-1} \times 10^2$)	Φ_{N_2O} (mol $einstein^{-1} \times 10^2$)
100.7	5.1	0.96	0.11
100.7	12.7	2.14	1.15
100.7	25.2	3.34	2.34
100.7	50.0	4.42	3.70
100.7	71.9	5.45	5.23
26.4	50.5	1.77	6.63
50.6	50.5	3.15	4.96
100.7	50.5	4.42	3.69
192.2	50.5	5.75	2.62
	($I_{abs} = 11.2$ μeinstein min^{-1})		

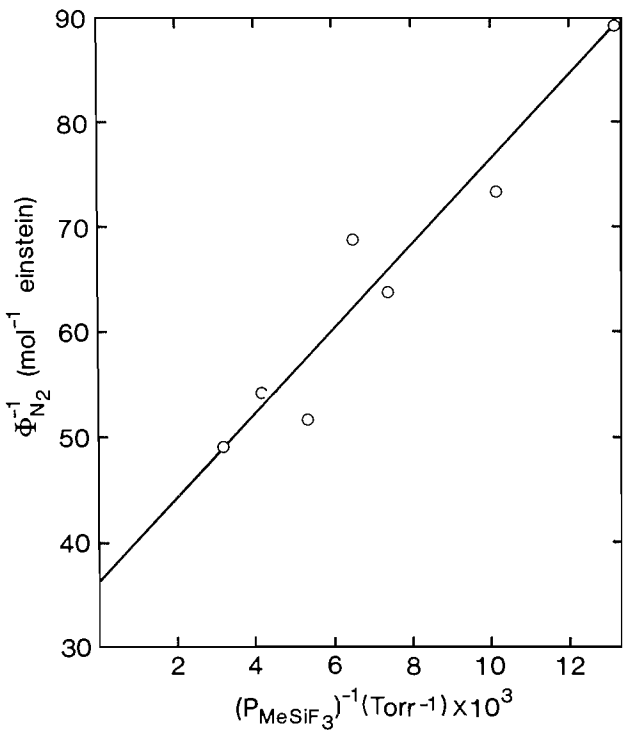

FIG. 1. Plot of reciprocal of quantum yield of N_2 vs. reciprocal of $MeSiF_3$ pressure. $P_{NO} = 98.4$ Torr.

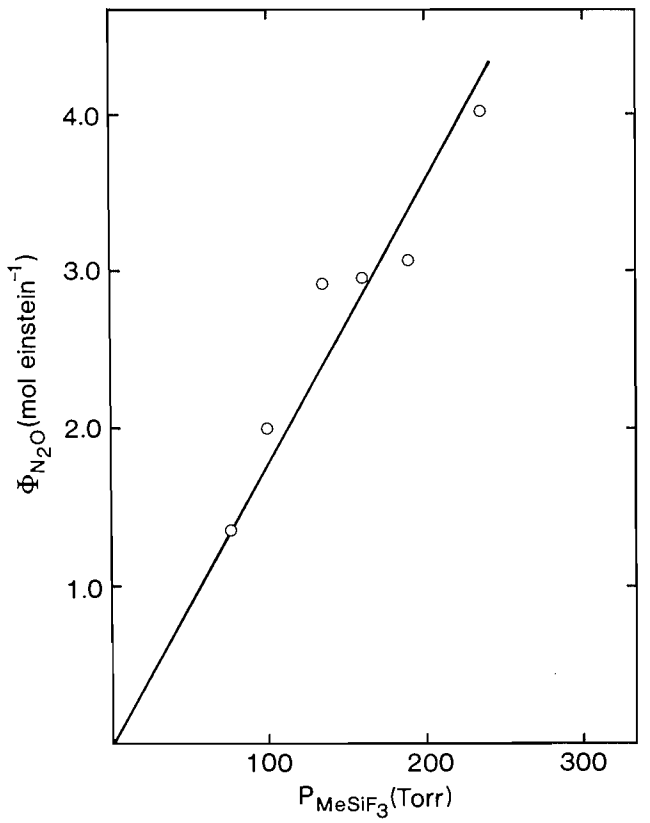

FIG. 2. Plot of quantum yield of N_2O vs. $MeSiF_3$ pressure. $P_{NO} = 98.4$ Torr.

of the silanes $MeSiF_3$ and Me_2SiF_2 but are unaffected by light intensity.

Strausz and Gunning (5), in their study of the $Hg(6^3P_1)$ + NO reaction, found that the sum of the quantum yields of N_2 and N_2O were independent of NO pressure in the complete quenching region. This observation clearly indicates that their mechanism, reactions [1] to [6], cannot also include the regeneration of NO from the excited dimer N_2O_2* by either a unimolecular dissociation or by reaction with NO.

Can. J. Chem. Downloaded from www.nrcresearchpress.com by 210.87.254.42 on 09/06/12
For personal use only.

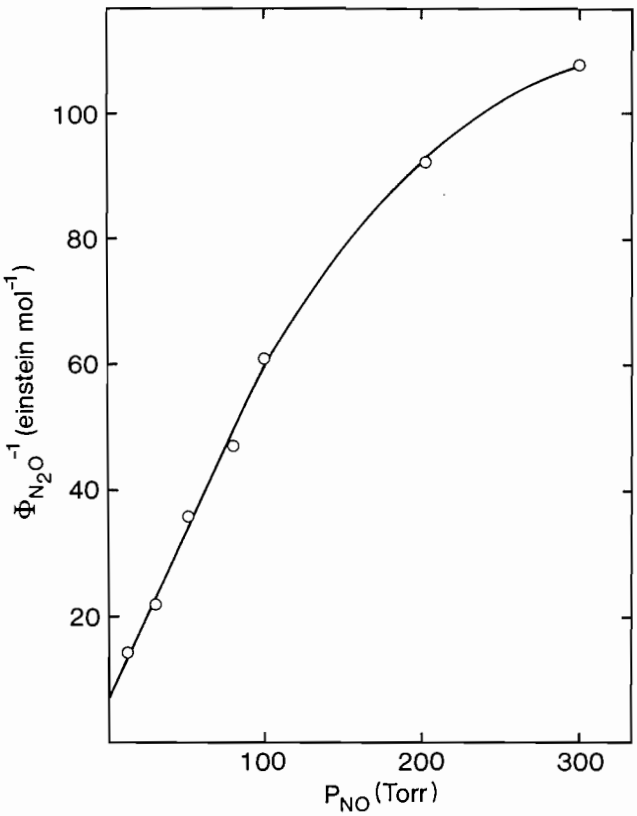

FIG. 3. Plot of reciprocal of quantum yield of N_2O vs. NO pressure. P_{MeSiF_3} = 100.2 Torr.

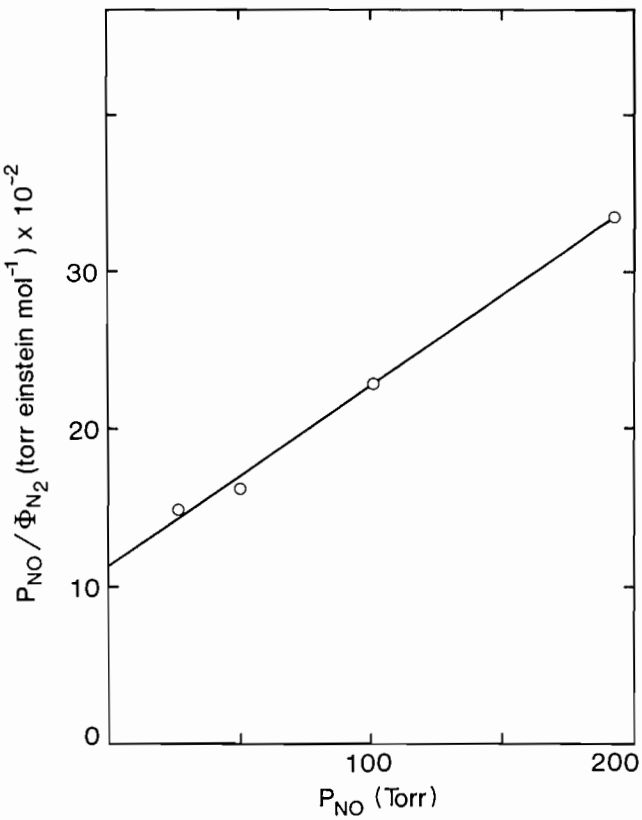

FIG. 4. Plot of P_{NO}/Φ_{N_2} vs. NO pressure. $P_{Me_2SiF_2}$ = 50.5 Torr.

The effect of added silanes cannot be a result of reaction of the silanes with N_2O_2* since this would not increase the yields of N_2 and N_2O. It seems likely that the silanes intervene in the mechanism through competition with reactions [3] and [4]. The data are consistent with an interpretation involving the formation of two different silane–NO complexes, each initiating a set of steps to yield one of the products of the reaction. The nature of these two complexes is conjectured upon later. They are designated SilNO† and SilNO†† in the proposed mechanism, where SilNO† leads to N_2 and SilNO†† leads to N_2O and where Sil represents either $MeSiF_3$ or Me_2SiF_2.

[7] $NO^* + Sil \rightarrow SilNO\dagger$

[8] $\rightarrow SilNO\dagger\dagger$

If these complexes are not interconvertible, their fates may be considered independently.

[9] $SilNO\dagger \rightarrow Sil + NO$

[10] $SilNO\dagger + NO \rightarrow Sil + N_2 + O_2$

[11] $SilNO\dagger + NO \rightarrow Sil + 2NO$

[12] $SilNO\dagger + Sil \rightarrow 2Sil + NO$

A steady state treatment of this mechanism yields the following expression for the quantum yield of N_2. The yield of N_2 by reaction [5] has been ignored because of the very low quantum yield for N_2 in the absence of silanes (5),

[*a*] $$\Phi_{N_2} = \frac{k_7k_{10}\,[Sil][NO]}{\{(k_3+k_4)[NO]+(k_7+k_8)[Sil]\}\{k_9+(k_{10}+k_{11})[NO]+k_{12}[Sil]\}}$$

The following reactions of the second complex are similarly considered.

[13] $SilNO\dagger\dagger \rightarrow Sil + NO$

[14] $SilNO\dagger\dagger + NO \rightarrow SilN_2O_2\dagger\dagger \xrightarrow{NO} Sil + N_2O + NO_2$

[15] $SilNO\dagger\dagger + NO \rightarrow Sil + 2NO$

[16] $SilNO\dagger\dagger + Sil \rightarrow 2Sil + NO$

A steady state treatment of these steps yields the following expression.

[*b*] $$\Phi_{N_2O} = \frac{k_8k_{14}\,[Sil][NO]}{\{(k_3+k_4)[NO]+(k_7+k_8)[Sil]\}\{k_{13}+(k_{14}+k_{15})[NO]+k_{16}[Sil]\}}$$

Tables 2 and 3 indicate differences between the effects of $MeSiF_3$ and Me_2SiF_2; thus, the two compounds are discussed separately.

$MeSiF_3$

The dependence of product quantum yields on reactants given in Table 2 requires modification to the above derived rate equations for Φ_{N_2} and Φ_{N_2O}. When the total data are considered together, the terms which must be dropped in order to fit the quantum yields to consistent and complementary kinetic schemes are self-selective.

Thus, $(k_7 + k_8)$[Sil] must be neglected in eq. [*a*] relative to $(k_3 + k_4)$[NO] and $(k_{10} + k_{11})$[NO] must be $\ll k_9 + k_{12}$[Sil]. These considerations reduce the equation for Φ_{N_2} to

$$\Phi_{N_2} = \frac{k_7k_{10}}{(k_3+k_4)}\,\frac{[Sil]}{(k_9+k_{12}[Sil])}$$

Can. J. Chem. Downloaded from www.nrcresearchpress.com by 210.87.254.42 on 09/06/12
For personal use only.

Can. J. Chem. Downloaded from www.nrcresearchpress.com by 210.87.254.42 on 09/06/12
For personal use only.

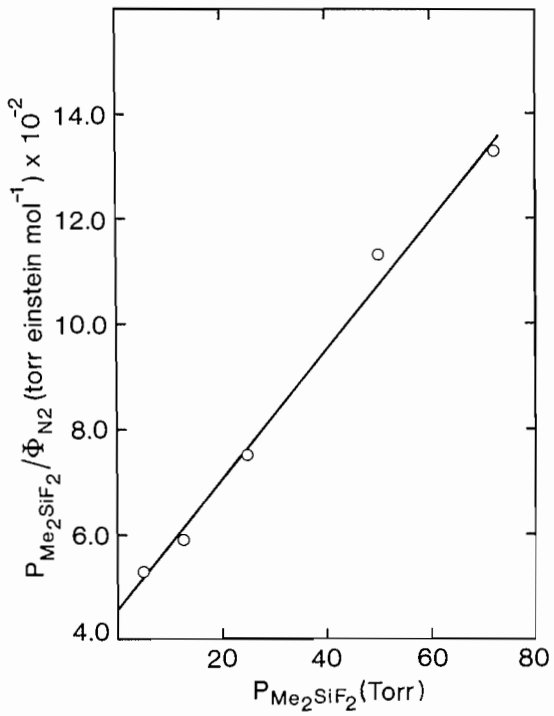

FIG. 5. Plot of $P_{Me_2SiF_2}/\Phi_{N_2}$ vs. Me_2SiF_2 pressure. P_{NO} = 100.7 Torr.

from which

$$\Phi_{N_2}^{-1} = \frac{(k_3 + k_4)}{k_7 k_{10}}\left(\frac{k_9}{[Sil]} + k_{12}\right)$$

As can be seen from Fig. 1, a plot of $\Phi_{N_2}^{-1}$ vs. $P_{MeSiF_3}^{-1}$ is a straight line and from the slope and intercept

$$k_9/k_{12} = 6.5 \times 10^{-3} \text{ mol L}^{-1}$$

The main fate of NO* is its deactivation to NO, both in the presence and absence of silane.

Since the conclusion that $(k_3 + k_4)[NO] \gg (k_7 + k_8)[Sil]$ has already been made in the $MeSiF_3$–NO system, the equation for Φ_{N_2O} is reduced to

$$\Phi_{N_2O} = \frac{k_8 k_{14}}{(k_3 + k_4)} \frac{[Sil]}{\{k_{13} + (k_{14} + k_{15})[NO] + k_{16}[Sil]\}}$$

A plot of Φ_{N_2O} vs. P_{MeSiF_3}, at constant P_{NO} (Fig. 2), is a straight line with zero intercept which indicates that $k_{16}[Sil]$ is negligible and so

$$\Phi_{N_2O} = \frac{k_8 k_{14}}{(k_3 + k_4)} \frac{[Sil]}{\{k_{13} + (k_{14} + k_{15})[Sil]\}}$$

or

$$\Phi_{N_2O}^{-1} = \frac{(k_3 + k_4)}{k_8 k_{14}} \frac{k_{13} + (k_{14} + k_{15})[NO]}{[Sil]}$$

Figure 3 shows that $\Phi_{N_2O}^{-1}$ is a linear function of P_{NO} at low pressures of NO. The fall-off of the graph at high NO pressures indicates that, as P_{NO} is increased beyond about 150 Torr, the yield of N_2O from reaction [6] becomes a significant source of N_2O which was not considered in the derivation of the equation for Φ_{N_2O}.

From the values of slope and intercept from Fig. 3 we have

$$\frac{k_{14} + k_{15}}{k_{13}} = 1.1 \times 10^3 \text{ mol L}^{-1}$$

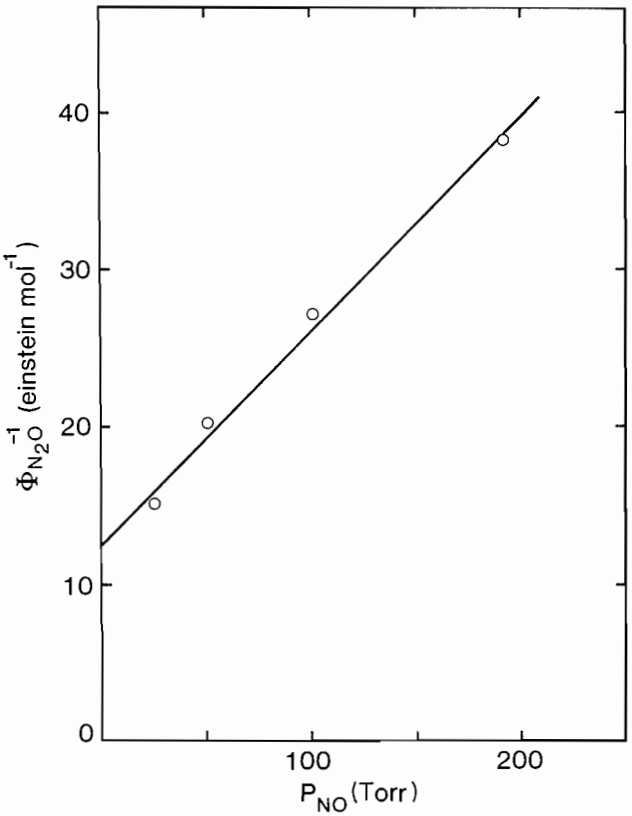

FIG. 6. Plot of reciprocal of quantum yield of N_2O vs. NO pressure. $P_{Me_2SiF_2}$ = 50.5 Torr.

Me_2SiF_2

In the case of Me_2SiF_2, there is a distinct dependence of Φ_{N_2} on the NO pressure. This would suggest that, in this case, $(k_7 + k_8)[Sil]$ is not negligible, compared with $(k_3 + k_4)[NO]$. Both terms are thus retained in the kinetic expression.

Retaining our arguments that $k_9 + k_{12}[Sil] \gg (k_{10} + k_{11})[NO]$ leads to a kinetic expression in agreement with experiment, provided $k_{12}[Sil]$ is sufficiently small and can be neglected relative to k_9; i.e., unimolecular dissociation of SilNO† is much faster than collisional deactivation by silane.

Thus, the expression for Φ_{N_2} becomes

$$\Phi_{N_2} = \frac{k_7 k_{10}[Sil][NO]}{k_9\{(k_3 + k_4)[NO] + (k_7 + k_8)[Sil]\}}$$

or

$$\frac{[NO]}{\Phi_{N_2}} = \frac{k_9}{k_7 k_{10}}\left\{(k_3 + k_4)\frac{[NO]}{[Sil]} + (k_7 + k_8)\right\}$$

A plot of P_{NO}/Φ_{N_2} versus P_{NO} at constant $P_{Me_2SiF_2}$ is a straight line and is shown in Fig. 4.

The appropriate equation for the dependence of Φ_{N_2} on [Sil] is

$$\frac{[Sil]}{\Phi_{N_2}} = \frac{k_9}{k_7 k_{10}}\left\{(k_3 + k_4) + (k_7 + k_8)\frac{[Sil]}{[NO]}\right\}$$

A plot of $P_{Me_2SiF_2}/\Phi_{N_2}$ vs. $P_{Me_2SiF_2}$ is a straight line and is shown in Fig. 5.

The formation of N_2O in the Me_2SiF_2/NO case must be in accord with the requirement for N_2 formation; i.e., $(k_7 + k_8)[Sil]$ is not negligible relative to $(k_3 + k_4)[NO]$.

The kinetic data then will fit with a kinetic expression, where

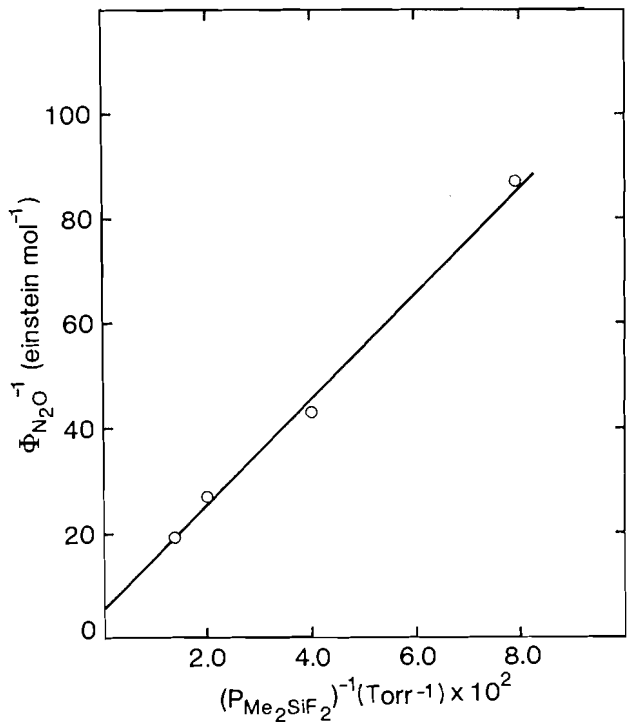

FIG. 7. Plot of reciprocal of quantum yield of N_2O vs. reciprocal of Me_2SiF_2 pressure. P_{NO} = 100.7 Torr.

deactivation and product formation via [15] and [14] are more important than the unimolecular decomposition of SilNQ††.

In such a case, the kinetic expression becomes

$$\Phi_{N_2O} = \frac{k_8 k_{14}[\text{Sil}]}{(k_{14} + k_{15})\{(k_3 + k_4)[\text{NO}] + (k_7 + k_8)[\text{Sil}]\}}$$

and

$$\Phi_{N_2O}^{-1} = \frac{k_{14} + k_{15}}{k_8 k_{14}}\left\{(k_3 + k_4)\frac{[\text{NO}]}{[\text{Sil}]} + (k_7 + k_8)\right\}$$

Figure 6 indicates that the plot of $\Phi_{N_2O}^{-1}$ vs. P_{NO}, at constant $P_{Me_2SiF_2}$, is linear, in agreement with the above expression.

Figure 7 is a plot of $\Phi_{N_2O}^{-1}$ vs. $P_{Me_2SiF_2}^{-1}$. It is also linear. The datum point for the lowest value of $P_{Me_2SiF_2}$ is not plotted. It lies far beyond the portion of the graph shown and the value of Φ_{N_2O} would be considerably larger than would be given by the straight line. Again, we conclude this is due to the increased importance of reaction [6] as a source of N_2O at low Me_2SiF_2 pressures.

Values of the ratio $(k_7 + k_8)/(k_3 + k_4)$ can be obtained from the slopes and intercepts of the four graphs of data from the Me_2SiF_2–NO system. The values are 2.0, 2.8, 1.8, and 0.5, respectively. The low value is derived from Fig. 7 and is the most uncertain, due to the small value of the intercept.

The mechanism proposed involves the formation of two non-interconvertible complexes of NO with silane.

If the reactive NO species were simply a vibrationally excited ground electronic state molecule, we would expect strong collisional deactivation with all species and it is hard to envisage vibrational deactivation together with complex formation. Further, we would anticipate interconversion of SilNO† and SilNO†† through the vibrational cascade, not in accord with the experimental kinetics.

We find the idea of a complex with $^4\pi$NO much more appealing and in line with the Strausz–Gunning proposal for the Hg-sensitized decomposition of NO itself. The $^4\pi$ state of NO lies 108 kcal above the ground state (9), permitting maximum vibrational excitation to $v = 1$; hence the two complexes must be structurally, rather than energetically, different.

The ability of Si to expand its coordination number to five, through the use of *d* orbitals, accounts for much of its chemistry different to that of carbon. In the present instance, we propose the two complexes are formed through Si—N and Si—O bonding; viz., Si—N—O and Si—O—N. We do not, however, conjecture which one leads to N_2 and which to N_2O.

Theoretical calculation by P. G. and K. A. Perkins[1] has indicated that, indeed, a minimum of the potential energy does occur in the interaction of silanes with NO in the ground state. This minimum of the potential lies between 3.0 and 3.5 angstroms separation distance. The complexes Si—N—O, for SiF_4, $MeSiF_3$, and Me_2SiF_2, lie energetically 2.7, 2.5, and 2.7 kcal below the ground state molecules, while the Si—O—N systems are 3.0, 3.4, and 4.5 kcal, respectively, below the ground state molecules.

In the quartet state, the only estimates available at this time are that SiF_4—NO lies 1.6 and SiF_4—ON 2.6 kcal below the separated molecules SiF_4 and $^4\pi$NO.[2]

Conclusions

The same mechanism yields rate equations in accord with experiment for the $MeSiF_3$—NO and the Me_2SiF_2—NO cases. Differences are due to differences in values of the rate constants.

The reactions in which the complexes are formed, reactions [7] and [8], are faster in the Me_2SiF_2 case. Indeed, they appear competitive with the deactivation reaction [3].

In both cases, a small fraction of the SilNO† complexes react to form N_2. Most dissociate to re-form Sil and NO. In the $MeSiF_3$ case, deactivating collision with Sil is also important.

Deactivation of SilNO†† by collision with Sil is of negligible importance in both the $MeSiF_3$ and Me_2SiF_2 cases. In the $MeSiF_3$ case, unimolecular dissociation to yield Sil + NO competes with reactions with NO, i.e., reactions [14] and [15]. In the Me_2SiF_2 case, the most important reactions of SilNO†† are those with NO. The data do not provide an estimate of the relative importance of [14] and [15] but [15] must be significant since, even in the Me_2SiF_2 case, where complex formation competes with the reaction [3], the quantum yield of N_2O is small.

Acknowledgements

We are grateful to the Natural Sciences and Engineering Research Council of Canada and the SFU President's fund for financial support.

1. W. A. NOYES, JR. J. Am. Chem. Soc. **53**, 544 (1931).
2. R. J. FALLON, J. T. VANDERSLICE, and E. A. MASON. J. Phys. Chem. **63**, 2082 (1959).
3. M. Z. HOFFMANN and R. B. BERNSTEIN. J. Phys. Chem. **64**, 1769 (1960).
4. J. L. COJAN and R. TABOVE. J. Phys. Radium, **19**, 960 (1958).
5. O. P. STRAUSZ and H. E. GUNNING. Can. J. Chem. **39**, 2549 (1961).

[1] P. G. Perkins and K. A. Perkins. Private communication.

[2] We are grateful to Drs. Perkins for providing these data which lend support to our proposal for complexes of this type.

Can. J. Chem. Downloaded from www.nrcresearchpress.com by 210.87.254.42 on 09/06/12
For personal use only.

6. R. J. CVETANOVIĆ. J. Chem. Phys. **23**, 1203 (1955); **23**, 1208 (1955).
7. A. J. YARWOOD, O. P. STRAUSZ, and H. E. GUNNING. J. Chem. Phys. **41**, 1705 (1964).
8. R. J. CVETANOVIC. Progress in reaction kinetics. Vol. 2. Pergamon Press, London, England. 1964. p. 39.
9. J. HEICKLEN and N. COHEN. Advances in photochemistry. Vol. 5. Intersciences, John Wiley, New York. 1969. p. 157.

Can. J. Chem. Downloaded from www.nrcresearchpress.com by 210.87.254.42 on 09/06/12
For personal use only.

Rotational relaxation of the $A^1\pi(v' = 13, J' = 13^+)$ state of $^{13}C^{16}O$ by various gases[1]

A. C. VIKIS[2]

Division of Chemistry, National Research Council of Canada, Ottawa, Ont., Canada K1A 0R6

Received July 13, 1982

This paper is dedicated to Professor Harry E. Gunning on the occasion of his 65th birthday

A. C. VIKIS. Can. J. Chem. **61**, 952 (1983).

Rotational relaxation of the $A^1\pi$ ($v' = 13, J' = 13^+$) state of $^{13}C^{16}O$ was studied in the presence of H_2, D_2, He, Ne, Ar, Xe, N_2, CO, $^{13}C^{16}O$, and $^{12}C^{18}O$. The rotational relaxation cross sections $\Sigma\sigma_{13\to J'}$, in $cm^2 \times 10^{16}$ and in the above order, were: 19 ± 1, 27 ± 1, 23 ± 1, 32 ± 1, 55 ± 2, 14 ± 1, 43 ± 3, 69 ± 5, 23 ± 1, and 100 ± 15. The rotational relaxation probabilities per gas-kinetic collision correlate with the square root of the reduced mass, except for Xe and the CO isotopic molecules. The latter molecules have several electronic states accessible at this energy. Their rotational relaxation cross sections depend on the magnitude of their respective electronic quenching cross sections, in a manner indicating preemption by fast electronic–electronic energy transfer.

A. C. VIKIS. Can. J. Chem. **61**, 952 (1983).

On a étudie la relaxation vibrationnelle de l'état $A^1\pi$ ($v' = 13, J' = 13^+$) du $^{13}C^{16}O$ en présence des gaz suivants: H_2, D_2, He, Ne, Ar, Xe, N_2, CO, $^{13}C^{16}O$ et $^{12}C^{18}O$. Les sections droites de relaxation vibrationnelle $\Sigma\sigma_{13\to J'}$ en $cm^2 \times 10^{16}$ sont, dans l'ordre des gaz mentionnés ci-dessous: 19 ± 1, 27 ± 1, 23 ± 1, 32 ± 1, 55 ± 2, 14 ± 1, 43 ± 3, 69 ± 5, 23 ± 1 et 100 ± 15. On a établi une corrélation entre les probabilités de relaxation rotationnelle par collision cinétique des gaz et la racine carrée de la masse réduite, sauf pour les molécules isotopiques de Xe et de CO. Ces dernières molécules ont plusieurs état électroniques accessibles à ce niveau d'énergie. Les sections droites de relaxation vibrationnelle dépendent de l'ordre de grandeur de leurs sections droites respectives de piégeage électronique d'une façon qui suggère une élimination préalable par transfert rapide d'énergie électronique–électronique.

[Traduit par le journal]

Introduction

Energy transfer from excited molecules in collisions with other molecules has been studied extensively because of the importance of such processes in chemical reactions and in lasers. Experimental and theoretical results have been summarized in several review articles (1–5) and in the books by Herzfeld and Litowitz (6) and Cottrell and McCoubrey (7). The bulk of the early data were obtained for ground electronic states, using techniques which yielded cross sections averaged over several vibrational and rotational states. Selective excitation of single molecular states can be achieved with monochromatic radiation from lasers or intense atomic resonance-lamps. Energy transfer from a selected state to others, monitored spectroscopically, can yield detailed cross sections which can be compared more easily with theoretical predictions. State detailed experiments (8–14) provided valuable information on how the dynamics and kinematics of the colliding pair affect the efficiency of energy transfer, and on how interconversion of energy among the various degrees of freedom occurs.

In this work the rotational relaxation of the $J' = 13^+$ state of $^{13}C^{16}O(A^1\pi, v' = 13)$ was studied in the presence of various gases. Selective excitation of this state, using sharp and unreversed radiation (123.58 nm) emitted by a krypton resonance-lamp, was demonstrated in a previous study (15). This fortuitous coincidence was used to enrich carbon-13 in the CO_2 and C_3O_2 products of the reaction of excited $^{13}C^{16}O$ with ground state CO (16, 17). Energy transfer from this state was studied for its own merits and also to assess the extent of destruction of the initial isotopic selectivity in the presence of high pressures of natural isotopic abundance CO, needed for practical reaction yields.

The electronic relaxation data for this state have already been reported in the literature (18). Even though $^{13}C^{16}O$ was also vibrationally excited, no detectable vibrational relaxation was observed due to the low cross sections for this process and the short lifetime (<10 ns) of the state with respect to emission and electronic quenching. Rotational relaxation cross sections were determined from measurements of the emission intensities of the parent $J' = 13^+$ state and the J' states populated by collisions with other molecules.

Experimental

The spectroscopic apparatus employed in this work was described elsewhere (15). Light source #2 (15) which emitted sharp and unreversed Kr resonance radiation (123.58 nm) was used. This radiation was absorbed selectively by the Q(13) transition of the $^{13}C^{16}O$ $A-X$ (13,0) band populating the $J' = 13^+$ component of the Λ-type doublet. The $A-X$ (13,21) band fluorescence at 237 nm was monitored in these experiments.

In the absence of rotational relaxation, selection rules applicable to this system (19) allow only a single Q(13) transition to be observed in fluorescence. Resolution of the Q(13) fluorescence from the relaxed fluorescence could be achieved with a spectrometer band width of 0.08 nm (Fig. 1). The ratio of the unrelaxed to the relaxed populations, $N(13^+)/\sum_{J'\neq 13^+} N(J')$, is equal to $2.0I_{Q(13)}/(\sum_{J'\neq 13^+} I(J') + 4.2I_{P(14)} + 3.9I_{R(12)}$, where the factors 2.0, 4.2, and 3.9 correspond to the degeneracy $(2J' + 1)$ divided by the rotational line strengths, $S_{J'}$, of the Q, P, and R transitions, respectively. In the present experiments the P(14) and R(12) transitions are not resolved from the rest ($J' \neq 13$) of the relaxed states. Therefore, the ratio $N(13^+)/\sum_{J'\neq 13^+} N(J')$ is approximated with $2.0I_{Q(13)}/\int_{J'\neq 13^+} I(J')$, where the denominator is the integrated intensity from all J' states except $J' = 13^+$. This approximation does not introduce a significant error because the intensities of the P(14) and R(12) transitions are not a significant

[1]NRCC No. 20746.

[2]Present address: Research Chemistry Branch, Chemistry and Materials Science Division, Atomic Energy of Canada Limited, Whiteshell Nuclear Research Establishment, Pinawa, Man., Canada R0E 1L0.

Can. J. Chem. Downloaded from www.nrcresearchpress.com by 210.87.254.5 on 09/06/12
For personal use only.

Can. J. Chem. Downloaded from www.nrcresearchpress.com by 210.87.254.5 on 09/06/12
For personal use only.

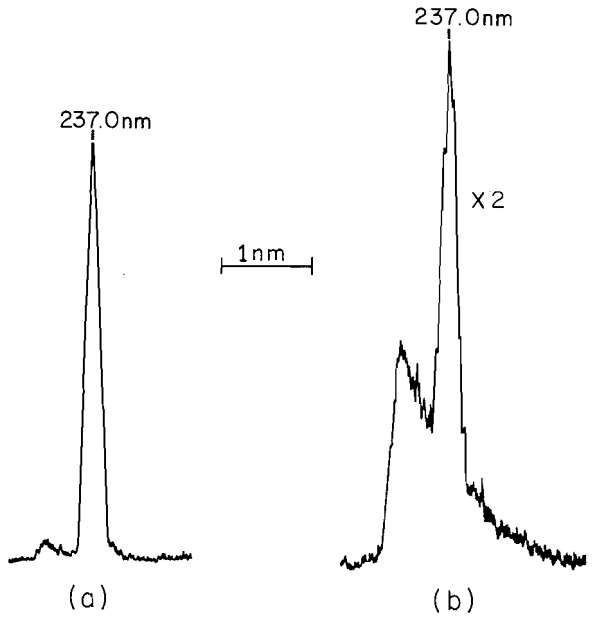

FIG. 1. (*a*) The $^{13}C^{16}O$ $A-X$ (13,21) band in the presence of 69 Pa $^{13}C^{16}O$, only; (*b*) the $^{13}C^{16}O$ $A-X$ (13,21) band in the presence of 69 Pa $^{13}C^{16}O$ and 2.5 kPa Ne.

fraction of the total relaxed intensity. It is shown later in this paper that the relaxed population of the $J' = 13$ state is ~12% of the total relaxed population. Also, within the narrow frequency range of the spectrum, corrections for the frequency dependence of emission and for the spectral response of the equipment were negligible.

The various gases and their purity, according to the manufacturer, were: Merck, Sharpe and Dohme ^{13}CO (92 atom% ^{13}C); Stohler Isotope Chemicals $C^{18}O$ (99 atom% ^{18}O); Matheson research grade CO (99.99% minimum), H_2 (99.9995%), He (<2 ppm impurities), Xe (99.9995% minimum); Airco research grade Ne (27 ppm He, <2 ppm of other impurities), Ar (<2 ppm impurities), N_2 (<2 ppm impurities); Bio-Rad D_2 (99.65 mol% D_2), N_2 (<24 ppm, O_2 <1 ppm).

In each experiment the partial pressure of $^{13}C^{16}O$ was kept constant at 66.7 ± 1.3 Pa. The various gases were added from their reservoirs to $^{13}C^{16}O$ through a needle valve. Pressures in the 0–133 Pa range were measured with an MKS (type-77 Baratron) pressure gauge. Higher pressures (up to 1.33 kPa) were measured with a Wallace and Tiernan mechanical pressure gauge.

Results

A higher resolution spectrum of the (13,21) emission band, obtained in the presence of 2.15 kPa of He, is shown in Fig. 2. Emission from J' levels other than $J' = 13^+$ was observed under these conditions. These levels were populated by both positive and negative $\Delta J'$ transitions. P and Q transitions originating from $J' > 12$ were sufficiently resolved to derive their relative population. The population of the rest of the rotational levels was obtained by computer simulation of the spectrum. The triangular distribution, shown in the insert of Fig. 2, seems to fit best the observed spectrum in this case.

From comparison of computed and observed spectra, it was concluded that all P, Q, and R transitions originating from relaxed levels are present, i.e., that collisions transfer molecules from the originally populated positive level of the $J' = 13^+$ Λ-type doublet to both positive and negative components of the other J' states. If an optical-like selection rule (+ ↔ −, + ↔ +, − ↔ −) (19) were obeyed in this collisional energy transfer case, no odd-numbered P, Q, and R transitions would have been observed except for Q(13). Transitions originating from P(21), P(19), P(17), P(15) + Q(19), and P(13) + Q(17) are well resolved and definitely present in the spectrum of Fig. 2. Optical-like propensities have been observed in other cases of rotational energy transfer (10).

Because of insufficient resolution, detailed cross sections, $\sigma_{13\to J'}$, were not determined. Instead, rotational relaxation cross sections, $\sigma_R = \sum\sigma_{13\to J'}$, were determined from the Q(13) intensity relative to the total intensity of the rest of the band, as a function of foreign-gas pressure. The steady-state ratio of the unrelaxed population ($J' = 13^+$, shown below by CO*) divided by the relaxed population ($J' \neq 13^+$, shown by CO′), as a function of foreign gas, M, was derived from the following mechanism:

[1] $CO + h\nu(\lambda = 123.58\ nm) \rightarrow CO^*$

[2] $CO^* + CO \rightarrow CO' + CO$

[3] $CO^* + CO \rightarrow$ electronic quenching products

[4] $CO^* + M \rightarrow CO' + M$

[5] $CO^* + M \rightarrow$ electronic quenching products

[6] $CO' + CO \rightarrow$ electronic quenching products

[7] $CO' + M \rightarrow$ electronic quenching products

[8] $CO^* \rightarrow CO + h\nu^*$ (unrelaxed emission)

[9] $CO' \rightarrow CO + h\nu'$ (relaxed emission)

In the above mechanism chemical reaction and electronic quenching to the ground and/or other electronic states were grouped together.

Repopulation of the unrelaxed state, due to collisional transfer from relaxed states (the reverse of [2] and [4]) was neglected in this analysis. If this effect were significant, rotational relaxation would be underestimated. An upper limit to the fraction of population of the unrelaxed state, which could be attributed to transfer from relaxed states, can be estimated from the relative populations of unrelaxed vs. relaxed states and the population distribution in the relaxed state. From the relaxed state population distribution given in Fig. 2 (triangular distribution in insert), the relaxed population for $J' = 13$ is ~10% of the total relaxed population. For the same experiment, the ratio of unrelaxed to total relaxed population calculated from the quenching curve is equal to 0.8. Thus, not more than ~12% of the population of the unrelaxed state can be attributed to transfer from relaxed states. This estimate is an upper limit, because a fraction of the relaxed population of $J' = 13$ is due to transfer from the unrelaxed component of the Λ-type doublet. At lower pressures, where the majority of data were obtained, collisional repopulation of the unrelaxed state would be even less important.

The steady-state ratio [CO*]/[CO′], derived from this mechanism, is:

$$[10]\quad [CO^*]/[CO'] = (1/\tau + k_6[CO] + k_7[M])/(k_2[CO] + k_4[M])$$

where τ is the radiative lifetime of the $A^1\pi$ state. With the exception of Xe, eq. [10] can be approximated by eq. [11] at the low and constant [CO] used in these experiments.

$$[11]\quad [CO^*]/[CO'] = k_7/k_4 + (1/\tau + k_6[CO])/k_4[M]$$

For Xe, $k_7[M] \sim (1/\tau + k_6[CO])$ and $k_4[M] \sim k_2[CO]$; therefore, the Xe data were fitted to eq. [10].

Can. J. Chem. Downloaded from www.nrcresearchpress.com by 210.87.254.5 on 09/06/12
For personal use only.

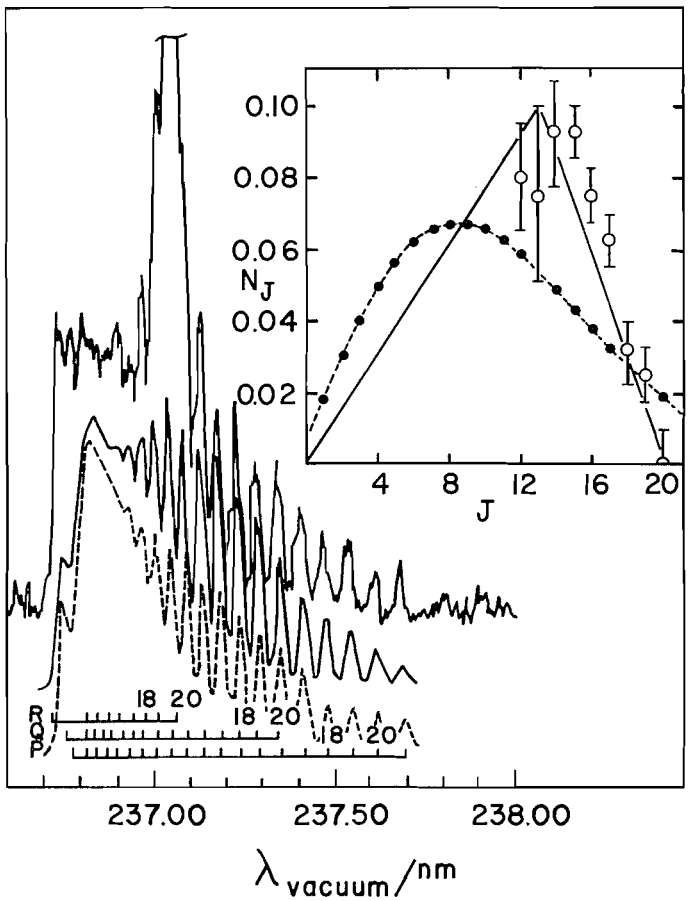

FIG. 2. The $^{13}C^{16}O$ $A-X$ (13,21) band (upper spectrum) at higher resolution in the presence of 190 Pa $^{13}C^{16}O$ and 2.1 kPa He. The insert gives the rotational population distribution for: (*a*) ○, determined from peak heights of resolved rotational transitions (upper spectrum); (*b*) —, corresponding to middle computed spectrum; (*c*) ·-·-·-·, Boltzmann distribution (T = 300 K) corresponding to lower computed spectrum.

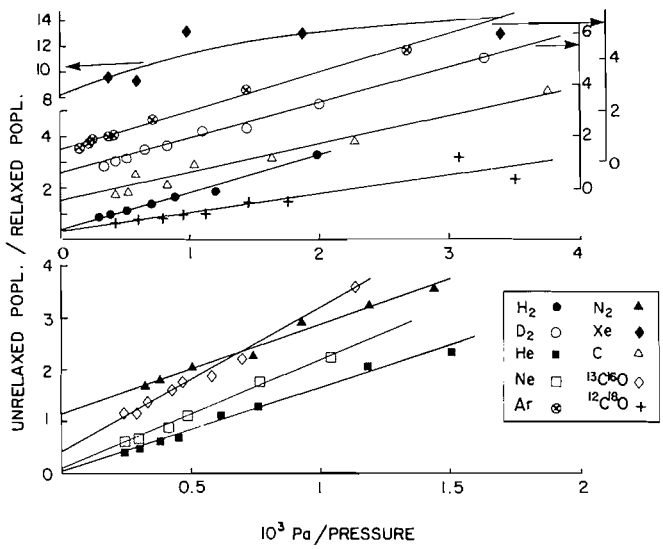

FIG. 3. Linear least-squares fits of rotational relaxation data for various molecules.

Graphs of [CO*]/[CO′] vs. $[M]^{-1}$ are shown in Fig. 3 for the various gases studied. The rotational relaxation rate constant, k_4, was determined from the slopes, $(1/\tau + k_6[CO])/k_4$, of these plots using τ = 10 ns and $k_6 = 7.83 \times 10^{11}$ dm^3 mol^{-1} s^{-1} (18).[3] The rotational relaxation cross sections, defined as $\sigma_R = k_4/\bar{c}$, are given in Table 1. The "hard-sphere" collision cross sections, $\sigma_{HS} = \pi\sigma^2_{CO^*-M}$, are also listed in Table 1 for comparison. Lennard–Jones potential parameters (22) derived from gas-viscosity data were used for σ_{CO^*-M}, assuming that $\sigma_{CO^*-M} = (\sigma_{CO^*} + \sigma_M)/2$. The σ_{CO^*} was approximated (9) with $\sigma_{CO} + \Delta r$, where Δr = 0.025 nm is the difference in bond lengths between the $X^1\Sigma^+$, v'' = 0 and $A^1\pi$, v' = 13 states of CO. Rotational relaxation probabilities, σ_R/σ_{HS}, are given in column 4 of Table 1 and are also plotted in Fig. 4 against the square root of the reduced mass of the CO*–M collision pair.

TABLE 1. Rotational relaxation (σ_R) and hard sphere (σ_{HS}) cross sections for $^{13}C^{16}O$ ($A^1\pi$, v' = 13, J' = 13$^+$) and various gases*

Molecule	σ_R (cm^2 × 10^{16})	σ_{HS} (cm^2 × 10^{16})	σ_R/σ_{HS}	$\mu^{1/2}$ (g$^{1/2}$ mol$^{-1/2}$)
H_2	19±1	38	0.50	1.37
D_2	27±1	38	0.71	1.87
He	23±1	34	0.67	1.87
Ne	32±1	36	0.89	3.45
N_2	43±3	47	0.93	3.77
Ar	55±2	43	1.3	4.10
Xe	14±1	52	0.27	4.87
CO	69±5	47	1.5	3.77
$^{13}C^{16}O$	23±1	47	0.48	3.81
$^{12}C^{18}O$	100±15	47	2.1	3.84

*The errors correspond to one standard deviation.

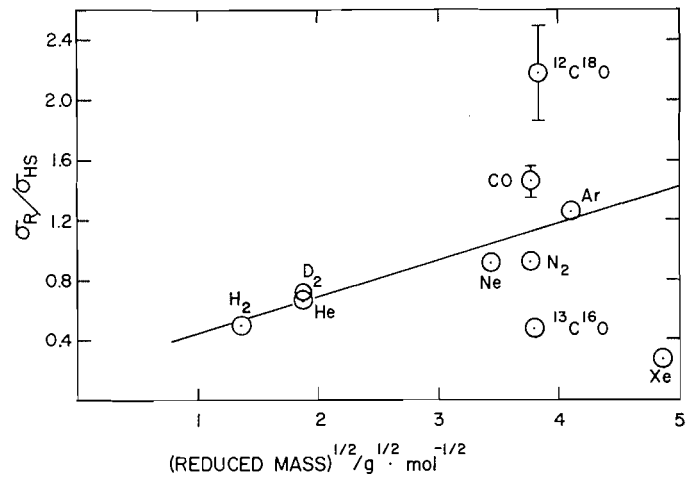

FIG. 4. Rotational relaxation probabilities ($\propto \sigma_R/\sigma_{HS}$) plotted against the square root of the reduced mass for the system $^{13}C^{16}O$ ($A^1\pi$, v' = 13, J' = 13) – various gases.

Discussion

In general the rotational relaxation cross section observed for $^{13}C^{16}O$ ($A'\pi$, v' = 13, J' = 13$^+$) are large, indicating an efficient energy-transfer process. This is in line with other experimental and theoretical evidence (6–9, 11, 14) on rotational ↔ translational energy transfer when the energy to be transferred is of the order of, or less than, kT.

[3]The natural lifetime of the $A^1\pi$, v' = 13 state of $^{13}C^{16}O$ has not been determined. The natural lifetime of the first seven vibrational levels of the $^{12}C^{16}O$ ($A^1\pi$) state varies from 9.0 ns to 10.5 ns (20, 21). Due to these uncertainties a natural lifetime of 10 ns was assumed.

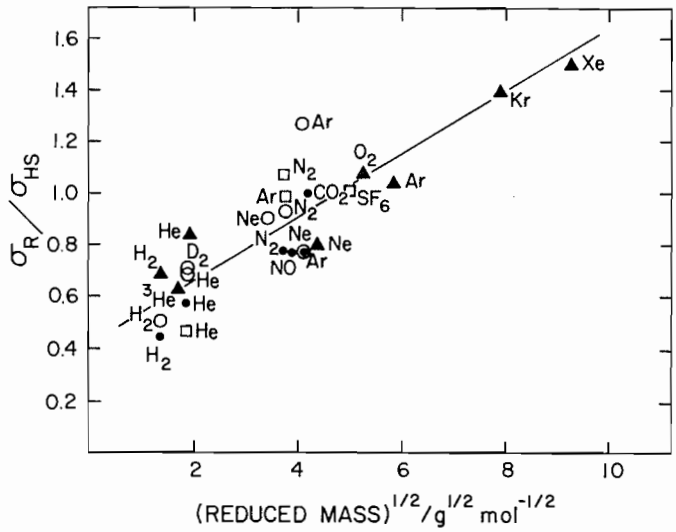

FIG. 5. Rotational relaxation probabilities ($\propto \sigma_R/\sigma_{HS}$) plotted against the square root of the reduced mass for the systems: ○, $^{13}C^{16}O$ ($A^1\pi$, $v' = 13$, $J' = 13$) − M; □, NO ($X^2\pi$, $v'' = 12$, $J'' = 2$) − M; ●, NO ($A^2\Sigma^+$, $v' = 1$, $K' = 13$) − M; ▲, I_2 ($B^3\pi_{0u^+}$, $v' = 25$, $J' = 34$) − M.

Also, for collisions between molecules which interact weakly and when $\Delta E \lesssim kT$ the rotational translational energy transfer probability varies proportionally with the square root of the reduced mass (9, 11). This mass effect was attributed (9, 23) to the relative momentum ($\bar{p} = \mu v \propto \mu^{1/2}$) of the collision. With the exception of Xe and the CO isotopic molecules, which are discussed below, the rest of the molecules studied conform well with this trend. Subtle changes in the dynamics (potential energy) of the collision are apparently unimportant, as far as the total rotational relaxation cross section is concerned. This is evidenced by the close similarity in both trend and magnitude (Fig. 5) between the present data and those for I_2 ($B^3\pi_{0u^+}$, $v' = 25$, $J' = 34$) (9), NO ($X^2\Sigma^+$, $v' = 1$, $K' = 13$) (8), and NO ($X^2\pi$, $v'' = 2$, $J'' = 10\frac{1}{2}$) (14).

The rather low cross section by Xe and the large variation between the cross sections by the three CO isotopic molecules are prominent. These molecules have electronic states accessible at this energy. Transfer from the $A^1\pi$ state to another electronic state can compete with rotational relaxation within the $A^1\pi$ state rotational manifold. Efficient electronic energy transfer to Xe ($^1P_1$, $^3P_{0,1,2}$) states must be the reason for the much larger electronic-quenching cross section by Xe (1.4×10^{-14} cm^2) (18) compared to the one by Ar (3.23×10^{-16} cm^2) (18). Argon has no accessible electronic states at this energy. Large electronic-quenching cross sections by Xe were also observed (24, 25) for the $A^1\pi$ state of $^{12}C^{18}O$ ($v' = 9$), $^{12}C^{16}O$ ($v' = 9$), and $^{12}C^{16}O$ ($v' = 14$). The Xe electronic-quenching cross sections for these states, compared to those by Kr given in parentheses, in the above order were: 110 (42), 91 (23), 170 (23) (cm$^2 \times 10^{16}$). Krypton has no electronic states accessible at these energies.

The variation of the rotational relaxation cross sections by the CO isotopic molecules must also be due to competition between rotational relaxation and electronic quenching. The electronic-quenching cross sections of the $^{13}C^{16}O$ ($A^1\pi, v' = 13$, $J' = 13$) state (18) (compared to the rotational ones given in parentheses) by $^{12}C^{16}O$, $^{13}C^{16}O$, and $^{12}C^{18}O$ are 57 (69), 198 (23), 38 (100) cm$^2 \times 10^{16}$, respectively. Preemption of the rotational relaxation channel by the more efficient electronic-quenching channel is most evident in the $^{13}C^{16}O$ case. The variation in the electronic-quenching cross sections which is assumed responsible for the rotational relaxation anomalies, was attributed (18) to electronic−electronic energy transfer processes from the $A^1\pi$ state to one or more of the electronic states ($A^3\pi$, $a'^3\Sigma^+$, $d^3\Delta_i$, $e^3\Sigma^-$, $I^1\Sigma^-$, $D^1\Delta$) accessible at this energy (26). Transfer of the system to another potential energy surface would depend on the symmetry of the states involved and on resonance (19). The latter depends heavily on isotopic substitution. Other large variations in electronic energy transfer involving isotopic combinations of the $A^1\pi$ state of CO have been observed (24, 25, 27) and support the above argument.

1. W. H. FLYGARE. Acc. Chem. Res. **1**, 121 (1968).
2. J. I. STEINFELD. *In* Physical chemistry series one. Vol. 9. Chemical kinetics. *Edited by* J. C. Polanyi. Butterworth and Co. Ltd., London. 1972.
3. D. SECREST. Ann. Rev. Phys. Chem. **24**, 379 (1973).
4. R. C. AMME. *In* Advances in chemical physics. Vol. 28. The excited state in chemical physics. *Edited by* J. Wm. McGowan. John Wiley and Sons, New York. 1975.
5. P. D. GAIT. Ann. Rep. Prog. Chem. Sect. A: Phys. Inorg. Chem. **73**, 5 (1976).
6. K. F. HERZFELD and T. A. LITOVITZ. Absorption and dispersion of ultrasonic waves. Academic Press, Inc., New York. 1959.
7. T. L. COTTRELL and J. C. MCCOUBREY. Molecular energy transfer in gases. Butterworths, London. 1961.
8. H. P. BROIDA and T. CARRINGTON. J. Chem. Phys. **38**, 136 (1963).
9. J. I. STEINFELD and W. KLEMPERER. J. Chem. Phys. **42**, 3475 (1965).
10. CH. OTTINGER, R. VELASCO, and R. N. ZARE. J. Chem. Phys. **52**, 1636 (1970).
11. M. RUBINSON, B. GARETZ, and J. I. STEINFELD. J. Chem. Phys. **60**, 3082 (1974).
12. J. C. POLANYI and N. SATHYAMURTHY. Chem. Phys. **29**, 9 (1978).
13. PH. BRECHIGNAC, A. PICARD-BERSELLINI, R. CHARNEAU, and J. M. LAUNAY. Chem. Phys. **53**, 165 (1980).
14. AA. S. SUDBO and M. M. T. LOY. J. Chem. Phys. **76**, 3646 (1982).
15. A. C. VIKIS. J. Chem. Phys. **69**, 697 (1978).
16. A. C. VIKIS. Chem. Phys. Lett. **53**, 565 (1978).
17. A. C. VIKIS. J. Photochem. **19**, 1 (1982).
18. A. C. VIKIS. J. Chem. Phys. **69**, 703 (1978).
19. G. H. HERZBERG. Molecular spectra and molecular structure, spectra of diatomic molecules. 2nd ed., Van Nostrand Reinhold, New York. 1950.
20. R. E. IMHOF and F. H. READ. Chem. Phys. Lett. **11**, 326 (1971).
21. M. J. MUMMA, E. J. STONE, and E. C. ZIPF. J. Chem. Phys. **54**, 2627 (1971).
22. J. O. HIRSCHFELDER, C. F. CURTIS, and R. B. BIRD. Molecular theory of gases and liquids. John Wiley and Sons, Inc. New York. 1967.
23. R. L. BROWN and W. KLEMPERER. J. Chem. Phys. **41**, 3072 (1964).
24. L. A. MELTON and K.-C. YIIN. J. Chem. Phys. **62**, 2860 (1975).
25. L. A. MELTON and H.-T. YAO. J. Chem. Phys. **64**, 4689 (1976).
26. S. G. TILFORD and J. D. SIMMONS. J. Phys. Chem. Ref. Data, **1**, 147 (1972).
27. A. C. VIKIS. Chem. Phys. Lett. **57**, 522 (1979).

Can. J. Chem. Downloaded from www.nrcresearchpress.com by 210.87.254.5 on 09/06/12
For personal use only.

Reaction topology of excited state potential energy hypersurfaces

PAUL G. MEZEY

Department of Chemistry, University of Saskatchewan, Saskatoon, Sask., Canada S7N 0W0

Received July 13, 1982

This paper is dedicated to Professor Harry E. Gunning on the occasion of his 65th birthday

PAUL. G. MEZEY. Can. J. Chem. **61**, 956 (1983).

Topology ("rubber geometry") is an exceptionally suitable mathematical framework for a global quantum chemical description of the fundamental relations between nonrigid molecular systems, chemical reactions, and many photochemical processes. In Reaction Topology the concept of nuclear geometry is replaced by open subsets of an abstract nuclear configuration space ^{n}R. The ground and various excited state energy expectation value functionals induce a sequence of topologies in the nuclear configuration space ^{n}R, leading to a consistent topological description of molecular structure, excimers, exciplexes, and reaction mechanisms. Utilizing earlier results on topological properties of the abstract nuclear charge space ^{n}Z, a theorem is proven on the ordering of excited state potential energy hypersurfaces for sequences of isoelectronic molecules.

PAUL. G. MEZEY. Can. J. Chem. **61**, 956 (1983).

La topologie ("géométrie de caoutchouc") est un cadre mathématique exceptionnellement adéquat pour une description de la chimie quantique globale des relations fondamentales entre les systèmes moléculaires non rigides, les réactions chimiques et plusieurs processus photochimiques. Dans la topologie des réactions, on remplace le concept de géométrie nucléaire par des sous ensembles ouverts de configurations spaciales nucléaires abstraites, ^{n}R. Les valeurs fonctionnelles attendues pour les énergies de l'état fondamental et de divers états excités induisent une suite de topologie dans les configurations spatiales nucléaires, ^{n}R, conduisant à une description topologique cohérente de la structure moléculaire, des excéplex et des mécanismes de réaction. Utilisant des résultats antérieurs sur les propriétés topologiques de charge spatiale nucléaire abstraite, ^{w}Z, on démontre un théorème sur la façon d'ordonner les hypersurfaces d'énergie potentielle des états excités pour des séquences de molécules isoélectroniques.

[Traduit par le journal]

Can. J. Chem. Downloaded from www.nrcresearchpress.com by 210.87.254.6 on 09/06/12
For personal use only.

Introduction

In most experimental and theoretical studies on photochemical processes the investigation is usually restricted to small domains of selected potential energy surfaces, and relatively little is known about the global properties of the corresponding energy expectation value functionals. There are good reasons for this. On the one hand, it is difficult to obtain reliable experimental information on molecular conformations which lie far from the equilibrium nuclear configurations. On the other hand, theoretical calculations of reasonably complete potential energy hypersurfaces are extremely costly even for the smallest of molecules. There is, however, a continuous and rather spectacular progress in computing capabilities where, significantly, it is the software development which lags behind the development of computer hardware. Without a doubt, the accelerating development of computing capabilities is expected to continue, paving the way for global analyses of potential surfaces of more and more complex molecules. Meanwhile, advanced mathematical methods which may simplify the global analysis are also expected to find more applications. Most advanced of the geometrical models is the theory of the intrinsic reaction coordinate, developed by Fukui (1,2), and Tachibana and Fukui (3,4). The intrinsic reaction coordinate represents the link between earlier geometrial models and the topological model discussed in the present study.

In recent years several studies have been carried out on the applications of topology and manifold theory to the problems of potential energy hypersurfaces (5–13). The theory of topological manifolds and differential topology (14, 15), as applied to energy expectation value functionals, leads to Reaction Topology, a topological – quantum mechanical model of conformational and reaction processes of molecules, and a mathematical framework for computer-aided quantum chemical synthesis design.

Consider a system of N nuclei and k electrons in a specified electronic state. In the Born–Oppenheimer model the energy expectation value functional $E(\boldsymbol{r})$ can be regarded as an energy hypersurface defined over an abstract nuclear configuration space $^{n}\tilde{R}$. We shall assume that this nuclear configuration space has the following properties.

(i) Over a subset ^{n}R of $^{n}\tilde{R}$

$$[1] \quad {}^{n}R \subset {}^{n}\tilde{R}$$

the energy expectation value functional $E(\boldsymbol{r})$

$$[2] \quad \boldsymbol{r} \in {}^{n}R$$

is a twice continuously differentiable functional.[1]

(ii) Furthermore, we shall assume that the negative gradient

$$[3] \quad -\boldsymbol{g}(\boldsymbol{r}),\ \boldsymbol{r} \in {}^{n}R$$

corresponds to the laboratory frame forces of relaxation acting upon the nuclei. The above conditions are equivalent to those in the definition of the intrinsic reaction coordinate as defined by Tachibana and Fukui (3,4).

As a consequence of the above conditions, at every noncritical point $\boldsymbol{r} \in {}^{n}R$ the steepest descent path $P_{\boldsymbol{r}}$ is well defined with respect to the energy hypersurface $E(\boldsymbol{r})$ of the given electronic state. Furthermore, the above conditions and the boundedness of the energy hypersurface $E(\boldsymbol{r})$ also imply that this path $P_{\boldsymbol{r}}$ has a unique extremity $\boldsymbol{e}\ (P_{\boldsymbol{r}})$ which is a critical point of $E(\boldsymbol{r})$:

[1]Throughout this paper we shall assume differentiability of $E(\boldsymbol{r})$. Note that this condition is not necessarily valid for more general hypersurfaces and in certain domains, denoted by D_{excl}, $E(\boldsymbol{r})$ is not well defined. For a treatment of more general hypersurfaces and for the description of D_{excl}, see refs. 5, 6, and 8.

[4] $\boldsymbol{e}(P_r) = \boldsymbol{c}^{(\lambda,i)} \in {}^nR$

[5] $\boldsymbol{g}(\boldsymbol{c}^{(\lambda,i)}) = \boldsymbol{0}$

Here we use similar notations as in refs. 5–13: λ is the number of negative eigenvalues of the Hessian matrix $H(\boldsymbol{c}^{(\lambda,i)})$ of second derivatives of $E(\boldsymbol{r})$, expressed at the critical point $\boldsymbol{c}^{(\lambda,i)}$. λ is referred to as the critical point index of $\boldsymbol{c}^{(\lambda,i)}$, whereas i is an index of ordering.

Consider the set P of all steepest descent paths of $E(\boldsymbol{r})$ in ${}^nR$:

[6] $P = \{P_r\}$

Set P is partitioned into equivalence classes $P^{c(\lambda,i)}$ according to the extremities of the paths:

[7] $P = \bigcup_{\lambda,i} P^{c(\lambda,i)}$

The $P^{c(\lambda,i)}$ equivalence class is defined as

[8] $P^{c(\lambda,i)} = \{P_r : \boldsymbol{e}(P_r) = \boldsymbol{c}^{(\lambda,i)}\}$

Since there is a one-to-one correspondence between each noncritical point $\boldsymbol{r} \in {}^nR$ and steepest descent path $P_r \in P$, the equivalence class partitioning of P, eq. [7], implies an equivalence class partitioning of ${}^nR$:

[9] ${}^nR = \bigcup_{\lambda,i} C^{c(\lambda,i)}$

Sets $C^{c(\lambda,i)}$ are referred to as catchment regions and are defined by

[10] $C^{c(\lambda,i)} = \{\boldsymbol{c}^{(\lambda,i)}, \boldsymbol{r}, \boldsymbol{r} : P_r \in P^{c(\lambda,i)}, \boldsymbol{r} \in {}^nR\}$

Note that each critical point $\boldsymbol{c}^{(\lambda,i)}$ belongs to its own catchment region. Alternatively, one could regard the critical points as degenerate "single point paths," thus elements of the corresponding $P^{c(\lambda,i)}$ equivalence classes.

The family of catchment regions,

[11] $\mathbf{C}' = \{C^{c(\lambda,i)}\}$

forms a cover of the entire space ${}^nR$. Similarly, the family of closures of catchment regions, where the closure refers to the metric topology $\mathbf{T}$ on ${}^nR$,

[12] $\mathbf{C}'' = \{\bar{C}^{c(\lambda,i)}\}$

is also a cover of the nuclear configuration space:

[13] ${}^nR = \bigcup_{\lambda,i} \bar{C}^{c(\lambda,i)}$

Evidently, the family $\mathbf{C}$ defined as

[14] $\mathbf{C} = \mathbf{C}' \cup \mathbf{C}''$

is also a cover for ${}^nR$.

Families $\mathbf{C}'$, $\mathbf{C}''$, and $\mathbf{C}$ are defining subbases for three topologies, $\mathbf{T}_{C'}$, $\mathbf{T}_{C''}$, and $\mathbf{T}_C$, respectively, on the nuclear configuration space ${}^nR$. Finite intersections of elements of $\mathbf{C}'$, $\mathbf{C}''$, and $\mathbf{C}$ form proper bases for topologies $\mathbf{T}_{C'}$, $\mathbf{T}_{C''}$, and $\mathbf{T}_C$, respectively, and for either of C', C'', or C, the three criteria of topology are fulfilled:

[15] (i) ${}^nR, \emptyset \in \mathbf{T}_X$ ($X = C'$, C'' or C)

[16] (ii) $\bigcup_{\beta} T_\beta \in \mathbf{T}_X$ if each $T_\beta \in \mathbf{T}_X$

[17] (iii) $\bigcap_{j=i}^{m} T_j \in \mathbf{T}_X$ if each $T_j \in \mathbf{T}_X$, m is finite

It has been demonstrated earlier that the concept of catchment regions gives a topological definition of molecular structure and reaction mechanism (5, 6, 8). Points from a given catchment region, i.e. from equivalence class $C^{c(\lambda,i)} \subset {}^nR$, are physically equivalent in the following sense: an ideal, "vibrationless relaxation" of the nuclear geometry from any of these points leads to the *same* extremity $\boldsymbol{c}^{(\lambda,i)}$, i.e. to the same distinguished point of the catchment region. Since any distortion of nuclear geometry within the catchment region $C^{c(\lambda,i)}$ retains the reference to the same critical point $\boldsymbol{c}^{(\lambda,i)}$, these distortions are not large enough to be regarded as chemical changes. In the topological representation of ${}^nR$ the identity of chemical structures is considered unchanged when geometry variations are confined to one catchment region. The topological molecular structure is defined as a catchment region, i.e. a $\mathbf{T}$-open set of defining subbase $\mathbf{C}$ of topology $\mathbf{T}_C$.

For all stable molecular structures the critical point index $\lambda = 0$, that is, the corresponding $\mathbf{T}_C$-open catchment regions are those of *minima* on the energy hypersurface. For all transition structures[2] ("transition states") the critical point index $\lambda = 1$, i.e. the corresponding $\mathbf{T}_C$-open catchment regions are those of saddle points with one negative canonical curvature. Structures with $\lambda \geq 1$ are unstable and those with $\lambda > 1$ are of lesser importance (1).

Relations between catchment region topologies of ground and excited electronic states

Consider a sequence of electronic states, a_1, a_2,..., a_s and the respective energy hypersurfaces $E^{(1)}(\boldsymbol{r})$, $E^{(2)}(\boldsymbol{r})$,..., $E^{(s)}(\boldsymbol{r})$, defined over ${}^nR$. The corresponding catchment region topologies $\mathbf{T}_C{}^{(1)}$, $\mathbf{T}_C{}^{(2)}$,..., $\mathbf{T}_C{}^{(s)}$ are defined in terms of subbases $\mathbf{C}^{(1)}$, $\mathbf{C}^{(2)}$,..., $\mathbf{C}^{(s)}$, respectively.

In any one of the resulting topological spaces $({}^nR,\mathbf{T}_C{}^{(1)})$, $({}^nR,\mathbf{T}_C{}^{(2)})$,..., $({}^nR,\mathbf{T}_C{}^{(s)})$ the general results on the topological properties of molecular structures, reaction mechanisms, and reaction networks (5–8) are equally applicable. We show now that the topological properties of the entire sequence of electronic states a_1, a_2,..., a_s can be described collectively within a *single* topological space. Family $\mathbf{C}^{(1,2,\ldots,s)}$, given as

[18] $\mathbf{C}^{(1,2,\ldots,s)} = \bigcup_{l=1}^{s} \mathbf{C}^{(l)}$

is a defining subbase for a unique topology $\mathbf{T}_C{}^{(1,2,\ldots,s)}$ on the nuclear configuration space ${}^nR$. Due to the construction of subbase $\mathbf{C}^{(1,2,\ldots,s)}$ topology $\mathbf{T}_C{}^{(1,2,\ldots,s)}$ is finer than any of the $\mathbf{T}_C{}^{(l)}$ topologies, i.e. for the respective topological spaces the following relation holds:

[19] $({}^nR, \mathbf{T}_C{}^{(l)}) \subset ({}^nR, \mathbf{T}_C{}^{(1,2,\ldots,s)})$

[20] $l = 1, 2,\ldots, s$

That is, any chemical structure or reaction mechanism of any of the energy hypersurfaces $E^{(l)}(\boldsymbol{r})$ being a $\mathbf{T}_C{}^{(l)}$-open set of the $({}^nR, \mathbf{T}_C{}^{(l)})$ topological space, ($l = 1, 2,\ldots, s$), is also a $\mathbf{T}_C{}^{(1,2,\ldots,s)}$-open set of the $({}^nR,\mathbf{T}_C{}^{(1,2,\ldots,s)})$ topological space. Consequently, all relations between chemical structures or reaction mechanisms in electronic states a_1, a_2,..., a_s of the system of N nuclei and k electrons can be described by *intersection and inclusion relations* between $\mathbf{T}_C{}^{(1,2,\ldots,s)}$-open sets of topological space $({}^nR,\mathbf{T}_C{}^{(1,2,\ldots,s)})$. Such intersection relations can be represented by intersection graphs, which graphs have been utilized earlier for the analysis of reaction networks defined for a single energy hypersurface (8). In special cases

[2]We prefer using the term "transition structure", as suggested by J. A. Pople, rather than the more conventional term "transition state".

Can. J. Chem. Downloaded from www.nrcresearchpress.com by 210.87.254.6 on 09/06/12
For personal use only.

Can. J. Chem. Downloaded from www.nrcresearchpress.com by 210.87.254.6 on 09/06/12
For personal use only.

where intersection relations are replaced by inclusion relations, as has been the case for level set topologies (5*c*), a concise description of these relations can be given in terms of incidence matrices.

Consider now the simplest nontrivial case of $s = 2$, i.e. a *pair* of energy hypersurfaces, $E^{(1)}(\boldsymbol{r})$ and $E^{(2)}(\boldsymbol{r})$, where a_1 is the electronic ground state and a_2 is an excited electronic state. Consider further a molecular structure $C^{c(\lambda,i,1)}$, with respect to $E^{(1)}(\boldsymbol{r})$, and another one, structure $C^{c(\lambda',i',2)}$, with respect to $E^{(2)}(\boldsymbol{r})$, where the third index in the superscript refers to the electronic state. Both catchment regions are open sets in the topological space $({}^{n}R, \mathbf{T}_C^{(1,2)})$:

[21] $C^{c(\lambda,i,1)} \in \mathbf{T}_C^{(1,2)}$

and

[22] $C^{c(\lambda',i',2)} \in \mathbf{T}_C^{(1,2)}$

Consequently, intersection and inclusion relations between them are topological relations in space $({}^{n}R, \mathbf{T}_C^{(1,2)})$.

There are five distinct possibilities:

[23] (*i*) $C^{c(\lambda,i,1)} \cap C^{c(\lambda',i',2)} = \phi$

[24] (*ii*) $C^{c(\lambda,i,1)} \cap C^{c(\lambda',i',2)} \neq \phi$

where

[25] $C^{c(\lambda,i,1)} \not\supset C^{c(\lambda',i',2)}$

and

[26] $C^{c(\lambda,i,1)} \not\subset C^{c(\lambda',i',2)}$

[27] (*iii*) $C^{c(\lambda,i,1)} \supset C^{c(\lambda',i',2)}$

where

[28] $C^{c(\lambda,i,1)} \not\subset C^{c(\lambda',i',2)}$

[29] (*iv*) $C^{c(\lambda,i,1)} \subset C^{c(\lambda',i',2)}$

where

[30] $C^{c(\lambda,i,1)} \not\supset C^{c(\lambda',i',2)}$

[31] (*v*) $C^{c(\lambda,i,1)} = C^{c(\lambda',i',2)}$

These five cases are shown schematically in Fig. 1.

Consider the special case of

[32] $\lambda = \lambda' = 0$

i.e. the relation between two stable molecules $C = C^{c(0,i,1)}$ and $C' = C^{c(0,i',2)}$ on the two energy hypersurfaces $E^{(1)}(\boldsymbol{r})$ and $E^{(2)}(\boldsymbol{r})$. An $a_1 \rightarrow a_2$ electronic excitation of molecule C cannot lead directly to C' in case (*i*), and can lead only to C' in cases (*iv*) and (*v*). In cases (*ii*) and (*iii*) C' is only one of the possible products. Note that for polyatomic systems cases (*i*)–(*iv*) are the most common and case (*v*), i.e. exact coincidence of C and C', is unlikely. However, for diatomic molecules case (*v*) is rather common, since whenever the two states a_1 and a_2 are nondissociative, the following relations are valid between the topological spaces over the nuclear configuration space ${}^{1}R$:

[33] $\mathbf{T}_C^{(1)} = \mathbf{T}_C^{(2)} = \mathbf{T}_C^{(1,2)} = \{\phi, {}^{1}R\}$

that is,

[34] $({}^{1}R, \mathbf{T}_C^{(1)}) = ({}^{1}R, \mathbf{T}_C^{(2)}) = ({}^{1}R, \mathbf{T}_C^{(1,2)})$

Relation [33] is a simple consequence of the usual shapes of Morse potentials.

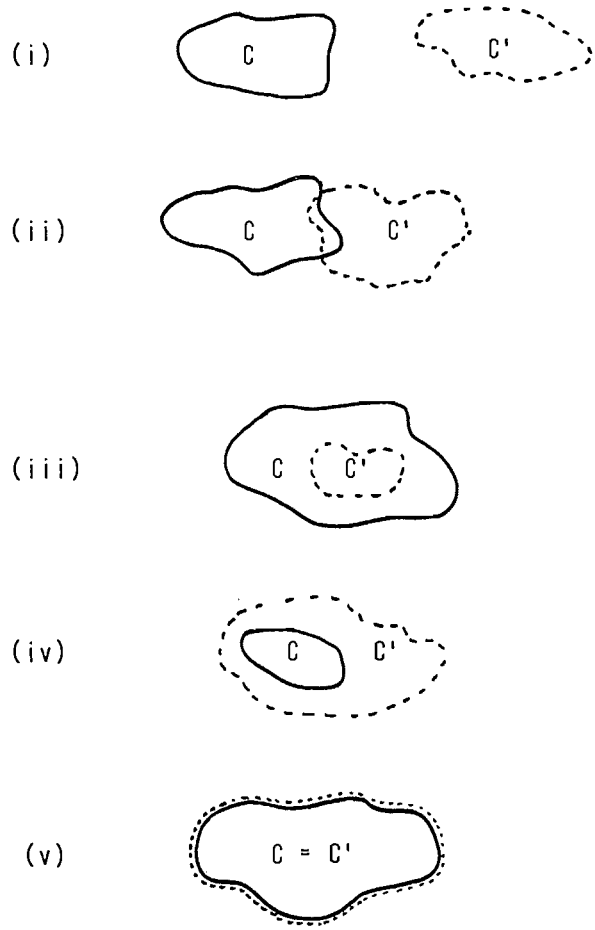

FIG. 1. The five topologically distinct cases, (*i*)–(*v*), for the relative positions of catchment regions $C = C^{c(\lambda,i,1)}$ and $C' = C^{c(\lambda',i',2)}$ of electronic states a_1 and a_2, respectively.

An $a_2 \rightarrow a_1$ de-excitation from structure C' can lead only to C in cases (*iii*) and (*v*). In cases (*ii*) and (*iv*) C is only one of the possible products, whereas in case (*i*) the de-excitation cannot lead directly to C. If chemical structure C is a single molecule (e.g. not a pair of dissociated fragments), then in cases (*iii*) and (*v*) C' *cannot* be an excimer (or exciplex). On the other hand, if case (*i*), that is relation [23], is valid for the given set C', $C' \in \mathbf{T}_C^{(2)}$ and for *every* $C \in \mathbf{T}_C^{(1)}$ where $C = C^{c(0,i,1)}$, then C' is an excimer (or exciplex) of electronic state a_2.

Photochemical relations in the abstract nuclear charge space ${}^{w}Z$. A topological "ordering rule" for the electronic states of isoelectronic molecules in product space ${}^{w}Z \otimes {}^{n}R$

We shall apply two theorems (12) on the topological properties of the abstract nuclear charge space ${}^{w}Z$ to obtain an ordering rule for excited state electronic energy hypersurfaces of isoelectronic molecules.

Space ${}^{w}\tilde{Z}$ has been defined (12) as

[35] ${}^{w}\tilde{Z} = \{z,\ z : z_i$ is the charge of the i-th nucleus, $i = 1,\ldots, w\}$

and usually a subset ${}^{w}Z$ of ${}^{w}\tilde{Z}$,

[36] ${}^{w}Z = \{z,\ z : z_i \geq 0\ (i = 1,\ldots, w),\ z \in {}^{w}Z\}$

is considered. Level sets of the electronic energy functional

Can. J. Chem. Downloaded from www.nrcresearchpress.com by 210.87.254.6 on 09/06/12
For personal use only.

$E_e(\boldsymbol{r},z)$ in ^{w}Z are defined for any fixed $\boldsymbol{r} \in {}^{n}R$ and energy value E^0 as

[37] $F_{E^0}(\boldsymbol{r}) = \{z, z : E_e(\boldsymbol{r},z) \geq E^0, z \in {}^{w}Z\}$

The first theorem of ref. 12 states that all such level sets in ^{w}Z are *convex* sets for *any* fixed $\boldsymbol{r} \in {}^{n}R$.

The second theorem of ref. 12 states that the electronic energy of molecule $M^{(1)}$ of nuclear charges $z^{(1)}$ is higher than that of molecule $M^{(2)}$ of nuclear charges $z^{(2)}$ ($M^{(2)}$ isoelectronic with $M^{(1)}$), if $z^{(2)}$ lies *outside* of a hypercube $C^0 \subset {}^{w}Z$ having one vertex the origin, and $z^{(1)}$ lies *within* a pyramid $P^0 \subset C^0$ with apex the origin.[3] Theorem 2 is valid for *any* geometries $\boldsymbol{r}^{(1)}$, $\boldsymbol{r}^{(2)} \in {}^{n}R$ if the electronic state considered is the *lowest* of a given manifold, i.e. the electronic wavefunctions $\psi^{(1)}$ and $\psi^{(2)}$ are variational.

It has been demonstrated earlier on many examples that the convexity theorem alone is often sufficient to establish electronic energy inequalities between molecules (9, 10, 12). Here we shall propose a trivial and a somewhat less trivial extension of these inequalities.

A simple *"rule of ordering"* for electronic hypersurfaces can be derived for isolectronic molecules $M^{(1)}$, $M^{(2)}$,..., $M^{(t)}$, fulfilling the conditions of Theorem 1 or Theorem 2.

Theorem: Consider a sequence of isoelectronic molecules $M^{(1)}$, $M^{(2)}$,..., $M^{(t)}$, and a sequence of electronic states a_1, a_2,..., a_s, all of which are the *lowest* of a given electronic manifold.

(*i*) If convexity of level sets in ^{w}Z implies the

[38] $E_e^{(1)} \geq E_e^{(2)} \geq \ldots \geq E_e^{(t)}$

order of electronic energies for a fixed geometry $\boldsymbol{r} \in {}^{n}R$ and for one of the electronic states, a_l ($1 \leq l \leq s$), then the ordering [38] is valid at *any* other geometry $\boldsymbol{r}' \in {}^{n}R$ and for any of the electronic states a_1, a_2,..., a_s.

(*ii*) If the sequence of points $z^{(1)}$, $z^{(2)}$,..., $z^{(t)}$ in ^{w}Z is such that the pyramid–cube separation applies for adjacent point pairs in the above order, in one of the electronic states a_l, then the ordering [38] is valid in any of the electronic states a_1, a_2,... a_s for *arbitrary geometries* $\boldsymbol{r}^{(1)}$, $\boldsymbol{r}^{(2)}$,..., $\boldsymbol{r}^{(t)} \in {}^{n}R$.

The proof of part (*i*) follows directly from Theorem 1 of ref. 12, since this theorem is applicable at any *common* geometry $\boldsymbol{r} \in {}^{n}R$. Since the electronic wavefunctions are variational for each of the a_1, a_2,..., a_s electronic states, ordering [38] is valid for any one of these states.

The proof of part (*ii*) follows from a repeated application of Theorem 2, ref. 12, on the sequence of point pairs $z^{(1)},z^{(2)}$; $z^{(2)},z^{(3)}$;..., $z^{(t-1)},z^{(t)}$. Since the above theorem gives a geometry-independent inequality for electronic energies, ordering [38] is valid for any *independent* choice of geometries $\boldsymbol{r}^{(1)}$, $\boldsymbol{r}^{(2)}$,..., $\boldsymbol{r}^{(t)}$ in any of the electronic states a_1, a_2,..., a_s.

Rephrased in terms of hypersurfaces, result (*i*) states that the electronic energy hypersurface $E_e(\boldsymbol{r})$ of molecule $M^{(j)}$ lies above that of $M^{(j')}$ over the entire ^{n}R if $j < j'$ in the sequence. Result (*ii*) is much stronger: if the conditions are fulfilled, then the *lowest* point of the electronic energy hypersurface $E_e^{(j)}(\boldsymbol{r})$ of molecule $M^{(j)}$ lies *above*[4] the *highest* point of the electronic energy hypersurface $E_e^{(j)}$ of $M^{(j')}$ if $j < j'$. Examples for cases (*i*) and (*ii*) are shown in Fig. 2.

[3] All but one of the faces of P^0 lie on the faces of C^0.

[4] In the special case of equality in [38] the lowest value of $E_e^{(j)}(\boldsymbol{r})$ may coincide with the highest value of $E_e^{(j')}(\boldsymbol{r})$.

Note that the result of Theorem 2, quoted above, can be further strengthened if geometry variations are restricted to various catchment regions $C^{c(\lambda,i)}$ of the nuclear configuration space (12), which restriction implies a constraint on homotopical variations of boundary sets of E_{E^0} level sets within cube C^0.

It has been shown (12), that for such limited geometry variations the boundary sets of level sets F_{E^0} are confined to a subset $T^{0(1)}$ of the closure of the relative complement T^0 of the pyramid P^0 in cube C^0:

[39] $T^{0(1)} \subset \overline{T^0} = \overline{C^0 \backslash P^0}$

This set $T^{0(1)}$, characteristic to a given catchment region of the nuclear configuration space ^{n}R, generates a partitioning of $\overline{T^0}$:

[40] $\overline{T^0} = \bigcup_{j=1}^{m} T^{0(j)}$, $m \geq 3$,

where $T^{0(2)}$ contains the center of cube C^0 and $T^{0(3)}$ contains the corner of C^0 with the longest distance from the origin (as measured in the metric topology $\mathbf{T}$ of ^{w}Z). For *any* two geometries within the catchment region,

[41] $\boldsymbol{r}^{(1)}, \boldsymbol{r}^{(2)} \in C^{c(\lambda,i)}$

and for any two points $z^{(1)}, z^{(2)} \in {}^{w}Z$ fulfilling conditions

[42] $z^{(1)} \in P^0 \cup T^{0(2)}$

and

[43] $z^{(2)} \in T^{0(3)} \cup ({}^{w}Z \backslash C^0)$

the inequality

[44] $E(\boldsymbol{r}^{(1)},z^{(1)}) \geq E_e(\boldsymbol{r}^{(2)},z^{(2)})$

applies.

The above result can be combined with the ordering rule and one can obtain a sequence of inequalities for the electronic energy functional $E_e(\boldsymbol{r},z)$ defined on the product space $^{n}R \otimes {}^{w}Z$. Taking the simplest nontrivial case of $t = 2$, in the $({}^{n}R,\mathbf{T}_C^{(1,2)})$ topological space, the union $C^{(1,2)}$ of catchment regions $C^{c(\lambda_1,i_1,l)}$ and $C^{c(\lambda_2,i_2,l)}$ of molecular structures $M^{(1)}$ and $M^{(2)}$ is an open set:

[45] $C^{(1,2)} \in \mathbf{T}_C^{(1,2)}$

where

[46] $C^{(1,2)} = C^{c(\lambda_1,i_1,l)} \cup C^{c(\lambda_2,i_2,l)}$

and

[47] $l = 1$ or 2

If the subsets $T^{0(1)}$, $T^{0(2)}$, and $T^{0(3)}$ of hypercube C^0 are defined with respect to set $C^{(1,2)}$, then relations [42] and [43] are sufficient to estabish the ordering

[48] $E_e^{(l)}(M^{(1)}) \geq E_e^{(l)}(M^{(2)})$

for both electronic states a_1 and a_2. Note that this result is stronger than the ordering relation obtained directly from Theorem 2, since here conditions [42] and [43] are less restrictive than the pyramid–hypercube separation of points $z^{(1)}$ and $z^{(2)}$.

Example:

We shall illustrate the application of the ordering rule, case (*ii*), on the following sequence of chemical systems:

$$M^{(1)} = \begin{matrix} COO^- \\ | \\ COO^- \end{matrix} + H_2O$$

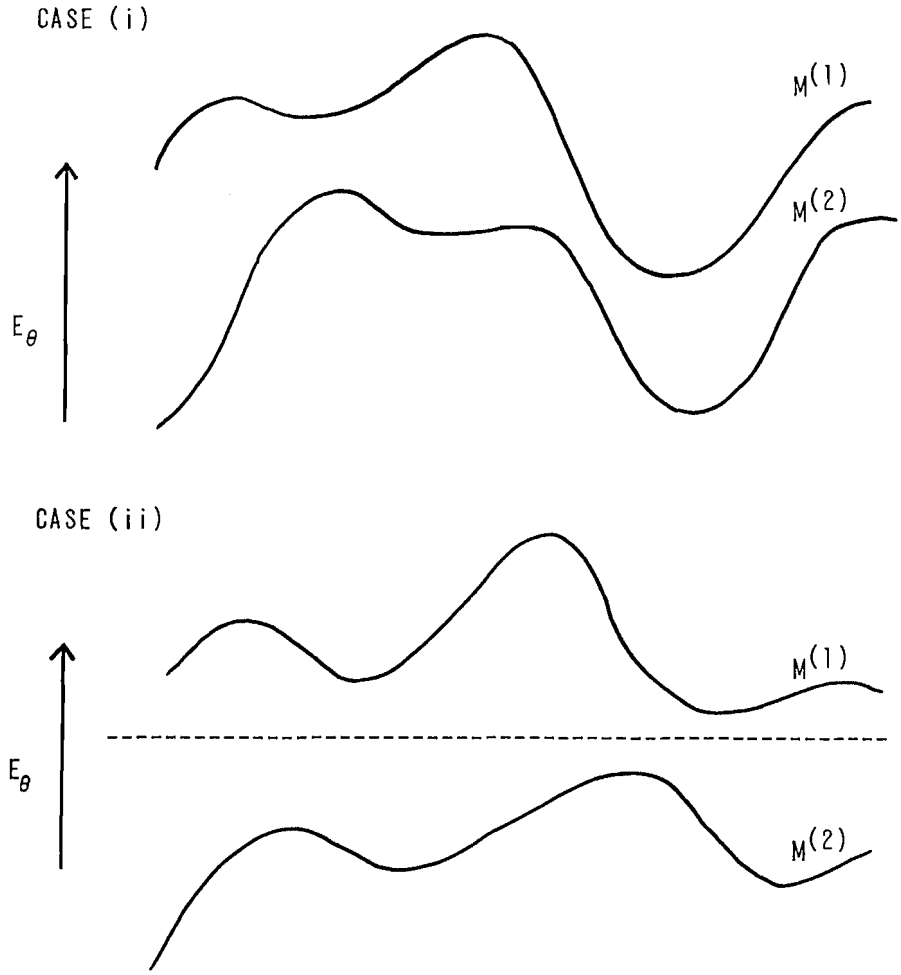

FIG. 2. The ordering rule, based on convexity of level sets of space ^{n}Z in case (*i*), implies that the electronic energy hypersurface of molecule $M^{(1)}$ lies above that of molecule $M^{(2)}$. A pyramid–hypercube separation of nuclear charge vectors $z^{(1)}$ and $z^{(2)}$ in ^{n}Z (see text for details) in case (*ii*) implies a stronger constraint, i.e. the existence of a constant energy value separating the two hypersurfaces. Both cases (*i*) and (*ii*) apply to any electronic state of sequence $a_1, a_2, \ldots, a_s$, which are the lowest states in their respective electronic manifolds.

$M^{(2)} = CsH$

$M^{(3)} = La^{+}$

Let us assume that the electronic states a_1, a_2, and a_3 are the lowest singlet, triplet, and quintuplet states, respectively. Not that case (*ii*) corresponds to the stronger conditions, consequently these systems also serve as examples for case (*i*).

Furthermore, the dimensions of both ^{n}Z and ^{n}R can be chosen such that they accommodate the largest chemical system, in our case $M^{(1)}$. For the rest of the chemical systems "dummy nuclei" with zero nuclear charges can be added in order to make up for the "missing" dimensions.

The above systems are isoelectronic ($k = 56$). Point $z^{(1)} \in {}^{9}Z$ falls within the largest pyramid $P^0 \subset C^0$ with apex the origin:

$$z^{(1)} \in P^0$$

where hypercube C^0 has the edge length of 54.5 protonic charge units, whereas point $z^{(2)}$ lies in the complement of C^0:

$$z^{(2)} \in ({}^{9}Z \setminus C^0)$$

On the other hand,

$$z^{(2)} \in P^{0'}$$

where pyramid $P^{0'} \subset C^{0'}$ is the largest pyramid in hypercube $C^{0'}$, the latter having an edge length of 56.5 protonic charge units. Point $z^{(3)}$ lies outside of both cubes,

$$z^{(3)} \in ({}^{9}Z \setminus C^{0'})$$
$$(C^0 \subset C^{0'})$$

Consequently, for both pairs $z^{(1)}, z^{(2)}$, and $z^{(2)}, z^{(3)}$ there exists a pyramid–cube separation in the 9-dimensional nuclear charge space ^{9}Z, and the ordering rule is applicable:

$$E_e(M^{(1)}) \geq E_e(M^{(2)}) \geq E_e(M^{(3)})$$

in *all three* electronic states a_1, a_2, and a_3. That is, the electronic energy hypersurfaces $E_e^{(j)}(\boldsymbol{r})$, ($j = 1, 2, 3$) must be separated by constant energy values over the entire nuclear configuation space ^{n}R, for each of the a_1, a_2, and a_3 electronic states.

Acknowledgement

The financial support of the Natural Sciences and Engineering Research Council of Canada is gratefully acknowledged.

1. K. FUKUI. J. Phys. Chem. **74**, 4161 (1970).
2. K. FUKUI. Acc. Chem. Res. **14**, 363 (1981).
3. A. TACHIBANA and K. FUKUI. Theor. Chim. Acta, **49**, 321 (1978).
4. A. TACHIBANA and K. FUKUI. Theor. Chim. Acta, **51**, 189

Can. J. Chem. Downloaded from www.nrcresearchpress.com by 210.87.254.6 on 09/06/12
For personal use only.

(1979); **51**, 275 (1979); **57**, 81 (1980).
5. (*a*) P. G. MEZEY. Theor. Chim. Acta, **54**, 95 (1980); (*b*) **58**, 309 (1981); (*c*) **60**, 97 (1981); (*d*) **62**, 133 (1982).
6. P. G. MEZEY. Int. J. Quantum Chem. SB, **8**, 185 (1981). Presented at the 1981 Sanibel Symposium.
7. P. G. MEZEY. Chem. Phys. Lett. **82**, 100 (1981); **86**, 562 (1982).
8. P. G. MEZEY. Theor. Chim. Acta, **60**, 409 (1982).
9. P. G. MEZEY. Int. J. Quantum Chem. SC, **15**, 279 (1981).
10. P. G. MEZEY. Theor. Chim. Acta, **59**, 321 (1981).
11. P. G. MEZEY. Chem. Phys. Lett. **87**, 277 (1982).
12. P. G. MEZEY. Int. J. Quantum Chem. **22**, 101 (1982).
13. P. G. MEZEY. Mol. Phys. **47**, 121 (1982).
14. E. H. SPANIER. Algebraic topology. McGraw–Hill, New York. 1966.
15. V. GUILLEMIN and A. POLLACK. Differential topology. Prentice Hall, Inc., Englewood Cliffs, NJ. 1974.

Can. J. Chem. Downloaded from www.nrcresearchpress.com by 210.87.254.6 on 09/06/12
For personal use only.

Photolyse du méthyl-3-butène-1 et du méthyl-2-butène-1 à 185 nm

DANIELLE HOUDE, HÉLÈNE DESLAURIERS ET GUY J. COLLIN[1]

Département des Sciences fondamentales, Université du Québec à Chicoutimi, Chicoutimi (Qué.) Canada G7H 2B1

Reçu le 19 juillet 1982

Cet article est dédié au Professeur Harry E. Gunning à l'occasion de son 65e anniversaire

DANIELLE HOUDE, HÉLÈNE DESLAURIERS et GUY J. COLLIN. Can. J. Chem. **61**, 962 (1983).

Nous avons étudié la photolyse du méthyl-3-butène-1 (M3B1) et du méthyl-2-butène-1 (M2B1) à 185 nm en phase gazeuse. Les processus primaires de fragmentation observés confirment la prépondérance de la fragmentation via la rupture de la liaison β(C—C) avec formation concomitante de radicaux méthyles et soit de radicaux α-méthallyles (cas du M3B1) soit de radicaux β-méthallyles (cas du M2B1). La comparaison de ces deux systèmes inspire une méthode très primitive quant à la détermination de l'énergie supportée par les radicaux méthallyles: 48% des radicaux C_4H_7* ainsi produits ont une énergie interne entre 42 et 58 kcal mol^{-1} à 185 nm. D'autres comparaisons sont faites avec ce qui a été observé précédemment à 163 et à 174 nm. Ces observations confirment la conclusion que l'énergie du photon est très probablement distribuée de façon statistique dans le tissu vibrationnel de la molécule photoexcitée avant sa fragmentation.

DANIELLE HOUDE, HÉLÈNE DESLAURIERS, and GUY J. COLLIN. Can. J. Chem. **61**, 962 (1983).

The gaseous photolysis of 3-methyl-1-butene (M3B1) and of 2-methyl-1-butene (M2B1) has been studied at 185 nm. The observed primary fragmentation processes of the photoexcited molecules confirm the leading role of the β(C—C) bond rupture, with formation of methyl radicals and either α-methallyl radicals (M3B1 system) or β-methallyl radicals (M2B1 system). The comparison of the two systems suggests a very simple method to evaluate the energy content of the methallyl excited radical: 48% of C_4H_7* radicals so produced have an energy content of 50 ± 8 kcal mol^{-1} at 185 nm. Other comparisons have been made with results previously obtained at 163 and 174 nm. These observations support the idea that the energy of the incident photon is very likely distributed among the vibrational frame of the photoexcited molecule before the occurrence of fragmentation processes.

Introduction

La photolyse du méthyl-2-butène-1 (M2B1) et du méthyl-3-butène-1 (M3B1) dans la région de l'ultraviolet sous vide a déjà fait l'objet d'études à différentes longueurs d'onde. À 147 nm, à 123,6 et à 104,8−106,7 nm, les produits principaux sont l'allène et le radical méthyle dans le cas du M2B1 (1) et le butadiène-1,3 et le radical méthyle dans le cas du M3B1 (2). Il faut mentionner en outre une isomérisation importante: formation de méthyl-2-butène-2 aux plus courtes longueurs d'onde, c'est-à-dire à des énergies supérieures aux potentiels d'ionisation du monomère et probablement associée à la photoionisation. À 174 et à 163 nm, la fragmentation observée a été expliquée sur la base de la rupture presque quantitative de la liaison C—C située en position β par rapport à la double liaison, suivie d'une importante fragmentation secondaire des radicaux α-méthallyles en butadiène-3 et un atome d'hydrogène (cas du M3B1) ou des radicaux β-méthallyles en allène et un radical méthyle (cas du M2B1) (3).

À 185 nm, les triméthyléthylène (méthyl-2-butène-2; M2B2) et tétraméthyléthylène ont montré un comportement similaire avec en outre formation d'isomères (4, 5). Le présent rapport a pour but de vérifier à 185 nm la validité du mécanisme réactionnel de fragmentation proposé à plus courtes longueurs d'onde. D'autre part, il est également pertinent de vérifier l'apparition éventuelle d'isomères, tout en poursuivant notre effort de réflexion sur la distribution de l'énergie dans la molécule photoexcitée (1−3).

Méthode expérimentale

Les techniques expérimentales utilisées ont été déjà abondamment décrites dans la littérature (1−5). Les méthylbutènes sont des produits A.P.I. de pureté moléculaire supérieure à 99,9%. L'analyse du M2B1 révèle les impuretés suivantes: méthyl-2-butène-2: 103 ± 3 ppm (échantillon A) ou 340 ± 10 ppm (échantillon B); butadiène-1,3: 1,2 ppm (A) ou 4 ppm (B). Celle du M3B1 montre la présence du butadiène-1,3 (2,0 ± 0,2 ppm), isoprène (0,6 ppm) et méthyl-2-butène-2 (3,8 ± 0,3 ppm). L'analyse du DI (Merck, Sharp, and Dohme of Canada) montre la présence de benzène: 300−500 ppm. Celle du D_2S montre de faibles signaux correspondants au méthane (20 ppm) et à l'acétylène (35 ppm).

Les analyses ont été réalisées par chromatographie en phase gazeuse (double flammes ionisantes). La lampe utilisée est une lampe à mercure "basse pression" achetée chez Philipps. Elle est vérifiée à l'aide d'un monochromateur d'un demi-mètre McPherson. L'actinométrie est réalisée en utilisant la photolyse de l'éthylène ($\Phi(C_2H_2)$ = 0,50) (6, 7).

Résultats

Les résultats exprimés sous la forme des rendements quantiques sont présentés dans les tableaux et figures qui accompagnent la discussion. À ces résultats il importe d'ajouter les remarques suivantes: (a) Les coefficients d'absorption de la lumière ont été mesurés à 185 nm: ϵ_{DI} = 140 ± 10% (8), ϵ_{D_2S} = 800 ± 5% (9), et $\epsilon_{M3B1} = \epsilon_{M2B1}$ = 7000 ± 15% L $mol^{-1}cm^{-1}$ (10). (b) En présence d'oxygène (10%) ou d'oxyde nitrique (5%), aucun produit, entre 133 et 16000 N m^{-2} (1−150 Torr), sauf le butadiène-1,3 (Fig. 1) et l'allène (Fig. 3), n'a un rendement quantique supérieur à 0,01. Ces mêmes rendements quantiques sont peu ou pas affectés par la variation de pression. (c) Nous n'avons pas pu mesurer de façon convenable la formation d'isomères provenant de la photolyse directe de chacun des deux monomères. Dans le cas du méthyl-2-butène-1, étant donné le niveau d'impuretés dans l'échantillon A, les rendements quantiques Φ(M3B1) et Φ(M2B2) sont inférieurs à 0,01 quelle que soit la pression du monomère. Aucun autre isomère n'a pu être mis en évidence. Dans le cas du méthyl-3-butène-1, la formation du M2B2 est plus évidente bien que l'incertitude expérimentale soit appréciable (Tableau 1).

[1]Auteur à qui toute correspondance doit être adressée.

Can. J. Chem. Downloaded from www.nrcresearchpress.com by 210.87.254.40 on 09/06/12
For personal use only.

TABLEAU 1. Photolyse du méthyl-3-butène-1 pur à 185 nm: rendements quantiques[a]

Produit	Pression (N m^{-2}) 133	350	1300	4000	6650
CH_4	$0{,}02_6$	0,02	$0{,}02_2$	$0{,}02_4$	0.03_4
$C_2H_4 + C_2H_2$[b]	$0{,}02_5$	0,03	$0{,}02_3$	$0{,}01_4$	$0{,}01_1$
C_2H_6	0,24	0,21	$0{,}24_7$	0,24	0,31
C_3H_6	$0{,}00_7$	$0{,}00_6$	$0{,}00_7$	$0{,}00_3$	$0{,}00_3$
$C_3H_4 + C_3H_8$	$0{,}00_5$	$0{,}00_5$	$0{,}00_3$	$0{,}00_4$	$0{,}00_5$
iso-C_4H_{10}	$0{,}00_6$	$0{,}00_4$	$0{,}00_4$	$0{,}00_7$	$0{,}00_7$
C_4H_6-1,3	0,20	0,18	$0{,}11_4$	$0{,}05_3$	0,03
C_4H_8-2[c]	0,04	0,02	$0{,}01_2$	$0{,}00_8$	Traces
X[d]	$0{,}01_3$	0,01	0,01	$0{,}01_4$	0,01
iso-C_5H_{12}	0,02	$0{,}00_7$	$0{,}00_4$	Traces	Traces
M2B2	n.m.[f]	$0{,}00_5$	$0{,}00_9$	0,04	0,02
C_5H_{10}-2[e]	$0{,}14_5$	0,16	$0{,}23_5$	0,21	$0{,}21_4$
C_6H_{14}[g]	0,10	0,07	$0{,}04_8$	$0{,}02_8$	$0{,}03_7$

[a]Incertitude expérimentale: ≤5%, sauf dans le cas du M2B2: $\Delta\Phi/\Phi \simeq \pm 20\%$.
[b]$C_2H_2/C_2H_4 < 0{,}2$.
[c]*cis/trans* = 0,55 ± 0,05.
[d]Composé inconnu apparaissant dans le pied du monomère sur la colonne de squalane (27); ce produit apparaît aussi en présence de O_2, NO, D_2S ou DI.
[e]*trans/cis* = 1,27; voir réf. 20.
[f]n.m.: non mesuré.
[g]Diméthyl-2,3-butane.

TABLEAU 2. Photolyse du méthyl-3-butène-1 à 185 nm en présence d'additifs: rendements quantiques[a]

Produit	Rendement quantique M3B1 1360 N m^{-2} D_2S[d] 150 N m^{-2}	M3B1 4000 N m^{-2} D_2S[d] 400 N m^{-2}	M3B1 1300 N m^{-2} DI[d] 150 N m^{-2}	M3B1 4000 N m^{-2} DI[d] 400 N m^{-2}
CH_4	0,35	0,6	1,0	1,1
$C_2H_2 + C_2H_4$	0,07	0,04	0,07	0,1
C_2H_6	0,16	0,11	$0{,}00_5$	0,01
C_3H_8	0,02	0,02	0,05	0,10
C_4H_6-1,3	0,00	0,03	0,10	0,08
C_4H_8-1	0,00	0,01	0,15	0,21
C_4H_8-2[b]	0,03	0,03	0,50	0,65
iso-C_5H_{12}	0,12	0,06	0,15	0,35
C_5H_{10}-2[c]	0,22	0,16	0,03	0,04

[a]$\Delta\Phi/\Phi \simeq \pm 15\%$.
[b]*cis/trans* ≃ 0,66 ± 0,1.
[c]*cis/trans* ≃ 0,70 ± 0,05.
[d]Additif.

Discussion

La fragmentation de la molécule photoexcitée

La photodécomposition des M3B1 et M2B1 à 185 nm est similaire à celle déjà observée à 163 nm que ce soit en l'absence ou en présence d'additifs: tableaux 1–4 (3). On ne rediscutera pas ici en détails cette photodécomposition si ce n'est pour en relever les principales caractéristiques et différences. Tout d'abord, dans les systèmes purs ou en présence d'oxygène ou d'oxyde nitrique ajoutés en vue d'éliminer la formation de produits via les recombinaisons radicalaires possibles, les rendements quantiques mesurés à 185 nm sont en première approximation les mêmes ou plus faibles que ceux mesurés à 163 nm. Dans les systèmes purs, le produit dont le rendement est le plus élevé est l'éthane. Conformément à la discussion présentée à 163 nm (3), et étant donnée l'absence de butane normal d'une part et la disparition de ce produit en présence soit d'oxygène, soit d'oxyde nitrique d'autre part, l'éthane est très probablement le résultat de la recombinaison des radicaux méthyles. On note aussi la formation importante de méthane (Tableaux 2 et 4), lorsque la photolyse a lieu en présence soit de D_2S, soit de DI:

[1] $CH_3 + RD \rightarrow CH_3D + R$ (où R ≡ I ou DS)

L'addition de D_2S ou de DI entraîne des modifications majeures sur la formation des produits (Tableaux 2 et 4). Cependant l'usage de l'un ou l'autre de ces deux additifs ne permet une interprétation très quantitative des résultats. Tout d'abord D_2S n'intercepte pas, ou mal, les radicaux allyliques de telle sorte que les radicaux α-méthallyles éventuellement formés dans le M3B1 ne sont pas interceptés. Lorsque le taux de

Can. J. Chem. Downloaded from www.nrcresearchpress.com by 210.87.254.40 on 09/06/12
For personal use only.

Can. J. Chem. Downloaded from www.nrcresearchpress.com by 210.87.254.40 on 09/06/12
For personal use only.

TABLEAU 3. Photolyse du méthyl-2-butène-1 pur à 185 nm: rendements quantiques[a]

Produit	Pression (N m^{-2}) 133	400	1330	6650
CH_4	0,04	0,06	0,06	0,09
$C_2H_4 + C_2H_2$[d,c]	$0,00_6$	$0,00_7$	$0,00_8$	$0,00_8$
C_2H_6[b]	0,55	0,64	0,58	0,65
C_3H_8[b] + propyne[b]	0,03	0,03	0,02	0,03
Allène (C_3H_4)[d]	0,08	0,09	$0,04_5$	$0,01_8$
C_3H_6[d]	n.m.	0,01	0,01	$0,01_2$
iso-C_4H_8[d]	$0,03_6$	$0,04_5$	$0,04_4$	0,03
iso-C_5H_{12}[b]	0,01	n.m.	$0,00_6$	$0,00_7$
C_6H_{12}[e,b]	n.m.	0,06	0,07	0,08
C_6H_{14}[f,b]	n.m.	0,04	0,04	0,04

[a]Incertitude expérimentale: $\Delta\Phi/\Phi \simeq \pm 5\%$ et $\pm 10\%$ dans le cas où la valeur absolue Φ est inférieure à 0,1.
[b]Produits dont les rendements sont inférieurs à 0,008 en présence de 10% d'oxygène ou d'oxyde nitrique.
[c]$C_2H_2/C_2H_4 \leq 0,1$.
[d]Produits peu ou pas affectés par la présence d'oxygène ou d'oxyde nitrique.
[e]C_6H_{12} ≡ méthyl-2-pentène-1 + éthyl-2-butène-1 en quantités similaires.
[f]C_6H_{14} ≡ diméthyl-2,2-butane.

conversion s'élève, les radicaux α-méthallyles entrent en compétition avec le deutérium sulfuré pour intercepter les radicaux méthyles, et l'on assiste à la formation de pentène-2 (Tableau 2). On sait en outre que le radical HS s'additionne probablement rapidement sur le butadiène-1,3 (11, 12). Ce dernier produit est alors consommé probablement dans un mécanisme en chaîne radicalaire.

De son côté l'iodure d'hydrogène est un bien meilleur intercepteur vis-à-vis des radicaux allyliques que l'hydrogène sulfuré (13):

[2] $CH_3\dot{C}HCH{=}CH_2 + DI \rightarrow$ 1- ou 2-$C_4H_7D + I$

[3] $CH_2{=}C(CH_3)\dot{C}H_2 + DI \rightarrow$ iso-$C_4H_7D + I$

Rappelons que les atomes d'iode ne sont pas insensibles à la présence du monomère insaturé (14, 15). Dans le cas particulier du M2B1 on observe une isomérisation du monomère avec production du M2B2 dans un mécanisme en chaîne radicalaire avec probablement apparition importante d'isopentane. En outre le dépôt d'iode sur la fenêtre inhérent à l'usage de DI, comme celui de soufre dans le cas de l'utilisation de D_2S, diminue sensiblement la précision expérimentale. On peut cependant qualitativement à partir des tableaux 2 et 4 confirmer la présence de radicaux α- et β-méthallyles.

L'analyse du tableau 1 permet de rationnaliser simplement la fragmentation du M3B1 selon le mécanisme déjà proposé à 163 nm (Fig. 1):

[4] M3B1 + $h\nu \rightarrow$ M3B1**

[5] M3B1** $\rightarrow CH_3\cdot + CH_3CH{=}C\dot{H}CH_2$* ou $CH_3\dot{C}HCH{=}CH_2$*
$\Delta H = 69$ kcal mol^{-1} (16)

[6] $CH_3\dot{C}HCH{=}CH_2$* ou $CH_3CH{=}C\dot{H}CH_2$* $\rightarrow$ H + $CH_2{=}CHCH{=}CH_2$
$\Delta H = 49$ kcal mol^{-1}
$E_A = 50,4$ kcal mol^{-1} (17, 18)

[7] $CH_3\dot{C}HCH{=}CH_2^* \xrightarrow{M} CH_3\dot{C}HCH{=}CH_2$ ...

On peut estimer le rendement quantique des radicaux α-méthallyles en considérant toutes leurs réactions possibles:

[A] $\Phi([5]) = \Phi(C_4H_6\text{-}1,3) + \Phi(C_5H_{10}\text{-}2) + \Phi(C_8H_{14})$

En effet les radicaux méthallyles stabilisés (issus de la réaction [7]) peuvent se recombiner ou dismuter entre eux (19) ou avec les radicaux méthyles (20). Si l'on sait mesurer le pentène-2, il faut aussi évaluer la fraction de la recombinaison méthyle + α-méthallyle qui reforme le monomère (20). Quant au C_8H_{14}, produit non analysé, on peut aussi l'estimer via la relation suivante (21):

[B] $$\frac{\Phi(CH_3 + \alpha\text{-}C_4H_7)}{\Phi(CH_3 + CH_3)^{\frac{1}{2}} \cdot \Phi(\alpha\text{-}C_4H_7 + \alpha\text{-}C_4H_7)^{\frac{1}{2}}} = 2,0$$

L'utilisation de cette équation de concert avec les remarques précédentes montre que le rendement de la réaction [5] est tel que: $\Phi([5]) = \Phi([7]) + \Phi(\text{butadiène-1,3}) = 0,8 \pm 0,2$ à toute pression entre 130 et 20 000 N m^{-2} (1 à 150 Torr). De la même manière, on peut estimer le rendement en radicaux méthyles: $\Phi(CH_3) = 0,85 \pm 0,10$ (3). On en conclut que la principale sinon la seule réaction importante de fragmentation de la molécule parente photoexcitée est la réaction [5]. Il s'ensuit que le système à 185 nm est beaucoup moins complexe qu'à 163 nm et que le radical méthyle a essentiellement la possibilité de réagir avec lui-même ou avec le radical α-méthallyle. Par exemple, le rendement en atomes d'hydrogène semble moins élevé à 185 nm qu'à 163 nm: la comparaison des rendements Φ_{DI}(iso-C_5H_{12}) confirme cette assertion.

Il faut aussi noter la formation d'isoprène qui pourrait être le résultat du mécanisme suivant (Fig. 2):

[8] M3B1** $\longrightarrow$ H + $(CH_3)_2\dot{C}CH{=}CH_2$*

[9] $(CH_3)_2\dot{C}CH{=}CH_2$* $\longrightarrow$ H + iso-C_5H_8

[10] $(CH_3)_2\dot{C}CH{=}CH_2^* \xrightarrow{(M)} (CH_3)_2\dot{C}CH{=}CH_2$

La rupture du β(C—H) serait donc faiblement en compétition avec la rupture β(C—C): $\Phi_0(C_5H_8) = 0,01$. Ce mécanisme a été observé dans le cas de la photolyse du M2B2 (22), et est probablement responsable en partie de la formation de l'isopentane en présence de D_2S ou de DI ou du diméthyl-2,3-butane dans le système pur.

L'alternative est d'admettre une élimination moléculaire d'hydrogène. Si tel est le cas, la figure 2 permettrait d'évaluer le temps de vie de la molécule photoexcitée. En effet l'interception de la droite avec l'axe des pressions permet d'évaluer la constante de vitesse de la réaction [11]: $k_{11} \simeq 2 \times 10^9$ s^{-1}. Cette constante de vitesse permettrait à son tour d'évaluer le temps de vie de la molécule photoexcitée à 5×10^{-10} s. C'est un temps comparable à celui mesuré dans le cas de la photolyse de l'hexène-1 à 184,9 nm (23). Ce mécanisme n'exclut cependant pas le précédent.

[11] M3B1** $\rightarrow H_2$ + iso-C_5H_8

[12] M3B1** + M3B1 $\rightarrow$ 2 M3B1

La situation est similaire dans le cas du méthyl-2-butène-1 et ne commande pas d'autres discussions (3). Il faut cependant rappeler l'importance de la formation de radicaux méthyles — formation de méthane en présence de D_2S ou de DI et d'éthane dans le produit pur — et de radicaux β-méthallyles — formation d'isobutène en présence de DI.

[13] $CH_2{=}C(CH_3)CH_2CH_3 + h\nu \rightarrow CH_2{=}C(CH_3)CH_2CH_3$**

[14] $CH_2{=}C(CH_3)CH_2CH_3$** $\rightarrow CH_3 + CH_2{=}C(CH_3)\dot{C}H_2$*
$\Delta H = 71$ kcal mol^{-1} (24)

TABLEAU 4. Photolyse du méthyl-2-butène-1 à 185 nm en présence d'additifs: rendements quantiques[a]

Produit	Rendement quantique M2B1 1330 N m^{-2} DI (10)[b]	M2B1 4000 N m^{-2} DI (10)[b]	M2B1 1360 N m^{-2} D_2S (16)[b]	M2B1 4260 N m^{-2} D_2S (10)[b]
CH_4	0,95	1,0	0,55	0,55
$C_2H_4 + C_2H_2$	0,07	0,06	0,12	0,04
C_2H_6	0,04	0,05	0,05	0,12
C_3H_6	0,03	0,04	0,03	$0,01_5$
C_3H_4 (allène)	0,01	$0,00_6$	0,01	0,05
C_3H_8	0,00	0,00	0,04	0,05
iso-C_4H_8	0,60	0,85	0,02	0,02
C_4H_8-2	0,05	0,04	Traces	Traces
iso-C_5H_{12}	0,7	1,0	0,06	0,07

[a]Voir note, tableau 2.
[b]Additif (%).

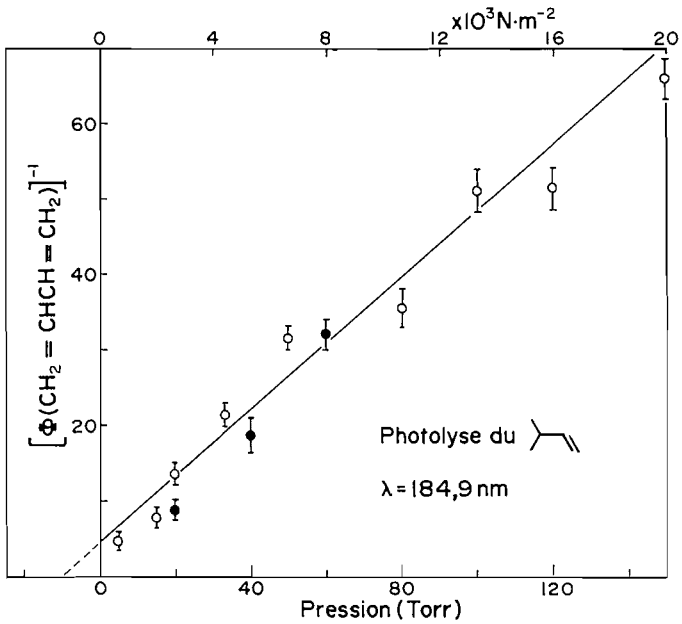

FIG. 1. Courbe de Stern–Volmer relative à la formation du butadiène-1,3 dans la photolyse du mélange M3B1/O_2 (100:10), ○; ou du mélange M3B1/NO (100:5), ●.

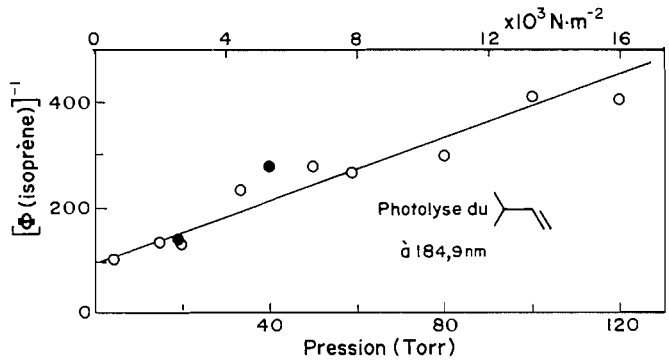

FIG. 2. Courbe de Stern–Volmer relative à la formation d'isoprène dans la photolyse du mélange M3B1/O_2 (100:10), ○; et du mélange M3B1/NO (100:5), ●.

[15] $CH_2{=}C(CH_3)\dot{C}H_2{}^* \xrightarrow{k_d} CH_2{=}C{=}CH_2 + CH_3$
ΔH = 49 kcal mol^{-1}
E_A = 56 kcal mol^{-1} (17)

[16] $CH_2{=}C(CH_3)\dot{C}H_2{}^* \xrightarrow{k_s[M]} CH_2{=}C(CH_3)\dot{C}H_2$

L'effet de la pression est aussi similaire à celui observé à plus courtes longueurs d'onde. L'effet le plus important porte sur la formation de l'allène (cas du M2B1) et du butadiène-1,3 (cas du M3B1). Les rendements quantiques de ces deux produits formés dans les réactions [5]–[7] et [14]–[16] sont susceptibles de suivre la loi de Stern–Volmer. Par exemple, dans le cas du M2B1 (Fig. 3),

[C] $[\Phi(\text{allène})]^{-1} = [\Phi_0(\text{allène})]^{-1} + [\Phi_0(\text{allène})]^{-1} k_s[M]/k_d$

où Φ_0 est le rendement du produit à pression nulle. Les figures 1 et 3 montrent la bonne linéarité obtenue pour les droites de Stern–Volmer. Ces droites permettent d'obtenir non seulement le rendement des produits à pression nulle, mais encore, via l'interception de la droite avec l'axe des abcisses, le rapport $-k_s/k_d$. En faisant l'hypothèse d'une unique collision pour stabiliser l'intermédiaire activé, c'est-à-dire en utilisant cette réaction de stabilisation comme horloge interne, on peut déterminer la constante de vitesse d'ordre 1 de la réaction de fragmentation du radical méthallyle. Cette particularité a été utilisée, via un calcul RRKM, pour évaluer l'énergie interne des méthallyles excités qui se fragmentent (25). Les résultats obtenus ne valent que pour les radicaux qui obéissent au mécanisme de Stern–Volmer. Ils ne permettent donc pas d'avoir une quelconque idée de l'énergie supportée par la majorité des $C_4H_7{}^*$ qui ne se fragmentent pas.

La distribution de l'énergie dans les fragments primaires

Il faut mentionner ici les différences ou ressemblances avec celles observées à plus courtes longueurs d'onde (Tableau 5). Tout d'abord, alors que la fragmentation primaire de la liaison β(C—C) devient la principale sinon la seule rupture primaire, il y a de moins en moins de ruptures secondaires du radical β-méthallyle avec l'accroissement de la longueur d'onde (Tableau 5). À 185 nm, à pression nulle, le rendement quantique de l'allène est de 0,04: il est donc tentant d'en déduire que le rendement des radicaux β-méthallyles activés qui ont au moins l'énergie interne suffisante pour permettre le passage au-dessus de la barrière de potentiel relatif à la réaction [12] est

Can. J. Chem. Downloaded from www.nrcresearchpress.com by 210.87.254.40 on 09/06/12
For personal use only.

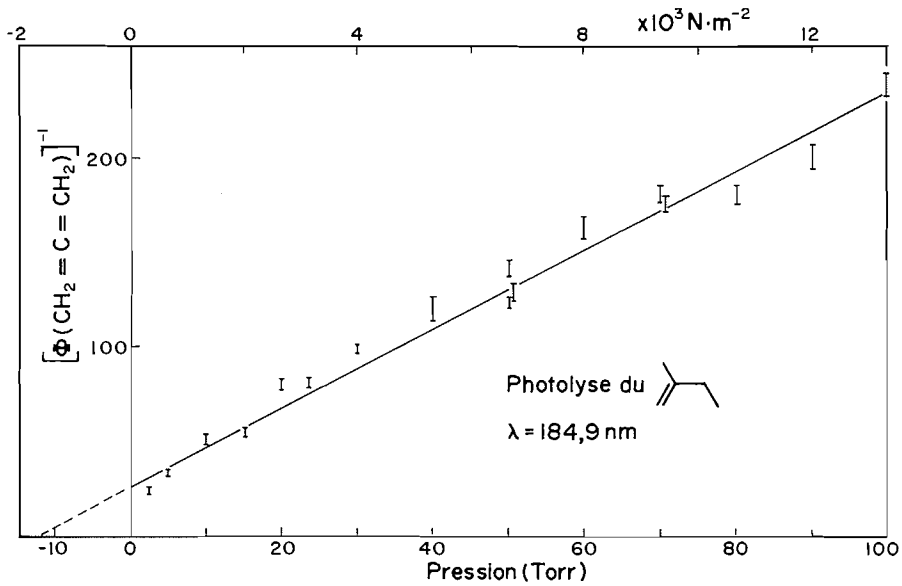

FIG. 3. Courbe de Stern–Volmer relative à la formation d'allène dans la photolyse du M2B1/O_2 (100:10).

TABLEAU 5. Photolyse de C_5H_{10} dans l'uv très lointain; fragmentation des radicaux méthallyles[a]

λ (nm)	r^2	a	b	a/b (Torr)	a^{-1} (Φ_0)
Méthyl-2-butène-1					
185	0,990	26	2,2	11 ± 1	0,04
174	0,984	7,0	0,9	8 ± 1	0,14
163	0,989	6,1	0,87	7 ± 1	0,165
147	0,98	1,67	0,05	35 ± 3	0,58
Méthyl-3-butène-1					
185	0,968	4,1	0,42	10 ± 1	0,24
174	0,99	2,1	0,2	11 ± 1	0,48
163	0,985	1,9	0,18	11 ± 1	0,58
147	0,99	1,1	0,022	49 ± 5	0,9
cis-Pentène-2					
174	0,986	[b]	[b]	13 ± 1	[b]
163	0,99	2,24	0,168	13 ± 1	0,45
147	0,98	1,56	0,02	63 ± 6	0,63

[a]Les données sont déterminées à partir des droites Stern–Volmer [C]; r^2 est le coefficient de corrélation, $a \equiv \Phi_0^{-1}$ et $b \equiv \Phi_0^{-1}\, k_s/k_d$.

[b]Les rendements quantiques n'ont pas été exactement mesurés (3).

de 0,04: E_{int} = 56 kcal mol^{-1}. Il s'ensuit, comme on l'a mentionné plus haut, qu'il est difficile d'obtenir une idée convenable de la distribution de l'excédent de l'énergie du photon dans la molécule photoexcitée puisqu'on n'a aucune idée de l'énergie supportée par 96% des radicaux β-méthallyles.[2] La situation semble un peu plus favorable dans le cas du butadiène-1,3 puisqu'à 185 nm environ 24% des radicaux α-méthallyles se fragmentent. En d'autres termes, le rendement des radicaux α-méthallyles qui ont l'énergie interne suffisante pour passer par-dessus la barrière de potentiel de la réaction [6] est voisin de 0,24: E_{int} = 50,4 kcal mol^{-1}. Ainsi l'importance de la fragmentation secondaire est plus grande dans le cas du M3B1 que dans celui du M2B1. Il est pertinent d'essayer de comprendre le pourquoi de cette différence. En fait ces deux systèmes sont très semblables. Les spectres d'absorption sont insuffisamment bien connus pour que l'on puisse sortir une quelconque différence entre 130 et 190 nm. Les deux molécules isomères absorbent à 185 nm avec formation concomitante d'une molécule excitée π,π* (26). On ne peut guère dire plus sur ce qui peut se passer entre l'absorption du photon et la fragmentation primaire, celle qui donne naissance au radical méthallyle. On peut raisonnablement penser que le cheminement de l'énergie dans les tissus électronique et vibrationnel des deux molécules est semblable. Dans les deux cas, il y a rupture primaire du lien β(C—C), tout comme dans les autres alcènes, et en particulier comme dans celui du *cis*-pentène-2 (3). Thermodynamiquement les différences sont vraiment mineures sauf peut-être entre les réactions secondaires de fragmentation des radicaux α- et β-méthallyles. Alors que les enthalpies sont les mêmes, la barrière de potentiel relative à l'addition du radical méthyle sur l'allène, $E_A(CH_3 + CH_2{=}C{=}CH_2)$ égale 8,1 kcal mol^{-1} (17) tandis que celle

[2]Pour la simplicité de la compréhension on a supposé implicitement que la fragmentation primaire de la liaison β(C—C) est quantitative à 185 nm.

Can. J. Chem. Downloaded from www.nrcresearchpress.com by 210.87.254.40 on 09/06/12
For personal use only.

relative à l'addition d'un atome d'hydrogène sur le butadiène-1,3 est de 1,3 kcal mol^{-1} (17). Cette différence entraîne une différence similaire dans l'énergie d'activation des processus inverse de fragmentation. Ainsi, si cette approche est correcte, le fait est que l'énergie requise pour la fragmentation du radical α-méthallyle requiert 7 kcal mol^{-1} d'énergie en moins. Puisqu'à 174 et à 163 nm, le comportement des radicaux α-méthallyles obtenus soit à partir du M3B1, soit à partir du *cis*-pentène-2 est le même, cela n'infirme pas cette approche. En considérant la photolyse des C_5H_{10} comme un même système on peut en déduire qu'à 185 nm 4% des radicaux C_4H_7* ont une énergie interne d'au moins 57 kcal mol^{-1}, que 24% ont au moins 50,4 et donc que 76% ont moins que 50,4 kcal mol^{-1}. À 174 nm, l'énergie du photon s'est enrichie de quelque 8 kcal $einstein^{-1}$. En faisant les hypothèses grossières que (a) le fragment primaire méthyle emporte à 174 nm la même énergie qu'à 185 nm et (b) l'énergie de recul des deux fragments primaires l'un par rapport à l'autre est similaire à ces deux longueurs d'onde, l'augmentation de 8 kcal mol^{-1} entraîne qu'à 174 nm, 14% des fragments C_4H_7* ont plus de 57 kcal mol^{-1}, 48% ont plus de 50,4 et donc 52% ont moins de cette valeur. L'enrichissement de 8 kcal mol^{-1} a donc déplacé 24% des radicaux C_4H_7* de la tranche la moins énergétique vers la tranche intermédiaire (celle comprise entre 50,4 et 57 kcal mol^{-1}). De son côté la tranche supérieure s'est gonflée de 4 à 24% du total. Par comparaison, on est donc amené à proposer qu'à 185 nm, 48% des radicaux C_4H_7* ont une énergie interne comprise entre 42 et 57 kcal mol^{-1}. Si l'on admet une distribution statistique de l'énergie du photon à travers le tissu vibrationnel de la molécule avant la fragmentation primaire, on devrait trouver une énergie moyenne voisine de 59 kcal mol^{-1} (25). Compte tenu des hypothèses faites, et surtout du caractère simpliste de ce raisonnement, on ne peut qu'être conduit à admettre cette distribution statistique de l'énergie du photon. En effet, la plus grande faiblesse de cette approche réside dans l'hypothèse faite que nécessairement si la fragment C_4H_7* a une énergie interne tout juste supérieure à ce qui est requis par la barrière de potentiel, il se fragmentera. Compte tenu de l'échelle de pression étudiée, il faut certainement déplacer les tranches énergétiques proposées de plusieurs kcal vers les valeurs supérieures pour avoir une vue plus réaliste.

Il serait aventureux de poursuivre la comparaison avec ce qui est obtenu à 163 nm. Cependant, ces comparaisons grossières confirment que le radical C_4H_7* libéré dans le processus primaire de fragmentation a une énergie relativement importante, distribuée largement autour de 55 ± 20 kcal mol^{-1}. On peut donc inférer une large distribution de l'énergie dans la molécule avant la rupture primaire.

Remerciements

Nous voulons remercier particulièrement le Conseil de Recherche en Sciences Naturelles et en Génie (CRSNG) de même que le Fonds FCAC pour l'aide apportée tout au long de ce projet.

1. H. Gagnon, G. J. Collin et C. Bertrand. J. Phys. Chem. **78**, 98 (1974).
2. G. J. Collin et C. Bertrand. J. Photochem. **3**, 123 (1974).
3. G. J. Collin, H. Deslauriers et S. Auclair. Can. J. Chem. **57**, 863 (1979).
4. G. J. Collin et H. Deslauriers. Nouv. J. Chim. **5**, 447 (1981).
5. G. J. Collin, H. Deslauriers et A. Więckowski. J. Phys. Chem. **85**, 944 (1981).
6. P. Potzinger, L. C. Glasgow et G. Von Bünau. Z. Naturforsch. A, **27**, 628 (1972).
7. H. Okabe. *Dans* Photochemistry of small molecules. Wiley–Interscience, New York. 1978. p. 126.
8. B. J. Huebert et R. M. Martin. J. Phys. Chem. **72**, 3046 (1968).
9. K. Watanabe et A. S. Jursa. J. Chem. Phys. **41**, 1650 (1964).
10. J. G. Calvert et J. N. Pitts, Jr. *Dans* Photochemistry. 2e éd. J. Wiley and Sons, Inc. New York. 1965. p. 494.
11. D. M. Graham, R. L. Mieville et C. Sivertz. Can. J. Chem. **42**, 2239 (1964).
12. G. J. Collin et P. M. Perrin. Can. J. Chem. **50**, 2400 (1972).
13. P. Ausloos, R. E. Rebbert et S. G. Lias. J. Photochem. **2**, 267 (1974).
14. Z. B. Alfassi, D. M. Golden et S. W. Benson. Int. J. Chem. Kinet. **6**, 155 (1973).
15. A. S. Rodgers et M. C. R. Wu. J. Am. Chem. Soc. **95**, 6913 (1973).
16. A. B. Trenwith. Trans. Faraday Soc. **66**, 2805 (1970).
17. P. I. Abell. Compr. Chem. Kinet. **18**, 111 (1976). *Edité par* C. H. Bamford et C. F. H. Tipper. Elsevier, Amsterdam.
18. W. Tsang, Int. J. Chem. Kinet. **5**, 929 (1973).
19. D. L. Baulch, P. K. Chown et D. C. Montague. Int. J. Chem. Kinet. **11**, 1055 (1979).
20. D. C. Montague. Int. J. Chem. Kinet. **5**, 513 (1973), et références citées.
21. R. E. Weston, Jr. et H. A. Schwarz. *Dans* Chemical kinetics. Prentice Hall, Englewood Cliffs, NJ. 1972. p. 90.
22. G. J. Collin, H. Deslauriers et J. Deschênes. Can. J. Chem. **57**, 870 (1979).
23. H. Deslauriers, G. J. Collin et B. Simard. J. Photochem. Sous presse.
24. A. B. Trenwith et S. P. Wrigley. J. Chem. Soc. Faraday Trans. I, **73**, 817 (1977).
25. G. J. Collin et H. Deslauriers. Int. J. Chem. Kinet. **12**, 17 (1980).
26. M. B. Robin. *Dans* Higher excited states of polyatomic molecules. Vol. II. Academic Press, New York. 1975. pp. 1–49.
27. R. A. Hively et R. E. Hinton. J. Gas Chromatogr. **6**, 203 (1968).

Can. J. Chem. Downloaded from www.nrcresearchpress.com by 210.87.254.40 on 09/06/12
For personal use only.

Mechanism of the reaction of oxygen atoms, $O(^3P)$ with dimethyl disulfide[1]

D. L. SINGLETON AND R. S. IRWIN

Division of Chemistry, National Research Council of Canada, Ottawa, Ont., Canada K1A 0R9

AND

R. J. CVETANOVIĆ[2]

Chemical Kinetics Division, National Bureau of Standards, Washington, DC 20234, U.S.A.

Received July 19, 1982

This paper is dedicated to Professor Harry E. Gunning on the occasion of his 65th birthday

D. L. SINGLETON, R. S. IRWIN, and R. J. CVETANOVIĆ. Can. J. Chem. **61**, 968 (1983).

The mechanism of the reaction of ground state oxygen atoms, $O(^3P)$, with CH_3SSCH_3 was studied by analysis of the final products. Oxygen atoms were generated by mercury photosensitized decomposition of N_2O such that $[CH_3SSCH_3] \gg [O]$. The only detected product was $CH_3S(O)_2SCH_3$, which accounted for close to 70% of the oxygen atoms reacted. Isomerization of small amounts of *cis*- or *trans*-2-butene added to the reaction mixture indicated the presence of CH_3S radicals. The results are consistent with the primary reaction $O + CH_3SSCH_3 \rightarrow CH_3SO + CH_3S$. The effect of small amounts of CH_3SH and H_2S on the yields of $CH_3S(O)_2SCH_3$ and the products formed provide further information on the nature of the secondary chemistry. A comprehensive reaction mechanism has been proposed.

D. L. SINGLETON, R. S. IRWIN et R. J. CVETANOVIĆ. Can. J. Chem. **61**, 968 (1983).

On a étudié, par l'analyse des produits finaux, le mécanisme de la réaction des atomes d'oxygène à l'état fondamental, $O(^3P)$, avec le CH_3SSCH_3. On génère les atomes d'oxygène par la décomposition photosensibilisée par le mercure du N_2O de telle sorte que $[CH_3SSCH_3] \gg [O]$. Le seul produit détecté est le $CH_3S(O)_2SCH_3$ qui compte presque pour 70% des atomes d'oxygène qui ont réagi. L'isomérisation de petites quantités de butène-2 *cis* et *trans* ajoutées au mélange réactionnel indique la présence de radicaux CH_3S. Les résultats sont en accord avec la réaction initiale $O + CH_3SSCH_3 \rightarrow CH_3SO + CH_3S$. L'effet de petites quantités de CH_3SH et de H_2S sur les rendements en $CH_3S(O)_2SCH_3$ et les produits formés fournissent une information plus poussée sur la nature de la chimie secondaire. On propose un mécanisme global de réaction.

[Traduit par le journal]

Introduction

Studies of the mechanisms of the gas phase reactions of oxygen atoms with thiols and organic sulfides indicate attack at the sulfur atom (1–3) with the formation of an energy rich adduct which subsequently fragments or which might be stabilized by collisions. We have recently carried out an extensive study of the kinetics (4) and mechanisms (5) of oxygen atom reactions with several organic sulfur compounds including CH_3SH, C_2H_5SH, CH_3SCH_3, and CH_3SSCH_3. From a detailed analysis of products observed in the reaction of single organic sulfur compounds and their mixtures (5), it was possible to arrive at substantial quantitative information on the primary and secondary reaction mechanisms. In the case of $O + CH_3SH$, the following reaction channels and their relative importance were indicated:

$$\begin{aligned} O + CH_3SH &\rightarrow CH_3 + HSO \ (60\%) \\ &\rightarrow H + CH_3SO \ (30\%) \\ &\rightarrow OH + CH_3S \ (10\%) \end{aligned}$$

For the reaction with methyl sulfide, our analysis of the stable products indicated that the major channel is

$$O + CH_3SCH_3 \rightarrow CH_3 + CH_3SO \ (>95\%)$$

There was no evidence of stabilization of a $CH_3S(O)CH_3$ adduct even at 1200 Torr.

In the $O + CH_3SSCH_3$ reaction, no volatile products were formed, and it was possible only to suggest by analogy with the thiol and sulfide a reaction mechanism with the following primary steps,

$$[1a] \quad O + CH_3SSCH_3 \rightarrow CH_3S + CH_3SO$$

$$[1b] \quad O + CH_3SSCH_3 \xrightarrow{[M]} CH_3S(O)SCH_3$$

In either case, on the basis of the postulated secondary reactions, it was expected that $CH_3S(O)_2SCH_3$ would be the final stable oxidation product. However, it was not possible to analyze for this compound by the analytical technique used, and the postulated mechanism was only tentative.

The present work was initiated to determine the products of the $O + CH_3SSCH_3$ reaction by an analytical procedure capable of recovering less volatile oxidation products. Also, several experiments were done to determine whether the reaction proceeded exclusively by addition–stabilization, reaction [1*b*], or whether fragmentation (or direct displacement), reaction [1*a*], occurred.

Experimental

Oxygen atoms were generated by mercury photosensitized decomposition of N_2O in a cylindrical quartz reaction cell (54 mm od × 81 mm) containing a few drops of mercury. Two short tubes fitted with septa extended from the side of the cell, which allowed the cell to be flushed with N_2O at atmospheric pressure and the reactants to be introduced by syringe. The source of the 253.7 nm radiation was a low pressure mercury lamp. A Corning 9-54 filter[3] removed the

[1]N.R.C.C. No. 20659.

[2]Visiting Scientist.

[3]Certain commercial materials and equipment are identified in this paper in order to specify adequately the experimental procedure. In no case does such identification imply recommendation or endorsement by the National Bureau of Standards, nor does it imply the material or equipment identified is necessarily the best available for the purpose.

Can. J. Chem. Downloaded from www.nrcresearchpress.com by 210.87.254.105 on 09/06/12
For personal use only.

Can. J. Chem. Downloaded from www.nrcresearchpress.com by 210.87.254.105 on 09/06/12
For personal use only.

184.9 nm line, and a neutral density filter reduced the intensity to acceptable levels. A rotating Teflon coated magnet agitated the mercury surface to help maintain a saturated vapor pressure of mercury. After irradiation, 0.5 cm^3-atm of propane was added as an internal standard, and aliquots were withdrawn by syringe and analyzed by gas chromatography with either thermal conductivity or flame ionization detection. A 1/8-in × 5-ft stainless steel column packed with Porapak QS was used for most analyses, and temperature programming up to 220°C was required. Analyses of *cis*- and *trans*-2-butene were done by gas chromatography on a 1/8 in × 10 ft column of Carbopak + 0.19% picric acid at room temperature. Analyses of N_2 and CH_4 were not made. After analysis of the gas phase, 1 cm^3 of acetone was injected into the reaction cell to dissolve any products adhering to the walls. Aliquots of the acetone solution were withdrawn by syringe and analyzed by gas chromatography using the Porapak QS column and the acetone as an internal standard. Response factors for the detectors were determined with standard mixtures. The response factor for $CH_3S(O)_2SCH_3$ determined for standard mixtures of 4 μmol and 40 μmol in 1 cm^3 of acetone showed a difference of about 16%, indicating that a small amount was lost on the chromatographic column at lower concentrations. The response factors were reproducible, and the appropriate values were used in the experiments.

Results

As in the previous work (5), no volatile products were detected in the O + CH_3SSCH_3 reaction. However, the product methyl methanethiosulfonate, $CH_3S(O)_2SCH_3$, was identified in the acetone used to rinse the reaction cell. Identification of the product was established by comparison of its gas chromatographic retention time with an authentic sample and by its mass spectrum obtained by gas chromatography – mass spectrometry. It was not formed in the absence of photolysis. In Table 1 the yield of $CH_3S(O)_2SCH_3$ is given as a function of reaction time. The yield increases linearly with time, as is evident in Fig. 1, indicating that it is not formed as a result of secondary oxygen atom reactions.

A series of experiments was done to determine the yield of $CH_3S(O)_2SCH_3$ per oxygen atom reacted, $\phi[CH_3S(O)_2SCH_3]$. The rate of production of oxygen atoms was determined by measuring the addition products, 1,2-epoxybutane, butanal, and 2-butanone produced in the O + 1-butene reaction at 1 atm of N_2O and ~30 Torr of 1-butene. Earlier measurements indicated that these products account for ~85% of the oxygen atoms reacted. The actinometry was done immediately before or after a measurement of the yield of $CH_3S(O)_2SCH_3$. The average value of $\phi[CH_3S(O)_2SCH_3]$ for 3 pairs of experiments was 0.34 ± 0.09, where the uncertainty is the 95% confidence interval. Thus the measured yield of $CH_3S(O)_2SCH_3$ accounts for close to 70% of the oxygen atoms reacted.

In order to determine whether the reaction proceeds solely by way of addition–stabilization as in reaction [1*b*], or whether reaction [1*a*] occurs to any extent, some experiments were done with small amounts of *cis*- or *trans*-2-butene added to the reaction mixture. Any CH_3S radicals formed in reaction [1*a*] would be expected to isomerize the olefin (6). The results in Table 2 indicate that isomerization occurs, and that the olefin does not significantly alter the yield of $CH_3S(O)_2SCH_3$. It was calculated that less than 6% of the oxygen atoms react with the olefin initially, but at long reaction times this would increase as the consumption of disulfide increases. This accounts for the trend in the amount of recovered butenes in Table 2. As the irradiation time increases, the mole fraction of *cis*-2-butene approaches the equilibrium value of 0.24 at 298 K, as shown in Fig. 2.

Addition of CH_3SH to the N_2O, Hg, CH_3SSCH_3 reaction mixture results in diminished yields of $CH_3S(O)_2SCH_3$, although less than 10% of the oxygen atoms react with CH_3SH in the experiment with the highest concentration of CH_3SH. The results are given in Table 3. The consumption of CH_3SSCH_3 is not as great as in the absence of CH_3SH, and in most cases the final amount of CH_3SSCH_3 exceeds the initial amount, i.e., CH_3SSCH_3 is actually formed from the added CH_3SH in the course of the reaction as has been observed in our earlier work (5). Addition of 80 μmol of CH_3SH decreases the yield of $CH_3S(O)_2SCH_3$ to about 30% of its value in the absence of CH_3SH. Complete suppression, however, is not approached until as much as 400 μmol of CH_3SH is added.

The recovery of the CH_3S groups (i.e., the mass balance) calculated from the analytical data is 86% in the absence of CH_3SH, and varies from 76% to 119%, with an average of 99 ± 5%, when CH_3SH is added to the reaction mixture, as seen in Table 3. The average value of $\Delta CH_3SH/\Delta CH_3S(O)_2SCH_3$ is 4.6 ± 0.5, where the uncertainty is the standard deviation of the mean, and $\Delta CH_3S(O)_2SCH_3$ is the difference between the yields with CH_3SH absent and present. The two runs in which CH_3SH was absent in the products and the run with the large initial amount of CH_3SH of 400 μmol were excluded from the average.

When H_2S is added to the reaction mixture of N_2O, Hg, and CH_3SSCH_3, the thiol CH_3SH appears as a product, as seen in

TABLE 1. The effect of irradiation time, *t*, on the yields of $CH_3S(O)_2SCH_3$ observed in the reaction of $O(^3P)$ with CH_3SSCH_3[a]

Run No.	*t* (min)	N_2O (Torr)	Amounts of products: CH_3SSCH_3 (μmol)	Amounts of products: $CH_3S(O)_2SCH_3$ (μmol)
129	5	762	57	1.2
102	15	753	53	4.5
103	30	739	37	9.9
142	30	758	47	10.7
145	30	742	48	11.7
128	60	738	27	25.
101	90	753	7	31.

[a]67 μmol of CH_3SSCH_3 were present initially; T = 24°C.

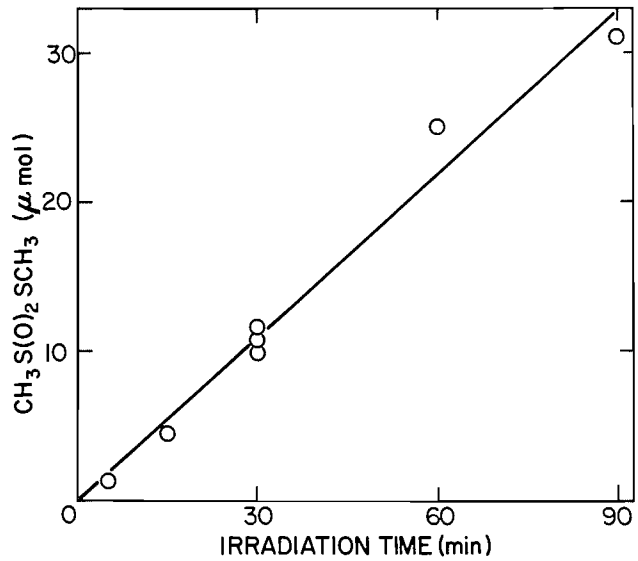

FIG. 1. The yield of $CH_3S(O)_2SCH_3$ as a function of irradiation time in the reaction of $O(^3P)$ with CH_3SSCH_3.

TABLE 2. Isomerization of 2-butenes in the reaction of $O(^3P)$ with CH_3SSCH_3[a]

Run No.	t (min)	Amounts of reactants: N_2O (Torr)	Amounts of reactants: *cis*-C_4H_8 (μmol)	Amounts of reactants: *trans*-C_4H_8 (μmol)	Amounts of products: *cis*-C_4H_8 (μmol)	Amounts of products: *trans*-C_4H_8 (μmol)	Amounts of products: MSSM (μmol)	Amounts of products: $MS(O)_2SM$ (μmol)	Recovery of C_4H_8 (%)	Recovery of MS (%)
120	5	768	4.2		4.6	0.5	62	nd[b]	(nd)	
121	5	769	4.1		nd	nd	60	1.9		92
119	5	759	20.		16.	2.5	61	nd	91	
122	15	757	20.		9.8	8.6	53	nd	90	
118	30	759	20.		5.6	10.2	45	nd	77	
123	60	763	21.		3.6	9.6	28	22.	64	74
126	5	760		20.	0.8	18.9	69	1.8	96	105
124	30	761		20.	4.1	14.2	50	5.7	89	83
125	60	760		20.	3.5	10.4	31	20.	68	76
127	30	760	10.	10.	4.9	12.2	53	8.9	84	92

[a]67 μmol of CH_3SSCH_3 were present intially; T = 24°C; MSSM = CH_3SSCH_3, etc.
[b]nd = not determined.

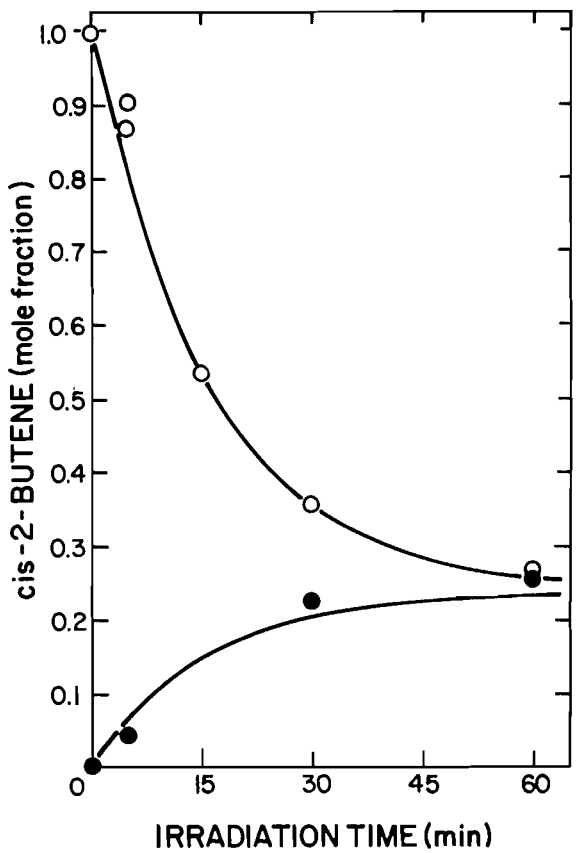

FIG. 2. Mole fraction of *cis*-2-butene as a function of irradiation time. Small amounts of either *cis* (○) or *trans* (●) isomer were added initially to the N_2O, Hg, CH_3SSCH_3 reaction mixture. The solid lines are the results of a steady state calculation.

Table 4. Also, H_2S and CH_3SSCH_3 are consumed, and the yield of $CH_3S(O)_2SCH_3$ is depressed in a similar fashion as in the experiments with CH_3SH initially added. The observed mass balance of the CH_3S group is not as good as in Table 3, with values of only 74% to 93%, and an average of 86 ± 3%. Although there was a very slow dark reaction between H_2S and CH_3SSCH_3 which formed CH_3SH, the correction to the measured yields of CH_3SH in the photolysis experiments due to the dark reaction was small, ranging from 7% to 12%.

Discussion

The notable feature of our previous study of the O + CH_3SSCH_3 reaction was the lack of any detectable volatile product (5). It was nevertheless possible to postulate tentatively a basic reaction mechanism by analogy with the O + CH_3SH and O + CH_3SCH_3 reactions studied at the same time, for which more experimental information on the products formed could be obtained. The postulated mechanism consisted of reactions [1]–[7] in Table 5, excluding disproportionation reactions. It was consistent with the absence of volatile products and also with the large consumption of CH_3SH and its partial conversion to CH_3SSCH_3 when CH_3SH was added in small amounts to the reaction mixture.The mechanism predicted formation of $CH_3S(O)_2SCH_3$, unobserved at the time, as the final stable product. The results of the present study confirm the formation of this compound as the major product and provide additional information on the reaction mechanism. The set of reactions listed in Table 5 includes the basic mechanism (reactions [1]–[7]) and a number of other reactions considered in connection with the additional experimental results obtained in the present work.

It was suggested previously (5) that some stabilization of the adduct could occur in reaction [1*b*]. The S—S bond in $CH_3S(O)SCH_3$ is 46 kcal/mol, and the S—O bond is about 80 kcal/mol. A simple RRK calculation indicates a lifetime similar to that calculated for the adduct in the O + CH_3SCH_3 reaction, i.e., about 10^{-10} s. Since the calculated lifetime of the initially formed $CH_3S(O)SCH_3$ is very small and is similar to that for $CH_3S(O)CH_3$ formed in the O + CH_3SCH_3 reaction, in which experiments showed (5) that stabilization is not important at 1 atm, it is likely that k_{1b}/k_{1a} is very small in our experiments.

The experiments in which *cis*- or *trans*-2-butene are isomerized provide evidence of significant formation of CH_3S radicals. The solid lines in Fig. 2 are calculated from a steady state expression having the functional form $X - X_{eq} = a \exp(-bt)$, where X is the mole fraction of *cis*-2-butene, X_{eq} is the value at equilibrium, and t is the irradiation time. It was assumed in the derivation that reaction [1*b*] was negligible, and that CH_3S radicals were consumed only in reaction [2]. The parameter b can be shown to be related to the equilibrium constant for *trans*- and *cis*-2-butene, the rate constants for reversible complex formation of CH_3S with the butenes, the rate constant for recombination of CH_3S radicals, and the rate of light absorption.

Can. J. Chem. Downloaded from www.nrcresearchpress.com by 210.87.254.105 on 09/06/12
For personal use only.

TABLE 3. The effect of CH_3SH on the yields of $CH_3S(O)_2SCH_3$ observed in the reaction of $O(^3P)$ with CH_3SSCH_3[a]

Run No.	Amounts of reactants		Amounts of products			Recovery of MS group (%)	ΔMSH/ ΔMS(O)$_2$SM
	N_2O (Torr)	MSH (μmol)	MSSM (μmol)	MSH (μmol)	MS(O)$_2$SM (μmol)		
142	758		47		10.7	86	
133	765	21	70	0.	11.7	105	
130	762	41	60	0.	6.4	76	9.4
131	763	82	79	49.	3.0	98	4.3
139	754	102	59	64.	2.1	79	4.4
141	756	102	62	76.	2.2	86	3.0
132	766	124	105	87.	4.4	119	5.8
135	750	162	107	129.	2.3	118	3.9
136	750	202	110	156.	3.0	113	5.9
137	744	400	97	315.	0.3	95	8.1

[a]67 μmol of CH_3SSCH_3 were present initially. Irradiation time = 30 min; T = 24°C; MSH = CH_3SH, etc.

TABLE 4. The effect of H_2S on the yields of $CH_3S(O)_2SCH_3$ observed in the reaction of $O(^3P)$ with CH_3SSCH_3[a]

Run No.	Reactants		Amounts of products				Recovery of MS (%)	Δ/ΔMS(O)$_2$SM[b]		
	N_2O (Torr)	H_2S (μmol)	MSSM (μmol)	H_2S (μmol)	MSH (μmol)	MS(O)$_2$SM (μmol)		MSSM	H_2S	MSH
142	758		47			10.7	86			
146	742	8	53	0.	0.	6.4	88	−3.2	−1.8	
144	760	20	53	1.5	7.8	3.3	89	−1.9	−2.5	1.0
143	760	41	56	21.	6.6	3.5	93	−1.5	−2.8	0.9
115	745	40	48	16.	10.	1.8	85	−2.1	−2.7	1.1
114	745	80	41	45.	17.	0.	74	−2.4	−3.3	1.6

[a]67 μmol of CH_3SSCH_3 were present initially. Irradiation time = 30 min; T = 24°C; MSSM = CH_3SSCH_3, etc.
[b]ΔMS(O)$_2$SM = 10.7 − amount of MS(O)$_2$SM in column 7.

The value of b which gives a reasonable fit to the experimental points is about 50% of that calculated using the rate constants in ref. 6. Although this may suggest that reaction [1b] is not negligible, the simplicity of the model calculation, the uncertainty in the rate constants, and the scatter of the data do not allow its quantitative determination.

The basic mechanism in Table 5 predicts a value of $\phi[CH_3S(O)_2SCH_3] = 0.5$ if disproportionation reactions are negligible. The lower value of 0.34 observed experimentally could be accounted for by assuming for reactions [3] and [4] the following disproportionation steps (written with their approximate[4] ΔH values in kcal/mol).

$$[3d_1]\quad CH_3SO + CH_3S \rightarrow CH_3SOH + CH_2S \quad -40$$

$$[3d_2]\quad CH_3SO + CH_3S \rightarrow CH_2SO + CH_3SH \quad -37$$

$$[4d_1]\quad CH_3SO + CH_3SO \rightarrow CH_2SO + CH_3SOH \quad -20$$

No experimental values for these disproportionation/recombination ratios appear to be available. If these are the only additional channels responsible for loss of oxygen atoms, the disproportionation reactions would account for 32% of the oxygen atoms, leading to an overall ratio of disproportionation/recombination of 0.47 for reactions [3] and [4]. For comparison, although earlier studies indicated a disproportionation/recombination ratio of 0.4 for CH_3S radicals (8), later work suggests that disproportionation is insignificant (9, 10).

The following alternative (or additional) pathway for loss of oxygen atoms can be postulated by analogy with the observation that aryl sulfinyl radicals, ArSO, can disproportionate in solution (11) to $ArSO_2$ and ArS, and the former radicals can, through a series of reactions, lead to a sulfonic anhydride (12).

$$[4d_2]\quad CH_3SO + CH_3SO \rightarrow CH_3SO_2 + CH_3S$$

$$CH_3SO_2 + CH_3SH \rightarrow CH_3SO_2H + CH_3S$$

$$CH_3SO_2H \rightarrow CH_4 + SO_2$$

The last two reactions are based, by analogy, on the report (13) that Cl_3CSO_2 can abstract hydrogen from $C_6H_{11}SH$ to give Cl_3SO_2H, which then decomposes into Cl_3CH and SO_2. This alternative pathway could, if valid, also account for the larger than expected yields of CH_4 in our earlier experiments (5) with CH_3SSCH_3/CH_3SH mixtures. It was found then that the yields of CH_4, although small, were about 2−10 times greater than could be explained by the minor secondary reaction of oxygen atoms with CH_3SH. (It should be pointed out that any CH_3SO_2 radicals formed in reaction [4d_2] would then also contribute to the isomerization of the 2-butenes in the experiments summarized in Table 2 (14).)

In another study, however, Block and O'Connor (15) found equal amounts of $CH_3S(O)_2SCH_3$ and CH_3SSCH_3 in the photochemical disproportionation of $CH_3S(O)SCH_3$ dissolved in either CH_2Cl_2 or C_6H_6, in contrast to the thermal disproportionation of $C_6H_5S(O)SC_6H_5$ for which the disulfide/

[4]Based on the similarity of $D(CH_3OO - H)$ and $D(HOO - H)$, the value of $D(CH_3SO - H)$ was estimated to be equal to $D(HSO - H)$, which was obtained from data in ref. 7.

Can. J. Chem. Downloaded from www.nrcresearchpress.com by 210.87.254.105 on 09/06/12
For personal use only.

TABLE 5. Elementary reactions involved in the reaction of $O(^3P)$ with CH_3SSCH_3, with mixtures of CH_3SSCH_3 and CH_3SH, and with mixtures of CH_3SSCH_3 and H_2S

	A. Basic reactions involved in the O + CH_3SSCH_3 reaction	
[1*a*]	$O(^3P) + CH_3SSCH_3$	$\rightarrow CH_3S + CH_3SO$
[1*b*]	$O(^3P) + CH_3SSCH_3$	$\xrightarrow{[M]} CH_3S(O)SCH_3$
[2]	$CH_3S + CH_3S$	$\rightarrow CH_3SSCH_3$
[3]	$CH_3S + CH_3SO$	$\rightarrow CH_3S(O)SCH_3$
[3*d*$_1$]	$CH_3S + CH_3SO$	$\rightarrow CH_2S + CH_3SOH$
[3*d*$_2$]	$CH_3S + CH_3SO$	$\rightarrow CH_3SH + CH_2SO$
[4]	$CH_3SO + CH_3SO$	$\rightarrow CH_3S(O)OSCH_3 \rightarrow CH_3S(O)_2SCH_3$
[4*d*$_1$]	$CH_3SO + CH_3SO$	$\rightarrow CH_2SO + CH_3SOH$
[5]	$2CH_3S(O)SCH_3$	$\rightarrow CH_3S(O)_2SCH_3 + CH_3SSCH_3$
	B. Major additional reactions involving CH_3SH	
[6]	$CH_3SH + CH_3S(O)SCH_3$	$\rightarrow CH_3SSCH_3 + CH_3SOH$
[7]	$CH_3SH + CH_3SOH$	$\rightarrow CH_3SSCH_3 + H_2O$
[8]	$CH_3SH + CH_3S(O)OSCH_3$	$\rightarrow CH_3S(O)SCH_3 + CH_3SOH$
[9]	$CH_3SH + CH_3SO$	$\rightarrow CH_3SOH + CH_3S$
[10]	$CH_3SOH + CH_3SOH$	$\rightarrow CH_3S(O)SCH_3 + H_2O$
	C. Major additional reactions involving H_2S	
[11]	$H_2S + CH_3S(O)SCH_3$	$\rightarrow CH_3SSH + CH_3SOH$
[12]	$H_2S + CH_3SOH$	$\rightarrow CH_3SSH + H_2O$
[13]	$H_2S + CH_3S(O)OSCH_3$	$\rightarrow CH_3SOH + CH_3S(O)SH$
[14]	$H_2S + CH_3SO$	$\rightarrow SH + CH_3SOH$
[15]	$H_2S + CH_3S$	$\rightarrow SH + CH_3SH$
[16]	$SH + CH_3SH$	$\rightarrow H_2S + CH_3S$
[17]	$SH + CH_3S$	$\rightarrow CH_3SSH$
[18]	CH_3SSH	$\rightarrow CH_3SH + S$
[19]	$S + CH_3SSCH_3$	$\rightarrow CH_3SS + CH_3S$

thiosulfonate ratio was greater than 1 (12). The results of Block and O'Connor suggest that under their conditions CH_3SO_2 radicals react only with CH_3S. It is clear that more information is needed on the reactions of these radicals.

The depletion of $CH_3S(O)_2SCH_3$ when small amounts of CH_3SH are added to the reaction mixture is consistent with reactions [6] and [7]. Addition of CH_3SH *after* irradiation of the N_2O, Hg, CH_3SSCH_3 mixture has no effect on the yield of $CH_3S(O)_2SCH_3$. Therefore CH_3SH must react with an intermediate such as $CH_3S(O)SCH_3$ formed in reaction [3], and not with $CH_3S(O)_2SCH_3$. But because addition of 400 μmol of CH_3SH leads to nearly complete depletion of $CH_3S(O)_2SCH_3$, CH_3SH must react also with the intermediate product of reaction [4], i.e.,

[8] $CH_3SH + CH_3S(O)OSCH_3 \rightarrow CH_3SOH + CH_3S(O)SCH_3$

Alternatively, the CH_3SH could potentially intercept the CH_3SO radical directly,

[9] $CH_3SH + CH_3SO \rightarrow CH_3SOH + CH_3S$

and prevent the formation of $CH_3S(O)_2SCH_3$ before reactions [3] and [4] occur. However, in estimating the rate constant of reaction [9] it should be remembered that this reaction may be endothermic (estimated $\Delta H = +9 \pm 10$ kcal/mol).

The basic mechanisms in Table 5 for the case with CH_3SH added to the reactants predict that $\Delta CH_3SH/\Delta CH_3S(O)_2SCH_3 = -4$. The experimental results in Table 3 average -4.6 ± 0.5 (neglecting runs 133, 130, and 137 for which the analytical error is large), which is in reasonable agreement with the predicted value in view of the precision with which this ratio can be determined.

Addition of H_2S to the N_2O, Hg, CH_3SSCH_3 reaction mixture decreases the yield of $CH_3S(O)_2SCH_3$ in a similar manner. Thus, H_2S must react with $CH_3S(O)SCH_3$ analogously to CH_3SH i.e.,

[11] $H_2S + CH_3S(O)SCH_3 \rightarrow CH_3SSH + CH_3SOH$

[12] $CH_3SOH + H_2S \rightarrow CH_3SSH + H_2O$

Also, because addition of 80 μmol of H_2S causes the yield of $CH_3S(O)_2SCH_3$ to be so small as to be undetectable, either one or both of reactions [13] and [14] (the analogs of reactions [8] and [9]) must occur, although reaction [14] may be endothermic.

[13] $H_2S + CH_3S(O)OSCH_3 \rightarrow CH_3SOH + CH_3S(O)SH$

[14] $H_2S + CH_3SO \rightarrow CH_3SOH + SH$

The fate of CH_3SSH is likely to be decomposition on the walls, as postulated in a different reaction sequence (16).

[18] $CH_3SSH \xrightarrow{\text{wall}} CH_3SH + S$

although it could conceivably react with H_2S, ultimately yielding the same products as reaction [18],

$CH_3SSH + H_2S \rightarrow CH_3SH + HSSH$

$HSSH \xrightarrow{\text{wall}} H_2S + S$

In either case, the formation of CH_3SH indicated in Table 4 would be accounted for. This reaction scheme, outlined in Table 5 predicts the ratios $-\Delta H_2S/\Delta CH_3S(O)_2SCH_3 = \Delta CH_3SH/\Delta CH_3S(O)_2SCH_3 = 4$, where ΔH_2S and ΔCH_3SH

Can. J. Chem. Downloaded from www.nrcresearchpress.com by 210.87.254.105 on 09/06/12
For personal use only.

Can. J. Chem. Downloaded from www.nrcresearchpress.com by 210.87.254.105 on 09/06/12
For personal use only.

are the consumption of reactant H_2S and the yield of product CH_3SH, and $\Delta CH_3S(O)_2SCH_3$ is the net difference in the yield of $CH_3S(O)_2SCH_3$ caused by adding H_2S to the reaction mixture. The observed ratios are $1.8 < -\Delta H_2S/\Delta CH_3S(O)_2SCH_3 < 3.3$ and $0.9 < \Delta CH_3SH/\Delta CH_3S(O)_2SCH_3 < 1.6$, with the ratios increasing with increasing H_2S. These ratios are smaller than the simple mechanism predicts because the product CH_3SH will compete with H_2S in reactions [6]–[9]. With increasing concentrations of H_2S, CH_3SH would be less competitive, and the ratios should increase, as observed. This mechanism is further supported by the observation that the consumption of CH_3SSCH_3 decreases when small amounts of H_2S are present, compared with the experiments where H_2S is absent, indicating that CH_3SSCH_3 is regenerated by reactions of the product CH_3SH in reactions [6] and [7].

The enhanced complexity of the O + CH_3SSCH_3 reactions with CH_3SH or H_2S added to the reaction mixture evidently requires inclusion of additional elementary steps in the reaction mechanism. The extended mechanism is summarized in Table 5. Its plausibility has been tested by computer simulation (17, 18) of the experimentally observed trends of product yields for different concentrations of reactants. Literature values of the required rate constants were used whenever available. However, for a number of reactions the rate constants are not known, and some plausible values had to be assumed. Thus, for the very fast radical–radical reactions, the statistical ratios $(k_3 + k_{3d_1} + k_{3d_2}) = 2k_2 = 2(k_4 + k_{4d_1} + k_{4d_2}) = 2k_{17}$ are adopted as was done previously (5). Sensitivity tests showed that appreciable variations in the absolute values of these and some of the other rate constants had only a minor effect on the results. The unknown disproportionation/recombination ratios (such as k_{3d_1}/k_3, k_{3d_2}/k_3, k_{4d_1}/k_4) were treated as curve fitting parameters as were also the rate constants for some other reactions shown to have an appreciable effect on the results. Whenever possible, the adopted values were scrutinized for thermodynamic and kinetic plausibility. The reactions O + CH_3SH and O + H_2S were included in the simulations but are not listed in Table 5 because they did not contribute significantly to the consumption of oxygen atoms.

The results of the computer simulation for the reactions in the presence of H_2S and CH_3SH, respectively, are presented in Figs. 3 and 4 in the form of standardized (per oxygen atom reacted) rate curves as a function of the initial concentration of the added compound (H_2S or CH_3SH).

The agreement between the computer simulated curves in Fig. 3 for $CH_3S(O)_2SCH_3$, CH_3SH, $-\Delta CH_3SSCH_3$, and ΔH_2S and the trends in the corresponding experimental points plotted is quite good in view of some unavoidable analytical error. No experimental data were obtained for H_2O and CH_2SO. The plot illustrates well the effect of H_2S addition to CH_3SSCH_3 on the character of the oxidation reaction products, which change from the oxygenated sulfur organics ($CH_3S(O)_2SCH_3$, CH_2SO) to water as the amount of added H_2S is increased, although the fraction of oxygen atoms reacting with the much less reactive H_2S remains very small.

Figure 4 shows the computer simulated rate curves for $CH_3S(O)_2SCH_3$, H_2O, CH_2SO, ΔCH_3SSCH_3, and ΔCH_3SH as a function of the amount of CH_3SH added. The experimental points are plotted only for $CH_3S(O)_2SCH_3$. Measurements have been made also for ΔCH_3SSCH_3 and ΔCH_3SH, but because of the large analytical uncertainty of the data (listed in Table 3) they are not plotted in Fig. 4. The data nevertheless illustrate

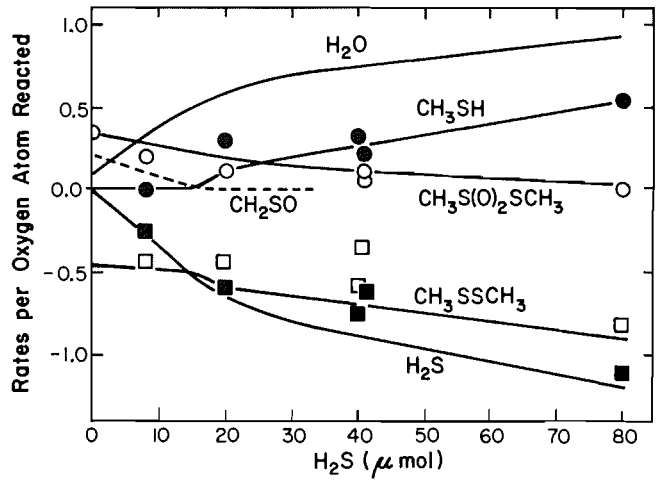

FIG. 3. Rate of product formation per oxygen atom reacted as a function of the initial amount of H_2S present. The lines are the results of computer simulations using the reactions in Table 5 and the experimental conditions in Table 4. The experimental results are indicated by symbols: ○ $CH_3S(O)_2SCH_3$; ● CH_3SH; □ CH_3SSCH_3; ■ H_2S.

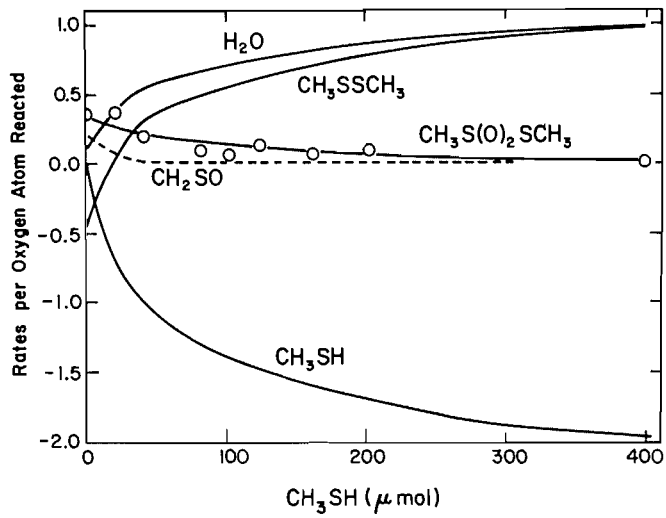

FIG. 4. Rate of product formation per oxygen atom reacted as a function of the initial amount of CH_3SH present. The lines are the results of computer simulations using the reactions in Table 5 and the experimental conditions in Table 3. ○ experimental yields of $CH_3S(O)_2SCH_3$.

clearly formation of CH_3SSCH_3 in the system at the expense of a large consumption of CH_3SH, although in this case also the fraction of oxygen atoms reacting with CH_3SH remains small. At sufficiently large CH_3SH addition, the net effect is the CH_3SSCH_3 catalyzed oxidation by oxygen atoms of two molecules of CH_3SH to form one molecule of CH_3SSCH_3 and one molecule of H_2O.

The computer simulations carried out demonstrate the plausibility of the mechanism summarized in Table 5. However, they do not eliminate the possibility of some variation of details, as for example the finer details of secondary chemistry in the presence of H_2S. Also, the question of the ratio k_{1a}/k_{1b} remains quantitatively unresolved, although the low $\phi[CH_3S(O)_2SCH_3] = 0.34$ measured in this work requires at least a substantial free radical formation in reaction [1*a*]. (Computer simulation with reaction [1*b*] alone predicts $\phi[CH_3S(O)_2SCH_3] = 0.5$, as expected.) This question reduces

Can. J. Chem. Downloaded from www.nrcresearchpress.com by 210.87.254.105 on 09/06/12
For personal use only.

to the effectiveness of collisional stabilization under different experimental conditions.

An addition–fragmentation–stabilization viewpoint has been applied originally to O + olefin reactions (19) and more recently by Lee *et al.* (1) to O + CH_3SCH_3 and by Slagle *et al.* (2) to O + CH_3SH and O + CH_3SCH_3 reactions. The most direct evidence of adduct formation was the detection of CH_3SOH^+ ions in the photoionization – mass spectrometry analysis of the products from high intensity crossed beams of oxygen atoms and CH_3SH (2). Supportive evidence for adduct formation was the similarity between the correlation of activation energies with ionization potentials of the sulfur compound (20) and the analogous correlation for O + olefin reactions which proceed by a major addition channel. Also, the curvature of the Arrhenius plots of O + thiol reactions (4, 20) and the negative Arrhenius activation energy for O + CH_3SCH_3 (1, 4, 20) are reminiscent of the O + olefin reactions (21). The correlation and behaviour of the Arrhenius parameters, however, cannot be considered as conclusive evidence.

Additional information on the nature of these reactions was provided by Tevault *et al.* (22), who photolyzed O_3 in an argon matrix at 10 K in the presence of CH_3SH or CH_3SCH_3 and analyzed the products by infrared spectroscopy. For O + CH_3SH, the products were consistent with fragmentation of a $CH_3S(O)H$ adduct in a matrix cage followed by recombination of the radical fragments. The products $CH_3S(O)H$, CH_3SOH and CH_3OSH were identified. In the CH_3SCH_3 reaction, only $CH_3S(O)CH_3$ was detected (as well as $CH_3S(O)_2CH_3$, presumed formed by stepwise addition of oxygen atoms to CH_3SCH_3). The presence of CH_3SOCH_3, which could have been formed by recombination of any CH_3 and CH_3SO radicals generated in the primary reaction, was not apparent. This molecule would have produced a band at 1084 cm^{-1} (C—O absorption), which may be at least partially obscured by the strong S=O band at 1091 cm^{-1}, and a band at about 767 cm^{-1} (S—O absorption), but no significant absorption is evident in this region in their Fig. 1. They interpreted their results as indicating that the adduct is stabilized for O + CH_3SCH_3 under their conditions, but that extensive fragmentation occurs for O + CH_3SH, in accord with the number of vibrational modes.

In our previous study (5) of the O + CH_3SCH_3 reaction, even at 1200 Torr at least 95% of the reaction results in breakage of the C—S bond. If $CH_3S(O)H$ were to be formed in our study of the O + CH_3SH reaction, it would not have been detected because of its instability. In view of the failure to stabilize any $CH_3S(O)CH_3$ adduct even at 1200 Torr in the O + CH_3SCH_3 reaction, it seems unlikely that a $CH_3S(O)H$ adduct would be important under our experimental conditions, and even less important at the very low pressures of molecular beam studies.

Further work is necessary to determine more quantitatively under a range of experimental conditions the relative importance of an addition–stabilization–fragmentation mechanism and a direct displacement ("pressure independent fragmentation") mechanism analogous to that occurring in the reaction of oxygen atoms with olefins (19) and possibly in the reaction of hydrogen atoms with organic sulfur compounds (16, 23). Further theoretical calculations would be expected to provide insight into the nature of the potential energy surfaces involved in such reactions.

1. J. H. LEE, R. B. TIMMONS, and L. J. STIEF. J. Chem. Phys. **64**, 300 (1976).
2. I. R. SLAGLE, R. E. GRAHAM, and D. GUTMAN. Int. J. Chem. Kinet. **8**, 451 (1976).
3. K. KIRCHNER, R. VETTERMANN, and H. INDRUCH. Ber. Bunsenges. Phys. Chem. **82**, 1223 (1978).
4. W. S. NIP, D. L. SINGLETON, and R. J. CVETANOVIĆ. J. Am. Chem. Soc. **103**, 3526 (1981).
5. R. J. CVETANOVIĆ, D. L. SINGLETON, and R. S. IRWIN. J. Am. Chem. Soc. **103**, 3530 (1981).
6. D. M. GRAHAM, R. L. MIEVILLE, and C. SIEVERTZ. Can. J. Chem. **42**, 2239 (1964).
7. S. W. BENSON. Chem. Rev. **78**, 23 (1978).
8. A. JONES, S. YAMASHITA, and F. P. LOSSING. Can. J. Chem. **46**, 833 (1968).
9. P. M. RAO and A. R. KNIGHT. Can. J. Chem. **50**, 844 (1972).
10. L. BRIDGES and J. M. WHITE. J. Phys. Chem. **77**, 295 (1973).
11. C. CHATGILIALOGLU, B. C. GILBERT, B. GILL, and M. D. SEXTON. J. Chem. Soc. Perkin Trans. 2, 1141 (1980).
12. P. KOCH, E. CIUFFARIN, and A. FAVA. J. Am. Chem. Soc. **92**, 5971 (1970).
13. E. S. HUYSER, H. SCHIMKE, and R. L. BURHAM. J. Org. Chem. **28**, 2141 (1963).
14. J. L. KICE. *In* Free radicals Vol. II. *Edited by* J. K. Kochi. Wiley, New York. 1973. Chapt. 24.
15. E. BLOCK and J. O'CONNOR. J. Am. Chem. Soc. **96**, 3929 (1974).
16. T. YOKOTA and O. P. STRAUSZ. J. Phys. Chem. **83**, 3196 (1979).
17. R. N. STABLER and J. P. CHESICK. Int. J. Chem. Kinet. **10**, 461 (1978).
18. R. L. BROWN. HICHM: a fortran code for homogeneous, isothermal chemical kinetics systems. NBSIR 81-2281, U.S. Dept. of Commerce, 1981.
19. R. J. CVETANOVIĆ. Adv. Photochem. **1**, 115 (1963).
20. I. R. SLAGLE, F. BAIOCCHI, and D. GUTMAN. J. Phys. Chem. **82**, 1333 (1978).
21. D. L. SINGLETON and R. J. CVETANOVIĆ. J. Am. Chem. Soc. **98**, 6812 (1976).
22. D. E. TEVAULT, R. L. MOWERY, and R. R. SMARDZEWSKI. J. Chem. Phys. **74**, 4480 (1981).
23. M. M. EKWENCHI, A. JODHAN, and O. P. STRAUSZ. Int. J. Chem. Kinet. **12**, 431 (1980).

Subpicosecond laser spectroscopy: strong field effects on molecular photophysics and dynamics

E. QUITEVIS, P. M. KROGER, C. KALPOUZOS, AND G. A. KENNEY-WALLACE

Picosecond Laser Laboratory, Lash Miller Laboratories, University of Toronto, Toronto, Ont., Canada M5S 1A1

Received August 10, 1982

This paper is dedicated to Professor Harry E. Gunning on the occasion of his 65th birthday

E. QUITEVIS, P. M. KROGER, C. KALPOUZOS, and G. A. KENNEY-WALLACE. Can. J. Chem. **61**, 975 (1983).

The possible role of strong field effects is discussed in the context of picosecond relaxation and reaction in polyatomic systems. The picosecond pulse diagnostics from an argon-ion synchronously pumped dye laser are then outlined in terms of cavity detuning and laser pumping parameters. A profile of auto-correlation data on ensemble-averaged pulses and streak camera data on single pulses is presented, from which the domain of stable, single pulse operation can be deduced. Finally data are presented on the photoionization and energy relaxation of pyrene in alcohols and micelles, and for the reorientational dynamics of liquid chlorobenzene, which illustrate different consequences of strong field phenomena in dense media.

E. QUITEVIS, P. M. KROGER, C. KALPOUZOS et G. A. KENNEY-WALLACE. Can. J. Chem. **61**, 975 (1983).

On discute du rôle que pourrait jouer des effets de champ fort dans le contexte de relaxation et de réaction de l'ordre de la picoseconde dans des systèmes polyatomiques. On décrit une méthode de diagnostique par impulsion de l'ordre de la picoseconde basée sur un laser à colorant activé d'une façon synchrone par de l'argon, en fonction d'un désajustement de la cavité et des paramètres de pompage du laser. On présente une courbe des données d'autocorrélation pour des impulsions ajustées au niveau de l'ensemble des données d'une caméra "streak camera" relatives aux impulsions uniques; à partir de ces données, on peut déduire le domaine d'opération stable d'un impulsion unique. Finalement on présente les données sur la photoionisation et sur la relaxation d'énergie du pyrène dans des alcools et des micelles et sur la réorientation dynamique du chlorobenzène liquide, qui illustrent les différentes conséquences du phénomène de champ fort dans les milieux denses.

[Traduit par le journal]

Can. J. Chem. Downloaded from www.nrcresearchpress.com by 210.87.254.105 on 09/06/12
For personal use only.

I. Introduction

The dramatic impact of tunable laser spectroscopy on our understanding of energy levels and dynamics in polyatomic molecules has shaped many of the contemporary theoretical attitudes towards the description of energy relaxation, energy transfer, and chemical reaction from electronically excited states (1). Picosecond laser spectroscopy (2) has opened up the realm of earliest events for polyatomic molecules, in which these central issues in photophysics and photochemistry can be directly examined during the lifetime of the event. Whether in condensed media, where the number density of molecules, intermolecular forces and torques, and collisional events become the determining factors, or isolated in the gas phase and characterised by a high density of states, molecular systems are a natural target for such fundamental studies of efficient and rapid inter- and intramolecular energy flow, using ultrashort laser pulses. Yet as we begin to explore laser-induced relaxation and reaction channels in molecules at shorter and shorter times, other issues arise which are unique to laser spectroscopy in the subpicosecond domain. These concern the preparation of optically excited states, local field effects, and nonlinear phenomena, to name a few specific examples, and the precision of measurement in general, as we approach the transform limits.

We present in this paper new spectroscopic and dynamic results selected to address strong field effects in particular from three different, ongoing research projects on multiphoton photoionization and electron transfer (3–5), on laser-induced photophysics and energy transfer (5, 6), and on the molecular dynamics of nonlinear optical phenomena in liquids (4, 7–9). Any problem of photochemical dynamics is really one of describing the photophysics (relaxation) and photochemistry (reaction) as competing channels, under precise conditions of the radiation field. Associated with all of these experiments is the need to fully characterise the laser pump and probe pulses, thus we outline new results from a comprehensive study of pulse generation and diagnostics that we have undertaken.

II. Optical interactions in the picosecond and femtosecond domain

A measurement using ultrashort laser pulses, whether information is recorded in time or frequency space, carries through a corresponding uncertainty that is a natural limitation to the interpretation of the experimental result. The limitation of subpicosecond measurements thus begins to appear in the energy resolution of the molecular event under study, through the simple relationship $\Delta E \Delta t \sim \hbar$. In picosecond (ps) and femtosecond (fs) laser spectroscopy, it makes little sense to try to distinguish the individual dynamical behavior of two close lying vibrational levels when the linewidth or frequency uncertainty of the subpicosecond laser pulse is greater than the frequency difference between the levels of interest. On the other hand, precisely such a situation can lead to the observation of interference effects when the two levels are *coherently* excited. This is the experimental prerequisite for studying quantum beats in the fluorescence decay of polyatomic molecules (10, 11). A pulse duration of 0.01 ps or 10 fs has associated with it an energy uncertainty corresponding to several eV or half the energy of a typical chemical bond. The shorter the duration of these visible laser pulses, the "whiter" they become. Therefore the region 10^{-13} to 10^{-9} s will probably remain the most productive in terms of new insights into dynamical theories or chemical kinetics and molecular energy transfer, because even if future advances in laser technology did allow us to probe and record even faster events, the uncertainty in the energy will be comparable to or greater than the energy measurement itself. For photochemistry, the time barrier beyond which our *current* questions begin to lose their practical significance is 10^{-13} s.

Can. J. Chem. Downloaded from www.nrcresearchpress.com by 210.87.254.105 on 09/06/12
For personal use only.

Nevertheless, we cannot anticipate the future results of the current picosecond and the most recent femtosecond (12) studies, and so new phenomena, requiring new theories rather than modified old theories, may be awaiting us. We will now briefly examine two specific areas which could constitute a source of new phenomena or new techniques.

(a) Laser pulses: profiles and propagation

Ideally, ps and fs experiments are performed with transform limited pulses, for which a theoretical limit on the product $\Delta\nu\Delta t$ can be established for a given temporal laser pulse profile, and hence the fwhm linewidth $\Delta\bar{\nu}$ cm^{-1} can be calculated. The significant difference between the bandwidth product of various pulse shapes, namely 0.4413 for Gaussian, 0.3148 for sech^2, and 0.1420 for an exponential (symmetric) intensity $I(t)$ profiles, immediately poses the problem of how one can determine $I(t)$, a topic addressed in the Experimental section. A Gaussian laser pulse of duration 0.3 ps at $\lambda = 600$ nm thus has a linewidth of 26 cm^{-1} and, if on resonance, the pulse will excite a subset of states within the molecule corresponding to that bandwidth. This raises the question of state-selective preparation as a feasible approach for studies of the earliest events in molecular photophysics at times $\ll 10^{-12}$ s. However, even if these ultrashort pulses were to propagate in transparent media, dispersion effects still play an important role and pulse broadening must be taken into account for every optical path in the system. Group velocity (V_g) must be used to calculate the propagation times of various frequency ($\omega = 2\pi\nu$) components of a laser pulse or of an absorption or emission spectrum. Low frequencies travel faster than high frequencies for $\lambda < 1.5$ μ and thus dispersion effects ($\partial V_g/\partial\lambda = \partial^2 k/\partial\omega^2$) are particularly limiting when trying to take (for example) simultaneous infrared and near-uv absorption data. Furthermore, it is not possible to spatially focus pulses of different frequency to exactly the same focal volume, nor to collect information at identically the same time from an image of finite size, since there will be an intrinsic uncertainty associated with the transit time of photons from different points on the image. A 100 μ image represents a ~0.3 ps limitation. Dispersion in quartz is such that a 600 nm, 100 fs pulse of 100 cm^{-1} bandwidth would experience 40 fs delay on propagating through a 1 cm lens. Every optical element leaves its imprint on the pulse characteristics.

Clearly, to do femtosecond spectroscopy, which we define operationally as the domain below 0.5 ps, we must first address fundamental issues of pulse propagation and optical measurements that are an integral part of the interactions of laser radiation with atoms and molecules. The nonlinear polarization interactions as well as dispersion are of paramount interest, and we will now briefly examine some of these in the more general context of strong field effects.

(b) Strong field effects

The strong field effects we wish to briefly summarise here are (*i*) the transient, laser $\boldsymbol{E}$ field-induced orientational alignment, studied as the ps optical Kerr effect, (*ii*) the static $\boldsymbol{E}$ field-gradient induced shifts in molecular energy levels, and (*iii*) the laser $\boldsymbol{E}$ field dressed-states concept in laser-induced chemistry.

(*i*) The nonlinear polarization (P) in dense media resulting from interaction with intense laser pulses is usually written as

$$[1] \quad P_i = \chi^{(1)}_{ij}E + \chi^{(2)}_{ijk}E_jE_k + \chi^{(3)}_{ijkl}E_jE_kE_l$$

an expansion in higher orders of the electric field (E^n) and the susceptibilities $\chi^{(n)}$ of the molecular system, as derived from a perturbation theory approach (13). While this expression does not explicitly include the time-dependence (8, 9, 15) of the medium susceptibility response nor of the laser pulse, it is illustrative of the origin of the nonlinear, strong field effects that we first discuss. The second-order term, which vanishes for isotropic material, describes the second harmonic generation (SHG) which is generally employed to measure ps pulse durations through second order autocorrelation techniques. Based on nonlinear sum or difference frequency mixing in biaxial crystals, for which no inversion centre of symmetry exists, SHG, or its higher order analogs, are the major source of information on laser pulse durations at times <50 ps. No electronic devices can match in speed such electronic polarization, which follows instantaneously the laser pulse intensity profile. We will return to SHG in the experimental section, but turn now to the third-order term $\chi^{(3)}_{ijkl}$, through which the laser field-induced orientational alignment occurs. The optical Kerr effect (OKE), frequently used as an ultrafast optical shutter technique (14), refers here to the transient birefringence $\delta n(t)$ induced in a system comprising non-spherically symmetric molecules, subjected to an intense ps laser pulse. The nonlinear polarization, third-order in the electric field, can be envisaged as a time-dependent, nonlinear refractive index (n_2) of the molecular system which relaxes after the laser pulse is over with a lifetime characteristic of the intrinsic orientational dynamics (τ_d) of the system. During the passage of the laser pulse, the molecules align such that the molecular axis of maximum polarizability is parallel to the propagating electric field vector. Of prime interest to us is the time-dependence of the rise and decay of the Kerr transients in response to the polarization selectivity of the $\chi^{(3)}$ coefficients and the fundamental molecular dynamics and time-dependent contributions to $\chi^{(3)}$ (7, 8, 15). Furthermore, we propose the possibility of using such laser-imposed orientational alignments to enhance or frustrate chemical reactions or energy transfer processes in which the geometry, or relative alignment of the molecules, is a deterministic factor on the time scale of the actual event.

(*ii*) While OKE is a transient external field phenomenon, clearly there are local, non-averaged internal field effects arising from polarizability fluctuations with which to contend on the ps time scale and this subject will be discussed elsewhere. One "local" field case, however, is of singular importance and that refers to the presence of a non-trivial field gradient, usually due to the presence of a charged interface. A few mV extending over several angstroms constitutes a field of about 10^5 V cm^{-1} and surface potentials of 100 mV are not unknown in biological interfaces. By analogy with Stark promoted field ionization of Rydberg states in atoms, we have proposed (3) that in molecules in close proximity to charged interfaces in micelles and vesicles, static, internal field gradient effects could lead to electron tunneling, to lowering of ionization potentials, or to the coupling of normally energetically disallowed processes by virtue of lowering the potential energy barriers. The influence of fields on charge detrapping in inorganic semiconductors (16) or the Poole–Frenkel effect, and the Schottky model of electron emission, touch upon similar concepts in solid state physics (17). More recently, the idea of using charged interfaces to assist the separation of ionic photoproducts in photosensitized electron transfer in aqueous media has been discussed (18) and data have been reported (18, 19) to show that quantum yields and kinetics have been correlated at least qualitatively with the surface charge and potential of micelles and the colloidal semi-

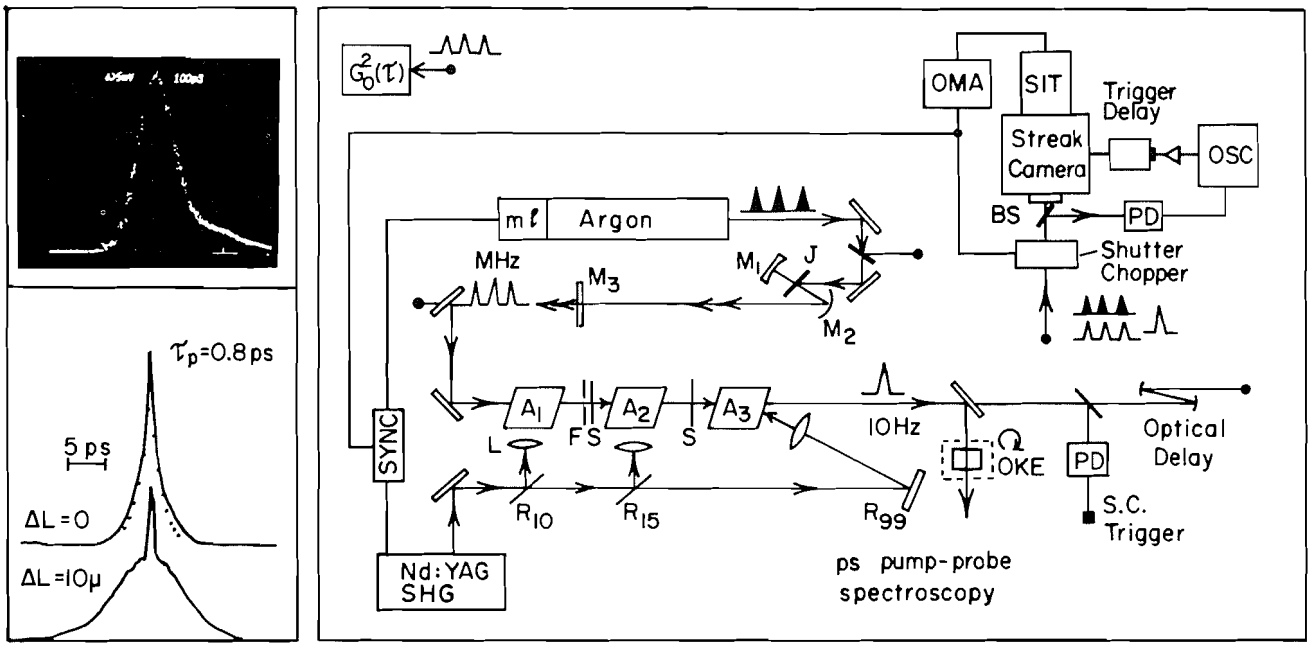

FIG. 1. Schematic of SML oscillator–amplifier dye laser system for picosecond absorption and emission studies, utilising a streak camera coupled to a SIT vidicon tube and optical multichannel analyser (OMA). See text for discussion and details on pulse diagnostics shown as inserts.

conductor material, SiO_2.

Picosecond laser spectroscopy allows us to directly examine these phenomena via a study of photoionization, electron transfer, and trapping processes across the interface. The results are of pivotal importance not only for basic understanding of these classic interfacial systems, but also for designing schemes which will produce rather practical and efficient solar energy cells.

(*iii*) The third, strong field effect refers to the dressed state concept, which has stimulated much theoretical interest in the description of potential energy surfaces within an intense laser radiation field (20). In principle, the molecular electronic state dressed (21) by an energy $\hbar\omega$, a quantum of the laser field, can couple to another electronic state to produce new reaction or relaxation channels otherwise inaccessible to the molecule. Thus the field can both distort the potential energy surfaces and, when two states can be coupled by photon exchange with the field, shift two potential energy surfaces with respect to each other, leading to new degeneracies. The intensity dependent effects we observe for laser-induced electron transfer originating from electrons in alcohol clusters (5) may well include type (*iii*) contributions. However, for the purposes of the present paper, we will focus on types (*i*) and (*ii*).

III. Experimental

(a) Pulse diagnostics and interpretation

Over the past year there have been some dramatic advances (12, 22, 23) in the generation of femtosecond laser pulses at 615 nm — the limit being 30 fs (22) at time of writing — and in obtaining significantly shorter subpicosecond pulses in general. By employing ring configurations for the dye laser, and using the colliding-pulse model (22) to determine the transit distances and times in the cavity for the counter-propagating pulses, it should be possible to gain a factor of at least 3 for the *tunable* pulses and to approach 300 fs.

Whatever the actual duration of the pulse, it is the pulse diagnostics which we emphasize here as the key to definitive and quantitative interpretation of the data. Figure 1 illustrates the oscillator–amplifier tunable dye laser system, which we have built for absorption and emission studies on the picosecond and subpicosecond time domain and whose pulse characteristics we describe here. The synchronously mode-locked (SML) dye laser oscillator is presently operating in a linear, extended cavity configuration and can generate pulses at 82 MHz of ≥0.8 ps with an average power of 150 mW, tunable from 580–620 nm. Full details of its operation and the 3-stage amplification, which is driven by the second harmonic output at 530 nm from a Q switched Nd:YAG laser operating at 10 Hz to generate trains of dye laser pulses ~800 μJ/pulse at 10 Hz in the visible, have been given elsewhere (4, 24); only the salient details will be repeated here.

We have measured the temporal profiles for both the pulse ensemble and a single pulse selected from the ensemble. Autocorrelation traces are inherently a part of an ensemble-averaged nature and thus may contain contributions from a distribution of pulse shapes. We employ our speaker–autocorrelator system (24) as a permanent on-line monitor to measure, in real time, the background-free second-order autocorrelation function ($G_o^{(2)}(\tau)$) of the unamplified pulses emerging at 82 MHz from the output coupler of the dye laser. A step-by-step measurement of $G_o^{(2)}(\tau)$ is taken for amplified pulses at 10 Hz, using translation stages capable of electronically-controlled ±1 μ precision to determine the delay time (τ) within ±35 fs in one arm of the correlator.

In order to determine the true single pulse profiles, we have taken unamplified and amplified pulse measurements using an Imacon 500 (Hadland Co.) streak camera, coupled to a 20/30 intensifier, with a minimum slit width of 25 μ, maximum streak speed of 20 ps/mm, and an intrinsic technical response time of 0.75 ps for a threshold flux of ~10^5 photons/event at the slits. In practice, before this minimum response of the camera can be fully evaluated, significant electronic triggering/synchronization has been necessary to coordinate the multiple functions of this laser oscillator–amplifier system. We summarise the main sequence of events below.

The intensifier is coupled via a f/1.2 1:2 lens to a SIT vidicon detector and OMA 2 system (P.A.R., Corp.) which can be operated to automate data acquisition and storage. Single shot measurements are made by passing the argon ion or dye laser beam through a chopper–shutter arrangement which produces one 60 μs burst of pulses upon command from the OMA. A fraction of this burst is diverted to a PIN diode (PD), the output of which is connected to a Tektronix 7904 (500 MHz) oscilloscope (OSC). The +GATE output of OSC, which is synchronized to the sweep, is amplified to give an 18 V pulse with a risetime of 0.5 V/ns which triggers the streak

Can. J. Chem. Downloaded from www.nrcresearchpress.com by 210.87.254.105 on 09/06/12
For personal use only.

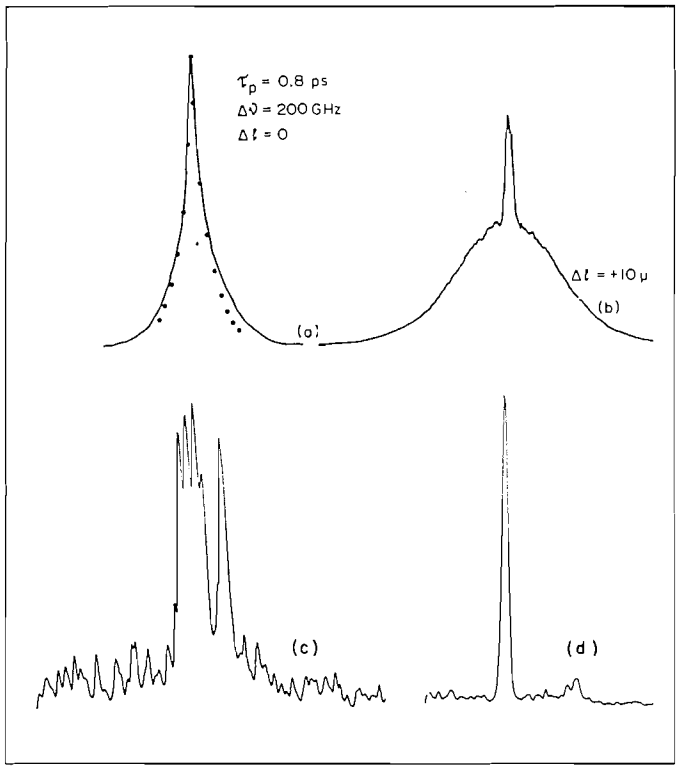

FIG. 2. Comparison of autocorrelation ensemble traces (*a*, *b*) and streak camera single pulse traces (*c*, *d*) for SML dye laser pulses as a function of cavity detuning. See text for details.

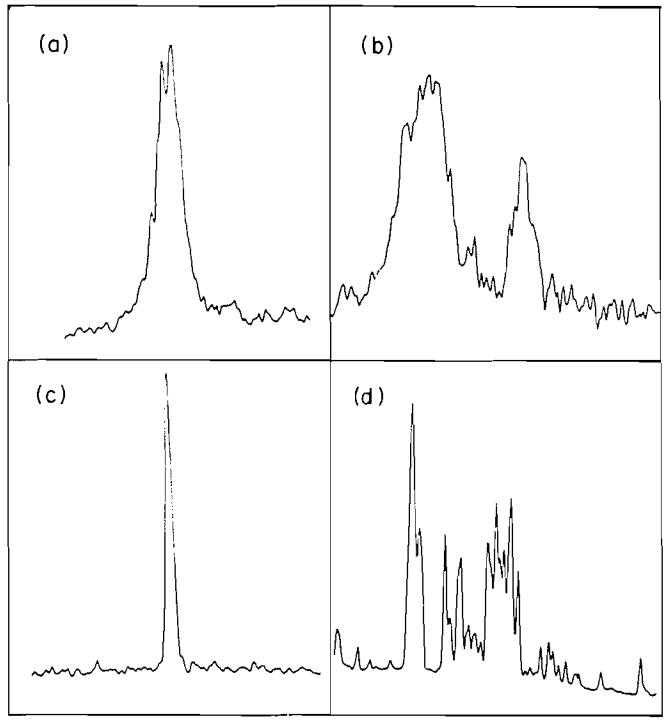

FIG. 3. Dependence of dye pulse profiles (*c*, *d*) on Ar^+ pump laser profiles (*a*, *b*) and cavity parameters. See text for details.

camera through an electronic delay. The trigger level on OSC is adjusted to select pulses from the burst and control jitter of streaks. Time calibration is accomplished with solid etalons.

Figure 2 illustrates the general effect of dye laser cavity detuning by 10 μ as revealed by the autocorrelation trace and the streak camera trace of the oscillator pulse. The effects of detuning on measurements of $G_o^{(2)}$ on synchronously-pumped dye laser systems have been reported earlier by us (24) and by others (25–27), but we are aware of only two other reports (26, 27) which have *compared* these effects with streak camera traces in the single shot mode, using a somewhat slower streak camera. Reproduced here to indicate that indeed apparent single pulse $G_o^{(2)}$ traces can actually include a major, if not dominant contribution, from multiple pulse structure, are selected data from a comprehensive survey of such effects that we are completing for the tunable SML laser system.

Trace (*a*) is obtained under optimum conditions, can be fitted (black dots) to an exponential pulse shape yielding τ_p = 0.8 ps ($\Delta\nu$ = 200 GHz) and is usually accepted as a "good" single pulse profile, while trace (*b*) represents the partial mode-locking case, which is seen following an increase in the dye laser cavity length of 10 μ. Under identical experimental conditions, the streak camera traces show that there is a significant population of multiple pulse structures, as typified in (*c*), hidden in the trace (*a*). In fact, the additional intensity in the wings of (*a*) above the theoretical fit is indeed a signature of some broader pulses within the ensemble. The pulse burst of (*c*) has a measured fwhm of 75.2 ps, with many narrower components. (This value is not corrected for streak camera resolution.) The analogous trace after detuning in (*d*) shows only single pulses with negligible satellite structures corresponding to the measured fwhm of (*b*), namely 10.3 ps.

The cavity detuning is not the sole parameter for determining single versus multiple pulse structure. If we can assign a probability P to the appearance of single pulses and thus $(1 - P)$ to the appearance of multiple structures, then for trace (*b*) $P \sim 1$, while for trace (*a*) $P < 1$ and has a weighted ratio of contributions from (*c*) and (*d*) type profiles. P is a complicated function related to the gain profile and at present we merely state $P = f(\omega,\omega_t,\omega_{ml},\nu_{ml},\Delta l,l...)$, where ω = average pumping power of argon ion laser, ω_t is the power threshold for the dye laser, ω_{ml} is the rf power, ν_{ml} the acousto-optic mode-locker frequency, and l the dye laser cavity length. We have separated out the intrinsic hydrodynamic behaviour of the ~300 μ thick dye jet, because although it is of most importance to the absolute duration and coherence quality of the subpicosecond laser pulses.

What determines the value of P in empirical terms? The four profiles in Fig. 3 illustrate the change in the Ar^+ pulse and the SML dye laser pulse as the laser operating conditions are varied. Trace (*a*) is a streak camera record of a single Ar^+ pulse (fwhm = 117 ps) from the 514 nm laser line just above threshold at 30 A, at W = 650 mW, and ν_{ml} = 41.1215 MHz, where P = 1 for single Ar^+ pulses. When l was adjusted to give good $G_o^{(2)}(\tau)$ traces (no wings), single pulse dye laser performance ($P \sim 1$) was obtained. Trace (*c*) (fwhm = 12 ps) is a typical streak camera record of such pulses. Increasing the ion current to 31 A where W = 800 mW and ν_{ml} = 41.1225 MHz lead to the Ar^+ double pulses seen in (*b*) with 259 ps separation between the major peaks. It is not surprising that under such conditions dye laser performance degrades to the trace in (*d*), a pulse burst of 168 ps where $P \sim 0.3$, even while cavity matching (Δl = 0) is maintained. One must be cautious in assessing true Ar^+ pulse shapes from ultrafast photodetectors and sampling techniques whose total response time averages out the vital information on the pulse substructure. The photograph inset to Fig. 1 shows such a photodiode signal of the argon ion pulse, where the diode total rise and fall time was specified to be 120 ps. There are three important conclusions from our studies so far which have general implications for all SML systems. (*1*) SML systems can generate multiple structure dye pulses with rather small changes in laser operating parameters. Single pulse operation is a very sensitive function of many variables. (*2*) These pulse bunches cannot be obviously recognized through autocorrelation traces, which averaged over millions of pulses could contain pulses of duration from typically 1 ps to 30 ps. This is because $G_o^{(2)}$ autocorrelation techniques based on second harmonic generation, while capable of indicating ultrafast subpicosecond and femtosecond components, are nevertheless fated to be symmetric in temporal profile and such pulse bunching appears as a somewhat dispersed contribution to the wings of the signal. (*3*) Streak camera traces reveal asymmetric and pulse

Can. J. Chem. Downloaded from www.nrcresearchpress.com by 210.87.254.105 on 09/06/12
For personal use only.

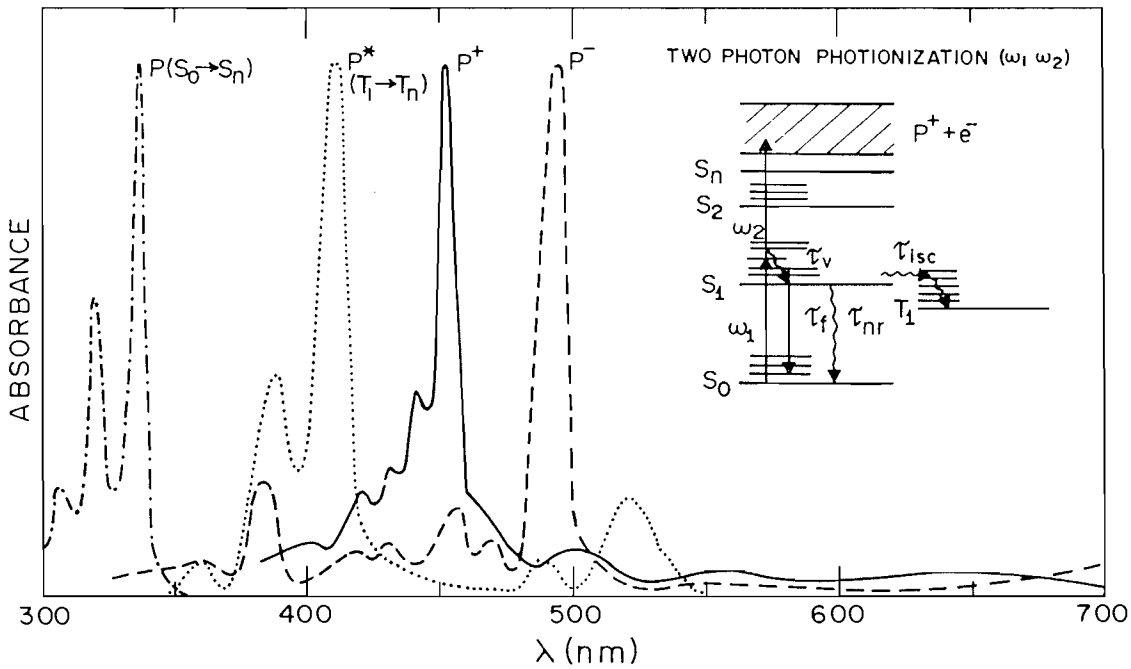

FIG. 4. Two photon photoionization of pyrene at $(\omega_1 + \omega_2)$ and competing intramolecular relaxation processes involving S_1, T_1 levels. Transient absorption spectra of the ions (P^+, P^-) and triplet [$P^*(T_1 \rightarrow T_n)$] are shown for comparison with singlet [$P^*(S_1 \rightarrow S_n)$] in Fig. 5. See text for discussion.

bunching or multiple structure very clearly, but nevertheless, at the present time, they cannot readily break the time barrier for subpicosecond resolution on a single shot on several technical accounts. These conclusions support earlier observations (26, 27) but indicate single pulse performance and the factor P to be a more sensitive function of cavity parameters than previously supposed. Such pulse diagnostics are the true beginning of reliable interpretations in photophysics and photochemistry, and for experiments exploiting excited states as probes of molecular and chemical dynamics. We have now succeeded in determining the domain of operating stability for single pulses from our SML oscillator–amplifier system and can deconvolute where necessary the excitation function from the dynamics of the molecular response under investigation.

(b) Picosecond and femtosecond pump-probe spectroscopy

Following excitation with a pump laser pulse, a weaker probe pulse (often of different frequency) monitors the transient absorbance, A. The intrinsic time resolution of an event is determined by varying the difference (τ) in arrival times of the pump and probe laser pulses, at both the sample and the detector. For recording the full optical absorption spectrum of ps transients, a ps continuum (28) is used in conjunction with a monochromator and calculations made for group velocity corrections and the SIT vidicon detector response of A (τ) where appropriate (4). For the photophysical studies both kinetics at single wavelengths and spectra were recorded for the transients following one or two photon laser excitation. For the pyrene absorption data reported here, purified and recrystallized pyrene (P) was used to prepare $\sim 10^{-4}$ M solutions in alcohols (distilled-in-glass quality) contained in 1, 2, or 10 mm pathlength quartz cells. Excitation and relaxation schemes are shown as an inset in Fig. 4. The amplified pulses at 615 nm were frequency-doubled to generate ω_1 (λ = 307 nm), which is absorbed strongly by pyrene undergoing a $S_0 \rightarrow S_2$ (^1L_a) transition, $\epsilon_{307} = 1.2 \times 10^4 M^{-1}\,cm^{-1}$. In other experiments, the 355 nm from the Nd:YAG laser was used to create population in the first excited singlet via excitation of a much weaker transition, $S_0 \rightarrow S_1$ (^1L_b) for which $\epsilon_{355} = 3.2 \times 10^2 M^{-1}\,cm^{-1}$. Subsequent excitations were for $\omega_1 = \omega_2$, or ω_2 tunable with $\lambda \geq 355$ nm. At these concentrations there was no evidence of excimer formation.

In the nonlinear optical experiments, chlorobenzene (spectroscopic grade) was used as a Kerr active medium and the measurements made in a collinear geometry for pump (ω_2) and probe (ω_1) pulses, as shown in the inset to Fig. 6*a*. The time-dependent transmission $T(\omega_1)$ of ω_1 through the Kerr cell contained within crossed polarizers (P_1, P_2) was measured during and after the passage of 300 fs pulses at 615 nm ($\omega_1 + \omega_2$). A double beam configuration was used as previously described (8) in order to normalise the data for laser pulse intensity fluctuations against the calibrated response from a CS_2 cell, where $n_2 = 2 \times 10^{-11}$ esu. The transmission of ω_1 through P_2 was detected by a fast photodiode coupled directly to a computer for the case of W_2 as linear and as circular polarized light, by manipulating a combination of wave plates and polarization rotators (represented by λ/n) at the entrance to the cell. Extreme care was taken to ensure the quality of polarized light and the absence of elliptical components in both ω_1 and ω_2, using techniques described earlier (8).

Organic molecular photophysics and dynamics

(a) Picosecond photophysics of pyrene

The influence of molecular motion such as vibration or rotation on the outcome of a chemical event depends on whether or not the nuclear kinetic energy terms can couple potential energy surfaces leading to new intramolecular relaxation or reaction channels. Such motion can enhance or impede the efficiency of the reactive channel. Multiphoton photoionization (29, 30) involving real intermediate stages S_1, S_2..., and thus sequential excitation to a higher S_n, level competes with vibronic relaxation (τ_v, τ_{nr}) intersystem crossing (τ_{isc}) and the onset of radiative relaxation (τ_f) from states already populated via ω_1, as shown for pyrene in Fig. 4 (inset). Tunable laser studies (3) of the multiphoton ionization mechanisms and measurement of the photoionization thresholds (IP) of molecules embedded in a range of environments can thus lead to important insights not only of intramolecular energy relaxation, but also of (*i*) the influence of intermolecular interactions, local fields, and phase density on the lowering of ionization potentials, (*ii*) the existence of molecular Rydberg states, and (*iii*) geminate ion recombination, electron trapping, and transfer processes. We

Can. J. Chem. Downloaded from www.nrcresearchpress.com by 210.87.254.105 on 09/06/12
For personal use only.

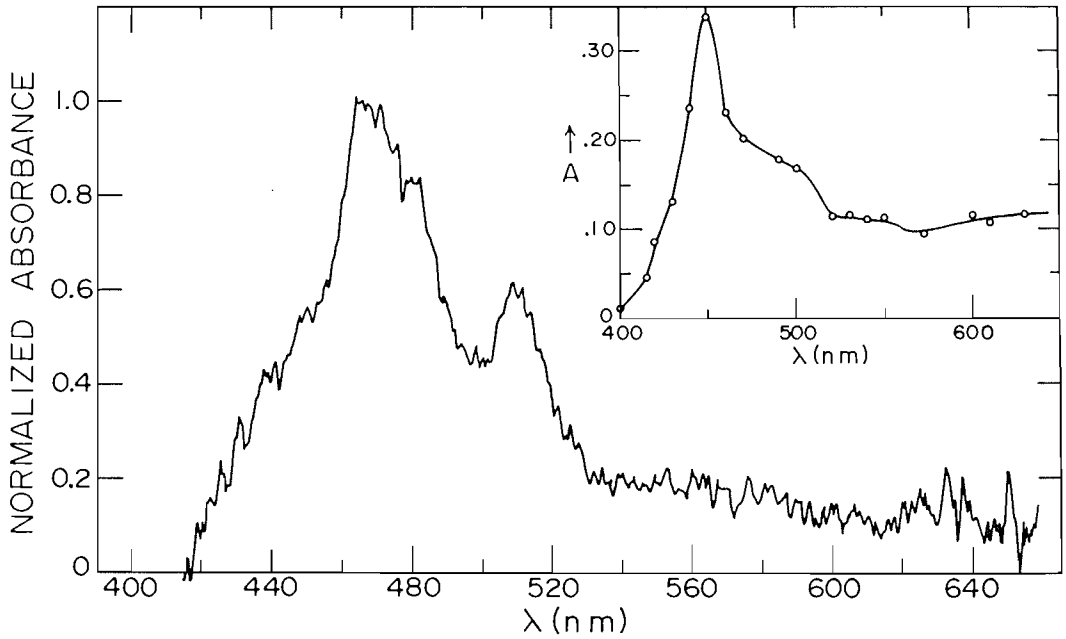

FIG. 5. Picosecond transient absorption: spectrum recorded at 2 ps in 10^{-4} *M* pyrene in ethanol following $S_o \rightarrow S_2$ excitation at 307 nm. Insert shows spectrum of P*($S_1 \rightarrow S_n$) recorded at 20 ns for 8×10^{-5} *M* pyrene in methanol, following $S_o \rightarrow S_1$ excitation at 347 nm.

report here the ps photophysics of pyrene in polar liquids as a prelude to ps photoionization studies of field-induced ionization and electron transfer in micelles.

Figure 4 shows the transient absorption spectra recorded in the $10^{-9}-10^{-6}$ s time domain following the two photon uv photoionization of pyrene in methanol at 355 nm and 347 nm (29). Note the relatively clear spectral separation of the radial ions P^+, P^-, and the triplet P*(T_1). The nanosecond spectrum of the singlet P*(S_1) and P^+ appear as an inset in Fig. 5, which shows the transient absorption spectrum in pyrene ethanol solutions following excitation with 300 fs pulse at 307 nm (31). The transient absorption was measured from 400 nm to 900 nm at 2 ps up to 50 ps delay, and within experimental resolution there were no significant spectral shifts, only loss of intensity over this interval. Absorption maxima occurred at 470 nm and 510 nm, corresponding to the singlet−singlet absorption at ns times (29). Under these experimental conditions, there was no evidence for the characteristic e_s^- absorption or the P^+ cation, which has a peak at 450 nm, and thus we conclude that only excited states have been formed. Furthermore, the triplet absorption ($^3P^*$) at 415 nm which grows significantly in $\sim 2 \times 10^{-6}$ s, is not apparent at these early times, eliminating suggestions of ultrafast triplet formation from this higher excited state of pyrene. The fact that the ps spectral profile of the P*($^1S_1 \rightarrow {}^1S_n$) transition is reminiscent of that measured in ns following 347 nm laser excitation of pyrene in cyclohexane (29), suggests that vibronic relaxation within the singlet manifold is very fast. However, current streak camera experiments designed to measure the ps fluorescence rise and decay in pyrene will confirm these qualitative observations and establish quantitative relaxation rates for $S_n \rightarrow S_1$ intramolecular radiationless transitions as a function of excess energy in the molecule. These are also important data for models of photoionization and electron transfer originating from high lying singlet states in pyrene in alcohols. The nature and lifetime of the ionizing state could well be important considerations in the interpretation of experiments which seek to measure the electron localization and solution time through the time-dependent appearance of e_s^- absorption (32−35). Clearly the pyrene photoionization step must be very efficient, and the lifetime of the ionizing state short, in order to complete effectively against ps vibronic relaxation. For electron localization times of 10^{-12} s, a lifetime of $\leq 10^{-12}$ s may determine the electron trapping rate.

The ionization potential of pyrene in a series of alcohols and micelles has been measured for ns times in double-pulse, tunable laser spectroscopy (3). The reduction in IP observed, from 7.7 eV in the gas phase to 6.6 eV in methanol, for example, is in agreement with the trends recently observed for other aromatic molecules such as benzene (30), and both sets of studies invoke the possibility of high-lying Rydberg states as the doorway states to ionization. Furthermore, this decrease of about 1.1 eV is within the 1.0−1.5 eV decrease commonly observed in photoemission studies of aromatic molecules in thin films, a shift assigned to valence electron interactions in the disordered media (36). While Rydberg states and valence states of gas phase atoms and small molecules exhibit different spectral features, discernible by observing the effects of perturber gases on the linewidth of the transitions, the number density of the condensed systems automatically ensures the high pressure limit and masks such distinctions. Nevertheless, ps emission and absorption studies of the onset of photoionization can provide quantitative dynamical data on the role of the *environment* in modifying the energetics and dynamics of the guest molecule. In a micelle, the charged interface could well be modelled as a type (*ii*) strong field effect. In sodium dodecyl sulphate micelles (SDS), which have a negative surface potential of about −85 mV and a radius of ~30 Å, the IP of pyrene is apparently lowered to 5.4 eV (3). This value was also later deduced from indirect measurements of the IP in cw illumination and conductivity experiments (37). Calculations of the polarization energies of the cation via the Born approximation and of V_o, the bottom of the conduction band for the excess, quasifree electron, are approximate but nevertheless cannot account for the further substantial decrease in IP on going from methanol to an aqueous SDS micelle (3). The unique contribution from the micelle could well be the charged

Can. J. Chem. Downloaded from www.nrcresearchpress.com by 210.87.254.105 on 09/06/12
For personal use only.

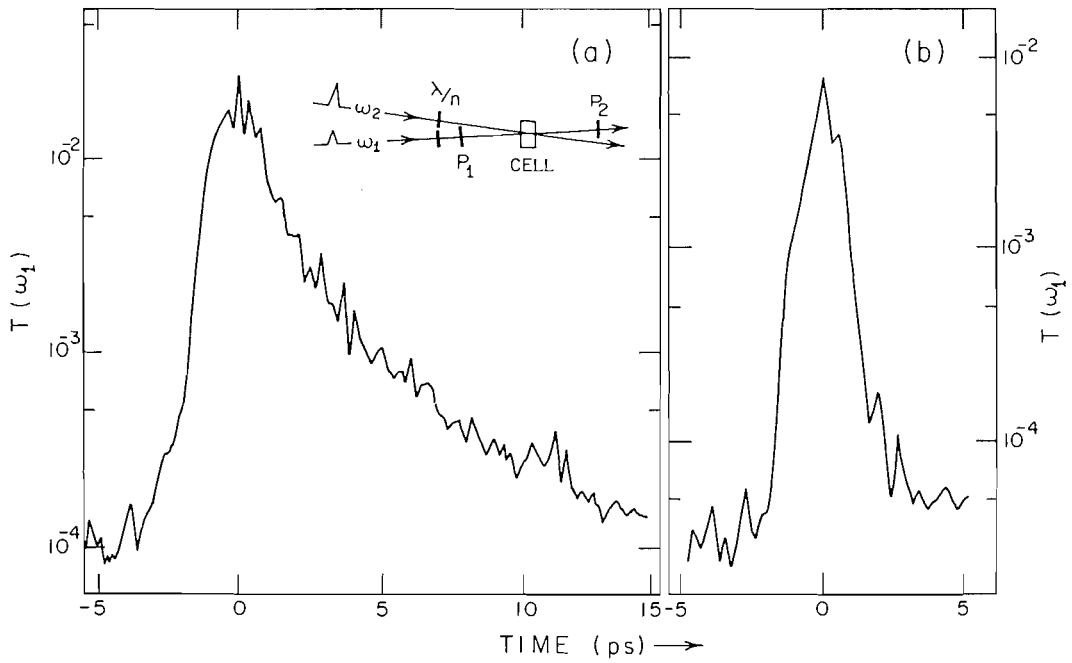

FIG. 6. Transient picosecond optical Kerr signals in chlorobenzene at 300 K, (*a*) linear pump polarization, linear probe polarization in collinear, travelling wave configuration, (*b*) circular pump polarization, linear probe polarization in identical configuration. Note transmission on log scales: see text for details.

interface, which leads to a distortion of the Coulomb potential and lowering of the effective barrier to ionization. The effect of the field gradient cannot be established quantitatively in the absence of a thorough understanding of the complex phase transitions and structural dynamics of these micelles, which are highly sensitive to the presence of a perturbing guest (5*a*), and it is from this perspective that we are now pursuing these interface studies in the picosecond domain.

(b) Femtosecond nonlinear optical responses

While several incoherent and coherent, linear and nonlinear optical techniques are employed to extract dynamical information on orientational relaxation times, vibrational relaxation (T_1), dephasing (T_2), and field-induced nonlinear phenomena, the motivation and results can all be traced back to a single, very basic question. What is the microscopic dynamical description of a liquid? Liquids can be viewed a structureless fluid with continuum, bulk properties at one extreme, which anticipates hydrodynamic behaviour (38), or, at the other extreme as molecular or (atomic) systems within which collisions, spatial correlations, and high frequency fluctuations in local properties determine the dynamics and structure. The latter approach is closely reminiscent of kinetic theory. Picosecond and femtosecond laser spectroscopy has a unique role to play in probing the nature of molecular dynamics of liquids in real time and testing such theories. We present here new results on the orientational dynamics in chlorobenzene ($n_2 = 6 \times 10^{-12}$ esu) at 300 K as illustrative of the optical Kerr effect and polarization memory (9) in liquids at femtosecond times. These data are part of a fs study on temperature dependence of rotational motion in CS_2 and C_6H_5Cl (8).

The transmission (T) of the optical Kerr shutter in the collinear geometry (8) described for Fig. 6 corresponds to:

$$T(\omega_1) \propto \int_{-\infty}^{+\infty} I\omega_1(t - t^1) \sin^2 \left\{\frac{\delta\phi(t)}{2}\right\} dt$$

for linearly polarized pump and probe pulses, where for small phase (ϕ) shifts:

$$\delta\phi(t) = \frac{2\pi}{\lambda_1}\delta n(t)\text{: } \delta\phi(t) \propto I\omega_2(t)$$

The peak transmission in Fig. 6(*a*) occurs at zero time delay ($t^1 = 0$), or total overlap of the 300 fs pump and probe pulses, and rapidly relaxes over about 20 ps. The decay has both fast and slow exponential components, the latter displaying a time constant of 12 ± 1 ps which can be assigned to the orientational relaxation time of chlorobenzene via collisional and diffusional events. This is in good agreement with $\tau = 11.1$ ps, measurements obtained from dielectric relaxation (39), and reflects the predominance of collective motions, as also observed in depolarized laser light scattering techniques (38). The fast component, which seems to follow the laser pulse profile, we assign to electronic nonlinear polarization with perhaps some vibrational contributions to $\chi^{(3)}$ too. In Fig. 6(*b*) is shown the transmission recorded for circular pump (ω_2) and linear probe (ω_1) pulses, in which the fast component clearly dominates. (The same transmission function was measured despite differences in the phase shift $\delta\phi(t)$ anticipated for the circular case (9).) The fwhm of this signal is ~300 fs and together with recent fs CS_2 data (8, 23) represents the fastest optical responses recorded to date in any liquid.

A full interpretation of these effects must take into account the simultaneous superposition of coherently scattered electric fields and polarization in the molecular ensemble, but this will be addressed in a future paper. In brief, we have shown theoretically that such polarization selectivity should reveal the only electronic Kerr response, which will be enhanced close to a two-photon resonance (15). However, since $\omega_1 = \omega_2$ in this experiment, it is also possible that some degenerate four wave mixing (8, 9, 13, 40, 41) is taking place. Thus the amplitude of the transmission signal must be studied in a tunable probe experiment before a definitive measurement of the magnitude

Can. J. Chem. Downloaded from www.nrcresearchpress.com by 210.87.254.105 on 09/06/12
For personal use only.

Can. J. Chem. Downloaded from www.nrcresearchpress.com by 210.87.254.105 on 09/06/12
For personal use only.

of $\chi^{(3)}_{elec}$ is established. Nevertheless, both effects find their roots in electronic hyperpolarization and if we deconvolute the electronic temporal contribution from that in Fig. 6(*a*) containing the molecular part too, it is clear that there is an asymmetry in the temporal response of the orientational component. Chlorobenzene is not a symmetric top and it is possible that anisotropic diffusional components are quire *E*-field sensitive. The rise time is faster than the decay, implying that the reorientation response of the molecules to the sudden imposition of a strong field is faster than the ~12 ps relaxation of the alignment when the field is off. This demonstrates that indeed strong field effects can influence molecular orientation via a memory of the prior statistical structure and interactions of the liquid. This memory becomes impressed upon the polarization properties of the transmitted later pulses. It is possible that intracavity Kerr experiments (4, 7) will reveal a sharper asymmetry in the orientational transients. With fs laser pulses, we can begin to probe spatial correlations in liquids on time scales approaching a relatively small number of collisional events and characterise the behaviour of the memory kernel or the correlation function of the random forces in liquids.

We are continuing these theoretical and experimental studies in order to examine the impact of these strong field and orientational effects on chemical dynamics for systems undergoing sterically specific reactions, isomerization, or dipole–dipole Forster energy transfer with prerequisite molecular alignments.

Acknowledgements

The collaboration of B. Greene and C. V. Shank on the initial pyrene experiments is gratefully acknowledged, as is the hospitality and collaboration of ENSTA, Ecole Polytechnique with G. A. Kenney-Wallace under the Canada–France exchange programme.

We also acknowledge the financial support of Natural Sciences and Engineering Research Council of Canada, the U.S. Office of Naval Research, and the Petroleum Research Fund, administered by the American Chemical Society, towards the different laser research projects discussed here.

1. J. JORTNER (*Editor*). Photoselective chemistry. Wiley, New York. 1981.
2. D. J. BRADLEY, G. PORTER, and M. H. KEY (*Editors*). Ultrashort laser pulses. The Royal Society, London. 1980.
3. S. C. WALLACE, G. E. HALL, and G. A. KENNEY-WALLACE. Chem. Phys. **49**, 279 (1980).
4. C. KALPOUZOS, G. A. KENNEY-WALLACE, P. M. KROGER, and E. QUITEVIS. *In* Picosecond lasers and applications. *Edited by* L. Goldberg SPIE. Vol. 322. 1982. pp. 188–198; to be published.
5. (*a*) L. HUNT BILLARD, K. BRINKER, C. HOLUBOV, and G. A. KENNEY-WALLACE. Unpublished data; (*b*) G. E. HALL, L. A. HUNT, G. A. KENNEY-WALLACE, and K. SARANTIDIS. J. Phys. Chem. **84**, 1145 (1980).
6. G. A. KENNEY-WALLACE, J. FLINT, and S. C. WALLACE. Chem. Phys. Lett. **32**, 71 (1975).
7. C. KALPOUZOS and G. A. KENNEY-WALLACE. To be published; C. KALPOUZOS. M.Sc. Thesis. University of Toronto. 1981.
8. J. ETCHEPARE, G. A. KENNEY-WALLACE, G. GRILLON, A. MIGUS, and J. P. CHAMBARET. IEEE J. Q. Elec. **18**, 1826 (1982).
9. C. KALPOUZOS, G. A. KENNEY-WALLACE, P. M. KROGER, E. QUITEVIS, and S. C. WALLACE. *In* Picosecond phenomena III, *Edited by* K. Eisenthal, R. M. Hochstrasser, W. Kaiser, and A. Laubereau. Springer-Verlag, New York. 1982. p. 221.
10. W. SHARFIN, M. IVANCO, and S. C. WALLACE. J. Chem. Phys. **76**, 2095 (1982).
11. W. LAMBERT, P. FELKER, and A. H. ZEWAIL. J. Chem. Phys. **75**, 5958 (1891).
12. R. FORK, B. GREENE, and C. V. SHANK. Appl. Phys. Lett. **38**, 671 (1981); C.V. SHANK *et al. In* Picosecond phenomena III, *Edited by* K. Eisenthal, R. M. Hochstrasser, W. Kaiser, and A. Laubereau. Springer-Verlag, New York. 1982. pp. 2–5.
13. N. BLOEMBERGEN. Non linear optics. Benjamin, New York. 1965; Rev. Modern Phys. **54**, 685 (1982).
14. (*a*) E. P. IPPEN and C. V. SHANK. Appl. Phys. Lett. **26**, 92 (1975); (*b*) K. L. SALA and M. C. RICHARDSON. Phys. Rev. A. **12**, 1036 (1975) and references therein.
15. B. A. GARETZ and G. A. KENNEY-WALLACE. To be published.
16. M. EICHHORN, F. WILLIG, K.-P. CHARLE, and K. BITTERLING. J. Chem. Phys. **76**, 4648 (1982).
17. N. MOTT and E. DAVIS. Electronic processes in non-crystalline materials. Clarendon Press. 1979.
18. M. CALVIN, I. WILLNER, C. LAANE, and J. OTVOS. J. Photochem. **17**, 195 (1981) and references therein.
19. (*a*) S. C. WALLACE and J. K. THOMAS. Rad. Res. **54**, 49 (1973); (*b*) P. P. INFELTA, M. GRATZEL, and J. H. FENDLER. J. Am. Chem. Soc. **102**, 1479 (1980) and references therein.
20. T. F. GEORGE, I. ZIMMERMAN, J.-M. YUAN, J. R. LAING, and P. DEVRIES. Acc. Chem. Res. **10**, 449 (1977).
21. C. COHEN-TANNOUDJI and S. HAROCHE. J. Phys. Paris, **30**, 153 (1969).
22. C. V. SHANK, R. L. FORK, R. YEN, R. STOLEN, and J. THOMLINSON. Appl. Phys. Lett. **40**, 761 (1982).
23. J. M. HALBOUT and C. L. TANG. Appl. Phys. Lett. **40**, 765 (1982); B. I. GREENE and R. C. FARROW. J. Chem. Phys. **77**, 4729 (1982).
24. K. SALA, G. A. KENNEY-WALLACE, and G. E. HALL. IEEE. J. Q. Elec. **16**, 990 (1980), and references on correlation techniques therein.
25. G. FLEMING. Adv. Chem. Phys. **49**, 1 (1982).
26. J. P. RYAN, L. GOLDBERG, and D. J. BRADLEY. Opt. Commun. **27**, 127 (1978).
27. S. L. SHAPIRO, R. CAVANAUGH, and J. C. STEPHENSON. Opt. Lett. **6**, 470 (1981).
28. R. R. ALFANO and S. L. SHAPIRO. Chem. Phys. Lett. **3**, 407 (1971).
29. (*a*) G. E. HALL and G. A. KENNEY-WALLACE. Chem. Phys. **28**, 205 (1978); Chem. Phys. **32**, 313 (1978); (*b*) G. E. HALL. Ph.D. Thesis. University of Toronto. 1980.
30. T. SCOTT, C. L. BRAUN, and A. C. ALBRECHT. J. Chem. Phys. **7**, 5195 (1982).
31. B. GREENE, G. A. KENNEY-WALLACE, and C. V. SHANK. Unpublished data.
32. Y. WANG, M. CRAWFORD, M. MCAULIFFE, and K. B. EISENTHAL. Chem. Phys. Lett. **74**, 160 (1980).
33. D. HUPPERT, G. A. KENNEY-WALLACE, and D. M. RENTZEPIS. J. Chem. Phys. **75**, 2265 (1981).
34. J. C. MIALOCQ, P. GOUJON, and J. SUTTON. J. Chem. Phys. **72**, 6338 (1980).
35. G. A. KENNEY-WALLACE and C. D. JONAH. J. Phys. Chem. **86**, 2572 (1982).
36. I. MAYER and C. DUKE. Phys. Rev. B**23**, 2111 (1981).
37. A. BERNAS, D. GRAND, S. HAUTECLOQUE, and A. CHAMBAUDET. J. Phys. Chem. **85**, 3684 (1981).
38. D. KIVELSON. Chem. Soc. Faraday Symp. **11**, 1 (1977).
39. J. M. SCHURR. Mol. Phys. **40**, 1025 (1980).
40. A. OWYOUNG. Ph.D. Thesis, Ca. Tech. 1972; J.-L. Oudar. To be published; Private communication.
41. VARDENNY and J. TAUC. Opt. Commun. **39**, 396 (1981).

Deviations from the $O_3-NO-NO_2$ photostationary state in tropospheric chemistry

JACK G. CALVERT and WILLIAM R. STOCKWELL

National Center for Atmospheric Research, P. O. Box 3000, Boulder, CO 80307, U.S.A.[1]

Received August 26, 1982

This paper is dedicated to Professor Harry E. Gunning on the occasion of his 65th birthday

JACK G. CALVERT and WILLIAM R. STOCKWELL. Can. J. Chem. **61**, 983 (1983).

A theoretical study of the magnitude and origin of deviations in the photostationary state relation, $[O_3]_t[NO]_t/[NO_2]_t \simeq (k_1/k_3)_t[I]$ has been carried out by computer simulation. Various homogeneous tropospheric mixtures were chosen with initial pollutant concentrations varied from those of highly polluted to very clean atmospheres. Even for the homogeneous conditions assumed here, strong negative deviations were observed ($[O_3]_t[NO]_t/[NO_2]_t < (k_1/k_3)_t$ for many of the conditions chosen. Failure of [I] in many cases resulted largely from the non-zero value of $d[O_3]/dt$. Many other factors, including significant rates of O_3 reaction with NO_2, alkene, HO_2, HO, and ozone photolysis, contribute significantly to the deviations seen in several cases considered.

JACK G. CALVERT et WILLIAM R. STOCKWELL. Can. J. Chem. **61**, 983 (1983).

Faisant appel à une simulation à l'aide de l'ordinateur, on a étudié théoriquement l'ampleur et l'origine des déviations de la relation de l'état stationnaire $[O_3]_t[NO]_t/[NO_2]_t \simeq (k_1/k_3)_t[I]$. On a choisi plusieurs mélanges troposphériques homogènes avec diverses concentrations initiales en polluant allant des atmosphères très polluées à des atmosphères très propres. Même dans les conditions homogènes utilisées dans ce travail, on a observé des fortes déviations négatives ($[O_3]_t[NO]_t/[NO_2]_t < (k_1/k_3)_t$ pour plusieurs des conditions choisies. Dans plusieurs cas, l'insuffisance de la relation [I] provient principalement de la valeur de $d[O_3]/dt$ différente de zéro. Plusieurs autres facteurs incluant les vitesses appréciables des réactions de O_3 avec le NO_2, l'alcène, le HO_2, le HO et la photolyse de l'ozone, contribuent de façon significative aux déviations observées dans plusieurs des cas considérés.

[Traduit par le journal]

Introduction

It has been recognized for many years that in a sunlight-irradiated, polluted troposphere reactions [1]–[3] are the dominant fates of the NO, O_3, and NO_2. For these conditions relation [I] is expected to hold reasonably well at any time t.

[1] $NO_2 + h\nu \rightarrow O + NO$

[2] $O + O_2 + M \rightarrow O_3 + M$

[3] $O_3 + NO \rightarrow NO_2 + O_2$

[I] $[NO]_t[O_3]_t/[NO_2]_t \simeq (k_1/k_3)_t$

There are a variety of qualitative studies which have helped define the conditions under which relation [I] holds or for which deviations are large. Both experiment and theory suggest that for conditions of high air pollution (high [NO] and strong sunlight) relation [I] is followed reasonably well (1–16). Large positive deviations of $[NO]_t[O_3]_t/[NO_2]_t$ from $(k_1/k_3)_t$ observed by Calvert for the early morning hours in Los Angeles (12) were attributed to the large heterogeneity of the morning air masses. It was suggested that pockets of NO-rich air that originated from pollution sources near ground level mixed turbulently with pockets of older O_3-rich air that came from aloft. It was reasoned that although the photostationary state relation [I] may apply reasonably well in each pocket, an apparent deviation from [I] may occur from the use of averaged values of [NO] and $[O_3]$. These are measured by the aircraft during some finite time period during which many diverse pockets are sampled. For these conditions the product $\langle[NO]\rangle\langle[O_3]\rangle$ must be greater than the true $[NO][O_3]$ product in each small pocket of air. This reasoning appears to be consistent with the results of more quantitative consideration of this phenomenon by Seinfeld (17), Feigley (18), Chock and Kumar (19), and Bilger (14).

It has been recognized by several workers that deviations from relation [I] may be anticipated even for well mixed, homogeneous air masses (1, 7, 10–12, 16, 20–22). These cases involve conditions for which either the rates of reactions of O_3 with other species (NO_2, alkene, etc.) may become competitive with that for reaction [3], or the steady-state assumption may not be justified because of a rapid change in sunlight intensity (early or late in the day, cloud development, etc.) or NO, NO_2, or O_3 concentrations. However, the general consensus in the existing literature is that relation [I] describes reasonably well the interrelationship of the [NO], $[O_3]$, and $[NO_2]$ data for the highly polluted and the moderately polluted troposphere.

The present work was initiated to better characterize the extent of the deviations from relation [I] for homogeneous tropospheric air masses with various degrees of contamination and to determine the magnitude and the reasons for its failure. Stedman and co-workers (16, 20, 21) have made an interesting suggestion that deviation of $[O_3]_t[NO]_t/[NO_2]_t$ from $(k_1/k_3)_t$ observed in the relatively clean tropospheric air may result largely from the importance of the reaction $HO_2 + O_3 \rightarrow HO + 2O_2$ for these conditions. We will test this hypothesis in this study. In addition, we will attempt to define those conditions where relation [I] is an adequate representation of the O_3, NO, NO_2 data. Such information is valuable to modelers in their attempts to simplify tropospheric simulations.

Discussion

In this work we have used a seemingly realistic reaction scheme (Table 1) to computer simulate the homogeneous chemistry which occurs in synthetic polluted atmospheres. The chemical reaction mechanism employed should describe well the interactions between the inorganic and carbonyl species.

[1]The National Center for Atmospheric Research is sponsored by the U.S. National Science Foundation.

Can. J. Chem. Downloaded from www.nrcresearchpress.com by 210.87.254.42 on 09/06/12
For personal use only.

TABLE 1. Reaction mechanism used in simulations of tropospheric chemistry

Reaction	Rate constant[a]
$NO_2 + h\nu \rightarrow O + NO$	6.2×10^{-1} [b]
$O + O_2 (+ M) \rightarrow O_3 (+ M)$	2.16×10
$O_3 + NO \rightarrow O_2 + NO_2$	2.59×10
$O_3 + h\nu \rightarrow O(^1D) + O_2$	3.00×10^{-3} [b]
$O_3 + h\nu \rightarrow O + O_2$	4.69×10^{-2} [b]
$O(^1D) + H_2O \rightarrow HO + HO$	2.40×10^5
$O(^1D) + M \rightarrow O + M$	7.40×10^4
$HO + NO (+ M) \rightarrow HONO (+ M)$	7.60×10^3
$HONO + h\nu \rightarrow HO + NO$	1.05×10^{-1} [b]
$HO + NO_2 (+ M) \rightarrow HONO_2 (+ M)$	1.48×10^4
$HO + CO (+ M) \rightarrow HO_2 + CO_2 (+ M)$	3.93×10^2
$H_2O + NO_2 + NO \rightarrow HONO + HONO$	5.50×10^{-10}
$HONO + HONO \rightarrow H_2O + NO + NO_2$	4.10×10^{-4}
$HO_2 + NO \rightarrow HO + NO_2$	1.20×10^4
$HO_2 + NO_2 (+ M) \rightarrow HO_2NO_2 (+ M)$	1.60×10^3
$HO_2NO_2 (+ M) \rightarrow HO_2 + NO_2 (+ M)$	4.10
$HO_2 + HO_2 \rightarrow H_2O_2 + O_2$	3.80×10^3
$HO_2 + HO_2 + H_2O \rightarrow H_2O_2 + O_2 + H_2O$	2.85×10^{-1}
$HO + \text{alkene} \rightarrow RO_2$ ($RO_2 = HOCH_2CHO_2CH_3$)	3.80×10^4
$RO_2 + NO \rightarrow RO + NO_2$	1.20×10^4
$RO \rightarrow HO_2 + CH_2O + CH_3CHO$	2.70×10^5
$CH_2O + h\nu \rightarrow HO_2 + HO_2 + CO$	1.80×10^{-3} [b]
$CH_2O + h\nu \rightarrow H_2 + CO$	2.38×10^{-3} [b]
$CH_3CHO + h\nu \rightarrow CH_3O_2 + HO_2 + CO$	2.12×10^{-4} [b]
Ketone (CH_3COCH_3) $+ h\nu \rightarrow CH_3COO_2 + CH_3O_2$	1.61×10^{-4} [b]
$CH_3O_2 + NO \rightarrow CH_2O + NO_2 + HO_2$	1.20×10^4
$O_3 + \text{alkene} \rightarrow CH_2OO\dagger + CH_3CHO$	7.50×10^{-3}
$O_3 + \text{alkene} \rightarrow CH_2O + CH_3CHOO\dagger$	7.50×10^{-3}
$CH_2OO\dagger + M \rightarrow CH_2OO + M$	2.54×10^5
$CH_2OO\dagger \rightarrow H_2 + CO_2$	1.10×10^{11}
$CH_2OO\dagger \rightarrow H_2O + CO$	1.90×10^{11}
$CH_2OO\dagger \rightarrow HCO_2H$	2.25×10^{10}
$CH_2OO + NO \rightarrow CH_2O + NO_2$	2.59×10
$CH_2OO + H_2O \rightarrow HCO_2H + H_2O$	1.55×10^{-3}
$CH_2OO + CH_2O \rightarrow HCO_2CH_2OH$	6.48
$CH_2OO + SO_2 \rightarrow H_2SO_4 + CH_2O$	2.59×10
$CH_2OO + CH_3CHO \rightarrow CH_3CO_2CH_2OH$	6.48
$CH_3CHOO\dagger + M \rightarrow CH_3CHOO + M$	2.54×10^5
$CH_3CHOO\dagger \rightarrow CH_4 + CO_2$	1.10×10^{11}
$CH_3CHOO\dagger + CH_3OH + CO$	1.90×10^{11}
$CH_3CHOO\dagger \rightarrow CH_3CO_2H$	2.25×10^{10}
$CH_3CHOO + H_2O \rightarrow CH_3CO_2H + H_2O$	1.55×10^{-3}
$CH_3CHOO + NO \rightarrow CH_3CHO + NO_2$	2.59×10
$CH_3CHOO + CH_2O \rightarrow CH_3CO_2CH_2OH$	6.48
$CH_3CHOO + CH_3CHO \rightarrow CH_3CO_2CH(CH_3)OH$	6.48
$CH_3CHOO + SO_2 \rightarrow H_2SO_4 + CH_3CHO$	2.59×10
$HO + CH_2O \rightarrow H_2O + HO_2 + CO$	2.10×10^4
$HO + CH_3CHO \rightarrow H_2O + CH_3COO_2$	2.20×10^4
$CH_3COO_2 + NO \rightarrow CH_3O_2 + CO_2 + NO_2$	4.90×10^3
$CH_3COO_2 + NO_2 \rightarrow CH_3COO_2NO_2$	1.60×10^3
$CH_3COO_2NO_2 \rightarrow CH_3COO_2 + NO_2$	2.20×10^{-2}
$HO + \text{alkane} \rightarrow H_2O + XO_2(CH_3CHO_2CH_3)$	4.40×10^3
$XO_2 + NO \rightarrow XO + NO_2$	1.20×10^4
$XO \rightarrow CH_3O_2 + CH_3CHO$	1.60×10^2
$XO + O_2 \rightarrow HO_2 + \text{ketone}$	3.20×10^{-1}
$CH_3O_2 + HO_2 \rightarrow CH_3O_2H + O_2$	1.92×10^3
$H_2O_2 + h\nu \rightarrow HO + HO$	6.19×10^{-4} [b]
$NO_2 + O_3 \rightarrow NO_3 + O_2$	5.00×10^{-2}
$HO + SO_2 (+ M) \rightarrow (HOSO_2O_2) \rightarrow SO_3(H_2SO_4) + HO_2$	1.60×10^3
$O + SO_2 (+ M) \rightarrow SO_3(H_2SO_4) (+ M)$	8.40×10
$NO_3 + NO_2 (+ M) \rightarrow N_2O_5 (+ M)$	5.60×10^3
$N_2O_5 (+ M) \rightarrow NO_3 + NO_2 (+ M)$	2.40×10
$NO_3 + NO \rightarrow NO_2 + NO_2$	1.30×10^4
$N_2O_5 + H_2O \rightarrow HONO_2 + HONO_2$	5.00×10^{-6}
Ketone $+ HO \rightarrow H_2O + YO_2(CH_3COCH_2O_2)$	1.48×10^3

Can. J. Chem. Downloaded from www.nrcresearchpress.com by 210.87.254.42 on 09/06/12
For personal use only.

TABLE 1 (*Concluded*)

Reaction	Rate constant[a]
$NO_3 + h\nu \rightarrow NO_2 + O$	1.08×10 [b]
$NO_3 + h\nu \rightarrow NO + O_2$	1.32 [b]
$HO + O_3 \rightarrow HO_2 + O_2$	1.00×10^2
$HO_2 + O_3 \rightarrow HO + O_2 + O_2$	2.3
$RO_2 + RO_2 \rightarrow RO + RO + O_2$	1.99
$CH_3O_2 + CH_3O_2 \rightarrow CH_3O + CH_3O + O_2$	2.36×10^2
$CH_3O_2 + CH_3O_2 \rightarrow CH_2O + CH_3OH + O_2$	3.10×10^2
$XO_2 + XO_2 \rightarrow XO + XO + O_2$	1.99
$YO_2 + YO_2 \rightarrow YO + YO + O_2$	1.47×10^2
$RO_2 + YO_2 \rightarrow RO + YO + O_2$	3.42×10
$XO_2 + RO_2 \rightarrow XO + RO + O_2$	1.99
$XO_2 + YO_2 \rightarrow XO + YO + O_2$	3.40×10
$YO_2 + HO_2 \rightarrow YO_2H + O_2$	1.92×10^3
$RO_2 + HO_2 \rightarrow RO_2H + O_2$	1.92×10^3
$XO_2 + HO_2 \rightarrow XO_2H + O_2$	1.92×10^3
$YO_2 + NO \rightarrow YO + NO_2$	1.20×10^4
$YO + O_2 \rightarrow MG(CH_3COCHO) + HO_2$	2.45
$MG + HO \rightarrow H_2O + CO + CH_3COO_2$	2.20×10^4
$MG + h\nu \rightarrow HO_2 + CO + CH_3COO_2$	8.84×10^{-3} [b]
$HO_2 + CH_2O \rightarrow HMO_2(O_2CH_2OH)$	2.50×10
$HMO_2 \rightarrow HO_2 + CH_2O$	9.00×10
$HMO_2 + HMO_2 \rightarrow OCH_2OH + OCH_2OH + O_2$	1.47×10^2
$HMO_2 + NO \rightarrow OCH_2OH + NO_2$	4.15×10^2
$HMO_2 + HO_2 \rightarrow HMO_2H + O_2$	2.60×10
$HMO_2 + XO_2 \rightarrow OCH_2OH + XO + O_2$	3.42×10
$HMO_2 + RO_2 \rightarrow OCH_2OH + RO + O_2$	3.42×10
$HMO_2 + YO_2 \rightarrow OCH_2OH + YO + O_2$	2.94×10^2
$HMO_2 + CH_3O_2 \rightarrow OCH_2OH + CH_3O + O_2$	5.88×10^2
$OCH_2OH + O_2 \rightarrow HCO_2H + HO_2$	2.20×10
$CH_3O_2 + XO_2 \rightarrow CH_3O + XO + O_2$	8.59×10
$CH_3O_2 + RO_2 \rightarrow CH_3O + RO + O_2$	8.59×10
$CH_3O_2 + YO_2 \rightarrow CH_3O + YO + O_2$	5.66×10^2
$HMO_2H + h\nu \rightarrow HO + OCH_2OH$	4.07×10^{-4} [b]
$CH_3O_2H + h\nu \rightarrow CH_3O + HO$	4.07×10^{-4} [b]
$CH_3O + O_2 \rightarrow CH_2O + HO_2$	9.0
$HO + HMO_2H \rightarrow H_2O + HMO_2$	1.88×10^3
$HO + H_2O_2 \rightarrow H_2O + HO_2$	1.94×10^3
$HO + CH_3O_2H \rightarrow H_2O + CH_3O_2$	1.88×10^3
$YO_2H + h\nu \rightarrow YO + HO$	4.07×10^{-4} [b]
$HO + YO_2H \rightarrow H_2O + YO_2$	1.88×10^3
$XO_2H + h\nu \rightarrow XO + HO$	4.07×10^{-4} [b]
$XO_2H + HO \rightarrow XO_2 + H_2O$	1.88×10^3
$RO_2H + h\nu \rightarrow RO + HO$	4.07×10^{-4} [b]
$RO_2H + HO \rightarrow RO_2 + H_2O$	1.88×10^3
$CH_3COO_2 + HO_2 \rightarrow CH_3COO_2H + O_2$	2.60×10
$CH_3COO_2 + CH_3COO_2 \rightarrow CH_3O_2 + CH_3O_2 + CO_2 + CO_2 + O_2$	1.45×10^2
$CH_3COO_2 + CH_3O_2 \rightarrow CH_3O_2 + CO_2 + CH_3O + O_2$	3.78×10^2
$CH_3COO_2 + HMO_2 \rightarrow CH_3O_2 + CO_2 + HMO + O_2$	1.47×10^2
$CH_3COO_2 + XO_2 \rightarrow CH_3O_2 + CO_2 + XO + O_2$	3.42×10
$CH_3COO_2 + YO_2 \rightarrow CH_3O_2 + CO_2 + YO + O_2$	3.42×10
$CH_3COO_2 + RO_2 \rightarrow CH_3O_2 + CO_2 + RO + O_2$	3.42×10
$HO + CH_3COO_2H \rightarrow H_2O + CH_3COO_2$	1.88×10^3
$CH_3COO_2H + h\nu \rightarrow CH_3O_2 + CO_2 + HO$	4.07×10^{-4} [b]
$CH_4 + HO \rightarrow H_2O + CH_3O_2$	1.14×10

[a] Units: second order constants, $ppm^{-1}\ min^{-1}$; first order, min^{-1}; third order, $ppm^{-2}\ min^{-1}$; pressure, 1 atm, temperature, 25°C.

[b] These rate constants vary with time to simulate the solar variation; the number shown is the value for 1200 h ($Z = 16.9°$, sea level, assumed 0.20 albedo).

Some shortcuts were adopted in the hydrocarbon reaction sequence adopted here in order to maintain some degree of control over the computer time for the simulations. Thus we have used only three hydrocarbon species, CH_4, "alkene", and "alkane". The reaction rate constants for HO and O_3 reactions with the alkene and alkane were adjusted averages (weighted by concentration, reactivity) which were derived from typical alkene, alkane, and aromatic hydrocarbon composition data from urban areas. The subsequent chemistry of the alkene and alkane was made to mimic that for propylene and propane,

Can. J. Chem. Downloaded from www.nrcresearchpress.com by 210.87.254.42 on 09/06/12
For personal use only.

Can. J. Chem. Downloaded from www.nrcresearchpress.com by 210.87.254.42 on 09/06/12
For personal use only.

respectively; thus CH_2O, CH_3CHO, and acetone (ketone) appear as the only carbonyl products. The sunlight intensity and the photolysis constants were picked to simulate a clear day in summer (July 1) at 40°N latitude, near sea level (temperature, 25°C). A surface albedo of 0.20 was assumed. The photolysis constants were varied to match reasonably well the diurnal variation of the sun through relation [II]:

$$[II]^2 \quad (k_x)_t = \exp\{\ln (k_x)_{noon}/\sin[(t - a)\pi/b]\}$$

Here $(k_x)_t$ is the apparent first-order rate constant for a given photochemical reaction x at time t (measured from midnight of the given day); a is the time for sunrise (0500, 300 min), and b is the time from sunrise to sunset (840 min). The $(k_x)_{noon}$ values for the eighteen different photochemical reactions in the simulation are shown in Table 1. All aspects of the mechanism chosen are based on current knowledge of the chemistry of these systems, but in those cases where experimental rate data are not available (e.g., the absolute rate constants for the reactions of the Criegee intermediates, CH_2O_2 and CH_3CHO_2), estimates were made using appropriate thermochemical and kinetic methods together with relative rate constant information. In most cases we have not included source terms for the pollutants, dilution of the reacting mixture, and ground loss of the reactants and products. The effects of adding these features are investigated in additional simulations as part of this study. Computer simulations were made using a variety of initial pollutant concentrations which are representative of a range of conditions from a highly polluted to a relatively clean tropospheric air mass. These initial concentrations are summarized in Table 2. The reactant, product − time distributions need not be considered here in detail, but they appear to be in qualitative accord with field data for conditions of similar pollutant contamination. Of special interest in the consideration of deviations from relation [I] are the reactants O_3, NO, NO_2, and alkene. A few examples of the time dependence during the daylight hours for cases *A*, *C*, *G*, and *H* can be seen in Figs. 3*a*, 4*a*, 8*a*, 11*a*–*c*, 13*a*, and 14*a*. Our analysis of these and other product and radical concentrations for cases *A*–*H* and other cases suggests that the present mechanism does a reasonably good job of simulating the gas phase chemistry of the troposphere, and our use of this mechanism to test for deviations from relation [I] should provide meaningful results.

The major reactions which control the ozone level in these simulations are as follows:

[1] $NO_2 + h\nu \rightarrow O + NO$

[2] $O + O_2 + M \rightarrow O_3 + M$

[3] $O_3 + NO \rightarrow O_2 + NO_2$

[4] $O_3 + h\nu \rightarrow O(^1D) + O_2$

[5] $O_3 + h\nu \rightarrow O + O_2$

[6] $O(^1D) + H_2O \rightarrow 2HO$

[7] $O(^1D) + M \rightarrow O + M$

[8] $O_3 + \text{alkene} \rightarrow \text{products}$

[9] $NO_2 + O_3 \rightarrow NO_3 + O_2$

[10] $HO + O_3 \rightarrow HO_2 + O_2$

[2]The function II is only for values in $\ln (k_x)_{noon} < 0$, for $\ln (k_x)_{noon} \geq 0$ a different function of similar form was used.

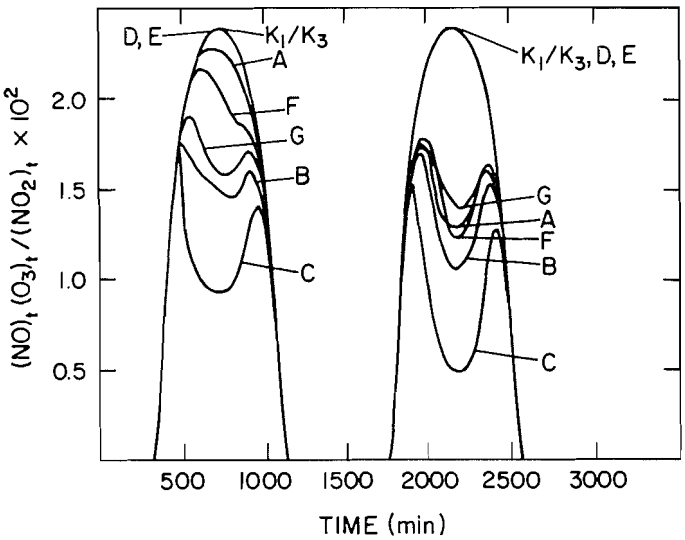

FIG. 1. Plot of the function $[O_3]_t[NO]_t/[NO_2]_t$ and $(k_1/k_3)_t$ for various times during a series of two-day computer simulations of the chemistry of tropospheric mixtures of varied pollutant composition; initial concentrations for the various cases A–G are given in Table 2.

[11] $HO_2 + O_3 \rightarrow HO + 2O_2$

Reaction [5] forming ground state $O(^3P)$ atoms is followed by an almost quantitative reformation of O_3 through reaction [2], so it is an insignificant O_3 loss mechanism in the lower troposphere. However, that fraction (Q) of the $O(^1D)$ formed in reaction [4] which ultimately reacts with H_2O, $Q = k_6[H_2O]/(k_6[H_2O] + k_7[M])$, results in O_3 loss. If we neglect dilution of the air mass and O_3 ground loss, then the rate of ozone generation in the system will be given by relation [III]:

$$[III] \quad \frac{d[O_3]}{dt} = k_1[NO_2] - [O_3][NO]k_3 - [O_3]k_4Q - [O_3][\text{alkene}]k_8 - [O_3][NO_2]k_9 - [O_3][HO]k_{10} - [O_3][HO_2]k_{11}$$

This relation can be recast into the form [IV] which reflects more directly the relation to the simplified steady state relation [I]:

$$[IV] \quad \frac{[O_3]_t[NO]_t}{[NO_2]_t} = \frac{(k_1)_t}{(k_3)_t}\left[1 + \frac{1}{(k_3)_t[NO]_t} \times \left\{\frac{k_4k_6[H_2O]_t}{k_6[H_2O]_t + k_7[M]_t} + k_8[\text{alkene}] + k_9[NO_2]_t + k_{10}[HO]_t + k_{11}[HO_2]_t + \frac{d[O_3]_t}{dt[O_3]_t}\right\}\right]^{-1} = (k_1/k_3)_tP$$

As we would expect the value of the function P approaches unity, and the relation [I] applies well, when $(k_3)_t[NO]_t$ is large compared to the other terms in relation [IV], that is, when reaction [3] is the dominant O_3 loss term. Of course deviations from [I] occur when alternative pathways of O_3 reaction become significant.

The instantaneous values of the function $[O_3]_t[NO]_t/[NO_2]_t$ were calculated as a function of time in the computer simulation of several one and two day scenarios using a range of typical impurity concentrations common in the troposphere. The magnitude of the deviations from the relation [I] were

TABLE 2. Initial concentrations of the pollutants for the simulations of various sunlight-irradiated tropospheric mixtures[a]

Pollutant	Concentration, ppb for the case shown							
	A	B	C	D	E	F	G	H
NO_2	25	2.5	0.25	25	25	2.5	0.25	0.025
NO	75	7.5	0.75	75	75	7.5	0.75	0.075
CO	2000	2000	2000	200	100	200	100	100
Alkene	100	100	100	10	1.0	10	1.0	0.1
Alkane	400	400	400	40	4.0	40	4.0	0.4
O_3	30	30	30	30	30	30	30	30
CH_2O	20	20	20	2.0	0.2	2.0	0.2	0.02
CH_3CHO	10	10	10	1.0	0.1	1.0	0.1	0.01
Ketone	5	5	5	0.5	0.05	0.5	0.05	0.005
SO_2	60	60	60	6	0.6	6	0.6	0.06
CH_4	2500	2500	2500	1400	1400	1400	1400	1400
H_2O (relative humidity)								
10% 3.12×10^6								
50% 1.56×10^7								
100% 3.12×10^7								

[a]These concentrations were assumed to be present at sunrise (0500) in simulations A–H shown.

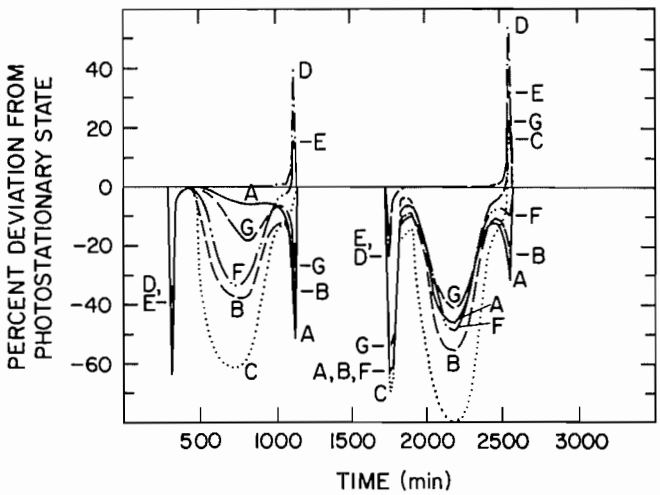

FIG. 2. Plot of the percentage deviation of the $[O_3]_t[NO]_t/[NO_2]_t$ function from $(k_1/k_3)_t$ for various times during a series of two-day computer simulations of the chemistry of various polluted tropospheric air masses; initial compositions are shown in Table 2.

calculated, and the contribution of each term of relation [IV] to this deviation was estimated. By "term" we refer to the individual terms within the { } signs multiplied by the quantity $1/(k_3)_t[NO]_t$. These deviations are seen in Fig. 1 for each of the initial conditions *A*–*G* (50% relative humidity) described in Table 2. Only in cases *D* and *E*, at the highest nitric oxide-to-hydrocarbon ratio, does the $[O_3]_t[NO]_t/[NO_2]_t$ time variation follow $(k_1/k_3)_t$ very closely during most of the daylight hours. In all other cases strong deviations are apparent. The percent deviation between the two terms at various times is shown in Fig. 2. Note that in all cases there is a strong negative deviation during the early morning hours. In the late afternoon hours all cases but *C* (first day) show another strong deviation, in some cases positive, some negative. The origin of the deviations has been determined from a detailed computer analysis of the systems. We will consider several of these cases which illustrate the results for different tropospheric mixtures.

(*a*) *The Highly Polluted Troposphere with a Relatively Low RH/NO_x Ratio, Case* A

The mixture chosen to represent highly polluted tropospheric air, case *A* (Table 2), has a relatively low hydrocarbon-to-nitrogen oxides ratio (5), which is typical of the early morning

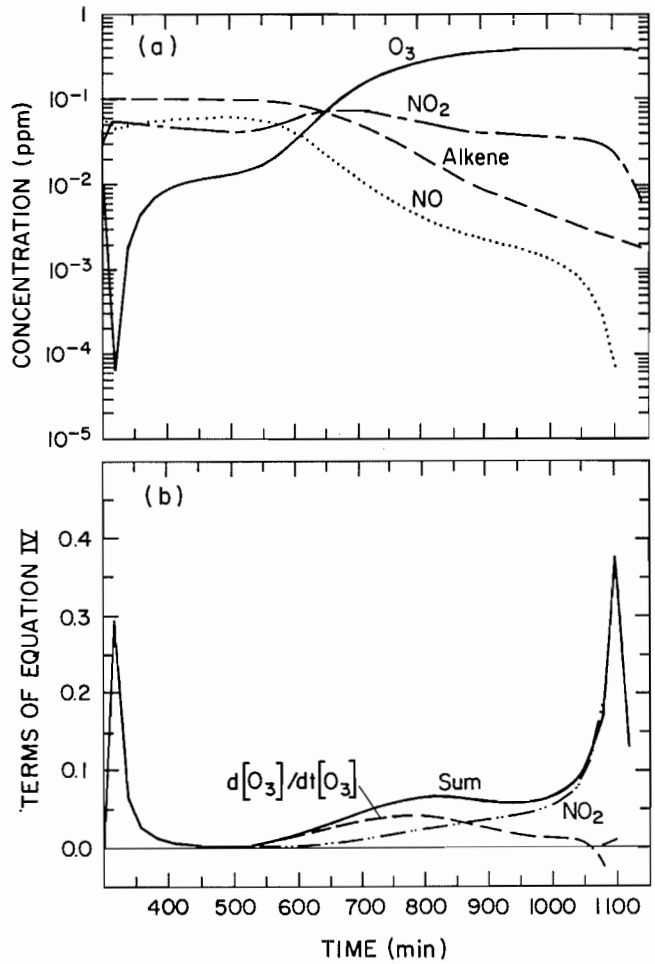

FIG. 3. (*a*) The time dependence of the various reactant concentrations during the first day of a computer simulation of the chemistry of a highly polluted tropospheric air mass (case *A*); (*b*) the magnitude of the individual terms of function [IV] and the sum of these terms for various times; the symbols shown with each curve give the reactant involved in the corresponding term in relation [IV].

Can. J. Chem. Downloaded from www.nrcresearchpress.com by 210.87.254.42 on 09/06/12
For personal use only.

Can. J. Chem. Downloaded from www.nrcresearchpress.com by 210.87.254.42 on 09/06/12
For personal use only.

urban air masses. During day 1 of this scenario, significant levels of ozone develop (about 0.39 ppm) late in the day; see Fig. 3*a*. In our simulation we have intentionally started the first morning with an imbalance in the $NO-NO_2-O_3$ mixture (with respect to relation [I]) which would be typical of the freshly mixed ozone-rich, older air from aloft and the NO-rich air from the early morning human activity near ground level. One sees a rapid decrease in the O_3 and NO as reaction [3] occurs forming NO_2. As the sunlight intensity increases, the hydrocarbons and aldehydes are oxidized, NO is converted to NO_2, and ozone development occurs; see Fig. 3*a*. The deviations from the steady state relation [I] for this case *A* are relatively small during most of the first day, but they become more serious the second day; see Figs. 1 and 2. Deviations seen near sunrise and sunset are the expected result of the rapidly changing concentrations of ozone, NO, and NO_2; for such conditions the steady-state relation [I] cannot be fulfilled at the very low NO_2 photolysis rates characteristic of the low solar flux at these hours.

In Fig. 3*b* we can learn the origin of the deviations seen from the plot of the magnitude of the individual terms of relation [IV]. The last term in relation [IV] involving $d[O_3]/dt[O_3]/k_3[NO]$ is the dominant source of the deviation during most of the day; in the afternoon hours, the third term of [IV] resulting from the O_3-NO_2 reaction [9] becomes important. At this time [NO] becomes very low and $[NO_2]$ relatively high. No other terms in [IV] are significant here.

Concentrations of reactants during the nighttime hours are not shown, but those starting with the sunrise the second day are plotted in Fig. 4*a*. The NO level is extremely low initially, although it climbs somewhat as NO_2 photolyzes to form NO. As a result reactions other than [3] are important in O_3 loss, and the second day deviations from relation [I] are much larger; Figs. 1 and 2. Several terms in relation [IV] cause the deviations in this case; see Fig. 4*b*. Large positive terms in [IV] come from both the HO_2-O_3 reaction [11] and the O_3 photolysis in process [4] followed by [6]; a large negative term results from the last term of [IV] involving $d[O_3]/dt[O_3]$. A smaller but observable contribution from the HO-reaction can be seen as well. Negative deviations of $[O_3]_t[NO]_t/[NO_2]_t$ from $(k_1/k_3)_t$ of the magnitude seen here for day 2 of case *A* have been observed in polluted tropospheric air masses by Kewley and Post (15) in the Sydney, Australia airshed, and by Stedman *et al.* (20) in Claremont, California. Both these groups have used alternative explanations to those advanced here in the explanation of these deviations.

We can see in Fig. 5 the effect of different humidities on the magnitude of the stationary state deviations starting with the initial *A* mixture composition. Note here that the deviations from relation [I] become larger with increasing humidity. From Fig. 6 it is apparent that the larger error enters by way of the increased significance of the $d[O_3]/dt[O_3]$ term. Other terms make observable contributions during the time near sunrise and sunset.

Real atmospheric mixtures of impurities have some degree of dilution as the dirty air mass diffuses turbulently into cleaner air, and the emission of new impurities into the air mass usually occurs as well near urban environments. To observe the effects of these more realistic conditions on the magnitude of the deviations from relation [I], we have made runs with case *A* initial conditions but with the inclusion of dilution of the reacting mixture (10^{-4} min^{-1}) and continued addition of new impurities (NO, NO_2, and alkene at 1.25×10^{-4}, 4.18×10^{-5}, and 1.67×10^{-4} ppm min^{-1}, respectively). These results are

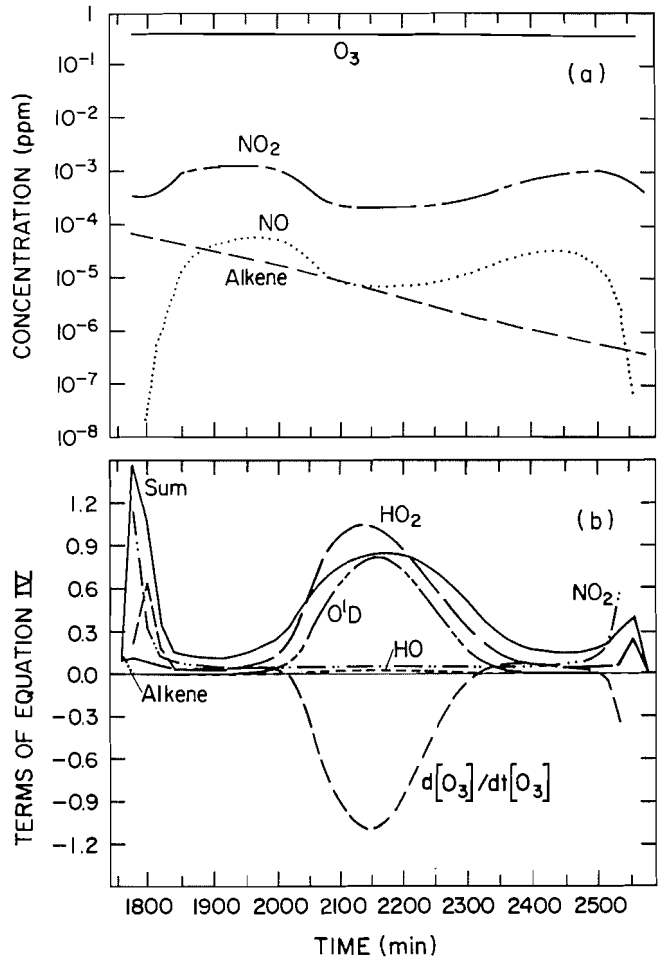

FIG. 4. (*a*) The time dependence of various reactant concentrations during the second day of a computer simulation of the chemistry of a highly polluted tropospheric air mass (case *A*); (*b*) the magnitude of the individual terms of the function [IV] and the sum of these terms for various times.

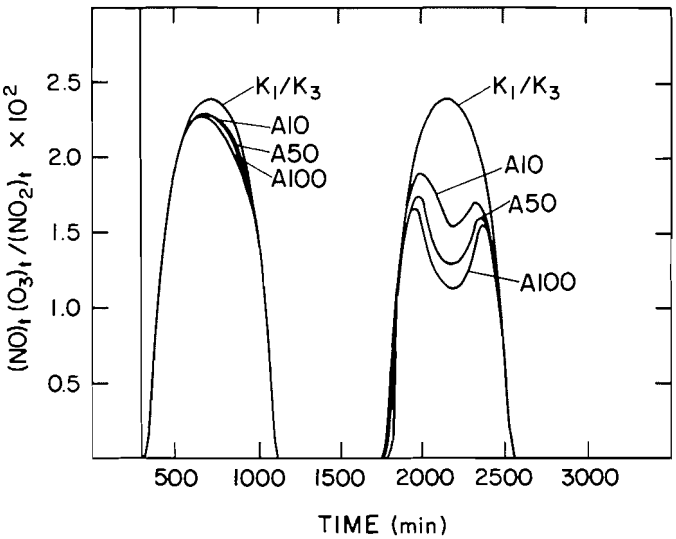

FIG. 5. The effect of humidity on the deviations of $[O_3]_t[NO]_t/[NO_2]_t$, from $(k_1/k_3)_t$, for a two-day computer simulation of the chemistry of a highly polluted tropospheric air mass (case *A*).

summarized in Figs. 7*a* and 7*b*. As one might expect a smaller deviation is seen for this case as a result of the higher NO levels

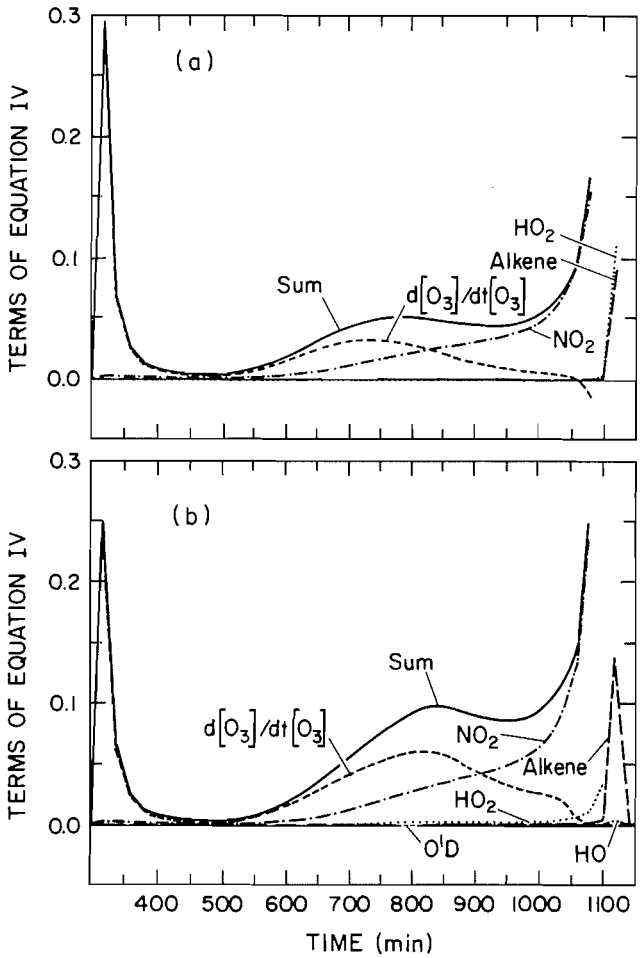

FIG. 6. The magnitude of the individual terms of the function [IV] and the sum of these terms for various times in the simulation of the highly polluted air mass (case *A*) for: (*a*) 10% and (*b*) 100% relative humidity. Compare with the similar results for case *A* at 50% relative humidity in Fig. 3*b*.

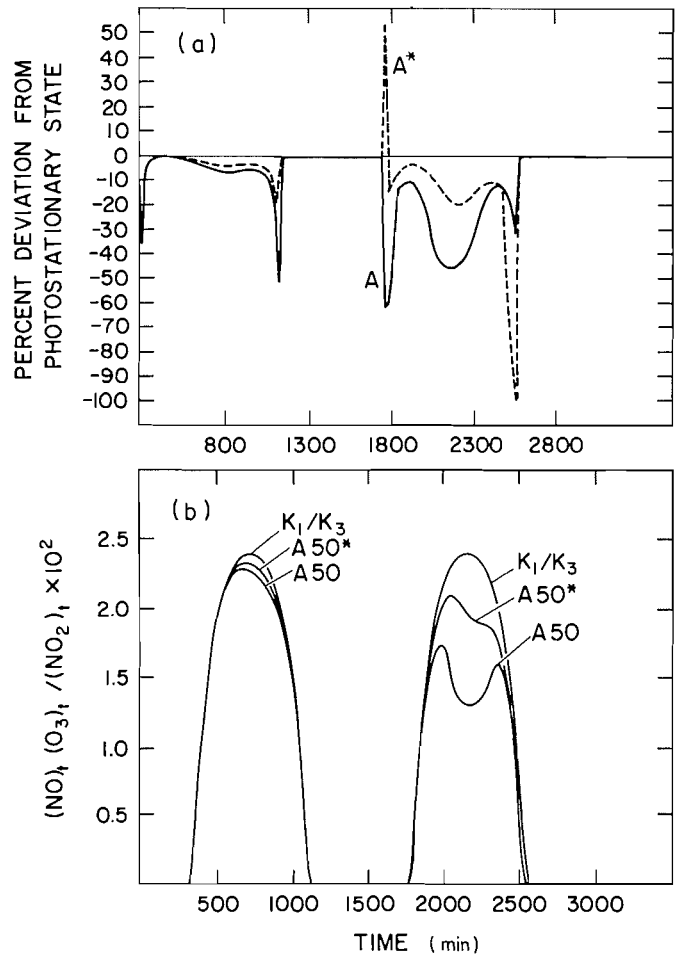

FIG. 7. (*a*) The percentage deviation of the $[NO]_t[O_3]_t/[NO_2]_t$ from $(k_1/k_3)_t$ for various times for the two scenarios of Fig. 7*a*. (*b*). Plot of the functions $[NO]_t[O_3]_t/[NO_2]_t$ and $(k_1/k_3)_t$ for various times during the computer simulation of the chemistry for case *A* (50% relative humidity) and with (A50*) and without (A50) pollutant dilution and continued pollutant additions.

maintained through continued NO emissions and the resulting enhanced rate of the $NO-O_3$ rate compared to other competitive O_3 reactions. It appears that for the highly polluted troposphere, the approximate relation [I] may apply reasonably well (within 20%) during the bulk of the daylight hours even over a several day period, provided that NO_x sources maintain a modest level of NO during the daylight hours. The use of relation [I] in simplifying computer simulations of highly polluted tropospheric mixtures such as case *A* at low RH/NO_x ratios, appears to be justified.

(*b*) *The Highly Polluted Troposphere at Very High RH-to-NO_x Ratio, case* C

In all of the studies made here the deviation from the relation [I] is greatest for case *C*. At the low levels of NO present in this case together with the high levels of impurities such as the hydrocarbons and aldehydes, the O_3 loss by reactants other than NO becomes very significant (Fig. 8*b*) from the onset of the simulation. The NO is titrated to NO_2 by O_3 during the early morning and late evening hours (Fig. 8*a*), and the O_3-NO_2 reaction leads to large positive deviations. The rate of change of ozone with time (last term of relation [IV]) leads to a much larger negative deviation at these times. During the vast portion of the daylight hours this same term is the source of the largest positive deviation. Smaller but significant deviations result from the O_3 loss by HO_2, O_3 photolysis, and alkene reactions. Obviously one cannot use relation [I] in simplifying tropospheric simulations for dirty air masses at high RH/NO_x ratios.

(*c*) *The Troposphere with Rather Low Pollution Levels, case* G

In this case NO_x, RH, RCHO, and SO_2 levels are only one-hundredth of those of the highly polluted troposphere (case *A*). Deviations from relation [I] are significant but not as serious as in case *C*; see Figs. 1 and 9. Again the deviations are sensitive to the humidity with the highest deviation occurring at the highest humidity; Fig. 9. In Fig. 10 we observe that during the first day events for case *G* the non-zero $d[O_3]/dt[O_3]$ term is the major error source for all humidities, but the loss of O_3 through its photolysis, and by its reactions with HO_2, HO, and NO_2 reactions becomes increasingly important for increased humidity. The results observed for the second day of case *G* at 100% relative humidity are interesting. NO is very low during the second day of case *G* (Fig. 11*c*), and the deviation seen during the day results from the sum of a large positive deviation from ozone loss by photolysis, a nearly equal term of negative sign from $d[O_3]/dt[O_3]$, and very significant positive terms which come from the HO_2 and HO reactions with O_3 (Fig. 11*d*). Obviously the deviation in this case results from

Can. J. Chem. Downloaded from www.nrcresearchpress.com by 210.87.254.42 on 09/06/12
For personal use only.

Can. J. Chem. Downloaded from www.nrcresearchpress.com by 210.87.254.42 on 09/06/12
For personal use only.

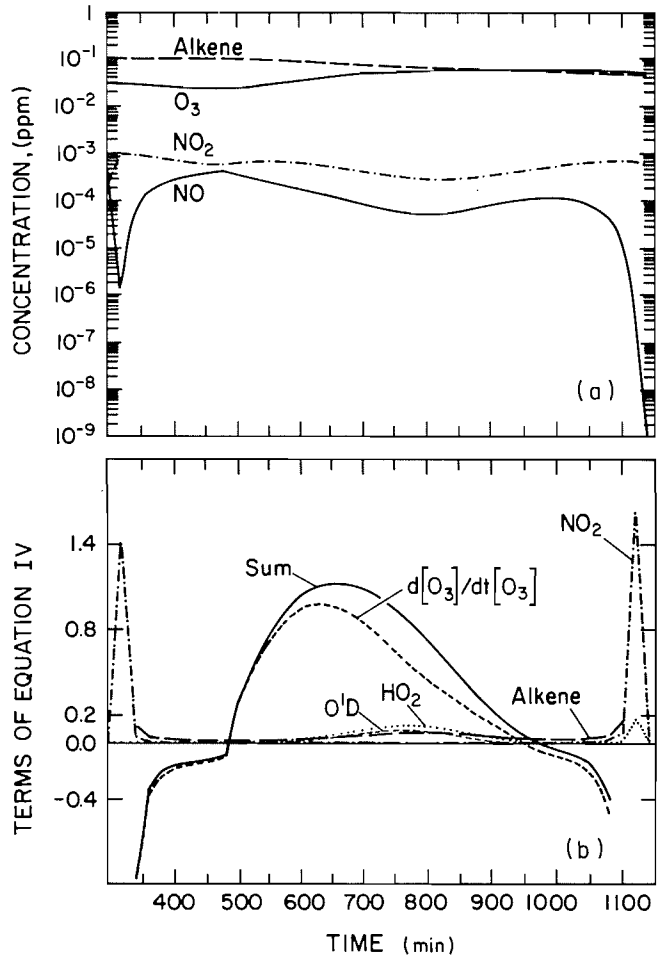

FIG. 8. (*a*) The time dependence of various reactant concentrations during the first day of the computer simulation of the chemistry of a polluted air mass of very low NO_x/RH ratio, case *C* of Table 2, 50% relative humidity; (*b*) the magnitude of the individual terms of function [IV] and the sum of these terms for various times in the simulation of case *C*.

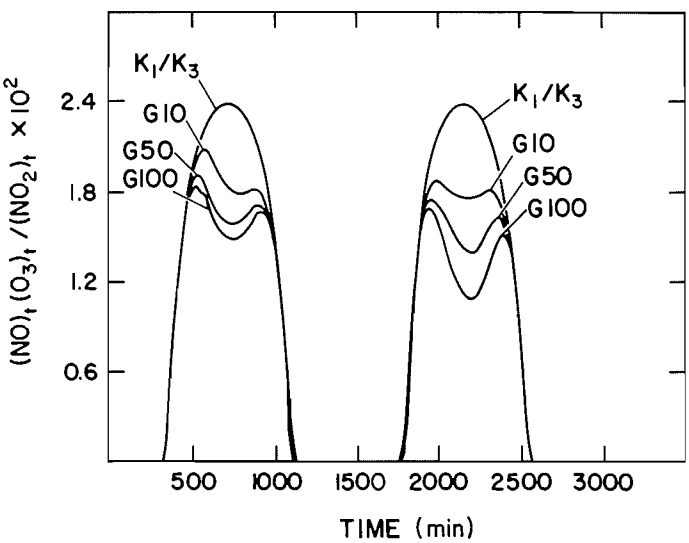

FIG. 9. A plot of the function $[NO]_t[O_3]_t/[NO_2]_t$ and $(k_1/k_3)_t$ versus time for the two-day computer simulation of the chemistry for a relatively clean tropospheric air mass (case *G* of Table 2) at various relative humidities.

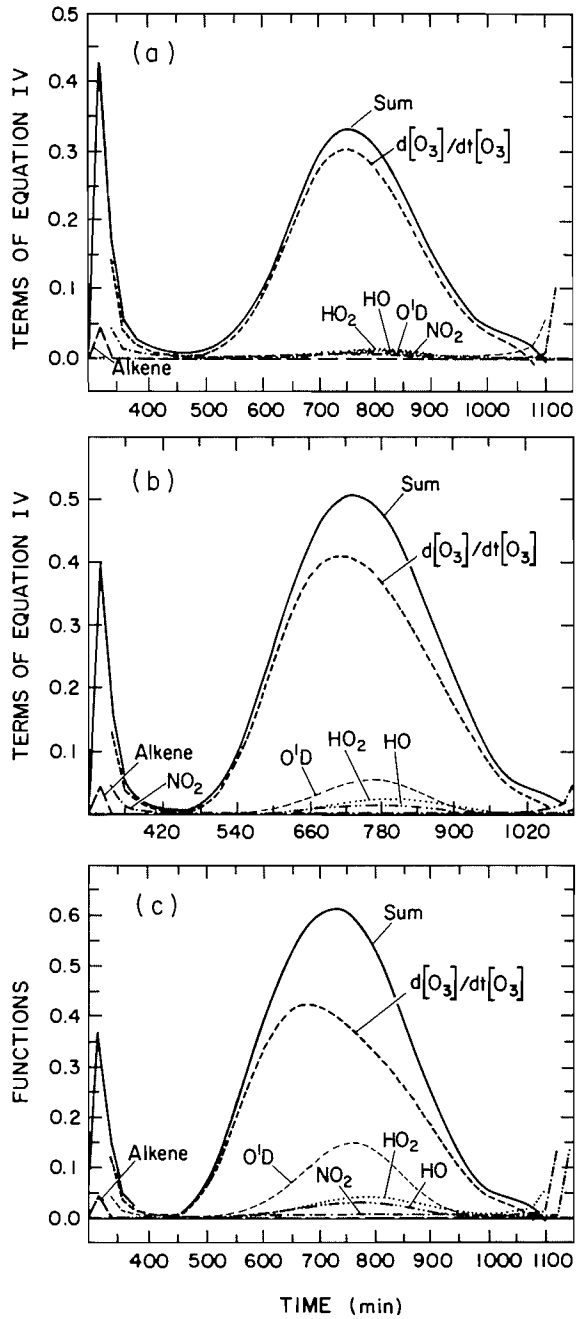

FIG. 10. The magnitude of the individual terms of the function [IV] and the sum of these terms for various times in the simulation of the relatively clean tropospheric air mass (case *G*): (*a*) day one, 10% relative humidity; (*b*) day one, 50% relative humidity; (*c*) day one, 100% relative humidity.

several significant contributing terms in relation [IV]; no single term dominates.

(*d*) *The Very Clean Tropospheric Air, case* H

To test the hypothesis of Stedman *et al.*, a five day scenario was studied using initial pollutant concentrations which are representative of very clean tropospheric air. The deviations of the $[NO]_t[O_3]_t/[NO_2]_t$ function from $(k_1/k_3)_t$ for this case can be seen in Fig. 12. After the first day little further change in the extent of the deviation can be seen. We have analyzed the origin of this deviation for the third and fourth days. The concentrations of O_3, NO, NO_2, and alkene during these

Can. J. Chem. Downloaded from www.nrcresearchpress.com by 210.87.254.42 on 09/06/12
For personal use only.

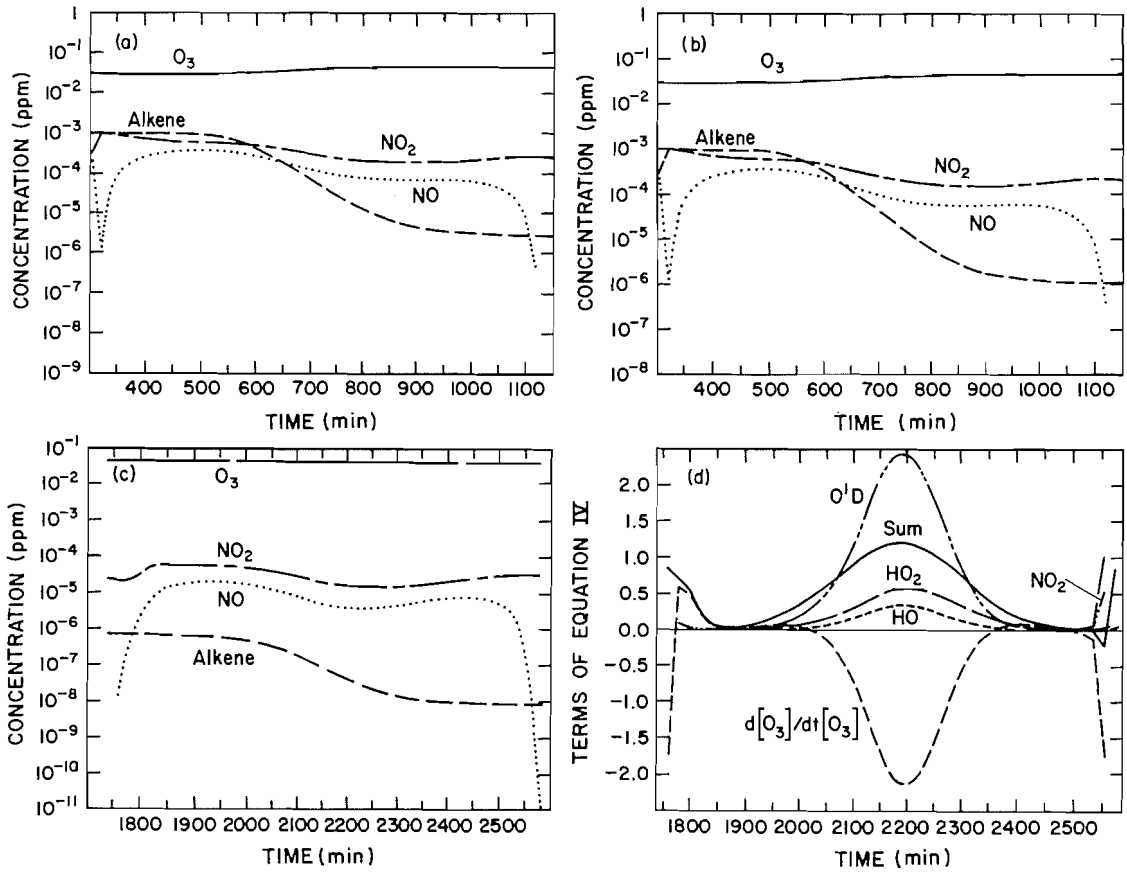

FIG. 11. The time dependence of various reactant concentrations during the computer simulation of the chemistry of a relatively clean tropospheric air mass (case *G*): (*a*) day 1, 50% relative humidity; (*b*) day 1, 100% relative humidity; (*c*) day two, 100% relative humidity.

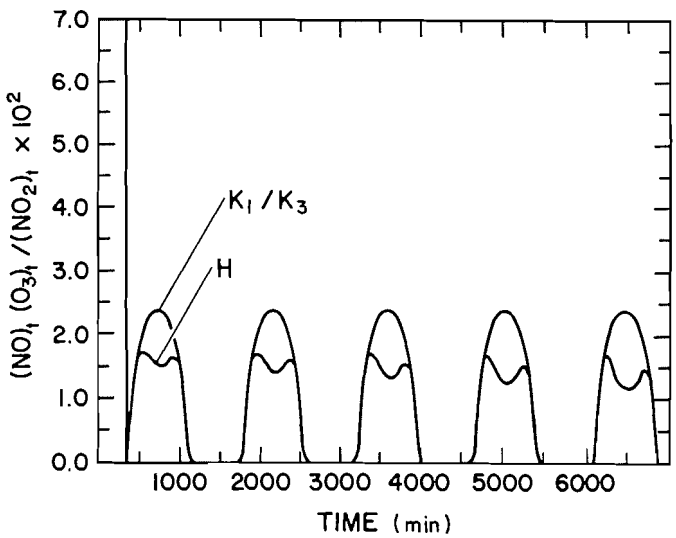

FIG. 12. Plot of the function $[NO]_t[O_3]_t/[NO_2]_t$ and $(k_1/k_3)_t$ versus time for a five-day simulation of the chemistry of a very clean tropospheric air mass (case *H*, 50% relative humidity).

periods are shown in Figs. 13*a* and 14*a*. The origin of the deviations are summarized in Figs. 13*b* and 14*b*. In each of these cases there is a near balance between the large negative term resulting from $d[O_3]/dt[O_3]$ and the positive term for O_3 loss by photolysis; O_3 loss from both HO_2 and HO reactions give relatively large positive terms. Note that near midday on the fourth day the total deviation is close to that for the HO_2-O_3 term alone; although other terms contribute significantly to the total deviation, a fortuitous near cancellation of the other terms results for this case. For this special case the suggestion of Stedman *et al.* (16, 20, 21) that observed deviations from [I] in relatively clean tropospheric air masses may reflect the occurrence of the HO_2-O_3 reaction is borne out. Note that during day 3 of case *H* this is not the case.

In most of the cases considered here several significant terms of relation [IV] control the deviation from the $O_3-NO-NO_2$ photostationary state. By far the largest term in most cases considered here is the last term of relation [IV] containing the $d[O_3]/dt[O_3]$ function. Several conclusions can be made in view of the present work. (*1*) The approximate steady-state relation applies well for NO-rich, highly polluted air masses at low RH/NO_x ratios. For this condition modellers will find that the use of relation [I] in the simplification of simulations is justified. (2) It is apparent that, in general, one cannot simply equate non-conformity of the O_3, NO, NO_2 concentration data to relation [I] with the influence of the HO_2-O_3 reaction alone; a reasonable interpretation can be made only through a knowledge of the level of all the potential O_3 reactant concentrations (NO, NO_2, alkene, HO_2, HO) as well the rate of change of O_3 with time; with this information in hand an investigator can make a meaningful interpretation of the magnitude of the several terms in relation [IV] and the extent of the deviation from [I]. We must conclude that the inference that HO_2 concentrations in the clean troposphere can be estimated from the measured deviations of $[O_3]_t[NO]_t/[NO_2]_t$ from $(k_1/k_3)_t$ is not of general validity, although there can be special circumstances where this appears to be a reasonably accurate hypothesis.

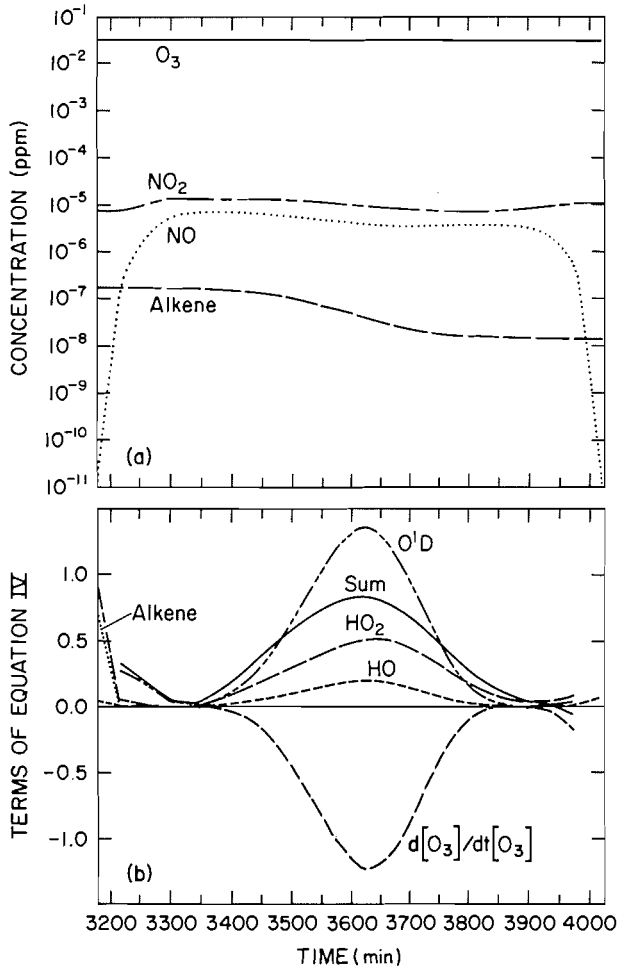

FIG. 13. (*a*) The time dependence of the various reactant concentrations during the computer simulation of the third day of the chemistry of the very clean tropospheric air mass (case *H*, 50% relative humidity); (*b*) the magnitude of the individual terms of function [IV] and the sum of these terms for various times during the third day of the simulation of case *H*, 50% relative humidity.

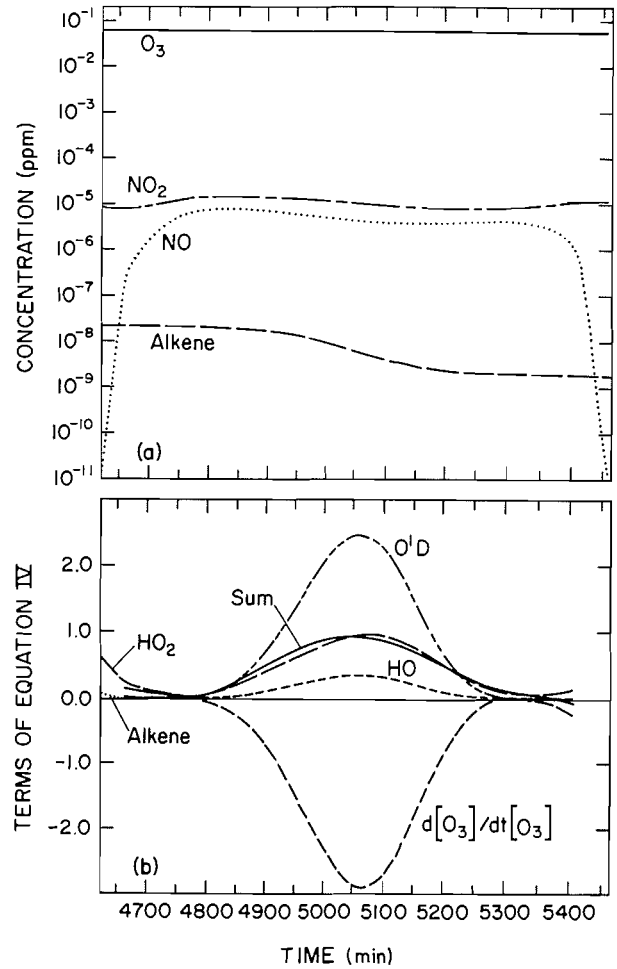

FIG. 14.(*a*) The time dependence of the various reactant concentrations during the computer simulation of the fourth day of the chemistry of the very clean tropospheric air mass (case *H*, 50% relative humidity); (*b*) the magnitude of the individual terms of function [IV] and the sum of these terms for various times during the fourth day of the simulation of case *H*, 50% relative humidity.

Acknowledgment

We are grateful to the National Center for Atmospheric Research for the award of a NCAR postdoctoral fellowship to one of us (W.R.S.) during the course of this study.

1. P. A. LEIGHTON. Photochemistry of air pollution. Academic Press, New York. 1961. pp. 152–157.
2. E. A. SCHUCK and E. R. STEVENS. Adv. Environ. Sci. Technol. **1**, 73 (1969).
3. K. WESTBERG, N. COHEN, and K. W. WILSON. Science, **171**, 1013 (1971).
4. D. H. STEDMAN, E. E. DABY, F. STUHL, and H. NIKI. J. Air Poll. Control Assoc. **22**, 260 (1972).
5. W. CHAMEIDES and J. C. G. WALKER. J. Geophys. Res. **78**, 8751 (1973).
6. D. H. STEDMAN and H. NIKI. Environ. Sci. Technol. **7**, 735 (1973).
7. R. J. O'BRIEN. Environ. Sci. Technol. **8**, 579 (1974).
8. K. L. DEMERJIAN, J. A. KERR, and J. G. CALVERT. Adv. Environ. Sci. Technol. **4**, 1 (1974).
9. J. G. CALVERT and R. D. MCQUIGG. Int. J. Chem. Kinet. Symp. **1**, 113 (1975).
10. D. H. STEDMAN and J. O. JACKSON. Int. J. Chem. Kinet. Symp. **1**, 493 (1975).
11. C. H. WU and H. NIKI. Environ. Sci. Technol. **9**, 46 (1975).
12. J. G. CALVERT. Environ. Sci. Technol. **10**, 248 (1976).
13. L. A. FARROW and T. E. GRAEDEL. J. Phys. Chem. **81**, 2480 (1977).
14. R. W. BILGER. Atm. Environ. **12**, 1109 (1978).
15. D. J. KEWLEY and K. POST. Atm. Environ. **12**, 2179 (1978).
16. J. A. RITTER, D. H. STEDMAN, and T. J. KELLEY. Nitrogenous air pollutants. *Edited by* D. Grosjean. Ann Arbor Science Publishers. 1979. Chapt. 20, p. 325.
17. J. H. Seinfeld. Environ. Sci. Technol. **11**, 1216 (1977).
18. C. E. FEIGLEY. Environ. Sci. Technol. **12**, 843 (1978).
19. D. P. CHOCK and S. KUMAR. Atm. Environ. **13**, 419 (1979).
20. D. H. STEDMAN, D. H. WEST, and R. E. SHETTER. Measurements related to atmospheric oxides of nitrogen. Final Report, Coordinating Research Council. 1981.
21. D. H STEDMAN and C. A. CANTRELL. Laboratory studies of an HO_2/RO_2 detector. Presented at 2nd Symp. on Composition of the Nonurban Troposphere, AMS/AGU/NASA, May 25–28, 1982, Williamsburg, VA.
22. J. G. CALVERT. The chemistry of the polluted troposphere. Proceedings of NATO Advanced Study Institute on Chemistry of the Unpolluted and Polluted Troposphere, Corfu, Greece, 1981; in press, Reidel Publishing Co., Dordrecht, Holland (1982).

Can. J. Chem. Downloaded from www.nrcresearchpress.com by 210.87.254.42 on 09/06/12
For personal use only.

Visible electronic absorption spectrum of vinyl radical

H. E. HUNZIKER, H. KNEPPE, A. D. MCLEAN, P. SIEGBAHN, AND H. R. WENDT
IBM Research Laboratory, 5600 Cottle Rd., San Jose, CA 95193, U.S.A.

Received August 26, 1982

This paper is dedicated to Professor Harry E. Gunning on the occasion of his 65th birthday

H. E. HUNZIKER, H. KNEPPE, A. D. MCLEAN, P. SIEGBAHN, and H. R. WENDT. Can. J. Chem. **61**, 993 (1983).

A simple, banded absorption spectrum has been detected by photochemical modulation spectroscopy in Hg-photosensitized reactions forming vinyl radicals. It starts at 499.5 nm, reaches maximum intensity ($\epsilon \approx 30\ M^{-1}\ cm^{-1}$) around 400 nm, and contains progressions of 1200 and 920 cm^{-1} vibrations. These features are compatible with the electronic structure, equilibrium geometries, and energies of the $^2A'$ ground and $^2A''$ first excited states of vinyl which were determined by *ab initio* SCF calculations. The upper state of the observed transition is analogous to the $\tilde{C}$ state of the isoelectronic formyl radical.

H. E. HUNZIKER, H. KNEPPE, A. D. MCLEAN, P. SIEGBAHN et H. R. WENDT. Can. J. Chem. **61**, 993 (1983).

Faisant appel à la spectroscopie de modulation photochimique, on a observé un spectre simple de bandes d'absorption lors des réactions photosensibilisées par le mercure conduisant à la formation de radicaux vinyles. Le spectre s'étale de 499,5 nm pour atteindre son maximum d'intensité ($\epsilon \approx 30\ M^{-1}\ cm^{-1}$) autour de 400 nm et contient des progressions de vibrations à 1200 et à 920 cm^{-1}. Ces caractéristiques sont compatibles avec la structure électronique, les géométries d'équilibre et les énergies de l'état fondamental $^2A'$ et du premier état excité $^2A''$ du vinyle que l'on a déterminé par des calculs *ab initio* de champ autocohérent. L'état supérieur de la transition observée est analogue à l'état $\tilde{C}$ du radical formyle isoélectronique.
[Traduit par le journal]

Introduction

It is surprising that a small hydrocarbon radical as common as vinyl has not yet been detected optically. Observation of this species has previously been accomplished only by mass spectroscopy (1) and electron spin resonance (2). The latter technique has been used to study reactions of substituted vinyl radicals in the liquid phase. Mass spectrometric detection of vinyl in gas phase reactions has been very limited (1, 3) and little is known about bimolecular rate processes involving the radical (4). This is unfortunate since vinyl radicals play a role in many chemical reactions, especially free radical addition to, and polymerization of, acetylenes. The simplest reaction of this type, reversible addition of H-atoms to acetylene, has been of interest to kineticists investigating falloff behavior of addition reactions (5). We have used this well-studied reaction as the basis of a search for the vinyl optical spectrum. The search was guided by *ab initio* SCF calculations for the ground and first excited electronic states of the radical. We hope that our identification of a visible spectrum of vinyl will be useful in future measurements of its gas phase reactivity.

Ab initio electronic structure calculations

SCF calculations show that the vinyl radical is planar in both its $1a'^2 \ldots 6a'^2 7a'^1 1a''^2, {}^2A'$ ground state and $1a'^2 \ldots 6a'^2 7a'^2 1a''^1, {}^2A''$ lowest excited state. The excitation moves one of the C—C π-bonding electrons into the in-plane orbital which is singly occupied and localized on the radical center in the ground state. In calculations with a basis set of double-zeta quality (6), the optimized geometries shown in Fig. 1 were determined. The largest relaxation effects following excitation are the expected lengthening of the C—C bond, 1.323 Å to 1.455 Å, and a change in the CCH angle at the radical center from 135° to 105°. The bond lengths shown in Fig. 1 are probably reliable to within 0.02 Å. These simple SCF calculations have taken advantage of compensating errors arising from lack of completeness in the basis set and neglect of correlation effects.

Excitation energies were computed with correlated wavefunctions at the geometries of Fig. 1. The wavefunctions, for both states, are CI expansions in a configuration state function (CSF) space of the dominant SCF configuration plus single and double replacement CSF's generated by replacing occupied orbitals in the dominant configuration by SCF unoccupied orbitals. Double replacement CSF's are restricted to those spanning the interacting space defined by McLean and Liu (7). In these correlated calculations the orbitals were expanded in a double-zeta plus polarization basis; one *d*-type function was added to each carbon and one *p*-type function to each hydrogen.

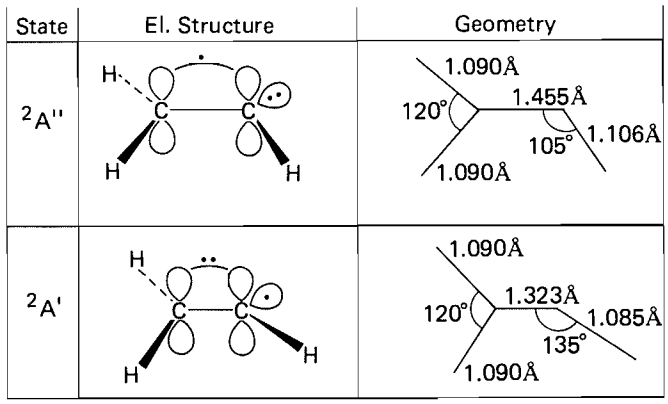

FIG. 1. Qualitative electronic structures and computed SCF geometries of the $^2A'$ ground state and $^2A''$ first excited state of vinyl radical.

The vertical excitation energy thus calculated is 3.24 eV, and the adiabatic excitation energy is 2.37 eV.

Photochemical modulation experiments

The optical absorption spectrum of the radical was measured by modulation spectroscopy of Hg-photosensitized reactions. An apparatus similar to one described previously was used (8), except that for the vinyl experiments it was equipped with a 12-pass White cell (9) affording a 2.4 m absorption path

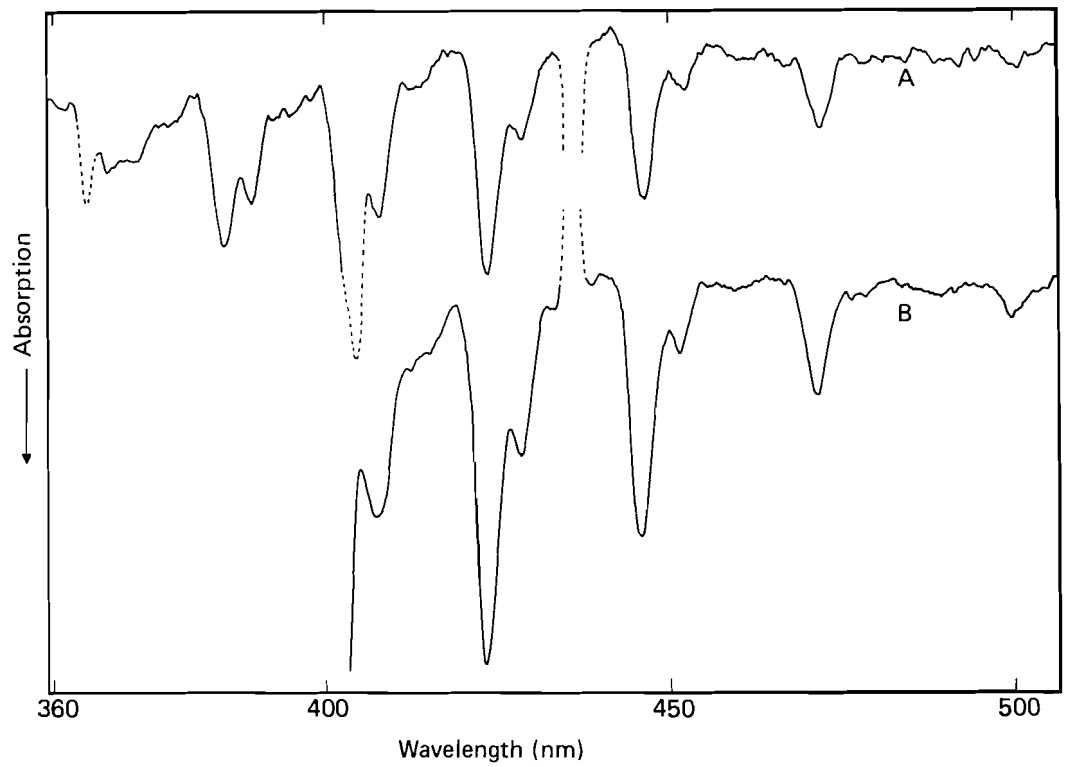

FIG. 2. Absorption spectrum of vinyl radical at 1.6 nm resolution. Reaction [3] was the H-atom source for Trace A (with RH = C_2H_6), and reaction [2] for Trace B. Dotted regions indicate interference by HgH absorption bands and Hg I straylight lines. The molar extinction coefficient at the 423.2 nm band maximum is approximately 30 L/mol cm (see text).

length, and with a cooled Si photodetector.[1] The photolysis source, an rf-excited, low pressure Hg arc, was modulated at 270 Hz and provided an average excitation rate of about 10^{-5} mol/L s inside the flow reactor. Experiments were carried out at 310 K and 1 atm total pressure, where the reaction

[1] $H + C_2H_2 + M \rightarrow C_2H_3 + M$

can be assumed to be in its high pressure limit with the polyatomic third bodies, M, used (5). H atoms were generated either by Hg-photosensitized decomposition of H_2,

[2] $Hg(6^3P_1) + H_2 \rightarrow 2\,H + Hg(6^1S_0)$

or of ethane or propane (RH),

[3] $Hg(6^3P_1) + RH \rightarrow H + R + Hg(6^1S_0)$

While reaction [2] yields more H-atoms and a larger vinyl signal, it also generates HgH as an intermediate (10) whose strong absorption spectrum interferes with that of vinyl below 405 nm. In this wavelength region reaction [3] is more useful since little HgH is formed and interference can be minimized by phase adjustment, making use of the shorter lifetime of HgH. Acetylene concentrations were approximately optimized for vinyl production, avoiding the possible side reactions $Hg(6^3P_1) + C_2H_2$ and H + RH. Accordingly 5 Torr of C_2H_2 were used with RH = C_3H_8 and 0.5 Torr with C_2H_6. With H_2 (used diluted, 1:30, in CH_4, which was the third body in this case) some removal of Hg was noted, increasing with C_2H_2 partial pressure and probably due to reaction of HgH with C_2H_2. Low C_2H_2 pressures (0.5 to 1 Torr) were therefore used.

Transient absorption spectra obtained with reactions [2] and [3] as H-atom sources are shown in Fig. 2, and positions of the band maxima are listed in Table 1. The phase shift of the transient absorption signal relative to the modulated photolysis light was about 45° at high acetylene concentrations, where reaction [1] is fast enough to contribute little to the shift. This corrresponds to a transient lifetime of about 1 ms which is expected when the decay occurs by radical–radical reactions. The bimolecular rate constant for the vinyl–vinyl reaction cannot be easily derived from this observation since vinyl–alkyl and vinyl–H encounters also contribute.

The 423.2 nm band was examined for rotational structure at twice the resolution of Fig. 2, but no clear evidence of structure was found. It was hoped that some K-subbands (11) could be detected on the long wavelength side of the band, where the geometries of Fig. 1 predict the subband spacings to become comparable with the 45 cm^{-1} resolution. No definite conclusion is possible as to whether the rotational structure is sharp or diffuse. The latter could be the case since the upper state lies above the H–C_2H_2 dissociation limit (770 nm) (12), although adiabatic dissociation into $C_2H_2(\tilde{X})$ + $H(^1S)$ is symmetry forbidden.

Experiments were also carried out using D_2 instead of H_2, and replacing C_2H_2 by C_2HD or C_2D_2. Spectra resembling those of Fig. 2, with ill-defined changes in the $v_2' = 1$ series, were obtained. It appeared that H–D exchange and increased polymer formation, the latter being especially severe in the C_2D_2/D_2 case, made it difficult to obtain clear-cut results with deuterated reactants.

In order to support the assignment of the observed spectrum the reaction

[4] $Hg(6^3P_1) + (C_2H_3)_2O \rightarrow Hg(6^1S_0) + C_2H_3 + C_2H_3O$

was investigated as an alternate vinyl source. Direct photolysis

[1]Model UV-444B, EG&G Inc., Salem, Mass.

TABLE 1. Observed positions of band maxima, in cm^{-1}, with band spacings in parentheses. The v_1' numbering is arbitrarily started at the first band observed.

	v_2'		
v_1'	0		1
0	20020		
	(1202)		
1	21222	(926)	22148
	(1205)		(1200)
2	22427	(921)	23348
	(1202)		(1204)
3	23629	(923)	24552
	(1186)		(1175)
4	24815*	(912)	25727
	(1166)		(1191)
5	25981	(937)	26918
	(1152)		
6	27137		

*Estimated position.

of divinyl ether is known to produce vinyl and "vinoxy" (α-oxo-ethyl) radicals (3). Several of the stronger bands of Fig. 2 were observed with reaction [4] together with the spectrum of C_2H_3O which starts at 347.7 nm (13). Hg-photosensitized decomposition of divinyl ether does not appear to proceed uniquely by reaction [4] since other transients absorbing in the region of the vinyl spectrum are also formed.

Since extinction coefficients for the "vinoxy" radical were determined previously (13), the divinyl ether experiment yields a direct estimate of the extinction of the vinyl bands, provided the two radicals are formed in a 1:1 ratio as in reaction [4]. $\epsilon = 24$ L/mol cm was thus obtained for the maximum of the 423.2 nm band. This value was checked by generating vinyl and "vinoxy" radicals separately, the former with reactions [1] and [3] ($RH = C_3H_8$) and the latter by Hg-photosensitized decomposition of methyl vinyl ether (13), under otherwise identical experimental conditions. Comparison of the absorption signals yielded a value of $\epsilon = 30$ L/mol cm based on an H-atom yield of 0.77 from propane (14). (With a yield of 1.0, $\epsilon = 24$ L/mol cm is obtained.) Including the uncertainty of the "vinoxy" reference, we estimate $\epsilon = (27 \pm 12)$ L/mol cm for the 423.2 nm band maximum at 1.6 nm resolution.

Discussion

The features of the observed absorption spectrum, Fig. 2 and Table 1, agree with the *ab initio* predictions for vinyl. From the equilibrium geometries of Fig. 1 we expect to see progressions of the upper state C—C stretching and CCH bending vibrations in the $^2A''-{}^2A'$ electronic transition. Two progressions with $\nu_1 \approx 1200$ cm^{-1} and $\nu_2 \approx 920$ cm^{-1} are indeed observed. These values are in reasonable agreement with those expected for C$\dot{-}$C and C$\dot{-}$C—H partial-bond stretching and bending motions, respectively,[2] as required by the upper state electronic structure. Similar frequencies have been found for the $\tilde{C}$ state of HCO where the corresponding modes give rise to intervals of 1200 cm^{-1} and 960 cm^{-1} (15). HCO is isoelectronic with C_2H_3 and the electronic structure of its $\tilde{C}$ state is analogous to that of the $^2A''$ state of C_2H_3 (16).

We cannot be certain whether the first band observed at 20 020 cm^{-1} is the 0–0 transition but it is not far from the predicted, adiabatic excitation energy, 18 300 cm^{-1}. The Franck–Condon maximum of the band system is located near the 24 815 cm^{-1} band which is again in reasonable agreement with the calculated, vertical excitation energy of 26 100 cm^{-1}. Since the matrix elements determining the strength of this $\pi \rightarrow n$ transition in vinyl are qualitatively similar to those of $n \rightarrow \pi^*$ transitions in aldehydes and ketones, we expect extinction coefficients of the same order of magnitude, i.e. $\epsilon(\text{max}) \approx 20$ L/mol cm (17). The observed value, $\epsilon(\text{max}) \approx 30$ L/mol cm, agrees with this expectation.

Conclusion

We have observed a transient absorption spectrum whose presence and kinetics in two simple reaction systems make it likely that it belongs to the vinyl radical, C_2H_3. While we were unable to obtain rotational and isotopic information, close agreement of the observed spectrum with *ab initio* predictions strongly favors its assignment to the $^2A''-{}^2A'$ lowest electronic transition of vinyl radical.

Acknowledgments

We want to thank Dr. J. Weber for assisting with the calculations, and Dr. J. V. Michael and Dr. B. Liu for helpful discussions.

1. A. G. HARRISON and F. P. LOSSING. J. Am. Chem. Soc. **82**, 519 (1960).
2. R. BENSASSON, K. LEIBLER, R. MARX, and H. SZWARC. Arch. Sci. **13**, 303 (1960); R. W. FESSENDEN and R. H. SCHULER. J. CHEM. PHYS. **39**, 2147 (1963); E. L. Cochran, F. J. Adrian, and V. A. BOWERS. J. Chem. Phys. **40**, 213 (1964).
3. K. O. MACFADDEN and C. L. CURRIE. J. Chem. Phys. **58**, 1213 (1973).
4. J. A. KERR and S. J. MOSS. Handbook of bimolecular and termolecular gas reactions. Vol. I. CRS Press, Boca Raton, FL. 1981. p. 301.
5. W. A. PAYNE and L. F. STIEF. J. Chem. Phys. **64**, 1150 (1976); D. G. KEIL, K. P. LYNCH, J. A. COWFER, and J. V. MICHAEL. Int. J. Chem. Kinet. **8**, 825 (1976), and earlier references cited in these two publications.
6. J. WEBER, M. YOSHIMINE, and A. D. MCLEAN. J. Chem. Phys. **64**, 4159 (1976).
7. A. D. MCLEAN and B. LIU. J. Chem. Phys. **58**, 1213 (1973).
8. H. E. HUNZIKER. IBM J. Res. Dev. **15**, 10 (1971).
9. J. U. WHITE. J. Opt. Soc. Am. **32**, 285 (1942).
10. A. B. CALLEAR and P. M. WOOD. J. Chem. Soc. Faraday Trans. II, **68**, 302 (1972).
11. G. HERZBERG. Molecular spectra and molecular structure. Vol. III. D. Van Nostrand Co., Princeton, NJ. 1966. p. 251.
12. S. W. BENSON. Thermochemical kinetics. J. Wiley & Sons, Inc., New York, NY. 1968. p. 204.
13. H. E. HUNZIKER, H. KNEPPE, and H. R. WENDT. J. Photochem. **17**, 377 (1981).
14. R. A. BACK. Can. J. Chem. **37**, 1834 (1954).
15. M. E. JACOX. Chem. Phys. Lett. **56**, 43 (1978).
16. R. N. DIXON. Trans. Faraday Soc. **65**, 3141 (1969).
17. J. G. CALVERT and J. N. PITTS. Photochemistry. J. Wiley & Sons, Inc., New York, NY. 1966. pp. 368, 369, and 377.

[2]Reference 12, p. 205.

The intermediate formation of ketocarbenes and the conformational control in the Wolff rearrangement of α-diazoketones

MANUEL TORRES, JUAN RIBO, ALLAN CLEMENT, AND OTTO P. STRAUSZ
Department of Chemistry, University of Alberta, Edmonton, Alta., Canada T6G 2G2

Received September 23, 1982

This paper is dedicated to Professor Harry E. Gunning on the occasion of his 65th birthday

MANUEL TORRES, JUAN RIBO, ALLAN CLEMENT, and OTTO P. STRAUSZ. Can. J. Chem. **61**, 996 (1983).

The conformational control of the Wolff rearrangement (WR) has been studied by means of a comparative study of the low temperature photolysis of argon-matrix isolated α-diazo ketones, **1**, and of vinylene thioxocarbonates, **2**. Under these conditions the *s-E*, *s-Z* conformational equilibrium of **1** will be hindered whereas **2** has a fixed *s-Z* conformation. The results indicate that the conformational control observed in the WR of α-diazo ketones is not per se a proof for a concerted mechanism and that a mechanism involving a ketocarbene intermediate is the most reasonable.

MANUEL TORRES, JUAN RIBO, ALLAN CLEMENT et OTTO P. STRAUSZ. Can. J. Chem. **61**, 996 (1983).

On a étudié le contrôle conformationnel de la transposition de Wolff (TW) au moyen d'une étude comparative de la photolyse à basse température des α-diazo cétones **1** et des thioxocarbonates de vinylène **2**, isolés dans une matrice d'argon. Dans ces conditions, l'équilibre conformationnel *s-E*, *s-Z* du composé **1** sera empêché tandis que le composé **2** a une conformation *s-Z* fixe. Les résultats indiquent que le contrôle conformationnel observé dans la TW des α-diazo cétones n'est pas en soi une preuve de l'existence d'un mécanisme concerté et qu'un mécanisme impliquant un cétocarbène comme intermédiaire est plus raisonnable.

[Traduit par le journal]

The Wolff rearrangement (WR) of α-diazo ketones and α-diazo esters to ketenes can be brought about either photolytically, thermally, or catalytically and ketocarbenes are generally thought to be implicated as short-lived reactive intermediates in the photochemical and thermal reactions (1–12).

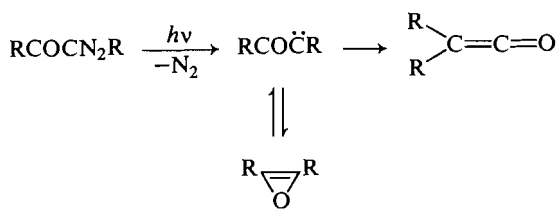

Unambiguous evidence for the intermediacy of ketocarbenes and carbalkoxycarbenes came from the detection of oxirenes as reactive intermediates in the WR (4, 10, 11) kinetic studies (7) as well as from the effects of the substituent upon nitrogen elimination (6). Moreover, molecular orbital computations predict a prohibitively high energy requirement for concerted nitrogen elimination (12). Also, the low temperature stabilization and direct esr detection of a series of triplet state ketocarbenes from the photolysis of α-diazo ketones has been reported (13–18). These observations are in agreement with molecular orbital predictions of a triplet ground state for these species, with a small singlet–triplet energy separation (19).

A concerted mechanism for the WR would be in clear contradiction to the now well established transient formation of oxirene in a large number of photochemical WR (for a recent review, see ref. 20). Recently, however, Kaplan and Mitchell (21) have restated an earlier suggestion (22) of an alternative concerted mechanism for the decomposition WR sequence of those α-diazo ketones in which the intermediacy of oxirene was not detected. The α-diazo ketones may exist as two rotational isomers of the type *s-E* and *s-Z* and the proposed mechanism is based on the conformational control observed in the photolysis and thermolysis of some α-diazo ketones. Accordingly, for α-alkyl α-diazo ketones, the *s-E* conformer leads preferentially to 1,2-hydrogen or alkyl migration whereas the *s-Z* conformer undergoes a concerted WR to the ketenes. A similar concerted approach has been proposed by Roth and Manion (23) based on CIDNP studies on α-diazoacetone. Direct photolysis of α-diazoacetone, which is known to undergo a WR to methylketene, failed to generate any nuclear spin polarization, whereas the triplet photosensitized reaction resulted in the observation of radical pairs derived from both triplet and singlet acetylmethylene. Tomioka *et al.* (24) have also advocated the occurrence of a concerted mechanism on the basis of their studies on the direct and triplet sensitized photolysis of α-diazo ketones in alcohols. The latter authors, however, were forced to invoke at least the partial participation of a nonconcerted mechanism via a ketocarbene intermediate to explain the experimental results.

Recently we have reported new source compounds for the study of the ketocarbene–ketene rearrangement, namely vinylene thioxocarbonates (25). This class of compounds features a rigid *s-Z* stereochemistry and hence comparison of their photolysis products with those of the analogous diazo ketones allows a better elucidation of the conformational effects associated with the WR. We wish to report here such a comparative study on the low temperature argon-matrix photolysis (coupled with ir spectroscopy) of α-diazo ketones **1** and on vinylene thioxocarbonates **2**. Under these conditions the conformational equilibrium of **1** will be hindered.

At room temperature 3-diazo-2-butanone, **1***a*, exists as a mixture of the *s-Z*, *s-E* conformers in equilibrium (26), and has been reported to lead to 100% oxirene formation in the gas-phase photolysis (11). Photolysis of argon-matrix isolated **1***a* using λ = 254 nm radiation resulted in the formation of dimethylketene, **3***a*, the WR product, and methylvinylketone, **4***a*, via 1,2-hydrogen shift; the latter is formed mostly in the *s-Z* conformation. Methylvinylketone, **4***a*, is known to exist in an *s-E*, *s-Z* equilibrium favouring the *s-E* conformation. Irradiation of **4***a* in an argon-matrix resulted in a change in the conformers' ratio leading to a photostationary state characterized by an increase in the *s-Z* conformer (27). The fact that the

Can. J. Chem. Downloaded from www.nrcresearchpress.com by 210.87.254.40 on 09/06/12
For personal use only.

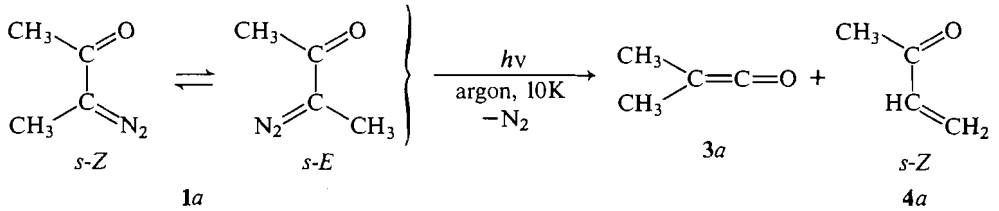

s-Z *s-E* 3*a* *s-Z*

1*a* 4*a*

methylvinylketone, 4*a*, obtained in the argon-matrix photolysis of 1*a* is formed in an *s-Z*/*s-E* ratio larger than expected from a photostationary state clearly suggests that it is formed from the *s-E* conformation of 1*a*. Photolysis, on the other hand, of dimethylvinylene thioxocarbonate 2*a* under the same conditions and using either λ = 270 or 254 nm radiation resulted in the exclusive formation of ketene 3*a* and no vinylmethylketone

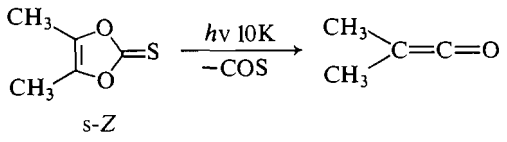

s-Z

2*a* 3*a*

4*a* could be detected. Although these results clearly indicate an *s-Z* preferred conformation for the WR, it is, however, difficult to visualize a concerted process for the COS elimination and ketene formation in the case of 2*a*.

Since the methyl group does not impose a strong steric hindrance we have carried out parallel studies for the bis(tert-butyl) substituted diazoketone and vinylene thioxocarbonate, 1*b* and 2*b* respectively, using λ = 254 nm radiation in both cases. The results showed the formation of α,β unsaturated ketone 4*b* and only traces of ketene 3*b* for the case of 1*b* and the formation of 3*b* and traces of 4*b* in the case of 2*b*. Although these results again parallel those of Kaplan and Mitchell (21), it is still difficult to visualize a concerted process for the formation of 3*b* from 2*b*.

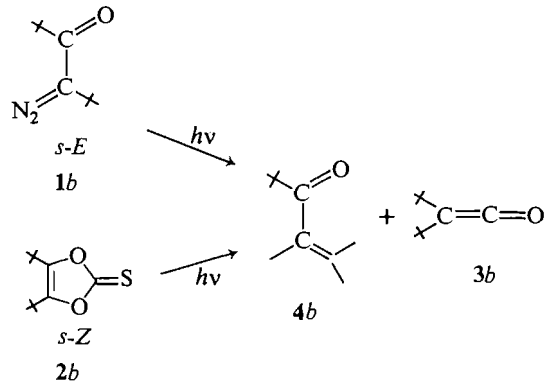

s-E *s-Z*

1*b* 2*b* 4*b* 3*b*

Finally, to confirm the transient formation of oxirene even under matrix conditions, and hence of ketocarbene, in the photolysis of 1*a*, we have carried out the photolysis of 1*a* ^{13}CO labelled under identical conditions as described above. Under these conditions no scrambling of the diazo ketone itself prior to nitrogen elimination was observed, in agreement with Blaustein and Berson (28). From the ir spectrum it could be estimated that the vinylmethylketone 4*a* was formed with ~5% scrambling whereas the dimethylketene 3*a* was formed with ≃30% scrambling. These results indicate that most of the ketene 3*a* is formed through a path that involves oxirene whereas 4*a* is not, and that the total oxirene formation, ~70% in argon-matrix conditions, is comparable to the reported 100% and 70% oxirene formation in the gas and solution phase, respectively (11).

From these results it can be concluded that of the two competing reactions that can take place upon photolysis of 1 and 2, the 1,2-hydrogen or alkyl shift and the WR, the former occurs preferentially from the *s-E* conformation and the latter from the *s-Z* conformation of the precursor. A concerted mechanism is difficult to envisage for the photolysis of vinylene thioxocarbonates 2 and, according to the ^{13}C labelling experiments, oxirene and ketocarbene are involved in the argon-matrix photolysis of 1*a*. Therefore, the observed conformational control must originate in the ketocarbene, that is, the conformational identity of the diazoketone must be preserved in the ketocarbene. Although *ab inito* MO calculations for the parent formylmethylene predict a geometry in which the methylene hydrogen lies perpendicular to the HCO plane with the consequent loss of *s-E*, *s-Z* conformational identity, the presence of substituents may change the situation and in fact, for 1*a*, three minima for the *s-E*, *s-Z*, and the perpendicular conformations are predicted.[1]

Preservation of the diazo ketone geometry in the ketocarbene is not unusual. We have observed in esr studies of triplet ketocarbenes that the conformation of the most abundant triplet is the same as the conformation of the diazo ketone precursor as determined by X-ray crystallography (29). Since it can be assumed that the triplet ketocarbene is formed most likely from the singlet ketocarbene via ISC then it follows that if the geometry is preserved in the triplet ketocarbene it must also be preserved in the singlet ketocarbene.

The fact that triplet sensitized decomposition of α-diazo ketones give rise to singlet ketocarbene reactions such as O—H insertion, but not necessarily to WR products (23) can be explained on the basis of the low vibrational energy content of the thermally populated singlet, which will favour the decay reaction requiring lower activation energy. Although *ab initio* MO calculations predict no activation energy for the ketocarbene–ketene rearrangement in the parent formylmethylene and only a small activation energy for the ketocarbene–oxirene ring closure, substituents will probably exert marked effects and could conceivably reverse the order.

In summary we have established that the conformational control of the WR of α-diazo ketones is also observed in cases such as the argon-matrix photolysis of 3-diazo-2-butanone in which oxirene, and hence a nonconcerted mechanism, is detected and in vinylene thioxocarbonates for which a concerted mechanism seems most unlikely. Therefore the conformational control in the decomposition WR of α-diazo ketones is not proof per se for the occurrence of a concerted mechanism and can be explained via ketocarbene intermediate.

Experimental

An Air-Products and Chemicals Inc. Model CS-202 Diplex closed-

[1]R. K. Gosavi and O. P. Strausz, unpublished results.

Can. J. Chem. Downloaded from www.nrcresearchpress.com by 210.87.254.40 on 09/06/12
For personal use only.

cycle-helium refrigeration system coupled to a high vacuum line was employed as described before (30). The light source was a 140 W Hanovia 30620 medium pressure mercury lamp equipped with a Vycor filter or a 270 nm interference filter, alternatively a low pressure mercury resonance lamp equipped with a Vycor filter was also used. Mass spectra were recorded on Metropolitan Vickers MS-12 and MS-50 spectrometers at an ionization potential of 70 eV, ir spectra were obtained on a Nicolet 7199 FT infrared spectrophotometer, and nmr spectra were recorded on Varian Associates Models A-60 and HR-100 spectrometers using TMS as internal standard. Values are given in δ units.

3-Diazo-2-butanone, **1***a* (31); 3-diazo-2-butanone ^{13}CO (11), 3,4-dimethylvinylenethioxocarbonate **2***a* (32), and 2,2,5,5-tetramethyl-4-diazo-3-hexanone **1***b* (33) were prepared according to described procedures.

4,5-Bis(*tert*-butyl)vinylenethioxocarbonate, **2***b*, was prepared according to the following sequence. 4,5-Bis(*tert*-butyl)vinylene

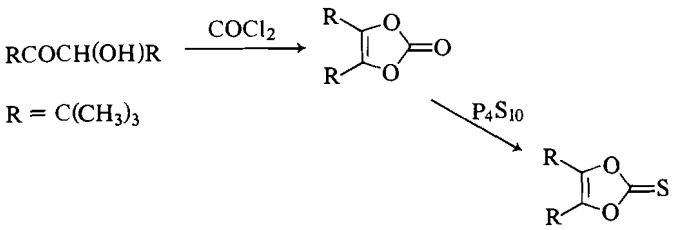

carbonate was prepared by reaction of pivaloin (21) with phosgene in the presence of dimethylaniline; ir (CCl_4): 1830 cm^{-1} (C=O); nmr (CCl_4): 1.31 (s); ms *m/e* (%): 198 (18), 183 (35), 97 (11), 69 (27), 57 (100). *Exact Mass* measured by high resolution mass spectrometry: 198.1257 ($C_{11}H_{18}O_3$). 4,5-Bis(*tert*-butyl)vinylene carbonate was subsequently converted to **2***b* by reaction with P_4S_{10}; mp 55–56°C; ir (CCl_4): 1325 cm^{-1} (C=S); nmr (CCl_4): 1.3 (s); ms *m/e* (%): 214 (100), 97 (69), 83 (15), 69 (97), 57 (89), 41 (39). *Exact Mass* measured by high resolution mass spectrometry: 214.1029 ($C_{11}H_{18}O_2S$). *Anal.* calcd. for $C_{11}H_{18}O_2S$: C 61.62, H 8.47, S 14.97%; found: C 61.46, H 8.52, S 15.01%.

Acknowledgments

The authors are grateful to the Natural Sciences and Engineering Research Council for continuing financial support and to Dr. E. M. Lown for helpful discussions.

1. W. KIRMSE. *In* Carbene chemistry. Academic Press, New York. 1971.
2. A. MELZER and E. F. JENNY. Tetrahedron Lett. 4503 (1968).
3. O. P. STRAUSZ, T. DOMINH, and H. E. GUNNING. J. Am. Chem. Soc. **90**, 1660 (1968).
4. I. G. CSIZMADIA, J. FONT, and O. P. STRAUZ. J. Am. Chem. Soc. **90**, 7360 (1968).
5. T. DOMINH, O. P. STRAUSZ, and H. E. GUNNING. J. Am. Chem. Soc. **91**, 1261 (1969).
6. W. JUNGELT and D. SCHMIDT. Tetrahedron, **25**, 269 (1969).
7. W. BARTZ and M. REGITZ. Chem. Ber. **103**, 1463 (1970).
8. T. DOMINH and O. P. STRAUSZ. J. Am. Chem. Soc. **92**, 1766 (1970).
9. D. E. THORNTON, R. K. GOSAVI, and O. P. STRAUSZ. J. Am. Chem. Soc. **92**, 1768 (1970).
10. G. FRATER and O. P. STRAUSZ. J. Am. Chem. Soc. **92**, 6654 (1970).
11. J. FENWICK, G. FRATER, K. OGI, and O. P. STRAUSZ. J. Am. Chem. Soc. **95**, 124 (1973).
12. I. G. CSIZMADIA, H. E. GUNNING, R. K. GOSAVI, and O. P. STRAUSZ. J. Am. Chem. Soc. **95**, 133 (1973).
13. A. M. TROZZOLO. Acc. Chem. Res. **1**, 329 (1968).
14. R. S. HUTTON and H. D. ROTH. J. Am. Chem. Soc.**100**, 4324 (1978).
15. H. MURAI, M. TORRES, and O. P. STRAUSZ. Chem. Phys. Lett. **70**, 358 (1980).
16. H. MURAI, M. TORRES, and O. P. STRAUSZ. J. Am. Chem. Soc. **102**, 1421 (1980).
17. H. MURAI, M. TORRES, and O. P. STRAUSZ. J. Am. Chem. Soc. **102**, 5104 (1980).
18. H. MURAI, J. RIBO, M. TORRES, and O. P. STRAUSZ. J. Am. Chem. Soc. **103**, 6422 (1981).
19. N. C. BAIRD and K. F. TAYLOR. J. Am. Chem. Soc. **100**, 1333 (1978).
20. M. TORRES, E. M. LOWN, H. E. GUNNING, and O. P. STRAUSZ. Pure Appl. Chem. **52**, 1623 (1980).
21. F. KAPLAN and M. L. MITCHELL. Tetrahedron Lett. 759 (1979).
22. F. KAPLAN and G. K. MELOY. J. Am. Chem. Soc. **88**, 950 (1966).
23. H. D. ROTH and M. L. MANION. J. Am. Chem. Soc. **98**, 3392 (1976).
24. H. TOMIOKA, H. OKUNO, and Y. IZAWA. J. Org. Chem. **45**, 5278 (1980).
25. M. TORRES, A. CLEMENT, and O. P. STRAUSZ, J. Org. Chem. **45**, 2271 (1980).
26. R. CURCI, F. DI FURIA, and V. LUCCHINI. Spectrosc. Lett. **7**, 211 (1974).
27. A. KRANTZ, T. D. GOLDFARB, and C. Y. LIN. J. Am. Chem. Soc. **94**, 4022 (1972).
28. M. A. BLAUSTEIN and J. A. BERSON. Tetrahedron Lett. 1081 (1981).
29. O. P. STRAUSZ, H. MURAI, and M. TORRES. J. Photochem. **17**, 207 (1981).
30. M. TORRES, A. CLEMENT, J. E. BERTIE, and O. P. STRAUSZ. J. Org. Chem. **43**, 2490 (1978).
31. A. L. WILDS and A. L. MEADER. J. Org. Chem. **13**, 763 (1948).
32. M. S. NEWMAN and A. ARKELL. J. Org. Chem. **24**, 385 (1959).
33. H. M. FISCHLER and W. HARTMAN. Chem. Ber. **105**, 2769 (1972).

Can. J. Chem. Downloaded from www.nrcresearchpress.com by 210.87.254.40 on 09/06/12
For personal use only.

On the chemistry of metastable species

E. F. HILINSKI, S. V. MILTON, C. RAMANA,[1] AND P. M. RENTZEPIS
Bell Laboratories, Murray Hill, NJ 07974, U.S.A.

Received December 1, 1982

This paper is dedicated to Professor Harry E. Gunning on the occasion of his 65th birthday

E. F. HILINSKI, S. V. MILTON, C. RAMANA, and P. M. RENTZEPIS. Can. J. Chem. **61**, 999 (1983).

The mechanisms of a variety of chemical, physical, and biological processes are now understood more clearly as a result of picosecond spectroscopic studies. The identification of metastable species and transient states and the measurement of their formation and decay kinetics are made possible by means of picosecond emission and absorption spectroscopy. The data from these studies provide detailed mechanistic information about a reaction as it evolves. In this paper, we describe a laser system used for picosecond spectroscopy along with several chemical applications of picosecond absorption and emission spectroscopy performed in our laboratories. These include studies on the photochemical generation of trimethylenemethane biradicals from azo compounds, excited-state relaxation dynamics of *p*-dimethylaminobenzonitrile, and photodissociation of haloaromatic compounds.

E. F. HILINSKI, S. V. MILTON, C. RAMANA et P. M. RENTZEPIS. Can. J. Chem. **61**, 999 (1983).

Les études spectroscopiques de l'ordre de la picoseconde permettent de mieux saisir les mécanismes de divers processus chimiques, physiques et biologiques. L'identification des espèces métastables et des états de transition, la mesure de leur formation et les cinétiques de la désintégration sont rendues possibles au moyen de spectroscopie d'émission et d'absorption de l'ordre de la picoseconde. Les données recueillies à partir de ces études fournissent une information détaillée sur le mécanisme de la réaction. Dans ce travail nous décrivons un système de laser utilisé pour la spectroscopie de l'ordre de la picoseconde ainsi que les applications chimiques de cette spectroscopie réalisées dans nos laboratoires. Ceci comprend les études sur la production photochimique des biradicaux triméthylène-méthane à partir des composés azo, les dynamiques de relaxation de l'état excité du *p*-diméthylaminobenzonitrile et la photodissociation des composés haloaromatiques.

[Traduit par le journal]

Can. J. Chem. Downloaded from www.nrcresearchpress.com by 210.87.254.105 on 09/06/12
For personal use only.

Introduction

Our understanding of chemical and biological reactions is based upon a knowledge of the sequence of events which transpires when one substance is transformed into another in a process induced by some external agent such as heat, light, or a chemical reagent. Many methods are available to the physical chemist for the elucidation of a reaction mechanism. Of these, picosecond spectroscopy has provided a means for identifying intermediates in reactions and measuring their formation and decay kinetics. The best time resolution of course will enable the greatest amount of detailed information to be obtained about a reaction and will therefore permit the best understanding of the microscopic events involved in the conversion of one species into another.

Direct observation of the ultrafast events involved in many chemical and biological reactions is provided by absorption, emission, and lately Raman spectroscopy with picosecond time resolution. Technological advances in lasers and optical detection systems have improved the original capabilities of picosecond spectroscopy and expanded its application to a wide variety of mechanistic problems. Currently several types of picosecond laser systems with time resolution of less than one picosecond to several picoseconds exist which can be used to monitor the dynamics of a photoinitiated chemical reaction while it is occurring.

We will briefly describe an experimental apparatus used for picosecond spectroscopy. Several applications of picosecond emission and absorption spectroscopy to mechanistic chemical problems which were performed in our laboratories will be presented. These include studies on the photochemical generation of trimethylenemethane biradicals from azo compounds, excited-state relaxation dynamics of *p*-dimethylaminobenzonitrile, and photodissociation of haloaromatics.

Experimental

Most commonly used picosecond laser systems currently rely on either solid-state oscillators or synchronously pumped dye lasers to generate picosecond light pulses initially. Passively mode-locked Nd^{3+}:YAG oscillators were the sources of the picosecond pulses used in the studies to be discussed later in this paper. This type of laser system has been described previously (1*a*,*b*). More recently, synchronously pumped dye laser systems have become popular as a result of their wavelength tunability and their capability of generating shorter pulses. While specific details of various laser systems differ, both the solid-state and synchronously pumped dye laser systems, in general, are the same after pulse generation and amplification has been accomplished. Because of their basic similarities, only a discussion of a synchronously pumped dye laser system will be described here.

The picosecond laser system illustrated in Fig. 1 is composed of an actively mode-locked argon ion laser which generates a train of 150-ps full-width-at-half-maximum (FWHM), 514.5-nm pulses at a repetition rate of 123 MHz. These pulses pump a ring dye laser which generates ~1-ps FWHM pulses with an average power of ~100 mW. Depending upon the dye used as a lasing medium, a wide range of wavelengths is available from the ring laser. The quality of the pulses is monitored by means of a background-free autocorrelator (1*c*).

On the basis of the specific requirements of a particular chemical or biological study, the train of low-energy ps-pulses emerging from the ring dye laser can be used directly or can be amplified by as much as $\sim 10^6$ times by means of flowing dye cells pumped by 10-ns pulses of the second harmonic, 532 nm, of a Nd^{3+}:YAG laser. The amplified pulse can then be used directly or now possesses sufficient energy to be converted, by means of frequency-doubling crystals and/or stimulated Raman scattering, to wavelengths other than the one originally generated by the ring laser. Appropriate direction and splitting of this

[1]Department of Chemistry, Yale University, New Haven, CT.

Can. J. Chem. Downloaded from www.nrcresearchpress.com by 210.87.254.105 on 09/06/12
For personal use only.

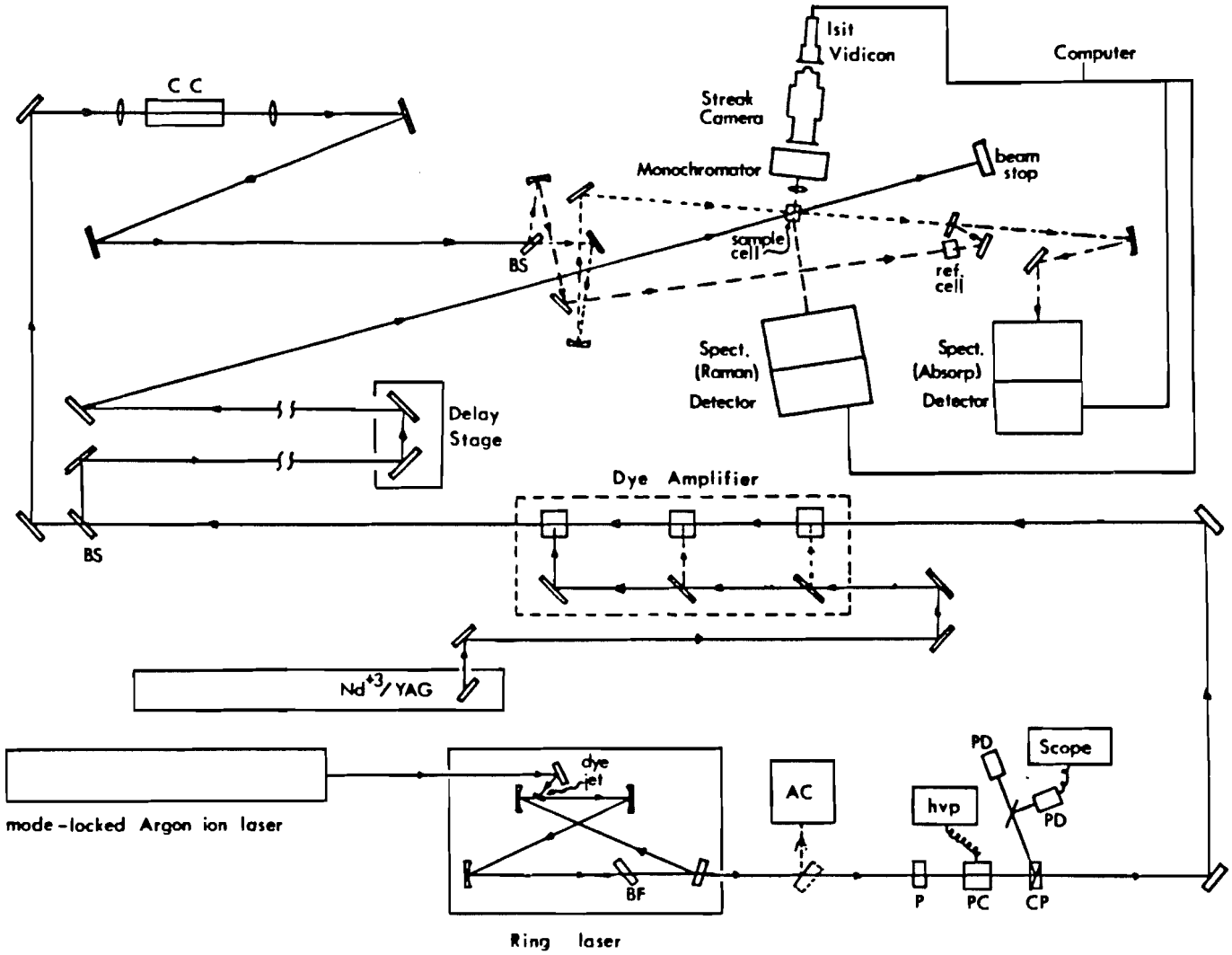

FIG. 1. Schematic diagram of a synchronously pumped dye laser system. AC: autocorrelation, P: polarizer, PC: Pockels cell, CP: crossed polarizer, bvp: high-voltage pulser, PD: photodiode, BS: beam splitter, CC: continuum cell.

ps pulse, as illustrated in Fig. 1, permits the detection and recording of the spectra of transient intermediates and measurement of their lifetimes by means of picosecond emission, absorption, and Raman spectroscopy.

Transient intermediates of a TMM derivative

A molecular species which has recently been studied by means of picosecond emission spectroscopy is the trimethylenemethane (TMM) derivative, 2-isopropylidenecyclopentane-1,3-diyl (**3**) (2). Many experimental and theoretical studies have been performed on the TMM biradical (3). Past spectroscopic studies have employed electron paramagnetic resonance to study the triplet ground-state of TMM (3*c*,*d*). Direct spectroscopic and kinetic information has been obtained only very recently by Kelley *et al.* (2) using picosecond fluorescence spectroscopy. Prior to this direct observation, evidence for the existence of singlet 2-isopropylidenecyclopentane-1,3-diyl (**3S**) was based upon the kinetic argument of Mazur and Berson (4).

Kelley *et al.* (2) observed the decay kinetics and emission spectra of transients generated by excitation of diazenes **1** and **2** with a 25-ps FWHM, 266-nm pulse in hexane solution at room temperature and in argon and xenon matrices at 4.2 K.

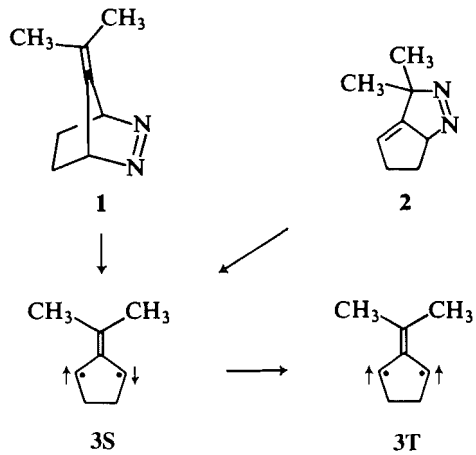

In hexane solution at room temperature, the fluorescence decay kinetics of both diazenes were found to exhibit biexponential decays with lifetimes, τ_1 and τ_2, of 38 ps and 280 ps for **1** and of 25 ps and 310 ps for **2** (Fig. 2). The short-lifetime components were assigned to emission from the predissociative states of **1** and **2**. The longer-lived component ($\tau \cong 300$ ps) was attributed to emission from an excited singlet

Can. J. Chem. Downloaded from www.nrcresearchpress.com by 210.87.254.105 on 09/06/12
For personal use only.

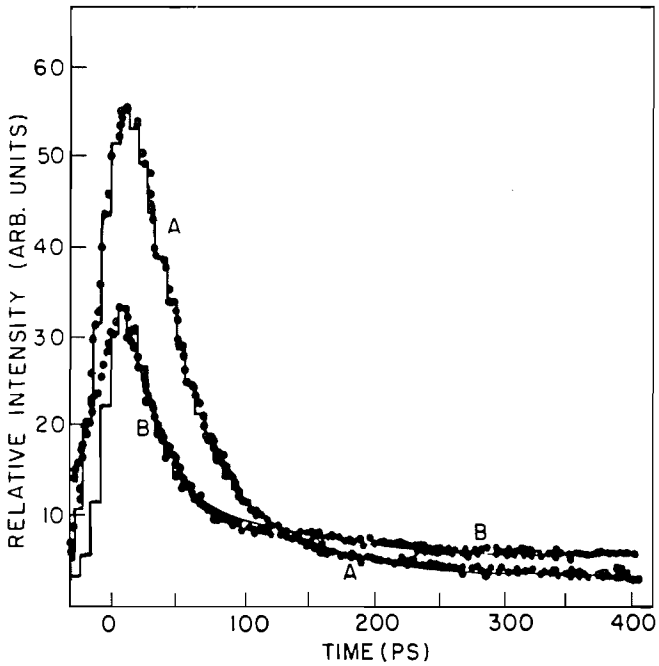

FIG. 2. Fluorescence intensity (>310 nm) versus time for diazene **1** (A) and diazene **2** (B) in hexane at room temperature. Solid lines are calculated biphasic curves with decay times of 38 ps and 280 ps for **1** and of 25 ps and 310 ps for **2**. No relationship between the two curves is implied since the curves are not normalized. (From ref. 2.)

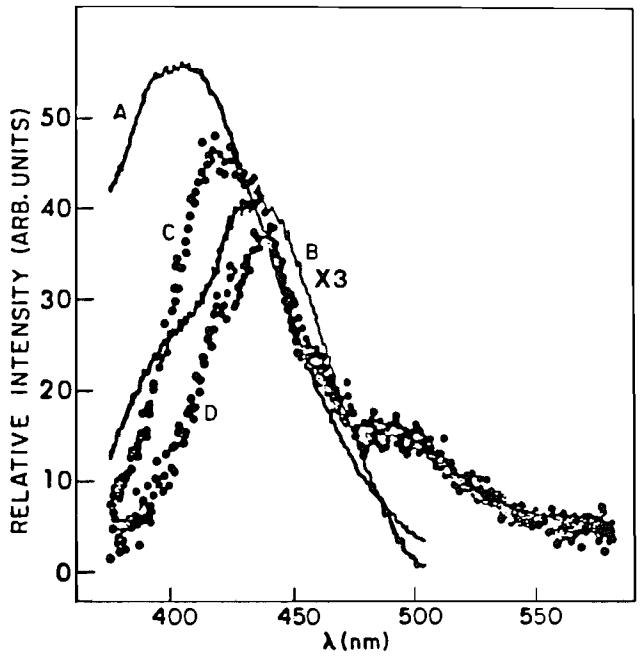

FIG. 3. Relative fluorescence intensity versus wavelength taken in hexane solution at room temperature. Spectra were recorded under the following conditions: (A) diazene **1**, fluorimeter; (B) diazene **2**, fluorimeter; (C) diazene **1**, laser-induced; (D) diazene **2**, laser-induced. Spectra A and B are normalized with respect to each other by multiplying the amplitude of B by a factor of three. (From ref. 2.)

state of the TMM biradical (**3S***). Room-temperature laser-induced emission spectra obtained by photolysis of either diazene was dominated by fluorescence from **3S***. In contrast, the laser-induced emission spectra obtained by photolysis of **1** or **2** in inert-gas matrices at 4.2 K were dominated by emission originating from the azo chromophores of the starting diazenes (Fig. 3). Kelley *et al.* (2) concluded that photochemical deazetation was partially suppressed under the conditions of matrix isolation and low temperature.

Biphasic fluorescence decays in argon matrices at 4.2 K were observed for **1** and **2**. The lifetimes of shorter-lived components (τ_1 = 5.0 ns and τ_1 = 3.1 ns for **1** and **2**, respectively) indicated a considerable increase from the room-temperature predissociative lifetimes. However, the predissociative lifetime of **1** remained longer than the corresponding value of **2**. The observed fluorescence lifetimes of the long-lived components ($\tau_2 \cong 30$ ns) of **1** and **2** correspond to the lifetime of **3S*** and are in accord with the expected natural radiative lifetime of **3S*** (5).

In xenon matrices at 4.2 K, monoexponential decays were observed for both **1** and **2** with identical lifetimes of 6.5 ns. The emission spectra of **1** or **2** in xenon matrices were very similar. This similarity was interpreted as indicating the occurrence of an isomerization of **2** → **1** which was fast compared to fluorescence decay. Little, if any, emission from **3S*** was observed in Xe matrices. This indicated that the lifetime **3S*** was <10 ns and supported the hypothesis that the major decay pathway for **3S*** was intersystem crossing to a triplet state, a process expected to be enhanced in the presence of the heavy atom, xenon.

The picosecond data obtained by Kelley *et al.* (2) provided direct evidence of the mechanism of predissociation and radical formation along with an identification of the several species by means of emission spectroscopy.

Relaxation dynamics of photoexcited *p*-dimethylaminobenzonitrile

Another problem of interest studied by means of picosecond spectroscopy is the anomalous dual fluorescence of *p*-dimethylaminobenzonitrile (DAB) in polar solvents. Many studies besides those utilizing picosecond spectroscopy have attempted to interpret the nature and kinetics of this anomalous phenomenon (6–10). The two fluorescence bands have been designated the *a* and *b* bands. The maxima of the *b* band occurs at ~350 nm in both polar and nonpolar solvents and exhibits an exceptionally large red shift of ~6000 cm^{-1} from the intense first absorption band at 295 nm. A highly polar excited state is believed to be responsible for the *a* band which has a fluorescence maxima at 470 nm in polar solvents. Both fluorescence bands are polarized parallel to the plane of the benzene ring (11). Recent steric evidence (12) favors the identification of the emitting state, a^*, with a strongly dipolar twisted internal charge-transfer singlet state, ^{1}(TICT), which relaxes torsionally to a conformation in which the phenyl ring and dimethylamino group are mutually perpendicular. These studies (11, 12) have also demonstrated that these emission bands do not correspond to the first absorption band of DAB, nor do they correspond to low-lying $^1(\pi,\pi^*)$ states.

High-pressure oxygen fluorescence quenching studies (13, 14) in acetonitrile suggest a consecutive rather than competitive formation of b^* and a^*, i.e. ground state $\xrightarrow{h\nu}$ $(X\rightarrow)$ $b^* \rightarrow a^*$. Results from previous studies (10, 12, 15) have shown that in most cases the activation energy for the $b^* \rightarrow a^*$ process follows closely the solvent viscosity, which suggest that the formation of the relaxed a^* state is viscosity-controlled. Using a reversible $b^* \rightleftarrows a^*$ kinetic model and results from the quenching experiments (13, 14), a reaction half-life as short as ~2 ps for DAB in methylene chloride is revealed. Alternatively, since

Can. J. Chem. Downloaded from www.nrcresearchpress.com by 210.87.254.105 on 09/06/12
For personal use only.

the solvent reorientation time of acetonitrile is ~1.5 ps (16), the fluorescence lifetime in this solvent (estimated to be ~10 ps) (13) appeared to be limited by the rate of internal rotation and not solvent viscosity.

Advances in the past decade in picosecond spectroscopy and streak camera technology now allow direct measurements of fluorescence decay rates which do not rely on a previously assumed kinetic model. Struve and Rentzepis (17), using a picosecond time-resolved CS_2 shutter apparatus, observed an ~40-ps risetime for the a^* fluorescence of DAB at ~470 nm in methanol, ethanol, and n-butanol, and a longer risetime in the more viscous cyclohexanol. More recently, Huppert *et al.* (18) have measured the a^* fluorescence risetimes and a^* formation kinetics of DAB by both direct measurement and by monitoring the b^* fluorescence decay rates. These results, which were not directly obtainable before (17, 19) because of picosecond spectrometer limitations, were obtained when Huppert *et al.* (18) used the fourth harmonic (266 nm, 20 ps FWHM) of a Nd^{3+}:YAG laser for sample excitation and a streak camera for detection of the ultrafast picosecond events.

With appropriate filters, both the a^* and b^* fluorescences could be observed and measured independently. The b^* state fluorescence was found to be biphasic and appeared within the pulse-width of the laser (risetime, $\tau_r^b < 10$ ps). This was true for all linear alcohols except methanol where τ_f^b was within the time resolution of the experiment. The long-component fluorescence lifetime was found to be linearly related to the respective solvent viscosity (Fig. 4). Pulse-limited fluorescence decay was also observed for the polar aprotic solvents, acetonitrile, *N*,*N*-dimethylformamide, and dimethyl sulfoxide, whose room-temperature viscosities are less than 2.5 cP. The fluorescence of the b^* state in the nonpolar aprotic solvents, methylcyclohexane and diethyl ether, showed no viscosity dependence (τ_f^b = 1.8 ns and 3.2 ns, respectively, at 25°C) and, as was known previously (6, 7), no a^* fluorescence was observed. It was further found by Huppert *et al.* (18) that the a^* fluorescence risetimes are the same as the b^* fluorescence decays within experimental error in the solvents, 1-pentanol, 1-hexanol, 1-decanol, and 1-dodecanol (Fig. 5). These results further confirmed that the b^* state is the kinetic precursor to the a^* state in many polar solvents as was previously concluded from the fluorescence quenching data (13). The a^* decay times were found to exhibit a marked temperature dependence and were measured to be single exponential with lifetimes of τ_f^a = 3.6 ns, 3.4 ns, 3.7 ns, and 1.4 ns in 1-dodecanol, 1-hexanol, acetonitrile, and methanol, respectively. This temperature dependence was attributed to a thermally activated nonradiative process. A similar observation for the TICT state of *p*-anthryl derivatives of dialkylanilines has also been reported elsewhere (20). The study by Huppert *et al.* (18) also revealed for the first time the biexponential character of the a^* risetimes and b^* decays. The short-time components were interpreted as reflecting the microscopic solvent reorientation required for solvation of the polar species, while the long-time component was attributed to the normal decay and risetimes of the bands.

Photodissociation of haloaromatics

Recent picosecond studies, by Struve and co-workers (21) and Huppert *et al.* (22), on the photodissociation of haloaromatics demonstrate the tremendous potential of picosecond spectroscopy for determining the detailed course of a reaction, specifying intermediate electronic states and the energy dissipation channels involved.

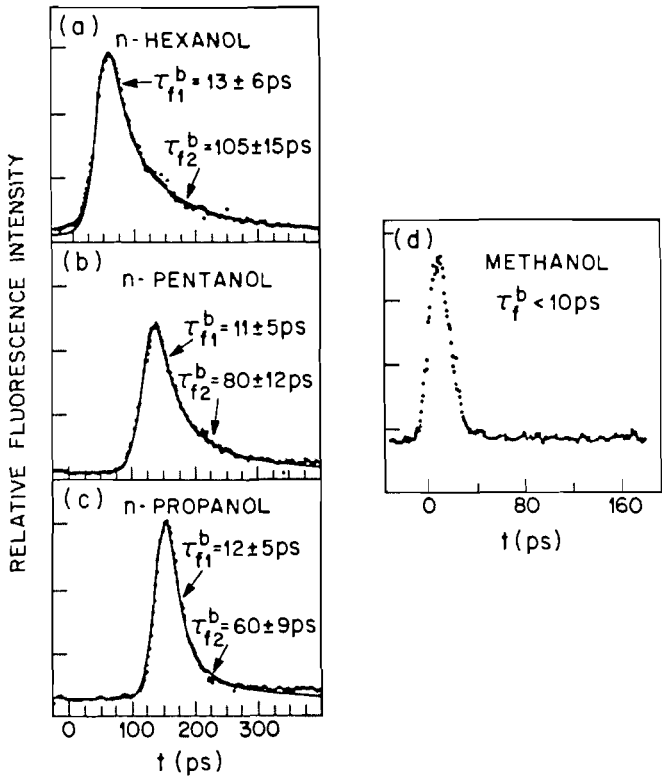

FIG. 4. Time-resolved b^* fluorescence intensities of $\sim 10^{-4}$ *M* solutions of DAB excited by 266-nm excitation pulses in 1-hexanol, 1-pentanol, 1-propanol, and methanol at 20°C. Each trace was averaged over five to eight laser pulses. (From ref. 18.)

Haloaromatics are known to photodissociate to the parent aromatic and halogen radicals. Ermolaev and Svitashev (23) have studied intersystem crossing from the excited singlet to a lower-lying triplet state by observing room-temperature fluorescence and low-temperature phosphorescence in rigid glasses. The quantum yields vary from $\phi_f < 0.0005$ and $\phi_p = 0.38$ for 1-iodonaphthalene to $\phi_f = 0.3$ and $\phi_p = 0.058$ for 1-chloronaphthalene. Phosphorescence spectra of some haloaromatics, studied by Pavlopous and El-Sayed (24), contain at least two "subspectra," which differ in their polarization, and are enhanced by heavy-atom substitution.

Pavlopoulos and El-Sayed (24) measured triplet decay rates by observation of $T_n \leftarrow T_1$ absorption for naphthalene, anthracene, and phenanthrene and their halogen derivates in cyclohexane and viscous paraffin (η = 170 cP) solutions at room temperature. Iodonaphthalene showed no $T_n \leftarrow T_1$ absorption while the bromo- and chloro-compounds showed maxima at 425 nm. They attributed the absence of triplet absorption in iodonaphthalene to either a low intersystem crossing probability or to a triplet lifetime less than 10^{-5} s. Sandros and Backstrom (25, 26) estimated the triplet lifetimes of 1-iodo- and 2-iodonaphthalene to be 10 ns and 1100 ns, respectively. Studies by Wilkinson (27) and Levy *et al.* (28) have shown that energy dissipation from the triplet state occurs by dissociation of the carbon–halogen bond, but that dissociation may occur from the singlet state as well. Temperatured dependence of the triplet lifetimes of 1-iodonaphthalene, 2-iodonaphthalene, and 4-iodobiphenyl was studied by Grieser and Thomas (29) using pulse radiolysis. The lifetimes were found to correlate well with the expression $\ln\left(\frac{1}{\tau}\right) = -E_a/RT + \ln A$. They attributed

Can. J. Chem. Downloaded from www.nrcresearchpress.com by 210.87.254.105 on 09/06/12
For personal use only.

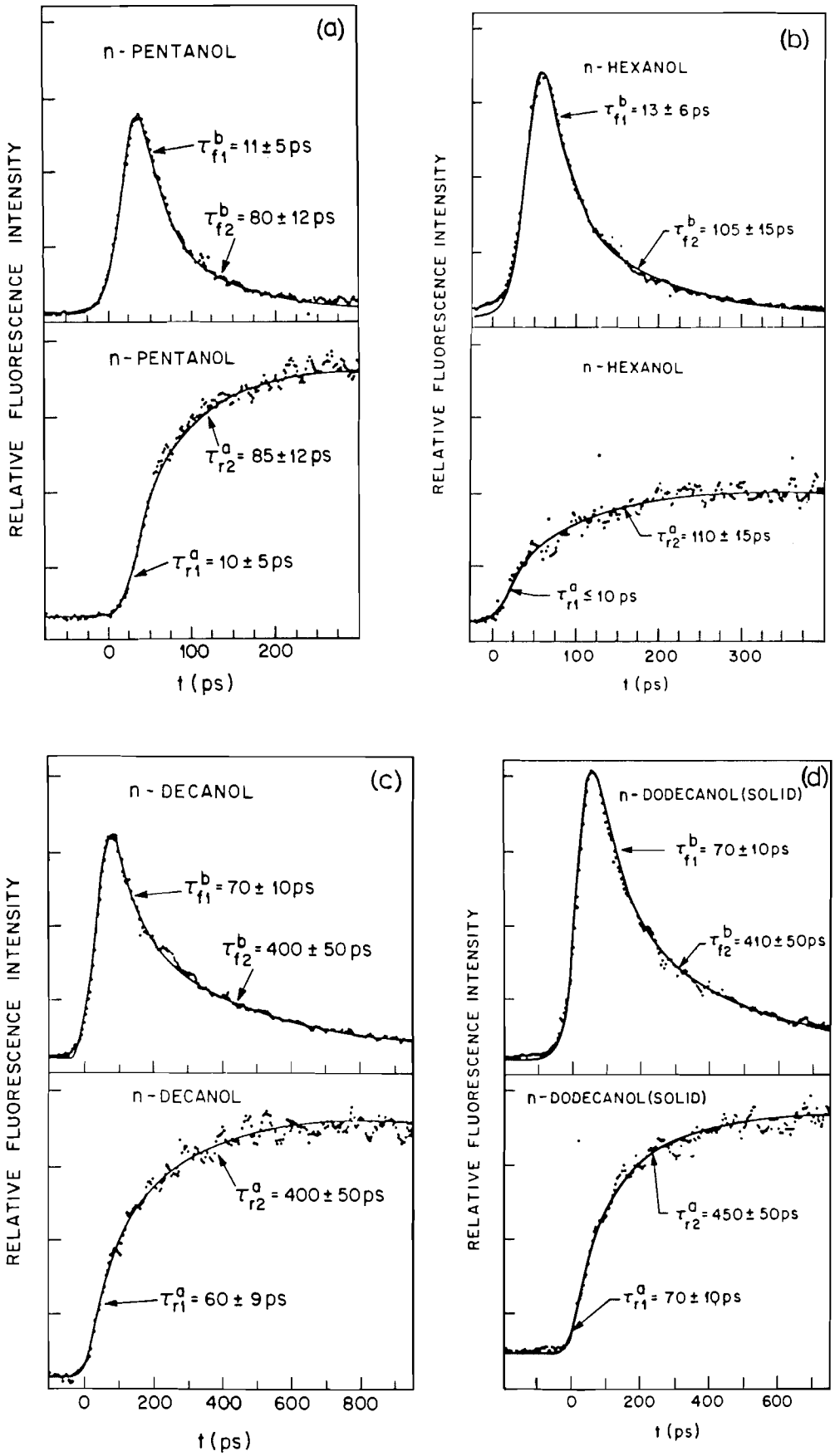

FIG. 5. Comparison of b^* fluorescence decay times τ_f^b to a^* fluorescence risetimes τ_r^a for DAB in (a) 1-pentanol; (b) 1-hexanol; (c) 1-decanol; (d) 1-dodecanol all at 20°C. (From ref. 18.)

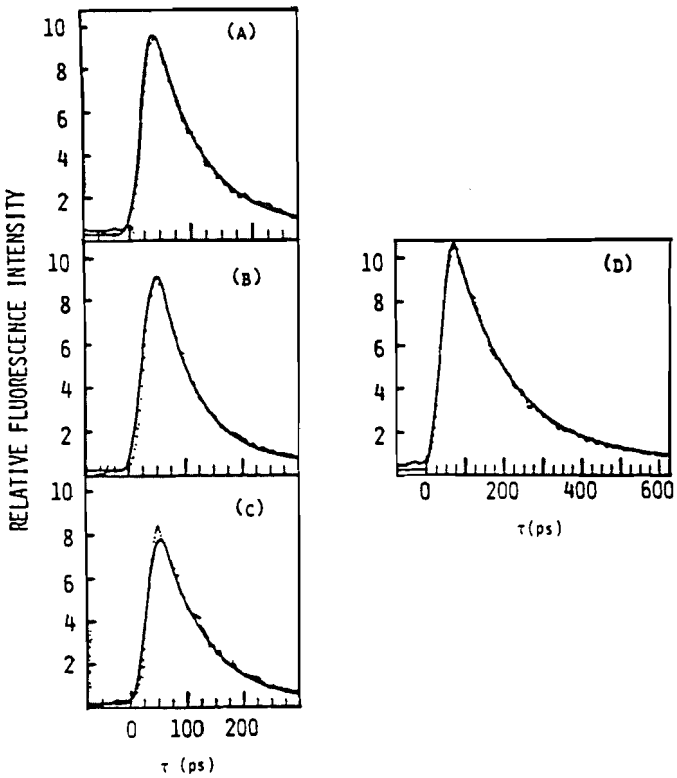

FIG. 6. Time-resolved emission of bromonaphthalenes in hexane at room temperature resulting from excitation by a 266-nm, 20-ps pulse. The emission is within the range of 310−550 nm. Plots of emission intensity vs. time (ps) for: (a) 1-bromonaphthalene; (b) 1-bromo-2-methylnaphthalene; (c) 1-bromo-4-methylnaphthalene; (d) 2-bromonaphthalene. (From ref. 22.)

this unusual dependence of lifetime on temperature to a crossing of the potential energy surfaces of the triplet state and the $T(\sigma,\sigma^*)$ dissociative state.

Saigusa *et al.* (30) measured the intersystem crossing (ISC) rates from the lowest excited singlet by picosecond emission spectroscopy. They found the ISC rates for 1-chloro- and 1-bromonaphthalene to be $(5.9 \pm 0.8) \times 10^8$ s^{-1} and $(1.5 \pm 0.3) \times 10^{10}$ s^{-1}, respectively. 1-Iodonaphthalene, as a result of its short lifetime, fluoresced only weakly, and its ISC rate could not be measured.

Haloaromatic photodissociation has also been studied in molecular beams by Bersohn and co-workers (31, 32). They estimated dissociation rates by determining β, the anisotropy parameter characterizing angular distribution of photofragments. The lifetimes of iodobenzene, 1-iodonaphthalene, and 2-iodonaphthalene were found to be ~0.5 ps. The lifetime of methyliodide is an order of magnitude smaller, 0.07 ps. The analogous aryl bromides were found to have lifetimes 2 orders of magnitude longer. They concluded that photodissociation occurs by intersystem crossing to the triplet state localized in the halogen bond: $S_0 \rightarrow S_2(\pi,\pi^*) \rightarrow S_1(\pi,\pi^*) \rightarrow T(\sigma,\sigma^*) \rightarrow$ fragments.

The bromoaromatics display an unusually long lifetime compared to the iodo-analogs, if intersystem crossing from $S(\pi,\pi^*)$, and therefore spin-orbit coupling, is the dominant parameter. Spin-orbit coupling energy is proportional to the $^2P_{3/2}-^2P_{1/2}$ fine structure splitting of the ground-state halogen atom. The lifetime of the bromoaryl should be longer by the square of the iodo−bromo splitting ratio. The bromoaryl lifetimes are approximately 10-fold longer − too long for spin-orbit coupling to be the dominant parameter. Bersohn reconciled this by including predissociation from the S_1 as another dissociation channel.

TABLE 1. Room temperature (~20°C) fluorescence lifetimes of haloaromatics in hexane for laser excitation at a given wavelength (λ_{ex}) (from ref. 22)

Sample	λ_{ex} (nm)	τ_f (ps)
4,4-Dibromobiphenyl	265	30
4-Bromobiphenyl	265	35
1-Bromonaphthalene	265	75
1-Bromo-4-methylnaphthalene	265	80
1-Bromo-2-methylnaphthalene	265	72
2-Bromonaphthalene	265	150
1-(Chloromethyl)naphthalene	265	490
2-(Bromomethyl)naphthalene	265	*
1-Chloronaphthalene	265	2400
2-Chloronaphthalene (zone refined >99%)	265	3300
2-Chloronaphthalene	265	3500
9-Bromoanthracene	355	100
9,10-Dibromoanthracene	355	1300
2-Iodoanthracene	265	14
9-Iodoanthracene	265	35
2-Iodoanthracene	355	17
9-Iodoanthracene	355	55

*Not detected.

The picosecond absorption and emission studies by Huppert *et al.* (22) clarify the mechanism of photodissociation of a number of haloaromatics. Their fluorescence measurements showed the expected heavy-atom effect due to spin-orbit coupling. Lifetimes of the chloronaphthalenes were the longest, 2.4 and 3.3 ns for 1-chloronaphthalene and 2-chloronaphthalene, respectively. The 1-bromo and 2-bromo compounds (see Fig. 6) had lifetimes of 75 ps and 150 ps, respectively. Iodo-substituted compounds had the shortest lifetimes, 14 ps and 35 ps for 2-iodoanthracene and 9-iodoanthracene, respectively. They found that the intersystem crossing rate is heavily influenced by the position of the substituent on the ring, as well as its spin-orbit couplings, as shown clearly by the lifetime data for 1- and 2-halonaphthalenes, 2- and 9-iodoanthracenes (see Table 1 for a summary of the fluorescence data).

Prompt risetimes and the absence of unrelaxed fluorescence ($\tau \cong 5$ ps) after excitation indicates that vibrational relaxation from hot S_1 levels to $S_1(v = 0)$ occurs within 5 ps. Fluorescence decay studies show the S_1 relaxation rate, but transient absorption spectra are needed to determine the identity of the several states involved in the relaxation process. Transient absorption spectra showing $S_n \leftarrow S_1$ disappearance and $T_n \leftarrow T_1$ appearance (see Fig. 7) give unequivocal proof of the dissociation pathway. Huppert *et al.* (22) concluded that photodissociation of these haloaromatics proceeds by fast relaxation from upper S_1 vibrational levels (6,000 cm^{-1} excess vibrational energy) to $S_1(v = 0)$ and intersystem crossing to an upper $T_1(v > 0)$ state. Fast vibrational relaxation to $T_1(v = 0)$, is followed by predissociation of a $T(\sigma,\sigma^*)$ state. Halo-substitution of the methyl group of the aromatics increased the intersystem crossing and predissociation rates which further supported Bersohn's proposals (31, 32). Though picosecond studies have provided detailed mechanistic information on the photodissociation of haloaromatics, questions remain, since,

Can. J. Chem. Downloaded from www.nrcresearchpress.com by 210.87.254.105 on 09/06/12
For personal use only.

Can. J. Chem. Downloaded from www.nrcresearchpress.com by 210.87.254.105 on 09/06/12
For personal use only.

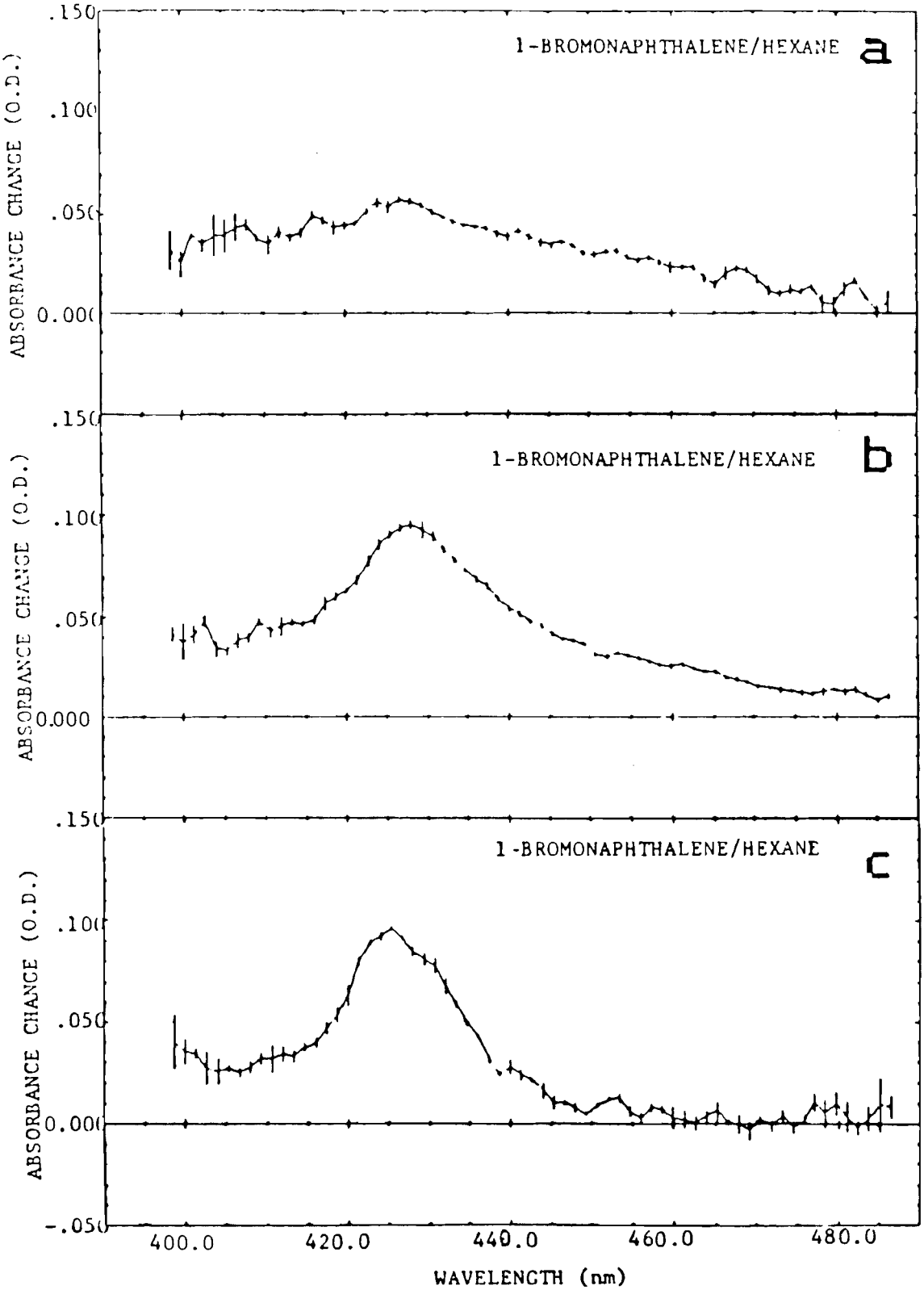

FIG. 7. Transient absorption spectra of 1-bromonaphthalene in hexane at room temperature excited with a 266-nm ps pulse, recorded (a) 25 ps after excitation; (b) 100 ps after excitation, (c) 500 ps after excitation. (From ref. 22.)

for example, Struve and co-workers have interpreted their data from picosecond studies of iodoanthracene differently (21).

Conclusion

From the examples of photoinitiated organic reactions discussed here, it is apparent that picosecond absorption spectroscopy and picosecond emission spectroscopy have provided data about the events which occur on this ultrafast time scale and which determine the path a reaction takes on its way to completion. Whether it be simply the mechanism of relaxation

from an excited state, as in the case of *p*-dimethylaminobenzonitrile, or an actual chemical change which takes place within a molecule, as in the studies of the photodissociation of haloaromatic or azo compounds, picosecond spectroscopy enables one to detect the intermediates involved and measure their kinetics in such a way as to give a detailed understanding of the mechanism of the occurring process. As picosecond Raman spectroscopy becomes a better-developed investigative tool, the structural information which it yields will enhance our understanding of chemical reactions at the molecular level and, in addition to general advances in technology, will increase the number of applications of picosecond spectroscopy to mechanistic chemical, physical, and biological problems.

1. (*a*) P. M. RENTZEPIS. Science, **202**, 174 (1978); (*b*) A. H. REYNOLDS and P. M. RENTZEPIS. Adv. Bot. Res. **8**, 1 (1980); (*c*) E. P. IPPEN and C. V. SHANK. *In* Ultrashort light pulses. *Edited by* S. L. Shapiro. Springer-Verlag, Heidelberg. 1971.
2. (*a*) D. F. KELLEY, M. R. MAZUR, P. M. RENTZEPIS, and J. A. BERSON. J. Am. Chem. Soc. **104**, 3764 (1982); (*b*) D. F. KELLEY and P. M. RENTZEPIS. J. Am. Chem. Soc. In press.
3. (*a*) J. A. BERSON. Acc. Chem. Res. **11**, 446 (1978); (*b*) J. A. BERSON. *In* Diradicals. *Edited by* W. T. Borden. John Wiley and Sons, New York, NY. 1982; (*c*) P. DOWD. Acc. Chem. Res. **5**, 242 (1972); (*d*) M. S. PLATZ, J. M. MCBRIDE, R. D. LITTLE, J. J. HARRISON, A. SHAW, S. E. POTTER, and J. A. BERSON. J. Am. Chem. Soc. **98**, 5725 (1976).
4. M. R. MAZUR and J. A. BERSON. J. Am. Chem. Soc. **103**, 684 (1981).
5. (*a*) J. H. DAVIS and W. A. GODDARD. J. Am. Chem. Soc. **99**, 4242 (1977); (*b*) S. J. STRICKLER and R. A. BERG. J. Chem. Phys. **37**, 814 (1962).
6. E. LIPPERT, W. LUDER, F. MOLL, W. NAGELE, H. BOOS, H. PR. H. PRIGGE, and I SEIBOLD-BLANKENSTEIN. Angew. Chem. **73**, 695 (1961).
7. E. LIPPERT, M. LUDER, and H. BOOS. *In* Advances in molecular spectroscopy. *Edited by* A. Mangini. Pergamon, New York, NY. 1962. p. 443.
8. A. SIEMIARCZUK, Z. R. GRABOWSKI, A. KROWCZYNSKI, M. ASHER, and M. OTTOLENGHI. Chem. Phys. Lett. **51**, 315 (1977).
9. E. M. KOSOWER and H. DODIUK. J. Am. Chem. Soc. **98**, 924 (1976).
10. Z. R. GRABOWSKI, K. ROTKIEWICZ, A. SIEMIARCZUK, D. J. CROWLEY, and W. BAUMANN. Nouv. J. Chim. **3**, 443 (1979).
11. K. ROTKIEWICZ, K.H. GRELLMANN, and Z. R. GRABOWSKI. Chem. Phys. Lett. **19**, 315 (1973).
12. K. ROTKIEWICZ, Z. R. GRABOWSKI, A. KROWCZYNSKI, and W. J. KUHLE. J. Lumin. **12–13**, 877 (1976).
13. K. ROTKIEWICZ, Z. R. GRABOWSKI, and J. JASNY. Chem. Phys. Lett. **34**, 55 (1975).
14. E. KIRKOR-KAMINSKA, K. ROTKIEWICZ, and Z. R. GRABOWSKI. Chem. Phys. Lett. **58**, 379 (1978).
15. Z. R. GRABOWSKI, K. ROTKIEWICZ, W. RUBASZEWSKA, and E. KIRKOR-KAMINSKA. Acta Phys. Pol. A, **54**, 767 (1975).
16. S. L. WHITTENBURG and C. H. WANG. J. Chem. Phys. **67**, 4255 (1977).
17. W. S. STRUVE and P. M. RENTZEPIS. J. Chem. Phys. **60**, 1533 (1974).
18. D. HUPPERT, S. D. RAND, P. M. RENTZEPIS, P. F. BARBARA, W. S. STRUVE, and Z. R. GRABOWSKI. J. Chem. Phys. **75**, 5714 (1981).
19. (*a*) W. S. STRUVE, P. M. RENTZEPIS, and J. JORTNER. J. Chem. Phys. **59**, 5014 (1973); (*b*) W. S. STRUVE and P. M. RENTZEPIS. Chem. Phys. Lett. **29**, 23 (1974).
20. A. SIEMIARCZUK, J. KOPUT, and A. POHORILLE. Z. Naturforsch. To be published.
21. R. L. PINEAULT, C. G. MORGANTE, and W. S. STRUVE. J. Photochem. **17**, 435 (1981).
22. D. HUPPERT, S. D. RAND, A. H. REYNOLDS, and P. M. RENTZEPIS. J. Chem. Phys. **77**, 1214 (1982).
23. V. L. ERMOLAEV and K. K. SVITASHEV. Opt. Spectrosc. USSR, **7**, 339 (1959).
24. T. PAVLOPOULOS and M. A. EL-SAYED. J. Chem. Phys. **41**, 1083 (1964).
25. K. SANDROS. Acta Chem. Scand. **18**, 235 (1964).
26. K. SANDROS and H. BACKSTROM. Acta Chem. Scand. **16**, 958 (1962).
27. F. WILKINSON. J.Phys. Chem. **66**, 2564 (1962).
28. A. LEVY, D. MEYERSTEIN, and M. OTTOLENGHI. J. Chem. Phys. **77**, 3044 (1973).
29. F. GRIESER and T. K. THOMAS. J. Chem. Phys. **73**, 2115 (1980).
30. H. SAIGUSA, T. AZUMI, M. SUMITANI, and K. YOSHIHARA. J. Chem. Phys. **72**, 1713 (1980).
31. A. FREEDMAN, S. C. YANG, M. KAWASAKI, and R. BERSOHN. J.Chem. Phys. **72**, 1028 (1980).
32. M. DZVONIK, S. YANG, and R. BERSOHN. J. Chem. Phys. **61**, 4408 (1974).

Can. J. Chem. Downloaded from www.nrcresearchpress.com by 210.87.254.105 on 09/06/12
For personal use only.

The use of insoluble benzoylated polystyrene beads (polymeric benzophenone) in photochemical reactions

JOSÉ LUIS BOURDELANDE, JOSEP FONT, AND FRANCISCO SÁNCHEZ-FERRANDO

Departament de Química Orgànica, Facultat de Ciències, Universitat Autònoma de Barcelona, Bellaterra, Spain

Received March 8, 1982[1]

This paper is dedicated to Professor Harry E. Gunning on the occasion of his 65th birthday

JOSÉ LUIS BOURDELANDE, JOSEP FONT, and FRANCISCO SÁNCHEZ-FERRANDO. Can. J. Chem. **61**, 1007 (1983).

Friedel–Crafts benzoylation of 2%-divinylbenzene (DVB) cross-linked polystyrene beads yielded insoluble polymeric analogs of benzophenone which were used as sensitizers in the |2 + 2| photocycloaddition of cyclohexene to maleic anhydride and in the $E-Z$ isomerization of (*E*)-1,3-pentadiene and methyl (*E*)-2,2-dimethyl-3,5-hexadienoate. In the first reaction, the use of the polymer-anchored sensitizers resulted in the separation of polymer-attached by-products by simple filtration, although the yield of photoadducts was less than three quarters of that obtained when using benzophenone itself, and the recovered polymers could not be reused. In the photoisomerizations, the compositions of the photostationary states reached when using the polymeric sensitizers (now reusable) were shown to depend on the degree of functionalization of the polymers via steric hindrance to the energy transfer process. Intrapolymerically sensitized $E-Z$ photoisomerization was also demonstrated on a polymer containing benzophenone and diene units. Photooxidation of secondary alcohols (isopropanol, cyclohexanol) to ketones and photooxygenation of 2,3-dimethyl-2-butene to 2,3-dimethyl-3-buten-2-yl hydroperoxide (in the presence of oxygen) were other reactions for which polymeric benzophenones could be used.

JOSÉ LUIS BOURDELANDE, JOSEP FONT et FRANCISCO SÁNCHEZ-FERRANDO. Can. J. Chem. **61**, 1007 (1983).

La benzolation selon Friedel et Crafts d'une résine de polystyrène réticulée à 2% de divinylbenzène (DVB) donne des polymères insolubles analogues de la benzophénone qu'on utilise comme sensibilisateur dans la photocycloaddition du type |2 + 2| du cyclohexène sur l'anhydride maléique et dans l'isomérisation du type $E-Z$ du pentadiène-1,3 (*E*) et du diméthyl-2,2 hexadiène-3,5 oate de méthyle (*E*). Dans la première réaction, l'utilisation d'un sensibilisateur fixé sur un polymère conduit à une séparation des produits secondaires fixés sur le polymère par simple filtration, bien que le rendement en photoadduits représente moins de 75% de celui que l'on obtient en utilisant la benzophénone elle-même et bien que les polymères récupérés ne soient pas réutilisables. Dans le cas des photoisomérisations, on montre que les compositions des états photostationnaires atteints lorsqu'on utilise les sensibilisateurs fixés sur un polymère (non réutilisable) dépendent du taux de fonctionnalisation des polymères via l'encombrement stérique qui gène le processus de transfert d'énergie. On a aussi démontré qu'un polymère contenant une benzophénone et un diène peut provoquer une photoisomérisation $E-Z$ sensibilisée à l'intérieur du polymère. La photoxydation des alcools secondaires (isopropanol, cyclohexanol) en cétones et la photoxygénation du diméthyl-2,3 butène-2 en hydroperoxyde de diméthyl-2,3 butène-3 yle-2 (en présence d'oxygène) sont d'autres réactions où il est possible d'utiliser des benzophénones fixées sur un polymère.

[Traduit par le journal]

Introduction

The well developed concept of solid-phase synthesis (1), i.e., the attachment of a reactant to an insoluble matrix (polymeric or inorganic) prior to its reaction (now in heterophase) with soluble reactants, offers the following possibilities when applied to photochemical reactions: (*i*) anchored substrate, soluble photoreagent (or sensitizer); (*ii*) anchored photoreagent, soluble substrate; (*iii*) both substrate and photoreagent anchored. We (2) and others (3) have described the photohalogenation of anchored *n*-alkanoic acids as an example of case (*i*). The present paper deals mainly with case (*ii*), although an example of case (*iii*) is also presented. Both cases offer great interest, since many of the current approaches to chemical storage or utilization of the energy of sunlight depend on the use of photoredox reagents or sensitizers physically adsorbed or chemically bound to solid insoluble particles of inorganic oxides or organic polymers, in order to produce separation of the individual reacting species involved in each step of the process (4). Actually, some insoluble polymeric (or polymer-bound) photosensitizers have been known for some time. After the pioneering work of Leermakers and James (5) on the use of polyvinyl phenyl ketone, prepared by bulk polymerization of the corresponding monomer, other authors used the solid phase concept and attached known sensitizers to insoluble resins, usually cross-linked polystyrene beads. Several resin-bound photosensitizers have been developed and tested, mainly by Neckers and co-workers, including both soluble and insoluble polystyrylmethyl 4-benzoylbenzoate (6), soluble poly(*p*-(trifluorovinyl)benzophenone) and poly(*p*-(trifluorovinyl)acetophenone) (7), rigid polydivinylbenzophenone (8), and the very useful P-Rose Bengal (9), which is the reagent of choice for the sensitized photochemical generation of singlet oxygen.

Benzophenone **1** is well known in organic photochemistry. With its convenient triplet energy of 288 kJ mol^{-1}, it sensitizes many photochemical reactions, such as |2 + 2| photocycloadditions and $Z-E$ photoisomerization of suitable alkenes. In addition, it can also act as a photoreagent, for instance in cycloadditions with alkenes (Paterno–Buchi reaction), or as photooxidant by hydrogen atom abstraction from appropriate donors. One polymeric analog of benzophenone, namely poly-*p*-styrylmethyl 4-benzoylbenzoate **2**, was found by Neckers to sensitize |2 + 2| photocycloadditions (6). However, in later work by the same group, some doubts were cast on this polymer as a true solid phase sensitizer (10). Another more closely related insoluble polymeric analog of **1**, namely polystyryl 4-(*N*,*N*-dimethylamino)phenyl ketone, was found to

[1]Revision received November 26, 1982.

Can. J. Chem. Downloaded from www.nrcresearchpress.com by 210.87.254.105 on 09/06/12
For personal use only.

Can. J. Chem. Downloaded from www.nrcresearchpress.com by 210.87.254.105 on 09/06/12
For personal use only.

sensitize the norbornadiene-quadricyclane photoisomerization with the same quantum yield as soluble 4-(*N*,*N*-dimethylamino)benzophenone, although at slightly slower rates (11). Quite surprisingly, the simplest polymeric analog of benzophenone, i.e., poly-*p*-styryl phenyl ketone **3**, has not been evaluated in photochemical reactions "because of the problem with $AlCl_3$ incorporation when polystyrene–divinylbenzene beads are benzoylated under Friedel–Crafts conditions" (6), in spite of the recorded successful uses of **3** in other types of reactions (12–14).

The purpose of the present work is to fill this gap by describing the preparation of $AlCl_3$-free cross-linked poly-*p*-styryl phenyl ketone **3** (polymeric benzophenone) and its use as sensitizer in the $|2 + 2|$ photocycloaddition of cyclohexene and maleic anhydride, and in the *E*–*Z* photoisomerization of two soluble conjugated dienes and one polymer-bound diene. Also described is the use of **3** in the photooxidation of two secondary alcohols and in the photooxygenation of an alkene to the corresponding hydroperoxide. Preliminary communications have been published on some of these subjects (15, 16).

Preparation and characterization of polymeric benzophenones

Beads of a (98:2) copolymer of styrene and divinylbenzene (DVB) were benzoylated by reaction with benzoyl chloride in carbon disulfide in the presence of $AlCl_3$ (17), a method which is also used for the benzoylation of soluble polystyrene (18). The degree of functionalization to be achieved was limited by the amount of benzoyl chloride and $AlCl_3$ used. The resulting polymeric benzophenones were thoroughly washed with a series of solvents and shown to be free of $AlCl_3$ by elemental analysis. The degree of functionalization was determined by conversion into the corresponding polymeric oximes **4** and elemental analysis for nitrogen in these derivatives.

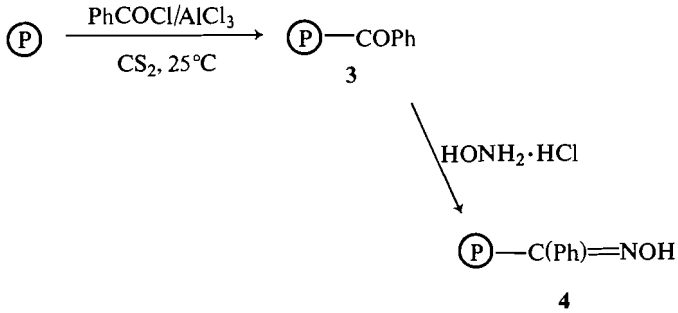

The three polymeric benzophenones prepared in this way were shown to contain 0.95, 2.2, and 3.2 mequiv. g^{-1} of carbonyl group. This can also be expressed as 11%, 29%, and 50% functionalization of the phenyl groups of the original polystyrene. For convenience, we shall refer to these three polymeric benzophenones as P-11, P-29, and P-50, respectively.

The photostability of all three polymers was checked by irradiation ($\lambda > 290$ nm) for 15 h in benzene or acetonitrile under nitrogen. This very prolonged irradiation released in soluble form less than 0.1% of a nonvolatile material which showed no peak of benzophenone by glc. The recovered irradiated polymers showed ir spectra almost identical to those of the starting materials, except for a very small broad absorption in the associated hydroxyl region. Furthermore, very little loss of activity was found when using P-29 pre-irradiated for 14 h in *Z*/*E* photoisomerizations (Fig. 2, curves 12 and 13). These data imply the occurrence of some (although very little) photodegradation of the polymers by backbone hydrogen atom abstraction, followed by cross-linking. Thus, P-11, P-29, and P-50 were shown to be rather photostable in the absence of substrates. These results should be compared with those obtained by Neckers (10) when evaluating his ester-type polymeric benzophenone **2** (6), which clearly showed the occurrence of up to 50% photodecarboxylation with release of up to 20% free benzophenone during irradiation for 6 h.

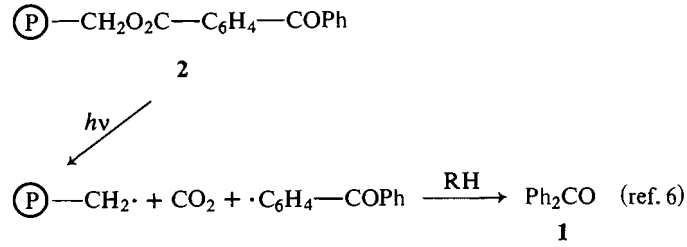

Polymeric benzophenones as sensitizers

(a) *Sensitized $|2 + 2|$ photocycloaddition of cyclohexene and maleic anhydride*

The photocycloaddition between cyclohexene **5** and maleic anhydride **6** gives mixtures of diastereomeric bicyclo|4.2.0|-octane-7,8-dicarboxylic anhydrides **7** and can be performed by unsensitized direct irradiation of the charge-transfer complex between **5** and **6** (19) or under sensitization by benzophenone **1** (20). We now describe the use of polymeric benzophenones as sensitizers for this reaction, the results being compared with those obtained when using **1** in the same conditions. In our hands, some by-products to be expected in the reaction sensitized by **1** were bi-2-cyclohexen-1-yl **8**, cyclohex-2-enyldiphenylmethanol **9**, and 7,7-diphenyl-6-heptenal **10**, as well as benzopinacol **11** and benzhydrol **12**. Of course, by-products of types **9**–**12**, if formed, could not be released to the solution when using the polymeric sensitizers P-11, P-29, or P-50. Thus, after filtration, the crude reaction mixture contained only adducts **7** and by-product **8**, besides starting materials.

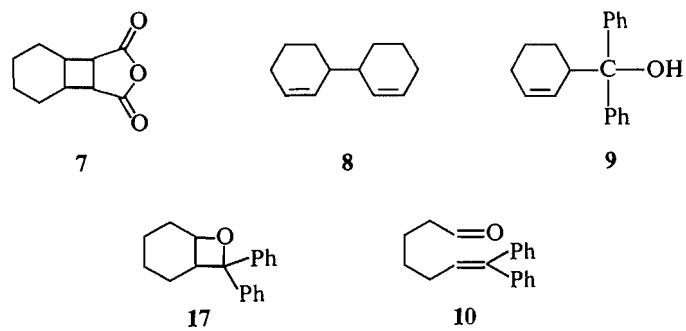

Formation of **7** as a function of irradiation time was determined by glc. The results are given in Fig. 1. As seen in this figure, the polymeric sensitizers were less efficient than **1**, and since the "concentrated" P-50 gave lower yields of **7** than the "diluted" P-11, steric hindrance is likely to play a major role. We conclude that energy transfer to the bulky charge-transfer complex between **5** and **6** is more sterically hindered when using the more highly functionalized polymeric sensitizer.

Other factors being the same, yields of **7** increased when performing these reactions in the presence of acetonitrile as a cosolvent, probably due to the low solubility of maleic anhy-

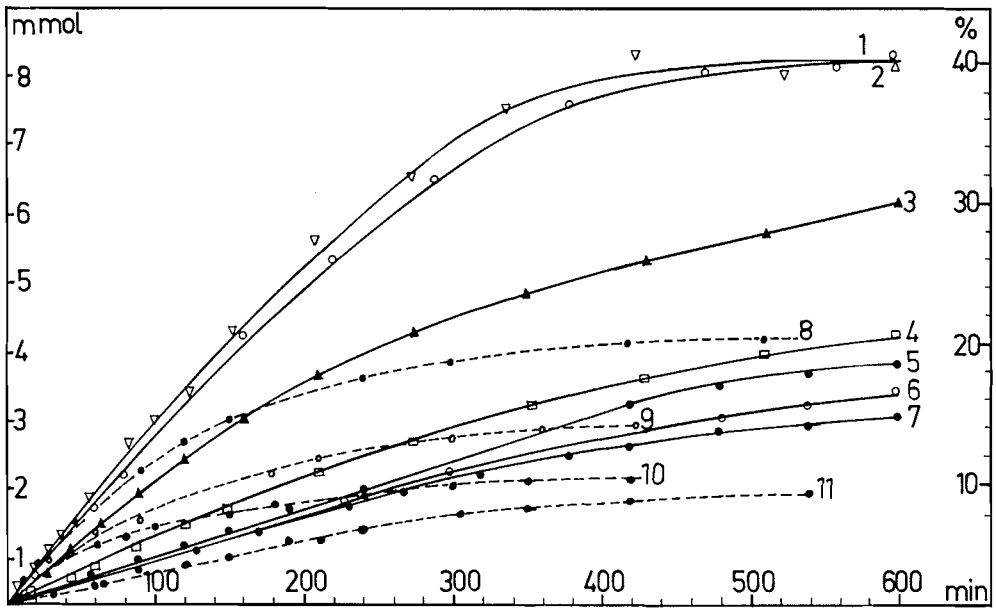

FIG. 1. Photocycloaddition of cyclohexene **5** and maleic anhydride **6**. Solid lines: yields of adducts **7** upon irradiation of **6** (2 g, 20.4 mmol) and **5** (10 mL) in acetonitrile (20 mL) in the presence of: curve 1, Ph_2CO (273 mg, 1.5 mmol); curve 2, Ph_2CO (273 mg, 1.5 mmol) and unfunctionalized polystyrene (2.38 g); curve 3, P-11 (2.7 g, 2.56 mequiv.); curve 4, P-50 (470 mg, 1.5 mequiv.); curve 5, unfunctionalized polystyrene (2.38 g); curve 6, no carbonyl compound; curve 7, P-11 recovered from experiment 3 (curve 3). Dashed lines: yields of adducts **7** upon irradiation of **6** (2 g, 20.4 mmol) in **5** (30 mL) in the presence of: curve 8, Ph_2CO (273 mg, 1.5 mmol); curve 9, P-11 (2.7 g, 2.56 mequiv.); curve 10, P-50 (470 mg, 1.5 mequiv.); curve 11, no carbonyl compound.

dride in cyclohexene.

Formation of the oxidative dimer **8** shows the photooxidizing ability of **1** and its polymeric analogs (see below).

The polymeric benzophenones recovered after their use in these sensitized cycloadditions did not show the original ketone carbonyl band in their ir spectra, bands at 1700–1780 (broad) and 1860 cm^{-1} as well as some associated hydroxyl bands at 3100–3600 cm^{-1} being observed instead. These recovered polymers could not be reused, and their 1780–1860 cm^{-1} bands, so similar to those of succinic anhydride, were taken as a clear indication of the anchoring of part of the maleic anhydride to the phenyl rings of the polymer units by $|2 + 2|$ photocycloaddition followed by conventional Diels–Alder cycloaddition, a process known to happen for benzene (21) and soluble polystyrene (22).

Attempts to determine the amount of polymer-bound maleic anhydride (by formation of the corresponding *p*-bromophenacyl ester, followed by Br analysis) failed, since most anhydride survived the treatment, as shown by ir.

(b) *Sensitized* E–Z *photoisomerization of conjugated dienes*

The *E–Z* photoisomerization of (*E*)-1,3-pentadiene, (*E*)-**13**, sensitized by **1**, is a well-known process (23) characterized by the triplet energies of substrate (*E*)-**13** (247 kJ mol^{-1}), product (*Z*)-**13** (238 kJ mol^{-1}), and sensitizer **1** (288 kJ mol^{-1}), and by a photostationary *Z/E* ratio of 0.82 ± 0.04 when using sensitizers having triplet energies well above those of the dienes, as is the case with **1**. We have performed this photoisomerization using polymeric benzophenones instead of **1**. The *Z/E* ratio was determined by glc as a function of irradiation time. The photoisomerization of methyl (*E*)-2,2-dimethyl-3,5-hexadienoate, (*E*)-**14**, prepared by known procedures (24), was also examined. The results of both series are given in Fig. 2. As shown in this figure, photostationary states were reached slightly more slowly when using polymeric benzophenones as sensitizers instead of **1**. The polymeric sensitizers could be reused without producing changes in the composition of the photostationary states, although these states were approached at somewhat smaller rates.[2] One important feature of the polymeric sensitizers was the decrease in the photostationary *Z/E* ratio which went along with the increase in the degree of functionalization of the polymer, clearly shown in the case of **14**. This effect appears to be of steric nature. Indeed, steric hindrance to energy transfer from triplet sensitizer to ground state alkene results in an increased photostationary proportion of the alkene isomer having the higher triplet energy (25). In our case such an effect should favour (*E*)-**13** over (*Z*)-**13**, according to the known triplet energies of these two isomers, and we assume that analogously (*E*)-**14** would also be favoured over (*Z*)-**14** . In the case of **13** this steric hindrance to energy transfer was operative only when using the more concentrated polymeric sensitizer, P-50. On the somewhat bulkier diene **14**, even the lightly functionalized polymer P-11 showed this effect. We therefore conclude that increasing the degree of functionalization of the polymeric benzophenones affects the photostationary *Z/E* ratios via steric hindrance of the energy transfer step. The same effect on the photostationary Z/E ratios can be obtained by means of the use of sensitizers with lower triplet energy, particularly if this energy approaches that of the phantom triplet of the alkene

[2]A referee points out that light transmittance/reflectance of the polymer beads changes on swelling in aromatic solvents, and that any change in this transmittance/reflectance ratio would affect the absorption of light and therefore the rate of the photochemical reaction. Nevertheless, the only type of reactions performed in benzene were these photoisomerizations and, although some changes could be observed in the *rates* of these reactions, the major finding was the change in the *composition* of the photostationary states, an effect which cannot be due to changes in transmittance/reflectance ratio.

Can. J. Chem. Downloaded from www.nrcresearchpress.com by 210.87.254.105 on 09/06/12
For personal use only.

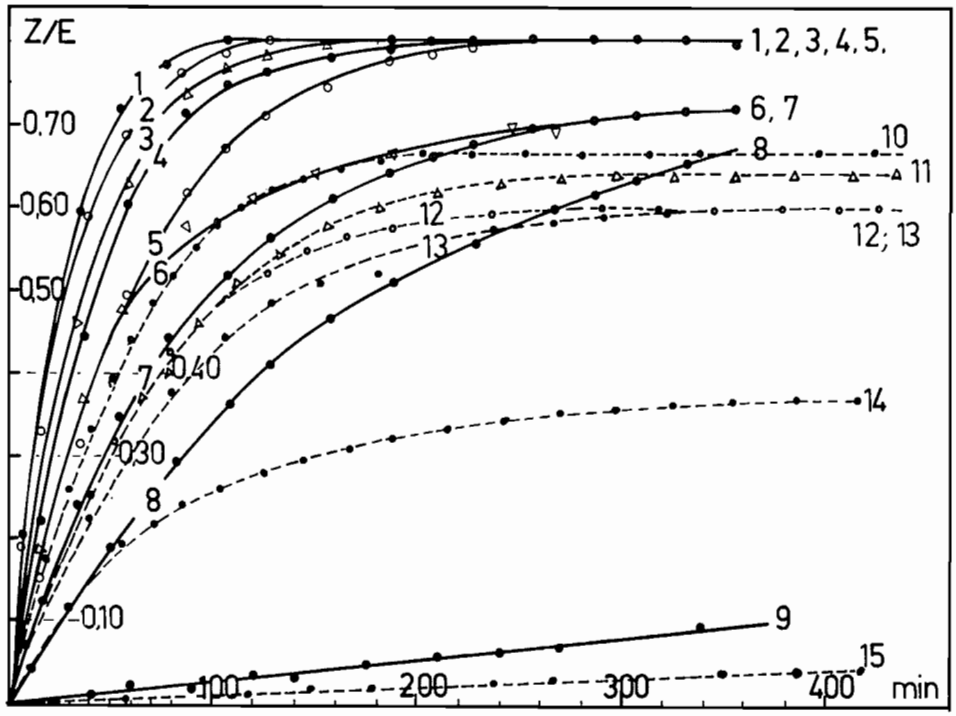

FIG. 2. $E-Z$ photoisomerization of conjugated dienes. Solid lines: Z/E ratio vs. irradiation time upon irradiation of (E)-**13** (0.20 mL, 135 mg, 2.0 mmol) in benzene (30 mL) in the presence of: curve 1, Ph_2CO (18 mg, 0.1 mmol); curve 2, P-11 (180 mg, 0.17 mequiv.); curve 3, Ph_2CO (9 mg, 0.05 mmol); curve 4, P-11 (90 mg, 0.085 mequiv.); curve 5, P-11 (90 mg) recovered from experiment 2; curve 6, P-50 (31 mg, 0.1 mequiv.); curve 7, P-50 (15 mg, 0.05 mequiv.); curve 8, P-50 (15 mg) recovered from experiment 6; curve 9, unfunctionalized polystyrene (161 mg). Dashed lines: Z/E ratio vs. irradiation time upon irradiation of (E)-**14** (462 mg, 3 mmol) in benzene (30 mL) in the presence of: curve 10, Ph_2CO (27 mg, 0.15 mmol); curve 11, P-11 (173 mg, 0.16 mequiv.); curve 12, P-29 (78 mg, 0.17 mequiv.); curve 13, P-29 (78 mg) preirradiated in benzene for 14 h; curve 14, P-50 (47 mg, 0.15 mequiv.); curve 15, no carbonyl compound.

(26). According to our results, we suggest the use of polymeric benzpohenones with an appropriate degree of functionalization as an alternative to lower triplet sensitizers for increasing the photostationary proportion of the olefin having the highest triplet energy.

(c) *The intrapolymerically sensitized* Z/E *isomerization of a resin-bound diene*[3]

The very encouraging results obtained in the isomerization of soluble dienes (above) suggested to us the feasibility of a similar intrapolymeric reaction, for which a difunctional polymer, containing both the sensitizer benzophenone and the diene units covalently linked to the same polymer lattice, was required. This type of reaction was already mentioned by us some years ago (2*a*).

There is little precedent in the literature of intrapolymeric reactions in insoluble difunctional polymers. One example is the directed mixed ester condensation of two acids (one of them non-enolizable in great excess) bound to a common polymer backbone, reported by Kraus and Patchornik in 1971 (27). Another example is the polymeric triphenylphosphine ligand containing both nickel and rhodium used by Pittman and Smith as a difunctional catalyst for sequential telomerization and hydrogenation reactions (28). In both cases the two different functional groups were introduced in a random array. A different approach was used by Leznoff and co-workers (29), who prepared difunctional polymers containing proximally located trityl and benzoyl chloride units by quenching polymeric phenyllithium with 4-benzoylphenyl ethyl carbonate and used these difunctional resins in the synthesis of insect sex attractants. In these three papers the feasibility of intrapolymeric reactions (transfer of substrate from one catalytic site to another, double binding of difunctional substrates, or actual bond formation between two different attached moieties) was demonstrated.

From the photochemical site, there is also precedent for the intramolecular energy transfer within a dichromophore, as demonstrated by Cowan and Baum for a series of phenyl ω-benzylidenealkyl ketones (30), in which light initially excited the acetophenone chromophore, which after intersystem crossing to the triplet state underwent energy transfer to the β-alkylstyrene moiety in an intramolecular process. The resulting triplet β-alkylstyrene moiety ultimately underwent Z/E isomerization (30), in what amounts to an intramolecularly sensitized photoisomerization.

We therefore tried the intrapolymeric reaction corresponding to photoisomerization of the soluble diene **14**, an excellent model which could be bound to chloromethylated resins as a benzylic ester. Two such difunctional polymers **15** were prepared by the sequence shown.

In the first step, the appropriate polymeric benzophenone (P-11 or P-29) was chloromethylated essentially as described by Merrifield for polystyrene (31), the only modification being the use of polymeric benzophenones precoordinated with $SnCl_4$ at all their carbonyl groups. The resulting chloromethylated polymers were analyzed for chlorine content and were then treated with (E)-2,2-dimethyl-3,5-hexadienoic acid **16** (24) in

[3]We gratefully thank a referee for his suggestions, particularly helpful in this section.

Can. J. Chem. Downloaded from www.nrcresearchpress.com by 210.87.254.105 on 09/06/12
For personal use only.

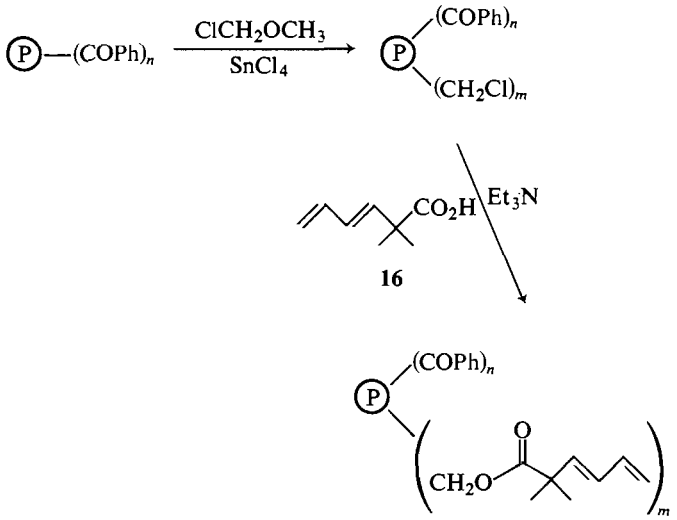

15*a* (n = 11%, m = 11%)

15*b* (n = 29%, m = 13%)

the presence of triethylamine, giving the desired difunctional polymers **15**, which were shown to be devoid of chlorine by elemental analysis. We assumed that the degree of ester functionalization of polymers **15** was the same as the chloromethyl contents of their immediate precursors. In this way, difunctional polymers **15***a* and **15***b* were prepared.

Both polymers released only the *E* diene ester (*E*)-**14** when transesterified with refluxing methanolic hydrochloric acid in dioxane (2). This shows the configurational stability of the double bond towards the transesterification conditions. On the other hand, the transesterification was far from complete, as shown by the low (<8%) yields of (*E*)-**14** obtained and by the prominent ester carbonyl absorption at 1725 cm^{-1} in the ir spectra of the recovered transesterified polymers. Other de-anchoring methods tested gave even worse results. Thus, neither sodium methoxide in anhydrous methanol – dioxane 1:1 at reflux nor sodium iodide in dioxane–acetone 1:6 at reflux, followed by treatment of the evaporated filtrate with diazomethane, gave the diene ester *E*-**14** (glc). One possible reason for the failure of the transesterification reaction could be the steric hindrance to attack at the ester carbonyl imposed by the neighbouring *gem*-dimethyl group (cf. ref. 2, where polymeric *n*-alkanoates were cleanly de-anchored by acid transesterification), coupled with instability of the diene esters **14** to prolonged heating. Actually, acid **16** is reported to polymerize spontaneously at room temperature within a few days, while it decarboxylates to 5-methylhexa-1,4-diene under pyrolytic conditions (24).

The difunctional polymers **15***a* and **15***b* were irradiated in benzene for up to 5 h. Bearing in mind the photodecarboxylation of **2** referred to above, we checked for the possible release of esters **14** or other derived compounds by glc on the filtrate after irradiation, but no peaks other than those of solvents were found. To make sure that no nonvolatile acids such as **16** had been released during irradiation, the filtrate was refluxed with methanolic hydrochloric acid in dioxane, and again glc showed the absence of esters **14**.

De-anchoring of the pendant ester groups from the irradiated difunctional polymers by refluxing them in methanolic hydrogen chloride in dioxane was quite incomplete even after long periods. However, this transesterification released not only

TABLE 1. Intrapolymerically sensitized photoisomerization of polymer-bound dienes **15**[a]

Polymer	Irradiation[b] (h)	Transesterification[c] (h)	Yield[d] (%)	Z/R ratio
15a	1	7	3.3	0.64
	1	20	5.4	0.58
	2	7	3.9	0.53
15*b*	0.5	1	2.0	0.38
	0.5	3	4.6	0.57
	0.5	5	3.7	0.54
	0.5	7	5.9	0.43
	0.5	20	6.2	0.39
	1	1	1.8	0.32
	1	3	3.3	0.57
	1	5	4.6	0.58
	1	7	5.4	0.49
	1	20	5.9	0.46
	2	5	2.9	0.89
	2	20	4.1	0.62

[a]The difunctional polymers **15** (300 mg) were irradiated in benzene (30 mL) under nitrogen bubbling.

[b]Irradiation for more than 2 h, followed by transesterification, resulted in very noisy chromatogrammes for the transesterification filtrates, in which peaks of esters **14** could no longer be resolved from background noise.

[c]The irradiated polymers were transesterified by refluxing them in a solution of 2 mL saturated methanolic HCl in 2 mL dioxane.

[d]Overall amount of esters **14** in the transesterification filtrate.

ester (*E*)-**14** but also (*Z*)-**14** (glc), undoubtedly formed from the polymeric esters **15** in a photoisomerization intrapolymerically sensitized by nearby benzophenone units. The results from these experiments are given in Table 1. From the data shown in this table we were unable to establish the photostationary Z/E ratio because of (*i*) the low yield of the transesterification step, and (*ii*) the dispersion of the experimental Z/E values. Nevertheless, the presence of (*Z*)-**14** in the transesterification mixtures proves unmistakably the occurence of the intrapolymerically sensitized $E-Z$ isomerization in what, to the best of our knowledge, appears to be the first example of such a process.

Polymeric benzophenones as photooxidizing reagents

Triplet benzophenone is known to abstract hydrogen atoms from suitable donors R—H, yielding hydroxybenzhydryl radicals $HOPh_2C\cdot$ (which ultimately couple to give benzopinacol) and radicals R· which can undergo further reactions, such as dimerization to R—R (cf. **8**) or loss of a second hydrogen atom, giving an unsaturated compound (i.e., oxidation of secondary alcohols to ketones). We have checked the photooxidizing ability of polymeric benzophenones in both types of reactions as described below.

(a) *Oxidative photodimerization of cyclohexene*

Previous work by Bradshaw (32) has shown that photolysis of benzophenone **1** in cyclohexene **5** gives oxetane **17** (13%), benzopinacol (47%), alcohol **9** (27%), and dimer **8** (6%). As mentioned above, some of these compounds were found as by-products of the photocycloaddition of **5** and **6** sensitized by **1**. We therefore investigated the products of the irradiation of **1** and its polymeric analogs in the presence of **5** but without added **6**. When using **1**, in our conditions (Pyrex equipment, 125 W lamp), the following compounds were isolated: benzopinacol (6.5%), alcohol **9** (9%), dimer **8** (26%), and aldehyde **10** (12%) (all yields relative to initial benzophenone). No oxe-

Can. J. Chem. Downloaded from www.nrcresearchpress.com by 210.87.254.105 on 09/06/12
For personal use only.

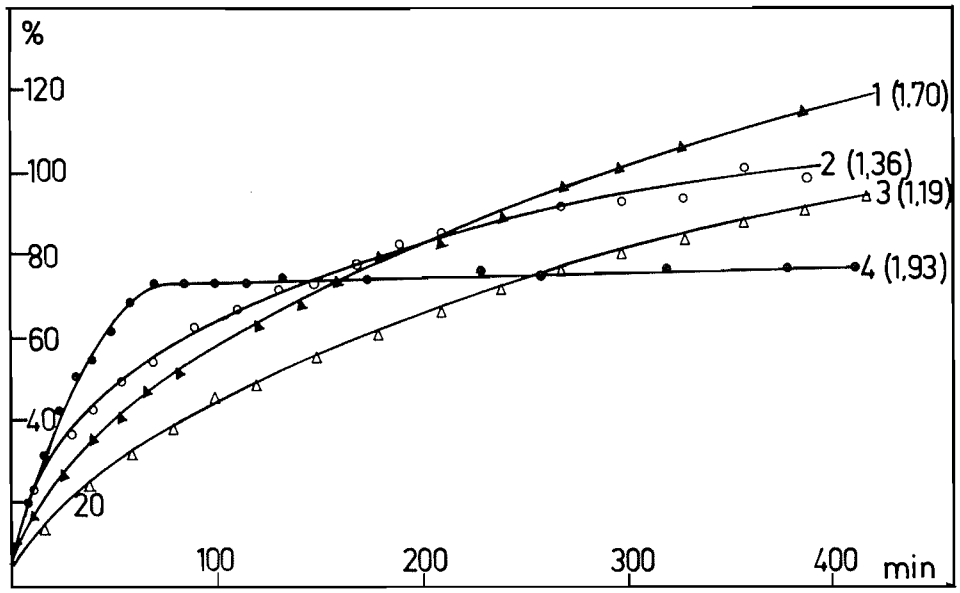

FIG. 3. Photooxidation of cyclohexanol. Yields (mmol cyclohexanone per mequiv. starting carbonyl compound) of cyclohexanone formed upon irradiation of cyclohexanol (10 mL) in CH_2Cl_2 (20 mL) in the presence of: curve 1, P-29 (0.64 g, 1.4 mequiv.); curve 2, P-11 (1.4 g, 1.3 mequiv.); curve 3, P-50 (390 mg, 1.25 mequiv.); curve 4, Ph_2CO (455 mg, 2.5 mmol). A complementary blank experiment, in which the irradiation was performed in the absence of any added carbonyl compound, gave a linear increase of the amount of cyclohexanone vs. irradiation time, with formation of 48 mg (0.5 mmol) after 7.5 h. Figures in parentheses give the mmol of cyclohexanone after 7.5 h irradiation.

tane **17** was found, although it was probably the precursor of aldehyde **10**. Formation of **8** was measured by glc as a function of irradiation time under sensitization by **1**, P-11, and P-50. The results reported elsewhere (15), showed that **1** was much more effective than P-11 or P-50 in promoting oxidative dimerization of **5** to **8**, while both polymeric benzophenones showed similar effectivities, particularly on a stoichiometric basis. The presence of acetonitrile as a cosolvent caused a decrease in the amount of **8** formed, probably due to the lower concentration of **5**.

The ir spectrum of a recovered polymer showed no carbonyl band. Instead, an associated hydroxyl band was present, and of course these recovered polymers could not be reused. This could conceivably be taken as an indication of the occurrence of a photoinduced additional cross-linking mechanism, known to take place in **2** (10), which starts by intrapolymeric hydrogen abstraction from benzylic positions, yielding macrodiradicals which ultimately collapse to a new C—C bond.

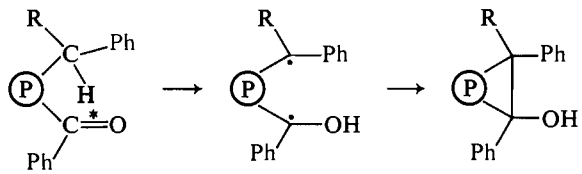

However, as described above, polymeric benzophenones themselves were shown to be rather stable towards irradiation. Finally, comparison of the ir spectra of polymers recovered from these photodimerizations and that of alcohol **9** supports the conclusion that most of the polymeric hydroxybenzhydryl radicals **18**, being unable for steric reasons to dimerize to a polymeric benzopinacol analog, collapse with cyclohexenyl radicals to end up as alcohols **19**, the polymeric analogs of **9**.

(b) *Photooxidation of secondary alcohols*

The photooxidation of secondary alcohols to ketones is one of the oldest applications of organic photochemistry. The well-

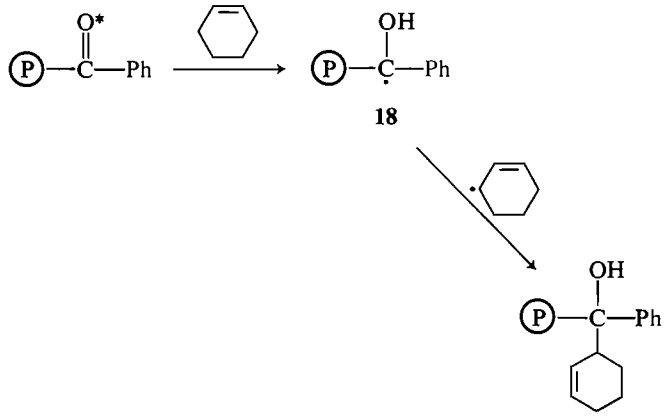

known benzopinacol mechanism of this reaction (33) requires the consumption of two moles of **1** per mole of ketone formed.

We have used polymeric benzophenone for the photooxidation of isopropyl alcohol **20** and cyclohexanol **21**. The results for **21** are given in Fig. 3, while similar results were obtained for **20**. As seen in this figure, the yield of ketone obtained, based on initial photooxidizing reagent, was higher than the 50% allowed by the stoichiometry of the benzopinacol mechanism, even after correction for the ketone formed in the blank experiments (except for the reaction between **20** and **1**, not shown in the figure, for which a 50% yield was obtained). For polymeric benzophenones, collapse of macroradicals **18** to a polymeric equivalent of benzopinacol should be sterically hindered, thus opening up the possibility of the alternative benzhydrol mechanism:

$$Ph—CO—Ph + h\nu \longrightarrow Ph—CO^*—Ph$$

$$Ph_2CO^* + R^1R^2CHOH \longrightarrow Ph_2(OH)C\cdot + R^1R^2(OH)C\cdot$$

$$Ph_2(OH)C\cdot + R^1R^2(OH)C\cdot \longrightarrow Ph_2CHOH + R^1R^2CO$$

$$Ph_2CO + R^1R^2CHOH + h\nu \longrightarrow Ph_2CHOH + R^1R^2CO$$

Can. J. Chem. Downloaded from www.nrcresearchpress.com by 210.87.254.105 on 09/06/12
For personal use only.

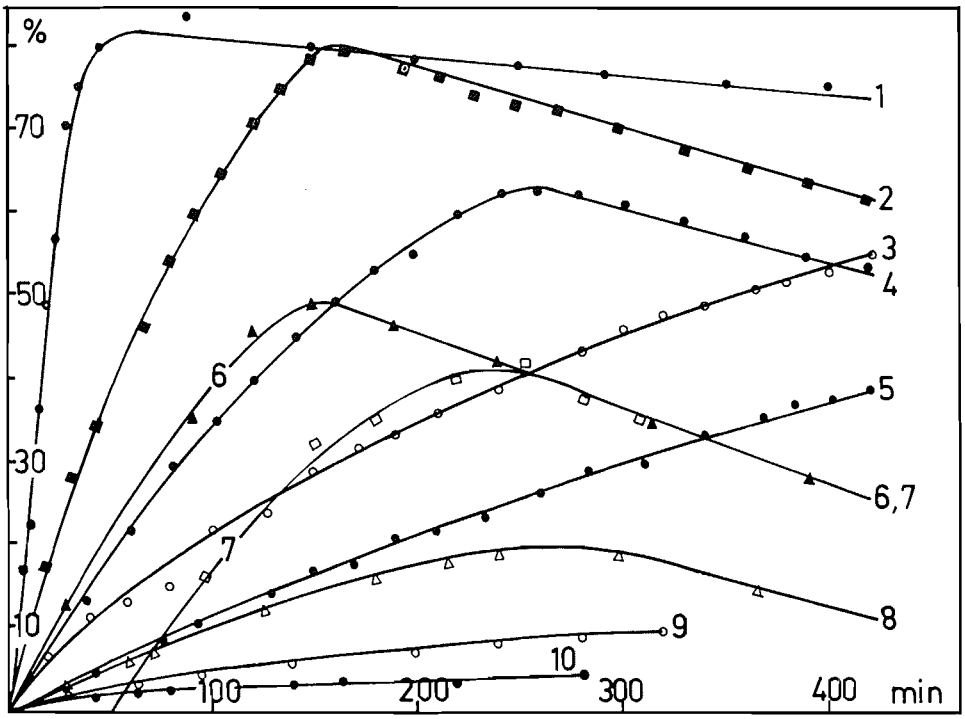

FIG. 4. Photooxygenation of 2,3-dimethyl-2-butene **22**. Yields of hydroperoxide **23** upon irradiation of **22** (0.42 mL, 340 mg, 4 mmol) in CH_2Cl_2 (30 mL) under oxygen bubbling in the presence of: curve 1, Rose Bengal (356 mg, 0.3 mmol; MeOH (ref. 36) instead of CH_2Cl_2 as solvent); curve 2, P-50 (94 mg, 0.3 mequiv.); curve 3, P-29 (156 mg) recovered from experiment 4; curve 4, P-29 (156 mg, 0.34 mequiv.); curve 5, P-11 (335 mg, 0.32 mequiv.); curve 6, P-29 (780 mg, 1.7 mequiv.; only 0.38 mL **22** used); curve 7, P-50 (94 mg, 0.3 mequiv.; 93 mg of 2,6-di-*tert*-butyl-*p*-cresol were also added; formation of **23** started after complete exhaustion of this radical inhibitor); curve 8, Ph_2CO (273 mg, 1.5 mmol); curve 9, no carbonyl compound (only 0.38 mL **22** used); curve 10, unfunctionalized polystyrene (102 mg).

This benzhydrol mechanism is known not to occur in the reaction between **20** and **1** (33). However, the results of our experiments (Fig. 3, curve 4) force us to conclude that this mechanism was operative (at least in part) in the reaction between **21** and **1**, although the second hydrogen transferred from cyclohexanol was possibly the α rather than the hydroxyl hydrogen.

The polymers recovered from these reactions no longer exhibited the carbonyl band in their ir spectra, and obviously could not be reused.

Photooxygenation of 2,3-dimethyl-2-butene

Irradiation of either benzophenone or polymeric benzophenones in solutions of 2,3-dimethyl-2-butene **22** in dichloromethane under oxygen bubbling resulted in the formation of 2,3-dimethyl-3-buten-2-yl hydroperoxide **23**, as shown by glc (Fig. 4). Unlike the singlet oxygen mediated reaction brought about by dyes such as Rose Bengal (Fig. 4, curve 1), formation of hydroperoxide **23** in the presence of **1** or its polymeric analogs is a radical reaction, inhibited by 2,6-di-*tert*-butyl-*p*-cresol (Fig. 4, curve 7). Effectivity in promoting formation of **23** increased in the order **1** ≪ P-11 < P-29 < P-50. When using soluble benzophenone **1**, most starting alkene **22** underwent a photocycloaddition with **1** (Paterno–Buchi reaction) to give 4,4-diphenyl-2,2,3,3-tetramethyloxetane **24**, a reaction which should be sterically hindered when using the polymeric benzophenones. This steric hindrance, which should be more acute for the more highly functionalized polymers, is probably responsible for the observed order of effectiveness in the formation of hydroperoxide **23**.

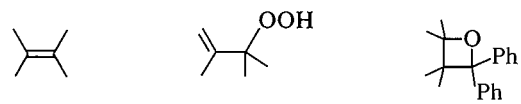

22 **23** **24**

Polymers recovered from these irradiations could be reused (Fig. 4, curve 3) and showed a broad range of carbonyl bands in their ir spectra (1770–1690 cm^{-1}), besides the expected band for the benzophenone-like carbonyl at 1665 cm^{-1}. Polystyrene is known (34) to degrade to carbonyl compounds under photooxygenation. Therefore, a similar process could originate the new carbonyl bands in the recovered polymers.

Conclusion

As seen in the preceding sections, insoluble poly-*p*-styryl phenyl ketones **3** (polymeric benzophenones) could be used as sensitizers or as photooxidizing reagents instead of benzophenone **1** itself. The sometimes noticeable differences between the results obtained with the two kinds of carbonyl compounds could be interpreted in terms of steric effects. Thus, steric hindrance to the energy transfer step, greater for the more highly functionalized polymeric benzophenones, resulted in a diminished efficiency of **3** in the photocycloaddition between cyclohexene and maleic anhydride, and in changes in the photostationary *Z*/*E* ratios from photoisomerization of olefins. On the other hand, steric hindrance of secondary reactions resulted in some cases in an increased efficiency of the polymeric benzophenones. For instance, we can quote that steric hindrance of formation of the polymeric

Can. J. Chem. Downloaded from www.nrcresearchpress.com by 210.87.254.105 on 09/06/12
For personal use only.

analog of benzopinacol went along with an increase in the yield of ketones for the photooxidation of secondary alcohols.

Experimental

The polystyrene used was a (98:2) copolymer of styrene–DVB, 200–400 mesh, purchased from Eastman–Kodak. Prior to its use, polystyrene (150 g) was sequentially washed with: ethanol–dioxane–water (30:4:1, v/v/v), 5 L; ethanol, 300 mL; ethanol–dioxane (2:1), 300 mL; ethanol–dioxane (1:1), 300 mL; dioxane, 1 L; dioxane–ether (1:1), 500 mL; dioxane–ether (1:2), 500 mL; and ether, 1 L. Drying (80°C, 2 Torr) to constant weight (149.5 g) over P_2O_5 gave a product with the following elemental analysis: C 92.34, H 7.99%.

Irradiations were performed in a small convential photochemical reactor, consisting of a three-necked 100 mL reaction vessel and a water-jacketed Pyrex immersion well, using a medium-pressure 125 W mercury lamp (Philips HPK-125), usually under a nitrogen atmosphere and with magnetic stirring. Except for irradiations under oxygen bubbling, nitrogen was bubbled through the solutions or suspensions to be irradiated for 30 min before switching the lamp on. For very volatile substrates, instead of nitrogen bubbling through the stirred mixtures, a nitrogen stream was passed very slowly over the reacting mixtures during irradiation. Except where otherwise stated, water was used for refrigeration of the immersion well jacket. Irradiations were stopped for taking aliquots (~50 μL) and resumed immediately after.

Gas–liquid chromatographic analyses were performed on a Perkin–Elmer Sigma 10 instrument, under fid detection, using the internal standard method. Results are the mean values of at least three nondeviating injections.

Polymeric benzophenones

P-11

To a stirred slurry of polystyrene (30.4 g, 291 mequiv.) and $AlCl_3$ (6.0 g, 45 mmol) in CS_2 (400 mL) was added dropwise a solution of benzoyl chloride (4.84 g, 34 mmol) in CS_2 (250 mL) over a 7 h period. After stirring overnight and filtering, the crude benzoylated polymer was washed with: 0.5 *M* HCl – dioxane (5:2), 4 L; water–dioxane (4:1), 4 L; water–dioxane (3:1), 1.5 L; water–acetone–dioxane (3:1:1), 1.5 L; water–acetone–dioxane (1:3:1), 2 L; acetone–dioxane (1:1), 500 mL; methanol–acetone–dioxane (1:1:1), 500 mL; methanol–dioxane (2:1), 500 mL; methanol–dioxane (1:2), 500 mL; methanol–dioxane (1:3), 500 mL; dioxane, 500 mL; dioxane–ether (2:1), 500 mL; dioxane–ether (1:1), 500 mL; dioxane–ether (1:2), 500 mL; dioxane–ether (1:3), 500 mL; ether, 1 L. The washed polymer was dried (80°C, 2 Torr) over P_2O_5 until constant weight. Yield, 33.0 g; ir (KBr): 1655 cm^{-1}. Elemental analysis: C 90.18, H 7.42%, Cl negative.[4]

Oxime of P-11

A suspension of P-11 (300 mg) in a solution of $NH_2OH \cdot HCl$ (3 g) and NaOH (5.6 g) in a mixture of ethanol (40 mL), dioxane (25 mL), and water (2 mL) was refluxed for 3 h. The mixture was then poured into 200 mL of a (1:1) mixture of 2 *N* HCl and dioxane containing 50 g of crushed ice, stirred for 30 min, and filtered. This washing was repeated twice. The acid-washed polymeric oxime was then washed with the sequence of solvents described above for the washing of P-11, from water–dioxane to ether, using 200 mL of each solvent or solvent mixture. Drying (80°C, 2 Torr) over P_2O_5 afforded 280 mg of the oxime of P-11. Infrared (KBr): 3700–3150 (broad) and 1600 cm^{-1}. Elemental analysis: C 90.08, H 7.22, N 1.31%, Cl negative.[4]

P-29 was prepared from 30.4 g (291 mequiv.) polystyrene and 15 g (112 mmol) of $AlCl_3$ in 400 mL CS_2 by addition of 12.1 g PhCOCl (86 mmol) in 200 mL CS_2. Yield: 37.5 g; ir (KBr): 1655 cm^{-1}. Elemental analysis: C 90.05, H 6.87, Cl negative.[4] Its oxime was prepared from 500 mg of P-29. Yield, 490 mg; ir (KBr): 3700–3150 (bd) and 1600 cm^{-1}. Elemental analysis: C 87.07, H 6.87, N 3.06%, Cl negative.[4]

P-50 was prepared from 26.0 g (249 mequiv.) polystyrene and 17 g (127 mmol) $AlCl_3$ in 250 mL CS_2 by addition of 20 g (142 mmol) PhCOCl in 125 mL CS_2. Yield, 38.0 g; ir (KBr): 1655 cm^{-1}. Elemental analysis: C 88.40, H 6.47%, Cl negative.[4] Its oxime was prepared from 320 mg of P-50. Yield, 310 mg; ir (KBr): 3700–3150 (bd) and 1600 cm^{-1}. Elemental analysis: C 84.19, H 6.68, N 4.23%, Cl negative.[4]

Stability towards irradiation

(a) A stirred suspension of P-29 (1.50 g, 3.29 mequiv.) in benzene (30 mL) was irradiated for 15 h under nitrogen. After filtration, the polymer was washed with benzene, benzene–ether, and ether and finally dried (80°C, 1 Torr) over P_2O_5 to constant weight (1.45 g). Infrared (KBr): 3600–3450 (very weak), other bands as in P-29. Evaporation of combined filtrate and washings gave 1.5 mg of an oil which , analyzed by glc, showed only peaks of retention time much higher than benzophenone. The ir spectrum of this oil, however, closely resembled that of benzophenone.

(b) Irradiation of P-50 (468 mg, 1.5 mequiv.) in acetonitrile (30 mL) for 10 h under nitrogen gave 430 mg of washed and dried polymer, similar to that described above, while the combined filtrates and washings showed no peaks other than those of the solvents by glc.

Photocycloaddition of cyclohexene and maleic anhydride

Materials

Cyclohexene was stirred overnight over neutral alumina, then refluxed over sodium for 24 h in a nitrogen atmosphere, and finally distilled over sodium under a slow nitrogen stream, bp 83°C. Acetonitrile was distilled twice over P_2O_5, bp 81°C. Maleic anhydride was recrystallized from chloroform and sublimed (70°C/14 Torr) before use, mp 58°C. Cycloadducts **7**, required as standards for quantitative glc determinations, were independently prepared following the method of Robson *et al.* (19).

Irradiations

The compositions of the mixtures to be irradiated are given in the caption of Fig. 1.

Analysis

Aliquots were analyzed by glc, using a 2 m × 1/8 in. column packed with 3% SE-30 on Chromosorb W-AW-DMCS (80–100 mesh) at 80–164°C (rate 3.5°C min^{-1}), then at 164–250°C (rate 10°C min^{-1}), and then 250°C (isotherm.) for 6 min, with nitrogen (25 mL min^{-1}) as the carrier gas. The internal standard used was diethyl adipate. Peaks for the individual stereoisomers of cycloadducts **7** could not be resolved completely, and therefore the overall envelope of cycloadducts **7** was integrated as a whole.

By-products

A peak from by-product **8** was detected in all the irradiations performed. Other peaks, from by-products **9** and **10**, were detected in irradiations in which benzophenone was used as sensitizer. The isolation and identification of these by-products is described under oxidative photodimerization of cyclohexene (see below).

Sensitized E–Z *photoisomerization of conjugated dienes*

Materials

(*E*)-1,3-pentadiene was purchased from Merck, showed a single peak in glc, and was used without further purification. Methyl (*E*)-2,2-dimethyl-3,5-hexadienoate was prepared following the procedure of Bigley and Weatherhead (24) and showed a single peak in glc. Thiophene-free benzene was used.

Irradiations

The compositions of the mixtures to be irradiated are given in the caption of Fig. 2.

Analysis

For 1,3-pentadiene irradiations, aliquots were analyzed by glc, using a 5.5 m × 1/8 in. column packed with 20% oxydipropionitrile

[4]A 15–20 mg sample was analyzed. Lower limit of detection is ≃ 0.5% Cl.

Can. J. Chem. Downloaded from www.nrcresearchpress.com by 210.87.254.105 on 09/06/12
For personal use only.

Can. J. Chem. Downloaded from www.nrcresearchpress.com by 210.87.254.105 on 09/06/12
For personal use only.

on Chromosorb P (80–100 mesh) at 70°C (isotherm.), with nitrogen (5 mL min^{-1}) as the carrier gas. The internal standard method was not used, since only *Z*/*E* ratios were determined. Equal response factors were assumed for both isomers. For methyl 2,2-dimethyl-3,5-hexadienoate irradiations, glc analyses were performed on a 2 m × 1/8 in. column, packed with 10% Carbowax 20M on Chromosorb W-HP (80–100 mesh) at 60–150°C (rate 3°C min^{-1}), with nitrogen (25 mL min^{-1}) as the carrier gas. No internal standard was used, since only *Z*/*E* ratios were determined. Equal response factors were assumed for both isomers.

Product identification

With both types of (*E*)-diene substrates, the peaks assigned to the *Z* isomers in glc analysis were confirmed by gc/ms to correspond to isomers of the starting materials.

Intrapolymerically sensitized E–Z *photoisomerization of difunctional polymers* ***15****a and* ***15****b*

Chloromethylation of P-29

To a stirred suspension of 2 g (4.4 mequiv.) of P-29 in anhydrous $CHCl_3$ (25 mL), kept at 0°C, was added 0.45 mL (1.0 g, 3.8 mmol) of $SnCl_4$ and, after 1 h, a solution (at 0°C) of 0.2 mL (0.44 g, 1.7 mmol) of $SnCl_4$ in 1.3 mL (1.4 g, 17 mmol) of methyl chloromethyl ether was added dropwise. After stirring at 0°C for another 30 min, the polymer was filtered and washed three times with 3 *N* HCl – dioxane (1:3), followed by the sequence described under benzoylation of polystyrene (see above). The polymer was then dried (100°C, 2 Torr) over P_2O_5 until constant weight. Yield, 2.1 g. Elemental analysis: C 87.15, H 6.68, 3.17%.

Chloromethylation of P-11 (2.0 g, 2.1 mequiv.) by methyl chloromethyl ether (1.3 mL, 1.4 g, 17 mmol) and $SnCl_4$ (0.4 mL, 0.9 g, 3.4 mmol overall) as above yielded 1.95 g of chloromethylated P-11. Elemental analysis: C 87.73, H 6.78, Cl 3.14%.

Difunctional polymer ***15****a*

A mixture of chloromethylated P-11 (1.4 g, 1.2 mequiv. CH_2Cl), (*E*)-2,2-dimethyl-3,5-hexadienoic acid **16** (21) (1.2 g, 8.6 mmol), and 1.4 mL (10 mmol) triethylamine was refluxed for 44 h. After filtration and washing as described above for the chloromethylated polymers, the product was dried (100°C, 1 Torr) over P_2O_5 for 20 h. Yield, 1.45 g; ir (KBr): 1725 and 1655 cm^{-1}. Elemental analysis: Cl negative, N negative.

Difunctional polymer ***15****b* was prepared similarly from 1.9 g (1.7 mequiv. CH_2Cl) of chloromethylated P-29. Yield: 1.9 g; ir (KBr): 1725 and 1655 cm^{-1}. Elemental analysis: Cl negative, N negative.

Transesterification of difunctional polymers ***15***

A suspension of **15***a* (300 mg, 0.26 mequiv. ester) in 2 mL dioxane and 2 mL saturated methanolic HCl was refluxed for 20 h. Aliquots taken after 7 h and 20 h were neutralized by addition of solid $NaHCO_3$, filtered, and analyzed for their contents in esters **14** by means of glc (see above, under sensitized *E*–*Z* photoisomerization of conjugated dienes, for the chromatographic conditions). Only the peak of (*E*)-**14** was detected. The transesterification yields measured using diethyl adipate as internal standard were 4% (7 h) and 7% (20 h). The remaining polymer was washed and dried (70°C, 1 Torr) to constant weight (280 mg), and showed ir bands (in KBr) at 1725 and 1655 cm^{-1}. The same treatment, applied on **15***b*, gave transesterification yields of 3% (1 h reflux), 7% (5 h), and 6% (20 h), without a peak for (*Z*)-**14**.

Irradiation of ***15***

A stirred suspension of **15***a* (300 mg) in benzene (30 mL) was irradiated under nitrogen bubbling for 1 h (longer irradiation resulted in the release of smaller amounts of esters **14** after transesterification). After filtering and washing (the washings were shown by glc to be devoid of esters **14**), the irradiated polymer was transesterified as described above, and the amount of ester (*E*)- and (*Z*)-**14**, as well as their ratio, was determined by glc. The results are given in Table 1, together with the conditions and results of other irradiations of difunctional polymers **15**.

Oxidative photodimerization of cyclohexene

Reaction of cyclohexene ***5*** *and benzophenone* ***1*** *under irradiation*

A stirred solution of **1** (2 g, 11 mmol) in cyclohexene (30 mL, 24.3 g) was irradiated for 4 h. On addition of hexane, benzopinacol (260 mg, 6.5%) crystallized out (mp 185–186°C). After filtration and removal of solvents the residue was chromatographed on silica gel, giving the following fractions.

Bi-2-cyclohexen-1-yl ***8****, eluted with hexane*

Yield 0.23 g (26% yield given according to the stoichiometry: 2 moles of **1** reacting with 2 moles of **5** to give one mole of **8**; the yield quoted is relative to initial **1**). The compound showed a single peak in glc, and showed spectra identical to those described by Strausz *et al.* (35).

2-Cyclohexen-1-yldiphenylmethanol ***9****, eluted with hexane–* CH_2Cl_2 *(3:1)*

Yield, 269 mg (9%). Its nmr spectrum was identical to that described by Bradshaw (32).

7,7-Diphenyl-6-heptenal ***10****, eluted with hexane–* CH_2Cl_2 *(1:1)*

Yield, 350 mg (12%); oil; ir (film): 3090, 3060, 2975, 2900, 2750, 1720, 1600, 1495, 1450, and 750 cm^{-1}; ^{1}Hmr ($CDCl_3$) δ: 1.3–2.7 (m, 8H), 6.1 (t, J = 7 Hz, 1H), 7.3 (m, 10H), and 9.85 (t, J = 1.5 Hz, 1H); ms at 70 eV, *m*/*e* (%): 264 (M, 26), 246 (7), 236 (17), 193 (93), 115 (100), 91 (44), and lower *m*/*e*.

Oxidative photodimerization of ***5*** *using polymeric benzophenones*

A stirred suspension of P-11 (2.7 g, 2.6 mequiv.) in cyclohexene (30 mL) was irradiated under nitrogen for 10 h. The amount of **8** formed was measured by analyzing aliquots by glc, with diethyl adipate as internal standard, under the chromatographic conditions described above for determination of cycloadducts **7**. The results were given in a preliminary communication (15).

Photooxidation of secondary alcohols

A suspension of P-11 (2.8 g, 2.7 mequiv.) in a solution of isopropyl alcohol or cyclohexanol (10 mL) in CH_2Cl_2 (20 mL) was irradiated for 7.5 h. The amount of ketone formed was measured by glc. Analytical conditions used when isopropyl alcohol was the substrate: 2 m × 1/8 in. column packed with 10% Carbowax 20M on Chromosorb W-HP (80–100 mesh), with nitrogen (8 mL min^{-1}) as the carrier gas, at 60°C (isotherm., 1 min), then 60 to 90°C (rate 5°C min^{-1}). Toluene was used as the internal standard. Analytical conditions used when cyclohexanol was the substrate: same column; nitrogen flow rate, 15 mL min^{-1}; temperatures: 60°C for 1 min, then 60–70°C (rate 5°C min^{-1}), then 70–110°C (rate 20°C min^{-1}), then 110°C for 3 min, then 110–150°C (rate 40°C min^{-1}), and finally 150°C for 3 min.

Photooxygenation of 2,3-dimethyl-2-butene ***22***

A stirred suspension of P-50 (95 mg, 0.3 mequiv.) in a solution of **22** (340 mg, 4.0 mmol) in CH_2Cl_2 (30 mL) was irradiated under oxygen bubbling for 7 h. Aliquots were analyzed by glc, using a 2 m × 1/8 in. column packed with 3% SE-30 on Chromosorb W-AW-DMCS (80–100 mesh), with nitrogen (5 mL min^{-1}) as the carrier gas, at 40°C for 2 min, then 40–90°C (rate 40°C min^{-1}), then 90°C for 3 min. Hydroperoxide **23**, independently prepared by a published procedure (36), was determined quantitatively, using toluene as the internal standard, for monitoring the progress of the reaction. Results are given in Fig. 4, as well as the compositions and results of other irradiations performed. In operations in which benzophenone **1** was used (Fig. 4, curve 8), a very late peak (beyond benzophenone), integrating for most of the reaction mixture, was identified (gc/ms) as 4,4-diphenyl-2,2,3,3-tetramethyloxetane **24** by comparison with the published mass spectrum (37) of this compound.

Acknowledgement

A grant from Plan de Formación del Personal Investigador, Ministerio de Educación y Ciencia, Spain (to J.L.B.) is gratefully acknowledged.

1. P. HODGE and D. C. SHERRINGTON (*Editors*). Polymer-supported

reactions in organic synthesis. Wiley, New York. 1980.
2. (*a*) P. BOSCH, J. FONT, A. MORAL, and F. SÁNCHEZ-FERRANDO. Tetrahedron, **34**, 947 (1978); (*b*) P. BOSCH, J. FONT, and F. SÁNCHEZ-FERRANDO. An. Quím. **75**, 392 (1979).
3. (*a*) N. C. DENO, R. FISHBEIN, and C. PEARSON. J. Am. Chem. Soc. **92**, 1451 (1970); (*b*) N. C. DENO, R. FISHBEIN, and J. C. WYCKOFF. J. Am. Chem. Soc. **92**, 5274 (1970); (*c*) C. EDEN and Z. SHAKED. Israel J. Chem. **13**, 1 (1975).
4. (*a*) M. CALVIN, I. WILLNER, C. LAANE, and J. W. OTVOS. J. Photochem. **17**, 195 (1981); (*b*) M. S. TUNULI and J. H. FENDLER. J. Am. Chem. Soc. **103**, 2507 (1981).
5. P. A. LEERMAKERS and F. C. JAMES. J. Org. Chem. **32**, 2898 (1967).
6. E. C. BLOSSEY and D. C. NECKERS. Tetrahedron Lett. 323 (1974).
7. N. ASAI and D. C. NECKERS. J. Org. Chem. **45**, 2903 (1980).
8. S. N. GUPTA, L. THIJS, and D. C. NECKERS. Macromolecules, **13**, 1037 (1980).
9. A. P. SCHAAP, A. L. THAYER, E. C. BLOSSEY, and D. C. NECKERS. J. Am. Chem. Soc. **97**, 3741 (1975).
10. D. C. NECKERS. Chemtech, **8**, 108 (1978).
11. R. R. HAUTALA, J. LITTLE, and E. SWEET. Sol. Energy, **19**, 503 (1977).
12. F. CRAMER and H. KÖSTER. Angew. Chem. Int. Ed. Engl. **7**, 473 (1968).
13. G. L. SOUTHARD, G. S. BROOKE, and J. M. PETEE. Tetrahedron Lett. 3505 (1969).
14. M. KAWANA and S. EMOTO. Tetrahedron Lett. 4855 (1972).
15. J. L. BOURDELANDE, J. FONT, and F. SÁNCHEZ-FERRANDO. Tetrahedron Lett. **21**, 3805 (1980).
16. J. L. BOURDELANDE, J. FONT, and F. SÁNCHEZ-FERRANDO. Polym. Photochem. **2**, 383 (1982).
17. A. I. VOGEL. A textbook of practical organic chemistry. 3rd ed. Longman, London. 1965. p. 733.
18. S. H. MERRILL, C. C. UNRUH, and E. M. ROBERTSON. U.S. Patent No. 2, 831,768 (Apr. 22, 1958); Chem. Abstr. **52**, 14400g (1958).
19. R. ROBSON, P. W. GRUBB, and J. A. BARLTROP. J. Chem. Soc. 2153 (1964).
20. (*a*) G. O. SCHENCK, W. HARTMANN, and R. STEINMETZ. Chem. Ber. **96**, 498 (1963); (*b*) G. O. Schenck, J. Kuhls, and S. H. KRAUCH. Justus Liebigs Ann. Chem. **693**, 20 (1966).
21. D. BRYCE-SMITH. Pure Appl. Chem. **16**, 47 (1968).
22. P. HRDLOVIC AND I. LUKAC. J. Polymer Sci. Symp. **47**, 319 (1974).
23. (*a*) D. F. Evans. J. Chem. Soc. 1351 (1957); (*b*) G. S. HAMMOND, N. J. TURRO, and P. A. LEERMAKERS. J. Phys. Chem. **66**, 1144 (1962).
24. D. B. BIGLEY and R. H. WEATHERHEAD. J. Chem. Soc. Perkin Trans. 2, 704 (1976).
25. W. G. HERKSTROETER, L. B. JONES, and G. S. HAMMOND. J. Am. Chem. Soc. **88**, 4777 (1966).
26. G. S. HAMMOND, J. SALTIEL, A. A. LAMOLA, N. J. TURRO, J. S. BRADSHAW, D. O. COWAN, R. C. COUNSELL, V. VOGT, and C. DALTON. J. Am. Chem. Soc. **86**, 3197 (1964).
27. M. A. KRAUS and A. PATCHORNIK. J. Am. Chem. Soc. **93**, 7325 (1971).
28. C. U. PITTMAN, JR. and L. R. SMITH. J. Am. Chem. Soc. **97**, 1749 (1975).
29. T. M. FYLES, C. C. LEZNOFF, and J. WEATHERSTON. Can. J. Chem. **56**, 1031 (1978).
30. D. O. COWAN and A. A. BAUM. J. Am. Chem. Soc. **92**, 2153 (1970); **93**, 1153 (1971).
31. R. B. MERRIFIELD. J. Am. Chem. Soc. **85**, 2149 (1963).
32. J. S. BRADSHAW. J. Org. Chem. **31**, 237 (1966).
33. G. S. HAMMOND and N. J. TURRO. Science, **142**, 1541 (1963).
34. B. RANBY and J. LUCKI. Pure Appl. Chem. **52**, 295 (1980).
35. O. P. STRAUSZ, G. J. A. KENNEPOHL, F. X. GARNEAU, T. DOMINH, B. KIM, S. VALENTY, and P. S. SKELL. J. Am. Chem. Soc. **96**, 5723 (1974).
36. G. O. SCHENCK and K. H. SCHULTE-ELTE. Justis Liebigs Ann. Chem. **618**, 185 (1958).
37. G. JONES II and L. P. MCDONNELL. Tetrahedron Lett. 4633 (1975).

Can. J. Chem. Downloaded from www.nrcresearchpress.com by 210.87.254.105 on 09/06/12
For personal use only.

Ligand exchange in the rhenium–quinone radical complexes: kinetics and mechanism

KATHERINE A. M. CREBER AND JEFFREY K. S. WAN
Department of Chemistry, Queen's University, Kingston, Ont., Canada K7L 3N6

Received July 12, 1982

This paper is dedicated to Professor Harry E. Gunning on the occasion of his 65th birthday

KATHERINE A. M. CREBER and JEFFREY K. S. WAN. Can. J. Chem. **61**, 1017 (1983).

The substitution of the labile carbonyl groups of the rhenium–quinone radical complexes by nitrogen, phosphorus, arsenic, antimony, and oxygen donor ligands was observed. The extent of substitution was evidenced from esr spectra, while the configuration of the ligands about the rhenium centre was deduced from infrared absorption spectra. Rate data was obtained for the mono-substitution reaction which can be best interpreted in terms of concurrent major dissociative (D) and minor dissociative interchange (I_d) pathways. The relative thermodynamic stability of a number of substituted rhenium–quinone radical complexes was also investigated by competitive ligand exchange reactions.

KATHERINE A. M. CREBER et JEFFREY K. S. WAN. Can. J. Chem. **61**, 1017 (1983).

On a observé la substitution des groupes carbonyles labiles des complexes radicalaires de rhénium–quinone par des ligands donneurs d'azote, de phosphore, d'arsenic, d'antimoine et d'oxygène. On a mis en évidence le degré de substitution à l'aide des spectres de rpe tandis qu'on a déduit la configuration des ligands autour du centre rhénium à partir des spectres d'absorption infrarouge. On a obtenu les données de vitesse pour la réaction de mono-substitution que l'on peut avantageusement interpréter en fonction d'un schéma d'interchange dissociatif principal D et d'un interchange dissociatif secondaire (I_d) concurrents. On a également étudié la stabilité thermodynamique d'un certain nombre de complexes radicalaires de rhénium–quinone substitués en faisant appel à des réactions compétitives d'échange de ligand.

[Traduit par le journal]

Can. J. Chem. Downloaded from www.nrcresearchpress.com by 210.87.254.6 on 09/06/12
For personal use only.

Introduction

Transition metal organometallic free radicals have received a considerable amount of attention in recent years, as they are known to have catalytic applications (1–3), as well as their potential to act as models for biological systems (4–7). The difficulty in studying these radicals is that they are usually very unstable and short-lived, making them very difficult to isolate. For example, the only 17-electron species for which a solid state crystal structure has been reported is $Mn(CO)(\eta^4\text{-}C_4H_6)$ (8).

Transition metal carbonyl radicals are easily formed by homolysis of metal–metal bonds, which can readily be accomplished by photolysis. These radical complexes are known to be very labile toward substitution (9). Hence, this type of organometallic radical complex offers an excellent opportunity for the study of organometallic radical reactions. In particular, the manganese and rhenium complexes have been examined by several groups with the aim of establishing a general mechanism for the substitution reactions of metal carbonyl radical complexes. While early controversy centered around the debate of a perfectly dissociative or an associative mechanism (10–14), recent consensus (15–17) emerged indicates that both mechanisms can be concurrently operative. Nevertheless, many of the metal carbonyl radicals are not totally stable in solution and they cannot be isolated for kinetic studies in the pure form. Thus, the recombination of the metal carbonyl radicals must be taken into consideration in the overall kinetic schemes (15).

In our earlier development of the HPLC-esr techniques (18, 19), we have found that *ortho*-quinones uniquely form very stable radical complexes with the rhenium carbonyls which can be isolated by the HPLC-esr technique for spectroscopic studies. However, a similar experiment with manganese carbonyls produced the radical complexes which decomposed while being eluted through a HPLC column. Since the rhenium carbonyl – quinone radical complexes undergo slow substitution reactions with a number of organometal donors (20–22), it follows that one could design kinetic experiments using the pure radical complexes. Furthermore, we have demonstrated (20, 21) that the ligand substitution reactions involving optically active organometals and/or optically active quinones led to the isolation of some interesting optically active radical complexes. These reactions are potentially highly stereo-specific and enantio-selective, it is important that some kinetics and mechanistic information of these rhenium carbonyl – quinone radical complexes involved in the substitution reactions be delineated.

Experimental

The HPLC-esr instrumentation has been previously described (18, 19).

The infrared absorption spectra were recorded on a Perkin-Elmer 598 spectrometer. The samples were run as chloroform solutions in NaCl cells having a path length of 0.25 cm.

A Perkin-Elmer 552 spectrometer was used for the kinetic runs. A specially constructed temperature accessory held the averaged sample temperature constant to ±0.1°C, within the temperature range 20–50°C. For the kinetic runs, the wavelength maximum of the DTBQ$^{\bullet}$—$Re(CO)_4$ radical complex (λ_{max} = 510 nm) was monitored at regular time intervals and the absorbance readings recorded.

The ligands triphenylphosphine (Aldrich), triphenylarsine (Aldrich), triphenylantimony (Aldrich), triphenylphosphite (Aldrich), triethylamine (Baker), pyridine (BDH), and dimethylsulphoxide (Baker) were found to be spectroscopically pure and were used as received. 3,5-Di-*t*-butyl-*o*-quinone was supplied by Aldrich and decacarbonyldirhenium was supplied by Strem.

Results and discussion

1. Kinetics and mechanism of the CO substitution reactions of DTBQ$^{\bullet}$—Re(CO)$_4$

The kinetics of the following reaction were investigated

$$[1]\quad DTBQ^{\bullet}\text{—}Re(CO)_4 + L \xrightarrow[\text{benzene}]{\text{dark}} DTBQ^{\bullet}\text{—}Re(CO)_3L + CO$$

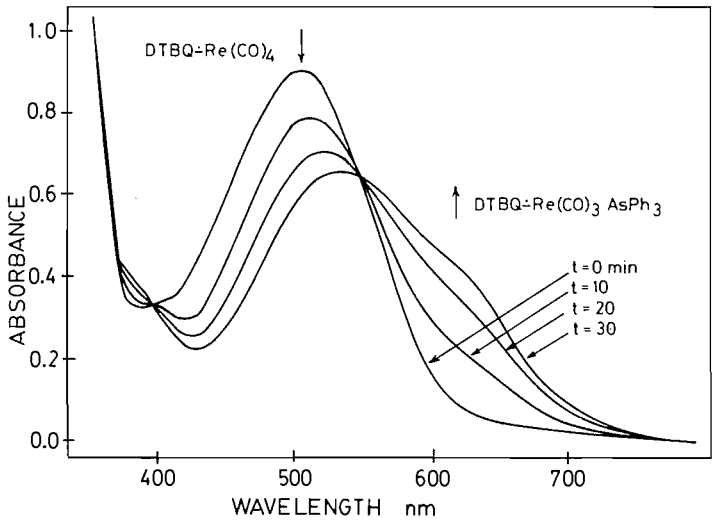

FIG. 1. Visible absorption spectrum of DTBQ—$^{\bullet}$—Re(CO)$_4$ in benzene at 25°C before and after the addition of a ten-fold excess of $AsPh_3$.

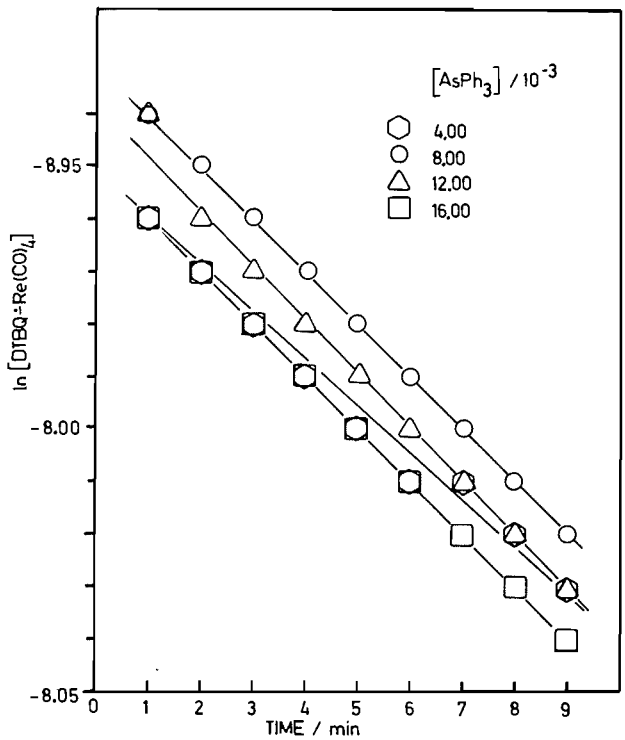

FIG. 2. Plot of ln [DTBQ—$^{\bullet}$—Re(CO)$_4$] vs. time for the reaction of DTBQ—$^{\bullet}$—Re(CO)$_4$ with $AsPh_3$ in benzene at 25°C.

where L represents PPh_3, $AsPh_3$, $SbPh_3$, and $P(OPh)_3$. The reaction was studied under pseudo-first order conditions, with the ligand (L) concentration being at least ten-fold in excess. The progress of the reaction was followed by visible absorption spectroscopy. In particular, the band at 510 nm, which corresponds to the $\pi \rightarrow \pi^*$ transition of the unsubstituted complex (18), was monitored at regular time intervals. Figure 1 shows a typical run where the entering ligand was $AsPh_3$.

The rate equation for reaction [1] can be written as a two-term rate law (15):

[2] Rate = $(k_1 + k_2[L])$[DTBQ—$^{\bullet}$—Re(CO)$_4$]

The rate constant k_1 is related to the first-order dissociative step while the rate constant k_2 describes the concurrent dissociative interchange process between the radical complex and the ligand. In our systems using pure DTBQ—$^{\bullet}$—Re(CO)$_4$ as well as the ligands to be substituted, it is possible to vary *independently* the initial concentrations of both reactants and to monitor the concentration of the DTBQ—$^{\bullet}$—Re(CO)$_4$ independently as a function of time.

For pseudo-first order treatment (which is valid for an initial concentration of the ligand being much higher than the radicals), eq. [2] can be rewritten as

[3] Rate = k'[DTBQ—$^{\bullet}$—Re(CO)$_4$]

where $k' = (k_1 + k_2[L])$. In our experiments, both the initial concentration of the radical complex, $[DTBQ—^{\bullet}—Re(CO)_4]_0$, and the instant concentration [DTBQ—$^{\bullet}$—Re(CO)$_4$], are monitored by either or both optical and esr measurements.

A plot of ln [DTBQ—$^{\bullet}$—Re(CO)$_4$], vs. time for the reaction with $AsPh_3$ at 25°C is shown in Fig. 2. The value of k' (slope = $-k'$) obtained at different experimental conditions are given in Table 1. A plot of log k' vs. log [L] indicates that within the experimental range of ligand concentrations the value of k' does not vary with [L]. Thus, it can be concluded that the reaction is first order, under the experimental conditions.

In order to obtain an approximate parameter for the Arrhenius activation energy, we assumed that the pre-exponential factor and the activation energy are constant over the experimental temperature range. The Arrhenius plots obtained for the four radical complexes studied are shown in Fig. 3 and the data obtained from the least squares analysis are given in Table 2. The k' values used in the plots are the average of all ligand concentrations at the particular temperature.

The thermodynamic parameters $\Delta H^{\ddagger}$ (enthalpy of activation), $\Delta S^{\ddagger}$ (entropy of activation), and $\Delta G^{\ddagger}$ (free energy of activation), were obtained from the following equations:

[4] $E_a = \Delta H^{\ddagger} + RT$

[5] $A = \frac{ekT}{h} \exp \frac{(\Delta S^{\ddagger})}{R}$

[6] $\Delta G^{\ddagger} = \Delta H^{\ddagger} - T\Delta S^{\ddagger}$

Can. J. Chem. Downloaded from www.nrcresearchpress.com by 210.87.254.6 on 09/06/12
For personal use only.

TABLE 1. Pseudo-first order kinetic data from the least squares fit of ln [DTBQ—$\overset{\bullet}{}$—Re(CO)$_4$] vs. time (min)

Ligand	Temperature /K	Concentration of ligand/10^{-3} M	Slope /10^{-3} min^{-1}	Standard deviation/10^{-3}	Correlation coefficient	k/10^{-4} s^{-1}
PPh_3	298.2	4.29	−7.05	0.60	−0.9997	1.2
		8.58	−8.27	1.25	−0.9989	1.4
		12.87	−9.57	0.78	−0.9997	1.6
		17.16	−12.1	1.28	−0.9996	2.0
	307.2	3.61	−21.98	0.68	−0.9999	3.7
		7.22	−22.45	1.10	−0.9998	3.7
		10.83	−23.51	7.93	−0.9911	3.9
		14.44	−24.54	1.99	−0.9995	4.1
	315.7	3.61	−69.86	1.21	−0.9999	11.6
		7.22	−61.94	1.35	−0.9998	10.3
		10.83	−67.32	2.59	−0.9994	11.2
		14.44	−71.33	6.74	−0.9964	11.9
$AsPh_3$	298.2	4.00	−8.02	1.74	−0.9984	1.3
		8.00	−9.13	3.04	−0.9962	1.5
		12.00	−10.18	1.77	−0.9989	1.7
		16.00	−10.27	0.82	−0.9998	1.7
	307.2	4.00	−25.08	3.57	−0.9982	4.2
		8.00	−26.90	9.08	−0.9900	4.5
		12.00	−34.97	7.59	−0.9958	5.8
		16.00	−32.80	5.69	−0.9973	5.5
	315.7	4.00	−73.67	3.92	−0.9989	12.3
		8.00	−71.36	4.01	−0.9987	11.9
		12.00	−76.10	5.55	−0.9979	12.7
		16.00	−84.52	1.83	−0.9998	14.1
$SbPh_3$	298.2	3.65	−9.66	1.27	−0.9993	1.6
		7.30	−10.03	1.48	−0.9992	1.7
		10.95	−10.59	0.97	−0.9997	1.8
		14.60	−11.13	1.69	−0.9992	1.9
	307.2	3.65	−26.74	1.57	−0.9998	4.5
		7.30	−29.18	2.51	−0.9995	4.9
		10.95	−29.19	4.01	−0.9987	4.9
		14.60	−31.65	3.60	−0.9991	5.3
	315.7	3.65	−89.74	4.60	−0.9989	15.0
		7.30	−93.97	3.87	−0.9993	15.7
		10.95	−67.04	6.14	−0.9966	11.2
		14.60	−82.42	5.74	−0.9980	13.7
$P(OPh)_3$	298.2	3.44	−2.57	0.37	−0.9990	0.4
		6.88	−2.49	0.66	−0.9967	0.4
		10.32	−2.43	0.32	−0.9992	0.4
		13.76	−2.10	0.92	−0.9916	0.4
	307.2	3.44	−6.63	0.58	−0.9991	1.1
		6.88	−6.29	0.34	−0.9997	1.1
		10.32	−5.24	1.23	−0.9968	0.9
		13.76	−5.67	1.42	−0.9964	1.0
	315.7	3.44	−23.90	4.10	−0.9925	4.0
		6.88	−20.57	1.58	−0.9980	3.4
		10.32	−12.24	1.23	−0.9983	2.0
		13.76	−19.05	2.93	−0.9917	3.2

where k is the Boltzman constant and all other parameters have their usual meaning. Table 3 gives the thermodynamic parameters for the various substitution reactions of DTBQ—$\overset{\bullet}{}$—Re(CO)$_4$.

Before discussing the mechanistic implications of the data obtained in this study, it is important that several concepts be made clear. The dissociative (S_N1, five-coordinate intermediate and rate of substitution independent of entering ligand) and associative (S_N2, seven coordinate intermediate and rate of substitution strongly dependent upon the nature and concentration of the entering ligand) mechanisms are extremes. Rarely is a mechanism a clear cut example of either an associative or dissociative mechanism. Tobe (23) has clearly described the extremes, as well as an intermediate case, known as an interchange mechanism. Both a dissociative interchange, I_d, and an associative interchange, I_a, are described. The main feature of the $I_{a,d}$ mechanism is that it is assigned when no evidence for an intermediate can be found, with the assumption that it is very short-lived.

The results of the study of the substitution of a CO group of DTBQ—$\overset{\bullet}{}$—Re(CO)$_4$ indicate that the reaction is mainly a dissociative process, with the loss of the CO group being the rate determining step. The lack of variation in the rate constants at

Can. J. Chem. Downloaded from www.nrcresearchpress.com by 210.87.254.6 on 09/06/12
For personal use only.

TABLE 2. The activation energies (E_a) and pre-exponential factors (A) of the Arrhenius Equation for the substitution reactions of DTBQ$^{\bullet-}$—Re(CO)$_4$; parameters are from the plot log k vs. T^{-1}

Ligand	k(ave)[a]/ 10^{-4} s^{-1}	log k	T^{-1}/ 10^{-3} K	Slope/ k	E_a/ kcal mol^{-1} (kJ mol^{-1})	log A
PPh_3	1.6±0.4	−3.80	3.353			
	3.9±0.2	−3.41	3.255	−4582	21.0	11.54
	11.3±1.0	−2.95	3.168		(87.9±5.7)	
$AsPh_3$	1.6±0.3	−3.80	3.353			
	5.1±0.9	−3.29	3.255	−4811	22.0	12.18
	12.8±1.1	−2.89	3.168		(92.0±6.8)	
$SbPh_3$	1.8±0.2	−3.74	3.353			
	4.9±0.4	−3.31	3.255	−4801	22.0	12.34
	13.9±2.7	−2.85	3.168		(92.0±5.9)	
$P(OPh)_3$	0.4±0.0	−4.40	3.353			
	1.0±0.1	−4.00	3.255	−4901	22.4	12.00
	3.2±0.8	−3.49	3.168		(93.6±5.4)	

[a]The k's at each temperature are the averaged values of the individual k's at different ligand concentrations as reported in Table 1.

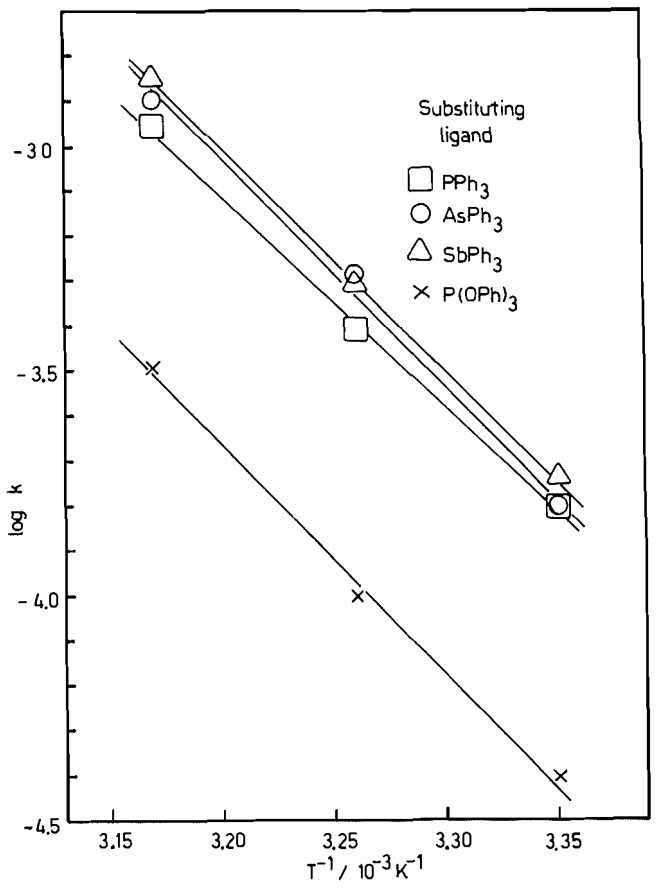

FIG. 3. Plot of log k vs. T^{-1} for the carbonyl substitution reactions of DTBQ$^{\bullet-}$—Re(CO)$_4$ by PPh_3, $AsPh_3$, $P(OPh)_3$, and $SbPh_3$.

differing ligand concentrations and the very small variation in the rates when different ligands were used is indicative of a dissociative mechanism. A similar, though associative, reaction involving the exchange of a CO group for various phosphine ligands on an iron–carbonyl complex was reported, having rate constants for the different phosphine ligand reactions which varied by as much as four orders of magnitude

TABLE 3. Thermodynamic parameters of the substitution reactions of DTBQ$^{\bullet-}$—Re(CO)$_4$ in benzene at 25°C

Ligand	$\Delta H^{\ddagger}$ (kJ/mol)	$\Delta S^{\ddagger}$ (J/mol)	$\Delta G^{\ddagger}$ (kJ/mol)
PPh_3	85.4±5.5	−31.8±16.5	95.1±5.5
$AsPh_3$	89.5±6.5	−19.7±20.0	95.3±6.5
$SbPh_3$	89.5±5.7	−16.3±17.0	94.5±5.7
$P(OPh)_3$	91.2±5.2	−23.0±16.0	97.9±5.2

(24).

The reactions at 25°C all had very small negative $\Delta S^{\ddagger}$ values. A large, negative value would be indicative of a purely associative mechanism, while a large positive value would indicate that the mechanism is purely dissociative in nature. In view of the error likely in the $\Delta S^{\ddagger}$ values (8 J mol^{-1} deg^{-1}) and their closeness to zero, it is reasonable to assume that the entering ligand probably approaches the radical complex within some defined distance before the dissociation of the CO group occurs.

Further evidence for the dissociative nature of the substitution reaction comes from the study of the reaction in benzene solutions which were saturated with carbon monoxide. For the three cases studied at 25°C, where the entering ligands were PPh_3, $AsPh_3$, and $SbPh_3$, the rate constants were found to be smaller by a factor of ten in the CO-saturated solutions than in the nitrogen-degassed solutions normally employed.

From the evidence accumulated here, it can be concluded that the mechanism which best describes the reaction is a dissociative reaction, with the loss of CO being the rate-determining step and with a small degree of I_d contribution between the ligand and the unsubstituted radical before CO dissociation occurs. A general scheme representing the reaction system and as suggested by a referee is given below:

[7] DTBQ$^{\bullet-}$—Re(CO)$_4$ ⇌ DTBQ$^{\bullet-}$—Re(CO)$_4$ + CO
DTBQ$^{\bullet-}$—Re(CO)$_4$ + L → DTBQ$^{\bullet-}$—Re(CO)$_4$L } D mechanism for major path

and

DTBQ$^{\bullet-}$—Re(CO)$_5$ + L → DTBQ$^{\bullet-}$—Re(CO)$_4$L + CO; I_d mechanism for minor path

Can. J. Chem. Downloaded from www.nrcresearchpress.com by 210.87.254.6 on 09/06/12
For personal use only.

TABLE 4. Carbonyl stretching frequencies and band assignments of some ligand substituted DTBQ$^{\bullet-}$—$Re(CO)_4$ radical complexes in chloroform solution at 25°C

Radical complex	Symmetry	Carbonyl stretching frequencies (± 2 cm^{-1}), relative intensities, and band assignments
DTBQ$^{\bullet-}$—$Re(CO)_3PPh_3$	C_{3v}	2020 (s, A_1); 1930 (s, E); 1894 (s, E)
DTBQ$^{\bullet-}$—$Re(CO)_3P(PhN(CH_3))_3$	C_{3v}	2006 (s, A_1); 1922 (s, E); 1886 (s, E)
DTBQ$^{\bullet-}$—$Re(CO)_3AsPh_3$	C_{3v}	2017 (s, A_1); 1927 (s, E); 1897 (s, E)
DTBQ$^{\bullet-}$—$Re(CO)_3SbPh_3$	C_{3v}	2009 (s, A_1); 1927 (s, E); 1900 (s, E)
DTBQ$^{\bullet-}$—$Re(CO)_3pY$	C_{3v}	1990 (s, A_1); 1911 (s, E); 1892 (s, E)
DTBQ$^{\bullet-}$—$Re(CO)_2[P(OCH_3)_3]_2$	C_{2v}	1935 (s, A_1); 1878 (s, B_1)

2. Substitution of ligands other than CO in the DTBQ—Re(CO)$_3$L radical complex

The exchange of ligands, other than CO, in radicals of the type DTBQ$^{\bullet-}$—$Re(CO)_3L$ by other ligands of similar type has also been investigated. Qualitative experiments, monitored by esr, were performed in which an excess of ligand, L′, was added to a toluene solution of a previously CO-substituted radical complex, as shown below:

[8] DTBQ$^{\bullet-}$—$Re(CO)_3L$ + L′ → DTBQ$^{\bullet-}$—$Re(CO)_3L'$ + L

Several interesting observations were made during the course of the reactions. When NEt_3 was the originally substituted ligand, the replacement of NEt_3 by $AsPh_3$ or $SbPh_3$ was very much faster than the substitution of CO in DTBQ$^{\bullet-}$—$Re(CO)_4$ by $AsPh_3$ or $SbPh_3$. Radical complexes substituted with pyridine, however, did not react with $AsPh_3$ or $SbPh_3$.

The results of this study can be summarized by listing the ligands in decreasing order of their ability to displace another ligand lower in the series. The series is:

$$PPh_3 > py > DMSO \approx AsPh_3 > SbPh_3 > NEt_3$$

It is clear from this series and the kinetic results of the previous section that the thermodynamic stability of a radical complex is not necessarily related to the rate of its formation.

The position of the substituting ligand in the octahedral radical complexes was investigated. In metal–quinone complexes, axial substitution (where the bidentate quinone defines the plane) has been reported for rhodium (25–27) and ruthenium (25) complexes, while equatorial substitution has been reported for platinum (25), palladium (25), and iridium (25–27) complexes, where PPh_3 was the entering ligand. Alberti *et al.* (28) have reported equatorial substitution of two triethylphosphite ligands on a manganese–quinone radical complex at 0°C which thermally rearranged to axial positions when the temperature was raised to 60°C. These results were based on esr data and the idea that an equatorial P atom is expected to have a smaller hyperfine coupling constants. This is due to the less efficient transmittance of spin density through the metal atom than an axial position where a direct overlapping with the unpaired spin π-orbitals of the quinone can occur.

Although positive esr data can provide information on the probable configuration, confirmation by another technique is, of course, valuable. Infrared absorption, particularly in the carbonyl region of the pure radical complex, was used to determine the configuration of the CO groups, and hence the other ligands, about the rhenium centre. Table 4 gives the carbonyl stretching frequencies and band assignments of the radical complexes. Again we were taking advantage of the valuable HPLC-esr technique which provides the pure radical complex (without the presence of parent compounds) which could mask the CO absorption region. The ir assignments were made assuming that the ligands were point charges (29), since they all have similar bonding properties (i.e., all are σ-donors and π-acceptors). It should be *emphasized* that the "point-charge" model is at best an approximation as the radical complexes will in fact exhibit some distortion from the ideal geometry. Nevertheless, the absorption of the CO groups is very strong in these complexes, making the resolution of the number of bands more unambiguous. Furthermore, the ir results are also consistent with the esr assignments.

The monosubstituted radical complexes could have been either of the two conformations shown below.

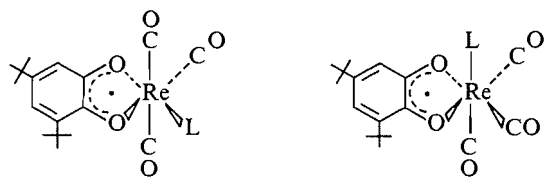

C_{2v} C_{3v}

The C_{2v} complex, with the ligand *trans* to the quinone, is expected to exhibit two bands in the carbonyl region, (A_1 + B_1). The C_{3v} complex should also exhibit two bands (A_1 + E), however, if the axial ligands are not identical, as is the case here, then the E band is expected to broaden or split as the symmetry of the molecule changes to C_5 (30). From the examination of the ir carbonyl bands, it can be concluded that the C_{3v} structure is the correct one for all of the monosubstituted radical complexes which were studied. This is in agreement with the rather large (~25 G) phosphorus coupling constants which were observed (21, 22).

There are three possible structures for the disubstituted rhenium radical complexes shown below.

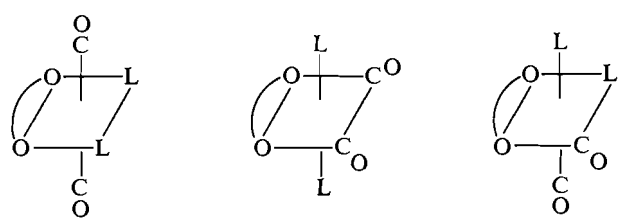

I (D_{4h}) II (C_{2v}) III (C_{2v})

The D_{4h} structure should exhibit only one ir band in the CO region (A_{2u}), hence can be ruled out as a possible structure. The esr spectrum showed that the two phosphite ligands were equiv-

Can. J. Chem. Downloaded from www.nrcresearchpress.com by 210.87.254.6 on 09/06/12
For personal use only.

alent, so that structure **III** can be eliminated. Structure **II** with *trans* phosphite ligands should have an ir spectrum with two bands of equal intensity ($A_1 + B_1$), which is exactly what was observed. The structure of the bisubstituted rhenium–quinone radical complexes can thus be assigned structure **II**.

Though the thermodynamically most favourable position for the substituting ligands has been shown to be in axial positions, this does not necessarily mean that the original CO group lost was in an axial position. It is well known that intramolecular rearrangement in transition metal carbonyl complexes can be very rapid (31). We were unable to observe a phosphorus ligand in an equatorial position, even when the complex was formed at 0°C.

Acknowledgments

This research is supported by the Natural Sciences and Engineering Research Council of Canada. K.A.M.C. gratefully acknowledges the award of an Ontario Graduate Fellowship.

1. R. L. SWEANY and J. HALPERN. J. Am. Chem. Soc. **99**, 8335 (1977).
2. R. F. HOWE. J. Chem. Soc. Faraday I, **71**, 1689 (1975).
3. C. F. BAMFORD and S. U. MULLIK. J. Chem. Soc. Faraday I, **71**, 625 (1975).
4. M. W. LYNCH, D. N. HENDRICKSON, B. J. FITZGERALD, and C. G. PIERPONT. J. Am. Chem. Soc. **103**, 3961 (1981).
5. K. D. MAGERS, C. G. SMITH, and D. T. SAWYER. Inorg. Chem. **19**, 492 (1980).
6. O. GANDOLFI, G. DOLCETTI, M. GHENDINI, and M. CAIS. Inorg. Chem. **19**, 1785 (1980).
7. C. C. FELIX, J. S. HYDE, T. SARNA, and R. C. SEALY. J. Am. Chem. Soc. **100**, 3922 (1978).
8. G. GUTTNER, D. NEWGEBAUER, and A. RAZARI. Angew. Chem. Int. Ed. Engl. **14**, 353 (1975).
9. T. L. BROWN. Ann. N.Y. Acad. Sci. **333**, 80 (1979).
10. A. POË. Inorg. Chem. **20**, 4029 (1981); **20**, 4032 (1981).
11. J. D. ATWOOD. Inorg. Chem. **20**, 4031 (1981).
12. J. P. FAWCETT, A. POË, and K. R. SHARMA. J. Chem. Soc. Dalton, 1887 (1979); J. P. FAWCETT, R. A. JACKSON, and A. POË. Chem Commun. 733 (1975).
13. R. W. WEGMAN, R. J. OLSEN, D. R. GARD, L. R. FAULKNER, and T. L. BROWN. J. Am. Chem. Soc. **103**, 6089 (1981).
14. B. H. BYERS and T. L. BROWN. J. Am. Chem. Soc. **99**, 2527 (1977); D. R. KIDD and T. L. BROWN. J. Am. Chem. Soc. **100**, 4095 (1978).
15. W. D. COVEY and T. L. BROWN. Inorg. Chem. **12**, 2820 (1973); S. B. MCCULLEN, H. W. WALKER, and T. L. BROWN. J. Am. Chem. Soc. **104**, 4007 (1982).
16. A. FOX, J. MALITO and A. POË. Chem. Commun. 1052 (1981).
17. Q. Z. SHI, T. G. RICHMOND, W. C. TROGLER, and F. BASOLO. J. Am. Chem. Soc. **104**, 4032 (1982).
18. K. A. M. CREBER and J. K. S. WAN. J. Am. Chem. Soc. **103**, 2101 (1981).
19. T. REICH, K. S. CHEN, and J. K. S. WAN. J. Chromatogr. **206**, 139 (1981).
20. T. I. HO, K. A. M. CREBER, and J. K. S. WAN. J. Am. Chem. Soc. **103**, 6524 (1981).
21. K. A. M. CREBER, T. I. HO, M. C. DEPEW, D. WEIR, and J. K. S. WAN. Can. J. Chem. **60**, 1504 (1982).
22. K. A. M. CREBER and J. K. S. WAN. Chem. Phys. Lett. **81**, 453 (1981).
23. M. L. TOBE. Inorganic reaction mechanisms. Thomas Nelson and Sons, London. 1972.
24. C. Y. CHANG, C. E. JOHNSON, T. G. RICHMOND, Y. T. CHEN, W. C. TROGLEV, and F. BASOLO. Inorg. Chem. **20**, 3167 (1981).
25. A. L. BALCH. J. Am. Chem. Soc. **95**, 2723 (1973).
26. Y. S. SOHN and A. L. BALCH. J. Am. Chem. Soc. **94**, 1144 (1972).
27. A. Y. GIRGIS, Y. S. SOHN, and A. L. BALCH. Inorg. Chem. **14**, 2327 (1975).
28. A. ALBERTI and C. M. CAMAGGI. J. Organomet. Chem. **161**, C63 (1978).
29. R. DOBSON and L. W. HAUK. Inorg. Chem. Acta, **1**, 287 (1967).
30. D. M. ADAMS. Metal–ligand and related vibrations. Edward Arnold Publishers, Ltd., London. 1967.
31. J. D. ATWOOD and T. L. BROWN. J. Am. Chem. Soc. **98**, 3160 (1976).

Can. J. Chem. Downloaded from www.nrcresearchpress.com by 210.87.254.6 on 09/06/12
For personal use only.

Photochemistry with high power ultraviolet lasers

R. J. DONOVAN, C. FOTAKIS,[1] A. HOPKIRK, C. B. MCKENDRICK, AND A. TORRE[2]
Department of Chemistry, University of Edinburgh, West Mains Road, Edinburgh, EH9 3JJ, Scotland

Received November 2, 1982

This paper is dedicated to Professor Harry E. Gunning on the occasion of his 65th birthday

R. J. DONOVAN, C. FOTAKIS, A. HOPKIRK, C. B. MCKENDRICK, and A. TORRE. Can. J. Chem. **61**, 1023 (1983).

Rotationally resolved photofragment fluorescence from $OH(A^2\Sigma^+)$ following the coherent two-photon excitation of H_2O with a KrF laser (248 nm), is reported and the dynamics of the dissociation process are discussed. Fluorescence from $CN(B^2\Sigma^+)$ following two-photon excitation of ICN is also described. In both cases the energy distribution in the photofragments is shown to differ significantly from that observed with single-photon excitation at closely similar energies.

Two further examples of multiphoton excitation, involving CS_2 and SO_2, are briefly discussed. In these cases absorption of a further photon, by fragments produced in the primary step, gives rise to strong laser-induced fluorescence.

R. J. DONOVAN, C. FOTAKIS, A. HOPKIRK, C. B. MCKENDRICK et A. TORRE. Can. J. Chem. **61**, 1023 (1983).

On rapporte la fluorescence de photofragment résolue rotationnellement à partir de $OH(A^2\Sigma^+)$ après excitation par deux photons cohérents de l'eau à l'aide d'un laser au KrF (248 nm) et on discute des dynamiques du processus de dissociation. On décrit également la fluorescence provenant de $CN(B^2\Sigma^+)$ qui suit l'excitation du ICN par deux photons. Dans les deux cas on montre que la distribution d'énergie des photofragments diffère de façon significative de celle observée lors d'une excitation à l'aide d'un photon unique à des énergies très semblables.

On discute brièvement de deux autres exemples d'excitations par multiphoton qui impliquent le CS_2 et le SO_2. Dans ces cas l'absorption d'un autre photon, par les fragments produits dans la première étage, donne lieu à une forte fluorescence induite par un laser.

[Traduit par le journal]

Introduction

The use of high power ultraviolet lasers to induce multiphoton excitation and bring about photochemical change offers a number of advantages over conventional techniques. Firstly, states which lie at energies equivalent to those for single-photon transitions in the vacuum ultraviolet can be populated without having to contend with the many practical difficulties associated with the evacuation of the optical path and the handling of materials that are transparent at vacuum ultraviolet wavelengths (the transmission of such materials is rapidly degraded by the slightest contamination and they are also susceptible to radiation damage). Secondly, the selection rules for multiphoton excitation differ from those for single-photon excitation and this allows access to a whole new range of electronically excited states. This point is well illustrated by the simplest of multiphoton excitation processes, i.e. two-photon excitation. The selection rules for two-photon excitation are equivalent to those for Raman scattering and thus complement the normal electric dipole selection rules.

A third difference which has not yet been much exploited is the ability to excite samples homogeneously that would otherwise be optically thick for single-photon absorption in the vacuum ultraviolet. Thus, using multiphoton excitation, a homogeneous distribution of radicals can be produced in systems where high reagent concentrations would render the sample opaque to vacuum ultraviolet radiation. The latter principle can be further exploited for the excitation and detection of atoms which by virtue of their high peak extinction coefficients become optically thick at very low concentrations.

[1]Permanent address: Department of Physics, University of Crete, Iraklion, P.O. Box 470, Crete, Greece.

[2]Permanent address: Department of Chemical Physics, University of Bilbao, Apartado 644, Bilbao, Spain.

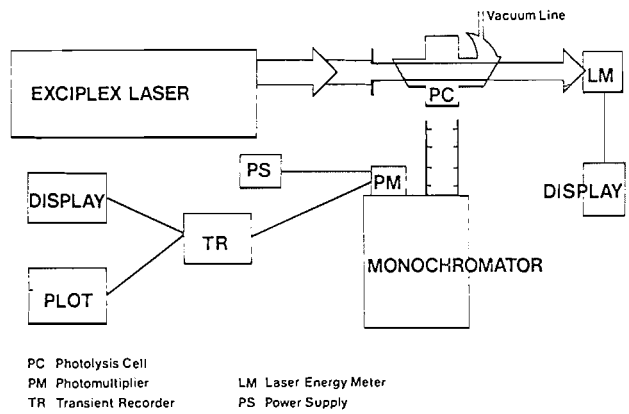

FIG. 1. Experimental arrangement for observing photofragment fluorescence and multiphoton excitation.

In the work presented below we demonstrate how a simple excimer laser can be used to induce multiphoton transitions in a number of small molecules and discuss the various mechanisms involved. The first example considered, that of the coherent two-photon excitation of H_2O, is the most clearly understood. We then discuss the two-photon excitation of ICN which involves a repulsive intermediate state at resonance with the first photon. Finally, we discuss two examples in which the primary photofragments are excited by absorption of a further photon from the laser pulse and give rise to strong *laser-induced* fluorescence spectra.

Experimental

The experimental arrangement (see Fig. 1) was similar in principle to that described previously (1) but differed in a number of important respects. For the multiphoton excitation of water the excimer laser used was a Lambda Physik EMG 201; this laser is capable of deliv-

Can. J. Chem. Downloaded from www.nrcresearchpress.com by 210.87.254.42 on 09/06/12
For personal use only.

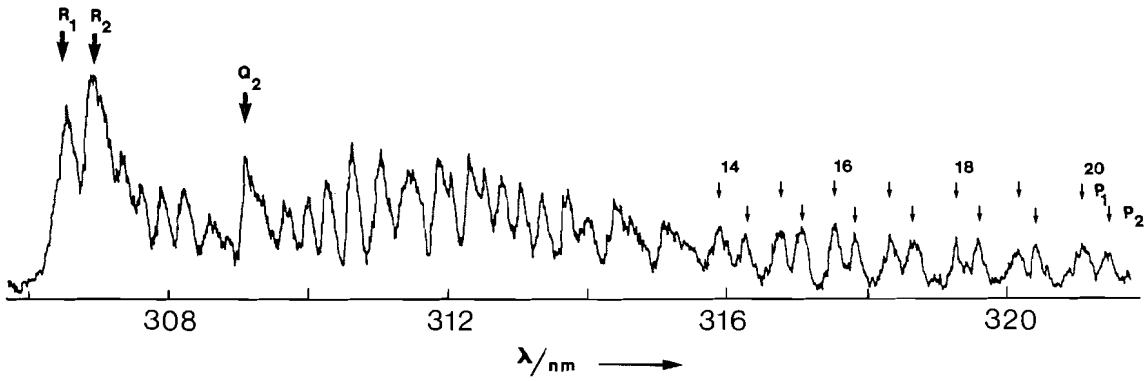

FIG. 2. Photofragment fluorescence from OH($A^2\Sigma^+$, $v' = 0 \rightarrow X^2\Pi$, $v'' = 0$) following two-photon excitation of H_2O (P_{H_2O} = 1.5 kN m^{-2}) with a KrF laser (248 nm). The heads of the R_1, R_2, and Q_2 branches, together with the resolved rotational lines of the P_1 and P_2 branches, are indicated by arrows.

ering 1 J per pulse on the KrF line at 248 nm. The laser output was focussed into the photolysis cell with a quartz lens of focal length 10 cm. The OH photofragment fluorescence was monitored at right angles to the laser beam and was dispersed with a Monospek 500 monochromator used in the second order. The observations on SO_2 excitation were also made with this arrangement.

The work with ICN and the other molecules discussed below was carried out with a Lambda Physik EMG 500 laser and an experimental arrangement that has been described previously (1, 2).

Results and discussion

(i) *Two-photon excitation of water*

The only photofragment fluorescence observed when water was subjected to the focussed output of the KrF laser was readily identified as due to OH($A^2\Sigma^+ \rightarrow X^2\Pi$). The intensity of the emission was found to increase slowly with increasing vapour pressure of water and at 1.5 kN m^{-2} pressure the intensity was sufficient to allow rotational structure to be resolved for levels with $K \geq 14$ (see Fig. 2). The spectrum could still be observed for pressures as low as 67 N m^{-2} and was essentially identical to that at the highest pressures. This is consistent with the large ratio for the cross-sections for electronic quenching versus rotational relaxation of OH($A^2\Sigma^+$) by water (3).

Water is completely transparent at 248 nm (i.e. for single-photon absorption) and as there is insufficient energy to dissociate the molecule we can be certain that this photofragment fluorescence must result from a coherent two-photon process or a higher order process. The intensity of the OH($A^2\Sigma^+$) fluorescence was found to increase quadratically with the laser intensity (1) which supports the two-photon mechanism.

The populations of the K levels, for K = 14–20, were readily determined using the known line strengths, as the P_1 and P_2 branches associated with these higher levels are clearly resolved. Careful analysis of the sharper features at shorter wavelength, several of which are blends of only two lines, allows a reasonable estimate to be made of populations below K = 14. These populations can then be fed into a computer program which simulates the fluorescence spectrum. Small adjustments are made to the populations until a good fit between the experimental and simulated spectrum is obtained. The best fit to the data in Fig. 2 was achieved with a distribution that peaked at about K = 16 and declined slowly up to K = 20. Below K = 16 the populations are fairly constant. This distribution is clearly very different to the one observed following single-photon excitation of H_2O at 123.6 nm where a monotonically

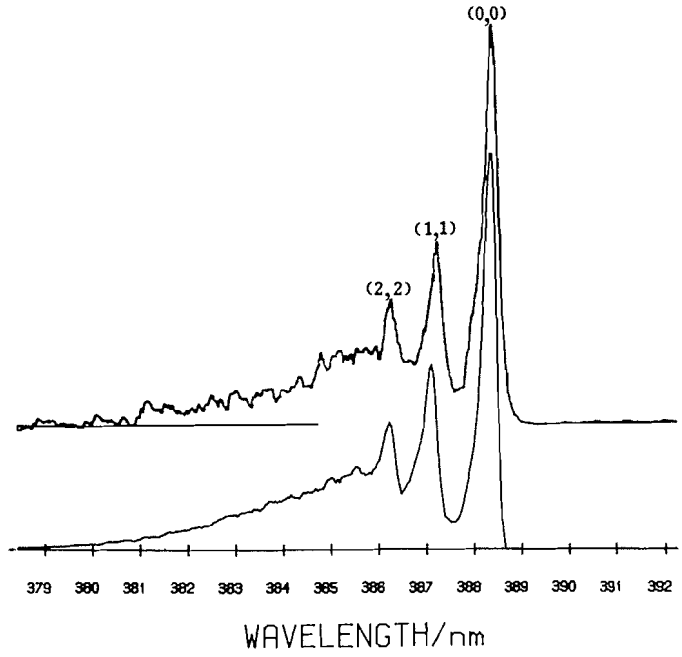

FIG. 3. Photofragment fluorescence from CN($B^2\Sigma^+ \rightarrow X^2\Sigma^+$) following two-photon excitation of ICN (P_{ICN} = 24 N m^{-2}) with a KrF laser (248 nm). The upper trace is the experimental spectrum and the lower trace a computer simulation.

rising population of K levels, up to the maximum possible level (i.e. K = 20), is observed (4). The rotational distribution produced by two-photon excitation is thus somewhat cooler than that produced by single-photon excitation but the OH($A^2\Sigma^+$) fragment still receives a considerable amount of angular momentum.

The different rotational distributions observed following single-photon and two-photon excitation suggest that different upper electronic states could be involved in the two absorption processes. In the case of single-photon excitation both the bound $\tilde{C}^1B_1$ and the repulsive $\tilde{B}^1A_1$ states are populated. The $\tilde{C}^1B_1$ state is known to be mixed with a close lying $^1A_2$ state, forming a Rydberg complex, and is also predissociated by the $\tilde{B}^1A_1$ state (5). Transitions to the $^1A_2$ state are forbidden for single-photon absorption, but allowed for two-photon absorption. Thus two-photon excitation of H_2O can directly populate the $^1A_2$ state which may therefore play a more important role in the two-photon process. As the $^1A_2$ state does not correlate

Can. J. Chem. Downloaded from www.nrcresearchpress.com by 210.87.254.42 on 09/06/12
For personal use only.

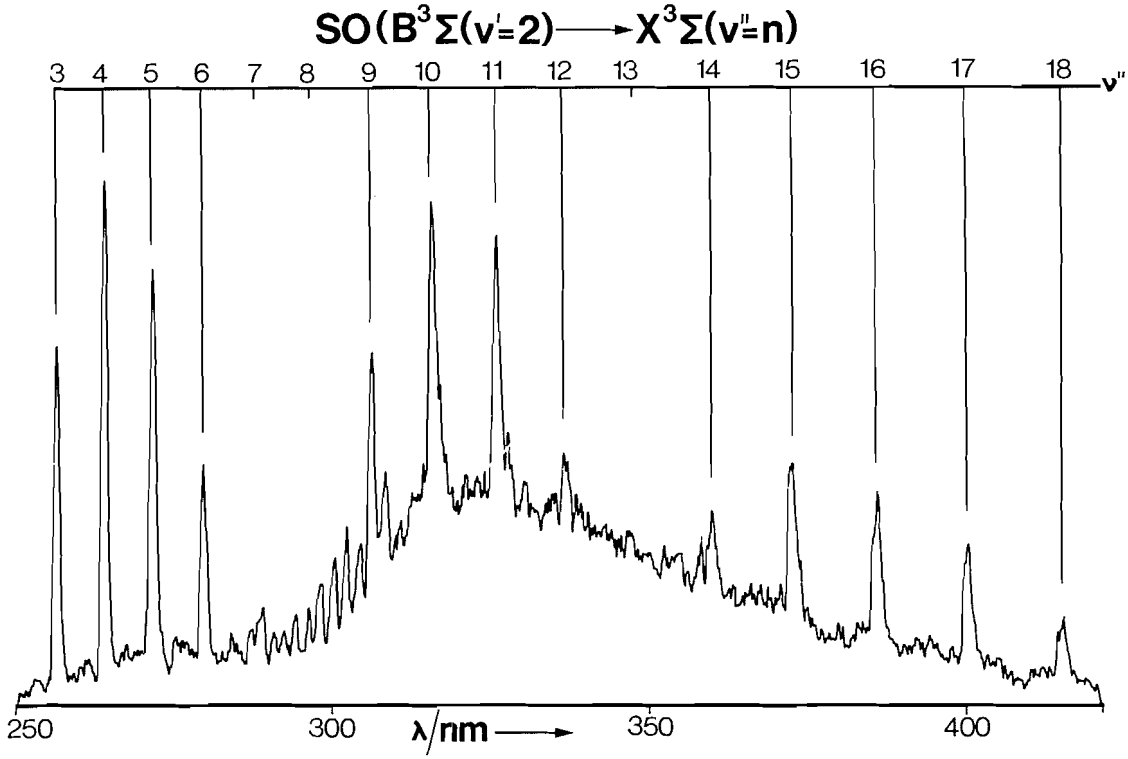

FIG. 4. Laser-induced fluorescence spectrum from SO following two-photon excitation of SO_2 (P_{SO_2} = 1.33 kN m^{-2}) with a KrF laser (248 nm). The broad continuous emission is due to fluorescence from SO_2 and the structure observed in the region 290–310 nm is due to *reabsorption* of this fluorescence by SO_2.

TABLE 1. Vibrational distributions (N_v/N_0) for CN($B^2\Sigma^+$) following two-photon and single-photon excitation of ICN

v'	Two-photon excitation ($\frac{1}{2}$ × 248 nm)	Single-photon excitation* (123.6 nm)
0	1.0	1.0
1	0.4	0.77
2	0.2	0.75
3	~0.1	0.52
4	<0.1	0.54

*Ashfold and Simons, private communication.

directly with OH($A^2\Sigma^+$), crossing to the $\tilde{B}\,^1A_1$ state is still required. If this crossing occurs in a different region of the hypersurface to that for the $\tilde{C}\,^1B_1$ state, as is likely to be the case, the dynamics of the dissociation process and the energy distribution in the products will differ from those for the single-photon excitation process, despite the similar total energies involved. We intend to examine this proposal in more detail in the future using the output of a tunable line-narrowed KrF laser.

(ii) *Two-photon excitation of ICN*

The photochemistry of the cyanogen halides has attracted considerable experimental and theoretical interest (6). Vacuum ultraviolet photolysis produces electronically excited (*A* and *B* state) CN radicals and this has facilitated the study of the photodissociation dynamics. The vibrational and rotational energy distribution in the CN radical has been shown to be very sensitive to the nature of the ICN state populated. In general the discrete (Rydberg) spectral features give rise to hot vibrational and rotational distributions, while the underlying continuum gives rise to a cold distribution (7).

In a recent study using two-photon excitation at 248 nm (KrF laser) we have shown (2) that CN($B^2\Sigma^+$) is formed with a relatively cold vibrational distribution (see Fig. 3) although the spectrum of ICN at 124 nm is dominated by a *discrete* transition to the $8s\sigma(^3\Pi)$ Rydberg state. This contrasts sharply with the hot distribution observed by Ashfold and Simons following single-photon excitation at 123.6 nm (Table 1). It was suggested by Hopkirk and Donovan (2) that this difference could result from the population of different electronic states of ICN by two-photon excitation, however, an alternative mechanism involving sequential excitation via a repulsive intermediate state could not be ruled out. The latter mechanism is expected to lead to a broader and cooler distribution of vibrational states, as the sequential pumping process can in principle sample a wide range of I—CN internuclear separations during dissociation on the repulsive intermediate surface. However, the probability of a molecule absorbing a second photon during this dissociation process is rather small, as the lifetime in the repulsive state will be $<10^{-12}$ s.

(iii) *Laser-induced fluorescence following multiphoton excitation and fragmentation*

Two-photon excitation of CS_2 with a KrF laser at 248 nm produces CS radicals in both the ground and excited $A^1\Pi$ electronic states (8). Ground electronic state radicals are formed in a range of vibrational levels and those in the $v'' = 2$ level absorb a further 248 nm photon, via the (2,2) band of the CS($A \leftarrow X$) system, leading to strong laser-induced fluorescence, viz:

$$CS_2 + 2h\nu\ (248\ \text{nm}) \rightarrow CS(X^1\Sigma^+, v'' = n) + S$$

$$CS(X^1\Sigma^+, v'' = 2) + h\nu\ (248\ \text{nm}) \rightarrow CS(A^1\Pi, v' = 2)$$

$$CS(A^1\Pi, v' = 2) \rightarrow CS(X^1\Sigma^+, v'' = n) + h\nu(248\text{–}290\ \text{nm})$$

Can. J. Chem. Downloaded from www.nrcresearchpress.com by 210.87.254.42 on 09/06/12
For personal use only.

A further example is seen in the two-photon *sequential* excitation of SO_2 at 248 nm which leads to the formation of SO in its ground electronic state, viz:

$$SO_2 + h\nu \rightarrow SO_2(\tilde{B}^1B_1)$$

followed by

$$SO_2(\tilde{B}^1B_1) + h\nu \rightarrow SO_2(\tilde{G}) \rightarrow SO + O$$

SO radicals produced in the $v'' = 2$ level then absorb a further photon (9, 10) which results in strong laser-induced $SO(B \rightarrow X)$ fluorescence (see Fig. 4), viz:

$$SO(X^3\Sigma, v'' = 2) + h\nu\ (248\ nm) \rightarrow SO(B^3\Sigma, v' = 2)$$

$$SO(B^3\Sigma, v' = 2) \rightarrow SO(X^3\Sigma, v'' = n) + h\nu\ (248-450\ nm)$$

A weaker contribution to this fluorescence from $SO(A^3\Pi_2, v' = 11)$ is also observed at the shorter wavelengths (11).

Conclusions

The main conclusion to be drawn from the above work is that the use of high power ultraviolet lasers allows the facile production of a range of electronically excited species which can now be readily studied using conventional time-resolved kinetic techniques. It should also be apparent that in most cases the detailed mechanism by which multiphoton excitation occurs is unclear and that much remains to be done in this new realm of photochemistry.

Acknowledgements

We thank Drs. A. Gibson and M. C. Gower and the S.E.R.C. for providing laser facilities at the Rutherford Appleton Laboratory. We also thank the S.E.R.C. for support for C.F. and A.H., the Patronato de la U.P.V. (Spain) for a fellowship for A.T., and the Carnegie Trust for support for C.B.McK.

1. C. FOTAKIS, C. B. MCKENDRICK, and R. J. DONOVAN. Chem. Phys. Lett. **80**, 598 (1981).
2. A. HOPKIRK and R. J. DONOVAN. J. Photochem. **19**, 101 (1982).
3. M. KANEKO, Y. MORI, and I. TANAKA. J. Chem. Phys. **48**, 4468 (1968).
4. K. H. BECKER and D. HAAKS. Z. Naturforsch. Teil A, **28**, 249 (1973).
5. J. W. C. JOHNS. Can. J. Phys. **41**, 209 (1963); **49**, 944 (1971).
6. M. N. R. ASHFOLD, M. T. MACPHERSON, and J. P. SIMONS. Top. Curr. Chem. **86**, 3 (1979).
7. M. N. R. ASHFOLD, A. S. GEORGIOU, A. M. QUINTON, and J. P. SIMONS. J. Chem. Soc. Faraday Trans. 2, **77**, 259 (1981).
8. M. MARTIN and R. J. DONOVAN. J. Photochem. **18**, 245 (1982).
9. C. FOTAKIS, A. TORRE, and R. J. DONOVAN. To be published.
10. M. W. WILSON, M. ROTHSCHILD, D. F. MULLER, and C. K. RHODES. J. Chem. Phys. **77**, 1837 (1982).
11. C. FOTAKIS. Chem. Phys. Lett. **82**, 68 (1981).

Can. J. Chem. Downloaded from www.nrcresearchpress.com by 210.87.254.42 on 09/06/12
For personal use only.

Radical cations of strained ring hydrocarbons. Cyclopropane derivatives

HEINZ D. ROTH AND MARCIA L. MANION SCHILLING
Bell Laboratories, Murray Hill, NJ 07974, U.S.A.

Received July 27, 1982

This paper is dedicated to Professor Harry E. Gunning on the occasion of his 65th birthday

HEINZ D. ROTH and MARCIA L. MANION SCHILLING. Can. J. Chem. **61**, 1027 (1983).

A series of radical cations has been generated from various cyclopropane derivatives by photoinitiated electron transfer to chloranil. Nuclear spin polarization effects observed during these reactions have been interpreted as evidence for the structure of these intermediates. Tri- and tetraalkylsubstituted cyclopropanes (**1**, **3**, **4**) form "trimethylene" radical cations in which the most highly substituted carbon–carbon bond is broken (or weakened). The benzocyclopropanorbornene (**12**) forms a radical cation in which spin and charge are located in the benzenoid ring; the tertiary cyclopropane protons are coupled by a homohyperconjugative interaction; otherwise, the cyclopropane ring is unaffected. To the radical cation derived from bismethanoparacyclophane (**17**) a trimethylene structure is assigned in which the benzylic carbons are pyramidal. Finally, benzonorcaradiene (**20**) forms a radical cation in which the two secondary–tertiary bonds are lengthened and in which the methylene group bears spin density.

HEINZ D. ROTH et MARCIA L. MANION SCHILLING. Can. J. Chem. **61**, 1027 (1983).

On a produit une série de cations radicalaires à partir de divers dérivés du cyclopropane en utilisant un transfert d'électron photoinduit sur le chloranil. On a interprété les effets de polarisation de spin nucléaire observés dans ces réactions comme une preuve de structure de ces intermédiaires. Les cyclopropanes portant des substituants tri et tétraalkyles (**1**, **3**, **4**) forment des cations radicalaires "triméthylène" dans lesquels la liaison carbone–carbone la plus substituée est rompue (ou affaiblie). Le benzocyclopropanorbornène (**12**) forme un cation radicalaire dans lequel le spin et la charge sont localisés dans le cycle benzénique; les protons tertiaires du cyclopropane sont couplés par une interaction homohyperconjuguée sans quoi le cycle cyclopropane n'est pas affecté. Au cation radicalaire provenant du biméthanoparacyclophane (**17**) on a attribué une structure triméthylène dans laquelle les carbones benzyliques sont pyramidaux. Finalement le benzonorcaradiène (**20**) forme un cation radicalaire dans lequel deux liaisons secondaire–tertiaires sont allongées et dans lequel le groupe méthylène porte la densité de spin.

[Traduit par le journal]

Can. J. Chem. Downloaded from www.nrcresearchpress.com by 210.87.254.42 on 09/06/12
For personal use only.

For several years we have been interested in photoinitiated electron transfer reactions and have utilized chemically induced nuclear polarization (CIDNP) effects to gain an insight into the structure and reactivity of short-lived radical cations which can be generated in this type of reaction (1, 2). The CIDNP technique is based on the interpretation of greatly enhanced nmr signals in either absorption or emission, which may be observed during reactions proceeding via pairs of radicals or radical ions (3). According to the generally accepted radical pair theory the directions and intensities of these effects are determined by several parameters, including the spin multiplicity of the precursor, the magnetic properties (electron g factor, hyperfine coupling constants) of the radical intermediates, and the type of reaction by which the polarized product is formed.

In recent publications we reported evidence for the structure of radical cations derived from substituted cyclopropanes such as diphenylcyclopropane (4) and quadricyclane (5). In order to evaluate the potential structures of the cyclopropane radical cations it is useful to consider the nature of the highest occupied molecular orbitals (HOMO's) of cyclopropane (6–11). One of its degenerate HOMO's is symmetrical and has appreciable bonding only between one pair of carbon atoms. Removal of an electron from this orbital would place spin and charge on two carbon atoms and would weaken the bond between them. The resulting radical cation could be described as a trimethylene species with a one-electron bond between the terminal methylene groups ($^2A_1$). The second HOMO has C_s symmetry; it is antibonding between two carbons and bonding between either of these and the third one. Removal of an electron from this orbital would generate a species which may be described as a π complex between ethylene and a methylene cation ($^2B_2$). This radical cation would have considerable spin density on the third carbon atom. Two of its carbon–carbon bonds would be weakened whereas the third one would be strengthened. A recent *ab initio* calculation of the cyclopropane radical cation (12) suggests that the lowest energy surface has low lying saddle points corresponding to the general structure types $^2A_1$ and $^2B_2$. The minima are of lower symmetry and have geometries intermediate between $^2A_1$ and $^2B_2$. The two degenerate HOMO's and schematic representations of the radical cations derived from them are shown in Scheme 1.

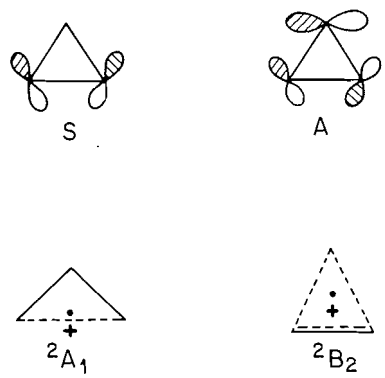

SCHEME 1

It is noteworthy that the lowest transition in the photoelectron spectrum of cyclopropane has been assigned to the ionization from the antisymmetrical orbital (8–11). However,

Can. J. Chem. Downloaded from www.nrcresearchpress.com by 210.87.254.42 on 09/06/12
For personal use only.

this conclusion does not necessarily have any bearing on the structure of the radical cations in solution. Photoelectron spectra reflect the energy differences of vertical transitions and do not reflect the energy differences between states. In addition, the relative energies of states in solution may be changed significantly by solvation. The generation of nuclear spin polarization effects requires radical (ion) pairs with lifetimes in the nanosecond range. This time scale is sufficient to allow the intermediates to dissipate excess energy. Accordingly, the CIDNP results can be expected to reflect the equilibrium geometry of the intermediates.

The general structure type which may be formed in cases of favorable interaction between aromatic/olefinic group and cyclopropane moiety is best illustrated for the isomers of 1,2-diphenylcyclopropane (4). The CIDNP results observed for these compounds suggest positive spin densities not only in the aromatic group but also on the benzylic carbons. These features are best accommodated in a structure in which the 3°−3° cyclopropane bond is broken or weakened, i.e. a structure of type $^2A_1$.

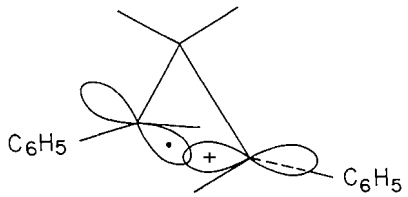

In continuing these studies we investigated the photoreactions of chloranil with several cyclopropane derivatives in which the three-membered ring is held in a well-defined position relative to olefinic and/or aromatic elements of unsaturation. These substrates should allow us to evaluate the factors influencing the interaction of the cyclopropane moiety with an unpaired spin in a π system and to identify the substitution patterns which would stabilize one structure type relative to the other. Among the factors likely to influence this interaction, we mention the relative ionization potentials of the two groups, the spatial relation between them, and the orbital symmetry of the aromatic/olefinic HOMO. The molecules to be discussed here were chosen primarily to evaluate geometric factors. The orbital symmetry effects will be discussed in a separate publication.

In some of the substrates to be discussed here, the cyclopropane ring is directly attached to the unsaturated moiety; in others the strained ring is separated from the unsaturated group by two or more single bonds. Further, the molecular architecture can force the 3°−3° cyclopropane bond into an orientation nearly parallel to the π orbitals of the element of unsaturation or into a position nearly orthogonal to them.

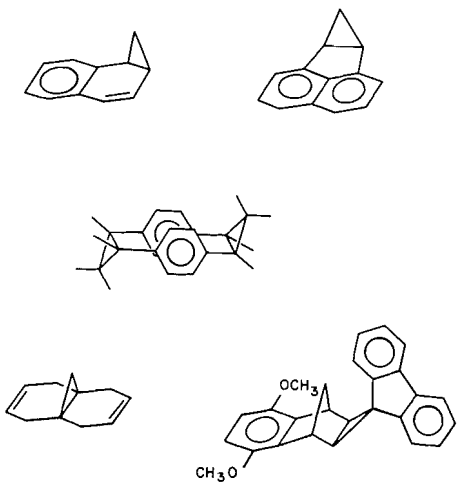

Molecules such as benzonorcaradiene or [9:10]methanoacenaphthene are examples for the orthogonal orientation whereas [1:2,9:10]bismethano[2.2]paracyclophane is an example for an essentially parallel orientation of π electrons and cyclopropane bond. Tricyclo[4.4.1.0^{1,6}]undeca-3,8-diene and a benzomethanonorbornene were chosen as examples for compounds in which cyclopropane moieties are held in a well-defined position relative to a π system but separated from it by more than one carbon−carbon bond. Finally, we studied a series of compounds, in which a cyclopropane ring is tetra-, tri-, or di-substituted without containing an element of unsaturation. We begin with a discussion of effects observed for two cyclopropanes which do not contain any element of unsaturation.

Methylsubstituted cyclopropanes

In an attempt to evaluate the donor potential of simple cyclopropane derivatives we studied the photoreactions of chloranil with a series of methylsubstituted cyclopropanes (13). These experiments failed to provide evidence for radical ion formation when dimethylcyclopropanes (**1***a*−*c*) were employed as substrates. However, in the case of 1,1,2-trimethylcyclopropane (**1***d*), pronounced CIDNP effects were found for all signals and in the case of 1,1,2,2-tetramethylcyclopropane (**1***e*) strong polarization was observed for the methyl groups and for the geminal cyclopropane protons. These results can

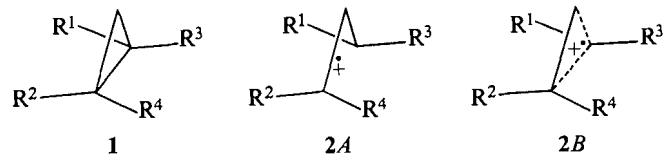

1 **2*A*** **2*B***

a R^1, R^2 = CH$_3$; R^3, R^4 = H
b R^1, R^4 = CH$_3$; R^2, R^3 = H
c R^1, R^3 = CH$_3$; R^2, R^4 = H
d R^1, R^2, R^3 = CH$_3$; R^4 = H
e R^1, R^2, R^3, R^4 = CH$_3$

be explained by a mechanism involving electron-transfer quenching of triplet chloranil by the cyclopropane derivatives, **1***d*,*e*. The resulting radical ion pairs can regenerate the reactants by reverse electron transfer after intersystem crossing. The finding that these simple cyclopropanes are electron donors is somewhat surprising. However, we note that the donor character is displayed only toward the excited state of a very strong electron acceptor and that it falls off rapidly with decreasing substitution. Thus, **1***d* shows only a small fraction of the effects observed for **1***e* (Fig. 1) and **1***a*−*c* fail to show any evidence for radical ion formation. In addition, neither uv nor nmr spectra showed any indication for charge transfer interactions in the ground state. These results characterize the cyclopropane moiety as only a marginal electron donor (13).

Evidence for the structure of the radical cations, **2**, derived from **1** is contained in the CIDNP pattern. The fact that the methyl groups at C-1 and the geminal cyclopropane protons at C-3 show the same signal direction (emission) and similar relative enhancements suggests that all protons occupy similar positions relative to the unpaired spin. The most likely structure

Can. J. Chem. Downloaded from www.nrcresearchpress.com by 210.87.254.42 on 09/06/12
For personal use only.

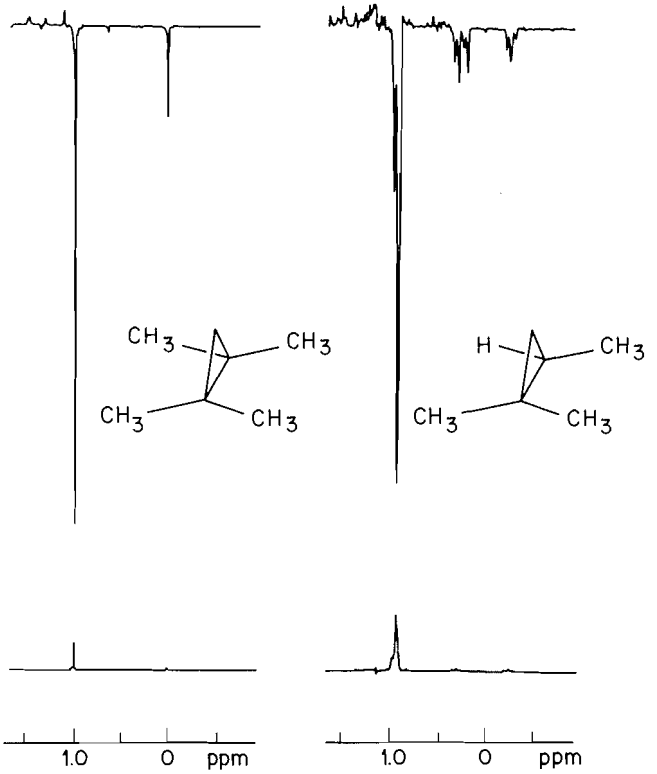

FIG. 1. The ^{1}H nmr spectra (90 MHz) of 0.02 *M* chloranil solutions in acetone-d_6 containing 0.02 *M* 1,1,2,2-tetramethylcyclopropane (**1***e*; left) or 1,1,2-trimethylcyclopropane (**1***d*; right) in the dark (bottom) and during uv irradiation. The gain for the spectra of **1***d* was 32 times as high as for the spectra of **1***e*.

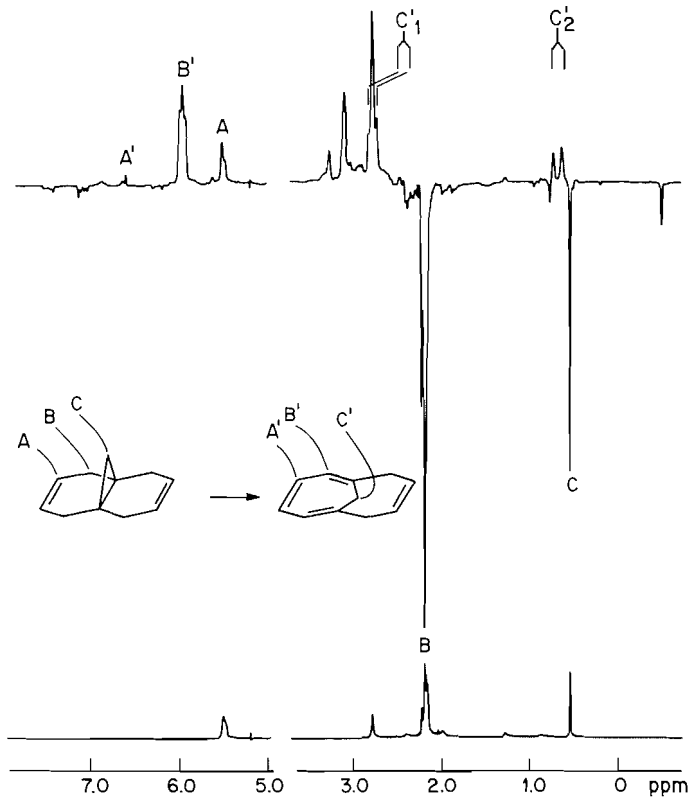

FIG. 2. The ^{1}H nmr spectra (90 MHz) of 0.02 *M* chloranil solutions in acetone-d_6 containing 0.02 *M* tricyclo[4.4.1.0^{1,6}]undeca-3,8-diene (**4**) in the dark (bottom) and during uv irradiation (top).

type is one in which the spin density is located on the quaternay cyclopropane carbons. This structure is related to the $^2A_1$ state of the cyclopropane molecular ion and is quite similar to the structure postulated for the diphenylcyclopropane radical cations.

Norcarene derivatives

In the norcar-3-ene system, a three-membered ring is arranged in a well-defined position relative to an olefinic π system but separated from it by more than one carbon–carbon bond. Two substrates of this type, 1,6-dimethylbicyclo[4.1.0]-hept-3-ene (**3**) and tricyclo[4.4.1.0^{1,6}]undeca-3,8-diene (**4**), were chosen to allow a comparative evaluation of the donor properties of the cyclopropane ring versus an olefinic moiety (13).

3 **4**

The results observed in these systems allow an unambiguous assignment. For example, the chloranil photosensitized reaction of the tricyclic diene, **4**, resulted in strong emission for the cyclopropane and the allylic protons but did not produce any polarization for the olefinic protons. Analogous results were observed for the bicyclic olefin, **3**. The observed polarization patterns establish the cyclopropane function as the better donor and, at the same time, eliminate any interaction of the olefinic groups with the unpaired spin of the radical cations, e.g. **5**.

The norcarene derivatives, **3** and **4**, also proved to be useful substrates to probe the mechanism of the photosensitized dehydrogenation of hydrocarbons. This reaction could be initiated by either electron transfer or hydrogen abstraction. For aromatic or hydroaromatic substrates it is difficult to differentiate between these pathways because both routes involve the same neutral radical. The primary intermediate of electron transfer, e.g. **6**, can be converted to the primary intermediate of hydrogen abstraction, e.g. **7**, by a simple deprotonation process.

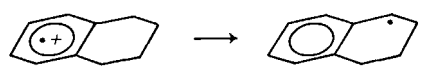

6 **7**

The substrates discussed here have the advantage that different radicals, e.g. **8** and **9**, are formed by the electron transfer/deprotonation route and by the dehydrogenation pathway, respectively. The hyperfine coupling patterns of these intermediates should be sufficiently different to allow an unambiguous assignment. Specifically, the olefinic protons are expected to have negligible hyperfine couplings in **8**, but sizeable couplings in **9**. The photoreaction of chloranil with **4** resulted in a characteristic polarization pattern for **10** (14); the bridge protons and the olefinic protons originating in the allylic position appeared in enhanced absorption but the remaining olefinic protons showed negligible polarization (Fig. 2). These results support the intermediacy of **8** and provide an unambiguous argument for the electron transfer induced mechanism.

A detailed examination of the CIDNP spectrum (Fig. 2) observed during this reaction also reveals the presence of a second dehydrogenation product. Emission multiplets near 7.2

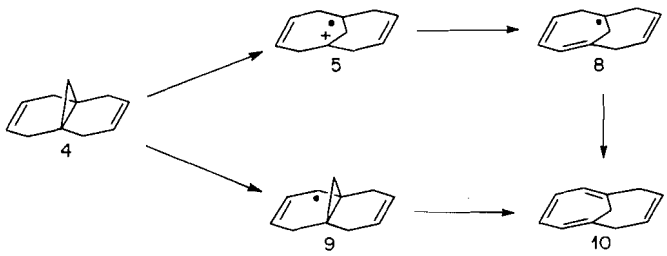

and 7.6 ppm and an emission singlet at −0.5 ppm indicate the formation of bicyclo[4.4.1]undecapentaene (**11**) (15–17). The detailed mechanism by which this product is generated, specifically the identity of the paramagnetic intermediate that gives rise to the observed polarization pattern, is not immediately obvious.

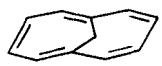

11

The [2.3]-benzo-[5:6]-methanonorbornene system

The bichromophoric compound, **12**, was originally synthesized to study the possibility of energy transfer between the fluorene and the dimethoxybenzene chromophores held in close propinquity but with orthogonal π systems (18, 19). Eventually, it was shown that energy transfer between the two π systems does occur readily (20). In the experiment described here, the radical cation of **12** is generated by reaction with photoexcited chloranil and the delocalization into the cyclopropane moiety is investigated. Of the two π systems contained in **12**, the dimethoxybenzene moiety is expected to be a better donor than the fluorene group because of the lower oxidation potential of the individual fragment.[1]

During the photoreaction, the two ^{1}H signals of the dimethoxybenzene moiety showed sizeable polarization: the aromatic singlet at 6.7 ppm appeared in enhanced absorption whereas the methoxy signal at 3.8 ppm appeared in emission (Fig. 3). In contrast, no polarization was observed for any signal of the fluorene subunit, confirming that the dimethoxybenzene group is the primary electron donor. The potential interaction between this radical cation and the cyclopropane ring can be evaluated on the basis of the polarization observed for the cyclopropane protons. During the photoreaction with chloranil, the signal near 2.0 ppm shows weak net emission. The relatively low intensity of this effect indicates a weak interaction. More importantly, the signal direction indicates a positive hyperfine coupling constant for the cyclopropane protons. This assignment rules out any delocalization of spin onto the tertiary cyclopropane carbons as in structure type **13** and is compatible

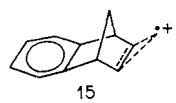

[1]The oxidation potential of dimethoxybenzene is 1.34 V vs. SCE (21), that of fluorene is 1.65 V vs. SCE (22).

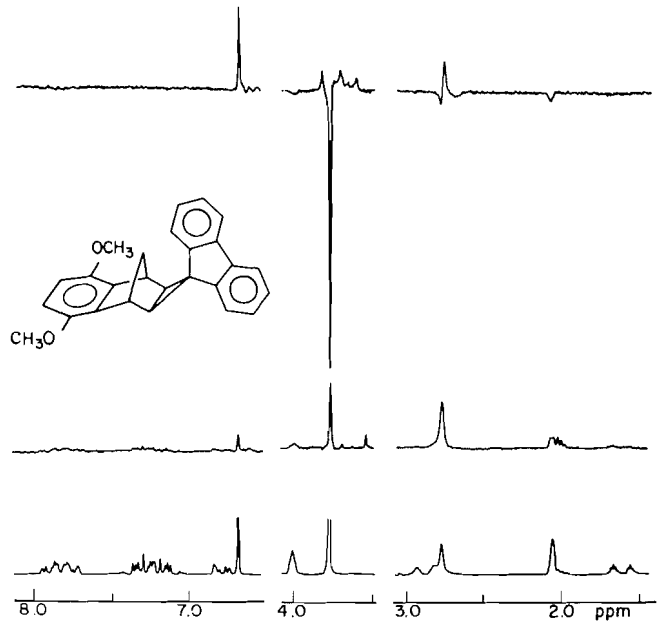

FIG. 3. The ^{1}H nmr spectra (90 MHz) of a concentrated acetone-d_6 solution (0.2 *M*) of the [1.2]benzo[5:6]cyclopropanorbornene, **12** (bottom) and net intensity changes ($I_{irr} - I_{dark}$) observed during uv irradiation of 0.02 *M* chloranil in an acetone-d_6 solution containing 0.02 *M* **12** (top).

either with a homohyperconjugative interaction (structure type **14**) or with a delocalization of spin onto the quaternary cyclopropane carbon (structure type **15**). The latter structure can be viewed as a π complex of a fluorenylidene radical cation with benzonorbornadiene, i.e. as a derivative of the $^2B_2$ structure (*vide supra*). The experimental results do not allow us to differentiate between structure types **14** and **15**.

As for the absence of delocalization of spin into the tertiary–tertiary carbon–carbon bond, a comparison with the polarization generated in the radical cation of benzonorbornadiene (**16**) is illuminating. In this molecule, the aromatic and olefinic π orbitals are in an orientation favoring delocalization. The polarization effects observed during the photoreaction of chloranil with **16** show identical signs and comparable magnitudes for olefinic and aromatic protons, indicating extensive delocalization of spin (and charge) into the olefinic moiety (Fig. 4). In contrast, the tertiary–tertiary bond of **12** is orthogonal to the aromatic π system. Hence the lack of delocalization.

Bismethanoparacyclophane

Having discussed several systems in which a cyclopropane group and an olefinic or aromatic π system are arranged in close proximity without being conjugated, we now proceed to compounds in which the two groups are conjugated. In principle, the two functionalities can be arranged so that the tertiary–tertiary cyclopropane bond is locked into a position nearly parallel to the normal axis of the aromatic π system or into a position nearly orthogonal to it. [1:2,9:10]Bismethano-[2.2]paracyclophane (**17**) is an interesting example for the parallel arrangement (23). This compound and its radical cation (**18**) obviously are highly strained. An insight into the spin density distribution of the intermediate might reveal how the strain is accommodated.

The CIDNP effects observed during the photoreaction of chloranil with **17** are, in principle, quite similar to those ob-

Can. J. Chem. Downloaded from www.nrcresearchpress.com by 210.87.254.42 on 09/06/12
For personal use only.

Can. J. Chem. Downloaded from www.nrcresearchpress.com by 210.87.254.42 on 09/06/12
For personal use only.

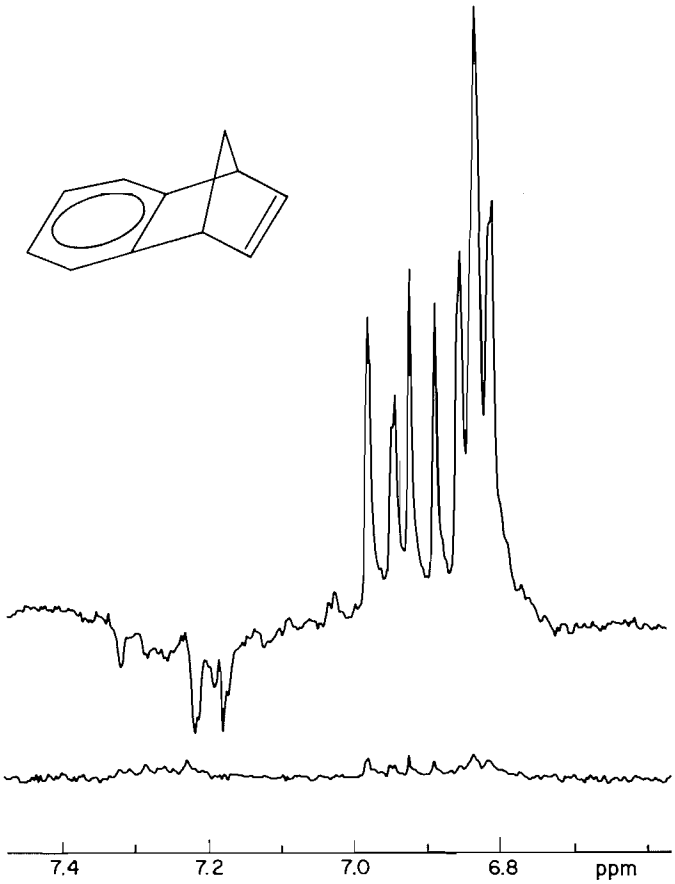

FIG. 4. The ^{1}H nmr spectra (90 MHz; olefinic/aromatic region) of a 0.02 *M* chloranil solution in acetone-d_6 containing 0.02 *M* of benzonorbornadiene (**15**) in the dark (bottom) and during uv irradiation (top).

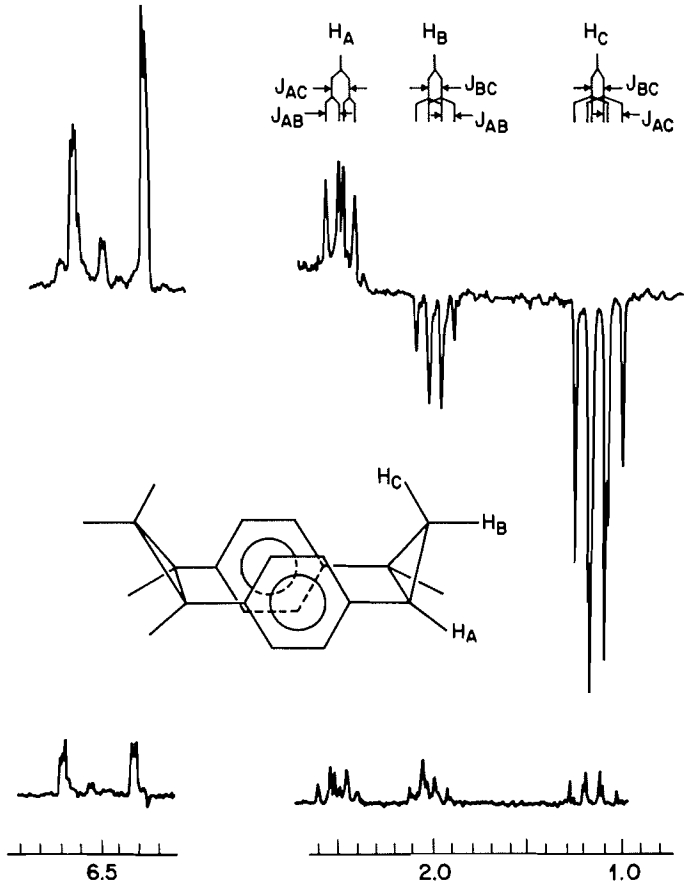

FIG. 5. The ^{1}H nmr spectrum (90 MHz) observed during the irradiation of chloranil (0.02 *M*) in acetone-d_6 solutions containing 0.01 *M* *syn*-[1:2.9:10]bismethano[2.2]paracyclophane. A dark spectrum of the hydrocarbon is shown as the lower trace.

served for *cis*-diphenylcyclopropane (4), indicating an intermediate with an open, delocalized structure not unlike that assigned to the diphenylcyclopropane radical cations. However, the relative signal intensities are noticeably different (Fig. 5). The secondary cyclopropane multiplet assigned to the *endo* proton (1.2 ppm) shows a considerably stronger enhancement than does the multiplet of the *exo* proton (2.0 ppm). In addition, the benzylic multiplet is comparably weaker than in the case of diphenylcyclopropane. The different enhancement factors observed for the two secondary protons are ascribed to nonidentical hyperfine coupling constants. This implies that the

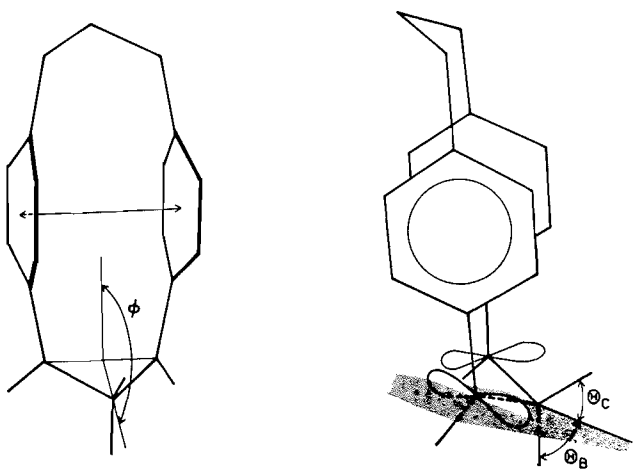

dihedral angles, θ_B and θ_C, between the singly occupied orbital and the two adjacent C—H bonds are different.

Nonidentical dihedral angles for the secondary cyclopropane protons can result if the angle, ϕ, between the plane of the three-membered ring and the plane defined by the benzylic and quaternary carbons, is increased in the radical cation relative to the parent hydrocarbon. The relative magnitude of the CIDNP effects and the chemical shifts of the corresponding protons are fully consistent with this interpretation. The *endo* proton, which in the diamagnetic molecule lies in the shielding cone of the aromatic moieties, has in the radical the smaller dihedral angle θ_C, with the benzylic π orbital and, therefore, the greater hyperfine coupling (24).

The comparably weak enhancement of the benzylic proton requires an additional explanation. This result, and the fact that ^{13}C polarization is observed only for the benzylic carbon signal, can be explained if the benzylic carbon adopts a pyramidal structure. Pyramidal carbon radicals are reasonably rare; most examples are derived from strained ring systems (25–28). For the radical cation discussed here, the change in the angle, ϕ, and the adoption of a pyramidal structure apparently relieve some of the strain in the carbon skeleton, yet maintain a reasonable degree of overlap between the benzylic carbons and the benzene rings (24).

The recent synthesis of [10:11]methano[3.2]paracyclophane (**19**)[2] allowed an extension of this study to a system which

[2]E. A. Truesdale, private communication.

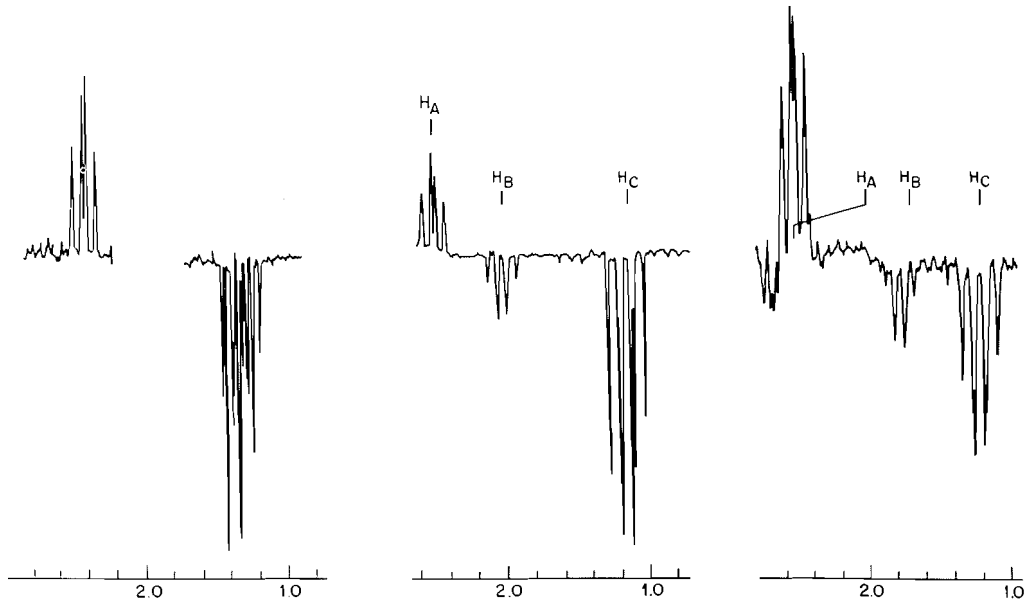

FIG. 6. A comparison of the CIDNP effects observed for the cyclopropane protons of *cis*-diphenylcyclopropane (left), [10:11]methano[3.2]-paracyclophane, **18** (center), and [1:2.9:10]bismethano[2.2]paracyclophane, **16** (right).

appears less strained than **17** yet more restricted than diphenylcyclopropane. The CIDNP effects observed for this hydrocarbon once again show different intensities for the two geminal cyclopropane protons. However, the enhancement pattern is closer to that of *cis*-diphenylcyclopropane than to that of **17** (Fig. 6). Obviously, a large fraction of the strain inherent in **17** is relieved by substituting a trimethylene bridge for one of the cyclopropane moieties (24).

Benzonorcaradiene

The final arrangement of cyclopropane ring and aromatic/olefinic group to be discussed in this paper is one in which the 3°−3° cyclopropane bond is essentially orthogonal to the π system. The benzonorcaradiene system (**20**) is a good example of this arrangement. This substrate is also of interest since its pattern of substitution may stabilize the alternative structure type for the cyclopropane radical cation. If spin and charge were localized on or near the methylene group, the remaining carbon frame would form a cyclic conjugated 10 π electron system whose stabilization may outweigh the potential lack of stability of the "methylene cation".

Benzonorcaradiene is one of four $C_{11}H_{10}$ hydrocarbons formally derived from naphthalene by addition of methylene to the four types of carbon−carbon bonds. Each of the hydrocarbons offers the possibility of an equilibrium between a bicyclic (cycloheptatriene) and a tricyclic (norcaradiene) valence isomer. However, the equilibria are decidedly one-sided: for three isomers the bicyclic structure is favored whereas for the fourth the tricyclic structure is preferred. The aromaticity of some of the valence isomers appears to be a key element in determining the preferred structure type: the four stable forms contain a cyclic conjugated system of either 6 or 10 π electrons whereas the unfavorable valence isomers are polyolefins. The four hydrocarbons can be interconverted through thermal, photochemical, or base-catalyzed reactions (29−31). Accordingly, the potential rearrangement of the radical cations cannot be neglected. Similarly, the deprotonation of the cations has to be considered, since it may play a role in the rearrangement of some of these radical cations.

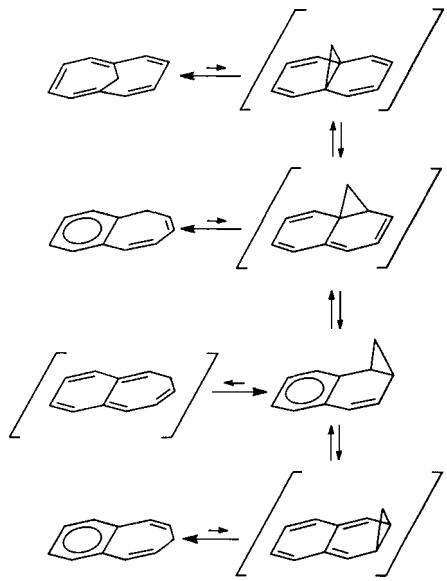

Three structure types can be envisioned for the radical cation of benzonorcaradiene. The first structure is essentially a styrene radical cation in which charge and spin are delocalized over eight carbon atoms and in which the cyclopropane ring is unaffected (**21**). In the second structure, the 3°−3° cyclopropane bond is broken and charge and spin are delocalized over ten carbon atoms (**22**). This structure implies a thorough reorganization of the three cyclopropane carbon atoms and its formation may require a substantial activation energy. The third structure is one in which the secondary cyclopropane carbon bears spin density and in which the two 3°−2° bonds are weakened. This structure is essentially a linear combination of structure **21** and the structure formed by removal of an electron from the antisymmetrical cyclopropane HOMO (**23**) and is related to the $^2B_2$ state of the cyclopropane molecular ion.

All three structures lead one to expect qualitatively the same result for the aromatic and olefinic protons. The unpaired spin density could be positive throughout the π system or could

Can. J. Chem. Downloaded from www.nrcresearchpress.com by 210.87.254.42 on 09/06/12
For personal use only.

Can. J. Chem. Downloaded from www.nrcresearchpress.com by 210.87.254.42 on 09/06/12
For personal use only.

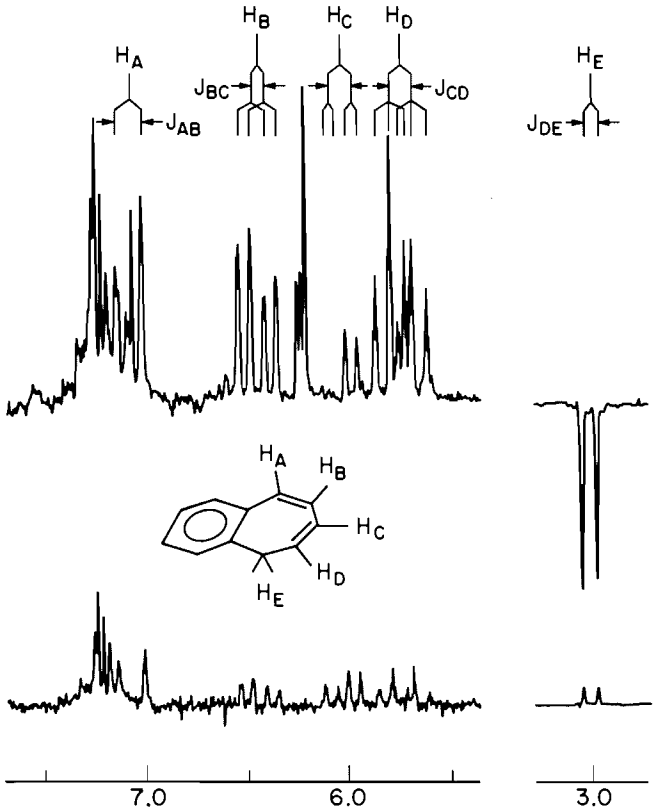

FIG. 7. The ^{1}H nmr spectra (90 MHz) of 0.02 *M* chloranil solutions in acetone-d_6 containing 0.02 *M* benzocycloheptatriene, **24**, in the dark (bottom) and during uv irradiation (top).

TABLE 1. Nuclear spin polarization observed for benzonorcaradiene and hyperfine coupling patterns of related radical ions

	21	**22**	**21 ↔ 23**	CIDNP
H_{arom}	−	−	−	A
H_{olef}	−	−	−	A
H_A	+	−	+	E
H_B	+	−	+	E
H_C		+	−	A
H_D		+	−	A

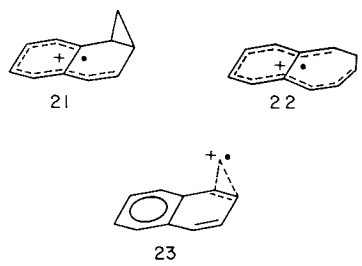

show an alternating pattern. The analogy with a related $C_{11}H_{10}$ system suggests the former spin density pattern. Benzocycloheptatriene (**24**) gives rise to a CIDNP spectrum in which essentially all aromatic/olefinic protons show enhanced absorption and in which the benzylic/allylic doublet shows strong emission (Fig. 7).

In contrast to the aromatic/olefinic protons, the four cyclopropane protons of **20** are expected to show characteristic differences. The polarization patterns expected for the first two structures are analogous to those discussed for the "closed" and

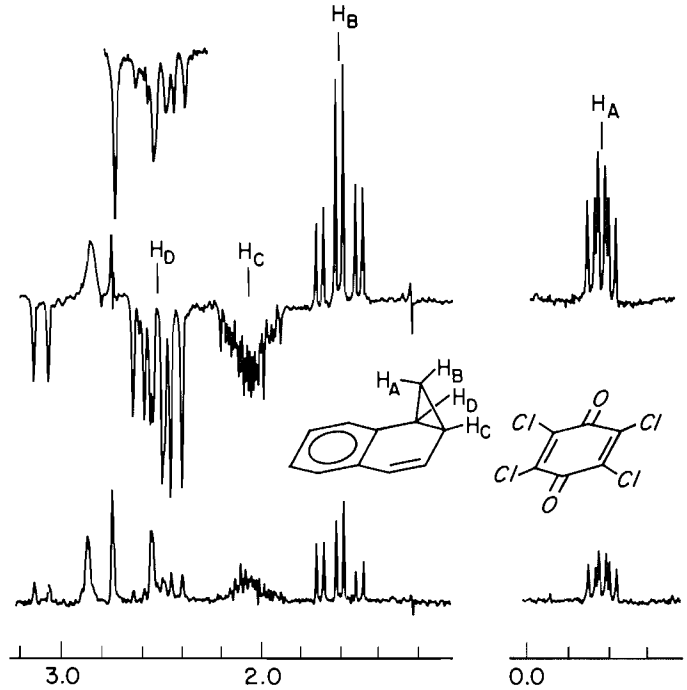

FIG. 8. The 90 MHz nmr spectra of 0.02 *M* chloranil solutions in acetone-d_6 containing 0.02 *M* benzonorcaradiene, **20**, in the dark (bottom) and during uv irradiation (center). The top trace (2.0−3.0 ppm) was recorded during the irradiation of 0.02 *M* chloranil in the presence of 0.002 *M* benzonorcaradiene.

"open" radical cation of diphenylcyclopropane (4). The third structure is unique since the secondary protons have negative hyperfine couplings whereas the tertiary ones have positive couplings. The hyperfine coupling patterns of these three structures are compared in Table 1.

The irradiation of chloranil in the presence of benzonorcaradiene results in substantial polarization for all ^{1}H signals of the substrate. The aromatic and olefinic protons appear in enhanced absorption as is expected for nuclei attached to carbons with positive spin density. Of the cyclopropane protons, the benzylic one (d of d of d; 2.5 ppm) and the allylic one (d of d of d of d; 2.1 ppm) appear in emission whereas the two geminal protons (d of t; 1.6 and −0.4 ppm) appear in enhanced absorption (Fig. 8). This polarization pattern is essentially that expected for the unique structure, **21** ↔ **23**, with spin density on the secondary carbon atom.

To make this assignment with confidence, an alternative explanation for the observed pattern must be eliminated. Nuclear spin polarization is occasionally observed for nuclei which do not possess a hyperfine coupling in the intermediate radial (ion). These effects are due to polarization transfer by dipolar or scalar cross relaxation (32−35). For the benzonorcaradiene radical cation, the polarization observed for the secondary protons (absorption) could be caused by dipolar cross relaxation of the tertiary protons (emission). Thereby, the radical cation of structure **21** would give rise to the same polarization pattern as that expected for **21** ↔ **23**.

Effects caused by cross relaxation can be identified by spin decoupling experiments. Closs and Czeropski have shown that primary polarization is not affected in these experiments but that secondary polarization vanishes when the nucleus with the primary polarization is irradiated (32, 33). For the system discussed here, the decoupling of the benzylic and the allylic

Can. J. Chem. Downloaded from www.nrcresearchpress.com by 210.87.254.42 on 09/06/12
For personal use only.

protons is crucial since they would be the logical source for any secondary polarization in the geminal protons. Accordingly, the transitions at 184 and 223 Hz and their average frequency were saturated while the photoreaction of chloranil with benzonorcaradiene was in progress. This caused the geminal multiplets to be simplified but did not cause the polarization of these multiplets to vanish. In the light of these results cross relaxation can be eliminated as an important contributor to the observed polarization and the structure **21** ↔ **23** is confirmed for the radical cation of benzonorcaradiene.

Further support for this assignment is derived from the observation of polarized 1- and 2-methylnaphthalene (emission, 2.7 and 2.5 ppm, respectively) at low benzonorcaradiene concentrations. The formation of these products is explained readily by transfer of a hydrogen atom from either the benzylic or the allylic position to the secondary cyclopropane carbon of **23**, followed by reverse electron transfer. The signal direction of the methyl groups is opposite to that of the geminal cyclopropane protons suggesting that the methylnaphthalenes are formed from the intermediate radical pair by a mechanism with a different electron spin dependence. This could be a mechanism involving the separation of the radical ions by diffusion or one involving triplet recombination of the intermediate pair. The information available at present does not permit us to identify the detailed chemical mechanism by which the methylnaphthalenes are formed.

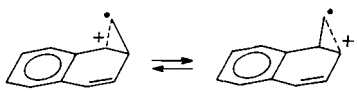

[9:10]Methanoacenaphthene

Another substrate in which an aromatic π electron system is arranged in a position orthogonal to the 3°−3° bond of a cyclopropane ring is [9:10]methanoacenaphthene (**25**) (36, 37). The principal geometric features of this molecule are similar to those of benzonorcaradiene. There is, however, an important difference. The radical cation structure resembling a π complex (**28**) does not appear to have the same stabilization for the cation of **25** that it has for the cation of **20**. Accordingly, a naphthalene type radical cation, **26**, is a more likely structure than is the cyclopropane radical cation, **28**. The alternative structure, **27**, in which the cyclopropane ring is opened and in which the benzylic carbons have positive spin density is unlikely because of the unfavorable (orthogonal) orientation of the 3°−3° cyclopropane bond relative to the naphthalene π system.

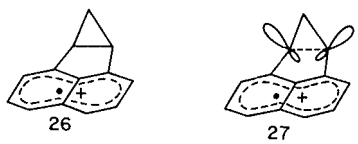

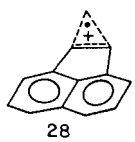

The CIDNP effects observed for this substrate during the photoreaction with chloranil are weak and they are observed only at low substrate concentrations. The aromatic multiplets show enhanced absorption whereas the multiplet representing the tertiary (benzylic) protons appears in emission. These findings are compatible with an intermediate of structure **26**, and they rule out an intermediate of structure **27**. However, it should be noted that they do not completely eliminate a contribution from structure **28**. An intermediate of this structure is likely to have negative hyperfine coupling constants for the secondary cyclopropane protons and thus should give rise to enhanced absorption for the multiplets representing them. The magnitude of the hyperfine coupling constants (and the intensity of the CIDNP effects) will depend on the contribution of structure **28** to the radical cation.

The absence of significant polarization for these protons rules out a dominant contribution due to that structure. *However, the overall low level of polarization does not allow us to set a low upper limit for its involvement.* One argument against the participation of structure **28** lies in the failure to observe cyclopropane ring opening and formation of 9-methylacenaphthylene. In the reaction of benzonorcaradiene (*vide supra*), we considered the observation of methylnaphthalenes an important argument in favor of structure **23**, the equivalent of structure **28**.

Accordingly, we identify **26** as the intermediate derived from **25**. However, we emphasize that the observed effects are weak and that the comparison with the results observed for benzonorcaradiene is an important factor in this assignment.

Conclusion

The radical cations of a series of hydrocarbons containing a cyclopropane moiety can be generated as short-lived intermediates by photoinduced electron transfer to chloranil. In general, the radical cations tend to favor the trimethylene structure type in which one carbon−carbon bond is broken or weakened. Steric factors may induce special features such as the pyramidal structure of the radical cation of bismethanoparacylcophane. In other cases, an interaction of the 3°−3° cyclopropane bond with the unpaired spin may be prevented. For example the benzomethanonorbornene (**12**) forms a radical cation in which the 3°−3° bond is unaffected and in which only the protons interact with the unpaired spin (possibly by a homohyperconjugative mechanism). Special substitution patterns may favor a radical cation structure, which can be described as a π complex between a methylene radical cation and an appropriate π system. An example of such a structure is the radical cation of benzonorcaradiene. The stability of this structure is ascribed to the aromaticity of the ten-carbon complement to the methylene radical cation.

The finding that tri- and tetraalkyl-substituted cyclopropanes are marginal donors and that they surpass disubstituted olefins, makes it possible to probe the mechanism of photosensitized dehydrogenation of appropriate substrates. For tricyclo-[4.4.1.$0^{1,6}$]undeca-3,8-diene and bicyclo[4.1.0]hept-3-ene, the polarization of the dehydrogenation products identifies cyclopropane radical cations as primary intermediates in the dehydrogenation reaction.

Acknowledgements

We are indebted to several colleagues for generous gifts of some of the donor molecules. A. A. Lamola provided the methanobenzonorbornene (19, 20), E. A. Truesdale the methanoparacyclophanes (23, 24), and R. Pagni the methanoacenaphthene (36−38).

1. H. D. ROTH and M. L. M. SCHILLING. J. Am. Chem. Soc. **102**, 4303 (1980).
2. H. D. ROTH and M. L. M. SCHILLING. J. Am. Chem. Soc. **103**, 7210 (1981).
3. H. D. ROTH. *In* Chemically induced magnetic polarization. *Edited by* L. T. Muus *et al*. Reidel, Dordrecht, The Netherlands. 1977. p. 39.
4. H. D. ROTH and M. L. M. SCHILLING. J. Am. Chem. Soc. **102**, 7956 (1980).
5. H. D. ROTH and M. L. M. SCHILLING. J. Am. Chem. Soc. **103**, 1246 (1981).
6. H. BASCH, M. B. ROBIN, N. A. KUEBLER, C. BAKER, and D. W. TURNER. J. Chem. Phys. **51**, 52 (1969).
7. R. S. BUENKER and S. D. PEYERIMHOFF. J. Phys. Chem. **73**, 1299 (1969).
8. D. W. TURNER, A. D. BAKER, C. BAKER, and C. R. BRUNDLE. Molecular photoelectron spectroscopy. Wiley–Interscience, New York. 1970.
9. E. LINDHOLM, C. FRIDH, and L. J. ASBRINK. Faraday Discuss. Chem. Soc. **54**, 127 (1972).
10. G. BIERI, F. BURGER, E. HEILBRONNER, and J. P. MAIER. Helv. Chim. Acta. **60**, 2213 (1977).
11. R. GLEITER. Top. Curr. Chem. **86**, 197 (1980).
12. J. R. COLLINS and G. A. GALLUP. J. Am. Chem. Soc. **104**, 1504 (1982).
13. H. D. ROTH and M. L. M. SCHILLING. Submitted for publication.
14. H. D. ROTH. Dissertation, University of Cologne, 1965.
15. E. VOGEL and H. D. ROTH. Angew. Chem. **76**, 145 (1964); Angew. Chem. Int. Ed. Engl. **3**, 228 (1964).
16. P. H. NELSON and K. G. UNTCH. Tetrahedron Lett. 4475 (1969).
17. E. VOGEL, W. KLUG, and A. BREUER. Org. Synth. **54**, 11 (1974).
18. J. R. DEMEMBER and N. FILIPESCU. J. Am. Chem. Soc. **90**, 6425 (1968).
19. N. FILIPESCU and J. R. DEMEMBER. Tetrahedron, **24**, 5181 (1968).
20. A. A. LAMOLA. J. Am. Chem. Soc. **91**, 4786 (1969).
21. T. M. MCKINNEY and D. H. GESKE. J. Am. Chem. Soc. **87**, 3013 (1965).
22. L. EBERSON and K. NYBERG. J. Am. Chem. Soc. **88**, 1686 (1966).
23. E. A. TRUESDALE and R. S. HUTTON. J. Am. Chem. Soc. **101**, 6476 (1979).
24. H. D. ROTH, M. L. M. SCHILLING, R. S. HUTTON, and E. A. TRUESDALE. J. Am. Chem. Soc. **105**, 153 (1983).
25. T. KAWAMURA, M. TSUMURA, Y. YOKOMICHI, and T. YONEGAWA. J. Am. Chem. Soc. **99**, 8251 (1977).
26. R. W. FESSENDEN. J. Phys. Chem. **71**, 74 (1967).
27. K. OHTA, H. NAKATSUJI, K. HIRAO, and T. YONEZAWA. J. Chem. Phys. **73**, 1770 (1980).
28. G. BEHRENS and D. SCHULTE-FROLINDE. Angew. Chem. **85**, 993 (1973).
29. E. VOGEL, D. WENDISCH, and W. R. ROTH. Angew. Chem. Int. Ed. Engl. **3**, 443 (1964).
30. M. POMERANTZ and G. W. GRUBER. J. Org. Chem. **33**, 4501 (1968).
31. M. POMERANTZ and G. W. GRUBER. J. Am. Chem. Soc. **89**, 6798 (1967); **89**, 6799 (1967).
32. G. L. CLOSS and M. S. CZEROPSKI. J. Am. Chem. Soc. **99**, 6127 (1977).
33. G. L. CLOSS and M. S. CZEROPSKI. Chem. Phys. Lett. **53**, 321 (1978).
34. R. KAPTEIN. Nature, **274**, 293 (1978).
35. G. J. GARSSEN, R. KAPTEIN, J. G. G. SCHOENMAKERS, and C. W. HILBERS. Proc. Natl. Acad. Sci. USA **75**, 5281 (1978).
36. G. WITTIG, V. RAUTENSTRAUCH, and F. WINGLER. Tetrahedron Suppl. **7**, 189 (1966).
37. J.-F. MULLER, D. MULLER, H. J. DEWEY, and J. MICHL. J. Am. Chem. Soc. **100**, 1629 (1978).
38. M. GISIN, E. ROMMEL, J. WIRZ, M. N. BURNETT, and R. M. PAGNI. J. Am. Chem. Soc. **101**, 2216 (1979).

Can. J. Chem. Downloaded from www.nrcresearchpress.com by 210.87.254.42 on 09/06/12
For personal use only.

The reaction of F atoms with CH_3SH. Vibrational spectroscopy and photochemistry of CH_3S and CH_2SH hydrogen-bonded to HF

MARILYN E. JACOX

Molecular Spectroscopy Division, National Bureau of Standards, Washington, DC 20234, U.S.A.

Received January 11, 1983

This paper is dedicated to Professor Harry E. Gunning on the occasion of his 65th birthday

MARILYN E. JACOX. Can. J. Chem. **61**, 1036 (1983).

When the products of the reaction between F atoms formed in a microwave discharge and methanethiol are frozen in a large excess of argon at 14 K, prominent absorptions of isolated and hydrogen-bonded HF appear, indicating that hydrogen abstraction occurs both in the deposition beam and in the solid. Secondary F-atom reactions play only a minor role. Studies of the partially deuterium-substituted methanethiols support the assignment of peaks at 3515 and 3672 cm^{-1} to the HF-stretching modes of HF hydrogen-bonded to CH_3S and CH_2SH, respectively, and indicate that CH_2SH is formed with enough excess energy to surmount the barrier for rearrangement to CH_3S. Although ground-state rearrangement of the thermochemically more stable isomer, CH_3S, to CH_2SH was not observed, when the sample was excited by radiation in the spectral region of a known electronic transition of CH_3S, isomerization to CH_2SH resulted. The present experiments cannot distinguish between direct isomerization and formation of CH_2SH by the cage recombination of CH_2S + H. Although peaks attributable to CH_3S isolated in solid argon are weak, the experiments provide some support for a recent assignment of vibrational fundamentals of CD_3S, based on photodetachment studies. A prominent, structured absorption at 424 cm^{-1} is assigned to the H_2CS "umbrella" deformation of CH_2SH, consistent with a recent *ab initio* calculation. The photodecomposition threshold of CH_2SH lies between 260 and 280 nm.

MARILYN E. JACOX. Can. J. Chem. **61**, 1036 (1983).

On observe des absorptions marquées dues au HF et au HF lié par des liaisons hydrogènes, lorsqu'on gèle dans un grand excès d'argon à 14 K les produits de la réaction entre les atomes de fluor issus d'une décharge de microonde, et le méthanethiol. Ces absorptions indiquent que l'élimination d'hydrogène se produit à la fois dans le faisceau de dépôt et dans le solide. La participation des réactions secondaires du fluor est minime. Des études portant sur le méthanethiol partiellement deutéré confirment l'attribution des pics à 3515 et à 3672 cm^{-1} aux modes d'élongation du HF des molécules de HF liées par des liaisons hydrogènes au CH_3S et au CH_2SH respectivement et indiquent que le CH_2SH formé a suffisamment d'énergie pour franchir la barrière de la transposition en CH_3S. Dans l'état stationnaire, on n'a pas observé la transposition de l'isomère le plus stable CH_3S en CH_2SH, cependant il s'isomérise en CH_2SH lorsqu'on excite un échantillon par une radiation de la région spectrale correspondant à la transition électronique du CH_3S. Ces expériences ne permettent pas d'établir une distinction entre l'isomérisation directe et la formation de CH_2SH par la recombinaison du CH_2S + H dans la cage. Bien que les pics attribuables au CH_3S isolé dans l'argon solide soient faibles, les expériences constituent un apport aux récentes attributions des vibrations fondamentales du CD_3S basées sur des études de photodétachement. On attribue une absorption marquée et structurée à 424 cm^{-1} à la déformation du H_2CS en "parapluie" en accord avec les récents calculs *ab initio*. Le désordre de la photodécomposition du CH_2SH se situe entre 260 et 280 nm.

[Traduit par le journal]

Introduction

Although an important role has been established for CH_3S free radicals in a variety of photolysis systems (1–3), their direct spectroscopic detection has been extraordinarily difficult. Flash photolysis studies by Callear *et al.* (4, 5) have provided chemical evidence for the assignment of a diffuse, unstructured absorption at 218.5 nm to the CH_3S free radical. Studies by Rosengren (6) and by Goldberg (7) had suggested that this radical should also have an electronic transition in the 400–370-nm spectral region. Their observations were confirmed by Tanaka and co-workers (8), who assigned an emission band system with origin near 378 nm to CH_3S and attributed a band spacing of 670 ± 75 cm^{-1} to the CS-stretching vibration. A similar band spacing was attributed to this fundamental of CH_3S in the photodetachment studies of Lineberger and co-workers (9), who assigned the CH_3 "umbrella" vibration at 1040 ± 80 cm^{-1}. In contrast, the photodetachment studies by Janousek and Brauman (10), which included studies of the deuterated molecule, suggested the assignment of these two fundamentals of CH_3S at 770 ± 50 cm^{-1} and 1360 ± 70 cm^{-1}, respectively.

The production of CH_3S in photolysis systems is complicated by the prevalence of secondary photodecomposition and by the multiplicity of the possible reactions of photodetached sulfur atoms. Such processes are important even for the mercury-arc photolysis of methanethiol isolated in inert solids at cryogenic temperatures (11). Recent studies by Dill and Heydtmann (12) and by Nesbitt and Leone (13) have provided evidence for the formation of both CH_3S and CH_2SH upon the reaction of fluorine or chlorine atoms with methanethiol. Although both of these studies were focused on the extent of vibrational excitation of the hydrogen halide product, the technique offers a promising route for generating the free radicals in sufficient concentration for direct spectroscopic characterization, without the complications which accompany photochemical generation of these species.

Recently, an experimental configuration has been developed in this laboratory which has permitted the trapping in solid argon at 14 K of a sufficient concentration of primary F-atom reaction products for study of their infrared spectra. In experiments on the F + CH_4 reaction (14), the principal product absorptions were assigned to isolated HF and CH_3 and to both

Can. J. Chem. Downloaded from www.nrcresearchpress.com by 210.87.254.105 on 09/06/12
For personal use only.

Can. J. Chem. Downloaded from www.nrcresearchpress.com by 210.87.254.105 on 09/06/12
For personal use only.

CH_3 and CH_3F hydrogen-bonded to HF. Although in a study of the F + CH_3OH system (15) only the lowest energy free radical, CH_2OH, was observed, in studies of the F + CH_3CHO reaction (16) infrared absorptions of both the acetyl and the vinoxy (formyl methyl) radical were prominent . These experiments also yielded photodecomposition thresholds and products for the free radicals formed in the primary reaction. The conduct of similar experiments on methanethiol not only may provide new spectral and photochemical data for the primary radical products but also may enhance our understanding of the dynamics of F-atom reaction. Although CH_2OH is thermodynamically somewhat more stable than is CH_3O, for the corresponding sulfur-containing radicals the reverse is true; CH_3S has been estimated (12) to be approximately 27 kJ/mol more stable than CH_2SH. This paper reports the results of such a study.

Experimental[1]

Samples of CH_3SH (Matheson Co., Inc.) and of CH_3SD, CD_3SH, and CD_3SD (Merck, Sharp, and Dohme of Canada, Ltd.) used for these experiments were freed of traces of relatively volatile impurities by pumping on the solid deposit at 77 K. Ar/CH_3SH-d_n samples of mole ratio 100 and 200 were prepared using standard manometric procedures. Ar/NF_3 samples of mole ratio 200 to 800 were used as F-atom sources. The Ar/NF_3 sample was introduced into the system through an Al_2O_3 tube with a pinhole having a diameter of between 1 and 2 mm. F atoms were produced in this discharge tube by microwave excitation, using 10 to 15% of the output of a 125-W, 2450-MHz microwave power supply. The Ar/CH_3SH-d_n sample was introduced into the system outside the discharge tube, in approximately the plane of the pinhole, and the reaction products were deposited on the cryogenic surface 2.5 cm downstream. The use of the Al_2O_3 tube completely eliminated SiF_4 from the reaction products, and there was no evidence for any aluminum-containing products. Studies in other experimental systems (14–16) have indicated that the primary hydrogen-abstraction reaction predominates under these experimental conditions, with a smaller yield, dependent on the F-atom concentration, of the product of the abstraction of a second hydrogen atom. There is no evidence for the participation of NF or NF_2 in secondary reactions; infrared absorptions of such species as HNF_2, HNF, *c*- and *t*-N_2F_2, and N_2F_4 have not been detected.

The cryogenic equipment and sample observation configuration (17) have previously been described. All observations were conducted at 14 K. After the infrared spectrum of the initial deposit had been recorded, the sample was subjected to the filtered radiation of a medium-pressure mercury arc in order to determine the threshold and products of secondary photodecomposition. Although observations were conducted with a variety of glass filters, the Corning filter of glass type 7740, with a short wavelength cutoff of 280 nm, was most useful for these studies.

Infrared spectra were recorded using a Beckman IR-9 spectrophotometer. Under the scanning conditions typical of these experiments, the relative and absolute frequency accuracies are estimated to be 1 cm^{-1} between 400 and 2000 cm^{-1} and 2 cm^{-1} between 2000 and 4000 cm^{-1}. The 275–400-cm^{-1} spectral region was also scanned for some of the deuterium-containing samples, using the CsI long wavelength interchange for this spectrophotometer. Because of the low signal level, the resolution and the relative and absolute frequency accuracies are estimated to be 5 cm^{-1} in this spectral region.

[1]Certain commercial instruments and materials are identified in this paper in order to specify adequately the experimental procedure. In no case does such identification imply recommendation or endorsement by the National Bureau of Standards, nor does it imply that the instruments or materials identified are necessarily the best available for the purpose.

Observations

In the previously reported (11) study of the photolysis of methanethiol in argon and nitrogen matrices, the most prominent product absorptions were those of H_2CS, CS, CS_2, and CH_4. However, several weaker absorptions which could not be definitively assigned may have been contributed by CH_3S or by CH_2SH. The positions and peak optical densities of the product absorptions in a typical study (designated as Experiment A) of the 121.6-nm photolysis of an Ar/CH_3SH = 200 sample are summarized in the first two columns of Table 1. Although the infrared spectrum of a previously unphotolyzed Ar/CH_3SH = 200 deposit was unchanged even on prolonged exposure of the sample to mercury-arc radiation of wavelength longer than 280 nm, marked changes occurred on exposure of the photolyzed deposit to radiation in this same spectral range. The peak optical densities which were observed at this stage of Experiment A are summarized in the third column of Table 1. There was little change in the intensities of the H_2CS and CH_4 absorptions under these photolysis conditions, but the absorption of CS diminished slightly in intensity and the 1479-cm^{-1} $^{13}CS_2$ peak and the 2180-cm^{-1} combination band of $^{13}CS_2$ grew, suggesting that some S-atom photodetachment occurred. Several unassigned absorptions diminished significantly in intensity, while a pair of relatively prominent absorptions at 424 and 431 cm^{-1} and a very weak absorption at 554 cm^{-1} grew substantially.

The peak optical densities of the product absorptions in a study (designated as Experiment B) of the reaction of a very low concentration of F atoms (Ar/NF_3 = 800) with CH_3SH are summarized in the fourth column of Table 1. Evidence for the occurrence of H-atom abstraction is provided by the appearance of infrared absorptions characteristic of HF isolated in solid argon (18) at 3886, 3922, and 3968 cm^{-1}. The moderately intense peak at 939 cm^{-1} corresponds to the strongest absorption of SF_6 in an argon matrix (19). Presumably this product results from the backstreaming of a small fraction of the methanethiol into the discharge region. There was little evidence for the infrared absorptions of other SF_n molecules (19) in the present series of experiments. The absorptions of CS and CS_2 which resulted from extensive secondary photodecomposition and S-atom reactions in Experiment A were completely absent from this and other F-atom reaction studies, and the most prominent peaks of H_2CS were diminished by a factor of approximately four. (The intensity of the 1056-cm^{-1} H_2CS absorption was relatively uncertain because of spectral interference by a nearby CH_3SH absorption.) A peak at 424 cm^{-1} was common to both systems. In the F-atom reaction study, its high-frequency satellite was shifted by 2 cm^{-1}, to 433 cm^{-1}. This peak is close to a band which has previously been attributed to HF aggregates in the solid (14), suggesting that their contribution may have led to the small but consistent frequency shift. Also common to both experimental systems was a weak absorption at 663 cm^{-1}. Because this peak lies very close to that of CO_2 isolated in solid argon, a contribution from a weakly absorbing photolysis or reaction product would be relatively uncertain. Prominent new absorptions appeared at 442, 569, 595, and 765 cm^{-1}, as well as between 3450 and 3700 cm^{-1}, the spectral region characteristic of the very strong HF-stretching absorptions of its hydrogen-bonded complexes.

Spectral regions in which major product absorptions appear are shown in the solid trace of Fig. 1 for an Ar/CH_3SH = 100 sample codeposited with a discharged Ar/NF_3 = 200 sample,

Can. J. Chem. Downloaded from www.nrcresearchpress.com by 210.87.254.105 on 09/06/12
For personal use only.

TABLE 1. Peak optical densities of 122-nm photolysis product absorptions compared to those of F-atom reaction product absorptions for CH_3SH isolated in solid argon[a]

	Experiment A		Experiment B	Experiment C		
cm^{-1}	Initial	$\lambda>280$	Initial	Initial	$\lambda>280$	Assignment
424	0.068	0.106	0.047	0.088	0.181	CH_2SH
431	0.052	0.078				CH_2SH
433			0.025	0.053	0.063	CH_3SH, $(HF)_n$
442			0.030	0.035	0.009	
462				0.014	0.011	$(HF)_n$
535			0.014	0.014	0.018	
554	0.009	0.027				
569			0.065	0.079	0.052	
595			0.049	0.043	0.018	
652			0.009	0.012	0.000	
663	0.021	0.019	0.009	0.014	0.018	CO_2, ?
765			0.076	0.091	0.071	
770			0.019	0.020	0.007	F_2CO, ?
776			0.019	0.010	0.014	
785					0.019	
804	0.034	0.014				
814				0.020	0.024	FNO_2, ?
815	0.149	0.111				
939			0.056	0.037	0.036	SF_6
988	0.115	0.113	0.035	0.038	0.054	H_2CS
994	0.207	0.207	0.046	0.050	0.061	H_2CS
1056	0.017	0.023	0.010	0.017	0.028	H_2CS
1063	0.018	0.024				H_2CS
1179	0.039	0.031				
1276	0.818	0.773				CS
1305	0.312	0.312		0.015	0.015	CH_4
1310				0.015	0.015	
1380					0.022	
1397			0.015	0.022	0.000	
1479	0.024	0.029				$^{13}CS_2$
1529	∞	∞				$^{12}CS_2$
1752	0.059	0.053				
2052	0.025	0.041				OCS
2180	0.033	0.038				CS_2
2972	0.030	0.043				H_2CS
3028	sh					CH_4, H_2CS
3478			0.025	0.035	0.029	
3515			0.267	0.258	0.218	$CH_3S\cdots HF$
3652			0.065	0.043	0.051	
3672			0.121	0.163	0.186	$CH_2SH\cdots HF$
3886			0.037	0.068	0.061	HF
3922			0.031	0.046	0.046	HF
3968			0.170	0.137	0.148	HF

[a]Experiment A, $Ar/CH_3SH = 200$ deposited with concurrent hydrogen-discharge photolysis; Experiment B, $Ar/CH_3SH = 200$ codeposited with discharged $Ar/NF_3 = 800$; Experiment C, $Ar/CH_3SH = 100$ codeposited with discharged $Ar/NF_3 = 200$.

and the peak optical densities of all of the F + CH_3SH reaction product absorptions observed in this experiment (designated as Experiment C) are summarized in the fifth column of Table 1. Trace atmospheric impurities in the NF_3 sample lead to the appearance of prominent FNO absorptions in all of the discharge experiments. In the more concentrated F-atom experiments, peaks of FNO_2, FCO, and F_2CO are also present. These peaks have been included in Table 1 only when they changed in intensity on photolysis, suggesting that another product absorption may overlap. Although the peak optical densities of most of the product absorptions were somewhat greater than in Experiment B, the only new absorptions to appear were weak to moderately intense peaks at 462, 814, 1305, and 1310 cm^{-1}. The 814-cm^{-1} peak, which corresponds closely to a prominent product absorption in the photolysis experiments, was contributed at least in part by FNO_2. The 462-cm^{-1} peak can be assigned to $(HF)_n$ (14) and the 1305-cm^{-1} peak to CH_4. Since the intensities of the H_2CS absorptions were low in the F-atom reaction studies, it is concluded that secondary processes play a relatively minor role.

The presence of O atoms in the discharge suggests that products of their reaction with CH_3SH may be detectable. Tevault *et al.* (20) have attributed numerous infrared absorptions to incompletely characterized products of the O + CH_3SH reaction. In the present experiments, only the weak absorption at 1397 cm^{-1} could be assigned to such a product.

Can. J. Chem. Downloaded from www.nrcresearchpress.com by 210.87.254.105 on 09/06/12
For personal use only.

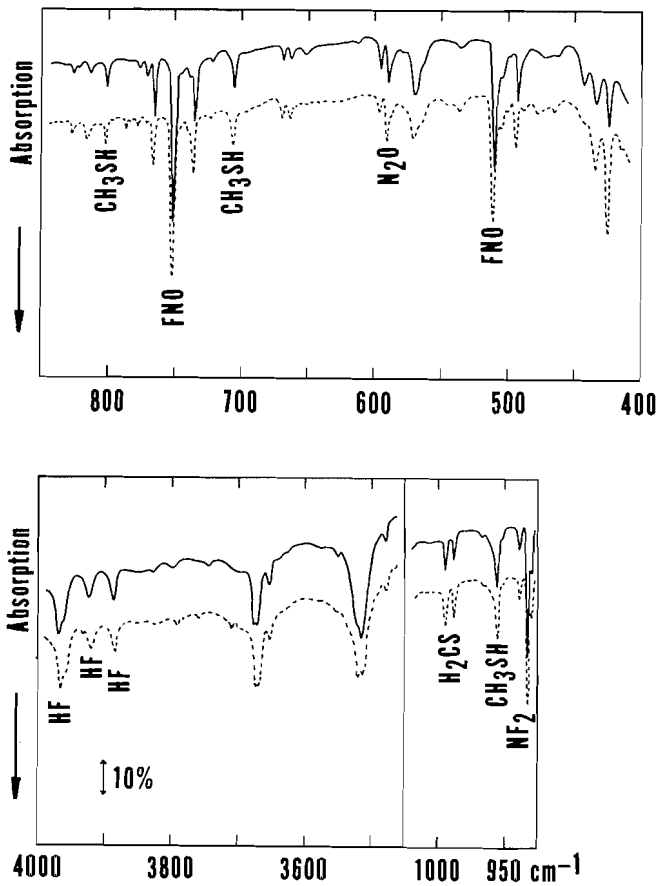

FIG. 1. Spectral regions for major product absorptions; ——— 4.71 mmol Ar/CH_3SH = 100 codeposited over period of 223 min with 3.21 mmol discharged Ar/NF_3 = 200. $[CH_3SH]/[NF_3]$ = 2.9; – – – – 120 min subsequent mercury-arc photolysis, $\lambda > 280$ nm.

When the sample of Experiment C was exposed to mercury-arc radiation with a 280-nm short wavelength cutoff, many of the product absorptions experienced changes in intensity. The spectrum observed at this stage of the experiment is shown in the broken-line trace of Fig. 1, for which the peak optical densities are summarized in the sixth column of Table 1. The marked growth in the intensity of the 424-cm^{-1} peak on 280-nm photolysis in both Experiment A and Experiment C supports its assignment to a common product. The more modest growth in the 433-cm^{-1} peak in the F-atom reaction system is consistent with spectral overlap by the absorption of $(HF)_n$. The 3672-cm^{-1} absorption also grew on 280-nm photolysis. The H_2CS absorptions grew somewhat, but absorptions of CS and CS_2 remained below the limits of detection. Within the experimental error, the intensities of the three absorptions of HF and of the weak CH_4 absorption were unchanged. The very prominent absorption at 3515 cm^{-1} diminished in intensity, as did the peaks at 442, 569, 595, 652, 765, 770, 1397, and 3478 cm^{-1}.

Two experiments were also conducted with the same samples used for Experiment C but with mercury-arc irradiation for a period of 1 to 3 h using a Type 7058 glass filter to give a photolysis cutoff of approximately 260 nm. After the 3-h irradiation, the peaks at 424, 433, 3652, and 3672 cm^{-1} were approximately halved in intensity, absorptions at 535 and 815 cm^{-1} grew to moderate intensity, broad, weak to moderately intense peaks grew in at 623 and 1380 cm^{-1}, the absorptions of H_2CS more than tripled in intensity, and weak to moderately intense absorptions of CH_4 and CS_2 appeared. While the peak optical density of the 3515-cm^{-1} absorption was almost unchanged, it was considerably broadened by the growth of one broad satellite absorption on the low frequency side and of two on the high frequency side.

The positions, peak optical densities, and direction of change on 280-nm photolysis of all of the product absorptions observed between 400 and 4000 cm^{-1} for Ar/CH_3SH-d_n = 200 samples codeposited with discharged Ar/NF_3 = 800 are summarized in Table 2, and the absorption patterns in the spectral regions typical of the HF- and DF-stretching vibrations of hydrogen-bonded complexes are shown in Fig. 2. The invariance of the 939-cm^{-1} peak on deuterium substitution is consistent with its assignment to SF_6.

Almost all of the product absorptions are common to both the Ar/CH_3SH study (Experiment B) and the Ar/CH_3SD experiment. Exchange of the deuterium atom at the walls of the vacuum system would lead to the formation of some CH_3SH in this latter experiment. However, a new, moderately intense peak at 2595 cm^{-1} which diminished in intensity on 280-nm photolysis has a frequency ratio of 0.74 to the 3515-cm^{-1} absorption, suggesting its assignment to the deuterium-stretching counterpart of the higher frequency peak. Furthermore, although in both systems the 424-, 433-, and 3672-cm^{-1} peaks grew significantly on photolysis, in the CH_3SD experiment a new pair of absorptions with a peak optical density of 0.038 appeared at 2700 and 2704 cm^{-1} in the spectrum of the photolyzed sample. (The spectrum was not scanned at this stage of the experiment for the CH_3SH sample of Fig. 2(a), but there was no absorption at this position in the spectra of other photolyzed CH_3SH samples.) The ratio of the mean frequency of this new absorption pair to the 3672-cm^{-1} absorption (which has a partially resolved component at 3666 cm^{-1}) is 0.74, appropriate for the assignment of the new doublet to the deuterium-stretching counterpart of the higher frequency absorption. A very weak absorption at 2898 cm^{-1} may be assigned to isolated DF. (Weak absorptions at 2854 and 2878 cm^{-1} were also present in the spectrum of a simple Ar/CH_3SD = 200 deposit.)

A supplementary experiment was conducted in which an Ar/CH_3SD sample codeposited with F atoms was successively photolyzed through glass filters with decreasing cutoff wavelengths, in order to determine the threshold for the growth in the 424–433-cm^{-1} absorptions on photolysis. The peak intensities of these two absorptions remained constant when filters with a short wavelength cutoff between 490 and 345 nm were used but grew significantly when a 300-nm cutoff filter was substituted.

In studies of the reaction of F atoms with CD_3SH and CD_3SD, the 424–433-cm^{-1} peaks were shifted below the range of the infrared scan with KBr optics. In supplementary experiments using the CsI optical interchange, a pair of product absorptions was reproducibly detected at 322–326 cm^{-1}. Unfortunately, the signal-to-noise ratio was too poor for meaningful comparison of the optical densities of these low frequency peaks before and after 280-nm photolysis. Since the frequency ratio of these two absorptions to that at 424 cm^{-1} is approximately 0.76, it is suggested that the vibration which contributes these absorptions is dominated by hydrogen-atom motion.

In the 430–2600-cm^{-1} spectral region, all of the F + CD_3SH and CD_3SD reaction product absorptions except a weak absorption at 447 cm^{-1} remained constant or diminished in intensity on 280-nm photolysis. The absorptions of both isolated DF and

Can. J. Chem. Downloaded from www.nrcresearchpress.com by 210.87.254.105 on 09/06/12
For personal use only.

TABLE 2. Peak optical densities of product absorptions and their behavior on 280-nm photolysis[a] in studies of the reaction of F atoms with Ar/CH_3SH-d_n = 200 samples

cm^{-1}	CH_3SH	CH_3SD	CD_3SH	CD_3SD	Assignment
424	0.047+	0.037+			CH_2SH
433	0.025+	0.031+			CH_2SH, $(HF)_n$
436			0.029−	0.035−	
442	0.030−	0.035−			
447			0.019+		
463			0.018	0.018	
477			0.014	0.023−	
535	0.014+	0.009+			
545				0.014−	
569	0.065−	0.059−	0.090−	0.087−	
593			0.089−	0.128−	$CD_3S\cdots HF$, DF
595	0.049−	0.053−			
620			0.028	0.049−	CD_3S ?
623		+			
652	0.009−	0.014−			
663	0.009+				
692				0.014−	
707			0.018−	0.028−	
760				0.019−	
765	0.076−	0.086−			
770	0.019−	0.019−		0.009	F_2CO, ?
776	0.019+	0.014			
779				0.010+	D_2CS
785				0.010	D_2CS
796			0.073−	0.083−	$CD_3S\cdots HF$, DF
815				0.014−	CD_3S ?
939	0.056	0.077	0.069	0.115	SF_6
988	0.035+	0.035+			H_2CS
994	0.046+	0.036+			H_2CS
1055	0.010+	0.005+			H_2CS
1093				0.011	$CD_3S\cdots DF$?
1397	0.015−	0.015−			CH_3SHO ?
2595		0.058−			$CH_3S\cdots DF$
2600			0.081	0.103	CH_3S-$d_n\cdots DF$
2618			+	+	
2690			0.063−	0.050−	
2700		+	0.098	0.092+	CH_2SH-$d_n\cdots DF$
2704		+			CH_2SH-$d_n\cdots DF$
2746				0.021−	
2898		0.012	0.022	0.036	DF
3478	0.025−				
3515	0.267−	0.179−	0.251−	0.233−	CH_3S-$d_n\cdots HF$
3580				0.029+	
3652	0.065+	0.068			
3672	0.121+	0.090+	0.017+	0.012+	CH_2SH-$d_n\cdots HF$
3760				0.044+	
3886	0.037	0.018	0.024	0.026	HF
3922	0.031	0.032	0.032	0.048	HF
3968	0.170	0.149	0.167	0.160	HF

[a]+, − indicate growth or decrease, respectively, on photolysis.

HF were observed in both systems; exchange of the sulfhydryl proton on the walls of the system led to the formation of CD_3SH in the CD_3SD experiments. The absorptions near 2600 and 2700 cm^{-1} and the 3515-cm^{-1} peak were prominent and had similar contours in both systems, but, as is shown in traces (c) and (d) of Fig. 2, the peaks at 2618 and 3672 cm^{-1} appeared with significant intensity only after 280-nm photolysis.

Discussion

F atoms may abstract either of the two different types of H atom from methanethiol:

[1] $F + CH_3SH \rightarrow CH_3SH + HF$

[2] $F + CH_3SH \rightarrow CH_2SH + HF$

While, as already noted, the first reaction is energetically somewhat more favorable, on the basis of stoichiometry the second reaction would be more probable. It has been estimated (21) that F atoms and the reactant molecule coexist in the beam for approximately 10^{-4} s before the sample reaches the cryogenic surface. At the concentrations used in these experiments, only one or two reactive collisions are likely to occur during this time. Products formed in the gas phase will generally be

Can. J. Chem. Downloaded from www.nrcresearchpress.com by 210.87.254.105 on 09/06/12
For personal use only.

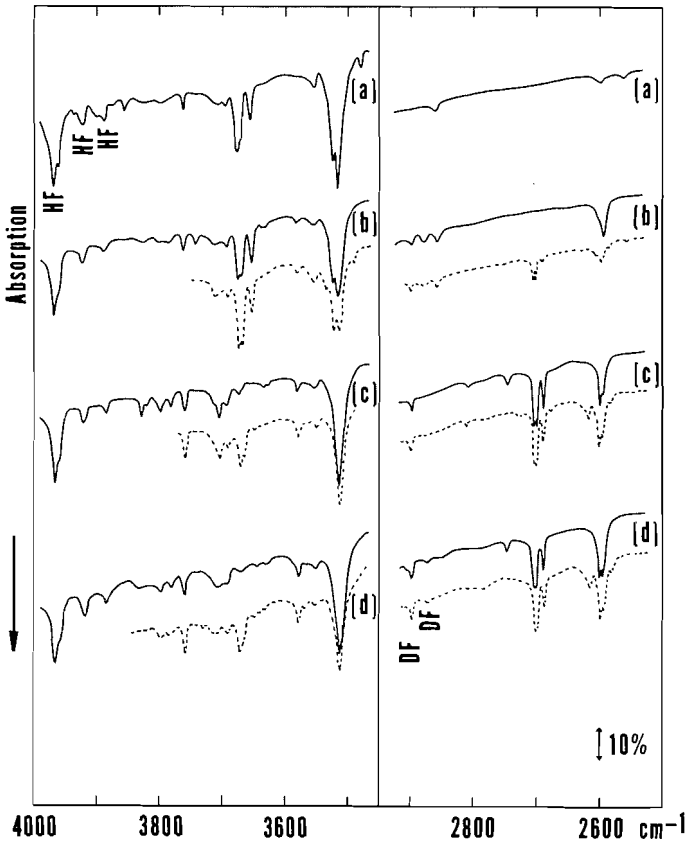

FIG. 2. Absorption patterns for (a) ——— 5.67 mmol Ar/CH_3SH = 200 codeposited over period of 260 min with 2.67 mmol discharged Ar/NF_3 = 800. $[CH_3SH]/[NF_3]$ = 8.5; ---- 107 min subsequent mercury-arc photolysis, $\lambda > 280$ nm; (b) ——— 4.92 mmol Ar/CH_3SD = 200 codeposited over period of 236 min with 3.00 mmol discharged Ar/NF_3 = 800. $[CH_3SD]/[NF_3]$ = 6.6.; ---- 107 min subsequent mercury-arc photolysis, $\lambda > 280$ nm; (c) ——— 5.03 mmol Ar/CD_3SH = 200 codeposited over period of 264 min with 3.64 mmol discharged Ar/NF_3 = 800. $[CD_3SH]/[NF_3]$ = 5.5; ---- 69 min subsequent mercury-arc photolysis, $\lambda > 280$ nm; (d) ——— 5.35 mmol Ar/CD_3SD = 200 codeposited over period of 281 min with 4.28 mmol discharged Ar/NF_3 = 800. $[CD_3SD]/[NF_3]$ = 5.0; ---- 104 min subsequent mercury-arc photolysis, $\lambda > 280$ nm.

trapped in isolated sites in the argon lattice. F atoms may also react with molecules on the surface of the deposit and, because of the exothermicity of the reaction, one or both of the product molecules may migrate from the site of the reaction, enhancing the probability for the trapping of the isolated species. Unreacted F atoms may diffuse through the argon lattice, where they may also react with methanethiol. However, HF formed in the solid cannot diffuse from the site of its production and will form a hydrogen bond with the free radical product:

[3] $F + CH_3SH\ (Ar) \rightarrow CH_3S\cdots HF$

[4] $F + CH_3SH\ (Ar) \rightarrow CH_2SH\cdots HF$

The six degrees of freedom lost by HF in forming the complex will contribute six new vibrational absorptions to the spectrum of the free radical (22). One of these, the H—F stretching mode, is generally very strongly infrared absorbing and appears at a somewhat lower frequency than the infrared absorption of isolated HF, often in the 3500–3800-cm^{-1} spectral region. The separation between these two absorptions provides a measure of the strength of the hydrogen bond in the complex. A pair of vibrational modes, doubly degenerate for a complex of cylindrical symmetry, is contributed by the H deformation motions in the hydrogen bond. These absorptions frequently have been observed in the 500–700-cm^{-1} spectral region, with a higher frequency associated with a stronger hydrogen bond. Three other vibrations appear in the far infrared, outside of the spectral region of these studies.

Secondary F-atom reactions may also occur. H-abstraction from either free radical product should lead to the formation of H_2CS. The strongest infrared absorptions of this product, observed at 988 and 993 cm^{-1} in an argon matrix (11), are of no more than weak to moderate intensity in these experiments, suggesting that such secondary F-atom reactions play a minor role. Secondary F-atom addition, forming CH_3SF or CH_2FSH, may also occur. The infrared spectrum of CH_3SF has not been reported. CH_2FSH should have a strong CF-stretching absorption in the 1000–1200-cm^{-1} spectral region. However, virtually no product absorption was present in this region. The conclusion that secondary F-atom reactions play a minor role under the conditions of these experiments parallels the similar conclusion drawn in the previously reported experiments (14–16, 21). On the basis of these earlier studies, it is also expected that the infrared spectra of products of the reaction of NF and NF_2 with methanethiol should be too weak to be detected in these experiments.

The presence of a rather prominent absorption of isolated HF indicates that reaction [1] and/or reaction [2] occur with significant probability, and the appearance of both isolated HF and isolated DF in the CD_3SH studies suggests that both occur. The relative prominence of the HF absorption in that experiment cannot be inferred to indicate that reaction [1] predominates, since the DF absorption is much weaker than is that of HF.

The appearance of very prominent absorptions at both 3515 and 3672 cm^{-1}, with differing photolysis behavior, suggests that both reaction [3] and reaction [4] also occur. In the CD_3SH study, the expected primary products should be $CD_3S\cdots HF$ and $CD_2SH\cdots DF$. The appearance of a single HF complex absorption at 3515 cm^{-1} supports the assignment of this peak to the complex of CH_3S-d_n with HF. However, in the CD_3SH experiments both DF complex absorptions appeared. The correlation of the lower frequency absorption with the complex of CH_3S suggests the assignment of the 2600-cm^{-1} absorption to $CHD_2S\cdots DF$. The 2700-cm^{-1} absorption would then be expected to be contributed by $CD_2SH\cdots DF$. Similarly, in the CH_3SD experiments, somewhat complicated by isotopic exchange, only the lower frequency DF-stretching absorption, assigned to $CH_3S\cdots DF$, was observed, but both HF stretching absorptions, assigned to $CH_2DS\cdots HF$ and $CH_2SD\cdots HF$, appeared. It is inferred that CH_2SH formed by reaction [2] or [4] possesses sufficient internal energy to surmount the barrier to its rearrangement to the thermochemically more stable CH_3S. However, the reverse rearrangement of CH_3S to form CH_2SH appears to be improbable under the conditions of these experiments.

The observed threshold for the appearance of the 2700-cm^{-1} absorption in the F + CH_3SD experiments and of the 3672-cm^{-1} absorption in the F + CD_3SH experiments, between 345 and 300 nm, lies within the expected absorption region for CH_3S-d_n corresponding to the emission band system reported for this molecule by Tanaka and co-workers (8). Therefore, it is suggested that photochemical rearrangement of CH_3S may occur:

Can. J. Chem. Downloaded from www.nrcresearchpress.com by 210.87.254.105 on 09/06/12
For personal use only.

[5] $CH_3S + h\nu \rightarrow CH_2SH$

The threshold for the photodecomposition of CH_2SH, forming H_2CS, lies near 280 nm. Alternatively, the primary photodecomposition of CH_3S may involve detachment of an H atom, with a significant probability of its cage recombination to form CH_2SH. Generally, there is a slight growth in the H_2CS absorption on 300- or 280-nm photolysis and a more marked growth on 260-nm photolysis. It is concluded that, while the experiments suggest the occurrence of reaction [5], they do not definitively establish it.

The spectra of isolated CH_3S and CH_2SH may contribute to the pattern of absorptions observed in both the vacuum-ultraviolet photolysis and the F-atom reaction studies. Only the 424–431-cm^{-1} absorption pair and the peaks near 663 and 815 cm^{-1} satisfy this criterion. While a 663-cm^{-1} peak, to which CO_2 is the major contributor, would lie within the experimental error of the assignment proposed for the CS-stretching fundamental of CH_3S by Tanaka (8) and by Lineberger (9) and their co-workers, it is outside of the range of uncertainty of the assignment suggested by Janousek and Brauman (10). Moreover, there is no absorption near 1040 cm^{-1}, the position estimated by Lineberger for the CH_3 "umbrella" mode of CH_3S. On the other hand, the peaks at 815 and 1397 cm^{-1} lie within the experimental error of the assignment proposed by Brauman for these two fundamentals. Because in the F-atom studies FNO_2 contributed to the absorption at 815 cm^{-1} and a product of the O + CH_3SH reaction may have contributed to that at 1397 cm^{-1}, further studies are required for a definitive assignment.

Brauman has also assigned the CD_3 "umbrella" vibration of CD_3S at 1100 ± 50 and the CS-stretching fundamental at 660 ± 60 cm^{-1}. The estimate of 1560 ± 50 cm^{-1} for the first overtone of the degenerate DCS deformation fundamental would place this mode near 780 cm^{-1}. Only the peaks at 545, 620, and 815 cm^{-1} in the F-atom experiments on CD_3SD lie close to product absorptions in the earlier Ar/CD_3SH photolysis study (11), and the latter two of these peaks lie within the experimental uncertainty estimated by Brauman for CD_3S fundamentals.

The vibrational fundamentals of CH_3S and CD_3S which are hydrogen-bonded to HF or DF would be expected to be somewhat shifted from those of the isolated molecule. Prominent peaks at 593 and 796 cm^{-1} in the CD_3SH and CD_3SD + F studies may have been contributed by these fundamentals of perturbed CD_3S.

Since analogy with the pattern of the fundamental vibrations of the methyl and methyl-d_3 halides (23) indicates that the CS-stretching vibration should be the lowest frequency fundamental of CH_3S and of CD_3S, the 424–431-cm^{-1} absorptions, also common to the F-atom and photolysis experiments, could not reasonably be assigned to CH_3S. On the other hand, both the torsional vibration and the CH_2S "umbrella" deformation vibration of CH_2SH are expected to lie at low frequencies; a very recent *ab initio* calculation by Schlegel[2] at the HF/3-21G level, using the HF/3-21G optimized geometry, gave a value of 426 cm^{-1} for the "umbrella" vibration and of 211 cm^{-1} for the torsion. The close correspondence of the 424–431-cm^{-1} peaks to the calculated value for the "umbrella" vibration is to some extent fortuitous, since anharmonicity and the low barrier to inversion were not taken into account. There should also be only a small dependence of the frequency of the "umbrella" mode on whether an H or a D atom is substituted on the sulfur atom, but a large dependence of the torsional vibration on the isotope in this position. Thus, the isotopic data also favor the assignment to the "umbrella" mode.

The correlation of the photochemical behavior of the 424–433-cm^{-1} peaks with that of the 3672-cm^{-1} peak, which the isotopic substitution experiments have tied to the product of the attack of the F atom on a C—H bond, further strengthens the assignment of the 424–433-cm^{-1} absorptions to CH_2SH. Since no new peaks parallel their behavior in the F-atom experiments, it is concluded that this vibration of CH_2SH is only slightly perturbed by the formation of a hydrogen bond with HF.

Because the HF stretching frequency experiences a greater shift in the formation of a hydrogen bond with CH_3S than with CH_2SH, it is inferred that the hydrogen bond of CH_3S with HF is the stronger, suggesting the localization of the unpaired electron on the S atom. A recent study of the structure of the $H_2S\cdots HF$ complex (24) has determined that the HF bond is almost exactly perpendicular to the plane of the H_2S moiety, consistent with the tendency of the S atom to form bonds at angles of approximately 90°. Therefore, it is likely that the HF bond in $CH_3S\cdots HF$ is approximately perpendicular to the C—S bond, implying that the degenerate CH stretching and bending vibrations and the degenerate HF deformation mode should be split. Taken together, these arguments suggest that there should be four HF-deformation absorptions in the 500–700-cm^{-1} region in the F-atom reaction studies and that the two absorptions contributed by the relatively strongly bound HF complex with CH_3S should lie at higher frequencies than those of the complex with CH_2SH. Only the weak 535- and 776-cm^{-1} absorptions have the appropriate photolytic behavior for assignment to $CH_2SH\cdots HF$. Assuming a very small interaction with vibrations of the CH_2SH-d_n moiety, the corresponding vibrations of the DF complex should lie near 400 and 580 cm^{-1}. Several absorptions behave appropriately for assignment to the HF-deformation vibrations of $CH_3S\cdots HF$. Noteworthy is the invariance of a rather prominent absorption at 569 cm^{-1} in all of the isotopic studies. The frequency ratio of the 569-cm^{-1} peak to that at 765 cm^{-1} is 0.74 and of the 436- to the 569-cm^{-1} peak is 0.77, suggesting that both an HF- and a DF-deformation vibration may contribute to the 569-cm^{-1} absorption. However, the present data do not suffice for a definitive assignment.

The 260-nm photolysis experiments indicate that the threshold for the photodecomposition of CH_2SH to produce H_2CS lies between 260 and 280 nm. Quite possibly the broadening of the 3515-cm^{-1} absorption of $CH_3S\cdots HF$ on prolonged irradiation through the 260-nm cutoff filter results from the superposition of the growing absorption of $H_2CS\cdots HF$.

Conclusions

Both CH_3S and CH_2SH are formed in primary F-atom reactions with CH_3SH. In argon-matrix sampling studies, the very prominent absorptions at 3515 and 2600 cm^{-1} can be assigned to the HF and DF complexes, respectively, with CH_3S-d_n, while the peaks at 3672 and 2700 cm^{-1} can be assigned to the corresponding complexes with CH_2SH-d_n. Studies on partially deuterium-substituted methanethiol indicate that CH_2SH is formed with enough excess energy to surmount the barrier for rearrangement to the thermochemically more stable CH_3S. In contrast, CH_2S has a relatively small probability of rear-

[2]H. B. Schlegel, private communication.

rangement to CH_2SH. The experiments suggest that the threshold for the photoinduced rearrangement of CH_3S to CH_2SH lies between 345 and 300 nm, in the region of a previously identified electronic transition of CH_3S. However, the observed rearrangement may result at least in part from the cage recombination of initially-formed H_2CS and H atoms. The infrared data support, but do not establish, the recent vibrational assignment for CD_3S based on the photodetachment studies of Janousek and Brauman (10). A prominent, structured absorption at 424 cm^{-1} has been assigned to the H_2CS "umbrella" deformation of CH_2SH. The threshold for the photodecomposition of CH_2SH lies in the 260–280-nm spectral region.

1. A. JONES, S. YAMASHITA, and F. P. LOSSING. Can. J. Chem. **46**, 833 (1968).
2. P. M. RAO and A. R. KNIGHT. Can. J. Chem. **50**, 844 (1972).
3. L. BRIDGES and J. M. WHITE. J. Phys. Chem. **77**, 295 (1973).
4. A. B. CALLEAR, J. CONNOR, and D. R. DICKSON. Nature, **221**, 1238 (1969).
5. A. B. CALLEAR and D. R. DICKSON. Trans. Faraday Soc. **67**, 1987 (1970).
6. KJ. ROSENGREN. Acta Chem. Scand. **16**, 1418 (1962).
7. P. GOLDBERG. J. Chem. Phys. **40**, 427 (1964).
8. K. OHBAYASHI, H. AKIMOTO, and I. TANAKA. Chem. Phys. Lett. **52**, 47 (1977).
9. R. C. ENGELKING, G. B. ELLISON, and W. C. LINEBERGER. J. Chem. Phys. **69**, 1826 (1978).
10. B. K. JANOUSEK and J. I. BRAUMAN. J. Chem. Phys. **72**, 694 (1980).
11. M. E. JACOX and D. E. MILLIGAN. J. Mol. Spectrosc. **58**, 142 (1975).
12. B. DILL and H. HEYDTMANN. Chem. Phys. **35**, 161 (1978).
13. D. J. NESBITT and S. R. LEONE. J. Chem. Phys. **75**, 4949 (1981).
14. M. E. JACOX. Chem. Phys. **42**, 133 (1979).
15. M. E. JACOX. Chem. Phys. **59**, 213 (1981).
16. M. E. JACOX. Chem. Phys. **69**, 407 (1982).
17. M. E. JACOX. Chem. Phys. **7**, 424 (1975).
18. M. G. MASON, W. G. VON HOLLE, and D. W. ROBINSON. J. Chem. Phys. **54**, 3491 (1971).
19. R. R. SMARDZEWSKI and W. B. FOX. J. Chem. Phys. **67**, 2309 (1977).
20. D. E. TEVAULT, R. L. MOWERY, and R. R. SMARDZEWSKI. J. Chem. Phys. **74**, 4480 (1981).
21. M. E. JACOX. Chem. Phys. **59**, 199 (1981).
22. R. K. THOMAS. Proc. R. Soc. London Ser. A, **325**, 133 (1971).
23. W. T. KING, I. M. MILLS, and B. CRAWFORD, JR. J. Chem. Phys. **27**, 455 (1957).
24. R. VISWANATHAN and T. R. DYKE. J. Chem. Phys. **77**, 1166 (1982).

Can. J. Chem. Downloaded from www.nrcresearchpress.com by 210.87.254.105 on 09/06/12
For personal use only.

ipso Halogenation. II.[1] Bromination of phenols, isomerization and disproportionation of bromophenols, and dienone–phenol rearrangement of bromodienones

ALFRED FISCHER AND GEORGE NARAYANAN HENDERSON
Department of Chemistry, University of Victoria, Victoria, B.C., Canada V8W 2Y2

Received July 22, 1982

ALFRED FISCHER and GEORGE NARAYANAN HENDERSON. Can. J. Chem. **61**, 1045 (1983).

Bromination of *p*-cresol, 2-bromo-*p*-cresol, 3,4-dimethylphenol, and mesitol in trifluoromethanesulfonic acid gives as the main product the bromo derivative with bromine *meta* to hydroxyl, a result attributed to the intermediate formation of a bromodienone and its rearrangement. Phenol does not give *m*-bromophenol in trifluoromethanesulfonic acid. 4-Bromo-2,4,6-trimethylcyclohexa-2,5-dienone rearranges to 3-bromomesitol in trifluoromethanesulfonic acid and, similarly, 2,4,6-tribromo-4-methylcyclohexa-2,5-dienone rearranges to 2,3,6-tribromo-4-methylphenol. Under appropriate conditions debromination of bromodienones is competitive with rearrangement. Tetramethylammonium bromide in trifluoromethanesulfonic acid is an effective reagent for isomerization and disproportionation of bromophenols. Tetramethylammonium iodide in trifluoromethanesulfonic acid is an effective reagent for selective debromination of bromophenols at the *ortho* and *para* positions.

ALFRED FISCHER et GEORGE NARAYANAN HENDERSON. Can. J. Chem. **61**, 1045 (1983).

La bromation de *p*-crésol, du bromo-2-*p*-crésol, du diméthyl-3,4 phénol et du mésitol dans l'acide trifluorométhanesulfonique donne comme produit principal le dérivé bromé portant un brome en position *méta* par rapport à l'hydroxyle. On attribue ce résultat à la formation intermédiaire d'une bromodiénone qui subirait ultérieurement une transposition. Le phénol ne donne pas le *m*-bromophénol dans l'acide trifluorométhanesulfonique. La bromo-4 triméthyl-2,4,6 cyclohexadiène-2,5 one se transpose en bromo-3 mésitol dans l'acide trifluorométhanesulfonique et d'une façon analogue la tribromo-2,4,6 méthyl-4 cyclohexadiène-2,5 one se transpose en tribromo-2,3,6 méthyl-4 phénol. Dans des conditions appropriées, la débromation des bromodiénones entre en compétition avec la transposition. Le bromure de tétraméthylammonium dans l'acide trifluorométhanesulfonique est un réactif efficace pour l'isomérisation et la disproportionation des bromophénols. L'iodure de tétraméthylammonium dans l'acide trifluorométhanesulfonique est un réactif efficace pour la débromation sélective des bromophénols en position *ortho* et *para*.

[Traduit par le journal]

Aromatic electrophilic substitution reactions can lead to unexpected products as a result of *ipso* attack and subsequent reaction of the *ipso* intermediate so obtained (1). Chlorination of *p*-cresol gives 4-chloro-4-methylcyclohexa-2,5-dienone as well as the expected 2-chloro-4-methylphenol (2). Reaction of the chlorodienone in trifluoromethanesulfonic (triflic) acid gives 3-chloro-4-methylphenol (3). We have now investigated the bromination of *p*-cresol in an attempt to obtain the corresponding bromodienone, and have studied other reactions involving bromodienones as potential intermediates.

Bromodienones have been known for a long time. Phenol, on reaction with bromine water, gives a tetrabromo derivative, first isolated by Benedikt in 1879 (4). The debate on the structure of this product, alternatively identified as 2,4,6-tribromophenol hypobromite or 2,4,4,6-tetrabromocyclohexa-2,5-dienone (5) continued into recent times (6). The dienone structure is now well established. The most comprehensive studies of the formation and reactions of bromodienones are those of Ershov *et al.* (7) involving 2,6-dialkyl and 2,4,6-trialkylphenols as substrates. The notion that halodienones could be formed only from phenols fully substituted in the *ortho* and *para* positions was prevalent in the past (7*a*). With the exception of 4-bromo-2,6-di-*tert*-butylcyclohexa-2,5-dienone, all of the known bromodienones are derived from 2,4,6-trisubstituted phenols. However, the bromination of α-*p*-tolyloxyisobutyric acid to the bromodiene **1** (8) provides a close analogue to the bromination of *p*-cresol to the corresponding bromodienone and provides support for the expectation that the bromodienone should be formed.

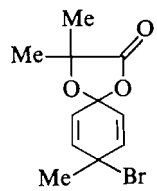

1

Jacquesy *et al.* have investigated the bromination of phenol, methylphenols (including *p*-cresol), and dimethylphenols in antimony pentafluoride – hydrogen fluoride (9, 10). They observed that *p*-cresol, 2,4-dimethylphenol, and 3,4-dimethylphenol gave 3- (or 5-) bromo derivatives in which the bromine atom is *meta* to the hydroxyl group. On the other hand, phenol, *o*-cresol, and *m*-cresol gave 4-bromo derivatives. The hydroxyl group is strongly *ortho–para* directing and they suggested that the *meta* orientations observed in the first reactions, and also in the bromination of 2,6-dimethylphenol under the same conditions, could be accounted for if the oxonium ion conjugate acid of the phenol was the actual substrate brominated. They assumed that the protonated hydroxyl group is *meta* directing. We thought that an alterantive explanation for these observations could be that bromination of *p*-cresol and the 2,4- and 3,4-dimethylphenols would give, via *ipso* bromination, the corresponding 4-bromo-4-methylcyclohexa-2,5-dienone, or derivative, which would rearrange by an acid-catalysed 1,2 shift of the bromine to give, after deprotonation, the 3-bromophenol derivative. We had demonstrated the analogous reaction for chlorination of *p*-cresol (2, 3). During our study, de la Mare and co-workers (11) reported their observations on the bromination of *p*-cresol in triflic acid and sug-

[1]For Part I, see ref. 2.

Can. J. Chem. Downloaded from www.nrcresearchpress.com by 210.87.254.6 on 09/06/12
For personal use only.

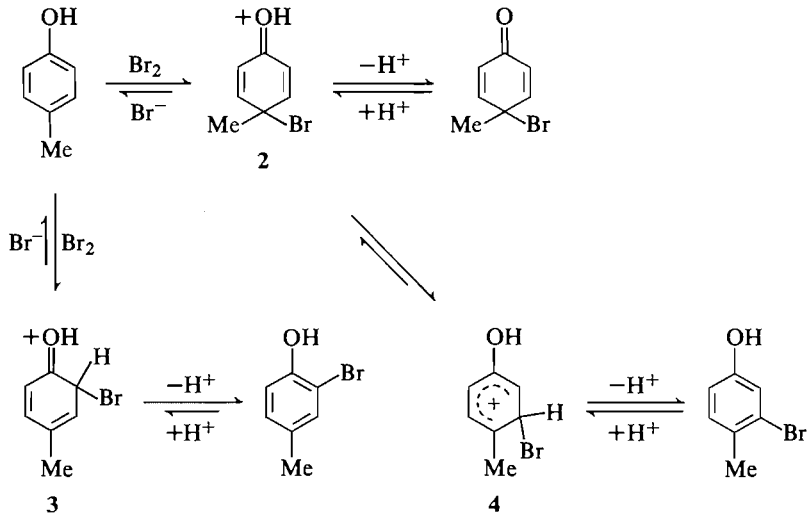

SCHEME 1. Bromination of *p*-cresol.

gested, amongst other possibilities, the pathway to 3-bromo-*p*-cresol involving the 1,2 bromine shift in the conjugate acid of 4-bromo-4-methylcyclohexa-2,5-dienone. De la Mare and co-workers have also investigated the polybromination of the cresols and of 3,4-dimethylphenol leading to the formation of tribromodienones (12, 13).

Results and discussion

Bromination of p*-cresol and 3,4,5-trimethylphenol*

p-Cresol was brominated under a number of different conditions in an attempt to detect the formation of 4-bromo-4-methylcyclohexadienone. Reactions were carried out, at 0°C or below, with bromine in deuteriochloroform containing pyridine, bromine in aqueous methanol, bromine in methanol, bromine in acetic anhydride, bromine in aqueous potassium bicarbonate, bromine in aqueous potassium carbonate, and bromine in ether. Only aromatic compounds were observed and no dienone was detected. 2-Bromo-4-methylphenol was the major product. Even at −50°C, under the conditions considered the most favourable for formation of bromodienones (ether–water–pyridine solvent), no dienone could be detected (7*h*).

Bromination of 3,4,5-trimethylphenol in ether containing a few drops of pyridine with a solution of bromine in aqueous potassium bromide gave only 2-bromo-3,4,5-trimethylphenol and no dienone was detected. Under the same conditions mesitol gave 4-bromo-2,4,6-trimethylcyclohexa-2,5-dienone in quantitative yield.

Bromination of phenols in acids

The products of bromination of *p*-cresol and of 2-bromo-*p*-cresol are shown in Table 1. Details of the results of bromination of other phenols are given in the experimental section. Sulfuric acid was unsatisfactory as a solvent for bromination of phenols since sulfonation occurred and no mono-brominated phenols were obtained. Bromination of *p*-cresol in methanesulfonic acid gave 2-bromo-*p*-cresol containing only small amounts of 3-bromo-*p*-cresol, and dibromo-*p*-cresol. In contrast, a substantial amount of *meta* bromination of *p*-cresol occurred in triflic acid, the amount increasing with reaction time.

De la Mare and co-workers have reported that bromination of *p*-cresol in triflic acid gives 3-bromo- as well as 2-bromo-*p*-cresol, the amount of the 3-bromo isomer increasing at the expense of the 2-bromo isomer on allowing the reaction mixture to stand (11). Our observations confirm and extend this report. We suggest, by analogy with the chlorination of *p*-cresol, that initial bromination can take place at both the 2-position and the 4-(*ipso*)position. The latter reaction would give 4-bromo-4-methylcyclohexa-2,5-dienone. Again by analogy with the chlorodienone, the conjugate acid of the bromodienone can rearrange by a 1,2 shift of bromine to give, after deprotonation, 3-bromo-*p*-cresol (Scheme 1). However, unlike chlorination, the *ipso* bromination is reversible, bromide ion being able to bring about the debromination of the bromodienone conjugate acid. In the very strongly acidic triflic acid the bromide ion concentration is low, as hydrogen bromide is only slightly dissociated. We suggest that, under this condition, the unimolecular rearrangement of the bromodienone conjugate acid **2** to **4** is able to compete with the bimolecular debromination to *p*-cresol and bromine and thus 3-bromo-*p*-cresol is obtained. In the less strong methanesulfonic acid, the bromide ion concentration is higher and the debromination reaction is favoured over the rearrangement. Although bromination at the (unsubstituted) 2-position is also reversible (Scheme 1) this would be expected to be much slower than debromination of the bromodienone. Protonation of the 2-bromo-*p*-cresol *ipso* to bromine, the first step of the reverse reaction, should be much less extensive than protonation of the bromodienone at the carbonyl oxygen atom. Thus on the time scale of the bromination–debromination at the *ipso* position, bromination at the unsubstituted 2-position is essentially irreversible. Hence bromination of *p*-cresol in methanesulfonic acid and in more weakly acidic conditions gives, essentially completely, 2-bromo-*p*-cresol, some of the *p*-cresol being cycled reversibly through the bromodienone before being converted into 2-bromo-*p*-cresol. In the stronger triflic acid debromination of 2-bromo-*p*-cresol is enhanced and, on standing, the 2-bromo isomer initially obtained isomerizes to 3-bromo-*p*-cresol and dibromo-*p*-cresols are also formed (see below).

Bromination of 2-bromo-*p*-cresol, 3,4-dimethylphenol, and mesitol in triflic acid, gave, in each case, the product of 3- (5-) substitution as the major (or only) component. As in the case of *p*-cresol, it is likely that these products are formed via *ipso* (4-) bromination followed by rearrangement of the bromine to the adjacent unsubstituted position. However, phenol gave only products of substitution at the 2- and 4-positions. Since it

Can. J. Chem. Downloaded from www.nrcresearchpress.com by 210.87.254.6 on 09/06/12
For personal use only.

Can. J. Chem. Downloaded from www.nrcresearchpress.com by 210.87.254.6 on 09/06/12
For personal use only.

TABLE 1. Products of bromination of *p*-cresol and bromo-*p*-cresols and of isomerization of bromo-*p*-cresol (mol%)

No.	Reactants			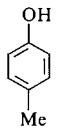	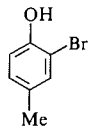	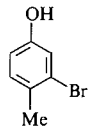	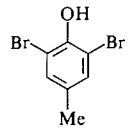	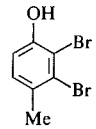	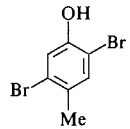	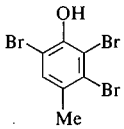
				OH Me	OH Br Me	OH Br Me	OH Br Br Me	OH Br Br Me	OH Br Br Me	OH Br Br Me
1[a]	Br_2	MeC_6H_4OH	CH_3SO_3H	11	84	1	3		1	
2[b]	Br_2	MeC_6H_4OH	CF_3SO_3H	30	41	11	5	1	9	
3[c]	Br_2	MeC_6H_4OH	CF_3SO_3H	29	24	18	10	2	16	
4[d]	Br_2	MeC_6H_4OH	CF_3SO_3H	26	26	28	5	1	14	
5[e]	Br_2	MeC_6H_4OH	CF_3SO_3H	13	8	61	1	2	15	
6[d]	Br_2	2-Br-4-MeC_6H_3OH	CF_3SO_3H	1	6	17	14	6	52	4
7[f]	Br_2	2-Br-4-MeC_6H_3OH	48% aq. HBr	15	70	4	8		3	
8[g]	NMe_4Br	2-Br-4-MeC_6H_3OH	CF_3SO_3H	8	84	3	2		3	
9[h]	NMe_4Br	2-Br-4-MeC_6H_3OH	CF_3SO_3H	13	75	4	4		4	
10[i]	NMe_4Br	2-Br-4-MeC_6H_3OH	CF_3SO_3H	11	8	63	2	2	14	
11[i]	NMe_4Br	3-Br-4-MeC_6H_3OH	CF_3SO_3H	9	6	62	2	2	18	1
12[i]	NMe_4Br	2-Br-6-Br-4-MeC_6H_2OH	CF_3SO_3H		1	10	16	6	57	10

[a]Bromine in methanesulfonic acid added over 10 min to *p*-cresol in methanesulfonic acid and the mixture worked up after further 10 min.
[b]Bromine solution added over 2.5 min and the mixture worked up after 0.5 min.
[c]Liquid bromine added rapidly and the mixture worked up after 5 min.
[d]Standard conditions described in the text of experimental section; bromine solution added over 15 min and worked up after 30 min.
[e]Liquid bromine added in a closed system to prevent the loss of HBr. Work-up after 24 h.
[f]The mixture of 2-bromo-*p*-cresol (1 mmol) and 48% HBr (10 cm^3) was heated under reflux in a closed system for 24 h. No reaction occurred when a similar mixture was stirred for 3 days at ambient temperature.
[g]Reaction time of 15 min.
[h]NMe_4Br added in 5 portions over 15 min; open system. Work-up after 30 min.
[i]Standard conditions described in the text of the experimental section; closed system. Work-up after 24 h.

Can. J. Chem. Downloaded from www.nrcresearchpress.com by 210.87.254.6 on 09/06/12
For personal use only.

lacks a methyl substituent, the *ipso* addition and rearrangement pathway is precluded. Again as expected, 3,4-dimethylphenol underwent bromination at only the 2- and 6-positions in aqueous acetic acid.

The above results do not rule out other pathways to *meta* brominated phenols that have been suggested. As mentioned in the introduction, Jacquesy and co-workers have proposed that it is the conjugate acid of the phenol that is substituted in strongly acidic conditions. However, de la Mare and co-workers observed that the OH_2^+ group should be *ortho*, *para* directing (11). Furthermore, bromination is extremely sensitive to substituent effects ($\rho = -12$ (14)) and it seems unlikely that the conjugate acid would be readily brominated. Indeed, we attribute the reduced reactivity of mesitol in the triflic acid to the fact that it is essentially completely protonated (probably at the ring rather than the hydroxyl group) and thus there is only a small amount of free mesitol available for reaction. Moreover, the fact that phenol does not give any 3-bromophenol on bromination in triflic acid is not readily explained if it is the conjugate acid that is brominated and if the OH_2^+ group is *meta* directing. De la Mare has also suggested that cation **3** can undergo a 1,2 bromine shift to give **4** (11). However, the same pathway should be available to phenol and should thus lead to the formation of 3-bromophenol.[2] An alternative pathway to the 3-brominated product would involve reversible *ipso* bromination followed by a slower but less reversible direct 3-bromination of the phenol. Bromination *meta* to the hydroxyl group is exceedingly slow. The difference between σ^+ for *p*-OH and σ ($= \sigma^+$) for *m*-OH is about -1, hence the relative rates of substitution in the *para* and *meta* positions of phenol are ca. 10^{12}:1. Such a calculation is at best crude and, moreover, in suitably substituted methylphenols the methyl groups can act in opposition to the directing effect of the hydroxyl. Nevertheless the reactivity difference is so great that it seems unlikely that direct *meta* substitution need be considered seriously. Experiments described in the next section involving a study of the reactions of the bromodienone from mesitol provide further evidence for ruling out this pathway.

Reaction of 4-bromo-2,4,6-trimethylcyclohexa-2,5-dienone with acids

When the dienone in deuteriochloroform at -20°C was treated with a few drops of triflic or sulfuric acid it immediately rearranged to 3-bromomesitol. This would appear to be an example of the acid-catalysed dienone–phenol arrangement observed for chlorodienones and illustrated for 4-bromo-4-methylcyclohexa-2,5-dienone in Scheme 1 (3). Reaction of the dienone in deuteriochloroform at -20°C with a solution of hydrogen bromide in ether gave, after 1 min, a mixture of 3-bromomesitol (78%) and mesitol (22%). The mesitol was slowly brominated to 3-bromomesitol, presumably via reformation of the dienone and its acid-catalysed rearrangement. Similar behaviour was exhibited when gaseous hydrogen bromide was passed into the bromodienone solution, and the characteristic colour of the liberated bromine was observed. Reaction with hydrogen chloride gave mainly 3-bromomesitol, while reaction with aqueous hydrogen iodide produced only mesitol. In the case of the reaction with iodide the iodine bromide formed in the debromination process reacts with excess iodide to form, irreversibly, iodine and bromide, thus preventing the rebromination reaction and leaving mesitol as the aromatic product.

The dienone did not react, within 10 min, with a solution of trifluoroacetic acid in deuteriochloroform (9% v/v) at 0°C. Evidently the acid is not strong enough to catalyse the 1,2 bromine shift under these conditions.

4-Methyl-2,4,6-tribromocyclohexa-2,5-dienone in deuteriochloroform gave 2,3,6-tribromo-*p*-cresol on treatment with a small amount of triflic or sulfuric acid. The same rearrangement in neat sulfuric acid has been reported by de la Mare and co-workers (13).

Methyl migration products were not observed in any of the reactions. Evidently migration of bromine is preferred over migration of methyl in the acid-catalysed dienone–phenol rearrangement, a result at least partially accounted for by the greater stabilizing effect of methyl than bromine on the positive charge developing in the transition state at the migration origin (cf. ref. 3).

Attempts were made to set up a competition between the 1,2-rearrangement reaction of 4-bromo-2,4,6-trimethylcyclohexadienone and the debromination to mesitol, by trapping the bromine released in the latter reaction. At -40°C no reaction occurred between the bromodienone and trimethoxybenzene in deuteriochloroform until hydrogen bromide was passed in, when rapid reaction to mesitol and bromotrimethoxybenzene ensued. Hydrogen bromide is a very effective debrominating reagent. However, addition of triflic acid (20% by vol) resulted in 78% of the bromodienone undergoing the rearrangement to 3-bromomesitol and 22% undergoing reaction to bromotrimethoxybenzene and mesitol. In strong acid and in the absence of a significant concentration of the bromide ion the rearrangement is faster than the debromination. The fact that in 20% triflic acid the 3-bromomesitol was formed in preference to bromotrimethoxybenzene from the bromodienone–trimethoxybenzene mixture indicates that the 3-bromomesitol is not formed by reversible debromination of the bromodienone followed by direct *meta* bromination, since bromination of trimethoxybenzene should be faster than *meta* bromination of mesitol.

The very ready debromination of bromodienones by the hydrogen bromide produced in the bromination accounts for the failure to observe the formation of bromodienones in the bromination of *p*-cresol and other simple phenols having at least one unsubstituted position *ortho* or *para* to the hydroxyl group. Thus bromination to bromodienone is rapidly reversible and the essentially irreversible bromination at the unsubstituted activated position is product determining.[3]

Isomerization and disproportionation of bromophenols

O'Bara *et al.* (16) showed that 4-bromo-*m*-cresol is converted into an equilibrium mixture of *m*-cresol, 2-, 4-, and 6-bromo-*m*-cresol, and 2,4-, 2,6-, and 4,6-dibromo-*m*-cresol on standing in chloroform saturated with hydrogen bromide, at 25°C, for several days. The same mixture was obtained when 2-bromo-*m*-cresol or when 6-bromo-*m*-cresol was used as substrate. O'Bara *et al.* proposed a reaction pathway involving the protodebromination of the bromocresol and the reversible rebromination of the resulting *m*-cresol and of the initial and

[2]Jacquesy and Jouannetaud (15) have recently demonstrated that direct rearrangement of **3** to **4** occurs in the superacid SbF_5–HF, but does not occur in triflic acid.

[3]Bromination at such a position is in fact reversible, but only on a time scale which is extremely long compared to the time of the forward bromination reaction.

Can. J. Chem. Downloaded from www.nrcresearchpress.com by 210.87.254.6 on 09/06/12
For personal use only.

product bromocresols. *p*-Bromophenol and 4-bromo-3,5-xylenol similarly isomerized and disproportionated. No *m*-bromophenols were detected in these reactions, in accord with the expectation that *meta* bromination of phenol is exceedingly slow compared to *ortho* or *para* bromination.

In preliminary experiments we established that solutions of hydrogen bromide or tetramethylammonium bromide in triflic acid provide a very effective means of bringing about isomerization and disproportionation of bromophenols. A solution of 2-bromo-*p*-cresol in deuteriochloroform saturated with hydrogen bromide was unreacted after 24 h at ambient temperature. Likewise 2-bromo-*p*-cresol was unchanged after stirring with 48% hydrobromic acid for 72 h at ambient temperature. In contrast, 16% of the 2-bromo-*p*-cresol had reacted after treatment with tetramethylammonium bromide in triflic acid for 15 min. *o*-Bromophenol isomerized and disproportionated on treatment with tetramethylammonium bromide in triflic acid but no *m*-bromophenol was formed, whereas 2-bromo-*p*-cresol gave a mixture of phenols in which 3-bromo-*p*-cresol predominated. A mixture of the same composition was obtained when 3-bromo-*p*-cresol was used as the substrate. This suggests that the mixture is close to an equilibrium or at least quasi-equilibrium distribution of components. When *p*-cresol was brominated in triflic acid in a closed system, to prevent the loss of hydrogen bromide, and the mixture stirred for 24 h, the product mixture had a similar composition. Clearly, the hydrogen bromide formed in the bromination had brought about the isomerization and disproportionation of the 2-bromo-*p*-cresol initially formed. Addition of tetramethylammonium iodide to the reaction mixture after the 24 h isomerization period resulted in the liberation of iodine. On work-up a mixture consisting mainly of 3-bromo-*p*-cresol was obtained from which pure 3-bromo-*p*-cresol could be obtained by preparative glc.

Further confirmation that bromine was liberated during the isomerization and disproportionation was provided by reacting 2-bromo-*p*-cresol with tetramethylammonium bromide in the presence of 3,4-dimethylphenol: 5-bromo-3,4-dimethylphenol was obtained in addition to 3-bromo-*p*-cresol. Again it is to be noted that the *m*-bromo isomers predominate.

Reaction of 4-bromo-2,6-dimethylphenol also gave mainly *meta* brominated products. In this case bromination occurs *ipso* to the 2-methyl group, followed by migration of the bromine to the adjacent 3-position. *o*-Bromination of 2,4,6-trisubstituted phenols to form 6-bromocyclohexa-2,4-dienones is a well established reaction (17). We have recently shown that 2,6-dimethylphenol, *o*-cresol, and other substituted *o*-cresols, are nitrated to form the corresponding 6-nitrocyclohexa-2,4-dienones.[4]

Experimental

Infrared spectra were obtained on Perkin–Elmer 283 and 1320 spectrometers. The ^{1}H nmr spectra at 90 and 250 MHz were determined using Perkin–Elmer R32 and Bruker WM250 spectrometers, respectively. The ^{13}C nmr at 15.1, 62.9, and 100.6 MHz were obtained on Nicolet-TT 14, Bruker WM250, and Bruker WH400 spectrometers, respectively. Mass spectra were obtained on a Hitachi Perkin–Elmer RMU 7 spectrometer. Combined gas chromatography and mass spectrometry was carried out on a Finnigan 3300 system. A Varian 5000 liquid chromatograph was used for analytical high pressure liquid chromatography. Analytical gas chromatography was performed on a Varian 3700 gas chromatograph, equipped with CDS 111 data system or Hewlett–Packard 3390A integrator. The 30 m glass capillary SE-54 and SP-2250 columns were from SUPELCO and the 25 m fused silica capillary SE30, OV-101, FFAP, and CW-20M columns from Varian. For preparative gas chromatography a Varian Aerograph 920 with a 3 m 3% SE-30 column was employed. Mixtures of bromo-*p*-cresol and of bromo-2,6-dimethylphenols were analysed on the SP-2250 and SE-54 or SE-30 columns. All other analyses, except that of the bromophenols, were carried out using the SE-54 column. In addition to the reported nmr data, appropriate infrared and mass spectral data, including the precise mass of the parent ion, were obtained for previously known bromophenols and methylbromophenols.

Phenol was obtained from British Drug Houses. 4-Bromo-, 4-methyl-, 2-bromo-4-methyl-, 2,6-dibromo-4-methyl-, 3,4-dimethyl-, and 2,4,6-trimethylphenol were from Aldrich, as were phloroglucinol dihydrate, methanesulphonic acid, and trifluoromethanesulphonic acid. 3-Bromo-, 2,4-dibromo-, 2,6-dibromo-, and 2,6-dimethylphenol were from Eastman. 2-Bromophenol was from Baker.

4-Bromo-2,6-dimethylphenol was obtained by bromination of 2,6-dimethylphenol in methylene chloride – pyridine. After recrystallization from ether it had mp 79°C (lit. (18) mp 79.5°C); ^{1}H nmr ($CDCl_3$) δ: 2.18 (s, CH_3), 4.55 (br s, O*H*), and 7.08 (s, 3-*H* and 5-*H*) ppm.

Addition of triflic acid (2 cm^3) to a stirred solution of 4-methyl-2,4,6-tribromocyclohexa-2,5-dienone (5.56 g) in methylene chloride (50 cm^3) at 0°C gave (<10 min) 2,3,6-tribromo-*p*-cresol. After crystallization from ether – methylene chloride the colourless crystals had mp 102°C (lit. (13, 19) mp 106°C, 101°C); ^{1}H nmr ($CDCl_3$) δ: 2.35 (s, CH_3), 5.87 (br s, O*H*), and 7.35 (s, 5-*H*) ppm; ^{13}C nmr ($CDCl_3$) δ_C: 23.9 (*C*H$_3$), 107.8 (*C*-6), 113.7 (*C*-2), 126.2 (*C*-3), 132.3 (*C*-5), 132.6 (*C*-4), and 148.4 (*C*-1) ppm.

3-Bromomesitol was obtained by addition of triflic acid to a solution of 4-bromo-2,4,6-trimethylcyclohexa-2,5-dienone in $CDCl_3$ at −40°C. Crystallization of the worked-up product from pentane yielded colourless needles, mp 83°C (lit. (20–22) mp 81°C, 84.5°C, 82°C); ^{1}H nmr ($CDCl_3$) δ: 2.16 (s, 6-CH_3), 2.29 (s, CH_3), 2.33 (s, CH_3) 4.54 (s, O*H*), and 6.87 (s, 5-*H*); ^{13}C nmr ($CDCl_3$) δ_C: 15.6 (6-*C*H$_3$), 16.3 (2-*C*H$_3$), 23.1 (4-*C*H$_3$), 121.8 (*C*-6), 123.8 (*C*-3), 125.2 (*C*-2), 129.5 (*C*-5), 129.7 (*C*-4), and 150.2 (*C*-1) ppm.

The literature procedure (12) for the preparation of 5-bromo-3,4-dimethylphenol was adapted for the preparation of 3-bromo-*p*-cresol. A mixture of 2,3,6-tribromo-*p*-cresol (3.5 g) and 54% HI (50 cm^3) was stirred and heated under reflux for 3 h. Work-up gave an oil (1.62 g) consisting of *p*-cresol (20%) and 3-bromo-*p*-cresol (80%). Preparative gc gave 3-bromo-*p*-cresol as a colourless oil which solidifed on standing, mp 55°C (lit. (23) mp 55.4°C); ^{1}H nmr ($CDCl_3$) δ: 2.28 (s, CH_3), 4.91 (s, O*H*), 6.17 (dd, J_{56} = 8 Hz, J_{26} = 2.5 Hz, 6-*H*), 7.03 (d, J_{26} = 2.5 Hz, 2-*H*), and 7.05 (d, J_{56} = 8 Hz, 5-*H*) ppm; ^{13}C nmr ($CDCl_3$) δ_C: 21.7 (*C*H$_3$), 114.5 (*C*-6), 119.2 (*C*-2), 124.8 (*C*-3), 130.2 (*C*-4), 131.3 (*C*-5), and 153.3 (*C*-1) ppm.

Bromination of 3,4-dimethylphenol in aqueous acetic acid gave a mixture of 3,4-dimethylphenol (18%), and 6-bromo- (58%), 2-bromo- (14%), and 2,6-dibromo-3,4-dimethylphenol (10%). 6-Bromo-3,4-dimethylphenol crystallized and had mp 78–79°C (lit. (12) mp 79°C); ^{1}H nmr ($CDCl_3$) δ: 2.14 (s, 3-CH_3 and 4-CH_3), 5.21 (s, O*H*), 6.79 (s, 2-*H*), and 7.17 (s, 5-*H*) ppm; ^{13}C nmr ($CDCl_3$) δ_C: 18.6 (3-*C*H$_3$) 19.5 (4-*C*H$_3$), 106.5 (*C*-6), 117.1 (*C*-2), 130.2 (*C*-4), 132.7 (*C*-5), 137.8 (*C*-3), and 150.0 (*C*-1) ppm.

1,3,5-Trimethoxybenzene was prepared by methylation of phloroglucinol with dimethyl sulfate. It had mp 53°C (lit.(24) mp 53°C); ^{1}H nmr ($CDCl_3$) δ: 3.72 and 6.06 ppm; ^{13}C nmr ($CDCl_3$) δ_C: 55.2 (O*C*H$_3$), 92.9 (*C*-2, *C*-4, *C*-6), and 161.6 (*C*-1, *C*-3, *C*-5) ppm. Bromination with *N*-bromosuccinimide in dimethylformamide gave 1-bromo-2,4,6-trimethoxybenzene, which was recrystallized from ether and had mp 98–99°C (lit.(25) mp 99°C); ^{1}H nmr ($CDCl_3$) δ: 3.79 (s, 4-OCH_3), 3.85 (s, 2- and 6-OCH_3), and 6.17 (s, 3-*H* and 5-*H*) ppm; ^{13}C nmr ($CDCl_3$) δ_C: 55.4 (4-O*C*H$_3$), 56.2 (2- and

[4]G. G. Cross, A. Fischer, G. N. Henderson, and T. A. Smyth. Unpublished work.

Can. J. Chem. Downloaded from www.nrcresearchpress.com by 210.87.254.6 on 09/06/12
For personal use only.

6-OCH_3), 91.6 (C-1, C-3, and C-5), 157.4 (C-4), and 160.5 (C-2 and C-6) ppm.

4-Bromo-2,4,6-trimethylcyclohexa-2,5-dienone (ref. 7a)

An ice-cold bromine solution prepared from bromine (1.6 g), potassium bromide (4.8 g), and water (to 20 cm^3) was added over 3 min, with stirring, to a solution of mesitol (1.36 g, 0.01 mol) and pyridine (5 drops) in ether (20 cm^3) at −15°C. The mixture was stirred for an additional 10 min, and allowed to warm to −10°C. The ethereal layer was extracted with aqueous sodium bicarbonate at −20°C, dried, and the ether evaporated at 0°C. Recrystallization of the residue from pentane at −25°C, followed by trituration with pentane, gave pale yellow crystals of the dienone which were dried under reduced pressure at 0°C. The purified dienone was dissolved at −20°C in $CDCl_3$ (5 cm^3) containing CH_2Cl_2 (50 mm^3). This gave a 0.71 mol dm^{-3} solution (calculated from the ^1H nmr spectrum using CH_2Cl_2 as internal standard) which was stored at −78°C and used in subsequent experiments. The solution was handled at −20°C or below. When the purified dienone was stored overnight as a solid at −20°C, it was found to have decomposed to 4-bromomethyl-2,6-dimethylphenol (74%), 3-bromomesitol (19%), and mesitol (3%), whereas the $CDCl_3$ solution at −20°C was stable for several days. 4-Bromo-2,4,6-trimethylcyclohexa-2,5-dienone had ^1H nmr ($CDCl_3$, −20°C) δ: 1.93 (s, 2- and 6-CH_3), 1.96 (s, 4-CH_3), and 6.89 (s, 3-H and 5-H) ppm; ^{13}C nmr ($CDCl_3$, −40°C) δ_C: 16.1 (2- and 6-CH_3), 30.7 (4-CH_3), 56.3 (C-4), 132.5 (C-2 and C-6), 146.2 (C-3 and C-5), and 186.2 (C-1) ppm. 4-Bromomethyl-2,6-dimethylphenol had ^1H nmr ($CDCl_3$) δ: 2.17 (s, 2- and 6-CH_3), 4.30 (br s, OH), 4.38 (s, CH_2Br), and 6.97 (s, 3- and 5-H) ppm.

2,4,6-Tribromo-4-methylcyclohexa-2,5-dienone

2,6-Dibromo-*p*-cresol (0.02 mol) was brominated in the presence of pyridine (2 cm^3), at −5°C, in a similar manner to mesitol. The bromine colour disappeared rapidly and a light yellow precipitate formed. After 10 min, the mixture was extracted with cold CH_2Cl_2, dried over $MgSO_4$, and the solvent removed at 10°C. The resulting yellow crystals (6.5 g), on recrystallization from CH_2Cl_2–ether at −20°C, gave pale yellow crystals of the dienone (4.6 g), mp 104°C (lit. (26, 27) mp 105°C); ir (KBr): 1673 (C=O), 1590, 1578, 1470, 1440, 1320, 1022, 910, and 690 (C—Br) cm^{-1}; ^1H nmr ($CDCl_3$, −20°C) δ: 2.02 (s, CH_3) and 7.54 (s, 3-H and 5-H) ppm; ^{13}C nmr ($CDCl_3$, −20°C) δ_C: 29.8 (CH_3), 54.3 (C-4), 121.0 (C-2 and C-6), and 150.4 (C-3 and C-5) ppm. The C-1 signal was not located.

Bromination of p*-cresol and 3,4,5-trimethylphenol (mild conditions)*

On a nmr scale, bromine solution (0.5 mmol in 200 mm^3) was added to the phenol solution (0.5 mmol in 200 mm^3) using the appropriate solvents. Some reactions were carried out on a larger scale (5 or 10 mmol). No dienone was observed in any of these reactions. Bromination of 3,4,5-trimethylphenol in ether–water–pyridine at −10°C gave only 2-bromo-3,4,5-trimethylphenol; ir (KBr): 3490 (OH), 1600, 1580, 1470, 1290, 1225 (C—O), 1200, 1155, 1100 1040, 990, and 900 cm^{-1}; ^1H nmr ($CDCl_3$) δ: 2.15 (s, 4-CH_3), 2.20 (s, 5-CH_3), 2.35 (s, 3-CH_3), 5.66 (s, OH), and 6.73 (s, 6-H) ppm; ^{13}C nmr ($CDCl_3$) δ_C: 16.0 (4-CH_3), 20.2 and 20.6 (3- and 5-CH_3), 111.1 (C-2), 114.6 (C-6), 128.0 (C-4), 135.5 (C-5), 136.7 (C-3), and 149.5 (C-1) ppm; ms m/e (relative intensity): 217 (12), 216 (97), 215 (25), 214.008 (100, M_r $^{12}C_9{}^1H_{11}{}^{79}Br^{16}O$: 213.999), 213 (18), 201 (55), 199 (53), 136 (13), 135 (59), 91 (27), 82 (11), 80 (13), 79 (14), and 77 (13).

Bromination of phenols in strong acids

Standard conditions of bromination, work-up, and analysis are described for *p*-cresol in triflic acid. Significant variations from these conditions are described in the text or in the footnotes to Table 1. Bromine (5 mmol) in triflic acid (10 cm^3) was added over 15 min, dropwise, with stirring, to a solution of *p*-cresol (0.54 g, 5 mmol) in triflic acid (5 cm^3). The bromine was immediately decolourized. After 30 min, the mixture was poured, with stirring, into ice-water (150 cm^3), neutralized with solid sodium bicarbonate (added in portions), saturated with solid NaCl, and extracted with ether (4 × 50 cm^3). After drying, evaporation gave an oil (0.88 g) which contained 3-bromo-*p*-cresol and other aromatic compounds. Analysis by temperature-programmed gc, using both 30 m SE-54 and 30 m SP-2250 capillary columns, and identification by both co-injection of authentic sample and by gc–ms (appropriate M + 1 peaks were obtained in all cases by chemical ionization) gave, in order of retention time in the indicated relative amount (mol%): *p*-cresol (26), 2-bromo-*p*-cresol (26), 3-bromo-*p*-cresol (28), 2,5-dibromo-*p*-cresol (14), 2,3-dibromo-*p*-cresol (1), 2,6-dibromo-*p*-cresol (5), and 2,3,6-tribromo-*p*-cresol (0.1). Identification of the 2,3-dibromo-*p*-cresol is tentative as an authentic sample was not available.

Bromine (5 mmol) in sulfuric acid (5 cm^3) was added dropwise over 5 min to a solution of *p*-cresol (5 mmol) in sulfuric acid (5 cm^3). The bromine decolourized slowly (1 h). The ^1H nmr spectrum showed that the isolated product (105 mg) was 56% 2,6-dibromo-*p*-cresol and 44% 2,3,6-tribromo-*p*-cresol.

Bromination of mesitol in sulfuric acid appeared to be incomplete even after 6 h at ambient temperature. Work-up gave 3,5-dibromomesitol (30%) mp 160–161°C; ir (KBr): 3370 (OH), 1563, 1375, 1300, 1240, 1183, 985, 955, and 810 cm^{-1}, ^1H nmr ($CDCl_3$) δ: 2.31 (s, 2- and 6-CH_3), 2.57 (s, 4-CH_3), and 4.72 (s, OH, disappeared on addition of D_2O) ppm; ^{13}C nmr ($CDCl_3$) δ_C: 17.1 (2- and 6-CH_3), 25.1 (4-CH_3), 123.1 (C-3 and C-5), 125.3 (C-2 and C-6), 129.7 (C-4), and 150.2 (C-1) ppm; ms m/e (relative intensity): 296 (47), 295 (15), 294 (100), 293 (14), 291.910 (51, M_r $^{12}C_9{}^1H_{10}{}^{79}Br_2{}^{16}O$: 291.910), 215 (63), 213 (63), 134 (14) 109 (12), 106 (35), 105 (25), 103 (14), 97 (18), 95 (18), 91 (27), 83 (18), 82 (12), 81 (20), 80 (12), 79 (18), 78 (14), and 77 (27).

Bromination of phenol (5 mmol) in triflic acid gave an oil (0.80 g) which was composed of phenol (22) and 2-bromo- (4), 4-bromo- (60), 2,4-dibromo- (13), and 2,6-dibromophenol (1). *m*-Bromophenol and *p*-bromophenol were inseparable by gc on any of the columns listed above. The two phenols have characteristic ^1H nmr spectra and the tallest peak of *m*-bromophenol at δ 7.02 ppm is clearly separated from peaks of *p*-bromophenol. *m*-Bromophenol had ^1H nmr δ: 5.89 (s, OH), 6.75 (m, 6-H), and 7.02 (m, 2-H, 4-H, and 5-H) ppm. *p*-Bromophenol had ^1H nmr δ: 5.22 (br s, OH), 6.70 (d, $J_{23} = J_{56} = 8.5$ Hz, 2-H and 6-H), and 7.34 (d, 3-H and 5-H). The component of the third gc peak, identified as *p*-bromophenol, was separated by preparative gc and the ^1H nmr showed the absence of *m*-bromophenol. No *m*-bromophenol was detected by analytical hplc of the reaction product, using a Varian reverse phase MCH-10 column and methanol–water 25:75 v/v eluent. The *m*- and *p*-bromophenols were shown to separate under this condition.

2,5-Dibromo-*p*-cresol, from the products of bromination of 2-bromo-*p*-cresol in triflic acid, was collected by preparative glc and was crystallized from pentane as colourless crystals, mp 60–61°C (lit. (19) mp 61°C); ^1H nmr ($CDCl_3$) δ: 2.26 (s, CH_3), 5.37 (s, OH), 7.20 (s, 6-H), and 7.29 (s, 3-H) ppm.

Bromination of 3,4-dimethylphenol (5 mmol) in triflic acid yielded a colourless solid (0.98 g), consisting largely 5-bromo-3,4-dimethylphenol (by ^1H nmr). Analyses by gc with identification by co-injection of authentic samples and by gc–ms showed the following composition (mol%): 3,4-dimethylphenol (20) and 6-bromo- (2), 2-bromo- (2), 5-bromo- (69), 5,6-dibromo- (4), and 2,6-dibromo-3,4-dimethylphenol (3). Crystallization of the crude product from carbon tetrachloride at −20°C gave colourless needles of 5-bromo-3,4-dimethylphenol, mp 101–102°C (lit. (12, 28) mp 101°C, 103°C); ^1H nmr ($CDCl_3$) δ: 2.24 (s, 3- and 4- CH_3), 4.56 (s, OH), 6.60 (d, J = 2.5 Hz, 2-H), and 6.92 (d, J = 2.5 Hz 6-H) ppm; ^{13}C nmr ($CDCl_3$) δ_C: 18.4 (3-CH_3), 21.5 (4-CH_3), 116.3 (C-2), 117.0 (C-6), 125.3 (C-5), 128.4 (C-4), and 139.3 (C-3) ppm.

Bromination of mesitol in triflic acid was carried out under the standard conditions except for an extended reaction time. After 3 h the solution was still reddish brown, indicative of the presence of unreacted bromine. Work-up gave a solid product (0.86 g) consisting of 3-bromomesitol (59%) and mesitol (41%) by ^1H nmr.

Reaction of bromodienones with acids

The formation of 2,3,6-tribromo-*p*-cresol, by addition of triflic acid

Can. J. Chem. Downloaded from www.nrcresearchpress.com by 210.87.254.6 on 09/06/12
For personal use only.

to 4-methyl-2,4,6-tribromocyclohexa-2,5-dienone, and of 3-bromomesitol by addition of triflic acid to 4-bromo-2,4,6-trimethylcyclohexa-2,5-dienone has been mentioned above. These reactions were also carried out for analytical purposes on a nmr scale. In a typical reaction five drops of triflic acid were added to a solution of 4-bromo-2,4,6-trimethylcyclohexa-2,5-dienone (61 mg, 0.28 mmol) in $CDCl_3$ (400 mm^3), containing as an internal nmr standard CH_2Cl_2, at −20°C. The solution turned reddish brown and a nmr spectrum recorded within 2 min showed that the dienone had aromatized completely to 3-bromomesitol. Work-up gave crystalline 3-bromomesitol (56 mg). A similar reaction with sulfuric acid (20 mm^3) as the reagent also gave 3-bromomesitol but no reaction occurred with trifluoroacetic acid (40 mm^3) over 10 min at 0°C.

When 2,4,6-tribromo-4-methylcyclohexa-2,5-dienone was used as substrate, 2,3,6-tribromo-*p*-cresol was obtained as the sole product on reaction with triflic acid and also with sulfuric acid.

A solution of hydrogen bromide (0.4 mmol) in ether (100 mm^3) was added to a solution of 4-bromo-2,4,6-trimethylcyclohexa-2,5-dienone (0.28 mmol) in $CDCl_3$ (400 mm^3) at −40°C. The mixture was warmed to −20°C and the reaction followed by nmr. All the dienone had disappeared when the first spectrum was measured (<1 min) to give ~22% mesitol and ~78% 3-bromomesitol. After 35 min there was 9% of mesitol and 91% of 3-bromomesitol and after 12 h only 3-bromomesitol was present.

Hydrogen bromide was passed for 10 s through a solution of the dienone at −40°C. The solution turned reddish brown. It was warmed to −20°C and ^1H nmr after 10 min showed 7% mesitol and 93% 3-bromomesitol. After 12 h at −20°C, the composition had changed to ~1% mesitol and ~99% 3-bromomesitol.

In a similar experiment in which hydrogen chloride was passed through the solution of the dienone at −55°C and the solution then warmed to −40°C for 10 min, the ^1H nmr spectrum showed that all of the dienone had reacted to give 3-bromomesitol (83%) and 3-chloromesitol (17%).

Aqueous hydroiodic acid (40 mm^3 of 55%) was added to a solution of the dienone in a nmr tube at −50°C and the mixture shaken well. The ^1H nmr spectrum, taken after 10 min at −50°C, showed that no dienone remained. Work-up gave mesitol, identified by ^1H nmr.

Reaction of 4-bromo-2,4,6-trimethylcyclohexa-2,5-dien-1-one with p-*cresol and 1,3,5-trimethoxybenzene*

p-Cresol (59 mm^2, 0.57 mmol) was added to a solution of the dienone (0.28 mmol) in $CDCl_3$ (400 mm^3) in a nmr tube at −40°C and the temperature then raised to −20°C. In 5 min the dienone was completely debrominated to give mesitol and 2-bromo-*p*-cresol.

1,3,5-Trimethoxybenzene (105 mg, 0.63 mmol) in $CDCl_3$ (300 mm^3) was added to a standard solution of the dienone (0.31 mmol in 400 mm^3) in a nmr tube at −40°C. The resulting solution was warmed to −20°C and the reaction was followed by ^1H nmr. Mesitol and 2-bromo-2,4,6-trimethoxybenzene were formed to the extent of ~45% in 10 min and 96% in 25 min.

A solution of 1,3,5-trimethoxybenzene (0.16 mmol) and the bromodienone (0.16 mmol) in $CDCl_3$ (400 mm^3) did not react in 30 min at −40°C. Hydrogen bromide was then passed for 15 s. The ^1H nmr spectrum measured within 5 min showed that complete reaction to give mesitol and bromotrimethoxybenzene had occurred. Similarly, addition of triflic acid (20 mm^3) in $CDCl_3$ (100 mm^3) to a solution of 1,3,5-trimethoxybenzene (0.53 mmol) and the bromodienone (0.31 mmol) at −50°C resulted in complete reaction to give mesitol and bromotrimethoxybenzene. 3-Bromomesitol was not detected by nmr. However, addition of triflic acid (150 mm^3) in $CDCl_3$ (150 mm^3) to a solution of the trimethoxybenzene 0.53 mmol) and the bromodienone (0.31 mmol) in $CDCl_3$ (500 mm^3) at −50°C resulted in part of the dienone (78%) rearranging to 3-bromomesitol and part of it debrominating (22%) to yield bromotrimethoxybenzene and mesitol.

The bromodienone did not react with trimethoxybenzene in $CDCl_3$ at −40°C. CD_3OD (75 mm^3) was added to a solution of trimethoxybenzene (59 mg, 0.35 mmol) and the dienone (0.23 mmol) in $CDCl_3$ (400 mm^3) at −50°C and the solution warmed to −40°C. In 30 min all of the dienone had reacted to give mesitol and bromotrimethoxybenzene.

Isomerization and disproportionation of bromophenols

Standard conditions of isomerization are described for 2-bromo-*p*-cresol. Significant variations from these conditions are described in the text or in the footnotes to Table 1. Tetramethylammonium bromide (309 mg, 2 mmol) was added to a stirred solution of 2-bromo-*p*-cresol (1 mmol) in triflic acid (5 cm^3) contained in a closed system to prevent the escape of HBr. After 24 h, the mixture was poured into ice-water (50 cm^3) and neutralized with solid $NaHCO_3$. The solution was saturated with NaCl and extracted with ether (3 × 50 cm^3). The combined extract solution was washed with saturated NaCl solution (50 cm^3) and dried ($MgSO_4$). Removal of solvent gave an oil (175 mg) whose composition (by gc and gc−ms) is listed in Table 1.

The reaction of 2-bromo-*p*-cresol was repeated in the presence of 3,4-dimethylphenol (2 mmol). Work-up after 24 h gave a product (412 mg) of composition (mol%): *p*-cresol (19), 3,4-dimethylphenol (62), 3-bromo-*p*-cresol (12), 5-bromo-3,4-dimethylphenol (4), plus unidentified products (total ~2%).

4-Bromo-2,6-dimethylphenol (1 mmol) was reacted with tetramethylammonium bromide in triflic acid and gave a solid product (196 mg) containing (mol%): 2,6-dimethylphenol (17) and 3-bromo- (56), 4-bromo- (5), and 3,5-dibromo-2,6-dimethylphenol (22). The components of the second and third peaks were separated by preparative gc. 3-Bromo-2,6-dimethylphenol (from the second peak) crystallized from pentane to give colourless needles, mp 61°C (lit. (18) mp 60−61°C); ^1H nmr ($CDCl_3$) δ 2.16 (s, 6-C*H*$_3$), 2.30 (s, 2-C*H*$_3$), 4.58 (s, O*H*), 6.81 (d, J = 8 Hz, 5-*H*), and 7.04 (d, J = 8 Hz, 4-*H*) ppm. The identity of 3,5-dibromo-2,6-dimethylphenol (from the fourth peak) was confirmed by mp, ^1H nmr, and ^{13}C nmr. Crystallization from $CHCl_3$ gave colourless crystals, mp 135°C (lit. (29) mp 132−133°C); ^1H nmr ($CDCl_3$) δ: 2.26 (s, 2- and 6-C*H*$_3$), 4.03 (br s, O*H*), and 7.39 (s, 4-*H*) ppm; ^{13}C nmr ($CDCl_3$, 100.6 MHz) δ_C: 15.8 (2- and 6-*C*H_3), 122.8 and 122.9 (*C*-2, *C*-3, *C*-5, and *C*-6), 127.7 (*C*-4), and 152.9 (*C*-1) ppm. 3,4-Dibromo-2,6-dimethylphenol has mp 86°C (ref. 30) and a less symmetrical ^1H nmr spectrum (ref. 31).

Reaction of 2-bromophenol (1 mmol) in triflic acid containing tetramethylammonium bromide gave product (162 mg) consisting of (mol%): phenol (24) and 2-bromo- (12), 4-bromo- (32), 2,4-dibromo- (29), and 2,6-dibromophenol (3). 4-Bromophenol was separated by preparative gc and found by ^1H nmr to contain no 3-bromophenol.

*Preparation of 3-bromo-*p*-cresol*

Liquid bromine (5 mmol) was added to a stirred solution of *p*-cresol (5 mmol) in triflic acid (5 cm^3) in a closed system. After 24 h, tetramethylammonium iodide (3 mmol) was added. After a further 30 min, work-up gave product (0.76 g) consisting of (mol%): 3-bromo-*p*-cresol (73), *p*-cresol (24), and dibromo-*p*-cresol (3). Pure 3-bromo-*p*-cresol was isolated from the mixture as a colourless solid by preparative gc.

1. R. B. MOODIE and K. SCHOFIELD. Acc. Chem. Res. **9**, 287 (1976).
2. A. FISCHER and G. N. HENDERSON. Can. J. Chem. **57**, 552 (1979).
3. A. FISCHER and G. N. HENDERSON. J. Chem. Soc. Chem. Commun. 1096 (1979).
4. R. BENEDIKT. Justus Liebigs Ann. Chem. **199**, 127 (1879).
5. A. HANTZSCH and K. SCHNETER. Chem. Ber. **20**, 2040 (1887).
6. V. V. ERSHOV, A. A. VOLOD'KIN, and G. N. BOGDANOV. Russ. Chem. Rev. **32**, 75 (1963).
7. (*a*) V. V. ERSHOV and A. A. VOLOD'KIN. Izv. Akad. Nauk SSSR Otd. Khim. Nauk, 730 (1962); (*b*) 1108 (1962); (*c*) 1292 (1962); (*d*) 2015 (1962); (*e*) 2022 (1962); (*f*) 2026 (1962); (*g*) 2150 (1962); (*h*) 893 (1963); (*i*) V. V. ERSHOV, A. A. VOLOD'KIN, G. A. NIKIFOROV, and K. M. DYUMAEV. Izv. Akad. Nauk SSSR Otd. Khim. Nauk, 1893 (1962); (*j*) V. V. ERSHOV and A. A. VOLOD'KIN. Izv. Akad. Nauk SSSR Ser. Khim. 336 (1965).

8. E. J. COREY, S. BARCZA, and G. KLOTMANN. J. Am. Chem. Soc. **19**, 4782 (1969).
9. J. C. JACQUESY, M. P. JOUANNETAUD, and S. MAKANI. J. Chem. Soc. Chem. Commun. 110 (1980).
10. J. C. JACQUESY and M. P. JOUANNETAUD. Tetrahedron, **37**, 747 (1981).
11. J. M. BRITTAIN, P. B. D. DE LA MARE, and P. A. NEWMAN. Tetrahedron Lett. 4111 (1980).
12. J. M. BRITTAIN, P. B. D. DE LA MARE, N. S. ISAACS, and P. D. MCINTYRE. J. Chem. Soc. Perkin Trans. 2, 933 (1979).
13. J. M. BRITTAIN, P. B. D. DE LA MARE, and P. A. NEWMAN. J. Chem. Soc. Perkin Trans. 2, 32 (1981).
14. L. M. STOCK and H. C. BROWN. *In* Advances in physical organic chemistry. Vol. 1. *Edited by* V. Gold. Academic Press, New York, NY. 1963. p. 35.
15. J. C. JACQUESY and M. P. JOUANNETAUD. Tetrahedron Lett. 1673 (1982).
16. E. J. O'BARA, R. B. BALSLEY, and I. STARER. J. Org. Chem. **35**, 16 (1970).
17. A. J. WARING. Adv. Alicyclic Chem. **1**, 176 (1966).
18. K. AUWERS and T. MAKOVITS. Chem. Ber. **41**, 2332 (1908).
19. G. BADDELEY and J. PLANT. J. Chem. Soc. 525 (1943).
20. O. JACOBSON. Justus Liebigs Ann. Chem. **195**, 265 (1879).
21. R. ADAMS and H. W. STEWART. J. Am. Chem. Soc. **63**, 2859 (1941).
22. R. C. FUSON, R. V. LINDSEY, and R. B. WELLDON. J. Am. Chem. Soc. **64**, 2888 (1942).
23. H. J. LUCAS and N. F. SCUDDER. J. Am. Chem. Soc. **50**, 244 (1928).
24. A. J. BIRCH, J. W. CLARK-LEWIS, and A. V. ROBERTSON. J. Chem. Soc. 3586 (1957).
25. E. HELGSTRAND. Acta Chem. Scand. **18**, 1616 (1964).
26. K. FRIES and G. OEHMKE. Justus Liebigs Ann. Chem. **462**, 1 (1928).
27. Y. BURSTEIN and A. PATCHORNICK. Biochemistry, **11**, 4641 (1972).
28. A. W. CROSSLEY and J. D. BARTLETT. J. Chem. Soc. 1297 (1913).
29. K. AUWERS and K. TRAUN. Chem. Ber. **32**, 3314 (1899).
30. S. W. GLEED and A. T. PETERS. J. Chem. Soc. 209 (1948).
31. W. G. B. HUYMANS, T. G. WESTRA, W. J. MIJIS, H. A. GAUR, J. VRIEND, and J. SMIDT. Tetrahedron Lett. 4345 (1968).

Can. J. Chem. Downloaded from www.nrcresearchpress.com by 210.87.254.6 on 09/06/12
For personal use only.

Preparation of some deuterium labelled 9- and/or 10-oxygenated derivatives of geraniol, geranial, nerol, and neral[1]

J. BALSEVICH

Prairie Regional Laboratory, National Research Council of Canada, Saskatoon, Sask., Canada S7N 0W9

Received October 26, 1982

J. BALSEVICH. Can. J. Chem. **61**, 1053 (1983).

The preparation of various deuterium labelled 9- and/or 10-oxygenated derivatives of geraniol, geranial, nerol, and neral is described. Wittig reaction of the tetrahydropyranyl ethers of (*E*)- and (*Z*)-1,1-dideutero-6-(triphenylphosphonium)-3-methyl-2-hexen-1-ol iodides (**23** and **24**) with the tetrahydropyranyl ethers of hydroxyacetone and 1,3-dihydroxyacetone afforded, after deprotection, C-1 dideuterated 9-hydroxygeraniol, 9-hydroxynerol, 9,10-dihydroxygeraniol, and 9,10-dihydroxynerol of high isomeric purity. Selective oxidation of these products allowed for the preparation of the corresponding derivatives possessing an aldehyde functionality at C-9 or C-1 and C-9. Wittig reaction of **23** and **24** with pyruvaldehyde dimethyl acetal followed by acidic hydrolysis afforded C-1 dideuterated 10-oxogeraniol and 10-oxonerol, oxidation of which yielded C-1 deuterated 10-oxogeranial and 10-oxoneral. Wittig reaction of (*E*)- and (*Z*)-1,1-dideutero-6-(triphenylphosphonium)-3-methyl-2-hexen-1-ol iodides (**49** and **50**) with 1,1,3,3-tetraethoxyacetone afforded C-1 dideuterated 9,9,10,10-tetraethoxygeraniol and 9,9,10,10-tetraethoxynerol, oxidation of which provided C-1 deuterated 9,9,10,10-tetraethoxygeranial and 9,9,10,10-tetraethoxyneral.

J. BALSEVICH. Can. J. Chem. **61**, 1053 (1983).

On décrit la préparation de plusieurs dérivés oxygénés en position 9 et/ou 10 du géraniol, du géranial, du nérol et du néral marqués au deutérium. Une réaction de Wittig des éthers tétrahydropyrannyles des iodures du dideutéro-1,1 (triphénylphosphonium)-6 méthyl-3 hexène-2 ol-1 (*E*) et (*Z*) (**23** et **24**) avec les éthers tétrahydropyrannyles de l'hydroxyacétone et de la dihydroxy-1,3 acétone conduit, après déprotection, aux hydroxy-9 géraniol, hydroxy-9 nérol, dihydroxy-9,10 géraniol et dihydroxy-9,10 nérol dideutérés en C-1 en une grane pureté isomérique. L'oxydation sélective de ces produits permet de préparer les dérivés correspondants ayant une fonction aldéhyde en C-9 ou en C-1 et en C-9. La réaction de Wittig des composés **23** et **24** avec le diméthyle acétal de la pyruvaldéhyde, suivie d'une hydrolyse acide, conduit à l'oxo-10 géraniol et à l'oxo-10 nérol dideutérés en C-1. Par oxydation, ces composés donnent l'oxo-10 géranial et l'oxo-10 néral dideutérés en C-1. La réaction de Wittig des iodures de dideutéro-1,1 (triphénylphosphonium)-6 méthyl-3 hexène-2 ol-1 (*E*) et (*Z*) (**49** et **50**) avec la tétraéthoxy-1,1,3,3 acétone permet d'obtenir le tétraéthoxy-9,9,10,10 géraniol et le tétraéthoxy-9,9,10,10 nérol dideutérés en C-1 qui, par oxydation fournissent le tétraéthoxy-9,9,10,10 géranial et le tétraéthoxy-9,9,10,10 néral deutérés en C-1.

[Traduit par le journal]

In the biosynthesis of monoterpene indole alkaloids, the "monoterpene portion" of the alkaloids has been shown to arise from the seco-iridoid glucoside secologanin (**1**) (1, 2) which in turn arises, via the cyclopentanoid derivative loganin (**2**) (3), from the acyclic monoterpenes geraniol (**3**) and nerol (**4**)

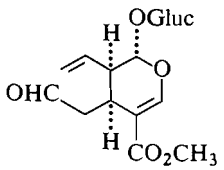

1

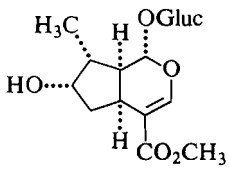

2

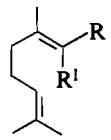

3 R = CH_2OH, R' = H
4 R = H, R' = CH_2OH

(4–6). The exact pathway between geraniol/nerol and loganin, however, remains uncertain. Previously, tracer studies had established that 10-hydroxygeraniol (**5**) and 10-hydroxynerol (**6**) were incorporated into loganin and indole alkaloids in *Cathar-*

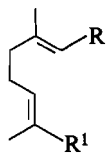

5 R = R' = CH_2OH
7 R = CH_2OH, R' = CHO
9 R = CHO, R' = CH_2OH
11 R = R' = CHO

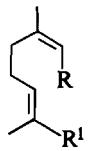

6 R = R' = CH_2OH
8 R = CH_2OH, R' = CHO
10 R = CHO, R' = CH_2OH
12 R = R' = CHO

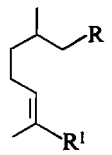

13 R = R', = CH_2OH
14 R = CHO, R' = CH_2OH
15 R = CH_2OH, R' = CHO
16 R = CH_2OH, R' = CH_3
17 R = CHO, R' = CH_3

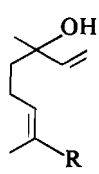

18 R = CH_3
19 R = CH_2OH

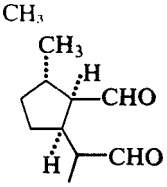

20

[1]NRCC No. 20574.

Can. J. Chem. Downloaded from www.nrcresearchpress.com by 210.87.254.5 on 09/06/12
For personal use only.

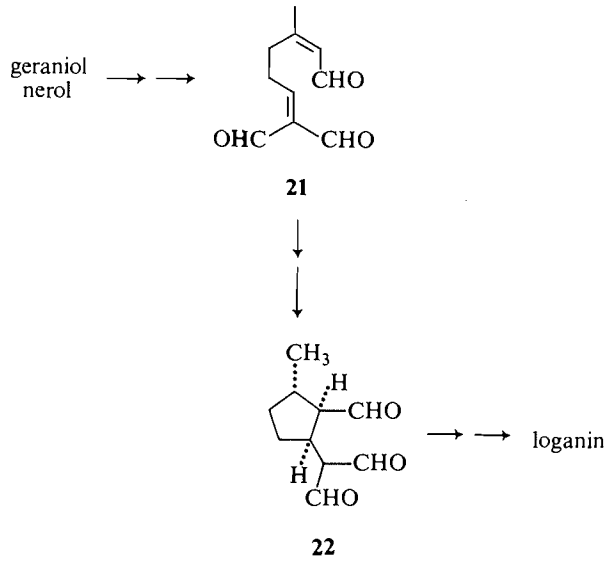

SCHEME 1

anthus roseus plants (7, 8). More recently, mixtures consisting of 10-oxogeraniol (**7**)/10-oxonerol (**8**), 10-hydroxygeranial (**9**)/10-hydroxyneral (**10**), and 10-oxogeranial (**11**)/10-oxoneral (**12**) were also shown to be incorporated (9), while such derivatives as 10-hydroxycitronellol (**13**), 10-hydroxycitronellal (**14**), 10-oxocitronellol (**15**), citronellol (**16**), citronellal (**17**), linalool (**18**), 10-hydroxylinalool (**19**), and iridodial (**20**) were not (7, 8, 10). These results coupled with the observation that an isotopic label at C-9 of geraniol becomes scrambled between C-9 and C-10 on conversion to loganin (3, 7, 11, 12) led to the hypothesis that the biosynthesis of loganin involves conversion of geraniol and nerol via several oxidative steps (and appropriate isomerizations) to 9,10-dioxoneral (**21**). Cyclization of **21** (to afford **22**) followed by further elaboration would then lead to loganin (Scheme 1) (7, 13).

In spite of the obtained evidence, however, definitive information regarding the importance of double bond geometries or direct evidence supporting the role of 9,10-oxygenated geraniol (nerol) derivatives is lacking. With the development of tissue culture methodology (which offers such advantages over the use of intact plants as having fewer problems associated with metabolite transport as well as greater control of experimental conditions) it was deemed that such questions could be resolved. Recently, it had been determined that 10-hydroxygeraniol and 10-hydroxynerol (labelled with deuterium) could be incorporated into indole alkaloids to the extent of 80% when a cell suspension culture of *C. roseus* was used for the tracer experiments (14). This incorporation was two orders of magnitude greater than that previously observed using intact plants, and augered well for further studies; however, a number of geraniol, geranial, nerol, and neral derivatives oxygenated at the 9 and/or 10 positions (i.e. hypothetical alkaloid precursors or analogs thereof) were required. Accordingly, the synthesis of these derivatives, possessing a deuterium label, was undertaken and the results presented here.

It was envisioned that the target compound could be conveniently prepared by Wittig reaction of isomerically pure phosphonium salts **23** and **24** with appropriately oxygenated derivatives of acetone (followed by deprotection and further functional group manipulation as required). To this end, 5-chloro-2-pentanone was coupled by Wittig–Horner reaction

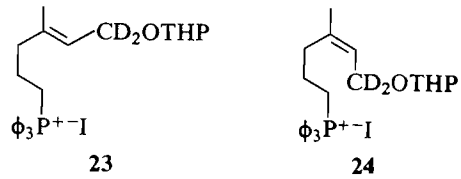

with trimethylphosphonoacetate to yield a mixture of (*E*)- and (*Z*)-methyl 6-chloro-3-methyl-2-hexenoates (**25** and **26**, *E*/*Z* = 1.8:1) in 91% yield. The assignments of stereochemistry were achieved by examination of the proton magnetic resonance spectra which exhibited characteristic signals for the olefinic methyl groups at δ 2.16 for the (*E*)-isomer **25** and δ 1.87 for the (*Z*)-isomer **26** (7). Separation, by spinning band distillation, afforded the individual esters in >98% isomeric purity as determined by glc analysis. Reduction of **25** and **26**

25 R = CO_2CH_3
27 R = CD_2OH
29 R = CD_2OTHP

26 R = CO_2CH_3
28 R = CD_2OH
30 R = CD_2OTHP

with lithium aluminum deuteride furnished the allylic alcohols **27** and **28** in 96% and 93% yields respectively. Alcohols **27** and **28** were converted to the tetrahydropyranyl ethers **29** (98% yield) and **30** (95% yield) via standard means and then treated with triphenylphosphine and sodium iodide in refluxing acetonitrile to afford the desired phosphonium salts **23** (86% yield) and **24** (89% yield) as crystalline solids.

Having the desired phosphonium salts in hand, their Wittig reactions with various substrates were examined. Wittig reaction of **23** with the tetrahydropyranyl ether of hydroxyacetone under "salt free conditions" (15) yielded, after removal of the protecting groups, 1,1-dideutero-9-hydroxygeraniol (**31**) in 85% yield. Correspondingly, **24** yielded 1,1-dideutero-9-hydroxynerol (**32**) in 91% yield. The Wittig reactions were highly stereoselective with only 3% contamination by the 10-hydroxy isomers.

Oxidation of **31** and **32** with manganese dioxide gave, after purification by thin-layer chromatography, 1,1-dideutero-9-oxogeraniol (**33**) and 1,1-dideutero-9-oxonerol (**34**) contaminated with ca. 5% of the 10-oxo isomers. The chemical shifts of the aldehyde protons of **33** and **34** (δ 10.13 and δ 10.09)

31 R = CD_2OH, R' = CH_2OH
33 R = CD_2OH, R' = CHO
35 R = CDO, R' = CHO

32 R = CD_2OH, R' = CH_2OH
34 R = CD_2OH, R' = CHO
36 R = CDO, R' = CHO

were consistent with the 9-oxo assignments (8). The observed preference for oxidation of the C-9 over the C-1 hydroxy groups was likely the result of the deuterium isotope effect wherein the rate-determining step of the oxidation would be the breaking of the C—H (C—D) bond.

Can. J. Chem. Downloaded from www.nrcresearchpress.com by 210.87.254.5 on 09/06/12
For personal use only.

Can. J. Chem. Downloaded from www.nrcresearchpress.com by 210.87.254.5 on 09/06/12
For personal use only.

Further oxidation of **33** and **34** using barium manganate afforded dialdehydes **35** and **36** in 71% and 75% yields respectively. In the case of **35**, no significant isomerization was noted during this oxidation. In the case of **36** a small amount (ca. 2%) of isomerization of the 2,3 double bond was observed.

For the preparation of some 10-oxygenated derivatives, the phosphonium salts **23** and **24** were coupled by Wittig reaction with the dimethyl acetal of pyruvaldehyde. Although the 9-acetal derivatives were formed initially, acidic hydrolysis of the protecting groups was accompanied by isomerization to

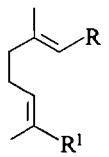

37 R = CD_2OH, R' = CHO
39 R = CDO, R' = CHO

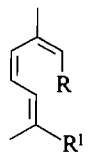

38 R = CD_2OH, R' = CHO
40 R = CDO, R' = CHO

afford 1,1-dideutero-10-oxogeraniol (**37**) contaminated with 2% of the 9-oxo isomer and 1,1-dideutero-10-oxonerol (**38**) contaminated with 7% of the 9-oxo isomer. The chemical shifts of the aldehyde protons of **37** and **38** (δ 9.36 and δ 9.38) were consistent with the 10-oxo assignments (8).

Further oxidation of **37** and **38** employing barium manganate afforded the dialdehydes **39** and **40**. The isomeric purity of these derivatives was essentially unchanged.

For the preparation of some 9,10-oxygenated derivatives two approaches were utilized. In the first, phosphonium salts **23** and **24** were coupled by Wittig reaction with ditetra-

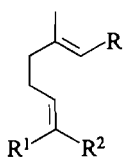

41 R = CD_2OH, R' = R^2 = CH_2OH
43 R = CD_2OH, R' = CHO, R^2 = CH_2OH
45 R = CD_2OH, R' = CH_2OH, R^2 = CHO

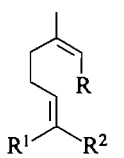

42 R = CD_2OH, R' = R^2 = CH_2OH
44 R = CD_2OH, R' = CHO, R^2 = CH_2OH
46 R = CD_2OH, R' = CH_2OH, R^2 = CHO

hydropyranyl ether of 1,3-dihydroxyacetone. After removal of the protecting groups 1,1-dideutero-9,10-dihydroxygeraniol (**41**) and 1,1-dideutero-9,10-dihydroxynerol (**42**) were obtained in 56% and 63% yields respectively.

Oxidation of triols **41** and **42** with manganese dioxide in tetrahydrofuran at 0°C was reasonably regioselective yielding 1,1-dideutero-9-oxo-10-hydroxygeraniol (**43**) contaminated with 12% of the 9-hydroxy-10-oxo isomer **45** and 1,1-dideutero-9-oxo-10-hydroxynerol (**44**) contaminated with 14% of the isomer **46**. The assignments of stereochemistry were based on the chemical shifts of the aldehyde protons. The major components of the two oxidations (i.e. **43** and **44**) exhibited resonances at δ 10.10 and δ 10.02 while the minor components (**45** and **46**) exhibited resonances at δ 9.41 and δ 9.37 (8). The yields of the oxidations were 72% and 66% respectively. Interestingly, when manganese dioxide in dichloromethane at ambient temperatures was used, poorer yields and lower regioselectivity were observed.

Attempted oxidation of **43** with barium manganate gave poor recovery of a complex mixture of products and was not further pursued, rather an alternative approach to other 9,10 oxygenated derivatives was employed. The second approach involved preparation of 1,1,3,3-tetraethoxyacetone (**47**) (16, 17) as the

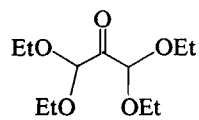

47

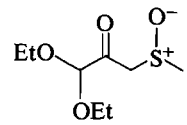

48

ketonic substrate for the Wittig reaction. Accordingly, ethyl diethoxyacetate was reacted with dimsyl sodium in dimethyl sulfoxide to furnish β-ketosulfoxide **48**. Treatment of **48** with mercuric oxide and boron trifluoride in refluxing ethanol effected Pummerer rearrangement and ethanolysis to yield **47**.[2]

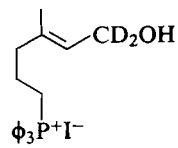

49

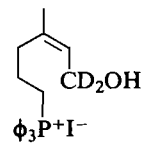

50

Wittig reaction of **47** (18) with phosphonium salts **49** and **50** (prepared from the chloroalcohols **27** and **28** by reaction with triphenylphosphine and sodium iodide in refluxing acetonitrile as before) furnished 1,1-dideutero-9,9,10,10-tetraethoxygeraniol (**51**) in 71% yield and 1,1-dideutero-9,9,10,10-tetraethoxynerol (**52**) in 55% yield.

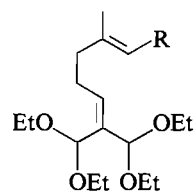

51 R = CH_2OH
53 R = CDO

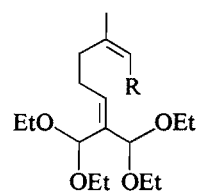

52 R = CH_2OH
54 R = CDO

Oxidation of **51** and **52** with barium manganate yielded the corresponding aldehydes **53** and **54**. Attempts to hydrolyse compounds **51** to **54** to afford the corresponding 9,10 dialdehydes were not successful, likely due to the instability of the vinyl dialdehyde system. This result, however, does not preclude the use of these derivatives for tracer experiments as the possibility of in vitro generation of the 9,10-dialdehyde functionality remains.

[2]The previous preparation of **47** (16, 17) involves reaction of pyruvaldehyde diethylacetal with ethyl nitrite in the presence of ethanolic hydrogen chloride, however, the product is generally contaminated with 5–10% of the corresponding ketal. The procedure employed gave essentially pure **47**.

Can. J. Chem. Downloaded from www.nrcresearchpress.com by 210.87.254.5 on 09/06/12
For personal use only.

Experimental

Melting points (mp) were obtained on a Koffler block and are uncorrected. Gas–liquid chromatography (glc) was carried out with a Hewlett–Packard model 5710A gas chromatograph equipped with an 8.6 meter capillary glass column containing OV-101. Ultraviolet (uv) spectra were obtained with samples in 95% ethanol using a Beckman model 35 spectrophotometer; absorption maxima are quoted in nanometers with log ϵ values in brackets. Infrared (ir) spectra were obtained with samples as neat films on sodium chloride plates using a Varian model 257B spectrophotometer; absorption maxima are quoted in centimeters^{-1}. Proton magnetic resonance (^{1}Hmr) spectra were obtained with samples in deuterochloroform (unless otherwise noted) using a Varian model EM-390 spectrometer. The position of peaks is listed in the δ scale relative to tetramethylsilane which was used as internal standard. Low resolution mass spectra (ms) were obtained on a Finnegan model 4000 spectrometer run at 70 eV. Microanalyses were performed by the Spang Microanalytical Laboratory, Eagle Harbor, Michigan, U.S.A. For thin-layer chromatography, Whatman PLK5F precoated silica gel plates were employed. For column chromatography, Aldrich silica gel, grade 12, 28–200 mesh was used.

Lithium aluminum deuteride and n-butyllithium were obtained from the Alfa Chemical Co. Manganese dioxide, barium manganate, and phenyllithium were obtained from the Aldrich Chemical Co. Potassium hexamethyldisilazide was prepared by the reaction of potassium hydride with hexamethyldisilazane in tetrahydrofuran. The tetrahydropyranyl ethers of hydroxyacetone (acetol) and 1,3-dihydroxyacetone were prepared from the alcohols via standard means. Anhydrous tetrahydrofuran was obtained by distillation from the sodium ketyl of benzophenone. Spinning band distillation was carried out with a Kontes model K-500400 spinning band micro still. Isomeric purities were determined from glc analyses or ^{1}Hmr spectra.

(E)-and (Z)-Methyl 3-methyl-6-chloro-2-hexenoates (25 and 26)

A suspension of sodium hydride (4.7 g of 50% NaH/mineral oil, 0.098 mol) in anhydrous tetrahydrofuran (150 mL) at 0°C was treated with a solution of trimethylphosphonoacetate (18.2 g, 0.099 mol) in dimethyl sulfoxide (25 mL) at a dropwise rate over 20 min. After a further 20 min 5-chloro-2-pentanone (10 mL, 0.087 mol) was added. The reaction mixture was stirred for 24 h at ambient temperature, diluted with petroleum ether (100 mL), and washed with 5% sodium bicarbonate solution (5 × 50 mL). The combined aqueous portion was back-extracted with petroleum ether (1 × 50 mL). The combined organic portion was dried (Na_2SO_4) and the solvent removed *in vacuo*. The residue was distilled at 10 Torr to afford a mixture of **25** and **26** (1.8:1, 13.92 g, 91%) as a colorless liquid; bp 112–119°C at 10 Torr. The two isomers were separated by spinning band distillation at 0.5 Torr (3×) yielding **25** and **26** in greater than 98% isomeric purity. (*E*)-Methyl 3-methyl-6-chloro-2-hexenoate (**25**); bp: 65°C at 0.5 Torr; glc retention time (80°C): 3.97 min; uv λ_{max}: 218 (4.41); ir ν_{max}: 1718, 1650, 1432, 1224, 1151, 1144; ^{1}Hmr δ: 5.67 (1H, bs), 3.65 (3H, s), 3.48 (2H, t, J = 6 Hz), 2.29 (2H, m), 2.16 (3H, d, J = 1.3 Hz), 1.96 (2H, m); ms m/e: 178 (^{37}Cl, M$^+$, 5%), 176 (^{35}Cl, M$^+$, 16%), 145 (39%), 127 (69%), 114 (100%), 95 (44%). (*Z*)-Methyl 3-methyl-6-chloro-2-hexenoate (**26**); bp: 61°C at 0.5 Torr; glc retention time (80°C): 3.07 min; uv λ_{max}: 217 (4.20); ir ν_{max}: 1716, 1648, 1430, 1224, 1152; ^{1}Hmr δ: 5.70 (1H, bs), 3.64 (3H, s), 3.52 (2H, t, J = 6 Hz), 2.73 (2H, m), 1.93 (2H, m), 1.87 (3H, d, J = 1.4 Hz); ms m/e: 178 (^{37}Cl, M$^+$, 7%), 176 (^{35}Cl, M$^+$, 20%), 145 (33%), 127 (100%), 114 (55%), 95 (72%). *Anal.* (mixture of *E* and *Z* isomers) calcd. for $C_8H_{13}O_2Cl$: C 54.39, H 7.42, Cl 20.07; found: C 54.43, H 7.42, Cl 20.10.

(E)-1,1-Dideutero-3-methyl-6-chloro-2-hexen-1-ol (27)

A solution of ester **25** (18 g, 0.10 mol) in anhydrous ether (150 mL) was treated with small portions of lithium aluminum deuteride (4.2 g, 0.10 mol) over a period of 30 min. After stirring for a further 4 h at ambient temperature, water (20 mL) was cautiously added over a period of 30 min. The reaction mixture was filtered and the solvent removed *in vacuo* to give **27** as a colorless liquid (14.5 g, 96%); ir ν_{max}: 3350, 2190, 2085, 1664, 1078; ^{1}Hmr δ: 5.44 (1H, bs), 3.51 (3H, t, J = 6 Hz), 2.3–1.7 (4H, m), 1.66 (3H, d, J = 1.3 Hz); ms m/e: 152 (^{37}Cl, M$^+$, 1.4%), 150 (^{35}Cl, M$^+$, 5.5%), 135 (15%), 133 (36%), 97 (15%), 83 (18%), 73 (100%). *Anal.* (of nondeuterated analog) calcd. for $C_7H_{13}OCl$: C 56.57, H 8.82, Cl, 23.85; found: C 56.32, H 8.77, Cl 23.75.

(Z)-1,1-Dideutero-3-methyl-6-chloro-2-hexen-1-ol (28)

A solution of ester **26** (13 g, 0.07 mol) in anhydrous ether (130 mL) was treated with lithium aluminum deuteride (3 g, 0.07 mol) as above to afford alcohol **28** as a colorless liquid (10.2 g, 93%); ir ν_{max}: 3350, 2190, 2082, 1664, 1078; ^{1}Hmr δ: 5.42 (1H, bs), 3.45 (3H, t, J = 6 Hz), 2.4–1.7 (4H, m), 1.71 (3H, d, J = 1.3 Hz); ms m/e: 152 (^{35}Cl, m$^+$, 0.9%), 150 (^{35}Cl, m$^+$, 3.1%), 135 (7%), 133 (13%), 97 (15%), 83 (30%), 73 (100%). *Anal.* calcd. for $C_7H_{11}D_2OCl$: C 55.83, Cl 23.54; found: C 55.11, Cl 23.25.

(E)-Tetrahydropyranyl ether 29

A solution of alcohol **27** (14.5 g, 0.096 mol) and *p*-toluenesulfonic acid monohydrate (300 mg, 1.6 mmol) in ether (100 mL) was treated with dihydropyran (11 mL, 0.13 mol) at a dropwise rate over a period of 2 h. The reaction mixture was stirred for a further 18 h at ambient temperature and then washed with 1 *N* sodium hydroxide solution (3 × 30 mL) and brine (2 × 30 mL). After drying (Na_2SO_4) the solvent was removed *in vacuo* to afford **29** as a colorless liquid (22 g, 98%); ir ν_{max}: 2155, 2075, 1662, 1020, 724; ^{1}Hmr δ: 5.39 (1H, bs), 4.59 (1H, t, J = 3 Hz), 3.9 (1H, m), 3.5 (1H, m), 3.49 (2H, t, J = 6 Hz), 2.4–1.4 (10H, m), 1.67 (3H, bs); ms m/e: 234 (M$^+$, 0.1%), 133 (33%), 85 (100%).

(Z)-Tetrahydropyranyl ether 30

A solution of alcohol **28** (9.5 g, 0.06 mol) and *p*-toluenesulfonic acid monohydrate (200 mg, 1.1 mmol) in ether (70 mL) was treated with dihydropyran (7.3 mL, 0.09 mol) as above to afford **30** as a colorless liquid (14 g, 95%); ir ν_{max}: 2158, 2074, 1661, 1020; ^{1}Hmr δ: 5.43 (1H, bs), 3.49 (1H, t, J = 6 Hz), 2.5–1.4 (10H, m), 1.75 (3H, bs); ms m/e: 234 (M$^+$, 0.1%), 133 (24%), 85 (100%). *Anal.* calcd. for $C_{12}H_{19}D_2O_2Cl$: C 61.39, Cl 15.12; found: C 61.73, Cl 15.02.

(E)-Phosphonium salt 23

A mixture of **29** (21.5 g, 0.092 mol), triphenylphosphine (25 g, 0.095 mol), and sodium iodide (27 g, 0.18 mol) in acetonitrile (60 mL) was heated at reflux. After 27 h the reaction mixture was cooled to 0°C, diluted with dichloromethane (130 mL), and filtered. The solvent was removed *in vacuo* and the resultant gum was washed with ether (3 × 50 mL), dissolved in acetone (50 mL), treated with ether (130 mL), and allowed to stand at 0°C for several days whereupon crystallization occurred. The solid mass was pulverized, filtered, further washed with ether and water, and dried *in vacuo* at 100°C to afford **23** as an off-white crystalline solid (48 g, 86%), mp 149–151°C (crystals soften at 119°C); ^{1}Hmr δ: 7.8 (15H, m), 5.35 (1H, bs), 4.55 (1H, m), 4.0–3.3 (4H, m), 2.73 (2H, t, J = 7.5 Hz), 2.2–1.3 (8H, m), 1.54 (3H, bs). *Anal.* calcd. for $C_{30}H_{37}D_2IOP$: C 61.23, I 21.57; found: C 61.40, I, 21.65.

(Z)-Phosphonium salt 24

A mixture of **30** (8 g, 0.034 mol), triphenylphosphine (9.4 g, 0.036 mol) and sodium iodide (10.2 g, 0.068 mol) in acetonitrile (25 mL) was heated at reflux. After 27 h the reaction mixture was cooled to 0°C, diluted with dichloromethane (100 mL), and filtered. The solvent was removed *in vacuo* and the resultant gum washed with ether (3 × 4 mL). The residue was treated with acetone (40 mL) and let stand at 0°C for 4 h whereupon cyrstallization occurred. The solid mass was pulverized, filtered, washed with ether, and dried *in vacuo* at 100°C to afford **24** as a white crystalline solid (17.8 g, 89%), mp 187–188°C; ^{1}Hmr δ: 7.8 (15H, m), 5.45 (1H, bs), 4.57 (1H, m), 4.0–3.2 (4H, m), 2.43 (2H, t, J = 7.5 Hz), 2.0–1.2 (8H, m), 1.59 (3H, bs). *Anal.* calcd. for $C_{30}H_{37}D_2IOP$: C 61.23, I 21.57; found: C 61.27, I 21.48.

Can. J. Chem. Downloaded from www.nrcresearchpress.com by 210.87.254.5 on 09/06/12
For personal use only.

1,1-Dideutero-9-hydroxygeraniol (31)

A suspension of phosphonium salt **23** (2.8 g, 4.76 mmol) in anhydrous tetrahydrofuran/hexamethylphosphoramide (10 mL/1 mL) under a nitrogen atmosphere was treated with a solution of potassium hexamethyldisilylazide in tetrahydrofuran (4.8 mL of 1 *M* solution, 4.8 mmol). After 15 min at ambient temperature the reaction mixture was cooled to −78°C and treated with the tetrahydropyranyl ether of hydroxyacetone (0.7 g, 4.7 mmol). The cooling bath was removed and the reaction mixture allowed to warm to ambient temperature. After a further 3 h at ambient temperature the reaction mixture was diluted with petroleum ether (10 mL) and filtered through a short column of silica gel using petroleum ether as eluent. After evaporation of the solvent, the residue was dissolved in methanol (50 mL), treated with *p*-toluenesulfonic acid monohydrate (80 mg), and stirred at ambient temperature for 18 h. Sodium hydroxide solution (2 *M*, 0.25 mL) was added and the solvent removed *in vacuo*. The residue was chromatographed on silica gel using ether as eluent to afford **31** (contaminated with 3% of the 10-hydroxy isomer) as a colorless liquid (690 mg, 85%); ir ν_{max}: 3340, 2180, 2090, 1080; ^{1}Hmr δ: 5.37 (1H, bs), 5.22 (1H, t, J = 7 Hz), 4.04 (2H, s), 2.70 (1H, bs), 2.2 (4H, m), 1.76 (3H, bs), 1.65 (3H, bs); ms m/e: 154 (M^+ − 18, 0.5%), 136 (3.2%), 121 (15%), 84 (28%), 70 (35%), 43 (100%). *Anal.* calcd. for $C_{10}H_{16}D_2O_2$: C 69.74; found: C 69.75.

1,1-Dideutero-9-hydroxynerol (32)

Reaction of phosphonium salt **24** (2 g, 3.4 mmol) with potassium hexamethyldisilazide (3.4 mL of 1 *M* solution in THF) and the tetrahydropyranyl ether of hydroxyacetone (0.5 g, 3.4 mmol) as above afforded **32** (contaminated with 3% of the 10-hydroxy isomer) as a colorless liquid (530 mg, 91%); ir ν_{max}: 3340, 2160, 2078, 1662, 1080; ^{1}Hmr δ: 5.40 (1H, bs), 5.26 (1H, t, J = 6.5 Hz), 4.02 (2H, s), 2.1 (4H, m), 1.77 (3H, bs), 1.71 (3H, bs); ms m/e: 154 (M^+ − 18, 0.3%), 139 (5%), 136 (5%), 121 (16%), 84 (27%), 70 (40%), 43 (100%).

1,1-Dideutero-9-oxogeraniol (33)

A solution of diol **31** (200 mg, 1.16 mmol) in dichloromethane (18 mL) at ambient temperature was treated with manganese dioxide (2.4 g). The resultant suspension was stirred for 1.5 h and filtered through Celite. The filtrate was concentrated *in vacuo* and the residue chromatographed on silica gel using ether/petroleum ether (1:1, v/v) as eluent to yield **33** (contaminated with 5% of the 10-oxo isomer) as a pale yellow oil (141 mg, 71%); uv λ_{max}: 237 nm (4.09); ir ν_{max}: 3420, 2180, 2078, 1672; ^{1}Hmr δ: 10.13 (1H, s), 6.48 (1H, t, J = 7 Hz), 5.43 (1H, bs), 2.71 (2H, q, J = 7 Hz), 2.18 (2H, t, J = 7 Hz), 1.88 (1H, s), 1.75 (3H, bs), 1.68 (3H, bs); ms m/e: 152 (M^+ − 18, 5%), 137 (9%), 123 (13%), 109 (11%), 95 (16%), 84 (35%), 82 (43%), 41 (100%).

1,1-Dideutero-9-oxonerol (34)

A solution of diol **32** (150 mg, 0.87 mmol) in dichloromethane (15 mL) was treated with manganese dioxide (1.5 g) as above to yield **34** (contaminated with 5% of the 10-oxo isomer) as a pale yellow oil (98 mg, 65%); uv λ_{max}: 237 (4.08); ir ν_{max}: 3420, 1674; ^{1}Hmr δ: 10.09 (1H, s), 6.46 (1H, t, J = 7 Hz), 5.47 (1H, bs), 1.74 (6H, bs); ms m/e: 170 (M^+, 0.1%), 152 (8%), 137 (12%), 109 (15%), 95 (30%), 84 (52%), 82 (94%), 42 (100%). *Anal.* calcd. for $C_{10}H_{14}D_2O_2$: C 70.55; found: C 70.05.

1-Dieutero-9-oxogeranial (35)

A solution of **33** (180 mg, 1.08 mmol) in dichloromethane (11 mL) was treated with barium manganate (1.9 g). The resultant suspension was stirred at ambient temperature for 2.5 days and filtered through Celite. The filtrate was concentrated *in vacuo* and the residue chromatographed on silica gel using ether/petroleum ether (1:1, v/v) as eluent to afford **35** as a pale yellow liquid (130 mg, 71%); uv λ_{max}: 237 (4.38); ir ν_{max}: 2100, 1663; ^{1}Hmr δ: 10.15 (1H, s), 6.43 (1H, t, J = 8 Hz), 5.89 (1H, bs), 3.0–2.2 (4H, m), 2.21 (3H, bs), 1.78 (3H, bs); ms m/e: 167 (M^+, 0.5%), 152 (7%), 149 (4%), 95 (36%), 82 (96%), 42 (100%). *Anal.* calcd. for $C_{10}H_{13}DO_2$: C 71.83; found: C 71.55.

1-Deutero-9-oxoneral (36)

A solution of **34** (120 mg, 0.71 mmol) in dichloromethane (8 mL) was treated with barium manganate (1.3 g) as above to afford **36** as a pale yellow liquid (88 mg, 75%); uv λ_{max}: 236 (4.35); ir ν_{max}: 2100, 1667, 1636; ^{1}Hmr δ: 10.11 (1H, s), 6.44 (1H, t, J = 7 Hz), 5.93 (1H, bs), 2.9–2.6 (4H, m), 2.00 (3H, bs), 1.77 (3H, bs); ms m/e: 167 (M^+, 0.4%), 152 (6%), 149 (4%), 95 (38%), 82 (96%), 42 (100%).

1,1-Dideutero-10-oxogeraniol (37)

A suspension of the (*E*)-phosphonium salt **23** (5.4 g, 9.2 mmol) in anhydrous tetrahydrofuran/hexamethylphosphoramide (30 mL/3 mL) under a nitrogen atmosphere was treated with a 1.9 *M* solution of phenyllithium in ether (5 mL, 9.5 mmol). After stirring for 10 min at ambient temperature the reaction mixture was cooled to −78°C and treated with pyruvaldehyde dimethyl acetal (1.05 g, 8.9 mmol). The reaction was allowed to warm to ambient temperature (ca. 30 min) and stirred for a further 3 h. Petroleum ether (30 mL) was added and the resultant mixture filtered through a short column of silica gel using ether/petroleum ether (1:1) as eluent. The filtrate was concentrated *in vacuo* and the residue dissolved in methanol (60 mL) containing *p*-toluenesulfonic acid monohydrate (50 mg). After stirring for 18 h at ambient temperature, water (70 mL) was added and stirring continued. After 30 min, the reaction mixture was concentrated *in vacuo* (to ca. one-half the original volume, made basic with 1 *N* sodium hydroxide, and extracted with ether (3 × 40 mL). The combined ether extract was dried and the solvent removed *in vacuo* to afford **37** (contaminated with 2% of the 9-oxo isomer) as a pale yellow oil (980 mg, 65%); uv λ_{max}: 229 (4.20); ir ν_{max}: 3400, 1683, 1640; ^{1}Hmr δ: 9.36 (1H, s), 6.46 (1H, t, J = 7 Hz), 5.43 (1H, bs), 2.7–2.0 (4H, m), 1.73 (3H, bs), 1.68 (3H, bs); ms m/e: 152 (M^+ − H_2O, 11%), 137 (26%), 123 (26%), 84 (60%), 42 (100%).

1,1-Deutero-10-oxonerol (38)

A suspension of the (*Z*)-phosphonium salt **24** (2.5 g, 4.3 mmol) in anhydrous tetrahydrofuran/hexamethylphosphoramide (13 mL/1.3 mL) under a nitrogen atmosphere was treated with a 1.9 *M* solution of phenyllithium in ether (2.4 mL, 4.6 mmol) as above to afford **38** (contaminated with 7% of the 9-oxo isomer) as a pale yellow oil (500 mg, 69%); uv λ_{max}: 229 (4.29); ir ν_{max}: 3400, 1672, 1644; ^{1}Hmr δ: 9.38 (1H, s), 6.48 (1H, t, J = 7 Hz), 5.48 (1H, bs), 2.4 (4H, m), 1.76 (6H, bs); ms m/e: 152 (M^+ − 18, 5%), 151 (6%), 137 (11%), 123 (16%), 109 (11%), 98 (26%), 95 (19%), 84 (76%), 55 (60%), 42 (100%). *Anal.* calcd. for $C_{10}H_{14}D_2O_2$: C 70.55; found: C 70.48.

1-Deutero-10-oxogeranial (39)

A solution of **37** (350 mg, 2.06 mmol) in dichloromethane (25 mL) was treated with barium manganate (3.3 g). The resultant suspension was stirred at ambient temperature for 3 days and then filtered through Celite. The solvent was removed *in vacuo* to give the dialdehyde **39** as a pale yellow liquid (272 mg, 80%); uv λ_{max}: 234 (4.42); ir ν_{max}: 2100, 1682, 1660, 1640; ^{1}Hmr δ: 9.39 (1H, s), 6.44 (1H, t, J = 7 Hz), 5.89 (1H, bs), 2.7–2.22 (4H, m), 2.22 (3H, bs), 1.76 (3H, bs); ms m/e: 167 (M^+, 0.2%, 166 (0.5%), 149 (8%), 121 (13%), 110 (33%), 82 (44%), 55 (100%). *Anal.* calcd. for $C_{10}H_{13}DO_2$: C 71.83; found: C 71.39.

1-Deutero-10-oxoneral (40)

A solution of **38** (114 mg, 0.67 mmol) in dichloromethane (8 mL) was treated with barium manganate (1 g) as above to afford the dialdehyde **40** as a pale yellow liquid (93 mg, 82%); uv λ_{max}: 229 (4.32), 235 sh (4.29); ir ν_{max}: 2100, 1681, 1662, 1638; ^{1}Hmr δ: 9.40 (1H, s), 6.45 (1H, t, J = 7 Hz), 5.93 (1H, bs), 3.0–2.4 (4H, m), 2.02 (3H, bs), 1.75 (3H, bs); ms m/e: 167 (M^+, 1%), 152 (3%), 149 (6%), 138 (12%), 122 (14%), 109 (27%), 95 (63%), 85 (66%), 82 (76%), 55 (100%).

1,1-Dideutero-9,10-dihydroxygeraniol (41)

A suspension of the (*E*)-phosphonium salt **23** (5.36 g, 9.1 mmol) in anhydrous tetrahydrofuran/hexamethylphosphoramide (30 mL/3 mL) under a nitrogen atmosphere was treated with a 1.9 *M* solution of

Can. J. Chem. Downloaded from www.nrcresearchpress.com by 210.87.254.5 on 09/06/12
For personal use only.

phenyllithium in ether/hexane (4.7 mL, 8.9 mmol). After stirring at ambient temperature for 15 min the reaction mixture was cooled to −78°C and treated with a solution of the ditetrahydropyranyl ether of 1,3-dihydroxyacetone (2.3 g, 8.9 mmol) in ether (3 mL). The reaction mixture was allowed to warm to ambient temperature and stirred for a further 3 h. Petroleum ether (20 mL) was added and the resultant mixture filtered through a short column of silica gel using petroleum ether/ether as eluent. The filtrate was concentrated *in vacuo* and the residue was dissolved in methanol (230 mL) containing *p*-toluenesulfonic acid monohydrate (150 mg). After standing at ambient temperature for 17 h, sodium hydroxide (50 mg) was added and the solvent removed *in vacuo*. The residue was chromatographed on silica gel using ether/methanol (20:1 then 10:1) as eluent to afford **41** as a colorless oil (940 mg, 56%); ir ν_{max}: 3340, 1005; ^{1}Hmr δ: 5.47 (1H, t, J = 7 Hz), 5.30 (1H, bs), 4.22 (2H, s), 4.14 (2H, s), 2.4–2.0 (4H, m), 1.66 (3H, bs). *Anal.* calcd. for $C_{10}H_{16}D_2O_3$: C 63.80; found: C 63.75.

1,1-Dideutero-9,10-dihydroxynerol (42)

A suspension of the (*Z*)-phosphonium salt **24** (3.4 g, 5.8 mmol) in anhydrous tetrahydrofuran/hexamethylphosphoramide (20 mL/2 mL) was treated with phenyllithium (3 mL of 1.9 *M* solution, 5.7 mmol) and the tetrahydropyranyl ether of 1,3-dihydroxyacetone (1.5 g, 5.7 mmol) as above to afford **42** as a colorless oil (680 mg, 63%); ir ν_{max}: 3340, 1008; ^{1}Hmr δ: 5.53 (1H, t, J = 7 Hz), 5.39 (1H, bs), 4.16 (2H, s), 4.10 (2H, s), 2.2–1.9 (4H, m), 1.73 (3H, bs).

*Oxidation of **41** with manganese dioxide*

A solution of **41** (100 mg, 0.53 mmol) in tetrahydrofuran (14 mL) at 0°C was treated with manganese dioxide (1 g). After 30 min at 0°C the reaction mixture was filtered through Celite and the filtrate concentrated *in vacuo* to afford 1,1-dideutero-9-oxo-10-hydroxygeraniol (**43**), contaminated with 12% of the 9-hydroxy-10-oxo isomer **45**, as a pale yellow liquid (72 mg, 72%); uv λ_{max}: 233 (4.04); ir ν_{max}: 3368, 1670; ^{1}Hmr δ: 10.10 (1H, s), 6.69 (1H, t, J = 7 Hz), 5.41 (1H, bs), 4.21 (2H, s), 2.75 (2H, q, J = 7 Hz), 2.23 (2H, t, J = 7 Hz), 1.67 (3H, bs).

*Oxidation of **42** with manganese dioxide*

A solution of **42** (150 mg, 0.81 mmol) in tetrahydrofuran (20 mL) at 0°C was treated with manganese dioxide as above to afford 1,1-dideutero-9-oxo-10-hydroxynerol (**44**), contaminated with 14% of the 9-hydroxy-10-oxo isomer **46**, as a pale yellow liquid (98 mg, 66%); uv λ_{max}: 234 (4.01); ir ν_{max}: 3380, 1668; ^{1}Hmr δ: 10.02 (1H, s), 6.70 (1H, t, J = 7 Hz), 5.44 (1H, bs), 4.19 (2H, bs), 2.71 (2H, q, J = 7 Hz), 2.32 (2H, t, J = 7 Hz), 1.73 (3H, bs). *Anal.* calcd. for $C_{10}H_{14}D_2O_3$: C 64.49; found: C 63.94.

*β-Ketosulfoxide **48***

A suspension of sodium hydride (4 g of 50% NaH/mineral oil, 83 mmol) in dimethyl sulfoxide (80 mL) was heated at 70°C for 1 h, cooled to ambient temperature, and treated with a solution of ethyl 1,1-diethoxyacetate (7 g, 39.8 mmol) in ether (5 mL) at a dropwise rate over 2 h. The reaction mixture was stirred for a further 17 h, diluted with water (50 mL), and washed with petroleum ether (3 × 50 mL). The aqueous portion was made neutral with acetic acid (5 mL) and extracted with dichloromethane (4 × 50 mL). The combined dichloromethane extract was dried (Na_2SO_4) and the solvent removed *in vacuo*. The residue was chromatographed on silica gel (250 g) using ethyl acetate/ethanol (100:1 then 10:1) as eluent to afford **48** as a yellow liquid (5 g, 60%); ir ν_{max}: 1729, 1110; ^{1}Hmr δ: 4.60 (1H, s), 4.00 (2H, AB quartet), 3.6 (4H, m), 2.,67 (3H, s), 1.23 (6H, t, J = 7 Hz). *Anal.* calcd. for $C_8H_{16}O_4S$: C 46.13, H 7.74, S 15.39; found: C 46.19, H 7.66, S 15.38.

1,1,3,3-Tetraethoxyacetone (47)

A suspension of red mercuric oxide (6.5 g, 0.03 mol) in ethanol (60 mL) was treated with boron trifluoride etherate (3.6 mL, 0.03 mol). After stirring for 5 min, a solution of **48** (4.4 g, 0.021 mol) in ether (5 mL) was added. The resultant mixture was heated at reflux for 45 min, cooled to ambient temperature, and stirred for a further 2 h. Petroleum ether (50 mL) was added and the mixture filtered through Celite. The filtrate was washed with 1 *N* sodium hydroxide (4 × 50 mL). The combined aqueous portion was back-extracted with petroleum ether (2 × 40 mL) and the combined organic portion dried (Na_2SO_4). The solvent was removed *in vacuo* and the residue distilled at 0.7 Torr to give **50** as a colorless liquid (3.5 g, 71%); bp 82°C at 0.7 Torr; ir ν_{max}: 1763, 1070; ^{1}Hmr δ: 5.02 (2H, s), 3.65 (8H, m), 1.24 (12H, t, J = 7 Hz).

*Phosphonium salt **49***

A mixture of the (*E*)-chloroalcohol **27** (5.2 g, 34.6 mmol), triphenylphosphine (9.2 g, 35.1 mmol), and sodium iodide (6 g, 40 mmol) in acetonitrile (80 mL) was heated at reflux. After 30 h, the reaction mixture was cooled to 0°C, diluted with dichloromethane (60 mL), and filtered. The filtrate was concentrated *in vacuo*, treated with ether (100 mL), and allowed to stand until crystallization was complete. The solid mass was pulverized, washed with ether, recrystallized from aqueous ethanol, and dried *in vacuo* at 100°C to give **49** as a white crystalline solid (14.4 g, 83%); mp 180–181°C; ^{1}Hmr δ: 7.8 (15H, m), 5.50 (1H, bs), 3.48 (2H, m), 2.28 (2H, t, J = 7 Hz), 1.8 (2H, m), 1.50 (3H, bs). *Anal.* (of nondeuterated analog) calcd. for $C_{25}H_{28}IPO$: C 59.77, H 5.62, I 25.26; found: C 59.91, H 5.62, I 25.32.

*Phosphonium salt **50***

A mixture of the (*Z*)-chloroalcohol **28** (7.3 g, 48.5 mmol), triphenylphosphine (13.1 g, 50 mmol), and sodium iodide (9 g, 60 mmol) in acetonitrile (100 mL) was treated as above to give **50** as a white crystalline solid (20.3 g, 83%); mp 149–150°C; ^{1}Hmr δ: 7.8 (15H, m), 5.59 (1H, bs), 3.57 (2H, m), 2.44 (2H, t, J = 7 Hz), 1.8 (2H, m), 1.49 (3H, bs). *Anal.* calcd. for $C_{25}H_{26}D_2IPO$: C 59.53, I 25.16; found: C 59.64, I 25.22.

1,1-Dideutero-9,9,10,10-tetraethoxygeraniol (51)

A suspension of phosphonium salt **49** (2.2 g, 4.38 mmol) in anhydrous tetrahydrofuran/hexamethylphosphoramide (15 mL/1.5 mL) under a nitrogen atmosphere was treated with a 2 *M* solution of n-butyllithium in hexane (4.4 mL, 8.8 mmol). After stirring for 15 min at ambient temperature the reaction was cooled to −78°C and treated with a solution of 1,1,3,3-tetraethoxyacetone (1 g, 4.27 mmol) in ether (2 mL). The reaction was allowed to warm to ambient temperature and stirred for a further 3 h. Water (5 drops) and petroleum ether (20 mL) were added, and the resultant mixture filtered through Celite. The filtrate was concentrated *in vacuo* and the residue chromatographed on silica gel using ether/petroleum ether (1:1) as eluent to give **51** as a colorless liquid (1 g, 71%); ir ν_{max}: 3450, 1056; ^{1}Hmr δ: 5.79 (1H, t, J = 7 Hz), 5.40 (1H, bs), 5.01 (1H, s), 4.77 (1H, s), 4.0–3.3 (8H, m), 2.7–2.0 (4H, m), 1.67 (3H, bs), 1.19 (12H, t, J = 7 Hz).

1,1-Dideutero-9,9,10,10-tetraethoxynerol (52)

A suspension of phosphonium salt **50** (2.2 g, 4.38 mmol) in tetrahydrofuran/hexamethylphosphoramide (15 mL/1 mL) was treated with a 2 *M* solution of n-butyllithium in hexane (4.4 mL, 8.8 mmol) and a solution of 1,1,3,3-tetraethoxyacetone (1 g, 4.27 mmol) in ether (2 mL) as above to afford **52** as a colorless oil (780 mg, 55%); ir ν_{max}: 3450, 1060; ^{1}Hmr δ: 5.81 (1H, t, J = 7 Hz), 5.43 (1H, bs), 5.00 (1H, s), 4.78 (1H, s), 4.0–3.3 (8H, m), 2.6–2.0 (5H, m), 1.72 (3H, bs), 1.18 (12H, t, J = 7 Hz). *Anal.* calcd. for $C_{18}H_{32}D_2O_5$: C 65.03; found: C 64.95.

1-Deutero-9,9,10,10-tetraethoxygeranial (53)

A solution of **51** (180 mg, 0.54 mmol) in dichloromethane (15 mL) was treated with barium manganate (1.7 g). The resultant suspension was stirred at ambient temperature for 3 days, filtered through Celite, and concentrated *in vacuo*. The residue was chromatographed on silica gel using ether/petroleum ether (1:1) as eluent to give **53** (86 mg, 48%) as a colorless liquid; uv λ_{max}: 238 (4.06); ir ν_{max}: 2096, 1665, 1064; ^{1}Hmr (CCl_4) δ: 5.74 (1H, bs), 5.53 (1H, t, J = 7 Hz), 4.79 (1H,

s), 4.53 (1H, s), 3.4 (8H, m), 2.8–2.1 (4H, m), 2.13 (3H, bs), 1.14 (6H, t, J = 7 Hz), 1.11 (6H, t, J = 7 Hz). *Anal.* calcd. for $C_{18}H_{31}DO_5$: C 65.62; found: C 65.56.

*1-Deutero-9,9,10,10-tetraethoxyneral (**54**)*

A solution of **52** (200 mg, 0.60 mmol) in dichloromethane (18 mL) was treated with barium manganate (1.9 g) as above to afford **54** as a colorless liquid (89 mg, 45%); uv λ_{max}: 237 (4.07); ir ν_{max}: 2092, 1663, 1062; ^{1}Hmr (CCl_4) δ: 5.74 (1H, bs), 5.60 (1H, t, J = 7 Hz), 4.81 (1H, s), 4.56 (1H, s), 3.4 (8H, m), 2.9–2.1 (4H, m), 1.95 (3H, bs), 1.15 (6H, t, J = 7 Hz), 1.12 (6H, t, J = 7 Hz).

Acknowledgements

The skilled assistance of Mr. K. B. Chatson, Mr. L. Hogge, Mr. W. Haid, and Mr. D. Olson is gratefully acknowledged.

1. A. R. BATTERSBY, A. R. BURNETT, and P. G. PARSONS. Chem. Commun. 1280 (1968).
2. A. R. BATTERSBY, A. R. BURNETT, and P. G. PARSONS. J. Chem. Soc. C, 1187 (1969).
3. A. R. BATTERSBY, R. T. BROWN, R. S. KAPIL, J. A. MARTIN, and A. O. PLUNKETT. Chem. Commun. 890 (1966).
4. A. R. BATTERSBY, R. S. KAPIL, and R. SOUTHGATE. Chem. Commun. 131 (1968).
5. A. R. BATTERSBY, E. S. HALL, and R. SOUTHGATE. J. Chem. Soc. C, 721 (1969).
6. S. BRECHBUHLER-BADER, A. J. COSCIA, P. LOEW, CH. VON SZCZEPANSKI, and D. ARIGONI. Chem. Commun. 136 (1968).
7. S. ESCHER, P. LOEW, and D. ARIGONI. Chem. Commun. 823 (1970).
8. A. R. BATTERSBY, S. H. BROWN, and T. G. PAYNE. Chem. Commun. 827 (1970).
9. A. R. BATTERSBY, M. THOMPSON, K.-H. GLÜSENKAMP, and L.-F. TIETZE. Chem. Ber. **114**, 3430 (1981).
10. R. M. BOWMAN and E. LEETE. Phytochemistry, **8**, 1003 (1969).
11. F. MCCAPRA, T. MONEY, A. I. SCOTT, and I. G. WRIGHT. Chem. Commun. 537 (1965).
12. H. GOEGGEL and D. ARIGONI. Chem. Commun. 538 (1965).
13. K. M. MADYASTHA and C. J. COSCIA. Recent Adv. Phytochemistry (Top. Biochem. Nat. Prod.), **13**, 85 (1979).
14. J. BALSEVICH, F. CONSTABEL, and W. G. W. KURZ. Planta Medica, **44**, 231 (1982).
15. C. SREEKUMAR, K. P. DARST, and W. C. STILL. J. Org. Chem. **45**, 4260 (1980).
16. A. MASCHKE and H. PASEDACH. DBP 1,905,603 (1969), BASF; Chem. Abstr. **73**, 87436a (1970).
17. C. REICHARDT and E.-U. WÜRTHWEIN. Synthesis, 1976, 248.
18. C. REICHARDT, W. PRESSLER, and E.-U. WÜRTHWEIN. Angew. Chem. Int. Ed. Engl. **15**, 112 (1976).

Can. J. Chem. Downloaded from www.nrcresearchpress.com by 210.87.254.5 on 09/06/12
For personal use only.

Tritium isotope fractionation between hydrogen sulphide and methanol

ANDRZEJ WAWER AND JERZY SZYDŁOWSKI[1]

University of Warsaw, Department of Chemistry, Zwirki i Wigury 101, 02-089 Warsaw, Poland

Received July 5, 1982

ANDRZEJ WAWER and JERZY SZYDŁOWSKI. Can. J. Chem. **61**, 1060 (1983).

Tritium isotope fractionation in the exchange reaction between methanol and hydrogen sulphide has been studied in the gaseous phase over the temperature range 283–373 K. It was found that the heavier isotope accumulates in methanol and that the tritium–protium isotope effect characterizing the exchange reaction studied reaches large values: from 2.70 at 373 K to 3.72 at 283 K. The temperature dependence can be described by the simple relation: $\ln \alpha = -0.1221 + 431.5/T$. Using observed vibrational frequencies, theoretical fractionation factors could be calculated and good agreement with the experimentally determined values was observed. The results presently obtained were also compared with those obtained for the CH_3SH-H_2S system.

ANDRZEJ WAWER et JERZY SZYDŁOWSKI. Can. J. Chem. **61**, 1060 (1983).

On a étudié le fractionnement isotopique du tritium dans la réaction d'échange entre le méthanol et le sulfure d'hydrogène en phase gazeuse dans l'intervalle de température allant de 283 à 373 K. On a trouvé que l'isotope le plus lourd s'accumule dans le méthanol et que l'effet isotopique tritium–protium caractérisant la réaction d'échange étudiée atteint de fortes valeurs qui vont de 2,70 à 373 K jusqu'à 3,72 à 283 K. On peut décrire l'effet de la température par la relation simple $\ln \alpha = -0,1221 + 431,5/T$. En utilisant les fréquences vibrationnelles observées, on peut calculer les facteurs de fractionnement théorique et on a observé un bon accord avec les valeurs déterminées expérimentalement. On compare également les résultats obtenus dans ce travail avec ceux du système CH_3SH-H_2S.

[Traduit par le journal]

In previous papers results of kinetic and thermodynamic studies on tritium isotope exchange between hydrogen sulphide and methyl thiol (1, 2) were reported. In this paper we present experimental and theoretical studies on tritium isotope fractionation between hydrogen sulphide and methanol in the gas phase. The knowledge of hydrogen isotope fractionation between compounds with OH and SH groups can play an important role in a better understanding of the physicochemical properties of biologically active structures containing OH and SH groups. Moreover, knowledge of the isotope effects in such exchange reactions may be interesting from a practical view point, especially in isotope enrichment technology.

Experimental

Reagents

Methanol used in the experiments was distilled over CaO, boiled with Mg + I_2, and redistilled. The water content in the alcohol was determined by means of the Fisher reagent; it did not exceed 0.02% (w/w).

The labelling, purification, and drying procedures for H_2S were the same as described earlier (1).

Procedure

Before each experiment the vacuum apparatus was carefully evacuated to a pressure of ca. 10^{-2} Pa. The reaction vessel was filled successively with hydrogen sulphide and methanol vapors. Exchange equilibrium was reached after 10 min. The reaction was quenched by condensation of the gas mixture at the temperature of liquid nitrogen. The components of the mixture were separated by vacuum distillation at 178 K (melting point of acetone). After distillation, the hydrogen sulphide contained less than 1% of methanol; this was verified by gas-chromatographic analysis. Furthermore, under the conditions of the vacuum distillation at 178 K no measurable isotope exchange between gaseous H_2S and liquid CH_3OH was observed.

The method of determination of tritium in H_2S was described previously (1, 3). However, in the present experiments the resolving time of the counter (2.0×10^{-4} s) was taken into account. This was done by standard method using the formula:

$$[1] \quad A_0 = A/(1 - A\tau)$$

where A_0 is the actual counting rate, A is the measured counting rate, and τ is resolving time of the counter.

The wall effect could be neglected as we are interested in the measurements of the relative specific radioactivities only. It should be added that the use of the isotope dilution method in the radioactivity measurements gave the same results.

Results and discussion

The tritium isotope fractionation in the gas phase exchange reaction:

$$[2] \quad H\overset{*}{S}H + CH_3OH = HSH + CH_3O\overset{*}{H}$$

can be defined as follows:

$$[3] \quad \alpha_{exp} = 2A_{m,\infty}/A_{s,\infty}$$

where $A_{m,\infty}$ and $A_{s,\infty}$ are the equilibrium specific radioactivities of methanol and hydrogen sulphide, respectively. $A_{m,\infty}$ was obtained from the material balance:

$$[4] \quad n_s A_{s,0} = n_s A_{s,\infty} + n_m A_{m,\infty}$$

where $A_{s,0}$ is the initial specific radioactivity of H_2S; n_m and n_s refer to the molar concentrations of methanol and hydrogen sulphide, respectively.

The tritium isotope fractionation factors α in the exchange reaction studied are presented in Table 1. The values listed in the second column are those obtained directly from experiments. In the third column the values with corrections for the resolving time of the counter are presented; the small corrections for the traces of radioactive CH_3OH in H_2S are also taken into account. Each separation factor reported represents the average of 5 to 7 separate determinations. The error limits cited in the table are the standard deviations of the measurements.

[1]To whom all correspondence should be addressed.

Can. J. Chem. Downloaded from www.nrcresearchpress.com by 210.87.254.6 on 09/06/12
For personal use only.

TABLE 1. The experimental fractionation factor in the tritium exchange reaction between CH_3OH and H_2S in the gas phase

T/K	α_{exp}	α_{corr}
283	3.58	3.78±0.10
293	3.40	3.59±0.08
308	3.22	3.39±0.10
323	3.02	3.18±0.10
339	2.84	2.99±0.08
353	2.70	2.85±0.12
373	2.56	2.70±0.08

It can be easily seen that the temperature dependence of the isotope effect is simple and that the experimental fractionation factors can be fitted by the least-squares method to the equation:

$$[5] \quad \ln \alpha = -0.1221 + 431.5/T$$

The molar enthalpy change of the exchange reaction [2] obtained from the relation [5] is equal to 3.6 kJ/mol.

It is worth noting that Khurma and Fenby (4) obtained similar values of the enthalpy change for the exchange reactions in the gas phase:

$$CH_3OD + CH_3SH = CH_3OH + CH_3SD$$

and

$$CH_3SH + HOD = CH_3SD + H_2O$$

They gave the values of 2.26 kJ/mol and 1.43 kJ/mol for the above reactions which gives approximately (5) 3.2 kJ/mol and 1.7 kJ/mol for the tritium exchange near room temperature.

Theoretical calculations of equilibrium constants for the isotope exchange reactions were initiated by Urey and Rittenberg (6) and developed further by Bigeleisen and Mayer (7) and Urey (8). Following the Bigeleisen and Mayer formulation (7) the isotope fractionation factor for the exchange reaction [2] can be expressed in terms of the reduced partition function ratios:

$$[6] \quad \alpha = (s/s')f_{CH_3OH}/(s/s')f_{HSH}$$

The equation for the isotopic reduced partition function ratio $(s/s')f$ in the harmonic approximation neglecting effects due to quantum-mechanical rotation is:

$$[7] \quad (s/s')f = \prod_i \left\{ \frac{u_i}{u_i'} \frac{1 - \exp(-u_i')}{1 - \exp(-u_i)} \exp \frac{u_i' - u_i}{2} \right\}$$

where $u_i = hc\omega_i/kT$, ω_i are the normal mode vibrational frequencies in cm^{-1}, and c, h, k, and T have their usual meanings; s is the symmetry number and the prime refers to the light isotopic species. The product is taken over all normal mode vibrational frequencies of the molecule. It is then evident that the reduced partition function ratio can be easily calculated by using the spectroscopic data of isotopic molecules.

The vibrational spectra of methanol and its isotopic species have been the subject of considerable interest. We mention here only the more recent experimental data and assignments; those by Falk and Whalley (9), Shimanouchi (10), Barnes and Hallam (11), Mallinson (12) and, the most important, those by Serrallach, Meyer, and Günthard (13). The assignments proposed in literature differ considerably from one another. In particular, the matrix data by Barnes and Hallam (11) showed

TABLE 2. Observed vibrational frequencies of gaseous CH_3OH and CH_3OD (13) used in the calculations of the reduced partition function ratios (frequencies in cm^{-1})

CH_3OH	CH_3OD	CH_3OH	CH_3OD
3681.5	2717.6	1454.5	1455
2999.0	3001.0	1334	864
2970	2970	1145	1142
2844.2	2840.8	1074	1224
1478	1479	1033	1038
1465.0	1463	271.5[a]	215.6[b]

[a]Matrix frequency.
[b]Calculated frequency.

that parts of the spectra are still not very well understood. Most disagreements in assignment concern the modes of the methyl group. Such discrepancies are not surprising in view of the difficulties arising in the interpretation of the spectra. Indeed the gas and matrix spectra can provide reliable information on the CH_3OH molecules; however, some difficulties in locating the fundamentals in the gas spectra still arise from frequent overlapping due to the broad rotational and complicated torsional structure as well as to Coriolis or Fermi resonances. The liquid and solid state spectra are even more complicated due to strong hydrogen bonding. Keeping all this in mind the vibrational data were carefully examined and the most reliable set, based on the Serrallach, Meyer, and Günthard data (Table 2) (and one which is consistent with the vibrational data for CH_3SeH (14) and CH_3SH (15)), was used in the calculation of the reduced partition function ratio of methanol. The results of the theoretical calculation of vibrational frequencies by the SCF method have been omitted due to their relatively large uncertainties (16).

Excellent data for the H_2S and D_2S molecules are available (17). However, to our knowledge there are no precise experimental vibrational data for HDS available but only the very old and incomplete data cited by Herzberg (18). Therefore, the vibrational frequencies of HDS must be calculated using the known force field for the H_2S molecule or by the following procedure (19) which enables one to evaluate the vibrational frequencies of HDS directly from the very precise data obtained for H_2S and D_2S. Thus the observed HS and DS stretching frequencies of HSD were taken as the average of ν_1 and ν_3 for H_2S and D_2S, respectively, while ν_2 was obtained from the equation:

$$[8] \quad \nu_2^2(HSD) = \frac{1}{2}\left[\nu_2^2(H_2S) + \nu_2^2(D_2S)\right]$$

These approximations require, of course, a negligible mixing among internal coordinates but seem to be justified when comparing the calculated and observed frequencies for HDO where only small errors are noted.

The following frequencies (in cm^{-1}): 2614.6, 1182.7, 2627.5, and 2621.0, 1032.0, 1901.0 for H_2S (13) and HDS, respectively, were used to calculate deuterium partition function ratios or hydrogen sulphide. It should be added that in this case such a calculation can be performed including force field analysis and anharmonic corrections. It is also possible to carry out these calculations using the procedure outlined by Bron, Chang, and Wolfsberg (20). In this procedure various correction factors to the harmonic approximation have been included and the reduced partition function ratios calculated by this method have been found to be very reliable. There are, of

Can. J. Chem. Downloaded from www.nrcresearchpress.com by 210.87.254.6 on 09/06/12
For personal use only.

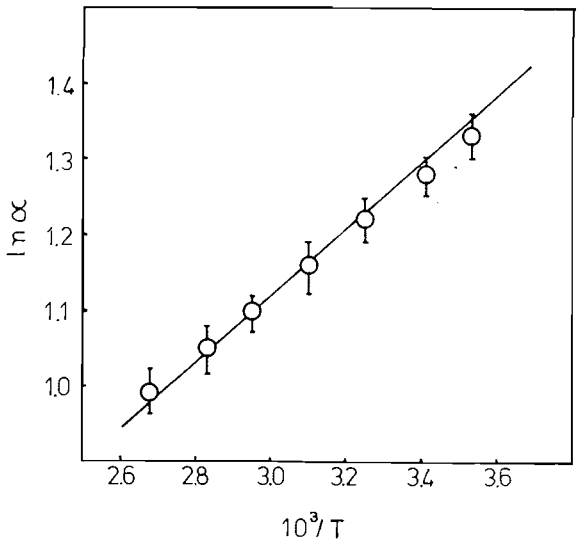

FIG. 1. Comparison of the calculated tritium isotope fractionation factors (solid line) with experimental results, α_{corr} (points) for the vapor phase exchange reaction: $CH_3OH + H\overset{*}{S}H = CH_3O\overset{*}{H} + HSH$. Uncertainties in the experimental values denoted by error bars are taken from Table 1.

course, some differences in the values of the partition function ratios calculated in this paper from the observed vibrational frequencies and resulting from the procedure mentioned above (20); thus at 283 K $(s/s')f(HDS/H_2S)$ is equal to 5.793 and 6.253 respectively. Taking into account that there is some cancellation in the correction factors to the harmonic approximation partition function ratios when equilibrium constants are obtained (20), and since in calculation of the deuterium reduced partition function ratio of methanol we used the observed vibrational frequencies without anharmonic corrections (the latter are not yet available), the same procedure was consequently applied in the case of H_2S. Hence the deuterium fractionation factor α_D for the reaction studied can be easily calculated. Then using the known relation of Swain (5*a*) and Bigeleisen (5*b*) we obtain the tritium fractionation factor characterizing the isotope effect in the exchange reaction studied. The values obtained are presented in Fig. 1 in comparison with the experimental results. It is seen that the agreement is good taking into account the approximations used in the calculations and the experimental error.

On the other hand, our experimental results can be correlated with those existing in the literature. Namely, from the known values of the fractionation factors for the exchange of hydrogen between H_2S and H_2O (21) and between CH_3OH and H_2O (22) we can calculate the fractionation factor for the $CH_3OH + H_2S$ reaction. Hence, the tritium isotope fractionation factor calculated in such a way (using also the Swain–Bigeleisen relation) is in the range of 3.46–3.65 at 298 K (these uncertainties arise from some scatter in the existing data). This result can be compared with our value at 298 K which is equal to 3.50 ± 0.08.

In conclusion it seems interesting to compare the two systems studied, i.e. CH_3SH/H_2S and CH_3OH/H_2S. It is immediately evident that there are pronounced differences in the values of the isotope effects accompanying above exchange reactions; thus at 293 K α is equal to 1.075 for the CH_3SH/H_2S and to 3.59 for the CH_3OH/H_2S systems. These differences can be explained taking into account the correlation between isotope effects and molecular structure. In particular we would like to emphasize here the role of the stretching vibrations and their contributions to the reduced partition function ratio. Thus in the case of CH_3SH/H_2S system the great similarity of SH bonds in the mercaptan and the sulphide and also similar values of the stretching vibrations frequencies result in a small value of the isotope effect.[2] On the other hand, in the CH_3OH/H_2S system the exchanging groups differ greatly and the frequencies of OH and SH stretching vibrations are far from each other. Consequently, we observe a large isotope effect in this exchange reaction. Such a behaviour is quite understandable, taking into account the discussion given by Bigeleisen on the relationship between the magnitude of isotope effects in polyatomic systems and bending and stretching force constants (23).

Finally, we should mention that considering the large value of the fractionation factor and its strong temperature dependence, as well as the acceptably rapid isotope exchange reaction, the system studied may be of some interest in the hydrogen isotope separation process.

Acknowledgement

The authors are greatly indebted to Professor J. Sobkowski for his interest and encouragement during the course of this work.

1. A. WAWER. Pol. J. Chem. **53**, 1917 (1979); **55**, 415 (1981).
2. A. WAWER and J. SZYDŁOWSKI. Radiochem. Radioanal. Lett. **48**, 193 (1981).
3. A. WAWER. Nukleonika, **26**, 35 (1981).
4. J. R. KHURMA and D. V. FENBY. Austral. J. Chem. **32**, 755 (1979).
5. (*a*) C. G. SWAIN, E. C. STIVERS, J. F. REUWER, and L. J. SCHAAD. J. Am. Chem. Soc. **80**, 5885 (1958); (*b*) J. BIGELEISEN. Tritium in the physical and biological sciences. Vol. 1. I.A.E.A., Vienna. 1962. p. 161; (*c*) R. E. WESTON, JR. Z. Naturforsch. **28**a, 177 (1973).
6. H. C. UREY and D. RITTENBERG. J. Chem. Phys. **1**, 137 (1933).
7. J. BIGELEISEN and M. G. MAYER. J. Chem. Phys. **15**, 261 (1947).
8. H. C. UREY. J. Chem. Soc. 562 (1947).
9. M. FALK and E. WHALLEY. J. Chem. Phys. **34**, 1554 (1961).
10. T. SHIMANOUCH. Tables of molecular vibrational frequencies. National Standard Reference Data Series, NBS, Washington, D.C. 1967. NSRDS-NBS 6.
11. A. J. BARNES and H. E. HALLAM. Trans. Faraday Soc. **66**, 1920 (1970).
12. P. D. MALLINSON. J. Mol. Spectrosc. **58**, 194 (1975).
13. A. SERRALLACH, R. MEYER, and HS. H. GÜNTHARD. J. Mol. Spectrosc. **52**, 94 (1974).
14. A. B. HARVEY and M. K. WILSON. J. Chem. Phys. **45**, 678 (1966).
15. I. W. MAY and E. L. PACE. Spectrochim. Acta, **24**A, 1605 (1968); H. WOLFF and J. SZYDŁOWSKI. To be published.
16. H. B. SCHLEGEL, S. WOLFE, and F. BERNARDI. J. Chem. Phys. **67**, 4181 (1977).
17. H. C. ALLEN, JR. and E. K. PLYLER. J. Chem. Phys. **25**, 1132 (1956); R. E. MILLER and D. F. EGGERS, JR. J. Chem. Phys. **45**, 3028 (1966); A. J. BARNES and J. A. R. HOWELLS. Trans. Faraday Soc. **68**, 729 (1972).
18. G. HERZBERG. Infrared and Raman spectra of polyatomic molecules. Van Nostrand Reinhold, New York. 1945.

[2]Similar effect is observed in the exchange reaction between methanol and water, where a small deuterium fractionation factor α = 1.16 at 298 K for the exchange between vapors is observed (22).

Can. J. Chem. Downloaded from www.nrcresearchpress.com by 210.87.254.6 on 09/06/12
For personal use only.

19. J. W. NIBLER and G. C. PIMENTEL. J. Mol. Spectrosc. **26**, 294 (1968).
20. J. BRON, C. F. CHANG, and M. WOLFSBERG. Z. Naturforsch. **28**a, 129 (1973).
21. J. BIGELEISEN. *In* Proc. Internat. Symp. Isot. Sep. *Edited by* J. Kistemaker, J. Bigeleisen, and A. O. C. Nier. North Holland Publ. Co., Amsterdam. 1958. p. 121; R. E. WESTON, JR. Z. Naturforsch. **28**a, 177 (1973).
22. D. E. CLEGG and J. H. ROLSTON. J. Chem. Soc. Chem. Commun. 1037 (1978) and references therein; D. V. FENBY. Austral. J. Chem. **30**, 2371 (1971).
23. J. BIGELEISEN and T. ISHIDA. J. Chem. Phys. **62**, 80 (1975).

Can. J. Chem. Downloaded from www.nrcresearchpress.com by 210.87.254.6 on 09/06/12
For personal use only.

Solvent and pH dependence of fluorescence spectra of 9-phenanthrylamine

MEENAKSHISUNDERAM SWAMINATHAN AND SNEH KUMAR DOGRA
Department of Chemistry, Indian Institute of Technology, Kanpur-208 016, U.P., India

Received July 27, 1982

MEENAKSHISUNDERAM SWAMINATHAN and SNEH KUMAR DOGRA. Can. J. Chem. **61**, 1064 (1983).

Fluorimetric titrations were carried out for various forms of 9-phenanthrylamine and pK_a^* values were determined. An unusual behaviour observed in the fluorimetric titration of the neutral form at moderate proton concentration is due to the quenching of the S_1 state of PNH_2 by H^+.

MEENAKSHISUNDERAM SWAMINATHAN et SNEH KUMAR DOGRA. Can. J. Chem. **61**, 1064 (1983).

On a réalisé des titrations par fluorométrie de différentes formes de la phénanthrylamine-9 et on a déterminé les valeurs du pK_a^*. On a observé un comportement inhabituel lors du titrage par fluorométrie de la forme neutre pour une concentration modérée en proton. Ceci est dû au piégeage de l'état S_1 du PNH_2 par H^+.

[Traduit par le journal]

Introduction

The information on the excited state pK_a^* values will be much more useful in understanding the mechanism of photoreactions (1) (photoreduction, photohydration etc.) if the excited state equilibrium constant (pK_a^*) is calculated with the help of fluorimetric titrations or time dependence fluorimetry. Tsutsumi *et al.* (2) have reported the excited state acidity constants of 2,3,4- and 9-phenanthrylamines, determined using the Förster cycle method and a semi-empirical SCF-MO-CI method for equilibrium [I]. The pK_a^*'s calculated using the Förster cycle method and the 0–0 transition energy, determined from absorption and fluorescence spectra, do not indicate whether the equilibrium in the excited state is actually attained. This information can be obtained from fluorimetric titration (3). Moreover, the technique also indicates the interactions of a proton with the molecules other than the simple proton transfer reaction in the excited state.

The present study was carried out to determine pK_a^* (S_1) using fluorimetric titrations for both the equilibria [I] and [II] of 9-phenanthrylamine (PNH_2). In addition we determined the influence of the solvent dependence on the absorption and the fluorescence,

[I] $PNH_3^+ \rightleftharpoons PNH_2 + H^+$

[II] $PNH_2 \rightleftharpoons PNH^- + H^+$

Experimental

PNH_2 was obtained from the Aldrich Chemical Co. and recrystallised from benzene. Analytical grade H_2SO_4 and NaOH were used to prepare acidic and basic solutions. A modified Hammett's scale (4) for H_2SO_4–H_2O mixtures and Yagil's basicity scale (5) for NaOH–H_2O mixtures were used for solutions below pH = 1 and above pH = 13, respectively. Methanol, acetonitrile, and hexane were of analytical grade and were purified further before use. Absorption spectra were recorded with a Cary 17D spectrophotometer and fluorescence measurements were made with a scanning spectrofluorimeter constructed in our laboratory. The details of the instrument are described elsewhere (6).

Results and discussion

Solvent effect on absorption and fluorescence spectra

Absorption and fluorescence spectra of PNH_2 were taken in different solvents and are shown in Figs. 1 and 2. The band

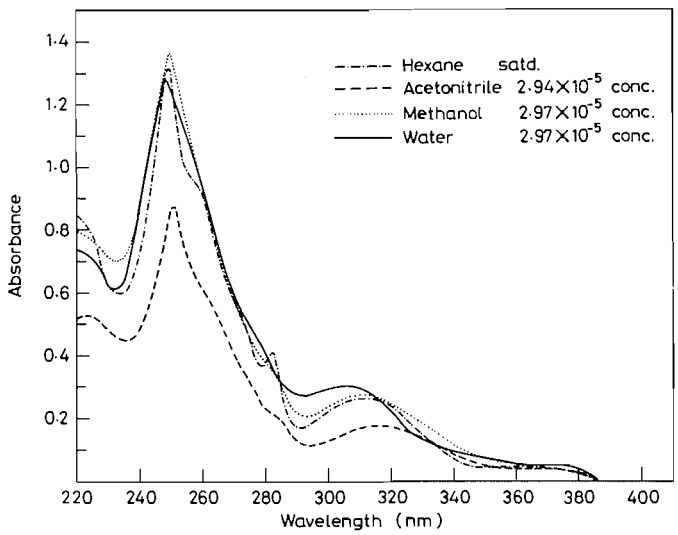

FIG. 1. Absorption spectra of 9-phenanthrylamine in different solvents.

maxima are listed in Table 1. The absorption and fluorescence spectra are structured in hexane and the structure is lost as the polarity and hydrogen bonding ability of the solvent increases. This structure loss is due to increased solute–solvent interaction.

A gradual blue shift in the absorption maxima was observed with an increase in the hydrogen bonding ability of the solvents with the exception of acetonitrile, whereas there is a continuous red shift in the fluorescence maxima for these conditions without exception.

An amino group attached to phenanthrene moiety can interact with a hydrogen donor solvent through its lone pair or it can interact with a hydrogen-acceptor solvent through its hydrogen atom. Due to this a blue shift in the former and a red shift in the latter relative to hexane are expected. The blue shifts in the absorption spectra in methanol and water relative to hexane show that only hydrogen–donor interaction of the solvent is taking place with the lone pair on the amino nitrogen atom. Acetonitrile, being a hydrogen-acceptor solvent, has little effect on the absorption spectra. But the red shift in the fluorescence maxima from hexane to water according to their hydrogen-acceptor capability shows that the availability of the

Can. J. Chem. Downloaded from www.nrcresearchpress.com by 210.87.254.6 on 09/06/12
For personal use only.

Can. J. Chem. Downloaded from www.nrcresearchpress.com by 210.87.254.6 on 09/06/12
For personal use only.

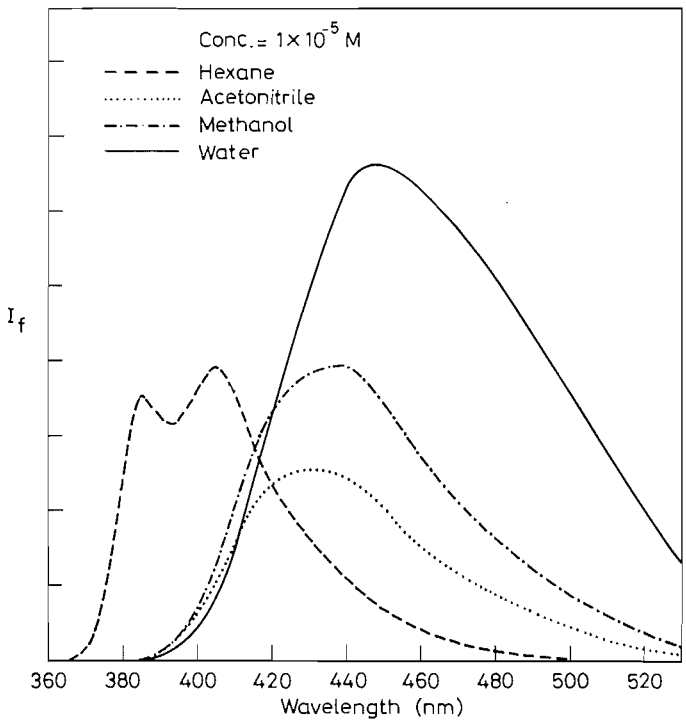

FIG. 2. Fluorescence spectra of 9-phenanthrylamine in different solvents.

TABLE 1. Absorption ($\bar{\nu}_a$) and fluorescence maxima ($\bar{\nu}_f$) of 9-phenanthrylamine in different solvents

	$\bar{\nu}_a$ (cm^{-1})	$\bar{\nu}_f$ (cm^{-1})
Hexane	45248	25974
	40008	
	38834	
	36832	24691
	35398	
	32051	—
Acetonitrile	39761	23201
	35335	
	31746	
Methanol	39920	22675
	32206	
Water	40080	22421
	32733	

lone pair in the excited state is much reduced by a greater charge transfer interaction of the lone pair of the amino group with the ring.

Prototropic phenomena in the ground and excited states

Equilibrium [II] showed a peculiar behaviour in absorption as well as in fluorescence. The absorption spectra of PNH_2 at different pH/H_- are shown in Fig. 3. It is found that there is no clear isosbestic point in this case; i.e. when the pH is increased above 14, the absorption maxima changes but the isosbestic point is constant only for solutions below $H_- = 15$. On further increase in H_- (>15), the isosbestic point changes without much change in the maximum for each solution. Due to this irregular dependence of the absorption spectrum on pH/H_- and a very narrow range of H_- over which one type of equilibrium is present, the pK_a for this equilibrium could not be determined.

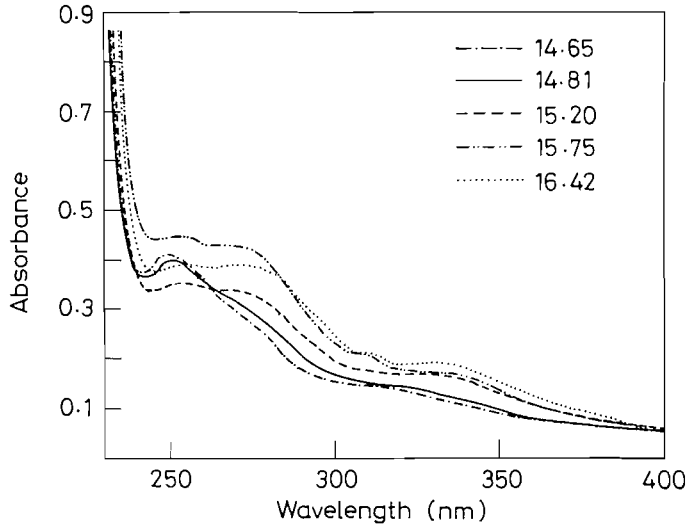

FIG. 3. Absorption spectra of 9-phenanthrylamine at different H values.

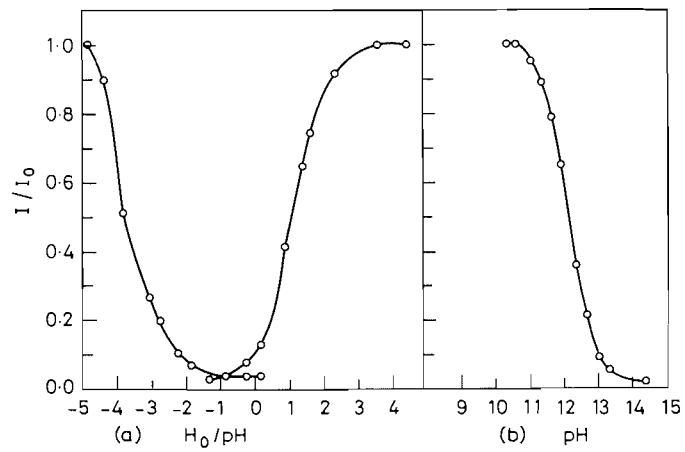

FIG. 4. Plot of relative fluorescence intensities of 9-phenanthrylamine versus pH/H_0; (*a*) cation and neutral form, (*b*) neutral form.

The fluorimetric titration curves are shown in Fig. 4 and the pK_a* values determined for different equilibria are reported in Table 2. It is clear from Fig. 4 that the fluorescence intensity of PNH_2 is quenched with a decrease in pH/H_0. The middle of this quenching occurs at pH 1.1 which could not be pK_a* [I] because PNH_3^+ starts fluorescing only from $H_0 \leq -1$ and its intensity increases with an increase in acidity. The mid-point of this rise occurs at $H_0 = -3.6$ which is in good agreement with the reported value of ($H_0 = -3.2$) (2). The sharp fluorimetric titration curve shows that the formation of PNH_3^+ is complete within the life time of the neutral species. The small difference of 0.4 units in the Förster cycle pK_a* might be due to the difference in the solvent relaxation of the excited conjugate acid – base pair in a highly concentrated acid solution. The lack of correspondence between quenching of fluorescence of PNH_2 and appearance of fluorescence of PNH_3^+ clearly indicates that the fluorimetric titration curves do not correspond to the simple two component (7) (i.e. conjugate acid – base pair) equilibrium in the lowest excited singlet state. Probably it is due to the proton-induced quenching of fluorescence of PNH_2^* at moderate H^+ concentration; it has been shown that this process competes with the proton transfer reaction (8). Similar behaviour has also been observed in many aromatic amino compounds. Under

TABLE 2. Excited singlet state acidity constants of 9-phenanthrylamine

Equilibrium	pK_a	pK_a^*[a]	pK_a^*(FT)[b]
[I]	3.5 (ref. 2)	−3.2 (ref. 2)	−3.6
[II]	>14.0	—	12.18

[a]Calculated using the Förster cycle and 0–0 band obtained from absorption and fluorescence data.
[b]FT = fluorimetric titration.

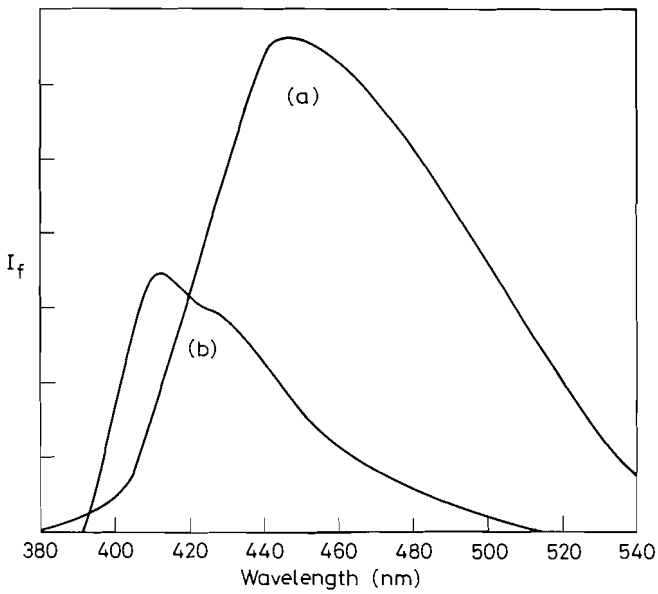

FIG. 5. Fluorescence spectra of 9-phenanthrylamine; (*a*) neutral form (pH ~ 7), (*b*) dianion (H_- 15.2).

such circumstances, accurate values of pK_a^*'s can only be calculated with the help of time-dependent fluorimetry; however, the mid-point of the rise of the PNH_3^+ fluorescence curve (9) will not be far from the true value.

The fluorescence of the neutral form is again quenched when the pH is increased above 10.5 due to the formation of the PNH^- anion. The mid-point of the quenching occurs at 12.8, which is the pK_a^* for the equilibrium between the neutral form and the anion. This indicates that PNH_2 has become more acidic in the excited singlet state as observed in other aromatic amino compounds (10, 11). When the pH is increased beyond 14, a new fluorescence peak appears at 410 nm which is blue-shifted relative to the neutral form. Figure 5 represents the fluorescence spectra of PNH_2 at pH 7 and at H_- = 16. This fluorescence could not be due to the monoanion of PNH_2 because (*i*) monoanions of other aromatic amines such as aminoquinolines (12), 5-aminoindazole (10), 2-aminobenzimidazole (11), etc. are nonfluorescent, and (*ii*) the maximum should be red-shifted relative to the fluorescence maximum of the neutral form as the amino group becomes more acidic in S_1. The intensity of this fluorescence increases up to H_- 16.75 (~8 *M* NaOH) and then decreases with further increase in concentration of NaOH. The appearance of this new fluorescence and the peculiar behaviour observed in the absorption spectra near this H_- range suggest the formation of a new fluorescent species which might be a dianion. α- and β-naphthylamines were also found to show a blue-shifted fluorescence under the similar conditions (10). Fluorimetric titration could not be used to calculate the pK_a^* for the equilibrium between the mono- and dianion because of the variation in the isosbestic point in this range. Similarly, the Förster cycle method cannot be used as the ground state pK_a is not known. But a blue shift in the band maxima when compared to the neutral form or PNH^- indicates qualitatively that PNH^- is a weaker acid in S_1 compared to S_0, i.e. the first dissociation of PNH_2 is strengthened in S_1 while the second dissociation is weakened.

Acknowledgement

One of the authors (M.S.) acknowledges the award of fellowship by University Grants Commission, New Delhi, under the Faculty Improvement Programme.

1. J. P. IRELAND and P. A. H. WYATT. *In* Advances in physical organic chemistry. Vol. 12. *Edited by* Av. Katrizky. Academic Press, New York. 1976. p. 131.
2. K. TSUTSUMI, A. AOKI, H. SHIZUKA, and T. MORITA. Bull. Chem. Soc. Jpn. **44**, 3245 (1971).
3. S. G. SCHULMAN and Q. FERNANDU. J. Phys. Chem. **71**, 2668 (1967).
4. M. J. JØRGENSON and D. R. HARTTER. J. Am. Chem. Soc. **85**, 878 (1963).
5. G. YAGIL. J. Phys. Chem. **71**(4), 1034 (1967).
6. M. SWAMINATHAN. Ph.D. Thesis, I.I.T., Kanpur. 1982.
7. K. TSUTSUMI, S. SEKIGUCHI, and H. SHIZUKA. J. Chem. Soc. Trans. Faraday I, **78**, 1087 (1982).
8. (*a*) K. TSUTSUMI and H. SHIZUKA. Chem. Phys. Lett. **52**, 485 (1977), Z. Phys. Chem. (N.F.) **111**, 129 (1978); (*b*) H. SHIZUKA, K. TSUTSUMI, H. TAKAUCHI, and I. TANAKA. Chem. Phys. **59**, 183 (1981); (*c*) S. TOBITA and H. SHIZUKE. Chem. Phys. Lett. **75**, 140 (1980).
9. S. G. SCHULMAN and P. LIEDKE. Z. Phys. Chem. N.F. **84**, 317 (1973).
10. M. SWAMINATHAN and S. K. DOGRA. Unpublished results.
11. A. K. MISHRA and S. K. DOGRA. Unpublished results.
12. (*a*) S. G. SCHULMAN and A. C. CAPOMACCHIA. Anal. Chim. Acta, **58**, 91 (1972); (*b*) S. G. SCHULMAN and L. B. SANDERS. Anal. Chim. Acta, **56**, 83 (1971); (*c*) S. G. SCHULMAN, K. ABATA, P. J. KOVI, A. C. CAPOMACCHIA, and D. JACKMAN. Anal. Chim. Acta, **65**, 59 (1973).

Can. J. Chem. Downloaded from www.nrcresearchpress.com by 210.87.254.6 on 09/06/12
For personal use only.

Adsorption of cycloalkane and cyclopentanealkyl acids at the air/water interface

JAN J. SPITZER AND LOUIS D. HEERZE[1]

Department of Chemistry, University of Lethbridge, Lethbridge, Alta., Canada T1K 3M4

Received September 10, 1982

JAN J. SPITZER and LOUIS D. HEERZE. Can. J. Chem. **61**, 1067 (1983).

Surface tensions of aqueous solutions of cyclopropane, cyclobutane, cyclopentane, and cycloheptane carboxylic acids, and of cyclopentaneacetic and cyclopentanepropionic acids were measured at 25°C by the drop volume method. The Traube constants for calculation of standard free energies of adsorption were estimated from second and third degree polynomial least-squares analyses, from nonlinear least-squares analysis using the Szyszkowsky equation, and graphically.

The standard free energies of adsorption at the air/solution interface of cycloalkane and cycloalkanealkyl carboxylic acids are less negative than those of the corresponding straight chain acids, but not by a constant amount; the standard free energy of the CH_2 group in a cycloalkane ring is -2.5 kJ mol^{-1} as compared to a value of -3.3 kJ mol^{-1} for straight chain acids.

JAN J. SPITZER et LOUIS D. HEERZE. Can. J. Chem. **61**, 1067 (1983).

On a mesuré les tensions de surface de solutions aqueuses d'acides carboxyliques cyclopropane-, cyclobutane-, cyclopentane- et cycloheptane-carboxyliques et des acides cyclopentane-acétique et -propionique, à 25°C, utilisant la méthode du volume de la goutte. On a évalué les constantes de Traube nécessaires pour le calcul des énergies libres standard d'absorption à partir d'analyses, par la méthode des moindres carrés de polynomes du second et du troisième ordre, à partir d'une analyse non linaire, par la méthode des moindres carrés, en utilisant l'équation de Szyszkowsky et par une méthode graphique.

Les énergies libres standard d'absorption au niveau de l'interface air/solution des acides cycloalcane- et cycloalcanealkyle-carboxyliques sont moins négatives que celles des acides correspondants à chaîne linéaire mais la différence n'est pas constante; l'énergie libre standard du groupe CH_2 d'un cycloalcane est de $-2{,}5$ kJ mol^{-1} alors qu'elle est de $-3{,}3$ kJ mol^{-1} pour les acides à chaînes linéaires.

[Traduit par le journal]

Introduction

The relationship between interfacial activity and the structure of the hydrophobic part of a surfactant molecule has not been much studied (1). In particular simple cycloalkane hydrophobic structures do not seem to have been investigated, most of the literature data dealing with surface properties of molecules with single or double n-alkyl chains. Recently we have investigated the free energy of adsorption and micellization behaviour of cyclohexanealkyl carboxylic acids and their salts in connection with their occurrence in petroleum (2). In this paper we report our further measurements of the standard free energies of adsorption of other cycloalkane and cyclopentanealkyl carboxylic acids in order to find out quantitatively how much the standard free energy of adsorption of the CH_2 group depends on the cyclic closure of a straight aliphatic chain.

For straight chain paraffinic compounds the free enregy of adsorption has been described by Traube's rule (1, 3) as

$$[1] \quad \Delta G^0_{ad} = A + BN$$

where N is the number of carbon atoms in the chain. The constant A is thought to depend only on the kind of hydrophilic group that is attached to the chain (ref. 3 and ref. 1, Chapt. 11). The constant B has been ascribed a value of -2.6 kJ mol^{-1}/CH_2 (ref. 3 and ref. 1, Chapt. 11), while later results on fatty acids (4) indicated a value of -3.3 kJ mol^{-1}/CH_2. A value of -3.1_5 kJ mol^{-1}/CH_2 based on straight chain alcohols has also been cited recently (5). It thus appears that the free energy of adsorption of the CH_2 group is about -3.2 kJ mol^{-1} for straight aliphatic chains. In this paper we show that the standard free energy of adsorption of the CH_2 group depends on the hydrophobic structure in which the CH_2 group is located.

[1]Present address: Department of Chemistry, University of Alberta, Edmonton, Alberta.

Experimental

The surface tensions were measured by the drop volume method using the Gilmont ultra-precision syringe (± 0.0001 cm^3). The syringe was mounted in a jacketed cell through which water that was thermostatted at 25.0 ± 0.1°C was circulated. The outside wetted diameter of the stainless steel tube from which drops were formed was measured with a travelling microscope to be 0.272 ± 0.001 cm. The surface tension of the water obtained from the Gelman Water I System was determined to be 71.9 mN m^{-1}, and this water was used for making up the solutions. The densities of solutions were measured with a vibrating tube Sodev densitometer to ± 0.00005 g cm^{-3}. The calculations of surface tensions using Harkins' corrections were done according to equations given in ref. 6.

The carboxylic acids were purchased from Pfaltz & Bauer or from Aldrich with stated purity of 96–99%. The general procedure for purifying these acids was as follows. The acids were converted to their sodium salts with a 1 molar aqueous solution of NaOH (pH ≃ 10.5), and the resulting solutions were filtered through 0.22 μm millipore filters to remove insoluble nonacidic impurities. The salts were then isolated in the solid state on a steambath, and then extracted with ether in a Soxhlet appartus for 3–4 days. After the salts were dried in a vacuum desiccator, they were converted back to acids with aqueous HCl (ph ≃ 2.5). Depending on the solubility of the acids in water, they were isolated either by liquid/liquid extraction (ether) or with a separating funnel. The acids were then redistilled once or twice under vacuum and used as such. Infrared and nmr spectra did not indicate presence of impurities.

The total uncertainty of individual measurements is estimated to be ± 0.3 mN m^{-1} or less. This larger uncertainty is partly due to aging phenomena in the equilibration of the drops (7).

Results

The Traube constants were estimated from the surface tension data by four independent methods: (*i*) graphically from the data in the low concentration region; (*ii*) as a limit at zero concentration of second degree polynomial least-squares fit.

Can. J. Chem. Downloaded from www.nrcresearchpress.com by 210.87.254.40 on 09/06/12
For personal use only.

TABLE 1. Traube constants and standard free energies of adsorption estimated graphically and from 2nd degree polynomial fit

Acid	Graphical method		2nd Degree polynomial fit				
	$\alpha\left(\frac{\text{mN m}^{-1}}{\text{mol dm}^{-3}}\right)$	$-\Delta G^0_{ad}$ (kJ mol^{-1})	$a_{0(2)}$	$\alpha = -a_{1(2)}$	$a_{2(2)}$	$-\Delta G^0_{ad}$ (kJ mol^{-1})	$-\Delta G^0_{ad}$(ave) (kJ mol^{-1})
$CH_2(CH_2)CH$-COOH	55	9.8	70.9	40.4	15.3	9.1	9.4
$CH_2(CH_2)_2CH$-COOH	150	12.3	71.5	142	151	12.1	12.2
$CH_2(CH_2)_3CH$-COOH	400	14.7	71.6	410	1680	14.7	14.7
$CH_2(CH_2)_4CH$-COOH	—	—	71.9	1180	13200	17.5	17.5
$CH_2(CH_2)_5CH$-COOH	2500	19.2	72.2	2650	68100	19.3	19.2
$CH_2(CH_2)_3CH(CH_2)$-COOH	1100	17.1	72.1	1270	13900	17.5	17.3
$CH_2(CH_2)_3CH(CH_2)_2$-COOH	5500	21.0	71.5	4370	153000	20.5	20.7

TABLE 2. Traube constants and standard free energies of adsorption estimated from 3rd degree polynomial fit and from Szyszkowsky fit

Acid	Szyszkowsky fit				3rd Degree polynomial fit					
	a	b	$\alpha = ab$	$-\Delta G^0_{ad}$ (kJ/mol)	$a_{0(3)}$	$\alpha = -a_{1(3)}$	$a_{2(3)}$	$-a_{3(3)}$	$-\Delta G^0_{ad}$ (kJ/mol)	$-\Delta G^0_{ad}$ (ave) (kJ/mol)
CH_2CH_2CH-COOH	12.6	5.67	71.4	10.5	71.9	55.8	49.7	16.5	10.2	10.3
$CH_2(CH_2)_2CH$-COOH	18.9	10.9	206	13.2	72.6	185	413	367	12.9	13.1
$CH_2(CH_2)_3CH$-COOH	17.3	30.3	524	15.5	72.2	460	2880	7100	15.2	15.3
$CH_2(CH_2)_4CH$-COOH	19.8	74.7	1480	18.1	72.4	1480	36400	428000	18.1	18.1
$CH_2(CH_2)_5CH$-COOH	19.1	160	3060	20.1	72.6	3050	13400	1930000	19.9	20.0
$CH_2(CH_2)_3CH(CH_2)$-COOH	25.3	57.0	1440	18.0	72.5	1500	33000	377000	18.0	18.0
$CH_2(CH_2)_3CH(CH_2)_2$-COOH	17.8	371	6600	21.8	72.6	5850	425000	1230000	21.4	21.6

[2] $\gamma = a_{0(2)} + a_{1(2)}C + a_{2(2)}C^2$

where C is molarity and (2) refers to second degree polynomial. In this case the Traube constant, defined by

[3] $\alpha = \lim_{C \to 0} \left(-\frac{d\gamma}{dC}\right)$

is given by $\alpha = a_{1(2)}$; (*iii*) as a zero concentration limit using a third degree polynomial least-squares fit

[4] $\gamma = a_0 + a_{1(3)}C + a_{2(3)}C^2 + a_{3(3)}C^3$

where (3) refers to third degree polynomial. The Traube constant is now equal to $a_{1(3)}$; (*iv*) from nonlinear least-squares analysis using Szyszkowsky's equation[2]

[5] $\pi = a \ln (1 + bC)$

where π is surface pressure that is defined by $\pi = \gamma_0 - \gamma$ where γ_0 is the surface tension of pure water and γ is the surface tension of the solution. The Traube constant is given now by $\alpha = ab$.

[2]Fortran program to fit interfacial data to Szyszkowsky's equation is available from the authors.

In this paper we define the standard free energy of adsorption ΔG^0_{ad} by the relation (8, 9)

[6] $\Delta G^0_{ad} = -RT \ln \alpha$

This definition has been applied to data for fatty acids (2, 4) but other definitions involving different standard states are possible (5, 10). In eq. [6] the implied standard states are the ideal solution of unit molarity for the bulk phase and the standard surface pressure of 1 mN m^{-1} for the surface phase. The least-squares derived coefficients, the Traube constants, and the standard free energies of adsorption are given in Tables 1 and 2.

Discussion

The estimation of Traube constants

From Tables 1 and 2 it is seen that two sets of Traube's constants can be derived from the data. The graphical method and the second degree polynomial fit (Table 1) give standard free energies precise to ±0.2 kJ mol^{-1} and in agreement with each other. The 3rd degree polynomial fit and Szyszkowsky's equation (11, 12) give concordant standard free energies of adsorption precise to ±0.1 kJ mol^{-1}. However, these two sets

Can. J. Chem. Downloaded from www.nrcresearchpress.com by 210.87.254.40 on 09/06/12
For personal use only.

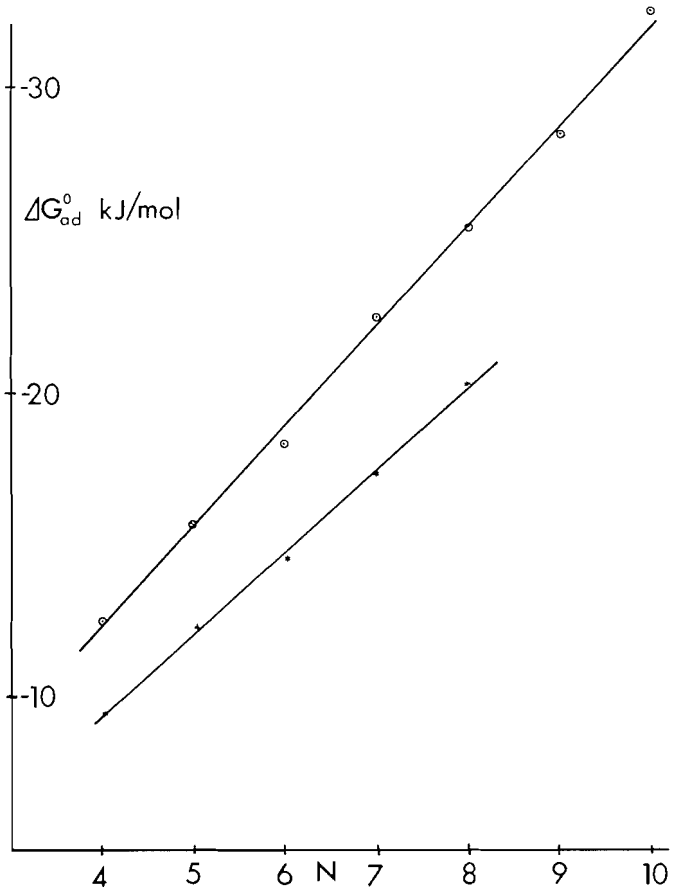

FIG. 1. Standard free energies of adsorption of straight chain paraffinic acids (○) and of cycloalkane carboxylic acids (*).

of data differ on average by 0.8 kJ mol^{-1}. For the purpose of the following correlations it does not matter which set of data is used since only the values of constant A in eq. [1] are affected. We have used the data from Table 1 for the sake of consistency for comparisons with previous work (2, 4).

The standard free energies of adsorption of CH_2 group

In Fig. 1 the standard free energies of adsorption of cycloalkane carboxylic acids are plotted against the number of carbon atoms, together with those for straight chain acids (2, 4). The standard free energies of adsorption of paraffinic acids were used to estimate the coefficients of the straight line (least-squares) as

[7] ΔG^0_{ad} (P.A.) = 0.7(±0.7) − 3.3(±0.1) N

where P.A. refers to straight chain paraffinic acids. The standard free energies of adsorption of cycloalkane carboxylic acids were found to obey eq. [8]

[8] ΔG^0_{ad} (C.P.A.) = 0.3(±0.7) − 2.5(±0.2) N

where C.P.A. refers to cycloparaffinic acids. The slope in eq. [8] is independent of the choice of the data given in Tables 1 and 2 within the experimental error. Clearly the free energy of adsorption of the CH_2 group (the slopes in eqs. [7] and [8] is by 0.8 kJ mol^{-1} less negative if the CH_2 group is located in a cycloparaffinic ring than if the CH_2 group is located in a straight paraffinic chain.

A further correlation is possible. The standard free energies of adsorption of cyclopentanealkyl and cyclohexanealkyl (2) carboxylic acids are shown in Fig. 2, where they are plotted against the number of carbon atoms. From these graphs the slope is estimated to be $-2.8(0.2_5)$ kJ mol^{-1} as the free energy of adsorption of the CH_2 group that is located in the alkyl portion of the cycloalkanealkyl moiety. These results may be summarized by saying that the standard free energy of adsorption of the CH_2 group located in a cycloalkanealkyl moiety is well described by the rule of three ($-RT$ ln 3), which gives -2.7 kJ mol^{-1}. The standard free energy of the CH_2 group in a straight paraffinic chain of alkanoic acids, however, does not follow this rule. The difference is likely to be due to the presence of a terminal methyl group in straight paraffinic chains and, since the slopes in Fig. 1 are different, the effect of the methyl group is not additive.

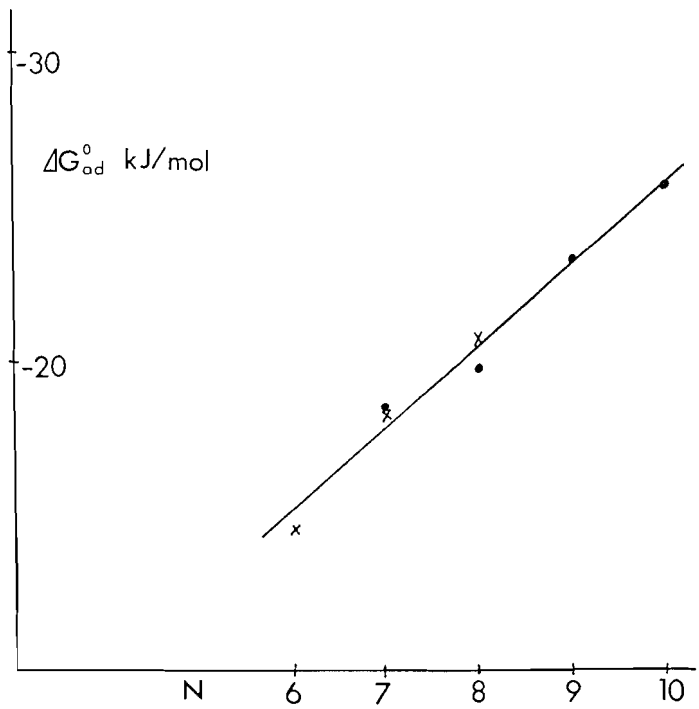

FIG. 2. Standard free energies of adsorption of cyclohexanealkyl carboxylic acids (●) and of cyclopentanealkyl carboxylic acids (×).

Acknowledgements

We thank Prof. Loren G. Hepler and Dr. Arne Skauge for useful comments during the course of this work, and the Natural Sciences and Engineering Research Council of Canada for financial support.

1. C. TANFORD. The hydrophobic effect: formation of micelles and biological membranes. J. Wiley & Sons, New York. 1973. Chapt. 9.
2. A SKAUGE and J. J. SPITZER. J. Phys. Chem. Submitted.
3. I. LANGMUIR. J. Am. Chem. Soc. **39**, 1848 (1917).
4. A. F. H. WARD. Trans. Faraday Soc. **42**, 399 (1946).
5. M. J. ROSEN and S. ARONSON. Colloids Surfaces, **3**, 201 (1981).
6. M. C. WILKINSON and R. L. KIDWELL. J. Colloid Interface Sci. **35**, 114 (1971).
7. A. LAKE, A. S. C. LAWRENCE, and O. S. MILLS. *In* Gas/liquid and liquid/liquid interface. Proceedings of the second international congress of surface activity. Butterworths, London. 1957. pp. 200–210.
8. R. AVEYARD and B. J. BRISCOE. Trans. Faraday. Soc. **64**, 2911 (1970).

Can. J. Chem. Downloaded from www.nrcresearchpress.com by 210.87.254.40 on 09/06/12
For personal use only.

9. N. H. SAGERT and W. LEE. Can. J. Chem. **58**, 2789 (1980).
10. E. H. LUCASSEN-REYNDERS. *In* Progress in surface and membrane science. Edited by D. A. Cadenhead and J. F. Danielli. Academic Press, New York. 1976. p. 253.
11. B. VON SZYSZKOWSKY. Z. Phys. Chem. **64**, 385 (1908).
12. A. FRUMKIN. Z. Phys. Chem. **116**, 466 (1925).

Can. J. Chem. Downloaded from www.nrcresearchpress.com by 210.87.254.40 on 09/06/12
For personal use only.

Reaction of 6,7-dimethoxy-3-isochromanone with hydrazine: a reinvestigation

PAUL BIRD AND MALCOLM SAINSBURY
School of Chemistry, University of Bath, Bath, BA2 7AY, U.K.

AND

DAVID I. C. SCOPES
Glaxo Group Research Ltd., Ware, Hertfordshire, SG12 ODJ, U.K.

Received November 2, 1982

PAUL BIRD, MALCOLM SAINSBURY, and DAVID I. C. SCOPES. Can. J. Chem. **61**, 1071 (1983).

We find that the product from the interaction of 6,7-dimethoxy-3-isochromanone and hydrazine, followed by treatment of the intermediate hydrazide with mineral acid, is not 6,7-dimethoxy-1,3-dihydro-3-(2*H*)isoquinolone as stated in the literature, but rather bis-2,2-(6,7-dimethoxy-1,4-dihydro-3(2*H*)isoquinolonyl). An explanation of the formation of this product is provided.

PAUL BIRD, MALCOLM SAINSBURY et DAVID I. C. SCOPES. Can. J. Chem. **61**, 1071 (1983).

Nous avons trouvé que la réaction entre la diméthoxy-6,7 isochromanone-3 et l'hydrazine, suivie de l'action d'un acide minéral sur l'hydrazide intermédiaire, donne la bis-2,2 (diméthoxy-6,7 dihydro-1,4 (2*H*) isoquinolonyle-3) et non pas la diméthoxy-6,7 dihydro-1,3 (2*H*) isoquinolone-3 comme mentionnée dans la littérature. Nous expliquons la formation de ce produit.

[Traduit par le journal]

In 1969 Rosen and Popp claimed (1) to have prepared 6,7-dimethoxy-1,4-dihydro-3(2*H*)isoquinolone (**3**, R = H) by reacting the isochromanone (**1**) with hydrazine, followed by treatment of the intermediate hydrazide (**2**) with 10% hydrochloric acid. We have repeated this preparation and now find that the product of the reaction is a colourless crystalline solid, which when first formed contains water of crystallization; this is not removed by recrystallization from ethanol, but is eliminated by azeotroping with toluene. When dry, our compound does not contain any protons which exchange with deuterium atoms from deuterium oxide and, unlike Rosen and Popp's product, it does not exhibit a band at 3400 cm^{-1} in the infrared spectrum.

We observe a slightly lower melting point for our compound (~215°C) than that quoted by Rosen and Popp (277–228°C, ethanol) and there are also differences between the published ^1H nmr data and ours; for example, in our product the aromatic protons resonate at δ 6.87 and δ 6.84, whereas Rosen and Popp observe a signal at δ 7.3 in the same solvent (DMSO-d_6). Thus we cannot be sure that we are dealing with the same compound, yet our chemical shift values correspond very closely with those of authentic 6,7-dimethoxy-2-methyl-1,4-dihydro-3(2*H*)isoquinolone (**3**, R = Me) (2).[1]

The mass spectrum of our product, recorded at an ionization potential of 70 eV, shows a weak molecular ion at m/z 412 (0.5%) which corresponds to $C_{22}H_{24}N_2O_6$ rather than to $C_{11}H_{13}NO_3$ (m/z 207) as required for the isoquinolone (**3**, R = H), but there are major fragmentation peaks at m/z 221 (30%), 208 (12%), 207 (26%), 206 (15%), 71 (30%), and 69 (100%). The molecular ion is further established by chemical ionization techniques (isobutane), which provide a $M + 1$ peak at m/z 413 (3%) and fragment ions at m/z 222 (7%), 208 (21%), and 71 (100%), and it is now clear that our compound is bis-2,2-(6,7-dimethoxy-1,4-dihydro-3(2*H*)isoquinolonyl) (**4**), i.e. the dehydrodimer of the isoquinolone (**3**, R = H). The low intensity of the molecular ion is readily understood in terms of scission of the N—N bond with transfer of a hydrogen atom via a cyclic transition state.

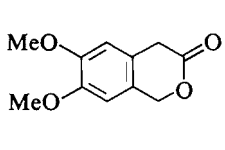

1

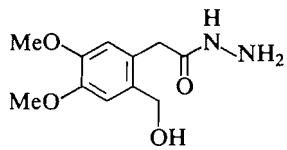

2

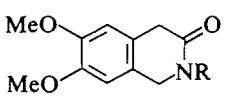

3

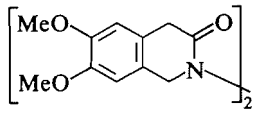

4

Both Rosen and Popp and ourselves have shown that under acidic conditions some of the hydrazide (**2**) is degraded back to the isochromanone (**1**), and it seems probable that these two compounds then react together to form the diacylhydrazide (**5**) which under the reaction conditions undergoes a double ring closure to the dehydrodimer (**4**). Such a sequence of reactions resolves the obvious difficulty which Rosen and Popp had in explaining why the least basic nitrogen in the hydrazine (**2**) was involved in the cyclization step, and also obviates the necessity to invoke a very unusual reductive N–N cleavage reaction in order to account for the formation of the "simple" isoquinolone (**3**, R = H) (3).

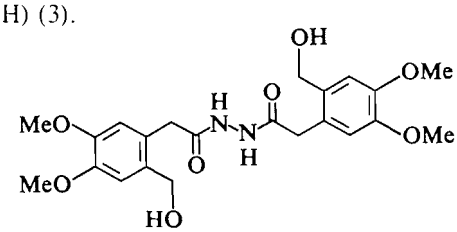

5

[1]*Note added in proof*: In the course of recent correspondence, Professor Popp confirms that the two samples are identical, and states that he has arrived at similar conclusions concerning the structure of the compound, although these observations have not been published.

Can. J. Chem. Downloaded from www.nrcresearchpress.com by 210.87.254.5 on 09/06/12
For personal use only.

We have repeated the reaction several times and on each occasion we have obtained the same result.

The ^{1}H nmr spectrum of our crude reaction product shows signals at similar chemical shifts to those of the refined compound, although the peaks are broadened and there is a signal of variable intensity due to water. At no time have we isolated a product which corresponds to the monomeric structure (**3**, R = H) (3).

Experimental

*Bis-2,2-(6,7-dimethoxy-1,4-dihydro-3(2H)-isoquinolonyl) (**4**)*

The hydrazide (**2**) (5 g), prepared as described previously (1), was heated in 10% hydrochloric acid solution (200 cm^3) for two hours. After cooling, water (50 cm^3) was added, and the solid product filtered off and crystallized from ethanol. Since this product had an indefinite mp it was then recrystallized twice more from toluene, allowing some of the solvent to boil off on each occassion. This afforded the title compound as colourless prisms (3.1 g), mp ~215°C (dec.); ν_{max} ($CHCl_3$): 1660, 1610 cm^{-1}; ^{1}H nmr δ (DMSO-d_6): 6.87, 6.84 (2 × s, 4H, 5-H, 8-H, 5′-H, 8′-H), 4.58 (s, 4H, 2 × CH_2N), 3.76 (s, 12H, 4 × CH_3O), 3.67 (s, 4H, 2 × CH_2CO); ^{13}C nmr δ (CF_3CO_2H): 174.2 (s, C=O), 150.7, 150.0 (2 × s, 4 × C—OCH_3), 123.7, 123.4 (2 × s, 4a-C, 8a-C, 4a′-C, 8a′-C), 112.9 (d, 8-C, 8′-C), 111.1 (d, 5-C, 5′-C), 57.3 57.2, (2 × q, 4 × OCH_3), 53.2 (t, 1-C, 1′-C), 37.2 (t, 4-C, 4′-C); *m/z* (EI): 412 (0.5%), 410 (2%), 221 (30%), 208 (12%), 207 (26%), 206 (15%), 192 (16%), 188 (16%), 149 (20%), 71 (30%), 69 (100%). *Mol. Wt.* calcd. for $C_{22}H_{24}N_2O_6$: C 64.1, H 5.9, N 6.8%; found: C 63.8, H 5.9, N 6.65%.

Acknowledgement

Paul Bird is a recipient of a CASE studentship jointly funded by the SERC and Glaxo Group Research Ltd.

1. G. Rosen and F. D. Popp. Can. J. Chem. **47**, 864, (1969).
2. J. Finkelstein and A. Brossi. J. Heterocycl. Chem. **4**, 315 (1967); cf. J. Wyatt, Ph. D. Thesis, Univ. of Bath (1978).
3. E. H. White, D. F. Roswell, I. R. Politzer, and B. R. Branchini. Methods Enzymol. **46**, 216 (1977).

Can. J. Chem. Downloaded from www.nrcresearchpress.com by 210.87.254.5 on 09/06/12
For personal use only.

Some alkali metal alkyl amides as alkyne isomerization reagents: selective isomerization of one triple bond of a diynol[1]

SUZANNE R. ABRAMS,[2] DONATO D. NUCCIARONE, AND WARREN F. STECK
Prairie Regional Laboratory, National Research Council of Canada, Saskatoon, Sask., Canada S7N 0W9

Received April 30, 1982[3]

SUZANNE R. ABRAMS, DONATO D. NUCCIARONE, and WARREN F. STECK. Can. J. Chem. **61**, 1073 (1983).

The lithium and sodium salts of 1,2-diaminoethane, 1,3-diaminopropane, n-butylamine, and the lithium salt of isobutylamine were studied as potential reagents for isomerization of triple bonds in alkyn-1-ols. The sodium salts of the diamines afforded high yields of the ω-alkyn-1-ol. Somewhat surprisingly, the sodium salt of n-butylamine also effects isomerization to the terminal position. The lithium salt of 1,3-diaminopropane gave the highest conversion of 2- to 3-alkyn-1-ol. A novel, selective rearrangement of one triple bond of a diynol, a 2,ω- to 3,ω-diyn-1-ol isomerization, was incorporated into a synthesis of the insect sex pheromone 3,13-octadecadienol acetate.

SUZANNE R. ABRAMS, DONATO D. NUCCIARONE et WARREN F. STECK. Can. J. Chem. **61**, 1073 (1983).

On a évalué l'utilisé des sels de sodium et de lithium du diamino-1,2 éthane, du diamino-1,3 propane, de la n-butylamine et du sel de lithium de l'isobutylamine en tant qu'agents potentiels d'isomérisation des triples liaisons des alcynols-1. Les sels de sodium des diamines donnent des rendements élevés en ω-alcynols-1. Par opposition le sel de sodium de la n-butylamine affecte aussi l'isomérisation vers la position terminale. Le sel de lithium du diamino-1,3 propane donne le plus fort pourcentage de transformation des alcyne-1 ols-1 en alcyne-3 ols-1. Dans le cadre de la synthèse de la phéromone sexuelle des insectes, l'acétate d'octadecadiène-3,13 ol, on a introduit une nouvelle transposition sélective d'une triple liaison d'un diynol à savoir l'isomérisation d'un 2,ω-diyne ol-1 en un 3,ω-diyne ol-1.

[Traduit par le journal]

Introduction

Isomerization of internal triple bonds of straight chain alkynes and alkyn-1-ols to the free terminus is effected by the sodium (1) and potassium (2) salts of 1,3-diaminopropane. This reaction is useful in synthesis as it makes α,ω-disubstituted long chain compounds readily available. We wish to report a study on the potential of some other alkali metal alkyl amides to isomerize triple bonds, and illustrate their application in a novel selective isomerization reaction.

Results and discussion

The isomeric linear decyn-1-ol system, which has been used in a previous study (3), was employed to compare potential isomerization reagents. The isomer with the triple bond furthest removed from the free terminus, 2-decyn-1-ol, was the starting material in this work. Four lithium reagents were prepared from 1,2-diaminoethane, 1,3-diaminopropane, n-butylamine, and isobutylamine. The sodio analogs of the two diamines and n-butylamine were also studied. Rearrangement reactions were carried out with 5.5 equivalents of reagent at 55°C. The reagents were formally 1.7 molar in the appropriate amine which also served as the solvent for the rearrangement reactions. In Fig. 1 is displayed the percentage of 9-decyn-1-ol, the isomer wherein the triple bond has migrated to the end of the chain, obtained with the lithium and sodium salts of 1,2-diaminoethane and 1,3-diaminopropane and with the sodium salt of n-butylamine. The lithium salts of n-butylamine and isobutylamine gave little 9-decyn-1-ol.

The sodium salts of 1,2-diaminoethane and 1,3-diaminopropane both prove to be excellent isomerization reagents. 9-Decyn-1-ol comprises over 95% of the total decyn-1-ol mixture after 0.5 hour and is obtained in 95% yield using the sodium salt of 1,2-diaminoethane for 1.0 hour. This reagent offers some practical advantages since it can be formed at a lower temperature and the solvent is dried by distillation at atmospheric pressure from BaO more conveniently. Solutions of both reagents can be stored in the freezer for over a month without loss of activity.

It is surprising that the sodium salt of n-butylamine is an effective isomerization reagent. The extremely fast reaction rates observed with the original isomerization reagents were attributed to a concerted, bimolecular mechanism involving the bidentate nature of the base (2). A cycle was postulated wherein the amide nitrogen would abstract a proton from the carbon next to the triple bond and the resultant allenic anion would abstract a proton from the other nitrogen of the base. The result obtained for the isomerization with sodium n-butylamide demonstrates that it is not necessary to invoke a concerted, cyclic mechanism.

While the rate of isomerization observed with the lithium salts is slower and thus not as useful for preparation of terminal acetylenes, it was thought that these milder reagents might be useful in selective rearrangements. Earlier work showed (3) that homopropargyl isomers are particularly stable and accumulate in rearrangement reactions even when the triple bond in the starting material was closer to the free terminus. It was hoped that high conversion of propargyl to homopropargyl compounds might be obtained. The rearrangement of 2- to 3-decyn-1-ol was studied with the different reagents at 10°C, just above the freezing point of 1,2-diaminoethane. In Table 1 is shown the maximum percentage of 3-decyn-1-ol observed. The lithium salts of the diamines gave the best conversions in the shortest times. The lithium salts of the monoamines reacted too slowly, while the sodium salts all led to further rearrangements to other products. The maximum conversion to the homopropargyl isomer is obtained with the lithium salt of 1,3-diaminopropane at −11°C.

[1]NRCC No. 20881.
[2]Author to whom correspondence may be addressed.
[3]Revision received November 12, 1982.

Can. J. Chem. Downloaded from www.nrcresearchpress.com by 210.87.254.105 on 09/06/12
For personal use only.

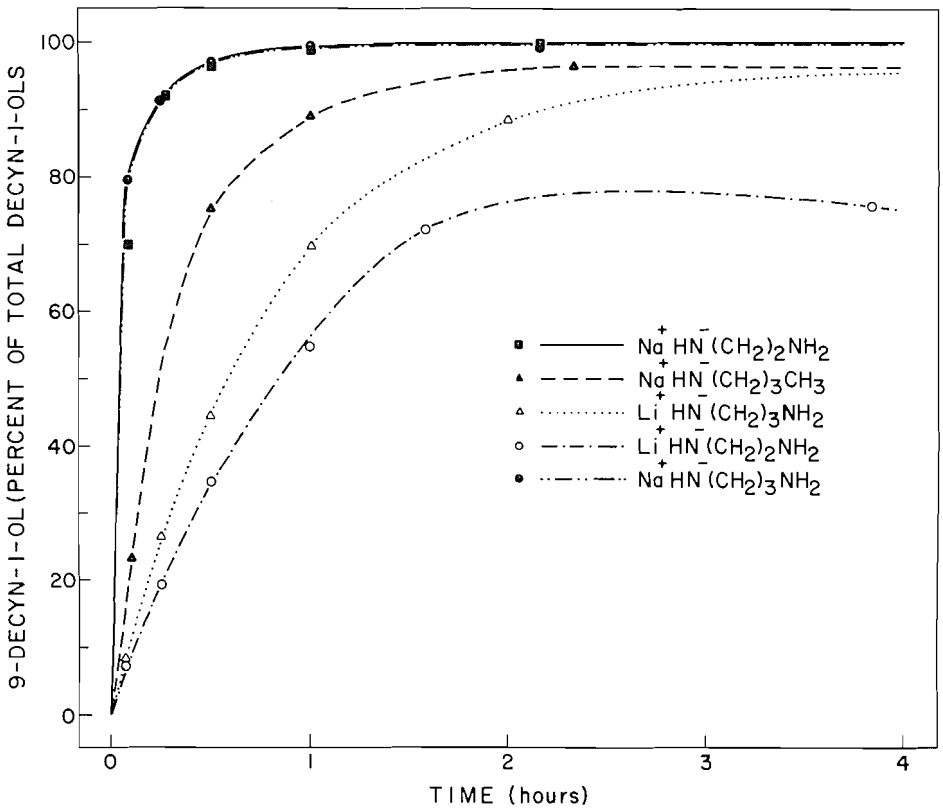

FIG. 1. Isomerization of 2-decyn-1-ol with some alkali metal amides at 55°C.[4]

TABLE 1. Rearrangement of 2- to 3-decyn-1-ol with alkali metal alkyl amides

Isomerization reagent	Reaction time (min)	Reaction temperature (°C)	% 3-Decyn-1-ol of total decyn-1-ols
Li^+ $H\bar{N}(CH_2)_2NH_2$	5	10	76
Li^+ $H\bar{N}(CH_2)_3NH_2$	5	10	78
	15	−11	82
Na^+ $H\bar{N}(CH_2)_3NH_2$	5	10	69
Na^+ $H\bar{N}(CH_2)_2NH_2$	5	10	47
Na^+ $H\bar{N}(CH_2)_3NH_2$	10	10	46
Li^+ $H\bar{N}(CH_2)_3CH_3$	60	10	55
Li^+ $H\bar{N}CH_2CH(CH_3)_2$	60	10	66

It was anticipated that, by employing a mild isomerization reagent, a unique selective isomerization of a one triple bond of a 2,ω-diynol might be possible. Such an isomerization has been incorporated as the key step in a new synthesis of *Z,Z*-3,13-octadecadienyl acetate (**5**) (Scheme 1), an insect sex pheromone of many clearwing moths including the cottonwood crown borer (4), the smaller clearwing moth (5), and the lesser peachtree borer (6). To our knowledge, this is the first report of a selective isomerization of one triple bond of a diyne independent of other acetylene groups in the molecule. Two triple bonds which are widely separated, as in α,ω-diynes, respond to base treatment as two separate monoacetylenes and diynes with triple bonds in close proximity tend to rearrange to give conjugated isomers (7, 8).

The synthesis is outlined in Scheme 1. The starting diyn-1-ol **2** was prepared by reaction of the monolithium salt of 1,12-tridecadiyne with paraformaldehyde. The selective rearrangement to **3** was carried out using 7.0 equivalents of isomerization reagent: 2 equivalents were employed to form the anion at each end of the molecule and 5 equivalents were available for the rearrangement reaction. With the lithium salt of 1,2-diaminoethane at ambient temperature, the ratio of **3** to **2** after 5 min was 7:1, and after 15 min was 12:1. By the latter time, some of the product had undergone further rearrangement, but still made up 61% of the total reaction mixture. Using the same conditions, but with the sodium salt of 1,2-diaminoethane, the ratio of **3** to **2** was only 1:1. To prevent side product formation the lithium salt of 1,3-diaminopropane at 0°C was used. The rearrangement proceeded more slowly: at 15 minutes the proportion of **3** to **2** was 3:1 but **3** made up 66% of the total diynol mixture. The propargylic and homopropargylic isomers were separable by silicic acid chromatography. The desired product was obtained in 53% isolated yield based upon consumed starting material.

[4]*Note added in proof*: The yields of 9-decyn-1-ol (glc) after 1.0 hour were greater than 70%. The lithium reagents gave lower yields: $LiNH(CH_2)_3NH_2$ (52%) and $LiNH(CH_2)_2NH_2$ (32%).

Can. J. Chem. Downloaded from www.nrcresearchpress.com by 210.87.254.105 on 09/06/12
For personal use only.

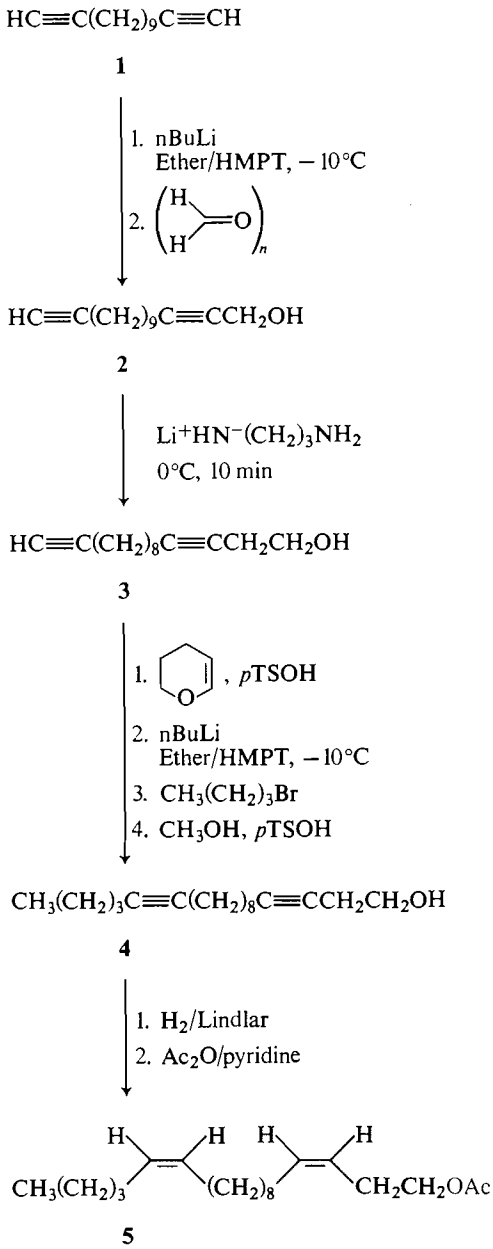

SCHEME 1

Alkylation of **3**, protected as the tetrahydropranyl ether, with butyl bromide and removal of the protecting group with methanol and *p*-toluenesulfonic acid gave **4** identical with authentic material (4, 9). Hydrogenation over Lindlar catalyst and acetylation gave the pheromone **5** (4).

Thus the sodium and lithium salts of amines can be useful isomerization reagents for different purposes. The sodium salts give high yields of terminal alkynes free of other isomers. The lithium salts can be employed in selective isomerizations as the reagents are strong enough bases to abstract the terminal acetylenic proton, trapping the triple bond at the end of the chain, and mild enough to effect the Δ2 to Δ3 rearrangement in good yield.

Experimental

The procedure for analysis of decyn-1-ol mixtures was the same as described in a previous paper: the alcohols were converted to the TMS ethers with *N,O*-bistrimethylsilylacetamide and analyzed by glc using a 30M SP 2100 capillary column. n-Decanol was added as internal standard in decyn-1-ol isomerization reactions. The amine solvents were distilled from BaO and stored over activated 4 Å molecular sieves. All reactions were carried out under a slight positive pressure of dry nitrogen in flame dried glassware.

Proton nmr spectra were recorded on an HA-100 spectrometer, with deuterochloroform as solvent and internal tetramethylsilane as reference. Carbon nmr spectra were recorded on an XL-100-15 spectrometer in the Fourier transform mode at 25.16 MHz with proton noise decoupling. Deuterochloroform served as solvent and internal deuterium lock.

Preparation of isomerization reagents

Lithium salt of 1,2-diaminoethane

According to the method of Reggel *et al.* (10), 1,2-diaminoethane (20 mL) was added to lithium wire (275 mg, 40 mmol). As the metal dissolved, the mixture turned blue and heat evolved as the salt formation began. Additional heating at 50°C was applied until the blue colour disappeared leaving a white suspension of the salt.

Lithium salt of 1,3-diaminopropane

The same procedure was used as for 1,2-diaminoethane.

Sodium salt of 1,2-diaminoethane

To sodium hydride (57% in mineral oil, 1.70 g, 40 mmol, washed free of oil with petroleum ether) was added 1,2-diaminoethane (20 mL). The mixture was stirred and heated to 50°C. After about a 5 min induction period, gas evolution was noted and the mixture turned to blue-grey and then to brown solution in 0.5 hour.

Sodium salt of 1,3-diaminopropane

The reagent was formed exactly as above except that heating to 70°C was required.

Sodium salt of n-butylamine

A mixture of sodium hydride (1.70 g, 40 mmol, washed free of oil) and n-butylamine (20 mL) was refluxed overnight to give a brown/purple mixture.

Lithium salt of n-butylamine

To n-butylamine (6.5 mL) at −10°C was added BuLi (in hexane, 0.6 *M*, 20 mL, 13 mmol). The hexane was removed by distillation at reduced pressure to give a yellow solution.

Lithium salt of isobutylamine

The lithium salt was prepared by reaction of isobutylamine (6.5 mL) with nBuli (in hexane, 0.6 *M*, 20 mL, 13 mmol) at −10°C. The hexane and isobutylamine were removed at reduced pressure and 6.5 mL isobutylamine added to the resultant solid.

General isomerization procedure

To the prepared reagent (nominally 40 mmol, in 20 mL solvent) at either 55° or 10°C was added a solution of 2-decyn-1-ol (900 mg, 6.0 mmol) and n-decanol (90 mg, 0.6 mmol) in solvent (4 mL). Samples of 1.0 mL were removed at intervals: 5 min, 15 min, 30 min, 1 h, 2 h, and 4 h; each was poured onto ice-water and extracted with ether (2×). The combined organic phases were washed with NaCl solution, dried over Na_2SO_4, filtered, and the solvent evaporated.

9-Decyn-1-ol

To the sodium of 1,2-diaminoethane (prepared from NaH (1.70 g, 40.0 mmol) and 1,2-diaminoethane, 20 mL) at 55°C was added 2-decyn-1-ol (925 mg, 60 mmol) in 1,2-diaminoethane (4.0 mL). After 1.0 h, the mixture was poured onto ice/water and extracted with ether (3×). The combined organic phases were washed with NaCl solution, dried over Na_2SO_4, filtered, and the solvent evaporated to yield 1.09 g crude product which was chromatographed over silica gel (Bio Rad 200–400 mesh), eluting with ether/hexane mixtures to separate residual mineral oil from the product 9-decyn-1-ol (880 mg, 95%).

2,13-Tetradecadiyn-1-ol (2)

To a solution of 1,12-tridecadiyne (1.0 g, 5.7 mmol) in diethylether (dry, 45 mL) and HMPT (dry, 5 mL) at −10°C was added n-butyllithium (5.7 mmol, 3.5 mL). After 0.5 h, paraformaldehyde (250 mg, 8.5 mmol) in ether (8 mL) was added. The mixture was stirred

Can. J. Chem. Downloaded from www.nrcresearchpress.com by 210.87.254.105 on 09/06/12
For personal use only.

and allowed to warm at room temperature overnight. Ice/water was added; the organic phase separated and the aqueous phase was extracted with ether (3×). The combined organic phases were washed successively with water and NaCl solution, then dried over Na_2SO_4, filtered, and the solvent evaporated. The crude product was chromatographed over silica gel, eluting with ether/hexane mixtures to give 1,12-tridecadiyne (500 mg) and desired product **2** (350 mg, 60%, based upon consumed starting material). The product was distilled (Kugelrohr oven temperature 110°C) at 0.1 Torr; ν_{max} (film): 3350 (s), 3280 (s), 2205 (w) and 2103 (w) cm^{-1}; ^1H ($CDCl_3$) δ: 4.21 (t, J = 1 Hz, 2H), 2.1–2.3 (m, 4H), 1.90 (t, J = 1.5 Hz, 1H), and 1.2–1.6 (m, 14H); ^{13}C ($CDCl_3$) δ: 86.56, 84.81, 78.45, 68.16, 51.38, 29.38, 29.09, 29.09, 28.87, 28.75, 28.65, 28.52, 18.78, and 18.44 ppm. *Anal.* calcd. for $C_{14}H_{22}O$: C 81.50, H 10.75; found: C 81.60, H 10.94%.

3,13-Tetradecadiyn-1-ol

To the lithium salt of 1,3-diaminopropane (prepared from lithium (150 mg, 21 mmol) and 1,3-diaminopropane, 12 mL) at 0°C was added a solution of **2** (600 mg, 3 mmol) in 1,3-diaminopropane (6 mL). The reaction was quenched after 10 min and worked up as usual to give 500 mg crude product which was chromatographed over silicic acid, eluting with ether/hexane mixtures to give recovered **2**, 80 mg, and **3**, 275 mg, 53% yield based upon consumed starting material. The product was distilled (Kugelrohr oven temperature 110°C) at 0.1 Torr; ν_{max} (film): 3350 (s), 3300 (s), and 2103 (w) cm^{-1}; ^1H nmr ($CDCl_3$) δ: 3.61, (t, J = 6.5 Hz, 2H), 2.38 (tt, J = 6.5, 1.5 Hz, 2H), 2.0–2.25 (m, 4H), 1.91 (t, J = 1.5 Hz, 1H), and 1.2–1.6 (m, 12H); ^{13}C nmr ($CDCl_3$) δ: 84.76, 82.65, 76.42, 68.15, 61.42, 29.01, 29.01, 29.01, 28.84, 28.72, 28.50, 23.22, 18.77, and 18.43 ppm; analyzed as the *p*-nitrobenzoate. *Anal.* calcd. for $C_{21}H_{25}NO_4$: C 70.95, H 7.10, N 3.94; found: C 71.08, H 7.09, N 3.92.

3,13-Octadecadiyn-1-ol

To **3** (380 mg, 1.85 mmol), cooled to 0°C, was added dihydropyran (5 mL) and 50 mg *p*-toluenesulfonic acid. After 1.5 h K_2CO_3 was added, the mixture was filtered, and the solid washed with ether. The solvents were evaporated and the crude THP ether was alkylated immediately, by dissolving it in diethyl ether (dry, 20 mL) and HMPA (dry 5 mL) and cooling to −10°C. A solution of n-butyllithium (in hexane, 2.2 mmol, 1.4 mL) was added, followed by n-butylbromide (0.4 mL, 2.3 mmol, 1.25 equivalent). The reaction was stirred at ambient temperature overnight, then ice/water was added. The phases were separated and the aqueous layer worked up with ether 3×. The combined organic phases were washed with water, then NaCl solution, dried over Na_2SO_4, filtered, and the solvent removed to yield a yellow oil which was suspended in methanol (100 mL) and *p*-toluenesulfonic acid (50 mg). The mixture was refluxed for 3.5 h and then the methanol evaporated. The residue was partitioned between ether and $NaHCO_3$ solution. The aqueous phase was extracted with ether (3×) and the combined organic phases were washed with water and NaCl solution, then dried over Na_2SO_4 and evaporated to give a brown oil which was chromatographed over silicic acid, eluting with ether/hexane mixtures to give 120 mg **4** (9) and 120 mg **3**. The yield based upon consumed starting material was 40%. Semihydrogenation and acetylation were carried out as previously described (4).

Acknowledgements

We wish to thank Mr. W. C. Haid and Mr. T. Mazurek for nmr measurements.

1. S. R. MACAULAY. J. Org. Chem. **45**, 734 (1980).
2. C. A. BROWN and A. YAMASHITA. J. Am. Chem. Soc. **97**, 891 (1975).
3. S. R. MACAULAY. Can. J. Chem. **58**, 2567 (1980).
4. E. W. UNDERHILL, W. STECK, M. D. CHISHOLM, H. A. WORDEN, and J. A. G. HOWE. Can. Entomol. **110**, 495 (1978).
5. S. VOERMAN. J. Chem. Ecol. **5**, 759 (1979).
6. J. H. TUMLINSON, C. E. YONCE, R. E. DOOLITTLE, R. R. HEATH, C. R. GENTRY, and E. R. MITCHELL. Science, **185**, 614 (1974).
7. R. J. BUSHBY. Q. Rev. Chem. Soc. **24**, 585 (1970).
8. F. THÉRON, M. VERNY, and R. VESSIÈRE. The chemistry of the carbon–carbon triple bond. *Edited by* Saul Patai. John Wiley and Sons, Toronto. 1978. Chapt. 10.
9. M. UCHIDA, K. NAKAGAWA, and K. MORI. Agric. Biol. Chem. **43**, 1919 (1979).
10. L. REGGEL, S. FRIEDMAN, and I. WENDER. J. Org. Chem. **23**, 1136 (1958).

Can. J. Chem. Downloaded from www.nrcresearchpress.com by 210.87.254.105 on 09/06/12
For personal use only.

A homoallyl radical rearrangement. Kinetics of the isomerization of the 2,2-dimethyl-3-buten-1-yl radical to the 1,1-dimethyl-3-buten-1-yl radical[1]

CHRYSSOSTOMOS CHATGILIALOGLU AND KEITH U. INGOLD[2]
Division of Chemistry, National Research Council of Canada, Ottawa, Ont., Canada K1A 0R6

AND

IRENE TSE-SHEEPY AND JOHN WARKENTIN[2]
Department of Chemistry, McMaster University, Hamilton, Ont., Canada L8S 4M1

Received September 1, 1982

CHRYSSOSTOMOS CHATGILIALOGLU, KEITH U. INGOLD, IRENE TSE-SHEEPY, and JOHN WARKENTIN. Can. J. Chem. **61**, 1077 (1983).

Rate constants for the overall rearrangement of the 2,2-dimethyl-3-buten-1-yl radical to the 1,1-dimethyl-3-buten-1-yl radical, $k^{C=C}$, have been measured from − 145°C to −101°C by kinetic epr spectroscopy and at 40°C by spin trapping with 1-methyl-4-nitroso-3,5-diphenylpyrazole. The temperature dependence can be represented by

$$\log (k^{C=C}/s^{-1}) = (12.5 \pm 0.6) - (6.6 \pm 0.4)/\theta$$

where $\theta = 2.3RT$ kcal mol^{-1}. This rearrangement, which must proceed via a 2,2-dimethylcyclopropylcarbinyl radical as an intermediate, is one of the fastest rearrangements involving a primary alkyl radical. At 25°C, $k^{C=C} = 4.3 \times 10^7$ s^{-1}, which makes this rearrangement about 10 000 times faster than the rearrangement of the simplest homoallyl radical, 3-buten-1-yl. This rate enhancement is attributed to steric acceleration of ring closure by the *gem* dimethyl groups (Thorpe–Ingold effect).

CHRYSSOSTOMOS CHATGILIALOGLU, KEITH U. INGOLD, IRENE TSE-SHEEPY et JOHN WARKENTIN. Can. J. Chem. **61**, 1077 (1983).

On a mesuré les constantes de vitesse de la transposition globale du radicale diméthyl-2,2 butène-3 yle-1 en radical diméthyl-1,1 butène-3 yle-1, $k^{C=C}$, de −145°C à −101°C en utilisant la spectroscopie de rpe cinétique et à 40°C par piégeage de spin avec le méthyl-1 nitroso-4 diphényl-3,5 pyrazole. On peut représenter l'effet de la température par:

$$\log (k^{C=C}/s^{-1}) = (12,5 \pm 0,6) - (6,6 \pm 0,4)/\theta$$

où $\theta = 2,3RT$ kcal mol^{-1}. Cette transposition qui ne peut se produire que par l'intermédiaire du radical diméthyl-2,2 cyclopropylcarbinyle est l'une des plus rapides impliquant un radical alkyle primaire. A 25°C, $k^{C=C} = 4,3 \times 10^7$ s^{-1}, ce qui rend cette transposition environ 10 000 fois plus rapide que la transposition du radical homoallyle le plus simple: le butène-3 yle-1. On attribue cette augmentation de vitesse à l'accélération stérique de la fermeture de cycle par les groupes *gem*-diméthyles (effet de Thorpe–Ingold).

[Traduit par le journal]

Introduction

Homoallylic rearrangements of free radicals, eq. [1], are well known and there is much evidence that cyclopropylcarbinyl radicals are discrete intermediates in the process, eq. [1].[3] Some of the evidence is direct, for cyclopropyl products can be isolated in a few cases (eq. [2] (2); eq. [3][4]), and some is indirect as, for example, in the *cis* ⇆ *trans*

[1] 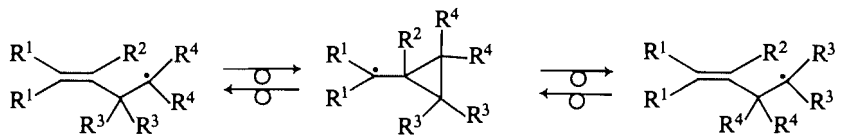

interconversion of eq. [4] (3), where there is no reasonable alternative mechanism.

[2] 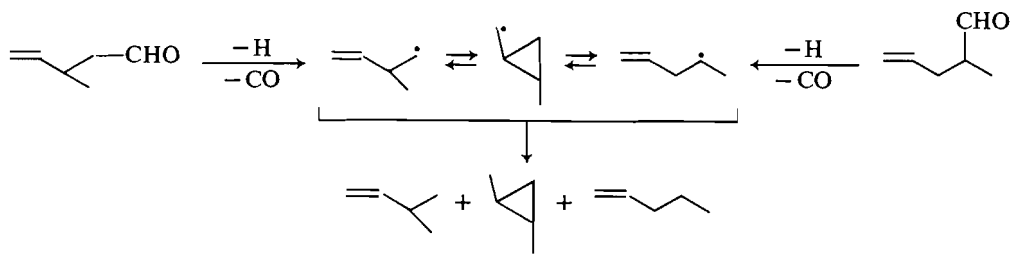

Although there is no longer any doubt about the mechanism of vinyl group transfer in free radical rearrangements, little is

[1]NRCC No. 20882.

[2]Correspondence may be addressed to either of these authors.

[3]For a recent general review of radical rearrangements, which includes rearrangements of homoallylic radicals, see ref. 1. Only selected background material on the latter subject is repeated here.

[4]K. U. Ingold, P. Schmid, and Y. Maeda. Unpublished results cited in ref. 1.

Can. J. Chem. Downloaded from www.nrcresearchpress.com by 210.87.254.42 on 09/06/12
For personal use only.

Can. J. Chem. Downloaded from www.nrcresearchpress.com by 210.87.254.42 on 09/06/12
For personal use only.

[3] 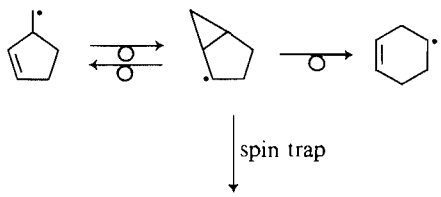

[4] 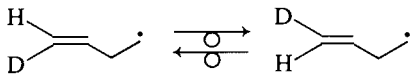

known about the kinetics of such processes. The rate constant for ring-closure of 1,1-dideuterio-3-buten-1-yl (eq. [5]) has the value 4.9×10^3 s^{-1} at 25°C (4)[5] and that for the overall irreversible rearrangement of eq. [6] is estimated to lie between

[5] 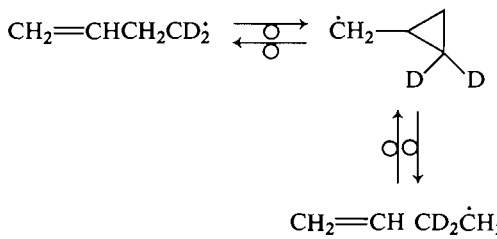

1×10^4 s^{-1} and 5×10^4 s^{-1} (5). These are the only known values for the overall process of vinyl migration, although a few rate constants for the ring opening step alone have been estimated (1).

[6] 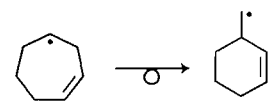

We wish to report the kinetics of rearrangement of the 2,2-dimethyl-3-buten-1-yl radical (**1**) to the 1,1-dimethyl-3-buten-1-yl radical (**2**), eq. [7]). This rearrangement rate is of

[7] 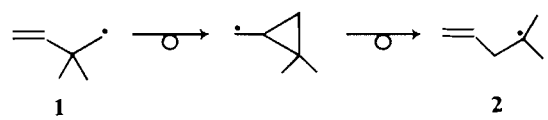

1 **2**

interest because of the question as to the magnitude of the "*gem* dimethyl acceleration factor" (cf. eq. [5]), which was found to be substantial in the analogous homopropargyl rearrangement (6). In addition, new "radical clocks" (7) are still required as aids to the quantitative study of free radical chemistry. That is, there is a need to increase the range of clock speeds, to fill in gaps in the existing range, and for clocks that are chemically compatible with as many reaction systems as possible.

Experimental

The steady state and kinetic epr techniques applicable to the study of radical rearrangements have been described (8–10). For direct epr studies, radicals **1** and **2** were generated by photolysis of 3,3-dimethyl-4-pentenoyl peroxide (**3**) in CF_2Cl_2 at low temperature. The region swept was 40 G wide and included lines of relative intensities 20, 30, 6, 15, and 12 from radical **2** and a line with relative intensity one from the 1:2:1 triplet spectrum of **1**. That line fell between the lines of relative intensity 20 and 30 from radical **2** (see parameters of Table 1) and was not well resolved from them. The total of these unresolved signals and the line of relative intensity 15 were doubly integrated. The latter integral was used to calculate the relative concentration of **2** and the former integral, corrected for the calculated contribution from **2**, was used to calculate the relative concentration of **1**. These relative concentrations were converted to absolute values in the usual way (8–10) through the use of the ruby signal and a solution of DPPH at a known concentration. For indirect epr studies, using the spin trapping technique, diacyl peroxide **3** was thermolyzed at 40°C in

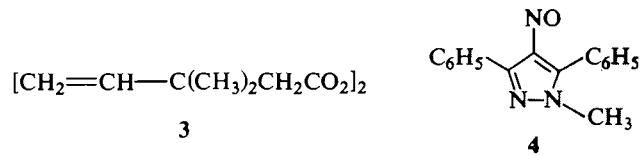

3 **4**

benzene or dichloromethane solutions containing 1-methyl-4-nitroso-3,5-diphenylpyrazole (**4**). The buildup of nitroxide spin adducts from addition of **1** and **2** to **4** was monitored by recording repeatedly a part of the spectrum containing the outer and center lines of one of the wing triplets in the spectrum of the spin adduct of **1**. That center line overlapped with a wing line of the 1:1:1 triplet from the spin adduct of **2**. Double integration and simple calculation gave the relative concentrations of the two adducts. The rearrangement rate constant was then determined from the known rate constant for trapping of **1** by **4**, assumed to be the same as that for trapping of undecyl radicals by **4** ($1.5 \times 10^7 M^{-1}$ s^{-1} at 40°C) (18), and the known concentration of **4**.

Peroxide **3** was prepared by the sequence of steps below.

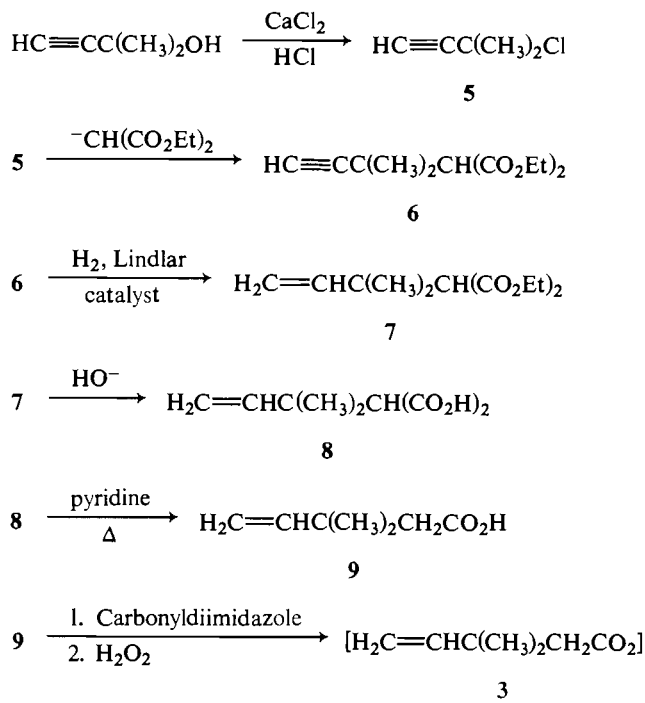

3-Chloro-3-methyl-1-butyne (5)

The published procedure (11) gave, from 84 g of 2-methyl-3-butyne-2-ol, 91.8 g of crude **5** which was distilled at 95–107 Torr, the fraction boiling at 27–30°C being collected. The distillate was redistilled at atmospheric pressure to afford, after a forerun boiling at 31–72°C, 37.4 g of pure **5**, bp 72–73°C (36% yield).

2,2-Dimethyl-3-butyne-1,1-dicarboxylic acid diethyl ester (6)

This compound was prepared from **5** by literature procedures (12,

[5]Barring large isotope effects, this means that the rate of overall rearrangement is $1/2 \times 4.9 \times 10^3$ s^{-1} (4).

TABLE 1. Electron paramagnetic resonance parameters in Cl_2CF_2

Radical	g-valuc	a^N(G)	a^{H_α}(G)	$a^{H_{other}}$(G)
$H_2C{=}CH\text{-}C(CH_3)_2CH_2^{\cdot}$ (**1**)	2.0026[a]		21.50(2H)	2.85(1H_γ) 2.85(1H_δ)
$H_2C{=}CH\text{-}CH_2\dot{C}(CH_3)_2$ (**2**)	2.0027[b]			23.04(6H_β) 17.22(2H_β)
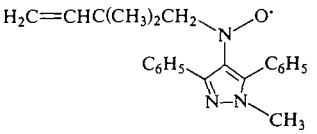		12.8[8]		8.09(2H_γ)
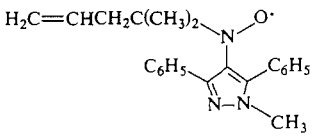	2.0067	13.2[5]		
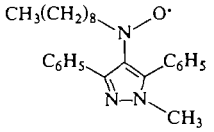	[c]	12.7		9.25(2H_γ)
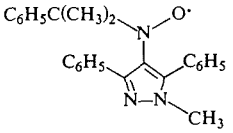	[c]	13.0[6]		

[a] At −140°C.
[b] at −70°C.
[c] Not measured.

13). From 24.96 g (243 mmol) of **5** was obtained 16.55 g (30%) of **6**, bp 63–68°C (0.2 Torr).

2,2-Dimethyl-3-butene-1,1-dicarboxylic acid diethyl ester (7)

Best results were obtained when **6** was hydrogenated over Lindlar catalyst at one atmosphere pressure in a solvent consisting of hexane and quinoline.

Lindlar catalyst (0.25 g) in 60 mL of hexane containing 0.3 mL of quinoline was exposed to H_2 at 1 atm for 30 min before **6** (4.55 g, 20.1 mmol) was added. When 20 mmol of H_2 had been taken up, the catalyst was filtered off and the hexane layer was washed with dilute acid and with dilute aqueous bicarbonate solution. It was dried over $MgSO_4$ and the hexane was evaporated to leave **7** as a colourless liquid (4.33 g, 94%).

2,2-Dimethyl-3-butene-1,1-dicarboxylic acid (8)

To diester **7** (4.27 g, 18.7 mmol) in ethanol (12 mL) was added 6 *N* NaOH (15 mL). The mixture was heated at 70°C for 2 h and at 85–90°C overnight. Hot water (40 mL) was added and the solution was concentrated on the rotary evaporator to remove ethanol. The aqueous solution was washed with CH_2Cl_2, acidified with 6 *N* HCl to pH = 1, and extracted with ethyl acetate. The extract was dried and evaporated to leave **8** as an off-white solid (3.11 g, 96%), mp 111–114.5°C.

3,3-Dimethyl-4-pentenoic acid (9)

Decarboxylation of **8** by heating it neat at 158°C for 3 min gave mostly β,β-dimethyl-γ-valerolactone, ir: ν_{CO} 1785 cm^{-1}. Cyclization could be avoided by heating **8** with pyridine at 145°C.

Diacid **8** (3.79 g, 22.0 mmol) was heated at 145°C with 374 μL of pyridine for 1 h. Distillation at 0.2 Torr, with the oil bath temperature between 94° and 100°C, gave **9** (2.81 g, 99%) as a colourless liquid; ^{1}H nmr ($CDCl_3$) δ: 1.20 (s, 6H), 2.37 (s, 2H), 4.82–5.22 (m, 2H), 5.78–6.30 (m, 1H), 11.9 (s, 1H).

3,3-Dimethyl-4-pentenoyl peroxide (3)

Acid **9** (1.72 g, 13.4 mmol) in 5 mL of dry tetrahydrofuran was added to a suspension of *N,N'*-carbonyldiimidazole in 15 mL of THF. After stirring for 1.5 h at room temperature, evolution of carbon dioxide had ceased. Hydrogen peroxide (0.77 mL of 30% solution, 6.8 mmol of peroxide) was added all at once and the resulting solution was stirred for 3 h at room temperature. The solvent was pumped off under vacuum, water and ether were added, and the ether extract was separated. It was washed with 5% H_2SO_4 and then with 5% $NaHCO_3$ before it was dried over $MgSO_4$. Evaporation of the ether without heating gave **3** (0.33 g, 19%) as a colourless oil; ^{1}H nmr ($CDCl_3$) δ: 1.20 (s, 6H), 2.37 (s, 2H), 4.80–5.17 (m, 2H), 5.67–6.17 (m, 1H).

Results and discussion

The epr parameters of **1** and **2**, as well as those of their spin adducts with **4**, are listed in Table 1. Table 2 gives measured concentrations of **1** and **2** and the rate data derived from the experiments carried out at low temperatures.

The observation of hyperfine splitting by just one of the δ-hydrogens in radical **1** was not unexpected, e.g. (14, 15), for the $CH_2{=}CHCH_2\dot{C}H_2$ radical, $a^H\gamma$ = 0.6 G and $a^H\delta$ (1H) = 0.35 G. Equivalence of the γ-H and δ-H splittings has also been observed previously in related radicals in the *cis* conformation, e.g. (16), for $RCH{=}CHCH_2\dot{C}H_2$ radicals, $a^H\gamma = a^H\delta$ (1H) = 0.7 G (R = CH_3) and = 0.61 G (R = c-C_3H_5 and OH).

Spectra of the spin adducts of **1** and **2** with **4** (Table 1) agree well with those of analogues (17, 18) and with those of the models which were prepared in this work (Table 1). This agreement provides assurance that the spin trapping reactions are not

Can. J. Chem. Downloaded from www.nrcresearchpress.com by 210.87.254.42 on 09/06/12
For personal use only.

TABLE 2. Rearrangement of **1** to **2** in CF_2Cl_2

T(K)	[**1**]$\times 10^7$ (M)	[**2**]$\times 10^7$ (M)	$[k^{C=C}/2k_t(\mathbf{2})]\times 10^7$ (M)	$2k_t$[a] (M^{-1} s^{-1})	$k^{C=C}$ (s^{-1})
172	1.5	12.1	110	10.9×10^8	11.9×10^3
159	4.3	10.8	37	6.6×10^8	2.5×10^3
149	13.3	8.7	14	4.0×10^8	0.58×10^3
128	35	1.7	1.8	1.2×10^8	0.02×10^3

[a]Values of $2k_t$ were calculated from the equation (ref. 10*g*):

$$\log 2k_t = 11.91 - 2.25/\theta$$

where $\theta = 2.3RT$ kcal mol^{-1}.

TABLE 3. Spin trapping with 0.986 M **4** in CH_2Cl_2 at 40°C ([**3**] = 0.175 M)

t(min)	[**2**/**4** adduct] / [**1**/**4** adduct]
(0)	(6)[a]
3	8.2
6	10.2
9	9.2
13	10.7
14.5	13.2
17	16.3
19	15.6
21	16.0

[a]Extrapolated, see text.

complicated by competitive O-alkylation of the nitroso compound or by rearrangements other than that of eq. [7]. It should perhaps be added that although the adduct from **4** and the 2,2-dimethylcyclopropylcarbinyl radical might not be distinguished from that of the **1**/**4** adduct, the lifetime of this intermediate will be far too short for it to be spin trapped. That is, although the rearrangement of cyclopropylcarbinyl to yield 3-butenyl is a rapid process ($k^{298\ K} = 1.3\times 10^8$ s^{-1} (10*g*)), the cyclopropylcarbinyl radical can at least be observed by epr at temperatures below ca. 153 K (10*g*, 15, 19). In contrast, when cyclopropylcarbinyls having one (20) or two (16, 19) methyl groups at the 2-position are generated, the epr spectrum of only the ring-opened alkylcarbinyls can be observed even at much lower temperatures, i.e., methyl substitution on the cyclopropane ring enhances the rate of ring opening of cyclopropylcarbinyls.

The [**2**/**4** spin adduct]/[**1**/**4** spin adduct] ratio increased slightly with time (Table 3), probably because of the greater persistence of the spin adduct of the tertiary alkyl radical. This ratio was therefore extrapolated back to time zero (defined as one minute after the cold tube was inserted into the epr cavity), a value of 6 being obtained. Using this extrapolated value of the ratio of the concentrations of the two spin adducts and assuming that the rate constant for trapping of **1** by **4** is the same as that for the trapping of the undecyl radical (18) yields $k^{C=C} = 8.8_7\times 10^7$ s^{-1} at 40°C.

Combination of the data from Tables 2 and 3 leads to the following equation for the temperature dependence of $k^{C=C}$, where $\theta = 2.3RT$ kcal mol^{-1}.

$$\log (k^{C=C}/s^{-1}) = (12.5 \pm 0.6) - (6.6 \pm 0.4)/\theta$$

Examination of the tables of rate constants for the clock reactions (7) of primary alkyl radicals reveals that the rearrangement reported herein is among the fastest yet discovered. In particular, we note that at 25°C rearrangement of **1** to **2** is about 2×10^4 times faster than the analogous rearrangement of the homoallyl radical itself (eq. [5]). The very substantial driving force for formation of three-membered rings by free radicals when *gem* dimethyl groups are present (Thorpe–Ingold effect) is demonstrated once again (6).

Acknowledgements

That portion of this work which was carried out at McMaster University was financed from a grant provided by NSERC. We are grateful to Professor M. J. Perkins for providing data from reference 18 prior to its publication and for donating a sample of **4**. Dr. A. J. Howard kindly provided a sample of azocumene.

1. A. L. J. BECKWITH and K. U. INGOLD. *In* Rearrangements in ground and excited states. Vol. 1. *Edited by* P. de Mayo. Academic Press Inc., New York. 1980. Essay #4.
2. L. K. MONTGOMERY, J. W. MATT, and J. R. WEBSTER. J. Am. Chem. Soc. **89**, 923 (1967).
3. (*a*) L. K. MONTGOMERY and J. W. MATT. J. Am. Chem. Soc. **89**, 3050 (1967); (*b*) J. Am. Chem. Soc. **89**, 6556 (1967).
4. A. EFFIO, D. GRILLER, K. U. INGOLD, A. L. J. BECKWITH, and A. K. SERELIS. J. Am. Chem. Soc. **102**, 1734 (1980).
5. E. C. FRIEDRICH and R. L. HOLMSTEAD. J. Org. Chem. **37**, 2550 (1972).
6. K. U. INGOLD and J. WARKENTIN. Can. J. Chem. **58**, 348 (1980).
7. D. GRILLER and K. U. INGOLD. Acc. Chem. Res. **13**, 317 (1980).
8. D. LAL, D. GRILLER, S. HUSBAND, and K. U. INGOLD. J. Am. Chem. Soc. **96**, 6355 (1974).
9. P. SCHMID, D. GRILLER, and K. U. INGOLD. Int. J. Chem. Kinet. **11**, 333 (1979).
10. (*a*) K. ADAMIC, D. F. BOWMAN, T. GILLAN, and K. U. INGOLD. J. Am. Chem. Soc. **93**, 902 (1971); (*b*) D. GRILLER and B. P. ROBERTS. Chem. Commun. 1035 (1971); (*c*) D. GRILLER and B. P. ROBERTS. J. Chem. Soc. Perkin Trans 2, 747 (1972); (*d*) A. G. DAVIES, D. GRILLER, and B. P. ROBERTS. J. Chem. Soc. Perkin Trans. 2, 993 (1972); (*e*) G. B. WATTS, D. GRILLER, and K. U. INGOLD. J. Am. Chem. Soc. **94**, 8784 (1972); (*f*) B. MAILLARD and K. U. INGOLD. J. Am. Chem. Soc. **98**, 1224 (1976); (*g*) B. MAILLARD, D. FORREST, and K. U. INGOLD. J. Am. Chem. Soc. **98**, 7024 (1976); (*h*) D. GRILLER and K. U. INGOLD. Acc. Chem. Res. **13**, 193 (1980).
11. G. F. HENNION, J. J. SHEEHAN, and D. E. MALONEY. J. Am. Chem. Soc. **72**, 3542 (1950).
12. O. K. BEHRENS, J. CORSE, D. E. HUFF, R. G. JONES, Q. F. SOPER, and E. W. WHITEHEAD. J. Biol. Chem. **175**, 771 (1948).
13. C. CORDES, V. PRELOG, E. TROXLER, and H. H. WESTEN. Helv. Chim. Acta, **51**, 1663 (1968).
14. R. W. FESSENDEN and R. H. SCHULER. J. Chem. Phys. **39**, 2147 (1963).
15. J. K. KOCHI, P. J. KRUSIC, and D. R. EATON. J. Am. Chem. Soc. **91**, 1877 (1969).

Can. J. Chem. Downloaded from www.nrcresearchpress.com by 210.87.254.42 on 09/06/12
For personal use only.

16. J. K. KOCHI, P. J. KRUSIC, and D. R. EATON. J. Am. Chem. Soc. **91**, 1879 (1969).
17. M. J. PERKINS. Adv. Phys. Org. Chem. **17**, 1 (1980); E. G. JANZEN. Free Radicals Biol. **4**, 115 (1980).
18. H. KAUR and M. J. PERKINS. Can. J. Chem. **60**, 1587 (1982).
19. K. S. CHEN, D. J. EDGE, and J. K. KOCHI. J. Am. Chem. Soc. **95**, 7036 (1973).
20. M. CASTAING, M. PEREYRE, M. RATIER, P. M. BLUM, and A. G. DAVIES. J. Chem. Soc. Perkin Trans 2, 287 (1979).

Can. J. Chem. Downloaded from www.nrcresearchpress.com by 210.87.254.42 on 09/06/12
For personal use only.

Conformations of simple disulfides and L-cystine

RUSSELL J. BOYD,[1] JOHN S. PERKYNS, AND R. RAMANI
Department of Chemistry, Dalhousie University, Halifax, N.S., Canada B3H 4J3

Received September 10, 1982

RUSSELL J. BOYD, JOHN S. PERKYNS, and R. RAMANI. Can. J. Chem. **61**, 1082 (1983).

ab initio Molecular orbital calculations at the STO-3G and STO-3G* levels on H_2S_2, $(CH_3)_2S_2$, $(CH_3CH_2)_2S_2$, and L-cystine show that the minimum energy conformation occurs at the angle at which the S—S overlap population is at a maximum. In agreement with experiment, the calculations favour a disulfide dihedral angle close to 90°. The variation of the S—S overlap population is essentially independent of substituents, whereas the *cis* barrier to rotation about the S—S bond increases relative to the *trans* barrier as the size of the substituents increases. These observations lead to the conclusion that electronic effects determine the disulfide dihedral angle and that both steric and electronic effects control the relative magnitude of the *cis* and *trans* barriers.

RUSSELL J. BOYD, JOHN S. PERKYNS et R. RAMANI. Can. J. Chem. **61**, 1082 (1983).

Les calculs *ab initio* d'orbitale moléculaire au niveau STO-3G et STO-3G* se rapportant au H_2S_2, au $(CH_3)_2S_2$, au $(CH_3CH_2)_2S_2$ et à la L-cystéine, montrent que la conformation d'énergie minimum s'établit à l'angle pour lequel la population de recouvrement S—S est maximum. En accord avec l'expérience, les calculs favorisent un angle dièdre pour le disulfure voisin de 90°. La variation de la population de recouvrement S—S est essentiellement indépendante des substituants alors que la barrière à la rotation autour de la liaison S—S du composé *cis* augmente avec la taille des substituants par rapport à la barrière du composé *trans*. Ces observations portent à conclure que les effets électroniques déterminent l'angle dièdre du disulfure et que les effets stériques et électroniques contrôlent l'amplitude relative des barrières des composés *cis* et *trans*.

[Traduit par le journal]

Can. J. Chem. Downloaded from www.nrcresearchpress.com by 210.87.254.42 on 09/06/12
For personal use only.

Introduction

There are two major covalent linkages between amino acids in proteins: the peptide bond of the linear backbone and the disulfide bond of cystine. The latter serves in some proteins as a cross-link between two separate polypeptide chains or between loops of a single chain. Thus the conformation of the disulfide bond affects the tertiary structure of some proteins. In open-chain molecules, the disulfide bond is known to have a nonplanar structure, similar to that of hydrogen peroxide, with the torsional angle around the S—S bond being about ±90°.

The purpose of this paper is to report the results of *ab initio* molecular orbital (MO) calculations on the S—S bond in H_2S_2, $(CH_3)_2S_2$, $(CH_3CH_2)_2S_2$, and L-cystine, and to examine the relationship between the overlap population (1) along the S—S bond and the conformational potential energy. Previous theoretical work includes some semi-empirical calculations on the conformation of disulfides (2, 3) and *ab initio* calculations on H_2S_2 (4, 5). As in the case of our study of the *cis* and *trans* conformations of natural dipeptides (6), our calculations on L-cystine, which are the first *ab initio* MO calculations, provide some insight into the structure of proteins.

Method

Standard single determinant *ab initio* MO theory was used in this work. All calculations were carried out on a CDC CYBER 170-720 system by use of the GAUSSIAN 76 program (7) at the STO-3G (8) and STO-3G* (9) levels. In order to reduce the requirements for computer time the following assumptions were introduced: H_2S_2 was assumed to have at least C_2 symmetry, model methyl groups (r(CH) = 1.09 Å and ∠HCH = 109.5°) were assumed for dimethyl disulfide, and standard bond lengths and angles (10) were assumed for diethyl disulfide and L-cystine. Only rigid rotations, corresponding to geometric model B of Radom and Pople (11), were carried out.

[1]Author to whom correspondence should be addressed.

TABLE 1. Calculated and experimental equilibrium geometries

Molecule	Geometrical parameter[a]	STO-3G	STO-3G*	Experimental[b]
H_2S_2	r(SS)	2.065	1.958	2.055
	r(SH)	1.334	1.327	1.327
	∠(SSH)	96.9	99.1	91.3
	∠(HSSH)	92.6	88.1	90.6
$(CH_3)_2S_2$[c]	r(SS)	2.064	1.950	2.038
	r(SC)	1.809	1.803	1.810
	∠(SSC)	100.0	102.9	102.8
	∠(CSSC)	90.6	87.4	84.7

[a]Bond lengths in angstroms and angles in degrees.
[b]Reference 19.
[c]Model methyl groups (r(CH) = 1.09 Å and ∠HCH = 109.5°) assumed.

TABLE 2. Total energies and net atomic charges[a]

Molecule	Total energy	Q_s	Q_{c_1}[b]	Q_{c_2}
H_2S_2	−787.49103	−0.035		
	−787.58720	−0.024		
$(CH_3)_2S_2$	−864.66267	+0.071	−0.272	
	−864.76180	+0.021	−0.209	
$(CH_3CH_2)_2S_2$[c]	−941.82012	+0.054	−0.177	−0.176
L-cystine[c]	−1420.23718	+0.037	−0.193	+0.018

[a]The STO-3G* values, where available, are listed below the STO-3G values. The energies are in atomic units (1 au = 627.5095 kcal/mol).
[b]The carbon adjacent to sulfur is denoted by the subscript 1.
[c]These are the results obtained with the CSSC dihedral equal to 90°.

Results and discussion

Equilibrium geometries calculated for H_2S_2 and $(CH_3)_2S_2$ are compared with the microwave spectroscopic structures in Table 1. The total energies and net atomic charges are listed in Table 2. With the exception of the ∠SSH, the STO-3G results

Can. J. Chem. Downloaded from www.nrcresearchpress.com by 210.87.254.42 on 09/06/12
For personal use only.

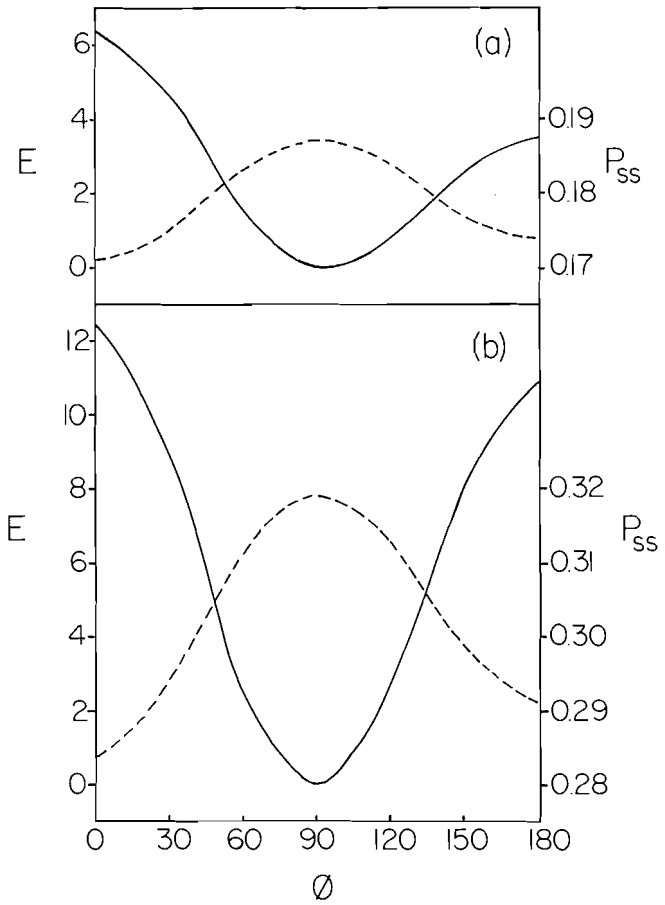

FIG. 1. One-dimensional cross-section of the conformational energy hypersurface for rigid rotation about the S—S bond of H_2S_2. The S—S overlap population, P_{SS}, is indicated by the dashed line. (a) STO-3G (b) STO-3G*.

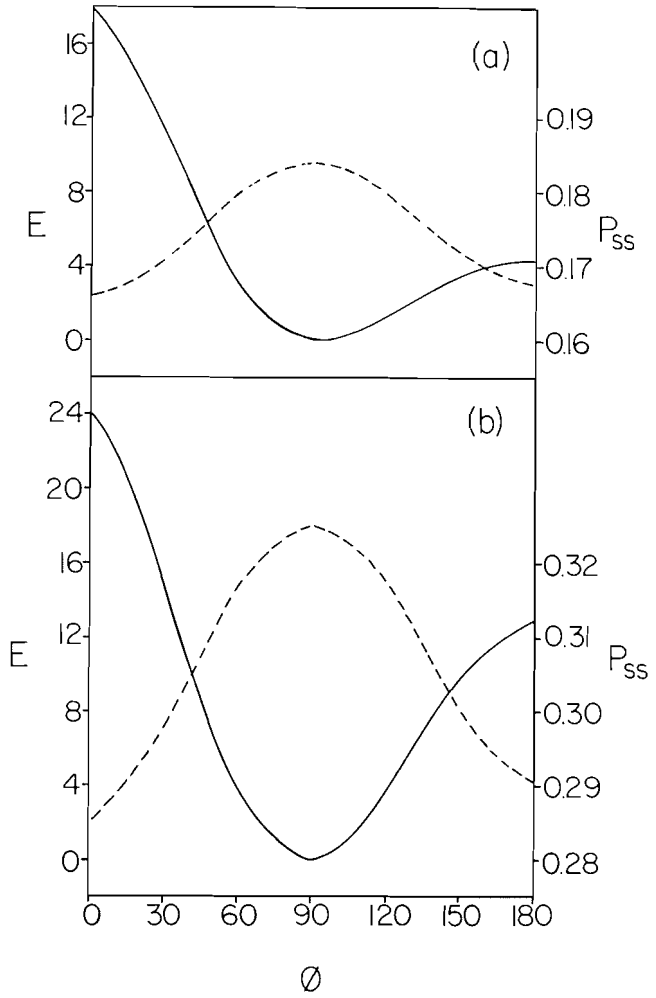

FIG. 2. One-dimensional cross-section of the conformational energy hypersurface for rigid rotation about the S—S bond of $(CH_3)_2S_2$. The S—S overlap population, P_{SS}, is indicated by the dashed line. (a) STO-3G (b) STO-3G*.

are excellent. In fact the STO-3G structure is in closer agreement with experiment than are the results obtained with split-valence basis sets (5). Adding polarization functions to the sulfurs leads to excessive shortening of the S—S bonds. The poor agreement between the STO-3G* and experimental S—S bond lengths stands in contrast to the results for hypervalent molecules containing sulfur. For the latter, the STO-3G* geometries are very much better than the STO-3G results (5, 9, 12, 13).

The one-dimensional cross-section of the conformational energy hypersurface for rigid rotation about the S—S bond of H_2S_2 is shown in Fig. 1. The variation of the overlap population as a function of the torsional angle is shown on the same graphs. Besides shortening the S—S bond by more than 0.1 Å, the addition of polarization functions to the basis set leads to larger barriers and overlap populations. Both basis sets lead to minimum energy conformations of about 90°, at which angle we note that the overlap population is at a maximum: 0.19 and 0.32[2] for STO-3G and STO-3G*, respectively. The *cis* and *trans* barriers obtained by rigid rotation are 6.4 and 3.5 kcal/mol, respectively, at the STO-3G level and 12.5 and 10.8 kcal/mol, respectively, at the STO-3G* level.

Similar results are shown in Fig. 2 for $(CH_3)_2S_2$. The overlap population is again a maximum at the minimum energy conformation. The effect of the methyl group is to raise the *cis* barrier relative to the *trans* barrier. The calculated barriers are 18.0 and 4.4 kcal/mol at the STO-3G level and 24.1 and 12.7 kcal/mol, respectively, at the STO-3G* level.

The asymmetry is even more pronounced in $(CH_3CH_2)_2S_2$ for which the *cis* and *trans* barriers are estimated to be 19.5 and 5.1 kcal/mol, respectively, at the STO-3G level (Fig. 3). Here we note that no geometry optimizations were carried out for diethyl disulfide and the CCSS dihedral angles were fixed at 180°C. Test calculations on H_2S_2 and $(CH_3)_2S_2$ indicate that the use of a model geometry will have only a very small effect on the results for $(CH_3CH_2)_2S_2$. Although the barriers in H_2S_2 have not been measured, Winneswisser *et al.* (14) have concluded that the two barriers are almost equal and that the barrier is much higher in H_2S_2 than in H_2O_2, for which the experimental value is 7.0 kcal/mol (15). From Fig. 1 it appears that the barrier is better described at the STO-3G* level than at the STO-3G level. Unfortunately the barrier in $(CH_3)_2S_2$ has not been studied experimentally, but the higher barrier for the *cis* conformation is readily attributed to a steric factor. In the absence of experimental values of the barriers, we can not decide which basis set provides a better description of internal rotation. Since the changes introduced into the hypersurfaces by replacing H by CH_3 are very similar for the two basis sets, we have not

[2]At the STO-3G equilibrium geometry, the STO-3G* overlap population between the sulfur atoms drops to 0.27 at the maximum.

Can. J. Chem. Downloaded from www.nrcresearchpress.com by 210.87.254.42 on 09/06/12
For personal use only.

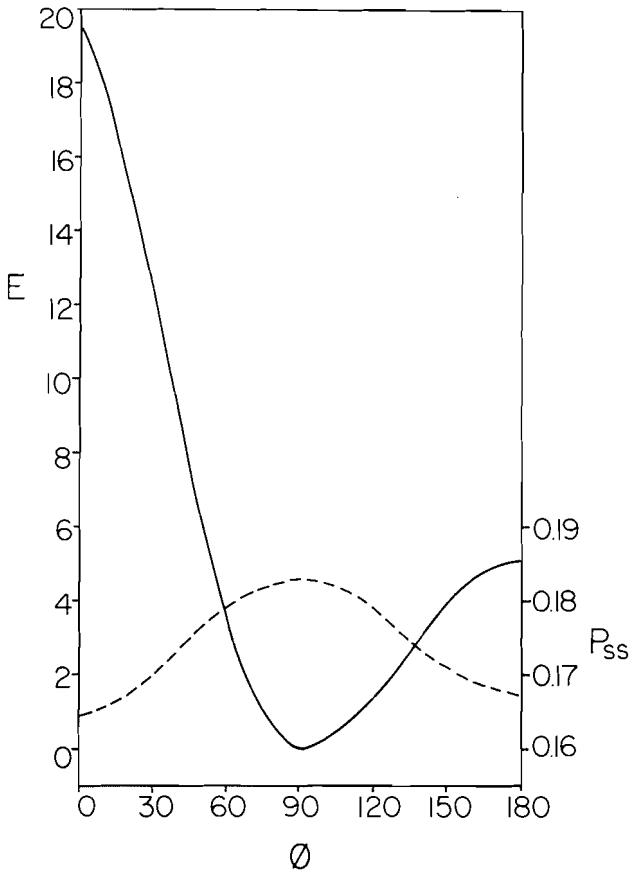

FIG. 3. One-dimensional cross-section of the conformational energy hypersurface for rigid rotation about the S—S bond of $(CH_3CH_2)_2S_2$. The S—S overlap population, P_{SS}, is indicated by a dashed line.

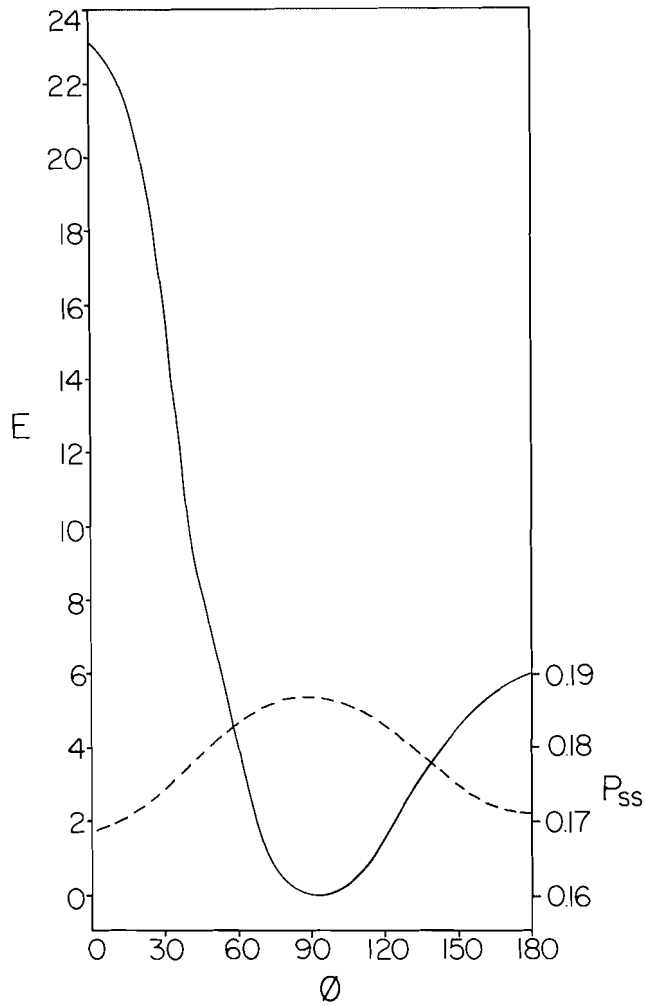

FIG. 4. One-dimensional cross-section of the conformational energy hypersurface for rigid rotation about the S—S bond of L-cystine. The S—S overlap population, P_{SS}, is indicated by a dashed line.

carried out the much more time-consuming STO-3G* calculations on diethyl disulfide.

The hypersurface for rigid rotation about the S—S bond of L-cystine is shown in Fig. 4. As in our previous studies of amino acids (6, 16), L-cystine was taken to be in the zwitterionic form (Fig. 5). With the CCSS dihedral angles fixed at 180°, as in diethyl disulfide,[3] the *cis* and *trans* barriers are 23.1 and 6.0 kcal/mol, respectively, at the STO-3G level. Thus, replacement of two hydrogens of the methyl groups by ammonium and carboxylate groups leads to a further increase in the barrier. Comparison of Figs. 1–4 reveals that the variation of the S—S overlap population is essentially independent of substituents in the disulfides, whereas the *cis* barrier increases relative to the *trans* barrier as the size of the substituent increases. In all cases the minimum energy and the maximum overlap population coincide at about 90°, which is the observed dihedral angle of the disulfide bond in the crystal structure of L-cystine.

Although only rigid rotations, corresponding to geometric model B of Radom and Pople (11), have been considered in this work, we would like to estimate the lowering of the barriers to be expected by allowing the molecule to undergo flexible rotations. Optimization of the CSS bond angles of the 0° and 180° conformations of $(CH_3)_2S_2$ at the STO-3G level leads to *cis* and *trans* barrier reductions of 7.4 and 0.7 kcal/mol, respectively, and optimized angles of 105.5° and 97.0°, respectively. At the STO-3G* level, the same procedure leads to reductions of 5.9 and 2.4 kcal/mol for *cis* and *trans* barriers, respectively, and

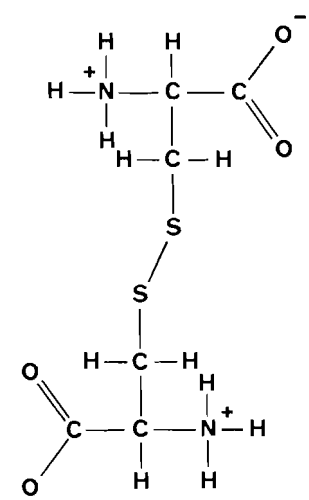

FIG. 5. Structural formula of cystine in the zwitterionic form.

[3]In both diethyl disulfide and L-cystine, the S—S bond was taken to be 2.06 Å and the C—S bond was fixed at 1.86 Å as observed in the crystal structure (see ref. 17).

optimized angles of 107.2° and 96.3°, respectively. Further relaxation of the structures, for example, by allowing the model methyl groups to distort or by re-optimization of the C—S and S—S bonds, would be expected to have only a secondary effect on the computed barriers. Even with the substantial reduction of the *cis* barriers due to relaxation of the CSS bond angles, the *cis* barriers are about 8 kcal/mol greater than the *trans* barriers at both the STO-3G and STO-3G* levels. From our inspection of molecular models, we expect the effect of optimizing the CSS bond angles in the larger disulfides to be comparable to the $(CH_3)_2S_2$ case. In summary, we suggest that the principal conclusions of this work would not be altered by carrying out completely flexible rotations rather than the rigid rotations illustrated in Figs. 1–4.

Conclusions

On the basis of the calculations reported in this paper, the following conclusions regarding the disulfide bond may be drawn.

1. The minimum energy conformation occurs at the angle at which the S—S overlap population is at a maximum. At the 6-31G** level (18) we have found the same conclusion applies to C_2H_6 and N_2H_4 but not to H_2O_2, in which the overlap population is at a maximum at about 90° but the energy minimum lies close to 115°.

2. All calculations favour an equilibrium dihedral angle close to 90° in agreement with microwave spectroscopic studies of small disulfides and an X-ray diffraction study of L-cystine dihydrobromide.

3. In contrast to the results for hypervalent sulfur moieties, the minimal STO-3G basis set leads to more accurate bond lengths than the STO-3G* basis set in which polarization functions are included in the sulfur basis set.

4. As the size of the substituents increases, the *cis* barrier to rotation about the S—S bond increases relative to the *trans* barrier. The variation of the S—S overlap population is essentially independent of substituents in the disulfides and is in fact lower in the *cis* conformation than in the energetically more favourable *trans* conformation. These observations suggest that the disulfide dihedral angle of the equilibrium conformation is determined by electronic effects, whereas the relative magnitudes of the *cis* and *trans* barriers are controlled by steric and electronic effects.

Acknowledgements

We wish to thank the Natural Sciences and Engineering Research Council of Canada for financial support in the form of an Operating Grant (to R.J.B) and an Undergraduate Summer Research Award (to J.S.P) and the Dalhousie University Computer Centre for computing facilities.

1. R. S. MULLIKEN. J. Chem. Phys. **23**, 1833, 1841 (1955); **23**, 1841 (1955).
2. D. PERAHIA and B. PULLMAN. Biochem. Biophys. Res. Commun. **43**, 65 (1971).
3. D. B. BOYD. Theoret. Chim. Acta, **30**, 137 (1973).
4. A. VEILLARD and J. DEMUYNCK. Chem. Phys. Lett. **4**, 476 (1970).
5. M. S. GORDON, J. S. BINKLEY, J. A. POPLE, W. J. PIETRO, and W. J. HEHRE. J. Am. Chem. Soc. **104**, 2797 (1982).
6. R. RAMANI and R. J. BOYD. Int. J. Quantum Chem. Quantum Biol. Symp. **8**, 117 (1981).
7. J. S. BINKLEY, R. A. WHITEHEAD, P. C. HARIHARAN, R. SEEGER, and J. A. POPLE. QCPE, **11**, 368 (1978).
8. W. J. HEHRE, R. F. STEWART, and J. A. POPLE. J. Chem. Phys. **51**, 2657 (1969).
9. J. B. COLLINS, P. VON R. SCHLEYER, J. S. BINKLEY, and J. A. POPLE. J. Chem. Phys. **64**, 5142 (1976).
10. J. A. POPLE and D. L. BEVERIDGE. Approximate molecular orbital theory, McGraw–Hill, New York. 1970.
11. L. RADOM and J. A. POPLE. J. Am. Chem. Soc. **92**, 4786,(1970).
12. R. J. BOYD, A. GUPTA, R. F. LANGLER, S. P. LOWNIE, and J. A. PINCOCK. Can. J. Chem. **58**, 331 (1980).
13. R. J. BOYD and J. P. SZABO. Can. J. Chem. **60**, 730 (1982).
14. G. WINNEWISSER, M. WINNEWISSER, and W. GORDY. J. Chem. Phys. **49**, 3465 (1968).
15. R. H. HUNT, R. A. LEACOCK, C. W. PETERS, and K. T. HECHT. J. Chem. Phys. **42**, 1931 (1965).
16. R. RAMANI and R. J. BOYD. Can. J. Chem. **59**, 3232 (1981).
17. J. PETERSON, L. K. STEINRAUF, and L. H. JENSEN. Acta Crystallogr. **13**, 104 (1960).
18. P. C. HARIHARAN and J. A. POPLE. Theoret. Chim. Acta, **28**, 213 (1973).
19. J. H. CALLOMON, E. HIROTA, K. KUCHITSU, W. J. LAFFERTY, A. G. MAKI, and C. S. POTE. Structure data of free polyatomic molecules. Landolt–Börnstein, New Series, Group II, Vol. 7. *Edited by* K. H. Hellwege and A. M. Hellwege. Springer-Verlag, Berlin. 1976.

Can. J. Chem. Downloaded from www.nrcresearchpress.com by 210.87.254.42 on 09/06/12
For personal use only.

Heterogeneous processes in the pyrolysis of ethane in contact with surfaces of SiO_2, C, KCl, and PbO

PHILIP D. PACEY AND JAYANTHA H. WIMALASENA[1]

Department of Chemistry, Dalhousie University, Halifax, N.S., Canada B3H 4J3

Received August 19, 1982

PHILIP D. PACEY and JAYANTHA H. WIMALASENA. Can. J. Chem. **61**, 1086 (1983).

Heterogeneous termination reactions in the pyrolysis of ethane have been investigated by three methods, involving measurements of the reductions in the steady state rates of formation of C_2H_4 and C_4H_{10} and of the reduction in the induction period in the presence of active surfaces. Equations were developed for the approach of the concentration of C_2H_5 to its steady state value when both first and second order termination reactions occur. Experiments have been performed at about 904 K with from 2.8×10^{-4} to 2.3×10^{-3} mol L^{-1} of C_2H_6 in the presence of surfaces of SiO_2, PbO, KCl, and C. Data from the literature have been reinterpreted. The data may be most simply explained if the main surface termination on most surfaces is first order with respect to gaseous C_2H_5. Collisional termination probabilities, γ, for this reaction were calculated to be: KCl, 905 K, 3×10^{-4}; C, 903 K, 3×10^{-4}; SiO_2, 894 K, 6×10^{-5}; 823 K, 10^{-5}; PbO, 833 K, 6×10^{-5}; Pyrex, 833 K, 4×10^{-6}.

PHILIP D. PACEY et JAYANTHA H. WIMALASENA. Can. J. Chem. **61**, 1086 (1983).

Nous avons étudié la pyrolyse de l'éthane en écoulement vers 904 K à des concentrations initiales comprises entre 2.8×10^{-4} et 2.3×10^{-3} mol L^{-1}. Le traitement des parois du réacteur à carbone a diminué la période d'induction et le rendement en C_2H_4. Le traitement des parois à C, à KCl ou à PbO a diminué le rendement en C_4H_{10}-*n*. Nos résultats, et la plupart de ceux de la littérature, sont compatibles avec un mécanisme radicalaire, dont les chaînes sont partiellement terminées par la destruction de radicaux C_2H_5. On obtient les rendements suivants de disparition de C_2H_5 par choc avec les parois suivantes: KCl, 905 K, 3×10^{-4}; C, 903 K, 3×10^{-4}; SiO_2, 894 K, 6×10^{-5}, 823 K, 10^{-5}; PbO, 833 K, 6×10^{-5}; Pyrex, 833 K, 4×10^{-6}.

Introduction

Studies of the pyrolysis of ethane have made important contributions to our understanding of kinetics (1–9), but complete acceptance of the results has been hindered by the knowledge that minor, heterogeneous reactions play a role in the mechanism (1–3). The nature of these reactions is unknown; it is known that they are most important at low temperatures and pressures (1) and in reactors coated with NaOH or PbO (2). Marshall and Quinn developed a detailed theory (10, 11). Lin and Back (1) and Scacchi, Martin, and Niclause (2) obtained experimental data which showed that the heterogeneous process was a chain termination reaction.

In principle, any of the three radical species present could react at the wall. Several authors (1, 2, 10, 11) have favoured the recombination of hydrogen atoms, since these species could diffuse most rapidly to the wall.

The object of this work is to learn more about the heterogeneous reaction. Experiments have been performed in flow reactors with surfaces of quartz, pyrolytic carbon, KCl, and PbO. The latter surface is known to be active in this and other pyrolyses (2, 12) and the carbon surface results from the process of "conditioning", which is sometimes used to obtain reproducible results (13). It has been found that the surfaces other than quartz result in reductions in the steady state rates of formation of C_2H_4 and *n*-C_4H_{10}; for the carbon surface there is a reduction in the induction period for establishment of the steady state. In the next section, the theory of these three phenomena is presented for six hypothetical surface termination reactions, for which the rate laws are listed in Table 1. A reduction in the steady state rates of formation of C_2H_4 and *n*-C_4H_{10} is predicted for each termination reaction; a reduction in the induction period, for five of the six. The reductions in the induction periods and steady state rates are in quantitative agreement with each other only if the termination is first order in gaseous C_2H_5 or H. The pressure dependence of the steady state rates is found to be correctly predicted only if the surface termination is dominated by a reaction first order in C_2H_5.

TABLE 1. Predicted orders of measurable quantities for various surface reactions

Rate of surface termination reaction, X	Kinetic control	Diffusion control
	Predicted orders of $R_{CH_4}^{\circ\,1/2}$ $(1 - ([C_2H_5]_{5+X}/[C_2H_5]_5)^2) \times [C_2H_5]_5/[C_2H_5]_{5+X}$	
$k_6[C_2H_5]$	0.0	−1.0
$k_{19}[H]$*	−0.5±0.1	−1.5±0.1
	Predicted orders of $([C_2H_5]_5/[C_2H_5]_{5+X})^2 - 1$	
$k_{20}[CH_3]$	−1.0	−2.0
$k_{22}[C_2H_5]^2$	0.0	—
$k_X[C_2H_5][H]$*	−0.5±0.1	—
$k_X[H]^2$*	−1.0±0.2	—

*k_3 has been assumed to have an order of 0.5 ± 0.1 (1).

Theory

The main features of the homogeneous pyrolysis of ethane are consistent with the following mechanism (1–9):

[1] $C_2H_6 \rightarrow 2CH_3$

[2] $CH_3 + C_2H_6 \rightarrow CH_4 + C_2H_5$

[3] $C_2H_5 \rightarrow C_2H_4 + H$

[4] $H + C_2H_6 \rightarrow H_2 + C_2H_5$

[5*a*] $2C_2H_5 \rightarrow C_4H_{10}$

[1]Present address: Department of Chemistry, University of Sri Jayewardenepura, Nugegoda, Sri Lanka.

Can. J. Chem. Downloaded from www.nrcresearchpress.com by 210.87.254.40 on 09/06/12
For personal use only.

Can. J. Chem. Downloaded from www.nrcresearchpress.com by 210.87.254.40 on 09/06/12
For personal use only.

[5b] $2C_2H_5 \rightarrow C_2H_6 + C_2H_4$

We shall assume at first that the additional, surface termination reaction is:

[6] $C_2H_5 \rightarrow$ Products

a process first order with respect to gaseous C_2H_5, and later shall consider the changes that should be made if other processes occur.

Making the steady state assumption for all three radicals and solving for $[C_2H_5]_{5+6}$, where reactions [5a], [5b], and [6] are considered to contribute to termination, and for $[C_2H_5]_5$, where only [5a] and [5b] contribute, one obtains

$$[7] \quad [C_2H_5]_{5+6}/[C_2H_5]_5 = (1 + k_6^2/a^2)^{1/2} - k_6/a$$

where $a = 4(k_1k_5[C_2H_6])^{1/2}$ and the rate constant $k_5 = k_{5a} + k_{5b}$.

Making the long chain assumption, the rate of formation of C_2H_4, when the steady state assumption is valid but before any secondary reactions become significant, is given by

$$R^\circ_{C_2H_4} = k_3[C_2H_5]$$

The ratio of rates in the presence or absence of reaction [6] then equals the ratio in eq. [7]:

$$[8] \quad R^\circ_{C_2H_4,5+6}/R^\circ_{C_2H_4,5} = [C_2H_5]_{5+6}/[C_2H_5]_5$$

Similarly, assuming reaction [5a] is the only source of C_4H_{10}, one obtains

$$[9] \quad R^\circ_{C_4H_{10},5+6}/R^\circ_{C_4H_{10},5} = ([C_2H_5]_{5+6}/[C_2H_5]_5)^2$$

Provided that reaction [2] is the only source of CH_4 and the only reaction of CH_3, it has been shown elsewhere (1–3) that

$$[10] \quad R^\circ_{CH_4} = 2k_1[C_2H_6]$$

Combining this result with the definition of a and with eq. [7] and rearranging, one obtains

$$[11] \quad k_6/k_5^{1/2} = (2R^\circ_{CH_4})^{1/2}\{1 - ([C_2H_5]_{5+6}/[C_2H_5]_5)^2\} \times [C_2H_5]_5/[C_2H_5]_{5+6}$$

By measuring the rates of formation of CH_4 and either C_2H_4 or C_4H_{10} in the presence and absence of a surface reaction, it should be possible, therefore, subject to the above assumptions, to determine the quotient $k_6/k_5^{1/2}$.

Pyrolysis before $[C_2H_5]$ is steady

If the steady state assumption is dropped for C_2H_5 but retained for CH_3 and H (8, 9) the net rate of formation of C_2H_5 becomes

$$d[C_2H_5]/dt = 2k_1[C_2H_6] - 2k_5[C_2H_5]^2 - k_6[C_2H_5]$$

Integrating this equation (14), taking $[C_2H_5] = 0$ when $t = 0$, one obtains

$$[12] \quad [C_2H_5] = a'/(4k_5)\tanh\{a't/2 + \tanh^{-1}(k_6/a')\} - k_6/(4k_5)$$

Here $a' = (a^2 + k_6^2)^{1/2}$.

Making the long chain assumption, the rate of formation of C_2H_4 is

$$[13] \quad d[C_2H_4]/dt = k_3[C_2H_5]$$

Substituting eq. [12] into eq. [13] and integrating, taking $[C_2H_4] = 0$ when $t = 0$, one obtains

$$[14] \quad \frac{[C_2H_4]}{t} = \frac{k_3}{2tk_5}\ln\{(a/a')\cosh[a't/2 + \tanh^{-1}(k_6/a')]\} - \frac{k_3k_6}{4k_5}$$

If $k_6 = 0$, this reduces to

$$[15] \quad \frac{[C_2H_4]}{t} = \frac{k_3}{2tk_5}\ln\cosh(at/2)$$

which is algebraically identical with the expression given in ref. 8. If $k_5 = 0$, eq. [14] does not apply, but it can be shown by similar methods (15) that

$$[16] \quad \frac{[C_2H_4]}{t} = \frac{2k_1k_3[C_2H_6]}{k_6}\{1 - \frac{1}{tk_6}[1 - \exp(-tk_6)]\}$$

In eqs. [14] to [16], the chordal rate of formation of C_2H_4 increases from zero and then approaches the steady state rate, given by eqs. [8] and [7]. A plot of $[C_2H_4]$ against t would approach a straight line at long residence times. If this line were extrapolated back it would intersect the time axis at $t_i = 2(a' - k_6)^{-1}\ln[2a'/(a' + k_6)]$. The induction period, t_i, approaches k_6^{-1} as k_5 approaches zero and $2a^{-1}\ln 2$ as k_6 approaches zero.

Control by diffusion or chemical reaction

Marshall and Quinn (10) have numerically solved the diffusion equation for second order removal of radicals in the gas phase and first order removal at a spherical vessel wall. They also obtained an approximate analytical solution which agreed with the numerical results within 13% or better. The approximate solution is identical in form to eq. [11], but with k_6 replaced by $(k_C^{-1} + k_D^{-1})^{-1}$. Here k_C is the rate constant for control by surface reaction, given by (16)

$$[17] \quad k_C = \gamma c(S/V)/4$$

where γ is the probability of reaction on each collision, c is the average molecular velocity of the radicals, and S/V is the surface-to-volume ratio of the vessel. Also, k_D is the effective rate constant for control by diffusion, which for laminar flow in a cylinder, is given by (16)

$$[18] \quad k_D = 0.915(S/V)^2D$$

Here D is the diffusion coefficient for the radical. For reaction in a sphere (10), the numerical factor becomes 5/3. The diffusion coefficient and k_D are inversely proportional to pressure, so if diffusion controls the rate of surface reaction, k_6 would have an apparent order of -1.

Nature of the surface reaction

We will now consider the effect of replacing reaction [6] by each of the five other reactions whose rate expressions are listed in Table 1.

As shown for eq. [11] in ref. 10, if the surface termination is

$$[19] \quad H \rightarrow \tfrac{1}{2}H_2$$

k_6 in eqs. [11], [14], and [16] would be replaced by $k_{19}k_3/(k_4[C_2H_6])$. Similar substitutions apply if H replaces C_2H_5 in reactions considered later.

The radical with the second highest concentration is CH_3. If reaction [6] is replaced by the surface termination

$$[20] \quad CH_3 \rightarrow \text{Products}$$

eq. [11] would be replaced by

$$[21] \quad k_{20}/k_2 = [C_2H_6](([C_2H_5]_5/[C_2H_5]_{5+20})^2 - 1)$$

If reaction [20] is significant, the induction period would become longer, whereas surface terminations involving C_2H_5 or H would shorten the induction period.

If reaction [6] is replaced by the second order surface reaction

$$[22] \quad 2C_2H_5 \rightarrow \text{Products}$$

making the same assumptions as previously, eq. [11] would be replaced by the following equation,

$$[23] \quad k_{22}/k_5 = ([C_2H_5]_5/[C_2H_5]_{5+22})^2 - 1$$

In eq. [15] and the expressions for a and t_i, k_5 would be replaced by $k_5 + k_{22}$. The first and second order terminations, reactions [6] and [22], affect the steady state rate and the induction period in different ways.

The predicted orders of the right hand sides of eqs. [11] and [23] for various surface reactions, calculated as above, are summarized in Table 1.

Experimental

A general description of the apparatus and experimental techniques has been given elsewhere (3, 8, 17). Reactors were constructed of cylindrical quartz tubing, with an axial thermocouple well 4 mm in outside diameter and with outer walls of either 17 mm inside diameter (S/V = 3.1 cm^{-1}) or 8 mm inside diameter (S/V = 9.9 cm^{-1}). Reactors described herein as clean quartz reactors were allowed to stand in concentrated HNO_3 overnight, washed with distilled water, and evacuated. One 17 mm diameter reactor was coated with carbon by filling it with 2.5×10^{-3} mol L^{-1} of propane and pyrolyzing at 900 K for 30 h. An 8 mm diameter reactor was coated with carbon by pyrolyzing 6.7×10^{-3} mol L^{-1} of ethane at 900 K for 20 h. A 17 mm diameter reactor was rinsed with a 10% KCl solution, drained for 2 min, and was heated to 373 K while evacuating slowly. A 17 mm diameter reactor was rinsed with a 1 mol L^{-1} solution of $Pb(NO_3)_2$ and then heated slowly to obtain a PbO deposit.

Products were analyzed on a 4.75 m, 10% squalane on chromasorb P (100/120 mesh) column, operated at 273 K for analysis of CH_4 and C_2H_4 and at 313 K for analysis of C_4H_{10}.

Results

Butane

Measurements[2] of yields of *n*-butane and methane have been determined for the pyrolysis of ethane at temperatures close to 904 K, at concentrations from 5.0×10^{-4} to 2.3×10^{-3} mol L^{-1}, for residence times from 1 to 7 s, in reactors of S/V equal to 3.1 cm^{-1}.

Product concentrations have been divided by residence times to obtain chordal rates. Chordal rates for experiments at constant temperature and pressure but differing residence times have been extrapolated to a residence time of zero to find initial rates, $R^\circ_{CH_4}$ or $R^\circ_{C_4H_{10}}$, following the method of ref. 17. Some results are presented in Table 2.

It can be seen that, for a constant C_2H_6 concentration, the rate of formation of C_4H_{10} drops by 28 to 77% as the reactor surface is changed from clean quartz to a coated surface. The rate of formation of CH_4 also appears to decline, but by a lesser amount.

[2]Tables of data are available, at a nominal charge, from the Depository of Unpublished Data, National Research Council of Canada, Ottawa, Ont., Canada K1A 0R6.

TABLE 2. Initial rates of formation of CH_4 and C_4H_{10} in reactors with S/V = 3.1 cm^{-1}

T (K)	Surface	$10^8 \times R^\circ_{CH_4}$ (mol L^{-1} s^{-1})	$10^8 \times R^\circ_{C_4H_{10}}$ (mol L^{-1} s^{-1})
$[C_2H_6] = 0.5 \times 10^{-3}$ mol L^{-1}			
904	SiO_2	1.7	0.44
903	C	1.2	0.22
905	KCl	1.2	0.17
$[C_2H_6] = 1.0 \times 10^{-3}$ mol L^{-1}			
904	SiO_2	4.8	1.4
903	C	3.4	0.81
903	C	3.7	0.69
905	KCl	3.3	0.77
907	PbO	3.8	0.32
$[C_2H_6] = 2.3 \times 10^{-3}$ mol L^{-1}			
904	SiO_2	12.1	3.6
903	C	9.7	2.3
905	KCl	8.7	2.4
905	KCl	9.5	2.6
907	PbO	11.1	1.7

Experiments have also been performed with clean quartz vessels of different S/V. In some cases an increase in S/V resulted in a small decline in $R^\circ_{C_4H_{10}}$, in others, an increase, and in yet others, no change. Evidently, any termination reaction on the quartz surface is too slow to be measured reproducibly by the present technique. As an approximation, the rate of such a reaction has been assumed to be zero in analyzing the present results.

The ratios of $R^\circ_{C_4H_{10}}$ in a coated reactor to $R^\circ_{C_4H_{10}}$ in a clean reactor in Table 2 were assumed to be equal to $([C_2H_5]_{5+6}/[C_2H_5]_5)^2$ as in eq. [9]. $R^\circ_{C_4H_{10}}$ in the clean reactor was adjusted to the same temperature as in the coated reactor using the Arrhenius law with an activation energy of 368 kJ mol^{-1}. $([C_2H_5]_{5+6}/[C_2H_5]_5)$ and $R^\circ_{CH_4}$ were then substituted in eq. [11] to calculate the quantity $k_6/k_5^{1/2}$.

The related quantity $k_6V/(Sk_5^{1/2})$ is plotted logarithmically as a function of C_2H_6 concentration as open circles (C surface), squares (KCl), and triangles (PbO) in the upper part of Fig. 1. It can be seen that the rates of surface termination on the C and KCl surfaces are similar, whereas the rate on the PbO surface is about three times faster. The data do not exhibit any clear trend with C_2H_6 concentration.

The data for each surface in Fig. 1 have been fitted by a least-squares method to a straight line. The slopes or orders which were found are quoted in the first three lines in the third column in Table 3. The quoted uncertainties are standard deviations. Within experimental uncertainty, the order for each surface is zero. From the upper part of Table 1, it can be seen that this result is consistent with a mechanism in which the dominant surface reaction is reaction [6], kinetically controlled.

The right hand side of eq. [23] has also been calculated from the data of Table 2. The order of this quantity, listed in the first three lines of the fourth column of Table 3, was found to vary from surface to surface.

Ethylene

Yields of CH_4 and C_2H_4 were measured in experiments at 902 K with 2.8×10^{-4} mol L^{-1} of ethane and residence times from 0.09 s to 2.2. s. Two reactors of S/V equal to 9.9 cm^{-1} were used; one reactor was of clean quartz, the other was

Can. J. Chem. Downloaded from www.nrcresearchpress.com by 210.87.254.40 on 09/06/12
For personal use only.

Can. J. Chem. Downloaded from www.nrcresearchpress.com by 210.87.254.40 on 09/06/12
For personal use only.

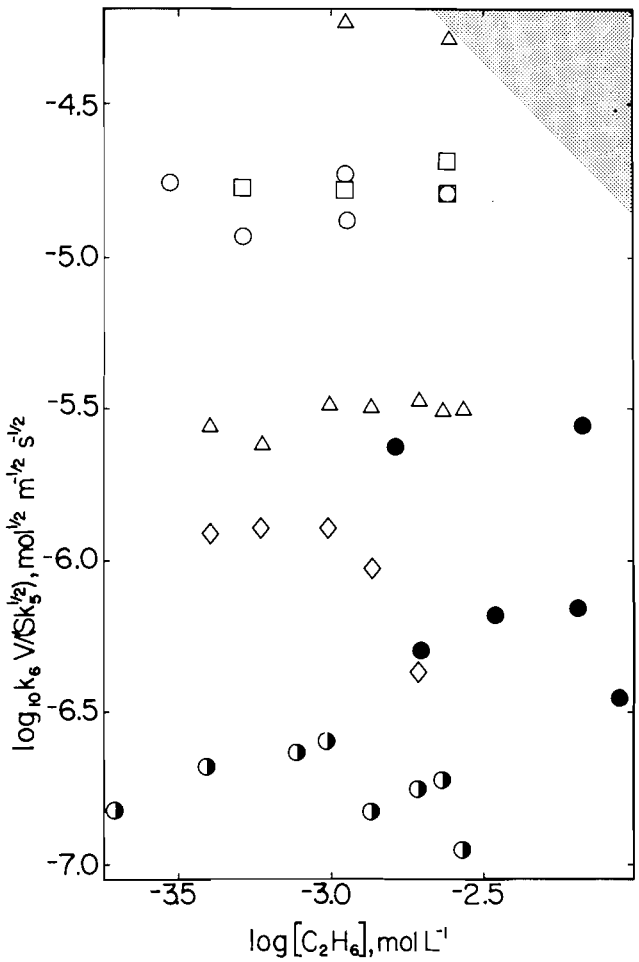

FIG. 1. Order plot for $k_6V/(Sk_5^{1/2})$: △, PbO surface, upper points, 907 K, this work, lower points, 833 K, ref. 2; □, KCl surface, 905 K, this work; ○, C surface, 903 K, this work; ●, SiO_2 surface, upper points, 894 K, lower points, 823 K, ref. 1; ◇, NaOH surface, 833 K, ref. 2; ◑, Pyrex surface, 833 K, ref. 2; the shaded area is above the limit set by diffusion for the conditions of this work.

coated with carbon. The results for C_2H_4 are shown in Fig. 2. In both reactors there is an initial increase in the chordal rate of formation of C_2H_4, followed by a plateau. This behaviour has been observed previously in clean quartz and Pyrex reactors (8, 9). In the C-coated reactor, however, the plateau is much lower and the leveling-out occurs at shorter residence times.

From the measured yields of CH_4, using eq. [10], k_1 was found to be 0.58×10^{-5} s^{-1} for the clean reactor and 0.68×10^{-5} s^{-1} for the C-coated reactor. These are within experimental uncertainty and may be averaged to obtain $k_1 = 0.63 \times 10^{-5}$ s^{-1}.

Equation [15] has been fitted by a nonlinear least-squares method (8) to the C_2H_4 data from the clean reactor; the results are shown as a smooth curve in Fig. 2. From the induction period, it was found that $4(k_1k_5[C_2H_6])^{1/2} = 19.7 \pm 1.2$ s^{-1} and hence that $k_5 = 1.43$ (± 0.17) $\times 10^{10}$ L mol^{-1} s^{-1}. From the plateau it was found that $k_3 = 810 \pm 110$ s^{-1}.

The other smooth curve in Fig. 2 shows the results of fitting eq. [14] to the data from the C-coated reactor. From the induction period, taking k_1 and k_5 as above, one finds $k_6 = 59 \pm 8$ s^{-1}. The ratio of the plateau rates in the two reactors, 0.155 ± 0.015, is equal, according to eq. [8], to $[C_2H_5]_{5+6}/[C_2H_5]_5$. From eq. [11], using the values of $R^\circ_{CH_4}$ and k_5 determined above, k_6 is found to be 62 ± 7 s^{-1}. These two values of k_6 are consistent. It was seen in the introduction that replacing reaction [6] by reaction [22] means that the establishment of the steady state is described by eq. [15], with k_5 replaced by $k_5 + k_{22}$. If the data for the C-coated reactor are fitted to this equation, one finds from the induction period that k_{22} would be 3.2 (± 0.5) $\times 10^{11}$ L mol^{-1} s^{-1} and from the plateau rate that k_{22} would be 6 (± 1) $\times 10^{11}$ L mol^{-1} s^{-1}. This discrepancy, a factor of two, is also found if other second order wall terminations are postulated.

The above values of k_5 and k_6 have been combined to obtain a value of $k_6V/(Sk_5^{1/2})$ of 1.6 (± 0.3) $\times 10^{-5}$ mol$^{1/2}$ m$^{-1/2}$ s$^{-1/2}$. This is in agreement with the average value obtained from the observation of C_4H_{10} yields with a C-coated surface, 1.5 (± 0.4) $\times 10^{-5}$ mol$^{1/2}$ m$^{-1/2}$ s$^{-1/2}$.

TABLE 3. Observed orders for the right hand sides of eqs. [11] and [23] and calculated collisional termination probabilities from eqs. [11] and [17]*

Surface	T (K)	Order Eq. [11]	Order Eq. [23]	$\gamma \times 10^4$
		This work		
C	903	−0.03±0.12	−0.48±0.18	2.8±0.6
KCl	905	+0.05±0.10	−0.79±0.13	3.2±0.4
PbO	907	−0.19	−1.40	≥10
		Reference 1		
SiO_2	823	−0.13±0.33	−0.77±0.37	0.11±0.03
SiO_2	894	+0.13	−0.47	0.6
		Reference 2		
Pyrex	833	+0.08±0.12	−0.81±0.12	0.04±0.01
PbO	833	+0.11±0.05	−0.98±0.09	0.6±0.1
NaOH	833	−0.56±0.26	−1.78±0.28	—

*Here and elsewhere, except in Table 1, quoted uncertainties are standard deviations.

Discussion

Data from the literature

Lin and Back (1) have reported yields of C_4H_{10} from ethane pyrolysis in quartz vessels with S/V equal to 0.6 cm^{-1} and 9.4 cm^{-1}. The yields were found to be reduced in the vessel of larger S/V. Assuming negligible surface reaction in the vessel of smaller S/V and applying eq. [9], the right hand sides of eq. [11] and eq. [23] have been calculated. Values of $k_6V/(Sk_5^{1/2})$ from eq. [11] are plotted in Fig. 1 as the filled circles. Calculated orders are listed in Table 3.

Scacchi, Martin, and Niclause (2) studied the overall reaction rate in clean Pyrex vessels with S/V of 0.8 cm^{-1} and 10.5 cm^{-1} and in reactors of S/V of 10.5 cm^{-1}, coated with NaOH or with PbO. Taking the overall rate as approximately equal to $R^\circ_{C_2H_4}$, and calculating the reduction in $[C_2H_5]$ from eq. [8], the right hand sides of eq. [11] and eq. [23] have been calculated; the results are shown in Fig. 1 and Table 3.

Nature of the surface reaction

If one compares the orders of the right hand side of eq. [11] in Table 3 with the predicted orders in the upper part of Table 1, one finds all the results but one are in agreement with the hypothesis that reaction [6], kinetically controlled, is the principal surface reaction. The lone exception is the NaOH surface, for which the order is −1/2.

In contrast, the orders of the right hand side of eq. [23] in

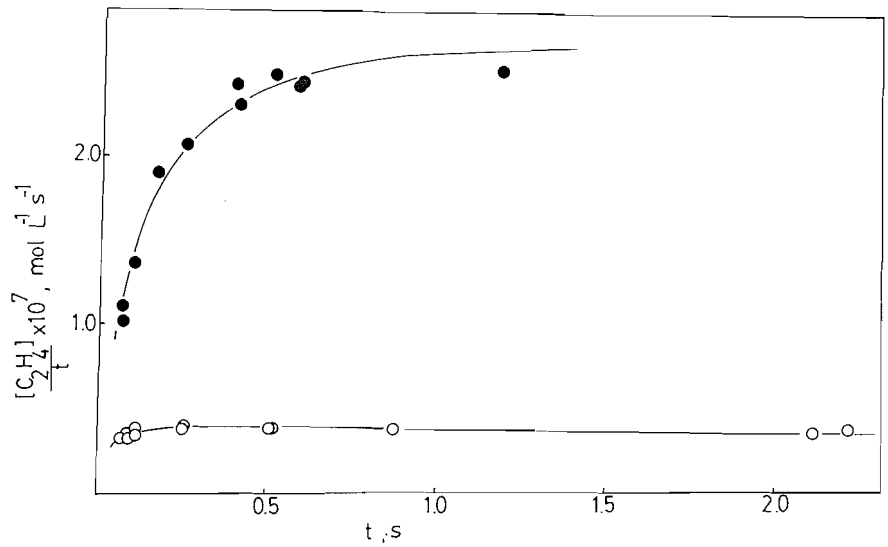

FIG. 2. Dependence of the chordal rate of formation of C_2H_4 on reactor residence time for pyrolysis of 2.8×10^{-4} mol L^{-1} of C_2H_6 at 902 K in reactors with $S/V = 9.9$ cm^{-1}: ●, SiO_2 surface; ○, C surface; —, least-squares fits to eqs. [15] and [14], respectively.

Table 3 vary considerably. It would be necessary to specify several different mechanisms to explain all the results by means of this equation.

A major contribution by reaction [21] can be ruled out because the induction period was observed to shorten in the presence of the C surface, instead of lengthening, as predicted in the Theory section. As seen in the Results section, if a second order wall termination is postulated, the rate constant, k_{22} or k_X, calculated from the induction period disagrees with that calculated from the plateau rate by a factor of two. The data in Fig. 2 can only be explained if reaction [6] or [19] is the principal heterogeneous termination.

Comparison of the predicted and observed orders in Tables 1 and 3 suggests that the reactions are kinetically controlled. This has been confirmed by calculating rate constants for diffusion control using eq. [18]. Diffusion coefficients were calculated using the methods of ref. 19. Lennard-Jones parameters for the radicals were assumed equal to those for the parent molecules. In all cases but one the diffusion rate was much faster than the observed reaction rate and hence could not be a limiting factor. The exception was the PbO surface at 907 K, for which k_D at 2.3×10^{-3} mol C_2H_6 L^{-1} was equal to the value of k_6 calculated from eq. [11] and for which, at 1.0×10^{-3} mol C_2H_6 L^{-1}, k_D was 50% greater than the value of k_6. This surface may exemplify combined kinetic and diffusion control.

It has been argued in the literature that H atoms may react at the wall, as they diffuse fastest (1, 2, 10, 11). However, it can be seen from the previous paragraph that C_2H_5 may also diffuse to the wall fast enough to account for the observed wall termination rates.

In predicting the orders in Table 1, only reactions first and second order in gaseous radical concentrations were considered. It would also be reasonable to consider intermediate, fractional orders or an inverse dependence on the concentration of reactant, which might absorb on the surface and block reaction sites. The observed orders for eq. [11] in Table 3 are randomly distributed about zero, so a fractional increase in order would not assist in interpreting the data with this equation. An inverse dependence on reactant concentration would have a similar effect to that shown in Table 1 for diffusion control. The predicted orders for diffusion control did not agree well with the experimentally observed orders.

For the above reasons, it is concluded that the simplest explanation of the data with all surfaces except NaOH is that the principal heterogeneous termination is reaction [6]. Using eq. [17], values of the collisional reaction probability, γ, have been calculated from the data of Figs. 1 and 2 and are listed in the final column in Table 3. These values may be compared with values of 5×10^{-4} at 843 K and 8×10^{-4} at 878 K which may be calculated from reported values of k_6 on a gold surface in very low pressure pyrolysis experiments (20). The values are smaller than some which have been quoted for hydrogen atom termination at similar temperatures (16), but the concentration of C_2H_5 is calculated to be several hundred times that of H at these conditions, allowing C_2H_5 to dominate the rate of surface termination.

The results of ref. 2 for the NaOH surface are more easily explained by first order termination by hydrogen atoms, reaction [19]. However, if the point furthest to the right for this surface in Fig. 1 were deleted, the order of $k_6V/(Sk_5^{1/2})$ would be -0.18 ± 0.14, similar to the values for the other surfaces in Table 3. Further work is necessary before the order of the termination on this surface can be established.

At the surface, C_2H_5 must react with species with unpaired electrons. Butane cannot be a major product of these processes as the rate of formation of butane was observed to decrease in the presence of active surfaces. Carbon is known to be formed when conversion is large, but no carbon deposition was observed in the experiments at small conversions. The detailed nature of the surface reactions cannot be determined from the present experiments.

Possible systematic errors

In this section we will consider certain assumptions which have been made and consider the influence they might have on our conclusions.

In our calculations, it has been assumed that only one reaction contributes to termination on each surface. In reality, several reactions probably contribute and the quoted values of γ for reaction [6] should be reduced.

In each calculation, it has been assumed that no surface reaction occurs in one reactor, used as a reference. Values of

Can. J. Chem. Downloaded from www.nrcresearchpress.com by 210.87.254.40 on 09/06/12
For personal use only.

Can. J. Chem. Downloaded from www.nrcresearchpress.com by 210.87.254.40 on 09/06/12
For personal use only.

γ calculated from the experiments of refs. 1 and 2 should be increased by 7 and 8%, respectively, to take surface reactions in the reference reactor into account. It is difficult to estimate the correction for the present experiments as the nature of the surface, not S/V, was changed. In Table 3, it can be seen that the value of γ for an SiO_2 surface at 894 K is about the same as the uncertainties in γ on the C and KCl surfaces at 903 and 905 K. This explains why we were unable to measure γ on SiO_2 in this work. If the value of γ for SiO_2 from the data of ref. 1, wherein the method of surface preparation was similar to that of the present work, is adjusted for the temperature difference and applied to the present work, values in Fig. 1 of $k_6V/(Sk_5^{1/2})$ for C and KCl surfaces from steady state measurements should be increased by about 25%. The value from the induction period measurement would not be significantly affected.

The long chain assumption would not introduce significant error. The shortest chain length, observed for the conditions of the lower curve in Fig. 2, was 25.

It has been assumed that C_4H_{10} is not formed at the surface. Calculations based on C_4H_{10} yields determined the rate of surface terminations forming products other than butane. Calculations based on C_2H_4 yields determined the total rate of surface termination.

Equation [10] will not be strictly true if the "atom-cracking" reaction (3) occurs. Reduction in the radical concentration by surface termination would be expected to reduce the influence of this process. Small reductions in $R^{\circ}_{CH_3}$ in the presence of active surfaces were observed in Table 1 but not in the experiments for Fig. 2 nor in refs. 1 and 2. If k_1 were reduced to allow for this reaction, values of k_6 calculated from steady state rates should be reduced but that from the induction period would be unchanged.

If a surface initiation occurs in parallel with the surface termination, the values of k_6 calculated from steady state rates should be increased, but that from the induction period would be unchanged.

A referee has suggested surface coating could affect radial heat transfer and hence gas temperatures. Flow rates have been kept to less than 5×10^{-5} mol s^{-1} to minimize this (21).

Elimination of some assumptions would increase the quoted surface rates, whereas elimination of others would decrease them. The values in Fig. 1 and Table 3 have not been adjusted, but the reader should be aware that the true uncertainties are greater than the quoted standard deviations and that the rates may depend on the method of surface preparation.

The preceding discussion illustrates the relative merits of static and flow systems for studies of surface effects. Static systems have the advantages that residence times are known precisely and that surface-to-volume ratios may be varied widely by packing reactors. In flow systems, packing reactors might create regions of stagnant gas, and residence times are less well known. Nevertheless, flow reactors do permit the use of shorter residence times, reducing the chance of reactions of products. In favourable circumstances, flow reactors enable the observation of induction periods. Rate parameters calculated from induction periods are subject to fewer of the foregoing assumptions than are those calculated from steady state rates.

It can be seen from eq. [7] that the ratio of heterogeneous to homogeneous termination is governed by the quantity $0.25k_6(k_1k_5[C_2H_6])^{-1/2}$. Ethane pyrolysis may be more influenced by surface effects than are other pyrolyses, because the initiation rate constant, k_1, is especially small.

We recommend that workers wishing to minimize surface termination use clean reactors of small S/V and keep conversion low so as to minimize carbon deposition. The opposite extreme, in which surface termination dominates, merits further study. Surface termination may be significant in industrial pyrolysis, in which conversions are large and carbon is known to be formed.

Acknowledgements

The authors thank the Natural Sciences and Engineering Research Council of Canada for a grant in support of this research, and Dr. M. H. Back for sending raw data for ref. 1. J.H.W. thanks the Dorothy J. Killam Trust for the award of a scholarship.

1. M. C. Lin and M. H. Back. Can. J. Chem. **44**, 505 (1966).
2. G. Scacchi, R. Martin, and M. Niclause. Bull. Soc. Chim. France, 731 (1971).
3. P. D. Pacey and J. H. Purnell. J. Chem. Soc. Faraday Trans. I, **68**, 1462 (1972).
4. J. A. Clark and C. P. Quinn. J. Chem. Soc. Faraday Trans. I, **72**, 706 (1976).
5. J. E. Taylor, D. A. Hutchings, and K. J. Frech. Int. J. Chem. Kinet. **5**, 455 (1973); D. M. Kulich and J. E. Taylor. Int. J. Chem. Kinet. **7**, 895 (1975).
6. A. B. Trenwith. J. Chem. Soc. Faraday Trans. 1, **75**, 614 (1979).
7. G. Pratt and D. Rogers. J. Chem. Soc. Faraday Trans. 1, **75**, 1089 (1979).
8. P. D. Pacey and J. H. Wimalasena. Chem. Phys. Lett. **76**, 433 (1980).
9. S. Corbel, P.-M. Marquaire, and G.-M. Côme. Chem. Phys. Lett. **80**, 34 (1981).
10. R. M. Marshall and C. P. Quinn. Trans. Faraday Soc. **61**, 2671 (1965).
11. M. C. Lin and M. H. Back. Can. J. Chem. **45**, 3165 (1967).
12. J. F. Foucaut and R. Martin. Int. J. Chem. Kinet. **9**, 789 (1979).
13. T. Haraguchi, F. Nakashio, and W. Sakai. ACS Symposium Series, No. 32, Industrial and Laboratory Pyrolyses. *Edited by* L. F. Albright and B. L. Crynes. American Chemical Society, 1976.
14. A. Shepp. J. Chem. Phys. **24**, 939 (1956).
15. R. M. Marshall and G. Shahkar. J. Chem. Soc. Faraday Trans. I, **77**, 2271 (1981).
16. J. Lede and J. Villermaux. J. Chim. Phys. **71**, 85 (1974).
17. P. D. Pacey. Can. J. Chem. **51**, 2415 (1973).
18. D. Jones, P. A. Morgan, and J. H. Purnell. J. Chem. Soc. Faraday Trans. I, **73**, 1311 (1977).
19. J. O. Hirschfelder, C. F. Curtiss, and R. B. Bird. Molecular theory of gases and liquids. Wiley, New York. 1954.
20. D. M. Golden, K. Y. Choo, M. J. Perona, and L. W. Piszkiewicz. Int. J. Chem. Kinet. **8**, 381 (1976).
21. H. Furue and P. D. Pacey. J. Phys. Chem. **84**, 3139 (1980).

Photochemical rearrangement of acetanilide, benzanilide, and ethyl phenyl carbonate in the presence of β-cyclodextrin

ROBERT CHÊNEVERT[1] AND RAYMOND PLANTE

Département de chimie, Faculté des sciences et de génie, Université Laval, Québec (Qué.), Canada G1K 7P4

Received July 21, 1982[2]

ROBERT CHÊNEVERT and RAYMOND PLANTE. Can. J. Chem. **61**, 1092 (1983).

The photorearrangement of acetanilide, benzanilide, and ethyl phenyl carbonate is changed in the presence of β-cyclodextrin (cycloheptaamylose). Addition of β-cyclodextrin alters the *para/ortho* migration ratio in favor of the *para* position and improves the rearrangement yield. The production of phenol (in the case of carbonate) and aniline (in the case of amides) falls significantly when irradiations are carried out in the presence of β-cyclodextrin.

ROBERT CHÊNEVERT et RAYMOND PLANTE. Can. J. Chem. **61**, 1092 (1983).

Le réarrangement photochimique de l'acétanilide, de la benzanilide et du carbonate d'éthyle et de phényle est modifié par la présence de la β-cyclodextrine (cycloheptaamylose). L'addition de β-cyclodextrine améliore le rendement du réarrangement et favorise la migration en *para* par rapport à la position *ortho*. La formation du phénol (dans le cas du carbonate) ou de l'aniline (dans le cas des amides) diminue sensiblement lorsque la photolyse a lieu en présence de β-cyclodextrine.

Introduction

Cyclodextrins form inclusion compounds in aqueous solution with a variety of smaller molecules and can catalyse several chemical reactions (1). These systems are considered to be enzyme models (2, 3) and some interesting rate enhancements or selectivity effects have been found. This last area, selective stereochemistry, is one of the most neglected areas of cyclodextrin chemistry. Breslow *et al.* (4) have reported a striking example of the use of complexation to alter the course of a reaction. When anisole was chlorinated by hypochlorous acid, *para* and *ortho* isomeric chloroanisoles were produced in the ratio 1.48:1. This ratio increased to 21.6:1 when α-cyclodextrin was added to the reaction. Cyclodextrins also modified product distribution in the rearrangement of dibenzylmethylsulfonium tetrafluoroborate in alkaline medium (5) and changed the *para* to *ortho* formylated phenol ratio of the Reimer–Tiemann reaction (6). Ohara and Watanabe (7) reported that β-cyclodextrin alters the *para* to *ortho*-hydroxyacetophenone ratio of the photochemical Fries rearrangement of phenyl acetate. We report here the influence of β-cyclodextrin on the photorearrangement of acetanilide, benzanilide, and ethyl phenyl carbonate.

Experimental

Reagents

Acetanilide and benzanilide (Aldrich Co.) were recrystallized until no further improvement in melting point was observed and dried in vacuum before use. Ethyl phenyl carbonate (Alfred Bader collection, Aldrich Co.) was shown to be pure by gas chromatography.

Irradiation; general procedure

The anilide or carbonate was dissolved in 500 mL of the chosen solvent. Concentrations were 10^{-2} *M* (acetanilide), 1.8×10^{-2} *M* (benzanilide), and 10^{-2} *M* (carbonate). When β-cyclodextrin was used, the molal proportion was 0.5 mol cyclodextrin per mol of substrate. The solution was placed in a cylindrical quartz reactor and irradiated with an immersion-type, 450-watt Ace–Hanovia uv lamp (medium pressure mercury arc). Degassed solvents were used and nitrogen was bubbled through the solution during the irradiation. When organic solvents were used, the solution was concentrated under vacuum (rotary evaporator) before analysis. When water was the solvent, the aqueous phase was thoroughly extracted with ether and the ether phase was dried and concentrated under vacuum. It was found that no loss of products occurred during these operations.

Analysis

The reaction mixtures were analyzed by quantitative vapor phase chromatography with a "7620 Research chromatograph Hewlett Packard" instrument using a 6 ft × 1/8 in., 10% Dexil 300 column on 80/100 Chromosorb W AW/DMSC support. In all cases, the injector and flame ionization detector were set at 250°C and the helium rate flow was 20.1 mL/min. The relative yields were determined by using the relative response ratio method with sulfolane as the internal standard. The retention times of all photoproducts were compared to those of authentic samples.

Acetanilide photoproducts analysis

Temperature program: 6°C/min (60°C to 125°C), 10 min; isotherm at 125°C, 10°C/min. (125°C to 210°C). Retention times (minutes): aniline (7.2), *o*-aminoacetophenone (18.0), acetanilide (24.6), *p*-aminoacetophenone (26.8).

Benzanilide photoproducts analysis

Temperature program: 6°C/min (60°C to 125°C), 10 min; isotherm at 125°C, 10°C/min. (125°C to 225°C), isotherm at 225°C. Retention times (minutes): benzoic acid (12.0), *o*-aminobenzophenone (31.6), benzanilide (34.0), *p*-aminobenzophenone (37.2).

Ethyl phenyl carbonate photoproducts analysis

Temperature program: same as for acetanilide. Retention times (minutes): phenol (5.6), ethyl phenyl carbonate (12.4), ethyl salicylate (14.6), ethyl *p*-hydroxybenzoate (25.0).

Results and discussion

Irradiations of acetanilide, benzanilide, and ethyl phenyl carbonate were first performed under conditions previously reported in the literature in order to set up experimental conditions and analysis techniques. The irradiations were then completed using water as the solvent with and without β-cyclodextrin. The results are summarized in eqs. [1]–[3] and compiled in Tables 1–3.

The photolysis of acetanilide in isopropyl alcohol and benzanilide in ethanol gave results identical to those reported by Hageman (8) and by Elad *et al.* (9). In both cases, the *ortho/para* ratio is 1.1. In our hands, photolysis of ethyl

[1]Author to whom correspondence should be addressed.

[2]Revision received December 2, 1982.

Can. J. Chem. Downloaded from www.nrcresearchpress.com by 210.87.254.42 on 09/06/12
For personal use only.

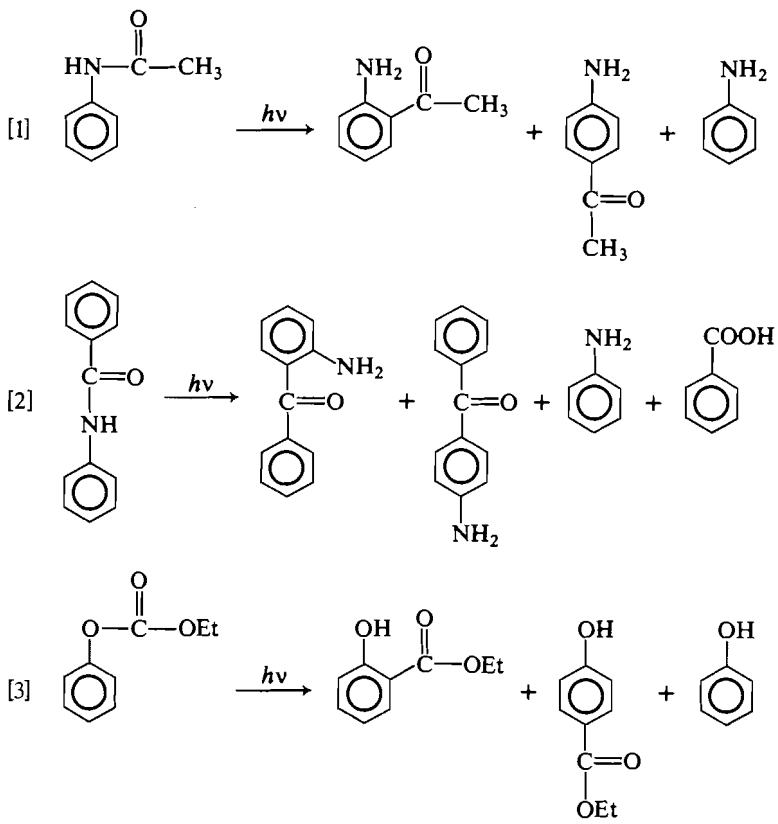

TABLE 1. Photolysis of acetanilide

Irradiation time (h)	Solvent	Yield (%) Aminoacetophenone *ortho*	Aminoacetophenone *para*	Aniline	Conversion of starting material (%)	*ortho*/*para* Ratio
8.0	Isopropanol[a]	35.5	31.6	32.9	10	1.1
8.0	Water	74.3	19.4	6.3	18	3.8
8.0	Water β-cyclodextrin	64.8	34.7	0.5	43	1.9

[a] Reference 8.

TABLE 2. Photolysis of benzanilide

Irradiation time (h)	Solvent	Yield (%) Aminobenzophenone *ortho*	Aminobenzophenone *para*	Benzoic acid	Conversion of starting material (%)	*ortho*/*para* Ratio
50.0	Ethanol[a]	52.6	47.1	0.3	3.7	1.1
24.0	Water	79.8	20.2	—	0.3	4.0
24.0	Water β-cyclodextrin	58.1	41.9	—	2.0	1.4

[a] Contrarily to ref. 9, we found no trace of aniline.

phenyl carbonate in ethanol gave an *ortho*/*para* ratio of 0.45. This value is lower than the value reported by Pac and Tsutsumi (10).

As seen from Tables 1–3, the presence of β-cyclodexetrin had three effects on the photolysis of the title compounds. (1) Conversion is increased by about 2.4-fold for acetanilide, 7-fold for benzanilide, and 1.5-fold for ethyl phenyl carbonate. (2) The migration to *para* position is preferred over the *ortho*-migration. (3) Formation of phenol or aniline is decreased.

These data can be explained by assuming that the substrate penetrates the cyclodextrin cavity and reacts according to the mechanism proposed for the photo-Fries reaction and related rearrangements (Scheme 1).

The primary mechanism involves fragmentation to give free radicals which undergo extensive geminate recombination (11, 12). In this mechanism, the carbon–heteroatom (oxygen or nitrogen) bond is cleaved homolytically giving acyl and phenoxy (or nitrogen equivalent) radicals which are held in close

Can. J. Chem. Downloaded from www.nrcresearchpress.com by 210.87.254.42 on 09/06/12
For personal use only.

TABLE 3. Photolysis of ethyl phenyl carbonate

Irradiation time (h)	Solvent	Yield (%) Ethyl hydroxybenzoate *ortho*	Ethyl hydroxybenzoate *para*	Phenol	Conversion of starting material (%)	*ortho*/*para* Ratio
24.0	Ethanol[a]	21.4	45.0	32.7	98	0.45
24.0	Water	15.0	71.9	13.1	15	0.21
24.0	Water β-cyclodextrin	6.8	90.9	2.3	22	0.078

[a]See also ref. 10.

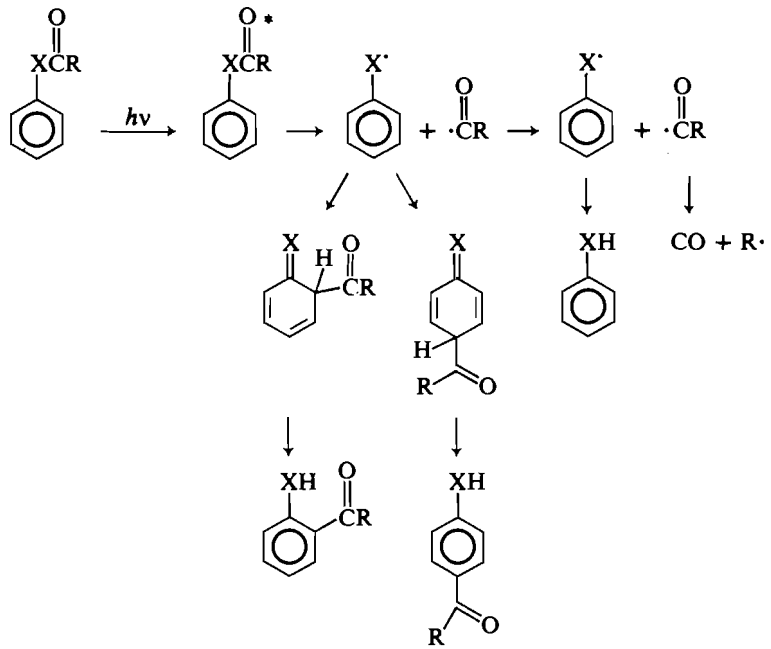

SCHEME 1

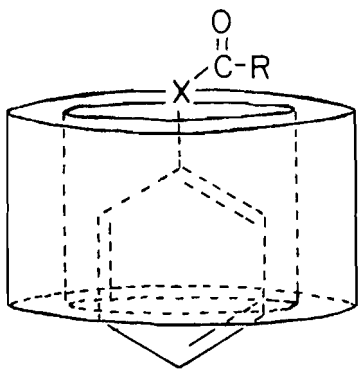

SCHEME 2

proximity to each other by the solvent cage. The lifetime of radical pairs should be very short in this solvent cage. Recombination of the two fragments by reestablishing the carbon–heteroatom bond would result in the regeneration of the starting material. On the other hand, recombination of the acyl radical at either *ortho* or *para* position of the aromatic radical would produce acyl cyclohexadienones (or nitrogen equivalent), tautomers of the final photoproducts. Alternatively, the radicals may escape from the solvent cage and diffuse to give separate products. Phenol (or aniline) is produced when the aromatic radical abstracts hydrogen from the solvent or otherwise.

During the photolysis in the presence of cyclodextrin, a substantial portion of substrate must react while bonded into the cavity of a cyclodextrin, otherwise no change in the aromatic substitution pattern would have been observed. The dissociation constants of cyclodextrin–aromatic complexes all lie close to 10^{-3} mol/L and are characteristic of weak intermolecular interactions (1). There is no correlation between the chemical properties (functional groups) of the guest molecules and dissociation constants. Thus, inclusion does not seem to depend primarily on the character of the substrate (13).

Better rearrangement yields in the presence of cyclodextrin can be explained by an increase in the solubility of the substances which are slightly soluble in water. It is a well-known fact that solubility of the guest component increases linearly with the amount of cyclodextrin added (1).

The change in the migration pattern in favor of the *para* position is the result of the geometric blocking role of the cyclodextrin. An aromatic nucleus bonded into the cavity of a cyclodextrin has its *ortho* and *meta* positions well shielded, while the *para* position is more accessible and might be involved in a reaction (Scheme 2). There is a well-known geometric requirement for binding aromatic compounds into the cavity, in which *para*-disubstituted aromatic compounds are well bound compared to *ortho*-disubstituted compounds (13).

Decrease in the formation of phenol or aniline can also be explained by the complex formation. The phenoxy radical (or

Can. J. Chem. Downloaded from www.nrcresearchpress.com by 210.87.254.42 on 09/06/12
For personal use only.

its nitrogen equivalent) has first to depart from the cyclodextrin cavity before leaving the solvent cage and abstracts hydrogen. This supplementary requirement slows down the process.

We are presently studying the influence of cyclodextrins on regio and stereoselectivity of other organic reactions.

Acknowledgements

This work was supported by research grants from the Natural Sciences and Engineering Research Council of Canada and by the Ministère de l'éducation du Québec.

1. W. SAENGER. Angew. Chem. Int. Ed. Engl. **19**, 344 (1980).
2. M. L. BENDER and M. KOMIYAMA. Cyclodextrin chemistry. Springer Verlag, Berlin. 1978.
3. I. TABUSHI. Acc. Chem. Res. **15**, 66 (1982).
4. R. BRESLOW, H. KOHN, and B. SIEGEL. Tetrahedron Lett. 1645 (1976).
5. M. MITANI, T. TSUCHIDA, and K. KOYAMA. J. Chem. Soc. Chem. Commun. 869 (1974).
6. M. OHARA and J. FUKUDA. Pharmazie, **33**, 467 (1978).
7. M. OHARA and K. WATANABE. Angew. Chem. Int. Ed. Engl. **14**, 820 (1975).
8. H. J. HAGEMAN. Recl. Trav. Chim. Pays-Bas, **91**, 1447 (1972).
9. D. ELAD, D. V. RAO, and V. I. STENBERG. J. Org. Chem. **30**, 3252 (1965).
10. C. PAC and S. TSUTSUMI. Bull. Chem. Soc. Jpn. **37**, 1392 (1964).
11. S. M. BECK and L. E. BRUS. J. Am. Chem. Soc. **104**, 1805 (1982).
12. (*a*) H. KOBSA. J. Org. Chem. **27**, 2293 (1962); (*b*) R. A. FINNIGAN and D. KNUTSON. J. Am. Chem. Soc. **89**, 1970 (1967); (*c*) H. SHIKUZA, T. MORITA, Y. MORI, and I. IANAKA. Bull. Chem. Soc. Jpn. **42**, 1831 (1969); (*d*) J. W. MEYER and G. S. HAMMOND. J. Am. Chem. Soc. **94**, 2219 (1972).
13. (*a*) R. BRESLOW and P. CAMPBELL. Bioorg. Chem. **1**, 140 (1971); (*b*) E. A. LEWIS and L. D. HANSEN. J. Chem. Soc. Perkin Trans. 2, 2081 (1973).

Can. J. Chem. Downloaded from www.nrcresearchpress.com by 210.87.254.42 on 09/06/12
For personal use only.

Tungsten carbonyl complexes of Main Group IV organometallic sulfides

C. Robert Lucas

Department of Chemistry, Memorial University of Newfoundland, St. John's, Nfld., Canada A1B 3X7

Received September 7, 1982

C. Robert Lucas. Can. J. Chem. **61**, 1096 (1983).

Vibrational spectroscopic data from the literature and from seven new compounds is treated by the methods of Cotton and Kraihanzel and of Graham. The results are interpreted as evidence that in $(R_3MSPh)W(CO)_5$ (R = Me, Ph; M = Si, Ge, Sn) there are W → S $d\pi-d\pi$ and S → M $p\pi \rightarrow d\pi$ components to the bonding, the extent of the latter varying in the order Si > Ge > Sn. It is concluded that changes in the carbonyl stretching spectra reflect changes in electron density on sulfur. Thus, the carbonyl spectra are affected both by the electronegativity of groups bound to sulfur and by the extent of S → M π-bonding. The fact that changing M affects spectroscopic properties of a bond three atoms away represents long range transmission of effects via multiple bonds but in a manner quite unlike that in conjugated organic systems.

C. Robert Lucas. Can. J. Chem. **61**, 1096 (1983).

Faisant appel aux méthodes de Cotton et Kraihanzel et de Graham, on traite les données spectroscopiques de vibration répertoriées dans la littérature ainsi que celles relatives à sept nouveaux composés. On interprète les résultats comme une preuve du fait que, dans le composé $(R_3MSPh)W(CO)_5$ (R = Me, Ph; M = Si, Ge, Sn), il y a des composantes de liaison W → S $d\pi-d\pi$ et S → M $p\pi \rightarrow d\pi$ l'importance de la dernière variant dans l'ordre suivant: Si > Ge > Sn. On conclut que les variations des spectres d'élongation du carbonyle réflètent les variations de la densité électronique du soufre. Ainsi l'électronégativité des groupes liés au soufre et le taux de liaison S → M affectent les spectres du carbonyle. Le fait que le remplacement de M affecte les propriétés spectroscopiques d'une liaison entre trois atomes éloignés, représente une transmission à longue distance des effets par l'intermédiaire des liaisons multiples. Ce comportement est complètement à l'opposé de celui des systèmes organiques conjugués.

[Traduit par le journal]

Can. J. Chem. Downloaded from www.nrcresearchpress.com by 210.87.254.5 on 09/06/12
For personal use only.

Introduction

Preparation and bonding studies of Main Group IV organometallic sulfides, R_3MSR' (M = C, Si, Ge, Sn, or Pb), have been undertaken by a variety of laboratories (1–4), as have studies of Group VI carbonyl complexes, $M(CO)_5L$ (M = Cr, Mo, or W), in which L is an organic sulfide (5, 6). Use of the organometallic sulfides as L, however, has been relatively infrequent (7–9). The purpose of this work, therefore, was to prepare a series of compounds $(R_3MSPh)W(CO)_5$ (R = Me, Ph; M = C, Si, Ge, or Sn) in which M is systematically varied in order to observe changes in the complexes as a function of M.

Experimental

All procedures were carried out under a nitrogen atmosphere and anhydrous conditions. Spectroscopic data (Tables 1 and 2) were obtained using the following instruments: ir, Perkin Elmer Model 283; Raman, Coderg laser; nmr, Varian EM-360 or Bruker WP 80 Fourier-transform; mass spectra, VG Micromass 7070 HS. Raman spectra were obtained from saturated hexane solutions of the complexes sealed *in vacuo*. Infrared spectra were obtained from dilute hexane solutions and are reproducible to ± 0.8 cm^{-1} on duplicate runs involving separate preparations of the same compound. Analyses were performed by Canadian Microanalytical Service Ltd. and by Analytical Laboratories, Elbach, West Germany.

(a) Preparation of ligands

Me_3CSPh was obtained in 58% yield by Ipatieff's method (16) involving addition of thiophenol to isobutene dissolved in cold 75% H_2SO_4.

Me_3SiSPh, Me_3GeSPh, and Ph_3CSPh were obtained in 65–85% yield using Abel's procedure (17) involving treatment of R_3MCl with $Pb(SPh)_2$ in refluxing benzene.

Me_3SnSPh, Ph_3GeSPh, and Ph_3SnSPh were prepared in 60–90% yield by Abel and Brady's method (18) of combining R_3MX with PhSH in presence of a base. (R = Me, M = Sn, solvent H_2O, base NaOH; R = Ph, M = Ge, Sn, solvent tetrahydrofuran, base pyridine.)

(b) Preparation of the complexes

Tungsten hexacarbonyl (4.6 g, 13 mmol) was dissolved in tetrahydrofuran (250 mL) in a Pyrex flask fitted with a double surface condenser, a magnetic stirrer, and a gas dispersion inlet tube. The top of the condenser was connected to an oil bubbler and the solution was irradiated with a 100 W uv lamp while stirring and passing a stream of N_2 bubbles. After 4 h, the lamp was switched off, the yellow solution chilled rapidly to 0°C, and ligand (13 mmol) added. The solution was stirred briefly, stored at −20°C in the dark overnight, filtered, and evaporated *in vacuo* at 40°C. The residue was extracted with hexane (3 × 100 mL) and the extracts were combined, concentrated, and placed on an Al_2O_3 column from which they were eluted with hexane. The yellow eluate was evaporated to dryness and the crystals that formed were ground to a fine powder, placed in a sublimer and the $W(CO)_6$ impurity sublimed at 40°C and 0.1 mm Hg. The residue was then recrystallized from hexane.

When the ligand was Me_3SiSPh the crude product was a yellow oil which was purified by distillation in a short path distillation apparatus at 0.01 mm Hg taking care that the heating bath temperature did not exceed 75°C.

$(Me_3CSPh)W(CO)_5$ mp 82°C (decomp.), yield 31%. *Anal.* calcd. for $C_{15}H_{14}O_5SW$: C 36.75, H 2.88, S 6.54, W 37.50; found: C 37.12, H 3.20, S 7.02, W 37.20.

$(Me_3SiSPh)W(CO)_5$ yield 18%. Decomposes in a few days at room temperature or rapidly above 75°C.

$(Me_3GeSPh)W(CO)_5$ mp 77°C (decomp.), yield 28%. *Anal.* calcd. for $C_{14}H_{14}GeO_5SW$: C 30.53, H 2.56, S 5.82; found: C 31.30, H 2.75, S 6.40.

$(Me_3SnSPh)W(CO)_5$ mp 81°C (decomp.), yield 43%. *Anal.* calcd. for $C_{14}H_{14}O_5SSnW$: C 28.17, H 2.36, S 5.37; found: C 28.51, H 2.64, S 5.23.

$(Ph_3CSPh)W(CO)_5$ mp 66°C (decomp.), yield 16%. *Anal.* calcd. for $C_{30}H_{20}O_5SW$: C 53.27, H 2.98, S 4.74, W 27.18; found: C 53.63, H 3.42, S 5.01, W 27.07. A second yellow band from the column contains a compound with carbonyl bands in the ir at 2040.3 vw,

TABLE 1. Vibrational data from hexane solutions of $W(CO)_5L$

L in $W(CO)_5L$	ν_{CO} ir (Raman) in cm^{-1}					Force constants (mdyn/Å)			Graham parameters (mdyn/Å)	
	A_1^1	B_1	E		A_1^2	k_1	k_2	k_i	$\Delta\sigma$	$\Delta\pi$
Me_3CSPh	2077.7	1988.0	1948.6	1945.5	1933.1	15.26	15.96	0.33	0	0
	(2080)	(1987)	(1942)		(1932)					
Me_3SiSPh	2078.2	1987.8	1949.6	1945.3	1934.0	15.30	15.96	0.32	−0.04	+0.04
	(2075)	(1981)	(1945)	(1938)	(1927)					
Me_3GeSPh	2075.8	1987.9	1946.5	1942.0	1927.6	15.06	15.96	0.35	+0.20	−0.20
Me_3SnSPh	2074.3	1986.0	1943.9	1938.2	1923.7	14.97	15.93	0.36	+0.23	−0.26
	(2073)	(1981)	(1936)		(1920)					
Ph_3CSPh	2077.4	1988.1	1949.8	1944.5	1932.3	15.24	15.96	0.32	−0.02	+0.02
Ph_3GeSPh	2075.0	1986.6	1947.8	1943.2	1923.6	15.09	15.94	0.33	+0.13	−0.15
	(2073)	(1982)	(1956)	(1943)	(1918)					
Ph_3SnSPh	2074.8	1987.4	1945.2		1923.0	15.03	15.95	0.34	+0.21	−0.22
	(2070)	(1979)	(1951)		(1915)					
HSPh[a]	2080	—	1948		1935.5	15.37	15.96	0.32	−0.11	+0.11
$(Me_3Ge)_2S$[b]	2074	1976	1937	1932	1919	15.16	15.77	0.33	−0.28	+0.09
$(Me_3Sn)_2S$[b]	2070	1975	1935	1928	1915	14.99	15.75	0.34	−0.15	−0.06
$(Me_3Pb)_2S$[b]	2065	1970	1930	1921	1909	14.86	15.67	0.35	−0.18	−0.11
$MeSCH_2Ph$[c]	2075	1983	1941		1934	15.28	15.88	0.33	−0.18	+0.10
C_4H_8S[a]	2075	—	1941.5		1930.5	15.29	15.86	0.32	−0.17	+0.07

[a]Graham parameters calculated from data in ref. 14.
[b]Force constants and Graham parameters calculated from data in ref. 7.
[c]Force constants and Graham parameters calculated from data in ref. 5.

TABLE 2. Methyl-hydrogen ^1H nmr data, δ in ppm from internal TMS

M	Me_3MSPh	$Me_3MSPh \cdot W(CO)_5$
C	1.28[a]	1.28[a]
Si	0.23	0.06
Ge	0.44	0.62
Sn	0.38[b]	0.56[c]

[a]In d^6-acetone. Others in $CDCl_3$.
[b]^2J $^{117}Sn - ^1H$ = 53.8 Hz; ^2J $^{119}Sn - ^1H$ = 56.3 Hz.
[c]^2J $^{117}Sn - ^1H$ = 53.6 Hz; ^2J $^{119}Sn - ^1H$ = 56.0 Hz.

1969.2 w, and 1953.8 w. It may be $(Ph_3CSPh)_2W(CO)_4$ but was not characterized further.

$(Ph_3GeSPh)W(CO)_5$ mp 95°C (decomp.), yield 55%. *Anal.* calcd. for $C_{29}H_{20}GeO_5SW$: C 47.26, H 2.74, S 4.35; found: C 47.17, H 2.98, S 4.13.

$(Ph_3SnSPh)W(CO)_5$ mp 95°C (decomp.), yield 62%. *Anal.* calcd. for $C_{29}H_{20}O_5SSnW$: C 44.48, H 2.57, S 4.09; found: C 44.69, H 2.90, S 3.94.

Mass spectra

Molecular ions were not detected except for $(Me_3GeSPh)W(CO)_5$ which gave a spectrum of the ions $[Me_3GeSPh \cdot W(CO)_5]^+$, $[Me_3GeSPh \cdot W(CO)_3]^+$, $[Me_3GeSPh \cdot W(CO)]^+$, $[Me_3GeSPh \cdot W]^+$, $[Me_3GeSPh]^+$, and various ligand fragments. Spectra of the other complexes consisted of peaks corresponding to $[ligand]^+$, $[R_3M]^+$, $[PhS]^+$, $[W(CO)_n]^+$ (n = 1−4), and ligand fragments.

Results

The new complexes prepared in this work were examined in hydrocarbon solutions in the carbonyl stretching region of their ir and Raman spectra (Table 1). The data obtained were treated according to Cotton and Kraihanzel (10) in order to obtain approximate carbonyl stretching force constants and then by Graham's method (11) to obtain $\Delta\sigma$ and $\Delta\pi$ factors. Results from these treatments are also given in Table 1 and are displayed graphically in Fig. 1. Force constant variation as a function of ligand Lewis basicity is plotted in Fig. 2. Results of a ^1H nmr study of the methyl resonances in $(Me_3MSPh)W(CO)_5$ are in Table 2.

Discussion

The ir and Raman spectra appeared as predicted by theory and as found previously for other molecules of idealized C_{4v} symmetry (10), except for the occurrence of a weak B_1 mode in the ir and splitting of the E mode. These anomalies suggest that the symmetry is actually somewhat lower than C_{4v}, probably because of non-equivalence of the two groups attached to sulfur in the ligand or because of crowding which causes distortion of the $W(CO)_5$-group.

Although the absolute values of the force constants derived from the ir data may be disputed, differences between them for a series of compounds of closely related structure are generally accepted as meaningful (12) and such differences were used here to calculate $\Delta\sigma$ and $\Delta\pi$ factors. As discussed by Graham (11), the possible error in these factors can be taken as ±0.08 for $\Delta\pi$ and ±0.12 for $\Delta\sigma$ although probable errors are considered to be smaller due to the excellent reproducibility of the data and the fact that any systematic errors would be eliminated during calculation of $\Delta\sigma$ and $\Delta\pi$.

For all the complexes in Table 1 and especially for the series of structurally related ones (L = R_3MSPh, HSPh), frequencies of the ν_{CO} bands are relatively constant, indicating that there are no drastic changes in carbonyl bonding throughout the series. This suggests that tungsten−sulfur bonding is similar throughout the series too and one may therefore conclude that varying M causes no qualitative changes in bonding within the S—W—$(CO)_5$ part of the complexes. However, when the data in Table 1 are plotted (Fig. 1) it becomes apparent that there is a definite relationship between the nature of the ligand and bonding in the carbonyls and one may therefore conclude that varying M causes quantitative changes in bonding within the

Can. J. Chem. Downloaded from www.nrcresearchpress.com by 210.87.254.5 on 09/06/12
For personal use only.

Can. J. Chem. Downloaded from www.nrcresearchpress.com by 210.87.254.5 on 09/06/12
For personal use only.

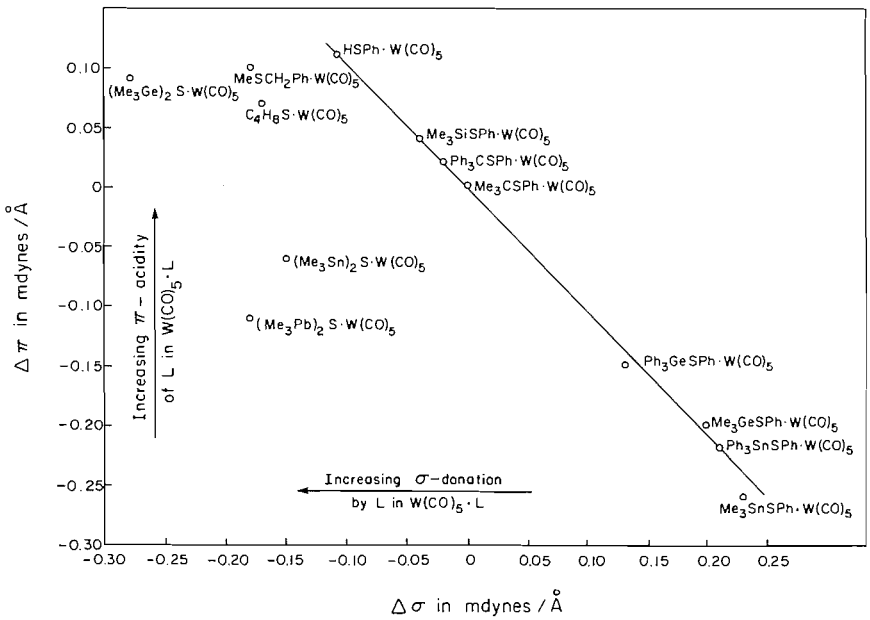

FIG. 1. Graham's $\Delta\sigma$ and $\Delta\pi$ factors.

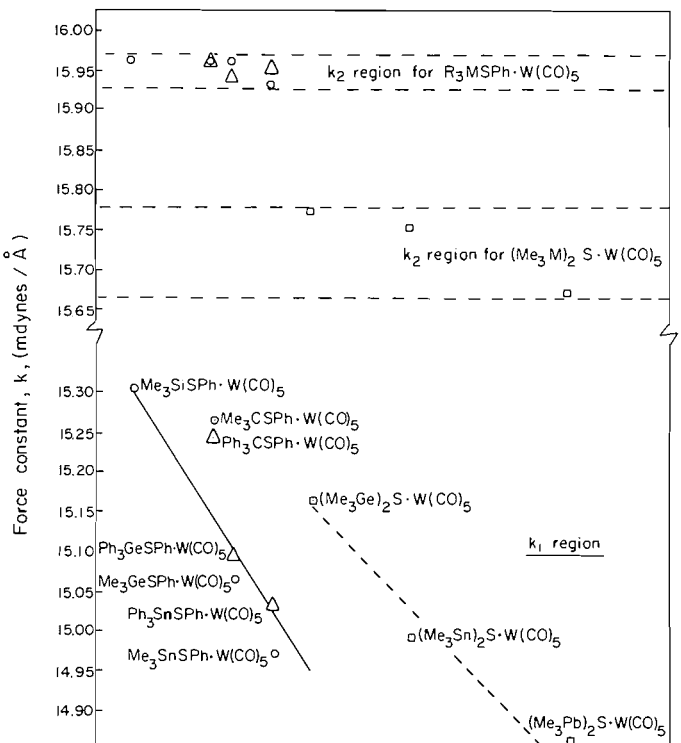

FIG. 2. Effect of ligand basicity on *cis* and *trans* CO bonding.

S—W—$(CO)_5$ part of the complexes.

It is generally accepted that the major route of influence on bonding in carbonyl ligands is the π-bond between the metal and CO (6). The effect of changing M could be transmitted by this route as a result of changes in either σ- or π-bonding (or both) between R_3MSPh and tungsten. The existence of a σ-bond between tungsten and sulfur, involving one of the unshared pairs of electrons on sulfur in the free ligand, is not a matter of dispute but the existence of a tungsten−sulfur π-bond is somewhat more contentious (5, 9). Observations on organic sulfide complexes and the results of this study are most conveniently understood, however, in terms of W → S, $d\pi-d\pi$ bonding of a type broadly similar to that already established for many other ligands (6). A similar question concerning π-bonding between M and sulfur in R_3MSPh has been addressed by several workers (1, 3, 13) and the evidence is again most readily interpretable in terms of multiple bonding involving some degree of S → M, $p\pi \rightarrow d\pi$ interaction. One must therefore acknowledge at least the possibility of a series of π-bonds in the complexes $(R_3MSPh)W(CO)_5$ extending from M to sulfur, from sulfur to tungsten, and from tungsten to the CO ligands. Conjugation, however, in the sense recognized in organic chemistry should not be assumed since different kinds of atomic orbitals are involved.

Notwithstanding the possibility of tungsten−sulfur $d\pi$-bonding, it is worthwhile to question whether the relationship displayed in Fig. 1 can be explained satisfactorily in terms of M—S—W σ-bond or inductive effects alone. Figure 2 is a plot of *cis*- and *trans*-carbonyl force constants in $W(CO)_5L$ as a function of Lewis basicity of L. (Lewis basicity is indicated by the shift, caused by the ligand, in ν(C—D) of $CDCl_3$ (2).[1]) Figure 2 demonstrates that changes in ligand basicity have a definite effect on the *trans*-carbonyl (k_1 region) but very little effect on those in *cis*-positions (k_2 regions). Furthermore, in Table 1 it may be noted that the largest changes in band position upon varying M are experienced by the A_1^2 mode which involves stretching of the *trans*-carbonyl. This effect can also be seen in values of k_1 (the *trans*-carbonyl force constant) which shows variation with M while k_2 (the *cis*-carbonyl force constant) remains relatively unchanged. These observations sug-

[1]Values of $\Delta\nu$ plotted for R_3MSPh are actually those for R_3MSMe because complete data for R_3MSPh are not available. Reference 2 indicates, however, that this practice will not change significantly the slopes of the lines in Fig. 2, although it would be expected to move entire lines left or right on the $\Delta\nu$ axis. Such horizontal movement of an entire line has no effect on arguments presented above since it is the slope, not the position, of a line which is significant in the present context.

Can. J. Chem. Downloaded from www.nrcresearchpress.com by 210.87.254.5 on 09/06/12
For personal use only.

gest that the effects of changing M are transmitted more efficiently to the *trans*- rather than the *cis*-positions. Since a purely inductive effect on tungsten by the ligand should be transmitted equally to both *cis*- and *trans*-positions, it is unlikely that effects of changing M are being transmitted to tungsten through the σ-bond framework alone. On the other hand, if the ligand were interacting with tungsten through a π-bond, the *trans*-carbonyl should be more sensitive than the *cis*-carbonyls to changes in the ligand. This is due to the fact that there are two tungsten *d*-orbitals of appropriate symmetry to interact with the ligand π-system and the π*-system of the *trans*-carbonyl but only one tungsten *d*-orbital to interact with the *cis*-carbonyls. It seems therefore that effects of changing M are transmitted through an S—W—CO π-system, but in a manner unlike that in organic compounds. Accompanying changes must also be occurring in the σ-system due to electronegativity changes in neighbouring groups and synergistic response to the π-system.

Based on this hypothesis, the spectroscopic results and the role of the M—S bond can be understood. Taking $(Me_3CSPh)W(CO)_5$, in which M—S π-bonding is unlikely, as reference ($\Delta\sigma$ and $\Delta\pi = 0$), one could argue that upon substituting carbon by silicon, which is more electron-donating, the electron density on sulfur would be increased. This should raise the energy of the sulfur *d*-orbitals (19) and make them less suitable for overlap with tungsten *d*-orbitals. Thus, if inductive effects alone are considered Me_3SiSPh should be a poorer π-acid and a better σ-donor than Me_3CSPh and $(Me_3SiSPh)W(CO)_5$ should appear lower in Fig. 1 and to the left of $(Me_3CSPh)W(CO)_5$ while in Fig. 2 it should appear lower and to the right. This is not, however, what is observed.

Therefore, there must be some mechanism, such as S → Si $p\pi \rightarrow d\pi$ bonding, which removes electron density from sulfur to an extent that causes contraction of the sulfur *d*-orbitals so that they overlap more, rather than less, effectively with tungsten *d*-orbitals. This would make Me_3SiSPh a better π-acid and synergistically a better σ-donor than Me_3CSPh, as observed.

The position of $(Me_3GeSPh)W(CO)_5$ in Fig. 1 can be understood similarly. Thus, germanium is probably a better σ-donor to sulfur than even silicon (6) but unlike silicon, the efficiency of S → M $p\pi \rightarrow d\pi$ bonding is not adequate to remove the extra electron density on sulfur. The sulfur *d*-orbital energies are therefore raised making the ligand a poorer π-acid and synergistically a poorer σ-donor than either Me_3SiSPh or Me_3CSPh.

The key to understanding the spectroscopic results in Figs. 1 and 2 seems to be the energy of the sulfur *d*-orbitals or, in other words, the π-acidity of the sulfide ligand. This in turn appears to be determined by the extent of both σ-donation to sulfur and $p\pi \rightarrow d\pi$ bonding from sulfur. Thus, changing R in R_3MSPh from Me to Ph or changing R_3M to H (14) should both decrease σ-donation to sulfur, causing movement upward and to the left in both figures, as observed. It should be noted, too, that while changes in R have some effect on the σ and π characteristics of the ligand, larger changes are caused by varying M. Thus, replacing Ph in R_3MSPh by a second R_3Ge or R_3Sn makes the ligands stronger π-acids and better σ-donors, implying that R_3M delocalizes sulfur-3*p* electron density more efficiently than Ph and does so in the order $R_3Ge > R_3Sn$. The positions of the benzylmethyl sulfide and tetrahydrothiophene complexes in Fig. 1 are also consistent with the explanation based on sulfur *d*-orbital energies. In these cases, the energies would be affected mainly by inductive effects since S → C $p\pi \rightarrow d\pi$ bonding is presumably absent.

The nmr results in Table 2 and, in particular, the observation that coordination of Me_3CSPh caused no change in the shift of the methyl resonance whereas coordination caused varying shifts for all other Me_3MSPh, make it tempting to suggest that the shift is dependent on the extent of S → M $p\pi \rightarrow d\pi$ bonding. However, such correlation is only meaningful if the magnetic anisotropic contributions to the shift are known to be constant or, at least, to vary linearly throughout the series. Unfortunately this is not known to be true for these complexes. In fact, since Me_4M (M = Ge, Sn, Pb) are known to have variable anisotropic contributions to the methyl resonance shift (15), it is possible the same applies to Me_3MSPh. Thus, until the anisotropic contribution to the methyl resonance shift in these complexes is understood any correlation between shift and other molecular properties must be viewed as suspect.

Acknowledgements

This work was supported in part by the Natural Sciences Engineering and Research Council of Canada and in part by the Department of Chemistry, Memorial University of Newfoundland. The assistance of Mr. J. Rendell with some of the preparations, of Dr. M. H. Brooker with the Raman spectra, and of Dr. B. Gregory and Miss M. Baggs who collected the mass spectra is gratefully acknowledged.

1. E. W. ABEL and D. A. ARMITAGE. Adv. Organomet. Chem. **5**, 1 (1967).
2. E. W. ABEL, D. A. ARMITAGE, and D. B. BRADY. Trans. Faraday Soc. **62**, 3459 (1966).
3. G. DISTEFANO, A. RICCI, R. DANIELI, A. FOFFANI, G. INNORTA, and S. TORRONI. J. Organomet. Chem. **65**, 205 (1974).
4. C. J. ATTRIDGE. Organomet. Chem. Rev. Sect. A. **5**, 323 (1970).
5. E. W. AINSCOUGH, E. J. BIRCH, and A. M. BRODIE. Inorg. Chim. Acta, **20**, 187 (1976).
6. F. A. COTTON and G. WILKINSON. Advanced inorganic chemistry. 4th ed. Wiley, New York. 1980.
7. H. SCHUMANN, O. STELZER, R. WEIS, R. MOHTACHEMI, and R. FISCHER. Chem. Ber. **106**, 48 (1973).
8. H. SCHUMANN, O. STELZER, and W. GICK. Angew. Chem. Internatl. Edit. **8**, 271 (1969).
9. J. PICKARDT, H. SCHUMANN, C. F. CAMPANA, and L. F. DAHL. J. Organomet. Chem. **216**, 245 (1981).
10. F. A. COTTON and C. S. KRAIHANZEL. J. Am. Chem. Soc. **84**, 4432 (1962).
11. W. A. G. GRAHAM. Inorg. Chem. **7**, 315 (1968).
12. F. A. COTTON. Inorg. Chem. **3**, 702 (1964).
13. D. R. EATON and W. R. MCCLELLAN. Inorg. Chem. **6**, 2134 (1967).
14. R. A. BROWN and G. R. DOBSON. Inorg. Chim. Acta, **6**, 65 (1972).
15. R. S. DRAGO. Physical methods in chemistry. Saunders, Philadelphia. 1977. p. 219.
16. V. N. IPATIEFF, H. PINES, and B. S. FRIEDMAN. J. Am. Chem. Soc. **60**, 2731 (1938).
17. E. W. ABEL. J. Chem. Soc. 4406 (1960).
18. E. W. ABEL and D. B. BRADY. J. Chem. Soc. 1192 (1965).
19. D. P. CRAIG and T. THIRUNAMACHANDRAN. J. Chem. Phys. **43**, 4183 (1965).

The determination of the stoichiometry and stability constant of weak complexes in solution: a restatement of the "straight-line" method

AURELIO BELTRÁN-PORTER AND JOSÉ A. RAMÍREZ

Departamento de Química Inorgánica, Facultad de Ciencias Químicas, Universidad de Valencia, Burjasot (Valencia), Spain

Received August 10, 1982

AURELIO BELTRÁN-PORTER AND JOSÉ A. RAMÍREZ. Can. J. Chem. **61**, 1100 (1983).

Usually, to establish the degree of condensation of a complex species in solution, primarily when it is a weak complex, is more cumbersome than to determine the stoichiometric ratio itself. The present work describes a modification of the Asmus method in order to render it suitable for the determination of the actual stoichiometric coefficients and the stability constant of weak complexes whatever the degree of condensation may be.

AURELIO BELTRÁN-PORTER ET JOSÉ A. RAMÍREZ. Can. J. Chem. **61**, 1100 (1983).

La détermination du degré de condensation des complexes relativement faibles dans dissolution présente souvent plus de difficultés que la détermination de leurs relations stoechimétriques. La modification de la méthode classique d'Asmus qui nous montrons dans ce travail-ci la rend utilisable pour établir les paramètres stoechiométriques réels du complex et, de cette façon, son degré de condensation. Également il est démontré que cette méthode permet de calculer la valeur de la constant de stabilité conditionelle du complex.

Can. J. Chem. Downloaded from www.nrcresearchpress.com by 210.87.254.42 on 09/06/12
For personal use only.

Introduction

The "straight-line method" was proposed by E. Asmus (1) as a suitable procedure for fixing the stoichiometric ratio and stability constant of relatively weak AB_n complexes in solution. It constituted an alternative to other classic methods which lead to uncertain results when the complex is not completely formed at the equivalence point.

Nevertheless, K. S. Klausen and F. J. Langmyhr (2) emphasized that while the applicability of the Asmus method to mononuclear systems seemed obvious, it was not clear whether it could be used for determining the composition of polynuclear A_mB_n complexes. Accordingly, assuming the same approximations introduced by Asmus, they developed a general equation which, in agreement with their discussion, made it possible, in some cases, to distinguish between mono and polynuclear species. In addition, calculation of the stoichiometric ratio and stability constant of the complex was also possible.

The fact that in the experimental part of the Klausen–Langmyhr work there are some contradictory aspects which make the procedure unreliable was recoginized later and an alternative procedure has been proposed (3). This fact not withstanding, it is our opinion that leaving aside the Klausen–Langmyhr speculative considerations, the equation derived by them *must* lead to the correct *m and n* values when it is strictly considered. In practice, we have often found serious difficulties in selecting the most likely degree of condensation of the complex from graphical plots of the equation.

The work reported here tries to avoid these troubles and shows an improved technique for applying the "straight-line" method to weak complexes in solution whatever its degree of condensation may be. The conditional stability constant of the complex and its specific value for the physical property measured can also be evaluated easily.

Theory

Let us assume a general equilibrium

$$[1] \quad \delta A + n\delta B \rightleftharpoons A_\delta B_{\delta n}$$

describing the formation of a weak complex in solution. In this equation δ and $n\delta$ are integral numbers whereas n may also be a fraction.

According to the practical procedure of Asmus and Klausen–Langmhyr, a constant volume v_0 of a standard solution of A (initial concentration a_0) and varying volumes v of a standard solution of B (concentration b_0) are introduced into a series of volumetric flasks of volume V. The samples are prepared in such a way that the reagent B always is in a great excess in relation to A. In this way δ represents the degree of condensation of the complex with respect to the deficient reagent, A. An inert saline solution is added until volume V and the pH are adjusted. Then, the variations of a physical property proportional to the complex concentration (i.e. the validity of the Lambert–Beer law is assumed (4)) are measured.

In these conditions the mass action law can be written as

$$[2] \quad K' = K^{1/\delta} = \frac{[A]\,[B]^n}{[A_\delta B_{\delta n}]^{1/\delta}}$$

The equilibrium concentrations of the reactants are related to the initial concentrations through

$$[3] \quad [A] = a - \delta[A_\delta B_{\delta n}] \qquad \text{and}$$

$$[B] = b - \delta n[A_\delta B_{\delta n}] = b - n(a - [A])$$

where $a = a_0v_0/V$ and $b = b_0v/V$.

If the Lambert–Beer law is obeyed

$$[4] \quad [A_\delta B_{\delta n}] = Y/\epsilon$$

(in which Y = variation of the physical property due to complex formation and ϵ = molar coefficient of proportionality[1]) and assuming, according to Asmus, that for a weak complex $a - [A] \simeq 0$ (or $[A_\delta B_{\delta n}] << b$),

$$[5] \quad [A] = a - \delta[A_\delta B_{\delta n}] = a - \delta\, Y/\epsilon$$

$$[B] \simeq b$$

Thus, the equation [2] is transformed into

$$[6] \quad K' = (a - \delta Y/\epsilon)\, b^n/(Y/\epsilon)^{1/\delta}$$

[1]It can be easily shown that the specific value of the physical property of the complex, ϵ_C, is related to ϵ through $\epsilon_C = \epsilon + \delta n\epsilon_B$

Can. J. Chem. Downloaded from www.nrcresearchpress.com by 210.87.254.42 on 09/06/12
For personal use only.

an expression that can be rearranged, after the substitution of a and b values, to yield

$$[7] \quad \frac{Y^{1/\delta}}{\nu^n} = \frac{a_0 b_0^n v_0}{V^{n+1}} \epsilon^{1/\delta} \frac{1}{K'} - \left(\frac{b_0}{V}\right)^n \cdot \delta \cdot \epsilon^{1/\delta - 1} \cdot \frac{1}{K'} \cdot Y$$

This equation, that easily can be transformed into that of Asmus when $\delta = 1$, will correspond to a straight line only if K' is truly a constant, that is to say when δ and δn values are the actual stoichiometric coefficients of the complex.

In this manner, from the graphical plots of $Y^{1/\delta}/\nu^n$ vs. Y we have the following relations.

(1) The correct δ and n values are those for which a plot of $Y^{1/\delta}/\nu^n$ vs. Y gives a straight line.

(2) For this straight line, (a) the abscissa at the origin (A.O.) provides us the ϵ value:

$$[8] \quad \text{A.O.} = (a_0 v_0/V)(\epsilon/\delta)$$

From this, ϵ_C is immediately calculated. (b) The K' value, and K consistently, can be calculated from:

$$[9] \quad \text{(i) slope} = -(b_0/V)^n \cdot \delta \cdot \epsilon^{1/\delta - 1} (1/K')$$

or

$$[10] \quad \text{(ii) ordinate at the origin} = (a_0 b_0^n v_0/V^{n+1}) \epsilon^{1/\delta} (1/K')$$

On the other hand, ϵ and K' can be simultaneously determined solving the system of eqs. [9] and [10].

In this way, contrary to Klausen and Langmhyr, a single experience is required in order to calculate the entire set of characteristic parameters of the complex. At the same time, eq. [8] enables us to check readily the reliability of our measurements: if only the $A_\delta B_{\delta n}$ complex has been formed in the solution the abscissa at the origin (A.O.) value must coincide with the upper limit value of the variation of the physical property measured.[2] In the same way, the fact that both ϵ and K' can be evaluated by two different means will allow us to estimate the meaning of our results.

Results and discussion

In order to demonstrate that the proposed technique can be used successfully to identify weak complexes in solution, studies were performed on previously well-characterized complexes.

Firstly we have considered it of interest to apply this procedure to the monomeric $[Fe(C_{13}H_{12}N_2)_3]^{2+}$ complex studied in the original work of Asmus. The experimental data used for our calculations are those tabulated in his paper.

When $(\text{absorbance})^{1/\delta}/\nu^n$ is plotted against (absorbance) for several δ and n values, a straight line is obtained only for $\delta = 1$ and $n = 3$. The coordinates at the origin of this straight line are:[3] abscissa $= 1.6 \pm 0.2$; ordinate $= 8.3 \pm 0.2 \times 10^4$. Its slope is equal to $-5.1 \pm 0.2 \times 10^4$. From these values, $\epsilon_C = 4.8 \pm 0.6 \times 10^3$ and $K = 4.6 \pm 0.4 \times 10^{-5}$ are calculated. As we see, our results are in excellent agreement with those reported by Asmus ($K = 4.3 \times 10^{-5}$, $\epsilon_C = 4.68 \times 10^3$).

TABLE 1. Mo(VI) – malic acid system pH = 4.00, excess of ligand

ν mL of ligand standard solution	Rotatory power measured[a]	Rotatory power due to the MH_2[a]	Corrected value
0.10	0.016	0.006	0.010
0.20	0.042	0.013	0.029
0.40	0.085	0.024	0.061
0.60	0.120	0.038	0.082
0.80	0.146	0.050	0.096
1.00	0.167	0.062	0.105
1.20	0.186	0.076	0.110
1.40	0.206	0.090	0.116
1.60	0.222	0.102	0.120
2.00	0.251	0.126	0.125
2.50	0.288	0.158	0.130
3.00	0.323	0.189	0.134
4.00	0.390	0.252	0.138
5.00	0.456	0.315	0.141

[a]All the samples are levorotatory at $\lambda = 436$ nm. Rotatory power values are expressed in degrees, $t = 30 \pm 0.05$°C.

Nevertheless, the main aim of the procedure described here lies in its applicability to polynuclear systems. In order to check this aim, the method has been applied, among others, to the system Mo(VI) – malic acid. When malic acid is in excess (reactant B), Mo(VI) (6), as well as W(VI) (7), gives rise to a dinuclear complex of stoichiometric ratio 1:1 which is stable in acidic medium.

A series of samples containing a constant amount of Na_2MoO_4 ($a = 2.00 \pm 0.01 \times 10^{-3}$ M) and varying concentrations of l(−)-malic acid (ν mL of a $b_0 = 1.2240 \pm 0.0001$ M solution) was prepared by dilution of the appropriate amounts of the standard solutions until $V = 25$ mL. All the solutions were made 1 M in $NaClO_4$ and their pH was adjusted to 4.00. The measured values of the rotatory power ($\lambda = 436$ nm, $t = 30 \pm 0.05$°C) of the solutions are summarized in Table 1.

In the Fig. 1 we show the plots of $(\text{rotatory power})^{1/\delta}/\nu^n$ vs. (rotatory power) as a function of δ and n values. The dimeric character of the complex ($\delta = 2$) and its stoichiometric ratio 1:1 ($n = 1$) are clearly inferred from it. The calculated values of the conditional stability constant, $K = 1.3 \pm 0.2 \times 10^{-6}$ (pH = 4.00), and specific molar rotation, $-(\delta)_{436}^{30°} = 1.5 \pm 0.2 \times 10^2$ agree (within experimental limits of error) with other values previously reported (8). On the other hand, the abscissa at the origin, A.O. $= 0.15 \pm 0.02$, is closer to the limiting value of the rotatory power.

Klausen–Langmhyr's equation could be applied in other ways, using the data in Table 1. It has the form

$$[11] \quad \frac{1}{\nu^n} = \frac{a_0^m v_0^m b_0^n}{V^{n+m} K} X_m - \frac{m^2}{K} \left(\frac{a_0 v_0}{V}\right)^{m-1} \left(\frac{b_0}{V}\right)^n$$

in which

$$[12] \quad X_m = \frac{1}{Y} + \left(\frac{m}{2}\right)\left(\frac{m}{a\epsilon}\right)^2 Y - \left(\frac{m}{3}\right)\left(\frac{m}{a\epsilon}\right)^3 Y^2 + \ldots + (-1)^m \left(\frac{m}{a\epsilon}\right)^m Y^{m-1}$$

m and n being the stoichiometric coefficients of the $A_m B_n$ complex. According to their considerations, the form and position of the curves obtained from eq. [11] varying m and n values are

[2]Occasionally, this limit value may be unaccessible in practice due to experimental hindrance (such as precipitation or a new complex formation, etc.). Equation [7] has the advantage that, unlike the Klausen–Langmhyr equation, previous knowledge of this value is not necessary.

[3]The line has been fitted according to the general method described by Lark *et al.* (5) and the confidence limits calculated at a 95% significance level.

Can. J. Chem. Downloaded from www.nrcresearchpress.com by 210.87.254.42 on 09/06/12
For personal use only.

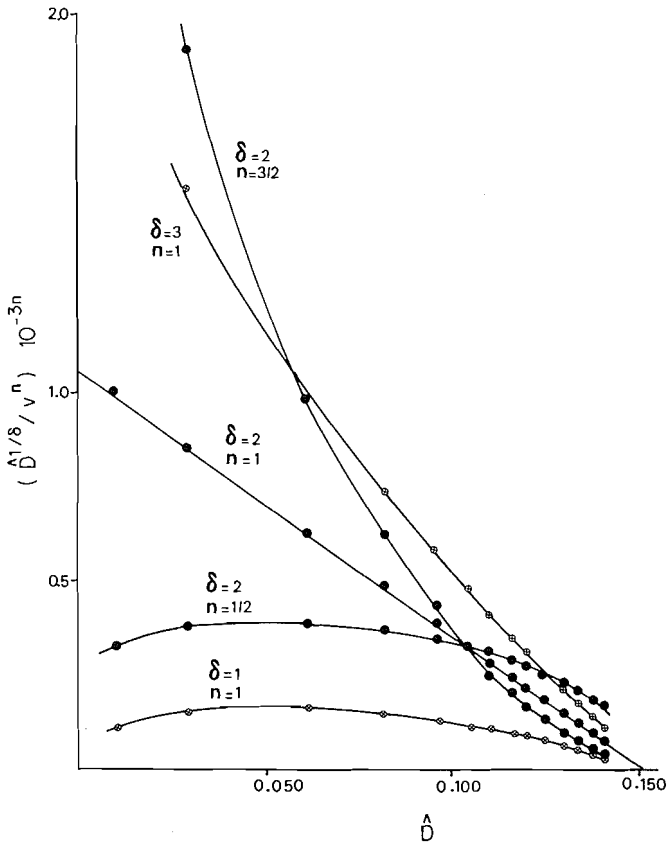

FIG. 1. Modified "straight-line" method for $[Mo_2O_5(C_4H_4O_5)_2(OH)_2]^{4-}$. $\hat{D}$ = rotatory power (Degrees). Curves have been plotted for some selected values of δ and n.

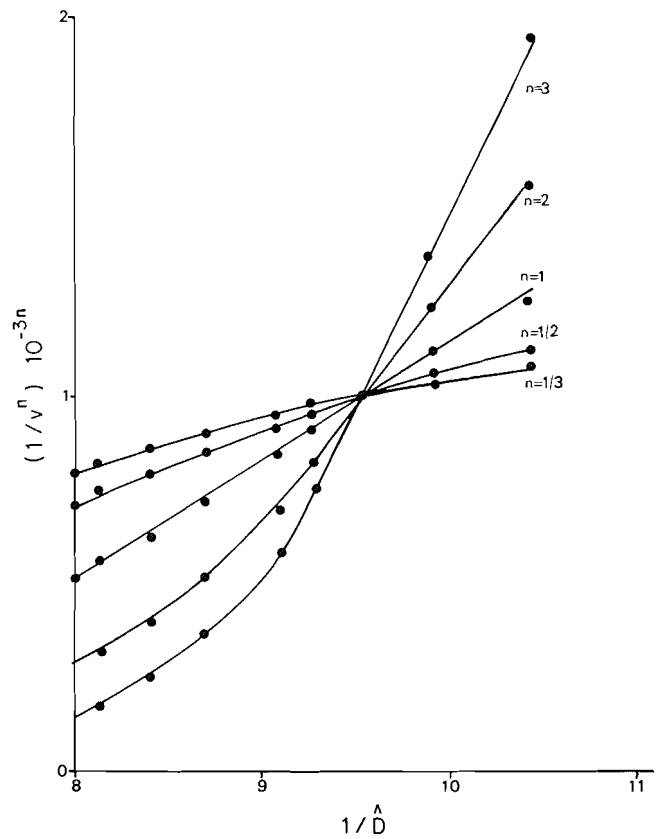

FIG. 2. Asmus "straight-line" method for $[Mo_2O_5(C_4H_4O_5)_2(OH_2)]^{4-}$.

determined mainly by the values of n. A straight line would be produced by the correct value of n irrespective of the value of m. Thus, the determination of m would require working with an excess of the reagent A.

However, it can be experimentally checked that this is not so. In agreement with our results, eq. [11] only leads to a straight line (through the entire interval of v considered) when $n = m = 2$, as expected if the approximations introduced hold. In spite of that, if we make $m = 1$, i.e. if we use an equation identical to that proposed by Asmus, the curves in Fig. 2 result. From these, it seems clear that a stoichiometry $m = n = 1$ might be erroneously deduced. This fact is an example of the statement made above: whereas the stoichiometric ratio of the complex can be inferred accurately from eq. [11], it does not seem equally obvious to distinguish its degree of condensation by visual examination of the graphs.

Conclusion

The modification of the straight-line method proposed here can be advantageously used in order to determine unambiguously the actual stoichiometric coefficients and the conditional stability constant of weak complexes in solution irrespective of their mono or polynuclear character.

A single experiment is required. When only one complex is formed, this experiment might be performed regardless of which reagent is in excess. If the composition of the prevailing species depends on the relation between concentrations of the reactants, this procedure could allow us to establish the stoichiometry of both species.

As it has been shown in Fig. 1, plotting *simultaneously* the curves[4] resulting from eq. [7] for different degrees of condensation (δ values) and stoichiometric ratios (n values), the possibility of getting an erroneous result is greatly lessened.

Experimental

The rotatory power of the samples has been measured with a Perkin–Elmer 141 digital reading photoelectric polarimeter. The precision of the measurements is ± 0.002 degrees.

The cell is thermostatically set at 30 ± 0.05°C and has a length of 10 ± 0.002 cm. The measurements can be taken at five different wavelengths (589, 578, 564, 436, and 365 nm). The results obtained for each one of these are comparable in all cases.

1. E. ASMUS. Z. Anal. Chem., **178**, 104 (1960).
2. K. S. KLAUSEN and F. J. LANGMYHR. Anal. Chim. Acta, **28**, 501 (1963).
3. A. HOLME and F. J. LANGMYHR. Anal. Chim. Acta, **36**, 383 (1966); see also J. A. THOMSON and G. F. ATKINSON. Anal Chim. Acta, **47**, 380 (1969).
4. K. KEITH and M. M. JONES. J. Phys. Chem. **62**, 1005 (1958).
5. P. D. LARK, B. R. CRAVEN, and R. C. L. BOSWORTH. The handling of chemical data. Pergamon Press, London. 1968. p. 142.
6. A. BELTRÁN, A. CERVILLA, and J. BELTRÁN. J. Inorg. Nucl. Chem. **43**, 1337 (1981).
7. A. CERVILLA, A. BELTRÁN, and J. BELTRÁN. Can. J. Chem. **57**, 773 (1979).
8. A. BELTRÁN. Doctoral Thesis, University of Valencia (Spain), 1979.

[4]The theoretical shapes of the curves obtained for wrong δ or n values may be predicted by working out the two first derivatives of eq. [7]. Although the procedure becomes tedious, it provides us a direct way to check the validity of our findings. Curves in Fig. 1 are as predicted.

Photolysis of polychlorinated benzenes in cyclohexane solution

NIGEL J. BUNCE,[1] PATRICK J. HAYES, AND MARY E. LEMKE
Department of Chemistry, University of Guelph, Guelph, Ont., Canada N1G 2W1

Received October 15, 1982

NIGEL J. BUNCE, PATRICK J. HAYES, and MARY E. LEMKE. Can. J. Chem. **61**, 1103 (1983).

Quantum yields of dechlorination and of intersystem crossing have been measured in cyclohexane for a series of chlorinated benzenes. The results are compatible with the reactions occurring predominantly from the triplet excited state. The quantum yield of reaction shows a concentration dependence on [ArCl], but the dependence is less for the more heavily chlorinated members of the series.

NIGEL J. BUNCE, PATRICK J. HAYES et MARY E. LEMKE. Can. J. Chem. **61**, 1103 (1983).

On a mesuré dans le cyclohexane, les moments quantiques de déchloration et de croisement intersystème de divers benzènes chlorés. Les résultats sont compatibles avec les réactions qui ont lieu de façon prédominante à partir de l'état excité triplet. Le rendement quantique de la réaction montre une influence de [ArCl] sur la concentration, mais l'influence est moindre dans le cas des composés de la série la plus fortement chlorée.

[Traduit par le journal]

Can. J. Chem. Downloaded from www.nrcresearchpress.com by 210.87.254.42 on 09/06/12
For personal use only.

We recently reported a study of the photodehalogenation of chlorobenzene in cyclohexane solution (1). For this compound the identity of the reactive excited state is difficult to determine. Energetic considerations would seem to suggest that the triplet state is not reactive, unless it is postulated that the vibrational energy content of the molecule becomes available for bond cleavage. Conventional sensitization studies are ruled out for this system because of the lack of suitably high energy sensitizers. Quenching experiments were not completely conclusive; simple alkenes failed to quench the reaction as would have been expected for a triplet state process (cf. ref. 2). However, xenon did accelerate decomposition slightly (cf. ref. 3), and the effect of oxygen was greater for reaction quenching than for fluorescence quenching. On balance, therefore, it was concluded that the triplet is the predominant reactive state for chlorobenzene.

The uncertainties in the above arguments prompted us to extend our studies to other members of the chlorobenzene family. The strategy was to obtain quantum yields of both dechlorination (ϕ_r) and intersystem crossing, in the hope that a photon balance would allow us to draw conclusions about the identity of the reactive excited state. The problem was complicated somewhat by the fact that we had previously found (1, 4) that ϕ_r for chlorobenzene is concentration dependent, with the photoefficiency greater at lower concentrations. This effect was ascribed to the intervention of an unreactive excimer of chlorobenzene.

Photodechlorination of chlorobenzene derivatives has received considerable attention because of the importance of a number of these compounds as environmental pollutants (5). The present work is mainly oriented mechanistically rather than environmentally, and the photolyses have been carried out at 254 nm.

Experimental

Chlorinated benzenes were reagent grade materials; their purities were checked by glc, and they were purified where necessary. Biacetyl was freshly distilled before use and was kept in the dark. Spectral grade cyclohexane was used throughout as the solvent.

The intersystem crossing quantum yields were determined as described previously (1) with solutions that were degassed in the dark at pressures $\leq 10^{-3}$ Torr using the freeze–pump–thaw method. Solutions for dechlorination were similarly degassed at 10^{-2} Torr. The concentration dependence of ϕ_r was determined as follows. Solutions in which all the light was absorbed were prepared at different concentrations in the range 0.01 to 0.06 *M* and their relative quantum yields were determined using the relationship $\phi_r = M_0 \ln (M_0/M)/$(einsteins absorbed), where M_0 is the initial concentration of the chlorobenzene, and *M* its concentration after photolysis (6). Then $\phi_r/\phi'_r = (M_0 \ln (M_0/M))/(M'_0 \ln (M'_0/M'))$ when several solutions are irradiated simultaneously using a "merry-go-round". To convert these relative values to an absolute scale, ϕ_r was determined by azoxybenzene actinometry at [ArCl] = 0.02 *M*. The azoxybenzene actinometer has $\phi = 0.017$ at 254 nm.[2] The methodology for correcting for the light that was not absorbed by ArCl was decribed previously for chlorobiphenyls (7).

The results of these studies are given in Table 1. Uncertainties on the ϕ_{ISC} data are ±20%, those on the ϕ_r's are ±10%. Experimental information about the analyses is given in Table 2.[3] The expected dechlorination products were formed, but were not analysed quantitatively.

Discussion

The following points emerge from an examination of Table 1.

1. Among isomers, higher quantum yields of reaction are seen when *ortho* chlorines are present. Probably this is a steric effect (cf. refs. 1 and 7). Quite wide variations are observed when different values of ϕ_r are available for comparison. Not only solvent changes, but also differences in the concentrations of the solutions photolysed probably explain most of these differences, especially in those cases, such as *p*-dichlorobenzene and 1,3,5-trichlorobenzene, where the concentration dependence of ϕ_r is particularly strong.

2. If the assumption is made that the whole series behaves similarly mechanistically, the results are incompatible with exclusively singlet reactivity. Thus, the triplet has to be involved in the case of 1,2,3-trichlorobenzene ($\phi_{ISC} = 0.7$

[1]Author to whom correspondence may be addressed.

[2]N. J. Bunce, J. LaMarre, and S. P. Vaish, unpublished observations.

[3]Table 2 is available at a nominal charge, from the Depository of Unpublished Data, CISTI, National Research Council of Canada, Ottawa, Ont., Canada K1A 0S2.

TABLE 1. Photochemical data for chlorinated benzenes in cyclohexane solution

Substituents	ϕ_{ISC}[a]	ϕ_r[b]	Concentration dependence[c] Slope, M^{-1}	Intercept	Intercept^{-1}	ϕ_r, Previous data (ref. no.)
Cl	0.6±0.1[d]	0.25[e]	36±4[f]	3.3[f]	0.31[f]	0.38(C_6H_{12}) (8), 0.13(MeOH) (9)
o-Cl_2	0.4±0.1	0.72	7±2	1.3	0.78	0.24(hexane) (10), 0.81(MeOH) (9), 0.64(ether) (9)
m-Cl_2	0.8±0.2	0.39	37±4	2.1	0.49	0.04(hexane) (10), 0.34(MeOH) (9), 0.22(ether) (9)
p-Cl_2	0.8±0.2	0.17	360±14	2.2	0.45	0.004(hexane) (10), 0.04(MeOH) (9)
1,2,3-Cl_3	0.7±0.3	1.0		Not determined		0.69(MeOH) (9), note *g*
1,2,4-Cl_3	0.8±0.2	0.63	16±5	1.4	0.70	0.59(MeOH) (9), 0.46(aerated isoPrOH) (11), note *g*
1,3,5-Cl_3	0.8±0.1	0.14	120±10	6.2	0.16	Note *g*
1,2,4,5-Cl_4	1.0±0.1	0.43	17±9	2.2	0.46	0.18(MeOH) (9)
Cl_5	0.9±0.1	0.67	−2±2	1.5	0.67	
Cl_6	0.5±0.1	0.21	24±64	4.7	0.21	0.62(MeOH) (9)

[a]Determined at concentrations ca. 10^{-4} *M*.
[b]Determined at concentrations ca. 10^{-2} *M*.
[c]Plotted as ϕ_r^{-1} vs. [ArCl]. Intercept^{-1} is the limiting ϕ_r.
[d]Previous value 0.64, ref. 1.
[e]Previous value 0.42, ref. 1. The difference is in the actinometry. In this work the azoxybenzene actinometer was used; this was easier than the previously used potassium ferrioxalate, because of the very high concentrations of ferrioxalate that were used previously.
[f]Recalculated from the data of ref. 1, using the new value for ϕ_r at 10^{-2} *M*.
[g]According to ref. 12, ϕ_r are in the order 1,2,4- > 1,2,3- ~ 1,3,5-Cl_3.

± 0.3, ϕ_r = 1.0) and in the case of 1,2,4,5-tetrachlorobenzene (ϕ_{ISC} = 1.0 ± 0.1). The only case where singlet reactivity would seem to be implicated definitely is that of *ortho*-dichlorobenzene (ϕ_{ISC} = 0.4 ± 0.1, $\phi_r \rightarrow$ 0.78). *o*-Dichlorobenzene is one of the two cases, together with hexachlorobenzene, where ϕ_{ISC} is unusually low; both values were rechecked, with the same result. However, the biacetyl quenching method is not easy to carry out; we found that many ampoules had to be discarded because they did not give the expected phosphorescence spectrum, either inexplicably, or because of the presence of traces of oxygen. Fortunately, this latter situation causes very clear-cut changes in the spectrum (a tailing at short wavelength). Thus the most economical explanation of the results is that most of the members of the series react predominantly from the triplet state.

Duality of mechanism, i.e. singlet and triplet reactivity, in the photodechlorination of aryl halides has been proposed previously. In the case of chlorobenzene, Augustyniak (13) has studied the direct and acetone sensitized photolyses. Despite an initial uncertainty as to what state was being sensitized by acetone, the current view is that triplet acetone acts as a triplet sensitizer although the rate constant is well below that for diffusion. Thus dechlorination can occur from the triplet state, in agreement with the present interpretation. Soumillion and De Wolf (14) likewise conclude that the dechlorination of chlorobenzene in methanol involves both states. They studied the competition between dechlorination and nucleophilic replacement of chlorine by CN^-, and found that acetone sensitization caused relatively more nucleophilic substitution. Consequently, both S_1 and T_1 must dechlorinate.

Both mechanisms also operate in the photodechlorination of 1,2,4-trichlorobenzene in methanol (11, 12). The direct and acetone-sensitized reactions give different proportions of *m*- and *p*-dichlorobenzene. The *m*-isomer arises predominantly from the triplet and most of the *p*-isomer comes from singlet excited trichlorobenzene.

3. The concentration dependence of ϕ_r drops off as the number of chlorine substituents increases, and is essentially lost for tetra-, penta-, and hexachlorobenzenes. Previously, we have explained this concentration dependence in terms of an unreactive excimer (4). The present results, if interpreted in the same way, suggest that excimer formation becomes less important with increasing chlorination. We cannot tell whether this is because of decreased excimer stability or perhaps because of an increased rate of intersystem crossing in more highly chlorinated benzenes. Among isomers, the concentration dependence is greater in the order *p* > *m* > *o* for dichlorobenzenes, and 1,3,5 > 1,2,4 for trichlorobenzenes. Perhaps this points to a steric factor affecting excimer stability, but we have no further information on this point.

Acknowledgements

We thank the Natural Sciences and Engineering Research Council for financial support.

1. N. J. BUNCE, J. P. BERGSMA, M. D. BERGSMA, W. DEGRAAF, Y. KUMAR, and L. RAVANAL. J. Org. Chem. **45**, 3708 (1980).
2. F. A. CARROLL and F. H. QUINA. J. Am. Chem. Soc. **98**, 1 (1976).
3. H. MORRISON and A. MILLER. Tetrahedron, **37**, 3405 (1981).
4. N. J. BUNCE and L. RAVANAL. J. Am. Chem. Soc. **99**, 4150 (1977).
5. J. R. PLIMMER and U. I. KLINGEBIEL. J. Agric. Food Chem. **24**, 721 (1976).
6. N. J. BUNCE. J. Photochem. **15**, 1 (1981).
7. N. J. BUNCE, C. T. DESCHUTTER, and E. J. TOONE. J. Chem. Soc. Perkin Trans. 2. In press.
8. M.-A. FOX, W. C. NICHOLS, and D. M. LEMAL. J. Am. Chem. Soc. **95**, 8164 (1973).
9. E. LATOWSKA and T. LATOWSKI. Rocz. Chem. **40**, 1977 (1966); A. BASINSKI and E. LATOWSKA. Rocz. Chem. **40**, 1747 (1966).
10. H. PARLAR and F. KORTE. Chemosphere, **8**, 797 (1979).
11. B. AKERMARK, P. BAECKSTRÖM, V. E. WESTLIN, R. GÖTHE, and C. A. WACHTMEISTER. Acta Chem. Scand. Ser. B, **30**, 49 (1976).
12. G. G. CHOUDHRY, A. A. M. ROOF, and O. HUTZINGER. Tetrahedron Lett. 2059 (1979).
13. W. AUGUSTYNIAK. Polish J. Chem. **52**, 841 (1978); W. AUGUSTYNIAK. Ser. Chem. (Univ. im Adama Mickiewicza, Posnan), 1980, **39**, 72 pp., through Chem. Abstr. **96**, 103465s (1982).
14. J. P. SOUMILLION and B. DE WOLF. J. Chem. Soc. Chem. Commun. 436 (1981).

Can. J. Chem. Downloaded from www.nrcresearchpress.com by 210.87.254.42 on 09/06/12
For personal use only.

Réactions des diazaphospholes et d'un diazaarsole avec les ylures de nitrile

Y. Y. C. Yeung Lam Ko et Robert Carrié[1]

Groupe de Physicochimie Structurale, E.R.A. no 389, Université de Rennes, 35042 Rennes Cedex, France

ET

Francesco De Sarlo et Alberto Brandi

Centro di studio sulla chimica e la struttura dei composti eterociclici e loro applicazioni, C.N.R., Istituto di Chimica organica, Universita de Firenze, 50121 Firenze, Italie

Reçu le 7 juillet 1982

Y. Y. C. Yeung Lam Ko, Robert Carrié, Francesco De Sarlo et Alberto Brandi. Can. J. Chem. **61**,1105 (1983).

Les ylures de nitriles **2** résultant de l'ouverture photochimique des azirines **1** s'additionnent aux diazaphospholes **3** et au diazaarsole **4** pour donner les adduits **6** et **7**. Le site d'addition et son orientation sont établis à l'aide de la rmn ^{1}H, ^{31}P et ^{13}C. La stéréochimie des adduits est discutée. Le triazole **5** ne réagit pas avec les ylures de nitrile **2**.

Y. Y. C. Yeung Lam Ko, Robert Carrié, Francesco De Sarlo, and Alberto Brandi. Can. J. Chem. **61**,1105 (1983).

Nitrile ylides **2** obtained by the photochemical ring-opening of azirines **1** react with diazaphospholes **3** and diazaarsole **4** yielding adducts **6** and **7**. The regiospecificity of the addition is established by nmr spectroscopy (^{1}H, ^{31}P, and ^{13}C). The stereochemistry of the adducts is discussed. The triazole **5** does not react with nitrile ylides **2**.

La chimie des composés du phosphore dicoordiné fait l'objet d'un intérêt croissant (1–3). Cependant la réaction des dipôles-1,3 avec la double liaison C=P a donné lieu à très peu de travaux. Deux études relativement ponctuelles ont été consacrées à l'addition de diazocomposés (4, 5) et récemment la cycloaddition de nitriles imines a été signalée (6). Par ailleurs, la réactivité de nitrones vis à vis de composés dicoordinés de l'arsenic a été aussi décrite (7).

Dans deux publications récentes nous avons étudié le comportement comparé des doubles liaisons N=C, P=C et As=C vis à vis des oxydes de nitriles (8, 9). L'objet du présent mémoire est de préciser la réactivité de diazaphospholes, d'un diazaarsole et du triazole correspondant avec les ylures de nitrile résultant de la photolyse d'azirine.

Resultats

Il est connu que l'ouverture photochimique des azirines **1** conduit d'une manière irréversible aux ylures de nitrile **2** qui ont été engagés dans de nombreuses cycloadditions (10).

Ces ylures de nitrile **2** s'additionnent sur la double liaison C=P et C=As des diazaphospholes **3** et du diazaarsole **4**. Les cycloadduits primaires **6** et **7** (schéma 1) sont isolés. Le triazole **5** ne réagit pas.

Les cycloadduits sont obtenus après irradiation d'une solu-

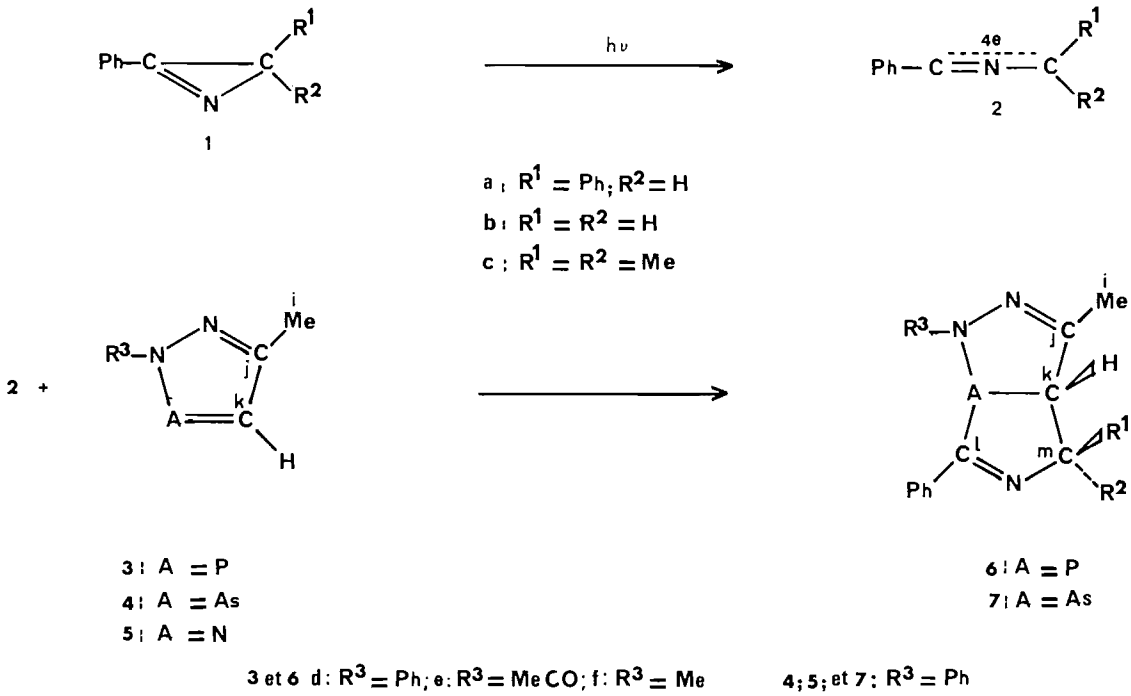

Schéma 1

[1]Auteur à qui adresser la correspondance.

Can. J. Chem. Downloaded from www.nrcresearchpress.com by 210.87.254.6 on 09/06/12
For personal use only.

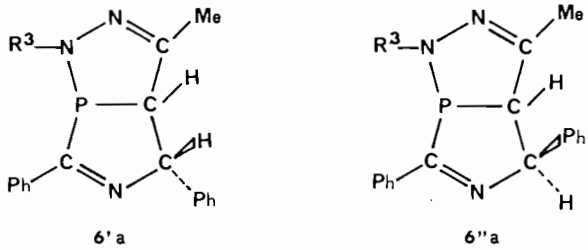

SCHÉMA 2

tion benzénique du composé **3** ou **4** et d'une azirine **1** dans un récipient en quartz (lampe Hanau HQ 80 ou Philips HPK 125 W). La chaleur dégagée par la lampe maintient la solution à l'ébullition. L'ylure de nitrile **2***a* dérivé de la phénylazirine **1***a* ($R^1 \neq R^2$) conduit avec les diazaphospholes **3** aux deux diastéréoisomères **6′***a* et **6″***a* (schéma 2) qui ont été complètement ou partiellement séparés.

Les points importants suivants doivent être soulignés.

(a) L'irradiation prolongée des composés **3***d*, **3***f* et **4** n'entraîne pas une dégradation sensible des dipolarophiles dans le benzène bouillant. Le composé **3***e* est plus sensible, il est complètement transformé après 18 h d'irradiation dans les mêmes conditions; cet inconvénient se trouve partiellement compensé par la réactivité plus grande de **3***e* (comparée à celle des autres dipolarophiles) vis à vis des ylures de nitrile.

(b) Les azirines donnent divers produits d'évolution lorsqu'elles sont irradiées (10*d*, 11). La formation de ces composés est d'autant plus importante que le dipolarophile est moins réactif et dépend de la nature de l'azirine (**1***b* est particulièrement sensible).

(c) Les adduits se dégradent d'une manière sensible sous l'influence du rayonnement ultra-violet. Ils ne sont pas thermiquement très stables et évoluent lentement à la température ambiante d'autant plus vite qu'ils sont moins purs.

Pour ces raisons, lors des réactions de cycloadditions, la proportion relative de l'azirine et du dipolarophile d'une part, la durée de la réaction d'autre part sont modulées en fonction de la stabilité des réactifs, de celle des produits formés et des difficultés rencontrées pour séparer l'adduit du mélange réactionnel. Les conditions opératoires et les résultats obtenus sont précisés dans la partie expérimentale. Les rendements sont en général faibles et la purification des adduits particulièrement difficile dans la plupart des cas.

Spectres de résonance magnétique nucléaire et structure des produits obtenus

Les principales caractéristiques de rmn ^1H et ^{31}P d'une part, ^{13}C d'autre part, figurent respectivement dans les tableaux 1 et 2. Les atomes d'hydrogène et de carbone sont référenciés comme il est indiqué dans le schéma 1.

(a) L'addition s'est effectuée sur la double liaision C=P ou C=As et non sur C=N. En effet, le phosphore des adduits **6** est considérablement blindé (δ ^{31}P 225 à 231, 4 pour les composés **3**), et la même observation est faite en ce qui concerne H_k et C_k (**3** et **4**: δ_{H_k} = 7,25 à 8,62, δ_{C_k} = 135,5 à 154,5). Les déplacements chimiques de H_i et C_j varient peu après la cycloaddition.

(b) Les observations suivantes permettent d'établir la structure des composés **6** et d'éliminer le sens inverse d'addition qui conduirait aux composés **8** (schéma 3). Le couplage entre $R^1 = R^2 = H$ et le phosphore (J = 2 à 7 Hz) est incompatible avec la structure **8**, le couplage $^2J_{PH_k}$ étant de l'ordre de 33 à 35 Hz; et le couplage entre le phosphore et le carbone 1 (J = 51 à 57 Hz) est en accord avec $^1J_{PC}$ et non avec $^2J_{PC}$. Nous avons trouvé des constantes du même ordre de grandeur lors de l'étude des composés **9** résultant de l'addition d'oxydes de nitrile à des diazaphospholes ($^1J_{PC_1}$ = 53 à 63 Hz) (8, 9).

La structure des composés **7** est attribuée par analogie avec les dérivés phosphorés **6** (déplacements chimiques, rmn ^1H et ^{13}C).

(c) La rmn donne également des renseignements intéressants quant à la stéréochimie des cycloadduits: la valeur élevée de $^2J_{PH_k}$ (32 à 36 Hz) indique que H_k est en *cis* de la paire libre du phosphore ($^2J_{PH_k}$ des composés **9** est nettement plus élevé: 44,2 à 50,0 Hz) (12). De plus il est possible de discuter la stéréochimie (schéma 4) des adduits phosphorés diastéréoisomères **6′***a* et **6″***a* obtenus à partir de l'azirine **1***a*.

Le méthyle i des composés **6′***a* est très blindé comparativement à ceux de **6″***a* (différence de déplacement chimique supérieure à 1 ppm); il est dans le cône de blindage du phényle substituant le carbone m. De ce fait, les hydrogènes k et m de **6′***a* sont en *cis* ($^3J_{H_kH_m}$ = 5 à 6,1 Hz). Ces deux hydrogènes sont en *trans* en ce qui concerne **6″***a*, la constante $^3J_{H_kH_m}$ est alors pratiquement nulle. La géométrie proposée est donc qualitativement en accord avec la relation de Karplus. On retrouve des résultats comparables avec les composés **6***b* ($R^1 = R^2 = H$) pour lesquels l'un des hydrogènes lié au carbone m est en *cis* de H_k et l'autre nécessairement en *trans*.

Un point intéressant doit être souligné. Lorsque H_m est en *trans* de la paire libre du phosphore, la constante de couplage $^3J_{PH_m}$ est de l'ordre de 6 à 7 Hz. Elle est nettement plus petite (0 à 2,5 Hz) si H_m est en *cis* de cette paire libre. Comme nous l'avons mentionné précédemment l'inverse est observé avec les constantes $^2J_{PH}$ des composés **6**.

Remarque

La spectrométrie de masse n'apporte pas de renseignements intéressants sur la structure (et donc l'orientation de l'addition du dipôle 1,3). La cycloréversion attendue est observée, l'ion moléculaire de l'azirine étant le pic de base dans la plupart des cas. On note également la fragmentation de l'ion moléculaire avec perte de benzonitrile (confirmée dans certains cas par l'étude de spectres MIKE).

Partie expérimentale

Les points de fusion sont pris au banc Kofler. Les spectromètres de rmn suivants sont utilisés: JEOL MH 100 (^1H, 100 MHz) et Bruker WP 80 DS (^1H: 80 MHz; ^{13}C: 20,115 MHz; ^{31}P: 32,38 MHz). Les spectres de masse sont enregistrés sur l'appareil Varian MAT 311 (géométrie Nier Johnson inversée) du Centre de Mesures Physiques de Rennes:[2] énergie des électrons 70 eV, intensité du faisceau électronique 300 μA, tension d'accélération des ions 3000 V, la température de la source T_s et celle de la sonde d'introduction directe T_i est précisée dans chaque cas, la détermination de la masse des ions moléculaires est effectuée à l'aide de la technique dite par "Peak Matching". Les spectres MIKE sont enregistrés sur le même appareil par balayage du champ électrique. Les analyses élémentaires ont été effectuées par le Service Central de Microanalyse du CNRS.

Préparation des azirines 1

Les azirines **1***a* et **1***b* d'une part, **1***c* d'autre part, sont préparées selon les méthodes décrites respectivement par Hassner et collaborateurs (13) et par Sato (14).

Ces méthodes ont été légèrement améliorées par Perrocheau (15).

[2]Les auteurs remercient P. Guenot pour l'enregistrement des spectres et ses remarques constructives.

Can. J. Chem. Downloaded from www.nrcresearchpress.com by 210.87.254.6 on 09/06/12
For personal use only.

TABLEAU 1. Caractéristiques de rmn ^1H et ^{31}P ($CDCl_3$, δ,[a] J Hz) des composés **6** et **7**

Composés	R^1	R^2	R^3	$(CH_3)_i$ δ	H_k[b] δ	$^2J_{PH}$	$^3J_{H_kR^1}$	R^1 δ	$^3J_{PR^1}$	R^2 δ	$^3J_{PR^2}$	$R^3 \neq Ph$ δ	$^3J_{PR^3}$	^{31}P δ
6′*ad*	H	Ph	Ph	1,20[c]	4,00[c]	32,4	5,5	5,78	1,8	—	—			58,2
6″*ad*	Ph	H	Ph	2,26	3,77	34,2	—	—	—	6,10	6,0			49,6
6′*ae*[d]	H	Ph	MeCO	1,14	4,05	33,6	6,1	5,91	2,4	—	—	2,29	—	55,4
6″*ae*[e]	Ph	H	MeCO	2,28[f]	3,68	35,7	—	—	—	6,12	5,4	2,32[f]	—	46,2
6′*af*	H	Ph	Me	1,14	4,10	32,7	5,1	5,82	[g]	—	—	3,18	9,9	70,0
6″*af*	Ph	H	Me	2,15	3,72	35,4	—	—	—	6,33	5,7	3,18	9,9	59,6
6*bd*	H	H	Ph	2,01	3,63	33,3	5,4	4,27	3,0[h]	4,57	7,2			49,4
6*be*	H	H	MeCO	2,07[f]	3,66	36,0	5,7	4,53	2,8[i]	4,77	6,3	2,28[f]	—	44,5[j]
6*bf*	H	H	Me	1,98	3,66	34,8	3,1	4,44	1,8[k]	4,68	7,2	3,15	10,2	58,8
6*cd*	Me	Me	Ph	2,20[c]	3,67[c]	32,1	—	1,40[f]	—	1,77[f]	—			63,3
746*ce*	Me	Me	MeCO	2,19[f]	3,63	34,2	—	1,42[f]	—	1,74[f]	—	2,28[f]	—	63,5
6*cf*	Me	Me	Me	2,10	3,68	32,4	—	1,38[f]	—	1,71[f]	—	3,12	9,9	76,1
7*b*	H	H	Ph	2,13	3,90	—	5,5	4,51[m]	—	4,93	—			—
7*c*	Me	Me	Ph	2,25	3,87	—	—	1,41[f]	—	1,80[f]	—			—

[a] Références ^1H: TMS; ^{31}P: H_3PO_4 85% les déplacements chimiques des protons aromatiques ne sont pas données.
[b] $^3J_{H_kR^2} \sim 0$ lorsque $R^2 = H$.
[c] $^4J_{HH} = 0,6$.
[d] Caractéristiques déduites du mélange **6′***ae*/**6″***ae* = 85:15.
[e] Caractéristiques déduites du mélange **6′***ae*/**6″***ae* = 30:70.
[f] La distinction entre $\delta(CH_3)_i$ et $\delta\ (CH_3)_{R^3}$ n'est pas possible avec certitude.
[g] Doublet dont chaque branche est élargie.
[h] $^2J_{HH} = 17,0$ ($R^1 = R^2 = H$).
[i] $^2J_{HH} = 17,2$ ($R^1 = R^2 = H$).
[j] Solvant C_6H_6 + 10% + C_6D_6.
[k] $^2J_{HH} = 17,0$ ($R^1 = R^2 = H$).
[l] R^1 ou R^2.
[m] $^2J_{HH} = 17,2$ ($R^1 = R^2 = H$).

TABLEAU 2. Caractéristiques de rmn ^{13}C ($CDCl_3$, δ, J_{PC} Hz) des composés **6** et **7**[a]

Composés	R^1	R^2	R^3	C_i δ	^3J	C_j δ	^2J	C_k δ	^1J	C_l δ	^1J	C_m δ	^2J	C_n δ	^2J	C_o δ	^2J
6′*ad*	H	Ph	Ph	17,5	2	152,2	3	62,7	8	179,2	51	78,8	3	135,2	21	145,5	14
6″*ad*	Ph	H	Ph	15,7	2	153,4	2	64,8	7	178,7	53	82,7	~0	135,0	22	145,6	15
6′*ae*	H	Ph	MeCO	17,7	2	157,5	4	61,0	11	178,4	51	80,1	~0	134,0	22	173,3[b]	12
6″*ae*	Ph	H	MeCO	16,0	2	158,7	3	63,3	10	177,8	53	83,6	~0	133,8	22	173,3[b]	12
6′*af*	H	Ph	Me	17,0	~0	149,3	2	64,3	8	178,8	57	79,8	~0	[c]		39,2	19
6″*af*	Ph	H	Me	15,4	~0	150,7	~0	66,4	7	179,0	57	83,6	~0	136,0	20	39,0	17
6*bd*	H	H	Ph	18,9	~0	153,9	2	55,7	6	177,9	54	65,7	2	135,2	21	145,6	12
6*be*	H	H	MeCO	15,5	~0	159,0	3	54,3	9	177,3	53	66,4	~0	133,9	23	173,4[d]	12
6*bf*	H	H	Me	14,8	~0	151,3	2	57,1	6	178,2	56	66,3	~0	136,2	20	38,8	16
6*cd*	Me	Me	Ph	18,9	~0	151,9	4	68,7	5	174,3	51	79,9	2	135,8	21	146,3[e]	15
6*ce*	Me	Me	MeCO	19,2	2	156,5	4	66,5	9	173,9	51	81,1	~0	134,9	22	172,5[f]	12
6*cf*	Me	Me	Me	18,8	2	149,4	2	70,6	6	175,1	52	81,1	~0	136,4	20	39,3[g]	19
7*b*	H	H	Ph	15,4	—	149,4[h]	—	61,4	—	180,6	—	69,4	—	136,0	—	148,2[h]	—
7*c*	Me	Me	Ph	19,4	—	148,2[h]	—	74,3	—	176,1	—	84,1	—	136,7	—	147,6[h]	—

[a] Référence TMS, les caractéristiques des carbones aromatiques ne sont pas données à l'exception de C_n lié à C_l et C_o lié à N.
[b] CH_3CO: δ = 22,5.
[c] Caractéristiques relevées sur le spectre du produit brut de la réaction δ_{C_n} ne peut être précisé avec certitude.
[d] CH_3CO: δ: 22,6.
[e] $R^1 = R^2 = CH_3$: δ = 28,5 et 34,1.
[f] $R^1 = R^2 = CH_3$: δ = 28,3 et 34,2 ($^3J_{PC} = 2$); CH_3CO: δ = 22,4 ($^3J_{PC} = 1$).
[g] $R^1 = R^2 = CH_3$: δ = 28,5 et 34,1.
[h] L'attribution de ces signaux n'est pas certain (C_j ou C_o).

Préparation des dipolarophiles

Les composés **3***a* et **3***c* sont préparés à l'aide de la méthode de Weinmaier *et al.* (16), **3***b* selon la réf. 17.

Le diazaarsole **4** est obtenu suivant la procédure de Märkl et Martin (18) modifiée (9). Le triazole **5** est préparé selon Henseke et Müller (19, 9).

Mode opératoire général utilisé pour les cycloadditions

Toutes les réactions sont réalisés sous gaz inerte (azote ou argon) et un solvant soigneusement séché. Après 15 minutes de dégazage une solution benzénique contenant $3,2 \times 10^2$ mol par litre des composés **3** ou **4** et 0,9 à 1,1 équivalents d'azirine **1** est irradiée. La lampe (Hanau HQ 80 (80 W) ou Philips HPK (125 W)) est placée dans un

Can. J. Chem. Downloaded from www.nrcresearchpress.com by 210.87.254.6 on 09/06/12
For personal use only.

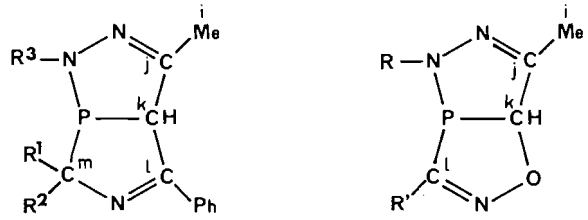

8 9

SCHÉMA 3

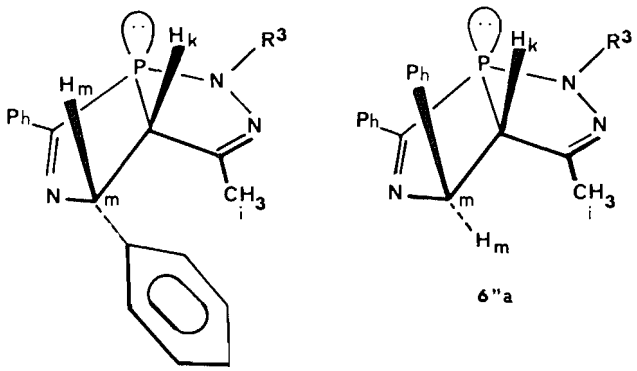

6'a 6"a

SCHÉMA 4

plongeur en quartz. La chaleur dégagée maintient le benzène à reflux. Après irradiation, le benzène est distillé et les cycloadduits isolés par cristallisation, cristallisation fractionnée ou chromatographie sur colonne.

La purification par recristallisation des adduits solides a échoué dans de nombreux cas en raison de l'instabilité de ces composés.

Les résultats sont donnés dans le tableau 3.

Réactions de l'azirine **1**a *avec les composés* **3**

(a) Diazaphosphole **3**d

La réaction est effectuée avec 1,00 g de **3***d* et 1,00 g de **1***a* dissous dans 175 cm^3 de benzène. Après distillation de ce dernier, l'addition d'éthanol à 95°C provoque la cristallisation de l'adduit impur (0,31 g). Il est essoré, dissous dans le dichlorométhane et la solution filtrée sur silice (Merck 60). La distillation sous vide du solvant donne 0,26 g de **6'***ad* pur (F = 141−143°C; Rdt = 12%). *Anal.* calc. pour $C_{23}H_{20}N_3P$: C 74,80 H, 5,42, N 11,38; trouvée: C 74,9, H 5,6, N 11,3%. Spectre de masse (T_i = 110°C; T_s = 140°C); masse moléculaire calculée: 369,139; trouvée: 369,138; *m/z* (intensité relative %): 369 (2,1); 193 (100,0; $\mathbf{1}a^{]+}$); 192 (6,5); 176 (14,1; $\mathbf{3}d^{]+}$); 165 (9,5); 122 (8,1); 91 (7,7); 90 (18,8); 89 (11,4); 77 (11,8); 51 (5,0).

Lorsque le produit brut de la réaction est directement chromatographié sur une colonne de silice (Merck 60) en utilisant le dichlorométhane comme éluant, l'une des fractions d'élution (60 à 90 cm^3 de CH_2Cl_2) donne 0,19 g de cycloadduit **6"***ad* impur qui est purifié (contrôle rmn) après lavage avec 2 cm^3 de méthanol. On obtient 0,10 g de **6"** *ad* pur (F = 155−157°C; Rdt = 5%).

(b) Diazaphosphole **3**e

L'irradiation d'une solution benzénique (220 cm^3) de diazaphosphole (1,00 g) et d'azirine **1***a* (1,22 g) est effectuée. Après élimination du benzène, l'addition de méthanol anhydre permet d'obtenir 3 jets successifs qui sont des mélanges dans des proportions différentes des diastéréoisomères **6'***ae* et **6"***ae*. Le 1er jet (0,21 g) dissous dans CH_2Cl_2 donne après filtration sur silice (Merck 60) 0,15 g du mélange **6'***ae*/**6"***ae* = 30:70 (F = 172−173°C). Le 2ème jet fond à 139−142°C (**6'***ae*/**6"***ae* = 85:15). Le 3ème jet est un mélange 50:50 des deux diastéréoisomères (F = 129−130°C). Le rendement global du mélange d'isomères est de 17%. Il n'a pas été possible de séparer **6'***ae* et **6"***ae* caractérisés à l'aide de la rmn ^1H et ^{13}C. Spectre de masse (mélange d'isomères F = 172−173°C; T_i = 105°C; T_s = 130°C; l'ion moléculaire n'est pas mis en évidence), *m/z* (intensité relative %): 232 (1,2; M − $PhCN^{]+}$); 193 (100,0; $\mathbf{1}a^{]+}$); 192 (7,4); 191 (2,7); 190 (4,9); 189 (10,1); 165 (8,8); 147 (2,5); 144 (3,0); 103 (4,3); 100 (5,1); 90 (14,6); 89 (12,4); 77 (4,0).

(c) Diazaphosphole **3**f

On irradie une solution de 0,90 g de **3***f* et de 1,00 g de **1***a* dans 250 cm^3 de benzène. Le produit brut de la réaction est chromatographié sur une colonne de silice (Florisil) en éluant successivement par l'éther de pétrole et des mélanges d'éther et d'éther de pétrole 30:70 et 40:60.

On elue 0,20 g de **6"***af* huileux pour (rmn) avec le mélange 40:60; 0,29 g d'huile sont obtenus après élution avec le mélange 30:70; l'addition de 1 à 2 cm^3 d'éther fait cristalliser le cycloadduit **6'***af* (0,09 g; Rdt = 4%; F = 130−131°C). Les adduits évoluent relativement rapidement à la température ambiante.

Composé **6"***af*

Spectre de masse (T_i = 70°C; T_s = 140°C), masse moléculaire calculée pour $C_{18}H_{18}N_3P$: 307,124; trouvée: 307,122; *m/z* (intensité relative %): 307 (1,3); 204 (1,1; M − $PhCN^{]+}$); 203 (4,1); 193 (100,0; $\mathbf{1}a^{]+}$); 192 (7,0); 166 (3,4); 165 (9,3); 127 (2,9); 114 (6,2; $\mathbf{3}f^{]+}$); 113 (3,0); 104 (2,3); 103 (2,9); 90 (14,3); 89 (12,9); 77 (3,7); 60 (8,0).

Réactions de l'azirine **1**b *avec les composés* **3** et **4**

(a) Diazaphosphole **3**d

Solution irradiée: 1,00 g de **3***d* et 0,73 g **1***b* dans 80 cm^3 de benzène. Le benzène distillé sous vide, le résidue cristallise. Après lavage au benzène froid 0,35 g du cycloadduit **6***bd* pur (rmn) est isolé (F = 160−162°C; Rdt = 21%). Le composé peut être recristallisé dans le méthanol. *Anal.* calc. pour $C_{17}H_{16}N_3P$: C 69,62, H 5,46, N 14,33; trouvée: C 69,7, H 5,5, N 14,1%. Spectre de masse (T_i = 85°C; T_s = 140°C), masse moléculaire calculée: 293,108; trouvée: 293,108; *m/z* (intensité relative %): 293 (16,0); 190 (21,0); M − $PhCN^{]+}$); 189 (10,6); 176 (4,0); 122 (21,0); 117 (100,0; $\mathbf{1}b^{]+}$); 103 (4,2); 90 (5,6); 78 (8,5); 77 (27,8) 51 (7,7).

(b) Diazaphosphole **3**e

On irradie une solution de 1,15 g de **3***e* et de 0,85 g de **1***b* dans 250 cm^3. Après élimination du solvant, on ajoute 10 cm^3 du mélange éther − éther de pétrole (50:50). Le produit solide est essoré est lavé avec 2 à 3 cm^3 de méthanol anhydre froid. On obtient ainsi 0,31 g de cycloadduit **6***be* relativement pur. Le filtrat après élimination du solvant est chromatographié sur une colonne de silice Merck 60 en éluant successivement avec des mélanges éther − éther de pétrole (40:60 et 60:40) puis avec de l'éther pur; 0,07 g d'adduit pratiquement pur sont récupérés de l'éluant éthéré.

La totalité du produit obtenu (0,38 g) est recristallisée dans 50 cm^3 d'un mélange éther − éther de pétrole à −20°C. On isole ainsi 0,24 g de **6***be* pur (F = 127−128°C; Rdt = 11%). Ce composé évolue lentement à la température ambiante. Spectre de masse (T_i = 55°C; T_s = 120°C, masse moléculaire pour $C_{13}H_{14}N_3OP$: 259,087; trouvée; 259,089; *m/z* (intensité relative %): 259 (10,3); 232 (10,3); 156 (21,7; M − $PhCN^{]+}$); 118 (10,3); 117 (100,0; $\mathbf{1}b^{]+}$); 115 (7,8); 114 (39,5); 103 (6,0); 102 (8,0); 90 (7,6); 77 (15,9); 73 (8,4).

(c) Diazaphosphole **3**f

Solution irradiée: 0,90 g de **3***f* et 0,85 g de **1***b* dans 250 cm^3 de benzène. Après élimination du solvant, on obtient 1,60 g d'une huile rouge qui est chromatographiée sur une colonne de silice (Merck 60) avec l'éther comme éluant. On isole 0,33 g (Rdt = 18%) de l'adduit **6***bf* pur (rmn). Le composé est une huile qu'il n'a pas été possible de faire cristalliser. Spectre de masse (T_i = 75°C; T_s = 150°C), masse moléculaire calculée pour $C_{12}H_{14}N_3P$: 231,092; trouvée 231,092; *m/z* (intensité relative %): 231 (12,9); 172 (5,9); 171 (3,3); 128 (38,7; M − $PhCN^{]+}$); 127 (21,3); 117 (100,0; $\mathbf{1}b^{]+}$); 116 (3,7); 114 (7,1); 113 (8,0); 105 (2,8); 104 (3,2); 103 (5,1); 101 (2,7); 99 (2,4); 91 (3,7); 90 (7,1); 89 (5,9); 87 (5,9); 86 (4,3); 77 (20,0); 76 (3,1); 60 (24,0).

Can. J. Chem. Downloaded from www.nrcresearchpress.com by 210.87.254.6 on 09/06/12
For personal use only.

TABLEAU 3. Réactions des ylures de nitrile avec les composés **3** et **4**. Conditions opératoires et rendements

Produits obtenus	R^1	R^2	R^3	n^a	Lampe utilisée	Durée d'irradiation (heures)	% relatif de **6′***a* et **6″***a*	C[b] / A + C	C / D + C	Rdt %[c]	*F*(°C) avec décomp.
6′*ad*	H	Ph	Ph	0,9	Phillips	1,25	75	1,00	0,50	12	141−143
6″*ad*	Ph	H	Ph				25			5	155−157
6′*ae*	H	Ph	MeCO	0,9	Phillips	0,5	60	0,80	1,00	17	139−142[d]
6″*ae*	Ph	H	MeCO				40				172−173[e]
6′*af*	H	Ph	Me	0,9	Phillips	4,5	60	1,00	0,25	4	130−131
6″*af*	Ph	H	Me				40			8	Huile
6*bd*	H	H	Ph	1,1	Hanau	24	—	0,50	0,44	21	160−162
6*be*	H	H	MeCO	0,9	Phillips	4	—	0,65	1,00	11	127−128
6*bf*	H	H	Me	1,1	Phillips	6	—	1,00	0,45	18	Huile
7*b*	H	H	Ph	0,9	Phillips	8	—	0,91	0,77	43	175−177
6*cd*	Me	Me	Ph	1,1	Hanau	24	—	0,61	0,58	18	109−110
6*ce*	Me	Me	MeCO	1,1	Phillips	1,5	—	0,57	1,00	28	119−120
6*cf*	Me	Me	Me	0,9	Phillips	6	—	0,80	0,53	9	74−76
7*c*	Me	Me	Ph	0,9	Phillips	31	—	0,72	0,43	15	Huile

[a] Nombre d'équivalents d'azirine engagée par rapport au phosphole.
[b] C: cycloadduit, A: azirine, D: dipolarophile, rapports déterminés par analyse rmn du produit brut de la réaction.
[c] Rendement en produit pur (rmn) calculé par rapport au dipolarophile engagé.
[d] Mélange **6′***ae*/**6″***ae* = 85:15.
[e] Mélange **6′***ae*/**6″***ae* = 30:70.

L'examen du spectre MIKE montre que les ions m/z = 128 et 117 proviennent de la fragmentation directe de l'ion moléculaire (m/z = 231).

Diazaarsole **4**

Solution irradiée: 1,75 g de **4** et 0,85 g de **1***b* dans 250 cm³ de benzène. Après distillation du benzène sous vide, le résidu solide est lavé avec 50 cm³ d'éther. On isole 1,50 g de produit cristallisé dans le mélange chloroforme−éther à −20°C; 1,15 g de **7***b* (F = 175−177°C; cristaux jaunes; Rdt = 43%) sont obtenus. *Anal.* calc. pour $C_{17}H_{16}N_3As$: C 60,54, H 4,75, N 12,46; trouvée C 60,6, H 4,8, N 12,4%. Spectre de masse (T_i = 65°C; T_s = 130°C), masse moléculaire calculée: 337,056; trouvée: 337,056; m/z (intensité relative %): 337 (53,6); 234 (100,0; M − $PhCN^{\cdot+}$); 233 (41,1); 220 (10,0; $\mathbf{4}^{\cdot+}$); 219 (5,2); 193 (6,8); 192 (19,6); 168,5 (2,3; M^{2+}); 167 (4,6); 166 (51,8); 159 (13,4); 152 (3,0); 151 (2,9); 145 (4,6); 144 (2,1); 139 (4,6); 138 (2,3); 129 (4,6); 127 (2,5); 118 (14,1); 117 (96,4); $\mathbf{1}b^{\cdot+}$); 116 (6,2); 115 (2,9); 105 (8,2); 104 (6,8); 103 (9,1); 102 (2,3); 101 (3,4); 91 (7,0); 90 (10,2); 89 (6,8); 78 (6,8); 77 (97,1); 76 (4,6); 65 (3,2); 64 (2,9); 63 (2,7); 51 (10,2).

L'examen du spectre MIKE montre que l'ion m/z = 234 provient de la fragmentation directe de l'ion moléculaire m/z = 337.

Réactions de l'azirine **1**c *avec les composés* **3** *et* **4**

(a) Diazaphosphole **3**d

Solution irradiée: 1,00 g de phosphole et 0,90 g de **1***c* dans 80 cm³ de benzène. Après élimination du solvant le résidu cristallise lentement et partiellement. Le produit solide est essoré et lavé avec très peu de benzène. On obtient ainsi 0,19 g de l'adduit **6***cd*. Le filtrat est repris au benzène. La formation de gouttelettes huileuses non solubles est observée; la phase benzénique est décantée et le solvant distillé sous vide. Après addition de méthanol au résidu huileux ont obtient 0,13 g de **6***cd*. Rendement total 18%; F = 109−110°C. Le composé peut être recristallisé dans le méthanol. *Anal.* calc. pour $C_{19}H_{20}N_3P$: C 71,03, H 6,23, N 13,08; trouvée: C 70,8, H 6,2, N 13,0%. Spectre de masse (T_i = 75°C; T_s = 150°C), masse moléculaire calculée: 321,139; trouvée; 321,139; m/z (intensité relative %): 321 (6,0); 176 (8,9; $\mathbf{3}d^{\cdot+}$); 146 (12,7); 145 (100,0; $\mathbf{1}c^{\cdot+}$) 122 (8,2); 104 (38,5); 103 (7,3); 77 (12,7).

(b) Diazaphosphole **3**e

Solution irradiée: 0,90 g de **3***e* et 1,00 g de **1***c* dans 200 cm³ de benzène. Le résidu après distillation du benzène sous vide cristallise après addition de méthanol (0,40 g); un second jet (0,11 g) est obtenu après refroidissement de la solution méthanolique à −20°C. Rendement total 28%; F = 119−120°C. *Anal.* calc. pour $C_{15}H_{18}N_3OP$: C 62,72, H 6,27, N 14,63; trouvée: C 62,6, H 6,3; N 14,5%. Spectre de masse (T_i = 70°C; T_s = 125°C), masse moléculaire calculée: 287,119; trouvée: 287,117; m/z (intensité relative %): 287 (1,8); 184 (2,0; M − $PhCN^{\cdot+}$); 146 (14,3); 145 (100,0; $\mathbf{1}c^{\cdot+}$); 142 (2,0; $\mathbf{3}e^{\cdot+}$); 141 (15,2); 127 (10,5); 104 (49,5); 103 (10,0); 100 (7,4); 77 (7,7).

(c) Diazaphosphole **3**f

Solution irradiée 0,90 g de **3***f* et 1,00 g de **1***c* dans 250 cm³ de benzène. Le benzène est distillé sous vide et le résidu repris à l'éther. Un solide pateux insoluble (évoluant à l'air) est éliminé par filtration. Après refroidissement à −20°C de la solution éthérée on obtient 0,18 g de **6***cf* pur (rmn); F = 74−76°C; Rdt = 9%. Le produit évolue assez rapidement à la température ambiante. Spectre de masse (T_i = 30°C; T_s = 140°C) masse moléculaire calculée pour $C_{14}H_{18}N_3P$: 259,124; trouvée: 259,122; m/z (intensité relative %): 259 (3,8); 145 (100,0; $\mathbf{1}c^{\cdot+}$); 144 (6,2); 141 (10,6); 114 (8,2; $\mathbf{3}f^{\cdot+}$); 113 (3,0); 105 (5,6); 104 (4,7); 103 (9,5); 77 (7,1); 76 (2,4); 71 (2,6); 60 (8,0).

(d) Diazaarsole **4**

Solution irradiée: 1,00 g de **4** et 0,60 de **1***c* dans 150 cm³ de benzène. Après élimination du solvant, le résidu est chromatographié sur une colonne de silice (Merck 60) avec comme éluant un mélange éther − éther de pétrole (50:50). On obtient ainsi 0,25 g d'adduit **7***c* pur (rmn). Le composé est une huile rouge qu'il n'a pas été possible de cristalliser (Rdt = 15%). Spectre de masse (T_i = 65°C; T_s = 120°C), masse moléculaire calculée pour $C_{19}H_{20}N_3As$: 365,087; trouvée; 365,084; m/z (intensité relative %): 365 (5,1); 262 (2,6; M − $PhCN^{\cdot+}$); 247 (8,5); 220 (9,0; $\mathbf{4}^{\cdot+}$); 206 (2,4); 166 (8,0); 145 (100,0; $\mathbf{1}c^{\cdot+}$); 144 (6,0); 130 (2,0); 105 (4,9); 103 (8,5); 78 (12,0); 77 (12,4); 75 (3,1).

Le spectre MIKE montre que les ions m/z = 262 et 145 proviennent de la fragmentation directe de l'ion moléculaire m/z = 365.

1. N. I. SHVETSOV-SHILOVSKII, R. G. BOBKOVA, N. P. IGNATOVA et N. N. MEL'NIKOV. Russ. Chem. Rev. **46**, 514 (1977).
2. E. FLUCK. *Dans* Topics in phosphorus chemistry. Vol. 10. Interscience publication, John Wiley and Sons. 1980. p. 193.
3. R. APPEL, F. KNOLL et I. RUPPERT. Angew. Chem. Int. Ed. Engl. **20**, 731 (1981).

Can. J. Chem. Downloaded from www.nrcresearchpress.com by 210.87.254.6 on 09/06/12
For personal use only.

4. E. NIECKE, N. W. SCHOELLER et D. A. WILDBREDT. Angew. Chem. Int. Ed. Engl. **20**, 131 (1981).
5. B. A. ARBUZOV et E. N. DIANOVA. Izv. Akad. Nauk SSSR, 1453 (1977).
6. A. SCHMIDPETER et J. HÖGEL. Communication au 8ème Congrès International de Chimie hétérocyclique, Graz, Autriche. 1981.
7. B. A. ARBUZOV, E. N. DIANOVA et N. A. CHADAEVA. Dokl. Akad. Nauk SSSR, **246**, 1130 (1979).
8. R. CARRIÉ, Y. Y. C. YEUNG LAM KO, F. DE SARLO et A. BRANDI. J. Chem. Soc. Chem. Commun. 1131 (1981).
9. Y. Y. C. YEUNG LAM KO, F. TONNARD, R. CARRIÉ, F. DE SARLO et A. BRANDI. Tetrahedron. Sous presse.
10. (*a*) A. PADWA, J. SMOLANOFF et S. I. WETMORE JR. Pure Appl. Chem. **33**, 269 (1973), et références citées; (*b*) P. CLAUS, T. DOPPLER, N. GAKIS, M. GEORGARAKIS, H. GIEZENDANNER, P. GILGEN, H. HEIMGARTNER, B. JACKSON, M. HARKY, N. S. NARASIMHAN, H. J. ROSENKRANG, A. WUNDERLI, H. J. HANSEN et H. SCHMID. Pure Appl. Chem. **33**, 339 (1973), et références citées; (*c*) A. PADWA. Acc. Chem. Res. **9**, 371 (1976), et références citées; (*d*) Chem. Rev. **77**, 37 (1977), et références citées.
11. A. PADWA, M. DHARAN, J. SMOLANOFF et S. I. WETMORE JR. J. Am. Chem. Soc. **95**, 1954 (1973); A. PADWA, J. SMOLANOFF et S. I. WETMORE JR. J. Org. Chem. **38**, 1333 (1973).
12. J. P. ALBRAND, D. GAGNAIRE, J. MARTIN et J. B. ROBERT. Bull. Soc. Chim. Fr. 40 (1969); J. P. ALBRAND, D. GAGNAIRE, M. PICARD et J. B. ROBERT. Tetrahedron Lett. 4593 (1970).
13. F. N. FOWLER, A. HASSNER et L. A. LEVY. J. Am. Chem. Soc. **89**, 2077 (1967).
14. S. SATO. Bull. Chem. Soc. Jpn. **41**, 1440 (1968).
15. J. PERROCHEAU. Thèse de 3ème Cycle, Rennes, France, 1979.
16. J. H. WEINMAIER, G. BRUNNHUBER et A. SCHMIDPETER. Chem. Ber. **113**, 2278 (1980).
17. N. I. SHVETSOV-SHILOVSKII, N. P. IGNATOVA et N. N. MEL'NIKOV. Zh. Obshch. Khim. **40**, 1501 (1970).
18. G. MÄRKL et C. MARTIN. Tetrahedron Lett. 4503 (1973).
19. G. HENSEKE et G. MÜLLER. J. Prakt. Chem. **18**, 47 (1962).

Can. J. Chem. Downloaded from www.nrcresearchpress.com by 210.87.254.6 on 09/06/12
For personal use only.

The chemistry of thujone. VII.[1] Thujone as a chiral synthon for the preparation of sesquiterpenes. Synthesis of β-elemol

JAMES P. KUTNEY AND ASHOK K. SINGH

Department of Chemistry, University of British Columbia, 2036 Main Mall, University Campus, Vancouver, B.C., Canada V6T 1Y6

Received September 14, 1982

JAMES P. KUTNEY and ASHOK K. SINGH. Can. J. Chem. **61**, 1111 (1983).

An efficient synthesis of β-elemol (**4**) from thujone (**1**) is described. The key intermediate **3** is readily prepared and described in previous studies within the synthesis of (+)-carissone (**2**).

JAMES P. KUTNEY et ASHOK K. SINGH. Can. J. Chem. **61**, 1111 (1983).

On décrit une synthèse efficace du β-élémol (**4**) à partir de la thujone. L'intermédiaire principal **3** se prépare facilement et il a été décrit antérieurement à la suite d'études sur la synthèse de la (+)-carissone (**2**).

[Traduit par le journal]

In previous studies from these laboratories, thujone (**1**)[2] has been shown to be a versatile synthon in the preparation of juvenoid (1, 2), pyrethroid (3), and steroidal (4) analogues as well as in the synthesis of the natural products (+)-β-cyperone (5) and (+)-carissone (**2**) (6). Here we wish to describe the synthesis of β-elemol (**4**) by elaboration of ring A in the intermediate **3** (mixture of C11 isomers) prepared earlier during our studies within the carissone synthesis (6).

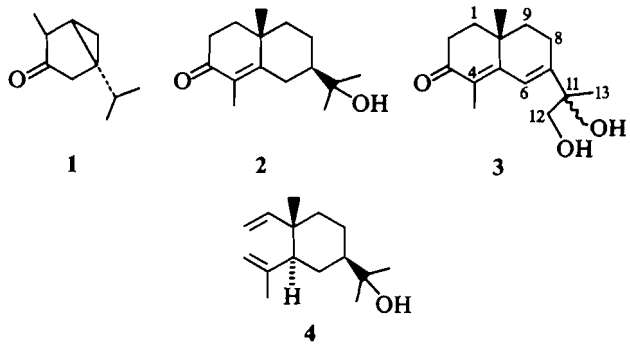

Controlled hydrogenation of **3** (ethanol, KOH, Pd) for 30 min as described earlier (6) provides the partially reduced intermediates **5** (72% yield) as an inseparable mixture of C11 isomers, and the fully reduced diols **6** (C11 isomers) as minor components (24% yield). On the other hand, reduction of **3** for an extended period (4 h) affords **6** in quantitative yield. Again efforts to separate the C11 isomers of **6** proved fruitless but it was found very convenient to utilize this mixture directly in the synthesis of β-elemol as described below.

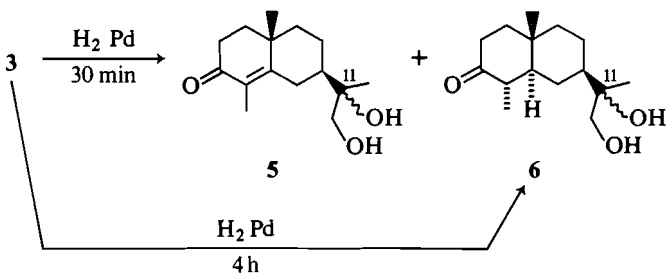

[1]For part VI, see ref. 4.

[2]Thujone is the major component (ca. 80%) of the steam distillate from the slash (waste) of Western red cedar.

Treatment of **6** with *p*-toluenesulfonyl chloride in pyridine provided the mixture of tosylates **7**. The latter on chromatography employing basic alumina (grade III) afforded the epoxyketone **8** in high yield. Direct reduction of **7** or **8** yielded a crystalline diol **9**. The preparation of **9** was more convenient from the tosylate **7** and this was the route selected for all subsequent studies.

Oxidation of **9** with chromium trioxide in pyridine afforded, in 92% yield, a crystalline product, mp 111−112°C, and with spectral characteristics identical with those published for (−)-*trans*-dihydrocarissone (**10**) (7).

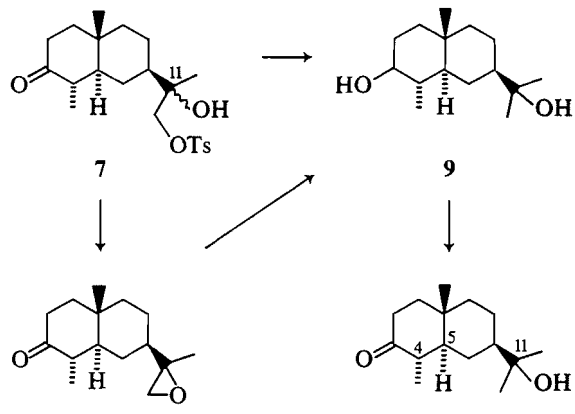

It is indicated (7) that the reduction of **2** affords the *trans* product **6**. We have confirmed the stereochemistry at C4 and C5 by a detailed nmr study at 400 MHz and a brief discussion of these results is appropriate. The C4 methine proton appeared at δ 2.23 (1H, sextet, J = 6 and 12 Hz) while the C4 methyl group revealed a doublet at δ 1.01 (J = 6 Hz). These assignments were established from decoupling studies which showed that C4-H becomes a doublet (J = 12 Hz) upon irradiation at the C4-methyl group frequency while, in turn, the latter becomes a singlet when the C4-H is irradiated. The *trans* diaxial relationship between C4-H and C5-H is consistent with initial *cis* reduction of **2** from the α face of the molecule followed by base-catalyzed epimerization of the C4-methyl group to the more stable 4α-(equatorial) orientation.

Treatment of **10** with BF_3 and tosylhydrazine in benzene gave an inseparable mixture of the isomeric hydrazones (see

Can. J. Chem. Downloaded from www.nrcresearchpress.com by 210.87.254.105 on 09/06/12
For personal use only.

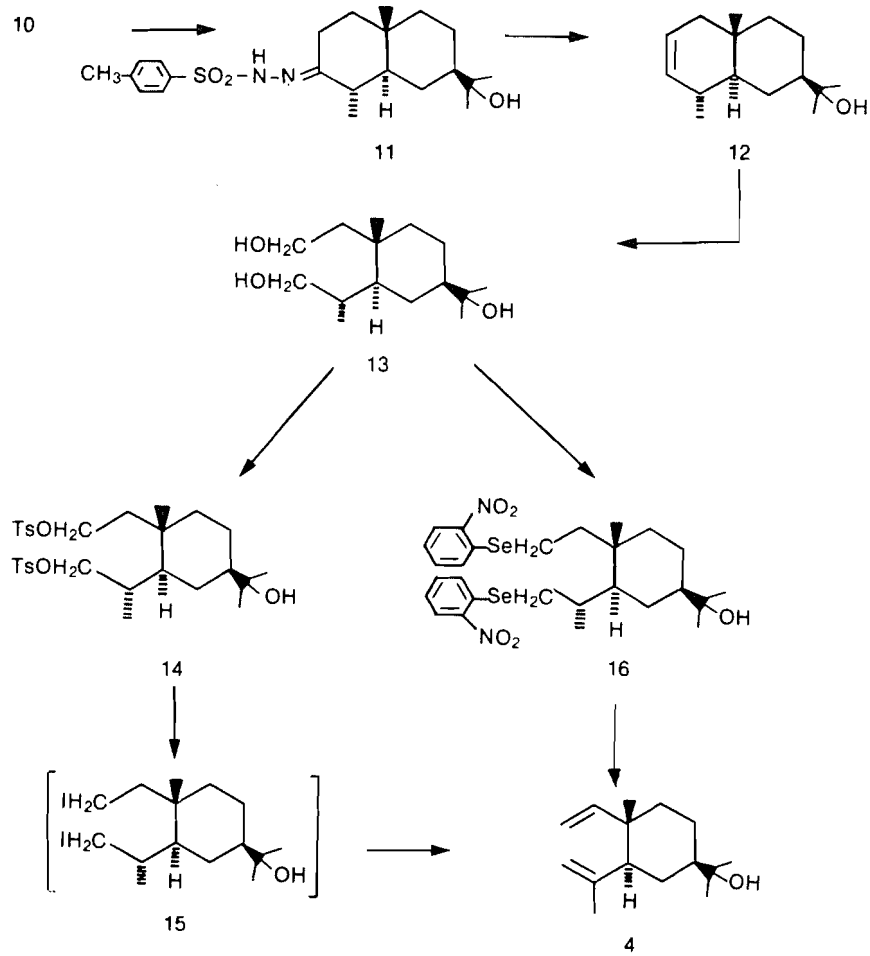

SCHEME 1

nmr data in Experimental) **11**, which was subjected directly to a modified Bamford–Stevens reaction (for a review of this reaction, see ref. 8) to provide the crystalline unsaturated alcohol **12** in 76% yield (Scheme 1).

Ozonolysis of **12** followed by treatment of the reaction mixture with sodium borohydride afforded the crystalline triol **13**, mp 117–118°C ($[\alpha]_D$ −9.4°) in 77% yield. The latter compound has been previously reported (9) as a glass ($[\alpha]_D$ −10°) and obtained from elemol.

Elaboration of **13** to the desired natural product **4** was considered via two synthetic routes as shown in Scheme 1. The initial study involved the sequence, **13** → **14** → **15**. Formation of ditosylate **14**, in 86% yield, proceeded without difficulty but unfortunately the intended conversion to di-iodide **15** and the subsequent elimination to **4** proceeded only in poor yield (see Experimental). The alternative sequence, **13** → **16** → **4** involving selenium intermediates is much preferred and is discussed in more detail.

Elimination of *o*-nitrophenylselenides to olefins is known (10) to proceed in excellent yields and this route was therefore evaluated with the triol **13**. The bis-*o*-nitrophenylselenide derivative **16** isolated as a crystalline product, mp 42–44°C (84% yield), was treated with sodium metaperiodate in an alkaline medium at room temperature and afforded β-elemol (**4**) in 72% yield. All the spectral data of the synthetic product are in acord with those published for the natural compound.

The previously reported syntheses of β-elemol (11, 12) provide low overall yields and/or racemic material. The present study affords a convenient route to optically active β-elemol in an overall yield of 35% from (−)-*trans*-dihydrocarissone (**10**).

Experimental

Melting points were determined on a Reichert hot stage apparatus and are uncorrected. Ultraviolet spectra were recorded on a Cary 15 spectrophotometer in methanol solution. Infrared spectra were measured on a Perkin–Elmer 710 spectrophotometer using chloroform as solvent. The ^{1}Hmr spectra were recorded on Bruker WH-400, Bruker WP-80, Varian XL-100, or Nicolet–Oxford H-270 instruments. Deuteriochloroform was used as the solvent with TMS as internal standard. Low resolution mass spectra were determined on either an AEI-MS-902 or an Atlas CH-4B spectrometer. High resolution mass measurements were made on an AEI-MS-50 spectrometer. Optical rotations were recorded on a Perkin–Elmer 141 polarimeter using a cell with a path length of 10 cm. Microanalyses were performed by Mr. P. Borda, Microanalytical Laboratory, University of British Columbia. Column chromatography utilized Merck silica gel 60 (70–230 mesh). Preparative and thin layer chromatography utilized Merck silica gel GF_{254}. Petroleum ether refers to the fraction with boiling range 30–60°C.

Ketodiols 6

A mixture of dienone **3** (400 mg), potassium hydroxide (80 mg), and 10% palladium charcoal (560 mg) in ethanol (80 mL) was hydrogenated at room temperature and atmospheric pressure. Hydrogen absorption ceased after 4 h. The mixture was filtered and the filtrate evaporated, water (10 mL) was added to the residue, extracted with methylene chloride, and dried ($MgSO_4$). Evaporation of solvent at reduced pressure left ketodiols **6** (393 mg, 97%) which were identical with previously reported samples (6).

Can. J. Chem. Downloaded from www.nrcresearchpress.com by 210.87.254.105 on 09/06/12
For personal use only.

Can. J. Chem. Downloaded from www.nrcresearchpress.com by 210.87.254.105 on 09/06/12
For personal use only.

Tosylates 7

p-Toluenesulfonyl chloride (279 mg) was added to a solution of the diols **6** (186 mg) in dry pyridine (4 mL). The mixture was stirred at ambient temperature for 44 h, then poured into water (10 mL) and extracted with methylene chloride (3 × 20 mL). The extracts were combined, dried ($MgSO_4$), and concentrated *in vacuo* to give a colourless solid. Recrystallization from ether – petroleum ether gave tosylates **7** (270 mg, 91%): mp 99–101°C; ir ν_{max}: 3563, 1706, 1460, 1385, 1180, 995 cm^{-1}; uv λ_{max}: 225 (ε 13 562), 257 (573), 262 (672), 267 (600), 273 (537), 285 (30) nm; ^{1}Hmr δ: 0.94, 0.97 (3H, d, J = 7 Hz, two sets), 1.05 (3H, s), 1.13, 1.15 (3H, s, two sets), 1.18–1.83 (10H, m), 1.88 (1H, bs, D_2O exchangeable), 2.19 (1H, m), 2.36 (1H, ddd, J = 12, 8, 2 Hz), 2.47 (3H, s), 2.53 (1H, dt, J = 12, 8 Hz), 3.91, 3.93 (1H, d, J = 10 Hz, two sets), 3.99, 4.00 (1H, d, J = 10 Hz, two sets), 7.36 (2H, d, J = 8 Hz), 8.00 (2H, d, J = 8 Hz); ms *m/e*: 408 (M^+), 393, 390, 378, 236, 223. High resolution molecular weight determination, calcd. for $C_{22}H_{32}O_5S$: 408.1970; found: 408.1985. *Anal.* calcd. for $C_{22}H_{32}O_5S$: C 64.70, H 7.84; found: C 64.74, H 8.00.

Epoxy ketone 8

Compound **7** (260 mg) was filtered through basic alumina activity III (25 g), using ether to elute the product. Evaporation of the solvent left epoxyketone **8** (146 mg, 97%) as a viscous oil; $[\alpha]_D$ −8.6° ($CHCl_3$, *c* 0.1635); ir ν_{max} (neat): 1706 cm^{-1}; uv λ_{max}: 280 (ε 34) nm; ^{1}Hmr δ: 1.00 (3H, d, J = 7 Hz), 1.09 (3H, s), 1.29 (3H, s), 1.40–1.80 (7H, m), 2.00–2.50 (4H, m), 2.53 (1H, d, J = 5 Hz), 2.62 (1H, d, J = 5 Hz); ms *m/e*: 236 (M^+), 221, 203, 189, 179. High resolution molecular weight determination, calcd. for $C_{15}H_{24}O_2$: 236.1776; found: 236.1777. *Anal.* calcd. for $C_{15}H_{24}O_2$: C 76.27, H 10.16; found: C 75.90, H 10.13.

Diol 9

A mixture of **7** (460 mg) and LAH (88 mg) in dry ether (50 mL) under an atmosphere of argon was refluxed for 5 h. Excess LAH was destroyed by careful addition of water. The mixture was extracted with ether (3 × 50 mL), the combined organic extracts were dried ($MgSO_4$) and evaporated to leave a colourless solid. Recrystallization from ether – petroleum ether afforded the diol **9** (258 mg, 95%); mp 138–139°C; ir ν_{max}: 3450, 1461, 1395 cm^{-1}; ^{1}Hmr δ: 0.84 (3H, s), 0.98 (3H, d, J = 7 Hz), 1.03–1.13 (2H, m), 1.19 (3H, s), 1.20 (3H, s), 1.23–1.63 (10H, m), 1.77–1.86 (2H, m), 3.13 (1H, m); ms *m/e*: 240 (M^+), 225, 222, 207. High resolution molecular weight determination, calcd. for $C_{15}H_{28}O_2$: 240.2089; found: 240.2088. *Anal.* calcd. for $C_{15}H_{28}O_2$: C 75.00, H 11.66; found: C 74.55, H 11.71.

A solution of **8** (654 mg) in dry ether (10 mL) under argon was added to a stirred suspension of LAH (162 mg) in ether (20 mL). The mixture was refluxed for 12 h. Work-up as described above afforded **9** (622 mg, 94%).

Hydroxyketone 10

To a magnetically stirred solution of chromium trioxide (300 mg) in pyridine (4 mL) was added a solution of diol **9** (87 mg) in pyridine (3 mL). After stirring for 3 h at room temperature, the mixture was diluted with water (15 mL) and extracted with benzene–ether (100 mL, 1:1 v/v). The extracts were dried and evaporated. Chromatography of the residue on silica gel (ether – petroleum ether, 1:1 v/v) gave hydroxyketone **10** (80 mg, 92%); mp 111–112°C (lit. (7) mp 109–110°C); $[\alpha]_D$ −11.8° ($CHCl_3$, *c* 0.153) (lit. (7) $[\alpha]_D$ −11.7° (*c* 2.0)); ir ν_{max}: 3463, 1702, 1460, 1390 cm^{-1}; uv λ_{max}: 282 (ε 28) nm; ^{1}Hmr δ: 1.01 (3H, d, J = 6 Hz), 1.08 (3H, s), 1.10–1.19 (3H, m), 1.21 (3H, s), 1.22 (3H, s), 1.31 (1H, dt, J = 12, 4 Hz), 1.37 (1H, m), 1.49 (1H, dt, J = 14, 6 Hz), 1.59–1.69 (3H, m, including 1.66 (1H, bs, D_2O exchangeable)), 1.74 (1H, ddd, J = 14, 6, 2 Hz), 1.82 (1H, dt, J = 12, 4 Hz), 2.23 (1H, sextet, J = 12, 6 Hz), 2.36 (1H, ddd, J = 14, 6, 2 Hz), 2.53 (1H, dt, J = 14, 6 Hz); ms *m/e*: 238 (M^+), 223, 220, 205, 180. High resolution molecular weight determination, calcd. for $C_{15}H_{26}O_2$: 238.1933; found: 238.1929. *Anal.* calcd. for $C_{15}H_{26}O_2$: C 75.63, H 10.92; found: C 75.62, H 11.01.

Hydrazones 11

A solution of hydroxyketone **10** (436 mg) in benzene (50 mL) together with *p*-toluenesulfonyl hydrazide (358 mg) and a drop of boron trifluoride etherate was stirred under argon at ambient temperature for 4 h. The reaction mixture was evaporated under reduced pressure, the residue diluted with water (10 mL) and extracted with THF–ether (100 mL, 1:4 v/v). The extracts were dried ($MgSO_4$) and evaporated to leave hydrazones **11** which was crystallized from ether – petroleum ether, yield (435 mg, 99%); mp 116–118°C; ir ν_{max}: 3550, 1610, 1460, 1390, 1340, 1270, 1110 cm^{-1}; uv λ_{max}: 226 (ε 14 135), 260 (2257), 273 (1129) nm; ^{1}Hmr δ: 0.90 (3H, s), 1.01, 1.02 (3H, d, J = 7 Hz, two sets), 1.19, 1.21 (3H, s, two sets), 1.20, 1.22 (3H, s, two sets), 1.25–1.70 (7H, m), 1.74 (1H, ddd, J = 14, 6, 2 Hz), 1.81 (1H, m), 1.97 (1H, dt, J = 14, 6 Hz), 2.08 (1H, m), 2.24 (1H, m), 2.35 (1H, ddd, J = 14, 6, 2 Hz), 2.44, 2.46 (3H, s, two sets), 2.53 (1H, m), 5.56 (1H, bs), 7.32, 7.37 (2H, d, J = 8 Hz, two sets), 7.81, 7.87 (2H, d, J = 8 Hz, two sets); ms *m/e*: 406 (M^+), 391, 251, 233, 204. High resolution molecular weight determination, calcd. for $C_{22}H_{34}N_2O_3S$: 406.2289; found: 406.2282. *Anal.* calcd. for $C_{22}H_{34}N_2O_3S$: C 65.02, H 8.37, N 6.89; found: C 65.57, H 8.89, N 6.34.

Hydroxy olefin 12

To a solution of hydrazone **11** (708 mg) in THF (25 mL) at 0°C under argon was added ethereal methyllithium (15 mL of a 1 *M* solution). The mixture was stirred 20 min at the same temperature. The cooling bath was removed and the mixture was stirred at room temperature for 3 h. The reaction was quenched by the addition of water (10 mL) and extracted with petroleum ether (3 × 50 mL). The combined extracts were dried and evaporated to furnish 375 mg crude product. Chromatography on 50 g silica gel (ether – petroleum ether, 1:4 v/v) gave hydroxy olefin **12** (294 mg, 76%) as a white solid; mp 47–48°C; $[\alpha]_D$ −35.5° ($CHCl_3$, *c* 0.945); ir ν_{max}: 3463, 1660, 1470, 1390 cm^{-1}; ^{1}Hmr δ: 0.80 (3H, s), 0.97 (3H, d, J = 7 Hz), 1.17 (3H, s), 1.18 (3H, s), 1.23–1.35 (4H, m), 1.50–1.90 (8H, m), 5.43 (1H, dd, J = 8, 2 Hz), 5.54 (1H, ddd, J = 10, 5, 2 Hz); ms *m/e*: 222 (M^+), 207, 204, 189, 164. High resolution molecular weight determination, calcd. for $C_{15}H_{26}O$: 222.1983; found: 222.1968. *Anal.* calcd. for $C_{15}H_{26}O$: C 81.08, H 11.71; found: C 81.34, H 11.62.

Triol 13

A stirred solution of **12** (268 mg) in methanol and methylene chloride (20 mL, 1:1 v/v) was cooled to −77°C and treated with 50 mL of a precooled (−77°C) saturated solution of ozone in methylene chloride. After 20 min sodium borohydride (100 mg) was added at −77°C. At 15 min intervals additional portions (3 × 100 mg) of $NaBH_4$ were added. The reaction mixture was warmed to room temperature and the solvent was removed *in vacuo*. The residue was diluted with water and the product isolated by ether extraction. After drying, the solvent was removed to give a viscous material. Chromatography on alumina (activity III, methanol–ether, 1:20 v/v) afforded the triol **13** (241 mg, 77%) as a coloured solid; mp 117–118°C; $[\alpha]_D$ −9.4° (MeOH, *c* 0.384) (lit. (9) $[\alpha]_D$ −10° (*c* 4.2)); ir ν_{max}: 3413, 1480, 1420, 1390 cm^{-1}; ^{1}Hmr δ: 0.78 (3H, d, J = 6 Hz), 0.88 (3H, s), 1.15 (3H, s), 1.17 (3H, s), 1.21–1.62 (10H, m), 1.71 (1H, m), 2.07 (1H, m), 2.66 (2H, bs, D_2O exchangeable), 3.33–3.40 (2H, m), 3.65 (1H, m), 3.80 (1H, m); ms *m/e*: 240 ($M^+ - H_2O$), 225, 222, 210, 207. High resolution molecular weight determination, calcd. for $C_{15}H_{30}O_3 - H_2O$: 240.2089; found: 240.2092. *Anal.* calcd. for $C_{15}H_{30}O_3$: C 69.76, H 11.62; found: C 70.08; H 11.70.

Ditosylate 14

To a solution of triol **13** (200 mg) in pyridine (10 mL) was added *p*-toluene sulfonylchloride (590 mg). The solution was stirred for 3 days at ambient temperature. Work-up as described in **7** gave crude material, which was purified by column chromatography on alumina

Can. J. Chem. Downloaded from www.nrcresearchpress.com by 210.87.254.105 on 09/06/12
For personal use only.

activity III. Elution with methanol – petrolcum ether – ether (1:4:5) gave pure **14** as a viscous oil, yield 376 mg (86%); $[\alpha]_D$ −5.8° ($CHCl_3$, *c* 0.651); ir ν_{max} (neat): 3475, 1600, 1460, 1360 cm^{-1}; uv λ_{max}: 225 (ε 24 553), 257 (958), 262 (1197), 267 (1117), 273 (1046) nm; ^{1}Hmr δ: 0.77 (3H, d, *J* = 6 Hz), 0.82 (3H, s), 1.01–1.08 (2H, m), 1.12 (3H, s), 1.14 (3H, s), 1.15–1.60 (8H, m, including 1.57 (1H, s, D_2O exchangeable)), 1.71 (1H, m), 2.03 (1H, m), 2.46 (6H, s), 3.74–3.78 (2H, m), 4.06–4.12 (2H, m), 7.36 (2H, d, *J* = 8 Hz), 7.37 (2H, d, *J* = 8 Hz), 7.79 (2H, d, *J* = 8 Hz), 7.81 (2H, d, *J* = 8 Hz); ms *m/e*: 548 ($M^+ - H_2O$), 376, 204, 189. High resolution molecular weight determination, calcd. for $C_{29}H_{42}O_7S_2 - H_2O$: 548.2266; found: 548.2282. *Anal.* calcd. for $C_{29}H_{42}O_7S_2$: C 61.48, H 7.42, S 11.30; found: C 61.43, H 7.48, S 11.15.

A mixture of compound **14** (71 mg) and NaI (160 mg) in dry acetone (6 mL) was heated to reflux in an oil bath for 5 h under argon. After removal of the acetone, the mixture was diluted with water and extracted with ether, and the ether layer was washed with water, dried ($MgSO_4$), and evaporated. The crude product **15** (55 mg) was used for subsequent reactions without further purification; ms *m/e*: 478 (M^+), 463, 420, 333. High resolution molecular weight determination, calcd. for $C_{15}H_{28}O^{127}I_2$: 478.0228, found: 478.0242.

The compound **15** (55 mg) was added to potassium *tert*-butoxide (300 mg) in DMSO (4 mL). The reactants were stirred for 12 h at room temperature and then poured into ice water. The mixture was extracted with ether (3 × 20 mL) and the combined ether extracts were washed with water, brine, and then dried over $MgSO_4$. Evaporation of the solvents left a semi-solid residue which was purified by preparative tlc on silica gel with ether – petroleum ether as the eluent. The yield was 1.2 mg (5%) of solid **4**.

Diselenide ***16***

A solution of triol **13** (61 mg), *o*-nitrophenyl selenocyanate (429 mg) (14) in THF (4 mL), and pyridine (4 mL) was treated with tri-*n*-butyl phosphine (338 mg). The mixture was stirred for 18 h at ambient temperature and concentrated *in vacuo*. The product was extracted with ether, dried ($MgSO_4$), evaporated, and chromatographed on silica gel (ether) to give diselenide **16** (125 mg, 84%) as a yellow solid; mp 42–44°C; $[\alpha]_D$ −32.1° ($CHCl_3$, *c* 0.461); ir ν_{max}: 3550, 1596, 1571, 1516, 1324, 1306, 1110, 870 cm^{-1}; uv λ_{max} ($CHCl_3$): 256 (ε 29 394), 272 (13 636) nm; ^{1}Hmr δ: 0.94 (3H, s), 1.05 (3H, d, *J* = 6 Hz), 1.20 (3H, s), 1.21 (3H, s), 1.30–1.73 (11H, m), 2.16 (1H, m), 2.74–2.84 (2H, m), 2.85–2.96 (2H, m), 7.18–7.30 (2H, m), 7.36–7.43 (4H, m), 8.11 (1H, d, *J* = 8 Hz), 8.25 (1H, d, *J* = 8 Hz); ms *m/e*: 628 (M^+), 426. High resolution molecular weight determination, calcd. for $C_{27}H_{36}N_2O_5{}^{80}Se_2$: 628.0953; found: 628.0934; *Anal.* calcd. for $C_{27}H_{36}N_2O_5{}^{80}Se_2$: C 51.59, H 5.73, N 4.45; found: C 51.65, H 5.83, N 4.63.

β-*Elemol* ***4***

The diselenide **16** (108 mg) was dissolved in a mixture of methanol (6 mL) and THF (6 mL), then water (0.9 mL), $NaHCO_3$ (51 mg), and $NaIO_4$ (258 mg) were added with vigorous stirring. After 6 h at room temperature, the reaction mixture was evaporated under *vacuo*, then diluted with saturated $NaHCO_3$ (5 mL), and extracted with ether (3 × 10 mL). The organic layer was washed with water, NaCl solution, and dried ($MgSO_4$). Solvent was removed and the residue chromatographed on alumina grade III (10 g) eluted with ether – petroleum ether (1:9, v/v) to give a crystalline solid (27.3 mg, 72%); mp 51–52°C (lit. (13) mp 51–52°C); $[\alpha]_D$ −4.6° ($CHCl_3$, *c* 0.5005) (lit. (13) $[\alpha]_D$ −4.5° ($CHCl_3$)); ir ν_{max}: 3438, 1643, 1473, 1448, 1383, 1116, 1011, 906, 891 cm^{-1}; ^{1}Hmr δ: 1.00 (3H, s), 1.22 (6H, s), 1.26–1.50 (5H, m), 1.55–1.70 (3H, m, including 1.56 (1H, bs, D_2O exchangeable)), 1.73 (3H, s), 1.98 (1H, dd, *J* = 12, 4 Hz), 4.62 (1H, bs), 4.83–4.96 (3H, m), 5.84 (1H, dd, *J* = 16, 12 Hz); ms *m/e*: 204 ($M^+ - H_2O$), 189, 163. High resolution molecular weight determination, calcd. for $C_{15}H_{26}O - H_2O$: 204.1878; found: 204.1887. *Anal.* calcd. for $C_{15}H_{26}O$: C 81.08, H 11.71; found: C 80.96, H 11.63.

Acknowledgements

Financial aid from the Science Council of British Columbia is gratefully acknowledged. The authors would also like to thank MacMillan Bloedel Limited and Mr. Alan Moss and Associates for generous samples of cedar leaf oil. We are grateful to Dr. Lewis S. L. Choi for helpful discussions and assistance.

1. J. P. KUTNEY, J. BALSEVICH, R. CARRUTHERS, A. MARKUS, M. J. MCGRATH, R. N. YOUNG, and B. R. WORTH. Bioorg. Chem. **7**, 289 (1979).
2. J. P. KUTNEY, M. J. MCGRATH, R. N. YOUNG, and B. R. WORTH. Can. J. Chem. **57**, 3145 (1979).
3. J. P. KUTNEY, M. K. CHOUDHURY, J. M. DECESARE, H. JACOBS, A. K. SINGH, and B. R. WORTH. Can. J. Chem. **59**, 3162 (1981).
4. J. P. KUTNEY, P. GRICE, K. O. PASCOE, K. PIOTROWSKA, S. J. RETTIG, J. SZYKULA, and J. TROTTER. Helv. Chim. Acta, **65**, 2345 (1982).
5. J. P. KUTNEY, J. BALSEVICH, and P. GRICE. Can. J. Chem. **58**, 2641 (1980).
6. J. P. KUTNEY and A. K. SINGH. Can. J. Chem. **60**, 1842 (1982).
7. D. C. HUMBER, A. R. PINDER, and R. A. WILLIAMS. J. Org. Chem. **32**, 2335 (1967).
8. R. H. SHAPIRO. Org. React. **23**, 205 (1976).
9. T. G. HALSALL, D. W. THEOBALD, and K.B. WALSHAW. J. Chem. Soc. 1029 (1964).
10. P. A. GRIECO and M. NISHIZAWA. J. Org. Chem. **42**, 1717 (1977), and references cited therein.
11. L. J. PATIL and A. S. RAO. Tetrahedron Lett. 2273 (1967).
12. E. J. COREY and E. A. BROGER. Tetrahedron Lett. 1779 (1969), and earlier papers cited therein.
13. R. V. H. JONES and M. D. SUTHERLAND. Chem. Commun. 1229 (1968).
14. H. BAUER. Ber. **46**, 92 (1913).

Solvent structure effects on electron thermalization ranges in water–alcohol mixed solvents; preferred E_{Amax} values for e^-_s in alcohols[1]

AH-DONG LEU,[2] KAMAL N. JHA,[2] AND GORDON R. FREEMAN
Chemistry Department, University of Alberta, Edmonton, Alta., Canada T6G 2G2

Received June 7, 1982

AH-DONG LEU, KAMAL N. JHA, and GORDON R. FREEMAN. Can. J. Chem. **61**, 1115 (1983).

Addition of 2 mol% of an alcohol to water or of 1 mol% of water to an alcohol increases the value of $G_{fi}\epsilon_{max}$ (e^-_s) above that in the pure solvent. The effect is attributed mainly to an increasing free ion yield G_{fi}. The increase of G_{fi} correlates with a "stiffening" of the solvent molecular rotational motions and a corresponding lower rate of energy loss by the epithermal electrons to dipole rotations. Thus the increase of G_{fi} is mainly attributed to a larger electron thermalization range b_{GP}. The value of $G_{fi}\epsilon_{max}$ passes through a maximum at 2 mol% of an alcohol in water; the maximum increases in the order methanol < ethanol < 1-propanol as additive. The solvent "stiffening" effect of these solutes increases in the same order.

Some of the published values of E_{Amax} and $W_{1/2}$ for solvated electrons in alcohols appear to be too low. A set of preferred values is reported herein.

AH-DONG LEU, KAMAL N. JHA et GORDON R. FREEMAN. Can. J. Chem. **61**, 1115 (1983).

L'addition de 2 mol% d'un alcool à l'eau ou de 1 mol% d'eau à un alcool augmente la valeur de $G_{fi}\epsilon_{max}$ (e^-_s) au dessus de celle du solvant pur. On attribue principalement cet effet à une augmentation du rendement de l'ion libre qui donne G_{fi}. L'augmentation de G_{fi} est en accord avec un raidissement des mouvements de rotation moléculaire du solvant et avec une vitesse correspondante plus faible de la perte d'énergie par les électrons épithermiques lors des rotations du dipole. Ainsi on attribue l'augmentation de G_{fi} principalement à un plus large distance de thermalisation de l'électron b_{GP}. La valeur de $G_{fi}\epsilon_{max}$ passe par un maximum à 2 mol% d'un alcool dans l'eau; le maximum augmentant dans l'ordre suivant: méthanol < éthanol < propanol-1 comme additifs. L'effet de raidissement du solvant de ces solutés augmente dans le même ordre.

Quelques unes des valeurs de E_{Amax} et de $W_{1/2}$ préférées pour les électrons solvatés dans des alcools semblent trop faibles. On rapporte qui ont été publié ici un ensemble de valeurs.

[Traduit par le journal]

Introduction

Addition of water to an alcohol has a large effect on the optical absorption energy and band shape of solvated electrons (1). The large effect of water was expected in tertiary and secondary alcohols, because the optical absorption energies, and presumably the electron trap depths, are greater in water than in these alcohols. However, water also has an unexpected, large effect on the spectra of solvated electrons in primary alcohols, where the absorption energies in the pure alcohols are greater than those in water. Furthermore, a distinct minimum in E_{Amax} exists at about 10 mol% water in a primary alcohol, which seems to imply that a particular solvent structure exists at that composition. No direct evidence about the nature of the structure is available, but speculation was offered about a hydrogen bonded cube of eight alcohol molecules reinforced by a water molecule at its center (1). Intermolecular solvent structure, rather than intramolecular structure by itself, has a dominating influence on the energy levels of solvated electrons.

The intensity of the e^-_s absorption, measured by $G\epsilon_{max}$, has now been found to display an unusual composition dependence in alcohol/water mixed solvents. The results are reported herein.

On a mundane level, there are significant discrepancies among reported values of E_{Amax} for solvated electrons in many alcohols at ~298 K (2–12). The discrepancies might be caused by the presence of impurities such as water in some of the alcohols. It seems less likely that the discrepancies, sometimes as much as 20% (5), were caused by malfunctioning monochromators. We present an internally consistent set of values of E_{Amax}, $W_{1/2}$, W_r, and W_b for $C_nH_{2n+2}O$, with $n = 0, 1, 2, ---, 8$.

Experimental

The materials and techniques were the same as those described earlier (1).

In brief, samples of purified alcohols and water in Spectrosil cells were given monitored 1.0 μs pulses of 1.8 MeV electrons (9×10^{16} eV/g). The optical absorbance at a given wavelength was measured as a function time after each pulse. The observed values of the absorbance A_{obs} at the end of a pulse were corrected for first order decay during the pulse to obtain A_e.

$$[1] \quad A_e = A_{obs}kt_p/[1 - \exp(-kt_p)]$$

where t_p is the pulse duration and $k = 0.69/t_{1/2}$ is the decay constant.

The pulse dose monitor was calibrated with 5 m*M* KCNS solution saturated with oxygen, using $G\epsilon_{max}$ = 21 000 (e^-_s/100 eV *M* cm) at 478 nm and 298 K.

Results and discussion

$G\epsilon_{max}$ and electron thermalization ranges

The value of $G\epsilon_{max}$ (e^-_s/100 eV *M* cm) was measured at 298 K in methanol, ethanol, and 1-propanol as functions of water concentration. There is a maximum in $G\epsilon_{max}$ at 98 mol% water in each system (Fig. 1). The height of the maximum increases in the order methanol < ethanol < 1-propanol, being 12, 16, and 24% greater than $G\epsilon_{max}$ in pure water. At the other end of the composition range, addition of 1 mol% water to alcohol also causes a significant increase of $G\epsilon_{max}$, by 6% in methanol, ~10% in ethanol, and 21% in 1-propanol.

The $G\epsilon$ curves in Fig. 1 show that the effects of water and alcohol are not additive. Between 10 and 98 mol% water the

[1]Assisted financially by the Natural Sciences and Engineering Research Council of Canada.

[2]Present address: Research and Development Division, Saskatchewan Oil and Gas Corp., Regina, Sask., Canada S4P 0B5.

Can. J. Chem. Downloaded from www.nrcresearchpress.com by 210.87.254.105 on 09/06/12
For personal use only.

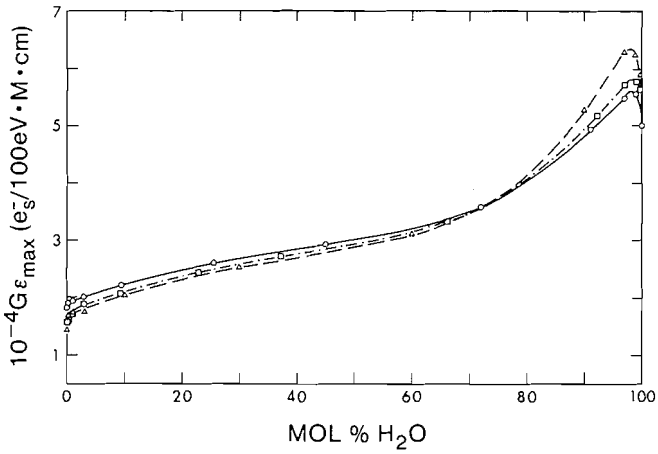

FIG. 1. Composition dependence of $G\epsilon_{max}$ in alcohol–water mixed solvents at 298 K. ○, methanol; □, ethanol; △, 1-propanol.

alcohols dominate the behavior of $G\epsilon$. This is the opposite of the effects on the optical band energy parameters, which were dominated by water (1).

The addition of 1 mol% of water to an alcohol or of 2 mol% of alcohol to water has greater relative effects on $G\epsilon_{max}$ than on the energy parameters of the absorption bands (Table 1). It is therefore probable that ϵ_{max} remained relatively constant for the small change of composition and that the increase of $G\epsilon_{max}$ was mostly due to an increase in G. The changes in G were analysed by the modified Onsager model (13, 14) to gain insight about electron behavior in the mixed solvents.

The approximate mechanism is as follows.

[2] $\mathrm{ROH} \rightsquigarrow [\dot{\mathrm{R}}\mathrm{OH}^+ + e^-]$

[3] $[e^- + n\mathrm{ROH}] \rightarrow [e^-_s]$

[4] $[\dot{\mathrm{R}}\mathrm{OH}^+ + m\mathrm{ROH}] \rightarrow [\mathrm{H}^+_s + \mathrm{RO}\cdot]$

[5] $[e^-, \dot{\mathrm{R}}\mathrm{OH}^+, e^-_s, \mathrm{H}^+_s] \rightarrow$ geminate neutralization

[6] $[e^-, \dot{\mathrm{R}}\mathrm{OH}^+, e^-_s, \mathrm{H}^+_s] \rightarrow e^-_s + \mathrm{H}^+_s$, free ions

Reaction [6] indicates that by the time electrons and ions have escaped from spurs the solvation processes [3] and [4] are complete (13). Under the conditions of the present measurements only the solvated electrons that had become free ions were measured.

The free ion yield in the single pair spur model is given by (13):

$$[7] \quad G_{fi} = G_{tot} \int_0^\infty F(y) \exp(-\xi^2/\epsilon_{ave} ykT)\, dy$$

where G_{tot} is the initial number of ionizations (reaction [2]) per 100 eV absorbed by the system, $F(y)dy$ is the fraction of electrons that travel distances between y and $y + dy$ from the parent ions during thermalization, ξ is the protonic charge, ϵ_{ave} is the average value of the time dependent dielectric constant during the competition between reactions [5] and [6], k is Boltzmann's constant, and T is the absolute temperature.

The $F(y)$ distribution function YGP (14), which has a Gaussian body and a power function tail, was used.

$$[8] \quad F(y)_1 = (3.84y^2/\pi^{1/2}b_{GP}^3) \exp(-y^2/b_{GP}^2), \quad y < 2.4\ b_{GP}$$

$$F(y)_2 = F(y)_1 + 0.48b_{GP}^2/y^3, \quad y > 2.4\ b_{GP}$$

A simple Gaussian would be adequate for alcohols and water because the power function tail is only needed to explain the electric field dependence of the small free ion yields ($G_{fi} < 0.2$) obtained in most hydrocarbons (14).

On the timescale of reaction [5] the dielectric constant of an alcohol, and probably that of water, is time dependent (13, 15, 16). Equation [7] would be more accurately represented as [7']:

$$[7'] \quad G_{fi} = G_{tot} \int_0^\infty \int_0^{t_{gn}(y)} F(y) \exp(-\xi^2/\epsilon(t) ykT)\, dy dt$$

where $\epsilon(t)$ is the dielectric constant of the medium between the ion and the electron as a function of time after the ionization event, and $t_{gn}(y)$ is the mean time required for geminate neutralization from an initial separation distance y. The value of $t_{gn}(y)$ is also a function of $\epsilon(t)$, so the complete calculation would be done iteratively. However, the range and relaxation parameters are not yet well enough known for such a treatment.

One can estimate crude values of ϵ_{ave} for use in eq. [7], for example, by assuming Debye-type relaxation with time constant τ (13):

$$[9] \quad \epsilon_{ave} = \epsilon_\infty + \frac{\epsilon_0 \tau}{t_{gn}} \ln\left(\frac{1 + [(\epsilon_\infty - \epsilon_0)/\epsilon_0] \exp(-\epsilon_\infty t_{gn}/\epsilon_0 \tau)}{1 + [(\epsilon_\infty - \epsilon_0)/\epsilon_0]}\right)$$

where ϵ_0 and ϵ_∞ are the values of ϵ at $t = 0$ and ∞, respectively. The values of τ and t_{gn} appear only as a ratio in eq. [9]. Addition of a small amount of alcohol to water or of a small amount of water to alcohol causes both τ (16) and the viscosity (17) to increase. Electron mobility in these liquids is ion like, so the mobilities are roughly inversely proportional to the viscosity and t_{gn} would be approximately proportional to the viscosity. These effects would tend to keep the ratio τ/t_{gn} constant.

Values of ϵ_∞ were obtained from ref. 18; the value for pure methanol in this reference was 3% low (17), so small corrections were applied for methanol containing <10 mol% water. The value of ϵ_0 changes negligibly upon the addition of a small amount of alcohol to water (16) or of water to alcohol (17).

The nitrogen yields from concentrated solutions (1–10 mol%) of nitrous oxide in water (19)[3] and the three alcohols (13, 20, 21) indicate that G_{tot} lies in the range 4.2–4.9. The value $G_{tot} = 4.6$ was used for all the liquids.

The free ion yields in water (22, 23) and the alcohols (13, 20, 24) were derived from scavenging yields, with the aid of models. The free ion yields in the mixed solvents were then estimated from the changes in $G_{fi}\epsilon_{max}$ (Table 1). Whether a bit of water was added to an alcohol or a bit of an alcohol was added to water, G_{fi} increased.

In our earlier study of electron scavenging in water by nitrous oxide we had added 3.3 mol% of ethanol to scavenge hydrogen atoms and hydroxyl radicals (19). The estimated free ion yield, 2.7, was therefore higher than would be obtained in pure water. For the present work we have chosen $G_{fi} = 2.6$, but the true value might be even lower.

It had been reported previously that addition of 2 mol% of ethanol to water increases G_{fi} (e^-_s) by 0.2 units, from 2.65 to 2.84 (23). The increase was attributed to the occurrence of reaction [10], thereby preventing reaction [11], and it was assumed that reaction [12] did not occur to an appreciable extent.

[10] $[\dot{\mathrm{O}}\mathrm{H} + \mathrm{RCH_2OH}] \rightarrow [\mathrm{H_2O} + \dot{\mathrm{R}}\mathrm{CHOH}]$

[3] $G_{tot} > 4.0$ because $G(N_2)$ did not reach a plateau (Fig. 1 of ref. 19).

Can. J. Chem. Downloaded from www.nrcresearchpress.com by 210.87.254.105 on 09/06/12
For personal use only.

TABLE 1. Free ion yields and electron ranges in ROH/H_2O solutions at 298 K

Solvent[a]	Solute[a] (mol%)	ϵ_s[b]	$E_{\lambda max}$[c] (eV)	$10^{-3}\ G_{fi}\epsilon_{max}$ (e^-_s/100 eV M cm)	$10^{-3}\ \epsilon_{max}$ (M^{-1} cm^{-1})	G_{fi} (e^-_s/100 eV)	$\epsilon_{ave} b_{GP}$[d] (nm)	$_{min}b_{GP}$[e] (nm)
W	—	78.5	1.73	50	19.2	2.6[f]	94	1.2
W	M, 2	77.0	1.75	56	19[g]	2.9[h]	~123	~1.6
W	E, 2	75.7	1.76	58	19[g]	3.0[h]	~129	~1.7
W	P, 2	74.3	1.76	62	19[g]	3.2[h]	~156	~2.1
W	P, 10	60.0	1.79	53	18[g]	2.9[h]	~120	~2.0
W	P, 40	31.3	1.79	31	18[g]	1.7[h]	~53	~1.7
M	—	32.6	1.97	18.2	9.6	1.9[i]	59	1.8
M	W, 1	32.8	1.94	19.3	9.6[g]	2.0[h]	62	1.9
E	—	24.3	1.82	15.6	10.4	1.5[j]	46	1.9
E	W, 1	24.4	1.78	16.9(17.5[l])	10.4[g]	1.6[h](1.7[m])	49(51)	2.0(2.1)
P	—	20.1	1.95	14.3	11.7	1.2[k]	36	1.8
P	W, 1	20.2	1.88	17.3	11.7[g]	1.5[h]	44	2.2

[a] W = water, M = methanol, E = ethanol, P = 1-propanol, 2 = 2 mol% and so on.
[b] Reference 18, with methanol values corrected from ref. 16.
[c] Reference 1.
[d] Calculated from eqs. [7] and [8], assuming $G_{tot} = 4.6$.
[e] Value that would be obtained if $\epsilon_{ave} = \epsilon_s$.
[f] References 22 and 23.
[g] Assumed.
[h] Obtained using assumed ϵ_{max}.
[i] References 20*a* and 24.
[j] Reference 20*b*.
[k] Reference 13.
[l] Estimated from Fig. 1.

[11] $[e^-_s + \dot{O}H] \rightarrow [OH^-_s]$

[12] $[e^-_s + R\dot{C}HOH] \rightarrow [RCHOH^-_s]$

Two mol% of alcohol in water corresponds to an alcohol concentration of 1 mol/dm^3. The values of the rate constant k_{10} (dm^3/mol s) in aqueous solution at ~295 K are ~9×10^8 for methanol, ~18×10^8 for ethanol, and ~27×10^8 for 1-propanol (25). The half-lives of reaction [10] in the 2% solutions are therefore ~1.1, ~0.6, and ~0.4 ns, respectively. Thus reaction [10] is negligible until well after the few ps required for reactions [3] and [4] to go to completion. However, reaction between the solvated intermediates in multipair spurs continues to be significant at several ns in water (26, 27), so [10] would influence the latter spur reactions. But reaction [12] should be included. It is probably exothermic, because gas phase radicals have positive electron affinities (28) and the solvation energy of the anion is probably greater than that of the electron.[4] The value of the rate constant k_{12} in the alcoholic aqueous solutions would be smaller than that of k_{11} in water solvent, because addition of an alcohol to water increases the viscosity η and the dielectric relaxation time τ of the system (16, 17). The diffusion coefficients of the radical and e^-_s (which is in a deeply localized state) in hydroxylic solvents decrease with increasing η and τ.

The decay rate of e^-_s during the time period 0.1–3.3 ns is 1.6-fold slower in 3 M ethanol/water than in pure water solvent (26). The value of η of the 3 M ethanol solvent is 1.7-fold larger than that of water (17), and the value of τ is ~1.5-fold larger (by comparison with the 1.74 factor for a 3 M 1-propanol aqueous solution, ref. 16). The values of k_{10} and k_{12} should therefore be about 1.6-fold smaller in the 3 M ethanol solvent than in water. This factor alone explains the difference between the e^-_s decay curves in water and 3 M ethanol shown in Figs. 2 and 3 of ref. 26. The 3 M ethanol curves superimpose the water curves if the times of the former are reduced 1.6-fold, taking the 0.1 ns normalization point as the zero of time. The signal heights, which are proportional to $G\epsilon(e^-_s)$, were normalized at 0.1 ns, so an increase of $G\epsilon$ caused by the addition of ethanol to water would not be observed. It therefore seems probable that the increase of $G_{fi}(e^-_s)$ reported by Fielden and Hart (23) was due mainly to events that occurred before 0.1 ns, namely, an increase of electron thermalization range.

Furthermore, reactions analogous to [10] could not explain the increase of $G_{fi}(e^-_s)$ caused by the addition of 1 mol% of water to the alcohols. The analogous reactions would be the reverse of reaction [10] and would be endothermic. Even if they did occur to an appreciable extent during the lifetime of the spur they would not cause $G_{fi}(e^-_s)$ to increase because the product $\dot{O}H$ radical is as efficient an electron scavenger as the $R\dot{C}HOH$ radical. The increase of $G_{fi}(e^-_s)$ when a little water is added to an alcohol is therefore due to something else.

The increase of $G_{fi}(e^-_s)$ caused by addition of 1 mol% of water to an alcohol, and at least a major portion of that caused by addition of 2 mol% of an alcohol to water, is attributed to an increase of the electron thermalization distance b_{GP}. The

[4] Dorfman and Taub reported that the lifetime of e^-_s was an order of magnitude smaller than that of $CH_3\dot{C}HOH$ in pulse irradiated 0.5 M ethanol in neutral water. They suggested that e^-_s and $CH_3\dot{C}HOH$ did not interact. The e^-_s lifetime would be dominated by reaction with H^+_s and H_2O_2 formed during the 5 μs (10 krad) pulse and possibly with H_2O_2 and acetaldehyde accumulated from previous pulses. The alcohol radicals would therefore be left to react mainly with each other. One cannot conclude from these results that $k(e^-_s + CH_3\dot{C}HOH)$ is small.

Can. J. Chem. Downloaded from www.nrcresearchpress.com by 210.87.254.105 on 09/06/12
For personal use only.

TABLE 2. Dielectric relaxation time and electron range at 298 K

Solvent	ϵ_∞	G_{fi}	$\epsilon_{ave} b_{GP}$ (nm)	$_{min}b_{GP}$ (nm)	τ^a (ps)	$(-dW/dt)_{dip}{}^b$ (eV/ps)
H_2O^c	78.5	2.6	94	1.2	8.4	8.2
D_2O	78.3	2.9[d]	118[e]	1.5[e]	10.7	6.3
H_2O + 2% P[e]	74.3	3.2	~156	~2.1	10.4	6.2

[a] Reference 16*a*.
[b] Estimated from eq. [13], using $\epsilon_{ir} = 5.5$ (16*a*), $d = 3.8 \times 10^{-8}$ cm, and $n = n_D = 1.333$ for each liquid.
[c] Table 1.
[d] Reference 33.
[e] See footnotes *d* and *e* in Table 1.

value of $\epsilon_{ave} b_{GP}$ for each of the liquids was calculated from eqs. [7] and [8] and is listed with the other pertinent data in Table 1. A lower limit for b_{GP} was estimated by taking $\epsilon_{ave} = \epsilon_\infty$; it is labelled $_{min}b_{GP}$ in Table 1.

The value of $_{min}b_{GP}$ increases progressively on going from methanol to ethanol to propanol as the 2% additive in water. The relative effect is greater for adding a bit of alcohol to water than for adding a bit of water to alcohol (Table 1). These changes correlate with the relative extents of changes in the liquid structures, as reflected by the viscosities (17). Furthermore, adding a few percent of an alcohol to water actually increases the partial molar volume of water, presumably due to enhancement of an icelike structure (29). At >10 mol% of alcohol the partial molar volume of water decreases, due to breaking of the icelike structure. There is a minimum in the partial molar excess volume of the alcohol in dilute aqueous solution. The minimum is deepest (-6.5 cm^3/mol) and lies at the lowest concentration (3 mol%) for 1-propanol, next deepest for ethanol (-5.7 cm^3/mol at 7 mol%), and shallowest for methanol (-3.3 cm^3/mol at 10 mol%) (29). Other thermodynamic parameters exhibit complex behavior that imply the existence of enhanced ordering of the liquid structure when a few mol% of an alcohol is added to water (30–32). For example, ethanol can form a clathrate $C_2H_5OH \cdot 17H_2O$, which is 6 mol% ethanol (31); there is a maximum in the velocity of sound and in the sound absorption coefficient around 7 mol% *t*-butanol in water (p. 55 of ref. 30); the critical micelle concentration of sodium dodecyl sulfate at 298 K has a minimum at 4 mol% *t*-butanol in water (30); in the hydrolysis of *t*-butyl chloride there are maxima in the enthalpy and entropy of activation for 3 mol% ethanol in water (32); and so on.

An increase of the icelike structure of water "hardens" the fluid and increases the rotational relaxation time τ (16). An increase in τ decreases the rate at which epithermal electrons lose energy W to dipole rotations (33):

$$[13] \quad \left(-\frac{dW}{dt}\right)_{dip} \approx \frac{\pi\xi^2(\epsilon_\infty - \epsilon_{ir})}{4dn^4\tau} \text{ erg/s}$$

where ϵ_{ir} = dielectric constant at frequencies sufficiently lower than the main infrared absorption frequency, d = intermolecular distance, and n = a suitable average optical refractive index; the units are ξ (esu) and d (cm). The thermalization time and therefore the value of b_{GP} is greater when τ is larger, other things being equal.

The liquid structure effect is also observed when comparing G_{fi} values in H_2O and D_2O (Table 2). The value of $G_{fi}(e^-_s)$ in D_2O is 11% greater than that in H_2O at ~298 K (34–36), which corresponds to a 25% greater value of $_{min}b_{GP}$ and correlates with the 27% larger τ in D_2O (Table 2 and ref. 37). The behavior in D_2O is similar to that in H_2O containing 2 mol% alcohol.

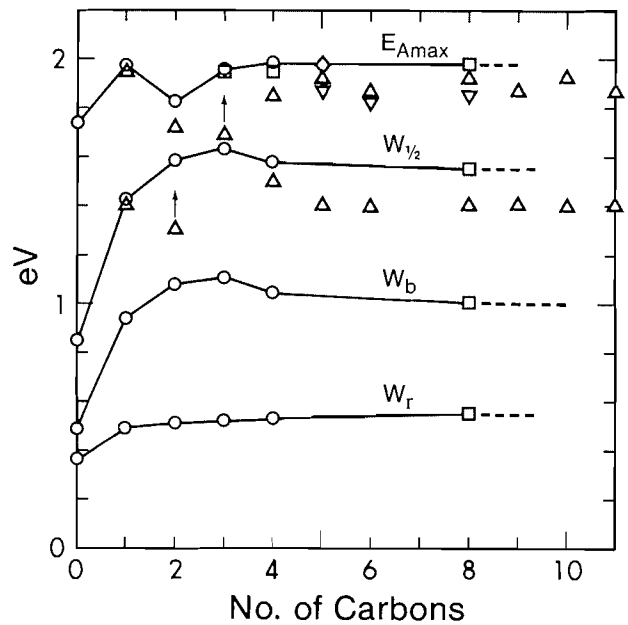

FIG. 2. Spectral parameter values as functions of the number of carbon atoms in 1-alcanols at 298 K. ○, this work; ◇, ref. 40; □, ref. 12; △, ref. 6; ▽, ref. 5. The E_{Amax} values from refs. 5, 6, and 12 were increased slightly to adjust to 298 K, using measured temperature coefficients for primary alcohols (40).

Critique

The preceding discussion is based upon a model in which there is only one ion–electron pair per spur (13). In reality, only about half of the ion–electron pairs are initially in single pair spurs; in water most of these become free ions. Most of the geminate reaction in water and much of it in alcohols occurs in spurs that initially contain more than one pair. Geminate neutralization yield calculations with an accurate multipair spur model are not yet possible (38). However, one may deduce that the above conclusions about structure effects in the mixed solvents and D_2O would be magnified in a multipair spur model. For example, the estimated increases of electron range would be larger.

Jonah and co-workers neglected solvent structure effects of solutes in their kinetic analysis of the e^-_s decay curves over the period 0.1–3.3 ns (26). Inclusion of the structure effects, which are large for the 1–3 mol/dm^3 that they used of ethanol, ammonia, sodium acetate, and sodium hydroxide, will greatly alter the diffusion coefficients and rate constants of the species. The conclusions drawn from the analysis will also be changed. In addition to those discussed above one might mention that

Can. J. Chem. Downloaded from www.nrcresearchpress.com by 210.87.254.105 on 09/06/12
For personal use only.

TABLE 3. Preferred values of $E_{\lambda max}$ and $W_{1/2}$ for e^-_s at 298 K

Solvent	$E_{\lambda max}$ (eV)	$W_{1/2}$ (eV)
Water	1.73	0.85
Methanol	1.97	1.43
Ethanol	1.82	1.59
1-Propanol	1.95	1.63
2-Propanol	1.52	1.45
1-Butanol	1.98	1.57
2-Methyl-1-propanol	1.97	1.61
2-Butanol	1.59	1.57
1-Pentanol	1.97	~1.57
1-Octanol	1.98	1.55

most of the effect of the sodium acetate at times up to 2 ns is attributable to the 1.4-fold increase of viscosity (39).

Reassessment of spectral parameter values in pure solvents

Recent measurements (1, 12, 40) indicate that some of the earlier reported values of $E_{\lambda max}$ and $W_{1/2}$ for solvated electrons in 1-alcanols (5, 6) are too low (Fig. 2). A possible cause of the low values, in addition to instrumental error, is the presence of a few mol% of water in the alcohols (1). Consistent with the wet alcohol interpretation is the relatively good agreement between the present and earlier (6) values for methanol, and the much smaller sensitivity to water of the parameters in methanol than those in other alcohols (1). Similar errors appear to exist for other alcohols as well (6), so preferred values are listed in Table 3.

Values of $E_{\lambda max}$ plotted against the number of carbon atoms in a 1-alcanol show a dip at ethanol (Fig. 2). In view of the discussion in the previous section, the dip is qualitatively attributed to a peculiarity of the liquid structure, without being able to say what it is.

Analogous plots show more variation in W_b than in W_r (Fig. 2).

1. A.-D. LEU, K. N. JHA, and G. R. FREEMAN. Can. J. Chem. **60**, 2342 (1982).
2. I. A. TAUB, D. A. HARTER, M. C. SAUER, JR., and L. M. DORFMAN. J. Chem. Phys. **44**, 979 (1964).
3. M. C. SAUER, JR., S. ARAI, and L. M. DORFMAN. J. Chem. Phys. **42**, 708 (1965).
4. K. N. JHA, G. L. BOLTON, and G. R. FREEMAN. J. Phys. Chem. **76**, 3876 (1972).
5. R. R. HENTZ and G. A. KENNEY-WALLACE. J. Phys. Chem. **76**, 2931 (1972).
6. R. R. HENTZ and G. A. KENNEY-WALLACE. J. Phys. Chem. **78**, 514 (1974).
7. G. G. TEATHER and N. V. KLASSEN. Int. J. Rad. Phys. Chem. **7**, 475 (1975).
8. F.-Y. JOU and G. R. FREEMAN. J. Phys. Chem. **81**, 909 (1977).
9. T. A. CHUBAKOVA and N. A. BAKH. High Engy. Chem. **12**, 315 (1977).
10. K. OKAZAKI and G. R. FREEMAN. Can. J. Chem. **56**, 2313 (1978).
11. F.-Y. JOU and G. R. FREEMAN. J. Phys. Chem. **83**, 261 (1979).
12. F.-Y. JOU and G. R. FREEMAN. Can. J. Chem. **57**, 591 (1979).
13. K. N. JHA and G. R. FREEMAN. J. Chem. Phys. **51**, 2839 (1969).
14. J.-P. DODELET, K. SHINSAKA, U. KORTSCH, and G. R. FREEMAN. J. Chem. Phys. **59**, 2376 (1973).
15. G. R. FREEMAN. Adv. Chem. Ser. **82**, 339 (1968).
16. (*a*) F. BUCKLEY and A. A. MARYOTT. Tables of dielectric dispersion data for pure liquids and dilute solutions. NBS Circular 589, US Dept. of Commerce, Washington, DC, 1958; (*b*) F. X. Hassion and R. H. Cole. J. Chem. Phys. **23**, 1756 (1955).
17. (*a*) J. TIMMERMANS. The physico-chemical constants of binary systems in concentrated solutions. Vol 4. Interscience, New York. 1960; (*b*) W. WEBER. Rheol. Acta, **14**, 1012 (1975); (*c*) R. L. KAY, G. P. CUNNINGHAM, and D. F. EVANS. *In* Hydrogen bonded solvent systems. Taylor and Francis, London. 1968. p. 249.
18. G. ÅKERLÖF. J. Am. Chem. Soc. **54**, 4125 (1932).
19. J. C. RUSSELL and G. R. FREEMAN. J. Chem. Phys. **48**, 90 (1968).
20. K. N. JHA and G. R. FREEMAN. J. Chem. Phys. (*a*) **48**, 5480 (1968); (*b*) **51**, 2846 (1969).
21. T. E. M. SAMBROOK and G. R. FREEMAN. Can. J. Chem. **53**, 1521 (1975).
22. M. HAISSINSKY. J. Chim. Phys. **62**, 1149 (1965).
23. E. M. FIELDEN and E. J. HART. Radiat. Res. **32**, 564 (1967).
24. K. N. JHA and G. R. FREEMAN. J. Am. Chem. Soc. **95**, 5891 (1973).
25. L. M. DORFMAN and G. E. ADAMS. NSRDS-NBS 46, U.S. Dept. of Commerce, Washington, DC. 1973.
26. C. D. JONAH, M. S. MATHESON, J. R. MILLER, and E. J. HART. J. Phys. Chem. **80**, 1267 (1976).
27. C. D. JONAH and J. R. MILLER. J. Phys. Chem. **81**, 1974 (1977).
28. G. R. FREEMAN. Radiat. Res. Rev. **1**, 1 (1968). Table 3.
29. G. C. BENSON and O. KIYOHARA. J. Solution Chem. **9**, 791 (1980).
30. F. FRANKS (*Editor*). Physico-chemical processes in mixed aqueous solvents. Elsevier, New York. 1967. See especially Chapt. 3 by F. Franks and Chapt. 6 by E. M. Arnett.
31. A. D. POTTS and D. W. DAVIDSON. J. Phys. Chem. **69**, 996 (1965).
32. A. Winstein and A. H. FAINBERG. J. Am. Chem. Soc. **79**, 5937 (1957).
33. H. FRÖHLICH and R. L. PLATZMAN. Phys. Rev. **92**, 1152 (1953).
34. D. A. ARMSTRONG, E. COLLINSON, and F. S. DAINTON. Trans. Faraday Soc. **55**, 1375 (1959).
35. E. M. FIELDEN and E. J. HART. Radiat. Res. **33**, 426 (1968).
36. K.-D. ASMUS and J. H. FENDLER. J. Phys. Chem. **73**, 1583 (1969).
37. C. H. COLLIE, J. B. HASTED, and D. M. RITSON. Proc. Phys. Soc. **60**, 145 (1948).
38. J.-P. DODELET and G. R. FREEMAN. Int. J. Radiat. Phys. Chem. **7**, 183 (1975).
39. R. H. STOKES and R. MILLS. Viscosity of electrolytes and related properties. Pergamon, Oxford. 1965. p. 143.
40. K. OKAZAKI, A.-D. LEU, and G. R. FREEMAN. Unpublished results.
41. L. M. DORFMAN and I. A. TAUB. J. Am. Chem. Soc. **85**, 2370 (1963).

Can. J. Chem. Downloaded from www.nrcresearchpress.com by 210.87.254.105 on 09/06/12
For personal use only.

Kinetics and mechanisms of the oxidation of ascorbic acid and benzene diols by nickel(III)tetraazamacrocycles in aqueous perchloric acid

A. McAuley,[1] T. Oswald,[2] and R. I. Haines

Department of Chemistry, University of Victoria, Victoria, B.C., Canada V8W 2Y2

Received February 12, 1982[3]

A. McAuley, T. Oswald, and R. I. Haines. Can. J. Chem. **61**, 1120 (1983).

The kinetics of reaction of ascorbic acid, hydroquinone, and catechol (H_2A) with nickel(III) macrocycles (NiL^{3+}) (L = cyclam, *meso*-(5,12)-7,7,14,14-Me_6-14-ane-1,4,8,11-N_4 (tet-*a*), and *rac*-(5,14)-7,7,12,12-Me_6-14-ane-1,4,8,11-N_4 (tet-*c*):

$$2NiL^{3+} + H_2A \rightarrow 2NiL^{2+} + A + 2H^+$$

have been investigated in aqueous perchloric acid solutions using the stopped-flow technique. The data are consistent with a rate-determining one-electron transfer reactions:

$$NiL^{3+} + H_2A \xrightarrow{k_1} NiL^{2+} + H_2A^+$$

$$NiL^{3+} + HA^- \xrightarrow{k_4} NiL^{2+} + HA^\cdot$$

$$H_2A \rightleftharpoons HA^- + H^+ \ (K_a)$$

followed by a rapid oxidation of the radical formed. In the reaction with ascorbic acid, for Ni(cyclam)$^{3+}$, $k_1 = 250\ M^{-1}\ s^{-1}$ (25°C), $k_4K_a = 680\ s^{-1}$; Ni(tet-*c*)$^{3+}$, $k_1 = 2.52 \times 10^3\ M^{-1}\ s^{-1}$, $k_4K_a = 1.06 \times 10^4\ s^{-1}$; and Ni(tet-*a*)$^{3+}$, $k_1 = 2.85 \times 10^3\ M^{-1}\ s^{-1}$ (21.95°C), $k_4K_a = 1.26 \times 10^4\ s^{-1}$. With catechol, $k_1 = 6.98 \times 10^2\ M^{-1}\ s^{-1}$, $1.73 \times 10^4\ M^{-1}\ s^{-1}$, and $3.3 \times 10^4\ M^{-1}\ s^{-1}$ respectively in reactions with Ni(cyclam)$^{3+}$, Ni(tet-*c*)$^{3+}$, and Ni(tet-*a*)$^{3+}$. With hydroquinone, $k_1 = 1.09 \times 10^4\ M^{-1}\ s^{-1}$ (Ni(cyclam)$^{3+}$) and $2.49 \times 10^5\ M^{-1}\ s^{-1}$ (20.9°C) (Ni(tet-*c*)$^{3+}$). The reactions are considered to take place via an outer-sphere mechanism and rate constants are discussed in terms of the Marcus cross correlation. Use has been made of predicted rate constants to identify reaction pathways in the hydrogen-ion dependent systems.

A. McAuley, T. Oswald et R. I. Haines. Can. J. Chem. **61**, 1120 (1983).

Faisant appel à la méthode de flux stoppé, on a étudié, dans des solutions aqueuses d'acide perchlorique, la cinétique de la réaction de l'acide ascorbique, de l'hydroquinone et du catéchol (H_2A) avec les macrocycles de Ni(III) (NiL^{3+}) (L = cyclam, *méso*-(5,12)-7,7,14,14-Me_6-ane-14-N_4-1,4,8,11 (tét-*a*) et *rac*-(5,14)-7,7,12,12-Me_6-ane-14-N_4-1,4,8,11 (tét-*c*):

$$2NiL^{3+} + H_2A \rightarrow 2NiL^{2+} + A + 2H^+$$

Les données s'accordent avec une étape de transition impliquant des réactions de transfert à un électron:

$$NiL^{3+} + H_2A \xrightarrow{k_1} NiL^{2+} + H_2A^+$$

$$NiL^{3+} + HA^- \xrightarrow{k_4} NiL^{2+} + HA^\cdot$$

$$H_2A \rightleftharpoons HA^- + H^+ \ (K_a)$$

qui serait suivi par une oxidation rapide du radical formé lors de la réaction de l'acide ascorbique avec le Ni(cyclam)$^{3+}$, $k_1 = 250\ M^{-1}\ s^{-1}$ (25°C), $k_4K_a = 680\ s^{-1}$; avec Ni(tét-*c*)$^{3+}$ $k_1 = 2{,}52 \times 10^3\ M^{-1}\ s^{-1}$, $k_4K_a = 1{,}06 \times 10^4\ s^{-1}$ et Ni(tét-*a*)$^{3+}$, $k_1 = 2{,}85 \times 10^3\ M^{-1}\ s^{-1}$ (21,95°C), $k_4K_a = 1{,}26 \times 10^4\ s^{-1}$; dans le cas du catéchol, ces valeurs sont respectivement $k_1 = 6{,}98 \times 10^2\ M^{-1}\ s^{-1}$; $1{,}73 \times 10^4\ M^{-1}\ s^{-1}$ et $3{,}3 \times 10^4\ M^{-1}\ s^{-1}$ pour les réactions avec le Ni(cyclam)$^{3+}$, Ni(tét-*c*)$^{3+}$ et Ni(tét-*a*)$^{3+}$; avec l'hydroquinone $k_1 = 1{,}09 \times 10^4\ M^{-1}\ s^{-1}$ (Ni(cyclam)$^{3+}$) et $2{,}49 \times 10^5\ M^{-1}\ s^{-1}$ (20,9°C) (Ni(tét-*c*)$^{3+}$). On considère que ces réactions se font via un mécanisme hors sphère et on discute des constantes de vitesse en fonction de la corrélation croisée de Marcus. Dans les systèmes où il existe une influence des ions hydrogènes on a utilisé les constantes de vitesse prévues pour identifier les schémas de réactions.

[Traduit par le journal]

Introduction

A variety of metal complexes have been studied as oxidants (1–7) in reaction with ascorbic acid and there is evidence for both inner- and outer-sphere redox behaviour. Intermediate complexes have been identified in the reactions with vanadium(V) (8) and aquo-iron(III) (9) where the redox process involves the formation of an ascorbate radical ion rather than a two-electron transfer to yield the dehydroascorbic acid. Among other complexes of iron(III), for example, the reaction of tris(phenanthroline)iron(III) and its derivatives (2), and the reactions involving thioureapentacyanoferrate(III) (10), the dif-

[1]To whom all correspondence should be addressed.

[2]Present address: Department of Chemistry, University of Calgary, Calgary, Alta., Canada T2N 1N4.

[3]Revision received November 9, 1982.

Can. J. Chem. Downloaded from www.nrcresearchpress.com by 210.87.254.42 on 09/06/12
For personal use only.

Can. J. Chem. Downloaded from www.nrcresearchpress.com by 210.87.254.42 on 09/06/12
For personal use only.

ferences in oxidation rates have been discussed in terms of free energy changes as related to the Marcus theory (11).

In previous studies from our laboratory, we have investigated redox reactions of nickel(III) macrocyclic complexes. Complex formation has been observed in the reactions of nickel(III) cyclam (cyclam = 1,4,8,11-tetraazacyclotetradecane) with Cl^-, Br^-, and NCS^- (12) but with I^- (12) and aromatic diols (13) a redox process occurs. These nickel(III) macrocycles with various ring substituents offer a wide range of oxidising potentials, but relatively few studies have been made of the kinetics and mechanisms of reactions with reducing substrates. In the present paper we report the results of a kinetic study of the oxidation of ascorbic acid by Ni(III)L^{3+} (L = cyclam, tet-*a*, and tet-*c*), and of the latter two complexes as oxidants in reactions with hydroquinone and catechol.

Experimental

Nickel(II)L^{2+} (L = cyclam, tet-*a*, tet-*c*) were prepared as described in the literature (14). Cyclam (Strem) was recrystallised from ethanol before use. For the latter two complexes, the Me_6-4,11- and Me_6-4,14-N_4 diene intermediates prepared initially were reduced to tet-*a* and tet-*c* respectively using Ni/Al alloy at 70°C. Solid samples of the Ni(III) complexes $NiL(CH_3CN)_2(ClO_4)_3$ were prepared by electrolysis (0.01 *M* $NaClO_4$) of the corresponding Ni(II) species in rigorously anhydrous acetonitrile (P_2O_5/CaH_2) at 5°C in the dark under dry N_2. The solids were stored at −15°C in the dark.

L-Ascorbic acid was used as received (Sigma) while catechol and hydroquinone were recrystallised from ethanol. $LiClO_4$ was prepared by neutralisation of Li_2CO_3 with $HClO_4$ and recrystallised three times from distilled water. Care was taken to ensure the absence of SO_4^{2-} ion, which was removed by adding a slight excess of $Ba(ClO_4)_2$.

The stopped-flow apparatus and data acquisition system used have been described previously (15). For some runs a modified Applied Photophysics instrument was used. Both reservoirs and the drive syringes were thermostatted by circulating water (controlled to ±0.05°C). Absorbance data were collected at desired time intervals and processed using a PCM 12 minicomputer. In general, for each run, 200 points were used and rate constants quoted are the least squares slopes of log ($OD_\infty - OD_t$) vs. time curves.

Solutions were prepared immediately before starting the experiments, which were carried out with an excess of reductant. Ionic strength (1.0 *M*) was maintained constant with $LiClO_4$. Solutions of Ni(III)L^{3+} (L = tet-*a*, tet-*c*) were prepared by adding the required amount of solid to the thermostatted solution immediately prior to reaction. This is especially important at lower acid concentrations where decomposition of the (NiL^{3+}) in the absence of reductant was complete in 10−15 min. The disappearance of Ni(III)cyclam^{3+} was observed at 380 nm and that of Ni(III)L^{3+} (L = tet-*a*, tet-*c*) at 408 nm, yielding pseudo-first order plots which were linear over at least three half-lives.

Results and discussion

Spectrophotometric titration of the ascorbic acid and of the diols with the nickel complexes showed a stoichiometry of 2.0 mol of nickel(III) reacting per mole of reductant within experimental error (±4%). The overall reaction may thus be written as

$$[1]\quad 2Ni(III)L^{3+} + H_2A \rightarrow 2Ni(II)L^{2+} + A + 2H^+$$

where L = cyclam, tet-*a*, tet-*c*, and H_2A = ascorbic acid, catechol, or hydroquinone and A is dehydroascorbic acid or the corresponding quinone.

At constant $[H^+]$, the reactions were first order with respect to both oxidant and reductant as indicated by the pseudo first-order disappearance of Ni(III)L^{3+} and the linear dependence of the observed rate constant, k_{obs}, on reductant concentration (Fig. 1).

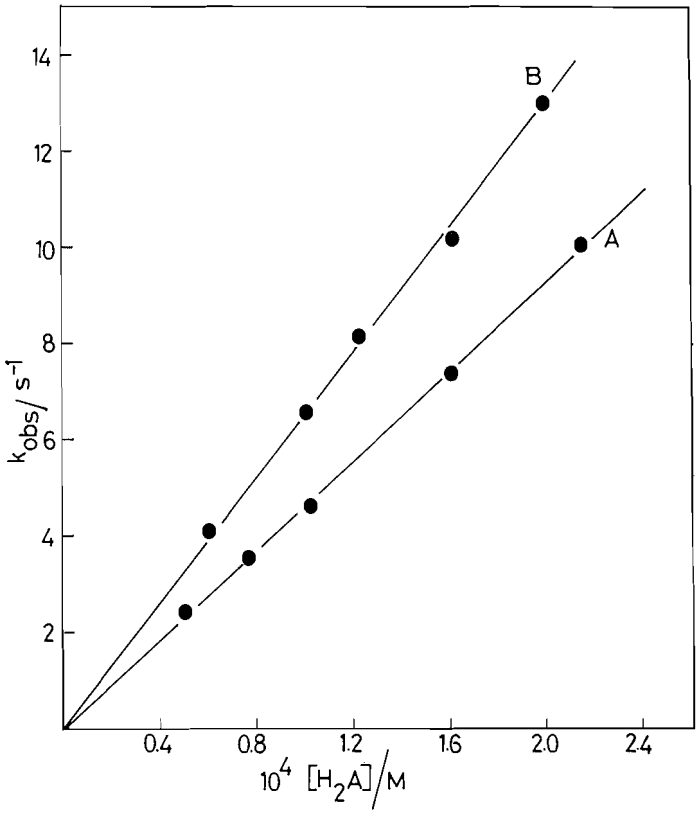

FIG. 1. First order substrate dependence: k_{obs} vs. [reductant]. (*A*) Nitet-c^{3+} + catechol, (*B*) Nitet-c^{3+} + ascorbic acid, T = 25°C, $HClO_4$ = 1.00 *M*.

Reaction with ascorbic acid

Hydrogen ion dependences of the rates were investigated for each oxidant. Although solutions of Ni(III) cyclam were sufficiently stable at pH 2 for kinetic measurements to be made, owing to the limited stability with respect to intramolecular decomposition of the tet-*a* and tet-*c* complexes at $[H^+] < 0.2$ *M*, hydrogen ion dependences for these species were studied over the range 0.2−1.0 *M*. Investigations were carried out in the temperature range = 5.1−31.1°C. For all three oxidants the rate of reaction was observed to be inversely dependent on $[H^+]$ with linear plots of the second order rate constant, k_2 (= $k_{obs}/2[H_2A]$) against $[H^+]^{-1}$ showing positive intercepts (Fig. 2).

These data are consistent with reaction of nickel(III) species with neutral and anionic forms of the ascorbic acid.

$$[2]\quad H_2A \rightleftharpoons H^+ + HA^- \quad (K_a)$$

$$[3]\quad Ni(III)L^{3+} + H_2A \xrightarrow{k_3} Ni(II)L^{2+} + (HA^\cdot + H^+)$$

$$[4]\quad Ni(III)L^{3+} + HA^- \xrightarrow{k_4} Ni(II)L^{2+} + (A^{\cdot -} + H^+)$$

followed by rapid oxidation of the radical intermediate

$$[5]\quad Ni(III)L^{3+} + A^{\cdot -}(HA^\cdot) \xrightarrow{fast} Ni(II)L^{2+} + A(+H^+)$$

An alternative mechanism, involving two-electron transfer reactions,

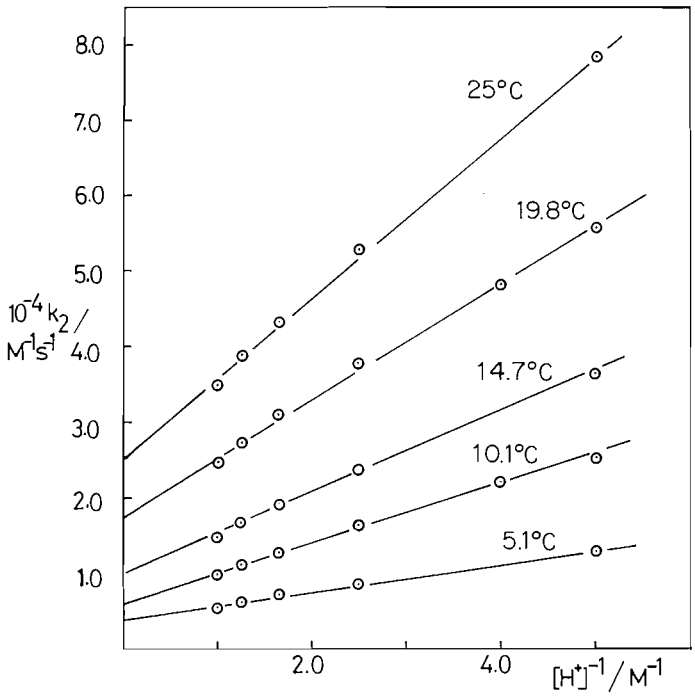

FIG. 2. Dependence of k_2 on $[H^+]^{-1}$ and temperature. Reaction of Ni tet-c^{3+} with ascorbic acid.

$$Ni(III)L^{3+} + H_2A \rightarrow Ni(I)L^{+} + A + 2H^{+}$$

$$Ni(I)L^{+} + Ni(III)L^{3+} \xrightarrow{fast} 2Ni(II)L^{2+}$$

is also consistent with the observed data. There is, however, no evidence for any concerted two-electron reduction of nickel(III). The redox potential for the couple

$$A + 2H^{+} + 2e \rightleftharpoons H_2A$$

has been determined as +0.39 V (30°C) in 1 *M* acid (16). For the reduction

$$Ni(II)tet\text{-}a^{2+} \rightarrow Ni(I)(tet\text{-}a)^{+}$$

in DMF, $E^0 = -1.295$ V (17*a*). Assuming a similar value in aqueous media, when combined with the reduction potential (1.23 V) for $Ni^{III/II}$ (17*b*), the overall Ni(III)L/Ni(I)L potential may be estimated at ~ -0.05 V, effectively ruling out any two-electron process. Using the data of Busch *et al.* (18), the $Ni^{III/I}$ potential is ~ -0.70 V (in CH_3CN versus a Ag/Ag^+ (0.1 *M*) reference electrode).

Although the reaction of the H_2A species (reaction [3]) may be assigned uniquely, there persists a "proton ambiguity" in the case of [4] since an equivalent representation, [7], may be presented:

[6] $$Ni(III)L(OH_2)_2^{3+} \rightleftharpoons Ni(III)L(OH)^{2+} + H^{+} \quad (K_h)$$

[7] $$Ni(III)L(OH)^{2+} + H_2A \xrightarrow{k_7} Ni(II)L^{2+} + HA^{\cdot}$$

There is evidence (19) for a pentacoordinate geometry of the hydroxo species for the tet-*a* and tet-*c* complexes whereas the cyclam complex has been shown (at pH ~10) to exist in the form $NiL(OH)_2^+$.

Using the reactions [3], [4], and [7] together with the associated equilibria, the rate expression is of the form

TABLE 1. Rate constants for reactions of ascorbic acid with Ni(III) macrocycles, $I = 1.00$ *M* ($HClO_4/LiClO_4$)

Oxidant	T/°C	$10^{-3}k_3/M^{-1}\,s^{-1}$	$10^{-3}(k_4K_a + k_7K_h)/s^{-1}$
Ni(III)cyclam^{3+}	11.5	0.15	0.26
	19.0	0.18	0.465
	25.0	0.25	0.68
	30.1	0.31	0.89
	$\Delta H^{\neq} = 6.5 \pm 0.8^a$		
	$\Delta S^{\neq} = -25.7 \pm 5^b$		
Ni(III)tet-c^{3+}	5.1	0.409	1.76
	10.1	0.72	3.92
	14.7	1.01	5.31
	19.8	1.83	7.65
	25.2	2.52	10.6
	$\Delta H^{\neq} = 14.4 \pm 1.1^a$		
	$\Delta S^{\neq} = 10.0 \pm 4^b$		
Ni(III)tet-a^{3+}	9.6	1.47	4.6
	15.0	1.76	7.66
	18.9	2.14	9.27
	21.9	2.85	12.6
	$\Delta H^{\neq} = 7.9 \pm 1.7^a$		
	$\Delta S^{\neq} = -11.4 \pm 5^b$		

[a] In kcal mol^{-1}.
[b] In cal deg^{-1} mol^{-1}.

[8] $$-d[Ni(III)]_{tot}/dt = \frac{2(k_3 + (k_4K_a + k_7K_h)/[H^+])[Ni(III)]_{tot}[H_2A]_{tot}[H^+]^2}{([H^+] + K_a)([H^+] + K_h)}$$

Since measurements were made in the range $[H^+] = 0.1-1.0$ *M* and $K_a \sim 10^{-4}$ *M* (1, 4, 20) and $K_h \sim 10^{-4}$ *M* (13, 21), the second order rate constant may be written as

[9] $$k_2 = k_3 + (k_4K_a + k_7K_h)/[H^+]$$

consistent with the experimental observations. There is no evidence for any $[H^+]^{-2}$ dependence attributable to the reaction of HA^- with $[Ni(III)L(OH)]^{2+}$ which may be expected at higher pH's. Rate data are shown in Table 1.

Nickel(III) species have been shown to form complexes with sulphate ions (21, 22). The reduction potentials associated with these systems are lower (by ~300 mV) than those for the aquo ions. We have examined the effect of sulphate on the reaction rates and find a marked decrease attributed to slower reactions of the sulphato complexes (Table 2). A similar effect has been observed previously in reactions of benzene diols (13) and in sulphate media an evaluation of the data based on reactions of nickel sulphate complexes as oxidants has been presented. In the present system, however, although the data are consistent with only monosulphato complexes reacting (as observed from the linear dependence of k_2^{-1} against $[SO_4^{2-}]_t$), the changes in rate with $[H^+]$ could not be assigned unambiguously and no extensive studies were therefore carried out.

Reactions with catechol and hydroquinone

Previous studies in these laboratories have dealt with the oxidation of these substrates by a variety of reagents (1, 13). In the present investigation we have extended the data on Ni(III) reactants to include the tet-*a* and tet-*c* complexes. Studies have been made at $[H^+] = 1.00$ *M* in order to limit reaction to only the $Ni(III)L^{3+}$ oxidant. In the range $[H^+] = 0.1-1.00$ *M* for reaction of these reductants, there is a fairly constant rate ob-

Can. J. Chem. Downloaded from www.nrcresearchpress.com by 210.87.254.42 on 09/06/12
For personal use only.

Can. J. Chem. Downloaded from www.nrcresearchpress.com by 210.87.254.42 on 09/06/12
For personal use only.

TABLE 2. Effect of sulphate ion on the rate of oxidation of ascorbic acid by Ni(III)cyclam^{3+} (in all experiments, [Ni(III)cyclam^{3+}] ~ 5 × 10^{-5} *M*, ascorbic acid = 5.0 × 10^{-4} *M*)

T/°C	[H$^+$]/*M*	[SO$_4^{2-}$]$_t$/*M*	k_2/*M*$^{-1}$ s^{-1}
11.5	0.1	0.0	2.76×10^3
	0.1	9.9×10^{-5}	2.56×10^3
	0.1	9.87×10^{-4}	1.59×10^3
	0.1	9.87×10^{-3}	0.51×10^3
	1.0	0.0	0.38×10^3
	1.0	9.9×10^{-4}	0.33$_4$×10^3
25	1.0	0.0×10^{-4}	9.7$_7$×10^2
	1.0	1.0×10^{-4}	9.6×10^2
	1.0	2.0×10^{-4}	9.4$_4$×10^2
	1.0	10.0×10^{-4}	9.00×10^2
	1.0	20.0×10^{-4}	8.2$_8$×10^2

TABLE 3. Rate constants for reaction of Ni(III)-tet-*a*$^{3+}$ and Ni(III)-tet-*c*$^{3+}$ complexes with catechol and hydroquinone, [H$^+$] = 1.00 *M*, *I* = 1.00 *M*[a]

(*a*) Ni(III)tet-*c*$^{3+}$

T/°C	k_2/*M*$^{-1}$ s^{-1}
Catechol	
5.90	0.84×10^4
11.61	1.01×10^4
16.00	1.18×10^4
20.90	1.35×10^4
25.60	1.73×10^4
$\Delta H^{\ddagger}$ = 5.4 ± 1.2 kcal mol^{-1}	
$\Delta S^{\ddagger}$ = −21 ± 8 cal deg^{-1} mol^{-1}	
Hydroquinone	
11.61	1.18×10^5
16.00	1.30×10^5
20.90	2.49×10^5

(*b*) Ni(III)tet-*a*$^{3+}$

T/°C	k_2/*M*$^{-1}$ s^{-1}
Catechol	
25	3.30×10^4
$\Delta G^{\ddagger}$ = 8.84 kcal mol^{-1}[b]	

[a]Rate constants corrected for protonated reductant present under these reaction conditions.
[b]Assuming $k = 10^{11}e^{-\Delta G^{\ddagger}/RT}$.

served with a small, reproducible retardation in rate becoming increasingly more pronounced in the range [H$^+$] ≥ 0.6 *M*. This is attributable to the protonation of the organic substrate,

[10] $H_3Q^+ \rightleftharpoons H^+ + H_2Q \qquad K_{10}$

where H_2Q represents the quinol. Values of K_{10} have been shown to lie in the range 1−10 *M* for alcohols with the constant K_{10} = 3.9 *M* for phenol (23). In the case of hydroquinone and catechol, values of 4.5 ± 1.2 *M* and 3.3 ± 0.9 *M* have been determined from kinetic measurements, and interpolation into the data of Pelizzetti (24) on the oxidation of catechol by $IrCl_6^{2-}$ is consistent with K_{10} = 5.3 ± 2 *M* for this species. At [H$^+$] = 1.00 *M* some of the reductant will be in the protonated form. There is no evidence from any study to date of H_3Q^+ reacting. Assuming only H_2Q to react,

[11] $Ni(III)L^{3+} + H_2Q \xrightarrow{k_{11}} Ni(II)L^{2+} + HQ^{\cdot} + H^+$

[12] $Ni(III)L^{3+} + HQ^{\cdot} \xrightarrow{fast} Ni(II)L^{2+} + Q + H^+$

The second order rate constant may be expressed in the form

[13] $k_2 = k_{obs}/2[H_2Q]_t = k_{11}K_{10}/([H^+] + K_{10})$

k_{11} values are presented in Table 3. The first order dependence of the rate on [H_2Q] is shown in Fig. 1 (*T* = 25.6°C) and the other data quoted are the mean values of constants derived using at least two differing reductant concentrations. In the reaction of Ni(III)tet-*a*$^{3+}$ with hydroquinone, however, the rate was too rapid to be observed in our apparatus. (Using solutions of 5 × 10^{-5} *M* [H_2Q] and 5 × 10^{-6} *M* [Ni(III)], [H$^+$] = 1.00 *M*, *T* = 25°C, $t_{1/2}$ ~ 3 ms.)

Although attempts were made to identify intermediate complexes formed, there is no evidence in any of the systems studied for axially coordinated precursors, suggesting an outer-sphere mechanism.

The Marcus theory (11) affords the possibility of correlating free energy changes with the rate data, and its applicability to redox reactions involving organic substrates has been verified in the case of ascorbic acid (3, 10) and quinols (1, 24, 25) oxidised by a variety of Ir(IV), Fe(III), and Co(III) ions. The relationship may be expressed in the form

[14] $\Delta G_{12}^{\ddagger} = w_{12} + \lambda(1 + \Delta G_c^0/\lambda)^2/4$

where $\Delta G_c^0 = \Delta G_{12}^0 + w_{12} - w_{21}$, $\lambda = 2(\Delta G_{11}^{\ddagger} - w_{11} + \Delta G_{22}^{\ddagger} - w_{22})$, and $k_{12} = Z\exp(-\Delta G_{12}^{\ddagger}/RT)$. $\Delta G_{11}^{\ddagger}$ and $\Delta G_{22}^{\ddagger}$ are free energies of activation of the self-exchange process and w_{11} and w_{22} represent the associated work terms involved. w_{12} and w_{21} are the work terms required to bring together the reactants or products in the activated complex (26, 27). In many of the systems under study, since one of the reactants (or products) is uncharged, work terms are considered to reduce to zero.

The free energy of activation for the self-exchange process for Ni(cyclam)$^{3+/2+}$ has been measured recently (13, 28). Both direct measurements involving esr and cross reactions with Fe(LL)$_3^{3+}$ yield a value of $\Delta G_{11}^{\ddagger}$ = 10.9 ± 1.0 kcal mol^{-1}. There are no experimental data available for the self-exchange rates for H_2Q/H_2Q^+ or for H_2A/H_2A^+. Estimates for the quinols have been made from cross reactions with $IrCl_6^{2-}$ and $Mo(CN)_8^{3-}$, however, with a value in the range $\Delta G_{22}^{\ddagger\ddagger}$ ~ 6−7 kcal mol^{-1} (29). We have used a value of $\Delta G_{22}^{\ddagger\ddagger}$ = 6.0 kcal mol^{-1} (k_{22} ~4 × 10^6 *M*$^{-1}$ s^{-1}). The complexities of ascorbate as a reductant have been described recently (30). From an analysis of emf data derived for the $A^{\cdot}/A^{2-}$ couple (31), a value for $E^0(HA^{\cdot}/HA^-)$ = 0.68 V has been proposed, somewhat lower than that suggested previously. Using data for the reaction with Fe(LL)$_3^{3+}$, the self-exchange rate for the reaction is calculated as 10^2−10^4 *M*$^{-1}$ s^{-1}, consistent with that (10^4 *M*$^{-1}$ s^{-1}) derived from the Fe^{III}(cyt-*c*)/HA^- reaction (32). It is considered that barriers to the electron exchange process derive from differences in C=C and possibly C—C bond lengths in the various species. The data for H_2A/H_2A^+ are more tentative, however, owing to a lack of a measured value for the second pK_a of the ascorbate radical ($H_2A^+ \rightleftharpoons HA^{\cdot} + H^+$). Since the value for p$K_{a1}$ ($HA^{\cdot} \rightleftharpoons H^+ + A^{\cdot-}$) is negative (−0.45), using the data of Steeken and Neta (31) for the one-electron potentials $E^0(A^{\cdot-}/A^{2-})$ at higher pH's (11, 13.5), an approximate value for $E^0(H_2A/H_2A^+)$ may be calculated from known p*K*'s and an assumed value of pK_{a2}. If pK_{a2} lies in the range −1 to −4,

TABLE 4. Comparison of calculated and experimental data

Reaction		$\Delta G_c^{0\,a}$	$\Delta G^{\ddagger}_{12\,(obs)}{}^{a}$	$Q^{a,d}$	$k_{exp}{}^{b}$	$k_{calc}{}^{b}$
(1) Ni cyclam^{3+}	+ H_2A	0.26	11.73	0.43	2.5×10^{2}	3.0×10^{2}
(2)	+ H_2cat	4.66	11.14	2.73	$7\times10^{2\,c}$	1.4×10^{3}
(3)	+ H_2Quin	2.59	9.54	1.29	$1.1\times10^{4\,c}$	1.0×10^{4}
(4)	+ HA^-	−6.73	5.73[c]	−4.52	$6.2\times10^{6\,c}$	$1.3\times10^{6\,c}$
(5) Ni tet-c^{3+}	+ H_2A	−6.18	10.37	−3.01	2.5×10^{3}	1.6×10^{3}
(6)	+ H_2cat	−1.79	9.12	−0.79	1.7×10^{4}	2×10^{4}
(7)	+ H_2Quin	−3.87	8.16	−2.45	2.5×10^{5}	1.0×10^{5}
(8)	+ HA^-	−13.19	4.12	−8.61	$9.7\times10^{7\,c}$	$5.3\times10^{6\,c}$
(9) Ni tet-a^{3+}	+ H_2A	−6.18	10.23	−3.15	3.2×10^{3}	1.6×10^{3}
(10)	+ H_2cat	−1.79	8.84	−1.18	3.3×10^{4}	2×10^{4}
(11)	+ HA^-	−13.19	4.03	−8.72	$1.1\times10^{8\,c}$	$5.3\times10^{6\,c}$

[a] kcal mol^{-1}.
[b] M^{-1} s^{-1}.
[c] Assuming no contribution from reaction [7], work term contribution included in evaluation of Q.
[d] See eq. [15].
[e] Reference 13.

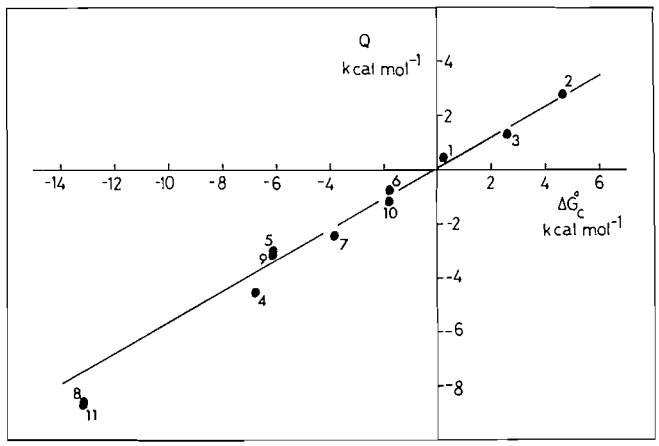

FIG. 3. Plot of Q against ΔG_c^0, eq. [15] for various systems. The numbers refer to reactions indicated in Table 4.

$E^0(H_2A/H_2A^+) = 0.98 \pm 0.10$ V. The rate of oxidation of H_2A by $Fe(LL)_3^{3+}$ (LL = 1,10-phenanthroline) has been measured recently (33) and from the observed rate ($1.73 \times 10^5\ M^{-1}$ s^{-1}) a self-exchange rate for H_2A/H_2A^+ of $\sim 10^2\ M^{-1}$ s^{-1} may be derived. We have used these data in our calculations. In the case of Ni(tet-c)$^{3+/2+}$ and Ni(tet-a)$^{3+/2+}$ we observed reasonable agreement with systems studied using a value $\Delta G_{11}^{**} = 14.0$ kcal mol^{-1} ($k_{11} \sim 2\ M^{-1}$ s^{-1}). Differences in ΔG_{11}^{*} have been observed previously with changes in ligand structure for the corresponding cobalt(III) complexes (34).

In Table 4, comparison is made of the calculated rate constants and those derived experimentally. In most cases the agreement is good when uncertainties in the self-exchange rates (~1 kcal mol^{-1}) are taken into account. Rearrangement of [14] leads to the expression

$$[15]\quad Q = \Delta G_{12}^{*} - w_{12} - \lambda/4 - (\Delta G_c^0)^2/4\lambda = 0.5\Delta G_c^0$$

and in Fig. 3 is shown a plot of ΔG_c^0 against Q. The least-squares slope (0.57) and intercept (0.03) are close to those predicted theoretically, with only the values for reaction of Ni(tet-c)$^{3+}$ and Ni(tet-a)$^{3+}$ with ascorbate ion (not included in the least-squares treatment) showing significant deviations. In these systems, however, very large free energy changes are involved and under such circumstances the Marcus approach may no longer hold. For other reactions, however, the agreement is consistent with an outer-sphere designation for these oxidations.

Adherence to the Marcus treatment enables some predictions to be made with respect to the relative rates of the hydrogen ion dependent pathways for ascorbic acid. Using $\Delta G_{11}^{*} = 9.55$ kcal mol^{-1} ($E^0 = 0.68$ V), the rate constants for the process $NiL^{3+} + HA^-$ (k_4) may be calculated (Table 4). In the reaction of Ni(cyclam)$^{3+}$ with HA^-, for example, k_4(calcd.) $= 1.3 \times 10^6\ M^{-1}$ s^{-1}. The composite constant observed, $(k_4K_a + k_7K_h) = 6.8 \times 10^2\ M^{-1}$ s^{-1}. If only the k_4 path is significant, using $K_a = 1.09 \times 10^4\ M$ (10), k_{obs} (= $6.2 \times 10^6\ M^{-1}$ s^{-1}) in reasonable agreement with the predicted value. It is known (35) that Ni(III)L(OH)$^{2+}$ is a weaker oxidant than Ni(III)L^{3+} so that the former species may be predicted to be less reactive. Also if the hydroxo species are pentacoordinated as seems likely, then an inner-sphere route may be a possibility in this instance. The hydrogen ion dependence of the reactions with ascorbic acid is therefore attributed to HA^- as the reducing ion. There are, in fact, very few instances where only the H_2A pathway predominates (36).

Further studies on redox reactions involving series of organic substrates such as those under consideration will be useful in providing a deeper insight into the use of the Marcus theory in the description of rate processes involved. Recently, data have been presented on the formation of nickel(III) complexes with a variety of polydentate (N_4 and N_5) macrocyclic ligands (37). Studies of the rates of redox reactions involving such species will be helpful in identifying contributions deriving from ligand effects on the metal centre. It is also inferred from the present study that significant changes in the rates of self-exchange reactions for the $NiL^{3+/2+}$ couples occur with ligand substitution. Electron spin resonance studies are planned to attempt to obtain a direct measure of these effects.

Acknowledgements

We thank the Natural Sciences and Engineering Research Council of Canada and the University of Victoria for financial support. Helpful discussions with Drs. D. H. Macartney and J. M. Winfield are acknowledged.

1. Z. AMJAD, J. C. BRODOVITCH, and A. MCAULEY. Can. J. Chem. **55**, 3581 (1977).
2. E. PELIZZETTI, E. MENTASTI, and E. PRAMAURO. Inorg. Chem.

Can. J. Chem. Downloaded from www.nrcresearchpress.com by 210.87.254.42 on 09/06/12
For personal use only.

15, 2898 (1976).
3. E. PELIZZETTI, E. MENTASTI, and E. PRAMAURO. Inorg. Chem. **17**, 1181 (1978).
4. M. M. TAQUI-KHAN and A. E. MARTELL. J. Am. Chem. Soc. **90**, 3386 (1968).
5. U. S. MEHROTRA, M. C. AGRAWAL, and S. P. MUSHRAN. J. Phys. Chem. **73**, 1996 (1969).
6. R. A. RICHMAN, R. L. SORENSON, K. O. WATKINS, and G. DAVIES. Inorg. Chem. **16**, 1570 (1977).
7. E. PELIZZETTI, E. MENTASTI, and E. PRAMAURO. J. Chem. Soc. Dalton Trans. 61 (1978).
8. K. KUSTIN and D. L. TOPPEN. Inorg. Chem. **11**, 1952 (1972).
9. G. S. LAURENCE and K. J. ELLIS. J. Chem. Soc. Dalton Trans. 1667 (1972).
10. D. H. MACARTNEY and A. MCAULEY. Can. J. Chem. **59**, 132 (1981).
11. R. A. MARCUS. J. Phys. Chem. **72**, 891 (1968).
12. R. I. HAINES and A. MCAULEY. Inorg. Chem. **19**, 719 (1980).
13. J. C. BRODOVITCH, T. OSWALD, and A. MCAULEY. Inorg. Chem. **21**, 3442 (1982).
14. B. BOSNICH, M. L. TOBE, and G. A. WEBB. Inorg. Chem. **4**, 1102 (1965); **4**, 1109 (1965); N. F. CURTIS, Y. M. CURTIS, and H. J. K. POWELL. J. Chem. Soc. A, 1015 (1966).
15. K. J. ELLIS and A. MCAULEY. J. Chem. Soc. Dalton Trans. 1533 (1973).
16. E. G. BALL. J. Biol. Chem. **118**, 219 (1937).
17. (*a*) R. R. GAGNÉ and D. M. INGLE. Inorg. Chem. **20**, 420 (1981); (*b*) T. OSWALD and A. MCAULEY. To be published.
18. F. V. LOVECCHIO, E. S. GORE, and D. H. BUSCH. J. Am. Chem. Soc. **96**, 3109 (1974).
19. E. ZEIGERSON, G. GINZBURG, J. Y. BECKER, L. J. KIRSCHENBAUM, H. COHEN, and D. MEYERSTEIN. Inorg. Chem. **20**, 3988 (1981).
20. A. E. MARTELL and R. M. SMITH. Critical stability constants. Vol. 3. Plenum Press, New York. 1977. p. 264.
21. E. ZEIGERSON, G. GINSBURG, N. SCHWARTZ, Z. LUZ, and D. MEYERSTEIN. J. Chem. Soc. Chem. Commun. 241 (1979).
22. E. ZEIGERSON, G. GINSBURG, D. MEYERSTEIN, and L. J. KIRSCHENBAUM. J. Chem. Soc. Dalton Trans. 1243 (1980).
23. C. F. WELLS. Trans. Faraday Soc. **62**, 2815 (1966).
24. E. PELIZZETTI, E. MENTASTI, and C. BAIOCCHI. J. Chem. Soc. Dalton Trans. 132 (1977); E. PELIZZETTI, E. MENTASTI, and E. PRAMAURO. J. Chem. Soc. Perkin Trans. II, 620 (1978).
25. E. MENTASTI and E. PELIZZETTI. Int. J. Chem. Kinetics, **9**, 215 (1977).
26. G. M. BROWN and N. SUTIN. J. Am. Chem. Soc. **101**, 883 (1979).
27. J. PHILLIPS and A. HAIM. Inorg. Chem. **19**, 76 (1980).
28. A. MCAULEY, D. H. MACARTNEY, and T. OSWALD. J. Chem. Soc. Chem. Commun. 274 (1982).
29. E. PELIZZETTI, E. MENTASTI, and E. PRAMAURO. Inorg. Chem. **17**, 1688 (1978).
30. C. CREUTZ. Inorg. Chem. **20**, 4449 (1981).
31. S. STEENKEN and P. NETA. J. Phys. Chem. **83**, 1134 (1979).
32. R. K. GUPTA, S. H. KOENIG, and A. G. REDFIELD. J. Mag. Res. **7**, 66 (1972).
33. M. KIMURA, M. YAMAMOTO (TSURUTA), and S. YAMABE. J. Chem. Soc. Dalton Trans. 423 (1982).
34. D. P. RILLEMA, J. F. ENDICOTT, and R. C. PATEL. J. Am. Chem. Soc. **94**, 394 (1972); D. P. RILLEMA and J. F. ENDICOTT. J. Am. Chem. Soc. **94**, 8711 (1972).
35. M. JAACOBI, D. MEYERSTEIN, and J. LILIE. Inorg. Chem. **18**, 429 (1979).
36. M. WOODS, C. A. HOENICH, and J. C. SULLIVAN. J. Inorg. Nucl. Chem. **40**, 1907 (1978).
37. A. BENCINI, L. FABBRIZZI, and A. POGGI. Inorg. Chem. **20**, 2544 (1981).

Can. J. Chem. Downloaded from www.nrcresearchpress.com by 210.87.254.42 on 09/06/12
For personal use only.

Synthetic approaches to haplophytine. 2. Synthesis of 4-methylamino-1-(2-furanyl)-2-phenyl-2-(2-pivaloylamidophenyl)butan-1-one[1]

DAVID AARON SCHWARTZ AND PETER YATES

Lash Miller Chemical Laboratories, University of Toronto, Toronto, Ont., Canada M5S 1A1

Received November 9, 1982

DAVID AARON SCHWARTZ and PETER YATES. Can. J. Chem. **61**, 1126 (1983).

Approaches to the synthesis of compounds related to the 7-aryl-7-[3-(1-hydroxy-2-aminophenyl)]-9-methylamino-5,6-dioxononanoic acid moiety (**3**) of the alkaloid haplophytine and its dihydrobromide are described. Treatment of the dianion of phenyl (*o*-pivaloylamidophenyl)methane with 2-furancarboxaldehyde followed by oxidation of the resulting alcohol gives 1-(2-furanyl)-2-phenyl-2-(2-pivaloylamidophenyl)ethanone (**14**). This on allylation gives 1-allyloxy-1-(2-furanyl)-2-phenyl-2-(2-pivaloylamidophenyl)ethene (**20**), which on being heated at 80–95°C undergoes an intramolecular Diels–Alder reaction. Heating the resulting product or **20** at 165°C converts them to the C-allylation product of **14**, 1-(2-furanyl)-2-phenyl-2-(2-pivaloylamidophenyl)pent-4-en-1-one (**22**). Oxidation of **22** gives 4-(2-furoyl)-1,2,3,4-tetrahydro-4-phenyl-1-pivaloyl-2-quinolinol, which on Boreh reduction gives 4-methylamino-1-(2-furanyl)-2-phenyl-2-(2-pivaloylamidophenyl)butan-1-one (**24**) and 2-(2-furanyl)-1-methyl-3-phenyl-3-(2-pivaloylamidophenyl)pyrrolidine. Compound **24** is a potential advanced intermediate for the synthesis of compounds related to **3**. Experiments directed to the incorporation of a methoxyl or methylthio substituent at the C-5 position of the furan ring of **24** are also described.

DAVID AARON SCHWARTZ et PETER YATES. Can. J. Chem. **61**, 1126 (1983).

On décrit des méthodes de synthèse des composés apparentés à l'unité acide aryl-7 [(hydroxy-1 amino-2 phényl)-3] méthylamino-9 dioxo-5,6 nonanoïque (**3**) de l'alcaloïde halophytine et son dibromhydrate. Le dianion du phényl(*o*-pivaloylamidophényl) méthane réagit avec le furanne-2 carboxaldéhyde en donnant un alcool qui, par oxydation, conduit à la (furannyl-2)-1 phényl-2 (pivaloylamido-2 phényle)-2 éthanone (**14**). Cette dernière, par allylation, conduit à l'allyloxy-1 (furannyl-2)-1 phényl-2 (pivaloylamido-2 phényl)-2 éthène (**20**) qui, par chauffage à 80–95°C, subit une réaction de Diels–Alder intramoléculaire. Le chauffage du produit obtenu ou du composé **20** à 165°C les transforme en un produit C-allylé du composé **14**, la (furannyl-2)-1 phényl-2 (pivaloylamido-2 phényl)-2 pentène-4 one-1 (**22**). L'oxydation du composé **22** donne le (furonyl-2)-4 tétrahydro-1,2,3,4 phényl-4 pivaloyl-1 quinolénol-2 qui, par une réduction de Boreh, donne la méthylamino-4 (furannyl-2)-2 phényl-2 (pivaloylamido-2 phényl)-2 butanone-1 (**24**) et la (furannyl-2)-2 méthyl-1-phényl-3 (pivaloylamido-2 phényl)-3 pyrrolidine. Le composé **24** est un intermédiaire avancé potentiel pour la synthèse des composés apparentés au composé **3**. On décrit également des expériences portant sur l'incorporation d'un substituant méthoxyl ou méthylthio en position C-5 du cycle furanne du composé **24**.

[Traduit par le journal]

We have discussed in the previous paper in this series (1) the presence of the moieties **1** and **2** in the structures of the alkaloid haplophytine and its dihydrobromide, respectively, and the relationship of these to compounds of type **3**. In an approach to the synthesis of haplophytine we undertook studies of the synthesis of compounds of type **4**, which are closely related models of **3**, and have described the synthesis of compounds **5** and **6**. These contain the amino (X) and α-oxoglutaryl (Y) residues

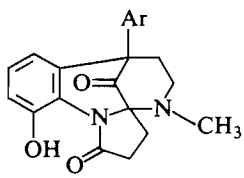

1

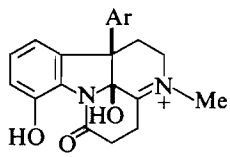

2

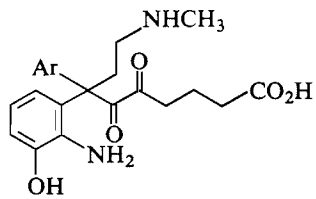

3

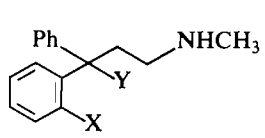

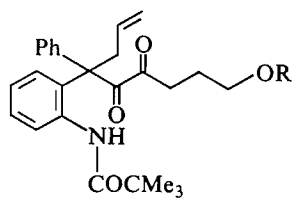

4 X = NH_2 equivalent
Y = $COCOCH_2CH_2CO_2H$ equivalent

5 R = H
6 R = Me

[1]For paper 1, see ref. 1.

Can. J. Chem. Downloaded from www.nrcresearchpress.com by 210.87.254.105 on 09/06/12
For personal use only.

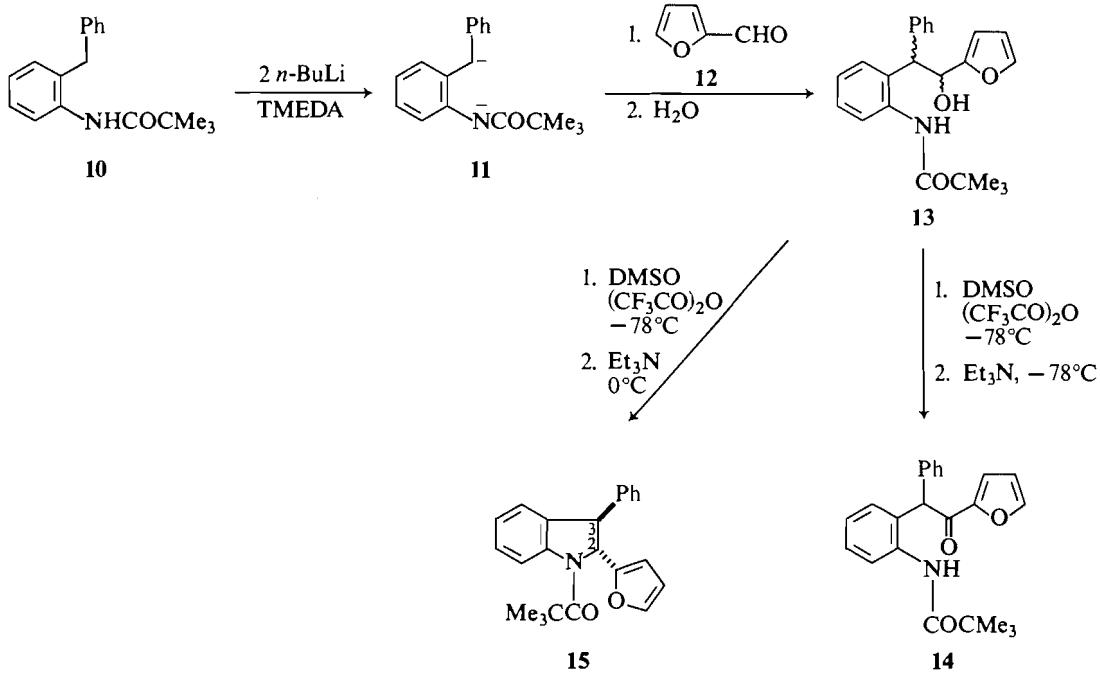

SCHEME 1

of **4**, but we were unable to convert the allyl group of **5** or **6** to the 2-(methylamino)ethyl group of **4**.

We now describe the synthesis of a compound of type **4** in which the group Y is an α-furoyl group **7**, which it is anticipated will serve as an equivalent of the -$COCOCH_2CH_2CHO$ group, itself an equivalent via oxidation of the α-oxoglutaryl group (Y).[2] We also discuss experiments directed towards the

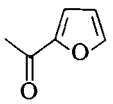

7

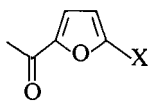

8 X = OMe
9 Y = SMe

incorporation of 5-substituted α-furoyl groups of type **8** and **9**, which would serve as α-oxoglutaryl equivalents without need of further oxidation.

The dianion **11** was formed from *o*-pivaloylamidodiphenylmethane (**10**) and two equivalents of *n*-butyllithium/TMEDA or of lithium diisopropylamide in tetrahydrofuran at −20°C (1). Treatment with 2-furancarboxaldehyde (**12**) gave a 1:1 mixture of diastereomeric alcohols **13** in 98% yield (Scheme 1). The oxidation of **13** to the corresponding ketone **14** was attempted with silver carbonate on Celite (3) but this did not affect **13**. Success was achieved by addition of **13** to a solution of dimethyl sulfoxide and trifluoroacetic anhydride followed by addition of triethylamine, both at −78°C (4); the ketone **14** was thus obtained in 99% yield.[3] If the reaction mixture was allowed to warm to 0°C before addition of the triethylamine, the indoline **15** was formed as a single diastereomer, considered to have the *trans* configuration. The structural assignments **13**–**15** are based on spectroscopic data (see Experimental) as are those of other products discussed in the sequel. In the case of **15** some comment is appropriate. In its ^1H nmr spectrum two one-proton broadened singlets at δ 4.42 and 5.60 ppm are assigned to the C-2 and C-3 protons, respectively: the band widths indicate that they are coupled with $J = 1-1.5$ Hz. Anet and Muchowski (6) have observed that for 2,3-dimethylindoline $J_{2,3\text{-}cis} = 8.83$ Hz and $J_{2,3\text{-}trans} = 8.85$ Hz, but that on substitution of a conjugative group on the nitrogen, $J_{2,3\text{-}trans}$ decreases to 2.7–3.0 Hz while $J_{2,3\text{-}cis}$ is little changed (8.6–8.7 Hz); we therefore assign the *trans* configuration to **15** which is in accord with the following mechanistic proposal.

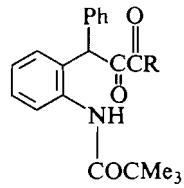

17

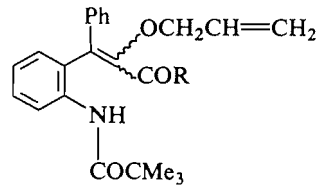

18

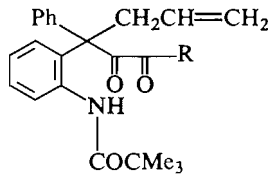

19

We interpret the formation of the indoline **15** as involving formation of the carbonium ion **16** from **13** (Scheme 2). This interpretation is substantiated by the fact that on addition of trifluoroacetic anhydride to a solution of **13** in deuteriochloroform the indoline **15** is formed as shown by ^1H nmr spectroscopy.

We have previously introduced an allyl group at the benzylic carbon of compounds of type **17** by reaction with allyl bromide and sodium carbonate in aqueous solution at 25°C to give an

[2]For example, cf. ref. 2.

[3]Another attempt to form the ketone **14** directly from the dianion **11** by treatment with methyl furan-2-carboxylate at −78°C led only to the recovery of starting materials, most probably because of deprotonation at the C-5 position of the furan by the dianion (5).

Can. J. Chem. Downloaded from www.nrcresearchpress.com by 210.87.254.105 on 09/06/12
For personal use only.

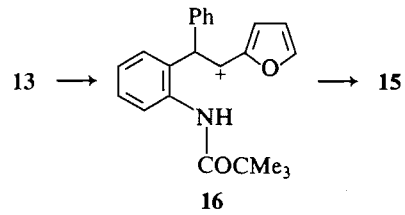

SCHEME 2

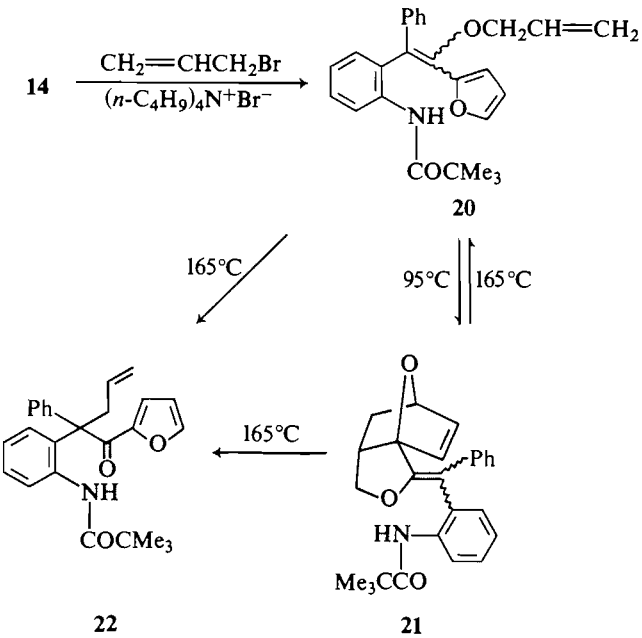

SCHEME 3

O-allyl vinyl ether of type **18** followed by thermolytic conversion of this to the C-allyl derivative **19** (1). In the case of **14** these reagents were ineffective for O-allylation, even at elevated temperatures. However, phase transfer alkylation (7) with tetra-*n*-butylammonium bromide as catalyst gave the O-allylation product **20** as a 7:3 mixture of geometrical isomers in 95% yield (Scheme 3). Thermolysis of **20** in toluene at 95°C led not to the desired C-allyl isomer but gave the intramolecular Diels–Alder adduct **21** as a mixture of stereoisomers; the same product was formed from **20** in boiling benzene. It was considered that this cycloaddition reaction would be reversible and that at higher temperatures such reversal might be followed by irreversible Claisen rearrangement to the desired C-allyl product. In fact it was found that heating of the mixture of stereoisomers **21** in mesitylene at 165°C gave the C-allyl product **22** in 95% yield; direct thermolysis of **20** under these conditions also gave **22**.

We next turned to the conversion of the allyl group to the 2-(methylamino)ethyl group. Attempted oxidative cleavage of the ethylenic double bond of **22** with ozone at −78°C led to degradation, but treatment with 2 equivalents of sodium periodate and a catalytic amount of osmium tetroxide (8) gave the hemiaminal **23** as a single diastereomer[4] in 91% yield (Scheme 4). Reaction of this with five molar equivalents of methylamine hydrochloride and one molar equivalent (three hydride equivalents) of sodium cyanoborohydride in methanol gave instead of the desired amine **24** a mixture of diastereomeric pyrrolidines **26**. This must have arisen via normal reductive amination (9) of **23** to **24** followed by a second reductive amination involving the intramolecular formation of the immonium ion **25**. In order to limit the occurrence of the second reductive amination, the hemiaminal **23** was treated with 25 molar equivalents of methylamine hydrochloride and 1.5 hydride equivalents of sodium cyanoborohydride. Under these conditions a 2:1 mixture of **24** and the diastereomeric pyrrolidines **26** was obtained from which the desired product **24** could be cleanly separated by chromatography.

Compound **24** represented our immediate synthetic goal since it contains the carbon skeleton of **4** with nitrogen and oxygen substituents appropriately situated. As noted earlier, the α-furoyl system is a latent α-oxoglutaryl group as required. However, its oxidation state is lower than that of the α-oxoglutaryl group and its successful utilization for further elaboration will require at some stage an increase in the oxidation state of the carbon atom corresponding to C-5 of the α-furoyl system. Of the several stages at which such a change might be effected, one could involve incorporating a suitable substituent at C-5 in the furan system before it is treated with the dianion **11**, and another could involve such incorporation immediately prior to manipulation of the allyl group. We conclude by describing approaches of these two types.

5-Methoxy-2-furancarboxaldehyde (**28**) was prepared from methyl 5-methoxy-2-furancarboxylate (**27**) (10) as outlined in Scheme 5. Reaction of **28** with the dianion **11** gave a mixture of diastereomeric alcohols **29**, the analogues of **13**, but oxidation of **29** under the conditions that had previously been used for the oxidation of **13** to the corresponding ketone **14** gave only the indoline **30**, as a single diastereomer (cf. **15**). The methoxyl group must sufficiently stabilize the carbonium ion analogue of **16**, which gives rise to **30** (cf. Scheme 2), to lead to formation of **30** even when the reaction is performed at −78°C. The synthesis of the ketone **31** was achieved in 50% yield by treatment of the ester **27** with the dianion **11**; here, in contrast to the case of methyl furan-2-carboxylate, the furan has no α hydrogen atom and proton exchange does not preempt attack of the dianion on the ester group. However, treatment of the ketone **31** under the phase transfer conditions that had previously been used successfully for the O-allylation of ketone **14** (Scheme 3) was ineffective in this case, as were the liquid–solid phase transfer conditions of Makosza and coworkers (11).

We were able to prepare an analogue of **22** with the C-5 carbon atom of the furan ring in a higher oxidation state by direct introduction of a methylthio substituent at this carbon as shown in Scheme 6. Compound **22** was converted to its dianion **32** and this was treated with dimethyl disulfide to give the methylthio derivative **33**. But we were unable to convert the allyl group of this to a 2(methylamino)ethyl group: attempted oxidative cleavage of the ethylenic double bond with osmium tetroxide and sodium periodate, as in the conversion of **22** to **23**, or with osmium tetroxide and *N*-methylmorpholine *N*-oxide (12) led to extensive destruction of the molecule presumably due to concomitant oxidation of the (methylthio)furan system.

Experimental

Melting points are uncorrected. Unless otherwise specified, the ir spectra were recorded for $CHCl_3$ solutions and the ^1H and ^{13}C nmr spectra for $CDCl_3$ solutions. Mass spectra were recorded at 70 eV and peak positions (m/e) are followed by relative abundances in parenthe-

[4]This is considered to have the phenyl group *trans* to the hydroxyl group as in the case of its 4-carbomethoxy analogue (1).

Can. J. Chem. Downloaded from www.nrcresearchpress.com by 210.87.254.105 on 09/06/12
For personal use only.

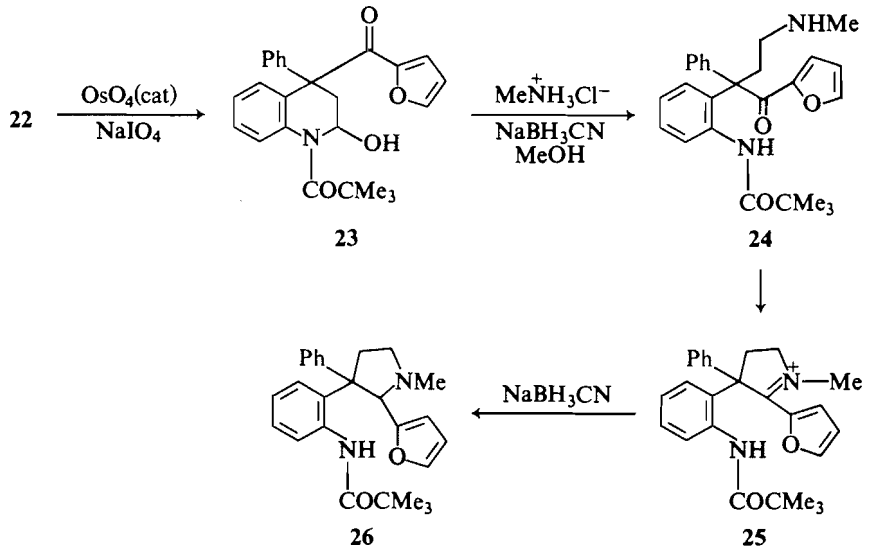

SCHEME 4

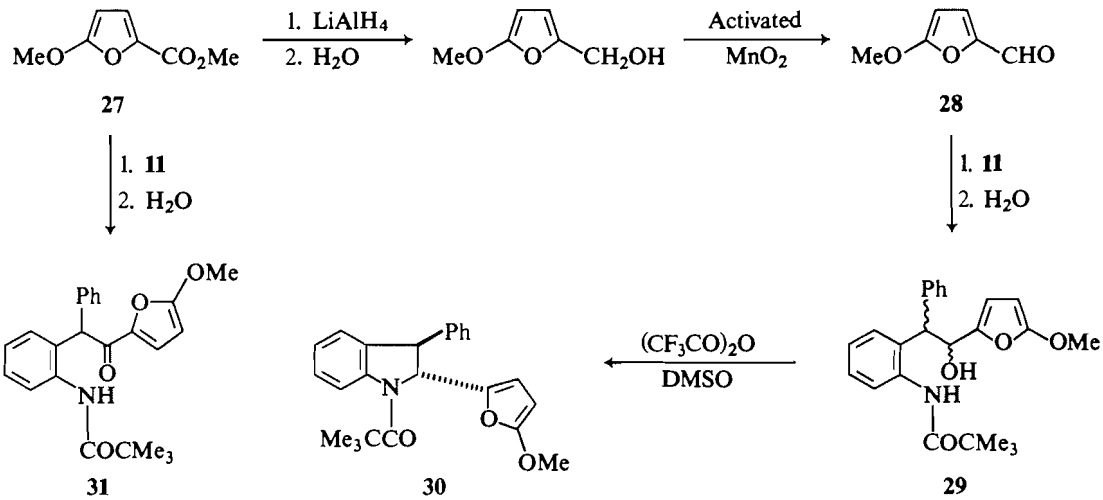

SCHEME 5

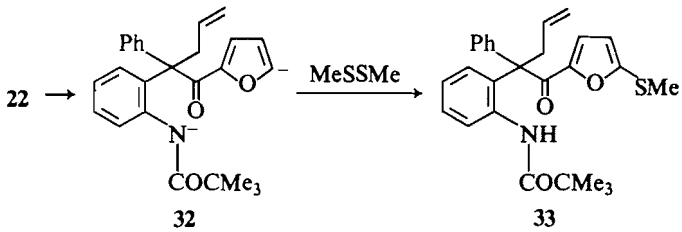

SCHEME 6

ses. Preparative thin layer chromatography was carried out on 20 × 20 × 1-mm or 20 × 20 × 2-mm Merck silica gel "60 PF_{254}" plates with uv visualization; the bands were extracted with MeOH, the residues obtained after filtration and evaporation were slurried with $CHCl_3$, and the solutions were filtered and evaporated to give the products. Solutions in organic solvents were dried over anhydrous $MgSO_4$ and evaporated by means of a rotary evaporator at water aspirator pressure.

*1-(2-Furanyl)-2-phenyl-2-(2-pivaloylamidophenyl)ethanol (**13**)*[5]

To a solution of dianion **11**, formed from amide **10** (4.00 g, 15 mmol), TMEDA (4.52 mL, 30 mmol), and 2.15 *M* *n*-BuLi in *n*-hexane (14.0 mL, 30 mmol) in THF (30 mL) at −30°C (1) was added 2-furancarboxaldehyde (**12**) (2.0 mL, 24 mmol) over 3 min. The color of the dianion was discharged upon completion of addition of the aldehyde. The reaction mixture was allowed to warm to room temperature. The standard work-up procedure (1) yielded 5.40 g (97%) of a crude mixture of diastereomeric alcohols **13** as a colorless oil. Crystallization from hexane–benzene yielded a single diastereomer, mp 127–128°C; ir λ_{max}: 3.00 (m), 6.00 μm; ^{1}H nmr δ: 1.27 (s, 9H), 3.2 (br s, 1H; D_2O exchangeable), 4.67 (d, J = 9 Hz, 1H), 5.43 (d, J = 9 Hz, 1H), 6.1 (m, 2H), 7.1–7.7 (m, 10H), 8.10 (br s, 1H); ^{13}C nmr δ: 27.6 (q), 39.4 (s), 51.1 (d), 70.5 (d), 107.6 (d), 110.2 (d), 125.5, 125.8, 126.8, 127.2, 128.4, 128.7, 128.8, 129.5, 134.3, 136.6, 140.1 (s), 141.7 (d), 155.2 (s), 177.4 (s); *m/e*: 363 (<1), 266 (100). *Anal.* calcd. for $C_{23}H_{25}NO_3$: C 76.00, H 6.93, N 3.85; found: C 75.62, H 6.93, N 3.70.

*1-(2-Furanyl)-2-phenyl-2-(2-pivaloylamidophenyl)ethanone (**14**)*[5]

To a solution of dimethyl sulfoxide (2.40 mL, 33.9 mmol) in dichloromethane (40 mL) cooled to −65°C was added dropwise with stirring a solution of trifluoroacetic anhydride (3.50 mL, 24.8 mmol) in dichloromethane (10 mL) at −60°C. After 15 min a solution of alcohol **13** (5.97 g, 16.4 mmol) in dichloromethane (10 mL) was added at −60°C. After a further 30 min trimethylamine (8 mL) was added at −60°C and stirring was continued for 5 min and the mixture

[5]This experiment was conducted under rigorously anhydrous conditions under a positive pressure of nitrogen.

Can. J. Chem. Downloaded from www.nrcresearchpress.com by 210.87.254.105 on 09/06/12
For personal use only.

Can. J. Chem. Downloaded from www.nrcresearchpress.com by 210.87.254.105 on 09/06/12
For personal use only.

was then allowed to warm to 23°C. Water (30 mL) was added, the phases were separated, and the organic layer was washed with saturated aqueous ammonium chloride (2 × 30 mL). The combined aqueous solutions were back-extracted with dichloromethane (30 mL). The combined organic extracts were dried and the solvent was removed to yield crude **14** (5.90 g, 99%) as a solid. Recrystallization from hexanes – ethyl acetate provided an analytical sample as colorless crystals, mp 176–177°C; ir λ_{max}: 3.00 (w), 5.99 μm; ^{1}H nmr δ: 1.00 (s, 9H), 5.98 (s, 1H), 6.53 (dd, J = 3.5–1.5 Hz, 1H), 7.0–7.5 (m, 9H), 7.6 (m, 1H), 7.9 (m, 1H), 8.5 (br s, 1H); ^{13}C nmr δ: 27.2 (q), 39.4 (s), 47.0 (d), 104.1 (d), 113.1 (d), 119.8, 125.1, 125.9, 127.3, 128.2, 128.7, 132.0, 136.9, 137.4, 147.8 (d), 152.5 (s), 177.0 (s), 189.3 (s); m/e: 361 (50), 266 (100). *Anal.* calcd. for $C_{23}H_{23}NO_3$: C 76.43, H 6.41, N 3.88; found: C 76.24, H 6.50, N 3.72.

*2-(2-Furanyl)-3-phenyl-1-pivaloylindoline (**15**)*[5]

Method A

A solution of trifluoroacetic anhydride (0.584 mL, 4.13 mmol) in dichloromethane (2 mL) was added dropwise to a stirred solution of dimethyl sulfoxide (0.390 mL, 5.51 mmol) in dichloromethane (10 mL) at −60°C. The reaction mixture was stirred at −60°C for 10 min and a solution of alcohol **13** (1.00 g, 2.75 mmol) in dichloromethane (7 mL) was added dropwise. The reaction mixture was stirred at −60°C for 10 min and allowed to warm to 0°C and then triethylamine (2 mL) was added. The reaction mixture was warmed to room temperature and washed with saturated aqueous ammonium chloride (2 × 10 mL). The organic solution was dried and concentrated to yield **15** (850 mg, 89%) as an oil; ir λ_{max}: 6.10 μm; ^{1}H nmr δ: 1.07 (s, 9H), 4.42 (br s, 1H), 5.62 (br s, 1H), 5.96 (d, J = 3 Hz, 1H), 6.15 (dd, J = 3, 2Hz, 1H), 6.9–8.2 (m, 9H), 8.27 (br d, J = 7 Hz, 1H); m/e: 345 (80), 255 (100). *Accurate mass* calcd. for $C_{23}H_{23}NO_2$: 345.1729; found: 345.1729.

Method B

A ^{1}H nmr tube was charged with alcohol **13** (50 mg) and deuteriochloroform containing 1% tetramethylsilane (~1 mL). Trifluoroacetic anhydride (0.25 mL) was added and the tube was shaken. The reaction mixture became deep blue in color. An ^{1}H nmr spectrum taken subsequently was identical to that of the product from Method A.

*1-Allyloxy-1-(2-furanyl)-2-phenyl-2-(2-pivaloylamidophenyl)ethene (**20**)*

A solution of ketone **14** (2.965 g, 8.2 mmol) and allyl bromide (1.0 mL, 11.6 mmol) in dichloromethane (25 mL) was added to a solution of sodium hydroxide (0.355 g, 8.88 mmol) and tetra-*n*-butylammonium bromide (0.55 g, 1.5 mmol) in water (25 mL). The heterogeneous mixture was stirred under nitrogen rapidly at 23°C for 18 h. The phases were separated and the aqueous phase was extracted with dichloromethane (15 mL). The combined organic solutions were concentrated to yield an oil. Treatment with ether (150 mL) effected precipitation of tetra-*n*-butylammonium bromide. Magnesium sulfate was added and the solution was filtered and concentrated to yield crude **20** (3.29 g, 99%) as an oil; ir λ_{max}: 2.90 (w), 5.96 μm; ^{1}H nmr δ: 1.08 and 1.18 (2 s, 9H), 4.15 and 4.33 (2 dd, J = 5, 1 Hz, 2H), 4.8–6.3 (m, 5H), 6.9–7.6 (m, 10H), 8.0–8.15 (m, 1H); m/e: 401 (26), 101 (100).

*6-[Phenyl(2-pivaloylamidophenyl)methylene]-5,10-dioxatricyclo-[4.2.1.0^{3,7}]dec-8-ene (**21**)*

A solution of allyl enol ethers **20** (600 mg, 1.5 mmol) in benzene was boiled under reflux under nitrogen for 26 h. The solution was allowed to cool to room temperature and the solvent was removed to yield an oil. The ^{1}H nmr analysis indicated the presence of three components. Compound **21** was isolated as a white crystalline solid (280 mg, 47%) by crystallization from hexanes – ethyl acetate; mp 156–158°C; ir λ_{max}: 2.95 (w), 5.96 μm; ^{1}H nmr δ: 1.20 (s, 9H), 1.3–2.6 (m, 2H), 3.83 (dd, J = 10, 8 Hz, 1H), 4.50 (t, J = 8 Hz, 1H), 5.22 (dd, J = 4, 2 Hz, 1H), 5.75 (d, J = 6 Hz, 1H), 6.20 (dd, J = 6, 2 Hz, 1H), 7.0–7.4 (m, 9H), 7.9 (br s, 1H), 8.15 (br d, J = 7 Hz, 1H); ^{13}C nmr δ: 27.5 (q), 30.4 (t), 39.5 (s), 45.9 (d), 74.7 (t), 81.2 (d), 90.0 (s), 121.9, 123.9, 127.0, 127.7, 128.3, 128.6, 129.8, 130.1, 130.7, 134.1, 135.4, 137.5, 176.3 (s); m/e: 401 (7), 180 (100). *Anal.* calcd. for $C_{26}H_{27}NO_3$: N 3.49; found: N 3.44.

*1-(2-Furanyl)-2-phenyl-2-(pivaloylamidophenyl)pent-4-en-1-one (**22**)*

A solution of allyl enol ethers **20** (5.37 g, 13.4 mmol) in mesitylene (55 mL) under nitrogen was immersed in an oil bath at 165°C for 3.5 h. The solution was then allowed to cool to room temperature and the solvent was removed to yield an oil. This was dissolved in hexanes – ethyl acetate (4:1) and eluted through a plug of silica gel (50 g) with hexanes – ethyl acetate. The eluate was concentrated to yield **22** as an oil (4.64 g, 86%), which crystallized on standing. Recrystallization from hexanes – ethyl acetate provided an analytical sample, mp 105–106°C; ir λ_{max}: 2.96, 6.00 μm; ^{1}H nmr δ: 0.90 (s, 9H), 3.38 (dd, J = 8, 2 Hz, 2H), 4.7–5.6 (m, 3H), 6.27 (dd, J = 4, 2 Hz, 1H), 6.75 (d, J = 4 Hz, 1H), 7.0–7.4 (m, 9H), 7.6–8.1 (m, 2H); ^{13}C nmr δ: 26.8 (q), 39.5 (s), 43.2 (t), 61.7 (s), 111.9 (d), 118.9, 119.9, 124.5, 125.2, 127.4, 128.0, 128.6, 128.9, 129.8, 130.4, 133.2, 137.5, 139.1, 145.8 (d), 151.6 (s), 176.4 (s), 187.9 (s); m/e: 401 (5), 180 (100). *Anal.* calcd. for $C_{26}H_{27}NO_3$: C 77.78, H 6.78, N 3.49; found: C 77.52, H 6.83, N 3.44.

*4-(2-Furoyl)-1,2,3,4-tetrahydro-4-phenyl-1-pivaloyl-2-quinolinol (**23**)*

To a stirred solution of olefin **22** (0.693, 1.72 mmol) in ether (15 mL) were added sequentially water (15 mL), osmium tetroxide (40 mg), and sodium periodate (0.734 g, 3.43 mmol) and the reaction mixture was stirred for 19 h at room temperature. The phases were separated and the ethereal solution was washed with water (10 mL). The combined aqueous solutions were back-extracted with ether (15 mL). The combined ethereal solutions were washed with aqueous 5% sodium hydroxide solution (2 × 15 mL), dried, and concentrated to yield **23** (635 mg, 91%) as a fluffy white solid, mp 147–149°C; ir λ_{max}: 2.70 (w), 6.00, 6.14 μm; ^{1}H nmr δ: 1.03 (s, 9H), 2.07 (dd, J = 13, 7 Hz, 1H), 3.50 (dd, J = 13, 7 Hz, 1H), 4.15 (br s, 1H; D_2O exchangeable), 5.75 (td, J = 7, 2.5 Hz, 1H), 6.35 (dd, J = 4, 2 Hz, 1H), 6.8–7.5 (m, 11H); ^{13}C nmr δ: 29.6 (q), 42.3 (s), 43.3 (t), 58.6 (s), 79.2(d), 112.0 (d), 119.8 (d), 125.5, 125.7, 126.9, 127.3, 127.6, 128.1, 128.3, 128.8, 136.4, 139.2, 146.0 (d), 152.4 (s), 185.2 (s), 187.0 (s); m/e: 403 (10), 306 (100). *Anal.* calcd. for $C_{25}H_{25}NO_4$: N 3.58; found: N 3.45.

*2-(2-Furanyl)-1-methyl-3-phenyl-3-(2-pivaloylamidophenyl)pyrrolidine (**26**)*

The general method of Borch *et al.* (9) was followed. A solution of hemiaminal **23** (0.052 g, 0.129 mmol), methylamine hydrochloride (0.045 g, 0.667 mmol), and sodium cyanoborohydride (0.009 g, 0.143 mmol) in methanol (5 mL) under nitrogen was allowed to stand overnight over 3 Å molecular sieves. The methanolic solution was decanted from the molecular sieves, the sieves were washed with methanol (3 × 5 mL), and the washings were decanted. The combined methanolic solution and washings were concentrated and the residue was treated with 1 *N* hydrochloric acid (5 mL) and extracted with ether (15 mL). The ethereal extract was extracted with 1 *N* hydrochloric acid (15 mL) and the combined acidic solutions were basified with powdered potassium hydroxide and extracted with ether (2 × 15 mL). The combined ethereal extracts were dried and concentrated to yield **26** (0.030 mg, 50%) as a colorless oil; ir λ_{max}: 2.92 (w), 5.97 μm; ^{1}H nmr δ: 0.90 and 1.08 (2 s, 9H), 2.18 and 2.45 (2 s, 3H), 2.0–3.4 (m, 4H), 4.25 and 4.662 (s, 1H), 5.15 and 5.80 (2 d, J = 3 Hz, 1H), 6.0 (dd, J = 3, 2 Hz, 1H), 6.6–8.0 (m, 11H); m/e: 402 (100). *Accurate mass* calcd. for $C_{26}H_{30}N_2O_2$: 402.2307; found: 402.2308.

*4-Methylamino-1-(2-furanyl)-2-phenyl-2-(2-pivaloylamidophenyl)-butan-1-one (**24**)*[5]

A solution of hemiaminal **23** (0.10 g, 0.25 mmol), methylamine hydrochloride (0.418 g, 6.19 mmol), and sodium cyanoborohydride (0.008 g, 0.127 mmol) in methanol (10 mL) was stirred overnight at room temperature. The reaction mixture was worked-up as in the case of **26** to yield an acid-soluble fraction as an oil that contained a 2:1 mixture of **24** and **26** by ^{1}H nmr spectroscopic analysis. Preparative thin-layer chromatography on silica gel with hexanes–ether (1:1) as

Can. J. Chem. Downloaded from www.nrcresearchpress.com by 210.87.254.105 on 09/06/12
For personal use only.

eluant gave **24** (R_f = 0, 20 mg, 20%) as a pale brown oil; ir λ_{max}: 2.95 (w), 6.00 μm; ^{1}H nmr δ: 1.31 (s, 9H), 2.2–3.2 (m, 4H), 2.67 (s, 3H), 6.05 (dd, J = 3, 2 Hz, 1H), 6.40 (d, J = 4 Hz, 1H), 6.6 (m, 1H), 6.8–7.4 (m, 9H); m/e: 400 (M − H_2O; 14), 343 (100). *Accurate mass* calcd. for $C_{26}H_{28}N_2O_2$ (M − H_2O): 400.2151; found: 400.2152.

Methyl 5-methoxy-2-furancarboxylate (27)

This compound was prepared from methyl 5-bromo-2-furancarboxylate, sodium methoxide, and sodium iodide in methanol according to the method of Torii *et al.* (10). The crude product was sublimed in a Kugelrohr appratus at 90–100°C/0.025 Torr; mp 50–51°C (lit. (10) 51–52°C); ir λ_{max}: 5.80 μm; ^{1}H nmr δ: 3.80 (s, 3H), 3.94 (s, 3H), 5.29 (d, J = 4 Hz, 1H), 7.08 (d, J = 4 Hz, 1H).

5-Methoxy-2-furancarboxaldehyde (28)

5-Methoxy-2-furanmethanol was prepared in 61% yield by lithium aluminum hydride reduction of the ester **27** in ether according to the method of Manly and Amstutz (13). The crude product was used directly in the subsequent step; ^{1}H nmr δ: 3.20 (br s, 1H; D_2O exchangeable), 3.80 (s, 3H), 4.37 (s, 2H), 5.05 (d, J = 3.5 Hz, 1H), 6.08 (d, J = 3.5 Hz, 1H).

Activated manganese dioxide (9.0 g) was added to a solution of the alcohol (0.880 g, 7.86 mmol) in dichloromethane (80 mL) and the reaction mixture was stirred for 16 h at room temperature. Celite was added and the reaction mixture was filtered. The filtrate was concentrated to yield aldehyde **28** (600 mg, 69%) as a colorless oil. The oil was molecularly distilled; bp 110–120°C/15 Torr; ir λ_{max}: 5.95 μm; ^{1}H nmr δ: 4.04 (s, 3H), 5.48 (d, J = 4 Hz, 1H), 7.20 (d, J = 4 Hz, 1H), 9.30 (s, 1H).

1-(2-(5-Methoxy)furanyl)-2-phenyl-2-(2-pivaloylamidophenyl)ethanol (29)[5]

To a stirred solution of dianion **11**, formed from amide **10** (0.250 g, 0.936 mmol), TMEDA (0.285 mL, 0.93 mmol), and 2.20 *M* *n*-BuLi in *n*-hexane (0.85 mL, 0.93 mmol) in THF (5 mL) at −30°C (1) was added a solution of **28** (0.118 g, 0.936 mmol) in THF (1.5 mL). The reaction mixture was stirred at −30°C for 30 min and at room temperature for 1 h. The standard work-up procedure (1) yielded **29** (0.312 g, 85%) as a colorless oil; ir λ_{max}: 2.90 (w), 5.96 μm; ^{1}H nmr δ: 1.10 (2 s, 9H), 2.3 (br s, 1H), 3.68 (2 s, 3H), 4.4–5.5 (m, 3H), 5.84 (d, J = 4 Hz, 1H), 6.8–7.6 (m, 9H), 8.3 (br s, 1H); m/e: 393 (<1), 266 (100). *Accurate mass* calcd. for $C_{24}H_{27}NO_4$: 393.1940; found: 393.1940.

2-(2-(5-Methoxy)furanyl)-3-phenyl-1-pivaloylindoline (30)[5]

A solution of trifluoroacetic anhydride (0.030 mL, 0.21 mmol) in dichloromethane (1 mL) was added dropwise to a stirred solution of dimethyl sulfoxide (0.018 mL, 0.25 mmol) in dichloromethane (5 mL) at −60°C. The mixture was stirred for 10 min and a solution of alcohol **29** (50 mg, 0.13 mmol) in dichloromethane (1 mL) was added dropwise at −60°C. After 20 min triethylamine (0.5 mL) was added at −60°C. The reaction mixture was allowed to warm to room temperature and stirred for 10 min. It was then washed with water (10 mL) and saturated aqueous ammonium chloride (10 mL), dried, and concentrated to yield **30** (36 mg, 75%) as a yellow oil; ir λ_{max}: 6.10 μm; ^{1}H nmr δ: 1.10 (s, 9H), 3.80 (s, 3H), 4.40 (br s, 1H), 4.90 (d, J = 4 Hz, 1H), 5.45 (br s, 1H), 5.84 (d, J = 4 Hz, 1H), 6.9–8.4 (m, 9H).

1-[2-(5-Methoxy)furanyl]-2-phenyl-2-(2-pivaloylamidophenyl)-ethanone (31)[5]

A solution of dianion **11**, formed from amide **10** (0.200 g, 0.75 mmol), TMEDA (0.230 mL, 1.53 mmol), and 2.05 *M* *n*-BuLi in *n*-hexane (0.80 mL, 1.64 mmol) in THF (5 mL) at −30°C (1) was added dropwise by cannula to a stirred solution of ester **27** (0.215 g, 1.49 mmol) in THF (5 mL) at −70°C. The reaction mixture became red-brown and was then stirred for 15 min. Saturated aqueous ammonium chloride (10 mL) was added and the heterogeneous mixture was extracted with ether (2 × 20 mL). The combined ethereal extracts were washed with saturated aqueous ammonium chloride (10 mL), dried, and concentrated. The residue was chromatographed on silica gel with hexanes – ethyl acetate as eluant to yield **31** (0.146 g, 50%) as a yellow oil. Crystallization from hexanes – ethyl acetate gave an analytical sample, mp 136–138°C; ir λ_{max}: 3.00 (w), 6.00 μm; ^{1}H nmr δ: 0.98 (s, 9H), 3.93 (s, 3H), 5.43 (d, J = 4 Hz, 1H), 5.78 (s, 1H), 6.9–7.4 (m, 9H), 7.47 (d, J = 4 Hz, 1H), 7.95 (m, 1H); m/e: 391 (32), 125 (100). *Anal.* calcd. for $C_{24}H_{25}NO_4$: C 73.64, H 6.44, N 3.58; found: C 73.89, H 6.33, N 3.29.

1-[2-(5-Methylthio)furanyl]-2-phenyl-2-(2-pivaloylamidophenyl)pent-4-en-1-one (33)[5]

A 1.95 *M* solution of *n*-BuLi in *n*-hexane (0.970 mL, 1.89 mmol) was added dropwise to a stirred solution of diisopropylamine (0.263 mL, 1.88 mmol) in tetrahydrofuran (10 mL) at −20°C. The mixture was stirred at −20°C for 10 min and a solution of **22** (0.250 g, 0.623 mmol) in tetrahydrofuran was added dropwise, when the solution became brown. The reaction mixture was stirred at −20°C for 15 min and dimethyl disulfide (0.10 mL, 1.11 mmol) was added dropwise. The reaction mixture became light brown after standing for 30 min at −20°C and for 5 h at room temperature. Saturated aqueous ammonium chloride (10 mL) was added and the hetergeneous mixture was extracted with ether (2 × 15 mL). The combined ethereal extracts were washed with saturated aqueous ammonium chloride (10 mL), dried, and concentrated to give crude **33** (250 mg, 89%) as an oil; ir λ_{max}: 2.95 (w), 6.00 μm; ^{1}H nmr δ: 0.95 (s, 9H), 2.33 (s, 3H), 3.4 (br d, 2H), 4.75–5.80 (m, 3H), 6.20 (d, J = 4 Hz, 1H), 6.90 (d, J = 4 Hz, 1H), 7.0–8.2 (m, 10H); m/e: 447 (19), 141 (100). *Accurate mass* calcd. for $C_{27}H_{29}NO_3S$: 447.1868; found: 447.1853.

Acknowledgement

We thank the Natural Sciences and Engineering Research Council of Canada for support of this work.

1. P. YATES and D. A. SCHWARTZ. Can. J. Chem. **61**, 509 (1983).
2. G. BÜCHI and H. WÜEST. J. Org. Chem. **31**, 977 (1966); L. CROMBIE, P. HEMESELY, and G. PATTENDEN. J. Chem. Soc. (C), 1024 (1969); M. A. TOBIAS. J. Org. Chem. **35**, 267 (1970); T. KAMETANI, M. TSUBUKI, and H. NEMOTO. Tetrahedron Lett. **22**, 2373 (1981).
3. M. FÉTIZON, F. GOMEZ-PARRA, and J.-M. LOUIS. J. Heterocycl. Chem. **13**, 525 (1976).
4. S. L. HUANG, K. OMURA, and D. SWERN. J. Org. Chem. **41**, 3329 (1976); A. J. MANCUSO and D. SWERN. Synthesis, 165 (1981).
5. V. RAMANATHAN and R. LEVINE. J. Org. Chem. **27**, 1216 (1962).
6. F. A. L. ANET and J. M. MUCHOWSKI. Chem. Ind. (London), 81 (1963).
7. G. W. GOKEL and H. D. DURST. Synthesis, 168 (1976).
8. R. PAPPO, D. S. ALLEN, JR., R. U. LEMIEUX, and W. S. JOHNSON. J. Org. Chem. **21**, 478 (1956).
9. R. F. BORCH, M. D. BERNSTEIN, and H. D. DURST. J. Am. Chem. Soc. **93**, 2897 (1971).
10. S. TORII, M. TANAKA, and T. OKAMOTO. Bull. Chem. Soc. Jpn. **45**, 2783 (1972).
11. M. FEDORYŃSKI, K. WOJCIECHOWSKI, Z. MATACZ, and M. MAKOSZA. J. Org. Chem. **43**, 4682 (1978).
12. V. VANRHEENEN, R. C. KELLY, and D. Y. CHA. Tetrahedron Lett. 1973 (1976).
13. D. G. MANLY and E. D. AMSTUTZ. J. Org. Chem. **21**, 516 (1958).

Purine complexes of platinum: synthesis, nmr, and crystal and molecular structures of *cis*-chloro(caffeine)bis(triethylphosphine)platinum(II) fluoroborate and *cis*-bis(isocaffeine)bis(triethylphosphine)platinum (II) fluoroborate

GORDON WILLIAM BUSHNELL, RODERICK JAMES DENSMORE, KEITH ROGER DIXON, AND ARTHUR CHARLES RALFS
Department of Chemistry, University of Victoria, Victoria, B.C., Canada V8W 2Y2

Received September 24, 1982

GORDON WILLIAM BUSHNELL, RODERICK JAMES DENSMORE, KEITH ROGER DIXON, and ARTHUR CHARLES RALFS. Can. J. Chem. **61**, 1132 (1983).

Synthesis and ^{31}P nmr spectra of the complex cations, *cis*-$[PtCl(L)(PEt_3)_2]^+$, L = theophylline, caffeine, or isocaffeine, and *cis*-$[Pt(isocaff)_2(PEt_3)_2]^{2+}$ are reported. The crystal structure of *cis*-$[PtCl(caffeine)(PEt_3)_2][BF_4]$ is determined, space group $P\bar{1}$, a = 1.1766(6), b = 1.4428(5), c = 0.9002(4) nm, α = 97.28(4)°, β = 97.69(4)°, γ = 100.96(5)°, D_m = 1.649 g cm^{-3}, the bond lengths are Pt—Cl = 233.4(4) pm, Pt—N = 215(1) pm, Pt—P = 225.4(5) pm (mean), and the residual R = 0.071. The crystal structure of *cis*-$[Pt(isocaffeine)_2(PEt_3)_2][BF_4]_2$ is orthorhombic, space group *Pbca*, a = 2.317(3), b = 1.717(3), c = 2.130(3) nm, D_m = 1.574 g cm^{-3}, with an opposing isocaffeine conformation, bond lengths Pt—N = 211(2) pm, Pt—P = 227.6(9) pm (mean), and R = 0.073. Both crystal structures contain approximately square planar Pt(II) coordination with the purine coordinated via an imidazole nitrogen. The structures are discussed as models for the possible involvement of N_7---O_6 chelation of guanine to platinum when platinum drugs act as antitumour agents, but there is no evidence that isocaffeine acts as an N_7---O_6 chelate.

GORDON WILLIAM BUSHNELL, RODERICK JAMES DENSMORE, KEITH ROGER DIXON et ARTHUR CHARLES RALFS. Can. J. Chem. **61**, 1132 (1983).

On rapporte la synthèse et les spectres de rmn du ^{31}P des cations complexes: $[PtCl(L)(PEt_3)_2]^+$ *cis*, L = théophylline, caféine ou isocaféine et $[Pt(isocaf)_2(PEt_3)_2]^{2+}$ *cis*. On a déterminé la structure du composé $[PtCl(caféine)PEt_3)_2][BF_4]$. Le cristal appartient au groupe d'espace $P\bar{1}$ avec a = 1,1766(6), b = 1,4428(5), c = 0,9002(4) nm, α = 97,28(4)°, β = 97,69(4)°, γ = 100,96(5)°, D_m = 1,649 g cm^{-3}. Les longueurs de liaison sont de Pt—Cl = 233,4(4) pm, Pt—N = 215(1) pm, Pt—P = 225,4(5) pm (moyenne) et la valeur conventionnelle de R est de 0,071. La structure cristalline du composé $[Pt(isocaféine)_2(PEt_3)_2][BF_4]_2$ *cis* est orthorhombique et appartient au groupe d'espace *Pbca* avec a = 2,317(3), b = 1,717(3), c = 2,130(3) nm, D_m = 1,574 g cm^{-3} avec une conformation isocaféine opposée. Les longueurs de liaison sont de Pt—N = 211(2) pm, Pt—P = 227,6(9) pm (moyenne) et R = 0,073. Dans chacune des deux structures cristallines, on retrouve du Pt(II) avec une coordination approximativement plan carrée avec la purine coordonnée au moyen de l'azote de l'imidazole. On discute des structures en tant que modèle pour l'implication de la chélation N_7---O_6 de la guanine sur le platine lorsque les drogues contenant du platine agissent comme agents antituméreux, mais il n'y a pas de preuve du fait que l'isocaféine agit comme un chélate N_7---O_6.

[Traduit par le journal]

Introduction

The use of platinum complexes as anti-tumour drugs is now well known and the subject has been extensively covered in recent reviews (1–5). One such complex, *cis*-$[PtCl_2(NH_3)_2]$, has passed into widespread clinical use (recent reports of the clinical status of the drug appear in a two-part issue (6)) but the design of more effective analogues, for example with greater solubility in body fluids and reduced toxicity, is hampered by the lack of detailed understanding of the mechanism of action of these drugs. It is widely accepted that the platinum becomes attached to DNA, most probably via coordination to the N_7 position of a guanine base, but the details of the attachment and the mechanism of its effect on the cancer cell are unknown. Several different models have been proposed (5, 7) and an especially important point is to account for the activity of *cis*-$[PtCl_2(NH_3)_2]$ relative to the corresponding *trans* isomer which is essentially inactive. An early proposal (8–12) which is still under discussion (5, 7, 13) involves chelation of the platinum by the N_7 and O_6 atoms of a guanine base attached to DNA. Assuming that it is the chloride ligands which are displaced by base coordination, such chelation is possible only for *cis*-$[PtCl_2(NH_3)_2]$ and not for the *trans* isomer (8–12).

Studies on model complexes have shown that unsubstituted purines normally coordinate to metals via the imidazole nitrogen atom which is protonated in the free, neutral ligand, i.e., N_9 for adenine, guanine, xanthine, and hypoxanthine and N_7 for theophylline. However, when N_9 is blocked, as it would be by the deoxyribose residue in DNA bound guanosine, N_7 is indeed the normal site of metal coordination (3).

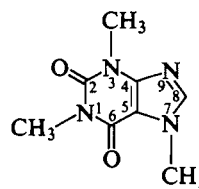

Caffeine[1]
(1,3,7-trimethylxanthine)

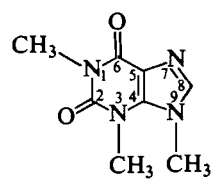

Isocaffeine[1]
(1,3,9-trimethylxanthine)

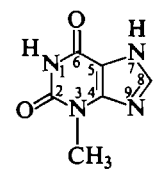

Theophylline[1]

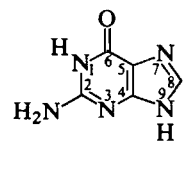

Guanine[1]

Unfortunately no platinum purine complexes have provided

[1]For a discussion of nomenclature and numbering of purines, see ref. 36.

Can. J. Chem. Downloaded from www.nrcresearchpress.com by 210.87.254.42 on 09/06/12
For personal use only.

TABLE 1. Nuclear magnetic resonance parameters for platinum–purine complexes

Complex	^{31}P spectrum[a]					^{1}H spectrum[a]	
	trans to N[b]		*trans* to Cl[b]				
	δ	^{1}J(Pt—P)	δ	^{1}J(Pt—P)	^{2}J(P—P)	δ(H_8)	^{3}J(Pt—H_8)
cis-[PtCl(theo)(PEt_3)$_2$][BF_4]	−136.5[c]	3291	−134.2	3520	21		
cis-[PtCl(caff)(PEt_3)$_2$][BF_4]	−134.3[d]	3290	−132.7	3388	20	8.08[e]	11.7
cis-[PtCl(isocaff)(PEt_3)$_2$][BF_4]	−135.7[d]	3334	−133.7	3505	21		
cis-[Pt(isocaff)$_2$(PEt_3)$_2$][BF_4]$_2$	−140.4[d]	3346				7.50[f]	14.0

[a]Chemical shifts in parts per million and coupling constants in Hertz. Positive shifts are downfield from the references: [$P(OCH_3)_3$] for ^{31}P and [$Si(CH_3)_4$] for ^{1}H.
[b]The assignment of these resonances is discussed in the Results sections.
[c]CH_3OH solution.
[d]CH_2Cl_2 solution.
[e]CD_2Cl_2 solution with CH_2Cl_2 lock.
[f]$SO(CD_3)_2$ solution with CH_2Cl_2 lock.

any structural evidence for metal interaction with O_6 in addition to N_7, although chelation has been suggested several times from spectroscopic evidence (8–12). Indeed the only crystallographic demonstration of a direct O_6–metal interaction is in a copper complex of the theophyllinate anion and even here the bond is very weak, Cu—O = 292 pm (14). More definite chelate interactions have been observed in 6-thio-purine complexes of both copper, Cu—S = 242 pm (15), and palladium, Pd—S = 231 pm (16).

We have chosen to study this problem by a structural comparison of platinum complexes of the caffeine and isocaffeine molecules. Isocaffeine is a close model for the guanine base with the same possibilities for N_7—O_6 chelation but with the other sites blocked by methylation. Caffeine is isomeric but the different methylation pattern limits coordination to N_9 where no possibility of oxygen chelation exists. At the same time the presence of the methyl group on N_3 in caffeine permits a direct comparison of the Pt—O distance in the isocaffeine complex with the Pt—C(N_3) distance in the caffeine complex. This comparison is expected to reveal any shortening of Pt—O_6 or other geometrical distortions caused by Pt—O_6 bonding interactions.

Several crystallographic studies of transition metal caffeine complexes have been reported previously (17, 18). Structures of isocaffeine complexes are very few, but a recent paper (19) gives two crystal structures containing the ion $[Pt(en)(isocaff)_2]^{2+}$.

Results

(A) Synthesis and spectroscopy

The bridge cleavage reaction represented by eq. [1] is a convenient route to complexes of the general type [PtCl(L)(PEt_3)$_2$][BF_4], and under controlled conditions usually leads to exclusively *cis* stereochemistry (20).

[1] [$Pt_2(\mu\text{-}Cl)_2(PEt_3)_4$][$BF_4$]$_2$ + 2L → 2*cis*-[PtCl(L)(PEt_3)$_2$][BF_4]

Our preliminary results with a range of purines (L = guanine, hypoxanthine, adenine, and theophylline) indicated that crystals suitable for X-ray diffraction study were likely to be obtained only if L was highly substituted. Moreoever, ^{31}P nmr studies showed that complex mixtures, apparently involving coordination to several different nitrogen sites, resulted from reactions of unsubstituted purines. Even when L was theophylline several minor products were formed in addition to *cis*-[PtCl(theo)(PEt_3)$_2$][BF_4] which was identified as the main product by ^{31}P nmr (see Table 1). In view of these results we decided to focus our structural studies on the trimethylated purines, caffeine and isocaffeine.

Reaction of caffeine according to eq. [1] proceeded smoothly under mild conditions to yield *cis*-[PtCl(caff)(PEt_3)$_2$][BF_4] which was initially identified by microanalysis, and by infrared and nmr spectroscopy and finally by a full structure determination as described below. The infrared spectrum showed the expected caffeine, triethylphosphine, and fluoroborate absorptions together with ν(Pt—Cl) at 290 cm^{-1}. The ^{31}P nmr spectrum recorded at 24.3 MHz showed an AB quartet (δ_{AB} = 38.5 Hz) with ^{2}J(P—P), 20 Hz, typical of a *cis*-P_2Pt arrangement (21). Sidebands attributable to the 33.8% of molecules containing ^{195}Pt were also observed and, as is expected in this type of spin system (22), the sideband patterns were not identical to the centre-band. The effective chemical shifts introduced by the different phosphorus coupling constants to platinum ($\delta_{EFF} = \delta_{AB} \pm (1/2)\{^{1}J(Pt—P_A) - {}^{1}J(Pt—P_B)\}$) result in a low-field sideband which is essentially an AX double doublet, and an up-field sideband which is an AB system so closely coupled that only a single line is observed. The spectra of *cis*-[PtCl(theo)(PEt_3)$_2$][BF_4] and *cis*-[PtCl(isocaff)(PEt_3)$_2$]-[BF_4] which were identified only by nmr, were closely similar to that for the structurally characterised *cis*-[PtCl(caff)(PEt_3)$_2$]-[BF_4] complex and nmr parameters for all these molecules are collected in Table 1. The assignment of phosphorus resonances in this table is based on the assumption that the nmr *trans*-influence of nitrogen ligands is generally greater than that of chloride and hence the phosphorus *trans* to chloride will be the one with the larger ^{1}J(Pt—P) value (23). In the present case where the platinum–phosphorus coupling constants are fairly closely similar, the assignment should be treated with caution. The ^{1}H nmr of *cis*-[PtCl(caff)(PEt_3)$_2$][BF_4] showed the expected caffeine and triethylphosphine resonances in the correct relative intensities and is mainly notable for the ^{195}Pt sidebands observed on the caffeine H_8 resonance. The coupling constant (^{3}J(Pt—H) = 11.7 Hz) is a typical value for a proton α to a coordinated nitrogen (24) and confirms that the platinum is attached in the imidazole ring.

The reaction of isocaffeine with [$Pt_2Cl_2(PEt_3)_4$][BF_4]$_2$ was slightly more complex. ^{31}P nmr of the initial crude products showed the presence of a small amount of *cis*-[$PtCl_2(PEt_3)_2$] (δ_P −130.7 ppm, ^{1}J(Pt—P) 3509 Hz) together with two new compounds in an approximately 2:1 ratio. The more intense new

Can. J. Chem. Downloaded from www.nrcresearchpress.com by 210.87.254.42 on 09/06/12
For personal use only.

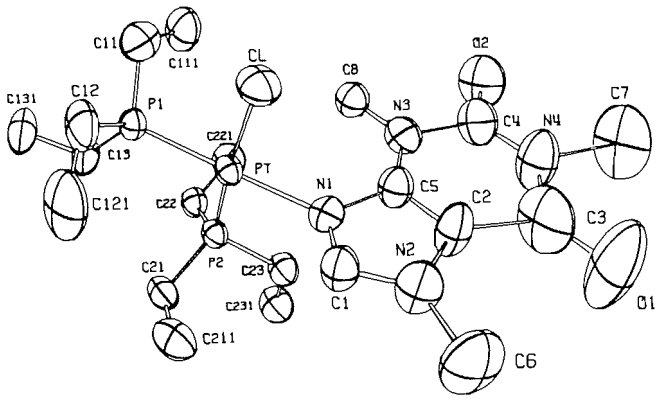

FIG. 1. The molecular structure of *cis*-[Pt(PEt$_3$)$_2$(caff)Cl][BF$_4$].

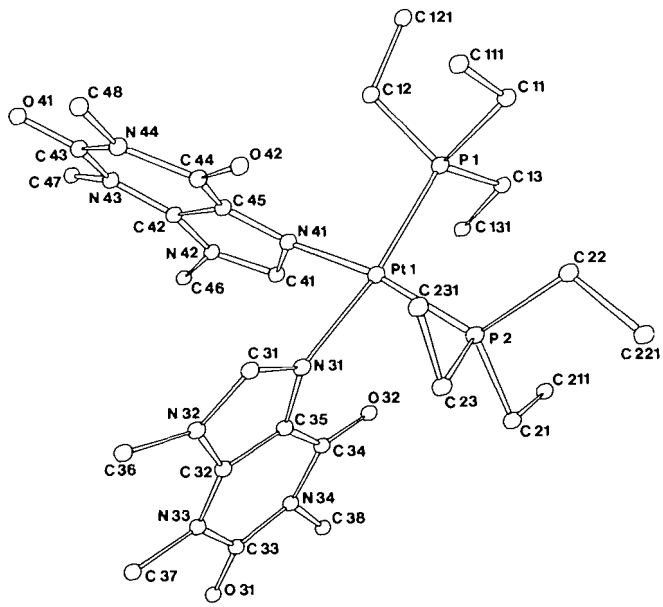

FIG. 2. The molecular structure of *cis*-[Pt(PEt$_3$)$_2$(isocaff)$_2$][BF$_4$]$_2$.

spectrum was very similar to that described above for the caffeine complex and is assigned to *cis*-[PtCl(isocaff)(PEt$_3$)$_2$]$^+$ while the less intense spectrum was a singlet with ^{195}Pt sidebands consistent with *cis*-[Pt(isocaff)$_2$(PEt$_3$)$_2$]$^{2+}$. An infrared spectrum of the mixture showed a ν(Pt—Cl) absorption at 275 cm^{-1}. However, various attempts at recrystallization to obtain high quality product for further analytical and crystallographic study resulted only in crystals of *cis*-[Pt(isocaff)$_2$(PEt$_3$)$_2$][BF$_4$]$_2$ and we were unable to obtain pure *cis*-[PtCl(isocaff)(PEt$_3$)$_2$]-[BF$_4$]. Mother liquors from these crystallizations contained no *cis*-[Pt(isocaff)$_2$(PEt$_3$)$_2$]$^{2+}$ but only *cis*-[PtCl(isocaff)(PEt$_3$)$_2$]$^+$ together with a much increased quantity of *cis*-[PtCl$_2$(PEt$_3$)$_2$]. Evidently *cis*-[PtCl(isocaff)(PEt$_3$)$_2$]$^+$ tends to disproportionate during crystallization and only the least soluble complex *cis*-[Pt(isocaff)$_2$(PEt$_3$)$_2$][BF$_4$]$_2$ is obtained.

(B) Description of structures

Both structures consist of discrete, essentially square planar cations and fluoroborate anions. The structures of the *cis*-[PtCl(caff)(PEt$_3$)$_2$]$^+$ and *cis*-[Pt(isocaff)$_2$(PEt$_3$)$_2$]$^{2+}$ cations are shown in Figs. 1 and 2 and the packing diagrams are given in Figs. 3 and 4. Fractional atomic coordinates, bond lengths, bond angles, and results of mean plane calculations are collected in Tables 2–9. Tables of anisotropic temperature parameters (Tables S12 and S13), mean plane coefficients (Tables S5 and S9), and bond lengths and angles of the BF$_4$ and PEt$_3$ groups (Tables S3, S4, S7, and S8) have been deposited for both structures.[2]

(i) cis-*[PtCl(caff)(PEt$_3$)$_2$][BF$_4$]*

The caffeine ligand is coordinated, as expected, through N$_9$ and is inclined at 97–98° (depending on the plane chosen for the ligand) to the coordination plane defined by the PtClP$_2$ unit. The platinum atom is significantly displaced (41.0 pm) from the plane of the imidazole ring. Similar displacements are not uncommon (e.g. [PtCl$_3$(caff)]$^-$, 4.9 pm (18), *cis*-[PtCl(naphthyridine)(PEt$_3$)$_2$]$^+$, 14.3 pm (25), and [CuCl$_2$(H$_2$O)(caff)], 31 pm (17)) but the present example seems unusually large. We have recently observed a similarly large displacement (34.8 pm) in a palladium pyrazole complex, *cis*-[PdCl(dimethylpyrazole)(PEt$_3$)$_2$]$^+$ (26). These displacements may simply be the result of steric factors such as interaction between the five-membered rings and the *cis*-PEt$_3$ ligands, but could also be indicative of some rehybridisation of the coordinating nitrogen. All the caffeine ligands in the crystal are parallel by symmetry and it may be seen in Fig. 3 that there is an intermolecular caffeine/caffeine contact halfway along the *b*-axis.

The bond lengths and bond angles within the caffeine ligand are essentially identical within experimental error with those reported previously in the complexes, [CuCl$_2$(H$_2$O)(caff)] (17) and [PtCl$_3$(caff)]$^-$ (18), the comparison with the latter being especially exact. The only slight discrepancy concerns the N$_7$—C$_8$—N$_9$ angle in the imidazole ring, where the present value of 109° is close to that found in [H(caff)]$^+$ (109.6°) rather than to the more usual value of 112–113° found in caffeine itself and in other N-bonded caffeine complexes (18). As in previous examples the caffeine shows significant departures from planarity, notably a slight dihedral angle (2.3°) between the 5- and 6-membered rings.

Within the platinum coordination sphere, the Pt—N distance is longer, 215 pm, in the present complex than in [PtCl$_3$(caff)]$^-$, 202 pm (18), reflecting the greater *trans* influence of phosphorus relative to chlorine. On the basis of *trans*-Pt—Cl bond lengths, the *trans* influence of caffeine itself has been suggested to be similar to that of simple nitrogen donors (18) and this view is confirmed by the Pt—P bond length *trans* to caffeine in the present complex. The value of 225.3 pm is very close to lengths observed *trans* to phenanthroline (27), naphthyridine (25), and phthalazine (28) ligands. Indeed, as Table 10 shows, the geometry of the *cis*-PtCl(PEt$_3$)$_2$ fragment remains very constant in a range of complexes and the *cis*-PdCl(PEt$_3$)$_2$ fragment in *cis*-[PdCl(dimethylpyrazole)(PEt$_3$)$_2$]$^+$ is also similar (26). The conformations of the triethylphosphine ligands are also the same in all these complexes.

(ii) cis-*[Pt(isocaff)$_2$(PEt$_3$)$_2$][BF$_4$]$_2$*

The two isocaffeine ligands are coordinated through N$_7$ and are inclined at 88.2 and 87.9° to the coordination plane defined by the PtP$_2$N$_2$ unit. The isocaffeines are arranged so that their 6-membered rings are away from each other, one above and one below the coordination plane. As in the *cis*-

[2]The structure factor tables for both **I** and **II** are available, at a nominal charge, from the Depository of Unpublished Data, CISTI, National Research Council of Canada, Ottawa, Ont., Canada K1A 0S2.

Can. J. Chem. Downloaded from www.nrcresearchpress.com by 210.87.254.42 on 09/06/12
For personal use only.

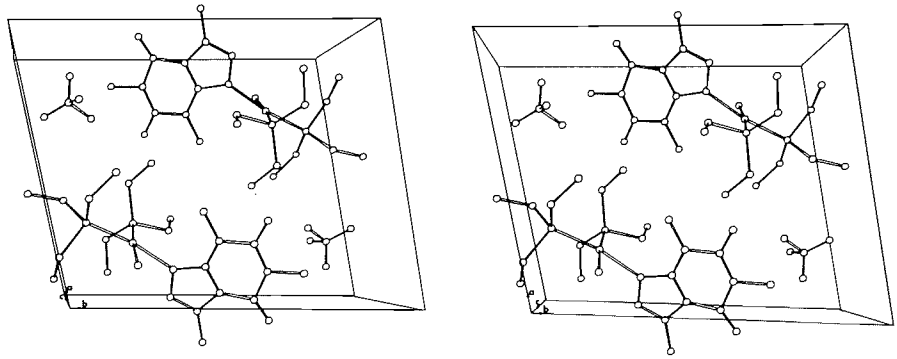

FIG. 3. The stereoscopic packing drawing for the caffeine complex, **I**.

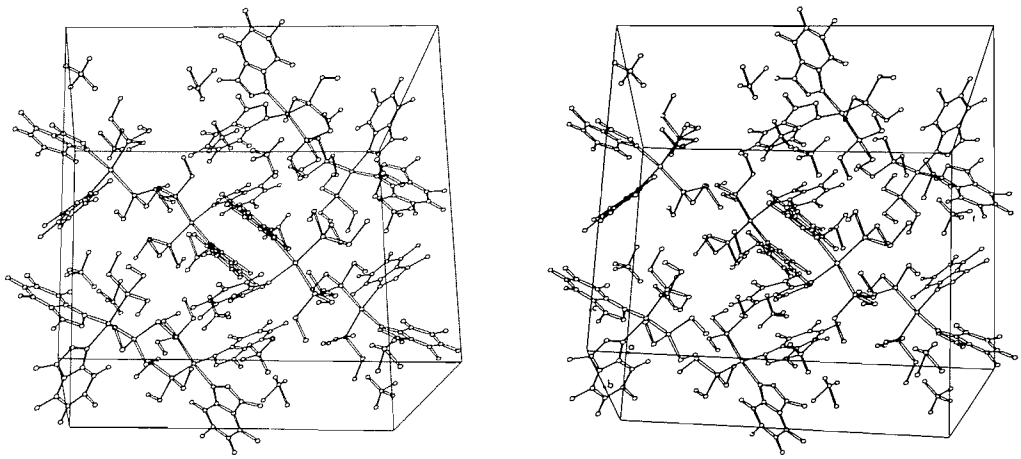

FIG. 4. The stereoscopic packing drawing for the isocaffeine complex, **II**.

$[PtCl(caff)(PEt_3)_2]^+$ structure the platinum atom is significantly displaced from the planes of the imidazole rings, by 22.6 pm from the more planar and by 44.7 pm from the less planar isocaffeine.

The bond lengths and bond angles in the isocaffeine ligands are generally similar within experimental error to those reported for the free ligand (29) but the puckering of the rings appears to be affected by coordination. One isocaffeine is fairly closely planar while the 5- and 6-membered rings in the other isocaffeine are inclined at ~8.9° to each other, possibly because of steric interactions with a PEt_3 ligand. Both base ligands of the complex are involved in intermolecular contacts with their planes parallel, as may be seen in Fig. 4. The hexafluorophosphate and nitrate salts of *cis*-$[Pt(en)(isocaff)_2]^{2+}$ studied by Orbell *et al.* (19) show structures similar to our isocaffeine complex in the general conformation of the *cis*-isocaffeine ligands and in departures of them from planarity, but differ in the base/base dihedral angles 70.6° (nitrate), 87.3° (hexafluorophosphate), 65.4° (this work). Hydrogen bonding cannot occur in our complex as it does in the structures containing ethylenediamine.

Within the platinum coordination sphere the Pt—N(isocaff) distances reported by Orbell *et al.* (19) are shorter than in *cis*-$[Pt(isocaff)_2(PEt_3)_2]^{2+}$ owing to the greater *trans* influence of PEt_3 over en, the mean values being 201.9(7) pm (19) and 211(1) pm (this work). The latter value is still slightly shorter than the corresponding distance, 215(1) pm, in the caffeine complex. If this is a reflection of greater donor strength towards platinum then it may explain the formation of the 2:1 complex in the isocaffeine/platinum case whereas we were able to obtain only the 1:1 complex for caffeine. Finally, we note that the geometry of the $Pt(PEt_3)_2$ unit in *cis*-$[Pt(isocaff)_2(PEt_3)_2]^{2+}$ is very similar to that in the complexes containing $PtCl(PEt_3)_2$ units (Table 10) and indeed the entire PtP_2N_2 geometry is closely comparable with other complexes containing $PtClNP_2$ and $PtCl_2P_2$ coordination spheres. The principal variable in these structures is the displacement of the coordinating nitrogen atom from the otherwise planar coordination geometry. In the phthalazine, naphthyridine, and phenanthroline complexes (Table 10), the displacement varies from 4 pm in *cis*-$[PtCl(phth)(PEt_3)_2]^+$ to 37 pm in *cis*-$[PtCl(phen)(PEt_3)_2]^+$. It correlates with the rate of metal shuttling between the two ligand nitrogens and serves as an index of potentially bidentate character (28). However, this does not appear to be a useful concept in the present case since the displacement (23 pm) in the caffeine complex, where there is no possibility of a chelate interaction, is larger than the displacements (+15 and −10 pm) in the isocaffeine complex.

Discussion

As noted in the Introduction, a primary motivation for this study was to seek evidence for or against the possibility of O_6—N_7 chelation in the isocaffeine complex. Two principal lines of evidence bear on this question.

Firstly, the Pt---O_6 distances in *cis*-$[Pt(isocaff)_2(PEt_3)_2]^{2+}$ are 334 pm and 322 pm. Szalda, Kirstenmacher, and Marzilli (14) have collected data for several 6-oxopurine complexes of copper in which they consider there is no Cu---O_6 interaction and the distances range from 328 to 383 pm. In contrast a complex with a weak Cu---O_6 interaction has a distance of 292 pm (14).

Can. J. Chem. Downloaded from www.nrcresearchpress.com by 210.87.254.42 on 09/06/12
For personal use only.

Can. J. Chem. Downloaded from www.nrcresearchpress.com by 210.87.254.42 on 09/06/12
For personal use only.

TABLE 2. Fractional atomic coordinates[a] ($\times 10^4$) for *cis*-[PtCl(caff)-$(PEt_3)_2$][BF_4]$_2$

	x	*y*	*z*
Pt	2361.7(4)	2313.2(4)	2473.7(6)
Cl	1580(4)	2186(3)	−86(4)
P(1)	3103(4)	1023(3)	1774(4)
P(2)	3109(3)	2580(3)	4970(4)
B	7600(29)	1299(22)	3718(51)
F(1)	7067(28)	478(17)	3857(46)
F(2)	8560(20)	1517(33)	4157(65)
F(3)	7648(44)	1531(24)	2358(38)
F(4)	6999(34)	1896(19)	4206(43)
N(1)	1381(11)	3416(10)	2800(15)
N(2)	−260(12)	3910(11)	2983(22)
N(3)	2426(11)	4821(10)	1861(15)
N(4)	1325(15)	6047(12)	1710(26)
O(1)	−525(18)	5873(14)	2358(39)
O(2)	3171(13)	6241(10)	1118(20)
C(1)	281(14)	3166(12)	3079(23)
C(2)	489(15)	4617(12)	2478(26)
C(3)	330(20)	5553(16)	2212(40)
C(4)	2345(17)	5738(12)	1524(24)
C(5)	1477(13)	4296(11)	2358(19)
C(6)	−1478(19)	3908(18)	3249(37)
C(7)	1298(27)	7041(18)	1400(45)
C(8)	3499(14)	4491(12)	1673(21)
C(11)	3929(22)	1195(16)	220(25)
C(12)	1864(21)	41(12)	866(24)
C(13)	3932(19)	520(14)	3178(23)
C(111)	4878(21)	2108(16)	492(30)
C(121)	1050(25)	−265(23)	2031(45)
C(131)	4177(22)	−481(17)	2641(28)
C(21)	2479(17)	1686(13)	6026(20)
C(22)	4699(14)	2745(12)	5492(19)
C(23)	2824(16)	3716(12)	5848(18)
C(211)	1134(18)	1506(17)	5843(26)
C(221)	5413(16)	3512(16)	4771(24)
C(231)	3291(18)	3991(15)	7572(21)

[a]Estimated standard deviations are given in parentheses.

TABLE 3. Bond lengths (pm) for *cis*-[PtCl(caff)$(PEt_3)_2$][BF_4]$_2$

(*a*) Platinum coordination

Bond	Length	Bond	Length
Pt—Cl	233.3(4)	Pt—P(1)	225.3(4)
Pt—N(1)	215(1)	Pt—P(2)	225.5(5)

(*b*) The caffeine ligand

Bond	Length	Bond	Length
C(3)—O(1)	120(3)	C(4)—O(2)	122(2)
N(4)—C(7)	149(3)	N(3)—C(8)	145(2)
C(2)—C(3)	145(3)	C(2)—C(5)	134(2)
C(3)—N(4)	142(3)	C(5)—N(3)	139(2)
N(4)—C(4)	138(2)	N(3)—C(4)	141(2)
N(1)—C(5)	137(2)	N(2)—C(2)	138(2)
N(1)—C(1)	134(2)	N(2)—C(1)	135(2)
		N(2)—C(6)	149(2)

Orbell *et al.* (19) find Pt---O_6 distances of 341.3(6), 336.6(6), and 335.4(6) pm in two *cis*-[Pt(en)(isocaff)$_2$]$^{2+}$ salts, the hexafluorophosphate and the nitrate, and this is interpreted as indicating no significant participation of the 6-oxo group in the metal binding. The Pt---O_6 distance in our isocaffeine complex may also be compared with the corresponding non-bonding Pt---CH_3 distance of 338 pm in *cis*-[PtCl(caff)$(PEt_3)_2$]$^+$. Bearing in mind that the van der Waals radius (30) for a methyl group (200 pm) is larger than that for oxygen (140 pm), it is clear that the Pt---O_6 distance in *cis*-[Pt(isocaff)$_2(PEt_3)_2$]$^{2+}$ is too long to represent a bonding interaction.

Secondly, the various angles collected in Table 11 are expected to reflect the degree of interaction between M and X. For [$PtCl_3$(caff)]$^-$ we see that angle *b* is greater than angle *a* and that relative to caffeine itself *c* has increased in the complex while *d* has decreased. These observations have been interpreted as indicative of steric repulsion between (X = CH_3) and the metal coordination sphere (18). The argument may be extended by examination of the three copper theophylline complexes. In [Cu(theophyllinato)(SME)] (31) the O_6 atom of theophylline is involved in inter-ligand hydrogen bonding and $b > a$, in contrast to the situation in [Cu(theophyllinato)(BDE)] (14) where there is a weak Cu---O_6 bond and $a > b$. In the other theophylline complex, [$Cu(NO_3)(H_2O)_2$(theophylline)$_2$]$^+$, there are no special interactions involving O_6 and the angles *a* and *b* are approximately equal (32). In the 6-thiopurine complexes of copper and palladium in Table 11 there is a full coordinate bond between the metal and the S_6 atom and this introduces even more marked distortion with $a \gg b$ (15, 16). The other angles, *c*, *d*, and *e*, also show some changes which are correlated with the M---X interaction, especially in the thiopurine complexes which are genuine chelates. However, examination of all the data in Table 11 shows that the relative size of angles *a* and *b* is much the most sensitive criterion of interaction, either repulsive or bonding. On this basis it is clear that *cis*-[PtCl(caff)$(PEt_3)_2$]$^+$ has a repulsive Pt---CH_3 interaction similar to that in [$PtCl_3$(caff)]$^-$ and that *cis*-[Pt(isocaff)$_2(PEt_3)_2$]$^{2+}$ has essentially no Pt---O_6 interaction, similar to the case of [$Cu(NO_3)(H_2O)_2$(theophylline)$_2$]$^+$. Thus we find no evidence of any tendency for isocaffeine to act as a chelating ligand.

Experimental section

(A) Synthesis and spectroscopic studies

Data relating to the characterization of the complexes are given in the Results section and under individual preparations below. Microanalyses were by Schwarzkopf Microanalytical Laboratory, Woodside, NY. Infrared spectra were recorded from 4000 to 250 cm^{-1} with an accuracy ±3 cm^{-1} on a Beckman IR20 spectrophotometer calibrated against polystyrene film and water vapour. Solid samples were examined as Nujol mulls between caesium iodide plates. ^1H nmr spectra were recorded at 90 MHz on a Perkin-Elmer R32 spectrometer. ^{31}P nmr spectra were recorded in dichloromethane solution at 24.29 MHz on a Nicolet TT14 Fourier transform spectrometer using a Varian HA60 magnet. Protons were decoupled by broad band ("noise") irradiation at appropriate frequencies. [$P(OCH_3)_3$] was used as external reference and C_6D_6 as external lock. In all nmr spectra *positive* chemical shifts are *downfield* from the reference.

Caffeine and isocaffeine were commercially available and [$Pt_2Cl_2(PEt_3)_4$][BF_4]$_2$ was prepared as previously described (33).

(i) cis-*[PtCl(caff)$(PEt_3)_2$][BF_4]*

A solution of caffeine (0.083 g, 0.427 mmol) in dichloromethane was added dropwise to a stirred solution of [$Pt_2Cl_2(PEt_3)_4$][BF_4]$_2$ (0.237 g, 0.214 mmol) in dichloromethane under a nitrogen atmosphere at 25°C. After stirring for 3 h, the solution was evaporated to small volume under reduced pressure and diethyl ether slowly added to give *cis*-[PtCl(caff)$(PEt_3)_2$][BF_4] as a white precipitate (0.279 g, 0.373 mmol). Colourless crystals suitable for both X-ray study and microanalysis were grown by vapour diffusion of diethyl ether into a solution of the complex in dichloromethane. *Anal.* calcd. for

TABLE 4. Bond angles (deg) for *cis*-[PtCl(caff)$(PEt_3)_2$][BF_4]$_2$

(*a*) Platinum coordination

Bonds	Angle	Bonds	Angle
P(1)—Pt—Cl	86.5(2)	N(1)—Pt—Cl	84.5(4)
P(1)—Pt—P(2)	98.4(1)	N(1)—Pt—P(2)	90.9(4)
P(1)—Pt—N(1)	169.1(4)	P(2)—Pt—Cl	174.7(2)

(*b*) The caffeine ligand

Bonds	Angle	Bonds	Angle
O(2)—C(4)—N(4)	122(2)	C(7)—N(4)—C(4)	116(2)
O(2)—C(4)—N(3)	120(2)	C(7)—N(4)—C(3)	117(2)
N(3)—C(4)—N(4)	118(2)	C(3)—N(4)—C(4)	128(2)
C(8)—N(3)—C(4)	118(1)	O(1)—C(3)—N(4)	124(2)
C(8)—N(3)—C(5)	124(1)	O(1)—C(3)—C(2)	126(2)
C(4)—N(3)—C(5)	118(1)	N(4)—C(3)—C(2)	110(2)
N(1)—C(5)—N(3)	128(1)	N(2)—C(2)—C(3)	129(2)
N(3)—C(5)—C(2)	122(2)	C(3)—C(2)—C(5)	124(2)
N(1)—C(5)—C(2)	110(1)	N(2)—C(2)—C(5)	107(1)
Pt—N(1)—C(5)	132.5(9)	C(6)—N(2)—C(2)	127(2)
Pt—N(1)—C(1)	118(1)	C(6)—N(2)—C(1)	125(2)
C(1)—N(1)—C(5)	106(1)	C(1)—N(2)—C(2)	107(1)
N(1)—C(1)—N(2)	109(1)		

TABLE 5. Mean plane results for *cis*-[PtCl(caff)$(PEt_3)_2$][BF_4]$_2$[a]

Plane	Description	Number of atoms	χ^2
1	The heavy atoms (Z = 15–78)	4	196
2	The 5-membered ring plus attached C-methyl	6	10
3	The 6-membered ring plus its 4 peripheral atoms	10	3.9
4	The caffeine ligand less N(1)	13	8.2

Perpendicular distances of atoms from the mean planes (pm)

Plane	Atom/distance list
1	Pt, −0.15(5); Cl, 4.8(5); P(1), 0.4(4); P(2), 3.5(4); N(1), −23(1)
2	Pt, 40.96(5); C(3), −6(3); N(3), 6(1)
3	N(1), −8(1); N(2), 1(2); C(1), 2(2); Pt, 26.74(5)
4	Pt, 25.60(5); N(1), −10(1)

[a]Angles between planes: *1,2* = 97.3°; *1,3* = 98.3°; *1,4* = 98.0°; *2,3* = 2.3°; *2,4* = 2.2°; *3,4* = 0.3°.

$\chi^2 = \sum_i (P_i^2/\sigma^2(P_i))$ where P_i = the perpendicular distance of atom *i* from the plane (atom *i* belongs to the plane defining set of atoms).

$C_{20}H_{40}BClF_4N_4O_2P_2Pt$: C 32.1, H 5.39, N 7.49%; found: C 32.0, H 5.42, N 7.58%.

(ii) cis-*[PtCl(isocaff)$(PEt_3)_2$][BF_4] and* cis-*[Pt(isocaff)$_2$$(PEt_3)_2$]-[$BF_4$]$_2$*

A solution of isocaffeine (0.100 g, 0.515 mmol) in acetone (60 mL) was added dropwise to a stirred solution of [$Pt_2Cl_2(PEt_3)_4$][BF_4]$_2$ (0.285 g, 0.257 mmol) in acetone (15 mL) under a nitrogen atmosphere at 25°C. After stirring for 90 min, the solution was evaporated under reduced pressure to about 15 mL and diethyl ether slowly added to give a white precipitate (0.350 g). As detailed in the Results section, ^{31}P nmr showed this precipitate to be an approximately 2:1 mixture of *cis*-[PtCl(isocaff)$(PEt_3)_2$][BF_4] and *cis*-[Pt(isocaff)$_2$-$(PEt_3)_2$][BF_4]$_2$. Recrystallization by vapour diffusion of diethyl ether into a solution of the mixture in methanol resulted in colourless crystals, which were identified as *cis*-[Pt(isocaff)$_2$$(PEt_3)_2$][$BF_4$]$_2$ by ^{31}P nmr and then fully characterised by an X-ray diffraction study. *Anal.* calcd. for $C_{28}H_{50}B_2F_8N_8O_4P_2Pt$: C 33.9, H 5.07, N 11.3%; found: C 32.9, H 5.11, N 10.6%.

A ^{31}P nmr spectrum of the mother liquors from the recrystallization showed only *cis*-[$PtCl_2(PEt_3)_2$] and *cis*-[PtCl(isocaff)$(PEt_3)_2$][BF_4].

(B) Crystal measurements

Crystals of *cis*-[PtCl(caff)$(PEt_3)_2$][BF_4] (**I**) and *cis*-[Pt(isocaff)$_2$-$(PEt_3)_2$][BF_4]$_2$ (**II**) were prepared as described above and examined by photographic methods using CuK_α radiation and Weissenberg and precession cameras. For **I** a primitive unit cell was chosen and then changed by use of the Delaunay reduction procedure. Both crystals were mounted approximately along the *c*-axis. The crystals were then transferred to a Picker 4-circle diffractometer automated with a PDP-11 computer and the orientation matrices were refined by least squares

Can. J. Chem. Downloaded from www.nrcresearchpress.com by 210.87.254.42 on 09/06/12
For personal use only.

Can. J. Chem. Downloaded from www.nrcresearchpress.com by 210.87.254.42 on 09/06/12
For personal use only.

TABLE 6. Atomic parameters × 10^3 (×10^4 for Pt and P)[a] for *cis*-[Pt(isocaff)$_2$(PEt$_3$)$_2$][BF$_4$]$_2$

Atom	x	y	z	U_{iso} (pm^2×10^{-4})
Pt	1250(1)	2168(1)	1576(1)	—
P(1)	1745(4)	2241(5)	2486(4)	—
P(2)	1929(4)	1557(5)	965(4)	—
B(1)	366(3)	308(4)	399(3)	0.18(3)
B(2)	39(4)	430(5)	376(4)	0.26(5)
F(11)	344(2)	364(2)	364(2)	0.23(2)
F(12)	345(2)	301(3)	459(2)	0.33(3)
F(13)	375(2)	239(3)	375(3)	0.32(3)
F(14)	421(2)	331(3)	409(2)	0.27(2)
F(21)	78(1)	432(2)	332(1)	0.16(1)
F(22)	66(1)	418(2)	433(1)	0.18(1)
F(23)	14(2)	363(2)	366(2)	0.24(2)
F(24)	5(2)	487(2)	385(2)	0.25(2)
O(31)	−5(1)	417(2)	−93(1)	0.119(9)
O(32)	125(1)	373(1)	64.4(9)	0.074(6)
O(41)	−151(1)	214(1)	294(1)	0.087(7)
O(42)	23(1)	117(1)	222.2(9)	0.073(6)
N(31)	66(1)	213(1)	81(1)	0.062(7)
N(32)	−10(1)	184(1)	28(1)	0.059(7)
N(33)	−14(1)	301(2)	−39(1)	0.076(8)
N(34)	61(1)	390(1)	−16(1)	0.079(8)
N(41)	57(1)	281(1)	198(1)	0.060(7)
N(42)	−6(1)	376(1)	212(1)	0.061(7)
N(43)	−83(1)	300(1)	258(1)	0.050(6)
N(44)	−67(1)	167(1)	253(1)	0.065(8)
C(31)	29(1)	160(2)	71(1)	0.051(8)
C(32)	10(1)	253(2)	6(1)	0.057(9)
C(33)	13(2)	369(2)	−54(2)	0.09(1)
C(34)	85(2)	349(2)	33(1)	0.070(9)
C(35)	56(1)	276(1)	40(1)	0.036(6)
C(36)	−58(2)	137(2)	6(1)	0.08(1)
C(37)	−65(2)	278(2)	−81(2)	0.10(1)
C(38)	88(2)	473(2)	−28(2)	0.11(1)
C(41)	51(1)	360(2)	189(1)	0.059(8)
C(42)	−34(1)	312(2)	232(1)	0.044(7)
C(43)	−103(2)	228(2)	270(1)	0.060(9)
C(44)	−9(1)	176(2)	227(1)	0.058(9)
C(45)	9(1)	252(2)	224(1)	0.056(8)
C(46)	−33(1)	459(2)	206(1)	0.070(9)
C(47)	−127(2)	370(2)	281(2)	0.09(1)
C(48)	−89(2)	82(2)	262(2)	0.10(1)
C(11)	214(2)	137(2)	274(2)	0.09(1)
C(111)	173(2)	67(2)	283(2)	0.11(1)
C(12)	125(2)	247(2)	314(2)	0.09(1)
C(121)	158(2)	253(3)	379(3)	0.14(2)
C(13)	231(2)	302(2)	250(2)	0.10(1)
C(131)	207(2)	381(2)	231(2)	0.09(1)
C(21)	228(2)	226(3)	46(2)	0.14(2)
C(211)	258(2)	294(3)	74(2)	0.11(1)
C(22)	255(2)	104(2)	135(2)	0.11(1)
C(221)	296(2)	63(3)	85(2)	0.13(2)
C(23)	163(3)	77(4)	43(3)	0.19(2)
C(231)	144(2)	13(2)	93(2)	0.12(2)

[a]Estimated standard deviations are given in parentheses. Temperature factor = exp $(-8\pi^2 U_{iso} \sin^2 \theta/\lambda^2)$.

using pairs of centred reflections and MoK$_\alpha$ radiation. The unit cell of **I** was refined by least squares from 2θ measurements in the range 26–45°, and that of **II** was obtained photographically. Crystal data for **I** are as follows:

$C_{20}H_{40}BClF_4N_4O_2P_2Pt$ mw = 747.90

Triclinic, space group $P\bar{1}$ (No. 2), a = 1.1766(6), b = 1.4428(5), c = 0.9002(4) nm, α = 97.28(4)°, β = 97.69(4)°, γ = 100.96(5)°, cell volume 1.469(1) nm^3, D_m = 1.694 g cm^{-3} (flotation), D_c = 1.690 g cm^{-3}, Z = 2.

TABLE 7. Bond lengths (pm) for *cis*-[Pt(isocaff)$_2$(PEt$_3$)$_2$][BF$_4$]$_2$[a]

(*a*) Platinum coordination

Bond	Length	Bond	Length
Pt—P(1)	225.7(8)	Pt—P(2)	229.4(9)
Pt—N(31)	212(2)	Pt—N(41)	210(2)

(*b*) Isocaffeine ligands

Bond	Length	Bond	Length
N(31)—C(31)	128(3)	N(41)—C(41)	138(3)
C(31)—N(32)	135(3)	C(41)—N(42)	143(4)
N(32)—C(32)	134(3)	N(42)—C(42)	134(3)
C(32)—N(33)	138(3)	C(42)—N(43)	128(3)
N(33)—C(33)	137(4)	N(43)—C(43)	134(3)
C(33)—N(34)	143(4)	C(43)—N(44)	138(3)
N(34)—C(34)	138(4)	N(44)—C(44)	146(4)
C(34)—C(35)	143(4)	C(44)—C(45)	138(4)
C(35)—N(31)	141(3)	C(45)—N(41)	134(3)
C(35)—C(32)	135(4)	C(45)—C(42)	145(4)
N(32)—C(36)	145(4)	N(42)—C(46)	157(4)
N(33)—C(37)	154(4)	N(43)—C(47)	164(4)
C(33)—O(31)	123(4)	C(43)—O(41)	125(3)
N(34)—C(38)	156(4)	N(44)—C(48)	154(4)
C(34)—O(32)	121(3)	C(44)—O(42)	127(3)

[a]Estimated standard deviations in parentheses.

Crystal data for **II** are as follows:

$C_{28}H_{50}B_2F_8N_8O_4P_2Pt$ mw = 993.40

Orthorhombic, space group *Pbca* (No. 61), a = 2.317(3), b = 1.717(3), c = 2.130(3) nm, cell volume 8.472(3) nm^3, D_m = 1.574 g cm^{-3}, D_c = 1.557, Z = 8.

Intensity measurements were obtained for the hemisphere $h \geq 0$ up to 48° in 2θ for **I** and up to 40° for **II**. Stepped scans with 50 steps of 0.04° in 2θ were used, counting for 1 s per step with a 25 s background count at each end. Each batch of 50 reflections was preceded by the measurement of three standard reflections (**I**: 4,0,0; 0,6,0; 0,0,4. **II**: 16,0,0; 2,5,0; 0,0,10). The Lorentz and polarisation factors were applied and each batch was scaled to maintain the sum of the standards constant. There was no marked decrease in the standard intensities during the measurements. An instrument instability constant of 0.020 was used to estimate σ(**I**). Absorption corrections were applied using numerical integration over 8×8×8 Gaussian grids with absorption coefficients 52.78 cm^{-1} (**I**) and 36.93 cm^{-1} (**II**) for MoK$_\alpha$ radiation. The crystal shapes were defined by perpendicular distances to seven crystal faces from central origins as follows: **I**, ±(1,0,0) 0.181 mm, ±(0,1,0) 0.087 mm, (0,0,1) 0.279 mm, (0,−1,−1) 0.104 mm, (0,1,−1) 0.145 mm; **II**, ±(1,0,0) 0,055 mm, ±(0,1,0) 0.105 mm, (0,0,−1) 0.350 mm, (0,1,1) 0.267 mm, (0,−1,1) 0.297 mm. The correction factors were in the ranges 0.16–0.43 (**I**) and 0.48–0.68 (**II**). The measurements were sorted and any duplicates averaged to give files containing 3749 (**I**) and 1893 (**II**) independent reflections.

(C) Crystal structure solution and refinement[2]

A set of programmes supplied by Penfold (34) was manly used. The programmes are based on ORFLS, ORFFE, ORTEP, and FORDAP. Platinum coordinates were found from the Patterson function and lighter atoms were located by means of difference maps. The refinement was by the method of least squares minimising $\Sigma w(|F_o| - |F_c|)^2$. The atomic scattering factors were corrected for dispersion (35).

Can. J. Chem. Downloaded from www.nrcresearchpress.com by 210.87.254.42 on 09/06/12
For personal use only.

TABLE 8. Bond angles (deg) for *cis*-$[Pt(isocaff)_2(PEt_3)_2][BF_4]_2$

(*a*) Platinum coordination

Bonds	Angle	Bonds	Angle
P(1)—Pt—P(2)	99.5(3)	N(31)—Pt—N(41)	81.4(9)
P(2)—Pt—N(31)	89.5(7)	N(41)—Pt—P(1)	90.0(7)
N(31)—Pt—P(1)	170.6(7)	N(41)—Pt—P(2)	169.5(6)

(*b*) Isocaffeine ligands

Bonds	Angle	Bonds	Angle
Pt—N(31)—C(31)	126(2)	Pt—N(41)—C(41)	123(2)
Pt—N(31)—C(35)	124(2)	Pt—N(41)—C(45)	127(2)
C(35)—N(31)—C(31)	109(2)	C(45)—N(41)—C(41)	110(3)
N(31)—C(31)—N(32)	110(3)	N(41)—C(41)—N(42)	104(3)
C(31)—N(32)—C(32)	106(3)	C(41)—N(42)—C(42)	114(3)
N(32)—C(32)—C(35)	110(3)	N(42)—C(42)—C(45)	102(3)
C(32)—C(35)—N(31)	104(2)	C(42)—C(45)—N(41)	111(3)
C(35)—C(32)—N(33)	121(3)	C(45)—C(42)—N(43)	123(3)
C(32)—N(33)—C(33)	120(3)	C(42)—N(43)—C(43)	122(3)
N(33)—C(33)—N(34)	116(3)	N(43)—C(43)—N(44)	117(3)
C(33)—N(34)—C(34)	128(3)	C(43)—N(44)—C(44)	124(3)
N(34)—C(34)—C(35)	110(3)	N(44)—C(44)—C(45)	114(3)
C(34)—C(35)—C(32)	125(3)	C(44)—C(45)—C(42)	117(3)
C(31)—N(32)—C(36)	123(3)	C(41)—N(42)—C(46)	121(2)
C(32)—N(32)—C(36)	131(3)	C(42)—N(42)—C(46)	126(3)
N(32)—C(32)—N(33)	128(3)	N(42)—C(42)—N(43)	134(3)
C(32)—N(33)—C(37)	124(3)	C(42)—N(43)—C(47)	124(3)
C(33)—N(33)—C(37)	116(3)	C(43)—N(43)—C(47)	114(3)
N(33)—C(33)—O(31)	126(4)	N(43)—C(43)—O(41)	124(3)
N(34)—C(33)—O(31)	118(4)	N(44)—C(43)—O(41)	119(3)
C(33)—N(34)—C(38)	117(3)	C(43)—N(44)—C(48)	120(3)
C(34)—N(34)—C(38)	115(3)	C(44)—N(44)—C(48)	116(3)
N(34)—C(34)—O(32)	124(3)	N(44)—C(44)—O(42)	120(3)
C(35)—C(34)—O(32)	127(3)	C(45)—C(44)—O(42)	125(3)
C(34)—C(35)—N(31)	131(3)	C(44)—C(45)—N(41)	129(3)

TABLE 9[a]

(*a*) Mean plane results for $[Pt(isocaff)_2(PEt_3)_2][BF_4]_2$

Plane	Description	Atoms	χ^2
1	Coordination plane Pt, P(1), P(2), N(31), N(41)	5	70.3
2	1st isocaffeine	14	36.4
3	2nd isocaffeine	14	252.0
4	5-ring and methyl substituent of 2nd isocaffeine	6	6.1
5	6-ring of the 2nd isocaffeine	6	24.1

(*b*) Perpendicular distances of atoms from the mean planes (pm)

Plane	Atom/distance list
1	Pt, −0.03(11); P(1), −0.9(8); P(2), 1.7(8); N(31), −10(2); N(41), 15(2)
2	O(32), −6(2); C(36), −8(3); Pt, −22.6(1)
3	N(41), −10(2); N(44), 10(2); C(45), −14(3); C(46), 27(3); C(47), −24(3); C(48), 24(4); Pt, 19.0(1)
4	Pt, 44.7(1)
5	C(42), 7(3); C(45), −9(3); O(41), −9(2); O(42), −11(2); C(47), −14(3); C(48), 7(4)

[a]Angles between planes *1,2* = 88.2°; *1,3* = 87.9°; *1,4* = 92.3°; *2,3* = 65.4°; *2,4* = 62.0°; *2,5* = 66.0°; *4,5* = 8.9°. χ^2 has been defined in Table 5.

(i) cis-*[PtCl(caff)(PEt$_3$)$_2$][BF$_4$]*

The 35 non-hydrogen atoms were treated anisotropically and the refinement was done using alternate cycles which refined the heavy atoms and the caffeine ligands, then the heavy atoms, the fluoroborate group, and the triethylphosphine ligands. The weighting scheme finally used was of the form $w = [A + Bx + Cx^2 + Dx^3]^{-1}$ where $x = |F_o|$, with values $A = 57.82$, $B = -2.006$, $C = 4.793 \times 10^{-2}$, $D = -1.04 \times 10^{-4}$. This gave approximately constant $\Sigma w\Delta^2$ as a function of $|F_o|$, the summations being over subsets of reflections. At convergence the maximum change/error ratio was 1.16, the mean change/error ratio was 0.13, the larger ratios being associated with the BF_4 group. The final difference map gave no evidence for any further atoms, the major peaks and troughs being close to the Pt atom. The final R-value was 0.071 and $R_w = \sqrt{(\Sigma(w\Delta^2)/\Sigma wF_o^2)}$ was 0.087. $\Sigma w\Delta^2 = 822$ for 3749 observations and 316 variables, hence $\sqrt{(\Sigma(w\Delta^2)/(NO - NV)} = 0.489$.

(ii) cis-*[Pt(isocaff)$_2$(PEt$_3$)][Bf$_4$]$_2$*

Both BF_4 groups were subjected to the contraints B—F = 136 ± 10 pm, F—F = 222 ± 10 pm, which were significant but did not totally dominate the X-ray intensities. There were 1893 X-ray observations and 228 parameters in the refinement. The weighting scheme was $w = 0.3346/(\sigma(F)^2 + 0.0166F^2)$. The R-value was 0.0731 and $R_w = \sqrt{(\Sigma w\Delta^2/\Sigma wF_o^2)} = 0.1010$. The refinement converged and the maximum (shift/sigma) was 0.15 in the final cycle. The final difference map had a maximum of 2.3×10^{-6} e pm^{-3} close to the position of the Pt atom; there were only 4 peaks above 1.0×10^{-6} e pm^{-3} and these were unsuitable as positions of new atoms.

TABLE 10. Comparison of metal coordination geometry

Bond	Distance (pm)						
	cis-$[MCl(L)(PEt_3)_2]^{+1 \text{ or } 0}$						
	M=Pt L[a]=phen[b]	M=Pt L=naph[c]	M=Pt L=phth[d]	M=Pt L=caff[e]	M=Pt L=Cl[f]	M=Pd L=DMP[g]	*cis*-$[Pt(isocaff)_2(PEt_3)_2]^{2+}$ [e]
Pt—Cl	236.1(6)	236.6(4)	235.4(9)	233.3(4)	236.6(1), 235.5(2)	235.2(4)	
Pt—N	214(2)	208(1)	208(1)	215(1)		210.2(2)	210(2), 215(2)
Pt—P(*trans* to Cl)	224.1(6)	225.2(4)	225.2(8)	225.3(4)	225.7(1), 226.2(1)	227.4(4)	
Pt—P(*trans* to N)	223.9(7)	225.4(4)	226.9(8)	225.5(5)		229.0(4)	230.0(8), 231.1(9)
Bonds	**Angle (deg)**						
	cis-$[MCl(L)(PEt_3)_2]^{+1 \text{ or } 0}$						
	M=Pt L[a]=phen[b]	M=Pt L=naph[c]	M=Pt L=phth[d]	M=Pt L=caff[e]	M=Pt L=Cl[f]	M=Pd L=DMP[g]	*cis*-$[Pt(isocaff)_2(PEt_3)_2]^{2+}$ [e]
Cl—Pt—P	85.5(2)	86.8(2)	86.5(4)	86.5(2)	83.5(1), 90.7(5)	84.9(1)	
P—Pt—P	99.5(2)	99.3(1)	98.9(3)	98.4(1)	99.2(1)	97.9(1)	100.6(3)
P—Pt—N	93.6(5)	90.6(3)	91.3(7)	90.9(4)		91.9(1)	88.3(7), 88.9(7)
N—Pt—Cl	81.2(5)	83.2(3)	83.4(7)	84.5(4)		85.5(1)	
N—Pt—N							82.4(9)
Cl—Pt—Cl					86.5(1)		
N—Pt—P(*trans*)	162.5(5)	169.7(3)	169.8(7)	169.1(4)		169.95(5)	170.8(7), 169.5(7)
Cl—Pt—P(*trans*)	174.8(3)	173.6(1)	174.3(3)	174.7(2)	176.2(1), 169.6(1)	176.02(7)	

[a]phen = 1,10-phenanthroline; naph = 1,8-naphthyridine; phth = phthalazine; caff = caffeine; DMP = 3,5-dimethylpyrazole; isocaff = isocaffeine.
[b]Reference 27.
[c]Reference 25.
[d]Reference 28.
[e]Present work.
[f]Lj. Manojlovic-Muir, K. W. Muir, and T. Solomun. Private communication.
[g]Reference 26.

TABLE 11. Bond angles as a criterion of chelation in metal purine complexes

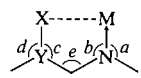

X = O, S, or CH_2
Y = C or N

Complex	Angles (deg)				
	a	*b*	*c*	*d*	*e*
Caffeine[a]			121.4	118.5	126.6
$[PtCl_3(caff)]^-$ [a]	119.4	135.8	124.7	116.7	128.3
cis-$[PtCl(caff)(PEt_3)_2]^+$ [b]	118	132.5	124	118	128
cis-$[Pt(isocaff)_2(PEt_3)_2]^{2+}$ [b,c]	124.5	125.5	126	122	130
cis-$[Pt(en)(isocaff)_2]^{2+}$ [d,c]	124.2	130.3	126.6	121.3	128.9
[Cu(theophyllinato)(SME)][e]	118.9	138.0	127.7	119.4	132.0
$[Cu(NO_3)(H_2O)_2(\text{theophylline})_2]^+$ [f]	127.2	127.9	125.8	122.1	129.6
[Cu(theophyllinato)(BDE)][g]	138.9	117.8	125.8	122.6	129.0
$[CuCl_2(6\text{-thio-9-methylpurine})]$[h]	142.0	113.3	119.6	128.4	126.2
[Pd(6-thio-9-benzylpurine][c,i]	146	110	116	124	128

[a]Reference 18.
[b]Present work.
[c]Average values.
[d]Reference 19.
[e]Reference 31. SME = *N*-salicylidene-*N'*-methylethylenediamine.
[f]Reference 32. Only the parameters for the theophylline which is not involved in hydrogen bonding are shown.
[g]Reference 14. BDE = *N*-3,4-Benzosalicylidene-*N'*,*N'*-dimethyl-ethylenediamine.
[h]Reference 15.
[i]Reference 16.

Acknowledgements

We thank the Natural Sciences and Engineering Research Council of Canada, and the University of Victoria for operating grants, Mr. Blaine Hawkins for illustrative photography, Mrs. Kathy Beveridge for technical assistance, and Mr. B. Brandon for chemical contributions.

1. M. J. CLEARE. Coord. Chem. Rev. **12**, 349 (1974).

Can. J. Chem. Downloaded from www.nrcresearchpress.com by 210.87.254.42 on 09/06/12
For personal use only.

2. S. J. LIPPARD. Accts. Chem. Res. **11**, 211 (1978).
3. D. J. HODGSON. Prog. Inorg. Chem. **23**, 211 (1977).
4. L. G. MARZILLI. Prog. Inorg. Chem. **23**, 255 (1977).
5. T. G. SPIRO. Nucleic acid: metal ion interactions. Wiley, New York. 1980.
6. J. Clin. Hematol. Oncol. **7** (1977).
7. R. FAGGIANI, C. J. L. LOCK, and B. LIPPERT. J. Am. Chem. Soc. **102**, 5418 (1980), and references therein.
8. J. P. MACQUET and T. THEOPHANIDES. Inorg. Chim. Acta, **18**, 189 (1976).
9. M. M. MILLARD, J. P. MACQUET, and T. THEOPHANIDES. Biochim. Biophys. Acta, **402**, 166 (1975).
10. J. P. MACQUET and T. THEOPHANIDES. Bio. Inorg. Chem. **5**, 59 (1975).
11. D. M. L. GOODGAME, L. JEEVES, F. L. PHILLIPES, and A. C. SKAPSKE. Biochim. Biophys. Acta, **378**, 153 (1975).
12. J. DEHAND and J. JORDANOV. J. Chem. Soc. Chem. Commun. 598 (1976).
13. B. ROSENBERG. Paper presented at the International Conference on the Chemistry of the Platinum Group Metals, Bristol, England. July 1981.
14. D. J. SZALDA, T. J. KIRSTENMACHER, and L. G. MARZILLI. J. Am. Chem. Soc. **98**, 8371 (1976).
15. E. SLETTEN and A. APELAND. Acta. Crystallogr. B**31**, 2019 (1975).
16. H. J. HEITNER and S. J. LIPPARD. Inorg. Chem. **13**, 815 (1974).
17. G. BANDOLI, M. C. BIAGINI, D. A. CLEMENTE, and G. RIZZARDI. Inorg. Chim. Acta, **20**, 71 (1976).
18. R. E. CRAMER, D. M. HO, W. VAN DORNE, J. A. IBERS, T. NORTON, and M. KASHIWAGI. Inorg. Chem. **20**, 2457 (1981), and references therein.
19. J. D. ORBELL, K. WILKOWSKI, B. DE CASTRO, L. G. MARZILLI, and T. J. KISTENMACHER. Inorg. Chem. **21**, 813 (1982).
20. K. R. DIXON, K. C. MOSS, and M. A. R. SMITH. Can. J. Chem. **52**, 692 (1974), and references therein.
21. R. J. GOODFELLOW and B. F. TAYLOR. J. Chem. Soc. Dalton Trans. 1676 (1974).
22. K. R. DIXON and T. W. DINGLE. Inorg. Chem. **13**, 846 (1974).
23. T. G. APPLETON, H. C. CLARK, and L. E. MANZER. Coord. Chem. Rev. **10**, 335 (1973).
24. K. R. DIXON. Inorg. Chem. **16**, 2618 (1977).
25. G. W. BUSHNELL, K. R. DIXON, and M. A. KHAN. Can. J. Chem. **56**, 450 (1978).
26. G. W. BUSHNELL, K. R. DIXON, D. T. EADIE, and S. R. STOBART. Inorg. Chem. **20**, 1545 (1981).
27. G. W. BUSHNELL, K. R. DIXON, and M. A. KHAN. Can. J. Chem. **52**, 1367 (1974).
28. G. W. BUSHNELL and K. R. DIXON. Can. J. Chem. **56**, 878 (1978).
29. H. RASMUSSEN and E. SLETTEN. Acta Chem. Scand. **27**, 2757 (1973).
30. F. A. COTTON and G. WILKINSON. Advanced inorganic chemistry. 2nd ed. Interscience, New York. 1966. p. 115.
31. T. J. KIRSTENMACHER, D. J. SZALDA, and L. G. MARZILLI. Inorg. Chem. **14**, 1686 (1975).
32. B. L. KINDBERG, E. A. H. GRIFFITH, E. L. AMMA, and E. R. JONES, JR. Cryst. Struct. Commun. **5**, 533 (1976).
33. K. R. DIXON and D. J. HAWKE. Can. J. Chem. **49**, 3252 (1971).
34. B. R. PENFOLD. University of Canterbury crystallographic programs, Christchurch, New Zealand.
35. International Tables for X-ray Crystallography. Vol IV. The Kynoch Press, Birmingham, England. p. 71 (f-curves), and p. 148 (dispersion).
36. J. H. LISTER. *In* The chemistry of heterocyclic compounds — fused pyrimidines. Part II. Purines. *Edited by* A. Weissberger and E. C. Taylor. Wiley, New York. 1971. pp. 4–7.

Can. J. Chem. Downloaded from www.nrcresearchpress.com by 210.87.254.42 on 09/06/12
For personal use only.

The reaction of trimethylamine in liquid hydrogen sulphide: an electrical conductivity study[1]

JAMES D. HALLIDAY AND PATRICK E. BINDNER

Physical Chemistry Branch, Atomic Energy of Canada Limited Research Company, Chalk River Nuclear Laboratories, Chalk River, Ont., Canada K0J 1J0

Received October 27, 1982

JAMES D. HALLIDAY and PATRICK E. BINDNER. Can. J. Chem. **61**, 1142 (1983).

The electrical conductivity of trimethylamine solutions (2.26×10^{-4} to 2.89×10^{-1} mol L^{-1}) in liquid hydrogen sulphide over the temperature range −72.5°C to +25.0°C has been measured. The data indicate that the trimethylamine behaves as a Brønsted base in liquid hydrogen sulphide [1] and is protonated to form trimethylammonium hydrogensulphide. The latter

[1] $(CH_3)_3N + H_2S \rightleftharpoons (CH_3)_3NH \cdot SH \rightleftharpoons (CH_3)_3\overset{+}{N}H + \bar{S}H$

behaves as a normal weak electrolyte in a solvent of low to medium dielectric constant ($\epsilon_{H_2S} = 9.05$ at −78.5°C). The conductance data as a function of temperature also show that trimethylamine exists both as a hydrogen bonded complex with H_2S and as an unassociated molecule in liquid H_2S.

JAMES D. HALLIDAY et PATRICK E. BINDNER. Can. J. Chem. **61**, 1142 (1983).

On a mesuré la conductivité électrique des solutions de triméthylamine ($2{,}26 \times 10^{-4}$ à $2{,}89 \times 10^{-1}$ mol L^{-1}) dans le sulfure d'hydrogène liquide dans un intervalle de température allant de −72,5°C à +25,0°C. Les données indiquent que la triméthylamine se comporte comme une base de Brønsted dans le sulfure d'hydrogène liquide [1]

[1] $(CH_3)_3N + H_2S \rightleftharpoons (CH_3)_3NH \cdot SH \rightleftharpoons (CH_3)_3\overset{+}{N}H + \bar{S}H$

et se protone pour former l'hydrogénosulfure de triméthylammonium. Ce dernier se comporte comme un électrolyte faible normal dans un solvant de constante diélectrique allant de faible à moyen ($\epsilon_{H_2S} = 9{,}05$ à −78,5°C). Les données de conductance en fonction de la température montrent également que la triméthylamine existe comme un complexe lié par des liaisons hydrogènes avec H_2S et comme une molécule non associée dans le H_2S liquide.

[Traduit par le journal]

Introduction

Relatively little information is available concerning the electrical conductivity of liquid H_2S and its solutions compared with that available from water and aqueous solutions. Even some of the physical properties of liquid H_2S such as the dielectric constant, ϵ, are not well documented as a function of temperature ($\epsilon_{H_2O,0°C} = 87.740$, $\epsilon_{H_2S,-78.5°C} = 9.05$). The dissociation of weak electrolytes in these two solvents is expected to differ due to the large difference in the magnitudes of their dielectric constants. The high dissociation of many electrolytes in water has allowed determinations of the limiting equivalent conductances, Λ_0, of these ions, but none have been determined for ions in liquid H_2S. However, trialkylamines are known to be protonated in liquid H_2S to yield conducting solutions (1, 2) (for example, trimethylamine, reaction [1])

[1] $(CH_3)_3N + H_2S \rightleftharpoons (CH_3)_3NH \cdot SH \rightleftharpoons (CH_3)_3\overset{+}{N}H + \bar{S}H$

Further evidence for this reaction is that trialkylammonium hydrogensulphides have been isolated and characterized from trialkylamine/H_2S reaction mixtures (e.g. $(CH_3)_3NH \cdot SH$, mp 28−30°C (3)). Earlier studies (1, 2) indicated that there was an abnormal electrical conductivity behaviour in these solutions in that the equivalent conductance, Λ, increased with increasing concentration of trialkylamine. This paper describes an electrical conductance study of the reaction of trimethylamine with liquid hydrogen sulphide, as a function of trimethylamine concentration and temperature, in an attempt to better understand the reaction of this base with hydrogen sulphide.

[1]AECL No. 7999.

Experimental

Variable temperature studies near ambient temperature with liquid H_2S require glass apparatus that can safely withstand the considerable vapour pressure of this liquid (2.1 MPa at 25°C) and handling techniques that take into consideration its very high toxicity (equivalent to that of HCN). For these reasons the conductance cells used in this study were hydrostatically tested to 5.0 MPa before use. Several failed this test, sometimes after being at high pressure for many hours. Cells containing liquid H_2S were kept behind scatter shields in a fumehood (air flow rate 52 L s^{-1}) whenever practical.

In addition to meeting the above pressure requirements the conductivity cell system was designed so that the concentrations of $(CH_3)_3N$ could be changed by direct transfer of the amine in the gas phase. This avoided the use of the large quantities of H_2S that would normally be required to dilute initial stock solutions. In addition the small volume of the cell itself (16.5 mL) minimized the total amount of H_2S being handled at any one time.

The final design of the conductivity cell is shown in Fig. 1. The walls are 3.8 mm thick Pyrex glass tubing with an ID of 23.5 mm. Construction was facilitated by the use of a glass cassette A that fitted snugly inside the cell and held the platinum electrodes B (18 × 18 × 0.5 mm, separated by a 2 mm glass spacer in the shape of a cross, C). Shiny platinum electrodes were used to minimize adsorption effects in the cell. The electrodes were held rigidly in the cassette by solid glass rods, D, ground flat on one side. The platinum electrode leads were spot-welded to short lengths of tungsten wire for passage through the cell walls. This enabled a good metal-to-glass seal to be made with the combination tungsten/uranium glass/Pyrex. A 4 mm Fischer and Porter flow control valve provided access to the solution containing approximately 6 mL of liquid H_2S.

The cell constant was determined as 0.08496 ± 0.00025 cm^{-1} at 25°C using a 0.000999 g equiv. L^{-1} aqueous KCl (Baker, Ultrex) solution, where Λ_{KCl} was obtained from the Fuoss equation (4).

Can. J. Chem. Downloaded from www.nrcresearchpress.com by 210.87.254.42 on 09/06/12
For personal use only.

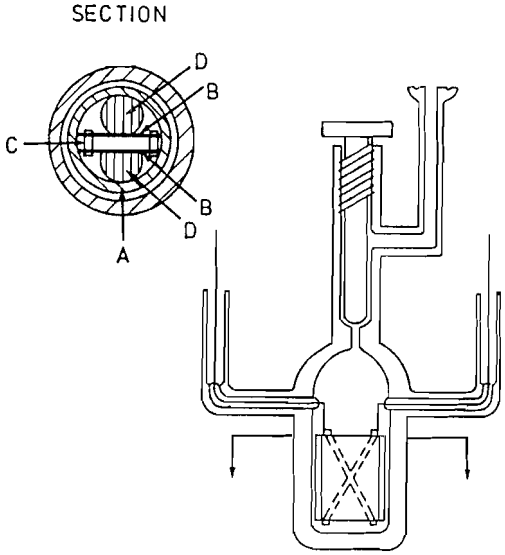

FIG. 1. Electrical conductance cell used for these experiments: wall (Pyrex) thickness 3.8 mm; platinum electrodes, 18 × 18 × 0.5 mm; cell constant, 0.08496 ± 0.00025 cm^{-1}. See text for description of the parts labelled with letters in the section view.

Conductance measurements were made using a Beckman RC-18A Conductivity Bridge at frequencies of 1 kHz and 3 kHz. The temperature of the cell was maintained to ±0.05°C by immersion in Neslab LT-9 and Haake FK2 constant temperature baths. The reagents were measured and transferred in the gas phase using a stainless steel/glass vacuum line equipped with calibrated gas volumes. Pressures were determined with either a 266 kPa (2000 Torr) Heise or an MKS Baratron 133 kla (1000 Torr) 170 Series pressure gauge. The reagents, H_2S (Matheson) and $(CH_3)_3N$ (Eastman), were purified by repeated cryogenic distillations on the vacuum line.

The solution concentrations were determined from the number of moles of trimethylamine added to the cell. Deviations due to solute in the vapour phase should be ≪1% since the trimethylamine was <0.012 mole fraction at the highest concentration. Changes in the H_2S liquid volume as a function of temperature were determined by an iterative technique using the following parameters: number of moles of H_2S in the cell, the vapour pressure (5) and density (6) of H_2S at each temperature, and the volume of the cell.

Results

The minimum measurable conductance value on our bridge with a 10 kΩ resistor in parallel with the cell is 9.9999×10^{-10} S. Conductances less than this, although they sometimes showed a small change in the bridge balance, could not be accurately determined. After repeated rinsings of the cell with liquid H_2S, the bridge consistently showed conductances $<9.9999 \times 10^{-10}$ S for the solvent at all the temperatures studied. This corresponds to a specific conductance for liquid H_2S of $<8.5 \times 10^{-11}$ S cm^{-1}.

Conductance data obtained from measurements made on solutions of $(CH_3)_3N$ in liquid H_2S are given in Table 1 and illustrated in Figs. 2 and 3. Small polarization effects were corrected for by taking measurements at 1 kHz and 3 kHz and then extrapolating the results to infinite frequency (by plotting frequency$^{-1/2}$ vs. resistance).

At the higher temperatures there was the possibility of solution decomposition since above 0°C polysulphide formation was reported (7) to occur in triethylamine solutions in liquid H_2S. The conductance data in this paper, even at 25°C, showed no changes over 24 h, which indicate that polysulphide formation was not a problem for trimethylamine solutions.

Discussion

As previously mentioned, few data have been reported from conductance measurements in liquid H_2S. The accepted literature values for the specific conductance of the pure liquid are given in Table 2. Our result of $<8.5 \times 10^{-11}$ S cm^{-1} for the specific conductance of liquid H_2S over the temperature range 25.0°C to −72.5°C is in good agreement with that of Satwalekar *et al.*, 3.7×10^{-11} S cm^{-1} (8). The conductance of pure H_2S would be expected to be low based on the self-dissociation constant of H_2S ($K = 2.5 \times 10^{-33}$ (2)) which is a factor of 10^{19} less than that of water. Higher literature values reported for the specific conductance of liquid H_2S are most likely due to trace impurities being present.

In aqueous solution trimethylamine behaves as a normal weak electrolyte (10) (dissociation constant, 5.45×10^{-5} (11)) in a solvent of high dielectric constant, i.e. the equivalent conductance initially decreases with increasing amine concentration. Cotton and Waddington (12) have shown for three concentrations of trimethylamine in liquid H_2S at −78.5°C a much different behaviour, in that the Λ appears to increase from the first addition of amine. Chipman and McIntosh (1) found similar behaviour for isopropylamine and *n*-butylamine in liquid H_2S, which led to Jander's (2) proposal that there was self-association of amine molecules in these solutions [2].

$$R_3NH\cdot SH + xR_3N \rightleftharpoons R_3\overset{+}{N}H + \bar{S}H + xR_3N$$

[2] $(x+1)R_3N + H_2S$ //

$$(R_3N)_x\cdot R_3NH\cdot SH \rightleftharpoons (R_3N)_x\cdot R_3NH^+ + \bar{S}H$$

R = alkyl

Such adducts have not been shown conclusively to exist but ammonium salts do coordinate H_2S loosely at low temperature (12, 13). For triethylammonium hydrogensulphide and tetramethylammonium hydrogensulphide the adducts have 2 and 3 moles of H_2S per mole of salt respectively at −78.5°C (13). These adducts do not form at significantly higher temperatures. Therefore an increase in Λ at higher concentrations may be interpreted as arising from the formation of triple ions and higher conducting agglomerates in solution, as predicted by the theory of Fuoss and Kraus (14).

However, our results, while confirming the increase in Λ at the higher concentrations, also show for the first time a minimum in Λ with decreasing trimethylamine concentration, Fig. 2. This behaviour is observed at all but the two highest temperatures studied. The minimum occurs at ~0.006 mol L^{-1} $(CH_3)_3N$. This implies that at the lowest concentrations $(CH_3)_3N$ in liquid H_2S is behaving like a normal weak electrolyte in this solvent of low to medium dielectric constant.

The conductances of a number of alkylammonium salts have been measured in liquid H_2S (15) and the Λ vs. concentration

Can. J. Chem. Downloaded from www.nrcresearchpress.com by 210.87.254.42 on 09/06/12
For personal use only.

TABLE 1. Experimental equivalent conductance, Λ (S cm^2 equiv.$^{-1}$) vs. concentration (mol L^{-1}) for trimethylamine solutions in liquid hydrogen sulphide at the temperature (°C) indicated

−72.5°C		−46.5°C		−27.5°C		−7.2°C		10.0°C		25.0°C	
10^4 Conc.	10^2 Λ	10^4 Conc.	10^2Λ	10^4 Conc.	10^2 Λ	10^4 Conc.	10^2 Λ	10^4 Conc.	10^2 Λ	10^4 Conc.	10^2 Λ
2.59	5.52	2.52	5.42	2.46	4.31	2.39	3.31	—	—	—	—
5.18	3.58	5.05	2.69	4.92	2.19	4.78	1.69	4.65	1.10	4.53	0.62
9.60	4.18	9.35	3.40	9.12	2.77	8.86	2.07	8.62	1.35	8.38	0.73
144	3.31	141	3.21	137	2.76	133	2.05	130	1.24	126	0.58
287	4.46	279	4.35	272	3.82	265	2.84	257	1.64	250	0.76
562	6.77	548	6.65	534	5.92	519	4.49	—	—	—	—
1120	13.8	1090	14.2	1070	13.0	1040	10.2	—	—	—	—
1710	26.7	1670	27.6	1630	26.2	1580	21.2	1540	12.7	1500.	4.61
2240	40.5	2190	42.8	2130	40.9	2070	34.0	—	—	—	—
3310	79.0	3230	87.2	3150	85.8	3060	75.9	2970	51.3	2890	20.0

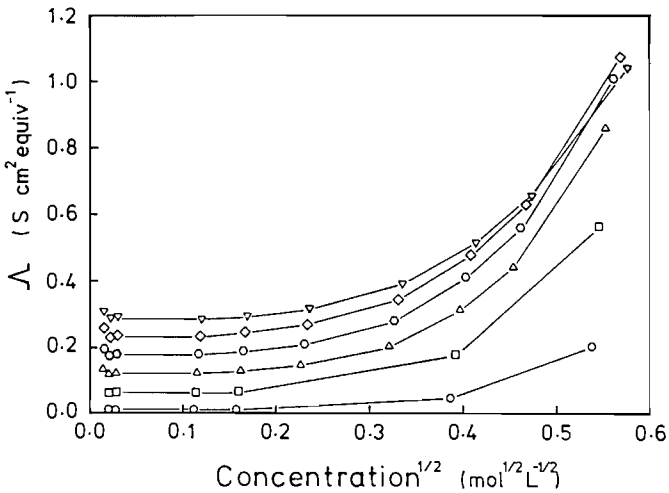

FIG. 2. Equivalent conductance vs. concentration$^{1/2}$ for $(CH_3)_3N$/liquid H_2S solutions: −72.5°C, ▽; −46.5°C, ◇; −27.5°C, ⬡; −7.2°C, △; +10.0°C, □; and +25.0°C, ○. For clarity, the *y*-axis for each succeeding data set from 25°C (○) is offset from 0 by successive 0.05 steps.

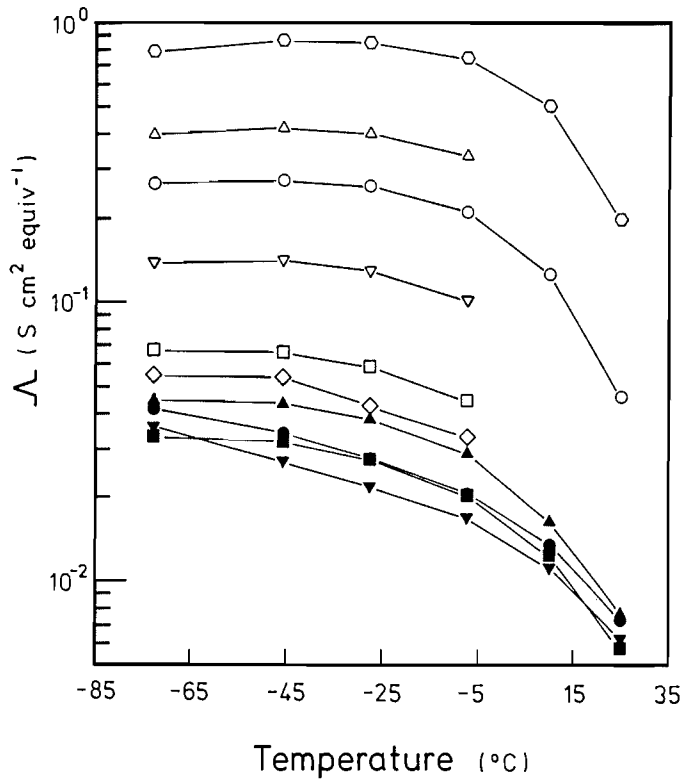

FIG. 3. Equivalent conductance vs. temperature for $(CH_3)_3N$/liquid H_2S solutions at the following concentrations of $(CH_3)_3N$ (mol L^{-1}): 2.89×10^{-1}, ⬡; 1.96×10^{-1}, △; 1.50×10^{-1}, ○; 9.80×10^{-2}, ▽; 4.91×10^{-2}, □; 2.50×10^{-2}, ▲; 1.26×10^{-2}, ■; 8.38×10^{-4}, ●; 4.53×10^{-4}, ▼; 2.26×10^{-4}, ◇.

curves nearly all show the Fuoss, Kraus (14) minimum in the same concentration range that we have observed for trimethylamine. However, no limiting equivalent conductance values, Λ_0, have been determined, even for solutions of tetraalkylammonium hydrogensulphides, which are among the most highly dissociated salts in liquid hydrogen sulphide (12). Even here though, unlike their analogues the tetraalkylammonium hydroxides in aqueous solution, these hydrogensulphide salts may not be fully dissociated due to the lower dielectric constant of liquid H_2S. A comparison of our Λ for trimethylammonium hydrogensulphide with those Λ available for tetramethylammonium hydrogensulphide from Cotton and Waddington (12) is given in Table 3.

This shows that the trimethyl compound is much less dissociated at the indicated concentrations. However, the Λ values need to be determined at concentrations $<2.26 \times 10^{-4}$ mol L^{-1} to allow fitting with the Fuoss−Shedlovsky equation (16) to determine Λ_0 and the dissociation constant for the ion pair accurately. Our lowest concentration was predetermined by the cell volume and the minimum transferable aliquot of $(CH_3)_3N$. To achieve lower concentrations much larger quantities of liquid H_2S would be required as a diluent. Handling such quantities in our apparatus would increase the safety hazards beyond an acceptable level.

Another interesting aspect to these solutions that illustrates the weak base character of this hydrogensulphide salt is the effect of temperature on Λ, Fig. 3. A decrease in Λ above −45.6°C was found, opposite to that expected if the dissociation constant increases with temperature. An analogy may be drawn here with the aqueous solutions of trialkylamines. Unlike the tetraalkylammonium hydroxides, which, as already mentioned, are strong bases in H_2O, the trialkylamines behave as very weak bases in aqueous solution. These amines, rather than forming highly ionized hydroxides, form unstable hydrates through hydrogen bonding (17). The amine can exist in two states, the more soluble hydrate and the unhydrated "free" amine. Triethylamine is 70% hydrated at 15°C, but less than 50% at 32.5°C (17). Thus hydrogen bonded and free tri-

Can. J. Chem. Downloaded from www.nrcresearchpress.com by 210.87.254.42 on 09/06/12
For personal use only.

TABLE 2. Specific conductance of pure liquid H_2S (S cm^{-1})

Reported value (−78.5°C)		Our best value (25.0 to −72.5°C)
Direct current (8)	5 kHz (9)	1 and 3 kHz
3.7×10^{-11}	1.17×10^{-9}	$<8.5\times10^{-11}$

TABLE 3. Comparison of Λ for $(CH_3)_4NSH$ and $(CH_3)_3NHSH$

Compound	Concentration (mol L^{-1})	Λ (s cm^2 equiv.$^{-1}$)	
$(CH_3)_4NSH$	0.0150	2.2 (12)	(−78.5°C)
	0.0782	8.7 (12)	(−78.5°C)
$(CH_3)_3NHSH$	0.0150	0.032	(−72.5°C)
	0.0782	0.094	(−72.5°C)

methylamine species may be considered to exist in H_2S solutions. The ratio of free to hydrogen bonded species would be expected to increase with temperature. Since hydrogen bonding is much weaker in H_2S than in H_2O most of the amine in our solutions must be present in the free state. This is consistent with the very low Λ values measured.

To summarize, although the conductivity data do not allow us to calculate the limiting equivalent conductance values in H_2S solutions and consequently the dissociation constant for trimethylammonium hydrogensulphide in liqud H_2S, investigations have been furthered into the reactions of the triamines with liquid H_2S. We have been able to show that trimethylamine dissolved in liquid H_2S appears to behave as a normal weak electrolyte, contrary to previous reports (1, 2, 12). The increased Λ at the higher concentrations may be attributed to the formation of triple ions and higher conducting agglomerates in solution. At the lower concentrations the Λ also increase in the expected manner due to the decline in the ratio of ion-pairs to free ions in solution. Two effects of temperature on these solutions have been observed: firstly, the solutions have been found to be thermally stable up to 25°C with no signs of thermal decomposition to polysulphides; secondly, there appears to be a significant change in the hydrogen bonded to unassociated amine ratio at the higher temperatures, evidenced by the lowering of Λ. Over the temperature range studied there was no observed effect of $HS^- - H_2S$ hydrogen bonding.

Acknowledgement

The authors would like to thank Dr. E. A. Symons for many helpful discussions.

1. H. R. CHIPMAN and D. MCINTOSH. Proc. Nova Scotian Inst. Sci. **16**, 189 (1926).
2. G. JANDER. Die Chemie in Wasserahnlichen Losungsmitteln. Springer-Verlag, Berlin. 1949.
3. M. ACHTERHOF, R. F. CONAWAY, and C. E. BOORD. J. Am. Chem. Soc. **53**, 2682 (1931).
4. J. E. LUND, JR., J. J. ZWOLENIK, and R. M. FUOSS. J. Am. Chem. Soc. **81**, 1557 (1959).
5. E. C. W. CLARKE and D. N. GLEW. Can. J. Chem. **48**, 764 (1970).
6. J. R. WEST. Chem. Eng. Prog. **44**, 287 (1948).
7. I. S. AKHMETZHANOV. Zhur. Obsh. Khim. **38**, 1090 (1968).
8. S. D. SATWALEKAR, L. W. BUTLER, and J. A. WILKINSON. J. Am. Chem. Soc. **52**, 3045 (1930).
9. W. G. BICKFORD and J. A. WILKINSON. Proc. Iowa Acad. Sci. **40**, 89 (1933).
10. G. BRUNI and C. SANDONNINI. Z. Elekt. **16**, 223 (1910).
11. H. S. HARNED and B. B. OWEN. J. Am. Chem. Soc. **52**, 5079 (1930).
12. J. D. COTTON and T. C. WADDINGTON. J. Chem. Soc. A, 785 (1966).
13. D. H. MCDANIEL and W. G. EVANS. Inorg. Chem. **5**, 2180 (1966).
14. R. M. FUOSS and C. A. KRAUS. J. Am. Chem. Soc. **55**, 2387 (1933).
15. E. E. LINEKIN and J. A. WILKINSON. J. Am. Chem. Soc. **62**, 251 (1940).
16. R. M. FUOSS and T. SHEDLOVSKY. J. Am. Chem. Soc. **71**, 1496 (1949).
17. I. T. MILLAR and H. D. SPRINGALL. A shorter Sidgwick's organic chemistry of nitrogen. Clarendon Press, Oxford. 1969. p. 41.

Can. J. Chem. Downloaded from www.nrcresearchpress.com by 210.87.254.42 on 09/06/12
For personal use only.

Neutral and anionic derivatives of toluene-3,4-dithiolatocadmium(II); the crystal structure of di(tetraphenylarsonium) bis(toluene-3,4-dithiolato)cadmate(II)

LUIS BUSTOS, MASOOD A. KHAN, AND DENNIS G. TUCK
Department of Chemistry, University of Windsor, Windsor, Ont., Canada N9B 3P4

Received July 29, 1982

LUIS BUSTOS, MASOOD A. KHAN, and DENNIS G. TUCK. Can. J. Chem. **61**, 1146 (1983).

Cadmium(II) chloride reacts with toluene-3,4-dithiol (H_2TDT) to give Cd (TDT), which is apparently a homopolymer in the solid state. Adducts with neutral monodentate and bidentate donors have been prepared. The structure of the salt $(Ph_4As)_2[Cd(TDT)_2]$ was determined by X-ray crystallography. Crystals of this compound are monoclinic ($P2_1/c$), with a = 23.032(4) Å, b = 12.396(4) Å, c = 22.529(5) Å, β = 111.106(2)°. The structure was refined by least-squares methods to a final R-value of 0.0469 for 2523 "observed" reflections. The anion is a distorted tetrahedral, mononuclear species with Cd—S bond distances ranging from 2.488(5) Å to 2.531(4) Å. This anion is also a Lewis acid, forming complexes of the type $[Cd(TDT)_2L]^{2-}$ with neutral bidentate ligands.

LUIS BUSTOS, MASOOD A. KHAN et DENNIS G. TUCK. Can. J. Chem. **61**, 1146 (1983).

Le chlorure de cadmium(II) réagit avec le toluènedithiol-3,4 (H_2TDT) en donnant le Cd(TDT) qui est apparemment un homopolymère à l'état solide. On a préparé des adduits avec des donneurs monodentate et didentate neutres. On a déterminé la structure du sel $(Ph_4As)_2[Cd(TDT)_2]$ par crystallographie de rayons-X. Les cristaux de ce composé sont monocliniques et appartiennent au groupe d'espace ($P2_1/c$) avec a = 23,032(4) Å, b = 12, 396(4) Å, c = 22,529(5) Å, β = 111,106(2)°. On a affiné la structure par la méthode des moindres carrés jusqu'à une valeur finale de R = 0,0469 pour 2523 réflexions "observées". L'anion qui est une espèce mononucléaire a une géométrie tétraédrique déformée avec des longueurs de liaison Cd—S allant de 2,488(5) Å à 2,531(4) Å. Cet anion est également un acide de Lewis qui forme des complexes du type $[Cd(TDT)_2L]^{2-}$ avec les ligands bidentates neutres.

[Traduit par le journal]

Introduction

Complexes of cadmium with sulphur donor ligands have received some measure of attention recently, and one obvious reason is the interest in the biological activity of cadmium compounds. Studies of the stereochemistry of these molecules are important features of such investigations, and both solid state (1) and solution studies (2, 3) have been reported. A general review of the stereochemistry of cadmium complexes has appeared elsewhere (4).

The present paper reports the preparation of neutral and anionic derivatives of the cadmium salt of toluene-3,4-dithiol (H_2TDT). The compound Cd(TDT) forms a series of adducts with neutral ligands, and the anion $[Cd(TDT)_2]^{2-}$, which has been shown by X-ray crystallography to have a distorted tetrahedral CdS_4 kernel. This anion is itself a Lewis acid, giving rise to anions such as $[Cd(TDT)_2bipy]^{2-}$ (bipy = 2,2′-bipyridine) with bidentate nitrogen donors.

Experimental

General

All materials were of Reagent grade; solvents were appropriately dried and stored over drying agents. Toluene-3,4-dithiol (Eastman Kodak) was used as supplied.

Infrared spectra were recorded between 400–4000 cm^{-1} with Beckman IR-12 and/or Perkin-Elmer 180 instruments, using Nujol mulls, KBr or CsI discs as appropriate. Proton nmr spectra were recorded on a Varian EM-360 instrument operating at 60 MHz.

Cadmium analysis was carried out by atomic absorption spectroscopy, using an IL-250 atomic absorption emission spectrophotometer. Microanalyses (carbon, hydrogen, and sulphur) were carried out by Guelph Chemical Laboratories Ltd., Guelph, Ont., Canada. Analytical results are given in Table 1.

TABLE 1. Analytical results

Compound	Metal analysis (%) Found	Calcd.
Cd(TDT)[a]	41.7	42.2
$Cd(TDT)(py)_2$	26.9	26.5
$Cd(TDT)(phen)_2$	17.7	17.9
Cd(TDT)(bipy)	26.7	26.6
Cd(TDT)(tmed)	29.9	29.4
Cd(TDT)(dmso)	33.2	32.6
$(Ph_4As)_2[Cd(TDT)_2]\cdot 2EtOH$[b]	9.6	8.8
$(Ph_4As)_2[Cd(TDT)_2(phen)]$	8.4	8.2
$(Ph_4As)_2[Cd(TDT)_2(bipy)]$	8.5	8.4
$(Ph_4As)_2[Cd(TDT)_2(tmed)]$	8.9	8.8

[a] Found C 30.7, H 2.4, S 23.7%; calcd. C 31.5, H 2.3, S 24.0%.
[b] Found C 61.9, H 4.6, S 10.9%; calcd. C 61.9, H 5.0, S 10.0%.

Preparative

(a) Toluene-3,4-dithiolato cadmium(II): This compound has been prepared from the reaction between H_2TDT and cadmium nitrate in aqueous solution (3). In the present work, anhydrous cadmium chloride (4.3 g) dissolved in ethanol (30 mL) was slowly added to a mechanically stirred solution of H_2TDT (1.1 g) in ethanol (20 mL). This mixture was stirred for approximately 12 h at 55°C, yielding a yellow precipitate which was collected, washed twice with ethanol, and dried *in vacuo*. The product is toluene-3,4-dithiolato cadmium(II) (mp 225–227°C), which is soluble in dimethylsulphoxide (dmso), pyridine (py), ethylenediamine (en), and *N,N,N′,N′*-tetramethylethylenediamine (tmed), but insoluble in acetone, chloroform, or methanol. Yield 2.1 g, 34%.

(b) Bis(pyridine)(toluene-3,4-dithiolato) cadmium(II): Cd(TDT) (0.43 g) was dissolved in pyridine (5 mL), with stirring. Diethyl ether was added dropwise until the solution became cloudy; a further small quantity of pyridine was added to redissolve the precipitate, and the solution cooled at 0°C for 24 h. The resultant yellow precipitate was collected and dried *in vacuo*. Analysis and ir spectra showed this solid

Can. J. Chem. Downloaded from www.nrcresearchpress.com by 210.87.254.40 on 09/06/12
For personal use only.

Can. J. Chem. Downloaded from www.nrcresearchpress.com by 210.87.254.40 on 09/06/12
For personal use only.

to be Cd(TDT)(py)$_2$. Yield 0.87 g, 40%.

(c) Dimethylsulphoxide(toluene-3,4-dithiolato) cadmium(II): Cd(TDT) (0.65 g) was dissolved in 7 mL of dimethylsulphoxide, and the excess solvent removed under vacuum over several hours. A brown heavy oil was collected and redissolved in chloroform. Dropwise addition of diethyl ether precipitated Cd(TDT) (dmso) as a white powder, soluble in chloroform. Yield 0.24 g, 30%.

(d) Bis(1,10-phenanthroline) (toluene-3,4-dithiolato) cadmium(II): To a solution of 0.54 g of 1,10-phenanthroline(phen) in 40 mL of ethanol was added 0.25 g Cd(TDT). The solution slowly changed colour from pale yellow to orange on being stirred over a period of 6 h; the suspended solid was then collected, washed twice with ethanol, and dried *in vacuo*. This procedure was carried out for three different reaction times (6, 14, and 30 h) but the same product was obtained in each case, namely Cd(TDT) (phen)$_2$. Yield 0.36 g, 52%.

(e) 2,2′-Bipyridine(toluene-3,4-dithiolato) cadmium(II): The preparative method was exactly the same as that for the phenanthroline complex. The colour of the solution changed from pale yellow to deep yellow. This reaction was done twice for different reaction times, 7 h and 16 h, with the product being Cd(TDT) (bipy) in both cases. Yield 0.23 g, 50%.

(f) (N,N,N′,N′-Tetramethylethylenediamine) (toluene-3,4-dithiolato) cadmium(II): Cd(TDT) was dissolved in tmed and excess solvent pumped off over several hours. The dropwise addition of petrolcum ether precipitated a yellow powder, which was dissolved in chloroform, reprecipitated with petroleum ether, collected, and dried *in vacuo*.

(g) Di(tetraphenylarsonium)bis(toluene-3,4-dithiolato)cadmate-(II): Sodium hydroxide (0.8 g) dissolved in 30 mL of ethanol was mixed with a stirred solution of H_2TDT in 15 mL of ethanol at room temperature, Cd(TDT) (1.03 g) added slowly, and the mixture stirred until complete dissolution took place (approx. 16 h). An ethanol solution of tetraphenylarsonium chloride was then added, and after 5 min a yellow powder slowly precipitated. This material was collected, washed twice with ethanol, redissolved in EtOH/CH_3CN, and the solution cooled overnight at 0°C. The resultant yellow crystals were collected and dried *in vacuo* (mp 230−232°C). Yield 0.32 g, 6%.

(h) Di(tetraphenylarsonium)bis(toluene-3,4-dithiolato) (1,10-phenanthroline) cadmate(II): 1,10-Phenanthroline (0.08 g) in 10 mL ethanol was added to a stirred solution of $(Ph_4As)_2[Cd(TDT)_2]$ (0.6 g) in 30 mL of acetonitrile; the solution changed colour from yellow to orange. Diethyl ether was added dropwise until the appearance of cloudiness in the solution, the solid redissolved in acetonitrile, and the resultant solution cooled for approximately 15 h. The final yellow precipitate was filtered off, washed with ethanol, and dried *in vacuo* (mp 256−258°C). Yield 0.35 g, 51%. The corresponding $(Ph_4As)_2$-[Cd(TDT)$_2$ (bipy)] was prepared in 63% yield by a similar procedure.

(i) Di(tetraphenylarsonium)bis(toluene-3,4-dithiolato) (N,N,N′,-N′-tetramethylethylenediamine) cadmate(II): 3 mL of tmed was added to a solution of 0.3 g of $(Ph_4As)_2[Cd(TDT)_2]$ in 10 mL of acetonitrile. The volume of the solution was reduced to approximately 5 mL, yielding a white precipitate which was collected, washed with ethanol, and dried *in vacuo* (mp 215−217°C). Yield 0.27 g, 81%.

Spectroscopic studies

Infrared and nmr (^{1}H) spectra served to establish the presence of the relevant ligand and/or cation in the complexes listed in Table 1. Integration of the proton resonance was also used to confirm the stoichiometry. Because of the insolubility of the neutral complexes in common non-donor solvents, all nmr spectra were run in d_6-dmso. It seems very probable that dissolution in this solvent involves removal of the donor molecule, so that the species in solution are then free ligand and Cd(TDT) (dmso)$_n$, where the latter represents a solvated Cd(TDT) species. Under these circumstances, the resonance frequencies of TDT are essentially constant, with the toluene methyl group giving rise to a sharp singlet at 2.15 ppm from TMS, and the aromatic protons giving a multiplet centred at 7.31 ppm. These frequencies are shifted only slightly from those in the parent acid (2.05, 7.1 ppm), for which the thiol protons resonances are at 3.90 ppm. The resonance frequencies of bipy, phen, etc. released on dissolving the adducts in d_6-dmso are essentially those of the parent ligand in the same solvent. Spectra run in other solvents were of too low an intensity to be used for structural interpretation.

TABLE 2. Summary of crystal data, intensity collection, and structural refinement for $C_{66}H_{64}As_2CdO_2S_4$, $[(C_6H_5)_4As]_2[Cd(CH_3C_6H_3S_2)_2]\cdot(C_2H_5OH)_2$

Cell constants	a = 23.032(4) Å b = 12.396(4) Å, β = 111.106(2)° c = 22.529(5) Å V = 6001(3) Å^3
Space group	$P2_1/c$ (C^5_{2h}; No. 14)
Z	4
M	1279.74 g mol^{-1}
ρ (calcd.)	1.410 g cm^{-3}
ρ (obsd.)	1.409 g cm^{-3}
Absorption coefficient (μ)	16.96 cm^{-1}
Cystal dimensions	0.1 × 0.2 × 0.2 mm
Radiation	MoK$_\alpha$ (λ = 0.71069 Å)
$2\theta_{max}$	45.0°
Scan type	coupled θ (crystal)/2θ (counter)
Scan width	Kα$_1$ − 1° to Kα$_2$ + 1°
Scan speed	2.02° − 4.88° min^{-1}
Background time/s time	0.5
Total reflections meas.	6884 (h, ±k, ±l)
Unique averaged data	2523[$(F^2_o) > 3\sigma(F_o)^2$] $R(I)$ = 0.034
$R = [\Sigma\Delta/\Sigma\lvert F_o\rvert]$	0.0469
$R_\omega = [\Sigma_\omega\Delta^2/\Sigma_\omega F_o^2]^{1/2}$	0.0486

Crystallographic measurements

Pale yellow irregularly shaped crystals of $(Ph_4As)_2[Cd(TDT)_2]$ were obtained by the slow evaporation of ethanol/acetonitrile solutions (see above). An initial attempt to collect data using a crystal attached to a thin glass fibre failed because of crystal decomposition within 24 h. A second crystal (approximate dimensions given in Table 2) was sealed in a thin-walled glass capillary in random orientation and used for subsequent data collection on a Syntex P2$_1$ diffractometer. Details of the procedure for data collections and processing were described previously (5). The crystal was stable under these conditions, and the intensities of three monitor reflections decreased by only 8.0% during the data collection process; this was corrected for by applying an appropriate scaling factor. The space group $P2_1/c$ (No. 14) was determined from systematic absences ($h0l$, $l = 2n + 1$; $0k0$, $k = 2n + 1$). The data were corrected for Lorentz and polarization effects, but no absorption corrections were applied in view of the low absorption coefficient and crystal dimensions.

Solution and refinement of the structure

All calculations were performed on the IBM 3031 computer at the University of Windsor. Programmes used during the structural analysis include CHECK, PROC, XANADU, ORTEP (5), and SHELX 77 (6). Scattering factors for all the non-hydrogen atoms, including anomalous dispersion correction terms $\Delta f'$ and $\Delta f''$, were taken from ref. 7, and scattering factors for hydrogen atom were obtained from ref. 8.

The positions of Cd and As atoms were determined from a sharpened three-dimensional Patterson synthesis. The coordinates of the remaining non-hydrogen atom were obtained from the subsequent difference Fourier syntheses. The structure was refined by blocked matrix least-squares refinement; one matrix contained all the coordinates for the anion, with Cd and S atoms treated anisotropically, and the other contained all the coordinates of the cations, with As atoms being refined anisotropically. Six cycles of least-squares refinement gave an R-value of 0.09. At this stage a difference Fourier map showed two areas of electron density which could be attributed to disordered solvent molecules. The proton nmr spectrum confirmed the

Can. J. Chem. Downloaded from www.nrcresearchpress.com by 210.87.254.40 on 09/06/12
For personal use only.

presence of two ethanol molecules in the crystal lattice, and since the two highest peaks in the difference map were ~3.0 e Å^{-3}, these were treated as the oxygen atoms of these C_2H_5OH units and were included in the least-squares refinement. Subsequent difference syntheses with various sin θ/λ cut-off values did not resolve the two carbon atoms of the ethanol molecules. From all the available evidence, we conclude that the two ethanol molecules are loosely held in the crystal lattice and are undergoing very high thermal motion. The S(4)—O(015) and S(1)—O(017) distances (see Table 4) are compatible with O—H---S bonding.[1]

No further attempt was made to resolve the carbon atoms, which were refined anisotropically in an averaged position to yield distances of 1.77(3) Å and 1.76(4) Å from the O(015) and O(017) atoms respectively. Eight cycles of block matrix least-squares refinement, with the coordinates of the solvent atoms being refined with the anion atoms coordinates, gave an R-value of 0.057. A difference Fourier synthesis then showed electron density maxima in some of the plausible hydrogen atom locations. All hydrogen atoms were subsequently included in idealized positions with C—H = 0.95 Å, HCH = 109.5°, and CCH = 120°; isotropic thermal parameters were refined for all the hydrogen atoms. After 10 more cycles of refinement, convergence was achieved, with the final R-value = 0.0469 and the final R_w = 0.0486 for the "observed" reflections. The function minimized during least-squares calculations was $\Sigma w(|F_o| - |F_c|)^2$. Unit weights were used in the initial stages of refinement, while in the final cycles of calculation a weighting scheme of the form $w = [1/\sigma^2(F) + pF^2]$ was employed, with a final p-value of 0.001. In the final cycle of refinement the largest shift/error ratio was ~0.2. The final difference map showed some features around the solvent molecules, with the largest peak being ~0.5 e$^-$ Å^{-3}. The function $\Sigma w(|F_o| - |F_c|)^2$ showed no appreciable dependence either upon (sin θ/λ) or upon $|F_o|$, so that the weighting scheme is satisfactory. There was no evidence for secondary extinction.

A table of observed and calculated structure factor amplitudes is available as supplementary data.[2] Positional and thermal parameters are given in Table 3, and interatomic distances and angles are listed in Table 4. Figure 1 shows the anion with the atomic numbering scheme, and Fig. 2 gives the cell packing; hydrogen atoms are excluded from both figures for the sake of clarity.

Results and discussion

The $[Cd(TDT)_2]^{2-}$ anion

The X-ray results show that the molecular structure of the $[Cd(TDT)_2]^{2-}$ anion is essentially distorted tetrahedral, with a mononuclear CdS_4 kernel. There is none of the intermolecular Cd—S interactions which are such a common feature of many other crystalline cadmium compounds (4), and this is presumably due both to the bulk of the cation and to the steric requirements of the TDT^{2-} ligand. The cation shows no unusual features which require comment.

The average Cd—S bond distance in the anion is 2.508(5) Å. By way of comparison, values in the range 2.51−2.62 Å have been reported for other four-coordinate CdS_4 species (4). The Cd—S distances in five-coordinate species lie in the same range (2.51−2.87 Å), but again any direct comparison is made difficult because of bridging, etc. The present value is thus one of the shortest Cd—S bonds reported to date. The S—Cd—S angle (average value 86.8(2)°) in the five-membered CdS_2C_2 ring is of course constrained by the nature of the bidentate ligand.

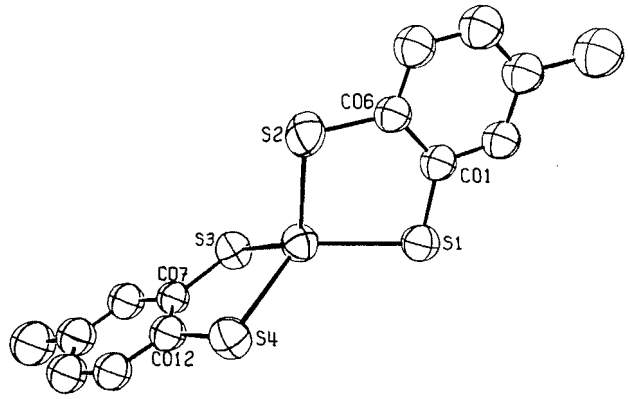

FIG. 1. The stereochemistry of the $[Cd(TDT)_2]^{2-}$ anion: ORTEP diagram, 50% probability for all atoms other than hydrogen. Hydrogen atoms omitted for clarity.

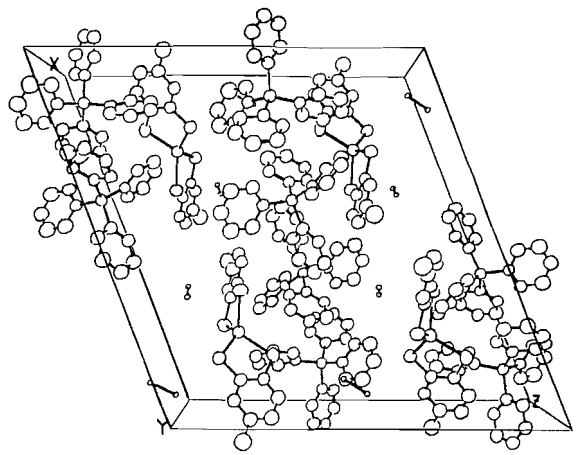

FIG. 2. Packing of Ph_4As^+ and $[Cd(TDT)_2]^{2-}$ in the unit cell. Hydrogen atoms omitted for clarity.

This anion is isoelectronic with $[In(TDT)_2]^-$ reported some years ago (9). One of the features of that complex is the easy conversion to $[In(TDT)_3]^{3-}$, but we were unable to obtain any analogous six-coordinate cadmium(II) species. It is also worth noting that the tetraphenylarsonium salt of $[Cd(TDT)_2]^{2-}$ was the only one which we were able to isolate. Attempts to synthesise a salt with the tetraethylammonium counterion, using procedures identical to those described above, were unsuccessful, since the product contained 29.8% cadmium; calcd. for $(Et_4N)_2[Cd(TDT)_2]$, $C_{30}H_{52}N_2S_4Cd$, Cd 16.5%. This result, together with the instability of $[Cd(TDT)_3]^{4-}$ in the solid state, appears to imply some special stability in the $Ph_4As^+/[Cd(TDT)_2]^{2-}$ lattice.

$[Cd(TDT)_2bipy]^{2-}$, and related anions

The tendency of indium(III) to expand its coordination number from four to six, as shown in the formation of $[In(TDT)_3]^{3-}$ from $[In(TDT)_2]^-$, is also evidenced in the formation of anionic species of the type $[In(TDT)_2(bipy)]^-$ (9). Exactly analogous behaviour is seen in the case of $[Cd(TDT)_2]^{2-}$, which readily forms 1:1 adducts with the bidentate ligands 2,2-bipyridine, 1,10-phenanthroline, and *N,N,N',N'*-tetramethylethylenediamine. These $[Cd(TDT)_2L]^-$ anions are formulated as mononuclear six-coordinate CdS_4N_2 species, isostructural with anionic indium(III) and neutral tin(IV) species (10−12) having this coordination kernel.

[1]We are grateful to a referee for pointing out this fact.

[2]Complete set of data is available, at a nominal charge, from the Depository of Unpublished Data, CISTI, National Research Council of Canada, Ottawa, Ont., Canada K1A 0S2.

TABLE 3.

(*a*) Final atomic coordinates[a] and isotropic thermal parameters for $[(C_6H_5)_4As]_2$-$[Cd(CH_3C_6H_3S_2)_2](C_2H_5OH)_2$

Atom	*x/a*	*y/b*	*z/c*	*U* (Å^2 × 10^3)
Cd	0.76113(5)	0.15966(10)	0.25303(5)	
As(1)	0.3968(1)	0.2018(1)	0.4772(1)	
As(2)	0.1213(1)	0.1035(1)	0.4315(1)	
S(1)	0.8249(2)	0.3094(3)	0.3204(2)	
S(2)	0.8221(2)	0.1846(4)	0.1825(2)	
S(3)	0.7487(2)	−0.0257(3)	0.2908(2)	
S(4)	0.6435(2)	0.1649(3)	0.2050(2)	
O(015)	0.6328(9)	0.2850(18)	0.3325(7)	
O(017)	0.9281(7)	0.2872(21)	0.4719(9)	
C(016)	0.6555(16)	0.4215(24)	0.3362(13)	
C(018)	0.8899(19)	0.3434(21)	0.5198(13)	
C(01)	0.8819(6)	0.3239(11)	0.2858(7)	57(4)
C(02)	0.9334(6)	0.3852(12)	0.3192(7)	64(4)
C(03)	0.9822(7)	0.4036(13)	0.2956(8)	72(5)
C(03A)	1.0357(9)	0.4830(16)	0.3320(10)	104(6)
C(04)	0.9812(8)	0.3584(13)	0.2417(8)	78(5)
C(05)	0.9319(7)	0.2932(12)	0.2077(8)	71(5)
C(06)	0.8822(6)	0.2751(11)	0.2281(6)	56(4)
C(07)	0.6698(6)	−0.0493(11)	0.2461(6)	53(4)
C(08)	0.6494(7)	−0.1557(13)	0.2476(7)	69(5)
C(09)	0.5897(8)	−0.1852(14)	0.2164(8)	78(5)
C(09A)	0.5671(10)	−0.3004(15)	0.2255(10)	110(7)
C(010)	0.5468(8)	−0.1102(13)	0.1812(7)	74(5)
C(011)	0.5665(7)	−0.0054(13)	0.1774(7)	65(5)
C(012)	0.6268(7)	0.0264(12)	0.2101(7)	59(4)
C(11)	0.4111(7)	0.1305(11)	0.5562(7)	51(4)
C(12)	0.3644(8)	0.0692(12)	0.5639(8)	66(5)
C(13)	0.3760(9)	0.0112(15)	0.6221(8)	91(6)
C(14)	0.4332(8)	0.0195(14)	0.6677(9)	82(5)
C(15)	0.4799(10)	0.0810(15)	0.6614(10)	97(6)
C(16)	0.4690(9)	0.1410(15)	0.6044(8)	87(6)
C(21)	0.4735(7)	0.2501(13)	0.4773(7)	61(4)
C(22)	0.5001(8)	0.3425(14)	0.5123(7)	71(5)
C(23)	0.5590(8)	0.3749(15)	0.5183(8)	83(6)
C(24)	0.5924(9)	0.3188(14)	0.4882(8)	82(5)
C(25)	0.5671(8)	0.2252(14)	0.4537(8)	77(5)
C(26)	0.5078(7)	0.1905(13)	0.4480(7)	62(5)
C(31)	0.3591(6)	0.0989(11)	0.4107(6)	47(4)
C(32)	0.3818(8)	−0.0054(13)	0.4194(8)	69(5)
C(33)	0.3560(8)	−0.0816(16)	0.3738(8)	82(5)
C(34)	0.3084(8)	−0.0537(16)	0.3209(9)	79(5)
C(35)	0.2859(8)	0.0478(14)	0.3098(9)	77(5)
C(36)	0.3118(7)	0.1288(14)	0.3565(7)	62(5)
C(41)	0.3444(6)	0.3230(11)	0.4664(7)	51(4)
C(42)	0.3129(6)	0.3410(12)	0.5070(7)	54(4)
C(43)	0.2734(8)	0.4314(14)	0.4973(9)	90(6)
C(44)	0.2653(7)	0.4985(14)	0.4458(7)	68(5)
C(45)	0.2975(7)	0.4808(13)	0.4055(8)	62(5)
C(46)	0.3366(7)	0.3905(12)	0.4155(7)	57(4)
C(51)	0.1337(6)	0.1665(12)	0.3597(7)	53(4)
C(52)	0.1604(7)	0.2667(13)	0.3623(8)	65(5)
C(53)	0.1698(7)	0.3082(15)	0.3096(8)	73(5)
C(54)	0.1510(7)	0.2504(14)	0.2541(8)	74(5)
C(55)	0.1250(7)	0.1512(15)	0.2511(9)	79(5)
C(56)	0.1151(7)	0.1043(15)	0.3036(7)	68(5)
C(61)	0.0389(7)	0.0454(12)	0.4044(7)	55(4)
C(62)	−0.0077(7)	0.0967(14)	0.3567(7)	66(5)
C(63)	−0.0677(8)	0.0522(14)	0.3389(9)	76(5)
C(64)	−0.0786(8)	−0.0356(13)	0.3694(7)	71(5)
C(65)	−0.0310(7)	−0.0845(14)	0.4159(8)	72(5)
C(66)	0.0285(8)	−0.0470(13)	0.4346(8)	68(5)
C(71)	0.1313(7)	0.2150(12)	0.4939(7)	57(4)

Can. J. Chem. Downloaded from www.nrcresearchpress.com by 210.87.254.40 on 09/06/12
For personal use only.

(*a*) (*Concluded*)

Atom	*x/a*	*y/b*	*z/c*	*U* (Å^2 × 10^3)
C(72)	0.0854(9)	0.2880(14)	0.4844(9)	82(5)
C(73)	0.0901(10)	0.3678(17)	0.5315(9)	104(7)
C(74)	0.1429(9)	0.3743(17)	0.5809(10)	93(6)
C(75)	0.1907(10)	0.3028(14)	0.5918(9)	91(6)
C(76)	0.1851(8)	0.2190(14)	0.5478(7)	66(5)
C(81)	0.1788(7)	−0.0092(12)	0.4665(7)	57(4)
C(82)	0.2087(7)	−0.0612(12)	0.4309(8)	63(5)
C(83)	0.2489(8)	−0.1430(14)	0.4574(8)	78(5)
C(84)	0.2598(8)	−0.1820(16)	0.5199(8)	88(6)
C(85)	0.2298(7)	−0.1294(13)	0.5533(9)	75(5)
C(86)	0.1893(7)	−0.0458(13)	0.5293(8)	67(5)
H(02)	0.9363	0.4161	0.3588	80(45)
H(3A1)	1.0294	0.5078	0.3692	66(50)
H(3A2)	1.0357	0.5428	0.3057	218(63)
H(3A3)	1.0746	0.4467	0.3439	225(90)
H(04)	1.0143	0.3711	0.2267	119(60)
H(05)	0.9316	0.2599	0.1696	27(29)
H(08)	0.6785	−0.2085	0.2711	61(40)
H(9A1)	0.5242	−0.3073	0.2003	139(75)
H(9A2)	0.5730	−0.3118	0.2690	220(81)
H(9A3)	0.5902	−0.3525	0.2123	74(49)
H(010)	0.5045	−0.1301	0.1599	74(45)
H(011)	0.5376	0.0456	0.1517	68(42)
H(12)	0.3247	0.0654	0.5309	60(40)
H(13)	0.3446	−0.0317	0.6284	157(82)
H(14)	0.4415	−0.0196	0.7061	112(58)
H(15)	0.5193	0.0840	0.6949	160(88)
H(16)	0.5002	0.1865	0.5995	84(48)
H(22)	0.4771	0.3832	0.5320	152(77)
H(23)	0.5770	0.4364	0.5433	178(82)
H(24)	0.6323	0.3434	0.4910	235(89)
H(25)	0.5905	0.1852	0.4341	95(52)
H(26)	0.4906	0.1272	0.4245	98(54)
H(32)	0.4155	−0.0240	0.4571	23(29)
H(33)	0.3716	−0.1533	0.3794	130(63)
H(34)	0.2897	−0.1078	0.2901	139(75)
H(35)	0.2531	0.0651	0.2711	152(77)
H(36)	0.2969	0.2009	0.3501	134(67)
H(42)	0.3177	0.2929	0.5413	52(37)
H(43)	0.2525	0.4463	0.5259	132(68)
H(44)	0.2373	0.5575	0.4381	128(65)
H(45)	0.2932	0.5291	0.3715	134(69)
H(46)	0.3577	0.3759	0.3871	63(42)
H(52)	0.1724	0.3075	0.4006	71(44)
H(53)	0.1892	0.3765	0.3119	172(87)
H(54)	0.1563	0.2799	0.2175	181(88)
H(55)	0.1129	0.1122	0.2122	86(53)
H(56)	0.0971	0.0349	0.3014	236(61)
H(62)	0.0002	0.1594	0.3365	150(78)
H(63)	−0.1011	0.0839	0.3051	154(73)
H(64)	−0.1197	−0.0629	0.3581	76(45)
H(65)	−0.0394	−0.1467	0.4361	102(54)
H(66)	0.0616	−0.0823	0.4669	130(65)
H(72)	0.0499	0.2863	0.4463	94(51)
H(73)	0.0563	0.4147	0.5275	219(73)
H(74)	0.1477	0.4317	0.6103	223(86)
H(75)	0.2273	0.3094	0.6286	135(69)
H(76)	0.2172	0.1669	0.5548	149(73)
H(82)	0.2010	−0.0397	0.3883	86(49)
H(83)	0.2706	−0.1754	0.4333	232(84)
H(84)	0.2867	−0.2414	0.5372	179(94)
H(85)	0.2372	−0.1520	0.5957	139(73)
H(86)	0.1687	−0.0127	0.5542	60(40)

[a]Estimated standard deviation in parentheses.

Can. J. Chem. Downloaded from www.nrcresearchpress.com by 210.87.254.40 on 09/06/12
For personal use only.

(*b*) Final anisotropic thermal parameters[a,b] ($Å^2 \times 10^3$)

Atom	U_{11}	U_{22}	U_{33}	U_{12}	U_{13}	U_{23}
Cd	60.6(8)	64.4(8)	57.7(7)	−4.4(7)	18.9(6)	−0.1(7)
As(1)	54(1)	49(1)	44(1)	−1(1)	15(1)	−2(1)
As(2)	55(1)	65(1)	50(1)	−4(1)	20(1)	7(1)
S(1)	63(3)	80(3)	63(3)	−5(2)	23(2)	−9(3)
S(2)	87(3)	85(4)	52(3)	−17(3)	26(2)	−8(2)
S(3)	64(3)	61(3)	70(3)	1(2)	17(2)	9(2)
S(4)	62(3)	66(3)	79(3)	8(3)	14(2)	12(3)
O(015)	235(19)	261(22)	140(14)	−3(17)	123(14)	−25(15)
O(017)	106(12)	437(32)	151(15)	26(16)	17(11)	108(19)
C(016)	348(42)	176(27)	163(26)	−71(28)	153(28)	7(22)
C(018)	511(59)	160(24)	147(25)	−208(33)	124(33)	−74(21)

[a] Estimated standard deviation in parentheses.

[b] The anisotropic thermal parameter is defined by the following expression:

$$\exp[-2\pi^2(U_{11}h^2a^{*2} + U_{22}k^2b^{*2} + U_{33}l^2c^{*2} + 2U_{12}hka^*b^* + 2U_{13}hla^*c^* + 2U_{23}klb^*c^*)]$$

TABLE 4. Interatomic distances (Å) and angles (deg), with standard deviations in parentheses[a]

(*a*) Bonding distances

Bond	Distance	Bond	Distance
Cd—S(1)	2.510(4)	CD—S(3)	2.502(4)
Cd—S(2)	2.488(5)	Cd—S(4)	2.531(4)
S(1)—C(01)	1.759(18)	S(3)—C(07)	1.757(13)
S(2)—C(06)	1.791(13)	S(4)—C(012)	1.773(15)
C(01)—C(02)	1.38(2)	C(07)—C(08)	1.41(2)
C(01)—C(06)	1.44(2)	C(07)—C(012)	1.39(2)
C(02)—C(03)	1.42(3)	C(08)—C(09)	1.35(2)
C(03)—C(03A)	1.56(2)	C(09)—C(09A)	1.56(3)
C(03)—C(04)	1.33(3)	C(09)—C(010)	1.38(2)
C(04)—C(05)	1.38(2)	C(010)—C(011)	1.39(2)
C(05)—C(06)	1.40(2)	C(011)—C(012)	1.37(2)
As(1)—C(11)	1.906(15)	As(2)—C(51)	1.907(16)
As(1)—C(21)	1.865(16)	As(2)—C(61)	1.913(15)
As(1)—C(31)	1.921(13)	As(2)—C(71)	1.926(15)
As(1)—C(41)	1.886(14)	As(2)—C(81)	1.890(14)
C—C(ave)Ph1	1.39(3)	C—C(ave)Ph5	1.38(2)
C—C(ave)Ph2	1.39(2)	C—C(ave)Ph6	1.38(2)
C—C(ave)Ph3	1.37(3)	C—C(ave)Ph7	1.38(4)
C—C(ave)Ph4	1.39(1)	C—C(ave)Ph8	1.39(3)

(*b*) Bond angles

Bonds	Angle	Bonds	Angle
S(1)—Cd—S(2)	87.3(2)	S(1)—Cd—S(3)	126.0(1)
S(1)—Cd—S(4)	122.9(1)	S(2)—Cd—S(3)	119.4(2)
S(2)—Cd—S(4)	119.1(1)	S(3)—Cd—S(4)	86.2(1)
Cd—S(1)—C(01)	100.1(5)	Cd—S(2)—C(06)	102.0(6)
Cd—S(3)—C(07)	100.4(5)	Cd—S(4)—C(012)	99.9(5)
S(1)—C(01)—C(02)	117(1)	S(1)—C(01)—C(06)	127(1)
C(02)—C(01)—C(06)	116(2)	C(01)—C(02)—C(03)	122(2)
C(02)—C(03)—C(03A)	119(2)	C(02)—C(03)—C(04)	121(1)
C(03A)—C(03)—C(04)	120(2)	C(03)—C(04)—C(05)	120(2)
C(04)—C(05)—C(06)	121(2)	S(2)—C(06)—C(01)	122(1)
S(2)—C(06)—C(05)	118(1)	C(01)—C(06)—C(05)	120(1)
S(3)—C(07)—C(08)	115(1)	S(3)—C(07)—C(012)	126(1)
C(08)—C(07)—C(012)	118(1)	C(07)—C(08)—C(09)	122(2)
C(08)—C(09)—C(09A)	120(1)	C(08)—C(09)—C(010)	120(2)
C(09A)—C(09)—C(010)	119(2)	C(09)—C(010)—C(011)	119(2)
C(010)—C(011)—C(012)	122(1)	S(4)—C(012)—C(07)	124(1)
S(4)—C(012)—C(011)	116(1)	C(07)—C(012)—C(011)	119(1)
C(11)—As(1)—C(21)	107.7(6)	C(11)—As(1)—C(31)	107.3(6)
C(11)—As(1)—C(41)	112.2(7)	C(21)—As(1)—C(31)	112.1(7)
C(21)—As(1)—C(41)	107.9(7)	C(31)—As(1)—C(41)	109.9(5)

Can. J. Chem. Downloaded from www.nrcresearchpress.com by 210.87.254.40 on 09/06/12
For personal use only.

(*b*) (*Concluded*)

Bonds	Angle	Bonds	Angle
C(51)—As(2)—C(61)	108.5(6)	C(51)—As(2)—C(71)	108.1(7)
C(51)—As(2)—C(81)	111.1(7)	C(61)—As(2)—C(71)	110.3(7)
C(61)—As(2)—C(81)	108.7(6)	C(71)—As(2)—C(81)	110.1(6)
C—C—C(ave)—Ph	120(2)		

(*c*) Non-bonding distances

Atom pair	Distance	Atom pair	Distance
O(015)---S(4)	3.322	O(017)---S(1)	3.396

"Estimated standard deviations on average values are calculated by using the "scatter" formula $\delta = [\Sigma(d_i - \bar{d})^2/(N-1)]^{1/2}$ where d_i is the ith and $\bar{d}$ is the mean of N "equivalent" measurements.

Cd(TDT), and neutral adducts

The parent compound Cd(TDT) has many of the properties expected of a homopolymer, especially in that it is insoluble in all but donor solvents, with which it forms a series of adducts. A CdS_2 species would be a Lewis acid, and therefore prone to polymerise by sulphur-bridging. Examples of such bridging are to be found in many cadmium–sulphur compounds (4), and it is worth noting that the related $Sn(TDT)_2$ is also a polymeric solid, soluble only in donor solvents (10, 13). There are several forms which this bridging might take, and there is no evidence at present as to which form is preferred. For discussion purposes only, we can consider an idealised structure in which all dithiolate ligands participate in bridging.

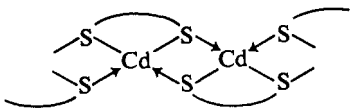

Since the adducts are insoluble in non-donor organic solvents, it seems that the polymeric structure is retained after addition of neutral donors. The simplest mode of adduct formation would then involve coordination of the neutral ligand at the cadmium to expand the coordination sphere without rupture of the polymeric chain, although other structures in which the chain undergoes some reorganisation are also easily envisaged.

One unusual feature is the different coordination behaviour of 2,2′-bipyridine and 1,10-phenanthroline towards Cd(TDT), in that 1:1 and 1:2 adducts (respectively) are formed. A number of different factors might be responsible for this effect, including differing rearrangements of the polymeric structure. An interesting system relevant to this point involves the adducts of zinc ethylxanthate (14), for which the number of donor nitrogen atoms per zinc varies between one (i.e. $Zn(Etxanthate)_2py$) and six (i.e. $Zn(Etxanthate)_2(phen)_3$). A detailed discussion of the factors which might govern the stoichiometry of adducts in such polymeric systems is beyond the scope of the present paper.

Acknowledgements

This work was supported in part by Operating Grants (to D.G.T) from the Natural Sciences and Engineering Research Council of Canada, and from Imperial Oil Limited.

1. A. J. CANTY, R. KISHIMOTO, G. B. DEACON, and G. J. FARQUHARSON. Inorg. Chim. Acta, **20**, 161 (1976).
2. P. A. W. DEAN. Can. J. Chem. **59**, 3221 (1981).
3. G. K. CARSON, P. A. W. DEAN, and M. J. STILLMAN. Inorg. Chim. Acta, **56**, 59 (1981).
4. D. G. TUCK. Rev. Inorg. Chem. **1**, 209 (1979).
5. M. A. KHAN, R. C. STEEVENSZ, D. G. TUCK, J. G. NOLTES, and P. W. R. CORFIELD. Inorg. Chem. **19**, 3407 (1980).
6. G. M. SHELDRICK. SHELX, a programme for least-squares refinement and Fourier calculations. University of Cambridge, 1977.
7. J. A. IBERS and W. C. HAMILTON. International tables for X-ray crystallography. Vol. 4. Kynoch Press, Birmingham. 1979. pp. 99, 149.
8. R. F. STEWART, E. R. DAVIDSON, and W. T. SIMPSON. J. Chem. Phys. **42**, 3175 (1965).
9. D. G. TUCK and M. K. YANG. J. Chem. Soc. A, 214 (1971).
10. R. C. POLLER and J. A. SPILLMAN. J. Chem. Soc. A, 958 (1966).
11. L. M. EPSTEIN and D. K. STRAUB. Inorg. Chem. **4**, 1551 (1965).
12. J. L. HENCHER, M. A. KHAN, F. F. SAID, R. SEILER, and D. G. TUCK. Inorg. Chem. **21**, 2787 (1982).
13. R. C. POLLER. Proc. Chem. Soc. 312 (1963).
14. G. WINTER. Rev. Inorg. Chem. **2**, 309 (1980).

Can. J. Chem. Downloaded from www.nrcresearchpress.com by 210.87.254.40 on 09/06/12
For personal use only.

The hydrogen–oxygen reaction on lanthanum oxide and europium oxide

JOHN F. READ, SANDRA J. AMIRAULT, YUK TONG CHAN, ALAN C. HIGGINS, DAPHNE G. IRVINE, VEDA C. STOREY, AND B. MICHAEL WHELTON

Department of Chemistry, Mount Allison University, Sackville, N.B., Canada E0A 3C0

Received April 21, 1982

JOHN F. READ, SANDRA J. AMIRAULT, YUK TONG CHAN, ALAN C. HIGGINS, DAPHNE G. IRVINE, VEDA C. STOREY, and B. MICHAEL WHELTON. Can. J. Chem. **61**, 1153 (1983).

The stoichiometric hydrogen–oxygen reaction has been studied in a static system over lanthanum oxide and europium oxide at an initial hydrogen pressure of approximately 200 N m^{-2} from 480 to 775 K, and at different initial hydrogen pressures from 70 to 750 N m^{-2} over the same temperature range. Nonstoichiometric reactions were conducted at five different temperatures over lanthanum oxide and four different temperatures over europium oxide, at hydrogen–oxygen ratios in the range 0.1 to 10. After detailed kinetic analysis it is shown that the results fit an equation of the form:

$$-\frac{dP_T}{dt} = \frac{k(b_{H_2}P_{H_2})^x b_{O_2}P_{O_2}}{(1 + b_{H_2}P_{H_2} + b_{O_2}P_{O_2})^{1+x}}$$

where k is a proportionality constant, b_{H_2} and b_{O_2} are the adsorption coefficients for hydrogen and oxygen, respectively, P_T is the total pressure of hydrogen plus oxygen, P_{H_2} and P_{O_2} are the partial pressures of hydrogen and oxygen, respectively, and x equals 2 for lanthanum oxide and 1 for europium oxide. The mechanism involves the competitive adsorption of molecular hydrogen and oxygen, with the rate-determining step involving the interaction between adsorbed hydrogen molecules and adsorbed oxygen or hydrogen peroxide (double hydroxide groups).

JOHN F. READ, SANDRA J. AMIRAULT, YUK TONG CHAN, ALAN C. HIGGINS, DAPHNE G. IRVINE, VEDA C. STOREY et B. MICHAEL WHELTON. Can. J. Chem. **61**, 1153 (1983).

On a étudié la réaction stoechiométrique hydrogène–oxygène dans un système statique sur de l'oxyde de lanthane et de l'oxyde d'europium à une pression initiale d'hydrogène de 200 N m^{-2} sur un intervalle de température allant de 480 à 775 K et à des pressions initiales variables d'hyrogène allant de 70 à 750 N m^{-2} pour le même intervalle de température. On a effectué des réactions nonstoechiométriques à 5 températures différentes sur de l'oxyde de lanthane et à quatre températures différentes sur de l'oxyde d'europium avec des rapports d'hydrogène–oxygène allant de 0,1 à 10. Après une analyse cinétique détaillée, on montre que les résultats s'ajustent à une équation de la forme:

$$-\frac{dP_T}{dt} = \frac{k(b_{H_2}P_{H_2})^x b_{O_2}P_{O_2}}{(1 + b_{H_2}P_{H_2} + b_{O_2}P_{O_2})^{1+x}}$$

où k est une constante de proportionnalité, b_{H_2} et b_{O_2} sont respectivement les coefficients d'adsorption de l'hydrogène et de l'oxygène, P_T est la pression totale (hydrogène + d'oxygène), P_{H_2} et P_{O_2} sont les pressions partielles d'hydrogène et d'oxygène respectivement; x égal 2 pour l'oxyde de lanthane et x égal 1 pour l'oxyde d'europium. Le mécanisme fait intervenir une adsorption compétitive de l'hydrogène et de l'oxygène moléculaire avec une étape déterminante impliquant une interaction entre les molécules d'hydrogène adsorbées et le peroxyde d'oxygène ou d'hydrogène adsorbé (groupes d'hydroxyde double).

[Traduit par le journal]

Introduction

Bakumenko (1) has studied the extreme nonstoichiometric hydrogen–oxygen reaction over lanthanum oxide at 2×10^3 N m^{-2} from 640 to 773 K. The activity decreased with time, with excess hydrogen having the greater deactivating effect; the activation energy in excess oxygen is 50 kJ mol^{-1} and in excess hydrogen is 70 kJ mol^{-1}. Barrett and Barry (2) investigated the adsorption of hydrogen and oxygen on europium oxide and the subsequent effect on the hydrogen–oxygen reaction. Hydrogen adsorption at 900 K and 133 N m^{-2} caused reduction to $EuO_{1.4928}$. Outgassing of this sample at 1100 K led to subsequent adsorption of oxygen down to 200 K, whereas after adsorption of oxygen on the pure oxide and outgassing at 1100 K, no further oxygen could be adsorbed. Hydrogen is strongly adsorbed and cannot be removed to any extent from the reduced oxide even after prolonged heating at 1100 K. This adsorption is weakened by re-oxidation. A cursory examination of the hydrogen–oxygen reaction at 3×10^4 N m^{-2} showed that pre-reduction in hydrogen increased the activity. The reaction on untreated europium oxide yielded kinetics which were first-order in hydrogen and zero-order in oxygen with an activation energy of 15 kJ mol^{-1}. Loginov *et al.* (3) studied the stepwise mechanism over lanthanum and europium oxides showing that the peroxide form of chemisorbed oxygen was an active participant.

A number of studies have been made, particularly on lanthanum oxide, concerning the nature of the active sites and the effect of pretreatment. Lanthanum oxide is one of the most basic lanthanide compounds, with the active reduction sites probably being O^{2-} surface ions, together with anion vacancies. These are produced by dehydration of the surface, which Rosynek and Fox (4) state is complete at 600 K; other workers give higher temperatures for this dehydration (5). Most studies, however, show that maximum activity is obtained after heating at higher temperatures than 600 K.

The reduction sites can be increased by exposure to hydrogen, eliminating hydroxyl groups and surface lattice oxygen, although extreme exposure can cause deactivation (6). Oxygen can adsorb as O_2^-, poisoning these sites (7), or creating lanthanum ion vacancies (8). The critical effect of pretreatment is illustrated by the two values obtained for the activation energy for the oxygen exchange reaction over lanthanum oxide of 46 kJ mol^{-1} (9) and 86 kJ mol^{-1} (10), where, in the latter case, the catalyst was heated in air at 900 K prior to the experiments. The acid sites on lanthanum oxide are generally considered to be the lanthanum ion, perhaps associated with an oxygen ion,

Can. J. Chem. Downloaded from www.nrcresearchpress.com by 210.87.254.105 on 09/06/12
For personal use only.

Can. J. Chem. Downloaded from www.nrcresearchpress.com by 210.87.254.105 on 09/06/12
For personal use only.

with hydrogen adsorbed in a polarised form (11).

For europium oxide, anion vacancies are readily produced (2), though they have a low mobility; the production of these sites increasing the activity towards the hydrogen–oxygen reaction. Ross and Delgass (12) showed, at 800 K, that oxygen adsorption was negligible but hydrogen adsorption considerable, causing surface reduction. Subba Rao *et al.* (8) have shown that, at low oxygen pressures and high temperatures, oxygen is lost from the surface and anion vacancies are produced giving rise to n-type characteristics, although under higher pressures, p-type characteristics result (8, 13).

Lanthanum oxide is one of the small group of lanthanide oxides with a stable hexagonal (A-type) structure whereas europium oxide has a cubic (C-type) structure (for example, ref 14). However, there is a tendency for europium oxide to transform to the monoclinic structure (B-type) (15) as the temperature increases, the change being slower in hydrogen than in oxygen atmospheres (16).

Experimental methods

The apparatus, experimental procedure, catalyst conditioning, method of analysis, and identification system for the reaction between hydrogen and oxygen are identical to those described in previous papers in this series (for example, ref. 17). The reaction was carried out in a batch reactor with a trap to remove water. The gas composition was analyzed by mass spectroscopy. Preliminary experiments excluded the possibility of transport domination. The catalysts were "specpure" grade lanthanum oxide and europium oxide (Johnson Matthey) each with a total surface area of 1.6 m^2 (determined by the BET method using krypton).

Twenty-six groups of experiments were conducted on lanthanum oxide. Groups 1 to 15 contain stoichiometric reactions at various temperatures in the range 480 to 775 K at an approximately constant initial hydrogen pressure in the range 185 to 239 N m^{-2}, three to five identical reactions being conducted in each group; groups 16 to 20 contain stoichiometric reactions at 474, 600, 776, 701, and 549 K, respectively, each group comprising from six to sixteen reactions at different initial hydrogen pressures from 70 to 742 N m^{-2}; groups 21 to 25 contain nonstoichiometric and standard stoichiometric (with an initial hydrogen pressure of approximately 210 N m^{-2}) reactions at 474, 599, 776, 698, and 548 K, respectively, and group 26 contains standard stoichiometric reactions at 598 K after pretreatment with hydrogen and oxygen (using the techniqc described previously (18)).

Similar experiments were performed on europium oxide. The first sixteen groups are stoichiometric at a constant initial pressure; groups 17 to 19 are stoichiometric at 624, 572, and 518 K, respectively, with varying initial pressures, and groups 20 to 23 are nonstoichiometric at 620, 544, 694, and 583 K, respectively.

Results

Analysis of data

The data were analyzed as before (for example, ref. 19) and are summarized below and in Tables 1, 2 and in the Depository of Unpublished Data.[1]

Summary of the results for the stoichiometric reactions

Reaction type

Three different types of log (rate) versus log (pressure) plots can be characterized (cf. ref. 19). Types *a* and *b* show three distinct regions: an inital section of short duration with a slope which is either greater than the second section (type *a*) or less than the second section (type *b*); a second linear section lasting for most of the reaction (the quoted orders with respect to time are calculated from this slope); and a third section with rapidly increasing slope. Type *c* does not show the "initial" section.

Most of the reactions over lanthanum oxide are type *c*. Type *a* appears at high initial pressures (>300 N m^{-2}) and *b* at low pressures. Type *b* also appears in some cases after exposure to excess of either gas. The reaction type over europium oxide is amost exclusively type *a*.

Catalyst activity

The initial rate and the time taken for 90% completion was calculated in all cases, as a measure of catalyst activity. For standard reactions over lanthanum oxide the initial rate is 1.5 ± 0.3 N m^{-2} s^{-1} with a negligible temperature effect. Over europium oxide the rate is 2.0 ± 0.3 N m^{-2} s^{-1} with a more marked temperature effect. Over both catalysts the rate decreases in runs preceded by nonstoichiometric reactions. The time taken for reactions to go to completion follows the expected pattern, with an average time of 700 s.

The rate of the central, linear portion increases with temperature and pressure for lanthanum oxide but is relatively constant over europium oxide with a value of 0.5 ± 0.2 N m^{-2} s^{-1}.

Orders with respect to time

These orders are calculated from the central, linear portion of each log (rate) versus log (pressure) plot and from the integrated *n*th order kinetic expression. For lanthanum oxide the order from groups 1 to 15 (with an initial hydrogen pressure of 210 ± 20 N m^{-2}) is 1.0 ± 0.4 and for the equivalent groups over europium oxide the order is 0.4 ± 0.1. The pressure dependent runs give orders which decrease to 0.2 for lanthanum oxide and 0 for europium oxide as the pressure increases. The temperature effect is more erratic, though for groups 16 to 20 over lanthanum oxide there is a definite decrease in order with a decrease in temperature. Pretreatment, or prior exposure to excess of either gas, does not affect the order.

Orders with respect to concentration

These orders, calculated from the pressure dependent runs, are 0.3 ± 0.2 for both oxides.

Temperature effects

Activation energies were calculated using zero-order and half-order rate constants. For lanthanum oxide there is a definite change with temperature giving activation energies of 13, 1, and 14 ± 2 kJ mol^{-1} in the temperature ranges 480–560, 560–650, and 650–770 K, respectively. For europium oxide the activation energy decreases from 8 ± 2 kJ mol^{-1} at low temperatures to a very low value above 550 K.

Summary of results for the nonstoichiometric reactions

Reaction type

For lanthanum oxide in hydrogen excess most reactions are of type *c*. In excess oxygen the pattern is more varied. At 474, 548, and 698 K, type *b* predominates under standard conditions (initial hydrogen pressure of approximately 200 N m^{-2}), with a tendency to give type *c* at 474 K, and type *a* at 548 and 698 K, when the initial hydrogen pressure is below 200 N m^{-2}. At 599 and 776 K most reactions are type *a*. The reaction type over europium oxide is almost exclusively type *a*.

Catalyst activity

For both oxides the initial rate generally decreases as the ratio becomes richer in hydrogen, and increases as the ratio

[1]Complete set of result is available at a nominal charge, upon request, from the Depository of Unpublished Data, CISTI, National Research Council of Canada, Ottawa, Ont., Canada K1A 0S2.

TABLE 1. Average values for the adsorption coefficients

Oxide	Group number	Temperature (K)	$x = 1, y = 1$		$x = 2, y = 1$	
			$b_{O_2} \times 10^2$ (N^{-1} m^2)	$b_{H_2} \times 10^2$ (N^{-1} m^2)	$b_{O_2} \times 10^2$ (N^{-1} m^2)	$b_{H_2} \times 10^2$ (N^{-1} m^2)
La_2O_3	21	474	10	6	5	6
	25	548	4	2	2	2
	22	599	3	2	2	2
	24	698	2	2	1	2
	23	776	3	1	1	1
Eu_2O_3	23	583	6	6	3	6
	20	620	5	3	3	3
	22	693	9	7	5	7

TABLE 2. Sample values for the proportionality constant, k

Oxide	Run	Temperature (K)	Proportionality constant (N m^{-2} s^{-1})	
			$x = 1$	$x = 2$
La_2O_3	15A2	501	9	11
	20A5	549	5	8
	14A3	552	6	11
	17A5	600	7	17
	19A5-8	700	10	26
Eu_2O_3	14A1	453	5	7
	15A1	571	5	8
	03A1	574	5	7
	04A2	603	4	6
	16A1	625	4	6
	09A2	656	5	8

becomes richer in oxygen, except at extreme ratios.

For both oxides the average rates for the major portion of the reactions at an initial hydrogen pressure of approximately 220 N m^{-2} show a decrease in hydrogen excess as the mixture becomes richer in hydrogen, whereas in excess oxygen the rate increases slightly and then decreases as the mixture becomes richer in oxygen. The rate in excess oxygen is higher than the rate in excess hydrogen. There is little temperature effect. The rates range from 0.1 to 1.2 N m^{-2} s^{-1}.

Orders with respect to concentration

These orders, calculated from the initial rates of the pressure dependent runs, are 0.4 ± 0.2 for both oxides, with no consistent temperature effects.

Orders with respect to time

For lanthanum oxide the orders for oxygen are close to unity, especially as the ratio diverges significantly from stoichiometry. The orders for hydrogen are more varied, changing from a low of 0.2 at 698 K near the stoichiometric mixture to a high of 1.7 at 474 K at extreme ratios. For europium oxide the orders for oxygen increase from 0.5 to 1.2 as the ratio becomes more extreme, and the orders for hydrogen increase from zero near the stoichiometric ratio to approximately 1.5 at extreme ratios.

Isobars

In all cases plots of log (rate) versus log (pressure of hydrogen or oxygen) with oxygen or hydrogen pressure being constant are smooth curves exhibiting maxima.

For lanthanum oxide the hydrogen–oxygen ratio at the maxima for the hydrogen isobars is 1.0 ± 0.2 and for the oxygen isobars is 1.4 ± 0.2. There is a slight tendency for the maxima to decrease as temperature increases and pressure decreases. The slopes on the low pressure side of the isobars are 1.2 ± 0.4 for the hydrogen isobars and 1.8 ± 0.4 for the oxygen isobars. The slopes on the high pressure side are 1.4 ± 0.8 for the hydrogen isobars and 1.2 ± 0.5 for the oxygen isobars. There is a tendency for the slope to increase with pressure, and decrease with temperature.

For europium oxide the ratio at the maxima for the hydrogen isobars is 1.0 ± 0.1 and for the oxygen isobars is 1.2 ± 0.2 with no obvious temperature or pressure effect. The slopes of the isobars give a value of 0.9 ± 0.2 for the low pressure side of the hydrogen isobars and the high pressure side of the oxygen isobars, and 0.9 ± 0.2 for the other sides. There is no pattern to the variation of these values with temperature or pressure.

Discussion

The overall results for both oxides fit the general pattern described previously for other lanthanide oxides (for example, ref. 19) and will be discussed on the same basis.

General characteristics

Reaction type

Type *a* appears to be the standard form. Europium oxide exhibits this type of curve almost exclusively, whereas for lanthanum oxide, it only appears for nonstoichiometric reactions at 599 and 776 K, at low hydrogen initial pressures at 548 and 698 K, and at high pressures for stoichiometric reactions. Type *b* appears in oxygen excess reactions at 474, 548, and 698 K and in low pressure stoichiometric reactions. Also, prior exposure to excess of either gas can give rise to type *b* plots.

Can. J. Chem. Downloaded from www.nrcresearchpress.com by 210.87.254.105 on 09/06/12
For personal use only.

Can. J. Chem. Downloaded from www.nrcresearchpress.com by 210.87.254.105 on 09/06/12
For personal use only.

Most other reactions are type *c*, especially for most stoichiometric and hydrogen excess reactions.

Catalyst activity

Generally, the initial rate is decreased by prior exposure to excess of either gas, with the effect being greater for lanthanum oxide than for europium oxide. This parallels the change in reaction type discussed above and indicates that both gases can deactivate some or all of the very active sites available at the start of the reaction. Hydrogen-excess nonstoichiometric reactions also decrease the initial rate, indicating a deactivation process. Oxygen-excess nonstoichiometric reactions generally increase the initial rate which is in contradistinction to the appearance of type *b* plots in oxygen excess over lanthanum oxide at 474, 548, and 698 K.

The rate of the central, linear, portion is relatively independent of temperature except for a slight increase for lanthanum oxide. For nonstoichiometric reactions the rate decreases in hydrogen excess, and increases and then decreases as the ratio becomes more extreme in oxygen excess. This, again, shows a deactivating effect for hydrogen and a mixed effect for oxygen.

Active sites

The "standard" form of reaction curve is type *a*, indicating at least two different sets of sites: a hyperactive set available at the start of the reaction, and a less active set on which most of the reaction occurs.

The hyperactive set is always present for europium oxide and usually present for lanthanum oxide, though some of the sites can be blocked by prior exposure to either gas. For nonstoichiometric reactions sites are deactivated in excess hydrogen but activated in excess oxygen. It is assumed that these sites could result from the loss of hydroxyl groups during conditioning.

The second set of sites is probably associated with anion vacancies (cf. ref. 12 for europium oxide). Hydrogen adsorbs more extensively than oxygen, accounting for the rate decrease in excess hydrogen and rate increase in slight excess of oxygen. This deactivating effect was observed by Bakumenko (1), with the activation energy being greater in hydrogen excess reactions (70 kJ mol^{-1}) than in oxygen excess reactions (50 kJ mol^{-1}). The larger values for the activation energy obtained by Bakumenko over lanthanum oxide, and the slightly larger values of 15 kJ mol^{-1} obtained by Barrett and Barry (2) over europium oxide, are explained by prior deactivation of the surface sites.

Kinetics

Analysis of the data shows that the results (after the short initial period) fit a kinetic expression similar to that obeyed by this reaction over other lanthanide oxides, namely

$$[1] \quad \frac{-dP_T}{dt} = \frac{k(b_{H_2}P_{H_2})^x(b_{O_2}P_{O_2})^y}{(1 + b_{H_2}P_{H_2} + b_{O_2}P_{O_2})^{x+y}}$$

where k is a proportionality constant, b_{H_2} and b_{O_2} are the adsorption coefficients for hydrogen and oxygen, respectively, P_T is the total pressure of hydrogen plus oxygen, P_{H_2} and P_{O_2} are the partial pressures of hydrogen and oxygen, respectively, and x and y are integers.

Orders with respect to time

For stoichiometric reactions eq. [1] reduces to

$$[2] \quad \frac{-dP_T}{dt} = \frac{(A_m P_T)^m}{(1 + BP_T)^m}$$

where A_m and B are temperature-dependent constants, with B decreasing as temperature increases; $m = 1$, 2, or 3; and $B = (2b_{H_2} + b_{O_2})/3$.

The apparent order over lanthanum oxide is 1.0 and over europium oxide is 0.4. This indicates that $(2b_{H_2} + b_{O_2}) \times 100$ is of the order of unity, with the adsorption coefficients over lanthanum oxide being smaller than over europium oxide. The temperature and pressure effects are as expected from eq. [2].

For nonstoichiometric reactions the apparent orders are difficult to obtain accurately because the ratio of hydrogen to oxygen is continuously changing. The most accurate assessment of the order will be obtained when one gas is in extreme excess, so that the pressure will remain effectively constant. For lanthanum oxide the order is unity in oxygen, and low in hydrogen near the stoichiometric point.This agrees well with the stoichiometric results. The order in hydrogen increases up to 1.7. For europium oxide the order is approximately 0.5 in oxygen and zero in hydrogen near the stoichiometric point, again collaborating the stoichiometric results. The order in oxygen increases up to 1.2 and in hydrogen up to 1.5 as the ratio diverges from stoichiometry.

Isobars

If the kinetic expression shown in eq. [1] is differentiated with respect to change in pressure of oxygen or hydrogen, keeping the other pressure constant, a smooth curve exhibiting a maximum should result. The slopes of these isobars give an indication of the value for x or y, with the most accurate results being expected from the positive slopes. The position of the maximum allows b_{O_2} and b_{H_2} to be calculated.

Isobars are obtained as expected, further verifying eq. [1]. For both oxides an order close to unity in oxygen is obtained. This is in agreement with the results discussed above. For lanthanum oxide the average order in hydrogen is 1.8 with a high of 2.2. This, together with the results discussed above, indicates that the order is 2. The order in hydrogen is much lower over europium oxide, with an average of 0.9, indicating that the order is unity. This agrees with the preliminary value obtained by Barrett and Barry (2).

Approximate values for the hydrogen and oxygen adsorption coefficients can be calculated from the hydrogen−oxygen ratio at the maximum of the isobars. Some values are shown in Table 1. These results are of the correct order of magnitude, and the relative values between the two oxides support the conclusion that $x = 2$ for lanthanum oxide and $x = 1$ for europium oxide. The adsorption coefficient is expected to decrease with increasing temperature. This is seen over lanthanum oxide (with the values being particularly high at 474 K) but the values over europium oxide are abnormally high at 693 K.

The oxygen and hydrogen adsorption coefficients are approximately equal, indicating that both gases are adsorbed equally strongly although the coverage by hydrogen is higher than by oxygen. In general, the adsorption coefficients over lanthanum oxide are lower than those over europium oxide.

An approximate value for the proportionality constant, k, can be calculated and sample results are given in Table 2. The values obtained for lanthanum oxide are relatively constant at the lower temperatures and then increase at the higher temperatures, whereas, the values obtained for europium oxide are independent of temperature. These results, together with the adsorption coefficients, indicate a slight change in heat of adsorption with temperature.

Finally, once values are obtained in this manner for k, b_{O_2}, and b_{H_2} at each temperature, the results are shown to obey

eq. [1] with $y = 1$, and $x = 2$ for lanthanum oxide and $x = 1$ for europium oxide. The results do not fit any simple variation of this equation.

Mechanism

The general mechanism over both oxides appears to follow the pattern proposed before (e.g. ref. 18):

[3] $H_2(g) \leftrightharpoons H_2(ads)$

[4] $O_2(g) \leftrightharpoons O_2(ads)$

[5] $H_2(ads) + O_2(ads) \rightarrow H_2O_2(ads)$

[6] $H_2O_2(ads) + H_2(ads) \rightarrow 2H_2O(ads)$

[7] $H_2O(ads) \leftrightharpoons H_2O(g)$

From kinetic data the rate-determining step for europium oxide is [5], possibly associated with low oxygen adsorption. The rate-determining step for lanthanum oxide is [6], with [5] being reversible.

It has been shown that both lanthanum oxide and europium oxide are active catalysts for the hydrogen–oxygen reaction. The kinetic data were analyzed in detail and shown to obey a relationship of the form shown in eq. [1]. Therefore, for simplicity of presentation, it has been shown in this paper that the results are, indeed, consistent with this expression. A general overall mechanism has been proposed which is consistent with the kinetic information.

Acknowledgement

The authors express their appreciation to the Natural Sciences and Engineering Research Council of Canada for financial support of their project.

1. T. T. BAKUMENKO. Kinet. Katal. **6**, 74 (1965).
2. M. F. BARRETT and T. I. BARRY. J. Inorg. Nucl. Chem. **27**, 1483 (1965).
3. A. YU. LOGINOV, N. SHEIKKRUSH, S. V. KOSTIKOV, and K. V. TOPCHIEVA. Vestn. Mosk. Univ. Khim. **17**, 653 (1976).
4. M. P. ROSYNEK and J. S. FOX. J. Catal. **49**, 285 (1977).
5. D. BLOOR and J. R. DEAN. J. Phys. C, **5**, 1237 (1972).
6. M. AKIMOTO and I. G. DALLA LANA. J. Catal. **62**, 84 (1980).
7. A. YU. LOGINOV, E. V. LUNINA, and K. V. TOPCHIEVA. Zhur. Fiz. Khim. **48**, 1553 (1974).
8. G. V. SUBBA RAO, S. RAMDAS, P. N. MEHROTRA, and C. N. R. RAO. J. Solid State Chem. **2**, 377 (1970).
9. E. R. S. WINTER. J. Chem. Soc. A, 1832 (1969).
10. KH. M. MINACHEV and G. V. ANTOSHIN. Dokl. Akad. Nauk. SSSR, **161**, 122 (1965).
11. KH. M. MINACHEV, Y. S. KHODAKOV, and V. S. NAKHSHUNOV. J. Catal. **49**, 207 (1977).
12. P. N. ROSS and W. N. DELGASS. J. Catal. **33**, 219 (1974).
13. E. G. VRIELAND and P. W. SELWOOD. J. Catal. **3**, 539 (1964).
14. L. EYRING and B. HOLMBERG. Adv. Chem. **39**, 46 (1963).
15. H. L. YAKEL. Acta Crystallogr. B**35**, 564 (1979).
16. H. SUZUKI, T. ISEKI, and T. MARUYAMA. J. Am. Ceram. Soc. **59**, 451 (1976).
17. J. F. READ, L. G. DUNFIELD, R. M. SHREVE, and E. A. SPINNEY. J. Catal. **33**, 335 (1974).
18. J. F. READ, S. J. AMIRAULT, and Y. T. CHAN. J. Catal. **59**, 188 (1979).
19. J. F. READ and E. W. PERKINS. J. Catal. **42**, 443 (1976).

Can. J. Chem. Downloaded from www.nrcresearchpress.com by 210.87.254.105 on 09/06/12
For personal use only.

A total synthesis of (±)-biotin

RALPH ALLEN WHITNEY
Department of Chemistry, Queen's University, Kingston, Ont., Canada K7L 3N6

Received November 15, 1982

RALPH ALLEN WHITNEY. Can. J. Chem. **61**, 1158 (1983).

A total synthesis of (±)-biotin **1** based on the photochemical cycloaddition reaction of 1,3-diacetylimidazolin-2-one **2** with 3,4-dihydro-2-methoxy-2*H*-pyran **3** is described. The photoadduct **4** was converted into the lactone **6**, which bears the complete carbon framework and all the requisite stereochemical features, via hydrolysis, Wittig olefination, and catalytic hydrogenation to the cyclobutanol **5** followed by oxidative rearrangement. Subsequent conversion of the lactone to (±)-biotin followed from literature precedent (5).

RALPH ALLEN WHITNEY. Can. J. Chem. **61**, 1158 (1983).

On décrit une synthèse totale de la (±) biotine **1** basée sur la cycloaddition photochimique de la diacétyl-1,3 imidazolinone-2 **2** sur le dihydro-3,4 méthoxy-2 2*H* pyranne **3**. On a transformé l'adduit photochimique **4** en la lactone **6** qui porte le squelette carboné complet et toutes les caractéristiques stéréochimiques requises en utilisant les étapes suivantes – hydrolyse, transformation en oléfine de Wittig et hydrogénation catalytique en cyclobutanol **5** suivie d'une transposition oxydante. On a transformé ensuite la lactone en (±) biotine selon la méthode décrite dans la littérature (5).

[Traduit par le journal]

Biotin, a vitamin of the B-complex, has been the goal of much synthetic activity (1) since its discovery in 1936 (2), particularly in the past decade. We have recently described a photochemical approach (3) to (±)-biotin **1** that gave an intermediate, n-pentyl biotin, which had previously been converted microbiologically to biotin itself (4). The purpose of this present report is to elaborate upon this photochemical route to provide directly a total synthesis of biotin that procedes via the previously described (5) 1,4-diol intermediate **9***b* as shown in Scheme 1.

1,3-Diacetylimidazolin-2-one **2** undergoes photochemical [2+2] cycloaddition with alkenes in acetone as solvent and sensitizer (6). Using commercially available 3,4-dihydro-2-methoxy-2*H*-pyran **3** as the alkene component, the photoadduct **4** was obtained in 75–80% yield, on chromatographic purification, as a mixture of four stereoisomers, presumably the two anomers of each of the *syn*- and *anti*-photoadducts, as evidenced by proton nmr. A single isomer was obtained by recrystallization for analytical purposes.

This readily available photoadduct required three basic modifications: exposure of the cyclobutanol portion of the compound, development of a five-carbon appendage functionalized at the terminal carbon, and oxidative rearrangement of the cyclobutanol to a fused butyrolactone suitable for elaboration to biotin. Liberation of the cyclobutanol portion of the photoadduct **4** was accomplished by the use of aqueous acetic acid to effect hydrolysis to the corresponding hemiacetal which was isolated by extraction and used without further purification. Treatment of the hemiacetal with cyanomethylenetriphenylphosphorane gave, via the isomeric hydroxyaldehyde, the α, β-unsaturated nitrile as the expected Wittig reaction product. Proton nmr indicated the product to be a mixture of (*E*)- and (*Z*)-alkene isomers so that, immediately upon chromatographic purification, the product was catalytically hydrogenated, then characterized as the saturated nitrile **5**. An overall yield of 54% from the photoadduct was obtained in accomplishing these modifications. The product was a mixture of two diastereomers as a consequence of the initial formation of *syn* and *anti* photoadducts. A single isomer was obtained for analytical purposes by recrystallization.

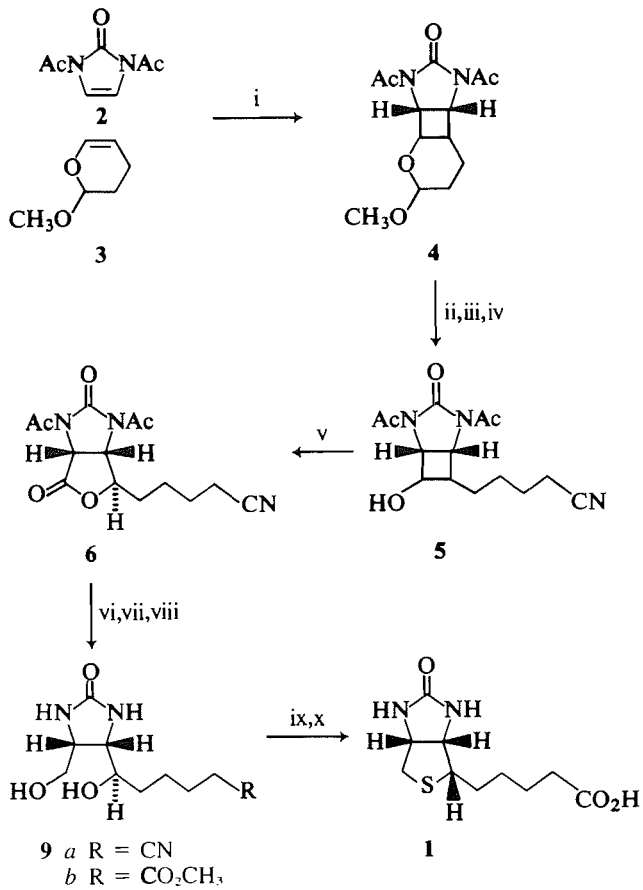

SCHEME 1. Reagents: (i) *hv*, CH_3COCH_3; (ii) CH_3CO_2H, H_2O; (iii) $Ph_3P{=}CHCN$, CH_2Cl_2; (iv) H_2, Pd/C, EtOAc; (v) $RuCl_3$, NaOCl, H_2O, CH_2Cl_2; (vi) $NaBH_4$, EtOH, H_2O; (vii) NaOH, H_2O; H_3O^+, (viii) CH_2N_2, Et_2O, CH_3OH; (ix) Na_2S, DMF; (x) NaOH, H_2O; H_3O^+.

Oxidative rearrangement of the cyclobutanol **5** to lactones was then examined under conditions similar to those previously employed (3). As expected, Jones oxidation gave rise to the

Can. J. Chem. Downloaded from www.nrcresearchpress.com by 210.87.254.105 on 09/06/12
For personal use only.

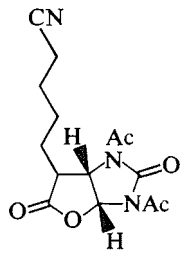

7

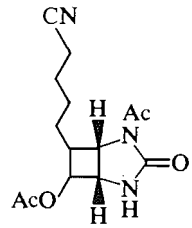

8

wrong regioisomeric lactone **7** as evidenced by proton nmr; the hydrogen at the γ-position of the lactone appeared at 6.35 δ (doublet, J = 7 Hz). Also present was a product **8** arising from acyl migration; the *N*-acetyl group appeared at 2.5 δ while the *O*-acetyl group appeared at 2.1 δ. As in our earlier experiences, the two-phase mixed oxidation system comprised of ruthenium tetroxide in the organic phase and sodium hypochlorite in the aqueous phase (7) again proved successful for obtaining the desired lactone. At moderate concentrations of hypochlorite (6–12%) in the aqueous phase, acyl migration was again observed so that the *N*-chloro derivative of **8** was obtained and converted to **8** upon bisulfite reduction. This problem was minimized by using low initial concentrations of hypochlorite, then adding additional hypochlorite only as necessary to regenerate the yellow ruthenium tetroxide. In this manner a mixture of rearrangement products was obtained from which the lactone **6** was recrystallized in 34% yield. A chemical shift of 5.38 δ for the hydrogen at the γ-position of the lactone ring indicated the correct regioisomer, while a coupling constant of 9 Hz between the hydrogens at the α- and β-positions indicated a *cis*-stereochemical relationship, and a negligible coupling (<0.5 Hz) between the hydrogens at the β- and γ-positions indicated a *trans*-stereochemical relationship. The structure of this important intermediate bearing the complete carbon framework and all the requisite stereochemical details was substantiated by other spectroscopic and analytical data. The structural assignment was verified by X-ray crystallographic analysis.[1]

Preliminary experiments designed to effect removal of the *N*-acetyl groups and reduction of the lactone in the presence of a nitrile were attempted using lithium borohydride (8) in ethereal solvents (tetrahydrofuran, diglyme). Products were obtained which, by proton nmr, appeared to include lactols arising from incomplete reduction of the lactone. Low solubility in ethereal solvents may have, in part, been responsible for the incomplete reduction. Complete reduction was achieved using sodium borohydride in aqueous ethanol (9) at reflux; however, the resulting dihydroxynitrile **9***a* proved difficult to purify so that conversion to the methyl ester **9***b* was effected to give, in 65% yield, material that could be purified by recrystallization and which was identical to that previously described (5).

Conversion of the diol **9***b* to biotin proceeded via the corresponding unstable bis-mesylate followed by treatment with sodium sulfide in dimethylformamide (5). Base hydrolysis followed by acidification then gave (±)-biotin **1**.

Experimental

General

Melting points were determined on a Fisher–Johns or a Thomas Hoover melting point apparatus and are uncorrected. Infrared spectra were recorded on either Perkin–Elmer 528 or Acculab 6 instruments. Proton and carbon magnetic resonance spectra were recorded on Varian EM 360, Bruker HX60, or Bruker CXP200 spectrometers. Chemical shifts are reported in δ values relative to tetramethylsilane. Column chromatography was performed with Merck silica gel 60 (70–230 mesh) while high performance liquid chromatography was performed on Merck Lobar columns. Unless otherwise stated, sodium sulfate was used as drying agent for organic solutions. Microanalyses were performed by Guelph Analytical Laboratories, Guelph, Ontario.

9,11-Diacetyl-4-methoxy-3-oxa-9,11-diazatricyclo[6.3.0.0^{2,7}] undecan-10-one ***4***

A solution of 1,3-diacetylimidazolin-2-one (3) (10 g, 59.5 mmol) in acetone (230 mL, distilled from $KMnO_4$) and 3,4-dihydro-2-methoxy-2*H*-pyran (70 mL) was placed in an immersion well photochemical reactor,[2] then deoxygenated with a stream of nitrogen for 0.5 h. The reaction mixture was then photolysed for 10 h with a 450 W Hanovia lamp filtered with Corex. Removal of the acetone by rotary evaporation under reduced pressure, drying overnight under high vacuum, then purification by column chromatography (hexanes – ethyl acetate) gave the photoadduct **4** (12.9 g, 77%) as a mixture of four stereoisomers; ^{1}Hmr ($CDCl_3$): 3.58, 3.40, 3.39, 3.33 (singlets, —OCH_3, four stereoisomers). One stereoisomer was obtained by recrystallization (ether – ethyl acetate), mp 128–129°C; ir ($CHCl_3$): 2930, 1750, 1700, 1360, 1270 cm^{-1}; ^{1}Hmr ($CDCl_3$): 4.88 (1H, m), 4.70 (1H, m), 4.47 (2H, m), 3.40 (3H, s, —OCH_3), 2.78 (1H, m), 2.61 (3H, s, —$COCH_3$), 2.60 (3H, s, —$COCH_3$), 1.95–1.42 (4H, m). *Anal.* calcd. for $C_{13}H_{18}N_2O_5$: C 55.3, H 6.4, N 9.9; found: C 55.5, H 6.4, N 10.1.

2,4-Diacetyl-7-(4-cyanobutyl)-6-hydroxy-2,4-diazabicyclo[3.2.0]-heptan-3-one ***5***

The photoadduct **4** (2.12 g, 7.45 mmol) was dissolved in acetic acid (10 mL) and water (30 mL), then heated on a steam bath for 1 h. Concentration by rotary evaporation under reduced pressure gave a residue that was dissolved in CH_2Cl_2 (100 mL), then the organic solution was washed with aqueous sodium bicarbonate, dried, filtered, and evaporated to dryness to give the crude hemiketal (1.9 g, 95%); ir ($CHCl_3$); 3600–3200 (OH), 3010, 2940, 1745, 1695, 1360, 1265 cm^{-1}.

The crude hemiketal (1.9 g, 7.1 mmol) was dissolved in CH_2Cl_2 (25 mL), then added to a solution of cyanomethylenetriphenylphosphorane (2.12 g, 8 mmol) in CH_2Cl_2 (25 mL) under a nitrogen atmosphere. The reaction mixture was stirred overnight at room temperature, then the organic solution was washed with water, dried, filtered, and evaporated to dryness. Column chromatography (Lobar, ethyl acetate) of the residue gave the unsaturated nitrile as a mixture of isomers; ir ($CHCl_3$): 3600–3200 (OH), 3000, 2940, 2220 (C≡N), 1760, 1700, 1370, 1275 cm^{-1}; ^{1}Hmr ($CHCl_3$): 6.90–6.45 (1H, m, —CH=CH—CN, (*E*)- and (*Z*)-isomers), 5.60–5.30 (1H, m, —CH=CH—CN, (*E*)- and (*Z*)-isomers), 4.85–4.23 (3H, m), 3.0–1.35 (12H, acetyl groups at 2.60–2.56).

The crude unsaturated nitrile was hydrogenated (5% Pd on charcoal, 150 mg, ethyl acetate) at atmospheric pressure, then filtered and the solution evaporated to dryness to give a mixture of isomeric nitriles (1.26 g, 3.8 mmol, 54% from the photoadduct) as a white solid. A single isomer was obtained by recrystallization (ether – ethyl acetate), mp 130–131°C; ir ($CHCl_3$): 3600, 2950, 2250 (C≡N), 1760, 1700, 1370, 1275 cm^{-1}; ^{1}Hmr ($CDCl_3$): 4.80–4.60 (3H, multiplet), 3.0–2.75 (1H, multiplet), 2.61 (3H, s, —$NCOCH_3$), 2.59 (3H, s, —$NCOCH_3$), 2.34 (2H, t, J = 6 Hz, —CH_2CN), 2.32 (1H, —OH), 1.8–1.1 (6H, multiplet); ^{13}Cmr ($CDCl_3$): 172.1, 171.2, 153.5, 119.8, 67.3, 53.0, 50.2, 43.5, 27.1, 25.4, 24.1, 24.0, 21.9, 17.1. *Anal.* calcd. for $C_{14}H_{19}N_3O_4$: C 57.3, H 6.5, N 14.3; found: C 57.4, H 6.5, N 14.4.

*(1*RS*,4*RS*,5*RS*)-6,8-Diacetyl-4-(4-cyanobutyl)-3-oxa-6,8-diazabicyclo [3.3.0]octan-2,7-dione* ***6***

To a mixture of CH_2Cl_2 (15 mL) and water (10 mL) containing

[1]A. S. Grant, P. S. White, and R. A. Whitney, unpublished results.

[2]Ace Glass Incorporated, Vineland, NJ 08360.

Can. J. Chem. Downloaded from www.nrcresearchpress.com by 210.87.254.105 on 09/06/12
For personal use only.

$RuCl_3 \cdot 3H_2O$ (100 mg) was added sufficient sodium hypochlorite solution (6%, commercial bleach) to generate a yellow RuO_4 solution in the organic phase. The cyclobutanol **5** (1.126 g, 3.8 mmol, mixture of stereoisomers) in CH_2Cl_2 (15 mL) was added dropwise to the rapidly stirred oxidizing solution; hypochlorite solution was added as required to maintain the yellow oxidizing solution. On completion of the addition the reaction mixture was stirred for 3 h, then the organic layer was separated, washed with dilute aqueous sodium metabisulfite, dried, filtered, and evaporated to dryness to give the crude product (1.01 g) as a mixture of rearrangement products. Recrystallization (ether − ethyl acetate) gave the desired lactone **6** (0.40 g, 1.3 mmol, 34%), mp 145−146°C; ir ($CHCl_3$): 3020, 2940, 2860, 2250 (CN), 1790 (lactone), 1770, 1705, 1370, 1350, 1310, 1270 cm^{-1}; ^{1}Hmr ($CDCl_3$): 5.38 (1H, d, J = 9 Hz), 4.65 (1H, d of d, J = 8 Hz, 5 Hz), 4.54 (1H, d, J = 9 Hz), 2.55 (6H, s, —$NCOCH_3$), 2.40 (2H, t, J = 6 Hz), 2.1−1.5 (6H, multiplet); ^{13}Cmr ($CDCl_3$): 171.4, 170.2, 169.0, 150.3, 119.1, 82.6, 56.3, 50.4, 33.5, 25.0, 24.1, 24.1, 23.9, 17.0. *Anal.* calcd. for $C_{14}H_{17}N_3O_5$: C 54.7, H 5.6, N 13.7; found: C 54.6, H 5.6, N 13.9.

*(4*RS,*5*SR,*6'*RS*)-5-Hydroxymethyl-2-imidazolidone-4-(6'-hydroxy)-hexanoic acid methyl ester 9*b

Sodium borohydride (800 mg, 21.1 mmol) was dissolved in aqueous ethanol, then the lactone (400 mg, 1.3 mmol) in ethanol was added. The reaction mixture was heated to reflux, then, after 2 h, additional sodium borohydride (300 mg, 8.4 mmol) in water was added. After an additional hour at reflux, the solution was cooled, acidifed to pH 2−3 with dilute sulfuric acid, then evaporated to dryness. The solid residue was triturated with absolute ethanol (3 × 30 mL), then the ethanol extracts were evaporated to dryness to give the crude diol contaminated with inorganic salts; ^{1}Hmr ($CDCl_3/CD_3OD$): 4.05−3.64 (5H, multiplet), 2.47 (2H, t, J = 6 Hz), 1.88−1.41 (m, 6H); ^{13}Cmr ($CDCl_3/CD_3OD$): 165.0 (C=O), 120.4 (C≡N), 69.3 60.8, 60.7, 57.5, 33.6, 25.7, 24.7, 17.1.

The crude product was dissolved in water, then sodium hydroxide (280 mg, 7 mmol) was added and the mixture refluxed for 6 h. After cooling, the solution was acidified with ion exchange resin (Amberlite IR-120H), then filtered and evaporated to dryness. The residue was dissolved in methanol, filtered, then treated with an excess of ethereal diazomethane. The resulting solution was concentrated by heating on a steam bath, filtered, and evaporated to dryness to give the methyl ester (221 mg, 65%), mp 165−168°C (chloroform−methanol) (lit. (5) mp 165−167°C); ^{1}Hmr ($CDCl_3/CD_3OD$): 3.98−3.45 (8H, multiplet, singlet located at 3.64), 2.33 (2H, triplet, J = 7.5 Hz), 1.8−1.2 (6H, multiplet); ^{13}Cmr ($CDCl_3/CD_3OD$): 175.2, 164.8, 69.4, 60.8, 60.6, 57.2, 55.1, 34.2, 34.0, 25.1, 25.0.

(±)-Biotin 1

To a solution of the diol **9***b* (200 mg, 0.77 mmol) in dry pyridine (5 mL), under a nitrogen atmosphere and cooled in an ice−salt bath, was added methanesulfonyl chloride (1.2 g, 10.5 mmol) dropwise with stirring. After 0.5 h the cooling bath was removed and the reaction mixture stirred at room temperature for 2.5 h. Evaporation to dryness and drying under high vacuum gave a residue that was dissolved in CH_2Cl_2 (50 mL), then washed with 1% aqueous HCl and 5% aqueous $NaHCO_3$, dried, filtered, and evaporated to dryness to give the crude bis-mesylate; ^{1}Hmr ($CDCl_3$): 6.2 (broad s, NH), 6.0 (broad s, NH), 5.0−3.6 (m), 3.63 (s, —CO_2CH_3), 3.10 (s, —OSO_2CH_3), 3.06 (s, —OSO_2CH_3), 2.32 (t, J = 7.5 Hz), 2.0−0.9 (m).

The crude mesylate was dissolved in dimethylformamide, then added to $Na_2S \cdot 9H_2O$ (0.25 g, 0.92 mmol) in dimethylformamide (5 mL) under a nitrogen atmosphere. The reaction mixture was heated to, then stirred at, 90°C for 2 h. The solution was cooled and the solvent removed under high vacuum, then the residue was heated at reflux in aqueous NaOH (2 *M*, 10 mL) for 3 h, decolourized with charcoal, and filtered. The filtrate was acidified with aqueous HCl, filtered, then concentrated under reduced pressure. The resulting residue was recrystallized from water to give (±)-biotin **1** (27 mg, 14%), mp 235−237°C (lit. (5) mp 236−237°C).

Acknowledgments

Financial assistance of the Aldrich Chemical Company, Queen's University, and the Natural Sciences and Engineering Research Council of Canada is gratefully acknowledged as is the technical assistance of the Heyding Magnetic Resonance Laboratory, Nuclear Division. The author is pleased to express his gratitude to Mr. Andrew Stuart Grant and Dr. Peter S. White, Department of Chemistry, University of New Brunswick for performing the X-ray crystallographic analysis.

1. D. D. MIKHNO and V. M. BEREZOVSKII. Chem. Nat. Comp. **16**, 313 (1980); E. G. BAGGIOLINI, H. L. LEE, G. PIZZOLATO, and M. R. USKOKOVIC. J. Am. Chem. Soc. **104**, 6460 (1982); PH. ROSSY, F. G. M. VOGEL, W. HOFFMANN, J. PAUST, and A. NURRENBACH. Tetrahedron Lett. **22**, 3493 (1981); P. N. CONFALONE, G. PIZZOLATO, D. LOLLAR-CONFALONE, and M. R. USKOKOVIC. J. Am. Chem. Soc. **102**, 1954 (1980).
2. F. KOGL and B. TONNIS. Z. Physiol. Chem. **242**, 43 (1936); P. GYORGY, R. KUHN, and E. LEDERER. J. Biol. Chem. **131**, 745 (1939).
3. R. A. WHITNEY. Can. J. Chem. **59**, 2650 (1981).
4. O. OGINO, S. FUJIMOTO, and Y. AOKI. Agric. Biol. Chem. **38**, 275 (1974); **38**, 707 (1974).
5. A. FLIRI and K. HOHENLOHE-OEHRINGEN. Chem. Ber. **113**, 607 (1980); H. OHRUI, N. SUEDA, and S. EMOTO. Agric. Biol. Chem. **42**, 865 (1978); T. OGAWA, T. KAWANO, and M. MATSUI. Carbohydr. Res. **57**, C31 (1977).
6. R. A. WHITNEY. Tetrahedron Lett. **22**, 2063 (1981); K.-H. SCHOLZ, J. HINZ, H.-G. HEINE, and W. HARTMANN. Ann. Chem. 248 (1981).
7. S. WOLFE, S. K. HASAN, and J. R. CAMPBELL. Chem. Commun. 1420 (1970).
8. H. C. BROWN, E. J. MEAD, and B. C. SUBBA RAO. J. Am. Chem. Soc. **77**, 6209 (1955).
9. G. S. BATES and M. A. VARELAS. Can. J. Chem. **58**, 2562 (1980).

Can. J. Chem. Downloaded from www.nrcresearchpress.com by 210.87.254.105 on 09/06/12
For personal use only.

The reaction of 1,6,6aλ⁴-trithiapentalenes with carbene and nitrene reagents

DAVID M. MCKINNON
Chemistry Department, University of Manitoba, Winnipeg, Man., Canada R3T 2N2

Received October 12, 1982

DAVID M. MCKINNON. Can. J. Chem. **61**, 1161 (1983).

The reaction of some 1,6,6aλ⁴-trithiapentalenes with ethyl azidoformate provides 1:1 adducts, formulated as 4-thioacylmethylene-1,3,2-dithiazine-2-carboxylic esters; and with diphenyldiazomethane, 1:2 adducts, formulated as 4-(3-propenylidene)-1,3-dithiins. In some cases 4-diphenylmethylenethiopyrans are isolated. The products arise by insertion at a disulfide type bond, or on a thione function of an initial reaction product.

DAVID M. MCKINNON. Can. J. Chem. **61**, 1161 (1983).

Les trithia-1,6,6aλ⁴ pentalènes réagissent avec l'azidoformate d'éthyle en donnant des adduits 1:1 auxquels on attribue une formule d'esters d'acide thioacyl-4 méthylènedithiazine-1,3,2 carboxylique-2, la même réaction avec le diphényldiazométhane donne des adduits 1:2 que l'on a identifié comme étant des (propénylidène-3)-4 dithiins-1,3. Dans certains cas on a isolé des diphényl-4 méthylènethiopyrannes. Les produits proviennent de l'insertion du produit de la réaction initiale dans une liaison du type disulfure ou dans une fonction thione.

[Traduit par le journal]

Can. J. Chem. Downloaded from www.nrcresearchpress.com by 210.87.254.6 on 09/06/12
For personal use only.

Introduction

The reactions of 1,6,6aλ⁴-trithiapentalenes (**1**) with various species have been described. Thus, nucleophilic attack occurs at the positions 2 or 5, and electrophilic substitution occurs at the positions 3 or 4, although alkylating agents react at 1 or 6 sulfur atoms leading to substituted 1,2-dithiolium cations (1). Also, certain radicals react with the trithiapentalenes **1** at position 1 or 6 to form substituted pentadienyl radicals (2). However, no reactions are reported for the attack of nitrene or carbene species on trithiapentalenes. Some 1,2-dithioles, with which the trithiapentalenes have some structural affinity, do react with nitrenes and carbenes to form insertion products (3, 4) in the disulfide bond.

Results and discussion

Accordingly, 2,5-diphenyl-1,6,6aλ⁴-trithiapentalene (**1***a*) was treated with ethyl azidoformate in refluxing carbon tetrachloride. A slow reaction was evident by the gradual disappearance of the typical deep red color of the trithiapentalene, and work-up gave a product whose analysis and nmr were consistent with a 1:1 trithiapentalene/nitrene adduct. Likewise, two other trithiapentalenes **1***b* and **1***c* also gave 1:1 adducts.

The adduct from **1***a* is assigned the structure **2***a* on the following basis; attack of the nitrene on other than a sulfur atom, whether on a heterocyclic ring carbon or on a carbon of an aryl substitutent, would produce a substituted trithiapentalene, with little change from the typical deep red color. A possible mechanism of formation is shown (Scheme 1).

The only other reasonable structure might be a thiaziridine, but such a structure would be expected to extrude sulfur rapidly to form an imine, as has been demonstrated for the attack of carbethoxynitrenes on thiones (4).

For the asymmetrical trithiapentalene **1***b* two monoadducts of the type above are possible, i.e. **2***b* and **2***c*. The latter is a thial. Although this has some structural resemblances to some thials which have been isolated (5), these types of compounds are notoriously unstable and may dimerize with subsequent elimination of sulfur (6, 7). On this basis the structure **2***b* is considered the more likely,

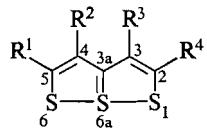

1

a $R^1 = R^4 = Ph$, $R^2 = R^3 = H$
b $R^1 = R^3 = Ph$, $R^2 = R^4 = H$
c $R^1 = Ph$, $R^2 = H$, $R^3/R^4 = -(CH{=}CH)_2-$

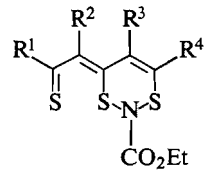

2

a $R^1 = R^4 = Ph$, $R^2 = R^3 = H$
b $R^1 = R^3 = Ph$, $R^2 = R^4 = H$
c $R^1 = R^3 = H$, $R^2 = R^4 = Ph$
d $R^1 = Ph$, $R^2 = H$, $R^3/R^4 = -(CH{=}CH)_2-$
e $R^1/R^2 = -(CH{=}CH)_2-$, $R^3 = H$, $R^4 = Ph$

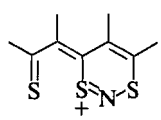

3

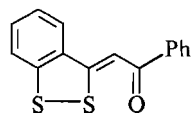

4

For the trithiapentalene **1***c*, again two monoadducts are possible, i.e. **2***d* and **2***e*. Compound **2***e* contains an *o*-quinonoid thione structure and is unlikely to exist as a monomer. Such types are related to intermediates in certain 1,2-benzodithiole reactions with amines (8), alkenes (9, 10), or trivalent phosphorus compounds (11). On this basis the structure **2***d* is considered the more likely and this formulation is in accord with carbene reactions described below. No differentiation could be made on the basis of mass spectrometry. In all of these products no ions corresponding to the parent were evident. They did however, exhibit $M - 73$ peaks, corresponding to loss of carbethoxy groups, i.e. the formation of ions of structure **3**.

The starting trithiapentalene **1***c* has been previously syn-

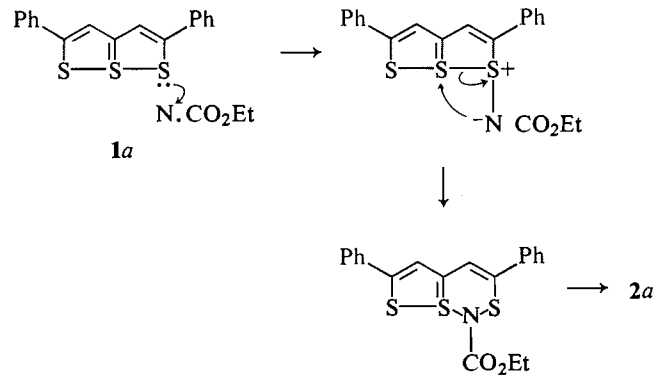

SCHEME 1

thesized from 1,2-benzodithiole-3-thione by condensation with benzoylacetonitrile and modification of the side chain (12) or in very low yield by direct reaction of dehydrobenzene with 5-phenyl-1,2-dithiole-3-thione (13), but an approach using reaction with phenacyl bromide, similar to that used for monocyclic 1,2-dithiole-3-thiones (14), was more convenient. The resulting 3-phenacylidene-1,2-benzodithiole (**4**) gave the trithiapentalene **1***c* on treatment with phosphorus pentasulfide.

The reaction of the trithiapentalene **1***a* with diphenyldiazomethane in the presence of copper acetylacetonate, to generate diphenylcarbene, gave a mixture from which was isolated tetraphenylethylene sulfide and a yellow oil which crystallized as yellow prisms. The properties of this were consistent with a trithiapentalene/carbene 1:2 adduct, less one atom of sulfur. This adduct is assigned the structure **5***a*. It could have been formed via a mechanism similar to that proposed for the nitrenes, with subsequent reaction at the thione function generated. The first stage is thus analogous to the insertion of carbenes in naphtho[1,8-*cd*]-1,2-dithiole (3) or 5-phenyl-1,2-dithiole-3-one (15), and the subsequent reaction is typical of thione functions in general (16–20).

When the reaction was performed with an excess of copper acetylacetonate, the thiopyran derivative **6***a* was obtained. Although trithiapentalenes may form complexes with various transition metals (21–23), treatment of the trithiapentalene **1***a* with only copper acetylacetonate gave no thiopyran products and therefore it may be that it is an initial carbene/trithiapentalene reaction product **7** that is the actual species undergoing rearrangement. Alternatively, a different reaction mechanism, e.g. attack of the carbene at carbon **3***a*, may be responsible.

The treatment of 2,4-diphenyl-1,6,6aλ^4-trithiapentalene (**1***b*) with diphenyldiazomethane and copper acetylacetonate gave a yellow oil which could not be crystallized, but had satisfactory analytical and spectral data for a 1:2 adduct, less one atom of sulfur. Two possible structures **5***b* and **5***c* must be derived from the 1:1 initial reaction products, **7***b* and **7***c* respectively. If the mechanism of the carbene reaction is similar to the nitrenes, then the former are favored, i.e. because **7***c* is a thial. It is possible that a metal carbenoid may be the actual attacking reagent (3), but this would also lead to the same intermediate **7***b*.

In these reactions the carbene (or carbenoid) may be considered as an electrophile, hence these reactions should have some parallels to the reactions of trithiapentalenes with electrophilic reagents, especially alkylating agents. In fact the trithiapentalene **1***b* reacts with methyl iodide at the 6 sulfur rather than the 2 sulfur atom (24).

From the reaction of 1,8,8aλ^4-2-phenylcyclopenta[*a*]indene (**1***c*) with diphenyldiazomethane, two yellow bands were separated by chromatography. One of these gave a satisfactory analysis and mass spectrum for a 1:2 adduct, minus one sulfur atom, and is assigned the structure **5***d* on the basis of the results for reaction of the trithiapentalene with ethyl azidoformate. This corresponds to an initial attack on the least hindered sulfur atom (24). The other material collected had the same mol. wt. (by mass spectrometry), but darkened rapidly on standing and could not be obtained sufficiently pure for analysis. This may be either a product **5***e* derived from an initial reaction at an alternate sulfur atom, or possibly a geometrical isomer of **5***d*. From the first band, a small amount of a yellow crystalline material separated on attempted crystallization. The analysis of

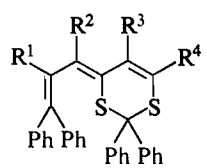

5

a $R^1 = R^4 = Ph$, $R^2 = R^3 = Ph$
b $R^1 = R^3 = Ph$, $R^2 = R^4 = H$
c $R^1 = R^3 = H$, $R^2 = R^4 = Ph$
d $R^1 = Ph$, $R^2 = H$, $R^3/R^4 = —(CH=CH)_2—$
e $R^1/R^2 = —(CH=CH)_2—$, $R^3 = H$, $R^4 = Ph$

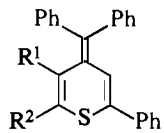

6

a $R^1 = H$, $R^2 = Ph$
b $R^1/R^2 = —(CH=CH)_2—$

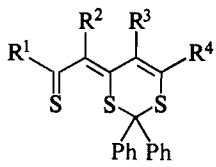

7

a $R^1 = R^4 = Ph$, $R^2 = R^3 = H$
b $R^1 = R^3 = Ph$, $R^2 = R^4 = H$
c $R^1 = R^3 = H$, $R^2 = R^4 = Ph$
d $R^1 = Ph$, $R^2 = H$, $R^3/R^4 = —(CH=CH_2)_2—$

Can. J. Chem. Downloaded from www.nrcresearchpress.com by 210.87.254.6 on 09/06/12
For personal use only.

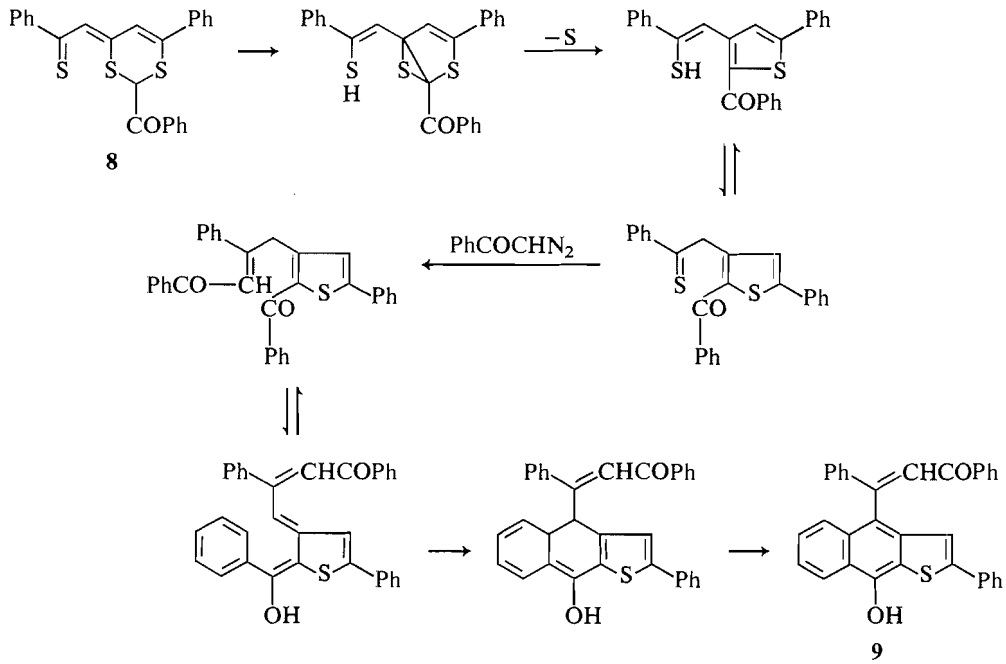

SCHEME 2

this was consistent with a 1:1 adduct minus two sulfur atoms. It was identified as the benzothiopyran structure **6***b*, and thus corresponds in type to the product **6***a* from the reaction of **1***a*, and may be formed by a similar mechanism. The compound **6***b* was made for reference by the reaction of 2-phenylbenzothiopyran-4-thione and diphenyldiazomethane, a typical reaction of thione functions (16–20).

The reaction of the trithiapentalene **1***a* with benzoyldiazomethane gave a pale yellow material whose data were consistent with a 1:2 adduct less two sulfur and two hydrogen atoms. This may arise by aromatization of an intermediate and the compound is tentatively assigned the structure **9**. An initial monoadduct of the type shown, **8**, in contrast to the products **2**, **5**, or **7** above, would possess an acidic hydrogen, and ready loss of a sulfur atom via an episulfide forming a benzoylthiophene is highly likely (Scheme 2). A plausible scheme for the eventual formation of a napththo[2,3-*b*]thiophene **9** by sequential tautomerism, electrocyclization, and aromatization is shown. Alternatively the monoadduct may form a diadduct prior to episulfide formation.

This reaction also gave traces of another product whose mass spectrum was consistent with a 1:1 adduct, minus one sulfur and two hydrogen atoms, indicating that at least the initial reaction product may lose sulfur readily.

The reaction of the other two trithiapentalenes **1***b* and **1***c* with benzoyldiazomethane gave only oily materials which could not be obtained sufficiently pure for analysis.

The nmr spectrum of the compound **2***a* exhibited two sharp single peaks at δ = 6.13 and 8.18 ppm respectively. Since the later is not much shifted from the heterocyclic proton peaks in the trithiapentalene **1***a* (1), it is assigned to the proton on the 1,3,2-dithiazine ring, and the former to the vinylic proton of the side chain. While the trithiapentalene **1***b* has the 3- and 5-heterocyclic protons at δ = 8.10 and 8.81 ppm respectively (26), the adduct **2***b* derived from it gave two apparent singlets at δ 6.60 and 7.13 ppm, the latter poorly resolved from aromatic protons. On the basis of the shift found from **1***a* to **2***a* above, the former is tentatively assigned to the proton on the thiophenacylidene side chain. The product **2** did not exhibit any proton in the range of 8.7 ppm (the heterocyclic proton of **1***c* (1)). An apparent single peak at 7.73 ppm cannot be discriminated from aromatic protons with certainty. No literature models of 1,3,2,-dithiazines are available and products from diphenylcarbene give only a complex series of aromatic peaks.

Experimental

Unless otherwise stated, ^{1}H nmr spectra were obtained in deuteriochloroform solution using tetramethylsilane as an internal standard, on a Varian model E. M. 360 spectrometer. Mass spectra were obtained on a Finnegan model 1015 spectrometer, and ir spectra on a Perkin–Elmer model 337 spectrophotometer. Thick-layer chromatography (tlc) was performed on "Camag" silica gel type D.S.F.S. supplied by Terochem Laboratories. All solutions were dried over anhydrous magnesium sulfate.

Preparation of 1,8,8aλ^4-2-phenylcyclopent[a]indene (1c)

1,2-Benzodithiole-3-thione (1.84 g, 10 mmol) and phenacyl bromide (2.39 g, 12 mmol) were intimately mixed and heated gently to form a homogenous red melt. This rapidly solidified to a yellowish solid which was triturated with tetrahydrofuran and filtered. The bright yellow salt was then heated in a mixture of tetrahydrofuran and propionic acid (2:1) (50 mL) until all solid material had dissolved and then for one further hour. The solution was poured into water and extracted with chloroform, washed with sodium bicarbonate solution, dried, and evaporated to give a yellow oil.

This was chromatographed on silica gel (60–200 mesh, Davison Chemical) in benzene. The second yellow band was collected and on evaporation gave a yellow oil which crystallized under ethanol. Recrystallization from nitromethane gave 3-phenacylidene-1,2-benzodithiole (**4**) as gritty orange prisms, mp 134–135°C (lit. (25) mp 135°C) (61%).

This compound was thionated in toluene to afford the trithiapentalene **3***c* (80%) as violet needles, mp 130–132°C (lit. (12) mp 130–132°C) (81%).

*Reactions of trithiapentalenes 1*a–c *with ethyl azidoformate*

Generally, the trithiapentalene (1 mmol) in carbon tetrachloride at reflux was treated with ethyl azidoformate (1 mL). Reflux was maintained 16 h, then a further 1 mL was added and reflux continued until a pale yellow solution resulted. The solutions were evaporated *in*

Can. J. Chem. Downloaded from www.nrcresearchpress.com by 210.87.254.6 on 09/06/12
For personal use only.

TABLE 1. Reactions of trithiapentalenes **1** with ethyl azidoformate or diphenyldiazomethane

Compound	Yield (%)	Melting point (°C)	Formula	Analysis (%) Calculated C	H	N	S	Found C	H	N	S
2*a*	51	60–65	$C_{20}H_{17}NO_2S_3$	60.15	4.26	3.51	24.06	60.30	4.40	3.36	23.89
2*b*	70	—	$C_{20}H_{17}NO_2S_3$	60.15	4.26	3.51	24.06	60.46	4.56	3.25	23.97
2*d*	45	90–92	$C_{18}H_{15}NO_2S_3$	57.91	4.02	3.75	25.74	58.27	4.16	3.74	25.43
5*a*	41	158–160	$C_{43}H_{32}S_2$	84.31	5.23		10.46	84.33	5.37		10.53
5*b*	62	—	$C_{43}H_{32}S_2$	84.31	5.23		10.46	84.21	5.48		10.19
5*d*	33	—	$C_{41}H_{30}S_2$	83.96	5.12		10.92	83.52	5.28		10.69
6*b*	5	168	$C_{25}H_{20}S$	86.60	5.15		8.25	86.27	5.49		8.00

vacuo to give viscous yellow oils. The products **2***a* and **2***d* crystallized under a benzene/petroleum ether 1:1 mixture at −20°C. The compound **2***b* did not crystallize, even after further purification by thick-layer chromatography.

Data are summarized in Table 1.

*Reactions of trithiapentalenes **1** with diphenyldiazomethane*

The trithiapentalenes (1 mmol) in dry benzene (10 mL) were treated at reflux with freshly prepared diphenyldiazomethane (27) (~0.5 g) and copper acetylacetonate (25 mg). After a few minutes the color of the solution became dark yellow. The solutions were evaporated and the yellow oils examined by chromatography using a benzene/petroleum ether 1:3 mixture as an eluent. The fastest running band in each case gave tetraphenylthiirane, mp 175°C (lit. (28) mp 175°C); mixture mp 175°C. A bright yellow band running next corresponded to the 1:2 adducts produced in the reaction; a single band for reactions of **1***a* and **1***b*, and two bands for **1***c*. Other bands appear to be only reaction products of the diphenyldiazomethane decomposition, e.g. benzophenone azine.

The yellow bands gave thick oils or glasses on separation and evaporation, which in some cases slowly crystallized from mixtures of benzene and petroleum ether at −20°C as pale yellow solids. The compound **5***d* did not crystallize, but was accompanied by small amounts (5%) of a material which separated in a crystalline form. These were recrystallized from benzene/petroleum ether as yellow needles identical (mixture mp) with compound **6***b* reported below. Also **5***d* was accompanied by another material of close R_f value which did not crystallize and darkened rapidly on standing. Data are summarized in the table.

*Reactions of trithiapentalenes **1** with benzoyldiazomethane*

The trithiapentalenes (0.5 mmol) in boiling benzene (10 mL) containing copper acetylacetonate (25 mg) were treated with excess benzoyldiazomethane (0.4 g) and refluxed 16 h. The mixtures were filtered and examined by chromatography. A reasonable separation of components was obtained for only the reaction products from the trithiapentalene **1***a*. Two yellow bands both crystallized from benzene/petroleum ether mixtures at −20°C. The first eluted gave pale yellow prisms (51 mg), mp 152–154°C, tentatively assigned structure **9**. The ir spectrum: 1679 cm^{-1} (C=O str). The mass spectrum M^+ calcd.: 482 M^+; found: 482. *Anal.* calcd. for $C_{33}H_{22}O_2S$: C 82.16, H 4.56, S 6.64%; found: C 81.87, H 4.65, S 6.88.

Traces (~5 mg) of another material crystallizing as a pale yellow powder, mp 155–160°C, were obtained. The mass spectrum M^+ found: 396; M calcd. for $C_{25}H_{16}S_2O$ is 396.

*Reaction of trithiapentalene **1**a with diphenyldiazomethane and excess acetylacetonate*

The reaction performed as above, but with copper acetylacetonate (100 mg), gave a yellow oil on work-up. Separation by chromatography using a benzene/petroleum ether 1:4 mixture as an eluent gave initially a colorless crystalline material, identified (mixed up) as tetraphenylethene, and **6***a* as a golden yellow solid which crystallized from toluene as yellow plates, mp 252°C (lit. (29) mp 252°C) (41%). The reaction also gave a reddish oil which could not be crystallized.

*Reaction of 2-phenylbenzothipyran-4-thione with diphenyldiazomethane forming 2-phenyl-4-diphenylmethylenebenzothiopyran (**6**b)*

The thione (254 mg, 1 mmol) in benzene (10 mL) and copper acetylacetonate (25 mg) were treated at reflux with diphenyldiazomethane (250 mg). After a few minutes the dark yellow-green solution had become dark yellow. The mixture was filtered, evaporated, and chromatographed. The first bright yellow band, on work-up, gave a yellow oil which crystallized under ethanol as yellow prisms, mp 168°C (83%).

Acknowledgements

Thanks are due to the Natural Sciences and Engineering Research Council of Canada (NSERC) for financial support of this work, and to Mr. W. Buchannon and Mr. K. Marat for the preparation of spectra.

1. N. LOZAC'H. Adv. Heterocycl. Chem. **13**, 161 (1971).
2. K. U. INGOLD, D. H. REID, and J. C. WALTON. J. Chem. Soc. Chem. Commun. 371 (1979).
3. S. TAMAGAKI and S. OAE. Bull. Chem. Soc. Jpn. **45**, 960 (1972).
4. M. S. CHAUHAN and D. M. MCKINNON. Can. J. Chem. **54**, 3879 (1976).
5. H. DAVY and J. VIALLE. Bull. Soc. Chim. Fr. 1635 (1975).
6. D. M. MCKINNON and J. M. BUCHSHRIBER. Can. J. Chem. **49**, 3299 (1971).
7. D. B. J. EASTON, D. LEAVER, and T. J. RAWLINGS. J. Chem. Soc. Perkin Trans. 1, 41 (1972).
8. KYUNG TAE KANG, R. OKAZAKI, and N. INAMOTO. Bull. Chem. Soc. Jpn. **52**, 3640 (1979).
9. P. DEMAYO and H. T. NG. Can. J. Chem. **55**, 3763 (1977).
10. R. OKAZAKI, F. ISHII, and K. OKAWA. J. Chem. Soc. Perkin Trans. 1, 270 (1975).
11. D. N. HARPP and J. G. GLEASON. J. Org. Chem. **35**, 3259 (1970).
12. H. BEHRINGER, M. RUFF, and R. W. WIEDENMANN. Ber. **97**, 1732 (1964).
13. D. PAQUER and R. POU. Bull. Soc. Chim. Fr. 120 (1976).
14. G. CAILLAUD and Y. MOLLIER. Bull. Soc. Chim. Fr. 2018 (1970).
15. M. A. ELKASCHEF, F. M. E. ABDEL-MEGEID, and A. A. ELBARBARY. Tetrahedron, **30**, 4113 (1974).
16. H. STAUDINGER and J. SIEGWART. Helv. Chim. Acta, **3**, 833 (1920); **3**, 840 (1920).
17. N. LATIF and I. FATHY. J. Org. Chem. **27**, 1633 (1962).
18. A. SCHONBERG and E. FREESE. Ber. **95**, 2810 (1962).
19. W. J. MIDDLETON, E. G. HAWARD, and W. H. SHARKEY. J. Org. Chem. **30**, 1375 (1965).

Can. J. Chem. Downloaded from www.nrcresearchpress.com by 210.87.254.6 on 09/06/12
For personal use only.

20. D. SEYFERTH and W. TRONICH. J. Am. Chem. Soc. **91**, 2138 (1969).
21. A. FURUHASHI, M. KAWANO, and A. OUCHI. J. Inorg. Nucl. Chem. **34**, 2960 (1972).
22. B. BOGDANOVIC, C. KRUEGER, and O. KUZMIN. Angew. Chem. **91**, 744 (1979).
23. B. BOGDANOVIC, C. KRUEGER, and P. LOCATELLI. Angew. Chem. **91**, 745 (1979).
24. E. KLINGSBERG. J. Org. Chem. **33**, 2915 (1968).
25. D. BARILLIER, C. GY, P. RIOULT, and J. VIALLE. Bull. Soc. Chim. Fr. 277 (1973).
26. J. G. DINGWALL, J. MCKENZIE, and D. H. REID. J. Chem. Soc. (C) 2543 (1968).
27. J. B. MILLER. J. Org. Chem. **21**, 560 (1959).
28. H. STAUDINGER and J. SIEGWART. Helv. Chim. Acta, **3**, 833 (1920).
29. A. SCHONBERG and R. VON ARDENNE. Ber. **101**, 346 (1968); F. EIDEN and M. PEGLOW. Arch. Pharm. **303**, 61 (1970).

Can. J. Chem. Downloaded from www.nrcresearchpress.com by 210.87.254.6 on 09/06/12
For personal use only.

Enantiomeric synthesis of 9-hydroxy-(*E*)-2-decenoic acid, a queen honeybee pheromone

ALI A. KANDIL AND KEITH N. SLESSOR
Department of Chemistry, Simon Fraser University, Burnaby, B.C., Canada V5A 1S6

Received August 25, 1982

ALI A. KANDIL and KEITH N. SLESSOR. Can. J. Chem. **61**, 1166 (1983).

S-(+)-, *R*-(−)-, and (±)-9-hydroxy-(*E*)-2-decenoic acid have been synthesized by organocuprate-catalyzed opening of *S*-(−)-, *R*-(+)-, and racemic methyl oxiranes. This acid, of unknown chirality, is an important constituent of the honeybee queen's mandibular gland.

ALI A. KANDIL et KEITH N. SLESSOR. Can. J. Chem. **61**, 1166 (1983).

On a synthétisé les acides (*E*) décèn-2 oïques *S*-(+)-, *R*-(−)-, ainsi que l'acide hydroxy-9 (*E*) décen-2 oïque au moyen de l'ouverture des méthyloxyrannes racémiques, *S*-(−)- et *R*-(+)- catalysée par un organocuprate. Cet acide, de chiralité inconnue, est un constituant important de la glande mandibulaire de la reine des abeilles.

[Traduit par le journal]

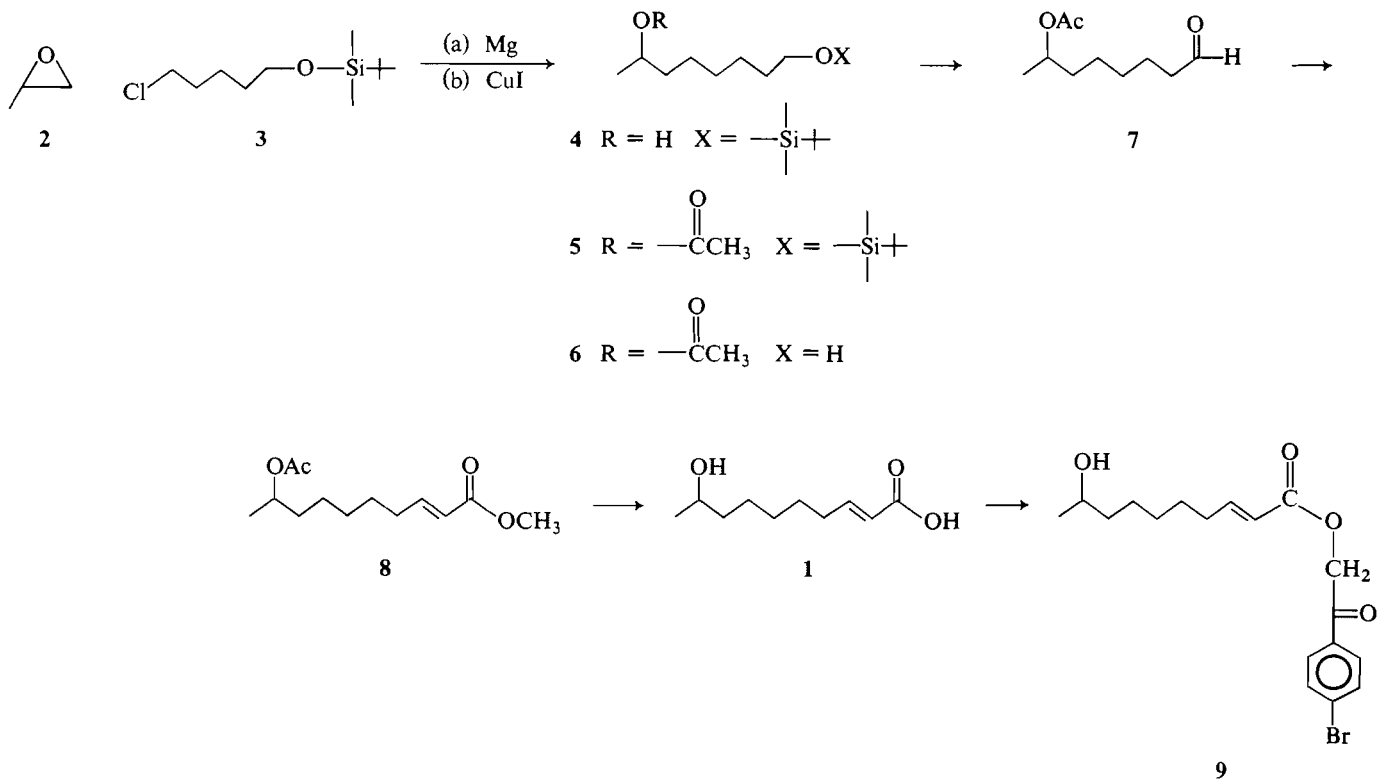

SCHEME 1

Introduction

It has been known for some time that queen honeybees produce 9-hydroxy-(*E*)-2-decenoic acid in their mandibular glands (1). There has been considerable controversy regarding the bioactivity of synthetic (±)-9-hydroxy-(*E*)-2-decenoic acid, especially in its role as a swarm-settling pheromone. The purity of some of the synthetic preparations has been questioned (2) since they were prepared from the biologically-active 9-keto analogue. It was evident to us that the chirality of the 9-hydroxyl group may further complicate the recognition of the material by worker bees. Inhibition of pheromonal response by the opposite enantiomers has been documented in several insects (3). The chirality of the natural pheromone has not been determined and may well not be racemic in accord with the vast majority of known chiral pheromones (4).

It was of interest, then, to prepare pure 9-hydroxy-(*E*)-2-decenoic acid in a manner which did not involve the 9-keto intermediate and which permitted the chiral synthesis of the two enantiomers as well as racemate. The problem was facilitated by our earlier work on the chiral synthesis of 6-methyl-5-hepten-2-ol, the aggregation pheromone of the two sympatric northwestern timber pests, *Gnathotrichus retusus* and *G. sulcatus* (5). Advantage was taken of the CuI-catalyzed opening of the chiral methyl oxiranes, both readily derived from ethyl *S*-(−)-lactate from the chiral pool (6). With an appropriately functionalized alkylating agent, oxirane ring opening should provide a direct route to the desired chiral unsaturated acids **1**, as outlined in Scheme 1.

Can. J. Chem. Downloaded from www.nrcresearchpress.com by 210.87.254.42 on 09/06/12
For personal use only.

Can. J. Chem. Downloaded from www.nrcresearchpress.com by 210.87.254.42 on 09/06/12
For personal use only.

Discussion

The utility of copper-catalyzed Grignard oxirane openings is well documented (7). The very high regioselectivity and consequent stereoselectivity displayed by these reagents on methyloxirane provide an excellent entry into molecules containing a chiral 2-ol functionality (5, 8). The availability of methyloxiranes of high chiral purity is facilitated by the transformation of commercially available ethyl *S*-(−)-lactate into either oxirane enantiomer. Crystalline intermediates in the synthesis of the chiral oxiranes from commercial ethyl lactate (9) provided these materials in high enantiomeric excess, >95% for (−)-**2** and >99% for (+)-**2**, as determined by rotation.

5-Chloropentan-1-ol was prepared by the treatment of tetrahydropyran with acetyl chloride and anhydrous zinc chloride (10) followed by acid hydrolysis. The *tert*-butyldimethylsilyl group (11) was chosen as an appropriate blocking group due to its stability under the coupling conditions and its ease of removal, whereas the trimethylsilyl ether was found to be labile under these conditions. Difficulty in promoting the formation of the Grignard reagent was experienced when tetrahydropyranyl ether was utilized as a blocking group. The identity of the final product was verified by formation of the known racemic *p*-bromophenacyl ester (12).

Biological testing of the racemic and enantiomeric acids has begun and we have shown that 9-hydroxy-(*E*)-2-decenoic acid is indeed effective in swarm settling, with the *R*-(−)-isomer substantially more active than other formulations (13). Further work will establish the chirality of the natural acid and any role this material may have in the sex attraction of the drones.

Experimental

General procedures and instrumentation were as described earlier (5) except that nmr data were obtained on a Varian EM360 and the Si-methyl signals of the *tert*-butyldimethylsilyl were assigned a zero for compounds **3** − **5**. Purification of intermediates and analytical samples was carried out using flash chromatography (14). Analyses were performed by M. K. Yang, of Simon Fraser University, on a Perkin−Elmer elemental analyzer, Model 240. High resolution mass spectra were obtained by Dr. G. Eigendorf, Chemistry Department, The University of British Columbia, on a DS-50 mass spectrometer.

1-O-tert-*Butyldimethylsilyl-5-chloropentanol (**3**)*

5-Chloropentanol (5.8 g) was stirred with imidazole (5.9 g, 2.5 equiv.) and *tert*-butyldimethylsilylchloride (6.2 g, 1.2 equiv.) in *N*,*N*-dimethylformamide (15 mL) at 25°C for 12 h. The mixture was poured into ice-cold water (50 mL), extracted with ether (2 × 20 mL) washed with brine (50 mL), and dried over sodium sulphate. Evaporation of solvent under reduced pressure followed by vacuum distillation afforded **3** (9.18 g, 82% yield), bp 72−74°C (0.025 Torr); i.r. (film) ν_{max}: 2942, 1461, 1255, 1105 cm^{-1}; δ (CCl_4): 3.65 (t, 2H, J = 5 Hz, —CH_2—O), 3.41 (t, 2H, J = 6 Hz, —CH_2Cl), 1.56 (m, 6H, —$(CH_2)_3$), 0.81 (s, 9H, *tert*-butyl), 0.00 (s, 6H, $(CH_3)_2$Si—).

1-O-tert-*Butyldimethylsilyl-1,7-octanediol (**4**)*

A three-necked flask (50 mL), containing magnesium turnings (1.4 g, 61 mg-atoms) and a stirring bar, was dried in an oven at 100°C for 2 h and cooled to room temperature under a stream of dry N_2. A portion of a solution of 1-*O*-*tert*-butyldimethylsilyl-5-chloropentanol (8.0 g, 33 mmol) in anhydrous tetrahydrofuran (15 mL) was introduced, the reaction initiated with a small crystal of iodine, and the remaining solution added over 30 min. Stirring was continued for a further 1 h at room temperature and the mixture was cooled to −30°C. Freshly prepared CuI (15) (0.63 g, 3.3 mmol) was added and the mixture stirred for 30 min. Methyl oxirane **2** (1.56 g, 27 mmol) was added dropwise over a 15 min period, the mixture warmed to 0°C, and stirred for 3 h. The reaction was quenched by addition of saturated aqueous ammonium chloride (15 mL) and the product isolated by extraction with ether to yield a colorless liquid (8.1 g). Flash chromatography on silica gel with ether − petroleum ether (30−60°C) (1:1) afforded a pure product **4** (7.2 g, 25 mmol, 92% yield); i.r. (film) ν_{max}: 3316, 1462, 1359, 1257, 1109, 785 cm^{-1}; δ (CCl_4): 3.72 (m, 1H, CH), 3.52 (t, 2H, J = 6 Hz, —CH_2O—), 2.98 (b, 1H, OH), 1.35 (m, 10H, —CH_2—), 1.18 (d, 3H, J = 6 Hz, —CH_3), 0.87 (s, 9H, $(CH_3)_3$C—), 0.00 (s, 6H, $(CH_3)_2$Si—).

1-O-tert-*Butyldimethylsilyl-7*-O-*acetyl-1,7-octanediol (**5**)*

The hydroxy silyl ether **4** (0.8 g, 3.2 mmol) was acetylated in pyridine (8 mL), using acetic anhydride (8 mL), at room temperature for 12 h. The solution was poured into ice water (20 mL), extracted with methylene dichloride (2 × 30 mL) washed with ice-cold 1 *N* hydrochloric acid (2 × 5 mL) and water (2 × 25 mL), dried over anhydrous sodium sulphate. Evaporation of the solvent afforded **5** (0.72 g, 93% yield); ir (film) ν_{max}: 1747, 1248, 1105 cm^{-1}; δ (CCl_4): 4.82 (m, 1H, CH), 3.58 (t, 2H, J = 5 Hz, —CH_2O—), 1.94 (s, 3H, $COCH_3$), 1.37 (m, 10H, —CH_2—), 1.21 (d, 3H, J = 6 Hz, CH_3), 0.86 (s, 9H, $(CH_3)_3$C—), 0.00 (s, 6H, $(CH_3)_2$Si—).

7-O-*Acetyl-1,7-octanediol (**6**)*

A solution of **5** (1 g, 3.3 mmol), in acetic acid − water−tetrahydrofuran (3:1:1, 34 mL), was stirred at 25°C for 24 h. The reaction was poured into ice water (50 mL), extracted with methylene dichloride (2 × 30 mL), and washed with cold water (2 × 10 mL) and with cold 5% aqueous sodium hydrogen carbonate (2 × 5 mL). The extract was given a final water wash, dried over anhydrous sodium sulphate, and evaporated. Flash chromatography on silica gel, using ether − petroleum ether (30−60°C) (1:1) afforded **6** (0.52 g) in 84% yield, ir (film) ν_{max}: 3405, 1742, 1262, 1248 cm^{-1}; δ (CCl_4): 4.74 (m, 1H, CH), 3.74 (s, 1H, OH), 3.53 (t, 2H, J = 4 Hz, —CH_2O—), 1.91 (s, 3H, CH_3CO—), 1.39 (m, 10H, —CH_2—), 1.29 (d, 3H, J = 6 Hz, CH_3).

*7-Acetoxy-octanol (**7**)*

A solution of **6** (0.28 g, 1.48 mmol), in methylene dichloride (1 mL) was added to a stirred suspension of pyridinium chlorochromate (0.48 g, 2.23 mmol) in methylene dichloride (4 mL) under nitrogen atmosphere. After 2 h, at room temperature anhydrous ether (20 mL) was added and the supernatant decanted from the black gum. The insoluble residue was washed thoroughly with ether (3 × 50 mL) and the combined extracts filtered through a short column of Florisil. The eluent was evaporated to yield **7** (0.26 g) in 96% yield, ir (film) ν_{max}: 2982, 2735, 1752, 1728, 1378, 1248 cm^{-1}; δ (CCl_4): 9.83 (t, 1H, J = 2 Hz, CHO), 4.82 (m, 1H, —CH—), 2.37 (m, 2H, —CH_2—CHO), 1.93 (s, 3H, $COCH_3$), 1.42 (m, 10H, —CH_2—), 1.24 (d, 3H, J = 6 Hz, CH_3).

Methyl-9-acetoxy-(E)-*2-decenoate (**8**)*

Trimethylphosphonoacetate (0.46 g, 2.52 mmol) and sodium hydride (0.13 g of 50% dispersion) were stirred together in anhydrous tetrahydrofuran (10 mL), under N_2, at room temperature, for 40 min. A solution of **7** (0.47 g, 2.5 mmol), in tetrahydrofuran (2 mL) was added and the stirring continued for 1.5 h. Water (10 mL) was added to the reaction mixture and the mixture immediately neutralized with 2 *N* hydrochloric acid. The aqueous suspension was extracted with ether, the extract dried over anhydrous sodium sulphate and evaporated to a crude product (0.51 g). This material was subjected to flash chromatography on silica gel and elution with ether − petroleum ether (30 − 60°C) (1:4) yielded the diester **8** (0.41 g, 70%); ir (film) ν_{max}: 3005, 1745, 1718, 1655, 1240, 960 cm^{-1}; δ (CCl_4): 6.85 (d of t, J = 15 Hz, 6 Hz, CH_2—C*H*=CH—), 5.65 (d, 1H, J = 15 Hz, CH=C*H*—$COOCH_3$), 4.78 (m, 1H, —CH—), 3.92 (s, 3H, —$COCH_3$), 3.62 (s, 3H, —OCH_3), 2.22 (d, 2H, J = 7 Hz, CH_2—C=C), 1.38 (m, 8H, —CH_2—), 1.21 (d, J = 6 Hz, CH_3).

9-Hydroxy-(E)-*2-decenoic acid ((±)-**1**)*

The acetoxy ester **8** (0.8 g, 3.3 mmol) was stirred with 5% sodium hydroxide in methanol−water (1:1) (8 mL), at room temperature, for 12 h. Evaporation and dissolution in water (5 mL), washing with

TABLE 1. Analytical data

Compound	Analysis	Calcd. for	Found	Yield from immediate precursor	$[\alpha]_D^{23}$	Melting point
4 (±)	$C_{14}H_{32}O_2Si$	C 64.56, H 12.4	C 64.61, H 12.23	82	—	—
S-(+)			64.64 12.02	83	+3.7 (*c*, 2.43 EtOH)	—
R-(−)			64.65 12.12	79	−3.6 (*c*, 11.3 EtOH)	—
5 (±)	$C_{16}H_{34}O_3Si$	C 63.57, H 11.35	C 63.81, H 11.40	93	—	—
S-(+)			63.61 11.60	69	+0.8 (*c*, 4.64 EtOH)	—
R-(−)			63.68 11.35	88	−0.7 (*c*, 12.2 EtOH)	—
6 (±)	$C_{10}H_{20}O_3$	C 63.81, H 10.71	C 64.12, H 10.88	84	—	—
S-(+)			63.95 10.72	72	+1.5 (*c*, 4.53 EtOH)	—
R-(−)			63.74 10.86	86	−1.8 (*c*, 8.79 EtOh)	—
7 (±)	$C_{10}H_{18}O_3$	*		96	—	—
S-(+)		*		76	+2.9 (*c*, 3.48 EtOH)	—
R-(−)		*		86	−3.1 (*c*, 5.88 EtOH)	—
8 (±)	$C_{13}H_{22}O_4$	C 64.44, H 9.15	C 64.61, H 9.51	70	—	—
S-(+)			64.62 9.29	64	+2.1 (*c*, 6.16 EtOH)	—
R-(−)			64.68 9.30	67	−1.8 (*c*, 7.17 EtOH)	—
1 (±)	$C_{10}H_{18}O_3$	C 64.49, H 9.74	C 65.05, H 9.51	68	—	—
S-(+)			64.58 9.58	79	+5.2 (*c*, 7.61 EtOH)	—
R-(−)			64.35 9.76	91	−5.4 (*c*, 21.0 EtOH)	—
9 (±)	$C_{18}H_{23}BrO_4$	C 56.40, H 6.06	C 56.69, H 6.21	56	—	73−74†
S-(+)			56.41 6.22	53	+6.1 (*c*, 5.21 EtOH)	96−97†
R-(−)			56.37 6.19	57	−6.4 (*c*, 6.61 EtOH)	96−97†

*Difficulty was experienced obtaining consistent C, H analyses. High resolution mass spectrometry gave a weak, consistent $(M-1)^{\dagger\bullet}$ and a strong $(M—COCH_3)^{\dagger\bullet}$. Calcd. for $C_8H_{15}O_2$: 143.1072; found: 143.1070(±), 143.1066(+), 143.1072(−).

†The melting point of the racemate is lower than both enantiomers and in agreement with the reported melting point 73−74°C from hexane (cf. ref. 12).

methylene dichloride (2 × 5 mL), yielded an aqueous solution which was acidified with ice-cold 2 *N* hydrochloric acid (5 mL). Extraction with methylene dichloride (3 × 30 mL), washing with water (2 × 10 mL), and drying over sodium sulphate gave a solution which was evaporated to give the racemic 9-hydroxy-2-decenoic acid (0.42 g, 68% yield); ir (film) ν_{max}: 3385, 3005, 1705, 1662, 1425, 1292, 965 cm^{-1}; δ ($CDCl_3$): 7.21 (s, 2H, OH, COOH), 6.98 (d of t, 1H, J = 15 Hz, 6 Hz, CH_2—*CH*=CH), 5.77 (d, 1H, J = 15 Hz, C=*CH*—COOH), 3.89 (m, 1H, —CH—), 2.24 (d, 2H, J = 6 Hz, CH_2—C), 1.38 (m, 8H, —CH_2—), 1.22 (d, 3H, J = 6 Hz, CH_3).

p-*Bromophenacyl-9-hydroxy*-(E)-*2-decenoate* (***9***)

A sample of the hydroxy acid **1** (186 mg) was converted into its sodium salt with 5% aqueous sodium hydroxide to which 0.9 mmol of *p*-bromophenacyl bromide (286 mg) in ethanol (5 mL) was added. The solution was reflexed for 3 h, cooled, filtered, and recrystallized from hexane to give the derivative (215 mg).

S-(+)-*9-Hydroxy*-(E)-*2-decenoic acid* (*(±)-**1***)

The free acid was prepared as described for the racemic material, except for the substitution of anhydrous 1,2-dimethoxyethane as the solvent in the Wittig/Horner condensation. All physical properties of the intermediate enantiomeric materials were identical to those observed for the racemate (±)-**1** with the exception of the optical rotations and melting points of the derivatives. Table 1 summarizes the salient information.

R-*(−)-9-Hydroxy-(E)-Z-decenoic acid* (*(−)-**1***)

The laevorotatory isomer was prepared in a manner identical to the racemate (Table 1).

Acknowledgements

We thank the Natural Sciences and Engineering Research Council of Canada for financial support (Operating Grant A3785) and K. Berkinshaw for technical assistance.

1. R. K. CALLOW, J. R. CHAPMAN, and P. N. PATON. J. Apic. Res. **3**, 77 (1964).
2. R. BOCH, D. A. SHEARER, and J. C. YOUNG. J. Chem. Ecol. **1**, 133 (1975).
3. (*a*) J. H. BORDEN, J. R. HANDLEY, J. A. MCLEAN, R. M. SILVERSTEIN, L. CHONG, K. N. SLESSOR, B. D. JOHNSTON, and H. R. SCHULER. J. Chem. Ecol. **6**, 445 (1980); (*b*) D. M. LIGHT and M. L. BIRCH. Naturwissenshaften, **66**, 159 (1979); (*c*) R. T. CARDE, C. C. DOANE, T. C. BAKER, S. IWAKI, and S. MARUMO. Environ. Entomol. **6**, 768 (1977).
4. R. ROSSI. SYNTHESIS, 413 (1978).
5. B. D. JOHNSTON and K. N. SLESSOR. Can. J. Chem. **57**, 233 (1979).
6. B. SEURING and D. SEEBACH. Helv. Chim. Acta, **60**, 1175 (1977).
7. G. H. POSNER. An introduction to synthesis using organocopper reagents. John Wiley and Sons, New York. 1980. p. 107.
8. C. HUYNH, F. DERGUINI-BOUMECHAL, and G. LINSTRUMELLE. Tetrahedron Lett. 1503 (1979).
9. K. HINTZER, R. WEBER, and V. SCHURIG. Tetrahedron Lett. **22**, 55 (1981).
10. M. E. SYNERHOLM. J. Am. Chem. Soc. **69**, 2581 (1947).
11. E. J. COREY and A. VENKATESWARLU. J. Am. Chem. Soc. **94**, 6190 (1972).
12. W. H. BROWN, E. E. FELAUER, and M. V. SMITH. Can. J. Chem. **40**, 1882 (1962).
13. M. L. WINSTON, K. N. SLESSOR, M. J. SMIRLE, and A. A. KANDIL. J. Chem. Ecol. **8**, 1283 (1982).
14. W. C. STILL, M. KAHN, and A. MITRA. J. Org. Chem. **43**, 2923 (1978).
15. H. O. HOUSE and M. J. UMEN. J. Org. Chem. **38**, 3893 (1973).

Can. J. Chem. Downloaded from www.nrcresearchpress.com by 210.87.254.42 on 09/06/12
For personal use only.

Enchaînements hétéroatomiques et leurs produits de cyclisation. VI.[1] Nouvelle synthèse de céphèmes: acétyl-3 méthyl-7 phtalimido-7 oxo-8 thia-5 aza-1 bicyclo[4.2.0]octènes-2 diastéréomères

JEAN-CLAUDE ROZÉ, JEAN-PAUL PRADERE, GUY DUGUAY, ANDRÉ GUEVEL ET HERVÉ QUINIOU[2]
Laboratoire de Chimie Organique 2, 2, rue de la Houssinière, 44072 Nantes, France

ET

SERGE POIGNANT
Laboratoire de Chimie Organique Physique, ERA CNRS 315, 2, rue de la Houssinière, 44072 Nantes, France

Reçu le 5 août 1982

JEAN-CLAUDE ROZÉ, JEAN-PAUL PRADERE, GUY DUGUAY, ANDRÉ GUEVEL, HERVÉ QUINIOU et SERGE POIGNANT. Can. J. Chem. **61**, 1169 (1983).

La synthèse totale de deux céphèmes diastéréomères est décrite avec trois étapes particulièrement originales: synthèse du cycle thiazinique-1,3 par cycloaddition (4+2), hydrogénations régiosélectives de la double liaison carbone–azote et lactamisation, en présence de BOP, avec d'excellents rendements.

JEAN-CLAUDE ROZÉ, JEAN-PAUL PRADERE, GUY DUGUAY, ANDRÉ GUEVEL, HERVÉ QUINIOU, and SERGE POIGNANT. Can. J. Chem. **61**, 1169 (1983).

The total synthesis of two diastereomeric cephems is described with three original steps in excellent yields: construction of the 1,3-thiazine ring via a (4+2) cycloaddition reaction, regioselective hydrogenation of the carbon–nitrogen double bond, and lactamization using BOP.

Can. J. Chem. Downloaded from www.nrcresearchpress.com by 210.87.254.40 on 09/06/12
For personal use only.

Introduction

L'accès aux céphèmes et céphalosporines par synthèse totale est conditionné par une double cyclisation: celle du β-lactame et celle du cycle thiazinique. Les deux cycles ont leurs difficultés de construction propres mais aussi relatives: l'ordre dans lequel il est préférable de les construire n'est pas évident.

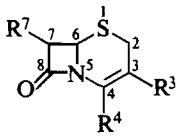

Céphèmes (céphalosporines: R^3 = substituant variable, R^4 = CO_2H, R^7 = RCONH)

Les travaux récents (2) ont généralement donné la préférence à l'ordre (*i*) lactame (*ii*) dihydrothiazine. Cette stratégie permet d'introduire au départ (et dans le meilleur des cas de conserver) la bonne stéréochimie autour des carbones 6 et 7. Elle exclut néanmoins, entre autre, l'usage ultérieur de réactifs nucléophiles susceptibles d'ouvrir le cycle lactamique. L'alternative, (*i*) dihydrothiazine (*ii*) lactame, a été suivie avec succès par Heymes *et al.* (3). Au total cette voie a été moins explorée sans doute en raison du caractère aléatoire prêté à une lactamisation placée à la fin d'une longue synthèse.

Nous avons eu l'occasion d'accéder aux thiazines par une réaction très générale de cycloaddition (4+2) (4).

A partir de ces thiazines convenablement substituées pour conduire aux céphèmes (et ultérieurement aux céphalosporines), il était tentant de mettre en oeuvre la seconde stratégie évoquée ci-dessus et notamment d'éprouver l'une des étapes qui pouvait sembler la plus délicate: l'hydrogénation

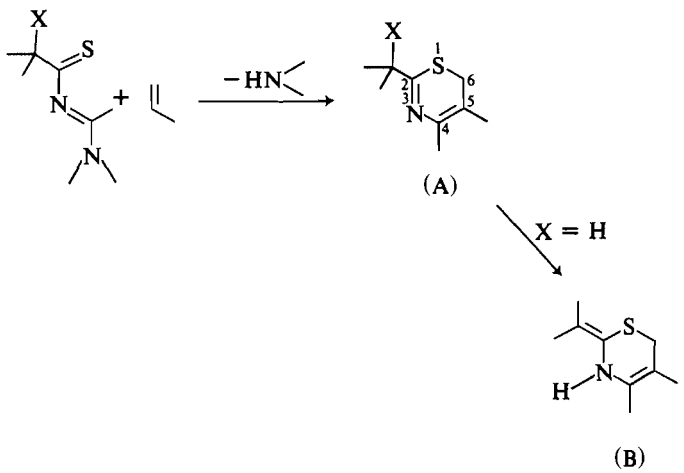

(B)

régiosélective de la thiazine sans ouverture de cycle. Un regain d'intérêt pour cette voie nous semblait aussi justifié par de nouvelles facilités offertes par le récent foisonnement des modes de couplage acide–amine que l'on relève en synthèse peptidique et que l'on peut espérer étendre aux lactames.

Les premiers essais d'hydrogénation pratiqués sur des modèles ont donné des résultats plus satisfaisants sur les structures de type (A) que sur les structures tautomères de type (B). Dans les réactions relatées ci-après nous avons donc maintenu les deux doubles liaisons dans le cycle en substituant le futur carbone 7 par un méthyle (A, X = CH_3).

Résultats

La nitrosation du cyanacétate de méthyle, obtenue avec un rendement de 85%, est suivie de l'hydrogénation de l'oxime **1** par l'amalgame d'aluminium dans le méthanol à 95% (Schéma 1). L'aminoester est traité par l'anhydride phtalique fournissant le cyano-2 phtalimido-2 acétate de méthyle **2**. Le rendement cumulé des deux étapes est de 50%. Les meilleurs rendements

[1]Mémoire précédent V, voir réf. 1.
[2]Auteur à qui adresser la correspondance.

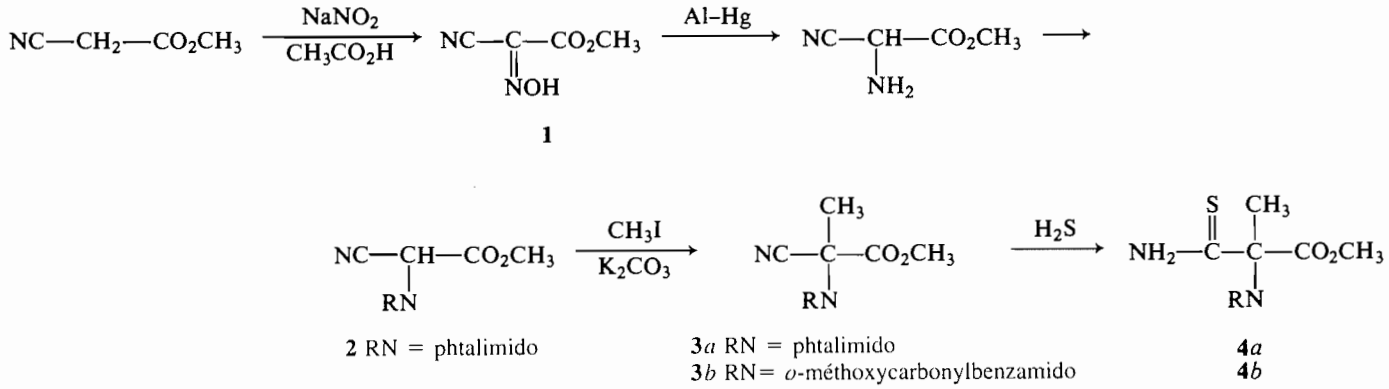

SCHÉMA 1

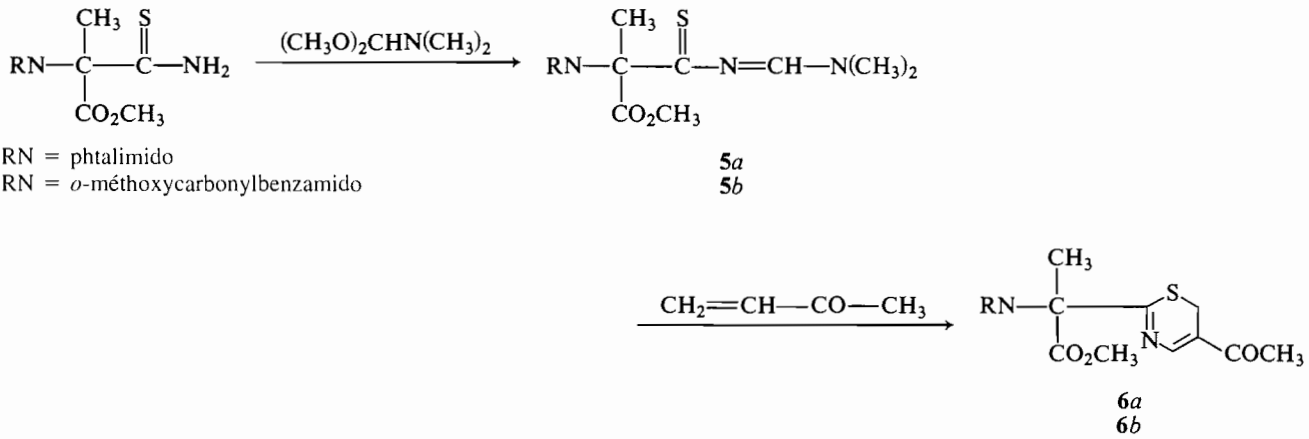

SCHÉMA 2

de méthylation (80%) sont obtenus en traitant par l'iodure de méthyle en excès l'ester-nitrile **2** en solution dans l'acétone anhydre, en présence de carbonate de potassium. A ce stade on peut provoquer l'ouverture du groupement phtalimido de **3***a* en dérivé *o*-méthoxycarbonylbenzamido **3***b* par action du méthanol en présence de triéthylamine. L'addition d'hydrogène sulfuré sur le groupement nitrile de **3***a* et **3***b* fournit les thioamides-esters correspondants **4***a* et **4***b* (80%).

La condensation de **4***a* sur le diméthylacétal du diméthylformamide, dans le benzène (Schéma 2) permet d'isoler la thioacylformamidine substitutée **5***a* (87%). A température ambiante, en solution benzénique, **5***a* réagit sur la méthylvinylcétone conduisant à la thiazine **6***a* (80%). Comme précédemment, la semi-alcoolyse de **6***a* par le méthanol, en présence de triéthylamine, convertit ce composé en son produit d'ouverture du groupement imide **6***b*. Ce produit **6***b* peut aussi être obtenu parallèlement à la voie précédente: réaction du thioamide **4***b* avec le diméthylacétal du diméthylformamide donnant **5***b* (87%) puis cyclisation de **5***b* sur la méthylvinylcétone aboutissant comme précédemment à **6***b* (80%).

La réduction de **6***a* par l'amalgame d'aluminium (Schéma 3) fournit trois composés. L'un d'entre eux **8** correspond à une double hydrogénation portant sur l'un des carbonyles du groupement phtalimido et sur la liaison C=N du cycle thiazinique. Les deux autres composés **9** (5) et **10** résultent vraisemblablement d'une élimination basique avant ou après réduction de l'un des carbonyles du groupement phtalimido. Ces complications nous avaient conduit à ouvrir le cycle phtalimido au niveau de **3***a* afin de rendre le carbonyle amidique restant moins réductible. Dans ce cas on observe effectivement la réduction régiosélective de **6***b* en **7***b* avec un rendement global de 95%. Nous avons séparé les deux racémates diastéréomères obtenus (*F* 112–114° et 182–184°C). La configuration de ces esters et des acides correspondants a été établie, comme il sera indiqué par la suite, à partir des lactames en dérivant.

Le cyanoborohydrure de sodium opposé à **6***a* et **6***b* apparaît comme un hydrogénant régiosélectif de la liaison C=N. Les composés **6***a* et **6***b* fournissent respectivement **7***a* et **7***b* (Schéma 4). Les rendements ne dépassent pas 45 à 50%. Dans les conditions expérimentales utilisées, il reste environ la moitié du composé initial qui n'as pas réagi quelle que soit la quantité d'hydrogénant. L'hydrogénation de **6***a* a aussi été effectuée par le triéthylsilane en présence d'acide trifluoroacétique: on obteint **7***a* avec un rendement de 86%.

A propos des saponifications décrites ci-après, on doit faire les remarques préliminaires suivantes. En plus de l'hydrolyse des fonctions esters de **7***a* et **7***b* (Schéma 5), on observe l'ouverture du groupement phtalimido de **7***a* (en *o*-carboxybenzamido) et une épimérisation au niveau du carbone 2. L'un ou l'autre des diesters **7***b* (ou leur mélange ou encore **7***a*) est saponifié par la lithine aqueuse 4 *N* dans le tétrahydrofuranne. Quel que soit le diester ou le monoester de départ, on obtient le mélange de deux diacides **11** approximativement dans le même rapport (Rdt global 95%).

Du mélange d'acides totalement solubles à chaud (acétone – acétate d'éthyle 50:50), le racémique *cis* (6*RS*, 7*RS*)[3] précipite

[3]Afin de faciliter l'exposition des résultats, la numérotation des atomes adoptée ici pour les esters et les acides est celle des céphèmes.

Can. J. Chem. Downloaded from www.nrcresearchpress.com by 210.87.254.40 on 09/06/12
For personal use only.

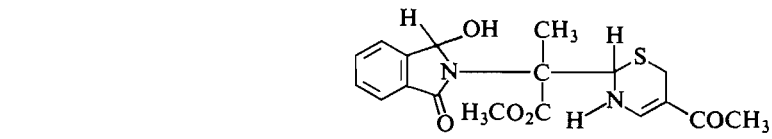

8

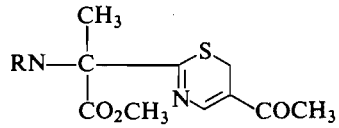

6a RN = phtalimido

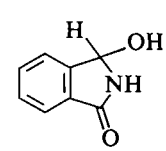

9

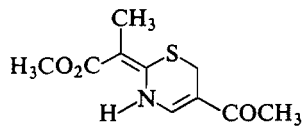

10

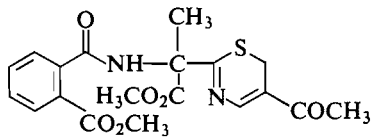

6b

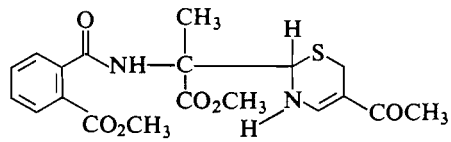

7b

SCHÉMA 3

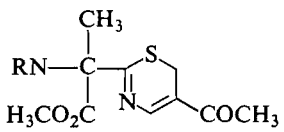

6a RN = phtalimido
6b

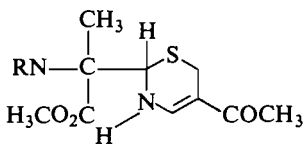

7a
7b

SCHÉMA 4

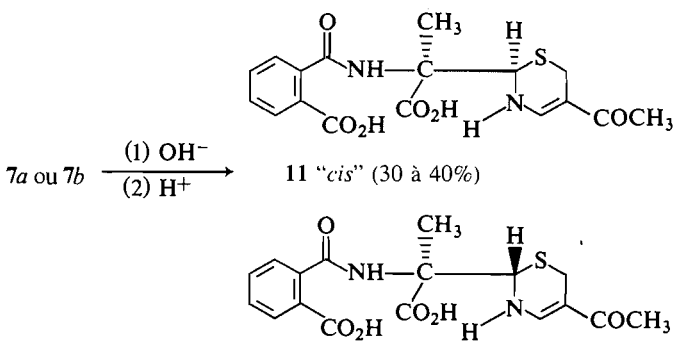

11 "*cis*" (30 à 40%)

11 "*trans*" (60 à 70%)

SCHÉMA 5

d'abord. En alcalinisant les eaux-mères, on peut provoquer une épimérisation partielle *trans*–*cis* et cristalliser, après acidification, une seconde fraction de racémique *cis*, etc...

La lactamisation des acides ci-dessus est accompagnée de la fermeture du substituant *o*-carboxybenzamido en groupement phtalimido. En opérant cette double cyclisation en présence de dicyclohexylcarbodiimide (DCC), dans une solution à parts égales de nitrométhane et de dichlorométhane, les rendements ne dépassent pas 20%. Les rendements ont été portés à 80% en employant l'hexafluorophosphate de benzotriazol-1-yl-oxy-tris(diméthylamino) phosphonium (BOP), agent de couplage intermoléculaire acide–amine utilisé en synthèse peptidique (6).

La lactamisation d'un mélange d'acides *cis*–*trans* (30:70) donne un mélange de céphèmes dans les mêmes proportions. L'acide *cis* pur donne un seul lactame **12** (6*RS*, 7*RS*) identifié comme étant l'isomère *cis* par effect nOe. L'irradiation du méthyle en position 7 produit un effect Overhauser nucléaire de

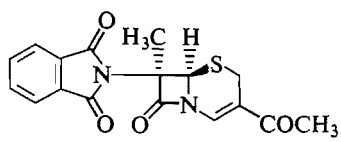

+ Enantiomère
12 "*cis*" (6*RS*, 7*RS*)

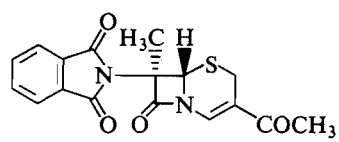

+ Enantiomère
12 "*trans*" (6*SR*, 7*RS*)

20% sur le proton lié au carbone 6. Le lactame diastéréomère **12** (6*SR*, 7*RS*) n'a pas été complètement purifié mais nous nous sommes assurés que son irradiation dans le mélange ne permettait pas de déceler d'effet nOe (7).

Comme on l'a remarqué, un diacide pur conduit par lactamisation à un céphème pur. L'autre diacide majoritaire dans un mélange conduit à l'autre céphème dans un mélange sous le même rapport. L'hypothèse d'une inversion complète de la configuration du carbone 6 en cours de lactamisation, inversion complète quelle que soit le configuration initiale *R* ou *S* étant peu vraisemblable, on a pu, à partir des céphèmes, attribuer les configurations des acides. Les attributions structurales (Tableau 1) ont été faites à partir d'enregistrements rmn du proton à 250 MHz en s'aidant du découplage homonucléaire.

En suivant la voie ascendante on peut aussi remarquer la similitude des déplacements chimiques des protons 6 du céphème *cis* et de l'ester **7***a* fondant à 195–200°C (5,19 ppm et 5,21 respectivement). Cet ester serait donc aussi *cis*. On peut faire la même observation relativement à leurs diastéréomères (5,36 ppm et 5,40 respectivement). L'ester **7***a* non isolé du mélange serait donc *trans*.

Can. J. Chem. Downloaded from www.nrcresearchpress.com by 210.87.254.40 on 09/06/12
For personal use only.

TABLEAU 1. Déplacements chimiques ^1H en ppm; constantes de couplage (Hz) (température: 25°C; référence: TMS; solvant CD_3COCD_3)*

Composés	$CH_3(7)$	$COCH_3(3)$	$CO_2CH_3(7)$	$CO_2CH_3(\phi)$	$CH_2(2)$	CH(4) $J(4-5)$	NH(5) $J(5-6)$	CH(6)	NH(7)		
										syst ABCD	
Ester **7***a* *cis*	2,01	2,06	3,76		3,40	7,66 (6,8)	6,76 (3,8)	5,21		7,89	
										syst ABCD	
Ester **7***a* *trans*	1,91	2,12	3,72		3,50	7,76 (6,75)	7,10 (4,6)	5,40		7,90	
										syst ABC	X
Diester **7***b* *cis*	1,68	2,10	3,78	3,82	3,56	7,74 (6,5)	7,10 (3,4)	5,06	8,16	7,56	7,81
										syst ABC	X
Diester **7***b* *trans*	1,69	2,12	3,76	3,82	3,50	7,76 (6,6)	7,04 (4)	5,18	8,08	7,58	7,76
										syst ABC	X
Diacide **11** *cis*	1,76	2,10			3,54	7,63 (6,6)	7,18 (3,4)	5,16	8,10	7,56	7,94
										syst ABC	X
Diacide **11** *trans*	1,78	2,13			3,52	7,68 (6,8)	7,16 (4)	5,20	8,11	7,62	7,92
										syst ABCD	
Céphème **12** *cis*	2,17	2,38			3,60	7,90		5,19		7,90	
										syst ABCD	
Céphème **12** *trans*	1,96	2,38			3,64	7,97		5,36		7,90	

*Voir la note no. 3 en bas de page 1170.

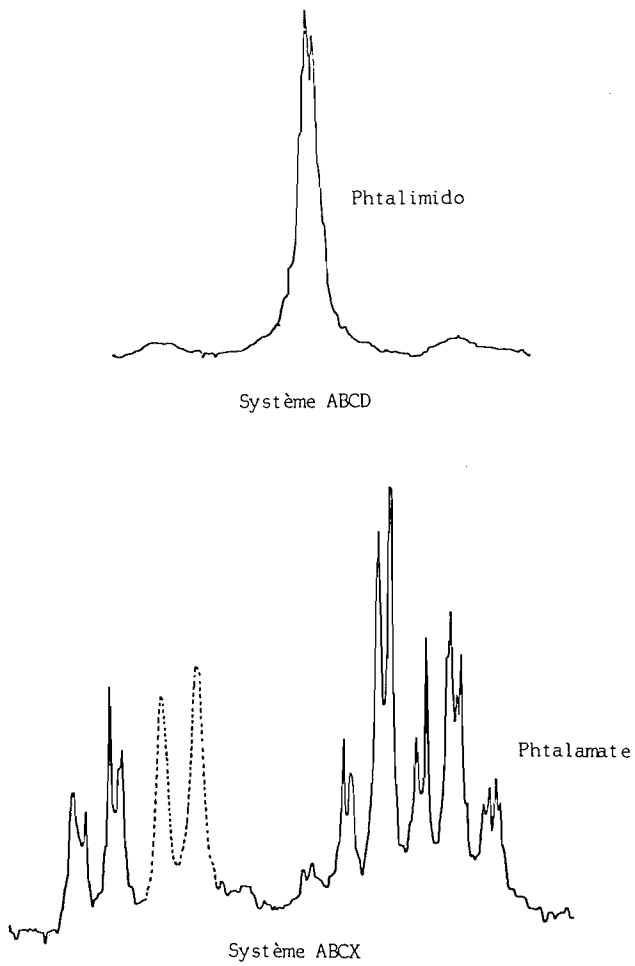

FIG. 1.

La similitude des couplages $J(5-6)$ entre les diacides et leurs diesters: 4 Hz d'une part permet d'attribuer la configuration *trans* à l'ester **7***b* fondant à 112–114°C, 3,4 Hz d'autre part permet d'attribuer la configuration *cis* à l'ester fondant à 182–184°C.

Notons aussi que l'ouverture du groupement phtalimido (méthanolyse et hydrolyse) est facilement repérée par rmn. La figure 1 montre les résonances comparées du cycle aromatique sous les deux formes: forme fermée phtalimido (système ABCD) et forme ouverte phtalamate N-substitué (système ABCX).

Conclusion

En résumé la rmn du proton (250 MHz) a permis d'établir les structures des précurseurs des céphèmes et des céphèmes eux-mêmes avec les configurations de leurs carbones asymétriques. La synthèse utilisée, originale à divers titres, peut être considérée comme stéréospécifique relativement à la production du racémique correspondant à la série naturelle active. En effet l'acide **11** *cis* moins soluble que son épimère peut être facilement isolé du mélange **11** *cis* + **11** *trans*. La solution acide, appauvrie en **11** *cis*, peut être rééquilibrée en milieu alcalin, une deuxième fraction de **11** *cis* précipite par acidification, etc... Finalement l'acide **11** *cis* est cyclisé en phtalimido-7 céphème, par l'intermédiare de BOP, avec de bons rendements et sans nouvelle épimérisation décelable.

Nous projetons d'utiliser les enseignements consignés dans ce mémoire à la synthèse de céphèmes méthoxylés en position 7 et des céphalosporines correspondantes (céphamycines). Les équivalents méthoxylés des composés **3**, inconnus à l'époque à laquelle nous avons commencé ce travail, ont été synthétisés dans l'intervalle dans notre laboratoire.

Partie expérimentale

Les points de fusion ont été déterminés à l'aide d'un microscope

Can. J. Chem. Downloaded from www.nrcresearchpress.com by 210.87.254.40 on 09/06/12
For personal use only.

Can. J. Chem. Downloaded from www.nrcresearchpress.com by 210.87.254.40 on 09/06/12
For personal use only.

Reichert à platine chauffante Kofler. Les chromatographies ont été effectuées sur des colonnes d'alumine neutre Prolabo désactivée par 5% d'eau ou sur gel de silice Merck (Kieselgel 60, 70–230 mesh ASTM). Les spectres ir ont été enregistrés sur un spectrophotomètre Unicam SP 1100. Les mesures sont faites sur les substances dispersées dans le bromure de potassium. Les spectres de rmn ont été enregistrés sur des spectromètres Perkin–Elmer R-24-B (60 MHz), Varian XL 100 et Cameca 250 MHz. Les spectres de masse ont été enregistrés sur un spectromètre Varian-mat à double focalisation (énergie d'ionisation: 70 eV).

Cyano-2 oximino-2 acétate de méthyle ***1***

Ce composé a été préparé suivant le mode opératoire décrit dans l'une de nos publications (4). Après cristallisation dans le benzène, on obtient des cristaux blancs fondant à 124°C, Rdt = 85%. *Anal.* calc. pour $C_4H_4N_2O_3$: C 37,50, H 3,15, N 21,87; tr.: C 37,63, H 3,00, N 21,94.

Amino-2 cyano-2 acétate de méthyle et cyano-2 phtalimido-2 acétate de méthyle ***2***

L'amalgame d'aluminium nécessaire au traitement de 12,8 g (0,1 mol) d'oxime **1** est préparé à partir de 4 g de métal (0.15 mol) recouvert d'une solution aqueuse de 5% de chlorure mercurique. On laisse réagir 5 à 7 min puis on décante. L'amalgame obtenu est lavé deux fois par de l'eau puis deux fois par le minimum de méthanol. On y ajoute alors 150 cm^3 de méthanol, 12,8 g d'oxime et 5 cm^3 d'eau. L'agitation est maintenue jusqu'à refroidissement du mélange réactionnel (environ 30 min) puis on filtre. Le résidu solide est lavé par de l'acétate d'éthyle. Après concentration, le filtrat fournit environ 10 g d'une huile jaune. L'amino-2 cyano-2 acétate de méthyle obtenu, peu stable, est aussitôt dissous dans 100 cm^3 de toluène. On y ajoute 0,9 cm^3 de triéthylamine et 15 g d'anhydride phtalique (0,1 mol). Le mélange réactionnel est porté à reflux à l'aide d'un bain d'huile préalablement chauffé à 180°C. Le reflux est maintenu 15 min, on filtre le contenu du ballon encore chaud et on concentre le filtrat. Le précipité cristallin obtenu est traité par environ 200 cm^3 d'eau bouillante afin d'éliminer l'anhydride phtalique en excès. Après essorage, le produit est cristallisé dans le méthanol. On obtient des cristaux blancs fondant à 139–141°C, Rdt de 50% sur l'ensemble des 2 réactions; ir: 2270 (C≡N), 1780 et 1730 (C=O phtalimido), 1768 (C=O ester) cm^{-1}; rmn ($CDCl_3$) δ: 3,98 (s, 3H, OCH_3), 5,90 (s, 1H, CH), 7,93 (s, 4H, phtalimido); sm *m/e*: 244 $(M)^{\ddagger}$, 200, 185 ($Pht\overset{+}{N}{=}CH{-}C{\equiv}N$), 160 ($Pht\overset{+}{N}{=}CH_2$), 132, 104 ($C_6H_4{-}C{\equiv}\overset{+}{O}\cdot$), 76 (benzyne). *Anal.* calc. pour $C_{12}H_8N_2O_4$: C 59,02, H 3,30; tr.: C 59,50, H 3,55.

Cyano-2 phtalimido-2 propionate de méthyle ***3***a

Dans un ballon surmonté d'un réfrigérant à reflux et contenant 13,8 g (0,1 mol) de carbonate de potassium en suspension dans 100 cm^3 d'acétone anhydre, on ajoute 0,1 mol de composé **2** à méthyler. Après 15 min d'agitation à température ambiante, on ajoute un léger excès d'iodure de méthyle puis on chauffe sous reflux pendant 1 h. Après refroidissement, le mélange réactionnel est filtré. Le précipité est lavé par de l'acétone. Après évaporation du filtrat, le résidu est dissous dans le minimum de benzène que l'on filtre à travers une colonne de gel de silice (h = 20 cm, ϕ = 1,5 cm, éluant: benzène). Après cristallisation dans le méthanol, on obtient des cristaux blancs fondant à 113°C, Rdt = 80%; ir: 1782 et 1725 (C=O phtalimido), 1760 (C=O ester) cm^{-1}; rmn ($CDCl_3$) δ: 2,27 (s, 3H, CH_3—C), 3,93 (s, 3H, OCH_3), 7,99 (s, 4H, phtalimido); sm *m/e*: 258 $(M)^{\ddagger}$, 214, 199 ($Pht\overset{+}{N}{=}C(CH_3)CN$), 172 ($Pht\overset{+}{N}{=}C{=}CH_2$), 132, 104 ($C_6H_4{-}C{\equiv}\overset{+}{O}\cdot$), 76. *Anal.* calc. pour $C_{13}H_{10}N_2O_4$: C 60,46, H 3,90, N 10,85; tr.: C 60,45, H 3,91, N 10,96.

Cyano-2 o*-méthoxycarbonylbenzamido-2 propionate de méthyle* ***3***b

A 14,5 g (0,05 mol) de ***3a*** dissous dans 30 cm^3 de méthanol, on ajoute 0,8 cm^3 de triéthylamine. On chauffe le mélange sous reflux pendant 1 h. Après évaporation des solvants, le résidu est chromatographié sur gel de silice (éluant: éther de pétrole – acétate d'éthyle 75:25). On obtient des cristaux blancs (acétate d'éthyle – éther diéthylique) fondant à 104–106°C, Rdt = 79%. *Anal.* calc. pour $C_{14}H_{14}N_2O_5$: C 57,92, H 4,86, N 9,65; tr.: C 57,74, H 4,84, N 9,46.

Amino-3 méthyl-2 phtalimido-2 thioxo-3 propionate de méthyle ***4***a

On fait barboter pendant 4 h, à température ambiante, de l'hydrogène sulfuré dans une solution de 12 g (0,04 mol) de **3** dans 80 cm^3 de pyridine et 40 cm^3 de triéthylamine. L'hydrogène sulfuré en excès est éliminé sous le vide partiel de la trompe à eau. La solution est concentrée et reprise plusieurs fois par du toluène pour éliminer totalement la pyridine. Le précipité blanc-rougeâtre ainsi obtenu peut être purifié éventuellement sur une colonne de gel de silice (élimination de soufre). La cristallisation dans le benzène ou l'acétate d'éthyle fournit des cristaux blancs fondant à 194–199°C, Rdt = 80%; ir: 3350 et 3180 (NH_2 thioamide), 1782 et 1725 (C=O phtalimido), 1750 (C=O ester) cm^{-1}; rmn (DMSO) δ: 2,09 (s, 3H, CH_3—C), 3,75 (s, 3H, OCH_3), 7,85 (s, 4H, phtalimido), 9,40 et 10,04 (2s, 2H, NH_2); sm *m/e*: 292 $(M)^{\ddagger}$, 233 ($Pht\overset{+}{N}{=}C(CH_3){-}CSNH_2$), 201, 172 ($Pht\overset{+}{N}{=}C{=}CH_2$), 132, 104 ($C_6H_4{-}C{\equiv}\overset{+}{O}\cdot$), 76, 58, 50, 43. *Anal.* calc. pour $C_{13}H_{12}N_2O_4S$: C 53,41, H 4,14, N 9,58, S 10,97; tr.: C 53,44, H 4,15, N 9,60, S 11,00.

Amino-3 méthyl-2 o*-méthoxycarbonylbenzamido-2 thioxo-3 propionate de méthyle* ***4***b

A 11,3 g de ***4a*** dissous dans 25 cm^3 de méthanol, on ajoute 0,5 cm^3 de triéthylamine. Le mélange est chauffé sous reflux et agitation pendant 1 h. Après évaporation des solvants, le résidu est chromatographié sur gel de silice (éluant: chloroforme – éther diéthylique 50:50). Après cristallisation dans le méthanol, on obtient ***4b*** sous forme de cristaux blancs fondant à 150–154°C. Rdt = 70%. Le composé ***4b*** est aussi obtenu par addition d'hydrogène sulfuré sur ***3b*** selon le même mode opératoire que celui décrit pour la préparation du thioamide-ester ***4a***, Rdt 80%; ir: 3370, 3280, 3200 (NH amide et NH_2 thioamide), 1730 et 1705 (C=O ester), 1660 (C=O amide) cm^{-1}; rmn (DMSO) δ: 1,86 (s, 3H, CH_3—C), 3,71 et 3,80 (2s, 6H, 2 OCH_3), 7,70 (s, 4H, benzamide), 8,83 (s, 1H, NH), 9,25 et 10,30 (2s, 2H, NH_2); sm *m/e*: 324 $(M)^{\ddagger}$, 163, 102, 77, 76, 55, 44, 43, 42, 41. *Anal.* calc. pour $C_{14}H_{16}N_2O_5S$: C 51,84, H 4,97, N 8,64, S 9,89; tr.: C 52,08, H 4,75, N 8,67, S 9,84.

(N,N-diméthylaminométhylène)amino-3 méthyl-2 phtalimido-2 thioxo-3 propionate de méthyle ***5***a

Le mode opératoire utilisé est celui décrit par Weidinger et Eilingsfeld (8). Des quantités équimoléculaires du diméthylacétal du diméthylformamide et du thioamide-ester précédent ***4a*** dissous dans le chloroforme sont maintenues sous agitation, à température ambiante, pendant 2 h. Après évaporation de la majeure partie du solvant, on filtre sur colonne de gel de silice en éluant par un mélange benzène – acétate d'éthyle 80:20. La cristallisation dans le méthanol donne des cristaux jaunes fondant à 156–159°C, Rdt 87%; ir: 1770 et 1720 (C=O phtalimido), 1738 (C=O ester), 1622 (C=N) cm^{-1}; rmn ($CDCl_3$) δ: 2,31 (s, 3H, CH_3—C), 2,95 et 3,19 (2s, 6H, $N(CH_3)_2$), 3,80 (s, 3H, OCH_3), 7,75 (s, 4H, phtalimido), 8,49 (s, 1H, N=CH); sm *m/e*: 347 $(M)^{\ddagger}$, 199 ($Pht\overset{+}{N}{=}C(CH_3)CN$), 172 ($Pht\overset{+}{N}{=}C{=}CH_2$), 115 ($\overset{+}{S}{\equiv}C{-}N{=}CH{-}N(CH_3)_2$), 44. *Anal.* calc. pour $C_{16}H_{17}N_3O_4S$: C 55,32, H 4,93, N 12,10, S 9,23; tr.: C 55,51, H 4,93, N 12,22, S 9,13.

(N,N-diméthylaminométhylène)amino-3 o*-méthoxycarbonylbenzamido-2 méthyl-2 thioxo-3 propionate de méthyle* ***5***b

Ce composé est obtenu à partir de ***4b*** selon de mode opératoire ci-dessus. Il a été purifié par chromatographie sur gel de silice (éluant: éther diéthylique – acétate d'éthyle 50:50). Après cristallisation dans un mélange éther de pétrole – acétate d'éthyle, on obtient des cristaux jaunes fondant à 126–127°C, Rdt 87%; ir: 3300 (NH), 1755 et 1735 (C=O ester), 1665 et 1635 (C=O amide) cm^{-1}; rmn ($CDCl_3$) δ: 1,90 (s, 3H, CH_3—C), 3,08 et 3,20 (2s, 6H, $N(CH_3)_2$), 3,69 et 3,81 (2s, 6H, 2 OCH_3), 7,48 (m, 3H, benzamido), 7,71 (m, 1H, benzamido), 8,39 et 8,52 (2s, 2H, NH et N=CH); sm *m/e*: 379 $(M)^{\ddagger}$, 163, 115, 77, 44, 42. *Anal.* calc. pour $C_{17}H_{21}N_3O_5S$: C 53,81, H 5,58, S 8,45; tr.: C 53,90, H 5,60, S 8,31.

Can. J. Chem. Downloaded from www.nrcresearchpress.com by 210.87.254.40 on 09/06/12
For personal use only.

*(Acétyl-5 6*H*-thiazine-1,3 yl-2)-2 phtalimido-2 propionate de méthyle* **6***a*

A 4 g de **5***a* en solution dans 30 cm^3 de benzène anhydre, on ajoute 0,1 g d'hydroquinone et 2 cm^3 de méthylvinylcétone fraîchement distillée. On chauffe sous reflux et agitation pendant 2 h puis on ajoute de nouveau un excès de diénophile (2 cm^3) en maintenant l'agitation et le chauffage. L'évolution de la réaction est contrôlée par chromatographie sur couches minces. On répète au besoin l'addition précédente jusqu'à disparition de **5***a*. L'évaporation du solvant sous pression réduite puis la chromatographie sur colonne de gel de silice, élution benzène – acétate d'éthyle 90:10, fournissent une huile jaune qui cristallise dans le méthanol ou l'éther diéthylique. On obtient des cristaux jaunes fondant à 155–157°C, Rdt 80%; ir: 1780 et 1723 (C=O phtalimido), 1760 (C=O ester), 1660 (C=O cétone), 1605 (cycle thiazinique) cm^{-1}; rmn ($CDCl_3$) δ: 2,21 (s, 3H, CH_3—C), 2,40 (s, 3H, CH_3CO), 3,66 (s, 2H, CH_2), 3,88 (s, 3H, OCH_3), 7,90 (s, 1H, CH en position 4 du cycle thiazinique), 7,90 (s, 4H, phtalimido); sm *m/e*: 372 $(M)^{\ddagger}$, 225 (M − PhtNH), 200, 193, 172 ($PhtN^{+}{=}C{=}CH_2$), 165, 145, 85, 71, 69, 57, 45, 43. *Anal.* calc. pour $C_{18}H_{16}N_2O_5S$: C 58,05, H 4,33, S 8,61; tr.: C 58,01, H 4,58, S 8,54.

*(Acétyl-5 6*H*-thiazine-1,3 yl-2)-2* o*-méthoxycarbonylbenzamido-2 propionate de méthyle* **6**b

Le mode opératoire est analogue au précédent mais on a procédé à température ambiante en 72 h d'agitation. Le produit brut a été chromatographié sur colonne de gel de silice (éluant: chloroforme – éther diéthylique 90:10). Le composé **6***b* est obtenu sous forme d'une huile jaune, Rdt 80%; ir: 3370 (NH), 1745 (C=O ester), 1675 (C=O amide) cm^{-1}; ir (CCl_4): 3400 (NH), 1745 (C=O ester), 1675 (C=O amide) cm^{-1}; rmn ($CDCl_3$) δ: 2,04 (s, 3H, CH_3—C), 2,40 (s, 3H, CH_3CO), 3,56–3,64 (m, 2H, CH_2), 3,84 et 3,86 (2s, 6H, OCH_3), 7,36–7,60 (m, 3H, benzamido), 7,72 (s, 1H, NH), 7,78–7,94 (m, 1H, benzamido et H en position 4); sm *m/e*: 404 $(M)^{\ddagger}$, 225, 163, 77, 43.

Hydrogénation de **6**a *par l'amalgame d'aluminium: (acétyl-5 dihydro-3,6 2*H*-thiazine-1,3 yl-2)-2 (hydroxy-3 phtalimidino)-2 propionate de méthyle* **8***, hydroxy-3 phtalimidine* **9** *et (acétyl-5 dihydro-3,6 2*H*-thiazine-1,3 ylidène-2)-2 propionate de méthyle* **10**

A 0,108 g (0,004 mol) d'aluminium décapé au préalable par le chlorure mercurique, on ajoute 0,372 g (0,001 mol) de **6***a* dissous dans 9 cm^3 de méthanol à 96% et 3 cm^3 de benzène. On agite 1 h à température ambiante. On filtre puis lave le précipité avec du méthanol. On évapore le filtrat puis on reprend le résidu par du benzène. Le composé **8** précipite déjà de cette solution benzénique. Le nouveau filtrat est chromatographié sur gel de silice (éluant: éther diéthylique – acétate d'éthyle 50:50).

8 (2 isomères) se présente sous forme de cristaux blancs; ir: 3360, 3250 (OH, NH), 1730, 1680, 1640 (C=O) cm^{-1}; sm *m/e*: 376 $(M)^{\ddagger}$, 235, 227, 217, 202, 186, *185*, 159, 158, 157, 143, 142, 133, 132, 130, 88, 77, 43.

9 se présente aussi sous forme de cristaux blancs (lit. (5) *F* 178°C); sm *m/e*: 149 $(M)^{\ddagger}$, 148, 132, 131, 130, 121, 105, 104, 103, 102, *77*, 76, 75, 74, 66, 65, 57, 52, 51, 50.

10 est une huile jaune; ir (CCl_4): 3190, 3130 (NH), 1665, 1640, 1585 (C=O, C=C) cm^{-1}; rmn ($CDCl_3$) δ: 1,93 (s, 3H, CH_3—C), 2,27 (s, 3H, CH_3CO), 3,60 (s, 2H, CH_2), 3,72 (s, 3H, OCH_3), 7,40 (d, J = 6,6 Hz, 1H, H en position 4), 11,44 (d, 1H, NH); sm *m/e*: 227 $(M)^{\ddagger}$, 195, 194, 184, 153, *152*, 124, 102, 99, 92, 91, 78, 71, 59, 45, 44, 43.

Hydrogénation de **6**b *par l'amalgame d'aluminium: (acétyl-5 dihydro-3,6 2*H*-thiazine-1,3 yl-2)-2* o*-méthoxycarbonylbenzamido-2 propionate de méthyle* **7**b

On ajoute 1,6 g de **6***b* (0,004 mol) dissous dans un mélange de 20 cm^3 de méthanol à 96% et de 20 cm^3 de benzène à 0,648 g (0,024 mol) d'aluminium décapé comme ci-dessus. On agite 2 h à température ambiante. Après filtration et lavage du précipité par du méthanol, le filtrat est concentré. Le résidu dissous dans le minimum d'acétate d'éthyle est chromatographié sur gel de silice. L'élution par de l'acétate d'éthyle fournit le mélange des deux isomères, séparés par cristallisation fractionnée. Une première cristallisation dans l'acétate d'éthyle conduit à un isomère fondant à 112–114°C (cristaux blancs). Les eaux mères concentrées sont reprises par du benzène et laissent déposer des cristaux blancs correspondant à l'isomère fondant à 182–184°C, Rdt global = 95%; ir: 3355 (NH), 1730 (C=O ester), 1655, 1635 (C=O amide et C=O cétone) cm^{-1}; rmn (CD_3COCD_3): voir Tableau 1; sm *m/e*: 406 $(M)^{\ddagger}$, 265 (M − cycle acétylthiazinique)$^+$, 227 (M − *o*-méthoxycarbonylbenzamido)$^+$, 173, 172, 163 ($CH_3OCOC_6H_4$—C≡O^+), 143, *142* (cycle acétylthiazinique)$^+$, 102, 98, 77, 56, 43. *Anal.* calc. pour $C_{19}H_{22}N_2O_6S$: C 56,14, H 5,46, S 7,89; tr.: C 55,98, H 5,50, S 7,75.

Hydrogénation de **6** *par le cyanoborohydrure de sodium: (acétyl-5 dihydro-3,6 2*H*-thiazine-1,3 yl-2)-2 phtalimido-2 propionate de méthyle* **7**a

On dissout 2,23 g (0,006 mol) de **6***a* dans 150 cm^3 d'éthanol bouillant. Après retour à la température ambiante, on ajoute 0,415 g (0,0066 mol) de cyanoborohydrure de sodium et quelques cristaux de vert de bromocrésol comme indicateur de pH. On maintient l'acidité en additionnant goutte à goutte de l'acide chlorhydrique concentré. L'agitation est maintenue 1,5 h. Après lavage à l'eau puis extraction par de l'acétate d'éthyle, une chromatographie sur gel de silice fournit un mélange de diastéréomères du produit attendu (éluant: benzène – acétate d'éthyle 80:20). Un échantillon cristallisé dans un mélange acétone – éther diéthylique puis recristallisé dans l'acétate d'éthyle fournit l'isomère ayant le point de fusion le plus élevé (195–200°C) sous forme de cristaux blancs. L'autre isomère, contenu dans les eaux-mères n'a pu être isolé à un degré de pureté suffisant, Rdt global = 45 à 50%; ir: 3415 (NH), 1782 et 1724 (phtalimido), 1745 (C=O ester), 1720 (C=O cétone), 1610 (C=C) cm^{-1}; rmn (CD_3COCD_3): voir Tableau 1; sm *m/e*: 374 $(M)^{\ddagger}$, 174 ($PhtN^{+}{=}CH{-}CH_3$), 143, *142* (cycle acétylthiazinique)$^+$, 132, 104, 98, 76, 43. *Anal.* calc. pour $C_{18}H_{18}N_2O_5S$: C 57,74, H 4,85, N 7,48, S 8,56; tr.: C 57,85, H 4,93, N 7,45, S 8,32.

Hydrogénation de **6**a *par le triéthylsilane: (acétyl-5 dihydro-3,6 2*H*-thiazine-1,3 yl-2)-2 phtalimido-2 propionate de méthyle* **7**a

On agite 1 h, à température ambiante, 0,372 g (0,001 mol) de **6***a* en solution dans 2,28 g (0,020 mol) d'acide trifluoroacétique. On ajoute ensuite 0,58 g (0,005 mol) de triéthylsilane. On maintient alors l'agitation 72 h à 60°C. On dilue par de l'eau puis neutralise par de la soude. Le composé hydrogéné **7***a* est extrait par du chlorure de méthylène puis chromatographié sur gel de silice (éluant: chlorure de méthylène-acétate d'éthyle 90:10), Rdt global des 2 isomères = 86%.

Sponification de **7**a *et* **7**b*: acides (acétyl-5 dihydro-3,6 2*H*-thiazine-1,3 yl-2)-2* o*-carboxybenzamido-2 propioniques* **11**

A 0,010 mol de **7***a* ou **7***b* en solution dans 50 cm^3 d'acétonitrile, on ajoute sous agitation 8 cm^3 de lithine 4 *N* (0,032 mol) à la température ambiante. On suit la réaction par chomatographie sur couches minces en effectuant périodiquement des prélèvements et l'on arrête la réaction lorsque tout l'ester a disparu. Après acidification du mélange réactionnel et extraction par l'acétate d'éthyle, l'acide obtenu est cristallisé dans l'acétate d'éthyle ou dans un mélange acétone – acétate d'éthyle. On obtient des cristaux blancs fondant à 158–160°C (décomposition), Rdt 95%; rmn (CD_3COCD_3): voir Tableau 1; sm *m/e*: 316 $(M - CO_2 - H_2O)^{\ddagger}$, *142* (cycle acétylthiazinique)$^+$. Ce composé est le seul parmi tous les composés décrits dans ce mémoire à ne pas présenter de pic moléculaire dans les conditions standard d'enregistrement. Les diacides subissent une décarboxylation et une déshydratation dans le spectromètre. *Anal.* calc. pour $C_{17}H_{18}N_2O_6S$: C 53,96, H 4,79, N 7,40, S 8,47; tr.: C 54,19, H 4,75, N 7,47, S 8,37.

Acétyl-3 méthyl-7 phtalimido-7 céphème **12***. Lactamisation en présence de DCC*

A 0,378 g (0,001 mol) d'acide **11** en suspension dans 20 cm^3 de chlorure de méthylène, sous agitation, on ajoute 0,3 g (0,015 mol) de dicyclohexylcarbodiimide (DCC). Le mélange réactionnel est agité à

température ambiante pendant 72 h. Après séparation de la majeure partie de la dicyclohexylurée qui a précipité, le filtrat est distillé sous pression réduite puis le résidu est repris par le minimum de chlorure de méthylène. On répète au besoin l'opération. Après chromatographie sur colonne de gel de silice (éluant: benzène – acétate d'éthyle 95:5), on cristallise dans le méthanol et l'on obtient ainsi **12** sous forme de cristaux blancs fondant à 227–229°C.

Lactamisation en présence de BOP

A 0,110 g (≃ 0,0003 mol) d'acide **11** *cis* en solution dans 9 cm^3 de chlorure de méthylène anhydre, on ajoute 0,12 g (0,0012 mol) de triéthylamine et 0,26 g (0,0006 mol) d'hexafluorophosphate de benzotriazol-1-yl-oxy-tris(diméthylamino) phosphonium (BOP). Le mélange réactionnel prend une coloration jaune. On agite à température ambiante pendant 4 h. On ajoute alors 9 cm^3 d'une solution aqueuse saturée de NaCl. On extrait ensuite trois fois par 30 cm^3 d'acétate d'éthyle. On lave trois fois par 10 cm^3 d'acide chlorhydrique 2 *N* puis trois fois par 10 cm^3 d'une solution aqueuse saturée de bicarbonate de sodium puis finalement deux fois par 10 cm^3 d'une solution aqueuse saturée de chlorure de sodium. La solution résultante est séchée sur sulfate de sodium puis distillée sous pression réduite. Le résidu est chromatographié (éluant: chlorure de méthylène). On obtient 0,080 g de lactame **12** *cis* (Rdt 80%) fondant à 227–229°C (méthanol); ir ($CHCl_3$): 1798 (C=O lactame), 1784 et 1726 (C=O phtalimido), 1664 (C=O cétone), 1617 (C=C) cm^{-1}; rmn (CD_3COCD_3): voir Tableau 1; sm *m/e*: 342 $(M)^{\ddagger}$, 218 $(PhtN(CH_3)CHC{\equiv}S^+)$, *201* $(PhtN(CH_3)C{=}C{=}O)^{\ddagger}$, 174 $(Pht\overset{+}{N}{=}CH{-}CH_3)$, 173 $(PhtN{-}CH{=}CH_2)^{\ddagger}$, 147 $(PhtNH)^{\ddagger}$, 132, 104 $(C_6H_4{-}C{\equiv}O)^{\ddagger}$, 76, 43 $(CH_3{-}C{\equiv}O)^+$. *Anal.* calc. pour $C_{17}H_{14}N_2O_4S$: C 59,63, H 4,12; tr.: C 59,51, H 4,18.

1. A. RELIQUET, F. RELIQUET, J. C. MESLIN et H. QUINIOU. Phosphorus Sulfur. Sous presse.
2. P. G. SAMMES. Topics in antibiotic chemistry. Vol. 4. John Wiley and Sons, New York. 1980.
3. R. HEYMES, J. MARTEL et G. NOMINE. Bull. Soc. Chim. Fr. 906 (1977); Fifth Int. Cong. Heterocycl. Ljubljana, 1975; R. BUCOURT. *Dans* Recent advances in the chemistry of β-lactam antibiotics. *Edited by* G. I. Gregory. Second International Symposium, Cambridge. 1980. p. 1.
4. G. DUGUAY, J. P. GUEMAS, J. C. MESLIN, J. P. PRADERE, F. RELIQUET, A. RELIQUET, C. TEA-GOKOU et H. QUINIOU. J. Heterocycl. Chem. 767 (1980).
5. A. REISSERT. Chem. Ber. **46**, 1488 (1913); A. DUNNET et A. WILLEMART. C. R. Acad. Sci. Paris, **226**, 821 (1948).
6. B. CASTRO, J. R. DORMOY, G. EVIN et C. SELVE. Tetrahedron Lett. 1219 (1975); J. Chem. Research (S), 182 (1977); B. CASTRO, J. DORMOY, B. DOURTOGLOU, G. EVIN et C. SELVE. Synthesis, 751 (1976); B. CASTRO, G. EVIN, C. SELVE et R. SEYER. Synthesis, 413 (1977); J. DORMOY et B. CASTRO. Tetrahedron Lett. 3321 (1979).
7. E. H. W. BOHME, H. E. APPLEGATE, J. B. EWING, P. T. FUNKE, M. S. PUAR et J. E. DOLFINI. J. Org. Chem. **38**, 230 (1973).
8. H. WEIDINGER et H. EILINGSFELD. Brevet Belge No 629972 (1963); Chem. Abstr. **61**, 1803 (1964).

Can. J. Chem. Downloaded from www.nrcresearchpress.com by 210.87.254.40 on 09/06/12
For personal use only.

Electrophilic cleavage of cyclopropanes. IV. The reaction of 2-nitrobenzenesulphenyl chloride with tetracyclo[3.2.0.0^{2,7}.0^{4,6}]heptane in methanol and acetic acid: the crystal structure of *exo*-3-(2′-nitrophenylthio)-*exo*-5-methoxytricyclo[2.2.1.0^{2,6}]heptane, $C_{14}H_{15}NO_3S$ [1]

DENNIS G. GARRATT[2]

Division of Chemistry, National Research Council of Canada, Ottawa, Ont., Canada K1A 0R6

AND

MARIA PRZYBYLSKA AND MIROSLAW CYGLER[3]

Division of Biological Sciences, National Research Council of Canada, Ottawa, Ont., Canada K1A 0R6

Received October 22, 1982

DENNIS G. GARRATT, MARIA PRZYBYLSKA, and MIROSLAW CYGLER. Can. J. Chem. **61**, 1176 (1983).

The electrophilic cleavage of a cyclopropane single bond in tetracyclo[3.2.0.0^{2,7}.0^{4,6}]heptane by 2-nitrobenzenesulphenyl chloride in methanol and acetic acid has been studied using both nmr and single crystal X-ray structural determination techniques. The orientation of ring opening has been shown to be inversion as a result of electrophilic corner attack. The crystal structure of one adduct allowed the unambiguous assignment of *exo*-3-(2′-nitrophenylthio)-*exo*-5-methoxytricyclo[2.2.1.0^{2,6}]-heptane, $C_{14}H_{15}NO_3S$. This species crystallizes in space group $P2_1/a$ with unit cell dimensions a = 10.633(1), b = 13.637(1), c = 9.938(1) Å, β = 115.36(1)°, Z = 4. The structure was solved by MULTAN 78. The parameters were refined by block-diagonal least squares to a final R = 0.039 for 2445 observed reflections. Of particular interest is an interaction between the sulphur atom and the oxygen atom of the nitro group with an S...O distance of 2.694(2) Å and C—S···O = 175.5(1)°. The data presented in this paper show errors in previous assignments based on ^{13}C nmr spectroscopy made in this laboratory and indicate the danger of basing assignments of configuration in nortricyclenes entirely upon this technique.

DENNIS G. GARRATT, MARIA PRZYBYLSKA et MIROSLAW CYGLER. Can. J. Chem. **61**, 1176 (1983).

Faisant appel à la détermination de structure par cristallographie de rayons-X sur un mono cristal et à la rmn, on a étudié le clivage électrophile d'une liaison simple du cyclopropane du tétracyclo[3.2.0.0^{2,7}.0^{4,6}]heptane par le nitro-2 benzène chlorure de sulphényle dans le méthanol et l'acide acétique. On montre que l'orientation de l'ouverture du cycle est une inversion résultant d'une attaque électrophile par l'arête. La structure du cristal d'un adduit permet d'identifier sans ambiguité l'*exo*-(nitrophényl-2′ thio)-3 *exo* méthoxy-5 tricyclo[2.2.1.0^{2,6}]heptane $C_{14}H_{15}NO_3S$. Ce composé cristallise dans le groupe d'espace $P2_1/a$ avec a = 10,633(1), b = 13,637(1), c = 9,938(1) Å, β = 115,36(1)°, Z = 4. On a résolu la structure selon la méthode MULTAN 78 et on l'a affinée par la méthode des moindres carrés ("block-diagonal") jusqu'à une valeur finale de R = 0,039 pour 2445 réflexions observées. L'interaction entre l'atome de soufre et l'atome d'oxygène du groupe nitro avec une distance S···O de 2,694(2) Å et d'un angle C—S···O 175,5(1)° est d'un intérêt particulier. Les données que l'on présente ici révèlent les erreurs qui se sont glissées dans les attributions antérieures fondées sur la spectroscopie de la rmn du ^{13}C et mettent en évidence le danger d'utiliser uniquement cette technique pour établir la configuration des nortricyclènes.

[Traduit par le journal]

Introduction

In an earlier paper of this series, we reported the reactions of a series of arenesulphenyl chlorides with tetracyclo-[3.2.0.0^{2,7}.0^{4,6}]heptane to give two or all three of the adducts **1**–**3** (eq. [1]), when methylene chloride is used as solvent at

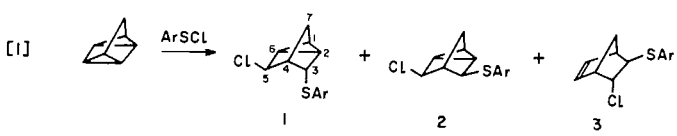

ambient temperature (1). Assignment of the nortricyclene adducts, **1** and **2**, was based upon previously defined criteria utilizing ^{1}H and ^{13}C nmr spectroscopy. For example, the ^{13}C nmr data for species **1** and **2** indicated three cyclopropyl methine carbons with characteristic high-field chemical shifts (2) and high $^1J_{^{13}C-^1H}$ values (3). The remaining carbon resonances, methine *geminal* to chlorine or sulphur and the lone methine, and methylene bridge, were readily identified on the basis of their respective chemical shifts and multiplicities. In addition we were able to compare these spectral data with those of authentic samples of **2** and **3** prepared during the analogous investigation using bicyclo[2.2.1]hepta−2,5-diene.

The structure of **1** was defined as the C(3) epimer of **2** on the basis of ^{13}C nmr analysis. The *endo* orientation of the arylthio moiety at C(3) follows from the observed paramagnetic shift of C(3) in **1** relative to **2**, and a diamagnetic shift of C(5), albeit a small one, in **1** relative to **2**. The small absolute value of this latter shift difference was unanticipated but presumably results from a combination of the expected γ−*gauche* interaction and an anisotropy effect from the phenyl ring operating in the opposite sense.

These assignments were further corroborated by the observations of Morrill *et al.* (4) that tetracyclo[3.2.0.0^{2,7}.0^{4,6}]-heptane-1,5-dicarboxylic acid **4***a* and its dimethyl ester **4***b*

[1]NRCC No. 21008.

[2]Current address: Research and Development Division, Eldorado Resources Limited, 400-255 Albert St., Ottawa, Ont., Canada K1P 6A9.

[3]Current address: Department of Biochemistry, University of Alberta, Edmonton, Alta., Canada T6G 2H7.

Can. J. Chem. Downloaded from www.nrcresearchpress.com by 210.87.254.40 on 09/06/12
For personal use only.

react with benzenesulphenyl chloride (eq. [2]) to give *exo*-5-chloro-*endo*-3-phenylthiotricyclo[2.2.1.$0^{2,6}$]heptane-2-*exo*-3-dicarboxylic acid, **5***a*, the C(3) epimer **6***a*, and the corresponding dimethyl esters, **5***b* and **6***b*, in approximately equal amounts. Both Bredt and later Cristol and LaLonde substantiated these results in their studies of the analogous addition of 4-toluenesulphenyl chloride to **4** (5).

[2] 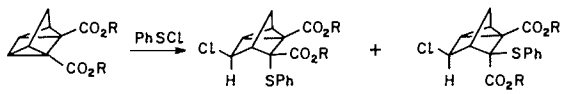

4 a R = H
b R = CH_3 5 6

A recent paper by Zefirov *et al.*, however, brings all of these results into question (6). They have shown on the basis of a single crystal X-ray structure determination that the nortricyclene adduct isolated in the reaction of arenesulphenyl chlorides with bicyclo[2.2.1]hepta-2,5-diene is not **2** as previously reported (7), but is in fact the species: *endo*-3-chloro-*exo*-5-arylthiotricyclo[2.2.1.$0^{2,6}$]heptane, **7** (eq. [3]). Since species **7**

[3] 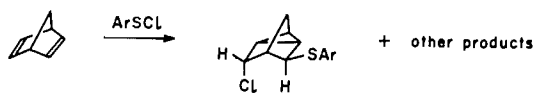

7

corresponds spectroscopically to species **2** in our work with tetracyclo[3.2.0.$0^{2,7}$.$0^{4,6}$]heptane it is obvious that there exists an error in our assignments. This brings into question the methodology based upon the use of ^{13}C nmr for assignment of configuration in nortricyclene products. The importance of these data is clearly evident in that numerous papers from this laboratory and elsewhere have been based upon the utility and ease of ^{13}C nmr based assignments.

The importance attached to correctly establishing the stereochemistry of the nortricyclene adducts stems from the controversy surrounding the mode of interaction of an electrophile EN with a strained carbon–carbon single bond. Conceptually there exist two distinct mechanisms as shown in Scheme 1. For example, the electrophile and the strained bond may approach each other orthogonally, i.e. edge-on attack. In the case of cyclopropane, one would anticipate the maximum interaction of orbitals to occur when the electrophile approaches the single bond in the same plane as the three carbons which define the ring, i.e. for $\theta = 0°$. In the case of a substituted cyclopropane, as is found in the substrate used in this investigation, the best angle of approach with respect to this plane may be significantly different. The major point to be noted is that this type of interaction leads to retention of configuration at the carbon atom, wherein the new bond is formed with the electrophilic portion of the reagent (E of EN or ArS of ArSCl).

Alternatively, the electrophile may approach the corner of the strained bond along an extended axis joining two of the carbon atoms of the ring, that is to say, collinearly or end-on, the interaction ultimately resulting in inversion of configuration at the carbon atom forming the new bond with E (ArS). The presence of diastereomeric products in this latter case requires that the subsequent nucleophilic attack on the cationic intermediate be nonstereospecific, the relative proportions of each product being dependent upon steric or other electronic effects.

Earlier studies carried out in these laboratories suggested that arenesulphenyl halides react with tetracyclo[3.2.0.$0^{2,7}$.$0^{4,6}$]-

Edge-on attack
retention of configuration at carbon
in plane $\theta = 0°$

Corner or end-on attack
inversion of configuration at carbon
in plane $\theta = 0°$, equivalent to collinear attack

SCHEME 1

heptane by both pathways described above. If the original assignments were incorrect a new mechanistic scenario would be required.

Results and discussion

In order to study this problem in more detail an investigation was undertaken wherein 2-nitrobenzenesulphenyl chloride was reacted with tetracyclo[3.2.0.$0^{2,7}$.$0^{4,6}$]heptane in protic solvents, in particular, methanol and anhydrous acetic acid.

The reaction in acetic acid is quite complex, yielding in addition to two 3-arylthio-5-acetoxy nortricyclenes **8** and **9**, the two known 3-arylthio-5-chloro species **1** and **2**, the known olefinic species **3**, 3-acetoxytricyclo[2.2.1.$0^{2,6}$]heptane, presumably from addition of acetic acid upon the substrate, and two species which were shown to be 2-chloro-3-arylthio-5-acetoxy and 2-chloro-3-arylthio-6-acetoxy substituted norbornanes.

Of primary interest is the assignment of the two nortricyclenes **8** and **9**. On the basis of ^{13}C nmr criteria these species may be tentatively assigned as **8***a* and **9***a* respectively (see Table 1). On the basis of ^{1}H nmr data, however, Zefirov has chosen to assign the same species as **8***b* and **9***b*. In both

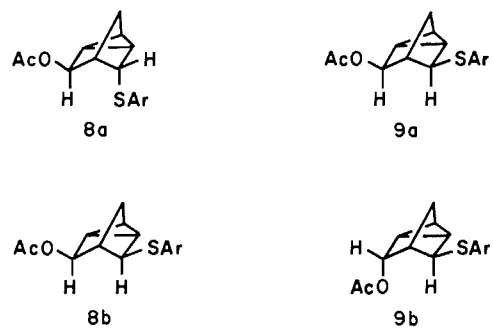

cases use has been made of the relative differences in chemical shifts. Thus, Zefirov and co-workers have argued for structures **8***b* and **9***b* on the basis of the observation that the ^{1}H nmr chemical shifts of the methine protons geminal to the acetoxy groups δ 4.9 and 4.7, respectively, indicate that the arylthio group in both isomers is found in the same position, whereas the difference in the proton chemical shifts of the methine protons geminal to the arylthio groups, δ 3.4 and 3.9, points to a difference in the configuration of the acetoxy group, the latter apparently being in the *endo* orientation in species **9**. On the basis of the greater probabililty of *exo* attack upon bicyclo-[2.2.1]hepta-2,5-diene, which yields the same two nortri-

Can. J. Chem. Downloaded from www.nrcresearchpress.com by 210.87.254.40 on 09/06/12
For personal use only.

Can. J. Chem. Downloaded from www.nrcresearchpress.com by 210.87.254.40 on 09/06/12
For personal use only.

TABLE 1. Carbon-13 and proton nmr parameters for nortricyclene adducts and model compounds

Compound	Spectra	Spectral coordinates δ (ppm, TMS) C(1)	C(2)	C(3)	C(4)	C(5)	C(6)	C(7)	OR	Aryl group
8	^{13}C	12.2	[18.5]	50.0	38.8	77.8	[16.7]	27.5	170.7 21.1	146.4, 138.1, 133.1, 127.6, 126.0, 124.3
	^{1}H			3.4		4.9				
9	^{13}C	14.1	[16.4]	50.3	38.8	79.9	[17.1]	28.0	170.7 21.1	146.3, 137.3, 127.3, 133.5, 126.1, 124.6
	^{1}H			3.9		4.7				
10	^{13}C	13.1	[19.2]	49.6	39.3	76.8	[18.3]	26.9		146.4, 138.0, 133.2, 127.5, 126.0, 124.3
11	^{13}C	15.6	[16.4]	50.5	39.3	79.3	[16.8]	27.8		146.7, 139.1, 134.8, 134.3, 125.8, 123.7
12	^{13}C	21.8	23.8	47.9	42.9	208.6	20.4	28.7		146.7, 135.0, 133.4, 127.9, 125.9, 125.4
13	^{13}C	10.6	14.4	50.2	33.9	[32.9]	11.9	[29.9]		145.8, 136.2, 133.4, 127.9, 125.7, 124.8
14		19.1	17.1	214.0	37.9	31.4	19.1	31.4		
15	^{13}C	12.3	16.7	47.8	37.5	84.5	18.1	27.2	56.7	146.7, 137.2, 133.2, 127.7, 126.0, 124.7
	^{1}H	1.481m	1.505m	3.348bq′	2.375bm	3.580bq′	1.528m	1.863q′ABq	3.322s	— — 7.56m
				$w_{1/2}$ = 16.4 Hz						7.52m, 8.183ddd, 7.267m
		$J_{1,5}$ = 1.56 Hz								
		$J_{1,3}$ = 1.56 Hz		$J_{3,5} \leq$ 0.5 Hz				$J_{7syn,\ 7anti}$ = −10.2 Hz		
			$J_{2,7anti}$ = 1.6 Hz				$J_{6,7syn}$ = 2.3 Hz			
16	^{13}C	14.4	[16.3]	47.7	37.6	86.5	[16.5]	28.3	56.9	146.5, 138.0, 133.3, 127.5, 126.1, 124.4
	^{1}H	1.60tdd	1.49m	3.902bs	2.260m	3.657dt	1.44m	1.949mABq	3.375s	— — 7.57ddd
				$w_{1/2}$ = 3.52 Hz						
					$w_{1/2}$ = 4.68 Hz			$J_{7syn,\ 7anti}$ = −10.9 Hz		7.655ddd, 8.163ddd, 7.53ddd
						$J_{5,4}$ = 1.78 Hz				
						$J_{5,7syn}$ = 0.46 Hz				

Abbreviations: bs = broad singlet, d = doublet, dm = doublet of a multiplet, bm = broad multiplet, bq′ = broad quintet, q′ABq = quintet of AB quartet, mABq = multiplet of AB quartet, δ values in [ ] may be reversed.

Can. J. Chem. Downloaded from www.nrcresearchpress.com by 210.87.254.40 on 09/06/12
For personal use only.

cyclene adducts, Zefirov ascribed an *exo* orientation to the arylthio moieties (6).

On the other hand, an examination of the ^{13}C nmr data in Table 1 shows that the chemical shifts of methine carbons bonded to sulpur in **8** and **9** are essentially identical (δ 50.0 and 50.3), whereas the chemical shifts of the methine carbons bonded to the acetoxy groups (δ 77.8 and 79.9) show a larger difference. If the adducts are epimeric at C(5) as per Zefirov's assignment one would expect, on the basis of the γ−*gauche* effect, to see little difference in the resonances at C(5) but a diamagnetic shift of the C(3) resonance in species **9***b* relative to **8***b*. If, however, the adducts are epimeric at C(3) as per the assignments **8***a* and **9***a*, the ^{13}C nmr data are readily interpretable.

Since both interpretations cannot be correct, another approach to the problem was necessary. Reduction of the two acetates **8** and **9** with sodium borohydride in the presence of lithium chloride in 2-propanol as solvent at reflux gave the corresponding alcohols **10** and **11**. An examination of the ^{13}C nmr parameters (Table 1) of these species indicates that no molecular rearrangements have occurred and that **8** yields clearly species **10**, while **9** yields species **11**. If the assignments as based on ^{13}C nmr are correct, oxidation of **10** and **11** should yield two different ketones. (eq. [4]). If, on the other hand,

[4]

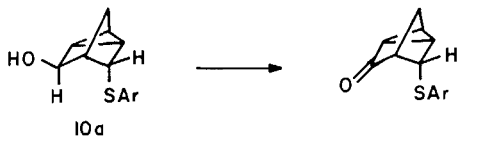

10a

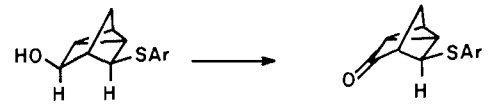

11a

the species are epimeric at C(5) as per the ^{1}H nmr assignment only one ketone should be formed on oxidation (eq. [5]).

[5]

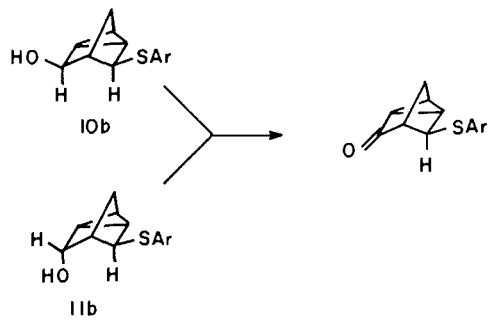

The reactions of **10** and **11** with Jones' reagent in acetone at room temperature yield a single ketone **12** which is readily converted to the known compound **13**: 3-arylthiotricyclo-[2.2.1.$0^{2,6}$]heptane by conversion first to its tosylhydrazone followed by reduction with sodium borohydride (eq. [6]) or 1 : 1 methyllithium and lithium bromide in diethyl ether. The

[6]

12 13

assignment is further corroborated by a comparison of the spectral parameters of **12** with those of **13** and species **14**: tricyclo[2.2.1.$0^{2,6}$]heptanone.

While this last series of experiments clearly shows that the assignments based on ^{13}C nmr spectroscopy are incorrect and that therefore the nortricyclene adducts are epimeric at C(5), the relative orientations of both the arylthio groups and the acetoxy groups are still in question.

To solve this latter problem the reaction of 2-nitrobenzenesulphenyl chloride with tetracyclo[3.2.0.$0^{2,7}$.$0^{4,6}$]heptane in methanol has been used as a model since the reaction is much cleaner (only 3 species are formed) and the adducts may be isolated in a much more facile manner. As per the reaction in acetic acid, two solvent-incorporated nortricyclenes, **15** and **16**, are formed. The third species has been tentatively assigned as *exo*-2-methoxy-*syn*-7-(2′-nitrophenylthio)bicyclo[2.2.1]-hepta-2,5-diene, **17** (eq. [7]).

[7]

15 + 16 17

The relationship of **15** and **16** to the acetoxy nortricyclenes was, furthermore, established through conversion of the alcohols **10** and **11** to their respective methyl ethers with diazomethane, thereby showing that the orientation of arylthio groups and solvent-incorporated functionalities (methoxy, hydroxy, acetoxy) are similarly oriented in species **15**, **10**, and **8** and in species **16**, **11**, and **9** (eq. [8]).

[8]

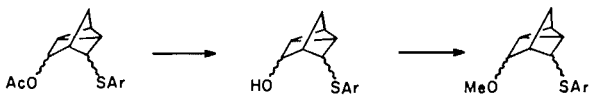

8 or 9 — 10 or 11 — 15 or 16

A detailed analysis of the ^{1}H nmr (250 MHz) and ^{13}C nmr spectra (20 MHz) of species **15** and **16** did not allow us to make unambiguous assignments. In order to unequivocally establish the configurational specificity of this reaction, we therefore undertook a single crystal X-ray structural determination of adduct **15**. The molecular conformation, the numbering scheme, and the bond lengths of species **15** are shown in Fig. 1. The refined positional parameters and isotropic temperature factors are listed in Table 2.[4] The angles are listed in Table 3. The C—H bonds vary from 0.93 to 1.00 Å (mean = 0.96 and esd ≤ 0.03 Å).

The C—C bonds of nortricyclene are in the range of 1.500 to 1.519 Å with the exception of the bonds to C(4), which are appreciably longer (1.528(2), 1.540(2), 1.548(2) Å). The substitution by a methoxy group at C(5) leads to a significant shortening of the C(5)—C(6) bond (1.500(3) Å) and the lengthening of the C(4)—C(5) bond to 1.548(2) Å as compared with the equivalent bonds in this moiety. The angles of the three-membered ring give a mean of 60.0°, and those of the

[4]Tables of observed and calculated structure factors and of temperature factors are available, at a nominal charge, from the Depository of Unpublished Data, CISTI, National Research Council of Canada, Ottawa, Ont., Canada K1A 0S2

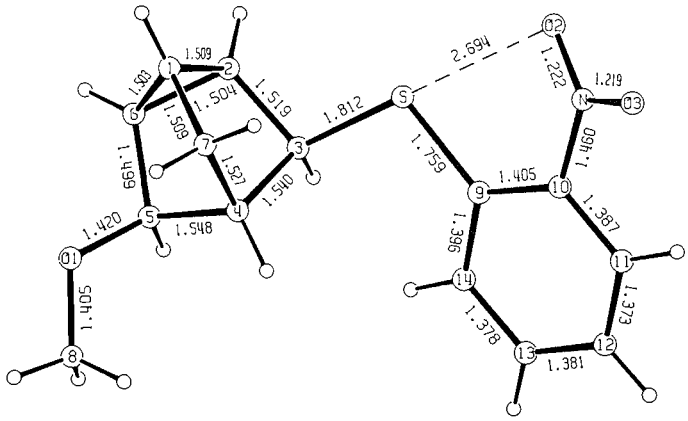

FIG. 1. ORTEP drawing (8) of the molecule **15** showing the bond lengths. The esd's are 0.002 Å except for bonds to C(1), C(12), and O(3) for which they are 0.003 Å.

TABLE 2. Final fractional coordinates with esd's in parentheses ($\times 10^4$ for non-hydrogen atoms and $\times 10^3$ for H) and isotropic temperature factors ($B_{eq} = (8\pi^2/3)\sum_i \sum_j U_{ij} a_i^* a_j^* \mathbf{a}_i \cdot \mathbf{a}_j$)

Atom	x	y	z	B_{eq} or B (Å^2)
S	6681(0)	928(0)	9754(0)	3.7
N	9774(2)	355(1)	11555(2)	4.3
O(1)	3580(1)	2972(1)	4946(1)	4.4
O(2)	8852(2)	−240(1)	11360(2)	5.6
O(3)	10959(2)	115(1)	11807(2)	6.6
C(1)	4191(2)	846(1)	6208(2)	4.2
C(2)	4068(2)	1052(1)	7639(2)	3.9
C(3)	5274(1)	1719(1)	8565(2)	3.2
C(4)	5419(1)	2227(1)	7255(1)	3.0
C(5)	3904(1)	2591(1)	6387(2)	3.5
C(6)	3201(2)	1619(1)	6251(2)	4.2
C(7)	5472(2)	1370(1)	6291(2)	3.8
C(8)	3995(2)	3951(1)	4957(2)	4.6
C(9)	8071(1)	1732(1)	10721(1)	3.0
C(10)	9444(2)	1397(1)	11509(2)	3.4
C(11)	10545(2)	2021(1)	12298(2)	4.0
C(12)	10304(2)	3008(1)	12333(2)	4.4
C(13)	8968(2)	3363(1)	11564(2)	4.1
C(14)	7881(2)	2743(1)	10759(2)	3.5
H(1, 1)	383(2)	27(2)	569(3)	5.8(0.5)
H(2, 1)	365(2)	61(2)	806(2)	4.9(0.4)
H(3, 1)	503(2)	218(1)	917(2)	3.2(0.3)
H(4, 1)	617(2)	273(1)	753(2)	3.2(0.3)
H(5, 1)	366(2)	309(1)	698(2)	3.7(0.3)
H(6, 1)	220(2)	156(2)	581(3)	5.6(0.5)
H(7, 1)	629(2)	100(1)	675(2)	4.2(0.4)
H(7, 2)	538(2)	158(1)	533(2)	4.6(0.4)
H(8, 1)	366(2)	415(2)	396(3)	5.5(0.5)
H(8, 2)	359(3)	436(2)	546(3)	6.2(0.5)
H(8, 3)	496(3)	404(2)	550(3)	7.1(0.6)
H(11, 1)	1147(2)	174(1)	1283(2)	4.4(0.4)
H(12, 1)	1107(2)	343(2)	1290(3)	5.4(0.5)
H(13, 1)	876(2)	404(2)	1160(3)	5.8(0.5)
H(14, 1)	700(2)	303(1)	1024(2)	4.4(0.4)

five-membered rings vary from 97.0 to 107.5° with the smallest at C(3), C(5), and C(7).

The dihedral angle between the plane of the benzene ring and that of the nitro group is 25.0°. This rotation of NO_2 about the C—N bond combined with the increase of the C(9)—C(10)—N angle (120.8° vs. 116.5° for C(11)—C(10)—N) gives rise to the S···O(2) distance of 2.694(2) Å. Since this distance is considerably smaller than the sum of O and S van der Waals radii (3.07 Å), a nonbonded interaction between these two atoms must be present, as otherwise a much larger rotation of the nitro group would be expected to lead to an adequate separation between them. Very large twists of the nitro groups to accommodate *ortho*-substituents have indeed been reported for 1-bromo-2,4-dinitrobenzene (40°) (9), 1,5-dinitronaphthalene (49°) (10), 9,10-dinitroanthracene (63.7°) (11), and nitromesitylene (66.4°) (12).

The C(3), S, and O(2) atoms are almost collinear with C(3)—S···O(2) = 175.5(1)°. This condition appears to ensure maximum hybridization utilizing empty *p*- and *d*-orbital participation in bonding. An examination of 69 structures containing divalent sulphur carried out by Rosenfield *et al.* (13) revealed that nucleophiles tend to make short contacts with S approximately along the extension of one of the covalent bonds to S.

A similar S···O interaction, although somewhat weaker, was observed in 1-chloromethyl-3-*endo*-(2′,4′-dinitrophenylthio)tricyclo[2.2.1.0^{2,6}]heptane (14), **18**, where S···O is 2.739(2) Å and C(3)—S···O = 166.3(1)°. This difference in strength is consistent with that found between S···O in other 2-nitrophenylthio compounds (15) (2.630, 2.634 Å) and 2,4-dinitrophenylthio derivatives (16) (2.657 Å).

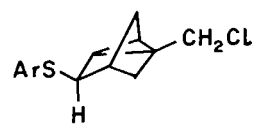

18

Ar = 2, 4-dinitrophenyl

Somewhat stronger S···O interactions were reported in compounds in which complex alicyclic moieties were replaced by either a phenyl or a thiophenyl group (17). The S···O distances vary in these compounds from 2.588 to 2.636 Å and the C—N rotations are 1° to 18.6°. In general the S···O distances can be correlated with the variations in the rotations of the nitro groups. There is no doubt therefore that the strength of the interaction depends on the nature of the substituents on S. This was demonstrated clearly by Kálmán and Párkányi (18) who compared intramolecular X—S···O=Y interactions in 26 structures. The shortest S···O contact of 2.034(5) Å was reported in S—S···O=N with S—S···O = 174.1(1) Å (19).

The energetic favourability of the above interaction between sulphur and an oxygen atom of the *ortho*-nitro substituent is corroborated both here and elsewhere by use of carbon-13 nmr spectroscopy (18, 20–22) to exist in the solution phase and thus is not a manifestation of the conformational changes often required during crystallization to give the energetically most stable packing arrangement in the crystal stucture.

The S—C (sp^3) and S—C (sp^2) bonds in **15** are 1.812(2) and 1.758(2) Å, respectively. The bonds along the chain S—C(9)—C(10)—N—O(2) show an alternate shortening and lengthening similar to that observed in **18**, the corresponding values being in agreement within 0.002 Å. The torsion angles for the nortricyclene moiety also agree well with the values for **18**, as is shown in Table 4. The attachment of the chloromethyl group at C(1) in **18** caused only a slight increase in the

Can. J. Chem. Downloaded from www.nrcresearchpress.com by 210.87.254.40 on 09/06/12
For personal use only.

TABLE 3. Bond angles (deg) and esd's

C(3)—S—C(9)	104.6(1)	O(1)—C(5)—C(4)	115.1(1)
O(2)—N—O(3)	122.9(2)	O(1)—C(5)—C(6)	109.7(1)
O(2)—N—C(10)	118.4(1)	C(4)—C(5)—C(6)	97.2(1)
O(3)—N—C(10)	118.7(2)	C(1)—C(6)—C(2)	60.3(1)
C(5)—O(1)—C(8)	113.6(1)	C(1)—C(6)—C(5)	107.2(1)
C(2)—C(1)—C(6)	59.9(1)	C(2)—C(6)—C(5)	106.6(1)
C(2)—C(1)—C(7)	107.5(1)	C(1)—C(7)—C(4)	97.0(1)
C(6)—C(1)—C(7)	107.0(1)	S—C(9)—C(10)	122.1(1)
C(1)—C(2)—C(3)	106.9(1)	S—C(9)—C(14)	122.2(1)
C(1)—C(2)—C(6)	59.8(1)	C(10)—C(9)—C(14)	115.7(1)
C(3)—C(2)—C(6)	105.9(1)	N—C(10)—C(9)	120.8(1)
S—C(3)—C(2)	106.6(1)	N—C(10)—C(11)	116.5(1)
S—C(3)—C(4)	117.8(1)	C(9)—C(10)—C(11)	122.7(1)
C(2)—C(3)—C(4)	97.0(1)	C(10)—C(11)—C(12)	119.6(2)
C(3)—C(4)—C(5)	99.1(1)	C(11)—C(12)—C(13)	119.2(2)
C(3)—C(4)—C(7)	103.3(1)	C(12)—C(13)—C(14)	121.0(2)
C(5)—C(4)—C(7)	101.8(1)	C(9)—C(14)—C(13)	121.7(1)

TABLE 4. Selected torsion angles (deg); esd's are ≤ 0.5°

(*a*) Endocyclic torsion angles of five-membered rings

Ring A: C(1), C(2), C(3), C(4), and C(7)
Ring B: C(2), C(3), C(4), C(5), and C(6)
Ring C: C(1), C(6), C(5), C(4), and C(7)

Bond	A	B	C	Mean	Mean*	C_s†
C(1)—C(2)	1.0					
C(2)—C(6)		0.0		0.7	1.7	0.0
C(1)—C(6)			− 1.0			
C(2)—C(3)	29.2	−33.4				
C(5)—C(6)		33.3	−30.1	31.5	31.4	25.0
C(1)—C(7)	−31.0		32.0			
C(3)—C(4)	−50.3	54.3				
C(4)—C(5)		−54.5	51.2	52.1	52.2	40.3
C(4)—C(7)	50.8		−51.6			

*Mean values for 1-chloromethyl-3-*endo*-(2′,4′-dinitrophenylthio)tricyclo[2.2.1.$0^{2,6}$]heptane (14).

†Calculated values for the envelope conformation with a puckering amplitude (q = 0.435 Å) determined from an electron diffraction study of cyclopentane (23).

(*b*) Exocyclic torsion angles

C(4)—C(5)—O(1)—C(8)	−81.9
C(4)—C(3)—S—C(9)	69.4
C(3)—S—C(9)—C(14)	14.7
C(9)—C(10)—N—O(2)	−24.5

mean value for the torsion angles along the C(1)—C(2), C(2)—C(6), and C(6)—C(1) bonds (1.7 vs. 0.7°).

The N—O(3) bond is 1.220(3) Å and the presence of a weak C(11)—H···O(3) intramolecular hydrogen bonding is indicated by the difference between the angles C(10)—C(11)—H(11, 1) and C(12)—C(11)—H(11, 1) (118.7(1.3)° vs. 121.6(1.3)°). O(3)···H(11, 1) = 2.41(2) Å and C(11)—H(11, 1)···O(3) = 97.9(1.4)°.

The benzene ring deviates significantly from planarity (χ^2 = 133) as C(9) is at −0.009 and C(14) at 0.011 Å from the plane calculated for the six atoms of the ring. S, N, and O(2) are situated at −0.049, −0.023, and −0.494 Å from that plane, respectively.

The molecules are held together by van der Waals forces. The shortest intermolecular O···H distance O(1)···H(12, 1) is 2.65(2) Å and the closest H···H contacts are 2.41(4) and 2.58(3) Å.

The use of the above X-ray structure data to assign **15** unambiguously as *exo*-3-(2′-nitrophenylthio)-*exo*-5-methoxytricyclo-[2.2.1.$0^{2,6}$]heptane allows us now to assign **8** as the di-*exo* species **8***b*. Since species **8** and **9** were shown to be epimeric at C(5), it is also clear that **9** must be *exo*-3-(2′-nitrophenylthio)-*endo*-5-acetoxytricyclo[2.2.1.$0^{2,6}$]heptane, **9***b*. Similarly, species **16** must be epimeric at C(5) and thus have an *endo*-5-methoxy moiety.

The question may now be raised as to the possible existence of an applicable heuristic method utilizing ^{13}C nmr spectroscopy for assigning configuration in 3,5-disubstituted tricyclo[2.2.1.$0^{2,6}$]heptanes. The behaviour of the compounds studied in this investigation is clearly anomalous relative to the normally anticipated γ−*gauche* effects of the model systems. Specifically, when the chemical shifts of the C(3) and C(5)

Can. J. Chem. Downloaded from www.nrcresearchpress.com by 210.87.254.40 on 09/06/12
For personal use only.

TABLE 5. A comparison of variations in the ^{13}C chemical shifts of C(3) and C(5) for various substituents

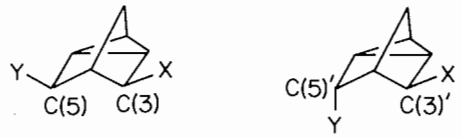

Substituents		Chemical shifts (δ, ppm)					
X	Y	C(5)	C(3)	C(5)′	C(3)′	$\Delta_{C(5)-C(5)'}$	$\Delta_{C(3)-C(3)'}$
ArS*	Cl	64.2	49.4	64.9	48.1	−0.7	1.3
ArS*	OAc	77.8	50.0	79.9	50.3	−2.1	−0.3
ArS*	OH	76.8	49.6	79.3	50.5	−2.5	−0.9
ArS*	OMe	84.5	47.8	86.5	47.7	−2.0	0.1
Br	Br	51.0	51.0	[54.3]†	[53.7]†	−3.3	−2.7
Br	OEt	80.3	53.1	83.7	55.2	−3.4	−2.1
Br	OMe	81.8	52.6	85.2	54.6	−3.4	−2.0

*ArS = 2-nitrophenylthio.
†Chemical shifts in brackets may be switched.

resonances are compared, a shift from *exo* to *endo* at C(5) uniformly gives rise to a diamagnetic shift of from 0.7 to 2.5 ppm, upon comparing **1**, **8**, **10**, and **15** to **2**, **9**, **11**, and **16**, respectively. The chemical shift difference of C(3) is generally smaller, being either slightly diamagnetic or paramagnetic. Comparing the chemical shift differences as per Table 5 indicates that as the variation in C(5) resonances becomes less negative, i.e. less diamagnetic, the variations at C(3) become more positive and paramagnetic.

While the behaviour of the arylthio systems seems quite general, its universality must still be tested. One possible set of compounds are the 3-bromo-5-substituted tricyclo[2.2.1.$0^{2,6}$]-heptanes prepared by the electrophilic cleavage of tetracyclo[3.2.0.$0^{2,7}$.$0^{4,6}$]heptane by molecular bromine and previously reported (24). Initial assignments were made on the basis of the γ-*gauche* effect which has now been shown to be inapplicable. If the bromination reaction is reinterpreted in terms of the model of Skell *et al.* (25), the variations in chemical shifts for C(3) and C(5) are as given in Table 5 and follow the observed behaviour of the arylthio compounds. The above correlations, while gratifying, do not, however, prove the universality of the new heuristic method, but suggest that further detailed studies in this area are warranted.

Summary

Our studies show that electrophilic cleavage of cyclopropane rings by arenesulphenyl chlorides in systems such as tetracyclo[3.2.0.$0^{2,7}$.$0^{4,6}$]heptane occurs by a single path leading to corner attack by the electrophile followed by proportioning between *exo* and *endo* attack by solvent in a second step. Previous work in this laboratory is thus in error and the preceding papers in this series must be reevaluated in terms of the new data. In particular, our work on the bromination of cyclopropanes (24) which questioned the interpretations of Skell *et al.* (25) must be reinvestigated in detail. If this system, too, can be shown to be epimeric at C(5), our data become compatible with those of Skell and will lead to a self-consistent theory of cyclopropane cleavage by bromine.

In conclusion, the assignment of configuration in nortricyclenes by use of ^{13}C nmr spectroscopy has been shown to be invalid in the absence of good models of known configuration. A heuristic method, utilizing ^{13}C nmr, based upon existing data has been suggested but requires further model compounds.

Experimental

General

The ^{1}H nmr spectra were recorded on a Bruker WM-250 spectrometer. The ^{13}C nmr spectra were recorded on a Bruker WP-80 spectrometer, using chloroform-*d* as an internal lock and reference. All spectral parameters are referenced to TMS as an internal standard.

Tetracyclo[3.2.0.0.^{2,7}.$0^{4,6}$]heptane was purchased from Aldrich and used without further purification. The purity was confirmed by nmr and glc.

2-Nitrobenzenesulphenyl chloride was purchased from Aldrich and recrystallized prior to use.

The general procedure for the reaction of tetracyclo-[3.2.0.$0^{2,7}$.$0^{4,6}$]heptane with sulphenyl chloride is as previously described (1). All reactions were carried out at 23°C, unless otherwise stated, on a 0.01 to 0.02 mole scale. When methanol was used as the solvent, recovery of the products was accomplished by distillation of the excess methanol under vacuum.

The resultant oil was separated into its components by preparative tlc on silica gel using in the first instance a 1:1 mixture of methylene chloride and 30−60 petroleum ether which yields six bands with R_f's of 0.71, 0.63, 0.53, 0.36, 0.27, and 0.16. No evidence for isomerization on the plates was observed. The combined fractions with R_f's of 0.53, 0.36, and 0.27 were rechromatographed on silica gel using a 1:4 mixture of ethyl acetate and toluene which yields three fractions with R_f's of 0.74, 0.56, and 0.47. The species with R_f's of 0.56 and 0.47 were shown by nmr to be the 5-methoxy-3-(2′-nitrophenylthio)-nortricyclenes.

Crystals of the species with R_f = 0.47 were obtained from a 1:1 mixture of ethyl acetate and chloroform. *Anal.* calcd. for $C_{14}H_{15}O_3NS$: C 60.63, H 5.45, N 5.05, S 11.56, O 17.31%; found: C 60.42, H 5.49, N 5.12, S 11.70%. Single crystal X-ray structural analysis showed this species to be exo-*3-(2′-nitrophenylthio)*-exo-5-*methoxytricyclo[2.2.1.$0^{2,6}$]heptane*, **15**. On the basis of spectral analysis, the species with R_f = 0.56 was shown to be exo-*3-(2′-nitrophenylthio)*-endo-*5-methoxytricyclo[2.2.1.$0^{2,6}$]heptane*.

When anhydrous acetic acid was used as solvent, recovery of the products was accomplished by distillation under vacuum using a liquid nitrogen condenser followed by dissolution in water, neutralization with sodium bicarbonate, and extraction with methylene chloride. The methylene chloride extracts were dried over anhydrous magnesium sulphate. Preparative tlc on silica gel using 1:3 ethyl acetate/65−110

Can. J. Chem. Downloaded from www.nrcresearchpress.com by 210.87.254.40 on 09/06/12
For personal use only.

Can. J. Chem. Downloaded from www.nrcresearchpress.com by 210.87.254.40 on 09/06/12
For personal use only.

petroleum ether gave six fractions with R_f's of 0.67, 0.62, 0.51, 0.37, 0.33, and 0.25, the latter two of which were identified by nmr as the 5-acetoxy-3-(2′-nitrophenylthio)nortricyclenes. Treatment of either acetoxynortricyclene with 1:1 sodium borohydride/lithium chloride in 2-propanol under reflux for 24 h gives the corresponding hydroxynortricyclene in 75–83% yields after standard work-up. Treatment of either hydroxynortricyclene with Jones' reagent in acetone at 25°C gives a single ketone with R_f = 0.27 on silica gel using 1:3 ethyl acetate/toluene. Yellow needles, mp 94–95°C, were obtained from 1:1 ethyl acetate/cyclohexane. *Anal.* calcd. for $C_{13}H_{11}NO_3S$: C 59.76, H 4.24, N 5.36, S 12.27%; found: C 60.02, H 4.35, N 5.02, S 12.31%.

The ketone was treated with one molar equivalent of tosylhydrazine in ethanol at reflux for 2 h to yield the corresponding tosylhydrazone in 78% yield. The tosylhydrazone was dissolved in anhydrous diethyl ether and reacted with 2 molar equivalents of 1:1 methyllithium/lithium bromide at 23°C for 4 h. Aqueous hydrolysis followed by extraction with methylene chloride gives 3-(2′-nitrophenylthio)-tricyclo[2.2.1.$0^{2,6}$]heptane in 69% yield based on the corresponding ketone.

X-ray structure determination

Crystal data are as follows.

$C_{14}H_{15}NO_3S$ fw = 277.3

Monoclinic, $P2_1/a$, a = 10.633(1), b = 13.637(1), c = 9.938(1) Å, β = 115.36(1)°, V = 1302.2 Å^3. Z = 4, ρ_c = 1.42 g cm^{-3}, λ(CuK$\bar{\alpha}$) = 1.54178 Å, μ(CuK$\bar{\alpha}$) = 22.0 cm^{-1}. Yellow prisms of **15** were obtained as described above. After establishing the space group from precession films, the data were collected at room temperature for a crystal of dimensions 0.34 × 0.34 × 0.39 mm with a Nonius CAD-4 diffractometer using Ni-filtered CuKα, at a take-off angle of 2.5°.

The intensities were collected by $\omega-2\theta$ scan techique using for ω scan angle 0.6° + 0.2 tan θ, with a maximum scan time of 90 s. Three standard reflections were used to monitor the intensity changes every 100 min of exposure time. Data were collected to 2θ limit of 152°. 2686 reflections were measured out of which 2445 (91%) were above threshold of $2\sigma(I_{net})$. The net intensities were corrected for Lorentz and polarization effects, but not for absorption.

The structure was solved by direct methods using the program MULTAN 78 (26). The E map revealed all the non-hydrogen atoms of the molecule.

Refinement was by block-diagonal least-squares with the weighting scheme:

$$\sqrt{w} = 1/\{1 + [(|F_o| - 10)/15]^2\}^{1/2} \text{ if } \sin^2\theta \geq 0.27$$

and

$$\sqrt{w} = [1/\{1 + [(|F_o| - 10)/15]^2\}^{1/2}](\sin^2\theta/0.27)$$

$$\text{if } \sin^2\theta < 0.27$$

The constants were chosen to make $\Sigma w(F_o - F_c)^2$ independent of $|F_o|$.

When R decreased to 0.07, the hydrogen atoms were located from a difference map. They were refined isotropically, but for all other atoms anisotropic temperature factors were used. The refinement was carried out only with the observed reflections, excluding three reflections which suffered form multiple diffraction ($\bar{2}56$, $\bar{2}75$, 407). Eight strongest reflections were corrected for extinction. In the final cycle, R = 0.039 and R_w = 0.040 and the mean and maximum parameter shifts for all atoms were 0.08σ and 0.48σ, respectively. The residual electron density distribution in the final difference map was within −0.41 (in the vicinity of S) to 0.22 e Å^{-3}. Scattering factors for non-hydrogen atoms were those of Hanson *et al.* (27) and for H those of Stewart *et al.* (28). Calculations were carried out with the NRCC system of programs by Ahmed *et al.* (29)

Acknowledgements

The authors wish to acknowledge the assistance of Mrs. H. M. Sheppard during the X-ray structure determination, and the aid of the Translation Bureau No. 798597, Multilingual Services Division, Department of the Secretary of State for translations of articles published in Russian.

1. P. L. Beaulieu, A. Kabo, and D. G. Garratt. Can. J. Chem. **58**, 1014 (1980).
2. (*a*) E. Lippmaa, T. Pehk, and J. Paasivirta. Org. Magn. Reson. **5**, 277 (1973); (*b*) Y. Marino, K. Kirchitau, and A. Yonazeki. Bull. Chem. Soc. Jpn. **40**, 1552 (1967).
3. (*a*) V. S. Watts and J. H. Goldstein. J. Chem. Phys. **46**, 4165 (1967); (*b*) K. Taci, R. Muneyuki, and H. Tanida. Can. J. Chem. **41**, 3142 (1963); (*c*) G. Schrumpf and W. Lüttke. Tetrahedron Lett. 2635 (1965).
4. T. C. Morrill, S. Malasanta, K. M. Warren,and B. E. Greenwald. J. Org. Chem. **40**, 3032 (1975).
5. (*a*) J. Bredt. J. Prakt. Chem. **121**, 153 (1929); (*b*) S. J. Cristol and R. T. LaLonde. J. Am. Chem. Soc. **80**, 4355 (1958).
6. N. S. Zefirov, N. K. Sadovaya, R. Sh. Akhmedova, I. V. Bodrikov, T. C. Morrill, A. M. Nersisyan, V. B. Rybakov, N. D. Saraceno, and Yu. T. Struchkov. Zh. Org. Khim. **16**, 580 (1980).
7. (*a*) D. G. Garratt and P. L. Beaulieu. J. Org. Chem. **44**, 3555 (1979); (*b*) N. S. Zefirov, N. K. Sadovaya, R. Sh. Akhmedova, and I. V. Bodrikov. Zh. Org. Khim. **14**, 662 (1978); Chem. Abstr. **89**, 42641 (1978); (*c*) S. J. Cristol, R. P. Arganbright, G. D. Brindell, and R. M. Heitz. J. Am. Chem. Soc. **79**, 6035 (1957); (*d*) W. A. Smit, N. S. Zefirov, I. V. Bodrikov, and M. Z. Krimer. Acta Chem. Res. **12**, 282 (1979); (*e*) A. S. Gybin, V. S. Bogdanov, M. Z. Krimer, V. A. Smit, L. A. Novgorodtseva, R. Sh. Akhmedova, N. K. Sadovaya, and N. S. Zefirov. Zh. Org. Khim. **15**, 1361(1979).
8. C. K. Johnson. ORTEP. Report ORNL-3794, revised. Oak Ridge National Laboratory, Tennessee.
9. K. J. Watson. Nature, **188**, 1102 (1960).
10. J. Trotter. Acta Crystallogr. **13**, 95 (1960).
11. J. Trotter. Acta Crystallogr. **12**, 232 (1959).
12. J. Trotter. Acta Crystallogr. **12**, 605 (1959).
13. R. E. Rosenfield, Jr., R. Parthasarathy, and J. D. Dunitz. J. Am. Chem. Soc. **99**, 4860 (1977).
14. M. Przybylska and D. G. Garratt. Can. J. Chem. **59**, 658 (1981).
15. (*a*) K. A. Potekhin, E. N. Kurkutova, Yu. T. Struchkov, V. N. Kirin, A. S. Koz'min, N. S. Zefirov, V. V. Ilyukhin, and N. V. Belov. Dokl. Akad. Nauk SSSR, **243**, 348 (1978); (*b*) **243**, 652 (1978).
16. (*a*) K. A. Potekhin, E. N. Kurkutova, Yu. T. Struchkov, R. Sh. Akhmedova, V. N. Kirin, A. S. Koz'min, and N. S. Zefirov. Dokl. Akad. Nauk SSSR, **242**, 341 (1978); (*b*) A. M. Nersisyan, S. V. Lindeman, V. G. Andrianov, Yu. T. Struchkov, R. Sh. Akhmedova, V. B. Rybakov, N. K. Sadovaya, and N. S. Zefirov. Cryst. Struct. Commun. **9**, 247 (1980).
17. (*a*) J. S. Ricci and I. Bernal. J. Am. Chem. Soc. (B), 806 (1970); (*b*) J. D. Korp, I. Bernal, R. F. Miller, J. C. Turley, L. Williams, and G. E. Martin. J. Cryst. Mol. Struct. **8**, 127 (1978); (*c*) J. D. Korp, I. Bernal, and G. E. Martin. J. Cryst. Mol. Struct. **11**, 11 (1981).
18. A. Kálmán and L. Párkányi. Acta Crystallogr. Sect. B, **36**, 2372 (1980).
19. P. L. Johnson, K. I. G. Reid, and I. C. Paul. J. Chem. Soc. (B), 946 (1971).
20. J. C. Turley and G. E. Martin. Spectrosc. Lett. **11**, 681 (1978).
21. G. E. Martin and J. C. Turley. J. Heterocycl. Chem. **15**, 609 (1978).
22. J. C. Turley and G. E. Martin. J. Heterocycl. Chem. **18**, 431 (1981).
23. W. J. Adams, H. J. Geise, and L. S. Bartell. Phys. Inorg.

Chem. **92**, 5013 (1970).
24. D. G. GARRATT. Can. J. Chem. **58**, 1327 (1980).
25. P. S. SKELL, J. C. DAY, and K. J. SHEA. J. Am. Chem. Soc. **98**, 1195 (1976).
26. P. MAIN, S. E. HULL, L. LESSINGER, G. GERMAIN, J. P. DECLERCQ, and M. M. WOOLFSON. MULTAN 78. A system of computer programmes for the automatic solution of crystal structures from X-ray diffraction data. Univs. of York, England, and Louvain-La-Neuve, Belgium. 1978.
27. H. P. HANSON, F. HERMAN, J. D. LEA, and S. SKILLMAN. Acta Crystallogr. **17**, 1040 (1964).
28. R. F. STEWART, E. R. DAVIDSON, and W. T. SIMPSON. J. Chem. Phys. **42**, 3175 (1965).
29. F. R. AHMED, S. R. HALL, M. E. PIPPY, and C. P. HUBER. NRC Crystallographic Programs for the IBM/360 System, Accession Nos. 133–147. J. Appl. Crystallogr. **6**, 309 (1973).

Can. J. Chem. Downloaded from www.nrcresearchpress.com by 210.87.254.40 on 09/06/12
For personal use only.

The reaction of tetrasulphur dinitride with norbornadiene; the crystal and molecular structure of $S_4N_2 \cdot C_7H_8$, an eight-membered $C_2S_4N_2$ heterocycle

HANS KOENIG AND RICHARD T. OAKLEY[1]
Department of Chemistry, University of Calgary, Calgary, Alta., Canada T2N 1N4

AND

A. WALLACE CORDES AND MARK C. NOBLE
Department of Chemistry, University of Arkansas, Fayetteville, AR 72701, U.S.A.

Received September 30, 1982

HANS KOENIG, RICHARD T. OAKLEY, A. WALLACE CORDES, and MARK C. NOBLE. Can. J. Chem. **61**, 1185 (1983).

The reaction of tetrasulphur dinitride with norbornadiene produces the 1:1 adduct $S_4N_2 \cdot C_7H_8$; X-ray crystallographic analysis of this compound reveals that olefin addition cleaves one of the sulphur–sulphur bonds of S_4N_2, yielding a novel eight-membered $C_2S_4N_2$ ring. Crystals of $S_4N_2 \cdot C_7H_8$ are monoclinic, space group $P2_1/c$, $a = 6.127(1)$, $b = 17.369(1)$, $c = 9.580(1)$ Å, $\beta = 106.74(1)°$, $V = 1003.8(5)$ Å^3, $Z = 4$. The structure was solved by direct methods and was refined by full-matrix least-squares procedures to $R = 0.039$. The S—S—N—S—N—S fragment of the $C_2S_4N_2$ ring is planar to within 0.15 Å. The S—C—C—S unit is folded out of this plane to produce a dihedral angle of 74.5°.

HANS KOENIG, RICHARD T. OAKLEY, A. WALLACE CORDES et MARK C. NOBLE. Can. J. Chem. **61**, 1185 (1983).

La réaction du dinitrure de tétrasoufre avec le norbonadiène donne l'adduit 1:1 $S_4N_2 \cdot C_7H_8$. L'analyse de ce composé par cristallographie de rayons-X révèle que l'addition d'oléfine clive une des liaisons soufre–soufre du S_4N_2 en donnant un nouveau cycle à 8 chaînons $C_2S_4N_2$. Les cristaux de $S_4N_2 \cdot C_7H_8$ sont monocliniques et appartiennent au groupe d'espace $P2_1/c$ avec $a = 6{,}127(1)$, $b = 17{,}369(1)$, $c = 9{,}580(1)$ Å, $\beta = 106{,}74(1)°$, $V = 1003{,}8(5)$ Å^3, $Z = 4$. On a résolu la structure par des méthodes directes et on l'a affinée par la méthode des moindres carrés (matrice entière) jusqu'à une valeur de $R = 0{,}039$. Le fragment S—S—N—S—N—S du cycle $C_2S_4N_2$ est plan à plus ou moins 0,15 Å. L'unité S—C—C—S est pliée hors de ce plan pour former un angle dièdre de 74,5°.

[Traduit par le journal]

Introduction

The orientation of the addition of 2*e*-olefins to tetrasulphur tetranitride S_4N_4 remained a controversial issue for many years (1). The correct mode of addition, in a 1,3-*S*,*S*-fashion, was finally confirmed by chemical degradation methods (2) and X-ray crystallography (3). A similar regiochemistry has since been observed for the addition of norbornadiene to phosphadithiatriazenes $R_2PS_2N_3$ (4). In the light of these findings and our recent report of the molecular and electronic structure of tetrasulphur dinitride S_4N_2 (5) we have investigated the reaction of S_4N_2 with olefins. In part, our work was stimulated by the observation that S_4N_2 forms a 1:1 adduct with dicyclopentadiene, for which the structure **1** was proposed (6). Esr spectroscopic analysis of the reaction suggested an alternative pathway, involving free radicals such as **2** (7). We report here that the reaction of S_4N_2 with norbornadiene produces an adduct of composition $S_4N_2 \cdot C_7H_8$. An X-ray crystal structure determination of this compound reveals that olefin addition cleaves the six-membered ring structure of S_4N_2, producing the novel eight-membered heterocycle **3**.

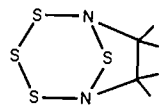

1

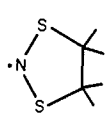

2

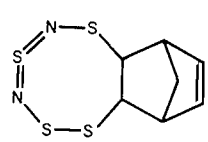

3

Experimental

Tetrasulphur dinitride was prepared in small quantities by the reaction of sulphur monochloride with aqueous ammonia (5). Ultraviolet–visible spectra were recorded on a Cary 219 spectrophotometer, and ^{1}H nmr spectra were recorded on an XL-200 NMR spectrometer. Chemical analyses were performed by Mr. Lada Malek.

Preparation of $S_4N_2 \cdot C_7H_8$ (3)

Equimolar solutions of S_4N_2 (freshly sublimed, 0.277 g, 1.78 mmol in 9 mL CS_2) and norbornadiene (0.166 g, 1.78 mmol in 9 mL CH_2Cl_2) were simultaneously added dropwise over a 10 h period (using a syringe pump) to a rapidly stirred reservoir of 200 mL of CH_2Cl_2. The resultant orange solution was evaporated to dryness and the residual oil eluted down a short (100 mm) silica column using 80:20 hexane:CH_2Cl_2 as eluting solvent. The orange–red band ($r_f \simeq 0.8$) was collected and the solvent removed from it to leave a semi-crystalline material which was further purified by chromatography down a 35 × 700 mm Bio-Beads S-X8 column using toluene as eluting solvent. Evaporation of the solvent from the orange–red fraction yielded orange crystals of $S_4N_2 \cdot C_7H_8$ **3** (68 mg, 0.276 mmol, 15%), which could be recrystallized from ether/toluene at −20°C as orange mica-like plates, mp 92–94°C. The compound is stable indefinitely in air as a solid and in solution (hexane). *Anal.* calcd. for $H_8C_7N_2S_4$: C 33.85, H 3.25, N 11.28; found: C 33.73, H 3.24, N 11.11. Ultraviolet and visible spectrum (CH_2Cl_2), λ_{max} (ϵ): 420 (2 × 10^3), 362 (3 × 10^3), 266 (4 × 10^3) nm (M^{-1} cm^{-1}). ^{1}H nmr ($CDCl_3$) δ: 6.45, 6.33 (m, $H_{5,6}$), 3.25, 3.21 (s, $H_{1,4}$), 2.81, 2.53 (d of d, $H_{2,3}$, J = 1.8, 6.6), 1.82, 1.68 (AB, $H_{7,7'}$, $J_{7-7'}$ = 9.5).

X-ray analysis of $S_4N_2 \cdot C_7H_8$ (3)

A small irregularly shaped crystal of $S_4N_2 \cdot C_7H_8$, mounted on a glass fiber, was used for data collection on an Enraf-Nonius CAD-4 diffractometer employing MoK_α ($\lambda = 0.71069$ Å) radiation. A least-squares calculation using the diffractometer settings for 25 carefully

[1]To whom all correspondence should be addressed.

Can. J. Chem. Downloaded from www.nrcresearchpress.com by 210.87.254.40 on 09/06/12
For personal use only.

Can. J. Chem. Downloaded from www.nrcresearchpress.com by 210.87.254.40 on 09/06/12
For personal use only.

TABLE 1. Atomic coordinates for $S_4N_2 \cdot C_7H_8$

Atom	x/a	y/b	z/c	B_{equiv}
S1	0.4940(1)	0.23912(3)	0.10672(6)	3.39(1)
S2	−0.0183(1)	0.27254(5)	−0.06300(6)	3.97(1)
S3	0.0010(2)	0.11024(4)	0.04595(7)	4.91(2)
S4	0.4846(1)	0.14045(4)	0.21291(7)	4.35(2)
N5	0.2401(4)	0.0947(1)	0.1490(2)	4.66(7)
N6	−0.0968(4)	0.1831(1)	−0.0353(3)	4.52(7)
C7	0.0885(5)	0.3187(1)	0.1096(3)	2.88(5)
C8	0.0808(6)	0.4064(2)	0.0757(3)	3.70(5)
C9	0.3467(6)	0.3061(1)	0.1896(3)	2.85(7)
C10	0.1246(6)	0.4459(2)	0.2193(3)	4.68(7)
C11	0.3098(6)	0.4185(2)	0.0477(3)	4.52(7)
C12	0.4459(5)	0.3887(2)	0.1925(3)	4.31(7)
C13	0.3403(8)	0.4348(2)	0.2868(3)	5.02(9)
H11	0.3375	0.4711	0.0327	
H11	0.3260	0.3884	−0.0285	
H10	0.0181	0.4732	0.2533	
H13	0.4155	0.4528	0.3789	
H12	0.6076	0.3907	0.2184	
H8	−0.0538	0.4227	0.0055	
H7	0.0019	0.2982	0.1661	
H9	0.3629	0.2832	0.2802	

centred reflections gave the following cell parameters (at 21°C):

$C_7H_8S_4N_2$ mw = 248.41

$a = 6.127(1)$, $b = 17.369(1)$, $c = 9.850(1)$ Å, $\beta = 106.74(1)°$, $V = 1003.8(5)$Å^3, $Z = 4$, $D_c = 1.64$ g cm^{-3}, $F_{000} = 512$, $\mu(MoK_\alpha) = 8.63$ cm^{-1}, space group $P2_1/c$.

Systematic absences of $h0l$ (l odd) and $0k0$ (k odd) uniquely indicated the space group $P2_1/c$. Reflections were measured using $\theta-\theta$ scans for 2θ from 4 to 50° (h = 0 to 7, k = 0 to 20, l = −11 to 11). The scan range was (1.3 + 0.35 tan θ) and the scan speed varied from 20 to 5 deg/min. Of the 1987 unique data collected, 399 reflections had $I < 3\sigma(I)$ and were considered unobserved. An empirical absorption correction based on psi scans gave correction factors which varied from 0.811 to 0.996. The intensities of three reflections (−1 13 −1, 2 5 −6, 3 5 −1) were measured periodically during the data collection; these varied by less than 4% and thus indicated crystal and electronic stability.

The structure was solved by direct methods (MULTAN80) (8) and refined by full-matrix least-squares techniques. The final cycle of refinement based on F^2 included 118 parameters (positional and anisotropic thermal parameters for all non-hydrogen atoms) and gave a parameter:reflection ratio of 1:13.5. Hydrogen atoms were included in the structure factor calculations at idealized positions (d(C—H) = 0.95 Å) with isotropic thermal parameters of 5.0 Å^2. The final R = 0.039 and R_w = 0.055. The weighting scheme used was $w = [\sigma^2(F) + 0.05F^2]^{-1}$ where $\sigma(F)$ was derived from counting statistics. The standard deviation of an observation of unit weight was 1.68. In the final cycle of refinement, the maximum shift/error was 0.42. The final difference map had maximum values of 0.6 e/Å^3. No secondary extinction correction was made. The atomic scattering factors for neutral atoms were those of Cromer and Waber (9) and the real and imaginary anomalous dispersion corrections were those of Cromer (10). The computer programs were those provided by the Enraf-Nonius SDP program package. Table 1 gives the atomic coordinates of all the atoms, and Table 2 provides the derived bond distances and valence angles. Table 3 (anisotropic thermal parameters) and the table of measured and calculated structure factors have been placed in the Depository of Unpublished Data.[2]

[2]The structure factor table and Table 3 are available, at a nominal charge, from the Depository of Unpublished Data, CISTI, National Research Council of Canada, Ottawa, Ont., Canada K1A 0S2.

TABLE 2. Bond distances and angles for $S_4N_2 \cdot C_7H_8$

Bond	Distance	Bond	Distance
S1—S4	2.017(1)	C7—C9	1.566(5)
S4—N5	1.651(3)	C9—12	1.555(4)
S3—N5	1.547(3)	C7—C8	1.557(4)
S3—N6	1.524(2)	C8—C11	1.520(6)
S2—N6	1.672(2)	C11—C12	1.521(4)
S1—C9	1.805(3)	C12—C13	1.506(5)
S2—C7	1.822(2)	C8—C10	1.525(4)
		C10—C13	1.311(5)

Bonds	Angle	Bonds	Angle
S4—S1—C9	102.7(1)	C7—C9—C12	102.3(2)
S1—S4—N5	111.7(1)	C8—C7—C9	102.0(2)
S4—N5—S3	138.6(2)	C9—C12—C13	105.5(2)
N5—S3—N6	130.1(1)	C9—C12—C11	101.0(2)
S2—N6—S3	140.3(2)	C7—C8—C10	104.8(2)
N6—S2—C7	107.4(1)	C7—C8—C11	101.7(2)
S1—C9—C7	115.2(2)	C8—C11—C12	93.9(2)
S2—C7—C9	116.6(2)	C11—C12—C13	100.4(3)
S1—C9—C12	111.1(2)	C12—C13—C10	108.3(3)
S2—C7—C8	104.4(2)	C13—C10—C8	106.7(3)
		C10—C8—C11	100.4(2)

Results and discussion

Reaction of S_4N_2 with 2e-olefins

The pericyclic reactions of conjugated sulphur–nitrogen rings provide an important means of analysing the nature of their frontier molecular orbitals. For example, the cycloaddition of 2e-olefins to S_4N_4 (11) and phosphadithiatriazenes (4) substantiates the theoretically predicted symmetries of their highest occupied and lowest unoccupied molecular orbitals. In contrast to these reactions, which afford virtually quantitative yields of $S_4N_2 \cdot$ 2olefin and $R_2PS_2N_3 \cdot$ olefin, the reaction of S_4N_2 with olefins (norbornadiene, dicyclopentadiene) is less specific, leading, primarily, to intractable polymeric materials of variable composition. However, soluble molecular species of formula $S_4N_2 \cdot$ olefin are also formed and, with appropriate preparative procedures, these compounds can be obtained in low to moderate yields.

The first such derivative was reported by Adkins and Turner, who were able to isolate and partially characterize a red–orange solid with the empirical formula $S_4N_2 \cdot C_{10}H_{12}$ from the reaction of S_4N_2 with dicyclopentadiene (6). On the basis of infrared and mass spectrometric results, they assigned to it a structure of the type **1**. They did not report the yield of the compound but, using their conditions, we have been unable to achieve yields better than 2–3%. We have focused our own synthetic work on the use of norbornadiene, in part because it affords an easily crystallizable product, but also because it avoids the possibility of a product which is a mixture of diastereomers (which appears to be the case for $S_4N_2 \cdot C_{10}H_{12}$). However, the major synthetic innovation involved not so much the choice of olefin as the method of mixing of the two reagents (S_4N_2 and norbornadiene). When high dilution addition techniques are employed instead of normal addition methods the proportion of intractable materials is markedly reduced. More importantly, the soluble fraction consists (based on tlc evidence) almost entirely of a single component, $S_4N_2 \cdot C_7H_8$ **3**, which can be purified by gel permeation chromatography and recrystallization to give yields of 15%.

Can. J. Chem. Downloaded from www.nrcresearchpress.com by 210.87.254.40 on 09/06/12
For personal use only.

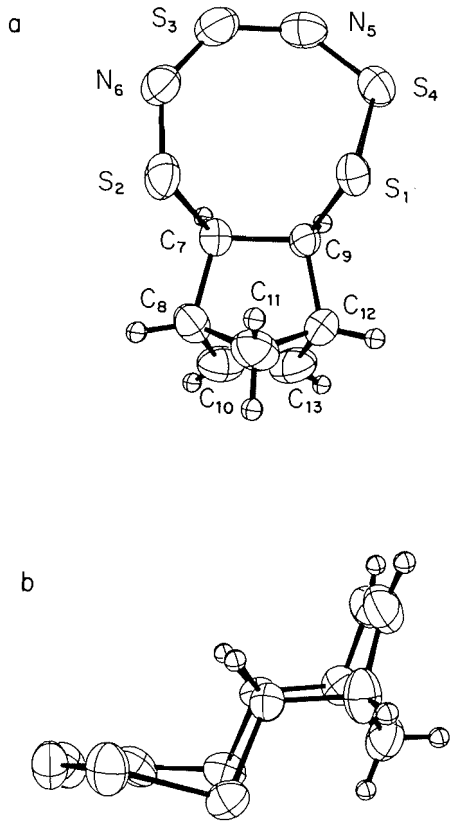

FIG. 1. (*a*) An ORTEP drawing of $S_4N_2 \cdot C_7H_8$ showing the atom numbering scheme, and (*b*) an alternative view illustrating the orientation of the C_7H_8 residue with respect to the S_4N_2 plane.

Some of the structural permutations possible for the cycloaddition of S_4N_2 and a 2*e*-olefin have been reviewed by Adkins and Turner (6). Many of these possibilities were immediately eliminated for $S_4N_2 \cdot C_7H_8$ by the appearance of its ^1H nmr spectrum, which shows a high multiplicity for the $H_{1,4}$, $H_{2,3}$, and $H_{5,6}$ resonances and thereby establishes an unsymmetrical mode of substitution for the norbornenyl group.[3] That the substituents are both sulphur is suggested by the δ-values of the $H_{2,3}$ signals (2.81, 2.53 ppm), which are quite different from those expected for *N*-substitution (ca. 4.5 ppm) (1*c*, 12). The relationship between **3** and the compound reported by Adkins and Turner cannot be established by ^1H nmr spectroscopy,[4] but can be inferred through a comparison of their uv–visible spectra. The dicyclopentadiene derivative exhibits an almost identical pattern of absorption bands (λ_{max} = 262, 350, and 420 nm) with the same relative extinction coefficients. Clearly the chromaphores in $S_4N_2 \cdot C_{10}H_{12}$ and $S_4N_2 \cdot C_7H_8$ are the same. However, while the spectroscopic information on the latter are consistent with the proposed structure **3**, absolute confirmation of this assignment has required the use of X-ray crystallography.

Molecular structure of $S_4N_2 \cdot C_7H_8$

Two ORTEP drawings of $S_4N_2 \cdot C_7H_8$ **3** are shown in Fig. 1. The structure (which exhibits no unusually short intermolecular contacts) reveals that the $S_4N_2 \cdot C_7H_8$ molecule is indeed formed via the *exo* addition of a S—S σ-bond of S_4N_2 across a π-bond of norbornadiene.[5] The molecule thus consists of an eight-membered $C_2S_4N_2$ ring. This ring possesses an approximately planar (to within 0.15 Å) S(1)—S(4)—N(5)—S(3)—N(6)—S(2) sequence with the S(1)—C(9)—C(7)—S(2) unit (which is itself planar to within 0.04 Å) folded out of this plane to produce a dihedral angle of 74.5°. Within the $C_2S_4N_2$ ring there are variations in the N—S distances which are reminiscent of those observed in S_4N_2 itself (5). Thus the bonds to S(3) (mean 1.536 Å) are significantly shorter than those to S(4) and S(2) (mean 1.662 Å). The S(1)—S(4) bond (2.017 Å) is slightly shorter than in S_4N_2 (2.061 Å). The S(1)—S(2) separation (3.156 Å) is shorter than expected for a normal non-bonded contact. The endocyclic angles at sulphur and nitrogen are all somewhat larger than in S_4N_2 itself, as would be expected following the expansion of the ring. The structural parameters of the norbornenyl residue are all normal.

Conclusion

The rupture of the cyclic skeleton of S_4N_2 by norbornadiene represents a surprising departure from other sulphur nitride/olefin electrocyclic reactions. Indeed the attack of the olefin at a sulphur–sulphur σ-bond is not easily rationalized on symmetry grounds; olefin addition across a disulphide linkage represents a forbidden $2_s + 2_s$ process. However, the generation of free radicals in the reaction (7) suggests that a non-concerted di-radical mechanism is involved. The need for high dilution addition techniques, which would suppress competitive bimolecular reactions and thereby favour ring closure, supports this conclusion. The intractable materials produced are probably the result of a radical polymerization.

Acknowledgments

We thank the Natural Sciences and Engineering Research Council of Canada, the Research Corporation, the National Science Foundation (EPSCOR grant ISP 8011447), and the State of Arkansas for financial support. We also acknowledge NSERC for a University Research Fellowship (to R.T.O.) and a Summer Undergraduate Scholarship (to H.K.).

1. (*a*) M. BECKE-GOEHRING and D. SCHLÄFER. Z. Anorg. Allg. Chem. **356**, 234 (1968). (*b*) R. GLEITER. J. Chem. Soc. A, 3174 (1970); (*c*) M. R. BRINKMAN and C. W. ALLEN. J. Am. Chem. Soc. **94**, 1550 (1972).
2. W. L. MOCK and I. MEHOTRA. J. Chem. Soc. Chem. Commun. 123 (1976).
3. (*a*) VON G. ERTT and J. WEISS. Z. Anorg. Allg. Chem. **420**, 155 (1976); (*b*) A. M. GRIFFIN and G. M. SHELDRICK. Acta Crystallogr. B**31**, 895 (1975).
4. N. BURFORD, T. CHIVERS, A. W. CORDES, W. G. LAIDLAW, M. C. NOBLE, R. T. OAKLEY, and P. N. SWEPSTON. J. Am. Chem. Soc. **104**, 1282 (1982).
5. (*a*) T. CHIVERS, P. W. CODDING, and R. T. OAKLEY. J. Chem. Soc. Chem. Commun. 584 (1981); (*b*) T. CHIVERS, P. W. CODDING, W. G. LAIDLAW, S. W. LIBLONG, R. T. OAKLEY, and M. TRSIC. J. Am. Chem. Soc. In press.
6. R. R. ADKINS and A. G. TURNER. Inorg. Chim. Acta, **25**, 233 (1977).

[3] ^1H nmr assignments were confirmed by homonuclear decoupling experiments.

[4] The ^1H nmr spectrum of $S_4N_2 \cdot C_{10}H_{12}$ is uninterpretable because of the superposition of multiplets arising from different stereoisomers. By contrast, the uv–visible spectra of these isomers will be, to a first approximation, independent of the organic moiety, since the transitions are confined to the S_4N_2 fragment.

[5] Specific *exo* addition is also observed in the reaction of S_4N_4 (3) and $R_2PS_2N_3$ molecules (4) with norbornadiene.

7. S. A. FAIRHURST and L. H. SUTCLIFFE. J. Chem. Soc. Faraday Trans. I, 1490 (1980).
8. P. MAIN, S. J. FISKE, S. E. HULL, L. LESSINGER, G. GERMAIN, J.-P. DECLERCQ, and M. M. WOOLFSON. 1980. MULTAN80 — a system of computer programs for the automatic solution of crystal structures from X-ray diffraction data. University of York, England and University of Louvain, Belgium.
9. D. T. CROMER and J. T. WABER. International tables for X-ray crystallography. Vol. IV. Kynoch Press, Birmingham. 1974.
10. D. T. CROMER. Acta Crystollogr. **18**, 17 (1965).
11. T. YAMABE, K. TANAKA, A. TACHIBANA, K. FUKUI, and H. KATO. J. Phys. Chem. **83**, 767 (1979).
12. (*a*) T. SHIELDS and A. N. KRANTZ. J. Am. Chem. Soc. **91**, 5415 (1969); (*b*) R. HIUSGEN, L. MÖBINS, G. MÜLLER, H. STANGEL, G. SZERMIER, and J. M. VERNON. Chem. Ber. **98**, 3992 (1965); (*c*) W. H. MUELLER and P. E. BUTLER. J. Am. Chem. Soc. **88**, 2867 (1966).

Can. J. Chem. Downloaded from www.nrcresearchpress.com by 210.87.254.40 on 09/06/12
For personal use only.

Échelle d'acidité dans les mélanges eau–oxydipropionitrile. II. Cas des mélanges eau–oxydipropionitrile. Application à l'extraction

J. Y. GAL, M. PERSIN ET B. CASTELAS

Laboratoire de chimie analytique de l'université des sciences et techniques du Languedoc, Place Eugène Bataillon, 34060 Montpellier Cedex, France

Reçu le 26 avril, 1982[1]

J. Y. GAL, M. PERSIN et B. CASTELAS. Can. J. Chem. **61**, 1189 (1983).

L'étude des réactions acide–base dans les mélanges eau–oxydipropionitrile à l'aide des électrodes de verre et à hydrogène permet de déterminer les pK_a de quelques couples dans ces milieux. Il est alors possible de disposer de tampons susceptibles de fixer le niveau d'acidité dans les mélanges se séparant lors de la démixtion. L'extraction de divers acides, bases et chélatants par l'oxydipropionitrile montre que les rendements de celles-ci sont très influencés par la nature des ions présents dans la phase aqueuse. La connaissance des paramètres de transfert des diverses espèces présentes constitue une donnée importante permettant d'orienter la recherche des conditions d'extraction les plus favorables.

J. Y. GAL, M. PERSIN, and B. CASTELAS. Can. J. Chem. **61**, 1189 (1983).

The study of acid–base reactions in water–oxydiproprionitrile mixtures using glass and hydrogen electrodes allows for the determination of the pK_a for some couples in these media. It then becomes possible to develop buffers capable of fixing the acidity level in mixtures undergoing separation during demixtion. The extraction with oxydiproprionitrile of various acids, bases, chelating agents shows that the yields are greatly influenced by the nature of the ions present in the aqueous phase. Knowing the transfer parameters of the various species is an important factor in orienting the research for the most favorable extraction conditions.

[Journal translation]

Can. J. Chem. Downloaded from www.nrcresearchpress.com by 210.87.254.105 on 09/06/12
For personal use only.

Introduction

Dans un précédent mémoire (1) nous avons décrit les propriétés de quelques couples acide–base dans l'oxydipropionitrile[2] pur. Ce solvant est intéressant car il est fortement dissociant et moins basique que l'eau. On peut donc y titrer des bases relativement faibles. Les mélanges eau–oxydipropionitrile présentent une importante lacune de miscibilité comprise entre 0,018 et 0,6 en fraction molaire d'oxydiopropionitrile, il était naturel de tenter d'utiliser ce solvant en extraction liquide–liquide. Au cours du présent mémoire, nous avons tout d'abord étudié les propriétés acido-basique de quelques couples dans les mélanges eau–oxydipropionitrile afin de pouvoir disposer de tampons efficaces dans les deux phases se séparant à la démixtion. Cette étude préliminaire permet alors d'envisager la réalisation d'extractions sélectives en milieu de pH contrôlé. La seconde partie de notre mémoire est consacrée à l'étude de différents effets de sels sur l'extraction d'acides, de bases et d'un chélatant: la 1,10-phénanthroline; on y met en particulier en évidence l'influence de l'anion associé lors de l'extraction de certains cations. La connaissance des paramètres de solvatation de divers ions déjà étudiés par ailleurs (2) permet d'orienter de façon judicieuse la mise au point d'extraction quantitative.

Partie expérimentale

Synthèse et purification du solvant

L'établissement d'une échelle d'acidité dans les mélanges eau–oxydipropionitrile nécessite l'obtention d'un solvant particulièrement propre. Le solvant a été synthétisé au laboratoire selon le protocole décrit dans un précédent mémoire (1). L'usage d'un tel solvant n'est cependant pas envisageable directement, celui-ci contenant une impureté amphotère acide–base à concentration voisine de 10^{-3} *M*. Une chromatographie du solvant sur colonne d'alumine neutre permet d'éliminer totalement cette impureté; le solvant obtenu a une conductivité spécifique voisine de 10^{-7} Ω^{-1} cm^{-1}, il est alors conservé sur tamis moléculaire 4 Å.

Réactif

Les acides et les bases utilisés sont des produits pour analyse Prolabo, les sels de tétraalkylammonium sont des produits des établissements K et K. Les agents extractants tripyridyl-symtriazine, dipyridyle et 1,10-phénanthroline proviennent des établissements Merck.

Réalisation des mesures

Les titrages acido-basique ont été réalisés en utilisant une électrode de verre Tacussel ou une électrode à hydrogène constituée d'un carré de platine platiné de 1 cm^2 de surface. Les mesures des potentiels ont été effectuées à l'aide d'un millivoltmètre Tacussel type S6; la température était régulée à 25°C. Les bases ont été titrées avec de l'acide perchlorique 0,1 *M* préparé directement dans le milieu étudié, les acides ont été titrés par la butylamine 0,1 *M*. Les potentiels sont rapportés par rapport à une électrode de référence $Ag \downarrow / Ag^+$ 10^{-2} *M* fonctionnant dans le milieu étudié.

Pour les manipulations d'extraction nous avons déterminé les concentrations des espèces dans chacune des phases par spectrophotométrie à l'aide d'un spectrophotomètre Jean et Constant. Les volumes respectifs des deux phases mises en contact initialement sont egaux.

Résultats expérimentaux

Étude de l'acidité dans les mélanges eau–oxydipropionitrile

Les résultats présentés ont été obtenus en utilisant les électrodes à hydrogène et de verre qui sont indicatrices de l'activité du proton dans tous les mélanges. Le fonctionnement de l'électrode à hydrogène s'avère cependant plus délicat surtout dans les milieux riches en solvant organique par suite de la lenteur de l'établissement des équilibres. Nous l'avons surtout utilisée pour la corrélation des diverses échelles, les titrages classiques ont été effectués à l'aide de l'électrode de verre après étalonnage de celle-ci au moyen de solutions tampons préparées dans les divers milieux.

[1]Révision reçue le 23 novembre, 1982.

[2]$C_6H_8N_2O$.

Can. J. Chem. Downloaded from www.nrcresearchpress.com by 210.87.254.105 on 09/06/12
For personal use only.

TABLEAU 1. Echelle d'acidité dans l'eau saturée d'oxydipropionitrile

Couple acide–base	pK_a $x = 0{,}018$	pK_a H_2O (4)
Acide perchlorique	Fort	Fort
Acide nitrique	Fort	Fort
Acide paratoluène-sulfonique	Fort	Fort
Acide benzoïque	4,2	4,2
Acide acétique	4,8	4,7
Ammoniaque	9,2	9,2
Pyridine	5,2	5,2
Butylamine	10,6	10,6

(a) *Cas des mélanges riches en eau*

L'ensemble des résultats expérimentaux montre que les pK_a mesurés dans les divers mélanges sont sensiblement identiques à ceux observés dans l'eau. Ceci s'explique avant tout par la nature très différente des deux cosolvants. Tous ces milieux présentent une basicité probablement voisine de celle de l'eau puisque les quantités ajoutées d'ODPN, solvant moins basique que l'eau, sont très faibles (1). L'espèce la plus acide se trouve pratiquement être toujours l'ion H_3O^+ et l'origine de l'échelle d'acidité est peu modifiée par rapport à l'eau. Dans le tableau 1 nous avons reporté les valeurs mesurées dans l'eau saturée d'oxydipropionitrile ($X_{ODPN} = 0{,}018$). En première approximation on peut donc utiliser les valeurs de $pK_a^{H_2O}$ pour estimer les pK_a dans l'eau saturée d'ODPN de nombreux couples acide–base (tableau 1).

Les comportements des acides et des bases dans les mélanges eau–oxydipropionitrile riches en eau sont voisins de ceux observés dans les mélanges similaires eau – carbonate de propylène de basicité sensiblement équivalente (3).

(b) *Cas des mélanges riches en solvant organique*

Au contraire du cas précédent les pK_a mesurés sont très dépendants de la quantité d'eau présente dans le mélange. Comme nous le verrons par la suite la basicité du milieu augmente avec la quantité d'eau ajoutée, l'origine de l'échelle d'acidité se déplace vers les milieux acides au fur et à mesure de la diminution de la concentration en eau du mélange. L'analyse de l'évolution du comportement des différents couples acide–base permet de formuler les remarques suivantes.

De tous les acides minéraux usuels étudiés seul l'acide perchlorique est toujours totalement dissocié quel que soit la composition du milieu ce qui est en bon accord avec la relativement bonne solvatation de l'anion perchlorate dans tous les mélanges (2). Pour les autres acides minéraux totalement dissociés dans l'eau (HCl, HNO_3, H_2SO_4) la dissociation n'est totale que pour les milieux les plus riches en eau, ce qui est également en accord avec la très faible solvatation des anions dans les mélanges H_2O–ODPN (2). L'ensemble des autres acides organiques se comportent de manière identique et présentent une élévation de leur pK_a au fur et à mesure de l'augmentation de la fraction molaire en ODPN (Tableau 2).

Pour les couples de type B/HB^+ la tendance est également à l'élévation du pK_a au fur et à mesure de la diminution de la teneur en eau. Nous avons examiné plus en détail les variations de la solvatation des espèces responsables de cette évolution des pK_a.

(c) *Corrélation des différentes échelles d'acidité*

La corrélation des échelles d'acidité de façon approximative n'est possible que par la connaissance du paramètre de solvatation $\gamma(H^+)$ du proton, celui-ci peut être obtenu en réalisant les piles suivantes dans l'eau et chacun des mélanges:

$$H^+/H_2 \mid \text{Pt platiné} \parallel Fc/Fc^+ \mid Pt$$

La mesure des potentiels normaux de cette pile dans chacun des milieux par rapport au couple de référence Ferrocène–Ferricinium permet de déterminer le coefficient d'activité de transfert $\gamma(H^+)$ du proton au moyen de la relation:

$$\log \gamma(H^+) = \frac{{}^{s}E^0_{H^+/H_2} - {}^{E}E^0_{H^+/H_2}}{0{,}059} \qquad \text{à } t = 25°C$$

ou ${}^{s}E^0_{H^+/H_2}$ est le potentiel normal apparent du couple H^+/H_2 dans le mélange et ${}^{E}E^0_{H^+/H_2}$ est le potentiel normal apparent du couple H^+/H_2 dans l'eau.

Nous avons pu vérifier le fonctionnement Nernstien de cette pile dans tous les milieux, cependant le temps de réponse est allongé à quelques minutes lorsque la fraction molaire en oxydipropionitrile augmente dans les milieux riches en solvant organique. L'ensemble des résultats est rassemblé dans le tableau 3.

Ceux-ci montrent que dans les milieux très riches en eau la présence d'oxydipropionitrile affecte peu log $\gamma(H^+)$. Par conséquent la basicité du mélange n'est pas modifiée par les traces d'oxydipropionitrile conformément à la faible basicité de ce solvant. Au contraire dans les milieux riches en oxydipropionitrile l'addition d'eau entraine une variation importante de log $\gamma(H^+)$ qui montre que la basicité du milieu augmente considérablement; le milieu de composition 0,6 correspondant à l'une des phases qui apparait à la démixtion présente une basicité très voisine de celle de l'eau pure. Il est dès lors possible de corréler entre elle les différentes échelles d'acidité; le décalage de chacune d'elles par rapport à l'eau étant donné par la valeur de log $\gamma(H^+)$, Fig. 1. On peut expliquer aisément l'affaiblissement général des acides HA ou HB^+ dans les milieux riches en oxydipropionitrile par la solvatation de plus en plus faible du proton.

L'ensemble des résultats mentionnés précédemment montre qu'il est possible de disposer de divers mélanges tampons dans une large gamme de pH. Nous allons maintenant étudier les possibilités d'utilisation de l'oxydipropionitrile pour réaliser des extractions à pH contrôlé; ce milieu est à priori intéressant car sa forte constante diélectrique rend possible l'emploi de méthodes électrochimiques d'analyse en phase organique, ce qui s'avère impossible lorsque l'on utilise des solvants comparables au chloroforme ou au tétrachlorure de carbone. Afin de préciser les conditions à réaliser nous aborderons dans ce mémoire le comportement de divers réactifs lors du processus d'extraction par l'oxydipropionitrile.

Extraction des acides et des bases par l'oxydipropionitrile

Une solution d'eau saturée d'oxydipropionitrile contenant un acide ou une base à la concentration C_0 est agitée avec le même volume de solution d'oxydipropionitrile saturé d'eau. Après séparation le dosage dans chacune des deux phases de l'acide ou de la base conduit au coefficient de distribution défini par

$$K_D = \overline{|A|}_s / |A|_E$$

(a) *Coefficient de distribution de quelques acides*

Les résultats du tableau 4 montrent que les acides sont plus ou moins extraits selon la nature de l'anion présent.

Dans le cas des acides totalement dissociés dans les deux phases de démixtion tel $HClO_4$, HNO_3, HCl ... l'équilibre d'extraction est du type:

$$H_E^+ + A_E^- \rightleftharpoons H_s^+ + A_s^-$$

Comme les données concernant la solvatation nous ont montré

Can. J. Chem. Downloaded from www.nrcresearchpress.com by 210.87.254.105 on 09/06/12
For personal use only.

TABLEAU 2. Échelles d'acidité dans les milieux riches en oxydipropionitrile

Couple acide–base	H_2O (4)	pK_a x = 0,6	x = 0,8	x = 0,9 ±0,1	x = 0,95	x = 0,998
Perchlorique	F	F	F	F	F	F
Nitrique	F	F	F	3,7	5,2	7,5
Chlorhydrique	F	F	F	4,1	5,4	7,6
Sulfurique (I)	F	F	F	F	F	5,1
Sulfurique (II)	1,9	5,6	8,1	7,5	8,5	11,5
Monochloracétique	2,9		8,3	10,0	11,1	14,5
Trichloracétique	0,7	3,2	4,5	4,8	5,7	9,1
Oxalique (I)	1,3	4,4	5,9	7,0	8,4	11,1
Oxalique (II)	4,3		9,6	10,2		14,3
Picrique	0,4	F	F	4,0	4,6	8,5
Benzoïque	4,2	6,6		11,5		16,4
Acétique	4,7					
Butylamine	10,6	10,8	12,1	14,1	14	16,8
Dibutylamine	11,3	11,1		13,6	14,6	17,4
Ammoniaque	9,2	9,6		12,1	12,6	15,0
Morpholine	8,7	9,5		11,9	13,0	14,9
N,*N*-diéthylaniline	6,5	6,1	6,6	7,9	8,7	11,0
Pyridine	5,2	4,9		8,0	8,8	10,9
Hydroxy-8-quinolèine	4,9	4,5		6,5	7,6	9,7
1,10-Phénanthroline	4,9	5,3	6,4	8,2	9,2	11,8
Aniline	4.6	4.0	4,9	5,9	6,6	8,9

TABLEAU 3. Variation de log $\gamma(H^+)$ dans différents mélanges eau–oxydipropionitrile

Fraction molaire x_{ODPN}	$^{s}E^{0}_{H^+/H_2}$ (volt)	log $\gamma(H^+)$ ±0,1
0	−0,396	0
0,006	−0,400	0
0,009	−0,400	0
0,012	−0,400	0
0,015	−0,400	0
0,018	−0,400	0
0,60	−0,400	0
0,70	Non déterminée	
0,80	−0,358	+0,6
0,90	−0,306	+1,5
0,95	−0,270	+2,1
0,998	−0,143	+3,95

que le proton est préférentiellement solvaté par la phase aqueuse on doit s'attendre à une extraction de l'acide d'autant plus prononcée que l'anion associé est mieux solvaté par la phase organique. Dans celle-ci l'ordre de solvatation a été déterminé (2):

$$ClO_4^- > NO_3^- > Cl^-$$

Ces données sont en bon accord avec l'importance des coefficients de distribution observés:

$$HClO_4 > HNO_3 > H_2SO_4 > HCl$$

On peut toutefois noter que parmi les acides minéraux usuels seul l'acide perchlorique est extrait de façon importante, la même conclusion s'applique à l'acide picrique dont l'anion très volumineux peut être relativement facilement solvaté par la phase organique, ces résultats sont en tous points analogues à ceux observés dans les mélanges eau – carbonate de propylène (5, 6).

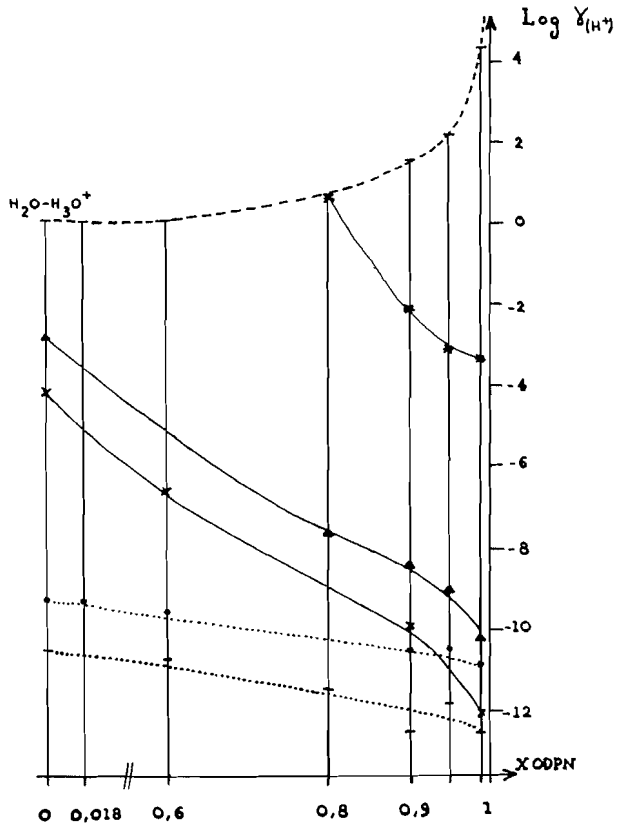

FIG. 1. Variation log $\gamma(H^+)$ et des pK_a de quelques acides dans les mélanges H_2O–ODPN; ● ammoniaque, × acide benzoique, – butylamine, *acide chlorhydrique, ▲ acide monochloracétique.

Dans le cas des autres acides peu dissociés dans les deux phases, ceux-ci sont extraits principalement à l'état de molécules, le coefficient de distribution rend compte de leur affinité pour chacune des deux phases. On peut remarquer que la pro-

Can. J. Chem. Downloaded from www.nrcresearchpress.com by 210.87.254.105 on 09/06/12
For personal use only.

TABLEAU 4. Extraction de quelques acides par l'oxydipropionitrile

Acide	log K_D	Taux de recouvrement %
Perchlorique	−0,18	98,7
Nitrique	−1,11	97
Chlorhydrique	−1,71	97
Sulfurique	−1,68	99
Picrique	+0,51	97
Acétique	−0,23	97
Monochloracétique	−0,36	99
Trichloracétique	−0,06	99
Phosphorique	−1,83	98

TABLEAU 5. Effet de la présence de cation sur le rendement d'extraction des acides forts

Acide	Sel		Rendement %
HCl 0,1 *M*	—		2
HCl 0,01 *M*	Bu_4NCl	0,1 *M*	3,5
HCl 0,01 *M*	NaCl	0,1 *M*	3,5
HNO_3 0,1 *M*	—		7
HNO_3 0,01 *M*	$NaNO_3$	0,1 *M*	12,5
$HClO_4$ 0,1 *M*	—		39
$HClO_4$ 0,01 *M*	Et_4NClO_4	0,1 *M*	20
$HClO_4$ 0,01 *M*	$NaClO_4$	0,1 *M*	51

portion d'acide passant dans la phase organique et loin d'être négligeable.

(b) *Effet de sel sur l'extraction des acides forts*

Le tableau 5 montre que la présence d'un sel dont l'anion est commun à l'acide extrait modifie considérablement le rendement d'extraction de ce dernier. Ce résultat est particulièrement net dans le cas de l'acide perchlorique où le rendement passe de 39% en l'absence de sel, à 20% en présence de perchlorate de tétraéthylammonium et 51% en présence de perchlorate de sodium. On peut expliquer ce phénomène par une compétition entre l'extraction de l'acide et du sel. Dans le cas d'un sel présentant un cation ammonium quaternaire il y a abaissement du rendement de l'extraction de l'acide et extraction préférentielle du sel dont le cation ammonium se trouve mieux solvaté par la phase organique que le cation H^+; au contraire l'utilisation d'un sel contenant un cation minéral augmente le rendement par suite de la mauvaise solvatation de ce dernier par la phase organique. Pour l'acide nitrique et l'acide chlorhydrique ces variations sont bien plus faibles à cause de la mauvaise solvatation des ions nitrate et chlorure par la phase organique.

Extraction d'une substance chélatante: la 1,10-phénanthroline

(a) *Étude de l'influence du pH de la phase aqueuse*

La 1,10-phénanthroline (oph) est une base de pK_a 4,9 en phase aqueuse et 5,3 dans l'ODPN saturé d'eau. Il en résulte que selon le pH elle sera extraite soit à l'état de molécule oph ou d'ion $ophH^+$, dans ce dernier cas la présence d'anions doit modifier les conditions d'extraction. L'analyse du tableau 6 montre qu'en milieu tampon ammoniacal de pH 9,2 l'extraction est peu sensible à la nature de l'ion associé au cation NH_4^+; on extrait la molécule de 1,10-phénanthroline. En milieu acide le rendement de l'extraction dépend de l'acide utilisé pour imposer le pH. Le rendement est d'autant plus élevé que l'anion de l'acide présente d'affinité pour la phase organique.

(b) *Modification du rendement en présence de sels*

En milieu acide perchlorique le rendement est peu affecté par

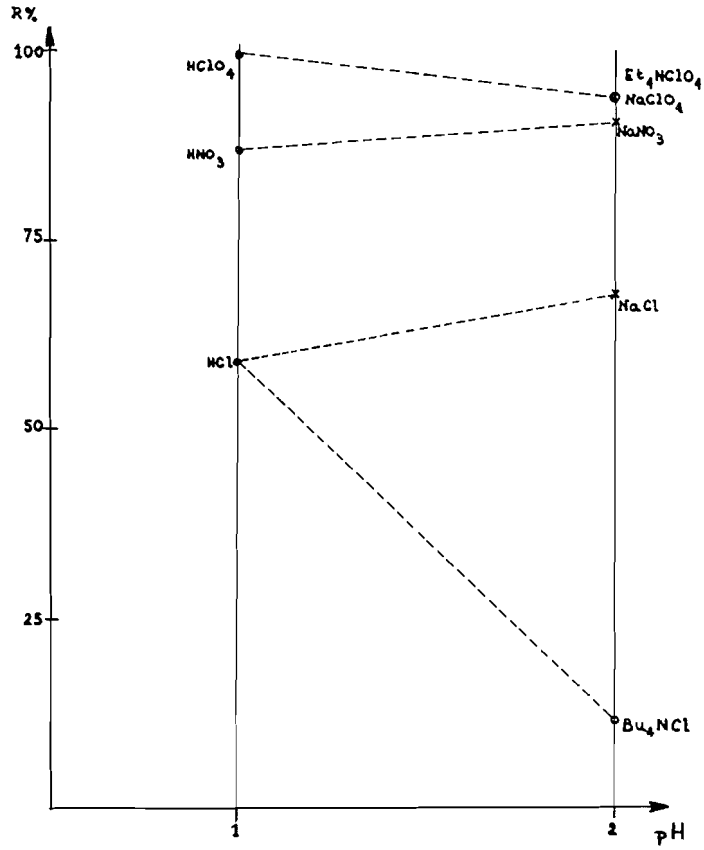

FIG. 2. Rendement d'extraction de la 1,10-phénanthroline en milieu acide en présence de divers sels à la concentration 0,1 *M*.

la présence de sels, les ions Et_4N^+ ou Na^+ ne perturbent pas l'extraction de $ophH^+$ ClO_4^-.

En milieu acide chlorhydrique la présence d'ion Bu_4N^+ diminue fortement le rendement d'extraction de $ophH^+$ Cl^- au profit de Bu_4N^+ Cl^-; la présence d'un petit cation Na^+ peu solvaté par la phase organique renforce au contraire l'extraction de $ophH^+$ Cl^- (Fig. 2). En milieu tamponné le rendement dépend de l'anion du sel ajouté si celui-ci présente un cation identique à celui de la base du tampon, ainsi en milieu tampon chloracétique on extrait le chloracétate de 1,10-phénanthrolinium, l'addition de perchlorate de sodium favorise l'extraction du perchlorate de 1,10-phénanthroline. Dans le cas d'un tampon imposant un pH en phase aqueuse supérieur au pK_a de la 1,10-phénanthroline les effets de sels sont moins nets, l'extraction s'effectuant à l'état de molécules.

Il apparait que l'incidence des cations ou anions parasites en solution peut être aisément prévue par la connaissance des grandeurs de transfert de ceux-ci entre les deux phases de démixtion, il est dès lors possible d'orienter les conditions optimales d'extraction de façon raisonnée. Les résultats obtenus constituent une bonne vérification des grandeurs de transfert de quelques anions déjà déterminées (1, 2).

Conclusions

Cette étude montre qu'il est possible d'utiliser certains couples acide−base comme substances tampons dans les deux zones de démixtion des mélanges eau oxydipropionitrile. L'étendue de l'échelle de pH utilisable dans les mélanges eau−oxydipropionitrile est réduite à une douzaine d'unités par suite de la basicité importante de l'eau par rapport à

TABLEAU 6. Extraction de la 1,10-phénanthroline 10^{-3} *M* dans différents milieux

Milieux tampons	Sels ajoutés 0,1 *M*	pH phase riche en eau	Rendement extraction %
$HClO_4$ 0,1 *M*	—	1	98
$HClO_4$ 0,01 *M*	Et_4NClO_4	2,1	94
$HClO_4$ 0,01 *M*	$NaClO_4$	2,1	94
HCl 0,1 *M*	—	1	59
HCl 0,01 *M*	Bu_4NCl	2,1	12
HCl 0,01 *M*	Et_4NClO_4	2,1	26
HCl 0,01 *M*	NaCl	2,1	68
HNO_3 0,1 *M*	—	1	87
HNO_3 0,01 *M*	$NaNO_3$	2,1	91
CH_2ClCO_2H/CH_2ClCO_2Na 0,1 *M*	—	2,8	71
CH_2ClCO_2H/CH_2ClCO_2Na 0,01 *M*	$NaClO_4$	2,8	98
CH_2ClCO_2H/CH_2ClCO_2Na 0,01 *M*	NaCl	2,8	80
CH_3CO_2H/CH_3CO_2Na 0,1 *M*	—	4,7	83
CH_3CO_2H/CH_3CO_2Na 0,01 *M*	$NaClO_4$	4,7	98
CH_3CO_2H/CH_3CO_2Na 0,01 *M*	NaCl	4,7	82
NH_3/NH_4Cl 0,1 *M*	—	9,2	90
NH_3/NH_4Cl 0,01 *M*	Bu_4NCl	9,2	84
NH_3/NH_4Cl 0,01 *M*	NaCl	9,2	95
NH_3/NH_4NO_3 0,1 *M*	—	9,2	89

l'oxydipropionitrile.

L'utilisation de l-oxydipropionitrile comme solvant d'extraction est intéressante par suite du caractère dissociant des milieux se séparant à la démixtion; ce qui constitue une originalité par rapport aux solvants inertes classiquement utilisés ($CHCl_3$, CCl_4). La possibilité d'extraire certaines substances sous forme ionique permet de jouer sur la nature du contre-ion extrait pour modifier les rendements d'extraction. Les prévisions de ces derniers à partir de la connaissance des paramètres de transfert γ sont vérifiées expérimentalement de façon satisfaisante. On dispose alors d'un paramètre supplémentaire qui permet d'orienter les séparations et de les rendre quantitatives dans certaines conditions par ajout d'un contre-ion bien solvaté par la phase organique se séparant lors de la démixtion.

1. J. Y. GAL et M. PERSIN. Can. J. Chem. **59**, 2491 (1981).
2. J. Y. GAL, D. DE BARROS, M. PERSIN et F. PERSIN. J. Electroanal. Chem. **99**, 347 (1979).
3. F. QUENTEL, J.Y. CABON, M. L'HER et J. COURTOT-COUPEZ. C. R. Acad. Sci. Paris Ser. C., **284**, 917 (1977).
4. G. CHARLOT. Chimie analytique générale. Tome I. Masson, Paris. 1967.
5. J. Y. CABON, M. L'HER et J. COURTOT-COUPEZ. J. Chem. Res. M, 4301 (1978).
6. J. Y. CABON, M. L'HER et J. COURTOT-COUPEZ. J. Chem. Res. M, 4310 (1978).

Can. J. Chem. Downloaded from www.nrcresearchpress.com by 210.87.254.105 on 09/06/12
For personal use only.

A partial synthesis of aconosine[1]

O. E. EDWARDS, R. J. KOLT, AND K. K. PURUSHOTHAMAN[2]

Chemistry Division, National Research Council of Canada, 100 Sussex Drive, Ottawa, Ont., Canada K1A 0R6

Received November 30, 1982

O. E. EDWARDS, R. J. KOLT, and K. K. PURUSHOTHAMAN. Can. J. Chem. **61**, 1194 (1983).

The diterpenoid alkaloid cammaconine, with known structure and stereochemistry, was converted into a base with the same properties as those reported for the alkaloid aconosine.

O. E. EDWARDS, R. J. KOLT et K. K. PURUSHOTHAMAN. Can. J. Chem. **61**, 1194 (1983).

On a transformé l'acaloïde diterpénique cammaconine, dont la strueture et la stéréochimie sont connues, en une base possédant les même propriétés que cells rapportées pour l'alcaloïde aconosine.

[Traduit par le journal]

In 1972 Murav'eva *et al.* (1) described a new diterpenoid alkaloid from *Aconitum nasutum*, which they named aconosine. It had a C_{18} skeleton, the first of its class, and they proposed that it had structure **1** (but with a 1β methoxy group), lacking the usual alkyl or oxyalkyl group on C-4. We report a simple transformation of the alkaloid cammaconine **2***a* into **1**, with properties very similar to those reported for aconosine by the Russian workers.[3,4]

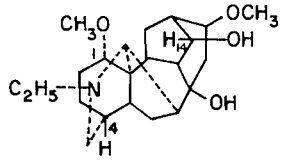

1

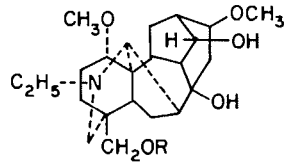

2a R=H
2b R=CH_3

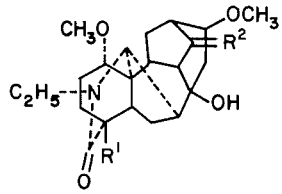

3 R^1 = CH_2OH, R^2 = H, OH
4 R^1 = CH_2OH, R^2 = O
5 R^1 = COOH, R^2 = H, OH
6 R^1 = COOH, R^2 = O

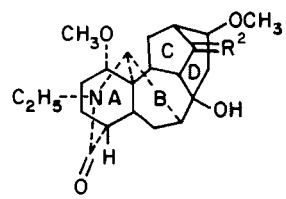

7 R=O
8 R=H,OH
HYDROXYL *syn* TO RING D

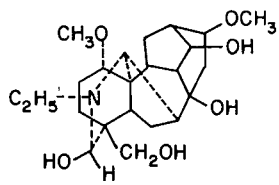

9

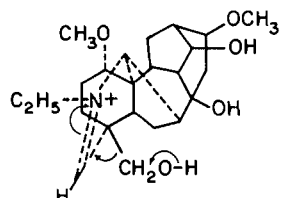

10

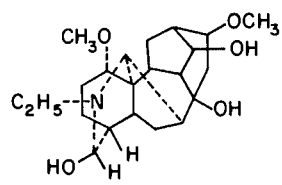

11

Early work in these laboratories had shown that the hydroxymethyl group on C-4 of lycoctonine could be replaced by hydrogen in two ways (2, 3). One of these routes was applicable

[1]NRCC No. 21086.

[2]NRCC postdoctoral fellow. Present address, Captain Srinavasa Murthi Research Institute, Madras, India.

[3]No comparison with authentic aconosine has yet been possible. However, since we are confident of the identity, we have named compounds **1** and **7**–**9** using the aconosine root name.

[4]Note added in proof: A ^1H nmr spectrum of aconosine kindly sent by Prof. M. S. Yunusov was nearly identical to that of **1** except for absence of the signals for the hydroxyl protons (deuterium exchange?).

TABLE 1. ^{13}C nuclear magnetic resonance assignments

Carbon, multiplicity	1*	2a*	3	4	6	7	8
C-1 d	86.3	86.1	83.7	84.1	82.7	84.1	84.1
C-2 t	26.6	26.3	26.5†	26.8	25.9	26.5	26.6
C-3 t	30.3	32.7	29.7	29.9	33.3	30.1	30.3
C-4 s	46.5(d)†	39.4	49.4	49.7	57.8	52.9(d)	53.8(d)
C-5 d	37.0	46.3†	52.6	52.2	52.5	48.9	49.2
C-6 t	29.8	25.4	25.7	25.8	30.4	25.4	25.5
C-7 d	46.2†	46.2†	45.4††	45.6†	43.8†	43.2	43.4
C-8 s	73.2	73.2	71.4	81.4	81.3	81.6	71.8
C-9 d	47.8	47.5	45.7††	54.4	54.2	54.6	46.0
C-10 d	39.1	38.5	36.9	44.2	44.0†	44.1	37.4
C-11 s	49.0	49.0	47.4	47.8	47.2	47.7	47.6
C-12 t	28.2	28.2	26.8†	24.7	24.4	24.7	27.2
C-13 d	45.7	45.9	45.7††	46.1†	46.0	46.1	46.0
C-14 d	76.0	75.9	74.9	214.0(s)	213.5(s)	214.2(s)	75.2
C-15 t	40.0	39.1	36.8	36.1	36.1	36.4	37.6
C-16 d	82.7	82.6	81.8	85.0	84.9	84.9	82.0
C-17 d	63.0	62.8	61.6	62.4	63.8	61.8	61.1
C-18 t	—	68.7	66.6	66.7	172.7(s)	—	—
C-19 s	50.8(t)	53.7(t)	174.3	174.3	172.7	171.0	171.2
N—CH_2 t	49.8	49.6	41.0	41.3	42.6	41.3	41.2
CH_3 q	13.8	13.8	12.9	13.1	12.8	13.2	13.2
16′ d	56.0	56.1	56.5	56.1	56.2	56.1	56.7
1′ d	55.8	55.7	55.6	55.8	56.2	55.9	55.9

*In benzene-d_6

†,††Values within a column may be interchanged.

( )Variation in multiplicity within a row.

to cammaconine. This alkaloid (4, 5) was oxidized by permanganate to oxocammaconine (**3**). The latter was converted to a mixture of oxocammaconic acid **5** and the corresponding 14-keto acid **6** by more vigorous permanganate oxidation. Jones' reagent in acetone completed the oxidation to 14-dehydrooxocammaconic acid **6**. This decarboxylated smoothly above 210°C to give 14-dehydroaconosine (**7**). Sodium borohydride reduction of **7** gave, with the usual high stereospecificity in the reduction of the 14-carbonyl (5), oxoaconosine **8**. Finally, lithium aluminum hydride reduced the lactam carbonyl, giving **1**.

Since cammaconine has been related to talatisamine (**2***b*) (6, 7), which has been synthesized (8), this leaves no ambiguity about the structure and stereochemistry of **1**. Its melting point, rotation, and spectra (in as far as they have been reported) agree with those of aconosine.

The natural occurrence of aconosine suggests that a carbinolamine such as **9** is involved in its biosynthesis. As in lycoctonine chemistry (2, 3), **9** could lose the hydroxymethyl group in a retro-aldol reaction (via the immonium salt **10**). This implies that a biochemical mechanism exists for the reduction of the resulting carbinolamine **11** to aconosine. The problem of highly strained intermediates with bridgehead double bonds in decarboxylation of acids such as **6** and in the retro-aldol reaction has been discussed elsewhere (3, 9). For very recent work on anti-Bredt olefins see ref. 10.

Contrary to the opinion of Pelletier *et al.* (11), we consider that oxygenation of the diterpenes in vivo proceeds from a methyl group on C-4 (e.g. sachaconitine, delpheline, and deltaline) to a hydroxymethyl group (e.g. cammaconine, lycoctonine) to carbinolamines such as **9**, then to the des(oxymethylene) type (aconosine).

The mass spectra criterion, on which basis the 1β-configuration was assigned to aconosine (1), is not reliable (12), hence the mass spectrum does not conflict with structure **1** for the alkaloid.

The ^{13}C nmr assignments in Table 1 are based on predicted chemical shifts, multiplicities determined using off-resonance decoupling, correlation with values for related molecules from our own laboratory, and the extensive correlations by Jones and Benn, and Pelletier and co-workers (13).

Experimental

Preparative chromatography was on 20 × 20 cm 1000 μ silica gel plates with fluorescent indicator. Iodine vapor could also be used to detect both bases and lactams. All ^1H nmr and ^{13}C nmr spectra were for solutions in deuteriochloroform unless otherwise noted, and were obtained on a Varian EM-360 or a Bruker WP-80 spectrometer operating at 20.15 MHz in the Fourier transform mode using 16K data points and a pulse flip angle of 35°. Off-resonance decoupling used ^1H irradiation at ca. 6 ppm upfield from TMS and power of 2 watts. Infrared spectra were of methylene chloride solutions and rotations were taken in chloroform unless otherwise noted.

Oxocammaconine (3)

A solution of 304 mg of cammaconine in 15 mL of acetone and 10 mL of water was stirred in a bath held at 15°C. During 5 min a solution of 300 mg of potassium permanganate in 20 mL of 50% acetone–water (V/V) was added to this. The permanganate was reduced rapidly. The suspension was filtered through Celite, then the filtrate reduced to a volume of 10 mL on a rotating evaporator. The solution was acidified using dilute sulfuric acid, then the neutral and acidic products extracted into chloroform. An aqueous sodium carbonate wash removed the acids, leaving a solution of 195 mg of neutral product. From the aqueous layers 11 mg of acids and 62 mg of base were recovered. The neutral product crystallized from acetone–hexane. After recrystallization from the same solvent it had mp 193–195°C and ν_{max} 3500 and 1610 cm^{-1}. It had R_f 0.45 on silica gel plates with 10% methanol in chloroform for development. It had

^{1}H nmr signals at δ 1.18 (3H, t, J = 7 Hz), 3.30 (3H, s), and 3.42 (3H, s). *Anal.* calcd. for $C_{23}H_{35}NO_6$: C 65.53, H 8.37; found: C 65.26, H 8.35.

Permanganate oxidation of oxocammaconine (3)

A solution of 134 mg of oxocammaconine (**7**) was prepared in 15 mL of acetone, 1.2 mL of water, and 0.3 mL of acetic acid. To the vigorously stirred solution at 50°C was added 10 mg of manganese dioxide and 104 mg of potassium permanganate. After 5 h heating a further 200 mg of the permanganate was added. Most of the permanganate had been reduced after 16 h at 50°C. A final 52 mg of permanganate was added and heating continued for 7 h. Excess reagent was destroyed using aqueous sodium hydrogen sulfite, then the manganese dioxide removed by filtration through Celite. The solid was washed with acetone and dichloromethane. The filtrates were evaporated to dryness, then the residue distributed between dichloromethane and 5% sodium carbonate solution. The organic layer yielded 25 mg of crude 14-dehydrooxocammaconine (**4**) while the carbonate solution yielded 103 mg of acids, mainly oxocammaconic (**5**) and 14-dehydrooxocammaconic acids (**6**).

14-Dehydrooxocammaconic acid 6

The mixture of acids from permanganate oxidation of oxocammaconine (370 mg) was dissolved in 20 mL of acetone, then Jones' reagent (14) diluted with acetone was added with stirring until an excess persisted for 10 min. Excess reagent was destroyed with methanol, the solids removed by decantation and filtration, then the solvent evaporated. The residue yielded 361 mg of acids which crystallized from aqueous acetone giving 176 mg (36% from oxocammaconine) of 14-dehydrooxocammaconic acid (**6**). This had mp ca. 210°C dec.; ν_{max}: 3580, 3460, 1750, and 1595 cm^{-1}; and $[\alpha]_D$ 16° (c 0.51). Its ^{1}H nmr spectrum gave signals at δ 3.34 (3H, s), 3.33 (3H, s), and 1.28 (t, J = 7 Hz). *Anal.* calcd. for $C_{23}H_{31}NO_7$: C 63.72, H 7.21, N 3.23; found: C 63.49, H 7.45, N 3.10.

Oxidation of oxocammaconine with Jones' reagent gave **6** directly, but in poorer yield.

14-Dehydrooxoaconosine 7

14-Dehydrooxocamaconic acid (**6**, 176 mg), in a glass bulb with a long outlet tube, was decarboxylated by immersion in a bath at 220–230°C under 15 Torr for 10 min. The cooled residue was dissolved in dichloromethane (20 mL). This solution was washed with 5% sodium carbonate solution, which removed a trace of acid. The organic layers yielded 155 mg of quite pure 14-dehydrooxoaconosine which crystallized from acetone–hexane, mp 202–203°C. It had ν_{max}: 3580, 3480, 1750, and 1670 cm^{-1} and $[\alpha]_D$ −44.5° (c 0.53). Its ^{1}H nmr spectrum had signals at δ 3.34 (3H, s), 3.30 (3H, s), and 1.21 (3H, t, J = 7 Hz). *Anal.* calcd. for $C_{22}H_{31}NO_5$: C 67.84, H 8.02, N 3.60; found: C 67.80, H 8.16, N 3.53.

Oxoaconosine 8

To a solution of 216 mg of 14-dehydrooxoaconosine (**7**), in 12 mL of methanol, 230 mg of sodium borohydride was added portionwise over 5 min. The mixture was left for 15 min, then concentrated under reduced pressure. The residue was distributed between water and dichloromethane. The organic layers gave 204 mg of crude product which crystallized from acetone–hexane giving 183 mg (84%) of oxoaconosine (**8**). This had mp 208–210°C; ν_{max}: 3530, 3410, and 1630 cm^{-1}; and $[\alpha]_D$ −4.6 (c 0.69). Its ^{1}H nmr spectrum had signals at δ 4.93 (1H, d, J = 4.5 Hz, exchangeable with D_2O), 3.68 (1H, s, exchangeable with D_2O), 3.38 (3H, s), 3.24 (3H, s), and 1.18 (3H, t, J = 7 Hz). *Anal.* calcd. for $C_{22}H_{33}NO_5$: C 67.49, H 8.50, N 3.58; found: C 67.69, H 8.62, N 3.39.

Aconosine 1

Lithium aluminum hydride (170 mg) was added to a solution of 100 mg of oxoaconosine (**8**) in 5 mL of dioxane. The mixture was refluxed for 2 h under argon. Excess reagent was destroyed by addition of methanol, then saturated sodium sulfate solution. After addition of solid anhydrous sodium sulfate, the solids were removed by filtration using a bed of Celite on sintered glass. The filter cake was washed with methanol and dichloromethane, then the filtrates concentrated to small volume. The residue was diluted with water, then acidified using 5 *N* sulfuric acid. Methylene chloride extraction removed a small amount of neutral product. The aqueous layer was made strongly alkaline (NaOH), then extracted with dichloromethane, giving 82 mg of base. This crystallized from aqueous methanol giving 68 mg (71%) of aconosine with mp 150°C (Lit. (1) mp 148°C). It had ν_{max}: 3520 and 3410 cm^{-1} and $[\alpha]_D$ −25°C (c 0.57, methanol) (Lit. (1) $[\alpha]_D$ −21°). Its ^{1}H nmr spectrum in $CDCl_3$ had signals at δ 4.56 (1H, d, J = 4 Hz, exchangeable with D_2O). 4.08 (1H, d of d, J = 4 Hz), 3.56 (1H, s, exchangeable with D_2O) 3.34 (3H, s), 3.26 (3H, s), and 1.05 (3H, t, J = 7 Hz). Its ^{1}H nmr spectrum in benzene-d_6 had signals at δ 4.56 (1H, d, J = 4 Hz, exchangeable with D_2O), 4.14 (1H, d of d, J = 4 Hz), 3.89 (1H, s, exchangeable with D_2O), 3.09 (3H, s), 2.87 (3H, s), and 1.04 (3H, t, J = 7 Hz). *Anal.* calcd. for $C_{22}H_{35}NO_4$: C 69.99, H 9.35, N 3.71; found: C 69.81, H 9.21, N 3.70. The hydriodide of aconosine crystallized as rods from methanol–acetone, mp 209°C. *Anal.* calcd. for $C_{22}H_{36}INO_4$: C 52.28, H 7.18, N 2.77; found: C 52.04, H 7.35, N 2.92. Its mass spectrum had peaks at m/e: 377 (M^+) (2%), 376 (2%), 348 (4%), 347 (26%), 346 (100%), 344 (2%), 332 (2%), 330 (3%), 328 (3%), 314 (2%), and 298 (3%).

1. D. A. Murav'eva, T. I. Plekhanova, and M. S. Yunusov. Khim. Prir. Soedin. **8**, 128 (1972).
2. O. E. Edwards and L. Marion. Can. J. Chem. **30**, 627 (1952).
3. O. E. Edwards, L. Marion, and D. K. R. Stewart. Can. J. Chem. **34**, 1315 (1956); O. E. Edwards, M. Los, and L. Marion. Can. J. Chem. **37**, 1996 (1959).
4. N. V. Mody, S. W. Pelletier, and N. M. Mollov. Heterocycles, **14**, 1751 (1980).
5. S. W. Pelletier and L. H. Keith. *In* The alkaloids. Vol. XII. *Edited by* R. H. F. Manske. Academic Press. New York. 1970. Chapt. I.
6. M. A. Khaimova, M. D. Palamareva, N. M. Mollov, and V. P. Krestev. Tetrahedron, **27**, 819 (1971).
7. O. E. Edwards, V. Boido, K. L. Handa, R. Kolt, and K. K. Purushothaman. In preparation.
8. K. Wiesner, T. Y. R. Tsai, K. Huber, S. E. Bolton, and R. Vlahov. J. Am. Chem. Soc. **96**, 4990 (1974).
9. O. E. Edwards. Can. J. Chem. **59**, 3039 (1981).
10. H. J. Bestmann and G. Schade. Tetrahedron Lett. 3543 (1982).
11. S. W. Pelletier, N. V. Mody, and N. Katsui. Tetrahedron Lett. 4027 (1977).
12. O. E. Edwards and M. Pryzbylska. Can. J. Chem. **60**, 2661 (1982).
13. J. Finer-Moore, N. V. Mody, S. W. Pelletier, N. A. B. Gray, C. W. Crandall, and D. H. Smith. J. Org. Chem. **46**, 3399 (1981).
14. K. Bowden, J. M. Heilbron, E. R. H. Jones, and B. C. Weedon. J. Chem. Soc. 39 (1946).

Tautomerism of pyrazoline-5-thione and triazoline-5-thione studied by variable temperature photoelectron spectroscopy[1]

CLAUDE GUIMON and GENEVIÈVE PFISTER-GUILLOUZO
Laboratoire de Physico-Chimie Moléculaire, ERA 895, Université de Pau et des Pays de l'Adour, Avenue Louis Sallevave, 64000 Pau, France

AND

MIKAEL BEGTRUP
Department of Organic Chemistry, The Technical University of Denmark, DK 2800 Lyngby, Denmark

Received October 26, 1982

CLAUDE GUIMON, GENEVIÈVE PFISTER-GUILLOUZO, and MIKAEL BEGTRUP. Can. J. Chem. **61**, 1197 (1983).

Photoelectron spectra at variable temperatures demonstrate that the rate of thermal isomerization of pyrazoline-5-thione (**1***a*) into methylthiopyrazole(s) in the gaseous phase is metal catalysed. Similar isomerizations of triazolethione (**2***a* and **3***a*) are at best only slightly so.

Furthermore, photoelectron spectra and MNDO calculations show that gaseous methylthiopyrazoles (**1***b* and **1***c*) and methylthiotriazoles (**2***b* and **2***c*) exist predominantly in planar form for the *b* isomer and in nonplanar form for the *c* isomer. The ΔH^0 for the rotameric equilibria is 2.7−4.2 kJ·mol^{-1}.

CLAUDE GUIMON, GENEVIÈVE PFISTER-GUILLOUZO et MIKAEL BEGTRUP. Can. J. Chem. **61**, 1197 (1983).

L'analyse des spectres photoélectroniques enregistrés à l'aide d'une "sonde à température variable" montre que la transformation en phase vapeur de la pyrazoline-thione-5 (**1***a*) en méthylthio-pyrazole(s) est catalysée par les parois métalliques de la sonde. Cette réaction d'isomérisation est, semble-t-il, nettement plus difficile dans le cas des triazolethiones (**2***a* et **3***a*).

D'autre part les spectres expérimentaux et les calculs théoriques réalisés à l'aide de la méthode MNDO montrent que les composés S-méthylés (**1***b*, **1***c*, **2***b* et **2***c*) existent préférentiellement sous une forme plane dans le cas des isomères *b* et une forme non plane dans celui des isomères *c* et qu'ils présentent un équilibre entre rotamères (ΔH^0 compris entre 2.7 et 4.2 kJ·mol^{-1}).

Introduction

Maquestiau *et al.* (1) recently showed that 1,2-dimethylpyrazoline-5-thione, with various substituents on the carbons (Me, ϕ) was rapidly transformed by thermal rearrangement (heating to around their melting point) into 1-methyl-3-methylthiopyrazoles and into 1-methyl-5-methylthiopyrazoles after longer periods of heating (Fig. 1).

The authors concluded from these data that form *b* is the kinetic product and that form *c* is the thermodynamic product of a reaction proceeding principally by an intermolecular mechanism.

Heating of 1,2-dimethylpyrazoline-5-thione (**1***a*, $R^1 = R^2 =$ H) suspended in benzene to 200°C for 5 h leads to its complete isomerization into a 1.04:1 mixture of 1-methyl-3-methylthiopyrazole (**1***b*) and 1-methyl-5-methylthiopyrazole (**1***c*). Similarly, 1,2-dimethyl-1,2,3-triazoline-5-thione (**2***a*) produces a 2.7:1 mixture of methylthiotriazoles (**2***b* and **2***c*) (Fig. 2) and anhydro-1,3-dimethyl-4-mercapto-1,2,3-triazolium hydroxide (**3***a*) generates a 1.6:1 mixture of methylthiotriazoles (**3***b* and **3***c*) (2) (Fig. 3). The product ratios remain unchanged by prolonging the reaction time and all single methylthio compounds are stable under the reaction conditions, indicating that the isomerizations are kinetically controlled.

In a general study of the electronic structure of thiocarbonyl compounds, we presented the photoelectron spectra of compounds **1***a*, **2***a*, and **3***a* (3). The spectrum of the first compound (**1***a*) shown here (Fig. 11-P_1) contains a minor band at around 9.15 eV. In the light of previous data, it could be due to the presence of small quantities of one or two SMe forms.

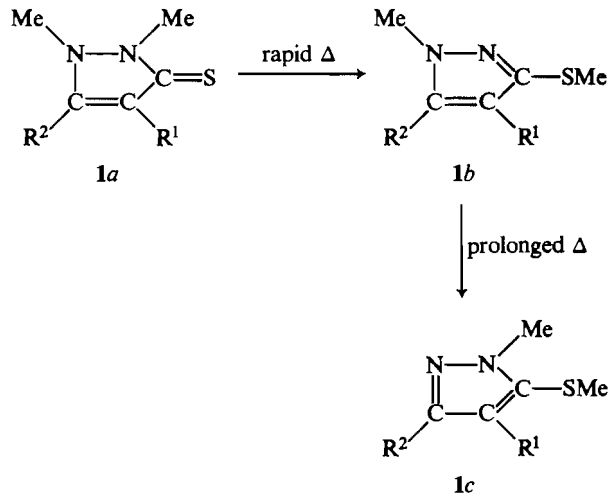

1*a* **1***b* **1***c*

FIG. 1.

Photoelectron spectroscopy has proven itself to be a good method to study equilibria in the gas phase (4). It was our desire to continue this initial work by using the variable temperature method, recently used by two of us (5). It has been previously used with success for studying conformational problems (6−10).

In order to be able to unambigously determine the existence of an equilibrium among forms *a*, *b*, and *c* in the vapor phase, however, it was necessary to record the spectra of the two SMe isomers (*b* and *c*) and to verify their structural characteristics.

[1]Part 11 of "Application of photoelectron spectroscopy to molecular properties". For Part 10, see ref. 20.

Can. J. Chem. Downloaded from www.nrcresearchpress.com by 210.87.254.40 on 09/06/12
For personal use only.

Can. J. Chem. Downloaded from www.nrcresearchpress.com by 210.87.254.40 on 09/06/12
For personal use only.

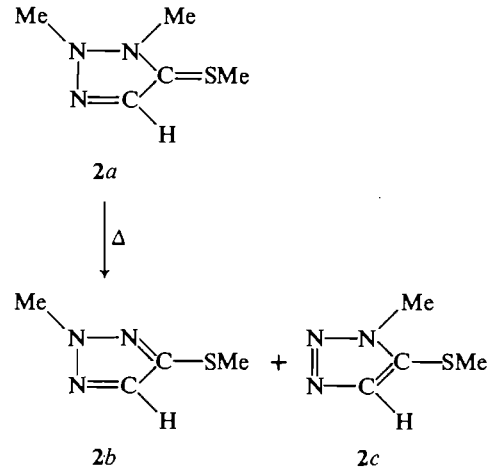

FIG. 2.

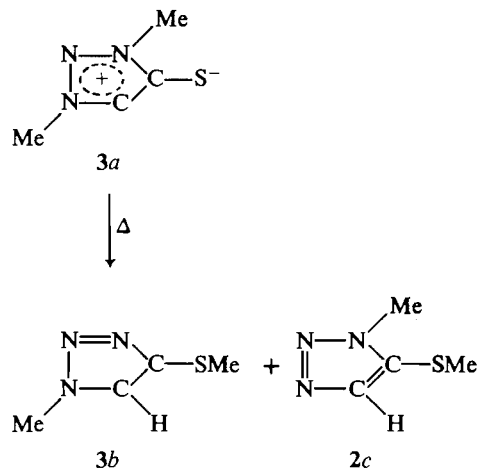

FIG. 3.

Experimental

Spectra were recorded with a Perkin–Elmer PS 18 photoelectron spectrometer with a HeI/HeII "Helectros" source. The HeI and HeII resonance lines at 21.22 eV and 40.21 eV served as the ionizing source. The spectra were calibrated with the $^2P_{1/2}$ and $^2P_{3/2}$ lines of Ar and Xe and were recorded with a resolution of 30 meV.

Results and discussion

Methylthiopyrazoles

The electronic structure of 1-methyl-3-methylthiopyrazole (**1***b*) and 1-methyl-5-methylthiopyrazole (**1***c*) derives from that of 1-methylpyrazole. According to MNDO (11) and previous *ab initio* calculations (12), the highest occupied orbitals in order of decreasing energy are π_3 and π_2, two π orbitals localized within the ring, and a σ orbital localized at N-2 (Table 1).

The introduction of a methylthio group at C-3 enables the n_S^{π} orbital to disturb the ring π-system. The π_3 orbital with a node at C-3 is hardly influenced while the π_2 orbital is disturbed to an extent depending on the angle θ between the ring plane and the C-3—S—Me plane (Fig. 4). Maximum disturbance occurs when $\theta = 0°$.

By introducing a methylthio group at C-5, the n_S^{π} orbital strongly disturbs the π_3 orbital, highly localized on C-5, while the π_2 orbital is hardly affected (Fig. 5).

The assignment of the photoelectron spectrum of 1-methyl-3-methylthiopyrazole (**1***b*) (Fig. 6) is evident from

TABLE 1. Calculated (MNDO) localization and energies of the two highest occupied MO's of 1-methylpyrazole

Localization	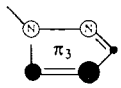	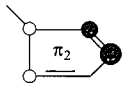
$-\epsilon_i$ (eV)	9.54	9.73
PI_{exp} (eV)	9.46	9.95

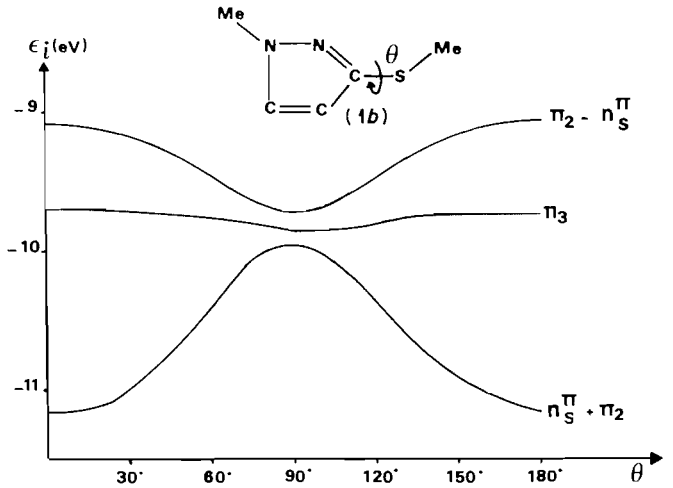

FIG. 4. Calculated (MNDO) evolution of the three π HOMO's of 1-methyl-3-methylthiopyrazole (**1***b*) as a function of the dihedral angle θ.

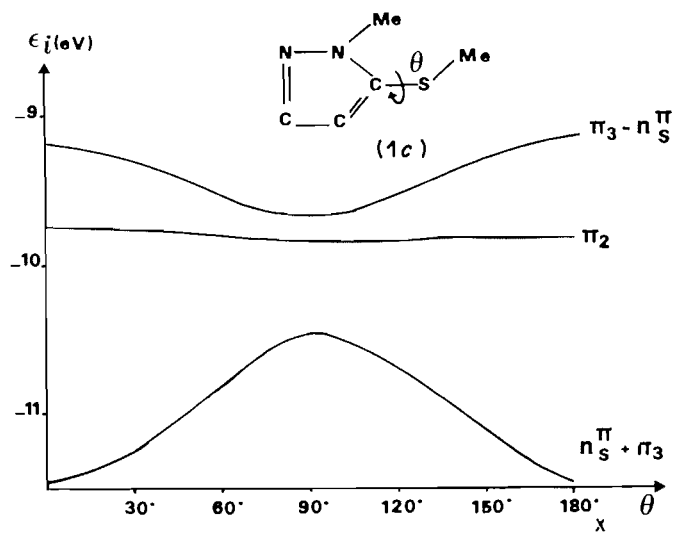

FIG. 5. Calculated (MNDO) evolution of the three π HOMO's of 1-methyl-5-methylthiopyrazole (**1***c*) as a function of the dihedral angle θ.

Table 2.The three strong and well-resolved low-energy bands are associated with the ionization of the π electrons localized within the ring. The assignment was confirmed by a spectrum recorded during HeII irradiation (40.81 eV) in which band number one, and particularly band number five, appear with reduced intensity while band number four becomes more intense. According to the empirical rules (13) successfully applied by spectrum assignment in several cases (14–18), bands number one and five would be associated with the ionization of electrons in the two orbitals highly localized on the sulfur atom,

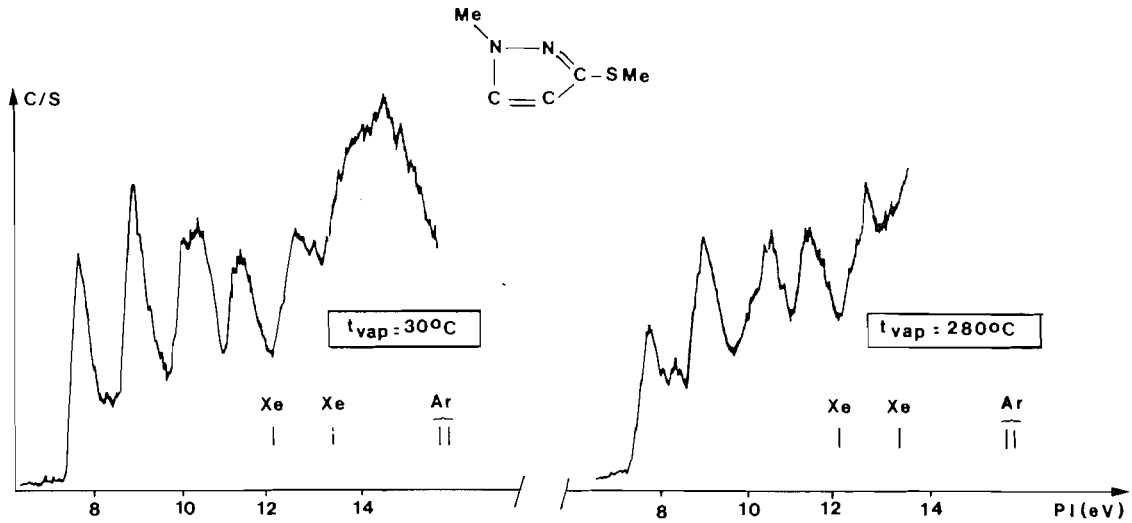

FIG. 6. Photoelectron spectra of 1-methyl-3-methylthiopyrazole (**1***b*).

TABLE 2. Calculated (MNDO) and experimental vertical ionization potentials (eV) for methylthiopyrazoles and mercaptopyrazoles

Compounds	θ[a]		Orbitals				
			π_1	π_2	π_3	n_N^{σ}	n_S^{σ}
1-Methyl-3-methylthiopyrazole (**1***b*)	0°	Calcd.	9.07	9.71	11.16	11.98	12.63
		Expt.	8.0	9.15	10.30	10.5	11.45
	90°	Calcd.	9.73	9.86	9.95	12.20	12.66
		Expt.	8.6				
1-Methyl-3-mercaptopyrazole (**4***b*)	0°	Calcd.	9.18	9.78	11.46	12.17	13.43
		Expt.	8.6	9.6	10.65	10.65	12.3
1-Methyl-5-methylthiopyrazole (**1***c*)	0°	Calcd.	9.18	9.74	11.45	11.92	12.77
		Expt.	8.3				
	76.81°	Calcd.	9.64	9.82	10.56	12.12	12.97
		Expt.	Between 8.7 and 9.5				
1-Methyl-5-mercaptopyrazole (**5***c*)	76.26°	Calcd.	9.74	9.90	10.83	12.21	13.55
		Expt.	9.1	9.45	10.0	10.9	>12

[a]θ refers to the dihedral angle between the pyrazole ring plane and the C—S—Me or C—SH plane.

while band number four would be due to the ionization of electrons in an orbital localized on N-2.

A comparison between experimental and calculated ionization potentials (Table 2) indicates that 1-methyl-3-methylthiopyrazole (**1***b*) preferentially adopts a planar conformation (θ ~ 0° or 180°) in the gas phase.

This conclusion is consistent with the molecular energy calculated by the MNDO method as a function of the dihedral angle θ between the heterocycle and the S—Me fragment (this energy is minimized versus all the structural parameters). The energy minimum (Fig. 7) corresponds to an angle θ equal to 0° whereas the maximum corresponds to 180°, with a rotation barrier of 8.78 kJ·mol^{-1} (for θ = 90°, the molecular energy increases of 3.85 kJ·mol^{-1}).

In addition to the strong bands from this species, a weak band is also observed at 8.6 eV, reflecting the presence of a small quantity of a second conformer in which θ is close to 90° (Fig. 4). The proportion of the minor conformer increases with higher temperatures (Fig. 6), denoting a temperature dependent equilibrium between the two conformers in the gas phase. A calculation based on Van't Hoff's law (4) furnishes an enthalpy difference between the conformers of 4.2 kJ·mol^{-1} (Table 3). It must be emphasized that this value is approximate since its determination can lead to systematic errors as shown by Honnegger and Heilbronner (19). Nevertheless its value is consistent with the result of the MNDO calculation.

In the photoelectron spectrum of 1-methyl-5-methylthiopyrazole (**1***c*) (Fig. 8) the strong band around 9.2 eV is attributed to the ionization of electrons in the ring π orbitals and that at 10.60 eV to the ionization of n_N electrons (see Table 2). The band at 11.75 eV is unambiguously associated with the ionization of n_S^{σ} electrons, since its relative intensity decreases markedly in a spectrum recorded with HeII irradiation. The best correlation between calculated and experimental ionization potentials is obtained when θ in 1-methyl-5-methylthiopyrazole (**1***c*) is at about 90°C (see Table 2 and Fig. 5). The same MNDO calculation on this molecule indicates a stable nonplanar conformation (θ = 76.8°) and two rotation barriers (5.52 kJ·mol^{-1} for θ = 0° and 27.71 kJ·mol^{-1} for θ = 180°) (Fig. 7). A weak band at 8.3 eV whose intensity increases with increasing temperature again indicates the presence of a minor quantity of the planar conformer (θ = 0°). Calculation of the free enthalpy for the conformational equilibrium is not feasible in this case, however, due to close spacing of the bands from each conformer.

At high temperatures, the proportions of the unfavored con-

Can. J. Chem. Downloaded from www.nrcresearchpress.com by 210.87.254.40 on 09/06/12
For personal use only.

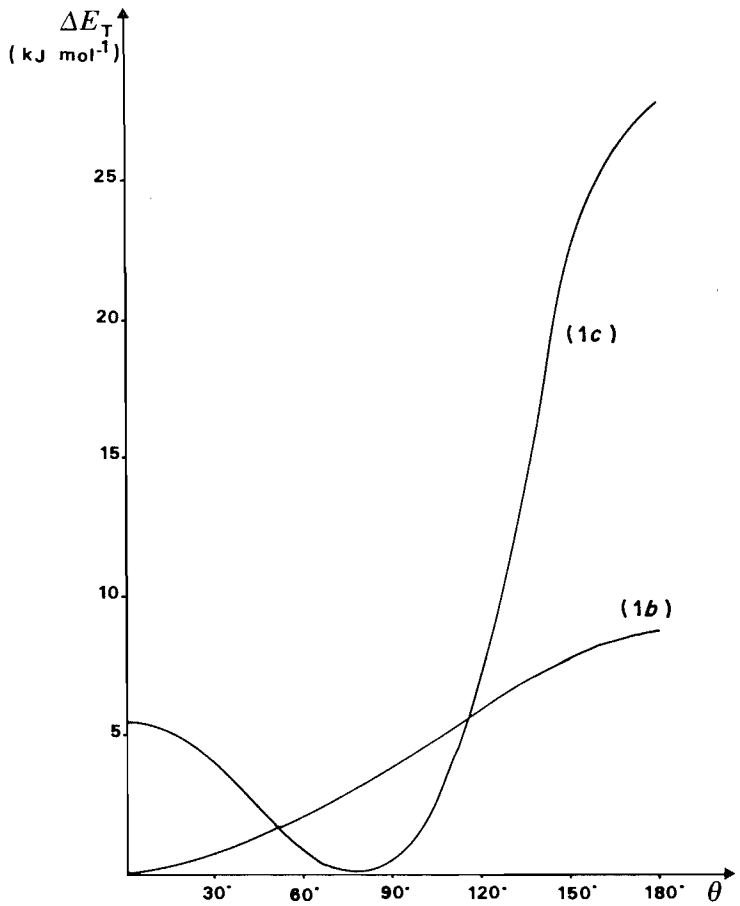

FIG. 7. Calculated (MNDO) evolution of the total energy of 1-methyl-3-methylthiopyrazole (**1***b*) and 1-methyl-5-methylthiopyrazole (**1***c*) as a function of the dihedral angle θ.

TABLE 3. Equilibrium constants K_T and differences in free enthalpy $\Delta H°$ for equilibria between planar and nonpolar conformers of methylthiopyrazoles and methylthiotriazoles

	Compounds		
Parameter	1-Methyl-3-methylthiopyrazole (**1***b*)	1-Methyl-4-methylthiotriazole (**3***b*)	1-Methyl-5-methylthiotriazole (**2***c*)
K_T[a]	0.22 (20°C) 0.42 (205°C)	0.68 (50°C) 1.02 (240°C)	4.(20°C) 2.38 (260°C)
$\Delta H°$ kJ·mol^{-1}[b]	4.2	2.9	−2.7

[a]K_T has been calculated assuming that the pair of rotamers exhibit the same cross section of ionization of the HOMO localized on the lone pair π orbital of the sulphur atom.
[b]Estimated limits of error are ±1.5 kJ·mol^{-1}.

TABLE 4. Experimental ionization potentials (eV) of methylthiotriazoles

Compounds	θ[a]	Ionization potentials (eV)					
1-Methyl-4-methylthiotriazole (**3***c*)	0°	8.33	10.	10.37	10.75	11.40	12.10
	~90°	8.75					
1-Methyl-5-methylthiotriazole (**2***c*)	0°	8.65					
	~90°	9.30	9.70	10.40	10.65	11.55	12.45

[a]Same footnote as Table 2.

formers increase. Equilibrium constants and free enthalpy differences for the conformational equilibria are given in Table 3. The parallel behavior of methylthiopyrazoles and triazoles suggests that a similar distribution of conformers is a feature of other methylthio substituted N-methylazoles.

Mercaptopyrazoles

1-Methyl-3-mercaptopyrazole (**4**) may adopt two tautomeric structures (**4***a*, *b*). In nonpolar solvents ($CDCl_3$), the SH form (**4***b*) is the sole detectable by ^1H nmr. This also obtains for other 1-substituted 3-mercaptopyrazoles (3). Comparison of the

Can. J. Chem. Downloaded from www.nrcresearchpress.com by 210.87.254.40 on 09/06/12
For personal use only.

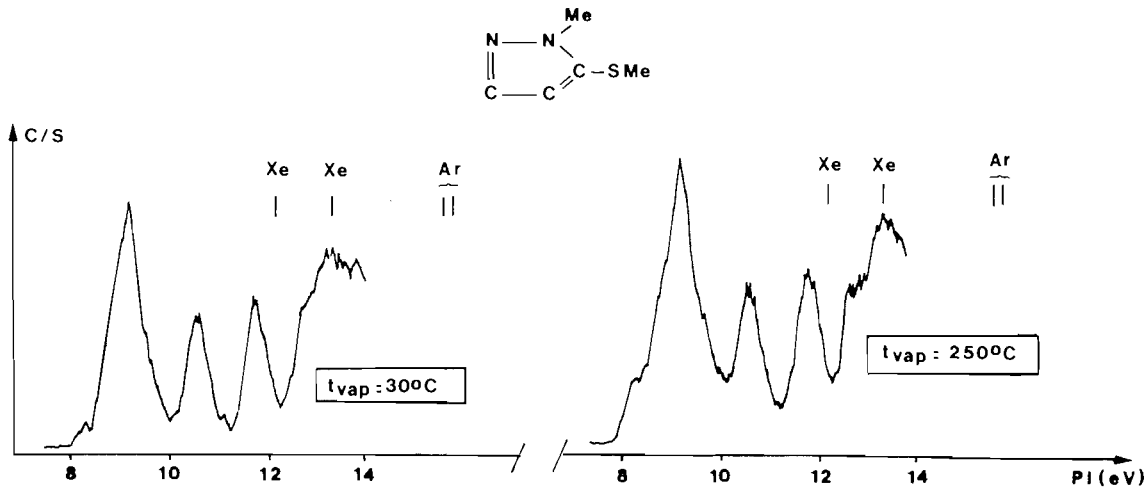

FIG. 8. Photoelectron spectra of 1-methyl-5-methylthiopyrazole (**1***c*).

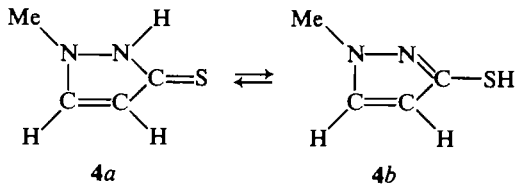

4*a* **4***b*

FIG. 9.

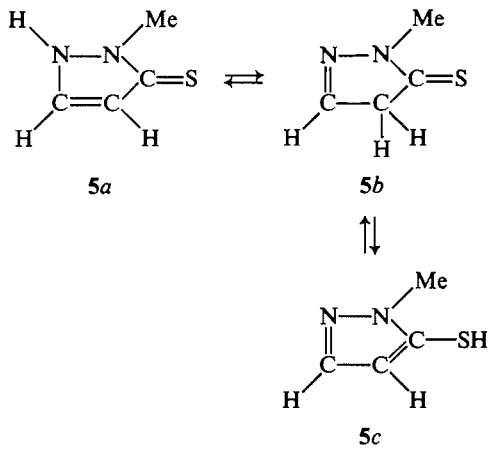

5*a* **5***b* **5***c*

FIG. 10.

photoelectron spectrum of 1-methyl-3-mercaptopyrazole (**4**) with the spectra of its N- and S-methyl derivatives (**1***a* and **1***b*) (Table 2) shows that only signals attributable to the SH form (**4***b*) are present. From the estimated detection limits it may be stated that the NH form (**4***a*) represents less than 5% of gaseous (**4**). Furthermore, the comparison of experimental and calculated ionization energies (Table 2) demonstrates that 1-methyl-3-mercaptopyrazole, as its S-methyl derivative (**1***b*), adopts a virtually planar conformation.

1-Methyl-5-mercaptopyrazole (**5**) may adopt three tautomeric structures (**5***a*–*c*). In nonpolar solvents, only the SH form (**5***c*) is observed by ^{1}H nmr. The addition of deuterium oxide, however, leads to the exchange of H-4 suggesting the presence of minute quantities of **5***b*. The photoelectron spectrum of **5** exhibits signals only from the SH form (**5***c*) (Table 2). Again, the NH form represents less than 5% of gaseous (**5**). The experimental ionization potentials are most consistent with those calculated for a conformer in which the angle between the ring and the C—S—H plane is close to 90°, as in the S-methyl derivative (**1***c*).

1,2-Dimethylpyrazoline-5-thione

The isomerization of 1,2-dimethylpyrazoline-5-thione (**1***a*) was studied by photoelectron spectroscopy using two probes. The first (P_1) was studied in the standard fashion (sample evaporated in ionization chamber) and the second (P_2) with the evaporation chamber separated by about 30 cm from the ionization chamber by a metallic guide in which the evaporated sample could be heated independently without affecting unvaporized material. Temperatures were measured at the two probes. The photoelectron spectra of 1,2-dimethylpyrazoline-5-thione obtained with the standard probe at a gas temperature between 100°C and 180°C corresponds to unchanged **1***a* (5) (Table 5) mixed with a minute quantity of methylthiopyrazole (**1***b*) and/or (**1***c*) giving rise to an additional weak band at 9.15 eV (Fig. 11 − P_1). The spectrum of **1***a* obtained with probe P_2 (same temperature) is devoid of pyrazolinethione bands and is similar to the spectrum of 1-methyl-3-methylthiopyrazole (**1***b*) (Fig. 6). No conclusions concerning the presence of 1-methyl-5-methylthiopyrazole (**1***c*) can be drawn, since its bands may be masked by those of the former compound (**1***b*). (In its stable conformation, **1***b* has a calculated energy 5.48 kJ·mol^{-1} lower than **1***c*). A similar spectrum is obtained by heating the gas to 360°C, the only difference being that the band at 8.7 eV, due to the nonplanar conformer of **1***b*, appears with enhanced intensity. Spectra reveal that both methylthiopyrazoles **1***b* and **1***c* are stable in the gas phase at 250°C. Hence, Fig. 11 − P_2 reflects the result of a kinetically controlled isomerization of the pyrazolinethione **1***a*.

The variable temperature experiment was terminated by recording a control spectrum of still unvaporized pyrazolinethione (**1***a*) at 80°C using probe P_1. The spectrum affirmed that the sample itself had not isomerized; neither did heating the solid sample to 160°C give rise to significant changes. Thus, isomerization of pyrazolinethione (**1***a*) into methylthiopyrazole (**1***b*) and probably **1***c* is more rapid in the gas phase than in the solid phase. Additional experiments showed that the rate of isomerization depended on dwell time in the guide rather than being a function of the temperature of the evaporated sample. This suggests a catalytic effect on isomerization brought about by contact between the metallic surfaces and the vapors.

Can. J. Chem. Downloaded from www.nrcresearchpress.com by 210.87.254.40 on 09/06/12
For personal use only.

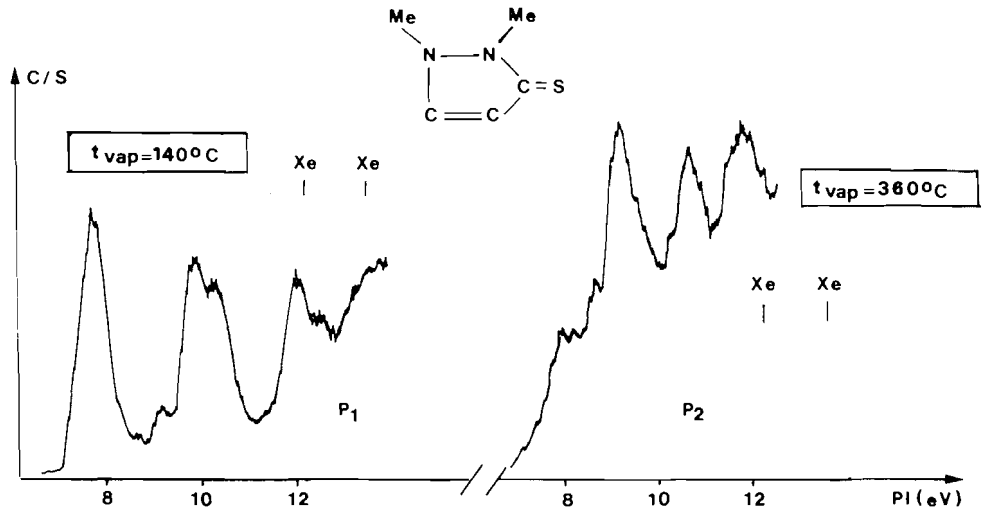

FIG. 11. Photoelectron spectra of 1,2-dimethylpyrazoline-5-thione (1*a*) using probes P_1 and P_2 (see text).

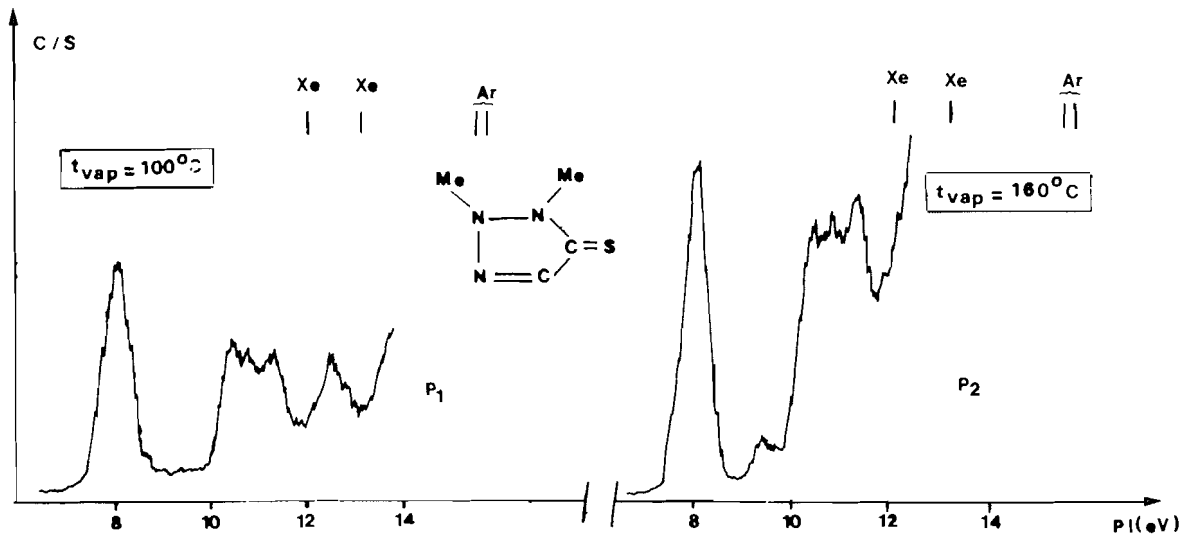

FIG. 12. Photoelectron spectra of 1,2-dimethyltriazoline-5-thione (2*a*) using probes P_1 and P_2 (see text).

TABLE 5. Calculated (MNDO) and experimental ionization potentials (eV) for 1,2-dimethylpyrazoline-5-thione (1*a*)

	Orbitals				
	$\pi_{C=S}$	n_S^{σ}	π	π	σ_{CS}
Calcd.	8.43	8.93	10.55	11.35	11.31
Expt.	7.6	7.6	9.78	10.22	11.96

The isomerization rate of gaseous 1,2-dimethyltriazoline-5-thione (2*a*) was only slightly enhanced compared to that of solid 2*a*. Thus, the spectra of just evaporated material obtained with probe P_1 indicate the presence of the unchanged thione even at 160°C (Fig. 12 − P_1). A spectrum recorded with probe P_2 after heating the evaporated sample to 160°C exhibits an additional minor band at 9.40 eV (Fig. 12 − P_2) which, according to Table 4, is most likely due to 2-methyl-4-methylthiotriazole (2*b*). The presence of 1-methyl-5-methylthiotriazole (2*c*) could not be demonstrated since its bands would be masked by those of its isomer (2*b*).

Isomerization of anhydro-1,3-dimethyl-4-mercaptotriazolium hydroxyde (3*a*) could not be detected even after heating the evaporated sample to 160°C.

Conclusion

This study indicates the power of photoelectron spectroscopy for the study of equilibria and isomerization phenomena in the gaseous phase. In our experimental conditions the isomerization of pyrazoline-5-thione and triazoline-5-thione into methylthiopyrazole seems to be a catalytic process. We have also shown that these methylthiopyrazoles exist under different rotamer forms.

1. A. MAQUESTIAU, Y. VAN HAVERBECKE, and J. D. VANOVERVELT. Bull. Soc. Chim. Belg. **86**, 961 (1977).
2. M. BEGTRUP. Acta Chem. Scand. **26**, 1243 (1972).
3. C. GUIMON, G. PFISTER-GUILLOUZO, and M. BEGTRUP. J. Am. Chem. Soc. **100**, 1275 (1978).
4. H. BOCK and B. SOLOUKI. Angew Chem. Int. Ed. Engl. **20**, 427 (1981), and refs. cited therein.
5. C. GUIMON, G. GARRABE, and G. PFISTER-GUILLOUZO. Tetrahedron Lett. 2585 (1979).
6. A. SCHWEIG and N. THON. Chem. Phys. Lett. **38**, 482 (1976).

Can. J. Chem. Downloaded from www.nrcresearchpress.com by 210.87.254.40 on 09/06/12
For personal use only.

7. C. MULLER, W. SCHAFER, A. SCHWEIG, N. THON, and H. VERMEER. J. Am. Chem. Soc. **98**, 5440 (1976).
8. A. SCHWEIG, N. THON, and H. VERMEER. J. Am. Chem. Soc. **101**, 80 (1979).
9. H. FRIEGE and M. KLESSINGER. J. Chem. Res. **208** (1977); Chem. Ber. **112**, 1614 (1979).
10. T. H. GAN, J. B. PEEL, and G. D. WILLET. Chem. Phys. **965** (1977); J. Mol. Struct. **44**, 211 (1978).
11. M. J. S. DEWAR and W. THIEL. J. Am. Chem. Soc. **99**, 4899 (1977); **99**, 4907 (1977).
12. S. CRADOCK, R. H. FINDLAY, and M. H. PALMER. Tetrahedron, **29**, 2173 (1973).
13. A. SCHWEIG and W. THIEL. J. Electron Spectrosc. **3**, 27 (1974), and refs. cited therein.
14. C. GUIMON, G. PFISTER-GUILLOUZO, A. BERNARDINI, and P. VIALLEFONT. Tetrahedron, **36**, 1071 (1980).
15. A. KATRIB, T. P. DEBIES, R. J. COLTON, T. H. LEE, and J. W. RABALAIS. Chem. Phys. Letts. **22**, 196 (1973).
16. C. GUIMON, D. GONBEAU, G. PFISTER-GUILLOUZO, L. ASBRINK, and J. SANDSTROM. J. Electron Spectrosc. **4**, 49 (1974).
17. T. H. GAN, J. P. PEEL, and G. D. WILLETT. Chem. Phys. Lett. **48**, 483 (1977).
18. H. DAAMEN and A. OSKAM. Inorg. Chim. Acta, **27**, 209 (1978).
19. E. HONEGGER and E. HEILBRONNER. Chem. Phys. Lett. **81**, 615 (1981).
20. C. GUIMON, G. PFISTER-GUILLOUZO, and E. ROSE. J. Organomet. Chem. **224**, 125 (1982).

Can. J. Chem. Downloaded from www.nrcresearchpress.com by 210.87.254.40 on 09/06/12
For personal use only.

The preparation of protected arabinonucleosides[1]

KELVIN K. OGILVIE,[2] DANNY P. C. MCGEE, SUZANNE M. BOISVERT, GHOLAM H. HAKIMELAHI, AND ZBIGNIEW A. PROBA

Department of Chemistry, McGill University, Montreal, P.Q., Canada H3A 2K6

Received October 28, 1982

KELVIN K. OGILVIE, DANNY P. C. MCGEE, SUZANNE M. BOISVERT, GHOLAM H. HAKIMELAHI, and ZBIGNIEW A. PROBA. Can. J. Chem. **61**, 1204 (1983).

A general procedure is described for the preparation of protected arabinonucleosides. Protection at the 5′-position involves triphenylmethyl groups (DMT and MMT) while the *tert*-butyldimethylsilyl (TBDMS) group is used to protect the 2′- or 3′-positions. The effects of novel catalysts on the position of silylation have been determined, leading to highly selective reactions at 2′- or 3′-positions.

KELVIN K. OGILVIE, DANNY P. C. MCGEE, SUZANNE M. BOISVERT, GHOLAM H. HAKIMELAHI et ZBIGNIEW A. PROBA. Can. J. Chem. **61**, 1204 (1983).

On décrit une méthode générale de préparation des arabinonucléosides protégés. On utilise le groupe triphénylméthyle (DMT et MMT) pour protéger la position 5′ tandis qu'on fait appel au groupe *tert*-butyldiméthylsilyle (TBDMS) pour protéger les positions 2′ ou 3′. On a déterminé les effets d'un nouveau catalyseur de silylation qui conduit à des réactions très sélectives au niveau des positions 2′ ou 3′.

[Traduit par le journal]

Can. J. Chem. Downloaded from www.nrcresearchpress.com by 210.87.254.6 on 09/06/12
For personal use only.

Introduction

Arabinonucleosides (1−5) and arabinonucleotides (6−12) have been shown to possess a wide range of biological activities including antiviral and antitumor activity. A number of reports (13−19) have appeared which describe hydroxyl-derivatized arabinonucleosides with real or potential biological activity. However, the only literature report describing a general attempt at incorporating arabinonucleosides into nucleotide chains is the pioneering work by Wechter (20). In this latter work, the 2′- and 3′-hydroxyls were left unprotected during nucleotide coupling steps. As a result, mixtures of 2′−5′ and 3′−5′ linked nucleotides were obtained which were difficult to separate. We wish to describe the first general procedure for the preparation of protected arabinonucleosides suitable for stepwise incorporation into nucleotide chains.

The overall objective was to prepare arabinonucleosides protected at the 5′-position with monomethoxytrityl (MMT) or dimethoxytrityl (DMT) groups and protected at either the 2′- or 3′-positions with the *tert*-butyldimethylsilyl (TBDMS) group. These protecting groups have been successfully developed in the ribonucleotide area (21−23) and have allowed the synthesis of oligoribonucleotide chains both in solution (24, 25) and on a solid support (26). A preliminary report of some of these results has appeared (27).

Discussion

Tritylation of arabinonucleosides

The methoxytritylation and dimethoxytritylation of arabinonucleosides was carried out (Scheme 1) using a modification of the general procedures originally developed by Khorana and co-workers for nucleosides (28). These modifications have been described for the ribonucleosides (23). In the case of arabinonucleosides, yields (see Table 1) were generally greater than 90%. The properties of the tritylated nucleosides are collected in Table 1.

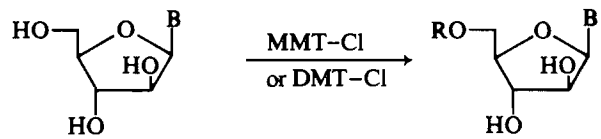

1*a* B = uracil
b B = cytosine
c B = *N*-benzoylcytosine
d B = adenine

2 R = MMT
3 R = DMT

SCHEME 1

Silylation of arabinouridine

The silylation of arabinouridine (araU, **1***a*) using the conditions developed for ribo- and deoxyribonucleosides (21, 22, 29) consisting of TBDMS-Cl and imidazole in DMF led to 51% of 3′,5′-diTBDMSaraU (**8***a*, 3′,5′-diSiaraU) and 18% of 2′,5′-diTBDMSaraU (**5***a*, 2′,5′-diSiaraU). Lesser amounts of the monosilyl derivative **4***a* and the trisilyl derivative **11***a* were obtained (Scheme 2).

The silylation of 5′-methoxytritylarabinouridine (**2***a*, 5′-MMTaraU) gave similar results (50% of **9***a*, 18% of **6***a*). One of the problems with the arabinouridine series was the difficulty of separating isomeric pairs such as **5***a* and **8***a* or **6***a* and **9***a*. Only the latter pair could be separated on a preparative scale and then with difficulty (Table 7). The isomers were generally isolated together from chromatography and the ratios determined by nmr (Table 5) as described below. Procedures were developed (below) that permit the isolation of the pure isomers.

One method that allowed the synthesis of the pure isomers was based on O^2,2′-cyclouridine (**14**). This compound is readily prepared from uridine in good yield (30). Compound **14** can be converted into 5′-methoxytrityl-3′-TBDMSarabinouridine (**9***a*) or into 3′,5′-diTBDMSaraU (**8***a*) in 70% and 80% yields respectively without the need to isolate the intermediates (e.g., **15**, **16**, and **17**). Selective acid catalyzed hydrolysis (21, 29) of either the methoxytrityl group or TBDMS group

[1]Part XXI in a series on silyl protecting groups in nucleoside and nucleotide chemistry. Part XX is ref. 27.

[2]Author to whom correspondence may be addressed.

TABLE 1. Preparation of tritylated arabinonucleosides*

Product		Yield (%)	Melting point (°C)	λ_{max} (nm) (95% EtOH)	R_f (tlc) b	R_f (tlc) e
MMT-araU	(**2***a*)	90	119–120	231, 264	0.21	
MMT-araC	(**2***b*)	90	150–152	230, 275	0.22	0.34
MMT-araC^{Bz}	(**2***c*)	90	154–157	230, 260, 307	0.37	
DMT-araU	(**3***a*)	90	123–125	231, 265	0.19	
DMT-araC	(**3***b*)	95	155–157	233, 275	0.19	
DMT-araC^{Bz}	(**3***c*)	98	162–163	233, 260, 307	0.37	
DMT-araA	(**3***d*)	70	139–140	232, 259	0.06	0.44

*General experimental conditions are described in the experimental section. Solvents used for tlc were b, $CHCl_3$/EtOH (9:1) and e, $CHCl_3$/EtOH (8:2).

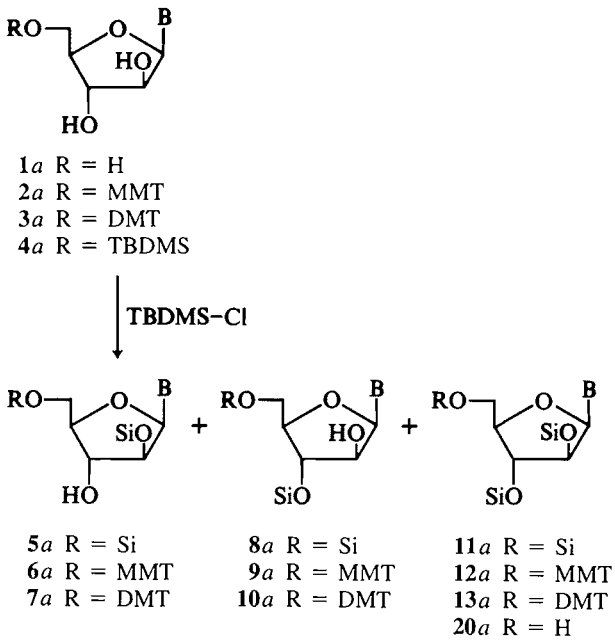

SCHEME 2

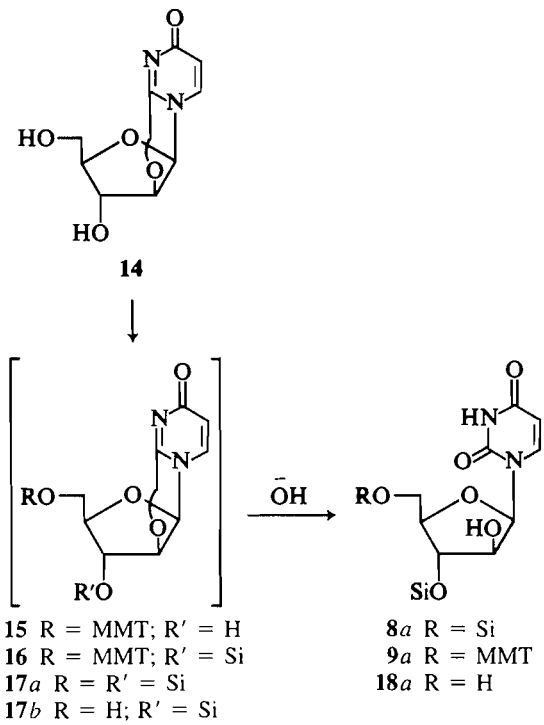

SCHEME 3

from **8***a* or **9***a* gave **18***a*.

The 5′-MMT-2′-TBDMSaraU (**6***a*) and 2′,5′-diTBDMS-araU (**5***a*) were also prepared from cyclouridine (**14**). Compound **14** was first converted to its bistetrahydropyranyl derivative (31). Base cleavage of the cyclouridine ring followed successively by silylation of the 2′-OH in DMF and the acid hydrolysis of the tetrahydropyranyl group (Scheme 4) gave 2′-TBDMSaraU (**19***a*, 31). The methoxytritylation or 5′-monosilylation of **19***a* led to the pure compounds **6***a* and **5***a*, respectively.

The cyclouridine route provided an unequivocal synthesis of the isomeric silylated arabinouridine derivatives. However, we wished to obtain a direct synthesis of these compounds. To this end we investigated the novel silylation methods that we have recently introduced in the ribo series (23, 32). The silylation of araU in THF using silver nitrate and pyridine with TBDMS-Cl gave high yields (70–80%) of the 3′,5′-diprotected derivatives (e.g., **8***a* and **10***a*). The 2′-silylated isomers (**5***a* and **7***a*) were always produced as well but in about 5% yields. If silver nitrate was omitted from this reaction only 5′-silylation occurred but in excellent yield (~90%). If pyridine was replaced by 3-methylpyridine *N*-oxide in the original reaction procedure, then the yields of 3′-silylated derivatives were nearly always above 90% (Table 2).

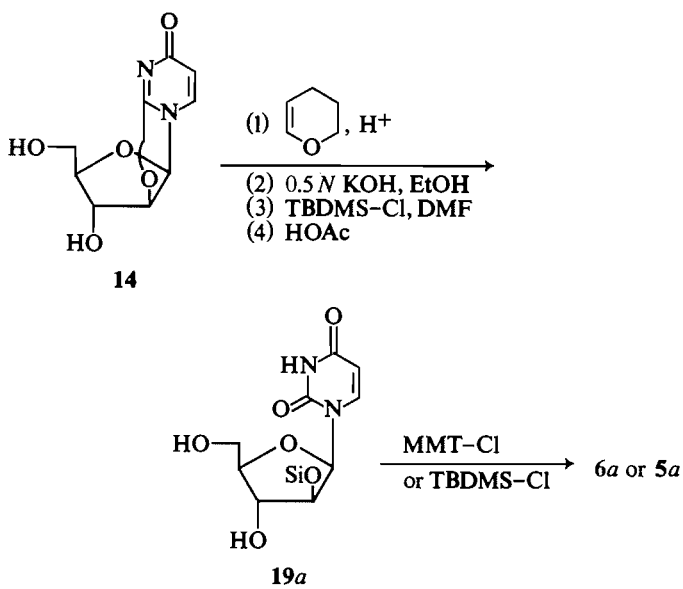

SCHEME 4

Can. J. Chem. Downloaded from www.nrcresearchpress.com by 210.87.254.6 on 09/06/12
For personal use only.

TABLE 2. Silylation of arabinouridines*

Starting material		TBDMS-Cl (equiv.)	Solvent	Base (equiv.)	Catalyst (equiv.)	Time (h)	% Yield 5′	2′,5′	3′,5′
AraU	(**1***a*)	1.3	DMF	Im (2.6)	—	40	90	2	6
AraU†	(**1***a*)	2.4	DMF	Im (4.8)	—	24	—	18*	51*
MMT-araU	(**2***a*)	1.3	DMF	Im (2.6)	—	40	—	18	50
DMT-araU	(**3***a*)	3	DME	Et_3N (8)	$AgNO_3$ (3)	5	—	70	5
DMT-araU	(**3***a*)	2	THF	Py (4)	$AgNO_3$ (2)	5	—	5	80
DMT-araU‡	(**3***a*)	1.2	THF	3-MPNO (1.5)	$AgNO_3$ (1.2)	5	—	5	90
AraU	(**1***a*)	2.5	DME	Et_3N (5)	$AgNO_3$ (2.5)	5	—	96	—
AraU	(**1***a*)	2.2	THF	Py (5)	$AgNO_3$ (2.2)	5	—	5	70
AraU	(**1***a*)	2.2	THF	3-MPNO (2.6)	$AgNO_3$ (2.2)	1.5	—	—	95
AraU	(**1***a*)	1.2	THF	3-MPNO (1.6)	$AgNO_3$ (1.2)	2	30	—	30
AraU	(**1***a*)	1.2	THF	3-MPNO (1.6)	—	2	—	—	—
AraU	(**1***a*)	3	THF	DABCO (6)	$AgNO_3$ (2.5)	3	—	75	5

*Experimental conditions are described in detail in the experimental section. Abbreviations used are DMF (dimethylformamide), DME (1,3-dimethoxyethane), THF (tetrahydrofuran), Im (imidazole), Et_3N (triethylamine), Py (pyridine), 3-MPNO (3-methylpyridine *N*-oxide), and DABCO (1,4-diazabicyclo[2.2.2]octane). Yields are based on isolated product except for * where yields were estimated from nmr spectra.
†14% of the trisilylderivative was also obtained in this experiment.
‡1.5 Equivalents of collidine included in this experiment.

TABLE 3. Silylation of arabinocytidines*

Starting material		TBDMS-Cl (equiv.)	Solvent	Base (equiv.)	Catalyst (equiv.)	Time (h)	% Yields 5′	2′,5′	3′,5′
AraC	(**1***b*)	1.3	DMF	Im (2.6)	—	5	64	2	7
AraC	(**1***b*)	2.3	DMF	Im (4.6)	—	24	—	11	65
AraC	(**1***b*)	6	DME	Et_3N (12)	—	24	—	51	27
$AraC^{Bz}$	(**1***c*)	2.3	DMF	Im (4.6)	—	12	—	15	75
MMT-araC	(**2***b*)	1.3	DMF	Im (2.6)	—	24	—	13	61
MMT-araC	(**2***b*)	3	Py		—	48	—	8	67
MMT-araC	(**2***b*)	4	DME	Et_3N (8)	—	24	—	75	5
$MMT\text{-}araC^{Bz}$	(**2***c*)	5	DMF	Im (10)	—	48	—	1	77
$MMT\text{-}araC^{Bz}$	(**2***c*)	15	Py		—	48	—	5	45
AraC	(**1***b*)	2.5	DME	Et_3N (5)	$AgNO_3$ (2.5)	3	—	90	5
AraC	(**1***b*)	2.2	DME	3-MPNO (2.6)	$AgNO_3$ (2.2)	2	—	5	90
AraC	(**1***b*)	1.3	DME	3-MPNO (1.6)	—	2	—	—	—
$AraC^{Bz}$	(**1***c*)	2.5	DME	Et_3N (5)	$AgNO_3$ (2.5)	3	—	50	35
DMTaraC	(**3***b*)	1.8	DME	Et_3N (4)	$AgNO_3$ (1.8)	3	—	92	4
AraC	(**1***b*)	2.5	THF	Py (5)	$AgNO_3$ (2.5)	3	—	5	90
AraC	(**1***b*)	2.2	THF	3-MPNO (2.6)	$AgNO_3$ (2.2)	2	—	—	95
$AraC^{Bz}$	(**1***c*)	2.5	THF	Py (5)	$AgNO_3$ (2.5)	3	—	20	70
$AraC^{Bz}$	(**1***c*)	2.2	THF	3-MPNO (2.6)	$AgNO_3$ (2.2)	2	—	—	91
$AraC^{Bz}$	(**1***c*)	1.3	THF	3-MPNO (1.6)	—	2	—	—	—
DMTaraC	(**3***c*)	1.8	THF	Py (4)	$AgNO_3$ (1.8)	3	—	10	80
DMTaraC	(**3***c*)	1.2	THF	3-MPNO (1.5) collidine (1.5)	$AgNO_3$ (1.2)	2	—	5	90
AraC	(**1***c*)	3	THF	DABCO (6)	$AgNO_3$ (2.5)	3	—	80	—

*Experimental conditions and abbreviations are as described in Table 4.

An amazing reversal of isomer distribution occurs on changing the solvent to dimethoxyethane (DME) containing triethylamine (Table 2). Using silver nitrate and TBDMS-Cl in this solvent gives virtually exclusive silylation at the 2′-position (e.g., **5***a* in 96% yield). High selectivity for the 2′-position is also observed in THF when DABCO and silver nitrate are used with TBDMS-Cl (Table 2, e.g., 75% of **5***a*, 5% of **8***a*). This latter result is a reversal of the situation in the ribo series where DABCO and silver ions provide a highly selective route to 3′,5′-silylation (23).

Silylation of arabinocytidine derivatives

A. *DMF and pyridine solvents*

The standard silylation procedures in DMF containing imidazole were applied to araC, *N*-benzoylaraC, and their derivatives. The results, collected in Table 3, show that using a slight excess of TBDMS-Cl led to the production of the 5′-TBDMS derivatives (**4**) in good yields. Using slightly more than two equivalents of TBDMS-Cl gave disilylated products. There was clearly a marked preference for silylation at the 3′-position relative to the 2′-position. Thus, 3′-5′-diTBDMSaraC (**8***b*) was obtained in 65% yield while the 2′-5′-isomer (**5***b*) was obtained in 11% yield. Similar results were obtained with $araC^{Bz}$ giving the 3′,5′-derivative **8***c* in 75% yield and the 2′,5′-derivative **5***c* in 15% yield. These results, along with those from araU, indicate that the 3′-hydroxyl is less sterically hindered than the 2′-hydroxyl which is in close proximity to the pyrimidine ring. The methoxytrityl derivatives **2***b* and **2***c* were

Can. J. Chem. Downloaded from www.nrcresearchpress.com by 210.87.254.6 on 09/06/12
For personal use only.

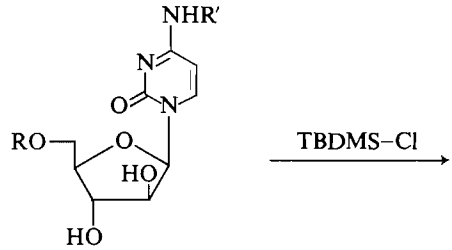

1*b* R = R′ = H
2*b* R = MMT, R′ = H
3*b* R = DMT, R′ = H
1*c* R = H, R′ = Bz
2*c* R = MMT, R′ = Bz
3*c* R = DMT, R′ = Bz
4*b* R = Si, R′ = H
4*c* R = Si, R′ = Bz

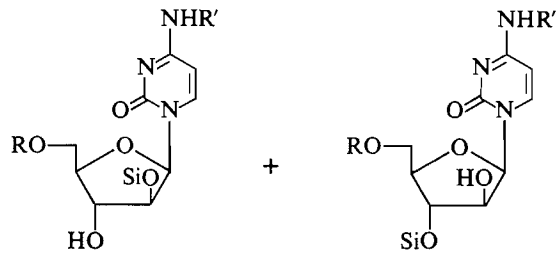

5*b* R = Si, R′ = H
5*c* R = Si, R′ = Bz
6*b* R = MMT, R′ = H
6*c* R = DMT, R′ = Bz
7*b* R = DMT, R′ = H
7*c* R = DMT, R′ = Bz
19*b* R = R′ = H

8*b* R = Si, R′ = H
8*c* R = Si, R′ = Bz
9*b* R = MMT, R′ = H
9*c* R = DMT, R′ = Bz
10*b* R = DMT, R′ = H
10*c* R = DMT, R′ = Bz
18*b* R = R′ = H

SCHEME 5

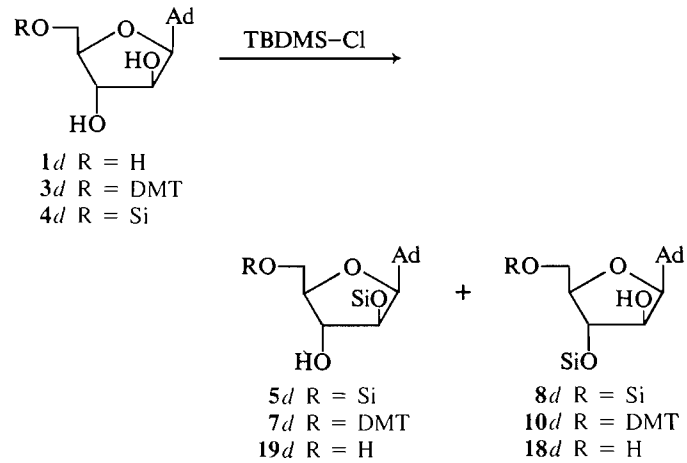

1*d* R = H
3*d* R = DMT
4*d* R = Si

5*d* R = Si
7*d* R = DMT
19*d* R = H

8*d* R = Si
10*d* R = DMT
18*d* R = H

SCHEME 6

also selectively silylated at the 3′-position (Table 3). Reactions in pyridine as solvent were much slower than those in DMF but showed a clear selectivity for the 3′-hydroxyl.

B. *Dimethoxyethane as solvent*

The silylation of araC nucleosides in DME gave an isomer distribution which was the reverse of that found in the DMF system (Table 3). Thus the silylation of either araC or methoxytritylaraC using TBDMS-Cl in DME containing triethylamine gave the 2′,5′-protected derivatives **5***b* and **6***b* as the major products.

When silver nitrate was added to the DME system there was a nearly exclusive silylation at the 2′-position for araC and DMTaraC. Thus **5***b* and **7***b* were produced in 90 and 92% yields, respectively. The selectivity toward the 2′-position was lower with $araC^{Bz}$ where the yield of the 2′,5′-diTBDMS$araC^{Bz}$ (**5***c*) was 50% and that of the 3′,5′-isomer (**8***c*) was 35%.

The replacement of triethylamine by 3-methylpyridine *N*-oxide (3MPNO) gave a complete reversal of isomer distribution (Table 3). Thus araC was 90% converted to the 3′,5′-disilyl derivative (**8***b*) under these conditions.

C. *Tetrahydrofuran as solvent*

The results here were similar to those obtained for arabinouridine. Silylation occurred nearly exclusively at the 3′- and 5′-positions when pyridine or 3MPNO were present along with silver nitrate (Table 3). Further, as in the case of araU, DABCO and silver nitrate gave a high degree of selectivity for silylation at the 2′-position.

Further proof of structure of silylated arabinocytidines

Notari *et al.* (33) have reported that the 2′-hydroxyl (but not the 3′-hydroxyl) of arabinocytidine participates in the acid catalyzed deamination of araC. As a result, of the isomeric pairs **18***b* and **19***b*, only the 3′-silylated araC, **18***b*, should undergo rapid acid catalyzed deamination. In acetic acid buffer (pH 4.6) at 87°C the 3′-SiaraC (**18***b*) was 10% deaminated after 25 min (by hplc) and 66% deaminated after 5 h. Under these same conditions the 2′-SiaraC (**19***b*) was unaffected after 25 min and only 6% deaminated after 5 h.

Silylation of arabinoadenosine derivatives

A. *Dimethoxyethane as solvent*

When silylation was carried out in DME containing triethylamine and silver nitrate the results were the reverse of those found in the pyrimidine series. Thus the 3′,5′-protected derivatives **8***d* and **10***d* were each obtained in 50% yields while their 2′,5′-isomers **5***d* and **7***d* were obtained in 30 and 35% yields, respectively (Table 4). When pyridine replaced triethylamine the isomer ratios switched back to favor the 2′,5′-derivative (Table 4) but the selectivity was not very great.

B. *Tetrahydrofuran as solvent*

When THF was used as solvent, silylations in the presence of nitrate or perchlorate salts gave highly selective reactions at the 2′-position providing pyridine was used as base. In the absence of base (e.g., pyridine) reaction occurred mainly at the 5′-position. The use of picoline *N*-oxide in THF with silver nitrate and TBDMS-Cl gave highly selective silylation at the 3′-position. It is interesting to note that 4-methoxy and 4-nitropyridine *N*-oxide gave mainly 5′-silylation.

Nuclear magnetic resonance analysis of arabinocytidine derivatives

The chemical shifts for protons and carbons from the sugar ring of silylated arabinonucleosides are collected in Tables 5 and 6. The ^{13}C assignments for araC and araA derivatives were made by selectively decoupling the 2′ and 3′-protons while measuring the nuclear Overhauser effect on the C-2′ and C-3′ signals. The proton assignments were made on the basis of homonuclear decoupling experiments.

From Table 5 it can be seen that while there are small trends arising from the position of silylation, spectra are best used for comparison when the spectra of both isomers of a pair of isomers are available. The methyl groups directly attached to silicon usually appear as two singlets. The difference in chem-

Can. J. Chem. Downloaded from www.nrcresearchpress.com by 210.87.254.6 on 09/06/12
For personal use only.

TABLE 4. Silylation of arabinoadenosines*

Starting material	TBDMS-Cl (equiv.)	Solvent	Base (equiv.)	Catalyst (equiv.)	Time (h)	% Yields 5′	2′,5′	3′,5′
AraA (**1***d*)	2.5	DME	Et_3N (5)	$AgNO_3$ (2.5)	3	—	30	50
AraA	2.5	DME	Py (5)	$AgNO_3$ (2.5)	3	—	50	40
MMT-araA (**2***d*)	1.5	DME	Et_3N (3)	$AgNO_3$ (1.5)	3	—	35	50
DMT-araA (**3***d*)	1.5	THF	Py (3)	$AgNO_3$ (1.5)	3	—	90	5
AraA	2.5	THF	Py (5)	$AgNO_3$ (2.5)	3	—	92	3
AraA	2.5	THF	Py (5)	$AgClO_4$ (2.5)	3	—	90	5
AraA	2.5	THF	Py (5)	$(nBU)_4NClO_4$[23] (2.5)	3	—	90	5
AraA	2.5	THF	Py (5)	$(nBU)_4NNO_3$[23] (2.5)	3	—	90	5
AraA	2.5	THF	Et_3N (5)	$AgNO_3$ (2.5)	3	—	40	40
AraA	2.2	THF	—	$AgNO_3$ (2.2)	4	60	—	20
AraA	2.2	THF	—	$AgClO_4$ (2.2)	4	55	—	20
AraA	2.2	THF	3-MPNO (2.6)	—	2	—	—	—
AraA	2.2	THF	3-MPNO (2.6)	$AgNO_3$ (2.2)	2	—	5	90
AraA	2.2	THF	4-MPNO (2.6)	$AgNO_3$ (2.2)	2	—	10	80
AraA	2.2	THF	4-MPNO (2.6)	$AgClO_4$ (2.2)	2		10	80
AraA	2.2	THF	4-MOPNO (2.6)	$AgNO_3$ (2.2)	3	85	—	—
AraA	2.2	THF	4-NOPNO (2.6)	$AgNO_3$ (2.2)	4	50	—	20

*Reaction conditions and abbreviations are as described in Table 1 with following additions: 4-MPNO (4-methylpyridine *N*-oxide), 4-MOPNO (4-methoxypyridine *N*-oxide), and 4-NOPNO (4-nitropyridine *N*-oxide).

TABLE 5. Chemical shifts of selected protons for tritylated and silylated arabinonucleosides*

Compound	H1′ ($J_{1',2'}$)	H2′	H3′	H4′	H5′	$-C(CH_3)_3$	$-Si(CH_3)_2$	$-OCH_3$
MMT-araU (**2***a*)	6.18 (8.2)	4.23	4.23	4.07	3.41			3.80
MMT-cU (**15**)	6.12 (6.7)	5.32	4.56	4.40	3.07			3.80
MMT-araC (**2***b*)	6.22 (4.4)	4.27	4.17	4.07	3.41			3.80
DMT-araA (**3***d*)	6.58 (4.2)	4.50	4.50	4.26	3.47			3.90
araU (**1***a*)	6.18 (5.2)	4.41	4.13	3.98	3.89			
2′-SiaraU (**19***a*)	6.17 (4.6)	4.33	4.16	3.92	3.80	0.84	0.12, −0.01	
3′-SiaraU (**18***a*)	6.12 (3.9)	4.15	4.31	3.94	3.83	0.92	0.15	
5′-SiaraU (**4***a*)	6.14 (4.0)	4.23	4.23	3.97	3.97	0.94	0.14	
2′,5′-SiaraU (**5***a*)	6.18 (4.8)	4.36	4.19	4.19	3.97	0.93, 0.84	0.12, 0.01	
3′,5′-SiaraU (**8***a*)	6.14 (4.3)	3.93	4.31	3.93	3.90	0.95, 0.92	0.16, 0.13	
5′-MMT-2′-SiaraU (**6***a*)	6.22 (4.0)	4.26	4.14	4.20	3.40	0.73	0.02, −0.08	3.80
5′-MMT-3′-SiaraU (**9***a*)	6.16 (4.0)	4.27	4.30	3.96	3.45	0.85	0.11, 0.04	3.80
5′-MMT-3′-SicU (**16**)	6.37 (5.0)	5.31	4.64	4.27	3.10	0.88	0.15, 0.08	3.80
3′-SicU (**12***b*)	6.42 (4.9)	5.30	4.71	4.19	3.48	0.94	0.22, 0.19	
araC (**1***b*)	6.20 (4.7)	4.43	4.15	4.02	3.90			
2′-SiaraC (**19***b*)	6.21 (3.6)	4.32	4.14	3.97	3.80	0.82	0.07, −0.10	
3′-SiaraC (**18***b*)	6.16 (3.7)	4.32	4.21	3.97	3.83	0.93	0.17	
5′-SiaraC (**4***b*)	6.19 (4.1)	4.27	4.18	3.94	3.94	0.93	0.13	
2′,5′-SiaraC (**5***b*)	6.24 (3.9)	4.37	4.15	3.90	3.90	0.93, 0.82	0.11(6H), 0.07, −0.09	
3′,5′-SiaraC (**8***b*)	6.17 (3.1)	4.29	4.29	3.89	3.93	0.93, 0.89	0.18, 0.16, 0.14(6H)	
2′,3′-SiaraC (**20***b*)	6.17 (3.1)	4.22	4.26	3.97	3.81	0.95, 0.84	0.19, 0.18, 0.10, −0.12	
5′-MMT-2′-SiaraC (**6***b*)	6.33 (3.0)	4.35	4.04	4.24	3.33	0.67	−0.04, −0.20	3.80
5′MMT-3′-SiaraC (**9***b*)	6.28 (4.2)	4.32	4.32	3.95	3.38	0.84	0.12, 0.03	3.79
araA (**1***d*)	6.54 (4.0)	4.38	4.55	4.16	4.00			
2′-SiaraA (**19***d*)	6.56 (4.7)	4.59	4.58	4.09	3.97	0.76	0.13, −0.17	
3′-SiaraA (**18***d*)	6.51 (4.4)	4.39	4.66	4.10	3.97	0.98	0.31	
5′-SiaraA (**4***d*)	6.54 (4.4)	4.15	4.51	4.10	4.10	1.05	0.24	
2′5′-SiaraA (**5***d*)	6.57 (4.9)	4.58	4.52	4.10	4.10	1.06, 0.79	0.12	
3′,5′-SiaraA (**8***d*)	6.52 (4.6)	4.46	4.60	4.08	4.08	1.08, 1.06	0.12	
2′,3′-SiaraA (**20***d*)	6.56 (3.9)	4.46	4.63	4.12	3.99	1.09, 0.82	0.33, 0.13, −0.27	
5′-DMT-2′-SiaraA (**7***d*)	6.64 (4.3)	4.46	4.40	4.36	3.56	0.73	0.12, 0.02	3.91
5′-DMT-3′-SiaraA (**10***d*)	6.56 (4.9)	4.50	4.68	4.14	3.55	1.00	0.27, 0.19	3.897, 3.896

*Spectra were recorded in acetone-d_6 (except for **1***a* and **1***b* which were in D_2O) on a Varian XL200 spectrometer except for **5***d*, **7***d*, **8***d*, and **10***d* which were recorde on a Bruker WH-400 spectrometer. Chemical shifts are in ppm relative to TMS. Coupling constants are in Hz.

ical shift for the nonequivalent methyl groups is usually larger for the 2′-silyl isomer than for the 3′-silyl isomer.

Some time ago Reese and co-workers (34) observed that in the ^1H nmr spectra of a pair of 2′- and 3′-isomers (position of substituent), the anomeric proton is at lower field (up to 0.25 ppm) for the 2′-isomer relative to the 3′-isomer. In addi-

Can. J. Chem. Downloaded from www.nrcresearchpress.com by 210.87.254.6 on 09/06/12
For personal use only.

TABLE 6. Arabinose ^{13}C chemical shifts*

Compound	C-1′	C-2′	C-3′	C-4′	C-5′
AraU (**1***a*)	85.03	75.27	75.48	84.60	60.70
5′-MMTaraU (**2***a*)	84.87	75.10	76.08	82.71	63.24
2′-SiaraU (**19***a*)	84.76	76.62	75.59	84.98	60.65
3′-SiaraU (**18***a*)	84.81	75.43	76.99	84.81	60.27
5′-SiaraU (**4***a*)	84.71	74.89	75.37	83.57	62.21
2′,5′-SiaraU (**5***a*)	84.82	76.67	75.43	83.90	62.10
3′,5′-SiaraU (**8***a*)	84.52	75.42	76.40	83.52	61.62
2′,3′-SiaraU (**20***a*)	86.49	76.45	77.37	85.73	60.70
5′-MMT-2′-SiaraU (**6***a*)	85.71	76.18	76.88	83.80	63.60
5′-MMT-3′-SiaraU (**9***a*)	85.45	75.40	77.08	82.00	62.58
cU (**14**)	90.05	88.81	74.78	89.24	60.86
3′-SicU (**17***b*)	89.67	88.86	76.29	89.02	60.32
5′-MMTcU (**15**)	89.72	88.48	74.73	86.70	62.91
5′-MMT-3′-SicU (**16**)	89.11	85.53	76.42	88.41	61.98
AraC (**1***b*)	85.81	74.83	76.45	84.81	61.19
2′-SiaraC (**19***b*)	86.54	76.40	76.99	85.84	61.67
3′-SiaraC (**18***b*)	85.79	75.05	77.91	85.17	60.81
5′-SiaraC (**4***b*)	85.25	75.00	75.48	83.52	62.43
2′,5′-SiaraC (**5***b*)	85.89	76.29	76.29	84.44	62.59
3′,5′-SiaraC (**8***b*)	85.25	75.00	76.97	83.74	61.89
2′,3′-SiaraC (**20***b*)	86.59	76.02	78.02	86.76	61.13
5′-MMTaraC (**2***b*)	85.41	74.73	76.72	82.66	63.67
5′-MMT-2′-SiaraC (**6***b*)	86.59	75.75	77.64	84.22	64.26
5′-MMT-3′-SiaraC (**9***b*)	85.25	75.16	77.80	82.33	62.80
araA (**1***d*)	84.07	75.67	75.00	83.57	60.87
2′-SiaraA (**19***d*)	85.13	77.09	74.96	83.51	60.77
3′-SiaraA (**18***d*)	84.29	75.73	76.55	83.51	60.63
5′-SiaraA (**4***d*)	83.14	75.70	74.40	83.14	62.54
2′,5′-SiaraA (**5***d*)	83.36	77.02	74.86	83.33	62.47
3′,5′-SiaraA (**8***d*)	83.25	75.64	76.02	83.25	61.94
2′,3′-SiaraA (**20***d*)	85.05	76.86	76.71	83.66	60.63
5′-DMT-2′-SiaraA (**7***d*)	84.11	76.51	76.78	83.36	64.32
5′-DMT-2′-SiaraA (**10***d*)	83.09	75.70	76.94	81.96	63.24

*Spectra were recorded in DMSO-d_6 (ppm relative to TMS).

tion, Reese found that $J_{1',2'}$ is greater for the 3′-isomer than for the 2′-isomer. From Table 2 it can be seen that for silylated arabinonucleosides the chemical shift for H1′ is slightly greater for the 2′-isomer than for the 3′-isomer ($\Delta\delta \sim 0.05$ ppm) in agreement with the rules (34). However, it is equally clear that $J_{1',2'}$ is generally greater for the 2′-silylated isomer than for the 3′-isomer, except for 5′-tritylated derivatives.

The ^{13}C chemical shifts for the pentose carbons relative to C-5′ are collected in Table 6. It is clear that silylation of a particular oxygen leads to a deshielding of the carbon to which it is attached by ~1 ppm. This is consistent with all previous results in the ribose series (35, 36).

Experimental

General methods

Products from preparative scale reactions were isolated by short column chromatography (23) or by thick layer plates. Reactions were monitored by thin-layer chromatography (tlc) using Merck Kieselgel 60F254 analytical sheets. Solvents used on thin- and thick-layer chromatography were: (a) ethyl ether/chloroform/ethanol (5:4:1); (b) ethyl ether/xylene/chloroform (9:2:1), two developments; (c) chloroform/ethanol (9:1); (d) chloroform/ethanol (4:1); (e) ethyl acetate/ethanol (3:1); (f) chloroform/dimethylformamide (7:3); and (g) chloroform/dimethylformamide (4:1).

Ultraviolet spectra were recorded using a Cary 17 spectrometer. Nuclear magnetic resonance spectra were recorded from the following spectrometers: a Bruker WH-90, a Varian XL-200, and a Bruker WH-400.

Reagents were purified as previously described (23).

Methoxytritylation of arabinonucleosides

The nucleoside was dissolved in pyridine (5 mL/mmol) and 1.25 equiv. of monomethoxytrityl chloride were added. The solution was stirred at 50°C for 24 to 48 h. The solution was poured into vigorously-stirred ice water. The resulting solid was collected by filtration, dissolved in a small volume of acetone, and applied to silica gel thick layer plates. The thick layer plates were developed first in ether or hexane and then in chloroform–ethanol mixtures (generally 9:1 or 8:3, v/v). The properties of the products are collected in Table 1.

Dimethoxytritylation of arabinonucleosides

The nucleoside was dissolved in pyridine–DMF (1:1, 5 mL/mmol, araA, araC, and $araC^{Bz}$) or pyridine (araU). A total of 1.2 equiv. of dimethoxytrityl chloride was added in 8 equal portions (1 h betwen additions) to the solution stirred at −5°C. One hour after the final addition the solution was poured into ice water. The solid product was collected by filtration and purified by short column chromatography. The product mixture was applied to a column of silica gel (2 cm in diameter) using 13 g of silica/g of mixture. The products from araA, araC, and $araC^{Bz}$ were separated using chloroform–methanol (9:1) while $CHCl_3$–MeOH (9.5:0.5) was used in the araU reaction. Product yields and properties are collected in Table 1.

General procedure for the silylation of arabinonucleosides in N,N-dimethylformamide (DMF), pyridine, and 1,2-dimethoxyethane (DME)

The nucleoside was dissolved in the solvent (DMF, pyridine, or DME, 5 mL/mmol). DMF reactions contained 2 equiv. of

Can. J. Chem. Downloaded from www.nrcresearchpress.com by 210.87.254.6 on 09/06/12
For personal use only.

Can. J. Chem. Downloaded from www.nrcresearchpress.com by 210.87.254.6 on 09/06/12
For personal use only.

TABLE 7. Properties of arabinouridine derivatives

Compound	Melting point (°C)	λ_{max} (nm) (95% EtOH)	R_f (tlc)* a	c	other
5′-SiaraU (**4***a*)	159–160	263	0.26	0.18	
2′-SiaraU (**19***a*)	176–178	264	0.28	0.17	
3′-SiaraU (**18***a*)	202–204	263	0.42	0.27	
2′,5′-SiaraU (**5***a*)	53–55	263	0.62	0.46	
3′,5′-SiaraU (**8***a*)	155–157	263	0.62	0.46	
2′,3′-SiaraU (**20***a*)	218–220	262	0.67	0.44	
2′,3′,5′-SiaraU (**11***a*)	Gum	263	0.38	0.27	
5′-MMT-2′-SiaraU (**6***a*)	99–101	229, 264	0.61	0.52	0.62[b]
5′-MMT-3′-SiaraU (**9***a*)	116–118	229, 265	0.61	0.52	0.55[b]
5′-DMT-2′-SiaraU (**7***a*)	103–105	229, 265	0.58	0.49	0.48[b]
5′-DMT-3′-SiaraU (**10***a*)	118–120	229, 265	0.58	0.49	0.48[b]
3′-SicU (**17***b*)	264–265	224, 249		0.17	0.50[d]
5′-MMT-3′-SicU (**16**)	84–86	228		0.39	0.59[g]

*Solvents are described in the experimental section.

TABLE 8. Properties of arabinocytidine derivatives

Compound	Melting point (°C)	λ_{max} (nm) (95% EtOH)	R_f (tlc)*
5′-SiaraC (**4***b*)	203–205	275	0.15[d], 0.14[f]
2′-SiaraC (**19***b*)	254 (dec.)	274	0.42[d], 0.46[f]
3′-SiaraC (**18***b*)	185 (dec.)	275	0.15[d], 0.34[f]
2′,5′-SiaraC (**5***b*)	248–249	275	0.63[f], 0.66[e]
3′,5′-SiaraC (**8***b*)	203–205	275	0.45[f], 0.59[e]
2′,3′-SiaraC (**20***b*)	114–116	275	0.85[f], 0.62
5′-MMT-2′-SiaraC (**6***b*)	253 (dec.)	230, 275	0.76[f], 0.58[d]
5′-MMT-3′-SiaraC (**9***b*)	228 (dec.)	230, 275	0.52[f], 0.54[d]
5′-DMT-2′-SiaraC (**7***b*)	257 (dec.)	230, 275	0.73[f], 0.57[d]
5′-DMT-3′-SiaraC (**10***b*)	232 (dec.)	230, 275	0.50[f], 0.52[d]
$AraC^{Bz}$ (**1***c*)	175–177	250, 307	0.10[a], 0.59[d]
$5'\text{-}SiaraC^{Bz}$ (**4***c*)	205–207	250, 307	0.30[c], 0.28[f]
$2',5'\text{-}SiaraC^{Bz}$ (**5***c*)	240–243	250, 307	0.69[d], 0.78[f]
$3',5'\text{-}SiaraC^{Bz}$ (**8***c*)	210–212	250, 307	0.61[d], 0.57[f]

*Solvents are described in the experimental section.

TABLE 9. Properties of arabinoadenosine derivatives

Compound	Melting point (°C)	λ_{max} (nm) (95% EtOH)	R_f (tlc)*
5′-SiaraA (**4***d*)	155–156	258	0.38[d], 0.15[g]
2′-SiaraA (**19***d*)	193–194	257	0.47[d], 0.16[g]
3′-SiaraA (**18***d*)	200–201	258	0.52[d], 0.21[g]
2′,5′-SiaraA (**5***d*)	189–190	258	0.86[f], 0.64[g]
3′,5′-SiaraA (**8***d*)	174–175	257	0.71[f], 0.51[g]
2′,3′-SiaraA (**20***d*)	240–241	257	0.57[g]
5′-DMT-2′-SiaraA (**7***d*)	116–117	234, 257	0.60[g]
5′-DMT-3′-SiaraA (**10***d*)	110–111	234, 258	0.46[g]

*Solvents are described in the experimental section.

imidazole/mmol of TBDMS-Cl while DME reactions contained 2 equiv. of Et_3N/mmol of TBDMS-Cl. TBDMS-Cl was added to the stirred solution. At the end of the reaction period the solution was poured into an ice/water mixture. The resulting solid was collected by filtration, dissolved in a small volume of acetone, and applied to thick layer plates. The reactions producing 5′-monosilylated nucleosides were quenched by the addition of ethanol. The solution was concentrated to a small volume and applied to thick layer plates. The results are collected in Tables 2 to 4, and physical properties are collected in Tables 7–9.

Preparation of 3′,5′-diTBDMSarabinouridine (8a) from cyclouridine

To a stirred solution containing O^2,2′-cyclouridine (250 mg, 1.1 mmol) and imidazole (6.6 mmol) in DMF (15 mL) was added TBDMS-Cl (500 mg, 3.3 mmol). The solution was stirred for 1 h and then poured into ice water. The precipitate was collected by filtration and then dissolved in 0.1 *M* ethanolic KOH ((10 mL). After 2 h, the solution was concentrated at reduced pressure to ~1/3 its original volume and poured into 100 mL of water. The solid was collected by filtration and the products were isolated from five thick layer plates developed once in chloroform/ethanol (9:1). The major band was

TABLE 10. Elemental analyses of representative compounds

Compound	Calculated (%)			Found (%)		
	C	H	N	C	H	N
5′-MMT-2′-SiaraU (**6***a*)						
$C_{35}H_{42}N_2O_7Si$	66.64	6.71	4.41	66.06	6.74	4.36
2′,5′-SiaraU (**5***a*)						
$C_{21}H_{40}N_2O_6Si_2$	53.36	8.53	5.93	53.07	8.78	5.80
5′-MMT-2′-SiaraC (**6***b*)						
$C_{35}H_{43}N_3O_6Si$	66.75	6.88	6.67	67.05	7.07	6.61
2′,5′-SiaraC (**5***b*)						
$C_{21}H_{41}N_3O_5Si_2$	53.47	8.76	8.91	53.61	8.88	9.03
3′,5′-SiaraA (**8***d*)						
$C_{22}H_{41}N_5O_4Si_2\cdot\frac{1}{2}EtOH$	53.25	8.54	13.50	53.55	7.77	13.16

eluted with ethanol, which on evaporation yielded 421 mg (81%) of 3′,5′-diTBDMSarabinouridine (**8***a*, see Table 7).

*Preparation of 5′-MMT-3′-TBDMSarabinouridine (***9**a*) from cyclouridine (**14**)*

To a solution of O^2,2′-cyclouridine (200 mg, 0.88 mmol) in pyridine (5 mL) was added monomethoxytrityl chloride (380 mg, 1.2 mmol). The solution was stirred for 24 h and poured into ice water. The product (5′-MMTcyclouridine (**15**, Table 8)) can be isolated from thick layer plates (31) or, as in this case, dried overnight under vacuum. The dried material was dissolved in DMF (6 mL) and TBDMS-Cl (330 mg, 2.2 mmol) and imidazole (300 mg, 4.4 mmol) were added. The solution was stirred for 25 h and the solution was concentrated at reduced pressure. The product, 5′-MMT-3′-TBDMS-cyclouridine (**16**, Table 7) can be isolated from thick layer plates or, as in this case, dissolved in 0.5 *M* ethanolic KOH (10 mL). After 30 min the solution was concentrated at reduced pressure and poured into ice water (100 mL). The solid product was collected by filtration and the products separated by thick-layer chromatography to give 5′-MMT-3′-TBDMSarabinouridine (**9***a*, 387 mg, 70%, Table 7).

*Preparation of 2′-TBDMSarabinouridine (**19**a) from O^2,2′-cyclouridine*

O^2,2′-Cyclouridine (1 mmol) was added to a solution of dihydropyran (10 equiv.) and toluenesulfonic acid (0.1 equiv.) in acetonitrile and the solution was stirred at room temperature for 3 h. The solution was neutralized, concentrated at reduced pressure, and diluted with 0.1 *M* ethanolic KOH (10 mL). After 3 h the solution was concentrated at reduced pressure and poured into ice water. The solid, collected by filtration, was dried under vacuum and dissolved in DMF (5 mL). TBDMS-Cl (2.5 mmol) and imidazole (5 mmol) were added and the solution was stirred at room temperature for 12 h. Again the product was collected by precipitation in ice water. Treatment with 80% HOAc (in water, 15 mL) at 20°C for 24 h yielded 2′-TBDMS-arabinouridine (**19***a*) in 66% overall yield (see Table 7).

Compound **19***a* was converted into 5′-MMT-2′-TBDMSarabinouridine (**6***a*, see Table 7) by the general procedure for methoxytritylation. Monosilylation of **19***a* by the general procedure gave 2′,5′-diTBDMSaraU (**5***a*, Table 7).

Silylation of arabinonucleosides in THF silver nitrate and pyridine

General procedure

The nucleoside or its derivative was added to THF (20 mL/mmol of nucleoside) and pyridine (generally 5 equiv.) was added. To this solution was added silver nitrate (see Tables 2–4) and after stirring for 1 h at 20°C, TBDMS-Cl (Tables 2–4) was added. At the end of the reaction period the mixture was filtered into a 10% sodium bicarbonate solution (aqueous). The product was extracted into methylene chloride and products were separated by short column chromatography (~13 g of silica/g of mixture). Ethyl acetate was used to elute products in the arabinouridine series as well as the product in the preparation of 5′-TBDMSaraC and 3′,5′-diTBDMSaraA. Chloroform–methanol (9:1) was used to elute products from all of the other araC reactions. Chloroform–methanol (9.5:0.5) was used for the preparations of 5′-TBDMSaraA and 5′-DMT-3′-TBDMSaraA, while a ratio of 9.7:0.3 was used for 2′,5′-diTBDMSaraA and 5′-DMT-2′-TBDMSaraA. It is important to note that the order in which reagents are added in this reaction is critical. Yields of products are collected in Tables 2 to 4 and product descriptions are collected in Tables 7 to 10.

Silylations in dimethoxyethane–triethylamine

General procedure

The procedure is identical to that described above, except that DME replaced THF and triethylamine replaced pyridine. Yields are collected in Tables 2 to 4.

Silylations using DABCO

General procedure

DABCO (6 mmol/mmol of nucleoside) was dissolved in dry THF (25 mL/mmol of nucleoside). Silver nitrate was added and the mixture was stirred for 5 min. TBDMS-Cl was then added and after an additional 5 min the nucleoside was added and the reaction mixture was stirred at 20°C. Ratios of reagents used are listed in Tables 2 to 4. Reagents must be added in the order described above.

At the end of the reaction period the solution was collected by filtration, diluted with 50 mL of water, and the product extracted into chloroform (~100 mL). The chloroform solution was dried and concentrated and the products isolated by short column chromatography as described above. Results are collected in Tables 2 to 4.

Silylations using 3-methylpyridine N-oxide (3-MPNO)

General procedure

Silver nitrate was suspended in THF (20 mL/mmol of nucleoside). 3-MPNO was added and after 5 min TBDMS-Cl was added. This mixture was stirred at room temperature for 1.5 h. (For the dimethoxytritylated derivatives collidine was also added to this mixture in an amount equal to the amount of 3-MPNO used.) The nucleoside was then added and stirring was continued for 2 to 3 h. The solution was collected by filtration, diluted with chloroform, and extracted three times with water. The organic layer was then dried over magnesium sulfate and concentrated at reduced pressure. Products were isolated by short column chromatography. Results are collected in Tables 2 to 4.

Acknowledgements

We gratefully acknowledge generous financial support from the Natural Sciences and Engineering Research Council of Canada, the Government of Quebec (FCAC), and the Faculty of Graduate Studies at McGill. We are also indebted to Dr. Françoise Sauriol for numerous nmr spectra and assistance in their interpretation.

1. R. S. K. YOUNG and G. A. FISCHER. Biochem. Biophys. Res. Commun. **32**, 23 (1968).

Can. J. Chem. Downloaded from www.nrcresearchpress.com by 210.87.254.6 on 09/06/12
For personal use only.

2. P. B. FARMER and R. J. SUHADOLNIK. Biochemistry, **11**, 911 (1972).
3. P. J. ORTIZ, M. I. MANDUKA, and S. S. COHEN. Cancer Res. **32**, 1512 (1972).
4. C. SHIPMAN, S. H. SMITH, and J. C. DRACH. Proc. Natl. Acad. Sci. USA, **69**, 1753 (1972).
5. D. FALKE, K. RONGE, J. ARENDES, and W. E. G. MULLER. Biochim. Biophys. Acta, **563**, 36 (1979).
6. R. L. MOMPARLER. Biochem. Biophys. Res. Commun. **34**, 465 (1979).
7. R. A. LONG, G. L. SZEKERES, T. A. KHWAJA, R. W. SIDWELL, L. N. SIMON, and R. K. ROBINS. J. Med. Chem. **15**, 1215 (1972).
8. M. STAUB, H. R. WARNER, and P. REICHARD. Biochem. Biophys. Res. Commun. **46**, 1824 (1972).
9. G. A. LEPAGE and E. M. HERSH. Biochem. Biophys. Res. Commun. **46**, 1918 (1972).
10. A. MIMIAN, R. HARRIS, R. W. SIDWELL, R. K. ROBINS, and T. A. KHWAJA. J. Med. Chem. **17**, 259 (1974).
11. G. HESS, W. ARNOLD, and K-H. MEYER ZUM BUSCHENTELDE. Antimicrob. Agents Chemother. **19**, 44 (1981).
12. J. F. GEPHART and A. M. LERNER. Antimicrob. Agents Chemother. **19**, 170 (1981).
13. D. T. GISH, R. C. KELLY, G. W. CAMIENER, and W. J. WECHTER. J. Med. Chem. **14**, 1159 (1971).
14. J. A. MONTGOMERY and H. J. THOMAS. J. Med. Chem. **15**, 116 (1972).
15. K. MIYAI, L. B. ALLEN, J. H. HUFFMAN, R. W. SIDWELL, and R. L. TOLMAN. J. Med. Chem. **17**, 242 (1974).
16. W. J. WECHTER, M. A. JOHNSON, C. M. HALL, D.T. WARNER, A. E. BERGER, A. H. WENZEL, D. T. GISH, and G. L. NEIL. J. Med. Chem. **18**, 339 (1975); D. T. WARNER, G. L. NEIL, A. J. TAYLOR, and W. J. WECHTER. J. Med. Chem. **15**, 790 (1972).
17. D. C. BAKER, T. H. HASKELL, and S. R. PUTT. J. Med. Chem. **21**, 1218 (1978).
18. D. C. BAKER, T. H. HASKELL, S. R. PUTT, and B. J. SLOAN. J. Med. Chem. **22**, 273 (1979).
19. W. E. G. MULLER. Jpn. J. Antibiot. S-104 (1977).
20. W. J. WECHTER. J. Med. Chem. **10**, 762 (1967).
21. K. K. OGILVIE, S. L. BEAUCAGE, A. L. SCHIFMAN, N. Y. THERIAULT, and K. L. SADANA. Can. J. Chem. **56**, 2768 (1978).
22. K. K. OGILVIE, A. L. SCHIFMAN, and C. L. PENNEY. Can. J. Chem. **57**, 2230 (1979).
23. G. H. HAKIMELAHI, Z. A. PROBA, and K. K. OGILVIE. Can. J. Chem. **60**, 1106 (1982).
24. K. K. OGILVIE and N. Y. THERIAULT. Can. J. Chem. **57**, 3140 (1979).
25. K. K. OGILVIE and M. J. NEMER. Can. J. Chem. **58**, 1389 (1980).
26. K. K. OGILVIE and M. J. NEMER. Tetrahedron Lett. **21**, 4159 (1980).
27. K. K. OGILVIE, G. H. HAKIMELAHI, Z. A. PROBA, and D. P. C. MCGEE. Tetrahedron Lett. **23**, 1997 (1982).
28. D. H. RAMMLER and H. G. KHORANA. J. Am. Chem. Soc. **84**, 3112 (1962); M. SMITH, D. H. RAMMLER, I. H. GOLDBERG, and H. G. KHORANA. J. Am. Chem. Soc. **84**, 430 (1962).
29. K. K. OGILVIE. Can. J. Chem. **51**, 3799 (1973).
30. A. HAMPTON and A. W. NICHOL. Biochemistry, **5**, 2076 (1966).
31. D. P. C. MCGEE. M.Sc. Thesis, McGill University, 1981.
32. (*a*) G. H. HAKIMELAHI, Z. A. PROBA, and K. K. OGILVIE. Tetrahedron Lett. **22**, 4775 (1981); (*b*) **22**, 5243 (1981).
33. R. E. NOTARI, M. L. CHIN, and A. CARDONI. Tetrahedron Lett. 3499 (1969).
34. H. P. M. FROMAGEOT, B. E. GRIFFIN, C. B. REESE, J. E. SULSTON, and D. R. TENTHAM. Tetrahedron, **22**, 205 (1966).
35. D. FLOCKERZI, G. SILBER, R. CHARUBALA, W. SCHLOSSER, R. S. VARMA, F. CREEGAN, and W. PFLEIDERER. Justus Liebigs Ann. Chem. 1568 (1981).
36. K. K. OGILVIE. Proceedings of the 5th International Round Table on Nucleosides and Nucleotides. October, 1982. In press.

Can. J. Chem. Downloaded from www.nrcresearchpress.com by 210.87.254.6 on 09/06/12
For personal use only.

The 1:1 adducts of 2,5-dimethyl-3,4-diphenylcyclopentadienone and dimethyl azodicarboxylate: a fourth isomer

DONALD MACKAY, DEANE DOUGLAS MCINTYRE, NICHOLAS J. TAYLOR, AND LICHIN L. WONG[1]

Guelph–Waterloo Centre for Graduate Work in Chemistry, Waterloo Campus, University of Waterloo, Waterloo, Ont., Canada N2L 3G1

Received September 8, 1982

DONALD MACKAY, DEANE DOUGLAS MCINTYRE, NICHOLAS J. TAYLOR, and LICHIN L. WONG. Can. J. Chem. **61**, 1213 (1983).

The 1,3,4-oxadiazine **2**, one of three known 1:1 adducts of 2,5-dimethyl-3,4-diphenylcyclopentadienone and dimethyl azodicarboxylate, is converted by MeO^-–MeOH into a fourth isomer, the 1,3-oxazolidone **4**, whose structure was determined by X-ray analysis. There is evidence, however, that one of the methoxy groups of **4** comes from the solvent.

DONALD MACKAY, DEANE DOUGLAS MCINTYRE, NICHOLAS J. TAYLOR et LICHIN L. WONG. Can. J. Chem. **61**, 1213 (1983).

L'un des trois isomères connus des adduits 1:1 de la diméthyl-2,5 diphényl-3,4 cyclopentadiénone et de l'azodicarboxylate de méthyle, la oxadiazine-1,3,4 **2** dans le MeO^-–MeOH se transforme en un quatrième isomère, la oxazolidone-1,3 **4** dont on a déterminé la structure par cristalographie de rayons-X. Les données que l'on possède suggèrent qu'un des groupes du méthoxy **4** provient du solvant.

[Traduit par le journal]

Introduction

Ten years ago we showed that the reaction of 2,5-dimethyl-3,4-diphenylcyclopentadienone with azo esters led to three structurally isomeric 1:1 adducts, formally the products of addition in a 4 + 2, 2 + 4, and 2 + 2 mode (1). Thus in the case of the dimethyl ester the initially formed bridged adduct **1** was thermally labile, giving reversibly the 1,3,4-oxadiazine **2**, and irreversibly the 1,2-diazetidine **3**; **3** was thus, remarkably, the thermodynamically most stable of the three isomers. Reversal of these reactions was also possible by photolysis, **2** or **3** being convertible into **1**.

We report here on the formation of yet another isomer of these adducts.

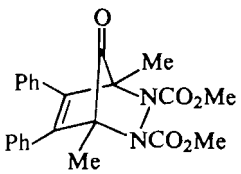

1

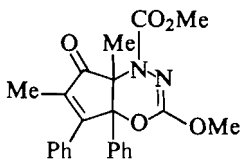

2

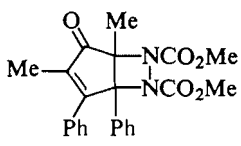

3

Results and discussion

Synthesis and isolation

In attempts to saponify the ester group of **2** we observed that a clean transformation took place when **2** was treated with KOH or NaOH in MeOH, satisfactory results being obtained with a 0.1 *M* solution over 5 h at reflux or a 1 *M* solution over 4 h at room temperature. Since the acidities of H_2O and MeOH are about equal, such dilute solutions of OH^- are converted nearly completely into H_2O and MeO^-. The latter is likely the catalyst since the reaction could be effected using a solution of NaOMe in dry MeOH. Inclusion of water, beyond trace amounts, led to profound decomposition of **2**.

Work-up of the reaction product by careful neutralization and ether extraction gave a good yield of a glassy solid. Its ^1H nmr spectrum ($CDCl_3$), which showed only trace impurities, had a *tert*-Me, a vinylic Me, two Ph groups, and two sharp OMe singlets (3.98, 3.74), thus resembling the spectrum of **2** rather closely (1). Strong ir peaks at 1775 and 1725 cm^{-1} implied the presence of at least one ester group, and the cyclopentenone chromophore, common to **2** and **3**, was inferred from the uv absorption at 282 nm. The mass spectrum had the parent peak at *m/e* 406 and a base peak at *m/e* 260 (cyclone). The product was thus unequivocally a fourth isomer of the adducts **1**–**3**.

All attempts to elucidate the structure of the new isomer by chemical means proved fruitless, in large measure due to its conversion with acids (hydrochloric, trifluoroacetic) into a demethylation product, $C_{23}H_{22}N_2O_5$, identical with the product obtained from any of **1**–**3** with acid (2). Its formation here was thus of little diagnostic value, other than confirming the preservation of the cyclopentenone ring system.

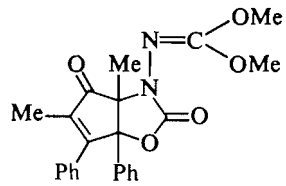

4

Crystallization and X-ray analysis

Sporadic efforts to crystallize the isomer since it was first prepared in 1971 were finally successful 10 years later, from a solvent mixture of ether and hexane. An X-ray analysis now shows it (Fig. 1) to be the dimethyl carbonate hydrazone, **4**, a functionality hitherto unreported in the literature.[2] The crystal

[1]MDS Health Group, Rexdale, Ont., Canada M9W 4Z9.

[2]A dimethyl carbonate azine has, however, been described (3, 4) as have phosgene hydrazones (5).

Can. J. Chem. Downloaded from www.nrcresearchpress.com by 210.87.254.42 on 09/06/12
For personal use only.

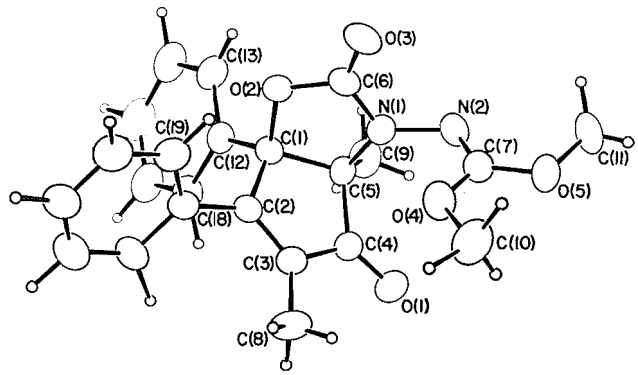

FIG. 1. ORTEP plot of compound **4**.

contained half an equivalent of solvated ether, this ratio being also confirmed by ^{1}H nmr spectroscopy. Crystals of **4** could not be obtained free of solvent, aromatic solvents being particularly easily incorporated (in preference to ether if both were present in the recrystallization medium). Thus crystals were readily obtained containing half an equivalent of any of toluene, *o*-xylene, mesitylene, or *p*-dichlorobenzene. The presence and proportion of the solvent could be determined by ^{1}H or ^{13}C nmr spectroscopy. All samples softened between 90 and 100°C and had no definable melting point.

Crystal data

$C_{23}H_{22}N_2O_5 \cdot 0.5(C_2H_5)_2O$ Mol. wt. 443.50

Monoclinic, $a = 16.522(3)$, $b = 14.062(3)$, $c = 20.761(5)$ Å, $\beta = 90.65(2)°$, $U = 4823(2)$ Å^3, space group $I2/c$ (non-standard setting of $C2/c$), $Z = 8$, $\rho_c = 1.221$ g cm^{-3}, $F(000) = 1880$, $\lambda = 0.71069$, μ (MoK$_\alpha$) = 0.936 cm^{-1}.

Data collection and reduction

A crystal (0.3 mm^3) of **4** was attached to a glass fibre and mounted on a eucentric goniometer. This was placed on a fully automated Syntex P2$_1$ diffractometer equipped with graphite monochromated molybdenum K$_\alpha$ radiation. Accurate cell dimensions were obtained from 15 well-distributed general reflections ($17 \leq 2\theta \leq 27°$). Data were collected by the $\theta-2\theta$ scan technique ($2\theta \leq 45°$) using variable scan speeds (3.9–29.3° min^{-1}), the rate being determined by a fast preliminary scan of each reflection. Of a total of 3179 unique reflections measured, 1871 with intensities $I \geq 3\sigma(I)$ were considered observed and used in the structure solution and refinement. The data were corrected for Lorentz and polarization effects.

Structure solution and refinement

The systematic absences hkl, $h + k + l = 2n + 1$ and $h0l$, h and $l = 2n + 1$ were consistent with the space groups Ic or $I2/c$. With $Z = 8$ and a centric E distribution, the latter was suggested and this choice was supported throughout the solution and refinement. The molecule was solved by direct methods (MULTAN 80) and refined by full-matrix least-squares methods. With anisotropic thermal parameters, an R of 0.13 was obtained ($R = \Sigma||F_o| - |F_c||/\Sigma|F_o|$). This very high residual was strongly suggestive of unaccounted- for electron density. A difference Fourier map at this stage revealed the presence of a solvent molecule about the two-fold axis at $0y\frac{1}{4}$. Although exact atomic centres were unresolved, the electron density was rationalized as being an ether solvate molecule exhibiting two-fold disorder about this axis. Hydrogen atoms of the principal molecule were also located at this stage. These atoms were then included in the refinement which converged at

TABLE 1. Atomic coordinates (fractional, $\times 10^4$)

Atom	*x*	*y*	*z*
O(1)	10461(1)	1529(2)	5153(1)
O(2)	8005(1)	2246(2)	6065(1)
O(3)	8410(2)	3521(2)	6635(1)
O(4)	10419(2)	2712(2)	6534(1)
O(5)	10982(2)	4058(2)	6195(1)
N(1)	9171(2)	2895(2)	5820(1)
N(2)	9762(2)	3637(2)	5775(2)
C(1)	8376(2)	1600(2)	5608(2)
C(2)	8771(2)	783(2)	5981(2)
C(3)	9564(2)	733(2)	5877(2)
C(4)	9812(2)	1474(3)	5421(2)
C(5)	9104(2)	2158(2)	5330(2)
C(6)	8536(2)	2960(2)	6213(2)
C(7)	10365(2)	3461(3)	6154(2)
C(8)	10177(3)	59(4)	6171(3)
C(9)	9028(3)	2563(4)	4652(2)
C(10)	11477(4)	2595(5)	6931(3)
C(11)	10929(3)	4920(3)	5818(3)
C(12)	7757(2)	1290(2)	5115(2)
C(13)	7090(2)	1843(3)	4971(2)
C(14)	6561(3)	1566(4)	4481(2)
C(15)	6700(3)	744(4)	4140(2)
C(16)	7351(3)	191(4)	4280(2)
C(17)	7874(2)	464(3)	4767(2)
C(18)	8293(2)	140(2)	6394(2)
C(19)	7888(3)	472(3)	6931(2)
C(20)	7465(3)	−139(3)	7321(2)
C(21)	7438(3)	−1091(3)	7172(2)
C(22)	7815(3)	−1431(3)	6637(2)
C(23)	8250(3)	−822(3)	6252(2)
Solvent*			
O(S)	266(7)	3399(8)	2819(5)
C(S1)	−216(9)	3961(13)	2601(9)
C(S2)	131(11)	4955(7)	2552(11)
C(S3)	10(13)	2393(12)	2878(7)
C(S4)	393(10)	1886(11)	2369(9)

*Occupancy 0.5.

$R = 0.042$ with $R_w = 0.051$ ($R_w = [\Sigma w||F_o| - |F_c||^2/\Sigma w|F_o|^2]^{\frac{1}{2}}$). An empirical weighting scheme of the form $w^{-1} = 2.36 - 0.052|F_o| + 0.0018|F_o|^2$ was used in the final cycles of refinement. A final difference Fourier map revealed several residual peaks of 0.1 e Å^{-3} in the vicinity of the solvent molecule. Programs used have been described elsewhere (6). Scattering factor tables for non-hydrogen atoms were taken from the usual source (7). Scattering factors for hydrogen were those of Stewart *et al.* (8). Non-hydrogen atomic positions are listed in Table 1. Selected bond lengths and angles are given in Table 2.[3]

The bond lengths and angles in **4** are quite unexceptional. The lactam bonds to the carbonyl carbon are very similar in length to those in other lactams (9, 10), and the imino bond length is typical for hydrazones (11). The hydrazone carbon is planar, its place being almost orthogonal (85.9°) to that of the C—N—C plane in the lactam ring.

[3]Tables of (*i*) observed and calculated structure factor amplitudes, (*ii*) bond lengths and angles of phenyl groups and solvent molecules, and C—H bond lengths, and (*iii*) temperature factors are available at a nominal charge from the Depository of Unpublished Data, CISTI, National Research Council of Canada, Ottawa, Ont., Canada K1A 0S2.

Can. J. Chem. Downloaded from www.nrcresearchpress.com by 210.87.254.42 on 09/06/12
For personal use only.

TABLE 2. Selected bond lengths (Å) and angles (°)

Bond	Length (Å)	Bond	Length (Å)
C(1)—O(2)	1.453(4)	C(5)—C(9)	1.522(6)
C(1)—C(2)	1.528(5)	C(6)—O(2)	1.367(4)
C(1)—C(5)	1.553(5)	C(6)—O(3)	1.199(4)
C(1)—C(12)	1.505(5)	C(6)—N(1)	1.341(5)
C(2)—C(3)	1.332(5)	N(1)—N(2)	1.421(4)
C(2)—C(18)	1.480(5)	N(2)—C(7)	1.285(5)
C(3)—C(4)	1.468(5)	C(7)—O(4)	1.318(5)
C(3)—C(8)	1.512(6)	C(7)—O(5)	1.322(5)
C(4)—O(1)	1.217(4)	O(4)—C(10)	1.461(6)
C(4)—C(5)	1.525(5)	O(5)—C(11)	1.445(6)
C(5)—N(1)	1.455(5)		

Bond	Angle (°)	Bond	Angle (°)
O(2)—C(1)—C(2)	108.6(1)	C(1)—C(5)—C(9)	118.5(2)
O(2)—C(1)—C(5)	105.2(1)	C(4)—C(5)—N(1)	108.1(1)
O(2)—C(1)—C(12)	109.7(1)	C(4)—C(5)—C(9)	114.0(2)
C(2)—C(1)—C(5)	103.9(1)	N(1)—C(5)—C(9)	112.6(2)
C(2)—C(1)—C(12)	114.2(1)	C(1)—O(2)—C(6)	109.4(2)
C(5)—C(1)—C(12)	114.7(1)	O(2)—C(6)—O(3)	122.2(1)
C(1)—C(2)—C(3)	111.8(1)	O(2)—C(6)—N(1)	108.5(1)
C(1)—C(2)—C(18)	121.7(1)	O(3)—C(6)—N(1)	129.3(1)
C(3)—C(2)—C(18)	126.4(1)	C(5)—N(1)—C(6)	114.8(2)
C(2)—C(3)—C(4)	110.5(2)	C(5)—N(1)—N(2)	121.1(1)
C(2)—C(3)—C(8)	128.6(2)	C(6)—N(1)—N(2)	122.2(1)
C(4)—C(3)—C(8)	120.9(2)	N(1)—N(2)—C(7)	110.9(2)
C(3)—C(4)—O(1)	126.5(1)	N(2)—C(7)—O(4)	123.9(1)
C(3)—C(4)—C(5)	107.9(1)	N(2)—C(7)—O(5)	121.1(1)
O(1)—C(4)—C(5)	125.6(1)	O(4)—C(7)—O(5)	115.0(1)
C(1)—C(6)—C(4)	103.4(1)	C(7)—O(4)—C(10)	118.5(2)
C(1)—C(5)—N(1)	98.8(1)	C(7)—O(5)—C(11)	117.2(2)

Reactions of 4

Compound **4** was slowly decomposed by prolonged treatment with MeO^- in MeOH and rapidly by aqueous alkali to a complex mixture. The acid catalyzed demethylation product formed from **4**, and from its isomers **1**–**3**, has previously been formulated as **5** (2) on the grounds that its methoxycarbonyl derivative showed two MeO singlets in its ^1H nmr spectra, as required for **6**. We assumed that the alternative formulation **7**,

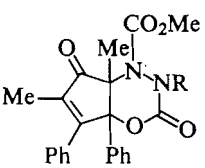

5 R = H
6 R = CO_2Me

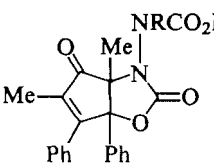

7 R = H
8 R = CO_2Me

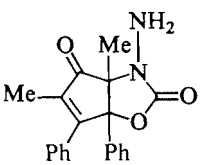

9

otherwise acceptable on the basis of the properties of the product, could be rejected, since in its methoxycarbonyl derivative, **8**, the diastereotopic MeO groups would give one singlet, due to rapid rotation of the N—N bond. In other polyacylated hydrazines, however, there is evidence that this rotation barrier may be rather high (12). Though the two MeO singlets did not coalesce, at least up to 120°C,[4] we felt that a re-examination of this demethylation product was warranted. It has now been subjected to X-ray analysis and shown in fact to have structure **7**.[5]

Because of its sensitivity to acid or base, difficulties were encountered in trying to exchange **4** into a different hydrazone or in converting it into the free hydrazine **9**. Thus **4** was inert to refluxing acetone and inclusion of acid led only to the demethylation product **7**. Similarly the latter was produced when **4** was heated with 1,1-dimethylhydrazine, even without an acid catalyst. However, the hydrazine **9** could be obtained in a good yield when a dilute solution of **4** was refluxed with *p*-toluene sulfonic acid in MeOH. The conversion of **4** into either **7** or **9** under different solvolysis conditions can be accommodated by Scheme 1 in which the N-protonated form is attacked either by, for example, trifluoroacetate or by MeOH. Attempts to reconvert **9** into **4** with tetramethyl orthocarbonate failed, but it readily gave an oily isopropylidene derivative when refluxed in acetone.

The hydrazone was thermally very stable, surviving a three day reflux in tetrachloroethylene. Its stability allowed an examination of the MeO region in the ^1H nmr spectrum at temperatures up to 120°C (CD_3SOCD_3). No change was observed. Considerable work has been done on the rotational barriers in imino carbonates of general formula **10** (4, 13, 14), which shows that the barrier height increases with the electro-

[4]In CD_3SOCD_3. The $\Delta\nu$ value of 8.1 Hz at 80 MHz puts a lower limit to the rotation barrier of $\Delta G^{\ddagger}$ = ca. 21 kcal mol^{-1}.

[5]Crystals of $C_{22}H_{20}N_2O_5$ are orthorhombic, a = 14.263(3), b = 16.229(4), c = 16.585(3) Å, space group *Pbca*, Z = 8. The structure was solved by direct methods, using 1527 observed reflections ($3\sigma(I)$), and has been refined with isotropic thermal parameters to an R of 0.109.

Can. J. Chem. Downloaded from www.nrcresearchpress.com by 210.87.254.42 on 09/06/12
For personal use only.

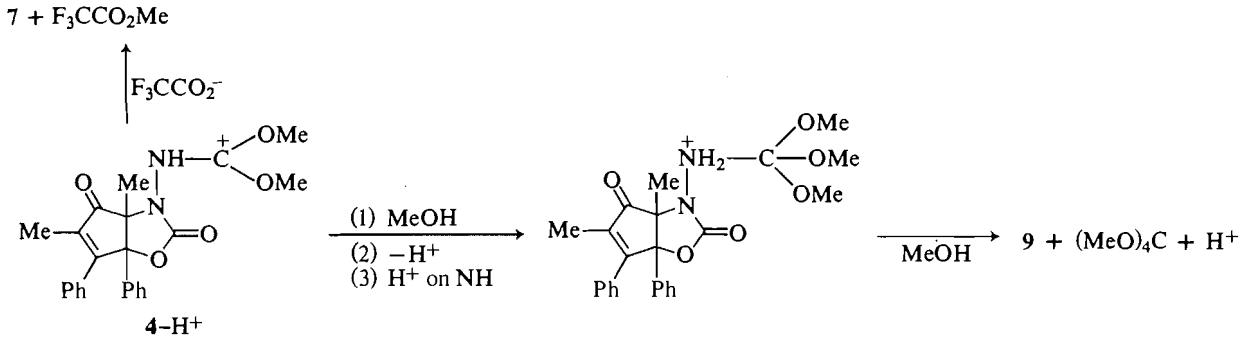

SCHEME 1

negativity of the directly bonded atom in Z (4). Thus for the anil **10** (Z = Ph) $\Delta G^{\ddagger}$ (0°C) is 14.3 kcal mol^{-1}, while for the chlorimine **10** (Z = Cl) or the azine **10** (Z = N=C(OMe)$_2$) $\Delta G^{\ddagger}$ is at least 23 kcal mol^{-1}. On this basis, rotation in **4** is expected to be too slow to affect the spectrum.

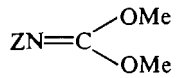

10

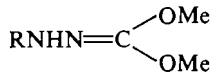

11 R = 2,4-$(NO_2)_2C_6H_3$
12 R = OEt

We found that simple hydrazone carbonates, e.g. **11** and **12**, could be routinely made from the hydrazine and tetramethyl orthocarbonate in the presence of acid. The MeO singlets in the ^{1}H nmr spectrum of each of **11** and **12** were nonequivalent. Those in **11** did not coalesce up to 150°C (CD_3SOCD_3).

Scope of the reaction

Attempts to extend the scope of the transformation of **2** → **4** met with very limited success. The nature of both the base and the solvent was crucial. The use of OH^- or EtO^- in EtOH caused rapid degradation of **2**, as did OH^- in water-rich media, e.g. 1 : 1 aqueous MeOH. MeOH was thus uniquely necessary. In place of OH^- or MeO^- the only other suitable bases found were CN^- and CO_3^{2-}, their effectiveness being, and presumably significantly so, in the order of their base strengths: $OH^- > CN^- > CO_3^{2-}$.

These results are strongly indicative of the incorporation of external MeOH in the hydrazone **4**. Confirmation of this was obtained by the behaviour of the oxadiazine **13**, obtained analogously from diethyl azodicarboylate. EtO^- in EtOH completely degraded **13**, but 0.2 *M* KOH in MeOH (effectively MeO^-) cleanly converted it into a mixture of two products, which resisted separation. The ^{1}H nmr spectrum was fully

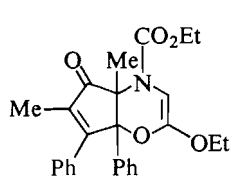

13

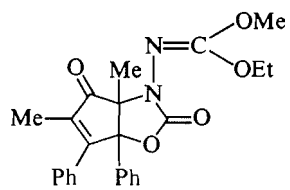

14

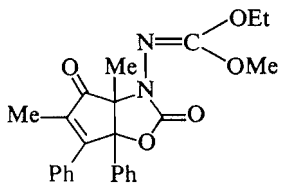

15

consistent with that of an approximately equimolar mixture of the two diastereomeric hydrazones **14** and **15**, having two MeO singlets at δ 3.96 and 3.72 (cf. the MeO singlets in **4**) and two overlapping OCH_2 quartets.

These results raise more questions than they answer concerning the transformation of **2** into **4**: which MeO group in **2** is lost; which N in **2** becomes the exocyclic N in **4**; why are the MeO groups in **4** scrambled with respect to their origin, one from **2** and one from the solvent (an implication to be drawn from the reaction of **13**); why is MeOH so specific to the reaction? Work on some of these details is well underway. At this stage we can only assert that the conversion of **2** into its isomer **4** is not in fact an isomerization.

Experimental

Infrared spectra were recorded on a Beckman IR-10 and uv spectra on a Hitachi Perkin–Elmer RM-UGE spectrometer. Nuclear magnetic resonance spectra were obtained on a Perkin–Elmer R-12B (^{1}H) or a Bruker WP-80 (^{1}H, ^{13}C) spectrometer with tetramethylsilane as internal standard. Mass spectra were determined on a Varian MAT-CH7 instrument. Melting points are uncorrected.

1-(Dimethoxymethanimino)-3a,4-diphenyl-5,6a-dimethyl-2,6-dioxo-1,2,3a,6,6a-pentahydrocyclopent[d][1,3]-oxazole (4)

A solution of the oxadiazine **2** (1) (205 mg, 0.505 mmol) in 1 *M* KOH in MeOH (from solid KOH and reagent grade MeOH with no added water, 10 mL) was kept for 4 h at room temperature and then neutralized with solid CO_2. Evaporation of the solution was carried out at room temperature to near dryness and ether and water were added. The ethereal layer was twice washed with water, dried ($MgSO_4$), and evaporated. The glassy residue (202 mg) had only trace impurities as indicated by its ^{1}H nmr spectrum.

Alternatively the reaction could be carried out at reflux with a 0.2 *M* solution for 3 h or a 0.1 *M* solution for 6 h. The work-up was the same. In any of these reactions KOH could be replaced by NaOH or NaOMe.

The hydrazone could be purified by dissolving it in carbon tetrachloride and adding hexane with stirring, which caused its precipitation as an amorphous powder; ν(CCl_4): 1775 (endocyclic CO), 1725 (exocyclic and, probably, ketone CO), 1638 (probably C=N) cm^{-1}; λ_{max} (EtOH): 284 nm; ^{1}H nmr ($CDCl_3$) δ: 7.6–6.8 (10H, m, Ph), 3.98 (s, OMe), 3.74 (s, OMe), 2.12 (s, vinylic Me), 0.94 (s, *tert*-Me); ^{1}H nmr (CD_3SOCD_3) δ: 3.90 and 3.70 (OMe singlets, unchanged up to 150°C); ^{13}C nmr ($CDCl_3$) δ: 201.3 (ketone CO), 162.7, 161.4, 151.8, 138.4, 135.8, 132.6, 129.5, 128.5, 128.3, 127.7, 126.9, 126.1, 89.9 (C5), 69.1 (C1), 57.0 (OMe), 55.7 (OMe), 13.9 (vinylic Me), 10.3 (*tert*-Me); *m/e*: 406 $M^{+\cdot}$, 260 cyclone$^{+\cdot}$.

Crystallization could be achieved only with incorporation of solvent (see Discussion); from ether–hexane the crystals corresponded to $C_{23}H_{22}N_2O_5 \cdot 0.5\ Et_2O$. *Anal.* calcd.: C 67.70, H 6.13, N 6.54; found: C 67.96, H 5.89, N 6.60%.

Reactions of 2 with other basic solutions

The following solutions of **2** (typically 100 mg in 10 mL) containing

Can. J. Chem. Downloaded from www.nrcresearchpress.com by 210.87.254.42 on 09/06/12
For personal use only.

Can. J. Chem. Downloaded from www.nrcresearchpress.com by 210.87.254.42 on 09/06/12
For personal use only.

0.2 *M* base were refluxed: (*i*) KCN in MeOH: **4** was slowly formed over about 9 h; (*ii*) Na_2CO_3 (saturated) in MeOH: **4** was very slowly formed, about 75% conversion in 17 h; (*iii*) NaOEt in EtOH: rapid decomposition; the ^{1}H nmr spectrum became very complex; (*iv*) KOH in EtOH: rapid decomposition; (*v*) KOH in 1:1 EtOH–H_2O: very rapid decomposition.

*Conversion of oxadiazine **13** into hydrazones **14** and **15***

Refluxing of **13** with 0.2 *M* KOH in EtOH, as described for the analogous reaction of **2** in MeOH, caused complete degradation.

A solution of **13** (200 mg, 0.46 mmol) in 0.2 *M* KOH in MeOH was refluxed for 4 h and then worked up as described for the synthesis of **4**. The residue (169 mg, 87%) contained only a trace of starting material, and its ^{1}H nmr spectrum was fully reconcilable with that of an approximately 1:1 mixture of **14** and **15**; ^{1}H nmr ($CDCl_3$) δ: 7.6–6.8 (10H, m, Ph), 4.40, 4.14 (two OCH_2, quartets, both J = 7.1 Hz), 3.96, 3.72 (two OMe, singlets), 2.13 (s, vinylic Me), 1.38, 1.22 (two OCH_2Me triplets), 0.94 (s, *tert*-Me).

Attempts to separate **14** and **15** by column chromatography (neutral Al_2O_3) or hplc (silica) caused degradation.

*Stability of **4***

A sample of **4** (50 mg) in tetrachloroethylene was heated at reflux (120°C) in an nmr tube. Its proton spectrum showed no change after 3 days.

*Demethylation of **4** to **7***

(*i*) *Trifluoracetic acid*

A solution of **4** (90 mg, 0.22 mmol) in carbon tetrachloride (1 mL) was made 5% v/v in trifluoroacetic acid and kept for 1 day at room temperature. After evaporating to dryness the residue was crystallized from carbon tetrachloride – hexane to give the known demethylation product **7** (50%), mp 232.5–234.5°C, undepressed in admixture with authentic material (2).

(*ii*) *Hydrochloric acid*

A solution of **4** as the hemi-etherate (30 mg, 0.068 mmol) in $CDCl_3$ (0.4 mL) in an nmr tube was shaken for 3 min with 2 drops of 12 *M* hydrochloric acid. The spectrum showed demethylation to be complete. The contents of the tube were neutralized and dried with solid Na_2CO_3, and the solution evaporated to give crude product (23 mg, 83%), which was washed with cold ether. Its ir spectrum was identical with that of an authentic sample.

*Reactions of **4** with alkali*

A solution of **4** (100 mg) in 0.2 *M* KOH in 1:1 H_2O–acetonitrile (50 mL) was refluxed for 1 h and then extracted with ether. The nmr spectrum of the residue from the ether solution showed that **4** had been completely degraded.

Attempted ketone exchange with acetone

The hydrazone **4** was recovered without change after refluxing for 12 h in acetone.

A sample of **4** (50 mg, 0.12 mmol), acetone (5 equiv.), and boron trifluoride etherate (5 equiv.) were refluxed for 2 h in chloroform (1 mL). The solution darkened and a precipitate formed. Evaporation to dryness and addition of ether gave an almost colorless solid identified as the demethylation product by its ir and ^{1}H nmr spectra.

Attempted exchange with 1,1-dimethylhydrazine

The etherate of **4** (93 mg, 0.21 mmol) and 1,1-dimethylhydrazine (38 mg, 0.63 mmol) were heated at reflux in $CDCl_3$ (0.5 mL) in an nmr tube, and the reaction monitored by proton spectroscopy. Reaction was complete after 4 days, the separation of solid being evident. Evaporation and trituration with ether gave the demethylation product, identified as before.

*The N-amino compound **9***

The hydrazone **4** (1.6 g, 0.39-mmol) and *p*-toluenesulfonic acid (1.5 g, 0.87 mmol) were refluxed together in MeOH (400 mL) for 30 min. The whole was then shaken with ether (600 mL) and water (400 mL), and the organic layer was separated, washed with water, and dried. Evaporation gave **9** as an oil (1.1 g, 80%), which slowly crystallized from ether–hexane. It was recrystallized from ether–hexane, mp 157.5–158.5°C; ν(film): 3360 (NH), 1764, 1712 (urethane, ketone CO) cm^{-1}; ^{1}H nmr ($CDCl_3$) δ: 7.6–7.2 (10H, m, Ph), 3.93 (2H, s, NH_2, exchangeable with D_2O), 2.13 (s, vinylic Me), 0.96 (*tert*-Me). *Anal.* calcd. for $C_{20}H_{18}N_2O_3$: C 71.84, H 5.42, N 8.38; found: C 71.80, H 5.33, N 7.97%.

Refluxing of **9** in acetone for 12 h without catalyst gave a quantitative conversion into the isopropylidene derivative, obtained on evaporation as an oil; ^{1}H nmr ($CDCl_3$) δ: 7.5–7.0 (10H, m, Ph), 2.17 (6H, s, CMe_2), 1.88 (s, vinylic Me), 1.04 (s, *tert*-Me); ^{1}H nmr (C_6D_6) δ: 1.74, 1.73 (two CMe_2 singlets).

*Dimethyl carbonate 2,4-dinitrophenylhydrazone (**11**)*

2,4-Dinitrophenylhydrazine (1.84 g, 0.01 mol), tetramethyl orthocarbonate (1.36 g, 0.01 mol), and 5 drops of trifluoroacetic acid were refluxed in benzene (20 mL) for 10 min. The product obtained on cooling was collected and then crystallized from benzene as orange-red needles (1.9 g, 70%), mp 191–192°C; ν (Nujol): 3315 (NH) cm^{-1}; λ_{max} ($CHCl_3$): 3740 Å (ε 17 800); ^{1}H nmr ($CDCl_3$) δ: 10.85 (NH), 9.08 (C3-H), 8.19 (C5-H), 7.61 (C6-H), 3.99 (two coincident OMe groups); ^{1}H nmr (C_6D_6 δ: 3.38, 3.04 (two OMe singlets); *m/e*: 270 (M^+). *Anal.* calcd. for $C_9H_{10}N_4O_6$: C 40.01, H 3.73, N 20.74; found: C 40.07, H 3.80, N 20.65%.

The OMe peaks were distinguishable in CD_3SOCD_3 and did not coalesce when the nmr probe was heated to 150°C.

*Dimethyl carbonate ethoxycarbonylhydrazone (**12**)*

The preparation was similar to that of **11**, but was more efficient in MeOH as solvent with a few drops of hydrochloric acid as catalyst; ^{1}H nmr ($CDCl_3$) δ: 7.2 (1H, bs, NH), 4.20 (2H, OCH_2, q, J = 7 Hz), 3.87 (s, OMe), 3.81 (s, OMe), 1.27 (3H, OCH_2Me, t); *m/e*: 176 (M^+).

Acknowledgement

We thank the Natural Sciences and Engineering Research Council of Canada for support of this work.

1. D. MACKAY, C. W. PILGER, and L. WONG. J. Org. Chem. **38**, 1043 (1973).
2. D. MACKAY and C. W. PILGER. Can. J. Chem. **52**, 1114 (1974).
3. J. THIELE. Ann. **303**, 57 (1898).
4. F. VOGTLE, A. MANNSCHRECK, and H. A. STAAB. Ann. **708**, 51 (1967).
5. D. SEYFERTH and H. SHIH. J. Org. Chem. **39**, 2329 (1974).
6. N. J. TAYLOR, S. E. JACOBSON, and A. J. CARTY. Inorg. Chem. **14**, 2648 (1975).
7. International Tables for X-ray Crystallography. Vol. 4. Kynoch Press, Birmingham, England. 1974.
8. R. F. STEWART, G. R. DAVIDSON, and W. T. SIMPSON. J. Chem. Phys. **42**, 3175 (1965).
9. J. W. TURLEY. Acta Crystallogr. Sect. B, **28**, 140 (1972).
10. P. GROTH. Acta Chem. Scand. **27**, 945 (1973).
11. H. O. HOUSE, C-C. YAU, and D. VANDERVEER. J. Org. Chem. **44**, 3031 (1979).
12. Y. SHVO. *In* The chemistry of the hydrazo, azo and azoxy groups. Part 2. *Edited by* S. Patai, John Wiley and Sons, London. 1975. Chapt. 21.
13. N. P. MARULLO and E. H. WAGENER. J. Am. Chem. Soc. **88**, 5034 (1966).
14. H. KESSLER, P. F. BLEY, and D. LEIBFRITZ. Tetrahedron, **27**, 1687 (1971).

Preparation and properties of tetrazinc μ_4-oxohexa-μ-carboxylates (basic zinc carboxylates)

RHIANYDD M. GORDON AND HOWARD B. SILVER

BP Research Centre, Chertsey Road, Sunbury-on-Thames, Middlesex TW16 7LN, U.K.

Received June 14, 1982

RHIANYDD M. GORDON and HOWARD B. SILVER. Can. J. Chem. **61**, 1218 (1983).

The compounds $(RCO_2)_6Zn_4O$ have not been widely reported in the literature, and in order to examine their little-known chemistry, a number of them have been synthesised by several methods. The simplest method of preparation, using the carboxylic acid and zinc oxide, was found to be restricted to branched chain acids. The reaction of these basic salts with primary and secondary amines led to a breakdown of their structures, with the formation of the amine complexes of the neutral carboxylates.

RHIANYDD M. GORDON et HOWARD B. SILVER. Can. J. Chem. **61**, 1218 (1983).

Dans la littérature on trouve peu de travaux relatifs aux composés du type $(RCO_2)_6Zn_4O$. Dans le but d'examiner leur chimie peu connue, on a synthétisé un certain nombre de ces composés selon plusieurs méthodes. On a trouvé que la méthode de préparation la plus simple qui utilise l'acide carboxylique et l'oxyde de zinc se limite aux acides ayant une chaîne secondaire. La réaction de ces sels basiques avec des amines primaires et secondaires conduit à une rupture de leurs structures avec formation de complexes d'amines de carboxylates neutres.

[Traduit par le journal]

Can. J. Chem. Downloaded from www.nrcresearchpress.com by 210.87.254.6 on 09/06/12
For personal use only.

Introduction

Basic beryllium acetate, $(CH_3CO_2)_6Be_4O$, with its tetrahedral symmetry consisting of four beryllium atoms at the apices and an oxygen atom at the centre, has been well characterised in the literature (1). A number of reports exist on other basic beryllium carboxylates (2) and their derivatives (3). However, very little is known of the isostructural zinc compounds.

The basic acetate, $(CH_3CO_2)_6Zn_4O$, was first prepared by Auger and Robin (4) by the vacuum distillation of the normal acetate, and its structure was established by Wyart (5) and by Koyama and Saito (6). Few reports exist of any other basic zinc carboxylates. In a limited study several years ago we described the preparation and mass spectra of the 2-ethylhexanoate and 3,5,5-trimethylhexanoate (7), and Charalambous and coworkers (8) discussed the mass spectra of the acetate, *n*-propionate, and *n*-butanoate, prepared by pyrolysis of the normal carboxylate (9). Recent interest in these compounds (10) as intermediates in the formation of complexes in the gelling of crude oil spillages, has led us to examine them further, and we report here some of our findings regarding their preparation and reactions with certain amines.

Experimental

Spectroscopic analysis

Infrared spectra were recorded on a Perkin Elmer Infracord Spectrometer. Mass spectra were obtained on a Kratos MS 12 single focussing mass spectrometer at low resolution, with a direct inlet system temperature of 250°C, ion source temperature of 250°C, and with ionising electron energy of 70 eV.

AnalaR zinc oxide and the solvents employed were used as received. The carboxylic acids and amines were generally distilled, or recrystallised, to give boiling points, or melting points, consistent with those reported in the literature. Zinc 2-methylpropionate, mp 226 (Calcd. Zn 27.3; found Zn 27.3) and 2-ethylhexanoate (Calcd. Zn 18.6; found Zn 17.7) were prepared from the oxide and the free acid in stoichiometric proportions.

Preparation of $(RCO_2)_6Zn_4O$

Three methods were used to prepare the basic carboxylates. These were (*a*) by the reaction between zinc oxide and the carboxylic acid in the appropriate proportions, (*b*) by the thermal decomposition of the neutral carboxylate, $(RCO_2)_2Zn$, and (*c*) by the reaction of zinc oxide with the neutral carboxylate.

Method (a)

In a typical experiment on a 0.1 *M* scale, a mixture of the acid (6 equiv.), zinc oxide (4 equiv.), and toluene (250 mL) was placed in a round-bottomed flask fitted with a stirrer and a Dean and Stark head for the removal of water. Heating and stirring were maintained until all of the water of reaction had been collected, and then continued for a further 2 to 3 h. The product was filtered and solvent removed from the filtrate. The basic carboxylate was then purified by distillation or recrystallisation.

Method (b)

The neutral carboxylate was placed in a single-necked flask equipped with an air condenser set at right angles to the neck of the flask, which was heated for 6 h at 250 ± 5°C and at 0.2 mm. The product was isolated as the sublimate, and by toluene extraction from the residue.

Method (c)

Neutral zinc 2-ethylhexanoate (105.5 g, 0.33 mol) in toluene (350 mL) was heated and stirred for 3 h with zinc oxide (8.1 g, 0.10 mol). The product was filtered and removal of solvent afforded a viscous liquid (115 g), n_D^{25} 1.4570, whose infrared spectrum showed it to be identical to that of the spectrum of basic zinc 2-ethylhexanoate.

The physical properties of the basic carboxylates prepared are summarised in Table 1.

Reaction between basic zinc 2-methylpropionate and 2-ethylhexanoic acid

Basic zinc 2-methylpropionate (30.0 g, 0.037 mol) in xylene (400 mL) was heated with stirring for 2 h with a solution of 2-ethylhexanoic acid (32.5 g, 0.225 mol) in xylene (100 mL). Water (0.65 mL) collected in a Dean and Stark column. Distillation of the reaction mixture afforded 2-methylpropionic acid (9.47 g, 0.107 mol, bp 153–154°C). The infrared and mass spectra identified the distillation residue as a mixture of neutral zinc 2-methylpropionate and neutral zinc 2-ethylhexanoate.

Reactions of (a) basic zinc carboxylates and (b) neutral zinc carboxylates with amines

(*a*) In a typical experiment a solution of cyclohexylamine (4.0 g, 0.04 mol) in ether (10 mL) was treated with basic zinc 2-ethylhexanoate (5.7 g, 0.005 mol) in the same solvent (20 mL) at ambient temperature. The reaction was slightly exothermic and produced a clear liquid, which was kept at room temperature for 24 h. Solvent was removed to afford a waxy solid (9.55 g), which was

TABLE 1. Tetrazinc μ_4-oxohexa-μ-carboxylates

Carboxylic acid	Method of preparation	Yield %	bp/mm (mp)°C	Found % C	Found % H	Found % Zn	Required % C	Required % H	Required % Zn	Carbonyl frequency cm^{-1}
Acetic	b	55	(243–250)	22.8	2.9	41.6	22.8	2.9	41.4	1607
Propionic	b	49	(200–202)	30.5	4.3	—	30.2	4.2	—	1545
2-Methylpropionic	a	69	(116)	35.5	5.2	32.4	36.0	5.3	32.7	1600
Trimethylacetic	a	83	(192–194)	40.8	6.1	28.4	40.7	6.2	29.6	1575
2-Ethylbutanoic	a	99	232°C/0.3 (98–100)	44.2	7.0	27.0	44.6	6.8	27.0	1590
2,2-Dimethylbutanoic	a	91	(190–192)	44.3	7.0	26.9	44.6	6.8	27.0	1600
3,3-Dimethylbutanoic	a	96	(148–150)	44.5	6.7	26.6	44.6	6.8	27.0	1607
2-Ethylhexanoic	a, c*	93	255/0.1	51.0	8.0	22.8	50.7	8.0	23.0	1590
3,5,5-Trimethylhexanoic	a†	99	282/0.05	54.1	8.7	—	53.2	8.5	—	—
3-Chloro-2,2-dimethylpropionic	a	81	(192–194)	33.2	4.6	23.4	33.0	4.4	23.9	1600

*a, n_D^{25} 1.4570; c, n_D^{25} 1.4570.
†n_D^{25} 1.4637.

crystallised from 40–60°C petroleum ether to give a crystalline solid, mp 130°C (*Anal.* Calcd. for $(C_7H_{15}CO_2)_2Zn.2C_6H_{11}NH_2$: C 61.1, H 10.3, N 5.1; found: C 61.1, H 10.3, N 5.1; *Anal.* Calcd. for $(C_7H_{15}CO_2)_6Zn_4O.8C_6H_{11}NH_2$: C 59.7, H 10.1, N 5.8).

(*b*) As in the above, THF or 40–60°C petroleum ether solutions of the normal carboxylates were added to the same series of amines at 2:1 equivalent ratios and on a similar molar scale. The products, crystalline solids, were isolated and purified from hydrocarbon solvents, to yield the 2:1 complexes of the amine and neutral carboxylates.

Results and discussion

Tetrazinc μ_4-oxohexa-μ-carboxylates

The compounds prepared in the present study by one of the three methods previously described are shown in Table 1. The preferred route was to heat zinc oxide with toluene solutions of the carboxylic acid. Examination of Table 1 shows that the basic carboxylates prepared in this way are from a fairly restricted range of acids, i.e. acids with branched hydrocarbon chains. Two alternatives to the formation of the basic carboxylates were observed. Straight chain acids, of carbon number up to ten, formed only the neutral salts, leaving an excess of zinc oxide. Examples of this reaction path were seen with acetic, *n*-propionic, *n*-hexanoic, *n*-octanoic, phenylacetic, and *n*-decanoic acids. Straight chain acids greater than C_{10} did not react at all with zinc oxide, e.g. dodecanoic, hexadecanoic, and oleic acids, and this was similarly the case with 2-methyl- and 4-*t*-butyl-benzoic acids.

The reasons for these results are far from clear. Since it was shown in the case of the 2-ethylhexanoate derivative that the basic salt could be formed via the neutral, it is reasonable to assume that the neutral salt is formed as an intermediate in the reaction, thus implying reaction between the insoluble zinc oxide and the neutral salt (reactions [1] and [2]). It was also established that the neutral salt was formed from the acid, rather than the anhydride, since it was found that under the conditions of the reaction, water cannot be removed by dehydration from the acid even in the presence of a catalytic amount of zinc oxide (reaction [3]).

[1] $6RCO_2H + 3ZnO \rightarrow 3(RCO_2)_2Zn + 3H_2O$

[2] $3(RCO_2)_2Zn + ZnO \rightarrow (RCO_2)_6Zn_4O$

[3] $6RCO_2H \not\rightarrow 3(RCO)_2O + 3H_2O$

Basic zinc acetate and propionate could only be prepared by the vacuum pyrolysis of the neutral salts (reaction [4]).

[4] $4(RCO_2)_2Zn \rightarrow (RCO_2)_6Zn_4O + (RCO)_2O$

This gives further support to the hypothesis that neutral zinc carboxylates are formed as intermediates. Somewhat unexpectedly, the higher molecular weight salts, e.g. zinc di-*n*-hexanoate and *n*-octanoate, did not afford the basic compounds when treated in this way. Although it is fair to cite the insolubility of the neutral acetate and propionate in the toluene solvent as inhibiting reaction with the oxide, this cannot be said for the more oleophilic zinc *n*-octanoate and *n*-decanoate, which were soluble in the heated solvent. The reason for the lack of reactivity of the higher acids towards zinc oxide is also not immediately apparent. It is doubtful whether this is because of steric factors, since the straight chain acids would offer less hindrance of approach to zinc oxide than the lower branched-chain (e.g., trimethylacetic) acids; neither can acid strength be considered a factor in this lack of reactivity since the difference in pK_a of the acids after C_4 is negligible.

Infrared examination of the basic zinc carboxylates

Examination of the infrared spectra of the basic carboxylates shows single strong absorption bands between 1570 and 1607 cm^{-1} except for the propionate (1545 cm^{-1}), see Table 2. These bands are not seen in the infrared spectra of the nuetral salts, and confirm the findings of Beattie and Gilson (11), who reported a value of 1598 cm^{-1} for the acetate and stated this C—O stretching vibration to be characteristic of bridging or chelate carboxylate groups. In the basic beryllium carboxylates, Semenenko and Kurdyumov (12) noted an intense band at 770–80 cm^{-1}, which they ascribed to the BeO_4 tetrahedron, but a similar, consistent band was not seen by us in the zinc system.

Mass spectra

All of the basic zinc carboxylates examined showed the most intense ion to be $(RCO_2)_5Zn_3O^+$, confirming our earlier results (7) and those of Charalambous (8), Vogel and Hobrock (13), and Sipachev *et al.* (14).

Transacidification of basic zinc carboxylates

Transacidification (carboxylic acid exchange) of basic zinc carboxylates was attempted to determine whether it was possible to prepare those compounds which were not available by simple zinc oxide – carboxylic acid interaction, i.e.

[5] $(RCO_2)_6Zn_4O + 6R'CO_2H \rightarrow (R'CO_2)_6Zn_4O + 6RCO_2H$

The basic zinc carboxylate chosen was the 2-methylpropionate

Can. J. Chem. Downloaded from www.nrcresearchpress.com by 210.87.254.6 on 09/06/12
For personal use only.

TABLE 2. Complexes formed between basic/neutral zinc carboxylates and amines

Carboxylate*		Amine	Melting point °C	Analytical results: Found C	H	N	Zn	Calculated† C	H	N	Zn	Carbonyl frequency cm^{-1}
2-Ethylhexanoate	(B)	*C*-Hexyl	130	61.1	10.6	5.2	12.2	59.7	10.1	5.8	13.5	1575
	(N)		130–132	61.7	10.5	5.3	11.2	61.1	10.3	5.1	11.9	1575
	(B)	*n*-Dodecyl	60–62	66.2	12.6	4.0	8.8	66.0	11.8	4.3	10.0	1587
	(N)		58–60	66.0	11.9	3.9	8.9	66.5	11.7	3.9	9.0	1560
	(B)	Morpholine	80–81	55.0	9.5	5.3	13.4	52.4	8.9	6.1	14.3	1610
	(N)		81	53.7	9.1	5.2	11.8	54.8	9.2	5.3	12.4	1626
2-Methylpropionate	(B)	*C*-Hexyl	160–162	53.9	9.2	6.3	14.9	54.2	9.2	7.0	16.4	1631
	(N)		164	54.6	9.2	6.4	14.4	54.8	9.2	6.4	14.9	1618
	(B)	4-Methyl	122–124 (decomp.)	54.2	9.5	6.2		54.2	9.2	7.0	16.9	1613
	(N)	piperidine	126 (decomp.)	54.4	9.4	6.8	14.8	54.8	9.2	6.4	14.9	1613

*B = basic, N = neutral.
†Calculated as the basic salt adduct and the neutral salt adduct.

TABLE 3. TBN values for reaction product of basic zinc carboxylates and amines

Basic zinc carboxylate	Amine	TBN (found)	TBN (calcd.) $(RCO_2)_2Zn.2RNH_2$	TBN (calcd.) $(RCO_2)_6Zn_4O.8RNH_2$
2-Ethylhexanoate*	Cyclohexylamine	416.7; 410.6	408	465
	n-Dodecyclamine	311.8; 313.5	311	342.6
	Morpholine	430.0; 430.0	426.6	489.5
2-Methylpropionate	4-Methylpiperidine	506.8; 508.8	512	563
	Cyclohexylamine	516.2; 521.5	512	563

*TBN from neutral zinc complex was 406.5; 411.0.

which was reacted with 2-ethylhexanoic acid. However, the above reaction did not take place. Instead, the basic structure was destroyed and water and the two neutral salts were obtained. A possible pathway is as follows:

[6] $(RCO_2)_6Zn_4O + 6R'CO_2H \rightarrow 3(R'CO_2)_2Zn + (RCO_2)_2Zn + 4RCO_2H + H_2O$

From these results it would appear that the basic carboxylate behaves as a mixture of zinc oxide and neutral carboxylate, which are both vulnerable to attack by higher molecular weight acid. These findings are consistent with those of Hardt and Stavenow (15) who reported that formic acid reacted with basic zinc acetate to afford the neutral zinc formate.

Reaction with amines

The coordination number of zinc in the basic zinc carboxylates is 4. It was therefore argued that addition compounds of the type $(RCO_2)_6Zn_4O.8RR'NH$ should be capable of existence. The reaction of the basic 2-ethylhexanoate and 2-methylpropionate with a number of primary and secondary amines proceeded smoothly to give crystalline products. Their elemental analyses were not, however, in line with compounds of the above structure, and molecular weight determinations by vapour pressure osmometry did not give consistent results. Further examination of the elemental analyses suggested that the complexes might be the addition products of the *neutral* carboxylates, $(RCO_2)_2Zn.2R'R''NH$. These compounds are well characterised in the literature (16–21) in contrast with the unknown complexes of the basic salts. In order to help clarify the situation the amine complexes of the corresponding neutral carboxylates were prepared, a full summary of the results obtained being given in Table 2. It will be noted that the melting points of the amine addition compounds from either the basic carboxylate or the corresponding neutral salt are very similar and the elemental analyses in both cases are very close and correspond with the addition product of the neutral amine. Examination of the infrared spectra of the products from the neutral and basic carboxylate with the same amine showed the same product was formed; Table 2 gives data of the carbonyl stretching frequencies.

Further evidence for the breakdown of the tetrahedral structure was provided by the determination of the Total Base Numbers (TBN) (22) of the addition compounds. This potentiometric titration of the total alkalinity of a compound proved to be a most effective way of distinguishing between the basic and neutral complexes. The breakdown by acids in the determination of the value is shown below:

[7] $(RCO_2)_2Zn.2R'R''NH + 4H^+ \rightarrow 2RCO_2H + Zn^{2+} + 2R'R''NH_2^+$

[8] $(RCO_2)_6Zn_4O.8R'R''NH + 16H^+ \rightarrow 6RCO_2H + 4Zn^{2+} + 8R'R''NH_2^+$

The results found for a representative number of complexes are shown in Table 3 from which it can be concluded that the addition compounds isolated from the interaction of the basic carboxylates with the amines are indeed the neutral salts.

Finally, the X-ray examination of the addition products from the interaction of the basic zinc 2-methylpropionate with both cyclohexylamine and 4-methyl piperidine confirmed that in both cases they were the diamino derivative of the neutral salts. This work will be reported elsewhere.

Can. J. Chem. Downloaded from www.nrcresearchpress.com by 210.87.254.6 on 09/06/12
For personal use only.

From the evidence of the above results, it would therefore appear that nucleophilic attack of the amines on the zinc atoms destroys the basic carboxylate structure, as did the reaction with carboxylic acids.

Acknowledgement

Permission to publish this paper has been given by the British Petroleum plc.

1. W. H. BRAGG. Nature, London, **111**, 532 (1923).
2. G. URBAIN and H. LACOMBE. Compt. Rend. **133**, 874 (1901); S. TANATAR and E. KUROVSKY. J. Russ. Phys. Chem. Soc. **39**, 936 (1907).
3. A. I. GRIGOR'EV, A. V. NOVOSELOVA, and K. N. SEMENENKO. Zh. Neorg. Khim. **3**, 1599 (1958).
4. V. AUGER and I. ROBIN. Compt. Rend. **178**, 1546 (1924).
5. J. WYATT. Bull. Soc. Fr. Mineral. **49**, 148 (1926).
6. H. KOYAMA and Y. SAITO. Bull. Chem. Soc. Jpn. **27**, 112 (1954).
7. W. L. MEAD, W. K. REID, and H. B. SILVER. J. Chem. Soc. Chem. Commun. 573 (1968).
8. J. CHARALAMBOUS, R. G. COPPERTHWAITE, S. W. JEFFS, and D. E. SHAW. Inorg. Chim. Acta, **14**, 53 (1975).
9. J. CHARALAMBOUS. Private communication.
10. BP European Patent Application 0023084. 23.1.81.
11. I. R. BEATTIE and T. GILSON. J. Chem. Soc. 2585 (1961).
12. K. N. SEMENENKO and G. M. KURDYUMOV. Zh. Neorg. Khim. **7**, 1512 (1962).
13. J. G. VOGEL and B. G. HOBROCK. 153rd Am. Chem. Soc. Meeting, Miami Beach, FL. April 1967.
14. V. A. SIPACHEV, L. N. RESHETOVA, Y. S. NEKRASOV, and S. YU. SIL'VESTROVA. Org. Mass Spectrosc. **15**, 192 (1980).
15. H. D. HARDT and F. STAVENOW. Z. Anorg. Allgem. Chem. **301**, 267 (1959).
16. K. N. SEMENENKO and G. M. KURDYUMOV. Vestik Moskov. Univ. Ser. Mat., McKh., Astron. F12., Khim. **13**, 207 (1958).
17. M. A. BARNARD, A. BUSNOT, and F. BUSNOT. Bull. Soc. Chim. Fr. 2867 (1970).
18. I. S. AHUJA and P. RASTOGI. Indian J. Chem. **8**, 88 (1970).
19. C. D. RAO, B. PAUL, B. K. MOHAPATRA, and S. GURU. J. Inorg. Nucl. Chem. **40**, 134 (1978).
20. C. D. RAO, B. K. MOHAPATRA, and S. GURU. J. Indian. Chem. Soc. **56**, 631 (1979).
21. F. N. MUSAOV, E. M. MOVSUMOV, AH.S MAMEDOV, I. R. AMIRASLANOV, and A. I. MAGERRARMOV. Koord. Khim. **4**, 1420 (1978).
22. IP Standards for Petroleum and its Products. Method IP276. Institute of Petroleum, Great Britain.

Can. J. Chem. Downloaded from www.nrcresearchpress.com by 210.87.254.6 on 09/06/12
For personal use only.

Structure of bis(*p*-bromophenyl)tellurium(IV) dichloride

RAJ K. CHADHA, JOHN E. DRAKE, AND J. L. HENCHER
Department of Chemistry, University of Windsor, Windsor, Ont., Canada N9B 3P4

Received October 15, 1982

RAJ K. CHADHA, JOHN E. DRAKE, and J. L. HENCHER. Can. J. Chem. **61**, 1222 (1983).

The X-ray crystal structure of bis(*p*-bromophenyl)tellurium(IV) dichloride has been determined: $R = 0.025$. The crystals were triclinic, $P\bar{1}$, $a = 8.000(7)$ Å, $b = 11.811(11)$ Å, $c = 7.978(6)$ Å, $\alpha = 101.85(7)°$, $\beta = 98.73(6)°$, $\gamma = 80.95(7)°$, and $Z = 2$. The compound exhibits a ψ-trigonal bipyramidal arrangement of ligands around tellurium with weak secondary interactions between tellurium and bromine atoms in adjacent molecules.

RAJ K. CHADHA, JOHN E. DRAKE et J. L. HENCHER. Can. J. Chem. **61**, 1222 (1983).

On a déterminé la structure cristalline du dichlorure de bis(*p*-bromophényl)tellure(IV) par diffraction de rayons-X: $R = 0{,}025$. Les cristaux sont tricliniques, $P\bar{1}$, $a = 8{,}000(7)$ Å, $b = 11{,}811(11)$ Å, $c = 7{,}978(6)$ Å, $\alpha = 101{,}85(7)°$, $\beta = 98{,}73(6)°$, $\gamma = 80{,}95(7)°$ et $Z = 2$. Le composé présente un arrangement bipyramidal ψ-trigonal du ligand autour du tellure avec des interactions secondaires faibles entre les atomes de tellure et de brome des molécules adjacentes.

[Traduit par le journal]

Introduction

Crystal structures of many compounds of the type R_2TeX_2 have been determined (1–8). They all have ψ-trigonal bipyramidal stereochemistry about tellurium, but several packing arrangements arise apparently from differing secondary Te----X interactions. We have communicated the crystal structure of phenyl(*p*-bromophenyl)tellurium dichloride (1) and have shown that two independent molecules of the compound pack into discrete tetramers. This combined with a recent report on the crystal structure of diphenyltellurium dichloride (2), wherein the monomers pack into chains, has prompted us to investigate the structure of bis(*p*-bromophenyl)tellurium dichloride.

Experimental

The title compound was prepared by Bergman's method (9) followed by recrystallisation by slow-evaporation of acetonitrile solution.

A single crystal with overall dimensions 0.11 × 0.23 × 0.34 mm was mounted on a Syntex $P2_1$ diffractometer equipped with a Mo X-ray tube and a highly oriented graphite monochromator. ($\lambda = 0.71069$ Å). The crystal data at 21°C were:

$C_{12}H_8Br_2TeCl_2$ mw = 510.4
$a = 8.000(7)$ Å, $b = 11.811(11)$ Å, $c = 7.978(6)$ Å, $\alpha = 101.85(7)°$, $\beta = 98.73(6)°$, $\gamma = 80.95(7)°$, $V = 723(1)$ Å^3, $F(000) = 472$, $Z = 2$, $D_c = 2.344$ g cm^{-3}, $\mu = 7.80$ mm^{-1}.

The data were collected in $\theta/2\theta$ mode, scan width $K_{\alpha 1} - 1°$ to $K_{\alpha 2} + 1°$, variable scan rate 2–5° min^{-1} over the range $4 < 2\theta < 45°$. The intensities of three monitor reflections did not change significantly during data collection. The space group $P\bar{1}$ was used and later assumed to be correct because of successful refinement of the structure. 2127 independent reflections were recorded and reduced to 1628 ($I > 3\sigma(I)$) unique reflections. Absorption correction factors obtained by an analytical procedure ranged from 2.36 to 4.23.

The structure was solved by direct methods using the program MULTAN. Phasing was carried out for 168 E's normalised according to parity groups, with magnitude greater than 1.2. The solution with largest overall figure of merit was used to calculate the E-map from which the five atoms Te, Br(1), Br(2), Cl(1), and Cl(2) were found. The carbon atoms C(11)—C(61) and C(12)—C(62) were located by difference Fourier synthesis. Full-matrix least-squares refinement was carried out for all non-hydrogen atoms. Anomalous scattering factors were used for Te and Br throughout and all non-hydrogen atoms were refined with anisotropic temperature factors. The hydrogen atom positions were recalculated before each cycle for CH bond length of 0.97 Å and standard geometry, with isotropic temperature factors 1.1 times the isotropic equivalent for the attached carbon atoms. The final discrepancy factors were $R = 0.025$ and $R_{WF} = 0.040$.

Wayne State University versions of the programs ABSORB (10) for analytical correction, MULTAN (11), SYNCOR (for data reduction by W. Schmonsees), FORDAP (for Fourier synthesis by A. Zalkin), ORFLS (12) for structure factor and least-squares calculations, ORFEE (12) for calculation of distances and angles, ORTEP (13) and HFINDER (hydrogen atom position calculation by A. Zalkin) were used.

The final atomic coordinates for non-hydrogen atoms are given in Table 1 and important distances and angles in Table 2.[1]

TABLE 1. Atomic coordinates and equivalent isotropic thermal parameters for non-hydrogen atoms of $(p\text{-}BrC_6H_4)_2TeCl_2$[a]

Atom	x/a	y/b	z/c	B_{iso}[b]
Te	0.37219(5)	−0.70264(3)	−0.71883(5)	2.40(1)
Br(1)	−0.38189(8)	−0.59581(6)	−1.20648(9)	3.47(2)
Br(2)	0.1828(1)	−1.16620(6)	−0.4447(1)	4.21(2)
Cl(1)	0.2437(2)	−0.5706(1)	−0.4682(2)	3.18(4)
Cl(2)	0.4901(2)	−0.8343(1)	−0.9703(2)	3.39(4)
C(11)	0.1358(8)	−0.6728(5)	−0.8782(8)	2.5(1)
C(21)	0.1340(8)	−0.6575(5)	−1.0454(8)	2.7(1)
C(31)	−0.0192(8)	−0.6349(5)	−1.1449(7)	2.7(1)
C(41)	−0.1667(8)	−0.6299(5)	−1.0736(8)	2.7(1)
C(51)	−0.1678(8)	−0.6447(6)	−0.9084(8)	3.0(1)
C(61)	−0.0150(8)	−0.6641(6)	−0.8078(8)	2.9(1)
C(12)	0.3126(7)	−0.8489(5)	−0.6339(8)	2.5(1)
C(22)	0.3386(8)	−0.8524(5)	−0.4607(8)	2.9(1)
C(32)	0.2985(8)	−0.9475(6)	−0.4056(8)	3.1(1)
C(42)	0.2362(8)	−1.0360(5)	−0.5223(9)	2.9(1)
C(52)	0.2097(8)	−1.0340(6)	−0.6978(8)	3.3(2)
C(62)	0.2492(9)	−0.9402(6)	−0.7526(8)	3.1(1)

[a]Estimated standard deviations are given in parentheses.

[b]B_{iso} is the equivalent isotropic thermal parameter obtained from the refined anisotropic thermal parameters (deposited) by the equation:

$$B_{iso} = \frac{1}{3}\sum_i\sum_j B_{ij}a_i^*a_j^*\bar{a}_i\cdot\bar{a}_j$$

[1]Factional coordinates for hydrogen atoms, equations for mean planes, lists of structure factors, and anisotropic thermal parameters have been deposited and are available, at a nominal charge, from the Depository of Unpublished Data, CISTI, National Research Council of Canada, Ottawa, Ont., Canada K1A 0S2.

Can. J. Chem. Downloaded from www.nrcresearchpress.com by 210.87.254.42 on 09/06/12
For personal use only.

TABLE 2. Bond lengths (Å) and angles (deg) for $(p\text{-}BrC_6H_4)_2TeCl_2$[a]

Bond	Length	Bonds	Angle	Bonds	Angle
Te—Cl(1)	2.516(3)	Cl(1)TeCl(2)	178.24(9)		
Te—Cl(2)	2.483(3)	Cl(1)TeC(11)	89.3(2)	Cl(1)TeC(12)	89.4(2)
Te—C(11)	2.136(6)	Cl(2)TeC(11)	89.2(2)	Cl(2)TeC(12)	90.0(2)
Te—C(12)	2.125(6)	C(11)TeC(12)	96.1(2)		
C—C(ring1)	1.377	CCC(ring1)	120.0		
C—C(ring2)	1.376	CCC(ring2)	120.0		
Br—C(41)	1.911(6)	Br(1)C(41)C(31)	119.4(5)	Br(1)C(41)C(51)	117.6(5)
Br—C(42)	1.900(6)	Br(2)C(42)C(32)	119.4(5)	Br(2)C(42)C(52)	119.0(5)

Dihedral angle	Value	Nearest intermolecular distance	Value
C(21)C(11)TeCl(1)	139.5(5)	Te----Cl(1)′	4.67
C(22)C(12)TeCl(1)	41.6(5)	Te----Cl(2)′	5.54
C(11)TeC(12)C(22)	130.8(5)	Te----Br(1)′	3.71
C(12)TeC(11)C(61)	51.6(5)	Te----Br(2)′	3.80

[a]Estimated standard deviations are given in parentheses.

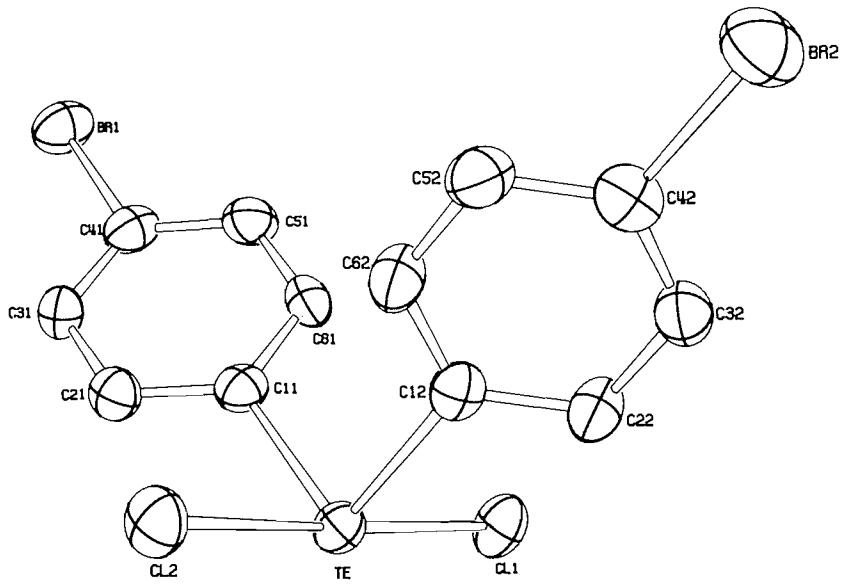

FIG. 1. ORTEP plot of $(p\text{-}C_6H_4Br)_2TeCl_2$. The atoms are drawn with the 50% probability ellipsoids.

Discussion

The atom labelling of the molecule, $(p\text{-}BrC_6H_4)_2TeCl_2$, is given in Fig. 1. The compound adopts a distorted trigonal bipyramidal arrangement with the chlorine atoms in axial positions and the two bromophenyl rings in the equatorial plane. The Cl—Te—Cl bond angle is close to 180° and the Cl—Te—C bond angles are close to right angles. The C—Te—C angle, 96.1(2)°, is typical of R_2TeCl_2 compounds and presumably indicates the presence of a stereochemically active non-bonding electron pair in the equatorial plane.

It is interesting to note that though Te—C and Te—Cl distances and angles are comparable to the observed distances and angles in other R_2TeCl_2 compounds (Table 3), the shortest non-bonded Te----Cl distance is considerably greater than the sum of van der Waals distances (4.0 Å). The ratio Te----Cl/Te—Cl is ~1.86, and as such, it must be presumed that the secondary Te----Cl interactions are insignificant in this compound. This is in contrast to three different kinds of secondary interactions observed in $(C_6H_5)(p\text{-}C_6H_4Br)TeCl_2$ (1) and one secondary interaction observed in $(C_6H_5)_2TeCl_2$ (2). However, the non-bonded Te----Br′ distances (3.71 Å and 3.80 Å) are comparable with the secondary Te----Br distances (3.93 Å) reported in $(C_6H_5)_2TeBr_2$ (6). This suggests that each tellurium atom may be interacting with two bromine atoms of the neighbouring molecules linking the molecules into chains (Fig. 2). The bromine atoms forming the secondary interactions are so positioned that the geometry about tellurium now appears as a distorted octahedral. Whether this indicates that the lone-pair is inactive or is still positioned, as assumed for the ψ-trigonal bipyramidal structure, between the two "secondary-bonds" is an open question.

The absence of Te----Cl interactions, which have been shown to be present in other R_2TeCl_2 compounds (1–5), could result from the availability of bromine atoms at more convenient positions for secondary interactions. Similar behaviour was observed in $(C_6H_5)_2TeF_2$ (8), where very weak Te----F interactions were attributed to the small size of the halogen atom as compared to the phenyl ring. The structure of (*p*-

Can. J. Chem. Downloaded from www.nrcresearchpress.com by 210.87.254.42 on 09/06/12
For personal use only.

TABLE 3. Bond lengths (Å) and bond angles (deg) in some R_2TeCl_2 compounds

Compound	Reference	Te—Cl	Te—C	Te----Cl	Cl—Te—Cl	C—Te—C
$(p\text{-}BrC_6H_4)_2TeCl_2$		2.516(3)	2.136(6)	4.67	178.2(1)	96.1(2)
		2.483(3)	2.125(6)	5.54		
$C_6H_5(p\text{-}BrC_6H_4)TeCl_2$	1	2.530(2)	2.114(9)	3.723(2)	176.0(1)	96.1(4)
		2.496(2)	2.110(11)	3.500(2)	176.6(1)	94.0(4)
		2.437(3)		3.413(3)		
		2.590(2)		3.592(2)		
$(C_6H_5)_2TeCl_2$	2	2.529(2)	2.111(7)	3.677(2)	175.5(1)	99.0(3)
		2.482(2)	2.102(7)			
$(CH_3)_2TeCl_2$	3	2.541(10)	2.10[a]	3.46[a]	172.3(5)	98.2(11)
		2.480(10)	2.08	3.52		
$(C_{12}H_8O)_2TeCl_2$	4	2.576(3)	2.087(3)	3.502(4)	176.8(1)	90.7(3)
		2.478(3)	2.103(3)	3.368(4)		
		2.501(3)		3.398(4)		
		2.563(3)		3.504(4)		
$(o\text{-}C_6H_{10}Cl)_2TeCl_2$	5	2.470(5)	2.18(1)	[b]	177.6(2)	103.0(5)
		2.515(6)	2.20(1)			
$(o\text{-}C_6H_{10}Cl)(p\text{-}CH_3C_6H_4)TeCl_2$	5	2.47(1)	2.24(2)	[b]	176.4(3)	101.0(6)
		2.50(1)	2.08(2)			

[a]Standard deviation not given in the reference.
[b]Packing distances not given in the reference.

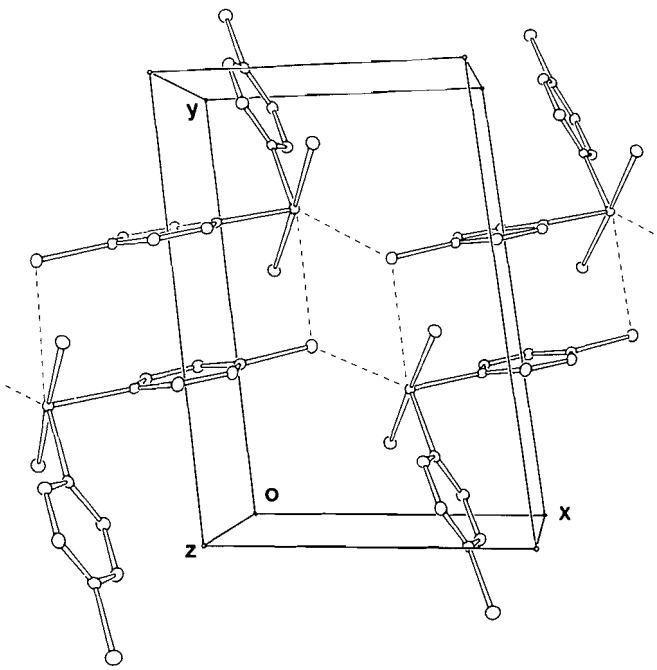

FIG. 2. Unit cell packing of $(p\text{-}C_6H_4Br)_2TeCl_2$. Hydrogen atoms are omitted for clarity.

$ClC_6H_4)_2TeI_2$ (7) which might have been assumed to be more closely related to $(p\text{-}BrC_6H_4)_2TeCl_2$ shows, an usual, Te----I′ interactions but no significant Te----Cl′ interactions (Te----Cl′ distance is 3.91 Å). This limited evidence suggests that the relationship of size and position of ligands and halides is quite subtle.

The angles between the TeCC plane and the bromophenyl rings are 51.6(5)° and 130.8(5)°, respectively, for the rings C(11)—C(61) and C(12)—C(62). The comparable angles in $(C_6H_5)(p\text{-}BrC_6H_4Br)TeCl_2$ are 41.9(10)° and 144.7(10)° for one molecule and 32.1(10)° and 129.4(10)° for the second molecule. The mean planes table[1] shows that the phenyl rings are both rotated by 140° with respect to plane C(11)TeCl(1)Cl(2) and C(12)TeCl(1)Cl(2) so that the rings are in a propeller rather than a butterfly arrangement. Neither substitution in the ring nor a change in the size or electronegativity of the halide apparently changes this arrangement. However, in $(C_6H_5)(p\text{-}BrC_6H_4)TeCl_2$ (1), the packing is such that the phenyl ring on one molecule lies parallel to the bromophenyl ring on the other, while the phenyl ring on the latter molecule lies normal to the bromophenyl ring on the former molecule. This arrangement presumably maximises the number of secondary Te----Cl interactions. By contrast, in $(C_6H_5)_2TeCl_2$ (2), the rings in adjacent molecules are parallel to one another as they are in $(p\text{-}BrC_6H_4)_2TeCl_2$. However, this present molecule is in a head-to-tail configuration in contrast to $(C_6H_5)_2TeCl_2$, where the molecules are linked in a sideways or end-on fashion.

Acknowledgements

This work was supported in part by Operating Grants from the Natural Sciences and Engineering Research Council of Canada. We thank Wayne State University for providing X-ray equipment and computer facilities.

1. R. K. CHADHA, J. E. DRAKE, and M. A. KHAN. Acta Crystallogr. B. In press.
2. N. W. ALCOCK and W. D. HARRISON. J. Chem. Soc. Dalton Trans. 251 (1982).
3. G. D. CHRISTOFFERSON, R. A. SPARKS, and J. D. MCCULLOUGH. Acta Crystallogr. **11**, 782 (1958).
4. J. D. KORP, I. BERNAL, J. C. TURLEY, and G. E. MARTIN. Inorg. Chem. **19**, 2556 (1980).
5. T. S. CAMERON, R. B. AMERO, and R. E. CORDES. Cryst. Struct. Commun. **9**, 533, (1980); **9**, 539 (1980).
6. G. D. CHRISTOFFERSON and J. D. MCCULLOUGH. Acta Crystallogr. **11**, 249 (1958).
7. G. Y. CHAO and J. D. MCCULLOUGH. Acta Crystallogr. **15**, 887 (1962).
8. F. J. BERRY and A. J. EDWARDS. J. Chem. Soc. Dalton Trans. 2306 (1980).
9. J. BERGMAN. Tetrahedron, **28**, 3323 (1972).
10. D. H. TEMPLETON and L. K. TEMPLETON. ABSORB. An analytical absorption correction program. University of California,

Can. J. Chem. Downloaded from www.nrcresearchpress.com by 210.87.254.42 on 09/06/12
For personal use only.

Berkley, CA.
11. G. GERMAIN, P. MAIN, and M. M. WOLFSON. MULTAN. Acta Crystallogr. B, **26**, 274 (1970).
12. W. R. BUSING, K. O. MARTIN, and H. A. LEVY. ORFLS and ORFFE. Report ORNL-TM-305. Oak Ridge National Laboratory, TN. 1962.
13. C. K. JOHNSON. ORTEP. Report ORNL-3794. Oak Ridge National Laboratory. TN. 1965.

Can. J. Chem. Downloaded from www.nrcresearchpress.com by 210.87.254.42 on 09/06/12
For personal use only.

Seven-membered ring annulation and spiro-annulation processes via preparation and thermal rearrangement of β-(2-vinylcyclopropyl) α,β-unsaturated ketones

EDWARD PIERS, HOWARD E. MORTON, ISAO NAGAKURA, AND RICHARD W. THIES[1]

Department of Chemistry, University of British Columbia, 2036 Main Mall, University Campus, Vancouver, B.C., Canada V6T 1Y6

Received November 8, 1982

EDWARD PIERS, HOWARD E. MORTON, ISAO NAGAKURA, and RICHARD W. THIES. Can. J. Chem. **61**, 1226 (1983).

Treatment of the β-iodo enones **4** and **26**–**28** with lithium (phenylthio)(2-vinylcyclopropyl)cuprate (**21**, mixture of epimers), followed by thermolysis (180°C, 30–45 min) of the initially formed β-(2-vinylcyclopropyl) enones, provided excellent yields of the seven-membered ring annulation products **25** and **30**–**32**, respectively. In similar fashion, the (*E*)-2-(iodomethylene)cycloalkanones **8** and **29** were transformed efficiently into the spiro-annulation products **34** and **35**, respectively. When compound **36** was treated with bromoform – sodium hydroxide in the presence of a phase-transfer catalyst, the dibromocyclopropane **37** was produced. The latter substance served as the starting material for a sequence of reactions (hydrolysis with hydrochloric acid in methanol, **37** → **38**; oxidation with pyridinium chlorochromate, **38** → **39**; Wittig reaction with methylenetriphenylphosphorane, **39** → **40**; reduction with zinc in acetic acid, **40** → **41**) culminating in the stereoselective formation of *cis*-1-bromo-2,2-dimethyl-3-vinylcyclopropane (**41**). On the other hand, treatment of compound **37** with *n*-butyllithium (ether, −90°C), followed by protonation of the presumed intermediate **43** and hydrolysis of the resultant product **44**, provided the bromo alcohol **45** in 70% yield. The latter substance was converted into *trans*-1-bromo-2,2-dimethyl-3-vinylcyclopropane (**47**). When the cuprate reagents **42** and **48** (prepared from the bromocyclopropanes **41** and **47**, respectively) were allowed to react with the iodo enones **4** and **26**, the β-(2-vinylcyclopropyl) α,β-unsaturated ketones **49**, **52**, **54**, and **56** were produced in high yields. The enone **49**, upon thermolysis in refluxing *n*-hexane, underwent facile Cope rearrangement to produce the annulation product **50** quantitatively. In contrast, the homolog **54** was notably resistant to [3,3]-sigmatropic rearrangement and, upon thermolysis in *o*-xylene, *o*-dichlorobenzene, or collidine at elevated temperatures produced, in varying ratios, the Cope rearrangement product **55** and the isomerization product **56**. Thermal rearrangement (*o*-dichlorobenzene, 220°C, sealed tube) of *trans*-3-(2,2-dimethyl-3-vinylcyclopropyl)-2-cyclohexen-1-one (**52**) provided the annulation product **51** (59% yield). In contrast, the corresponding homolog **56**, under very similar conditions, produced only a minor amount of the annulation product **55**. In this case, the major product (trienone **57**) was that resulting from a [1,5]-sigmatropic hydrogen migration (ratio of **55**/**57** ≈ 1:4).

EDWARD PIERS, HOWARD E. MORTON, ISAO NAGAKURA et RICHARD W. THIES. Can. J. Chem. **61**, 1226 (1983).

La réaction des β-iodoénones **4**, **26** et **28** avec le cuprate de (phénylthio)(vinyl-2 cyclopropyle) (**21**, mélange épimère) suivie de la thermolyse (180°C, 30–45 min) des β-(vinyl-2 cyclopropyle) énones formées initialement conduit avec d'excellents rendements à des produits d'annellation à 7 chaînons, **25**, **30** et **32** respectivement. D'une façon analogue on transforme efficacement les (*E*) (iodométhylène)-2 cycloalcanones **8** et **29** en des produits de spiro annellation **34** et **35** respectivement. Le composé **36** réagit avec un mélange de bromoforme – hydroxyde de sodium en présence d'un catalyseur de transfert de phase en donnant le dibromocyclopropane **37**. Ce dernier sert de produit de départ pour cette suite de réactions (hydrolyse avec l'acide chlorhydrique dans le méthanol, **37** → **38**; oxydation par le chlorochromate de pyridinium, **38** → **39**; réaction de Wittig avec le méthylènetriphénylphosphorane, **39** → **40**; réduction par le zinc dans l'acide acétique **40** → **41**) se terminant par la formation stéréosélective du bromo-1 diméthyl-2,2 vinyl-3 cyclopropane *cis* (**41**). D'autre part la réaction du composé **37** avec le *n*-butyllithium (éther à −90°C), suivie de la protonation de l'intermédiaire présumé **43** et de l'hydrolyse du produit résultant **44** permet d'accéder à l'alcool bromé **45** avec un rendement de 70%. On transforme cet alcool en bromo-1 diméthyl-2,2 vinyl-3 cyclopropane *trans* (**47**). Quand on fait réagir les réactifs cuprate **42** et **48** (préparés respectivement à partir des bromocyclopropanes **41** et **47**) avec les iodoénones **4** et **26** on obtient avec de bons rendements les β-(vinyl-2 cyclopropyl) cétones α,β insaturées **49**, **52**, **54** et **56**. Par thermolyse dans le *n*-hexane au reflux l'énone **49** subit facilement une transposition de Cope en donnant quantitativement le produit d'annellation **50**. L'homologue **54** au contraire résiste de façon marquée à la transposition sigmatropique [3,3] et par thermolyse dans le *o*-xylène, le *o*-dichlorobenzène où la collidine à température élevée donne dans des proportions variées le produit de transposition de Cope **55** et le produit d'isomérisation **56**. La transposition thermique (*o*-dichlorobenzène, 220°C en tube scellé) de la (diméthyl-2,2 vinyl-3 cyclopropyl)-3 cyclohexène-2 one-1 *trans* **52** conduit au produit d'annellation **51** (seulement 59%). Au contraire l'homologue correspondant **56** dans des conditions très semblables donne le produit d'annellation **55** en faible quantité seulement. Dans ce cas le produit majoritaire (la triénone **57**) provient d'une migration d'hydrogène sigmatropique [1,5] (le rapport de **55**/**57** est d'environ 1:4).

[Traduit par le journal]

Introduction

The thermal $_{\pi}2_s + _{\sigma}2_s + _{\pi}2_s$ (Cope) rearrangement of *cis*-1,2-divinylcyclopropane (**1**) to 1,4-cycloheptadiene (**2**) (eq. [1]) was first described by Vogel more than twenty years ago (1–3). This transformation is extremely facile and, in fact, in Vogel's early experiments, compound **1** was not isolated but rearranged to **2** under the conditions of its formation. Indeed, it was not until more than a decade later that **1** was isolated and shown to rearrange to **2** with a half-life of approximately 90 seconds at 35°C (4–6). In contrast to the *cis* isomer **1**, *trans*-1,2-divinylcyclopropane (**3**) is a stable, isolable compound. However, at elevated temperatures (e.g. 190°C), this substance

[1]Professor Thies' contribution to this work was carried out while he was on sabbatical leave from the Department of Chemistry, Oregon State University, Corvallis, Oregon.

Can. J. Chem. Downloaded from www.nrcresearchpress.com by 210.87.254.42 on 09/06/12
For personal use only.

Can. J. Chem. Downloaded from www.nrcresearchpress.com by 210.87.254.42 on 09/06/12
For personal use only.

[1] ≤ room temperature

1 A 2

[2] 190°C 1 → [A] → 2

3

also rearranges cleanly and efficiently to 1,4-cycloheptadiene (**2**) (eq. [2]) (1, 3).

Since 1960, the 1,2-divinylcyclopropane → cycloheptadiene rearrangement has been studied extensively from a mechanistic point of view.[2] In general, it has been concluded that the rearrangement of **1** (and of other *cis*-1,2-divinylcyclopropanes) takes place in a concerted fashion via a boat-like transition state in which the two vinyl groups are folded back over the cyclopropane ring (see **A** in eq. [1]), thus providing cycloheptadiene systems in which the two double bonds have a (*Z*) geometry. On the other hand, thermal conversion of *trans*-1,2-divinylcyclopropanes into the corresponding 1,4-cycloheptadienes is thought to involve initial isomerization (usually rate-determining) into the *cis* isomer, followed by "normal" concerted rearrangement (e.g. **3** → **1** → [**A**] → **2**, eq. [2]).

During the first fifteen years after its discovery, the Cope rearrangement of 1,2-divinylcyclopropane systems had found only sporadic use in organic synthesis. However, more recently, this interesting transformation has been employed with increasing frequency by synthetic organic chemists, and its synthetic potential has begun to receive considerable recognition and attention (19–35).

Recently, we reported on a new five-membered ring annulation method based on the preparation and thermal vinylcyclopropane-to-cyclopentene rearrangement of β-cyclopropyl α,β-unsaturated ketones (36). For example (see eq. [3]), reaction of 3-iodo-2-cyclohexen-1-one (**4**) with lithium (phenylthio)(cyclopropyl)cuprate (**5**) provided, in 82% yield,

[3] [*c*-$C_3H_5CuSC_6H_5$]Li (**5**)

4 6

(1) 425°C
(2) basic alumina

7

3-cyclopropyl-2-cyclohexen-1-one (**6**). Thermolysis (~425°C) of the latter substance, followed by base-catalyzed isomerization of the crude product, produced the annulation product **7** in 88% yield. A subsequent paper (37) described the results of a similar study as applied to a new five-membered ring spiro-annulation procedure. Thus, for example, conversion of (*E*)-2-(iodomethylene)cyclohexanone (**8**) into the cyclopropyl enone **9** and thermolysis of the corresponding enol silyl ether

8 **5** 9

[4] (1) $LiN(i\text{-}Pr)_2$
(2) Me_3SiCl

11 (1) 425°C (2) H_3O^+ Me_3SiO 10

10 gave, after acid hydrolysis of the crude thermolysate, the spiro enone **11** in ~40% overall yield (see eq. [4]).

The results summarized above, along with the fact that thermal rearrangements of 1,2-divinylcyclopropane systems are often very efficient, easily executed transformations, encouraged us to extend our studies to include the possibility of carrying out seven-membered ring annulation and spiro-annulation processes. More explicitly, it seemed eminently reasonable to propose that treatment of a cyclic β-iodo enone **12** (see eq. [5]) with a suitable (2-vinylcyclopropyl)cuprate reagent would provide the corresponding β-(2-vinylcyclopropyl) enone **13** which, upon successful subjection to Cope rearrangement, would give the annulation products **14** and/or (if R = H) **15**. A similar sequence of reactions employing a

12 13

[5]

15 and/or (R = H) 14

16 17

[6]

18

[2]For review articles, see refs. 7 and 8. For more recent reports, see refs. 9–18, and citations therein.

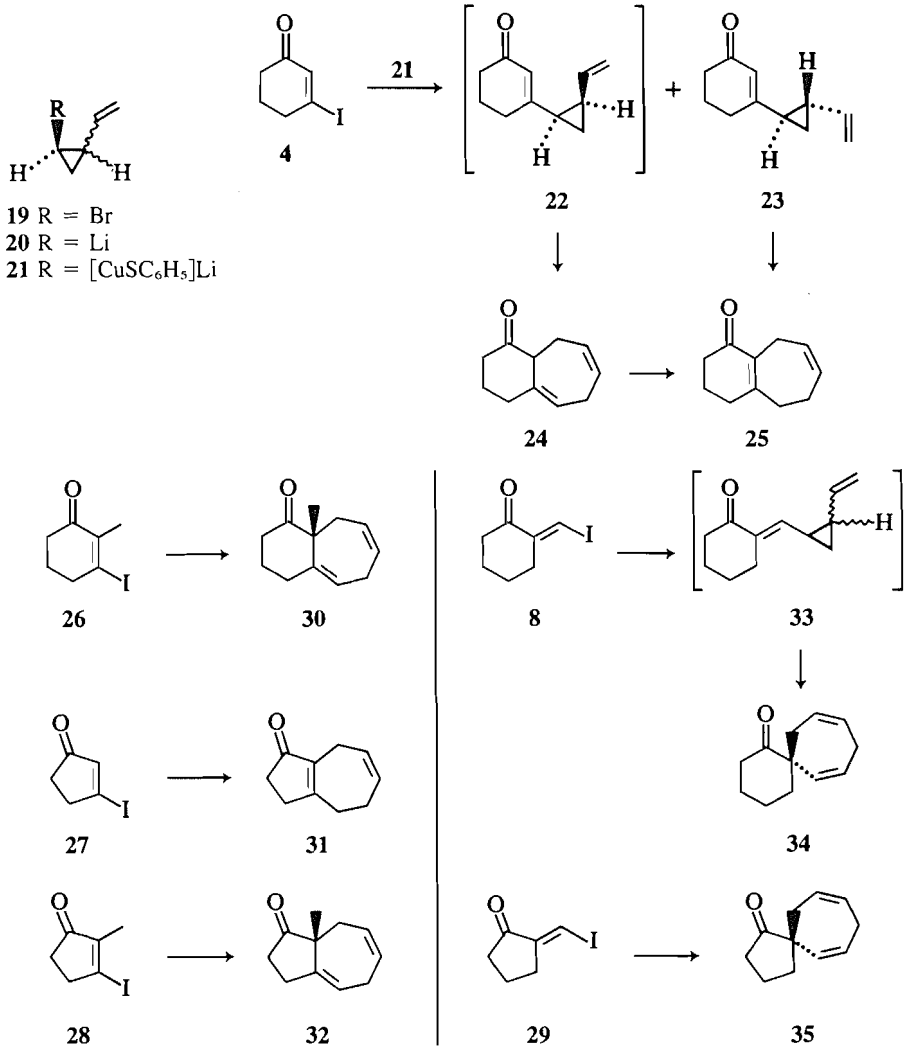

SCHEME 1

cyclic α-(iodomethylene) ketone **16** as the starting material would produce, via the intermediate **17**, the spiroannulation product **18** (see eq. [6]). We report herein the results of some of our studies in this area.[3] In the accompanying paper (38) we describe the application of this new annulation method to a total synthesis of the bicyclic sequiterpenoid (±)-β-himachalene.

Results and discussion

(a) *Reaction of the β-iodo enones **4**, **8**, and **26–29** with lithium (phenylthio)(2-vinylcyclopropyl)cuprate (**21**). Preparation of the annulation products **25**, **30–32**, **34**, and **35** (see Scheme 1)*

Addition of a pentane solution of *tert*-butyllithium (3 mmol) to a cold (−78°C) ethereal solution of 1-bromo-2-vinylcyclopropane (**19**, 1.5 mmol, mixture of diastereomers, *cis*/*trans* 7:3),[4] followed by dilution of the resultant mixture (containing suspended lithium bromide) with tetrahydrofuran (THF), gave a solution of 2-vinylcyclopropyllithium (**20**),[5] which upon treatment with solid phenylthiocopper (44, 45) (1.5 mmol) produced a clear yellow solution of lithium (phenylthio)(2-vinylcyclopropyl)cuprate (**21**).[6] When the latter reagent was allowed to react (−78°C, 1 h; − 20°C, 1 h; 0°C, 1 h) with 1.0 mmol of 3-iodo-2-cyclohexen-1-one (**4**) (50), and the crude product was distilled (~65–90°C) under reduced pressure, a clear oil was obtained in 90% yield. Analysis of this material by gas–liquid chromatography (glc) and proton nuclear magnetic resonance (^{1}H nmr) spectroscopy indicated that it consisted of a mixture of substances which appeared to be the annulation products **24** (minor) and **25** (major), along with 3-(*trans*-2-vinylcyclopropyl)-2-cyclohexen-1-one (**23**).[7] Thus, it was clear that the initially formed *cis*-cuprate product **22** had, under the conditions of work-up and/or distillation, rearranged to the bicyclic dienone **24** which, in turn, had largely isomer-

[3]For preliminary reports, see refs. 20 and 25.

[4]This material was prepared by tri-*n*-butyltin hydride reduction (39, 40) of 1,1-dibromo-2-vinylcyclopropane (41, 42).

[5]For a coincident, independent preparation of this reagent (*cis*/*trans* = 1:4), see ref. 43.

[6]It appears that Hahn and Jones (46) were the first to report the use of a (cyclopropyl)copper reagent for the conjugate addition of a cyclopropyl group to an enone. For subsequent reports, which demonstrate the synthetic utility of these versatile reagents, see refs. 47, 48, 20, 21, 49, 25, 26, 29, and 36–38.

[7]The preparation, via a route quite different from that described herein, and thermal rearrangement of a mixture of compounds **22** and **23** had been reported previously by Marino and Kaneko (19). See also ref. 22.

Can. J. Chem. Downloaded from www.nrcresearchpress.com by 210.87.254.42 on 09/06/12
For personal use only.

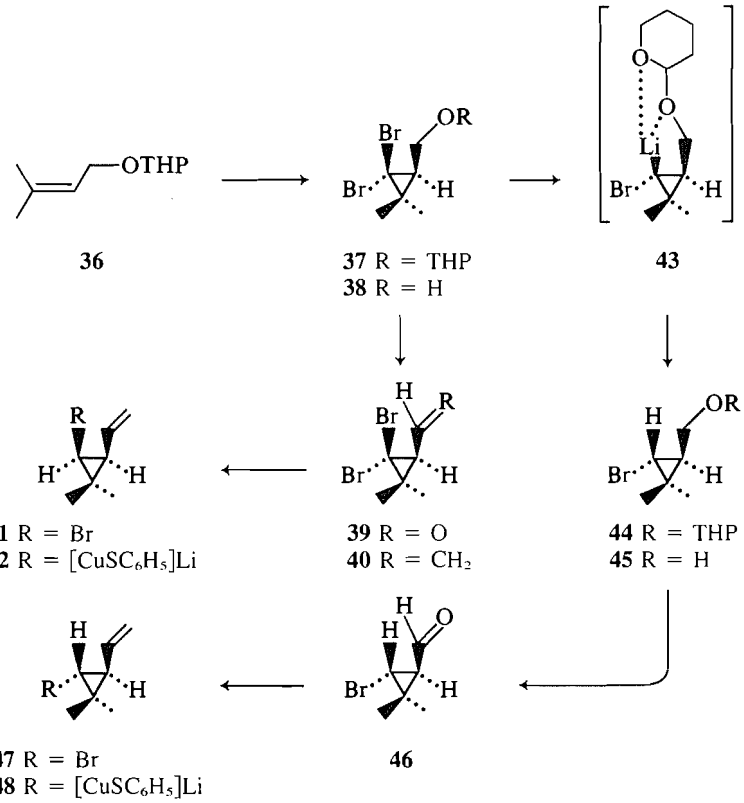

SCHEME 2

ized to the conjugated isomer **25**. In contrast, as would be expected, the product **23** derived from the *trans* cuprate reagent was stable to the work-up and distillation conditions. However, tedious separation of the mixture of products could be avoided, since the *trans* divinylcyclopropane **23** was known (19) to rearrange smoothly to the annulation product **25**. Thus, when the mixture of **23**, **24**, and **25** was heated at 180°C (neat, 30 min) and the resultant material was redistilled, the conjugated dienone **25** (19,22) was obtained in 75% overall yield.

Treatment of 3-iodo-2-methyl-2-cyclohexen-1-one (**26**) (50) with lithium (phenylthio)(2-vinylcyclopropyl)cuprate (**21**) under conditions similar to those described above for the β-iodo enone **4**, followed by direct thermolysis (180°C) of the initially formed products, provided, in 82% yield, the bicyclic dienone **30**.[8] In similar fashion, the β-iodo enones **27** and **28** could be converted smoothly and efficiently into the annulation products **31** (80%) and **32**[9] (84%), respectively.

Application of the reactions outlined above to the (*E*)-2-(iodomethylene)cycloalkanones **8** and **29** also proved successful. Thus, treatment of compound **8** with 1.5 equivalents of the cuprate reagent **21**, followed by thermal rearrangement of the resultant products **33**, produced spiro-[5.6]dodeca-7,10-dien-1-one (**34**) in 77% yield. Similarly, the (iodomethylene)cyclopentanone **29** was converted into the spiro dienone **35** in 64% yield.

It is clear from the results summarized above that the originally proposed annulation sequences (eqs. [5] and [6]) are indeed viable processes which are easily and smoothly executed. Since the β-iodo enones (**4**, **8**, **26**–**29**) are conveniently prepared from the corresponding β-dicarbonyl compounds (50) and the cuprate reagent **21** is obtained via a separate synthetic route, the overall annulation sequences are short, convergent, and efficient. Furthermore, although separation of *cis*- and *trans*-1-bromo-2-vinylcyclopropane (**19**) is possible (22, 29) and, thus, stereochemically homogeneous lithium (phenylthio)(2-vinylcyclopropyl)cuprate reagents can be prepared (29), the sequences outlined above do not require these (rather tedious) experimental operations. In each case, both the β-(*cis*-2-vinylcyclopropyl) α,β-unsaturated ketone and the corresponding *trans* isomer rearrange smoothly to provide the same annulation product.

(b) *Synthesis of* cis-*(41) and* trans-*1-bromo-2,2-dimethyl-3-vinylcyclopropane (47), and their conversion into the cuprate reagents 42 and 48, respectively (see Scheme 2)*

In order to obtain information regarding the effect of structural variations on the course of the thermal rearrangement of β-(2-vinylcyclopropyl) enones and to produce annulation products which might prove useful as synthetic precursors for natural product syntheses, we decided to extend the present study to include the preparation and use of (2-vinylcyclopropyl)cuprate reagents more highly functionalized than **21**. This section of the paper outlines the stereoselective preparation of *cis*-(**41**) and *trans*-1-bromo-2,2-dimethyl-3-vinylcyclopropane (**47**), and their transformation into the highly substituted (cyclopropyl)cuprate reagents **42** and **48**, respectively. The next section describes the reactions of the latter species with β-iodocyclohexenones and the thermal rearrangement of the resultant products.

Treatment of the tetrahydropyranyl ether of 3-methyl-2-

[8]An alternative preparation of 2-methyl-3-(2-vinylcyclopropyl)-2-cyclohexen-1-one and its rearrangement to compound **30** were reported independently by Wender and Filosa (22).

[9]For an alternative method of preparation of 2-methyl-3-(2-vinylcyclopropyl)-2-cyclopenten-1-one and its conversion into compound **32**, see refs. 21 and 22. These studies were coincident with those described herein.

Can. J. Chem. Downloaded from www.nrcresearchpress.com by 210.87.254.42 on 09/06/12
For personal use only.

Can. J. Chem. Downloaded from www.nrcresearchpress.com by 210.87.254.42 on 09/06/12
For personal use only.

buten-1-ol (**36**) with bromoform and aqueous sodium hydroxide in the presence of a phase-transfer reagent (51) provided the dibromocyclopropane **37** in 72% yield. The latter material served as a convenient starting material for the synthesis of both of the diasteromeric monobromocyclopropanes **41** and **47**. Thus, hydrolysis of **37** with hydrochloric acid in methanol, followed by oxidation of the resultant crystalline alcohol **38** with pyridinium chlorochromate in dichloromethane (52) gave, in 74% overall yield, the aldehyde **39**. When the latter substance was allowed to react with methylenetriphenylphosphorane in THF at room temperature, 1,1-dibromo-2,2-dimethyl-3-vinylcyclopropane (**40**) was obtained in 61% yield. Although this material could be distilled, it was quite unstable and tended to produce small amounts of decomposition products, especially if the distillation was carried out at temperatures above ~70°C. Therefore, a pure sample of **40** was difficult to obtain, and, typically, the undistilled product was used directly for the next synthetic step.

Reduction of compound **40** with zinc in acetic acid (53) at room temperature for 3 h afforded, in 66% yield, a mixture of *cis*-(**41**) and *trans*-1-bromo-2,2-dimethyl-3-vinylcyclopropane (**47**), in a ratio of approximately 20:1. This reaction was carried out a number of times and, in each case, compound **41** was the greatly predominant product. Presumably, since the less hindered bromine atom in **40** was preferentially removed in the reduction process, the stereoselective nature of the conversion was at least partially due to steric factors. However, it should be noted that the ratio of the two products **41** and **47** varied somewhat from one experiment to another. Although the reasons for this phenomenon were not fully delineated, it appeared that reaction time was a contributing factor. Shorter reaction times gave, in addition to some starting material,[10] a somewhat higher yield of products containing proportionately more of the *trans* product **47**, while longer reaction times produced, in decreased yields, a product which contained very little if any of compound **47**. Thus, it appears that further reductive removal of the bromine atom from **47**, to produce the highly volatile and therefore unisolated 1,1-dimethyl-2-vinylcyclopropane, occurred at a rate faster than (further) reduction of the more hindered bromine atom in **41**. In any case, the synthetically satisfying, highly stereoselective production of the *cis* monobromocyclopropane **41** could be accomplished very readily.[11]

Treatment of a cold (−90°C) ethereal solution of the tetrahydropyranyl ether **37** with 1 equivalent of *n*-butyllithium, followed by protonation of the resultant intermediate lithio carbenoid (54) and acid hydrolysis of the initially formed product **44**, provided (70% yield) a single bromo alcohol to which was assigned structure **45**. The lithium–halogen exchange reaction would be expected to involve the bromine atom which was *cis* to the group bearing the tetrahydropyranyl ether function, thus giving rise to a stabilized intermediate represented by **43**. Protonation of this species would then afford the observed product **44**.

Oxidation (pyridinium chlorochromate, dichloromethane (52)) of the alcohol **45** gave the corresponding aldehyde **46** which, upon reaction with methylenetriphenylphosphorane in THF, was converted into *trans*-1-bromo-2,2-dimethyl-3-vinylcyclopropane (**47**) (63% overall yield).

[10]The rate of this heterogeneous reduction reaction varied somewhat with the nature and source of the zinc metal.

[11]Reduction of compound **40** with tri-*n*-butyltin hydride afforded the products **41** and **47** in a ratio of approximately 3.7:1, respectively.

The ^{1}H nmr spectra of the epimeric substituted cyclopropanes **41** and **47** fully corroborated the stereochemical assignments. In the spectrum of compound **41**, the proton geminal to the bromine atom appeared as a doublet (δ 3.05) with a coupling constant of 7.5 Hz, while the corresponding proton in the epimer **47** gave rise to a doublet (δ 2.80) with J = 4 Hz. It is well known (55) that coupling constants associated with *cis* vicinal protons on cyclopropane systems are larger than those related to corresponding *trans* protons and, therefore, the stereochemical assignments appear to be secure.

Treatment of each of the bromocyclopropanes **41** and **47** with 2 equivalents of *tert*-butyllithium (ether, −78°C), followed by reaction of the resultant lithio cyclopropanes with phenylthiocopper (44, 45) (ether – THF, −20°C), afforded yellow-brown solutions of the corresponding cuprate reagents **42** and **48**, respectively. The latter species were employed in the next phase of the present study.

(c) *Reaction of the cuprate reagents **42** and **48** with the β-iodo enones **4** and **26**. Thermal rearrangement of the resultant products **49**, **52**, **54**, and **56** (see Scheme 3)*

When 3-iodo-2-cyclohexen-1-one (**4**) (50) was allowed to react (−78°C → room temperature, 2.5 h) with the cuprate reagent **42**, the expected substituted cyclohexenone **49** was obtained in 88% yield. The latter substance was quite unstable and already at room temperature underwent slow bond reorganization to give the Cope rearrangement product **50** (*vide infra*). However, samples of **49** containing only small amounts of **50** could be obtained and these exhibited spectral data in full accord with those expected for the enone **49**.

Treatment of the β-iodo enone **4** with the *trans* cuprate reagent **48**, under conditions identical with those employed for the conversion of **4** into **49**, provided a nearly quantitative yield of compound **52**. In similar fashion, reaction of 3-iodo-2-methyl-2-cyclohexen-1-one (**26**) (50) with the two cuprate reagents **42** and **48** produced the highly substituted cyclohexenones **54** and **56**, respectively. It is interesting to note that even though the copper-bearing carbon atom of the *cis* cuprate reagent **42** is quite hindered, the reaction of this species with the β-iodo enone **26** to produce the sterically congested vinylcyclopropane system in **54** is smooth and efficient (76% yield).

As mentioned above, the enone **49** undergoes rearrangement slowly at room temperature to give the bicyclic dienone **50**. When a solution of **49** in *n*-hexane (bp 69°C) was refluxed for 4 h, product **50** was produced in essentially quantitative yield. Furthermore, subjection of neat samples of **49** and **50** to brief (~10–15 min) heating at 110°C provided, in each case, a high yield of the conjugated enone **51**. Thus, as one might expect, the [3,3]-sigmatropic rearrangement of **49** is a very facile process.

With respect to the thermolysis of the *trans*-divinylcyclopropane **52**, it is pertinent to note that, in theory, this substance can undergo bond reorganization via one (or both) of two alternative pathways. That is to say, "normal" Cope rearrangement could occur to provide, presumably by way of the stabilized diradical **B** and the *cis* isomer **49**, the same product (dienone **51**) as that derived from direct thermolysis of **49**. On the other hand, a [1,5]-sigmatropic hydrogen shift[12] from the appropriate cyclopropyl methyl group to the terminal carbon of

[12]For reviews regarding this type of rearrangement process, see refs. 8 and 56.

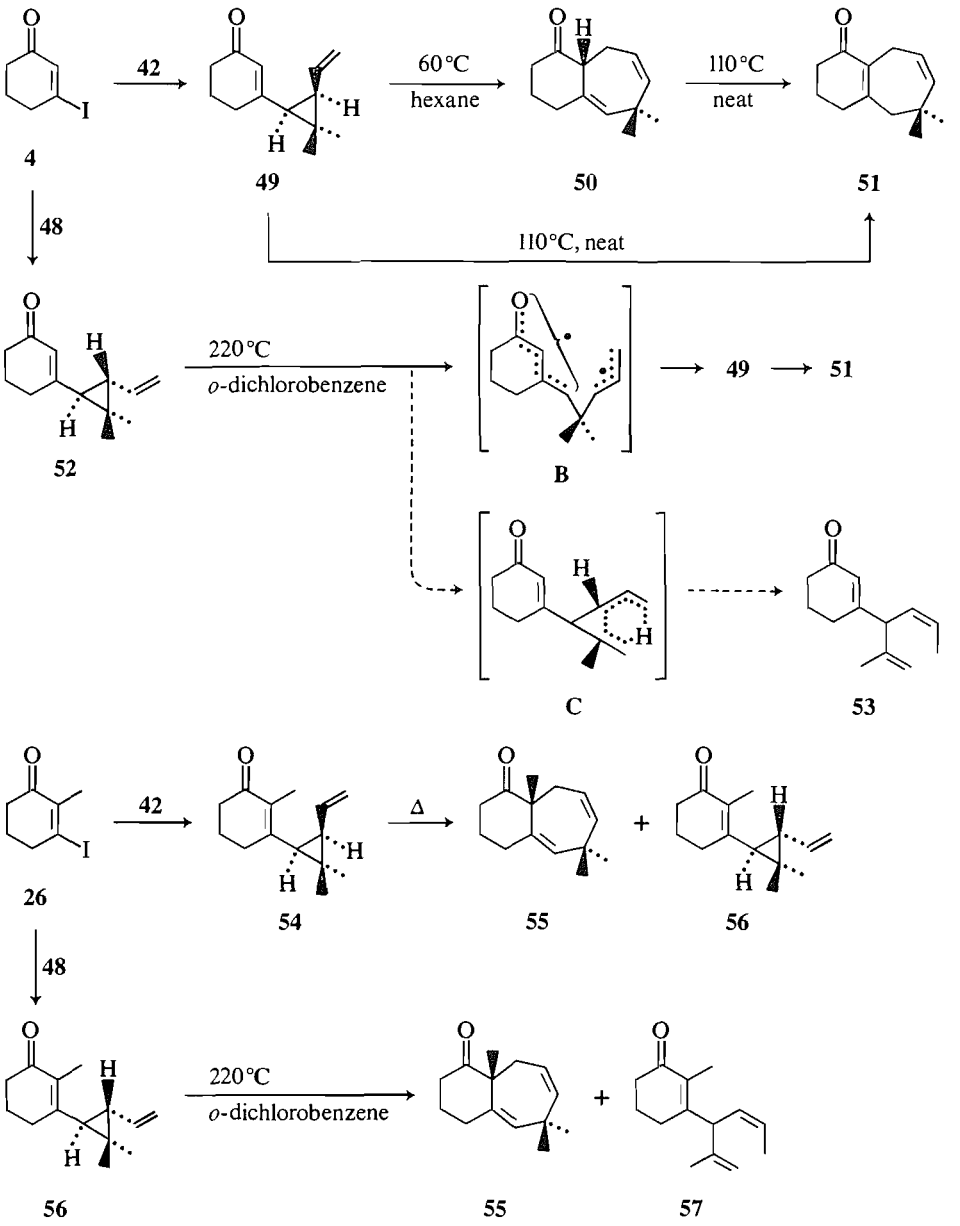

SCHEME 3

the vinyl function (via a transition state which might be represented by **C**), would produce the trienone **53**. In the event, thermolysis of compound **52** in *o*-dichlorobenzene (sealed tube, 220°C, 14 h) afforded very largely a single product, the bicyclic dienone **51** (59% yield of isolated, distilled material). Analysis of the initially obtained reaction mixture by glc and thin-layer chromatography (tlc) indicated that the product **51** was accompanied by only small amounts of unidentified compounds, along with traces of starting material. Thus, in this case, the Cope rearrangement pathway (**52** → [**B**] → **49** → **51**) is energetically favored over the alternative process involving a [1,5]-sigmatropic hydrogen shift (**52** → [**C**] → **53**).

Compared to the enone **49**, the homolog **54** was found to be remarkably stable and to exhibit notable resistance to undergoing the Cope rearrangement. In fact, when compound **54** was subjected to thermolysis at elevated temperatures, "simple" isomerization to the *trans* isomer **56** was competitive with sigmatropic rearrangement to **55**. For example, when a solution of **54** in *o*-xylene (bp 144°C) was refluxed for 48 h, the two products **55** and **56**[13] were produced in a ratio of ~2:1. On the other hand, subjection of **54** to thermolysis in a higher boiling solvent (*o*-dichlorobenzene, bp 179°C, reflux 3 h), provided compounds **55** and **56**[13] in a ratio of about 0.8:1, respectively.

A more detailed investigation of the thermolysis of enone **54** in *o*-xylene revealed that this was a frustratingly capricious reaction, since the ratio of the two products **55** and **56** varied significantly (~1.1:1 to ~2.7:1) from one experiment to another. Although the reasons underlying this difficulty have not been investigated thoroughly, it appeared that the presence of small amounts of the iodo enone **26** in the starting material **54** resulted in the production of mixtures containing relatively more of the isomerization product **56**. Perhaps the presence of trace amounts of hydrogen iodide was responsible for catalyzing the conversion of **54** into **56**. In any case, it was found that the relative amounts of the Cope rearrangement product **55**

[13]Under these conditions, the *trans*-divinylcyclopropane **56** was stable.

Can. J. Chem. Downloaded from www.nrcresearchpress.com by 210.87.254.42 on 09/06/12
For personal use only.

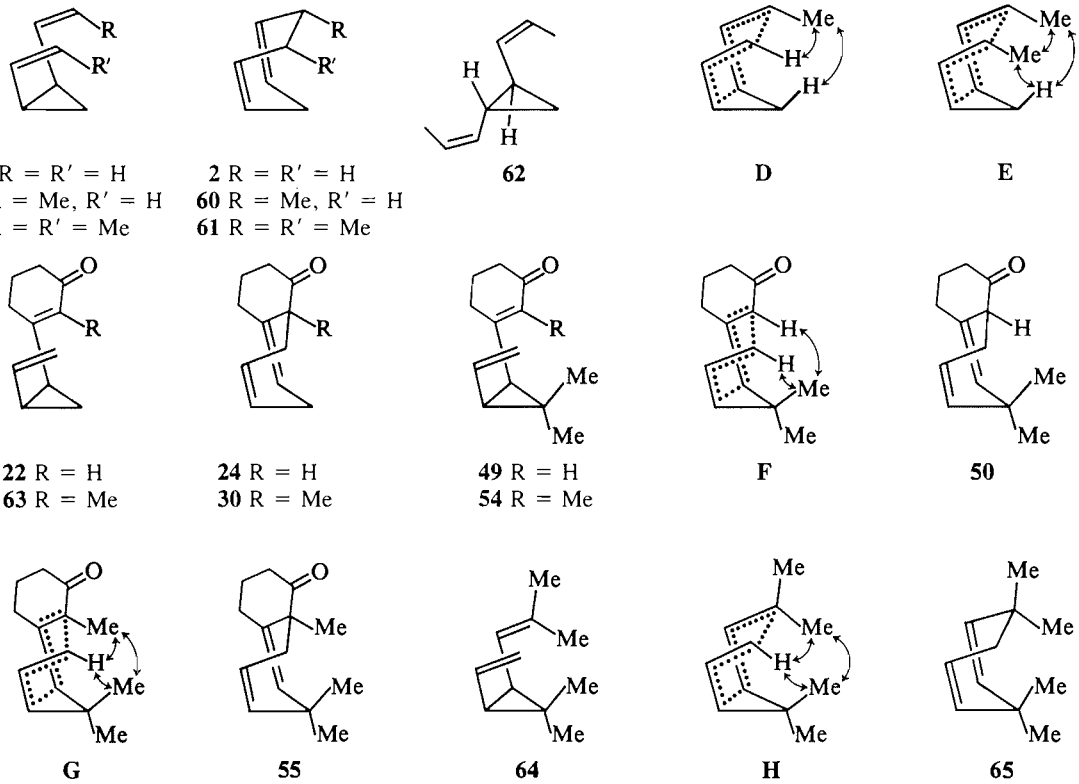

CHART 1

were greater, and the thermolysis results were somewhat more consistent, when care was taken to ensure that the starting material **54** was devoid of the iodo enone **26**, and when **54** was washed through basic alumina just prior to thermolysis.

Thermal rearrangement of the enone **54** in the weakly basic solvent collidine was also investigated. These reactions were carried out at 140–150°C for 42–44 h. Although the ratio of the two products **55** and **56** (~1.9:1 to ~2.4:1, respectively) still varied somewhat from one experiment to another, the results were more consistent than those obtained from thermolysis in *o*-xylene. Application of this procedure to the rearrangement of 10 mmol of compound **54** produced the annulation product **55** and the isomerization product **56** in isolated yields of 49 and 21%, respectively.

Subjection of the *trans*-divinylcyclopropane **56** to thermolysis (*o*-dichlorobenzene, sealed tube, 220°C, 16 h) under conditions similar to those used for the structurally similar substrate **52** produced a mixture of products which consisted largely of two components in a ratio of approximately 4:1. The minor product was shown to be the dienone **55**, while the major component was identified as the trienone **57**. Thus, in this case, the process involving a [1,5]-sigmatropic hydrogen migration is energetically more favorable than the alternative Cope rearrangement pathway.

It is appropriate to comment briefly regarding the relative ease of Cope rearrangement of the β-(*cis*-2-vinylcyclopropyl) enones **22**, **63**, **49**, and **54** and to compare these results with some related observations recorded in the literature (see Chart 1). It is known that the rate of rearrangement of *cis*-1,2-divinylcyclopropanes is affected quite dramatically by the presence of alkyl substituents on the terminal carbon atoms of the vinyl groups, particularly when these have a *cis* orientation. For example, it has been shown (16) that, at 40°C, the transformation of *cis*-2-(*cis*-1-propenyl)-1-vinylcyclopropane (**58**) into 6-methyl-1,4-cycloheptadiene (**60**) occurs at a rate ~5800 times slower than the conversion of **1** into **2**. Furthermore, the dimethyl analog **59** fails to undergo sigmatropic rearrangement to the dimethylcycloheptadiene **61**. Rather, at elevated temperatures, reversible isomerization takes place and an equilibrium mixture of **59** and **62** is produced (9, 16). These notable rate differences have been attributed to steric factors. Thus, it has been proposed (16) that the conversion of **58** into **60** proceeds by way of a transition state which is destabilized (relative to that for the transformation **1** → **2**) mainly by steric repulsion between the propenyl methyl group and the *cis* cyclopropyl proton ("methyl–ring interaction" (16), see **D**).[14] On the other hand, the transition state for the [3,3]-sigmatropic rearrangement of compound **59** would be destabilized by two such interactions, as well as by steric repulsion between the two methyl groups ("methyl–methyl interaction" (16), see **E**].[15] In this case, the combination of these deactivating features results in "simple" isomerization being energetically favored over the Cope rearrangement process.

Even though compound **58** undergoes bond reogranization at a rate considerably slower than **1**, both of these substances rearrange smoothly to produce the products **60** and **2**, respectively. Therefore, it is not surprising to find that thermolysis of the structurally analogous enones **22** and **63** results in the efficient production of the corresponding bicyclic dienones **24** and **30**, respectively.

If one assumes that [3,3]-sigmatropic rearrangement of the

[14]The deactivating energy ($\Delta\Delta G^{\ddagger}$) of the methyl-ring interaction has been estimated to be 4.55 kcal/mol. The other steric repulsion indicated in **D** ("methyl–hydrogen interaction") is, apparently, quite small, corresponding to ~0.84 kcal/mol (16).

[15]The $\Delta\Delta G^{\ddagger}$ value for the methyl–methyl interaction has been estimated to be 1.03 kcal/mol (16).

Can. J. Chem. Downloaded from www.nrcresearchpress.com by 210.87.254.42 on 09/06/12
For personal use only.

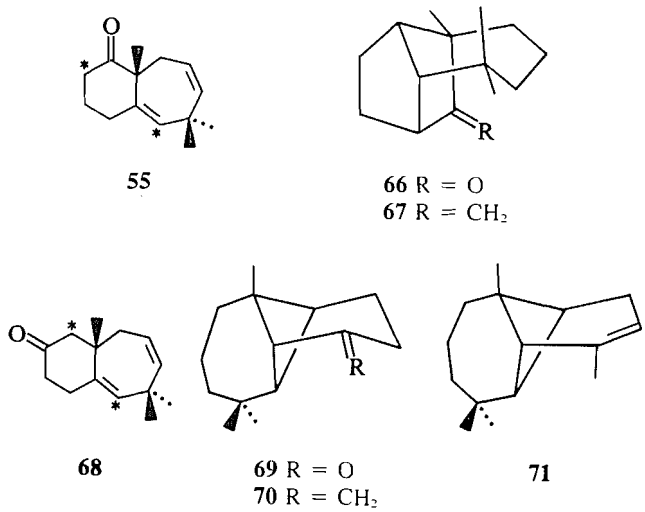

55

66 R = O
67 R = CH_2

68

69 R = O
70 R = CH_2

71

CHART 2

enone **49** proceeds via the transition state **F**, it can be seen that destabilization (relative to the transition state involved in the conversion of **22** into **24**) would be caused by steric repulsions between one of the cyclopropyl methyl groups and two of the vinyl protons (see **F**). At first sight, it would appear that these repulsions are similar to the methyl–ring interactions in transition state **E** and since the destabilizing effect of the methyl–methyl interaction (present in **E**, but absent in **F**) is quite small[15] the ease with which the enone **49** undergoes Cope rearrangement is surprising. However, it should be emphasized that in compound **49**, one of the "vinyl" groups is incorporated into a cyclohexenone ring and, thus, the substitution pattern of **49** is quite different from that of **59**. Certainly, the possibility that the conjugative effect of the carbonyl group in **49** influences the rate and/or mechanism of the reaction cannot be discounted.[16]

Again assuming a "normal" concerted mechanism, the Cope rearrangement of the highly substituted divinylcyclopropane **54** would proceed by way of the transition state **G**. Of the steric repulsions present in this species (see **G**), molecular models clearly show that the one involving the two methyl groups is particularly severe. Thus, on this basis, it is possible to rationalize, in a qualitative way, the striking difference between the relative ease of [3,3]-sigmatropic rearrangement of compounds **49** and **54** (compare **F** and **G**). However, it should be noted that the substituted divinylcyclopropane **64**, upon thermolysis at 180°C, fails to undergo Cope rearrangement to **65**. Instead, as in the case of substrate **59**, only reversible *cis* and *trans* isomerization is observed (58). Therefore, since the transition states for the conversions **54** → **55** and **64** → **65** would experience the same steric repulsions (see **G** and **H**), the fact that **54** undergoes [3,3]-sigmatropic rearrangement at all is, again, unexpected.

Conclusion

The results reported in this paper clearly demonstrate the viability of effecting seven-membered ring annulation and spiro-annulation via the preparation and thermolysis of β-(2-vinylcyclopropyl) α,β-unsaturated ketones. Indeed, it is appropriate to mention explicitly that this general method has been applied elegantly by Wender *et al.* to the synthesis of the sesquiterpenoids (±)-damsinic acid and (±)-confertin (27) and to the preparation of an intermediate containing the basic carbon skeleton found in the tigliane, daphnane, and ingenane families of diterpenoids (32). Furthermore, as mentioned previously, the accompanying paper (38) describes the details of a synthesis of the sesquiterpenoid (±)-β-himachalene via a route in which this new method played a key role.

We had mentioned earlier that one of the goals of the present study was to prepare substances which might prove useful as precursors for natural product syntheses. In this connection, the successful Cope rearrangement of the highly substituted divinylcyclopropanes **49** and **54** was particularly gratifying, since, for example, the annulation product **55** could, in theory, serve as a suitable intermediate for the synthesis of the well-known sesquiterpenoids (±)-longifolene (**67**), (±)-β-longipinene (**70**), and (±)-α-longipinene (**71**) (see Chart 2). Thus, subjection of **55** to a sequence of reactions involving at some stage bond formation between the appropriate carbon centers (* in **55**) would provide the tricyclic ketone **66**, a well-known precursor for the preparation of the natural product **67**. On the other hand, conversion of **55** into **68** (1,2-ketone transposition), followed by appropriate synthetic manipulations, including bond formation between the carbon atoms marked * in **68**, would produce the ketone **69**. The latter substance has been converted into the two longipinenes **70** and **71**.

Experimental

General[17]

Melting points and distillation temperatures are uncorrected. Ultraviolet (uv) spectra were recorded on a Cary 15 spectrophotometer, while infrared (ir) spectra were taken on Perkin–Elmer models 710 or 710B spectrophotometers. Proton nuclear magnetic resonance (^{1}H nmr) spectra (deuterochloroform solution) were measured using Varian Associates spectrometers, models HA-100 or XL-100. Signal positions are given in δ units, with tetramethylsilane as the internal standard. High resolution mass spectrometric measurements were recorded on a Kratos MS-50 mass spectrometer. Gas–liquid chro-

[16]It is interesting to point out that a conjugative substituent at C-1 of 1,5-hexadienes has been predicted to *decrease* the rate of Cope rearrangement of these substances (57). How this prediction relates to the work reported herein is, at least to us, unclear.

[17]This general section is applicable to the accompanying paper (38) as well as to the present paper.

Can. J. Chem. Downloaded from www.nrcresearchpress.com by 210.87.254.42 on 09/06/12
For personal use only.

Can. J. Chem. Downloaded from www.nrcresearchpress.com by 210.87.254.42 on 09/06/12
For personal use only.

matography (glc) was carried out with a Hewlett–Packard model 5832A gas chromatrograph (analytical) or with a Varian Aerograph model 90-P instrument (preparative). Thin-layer chromatography was carried out on commercial silica gel plates (Eastman Chromagram Sheet, No. 13181, analytical) or on 20 × 20 cm glass plates coated with 0.9 mm of silica gel (E. Merck, Silica Gel 60, preparative). Column chromatography was carried out on 70–230 mesh silica gel (E. Merck) while flash chromatography was accomplished using 230–400 mesh silica gel (E. Merck) according to the procedure developed by Still *et al.* (59).

Solutions of methyllithium, *n*-butyllithium, and *tert*-butyllithium, purchased from the Alfa Division of Ventron Corporation, were standardized by the method of Gilman and Cartledge (60). Bromoform and methyl iodide were passed through a short column of basic alumina (activity I) just prior to use. Tetrahydrofuran (THF) and ether were distilled under an atomsphere of nitrogen from sodium benzophenone ketyl. Diisopropylamine and hexamethylphosphoramide were distilled from calcium hydride and barium oxide, respectively, and were stored over molecular sieves. Dichloromethane was distilled from phosphorous pentoxide. *o*-Xylene was distilled, under an atmosphere of nitrogen, from sodium metal, while collidine and *o*-dichlorobenzene were freshly distilled before use.

Microanalyses were performed by Mr. P. Borda, Microanalytical Laboratory, University of British Columbia, Vancouver, B.C.

*Reaction of the β-iodo enones **4**, **8**, and **26–29** with lithium (phenylthio)(2-vinylcyclopropyl)cuprate (**21**). Preparation of the annulation products **25**, **30–32**, **34**, and **35***

A flame-dried 25 mL three-necked flask equipped with a bent side-arm tube containing solid phenylthiocopper (44, 45) (for the β-iodo enones **4**, **8**, **27**, and **29**: 260 mg, 1.5 mmol; for the β-iodo enones **26** and **28**: 345 mg, 2 mmol) was evacuated (vacuum pump) and filled with nitrogen (process repeated 3 times). A solution of 1-bromo-2-vinylcyclopropane (**19**, *cis*/*trans* ~7:3; for **4**, **8**, **27**, and **29**: 220 mg, 1.5 mmol; for **26** and **28**: 294 mg, 2 mmol) in anhydrous ether (3 mL) was added (syringe) to the flask via a septum cap. After the solution had been cooled to −78°C, it was treated with a solution of *tert*-butyllithium in pentane (1.2 *M*; for **4**, **8**, **27**, and **29**: 2.5 mL, 3 mmol; for **26** and **28**: 3.34 mL, 4 mmol), and the resulting mixture was stirred at −78°C under an atmosphere of nitrogen for 1 h. During this time, a white precipitate (lithium bromide) appeared. Successive addition of dry THF (10 mL, the white precipitate dissolved) and the phenylthiocopper (rotation of the bent tube) gave a yellow suspension which, when warmed to −20°C and then stirred for 10 min, produced a clear yellow solution of the cuprate reagent **21**. After this solution had been recooled to −78°C, a solution of the appropriate β-iodo enone (**4**, **28**, **29**: 222 mg, 1 mmol; **8**, **26**: 236 mg, 1 mmol; **27**: 208 mg, 1 mmol) in 2 mL of dry THF was added and the resultant reaction mixture was stirred at −78°C for 1 h, at −20°C for 1 h, and at 0°C for 1 h (**4**, **8**, **27**, and **29**) or 2 h (**26** and **28**). During this time the color of the reaction mixture changed from yellow to brown. Methanol (1 mL) and ether (10 mL) were added and the suspension thus obtained was filtered through a short column of silica gel (~10 g). The column was eluted with ether (200 mL) and the combined eluate was concentrated under reduced pressure. Distillation (~60–90°C/~0.5 Torr) of the residual material provided a clear, colorless oil which was subjected to thermolysis (neat, 180°C, 30–45 min) under an atmosphere of nitrogen. Distillation of the thermolysate provided the final product, which, in each case, consisted very largely or totally of one compound. In those cases in which the product was accompanied by small amounts of unidentified impurities, a sample of the desired annulation product was collected by preparative glc. The following products were obtained via this general procedure.

*Dienone **25*** (75% from **4**); uv (methanol) λ_{max}: 246 nm (ε 7 850); ir (film): 1665, 1638 cm^{-1}; ^1H nmr δ: 1.80–2.12 (m, 2H), 2.12–2.78 (m, 8H), 3.04–3.32 (broad s, 2H), 5.40–5.76 (m, 2H). *Exact Mass* calcd. for $C_{11}H_{14}O$: 162.1044; found: 162.1039.

*Dienone **30*** (82% from **26**); ir (film): 1710, 1665, 1635 cm^{-1}; ^1H nmr δ: 1.26 (s, 3H), 1.4–2.8 (diffuse m, 10H), 5.50 (broad t, 1H, J = 5 Hz), 5.64–6.00 (m, 2H). *Exact Mass* calcd. for $C_{12}H_{16}O$: 176.1200; found: 176.1213.

*Dienone **31*** (80% from **27**); uv (methanol) λ_{max}: 236 nm (ε 9 650); ir (film): 1700, 1645 cm^{-1}; ^1H nmr δ: 2.22–2.62 (m, 8H), 2.86–3.04 (broad s, 2H), 5.64–6.02 (m, 2H). *Exact Mass* calcd. for $C_{10}H_{12}O$: 148.0887; found 146.0886.

*Dienone **32*** (84% from **28**); ir (film): 1742, 1685 cm^{-1}; ^1H nmr δ: 1.14 (s, 3H), 2.18–2.70 (diffuse m, 6H), 2.80–2.98 (unresolved m, 2H), 5.48 (broad t, 1H, $J \approx 4$ Hz), 5.60–5.75 (m, 2H). *Exact Mass* calcd. for $C_{11}H_{14}O$: 162.1044; found: 162.1047.

*Spiro dienone **34*** (77% from **8**); ir (film): 1710, 1660, 1645 cm^{-1}; ^1H nmr δ: 1.60–2.04 (m, 6H), 2.12–2.72 (m, 4H), 2.72–2.94 (m, 2H), 5.52–5.92 (m, 4H). *Exact Mass* calcd. for $C_{12}H_{16}O$: 176.1200; found: 176.1215.

*Spiro dienone **35*** (64% from **29**); ir (film): 1738, 1640 cm^{-1}; ^1H nmr δ: 1.74–2.70 (diffuse m, 8H), 2.76–3.02 (m, 2H), 5.34–5.96 (m, 4H). *Exact Mass* calcd. for $C_{12}H_{14}O$: 162.1044; found: 162.1043.

*Tetrahydropyranyl ether of (2,2-dibromo-3,3-dimethylcyclopropyl)-methanol (**37**)*

To a mechanically stirred mixture of the tetrahydropyranyl ether of 3-methyl-2-buten-1-ol (**36**, 6.8 g, 40 mmol), benzyltriethylammonium chloride (0.16 g, 0.7 mmol), ethanol (0.32 mL, 5.5 mmol), and bromoform (21 g, 83 mmol) was added slowly 40 mL of 50% aqueous sodium hydroxide. After a period of 4 h, the dark reaction mixture was diluted with water and extracted three times with ether. The combined ether extract was washed sequentially with water, 1 *N* hydrochloric acid, water, saturated aqueous sodium bicarbonate, and brine, and then was dried over anhydrous magnesium sulfate. Removal of the solvent, followed by distillation (air-bath temperature 100–118°C/0.3 Torr) of the residual material gave 9.4 g of a viscous oil. Analysis of this material by spectroscopy (ir, ^1H nmr) and glc indicated that it was composed of a mixture of the desired tetrahydropyranyl ether **37**, along with some of the corresponding alcohol **38** (ratio ≈ 84:16, respectively).[18] Therefore, a mixture of this material, dihydropyran (4.5 g), and *p*-toluenesulfonic acid monohydrate (80 mg) was stirred at room temperature for 4 h. The mixture was diluted with ether and the resultant solution was passed through a short column of basic alumina (Woelm, activity III). The column was washed with additional portions of ether. Removal of the solvent from the combined eluate, followed by bulb-to-bulb distillation of the residual oil, gave 9.9 g (72%) of compound **37**; ^1H nmr δ: 1.23, 1.40 (s, s, 3H each), ~1.1–2.1 (diffuse m, 7H), 3.32–4.04 (diffuse m, 4H), 4.52–4.74 (m, 1H). *Anal.* calcd. for $C_{11}H_{18}Br_2O_2$: C 38.62, H 5.30; found: C 38.90, H 5.41.

*(2,2-Dibromo-3,3-dimethylcyclopropyl)methanol (**38**)*

To a stirred solution of the tetrahydropyranyl ether **37** (6.8 g, 19.9 mmol) in 50 mL of methanol, under an atmosphere of nitrogen, was added 10 mL of 1 *N* hydrochloric acid. After the resultant mixture had been stirred at room temperature overnight, most of the methanol was removed under reduced pressure. The remaining material was diluted with water and extracted thoroughly with ether. The combined extract was washed sequentially with water, saturated aqueous sodium bicarbonate, and brine, and then was dried over anhydrous magnesium sulfate. Removal of the solvent, followed by distillation (air-bath temperature 60–90°C/0.15 Torr) of the residual oil gave 4.6 g (90%) of the alcohol **38** as a viscous oil which solidified on standing (refrigerator). Recrystallization of a sample of this material from pentane containing a small amount of ether provided colorless crystals which exhibited mp 35.5°C; ir ($CHCl_3$): 3630, 3470 cm^{-1}; ^1H nmr δ: 1.29, 1.45 (s, s, 3H each), 1.62 (t, 1H, J = 7 Hz), 1.89 (s, 1H), 3.77 (d, 2H, J = 7 Hz). *Anal.* calcd. for $C_6H_{10}Br_2O$: C 27.94, H 3.91; found: C 28.07, H 3.89.

[18]The amount of alcohol **38** present in the mixture varied somewhat from one experiment to another. Clearly, if **38** was the required product (see next experiment), the dihydropyran-*p*-toluenesulfonic acid treatment was not carried out.

Can. J. Chem. Downloaded from www.nrcresearchpress.com by 210.87.254.42 on 09/06/12
For personal use only.

*2,2-Dibromo-3,3-dimethylcyclopropanecarboxaldehyde (**39**)*

To a stirred suspension of pyridinium chlorochromate (8.37 g, 38.6 mmol) in 190 mL of dry dichloromethane was added rapidly a solution of the alcohol **38** (4.97 g, 19.3 mmol) in 10 mL of the same solvent. The dark mixture was stirred at room temperature for 2 h. Ether (~800 mL) was added and the resultant mixture was passed through a short column of basic alumina (Woelm, activity III). The column was washed with additional volumes of ether. Removal of the solvent from the combined eluate, followed by distillation (air-bath temperature 67–81°C/0.4 Torr) of the residual material provided 4.17 g (84%) of the aldehyde **39** as a colorless oil which crystallized on standing (refrigerator) and exhibited mp ~27.5°C; ir (film): 1705 cm^{-1}; ^1H nmr δ: 1.54, 1.61 (s, s, 3H each), 2.10 (d, 1H, J = 5.5 Hz), 9.38 (d, 1H, J = 5.5 Hz). The 2,4-dinitrophenylhydrazone derivative of the aldehyde **39** was recrystallized from methanol and exhibited mp 112–113°C (dec.). *Anal.* calcd. for $C_{12}H_{12}Br_2N_4O_4$: C 33.05, H 2.77, N 12.85; found: C 33.28, H 2.80, N 12.82.

*1,1-Dibromo-2,2-dimethyl-3-vinylcyclopropane (**40**)*

To a cold (−78°C) stirred suspension of methyltriphenylphosphonium bromide (6.24 g, 17.6 mmol) in 80 mL of dry THF under an atmosphere of nitrogen was added a solution of *n*-butyllithium in hexane (6.5 mL, 2.7 *M*, 17.5 mmol). The mixture was allowed to warm to room temperature and stirred for an additional 30 min. A solution of the aldehyde **39** (4.08 g, 16 mmol) in 5 mL of dry THF was added, the reaction mixture was stirred at room temperature for 1 h, and then was poured into 400 mL of pentane. The resultant mixture was filtered through a short column of silica gel (Woelm, activity III) and the column was eluted with further volumes of pentane. Removal of the solvents from the combined eluate, followed by distillation (air-bath temeprature 52–59°C/0.8 Torr) of the residual oil gave 2.48 g (61%) of the substituted vinylcyclopropane **40** as a colorless oil; ir (film): 3100, 1635, 905 cm^{-1}; ^1H nmr δ: 1.27, 1.45 (s, s, 3H each), 1.93–2.11 (m, 1H), 5.19–5.77 (m, 3H). This material was somewhat unstable and, therefore, it was used directly for the next step of the synthetic sequence.

cis-*1-Bromo-2,2-dimethyl-3-vinylcyclopropane (**41**)*

To a vigorously stirred solution of the substituted dibromocyclopropane **40** (5.7 g, 22.4 mmol) in 53 mL of glacial acetic acid, under an atmosphere of nitrogen, was added, in small portions over a period of 2 h, 16.0 g (24.5 mg atoms) of zinc dust. The mixture was stirred for an additional period of 1 h and then was filtered. The filtrate was diluted with brine and the resultant mixture was extracted thoroughly with a 1:10 mixture of ether and petroleum ether (bp 30–60°C). The combined extract was washed three times with 1 *N* aqueous sodium hydroxide and once with brine, and then was dried over anhydrous magnesium sulfate. Removal of the solvent by distillation at atmospheric pressure, followed by bulb-to-bulb distillation (air-bath temperature ~40°C/0.4 Torr; collecting bulb cooled with a Dry Ice – acetone bath) of the residual material gave 2.6 g (66%) of a colorless oil. Analysis (glc, ^1H nmr) of this material indicated that it consisted of a mixture of *cis*-(**41**) and *trans*-1-bromo-2,2-dimethyl-3-vinylcyclopropane (**47**) (*vide infra*), in a ratio of about 20:1. Subjection of this material to column chromatography on silica gel (elution of the column with pentane) provided the pure *cis* isomer **41**; ir (film): 3090, 1630, 900 cm^{-1}; ^1H nmr δ: 1.16, 1.18 (s, s, 3H each), 1.49 (overlapped d of d, appears as a triplet, 1H, J = 7.5 Hz), 3.05 (d, 1H, J = 7.5 Hz), 5.10–5.34 (m, 2H), 5.44–5.83 (m, 1H). *Exact Mass* calcd. for $C_7H_{11}{}^{79}Br$: 174.0044; found: 174.0031.

trans-*(2-Bromo-3,3-dimethylcyclopropyl)methanol (**45**)*

To a cold (−90°C) stirred solution of the tetrahydropyranyl ether **37** (12.31 g, 36 mmol) in 30 mL of dry ether, under an atmosphere of nitrogen, was added a solution of *n*-butyllithium in hexane (15.7 mL, 2.3 *M*, 36 mmol) and the resultant solution was stirred at −90°C for 15 min. Methanol (6 mL) was added, the mixture was allowed to warm to room temperature, and then was diluted with brine and extracted thoroughly with pentane. The combined extract was washed with water and dried over anhydrous magnesium sulfate. Removal of the solvent, followed by distillation (air-bath temperature 58–90°C/0.6 Torr) of the crude product gave 8.42 g of a colorless oil. Analysis of this material by glc indicated that it was composed of a mixture of the tetrahydropyranyl ether **44** and the corresponding alcohol **45**, in a ratio of ~4:1. The oil was dissolved in methanol (80 mL) containing 16 mL of 1 *N* hydrochloric acid and the resultant solution was stirred overnight at room temperature under an atmosphere of nitrogen. Most of the methanol was removed under reduced pressure. The residual oil was diluted with brine and extracted thoroughly with ether. The combined extract was washed sequentially with water, saturated aqueous sodium bicarbonate, and brine, and then was dried over anhydrous magnesium sulfate. Removal of the solvent, followed by distillation (air-bath temperature 50–60°C/0.04 Torr) of the residual material gave 4.48 g (70%) of the desired alcohol **45** as a colorless oil; ir (film): 3400 cm^{-1}; ^1H nmr δ: ~1.1–1.45 (m, 1H), 1.14, 1.26 (s, s, 3H each), 1.96 (s, 1H), 2.69 (d, 1H, J = 4 Hz), 3.43–3.84 (m, 2H). *Anal.* calcd. for $C_6H_{11}BrO$: C 40.25, H 6.19; found: C 40.39, H 6.11.

trans-*2-Bromo-3,3-dimethylcyclopropanecarboxaldehyde (**46**)*

To a stirred suspension of pyridinium chlorochromate (7.29 g, 33.6 mmol) in 150 mL of dry dichloromethane, under an atmosphere of nitrogen, was added a solution of the alcohol **45** (3.0 g, 16.8 mmol) in 10 mL of the same solvent. After the dark reaction mixture had been stirred at room temperature for 2 h, it was poured into 800 mL of ether and the resultant mixture was filtered through a short column of basic alumina (Woelm, activity III). The column was washed with additional volumes of ether. Removal of the solvents from the combined eluate, followed by distillation (air-bath temperature 60–80°C/0.6 Torr) of the crude product, gave 2.7 g (91%) of the desired aldehyde **46** as a colorless oil; ir (film): 2850, 2750, 1705 cm^{-1}; ^1H nmr δ: 1.29, 1.44 (s, s, 3H each), 2.12 (d of d, 1H, J = 4.5, 3.5 Hz), 3.61 (d, 1H, J = 4.5 Hz), 9.67 (d, 1H, J = 3.5 Hz). *Exact Mass* calcd. for $C_6H_9{}^{79}BrO$: 175.9836; found: 175.9844.

trans-*1-Bromo-2,2-dimethyl-3-vinylcyclopropane (**47**)*

To a cold (−78°C) stirred suspension of methyltriphenylphosphonium bromide (5.5 g, 15.5 mmol) in 70 mL of dry THF, under an atmosphere of nitrogen, was added a solution of *n*-butyllithium in hexane (6.73 mL, 2.3 *M*, 15.5 mmol). The mixture was allowed to warm to room temperature and then was stirred for an additional 30 min. A solution of the aldehyde **46** (2.5 g, 14.1 mmol) in 5 mL of dry THF was added, the reaction mixture was stirred at room temperature for 1 h, and then was poured into 400 mL of pentane. The resultant mixture was filtered through a short column of Florisil, and the column was eluted with further volumes of pentane. Removal of the solvents from the combined eluate (distillation at atmospheric pressure), followed by bulb-to-bulb distillation (air-bath temperature ~40°C/0.1 Torr; collecting bulb cooled with a Dry Ice – acetone bath) of the crude product, gave 1.7 g (69%) of the substituted bromocyclopropane **47**; ir (film): 3110, 1635, 900 cm^{-1}; ^1H nmr δ: 1.10, 1.20 (s, s, 3H each), ~1.5–1.9 (m, 1H), 2.80 (d, 1H, J = 4 Hz), 4.83–5.84 (m, 3H). *Exact Mass* calcd. for $C_7H_{11}{}^{79}Br$: 174.0044; found: 177.0042.

*Reaction of the cuprate reagents **42** and **48** with the β-iodo enones **4** and **26**. Preparation of the 3-(2,2,-dimethyl-3-vinylcyclopropyl)-2-cyclohexen-1-ones **49**, **52**, **54**, and **56***

To a cold (−78°C) stirred solution of *cis*-(**41**) or *trans*-1-bromo-2,2-dimethyl-3-vinylcyclopropane (**47**) (132 mg, 0.75 mmol) in dry ether (3 mL), under an atmosphere of nitrogen, was added a solution of *tert*-butyllithium in pentane (0.71 mL, 2.1 *M*, 1.5 mmol). After the tan-colored slurry had been stirred at −78°C for 1 h, dry ether (7 mL), dry THF (2 mL), and solid phenylthiocopper (132 mg, 0.75 mmol) were added sequentially. The reaction mixture was allowed to warm to −20°C and then was stirred for an additional period of 1 h. After the resulting yellow-brown solution had been recooled to −78°C, a solution of the appropriate β-iodo enone (**4**: 111 mg, 0.5 mmol; **26**: 118 mg, 0.5 mmol) in dry ether (1 mL) was added. The reaction mixture was allowed to warm to room temperature and was stirred for an additional period of 2.5 h. Methanol (0.5 mL) and ether (10 mL)

Can. J. Chem. Downloaded from www.nrcresearchpress.com by 210.87.254.42 on 09/06/12
For personal use only.

were added and the resultant slurry was filtered through a short column of Florisil (~10 g). The column was washed with additional volumes of ether. Removal of the solvent from the combined eluate provided the crude product. The following compounds were obtained by means of this general procedure.

cis-*3-(2,2-Dimethyl-3-vinylcyclopropyl)-2-cyclohexen-1-one (49)*

The crude product (84 mg, 88%) obtained from reaction of 3-iodo-2-cyclohexen-1-one (**4**) with the cuprate reagent **42** was not distilled, since compound **49** rearranged slowly at room temperature to afford the bicyclic enone **50**. Although a sample of **49** totally devoid of the rearrangement product **50** was not obtained, material acquired by means of a quick, careful work-up procedure exhibited the following spectral data: ir (film): 1672, 1625, 890 cm^{-1}; ^1H nmr δ: 1.06, 1.17 (s, s, 3H each), ~1.4–2.5 (diffuse m, 8H), 4.92–5.82 (m, 3H), 5.90–6.01 (m, 1H). *Exact Mass* calcd. for $C_{13}H_{18}O$: 190.1357; found: 190.1352.

trans-*3-(2,2-Dimethyl-3-vinylcyclopropyl)-2-cyclohexen-1-one (52)*

Distillation (air-bath temperature 120–130°C/0.2 Torr) of the crude product obtained from reaction of the β-iodo enone **4** with the cuprate reagent **48** provided 90 mg (95%) of compound **52**; uv (methanol) λ_{max}: 256 nm (ε 14 900); ir (film): 1670, 1622, 882 cm^{-1}; ^1H nmr δ: 1.00, 1.20 (s, s, 3H each), ~1.4–2.5 (diffuse m, 8H), 4.99–5.26 (m, 2H), 5.47–5.82 (m, 1H), 5.79–5.85 (m, 1H). *Exact Mass* calcd. for $C_{13}H_{18}O$: 190.1357; found: 190.1350.

cis-*2-Methyl-3-(2,2-dimethyl-3-vinylcyclopropyl)-2-cyclohexen-1-one (54)*

Distillation (air-bath temperature 85–100°C/0.02 Torr) of the crude product obtained from reaction of 3-iodo-2-methyl-2-cyclohexen-1-one (**26**) with the cuprate reagent **42** gave 98 mg of a viscous oil. Analysis of this material by tlc and glc indicated the presence of ~5% of the starting material **26**. Subjection of the mixture to preparative tlc (silica gel, 5:1 pentane–ether) afforded 78 mg (76%) of the enone **54** as a colorless oil; uv (methanol) λ_{max}: 257 nm (ε 10 970); ir (film): 1660, 1625, 900 cm^{-1}; ^1H nmr δ: 1.00, 1.23, 1.79 (s, s, broad s, 3H each), ~1.5–2.05 and 2.1–2.5 (diffuse multiplets, 8H), 4.95–5.70 (m, 3H). *Exact Mass* calcd. for $C_{14}H_{20}O$: 204.1514; found: 204.1522.

trans-*2-Methyl-3-(2,2-dimethyl-3-vinylcyclopropyl)-2-cyclohexen-1-one (56)*

Distillation (air-bath temperature 90–100°C/0.02 Torr) of the crude product obtained from reaction of the β-iodo enone **26** with the cuprate reagent **48** provided 100 mg of a colorless oil. Analysis of this material by tlc and glc indicated that the starting material **26** and the desired product **56** were present in a ratio of ~1:30, respectively. The mixture also contained small amounts of unidentified compounds. Purification by preparative tlc (silica gel, 5:1 pentane–ether) gave 84 mg (82%) of the enone **56** as a colorless oil; uv (methanol) λ_{max}: 257 nm (ε 12 200); ir (film): 1670, 1642, 1622, 895 cm^{-1}; ^1H nmr δ: 0.95, 1.20, 1.80 (s, s, broad s, 3H each), ~1.5–2.05 and 2.15–2.5 (diffuse multiplets, 8H), 4.98–5.26 (m, 2H), 5.48–5.90 (m, 1H). *Exact Mass* calcd. for $C_{14}H_{20}O$: 204.1514; found: 204.1494.

Thermal rearrangement of compound 49

(a) *Neat*

A sample of crude enone **49** (obtained from 111 mg, 0.5 mmol of the β-iodo enone **4**, as described above) was placed under an atmosphere of nitrogen and heated at 110°C for 10 min. Direct distillation (air-bath 110–140°C/0.3 Torr) of the resultant material gave 88 mg (93% from **4**) of the conjugated dienone **51** as a clear oil; uv (methanol) λ_{max}: 248 nm (ε 6 800); ir (film): 1665, 1635 cm^{-1}; ^1H nmr δ: 1.05 (s, 6H), 2.01 (m, 2H), 2.30–2.54 (diffuse m, 4H), 2.48 (s, 2H), 3.11 (broad d, 2H, J = 5 Hz), 5.26 (broad d, 1H, J = 12 Hz), 5.39–5.65 (d of t, 1H, J = 5, 12 Hz). *Exact Mass* calcd. for $C_{13}H_{18}O$: 190.1357; found: 190.1349.

(b) *In hexane*

A solution of the crude enone **49** (67 mg) in dry hexane (1 mL) was refluxed under an atmosphere of nitrogen for 4 h. Removal of the solvent afforded 65 mg of a light yellow oil which consisted very largely of the dienone **50**; ir (film): 1712 cm^{-1}; ^1H nmr δ: 1.14, 1.18 (s, s, 3H each), ~1.65–2.05 (m, 2H), 2.28–2.64 (m, 6H), 3.12–3.36 (m, 1H), 5.38 (m, 1H), 5.49 (d, 1H, J = 12 Hz), 5.77 (d of t, 1H, J = 6, 12 Hz). When this material was heated briefly at 110°C (neat) under an atmosphere of nitrogen, and then distilled (see above), 59 mg (88%) of the conjugated dienone **51** was obtained.

Thermal rearrangement of compound 52

A solution of the enone **52** (59 mg, 0.31 mmol) in dry *o*-dichlorobenzene (0.5 mL) was placed on a thick-walled Pyrex tube and then was thoroughly purged with a stream of dry nitrogen. After the tube had been sealed (−78°C, vacuum), it was heated at ~220°C for 14 h. Removal of the solvent from the cooled solution provided a brown oil which was purified by preparative tlc (silica gel, 1:9 ether – petroleum ether). Distillation (air-bath temperature 120–137°C/0.2 Torr) of the material thus obtained afforded 35 mg (59%) of the conjugated enone **51**, which exhibited spectral data identical with those summarized above.

Thermal rearrangement of compound 54

(a) *In o-xylene*

A solution of the enone **54** (50 mg, 0.25 mmol) in dry ether (~1.0 mL) was passed through a small column of basic alumina (~1 g, activity I). The column was eluted with dry ether (~2 mL). The oil remaining after removal of the ether from the eluate was dissolved in dry, degassed *o*-xylene (3 mL) and the resultant solution was refluxed under an atmosphere of argon for 48 h. Removal of the solvent, followed by distillation (air-bath temperature 90–110°C/0.2 Torr) of the residual material gave 42 mg (84%) of a colorless oil. Analysis of this material by glc indicated that it consisted of a small amount of starting material (~2%) along with the Cope rearrangement product **55** and the isomerization product **56**, in a ratio of ~2.7:1.[19] Separation of the two products was effected by preparative tlc (silica gel, 98:2 benzene – ethyl acetate). The dienone **55** (24 mg, 48%) exhibited ir (film): 1715 cm^{-1}; ^1H nmr δ: 1.13, 1.15, 1.26 (s, s, s, 3H each), ~1.64–2.68 (diffuse m, 8H), 5.24 (broad s, 1H), 5.42–5.80 (m, 2H). *Exact Mass* calcd. for $C_{14}H_{20}O$: 204.1514; found: 204.1516.

The enone **56** (8.5 mg, 17%) exhibited spectra identical with those obtained previously (*vide supra*).

(b) *In o-dichlorobenzene*

A sample compound **54** (68 mg, 0.33 mmol) was subjected to rearrangement in refluxing *o*-dichlorobenzene (4 mL) via a procedure identical with that described above. The reaction time was 3 h. Distillation of the crude product provided 62 mg (91%) of a colorless oil which consisted largely (glc analysis) of compounds **55** and **56** in a ratio of approximately 0.8:1, respectively.

(c) *In collidine (small scale)*

Following the procedure outlined above, a sample of the enone **54** (53 mg, 0.26 mmol) was subjected to rearrangement in refluxing collidine (1.5 mL). The reaction time was 42.5 h. The cooled solution was dissolved in 40 mL of ether and the resultant solution was washed successively with 10% aqueous sulfuric acid (4 × 10 mL), saturated aqueous sodium bicarbonate, and brine, and then was dried over anhydrous magnesum sulfate. Removal of the solvent, followed by bulb-to-bulb distillation of the residual oil, gave 39 mg (73%) of a colorless liquid. Analysis of this material by glc indicated that it

[19]As noted in the Results and discussion section of the paper, the ratio of **55**/**56** varied somewhat from one experiment to another. It ranged from ~1.1:1 to ~2.7:1 and was typically at approximately 2:1.

contained, in addition to ~15% of an unidentified compound, the rearrangement products **55** and **56** in a ratio of ~2.4:1.[20]

(d) *In collidine (larger scale)*

A solution of the enone **54** (2.04 g, 10 mmol) in 70 mL of dry, degassed collidine, under an atmosphere of argon, was refluxed for 43.5 h. The cooled reaction mixture was taken up in 1 L of ether and the resultant solution was washed successively with 10% aqueous sulfuric acid (3 × 500 mL), saturated aqueous sodium bicarbonate, and brine, and then was dried over anhydrous magnesium sulfate. Removal of the solvent gave a crude oil which was subjected to flash chromatography on silica gel (59). Elution of the column with hexanes containing 7% ethyl acetate gave 1 g (49%) of the dienone **55** and 420 mg (21%) of the enone **56**. Other substances appearing in certain fractions as mixtures with **55** and/or **56** were not identified.

Thermal rearrangement of compound ***56***

Thermolysis of the enone **56** (50 mg, 0.24 mmol) in dry *o*-dichlorobenzene (0.5 mL) at 220°C for 16 h was carried out via a procedure identical with that described for the thermolysis of compound **52** (*vide supra*). A solution of the crude product in ether (1 mL) was passed through a short column of silica gel (~1 g). The column was washed with additional ether (3 mL). Removal of the solvent from the combined eluate, followed by distillation (air-bath temperature 120–140°C/0.2 Torr) of the residual liquid gave 43.5 mg (87%) of a colorless oil. Analysis of this material by glc showed that it consisted largely of two components, **55** and **57**, in a ratio of about 1:4, respectively. Samples of each substance were obtained by preparative glc. The ir spectrum of **55** was identical with that of the same compound obtained previously, while the trienone **57** exhibited uv (methanol) λ_{max}: 245 nm (ϵ 13 000); ir (film): 1665, 1615, 895 cm^{-1}; ^1H nmr δ: 1.63 (d, 3H, J = 5 Hz), 1.69 (broad s, 3H), 1.86 (t, 3H, J = 2 Hz), 2.12–2.52 (m, 4H), 4.26 (broad d, 1H, J = 7 Hz), 4.81 (broad s, 1H), 4.92 (q, 1H, $J \approx$ 1.5 Hz), 5.38–5.86 (m, 2H). *Exact Mass* calcd. for $C_{14}H_{20}O$: 204.1514; found: 204.1510.

Acknowledgements

Financial support for this study from the Natural Sciences and Engineering Research Council of Canada (N.S.E.R.C.C.), an N.S.E.R.C.C. postgraduate scholarship (to H.E.M.), and a Senior Fellowship awarded to R.W.T. by the Senior Scientists Programme of the North Atlantic Treaty Organization are gratefully acknowledged.

1. E. VOGEL. Angew. Chem. **72**, 4 (1960).
2. E. VOGEL, K.-H. OTT, and K. GAJEK. Justus Liebigs Ann. Chem. 644 (1961).
3. E. VOGEL. Angew. Chem. Int. Ed. Engl. **2**, 1 (1963).
4. J. M. BROWN, B. T. GOLDING, and J. J. STOFKO, JR. J. Chem. Soc. Chem. Commun. 319 (1973); J. Chem. Soc. Perkin Trans. 2, 436 (1978).
5. M. P. SCHNEIDER and J. REBELL. J. Chem. Soc. Chem. Commun. 283 (1975).
6. M. SCHNEIDER. Angew. Chem. Int. Ed. Engl. **14**, 707 (1975).
7. S. J. RHOADS and N. R. RAULINS. Org. React. **22**, 1 (1975).
8. E. M. MIL'VITSKAYA, A. V. TARAKANOVA, and A. F. PLATE. Russ. Chem. Rev. **45**, 469 (1976).
9. J. E. BALDWIN and C. ULLENIUS. J. Am. Chem. Soc. **96**, 1542 (1974).
10. J. A. BERSON, T. MIYASHI, and G. JONES II. J. Am. Chem. Soc. **96**, 3468 (1974).
11. J. A. BERSON, P. B. DERVAN, R. MALHERBE, and J. A. JENKINS. J. Am. Chem. Soc. **98**, 5937 (1976).
12. E. VEDEJS, W. R. WILBER, and R. TWIEG. J. Org. Chem. **42**, 402 (1977).
13. J. E. BALDWIN and K. E. GILBERT. J. Am. Chem. Soc. **98**, 8283 (1976).
14. M. P. SCHNEIDER and B. CSACSKO. J. Chem. Soc. Chem. Commun. 330 (1977).
15. D. L. GARIN. Tetrahedron Lett. 3035 (1977).
16. M. P. SCHNEIDER and A. RAU. J. Am. Chem. Soc. **101**, 4426 (1979).
17. D. BRULÉ, J.-C. CHALCHAT, R.-P. GARRY, B. LACROIX, A. MICHET, and R. VESSIÈRE. Bull. Soc. Chim. Fr. II-57 (1981).
18. S. SAREL, A. SCHLOSSMAN, and M. LANGBEHEIM. Tetrahedron Lett. **22**, 691 (1981).
19. J. P. MARINO and T. KANEKO. Tetrahedron Lett. 3975 (1973); J. Org. Chem. **39**, 3175 (1974).
20. E. PIERS and I. NAGAKURA. Tetrahedron Lett. 3237 (1976).
21. J. P. MARINO and L. J. BROWNE. Tetrahedron Lett. 3245 (1976).
22. P. A. WENDER and M. P. FILOSA. J. Org. Chem. **41**, 3490 (1976).
23. R. E. MOORE. Acc. Chem. Res. **10**, 40 (1977).
24. M. SCHNEIDER and A. ERBEN. Angew. Chem. Int. Ed. Engl. **16**, 192 (1977).
25. E. PIERS, I. NAGAKURA, and H. E. MORTON. J. Org. Chem. **43**, 3630 (1978).
26. E. PIERS and E. H. RUEDIGER. J. Chem. Soc. Chem. Commun. 166 (1979).
27. P. A. WENDER, M. A. EISSENSTAT, and M. P. FILOSA. J. Am. Chem. Soc. **101**, 2196 (1979).
28. T. AKINTOBI, L. JAENICKE, F.-J. MARNER, and S. WAFFENSCHMIDT. Justus Liebigs Ann. Chem. 986 (1979).
29. E. PIERS and H.-U. REISSIG. Angew. Chem. Int. Ed. Engl. **18**, 791 (1979).
30. E. PIERS and E. H. RUEDIGER. J. Org. Chem. **45**, 1725 (1980).
31. M. P. SCHNEIDER and M. GOLDBACH. J. Am. Chem. Soc. **102**, 6114 (1980).
32. P. A. WENDER, C. L. HILLEMANN, and M. J. SZYMONIFKA. Tetrahedron Lett. **21**, 2205 (1980).
33. J. P. MARINO and M. P. FERRO. J. Org. Chem. **46**, 1912 (1981).
34. W. ADAM, O. DE LUCCHI, and D. SCHEUTZOW. J. Org. Chem. **46**, 4130 (1981).
35. P. M. CAIRNS, L. CROMBIE, and G. PATTENDEN. Tetrahedron Lett. **23**, 1405 (1982).
36. E. PIERS, J. BANVILLE, C. K. LAU, and I. NAGAKURA. Can. J. Chem. **60**, 2965 (1982).
37. E. PIERS, C. K. LAU, and I. NAGAKURA. Can. J. Chem. **61**, 288 (1983).
38. E. PIERS and E. H. RUEDIGER. Can. J. Chem. **61**, 1239 (1983).
39. D. SEYFERTH, J. YAMAZAKI, and D. L. ALLESTON. J. Org. Chem. **28**, 703 (1963).
40. J. A. LANDGREBE and L. W. BECKER. J. Org. Chem. **33**, 1173 (1968).
41. R. C. WOODWORTH and P. S. SKELL. J. Am. Chem. Soc. **79**, 2542 (1957).
42. L. SKATTEBOL. J. Org. Chem. **29**, 2951 (1964).
43. J. P. MARINO and L. J. BROWNE. Tetrahedron Lett. 3241 (1976).
44. G. H. POSNER, C. E. WHITTEN, and J. J. STERLING. J. Am. Chem. Soc. **95**, 7788 (1973).
45. G. H. POSNER, D. J. BRUNELLE, and L. SINOWAY. Synthesis, 662 (1974).
46. R. C. HAHN and G. W. JONES. J. Am. Chem. Soc. **93**, 4232 (1971).
47. R. G. CARLSON and W. S. MARDIS. J. Org. Chem. **40**, 818 (1975).
48. J. P. MARINO and L. J. BROWNE. J. Org. Chem. **41**, 3629 (1976).
49. E. PIERS, I. NAGAKURA, and J. E. SHAW. J. Org. Chem. **43**, 3431 (1978).

[20]This ratio was not constant from one experiment to another, although the variation (~1.9:1 to ~2.4:1) was not as great as when *o*-xylene was employed as the thermolysis solvent.

Can. J. Chem. Downloaded from www.nrcresearchpress.com by 210.87.254.42 on 09/06/12
For personal use only.

50. E. PIERS, J. R. GRIERSON, C. K. LAU and I. NAGAKURA. Can. J. Chem. **60**, 210 (1982).
51. M. MAKOSZA and M. FEDORYNSKI. Synth. Commun. **3**, 305 (1973).
52. E. J. COREY and J. W. SUGGS. Tetrahedron Lett. 2647 (1975).
53. C. L. OSBORN, T. C. SHIELDS, B. A. SHOULDERS, J. F. KRAUSE, H. V. CORTEZ, and P. D. GARNER. J. Am. Chem. Soc. **87**, 3158 (1965).
54. K. KITATANI, T. HIYAMA, and H. NOZAKI. J. Am. Chem. Soc. **97**, 949 (1975); Bull. Chem. Soc. Jpn. **50**, 3288 (1977).
55. D. H. WILLIAMS and I. FLEMING. Spectroscopic methods in organic chemistry. 2nd ed. McGraw Hill Book Co. (U.K.) Ltd., London. 1973. pp. 107–108.
56. C. W. SPANGLER. Chem. Rev. **76**, 187 (1976).
57. B. K. CARPENTER. Tetrahedron, **34**, 1877 (1978).
58. T. SASAKI, S. EGUCHI, and M. OHNO. J. Org. Chem. **37**, 466 (1972).
59. W. C. STILL, M. KAHN, and A. MITRA. J. Org. Chem. **43**, 2923 (1978).
60. H. GILMAN and F. K. CARTLEDGE. J. Organomet. Chem. **2**, 447 (1964).

Can. J. Chem. Downloaded from www.nrcresearchpress.com by 210.87.254.42 on 09/06/12
For personal use only.

Preparation and thermal rearrangement of *trans*-3-[1-methyl-2-(2-methyl-1-propenyl)cyclopropyl]-2-cyclohexen-1-one. A synthesis of (±)-β-himachalene

EDWARD PIERS AND EDWARD H. RUEDIGER

Department of Chemistry, University of British Columbia, 2036 Main Mall, University Campus, Vancouver, B.C., Canada V6T 1Y6

Received November 8, 1982

EDWARD PIERS and EDWARD H. RUEDIGER. Can. J. Chem. **61**, 1239 (1983).

A total synthesis of the sesquiterpenoid (±)-β-himachalene (**2**) is described. Treatment of 5,5-dimethyl-2-vinyl-1,3-dioxane (**24**) with bromoform and aqueous sodium hydroxide in the presence of a phase-transfer catalyst afforded the dibromocyclopropane **25**. When the latter substance was allowed to react (tetrahydrofuran–hexamethylphosphoramide, −95°C) with *n*-butyllithium in the presence of methyl iodide, a mixture of the epimeric products **26** (87–93%) and **27** (7–13%) was produced in high yield. Compound **26** was converted via a two-step sequence (hydrolysis with 88% formic acid, **26** → **28**; Wittig reaction with isopropylidenetriphenylphosphorane, **28** → **16**) into the bromocyclopropane **16**, which was transformed into the cuprate reagent **17**. Reaction of 3-iodo-2-cyclohexen-1-one (**4**) with reagent **17**, followed by thermolysis (xylene, reflux) of the resultant product **18** (the title compound), afforded, in quantitative yield, the dienone 12. Methylation of **12** furnished compound **29** which, upon hydrogenation in the presence of tris(triphenylphosphine)chlororhodium, gave the ketone **32**. Conversion of compound **32** into the corresponding enol phosphate **33**, followed by reduction (lithium, ethylamine–tetrahydrofuran, *tert*-butyl alcohol) of the latter material, provided (±)-β-himachalene (**2**).

EDWARD PIERS et EDWARD H. RUEDIGER. Can. J. Chem. **61**, 1239 (1983).

On décrit une synthèse totale de sesquiterpène (±) β-himachalène (**2**). Le diméthyl-5,5 vinyl-2 dioxanne-1,3 (**24**) réagit avec le bromoforme dans l'hydroxyde de sodium aqueux en présence d'un catalyseur de transfert de phase pour donner le dibromocyclopropane **25**. Ce dernier réagit (tétrahydrofuranne–hexaméthylphosphoramide, −95°C) avec le *n*-butyllithium en présence de l'iodure de méthyle en donnant des produits épimères **26** (87–93%) et **27** (7–13%) avec un fort rendement. On a, en deux étapes, (hydrolyse par l'acide formique à 88%, **26** → **28**; réaction de Wittig avec l'isopropyllidène triphénylphosphorane, **28** → **16**) transformé le composé **26** en bromocyclopropane **16** que l'on transforme en cuprate **17**. La réaction de l'iodo-3 cyclohexène-2 one-1 (**4**) avec la réactif **17** suivie de la thermolyse (xylène, reflux) du produit résultant **18** (le composé mentionné dans le titre) donne avec un rendement quantitatif la diénone **12**. La méthylation de cette dernière conduit au composé **29** qui par hydrogénation en présence du tris(triphénylphosphine)chlororhodium donne la cétone **32**. La transformation de cette cétone en phosphate d'énol correspondant **33**, suivie d'une réduction (lithium, éthylamine–tétrahydrofuranne, alcool *tert*-butylique) permet d'accéder à la (±) β-himachalène (**2**).

[Traduit par le journal]

Introduction

The bicyclic $C_{15}H_{24}$ hydrocarbons (−)-α- and (+)-β-himachalene were first isolated some 30 years ago from the essential oil of Himalayan deodar (*Cedrus deodara* Loud.) (1). Approximately 9 years later, reports (2, 3) concerning structural elucidation work carried out independently by two research groups revealed that these two natural products possess the structures represented by formulas **1** and **2**, respectively. As such, these

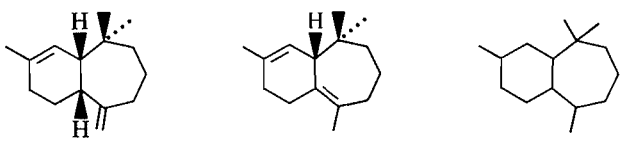

1 **2** **3**

compounds represented the first two known members of a new class of sesquiterpenoids containing the himachalane carbon skeleton **3**. Later, in 1968, Joseph and Dev (4) determined that the absolute stereostructures of (−)-α- and (+)-β-himachalene are as shown in **1** and **2**, respectively.

In the accompanying paper (5) we described a new seven-membered ring annulation method based on the preparation and thermal (Cope) rearrangement of β-(2-vinylcyclopropyl) α,β-unsaturated ketones. For example, treatment of 3-iodo-2-cyclohexen-1-one (**4**) with lithium (phenylthio)(2-vinylcyclopropyl)cuprate (**5**, mixture of epimers), followed by thermolysis of the resultant products **6**, afforded, in 75% yield, the bicyclic dienone **8** (see eq. [1]). Under the conditions necessary to effect complete bond reorganization of both isomers of **6**, the initially formed Cope rearrangement product **7** isomerized to the more stable α,β-unsaturated ketone **8**. Various extensions of our study to other systems revealed that syntheses of seven-membered ring annulation products via this method are gener-

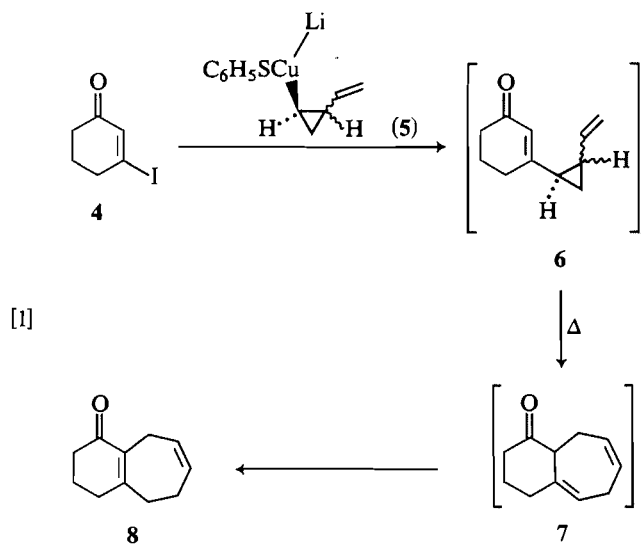

[1]

Can. J. Chem. Downloaded from www.nrcresearchpress.com by 210.87.254.105 on 09/06/12
For personal use only.

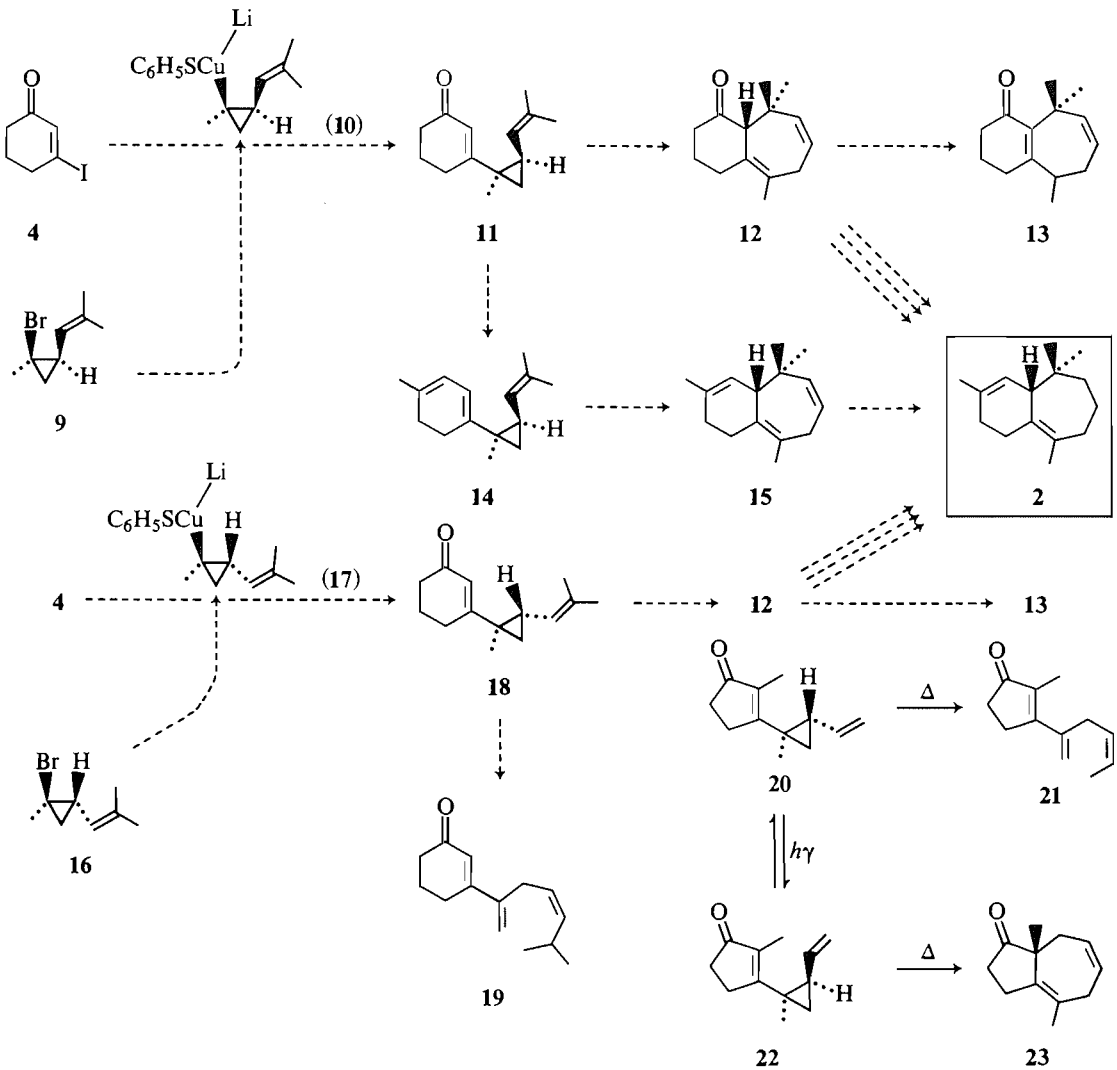

SCHEME 1

ally smooth and efficient (5). We report herein the application of this new annulation procedure to a total synthesis of racemic β-himachalene (**2**).[1,2]

Results and discussion

(a) *General considerations*

In principle, based on the work reported in the accompanying paper (5), the key step of the projected synthesis of (±)-β-himachalene (**2**) could involve thermal rearrangement of either of two possible substrates, *cis*-3-[1-methyl-2-(2-methyl-1-propenyl)cyclopropyl]-2-cyclohexen-1-one (**11**) or the corresponding *trans* isomer **18** (see Scheme 1). Thus, for example, treatement of 3-iodo-2-cyclohexen-1-one (**4**) with the substituted cyclopropylcuprate reagent **10** (presumably derived from the requisite bromide **9**) should afford the intermediate **11**. The latter substance would be expected (5) to undergo Cope rearrangement at, or slightly above, ambient temperatures to afford the required bicyclic dienone **12**. Reductive removal of the "extra" double bond in **12**, and use of the carbonyl group as a "handle" for introduction of the necessary methyl group and the alkene function would provide (±)-β-himachalene (**2**).

Alternatively, conversion of the cyclopropyl bromide **16** into the corresponding cuprate **17**, followed by reaction of this reagent with the β-iodo enone **4**, would afford the *trans* divinylcyclopropane **18**. The latter intermediate would be much more stable than the isomer **11** and, presumably, would be readily amenable to isolation at ambient temperatures. However, at elevated temperatures, compound **18** would be expected to undergo rearrangement and, if this bond reorganization were to proceed in the desired (Cope) sense, the product would again be the desired dienone **12**.

A potential problem associated with both of the sequences outlined above concerns the possibility of isomerization of the intermediate dienone **12**. Thus, in each case, the Cope rearrangement step (**11**---→**12** or **18**---→**12**), as well as some of the synthetic steps involved in the conversion of **12** into (±)-**2**, would have to be accomplished under conditions which would not effect isomerization of the tetrasubstituted double bond in **12** into conjugation with the carbonyl group (**12**---→**13**). If this isomerization, a clearly undesirable transformation, were to present a problem in either sequence, one would have to convert, prior to thermal rearrangement, the divinylcyclopropane intermediate (**11** or **18**) into a substance lacking the carbonyl group. One possibility, for example, would be to transform the intermediate **11** into the triene **14**. Cope rearrangement of the

[1]For a preliminary account of this work, see ref. 6.

[2]For other reported syntheses of (±)-β-himachalene, see refs. 7–9.

Can. J. Chem. Downloaded from www.nrcresearchpress.com by 210.87.254.105 on 09/06/12
For personal use only.

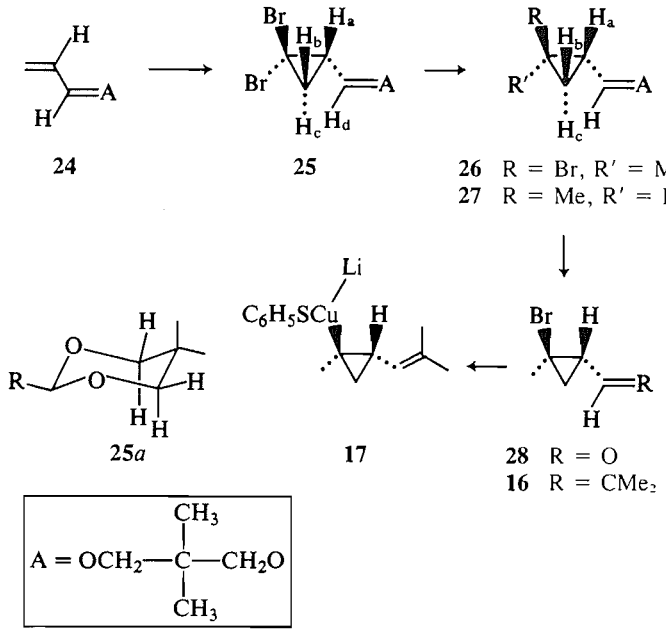

SCHEME 2

latter material would be expected to be a very facile process. Selective hydrogenation of the resultant product **15** would provide (±)-β-himachalene (**2**). It should be pointed out, however, that the anticipated ease with which the *cis*-divinylcyclopropane system in compound **11** would undergo bond reorganization could well preclude, or at least make very tricky, the possibility of transforming **11** into **14** or another suitable prerearrangement derivative. This potential difficulty could, therefore, represent a significant drawback to the synthesis of (±)-**2** via the route employing **11** as the key intermediate. On the other hand, conversion of the stable *trans*-divinylcyclopropane **18** into a suitable derivative lacking the carbonyl group should present no major difficulties.

Another potential problem attending the possible use of intermediate **18** in a synthesis of (±)-**2** should be mentioned, however. Although successful Cope rearrangement of this substance could provide the necessary bicyclic product **12**, it is clear that intermediate **18** could undergo another mode of rearrangement. That is to say, thermolysis of **18** at elevated temperatures could afford, instead of (or in addition to) the desired Cope rearrangement product **12**, a trienone **19** resulting from a [1,5]-sigmatropic hydrogen shift.[3] Indeed, it had been shown (10) that thermolysis of *trans*-2-methyl-3-(1-methyl-2-vinylcyclopropyl)-2-cyclopenten-1-one (**20**) produces nearly exclusively the trienone **21**. Subsequently, however, Wender *et al.* showed (11) that **20** could be converted cleanly into the Cope rearrangement product **23** by subjecting the former substance to simultaneous photolysis and thermolysis at 98°C. Under these conditions, a photo-induced equilibration between **20** and the isomeric material **22** occurs and, although compound **20** is *thermally* stable at 98°C, the isomer **22** readily undergoes Cope rearrangement at this temperature. This elegant procedure might also be applicable to the conversion of **18** into **12**, if high temperature thermolysis of **18** were to produce significant amounts of product **19**, resulting from a [1,5]-sigmatropic hydrogen migration.

[3]For examples of this type of rearrangement, along with appropriate citations, see ref. 5.

The analysis outlined above indicated that potential difficulties could well accompany both of the possible projected synthetic routes to (±)-β-himachalene (**2**). Therefore, the decision regarding the choice of a particular route was not straightforward. In fact, the choice as to which pathway to investigate first was made on the basis of a factor somewhat unrelated to the above discussion. More explicitly, at the outset of our work, we were not able to propose a suitable synthetic pathway which would, with a reasonable degree of certainty, result in an efficient, *stereoselective* preparation of *cis*-1-bromo-1-methyl-2-(2-methyl-1-propenyl)cyclopropane (**9**). This substance would serve as the precursor of the cuprate reagent **10**, which was to be employed to convert the β-iodo enone **4** into the possible key intermediate **11**. On the other hand, based on literature precedent (*vide infra*), it appeared that a convenient, stereoselective synthesis of the substituted bromocyclopropane **16** would be relatively straightforward. Therefore, we chose to study initially the possibility of carrying out the total synthesis of (±)-β-himachalene (**2**) via the general route **4**---→**18**---→**12**---→(±)-**2**.

(b) *Synthesis of* trans-*1-bromo-1-methyl-2-(2-methyl-1-propenyl)cyclopropane (**16**) and its converison into the cuprate **17** (see Scheme 2)*

Conversion (2,2-dimethyl-1,3-propanediol, *p*-toluenesulfonic acid, dichloromethane, anhydrous magnesium sulfate) of acrolein into the corresponding acetal **24**, followed by reaction of the latter substance with bromoform − sodium hydroxide in the presence of a phase-transfer catalyst (12), gave the crystalline dibromocyclopropane derivative **25**. Although the yield of the transformation of **24** into **25** was quite low (27%), this inefficiency was not entirely unexpected. It is well established (13) that in their reaction with alkenes dihalocarbenes behave as electrophilic reagents and, therefore, addition of these species to "electron rich" carbon−carbon double bonds is significantly faster than the corresponding process involving "electron poor" alkenes. Clearly, compound **24** belongs to the latter category and the sluggish nature of the addition of dibromocarbene to this material was shown by the observation

Can. J. Chem. Downloaded from www.nrcresearchpress.com by 210.87.254.105 on 09/06/12
For personal use only.

TABLE 1. The ^{1}H nmr signals of the cyclopropyl protons of compounds **25**, **26**, and **27**

Compound	H_a	H_b	H_c
25	δ 2.01; overlapped d of d of d; $J_{a,b}$ = 11 Hz, $J_{a,c} = J_{a,d}$ = 6 Hz	δ 1.84; d of d; $J_{a,b}$ = 11 Hz, $J_{b,c}$ = 6 Hz	δ 1.61; overlapped d of d; $J_{a,c} = J_{b,c}$ = 6 Hz
26	δ 1.7–2.0; m obscured by singlet due to cyclopropyl methyl group	δ 1.36; d of d; $J_{a,b}$ = 10 Hz, $J_{b,c}$ = 6.5 Hz	δ 0.92; overlapped d of d; $J_{a,c} = J_{b,c}$ = 6.5 Hz
27	The three protons appeared as a multiplet between δ 1.04–1.18.		

that starting material remained even after a reaction time of 20 h. Furthermore, the fact that analysis of the crude product by gas–liquid chromatography (glc) showed the presence of a number of components indicated that alternative processes (e.g. insertion reactions (14)) were competing with the desired addition reaction. Fortunately, however, it was found that the required dibromocyclopropane **25** could be crystallized directly from a pentane solution of the crude reaction product, Therefore, since the acetal **24** was readily available, appreciable quantities of compound **25** could be obtained quite easily.

When a cold (−95°C) solution of compound **25** in 5:1 tetrahydrofuran–hexamethylphosphoramide containing 2 equivalents of methyl iodide was treated (dropwise) with 1 equivalent of *n*-butyllithium (hexane solution) and the resultant mixture was warmed to room temperature (15), a mixture of the diastereomeric methylated derivatives **26** and **27** was obtained in excellent yield. The relative amounts of the two products varied slightly with the scale of the reaction. For example, when the transformation was carried out on a small scale (~1 mmol), the two products were obtained in a ratio of about 93:7, respectively, while a reaction involving 25 mmol of the dibromocylopropane **25** produced the two methylated substances in a somewhat lower ratio (~87:13). However, separation of the two epimers could be achieved readily by subjection of the mixture to column chromatography on silica gel and, thus, the two crystalline products **26** and **27** were obtained in yields of 74 and 11%, respectively.

Although, on the basis of analogy (15), the major product of the methylation reaction was expected to have the newly introduced methyl group *cis* to the acetal function (compound **26**), it is pertinent to mention that this expectation was fully corroborated by a comparison of the proton nuclear magnetic resonance (^{1}H nmr) spectrum of the starting material **25** with those of the two products **26** and **27**. The data related to the ^{1}H nmr resonance of the three cyclopropyl protons (H_a, H_b, H_c) of each of the compounds **25**, **26**, and **27** is summarized in Table 1. In the spectrum of **25**, these signals are well separated and, therefore, are readily assigned.[4] Not unexpectedly, the resonances due to H_a, H_b, and H_c of the major methylation product **26** are all found upfield as compared to the corresponding signals of **25**. However, the upfield shift (0.69 ppm) of one of the protons (H_c) is significantly larger than those of the other protons (H_a, 0.16 ppm; H_b, 0.48 ppm). On the other hand, in going from the starting material **25** to the minor methylated product **27**, two of the cyclopropyl protons (H_a, H_b) experience upfield shifts (~0.9 and 0.75 ppm, respectively) significantly greater than that of the third proton (H_c, ~0.5 ppm). On the basis of these data, it seems very reasonable to conclude that the major product (see **26**) has the newly introduced methyl group *cis* to one cyclopropyl proton (H_c), while in the minor product (see **27**) the methyl group is *cis* to two protons (H_a, H_b).

Initially, hydrolysis of the acetal function of compound **26** proved to be frustratingly problematic. For example, when this substance was treated with 1 *N* hydrochloric acid in methanol (room temperature) or with hot glacial acetic acid, only starting material was recovered. On the other hand, although the acetal appeared to be hydrolyzed partially by subjection of **26** to trifluoroacetic acid or titanium tetrachloride in wet dichloromethane, these reactions were not reproducible and gave poor yields of the desired product. Therefore, it was gratifying to find (eventually) that the conversion of **26** into the aldehyde **28** could be accomplished reproducibly and efficiently (72% yield) by treatment of the former material with 88% formic acid at room temperature (18). Since the aldehyde **28** is not a very stable compound, it was characterized as the corresponding 2,4-dinitrophenylhydrazone derivative and was used directly for the next step of the synthetic sequence.

When the aldehyde **28** was allowed to react with isopropylidenetriphenylphosphorane in tetrahydrofuran at room temperature, the desired *trans*-1-bromo-1-methyl-2-(2-methyl-1-propenyl)cyclopropane (**16**) was produced in 70% yield. Treatment of compound **16** with 2 equivalents of *tert*-butyllithium in cold (−78°C) ether–tetrahydrofuran (1:1), followed by addition of solid phenylthiocopper (19, 20) and warming of the resultant mixture to −20°C, furnished a reddish-brown solution of the required cuprate reagent **17**. The latter species was employed in the next phase of the projected synthesis.

(c) *Synthesis of* trans-*3-[1-methyl-2-(2-methyl-1-propenyl)-cyclopropyl]-2-cyclohexen-1-one (18) and its conversion into (±)-β-himachalene (2) (see Scheme 3)*

When 3-iodo-2-cyclohexen-1-one (**4**) (21) was allowed to react with 1.5 equivalents of the cuprate reagent **17** in tetrahydrofuran–ether (−78°C → room temperature), the substituted cyclohexenone **18** was produced in nearly quantitative yield. When a solution of this material in xylene was heated (reflux) for 3 h, rearrangement occurred smoothly and a single product was obtained in quantitative yield. The infrared (ir)

[4]It is well known (16) that coupling constants associated with *cis* vicinal protons on cyclopropane systems are normally significantly larger than those related to corresponding *trans* protons. Thus, in the case of compound **25**, $J_{a,b}$ = 11 Hz, while $J_{a,c}$ = 6 Hz. Another feature of the ^{1}H nmr spectrum of **25** which deserves mention is the interesting pattern associated with the methylene protons of the 1,3-dioxane ring. The two axial protons (see **25***a*, R = 2,2-dibromocyclopropyl) produced a pair of doublets (δ 3.41, 3.47, J = 10 Hz in each case), while the equatorial protons gave rise to a pair of doublet of doublets (δ 3.63, 3.70, J = 10 and ~2 Hz in each case). This spectral pattern, which is not uncommon for 2-substituted 5,5-dimethyl-1,3-dioxanes, has been discussed in more detail previously (17).

Can. J. Chem. Downloaded from www.nrcresearchpress.com by 210.87.254.105 on 09/06/12
For personal use only.

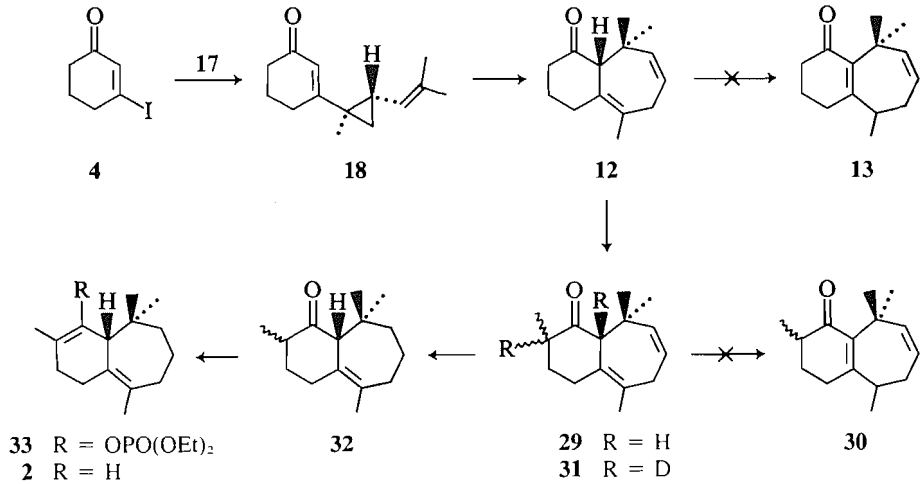

SCHEME 3

spectrum of the product exhibited a strong carbonyl absorption at 1700 cm^{-1}, while the ^1H nmr spectrum showed, along with other appropriate resonances, 3-proton singlets at δ 1.02, 1.08, and 1.80. Therefore, it was possible to draw the gratifying conclusion that the thermolysis product possessed structure **12** and, thus, both of our main misgivings with respect to the possibility of using compound **18** as a key intermediate in the projected synthesis of (±)-β-himachalene proved to be unfounded in fact.[5] Firstly, intermediate **18** underwent thermal bond reorganization exclusively in the desired Cope rearrangement sense, with no competition from the alternatively possible mode of rearrangement involving a [1,5]-sigmatropic hydrogen migration. Secondly, under the conditions of the thermolysis, the β,γ-unsaturated ketone function of the product **12** did not rearrange to the α,β-unsaturated ketone **13**.

With respect to the first point mentioned above, it is interesting to compare the thermal behaviour of compound **18** with that of 2-methyl-3-(1-methyl-2-vinylcyclopropyl)-2-cyclopenten-1-one (**20**) (10, 11). More explicitly, why does substrate **18** undergo exclusively a Cope rearrangement to furnish the bicyclic dienone **12**, while, under similar conditions, bond reorganization of compound **20** proceeds nearly entirely via a [1,5]-sigmatropic hydrogen shift pathway to afford the trienone **21**? Scheme 4 outlines the various reactions which could be involved in the thermolyses of **18** and **20**. If one assumes that the Cope rearrangement of substrate **20** would proceed by way of the corresponding *cis* isomer **22** (11),[6] and if one recalls that the latter substance undergoes Cope rearrangement very readily at relatively low temperatures (10, 11), then it is clear that the rate-determining step of the overall conversion of **20** into **23** would be the transformation (presumably by way of the diradical intermediate **A**) of **20** into **22**. Furthermore, a comparison of the transition states (see **B** and **E**) involved in the Cope rearrangement of the *cis*-divinylcyclopropanes **22** and **11**, respectively, reveals that these two states should be of very similar stability. Thus, the combined destabilizing energy associated with the steric repulsions labelled *a* and *b* in **B** should be equal (or nearly equal) to that related to the corresponding interactions in **E**, and the destabilizing energy connected with the interaction *c* (present in **E**, but absent in **B**) would be expected to be quite small.[7] Therefore, the rate-determining step of the overall conversion of **18** into **12** should also involve thermal isomerization of the *trans* isomer **18** into the *cis* isomer **11**, presumably via the diradical intermediate **D**.

The [1,5]-sigmatropic hydrogen migration associated with the thermolysis of compound **20** should, presumably, proceed by way of a transition state which can be represented by **C** (23). Since rearrangement of **20** furnishes nearly exclusively the trienone **21** (10, 11), it is clear that the hydrogen migration pathway (**20** → **C** → **21**) is energetically favored over the alternative route (**20** → **A** → **22**). Why, then, is the opposite true for substrate **18**? Based on the brief discussion given above, it is possible to propose two factors which could well contribute to the difference between the thermal behaviour of compounds **18** and **20**. Firstly, due to the presence of the two methyl groups on the 2-methyl-1-propenyl group of **18**, it seems reasonable to postulate that the diradical **D** would be more stable than the corresponding species **A**. Therefore, if this relative order of stability is reflected in the transition states giving rise to **D** and **A**, one would expect that the process **18** → **D** would be energetically favored over the conversion of **20** into **A**. Secondly, it is pertinent to compare the two transition states involved in the [1,5]-sigmatropic hydrogen migration reactions. While the transition state **C** lying between **20** and **21** has no serious steric interactions, the corresponding species **F** involved in the transformation of **18** and **19** suffers from a notable interaction between one of the vinyl methyl groups and one of the cyclopropyl protons (see *d* in **F**). Energetically speaking, these two effects are additive and it is therefore possible to rationalize, at least qualitatively, why thermolysis of **18** proceeds via the Cope rearrangement pathway.

Treatment of the ketone **12** with lithium diisopropylamide, followed by alkylation of the resultant enolate anion with methyl iodide, furnished, in 90% yield, the methylated derivative **29** (Scheme 3). The ir and ^1H nmr spectra of **29** showed unambiguously that the tetrasubstituted double bond had remained exocyclic to the six-membered ring. Indeed, experi-

[5]It is delightful to discover that, on occasion, one observes exceptions even to "Murphy's Law".

[6]For a brief discusison regarding the possible mechanism of the Cope rearrangement of *trans*-divinylcyclopropanes, see ref. 5 and citations therein.

[7]For a discussion concerning the approximate destabilizing energy values associated with steric interactions in the transition states of Cope rearrangement of *cis*-divinylcyclopropanes, see ref. 22. See also ref. 5.

Can. J. Chem. Downloaded from www.nrcresearchpress.com by 210.87.254.105 on 09/06/12
For personal use only.

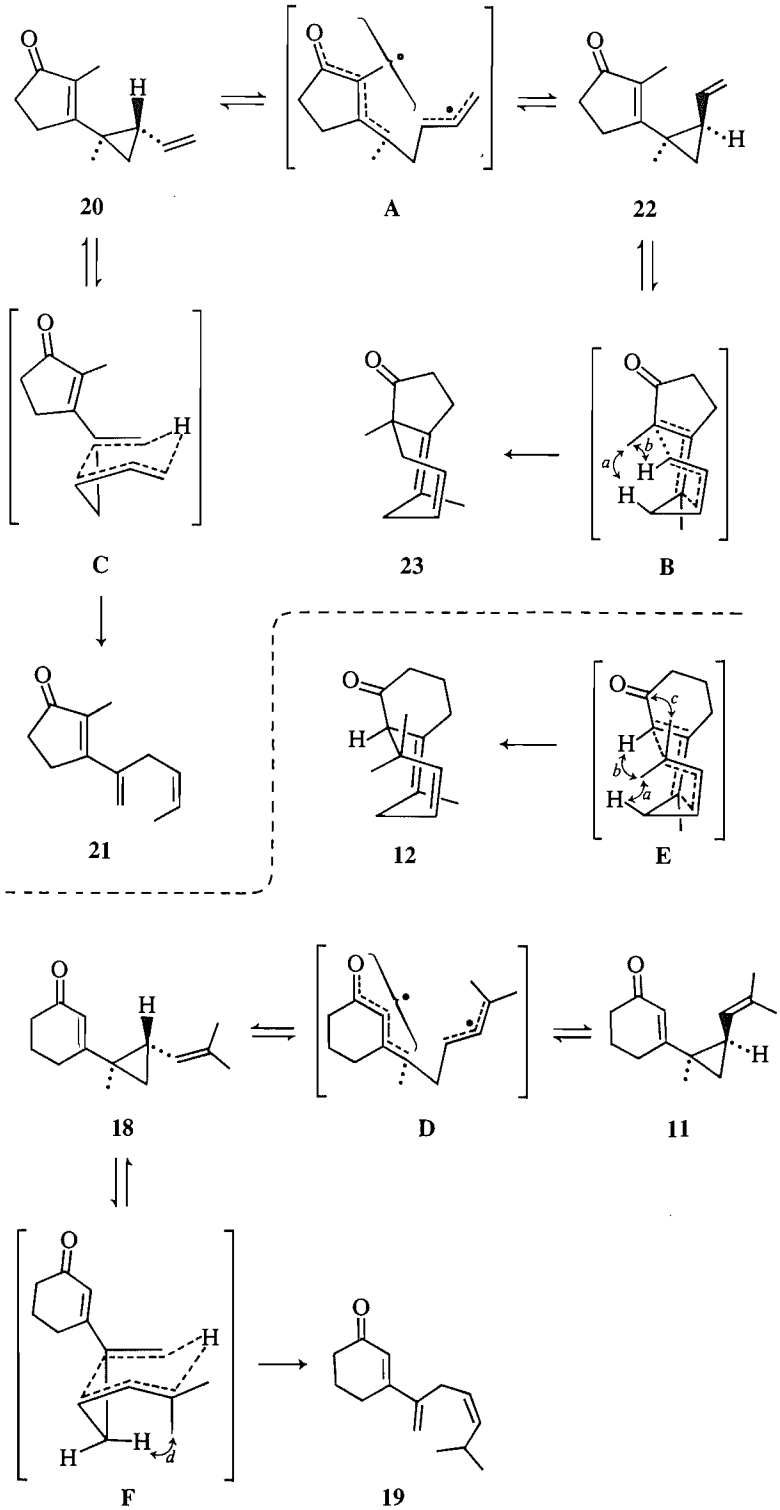

SCHEME 4

ments designed to deliberately effect iosmerization of compounds **12** and **29** into **13** and **30**, respectively, failed. Thus, both **12** and **29** were recovered essentially unchanged when solutions of these materials in methanol containing sodium methoxide were warmed for several hours. Furthermore, treatment of compound **29** with sodium methoxide in refluxing methanol-d_1 (30 h) provided, as the sole product, the dideuterio derivative **31**. The ^{1}H nmr spectrum of compound **31** showed that the broad singlet at δ 3.84 due to the bridgehead proton in **29** had disappeared, that the 3-proton doublet (δ 1.06) due to the secondary methyl group in **29** had collapsed to a singlet, and that the signal due to the vinyl methyl group (δ 1.78) had remained unchanged. It is not clear what factors underlie the fact that the β,γ-unsaturated ketones **12** and **29** are significantly more stable than their α,β-unsaturated counterparts **13** and **30**, respectively. However, an examination of molecular models suggests that in what appear to be the most stable conformations of **13** and **30** (secondary methyl group adjacent to the

Can. J. Chem. Downloaded from www.nrcresearchpress.com by 210.87.254.105 on 09/06/12
For personal use only.

Can. J. Chem. Downloaded from www.nrcresearchpress.com by 210.87.254.105 on 09/06/12
For personal use only.

carbonyl in a pseudoequatorial orientation), there exists a significant steric repulsion between one of the geminal methyl groups and the carbonyl oxygen atom. On the other hand, in the (apparently) most stable conformations of **12** and **29**, the oxygen atom is staggered between the two geminal methyl groups. In any case, the fact that compounds **12** and **29** showed no inclination to undergo isomerization was synthetically very satisfying and, presumably, made our synthetic work considerably less troublesome. In fact, the remainder of the synthetic sequence proceeded in a straightforward manner.

Hydrogenation of the dienone **29** in the presence of tris-(triphenylphosphine)chlororhodium gave, in 95% yield, the bicyclic enone **32**. Treatment of the latter substance with lithium diisopropylamide and trapping of the resultant enolate anion with diethyl bromophosphate (24)[8] afforded, in good yield, the enol phosphate **33**. Reduction of this material with lithium in ethylamine–tetrahydrofuran containing *tert*-butyl alcohol (25) furnished (±)-β-himachalene (**2**) in 38% yield.[9] The spectral and chromatographic properties of (±)-**2** were identical with those of authentic samples of the natural product.[10]

Experimental[11]

*Preparation of 5,5-dimethyl-2-vinyl-1,3-dioxane (**24**)*

To a solution of 2,2-dimethyl-1,3-propanediol (104 g, 1.0 mol) and *p*-toluenesulfonic acid (0.2 g) in 500 mL of dry dichloromethane was added successively acrolein (56 g, 1.0 mol) and anhydrous magnesium sulfate (~10 g). After the resulting mixture had been stirred at room temperature for 5 h, it was filtered through a short column of basic alumina (activity I, 100 g). The column was washed with additional dry dichloromethane (100 mL), and the solvent was removed carefully (rotary evaporator) from the combined eluate. Bulb-to-bulb distillation (air-bath 28°C/0.1 Torr, receiving bulb cooled to −78°C) of the remaining yellow liquid gave 114 g (80%) of the acetal **24** as a colorless liquid; tlc analysis: one spot; glc analysis: >99% one peak; ir(film): 2975, 2860, 1100 cm^{-1}; ^1H nmr δ: 0.74, 1.22 (s, s, 3H each), 3.52, 3.68 (d, d, 2H each, J = 11 Hz in each case), 4.86 (d, 1H, J = 5 Hz), 5.33 (broad d, 1H, J = 10 Hz), 5.48 (broad d, 1H, J = 17 Hz), 5.95 (d of d of d, 1H, J = 17, 10, 5 Hz). *Exact Mass* calcd. for $C_8H_{14}O_2$: 142.0994; found: 142.0994.

*Preparation of the dibromocyclopropane **25***

To a rapidly stirred mixture of 5,5-dimethyl-2-vinyl-1,3-dioxane (**24**) (4.26 g, 30 mmol), bromoform (15.2 g, 60 mmol), benzyltriethylammonium chloride (0.15 g), and ethanol (0.25 mL) was added dropwise 25 mL of 50% aqueous sodium hydroxide, and stirring was continued for 20 h. The resultant dark, tarry mixture was diluted with cold water (250 mL) and extracted thoroughly with pentane. The combined extract was washed with water until the aqueous phase remained neutral, and then was dried over anhydrous magnesium sulfate. Removal of the solvent and excess bromoform gave a dark brown oil. This material was taken up in pentane and the resultant solution was passed through a short column of neutral alumina (activity I). The column was washed with pentane. Removal of the solvent from the combined eluate gave a yellow oil which was subjected to crystallization from pentane at −15°C. Recrystallization from pentane provided 2.5 g (27%) of the dibromocyclopropane **25** as colorless crystals, mp 75–77°C; ir ($CHCl_3$): 2975, 2870, 1100 cm^{-1}; ^1H nmr (270 MHz) δ: 0.73, 1.23 (s, s, 3H each), 1.61 (overlapped d of d, 1H, J = 6, 6 Hz), 1.84 (d of d, 1H, J = 11, 6 Hz), 2.01 (overlapped d of d of d, 1H, J = 11, 6, 6 Hz), 3.41, 3.47 (d, d, 1H each, J = 10 Hz in each case), 3.63, 3.70 (d of d, d of d, 1H each, J = 10, ~2 Hz in each case), 4.20 (d, 1H, J = 6 Hz). *Anal.* calcd. for $C_9H_{14}Br_2O_2$: C 34.42, H 4.50; found: C 34.63, H 4.70.

*Preparation of the methylated monobromocyclopropanes **26** and **27***

To a cold (−95°C) stirred solution of the dibromocyclopropane **25** (8.00 g, 25.5 mmol) in a mixture of dry THF (125 mL), dry hexamethylphosphoramide (25 mL), and methyl iodide (7.2 g, 51 mmol), under an atmosphere of nitrogen, was added, dropwise, a solution of *n*-butyllithium (30.6 mmol) in hexane. The pale yellow solution was allowed to warm slowly to room temperature, at which time most of the volatile material was removed under reduced pressure. The remaining oil was poured into brine and the resultant mixture was extracted thoroughly with pentane. The combined extract was washed with brine and dried over anhydrous magnesium sulfate. Removal of the solvent gave 7.1 g of a pale yellow oil which, on the basis of analysis by glc, consisted mainly of two components in a ratio of approximately 87:13. This material was subjected to column chromatography on silica gel. The column was eluted with 1:10 ether – petroleum ether. Distillation (air-bath temperature 63°C/0.1 Torr) of the major product, which was eluted from the column first, provided 4.90 g (74%) of the monobromocyclopropane **26**. Crystallization of a small amount of this material from pentane gave colorless crystals, mp 24.5–26°C; ir(film): 2975, 2870, 1100, 1020, 785 cm^{-1}; ^1H nmr (270 MHz) δ: 0.72, 1.21, 1.84 (s, s, s, 3H each), 0.92 (overlapped d of d, 1H, J = 6.5, 6.5 Hz), 1.36 (d of d, 1H, J = 10, 6.5 Hz), 1.7–2.0 (m, 1H), 3.42 (d, 2H, J = 11 Hz), 3.65, 3.68 (overlapped d of d, overlapped d of d, 1H each, J = 11, ~2 Hz in each case), 4.25 (d, 1H, J = 6.5 Hz). *Anal.* calcd. for $C_{10}H_{17}BrO_2$: C 48.21, H 6.88; found: C 48.38, H 6.86.

Recrystallization of the minor product from pentane gave 0.72 g (11%) of the monobromocyclopropane **27** as colorless crystals, mp 52–53°C; ir ($CHCl_3$): 2970, 2865, 1470, 1170, 1095 cm^{-1}; ^1H nmr (270 MHz) δ: 0.74, 1.24, 1.78 (s, s, s, 3H each), 1.04–1.18 (m, 3H), 3.49, 3.53, (d, d, 1H each, J = 11 Hz in each case), 3.68, 3.72 (overlapped d of d, overlapped d of d, 1H each, J = 11 Hz, ~2 Hz in each case), 4.29 (d, 1H, J = 6.5 Hz). *Anal.* calcd. for $C_{10}H_{17}BrO_2$: C 48.21, H 6.88; found: C 48.16, H 7.00.

*Preparation of the cyclopropanecarboxaldehyde **28***

To 100 mL of degassed 88% formic acid was added 10.8 g (43 mmol) of the acetal **26**. After the mixture had been stirred under an atmosphere of nitrogen for 1.5 h at room temperature, it was poured into ice and the resulting mixture was extracted thoroughly with pentane. The combined extract was washed with saturated aqueous sodium bicarbonate until neutral and dried over anhydrous magnesium sulfate. Careful removal of the solvent, followed by distillation (air-bath temperature ~25–30°C/0.1 Torr, receiving bulb cooled with liquid nitrogen) of the remaining pale yellow oil, gave 5.05 g (72%) of the aldehyde **28** as a colorless, volatile liquid. This material, which showed one peak by glc analysis and exhibited ir(film): 2875, 2780, 1710 cm^{-1}, was used directly for the next step of the reaction sequence.

The 2,4-dinitrophenylhydrazone derivative of the aldehyde **28** was recrystallized from ethanol–water, mp 160–161.5°C (dec.); ^1H nmr δ: 1.40 (overlapped d of d, 1H, J = 6.5, 6.5 Hz), 1.76 (d of d, 1H, J = 10, 6.5 Hz), 1.88 (s, 3H), 2.50 (overlapped d of d of d, 1H, J = 10, 6.5, 6.5 Hz), 7.38 (d, 1H, J = 6.5 Hz), 7.93 (d, 1H, J = 10 Hz), 8.34 (d of d, 1H, J = 10, 3 Hz), 9.12 (d, 1H, J = 3 Hz), 9.34 (broad s, 1H). *Anal.* calcd. for $C_{11}H_{11}BrN_4O_4$: C 38.50, H 3.23, N 16.33; found: C 38.58, H 3.11; N, 16.25.

[8]Use of the less reactive although more normally employed diethyl chlorophosphate failed to produce any of the desired enol phosphate **33**.

[9]Examination (glc) of the crude reduction product indicated that it consisted very largely of (±)-β-himachalene. The low yield of isolated material, obtained by purification of the crude product by preparative tlc, was probably a function of the volatility of the racemic natural product.

[10]We are very grateful to Drs. V. Lukes (Czechoslovakia) and T. Norin (Sweden) for generous samples of (+)-β-himachalene.

[11]For general information, see the preceding, accompanying paper (5).

Can. J. Chem. Downloaded from www.nrcresearchpress.com by 210.87.254.105 on 09/06/12
For personal use only.

Preparation of the alkene ***16***

To a cold (−78°C) stirred suspension of isopropyltriphenylphosphonium iodide (6.2 g, 14.4 mmol) in dry THF (50 mL), under an atmosphere of nitrogen, was added dropwise a solution of methyllithium (14.4 mmol) in ether. The mixture was warmed to room temperature and stirred until a clear, dark red solution of the phosphorane was obtained. After the solution had been recooled to −78°C, a solution of the aldehyde **28** (2.0 g, 12.3 mmol) in 5 mL of dry THF was added. The reaction mixture was warmed slowly to room temperature, was allowed to stir for 2 h, was diluted with pentane (50 mL), and then was filtered through a short column of silica gel. The column was eluted with further volumes of pentane. Careful removal of the solvent from the combined eluate, followed by distillation (air-bath temperature ~40−50°C/0.1 Torr, receiving bulb cooled with a Dry Ice − acetone bath) of the residual material, gave 1.6 g (70%) of the alkene **16** as a colorless, volatile oil; ir(film): 3010, 2960, 1440, 1385, 1150 cm^{-1}; ^1H nmr δ: 0.64 (overlapped d of d, 1H, J = 6.5, 6.5 Hz), 1.46 (d of d, 1H, J = 10, 6.5 Hz), 1.70 (s, 3H), 1.72, 1.78 (broad singlets, 3H each), 2.12 (m, 1H), 4.76 (d of septuplets, 1H, J = 7.5, 1.5 Hz). *Exact Mass* calcd. for $C_8H_{13}{}^{81}Br$: 190.0181 found: 190.0157.

Preparation of the enone ***18***

To a cold (−78°C) stirred solution of the bromocyclopropane **16** (1.03 g, 5.4 mmol) in 50 mL of dry THF−ether (1:1), under an atmosphere of nitrogen, was added dropwise a solution of *tert*-butyllithium (10.8 mmol) in pentane. After the pale yellow solution had been stirred at −78°C for 30 min, phenylthiocopper (0.93 g, 5.4 mmol) was added from a bent tube attached to the reaction flask. When the resulting suspension was warmed to −20°C and stirred at this temperature for 30 min, a dark reddish-brown solution of the cuprate reagent **17** was formed. The solution was recooled to −78°C, and then a solution of 3-iodo-2-cyclohexen-1-one (**4**) (0.80 g, 3.6 mmol) in 5 mL of dry THF was added. The reaction mixture was stirred at −78°C for 10 min, at −20°C for 15 min, and then at room temperature for 2 h. Methanol (2 mL) and ether (50 mL) were added, and the resulting orange-yellow suspension was filtered through a short column of Florisil. The column was eluted with ether. Removal of the solvents from the combined eluate, followed by distillation (air-bath temperature 110−125°C/0.3 Torr) of the residual material gave 0.73 g (99%) of the enone **18** as a pale yellow oil; ir(film): 1660, 1600 cm^{-1}; ^1H nmr (270 MHz) δ: 0.64 (overlapped d of d, 1H, J = 5, 5 Hz), 1.18 (s, 3H), 1.36 (d of d, 1H, J = 10, 5 Hz), 1.6−1.8 (m, 1H), 1.68, 1.74 (broad singlets, 3H each), 1.96 (m, 2H), 2.18 (m, 2H), 2.34 (t, 2H, J = 8 Hz), 4.92 (broad d, 1H, J = 10 Hz), 5.92 (s, 1H). *Anal.* calcd. for $C_{14}H_{20}O$: C 82.30, H 9.87; found: C 82.06, H 9.90.

Preparation of the bicyclic dienone ***12***

A solution of the enone **18** (274 mg, 1.34 mmol) in 30 mL of dry, degassed xylene was refluxed under an atmosphere of nitrogen for 3 h. After the solution had been cooled to room temperature, the solvent was removed under reduced pressure. Analysis of the remaining pale yellow oil (275 mg) by tlc and glc indicated that this material was >99% pure and, consequently, it was used directly for the next step. Distillation (air-bath temperature 87−100°C/0.1 Torr) of a small amount of the oil provided an analytically pure sample of the bicyclic dienone **12**; ir(film): 1700 cm^{-1}; ^1H nmr δ: 1.02, 1.08, 1.80 (s, s, broad s, 3H each), 1.90−2.54 (diffuse m, 6H), 2.74 (m, 1H), 3.28 (broad d, 1H, J = 18 Hz), 3.74 (broad s, 1H), 5.14 (d of d, 1H, J = 12, 3 Hz), 5.50 (d of d of d, 1H, J = 12, 8, 3 Hz). *Anal.* calcd. for $C_{14}H_{20}O$: C 82.30, H 9.87; found: C 82.06, H 9.90.

Preparation of the bicyclic dienone ***29***

To a cold (−78°C), stirred solution of lithium diisopropylamide (1.76 mmol) in 20 mL of dry THF under an atmosphere of argon was added a solution of the dienone **12** (276 mg, 1.35 mmol) in 5 mL of dry THF. After the solution had been stirred at −78°C for 30 min and at 0°C for 30 min, dry hexamethylphosphoramide (2.7 mmol) was added. The resulting orange solution was recooled to −78°C, methyl iodide (5.4 mmol) was added, and stirring was continued at −78°C for 30 min and then at room temperature for 30 min. The reaction mixture was diluted with brine and extracted thoroughly with petroleum ether. The combined organic extract was washed with brine and dried over anhydrous magnesium sulfate. Removal of the solvent, followed by distillation (air-bath temperature 100−108°C/0.1 Torr) of the residual liquid gave 265 mg (90%) of the bicyclic dienone **29** as a pale yellow oil. Analysis of this material by glc − mass spectrometry indicated that it consisted of a mixture of two diastereomeric ketones, in a ratio of approximately 92:8; ir(film): 1700 cm^{-1}; ^1H nmr δ: 0.96, 1.09, 1.78 (s, s, broad s, 3H each), 1.06 (d, 3H, J = 6 Hz), 1.90−2.64 (diffuse m, 5H), 2.7−3.0 (m, 1H), 3.1−3.5 (m, 1H), 3.84 (broad s, 1H), 5.14 (d of d, 1H, J = 12, 3 Hz), 5.48 (d of d of d, 1H, J = 12, 8, 3 Hz). *Anal.* calcd. for $C_{15}H_{22}O$: C 82.52, H 10.16; found: C 82.17, H 10.20.

Treatment of the bicyclic dienone ***29*** *with NaOMe−DOMe*

To a solution of the bicyclic dienone **29** (12 mg, 92:8 mixture of diastereomers) in 2 mL of methanol-d_1 was added a small amount of dry sodium methoxide and the resulting mixture was refluxed under an atmosphere of nitrogen for 30 h. The reaction mixture was cooled to room temperature, diluted with D_2O, and then was extracted thoroughly with petroleum ether. The combined extract was washed with brine and dried over anhydrous magnesium sulfate. Removal of the solvent, followed by distillation (air-bath temperature 100−110°C/0.1 Torr) of the residual material gave 8 mg of a colorless oil. Analysis of this oil by glc and by glc − mass spectrometry showed that it consisted of a mixture of two components (ratio approximately 80:20), each exhibiting a molecular ion of m/e 220. The glc retention times of the major and minor isomers corresponded to those of the major and minor components in the starting material **29**. The ir spectrum of the distilled material exhibited a strong absorption at 1700 cm^{-1}. The ^1H nmr spectrum showed that the signal (broad singlet at δ 3.84) due to the bridgehead proton in **29** had disappeared, that the 3-proton doublet (δ 1.06) had collapsed to a singlet, and that the signal (broad singlet at δ 1.78) due to the vinyl methyl group had remained unchanged. On the basis of these data, the product could be identified as the dideuterated ketone **31**.

Preparation of the bicyclic enone ***32***

To a solution of the bicyclic dienone **29** (170 mg, 0.78 mmol) in 30 mL of dry, degassed benzene was added 35 mg of tris(triphenylphosphine)chlororhodium and the resulting solution was stirred under an atmosphere of hydrogen for 22 h. The reaction mixture was diluted with petroleum ether and filtered through a short column of silica gel. The column was eluted with petroleum ether. Removal of the solvent from the combined eluate, followed by distillation (air-bath temperature 100−112°C/0.1 Torr) of the remaining brown liquid gave 163 mg (95%) of the bicyclic enone **32** as a colorless oil. Analysis of this material by glc − mass spectrometry indicated that it consisted of a mixture of two diastereomers in a ratio of about 85:15; ir(film): 1700 cm^{-1}; ^1H nmr δ: 0.86, 1.00, 1.74 (s, s, broad s, 3H each), 1.05 (d, 3H, J = 6 Hz), 1.4−1.6 (m, 4H), 1.84−2.90 (diffuse m, 7H), 3.42 (broad s, 1H). *Anal.* calcd. for $C_{15}H_{24}O$: C 81.76, H 10.98; found: C 81.67, H 11.00.

Preparation of the enol phosphate ***33***

To a cold (−78°C), stirred solution of lithium diisopropylamide (0.42 mmol) in 4 mL of dry THF under an atmosphere of nitrogen, was added dropwise a solution of the bicyclic enone **32** (61 mg, 0.28 mmol) in 2 mL of dry THF. After the solution had been stirred at −78°C for 30 min and at 0°C for 15 min, it was recooled to −78°C and dry tetramethylethylenediamine (1.5 mL) was added. Diethyl bromophosphate (200 mg, 0.56 mmol) was added dropwise, the reaction mixture was stirred at −78°C for 30 min and at room temperature for 1 h, and then was poured into brine. The resultant mixture was extracted thoroughly with ether. The combined extract was washed thrice with brine and dried over anhydrous magnesium sulfate. Removal of the solvent gave ~100 mg of a yellow oil. This crude material, the ir spectrum of which showed no carbonyl absorption,

was used directly for the next step of the synthetic sequence. However, subjection of a small amount of this material to preparative tlc, followed by distillation (air-bath temperature 155–165°C/0.1 Torr) of the oil thus obtained, provided an analytical sample of the enol phosphate **33**; ir(film): 1450, 1275, 1040, 975 cm^{-1}; ^1H nmr δ: 0.80, 1.06, 1.70, 1.78 (s, s, broad s, broad s, 3H each), 1.34 (d of t, 6H, J = 8, 2 Hz), 1.1–1.6 (diffuse m, 6H), 1.9–2.6 (m, 4H), 3.39 (broad s, 1H), 4.17 (overlapped d of q, 4H, J = 8, 8 Hz). *Anal.* calcd. for $C_{19}H_{33}O_4P$: C 64.02, H 9.33; found: C 64.27, H 9.39.

Preparation of (±)-β-himachalene (2)

To a cold (0°C), stirred solution of lithium metal (9 mg) in ethylamine (25 mL, freshly distilled from lithium metal) under an atmosphere of nitrogen was added, dropwise, a solution of the enol phosphate **33** (46 mg, 0.13 mmol) and dry *tert*-butyl alcohol (38.5 mg, 0.52 mmol) in 2 mL of dry THF. The reaction mixture was stirred at 0°C for 20 min and then was quenched cautiously with water. The resulting mixture was extracted thoroughly with petroleum ether. The combined extract was washed with brine and dried over anhydrous magnesium sulfate. Removal of the solvent gave 18 mg of a pale yellow oil which was subjected to purification by preparative tlc. Distillation (air-bath temperature 70–80°C/0.1 Torr) of the material thus obtained gave 10 mg (38%) of (±)-β-himachalene (**2**) as a colorless oil which was spectrally (ir, ^1H nmr) and chromatographically (tlc, glc) identical with authentic samples of natural β-himachalene kindly supplied by Drs. V. Lukes (Czechoslovakia) and T. Norin (Sweden); ir(film): 2950, 1450, 1380, 1360 cm^{-1}; ^1H nmr δ: 0.74, 0.98 (s, s, 3H each), 1.2–2.7 (diffuse m, 10H), 1.74 (broad s, 6H), 2.90 (broad s, 1H), 5.45 (m, 1H).

Acknowledgements

Financial support for this work from the Natural Sciences and Engineering Research Council of Canada (N.S.E.R.C.C.) and an N.S.E.R.C.C. postgraduate scholarship (to E.H.R.) are gratefully acknowledged.

1. G. S. Krishna Rao, S. Dev, and P. C. Guha. J. Indian Chem. Soc. **29**, 721 (1952).
2. T. C. Joseph and S. Dev. Tetrahedron Lett. 216 (1961); Tetrahedron, **24**, 3809 (1968).
3. J. B. Bredenberg and H. Erdtman. Acta Chem. Scand. **15**, 685 (1961).
4. T. C. Joseph and S. Dev. Tetrahedron, **24**, 3841 (1968).
5. E. Piers, H. E. Morton, I. Nagakura, and R. W. Thies. Can. J. Chem. **61**, 1226 (1983).
6. E. Piers and E. H. Ruediger. J. Chem. Soc. Chem. Commun. 166 (1979).
7. B. D. Challand, G. Kornis, G. L. Lange, and P. de Mayo. Chem. Commun. 704 (1967); B. D. Challand, H. Hikino, G. Kornis, G. Lange, and P. de Mayo. J. Org. Chem. **34**, 794 (1969).
8. E. Wenkert and K. Naemura. Synth. Commun. **3**, 45 (1973).
9. H. J. Liu and E. N. C. Browne. Can. J. Chem. **59**, 601 (1981).
10. J. P. Marino and L. J. Browne. Tetrahedron Lett. 3245 (1976).
11. P. A. Wender, M. A. Eissenstat, and M. P. Filosa. J. Am. Chem. Soc. **101**, 2196 (1979).
12. M. Makosza and M. Fedorynski. Synth. Commun. **3**, 305 (1973).
13. W. Kirmse. Carbene chemistry. 2nd ed. Academic Press, New York, NY. 1971.
14. K. Steinbeck. Tetrahedron Lett. 1103 (1978).
15. K. Kitatani, T. Hiyama, and H. Nozaki. J. Am. Chem. Soc. **97**, 949 (1975); Bull. Chem. Soc. Jpn. **50**, 3288 (1977).
16. D. H. Williams and I. Fleming. Spectroscopic methods in organic chemistry. 2nd ed. McGraw–Hill Book Co. (U.K.) Ltd., London, 1973. pp. 107–108.
17. E. Piers and T. W. Hall. Can. J. Chem. **23**, 2613 (1980).
18. A. Gorgues. Bull. Soc. Chim. Fr. 529 (1974); D. R. Morton and R. A. Morge. J. Org. Chem. **43**, 2093 (1978).
19. G. H. Posner, C. E. Whitten, and J. J. Sterling. J. Am. Chem. Soc. **95**, 7788 (1973).
20. G. H. Posner, D. J. Brunelle, and L. Sinoway. Synthesis, 662 (1974).
21. E. Piers, J. R. Grierson, C. K. Lau, and I. Nagakura. Can. J. Chem. **60**, 210 (1982).
22. M. P. Schneider and A. Rau. J. Am. Chem. Soc. **101**, 4426 (1979).
23. C.W. Spangler. Chem. Rev. **76**, 187 (1976).
24. A. Gorecka, M. Leplawy, J. Zabrocki, and A. Zwierzak. Synthesis, 474 (1978).
25. R. E. Ireland and G. Pfister. Tetrahedron Lett. 2145 (1969).

Can. J. Chem. Downloaded from www.nrcresearchpress.com by 210.87.254.105 on 09/06/12
For personal use only.

Synthesis and vibrational spectra of 1:1 stoichiometric complexes of nitronium and nitrosonium tetrafluoroborate with 18-crown-6

RODRIGUE SAVOIE,[1] MARIE PIGEON-GOSSELIN, ANDRÉ RODRIGUE, AND ROBERT CHÊNEVERT[1]

Département de chimie et Centre de recherche sur les atomes et les molécules, Université Laval, Québec (Qué.), Canada G1K 7P4

Received June 25, 1982

RODRIGUE SAVOIE, MARIE PIGEON-GOSSELIN, ANDRÉ RODRIGUE, and ROBERT CHÊNEVERT. Can. J. Chem. **61**, 1248 (1983).

The macrocyclic ether 18-crown-6 can form 1:1 stoichiometric complexes with $NOBF_4$ and NO_2BF_4. These complexes, which are soluble in organic media, have been isolated and studied by infrared and Raman spectroscopy. The spectra suggest that the conformation of the ether in these complexes is essentially that of the highly regular crown of D_{3d} symmetry, the NO^+ and NO_2^+ ions being stuck into the ether cavity.

RODRIGUE SAVOIE, MARIE PIGEON-GOSSELIN, ANDRÉ RODRIGUE et ROBERT CHÊNEVERT. Can. J. Chem. **61**, 1248 (1983).

L'éther macrocyclique "18-crown-6" peut former des complexes de stoéchiométrie 1:1 avec les tétrafluoroborates de nitronium et de nitrosonium. Ces complexes, qui sont solubles en milieu organique, ont été isolés et étudiés par spectroscopie infrarouge et Raman. Les données spectrales indiquent que la conformation de l'éther dans ces complexes est essentiellement celle très régulière de symétrie D_{3d}, les ions NO^+ et NO_2^+ étant localisés dans la cavité centrale de l'éther.

Introduction

Macrocyclic polyether molecules are characterized by an internal cavity lined with electronegative oxygen atoms. The accumulation of partial negative charges around this cavity explains the remarkable complexing ability of these molecules, particularly towards positive ions. Neutral polar guest compounds are also complexed, especially those which can form hydrogen bonds with the oxygen atoms of the ether (see, for example, refs. 1–3). When both conditions are simultaneously met, e.g. with cations which can form H-bonds with the ether, particularly stable complexes are obtained. We have recently reported on the synthesis and vibrational spectra of such a complex, $H_3O^+BF_4^- \cdot 18C6$[2] (4), whose crystal structure is now being examined by X-ray crystallography.[3]

In an attempt to solubilize nitronium tetrafluoroborate (NO_2BF_4) and the corresponding nitrosonium salt ($NOBF_4$), which are useful organic reagents but noteworthily insoluble in most organic solvents, we found that this could easily be achieved by complexation with 18C6, although the reactivity of the cations was then strongly modified. The complexes formed between 18C6 and the tetrafluoroborates were isolated, and we present here the results of various measurements aimed at specifying their structure.

Experimental

All of the solvents used in the preparation of the complexes were thoroughly dried, as both the starting tetrafluoroborates and the resulting complexes are highly hygroscopic and readily hydrolyzed. The $NOBF_4 \cdot 18C6$ and $NO_2BF_4 \cdot 18C6$ complexes were prepared by mixing equimolar amounts of the tetrafluoroborate salt and the ether in $CHCl_3$ or CH_2Cl_2, and shaking the resulting mixture until complete dissolution of the salt (~10 min). The synthesis was also carried out with an excess of the salt, the extra material being filtered off after the complexation was complete. The complexes were then crystallized from the chloroform solution by adding a small amount of diethyl ether. Both complexes can be hydrolyzed to the corresponding hydronium complex, $H_3O^+BF_4^- \cdot 18C6$ (4), with a >95% yield. The hydrolysis takes place readily in acetonitrile, upon addition of a small amount of water. The solvent is then evaporated under reduced pressure and the residual hydronium complex is recuperated by filtration after being washed with diethyl ether.

Characteristics of the complexes

$NOBF_4 \cdot 18C6$: slightly yellow solid (mp 113–113.5°C); yield: 93%; ^1H nmr, δ: 3.67 ppm; ^{13}C nmr: 70.327 ppm (compared to 70.755 for the free ether in $CDCl_3$). *Anal.* calcd.: C 37.81%, H 6.35%, N 3.67%; found: C 38.4%, H 6.2%, N 3.5%.

$NO_2BF_4 \cdot 18C6$: colorless solid (mp 95°C); yield 81%; ^1H nmr, δ: 3.67 ppm; ^{13}C nmr: 70.463 ppm. *Anal.* calcd.: C 36.29%, H 6.08%, N 3.52%; found: C 37.5–40.3%, H 5.9–6.6%, N 2.8–3.6%.

The elementary analysis for the nitronium complex is not very satisfactory, as large variations were obtained, even from samples from the same batch (the values given above are extremes). This reflects the instability of the complex, particularly towards moisture. Although the analysis suggests an incomplete complexation between NO_2BF_4 and 18C6, the Raman spectrum of the solid complex, which is discussed below, gives no evidence for the presence of uncomplexed 18C6, whose spectrum is very characteristic (4).

For the infrared, hexachlorobutadiene, Fluorolube, and Nujol mulls contained between Irtran-4 (ZnSe) and AgCl windows were used. The spectra were recorded on a Beckman Model IR 4250 spectrophotometer, at a slit width of 2 cm^{-1}. For the Raman measurements, the samples were contained in sealed glass capillaries. These were mounted on a motor shaft and rotated at high speed when placed in the laser beam, to prevent sample decomposition. The solids and the nitronium complex in solution in chloroform were studied at ~200 mW laser power. In the case of the nitrosonium complex solution, however, the laser power had to be kept down to ~20 mW at the sample. The slit width then had to be fixed at 5 cm^{-1} in order to get a reasonably intense spectrum, whereas the solution of the nitronium complex could be studied at 3 cm^{-1} and the solids at 1 cm^{-1} slit widths. The spectra were recorded on a microcomputer-controlled Spex Model 1400 spectrometer (5), using the 514.5 nm exciting line from a Spectra Physics Model 165 argon ion laser. Data points were gathered by steps of 1 cm^{-1}, at 1 second intervals.

The ^1H nmr spectra were taken on a Bruker HX-90 (90 MHz) with TMS as an internal standard and, for ^{13}C, on a Bruker WP-80 spectrometer working at 20 MHz.

Results and discussion

The infrared spectra of the $NOBF_4 \cdot 18C6$ and $NO_2BF_4 \cdot 18C6$ complexes are reproduced in Fig. 1, and the corresponding Raman spectra of these solids and their solutions in chloroform are compared with those of the free tetrafluoroborate salts in Figs. 2 and 3 respectively.

Among the characteristic vibrations of the tetrahedral BF_4^-

[1]Author to whom correspondence should be addressed.

[2]18C6 will be used as an abbreviation of 18-crown-6 throughout the text.

[3]F. Brisse. Personal communication.

Can. J. Chem. Downloaded from www.nrcresearchpress.com by 210.87.254.6 on 09/06/12
For personal use only.

Can. J. Chem. Downloaded from www.nrcresearchpress.com by 210.87.254.6 on 09/06/12
For personal use only.

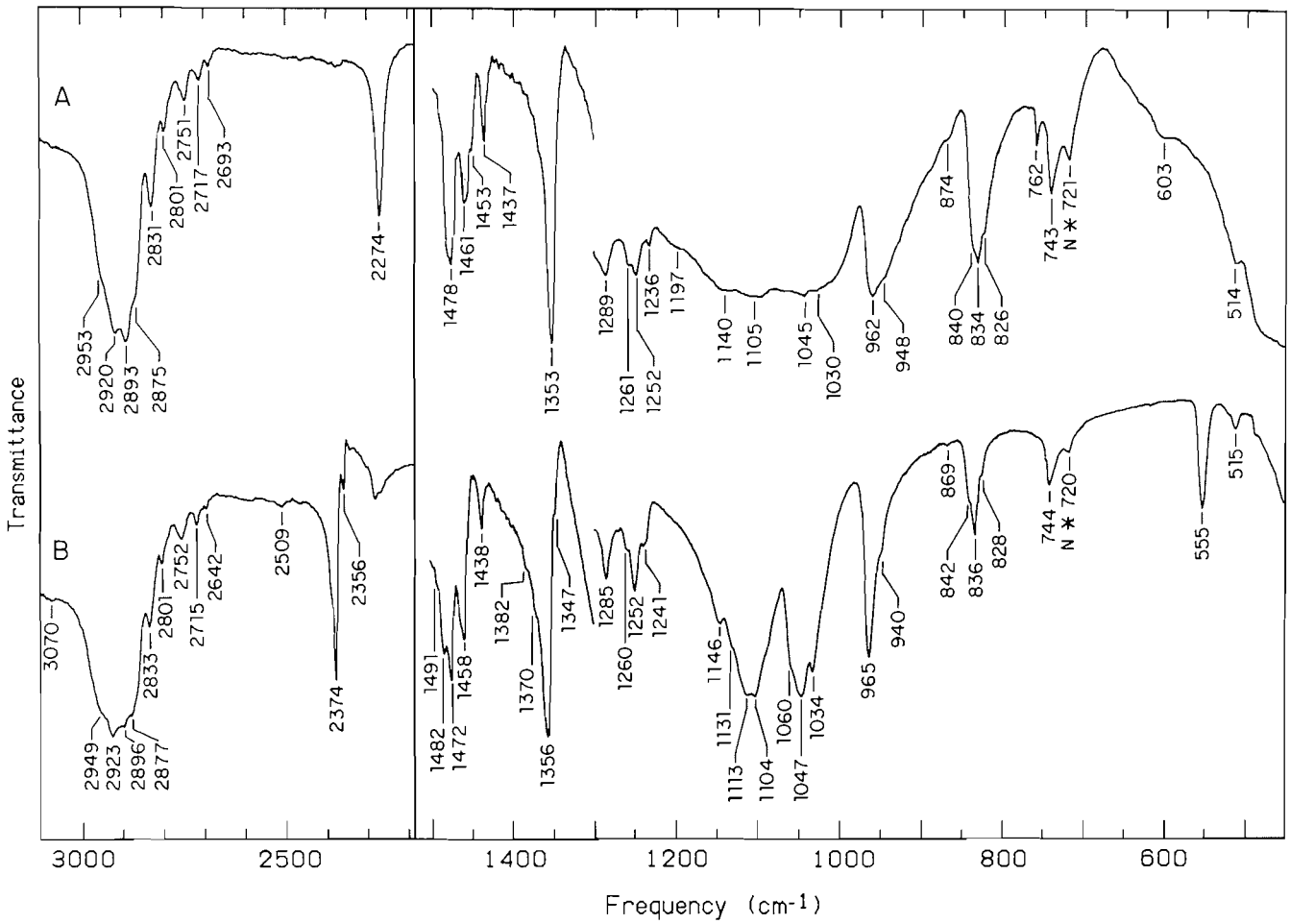

FIG. 1. Infrared spectra of hexachlorobutadiene (1300−3100 cm^{-1}) and Nujol (500−1300 cm^{-1}) mulls of the (A) $NOBF_4 \cdot 18C6$ and (B) $NO_2BF_4 \cdot 18C6$ complexes at room temperature.

ion (6−8), the totally symmetric stretching mode ν_1 gives a very sharp and strong line in the Raman spectra. From 771 and 778 cm^{-1} in the spectra of $NOBF_4$ and NO_2BF_4, respectively, this vibration is shifted to 764 cm^{-1} in the 18C6 complexes, both in $CHCl_3$ solution and in the crystalline state. The activity of this normally infrared-inactive vibration in the ir spectrum of the $NOBF_4 \cdot 18C6$ complex, where a weak band is definitely present at 762 cm^{-1} (Fig. 1A), points to some departure from tetrahedral symmetry of this ion in the nitrosonium complex. The same effect is not detected in the nitronium complex, suggesting a higher symmetry of the BF_4^- ion in the latter. It should be noted that the ν_1 band of BF_4^- is also present in the ir spectra of both free $NOBF_4$ and NO_2BF_4 (9). The decrease in the infrared intensity of this band upon complexation indicates a higher symmetry of these ions in the complexes. This is also suggested in $NOBF_4$ from the fact that the ν_4 band is split at 526/533 cm^{-1} in the salt, but not in the complex (521 cm^{-1}). The nearby band at 549 cm^{-1} in the spectrum of the complex, as well as the 368 cm^{-1} peak which is very close to the ν_2 band at 357 cm^{-1}, are most likely attributable to ether vibrations as they are also present in the spectrum of the $KBr \cdot 18C6$ complex (10).

Very little information can be obtained from the very strong infrared band near 1050 cm^{-1}, due to the asymmetric stretch (ν_3) of the BF_4^- ion. As in other tetrafluoroborate salts (6−8), this band is broadened by Fermi resonance with $2\nu_4$ and by reflection, a phenomenon often associated with transitions characterized by large $\partial\mu/\partial Q$ values. In the Raman spectrum, the corresponding band is also very broad, although extremely weak.

The stretching vibration of the NO^+ ion usually occurs in the 2300−2350 cm^{-1} frequency range, e.g. 2340 cm^{-1} in $NOBF_4$ (9), 2326 cm^{-1} in $NOAuF_6$ (11), and 2298 cm^{-1} in sulfuric acid solutions (12). The very large frequency shift, from 2342 to 2274 cm^{-1}, occurring upon complexation of $NOBF_4$ with 18C6 suggests a weakening of the N—O^+ bond in this process. This could result from a partial transfer of electronic charge from the lone pairs on the oxygen atoms of the crown ether into the vacant π^* antibonding orbitals of the nitrosonium ion. Note that if a complete transfer of the equivalent of one electron were to occur, then the N—O stretching frequency would drop to ~1875 cm^{-1}, which is the value for a neutral NO molecule isolated in an argon matrix (13).

Although the exact location of the NO^+ ion in the $NOBF_4 \cdot 18C6$ complex cannot be determined with certainty from the present results, it appears likely that it penetrates the ring of the macrocyclic ether. The cylindrical diameter of the NO^+ ion should be very similar to that of the diazonium group —N≡N^+ (~2.4 Å), and the latter has been shown by X-ray diffraction to project into the hole of the 21-crown-7 ether, the corresponding complex with 18C6 being less stable but presumably of a similar nature (14).

The N—O^+ stretching band in the Raman spectrum of the $NOBF_4 \cdot 18C6$ complex in solution in $CHCl_3$ (Fig. 2A) is rela-

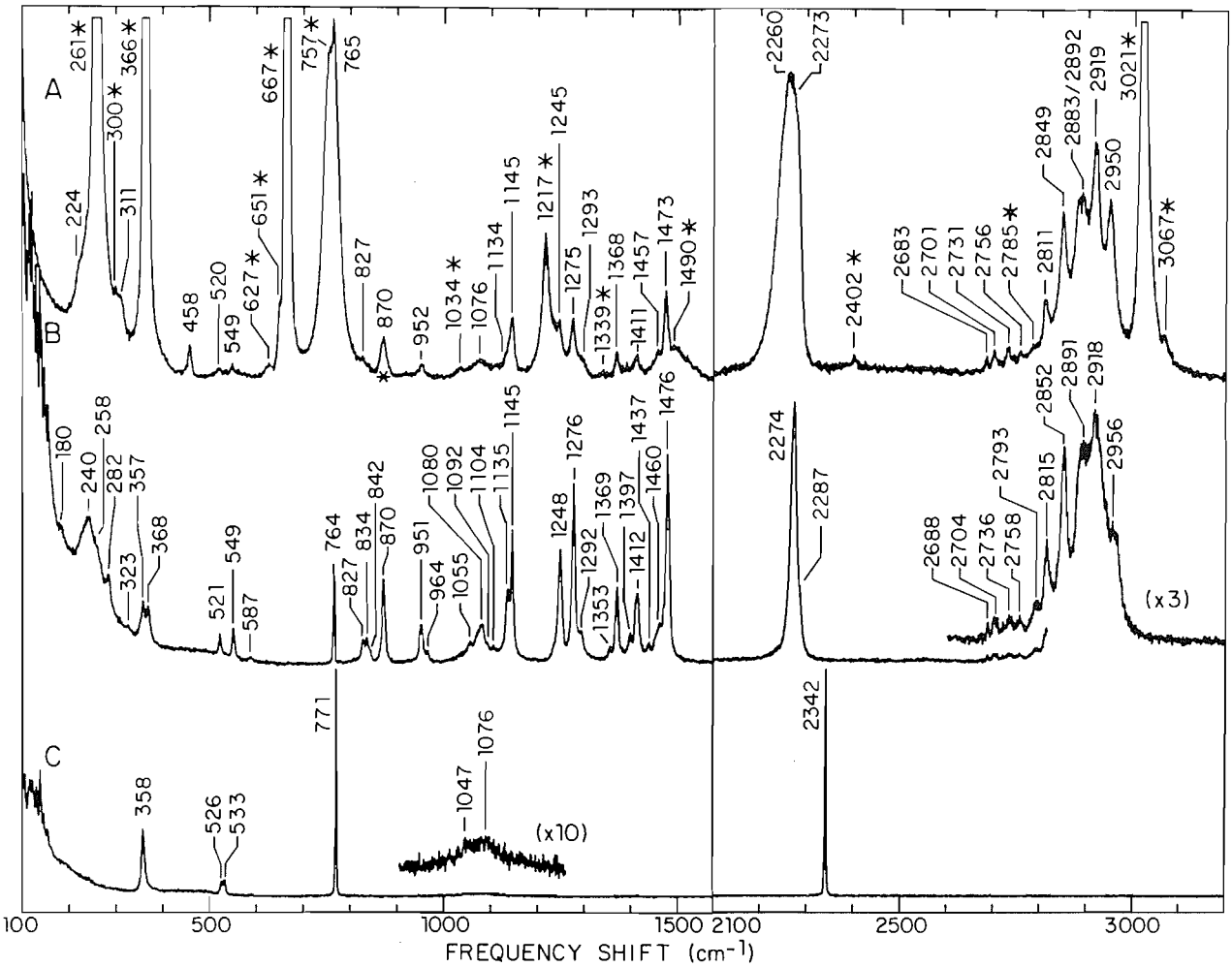

FIG. 2. Raman spectra of the $NOBF_4 \cdot 18C6$ complex (A) in solution in chloroform (solvent peaks indicated by *) and (B) in the crystalline state. The spectrum of the free $NOBF_4$ salt is shown in (C).

tively broad and appears to contain two distinct peaks separated by 15 cm^{-1}. This possibly indicates the presence in the solution of two types of complexed species. If indeed the rod-like NO^+ cation is stuck into the ether cavity, like the axle in a wheel, then it seems logical to assume that the accompanying BF_4^- counterion can be located on either side of the $NO^+ \cdot 18C6$ moiety, thus giving two different types of ion pairs: $NO^+BF_4^-$ and $ON^+BF_4^-$. In the solid complex, although the NO stretching Raman band is sharper than in the solution, it is still considerably broader than in the $NOBF_4$ salt. The main peak at 2274 cm^{-1}, with an associated low-frequency shoulder at ~2269 cm^{-1} in the spectrum at room temperature, is transformed into a well resolved doublet at 2270/2274 cm^{-1} at liquid nitrogen temperature (spectrum not shown). This splitting probably arises from intermolecular vibrational coupling, although some two-dimensional orientational disorder of the NO^+ ions, similar to that found in solid neutral NO, could be present in the solid and possibly explain the broad shoulder at ~2287 cm^{-1} on the high-frequency side of the main peak. It is noteworthy that the ν_1 vibration of the BF_4^- ion is also split, at 767/769 cm^{-1}, in the Raman spectrum at liquid nitrogen temperature. Such a fine splitting associated with very narrow vibrational components is best explained by a factor group effect, which would indicate that the primitive cell of the crystal contains at least two $NOBF_4 \cdot 18C6$ formula units.

The vibrational frequencies of the linear and centrosymmetric NO_2^+ ion are well known from its infrared and Raman spectra (9, 15–17). In the $NO_2BF_4 \cdot 18C6$ complex, the totally symmetric stretch gives a sharp Raman peak at 1397 cm^{-1}, slightly shifted from its 1407 cm^{-1} value in the free salt, whereas the corresponding asymmetric mode and the bending vibration occur at 2374 and 555 cm^{-1}, respectively, in the infrared spectrum. The mutual exclusion rule for the infrared and Raman activity of the vibrations of this ion in the complex appears to hold, which suggests that it is essentially of $D_{\infty h}$ symmetry in solid $NO_2BF_4 \cdot 18C6$. As in the case of the nitrosonium compound, it is likely that the nitronium ion is stuck into the ether cavity in the complex. Such a structure has been proposed for CdX_2 and HgX_2 adducts of 18C6 (18).

Both the infrared and Raman spectra of the crown ether in the nitronium and nitrosonium complexes are very similar to those of other complexes, such as with KSCN, RbSCN, and CsSCN (10) in which the ether has the highly symmetrical D_{3d} symmetry (19). This is also the case with the KBr complex, whose infrared (10, 20, 21) and Raman (10) spectra have been extensively studied, and with the nitromethane · 18C6 complex whose single crystal spectrum has been reported (22).

Except for the characteristic bands of the cation, the Raman spectrum of $NO_2BF_4 \cdot 18C6$ is practically identical to those of the alkaline thiocyanates (10). In the spectrum of the corre-

Can. J. Chem. Downloaded from www.nrcresearchpress.com by 210.87.254.6 on 09/06/12
For personal use only.

Can. J. Chem. Downloaded from www.nrcresearchpress.com by 210.87.254.6 on 09/06/12
For personal use only.

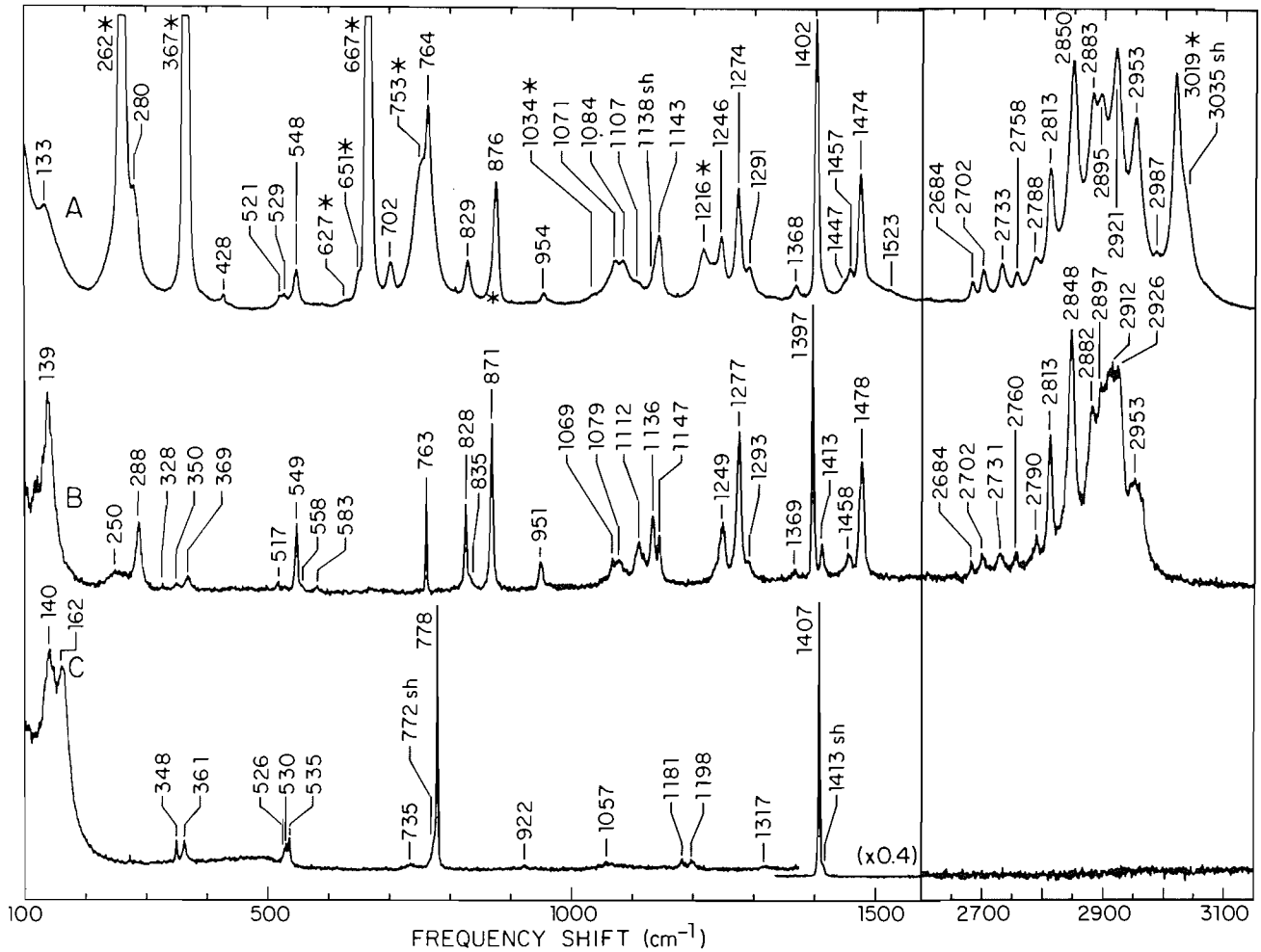

FIG. 3. Raman spectra of the $NO_2BF_4 \cdot 18C6$ complex (A) in solution in chloroform (solvent peaks indicated by *) and (B) in the crystalline state. The spectrum of the free NO_2BF_4 salt is shown in (C).

sponding nitrosonium complex, some weak extra features are present, for example at 964 cm^{-1} and in the 835 cm^{-1} region. The infrared spectra of both complexes also show weak bands, such as those at 1482 and 826 cm^{-1}, which do not appear to be present in the spectra of the KBr and alkaline thiocyanate complexes (10, 20, 21). (A stronger peak at 743 cm^{-1} in the spectra of both complexes is left unexplained as it does not belong to any of the known vibrations of the species present in these compounds.) These observations suggest that the shape of the 18C6 ether in the complexes described here is essentially that of a regular crown of symmetry D_{3d}, although some distortion is probably present, especially in the nitrosonium complex. The similarity between the Raman spectra of the solid complexes and those of the corresponding solutions also indicates that the 18C6·salt complex unit is retained upon dissolution, with little change in its basic structure.

The complexation of $NOBF_4$ and NO_2BF_4 by 18C6 strongly modifies their reactivity. For example, when the $NOBF_4 \cdot 18C6$ complex is allowed to react with benzamide in ice-cold acetonitrile, an homogeneous solution is obtained, from which no nitrogen evolution takes place and all of the starting materials can be recuperated, indicating that no reaction has occurred. This contrasts with the reaction in the absence of the crown ether: heterogeneous conditions then prevail, and the amide is transformed into the corresponding acid with a >90% yield, a behaviour consistent with the very low solubility of free $NOBF_4$ and the oxidizing nature of this salt under mild conditions (23). Similarly, free NO_2BF_4 (4 equivalents) reacts with toluene (1 equivalent) in dichloromethane, at −60°C under heterogeneous conditions, to yield 85% of a mixture of *o*- and p-nitrotoluene through a Friedel–Crafts type of reaction (24). However, when the reaction is repeated in the presence of 18C6 at a molar concentration equal to that of the salt, the nitration is completely suppressed in the resulting homogeneous solution. The reaction does, however, take place with good yield at room temperature or above, showing that the process is not completely hindered, although considerably slowed down.

Acknowledgements

Financial support of this work by the Natural Sciences and Engineering Research Council of Canada and by the Ministère de l'éducation du Québec is gratefully acknowledged.

1. J. S. BRADSHAW, S. L. BAXTER, J. D. LAMB, R. M. IZATT, and J. J. CHRISTENSEN. J. Am. Chem. Soc. **103**, 1821 (1981).
2. P. GROTH. Acta Chem. Scand. Ser. A, **36**, 109 (1982).
3. G. R. NEWKOME, H. C. R. TAYLOR, F. R. FRONCZEK, T. J. DELORD, D. K. KOHLI, and F. VÖGTLE. J. Am. Chem. Soc. **103**, 7376 (1981).
4. R. CHÊNEVERT, A. RODRIGUE, M. PIGEON-GOSSELIN, and R. SAVOIE. Can. J. Chem. **60**, 853 (1982).
5. R. SAVOIE, B. BOULÉ, G. GENEST, and M. PÉZOLET. Can. J. Spectrosc. **24**, 112 (1979).

6. J. B. BATES and A. S. QUIST. Spectrochim. Acta, Part A, **31**, 1317 (1975).
7. A. S. QUIST, J. B. BATES, and G. E. BOYD. J. Chem. Phys. **54**, 4896 (1971).
8. J. B. BATES. J. Chem. Phys. **55**, 489 (1971).
9. J. C. EVANS, H. W. RINN. S. J. KUHN, and G. A. OLAH. Inorg. Chem. **3**, 857 (1964).
10. M. FOUASSIER and J.-C. LASSEGUES. J. Chim. Phys. **75**, 865 (1978).
11. J. E. GRIFFITHS and W. A. SUNDER. Spectrochim. Acta, Part A, **35**, 1329 (1979).
12. D. J. MILLEN. J. Chem. Soc. 2606 (1950).
13. W. G. FATELEY, H. A. BENT, and B. CRAWFORD, JR. J. Chem. Phys. **31**, 204 (1959).
14. P. GROTH. Acta Chem. Scand. Ser. A, **35**, 541 (1981).
15. T. CHAUSSE, J.-L. PASCAL, A. POTIER, and J. POTIER. Nouv. J. Chim. **5**, 261 (1981).
16. D. COOK. *In* Friedel–Crafts and related reactions. Vol. I. *Edited by* G. A. Olah. Interscience. 1963. p. 769.
17. D. COOK, S. J. KUHN, and G. A. OLAH. J. Chem. Phys. **33**, 1669 (1960).
18. G. WULFSBERG and A. WEISS. J. Chem. Soc. Dalton Trans. 1640 (1977).
19. J. D. DUNITZ, M. DOBLER, P. SEILER, and R. P. PHIZACKERLEY. Acta Crystallogr. Sect. B, **30**, 2733 (1974).
20. J. DALE and P. O. KRISTIANSEN. Acta Chem. Scand. **26**, 1471 (1972).
21. R. M. COSTES, G. FOLCHER, P. PLURIEN, and P. RIGNY. Inorg. Nucl. Chem. Lett. **12**, 13 (1976).
22. R. D. MCLACHLAN. Spectrochim. Acta, Part A, **30**, 2153 (1974).
23. G. A. OLAH and J. A. OLAH. J. Org. Chem. **30**, 2386 (1965).
24. G. A. OLAH, S. J. KUHN, S. H. FLOOD, and J. C. EVANS. J. Am. Chem. Soc. **84**, 3687 (1962).

Can. J. Chem. Downloaded from www.nrcresearchpress.com by 210.87.254.6 on 09/06/12
For personal use only.

On the interpretation of vibrational relaxation times

HESHEL TEITELBAUM

Department of Chemistry, University of Ottawa, Ottawa, Ont., Canada K1N 9B4

Received April 27, 1982

H. TEITELBAUM. Can. J. Chem. **61**, 1253 (1983).

Rate laws for the evolution of vibrational energy level populations are derived when the Bethe–Teller law is obeyed. It is assumed that a Boltzmann distribution is maintained via rapid V–V processes. A variety of different rate laws result depending on the size and direction of the perturbation, the extent from equilibrium, and how classical the oscillator is at the initial and final conditions. An earlier analysis by Breshears is shown to be a special case. A prescription is given for procedures to compare relaxation times obtained from shock tube experiments and from laser-induced fluorescence experiments, when T–V energy transfer processes are rate-determining. Corrections for thermal effects are included. Shock tube, fluorescence, and chemical activation experiments are proposed which provide meaningful conditions for testing the Bethe–Teller law and for testing the existence of a Boltzmann distribution.

H. TEITELBAUM. Can. J. Chem. **61**, 1253 (1983).

On a déduit les lois de vitesse de l'évolution des populations du niveau d'énergie vibrationnel lorsque la loi de Bethe–Teller se vérifie. On pense que la distribution de Boltzmann est maintenue par l'intermédiaire d'un processus rapide du type V–V. Il en résulte diverses lois de vitesse suivant l'amplitude et le sens de la perturbation suivant la position par rapport à l'équilibre et suivant le comportement classique ou non de l'oscillateur dans les conditions initiales et finales. On montre qu'une analyse antérieure de Breshears n'est qu'un cas spécial. On décrit la façon de procéder pour comparer les temps de relaxation obtenus à partir d'expérience en tube blindé et à partir d'expériences de fluorescence induite au laser, lorsque les processus de transfert d'énergie du type T–V sont les étapes déterminantes. On y inclut les corrections pour tenir compte des effets thermiques. On propose des expériences d'activation chimique, de fluorescence en tube blindé qui fournissent des conditions propices pour vérifier la loi de Bethe–Teller et pour vérifier l'existence d'une distribution de Boltzmann.

[Traduit par le journal]

Introduction

In an earlier study Breshears showed that the nature and extent of the departure from equilibrium determines the relative relaxation rates of vibrational level populations (1). In particular, the fluorescent intensities from vibrational levels v decay with rate coefficients proportional to v, whereas all vibrational levels in shock wave experiments decay with the same rate coefficient. These results were shown to be natural consequences of the existence of a Boltzmann vibrational distribution and a corresponding temperature T_{vib} within a single mode of a harmonic oscillator. Although not clearly stated, they are also a consequence of the vibrational levels subsequently exchanging energy ϵ_{vib} with translational energy according to the Bethe–Teller law (2) where ϵ_T is the statistical-thermodynamic vibrational energy at the translational temperature T (which in principle also varies with time).

$$[1] \qquad \frac{d\epsilon_{vib}}{dt} = \frac{1}{\tau}(\epsilon_T - \epsilon_{vib})$$

The first condition is generally supposed to be fulfilled by rapid vibration–vibration (V–V) energy transfer processes for sufficiently non-diluted gases:

$$[2] \qquad A(v) + A(v') \rightleftarrows A(v-1) + A(v'+1)$$

However the rapidity is not guaranteed if the gas A is very dilute in say Ar. The second condition (eq. [1]) is theoretically sound for small perturbations (3), i.e. near equilibrium. It is also theoretically sound for a special relaxation mechanism (harmonic oscillators subject to single quantum translation-to-vibration (T–V) Landau–Teller type transitions) (2, 4, 5). Thus [1] is by no means generally true. Nevertheless its validity is assumed by those who plot log (fluorescence intensity) or log (dE/dt) vs. time and extract single relaxation times from the slopes of such plots. That this procedure appears to work for most cases has led to its acceptance. Yet [1] has really only been confirmed experimentally for a very limited range of conditions (6, 7) based on the quasi-exponential decay of vibrational energy. Thus it is clear that without a complete theoretical base [1] must be examined more carefully.

Breshears (1) analyzed the case $\theta = h\nu/k \gg T_{vib}$ and $\theta \gg T$, where ν is the fundamental frequency. We wish to continue the analysis for other cases which are extreme but which would provide more meaningful conditions under which the Bethe–Teller law should be tested. In so doing, definitive experiments will be proposed.

Breshears' study lays the foundation for making comparisons of vibrational relaxation times as obtained from laser-induced fluorescence and from shock wave studies. We extend the analysis to give prescriptions for adjusting one or the other result, including thermal effects which are generally ignored.

Relaxation model

The fractional vibrational level population n_v/n for quantum number v of a harmonic oscillator is given by the Boltzmann distribution if processes such as [2] are rapid:

$$[3] \qquad n_v/n = \exp(-v\theta/T_{vib}) - \exp[-(v+1)\theta/T_{vib}]$$

Can. J. Chem. Downloaded from www.nrcresearchpress.com by 210.87.254.42 on 09/06/12
For personal use only.

A similar expression exists at equilibrium when the translational temperature T replaces T_{vib}, and n_v^e/n represents the equilibrium fraction. As long as the translational temperature does not vary significantly, the quasi-first order rate coefficient $d \ln |n_v - n_v^e|/dt$ is (1):

$$[4] \quad \frac{d \ln |n_v - n_v^e|}{dt} = \frac{\theta}{T_{vib}^2} \frac{dT_{vib}}{dt} \times \frac{v - (v+1)\exp(-\theta/T_{vib})}{1 - \exp(-\theta/T_{vib}) - [1 - \exp(-\theta/T)]\left[\exp\left\{-v\theta\left(\frac{1}{T} - \frac{1}{T_{vib}}\right)\right\}\right]}$$

The second factor on the right hand side is denoted F, as in ref. 1. The first factor is determined by the rate law which is here assumed to be given by [1]. It was not evaluated in ref. 1. For a Boltzmann distribution of vibrational level populations of a pure gas of n harmonic oscillators at the equilibrium translational temperature T

$$[5] \quad \epsilon_T = nh\nu\,[\exp(\theta/T) - 1]^{-1}$$

Similarly

$$[6] \quad \epsilon_{vib} = nh\nu\,[\exp(\theta/T_{vib}) - 1]^{-1}$$

Substituting [5] and the derivative of ϵ_{vib} with respect to T_{vib} into [1], we obtain the rate law in terms of temperatures. τ is the vibrational energy relaxation time.

$$[7] \quad \frac{\theta}{T_{vib}^2} \frac{dT_{vib}}{dt} = \frac{1}{\tau}\left\{\exp\left[-\theta\left(\frac{1}{T} - \frac{1}{T_{vib}}\right)\right] - 1\right\} \times \left\{\frac{1 - \exp(-\theta/T_{vib})}{1 - \exp(-\theta/T)}\right\}$$

We now examine the behaviour of [4] for the special cases of shock tube experiments and fluorescence experiments. In the former $T \geq T_{vib}$, with T_{vib} varying from an initial value usually ~300 K to T; in the latter $T_{vib} \geq T$, with T_{vib} varying from an arbitrary initially high value to T. In both cases the perturbations are considered large, but shock wave experiments are usually but not always made near equilibrium, whereas fluorescence is almost always measured within the first 2 or 3 decay units i.e. $t/\tau \leqslant 3$. In both cases T varies with time according to whether vibrational energy is lost or gained. As will be seen the results depend on whether or not the molecule behaves as a classical oscillator ($\theta \ll T$) during relaxation.

Fluorescence

A. $\theta \gg T_{vib} \gg T$

$$[8] \quad \frac{\theta}{T_{vib}^2} \frac{dT_{vib}}{dt} \rightarrow -\frac{1}{\tau}$$

Furthermore $F \rightarrow v$ as shown in ref. 1, and all levels relax with rates proportional to v. If we assume a mechanism, the proportionality constant can be identified from [7]: $v = 1$ may relax by the T–V process

$$A(v = 1) + M \rightarrow A(v = 0) + M$$

with a rate constant k_{10}. Since the vibrational temperature is so high the population of $v = 0$ is much less than that at equilibrium, and the reverse process is not important. Thus $\tau = 1/k_{10}$, and

$$[9] \quad d \ln |n_v - n_v^e|/dt = -vk_{10}$$

The fluorescence intensity I_f is given by ref. 8:

$$I_f \propto \sum_{v=1} v n_v \propto \epsilon_{vib}$$

and relaxation times measured in this way are thus energy relaxation times. It is instructive to note that the solution to eq. [8] is

$$[10] \quad \frac{\theta}{T_{vib}} = \frac{\theta}{T_{vib}^0} + k_{10}t$$

Thus

$$\begin{aligned} I_f \propto \epsilon_{vib} &= nh\nu/[\exp(\theta/T_{vib}) - 1] \simeq nh\nu[\exp(-\theta/T_{vib})] \\ &= nh\nu[\exp(-\theta/T_{vib}^0)]\,[\exp(-k_{10}t)] \\ &= I_f^0 \exp(-k_{10}t) \end{aligned}$$

If the sample gas is optically thin to radiation from all levels then the effective rate constant is k_{10}. Breshears has dealt (1) with cases which are not optically thin for all v.

B. $T_{vib} \gg \theta \gg T$

The initial value of T_{vib} can be determined from

$$[11] \quad \epsilon_{vib}^0 = \frac{nh\nu}{\exp(\theta/T_{vib}^0 - 1)} \approx nkT_{vib}^0$$

Can. J. Chem. Downloaded from www.nrcresearchpress.com by 210.87.254.42 on 09/06/12
For personal use only.

It is quite clear that if all of the $v = 0$ population were laser-excited into $v = 1$, i.e. $\epsilon^0_{vib} \approx nh\nu$, then T^0_{vib} could only be as much as $\theta/\ln 2$. Thus $T_{vib} \gg \theta$ can usually be achieved realistically only as the result of a production from an exothermic chemical reaction. The population levels can be monitored by, e.g., infrared chemiluminescence. After sufficient time the situation degenerates to case *A*. Otherwise

$$\frac{\theta}{T_{vib}^2}\frac{dT_{vib}}{dt} \rightarrow -\frac{1}{\tau}\frac{\theta}{T_{vib}}$$

i.e.

[12] $$T_{vib} = T^0_{vib}\, e^{-t/\tau}$$

$T_{vib} \gg \theta$ prevails only for $t/\tau \ll \ln (T^0_{vib}/\theta)$

$$F \rightarrow \frac{-1}{\theta/T_{vib} - e^{-v\theta/T}}$$

There exists a characteristic temperature T_* which determines the sign of F, and hence the form of the relaxation rate law. T_* is given by

[13] $$T_* = \theta e^{v\theta/T} > \theta$$

For $T_{vib} \gg T_*$,

[14] $$F \rightarrow e^{v\theta/T}$$

For $T_{vib} \ll T_*$,

[15] $$F \rightarrow -T_{vib}/\theta$$

We note that a variation in T_{vib} represents a time history. If $T^0_{vib} \gg T_*$ then relaxation will proceed according to [14], but eventually ($t/\tau > \ln [T^0_{vib}/T_*]$) the relaxation will proceed according to [15]. Thus

(a) $T_{vib} \gg T_* \gg \theta \gg T$

$$d \ln |n_v - n^e_v|/dt \rightarrow -\frac{1}{\tau}\frac{\theta\, e^{v\theta/T}}{T_{vib}} = -\frac{1}{\tau}\frac{T_*}{T_{vib}}$$

Using expression [12] for the time-variation of T_{vib},

$$d \ln |n_v - n^e_v|/dt = -\frac{1}{\tau}\frac{T_*}{T^0_{vib}} e^{t/\tau}$$

which integrates to

[16] $$\ln\left\{\frac{n_v - n^e_v}{n^0_v - n^e_v}\right\} = -\frac{T_*}{T^0_{vib}} e^{t/\tau} = -\frac{T_*}{T_{vib}}$$

The relaxation amplitude is rather small, but the vibrational levels approach their equilibrium values with a stronger-than-exponential variation strongly dependent on v. If the gas sample is optically thin to radiation from all levels v, and if the chemiluminescence itself does not significantly affect the level populations, then $I_f \propto \epsilon_{vib}$. Note that $\theta \ll T_{vib}$ really means that the oscillator behaves classically during the relaxation of T_{vib} towards θ.
Therefore

$$I_f \propto kT_{vib}$$

or

[17] $$I_f = I^0_f\, e^{-t/\tau}$$

If in addition to $t/\tau \ll \ln (T^0_{vib}/T_*)$, we choose $t/\tau \ll 1 \ll \ln (T^0_{vib}/T_*)$, then [16] simplifies to

$$\ln\left\{\frac{n_v - n^e_v}{n^0_v - n^e_v}\right\} = -\frac{T_*}{T^0_{vib}} - \left(\frac{T_*}{T^0_{vib}}\right)\frac{t}{\tau}$$

and the vibrational levels relax with time constants $= \tau(T^0_{vib}/\theta)e^{-v\theta/T}$. This should serve as a good test of the Bethe–Teller law for strong departures from equilibrium. If we consider HF at $T = 300$ K, $\theta \simeq 5700$ K, $T_* = 10^{12}$ K; but for a molecule with reasonably small fundamental frequency such as the bending frequency of N_2O ($\bar{\nu}_2 = 589$ cm^{-1}), θ is reasonable. In this case $\theta = 848$ K, and $T_* = 14\,340$ K for $v = 1$ and 242 000 K for $v = 2$. Halogens are even more favourable.

(b) $T_* \gg T_{vib} \gg \theta \gg T$

T_{vib} eventually decreases below T_*, and even if the experimental conditions for case (*a*) are hard to attain (*b*) is feasible.

[18] $$F \rightarrow -\frac{T_{vib}}{\theta}$$

Can. J. Chem. Downloaded from www.nrcresearchpress.com by 210.87.254.42 on 09/06/12
For personal use only.

Can. J. Chem. Downloaded from www.nrcresearchpress.com by 210.87.254.42 on 09/06/12
For personal use only.

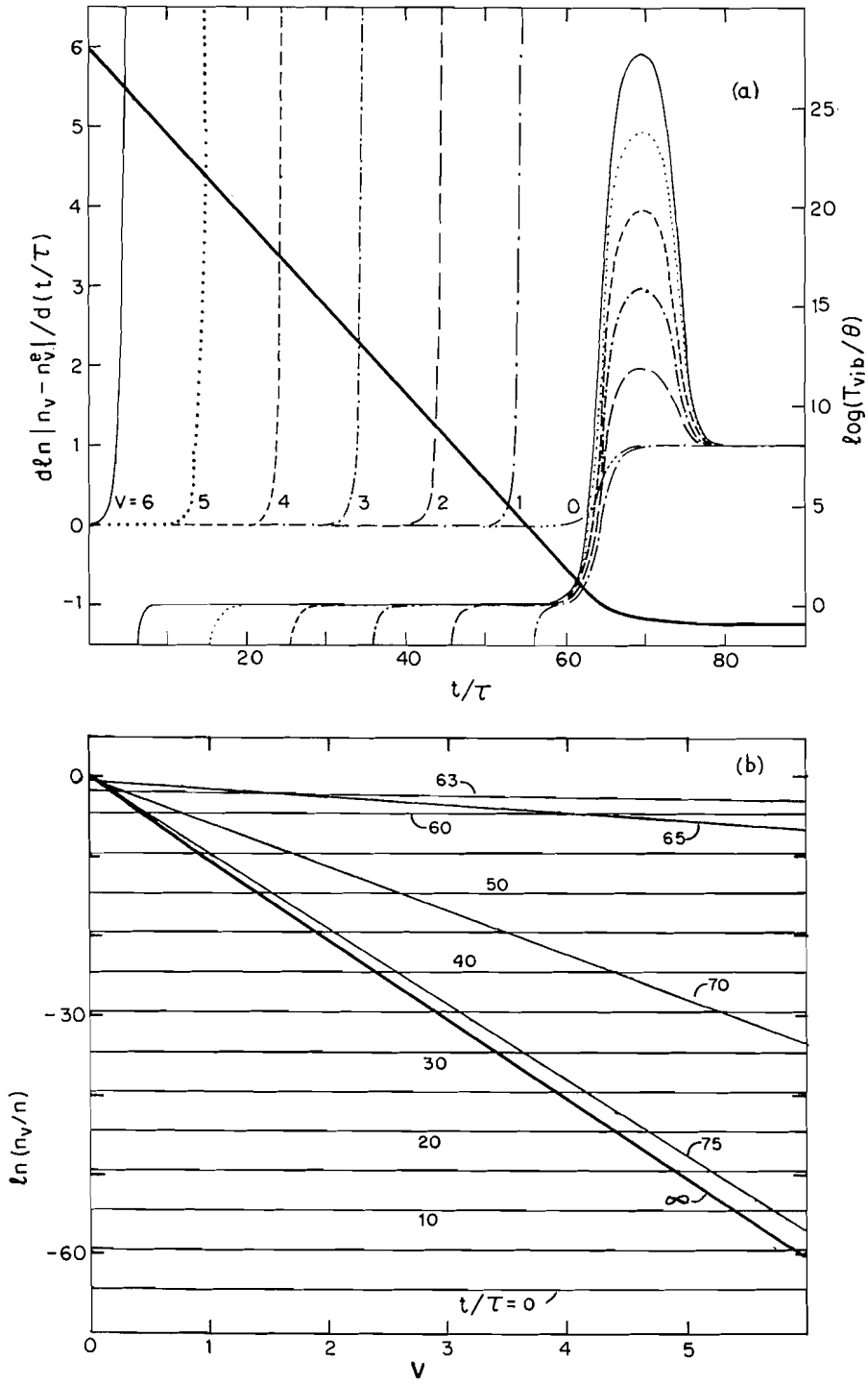

FIG. 1. Relaxation of a quantum harmonic oscillator obeying the Bethe–Teller law. Here $T^0_{vib}/\theta = 10^{28}$ K and $\theta/T = 10$. (*a*) Phenomenological rate coefficient k' as a function of reduced time and vibrational level. The thick solid curve is the variation of the vibrational temperature with time. The time origin for any real fluorescence experiment can be displaced arbitrarily to any point on the abscissa by first locating the initial vibrational temperature on the ordinate. Breshears' special case analysis (1) applies to the narrow region centred at the peaks. An ordinate of 1.0 means $k' = \tau^{-1}$. (*b*) Time evolution of the fractional level populations as a function of v (drawn as continuous curves for clarity). The thick line is the final population distribution. At the earliest time all v levels shown are underpopulated and approach equilibrium rapidly. Each level in turn becomes overpopulated, except $v = 0$, and deviate from equilibrium with a time constant τ until $t/\tau \sim 63$, whereupon the entire distribution proceeds to steepen and all level populations approach their equilibrium values at rates $\propto v$. Near equilibrium ($t/\tau > 78$) all levels relax with identical rate constants.

$$\mathrm{d}\ \ln\ |n_v - n_v^e|/\mathrm{d}t \rightarrow \frac{1}{\tau}$$

Equation [12] still expresses the time-variation of T_{vib}. The solution to [18] is

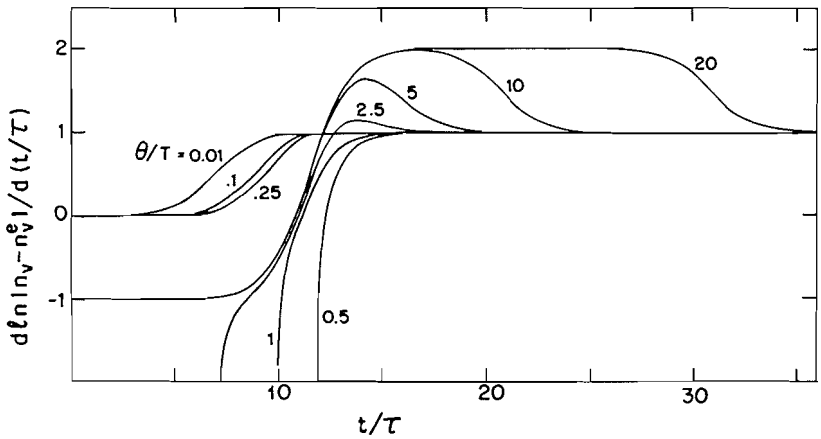

FIG. 2. Phenomenological rate coefficient for a fluorescence experiment as a function of reduced time and θ/T, which represents how close to the classical limit the relaxing molecule is. Here $v = 2$, and $T^0_{vib}/\theta = 10^5$, so that all reasonable-sized perturbations are represented by displacing the time origin. (Except near equilibrium $T_{vib} = T^0_{vib} \exp(-t/\tau)$.) Breshears' analysis applies only to $\theta/T \gg 1$, when the rate coefficient is $2\tau^{-1}$. For clarity the portions of curves for $\theta/T = 2.5, 1, 0.5$ are not drawn at times earlier than those for which the coefficients pass through $\pm\infty$. As in Fig. 1 a Boltzmann distribution is always maintained.

$$[19] \quad \ln\left|\frac{n_v - n_v^e}{n_v^0 - n_v^e}\right| = \frac{t}{\tau}$$

Evidently the level populations deviate increasingly from their equilibrium values until T_{vib} approaches θ, i.e. until t/τ approaches $\ln(T^0_{vib}/\theta)$. The fluorescence intensity and the vibrational energy both decrease exponentially with time. At first sight this might seem contradictory. Actually for most v the populations increasingly deviate from equilibrium values. They do so temporarily, only because the population distribution is essentially flat. As the vibrational temperature decreases, and the distribution steepens, the level populations increase because the number of states contributing to the partition function decrease faster yet. The same situation occurs for case (*a*); however there the population distribution is initially even flatter, and the partition function so large that all levels are almost equally populated at far below the equilibrium population of most other v and cannot help but approach n_v/n_v^e. Figures 1 and 2 display this phenomenon graphically. This behaviour is a consequence of the Bethe–Teller law, and as such lays the foundation for a test of this law. As long as $T^0_{vib} \gg \theta \gg T$, any molecule should show this behaviour, and can be used to test [1].

Shock waves

A. $\theta \gg T \geq T_{vib}$

$$F \to \frac{v}{1 - \exp\left[-v\theta\left(\frac{1}{T} - \frac{1}{T_{vib}}\right)\right]}$$

With most sensitive shock tube techniques, the relaxation zone is detected currently by measuring density gradients near equilibrium. Then $T \simeq T_{vib}$. If $(T - T_{vib}) \ll T^2/v\theta$ in addition, then as in ref. 1

$$[20] \quad F \to \theta^{-1}\left(\frac{1}{T} - \frac{1}{T_{vib}}\right)^{-1}$$

and

$$[21] \quad \frac{\theta}{T_{vib}^2}\frac{dT_{vib}}{dt} \to -\frac{\theta}{\tau}\left(\frac{1}{T} - \frac{1}{T_{vib}}\right)$$

so that $d \ln|n_v - n_v^e|/dt \to -1/\tau$, and there is a unique decay constant for all v. This constant can be identified by referring to the same model for relaxation of a harmonic oscillator by T–V processes as discussed in the fluorescence case. In the equilibration process of many levels such as

$$A(v = 0) + M \underset{10}{\overset{01}{\rightleftarrows}} A(v = 1) + M$$

the rate coefficient is $k_{10} - k_{01}$, where k_{10} is the downhill rate constant and k_{01} is the reverse uphill rate constant (4, 5). Using detailed balancing,

$$[22] \quad \tau^{-1} = k_{10}(1 - e^{-\theta/T})$$

Thus there is a basic difference between fluorescence results and shock wave results. It should be noted however that the difference exists because of the difference in perturbation sizes. It is quite feasible, for example, to measure vibrational relaxation times behind shock waves at early times, when $T \gg T_{vib}$. Then

Can. J. Chem. Downloaded from www.nrcresearchpress.com by 210.87.254.42 on 09/06/12
For personal use only.

$$\frac{\theta}{T_{vib}^2}\frac{dT_{vib}}{dt} \rightarrow \frac{\exp(\theta/T_{vib})}{\tau}$$

whose solution is

[23] $$\exp(-\theta/T_{vib}) = \exp(-\theta/T_{vib}^0) + t/\tau$$

T remains $\gg T_{vib}$ for times $t/\tau < e^{-\theta/T} \ll 1$.

$$F \rightarrow -v[\exp(-\theta/T_{vib})]$$

Thus

[24] $$d \ln |n_v - n_v^e|/dt \rightarrow -v/\tau$$

and each level relaxes at a rate proportional to v, just as in the fluorescence case. It is interesting to note that the Landau–Teller model (4) for T → V processes uses $k_{v-1\rightarrow v} \propto v$ on theoretical grounds in order to derive the Bethe–Teller law (2) for large perturbations, but the factor of v appearing in the above rate expression arises from the Boltzmann distribution itself. Here τ^{-1} can be identified as k_{01}, because the individual levels are subjected to generally uphill transitions at early times. A cryogenic shock tube would have to be used to achieve $\theta \gg T \gg T_{vib}$.

B. $T \gg \theta$

Here we extend the study to temperatures where the molecule behaves as a classical oscillator at equilibrium. From [4]

[25] $$F \rightarrow \frac{v - (v+1)[\exp(-\theta/T_{vib})]}{1 - \left[\exp\left(-\frac{\theta}{T_{vib}}\right)\right] - \frac{\theta}{T}\left[\exp\left\{-v\theta\left(\frac{1}{T} - \frac{1}{T_{vib}}\right)\right\}\right]}$$

and from [7]

[26] $$\frac{\theta}{T_{vib}^2}\frac{dT_{vib}}{dt} \rightarrow \frac{1}{\tau}\frac{T}{\theta}\left[1 - \exp\left(-\frac{\theta}{T_{vib}}\right)\right]\left\{\exp\left[-\theta\left(\frac{1}{T} - \frac{1}{T_{vib}}\right)\right] - 1\right\}$$

There are two special cases depending on whether the molecule behaves initially as a classical oscillator or not: (*a*) $T \gg \theta \gg T_{vib}$, (*b*) $T > T_{vib} \gg \theta$. Eventually T_{vib} approaches T, so that case (*b*) can be considered as a late time version of case (*a*). These two cases commonly occur: many molecules (excluding hydrogen-containing compounds) are nearly classical oscillators particularly at the shock tube temperatures where they relax at measurable speeds (e.g. θ = 309 K for I_2, θ = 806 K for Cl_2, etc.).

(a) $T \gg \theta \gg T_{vib}$

The rate law for vibrational temperature reduces to

$$\frac{\theta}{T_{vib}^2}\frac{dT_{vib}}{dt} = \frac{1}{\tau}\frac{T}{\theta}\exp\frac{\theta}{T_{vib}}$$

i.e.

[27] $$\exp\left(-\frac{\theta}{T_{vib}}\right) = \exp\left(-\frac{\theta}{T_{vib}^0}\right) + \frac{T}{\theta}\frac{t}{\tau}$$

and it is valid when $t/\tau < \theta/eT$.

$$F \rightarrow \frac{v}{1 - \frac{\theta}{T}\exp\frac{v\theta}{T_{vib}}}$$

and

[28] $$d \ln |n_v - n_v^e|/dt \rightarrow \frac{v}{\tau}\frac{T}{\theta}\left(1 - \frac{\theta}{T}\exp\frac{v\theta}{T_{vib}}\right)^{-1}$$

Just as in fluorescence experiments, there exists for each v a critical vibrational temperature T_c given by $T = \theta \exp v\theta/T_c$ which determines the way the level population evolves. If $T_{vib} > T_c$ the level population deviates further from its equilibrium value, i.e. overshoots it; if $T_{vib} < T_c$ the level population relaxes directly towards equilibrium. The physical explanation for this behaviour lies in the properties of the Boltzmann distribution: If the temperature is high the levels relax from a steep distribution to an essentially flat distribution wherein the populations of all levels are less than the initial population of most any level of sufficiently small v. In the flattening process most levels will first increase in population until the Boltzmann distribution approaches a classical distribution, at which point the molecule relaxes as in case *A*. In cases where the temperature is not so critically high but where the final distribution is still essentially flat, some levels of low v are overpopulated, but some at large v are underpopulated. At early times the flattening process occurs, and all level populations must approach equilibrium values. The higher v states relax most quickly, so that eventually most v states are overpopulated. The flattening process continues as in the very high temperature case with most levels increasing in population until the population distribution becomes classical. If the temperature is relatively low, but still $>\theta$, almost all levels are underpopulated. The flattening process does not result in overpopulation. These situations are

Can. J. Chem. Downloaded from www.nrcresearchpress.com by 210.87.254.42 on 09/06/12
For personal use only.

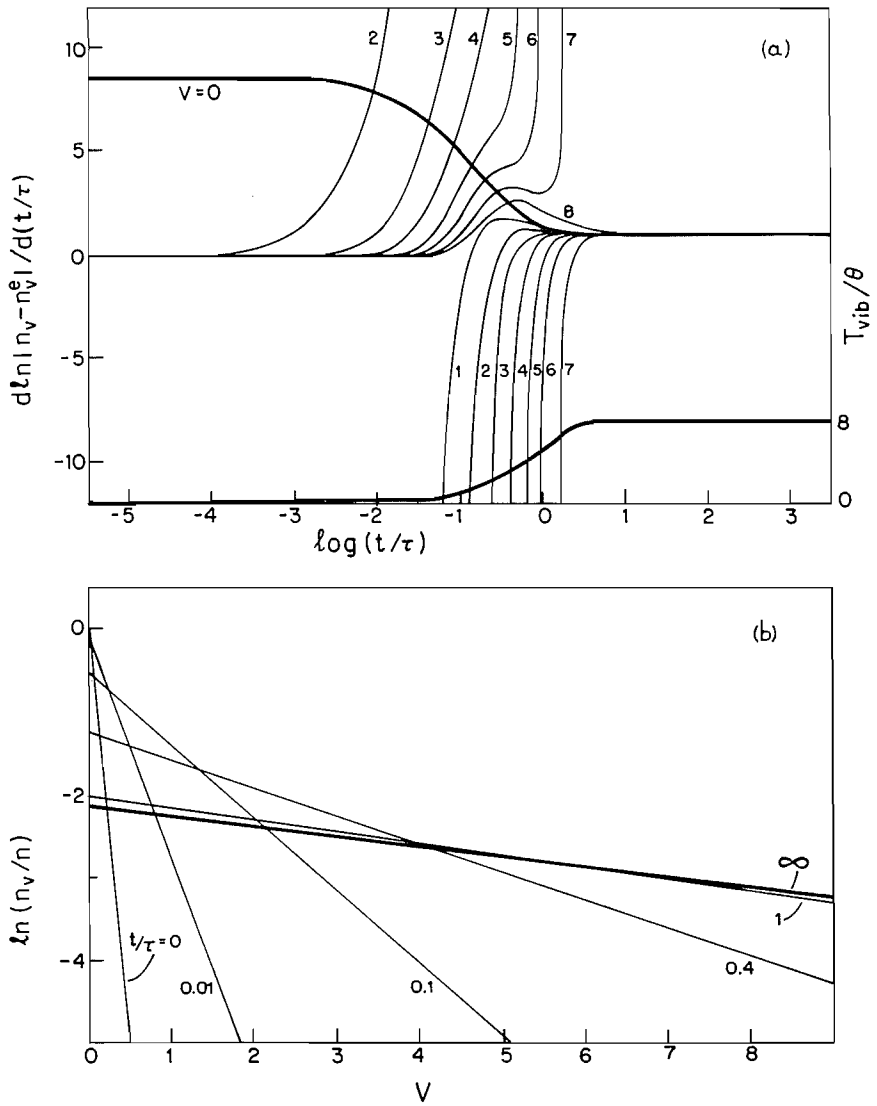

FIG. 3. Relaxation of a quantum oscillator obeying the Bethe–Teller law. Here $\theta/T^0_{vib} = 10$, $\theta/T = 0.125$. (*a*) Phenomenological rate coefficient k' as a function of reduced time and vibrational level. The thick solid curve is the vibrational temperature variation with time. In a real shock wave experiment, the vibrational temperature is within 5% of its equilibrium value T at times when most of the levels shown relax with the same rate coefficients. An ordinate of 1.0 means $k' = \tau^{-1}$. (*b*) Time evolution of the fractional level populations as a function of v (drawn as continuous lines for clarity). The thick line is the final population distribution. Note that $v \geq 8$ is never overpopulated at these conditions. By $t/\tau = 2.5$ all other levels are approaching equilibrium.

represented graphically in Figs. 3 and 4, and summarized below.

(i) $\theta\ exp\ (v\theta/T_{vib}) > T \gg \theta \gg T_{vib}$

$$F \rightarrow -\frac{vT}{\theta}\left[\exp\left(-\frac{v\theta}{T_{vib}}\right)\right]$$

i.e.

$$[29] \qquad \frac{\theta}{T_{vib}^2}\frac{dT_{vib}}{dt} = \frac{1}{\tau}\frac{T}{\theta}\exp\frac{\theta}{T_{vib}}$$

$$[30] \qquad \exp\left(-\frac{\theta}{T_{vib}}\right) = \left[\exp\left(-\frac{\theta}{T^0_{vib}}\right)\right] + \frac{T}{\theta}\frac{t}{\tau}$$

$$\frac{d\ln|n_v - n_v^e|}{dt} \rightarrow -\frac{v}{\tau}\left(\frac{T}{\theta}\right)^2 \exp\left[-\frac{(v-1)\theta}{T_{vib}}\right]$$

$$[31] \qquad \ln\left(\frac{n_v - n_v^e}{n_v^0 - n_v^e}\right) = \left(\frac{T}{\theta}\right)^{v+1}\left\{\left[\frac{\theta}{T}\exp\left(-\frac{\theta}{T^0_{vib}}\right)\right]^v - \left[\frac{t}{\tau} + \frac{\theta}{T}\exp\left(-\frac{\theta}{T^0_{vib}}\right)\right]^v\right\}$$

Can. J. Chem. Downloaded from www.nrcresearchpress.com by 210.87.254.42 on 09/06/12
For personal use only.

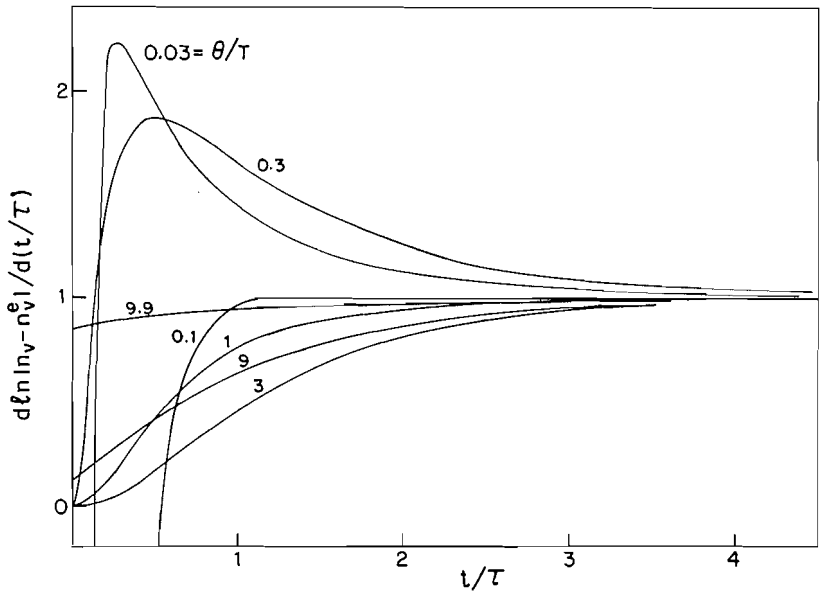

FIG. 4. Phenomenological rate coefficient k' for shock-wave experiments as a function of reduced time and θ/T. Here $\theta/T^0_{vib} = 10$ (a typical quantum oscillator). The population of $v = 4$ is shown evolving for various extents from equilibrium. It is only for a very narrow region of temperatures ($T \approx T^0_{vib}$) to which Breshears' results (1) apply, $k' = \tau^{-1}$. The figure also shows the effects of nearness to classical behaviour ($\theta/T < 1$). The early time-history related to overpopulation of $v = 4$ for $\theta/T < 0.1$ is not shown (see Fig. 3).

The levels (of large enough v) relax at rates which depend strongly on v. At the very earliest times the time-dependence approaches exponential with rate constants $\{v \exp[-(v-1)\theta/T^0_{vib}]\}(T/\theta)^2\tau^{-1}$. In terms of the critical vibrational temperature $T_c = v\theta/\ln(T/\theta)$, this situation represents $T_{vib} < T_c$ and encompasses the cases $T_c > T > \theta > T_{vib}$; $T > T_c > \theta > T_{vib}$; $T > \theta > T_c > T_{vib}$. The first two possibilities are satisfied until T_{vib} approaches θ, $t/\tau \ll e^{-1}\,\theta/T$. The third possibility is satisfied only until T_{vib} approaches T_c, i.e.

$$\frac{T}{\theta}\frac{t}{\tau} \ll \exp\left(-\frac{\theta}{T_{vib}}\right) < \exp\left(-\frac{\theta}{T_c}\right) = \left(\frac{T}{\theta}\right)^{-1/v}$$

or

$$\frac{t}{\tau} \ll \left(\frac{\theta}{T}\right)^{(1+1/v)}$$

Afterwards, $T_{vib} > T_c$, i.e. $\theta \exp(v\theta/T_{vib}) < T$.

(ii) $T > \theta\ exp\ (v\theta/T_{vib}) \gg \theta \gg T_{vib}$

$$F \to v$$

The vibrational temperature and its derivative are still given by [30] and [29], but

$$[32] \qquad \mathrm{d}\ln|n_v - n_v^e|/\mathrm{d}t \to \frac{v}{\tau}\frac{T}{\theta}\exp\frac{\theta}{T_{vib}}$$

Thus the level populations (of sufficiently small v) will deviate from their equilibrium values until T_{vib} approaches θ. This will actually occur at very early times becase $t/\tau \ll e^{-1}\,\theta/T$ and T is enormous (e.g. for $T^0_{vib} = 300$ K, $\theta = 1000$ K, T must be $>$ 28 000 K and $t/\tau \ll 0.036$). The solution of [32] is

$$[33] \qquad \frac{n_v - n_v^e}{n_v^0 - n_v^e} = \left(\frac{t}{\tau}\frac{T}{\theta}\exp\frac{\theta}{T^0_{vib}} + 1\right)^v$$

For both cases (*i*) and (*ii*) involving high and low v, a measurement of the time dependence is a good test of the Bethe–Teller law; and measurement of the v-dependence is a good test of the existence of a Boltzmann distribution. At high temperatures it is quite possible that the V–T relaxation rate approaches that of the V–V equilibration rates, and it would indeed be worthwhile testing the assumption of a Boltzmann distribution.

A feasible experiment would involve a cryogenic shock tube with $T^0_{vib} < 100$ K, $\theta \sim 300$ K, and $T \geqslant 6000$ K, for which $t/\tau < 0.050$. The molecule would have to relax slowly: N_2 would provide such an example. In such a case the level populations would have to be monitored by a Raman scattering technique.

(b) $T > T_{vib} \gg \theta$

In this case the molecule always behaves like a classical oscillator. The rate law for vibrational temperature reduces to

Can. J. Chem. Downloaded from www.nrcresearchpress.com by 210.87.254.42 on 09/06/12
For personal use only.

[34] $$\frac{\theta}{T_{vib}^2}\frac{dT_{vib}}{dt} = -\frac{\theta}{\tau}\left(\frac{1}{T} - \frac{1}{T_{vib}}\right)\frac{T}{T_{vib}}$$

i.e.

$$\frac{dT_{vib}}{dt} = \frac{T - T_{vib}}{\tau}$$

[35] $$T - T_{vib} = (T - T_{vib}^0)\exp(-t/\tau)$$

[36] $$F \rightarrow -\left\{\theta\left(\frac{1}{T_{vib}} - \frac{1}{T}\right)\left(1 - \frac{v\theta}{T}\right)\right\}^{-1} \text{ for } v \ll (T_{vib}/\theta)T/(T - T_{vib})$$

We may be somewhat more restrictive with respect to v. If $v \ll T_{vib}/\theta$, then v is also $\ll T/\theta$, and $F \rightarrow -\theta^{-1}(1/T_{vib} - 1/T)^{-1}$.

[37] $$d \ln |n_v - n_v^e|/dt = -\frac{1}{\tau}\frac{T}{T_{vib}}$$

Thus the populations relax with rates independent of v. Unlike a quantum oscillator this conclusion does not depend on the extent of departure from equilibrium, and should be valid for $v \leqslant 10$. Nevertheless, the value of the effective rate coefficient $\tau^{-1}(T/T_{vib})$ approaches the quantum oscillator rate constant τ^{-1} as equilibrium is approached. The actual level population dependence is given by solving [36]:

[38] $$\frac{n_v - n_v^e}{n_v^0 - n_v^e} = \frac{T_{vib}^0 e^{-t/\tau}}{T - (T - T_{vib}^0)e^{-t/\tau}}$$

It should be noted that as time increases the number of levels contributing to the partition function increases dramatically. Initially, the partition function increases faster than relative level populations change. As a result the lower levels approach equilibrium while the upper levels appear to deviate even if [36] is valid for some of them. When [36] is not valid, a more general but intractable equation must be solved:

[39] $$d \ln |n_v - n_v^e|/dt = -\frac{1}{\tau}\frac{T}{T_{vib}}\frac{(T - T_{vib})}{(T - T_{vib}\exp\{v\theta[1/T_{vib} - 1/T]\}}$$

Equation [38] should be applicable to many molecules, and represents a good test of the Bethe–Teller law; e.g. for I_2 whose level populations can be monitored by uv absorption, $\theta \simeq 309$ K. It can be shock heated to attain an initial temperature of ~1500 K, and perturbed by a reflected shock wave at T ~3000 K.

It is interesting to note that [37] would also be applicable to a laser-induced fluorescence experiment. In this case $T < T_{vib}$, and the vibrational temperature would decrease according to

[40] $$T_{vib} - T = (T_{vib}^0 - T)\exp(-t/\tau)$$

and the level populations would vary according to

[41] $$\frac{n_v - n_v^e}{n_v^0 - n_v^e} = \frac{T_{vib}^0 e^{-t/\tau}}{T + (T_{vib}^0 - T)e^{-t/\tau}}$$

A particularly good test of the Bethe–Teller law would involve laser-exciting an infrared active molecule after it is shock heated and studying its fluorescence (e.g. BrCl) or its uv absorption (e.g. NO). In this way one could achieve an experimental situation for which $T_{vib} \gg T \gg \theta$.

Thermal effects

The relaxation of molecules by V ↔ T processes is always accompanied by an evolution of heat in laser-excited fluorescence or chemical activation studies, or else by translational cooling in shock tube studies. The analysis is straightforward, and it has been recognized as a problem for a very long time. It has been discussed in some detail by Hunter (9) for spectrophone or phase-lag techniques, and Yardley has given a simple expression (10) for a linearized version applicable to small perturbations. Nevertheless the correction factors are usually small in such cases, and the effect is therefore generally ignored. In practice, however, perturbations *are* large. Vibrational temperatures vary between 2000 K and 300 K in a single experiment, and correction factors can become quite significant especially if the heat content or temperature of the gas is low to start with, as in e.g. ref. 11. We present analytical expressions for these correction factors.

Four subtle but distinguishable effects can be recognized: (*a*) τ is not a constant because it depends on a time-varying temperature. Curved log-plots with respect to time indicate the presence of this effect. (*b*) If the process is a true equilibration, then the forward and reverse processes are affected differently, and a correction factor must be applied to account for the relative temperature dependence of rate coefficients. (*c*) The Boltzmann factor varies during the relaxation, so that the equilibrium level populations themselves change as equilibrium is approached. Even if a particular level population is not changing significantly, it will appear to be closer to its final equilibrium value. (*d*) Similarly, the total vibrational energy appears to relax more rapidly, since it need only relax to a value determined by a translational temperature which is less perturbed.

In the following analysis we treat only the most common experimental situations, $\theta \gg T_{vib} \gg T$ and $\theta \gg T \gtrsim T_{vib}$ in detail. The method is directly applicable to other situations. We use the Bethe–Teller law [7] for the time-dependence of the vibrational temperature:

Can. J. Chem. Downloaded from www.nrcresearchpress.com by 210.87.254.42 on 09/06/12
For personal use only.

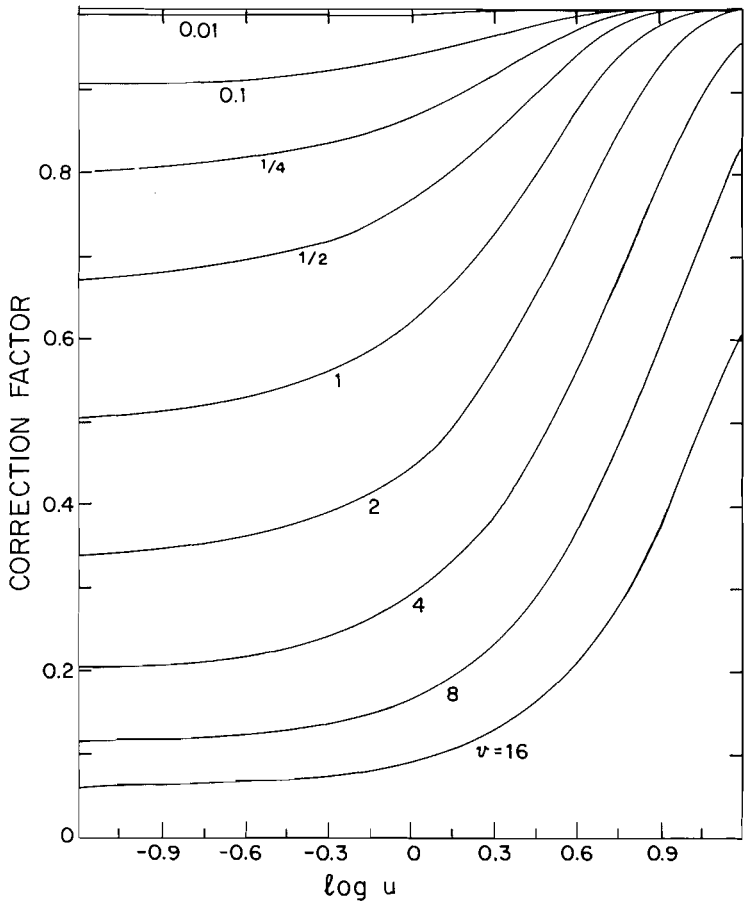

FIG. 5. Correction factor for thermal effect (b) as a function of $u = y = \theta/T_e$ and $\nu = x(T_0 - T_e)/T_e$ for shock tube studies, or alternatively as a function of $u = \theta/T_0$ and $\nu = (T_e - T_0)(1 - x)/T_0$ for fluorescence decay studies. x represents the departure from equilibrium.

$$[42] \quad \frac{\theta}{T_{vib}^2}\frac{dT_{vib}}{dt} = \frac{1}{\tau}\left[\exp\left(-\theta[1/T - 1/T_{vib}]\right) - 1\right]$$

Secondly, we consider the energy balance between the translational–rotational and the vibrational degrees of freedom. Shock tube experiments can be considered to be at constant pressure and enthalpy. This is an approximation, and indeed one analyzes data more carefully (13); however for a first-order determination of the thermal effect, the approximation is good. The gas enthalpy $H = \int_0^{T_e} C dT$ is a constant, where T_e is the true final temperature and C is the constant-pressure heat capacity $= \Sigma X_i C_i$. Here X_i is the mole fraction of species i, and C_i is the heat capacity of species i. The relaxing molecules A can release or take up heat from an inert buffer gas M. Then $C = X_A C_A + X_M C_M$, i.e. $C = X_A(C_A - C_M) + C_M$. The enthalpy is composed of translational and rotational contributions denoted by $\int(C - C_{vib})dT$ plus a vibrational term given by [6] for n molecules. On a per-molecule basis $C - C_{vib} = C_M(1 - X_A) + X_A(5k/2) + k$ for a linear molecule A; $C - C_{vib} = C_M(1 - X_A) + 3kX_A + k$ for a non-linear molecule A. If some of the A molecules' vibrational modes have already relaxed independently on a shorter time scale, then a corresponding term is added. Otherwise, and if the buffer is an atom such as Ar, then

$$[43a] \quad C - C_{vib} = k(X_A + 5/2)$$

$$[43b] \quad C - C_{vib} = k(3X_A/2 + 5/2)$$

for linear and non-linear relaxing molecules, respectively. Thus

$$H = \int(C - C_{vib})dT + X_A \epsilon_{vib}/n$$

$$X_A d\epsilon_{vib}/n dt = -(C - C_{vib})dT/dt$$

For $\theta \gg T_{vib}$ this becomes

$$[44] \quad X_A h\nu \left(\frac{\theta}{T_{vib}^2}\right)\exp\left(-\frac{\theta}{T_{vib}}\right)\frac{dT_{vib}}{dt} = -(C - C_{vib})\frac{dT}{dt}$$

This expression is also valid for laser or chemically activated systems if heat loss to the walls of the cell is not significant. In this case C is a constant-pressure heat capacity only at relatively high pressures, but is a constant volume heat capacity at low pressures where the excitation energy diffuses over the whole cell (10).

Can. J. Chem. Downloaded from www.nrcresearchpress.com by 210.87.254.42 on 09/06/12
For personal use only.

Equations [42] and [44] must be solved simultaneously for $T(t)$ and $T_{vib}(t)$. In practice this is difficult, but one can obtain a good first-order approximation to $T(t)$ by using the Blackman procedure (12). This procedure does not linearize the problem, i.e. does not assume a weak perturbation, but does assume that C is not very temperature-dependent. It leads to

[45] $$dT/dt = (T_e - T)/\tau'$$

where

$$\tau' = \tau(C - C_{vib})/C$$

The temperature varies exponentially with time. In shock tube experiments the initial post-shock temperature T_0 is typically anywhere between 400 and 3000 K, and the final temperature can be smaller by amounts ranging up to 1000 K or more. In laser-fluorescence experiments the initial temperature T_0 is typically room temperature plus a change corresponding to the release of heat by rapidly-relaxing modes of vibration on an immeasurably shorter time scale. The final temperature T_e can be as much as 1000 K higher. In shock tube experiments large temperature changes can be correlated well with a time-varying relaxation time (effect (*a*)), but the latter must be recognized as $\tau'(T(t))$ rather than $\tau(T(t))$ if a simple log-plot analysis of gas density is used. The correction factor for this effect is most significant for pure gas A, and for high temperatures. For a diatomic molecule A it approaches 7/9; for a linear triatomic molecule it approaches 7/15, etc., if all modes relax simultaneously. In fluorescence experiments, as long as the gas is optically thin to all transitions, the light intensity is proportional to the vibrational energy, which is closely associated with τ itself.

Effect (*b*) is important for high-temperature relaxation experiments near equilibrium, when both forward and reverse reactions are important. Usually only shock tube experiments are affected. For T–V mechanisms $1/\tau$ can be identified with $k_{10}(1 - e^{-\theta/T})$. When one compares fluorescence data with shock tube data one ultimately wishes to compare their corresponding k_{10}'s. The adjustment factor depends on the portion of the relaxation zone measured. At equilibrium one has a true handle on k_{10}. Over the time range $n\tau$ to $m\tau$, the average time $(n + m)\tau/2$ corresponds to an average temperature $\bar{T}$ given by $(\bar{T} - T_e)/T_0 - T_e) = \exp[-(m + n)/2]$. Referred to equilibrium for shock tube studies, and to the intial temperature for fluorescence studies, the measured rate coefficient is always smaller by factors which depend on the parameters $y = \theta/T_e$, $z = \theta/T_0$, and $x = \exp[-(m + n)/2]$. Figure 5 summarizes the adjustment factors, and is applicable to any size perturbation or relative value of θ, or the relaxation regime studied. For classical oscillators the factor approaches $T_e/(T_e + [T_0 - T_e]x)$.

In order to examine effect (*c*), eq. [4] must be rewritten to explicitly account for the temperature variation.

[46] $$\frac{d \ln |n_v - n_v^e|}{dt} = \frac{\frac{\theta}{T_{vib}^2}\frac{dT_{vib}}{dt}\left\{v - \left[(v+1)\exp\left(-\frac{\theta}{T_{vib}}\right)\right]\right\}\left[\exp\left(-\frac{v\theta}{T_{vib}}\right)\right] - \frac{\theta}{T^2}\frac{dT}{dt}\left\{v - \left[(v+1)\exp\left(-\frac{\theta}{T}\right)\right]\right\}\left[\exp\left(-\frac{v\theta}{T}\right)\right]}{\left[\exp\left(-\frac{v\theta}{T_{vib}}\right)\right]\left[1 - \exp\left(-\frac{\theta}{T_{vib}}\right)\right] - \left[\exp\left(-\frac{v\theta}{T}\right)\right]\left[1 - \exp\left(-\frac{\theta}{T}\right)\right]}$$

In order to proceed we must specify the type of experiment.

Fluorescence

We can simplify eq. [46] by using the adiabaticity relationship [44] and dividing through with $\exp(-v\theta/T_{vib})$, and using $\theta \gg T_{vib}$, $\theta \gg T$.

[47] $$\frac{d \ln |n_v - n_v^e|}{dt} = \left\{\frac{v + v\left\{\exp\left[-v\theta\left(\frac{1}{T} - \frac{1}{T_{vib}}\right)\right]\right\}\frac{\theta^2}{T^2}\frac{kX_A\left[\exp\left(-\frac{\theta}{T_{vib}}\right)\right]}{C - C_{vib}}}{1 - \left\{\exp\left[-v\theta\left(\frac{1}{T} - \frac{1}{T_{vib}}\right)\right]\right\}}\right\}\frac{\theta}{T_{vib}^2}\frac{dT_{vib}}{dt}$$

It is clear from [44] that if the translational temperature varies with time constant τ' then so will the vibrational temperature. The solution of [45] is

[48] $$T = T_0 + (T_e - T_0)(1 - \exp[-t/\tau'])$$

which has a value $\approx T_0$ during the observation region. The final temperature depends on the amount of photon- or chemical-excitation. If e.g. each molecule had absorbed v_0 quanta of laser energy initially, then $\int_{T_0}^{T_e} C dT = v_0 h\nu X_A$.
Under the present assumption that C is constant during the relaxation process

[49] $$(T_e - T_0) = X_A v_0 h\nu/C$$

Use of [48] and [49] simplifies the adiabaticity relationship to

$$\frac{\theta}{T_{vib}^2}\frac{dT_{vib}}{dt}\left[\exp\left(-\frac{\theta}{T_{vib}}\right)\right] = -\frac{v_0}{\tau}\left[\exp\left(-\frac{t}{\tau'}\right)\right]$$

i.e.

$$\exp\left(-\frac{\theta}{T_{vib}}\right) = \exp\left(-\frac{\theta}{T_{vib}^0}\right) - \left(\frac{\tau'}{\tau}\right)v_0\left[1 - \exp\left(-\frac{t}{\tau'}\right)\right]$$

Can. J. Chem. Downloaded from www.nrcresearchpress.com by 210.87.254.42 on 09/06/12
For personal use only.

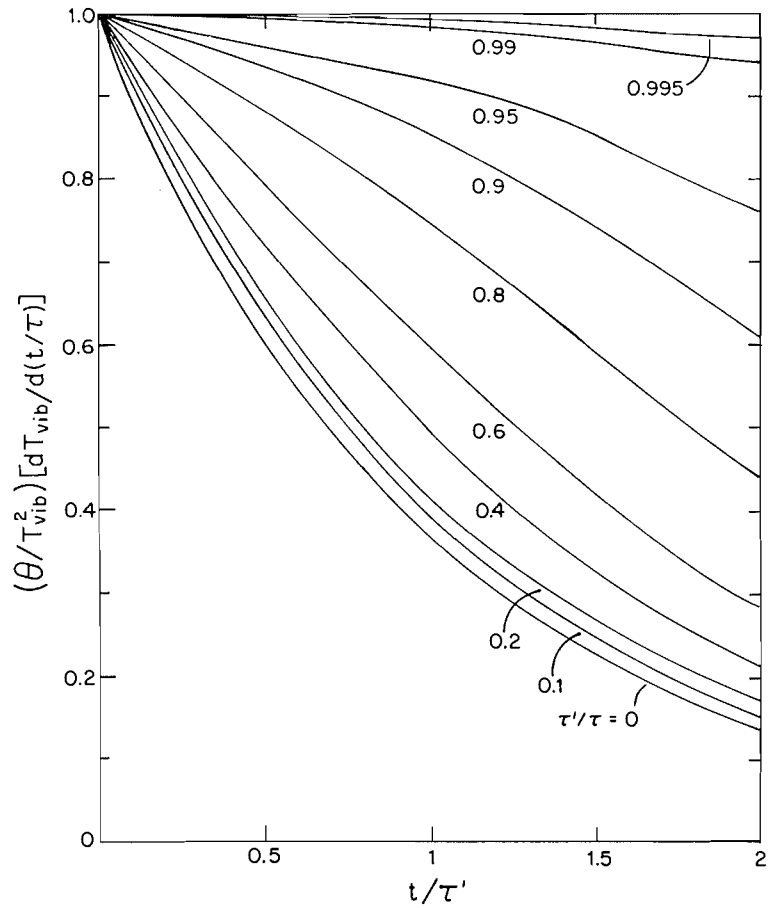

FIG. 6. Correction for thermal effect (d) as a function of reduced time t/τ' and as a function of $\tau'/\tau = (C - C_{vib})/C$. The latter depends essentially on the temperature and on the mole fraction of relaxing gas. An ordinate of 1.0 means $(\theta/T_{vib}^2)\,(dT_{vib}/dt) = \tau^{-1}$.

A more general expression allowing for other kinds of excitation can be obtained by noting that the change in vibrational energy per molecule due to the initial excitation is

$$X_A h\nu \left\{\left[\exp\frac{\theta}{T_{vib}^0} - 1\right]^{-1} - \left[\exp\frac{\theta}{T_0} - 1\right]^{-1}\right\}$$

Thus

$$T_c - T_0 \approx X_A h\nu \left[\exp\left(-\frac{\theta}{T_{vib}^0}\right) - \exp\left(-\frac{\theta}{T_0}\right)\right]\Big/C$$

and

$$\exp\left(-\frac{\theta}{T_{vib}}\right) = \exp\left(-\frac{\theta}{T_{vib}^0}\right) - \left(\frac{\tau'}{\tau}\right)\left\{\left[\exp\left(-\frac{\theta}{T_{vib}^0}\right)\right] - \left[\exp\left(-\frac{\theta}{T_0}\right)\right]\right\}\left\{1 - \left[\exp\left(-\frac{t}{\tau'}\right)\right]\right\}$$

and

$$\frac{\theta}{T_{vib}^2}\frac{dT_{vib}}{dt} = -\frac{\left\{\left[\exp\left(-\frac{\theta}{T_{vib}^0}\right)\right] - \left[\exp\left(-\frac{\theta}{T_0}\right)\right]\right\}\tau^{-1}\left[\exp\left(-\frac{t}{\tau'}\right)\right]}{\left[\exp\left(-\frac{\theta}{T_{vib}^0}\right)\right] - \left(\frac{\tau'}{\tau}\right)\left\{\left[\exp\left(-\frac{\theta}{T_{vib}^0}\right)\right] - \left[\exp\left(-\frac{\theta}{T_0}\right)\right]\right\}\left(1 - \exp\left(-\frac{t}{\tau'}\right)\right)}$$

We note that in fluorescence studies $T_{vib} \gg T > T_0$. Thus

$$[50] \qquad \frac{\theta}{T_{vib}^2}\frac{dT_{vib}}{dt} = -\frac{e^{-t/\tau'}}{\tau - \tau'(1 - e^{-t/\tau'})}$$

In the limit of no thermal effects this reduces simply to $-1/\tau$ as in [8]. Figure 6 shows that it is otherwise time-dependent. Not recognizing this can lead to significant errors! Even for modest thermal effects (i.e. $\tau' \to \tau$)

$$\frac{\theta}{T_{vib}^2}\frac{dT_{vib}}{dt} = -\frac{e^{-t/\tau'}}{(\tau - \tau') + \tau' e^{-t/\tau'}} \to -\frac{1}{\tau'}$$

We can now proceed with eq. [47]. For fluorescence studies, $\theta \gg T_{vib} > T$,

Can. J. Chem. Downloaded from www.nrcresearchpress.com by 210.87.254.42 on 09/06/12
For personal use only.

$$[51] \quad \frac{\mathrm{d} \ln |n_v - n_v^e|}{\mathrm{d}t} \rightarrow v\left\{1 + \left[\exp\left(-\frac{v\theta}{T}\right)\right]\frac{\theta^2}{T^2}\frac{kX_A\left[\exp\left(-\frac{\theta}{T_{vib}}\right)\right]}{C - C_{vib}}\right\}\frac{\theta}{T_{vib}^2}\frac{\mathrm{d}T_{vib}}{\mathrm{d}t}$$

For a good first estimate of the adjustment factor in parentheses we set $T = T_0$, and $T_{vib} = T_{vib}^0$, which should be valid for initial rates. The factor is strongly dependent on v. For example for $\theta = 1000$ K, $T_{vib}^0 = 600$ K, $T_0 = 300$ K, $C - C_{vib} = 7/2k$, $X_A = 1$, it is 1.600 for $v = 0$, 1.021 for $v = 1$, and 1.001 for $v = 2$. It is thus not very important for moderate conditions. However in extreme cases of very low temperatures, e.g. 150 K (11), it is as large as 3.40 for $v = 0$. The linear relationship between fluorescence intensity and vibrational energy still holds approximately for gases which are optically thin to radiation from all v. Except for $v = 0$ all levels relax at rates proportional to v to a good approximation. The adjustment factor can be compared to that of Yardley and Moore (10) applicable to phase-lag measurements. Except for the dependence on v we obtain a similar adjustment factor without having to limit the analysis to small perturbations or to the phase-lag technique. More important however is the $(\theta/T_{vib}^2\ \mathrm{d}T_{vib}/\mathrm{d}t)$ factor which is time-dependent. It implies that log-plots are not all appropriate. We integrate

$$\frac{\mathrm{d} \ln |n_v - n_v^e|}{\mathrm{d}t} \approx \frac{-v\,\mathrm{e}^{-t/\tau'}}{(\tau - \tau') + \tau'\,\mathrm{e}^{-t/\tau'}} \qquad v \neq 0$$

and obtain

$$[52] \quad \left(\frac{n_v - n_v^e}{n_v^0 - n_v^e}\right)^{1/v} = \frac{(\tau - \tau') + \tau'\,\mathrm{e}^{-t/\tau'}}{\tau}$$

We note that $\tau'/\tau = (C - C_{vib})/C$. Thus a plot of $\ln\{[(n_v - n_v^e)/(n_v^0 - n_v^e)]^{1/v} - C_{vib}/C\}$ against t will give a straight line whose slope is $-1/\tau'$. For $v = 1$ this is the same as the usual procedure except for the thermal term C_{vib}/C. Not following this modified procedure will lead to the large errors noted in Fig. 4. A similar procedure applies to fluorescence intensity.

Analogous reasoning applies to more extreme, yet common situations: $T_{vib} \gg \theta \gg T$. The adiabaticity relationship is modified because the oscillator is classical. Thus

$$[53] \quad X_A k \mathrm{d}T_{vib}/\mathrm{d}t = -(C - C_{vib})\mathrm{d}T/\mathrm{d}t$$

Equation [49] for $(T_e - T_0)$ is also modified

$$[54] \quad (T_e - T_0) \simeq X_A k T_{vib}^0/C$$

However, the temperature still varies exponentially with time constant τ'. So

$$\frac{\mathrm{d}T_{vib}}{\mathrm{d}t} = -\frac{T_{vib}^0}{\tau}\,\mathrm{e}^{-t/\tau'}$$

i.e.

$$T_{vib} = T_{vib}^0 - T_{vib}^0\,(\tau'/\tau)\,(1 - \mathrm{e}^{-t/\tau'})$$

and the factor

$$\frac{\theta}{T_{vib}^2}\frac{\mathrm{d}T_{vib}}{\mathrm{d}t} = -\frac{T_{vib}^0}{\tau}\frac{\mathrm{e}^{-t/\tau'}}{T_{vib}^2}$$

is smaller than that for the limit of no thermal effects by a factor $\mathrm{e}^{-t/\tau'}\,\mathrm{e}^{-t/\tau}\,[1 - (\tau'/\tau)\,(1 - \mathrm{e}^{-t/\tau'})]^2$. Furthermore, F is reduced in magnitude by the factor $[1 - v\mathrm{e}^{-v\theta/T}\,(T_{vib}/T)^2 kX_A/(C - C_{vib})]$, which is also significant. For $T_{vib}^0 = 3000$, $\theta = 1000$ K, $T_0 = 300$ K, $X_A = 1$, $C - C_{vib} = 7k/2$, it has a value of 1.000 for $v = 0$; -0.0193 for $v = 1$; 0.927 for $v = 2$. Without thermal effects, $F > 0$ for $v = 0$; $F < 0$ for $v \geq 1$. With thermal effects $F > 0$ for $v = 0, 1$; $F < 0$ for $v \geq 2$. Thus the temporary, yet increasing deviation from equilibrium for sufficiently large v noted earlier still occurs but it affects a smaller number of levels. Since the absolute value of the correction factor is <1, the apparent rate coefficients are smaller than in the absence of thermal effects, just as in the less extreme case $\theta \gg T_{vib} \gg T$. Modified log-plots would also be necessary.

Shock waves

For the usual condition $\theta \gg T \geq T_{vib}$, $(\theta/T_{vib}^2)\ (\mathrm{d}T_{vib}/\mathrm{d}t)$ is still given by eq. [21]. Use of this equation together with the adiabaticity relationship allows one to obtain an expression for $T(t)$ and $T_{vib}(t)$ in principle. However, this is not necessary, since under shock wave conditions near equilibrium $\theta v(1/T - 1/T_{vib}) \ll 1$. Thus we directly obtain

$$F \rightarrow \frac{1 + \left(\frac{\theta}{T}\right)^2 kX_A\left[\exp\left(-\frac{\theta}{T_{vib}}\right)\right](C - C_{vib})^{-1}}{\theta\left(\frac{1}{T} - \frac{1}{T_{vib}}\right)}$$

and hence

$$[55] \quad \frac{\mathrm{d} \ln |n_v - n_v^e|}{\mathrm{d}t} = -\frac{1}{\tau}\left\{1 + \frac{\theta^2}{T^2}\frac{X_A k\left[\exp\left(-\frac{\theta}{T_{vib}}\right)\right]}{C - C_{vib}}\right\}$$

Can. J. Chem. Downloaded from www.nrcresearchpress.com by 210.87.254.42 on 09/06/12
For personal use only.

without requiring an explicit expression for $T_{vib}(t)$. At or near equilibrium ($T_{vib} \simeq T \simeq T_e$), the correction factor to τ,

$$1 + \frac{\theta^2}{T_e^2}\left\{\frac{X_A k\left[\exp\left(-\frac{\theta}{T_e}\right)\right]}{C - C_{vib}}\right\}$$

is substantial. Noting that $C_{vib} = X_A h\nu(\theta/T_e^2)\exp(-\theta/T_e)$, we see that the correction factor for the population decay time is identical to that for the decay time of the measured temperature, $C/(C - C_{vib})$. For $X_A = 1$; $(C - C_{vib}) = 7/2k$; $\theta = 3000$, $T_e = 1000$, the populations of all levels decay 1.13 times faster than in the absence of thermal effects.

For the more extreme situation where the relaxing molecule always behaves like a classical oscillator, i.e. $T \gg T_{vib} \gg \theta$, $(\theta/T_{vib}^2)(dT_{vib}/dT)$ is given by eq. [34], the adiabaticity relationship by eqs. [53] and [54] and for $v < T_{vib}/\theta$.

$$F \rightarrow \frac{-\left\{1 + \frac{T_{vib}^2}{T^2}\frac{X_A k}{(C - C_{vib})}\right\}}{\theta(1/T_{vib} - 1/T)}$$

Thus

$$[56] \qquad \frac{d \ln |n_v - n_v^e|}{dt} = -\frac{1}{\tau}\left\{1 + \frac{X_A k}{C - C_{vib}}\right\}$$

Again noting that for a classical oscillator $C_{vib} = X_A k$, the decay time is just τ'. However, for a classical oscillator the correction factor can be quite substantial, e.g. if $(C - C_{vib}) = 7/2k$, $\tau' = 0.778\tau$.

Conclusions

In generalizing Breshears' analysis of the relaxation of a harmonic oscillator we have shown that the form of the rate law for the equilibration of vibrational energy level populations depends on many factors: the size and direction of the perturbation, the extent from equilibrium, and how classical the oscillator is at the initial and at the final conditions. The fluorescence decay rate coefficients are proportional to v only for a narrow range of experimental conditions. They are independent of v under shock tube conditions near equilibrium if the molecule is a quantum oscillator, but also for any size shock perturbation if the molecule is always a classical oscillator. All forms of the rate law are based on the validity of the Bethe–Teller law and on the existence of a rapid V–V energy transfer mechanism which assures a Boltzmann distribution throughout the relaxation zone. Generally, the Bethe–Teller law has been tested only under relatively mild conditions. We have proposed shock tube and laser-induced fluorescence or chemical activation experiments to test this under more extreme yet realistic conditions by observing the form of the time-dependence of the evolution of individual level populations. The rapidity of V–V processes can be tested by checking the v-dependence. (eqs. [17], [24], [32], [38], [41]).

When comparing fluorescence (fl) and shock tube (st) relaxation times, it should be noted that $\tau_{fl}/\tau_{st} = (k_{10} - k_{01})/k_{10}$ for the usual conditions, as long as a T ↔ V energy transfer mechanism prevails. Thermal effects must be accounted for, particularly in shock tube studies, where the rate coefficient $> 1/\tau$. Point-by-point analyses must be undertaken in order to obtain a true $\tau'(T(t))$, and hence a true $k_{10}(T(t))\,(1 - e^{-\theta/T(t)})$. If a relaxing gas sample is not optically thin to radiation from all levels then the rate law in fluorescence studies can be very complicated and can depend strongly on v. One must take great care in noting the extremity of the conditions. For example, for $v = 2$, if $\theta \gg T_{vib} \gg T$, $k' = 2\tau^{-1}$; if $T_{vib} \gg \theta \gg T$, $k' = \tau^{-1}(T_{vib}^0/\theta)^{-1} e^{20/T}$ when $t/\tau \ll 1$, and $k' = -\tau^{-1}$ when $\ln(T_{vib}^0/T_*) \ll t/\tau \ll \ln(T_{vib}^0/\theta)$; if $T_{vib} \gg \theta \sim T$, $k' = \tau^{-1}$. In such cases one would also have to account for thermal effects rather precisely. Simple log-plots of fluorescence intensities vs. time would not be appropriate. A proper analysis would yield τ', not τ. The ratio τ'/τ can be close to 1 if the gas is very dilute in say Ar, but the ratio can be as small as 0.78 for a single classical mode of oscillation, or even less if several modes are involved. Under some conditions, thermal effects can lead to curious ratios: e.g. −0.0193 cited above.

In summary, great care is needed in interpreting vibrational relaxation times.

Acknowledgement

The author gratefully acknowledges support from the Natural Sciences and Engineering Research Council of Canada.

1. W. D. Breshears. Chem. Phys. Lett. **20**, 429 (1973).
2. H. A. Bethe and E. Teller. Ballistic Research Labs, Rept. X-117 (1941).
3. H.-J. Bauer. *In* Physical acoustics. Vol. 2A. *Edited by* W. P. Mason. Academic Press, New York. 1965. p. 47.
4. J. F. Clarke and M. McChesney. The dynamics of real gases. Butterworths, London. 1964.
5. J. W. Rich and R. G. Rehm. *In* Proceedings of the 11th Symposium Internat. on Combustion, The Combustion Inst., Pittsburgh. 1967. p. 37.
6. R. W. Lutz and J. H. Kiefer. Phys. Fluids, **9**, 1638 (1966).
7. J. E. Dove and H. Teitelbaum. Chem. Phys. **6**, 431 (1974).
8. J. C. Decius. J. Chem. Phys. **32**, 1262 (1960).
9. E. Avramides and T. F. Hunter. J. Chem. Soc. Faraday Trans. II, **75**, 515 (1979).
10. J. T. Yardley and C. B. Moore. J. Chem. Phys. **49**, 1111 (1968).
11. J. C. Stephenson and C. B. Moore. J. Chem. Phys. **56**, 1295 (1972).
12. V. Blackman. J. Fluid Mech. **1**, 61 (1956).
13. J. H. Kiefer and R. W. Lutz. J. Chem. Phys. **44**, 658 (1965).

Can. J. Chem. Downloaded from www.nrcresearchpress.com by 210.87.254.42 on 09/06/12
For personal use only.

Generalized rate law for vibrational relaxation of a pure diatomic gas

HESHEL TEITELBAUM

Ottawa–Carleton Institute for Research and Graduate Studies in Chemistry, Department of Chemistry, University of Ottawa, Ottawa, Ont., Canada K1N 9B4

Received August 3, 1982

HESHEL TEITELBAUM. Can. J. Chem. **61**, 1267 (1983).

The master equation for the vibrational relaxation of a pure gas of diatomic molecules AB is reduced to a simple analytical rate law. Anharmonicity is accounted to first order, and both T–V and near-resonant V–V energy transfer processes are included with the limitation that $\Delta v = \pm 1$. Landau–Teller type transition probabilities are used to scale the rate constants. The rate law consists of a pair of simultaneous first order non-linear differential equations — one for the mean vibrational energy, $\bar{E}$, and one for the mean squared vibrational energy $\overline{E^2}$; or equivalently a non-linear second order differential equation for $\bar{E}$ with respect to time, t, plus an algebraic equation for $\overline{E^2}$. These lead to

$$\frac{d\bar{E}}{dt} = -\frac{(\bar{E} - \overline{E^\infty})}{\tau} - \chi_e h\nu_e k_{1,1}^{2,0} N\left[2\left(\frac{\bar{E}}{h\nu'}\right)^2 - \frac{\overline{E^2}}{(h\nu')^2} + \frac{\bar{E}}{h\nu'}\right]_0 e^{-\alpha t}$$

where χ_e is the anharmonicity factor, N the molecular concentration, ν_e the spectroscopic vibrational frequency; $\nu' = \nu_e(1 - \chi_e)$; $\nu'' = \nu_e(1 - 3\chi_e)$; $\alpha = Nk_{1,1}^{2,0}/(1 - \chi_e) + 2/\tau$; $1/\tau = Nk_{1,0}(1 - e^{-h\nu''/kT})$; $k_{1,0}$ the rate constant for the process $AB(v = 1) + AB(v) \rightarrow AB(v = 0) + AB(v)$; and $k_{1,1}^{2,0}$ the rate constant for the process $2AB(v = 1) \rightarrow AB(v = 0) + AB(v = 2)$. It is shown that the Bethe–Teller law, $d\bar{E}/dt = -(E - \bar{E}^\infty)/\tau$, is valid only in the limit of zero anharmonicity or slow V–V processes, or when the initial population is Boltzmann, such as in shock tube experiments. Furthermore, a population distribution which is initially Boltzmann will remain so; whereas a non-Boltzmann distribution rapidly becomes a Boltzmann distribution on a time scale determined by the sum of T–V and V–V rate constants. The present study allows one to gauge the importance of two common assumptions: the validity of the Bethe–Teller law and the existence of a Boltzmann distribution or vibrational temperature during the relaxation.

HESHEL TEITELBAUM. Can. J. Chem. **61**, 1267 (1983).

L'équation "master" qui décrit la relaxation vibrationelle d'un gaz pur de molécules diatomiques est simplifiée afin d'obtenir une loi analytique simple. On tient compte de l'anharmonicité. Les processus T–V et les processus V–V presque-resonants sont inclus, avec la limitation $\Delta v = \pm 1$. On réduit les probabilités de transition de la sorte Landau–Teller à une échelle commune. La loi de la vitesse qui en résulte consiste en une paire simultanée d'équations différentielles non-linéaires de première ordre — l'une pour l'énergie moyenne, $\bar{E}$, et l'autre pour la moyenne des énergies carrées, $\overline{E^2}$. Cela équivaut a une équation différentielle non-linéaire de deuxième ordre pour $\bar{E}$ par rapport aux temps, t, plus une équation algébrique pour $\overline{E^2}$. Ces deux donnent

$$\frac{d\bar{E}}{dt} = -\frac{(\bar{E} - \overline{E^\infty})}{\tau} - \chi_e h\nu_e k_{1,1}^{2,0} N\left[2\left(\frac{\bar{E}}{h\nu'}\right)^2 - \frac{\overline{E^2}}{(h\nu')^2} + \frac{\bar{E}}{h\nu'}\right]_0 e^{-\alpha t}$$

ou χ_e est la facteur d'anharmonicité, N la concentration moléculaire, ν_e la fréquence vibrationelle spectroscopique; $\nu' = \nu_e(1 - \chi_e)$; $\nu'' = \nu_e(1 - 3\chi_e)$; $\alpha = Nk_{1,1}^{2,0}/(1 - \chi_e) + 2/\tau$; $1/\tau = Nk_{1,0}(1 - e^{-h\nu''/kT})$; $k_{1,0}$ est la constante de vitesse pour $AB(v = 1) + AB(v) \rightarrow AB(v = 0) + AB(v)$; et $k_{1,1}^{2,0}$ est la constante de vitesse pour $2AB(v = 1) \rightarrow AB(v = 0) + AB(v = 2)$. On montre que la loi de Bethe–Teller, $d\bar{E}/dt = -(E - \bar{E}^\infty)/\tau$, est valable seulement dans la limite de nul anharmonicité et des processus V–V extrémement lents, ou quand la répartition de la population initialle est Boltzmann, telle qui existe dans les expériences de tube de choc. En plus, une répartition de population qui est initiallement Boltzmann restera toujours Boltzmann; tandis qu'une répartition non-Boltzmann devient Boltzmann rapidement avec une échelle de temps déterminée par la somme des constantes de vitesse T–V et V–V. L'étude actuelle nous permet d'estimer l'importance de deux suppositions utilisées par les chercheurs: la validité de la loi de Bethe–Teller et l'existence d'une répartition Boltzmann ou d'une température vibrationelle.

Introduction

In the analysis of measurements of vibrational relaxation times of diatomic molecules it is often assumed that the rate of equilibration of the vibrational energy E is given by

$$[1] \quad -\frac{dE}{dt} = \frac{1}{\tau}[E - E^\infty]$$

where E^∞ is the thermodynamically expected equilibrium vibrational energy at the temperature T (which may also be a function of time). This equation is strictly valid for small departures from equilibrium (1). However, it can be shown that for special mechanisms of the relaxation process (viz. translation-to-vibration mechanisms, T–V, even large departures from equilibrium lead to eq. [1] being valid regardless of the initial distribution of vibrational level populations as long as this distribution is Boltzmann (2) initially. If the relaxing molecules can be represented by simple harmonic oscillators then τ is related simply to the rate constant k_{10} for the process

$$AB(v = 1) + M \rightleftarrows AB(v = 0) + M$$

by

$$\tau^{-1} = k_{10}[M](1 - e^{-\theta/T})$$

Can. J. Chem. Downloaded from www.nrcresearchpress.com by 210.87.254.5 on 09/06/12
For personal use only.

where $\theta = h\nu/k$, ν is the fundamental oscillator frequency, and [M] is the concentration of the vibrationally inert collision partner M. When the initial distribution is non-Boltzmann, such as can occur if the molecules are laser-exited or if they are products of an exothermic chemical reaction, it is often further additionally supposed (3) that the distribution rapidly becomes Boltzmann in form via vibration-to-vibration, V–V, energy transfer steps:

$$AB(v) + AB(v') \rightleftarrows AB(v + n) + AB(v' - n)$$

For harmonic oscillators this is a resonant process, and the resonance supposedly accounts for the rapidity of the V–V processes. Thus eq. [1] is universally used to analyze measurements of vibrational relaxation of diatomic molecules. To some extent polyatomic molecules may be included, particularly if the modes of vibration relax independently (4). Otherwise, it is generally recognized that more care is required. In fact experiments bear out the validity of eq. [1] over a limited range of conditions (5, 6). In a recent paper we discussed the consequences of the above two assumptions and thereby suggested experiments whereby they could be tested. Indeed it is clear that the above assumptions cannot always hold. For example, when the relaxing molecule encounters inert species, e.g., argon, almost exclusively, then V–V processes cannot occur. Secondly, V–V processes are second-order in [AB(v)], whereas T–V processes are first order in [AB(v)]. Thus we might expect that inclusion of only moderately rapid V–V steps into the mechanism which normally leads to eq. [1] would now lead to an analogous one which is non-linear in E. Thus by including V–V processes of finite rate, both approximations are affected: Boltzmann distributions and the validity of eq. [1]. Under most experimental conditions small non-linearities are hard to detect even if they exist. Yet they may throw light on the mechanism of vibrational relaxation. Thus it is important to know when they might be expected. In this work we examine the influence of V–V steps on the energy rate law. In so doing we determine the conditions which enable us to measure non-linearities, and which allow us to interpret vibrational relaxation measurements in more detail, and which give us an alternative rate law valid even when non-Boltzmann distributions persist.

The relaxation model

In the simplest approach we consider a set of harmonic oscillator energy levels, m. The rate of change of population of the individual levels N_m can be expressed by a master equation which includes contributions from T–V and V–V processes. For the moment we consider the V–V portion only. Then

$$[2]\quad \frac{dN_m}{dt} = -k_{m,1}^{m+1,0}N_mN_1 + k_{m+1,0}^{m,1}N_{m+1}N_0 + k_{m-1,1}^{m,0}N_{m-1}N_1 - k_{m,0}^{m-1,1}N_mN_0$$

where $k_{i,j}^{k,l}$ are the rate constants for the process

$$AB(v = i) + AB(v = j) \rightleftarrows AB(v = k) + AB(v = l)$$

In eq. [2] we have considered only those processes which are most likely, namely, resonant energy transfer ($i + j = k + l$), and $\Delta v = \pm 1$ for an individual molecule. Furthermore, a molecule will collide most likely with another which exists either in $v = 0$ or $v = 1$, particularly if a Boltzmann or near-Boltzmann distribution is applicable. This last assumption will be eliminated below. The reasoning is identical for all other possible collison partners. Equation [2] applies to all v except $v = 0$, 1:

$$[3]\quad \frac{dN_0}{dt} = k_{1,1}^{2,0}N_1^2 - k_{2,0}^{1,1}N_2N_0 + k_{2,1}^{3,0}N_2N_1 - k_{3,0}^{2,1}N_3N_0 + \ldots$$

$$[4]\quad \frac{dN_1}{dt} = 2k_{2,0}^{1,1}N_2N_0 - 2k_{1,1}^{2,0}N_1^2 + k_{3,0}^{2,1}N_3N_0 - k_{2,1}^{3,0}N_2N_1 + \ldots$$

At any given instant, the total vibrational energy is proportional to $\sum_0^\infty mN_m$. Thus we multiply eqs. [2], [3], and [4] by the appropriate value of m and perform the summation:

$$\frac{d}{dt}\sum_0^\infty mN_m\Big|_{V-V} = -\sum_1^\infty mk_{m,1}^{m+1,0}N_mN_1 + \sum_1^\infty mk_{m+1,0}^{m,1}N_{m+1}N_0 + \sum_2^\infty mk_{m-1,1}^{m,0}N_{m-1}N_1 - \sum_2^\infty mk_{m,0}^{m-1,1}N_mN_0 - \sum_1^\infty 1k_{m,1}^{m+1,0}N_mN_1 + \sum_1^\infty 1k_{m+1,0}^{m,1}N_{m+1}N_0$$

$$= -\sum_1(m+1)k_{m,1}^{m+1,0}N_mN_1 + \sum_1(m+1)k_{m+1,0}^{m,1}N_{m+1}N_0 + \sum_2 mk_{m-1,1}^{m,0}N_{m-1}N_1 - \sum_2 mk_{m,0}^{m-1,1}N_mN_0$$

which, upon relabelling in the latter two sums, gives

$$\frac{d}{dt}\sum_0^\infty mN_m\Big|_{V-V} = -\sum_1(m+1)k_{m,1}^{m+1,0}N_mN_1 + \sum_1(m+1)k_{m+1,0}^{m,1}N_{m+1}N_0 + \sum_1(m+1)k_{m,1}^{m+1,0}N_mN_1 - \sum_1(m+1)k_{m+1,0}^{m,1}N_{m+1}N_0$$

$$= 0$$

Thus, V–V processes do not contribute to the rate of change of vibrational energy. Including other collision partners in addition to those with $v = 0$ and 1 would not change this conclusion, nor would allowing $|\Delta v| > 1$. This result is to be expected for resonant

Can. J. Chem. Downloaded from www.nrcresearchpress.com by 210.87.254.5 on 09/06/12
For personal use only.

energy transfer. If individual collisions do not change the total vibrational energy, then neither will the sum of any number of such collisions. Resonant energy transfer can at best redistribute energy among the levels but not increase or decrease it on the whole. We have ignored non-resonant processes because they can be considered as a sum of two processes — a resonant V–V process plus a non-resonant T–V process, and therefore their probabilities are much less than the product of the two components. Thus, if we wish to study the effect of V–V processes on the form of the energy rate law we must consider either these second order effects or else a more realistic model, namely, an anharmonic oscillator model. We expect the near-resonant V–V processes of anharmonic oscillators to be nearly as important as the resonant V–V processes of harmonic oscillators. Furthermore, each collision results in a small but net energy gain or loss. Thus, the near-resonant V–V processes will give a non-zero contribution to dE/dt, and we consider them to be the dominant V–V effect.

In what follows, we shall evaluate dE/dt for anharmonic oscillators using Landau–Teller type rate constants, including both T–V and "resonant" V–V processes. In a sense, this work can be considered to be an extension of the early Shuler studies (2, 7) which did not treat non-linear situations.

It should be borne in mind that while our molecules are considered anharmonic oscillators as far as energetics and detailed balancing are concerned, we retain Landau–Teller type rate constants of harmonic oscillators. We believe that this will be a reasonable representation of anharmonic oscillator transition rate constants at least with respect to their dependence on quantum number m, especially for the low-lying vibrational levels containing most of the vibrational energy.

The energy of an anharmonic oscillator in a vibrational state m referred to the ground state is given to a good approximation by

$$[5] \quad \epsilon_m = mh\nu_e(1 - \chi_e) - m^2 h\nu_e\chi_e$$

where χ_e is the anharmonicity constant. Clearly, for an anharmonic oscillator we must sum m^2N_m as well as mN_m in order to obtain $E = \sum N_m\epsilon_m$. The summation contains a finite number of terms, just as for the case of a harmonic oscillator truncated at the dissociation limit. We have shown in an earlier study (8) that this finiteness leads simply to the same result as that for a sum of infinite terms plus a truncation error or term which accounts for molecular dissociation. Under conditions where dissociation is not important to the relaxation we may ignore this term. Hence the following summations are described only by the lower limit to m.

A, T–V rates

For collisions of AB(m) with an inert species (whose vibrational energy, if any, does not change upon collision) we consider only $\Delta m = \pm 1$

$$\left.\frac{-dN_m}{dt}\right|_{T-V} = (k_{m,m+1}N_m + k_{m,m-1}N_m - k_{m+1,m}N_{m+1} - k_{m-1,m}N_{m-1})\sum_0 N_m$$

Here we have assumed that all AB(m) are equally efficient at (de-) exciting a molecule and that the collision frequencies for all AB(m) are the same. Thus, the rate of change of vibrational energy E is given by

$$[6] \quad \left.\frac{dE}{dt}\right|_{T-V} = h\nu_e(1 - \chi_e)\sum_0 m\left.\frac{dN_m}{dt}\right|_{T-V} - h\nu_e\chi_e\sum_0 m^2\left.\frac{dN_m}{dt}\right|_{T-V}$$

in which

$$[7] \quad -\sum_0 m\left.\frac{dN_m}{dt}\right|_{T-V} = N\left[\sum_0 mk_{m,m+1}N_m - \sum_1 mk_{m-1,m}N_{m-1} + \sum_1 mk_{m,m-1}N_m - \sum_0 mk_{m+1,m}N_{m+1}\right]$$

$$= N\left[\sum_0 mk_{m,m+1}N_m - \sum_0 (m+1)k_{m,m+1}N_m + \sum_0 (m+1)k_{m+1,m}N_{m+1} - \sum_0 mk_{m+1,m}N_{m+1}\right]$$

$$= -N\sum_0 k_{m,m+1}N_m + N\sum_0 k_{m+1,m}N_{m+1}$$

where $\sum_0 N_m = N$.

The V–T transition probabilities are known to some extent, namely their dependence on m. According to Landau and Teller (9, 10) both $k_{m+1,m}$ and $k_{m,m+1}$ are proportional to $(m+1)$. Note that in the derivation of these results microscopic reversibility had been neglected. The standard remedy, often called symmetrization (11), is to introduce the factor $e^{\pm\Delta\epsilon/2kT}$, where $\Delta\epsilon$ is the energy difference (constant for harmonic oscillators) between the levels m and $(m+1)$. Thus $k_{m+1,m} \propto (m+1)e^{\Delta\epsilon/2kT}$, and $k_{m,m+1} \propto (m+1)e^{-\Delta\epsilon/2kT}$. This procedure guarantees detailed balance, i.e. $k_{m,m+1}/k_{m+1,m} = e^{-\Delta\epsilon/kT}$, and hence the proper equilibrium populations. For anharmonic oscillators, $\Delta\epsilon$ can be found from eq. [5], viz.

$$\Delta\epsilon = (1 - 2\chi_e)h\nu_e - 2mh\nu_e\chi_e$$

Therefore

$$k_{m+1,m} = k_{1,0}(m+1)e^{-m\phi}$$

$$k_{m,m+1} = k_{0,1}(m+1)e^{m\phi}$$

and

Can. J. Chem. Downloaded from www.nrcresearchpress.com by 210.87.254.5 on 09/06/12
For personal use only.

$$k_{0,1}/k_{1,0} = e^{-\theta'/T+\phi}$$

where $\theta' = h\nu_e(1 - \chi_e)/k$ and $\phi = h\nu_e\chi_e/kT$. Using these results, [7] becomes

$$-\sum_0 m\frac{dN_m}{dt}\bigg|_{T-V} = N\left[-\sum_0 k_{m,m+1}N_m + \sum_1 k_{m,m-1}N_m\right] = N\left[-k_{0,1}\sum_0(m+1)N_m e^{m\phi} + k_{1,0}\sum_0 mN_m e^{-m\phi}\right]$$

Similarly, the contribution quadratic in m becomes

$$-\sum_0 m^2\frac{dN_m}{dt}\bigg|_{T-V} = N\left[\sum_0 m^2k_{m,m+1}N_m + \sum_1 m^2k_{m,m-1}N_m - \sum_0 m^2k_{m+1,m}N_{m+1} - \sum_1 m^2k_{m-1,m}N_{m-1}\right]$$

$$= N\left[-k_{0,1}\sum_0(2m+1)(m+1)N_m e^{m\phi} + k_{1,0}\sum_0 m(2m-1)N_m e^{-m\phi}\right]$$

We can combine these two results with eq. [6] to determine the T–V contribution to dE/dt. However, it is instructive to consider first the magnitude of $m\phi$. The quantity ϕ itself is typically of the order of 0.001 to 0.03; m may be anywhere between 1 and 100. It suffices to consider the largest m which might be important, and we arbitrarily define this level p as being one whose relative population at equilibrium is less than 1% or $\sim e^{-5}$. Thus

$$e^{-p\theta'/T}(1 - e^{-\theta'/T}) \simeq e^{-5}$$

Two limiting cases may be considered, depending on the magnitude of θ/T. For $\theta/T \to \infty$ then $p\theta/T = 5$, and $e^{\pm p\phi} = e^{\pm 5\chi_e}$. At worst, then, $e^{\pm m\phi}$ is not far from unity. For $\theta/T \to 0$, $e^{-p\theta/T} = e^{-5}T/\theta$, and $e^{\pm p\phi} = Te^{\pm 5\chi_e}/\theta$. Even if θ/T is as low as 0.001, $p\phi$ is only as large as 0.12. Typically, for temperatures where vibrational relaxation times are measureable, $\theta/T \sim 1$–3. Therefore we feel justified in replacing $e^{\pm m\phi}$ by $(1 \pm m\phi)$. This approximation is certainly good for all levels $m < p$ which contribute significantly to the energy at equilibrium and therefore even more so when far from equilibrium, particularly for shock tube experiments. Using this approximation

$$\frac{dE}{dt}\bigg|_{T-V} = k\theta'\sum_0 m\frac{dN_m}{dt} - \phi kT\sum_0 m^2\frac{dN_m}{dt}$$

can be simplified:

$$\frac{dE}{dt}\bigg|_{T-V} \approx NkT\left\{k_{1,0}\left(\frac{\theta'}{T} - \phi\right)e^{-(\theta'/T-\phi)}\sum_0 N_m - \left[\frac{\theta'}{T}(k_{1,0} - e^{\phi}k_{0,1}) + \phi(3k_{0,1} + k_{1,0}) + \phi^2k_{0,1}\right]\sum_0 mN_m\right.$$
$$\left. + \phi\left[\frac{\theta'}{T}(k_{0,1} + k_{1,0}) + 2(k_{1,0} - k_{0,1}) - \phi(2k_{1,0} - 3k_{0,1})\right]\sum m^2N_m - 2\phi^2(k_{0,1} + k_{1,0})\sum m^3N_m\right\}$$

Noting that $\phi \ll 1$ and $\phi \ll \theta'/T$, and rearranging:

$$\frac{dE}{dt}\bigg|_{T-V} \approx NkT\left\{k_{1,0}\left(\frac{\theta'}{T} - \phi\right)e^{-(\theta'/T-\phi)}\sum_0 N_m - (k_{1,0} - e^{\phi}k_{0,1})[(\theta'/T)\sum_0 mN_m - \phi\sum_0 m^2N_m]\right.$$
$$\left. + \phi[(\theta'/T)(k_{0,1} + k_{1,0}) + k_{1,0}e^{-\theta'/T}]\sum_0 m^2N_m\right\}$$

Using the conservation of mass and energy, which gives $\sum_0 N_m = N$ and

[8] $$k\theta'\sum_0 mN_m - \phi kT\sum_0 m^2N_m = E$$

allows the above results to be re-expressed as

[9] $$\frac{dE}{dt}\bigg|_{T-V} = -Nk_{1,0}[1 - e^{-(\theta'/T-2\phi)}]\left[E - \frac{Nh\nu_e(1 - 2\chi_e)e^{-(\theta'/T-\phi)}}{1 - e^{-(\theta'/T-2\phi)}}\right]$$
$$+ Nk_{1,0}h\nu_e\chi_e[(\theta'/T)(1 + e^{-(\theta'/T-\phi)}) + (1 - e^{-\theta'/T})]\sum_0 m^2N_m)$$

We recognize the term subtracting from E as being, to a good approximation (12), simply the equilibrium vibrational energy of an ensemble of N anharmonic oscillators, i.e., E^{∞}_{anh}. The last term is of the order of χ_e times the first term on the right hand side, and to the same level of approximation as heretofore, it may be absorbed into E or even neglected. Thus

[10] $$\frac{dE}{dt}\bigg|_{T-V} \approx -\frac{(E - E^{\infty}_{anh})}{\tau}$$

where

[11] $$(N\tau)^{-1} = k_{10}[1 - e^{-(\theta'/T-2\phi)}]$$

Apart from the interpretation of τ, this is experimentally indistinguishable from the Bethe–Teller law (eq. [1]).

B, V–V rates

We have shown earlier that

Can. J. Chem. Downloaded from www.nrcresearchpress.com by 210.87.254.5 on 09/06/12
For personal use only.

$$\sum_0 m \frac{dN_m}{dt}\bigg|_{V-V}$$

makes no contribution to the rate of energy change. Thus we need only evaluate

$$\sum_0 m^2 \frac{dN_m}{dt}$$

We use the same formalism as above, this time explicitly allowing for

$$AB(v = m) + AB(v = n) \rightleftarrows AB(v = m + 1) + AB(v = n - 1)$$

As pointed out by Shuler (7*d*, *e*), collisions resulting in $\Delta v \geq 2$ do not contribute significantly to the overall relaxation behaviour; thus, we need consider only $\Delta v = \pm 1$.

$$[12] \quad \frac{d}{dt}\sum_0 m^2 N_m\bigg|_{V-V} = -\sum_1 m^2 k_{m,n}^{m+1,n-1} N_m N_n + \sum_1 m^2 k_{m+1,n-1}^{m,n} N_{m+1} N_{n-1} + \sum_1 m^2 k_{m-1,n}^{m,n-1} N_{m-1} N_n - \sum_1 m^2 k_{m,n-1}^{m-1,n} N_m N_{n-1}$$

where the summation is from $n = 1$ and $m = 1$, and where we have accounted for all possible V–V transitions subject to $\Delta v = \pm 1$ with collision partners changing v in opposite directions. Formally this includes such processes as

$$AB(v = m) + AB(v = m - 1) \rightarrow AB(v = m - 1) + AB(v = m)$$

and their reverse processes whose contributions to dN_m/dt are obviously zero. Those terms as well as a large number of others in [12] cancel out. It is easily shown that

$$[13] \quad \frac{d}{dt}\sum_0 m^2 N_m\bigg|_{V-V} = \sum_{\substack{m=0 \\ n=1}} (2m + 1) k_{m,n}^{m+1,n-1} N_m N_n - \sum_{\substack{m=0 \\ n=1}} k_{m+1,n-1}^{m,n} N_{m+1} N_{n-1} (2m + 1)$$

Noting that $\sum_{\substack{m=0 \\ n=1}} k_{m,n}^{m+1,n-1} N_m N_n - \sum_{\substack{m=0 \\ n=1}} k_{m+1,n-1}^{m,n} N_{m+1} N_{n-1}$ is just $\sum_{n=0} \frac{dN_n}{dt} = 0$ when dissociation is unimportant, then

$$[14] \quad \sum_0 m^2 \frac{dN_m}{dt}\bigg|_{V-V} = 2\sum_{\substack{m=1 \\ n=1}} m k_{m,n}^{m+1,n-1} N_m N_n - 2\sum_{\substack{m=1 \\ n=1}} m k_{m+1,n-1}^{m,n} N_{m+1} N_{n-1}$$

The usual Landau–Teller probabilities for V–V transfer of energy are:

$$k_{m,n}^{m+1,n-1} = (m + 1) n k_{0,1}^{1,0}$$

$$k_{m+1,n-1}^{m,n} = (m + 1) n k_{1,0}^{0,1}$$

These rules obviously do not satisfy detailed balance. As above, we symmetrize the rate constants to account for this. Thus

$$k_{m,n}^{m+1,n-1} = (m + 1) n k_{VV} e^{(m+1-n)\phi}$$

and

$$k_{m+1,n-1}^{m,n} = (m + 1) n k_{VV} e^{-(m+1-n)\phi}$$

where $k_{VV} \equiv k_{0,1}^{1,0} = e^{-\phi} k_{1,1}^{2,0}/2$.

The exponential factor ensures the correct relative level populations at equilibrium, e.g., $k_{1,1}^{2,0}/k_{2,0}^{1,1} = (N_2 N_0/N_1^2)_{eq} = e^{2\phi}$. Using these relationships, eq. [14] becomes

$$\sum_0 m^2 \frac{dN_m}{dt}\bigg|_{V-V} = 2k_{VV}\left[\sum_{m=1} e^{\phi} m(m + 1) e^{m\phi} N_m \left(\sum_{n=1} n e^{-n\phi} N_n\right) - \sum_{m=1} m(m + 1) e^{-m\phi} N_{m+1} \left(\sum_{n=1} n e^{n\phi} N_{n-1}/e^{\phi}\right)\right]$$

Again, we expand the exponentials to two terms. Then, after considerable algebraic manipulation, and neglecting terms of the order of ϕ, we obtain

$$[15] \quad \sum_0 m^2 \frac{dN_m}{dt}\bigg|_{V-V} \approx 2k_{VV} e^{\phi}\left[2\left(\sum_0 m N_m\right)^2 - N\left(e^{\phi}\sum_0 m^2 N_m - \sum_0 m N_m\right)\right]$$

Now, since $\frac{d}{dt}\sum m N_m\Big|_{V-V} = 0$, the V–V contribution to the rate of energy change is:

$$[16] \quad \frac{dE}{dt}\bigg|_{V-V} = -2\phi k T k_{VV} e^{\phi}\left[2\left(\sum_0 m N_m\right)^2 - N\left(e^{\phi}\sum_0 m^2 N_m - \sum_0 m N_m\right)\right]$$

Can. J. Chem. Downloaded from www.nrcresearchpress.com by 210.87.254.5 on 09/06/12
For personal use only.

Can. J. Chem. Downloaded from www.nrcresearchpress.com by 210.87.254.5 on 09/06/12
For personal use only.

Rate law for vibrational relaxation

Both T–V and V–V processes contribute to the rate of change of vibrational energy. The net rate is given by the sum of eqs. [10] and [16].

$$\frac{dE}{dt} = \frac{-(E - E^{\infty})}{\tau} - 2\phi kTk_{VV}e^{\phi}\left[2\left(\sum_0 mN_m\right)^2 - N\left(e^{\phi}\sum_0 m^2N_m - \sum_0 mN_m\right)\right]$$

The term $\sum_0 mN_m$ is proportional to the vibrational energy of a set of harmonic oscillators and it forms the major portion of the vibrational energy of our set of anharmonic oscillators. It can be expressed in terms of E and $\sum_0 m^2N_m$ by using eq. [8]:

$$[17]\quad \sum_0 mN_m = [E + \phi kT\sum_0 m^2N_m]/k\theta' \approx E/k\theta'$$

Therefore

$$[18]\quad \frac{dE}{dt} \approx -\frac{(E - E^{\infty})}{\tau} - 2\phi kTk_{VV}e^{\phi}\left[2\left(\frac{E}{k\theta'}\right)^2 - N\left(\sum_0 m^2N_m - \frac{E}{k\theta'}\right)\right]$$

The second moment, $\sum_0 m^2N_m$, is more difficult to evaluate. Recourse is needed to the differential equation whose T–V and V–V components were discussed above, i.e.

$$\frac{d}{dt}\sum_0 m^2N_m = N[k_{0,1}\sum_0 (2m + 1)(m + 1)N_m e^{m\phi} - k_{1,0}\sum_0 m(2m - 1)N_m e^{-m\phi}] + 2k_{VV}e^{\phi}[2E^2/k^2\theta'^2 - N(e^{\phi}\sum_0 m^2N_m - E/k\theta')]$$

Using $e^{\pm m\phi} \approx 1 \pm m\phi$, and after some rearrangement of terms,

$$[19]\quad \frac{d}{dt}\sum_0 m^2N_m \approx Nk_{1,0}[Ne^{\phi-\theta'/T} + (1 + 3e^{\phi-\theta'/T})E/k\theta' - 2(1 - e^{\phi-\theta'/T})\sum_0 m^2N_m] + 2k_{VV}e^{\phi}[2E^2/k^2\theta'^2 + NE/k\theta' - N\sum_0 m^2N_m]$$

Together with eq. [18] this comprises the general rate law for vibrational relaxation. These equations must be solved simultaneously. Since this is not very practical for the analysis of experimental results, we attempt to combine them into a single differential equation. Before doing so, we note that $\sum_0 m^2N_m$ can be written as $N\overline{E^2}/k^2\theta'^2$, i.e., it is an average of the square of the molecular vibrational energies of harmonic oscillators and approximately so for anharmonic oscillators. Secondly, for harmonic oscillators at equilibrium

$$\frac{2\bar{E}^2}{k\theta} + \bar{E} = h\nu e^{-u}(1 + e^{-u})/(1 - e^{-u})^2$$

where $u = h\nu/kT$. Furthermore

$$\overline{E^2}/k\theta = h\nu\sum_0 m^2N_m/N = h\nu\sum_0 m^2e^{-mu}/Q \text{ at equilibrium}$$

where Q, the partition function, is $(1 - e^{-u})^{-1} = \sum_0 e^{-mu}$. Noting that $d^2Q/du^2 = \sum m^2e^{-mu}$, then at equilibrium $\overline{E^2}/k\theta$ also becomes $h\nu e^{-u}(1 + e^{-u})/(1 - e^{-u})^2$, and the second term on the right hand side of eq. [19] approaches zero at equilibrium. Taking the anharmonicity into account to first order, the first term also becomes zero. Thus, both $d\bar{E}/dt$ and $\sum m^2dN_m/dt$ approach zero at equilibrium, as is proper. We also note that $k_{VV} \gg k_{1,0}$ (V–V transition probabilities per collision are $\sim 10^{-3}$, whereas T–V transition probabilities per collision are several orders of magnitude smaller). Therefore we are tempted to ignore the first term on the right hand side of eq. [19]. However, the factor $(2E^2/k^2\theta'^2 + NE/k\theta' - N\sum m^2N_m)$ can be very small not only near equilibrium, but also at other times. In fact, any time that a Boltzmann distribution exists during the relaxation, this factor is exactly zero. Such a stituation will occur for example at $t = 0$ in a shock tube experiment; at $t = 0$ the first term $\neq 0$, and can therefore not be ignored. Thus, on a per molecule basis, eqs. [18] and [19] become:

$$[20]\quad \frac{d\bar{E}}{dt} = -\frac{(\bar{E} - \bar{E}^{\infty})}{\tau} - \chi_e'k_{1,1}^{2,0}N\left[\frac{2\bar{E}^2}{k\theta'} - \frac{\overline{E^2}}{k\theta'} + \bar{E}\right]$$

$$[21]\quad \frac{d\overline{E^2}}{dt} = Nk_{1,0}\left[e^{\phi-\theta'/T} + (1 + 3e^{\phi-\theta'/T})\frac{\bar{E}}{k\theta'} - 2(1 - e^{\phi-\theta'/T})\frac{\overline{E^2}}{k^2\theta'^2}\right]k^2\theta'^2 + k_{1,1}^{2,0}N\left[\frac{2\bar{E}^2}{k\theta'} - \frac{\overline{E^2}}{k\theta'} + \bar{E}\right]k\theta'$$

where $\chi_e' = \chi_e/(1 - \chi_e)$, and $k_{1,1}^{2,0} = 2k_{VV}e^{\phi}$ is the rate constant for the process

$$AB(v = 1) + AB(v = 1) \rightarrow AB(v = 2) + AB(v = 0)$$

We proceed to eliminate $\overline{E^2}$ by differentiating eq. [20] with respect to time and then substituting eq. [21] into the result. To simplify matters we consider τ, $k_{1,1}^{2,0}$, and $\bar{E}^{\infty}$ not to depend strongly on time, i.e. the temperature, on which each depends, does not vary significantly during the relaxation. Strictly speaking this cannot be true for gases of finite composition and of sufficient concentration for V–V processes to be important. However, these secondary matters will be discussed in subsequent papers dealing with solutions of the rate law. Here, we consider the main effects. We obtain (with $\chi_e \ll 1$)

$$[22]\quad \chi_e' N k_{1,1}^{2,0} \frac{\overline{E^2}}{k\theta'}\left[N k_{1,1}^{2,0} + \frac{2}{\tau}\right] = -\frac{d\bar{E}}{dt}\left[\chi_e' N k_{1,1}^{2,0} + \frac{1}{\tau}\right] - 4\chi_e' N k_{1,1}^{2,0} \frac{\bar{E}}{k\theta'}\frac{d\bar{E}}{dt} - \frac{d^2\bar{E}}{dt^2}$$
$$+ \chi_e' N k_{1,1}^{2,0} k\theta' \left\{N k_{1,0}\left[e^{-u} + \frac{\bar{E}}{k\theta'}(1 + 3e^{-u})\right] + N k_{1,1}^{2,0} \frac{\bar{E}}{k\theta'}\left(1 + \frac{2\bar{E}}{k\theta'}\right)\right\}$$

or

$$[23]\quad \frac{d\bar{E}}{dt}\left[\frac{N k_{1,1}^{2,0}}{1 - \chi_e} + \frac{3}{\tau}\right] = -\frac{(\bar{E} - \bar{E}^{\infty})}{\tau}\left[N k_{1,1}^{2,0} + \frac{2}{\tau}\right] - \chi_e' N k_{1,1}^{2,0}\left[\left(\frac{\bar{E} - \bar{E}^{\infty}}{\tau}\right)\left(1 + \frac{4\bar{E}}{k\theta'}\right) + \frac{4\bar{E}}{k\theta'}\frac{d\bar{E}}{dt}\right] - \frac{d^2\bar{E}}{dt^2}$$

Equation [23] is the generalized rate law for the vibrational relaxation of a pure gas of diatomic molecules. Three important conclusions are evident:

(*a*) Equation [23] is a second order differential equation. Its solution depends explicitly not only on the initial energy (or population distribution) but also on the initial *rate* of energy change. Thus, unlike the Bethe–Teller law (eq. [1]) the *form* of the expression for $d\bar{E}/dt$ will depend on the initial rate of relaxation. Physically this must be so. For example, if initially all molecules are in $v = 0$, then it is impossible for V–V processes to contribute to the relaxation mechanism: a molecule in $v = 0$ can be excited to $v = 1$ only via a T–V process. This can be seen by putting $\bar{E} = 0$, $\overline{E^2} = 0$ in eq. [20]. The initial rate will be small. Thereafter, when substantial numbers of molecules exist in $v > 1$, V–V processes will compete and possibly eventually dominate. Therefore an incubation period will exist. Such transience will not necessarily be a feature of the relaxation if, choosing a second example, half the molecules were laser-excited into $v = 1$. Then V–V processes could contribute even at $t = 0$. It is interesting to note that it is not necessary to actually specify the entire initial population distribution, but rather the initial energy, and the next higher initial moment!

(*b*) Equation [23] is non-linear in $\bar{E}$ and in $d\bar{E}/dt$. There is a term in $\bar{E}^2$ and in $\bar{E}\,d\bar{E}/dt$. This implies that in general, a quasi-first order time constant does not exist: that phenomenological time constants, τ' and τ'' defined as

$$[24]\quad \tau' = -\frac{(\bar{E} - \bar{E}^{\infty})}{d\bar{E}/dt}$$

$$[25]\quad \tau'' = -\left[\frac{d \ln (d\bar{E}/dt)}{dt}\right]^{-1}$$

are not constants, but rather vary with time, t. Actually, since eq. [23] can be written exactly in term of Nt, then $N\tau'$ and $N\tau''$ are functions of Nt (an experimentalist would write Pt where P is the gas pressure). The non-linearity in Pt gives rise to an insidious effect. For example, doubling the gas pressure ought to half the time scale, at which point τ' and τ'' would be different. This implies that τ' and τ'' are not inversely proportional to N or P. It is quite common in shock tube experiments to vary the initial gas pressure as a means of varying the temperature. It can now be seen that this is a dangerous practice, since $P\tau'$ and $P\tau''$ depend on both T and P. Spurious temperature dependences may result, particularly if some of the experiments within the temperature range sample the transient period and some beyond the transient period.

(*c*) The steady-state solution of eq. [23] corresponds to times beyond the transient period. Then $d^2E/dt^2 \approx 0$ and the vibrational energy will relax exponentially. However the time constant, if one can be said to exist, is not simply τ but is in general related to $k_{1,1}^{2,0}$ as well. Two special cases can be distinguished.

(*i*) $k_{1,1}^{2,0} \gg k_{1,0}$

The transient period is very short. After this period,

$$\frac{d\bar{E}}{dt} = -\frac{(\bar{E} - \bar{E}^{\infty})}{\tau}(1 - \chi_e) - \chi_e\left[\left(\frac{\bar{E} - \bar{E}^{\infty}}{\tau}\right)\left(1 + \frac{4\bar{E}}{k\theta'}\right) + \frac{4\bar{E}\,d\bar{E}}{k\theta'\,dt}\right]$$

It is easy to show that eq. [1] is an exact solution of this equation. Therefore, assuming that the transient period is not being probed, the rate law is identical to the Bethe–Teller law, with the rate being determined by the slowest process, T–V. The success of such a simple rate law under limited conditions (5, 6) may be due to an inability to probe into the incubation zone. The incubation zone itself will be discussed below for shock tube experiments, and in a subsequent paper for arbitrary initial population distributions.

(*ii*) $k_{1,1}^{2,0} \ll k_{1,0}$

It is unlikely that V–V transition probabilities are smaller than T–V probabilities. Yet, were this situation to exist, then the incubation period would be so long as to prevent use of the steady state assumption. Then eq. [23] reduces to

$$\frac{3\,d\bar{E}}{\tau\,dt} = -\frac{2(\bar{E} - \bar{E}^{\infty})}{\tau^2} - \frac{d^2\bar{E}}{dt^2}$$

whose solution is again exactly eq. [1], as is to be expected.

Summarizing, both for fast V–V processes beyond the transient period and for slow V–V processes during the transient period, the rate constant will be $1/\tau$. Between these limiting cases, the situation may be very different. In order to examine the form of the rate law's dependence on $k_{1,1}^{2,0}/k_{1,0}$ and to examine the conditions whereby eq. [1] is valid we must actually solve eq. [23] and obtain $\bar{E}(t/\tau)$, $\overline{E^2}(t/\tau)$, τ'/τ, and τ''/τ for various values of the parameters $k_{1,1}^{2,0}/k_{1,0}$, ϕ, and θ'/T. In general, eq. [23] can be solved numerically. However, it turns out (see below) that for all conditions of interest in shock excitation or laser excitation or chemical activation studies, exact analytical solutions are possible. These will be outlined in a subsequent paper.

To solve eq. [23] we must specify initial values of $\bar{E}$, $d\bar{E}/dt$, and $\overline{E^2}$. Equivalently instead of $\overline{E^2}(t = 0)$, we may specify the

Can. J. Chem. Downloaded from www.nrcresearchpress.com by 210.87.254.5 on 09/06/12
For personal use only.

initial value of $[2\bar{E}^2/k\theta' - \overline{E^2}/k\theta' + \bar{E}]$. It is instructive to consider the special case of a distribution which is initially Boltzmann. As mentioned earlier, this is equivalent to setting the initial value of $[2\bar{E}^2/k\theta' - \overline{E^2}/k\theta' + \bar{E}]$ equal to 0. Shuler has shown (7*c*) that when T–V processes alone are important *and* when the population distribution is initially Boltzmann, the relaxation proceeds through a continuous series of Boltzmann distributions. We would then expect $[2\bar{E}^2/k\theta' - \overline{E^2}/k\theta' + \bar{E}]$ to remain at zero during the relaxation. However, is it not known whether this is still the case when V–V processes contribute to the relaxation of a pure gas. Nor is it known how quickly an initially non-Boltzmann distribution becomes Boltzmann. Therefore our solution for $[2\bar{E}^2/k\theta' - \overline{E^2}/k\theta' + \bar{E}]$ is an important gauge for the existence of a time-dependent vibrational temperature — a concept which is widely used. We put

$$[26]\quad \frac{d\bar{E}}{dt} = -\frac{(\bar{E} - \bar{E}^{\infty})}{\tau} + f(t)$$

and substitute into eq. [23]. The result is

$$[27]\quad \left(\frac{Nk_{1,1}^{2,0}}{1 - \chi_e} + \frac{2}{\tau}\right) = -4\chi_e' Nk_{1,1}^{2,0}\frac{\bar{E}}{k\theta'} - \frac{d\ln f}{dt}$$

Equations [26] and [27] are equivalent to and more amenable to use than eq. [23]. We examine the magnitude of $4\chi_e'\bar{E}/k\theta'$, and note that the largest vibrational energy that any molecule can have is D_e, the bond dissociation energy. In fact it would be extremely rare if *all* molecules had that much energy, even at the start of relaxation. Normally $\bar{E} \ll D_e$ regardless of the type of experiment. Thus

$$4\chi_e'\frac{\bar{E}}{k\theta'} \ll \frac{4\chi_e' D_e}{h\nu_e(1 - \chi_e)} = \frac{4\chi_e D_e}{h\nu_e(1 - \chi_e)^2}$$

The anharmonicity factor is given for a Morse oscillator, and to a good approximation for a real anharmonic oscillator, by $\chi_e \equiv h\nu_e/4D_e$. Therefore $4\chi_e' Nk_{1,1}^{2,0}\bar{E}/k\theta' \ll Nk_{1,1}^{2,0}/(1 - \chi_e)$. We conclude that for all conditions which are conceivably attainable, the term $4\chi_e' Nk_{1,1}^{2,0}\bar{E}/k\theta'$ represents a minor perturbation in eq. [27]. Thus, eq. [27] is easily integrable. We obtain

$$[28]\quad f(t) = f(0)\exp\left[-\left(\frac{Nk_{1,1}^{2,0}}{1 - \chi_e} + \frac{2}{\tau}\right)t\right]$$

The initial value of the function $f(t)$ can be seen from eq. [26] to be related to the initial rate and amplitude of the relaxation. Indeed, by comparing eq. [20] with eq. [26] we recognize that $f(t)$ is nothing more than our Boltzmann distribution gauge function, and that $f(0)$ represents the non-Boltzmann nature of the initial distribution function.

$$[29]\quad \left[\frac{2\bar{E}^2}{k\theta'} - \frac{\overline{E^2}}{k\theta'} + \bar{E}\right] = \left[\frac{2\bar{E}^2}{k\theta'} - \frac{\overline{E^2}}{k\theta'} + \bar{E}\right]_0 \exp\left[-\left(\frac{Nk_{1,1}^{2,0}}{1 - \chi_e} + \frac{2}{\tau}\right)t\right]$$

and

$$[30]\quad \frac{d\bar{E}}{dt} = -\frac{(\bar{E} - \bar{E}^{\infty})}{\tau} - \chi_e' k_{1,1}^{2,0} N\left[\frac{2\bar{E}^2}{k\theta'} - \frac{\overline{E^2}}{k\theta'} + \bar{E}\right]_0 \exp\left[-\left(\frac{Nk_{1,1}^{2,0}}{1 - \chi_e} + \frac{2}{\tau}\right)t\right]$$

We come to some very interesting conclusions:

(*a*) A population distribution which is initially Boltzmann will remain so, regardless of the importance of V–V processes!

(*b*) Furthermore, there is no incubation period in a shock tube experiment: the energy will relax exponentially with a time constant given by τ, the T–V relaxation time.

(*c*) If a non-Boltzmann distribution exists initially, it decays rapidly to a Boltzmann distribution with a rate constant = $(Nk_{1,1}^{2,0} + 2/\tau)$, i.e. *faster* than the energy itself is relaxing rather than at similar rates.

Detailed solutions of eq. [30] will be given in a subsequent paper.

Conclusions

V–V processes as well as molecular anharmonicity are responsible for deviations of the derived rate law from the now superceded Bethe–Teller law. The initial conditions applicable to any individual type of experiment are explicitly accounted for.

Our derivation involved 3 main assumptions:

(*a*) The anharmonicity is not severe. Even for H_2 ($\chi_e = 0.027$) it appears that our approximation $e^{\pm m\phi} = 1 \pm m\phi$ is valid, as explained in the text.

(*b*) The T–V and V–V transition probabilities are given by Landau–Teller harmonic oscillator probabilities. Whereas such a theory may not be totally valid (it is known, e.g., that anharmonicity strongly influences the T–V probabilities (7*e*, 13, 14) we expect that at least with respect to the dependence on vibrational quantum number, m, the assumption is realistic. Essentially the Landau–Teller theory claims that energy transfer becomes more probable the higher the energy of the molecule. For T–V this probability increases linearly with m; for V–V nearly as mn. We related ΣmN_m to $\bar{E}$ and Σm^2N_m to $\overline{E^2}$, and this resulted in a simple rate law involving only $\bar{E}$ and $\overline{E^2}$. If such data were to become available, it would perhaps be better to use empirical scaling laws, and it would be interesting to see if these would lead to substantially different rate laws.

(*c*) Changes of only ± 1 in the quantum number are considered for T–V processes. Similarly $\Delta m = \pm 1$ for V–V processes in opposite directions for each collision partner alone are considered, such that transitions are near-resonant. While this limits our

Can. J. Chem. Downloaded from www.nrcresearchpress.com by 210.87.254.5 on 09/06/12
For personal use only.

model, it is known that for $\Delta m \geq 2$, transition probabilities decrease dramatically (10, 11), and that as a result they contribute little to the relaxation mechanism (7*e*). However, it would be interesting to do a full numerical solution of the master equation to compare with our predictions.

(*d*) The rotational substructure has been ignored. Since V–V probabilities can be as large as 0.01, and R–T as low as 0.01, future modelling should include rotation.

Our main results are that, in general,

(*a*) Initial experimental conditions are important.

(*b*) Transient periods exist such that great care is needed in citing results of experimental measurements. Without recognizing the transient period it is possible that one would conclude τ is not inversely proportional to the pressure. It is suggested that $P\tau$ be quoted not only as a function of temperature, but also as a function of t/τ, so as to facilitate comparison between different experiments. This requirement appears to be unnecessary for shock tube studies of pure diatomic molecules for which the Bethe–Teller law applies exactly. However, the situation is not yet clear for gas mixtures or for pure polyatomic molecules, and therefore it is safest if shock tube studies were included as well.

(*c*) The present rate law permits the experimentalist to test two common assumptions — the validity of the Bethe–Teller law and the existence of a Boltzmann distribution during relaxation.

Acknowledgement

Financial support from the Natural Sciences and Engineering Research Council of Canada is gratefully acknowledged.

1. H. J. BAUER. *In* Physical acoustics. Vol. 2A. *Edited by* W. P. Mason. Academic Press, NY. 1965.
2. J. F. CLARKE and M. MCCHESNEY. The dynamics of real gases. Butterworths, London. 1964. Chapt. 7.
3. W. D. BRESHEARS. Chem. Phys. Lett. **20**, 429 (1973).
4. W. D. BRESHEARS and L. S. BLAIR. J. Chem. Phys. **59**, 5824 (1973).
5. J. E. DOVE and H. TEITELBAUM. Chem. Phys. **6**, 431 (1974).
6. R. W. LUTZ and J. H. KIEFER. Phys. Fluids, **9**, 1638 (1966).
7. (*a*) R. J. RUBIN and K. E. SHULER. J. Chem. Phys. **25**, 59 (1956); (*b*) R. J. RUBIN and K. E. SHULER. J. Chem. Phys. **25**, 68 (1956); (*c*) E. W. MONTROLL and K. E. SHULER. J. Chem. Phys. **26**, 454 (1957); (*d*) N. W. BAZLEY, E. W. MONTROLL, R. J. RUBIN, and K. E. SHULER. J. Chem. Phys. **28**, 700 (1958); (*e*) N. W. BAZLEY, E. W. MONTROLL, R. J. RUBIN, and K. E. SHULER. J. Chem. Phys. **29**, 1185 (1958); (*f*) E. W. MONTROLL and K. E. SHULER. Adv. Chem. Phys. **1**, 361 (1958); (*g*) K. E. SHULER. J. Chem. Phys. **32**, 1692 (1960).
8. H. TEITELBAUM. Can. J. Chem. **60**, 2927 (1982).
9. L. LANDAU and E. TELLER. Phys. Z. Sowjet. **10**, 34 (1936).
10. K. F. HERZFELD and T. A. LITOVITZ. Absorption and dispersion of ultrasonic waves. Academic Press, NY. 1959.
11. D. RAPP and T. KASSAL. Chem. Rev. **69**, 61 (1969).
12. L. HAAR, A. S. FRIEDMAN, and C. W. BECKET. NBS Monograph **20**, (1961).
13. F. H. MIES. J. Chem. Phys. **41**, 903 (1964).
14. H. S. HEAPS and G. HERZBERG. Z. Phys. **133**, 48 (1952).

Can. J. Chem. Downloaded from www.nrcresearchpress.com by 210.87.254.5 on 09/06/12
For personal use only.

Solutions of the generalized rate law for vibrational relaxation of a pure diatomic gas

HESHEL TEITELBAUM

Ottawa–Carleton Institute for Research and Graduate Studies in Chemistry, University of Ottawa, Ottawa, Ont., Canada K1N 9B4

Received August 3, 1982

Can. J. Chem. Downloaded from www.nrcresearchpress.com by 210.87.254.5 on 09/06/12
For personal use only.

HESHEL TEITELBAUM. Can. J. Chem. **61**, 1276 (1983).

The generalized rate law for the relaxation of the vibrational energy of a pure diatomic gas, AB, derived earlier, is solved analytically for a variety of initial conditions corresponding to shock tube, laser-excited fluorescence, and chemical activation experiments. The resulting expressions can be used to easily predict whether a given system will relax according to a V–V or a T–V mechanism or both. The initial conditions and the molecular anharmonicity are shown to be as important, if not more important, for this purpose than the ratio of T–V and V–V rate constants. Behind shock waves the energy relaxes exponentially with a T–V time constant. The initial distribution remains Boltzmann. In laser or chemical activation experiments the energy does not relax exponentially, leading to phenomenological time "constants" $-(\bar{E} - \bar{E}^{\infty})/(d\bar{E}/dt)$ or $-[d \ln (d\bar{E}/dt)/dt]^{-1}$ which are not constant in time and prevent direct comparisons with shock tube data. It is only after an incubation period during which the vibrational energy is redistributed via V–V processes that the energy then exchanges with translational energy and decays. Prescriptions are given to extract T–V and V–V rate constants from such data. The initial degree of laser excitation, α, and the time regime probed, t/τ, must be known for this purpose. However, when direct overtone excitation is used, a careful choice of α can lead to extraction of the T–V constant directly. Even though the vibrational energy itself does not relax exponentially, it is shown that the mean energy, $\bar{E}/h\nu'$, and the mean squared energy, $\overline{E^2}/(h\nu')^2$, relax in such a way that the quantity $[2(\bar{E}/h\nu')^2 + \bar{E}/h\nu' - \overline{E^2}/(h\nu')^2]$ does decrease exponentially with a time constant very closely related to the V–V rate constant for $2AB(v = 1) \rightarrow AB(v = 0) + AB(v = 2)$. A short survey of various laser and chemical excitations in the literature is presented and analyzed in terms of initial conditions. In general, the larger the degree of excitation and the higher the quantum numbers of the excited levels, the more V–V character does the energy relaxation have.

The master equation for the time evolution of individual level populations is reduced to a simple form for times applicable to the early V–V redistribution of vibrational energy. This leads to a simple prescription for extrapolating measured population distributions back towards the initial distributions produced by a chemical reaction. The general features of the time–evolution profiles are found by numerical integration to show an initial broadening of the distribution simultaneous with a shift towards $v = 0$.

HESHEL TEITELBAUM. Can. J. Chem. **61**, 1276 (1983).

On résoude analytiquement la loi génerale dérivant la vitesse de la relaxation de l'énergie vibrationelle d'un gaz diatomique pur, AB — ceci pour une variété de conditions initiales correspondant aux expériences dans les tubes de choc, à la fluorescence induite par laser et à l'activation chimique. On peut utiliser les expressions qui en résultent afin de prédire facilement si un système quelconque s'équilibra selon un mécanisme V–V ou T–V. On montre que les conditions initiales et l'anharmonicité moléculaire sont aussi importantes que le rapport des constantes de vitesse T–V et V–V. Dans les ondes de choc l'énergie s'équilibre exponentiellement avec un temps de vitesse T–V. La répartition des populations des niveaux reste Boltzmann. Dans les expériences d'excitation par laser ou par réaction chimique, l'énergie ne s'équilibre pas exponentiellement — ce qui empêche que les "constantes" phénomenologiques $-(\bar{E} - \bar{E}^{\infty})/(d\bar{E}/dt)$ ou $-[d \ln (d\bar{E}/dt)/dt]^{-1}$ soient des vraies constantes par rapport au temps, et ce qui empêche une comparaison directe avec les résultats determinés par moyen de tube de choc. Il n'est qu'après une période d'incubation, pendant laquelle l'énergie vibrationelle se rédistribue via les processus V–V que l'énergie puisse se transformer en une énergie translationelle et diminuer. On donne une prescription pour tirer les constantes T–V et V–V à partir de tels mesures. Le degré d'excitation initiale, α, et le régime du temps étudié, t/τ, doivent être connus en générale pour ce but. Par contre, quand l'excitation overtone directe est utilisée une choix soigneuse de α peut mener à une extraction directe de la constante T–V. Bien que l'énergie vibrationelle même ne s'équilibre pas exponentiellement on montre que l'énergie vibrationelle moyenne, $\bar{E}/h\nu$, et l'énergie vibrationelle carrée moyenne, $\overline{E^2}/(h\nu')^2$, s'equilibrent d'une telle manière que la quantité $[2(\bar{E}/h\nu')^2 + \bar{E}/h\nu' - \overline{E^2}/(h\nu')^2]$ se décroît exponentiellement avec une constante de temps liée très étroitement à la constante de vitesse V–V pour le processus $2AB(v = 1) \rightarrow AB(v = 0) + AB(v = 2)$. Un résumé bref de plusieurs excitations par laser ou par réaction chimique décrites dans la litérature est donné. Il est analysé selon les conditions initiales des expériences individuelles. En générale on trouve que plus sévère l'excitation et que plus élevés les nombres quantiques des niveaux excités, alors plus de caractère V–V aura la relaxation.

L'équation "master" décrivant le changement des populations des niveaux vibrationels individuels par rapport au temps est simplifié pour le régime du temps qui correspond à la rédistribution rapide V–V de l'énergie. Ceci mène à une technique simple pour extrapoler les répartitions des populations observées vers la répartition initiale produite par une réaction chimique. Une intégration numérique montre qu'en générale la répartition s'applâtit simultanément avec un mouvment du pic vers $v = 0$.

A. Introduction

In a previous paper (1), we derived a rate law which describes the rate of change of the vibrational energy of pure diatomic molecules with respect to time. Both T–V and V–V processes were included, and the result was applicable to the relaxation subsequent to shock excitation, laser excitation, or chemical activation. It was shown that two common assumptions are not generally valid — the Bethe–Teller law, and the existence of a Boltzmann distribution during the relaxation. In this study we wish to demonstrate the far-reaching consequences of the unbridled use of these assumptions.

Shock tube studies of vibrational relaxation rely on measurements of the time-variation of the translational temperature of the relaxing gas. This is intimately related to the time-variation of the vibrational energy (2). The fluorescence intensity of laser-excited gases is directly proportional to the

Can. J. Chem. Downloaded from www.nrcresearchpress.com by 210.87.254.5 on 09/06/12
For personal use only.

vibrational energy (3) when the gas is optically thin to radiation from all levels (but see ref. 4). Similarly, photoacoustic detection of laser-induced relaxation is directly related to the vibrational energy. Thus the present study should be significant for enabling meaningful comparisons to be made between shock tube and laser-excitation data.

Many chemical reactions, particularly exothermic ones, produce molecules in vibrationally excited states. Infrared chemiluminescence is used to study the nascent population distributions (5–7). Yet rapid vibrational relaxation may prevent direct measurement of the initial populations. Simple extrapolation backwards in time gives a good indication of the initial distribution. It would be useful to know the relaxation rate law in order to best accomplish the extrapolation or to make checks on existing techniques. Our previous studies show (1) that the mean vibrational energy, $\bar{E}$, and the mean squared vibrational energy, $\overline{E^2}$, are constrained to relax in a certain way. This suggests the necessary guidelines for extrapolation.

We proceed by solving the generalized rate law, as applied to each of the three types of experiment. They are naturally divided into two groups: those for which the initial vibrational population distribution is Boltzmann and those which are not. To simplify matters we treat the relaxation as near-isothermal. For diatomic molecules thermal effects are not considered severe. A complete thermal analysis is presented in a subsequent study.

B. Isothermal relaxation of vibrational energy

When the translational temperature, the rate constants, and the equilibrium vibrational energy, $\bar{E}^{\infty}$, do not vary significantly with time, the generalized rate law for the relaxation of vibrational energy is given by (1)

$$[1]\quad \frac{d\bar{E}}{dt} = -\frac{(\bar{E}-\bar{E}^{\infty})}{\tau} - \chi_e h\nu_e k_{1,1}^{2,0} N[2(\bar{E}/h\nu')^2 + \bar{E}/h\nu' - \overline{E^2}/(h\nu')^2]_0 e^{-at}$$

where χ_e is the anharmonicity factor, N the molecular concentration, ν_e the spectroscopic vibrational frequency; $\nu' = \nu_e(1-\chi_e)$; $\nu'' = \nu_e(1-3\chi_e)$; $a = Nk_{1,1}^{2,0}/(1-\chi_e) + 2/\tau$; $1/\tau = Nk_{1,0}(1 - e^{-h\nu''/kT})$; $k_{1,0}$ the rate constant for the process $AB(v=1) + AB(v) \rightarrow AB(v=0) + AB(v)$; and $k_{1,1}^{2,0}$ the rate constant for the process $2AB(v=1) \rightarrow AB(v=0) + AB(v=2)$. Equation [1] applies strictly to a pure diatomic gas. The quantity $[2(\bar{E}/h\nu')^2 + (\bar{E}/h\nu') - \overline{E^2}/(h\nu')^2]$ subscripted with a zero is characteristic of the initial population distribution and thus identifies the type of experiment. At subsequent times this quantity decays to zero:

$$[2]\quad [2(\bar{E}/h\nu')^2 + \bar{E}/h\nu' - \overline{E^2}/(h\nu')^2] = [2(\bar{E}/h\nu')^2 + \bar{E}/h\nu' - \overline{E^2}/(h\nu')^2]_0 e^{-at}$$

1. Shock tubes

Using $\bar{E}_0/h\nu' = e^{-u}/(1-e^{-u})$ and $\overline{E_0^2}/(h\nu')^2 = e^{-u}(1+e^{-u})/(1-e^{-u})^2$ it is easily seen that $[2(\bar{E}/h\nu')^2 + \bar{E}/h\nu' - \overline{E^2}/(h\nu')^2]_0 = 0$. Here $u = h\nu'/kT_0$ where T_0 is the initial temperature (usually room temperature). The rate constants, $k_{1,0}$, $k_{1,1}^{2,0}$, and the equilibrium vibrational energy, $\bar{E}^{\infty}$, correspond to a final, higher temperature, T, to which the gas is exposed. Equation [1] becomes

$$[3]\quad \frac{d\bar{E}}{dt} = -\frac{(\bar{E}-\bar{E}^{\infty})}{\tau}$$

whose solution is

$$[4]\quad \bar{E} - \bar{E}^{\infty} = (\bar{E}_0 - \bar{E}^{\infty})e^{-t/\tau}$$

Clearly a single relaxation time exists. The phenomenological time constants, τ' and τ'', defined as

$$[5]\quad \tau' \equiv -\frac{(\bar{E}-\bar{E}^{\infty})}{d\bar{E}/dt}$$

and

$$[6]\quad \tau'' \equiv -\left[\frac{d\ \ln\ (d\bar{E}/dt)}{dt}\right]^{-1}$$

are both true constants and equal to τ. Therefore, shock tube studies are amenable to determining T–V rate constants exclusively. Furthermore, the Boltzmann distribution remains Boltzmann; at all times a vibrational temperature is defined, and the vibrational level populations are given by the expressions in ref. 5.

2. Non-Boltzmann initial distributions

We set

$$[7]\quad b \equiv \chi_e h\nu_e k_{1,1}^{2,0} N[2(\bar{E}/h\nu')^2 + \bar{E}/h\nu' - \overline{E^2}/(h\nu')^2]_0$$

The solution to eq. [1] is straightforward. Using the initial condition $\bar{E} = \bar{E}_0$ at $t = 0$, then

$$[8]\quad (\bar{E}-\bar{E}^{\infty}) = (\bar{E}_0 - \bar{E}^{\infty})e^{-t/\tau} + \frac{b(e^{-at} - e^{-t/\tau})}{(a - 1/\tau)}$$

Clearly this is not a simple decay process. Phenomenological time constants are not true constants in time. It is only at late times when the term e^{-at} has decayed that the apparent time constant is τ. At earlier times τ' and τ'' are given by

$$[9]\quad \frac{\tau'}{\tau} = \frac{be^{-at} + [(\bar{E}_0 - \bar{E}^{\infty})(a - 1/\tau) - b]e^{-t/\tau}}{ab\tau e^{-at} + [(\bar{E}_0 - \bar{E}^{\infty})(a - 1/\tau) - b]e^{-t/\tau}}$$

and

$$[10]\quad \frac{\tau''}{\tau} = \frac{ab\tau e^{-at} + [(\bar{E}_0 - \bar{E}^{\infty})(a - 1/\tau) - b]e^{-t/\tau}}{a^2 b\tau^2 e^{-at} + [(\bar{E}_0 - \bar{E}^{\infty})(a - 1/\tau) - b]e^{-t/\tau}}$$

These measureables are shown in Figs. 1–3 for various values of the parameters

$$\gamma = k_{1,1}^{2,0}/(k_{1,0} - k_{0,1})$$

and

$$\delta = (\bar{E}_0 - \bar{E}^{\infty})/\{h\nu_e\chi_e[2(\bar{E}/h\nu')^2 + \bar{E}/h\nu' - \overline{E^2}/(h\nu')^2]_0\}$$

as a function of the reduced time, t/τ. The first parameter represents the relative importance of V–V and T–V rate constants; the second parameter represents the relative initial deviations from equilibrium and from the Boltzmann distribution. The latter parameter can be either positive or negative; its magnitude can be $\ll 1$ or $\gg 1$, depending very sensitively on initial conditions. For example, if the initial energy is close to $\bar{E}^{\infty}$, or if the initial distribution is strongly non-Boltzmann weighted towards high vibrational levels, then $|\delta| \ll 1$; otherwise $|\delta|$ can be $\gg 1$. If the initial energy is $< \bar{E}^{\infty}$, or if the initial distribution is doubly peaked such that $\bar{E} > \bar{E}^{\infty}$ yet $[2\bar{E}^2/(h\nu')^2 + \bar{E}/h\nu' - \overline{E^2}/(h\nu')^2] < 0$, then $\delta < 0$; otherwise δ can be > 0. Thus the vibrational energy can approach equilibrium from above or below, and may overshoot or undershoot $\bar{E}^{\infty}$ before attaining $\bar{E}^{\infty}$. Overshooting (undershooting) indicates

Can. J. Chem. Downloaded from www.nrcresearchpress.com by 210.87.254.5 on 09/06/12
For personal use only.

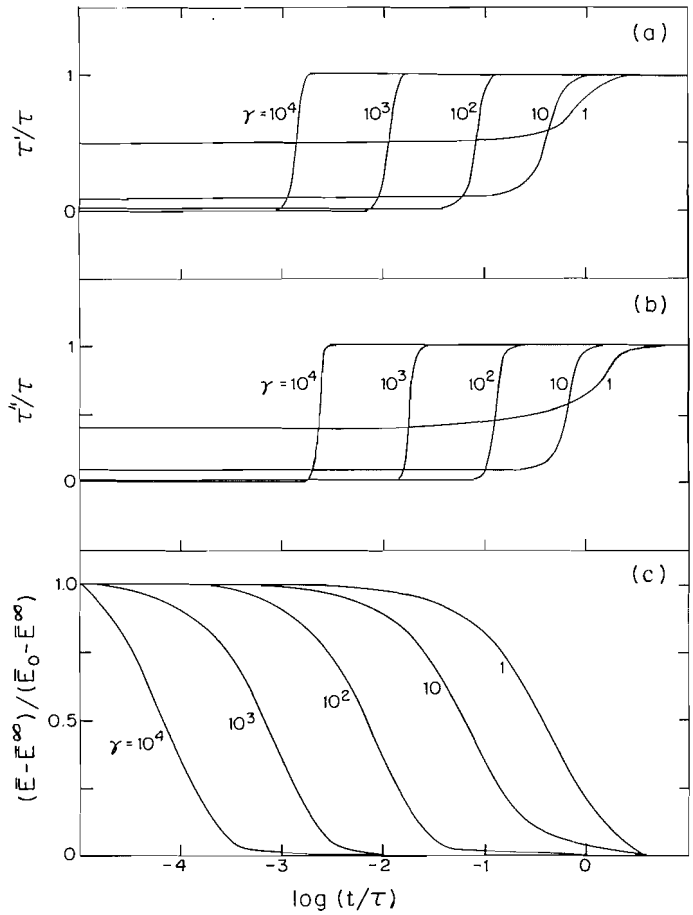

FIG. 1. Reduced phenomenological relaxation times, τ'/τ and τ''/τ, as defined by eqs. [5] and [6], and reduced vibrational energy as a function of reduced time for the relaxation of a gas of pure diatomic molecules. $\tau'/\tau = 1$ or $\tau''/\tau = 1$ mean that the time constant originates entirely from T–V processes. Here $\chi_e = 0.01$. Effect of $\gamma = k_{1,1}^{2,0}/(k_{1,0} - k_{0,1})$ on (*a*) τ'/τ, (*b*) τ''/τ, and (*c*) $(\bar{E} - \bar{E}^{\infty})/(\bar{E}_0 - \bar{E}^{\infty})$ for $\delta = 1$ where δ is given by $\delta = (\bar{E}_0 - \bar{E}^{\infty})/\{h\nu_e\chi_e[2(\bar{E}/h\nu') + (\bar{E}/h\nu') - \bar{E}^2/(h\nu')^2]_0\}$. The process which is responsible for the relaxation can be deduced by finding τ' or τ'' at a time when the energy is, say, 50% equilibrated: e.g. for $\gamma = 10$, $\tau' = 0.10\tau$, $\tau'' = 0.084\tau$, i.e. V–V is responsible; for $\gamma = 1$, $\tau' = 0.59\tau$, $\tau'' = 0.50$, i.e. V–V and T–V are roughly equally responsible.

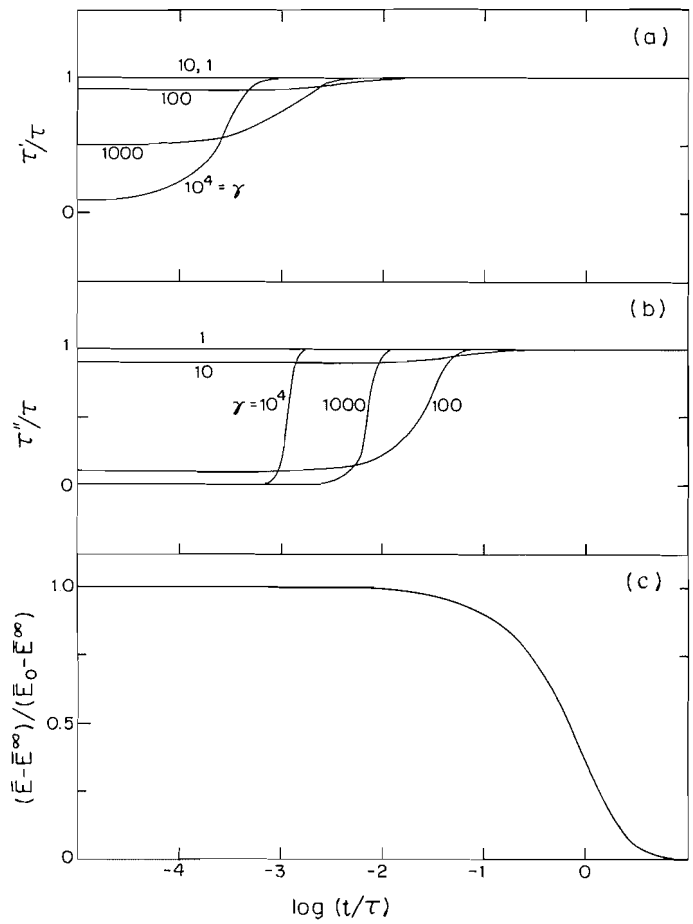

FIG. 2. Same as in Fig. 1, but with $\delta = 1000$. Note that at practically all times during which the vibrational energy changes substantially, $\tau' \simeq \tau$ and $\tau'' \simeq \tau$ for all γ. As a result, the energy relaxes almost purely exponentially at a rate determined by T–V processes.

the system's preference to readjust the population distribution without much regard to its effect on the deviation from equilibrium. A lack of overshooting (undershooting) indicates that the redistribution occurs without affecting the energy substantially. The function $(\bar{E} - \bar{E}^{\infty})/(\bar{E}_0 - \bar{E}^{\infty})$ shown in Figs. 1*c*, 2*c*, and 3*c* displays these features. Such complicated behaviour makes analysis of experimental results difficult, particularly if simple exponential behaviour is assumed, i.e. if the Bethe–Teller law, eq. [3], is assumed to be valid.

Figures 1*a*, 1*b*, 2*a*, 2*b*, 3*a*, and 3*b*, showing τ'/τ and τ''/τ as functions of the reduced time, t/τ, indicate the possible errors involved. We might expect the error in τ' and τ'' to be unimportant if γ is large, i.e. if V–V processes are dominant such that the populations redistribute themselves on a short time scale without affecting the energy much; thereafter the energy would relax on a time scale determined by T–V processes. This is indeed seen to be the case in Fig. 2. For example, by the time τ'' has reached 95% of its final value, τ, only 1% of the energy has relaxed when $\gamma = 1000$. However, it should be noted that this result corresponds to $\delta = 1000$, i.e. when the initial distribution is near-Boltzmann. Figure 1 leads to quite the opposite conclusion. Here, $\delta = 1$, i.e. the initial distribution is strongly non-Boltzmann. It is seen that regardless of the value of γ, nearly all the energy has relaxed during the transient period! In fact, τ'/τ and τ''/τ can be shown from eqs. [9] and [10] to have approximately their values at $t = 0$, i.e. $\delta/(\delta + \gamma)$ and $\delta/[\gamma(\gamma + 3)]$ respectively. Figures 1 and 2 therefore indicate that the initial conditions are far more important in determining the process responsible for relaxation than is the factor γ itself! The experimentalist should be aware of this fundamental result when interpreting his data. Indeed he can exploit this result by manipulating his conditions to give $\delta \lesssim 1$ in order to directly determine $k_{1,1}^{2,0}$. Alternatively $\delta \gg 1$ will lead to a direct determination of τ.

The influence of δ on τ' and τ'' is summarized in Fig. 3 for a typical $\gamma = 100$. We note that the smaller the value of δ, the more V–V character the energy relaxation has. For $\delta \geq 10$, only 3% of the energy or less has relaxed via V–V processes by the time $\tau' = 0.95\tau$. When $\delta < 10$, V–V relaxation becomes more important. When $0 < \delta < 1$, the energy rapidly approaches and overshoots (undershoots) equilibrium via V–V processes and then slowly reapproaches equilibrium via T–V processes. For $\delta < 0$, the energy initially deviates even further from equilibrium rapidly before finally approaching equilibrium slowly.

Can. J. Chem. Downloaded from www.nrcresearchpress.com by 210.87.254.5 on 09/06/12
For personal use only.

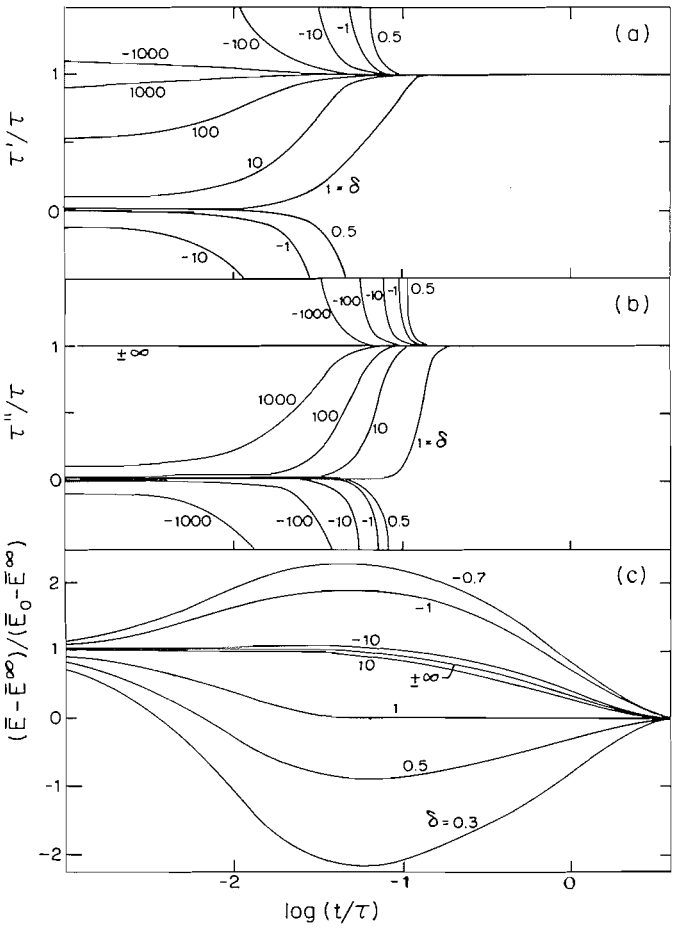

FIG. 3. Reduced phenomenological relaxation times and vibrational energy as a function of reduced time. Effect of initial conditions, i.e. of δ as defined in Fig. 1 on (*a*) τ'/τ, (*b*) τ''/τ, and (*c*) $(\bar{E} - \bar{E}^{\infty})/(\bar{E}_0 - \bar{E}^{\infty})$. Here $\chi_e = 0.01$, $\gamma = k_{1,1}^{2,0}/(k_{1,0} - k_{0,1}) = 100$. Note that only when $\delta = \pm\infty$, does the energy relax exponentially with the time constant $= \tau$. The closer δ approaches 0, i.e. the more non-Boltzmann the distribution, the larger the overshoot (undershoot) in energy.

It is also interesting to note that the transient period lasts longer for τ'' than it does for τ'.

There are several arbitrary ways to evaluate the above results. One can ask how much energy has relaxed (1%, 5%, 10%, 50% etc.) by the time t/τ has reached a certain value (0.5, 1, 2, etc.) or by the time either τ' or τ'' has reached a certain percentage of τ (50%, 90%, 95%, 99% etc.). Faced with such nonstandard criteria, an experimentalist must additionally decide with what to actually reduce his time scale (since it is not τ which he measures but rather τ' or τ''). Furthermore, the accessible range of t/τ is limited by experimental time resolution (0.1 μs for shock tubes or 1 μs for fluorescence), and transient behaviour near $t = 0$ may or may not be measurable. In other words, an experimentalist will not know unambiguously to which regime of t/τ his data correspond unless he measures τ' or τ'' over a long time scale. As an example, suppose the initial conditions are such that $\delta = 1$. Then a measurement of the phenomenological relaxation time, τ' as a function of t/τ', would result in Fig. 4, except for the scaling factor τ, rather than in Fig. 1*a*. The curves in Fig. 4 are very distinctive. By comparing both form and magnitude of experimental data with curves such as those in Fig. 4, the

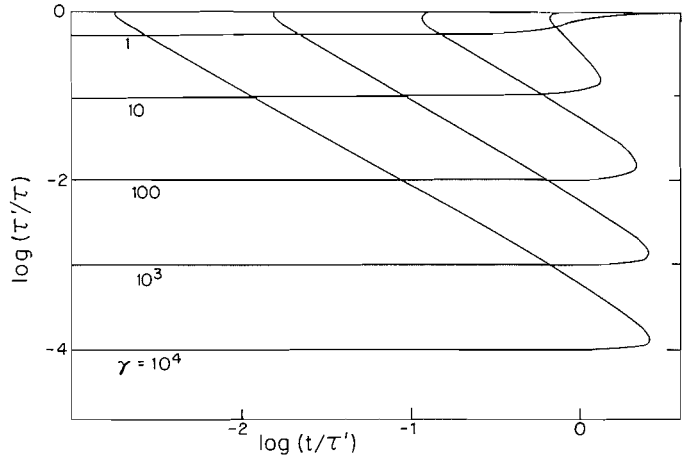

FIG. 4. Same as in Fig. 1(*a*) but with the time scale reduced by τ' instead of τ. This corresponds to what an experimentalist might plot. Note that the phenomenological relaxation time, τ', measured at a given t/τ' corresponds to three possible choices for τ. The ambiguity is cleared up when measurements are made at more than one t/τ'.

experimentalist could determine both γ and τ, as an alternative method to manipulating δ. We note that it may not be necessary to vary the time scale over many orders of magnitude: even for $\gamma = 10^4$ where the interesting region of t/τ' varies from 1.74×10^{-3} to 2.63, the absolute time scale, t, only varies by a factor of 4.7 (the region of rapid rise in Fig. 1*a*). Therefore even if the flat regions of Fig. 1*a* are not accessible by choosing δ appropriately, it is still feasible to obtain γ and τ by modest variation of the time scale, or equivalently the gas pressure (see below).

We note further that t/τ can be written at $Nt/N\tau$, where $N\tau$ is just $(k_{1,0} - k_{0,1})^{-1}$. N is the gas concentration and is proportional to the gas pressure, p. Therefore Figs. 1–3 can be considered either as functions of absolute time at a given pressure or as a function of pressure at a given absolute time. In the latter case they demonstrate an apparent deviation of the expected inverse dependence of τ' or τ'' on p. This has been observed (6).

Yet a third method to determine τ experimentally is to completely eliminate the influence of V–V processes by sufficiently diluting the relaxing gas in an inert species, such that AB–AB collisions are rare and thus negligible. This will be discussed in a subsequent article concerning mixture rules.

C. Determination of initial conditions

1. Shock waves

As mentioned above, the initial distribution is Boltzmann. Hence $\delta = \infty$, and the vibrational energy relaxes exponentially regardless of the deviation from equilibrium.

2. Fluorescence intensity measurements

Such experiments involve exciting molecules from a single vibrational level to another, v. Usually the initial level is $v = 0$. Therefore the initial values of $\bar{E}$ and $\overline{E^2}$ are larger than they would be without excitation. We note that $\bar{E}/h\nu'$ and $\overline{E^2}/(h\nu')^2$ were originally defined as $\sum_0 m(N_m/N)$ and $\sum_0 m^2(N_m/N)$. (They represent true average energies at modest temperatures when the anharmonicity does not influence the molecular energy much.) Let α be the fraction of molecules, initially in $v = 0$, which are excited into level v, then

TABLE 1. Initial conditions, δ, for vibrational relaxation of laser-excited molecules

Molecule	$\bar{\nu}_e$ (8) (cm^{-1})	χ_e (8)	T (K)	α = 0.01	α = 0.1	α = 0.5	v	Reference
HF	4138	0.0217	~300	2300	230	46.1	1	9, 6, 11
	4138	0.0217	~300	−48.0	−76.8	46.1	2	9, 12
	4138	0.0217	~300	−23.8	−32.9	46.1	3	9
	4138	0.0217	~1030	1280	213	45.4	1	10
DF	2998	0.0153	295	3270	327	65.4	1	13
	2998	0.0153	295	−68.1	−109	65.4	2	13
	2998	0.0153	295	−34.0	−46.7	65.4	3	13
	2998	0.0153	295	−22.4	−29.7	65.4	4	13
	2998	0.0153	200	3270	327	65.4	1	14
	2998	0.0153	200	−34.0	−46.7	65.4	3	14
$H^{35}Cl$	2991	0.0177	192	2820	282	56.5	1	15
	2991	0.0177	632	2210	275	56.2	1	15
$H^{81}Br$	2649	0.0171	~300	2920	292	58.5	1	16–18
	2649	0.0171	~300	−60.9	−97.5	58.5	2	16
HD	3813	0.0240	100	2080	208	41.7	1	7
	3813	0.0240	100	−43.4	−69.4	41.7	2	7, 19
	3813	0.0240	100	−14.3	−18.9	41.7	4	7, 19
	3813	0.0240	100	−8.54	−11.0	41.7	6	7, 19
	3813	0.0240	400	2080	208	41.7	1	7
	3813	0.0240	400	−43.4	−69.4	41.7	2	7, 19
	3813	0.0240	400	−14.3	−18.9	41.7	4	7, 19
	3813	0.0240	400	−8.54	−11.0	41.7	6	7, 19
H_2	4401	0.0276	300	1810	181	36.2	1	20*a*
	4401	0.0276	50	1810	181	36.2	1	20*b*
D_2	3116	0.0198	300	2530	253	50.5	1	21*a*
	3116	0.0198	40	2530	253	50.5	1	21*b*
OH	3738	0.0227	298	2200	220	44.1	1	22
CO	2170	0.00612	100	8170	817	163	1	23
	2170	0.00612	400	7500	810	163	1	23
	2170	0.00612	700	2360	655	158	1	23
$NO(X^2\Pi)$	1904	0.00739	300	6690	676	135	1	24
$NO(A^2\Sigma^+)$	2374	0.00678	300?	7370	737	148	1	25
$NO(B^2\Pi)$	1037	0.0074	300	−70.7	−98.6	131	3	26
	1037	0.0074	300	−46.8	−62.3	131	4	26
	1037	0.0074	300	−17.3	−21.9	131	9	27
$SO(A^3\Pi)$	413.3	0.0039	300	383	302	155	1	28
$I_2(^3\Pi_{0+u})$	125.7	0.0061	310?	−4.55	−5.80	—	43	29
$Br_2(A^3\Pi)$	153	0.018	300?	−8.08	−11.8	11.4	12	30
	153	0.018	300	−55.9	645	11.4	6	30
	153	0.018	300	14.2	13.6	11.4	1	30
$Br_2(B^3\Pi)$	168	0.0098	300?	−15.8	−22.8	23.6	11	31
	168	0.0098	300	−13.7	−19.3	23.6	12	31
	168	0.0098	300	−9.83	−13.3	23.6	15	31
$^{35}Cl_2(B^3\Pi)$	260	0.0204	300?	−22.6	−38.7	17.9	5	32
	260	0.0204	300	−8.05	−11.0	17.9	9	32
	260	0.0204	300	−6.94	−9.31	17.9	10	32
	260	0.0204	300	−6.09	−8.08	17.9	11	32
	260	0.0204	300	−5.43	−7.14	17.9	12	32
$^9BrF(B^3\Pi_{0+u})$	372	0.0094	300?	124	102	57.8	1	33
	372	0.0094	300	−889	443	57.8	2	33
	372	0.0094	300	−51.2	−78.2	57.8	4	33
	372	0.0094	300	−17.7	−23.3	57.8	8	33
$Na_2(B'\Pi_u)$	124.09	0.00564	673	14.3	13.9	—	2	34
	124.09	0.00564	673	21.0	18.6	—	6	34
	124.09	0.00564	673	23.7	20.3	—	7	34
	124.09	0.00564	673	32.2	24.9	—	9	34
	124.09	0.00564	673	39.1	28.0	—	10	34

Can. J. Chem. Downloaded from www.nrcresearchpress.com by 210.87.254.5 on 09/06/12
For personal use only.

TABLE 1 *(Concluded)*

Molecule	$\bar{\nu}_e$ (8) (cm^{-1})	χ_e (8)	T (K)	$\alpha = 0.01$	$\alpha = 0.1$	$\alpha = 0.5$	v	Reference
	124.09	0.00564	673	−14.6	−24.4	—	27	34
$Li_2(B'\Pi_u)$	270.12	0.00990	893	15.4	14.6	—	2	35
	270.12	0.00990	893	18.1	16.5	—	3	35
	270.12	0.00990	893	22.0	19.0	—	4	35
	270.12	0.00990	893	−330	76.9	—	9	35

Note: α is the fraction of molecules excited into the given indicated level v from the ground state $v = 0$. If not otherwise indicated the electronic state is the ground state. The molecules have been prepared in the specified levels by methods explained in the references cited, but their relaxation rates have not necessarily been measured, nor is α always given. δ is defined as $\delta = (\bar{E}_0 - \bar{E}^\infty)/\{h\nu_e\chi_e[2(\bar{E}/h\nu')^2 + \bar{E}/h\nu' - \overline{E^2}/(h\nu')^2]_0\}$ and is evaluated here using eq. [12].

$$[11]\quad \left[2\left(\frac{\bar{E}}{h\nu'}\right)^2 + \frac{\bar{E}}{h\nu'} - \frac{\overline{E^2}}{(h\nu')^2}\right]_0$$

$$= 2\left(\frac{\bar{E}_B}{h\nu'} + \alpha v\right)^2 + \left(\frac{\bar{E}_B}{h\nu'} + \alpha v\right) - \left(\frac{\overline{E_B^2}}{(h\nu')^2} + \alpha v^2\right)$$

$$= \left[2\left(\frac{\bar{E}}{h\nu'}\right)^2 + \frac{\bar{E}}{h\nu'} - \frac{\overline{E^2}}{(h\nu')^2}\right]_B + \alpha v\left(\frac{4\bar{E}_B}{h\nu'} + 1 + 2\alpha v - v\right)$$

where the subscript B refers to a Boltzmann distribution at the initial temperature T_0. Thus the first term on the right hand side of eq. [11] is zero. The average energy $\bar{E}_B/h\nu'$ is given to a good approximation by $e^{-u}/(1 - e^{-u})$ where $u = h\nu_e(1 - 2\chi_e)/kT_0$. The largest value α can have is the initial fraction of molecules in $v = 0$ prior to excitation, i.e. $(1 - e^{-u})$. Furthermore, the initial temperature is practically the same as the equilibrium temperature under our assumption of near-isothermal relaxation. Thus $(\bar{E}_0 - \bar{E}^\infty) = \alpha v$. (For an experiment involving simultaneous shock heating and laser excitation this is not true, and an additional term would be needed.) Combining this result with eq. [11], we obtain

$$[12]\quad \delta^{-1} \simeq \chi_e[(1 + 3e^{-u})/(1 - e^{-u}) + v(2\alpha - 1)]$$

Typically the excitation is directly into $v = 1$. Then

$$[13]\quad \delta^{-1} \simeq \chi_e[4e^{-u}/(1 - e^{-u}) + 2\alpha]$$

We can see that $\delta > (1 - e^{-u})/|2\chi_e(1 + e^{-2u})|$. For a classical oscillator ($u \to 0$), $\delta > D_e/kT$, where D_e is the Morse dissociation energy; for a quantum oscillator ($u \to \infty$) then $\delta > (2\chi_e)^{-1}$. Referring to Fig. 3 as a guide, it thus apears that the relaxation is significantly T–V in character when $v = 1$. However, when $v > 1$, eq. [12] shows that δ can be small or even negative. The relaxation then becomes V–V in character. Rabitz (7) has recently come to a similar conclusion for the special case of HD by numerically integrating the rate equations and scaling the individual rate constants in terms of $k_{1,1}^{2,0}$ and τ more elaborately than we do but using a much smaller number of V–V processes than we consider (1).

Table 1 shows the variety of values δ can have for selected molecules and therefore the special care needed in interpreting relaxation data. The molecules chosen are some which have actually been excited into the indicated levels by other workers, and whose relaxation times have either been measured or are conceivably measurable. Indeed some of these molecules exist in highly excited states in molecular lasers, and it is therefore of particular interest to understand their relaxation behaviour.

We note how sensitively the relaxation mechanism depends on initial conditions. In general, the larger the fraction of molecules initially excited into level v or the larger the value of v, the more V–V character the relaxation has (smaller $|\delta|$). Any experiment designed to measure the T–V rate constant, $k_{1,0}$, is best done by exciting few molecules into $v = 1$ and making the corrections suggested by Figs. 1–4; alternatively, any experiment designed to measure the V–V rate constant, $k_{1,1}^{2,0}$, is best done by direct excitation into the highest overtone level possible and applying the corresponding correction factors. In all cases it is crucial to measure α in order to measure δ. Yet, with rare exception (17, 20), in the experiments cited in Table 1 α has not been estimated. Certainly the need for detailed knowledge of absorption coefficients and line shapes makes this a difficult matter; however, it appears to be a necessity. For example, exciting only 1% of all HF molecules into $v = 1$ results in an essentially T–V mechanism, whereas a 50% excitation introduces V–V character. On the other hand, 1% of all HD excited into $v = 6$ results in more V–V character than does 50% excitation. If one were able to measure and control α reliably, then it would be a simple matter to arrange that the relaxation mechanism be totally T–V. Figure 5 shows the value of α necessary to make $\delta = \infty$ for this purpose.

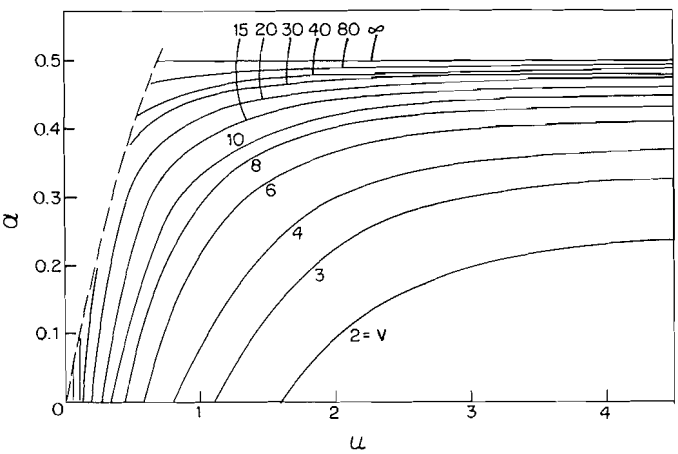

FIG. 5. The fraction of molecules, α, initially in the ground vibrational level, $v = 0$, which must be excited into level v in order to ensure pure exponential T–V relaxation, as a function of the reduced variable $u = h\nu_e(1 - 2\chi_e)/kT$. The dashed line is the function $(1 - e^{-u})$, the fraction of molecules in $v = 0$ prior to excitation, and therefore the maximum value of α physically possible.

Thermal excitation generally has little influence on δ itself (see Table 1). However, γ decreases strongly with temperature ($k_{1,0}$ increases with temperature usually according to exp $\{-cT^{-1/3}\}$, whereas $k_{1,1}^{2,0}$ is relatively temperature independent).

Can. J. Chem. Downloaded from www.nrcresearchpress.com by 210.87.254.5 on 09/06/12
For personal use only.

Can. J. Chem. Downloaded from www.nrcresearchpress.com by 210.87.254.5 on 09/06/12
For personal use only.

TABLE 2. Initial conditions, δ, for vibrational relaxation of chemically activated molecules

Diatomic[b]	Reagents	$\bar{\nu}_e$/cm (8)	χ_e (8)	T/K	N_v/N													$\frac{\bar{E}_v - \bar{E}^*_v}{h\nu'}$	$2\left(\frac{\bar{E}_v}{h\nu'}\right)^2_v + \frac{\bar{E}_0}{h\nu'} - \frac{\overline{E_0^2}}{(h\nu')^2}$	δ	Reference
					0	1	2	3	4	5	6	7	8	9	10	11	12				
HF	H + F_2	4138	0.0217	300		0.0322	0.055	0.081	0.134	0.240	0.253	0.127	0.076					5.136	28.57	8.28	36
HF	F + HBr	4138	0.0217	275		0.48	0.28	0.15	0.09									1.85	4.31	19.8	37
HF	F + H_2	4138	0.0217	300	0.03	0.16	0.52	0.29										2.07	5.79	16.5	38
DF	F + D_2	2998	0.0153	300	0.03	0.10	0.24	0.37	0.26									2.73	9.09	19.6	39
HCl	H + ICl	2991	0.0177	300	0.03	0.06	0.12	0.15	0.15	0.17	0.18	0.14						4.26	18.7	12.9	40
I_2	$I_2(B) - h\nu$	215	0.00287	300	[a]													81.3	6767	4.19	29
BrF	BrF(11) − $h\nu$	671	0.00604	298	0.958	0.0401	0.00168											0.001	0.000485	341	33
BaF	Ba + HF	469	0.00382	1050	0.333	0.32	0.23	0.093	0.02	0.003								0.034	1.345	6.62	41
BaCl	Ba + HCl	279	0.0032	1050	0.078	0.10	0.12	0.153	0.15	0.14	0.11	0.075	0.040	0.018	0.008	0.003		1.72	13.3	40.4	41
BaBr	Ba + HBr	194	0.0022	1050	0.009	0.018	0.029	0.044	0.056	0.073	0.081	0.088	0.096	0.096	0.086	0.080	0.067[b]	5.41	69.3	35.5	41
BaI	Ba + HI	152	0.00177	1050	0.013	0.015	0.021	0.023	0.023	0.032	0.044	0.050	0.056	0.064	0.071	0.077	0.079[b]	7.09	117.9	34.0	41
CN	C_2N_2 + $h\nu$	2069	0.00633	295–376	0.214	0.18	0.14	0.12	0.20	0.14								2.32	4.56	80.4	42
CO	Hg* + CO	2170	0.00612	300[c]	0.025	0.051	0.10	0.19	0.25	0.20	0.13	0.051						3.96	17.0	38.1	43
CO	O + CS	2170	0.00612	300					0.01	0.01	0.02	0.02	0.04	0.08	0.11	0.13	0.17[d]	13.1	193	11.1	44
CO	O + CN	2170	0.00612	298	0.336	0.174	0.113	0.065	0.049	0.032	0.027	0.029	0.045	0.049	0.045	0.027	0.010	2.98	−0.200	−2435	45
CO	O + CS	2170	0.00612	95[e]	0.114	0.107	0.094	0.083	0.077	0.075	0.086	0.088	0.080	0.068	0.046	0.037	0.019[f]	5.07	17.2	48.2	46
NO	Hg* + NO	1904	0.00739	300	0.19	0.13	0.10	0.081	0.075	0.072	0.066	0.059	0.056	0.050	0.039	0.031	0.022[g]	4.44	8.8	68	47
AlO	Al + O_2	979	0.00712	1000	0.49	0.30	0.12	0.06	0.03									0.51	0.45	159	48
BaO	Ba + O_2	670	0.00303	600	0.28	0.19	0.19	0.17	0.17									0.90	−1.41	−211	49
OH	H + O_3	3738	0.0227	300								0.18	0.37	0.45				8.27	76.1	4.79	50
OH	H + NO_2	3738	0.0227	300	0.27	0.35	0.35	0.03										1.14	1.72	29.2	50
H_2	Hg* + H_2	4401	0.0276	300[c]	0.10	0.27	0.38	0.17	0.08									1.86	4.18	16.1	43
D_2	Hg* + D_2	3116	0.0198	300[c]	0.04	0.10	0.26	0.36	0.16	0.08								2.74	8.82	15.7	43
O_2	Hg* + O_2	1580	0.00758	300[c]	0.021	0.042	0.053	0.063	0.074	0.11	0.14	0.17	0.17	0.15	0.021			6.13	38.1	21.2	43
N_2	Hg* + N_2	2359	0.00607	300[c]		0.024	0.18	0.24	0.20	0.16	0.12	0.082						4.00	17.6	37.4	43

Initial relaxation conditions for diatomic molecules produced by a variety of techniques described in the cited references: chemical reaction, Hg-sensitization, molecular beams, photolysis, laser-induced fluorescence. All molecules are in the ground electronic state unless otherwise specified. N_v/N is the fraction of molecules produced in the indicated levels v. δ is calculated from $\delta = (\bar{E}_0 - \bar{E}^*_v)/\{h\nu_e\chi_e[2(\bar{E}/h\nu')^2 + \bar{E}/h\nu' - \overline{E^2}/(h\nu')^2]_0\}$ where $\bar{E}/h\nu' = \sum vN_v/N$, $\overline{E^2}/(h\nu')^2 = \sum v^2N_v/N$, $\bar{E}/kT = ue^{-u}(1 - e^{-u})^{-1}$ and $u = h\nu_e(1 - 2\chi_e)/kT$. The temperature, T, used is that cited in the references except for molecular beam experiments where T is calculated from the cited average collision energy, $\bar{E}_c$, using $\bar{E}_c = 3kT/2$. It is only for such high energy experiments that the equilibrium vibrational energy, $\bar{E}$, is similar to the initial product vibrational energy, $\bar{E}_0$.

[a]The fluorescence intensities for final v = 76, 78, 79, 81, and 83 of I_2 are 0.035, 0.047, 0.023, 0.0351, and 0.585 respectively. The large values of v ensure a small δ.

[b]The remaining fractional level populations of BaBr in v = 13–20 are 0.057, 0.047, 0.031, 0.021, 0.011, 0.007, 0.004, and 0.002 respectively. Those for BaI in v = 13–23 are 0.077, 0.077, 0.069, 0.060, 0.047, 0.036, 0.025, 0.018, 0.013, 0.007, and 0.005 respectively.

[c]In the Hg-sensitization of CO, H_2, D_2, O_2, and N_2 the product energy has been ascribed to vibrational energy although the data cannot distinguish between vibrational and rotational energy. Also the E–V energy transfer occurs with a background Boltzmann distribution. Thus these data are akin to those in Table 1.

[d]The remaining fractional level populations of CO in v = 13, 14, 15 are 0.18, 0.17, and 0.16 respectively.

[e]95 K is the rotational temperature for the partially relaxed rotational distribution. It is assumed here that the rotational temperature was approaching the translational temperature.

[f]The remaining fractional level populations of CO in v = 13, 14, 15 are 0.011, 0.008, and 0.007 respectively.

[g]The remaining fractional level populations of NO in v = 13–17 are 0.016, 0.011, 0.006, 0.002, and 0.001, respectively.

[h]Note the bimodal distribution for CN as well as for CO produced by 3 different methods.

Can. J. Chem. Downloaded from www.nrcresearchpress.com by 210.87.254.5 on 09/06/12
For personal use only.

Then if δ is large (Fig. 2), an essentially T–V rate acquires V–V character; if δ is small (Fig. 4), an essentially V–V rate acquires T–V character.

3. Chemical activation

Exothermic chemical reactions produce molecules in vibrationally, rotationally and, sometimes, electronically excited states. The distribution of these states is unique for each reaction, and no general mathematical relationship can as yet be written down. Therefore δ must be evaluated for each individual case, which may additionally depend on the reagents' collisional energy (or temperature) and internal energy. In Table 2 we summarize the vibrational distributions for some selected reactions. Generally, such studies are not concerned with the energy relaxation rates themselves; however, the initial product distributions relax rapidly, and it is useful to know the relaxation mechanism in order to correct for these collisional effects. Further, as shown below, the manner in which any given individual level population relaxes depends explicitly on the bulk vibrational energy and the way *it* relaxes. Thus it is crucial to determine δ. For this purpose, δ is also given in Table 2.

We see that, with a couple of exceptions, $|\delta|$ is greater than 10 for the distributions shown, implying that despite the large excursions from equilibrium the vibrational energy relaxes essentially via T–V processes if the molecules encounter only like molecules. The vibrational level populations redistribute themselves rapidly via V–V processes without significantly affecting the energy itself; subsequently the energy relaxes via T–V processes. In one case (45), CO appears to have already attained a Boltzmann distribution by the time the distribution was measured. However, the vibrational temperature, T_{vib}, is 4750 K, and $\bar{E}_0$ is still fa away from $\bar{E}^z$. Similarly the BrF distribution is almost perfectly Boltzmann. However, in this case $T_{vib} \simeq 298$ K, so the cited distribution is likely already the equilibrium distribution. The T–V character of the relaxation will also be enhanced by the presence of inert colliders. The question of mixtures will be examined in detail in a subsequent paper.

On the other hand, I_2, HF (36), and OH have been produced with very strong non-Boltzmann distributions centred at high quantum numbers, v. The departure from equilibrium, though substantial, is not sufficient to compensate this effect. Thus $|\delta|$ is small, and the relaxation has considerable V–V character. Indeed, in one case (BaF) the vibrational energy is by chance almost identical to that needed for equilibrium at 1050 K. Thus, the small energy deficit relaxes during the V–V redistribution.

One of the main aims of the experiments cited in Table 2 is to determine the nascent vibrational level populations. Subsequent relaxation masks the initial distribution. If it is not possible to arrest the relaxation by decreasing the gas pressure (and hence the collision frequency), then extrapolation techniques are required. This is particularly important for rapid V–V relaxation, which is difficult to arrest. Guidelines for extrapolation are required. The present results indicate not only how simple a matter it is to determine the mechanism of vibrational relaxation of pure diatomic molecules but also suggest a simple procedure to extract $K_{1,1}^{2,0}$ and τ. The procedure leads additionally to exact constraints on the initial population distribution:

(*a*)Evaluate $2(\sum \nu N_\nu/N)^2 + \sum \nu N_\nu/N - \sum \nu^2 N_\nu/N$ at times when the vibrational level populations are being rapidly redistributed. Equation [2] shows that this quantity decays exponentially. In the present context this is more important than the question of exponential time-evolution of energy itself.

(*b*) Plot the logarithm of this quantity as a function of time, and extrapolate back to the presumed time origin in order to give the true initial value of $[2(\bar{E}/h\nu')^2 + \bar{E}/h\nu' - \overline{E^2}/(h\nu')^2]$. This does not give the actual initial distribution, but it can be used as a constraint to ensure the reasonableness of any existing extrapolation procedure for individual level populations.

(*c*) As a bonus, the slope of such a plot gives $N[k_{1,1}^{2,0}/(1 - \chi_e) + 2/\tau]$. Conceivably, the V–T rate constant could approach the V–V rate constant at extremely high translational temperatures; however, the author knows of no physical system to which this applies, certainly not at the low temperatures found in chemiluminescence experiments. In other words, $\gamma \gg 1$ in practice, and the slope should give a direct measure of $k_{1,1}^{2,0}$. The time constant for the energy relaxation rate should give τ, and this can be used to check the above assumption. It would be interesting to re-examine the data of the experiments in Table 2 in order to obtain $k_{1,1}^{2,0}$.

In order to further expound on the power of the present formulation, we show that the time evolution of the individual levels can be expressed easily for certain conditions. We refer to the earlier paper (1) which introduces the notation for the master equation. We begin with the master equation in the form

$$[14] \quad dN_m/dt = dN_m/dt|_{T-V} + dN_m/dt|_{V-V}$$

in which the two terms on the right-hand side are expressed as

$$[15] \quad dN_m/dt|_{T-V} = -(k_{m,m+1}N_m + k_{m,m-1}N_m - k_{m+1,m}N_{m+1} - k_{m-1,m}N_{m-1})\sum_0 N_m$$

and

$$[16] \quad \left.\frac{dN_m}{dt}\right|_{V-V} = -\sum_1 k_{m,n}^{m+1,n-1}N_mN_n + \sum_1 k_{m+1,n-1}^{m,n}N_{m+1}N_{n-1} + \sum_1 k_{m-1,n}^{m,n-1}N_{m-1}N_n - \sum_1 k_{m,n-1}^{m-1,n}N_mN_{n-1}$$

where $k_{m,m+1}$ is the rate constant for the T–V process $AB(m) + AB \rightarrow AB(m + 1) + AB$, and $k_{m,n}^{m+1,n-1}$ is the rate constant for the V–V process

$$AB(m) + AB(n) \rightarrow AB(m + 1) + AB(n - 1)$$

We use the scaling relationships

$$k_{m+1,m} = k_{1,0}(m + 1)e^{-m\phi}$$

$$k_{m,m+1} = k_{0,1}(m + 1)e^{m\phi}$$

$$k_{m,n}^{m+1,n-1} = (m + 1)nk_{0,1}^{1,0}e^{(m+1-n)\phi}$$

and

$$k_{m+1,n-1}^{m,n} = (m + 1)nk_{0,1}^{1,0}e^{-(m+1-n)\phi}$$

where

$$\theta' = h\nu_e(1 - \chi_e)/k$$

and

$$\phi = h\nu_e\chi_e/kT$$

These relationships satisfy microscopic reversibility. Equations [15] and [16] become

$$[17] \quad \left.\frac{dN_m}{dt}\right|_{T-V} = -Nk_{1,0}[(m + 1)e^{-\theta'/T}e^{(m+1)\phi}N_m + me^{-(m-1)\phi}N_m - (m + 1)e^{-m\phi}N_{m+1} - me^{-\theta'/T}e^{m\phi}N_{m-1}]$$

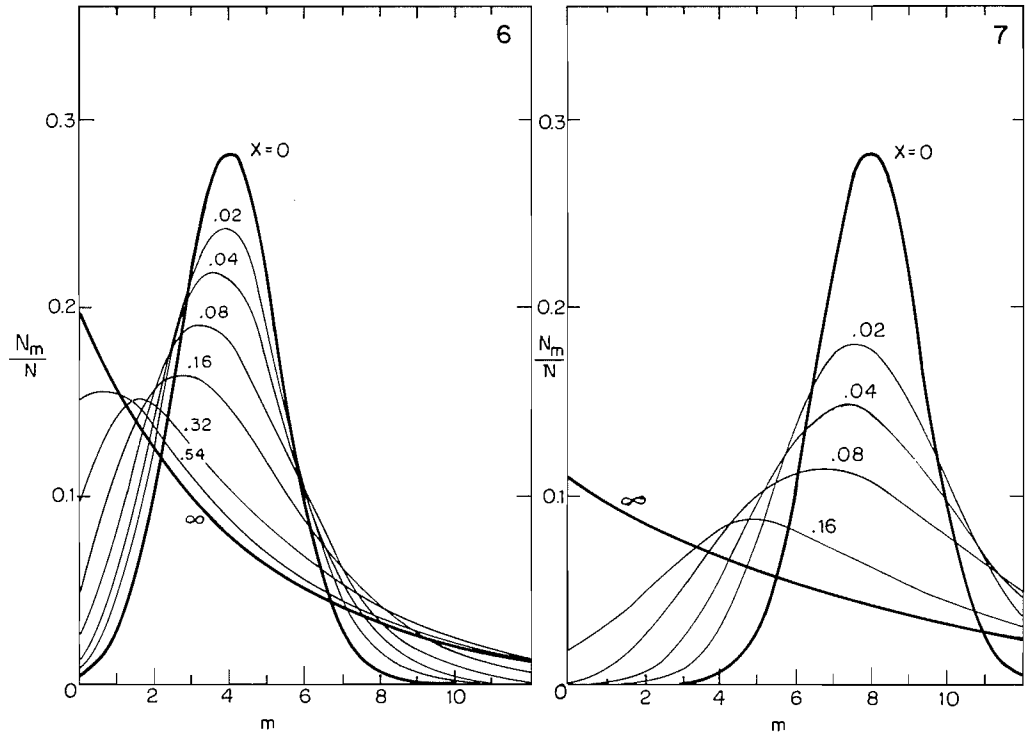

FIG. 6. Time evolution of the fractional level populations N_m/N of levels m as a function of the reduced time, $x = Nk_{1,0}^{0,1}t$. N_m/N has meaning only at integral levels of m; however, the distribution is drawn as continuous for clarity. The initial distribution ($x = 0$) and the final distribution ($x = \infty$) are indicated by thicker lines. The initial distribution is $N_m/N \propto \exp[-0.25(m - 4)^2]$, normalized so that $\sum N_m/N = 1$. At all subsequent times $\sum N_m/N$ remains at 1, and $\sum mN_m/N = 4.0025$, corresponding to a final vibrational temperature, T_{vib}, given by $h\nu/kT_{vib} = 0.2230$. The evolution is for times $\ll\tau$, and $\delta > 10$.

FIG. 7. Same as in Fig. 6, but with the initial distribution shifted to $m_0 = 8$: $N_m/N \propto \exp[-0.25(m - 8)^2]$. Here $\sum mN_m/N = 7.9992$, corresponding to a final $h\nu/kT_{vib} = 0.1178$.

$$[18]\quad \left.\frac{dN_m}{dt}\right|_{V-V} = k_{0,1}^{1,0}\{-\sum(m+1)N_m e^{(m+1-n)\phi}nN_n + \sum(m+1)N_{m+1}e^{-(m-n)\phi}nN_n + \sum mN_{m-1}e^{(m-n)\phi}nN_n - \sum mN_m e^{-(m-n-1)\phi}nN_n + \sum(m+1)N_{m+1}e^{-(m-n)\phi}N_n - \sum mN_m e^{-(m-n-1)\phi}N_n\}$$

where the summations start at $n = 0$.

Those interested in following the entire time evolution of the level populations up to equilibrium must solve the complicated set of differential equations [14], i.e. the sum eqs. [17] and [18]. In comparing eqs. [17] and [18] we note that our assumption $k_{1,1}^{2,0}(= 2e^{\phi}k_{0,1}^{1,0}) \gg k_{1,0}$ implies that we need only consider eq. [18] as the main contribution to dN_m/dt. We must be careful to recognize that this is not generally true, particularly near equilibrium, when the V–V contributions have decayed leaving T–V processes to relax the energy. However, Figs. 1–4 show that V–V processes do dominate at early times. If the experiment in question here has preserved much of the nascent distribution, then presumably not much redistribution has occurred; any modest redistribution that has occurred is V–V in character. Thus eq. [14] reduces for early times (even for $m = 0$) to

$$[19]\quad \frac{dN_m}{dt} \simeq Nk_{0,1}^{1,0}\{[(m+1)N_{m+1} - mN_m] + (\bar{E}/h\nu')[mN_{m-1} + (m+1)N_{m+1} - (2m+1)N_m]\}$$

where we have made the approximations $e^{\pm m\phi} \simeq 1$ and $e^{\pm n\phi} \simeq 1$, valid because the anharmonicity factor is so small, and where we have made use of $\sum_0 N_n = N$ and $\sum_0 nN_n \simeq N\bar{E}/h\nu'$. Whereas the vibrational energy in such experiments relaxes essentially via T–V processes ($|\delta| > 10$ in Table 2), it does so at relatively later times. At the early times in question we may consider $\bar{E}$ to be a constant and equal to the value given by the initial distribution, $\bar{E}_0$. We treat it as unknown but obtainable from an appropriate extrapolation of eq. [8] from late time measurements (the intercept of a plot of $\ln|\sum nN_n h\nu'/N - \bar{E}^{\infty}|$ vs. time, t, gives $\ln|\bar{E}_0 - \bar{E}^{\infty}|$), or else $\bar{E}/h\nu'$ can be evaluated directly from $\sum nN_n$ at each time.

The asymptotic solution ($t \to \infty$) of eq. [19] is $N_m/N = e^{-mw}(1 - e^{-w})$, as can be verified by direct substitution, with $\bar{E}/h\nu'$ given by $e^{-w}/(1 - e^{-w})$ and dN_m/dt set to zero. In other words, an arbitrary initial distribution relaxes towards a Boltzmann distribution — a particular one which is not the final equilibrium one. If $\bar{E}/h\nu'$ is considered constant (as it must be when V–V processes alone are important), then e^{-w} is determined by $\bar{E}_0/h\nu' = e^{-w}/(1 - e^{-w})$. In an example considered below, $\bar{E}_0/h\nu' = 8$; then $w = 0.1178$. For $\nu' = 4000\ cm^{-1}$ this corresponds to a vibrational temperature of 48,890 K; for $\nu' = 400\ cm^{-1}$ to 4890 K. Of course this is reached only at $t = \infty$, in principle. Before then, T–V processes will interfere and eventually dominate; $\bar{E}/h\nu'$ will change with time, and the distribution will relax according to the T–V rate law, i.e. constrained by $\bar{E} \to \bar{E}^{\infty}$. However, here we consider only the early redistribution which might be of interest for extrapolating experimental data. Equation [19] is the exact prescription nec-

Can. J. Chem. Downloaded from www.nrcresearchpress.com by 210.87.254.5 on 09/06/12
For personal use only.

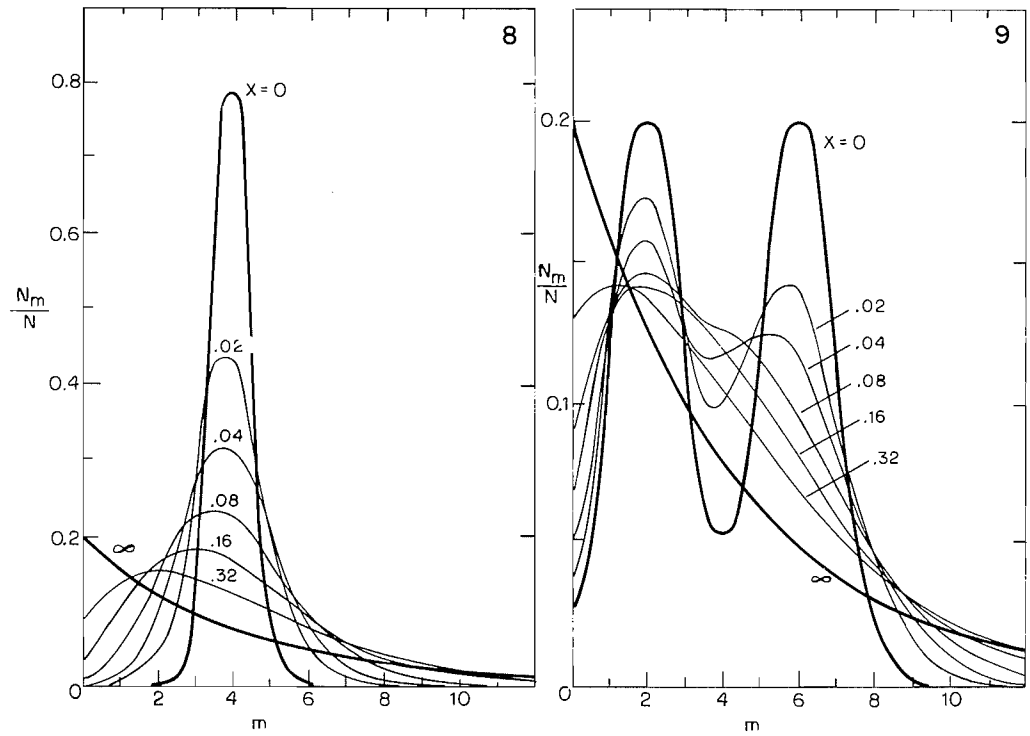

FIG. 8. Same as in Fig. 6, but with a narrower initial distribution: $N_m/N \propto \exp[-2(m-4)^2]$. Here $\sum mN_m/N = 3.9996$, corresponding to a final $h\nu/kT_{vib} = 0.2232$.

FIG. 9. Same as in Fig. 6, but with the initial distribution given by $N_m/N \propto \exp[-0.5(m-2)^2] + \exp[-0.5(m-6)^2]$. Here $-\sum mN_m/N = 4.0116$, corresponding to a final $h\nu/kT_{vib} = 0.2226$.

essary for the extrapolation. We note that any arbitrary distribution (here the first measured one) can be considered the initial distribution; and eq. [19] can be integrated backwards in time to a known time origin. The extrapolation is most conveniently carried out graphically. Equation [19], divided by N, gives the local slope of a graph of the fractional level populations vs. the reduced time, $Nk_{0,1}^{1,0}t$. (Recall that $k_{0,1}^{1,0} = e^{-\phi}k_{1,1}^{2,0}/2$ has essentially been determined in advance by the procedure described above.) Carried out in small steps of, say, 0.001 abscissa units, the initial distribution can be easily reconstructed. The slopes of such plots are, in general, not constant, underscoring the need to improve upon previous linear extrapolations. Whereas short extrapolations can be carried out in this way to correct experimental data, the entire time-evolution of the fractional level populations is best determined by numerical integration of eq. [19]. In order to proceed with examples, we must specify initial distributions. Figures 6–9 are the results of such integrations for Gaussian-like distributions peaked initially at level m_0. In these examples $\bar{E}/h\nu'$ is evaluated by direct summation, $\sum mN_m/N$, and is guaranteed by our choice of initial distributions to be substantial and thus consistent with V–V redistribution ($|\delta| \gg 1$).

As seen in Fig. 6 ($m_0 = 4$), the distribution broadens at first and develops a long exponential tail; at the same time the peak of the distribution moves towards $m = 0$. By the time the fractional level population in $m = 0$ becomes substantial most levels are overpopulated. Thereafter the populations approach their asymptotic values monotonically. It is because of the linear dependence of the V–V rate coefficients on m that the upper levels relax and spread out relatively rapidly. For this same reason the same distribution (this time peaked at $m_0 = 8$) relaxes in the same manner but more than twice as fast initially as it does when $m_0 = 4$ (see Fig. 7). We note that the reduced time scale, $Nk_{0,1}^{1,0}t$, refers to a progress variable identified as the total number of transitions. Since typical V–V collision probabilities are of the order of 0.01 transitions per collision (51), a value of 0.01 for $Nk_{0,1}^{1,0}t$ corresponds roughly to one single collision. It is therefore quite striking to see in Figs. 6–9 how the population distribution can change its character markedly even after only a few collisions!

Figure 8 compared with Fig. 6 shows that the initial width of the distribution has little or no effect on how the distribution approaches a Boltzmann one. Finally, it is interesting to see how a doubly peaked distribution (such as for the bimodal production (42–46) of CN or CO) evolves. The peak at low vibrational levels broadens but does not shift until the second peak at higher vibrational levels broadens and merges into the tail of the first one. Thereafter the resulting single peak relaxes as in Fig. 6 (See Fig. 9).

D. Summary and conclusions

We have solved analytically the rate law for the relaxation of the vibrational energy of a pure diatomic gas. We showed that it is easy to predict whether the vibrational energy in a given system will relax according to a V–V mechanism or according to a T–V mechanism or both. Surprisingly, the outcome is determined not so much by the ratio, γ, of the corresponding rate constants as it is by the specification of the initial conditions, δ (initial principal moments of the population distribution, equilibrium temperature, and anharmonicity are involved). With careful mapping out of some of the time history of the phenomenological time "constant", both the T–V constant, $k_{1,0}$, and the V–V constant, $k_{1,1}^{2,0}$, can be extracted in principle by the guidelines presented. Even time-evolution of

Can. J. Chem. Downloaded from www.nrcresearchpress.com by 210.87.254.5 on 09/06/12
For personal use only.

the individual level populations can be deduced; however, a numerical integration is required here.

Implications for comparison of shock tube results with fluorescence intensity results are clear. Whereas the former lead to $1/\tau = k_{1,0} - k_{0,1}$ directly, the latter lead to a complicated average of $k_{1,0}$ and $k_{1,1}^{2,0}$. Fluorescence data can be considered to be one of two types depending on the time resolution of the experiment: a rapid rise or drop in intensity followed by a slower decay; or else a simple decay. The former, by its nature, is usually analyzed according to a realistic V–V and T–V mechanism, and rate constants are reported. The latter type is deceptively simple and usually single time constants are reported which are often compared directly, but misguidedly, with shock tube data. In view of our results we should not be surprised at disagreement since fluorescence values of τ' are not constants in time or pressure. Using Figs. 1–4 the experimentalist could deduce τ. However, to do this the initial conditions (in this case α) and the regime of t/τ' probed must be known. These are not trivial but necessary requirements. Even then, the experimentalist will be uncertain as to which of the three choices of τ'/τ is actually appropriate, unless he measures τ' as a function of time or pressure. A survey of a variety of experiments (Table 1) suggests that fortunately many experimental conditions probably correspond to a T–V relaxation, particularly when $v = 1$ is laser-excited. However, in view of the fact that the degree of laser excitation is rarely known, this conclusion is not certain, and it would be worthwhile checking the data.

Even though they produce distinctly different initial distributions, both laser excitation and chemical activation can produce the entire range of values of δ. Particular values of α are suggested (Fig. 5) which ensure a pure T–V energy relaxation rate for fluorescence experiments involving direct overtone excitation. Of course, such external control is not possible for a chemical reaction, and it is found that the excited products of a chemical reaction ought to relax according to a mixed mechanism with the energy remaining roughly constant until the population distribution becomes essentially Boltzmann at a high vibrational temperature. Prescriptions are given for extracting rate constants simply from such data, and it would be interesting to actually carry out the analysis. A prescription is also given by extrapolating product distributions to their initial ones. Although the present technique is valuable for pure diatomic gases, the presence of relatively inert colliders in chemical activation experiments introduces an additional complexity. This will be examined in a subsequent article on mixture rules.

The present formalism should also serve as a guideline for future analysis of data from laser-assisted shock tube studies.

Acknowledgement

Financial support from the Natural Sciences and Engineering Research Council of Canada is gratefully acknowledged.

1. H. TEITELBAUM. Can. J. Chem. **61**, 1267 (1983).
2. J. H. KIEFER and R. W. LUTZ. J. Chem. Phys. **44**, 658 (1965).
3. J. C. DECIUS. J. Chem. Phys. **32**, 1262 (1960).
4. W. D. BRESHEARS. Chem. Phys. Lett. **20**, 429 (1973).
5. H. TEITELBAUM. Can. J. Chem. **61**, 1253 (1983).
6. J. K. HANCOCK and W. H. GREEN. J. Chem. Phys. **57**, 4515 (1972).
7. E. A. ROHLFING, H. RABITZ, J. GELFAND, R. B. MILES, and A. E. DEPRISTO. Chem. Phys. **51**, 121 (1980).
8. K. P. HUBER and G. HERZBERG. Molecular spectra and molecular structure. Vol. 4. Constants of diatomic molecules. Van Nostrand, NY. 1979.
9. J. F. BOTT. J. Chem. Phys. **65**, 4239 (1976).
10. J. F. BOTT. J. Chem. Phys. **57**, 96 (1972).
11. R. M. OSGOOD, JR., P. B. SACKETT, and A. JAVAN. Appl. Phys. Lett. **20**, 469 (1972).
12. M. BINA and C. JONES. Appl. Phys. Lett. **22**, 44 (1973).
13. J. F. BOTT. J. Chem. Phys. **70**, 4123 (1979).
14. J. F. BOTT. J. Chem. Phys. **74**, 2827 (1981).
15. A. B. HORWITZ and S. R. LEONE. J. Chem. Phys. **70**, 4916 (1979).
16. C. C. BADCOCK, W. C. HWANG, and J. F. KALSCH. Chem. Phys. Lett. **50**, 381 (1977).
17. I. BURAK, Y. NOTER, A. M. RONN, and A. SZÖKE. Chem. Phys. Lett. **16**, 306 (1972).
18. B. M. HOPKINS and H-L. CHEN. Chem. Phys. Lett. **17**, 500 (1972).
19. M. MARGOTTIN-MACLOU, L. DOYENNETTE, and L. HENRY. Appl. Opt. **10**, 1768 (1971).
20. (*a*) F. DEMARTINI and J. DUCUING. Phys. Rev. Lett. **17**, 117 (1966); (*b*) M. M. AUDIBERT, C. JOFFRIN, and J. DUCUING. Chem. Phys. Lett. **25**, 158 (1974).
21. J. LUKASIK and J. DUCUING. (*a*) J. Chem. Phys. **60**, 331 (1974); (*b*) Chem. Phys. Lett. **27**, 203 (1974).
22. G. C. LIGHT and J. H. MATSUMOTO. Chem. Phys. Lett. **58**, 578 (1978).
23. M. MARGOTTIN-MACLOU, L. DOYENNETTE, and L. HENRY. J. Chem. Phys. **67**, 3360 (1977).
24. J. KOSANETZKY, U. LIST, W. URBAN, H. VORMANN, and E. H. FINK. Chem. Phys. **50**, 361 (1980).
25. A. B. CALLEAR and I. W. M. SMITH. Trans. Faraday Soc. **61**, 2383 (1965).
26. L. A. MELTON and W. KLEMPERER. J. Chem. Phys. **59**, 1099 (1973).
27. T. HIKIDA, S. NAKAJIMA, T. ICHIMURA, and Y. MORI. J. Chem. Phys. **65**, 1317 (1976).
28. M. A. A. CLYNE and I. S. MCDERMID. J. Chem. Soc. Faraday II, **75**, 905 (1979).
29. J. B. KOFFEND, F. J. WODARCZYK, R. BACIS, and R. W. FIELD. J. Chem. Phys. **72**, 478 (1980).
30. M. A. A. CLYNE and I. S. MCDERMID. J. Chem. Soc. Faraday II, **76**, 961 (1980).
31. M. A. A. CLYNE and I. S. MCDERMID. J. Chem. Soc. Faraday II, **75**, 1313 (1979).
32. M. A. A. CLYNE and I. S. MCDERMID. J. Chem. Soc. Faraday II, **74**, 1935 (1978).
33. M. A. A. CLYNE and I. S. MCDERMID. J. Chem. Soc. Faraday II, **74**, 1376 (1978).
34. K. BERGMANN and W. DEMTRÖDER. J. Phys. B, **5**, 1386 (1974).
35. (*a*) CH. OTTINGER, R. V. VELASCO, and R. N. ZARE. J. Chem. Phys. **52**, 1636 (1970); (*b*) G. ENNEN and CH. OTTINGER. Chem. Phys. **3**, 404 (1974).
36. J. C. POLANYI and J. J. SLOAN. J. Chem. Phys. **57**, 4988 (1972).
37. D. BRANDT, L. W. DICKSON, L. N. Y. KWAN, and J. C. POLANYI. Chem. Phys. **39**, 189 (1979).
38. D. S. PERRY and J. C. POLANYI. Chem. Phys. **12**, 419 (1976).
39. J. C. POLANYI and K. B. WOODALL. J. Chem. Phys. **57**, 1574 (1972).
40. J. C. POLANYI and W. SKRLAC. Chem. Phys. **23**, 167 (1977).
41. H. W. CRUSE, P. J. DAGDIGIAN, and R. N. ZARE. Faraday Discuss. Chem. Soc. **55**, 277 (1973).
42. H. SCHACKE, H. GG. WAGNER, and J. WOLFRUM. Ber. Bunsen Ges. Phys. Chem. **81**, 670 (1973).
43. I. V. HERTL, H. HOFMANN, and K. J. ROST. Phys. Rev. Lett. **36**, 861 (1976).
44. G. HANCOCK, B. A. RIDLEY, and I. W. M. SMITH. J. Chem. Soc. Faraday II, **68**, 2117 (1972).
45. K. J. SCHMATJKO and J. WOLFRUM. Ber. Bunsen Ges. Phys.

Can. J. Chem. Downloaded from www.nrcresearchpress.com by 210.87.254.5 on 09/06/12
For personal use only.

Chem. **82**, 419 (1978).
46. J. W. HUDGENS, J. T. GLEAVES, and J. D. MCDONALD. J. Chem. Phys. **64**, 2528 (1976).
47. G. KARL, P. KRUUS, and J. C. POLANYI. J. Chem. Phys. **46**, 224 (1967).
48. P. J. DAGDIGIAN, H. W. CRUSE, and R. N. ZARE. J. Chem. Phys. **62**, 1824 (1975).
49. A. SCHULTZ, H. W. CRUSE, and R. N. ZARE. J. Chem. Phys. **57**, 1354 (1972).
50. J. C. POLANYI and J. J. SLOAN. Inernat. J. Chem. Kinet. (Suppl.) **1**, 51 (1975).
51. J. L. STRETTON. *In* Transfer and storage of energy by molecules. Vol. 2. *Edited by* G. M. Burnett and A. M. North. Wiley and Sons, Inc., NY. 1969. p. 58.

Can. J. Chem. Downloaded from www.nrcresearchpress.com by 210.87.254.5 on 09/06/12
For personal use only.

COMMUNICATIONS

The autoxidation of unsaturated lipids in micelles. Synergism of inhibitors vitamins C and E

LAWRENCE ROSS COATES BARCLAY,[1] STEVEN JEFFREY LOCKE, AND JOSEPH MARK MACNEIL
Department of Chemistry, Mount Allison University, Sackville, N.B., Canada E0A 3C0

Received January 3, 1983

LAWRENCE ROSS COATES BARCLAY, STEVEN JEFFREY LOCKE, and JOSEPH MARK MACNEIL. Can. J. Chem. **61**, 1288 (1983).

The kinetics of thermally (30°C) initiated autoxidations of unsaturated lipids, linoleic acid, and methyl linoleate are studied in 0.50 *M* sodium dodecyl sulfate (SDS) micelles. The rate of chain initiation, R_i, was controlled by using known amounts of the thermal initiator, di-*tert*-butylhyponitrite (DBHN). The initiator efficiency, e, determined by the induction period method with ∝-tocopherol, was 0.30 for linoleic acid and varied (0.30 to 0.36) for methyl linoleate autoxiation as the concentration of the ester increased. The rate of autoxidation of linoleic acid follows the classical rate law since it is proportional to the substrate concentration and to the square root of chain initiation. The oxidizability of linoleic acid measured in micelles is $4.09 \times 10^{-2}\ M^{-1/2}\ s^{-1/2}$. The oxidizability of methyl linoleate varied from 2.37×10^{-2} to $6.92 \times 10^{-2}\ M^{-1/2}\ s^{-1/2}$ as the amount of solubilized ester increased. The latter results are indicative of pooling of the ester in the micellar phase. Additions of aqueous solutions of ascorbic acid to ∝-tocopherol-inhibited micellar autoxidations result in very significant extensions of the efficient inhibition period compared to that obtained with ∝-tocopherol alone. The mechanism of this synergism is briefly discussed.

LAWRENCE ROSS COATES BARCLAY, STEVEN JEFFREY LOCKE et JOSEPH MARK MACNEIL. Can. J. Chem. **61**, 1288 (1983).

On a étudié la cinétique de l'autoxydation initiée thermiquement (30°C) des lipides insaturés, l'acide linoléique et le linoléate de méthyle, dans des micelles de sulfate de dodécyl sodium (SDS) (0,50 *M*). On a contrôlé la vitesse d'initiation de la chaîne, R_i, en utilisant des quantités connues de l'initiateur thermique, le di-*tert*-butylhyponitrite (DBHN). L'efficacité de l'initiateur, e, déterminée par la méthode de la période d'induction avec l'α-tocophérol, est de 0,30 pour l'acide linoléique et varie (de 0,30 à 0,36) pour l'autoxydation du linoléate de méthyle lorsque la concentration de l'ester augmente. La vitesse d'autoxydation de l'acide linoléique obéit à la loi de vitesse classique puisqu'elle est proportionnelle à la concentration du substrat et à la racine carrée de l'initiation de la chaîne. L'oxydabilité de l'acide linoléique mesurée dans des micelles est de $4{,}09 \times 10^{-2}\ M^{-1/2}\ s^{-1/2}$. L'oxydabilité du linoléate de méthyle varie de $2{,}37 \times 10^{-2}$ à $6{,}92 \times 10^{-2}\ M^{-1/2}\ s^{-1/2}$ lorsque la quantité d'ester solubilisé augmente. Ces derniers résultats sont une indication de l'entassement de l'ester dans la phase micellaire. Des additions de solutions aqueuses d'acide ascorbique à l'autoxydation micellaire inhibée par l'α-tocophérol conduisent à une augmentation marquée de l'efficacité de la période d'induction par rapport à celle obtenue avec l'α-tocophérol seul. On discute brièvement du mécanisme de ce synergisme.

[Traduit par le journal]

The free radical autoxidation of organic molecules organized in amphiphilic microenvironments is important to various biological processes, but has been lacking in *quantitative* kinetic data. In this communication we report some results from a kinetic study of the controlled thermally initiated autoxidation of linoleic acid and of methyl linoleate in sodium dodecyl sulfate (SDS) micelles. The results show *(1) that the kinetic rate law is compatible with that well established* (1) *for the autoxidation of organic substrates in homogeneous solution; namely*

$$-\frac{d[O_2]}{dt} = \frac{k_p[RH]R_i^{1/2}}{(2k_t)^{1/2}}$$

and (2) that there is a remarkable synergistic effect in the antioxidant activity of ∝-tocopherol (∝-T) and ascorbic acid (C) when both inhibitors are present.

The apparatus and techniques employed were similar to those described (2). The mole ratio of thermal initiator, di-*tert*-butyl hyponitrite (DBHN), to SDS was varied from 0.001 to 0.01 while that of substrate to SDS ranged from 0.01 to 0.1.[2] Molar concentrations were calculated by assuming a molar volume of reaction of 0.25 liters per mole of SDS, which is the molar volume of SDS obtained from density measurements (3). The rate of chain initiation, $R_i = 2[ArOH]/\tau$ was measured by the ∝-T induction period method assuming a stoichiometric factor of 2 (4). The initiator efficiency (cage effect), $e = R_i/2k_i[DBHN]$, was calculated using $k_i = 3.2 \times 10^{-6}\ s^{-1}$ for the DBHN decomposition rate constant (2).

The experimental substrate orders obtained in 0.50 *M* SDS at 30°C are 1.02 ± 0.01 for linoleic acid in phosphate buffer (pH = 7.0) and 0.1 m*M* EDTA, and 1.34 ± 0.02 for methyl linoleate[3]. The corresponding DBHN orders are 0.53 ± 0.03 and 0.61 ± 0.05. The efficiency of DBHN in linoleic acid autoxidations was found to be 0.30 ± 0.03, independent of acid concentration, while in runs on the ester it increased measurably from 0.30 to 0.36 as the concentration of ester was increased.

These micellar autoxidations exhibited several interesting characteristics. *(1)* The initiator (DBHN) efficiency drops from 66% observed (2) in homogeneous solution to 30%. This is expected of a free radical reaction initiated in a micellar microenvironment where the higher microviscosity (5) would cause a greater extent of cage recombination (6). *(2)* The autoxidation of linoleic acid follows the classical rate law, being first order in substrate and half order in DBHN concentrations. The substrate oxidizability, $k_p/(2k_t)^{1/2} = 4.09 \pm 0.29 \times 10^{-2}\ M^{-1/2}$

[1]Author to whom correspondence should be addressed.

[2]Typically experiments were performed by adding substrate to 2 mL of 0.50 *M* SDS containing DBHN and the rate measured by a recording gas absorption apparatus (2) followed by induction periods (30 to 120 min) obtained by adding 10^{-7} to 10^{-8} mol of ∝-tocopherol in the form of a 0.50 *M* SDS solubilized ∝-T stock solution.

Can. J. Chem. Downloaded from www.nrcresearchpress.com by 210.87.254.42 on 09/06/12
For personal use only.

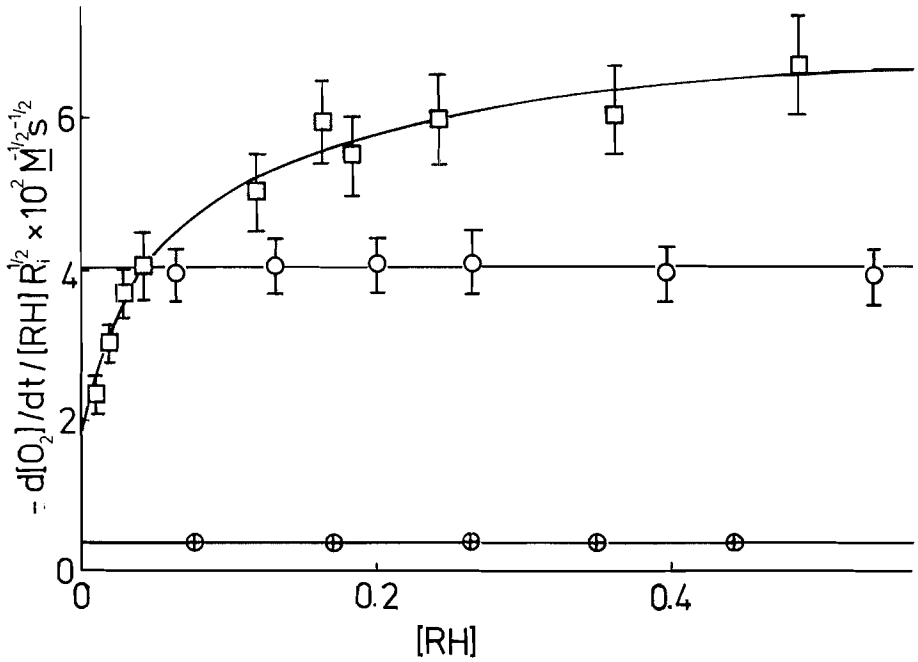

FIG. 1. Variation of the oxidizability of linoleic acid (○), pH 7.0; methyl linoleate, □; and tetralin ⊕; in 0.50 *M* SDS at 30°C. [RH] is the concentration, M L^{-1}, in the micellar phase.

$s^{-1/2}$, is constant over the concentration range used. Methyl linoleate autoxidations exhibit somewhat higher orders,[3] slightly variable *e*, and oxidizabilities which increase from 2.37×10^{-2} to 6.92×10^{-2} $M^{-1/2}$ $s^{-1/2}$ with increasing concentration (see Fig. 1).[4] We suggest that these substrates are incorporated differently in the micellar structure; the linoleate anion with its negatively charged head group is homogeneously dispersed, whereas a more complicated solubilization of the non-ionic ester, involving "pooling" at higher concentration, would decrease the volume of reaction and cause partitioning of the initiator.[4] The agreement between the limiting ester oxidizability at low concentration with the literature value of 2.1×10^{-2} $M^{-1/2}$ $s^{-1/2}$ (7) supports this viewpoint. The results contrast with trends in the oxidizability of a phosphatidylcholine which showed a marked *decrease* when dispersed in a bilayer compared to values in homogeneous solution (2). *(3)* The chain lengths exceed the number of substrate molecules per micelle, a value of 65 resulting for an average of 2.5 methyl linoleate molecules per micelle, based on a micelle aggregation number of 54 (8). This is attributed to a relatively long lifetime of *polar* (2, 9) peroxyl radicals compared to the very rapid monomer−micelle equilibrium (10), so that a peroxyl radical can propagate a chain reaction in several micelles. Thus, the chain reaction is *not* restricted by a particle size boundary that reflects the diffusing peroxyls back toward a cage encounter (11).

Finally we report a remarkable synergistic effect exerted by ascorbic acid (C), when injected into the aqueous phase, on the ∝-T-inhibited reaction in the micellar phase. ∝-T is an efficient inhibitor of micellar autoxidation when it is solubilized in SDS micelles before being injected into the reaction (Fig. 2 (C)). This is expected from the known antioxidant activity of ∝-T and the dynamic nature of micellar systems (*vide infra*). In contrast, C is a very poor inhibitor (Fig. 2 (B)). The combination of C (hydrophilic) with ∝-T (hydrophobic) results in a *very substantial extension of the efficient inhibition period observed when ∝-T is used alone* (compare Figs. 2 (D) and 2 (C)). A stoichiometric value for C as large as 0.50, relative to a value of 2 for ∝-T, was obtained at pH 4.5 and a mole ratio of C/∝-T = 4.6. The hplc analyses of samples taken from reactions inhibited with both C and ∝-T reveal that the concentration of the latter remains essentially constant throughout most of the inhibition period. Thus it appears that C in the aqueous phase serves to regenerate ∝-T in the micellar phase. Tentatively we propose the following general mechanism to account for this synergism.

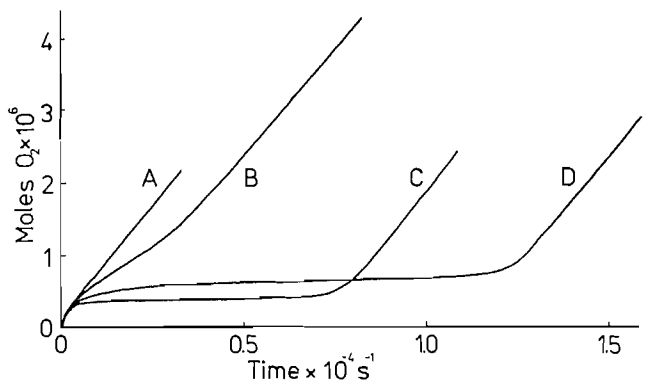

FIG. 2. Autoxiation of linoleic acid (6.4×10^{-5} mol) in 0.50 *M* SDS (2.0 mL) at pH 7.0 initiated with DBHN (7.2×10^{-6} mol): A, uninhibited reaction; B, inhibited with ascorbic acid (1.95×10^{-7} mol); C, inhibited with ∝-tocopherol (5.14×10^{-8} mol); D, inhibited with ∝-tocopherol (5.14×10^{-8} mol) and ascorbic acid (1.95×10^{-7} mol).

[3]The somewhat anomalous behaviour of methyl linoleate in this regard will be dealt with in a more complete kinetic analysis.

[4]Preliminary results shown for tetralin indicate it exhibits a constant oxidizability ($3.7 \pm 0.6 \times 10^{-3}$ $M^{-1/2}$ $s^{-1/2}$). We have no independent evidence on the *exact* location of the initiator; the lower efficiency and the approximate order, $[DBHN]^{1/2}$, indicate it is in the micellar phase.

Can. J. Chem. Downloaded from www.nrcresearchpress.com by 210.87.254.42 on 09/06/12
For personal use only.

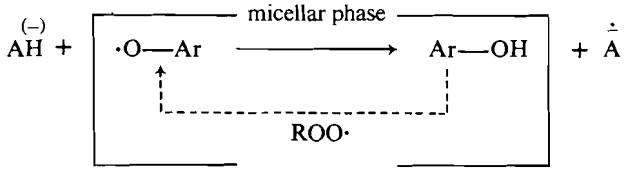

∝-T is known to rapidly transfer H-atoms to peroxyl radicals in homogeneous solution where $k_{-H\cdot} = 2.35 \times 10^6\ M^{-1}\ s^{-1}$ (4) and the effective antioxidant activity of ∝-T observed herein indicates this is also rapid in the micellar phase. Now if the polar phenolic head group, ArOH, of ∝-T is positioned in the micelle near the aqueous phase, the derived radical, ArO·, could readily regenerate ∝-T by hydrogen atom transfer from ascorbate, $\bar{A}H$, positioned in the aqueous phase. This proposal is in agreement with the known rapid hydrogen atom transfer between ∝-T radical and C ($k = 1.55 \times 10^6\ M^{-1}\ s^{-1}$) (12) and with recent esr studies of the interaction of ∝-T radicals with C and glutathione (13). The above mechanism could lead to a higher stoichiometric factor for ascorbate (a maximum of 1 compared to our observed 0.50). However, the chemistry of ascorbic acid, ascorbate ion, and derived radical ($\dot{\bar{A}}$) is known to be rather complex (14) and other radical reactions could deplete ascorbic acid.

These results provide the first definitive evidence for the synergistic effect of vitamins C and E as inhibitors in controlled autoxidations in a microenvironment. We plan to extend this study to bilayers with the expectation of clarifying the important role of natural inhibitors in autoxidations of biological membranes.

Acknowledgements

We thank Dr. G. W. Burton and Dr. K. U. Ingold for their help and advice. Financial assistance provided by the Natural Sciences and Engineering Research Council of Canada (L.R.C.B.) is gratefully acknowledged.

1. (*a*) K. U. INGOLD. Acc. Chem. Res. **2**, 1 (1969); (*b*) J. A. HOWARD. Adv. Free Radical Chem. **4**, 49 (1972).
2. L. R. C. BARCLAY and K. U. INGOLD. J. Am. Chem. Soc. **103**, 6478 (1981).
3. G. M. MUSBALLY, G. PERRON, and J. E. DESNOYERS. J. Colloid Interface Sci. **48**, 494 (1974).
4. G. W. BURTON and K. U. INGOLD. J. Am. Chem. Soc. **103**, 6472 (1981).
5. N. J. TURRO and T. OKUBO. J. Am. Chem. Soc. **103**, 7224 (1981).
6. H. KIEFER and T. G. TRAYLOR. J. Am. Chem. Soc. **89**, 6667 (1967).
7. J. A. HOWARD and K. U. INGOLD. Can. J. Chem. **45**, 793 (1967).
8. J. H. FENDLER and E. J. FENDLER. Catalysis in micellar and macromolecular systems. Academic Press, New York, 1975.
9. A. F. DMITRUK and I. A. OPEIDA. Zh. Strukt. Khim. **18**, 962 (1977).
10. J. M. BROWN. Colloid Sci. **3**, 253 (1979).
11. N. J. TURRO and B. KRAEUTLER. Acc. Chem. Res. **13**, 369 (1980).
12. J. E. PACKER, T. F. SLATER, and R. L. WILLSON. Nature, **278**, 737 (1979).
13. E. NIKI, J. TSUCHIYA, R. TANIMURA, and Y. KAMIYA. Chem. Soc. Jpn. Chem. Lett. 789 (1982).
14. B. H. J. BIELSKI. *In* Ascorbic acid: chemistry, metabolism, and uses. *Edited by* P. A. Seib and B. M. Tolbert. A.C.S. Adv. in Chem. Ser. **200**, 1982. Chapt. 4.

Can. J. Chem. Downloaded from www.nrcresearchpress.com by 210.87.254.42 on 09/06/12
For personal use only.

ADDITIONS AND CORRECTIONS / AJOUTS ET CORRECTIONS

Vol. 61, 1983

M.-T Béraldin and S. Fliszár. Charge distributions and chemical effects. XXXI. Molecular energies of ethylenic compounds.

Page 197. A systematic error in Table 3 indicates $\Sigma_i\Sigma_j a_{ij}\Delta q_i$ values which are too low by 2.13 kcal mol^{-1} and $\Sigma\epsilon_{ij}^0$'s too large by the same amount — an error which is of no consequences as regards the final ΔE_a^* results given for the olefins.

Jayati Datta and Kiron K. Kundu. Transfer thermodynamics of *p*-nitroaniline in aqueous solutions of some ionic and non-ionic cosolvents and the structuredness of the solvents.

Page 625. Due to a computational error, the ΔG_t^0(*p*NA) values for urea–water mixtures reported in Table 1 are wrong. The correct values are −1.37, −2.50, −3.49, and −4.26 kJ mol^{-1} for increasing urea concentration. As a result, the corresponding profile for urea in Fig. 1 should be increasingly negative instead of increasingly positive, as shown.

Consequently, the earlier contention that the increased destabilization of *p*NA is governed by the salting-out type interactions by the predominant zwitterionic forms of urea is not valid. Instead, the increased stabilization of *p*NA, as the corrections indicate, is chiefly governed by possible "acid–base" type interactions through $=NH_2^+$ and $—NO_2^-$ charge centres of *p*NA with zwitterionic forms of urea.

B. A. Keay and R. Rodrigo. An exceptional 5-*endo*–*trig* reversal; a convergent synthesis of daunomycinone.

Page 639. The first part of ref. 3 should read: T. R. KELLY, J. VAYA, and L. ANANTHASUBRAMANIAM. J. Am. Chem. Soc. **102**, 5983 (1980), and references therein; S. D. KIMBALL, D. R. WALT, and F. JOHNSON. J. Am. Chem. Soc. **103**, 1561 (1981); etc.

The last part of ref. 4 should read: B. A. KEAY, H. P. PLAUMANN, D. RAJAPAKSA, and R. RODRIGO. Can. J. Chem. In press.

Can. J. Chem. Downloaded from www.nrcresearchpress.com by 210.87.254.42 on 09/06/12
For personal use only.

Effect of interface mass transfer on the liquid-phase oxidation of acetaldehyde

TSE-CHUAN CHOU[1] AND FWU-SHING LIN
Department of Chemical Engineering, National Chenu Kung University, Taiwan

Received May 18, 1982

TSE-CHUAN CHOU and FWU-SHING LIN. Can. J. Chem. **61**, 1295 (1983).

Partial oxidation of acetaldehyde by oxygen in the liquid phase was studied in the temperature range from −10°C to 34°C, oxygen flow rate from 90 to 100 mL/min, concentration of acetaldehyde from 3.0 to 34.0 volume percent, and at different partial pressures of oxygen. Cobalt acetate was used as catalyst. It was found that the reaction rate was governed by two types of rate equations depending on the operating conditions as well as the loading of catalyst.

In the region of higher oxygen mass transfer, the rate

[1] $r = K_1 (Co^{+++})^{0.5} (CH_3CHO)^{1.5}$

where $K_1 = 6.9 \times 10^{-3}$ L mol^{-1} s^{-1} at the temperature −10°C.

In other conditions,

[2] $r = k_2 P_{O_2}$

where $k_2 = 5.7 \times 10^{-4}$ mol L^{-1} atm^{-1} s^{-1}, and is a pseudo rate constant which depends on the dispersion of oxygen in the reactor. The experimental results appeared to support a theoretical analysis. The key reaction steps of the reaction mechanisms were also identified.

TSE-CHUAN CHOU et FWU-SHING LIN. Can. J. Chem. **61**, 1295 (1983).

On a étudié l'oxydation partielle de l'acétaldéhyde par l'oxygène en phase liquide dans l'intervalle de température allant de −10°C à 34°C, avec un débit d'oxygène de 90 à 100 mL/min, pour une concentration d'aldehyde allant de 3,0 à 34 pour cent en volume et à différentes pressions partielles d'oxygène. On a utilisé l'acétate de cobalt comme catalyseur. On a trouvé que la vitesse de réaction dépend de deux types d'équations de vitesse selon les conditions opératoires et la charge du catalyseur.

Dans la région de plus forte vitesse de transfert de masse d'oxygène

[1] $r = K_1 (Co^{+++})^{0.5} (CH_3CHO)^{1.5}$

où $K_1 = 6{,}9 \times 10^{-3}$ L mol^{-1} s^{-1} à −10°C.

Dans d'autres conditions,

[2] $r = k_2 P_{O_2}$

où $k_2 = 5{,}7 \times 10^{-4}$ mol L^{-1} atm^{-1} s^{-1}. k_2 est une constante de pseudo vitesse qui dépend de la dispersion d'oxygène dans le réacteur. Les résultats expérimentaux semblent confirmer l'analyse théorique. On a également identifié les étapes déterminantes des mécanismes de la réaction.

[Traduit par le journal]

Introduction

Peracetic acid (PAA), a very powerful organic oxidation reagent, can be prepared by many methods (1–4). However, only a few have been commercialized. One of them is the catalytic liquid-phase oxidation of acetaldehyde (2, 4).

Although catalytic liquid-phase oxidation of acetaldehyde has been investigated by several investigators (1–11), the kinetics of the oxidations, as well as the factors which affect the yield of PAA, are not adequately illustrated and past investigators proposed two different reaction mechanisms. Thus, Bawn and Williamson (12) and others (2, 13) found that the primary product of liquid-phase oxidation of acetaldehyde was peracetic acid. The secondary reaction was the reaction of peracetic acid with acetaldehyde to form another peroxide, acetaldehyde monoperoxyacetate (AMP), which was then decomposed into acetic acid or acetic acid anhydride. However, several authors (4) proposed that the primary reaction product was AMP which decomposed in acid solution to form peracetic acid and acetaldehyde.

Starcher *et al.* (14) determined the structure of AMP by ir spectroscopy. Furthermore, they indicated that both PAA and AMP in the products were peroxides. Various analytical results of these two peroxides in solution were presented by different investigators (8, 12, 14).

Backstrom and Beatty (15) first determined that the liquid-phase catalytic oxidation of acetaldehyde was a free-radical chain reaction. However, Imamura *et al.* (5) found that the secondary reaction of PAA with acetaldehyde was a series of ionic reactions. In general, ozone, ultraviolet, and metal catalysts are used as the initiator of free radical reactions (2, 8). Cobalt and iron are the most powerful metal catalysts for preparing PAA from the oxidation of acetaldehyde. By using cobalt as catalyst, Bawn and Williamson (12) found that the rate of formation of PAA was of a first order reaction with respect both to the concentration of catalyst and the concentration of acetaldehyde. They also found that the concentration or partial pressure of oxygen did not affect the reaction rate of formation of peracetic acid. On the other hand, several investigators found that the rate of reaction was 0.5 order with respect to the concentration of catalyst, 1.5 order with respect to the concentration of acetaldehyde, and zero order with respect to partial pressure of oxygen. However, Sadana (16) found that the catalyzed free-radical liquid-phase oxidation of hydrocarbons and/or oxygenated compounds might be dependent on the concentration of oxygen. Ramage and Eckert (17) indicated that mass transfer of gas-phase reactants affected

[1]Visiting Professor, Department of Chemical Engineering, Rensselaer Polytechnic Institute, Troy, New York 12181, U.S.A.

Can. J. Chem. Downloaded from www.nrcresearchpress.com by 210.87.254.42 on 09/06/12
For personal use only.

Can. J. Chem. Downloaded from www.nrcresearchpress.com by 210.87.254.42 on 09/06/12
For personal use only.

both the selectivity and the reaction rate of liquid-phase free-radical reactions. Unfortunately, there are few investigations concerning the effects of mass transfer of oxygen on the rate of acetaldehyde oxidation in the liquid phase.

In this research work, the kinetics of liquid-phase oxidation of acetaldehyde by cobalt catalyst were systematically studied. The effect of the mass transfer rate of oxygen on the rate of oxidation of acetaldehyde was explored.

Theoretical analysis

Several investigators (2, 4, 8, 11) proposed that the role of metallic catalyst is to initiate the free radical chain reactions as follows.

Initiation:

[3] $Co^{3+} + CH_3CHO \xrightarrow{k_1} CH_3\dot{C}O + H^+ + Co^{2+}$

The oxygen of the gas phase is dissolved and is absorbed in the liquid phase before it reacts with the free radicals. The process of oxygen absorption is proposed as:

O_2 absorption:

[4] $O_{2(gas)} \underset{k_{-2}}{\overset{k_2}{\rightleftharpoons}} O_{2(abs.)}$

The absorbed oxygen reacts with the free radicals. The chain reactions are given as follows.

Propagation:

[5] $CH_3\dot{C}O + O_{2(abs.)} \xrightarrow{k_3} CH_3CO_3^{\cdot}$

[6] $CH_3CO_3^{\cdot} + CH_3CHO \xrightarrow{k_4} CH_3CO_3H + CH_3\dot{C}O$

Formation of AMP:

[7] $CH_3CO_3H + CH_3CHO \underset{k_{-5}}{\overset{k_5}{\rightleftharpoons}} AMP$

Imamura *et al.* (5) proposed and discussed step [7] in detail. Their results indicated that the formation of AMP was due to ionic reactions which are expressed as:

[8] $CH_3CO_3H \rightleftharpoons CH_3CO_3^- + H^+$

[9] $CH_3CHO + H^+ \rightleftharpoons CH_3C^+H_2O$

[10] $CH_3CO_3^- + CH_3C^+H_2O \rightarrow AMP$

Bawn and Williamson (12) and Philips *et al.* (10, 14) studied the decomposition of AMP.

[11] $AMP \rightarrow 2CH_3CO_2H$ or $(CH_3CO)_2O + H_2O$

The by-products, AMP, acetic acid, and acetic anhydride, are produced in reaction steps [7] and [11].

There are at least two main types of free radicals in the liquid phase. Thus the termination steps are expressed in [12] to [14] (18).

Termination:

[12] $2CH_3\dot{C}O \xrightarrow{k_7} (CH_3CO)_2$

[13] $CH_3\dot{C}O + CH_3CO_3^{\cdot} \xrightarrow{k_8} (CH_3CO_2)_2$

[14] $2CH_3CO_3^{\cdot} \xrightarrow{k_9}$ terminated products

In addition to steps [12] to [14], Chou and Albright (19) indicated that the termination might occur by the collision of the free radicals with a third body. Matsuzaki and Imamura (8) showed that the wall of the reactor also affected the oxidation reactions.

The regeneration of catalyst automatically occurs in the system and is expressed as

[15] $CH_3CO_3H + Co^{2+} \xrightarrow{k_{10}} CH_3CO_2^{\cdot} + OH^- + Co^{3+}$

Theoretically, free-radical reactions may include many intermediate reaction steps, which give rise to a complicated model for the reaction mechanisms. However, Chou *et al.*.(19, 20) pointed out that a simplified model could adequately express the reaction phenomena of the system by considering only the main reaction steps. The reaction model for the partial oxidation of acetaldehyde to form PAA described by the above equations could be simplified as follows.

Case i

If $(CH_3CO_3^{\cdot}) \gg (CH_3\dot{C}O)$, i.e. at high partial pressures of oxygen, the termination product concentrations can be approximately expressed by step [14]. The changes in free-radical concentrations are expressed as

$$[16]\quad \frac{d(CH_3\dot{C}O)}{dt} = k_1(Co^{3+})(CH_3CHO) - k_3(CH_3\dot{C}O)(O_{2(abs.)}) + k_4(CH_3CO_3^{\cdot})(CH_3CHO)$$

$$[17]\quad \frac{d(CH_3CO_3^{\cdot})}{dt} = k_3(CH_3\dot{C}O)(O_{2(abs.)}) - k_4(CH_3CHO)(CH_3CO_3^{\cdot}) - 2k_9(CH_3CO_3^{\cdot})^2$$

Assuming pseudo steady state conditions, we obtain from [16] and [17]

$$[18]\quad (CH_3CO_3^{\cdot}) = \left(\frac{k_1}{2k_9}\right)^{1/2}(Co^{3+})^{1/2}(CH_3CHO)^{1/2}$$

The rate of reaction is expressed as

$$[19]\quad r = \frac{d(O_{abs.})}{dt} = 2\frac{d(O_{2(abs.)})}{dt} = 2k_3(CH_3\dot{C}O)(O_{2(abs.)}) = 2k_4(CH_3CHO)(CH_3CO_3^{\cdot}) + 4k_9(CH_3CO_3^{\cdot})^2$$

Since $(CH_3CO_3^{\cdot})^2 \ll (CH_3CHO)(CH_3CO_3^{\cdot})$

$$[20]\quad r = 2k_4(CH_3CHO)(CH_3CO_3^{\cdot}) = \left(\frac{2k_1k_4^2}{k_9}\right)^{1/2}(Co^{3+})^{1/2}(CH_3CHO)^{3/2}$$

The above rate equation [20] indicates that the reaction rate is independent of the partial pressure of oxygen. The rate of mass transfer of oxygen is faster than the rate of chemical reaction.

Case ii

If $(CH_3\dot{C}O) \gg (CH_3CO_3^{\cdot})$, i.e. at moderately low partial pressures of oxygen or if the formation of $CH_3CO_3^{\cdot}$ free radical is slow, the termination can be approximately expressed by reaction step [12]. The changes of free radical concentrations are then expressed as

$$[21]\quad \frac{d(CH_3\dot{C}O)}{dt} = k_1(CH_3CHO)(Co^{3+}) - k_3(CH_3\dot{C}O)(O_{2(abs.)}) + k_4(CH_3CO_3^{\cdot})(CH_3CHO) - 2k_7(CH_3\dot{C}O)^2$$

Can. J. Chem. Downloaded from www.nrcresearchpress.com by 210.87.254.42 on 09/06/12
For personal use only.

$$[22]\quad \frac{d(CH_3CO_3^{\cdot})}{dt} = k_3(CH_3\dot{C}O)\,(O_{2(abs.)}) - k_4(CH_3CO_3^{\cdot})\,(CH_3CHO)$$

At pseudo steady state, from eqs. [21] and [22], we obtain

$$[23]\quad (CH_3\dot{C}O) = \left(\frac{k_1}{2k_7}\right)^{1/2}(CH_3CHO)^{1/2}\,(Co^{3+})^{1/2}$$

By Henry's law:

$$[24]\quad (O_{2(abs.)}) = k_2 P_{O_2}$$

where $k_2 = \kappa_2 k_{-2}$ and κ_2 is the equilibrium constant of oxygen, and P_{O_2} is the partial pressure of oxygen.

If eq. [5] is assumed to be the controlling step, then the rate of reaction can be expressed as

$$[25]\quad r = 2k_3(CH_3\dot{C}O)\,(O_{2(abs.)}) = \left(\frac{2k_1k_3^2k_2^2}{k_7}\right)^{1/2}(CH_3CHO)^{1/2}\,(Co^{3+})^{1/2}\,P_{O_2}$$

Case iii

If the rate of mass transfer of oxygen is less than that of the chemical reactions, the rate of reaction can be expressed as

$$[26]\quad r = k_2 P_{O_2}$$

Experimental

The reactor consisted of a Pyrex glass tube, 34 cm in length and 3.0 cm in outside diameter. At the bottom of the tube was a porous gas disperser which contained 100/160 mesh sintered glass powder. A condenser was installed above the reactor and its temperature was maintained at about −10°C by a cooling system. Oxygen entered from the bottom of the reactor and was bubbled through the solution in the reactor. The oxygen flow rate was measured by a flowmeter with a precision of ±0.2%. The temperature of the reactor was controlled within ±0.1°C by placing the entire reactor system in a constant temperature bath.

The chemicals used were of reagent grade. The catalyst solutions were prepared by dissolving cobalt acetate in distilled water. The desired concentrations of acetaldehyde solution were obtained by mixing acetaldehyde with solvent. After the acetaldehyde solution was introduced into the reactor, the catalyst solution was added to the reactor using a syringe. Then the cooling system of the condenser was started and the flow rate of oxygen was adjusted to the desired levels. Samples were taken periodically from the reactor and analyzed using iodometry titration and gas chromatography.

The concentrations of the organic peroxides were analyzed by iodometric methods. Both peroxides, PAA and AMP, in the products were oxidation reagents of iodide ions. The titration reactions were expressed as follows.

$$[27]\quad \text{PAA: } CH_3CO_3H + 2H^+ + 2I^- \rightarrow CH_3CO_2H + H_2O + I_2$$

$$[28]\quad \text{AMP: } C_4H_8O_4 + 2H^+ + 2I^- \rightarrow CH_3CO_2H + CH_3CHO + H_2O + I_2$$

$$[29]\quad I_2 + 2S_2O_3^{2-} \rightarrow 2I^- + S_4O_6^{2-}$$

The ability of PAA and AMP to oxidize iodide ion depended on the operating conditions which included pH value, temperature, and types of solutions, etc. The concentrations of PAA and AMP could be obtained by analysis of the total peroxides (TPO, i.e. the sum of PAA and AMP) and PAA in the solution by choosing different operating conditions. The ability of PAA to oxidize iodide ion did not depend on temperature; however, the ability of AMP to oxidize iodide ion was noted to be a function of temperature (21). AMP could not be reduced by iodide ion at temperatures below −2.0°C and could be completely reduced by iodide ion at temperatures above 30°C. Accordingly, the concentrations of PAA and TPO could be obtained by idometric analysis of the samples operating at the temperatures −2.0°C and 30.0°C, respectively. The concentration of AMP was the difference between TPO and PAA.

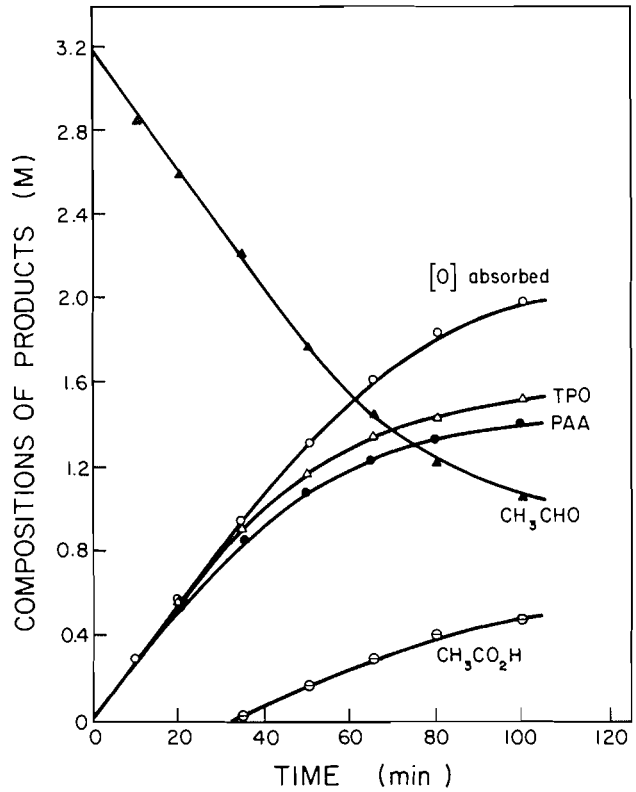

FIG. 1. The compositions of products vs. time. $[Co^{3+}] = 4 \times 10^{-4}$ M; O_2 flow rate = 100 mL/min; solvent = CH_3COCH_3; temperature = −10°C.

TABLE 1. Effect of catalyst loading on the formation of total peroxides*

Catalyst loading $M \times 10^4$	Concentration of TPO M/L			
	Reaction time, min			
	10	20	30	40
0.5	0.10	0.18	0.26	0.34
1.0	0.14	0.25	0.35	0.45
2.0	0.19	0.34	0.47	0.60
4.0	0.26	0.46	0.62	0.76
8.0	0.32	0.58	0.81	0.95
12.0	0.33	0.64	0.85	1.02

* Experimental conditions: concentration of CH_3CHO, 2.65 M; oxygen flow rate, 100 mL/min; solvent, CH_3COCH_3; temperature, −10°C.

Unreacted acetaldehyde was analyzed by gas chromatography. However, acetaldehyde could be generated by the decomposition of AMP. Thus, the actual unreacted acetaldehyde was given by the difference of acetaldehyde obtained by gas chromatography and the concentration of AMP. Errors were avoided by allowing time for the complete decomposition of AMP, subsequent to TPO analysis.

The amount of oxygen reacted was equal to the amounts of TPO and acetic acid which was calculated by

$$[30]\quad [CH_3CO_2H] = [CH_3CHO]_0 - [CH_3CHO] - 2[TPO] + [PAA]$$

where $[CH_3CHO]_0$ was the initial concentration of acetaldehyde and $[CH_3CHO]$ was the concentration of the unreacted acetaldehyde.

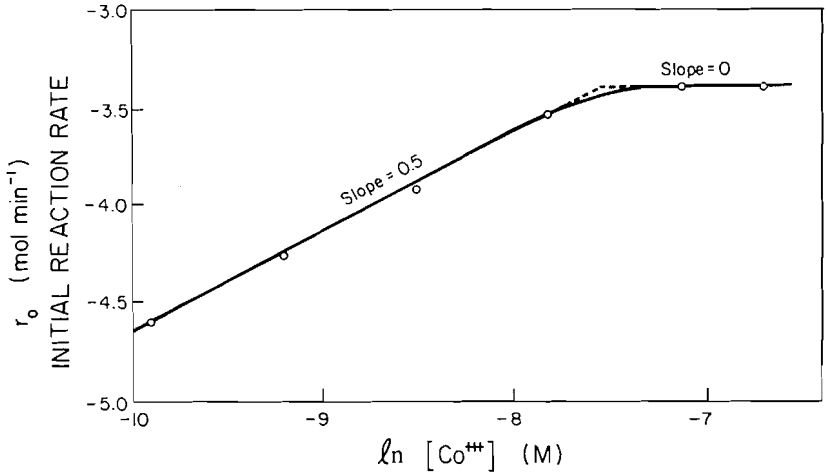

FIG. 2. Effect of the loading of catalyst on the initial reaction rate. [CH_3CHO] = 2.65 M; O_2 flow rate = 100 mL/min; solvent = CH_3COCH_3; temperature = −10°C.

TABLE 2. Effect of the concentration of acetaldehyde on the formation of total peroxides*

Concentration of CH_3CHO, M	Concentration of TPO, M/L				
	Reaction time, min				
	5	10	20	30	40
0.53	0.03	0.04	0.07	0.08	0.11
0.89	0.06	0.08	0.14	0.18	0.22
1.77	0.10	0.17	0.30	0.39	0.49
2.65	0.15	0.26	0.45	0.62	0.77
3.54	0.17	0.33	0.63	0.88	1.10
5.84	0.17	0.35	0.71	1.18	1.38

* Experimental conditions: catalyst loading, 4×10^{-4} M; oxygen flow rate, 100 mL/min; solvent, CH_3COCH_3; temperature, −10°C.

Results

The compositions of products for a typical run are shown in Fig. 1. The by-product acetic acid as well as AMP was generated during an interval of 0.5 hour. As shown in the figure, the intial peroxide product was PAA only. The amounts of TPO or PAA were equal to the amounts of oxygen absorbed at the initial stage. The difference of TPO and PAA was AMP; AMP increased slightly with conversion.

The effects of catalyst loading on the initial reaction rate are shown in Table 1 and Fig. 2. The reaction rate increased with the concentration of catalyst. But the effects of catalyst loading became insignificant when the concentration of catalyst exceeded a limiting value. At the operating conditions of 2.65 M acetaldehyde, oxygen flow rate of 100.0 mL/min, temperature of −10.0°C, and acetone as the solvent, the limiting value of catalyst loading was found to be 8.0×10^{-4} mole per liter. The reaction order was shown to be 0.5 ± 0.1 and 0, below and above the limiting value of catalyst loading, respectively.

Table 2 and Fig. 3 indicate the effect of acetaldehyde concentration on the initial rate of formation of PAA. The initial reaction order was 1.4 (±0.2) with respect to the concentration of acetaldehyde in a low concentration range (1.0 M and less). Further increases in the concentration of acetaldehyde above 1.0 M did not result in further increases of PAA, and the reaction became zero order with respect to acetaldehyde.

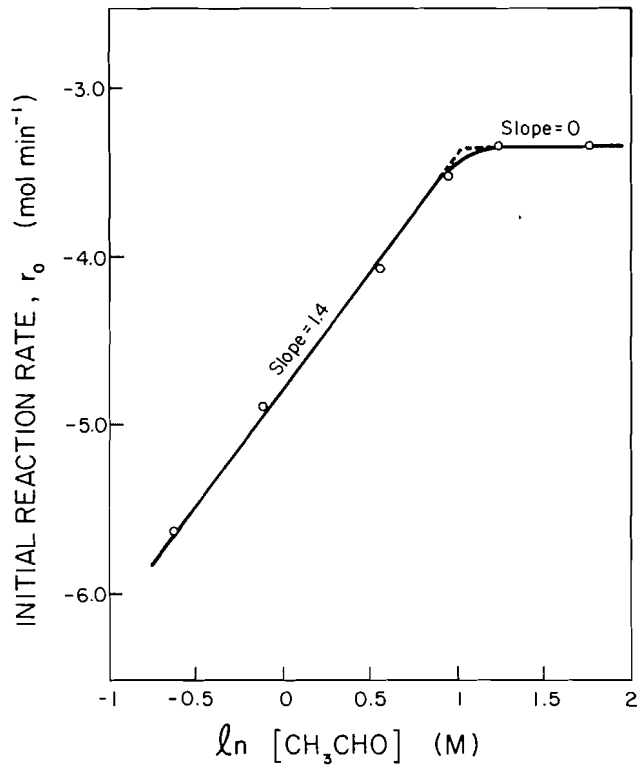

FIG. 3. Effect of the concentration of acetaldehyde on the initial reaction rate. [Co^{3+}] = 4×10^{-4} M; solvent = CH_3COCH_3; O_2 flow rate = 100 mL/min; temperature = −10°C.

At pseudo steady state, the reaction rate was equal to the rate of oxygen absorbed or reacted. At low catalyst loadings and low concentrations of acetaldehyde, the reaction rate was independent of the partial pressure of oxygen, as shown in Table 3(b) and curve I of Fig. 4. It was found that even at rather low partial pressures, the dissolved oxygen was sufficient for the oxidation reaction. The rate-determining step was reaction controlled in this case. At high catalyst loadings and high concentrations of acetaldehyde, the rate-determining step was mass-transfer controlled. In this case, the rate of reaction was a function of the partial pressure of oxygen only. However, the rate of reaction became independent of the partial pressure of oxygen at rather high partial pressures of oxygen (greater than

Can. J. Chem. Downloaded from www.nrcresearchpress.com by 210.87.254.42 on 09/06/12
For personal use only.

TABLE 3. Effect of the partial pressure of oxygen on the formation of total peroxides

(a) Concentration of CH_3CHO: 2.65 *M*

Partial pressure of O_2, atm	Concentration of TPO M/L* Reaction time, min 10	20	30	40
0.25	0.09	0.18	0.27	0.36
0.50	0.17	0.32	0.45	0.56
0.75	0.24	0.43	0.59	0.73
1.00	0.27	0.45	0.62	0.75

(b) Concentration of CH_3CHO: 1.00 *M*

Partial pressure of O_2, atm	Concentration of TPO M/L† Reaction time, min 10	20	30	40
0.25	0.10	0.19	0.27	0.33
0.50	0.11	0.22	0.31	0.36
1.00	0.11	0.21	0.29	0.35

* Other experimental conditions: oxygen flow rate, 100 mL/min; solvent, CH_3COCH_3; temperature, −10°C; and catalyst loading, 4.0×10^{-4} *M*.

† Other experimental conditions: oxygen flow rate, 100 mL/min; solvent, CH_3COCH_3; temperature, −10°C; and catalyst loading, 2.0×10^{-4} *M*.

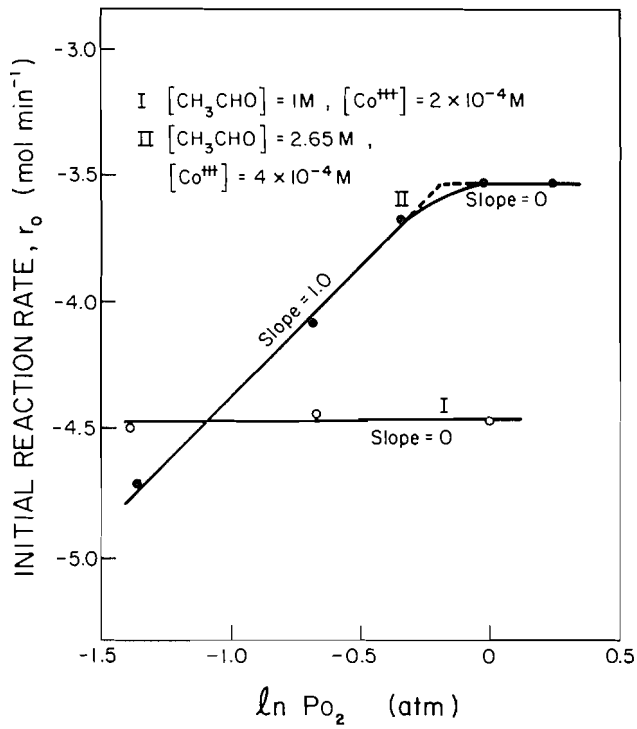

FIG. 4. Effect of the partial pressure of oxygen on the initial reaction rate. O_2 flow rate = 100 mL/min; temperature = −10°C.

0.75 atm) and at fixed catalyst loadings and concentration of acetaldehyde, as shown in Table 3(a) and curve II of Fig. 4. The rate of reaction was reaction controlled again, in this case.

Accordingly, the reaction rates for the formation of peracetic acid can be expressed in two forms. When the rate-determining step is reaction controlled, the rate equation can be written as

$$r = K_1(Co^{3+})^{0.5}\,(CH_3CHO)^{1.4}$$

where K_1 was 6.9×10^{-3} L mol^{-1} s^{-1} at the temperature −10.0°C. On the other hand, when the rate-determining step was mass-transfer controlled, the rate equation can be written as

$$r = k_2 P_{O_2}$$

where k_2 is a pseudo rate constant and equal to 5.7×10^{-4} mol L^{-1} atm^{-1} s^{-1}.

Discussion and conclusion

The reaction orders of the oxidation of acetaldehyde in the liquid phase using Co catalyst depended on the reaction conditions. At higher oxygen transfer rates, the rate of reaction was dependent on the concentrations of catalyst and acetaldehyde. As shown in Table 4, the experimental results correlated well with case (*i*) of the theoretical analysis. Several investigators (4, 11) also obtained similar results, indicating that the reaction order with respect to Co catalyst was 0.5 and to acetaldehyde was 1.5. However, Bawn and Williamson (12) obtained different results which showed that the reaction order was 0.4 with respect to Co catalyst and was 1.0 to acetaldehyde.

When the oxygen transfer rate was low, the reaction rate was dependent on the partial pressure of oxygen only. As shown in Table 4, the experimental results correlated well with case (*iii*) of the theoretical analysis. In this operating range, the rate constant for mass transfer was a pseudo rate constant, depending on the dispersion of oxygen bubbles as well as the composition of the liquid phase. Ramage and Eckert (17) obtained similar results for the free-radical reactions in the liquid phase.

The theoretical analysis and the experimental results of this work both show that $CH_3CO_3^{\cdot}$ was the main free radical in the liquid phase. It was observed that the dissolved oxygen molecules combined with the free radical CH_3CO at a fast rate to

TABLE 4. Comparison of experimental results and theoretical analysis of reaction kinetics for the oxidation of acetaldehyde

Parameters	Reaction order: Experimental results, High oxygen-transfer rate	Experimental results, Low oxygen-transfer rate	Theoretical analysis, Case *i*	Case *ii*	Case *iii*
Co^{3+}	0.5	0	0.5	0.5	0
CH_3CHO	1.4	0	1.5	0.5	0
P_{O_2}	0	1	0	1	1

Can. J. Chem. Downloaded from www.nrcresearchpress.com by 210.87.254.42 on 09/06/12
For personal use only.

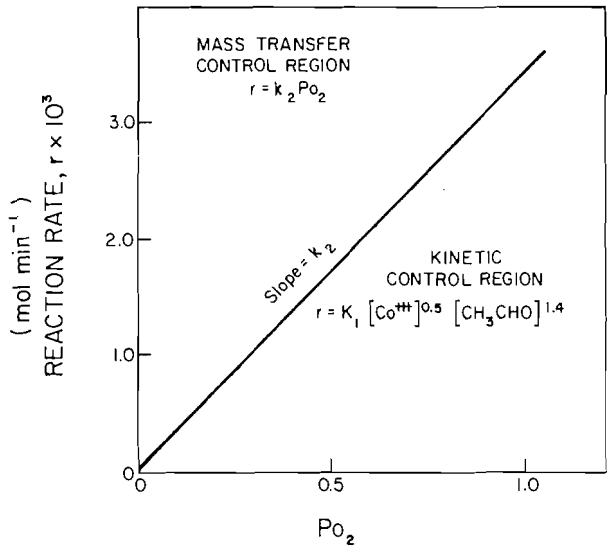

FIG. 5. The effect of the partial pressure of oxygen on the kinetics. Temperature = −10°C; solvent = CH_3COCH_3.

form the free radical $CH_3CO_3^{\cdot}$. Traylor and co-workers (18) found that several products, as well as several reaction steps, were included in the termination step involving $CH_3CO_3^{\cdot}$ free radicals.

As shown in Fig. 5, one criterion for choosing between the two rate equations might be the slope, which equals k_2 in eq. [2]. The region below the critical line represents high oxygen-transfer rates, i.e. the ratio of $(k_2P_{O_2})$ to $(K_1(Co^{3+})^{0.5}(CH_3CHO)^{1.4})$ is greater than one, and the reaction rate can be expressed by eq. [1]. The region above the same line represents low oxygen mass-transfer rates and the reaction rate can be expressed by eq. [2]. The pseudo rate constant k_2 was related to the dispersion of oxygen, the solvent used in the solution, and the flow pattern of the system.

1. J. F. BLACK. J. Am. Chem. Soc. **100**, 527 (1978).
2. A. G. DAVIES. Organic peroxides. Vol. 1. John Wiley & Sons, New York. 1970. p. 59.
3. E. KOUBCK and J. O. EDWARDS. J. Org. Chem. **28**, 2157 (1963).
4. S. TAKSOKA. Hydrogen peroxide and peracetic acid. Report No. 68AI. Stanford Reasearch Institute. 1976. p. 27.
5. J. IMAMURA, *et al*. Peracetic acid synthesis by liquid phase autoxidation of acetaldehyde. Nippon Sangyo Gijitsu Shinke Kyokai Gijitsu Shigyo, **13**, 17 (1970).
6. S. A. MASLOV and E. A. BLYUMBERG. Liquid-phase oxidation of aldehydes. Russ. Chem. Rev. **45**, 155 (1976).
7. A. M. NEMECEK, C. F. HENDRICKS, and C. A. HENDRICK. Ind. Eng. Chem. Prod. Res. Dev. **2**, 218 (1980).
8. T. MATSUZAKI and J. IMAMURA. J. Chem. Soc. Jpn. **8**, 1377 (1975).
9. J. R. MCUBEK and C. A. HELLER, JR. Chem. Rev. **54**, 325 (1954).
10. B. PHILIPS, F. C. FROSTICK, JR., and P. S. STARCHER. J. Am. Chem. Soc. **79**, 5982 (1957).
11. K. TANAKA, *et al*. J. Ind. Chem. Jpn. **73**, 938 (1970).
12. E. H. BAWN and J. B. WILLIAMSON. Trans. Faraday Soc. **47**, 721 (1951).
13. M. J. GAGAN and G. D. LUBARSKY. J. Phys. Chem. **39**, 837 (1935).
14. P. S. STARCHER, B. PHILIPS, and F. C. FROSTICK, JR. J. Org. Chem. **26**, 3568 (1961).
15. H. L. BACKSTROM and H. A. BEATTY. J. Phys. Chem. **35**, 2530 (1931).
16. A. SADANA. Ind. Eng. Chem. Process Des. Dev. **18**, 50 (1979).
17. M. P. RAMAGE and R. E. ECKERT. Ind. Eng. Chem. Process Des. Dev. **12**, 248 (1973).
18. N. A. CLINTON, R. A. KENLEY, and T. G. TRAYLOR. J. Am. Chem. Soc. **97**, 3746 (1975).
19. T. C. CHOU and L. F. ALBRIGHT. Ind. Eng. Chem. Process Des. Dev. **17**, 454 (1978).
20. T. C. CHOU and J. C. CHANG. Chem. Eng. Sci. **35**, 1581 (1980).
21. T. C. CHOU and F. S. LIN. Anal. Chem. Submitted.

Can. J. Chem. Downloaded from www.nrcresearchpress.com by 210.87.254.42 on 09/06/12
For personal use only.

Hydrogen isotope exchange between fluoroform (CF_3H) and water. 3. Catalysis by ^-OH-type anion exchange resins, and the effect of added dimethyl sulfoxide[1]

E. ALLAN SYMONS,[2] JOHN H. ROLSTON, LORRAINE A. BALDISERA, JOHN C. G. DROVER, AND J. DOUGLAS BONNETT

The Physical Chemistry Branch, Atomic Energy of Canada Limited, Chalk River Nuclear Laboratories, Chalk River, Ont., Canada K0J 1J0

Received July 26, 1982

E. ALLAN SYMONS, JOHN H. ROLSTON, LORRAINE A. BALDISERA, JOHN C. G. DROVER, and J. DOUGLAS BONNETT. Can. J. Chem. **61**, 1301 (1983).

Anion exchange resins like Rexyn 201(OH) and Amberlyst A-26 have been shown to be active catalysts for deuterium transfer between water and fluoroform. Under stirred slurry conditions at 50°C the Rexyn 201 is 25× more effective than NaOH on a per-hydroxide-ion basis. Addition of DMSO to the aqueous slurry produces an increase in Rexyn 201 reactivity, but the resin advantage over homogeneous ^-OH declines to zero by ~30 mol% DMSO. At 70 mol% DMSO the resin is *less* effective by a factor of ~100. Local fluoroform solubility and hydroxide ion solvation effects, including phase separation, in the pore liquid of the resin beads appear to be responsible for the observed behaviour.

E. ALLAN SYMONS, JOHN H. ROLSTON, LORRAINE A. BALDISERA, JOHN C. G. DROVER et J. DOUGLAS BONNETT. Can. J. Chem. **61**, 1301 (1983).

On a montré que les résines échangeuses d'anion du type Réxyne 201(OH) et Amberlyst A-26 sont des catalyseurs actifs pour le transfert de deutérium entre l'eau et le fluoroforme. Sous forme de pâte, agitée à 50°C, la Réxyne 201 est 25 fois plus efficace que la NaOH si on les compare sur la bases des ions hydroxydes présents. L'addition de DMSO à la pâte aqueuse provoque une augmentation de la réactivité de la Réxyne 201, mais l'avantage de la résine sur le OH^- homogène tend vers zéro lorsqu'on approche de 30 mol% de DMSO. A 70 mol% de DMSO, la résine est moins efficace par un facteur d'environ 100. La solubilité locale du fluoroforme et les effets de solvatation de l'ion hydroxyde, y compris une séparation de phase dans le liquide poreux des billes de résine, semblent être responsable du comportement observé.

[Traduit par le journal]

Introduction

Our interest in efficient catalysis of hydrogen isotope exchange between fluoroform and water was outlined previously (1). The use of dimethyl sulfoxide (DMSO) as co-solvent with water has been shown to enhance the relatively poor catalytic activity of the hydroxide ion (1) for this reaction by a factor of 10^6 (2). Such a base-catalyzed deuterium exchange step could be employed in the CF_3H redeuteration stage of a heavy water production process based on isotope-selective, infrared-laser-induced, multiphoton dissociation of CF_3D/CF_3H mixtures (3). However, on an industrial scale NaOH addition to and recovery from a large process water stream, although technically feasible, would add significantly to the overall cost of plant operation. Therefore, we have been looking for a more easily recoverable form of strongly basic catalyst.

Anion exchange resins have been used for many years as catalysts for various types of organic reactions (e.g. hydrolyses (ref. 4, Chapt. 3)), and as supports for organic reagent anions (ref. 4, Chapt. 2), but no reference has been found to their application as catalysts for hydrogen isotope exchange. In addition, although dipolar aprotic solvents like DMSO are known to increase ^-OH ion basicity in homogeneous aqueous solution (5, 6), the behaviour of *resin-bound* ^-OH ions in such mixed solvent systems has yet to be reported.

In this paper we present the results of a study of deuterium exchange between fluoroform and water catalyzed by several commercial anion exchange resins in the ^-OH form, in both water and aqueous DMSO mixtures. Some other types of heterogeneous catalyst were also tested. Unfortunately, carbon-supported metals like Pt, Pd, Ir, and Os, although quite effective for HD/H_2O exchange (7), were found to be completely inactive for CF_3D/H_2O exchange. Thus dissociation of fluoroform to give surface-adsorbed hydrogen atoms by analogy with HD/H_2O exchange (7) is an improbable route for exchange in such a weak hydrocarbon acid.

Experimental

Reagents

Deionized distilled water was used. DMSO (Fisher Certified) was distilled from 4A molecular sieves at reduced pressure, the central fraction then being stored over CaH_2. Water–DMSO solvent mixtures were prepared by weight. The resin Rexyn 201(OH) (Fisher Scientific) was used in the ^-OH form as received. The resins Amberlyst A-26 and A-27, and Amberlite 904 (BDH Chemicals) were obtained as the chlorides, and were exchanged in packed columns by treatment with NaOH solution and then water. The preparation of CF_3D from CF_3H (Matheson) has been described (2).

CF_3H gas solubility

Our general gas chromatographic method (1) was utilized, with the following modification. To prevent clogging of the syringe needle by fine resin particles in the slurries, the gas/liquid equilibration flask was equipped with an adjustable depth dip-tube assembly having a fritted disc.

Deuterium exchange runs

Essentially the same stirred gas/liquid reactor and kinetic procedure were used as before (1). The legs of the hollow stirrer shaft were changed from 1 mm capillary to 5 mm bore tubing, to prevent blockage of these gas dispersal legs by swollen resin beads. About 50–60 mL of resin slurry replaced the homogeneous catalyst solution. "Wet" resin was used to prepare the aqueous slurries, whereas vacuum-dried resin (to constant weight) was employed for the water–DMSO slurries. The Rexyn 201(OH) resin generally lost 50–51% by weight upon drying. Stirring rates up to 800 r/min were necessary to obtain rate constant data independent of stirring rate. Pseudo-first order kinetic plots were linear up to the three half-lives covered for the fastest runs, with correlation coefficients ranging from

[1]AECL Report No. 7998.

[2]To whom all correspondence should be addressed.

Can. J. Chem. Downloaded from www.nrcresearchpress.com by 210.87.254.105 on 09/06/12
For personal use only.

TABLE 1. Solubility of CF_3H in water–DMSO mixtures: the effect of added anion exchange resin

Mol% DMSO	System	CF_3H solubility, mole fraction $\times 10^4$ 25.0°C	50.0°C	% change relative to neat solvent at 25, 50°C
0.0	Pure water	2.31	1.42	—
	Rexyn slurry[a]	2.12	1.25	−8, −12
	0.8 mol L^{-1} NaOH[b]	1.69	1.03	−27, −27
28.9	Pure solvent	8.7	6.5	—
	Rexyn slurry[c]	8.4	6.8	−4, +5
58.1	Pure solvent	47.5	34.5	—
	Rexyn slurry[c]	45.5	36.2	−4, +5

[a]Ratio of ~15 g dry Rexyn 201(OH) resin/50 mL solvent.
[b]Moles of ^-OH in system comparable to resin slurry a.
[c]Ratio of 5 g dried resin/50 mL solvent.

0.997 to 0.9999. The experimental error for rate constants from multiple kinetic runs with the same catalyst charge was $<\pm 5\%$.

Confirmation that diffusion of CF_3D through the bulk liquid to the resin beads was not rate limiting was obtained as follows. A sample of 31 g wet (H_2O) Rexyn 201(OH) resin was suspended in a steel mesh bag in the vessel; no water, only CF_3D was added before the stirrer ws started. The "vapour" exchange rate constants measured at 47, 55, and 64°C (resin temperature by thermocouple) for the supported resin were comparable to those obtained for slurry conditions, after correction for the difference in vapour space volume.

Some of the resins, and also a sample of Ionac Chemical Company's MA-3475 anion resin membrane, were tested under countercurrent gas/liquid trickle flow conditions in a jacketed glass column of 5 cm id and 1.5 m overall height (including humidifier, catalyst, and dehumidifier sections). The resin beads were supported in fine mesh plastic or steel screen bags.

The wet (water) Rexyn resin is golden brown in colour, whereas the vacuum-dried beads are very dark brown. On contact with aqueous DMSO the dried beads remain almost black in colour, and are much more resistant to physical disintegration under the stirred slurry conditions than in pure water. The resin beads should swell in the mixed solvent, since it has been noted that the precursor resin, *p*-chloromethylstyrenedivinylbenzene co-polymer, swells readily in DMSO (8).

One batch of vacuum-dried Rexyn resin was tested for residual water, as follows. A calibration curve for water in aqueous DMSO was prepared using the H_2O peak intensity at 1942 nm in the near infrared spectrum (9) (Cary 17 spectrophotometer). A sample of the dried resin was contacted with CaH_2-dried DMSO, the slurry being gently stirred for 17 h at 21°C. The water content of the DMSO rose from 0.03 to 0.36 wt%, which corresponds to an additional ~1 wt% water in the original wet resin.

The possibility of a different solvent composition in the liquid and resin phases of a slurry was examined using the same near ir technique. Liquid samples after 22 and 88 h from a slurry of 8.9 g dried Rexyn resin in 89 g 50.94 mol% DMSO contained 51.70 and 51.90 mol% DMSO, respectively. This small *decrease* in water content of the bulk solvent reflects an in-resin solvent composition of ~43.5 mol% DMSO at equilibrium. Thus there is an "enrichment" of the water component of the solvent within the resin pores. A similar effect was reported for several types of ion exchange resin in acetone–water and dioxan–water systems (10).

Results

CF_3H gas solubility

CF_3H, only slightly soluble in water, is salted out of aqueous solution by NaOH (1). In contrast to the homogeneous distribution of ^-OH ions in NaOH solution, the ^-OH ions in a resin slurry are restricted to solvent at the surface of bead pores, so that the salting out effect in the bulk liquid for a comparable number of ions per unit volume of slurry should be reduced. As can be seen from the data in Table 1, this was found to be the case.

TABLE 2. Solvent dependence of k_{obs}(slurry) and E_a(slurry)

Mol% DMSO	k_{obs}[a] s^{-1}	E_a kJ mol^{-1}
0.0	7.4×10^{-5}	115
10.3	2.2×10^{-4}	101
30.1	1.3×10^{-3}	71
46.7	3.3×10^{-3}	63
68.2	$>8\times10^{-3}$	63

[a]For 5 g dried Rexyn 201(OH)/50 mL solvent at 49°C.

For the water–DMSO slurries a smaller ratio of resin weight to liquid volume was used (for reasons related to the kinetics of the deuterium exchange runs). As shown in Table 1, for both the 28.9 and 58.1 mol% DMSO slurry systems the CF_3H solubility is slightly lower at 25°C and slightly higher at 50°C, relative to the pure solvent mixtures. Overall, the effect of the resin on CF_3H solubility in the bulk water–DMSO solutions is slight. These small corrections were applied to the available solubility data for the pure solvent mixtures (2), to obtain the in-slurry solubilities (actually for the bulk liquid) required for calculation of in-slurry exchange rate constants (see below).

CF_3D/H_2O exchange runs

As in the case of homogeneous ^-OH catalysis of fluoroform–water exchange (1, 2), the experimental rate constants obtained are for change in CF_3D/CF_3H composition in the vapour space over the catalyst solution. The temperature- and solvent-dependent factor required for conversion of k_{obs}(vapour) to k_{obs}(slurry) is equal to the moles of fluoroform in the reaction vessel divided by the moles of gas dissolved in the bulk liquid, and ranged between about 30 and 2. In-slurry rate constants calculated on this basis do not contain a correction for any possible difference in CF_3D solubility between bulk liquid and pore liquid.

Most work was done with 5 g of dried Rexyn 201(OH) resin (average 1 mm beads) per 50 mL of solvent in the stirred reactor. In-slurry rate constant and Arrhenius activation energy data are recorded in Table 2 for the aqueous DMSO system.

For some parts of the study, the k_{obs}(vapour) data were compared directly. The dependence of k_{obs}(vapour) on weight of resin in the slurry was determined in 38 mol% DMSO. The rate

Can. J. Chem. Downloaded from www.nrcresearchpress.com by 210.87.254.105 on 09/06/12
For personal use only.

TABLE 3. Comparison of anion exchange resins for catalysis of deuterium transfer between CF_3D and H_2O at 49°C

Resin ($^-$OH form)	Type	Stirred slurry[a,d]	Trickle column[a,e]
Rexyn 201	Gel[b]	4×10^{-3}	9×10^{-4}
Amberlyst A-26	Macro[c]	1×10^{-3}	—
Amberlyst A-27	Macro[c]	2×10^{-3}	3×10^{-4}
Ionac MA-3475	Membrane	—	5×10^{-4}

[a]k_{obs}(vapour), s^{-1}, per mole $^-$OH.
[b]Irregular pore structure, <30 Å.
[c]Macroreticular structure, 175 and 375 Å average pore diameter.
[d]Corresponding value for 0.011 mol L^{-1} NaOH/H_2O data is 1.5×10^{-4} s^{-1}/mole $^-$OH.
[e]Corrected to same vapour/slurry volume ratio as in stirred reactor.

constant was proportional to dried resin loading up to ~10 g per 50 mL of solvent at 49°C; above this level the slurry could not be stirred fast enough to obtain values independent of stirring rate.

Only slight increases in k_{obs}(vapour) were observed for exchange runs with 5 g of smaller diameter (sieved, ~0.5 mm) beads or crushed beads in tests done at 49°C in 38 mol% DMSO. The rate constant is therefore not significantly dependent on the surface area of these gel-type resin beads. In fact, the total $^-$OH available is the key parameter. The hydroxide ion "concentration" in each of the tested resin types was about 4 mmol g^{-1} dry resin, while the value for the membrane was somewhat lower at 0.7 mmol g^{-1}. Based on representative data given in Table 3, k_{obs}(vapour) *per mole of $^-$OH* is very similar, within experimental error (problem of resin contamination by contact with CO_2 in air) for the various resins studied in water, including gel and macroreticular types. Data are included in Table 3 for the exchange column tests; the order of magnitude lower reactivity noted for resins in the column compared to the vigorously stirred reactor most probably arises from less efficient gas/solvent/resin bead contact in the column.

In 50 mol% DMSO slurry at 49°C the catalytic activities of the Amberlite 904 resin (macroreticular type) and the Rexyn 201 resin were found to be comparable. Therefore, even in the mixed solvent there is no advantage in using the large pore size resins.

Discussion

Resin versus NaOH in water

It has been found that, on a per-hydroxide-ion basis, the Rexyn 201(OH) resin is more effective than NaOH in water for catalysis of CF_3D-H_2O exchange. The factor is ~100 at 49°C, based on the vapour phase rate constant data in the stirred reactor. The temperature dependence of this factor arises from the larger apparent Arrhenius activation energy for the NaOH case, ~115 vs. ~99 kJ mol^{-1} for the resin. The corresponding in-liquid factor is ~25 at 49°C, with E_a(liquid) values of 125 and 115 kJ mol^{-1} for NaOH and resin, respectively.

The greater reactivity of the resin compared to NaOH can arise from at least two effects, differential reactant concentrations and changes in the second order rate constants. In general, reaction rates observed for homogeneous systems tend to be higher than for the corresponding ion exchange resin catalysts (11). However, Frisch notes that adsorption of a reactant on the resin particles can sometimes lead to a reversal of the normal case, by raising the concentration of the reactant at the catalyst surface (11). In the present system, because fluoroform solubility in water is so low (ca. 2×10^{-4} mole fraction, see Table 1), any adsorption of CF_3D molecules in the resin beads would lead to an increased rate of deuterium exchange if mass transfer effects for gas transport through the solvent to and from the catalyst surface are not limiting.

The fluoroform concentration effect noted above can be expressed mathematically (12), according to the two-phase model of catalysis,[3] as the *distribution coefficient* for reactant R between the two phases, with $\lambda_R = \bar{m}_R/m_R$; $\bar{m}_R$ and m_R represent the molal concentrations of R in the resin and homogeneous phases, respectively. The term *efficiency*, q, is used to compare the observed catalytic activity of the resin and homogeneous systems. Here, q is the ratio of the rate for the anion resin-catalyzed reaction to the rate for the NaOH-catalyzed reaction with the same bulk concentration of hyroxide ion. Thus $q = (\bar{k}_{OH^-}/k_{OH^-})\lambda_{CF_3D}$ (12), where $\bar{k}_{OH^-}$ represents the second order rate constant for catalysis in the resin pores and k_{OH^-} the value for NaOH solution. In general, for reactions involving small substrate molecules and a first order dependence on the catalyst ion concentration, $\bar{k}$ and k should be similar to one another (12).[4] Therefore, in the case of base-catalyzed deuterium transfer between fluoroform and water it is probable that most of the observed enhancement for Rexyn 201(OH) resin over NaOH is due to an increased concentration of fluoroform near the active sites within the resin pores (i.e. $q \sim \lambda_{CF_3D}$).

An experimental test of this argument was carried out. A stirred Rexyn resin aqueous slurry was contacted with CF_3H gas of known volume and initial pressure at 25°C. When the pressure had dropped to a constant value, the moles of CF_3H transferred into the slurry were calculated. After correction for the moles of gas expected to be in the bulk water at the final pressure, the "concentration" of CF_3H in the resin pore water (50 wt% of the wet resin) was found to be a factor of about five higher than in the bulk water. Since most of this gas could not be contained in the pore water itself, the local CF_3H concentration in the resin structure near the catalyst sites must be

[3]These arguments were developed for *cation* exchange resin catalysis via H^+ (12), but should be equally valid for the anion resin case.

[4]It can be argued that because of a high local concentration of $^-$OH ions inside the pores some enhanced $^-$OH reactivity might be expected, which would result in $\bar{k} > k$ (see H_- basicity function data for concentrated alkaline solutions (13)). An analogous situation would exist for H^+ ions in cationic exchange resins (H_0 acidity function). However, in practice, ion exchange resins tend to be *less* effective for most reactions than the corresponding homogeneous catalysts (11). A possible explanation is that reactant molecule size is more important than currently believed (12); diffusion of larger molecules into the pores could be rate-limiting, whereas smaller molecules like fluoroform could diffuse in easily and take advantage if $\bar{k} > k$.

Can. J. Chem. Downloaded from www.nrcresearchpress.com by 210.87.254.105 on 09/06/12
For personal use only.

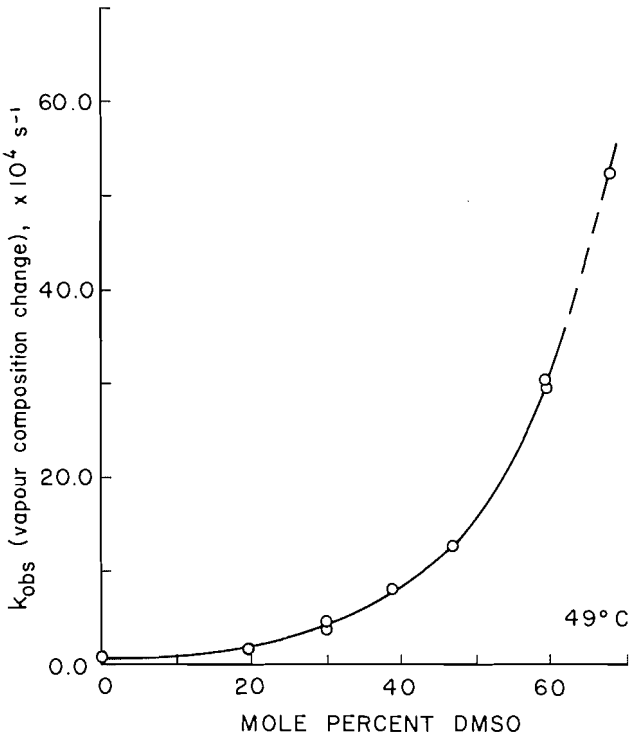

FIG. 1. Dependence of CF_3D/H_2O exchange rate constant on $DMSO/H_2O$ composition, catalyzed by 5 g Rexyn 201(OH) resin per 50 mL of solvent.

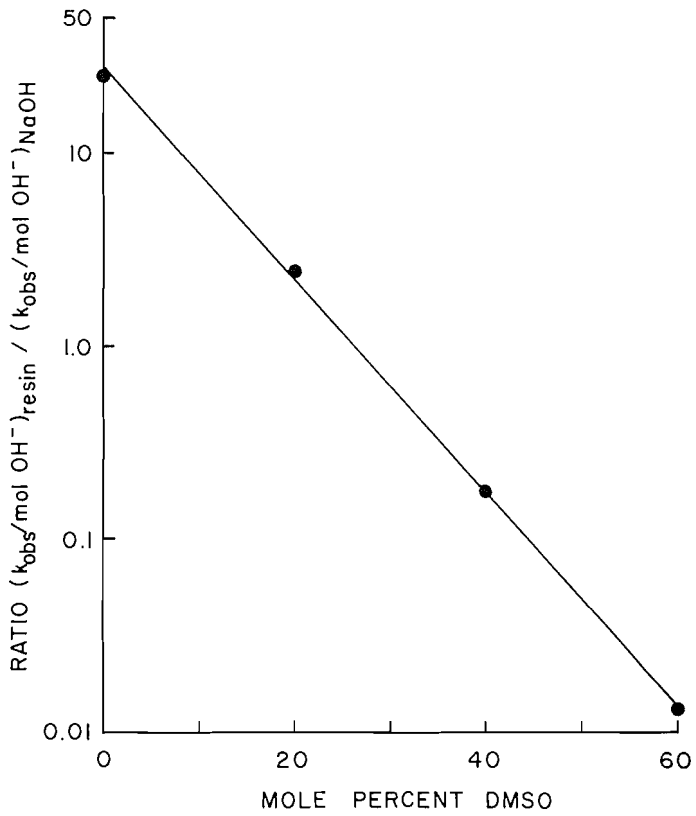

FIG. 2. Dependence of relative Rexyn 201(OH) resin ^-OH/NaOH catalytic reactivity for CF_3D/H_2O exchange on $DMSO/H_2O$ solvent composition at 49°C.

considerably higher. An observation consistent with this hypothesis is that CF_3H is ~50 times more soluble in toluene (1.06×10^{-2} mole fraction at 25°C) than in water; the similarity between the C_6H_5—CH_3 molecule and the backbone groups —C_6H_4—$CH_2\overset{+}{N}(CH_3)_4$ in the resin is clear.

Effect of DMSO addition

When DMSO is added as co-solvent, the observed in-slurry rate constant for CF_3D/H_2O exchange does increase, as shown in Fig. 1. The factor is ~100 between 0 and 70 mol% DMSO at 49°C, for 5 g dried Rexyn 201(OH) resin per 50 mL of solvent. Although this factor is significant, it falls well short of the value 10^6 measured for the homogeneous hydroxide ion case, with 0.011 mol L^{-1} ^-OH (2). As a result, the per ^-OH advantage noted above for resin over NaOH in water decreases as DMSO is added. This effect is clearly seen in Fig. 2; the resin advantage is lost by 30 mol% DMSO, and by 70 mol% DMSO the resin is *less* effective by >100×. Why?

If fluoroform adsorption in the resin particles *is* responsible for the rate enhancement over NaOH in water (see above), then the progressively greater solubility of the gas in the mixed solvent as DMSO is added (2) (Table 1) might be expected to lessen this effect. However, the ratio plotted in Fig. 2 should only gradually approach 1.0 as a result. That it falls to well below 1.0 suggests at least one other factor is also involved. It is known that for homogeneous hydroxide ion solution the addition of a dipolar aprotic solvent like DMSO to water causes reduced solvation of the ^-OH ions, and hence increased solution basicity, as measured by the H_- basicity function (5). This solvation effect is also reflected in the rapid decrease in NaOH solubility with increasing DMSO content (14). An important complication that occurs in the homogeneous system is phase separation over much of the solvent composition range (14), whereby a DMSO-poor/NaOH-rich phase forms below a DMSO-rich/NaOH-poor layer when the NaOH concentration is raised above a critical level.

The NaOH solubility (without phase separation) drops from ~29 mol L^{-1} in water to ~0.2 mol L^{-1} in 40 mol% DMSO and ~2×10^{-3} mol L^{-1} in 70 mol% DMSO (14). At 5 g dried Rexyn 201(OH) resin per 50 mL of solvent, the average ^-OH distribution in the slurry is ~0.4 mol L^{-1} and in the pore liquid itself ~4 mol L^{-1}. However, the ions are actually restricted to the even smaller liquid volume associated with the surface of the pores in the resin beads. The result will be a much higher *local* ^-OH concentration, which tends to favour a water-rich environment around the ions. If this leads to some "phase separation" at the catalyst surface in the pores, then enhanced basicity in the presence of aqueous DMSO solvent will be partially offset by a decrease in the amount of fluoroform dissolved in the region nearest the ions. The net effect would be that the calculated in-slurry rate constants would be proportionately low with increasing DMSO content, since the vapour/liquid conversion factor is based on CF_3H solubility in the bulk solvent.

It should be noted that the somewhat lower % DMSO in the resin pore liquid compared to the bulk mixed solvent (see Experimental section) will also cause a reduction in the observed in-slurry rate constant relative to the NaOH system; for example, the factor would be about four in 50 mol% DMSO at 50°C. This value is based on the reasonable assumption that the second order rate constant for ^-OH catalysis is essentially the same for the resin and NaOH solution environments. However, this factor of four is only part of the overall factor of ~20 lower reactivity for resin ^-OH versus NaOH in the 50 mol%

Can. J. Chem. Downloaded from www.nrcresearchpress.com by 210.87.254.105 on 09/06/12
For personal use only.

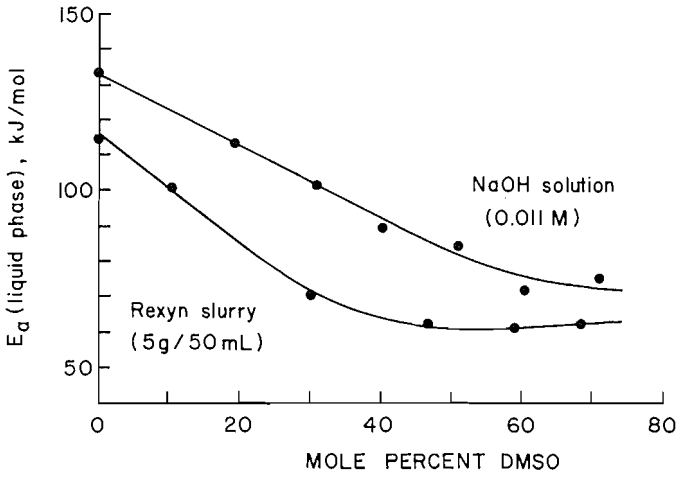

FIG. 3. Dependence of Arrhenius activation energy for Rexyn 201(OH) resin- and NaOH-catalyzed deuterium exchange between CF_3D and H_2O on DMSO/H_2O solvent composition.

DMSO case. The balance of the loss can be accounted for by the "phase separation" effect discussed above.

Mechanism of resin catalysis

By analogy with the homogeneous catalyst systems (1, 2), anion exchange resin catalysis of deuterium transfer between CF_3D and H_2O most likely involves attack by the hydroxide ion on the weak hydrocarbon acid CF_3D. However, this reaction can occur only in the solution inside the beads. Thus a better description for the resin would be a supported homogeneous, rather than hetergeneous, catalyst; homogeneous catalysis within the resin pore liquid is a common concept (12, 15).

The solvent dependence of the in-slurry Arrhenius activation energy is shown in Fig. 3; included are corresponding data for the NaOH system (2). For the slurries, k_{obs} was measured over 20–25°C within the overall range 25 to 72°C. Correlation coefficients for the Arrhenius plots were all >0.998. Although the resin and NaOH curves are similar, the resin E_a values are significantly lower. In each case E_a drops markedly as the % DMSO is raised, and then levels off by 50–60 mol% DMSO, as the $^-$OH ion becomes more reactive.

Acknowledgements

The authors wish to thank J. den Hartog for his contribution to the design of the Pyrex countercurrent exchange column, and J. G. Wesanko for construction of the column.

1. E. A. SYMONS and M. J. CLERMONT. J. Am. Chem. Soc. **103**, 3127 (1981).
2. E. A. SYMONS, M. J. CLERMONT, and L. A. CODERRE. J. Am. Chem. Soc. **103**, 3131 (1981).
3. J. B. MARLING, I. P. HERMAN, and S. J. THOMAS. J. Chem. Phys. **72**, 5603 (1980).
4. P. HODGE and D. C. SHERRINGTON (*Editors*). Polymer-supported reactions in organic synthesis. John Wiley and Sons, New York. 1980.
5. D. DOLMAN and R. STEWART. Can. J. Chem. **45**, 911 (1967).
6. J. R. JONES. Prog. Phys. Org. Chem. **9**, 241 (1972).
7. J. P. BUTLER, J. H. ROLSTON, and W. H. STEVENS. Am. Chem. Soc. Symp. Ser. **68**, 1978. p. 93; J. H. ROLSTON and J. W. GOODALE. Can. J. Chem. **50**, 1900 (1972).
8. J. T. AYRES and C. K. MANN. Polymer Lett. **3**, 505 (1965).
9. R. L. MEEKER, F. E. CRITCHFIELD, and E. T. BISHOP. Anal. Chem. **34**, 1510 (1962).
10. C. W. DAVIES and B. D. R. OWEN. J. Chem. Soc. 1676 (1956).
11. N. W. FRISCH. Chem. Eng. Sci. **17**, 735 (1962).
12. V. GOLD, C. J. LIDDIARD, and G. D. MORGAN. *In* Proton-transfer reactions. *Edited by* E. Caldin and V. Gold. Chapman and Hall, London. 1975. Chapt. 13.
13. K. BOWDEN. Chem. Rev. **66**, 119 (1966).
14. J. RICHARD, G. FERRONI, and J. GALÉA. Ann. Chim. **10**, 307 (1975).
15. F. HELFFERICH. Ion exchange. McGraw-Hill, New York. 1962. Chapt. 11.

Can. J. Chem. Downloaded from www.nrcresearchpress.com by 210.87.254.105 on 09/06/12
For personal use only.

Methanation of carbon monoxide and dioxide by supported metal carbonyl clusters

H. E. FERKUL, J. M. BERLIE, D. J. STANTON, J. D. MCCOWAN, AND M. C. BAIRD[1]

Department of Chemistry, Queen's University, Kingston, Ont., Canada K7L 3N6

Received July 26, 1982

H. E. FERKUL, J. M. BERLIE, D. J. STANTON, J. D. MCCOWAN, and M. C. BAIRD. Can. J. Chem. **61**, 1306 (1983).

The catalysis of carbon monoxide hydrogenation by supported cobalt and ruthenium clusters is studied, and an unusually specific cobalt methanation catalyst is described. A variety of ruthenium carbonyl clusters catalyzes carbon monoxide methanation, irrespective of support, and $Ru_3(CO)_{12}$ on γ-alumina is found to be a potentially useful carbon dioxide methanation catalyst.

H. E. FERKUL, J. M. BERLIE, D. J. STANTON, J. D. MCCOWAN et M. C. BAIRD. Can. J. Chem. **61**, 1306 (1983).

On étudie la catalyse d'hydrogénation du monoxyde de carbone par des amas de cobalt et de ruthénium fixés sur un support et on décrit un catalyseur de méthanation à base de cobalt qui est exceptionnellement spécifique. Un certain nombre d'amas de ruthénium carboxyle catalyse la méthanation du monoxyde de carbone indépendamment du support, et on a trouvé que le $Ru_3(CO)_{12}$ fixé sur de l'alumine γ est en catalyseur de méthanation du bioxyde de carbone potentiellement utile.

[Traduit par le journal]

Can. J. Chem. Downloaded from www.nrcresearchpress.com by 210.87.254.5 on 09/06/12
For personal use only.

The utilization of transition metals on various supports as catalysts for the hydrogenation of carbon monoxide to hydrocarbons (Fischer–Tropsch synthesis) has been well reviewed (refs. 1, 2; ref. 3, p. 29). Recently, influenced no doubt by the apparent similarities between metal carbonyl clusters and the metal particles of many heterogeneous catalysts (4–6), several attempts have been made to use cluster compounds as *homogeneous* Fischer–Tropsch catalysts, with mixed success (7). Rather more useful have been *heterogeneous* catalysts prepared by depositing metal carbonyl clusters on, for instance, oxide supports. By the late 1970's, it had been shown that cobalt (8) and rhodium (9) carbonyls can be used as very interesting precursors to a variety of Fischer–Tropsch catalysts, the product distributions from CO hydrogenation varying significantly as the supposedly inert supports were varied.

The potential for preparing novel catalysts by supporting metal carbonyl clusters on various materials seemed clear, and we have accordingly embarked on a program to investigate the use of cobalt and ruthenium carbonyl compounds in this way. The former has long been known as a versatile, low pressure catalyst (3), while the latter has been shown to be very active as a CO methanation catalyst (10) and to show interesting Fischer–Tropsch properties (11–13). We now report the results of our investigations to date; some of this work has been previously communicated (14).

Experimental

The compounds $Ru_3(CO)_{12}$ (15), $H_2Ru_4(CO)_{13}$ (16), $H_2FeRu_3(CO)_{13}$ (16), $[(Ph_3P)_2N][CoRu_3(CO)_{13}]$ (17), and $Co_4(CO)_{12}$ (18) were prepared as in the literature. The compounds $Fe(CO)_5$ and $Co_2(CO)_8$ were purchased from Strem Chemicals, as were γ-alumina (1/8 in. pellets), "large pore" silica gel (8 mesh granules), and Na–Y zeolite (1/16 in. pellets). The $RuCl_3.3H_2O$ was obtained from Johnson Matthey, Ltd.

The catalyst systems were prepared by dissolving a known amount of compound in ethyl ether ($[(Ph_3P)_2N][CoRu_3(CO)_{13}]$), *n*-pentane (other clusters), or acetone ($RuCl_3.3H_2O$). The solutions were mixed under nitrogen for several hours with a sample of the solid support (approximately 10 g) which had previously been dried at 400–500°C, the solvent was removed under reduced pressure, and the supported compounds (typically about 1–2% by weight of metal) were placed in a tubular glass reactor (length 18 cm, diameter 1 cm) under nitrogen. The catalysts were then activated by heating to 200°C in a stream of hydrogen (1 atm) for 2 h (cobalt) or 12 h (ruthenium).

Catalytic runs were carried out by passing synthesis gas mixtures through the catalysts at 1 atm. Typical reaction conditions involved H_2:CO ratios of 1.85 to 4.0, temperatures varying from 185–400°C, and space velocities of 300–600 h^{-1} for the cobalt, 1000–3750 h^{-1} for the ruthenium systems. Product water was collected by passing the reactor effluents through a water-cooled Liebig condenser; gaseous effluents were then collected and hydrocarbon distributions were determined using a Hewlett Packard 5880A gas chromatograph equipped with a 2 m column packed with Porapak Q and a flame ionization detector. Methane, H_2, CO, and CO_2 were determined using a Hewlett Packard F & M Scientific 700 gas chromatograph equipped with a 4 m Porapak Q column and a thermal conductivity detector. X-ray powder diffraction studies were carried out on Guinier-de Wolff Focussing Powder Diffraction Camera, SEM studies on a Hitachi H-450 Scanning Electron Microscope.

Results and discussion

Ruthenium catalysts

An extensive investigation of potential ruthenium catalysts was undertaken, involving two ruthenium clusters, $Ru_3(CO)_{12}$ and $H_2Ru_4(CO)_{13}$, and two mixed metal clusters, $H_2FeRu_3(CO)_{13}$ and $[(Ph_3P)_2N][CoRu_3(CO)_{13}]$, on three different supports, γ-alumina, silica gel, and Na–Y zeolite. Although quite significant differences in activity were found, the main product of CO hydrogenation was in all cases methane, formed as in reaction [1].

$$[1] \quad 3H_2 + CO \rightarrow CH_4 + H_2O$$

The oxygen-containing by-products included CO_2, however, suggesting that the water produced in reaction [1] could react further via the water gas shift reaction, [2].

$$[2] \quad H_2O + CO \rightarrow H_2 + CO_2$$

Representative data for the four clusters on the various supports are shown in Table 1. As can be seen, the best yields under these conditions were obtained using alumina as the support, but the differences between experiments were often not large. The mixed cobalt–ruthenium cluster on silica and zeolite exhibited anomalously low activities, for reasons which are not clear. It seems possible that the iminium cation decomposed during the "activation" procedure, coating the metal surface.

In an effort to better understand the effects of changing the

[1]To whom all correspondence should be addressed.

Can. J. Chem. Downloaded from www.nrcresearchpress.com by 210.87.254.5 on 09/06/12
For personal use only.

TABLE 1. Methane yields at 350°C; H_2:CO = 2:1

Catalyst precursor	Methane yields (%, ±5%)		
	γ-Al_2O_3	SiO_2	Na–Y Zeolite
$Ru_3(CO)_{12}$	56	27	43
$H_2Ru_4(CO)_{13}$	56	35	38
$H_2FeRu_3(CO)_{13}$	42	43	40
$[(Ph_3P)_2N][CoRu_3(CO)_{13}]$	60	Inactive	12

temperature and H_2:CO ratio, the $Ru_3(CO)_{12}/Al_2O_3$ system was studied in more detail. Representative data are shown in Table 2, and can be compared with similar data obtained under identical conditions for $RuCl_3.3H_2O$ on alumina, a recognized CO methanation catalyst (10).

Below 300°C, $Ru_3(CO)_{12}$ on alumina is not very active. As can be seen from Table 2, however, activities above 320°C are quite high, although increasing the temperature up to 400°C causes only small increases in activity. Interestingly, while the $RuCl_3.3H_2O/Al_2O_3$ system exhibited useful activity well below 300°C, there was little to choose between the two systems in the temperature range 350–400°C. In addition, while both lost activity over 8–10 h, the $Ru_3(CO)_{12}/Al_2O_3$ catalyst could be regenerated under a flow of hydrogen overnight at 300–400°C. The $RuCl_3.3H_2O/Al_2O_3$ system could not be regenerated as efficiently, and thus the catalyst life time was shorter in this case.

As mentioned above, the oxygen-containing by-products were water and CO_2; interestingly, the amounts of the latter decreased essentially to zero as the H_2:CO ratio increased to 4:1. These results suggested the possibility that the ruthenium was also behaving as a CO_2 methanation catalyst (reaction [3]),

[3] $4H_2 + CO_2 \rightarrow CH_4 + 2H_2O$

and the $Ru_3(CO)_{12}/Al_2O_3$ system was therefore investigated as a catalyst for CO_2 methanation, with typical results shown in Table 3. As can be seen, $Ru_3(CO)_{12}/Al_2O_3$ is an active CO_2 methanation catalyst at a much lower temperature than is the recognized high pressure methanation catalyst, $RuCl_3$ (11). It is to be anticipated that much higher yields of methane will be possible at higher pressures, a result which would be of great potential significance in view of current interest in the conversion of CO_2 to useful organic compounds (19).

While this work was in progress, several other groups reported the use of supported ruthenium carbonyl clusters as CO hydrogenation catalysts (20–24). In the work apparently most comparable to ours (19), it is claimed that $Ru_3(CO)_{12}$ on alumina is very active at 260°C for the hydrogenation of CO to olefins (C_2–C_6). While our system does produce small amounts of C_2–C_5 hydrocarbons below 200°C, as we have shown, methane is the sole product at higher temperatures. Indeed, we find, as have others (25), that $Ru_3(CO)_{12}$ on alumina is a very effective hydrogenolysis catalyst at 260°C, converting hexane smoothly to methane. The reasons for the different behaviour presumably involve subtle variations in the nature of the support surface. Under the conditions used here, the ruthenium exists almost certainly in the 0 oxidation state, but in aggregates of unknown size (25–27).

Cobalt catalysts

As indicated above, it is anticipated that adsorption of different clusters on different supports might give catalysts with different properties. Both $Co_2(CO)_8$ and $Co_4(CO)_{12}$ could be deposited from pentane solution onto silica and alumina, the materials so formed retaining the colouration of the carbonyls used and, presumably, their molecularity. Slow passage of hydrogen (or nitrogen) over the materials at 200°C then resulted in thermal decomposition to the metals via loss of CO. If the flow rate were too high at this point, a metallic mirror formed in the reactor tube, probably because of partial sublimation of $Co_2(CO)_8$ prior to decomposition.

On passing synthesis gas through alumina-supported systems under various conditions, a somewhat typical, for cobalt (refs. 1, 2; ref. 3, p. 29), distribution of saturated hydrocarbons was obtained. These results were similar to those reported previously (8), and work in this direction was discontinued.

Using $Co_2(CO)_8$ and $Co_4(CO)_{12}$ on the silica, however, quite different results were obtained. Using a H_2:CO ratio of 2:1 (space velocity = 482 h^{-1}), the catalyst systems were rather inactive below about 250°C and produced only small amounts of C_1–C_5 hydrocarbons. In the temperature range 300–450°C, however, the catalysts were both extremely active and selective, essentially all the CO reacting to form methane as the *sole* hydrocarbon. Interestingly carbon dioxide was also formed, in amounts equal to 60–80% of the amounts of methane, while water yields were < 5%. This behaviour, both with respect to the selectivity to methane and with respect to the formation of CO_2 as the oxygen-containing by-product, is unprecedented for cobalt-based CO hydrogenation catalysts (refs. 1, 2; ref. 3, p. 29).

It seems likely that the major reactions are as in [1] and [2], methanation of CO followed by the water gas shift reaction. Separate experiments which involved passage of water-saturated CO over fresh catalyst showed that the system does catalyze the water gas shift reaction, and the resulting increase in the concentration of H_2 may be a factor in selectivity to methane.

The unprecedented selectivity may, however, also be a result

TABLE 2. Product distributions as functions of temperature and H_2:CO ratio

Catalyst precursor	T (°C)	H_2/CO	% Conversion (±5%)	Production distribution	
				CH_4	CO_2
$Ru_3(CO)_{12}$	320	1.9	77	49	28
$Ru_3(CO)_{12}$	360	1.9	79	56	23
$Ru_3(CO)_{12}$	360	3	85	77	7
$Ru_3(CO)_{12}$	360	4	81	81	0
$RuCl_3.3H_2O$	266	3	86	67	18
$RuCl_3.3H_2O$	295	3	81	68	13
$RuCl_3.3H_2O$	360	3	84	70	14

TABLE 3. Product distributions as functions of temperature and $H_2:CO_2$ ratio

Catalyst precursor	T (°C)	H_2/CO_2	% Conversion to CH_4 (±5%)
$Ru_3(CO)_{12}$	280	2	57[a]
$Ru_3(CO)_{12}$	280	3	72[a]
$Ru_3(CO)_{12}$	280	4	82[a]
$RuCl_3.3H_2O$	365	2	22
$RuCl_3.3H_2O$	365	3	28
$RuCl_3.3H_2O$	365	4	52

[a]Production of CO was below the detectable limit. Water yields, based on CO_2 reacted, were about 90%.

of more subtle factors. For instance, hydrocarbon size limitation can result from shape selective catalysis if the pores in the support are sufficiently small (28), although this cannot be a factor here as the pores in the silica used are of the order of 100 Å or more in diameter.[2] A better explanation may centre around the metal particle size in the catalysts used, as there seems to exist a general relationship between particle size and molecular weight of Fischer-Tropsch products (29). We do not know the size(s) of the metal particles in the catalyst systems described here; X-ray diffraction and SEM studies on powdered samples of the catalyst were only consistent with the particles being <100 Å in diameter. However, the high selectivities to methane are certainly consistent with the formation of *small* crystallites on decomposition of the $Co_4(CO)_{12}$. The fact that the $Co_2(CO)_8$ on silica catalyst system also gives methane is not inconsistent with this hypothesis, as $Co_2(CO)_8$ is known to form $Co_4(CO)_{12}$ on mild heating (18). Furthermore, a very recent combined ir and temperature programmed decomposition study of $Co_2(CO)_8$ on silica and alumina, treated much as in this investigation, showed that $Co_2(CO)_8$ on SiO_2 formed adsorbed $Co_4(CO)_{12}$ on mild heating. This contrasted with $Co_2(CO)_8$ on γ-Al_2O_3, which seemed to form predominantly Co_2 moieties (30). While the extent of sintering at higher temperatures was not studied, it is clear that the nature of the metal species on the two supports can be quite different.

Another mode of formation of CO_2 is via the disproportion of CO (reaction [4]) (ref. 3, p. 1).

[4] $2CO \rightarrow C + CO_2$

While we have not assessed this process as a possible source of CO_2, it probably provides a route to catalyst deactivation; solid carbon was generally observed on used catalysts. Interestingly, overnight treatment of the catalyst systems with hydrogen at 400°C generally resulted in almost total renewal of catalyst activity, although no attempts have been made to ascertain the number of times a particular catalyst could be renewed. The cobalt system is unfortunately susceptible to sulphur poisoning, as the addition of 0.5% H_2S to the synthesis gas stream resulted in rapid (1 h) deactivation of the catalyst, presumably because of the formation of cobalt sulphide.

[2]Technical information from the manufacturer, W. R. Grace and Co.

Acknowledgements

Financial support from Queen's University and the Natural Sciences and Engineering Research Council of Canada made this research possible. We thank Johnson Matthey, Ltd., for a loan of $RuCl_3.3H_2O$, and Doctors R. D. Heyding and R. Barnett for assistance with the X-ray diffraction and SEM measurements, respectively.

1. H. H. STORCH. Adv. Catal. **1**, 115 (1948).
2. H. PICHLER. Adv. Catal. **4**, 271 (1952).
3. R. B. ANDERSON. *In* Catalysis. Vol. 4. *Edited by* P. H. Emmett. Reinhold, New York. 1956.
4. E. L. MUETTERTIES. Bull. Soc. Chim. Bel. **84**, 959 (1975).
5. R. MASON. Isr. J. Chem. **15**, 174 (1976/77).
6. E. SHUSTOROVICH and R. C. BAETZOLD. J. Am. Chem. Soc. **102** 5989 (1980).
7. C. MASTERS. Adv. Organomet. Chem. **17**, 61 (1979).
8. M. BLANCHARD and R. BONNET. Bull. Chem. Soc. Fr. 7 (1977).
9. M. ICHIKAWA. Bull. Chem. Soc. Jpn. **51**, 2268 (1978); **51**, 2273 (1978); J. Chem. Soc. Chem. Commun. 566 (1978).
10. M. A. VANNICE. J. Catal. **37**, 449 (1975).
11. F. S. KARN, J. F. SCHULTZ, and R. B. ANDERSON. I EC Prod. Res. Dev. **4**, 265 (1965).
12. R. C. EVERSON, E. T. WOODBURN, and A. R. M. KIRK. J. Catal. **53**, 186 (1978).
13. H. J. NIJS, P. A. JACOBS, and J. B. UYTTERHOEVEN. J. Chem. Soc. Chem. Commun. 180 (1979); 1095 (1979).
14. H. E. FERKUL, D. J. STANTON, J. D. MCCOWAN, and M. C. BAIRD. J. Chem. Soc. Chem. Commun. 955 (1982).
15. C. R. EADY, P. F. JACKSON, B. F. G. JOHNSON, J. LEWIS, M. C. MALATESTA, M. MCPARTLIN, and W. J. N. NELSON. J. Chem. Soc. Dalton Trans. 383 (1980).
16. G. L. GEOFFROY and W. L. GLADFELTER. J. Am. Chem. Soc. **99**, 7565 (1977).
17. P. C. STEINHARDT, W. L. GLADFELTER, A. D. HARLEY, J. R. FOX, and G. L. GEOFFROY. Inorg. Chem. **19**, 332 (1980).
18. R. B. KING. Organometallic syntheses. Vol. 1. Academic Press, New York. 1965. p. 103.
19. J. HAGGIN. Chem. Eng. News, **60**(6), 13 (1982).
20. G. B. MCVICKER and M. A. VANNICE. J. Catal. **63**, 25 (1980).
21. L. GUCZI, Z. SCHAY, K. LÁZÁR, A. VIZI, and L. MARKÓ. Surf. Sci. **106**, 516 (1981).
22. C. S. KELLNER and A. T. BELL. J. Catal. **70**, 418 (1981).
23. D. BALLIVET-TKATCHENKO and I. TKATCHENKO. J. Mol. Catal. **13**, 1 (1981).
24. T. OKUHARA, K. KOBAYASHI, T. KIMURA, M. MISONO, and Y. YONEDA. J. Chem. Soc. Chem. Commun. 1114 (1981).
25. A. F. SIMPSON and R. WHYMAN. J. Organomet. Chem. **213**, 157 (1981).
26. A. ZECCHINA, E. GUGLIELMINOTTI, A. BOSSI, and M. CAMIA. J. Catal. **74**, 225 (1982); **74**, 240 (1982); **74**, 252 (1982).
27. V. L. KUZNETSOV, A. T. BELL, and Y. I. YERMAKOV. J. Catal. **65**, 374 (1980).
28. D. VANHOVE, P. MAKAMBO, and M. BLANCHARD. J. Chem. Soc. Chem. Commun. 605 (1979).
29. H. H. NIJS and P. A. JACOBS. J. Catal. **65**, 328 (1980).
30. R. NAKAMURA, A. OOMURA, N. OKADA, and E. ECHIGOYA. Chem. Lett. 1463 (1982).

Can. J. Chem. Downloaded from www.nrcresearchpress.com by 210.87.254.5 on 09/06/12
For personal use only.

The regiospecific phase transfer catalyzed reductive carbonylation of azadienes

HOWARD ALPER[1] AND SHIYAMALIE AMARATUNGA

The Ottawa–Carleton Institute for Research and Graduate Studies in Chemistry, University of Ottawa Campus, Department of Chemistry, Ottawa, Ont., Canada K1N 9B4

Received July 30, 1982

HOWARD ALPER and SHIYAMALIE AMARATUNGA. Can. J. Chem. **61**, 1309 (1983).

Reaction of an azadiene with cobalt carbonyl, carbon monoxide, and methyl iodide under phase transfer catalysis conditions (benzene, water or aqueous NaOH, benzyltriethylammonium chloride) affords allylic amides in reasonable yields. This regiospecific reaction is sensitive to the concentration of base. One can also effect this transformation using acidic catalysis. A mechanism is proposed for the reductive carbonylation reaction.

HOWARD ALPER et SHIYAMALIE AMARATUNGA. Can. J. Chem. **61**, 1309 (1983).

La réaction de l'azadiène avec le cobalt carbonyle, le monoxyde de carbone et l'iodure de méthyle dans des conditions catalytiques de transfert de phase (benzène, eau ou NaOH aqueux, chlorure de benzyltriéthylammonium) conduit aux amides allyliques avec des rendements raisonables. Cette réaction régiospécifique est sensible à la concentration de base. On peut également effectuer cette transformation en présence d'un catalyseur acide. On propose un mécanisme pour cette réaction de carbonylation réductrice.

[Traduit par le journal]

Can. J. Chem. Downloaded from www.nrcresearchpress.com by 210.87.254.5 on 09/06/12
For personal use only.

Investigations during the past six years have established phase transfer catalysis as a cheap method for the generation of anionic metal species from neutral precursors under very gentle conditions (1, 2). The formed anions, being relatively unsolvated in the organic phase, display high reactivity towards appropriate substrates. Not only can phase transfer catalysis enable one to effect reactions under much milder conditions than by conventional methods, in certain cases, the reaction course can be altered as well, leading to more useful transformations (3, 4).

A particularly valuable phase transfer process is the conversion of cobalt carbonyl to the mononuclear cobalt tetracarbonyl anion using aqueous sodium hydroxide, benzene or toluene as the organic phase, and benzyltriethylammonium chloride or cetyltrimethylammonium bromide as the phase transfer agent. Subsequent reaction of $Co(CO)_4^-$ with methyl iodide and carbon monoxide gives acetylcobalt tetracarbonyl. The latter can be intercepted by carrying out the reaction in the presence of suitable unsaturated substrates. Examples include the cobalt carbonyl catalyzed acylation of dienes (e.g. **1** → **2**), trienes (5), and fulvenes (e.g. **3** → **4**) (6). These reactions are completely regiospecific.

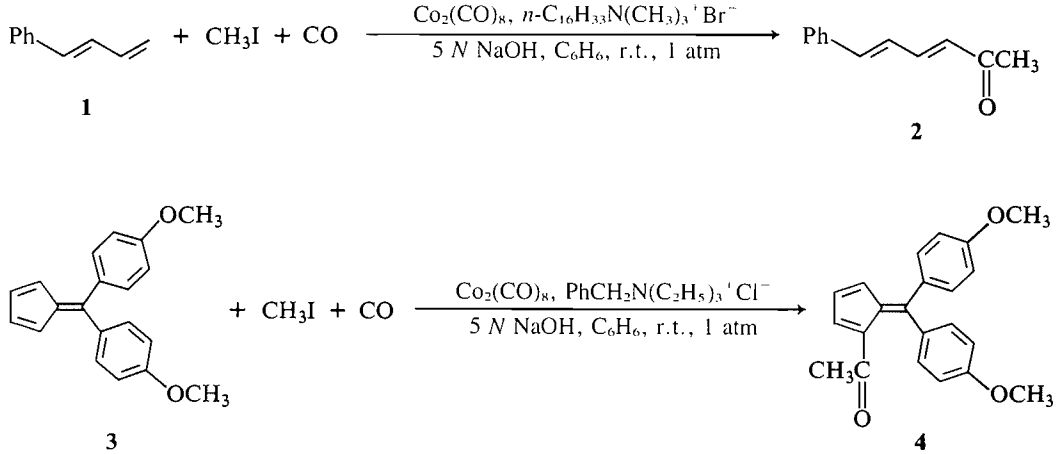

1 **2** **3** **4**

Azadienes are well known compounds, readily prepared by condensation of α,β-unsaturated carbonyls with amines (7). It was of interest to learn what effect, if any, the nitrogen heteroatom of the azadiene would have on the phase transfer catalyzed acylation reaction. We now describe the results of this investigation.

Results and discussion

Treatment of the azadiene **5**, R = Ph, R′ = H, R″ = *p*-$CH_3C_6H_4$, wih methyl iodide, carbon monoxide, benzene, water, benzyltriethylammonium chloride as the phase transfer catalyst, and cobalt carbonyl as the metal catalyst (10:1 ratio of **5**:$Co_2(CO)_8$), at room temperature for 60 h, afforded the allyl amide in 17% yield, with the remainder being recovered starting material. When the ratio of **5**/$Co_2(CO)_8$ was increased to 1:1, and the reaction time reduced to 6 h, the allylic amide (**6**) was formed in good yield (65%), and the amide **7**, R″ = *p*-$CH_3C_6H_4$, was isolated in 33% yield. Compounds **6** and **7** were obtained in the same yield when the reaction was repeated in the dark (using aluminum foil). The reaction was very fast at 60°C (2 min) but the yield of **6** decreased to 40% and **7**, R″ = *p*-$CH_3C_6H_4$ was isolated in 39% yield.

[1]E. W. R. Steacie Fellow, 1980–1982. To whom all correspondence should be addressed.

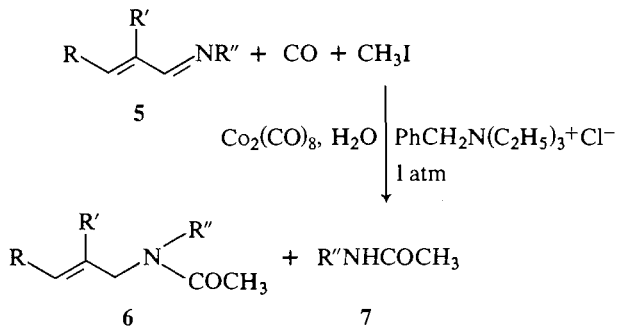

A variety of reaction conditions was used with the substrate **5**, R = Ph, R′ = H, R″ = *p*-$CH_3C_6H_4$ in order to determine the effect of the phase transfer catalyst, metal carbonyl, organic phase, and base concentration on the yield of allylic amides. In the absence of a phase transfer catalyst, the yield of allyl amide decreased from 65% to 21% (18 h reaction time), while *p*-methylacetanilide was formed in 61% yield. Benzyltriethylammonium chloride is a better phase transfer agent than Aliquat 336 (tricaprylmethylammonium chloride), since reaction using the latter was slower (18 h) and afforded the allyl amide in 41% yield. Only starting material was recovered when the reaction was run in the absence of cobalt carbonyl, but in the presence of benzyltriethylammonium chloride. Methylene chloride can be used as the organic phase in place of benzene, but the yield of **6**, R = Ph, R′ = H, R″ = *p*-$CH_3C_6H_4$ was poor (12%) while the less important **7**, R″ = *p*-$CH_3C_6H_4$ was isolated in 60% yield. When the reaction was effected for 2.5 days under homogeneous conditions (i.e. without water and a phase transfer catalyst), no allyl amide was formed. Rather, **7**, R″ = *p*-$CH_3C_6H_4$, was obtained in 35% yield with the remainder being recovered starting material. The extra hydrogen in **7** arises during work-up of the reaction mixture.

TABLE 1. Effect of base concentration on the phase transfer catalyzed reaction of **5**, R = Ph, R′ = H, R″ = *p*-$CH_3C_6H_4$ with $Co_2(CO)_8$, CH_3I, and CO

NaOH concentration *N*	Reaction time h	% Yield **6**	% Yield **7**
12.5	18	—	48[a]
5.0	3	8	88
2.0	8	22	71
0.5	8	48	36
0.1	6.5	56	38
H_2O	6	65	33

[a]50% of **5** was recovered.

The phase transfer reaction shows an interesting dependence on the base concentration of the aqueous phase (Table 1). At very high base concentration, i.e. 12.5 *N* NaOH, only **7**, R″ = *p*-$CH_3C_6H_4$ is formed. At 5 *N* NaOH, a small amount of **6** is obtained, the major product being **7**. As the concentration of base is decreased, the yield of the allylic amide increases to reasonable levels and **7**, the product of cleavage of the azadiene, is obtained in reduced yield.

Substitution of methanol for water or aqueous NaOH gives **6** in only 20% yield (and **7** in 61% yield). One can use an acid phase transfer catalyst, *p*-toluenesulfonic acid, for the conversion of **5** to **6** (water as the aqueous phase), the yield being somewhat lower (51%) than when a quarternary ammonium salt was employed as the catalyst.

On the basis of the above results, the highest yield of allylic amide **6**, R = Ph, R′ = *p*-$CH_3C_6H_4$ was realized using water as the aqueous phase, benzene as the organic phase, and benzyltriethylammonium chloride as the phase transfer catalyst. These conditions were then applied to the reactions of a series

TABLE 2. Reaction of azadienes (**5**) with $CO/CH_3I/Co_2(CO)_8/H_2O/C_6H_6/PhCH_2N(C_2H_5)_3{}^+Cl^-$

5, R =, R′ =, R″ =	Reaction temperature °C	Reaction time	Products	Yield[a] %
Ph,H,*p*-$CH_3C_6H_4$	r.t.	6 h	**6**	65
			7	32
	60	2 min	**6**	40
			7	39
Ph,H,*p*-$CH_3OC_6H_4$	r.t.	8 h	**6**	50
			7	33
p-$(CH_3)_2NC_6H_4$,H,*p*-$CH_3OC_6H_4$	r.t.	8 h	**6**	59
			7	39
2-Furyl,H,*p*-$CH_3C_6H_4$	r.t.	2 h	**6**	62
			7	34
	60	2 min	**6**	31
			7	66
2-Furyl,H,2,4-$(CH_3)_2C_6H_3$	r.t.	3 h	**6**	50
			7	50
Ph,CH_3,*p*-$CH_3C_6H_4$	60	8 h	**6**	41
			7	50
Ph,CH_3,*p*-ClC_6H_4	r.t.	6 h	—	—
	60	6 h	**8**	50
			5	50

[a]Isolated, not gc, yields.

Can. J. Chem. Downloaded from www.nrcresearchpress.com by 210.87.254.5 on 09/06/12
For personal use only.

Can. J. Chem. Downloaded from www.nrcresearchpress.com by 210.87.254.5 on 09/06/12
For personal use only.

TABLE 3. Melting points, analytical, and pertinent spectral data for the allylic amides (**6** and **8**)

6, R =, R′ =, R″ =, or **8**	Melting point (°C)	Anal. calcd. (found)			Ir, ν_{CO}[a] cm^{-1}	MS *m/e*	nmr, δ ppm
		C	H	N			
Ph,H,*p*-$CH_3C_6H_4$	212–215	81.47 (81.10)	7.22 (7.01)	5.28 (5.11)	1655	265$[M]^+$ 222$[M - COCH_3]^+$	1.87 (s, 3H, $COCH_3$), 2.43 (s, 3H, CH_3), 3.90 (m, 2H, CH_2), 6.20 (m, 1H, CH=), 6.50–7.50 (m, 10H, aromatic and olefinic protons)
Ph,H,*p*-$CH_3OC_6H_4$	188–190	76.84 (76.81)	6.81 (6.58)	4.98 (4.89)	1655	281$[M]^+$ 238$[M - COCH_3]^+$	1.73 (s, 3H, $COCH_3$), 1.83 (s, 3H, $COCH_3$), 3.82 (s, 3H, OCH_3), 3.85 (s, 3H, OCH_3), 3.93 (m, 2H, CH_2), 6.30 (m, 1H, CH=), 6.40–7.40 (m, 10H, aromatic and olefinic protons)[c]
Ph,CH_3,*p*-$CH_3C_6H_4$	Oil	81.68 (82.00)	7.58 (7.42)	5.01 (4.80)	1650		1.85 (s, 3H, $COCH_3$), 2.12 (s, 3H, CH_3C=), 2.32 (s, 3H, CH_3), 3.63 (m, 2H, CH_2), 6.80–7.50 (m, 10H, aromatic and olefinic protons)
p-$(CH_3)_2NC_6H_4$,H,*p*-$CH_3OC_6H_4$	100–104	74.04 (74.56)	7.46 (7.51)	8.63 (8.24)	1650		1.70 (s, 3H, $COCH_3$), 2.83 (s, 6H, $N(CH_3)_2$), 3.70 (m, 2H, CH_2), 3.75 (s, 3H, OCH_3), 6.20 (m, 1H, CH=), 6.30–7.35 (m, 9H, aromatic and olefinic protons)
2-Furyl,H,*p*-$CH_3C_6H_4$	184 decomp.	75.27 (74.98)	6.71 (6.66)	5.48 (5.71)	1645	255$[M]^+$ 212$[M - COCH_3]^+$	1.78 (s, 3H, $COCH_3$), 2.45 (s, 3H, CH_3), 3.98 (m, 2H, CH_2), 5.63 (d, 1H, J = 3.0 Hz, H3 of furan), 6.10 (m, 1H, CH=), 6.75–7.45 (m, 7H, remaining protons)
2-Furyl,H,2,4-$(CH_3)_2C_6H_3$	130 decomp.	75.81 (75.32)	7.11 (6.97)	5.20 (5.22)	1655		1.96 (s, 3H, $COCH_3$), 2.35 (s, 3H, CH_3), 2.38 (s, 3H, CH_3), 3.95 (m, 2H, CH_2), 5.63 (d, 1H, J = 3.5 Hz, H-3 of furan), 6.08 (m, 1H, CH=), 6.75–7.49 (m, 6H, remaining protons)
8	Oil	70.27 (70.64)	5.90 (5.89)	4.10 (4.02)	1720 1650	343, 341$[M]^+$ 300, 298 $[M - COCH_3]^+$	1.63 (s, 3H, $COCH_3$), 1.87 (s, 3H, $COCH_3$), 2.27 (s, 3H, CH_3C=), 5.70 (s, 1H, *CH*$COCH_3$), 6.77–7.43 (m, 10H, remaining protons)

[a]In $CHCl_3$.
[b]$CDCl_3$ with tetramethylsilane (TMS) as internal standard.
[c]Mixture of *cis* and *trans* isomers.

Can. J. Chem. Downloaded from www.nrcresearchpress.com by 210.87.254.5 on 09/06/12
For personal use only.

of azadienes with carbon monoxide, methyl iodide, and cobalt carbonyl. Fair to good yields (Table 2) of **6** were obtained in all but one reaction, and the products were identified on the basis of analytical and spectral data (Table 3). The exceptional case was **5**, R = Ph, R′ = CH_3, R″ = *p*-ClC_6H_4, where **8**, an unanticipated product of diacylation of the azadiene, was formed. With this one exception, the reactions were quite

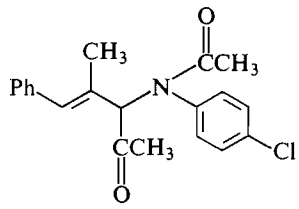

8

rapid, particularly at 60°C. What makes the conversion of **5** to **6** a useful one is its complete regiospecificity. Neither enamides (**9**) nor isomeric iminoketones (**10**, **11**) were detected in any of these reactions.

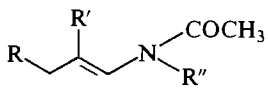

9

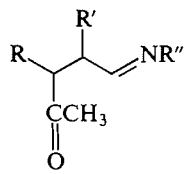

10

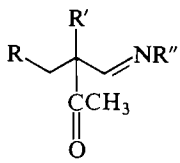

11

A possible mechanism for allylic amide formation is outlined in Scheme 1. 1,2-Addition of the *in situ* generated acetylcobalt

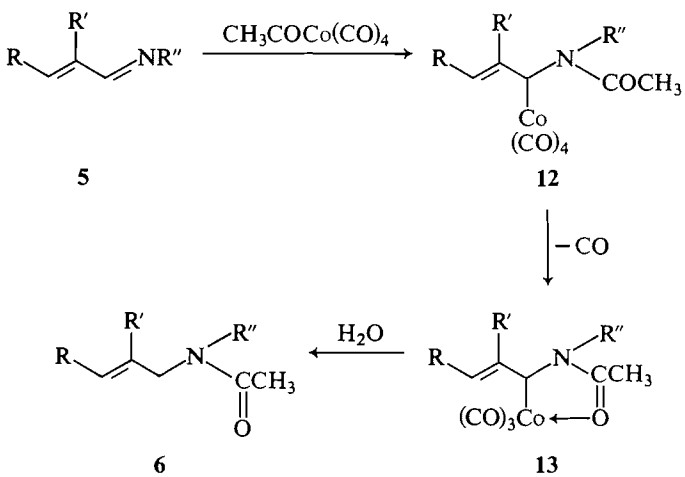

SCHEME 1

tetracarbonyl to the carbon–nitrogen double bond of **5** would give the σ-allylcobalt complex **12**. Such a 1,2-addition likely occurs at the least substituted double bond of a 1,3-diene affording a σ-allyl complex which is convertible to a π-allyl complex on subsequent loss of carbon monoxide (1). Rather than forming an analogous π-allyl complex on loss of carbon monoxide, coordination of the amide oxygen of **12** to the metal may occur to give **13**. The oxygen of an amide is more basic than that of a ketone (the intermediate σ-allyl complex formed using 1,3-dienes as substrates contains a ketone functionality). The allylic amide can then arise by hydrolytic cleavage of the carbon–cobalt bond of **13**. Although the generation of a π-allyl intermediate cannot be ruled out, one would have expected, in such an event, the enamide **9** to have been formed along with **6**.

Finally the mechanism of the cleavage and carbonylation of **5** to **7** is not known. The question, of course, arises as to the fate of the three-carbon unit of the azadiene. Repeated attempts to isolate an organic by-product (e.g. cinnamaldehyde from **5**, R = Ph, R′ = H, R″ = *p*-$CH_3C_6H_4$) failed.

In conclusion, the regiospecific phase transfer catalyzed reductive carbonylation of azadienes using $Co_2(CO)_8$ affords allylic amides in 31–65% yields. Allylic amides are valuable compounds, being precursors to a variety of acyclic and heterocyclic systems. For example, isomerization to enamides can be catalyzed by rhodium and ruthenium hydride complexes under thermal conditions (7), and by iron carbonyl under photolytic conditions (8).

Experimental section

General

Elemental analyses were carried out by Canadian Microanalytical Service Limited, Vancouver, and by Schwarzkopf Microanalytical Laboratory, Woodside, NY. The following instrumentation was used for spectral analyses: Varian T60 or HA-100 (NMR), Unicam SP-1100(IR), and VG Micromass 7070E (mass). Tetramethylsilane was the internal standard for nmr measurements. Melting points were recorded on a Fisher-Johns apparatus and are uncorrected.

The required azadienes (**5**) were synthesized by treatment of an α,β-unsaturated aldehyde with an equimolar amount of an amine, according to the procedure of Cardaci and Bellachioma (9). Cobalt carbonyl (Pressure Chemical Co.), the quarternary ammonium salts (Aldrich Chemical Co.), and methyl iodide (Eastman Kodak Co.) were commercial products and were used as received. Organic solvents were dried and distilled prior to use. All reactions were effected using dry nitrogen.

General procedure: phase transfer catalyzed reductive carbonylation of azadienes

Nitrogen gas was passed, for a period of 1 h, through a mixture of benzene (20 mL), distilled water (20 mL), and benzyltriethylammonium chloride (0.5 mmol). The gas was changed to carbon monoxide, and cobalt carbonyl (2.0 mmol) was added along with methyl iodide (1.0 mL). This mixture was stirred and then the azadiene (2.0 mmol) was added under a fast stream of carbon monoxide. The reaction mixture was stirred at room temperature or at 60°C (Table 2) until the solution became bright red, indicating completion of the reaction. The layers were separated, and the aqueous layer was extracted several times with 25 mL portions of methylene chloride. The methylene chloride extracts were combined with the organic phase (benzene), dried ($MgSO_4$), and then concentrated (rotary evaporation) to give the crude products. The products (**6** and **7**) were easily separated by column chromatography on silica gel using hexane–ether as the eluant, and recrystallized to give analytically pure materials. Product yields are given in Table 2, and melting points and spectral data for **6** (and **8**) are listed in Table 3. The acetanilide derivatives (**7**) were characterized by comparison of spectral properties with those for authentic samples.

The use of other conditions for the reductive carbonylation of azadienes

(a) Catalytic amount of $Co_2(CO)_8$

Repetition of the general procedure using 0.2 mmol of $Co_2(CO)_8$

(i.e. a 10:1 ratio of **5**, R = Ph, R′ = H, R″ = *p*-$CH_3C_6H_4$) afforded **6** in 17% yield and recovered **5**.

(b) Reaction in the absence of a quarternary ammonium salt

When the general procedure was carried out, without benzyltriethylammonium chloride, and for an extended period of time (18 h at room temperature), **6** (R = Ph, R′ = H, R″ = *p*-$CH_3C_6H_4$) was formed in 21% yield, the major product (61%) being **7**, R″ = *p*-$CH_3C_6H_4$.

(c) Using Aliquat 336 as the phase transfer agent

Substitution of 0.5 mmol of Aliquat 336 for benzyltriethylammonium chloride resulted in a more sluggish reaction (18 h) giving **6**, R = Ph, R′ = H, R″ = *p*-$CH_3C_6H_4$ in 41% yield.

(d) Reaction in the absence of $Co_2(CO)_8$

The azadiene **5**, R = Ph, R′ = H, R″ = *p*-$CH_3C_6H_4$ was completely recovered when the reaction was effected without $Co_2(CO)_8$.

(e) Using CH_2Cl_2 as the organic phase

Reaction of **5**, R = Ph, R′ = H, R″ = *p*-$CH_3C_6H_4$ at room temperature for 6 h, using methylene chloride as the organic phase, afforded **7** in 60% yield, with the desired **6** only obtained in 12% yield.

(f) At different base concentrations

The general procedure was applied to **5**, R = Ph, R′ = H, R″ = *p*-$CH_3C_6H_4$ with aqueous NaOH (0.1–12.5 *N*) used instead of water (see Table 1).

Reaction using acidic phase transfer catalysis

A degassed mixture of pentane (20 mL), water (20 mL), and *p*-toluenesulfonic acid (1.0 nmol) was treated with cobalt carbonyl (2.0 nmol) and methyl iodide (1.0 mL) under a carbon monoxide atmosphere for 4 h. Then **5**, R = Ph, R′ = H, R″ = *p*-$CH_3C_6H_4$ (2.0 nmol) was added and the reaction mixture was stirred overnight. Work-up following the general procedure gave **6** in 51% yield, and recovered starting material.

Acknowledgments

We are grateful to the Natural Sciences and Engineering Research Council of Canada for support of this research. Mrs. Amaratunga is a Commonwealth Scholarship recipient.

1. H. ALPER. Adv. Organomet. Chem. **19**, 183 (1981).
2. L. CASSAR. Ann. N.Y. Acad. Sci. **333**, 208 (1980).
3. H. ALPER, J. K. CURRIE, and H. DES ABBAYES. J. Chem. Soc. Chem. Commun. 311 (1978).
4. H. ALPER, K. E. HASHEM, and J. HEVELING. Organometallics, **1**, 775 (1982).
5. H. ALPER and J. K. CURRIE. Tetrahedron Lett. 2665 (1979).
6. H. ALPER and D. E. LAYCOCK. Tetrahedron Lett. **22**, 33 (1981).
7. J. K. STILLE and Y. BECKER. J. Org. Chem. **45**, 2139 (1980).
8. A. J. HUBERT, P. MONIOTTE, G. GOEBBELS, R. WARIN, and P. TEYSSIE. J. Chem. Soc. Perkin II, 1954 (1973).
9. G. CARDACI and G. BELLACHIOMA. J. Chem. Soc. Dalton Trans. 1735 (1976).

Can. J. Chem. Downloaded from www.nrcresearchpress.com by 210.87.254.5 on 09/06/12
For personal use only.

A kinetic study of the hydrogenation of hexene-1 catalyzed by a ferrocenyl-phosphine derivative of ruthenium(II)

GLEN E. RODGERS,[1] WILLIAM R. CULLEN, AND BRIAN R. JAMES
Department of Chemistry, University of British Columbia, Vancouver, B.C., Canada V6T 1Y6

Received August 9, 1982

GLEN E. RODGERS, WILLIAM R. CULLEN, and BRIAN R. JAMES. Can. J. Chem. **61**, 1314 (1983).

The complex, dichloro(triphenylphosphine){1-[*N*,*N*-α-dimethylaminoethyl]-2-diphenylphosphinoferrocene}ruthenium(II), prepared from $RuCl_2(PPh_3)_3$ by ligand displacement, catalyzes the hydrogenation of terminal olefins under mild conditions. The experimental rate-law for hydrogenation of hexene-1 in *n*-butanol at 40°C shows a first-order dependence on both olefin and hydrogen, and an inverse dependence to added triphenylphosphine. The dependence on ruthenium goes from first- to half-order with increasing metal concentration. The kinetic data, together with spectroscopic data, and studies on reactivity of the complex toward hydrogen, are interpreted in terms of catalysis via a ruthenium(I) complex that dissociates a phosphine ligand to generate the active species.

GLEN E. RODGERS, WILLIAM R. CULLEN et BRIAN R. JAMES. Can. J. Chem. **61**, 1314 (1983).

Le complexe de dichloro(triphénylphosphine){[*N*,*N*-α-diméthylaminoéthyl]-1 diphénylphosphinoferrocène-2}ruthénium(II), préparé à partir du $RuCl_2(PPh_3)_3$ par déplacement de ligand, catalyse l'hydrogénation des oléfines terminales dans des conditions douces. La loi de vitesse expérimentale d'hydrogénation de l'hexène-1, dans le *n*-butanol à 40°C, montre une dépendance d'ordre un vis-à-vis de l'oléfine et de l'hydrogène, et une dépendance inverse vis-à-vis de la triphénylphosphine ajoutée. L'influence du ruthénium va d'un ordre un à un ordre de $\frac{1}{2}$ lorsque la concentration du métal augmente. On interprète les données cinétiques ainsi que les données spectroscopiques et les études de réactivité du complexe envers l'hydrogène, en fonction de la catalyse par l'intermédiaire du complexe de ruthénium(I) qui dissocie un ligand phosphine pour produire l'espèce active.

[Traduit par le journal]

Introduction

Of all homogeneously catalyzed processes, hydrogenation has been the most intensely studied, and several systems particularly based on rhodium phosphine complexes, including some that are effective for asymmetric hydrogenation, are now understood at a remarkably sophisticated level (1–3). These rhodium systems operate via dihydride species that are formed by oxidative addition of dihydrogen at rhodium(I) centres. Catalysts based on the currently less expensive ruthenium metal are less thoroughly understood, even the well-studied and extremely active $RuHCl(PPh_3)_3$ complex (4). One unsolved problem with catalysis at ruthenium(II) centres is the accessibility of the Ru(IV) oxidation state; for example, does reaction [1], a *net* heterolytic cleavage of H_2, involve oxidative addition to give a $Ru^{IV}H_2$ intermediate followed by reductive elimination of HCl, or a transition state in which coordinated chloride stabilizes the released proton (1, 5)? Activation parameter data

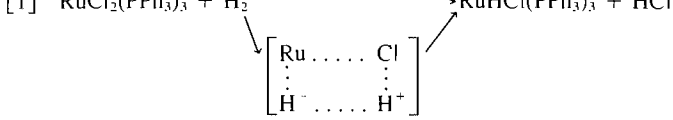

for several ruthenium(II) systems provide indirect support for a rate-determining oxidative addition (1).

Incorporation of an amino group into a phosphine, in which a coordinated nitrogen atom can play the role of proton acceptor (6), should allow for a further more direct probing of the dichotomy, and this coupled with our experience with the 1-[*N*,*N*-α-dimethylaminoethyl]-2-diphenylphosphinoferrocene ligand (**I**) (7, 8) led us to synthesize and characterize a ruthenium(II) derivative and study its reactivity toward H_2 in the absence and presence of olefinic substrates.

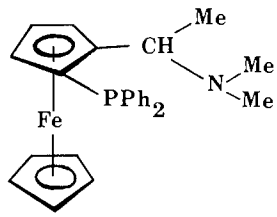

I

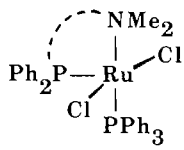

II

A range of other aminophosphine ligands has been used in catalytic hydrogenation systems, particularly with rhodium and iridium (6, 9),[2] but only qualitative rate data have been reported. There is in general a growing interest in ligand systems containing both "soft" and "hard" donor atoms (10, 11). The fact that rhodium systems such as $Rh(bipyridyl)_2^+$ can selectively catalyze hydrogenation of a ketone in ketone/olefin mixtures (12), while analogous systems with chelated diphosphines preferentially reduce olefins (13), encouraged further research into mixed PN donor systems.

Ligand **I**, abbreviated PPFA, possessing a planar element of chirality as well as chirality at the carbon substituent, is one of a range of ferrocenyl-phosphine ligands that have been used for asymmetric hydrosilylation (14) and hydrogenation (8, 15, 16). The asymmetric hydrogenation systems have used rhodium catalysts, but to our knowledge no reports on ruthenium systems have appeared. The studies reported in this present paper were carried out with the racemic ligand because of the interest noted above; they are also considered exploratory for future work using chiral systems.

Experimental

Air-sensitive materials were manipulated using a double-manifold

[1]On leave 1981–1982 from Chemistry Department, Allegheny College, Meadville, PA 16335, U.S.A.

[2]See also ref. 1, pp. 297, 339, and ref. 4, p. 384.

Can. J. Chem. Downloaded from www.nrcresearchpress.com by 210.87.254.5 on 09/06/12
For personal use only.

Can. J. Chem. Downloaded from www.nrcresearchpress.com by 210.87.254.5 on 09/06/12
For personal use only.

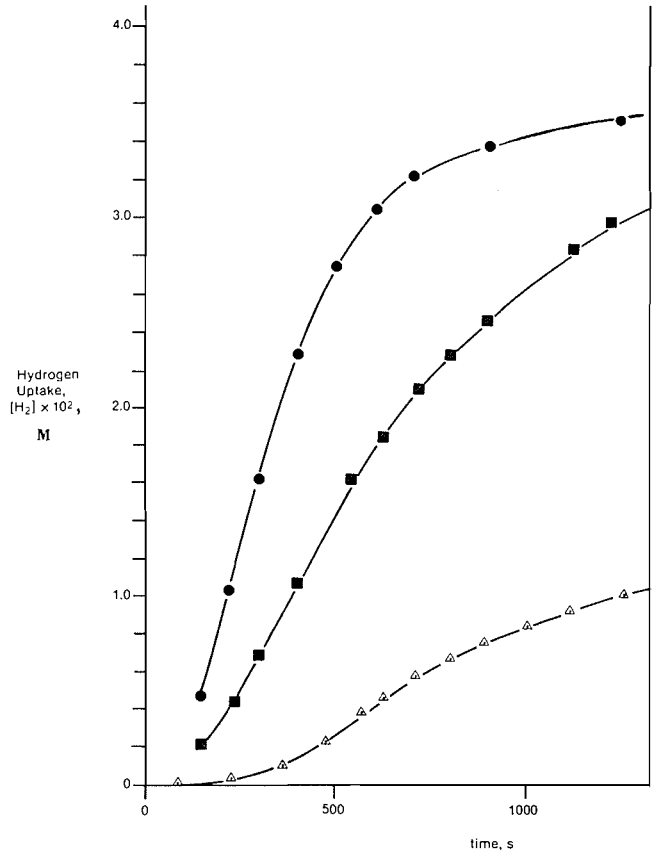

FIG. 1. Selected H_2 uptake plots for the hydrogenation of hexene-1 catalyzed by **II** in *n*-butanol at 40°C, 0.04 *M* hexene, 1 atm total pressure: ● 10×10^{-4} *M* Ru, ■ 2.47×10^{-4} *M* Ru, △ 1.23×10^{-4} *M* Ru.

vacuum system and standard Schlenk techniques. Nuclear magnetic resonance spectra were run on Varian XL100 or Bruker WM 400 instruments. Other instruments used were as follows: Perkin–Elmer 598 infrared spectrophotometer, Cary 17D uv/vis spectrophotometer, AEI-MS902 mass spectrometer, and a Hewlett Packard 5880A gas chromatograph.

Ruthenium(III) trichloride trihydrate was obtained as $RuCl_3 \cdot 3H_2O$ (40.59% Ru) from Johnson Matthey Limited. Olefinic substrates were obtained as CP grade; solids were recrystallized and liquids redistilled before use. Peroxide impurities in liquid olefins were removed by passage through an alumina column under N_2. *n*-Butanol was refluxed with magnesium metal/iodine to remove traces of water. Other materials used and the procedure used for following H_2-uptake at constant pressure have been described previously (17, 18).

*Preparation of dichloro(triphenylphosphine){1-[*N,N*-α-dimethylaminoethyl]-2-diphenylphosphinoferrocene}ruthenium(II), $RuCl_2(PPh_3)PPFA$, (II)*

Dichlorotris(triphenylphosphine)ruthenium(II) (1.24 mmol), prepared from $RuCl_3 \cdot 3H_2O$ (19), and 1-[*N*,*N*-α-dimethylaminoethyl]-2-diphenylphosphino-ferrocene (0.73 mmol), prepared from ferrocene carboxaldehyde (7), were refluxed in 75 mL of hexane for 18 h. The $RuCl_2(PPh_3)_3$ is present as a suspension in the hexane, but the slow reaction gives a resulting dark-green solid that was filtered and washed with small quantities of cold hexane. The product was dissolved in hot benzene (70°C) and, after a filtration step, the solid product was reprecipitated by adding hexane. The dark-green product, mp > 210°C dec., was isolated by filtration after the mixture had been stored at −20°C for 12 h. Infrared: 310 cm^{-1}, ν(Ru—Cl); λ_{max}, nm (ε, M^{-1} cm^{-1}) in BuOH: 628 (420), 457 (1100); ^1H nmr ($CDCl_3$) δ: 1.52 (d, 3, *J* = 7, C—CH_3), 2.44, 2.66 (2d, 6, *J* = 2.4, N—$(CH_3)_2$), 3.56 (s, 5, Fe—C_5H_5), 4.12, 4.27, 4.48 (s, t, s, 3, *J* = 2, Fe—C_5H_3), 6.23

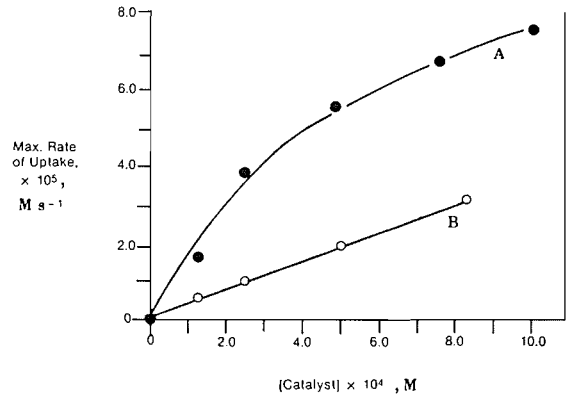

FIG. 2. A. Dependence of maximum hydrogenation rate on [Ru] in *n*-butanol at 40°C, 0.04 *M* hexene, 1 atm total pressure. B. As for A in the presence of 11.9×10^{-4} *M*, added PPh_3.

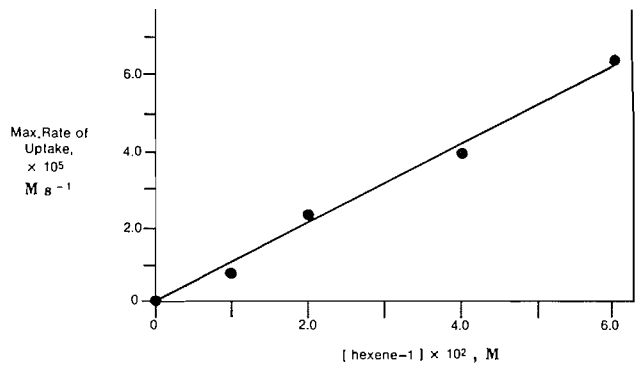

FIG. 3. Dependence of maximum hydrogenation rate on [hexene-1] in *n*-butanol at 40°C, 1 atm total pressure, [Ru] = 2.47×10^{-4} *M*.

(q, 1, *J* = 6.4, CH_3C—*H*), 6.9–7.8 (m, 25, P—$(C_6H_5)_2$, P—$(C_6H_5)_3$); $^{31}P\{^1H\}$ nmr (C_6D_6) δ (downfield from $P(OMe)_3$): 170.5 (d, 1, *J* = 38.0), 137.0 (d, 1, *J* = 38.9); ($(CD_3)_2CO$) δ: 174 (d, 1, *J* = 37.7), 140 (d, 1, *J* = 39.3); ms *m/e*: 398, 262, 183, 108. *Anal.* calcd. for $C_{44}H_{43}Cl_2FeNP_2Ru$: C 60.36, H 4.95, N 1.60, Cl 8.10; found: C 60.34, H 5.03, N 1.49, Cl 7.95. *Mol. Wt.* calcd.: 876; found ($CHCl_3$): 859.

Results

The $RuCl_2(PPh_3)$(PPFA) complex (**II**) in *n*-butanol was found to be an efficient catalyst for the hydrogenation of terminal olefins under mild conditions (30–60°C, ≤ 1 atm H_2). Under these conditions, hexene-1 as substrate gave conveniently measurable rates for kinetic studies at 40°C ([**II**] = $10^{-4} - 10^{-3}$ *M*, [hexene-1] = $(1.0–6.0) \times 10^{-2}$ *M*, added [PPh_3] = $(0.0–12.0) \times 10^{-4}$ *M*). Figure 1 shows selected uptake plots at the conditions noted using 5 mL solution volume. Hydrocarbon solvent systems gave much lower hydrogenation rates.

The total gas uptake corresponded to stoichiometric reduction of the hexene to hexane, as checked by gas chromatography. The hydrogenation rate of internal alkenes such as hexene-2, as well as of disubstituted olefins such as styrene and the prochiral substrate *N*-acetamidoacrylic acid, was negligible at 40°C. Hexene-2 was not detected at any stage during the hydrogenation, and thus there is no evidence for accompanying isomerization of the hexene-1.

The uptake plots (e.g. Fig. 1) show initially autocatalytic-type behaviour prior to reaching a maximum rate after

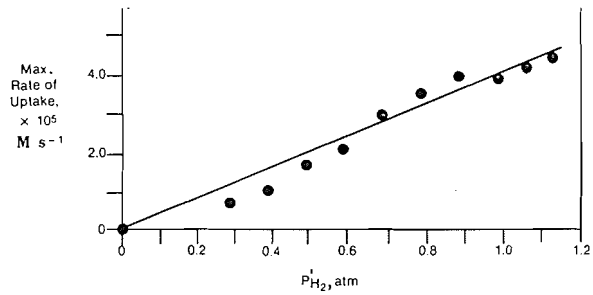

FIG. 4. Dependence of maximum hydrogenation rate on partial pressure of H_2 in *n*-butanol at 40°C, 0.04 *M* hexene, [Ru] = 2.47 × 10^{-4} *M*. Pressure reading is corrected for vapour pressure of *n*-butanol, 0.02 atm at 40°C (ref. 38*a*, p. 219).

200–800 s; the rates then gradually fall off. The "induction period" prior to the region of maximum rate increased with decreasing H_2 pressure (from 1 to 0.3 atm), and with decreasing ruthenium concentration (Fig. 1), but was largely independent of hexene-1 concentration. The maximum rates, which are readily measured, were used to determine the kinetic dependences. The data are summarized in Figs. 2–5 and reveal a complex dependence on Ru (Fig. 2A), first-order in hexene-1 (Fig. 3) and partial pressure of H_2 (Fig. 4), and an inverse dependence on added phosphine that is plotted as $(\text{rate})^{-1}$ vs. $[PPh_3]$ in Fig. 5. The dependence on Ru is first-order at low concentrations but becomes less than one with increasing concentration and, in fact, approaches half-order above 8 × 10^{-4} *M* (Fig. 2A); in the presence of excess phosphine, the dependence on Ru becomes strictly first-order (Fig. 2B).

In the absence of organic substrate, butanol solutions of **II** absorb slightly more than 0.5 mol of H_2 per Ru at several pressures. These reactions follow pseudo first-order behaviour at the constant H_2 pressure used and yield, for example, k_{obs} = 1.3 × 10^{-3} s^{-1} using 0.7 atm H_2 at 40°C. The gas uptake is accompanied by a colour change from green to orange-red. The intensity of the initial 628 nm band decreases, while increasing absorption in the 350–450 region washes out the initial 457 nm band; these spectral changes reveal isosbestic points at 435 and 530 nm. There was no evidence (ir, nmr) for the presence of a ruthenium-hydride species in the alcohol (or deuterated alcohol) solvents; reactivity toward H_2 in benzene was slow and incomplete, and again no metal hydride was detected. Of interest, the orange-red hydrogenated solutions gave no ^{31}P nmr signals, although the percursor green solutions of **II** at the same concentrations yielded a ^{13}P nmr spectrum (see Experimental and Discussion). Attempts to isolate solids from the orange-red solutions by evaporation of the solvent even under H_2 led to a slow regeneration of the green colour and partial formation of **II**; again, no metal hydride was detected in the solid residue.

Addition of hexene-1 to the orange-red solutions under H_2 caused further very slight visible spectral changes, the absorption in the 350–450 nm region decreasing somewhat; the spectrum shows only a broad shoulder from 420–450 nm ($\epsilon \sim 1000$ M^{-1} cm^{-1}), and is typical of that present during the region of maximum catalytic hydrogenation rate.

Solutions of $RuCl_2(PPh_3)$(PPFA) were unreactive toward hexene-1, although with *N*-acetamidoacrylic acid (a nonreducible substrate) a colour change from green to reddish was noted.

Suspensions of the hydridocomplex $RuHCl(PPh_3)_3$ (20) in hexane were unreactive toward the PPFA ligand (ligand/metal ratio = 2.5), even under reflux.

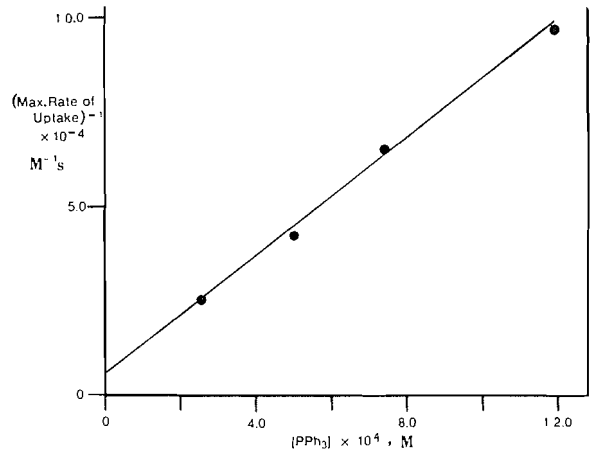

FIG. 5. Inverse dependence of maximum hydrogenation rate on added phosphine concentration in *n*-butanol at 40°C, 0.04 *M* hexene, 1 atm total pressure, [Ru] = 2.47 × 10^{-4} *M*.

Discussion

Characterization of $RuCl_2(PPh_3)$(PPFA), (II)

Complex **II** is obtained by the simple ligand exchange reaction outlined in eq. [2] using a ligand-to-complex ratio of less than one:

[2] $RuCl_2(PPh_3)_3 + PPFA \rightarrow RuCl_2(PPh_3)(PPFA) + 2P\dot{P}h_3$

Such a metathesis reaction but using excess ligand has been used previously, particularly with chelating ditertiary phosphine type ligands, to yield isolable complexes of the type $RuCl_2(\text{diphosphine})_2$, in which three or four of the phosphorus atoms are coordinated (21, 22), or of the type $Ru_2Cl_4(\text{diphosphine})_3$ containing a bridging diphosphine (22). The $CHCl_3$ solution molecular weight of **II** shows it to be a monomer, and since a visible spectrum of a Nujol sample shows the same absorption maxima as the solution spectrum (that is invariant with solvent), the same monomeric structure is indicated in the solid state; structure **II**, being either a square pyramid or distorted trigonal bipyramid, is consistent with the spectroscopic data.

The two N—CH_3 resonances in the room temperature ^1H nmr indicate that the nitrogen is coordinated as in the rhodium complex $[Rh(PPFA)(\text{norbornadiene})]^+ClO_4^-$ (7). These N—CH_3 resonances show small splittings that are field independent and are probably due to coupling to a single *trans* phosphorus. The nonproton-decoupled ^{31}P spectrum was too broad to detect this coupling. The ^1H nmr spectrum in toluene-d^8 is invariant from 0–100°C and shows the same nonequivalent methyl groups. (In a cationic rhodium complex with the arsenic analogue of PPFA, exchange between the two nonequivalent N—CH_3 groups is rapid at ambient temperatures (11).)

The ^{31}P nmr spectrum in C_6D_6 at room temperature shows two nonequivalent phosphorus atoms, the small coupling constant indicating a *cis*-geometry (22–24); the spectrum in $(CD_3)_2CO$ is invariant from −60°C to ambient temperatures.

The two-band visible spectrum with the more intense higher energy band resembles closely those of square-pyramidal $RuCl_2P_3$ species with *trans* chlorides and three phosphine (P) donors (22, 23).

Finally, the infrared spectrum shows a single band at 310 cm^{-1} that is characteristic of ν(Ru—Cl) with mutually *trans* chlorides (22, 25).

Can. J. Chem. Downloaded from www.nrcresearchpress.com by 210.87.254.5 on 09/06/12
For personal use only.

Can. J. Chem. Downloaded from www.nrcresearchpress.com by 210.87.254.5 on 09/06/12
For personal use only.

We are unaware of any studies akin to reaction [2], but using other chelating PN donor systems. A 1:1 stoichiometric reaction of $RuCl_2(PPh_3)_3$ with diop, the well-known chelating chiral diphosphine (22), has been shown to yield $RuCl_2(PPh_3)$(diop) that has an ABX pattern in the ^{31}P nmr, consistent with a structure such as **II** (26).

The nonreactivity of $RuHCl(PPh_3)_3$ toward excess PPFA is surprising in view of the success of reaction [2] and considering that chelating ditertiary-phosphines and -arsines, and chelating diamines readily yield complexes such as $RuHCl(chelate)_2$ or $RuHCl(PPh_3)_2$(chelate), under identical conditions (21, 27). The lack of reactivity may be related to solubility factors since the usual precursor and product hydrides have very low solubilities in the hexane medium (21, 26). Alternatively a hydridoruthenium(II) complex containing PPFA just may not form readily; formation of a detectable hydride via reaction of **II** with H_2 is not observed (see below), in spite of the possibility of a reaction such as [3] with the released proton being associated with a dissociated chloride or arsine donor (cf. eq. [1]).

$$[3]\quad Ru^{II} + H_2 \rightleftharpoons Ru^{II}H^- + H^+$$

Hydrogenation studies

The stoichiometry of the reaction of $RuCl_2(PPh_3)$(PPFA) with H_2, together with lack of evidence for hydride formation, is tentatively but best interpreted in terms of production of ruthenium(I) species:

$$[4]\quad Ru^{II} + \frac{1}{2}H_2 \rightleftharpoons Ru^{I} + H^+$$

The lack of ^{31}P nmr signals could be consistent with the presence of paramagnetic mononuclear Ru(I) d^7 species. No esr signal has yet been detected, but this is not uncommon for paramagnetic ruthenium species because of relatively fast relaxation rates of the quadrupolar nucleus (28). Ruthenium(I) phosphine complexes stabilized by carbonyl ligands have been known for some time (29), while evidence has been presented more recently for $[RuCl(PPh_3)_3]_n$, $[RuCl(PPh_3)_2]_2$, $[RuCl(PMe_3)_2]_2$, and $[RuCl(PPh_2(CH_2)_3PPh_2)_2]$ species (30–33).

Earlier work from this laboratory reported on the use of chlororuthenate(I) solutions for catalyzing hydrogenation of unsaturated carboxylic acids (34). Further indirect evidence against formation of a catalytically active ruthenium(II) hydride system (cf. eqs. [1], [3]) is the lack of accompanying isomerization of hexene-1 during the catalytic hydrogenation. Such monohydride catalysts are usually quite active for isomerization via the usual metal hydride addition – elimination sequence involving a metal alkyl intermediate (1, 35). Presumably, reduction to the ruthenium(I) state involves hydride formation (eq. [3]), followed by a reaction such as [5]. Such dihydrogen reduction of Ru(III) and Ru(II) species to Ru(II)

$$[5]\quad Ru^{II}H \text{ (or } Ru^0 + H^+) + Ru^{II} \rightarrow 2Ru^{I} + H^+$$

and Ru(I) species, respectively, has been studied previously (36, 37) and found to be promoted by base (cf. eqs. [1], [3], [5]). Enhanced reactivity here in butanol compared with benzene suggests solvent polarity is important, perhaps in stabilizing transition states akin to that shown in eq. [1].

The partial re-formation of complex **II**, on attempting to work up the "ruthenium(I)" solutions, implies some reversibility of reaction [4], although the gas uptake and visible spectral data show that reaction of **II** with H_2 is "complete" over the pressure range studied (0.5–1.0 atm).

The initial autocatalytic type profile of the hexene-1 hydrogenation plots is attributed to formation of the active Ru(I) catalyst, and the kinetics measured in the maximum rate region are consistent with catalysis via this species in mechanisms outlined in eqs. [6] and [7].

Pre-formation of the Ru(I) species, prior to addition of hexene-1, removed the autocatalytic region and led to initial hydrogenation rates very close to those measured in the region of maximum rate for uptake curves of the type illustrated in Fig. 1 under corresponding conditions.

$$[6]\quad Ru(I)(PPh_3) \overset{K_p}{\rightleftharpoons} Ru(I) + PPh_3$$

$$[7]\quad \begin{array}{ccc} Ru(I) + H_2 & \overset{K_1}{\rightleftharpoons} & Ru(III)H_2 \\ {\scriptstyle K_2\ \text{hexene}}\ \Big\Vert & & \Big|\ {\scriptstyle k_1\ \text{hexene}} \\ Ru(I)(\text{hexene}) & \xrightarrow[H_2]{k_2} & Ru(I) + \text{hexene} \end{array}$$

The nature of Ru(I) is uncertain but dissociation of a phosphine ligand prior to the rate-determining step is essential in order to account for the observed kinetic dependences.

If the ruthenium in solution is present as just $Ru(I)PPh_3$ and Ru(I), then the rate-law by both the K_1k_1 and K_2k_2 paths approximates to:

$$[8]\quad \frac{-d}{dt}[H_2] = \frac{(k_1K_1 + k_2K_2)K_p[Ru_T][H_2][\text{hexene}]}{K_p + [PPh_3]}$$

where subscript T refers to total concentration. This rate-law requires that K_1 and K_2 are sufficiently small such that there are no detectable hydrido or olefinic species based on the Ru(I) catalytic cycle, and this is supported by the experimental data. At sufficiently low ruthenium concentration $PPh_3 < K_p$, and rate-law [8] leads to a first-order dependence on Ru_T; at the higher ruthenium concentrations $[PPh_3] > K_p$, and in the absence of added phosphine is equated to [Ru(I)] (which is given by $[K_pRu_T]^{1/2}$). Thus the rate law then becomes:

$$[9]\quad \frac{-d}{dt}[H_2] = (k_1K_1 + k_2K_2)K_p^{1/2}[Ru_T]^{1/2}[H_2][\text{hexene}]$$

The complex dependence on Ru is thus accounted for by the K_p equilibrium, i.e. in terms of the relative magnitude of K_p and $[PPh_3]$ in the denominator of eq. [8] as Ru_T increases. In the presence of sufficient added phosphine ($[PPh_3] \gg K_p$ in eq. [8]), a first-order dependence on catalyst obtains.

The general dependence on added phosphine can by analyzed by taking the reciprocal form of eq. [8] and plotting $(\text{rate})^{-1}$ vs. $[PPh_3]$ (Fig. 5).

The mechanisms outlined in eq. [7] correspond to the well-established "hydride" (K_1k_1) and "unsaturate" (K_2k_2) routes.[3] K_1k_1 becomes zero if the k_2 unsaturate path predominates and vice versa. The very slight visible spectral change on adding hexene to the Ru(I) solutions gives some evidence for the K_2 equilibrium but the amount of Ru(I) (hexene) species present in solution is estimated to be <10% at the highest hexene concentration used (0.06 *M*). Significant amounts of this species would be evidenced kinetically by a fall-off in rate with increasing [hexene] (see Fig. 3), that is, by a less than first-order dependence as reflected in the addition of a K_2[hexene] term in the denominator of eq. [8].

[3]Reference 9, p. 400.

Can. J. Chem. Downloaded from www.nrcresearchpress.com by 210.87.254.5 on 09/06/12
For personal use only.

The data summarized in Figs. 2–5 are internally reasonably consistent, and lead to numerical values of $(k_1K_1 + k_2K_2)$ and K_p at 40°C (the solubility of H_2 in butanol is taken as 4.0×10^{-3} M atm^{-1} at 40°C (38)). A $(k_1K_1 + k_2K_2)$ value of about 1.3×10^3 M^{-2} s^{-1} is calculated from the initial slope of Fig. 2A, while a rate vs. $[Ru_T]^{1/2}$ plot for the higher ruthenium concentrations (see eq. [9]) yields a $(k_1K_1 + k_2K_2)K_p^{1/2}$ value of about 15 $M^{-3/2}$ s^{-1}; thus K_p is estimated to be about 1.3×10^{-4} M^{-1}. The slope of Fig. 5 yields a $(k_1K_1 + k_2K_2)K_p$ value of 0.3 M^{-3} s^{-1}, although the large error in the intercept value does not allow for a reliable $(k_1K_1 + k_2K_2)$ value. The data of Figs. 3 and 4 are measured at a ruthenium concentration in which the rates are closer to first-order in catalyst (i.e. the rates approximate to $(k_1K_1 + k_2K_2)[Ru_T][H_2][hexene]$); the slopes yield $(k_1K_1 + k_2K_2)$ values of 1.1×10^3 and 1.0×10^3 M^{-2} s^{-1}. The slope of Fig. 2B at the added phosphine concentration of 11.9×10^{-4} M ($\gg K_p$) gives a $(k_1K_1 + k_2K_2)K_p$ value of 0.25 M^{-3} s^{-1}.

More detailed kinetic studies using other olefinic substrates, coupled together with isolation of the suggested Ru(I)(PPh_3) catalyst, are required to further substantiate the admittedly rather speculative mechanism outlined in eqs. [6] and [7]. Modified schemes in which phosphine dissociation occurred at the time of dihydride or olefin complex formation could satisfy the kinetics equally well. A key test for the suggested mechanism would be an independent measurement of K_p, following isolation of the Ru(I) complex; labile phosphine exchange within the K_p equilibrum could also contribute to line-broadening in the ^{31}P nmr spectrum (see above).

Catalytic hydrogenation via Ru(I) monohydride intermediates requires more elaborate reaction schemes, and would also be expected to be accompanied by some isomerization (see above).

Our initial objectives in this study, regarded as preliminary, have not been fulfilled. Apparent reduction to ruthenium(I) complicates the probing of heterolytic cleavage of H_2 by Ru(II), while the catalytic hydrogenation system discovered seems inactive, at least under mild conditions, for hydrogenation of the prochiral amino acid precursors, although this may be due to strong chelation to the $RuCl_2(PPh_3)$(PPFA) complex. Nevertheless, catalytic hydrogenation via the relatively rare ruthenium(I) state is strongly indicated, and further efforts are in hand to isolate the active complex. The activity of the system for hydrogenation of hexene-1 is comparable to that of the $RuHCl(PPh_3)_3$ catalyst, which is one of the most active known for terminal olefins.[4]

Acknowledgements

This work was supported by the Natural Sciences and Engineering Research Council of Canada in the form of operating grants to W.R.C. and B.R.J. In addition, G.E.R. was supported by a Science Faculty Professional Development Award (Grant Number SPI-8165033) from the National Science Foundation, U.S.A. We thank Johnson Matthey Limited for the loan of ruthenium, and Mr. T-J. Kim and Dr. I. Butler for assistance with some of the experiments.

1. B. R. JAMES. *In* Comprehensive organometallic chemistry. Vol. 8. *Edited by* G. Wilkinson. Pergamon, Oxford. 1982. Chapt. 51.
2. H. B. KAGAN. *In* Comprehensive organometallic chemistry. Vol. 8. *Edited by* G. Wilkinson. Pergamon, Oxford. 1982. Chapt. 53.
3. P. S. CHUA, N. K. ROBERTS, B. BOSNICH, S. J. OKRASINSKI, and J. HALPERN. J. Chem. Soc. Chem. Commun. 1278 (1981), and references therein.
4. B. R. JAMES. Adv. Organomet. Chem. **17**, 319 (1979).
5. P. J. BROTHERS. Prog. Inorg. Chem. **28**, 1 (1981).
6. C. PRADAT, J. G. RIESS, D. BONDOUX, B. F. MENTZEN, I. TKATCHENKO, and D. HOUALLA. J. Am. Chem. Soc. **101**, 2234 (1979).
7. W. R. CULLEN, F. W. B. EINSTEIN, C-H. HUANG, A. C. WILLIS, and E-S. YEH. J. Am. Chem. Soc. **102**, 988 (1980).
8. W. R. CULLEN and E-S. YEH. J. Organomet. Chem. **139**, C13 (1977).
9. B. R. JAMES. Homogeneous hydrogenation. Wiley, New York. 1973. See *aminophosphine ligands* in Index.
10. M. D. FRYZUK and P. A. MACNEIL. J. Am. Chem. Soc. **103**, 3592 (1981).
11. W. R. CULLEN and J. D. WOOLLINS. Can. J. Chem. **60**, 1793 (1982).
12. G. MESTRONI, G. ZASSINOVICH, and A. CAMUS. J. Organomet. Chem. **140**, 63 (1977).
13. B. R. JAMES and D. MAHAJAN. Can. J. Chem. **57**, 180 (1979), and unpublished results.
14. T. HAYASHI, M. TAJIKA, K. TAMAO, and M. KUMADA. J. Am. Chem. Soc. **98**, 3718 (1976), and references therein.
15. T. HAYASHI, T. MISE, S. MITACHI, K. YAMAMOTO, and M. KUMADA. Tetrahedron Lett. 1133 (1976).
16. L. MARKO and J. BAKOS. *In* Aspects of homogeneous catalysis. Vol. 4. *Edited by* R. Ugo. Reidel, Dordrecht. 1981. p. 145.
17. B. R. JAMES and G. L. REMPEL. Discuss. Faraday Soc. **46**, 48 (1968); Can. J. Chem. **44**, 233 (1966).
18. B. R. JAMES and D. MAHAJAN. Isr. J. Chem. **15**, 214 (1977).
19. T. A. STEPHENSON and G. WILKINSON. J. Inorg. Nucl. Chem. **28**, 945 (1966).
20. B. R. JAMES and L. D. MARKHAM. J. Catal. **27**, 442 (1972).
21. B. R. JAMES and D. K. W. WANG. Inorg. Chim. Acta, **19**, L17 (1976), and references therein.
22. B. R. JAMES, R. S. MCMILLAN, R. H. MORRIS, and D. K. W. WANG. Adv. Chem. Ser. **167**, 123 (1978), and references therein.
23. P. R. HOFFMAN and K. G. CAULTON. J. Am. Chem. Soc. **97**, 4221 (1975).
24. P. W. ARMIT, A. S. F. BOYD, and T. A. STEPHENSON. J. Chem. Soc. Dalton Trans. 1663 (1975).
25. M. S. LUPIN and B. L. SHAW. J. Chem. Soc. A, 741 (1968).
26. D. K. W. WANG. Ph.D. dissertation. University of British Columbia, 1978.
27. R. G. BALL, B. R. JAMES, J. TROTTER, D. K. W. WANG, and K. R. DIXON. J. Chem. Soc. Chem. Commun. 460 (1979).
28. D. DOLPHIN, B. R. JAMES, A. J. MURRAY, and J. R. THORNBACK. Can. J. Chem. **58**, 1125 (1980), and references therein.
29. R. MASON, K. M. THOMAS, D. F. GILL, and B. L. SHAW. J. Organomet. Chem. **40**, C67 (1972).
30. J. M. TOWARNICKY and E. P. SCHRAM. Inorg. Chim Acta. **41**, 55 (1980).
31. R. A. JONES, F. M. REAL, G. WILKINSON, A. M. R. GALAS, M. B. HURSTHOUSE, and K. M. A. MALIK. J. Chem. Soc. Dalton Trans. 511 (1980).
32. B. R. JAMES and D. K. W. WANG. *In* Fundamental research in homogeneous catalysis. Vol. 2. *Edited by* M. Tsutsui and Y. Ishii. Plenum Press, New York. 1978. p. 35.
33. G. ZOTTI, G. PILLONI, M. BRESSAN, and M. MARTELLI. J. Electroanal. Chem. **75**, 607 (1977).
34. B. C. HUI and B. R. JAMES. Can. J. Chem. **52**, 3760 (1974).
35. J. P. COLLMAN and L. S. HEGEDUS. Principles and applications of organotransition metal chemistry. University Science, Mill Valley, CA. 1980. Chapt. 6.
36. B. C. HUI and B. R. JAMES. Can. J. Chem. **52**, 348 (1974).
37. B. R. JAMES, A. D. RATTRAY, and D. K. W. WANG. J. Chem. Soc. Chem. Commun. 792 (1976).
38. (*a*) International Critical Tables. Vol. III. McGraw–Hill, New York. 1928. p. 262; (*b*) D. MAHAJAN. Ph.D. dissertation. University of British Columbia, 1979.

[4]Reference 9, p. 83.

Organo-transition metal clusters: rational approaches to synthesis, structure, fluxionality, and reactivity

MICHAEL J. MCGLINCHEY,[1] MICHAEL MLEKUZ, PETER BOUGEARD, AND BRIAN G. SAYER
Department of Chemistry, McMaster University, Hamilton, Ont., Canada L8S 4M1

ANGELA MARINETTI AND JEAN-YVES SAILLARD
Laboratoires de Chimie du Solide et Inorganique Moléculaire, ERA 477, Université de Rennes I, 35042 Rennes Cedex, France

AND

GÉRARD JAOUEN
École Nationale Supérieure de Chimie, Rue Pierre et Marie Curie, 75231 Paris Cedex 05, France

Received August 10, 1982

MICHAEL J. MCGLINCHEY, MICHAEL MLEKUZ, PETER BOUGEARD, BRIAN G. SAYER, ANGELA MARINETTI, JEAN-YVES SAILLARD, and GÉRARD JAOUEN. Can. J. Chem. **61**, 1319 (1983).

By using the isolobality principle, it is shown that the electronic structures of the 4- through 9-atom organo-transition metal clusters are closely analogous to the corresponding boranes. This parallelism is extended beyond simple structural similarities and is used to account for the high reactivity and nmr fluxionality of clusters which possess a vacant site on the polyhedral surface. Comparisons are also drawn with main group anionic and cationic clusters. Finally, it is shown that clusters containing gold atoms can, under certain circumstances, also follow the structural patterns of the boranes.

MICHAEL J. MCGLINCHEY, MICHAEL MLEKUZ, PETER BOUGEARD, BRIAN G. SAYER, ANGELA MARINETTI, JEAN-YVES SAILLARD et GÉRARD JAOUEN. Can. J. Chem. **61**, 1319 (1983).

Faisant appel au principle d'isolobalité, il est démontré que les structures électroniques des clusters organo-métalliques possédant de 4 à 9 atomes sont très analogues aux boranes correspondants. Ce parallèle est étendu au delà des similarités structurelles simples et est utilisé pour expliquer la haute réactivité et la fluxionalité en rmn des clusters qui possèdant un site vacant à la surface du polyèdre. On fait également des comparaisons avec des clusters anioniques et cationiques des éléments des groupes principaux. Finalement, il est montré que les clusters incluant des atomes d'or, peuvent dans certaines circonstances, avoir un comportement semblable à celui des boranes.

[Traduit par le journal]

Introduction

Practitioners of industrial catalysis generally prefer to use heterogeneous systems for efficiency and ease of product separation; in contrast, academics are more likely to study homogeneous systems containing only one or two metal atoms which, while sometimes not as effective catalytically, can be more easily studied so as to yield fine details of the mechanisms involved (1–3). Over the past several years a great deal of attention has focussed on metal clusters which may be viewed as a bridge between the intensively studied monometallic systems and the less well understood reactions occurring on surfaces (4). In particular, much activity has been directed towards the search for an efficient homogeneous Fischer-Tropsch catalyst. However, such efforts have thus far met with only limited success (5).

Early cluster syntheses were, to some extent, serendipitous and involved such procedures as pyrolysis of di- or tri-metallic species to produce polymetallic clusters in a relatively uncontrolled fashion (6, 7). Some early syntheses typifying this approach are shown in Scheme 1.

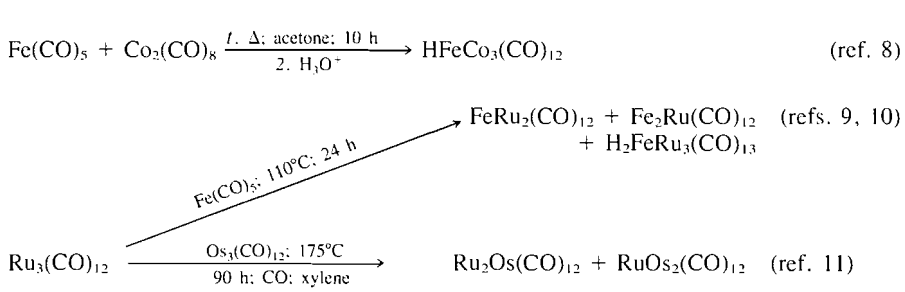

SCHEME 1

The pioneering syntheses of these mixed metal clusters prompted the search for other routes which avoided the forcing conditions previously used. Indeed, it was soon realised that treatment of the readily available simple metal carbonyls with metal carbonyl anions could lead to triangular, tetrahedral, or even trigonal bipyramidal clusters as shown in Scheme 2 (12, 13).

It had long been realised by organic chemists that the dimerisation of acetylenes might yield tetrahedrane but, even though the parent molecule C_4H_4 as yet remains elusive (18), the reac-

[1]To whom correspondence should be addressed.

Can. J. Chem. Downloaded from www.nrcresearchpress.com by 210.87.254.6 on 09/06/12
For personal use only.

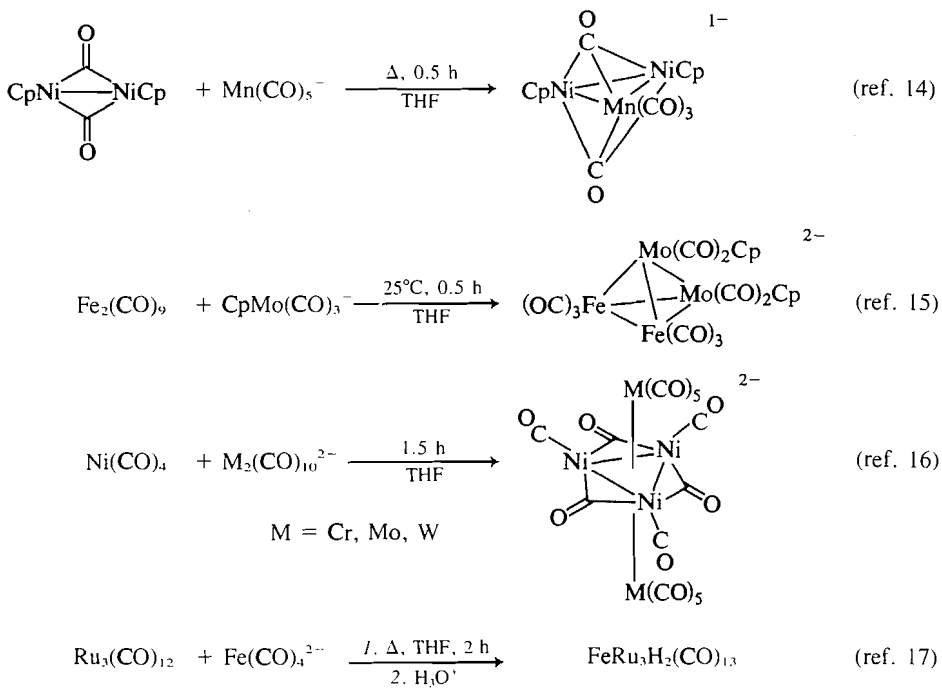

SCHEME 2

tion of alkynes with $Co_2(CO)_8$ to yield tetrahedral clusters of the type $R_2C_2Co_2(CO)_6$ was a well-established process (19) and indeed was even used to protect the alkyne linkage while another functional group in the molecule was being chemically modified (20, 21). It was, of course, realised that a metal–metal triple bond might be implicated and indeed the addition of alkynes to well-characterized metal–metal triple-bonded species provides an excellent route to a variety of tetrahedral systems (22). Scheme 3 contains several examples of this synthetic methodology in which a metal–metal multiple bond (either in an isolable molecule, or merely generated *in situ* by elimination of carbonyl groups) reacts with suitable addenda.

It has also been known for a number of years that $Co_2(CO)_8$ and $RCCl_3$ yield the tricobalt cluster complexes with a triple-bridging carbyne moiety (32), and speculation centred on the possible involvement of metal carbyne complexes, $L_nM{\equiv}CR$, which might behave analogously to alkynes. This idea has been

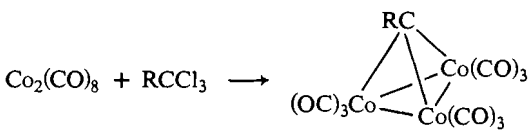

brilliantly exploited by Stone and colleagues (33, 34) who have characterised a tremendous variety of mixed clusters as typified by the sequences depicted in Scheme 4.

Stone's elegant work has placed this field on a firm foundation and currently provides the most logical routes to small clusters.

We next outline some underlying principles which rationalise these approaches to cluster synthesis and also account for the structures, fluxionality, and reactivity of many of these complexes. Finally, we describe some recent synthetic, structural, and spectroscopic results which support these assertions.

The Wade–Mingos bonding model

The realisation that transition metals in low oxidation states can use all nine ($1 \times s$, $3 \times p$, $5 \times d$) valence orbitals for bonding led to the widespread adoption of the "Effective Atomic Number" (E.A.N.) Rule (41). This concept has been remarkably successful in accounting for the behaviour of many catalytic intermediates, and the idea of 16-electron to 18-electron interconversions was very clearly expounded in a now classic review by Tolman (42). Thus, organo-transition metal complexes in which the central metal was assigned a 16-electron configuration could be regarded as coordinatively unsaturated; in contrast, a metal possessing an 18-electron configuration could not function as a catalytic centre without either losing or migrating a ligand or by decreasing the hapticity of a polyhapto substituent so as to generate a vacant site (43). Following this definition, complexes such as $(RC{\equiv}CR)Co_2(CO)_6$, whose structures are based on a tetrahedron, would be regarded (44) as being coordinatively saturated — a viewpoint which is belied by their surprisingly high reactivity even under mild reaction conditions. We shall return to this point presently.

Typical metal carbonyls such as **1** through **5** can all be assigned 18-electron configurations while the hexanuclear clusters **6** and **7** would, using the normal electron-counting formalism, place $18\frac{1}{3}$ electrons on each metal atom. That is, the octahedral clusters might be expected to have 84 valence elec-

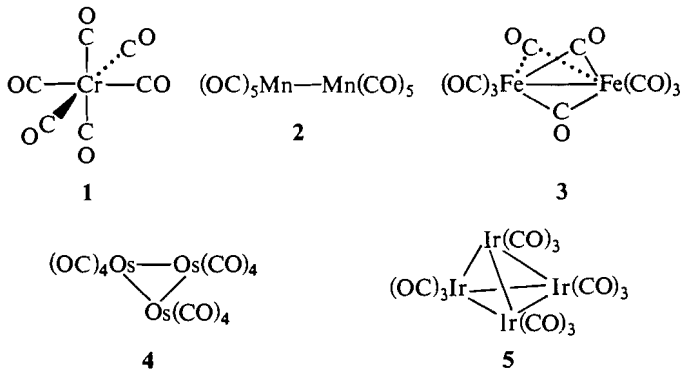

1 **2** **3**

4 **5**

Can. J. Chem. Downloaded from www.nrcresearchpress.com by 210.87.254.6 on 09/06/12
For personal use only.

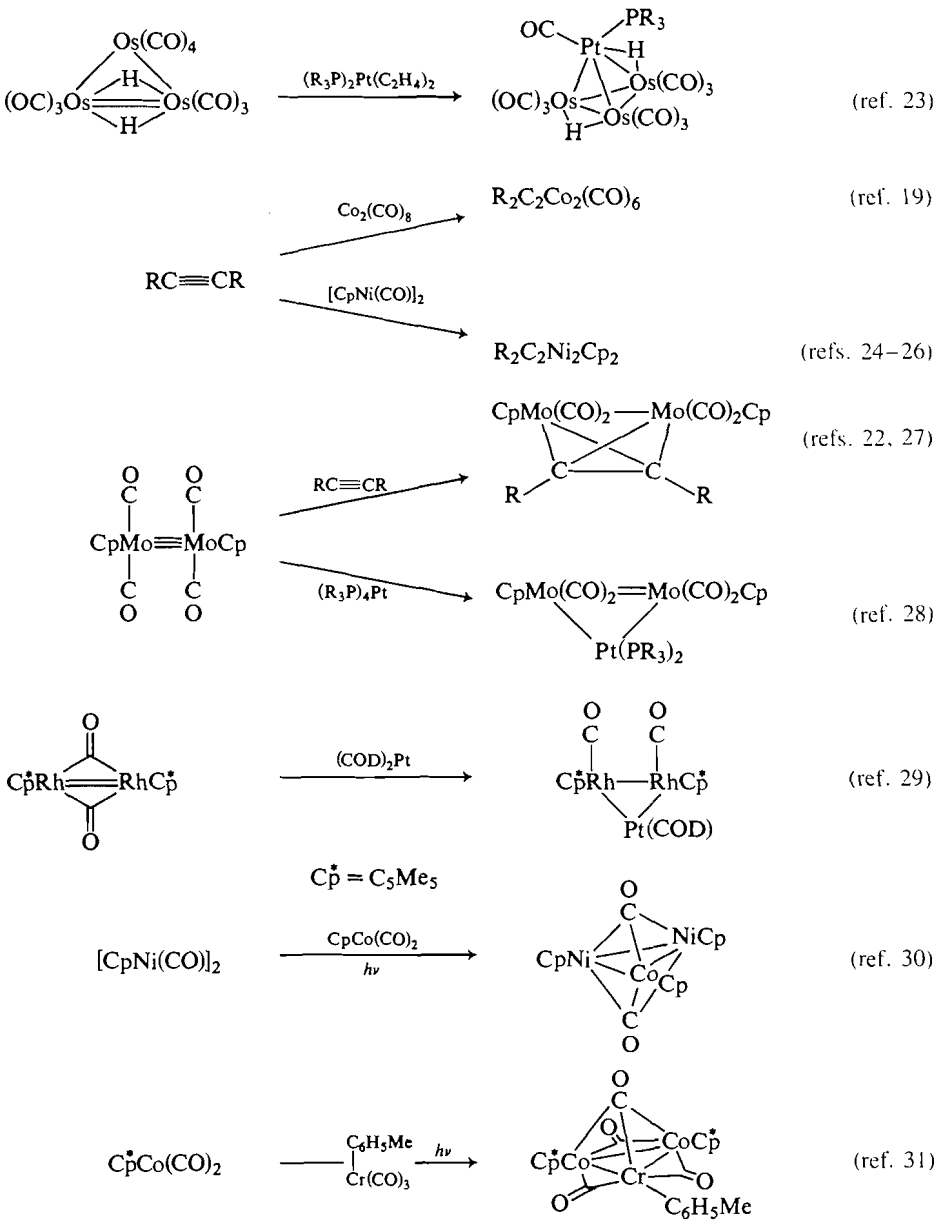

SCHEME 3

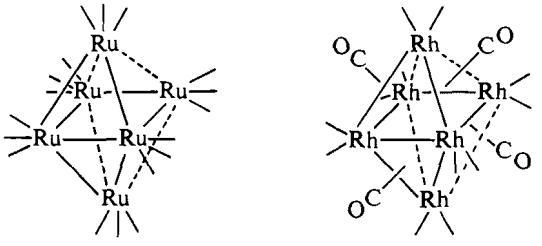

$Ru_6(CO)_{18}^{2-}$ **6**

$Rh_6(CO)_{16}$ **7**

trons (24 of them assigned to the 12 metal–metal bonds along the polyhedral edges) whereas in fact they have 86 valence electrons. In an apparent paradox, these seemingly *electron-rich* clusters may be conveniently rationalized as being *electron-deficient*.

We pause here a moment to clarify our nomenclature since much of one's thinking is based on the Lewis concept (45) of all bonded atoms being joined by at least one electron pair. Thus, in a system such as $B_6H_6^{2-}$ which has 26 valence electrons (12 of which are needed to form the six exo-skeletal B—H bonds) only 14 electrons, i.e., 7 electron pairs, are left with which to bond together the six borons in the cluster. Since the octahedron has 12 edges, 12 electron pairs would be required to bond the borons in a Lewis-type fashion; historically, this has been termed an electron-deficient molecule (46). Nevertheless, in molecular orbital terms no such problem exists since, from a basis set of sp_z, p_x, and p_y orbitals on each boron, one can readily construct an energy level scheme with seven strongly bonded orbitals (see Fig. 1) (47). King (48) has proposed that such systems be termed "globally delocalised" as opposed to "edge-localised". Hence, the octahedral cluster $B_6H_6^{2-}$ has seven skeletal electron pairs and is globally delocalised while the cluster C_8H_8 (cubane) has twelve skeletal electron pairs and is edge-localised.

Can. J. Chem. Downloaded from www.nrcresearchpress.com by 210.87.254.6 on 09/06/12
For personal use only.

Can. J. Chem. Downloaded from www.nrcresearchpress.com by 210.87.254.6 on 09/06/12
For personal use only.

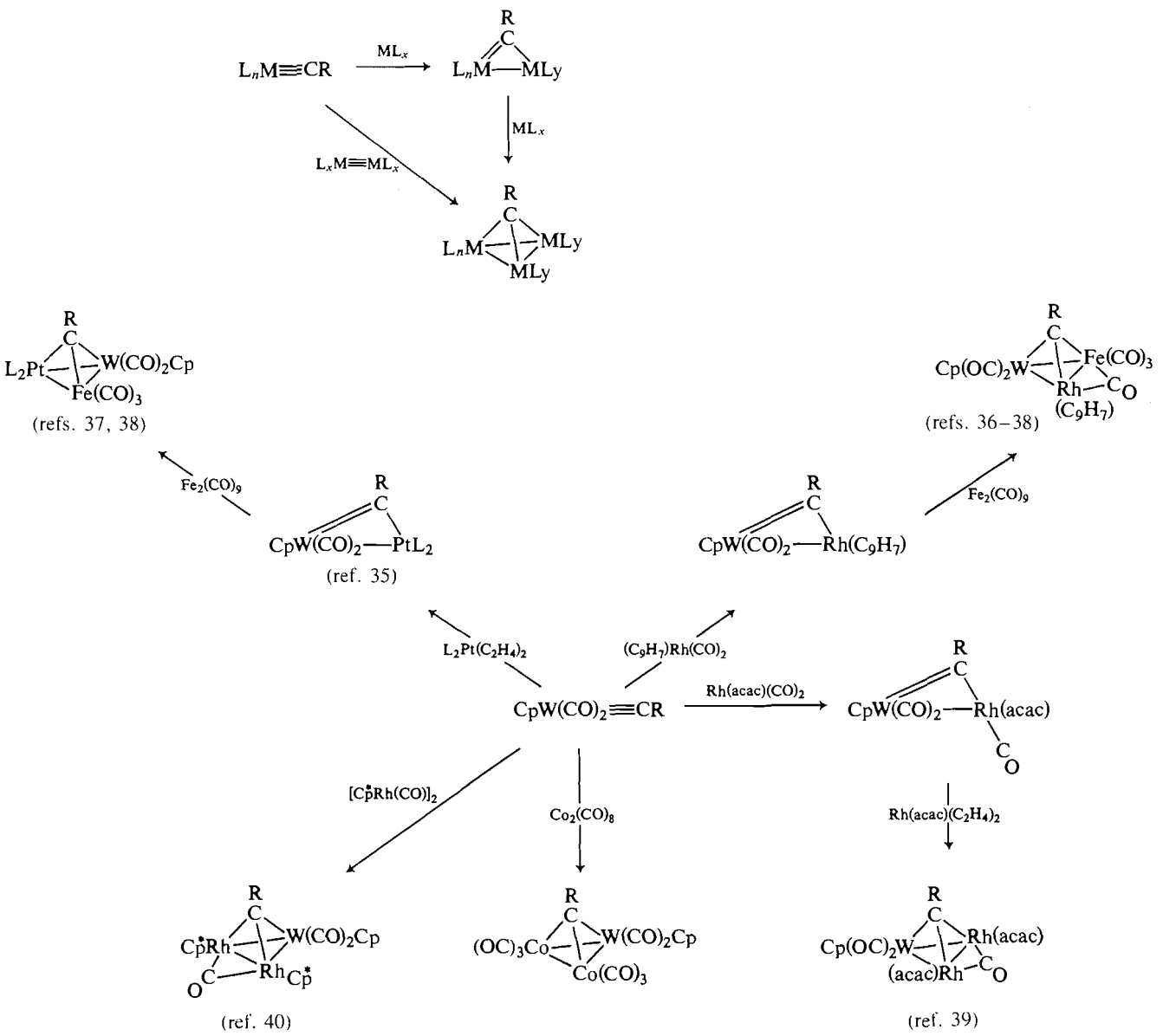

SCHEME 4

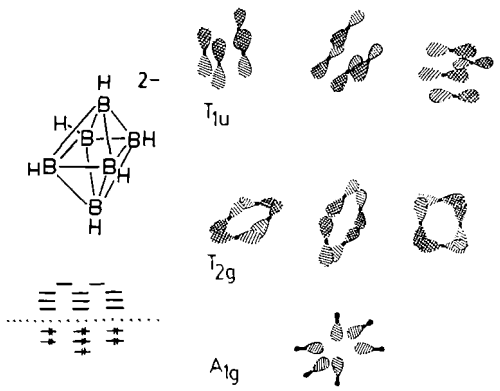

FIG. 1. The bonding molecular orbitals of $B_6H_6^{2-}$.

Returning to the case of $Ru_6(CO)_{18}^{2-}$, **6**, it has been shown in an important paper by Mingos (49) that a parallelism exists between the symmetry-adapted linear combinations of *p* and *sp*-hybridized orbitals of the boranes and those derivable from the *d* orbitals of metal carbonyl fragments. Several of these are shown in Fig. 2 and they provide a solid basis for the electron-counting schemes proposed by Wade (50) for boranes, carboranes, and transition metal clusters. The general conclusions which emerged from these considerations have a profound yet greatly simplifying effect on our view of clusters. The bonding in the six-vertex $B_6H_6^{2-}$ molecule is readily visualized as involving seven globally delocalised electron pairs. Indeed it has been shown (50, 51) that each of the $B_nH_n^{2-}$ systems gives rise to $n + 1$ bonding orbitals and some typical geometries and electron counts are shown in Fig. 3. As a corollary, one can invert this reasoning so as to state that a given number of skeletal electron pairs is associated with a particular molecular geometry. Typically, the clusters possessing 16 skeletal electrons are predicted to be based on the pentagonal bipyramid. This is indeed the case as exemplified by the boranes $B_7H_7^{2-}$, B_6H_{10} (≡ $B_6H_6^{4-}$) and B_5H_{11} (≡ $B_5H_5^{6-}$) shown in Fig. 4. These molecules may all be considered to be based on the same

Can. J. Chem. Downloaded from www.nrcresearchpress.com by 210.87.254.6 on 09/06/12
For personal use only.

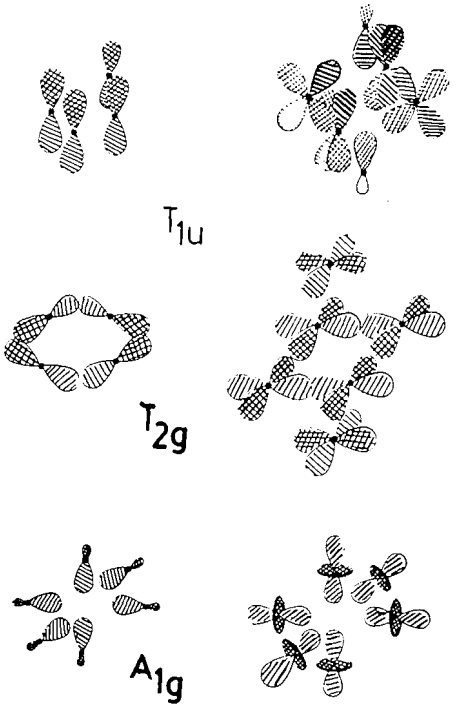

FIG. 2. Symmetry-adapted linear combinations of orbitals derived from BH and $M(CO)_3$ fragments.

deltahedron[2] but with zero, one, and two unoccupied vertices, respectively. These have been termed *closo* (closed cage), *nido* (nest), and *arachno* (cobweb) molecules, respectively; although the more open structures would imply that electron density is being positioned in regions of space not proximate to nuclei (a physically unrealistic circumstance (52)) such is not really the case since in the neutral boranes the open faces are stitched up by bridging protons as in **8**.

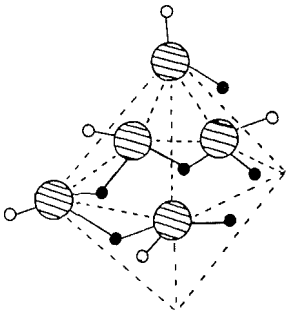

8

We can now clearly draw the parallel between the HB unit which presents three orbitals and two electrons and the $(OC)_3Fe$ moiety which likewise donates three orbitals and two electrons to the cluster (see Fig. 5). Of course, the HB unit is really a 4-electron system with two *exo*-skeletal electrons in the HB bond; the $(OC)_3Fe$ moiety is a 14-electron system which uses twelve *exo*-skeletal electrons to form a σ and a π bond between the metal and each of the three carbonyl ligands. Indeed, in several important papers by Fehlner (53, 54), the interchangeability of BH and $Fe(CO)_3$ moieties has been nicely

[2]A deltahedron is a convex polyhedron of maximum compactness, i.e., all the faces are triangular.

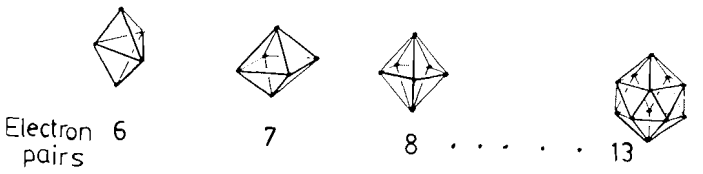

FIG. 3. Polyhedra corresponding to a particular number of skeletal electron pairs.

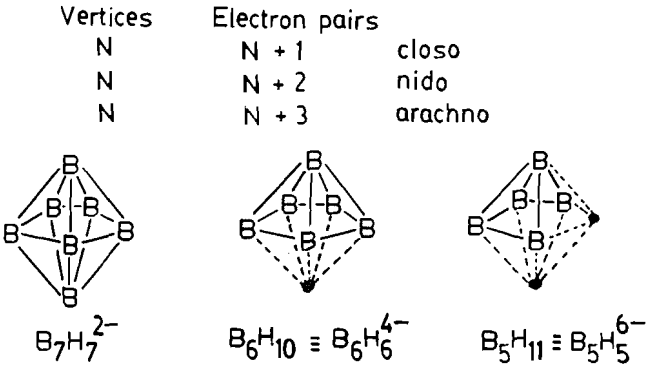

FIG. 4. Examples of boranes possessing eight skeletal electron pairs.

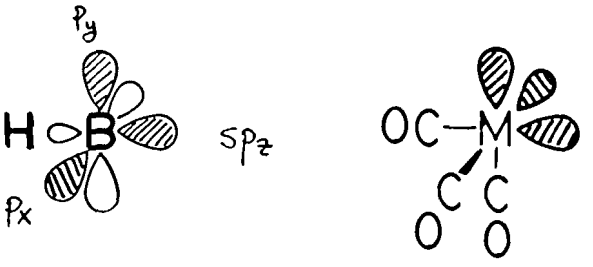

FIG. 5. The isolobal moieties BH and $M(CO)_3$.

exemplified. Thus, the series $B_nH_{n+4}(Fe(CO)_3)_{5-n}$ exists for $n = 5$, 4, and 3 and they adopt the square-based pyramidal (i.e., *nido*-octahedral) geometry as typified (55) by $B_4H_8Fe(CO)_3$):

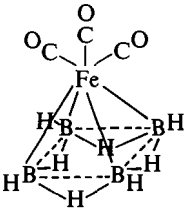

The situation in which chemically very different groups provide frontier orbitals of similar number, symmetry, extent in space, and energy has been skillfully exploited by Hoffmann (56, 57); thus one can regard the pentacarbonylmanganese and methyl radicals as being "isolobal" (58–60), each providing a single orbital containing one electron. Likewise, a parallel may be drawn between the tricarbonylcobalt moiety and the CH fragment which each provide three orbitals and three electrons to a cluster.

So, using these ideas developed by Wade (61, 62) and Mingos (63) one can classify cluster vertices as being *n*-electron donors to the cluster skeleton, as listed in Table 1.

Thus far we have for the most part summarized the ideas

TABLE 1. Some typical cluster vertices and their electron counts

Fragment	Total number of electrons	Number donated to cluster
HB	4	2
HC	5	3
$(OC)_3Cr$	12	0
$(OC)_3Fe$	14	2
$(OC)_3Co$	15	3
CpCo	14	2
CpNi	15	3
$CpMo(CO)_2$	15	3

TABLE 2. Electron counting in clusters

Cluster	Total valence electrons	=	*Exo*-skeletal electrons	+	Cluster electrons	
$B_6H_6^{2-}$	26		6×2		14	*closo*
$Ru_6(CO)_{18}^{2-}$	86		6×12		14	*closo*
$Rh_6(CO)_{16}$	86		6×12		14	*closo*
$Fe_5(CO)_{15}C^a$	74		5×12		14	*nido*
$Os_5(CO)_{15}^{2-}$	72		5×12		12	*closo*
$Co_4(CO)_{12}$	60		4×12		12	*nido*
$Fe_4(CO)_{13}^{2-}$	60		4×12		12	*nido*

"This molecule has a square-based pyramidal arrangement of $Fe(CO)_3$ groups with the carbon atom slightly displaced below the centre of the basal plane.

developed by others; there are two reasons for this. Firstly, the transition metal chemist with a primary interest in catalysis frequently has little time to follow the intricacies of borane chemistry and the different approaches to bonding and electron-counting which derive therefrom. Secondly, we shall show that these ideas are not restricted merely to a prediction of molecular geometry but can also be used to rationalise reactivity and molecular dynamics.

Fluxionality and reactivity in clusters

Table 2 shows the application of the Wade–Mingos theory to various clusters which are then categorised as being *closo*, *nido*, or *arachno* molecules.

Now tetrahedral clusters with twelve skeletal electrons can be viewed in two ways. One could regard them as having localised bonding with one electron pair along each of the six edges of the tetrahedron. Conversely, one might regard the six electron pairs as being delocalised and hence the molecule is formally a *nido* trigonal bipyramid. Of course, such a point of view may be a purely semantic difference but photoelectron data (64) on the $RCCo_3(CO)_9$ systems support the idea of electron delocalisation. Furthermore, in $Fe_4(CO)_{13}^{2-}$, **9**, the triply bridging carbonyl (65) seems to serve the same purpose as do bridging hydrogens in *nido*-boranes.

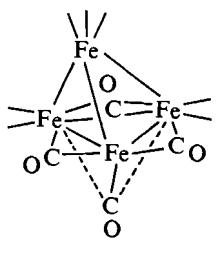

9

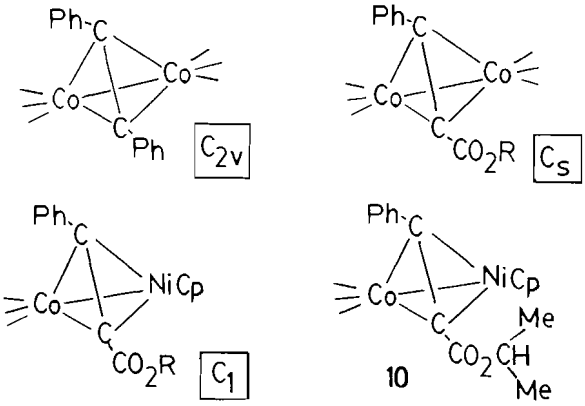

FIG. 6. Tetrahedral alkyne-bimetallic clusters.

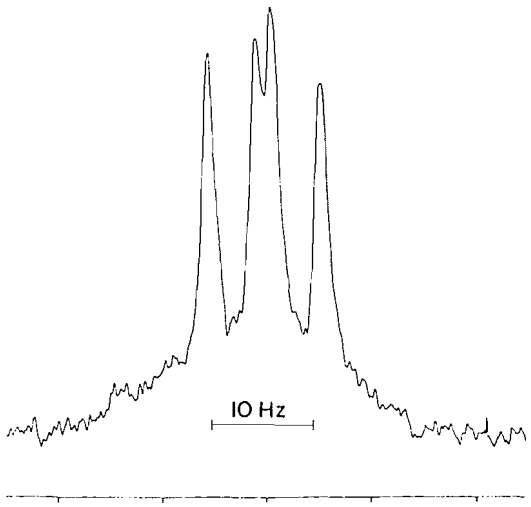

FIG. 7. 400 MHz ^1H nmr spectrum of **10**.

Now, if the tetrahedral clusters are viewed as *nido*-trigonal bipyramids they have a vacant coordination site on the surface of the polyhedron and may thus be regarded as being coordinatively unsaturated. The presence of a vacant site suggests that such clusters might be capable of reversibly coordinating suitable addenda and so may be of much higher reactivity than their formal 18-electron count would indicate. Furthermore, one could visualise that the vacancy might permit some structural flexibility with only a low activation energy barrier to rearrangement. A viable analogy may be drawn with SF_4 which in VSEPR terms is a trigonal bipyramid with a lone pair in an equatorial position (66). The detection of fluxionality in tetrahedral organotransition metal clusters is by no means a trivial undertaking although several previous studies (67, 68) had suggested that it might be possible. As shown in Fig. 6, one can systematically reduce the symmetry of the $(RC{\equiv}CR)Co_2(CO)_6$ (C_{2v}) to C_s by using an unsymmetrical alkyne and to C_1 by using two different metals as in $(RC{\equiv}CR')CpNiCo(CO)_3$ (69). This molecule is now chiral and so incorporation of an isopropyl group as in **10** provides a pair of diastereotopic methyl groups which can only be equilibrated via a process which racemises the chiral cluster.

Figure 7 shows the 400 MHz ^1H nmr spectrum of the isopropyl methyl groups of **10**. At room temperature interconversion of the diastereotopic methyls is slow on the nmr time scale and so each methyl appears as a doublet. At 100°C the peaks coalesce and the activation energy for the process is

Can. J. Chem. Downloaded from www.nrcresearchpress.com by 210.87.254.6 on 09/06/12
For personal use only.

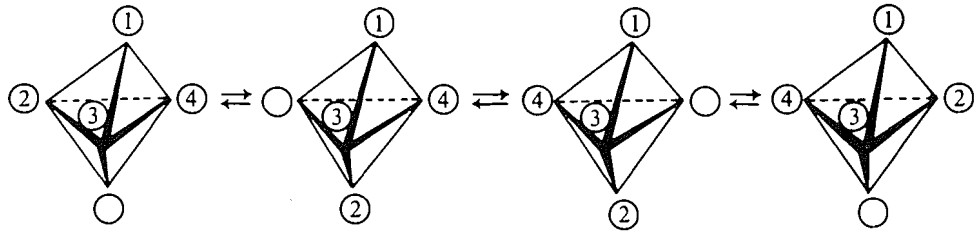

SCHEME 5

~21 kcal/mol. Hoffmann (70) has calculated a barrier of 20.5 kcal/mol for the tetrahedral–planar interconversion process shown below.

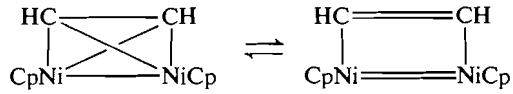

However, one could also visualise that racemisation might proceed via the mechanism in Scheme 5; this process would not involve scission of a formal bond, merely the migration of a cluster vertex into a vacant site on a surface. Nevertheless, more examples must be studied before a clear mechanistic understanding emerges.

This phenomenon of fluxionality of *vertices* is gradually gaining credence as more examples emerge; in contrast, fluxionality of peripheral *ligands*, such as carbonyls, which can migrate over cluster surfaces, is a well-established and widely-studied process (71). Nevertheless, Johnson has proposed (72, 73) that in molecules such as $Fe_3(CO)_{12}$ the fluxionality can be rationalised in terms of rotation of the metal triangle within a polyhedron of carbonyl groups. Indeed, solid state ^{13}C nmr studies by Hanson (74) and crystallographic data by Bruce (75) give some support to this proposal. Furthermore, a perusal of the literature reveals that fluxionality of vertices was observed some years ago but its potential generality was not appreciated.

Typically, in the molecule $(CpCo)_2C_4H_4$, the two CpCo groups are equilibrated at high temperature (76). We see now that this molecule can be classified as a *nido*-pentagonal bipyramid (eight skeletal electron pairs); its nmr fluxionality is now readily explicable — perhaps via the alternative *nido*-structure shown below:

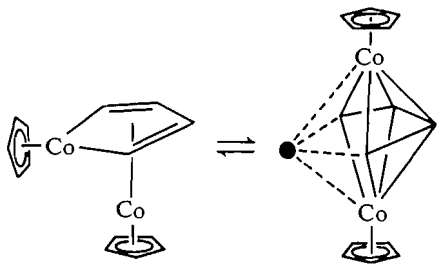

Analogous reasoning can be applied to the facile racemisation of Whiting's (77) ferro-ferradiene:

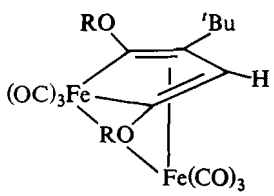

A particularly interesting reaction in this vein is that reported by Vollhardt (78), in which acetylenes and $CpCo(CO)_2$ react to furnish *closo*-clusters in which the two carbon atoms are no longer contiguous. One might speculate that in the initial product the carbon atoms are proximate but that rotation of a triangular face or reversible distortion to a square-based pyramid yields the thermodynamically favored isomer with two axial carbons; this structure also satisfies the requirements of eighteen electrons for cobalt and eight for carbon. (It has recently been suggested (79) that the rearrangement and acetylene-splitting may actually occur at the $Cp_3Co_3R_2C_2(CO)$ stage.)

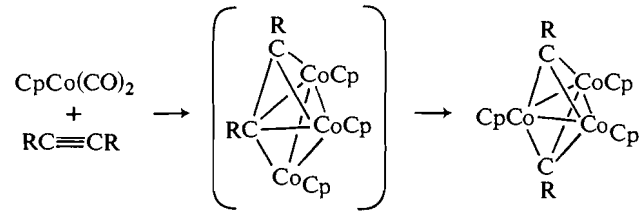

Of course, rearrangements of *closo*-clusters require much higher activation energies than do those of *nido*-clusters which possess a vacancy on the polyhedral surface; this is exemplified in the icosahedral carborane series, $C_2B_{10}H_{12}$ (80):

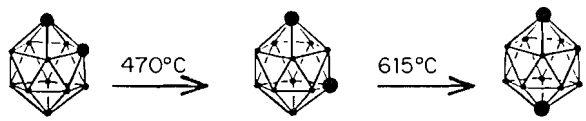

In keeping with this view, Geoffroy (81) has shown that a *closo*-transition metal cluster can rearrange but only on the (slow) chemical time-scale rather than the much faster nmr time-scale.

Another consequence of the vacant coordination site in a formally *nido*-cluster is the expectation of high reactivity. In accord with this prediction (82) the clusters **10** through **12**, when stirred with $Fe_2(CO)_9$ in refluxing tetrahydrofuran, undergo very facile addition of an $Fe(CO)_3$ moiety as shown in Scheme 6. The products **13** through **15** have been characterised crystallographically and, as befitting their fourteen skeletal electron count, they have the square-based pyramidal geometry appropriate for a *nido*-octahedral molecule. It is noticeable, however, that in **13** and **14** the $Fe(CO)_3$ unit caps the base which is comprised of the four original vertices; furthermore the electronic configuration at each atom follows the E.A.N. formalism. In contrast, in **15** the $CpMo(CO)_2$ moiety is the capping unit and the iron, nickel, and molybdenum atoms have 17-, 18-, and 19-electron counts, respectively. This difficulty is removed and the E.A.N. rule may be disregarded when we

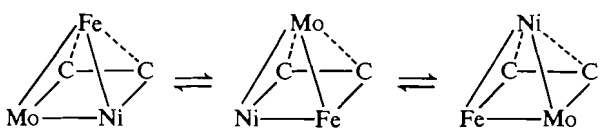

15*a* **15***b* **15***c*

Can. J. Chem. Downloaded from www.nrcresearchpress.com by 210.87.254.6 on 09/06/12
For personal use only.

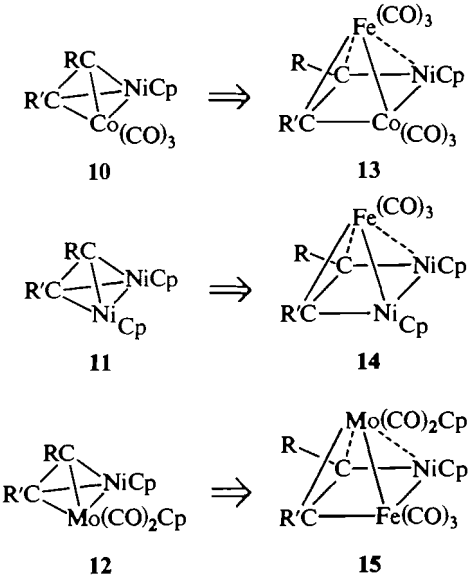

SCHEME 6

realise that the molecule has seven globally delocalised electron pairs. The particular orientation, **15***a*, *b*, or *c*, which occurs in the solid state should not particularly worry us since in solution the molecules **13** through **15** are fluxional. Typically, the variable-temperature ^{1}H nmr spectra of the cyclopentadienyl protons of **14** are shown in Fig. 8 and reveal a fluxional process with a barrier of 15 kcal/mol. Formally, one could view this rearrangement as a rotation of the alkyne moiety relative to the triangle of metal atoms. Such phenomena have been observed previously (83–88) and are usually interpreted in terms of the alkyne being σ-bonded to two atoms and π-bonded to a third. However, these are merely valence bond representations designed to satisfy the E.A.N. formalism and are unnecessary in the approach used here. Gratifyingly, other systems have been described (89) for which the 18-electron rule is inappropriate but which are well accommodated by the present model. A particularly nice example is provided by the molecule $Cp_2W_2Os(CO)_7R_2C_2$, **16**, recently studied by Stone (90); in this case the square-based pyramid (i.e., *nido*-octahedron) can have either osmium, **16***a*, or tungsten, **16***b*, as the capping atom and the crystallographic data show both rotamers to be present in the same crystal.

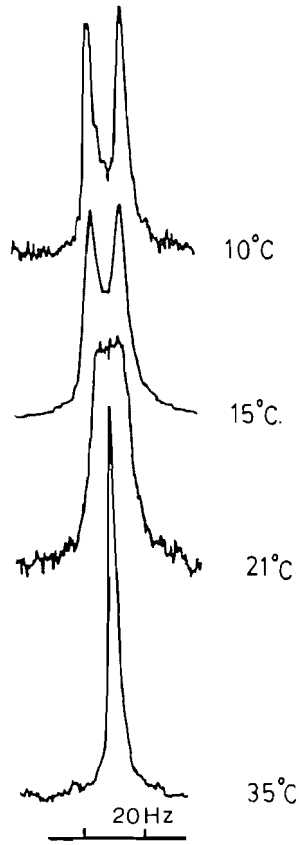

FIG. 8. Variable-temperature 80 MHz ^{1}H nmr spectra of the C_5H_5 protons of **14**.

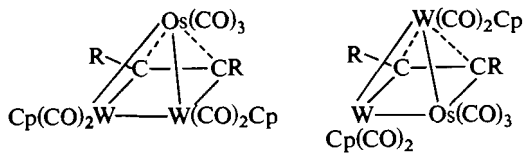

Expansion and substitution reactions in clusters

We can, therefore, summarise the reactivity patterns of *nido*-clusters by stating that they undergo addition reactions with 2-electron donors (e.g., $Fe(CO)_3$, $Os(CO)_3$, etc.) to produce the homologous *nido*-cluster with one more vertex. Scheme 7

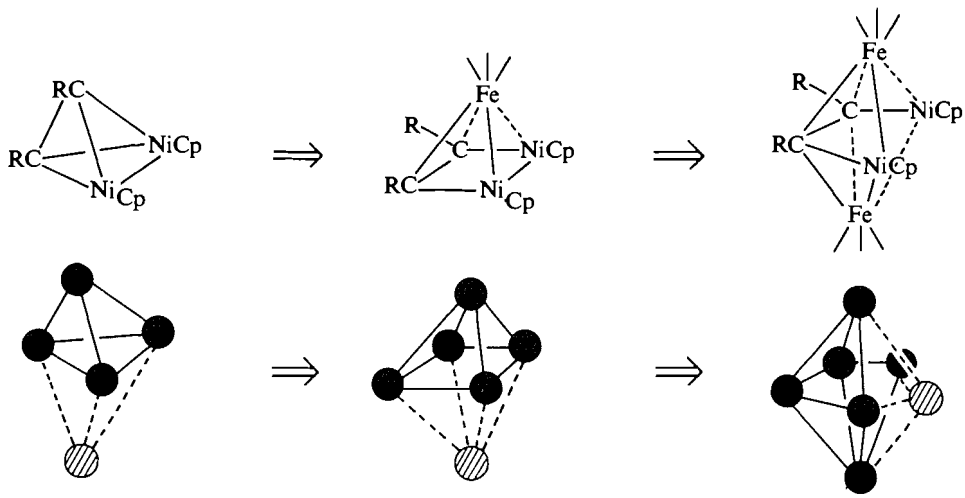

SCHEME 7

Can. J. Chem. Downloaded from www.nrcresearchpress.com by 210.87.254.6 on 09/06/12
For personal use only.

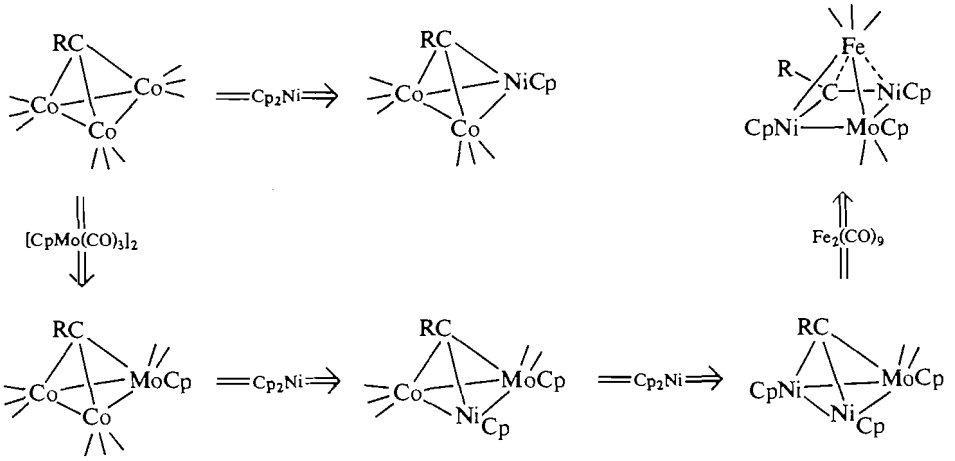

SCHEME 8

exemplifies this concept for the successive addition of $Fe(CO)_3$ moieties to the $(RC{\equiv}CR)Ni_2Cp_2$ molecule (82, 91).

We next consider the reactions of 3-electron donor reagents with *nido*-clusters. It is apparent that addition of such a moiety, such as CpNi or $CpMo(CO)_2$, would lead initially to expansion of the cluster giving the next highest *nido*-molecule. However, the extra electron must now reside in an orbital possessing some anti-bonding character and so would destabilise the cluster. Clearly elimination of the original or another 3-electron unit would regenerate a molecule of the original *nido*-geometry. The net result would be substitution of one 3-electron donor by another. Scheme 8 gives some of our synthetic results which support this assertion. Note that the final unit added is the 2-electron donor $Fe(CO)_3$ which, of course, results in cluster expansion. The elegant work of Vahrenkamp (92–94) is also entirely consistent with this picture.

It is also possible to rationalise other synthetic results within this framework. Thus, Geoffroy has replaced a $Co(CO)_3$ unit by the isolobal $Fe(CO)_3^-$ moiety in a tetrahedral cluster (95). Furthermore, recent Russian work (96) has described the addition of $Fe_2(CO)_9$ to a $CpMn(CO)_2$ ($RC{\equiv}CR'$) complex. Formally, one could regard the starting material as being a *nido* tetrahedron;[3] now successive addition of two $Fe(CO)_3$ units leads to the 14-skeltal electron species **17** which satisfies the criteria for a *nido*-octahedral complex. The isolobal analogy relates the first reaction to Stone's synthetic pathway exemplified in Scheme 4.

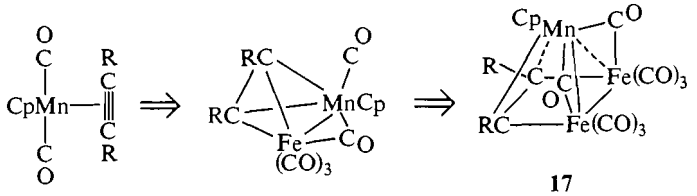

17

Now, in principle, it should be possible to cap a *nido* organo-transition metal cluster by the addition of a zero-electron donor such as $Cr(CO)_3$ or CpMn. Recently, Italian workers (97) have essentially achieved this goal in an indirect manner by adding a 13-electron unit (i.e., a 1-electron donor) and eliminating a hydrogen atom. Reaction of the cluster **18** with $[CpFe(CO)_2]_2$ provides a CpFe moiety to cap the open pentagonal face while loss of the bridging hydrogen atom leaves the skeletal electron

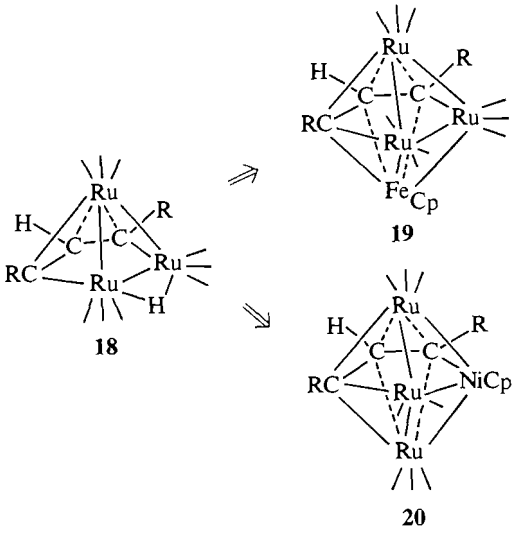

18 **19** **20**

count at 16 but now describable as a *closo* cluster, **19**. Analogously, treatment of **18** — with $[CpNi(CO)]_2$, a source of the 3-electron donor CpNi — leads to the *closo* cluster **20** with concomitant loss of CO and a hydrogen atom.

Epilogue

It is clear from the work of numerous laboratories that the analogy between the structures of boranes and transition metal clusters is an exceedingly useful one. There are, however, some limitations which must be recognized. Thus, the gradually accumulating data on large clusters, such as those obtained in the pioneering studies by Chini and colleagues (98), are more reminiscent of close-packed metal atoms surrounded by a surface coating of ligand than of borane analogues. Molecular orbital studies by Lauher (99) have analysed the changes involved in proceeding gradually from trimetallic systems to large multi-metallic clusters. Indeed, it is of interest to find out at what point the nature of cluster bonding begins to deviate from that rationalizable using the Wade–Mingos approach.

We have discussed already the dichotomy with tetrahedral molecules which could be regarded either as having six edge-localised skeletal electron pairs or six globally-delocalised electron pairs giving rise to a *nido*-trigonal bipyramid. For 5-, 6-, and 7-vertex clusters the borane analogy seems to hold up well but inevitably with large clusters the model will tend to break down as the central core becomes more like a close-packed metal fragment.

[3]The $CpMn(CO)_2$ unit is isolobal with CH_2 and so the starting material could also be regarded as being analogous to cyclopropene.

Can. J. Chem. Downloaded from www.nrcresearchpress.com by 210.87.254.6 on 09/06/12
For personal use only.

Can. J. Chem. Downloaded from www.nrcresearchpress.com by 210.87.254.6 on 09/06/12
For personal use only.

We note, however, that even a 9-vertex cluster can still behave according to the concepts described in this article. The cluster $[Rh_9P(CO)_{21}]^{2-}$, **21**, does not satisfy the E.A.N. rule but is well accounted for by the Wade–Mingos model. $[Rh_9P(CO)_{21}]^{2-}$ has 130 valence electrons and subtraction of 9 × 12 (= 108) electrons for the *exo*-skeletal ligands leaves 11 electron pairs for cluster bonding. We expect then that the molecule should adopt the shape of the 10-vertex deltahedron, viz., the bi-capped square antiprism, but with a vertex missing since this should be a *nido* molecule.

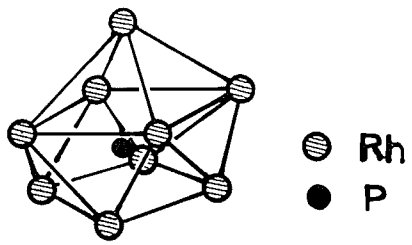

21

This structural prediction has been confirmed crystallographically (100) and, furthermore, our assertion that a *nido* molecule should be fluxional also has experimental support. In a very fine demonstration of the growing awareness of transition metal nmr spectroscopy, it has been shown by variable-temperature ^{103}Rh nmr that the molecule exhibits a 4:4:1 pattern of rhodium environments at low temperature but only a single line at room temperaure (101). Although no precise exchange mechanism has been elucidated for the Rh complex, we note the resemblance to another set of 9-vertex clusters, viz., Bi_9^{5+}, **22** and Sn_9^{4-}, **23** (102, 103).

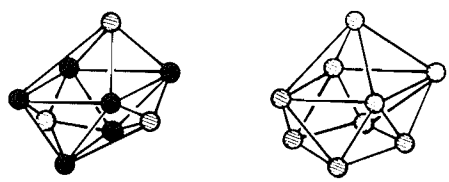

22 **23**

In **22** and **23** both clusters are classifiable as *nido* molecules[4] and it is known that the interconversion barrier for a monocapped square antiprism (C_{4v} symmetry) and the tricapped trigonal prism (D_{3h} symmetry) is rather low (103, 104). Indeed, Sn_9^{4-} has been shown to be fluxional using ^{119}Sn nmr spectroscopy (105); the analogy to the rhodium cluster **21** is thus readily apparent.

Finally, we turn to the fascinating question of the bonding modes available to the phosphine–gold moiety which has recently been incorporated into a number of systems. The simplest view of the R_3P—Au functionality is that it is isolobal with a hydrogen atom, that is, it provides a single orbital contributing only one electron to a cluster. This picture is given credence by recent work from the Lewis–Johnson group at Cambridge who have elucidated the structures of a series of Gp VIII metal clusters with phosphine–gold bridges (106, 107). Typically, in $Fe_5(CO)_{14}C(AuPPh_3)_2$, **24**, the molecule adopts essentially octahedral geometry and the 14 skeletal electron count requires only a single electron from each gold whether they be bridging or capping atoms. Similarly, Bruce (108) has developed a route to gold-containing clusters; for example, $HCoRu_3(CO)_{13}$ and $(Ph_3PAu)_3O^+$ react to give $CoRu_3(CO)_{12}(AuPPh_3)_3$, **25**, in which the Ph_3P—Au moieties have replaced bridging hydride and carbonyl units in the original cluster.

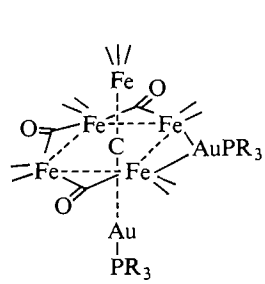

24

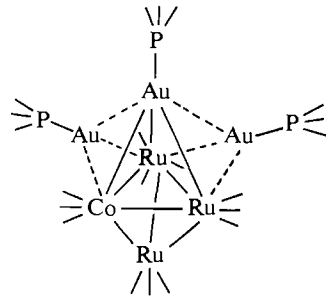

25

Nevertheless, other structures are extant in which this simple view is more problematical. Thus, Mingos (109) has pointed out that "although to a first approximation the $Au(PH_3)$ fragment can be considered to be isolobal with fragments such as CH_3, $Mn(CO)_5$, and $Co(CO)_4$ which have only a single frontier orbital available for bonding, it is necessary to also take into account the secondary contributions made by the $6p_x$ and $6p_y$ orbitals of gold". In spite of this, Mingos chose to describe $(Ph_3PAu)_3V(CO)_5$, **26** (110), as possessing only a single skeletal electron pair to hold together the tetrahedral cluster. However, if one were to regard the R_3P–Au unit as a three frontier orbital,[5] three-electron moiety (i.e., isolobal with CH) it can be more plausibly viewed as possessing 8 skeletal electrons, as follows: the $(R_3PAu)_3^+$ framework is an 8 electron unit isolobal with the cyclopropenium ion, $C_3H_3^+$; this can now be capped by $V(CO)_5^-$ which is isolobal with CH_3^+ (or CH_2 or CH^-) (57). In its simplest isolobal terms, $(R_3PAu)_3V(CO)_5$ corresponds to $C_4H_6^{2+}$, i.e., diprotonated tetrahedrane.

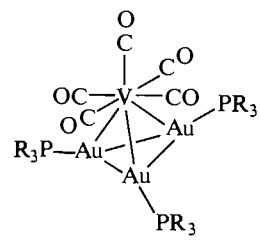

26

Indeed, to extend the analogy of gold clusters and boranes, one can consider the $Au_{11}(R_3P)_7I_3$ molecule which has a central gold atom (111). If the seven R_3P—Au fragments each contribute 3 skeletal electrons, the three Au—I vertices donate 2 skeletal electrons each and the central gold atom only 1 (i.e., it retains its d^{10} shell), we have 28 skeletal electrons and so the cluster should be based on the 13-vertex polyhedron. This polyhedron has been described by Lipscomb (112) and is produced by inserting a vertex of order 4 into any edge of the

[4]Each molecule has 40 valence electrons. Subtraction of an *exo*-skeletal lone pair for each of these main group atoms leaves 22 electrons for cluster bonding.

[5]These three orbitals are p_x, p_y, and the hybrid sd_{z^2}.

icosahedron, as in **27**. Now the Au_{11} complex must be a *hypho*-cluster and removal of three vertices yields the observed geometry **29**. However, the presence of the three iodide ligands gives the impression of threefold symmetry although, as the original authors have indicated (111), it is slightly distorted from idealised C_{3v} symmetry. One might venture a prediction that the analogous $(R_3P)_{10}Au_{11}^{3+}$ molecule would adopt the C_{2v} structure, **28**.

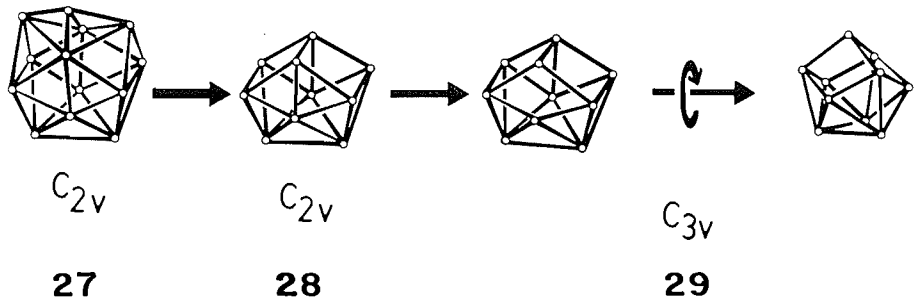

27 **28** **29**

Taking this analogy to its extreme, one could assign to the $(R_3P{-}Au)_6^{2+}$ molecule 16 skeletal electrons. We note that the geometry is not that of a regular octahedron but in fact the molecule is distorted along a threefold axis (113). This is somewhat reminiscent of XeF_6 (114) which in VSEPR terms (66) is an AX_6E case with two electrons too many for the regular octahedral structure.

To conclude, the current picture of metal clusters reveals that for a low nuclearity cluster with a high ligand-to-metal ratio the E.A.N. rule applies and we can assign each transition metal 18 electrons in localised bonds. As the ligand-to-metal ratio decreases we see a gradual increase in the delocalisation of electron density within the cluster framework; this behaviour parallels that observed in borane, carborane, and main group cluster chemistry. Finally, with even larger clusters of transition metal atoms, the regions of delocalised electron density are seen to merge almost into a conventional metallic structure in the centre of the cluster while the ligands merely coat the molecular periphery; the relationship to surface chemistry thus becomes more pronounced. A very nice example of the gradual transition from a cluster to a conventional metal is provided by the tetra-capped *closo*-octahedral cluster $Os_{10}C(CO)_{24}^{2-}$, for which the relationship to the face-centred cubic unit cell is readily apparent (115).

Acknowledgements

We thank N.S.E.R.C. (Canada) and C.N.R.S. (France) for financial support and Professor Roald Hoffmann for valuable discussions on isolobality. G.J. thanks the France–Canada Scientific Exchange Program for a Visiting Professorship.

1. J. P. COLLMAN and L. S. HEGEDUS. Principles and applications of organotransition metal chemistry. University Science Books, Mill Valley, CA. 1980. pp. 316–401.
2. B. R. JAMES. Homogeneous hydrogenation. John Wiley, New York. 1974.
3. G. PARSHALL. Homogeneous catalysis. Wiley–Interscience, New York. 1980.
4. V. W. DAY, M. F. FREDRICH. G. S. REDDY, A. J. SIVAK, W. R. PRETZER, and E. L. MUETTERTIES. J. Am. Chem. Soc. **99**, 8091 (1977) and references therein.
5. Ref. 1, pp. 434–452.
6. B. F. G. JOHNSON (*Editor*). Transition metal clusters. Wiley-Interscience, New York. 1980.
7. M. H. CHISHOLM and I. P. ROTHWELL. Progr. Inorg. Chem. **29**, 1 (1982).
8. P. CHINI, L. COLLI, and M. PERALDO. Gazz. Chim. Ital. **90**, 1005 (1960).
9. J. KNIGHT and M. J. MAYS. Chem. Ind. London, 1159 (1968).
10. D. B. W. YAWNEY and F. G. A. STONE. J. Chem. Soc. A, 502 (1968).
11. B. F. G. JOHNSON, R. D. JOHNSTON, J. LEWIS, I. G. WILLIAMS, and P. R. KILTY. J. Chem. Soc. Chem. Commun. 861 (1968).
12. G. L. GEOFFROY. Acc. Chem. Res. **13**, 469 (1980).
13. W. L. GLADFELTER and G. L. GEOFFROY. Adv. Organomet. Chem. **18**, 207 (1980).
14. A. T. T. HSIEH and J. KNIGHT. J. Organomet. Chem. **26**, 125 (1971).
15. A. T. HSIEH and M. J. MAYS. J. Organomet. Chem. **39**, 157 (1972).
16. J. K. RUFF, R. P. WHITE, JR., and L. F. DAHL. J. Am. Chem. Soc. **93**, 2159 (1971).
17. G. L. GEOFFROY and W. L. GLADFELTER. J. Am. Chem. Soc. **99**, 7565 (1977).
18. G. MAIER, S. PFRIEM, U. SCHÄFER, and R. MATUSCH. Angew. Chem. Int. Ed. Engl. **17**, 520 (1978).
19. H. W. STERNBERG, H. GREENFIELD, R. A. FRIEDEL, J. WOTIZ, R. MARKBY, and I. WENDER. J. Am. Chem. Soc. **76**, 1457 (1954).
20. D. SEYFERTH and A. T. WEHMAN. J. Am. Chem. Soc. **92**, 5520 (1970).
21. K. M. NICHOLAS and R. PETTIT. Tetrahedron Lett. 3475 (1971).
22. D. S. GINLEY, C. R. BROCK, and M. S. WRIGHTON. Inorg. Chim. Acta, **23**, 85 (1977).
23. L. J. FARRUGIA, J. A. K. HOWARD, P. MITRPRACHACHON, J. L. SPENCER, F. G. A. STONE, and P. WOODWARD. J. Chem. Soc. Chem. Commun. 260 (1978).
24. P. L. STANGHELLINI, R. ROSSETTI, O. GAMBINO, and G. CETINI. Inorg. Chim. Acta, **7**, 445 (1973).
25. E. ROSENBERG, E. W. RANDALL, L. MILONE, P. L. STANGHELLINI, and R. ROSSETTI. J. Organomet. Chem. **64**, 271 (1974).
26. P. L. STANGHELLINI and R. ROSSETTI. Inorg. Chim. Acta, **15**, 149 (1975).
27. W. I. BAILEY JR., M. H. CHISHOLM, F. A. COTTON, and L. A. RANKEL. J. Am. Chem. Soc. **100**, 5764 (1978).
28. M. D. CURTIS and R. J. KLINGLER. J. Organomet. Chem. **161**, 23 (1978).
29. M. GREEN, R. M. MILLS, G. N. PAIN, F. G. A. STONE, and P. WOODWARD. J. Chem. Soc. Dalton Trans. 1309 (1982).
30. L. R. BYERS, V. R. UCHTMAN, and L. F. DAHL. J. Am. Chem. Soc. **103**, 1942 (1981).
31. L. M. CIRJAK, J. S. HUANG, Z. H. ZHU, and L. F. DAHL. J. Am. Chem. Soc. **102**, 6623 (1980).
32. D. SEYFERTH. Adv. Organomet. Chem. **14**, 97 (1976).
33. F. G. A. STONE. Inorg. Chim. Acta, **50**, 33 (1981).
34. F. G. A. STONE. Acc. Chem. Res. **14**, 318 (1981).

Can. J. Chem. Downloaded from www.nrcresearchpress.com by 210.87.254.6 on 09/06/12
For personal use only.

Can. J. Chem. Downloaded from www.nrcresearchpress.com by 210.87.254.6 on 09/06/12
For personal use only.

35. T. V. ASHWORTH, J. A. K. HOWARD, and F. G. A. STONE. J. Chem. Soc. Dalton Trans. 1609 (1980).
36. M. J. CHETCUTI, M. GREEN, J. C. JEFFERY, F. G. A. STONE, and R. WILSON. J. Chem. Soc. Chem. Commun. 948 (1980).
37. M. J. CHETCUTI, M. GREEN, J. A. K. HOWARD, J. C. JEFFERY, R. M. MILLS, G. N. PAIN, S. J. PORTER, F. G. A. STONE, A. A. WILSON, and P. WOODWARD. J. Chem. Soc. Chem. Commun. 1057 (1980).
38. M. J. CHETCUTI, J. A. K. HOWARD, R. M. MILLS, F. G. A. STONE, and P. WOODWARD. J. Chem. Soc. Dalton Trans. 1757 (1982).
39. M. J. CHETCUTI, P. A. M. CHETCUTI, J. C. JEFFERY, R. M. MILLS, P. MITRPRACHACHON, S. J. PICKERING, F. G. A. STONE, and P. WOODWARD. J. Chem. Soc. Dalton Trans. 699 (1982).
40. M. GREEN, J. C. JEFFERY, S. J. PORTER, H. RAZAY, and F. G. A. STONE. J. Chem. Soc. Dalton Trans. 2475 (1982).
41. G. E. COATES, M. L. H. GREEN, and K. WADE. Organometallic compounds. Vol. 2. 3rd ed. The transition metals. Methuen. 1968.
42. C. A. TOLMAN. Chem. Soc. Rev. **1**, 337 (1972).
43. R. F. HECK. Organotransition metal chemistry: a mechanistic approach. Academic Press, New York. 1974.
44. E. L. MUETTERTIES, W. R. PRETZER, M. G. THOMAS, B. F. BEIER, D. L. THORN, V. W. DAY, and A. B. ANDERSON. J. Am. Chem. Soc. **101**, 2090 (1978).
45. G. N. LEWIS. J. Am. Chem. Soc. **38**, 762 (1916).
46. K. WADE. Electron deficient compounds. Nelson, London. 1971.
47. H. C. LONGUET-HIGGINS. Q. Rev. Chem. Soc. **11**, 121 (1957).
48. R. B. KING and D. H. ROUVRAY. J. Am. Chem. Soc. **99**, 7834 (1977).
49. D. M. P. MINGOS. J. Chem. Soc. Dalton Trans. 133 (1974).
50. K. WADE. Adv. Inorg. Chem. Radiochem. **18**, 1 (1976).
51. K. WADE. Chem. Brit. **11**, 177 (1975).
52. R. F. W. BADER, T. T. NGUYEN-DANG, and Y. TAL. Rep. Prog. Phys. **44**, 893 (1981).
53. K. J. HALLER, E. L. ANDERSEN, and T. P. FEHLNER. Inorg. Chem. **20**, 309 (1981).
54. C. E. HOUSECROFT and T. P. FEHLNER. Inorg. Chem. **21**, 1739 (1982) and references therein.
55. N. N. GREENWOOD, C. G. SAVORY, R. N. GRIMES, L. G. SNEDDON, A. DAVISON, and S. S. WREFORD. J. Chem. Soc. Chem. Commun. 718 (1974).
56. R. HOFFMANN. Science, **211**, 995 (1981).
57. R. HOFFMANN. Angew. Chem., Int. Ed. Engl. **21**, 711 (1982).
58. M. ELIAN and R. HOFFMANN. Inorg. Chem. **14**, 1058 (1975).
59. M. ELIAN, M. M. L. CHEN, D. M. P. MINGOS, and R. HOFFMANN. Inorg. Chem. **15**, 1148 (1976).
60. B. E. R. SCHILLING, R. HOFFMANN, and D. L. LICHTENBERGER. J. Am. Chem. Soc. **101**, 585 (1979).
61. K. WADE. *In* Transition metal clusters. *Edited by* B. F. G. Johnson. Wiley-Intersience, New York. 1980. pp. 193–264.
62. C. E. HOUSECROFT and K. WADE. Gazz. Chim. Ital. **110**, 87 (1980).
63. D. M. P. MINGOS. Adv. Organomet. Chem. **15**, 1 (1977).
64. S. F. XIANG, A. A. BAKKE, H. W. CHEN, C. J. EYERMANN, J. L. HOSKINS, T. H. LEE, D. SEYFERTH, H. P. WITHERS, and W. L. JOLLY. Organometallics, **1**, 699 (1982).
65. R. J. DOEDENS and L. F. DAHL. J. Am. Chem. Soc. **88**, 4847 (1966).
66. R. J. GILLESPIE. Molecular geometry. Van Nostrand Reinhold, London. 1972. p. 150.
67. R. S. DICKSON and G. N. PAIN. J. Chem. Soc. Chem. Commun. 277 (1979).
68. N. M. BOAG, M. GREEN, and F. G. A. STONE. J. Chem. Soc. Chem. Commun. 1281 (1980).
69. G. JAOUEN, A. MARINETTI, J-Y SAILLARD, B. G. SAYER, and M. J. MCGLINCHEY. Organometallics, **1**, 225 (1982).
70. R. HOFFMANN and D. HOFFMAN. Personal communication.
71. B. F. G. JOHNSON and R. E. BENFIELD. *In* Transition metal clusters. *Edited by* B. F. G. Johnson. Wiley-Interscience. New York. 1980. p. 471.
72. B. F. G. JOHNSON. J. Chem. Soc. Chem. Commun. 703 (1976).
73. B. F. G. JOHNSON and R. E. BENFIELD. J. Chem. Soc. Dalton Trans. 1554 (1978).
74. H. DORN, B. E. HANSON, and E. MOTELL. Inorg. Chim. Acta, **54**, L71 (1981).
75. M. I. BRUCE, B. K. NICHOLSON, and A. H. WHITE. J. Organomet. Chem. **240**, C33 (1982).
76. M. ROSENBLUM, B. NORTH, D. WELLS, and W. P. GIERING. J. Am. Chem. Soc. **94**, 1239 (1972).
77. R. CASE, E. R. H. JONES, N. V. SCHWARTZ, and M. C. WHITING. Proc. Chem. Soc. 256 (1962).
78. J. R. FRITCH and K. P. C. VOLLHARDT. Angew. Chem. Int. Ed. Engl. **19**, 559 (1980).
79. A. D. CLAUSS, J. R. SHAPLEY, C. N. WILKER, and R. HOFFMANN. Unpublished results communicated by Professor Hoffmann.
80. W. N. LIPSCOMB. Science, **153**, 373 (1966) and references therein.
81. J. R. FOX, W. L. GLADFELTER, G. L. GEOFFROY, I. TAVANAIEPOUR, S. ABDEL-MEQUID, and V. W. DAY. Inorg. Chem. **20**, 3230 (1981).
82. G. JAOUEN, A. MARINETTI, B. MENTZEN, R. MUTIN, J-Y. SAILLARD, B. G. SAYER, and M. J. MCGLINCHEY. Organometallics, **1**, 753 (1982).
83. J. EVANS. Adv. Organomet. Chem. **16**, 319 (1977).
84. J. EVANS, B. F. G. JOHNSON, J. LEWIS, and T. W. MATHESON. J. Organomet. Chem. **97**, C16 (1975).
85. A. J. DEEMING, R. E. KIMBER, and M. J. UNDERHILL. J. Chem. Soc. Dalton Trans. 2859 (1973).
86. L. J. TODD, J. R. WILKINSON, M. D. RAUSCH, and R. S. DICKSON. J. Organomet. Chem. **101**, 133 (1975).
87. A. J. DEEMING, I. P. ROTHWELL, M. B. HURSTHOUSE, and J. D. J. BACKER-DIRKS. J. Chem. Soc. Dalton Trans. 1879 (1981).
88. B. E. R. SCHILLING and R. HOFFMANN. Acta Chem. Scand. Ser. B, **33**, 231 (1979).
89. F. W. B. EINSTEIN, B. H. FREELAND, K. G. TYERS, D. SUTTON, and J. M. WATEROUS. J. Chem. Soc. Chem. Commun. 371 (1982).
90. L. BUSETTO, M. GREEN, J. A. K. HOWARD, B. HESSNER, J. C. JEFFERY, R. M. MILLS, F. G. A. STONE, and P. WOODWARD. J. Chem. Soc. Chem. Commun. 1101 (1981).
91. A. MARINETTI, E. SAPPA, A. TIRIPICCHIO, and M. CAMELLI-TIRIPICCHIO. Inorg. Chim. Acta, **44**, L183 (1980).
92. H. BEURICH and H. VAHRENKAMP. Angew. Chem. Int. Ed. Engl. **20**, 98 (1981).
93. H. VAHRENKAMP and E. J. WUCHERER. Angew. Chem. Int. Ed. Engl. **20**, 680 (1981).
94. F. RICHTER and H. VAHRENKAMP. Organometallics, **1**, 756 (1982) and references therein.
95. R. A. EPSTEIN, H. W. WITHERS, and G. L. GEOFFROY. Inorg. Chem. **18**, 942 (1979).
96. N. E. KOBOLOVA, L. L. IVANOV, O. S. ZHVANKO, A. S. BATSANOV, and YU. T. STRUCHKOV. J. Organomet. Chem. **231**, 37 (1982).
97. S. AIME and D. OSELLA. Inorg. Chim. Acta, **57**, 207 (1982).
98. P. CHINI. J. Organomet. Chem. **200**, 37 (1980).
99. J. W. LAUHER. J. Organomet. Chem. **213**, 25 (1981).
100. J. L. VIDAL, W. E. WALKER, R. L. PRUETT, and R. C. SHOENING. Inorg. Chem. **18**, 129 (1979).
101. O. A. GANSOW, D. S. GILL, F. J. BENNIS, J. R. HUTCHINSON, J. L. VIDAL, and R. C. SHOENING. J. Am. Chem. Soc. **102**, 2449 (1980).
102. R. M. FRIEDMAN and J. D. CORBETT. Inorg. Chem. **12**, 1134 (1973).
103. J. D. CORBETT and P. A. EDWARDS. J. Am. Chem. Soc. **99**,

3313 (1977).
104. R. C. BURNS, R. J. GILLESPIE, J. A. BARNES, and M. J. MCGLINCHEY. Inorg. Chem. **21**, 799 (1982).
105. R. W. RUDOLPH, W. L. WILSON, F. PARKER, R. CRAIG TAYLOR, and D. C. YOUNG. J. Am. Chem. Soc. **100**, 4629 (1978).
106. B. F. G. JOHNSON, D. A. KANER, J. LEWIS, P. R. RAITHBY, and M. J. TAYLOR. J. Chem. Soc. Chem. Commun. 314 (1982).
107. B. F. G. JOHNSON, D. A. KANER, J. LEWIS, and M. J. ROSALES. J. Organomet. Chem. **238**, C73 (1982) and references therein.
108. M. I. BRUCE and B. K. NICHOLSON. J. Chem. Soc. Chem. Commun. 1141 (1982).
109. D. G. EVANS and D. M. P. MINGOS. J. Organomet. Chem. **232**, 171 (1982).
110. J. E. ELLIS. J. Am. Chem. Soc. **103**, 6106 (1981).
111. P. BELLON, M. MANASSERO, and M. SANSONI. J. Chem. Soc. Dalton Trans. 1481 (1972).
112. L. D. BROWN and W. N. LIPSCOMB. Inorg. Chem. **16**, 2989 (1977).
113. P. L. BELLON, M. MANASSERO, L. NALDINI, and M. SANSONI. J. Chem. Soc. Chem. Commun. 1035 (1972).
114. L. S. BARTELL and R. M. GAVIN. J. Chem. Phys. **48**, 2470 (1968).
115. P. F. JACKSON, B. F. G. JOHNSON, J. LEWIS, W. J. H. NELSON, and M. MCPARTLIN. J. Chem. Soc. Dalton Trans. 2099 (1982).

Can. J. Chem. Downloaded from www.nrcresearchpress.com by 210.87.254.6 on 09/06/12
For personal use only.

Selective catalytic oxidation using hydrogen/oxygen mixtures with solutions of iridium and rhodium complexes

MARK T. ATLAY, MICHAEL PREECE, GIORGIO STRUKUL,[1] AND BRIAN R. JAMES[2]
Department of Chemistry, University of British Columbia, Vancouver, B.C., Canada V6T 1Y6

Received August 17, 1982

MARK T. ATLAY, MICHAEL PREECE, GIORGIO STRUKUL, and BRIAN R. JAMES. Can. J. Chem. **61**, 1332 (1983).

An iridium(III) hydride complex has been used in solution under a hydrogen/oxygen atmosphere at ambient temperatures to catalyze slowly the selective oxygenation of cyclooctene to cyclooctanone. The H_2 acts as a two-equivalent reducing agent in accepting the second oxygen atom of the O_2 molecule to generate water. The overall reaction shows similarities to catalytic oxygenation reactions performed by a class of P450 enzymes. Spectroscopic evidence for the iridium system indicates an oxygen atom transfer to the olefin via a hydroperoxide intermediate (IrOOH), formed by insertion of O_2 into the metal hydride bond; the hydride is thought to be regenerated, together with formation of water, by hydrogenolysis of the resulting iridium-hydroxo species. Catalytic hydrogenation of the monoene as well as hydrogenolysis of oxygen to water are observed as competing reactions. Some related rhodium systems do not give selective oxidation products.

MARK T. ATLAY, MICHAEL PREECE, GIORGIO STRUKUL et BRIAN R. JAMES. Can. J. Chem. **61**, 1332 (1983).

On a utilisé un complexe d'hydrure d'iridium(III) en solution sous atmosphère d'hydrogène/oxygène à la température ambiante pour catalyser lentement l'oxygénation sélective du cyclooctène en cyclooctanone. Le H_2 agit comme deux équivalents d'agent réducteur en acceptant le second atome d'oxygène de la molécule de O_2 pour produire de l'eau. La réaction globale montre des similitudes avec les réactions d'oxygénation catalytique réalisées par une classe d'enzymes P450. Les preuves spectroscopiques dans le cas du système iridium indiquent un transfert d'atome d'oxygène sur l'oléfine via un intermédiaire hydroperoxyde (IrOOH), formé par insertion de O_2 dans la liaison hydrure métallique. On pense que l'hydrure est regénéré de concert avec formation d'eau, par hydrogénolyse de l'espèce iridiumhydroxo résultant. On observe comme réaction de compétition une hydrogénation catalytique du monoène aussi bien qu'une hydrogénolyse de l'oxygène en eau. Quelques systèmes apparentés de rhodium ne donnent pas de produits d'oxydation sélective.

[Traduit par le journal]

Introduction

The chemical behaviour of O_2 after coordination, that is the activation of O_2, is a complex subject because of the many pathways available for O_2 reactions (1, 2). The search for more selective oxidations, especially using O_2, is a prime goal that has immense potential on an industrial scale (1–4), and is thus an important research area. The ultimate aim would be to mimic the O_2-activation properties of enzyme systems, for example, the ability of cytochrome P450 to catalyze the general reaction [1] of monooxygenases, where **S** can be a saturated or olefinic hydrocarbon (5–7). The preferred electron donor in the enzyme systems is the hydride of NADH.

$$[1] \quad \mathbf{S} + O_2 + 2c \xrightarrow{2H^+} \mathbf{SO} + H_2O \ (\mathbf{S} = \text{substrate})$$

The selective O_2-oxidation of olefins to ketones by a single oxygen atom transfer process catalyzed by rhodium complexes is well documented (7, 8); in some of these systems the second oxygen atom of the O_2 molecule is reduced concomitantly by a two-equivalent reducing agent (for example, added triphenylphosphine that is oxidized to the oxide (9), or two olefinic hydrogen atoms that are converted to water (8)), and analogies have been drawn to reaction [1].

An accidental finding in this laboratory over a decade ago (10) has led us to study the use of H_2 as the coreductant for monoxygenase-type activity. Heterolytic cleavage of the molecular hydrogen via a transition metal complex, reaction [2] (11, 12), can in principle furnish the hydride requirement of the metalloenzyme system.

$$[2] \quad M + H_2 \rightleftharpoons MH^- + H^+$$

Some aspects of the early studies (10) are presented here for they are important in terms of mechanistic considerations to be discussed later. While studying solvent effects on catalytic hydrogenation, we discovered a Rh(III)-catalyzed H_2 reduction of dimethylsulfoxide (DMSO) to the sulfide and water, and suggested a mechanism involving a hydrido-rhodium(III) intermediate containing a S-bonded sulfoxide (cf. reaction [2]). The reaction rates eventually decreased because of a buildup of inactive Rh(I), formed according to reaction [3], and stabilized by the dimethylsulfide produced.

$$[3] \quad HRh(III) \rightarrow H^+ + Rh(I)$$

In an attempt to maintain catalytic activity by reoxidation of the Rh(I), some O_2 gas was added to the H_2 atmosphere. This led to a surprising catalytic oxidation of the sulfoxide to the sulfone and water according to reaction [4] (10).

$$[4] \quad Me_2SO + O_2 + H_2 \ (\text{or } H^- + H^+) \rightarrow Me_2SO_2 + H_2O$$

Neither the Rh(III) nor Rh(I) species under O_2 alone performed the catalytic oxygenation of sulfoxide to sulfone, implying strongly that a rhodium hydride was the effective O_2 carrier. Trocha-Grimshaw and Henbest (13) also had found that isopropanol solutions of Rh(III) and Ir(III) salts carried out the same oxidation using just O_2, and such a medium is known to be effective for promoting formation of metal hydride species (14).

Our increasing interest in, and awareness of, P450 enzymes and some nonprotein model systems (15, 16), coupled with the earlier observations outlined above, encouraged us to test rhodium(III) and iridium(III) complexes as catalysts for the O_2 co-oxidation of olefins and molecular hydrogen. This paper

[1]On leave from Istituto di Chimica Generale, Universita di Venezia, Calle Larga S. Marta, 30123 Venezia, Italy.

[2]To whom all correspondence should be addressed.

Can. J. Chem. Downloaded from www.nrcresearchpress.com by 210.87.254.40 on 09/06/12
For personal use only.

Can. J. Chem. Downloaded from www.nrcresearchpress.com by 210.87.254.40 on 09/06/12
For personal use only.

reports on the successful catalytic oxidation of cyclooctene to cyclooctanone according to reaction [5], using the 1,5-cyclooctadiene (cod) dimer, $[IrHCl_2(C_8H_{12})]_2$ (17).

[5] $C_8H_{14} + O_2 + H_2 \rightarrow C_8H_{14}O + H_2O$

A communication on some of the work described here has been published previously (18).

Experimental

The iridium and rhodium were obtained mainly from Johnson Matthey Ltd. as hydrated trichlorides containing 51.76% and 41.37% of the metal, respectively, while $RhBr_3 \cdot 2H_2O$ was a Platinum Chemicals product. The dimeric 1,5-cyclooctadiene (cod) and cyclooctene complexes $[IrHCl_2(C_8H_{12})]_2$, $[MCl(C_8H_{12})]_2$, and $[MCl(C_8H_{14})_2]_2$ (M = Ir, Rh) were prepared according to literature procedures (17, 19–21). The complexes $IrHCl_2(DMSO)_3$ (22) and $RhCl_3(DMSO)_3$ (23) with meridional dimethylsulfoxide ligands were also synthesized via published methods. 1,5-Cyclooctadiene, cyclooctene, cyclooctanone, and other organic compounds (Aldrich) were distilled or recrystallized before use; peroxide impurities in liquid olefins were removed by passage through an alumina column under N_2. Professor C. B. Anderson kindly provided a sample of 4-cyclooctene-1-one.

Other materials used and the procedure used for following gas-uptake at constant pressure have been described previously (24); the metal complexes could be added if necessary from a glass bucket held over the substrate solutions via use of side-arms on the reaction vessel. N,N′-Dimethylacetamide (DMA) was stirred with CaH_2 overnight and then vacuum-distilled. A convenient way of adding HCl quantitatively was in the form of the solid dimethylacetamide adduct DMA·HCl, that is readily made by bubbling HCl gas through the amide solvent (25).[3] Matheson O_2 and H_2 (99.99% grade) were used as such.

Organic products were identified by gc and ms; OV-101/chromasorb and Porapak Q were the gc column materials for the organic products and water, respectively, using 2-bromomesitylene and methanol as internal standards.

Results and discussion

Of a range of systems tested for selective oxidation of olefins (see below), the most interesting proved to be one based on iridium. Although the catalysis, the selective conversion of cyclooctene to cyclooctanone, is very slow and inefficient, it has allowed for some mechanistic studies that demonstrate, for the first time, oxygen atom transfer to an olefin from a metal hydroperoxide intermediate.

Dimethylacetamide solutions of $[IrHCl_2(C_8H_{12})]_2$ (**I**) (0.01–0.03 *M*) in the presence of at least a ten-fold excess of cyclooctene and a five-fold excess of HCl (added as DMA·HCl) absorb gas from hydrogen/oxygen mixtures at a total pressure of 1 atm and temperatures between 5–30°C to generate catalytically cyclooctanone and water as products (reaction [5]). At 5°C with 350 Torr of each gas, the turnover for cyclooctanone per iridium is about two per day based on week-long experiments. Gas-uptake measurements, that usually provide a convenient method for studying the kinetics and stoichiometry of such homogeneous catalytic reactions, proved to be of little value in studying reaction [5], because it is accompanied by a competing catalytic hydrogenolysis of the oxygen:

[6] $2H_2 + O_2 \rightarrow 2H_2O$

[3] Details on this adduct will be published later; a crystal structure reveals protonation at the oxygen atom and essential planarity at the carbonyl carbon atom [$-C(O^-)=N^+<$].

The net gas uptake is very much greater than that expected for the stoichiometry of reaction [5], as determined by the concentration of cyclooctanone (the sole organic product seen by gc). Indeed, the gas-uptake stoichiometry corresponds within experimental error to that expected for reaction [6], because the H_2O:cyclooctanone ratio at the early stages of the reaction (5°C, 350 Torr H_2, 350 Torr O_2) was about 40 and decreased to a steady value of about 10 after one day. At 30°C, the initial rate of formation of cyclooctanone is higher, but the overall turnover number after a few days is much the same as that noted at 5°C; the oxygen hydrogenolysis reaction, however, is now even more dominant and the H_2O:cyclooctanone ratio remains at about 50.

Most important observations are that radical inhibitors have no inhibitory effect on the oxidation, and that in the absence of H_2 (at 1 atm O_2, 5°C) no oxygenation of cyclooctene occurs at all. The non-selective oxidation of cyclic olefins to mixtures of epoxide, ene-one, and ene-ol (reaction [7]) via a metal-catalyzed free-radical autoxidation reaction is well-documented for iridium(I) (and rhodium(I)) complexes (1, 2, 7); the complexes initiate the reaction by decomposing an enyl hydroperoxide (reactions [8], [9]), formed *in situ* by attack of O_2 on the radical produced by allylic hydrogen abstraction (reaction [7]).

[7] 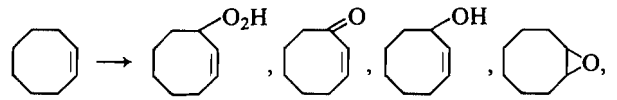

etc.

[8] $M^{n+} + ROOH \rightarrow M^{(n+1)+} + RO^{\cdot} + OH^-$

[9] $M^{(n+1)+} + ROOH \rightarrow M^{n+} + RO_2^{\cdot} + H^+$

A possible role of the H_2, reduction of the iridium(III) to iridium(I) that then initiates the oxidation (reactions [7]–[9]), is ruled out by the radical addition experiments and the product selectivity observed.

Evidence for a plausible mechanism for the oxidation comes from reaction of the hydride dimer **I** with oxygen, but before discussing this reaction it is necessary to consider the nature of **I** in solution. The dimer dissolves only in polar aprotic solvents of high donor number (26), and the solvated monomeric species $IrHCl_2(C_8H_{12})$(DMA), **II**, is considered to be present in dimethylacetamide solution (λ_{max} 395 nm, ϵ = 1480 M^{-1} cm^{-1}); the same solvated species is formed by addition of DMA·HCl to DMA solutions of $[IrCl(C_8H_{12})]_2$ and we have established the existence of equilibrium [10] by spectrophotometry.

[10] $IrCl(C_8H_{12})(DMA) + HCl \overset{K}{\rightleftharpoons} IrHCl_2(C_8H_{12})(DMA)$
III **II**

The $[IrCl(C_8H_{12})]_2$ complex remains as a dimer in toluene solution as evidenced by molecular weight data (19), and spectrophotometric data (λ_{max}(toluene) 454 nm, ϵ = 3600 M^{-1} cm^{-1}; λ_{max} (Nujol) 454 nm), but a quite different spectrum in DMA (λ_{max} 395 nm, ϵ = 1250 M^{-1} cm^{-1}) is again attributed to a solvated monomer **III**. Although the uv/vis spectra of **II** and **III** are remarkably similar (presumably, the common 395 nm maximum is associated with a charge transfer process involving the DMA ligand), there is a sufficient difference in the extinction coefficients to approximately estimate *K* for equilibrium [10] by a standard spectrophotometric titration pro-

Can. J. Chem. Downloaded from www.nrcresearchpress.com by 210.87.254.40 on 09/06/12
For personal use only.

cedure. Knowledge of this value, about 10^4 M^{-1} at ambient temperatures, is important for it is necessary to maintain the hydride species in solution for effective catalysis of reaction [5]. The iridium(I) species **III** is not effective for the catalytic oxidation using a H_2/O_2 atmosphere, and indeed at 1 : 1 gaseous mixtures the solution tends to precipitate metal; reaction of the cyclooctene dimer $[IrCl(C_8H_{14})_2]_2$ with H_2 in DMA to give metal has been noted previously (27). One role of the excess acid in the successful catalysis using **II** is undoubtedly to shift equilibrium [10] to the right. The basicity of the DMA solvent promotes reductive elimination of HCl from **II**; Winkhaus and Singer (28) have reported on the oxidative addition of HCl to the $[IrCl(C_8H_{12})]_2$ dimer in chloroform solution with resulting precipitation of $[IrHCl_2(C_8H_{12})]_2$.

DMA solutions of **II** (1.0–5.0) 10^{-2} M at 5°C containing an equal concentration of DMA·HCl absorb 1.0 mol of O_2 per iridium at oxygen pressures from 0.3–1.0 atm, but no free oxygenated organic compound is detected. A suspension of the hydride dimer I in CH_2Cl_2 at 20°C similarly absorbs O_2 to a 1 : 1 ratio to give a deep red solution that is conveniently monitored by ir. During the dissolution process (about 20 min), the ν(Ir—H) band (at 2260 cm^{-1} in the solid) is replaced by a strong band at 3495 cm^{-1}, considered to be the ν(O—H) of hydroperoxide (29). This band decreases in intensity and disappears with time as new bands grow in at 3680 and 3605 cm^{-1} (attributed to ν(O—H) of hydroxide), and at 1692 and 1607 cm^{-1} (attributed to ν(C—O) of free (30) and coordinated 4-cyclooctene-1-one, respectively). Addition of excess triphenylphosphine replaces the coordinated ketone which is accompanied by a corresponding decrease of the 1607 cm^{-1} band. The gas uptake stoichiometry, together with the ir data, are consistent with reaction [11] written for a monomer, and showing oxygen-atom transfer to the diene from an iridium hydroperoxide intermediate.

$$[11]\quad IrHCl_2(C_8H_{12}) \xrightarrow{O_2} Ir(OOH)Cl_2(C_8H_{12}) \rightarrow \text{“}Ir(OH)Cl_2\text{”} + C_8H_{12}O$$

Figure 1 shows changes in the 3500 cm^{-1} region as a function of time following the dissolution process; the isosbestic points are considered to arise from the constant total iridium concentration of hydroperoxide and hydroxide. Insertion of O_2 into metal hydride bonds is known for $RhH(NH_3)_5^{2+}$ (31), *trans*-$RhH(OH)(en)_2^+$ (32), and $RhH(CN)_4(H_2O)^{2-}$ (33); the presence of only ligands relatively insensitive to oxidation presumably accounts for isolation of the hydroperoxides.

The inorganic iridium product of reaction [11] has not been characterized, although after the triphenylphosphine treatment, the iridium was recovered as $IrCl(PPh_3)_3$ (34), while the phosphine oxide is indicated by the presence of a strong ir band at 1200 cm^{-1} in solid residues (35); these data provide further indirect evidence for a hydroxoiridium(III) product, reaction [12].

$$[12]\quad \text{“}Ir(OH)Cl_2\text{”} + PPh_3 \rightarrow \text{“}IrCl\text{”} + OPPh_3 + HCl$$
$$\downarrow\ 3PPh_3$$
$$IrCl(PPh_3)_3$$

Such a stoichiometric two-electron reduction using tertiary phosphines in the presence of hydroxide has been demonstrated for a platinum(IV) → platinum(II) process (36).

A metal-catalyzed oxygen-atom transfer, such as that outlined in reaction [11], has been postulated (7, 8, 29), but not previously demonstrated, although transfer from alkyl peroxides (M—OOR) is well-documented, and is usually considered to go via pseudo five-membered peroxometallocyclic intermediates (2, 8, 37). A closely similar pathway for the transfer from the hydroperoxide is suggested in equation [13].

[13] 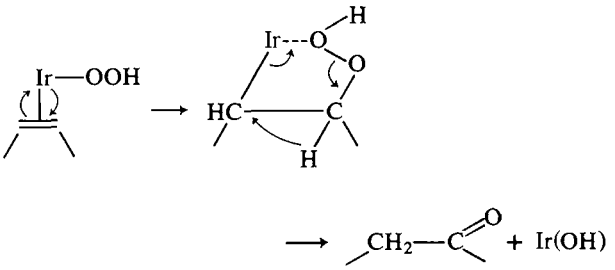

Mimoun (8) has proposed that the nature of the products that result from decomposition of the peroxometallocycle depends on the electrophilicity of the metal and the nature of the substrate. Epoxides are formed with highly electrophilic systems such as Mo(VI) that orient the electron transfer from the O—O bond towards the alkyl carbon atom; the less electrophilic rhodium(III), and therefore iridium(III), are considered to direct the electron transfer towards the β-carbon atom, hydride transfer from which yields the ketone, as illustrated in equation [13].

Some further indirect evidence for the role of the hydride ligand in reaction [11] is that treatment of the nonhydridic iridium(I) dimer $[IrCl(C_8H_{12})_2]_2$ with dioxygen does not give any ene-one or other characterizable oxidation product. Bonnaire and Fougeroux (38) first reported on reaction of the dimer with *air* in dichloromethane or benzene and suggested formation of a hydroxo-iridium species with the diene still coordinated, while Louw and Hepner (39) noted that such dimer solutions were stable toward oxygen. Our findings are contrary to the latter workers. As a dimer in benzene or toluene solutions or as a solvated monomer in DMA, the iridium(I)-cod species is sensitive to O_2. The extent of O_2 absorption at 5°C is about 0.65 mol O_2 per iridium. A mixture of yellow and brown iridium-containing solids, as yet uncharacterized, has been isolated from the solutions; elemental analyses and ir data are variable but indicate the presence of coordinated water and a C_8 fragment (40). Further studies on the $[IrCl(C_8H_{12})_2]_2/O_2$ system are in progress.

The 4-cyclooctene-1-one product of reaction [11] is detected also in the catalytic cyclooctene oxygenation described above; presumably removal of the diene by reaction [11] provides vacant or solvated sites for subsequent coordination of the monoene. The catalysis requires regeneration of the hydride from the “$Ir(OH)Cl_2$” species, and this could involve a net heterolytic splitting of H_2 by such an iridium(III) species, either before (step *a*) or after (step *b*) a protonation step, reaction [14].

$$[14]\quad Ir(OH)Cl_2 + H_2 \xrightarrow[-H_2O]{a} IrHCl_2 \overset{d}{\rightleftharpoons} IrCl + HCl$$
$$H^+ \swarrow\!\!\!\swarrow\ b \qquad -H^+ \nearrow\!\!\!\nearrow\ +H_2,\ c$$
$$Ir(H_2O)Cl_2$$

A step such as *a* is normally favoured since the released proton in heterolytic cleavage of H_2 is often stabilized by the leaving nucleophilic ligand (11, 12), in this case, hydroxide; however,

Can. J. Chem. Downloaded from www.nrcresearchpress.com by 210.87.254.40 on 09/06/12
For personal use only.

in the acid conditions used, the *b* equilibrium would be very much favoured towards the aquo species. The cyclooctene would then have to coordinate prior to hydride formation, that is, to the "$Ir(OH)Cl_2$" species, or to the hydride, to generate a monoene or possibly bis(monoene) intermediate corresponding to **II**. A further possible pathway to such an intermediate is reduction of the "$Ir(OH)Cl_2$" by H_2 to generate iridium(I), steps *a* and *d*, followed by coordination of monoene and then oxidative addition of HCl (cf. reaction [10]). Of interest, addition of cyclooctadiene instead of cyclooctene to the $IrHCl_2$(cod)-(DMA) system under H_2/O_2 does not result in catalytic oxidation to the cyclooctene-one. It is possible that compared to a monoene, the more strongly coordinating diene inhibits hydride regeneration. Since HCl readily adds to the iridium(I) diene complex (equilibrium [10]), this would require that the diene inhibits reactions such as step *a* or *c*.

The nature of the reactions that regenerate the hydride, reaction [14], is of critical importance, because this process is probably the rate-determining step in the overall catalysis. The kinetics of formation of the hydroxide, reaction [11], have been studied in DMA at 30°C by both a gas-uptake and more conveniently by a spectrophotometric technique (the absorption maximum at 395 nm decreases to give a continuum spectrum in the 500–300 nm region, with ϵ at 395 nm being 495 M^{-1} cm^{-1}). At about 5×10^{-4} *M* $IrHCl_2(C_8H_{12})$(DMA) and a 100-fold excess of HCl, under 0.3–1.0 atm O_2, conditions being chosen such that the $[O_2]$ is in large excess (the solubility of O_2 at 30°C was determined to be 7.6×10^{-3} *M* atm^{-1}, with Henry's Law being obeyed), the spectral changes analyzed for a standard pseudo first-order process with observed rate constants at 30°C, k_{obs}, equal to $(1.04 \pm 0.10)10^{-4}$ s^{-1} at 1.0 atm O_2. These pseudo first-order constants are proportional to the O_2 pressure from 0.3–1.0 atm, and thus the rate-law for the reaction is simply $k'[IrH][O_2]$, with k' being $(1.36 \pm 0.13) \times 10^{-2}$ M^{-1} s^{-1}. We have not been able to determine in DMA if these spectral measurements refer to production of the hydroperoxide or the hydroxide; the latter seems likely since only one set of first-order spectral changes are observed. The half-life for formation of the hydroxide following dissolution of the hydride as hydroperoxide in CH_2Cl_2 at 20°C is about 60 min (Fig. 1), comparable to that of the process measured in DMA (see below), but the coordination sphere of the iridium in the two solvents will be different. The k' rate constant is thus tentatively assigned as kK_{O_2}, where k is the rate constant for the oxygen atom transfer step, and K_{O_2} is a constant for the hydride/hydroperoxide equilibrium, that lies well to the side of hydride formation at the O_2 pressures used. Under the catalytic conditions at 30°C with 0.5 atm O_2, this would correspond to a half-life of about 3 h; some slower step appears to control the overall catalysis. A serious limitation in drawing such a conclusion, of course, is that the kinetic data determined for reaction [11] refer to the stoichiometric cyclooctadiene substrate and not the catalytic cyclooctene substrate. Nevertheless, during the cyclooctene oxidation, the visible spectrum of the solution is a continuum in the 500–350 nm region typical of that resulting from reaction [11] with no evidence for the presence of a hydride; this again implies the presence of "$Ir(OH)Cl_2$" and a process of reaction [14] being rate-determining. The monohydride formation is basically a ligand substitution process (11) (hydride for hydroxide or water) and substitution at iridium(III) is notoriously slow (41). Mechanistic aspects of reactions of O_2 with transition metal hydrides to give hydroperoxides have not been explored, and we know of no prior kinetic studies on such

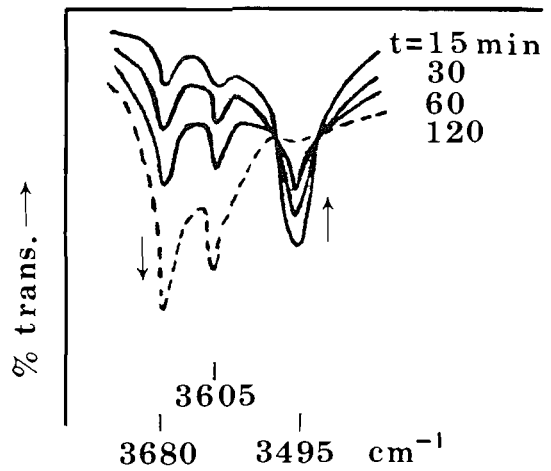

FIG. 1. Infrared changes in the 3500 cm^{-1} region in CH_2Cl_2 as a function of time (t) at 20°C, attributed to hydroperoxide to hydroxide conversion (reaction [11], see text).

systems. The possibility of protonation of an intermediate dioxygen complex, reaction [15], cannot be ruled out (ref. 1, p. 79 and see reaction [22] below).

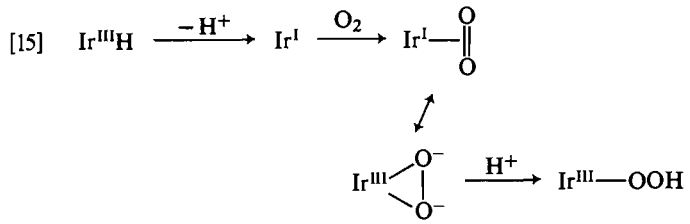

The net hydrogenolysis reaction shown in [16], studied by Reed and Roper (42), is of interest in that it demonstrates formation of a hydride from a hydroxo complex with liberation of water:

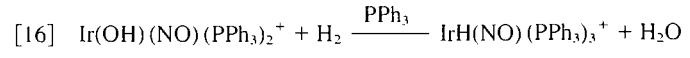

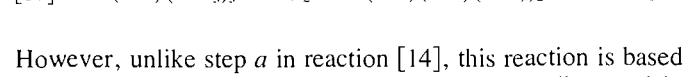

However, unlike step *a* in reaction [14], this reaction is based on a formal iridium(I) oxidation state, and was discussed in terms of oxidative addition of hydrogen followed by reductive elimination of water. Of further interest in this paper (42) is reaction [17], the overall process of which parallels closely that of reaction [11], although the oxidation state is again one, and oxidation of the phosphine was considered to proceed by way of a dioxygen species rather than a hydroperoxide, which was considered (42). Coupling of reactions [16] and [17] led to the overall catalytic hydrogenolysis of dioxygen to water with co-oxidation of triphenylphosphine (42), reaction [18],

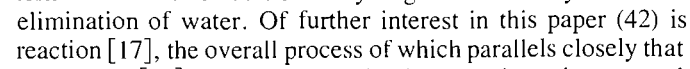

which is to be compared with reaction [5] in the present work.

The fact that molecular hydrogen can reduce cyclic peroxo complexes (43) led Sheldon and Van Doorn (44) to test reaction [19] with the known platinum(II) peroxometallocycle:

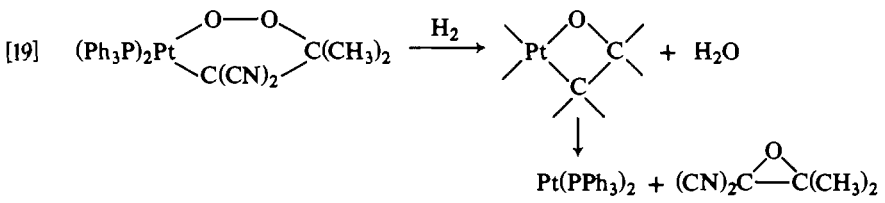

A similar hydrogenolysis process could be envisioned with the pseudo-peroxometallocycle intermediate suggested in equation [13], the reaction leading directly to epoxide (or ketone), water, and iridium(III) hydride (epoxides are readily isomerized to ketones in the presence of Lewis acids (45), but this has not been tested for in the presence of the iridium systems being studied here). However, reaction [19] did not occur under mild conditions, and the evidence for the presence of hydroxo-iridium species provides strong support for hydride regeneration via steps of reaction [14].

There is no evidence to suggest that H_2 and O_2 could produce hydrogen peroxide under the catalytic conditions, reaction [20], although the peroxide is readily formed from acid treatment of hydroperoxides.

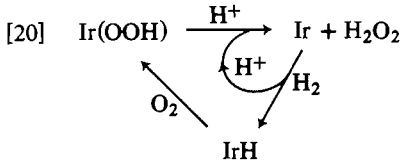

In any case, free hydrogen peroxide under the conditions used does not oxidize unactivated monoenes such as cyclooctene.

The competing oxygen hydrogenolysis[4] reaction, [6], is poorly understood but needs to be minimized for effective olefin oxygenation. In essence, the H_2 molecule is competing with the olefin for an oxygen atom. The simplified catalytic cycle shown in Fig. 2 encompasses reactions [6], [11], and [14]; the substrate **S** may be coordinated olefin, or H_2, although we know of no precedent for reaction of H_2 with M—OOH, or OM(OH) (see below), to generate water. Attempts to study this "blank water reaction" in the absence of olefinic substrate were thwarted by the system tending to precipitate metal, particularly at higher H_2/O_2 ratios; iridium(I) under H_2, in the absence of stabilizing π-acceptor ligands (cf. reaction [14]), readily gives metal (27). An earlier study from this laboratory using a ruthenium catalyst revealed a rate-law showing a first-order dependence on H_2, and an independence of O_2 (48), which is again consistent with regeneration of an intermediate hydride being the rate-determining step. A further report using a range of platinum metal phosphine complexes as catalysts (49) noted a rate-law showing first-order in both gases but mechanisms were not considered. Use of the 1 atm H_2/O_2 mixtures at ratios ≥ 1.5 for the cyclooctene oxidation produces also some cyclooctane, in amounts comparable to the cyclooctanone; such hydrogenation must involve intermediate alkyls and reaction of these with O_2 by a net insertion to give alkylperoxides, M—OOR (ref. 1, pp. 81, 100), also could provide a pathway for the oxygenation. However, the experimental evidence for reaction [11] leads us to a working hypothesis shown in Fig. 2 for the net catalysis. Although the use of H_2/O_2 mixtures sounds alarming, we have experienced no difficulties under the mild conditions used.

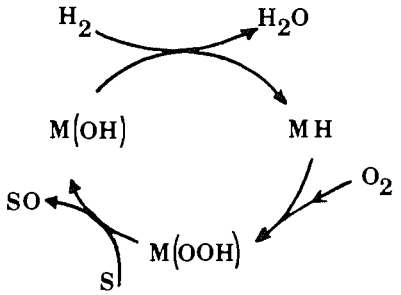

FIG. 2. Suggested catalytic cycle for selective oxygenation using H_2/O_2 mixtures; the substrate **S** may be olefin or H_2, while M represents Ir(III). MH could be written alternatively for this system as Ir(I) + H^+ (see reaction [15]).

A wide variety of related platinum metal complexes in several solvents (DMA, toluene, chlorobenzene) were tested for oxygenase-type activity with olefinic substrates. Rhodium systems in DMA included *in situ* $RhHCl_2(cod)(DMA)$ species formed from the cod dimer and HCl, $RhCl_3 \cdot 3H_2O$, $RhBr_3 \cdot 2H_2O$, $RhCl_3(DMSO)_3$, and a $[RhCl(C_8H_{14})_2]_2$/HCl mixture. Under comparable conditions (1:1 H_2/O_2 mixtures at 1 atm with cyclic olefins at 20°C), only trace amounts of several oxidation products were detected after reaction times of 2–5 days; however, extensive catalytic hydrogenation was commonly observed. Many of the above systems are known to be active hydrogenation catalysts that operate via rhodium(I) species (11, 50). Compared to iridium, the metal–hydride bond in corresponding rhodium systems is weaker (51), and hydrogen reduction to the rhodium(I) state is more likely (reactions [3], [14] step *d*); this would explain the preferred hydrogenation process, and also the formation of trace oxidation products via nonselective free-radical pathways (7), see reactions [7]–[9]. Use of the $RhCl_3(DMSO)_3$ complex in DMA, which readily generates $RhCl_3(DMSO)_2(DMA)$ containing two S-bonded DMSO ligands (23), yielded also some sulfone ($DMSO_2$) and sulfide (DMS) by oxygenation and hydrogenation, respectively. Using DMSO as solvent with olefinic substrates gave only sulphone formation according to reaction [4], presumably because the olefin is unable to compete with DMSO for a coordination site. The DMSO appears to stabilize the rhodium(III) hydride, rather than the rhodium(I) state (reaction [3]), as observed in synthetic studies (23). The oxygen atom transfer to the sulfoxide is again considered to involve a hydroperoxide intermediate rather than free hydrogen peroxide; coordination of the sulfoxide may not be essential, since the mechanism outlined in equation [21], which is exactly analogous to that suggested for the metal-catalyzed alkylhydroperoxide oxidation of sulfides to sulfoxides (52), seems plausible:

[4]The reversal of reaction [6] by photochemical means demands intense current interest (46), although catalysts were developed for disposal of the explosive 2:1 mixture of hydrogen and oxygen resulting from radiolytic decomposition of water in atomic reactors (47).

Can. J. Chem. Downloaded from www.nrcresearchpress.com by 210.87.254.40 on 09/06/12
For personal use only.

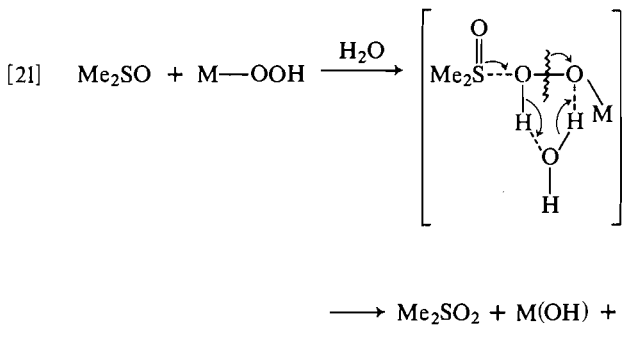

A DMA solution of $IrHCl_2(DMSO)_3$ at 20°C absorbs 1.0 mol O_2 per iridium (cf. reactions [11] and [21]), but the reaction products have not yet been identified.

We have also used ethanol and isopropanol as solvents and possible sources of hydride with the iridium(III) and rhodium(III) complexes, using just an O_2 atmosphere. However, no catalytic oxygenation of olefins is observed.

Of considerable interest to the present studies are the reports from Tabushi's group on catalytic epoxidation of olefins using a manganese(III) porphyrin under O_2 with borohydride (6) or H_2/colloidal platinum (53) as co-reductant. Non free-radical pathways involving a strongly electrophilic oxygen-containing species formed via a hydroperoxide were invoked (6):[5]

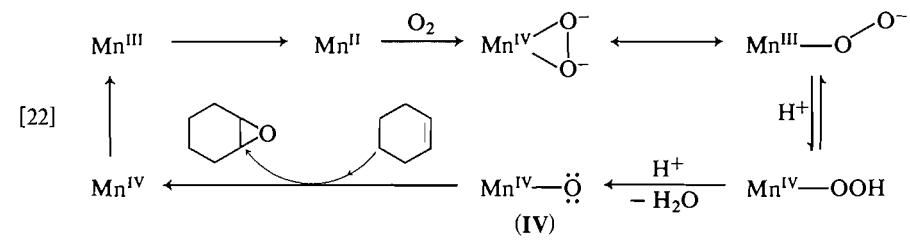

The net cycle shown in equation [22] again incorporates the overall stoichiometry of the P450 system (reaction [1]), the two electrons being provided by BH_4^- or H_2/Pt. The suggested mechanism is close to that postulated for the enzyme systems that appear (16, 54) to involve an iron porphyrin intermediate analogous to **IV**, namely $[Fe^{III}—\ddot{O}]$ (or one of its resonance forms, including porphyrin cation radical formulations). The overall analogy of the postulated mechanisms for the manganese porphyrin and P450 systems, with that for our iridium system is quite striking (cf. equations [22], [11], and [13]). Both involve hydroperoxide intermediates, but formed either by protonation of coordinated reduced dioxygen species, or by insertion of dioxygen into a metal–hydride bond. The subsequent oxygen transfer to substrate, however, is pictured quite differently. The P450 systems also incorporate an oxygen atom into a saturated C—H bond and this certainly requires a strongly electrophilic oxene-type species such as $[Fe^{III}—\ddot{O}] \leftrightarrow [Fe^{V}=O]$, probably via an initial hydrogen atom abstraction (5, 16, 54). The iridium system will not oxygenate saturated hydrocarbons, and on analogy with oxygen atom transfer from coordinated alkyl peroxide, the process via the pseudo peroxometallocycle seems plausible. Protonation of $[Ir^{III}—OOH]$ to yield $[Ir^{III}—\ddot{O}] \leftrightarrow [Ir^{V}=O]$ (cf. equation [22]) seems highly unlikely; there are no known examples of oxo complexes of even iridium(III), let alone iridium(V) (or rhodium analogues).

Concluding remarks

In summary, we have discovered that catalytic selective oxygenation of a cyclic olefin to give the ketone can be effected using H_2/O_2 mixtures with an iridium complex under mild conditions. Although the reaction is very inefficient, it does prove the potential of using H_2, activated as a metal–hydride, as the coreductant in monoxygenase-type catalysis. Tabushi and Yazaki (53) have recently used colloidal platinum to catalyze the necessary two-electron transfer from H_2 in the presence of a manganese porphyrin to effect similar oxygenation to give the epoxide. The studies with the iridium systems have concentrated thus far on a single substrate (cyclooctene) and a single precursor complex $[IrHCl_2(C_8H_{12})]_2$. The rate-determining step appears to be regeneration of the hydride at a substitution-inert iridium(III) centre. Studies are in progress to investigate the scope of the present catalytic system in terms of other olefinic substrates, and also to modify and "improve" the iridium centre by variation (and removal) of the chloride ligands.

Acknowledgements

We thank Johnson Matthey Ltd. for the loan of iridium and rhodium, Professor C. B. Anderson for a sample of 4-cyclooctene-1-one, and the Natural Sciences and Engineering Council of Canada, Imperial Oil Ltd., and N.A.T.O. for financial support.

1. R. A. SHELDON and J. K. KOCHI. Metal-catalyzed oxidations of organic compounds. Academic Press, New York. 1981.
2. J. E. LYONS. *In* Aspects of homogeneous catalysis. Vol. 3. *Edited by* R. Ugo. Reidel, Dordrecht. 1977. p. 1.
3. G. MODENA, K. B. SHARPLESS, G. COSTA, J. HALPERN, Y. ISHII, B. R. JAMES, J. E. LYONS, H. MIMOUN, P. ROSSI, R. A. SHELDON, P. TEYSSIE. *In* Fundamental research in homogeneous catalysis. *Edited by* M. Tsutsui and R. Ugo. Plenum, New York. 1977. p. 193.
4. Workshop on Fundamental Research in Homogeneous Catalysis as Related to United States Energy Problems. Stanford University, Stanford, California. 1974.
5. M. J. COON and R. E. WHITE. *In* Metal ion activation of dioxygen. *Edited by* T. G. Spiro. Wiley, New York. 1980. p. 73.
6. I. TABUSHI and N. KOGA. Adv. Chem. Ser. **191**, 291 (1980).
7. B. R. JAMES. Adv. Chem. Ser. **191**, 253 (1980), and references therein.
8. H. MIMOUN. J. Mol. Catal. **7**, 1 (1980); F. IGERSHEIM and H. MIMOUN. Nouv. J. Chim. **4**, 161 (1980).
9. G. READ and P. J. C. WALKER. J. Chem. Soc. Dalton Trans. 883 (1977).
10. B. R. JAMES, F. T. T. NG, and G. L. REMPEL. Can. J. Chem. **47**, 4521 (1969).
11. B. R. JAMES. *In* Comprehensive organometallic chemistry. *Edited by* G. Wilkinson. Pergamon, Oxford. 1982. Chapt. 51.
12. P. J. BROTHERS. Prog. Inorg. Chem. **28**, 1 (1981).

[5] Equation [22] is adapted from Fig. 20 of ref. 6, that contains an error in writing the hydroperoxide as $Mn^{III}—OOH$.

Can. J. Chem. Downloaded from www.nrcresearchpress.com by 210.87.254.40 on 09/06/12
For personal use only.

13. J. TROCHA-GRIMSHAW and H. B. HENBEST. J. Chem. Soc. Chem. Commun. 1035 (1968).
14. Y. M. Y. HADDAD, H. B. HENBEST, and J. TROCHA-GRIMSHAW. J. Chem. Soc. Perkin Trans. I, 592 (1974).
15. D. DOLPHIN, B. R. JAMES, and C. H. WELBORN. J. Mol. Catal. 7, 201 (1980).
16. D. DOLPHIN, B. R. JAMES, and H. C. WELBORN. Adv. Chem. Ser. **201**, 563 (1982).
17. S. D. ROBINSON and B. L. SHAW. J. Chem. Soc. 4997 (1965).
18. M. J. ATLAY, M. PREECE, G. STRUKUL, and B. R. JAMES. J. Chem. Soc. Chem. Commun. 406 (1982).
19. J. L. HERDE, J. C. LAMBERT, and C. V. SENOFF. Inorg. Synth. **15**, 18 (1974).
20. A VAN DER ENT and A. L. ONDERDELINDER. Inorg. Synth. **14**, 92 (1973).
21. J. CHATT and L M. VENANZI. J. Chem. Soc. 4735 (1957).
22. B. R. JAMES and R. H. MORRIS. J. Chem. Soc. Chem. Commun. 929 (1978).
23. B. R. JAMES and R. H. MORRIS. Can. J. Chem. **58**, 399 (1980).
24. B. R. JAMES and G. L. REMPEL. Discuss. Faraday Soc. **46**, 48 (1968); Can. J. Chem. **44**, 233 (1966).
25. B. R. JAMES, R. S. MCMILLAN, S. J. RETTIG, and J. TROTTER. To be published.
26. V. GUTMANN. Coord. Chem. Rev. **2**, 239 (1967).
27. B. R. JAMES and C. Y. CHAN. Inorg. Nucl. Chem. Lett. **9**, 135 (1973).
28. G. WINKHAUS and H. SINGER. Chem. Ber. **99**, 3610 (1966).
29. G. STRUKUL, R. ROS, and R. A. MICHELIN. Inorg. Chem. **21**, 495 (1982).
30. C. B. ANDERSON, B. J. BURRESON, and J. T. MICHALOWSKI. J. Org. Chem. **41**, 1990 (1976).
31. L. E. JOHNSTON and J. A. PAGE. Can. J. Chem. **47**, 4241 (1969).
32. R. D. GILLARD, B. H. HEATON, and D. H. VAUGHAN. J. Chem. Soc. A, 3126 (1970).
33. H. L. ROBERTS and W. R. SYMES. J. Chem. Soc. A, 1450 (1968).
34. M. A. BENNETT and D. L. MILNER. J. Am. Chem. Soc. **91**, 6983 (1969).
35. F. A. COTTON, R. D. BARNES, and E. BANNISTER. J. Chem. Soc. 2199 (1960).
36. A. SEN and J. HALPERN. J. Am. Chem. Soc. **99**, 8337 (1977).
37. R. A. SHELDON. *In* Aspects of homogeneous catalysis. Vol. 4. *Edited by* R. Ugo. Reidel, Dordrecht. 1981. p. 3.
38. R. BONNAIRE and P. FOUGEROUX. C.R. Acad. Sci. Ser. C, **280**, 767 (1975).
39. W. J. LOUW and C. E. HEPNER. Inorg. Chem. **19**, 7 (1980).
40. M. T. ATLAY and B. R. JAMES. Unpublished results; work in progress.
41. F. A. COTTON and G. WILKINSON. Advanced inorganic chemistry. 4th ed. Wiley, New York. 1980. p. 943.
42. C. A. REED and W. R. ROPER. J. Chem. Soc. Dalton Trans. 1014 (1973).
43. P. J. HAYWARD, D. M. BLAKE, G. WILKINSON, and C. J. NYMAN. J. Am. Chem. Soc. **92**, 5873 (1970).
44. R. A. SHELDON and J. A. VAN DOORN. J. Organomet. Chem. **94**, 115 (1975).
45. D. N. KIRK. Chem. Ind. London, 109 (1973).
46. J. R. DARWENT, P. DOUGLAS, A. HARRISON, G. PORTER, and M.-C. RICHOUX. Coord. Chem. Rev. **44**, 83 (1982) and references therein.
47. H. F. MCDUFFIE, E. L. COMPERE, H. H. STONE, L. F. WOO, and C. H. SECOY. J. Phys. Chem. **62**, 1030 (1958).
48. B. C. HUI and B. R. JAMES. Can. J. Chem. **52**, 348 (1974).
49. L. VASKA and M. E. TADROS. J. Am. Chem. Soc. **93**, 7099 (1971).
50. B. R. JAMES. Adv. Organomet. Chem. **17**, 319 (1979).
51. J. A. OSBORN, F. H. JARDINE, J. F. YOUNG, and G. WILKINSON. J. Chem. Soc. A, 1711 (1966).
52. R. CURCI, F. DI FURIA, R. TESTI, and G. MODENA. J. Chem. Soc. Perkin II, 752 (1974).
53. I. TABUSHI and A. YAZAKI. J. Am. Chem. Soc. **103**, 7371 (1981).
54. J. T. GROVES, R. C. HAUSHALTER, M. NAKAMURA, T. E. NEMO, and B. J. EVANS. J. Am. Chem. Soc. **101**, 1032 (1979) and references therein.

Can. J. Chem. Downloaded from www.nrcresearchpress.com by 210.87.254.40 on 09/06/12
For personal use only.

Synthesis and reactivity of iron nitrosyl hydrides substituted with triphenyl phosphine

JEAN-LOUIS A. ROUSTAN,[1] ALAIN FORGUES, JEAN-YVES MEROUR, NARINDER D. VENAYAK, AND B. A. MORROW

Ottawa–Carleton Institute for Research and Graduate Studies, University of Ottawa Campus, Ottawa, Ont., Canada K1N 9B4

Received August 17, 1982[2]

JEAN-LOUIS A. ROUSTAN, ALAIN FORGUES, JEAN-YVES MEROUR, NARINDER D. VENAYAK, and B. A. MORROW. Can. J. Chem. **61**, 1339 (1983).

Protonation of anion **1** $[Fe(CO)_3(NO)]^-$, (Na^+) in the presence of $P(C_6H_5)_3$ yielded the iron nitrosyl hydrides **3** $FeH(CO)_2(NO)(P(C_6H_5)_3)$ and **4** $FeH(CO)(NO)(P(C_6H_5)_3)_2$ or the iron nitrosyl cation **5** $[Fe(CO)_2(NO)(P(C_6H_5)_3)_2]^+$, (BF_4^-) depending upon the conditions. Anions **12** $(Li^+),[Fe(CO)(NO)(P(C_6H_5)_3)_2]^-$ and **15** $(Li^+),[Fe(CO)_2(NO)(P(C_6H_5)_3)]^-$ were formed in the reactions of $Li^+,{}^-HB(C_2H_5)_3$ **13** with hydrides **4** and **3** respectively. Anions **15** resulted also from the reaction of cation **5** with an excess (at least 6 equivalents) of boron hydride **13** and from the reaction of anion **12** with CO at atmospheric pressure. Hydrides **3** and **4** were prone to ligand exchange reactions and could be interconverted easily. This is in contrast to the reluctance of the isoelectronic cobalt hydride $CoH(CO)_3(P(C_6H_5)_3)$ to undergo further reaction with $P(C_6H_5)_3$. Another striking difference between the iron nitrosyl hydrides and the isoelectronic cobalt carbonyl hydrides was found when the reactions which normally yield bimetallic derivatives were investigated. The nature of the decomposition products formed in the thermolysis of **3** and **4**, in the reactions of **3** with olefins and dioxygen, and in the reduction reactions of cation **5** suggests that metallic dimers containing a $(Fe(NO))_2$ unit are prone to fast CO and NO exchanges triggering an irreversible fragmentation into monometallic decomposition products, comprising invariably iron dinitrosyl derivatives.

JEAN-LOUIS A. ROUSTAN, ALAIN FORGUES, JEAN-YVES MEROUR, NARINDER D. VENAYAK et B. A. MORROW. Can. J. Chem. **61**, 1339 (1983).

La protonation de l'anion **1** $[Fe(CO)_3(NO)]^-,(Na^+)$ en présence de $P(C_6H_5)_3$ conduit aux hydrures fer nitrosyles **3** $FeH(CO)_2(NO)(P(C_6H_5)_3)$ et **4** $FeH(CO)(NO)(P(C_6H_5)_3)_2$ ou au cation fer nitrosyle **5** $[Fe(CO)_2(NO)(P(C_6H_5)_3)_2]^+,(BF_4^-]$ suivant les conditions. Les anions **12** $(Li^+),[Fe(CO)(NO)(P(C_6H_5)_3)_2]^-$ et **15** $(Li^+),[Fe(CO)_2(NO)(P(C_6H_5)_3)]^-$ resultent de la réaction de $Li^+,{}^-HB(C_2H_5)_3$ **13** avec les hydrures **4** et **3** respectivement. L'anion **15** est aussi formé dans la réaction du cation **5** avec un excés (au moins 6 equivalents) du borohydrure **13**, et dans la réaction de l'anion **12** avec CO à pression atmosphérique. Les hydrures **3** et **4** se prêtent bien à des réactions d'échanges de ligandes et sont facilement interconvertibles. Par opposition l'hydrure du cobalt isoélectronique $CoH(CO)_3(P(C_6H_5)_3)$ ne réagit pas avec un excés du $P(C_6H_5)_3$. Une autre différence nette entre les hydrures fer nitrosyles et les hydrures cobalt carbonyles isoélectroniques apparait quand on s'intéresse à des réactions qui conduisent habituellement à des dérivés bimétalliques. La nature des produits de décomposition issus de la thermolyse de **3** et **4**, de la réaction de **3** avec des oléfines ou l'oxygène moléculaire, et des réactions de réduction du cation **5**, suggère que les dimères métalliques comportant un fragment $(Fe(NO))_2$ sont sujets à des échanges rapides de CO et de NO qui déclenchent une fragmentation irreversible en des produits de décomposition monométalliques, parmi lesquels figurent invariablement des dérivés du fer dinitrosyle.

Introduction

The recently discovered catalytic activity of the iron nitrosyl anion $[Fe(CO)_3(NO)]^-,Na^+$ **1** in the alkylation of allylic acetates (1) prompted us to extend the scope of our studies to other derivatives containing a $[FeNO]^x$ moiety (x = 8, 10)[3] which might serve as progenitors of other catalytically active species.

The pivotal role of transition metal hydrides, such as $CoH(CO)_4$ (3), in many reactions of current interest (4, 5) was the incentive to explore the chemistry of iron nitrosyl hydrides.

Prior to our work in this area, only one iron nitrosyl carbonyl hydride had been reported, the very thermolabile $FeH(CO)_3(NO)$ (dec. −45°C, sometimes explosively) (6). Starting with the readily available anion **1** (6), we had reported already that its protonation in the presence of an excess of triphenyl phosphine yielded the new hydride $FeH(CO)(NO)(P(C_6H_5)_3)_2$ which could be isolated easily in the solid state (7); the single crystal structure was obtained recently (8). In this paper, we report our results on protonation reactions of anion **1** in a variety of conditions, on reactions promoting the cleavage of the iron–hydrogen bond in the hydrides, and on reduction reactions of the iron nitrosyl cation $[Fe(CO)_2(NO)(P(C_6H_5)_3)_2)]^+$.

Altogether, the results provide new information useful for a better understanding of the chemistry of these nitrosyl complexes.

Experimental

All the operations were done under argon, carbon monoxide, or in vacuum. THF (tetrahydrofuran) was refluxed, then distilled from sodium/benzophenone under nitrogen and used immediately. All solvents were saturated with argon before use. Anhydrous ether (Mallinkrodt), acetic anhydride (J. T. Baker), trifluoroacetic acid (J. T. Baker or MCIB), aqueous 37% tetrafluoroboric acid (Applied Chemicals), lithium triethyl borohydride (1 *M* solution in THF), triphenyl phosphine (Aldrich), sodium nitrite (B.D.H.), iron pentacarbonyl (Pressure Chemical), and CO (Matheson, CO C.P. 99.5% min.) were used as received. The olefins (Aldrich) were passed through a short alumina column before use. SiO_2 plates for analytical chromatography were from Analtech Inc., those for preparative chromatography from Macherey Nagel; neutral alumina, activity II–III, from Merck was used for column chromatography. The ir spectra were recorded on a Unicam SP 1100 calibrated with a polystyrene film or on a Perkin–Elmer 283 (abbreviations: vs = very strong, s = strong, ν are given in cm^{-1}). The nmr spectra were recorded on a Varian HA 100 for proton (TMS internal reference) and on a Varian FT 80 operating at 32.2 MHz for phosphorus (85% H_3PO_4 external reference); a

[1]Author to whom correspondence may be addressed.

[2]Revision received January 25, 1983.

[3]$\{MNO\}^x$ represents a metal nitrosyl complex in which the nitrosyl ligand is formally considered as NO^+ and the metal to have x d electrons (2). In the present work, all the complexes which have been prepared correspond to x = 8 or 10.

Can. J. Chem. Downloaded from www.nrcresearchpress.com by 210.87.254.6 on 09/06/12
For personal use only.

Can. J. Chem. Downloaded from www.nrcresearchpress.com by 210.87.254.6 on 09/06/12
For personal use only.

positive chemical shift (ppm) indicates a resonance downfield from the reference. Elemental analyses were performed by M.H.W. Laboratories, Phoenix, Arizona, U.S.A. Published procedures were used to prepare authentic samples of $Fe(CO)_4(P(C_6H_5)_3)$ (10), $Fe(CO)_3(P(C_6H_5)_3)_2$ (11), and $Fe(CO)_2(NO)_2$ (12). $Fe(NO)_2(P(C_6H_5)_3)_2$ (13) was obtained from the thermal decomposition of the cation $[Fe(CO)(NO)(CH_3CN)(P(C_6H_5)_3)_2]^+,BF_4^-$ (14) in acetonitrile at 50°C, and crystallized out from the solution. $Fe(NO)_2(CO)(P(C_6H_5)_3)$ (13) was obtained from the reaction of $Fe(CO)_2(NO)_2$ with $P(C_6H_5)_3$ in hexane or ether at room temperature. Samples of (η^3-propenyl)-$Fe(CO)(NO)(P(C_6H_5)_3)$ were obtained from the reaction of (η-^{3}propenyl)$Fe(CO)_2(NO)$ with $P(C_6H_5)_3$ (9). The cation $[Fe(CO)_2(NO)(P(C_6H_5)_3)_2]^+,(BF_4^-)$ used in the reduction reactions was prepared either from the carbonylation at room temperature and atmospheric pressure of solid $[Fe(CO)(NO)(P(C_6H_5)_3)_2]^+,BF_4^-$ (14) or from the protonation of anion **1** as described below or from the direct nitrosylation of $Fe(CO)_3(P(C_6H_5)_3)$ with NO^+,BF_4^- (15). Whatever the method used for preparing the compound, the same dependency of the final distribution of the reduction products upon the excess of reductant used was observed.

Anion **1** $Fe(CO)_3(NO)^-Na^+$ was prepared by reacting $Fe(CO)_5$ with $NaNO_2$ in absolute methanol, in the presence of $NaOCH_3$, as described previously (6, 8).

*Protonation of anion **1** in THF in the presence of triphenyl phosphine*

A stock solution of anhydrous HBF_4 (17) was prepared just before use by dropwise addition of 2 mL of aqueous 37% HBF_4 (≃11 mmol of HBF_4) to 10 mL of acetic anhydride stirred and maintained at 0°C with an ice bath.

*Formation of $FeH(CO)(NO)(P(C_6H_5)_3)_2$ **4***

Anion **1** (0.7 g, 3.1 mmol) and $P(C_6H_5)_3$ (2.0 g, 7.6 mmol, ≃ 2.5 equivalents) were dissolved in 70 mL of THF cooled in an ice bath. To the stirred solution, 5 mL of the HBF_4 stock solution (≃1.5 equiv. of HBF_4) were added dropwise. Stirring was discontinued after two hours, and the homogeneous solution was brought to dryness in vacuum at room temperature. The residue was washed with 20 mL of ether, extracted with benzene, and crystallized in benzene/pentane to yield 0.66 g (30%) of hydride **4** identified by comparison with an authentic sample (7) (νCO = 1915, νNO = 1690 (THF); δ(Fe-H) = −5 pm, triplet, J_{P-H} = 79 ± 1 Hz; δP = 77.0 ppm ($CDCl_3$)).

*Formation of $[Fe(CO)_2(NO)(P(C_6H_5)_3)_2]^+,BF_4^-$ **5***

Anion **1** (0.37 g, 1.6 mmol) and $P(C_6H_5)_3$ (2.1 g, 5 equiv.) in 50 mL of THF were protonated, as described above, with 10 mL of the HBF_4 stock solution (≃5.5 equiv.) Infrared analysis of the solution, shortly after acidification, indicated complete disappearance of anion **1** and formation of an intermediate with νCO's identical to those of hydride **3**. Stirring of the solution, in the ice bath, was maintained an additional two hours, by which time a yellow precipitate had started to form. After additional stirring at room temperature for 6 hours, the solid was separated by filtration, washed with THF, dried, and extracted with $CHCl_3$. Crystallization in $CHCl_3$/pentane yielded 0.6 g (50%) of cation **5**, identical with an authentic sample prepared from the reaction of $Fe(CO)_3(P(C_6H_5)_3)_2$ with NO^+,BF_4^- (15). Infrared νCO = 2050 (s), 1990 (vs), νNO = 1790 (vs) ($CHCl_3$); reported (15): 2050 (s), 1993 (vs), 1788 (vs). *Anal.* calcd. for $C_{38}H_{30}BF_4FeNO_3P_2$: C 60.6, H 4.0, N 1.9, P 8.2; found: C 60.4, H 4.0, N 1.9, P 8.2.

*$FeH(CO)_2(NO)(P(C_6H_5)_3)$ **3***

Synthesis in solution

A typical preparation is described. Trifluoroacetic acid (0.13 mL, 1.8 mmol) was added dropwise to a stirred solution of anion **1** (0.33 g, 1.5 mmol) and $P(C_6H_5)_3$ (0.45 g, 1.7 mmol) in 35 mL of ether cooled at −15°C. An ir spectrum, recorded shortly after the addition (≃2 minutes), indicated the formation of hydride **3**. The solution was cooled to −78°C and sodium trifluoroacetate was decanted by gravity. The clear orange supernatant was used for ir, ^{1}H and ^{31}P nmr analyses (νCO = 2020, 1960; νNO = 1755; δ(Fe-H) = −3.5 ppm, doublet, J_{P-H} = 12 Hz; δP = 62.0 ppm). Heating the solution at reflux for a few minutes resulted in the decomposition of hydride **3** and precipitation of the degradation products $Fe(NO)_2(P(C_6H_5)_3)_2$ **8**, $Fe(NO)_2(CO)(P(C_6H_5)_3)$ **9**, $Fe(CO)_4(P(C_6H_5)_3)$ **10**, and $Fe(CO)_3(P(C_6H_5)_3)_2$ **11**, sparingly soluble in ether. Infrared (THF or CH_2Cl_2, numbers in parentheses correspond to literature values), **8**: νNO = 1720 (s), 1680 (vs) (1724, 1678 (13)); **9**: νCO = ~2000 (s); νNO = 1760 (s), 1720 (vs) (2009, 1764, 1722 (13)); **10**: νCO = 2060, 1975, 1945 (2059, 1978, 1938 (11)); **11** (νCO = 1890 (1887(11)). The mixtures were also analysed on tlc plates and the R_f values compared to those of authentic samples of **8**, **9**, **10**, and **11** (elution with benzene/hexane (1:4)). The same decomposition took place when ether solutions of hydride **3** were allowed to stand at room temperature for 4 hours. In that case, hydride **4** was also present in the precipitate (very likely it resulted from the reaction of hydride **3** still present with triphenyl phosphine released in solution as the decomposition was in progress). The solutions were also very air sensitive. Upon contact with air they darkened instantaneously to yield a mixture of the degradation products **8**, **9**, **10**, and **11**. The procedure given above was also used to prepare hydride **3** in toluene.

*Reaction of hydride **3** with triphenyl phosphine, formation of hydride **4***

Hydride **3** was prepared in ether, as described above, starting from 0.25 g (1.1 mmol) of anion **1**. Solid $P(C_6H_5)_3$ (1.36 g, 5.2 mmol, 5 equiv.) was added to the stirred solution. The temperature was allowed to rise to 5°C and maintained at this value with a water–ice bath. Precipitation of hydride **4** occured with gas evolution and no hydride **3** was present after 40 min (ir monitoring of the solution). The solid was filtered out, washed with 20 mL of ether, and extracted with benzene. Crystallization in benzene/pentane afforded 0.51 g of hydride **4** (64%) identified by ir and nmr.

*Reaction of hydride **4** with CO, partial conversion into hydride **3***

Hydride **4** (0.25 g)was dissolved in 10 mL of THF under argon. The orange solution darkened rapidly when CO, at atmospheric pressure, was passed into solution maintained at ~20°C with a water bath. After 20 min, there was no change in the relative intensities of the νCO's and the νNO's of **4** and **3**, which was formed in the reaction (the νNO's were in 1:1 ratio). The same experiment was done directly in an nmr tube with toluene as solvent. The ^{31}P resonance of **4** appeared at 77.4 ppm and that of **3** at 62.6 ppm.

*Stoichiometric hydrogenations with $FeH(CO)_2(NO)(P(C_6H_5)_3)$ **3***

in situ *Preparation of hydride **3** from $Fe(CO)_3(NO)^-,Na^+$*

Hydride **3** was prepared in ether as described above, starting with ~1.3 g of anion **1** for each of the reactions studied. The ir analysis of the solution was performed after the protonation step to make certain that hydride **3** was present in the solution. The stoichiometric amount of the olefin (olefin/anion **1** = 1:2) was then added, and the solution was stirred at room temperature until the disappearance of hydride **3** (15 min with 1,1-diphenyl ethylene, 2 hours with the other reactive olefins). By that time, a precipitate composed of the usual mixture of degradation products **8**, **9**, **10**, and **11** had formed. The solids were separated by filtration and the solution was concentrated to a volume of ~10 mL by distillation of the solvent at atmospheric pressure. After calibration with toluene, the solutions were subjected to vpc analysis (SE 30, 10% on Chromosorb W). In the case of 1,1-diphenyl ethylene, the organic products were separated from the metallic by-products by preparative thin-layer chromatography (elution with hexane) and analysed by ^{1}H nmr.

in situ *Generation of hydride **3** from $FeH(CO)(NO)(P(C_6H_5)_3)_2$ **4***

Hydride **4** (1 g, 1.5 mmol) was dissolved in 30 mL of THF (or benzene) under one atmosphere of CO. When ir analysis of the solution indicated the formation of hydride **3**, an excess of 1,1-diphenyl ethylene (olefin/hydride **4** = 1:1) was added at once. After 15 min, neither **4** nor **3** were detected in solution by ir. The mixture was treated as described above.

*$Li^+[Fe(CO)(NO)(P(C_6H_5)_3)_2]^-$ **12** and reaction with allyl chloride*

One mL of a 1 *M* THF solution of $LiBH(C_2H_5)_3$ (1.3 equiv.) was added to a stirred solution of hydride **4** (0.5 g, 0.78 mmol) in 5 mL of THF. Reduction into anion **12** (νCO = 1830 cm^{-1}; νNO obscured

Can. J. Chem. Downloaded from www.nrcresearchpress.com by 210.87.254.6 on 09/06/12
For personal use only.

by solvent absorptions; δP = 79.7 ppm) occurred within two hours at 50°C. After cooling to room temperature allyl chloride (0.1 mL, 1.24 mmol) was added dropwise. After stirring an additional 5 min the solvent was removed under reduced pressure and the residue was chromatographed on alumina (elution benzene/hexane 1:1) to afford 0.22 g (67%) of the known (η^3-propenyl)Fe(NO)(CO)($P(C_6H_5)_3$) **14** (9).

$Li^+[Fe(CO)_2(NO)(P(C_6H_5)_3)]^-$ 15 and reaction with allyl chloride

Anion **12** was prepared as described previously, starting with 1.26 g (1.97 mmol) of hydride **4** in 10 mL of THF. Conversion into anion **15** (νCO = 1920, 1885, 1850, 1820; νNO = 1600, 1530; δP = 76.7 ppm) was achieved upon passing CO at atmospheric pressure through the solution at room temperature for 15 min. Allyl chloride (0.21 mL, 2.7 mmol) was added and the solution was stirred overnight to yield a mixture of the known allyl complexes (η^3-propenyl)Fe(CO)(L)(NO) (L = CO, **16**; L = $P(C_6H_5)_3$, **14** (9)) in an approximate 2:1 ratio (based on the intensities of the νNO's).

Complex **16** was derivatized *in situ* into **14** by adding triphenyl phosphine (2.21 g, 7.9 mmol) and heating at reflux for 12 h. The η^3-allyl complex **14** was subsequently isolated as described above (0.53 g, 65%).

The reduction of hydride **4** (0.05 g, 0.08 mmol in 4.5 mL of THF) was also performed directly in a nmr tube to minimize material loss due to oxidation of the air-sensitive anions. With an excess of $LiHB(C_2H_5)_3$ (0.4 mL, 5 equiv.) the reduction into **12** took place at room temperature in less than 2 hours. After carbonylation of **12** to yield **15**, the ^{31}P nmr spectrum of the solution was composed of the peaks corresponding to anion **15** and $P(C_6H_5)_3$. They were in a 1:1 ratio, as expected for a 100% overall conversion of hydride **4** into anion **15**.

The lithium salt of anion **15** could also be formed by the fast reaction (upon mixing at 0°C) of hydride **3** in ether with one molar equivalent of the boron hydride.

Reduction of $[Fe(CO)_2(NO)(P(C_6H_5)_3)_2]^+,BF_4^-$ 5

A general procedure is given. A suspension of cation **5** (0.05 to 0.1 g) in THF (5 to 10 mL) was frozen under argon at −196°C. The required amount of boron hydride $Li^+,{}^-HB(C_2H_5)_3$ **13** (between 1 and 10 molar equivalents, depending upon the experiment) was added at once, and the temperature was raised. Stirring commenced when thawing occurred. Gas evolution began at ~−20°C and became vigorous at 0°C as the solid passed slowly into the solution. At the end of the reaction, the solutions (now homogeneous) were analyzed by ir, ^{31}P nmr, and, when anion **15** was not present, by thin-layer chromatography. In the low temperature nmr experiments, a CH_2Cl_2/THF solution of cation **5** was prepared in the nmr tube and cooled to −78°C. The required amount of reducing agent was added through the septum securing the tube, which was then transferred quickly into the probe of the spectrometer cooled at −70°C. When at least 6 equivalents of boron hydride **13** were used, anion **15** was the sole metallic product to be characterized by ^{31}P nmr and ir. For those reactions leading to anion **15**, in the absence of the degradation products, a spectroscopic yield of ≈80% was obtained when the intensity of the νCO of **15** at 1920 cm^{-1} was compared to that of calibrated solutions of anion **15** prepared from hydride **4**, as described previously. A Perkin–Elmer 283 operating in the absorbance mode was used for those mesurements.

Results

1. *Synthesis and reactions of iron nitrosyl hydrides substituted with triphenyl phosphine*

The protonation of metallic anions offers a convenient route to metallic hydrides. However, the success of the preparation might depend upon "a careful control of the reaction conditions" (18). We found this statement very appropriate in the case of the protonation reactions of the iron nitrosyl anion $[Fe(CO)_3(NO)]^-,Na^+$ **1**. In the presence of a phosphine ligand, the nature of the products formed after protonation was critically influenced by the nature of the solvent as well as the nature and the excess of both the acid and the phosphine. In the present work, triphenyl phosphine was used.

In THF, the reaction of anion **1** with ≈1.5 equiv. of anhydrous HBF_4 in the presence of 2.5 equiv. of triphenyl phosphine yielded the disubstituted nitrosyl hydride $FeH(CO)(NO)(P(C_6H_5)_3)_2$ **4** (7) (Scheme 1) in 30% yield. When 5 equiv. of both the acid and the phosphine were used, no evidence for the formation of hydride **4** was obtained. Instead, the ionic nitrosyl complex $[Fe(CO)_2(NO)(P(C_6H_5)_3)_2]^+,BF_4^-$ **5** precipitated slowly from the solution, and could be isolated in 50% yield. Shortly after acidification, ir analysis of the solution indicated the formation of an intermediate with νCO's at 2020 and 1960 cm^{-1} (solvent absorption obscured the region 1800–1700 cm^{-1} where the νNO was expected). Independently, protonation of a THF solution of the sodium salt of the anion $[Fe(CO)_2(NO)(P(C_6H_5)_3)]^-$ (7) with HBF_4 resulted in the formation of a compound with identical νCO's, and we suspected that it could be the dicarbonyl nitrosyl hydride $FeH(CO)_2(NO)(P(C_6H_5)_3)$ **3**. A cleaner synthesis of this previously unknown hydride was sought, and tri-

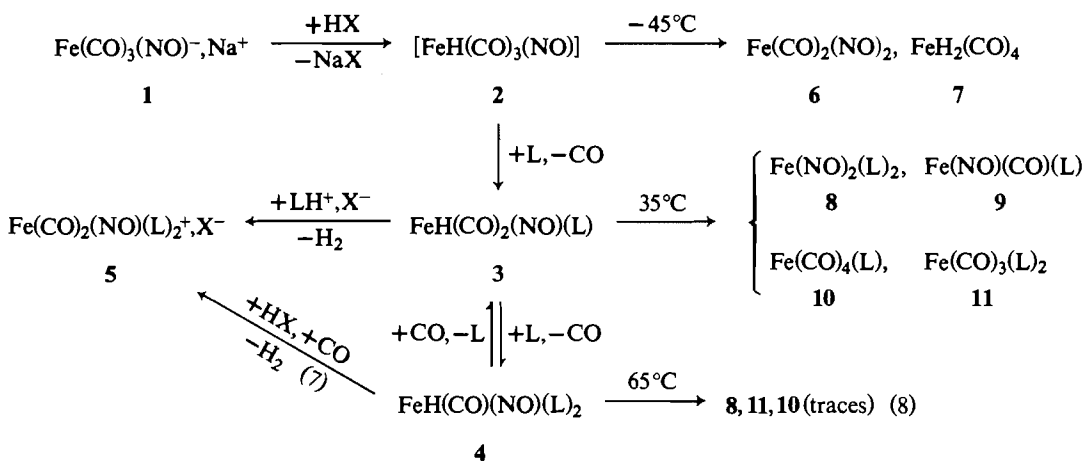

SCHEME 1 (L = $P(C_6H_5)_3$, X^- = BF_4^-)

TABLE 1. Selected νCO and νNO frequencies (cm $^{-1}$) of some iron carbonyl nitrosyl complexes substituted with triphenyl phosphine (L = $P(C_6H_5)_3$)

Compound	νCO	νNO	Solvent	Reference
$FeH(CO)_2(NO)(L)$ **3**	2020,1960	1755	Et_2O,THF, toluene, benzene	[a]
$Fe(CH_2CN)(CO)_2(NO)(L)$	2020,1976	1751	CCl_4	16
$Fe(SnCl_3)(CO)_2(NO)(L)$	2023,1980	1781	CS_2	43
$Fe(SnPh_3)(CO)_2(NO)(L)$	1988,1928	1732	CS_2	43
$(Fe(CO)_2(NO)(L))_2Hg$	1989,1963, 1924,1917	1725,1715	KBr	44
$Fe(HgI)(CO)_2(NO)(L)$	2000,1943	1746	$CHCl_3$	44
$Fe(CN)(CO)(NO)(L)_2$	1930	1700	Nujol	45
$Fe(Cl)(CO)(NO)(L)_2$	1922	1690	CH_2Cl_2	46

[a]This work.

fluoroacetic acid was selected as a more convenient reagent.

With trifluoroacetic acid, THF as a solvent was unsatisfactory. Even in the absence of phosphine, there was no significant reaction between anion **1** and one equivalent of acid. In sharp contrast to this result, in diethyl ether the anion reacted at 0°C upon mixing with the acid, and afforded the volatile dinitrosyl $Fe(CO)_2(NO)_2$ **6** (12), one of the reported decomposition products of the very thermolabile unsubstituted hydride $FeH(CO)_3(NO)$ **2** (6) (the other reported decomposition product, $FeH_2(CO)_4$ **7**, was not detected in our reaction conditions). In the presence of one molar equivalent of triphenyl phosphine, the course of the protonation reaction was dramatically altered. The new hydride $FeH(CO)_2(NO)(P(C_6H_5)_3)$ **3** was formed in yields at least equal to 70% (estimate based on the yields of products derived from **3** as shown below). This reaction could be conducted in ether as well as in toluene, under CO or argon, in the temperature range −15°C to 0°C. The solutions thus obtained were extremely reactive. Brief exposure to air, or heating for a few minutes at 35°C, induced a complete decomposition of hydride **3** into a mixture of products. The only metallic complexes which could be characterized were $Fe(NO)_2(P(C_6H_5)_3)_2$ **8** (13), $Fe(NO)_2(CO)(P(C_6H_5)_3)$ **9** (13), $Fe(CO)_4(P(C_6H_5)_3)$ **10** (11), and $Fe(CO)_3(P(C_6H_5)_3)_2$ **11** (11) (abbreviated hereafter as the degradation products). The stability of hydride **3** in solution appeared also to be affected by the presence of metallic impurities. In particular, when partially oxidized samples of anion **1** were used in the protonation reaction, the reaction afforded only the degradation products. Similarly, every attempt to isolate this hydride in a pure state was frustated by decomposition during the work-up. Therefore, the molecular structure was inferred from classical spectroscopic studies of the solutions containing the hydride. In ir, the νCO and νNO values (Table 1) compared well with those of other selected complexes containing the neutral $Fe(CO)_2(NO)(P(C_6H_5)_3)$ metallic fragment. The νNO value of 1755 cm^{-1} was indicative of a linearly bounded NO, this bonding mode was also found in the single crystal structure of a related complex, the mercuric derivative $(Fe(CO)_2(NO)(P(C_6H_5)_3)_2Hg)$ (19). In the ^{1}H nmr, the resonance of the hydride occurred at high field as a doublet ($\delta = -3.5$ ppm, $J_{P-H} = 12$ Hz), which is the best single diagnosis for its presence (20). Extensive and reversible broadening was observed upon raising the temperature from −30°C to 0°C. When freshly prepared samples of anion **1** were used in the preparation of hydride **3**, the $^{31}P\{^1H\}$ nmr spectrum was composed of a single line at $\delta = 62.0$ ppm, with no evidence for the presence of the degradation products.

Additional support for the formulation given came from observations pertaining to the chemical reactivity (Scheme 2).

Addition of an excess of triphenyl phosphine to ether solutions of hydride **3** caused gas evolution along with the precipitation of the sparingly soluble disubstituted hydride $FeH(CO)(NO)(P(C_6H_5)_3)_2$ **4** (64% yield) (7). The ligand exchange reaction took place also in the opposite direction. Exposure of THF solutions of hydride **4** to CO at atmospheric pressure resulted in the partial conversion of **4** into hydride **3**, as shown by ir and ^{31}P nmr analysis of the solutions. The maximum conversion was reached after twenty minutes of exposure to CO, the intensities of the νNO's of **3** and **4** being in a 1:1 ratio at that point. Not surprisingly, no reaction was apparent in the presence of at least a five-fold excess of triphenyl phosphine.

The monsubstituted hydride **3** was also active in the stoichiometric hydrogenation of some unsaturated molecules at room temperature. The results are summarized in Table 2. Only double bonds which were part of a conjugated system were hydrogenated successfully. No reduction of an isolated double bond such as in cyclohexene or in 1-octene was observed after two hours. 1,1-Diphenyl ethylene was the most reactive, the hydride was consumed totally in less than 15 minutes, but with the other reactive substrates, significantly longer reaction times were needed (~2 hours). At the end of each reaction the usual mixture of the degradation products was formed, with no evidence for the presence of other complexes containing CO and/or NO ligands. The disubstituted hydride **4**, which is easily handled at room temperature in the solid state with no precaution taken to exclude air, could also be used as a "stabilized" precursor of hydride **3**. For example, hydride **4**, in THF or benzene, was reacted with CO at atmospheric pressure at room temperature. When ir analysis of the solution indicated the presence of hydride **3**, 1,1-diphenyl ethylene was added. The hydrogenation of the olefin and the formation of the degradation products proceeded as in the direct reaction with hydride **3** prepared from anion **1**. Reaction with butadiene might also proceed in a similar way. Hydride **4** in THF under argon was unreactive towards one to ten equivalents of butadiene at 25°C. However, when CO was passed into the solution, rapid formation of a mixture of the degradation products occurs. No evidence for the concomitant formation of a η^3-allyl derivative was obtained. This is in contrast to the formation of a (η^3-crotyl)iron nitrosyl complex upon reaction of butadiene with the parent iron nitrosyl hydride $FeH(CO)_3(NO)$ (16).

The facile replacement of one triphenyl phosphine ligand by

Can. J. Chem. Downloaded from www.nrcresearchpress.com by 210.87.254.6 on 09/06/12
For personal use only.

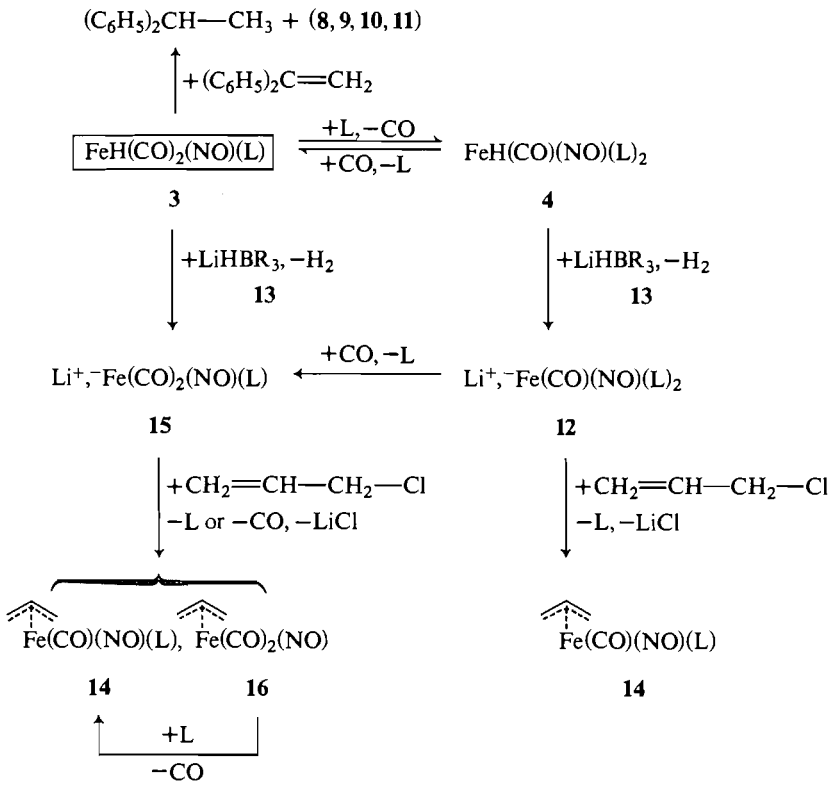

SCHEME 2 (L = $P(C_6H_5)_3$, R = C_2H_5)

TABLE 2. Stoichiometric hydrogenations with $FeH(CO)_2(NO)(P(C_6H_5)_3)$ **3**

Olefin	Hydrogenation product	Yield(%)
1,1-Diphenyl ethylene	1,1-Diphenyl ethane	75
1,1-Diphenyl ethylene	1,1-Diphenyl ethane	80[a]
1,1-Diphenyl ethylene	1,1-Diphenyl ethane	90[b]
α-Methyl styrene	Cumene	70
1,3-Cyclohexadiene	Cyclohexene	55
Cyclohexene	No reaction	0
1-Octene	No reaction	0

[a]Hydride **3** generated from hydride **4** in THF under CO.
[b]Hydride **3** generated from hydride **4** in benzene under CO.

CO was not limited to the neutral hydride $FeH(CO)(NO)(P(C_6H_5)_3)_2$ **4**. Its reduction product was also prone to the same facile substitution reaction.

In THF, hybride **4** was slowly reduced (2 hours at 50°C) to the lithium salt of the anion $[Fe(CO)(NO)(P(C_6H_5)_3)_2]^-$ **12** upon reaction with 1.3 molar equivalents of $LiHB(C_2H_5)_3$ **13**. The reactivity of the reduced species was very much like that of the sodium salt of the same anion, synthesized previously (7). The almost instantaneous reaction with allyl chloride at 0°C gave the allyl complex (η_3-propenyl)$Fe(CO)(NO)(P(C_6H_5)_3)$ **14** (9) in 67% yield. Furthermore, bubbling CO at atmospheric pressure through a THF solution of anion **12** at 20°C induced its irreversible conversion into the lithium salt of the dicarbonyl nitrosyl anion $[Fe(CO)_2(NO)(P(C_6H_5)_3)]^-$ **15**. Another more direct route to the same anion **15** involved the direct reduction of the dicarbonyl nitrosyl hydride **3** in ether. In that case, the reaction was fast at 0°C and occurred as soon as the reducing agent was added. The ir spectra of THF solutions of anion **15** were composed of four νCO's (1920, 1850 cm^{-1} strong and 1895, 1820 cm^{-1} weak) and two νNO's (1530 cm^{-1} strong and 1600 cm^{-1} weak). When THF was replaced by acetonitrile, only two νCO's (1895 and 1820 cm^{-1} strong) and one νNO (1600 cm^{-1}) were present. The shift towards higher wave numbers of the strong absorptions corresponding to the νNO and in the opposite direction for those corresponding to the νCO's under the influence of a good coordinating solvent was also observed with the sodium salts of the same anion **15** (7) and of the unsubstituted one $[Fe(CO)_3(NO)]^-$ **1** (21). This was taken as evidence for the occurence in THF of an equilibrium between loose and tight ion pairs, and for a specific cation...O-nitrosyl interaction in the tight ion pairs. In THF, anion **15** reacted with allyl chloride to yield a mixture of (η^3-propenyl)$Fe(CO)(NO)(P(C_6H_5)_3)$ **14** and the volatile (η^3-propenyl)$Fe(CO)_2(NO)$ **16** in a 1:2 ratio (based on the relative intensities of the NO's). The *in situ* transformation of **16** into **14** was accomplished by reaction with an excess of triphenyl phosphine, and **14** was isolated subsequently in a 65% overall yield.

2. *Reduction of the iron nitrosyl cation* $[Fe(CO)_2(NO)(P(C_6H_5)_3)_2]^+,BF_4^-$ **5**

These reactions were investigated to probe the utility of iron nitrosyl cations to serve as precursors of other iron nitrosyl derivatives. Cation **5** was already known to react with methoxide ion to yield a neutral carbomethoxy derivative (15). In the reaction with the boron hydride $LiHB(C_2H_5)_3$ **13** two competitive reactions were identified (Scheme 3).

Cation **5**, in suspension in THF, reacted with one to three molar equivalents of boron hydride **13** between −20°C and 0°C. Once the reaction reached completion (15 min), ir, ^{31}P nmr, and thin-layer chromatography revealed the formation of the degradation products **8**, **10**, and **11** (**9** was not detected) which were the only carbonyl and nitrosyl complexes to be

Can. J. Chem. Downloaded from www.nrcresearchpress.com by 210.87.254.6 on 09/06/12
For personal use only.

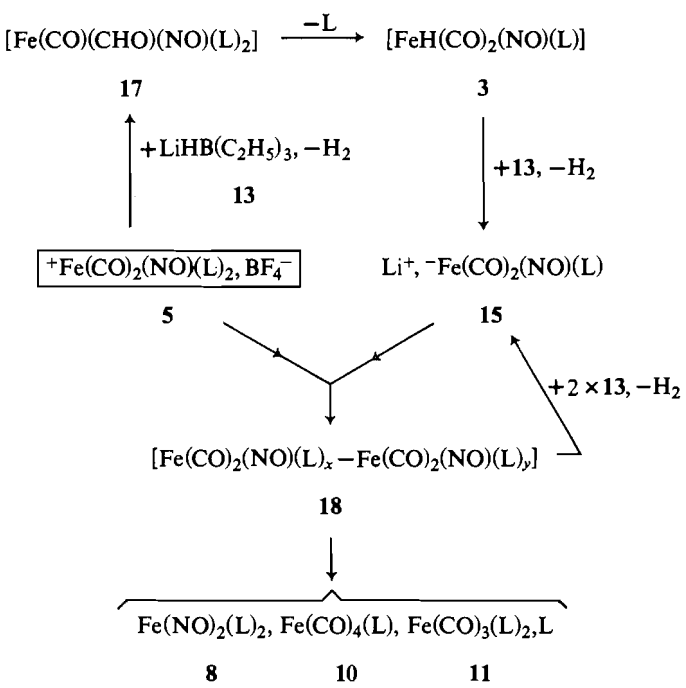

In **18**, $x + y \leq 4$ depending upon the coordination mode of the NO ligands

SCHEME 3 (L = $P(C_6H_5)_3$)

identified. Upon going from 3 to 6 equivalents of the reductant **13**, increasing amounts of the lithium salt of anion **15** were produced at the expense of the degradation products. With at least 6 equivalents of **13**, anion **15** was the sole metallic product to be characterized (≃80% spectroscopic yield). Although the distribution of the final reduction products was strongly affected by the amount of reducing agent used, there was no significant influence on the time required for the complete disappearance of cation **5**. Another characteristic of this reaction was the ability of one of the reduction products (anion **15**) to react rapidly with the complex subjected to the reduction (cation **5**). This was demonstrated by the following experiment. The same anion **15** (generated in two steps from an equimolar mixture of hydride **4** and reductant **13**, as described previously) reacted in THF at 0°C with the stoichiometric amount of cation **5**, added as a solid. In a few seconds, the same mixture of degradation products was produced as in the direct reduction of cation **5** with **13**. Considering previous results on related systems (22–26), an attractive route to anion **15** was to postulate the formation of the formyl complex **17** in the first step, followed by its decomposition into hydride **3** which had been found to undergo a rapid reduction upon reaction with borohydride **13**. Therefore, in an attempt to delineate the nature of the primary processes implicated in the reduction of cation **5**, its low temperature reactions in methylene chloride – THF solutions were monitored by ^1H and ^{31}P nmr. With $^{31}P\{^1H\}$ nmr, the only intermediate to be detected right after the reaction of cation **5** gave a single peak in the range δP = 61.8–62.3 ppm, depending upon the reaction conditions. Its transformation into anion **15** was fast. When an excess of reductant **13** was used, the reaction leading to **15** started at −60°C and was completed within 15 min upon raising the temperature to −40°C. In these conditions, anion **15** was the sole metallic product to be found at the end of the reaction. The nature of the intermediate remains speculative. The ^1H nmr of the solutions failed to reveal any proton resonance which could be assigned to hydride **3**. Instead, a low field triplet with 10 Hz separation between consecutive peaks was detected at δ = 13.6 ppm. The ^1H nmr data are comparable to those of the formyl complex $Ir(CO)(CHO)(P(C_6H_5)_3)_2$ (24). On that basis, the compound is tentatively formulated as the formyl derivative $Fe(CO)(NO)(CHO)(P(C_6H_5)_3)_2$ **17**. However, in the absence of low temperature ir data, the alternate formulation $Fe(CO)_2(NHO)(P(C_6H_5)_3)_2$ cannot be ruled out at present.

Discussion

In the protonation of anion **1** in THF with an excess of both the acid and the phosphine (Scheme 1), the intermediate detected by ir was likely the monosubstituted hydride **3**, on the basis of the νCO values. Probably, in those conditions, not enough free (unprotonated) phosphine was available for a rapid conversion into the disubstituted hydride **4**. The evolution towards the formation of cation **5** appears to be similar to the protonation of hydride **4** which led also to cationic complexes, and in particular to **5** when CO was present (7). In the appropriate acidic conditions, the formation of cationic derivatives indicates that the H ligand of both hydrides **3** and **4** can be removed formally as an H^-. The reductions into anions **12** and **15** demonstrate also that it can be removed easily as an H^+. Finally, the hydride ligand of hydride **3** can be transferred to an organic substrate, as shown by the stoichiometric hydrogenation reactions. The mechanisms of these reactions are not known at present, However, one should observe that, under our mild conditions, the reactive substrates were those capable of generating a resonance stabilized hydrocarbon radical. Thus, very much like the situation encountered with $MnH(CO)_5$ (27) or $CoH(CO)_4$ (3), the question of radical involvement in the hydrogenations with $FeH(CO)_2(NO)(P(C_6H_5)_3)$ should deserve further consideration.

Can. J. Chem. Downloaded from www.nrcresearchpress.com by 210.87.254.6 on 09/06/12
For personal use only.

Can. J. Chem. Downloaded from www.nrcresearchpress.com by 210.87.254.6 on 09/06/12
For personal use only.

Comparing further the reactivity of the iron nitrosyl complexes to that of the isoelectronic cobalt carbonyl hydrides reveals interesting differences; at least two are noteworthy.

The first difference resides in the substitution reactions. In particular, the substitutional lability of the monosubstituted hydride $FeH(CO)_2(NO)(P(C_6H_5)_3)$ **3**, reflected by its reaction with triphenyl phosphine to afford the disubstituted hydride $FeH(CO)(NO)(P(C_6H_5)_3)_2$, **4**, contrasts sharply with the reported lack of reaction of the isoelectronic cobalt hydride $CoH(CO)_3(P(C_6H_5)_3)$ with an excess of the same phosphine (28). This might be an indication of a greater accessibility of the metal coordination sphere in the iron complexes, possibly a consequence of the presence of the NO ligand.

The second major difference has to be found in the nature of the products resulting from thermal degradation. Decomposition of monohydrido complexes generally yields metallic dimers, as exemplified by the thermolysis of the cobalt hydrides $CoH(CO)_3(L)$ (L = CO (29), L = $P(OC_6H_5)_3$ (30), L = $P(C_6H_5)_3$ (31)). In no case could we detect the formation of metallic dimers containing a $(Fe(NO))_2$ unit in the thermolysis of the iron nitrosyl complexes $Fe(CO)_u(NO)(P(C_6H_5)_3)_v$ ($u + v = 3$, $v = 0$, 1, 2). Instead, a mixture of monometallic degradation products was formed. This difference in behavior is not restricted to thermolysis and appears to be general. For instance, metallic dimers were formed in the electrochemical one-electron oxidation of $[Co(CO)_4]^-$ (32), in the oxidation of $CpMo(CO)_3H$ (33) with molecular oxygen, in the reactions of olefins with $CpMo(CO)_3H$ (34), $MnH(CO)_5$ (27), or $CoH(CO)_4$ (3) (among others (35)), or in the reactions of a variety of cobaltates with cationic cobalt complexes (36). In contrast, $Fe(CO)_2(NO)_2$ resulted from the one-electron oxidation of the anion $[Fe(CO)_3(NO)]^-$ (37), and a mixture of the degradation products **8**, **9**, **10**, and **11** was formed in the reactions of $FeH(CO)_2(NO)(P(C_6H_5)_3)$ **3** with either molecular oxygen or olefins, and in the reaction of cation **5** with anion **15**.

All of these reactions have in common the persistent formation of monometallic dinitrosyl complexes (**2**, **8**, **9**, depending upon the reaction) which points to the occurrence of a nitrosyl exchange reaction at some stage of the reaction pathway. For such a reaction to take place, the formation of metal–metal bonded species appears to be a prerequisite (38, 39). This leads to the proposal that, in all these reactions, metallic dimers are actually formed, but they are transient intermediates because NO and CO exchange reactions promote fast and irreversible fragmentations into monometallic degradation products.[4]

This hypothesis offers an attractive and simple rationalization of the distribution of products found in the reduction of cation **5** (Scheme 3). The low temperature experiments have indicated that formation of anion **15** is a facile process at −40°C. Thus, in the temperature range −20°C to 0°C, when reduction of cation **5** in suspension in THF proceeded at a significant rate, anion **15** should have been present in solution before all of the cation had reacted with the reductant. It follows that, in parallel to the direct reduction of cation **5**, its rapid reaction with anion **15** should have occurred also to yield an unstable dimer such as **18**. Boron hydride **13** is known for its ability to reductively cleave metal–metal bonds (40). Therefore, reductive cleavage of dimer **18** back to anion **15** becomes an alternative to the irreversible evolution towards the degradation products. This model, which places the emphasis on the occurrence of a trapping reaction of the dimeric species **18** prior to its irreversible decomposition, has an obvious implication which is borne out by the results. As the excess of boron hydride **13** is increased, conversion of dimer **18** into anion **15** is expected to be favored at the expense of the degradation products, in agreement with the observations.

The question as to whether molecular hydrogen can perform also as an efficient trapping agent is then of prime importance in the context of catalytic reactions such as hydrogenation of hydroformylation. Very likely the unequivocal evaluation or the activity of the iron nitrosyl hydrides in those reactions will require conditions favoring an effective hydride regeneration step from a diiron dinitrosyl dimer, a reaction intermediate which is likely to be expected in the light of the known reactivity patterns (41, 42) of related systems. Experiments directed along those lines are underway.

[4]Extensive NO, CO, and phosphine exchanges were observed also in the reactions of halide complexes with metallates (47).

Acknowledgements

The authors wish to thank the Natural Sciences and Engineering Research Council of Canada for their financial support.

1. J. L. A. ROUSTAN, J. Y MEROUR, and F. HOULIHAN. Tetrahedron Lett. 3721 (1979).
2. J. H. ENEMARK and R. S. FELTHAM. Coord. Chem. Rev. **13**, 339 (1974).
3. M. ORCHIN. Acc. Chem. Res. **14**, 259 (1981).
4. B. R. JAMES. Adv. Organomet. Chem. **17**, 319 (1979).
5. I. WENDER and P. PINO (*Editors*). Organic synthesis via metal carbonyls. Vol. II. John Wiley and Sons, New York. 1977.
6. W. HIEBER and H. BUETNER. Z. Anorg. Allg. Chem. **320**, 91 (1963).
7. J. L. A. ROUSTAN and F. FORGUES. J. Organomet. Chem. **184**, C13 (1980).
8. M. CYGLER, F. AHMED, A. FORGUES, and J. L. A. ROUSTAN. Inorg. Chem. In press.
9. G. CARDACI. J. Chem. Soc. Dalton. Trans. 2452 (1974), and references therein.
10. O. SIEGLE. J. Organomet. Chem. **92**, 321 (1975).
11. A. F. CLIFFORD and A. K. MUKHERJEE. Inorg. Synth. **8**, 186 (1966).
12. R. B. KING. Organometallic synthesis. Vol. 1. Academic Press, New York. 1965. p. 157.
13. D. W. MCBRIDE, S. L. STAFFORD, and F. G. A. STONE. Inorg. Chem. **1**, 386 (1962).
14. J. L. A. ROUSTAN, J. Y MEROUR, and F. A. FORGUES. J. Organomet. Chem. **186**, C23 (1980).
15. B. F. G. JOHNSON and J. A. SEGAL. J. Chem. Soc. Dalton Trans. 1268 (1972), and references therein.
16. F. M. CHAUDARI, G. R. KNOX, and P. L. PAUSON. J. Chem. Soc. (C), 2255 (1967).
17. J. E. MAHLEN, D. H. GIBSON, and R. PETTIT. J. Am. Chem. Soc. **85**, 3959 (1963).
18. R. A. SCHUNN. *In* Transition metal hydrides. Vol. 1. *Edited by* E. L. Muetterties. Marcel Dekker, New York. 1971. Chapt. 5.
19. F. P. STEPHENS. J. Chem. Soc. Dalton Trans 2257 (1972).
20. J. P. MCCUE. Coord. Chem. Rev. **10**, 265 (1973); H. D. KAEZ and R. B. SAILLANT. Chem. Rev. **72**, 231 (1972); J. P. JESSON. *In* Transition metal hydrides, Vol. 1. *Edited by* E. L. Muetterties. Marcel Dekker, New York. 1971. Chapt. 4.
21. K. H. PANNEL, YU SEN CHEN, and K. L. BELKNAP. J. Chem. Soc. Chem. Commun. 362 (1977).
22. J. R. SWEET and W. A. G. GRAHAM. J. Organomet. Chem. **173**, C9 (1979).
23. C. P. CASEY, M. A. ANDREW, D. R. MCALLISTER, and J. E.

RINZ. J. Am. Chem. Soc. **102**, 1927 (1980).
24. W. TAM, WONG WAI KWOK, and J. A. GLADYSZ. J. Am. Chem. Soc. **101**, 1589 (1979).
25. P. LEGZDINS and D. T. MARTIN. Inorg. Chem. **18**, 1250 (1979).
26. B. F. G. JOHNSON and J. A. SEGAL. J. Chem. Soc. Dalton Trans. 478 (1973).
27. R. W. SWEANY and J. HALPERN. J. Am. Chem. Soc. **99**, 8335 (1977).
28. R. F. HECK. J. Am. Chem. Soc. **87**, 2572 (1965).
29. R. W. WEGMAN and T. L. BROWN. J. Am. Chem. Soc. **102**, 2494 (1980).
30. C. L. REICHEL and M. S. WRIGHTON. J. Am. Chem. Soc. **101**, 6771 (1979).
31. R. F. HECK. J. Am. Chem. Soc. **85**, 657 (1963).
32. V. A. VLCEE. Collect. Czechv. Chem. Commun. **24**, 1478 (1959).
33. R. B. KING and F. G. A. STONE. Inorg. Synth. **7**, 99 (1963).
34. A. MIAKE and H. KONO. Angew. Chem. Int. Ed. Engl. **7**, 631 (1968).
35. G. DOLCETTI and N. W. HOFFMAN. Inorg. Chem. Acta, **9**, 269 (1974).
36. M. SAMIR-ARABI, A. MOISONNAT, S. ATTALI, and R. POILBLANC. J. Organomet. Chem. **67**, 109 (1974).
37. S. M. MURGIA, G. PALIANI, and G. CARDACCI. Z. Naturforsch. Teil B, **27**, 134 (1972).
38. C. B. UNGERMANN and K. G. CAULTON. J. Am. Chem. Soc. **98**, 3862 (1975).
39. A. SACCO, G. VASAPOLLO, and P. GIANNOCARO. Inorg. Chem. Acta, **32**, 171 (1979).
40. J. A. GLADYSZ, G. M. WILLIAMS, W. TAM, D. L. JOHNSON, D. W. PARKER, and J. C. SELOVER. Inorg. Chem. **18**, 553 (1979).
41. R. B. KING, A. D. KING JR., M. Z. IQBAL, and C. C. FRASER. J. Am. Chem. Soc. **100**, 1687 (1978).
42. W. D. JONES and R. G. BERGMAN. J. Am. Chem. Soc. **101**, 5447 (1979).
43. M. CASEY and A. R. MANNING. J. Chem. Soc. (A), 256 (1971).
44. M. CASEY and A. R. MANNING. J. Chem. Soc. (A), 2258 (1970).
45. G. DOLCETTI, L. BUSETTO, and P. A. PALAZZI. Inorg. Chem. **13**, 222 (1974).
46. W. E. CAROLL, F. A. DEENEY, and F. J. LALOR. J. Chem. Soc. Dalton Trans. 1430 (1974).
47. P. BRAUNSTEIN, J. DEHAND, and B. MUNCHENBACH. J. Organomet. Chem. **124**, 71 (1977).

Can. J. Chem. Downloaded from www.nrcresearchpress.com by 210.87.254.6 on 09/06/12
For personal use only.

Synthesis and catalytic potential of coordinatively unsaturated rhodium hydride clusters incorporating chelating bidentate ligands

MICHAEL D. FRYZUK

Department of Chemistry, University of British Columbia, 2036 Main Mall, Vancouver, B.C., Canada V6T 1Y6

Received August 20, 1982

MICHAEL D. FRYZUK. Can. J. Chem. **61**, 1347 (1983).

The synthesis of three coordinatively unsaturated clusters of the formula $[\{R_2PCH_2CH_2PR_2\}RhH]_x$ (R = OMe and OEt: $x = 4$; R = O-*i*-pr: $x = 2$) is described starting from the appropriate 2-methylallylrhodium(I) derivatives and H_2. The reaction of PMe_3 with these clusters results in the formation of mononuclear complexes of the formula $HRh(PMe_3)_2(R_2PCH_2CH_2PR_2)$. Olefins such as 1-hexene do not appear to react with the clusters although a slow isomerization to internal hexenes takes place. The tetranuclear clusters do not form a detectable adduct with H_2 up to 4 atm, although exchange with D_2 is observed. However, the dinuclear cluster adds one equivalent of H_2 per dimer to generate, in situ, $[\{(i\text{-prO})_2PCH_2CH_2P(O\text{-}i\text{-pr})_2\}_2Rh_2H_4]$. These clusters are catalytically active in the hydrogenation of 1-hexene with isomerization to internal hexenes being a competitive process. Although the evidence suggests that the dinuclear derivative does not fragment during the catalytic cycle, the catalytic activity of the tetranuclear clusters may be due to a smaller cluster present in low concentration, generated by fragmentation.

MICHAEL D. FRYZUK. Can. J. Chem. **61**, 1347 (1983).

On décrit la synthèse de trois agrégats insaturés coordonnés de formule $[\{R_2PCH_2CH_2PR_2\}RhH]_x$ (R = OMe et OEt; $x = 4$, R = O-*i*-pr: $x = 2$) à partir des dérivés appropriés du méthyl-2 allylrhodium(I) et du H_2. La réaction de PMe_3 avec ces groupes conduit à la formation des complexes mononucléaires de formule $HRh(PMe_3)_2(R_2PCH_2CH_2PR_2)$. Les oléfines, tel l'hexène-1, ne semblent pas réagir avec ces agrégats bien qu'il se produise une isomérisation lente en hexènes internes. L'agrégat tétranucléaire ne donne pas d'adduit décelable avec H_2 jusqu'à 4 atm en dépit du fait qu'on observe un échange avec D_2. Cependant l'agrégat binucléaire capte un équivalent de H_2 par dimère pour produire "in situ" le $[\{(i\text{-prO})_2PCH_2CH_2P(O\text{-}i\text{-pr})_2\}_2Rh_2H_4]$. Ces agrégats sont actifs catalytiquement lors de l'hydrogénation de l'hexène-1 avec une isomérisation en hexènes internes comme processus compétitif. Bien que les preuves suggèrent que le dérivé binucléaire ne se fragmente pas pendant le cycle catalytique, l'activité catalytique de l'agrégat tétranucléaire peut être dû à un agrégat plus petit présent à faible concentration et qui est produit par la fragmentation.

[Traduit par le journal]

Can. J. Chem. Downloaded from www.nrcresearchpress.com by 210.87.254.42 on 09/06/12
For personal use only.

Introduction

The design of a transition metal based homogeneous catalyst for a particular chemical transformation requires the incorporation of many subtle features. Of these, coordinative unsaturation has long been recognized (1) as crucial since one must insure that the substrate molecule can coordinate to the metal complex at some point in the catalytic cycle. There are, of course, other properties that a catalyst must have, depending on the particular transformation of interest, but these can be largely overcome by a suitable choice of the metal and the ancillary ligands.

Rhodium(I) hydride complexes containing phosphorus ligands are well known (2) catalysts for olefin hydrogenation and isomerization type transformations. One of the earliest systems of this genre to be investigated (3) was P_4RhH where P = PPh_3. Using simple electron counting rules (4), P_4RhH is an 18 electron complex, and therefore coordinatively saturated, yet this particular derivative is catalytically active for the hydrogenation of olefins (5). This is not an exception to the requirement for coordinative unsaturation since it has been established (5) that phosphine dissociation occurs in solution to generate the 16 electron, coordinatively unsaturated species P_3RhH (reaction [1]) which is the active catalyst (6)

[1] $P_4RhH \rightleftharpoons P_3RhH + P$

Indeed, P_3RhH can be specifically synthesized (3, 6) and isolated and, not surprisingly, its catalytic activity was found to be greater than P_4RhH (7). It was initially believed (5) that the catalytic activity of P_3RhH also required dissociation to a 14 electron species P_2RhH (reaction [2]); however, this equilibrium was found (8, 9) to lie far to the left. Nonetheless, a

[2] $P_3RhH \rightleftharpoons P_2RhH + P$

number of groups have investigated the synthesis and reactivity of 14 electron fragments of empirical formula P_2RhH. For instance (10), the use of bulky, monodentate phosphines such as tri-*tert*-butylphosphine, $P(t\text{-}Bu)_3$, and tricyclohexylphosphine, $P(C_6H_{11})_3$, generates mononuclear 14 electron fragments via dissociation of dinitrogen from $[P(t\text{-}Bu)_3]_2RhH(N_2)$ and $\{[P(C_6H_{11})_3]_2RhH\}_2\text{-}\mu\text{-}N_2$ (reaction [3]).

[3] $\frac{1}{x}[P_2RhH]_x(N_2) \xrightarrow{-N_2} P_2RhH$

$x = 1$, P = $P(t\text{-}Bu)_3$
$x = 2$, P = $P(C_6H_{11})_3$

Solution ^1H nmr studies indicate that these particular 14 electron complexes are T-shaped with *trans* disposed phosphines (Fig. 1, structure **A**); this agrees with MO calculations (11) which indicate that the Y-shaped structure (Fig. 1, **B**) is higher in energy. Interestingly, if phosphites ($P(OR)_3$) are used as ligands, a series of coordinatively unsaturated clusters of the formula $[\{P(OR)_3\}_2RhH]_x$ can be synthesized (12). Although the nuclearity of the cluster depends on the choice of $P(OR)_3$, these derivatives can be formulated, albeit simplistically, as overlapping hydride-bridged T-shaped fragments of structure **C** (Fig. 1).

Our strategy was to attempt to generate 14 electron complexes with structure **C** by the use of chelating bidentate ligands. In this manner we hoped to synthesize reactive, coordinatively unsaturated catalysts with the necessary active site *cis* to the hydride ligand by virtue of the fact that the phosphorus donors were constrained to be *cis* disposed. In fact, we were unable to isolate the proposed mononuclear fragments, but rather tetranuclear and dinuclear clusters of the formula $[\{R_2PCH_2CH_2PR_2\}RhH]_x$ (R = OMe and OEt: $x = 4$; R =

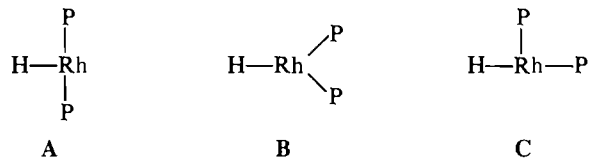

A B C

FIG. 1. Geometrical shapes available to the 14 electron fragments P_2RhH.

O-*i*-pr: $x = 2$) were generated. Fortunately, these clusters are catalytically active due to the fact that even as a cluster these derivatives are coordinatively unsaturated. We report here the syntheses of three such clusters and a portion of their reaction chemistry. A preliminary report of this work has appeared (13).

Cluster synthesis

The precursor to all the clusters of the formula $[\{R_2PCH_2CH_2PR_2\}RhH]_x$ is 2-methylallyl-1,5-cyclooctadienerhodium(I), $[\eta^3$-(2-Me-C_3H_4)Rh(COD)] (14). Substitution of the COD ligand by chelating phosphines or phosphinites is facile at room temperature (reaction [4]) to generate complexes

[4] 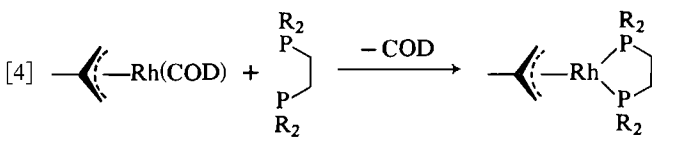

R = OMe **1***a*
R = OEt **1***b*
R = O-*i*-pr **1***c*

of the type **1** which react with medium pressures of hydrogen (2–4 atm) according to reaction [5].

[5] 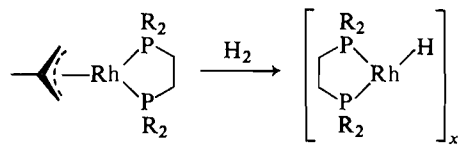

R = OMe; $x = 4$ **2***a*
R = OEt; $x = 4$ **2***b*
R = O-*i*-pr; $x = 2$ **2***c*

For example, the addition of one equivalent of 1,2-bis(dimethoxyphosphino)ethane (dmope) to $[\eta^3$-(2-Me-C_3H_4)Rh(COD)] in hexane, results in the formation of $[\eta^3$-(2-Me-C_3H_4)-Rh(dmope)] (**1***a*). **1***a* can be isolated (14) and stored under nitrogen indefinitely; however, it is more convenient to immediately subject **1***a* to 2–4 atm of hydrogen in toluene solution. Over a period of a few hours, the bright yellow colour of **1***a* darkens to a deep, black–red from which dark maroon crystals of the tetranuclear cluster $[(dmope)RhH]_4$ (**2***a*) can be isolated in 60–70% yield. The nuclearity of the cluster is evident from the hydride resonance (13) which appears as an overlapping quintet of nonets due to coupling with four magnetically equivalent rhodium nuclei and eight magnetically equivalent phosphorus nuclei; a solution molecular weight determination confirms this tetrameric formulation. With the use of 1,2-bis(diethoxyphosphino)ethane (deope), a similar sequence generates the closely related tetranuclear cluster $[(deope)RhH]_4$ (**2***b*), although in this case crystalline material could not be obtained. At room temperature, the hydride resonance of **2***b* is broad, but sharpens upon heating to >40°C to an identical 23 line multiplet as is observed for **2***a*.

With the isopropyl-substituted chelating phosphinite, $(i\text{-prO})_2PCH_2CH_2P(O\text{-}i\text{-pr})_2$ (dipope), a dinuclear cluster, $[(dipope)RhH]_2$ (**2***c*), is obtained as bright red crystals from the reaction of $[\eta^3$-(2-Me-C_3H_4)Rh(dipope)] (**1***c*) with hydrogen. Once again the nuclearity of the cluster is evident from the phosphorus decoupled proton nmr wherein the hydride resonance appears as a triplet due to coupling with two magnetically equivalent rhodium nuclei.

All of these clusters are extremely air- and moisture-sensitive in solution and in the solid state. The thermal stability of these derivatives in solution appears to be quite high; at 60°C, no change is observed for **2***c* in C_6D_6 by ^1H nmr over 24 h, with similar behaviour shown for the tetranuclear derivatives **2***a* and **2***b*.

The use of infrared spectroscopy to aid in the analysis of the clusters has been rather disappointing; the Rh—H stretching frequency for the tetranuclear clusters cannot be assigned as the ir's of $[(deope)RhH]_4$ and its deuterated analogue, $[(deope)RhD]_4$, are superimposable. A medium absorption at 1180 cm^{-1} is assigned to ν_{Rh-H} for the dinuclear derivative $[(dipope)RhH]_2$ (ν_{Rh-D} = 870 cm^{-1}).

Reaction chemistry

The addition of excess trimethylphosphine, PMe_3, to **2***a* results in the slow loss of the deep red colour of the tetranuclear cluster, to generate a light yellow solution. By ^1H and $^{31}P\{^1H\}$ nmr, the species formed in quantitative yield is the mononuclear complex $[HRh(PMe_3)_2(dmope)]$ (**3***a*) (reaction [6]).

[6] 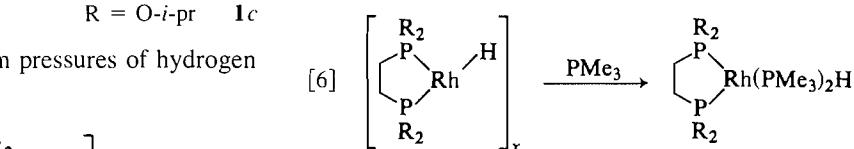

R = OMe **3***a*
R = O-*i*-pr **3***b*

For the tetranuclear cluster, this reaction is remarkably slow, proceeding to completion over a period of 2–3 h. Monitoring the reaction by ^1H nmr indicates only the presence of the starting cluster and the mononuclear product. In contrast, the reaction of PMe_3 with the dinuclear complex **2***c* is immediate upon mixing to generate **3***c*.

The hydride resonances of **3***a* and **3***c* are virtually identical; for example, at room temperature the hydride portion of the ^1H nmr spectrum of **3***a* appears as a well resolved triplet of double triplets centered at −9.8 ppm with the following parameters: $^1J_{Rh}$ = 10.6 Hz; $^2J_{PMe_3}$ = 22.6 Hz; $^2J_{P(OMe)_2}$ = 88.5 Hz. Based on the known (15) structure of $\{P(OEt)_3\}_4RhH$, a similar pseudotetrahedral structure for **3** is reasonable with the hydride undergoing "tunneling" (15) between tetrahedral faces.[1]

A reaction which is remarkably dependent on the nuclearity of the cluster involves H_2. No reaction between the tetranuclear clusters, **2***a* and **2***b*, and H_2 is observed even up to 4 atm. Thus

[1]It is interesting to note that these mononuclear derivatives, **3**, have two types of tetrahedral faces due to the two types of ligands, unlike $\{P(OEt)_3\}_4RhH$ for which all the tetrahedral faces are identical. Based on coupling constants measured for **3***a*, it is conceivable that the hydride preferentially occupies that set of tetrahedral faces *trans* to the $P(OMe)_2$ donors since $^2J_{P(OMe)_2}$ = 88.5 Hz is typical of an "averaged" *trans* coupling (15) whereas $^2J_{PMe_3}$ = 22.6 Hz is consistent with a *cis* coupling constant.

Can. J. Chem. Downloaded from www.nrcresearchpress.com by 210.87.254.42 on 09/06/12
For personal use only.

a sealed nmr tube of **2***a* under ≈4 atm of H_2 indicates only the presence of the starting tetranuclear cluster even down to −80°C. However, the hydrides of both tetranuclear clusters exchange with D_2 gas (1 atm) at room temperature over a period of 30−40 min. In contrast, the dinuclear complex **2***c* reacts immediately with H_2 to produce a new, dinuclear tetrahydride, $[(dipope)_2Rh_2H_4]$ (**4**) in quantitative yield (by ^1H nmr) (reaction [7]).

[7] 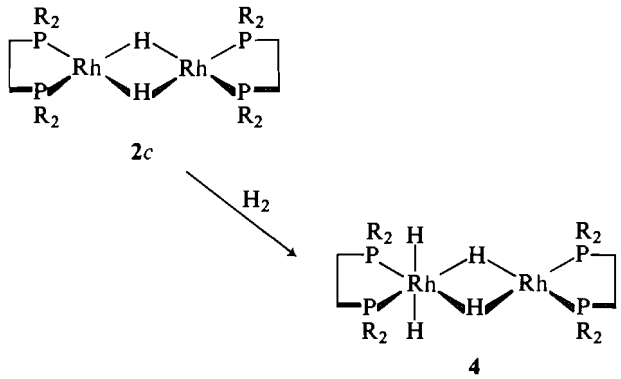

2*c*

4

R = O-*i*-pr

Attempts to isolate **4** have so far proved unsuccessful as dehydrogenation to regenerate **2***c* appears to be facile. The structure of **4** shown is based on low temperature ^1H nmr studies (see Experimental section) wherein two hydride resonances of equal area are observed: a doublet of broad multiplets at −7.25 ppm (J_P = 148 Hz) and a broad multiplet at −12.0 ppm, at −50°C in C_7D_8. Further cooling to −90°C only results in slight broadening of these resonances. Based on other closely related dinuclear rhodium hydride complexes (12, 16), **4**, may not be the ground state structure of $[(dipope)_2Rh_2H_4]$; rather, a similar structure to that proposed (12) for $[\{P(O\text{-}i\text{-}pr)_3\}_4Rh_2H_4]$ (**5**) may be implicated.

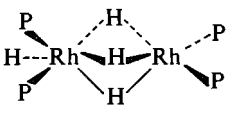

P = P(O-*i*-pr)$_3$

5

Unfortunately, no corroborating evidence for the triply bridging hydride type structure was obtained for **4**.

Both tetranuclear clusters **2***a* and **2***b* appear inert to olefins such as 1-hexene, ethylene, butadiene, and 1,5-cyclooctadiene, although with 1-hexene, a very slow isomerization reaction is observed (vide infra). The dinuclear cluster **2***c* also appears, by ^1H nmr, indifferent to mono-olefins such as 1-hexene and ethylene whereas diolefins react quite rapidly (17).[2] Again, a very slow isomerization of 1-hexene is observed with **2***c*.

Hydrogenation of 1-hexene

The tetranuclear cluster **2***a* is an efficient catalyst for the hydrogenation of 1-hexene at 1 atm pressure and 22°C. Turnover numbers[3] are of the order of 150 h^{-1}. Concomitant with hydrogenation is an isomerization process which converts 1-hexene to *cis*- and *trans*-2-hexene in a ≈1:3 ratio; the turnover numbers for isomerization are ≈600 h^{-1} for *trans*-2-hexene formation and ≈180 h^{-1} for *cis*-2-hexene. In the absence of hydrogen, isomerization occurs with a turnover number of ≈3 h^{-1} with ratio of *trans*-2-hexene to *cis*-2-hexene being 2:1. It appears that a small amount of *cis*- and *trans*-3-hexene is also produced, but our method of analysis (see Experimental section) did not allow us to distinguish these particular stereoisomers from *cis*- and *trans*-2-hexene, respectively. It should be noted that although these turnover numbers are reproducible, extreme care must be taken to avoid oxygen contamination.

The corresponding turnover numbers for the dinuclear cluster **2***c* are higher; hydrogenation proceeds with turnover numbers of ≈700 h^{-1} while isomerization occurs with a turnover number of ≈1000 h^{-1} for *trans*-2-hexene and ≈300 h^{-1} for *cis*-2-hexene. In the absence of hydrogen, isomerization proceeds with a turnover number of ≈5 h^{-1}.

The tetranuclear cluster, **2***a*, and the dinuclear cluster, **2***c*, hydrogenate both terminal olefins and internal olefins with little or no selectivity; this is evidenced by the fact that hexane formation is relatively constant even after the disappearance of 1-hexene, leaving internal hexenes.

Discussion

Although our strategy to generate mononuclear 14 electron complexes was unsuccessful, we were able to isolate three new members of the family of coordinatively unsaturated clusters having the formula $[P_2RhH]_x$ (12, 13, 16). The nuclearity of the cluster appears to be a function of the bulkiness of the phosphorus donor ligand. The use of the bidentate ligand $(MeO)_2PCH_2CH_2P(OMe)_2$ allows for the formation of the tetranuclear cluster **2***a*, the largest member of this family of clusters; this contrasts the use of $P(OMe)_3$ as a monodentate ligand for which the trinuclear cluster $[\{(MeO)_3P\}_2RhH]_3$ is generated (12). In an attempt to generate a trinuclear cluster incorporating chelating bidentate phosphinite ligands, the use of $(EtO)_2PCH_2CH_2P(OEt)_2$ was investigated; however, only the tetranuclear cluster **2***b* was detected. The bulkier chelating phosphinite ligand $(i\text{-}prO)_2PCH_2CH_2P(O\text{-}i\text{-}pr)_2$ yields the dinuclear cluster **2***c*, analogues of which are known using monodentate phosphorus donors (12, 16).

The reactivity patterns of these clusters are beginning to take shape even though numerous reaction types other than those described are conceivable. The reaction of a strong ligand such as PMe_3 results in fragmentation of the cluster and the production of the mononuclear species **3**; the outcome of this reaction is independent of the cluster size, although the tetranuclear cluster is notably slower, and in line with these derivatives being coordinatively unsaturated (13). In contrast, mono-olefins do not form adducts which can be detected, and the cluster remains intact; however, the fact that isomerization is observed suggests either some type of weak interaction, or the generation of a reactive adduct in very small concentration.

Whereas the dinuclear cluster **2***c* oxidatively adds one equivalent of H_2 to generate the dinuclear tetrahydride **4**, no reaction with H_2 is observed with the tetranuclear clusters **2***a* and **2***b*. Yet, the hydrides of **2***a* and **2***b* exchange with D_2, again suggestive of a reactive intermediate present in very low concentration.

The differences in the reactivities of the tetranuclear clusters as compared to the dinuclear derivative are further observed

[2]For instance, 2,5-norbornadiene and 1,5-cyclooctadiene react instantaneously to generate new complexes which are under investigation.

[3]Turnover numbers for a given transformation, either hydrogenation or isomerization, are defined as: number of moles product per mole of cluster per hour.

Can. J. Chem. Downloaded from www.nrcresearchpress.com by 210.87.254.42 on 09/06/12
For personal use only.

Can. J. Chem. Downloaded from www.nrcresearchpress.com by 210.87.254.42 on 09/06/12
For personal use only.

under catalytic hydrogenation conditions wherein the tetranuclear cluster exhibits lower turnover numbers for both hydrogenation and isomerization of 1-hexene.

It has been proposed (12, 16) that the mechanism of hydrogenation of olefins by dinuclear rhodium hydrides of the type $[P_2RhH]_2$, where P is a *monodentate* ligand such as $P(O\text{-}i\text{-}pr)_3$ or $P(NMe_2)_3$, proceeds without fragmentation of the binuclear framework to mononuclear species; the first step involves oxidative addition of H_2 to generate the dinuclear tetrahydride $[P_4Rh_2H_4]$, followed by olefin coordination and subsequent hydride transfers to give the alkane. The turnover numbers for hydrogenation by these dinuclear systems having monodentate ligands are approximately 10 times higher ($\approx$7200 h^{-1}) than our dinuclear cluster incorporating chelating ligands. Since the reaction conditions are comparable, it is tempting to suggest that the bidentate ligand influences the course of the reaction. Support for this comes from a recent X-ray study (16) of the dinuclear tetrahydride $[\{P(NMe_2)_3\}_4Rh_2H_4]$, wherein the phosphorus donors on one rhodium are *trans* disposed as in **6**, a stereochemistry which cannot be attained using the bidentate ligand strategy (cf. **4**).

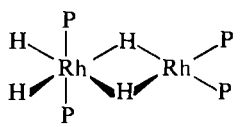

$P = P(NMe_2)_3$

6

Although it is not clear as yet how the tetrahydride **6** could be more reactive than our tetrahydride **4**, it should be noted that, if hydrogenation and isomerization are competitive processes in the catalytic cycle, then a change in the stereochemistry of the tetrahydride intermediate may allow one process to dominate. This is in fact observed in our dinuclear system where turnover numbers for isomerization are higher than for hydrogenation.

Unfortunately, little can be deduced about the mechanism of hydrogenation of 1-hexene by the tetranuclear cluster **2***a*. It is possible that the active species, present in low concentration, is generated by fragmentation of the cluster. One possible stepwise fragmentation reaction would generate a trinuclear cluster in addition to a mononuclear fragment (reaction [8]); another possibility (reaction [9]) involves formation of dinuclear deriv-

[8] $[(dmope)RhH]_4 \rightleftharpoons [(dmope)RhH]_3 + \text{"(dmope)RhH"}$

[9] $[(dmope)RhH]_4 \rightleftharpoons 2[(dmope)RhH]_2$

atives. The presence of some undetectable reactive impurity in the tetranuclear cluster is also a possibility, although very little change in turnover numbers is observed for different batches of **2***a*. The fragmentation aspect of cluster catalysis is extremely important. For the dinuclear hydride systems, fragmentation does not appear to be a necessary component for catalysis; however, for the tetranuclear cluster, fragmentation to generate smaller clusters still remains as a possible mode of activation.

Another important facet which we are presently involved in is the following: if the cluster remains intact during the catalytic cycle, do the metal centers act synergistically (that is, substrate coordination by one metal, H_2 activation by another, and subsequent migration of the organic intermediates between metal centers), or, do the metal centers act independently within the cluster?

Experimental section

General procedures and precautions were identical to that previously described (14). Infrared spectra were recorded on a Pye-Unicam SP-1100 in matched solution cells (0.1 mm, NaCl). $[\eta^3\text{-}(2\text{-}Me\text{-}C_3H_4)Rh(dmope)]$ (**1***a*) was prepared by the literature procedure (14).

Ligand syntheses

All of the chelating phosphinite ligands were synthesized by King's method (18) from $Cl_2PCH_2CH_2PCl_2$ (19) and the appropriate alcohol, ROH (dried over $Mg(OR)_2$).

$(MeO)_2PCH_2CH_2P(OMe)_2$ (dmope): ^1H nmr (C_6D_6, ppm): PCH_2CH_2P, 1.72 (t, J_P = 6.2 Hz); $P(OCH_3)_2$, 3.32 (complex doublet, J_P = 11.0 Hz).

$(EtO)_2PCH_2CH_2P(OEt)_2$ (deope): ^1H nmr (C_6D_6, ppm): PCH_2CH_2P, 1.83 (t, J_P = 6.0 Hz); $P(OCH_2CH_3)_2$, 3.68 (m); $P(OCH_2CH_3)_2$, 1.00 (t, J_{CH_2} = 7.0 Hz).

(i-prO)$_2$PCH$_2$CH$_2$P(O-i-pr)$_2$ (dipope): ^1H nmr (C_6D_6, ppm): PCH_2CH_2P, 1.92 (t, J_P = 6.0 Hz); $P(OCH(CH_3)_2)_2$, 4.12 (m); $P(OCH(CH_3)_2)_2$, 1.22, 1.15 (d, J_{CH} = 6.0 Hz).

$[\eta^3$-(2-Me-C$_3$H$_4$)Rh(deope)] (1b): This complex was synthesized as previously described (14) for $[\eta^3\text{-}(2\text{-}Me\text{-}C_3H_4)Rh(dmope)]$. It was obtained as a yellow oil and characterized by its ^1H nmr. ^1H nmr (C_6D_6, ppm): H_{syn}, 3.83 (s, 2); H_{anti}, 2.29 (d, 2, J_P = 7.0 Hz); 2-CH_3, 1.57 (d, 3, J_{Rh} = 2.0 Hz); PCH_2CH_2P, 1.81 (m, 4); $P(OCH_2CH_3)_2$, 3.89 (m, 8); $P(OCH_2CH_3)_2$, 1.13 (t, 6, J_{CH_2} = 7.1 Hz), 1.08 (t, 6, J_{CH_2} = 7.1 Hz).

$[\eta^3$-(2-Me-C$_3$H$_4$)Rh(dipope)] (1c): This was synthesized as described above for **1***c*, and isolated as a yellow–green oil. ^1H nmr (C_6D_6, ppm): H_{syn}, 3.79 (s, 2); H_{anti}, 2.33 (br d, 2, J_P = 6.5 Hz); 2-CH_3, 1.59 (d, 3, J_{Rh} = 2.0 Hz); PCH_2CH_2P, 1.78 (m, 4); $P(OCH(CH_3)_2)_2$, 4.58 (m, 4, $J_P = J_{CH_3}$ = 6.1 Hz); $P(OCH(CH_3)_2)_2$, 1.26 (d, 12), 1.12 (d, 6), 1.03 (d, 6).

Cluster syntheses

The reaction of the 2-methylallylrhodium derivatives with hydrogen (purified by passage over MnO on vermiculite and activated 4 Å molecular sieves) was carried out in a 180 mL thick-walled glass vessel, which could be attached directly to a vacuum line, and was equipped with an 8 mm Kontes Teflon needle valve and a magnetic stirring bar.

[(dmope)RhH]$_4$ (2a): A yellow solution of **1***a* (0.700 g, 1.88 mmol) in toluene (10 mL) was degassed on the vacuum line, then cooled to −196°C and placed under 1 atm pressure of H_2. The needle valve was closed and the vessel allowed to warm to room temperature and then vigorously stirred for 24 h. The colour deepens over this time to generate a black–red solution. The excess H_2 was removed and the volume of the solution reduced to $\approx$1 mL. Hexanes (2–3 mL) was slowly added and the solution cooled at −30°C for 12 h. Large, maroon prisms formed and were filtered, washed with cold hexane, and dried under vacuum. Yield: 0.410 g (68%). mp 183°C (decomp.). Molecular weight (Signer): 1280 ± 50; theoretical: 1272. ^1H nmr (C_6D_6, ppm): $P(OCH_3)$, 3.83 (d, 48, J_P = 11.7 Hz); PCH_2CH_2P, 1.51 (br d, 16, J_P = 21.0 Hz); Rh*H*, −6.52 (q of nonets, 4, J_{Rh} = 10.7 Hz, J_P = 16.1 Hz). $^{31}P\{^1H\}$ nmr (C_6D_6, relative to $P(OMe)_3$ at +141.0 ppm): 199 (d of complex multiplets separated by $\approx$230 Hz). *Anal.* calcd. for $C_6H_{17}O_4P_2Rh$: C 22.66, H 5.39; found: C 22.91, H 5.32. ^1H nmr analysis of the filtrate from the recrystallization indicates the presence of an as yet unidentified trinuclear cluster in addition to the tetranuclear cluster: $^1H\{^{31}P\}$ nmr: (C_6D_6, ppm): Rh*H*, −6.5 (quartet, J_{Rh} = 16.5 Hz).

[(deope)RhH]$_4$ (2b): A yellow solution of **1***b* (0.900 g, 2.10 mmol) in toluene (12 mL) was treated with H_2 as described above for **2***a*. Stirring was maintained for 48 h to give a dark red–brown solution. Removal of the hydrogen and the toluene *in vacuo* gave an oily, dark red–brown solid which could not be purified further. Analysis by ^1H nmr indicates no other products are present. ^1H nmr (50°C, C_6D_6, ppm): $P(OCH_2CH_3)_2$, 4.31 (m, 32); PCH_2CH_2P, 1.56 (br d, 16); $P(OCH_2CH_3)_2$, 1.25 (t, 48, J_{CH_2} = 6.8 Hz); Rh*H*, −6.85 (q of nonets,

Can. J. Chem. Downloaded from www.nrcresearchpress.com by 210.87.254.42 on 09/06/12
For personal use only.

4, J_{Rh} = 10.7 Hz, J_P = 16.1 Hz). $^{31}P\{^1H\}$ nmr (C_6D_6, relative to $P(OMe)_3$ at +141.0 ppm): 191.8 (d of complex multiplets separated by ≈230 Hz). *Anal.* calcd. for $C_{10}H_{25}O_4P_2Rh$: C 32.19, H 6.74; found: C 32.29, H 6.60.

[(dipope)RhH]$_2$ (2c): To a solution of [η^3-(2-Me-C_3H_4)Rh(COD)] (14) (0.534 g, 2.0 mmol) in hexanes (4 mL) was added dipope (0.653 g, 2.0 mmol) in hexanes (3 mL) dropwise with swirling to generate a clear olive-coloured solution. After 0.5 h, the hexanes were removed to yield an oily green–brown material which was dissolved in toluene (8 mL) and treated with H_2 as described above. After stirring for 48 h, the toluene was removed to give an oily dark-red solid which was dissolved in minimum hexanes (≈3 mL) and cooled at −30°C for 12 h. Red crystals deposited. Yield: 0.490 g (two crops, 57%). mp 153°C (decomp.). The filtrate appears to contain only the dimer contaminated by unreacted starting material. Molecular weight (Signer): 830 ± 30; theoretical: 861. ^1H nmr (C_7D_8, ppm): $P(OCH(CH_3)_2)_2$, 5.35 (m, 9, J_{CH_3} = 6.4 Hz); PCH_2CH_2P, 1.49 (br m, 8); $P(OCH(CH_3)_2)_2$, 1.45 (d, 24), 1.35 (d, 24); Rh*H*, −4.30 (br sep, 2, J_{Rh} = 34.1 Hz, J_P = 33–35 Hz). $^{31}P\{^1H\}$ nmr (C_6D_6, relative to $P(OMe)_3$ at +141.0 ppm): 196.4 (AA′A″A‴XX′, $|^1J_{Rh} + {}^3J_{Rh}|$ = 212.4 Hz). Infrared (hexane, cm^{-1}): ν_{Rh-H}, 1180 (m); ν_{Rh-D}, 870 (m). *Anal.* calcd. for $C_{14}H_{33}O_4P_2Rh$: C 39.08, H 7.73; found: C 39.01, H 7.62.

[HRh(PMe$_3$)$_2$ (dmope)] (3a): To a solution of **2***a* (0.100 g, 0.079 mmol) in toluene (3 mL) was added PMe_3 (0.100 g, 1.31 mmol) in toluene (3 mL) with swirling. The reaction mixture was allowed to stand for 2 h during which time the original deep red colour faded to give a light yellow solution. The toluene and excess PMe_3 were removed *in vacuo* to give a yellow oil which could not be crystallized. ^1H nmr (C_6D_6, ppm): $P(OCH_3)_2$, 3.44 (d, ^3J_P = 6.0 Hz); PCH_2CH_2P, 1.73 (d of m); $P(CH_3)_3$, 1.38 (br t); Rh*H*, −9.80 (t of dt, $^1J_{Rh}$ = 10.6 Hz, $^2J_{P(OMe)_2}$ = 88.5 Hz, $2J_{PMe_3}$ = 22.6 Hz). $^{31}P\{^1H\}$ nmr (C_6D_6, relative to $P(OMe)_3$, at +141.0 ppm): PMe_3, −22.6 (overlapping doublet of triplets, $^1J_{Rh}$ = 141 Hz, ^2J_P = 70.5 Hz); $P(OMe)_2$, 228.7 (d of t, $^1J_{Rh}$ = 185 Hz).

[HRh(PMe$_3$)$_2$ (dipope)] (3c): To a solution of **2***c* (0.065 g, 0.038 mmol) in hexanes (3 mL) was added PMe_3 (0.060 g, 0.790 mmol) in hexanes (3 mL) dropwise with swirling. The colour change was immediate to give a light yellow solution which was immediately pumped down under vacuum to given an off-white solid. Recrystallization from minimum hexanes gave colourless plates. Yield: 0.080 g (91%). ^1H nmr (C_6D_6, ppm): $P(OCH(CH_3)_2)_2$, 4.57 (m, $J_{CH_3} = J_P$ = 6.1 Hz); PCH_2CH_2P, 1.71 (br d., J_P = 23.0 Hz); $P(CH_3)_3$, 1.40 (br s); $P(OCH(CH_3)_2)_2$, 1.24, 1.18 (d, J_{CH} = 6.1 Hz); Rh*H*, −10.4 (t of dt, $^1J_{Rh}$ = 10.7 Hz, $^2J_{P(OMe)_2}$ = 85.4 Hz, $^2J_{PMe_3}$ = 21.1 Hz).

[(dipope)$_2$Rh$_2$H$_4$] (4): The dinuclear cluster **2***c* (0.030 g, 0.035 mmol) was dissolved in C_7D_8 (0.40 mL) and placed in an nmr tube sealed to a ground glass joint and fitted with a Teflon needle valve adapter. The nmr tube assembly was attached to a vacuum line and the solution degassed. At −196°C, H_2 (600 Torr) was introduced and the tube sealed with a toreh. After warming to room temperature, the nmr tube was cooled to −50°C in the nmr spectrometer. ^1H nmr (C_7D_8, −50°C): $P(OCH(CH_3)_2)_2$, 5.48, 5.03 (m); PCH_2CH_2P. 1.84, 1.67 (br d, J_P ≈ 20 Hz); $P(OCH(CH_3)_2)_2$, ≈1.36, 1.19 (overlapping doublets, J_{CH} = 6.0 Hz); Rh*H*, −7.25 (d of m, bridging, J_P = 148 Hz), −12.0 (br s, terminal).

Hydrogenation of 1-hexene

The hydrogenation apparatus was similar to that described for the reactor used to synthesize the clusters. A 250 mL thick-walled glass vessel fitted with a Kontes 8 mm Teflon needle valve and an efficient magnetic stirring bar was loaded with 1-hexene (Aldrich, purified by drying over activated 4 Å molecular sieves, then vacuum transferred and degassed, followed by passage through neutral alumina; the purified material was stored under N_2 in the glove box) and the cluster (ratio of substrate to cluster: ≈1500–2000:1) in the glove box and transferred to a vacuum line which had access to purified H_2. After the solution was degassed, a constant temperature bath maintained at 22.0°C was placed around the flask and hydrogen admitted to 1 atm. Samples were withdrawn periodically via the Teflon needle valve port using an argon-flushed syringe, vacuum transferred away from the catalyst, and analyzed by gas chromatography. A Varian 6000 instrument equipped with FID detectors, a 20% tri-*o*-cresylphosphate on 60/80 chromosorb-P column (20′ × 1/8″ SS) operating at 50°C was used. The identities of the gc traces were established by "spiking" with the pure materials (Aldrich).

Acknowledgments

Financial support for this reseach was generously provided by the Department of Chemistry (U.B.C.), the Natural Sciences and Engineering Research Council of Canada, and Research Corporation. The generous loan of rhodium chloride by Johnson-Matthey is also acknowledged.

1. J. P. COLLMAN. Acc. Chem. Res. **1**, 136 (1968).
2. B. R. JAMES. Homogeneous hydrogenation. Wiley, New York. 1973; Adv. Organomet. Chem. **17**, 319 (1979).
3. K. C. DEWHIRST, W. KEIM, and C. A. REILLY. Inorg. Chem. **7**, 546 (1968).
4. J. P. COLLMAN and L. S. HEGEDUS. Principles and applications of organotransition metal chemistry. University Science, Mill Vally, CA. 1980. p. 17.
5. J. JHORTKJAER. Adv. Chem. Ser. No. 132, 133 (1974).
6. S. H. STRAUSS, S. E. DIAMOND, F. MARES, and D. F. SHRIVER. Inorg. Chem. **17**, 3064 (1979).
7. S. H. STRAUSS and D. F. SHRIVER. Inorg. Chem. **17**, 3069 (1978).
8. D. BUDD, D. G. HOLAH, A. N. HUGHES, and B. C. HUI. Can. J. Chem. **52**, 775 (1974).
9. D. G. HOLAH, I. M. HOODLESS, A. N. HUGHES, B. C. HUI, and D. MARTIN. Can. J. Chem. **52**, 3758 (1974).
10. T. YOSHIDA, T. OKANO, D. L. THORN, T. H. TULIP, S. OTSUKA, and J. A. IBERS. J. Organomet. Chem. **181**, 183 (1979).
11. S. KOMIYA, T. A. ALBRIGHT, R. HOFFMANN, and J. K. KOCHI. J. Am. Chem. Soc. **98**, 7255 (1976).
12. A. J. SIVAK and E. L. MUETTERTIES. J. Am. Chem. Soc. **101**, 4878 (1979).
13. M. D. FRYZUK. Organometallics, **1**, 408 (1982).
14. M. D. FRYZUK. Inorg. Chem. **21**, 2134 (1982).
15. P. MEAKIN, E. L. MUETTERTIES, and J. P. JESSON. J. Am. Chem. Soc. **94**, 5271 (1972).
16. E. B. MEIER, R. R. BURCH, E. L. MUETTERTIES, and V. W. DAY. J. Am. Chem. Soc. **104**, 2661 (1982).
17. R. R. BURCH, E. L. MUETTERTIES, and V. W. DAY. Organometallics, **1**, 188 (1982).
18. R. B. KING and W. M. RHEE. Inorg. Chem. **17**, 2961 (1978).
19. R. J. BURG, J. CHATT, W. HUSSAIN, and G. J. LEIGH. J. Organomet. Chem. **182**, 203 (1979).

Preparation, characterization, and some reactions of hydridobis(tri-*tert*-butyl)phosphineplatinum(II) cation containing three-coordinate platinum

RAM G. GOEL[1] AND RAMESH C. SRIVASTAVA[2]

The Guelph–Waterloo Centre for Graduate Work in Chemistry, Department of Chemistry, University of Guelph, Guelph, Ont., Canada N1G 2W1

Received September 7, 1982

RAM G. GOEL and RAMESH C. SRIVASTAVA. Can. J. Chem. **61**, 1352 (1983).

Removal of the chloride ligand from *trans*-PtHCl[P(*t*-Bu)$_3$]$_2$ by a noncoordinating anion affords the complexes *trans*-[PtH{P(*t*-Bu)$_3$}$_2$]X (X = PF_6, BF_4, ClO_4, SO_3CF_3), **1***a*, **1***b*, **1***c*, and **1***d* respectively, which contain the cationic hydride in which platinum is formally three-coordinate. Complexes **1** react with several σ-donor neutral ligands, L, to give the square-planar complexes *trans*-[PtHL{P(*t*-Bu)$_3$}$_2$]X. No reaction occurs with $H_2C{=}CH_2$ or $F_2C{=}CF_2$ but $(NC)_2C{=}C(CN)_2$ reacts with **1***c* to give an air-stable complex *trans*-[PtH{$(NC)_2C{=}C(CN)_2$}{P(*t*-Bu)$_3$}$_2$]ClO_4 which is indicated to contain π-bonded $(NC)_2C{=}C(CN)_2$. Neither PhC≡CPh nor $MeO_2CC{\equiv}CCO_2$ reacts with **1** but HC≡CH seems to react reversibly to form the four-coordinate species *trans*-[PtH(HC≡CH){P(*t*-Bu)$_3$}$_2$]$^+$, which could not be isolated. In marked contrast to the behaviour of previously reported cationic platinum(II) hydrides, addition of an equivalent of PCy_3 of P(*t*-Bu)$_3$ to an acetone solution of **1** results in its deprotonation and gives the platinum(0) complex Pt[P(*t*-Bu)$_3$]$_2$ quantitatively. Deprotonation of **1** also occurs upon treatment with NH_3, Me_2S, and NaOMe in acetone.

RAM G. GOEL et RAMESH C. SRIVASTAVA. Can. J. Chem. **61**, 1352 (1983).

L'élimination d'un ligand chlorure du PtHCl[P(*t*-Bu)$_3$]$_2$ par un anion coordonnant conduit aux complexes de [PtH{P(*t*-Bu)$_3$}$_2$]X *trans* (X = PF_6, BF_4, ClO_4, SO_3CF_3), **1***a*, **1***b*, **1***c* et **1***d* respectivement, qui contiennent l'hydrure cationique dans lequel le platine est formellement tricoordonné. Le complexe **1** réagit avec plusieurs ligands neutres σ-donneurs, L, en donnant des complexes carrés-plans de [PtHL{P(*t*-Bu)$_3$}$_2$]X *trans*. Il n'y a pas de réaction avec $H_2C{=}CH_2$ ou $F_2C{=}CF_2$ mais le $(NC)_2C{=}C(CN)_2$ réagit avec **1***c* en donnant un complexe de [PtH{$(NC)_2C{=}C(CN)_2$}{P(*t*-Bu)$_3$}$_2$]ClO_4 *trans* stable à l'air qui contient le $(NC)_2C{=}C(CN)_2$ lié par une liaison π. Ni le PhC≡CPh ni le $MeO_2CC{\equiv}CCO_2$ ne réagit avec le composé **1** mais le HC≡CH semble réagir de façon réversible en donnant des complexes tétracoordonnés de [PtH(HC≡CH){P(*t*-Bu)$_3$}$_2$]$^+$ *trans* que l'on ne peut isoler. Contrastant de façon marquée avec le comportement des hydrures cationiques de platine(II) rapportés antérieurement, l'addition d'un équivalent de PCy_3 ou de P(*t*-Bu)$_3$ sur le composé **1** en solution dans l'acétone conduit à sa déprotonation et donne quantitativement le complexe de platine(0): le Pt[P(*t*-Bu)$_3$]$_2$. La déprotonation du composé **1** se produit également lorsqu'on le fait réagir avec le NH_3, le Me_2S ou le NaOMe dans l'acétone.

[Traduit par le journal]

Introduction

Several cationic platinium(II) hydrides stabilized by tertiary phosphine ligands have been prepared (1) by removing the halide, X, in the complexes $PtHX(PR_3)_2$, by a poorly coordinating anion (such as ClO_4^-, BF_4^-, or PF_6^-) in the presence of either a neutral ligand or a donor solvent. Cations of the type $[PtHL(PR_3)_2]^+$, where L is a donor solvent, have often been generated and used *in situ*. All such cationic hydrides, including the complexes (1*f*) *trans*-$[PtHL(PCy_3)_2]^+$ (L = PCy_3 or P(*o*-tolyl)$_3$), invariably contain formally four-coordinate platinum(II).

As part of our continuing investigation on steric and electronic effects in platinum metal complexes of tertiary phosphines (2–7) and arsines (8–10), stabilization of platinum(II) (4, 8) and palladium(II) (9) hydrides by tri-*tert*-butylphosphine and -arsine ligands has been investigated in this laboratory. Tri-*tert*-butylphosphine has a larger steric requirement (11) than tricyclohexylphosphine as shown by the P—Pt—P angles in the two-coordinate complexes Pt{P(*t*-Bu)$_3$}$_2$ (6*a*) and Pt[PCy_3]$_2$ (12); unlike the tris(tricyclohexylphosphine)-platinum(II)$^+$ complex [PtH(PCy_3)$_3$], no metal complex containing more than two P(*t*-Bu)$_3$ ligands bonded to a metal has been isolated. The present work was undertaken to explore the possibility of stabilizing the formally three-coordinate platinum(II) hydride by tri-*tert*-butylphosphine. Coordinatively unsaturated transition metal hydrides are invariably involved in homogeneous catalytic hydrogenation and isomerization of olefins. Thus, knowledge of their chemistry is essential for a better understanding of the above-mentioned catalytic processes (13, 14). A preliminary report (15) on this work has appeared.

Results and discussion

Treatment of *trans*-PtHCl[P(*t*-Bu)$_3$]$_2$ with AgX (X = PF_6, BF_4, ClO_4, SO_3CF_3) in acetone or methanol, according to eq. [1], affords the cationic hydridoplatinum(II) complexes *trans*-[PtH{P(*t*-Bu)$_3$}$_2$]X (X = PF_6 (**1***a*), BF_4 (**1***b*), ClO_4 (**1***c*), SO_3CF_3 (**1***d*)), in almost quantitative yields.

[1] *trans*-PtHCl{P(*t*-Bu)$_3$}$_2$ + AgX → *trans*-[PtH{P(*t*-Bu)$_3$}$_2$]X + AgCl

(X = PF_6, BF_4, ClO_4, SO_3CF_3)

The compounds **1***a*–**1***d* are moisture-sensitive yellow solids which are soluble in polar solvents such as acetone, acetonitrile, and dichloromethane. Conductivity measurements on their 10^{-3} *M* solutions in dichloromethane gave Λ_M values ~50 M^{-1} ohm^{-1} cm^{-1} which are consistent with their formulation as 1:1 electrolytes (16). Analytical data and the characteristic infrared frequencies for the four compounds are given in Table 1. Their ^{1}H and ^{31}P-{^{1}H} nmr parameters are listed in Table 2.

The ^{31}P-{^{1}H} nmr spectra for all the four compounds in CH_2Cl_2 (containing 20% C_6D_6) consist of a main resonance (86.2–86.7 δ) and a pair of satellite resonances showing ^{195}Pt—^{31}P spin–spin coupling (^1J(Pt—P) = ~2625 Hz); the spectrum of **1***a* also shows a characteristic septet at −144.7 δ

[1]Deceased November 8, 1982.

[2]To whom correspondence should be addressed. On leave from the Department of Chemistry, University of Lucknow, Lucknow, India.

Can. J. Chem. Downloaded from www.nrcresearchpress.com by 210.87.254.5 on 09/06/12
For personal use only.

Can. J. Chem. Downloaded from www.nrcresearchpress.com by 210.87.254.5 on 09/06/12
For personal use only.

TABLE 1. Analytical and infrared spectral data

Compound[a]	C (%) Found	C (%) Calcd.	H (%) Found	H (%) Calcd.	ν(Pt—H)	Frequencies due to X	Other frequencies
trans-[PtH{P(*t*-Bu)$_3$}$_2$]PF$_6$,[b] **1***a*	38.80	38.65	7.40	7.45		840vs, 560s	
trans-[PtD{P(*t*-Bu)$_3$}$_2$]PF$_6$	38.30	38.59	7.46	7.57	2060mw	840vs, 555s	
trans-[PtH{P(*t*-Bu)$_3$}$_2$]BF$_4$, **1***b*	42.10	41.92	7.88	8.08		1060vs, 510s	
trans-[PtH{P(*t*-Bu)$_3$}$_2$]ClO$_4$,[c] **1***c*	41.22	41.16	7.86	7.93		1095vs, 615s	
trans-[PtH{P(*t*-Bu)$_3$}$_2$]SO$_3$CF$_3$, **1***d*	39.68	40.04	7.60	7.41		1265vs, 1135s, 1035s	
trans-[PtH(H$_2$O){P(*t*-Bu)$_3$}$_2$]PF$_6$, **2***a*					2440mw	845vs, 560s	ν(OH) = 3400s, b δ(HOH) = 1625m
trans-[PtH(H$_2$O){P(*t*-Bu)$_3$}$_2$]BF$_4$, **2***b*					2440mw	1060vs, 510s	ν(OH) = 3400s, 3240w δ(HOH) = 1625m
trans-[PtH(H$_2$O){P(*t*-Bu)$_3$}$_2$]ClO$_4$, **2***c*						1090vs, 620s	ν(OH) = 3380s, 3240w δ(HOH) = 1630m
trans-[PtH(H$_2$O){P(*t*-Bu)$_3$}$_2$]SO$_3$CF$_3$, **2***d*						1265vs, 1130s, 1030s	ν(OH) = 3370s, 3230w δ(HOH) = 1640w
trans-[PtH(NH$_3$){P(*t*-Bu)$_3$}$_2$]PF$_6$,[d] **4***a*	37.66	37.99	7.60	7.68	2362m	840vs, 550s	ν(NH$_3$) = 3390m, 3300m δ(NH$_3$) = 1625m
trans-[PtH(NH$_3$){P(*t*-Bu)$_3$}$_2$]ClO$_4$, **4***c*	40.24	40.18	8.22	8.17	2360m	1090vs, 618s	ν(NH$_3$) = 3340m, 3265m δ(NH$_3$) = 1620m
trans-[PtH(CH$_3$CN){P(*t*-Bu)$_3$}$_2$]PF$_6$, **5***a*	39.72	39.68	7.50	7.45	2375w	840vs, 555s	ν(CN) = 2278w, sp
trans-[PtH(CH$_3$CN){P(*t*-Bu)$_3$}$_2$]BF$_4$, **5***b*	42.78	42.85	8.20	8.04	2375w	1650vs, 510s	ν(CN) = 2278w, sp
trans-[PtH(CH$_3$CN){P(*t*-Bu)$_3$}$_2$]ClO$_4$, **5***c*	42.06	42.12	8.01	7.90	2375w	1080vs, 620s	ν(CN) = 2280w, sp
trans-[PtH(*t*-BuCN){P(*t*-Bu)$_3$}$_2$]ClO$_4$, **6***c*	44.50	44.46	8.32	8.25	2375mw	1090vs, 622s	ν(CN) = 2260w, sp
trans-[PtH(C$_6$F$_5$CN){P(*t*-Bu)$_3$}$_2$]PF$_6$,[e] **7***a*	39.28	39.66	5.80	5.92	2375w	840vs, 555s	ν(CN) = 2260w, sp
trans-[PtH(*t*-BuNC){P(*t*-Bu)$_3$}$_2$]PF$_6$, **8***a*	41.73	42.02	7.64	8.0	2270mw	835vs, 555s	ν(CN) = 2155ms
trans-[PtH(*t*-BuNC){P(*t*-Bu)$_3$}$_2$]ClO$_4$,[f] **8***c*	44.34	44.46	8.05	8.25	2270mw	1090vs, 622s	ν(CN) = 2155ms
trans-[PtH(CO){P(*t*-Bu)$_3$}$_2$]PF$_6$, **9***a*	38.91	38.80	7.00	7.18	2240m	835vs, 555s	ν(CO) = 2040s
trans-[PtH(CO){P(*t*-Bu)$_3$}$_2$]BF$_4$, **9***b*	42.02	41.96	7.60	7.76	2240w	1050vs, 510s	ν(CO) = 2040s
trans-[PtH(CO){P(*t*-Bu)$_3$}$_2$]ClO$_4$, **9***c*	41.15	41.23	7.58	7.63	2240m	1090vs, 620s	ν(CO) = 2040s
trans-[PtH(CO){P(*t*-Bu)$_3$}$_2$]SO$_3$CF$_3$, **9***d*	39.86	40.14	6.96	7.14	2240w	1260vs, 1135s, 1025s	ν(CO) = 2040s
trans-[PtH{(CN)$_2$C=C(CN)$_2$}{P(*t*-Bu)$_3$}$_2$]ClO$_4$, **10***c*	43.01	43.50	6.67	6.71		1090vs, 620s	ν(CO) = 2250ms, 2210m

[a] All the compounds decompose on melting between 190–220°C.
[b] %F found, 14.88 (calcd. 15.29).
[c] %Cl found 4.85 (calcd. 5.06).
[d] %N found, 1.80 (calcd. 1.84).
[e] %N found 1.42 (calcd. 1.49).
[f] %N found, 1.70 (calcd. 1.79).

Can. J. Chem. Downloaded from www.nrcresearchpress.com by 210.87.254.5 on 09/06/12
For personal use only.

TABLE 2. ^{1}H and ^{31}P-{^{1}H} nmr data

Compound[t]	^{1}H nmr data						^{31}P-{^{1}H} nmr data				
	Solvent[a]	δ(Pt—H) (ppm)	^1J(Pt—H) (Hz)	^2J(P—H) (Hz)	δ(*t*-Bu) (ppm)	^3J(P—H) + ^5J(P—H) (Hz)	Solvent[b]	δ(Pt—P) (ppm)	^1J(Pt—P) (Hz)	δ(P—F) (ppm)	^1J(P—F) (Hz)
$[PtH\{P(t\text{-}Bu)_3\}_2]PF_6$,[c] **1***a*	CD_2Cl_2	−36.3*t*	2592	8.8	1.54*t*	13.7	CH_2Cl_2	86.7	2623	−144.7	710
	$(CD_3)_2CO$	−27.9*t*	1510	12.2	1.53*t*	12.7	$(CH_3)_2CO$	83.0	2811	−144.8	707
$[PtH\{P(t\text{-}Bu)_3\}_2]BF_4$, **1***b*	CD_2Cl_2	−36.3*t*	2567	8.5	1.55*t*	13.4	CH_2Cl_2	86.2	2627	—	—
	$(CD_3)_2CO$	−27.4*t*	1458	12.2	1.52*t*	12.7	$(CH_3)_2CO$	82.1	2830	—	—
$[PtH\{P(t\text{-}Bu)_3\}_2]ClO_4$, **1***c*	CD_2Cl_2	−36.2*t*	2571	8.6	1.51*t*	13.4	CH_2Cl_2	86.1	2626	—	—
	$(CD_3)_2CO$	−27.6*t*	1465	12.2	1.53*t*	12.2	$(CH_3)_2CO$	81.2	2857	—	—
$[PtH\{P(t\text{-}Bu)_3\}_2]SO_3CF_3$, **1***d*	CD_2Cl_2	−36.2*t*	2575	8.7	1.52*t*	13.5	CH_2Cl_2	86.2	2620	—	—
	$(CD_3)_2CO$	−27.4*t*	1455	12.2	1.53*t*	12.7	$(CH_3)_2CO$	81.8	2830	—	—
$[PtH(H_2O)\{P(t\text{-}Bu)_3\}_2]BF_4$, **2***b*	$CDCl_3$	−29.7*t*	1757	10.6	1.54*t*	12.5	CH_2Cl_2	85.3	2664		
$[PtH(NH_3)\{P(t\text{-}Bu)_3\}_2]PF_6$, **4***a*	$CDCl_3$	−19.3*t*	955	11.6	1.52*t*	12.6	CH_2Cl_2	79.0	2848	−144.7	714
$[PtH(NH_3)\{P(t\text{-}Bu)_3\}_2]BF_4$, **4***b*	CD_2Cl_2	−19.2*t*	956	12.2	1.51*t*	12.7					
$[PtH(NH_3)\{P(t\text{-}Bu)_3\}_2]ClO_4$, **4***c*	CH_2Cl_2	−19.2*t*	940	11.6	1.51*t*	12.7	CH_2Cl_2	79.0	2856	—	—
$[PtH(CH_3CN)\{P(t\text{-}Bu)_3\}_2]PF_6$, **5***a*	$CDCl_3$	−19.3*t*	1056	11.6	1.52*t*	12.7	$(CH_3)_2CO$	79.3	2808	−145.3	707
$[PtH(CH_3CN)\{P(t\text{-}Bu)_3\}_2]BF_4$, **5***b*	$CDCl_3$	−19.2*t*	1052	11.7	1.52*t*	12.7	CH_2Cl_2	79.9	2808	—	—
$[PtH(CH_3CN)\{P(t\text{-}Bu)_3\}_2]ClO_4$, **5***c*	$CDCl_3$	−19.2*t*	1053	11.7	1.51*t*	12.7	$(CH_3)_2CO$	79.4	2810	—	—
$[PtH(CH_3CN)\{P(t\text{-}Bu)_3\}_2]SO_3CF_3$, **5***d*	CD_2Cl_2	−19.2*t*	1056	11.7	1.50*t*	12.7	CH_2Cl_2	79.9	2805	—	—
$[PtH(t\text{-}BuCN)\{P(t\text{-}Bu)_3\}_2]ClO_4$, **6***c*	$(CD_3)_2CO$	−19.2*t*	1041	12.1	1.60*t*	13.2	CH_2Cl_2	79.7	2810	—	—
$[PtH(C_6F_5CN)\{P(t\text{-}Bu)_3\}_2]PF_6$, **7***a*	$CDCl_3$	−18.8*t*	1077	11.6	1.55*t*	12.2	CH_2Cl_2	81.2	2752	−145.1	710
$[PtH(t\text{-}BuNC)\{P(t\text{-}Bu)_3\}_2]PF_6$, **8***a*	$CDCl_3$	−8.8*t*	660	12.3	1.55*t*	13.4	CH_2Cl_2	84.8	2634	−144.5	710
$[PtH(t\text{-}BuNC)\{P(t\text{-}Bu)_3\}_2]ClO_4$, **8***c*	CD_2Cl_2	−8.8*t*	665	12.3	1.54*t*	13.2	CH_2Cl_2	84.8	2632	—	—
	$CDCl_3$	−8.9*t*	661	12.2	1.55*t*	13.6					
$[PtH(CO)\{P(t\text{-}Bu)_3\}_2]PF_6$,[d] **9***a*	$(CD_3)_2CO$	−5.2*t*	742	9.6	1.69*t*	13.2	$(CH_3)_2CO$	89.4	2416	−145.0	704
$[PtH(CO)\{P(t\text{-}Bu)_3\}_2]BF_4$, **9***b*	$(CD_3)_2CO$	−5.3*t*	742	9.9	1.65*t*	13.6	$(CH_3)_2CO$	89.4	2412	—	—
$[PtH(CO)\{P(t\text{-}Bu)_3\}_2]ClO_4$, **9***c*	$(CD_3)_2CO$	−5.3*t*	742	9.8	1.67*t*	13.4	$(CH_3)_2CO$	89.7	2415	—	—
$[PtH(CO)\{P(t\text{-}Bu)_3\}_2]SO_3CF_3$, **9***d*	CD_2Cl_2	−5.3*t*	744	9.9	1.62*t*	13.3	CH_2Cl_2	89.1	2408	—	—
$[PtH(CN)_2C{=}C(CN)_2\{P(t\text{-}Bu)_3\}_2]ClO_4$, **10***c*	$(CD_3)_2CO$	−19.0*t*	1013	12.2	1.62*t*	12.7	CH_2Cl_2	81.4	2739	—	—
$[PtH(CH{\equiv}CH\{P(t\text{-}Bu)_3\}_2]ClO_4$, **11***c*	CD_2Cl_2	−33.0*t*	2168	9.2	1.51*t*	13.4					

[a] The solvent was also used as the reference.
[b] Containing 20% C_6D_6.
[c] ^{2}H nmr data for $[PtD\{P(t\text{-}Bu)_3\}_2]PF_6$: (*a*) in CH_2Cl_2, δ(Pt—D) = −36.2 ppm, ^1J(Pt—D) = 391 Hz, (*b*) in $(CH_3)_2CO$, δ(Pt—D) = −27.9 ppm, ^1J(Pt—D) = 248 Hz.
[d] ^{2}H nmr data for $[PtD(CO)\{P(t\text{-}Bu)_3\}_2]PF_6$ in CH_2Cl_2, δ(Pt—D) = −5.6 ppm, ^1J(Pt—P) = 114 Hz.

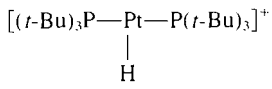

FIG. 1. T-shaped cationic hydride.

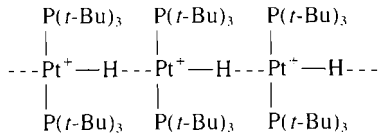

FIG. 2. Polymeric structure of cationic hydride.

(^1J(P—F) = 710 Hz) due to PF_6^-. The ^{1}H nmr spectra of **1***a*–**1***d*, in CD_2Cl_2, exhibited a 1:2:1 triplet due to the *t*-butyl protons (1.52 δ, $|^3J$(P—H) + ^5J(P—H)$|$ ≃ 13.5 Hz); a high-field triplet (~−36.2 δ, ^2J(P—H) ≃ 8.7 Hz), flanked on each side by a satellite triplet (^1J(Pt—H) ≃ 2570 Hz, ^2J(P—H) ≃ 8.7 Hz) of relative intensity 0.25, was observed due to the proton bonded to platinum. The appearance of the *t*-butyl resonance as a 1:2:1 triplet is indicative of "virtual coupling" (17) showing that the two phosphines are mutually *trans*.

The infrared spectra for **1***a*–**1***d*, in the solid state, showed characteristic bands due to the free anion (18), X, and coordinated P(*t*-Bu)$_3$ (19). It also showed a medium band at 1080 cm^{-1} which can be assigned to the Pt—H bending mode. The Pt—H stretching frequency for the three-coordinate *trans*-[PtH{P(*t*-Bu)$_3$}$_2$]$^+$ is expected to be above 2400 cm^{-1} because ν(Pt—H) for the four-coordinate *trans*-PtHX[P(*t*-Bu)$_3$]$_2$ complexes (4*a*) is in the 2400 cm^{-1} region. No band which can be assigned to ν(Pt—H) was evident in the spectra of **1***a*–**1***d*. It is very likely that ν(Pt—H) for these compounds overlaps with the C—H stretching vibrations of P(*t*-Bu)$_3$ which fall in the 2800 to 2900 cm^{-1} region. Support for this proposal is provided by the infrared spectrum of the deuterated analogue of **1***a* which shows a weak band at 2060 cm^{-1} attributable to ν(Pt—D). On this basis, ν(Pt—H) for ***1*** is expected to occur at ca. 2860 cm^{-1}.

The structure of **1***c* in the solid state was probed further by recording its high resolution ^{31}P-{^{1}H} nmr spectrum in the solid state by using magic-angle spinning technique (20). The spectrum was very similar to that observed in solution in CD_2Cl_2 and showed a main resonance at 89.08 accompanied by a pair of satellite resonances giving the ^1J(Pt—P) value of 2600 Hz which is very close to that observed in solution in CD_2Cl_2. Thus the structure of the cation *trans*-[PtH{P(*t*-Bu)$_3$}$_2$]$^+$ in the solid state cannot be markedly different than that in solution.

The δ(Pt—H), ^1J(Pt—H), and ν(Pt—H) values for **1***a*–**1***d* are the largest known for a platinum(II) hydride. Furthermore, these values are invariant of the nature of the anion X. On the basis of the spectral and conductance data and the diamagnetism[3] of the compounds, all of the four compounds are assigned an ionic structure containing the formally three-coordinate T-shaped cationic hydride as shown in Fig. 1. A polymeric structure such as shown in Fig. 2 can be ruled out on the basis of the very large values of δ(Pt—H), ^1J(Pt—H), and ν(Pt—H) as well as the absence of infrared bands attributable to ν(Pt—H—Pt). For example, the δ(Pt—H) and ^1J(Pt—H) values for the bridging hydride in the complex [Ph(PEt$_3$)$_2$Pt^a—H—Pt^b(PEt$_3$)$_2$H]$^+$ have been reported to be −9.46 δ, and ≃500 Hz [^1J(Pt^a—H) ≃ ^1J(Pt^b—H)], respectively (21).

Complexes **1** react according to eq. [2] with a variety of neutral ligands (L) to give the four-coordinate hydrides *trans*-[PtHL{P(*t*-Bu)$_3$}$_2$]X.

[2] *trans*-[PtH{P(*t*-Bu)$_3$}$_2$]X + L ⇌ *trans*-[PtH{P(*t*-Bu)$_3$}$_2$L]X

(L = H_2O, $(CH_3)_2O$, NH_3, RCN (R = Me, *t*-Bu, C_6F_5), *t*-BuNC, and CO)

*Reactions of **1** with σ-donor neutral ligands*

If either the silver salt or the solvent used for reaction [1] is not completely dry, the reaction affords the aquo complexes *trans*[PtH(OH$_2$){P(*t*-Bu)$_3$}$_2$]X, **2***a* (X = PF_6), **2***b* (X = BF_4), **2***c* (X = ClO_4), and **2***d* (X = SO_3CF_3). Complexes **2***a* and **2***c* were also obtained readily by treating Pt{P(*t*-Bu)$_3$}$_2$ with aqueous solutions of HPF_6 and $HClO_4$ as represented by eq. [3].

[3] Pt{P(*t*-Bu)$_3$}$_2$ + H_3O^+ + X^- → *trans*-[PtH{P(*t*-Bu)$_3$}$_2$OH$_2$]X

(X = PF_6, ClO_4)

The C and H analyses for complexes **2** and their anhydrous analogues, **1**, are not expected to be significantly different. Complexes **2** are, however, unequivocally characterized by their spectral data. As shown in Table 1, the infrared spectra for **2***a*–**2***c*, in the solid state, show bands at ca. 3340–3370, 3240–3230, and 1620–1640 cm^{-1} attributable to the antisymmetric and symmetric O—H stretching and H—O—H bending frequencies (18), respectively. The nmr data which are given in Table 2 show that the hydride chemical shift for the aquo complex **2***b* is 6.5 ppm downfield from that for the anhydrous analogue **1***b*; the ^1J(Pt—H) for **2***b* is 810 Hz less than that for **1***b*. The ^{31}P-{^{1}H} nmr parameters for **2** are also different than those for the anhydrous analogues.

The data given in Table 2 show that the hydride chemical shifts for **1***a*–**1***d* move ca. 8.5 ppm downfield and the ^1J(Pt—H) values decrease by ca. 1000–1100 Hz when the spectra are measured in $(CD_3)_2CO$ instead of CD_2Cl_2; the ^{31}P chemical shifts and the ^1J(Pt—P) values for the acetone and dichloromethane solutions are also different. The observed changes in the nmr spectral parameters in going from dichloromethane to acetone are best accounted for in terms of the reaction of the three-coordinate species with acetone to form the four-coordinate hydride *trans*-[PtH{P(*t*-Bu)$_3$}$_2$OC(CH$_3$)$_2$]$^+$, **3**.

The ^{1}H nmr spectra of **1** and **2** in acetone-d_6, were identical except that the spectra for **2** showed an additional resonance at ~3.0 δ which is attributable to H_2O displaced by acetone-d_6. Attempts to isolate the acetone complexes **3**, however, failed; removal of acetone afforded the starting materials **1** or **2**. It appears therefore that the equilibrium in eq. [2] lies far to the left when L = acetone and that the water is replaced only because of the high concentration of acetone when it is used as a solvent. This is presumably due to the larger steric requirement of acetone than H_2O.

The yellow colour of dichloromethane solutions of **1** was discharged completely when gaseous NH_3 was passed through them. The resulting colourless solutions afforded the ammine complexes *trans*-[PtH(NH$_3$){P(*t*-Bu)$_3$}$_2$]X, **4***a* (X = PF_6), **4***b* (X = BF_4), **4***c* (X = ClO_4) quantitatively. The infrared (Table 1)

[3]In a trigonal planar structure the *d* orbitals of platinum will split in the order d_{xz}, d_{yz} < d_{z^2} < d_{xy}, $d_{x^2-y^2}$ giving rise to two unpaired 5*d* electrons (33).

Can. J. Chem. Downloaded from www.nrcresearchpress.com by 210.87.254.5 on 09/06/12
For personal use only.

Can. J. Chem. Downloaded from www.nrcresearchpress.com by 210.87.254.5 on 09/06/12
For personal use only.

and the ^1H and ^{31}P-$\{^1H\}$ nmr spectral data (Table 2) for **4***a*–**4***c* were identical to those of authentic samples prepared by the reaction of $Pt[P(t\text{-}Bu)_3]_2$ with NH_4X (22).

Treatment of dichloromethane solutions of **1** with nitriles, *t*-butylisonitrile, and carbon monoxide gave the four-coordinate hydrides *trans*-$[PtHL\{P(t\text{-}Bu)_3\}_2]X$, **5** (L = CH_3CN, *a* (X = PF_6), *b* (X = BF_4), *c* (X = ClO_4)), **6***c* (L = (*t*-Bu)CN, X = ClO_4), **7***a* (L = C_6F_5CN, X = PF_6), **8** (L = *t*-BuNC, *a* (X = PF_6), *c* (X = ClO_4)), **9** (L = CO, *a* (X = PF_6), *b* (X = BF_4), *c* (X = ClO_4), *d* (X = SO_3CF_3)). Complexes **5**–**9** were also obtained by displacement of the aquo ligand in **2** with nitriles, *t*-butylisonitrile, and carbon monoxide. They are air-stable white solids. All of them were characterized by elemental analyses (Table 1) and by infrared and ^1H and ^{31}P nmr measurements.

The ν(Pt—H), ν(CN), ν(CO), and the anion frequencies for **5**–**9** are tabulated in Table 1. The Pt—H stretching frequency can couple with ν(CN) or ν(CO). The CO stretching frequency for the deuterated analogue of **9***a* was observed to increase by 20 cm^{-1} indicating that the perturbation of ν(CO) by ν(Pt—H) is ca. 20 cm^{-1}. The ν(CN) values for **5**–**7** are comparable to those reported for the cationic methylplatinum(II)–nitrile complexes (23) suggesting little coupling between ν(Pt—H) and ν(CN) in the former compounds. The ν(Pt—H) for the nitrile complexes **5**–**7** is very similar to that for the ammine complexes **4**. For the isonitrile and carbonyl complexes this frequency decreases by 100–130 cm^{-1}.

The ^1H and ^{31}P-$\{^1H\}$ nmr spectra for **5**–**9** show the same features as described for **1**–**4**; the spectral parameters are given in Table 2. The hydride chemical shifts for the nitrile complexes are very similar to those for the ammine complexes but the ^1J(Pt—H) values for the former complexes are higher. The isonitrile and carbonyl complexes are characterized by very low upfield hydride chemical shifts (ca. −5.0 to −9.0 δ) as well as very low ^1J(Pt—H) values (660 to 740 Hz). The ^{31}P-$\{^1H\}$ nmr parameters for **5**–**9**, like those for the other four-coordinate complexes **2**–**4** also differ from those for **1**. However, the changes are not as marked as in the ^1H nmr parameters.

Unlike the aquo complexes, the nmr parameters for the ammine, nitrile, isonitrile, and carbonyl complexes did not change significantly when solvent was changed to acetone or acetone-d_6. Thus, the ammine, nitrile, isonitrile, or CO are not displaced by acetone. The ammine and the nitrile complexes were readily converted to the corresponding carbonyl complexes when CO was bubbled through their solutions in dichloromethane.

Facile deprotonation of ***1***

In marked contrast to the formation (1) of the complexes such as *trans*-$[PtHL(PR_3)_2]^+$, where R = Et or PCy, L = a tertiary phosphine or arsine, facile deprotonation of complexes **1** according to eq. [4] occurred when an equimolar amount of either Pcy_3 or $P(t\text{-}Bu)_3$ was added to their solutions in acetone.

$$[4]\quad \textit{trans}\text{-}Pt[H\{P(t\text{-}Bu)_3\}_2]^+ + B \rightleftharpoons Pt[P(t\text{-}Bu)_3] + BH^+$$

$$(B = NH_3,\ Pcy_3,\ P(t\text{-}Bu)_3,\ SMe_2,\ OMe^-)$$

The platinum(0) complex $Pt[P(t\text{-}Bu)_3]_2$ was also obtained almost quantitatively when NH_3 was passed through acetone solutions of **1**. Complex **1***c* was also deprotonated upon adding excess dimethylsulfide to its solution in acetone. It is very unlikely that deprotonation of **1** by Pcy_3 or $P(t\text{-}Bu)_3$ proceeds via coordination of the phosphine to platinum and subsequent reductive elimination of the protonated phosphine from the resulting four-coordinate hydride. A plausible reaction pathway for the observed deprotonation seems to be attack of the nucleophile on the hydride which apparently behaves as a proton. The reaction is perhaps driven to completion due to the insolubility of $Pt[P(t\text{-}Bu)_3]_2$ in the reaction medium.

Reactions of ***1*** *with alkenes and alkynes*

^1H nmr measurements showed that no reaction occurred when $H_2C{=}CH_2$ or $F_2C{=}CF_2$ was passed through solutions of **1** in CD_2Cl_2 or $(CD_3)_2CO$ at room temperature. No reaction also occurred when dichloromethane solution of **1** was treated with PhC≡CPh or $MeO_2CC{\equiv}CCO_2Me$ for several hours. Lack of reactivity of **1** towards the above-mentioned alkenes or alkynes is in marked contrast to the facile insertion of olefins (1*d*, *e*) and acetylenes (24) into the Pt—H bond of the cationic platinum(II) hydrides *trans*-$[PtHL(PEt_3)_2]^+$. The lack of reactivity of the three-coordinate hydride is undoubtedly attributable to the steric crowding around platinum caused by the two very bulky $P(t\text{-}Bu)_3$ ligands.

Treatment of **1***c* with tetracyanoethylene in dichloromethane, however, afforded *trans*-$[PtH\{(NC)_2C{=}C(CN)_2\}\{P(t\text{-}Bu)_3\}_2]ClO_4$, **10***c*, in high yield. It is a red-brown air-stable solid, soluble in dichloromethane and acetone. Its infrared spectrum (Nujol mull) shows a medium-strong band at 2250 cm^{-1} and a medium band at 2210 cm^{-1} which are similar to the CN stretching bands observed at 2260 and 2230 cm^{-1} for the free $(NC)_2C{=}C(CN)_2$. Since coordination of nitriles (25) through the nitrogen atom usually results in an increase in the CN stretching frequency, the tetracyanoethylene in **10***c* is indicated to be bonded to platinum by a π-bond. Thus, it represents a rare and important class of compounds (1*d*, 26) which contain both olefin and hydride bonded to the metal. It has been demonstrated (13, 14, 27) that insertion of an olefin or diene into a transition metal – hydride bond proceeds via coordination of the C=C bond to the metal in a position *trans* to the hydride ligand.

The ^1H and ^{31}P-$\{^1H\}$ nmr spectra for **10***c* showed features similar to those observed for the other complexes examined in this work. The hydride chemical shift for **10***c* is 17 ppm downfield than that for the three-coordinate complex **1***c*; the ^1J(Pt—H) value is reduced by 1580 Hz. Nuclear magnetic resonance measurements showed that tetracyanoethylene in **10***c* is displaced by CH_3CN as well as by CO but not by $(CD_3)_2CO$.

The yellow solution of **1***c* in CD_2Cl_2 became colourless when HC≡CH was passed through it at room temperature. As shown in Table 2, the ^1H nmr spectrum of the resulting solution showed features similar to those seen for **1***c* except that the hydride chemical shift was 3.2 ppm downfield and the magnitude of ^1J(Pt—H) was 400 Hz less. The infrared spectrum of the solution showed a weak band at 2580 cm^{-1} and a sharp medium band at 2200 cm^{-1} attributable to ν(Pt—H) and ν(C≡C), respectively. The spectral data are thus indicative of the presence of four-coordinate species *trans*-$[PtH(HC{\equiv}CH)\{P(t\text{-}Bu)_3\}_2]^+$, **11***c*. Acetylene complexes of the type $[PtH(RC{\equiv}CR)(PR_3)_2]^+$, like their olefin analogues, have been proposed (24, 28) as intermediates in reactions involving insertion of acetylenes into Pt—H bond but direct evidence for the proposed intermediates has been lacking. Spectral characterization of **11***c* provides support for the proposed intermediates. Attempts to isolate **11***c* were, un-

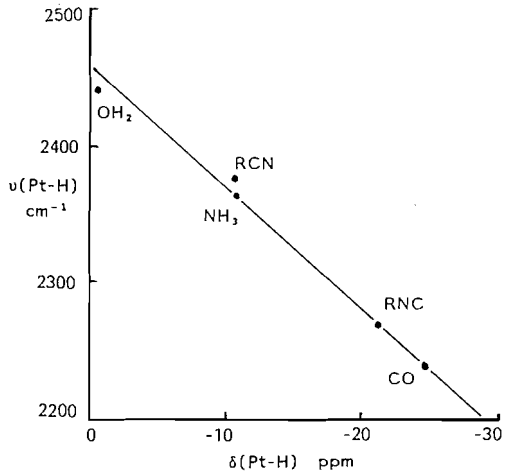

FIG. 3. A plot of ν(Pt—H), cm^{-1}, versus δ(Pt—H), ppm, for the *trans*-[PtHL{P(*t*-Bu)$_3$}$_2$]X complexes (L = H_2O, NH_3, RCN, RNC, CO).

fortunately, not successful; starting material **1***c* was recovered unchanged upon removing the volatiles. Lack of reaction of HC≡CH with the Pt—H bond in **1** is indeed remarkable and further demonstrates the extent of the kinetic stabilization provided by the steric bulk of the two P(*t*-Bu)$_3$ ligands.

The effects of the ligand *trans* to the hydride on δ(Pt—H), ^1J(Pt—H), and ν(Pt—H) have been examined (1*a*, *b*) for the series *trans*-[PtHL{E(Et)$_3$}$_2$]$^+$, where E = P or As and L = a neutral σ-donor ligand. It has been concluded that the ν(Pt—H) and ^1J(Pt—H) for the above-mentioned complexes decrease with increasing σ-donor strength of L. In the present work, ν(Pt—H) for the four-coordinate hydrides *trans*-[PtHL{P(*t*-Bu)$_3$}$_2$]$^+$ decreases in the order: H_2O > RCN > NH_3 > (*t*-Bu)NC > CO; the Pt—H coupling constants decrease in the order:

$$HC{\equiv}CH > H_2O > (CD_3)_2CO >> RCN > (NC)_2C{=}C(CN)_2 > NH_3 > CO > (t\text{-Bu})NC$$

The upfield hydride chemical shift falls in the order:

$$HC{\equiv}CH > H_2O > (CD_3)_2CO >> RCN \simeq (NC)_2C{=}C(CN)_2 \simeq NH_3 >> (t\text{-Bu})NC > CO$$

According to Buckingham and Stephens (29), the main contribution to δ(Pt—H) in platinum(II) hydrides is from the paramagnetic shielding of the proton by the platinum 5*d*-electrons. Thus, a linear correlation is expected between δ(Pt—H) and ν(Pt—H). As shown in Fig. 3, a plot of δ(Pt—H) against ν(Pt—H) for **2**, **4**–**9** gives a straight line. A linear correlation between δ(Pt—H) and ν(Pt—H) is also found (30) for the series *trans*-PtHX(PPh$_2$Me)$_2$ but there is no such correlation for the series *trans*-[PtHL{E(Et$_3$)$_3$}$_2$]$^+$ (1*a*, *b*).

Neither the ^{31}P nmr chemical shifts nor the Pt—P couplings for the *trans*-[PtHL{P(*t*-Bu)$_3$}$_2$]$^+$ complexes seem to show any systematic dependence upon the nature of L. The ammine and the nitrile complexes have the lowest chemical shifts which are upfield from those for **1**. The carbonyl complexes have the highest chemical shifts, and these are downfield from those for **1**. The spread between the lowest and the highest δ value is, however, only 10.0 ppm. The acetone complex exhibits the highest ^1J(Pt—P) value (2830 Hz) and the carbonyl complex the lowest (2408 Hz).

Experimental section

General

Tri-*tert*-butylphosphine and all other air- and moisture-sensitive materials were manipulated under an atmosphere of oxygen-free dry nitrogen or argon using a Vacuum Atmospheres Corporation glovebox and standard vacuum line techniques.

Materials

P(*t*-Bu)$_3$ (31), K_2PtCl_4 (32), Pt[P(*t*-Bu)$_3$]$_2$ (6*b*), *trans*-PtHCl[P(*t*-Bu)$_3$]$_2$ (4*b*), and *trans*-[P(*t*-Bu)$_3$]$_2$PtDCl were prepared by reported methods. Spectrograde acetone was stored over molecular sieve (3-Å) and distilled prior to use. Dichloromethane, benzene, and pentane were treated with sodium wire, distilled, and stored over molecular sieve. Reagent grade CO (Matheson) was purified by passing through a column of KOH pellets. Other chemicals were used as received.

Physical measurements

Elemental analyses were performed by Guelph Chemical Laboratory, Guelph, Ont. Melting points were determined with a Gallenkamp apparatus. Conductivity measurements were made with a Yellow Spring Instrument conductivity meter using a glass cell with platinized platinum electrodes. Infrared spectra were measured with a Perkin-Elmer 180 double-beam spectrophotometer using KRS-5 and polyethylene discs for solid samples (Nujol mull) and sealed NaCl cells for solutions. Nuclear magnetic resonance spectra in solution were recorded with a Bruker WP60 (^{1}H and ^{31}P nmr) or a Bruker WH400 spectrometer operating in the Fourier transform mode. High-resolution solid-state ^{31}P nmr spectra were obtained with a Bruker XL100 Spectrometer using a recently reported procedure (20). Hydrogen chemical shifts are relative to internal TMS. All ^{31}P chemical shifts (solution and solid state) are relative to external 85% H_3PO_4; positive δ values are downfield from 85% H_3PO_4.

Preparation of trans-*[PtH{P(t-Bu)$_3$}$_2$]X (X = PF_6, BF_4, ClO_4, SO_3CF_3)* **1**a–**1**d

To a suspension of *trans*-PtHCl[P(*t*-Bu)$_3$]$_2$ (1 mmol) in acetone (5 mL) was slowly added, with stirring, a solution of AgX (1 mmol) in acetone (2 mL). The precipitated AgCl was filtered off. The filtrate was evaporated *in vacuo* to give a yellow solid which was dissolved in dichloromethane (~3 mL). The solution was passed through a short florisil column. Pentane was added to the collected solution to give yellow [PtH{P(*t*-Bu)$_3$}$_2$]X in over 90% yield. A similar procedure was used to prepare *trans*-[PtD{P(*t*-Bu)$_3$}$_2$]PF_6.

Preparation of trans-*[PtH(H$_2$O){P(t-Bu)$_3$}$_2$]X (X = PF_6, BF_4, ClO_4, SO_3CF_3)* **2**a–**2**d

(*a*) Reaction of *trans*-PtHCl[P(*t*-Bu)$_3$]$_2$ with AgX following the above described procedure was carried out using reagent grade undried acetone.

(*b*) To a suspension of Pt[P(*t*-Bu)$_3$]$_2$ (0.5 mmol) in acetone was added equimolar amount of aqueous HPF_6 or $HClO_4$ at 0°C. Removal of volatiles under reduced pressure and recrystallization of the residue from dichloromethane/hexane gave very pale yellow crystals of **2***a* or **2***c* in 80% yield.

Reactions of ***1*** *with* NH_3

(*a*) Ammonia was bubbled through a solution of [PtH{P(*t*-Bu)$_3$}$_2$]X (0.5 mmol) in dichloromethane (10 mL) until the yellow colour disappeared. The solvent was removed under reduced pressure and the resulting solid was recrystallized with dichloromethane/pentane to give white crystalline *trans*-[PtH(NH_3){P(*t*-Bu)$_3$}$_2$]X, **4**, in >90% yield.

(*b*) Pt[P(*t*-Bu)$_3$]$_2$ was precipitated almost quantitatively when ammonia was passed through an acetone solution of **1***c* until the yellow colour was completely discharged. It was filtered, weighed, and characterized by ^{31}P-{^{1}H} nmr measurements.

Reactions of ***1*** *and* ***3*** *with nitriles*

(*a*) Excess CH_3CN (>1 mol equiv.) was added to a solution of **1** or **3** (0.5 mmol) in dichloromethane (2 mL). Removal of the volatiles *in vacuo* gave white *trans*-[PtH($NCCH_3$){P(*t*-Bu)$_3$}$_2$]X in quantitative

Can. J. Chem. Downloaded from www.nrcresearchpress.com by 210.87.254.5 on 09/06/12
For personal use only.

Can. J. Chem. Downloaded from www.nrcresearchpress.com by 210.87.254.5 on 09/06/12
For personal use only.

yields. The products were recrystallized from dichloromethane/pentane.

(*b*) A solution of (*t*-Bu)CN (0.5 mmol) in dichloromethane (1 mL) was slowly added to a solution of **1** (0.5 mmol) in the same solvent (~5 mL). The yellow colour of the solution disappeared immediately. Concentration of the colourless solution to ~1 mL, dilution of the concentrate by pentane, and cooling of the resulting solution gave colourless crystals of *trans*-[PtH{NC(*t*-Bu)}{P(*t*-Bu)$_3$}$_2$]X in ~90% yield.

(*c*) Treatment of **1***a* (0.5 mmol) with C_6F_6CN (0.5 mmol) in either methanol or dichloromethane according to the procedure (*b*) gave colourless needles of *trans*-[PtH(NCC$_6$F$_5$){P(*t*-Bu)$_3$}$_2$]PF$_6$ in ~90% yield.

Reactions of ***1*** *with (t-Bu)NC*

A solution of (*t*-Bu)NC in dichloromethane (0.5 mmol in 2 mL) was added dropwise to a stirred solution of **1***a* or **1***c* (0.5 mmol) in the same solvent at 0°C. The colourless solution was warmed to room temperature and then evaporated *in vacuo*. Recrystallization of the resulting solid from dichloromethane/pentane gave colourless crystals of *trans*-[PtH{CN(*t*-Bu)}{P(*t*-Bu)$_3$}$_2$]X (yield: ~80%).

Reactions of ***1****,* ***3****, and* ***5*** *with CO*

Carbon monoxide was passed through a solution of the platinum(II) complex in dichloromethane (0.5 mmol in 5 mL) for ~5 min at room temperature. The resulting colourless solution was concentrated *in vacuo* (to ~1 mL), diluted with pentane, and then cooled in an ice bath to give white needles of *trans*-[PtH(CO){P(*t*-Bu)$_3$}$_2$]X in over 90% yield.

Reactions of ***1*** *with P(t-Bu)$_3$, PCy$_3$, As(t-Bu)$_3$, Me$_2$S, and NaMeO*

(*a*) Dropwise addition of an acetone solution of P(*t*-Bu)$_3$, Pcy$_3$, or NaMeO (0.5 mmol in 2 mL) to a stirring solution of **1***c* (0.5 mmol) in the same solvent gave a white precipitate of Pt[P(*t*-Bu)$_3$]$_2$ which was filtered, washed with acetone, dried, and characterized by ^{1}H and ^{31}P-{^{1}H} nmr measurements in benzene (yield: >90%).

(*b*) Treatment of **1***c* with As(*t*-Bu)$_3$ in a similar manner did not result in any reaction.

(*c*) Addition of excess Me$_2$S (>1.5 mmol) to an acetone solution of **1***c* (0.5 mmol) resulted in the precipitation of Pt[P(*t*-Bu)$_3$]$_2$ in almost quantitative amount.

Reaction of ***1*** *with tetracyanoethylene*

A solution of tetracyanoethylene in dichloromethane was slowly added to an equimolar amount of **1***c* in the same solvent. Initial yellow colour changed to red–violet instantaneously. After stirring the reaction mixture for 30 min, the solvent was removed *in vacuo* to give a red–brown residue which was dissolved in minimum amount of dichloromethane. The solution was passed through a florisil column. Addition of pentane to the collected solution gave red–brown *trans*-[{P(*t*-Bu)$_3$}$_2$Pt{C$_2$(CN)$_4$}H]ClO$_4$, **10***c*, in ~85% yield.

Reactions of ***10****c with CH$_3$CN and CO*

(*a*) To a solution of **10***c* in dichloromethane was added an excess (>1 mol) of acetonitrile. The red colour of the solution disappeared. Removal of the solvent and washing of the resulting solid with benzene gave *trans*-[PtH(NCMe){P(*t*-Bu)$_3$}$_2$]ClO$_4$ which was characterized by ^{1}H and ^{31}P-{^{1}H} nmr measurements.

(*b*) Carbon monoxide was bubbled into a solution of **10***c* in dichloromethane until the red colour disappeared. Removal of the solvent and recrystallization of the resulting solid from dichloromethane/pentane gave colourless *trans*-[PtH(CO){P(*t*-Bu)$_3$}$_2$]ClO$_4$ in 90% yield.

Reactions of ***1*** *with HC≡CH*

Acetylene was bubbled through a solution of **1***a* or **1***c* in CD_2Cl_2 until the yellow colour of the solution was completely discharged. The ^{1}H nmr and infrared spectra of the resulting colourless solution were examined which indicated the formation of *trans*-[PtH(HC≡CH){P(*t*-Bu)$_3$}$_2$]ClO$_4$. Removal of the solvent, however, gave the starting material **1***c*.

Acknowledgements

The financial support of the Natural Sciences and Engineering Research Council of Canada is gratefully acknowledged. Thanks are due to Professor C. A. Fyfe for recording the solid-state ^{31}P-{^{1}H} nmr spectra and to Mr. Bruce Macdonald for recording the ^{2}H nmr spectra which were obtained at the South-Western Ontario NMR Facility, funded by a Major Installation grant from N.S.E.R.C. R.C.S. is thankful to the University of Lucknow for a leave of absence.

1. (*a*) M. J. Church and M. J. Mays. J. Chem. Soc. A, 3074 (1968); (*b*) M. J. Church and M. J. Mays. J. Chem. Soc. A, 1938 (1970); (*c*) L. Toniolo, M. Giustiniani and U. Belluco. J. Chem. Soc. A, 2666 (1969); (*d*) H. C. Clark and H. Kurosawa. Inorg. Chem. **11**, 1275 (1972); (*e*) H. C. Clark, C. R. Jablonski, and C. S. Wong. Inorg. Chem. **14**, 1332 (1975); (*f*) T. G. Attig and H. C. Clark. Can. J. Chem. **53**, 3466 (1975); (*g*) D. F. Christian, H. C. Clark, and R. F. Stepaniak. J. Organomet. Chem. **112**, 209 (1976); (*h*) T. Miyamoto. J. Organomet. Chem. **134**, 335 (1977); (*i*) G. Minghetti, G. Banditelli, and A. L. Bandini. J. Organomet. Chem. **139**, C80 (1977); (*j*) H. C. Clark, M. J. Dymarski, and J. D. Oliver. J. Organomet. Chem. **154**, C40 (1979).
2. R. G. Goel and R. G. Montemayor. Inorg. Chem. **16**, 2183 (1977).
3. (*a*) R. G. Goel, R. G. Montemayor, and W. O. Ogini. J. Am. Chem. Soc. **100**, 3629 (1978); (*b*) R. G. Goel and W. O. Ogini. Organometallics, **1**, 654 (1982).
4. (*a*) H. C. Clark, A. B. Goel, R. G. Goel, and W. O. Ogini. J. Organomet. Chem. **157**, C16 (1978); (*b*) R. G. Goel, W. O. Ogini, and R. C. Srivastava. Organometallics, **1**, 819 (1982).
5. (*a*) H. C. Clark, A. B. Goel, R. G. Goel, S. Goel, and W. O. Ogini. Inorg. Chim. Acta, **31**, L441 (1978); (*b*) H. C. Clark, A. B. Goel, R. G. Goel, and S. Goel. Inorg. Chem. **19**, 3220 (1980).
6. (*a*) K. J. Moynihan, C. Chieh, and R. G. Goel. Acta Crystallogr. B**35**, 3062 (1979); (*b*) R. G. Goel, W. O. Ogini, and R. C. Srivastava. J. Organomet. Chem. **214**, 405 (1981).
7. R. G. Goel. Inorg. Nucl. Chem. Lett. (1979).
8. (*a*) R. G. Goel and W. O. Ogini. J. Organomet. Chem. **186**, C67 (1980); (*b*) R. G. Goel, W. O. Ogini, and R. C. Srivastava. Inorg. Chem. **21**, 1627 (1982).
9. R. G. Goel and W. O. Ogini. Inorg. Chem. Acta, **44**, L165 (1980).
10. R. G. Goel, W. O. Ogini, and R. C. Srivastava. Inorg. Chem. **20**, 3611 (1981).
11. C. A. Tolman. Chem. Rev. **77**, 313 (1977).
12. A. Immirzi, A. Musco, P. Zambelli, and G. Carturan. Inorg. Chim. Acta, **13**, L12 (1975).
13. J. P. Collman and L. S. Hegedus. Principles and applications of organotransition metal chemistry. University Science Books, CA. 1980.
14. G. W. Parshall. Homogeneous catalysis. Wiley-Interscience, New York. 1980.
15. R. G. Goel and R. C. Srivastava. J. Organomet. Chem. **204**, C13 (1981).
16. W. J. Greary. Coord. Chem. Rev. **7**, 110 (1971).
17. (*a*) B. E. Mann, B. L. Shaw, and R. M. Slade. J. Chem. Soc. A, 2976 (1971); (*b*) A. W. Verstuyft, J. H. Nelson, and L. W. Cary. Inorg. Chem. **15**, 732 (1976).
18. K. Nakamoto. Infrared and Raman spectra of inorganic and coordination compounds. Wiley, New York. 1978.
19. H. Schumann and L. Rosh. Chem. Ber. 854 (1974).
20. L. Bemi, H. C. Clark, J. A. Davies, C. A. Fyfe, and R. E. Wasylishen. J. Am. Chem. Soc. **104**, 438 (1982).
21. G. Bracher, D. M. Grove, L. M. Venanzi, F. Bachechi, P. Mura, and L. Zambonelli. Angew. Chem. Int. Ed. Engl. **17**, 778 (1978).

22. R. G. GOEL and R. C. SRIVASTAVA. J. Organomet. Chem. In press.
23. H. C. CLARK and L. E. MANZER. Inorg. Chem. **10**, 2699 (1971).
24. H. C. CLARK, P. L. FIESS, and C. S. WONG. Can. J. Chem. **55**, 177 (1977) and references cited therein.
25. J. GRUNDONES and P. KLABOE. *In* The chemistry of the cyano group. *Edited by* Z. Rappoport. Interscience, New York. 1970. p. 123, and references cited therein.
26. (*a*) P. UGUAGLIATI and W. H. BADDLEY. J. Am. Chem. Soc. **90**, 5446 (1968); (*b*) A. J. DEEMING, B. F. G. JOHNSON, and J. LEWIS. J. Chem. Soc. Dalton, 1848 (1973); (*c*) H. C. CLARK, M. J. DYMARSKI, and N. C. PAYNE. J. Organomet. Chem. **165**, 117 (1979).
27. H. C. CLARK and C. S. WONG. J. Am. Chem. Soc. **96**, 7213 (1974).
28. T. G. ATTIG, H. C. CLARK, and C. S. WONG. Can. J. Chem. **55**, 189 (1977).
29. A. D. BUCKINGHAM and P. J. STEPHENS. J. Chem. Soc. 4583 (1964).
30. H. C. CLARK and H. KUROSAWA. J. Organomet. Chem. **36**, 399 (1972).
31. E. C. ALYEA, G. FEY, and R. G. GOEL. J. Coord. Chem. **5**, 143 (1976).
32. Inorg. Synth. **7**, 239 (1963).
33. Y. W. YARED, S. L. MILES, R. BAU, and C. A. REED. J. Am. Chem. Soc. **99**, 7076 (1977).

Can. J. Chem. Downloaded from www.nrcresearchpress.com by 210.87.254.5 on 09/06/12
For personal use only.

Initial state and transition state solvation effects in the oxidation of iodide and catechol by hexachloroiridate(IV) in binary aqueous solvent mixtures

MICHAEL J. BLANDAMER, JOHN BURGESS,[1] STEPHEN J. HAMSHERE, AND COLIN WHITE
Chemistry Department, University of Leicester, Leicester, LE1 7RH, U.K.

AND

ROBERT I. HAINES AND ALEXANDER MCAULEY[1]
Chemistry Department, University of Victoria, Victoria, B.C., Canada V8W 2Y2

Received January 11, 1981[2]

MICHAEL J. BLANDAMER, JOHN BURGESS, STEPHEN J. HAMSHERE, COLIN WHITE, ROBERT I. HAINES, and ALEXANDER MCAULEY. Can. J. Chem. **61**, 1361 (1983).

Rate constants are reported for hexachloroiridate(IV) oxidation of iodide in methanol–, ethanol–, *t*-butyl alcohol–, ethylene glycol–, glycerol–, acetone–, acetonitrile–, and dimethyl sulphoxide – water solvent mixtures, and for the hexachloroiridate(IV) oxidation of catechol in methanol–water mixtures. With the aid of ancillary solubility data and measurements, solvent effects on reactivity have been analysed into initial state and transition state components. In the latter, there are probably both electron transfer and diffusion contributions since it is not possible to identify uniquely the separate kinetic steps associated with the activation process. In these redox systems, however, transition state solvation changes dominate. This conclusion is compared with initial state – transition state effects in the reaction of catechol with hexahydroxoantimonic acid, in the bromate oxidation of bromide, the peroxodisulphate oxidation of iodide, and with patterns established earlier for substitution at inorganic centres. In view of some disagreements and uncertainties in the literature concerning the number of molecules of water of crystallisation in potassium hexachloroiridate(III) and hexachloroiridate(IV), this matter, of considerable importance to hexachloroiridate transfer parameter estimation, is briefly reviewed.

MICHAEL J. BLANDAMER, JOHN BURGESS, STEPHEN J. HAMSHERE, COLIN WHITE, ROBERT I. HAINES et ALEXANDER MCAULEY. Can. J. Chem. **61**, 1361 (1983).

On rapporte les constantes de vitesse d'oxydation de l'iode par l'hexachloroiridate(IV) dans le méthanol, l'éthanol, l'alcool *tert*-butylique, l'éthylène glycol, le glycérol, l'acétone, l'acétonitrile et le diméthylsulfoxyde mélangés à l'eau comme solvants et les constantes de vitesse d'oxydation du cathécol par l'hexachloroiridate(IV) dans des mélanges méthanol–eau. Faisant appel aux mesures et aux données de solubilité secondaires, on a analysé les effets de solvant sur la réactivité des composants à l'état initial et dans l'état de transition. Dans ce dernier cas, il y a probablement à la fois un transfert d'électron et des contributions de diffusion, puisqu'il n'est pas possible d'identifier uniquement les étapes cinétiques séparées associées aux processus d'activation. Dans ces systèmes redox, cependant les changements de solvatation de l'état de transition dominent. On a comparé cette conclusion avec les effets de l'état initial et de l'état de transition dans la réaction du cathécol avec l'acide hexahydroxcantimonique, dans l'oxydation du bromure par le bromate, dans l'oxydation de l'iodure par le peroxodisulfate et avec les schémas établis antérieurement pour la substitution des centres inorganiques. Tenant compte des désaccords et des incertitudes relevés dans la littérature au sujet du nombre de molécules d'eau de cristallisation dans l'hexachloroiridate(III) et l'hexachloroiridate(IV) de potassium, on a revu brièvement cet aspect qui est d'une importance considérable pour l'évaluation du paramètre de transfert de l'hexachloroiridate.

[Traduit par le journal]

Introduction

The dissection of solvent effects on reaction rates into initial state and transition state components has been achieved for a number of inorganic and organic reactions (1). The majority of these systems have involved substitution processes. Some peroxodisulphate oxidations have been analysed in this manner but the central part played by peroxodisulphate oxygen–oxygen bond breaking in determining reactivity makes these reactions complicated to discuss. In this study, therefore, we have investigated solvent effects on reactivity for two relatively well characterised outer-sphere electron transfer reactions. With the aid of the necessary ancillary thermodynamic data and experimental results, it is possible to examine the influence of initial state and transition state solvation changes in determining overall reactivity. The electron transfer reactions chosen are the oxidations of iodide and of catechol (1,2-dihydroxybenzene) by hexachloroiridate(IV). Preliminary reports on the former reaction (2) have been followed recently by a full study (3) where the rate constant data have been rationalised in terms of the Marcus theory (4). In the catechol reaction (5), the kinetic parameters in aqueous media are consistent with a bimolecular outer-sphere redox reaction obeying straightforward second-order rate laws. Moreover, it is known that $IrCl_6^{2-}$ undergoes aquation very much more slowly (6) than it oxidises these substrates.

We have studied the $IrCl_6^{2-}/I^-$ reaction in a wide variety of binary aqueous solvent mixtures to enable us to attempt to identify the importance of solvation, dielectric, ion-pairing, and other possibly relevant factors. Organic co-solvents used ranged from monohydric alcohols[3] through such liquids as glycerol and acetone to the dipolar aprotic solvents dmso and acetonitrile. We have thus employed solvent mixtures in which co-solvent–water interactions are thermodynamically favourable and those in which such interactions are thermodynamically unfavourable. Co-solvents such as methanol, ethanol, and acetone give "typically aqueous" mixtures in which entropy effects dominate (G^E positive; $|TS^E| > |H^E|$); acetonitrile gives "typically non-aqueous positive" mixtures (G^E

[1]To whom correspondence should be addressed.
[2]Revision received December 10, 1982.

[3]Oxidation of methanol by hexachloroiridate(IV) is very much slower than oxidation of iodide or of catechol (32).

Can. J. Chem. Downloaded from www.nrcresearchpress.com by 210.87.254.40 on 09/06/12
For personal use only.

Can. J. Chem. Downloaded from www.nrcresearchpress.com by 210.87.254.40 on 09/06/12
For personal use only.

positive; $|H^E| > |TS^E|$) and dmso and glycerol give "typically non-aqueous negative" mixtures (G^E negative; $|H^E| > |TS^E|$) (7). As outlined below, the $IrCl_6^{2-}$ anion neither aquates nor is reduced to any significant extent on our experimental time scales for any of the co-solvents employed.

In view of the recognised importance (8) of electrostatic effects in determining reactivities in redox reactions, it is desirable to study systems involving a variety of charge combinations. Implicit in our approach is that certain assumptions to be made regarding the extent of ion-pairing in the various solvent systems. The initial approach has been to use a ground/transition state model which although explaining our data is probably not completely adequate owing to our neglect of some of the pre-equilibria involved.[4] Also included in the present investigation, therefore, is a limited investigation of solvent effects on the corresponding oxidation of catechol where ion-pairing effects would be much less pronounced. We have also analysed solvent effects on the iodide–peroxodisulphate and catechol–antimony(V) reactions into initial state and transition state components for the purposes of comparative discussion.

Results and discussion

Oxidation of iodide by hexachloroiridate(IV)

Reaction in aqueous media

The oxidation of I^- by several complexes has been analysed recently in terms of differing kinetic pathways. In some instances ($Fe(di\text{-}imine)_3^{3+}$ and related oxidants) (3) there is evidence for two reaction sequences involving formation of either I_2^- or I·, consistent with the first- and second-order dependences on $[I^-]$ observed. A bimolecular (two-electron) transfer has also been reported in the case of a Ni(III) peptide (9). For other oxidants, however, $(Co(III)_{aq}$ (10), Cu(III) peptide (9), $Mo(CN)_8^{3-}$ (12), and 12-tungstocobaltoate(III) (11)) only a first order term in iodide is observed.

Previous studies (2, 3) on the present reaction indicate a simple second-order rate law $-d[IrCl_6^{2-}]/dt = k_2[I^-][IrCl_6^{2-}]$. These data were obtained in a reaction medium of 0.5 *M* H_2SO_4. In order to have a sufficiently documented basis in aqueous media we have re-investigated the effects of hydrogen ion and chloride ion at $I = 1.0$ *M* and confirmed at $I = 0.01$ *M*, the iodide dependence. Temperature dependence studies have also been completed. In general, measurements were made at as low an ionic strength as possible in order to minimise ion-pairing, especially in mixed solvents where the dielectric constants are markedly lower than that of water. The data agree reasonably well with those derived previously, after account is taken of the effects of ionic strength in these reactions, with $k_2 = 1.38 \times 10^3\ M^{-1}\ s^{-1}$ (0.5 *M* H_2SO_4) (3), $k_2 = 7.09 \times 10^2\ M^{-1}\ s^{-1}$ (1.0 *M* $HClO_4$), and $k_2 = 3.2 \times 10^2\ M^{-1}\ s^{-1}$ (0.01 *M* $LiClO_4$) (Table 1). Also at constant ionic strength, there is no $[H^+]$ or $[Cl^-]$ dependence observed. A similar lack of variation of rate with $[SO_4^{2-}]$ has also been observed (3). The ionic strength effects parallel those of the reactions of iodide with 12-tungstocobaltate(III) (11) and with octacyanomolybdate(V) (12). In the latter system, the study at low ionic strength ($I \leq 0.01$ *M*) has suggested that ion pairs may not play an important role in this reaction.

The temperature dependence of the rate constant yields the activation parameters $\Delta H^{\ddagger} = 27.6 \pm 0.8$ kJ mol^{-1}, $\Delta S^{\ddagger} = -105 \pm 8$ J K^{-1} mol^{-1} for the oxidation reaction. These values may be compared with those for other outer-sphere reactions, e.g. for the corresponding reaction of $Mo(CN)_8^{3-}$ which also exhibits a first order dependence on $[I^-]$, the constants are $\Delta H^{\ddagger} = 21 \pm 10$ kJ mol^{-1} and $\Delta S^{\ddagger} = -160 \pm 30$ J K^{-1} mol^{-1}. One reaction scheme proposed (3) for these reactions where rates may be rationalised in terms of the Marcus theory involves the formation of a weak ion pair ($K_{ip} = 0.3$ *M*) with a rate-determining electron transfer from the iodide ion to the metal centre, leading to formation of I·. Direct electron transfer cannot, however, be excluded.

A similar rate law could result from the rapid (pre-equilibrium) formation of an active ion-pair species which undergoes unimolecular electron transfer. Under these conditions the rate constant would be a composite k_2K_{ip}. It is interesting to note that a transient $[IrCl_6.IO_3]^{4-}$ intermediate has been suggested in the hexachloroiridate(III)–iodate reaction (13).

The detailed oxidation mechanism may thus be written in the form

$$IrCl_6^{2-} + I^- \overset{K_{os}}{\rightleftharpoons} [IrCl_6^{2-}:I^-] \underset{k_b}{\overset{k_a}{\rightleftharpoons}} [IrCl_6^{3-}.I^{\cdot}] \overset{k_c}{\rightarrow}$$

$$[IrCl_6]^{3-} + I^{\cdot} \xrightarrow[+I^-]{\text{fast}} I_3^-$$

As has been noted, the redox step is thermodynamically unfavourable. Using available $E^{\ominus}$ values[3] ($IrCl_6^{2-/3-}$, $I^-/I^{\cdot}$ 0.96 V and 1.40 V respectively) the rate k_a/k_b may be computed as $\approx 4 \times 10^{-8}\ M^{-1}$. The observed composite rate constant is of the form $k_2 = k_ak_c/(k_b + k_c)$. Also $k_bk_c/(k_b + k_c) \approx 8 \times 10^9$ s^{-1} The situation thus exists that after the initial redox reaction,

TABLE 1.

(*a*) Dependence of observed first order rate constants[a] for the oxidation of I^- by $IrCl_6^{2-}$ in aqueous media at 298.2 K, $[IrCl_6^{2-}] = 2.4 \times 10^{-5}$ *M*, $I = 0.01$ *M* (ClO_4^-), the $[Na^+]$ concentration was quoted for I^- and the ionic strength was maintained using $LiClO_4$

$[I^-]/M$[b]	k_{obs}/s^{-1}	T/K	$k_2/M^{-1}\ s^{-1}$[d]
0.001	0.32[c]	283.2	158
0.002	0.66	289.3	209
0.003	0.97	291.7	236
0.004	1.30	298.4	320
		302.3	350
		309.3	472

Mean $k_2 = 325 \pm 4\ M^{-1}\ s^{-1}$
$\Delta H^{\ddagger} = 6.6 \pm 0.2$ kcal mol^{-1}
$\Delta S^{\ddagger} = -25 \pm 2$ cal deg^{-1} mol^{-1}

(*b*) Hydrogen ion and chloride ion dependence studies,[e] $I = 1.00$ *M*, $T = 291.4$ K

$[H^+]/M$	$k_2/M^{-1}\ s^{-1}$	$[Cl^-]/M$	$k_2/M^{-1}\ s^{-1}$
0.00	695	0.00	695
0.50	730	0.50	710
1.00	709	1.00	700
	Mean 711±12		Mean 702±5

[a] From $-d[IrCl_6^{2-}]/dt$.
[b] These results for NaI give $k_2 = 325 \pm 10\ M^{-1}\ s^{-1}$.
[c] $k_{obs} = 0.28\ s^{-1}$ from $d[I_3^-]/dt$.
[d] $[I^-] = 10^{-2}$ *M*, $[IrCl_6^{2-}] = 5 \times 10^{-5}$ *M*, $I = 10^{-2}$ *M* ($LiClO_4$).
[e] H^+/Li^+ mixtures.

[4] Also in view of the unfavourable $\Delta G^{\ominus}$ for the iodide reaction, dynamic processes involving the successor complex must be taken into account.

TABLE 2. Second order rate constants (k_2/M^{-1} s^{-1}) for the $IrCl_6^{2-}/I^-$ reaction in binary aqueous solvent mixtures, T = 298.2 K, $[IrCl_6^{2-}] = 2.4 \times 10^{-5}$ M; $[I^-] = 5 \times 10^{-3}$ M

Co-solvent[a]	k_2 when co-solvent (% by vol) is					
	0	10	20	30	40	80
Methanol			64		24	
Ethanol		128	46	19	10	8
t-Butyl alcohol					(ca. 60)	
Ethylene glycol	324	128	62	27	12	
Acetone		80	30	20	7	
Acetonitrile		88	56	27	14	3
Dimethyl sulphoxide		96	30	5		

[a]Results for glycerol/water mixtures given in text.

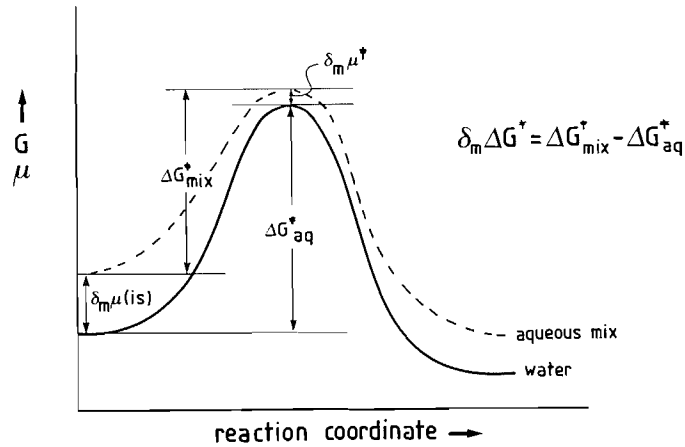

FIG. 1. Inter-relations between the kinetic and thermodynamic transfer parameters.

the recombination (k_b) within the solvent cage competes with the diffusion (k_c) of I$^{\cdot}$. It is not possible to separate the individual rate constants but since these reaction rates are close to the diffusion controlled limit, it can be shown that $k_b \approx k_c$ to within a factor of about 3. Assuming $k_b \approx k_c$ then the observed rate constant $k_2 \approx 0.5k_a$. We have, therefore, a measure of the rate of the initial redox process.

In the case of catechol reaction (*vide infra*) where $\Delta E^0 \sim -0.2$ V (69), if $k_c \approx 8 \times 10^9$ s^{-1} as above then $k_c \gg k_b$ leading to $k_{obs} = k_a$. This approach is justified since $k_a/k_b \approx 3 \times 10^{-4}$ M^{-1} leading to a value of $k_b \approx 5 \times 10^7$ s^{-1}. The rate of this outer-sphere redox recombination would be expected to be lower on Marcus theory grounds since there is a lower driving force than in the case of the iodide. Since the findings for catechol are broadly similar to those for I^- we feel that the assumptions made in the iodide reactions are tenable although inevitably in a rigorous treatment of transition state there are components of both redox recombination and diffusion.

Reaction in binary aqueous mixtures

The second order rate constants for the $[IrCl_6^{2-}]/[I^-]$ reaction are presented in Table 2. The overall pattern of reactivity is of a steady decrease in rate as the proportion of organic co-solvent is increased, e.g., k_2 (M^{-1} s^{-1}) for the reaction falls from 182 to 108 (at 298 K) in going from 24.3 to 51.9% by weight of glycerol.

Dielectric constants and ion-pairing

In this study we have assumed that direct transfer of the electron takes place when the iodide and hexachloroiridate(IV) are in "contact". This direct transfer may be contrasted with indirect transfer across intervening solvent molecules. The model is thus consistent with that of Adegite (3) and other workers (14–16) who have considered contact ion-pair precursors in such redox reactions. The dielectric properties of the solvent mixtures might be considered to have a significant effect owing to their influence on the formation of ion-paired species between the alkali metal counter ions and the negatively charged reactants. This would be true especially of the $[IrCl_6^{2-}]$ ion. It is well established that electron transfer from one anion to another may be facilitated by the role of the cation in reducing the electrostatic repulsion between the species (8, 17, 18). In general, such effects become apparent at much higher alkali metal ion concentrations than are used here. Ion association constants calculated from the standard equations (19) using the Debye–Hückel interaction potential, or estimated via known ion-pairing constants for our experimental conditions (20) suggest these effects to be sufficiently small as to contribute only slightly to the overall reactivity in the redox reaction. The relatively small specific ion effects (Table 1) and the fact that ion-pairing should lead to an increase in rate with decreasing dielectric constant (the opposite of the observed trend) substantiates our considerations in this regard. If the reactive ion-pairs are $[IrCl_6^{2-}.I^-]$ or $[M^+.IrCl_6^{2-}].I^-$, however, these species will be less favoured by increasing dielectric constant. This is consistent with the present data where the rates decrease with increasing concentrations or organic substrate in solution.

Solvation effects

The solvation and hence the chemical potentials of I^-, $IrCl_6^{2-}$ and the transition state will vary as solvent composition varies. Insofar as these determine the barriers to activation, they will determine the observed reactivity trend (Fig. 1) (1). The present data are analysed in these terms. If the Gibbs free energies of transfer of the iodide and hexachloroiridate(IV) ions, $\delta_m\mu^{\ominus}(I^-)$ and $\delta_m\mu^{\ominus}(IrCl_6^{2-})$ are known, and as the transfer function $\delta_m\Delta G^{\ddagger}$ may be derived from the rate constant variation, so the transfer function for the transition state $\delta_m\mu^{\ddagger}$ may be calculated. The transfer parameters $\delta_m\mu^{\ominus}(I^-)$ and $\delta_m\mu^{\ominus}(IrCl_6^{2-})$ must be derived from the appropriate thermodynamic data, generally coming from measurements on electrical cells or of solubilities. Unfortunately it is necessary to make assumptions in deriving the transfer parameters for individual ions. This is still an area of some discussion and concern and in this paper we have attempted to use values from consistent sources and to indicate where assumptions have been made in deriving single ion quantities.

There is a substantial body of information published on $\delta_m\mu^{\ominus}(I^-)$ values for transfer from water into binary aqueous mixtures. Two different Born-related approaches have been used (21, 22), however, and two different "large ion" assumptions employed for various ranges of mixtures by various authors, with little overlap to help in assessing consistency. We refer the reader to the sources cited (21–27) for the $\delta_m\mu^{\ominus}(I^-)$ values used below for details of calculations, conventions, and assumptions. The molar scale has also been used throughout and where necessary published values have been converted to this scale.

No transfer parameters are known for $[IrCl_6^{2-}]$, though a few are available for the closely related hexachlororhenate(IV) ion (28). Solubilities of K_2IrCl_6 have therefore been determined in

Can. J. Chem. Downloaded from www.nrcresearchpress.com by 210.87.254.40 on 09/06/12
For personal use only.

Can. J. Chem. Downloaded from www.nrcresearchpress.com by 210.87.254.40 on 09/06/12
For personal use only.

TABLE 3. Derivation of $\delta_m\mu^{\ominus}(IrCl_6^{2-})$ for transfer from water into binary aqueous solvent mixtures, at 298.2 K

Solvent[a]	OD[b]	$K_{sp}(K_2IrCl_6)$ / mol^2 dm^{-6}	$\delta_m\mu^{\ominus}(K_2IrCl_6)$[c] / kJ mol^{-1}	$\delta_m\mu^{\ominus}(K^+)$[c,d] / kJ mol^{-1}	$\delta_m\mu^{\ominus}(IrCl_6^{2-})$ / kJ mol^{-1}
Water	42.7[e]	10.2×10^{-6}[e]			
Methanol: 20%	7.7	3.6×10^{-7}	8.3	0.9 (19)	6.5
40%	0.62	1.6×10^{-8}	14.4	1.6 (19)	11.2[h]
Ethanol: 40%	0.84	2.2×10^{-8}	15.2	0.5[g] (29)	14.2
80%	0.68[f]	1.9×10^{-11}	33	5.6 (29)	22
Acetone: 40%	5.6	2.3×10^{-7}	9.4	−7 (30) or −3 (31)[i]	23 or 15
Acetonitrile: 40%	21.0	2.1×10^{-6}	3.9	−1.5 (23)	7
DMSO: 40%	21.0	2.1×10^{-6}	3.9	−0.5 (24)	5
Glycerol: 24.3%	27.5	3.7×10^{-6}	2.5	0.5_5 (25)	1.4
51.9%	20.5	2.1×10^{-6}	3.9	1.0 (25)	1.9

[a]Percentages by volume (before mixing), except for aqueous glycerol (percentages by weight).
[b]Saturated solution in 0.01 *M* KCl unless otherwise stated.
[c]Molar scale.
[d]References given in parentheses.
[e]The solubility of K_2IrCl_6 measured here at 298.2 K compares satisfactorily with the published value of 1.25 g/100 g water at ca. 292 K (refs. 34, 40).
[f]No added KCl.
[g]Use of the ref. 24 value of 2 kJ mol^{-1} does not significantly affect our deductions for this solvent mixture.
[h]Or 6 kJ mol^{-1} using $\delta_m\mu^{\ominus}(K^+)$ from ref. 22.
[i]Neither estimate for $\delta_m\mu^{\ominus}(K^+)$ here is attractive, in view of nmr and other evidence on selective solvation in acetone–water mixtures (ref. 35).

TABLE 4. Initial state and transition state solvation contributions to reactivity for the $I^-/IrCl_6^{2-}$ reaction in binary aqueous mixtures

	Value when co-solvent (% v/v) is							
	Methanol		Ethanol		MeCN	DMSO	Glycerol	
Parameter	20	40	40	80	40	40	24.3[a]	51.9[a]
k_2/dm^3 mol^{-1} s^{-1}	64	23	10.4	8	13.8	0.8	182	108
$\therefore\delta_m\Delta G^{\ddagger}$/kJ mol^{-1}	+4	+6.6	+8.5	+9.2	+7.8	+10.9	+1.4	+2.7
$\delta_m\mu^{\ominus}(I^-)$/kJ mol^{-1}	+1.6[b]	+3.3[b]	+2.6[c]	+3.0[c]	+0.8[d]	+2.1[e]	−0.2[f]	−0.7[f]
$\delta_m\mu^{\ominus}(IrCl_6^{2-})$/kJ mol^{-1}	+6.5	+11.2	+14.2	+22	+7	+5	+1.4	+1.9
$\therefore\delta_m\mu^{\ominus}$(is)/kJ mol^{-1}	+8.1	+14.5	+16.8	+25	+8	+7	+1.2	+1.2
$\therefore\delta_m\mu^{\ddagger}$/kJ mol^{-1}	+12.1	+21.1	+25.3	+34	+16	+18	+2.6	+3.9

[a]Percentage composition by weight.
[b]Reference 21.
[c]From potassium iodide solubilities (ref. 21) and ref. 22.
[d]Reference 25.
[e]Reference 26.
[f]Reference 27.

order to calculate $\delta_m\mu^{\ominus}(K_2IrCl_6)$ and hence estimate, using published values of $\delta_m\mu^{\ominus}(K^+)$ (19), values for $\delta_m\mu^{\ominus}(IrCl_6^{2-})$. In order to avoid any hydrolysis of the $IrCl_6^{2-}$ ion during solid–solution equilibrium, the measurements were made in potassium chloride solutions (29), except in 80% ethanol where K_2IrCl_6 is very sparingly soluble and the $IrCl_6^{2-}$ ion is known to hydrolyse only very slowly. Measured optical densities of suitably diluted samples of saturated solutions of K_2IrCl_6 in 0.01 *M* KCl are reported in Table 3. Data were obtained at 487 nm (ϵ = 4075 M^{-1} cm^{-1}), the extinction coefficient being in good agreement with that in the literature (30). Table 3 also includes values for the solubility product, and calculated values of $\delta_m\mu^{\ominus}(K_2IrCl_6)$ together with the transfer prameters for K^+ used (21, 25–27, 31, 33–35) and hence estimated values of $\delta_m\mu^{\ominus}(IrCl_6^{2-})$ (see also following sub-section).

The dissection of the observed reactivity variation with solvent composition is presented in Table 4, and illustrated diagrammatically in Fig. 2. The overall picture which emerges is that the transition state is more sensitive to solvent variation than the initial state. This behaviour differs from that of the majority of substitution reactions, but parallels that found recently (36) for the reaction of $S_2O_8^{2-}$ with the iron(II) complex $Fe(bipy)_2(CN)_2$, another outer-sphere electron transfer process.

One possible explanation of the greater sensitivity of the transition state to its solvent environment may be the result of its greater charge. To investigate this, we have estimated values of $\delta_m\mu^{\ominus}(IrCl_6^{3-})$ in order to compare these with $\delta_m\mu^{\ddagger}$ i.e., $\delta_m\mu^{\ominus}(I\ldots IrCl_6^{\ddagger 3-})$. Values of $\delta_m\mu^{\ominus}(IrCl_6^{3-})$ were derived as above from solubility data of K_3IrCl_6 (see below) in 0.10 *M* KCl to avoid any competing hydrolysis (37). Measurements were made in water and aqueous methanol (Table 5). The transfer parameters for $IrCl_6^{2-}$, $IrCl_6^{3-}$, and the transition state are shown in Fig. 3. It is noteworthy that the transition state is less sensitive than the $IrCl_6^{3-}$ anion; both have the same charge, but the $IrCl_6\ldots I^{3-}$ transition state is of course larger than the $IrCl_6^{3-}$ model.

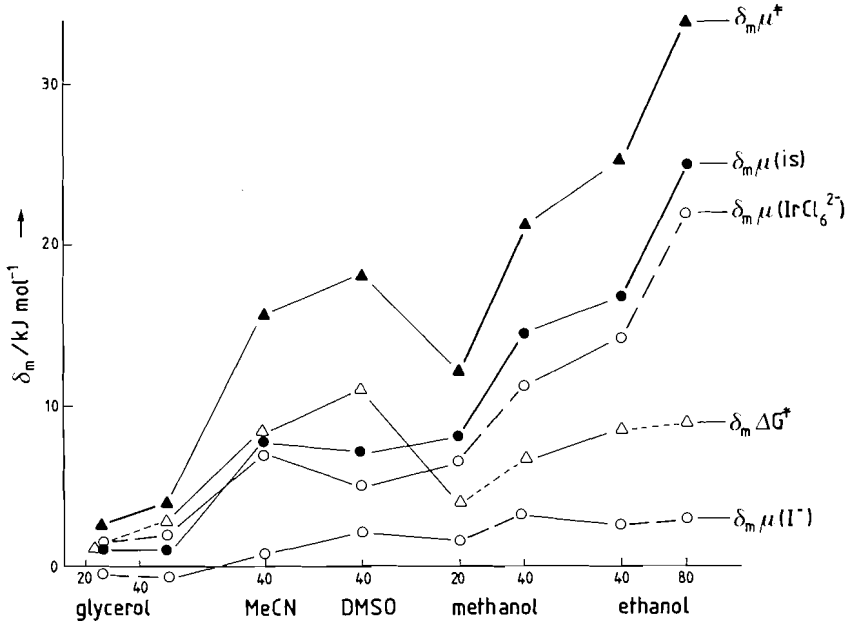

FIG. 2. Dissection of solvent effects on reactivity into initial state and transition state components for the hexachloroiridate(IV)–iodide reaction.

TABLE 5. Derivation of $\delta_m\mu^{\ominus}(IrCl_6^{3-})$ for transfer from water into binary aqueous solvent mixtures, at 298.2 K

		Methanol[a]	
Parameter	Water	20	40
Solubility (K_3IrCl_6)/mol dm^{-3}[b]	0.28[c]	0.057	0.0053
$\therefore K_{sp}(K_3IrCl_6)$/mol^4 dm^{-12}	0.166	2.85×10^{-4}	2.13×10^{-8}
$\therefore\delta_m\mu^{\ominus}(K_3IrCl_6)$/kJ mol^{-1}[c]		+15.8	+39.3
$\therefore\delta_m\mu^{\ominus}(IrCl_6^{3-})$/kJ mol^{-1}[c,d]		+13.1	+34.5

[a]Percentage composition in volume % (before mixing).
[b]Solubilities measured in 0.10 *M* KCl; solid in equilibrium is trihydrate $K_3IrCl_6.3H_2O$ in each case.
[c]Molar scale.
[d]Using $\delta_m\mu^{\ominus}(K^+)$ from ref. 21.
[e]Cf. approximately 0.14 *M* at 292 K (p. 326 of ref. 40).

Hydrates of K_2IrCl_6 and K_3IrCl_6

The correct deduction of such quantities as Gibbs free energies and enthalpies of transfer of salts requires knowledge of their state of hydration. For the former it is necessary to make a correction involving the Gibbs free energy of transfer of water if the number of molecules of water of hydration in the solid in equilibrium with saturated solutions changes with solvent composition. For the latter, one has to correct for the enthalpy of transfer of the appropriate number of water molecules if one measures enthalpies of solution of a hydrate rather than of an anhydrous salt. During the present investigation we have found that there is some confusion in the literature concerning the state of hydration of both the hexachloroiridates K_2IrCl_6 and K_3IrCl_6.

In the case of the iridium(IV) salt, the confusion stems from a discussion of spectra of hexachloroiridates which includes mention of an alleged hexahydrate $K_2IrCl_6.6H_2O$ (38). The earliest papers on K_2IrCl_6 indicate that it is, like the caesium and rubidium salts but unlike the sodium and lithium salts (both have $6H_2O$), anhydrous, on the basis of chemical analysis (34, 39–41). Griffiths (42) states that K_2IrCl_6 is isomorphous with K_2PtCl_6, which is undoubtedly anhydrous. Discussions of magnetic properties (43), paramagnetic resonance (44), nqr (45), neutron diffraction (46), and vibrational spectra (47) all assume that this salt is anhydrous, as does the paper reporting its specific heat (48). We must conclude that K_2IrCl_6 is indeed anhydrous; the solitary reference (38) to the hexahydrate gives no evidence of characterisation.

Various sources imply that K_3IrCl_6 crystallises with 0, 1, or $3H_2O$. First reports of this salt described it as a trihydrate (49–51). Subsequently the separation of the monohydrate from boiling hydrochloric acid was reported (52). Delépine's extensive review of hexachloroiridates (41) recognises both tri- and mono-hydrates. X-ray diffraction data have been reported (d and I/I_0) for a powdered sample (53) but it is not apparent whether this was anhydrous or one of the hydrates. The data are indexed (54) (and referenced incorrectly) under the formula of the anhydrous salt, but the description of the solid (53) suggests the monohydrate. We believe, on the basis of appearance and of thermogravimetric experiments, that the solid in equilibrium with saturated solutions in water and in water-rich aqueous methanol at 298.2 K is the trihydrate.

Can. J. Chem. Downloaded from www.nrcresearchpress.com by 210.87.254.40 on 09/06/12
For personal use only.

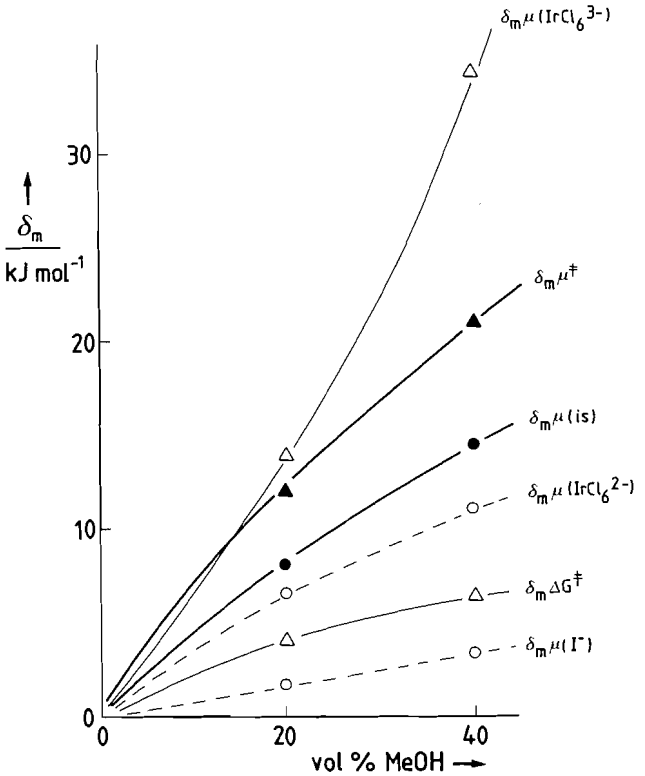

FIG. 3. Solvent effects on reactivity for the hexachloroiridate(IV)–iodate reaction in aqueous methanol; illustration of hexachloroiridate(III) as transition state model.

Oxidation of catechol by hexachloroiridate(IV)

Reaction in aqueous media

The kinetics of the oxidation have been studied under a variety of conditions in aqueous solution (5). These earlier results established a second-order rate law

$$-\mathrm{d[catechol]}/\mathrm{d}t = k_2[\mathrm{catechol}][IrCl_6^{2-}]$$

the reaction being considered as outer-sphere. These data were obtained at $I = 1.0\ M$ and a slight dependence on $[H^+]$ was observed, the reaction rate increasing with decreasing acidity. We have repeated the measurements at $I = 0$, and confirmed the second-order reaction overall. The k_2 value obtained ($1.39 \times 10^4\ M^{-1}\ s^{-1}$) at low ionic strength may be compared with an extrapolated value of $9.5 \times 10^3\ M^{-1}\ s^{-1}$ at $I = 1.0\ M$.

Reaction in binary aqueous mixtures

Rate constants (k_2) have been determined in 10, 20, and 30% methanol and solubility data on catechol has also been derived in order to calculate Gibbs free energies of transfer for this reactant. Analysis of solvents effects is shown in Table 6 with conclusions presented in Fig. 4. The pattern is similar to that for the corresponding reaction with iodide, except in that the catechol is somewhat stabilised in going from water into aqueous methanol in contrast to the de-stabilisation of the iodide ion. This finding where the extent of ion-pairing with the neutral molecule would be expected to be less than for the charged reactants may substantiate our view of the principal pathways involving only the reactants as described. Again, as with the iodide reaction the transition state for catechol is more affected by solvent than is the initial state. It would be interesting to assess how generally this pattern applies to hexachloroiridate(IV) oxidations. Several kinetic studies have been reported for this oxidant, of which a few appear attractive candidates in the present context. Thus oxidation of thiourea (55) commends itself by the availability of transfer data for the thiourea, while oxidation of the hydrazinium cation (56) would give an example of a reaction involving reactants of opposite charge, to complement the iodide and catechol systems described above. Unfortunately in these, and related reactions, the mechanisms prove not to be simple, and thus initial state – transition state dissections are hardly feasible.

We have established thus far a greater sensitivity for the transition state than for the initial state in redox reactions involving both $IrCl_6^{2-}$ and the $Fe(bipy)_2(CN)_2/S_2O_8^{2-}$ (36) system. In order to examine further the generality of this pattern[5] and the difference from the normal substitution behaviour, the hexahydroxoantimonate(IV)–catechol substitution process has been investigated and published data on other related redox reactions have been analysed. Details of experiments and calculations are presented below.

Reaction of antimony(V) with catechol

This reaction has been examined in aqueous solution (57) and the formation of 1:1 and 2:1 complexes established. The kinetics of the first stage have been investigated

the mechanism having been established as S_N1 in character.

In the present study, kinetic data for the above reaction have been obtained in several aqueous alcohol mixtures. First order rate constants were derived by monitoring the absorbance increase at 290 nm consequent on complex formation. Studies were carried out in the presence of excess catechol, and at a pH of 2.0 where the form of antimony(V) predominating is the neutral complex $HSb(OH)_6$ rather than the hexahydroxoantimonate(V) anion (57). The experimental data are presented in Table 7. The concentrations of antimony in saturated solutions containing 30% methanol and 30% *t*-butyl alcohol at pH 2 and pH 7 were determined. The results at pH 2 are included in Table 8. The solubility decreases much more dramatically on going from water to the aqueous alcohol mixtures at pH 7 than at pH 2. This is presumably attributable to the non-electrolyte form $NSb(OH)_6$ being present in more acid media. The analysis of initial state and transition state effects on the reaction are included in Table 8. The small solvent effect on reactivity contrasts with the trends in the $IrCl_6^{2-}$ reactions. The marked effects in these oxidations may be attributable to the large effects of solvent variation on the chemical potentials of the reactant ions $IrCl_6^{2-}$ and I^-. Catechol and $HSb(OH)_6$, both non-electrolytes, have small free energies of transfer from water into aqueous alcohols and there is not therefore an important contribution to reactivity variation from this source. In the catechol–antimony(V) reaction a large contribution from transition state solvation would not be expected since transition state generation does not involve charge separation or cancellation. Indeed it could be presumed that the state is reached by the stretching of an antimony to oxygen bond and the removal of water as a leaving group.

$$HSb(OH)_6 \rightarrow [(HO)_5Sb.....OH_2]^{\ddagger}$$

[5]It would be interesting to carry out an initial state-transition analysis of hexachloroiridate(IV) oxidation of oxalate, whose kinetics have recently been established in dioxan–water mixtures (70) to further examine this pattern.

Can. J. Chem. Downloaded from www.nrcresearchpress.com by 210.87.254.40 on 09/06/12
For personal use only.

TABLE 6. Initial state and transition state solvation contributions to reactivity for the catechol/$IrCl_6^{2-}$ reaction in aqueous methanol[a]

Parameter	Value when % methanol (v/v) is			
	0	10	20	30
k_2/dm^3 mol^{-1} s^{-1}[b]	13900	10000	6190	3850
$\therefore\delta_m\Delta G^{\ddagger}$/kJ mol^{-1}		+0.82	+2.00	+3.18
Solubility catechol/mol^{-1} dm^{-3}	5.6	6.5	7.2	8.6
$\therefore\delta_m\mu^{\ominus}$(catechol)/kJ mol^{-1}		−0.37	−0.62	−1.06
$\delta_m\mu^{\ominus}(IrCl_6^{2-})$/kJ mol^{-1}		+3.5	+6.5	+9.3
$\therefore\delta_m\mu^{\ominus}$(is)/kJ mol^{-1}		+3.1	+5.9	+8.2
$\therefore\delta_m\mu^{\ddagger}$/kJ mol^{-1}		+3.9	+7.9	+11.4

[a]All transfer parameters on the molar scale.
[b]Measured at 298.2 K, initial concentrations of catechol and of K_2IrCl_6 10^{-4} mol dm^{-3} and 4.7×10^{-6} mol dm^{-3} respectively.

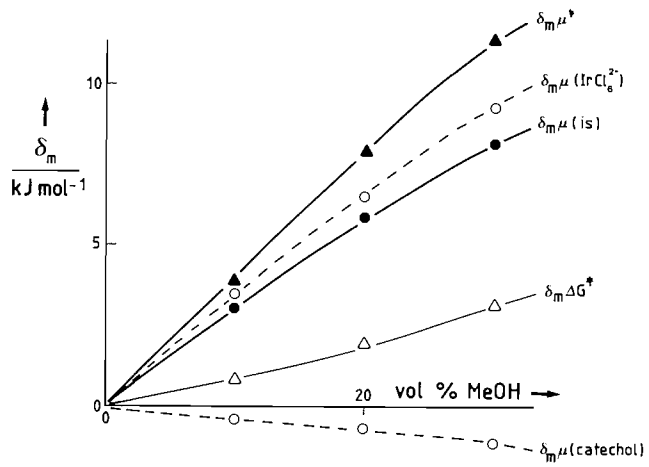

FIG. 4. Dissection of solvent effects on reactivity into initial state and transition state components for the hexachloroiridate(IV)–catechol reaction.

TABLE 7. Observed first-order rate constants (k_{obs}/s^{-1}) for the complex formation reaction of catechol with antimony(V) in aqueous alcohols at 298.2 K. Initial concentrations: antimony(V) 2.5×10^{-4}, catechol 1.5×10^{-2}, [HCl] = 10^{-2} mol dm^{-3}

Co-solvent	k_{obs}/s^{-1} when % co-solvent (v/v) is			
	0	10	30	50
Methanol	0.011	0.018	0.022	0.045
Ethanol			0.027	
t-Butyl alcohol			0.019	

Oxidation of iodide by peroxodisulphate

There is some kinetic information on this reaction in binary aqueous solvent mixtures, specifically in aqueous acetonitrile (58) and in aqueous *t*-butyl alcohol (59). Unfortunately, earlier estimates of Gibbs free energies of transfer of the peroxodisulphate anion into binary aqueous solvent mixtures included only the co-solvents methanol and acetone (60). We have therefore measured solubilities of potassium peroxodisulphate in several aqueous acetonitrile and in aqueous *t*-butyl alcohol solvent mixtures, thence estimating $\delta_m\mu^{\ominus}(S_2O_8^{2-})$ (Table 9) as before (60, 61).

Our analysis of solvent effects on the iodide–peroxodisulphate redox reaction is set out in Table 10 (58–63). Figure 5 shows the trends for the reactants and the transition state, and may be compared with Figs. 2 and 3 for the iodide–hexachloroiridate(IV) reaction. The patterns for the two similar reactions, both involving a dinegative and uninegative ion, are very similar in aqueous alcohols and in aqueous acetonitrile. Most significantly, the transition state for the iodide–peroxodisulphate reaction is again somewhat more affected by solvent composition variation, as in the other redox reactions cited earlier in this paper.

TABLE 8. Initial state and transition state solvation contributions to reactivity for the catechol–antimony(V) reaction in aqueous alcohols[a]

Parameter	Value when solvent (% ROH by vol) is		
	Water	30% methanol	30% *t*-butyl alcohol
k_{obs}/s^{-1}	0.011	0.022	0.019
$\therefore\delta_m\Delta G^{\ddagger}$/kJ mol^{-1}		−1.72	−1.35
Solubility Sb^V/mol dm^{-3}	4.5	2.6	1.8
$\therefore\delta_m\mu^{\ominus}(HSb(OH)_6)$/kJ mol^{-1}		+1.3	+2.2
$\therefore\delta_m\mu^{\ddagger}$/kJ mol^{-1}		−0.4	+0.8

[a]Compositions expressed in volume % (before mixing). For reaction concentrations see Table 7.

Oxidation of bromide by bromate

The small variation in rate with solvent composition for this reaction in ethanol–water mixtures has been discussed previously (64) in terms of dielectric constant effects. The overall solvent effect pattern is markedly different here from the $S_2O_8^{2-}$ or $IrCl_6^{2-}$ reactions. Whereas for these latter oxidants the rates of oxidation decrease as the proportion of organic co-solvent increases, for the bromate(V) oxidation of bromide the rate increases slightly with the higher proportions of ethanol. The analysis of the data indicates that this small difference probably represents a balance between larger effects on the initial state and transition state. It is not possible to carry out a quantitative determination of the rate trend into the initial state and transition state components since $\delta_m\mu^{\ominus}(H_2BrO_3^+)$ cannot be estimated satisfactorily. However, it is clear that the overall solvent effect pattern must be different. Under the conditions employed the reactants (Br^- and $H_2BrO_3^+$) are ionic and it is likely that their chemical potentials will increase with the proportion of organic co-solvent. The small change observed in rate constant then requires that the chemical potential of the transition state should increase by slightly less than that of the

Can. J. Chem. Downloaded from www.nrcresearchpress.com by 210.87.254.40 on 09/06/12
For personal use only.

TABLE 9. Derivation of $\delta_m\mu^{\ominus}(S_2O_8^{2-})$ for transfer from water into binary aqueous solvent mixtures, at 298.2 K

	Value when co-solvent (% v/v) is					
	t-Butyl alcohol			Acetonitrile		
Parameter	10	20	30	10	20	25
Solubility $(K_2S_2O_8)$/mol dm^{-3} [a]	0.152	0.108	0.077	0.232	0.224	0.213
$\therefore\delta_m\mu^{\ominus}(K_2S_2O_8)$/kJ mol^{-1} [b]	+3.4	+5.9	+8.5	+0.2	+0.5	+0.9
$\therefore\delta_m\mu^{\ominus}(S_2O_8^{2-})$/kJ mol^{-1} [b]	+6.2[c]	+12.9[c]	+15.9[c]	+0.4[d]	+0.7[d]	+1.3[d]

[a] Solubility in water 0.240 mol dm^{-3}
[b] Molar scale.
[c] Using $\delta_m\mu^{\ominus}(K^+)$ from ref. 61.
[d] Using $\delta_m\mu^{\ominus}(K^+)$ from ref. 25.

TABLE 10. Initial state and transition state solvation contribution to reactivity for the $I^-/S_2O_8^{2-}$ reaction in binary aqueous mixtures

	Value when x_2[a] (co-solvent) is								
	t-Butyl alcohol				Acetonitrile				
Parameter	0.013	0.027	0.042	0.080	0.016	0.034	0.052	0.073	0.095
k_2/dm^3 mol^{-1} s^{-1} [b]	32	25	20	17	15.3	12.1	9.8	4.0	2.5
$\therefore\delta_m\Delta G^{\ddagger}$/kJ mol^{-1}	+0.36	+0.97	+1.52	+1.93	+1.3	+1.9	+2.4	+4.6	+5.8
$\delta_m\mu^{\ominus}(I^-)$/kJ mol^{-1} [c, d]	+1.3	+2.8	+4.8	+8.0	0	0	+0.1	+0.1	+0.2
$\delta_m\mu^{\ominus}(S_2O_8^{2-})$/kJ mol^{-1} [c]	+4	+8	+13	+16	+0.2	+0.4	+0.6	+0.8	+1.2
$\therefore\delta_m\mu^{\ominus}$(is)/kJ mol^{-1}	+5	+11	+18	+24	+0.2	+0.4	+0.7	+0.9	+1.4
$\therefore\delta_m\mu^{\ddagger}$/kJ mol^{-1}	+5	+12	+20	+26	+1.5	+2.3	+3.1	+5.5	+7.2

[a] Mole fraction organic co-solvent.
[b] Rate constants from ref. 59 (*t*-butyl alcohol mixtures) and ref. 39 (acetonitrile mixtures).
[c] From ref. 42 (*t*-butyl alcohol mixtures) and ref. 25 (acetonitrile mixtures).
[d] Values for transfer to aqueous *t*-butyl alcohol obtained by a simultaneous extrapolation procedure (ref. 43) are rather larger, but their use in this dissection would not affect the general picture of relative importance of initial state and transition state solvation (cf. also ref. 63).
[e] Estimated from values in Table 9.

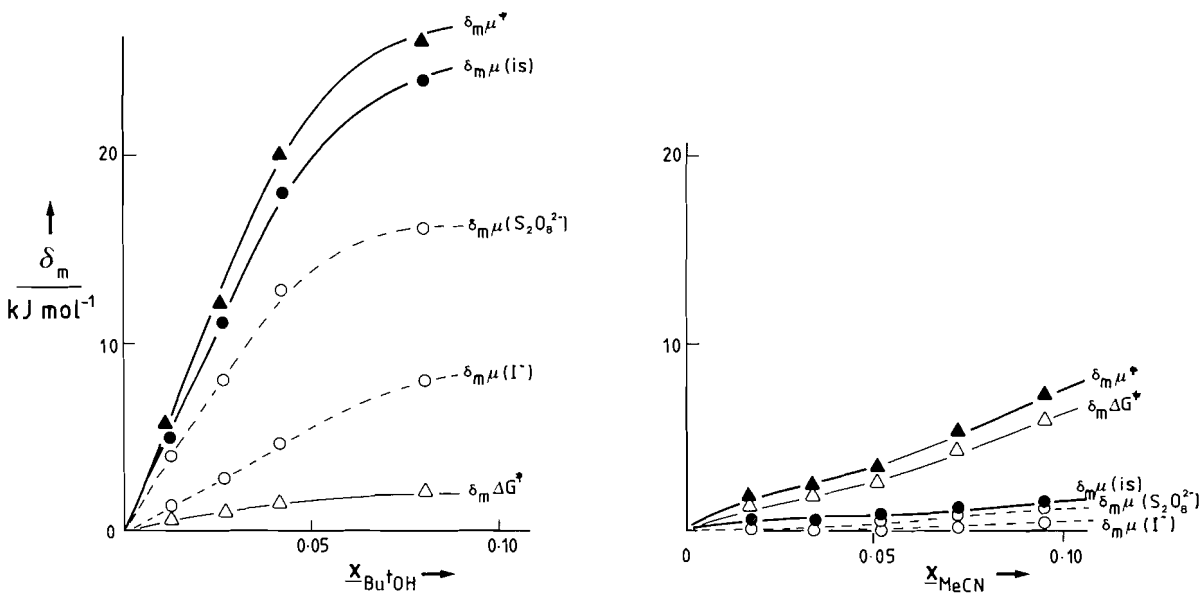

FIG. 5. Dissection of solvent effects on reactivity into initial state and transition state components for the peroxodisulphate–iodide reaction.

initial state. The pattern contrasts with that for $IrCl_6^{2-}$ oxidations. One difference, however, is that the charges of the reactant ions are now opposite in sign and this may be reflected in a transformation of solvation as a result of charge neutralisation in the transition state, a feature not present in the systems described above. In this way the behaviour is more reminiscent of substitution process such as those involving mercury(II) (65). There is an interest in establishing whether redox and substitution reactions behave in a similar manner and comparison of the mercury(II)-catalysed aquation and chromium(II) reduction of chlorotransition metal complexes (66) may be fruitful areas of study in this regard.

Can. J. Chem. Downloaded from www.nrcresearchpress.com by 210.87.254.40 on 09/06/12
For personal use only.

Oxidation of iodide by 12-tungstocobaltate(III)

We have recently shown that, in methanol–, acetonitrile–, and dimethyl sulphoxide–water mixtures, solvent effects on reactivity are dominated by destabilisation of the transition state on adding organic co-solvent, just as in the hexachloroiridate(IV) oxidations dealt with in the present paper (67).

Experimental

For experiments in aqueous solution, all solutions were prepared with water de-ionised then distilled from an all-glass apparatus. K_2IrCl_6 (Aldrich) was used without further purification. Potassium and sodium iodide were AnalaR grade. Acetonitrile (Anachem) was treated with calcium hydride, and distilled over P_2O_5. Acetone (Anachem), dimethylsulphoxide (Eastman), glycerol (Fisher), and ethylene glycol (Fisher) were reagent grade and used without further purification.

Spectra were recorded on a Varian Techtron Model 635 uv–visible instrument which when thermostatted was also used for monitoring the slower kinetic runs. The stopped-flow apparatus used has been described previously (68). Rate data were derived either from photographic analysis of oscilloscope traces or from the output of a PCM computer coupled to the photomultiplier tube of the instrument. Under pseudo-first order conditions, plots were linear to the greater than 80% reaction. Reproducibility between runs was ±3%.

Acknowledgements

We thank NSERC and the University of Victoria Research Fund for financial assistance, the Royal Society for support, and (J.B.) the Universities of Victoria and Leicester for hospitality and leave of absence respectively.

1. M. J. BLANDAMER and J. BURGESS. Coord. Chem. Rev. **31**, 93 (1980).
2. J. E. BYRD, J. Y. CHEN. H. PO, C.-P. CHUA, and W. K. WILMARTH. Am. Chem. Soc. Meeting 167, INOR 102.
3. C. O. ADEDINSEWO and A. ADEGITE. Inorg. Chem. **18**, 3597 (1979).
4. R. A. MARCUS. J. Phys. Chem. **67**, 853 (1963); **67**, 2889 (1963).
5. E. MENTASTI, E. PELIZZETTI, and C. BAIOCCHI. J. Chem. Soc. Dalton Trans. 132 (1977); D. F. C. MORRIS and T. J. RITTER. Intern. J. Chem. Kinet. **11**, 1081 (1979).
6. L. MOGGI, G. VARANI, M. F. MANFRIN, and V. BALZANI. Inorg. Chim. Acta, **4**, 335 (1970).
7. M. J. BLANDAMER and J. BURGESS. Chem. Soc. Rev. **4**, 55 (1975).
8. A. D. PETHYBRIDGE and J. E. PRUE. *In* Progress in inorganic chemistry. Vol. 17. *Edited by* J. O. Edwards. 1972. p. 327.
9. J. M. T. RAYCHEBA and D. W. MARGERUM. Inorg. Chem. **20**, 1441 (1981).
10. G. DAVIES and K. O. WATKINS. J. Phys. Chem. **74**, 338 (1970).
11. J. C. BRODOVITCH, R. I. HAINES, and A. MCAULEY. To be published.
12. M. H. FORD-SMITH and J. H. RAWSTHORNE. J. Chem. Soc. A, 160 (1969).
13. J. P. BIRK. Inorg. Chem. **17**, 1372 (1978).
14. G. NORD, B. PEDERSEN, and O. FARVER. Inorg. Chem. **17**, 2233 (1978).
15. M. KIMURA and G. WADA. Inorg. Chem. **17**, 2239 (1978).
16. R. D. CANNON. Inorg. React. Mech. **6**, 15 (1979).
17. F. FERRANTI. J. Chem. Soc. A, 134 (1970).
18. D. V. S. JAIN and F. S. NANDEL. J. Chem. Soc. Dalton Trans. 949 (1977).
19. R. G. WILKINS. Study of kinetics and mechanism of reactions of transition metal complexes. Allyn and Bacon, Boston, MA. 1974. p. 183.
20. M. T. BECK. Coord. Chem. Rev. **3**, 91 (1968).
21. C. F. WELLS. J. Chem. Soc. Faraday Trans. I, **69**, 984 (1973).
22. C. L. DE LIGNY and M. ALFENAAR. Rec. Trav. Chim. **84**, 81 (1965).
23. H. E. ARMSTRONG, J. V. EYRE, A. V. HUSSEY, and W. P. PADDISON. Proc. R. Soc. A, **79**, 564 (1907).
24. D. BAX, C. L. DE LIGNY, and A. G. REMIJNSE. Rec. Trav. Chim. **91**, 965 (1972).
25. B. G. COX, R. NATARAJAN, and W. E. WAGHORNE. J. Chem. Soc. Faraday Trans. I, **75**, 86 (1979).
26. B. G. COX, R. NATARAJAN, and W. E. WAGHORNE. J. Chem. Soc. Faraday Trans. I, **75**, 1780 (1979).
27. C. F. WELLS. J. Chem. Soc. Faraday Trans. I, **70**, 694 (1974).
28. J. BURGESS and S. J. CARTWRIGHT. J. Chem. Soc. Dalton Trans. 100 (1975); J. BURGESS, N. MORTON, and J. C. MCGOWAN. J. Chem. Soc. Dalton Trans. 1775 (1977); R. I. HAINES. Ph.D. Thesis, University of Leicester. 1977.
29. E. H. ARCHIBALD and J. W. KERN. Trans. R. Soc. Can. **11**, 7 (1917).
30. I. A. POULSEN and C. S. GARNER. J. Am. Chem. Soc. **84**, 2032 (1962); F. BOZON-VERDURAZ and C. LECLERE. Bull. Soc. Chim. Fr. I, 101 (1980).
31. O. POPOVYCH and A. J. DILL. Anal. Chem. **41**, 456 (1969).
32. K. K. SEN GUPTA and U. CHATTERJEE. J. Inorg. Nucl. Chem. **43**, 2491 (1981).
33. C. L. DE LIGNY, D. BAX, M. ALFENAAR, and M. G. L. ELFERINK. Rec. Trav. Chim. **88**, 1183 (1969); D. BAX, M. ALFENAAR, and C. L. DE LIGNY. Rec. Trav. Chim. **90**, 1002 (1971); D. BAX, C. L. DE LIGNY, and A. G. REMIJNSE. Rec. Trav. Chim. **91**, 1225 (1972).
34. M. DELEPINE. Bull. Soc. Chim. **3**, 901 (1908).
35. J. BURGESS. Metal ions in solution. Ellis Horwood, Chichester. 1978. Chapt. 6.
36. M. J. BLANDAMER, J. BURGESS, and R. I. HAINES. J. Chem. Soc. Chem. Commun. 963 (1978).
37. S. M. ZIMINA, G. P. TSAYUN, V. I. KRAVTSOV, and L. YA. SMIRNOVA. Elektrokhimiya, **15**, 578 (1979); Chem. Abstr. **90**, 210761*h* (1979).
38. A. J. MCCAFFERY, M. D. ROWE, and D. A. RICE. J. Chem. Soc. Dalton Trans. 1605 (1973).
39. M. DELÉPINE. Compt. Rend. Acad. Sci. **146**, 1267 (1908).
40. M. DELÉPINE. Compt. Rend. Acad. Sci. **147**, 198 (1908).
41. M. DELÉPINE. Ann. Chim. 9 **7**, 277 (1917).
42. W. P. GRIFFITH. The chemistry of the rarer platinum metals. Interscience, New York. 1967. p. 233.
43. A. D. WESTLAND and N. C. BHIWANDKER. Can. J. Chem. **39**, 2353 (1961).
44. J. H. E. GRIFFITHS, J. OWEN, J. G. PARK, and M. F. PARTRIDGE. Proc. R. Soc. London, **250**A, 84 (1959).
45. A. J. LINDOP. J. Phys. C. **3**, 1984 (1970).
46. M. T. HUTCHINGS and C. G. WINDSOR. Proc. Phys. Soc. London, **91**, 928 (1967).
47. D. M. ADAMS and H. A. GEBBIE. Spectrochim. Acta, **19**, 925 (1963); P. J. HENDRA and P. J. D. PARK. Spectrochim. Acta, **23**A, 1635 (1967).
48. C. A. BAILEY and P. L. SMITH. Phys. Rev. **114**, 1010 (1959).
49. C. CLAUS. J. Prakt. Chem. **39**, 100 (1846); **42**, 352 (1847); **80**, 282 (1860).
50. M. JOLY. Compt. Rend. Acad. Sci. **110**, 1132 (1890).
51. M. DUFET. Bull. Soc. Fr. Minér. **13**, 206 (1890).
52. A. DUFFOUR. Compt. Rend. Acad. Sci. **155**, 222 (1912).
53. G. W. WATT, E. P. HELVENSTON, and L. E. SHARIF. J. Inorg. Nucl. Chem. **24**, 1067 (1962).
54. Powder Diffraction File, JCPDS, International Centre for Diffraction Data, Swathmore, PA. 1978.
55. H. N. PO, H. E. ERAN, Y. KIM, and J. E. BYRD. Inorg. Chem. **18**, 197 (1979).
56. K. K. SENGUPTA and P. K. SEN. Inorg. Chem. **18**, 979 (1979).
57. J. MAZIÈRES and J. LEFEBVRE. Rev. Chim. Minér. **13**, 470 (1976).
58. J. BURGESS. J. Chem. Soc. A, 2351 (1970).

Can. J. Chem. Downloaded from www.nrcresearchpress.com by 210.87.254.40 on 09/06/12
For personal use only.

59. J. BURGESS. J. Chem. Soc. A, 2571 (1968).
60. M. J. BLANDAMER, J. BURGESS, and R. I. HAINES. J. Inorg. Nucl. Chem. **41**, 258 (1979).
61. C. F. WELLS. J. Chem. Soc. Faraday Trans. I, **72**, 601 (1976).
62. K. BOSE, K. DAS, A. K. DAS, and K. K. KUNDU. J. Chem. Soc. Faraday Trans. I, **74**, 1051 (1978).
63. Y. POINTUD, J. JUILLARD, J. P. MOREL, and L. AVEDIKIAN. Electrochim. Acta, **19**, 229 (1974); M. J. BLANDAMER, J. BURGESS, and J. G. CHAMBERS. J. Chem. Soc. Dalton Trans. 606 (1976).
64. M. S. SUBHANI. Rev. Roum. Chim. **23**, 719 (1978).
65. M. J. BLANDAMER, J. BURGESS, and R. I. HAINES. J. Chem. Soc. Dalton Trans. 607 (1980).
66. J. H. ESPENSON and S. R. HUBBARD. Inorg. Chem. **5**, 686 (1966).
67. M. J. BLANDAMER, J. BURGESS, P. P. DUCE, R. I. HAINES, and A. MCAULEY. Transition Metal Chem. **7**, 10 (1982).
68. K. J. ELLIS and A. MCAULEY. J. Chem. Soc. Dalton Trans. 1533 (1973).
69. S. STEENKEN and P. NETA. J. Phys. Chem. **83**, 1134 (1979).
70. U. CHATTERJEE, S. MAITI, and K. K. SENGUPTA. Z. Phys. Chem. Leipzig, **261**, 1231 (1980).

Can. J. Chem. Downloaded from www.nrcresearchpress.com by 210.87.254.40 on 09/06/12
For personal use only.

Coordinence 2 du phosphore: étude quantochimique des systèmes P=N et P=C

D. GONBEAU ET G. PFISTER-GUILLOUZO
Laboratoire de Physico-Chimie Moléculaire, ERA 895, I.U.R.S., Avenue Philippon, 64000 Pau, France

ET

J. BARRANS
ERA 926, Université Paul Sabatier, 31062 Toulouse Cedex, France

Reçu le 29 octobre, 1982

D. GONBEAU, G. PFISTER-GUILLOUZO et J. BARRANS. Can. J. Chem. **61**, 1371 (1983).

Nous avons réalisé en base *ab initio* double zeta de valence une approche quantochimique sur des entités modèles HP=NH et HP=CH_2. Un processus de minimisation à métrique variable a été utilisé pour la détermination des paramètres géométriques.

Les "forces" des liaisons $2p_\pi-3p_\pi$ pour P=N et P=C ont été estimées par évaluation des barrières obtenues en réalisant une rotation de 90° d'une partie de la molécule vis à vis de l'autre. L'essentiel des effets de corrélation a été pris en compte et pour la détermination des états à 90° de plus basse énergie un formalisme rigoureux RHF a été utilisé.

Nous avons ainsi mis en évidence des caractéristiques électroniques différentes pour les deux motifs et à partir de ces résultats nous avons interprété leur comportement réactionnel: dimérisation, addition de réactifs polaires et site de protonation dans le cas de HP=NH.

D. GONBEAU, G. PFISTER-GUILLOUZO, and J. BARRANS. Can. J. Chem. **61**, 1371 (1983).

Using *ab initio* valence double zeta as a basis, a quantum-chemical approach was developed for the models HP=NH and PH=CH_2. The geometric parameters were determined by a variable metrics minimization process.

The $2p_\pi-3p_\pi$ bond forces for P=N and P=C were estimated by evaluating the barriers obtained by a 90° rotation of one part of the molecule with respect to the other. The essential correlation effect was considered and a rigourous RHF formalism was used to determine the state at 90° of lower energy.

Different electronic characteristics were found for both motives and according to these results, their reaction behaviour was interpreted: dimerization, addition of polar reactants, and protonation site for HP=NH.

[Journal translation]

Can. J. Chem. Downloaded from www.nrcresearchpress.com by 210.87.254.5 on 09/06/12
For personal use only.

1. Introduction

La synthèse et la caractérisation de composés du phosphore à coordinence 2 est un domaine actuellement en plein développement (1–8). A notre connaissance, seules deux approches théoriques parallèles à la notre (9, 10) sur la structure électronique d'intermédiaires phosphorés présentant une liaison $p_\pi-p_\pi$ ont été réalisées contrairement aux nombreux travaux existants sur le silaéthylène (11). Le présent travail a pour but d'analyser la nature et la stabilité des doubles liaisons P=C et P=N dans les systèmes acycliques par une approche quantochimique. Dans ce but, nous avons choisi comme modèle d'une part la molécule HP=CH_2 détectée par pyrolyse de la diméthylphosphine (12)

$$(CH_3)_2PH \xrightarrow[1000°C]{} H_2C{=}PH + CH_4 \xrightarrow[-H_2]{} H{-}C{\equiv}P$$

et plus récemment de $Me_3SiCH_2PH_2$ (13), d'autre part le motif HP=NH qui bien qu'actuellement non isolé représente le plus simple des composés présentant la double liaison P=N.

2. Conditions de calcul

Tous les calculs ont été réalisés à l'aide du programme MONSTERGAUSS 80 (14*a*).

Une base double zeta de valence 4-31G (15) avec orbitales de polarisation de type *d* sur tous les hétéroatomes a été utilisée (une orbitale gaussienne de type *d* $\xi^d_P = 0{,}57$, $\xi^d_N = 0{,}8$, $\xi^d_O = 0{,}8$).

Nous avons vérifié que nos résultats essentiels n'étaient pas modifiés par introduction de fonction de polarisation de type *p* sur les hydrogènes.

Les paramètres géométriques ont été optimisés grâce à un processus de minimisation à métrique variable avec évaluation du gradient selon la méthode de Broyden–Fletcher–Goldfarb–Shanno (14*b*).

Tous les calculs sur les états couches ouvertes ont été menés à l'aide du formalisme RHF.

De plus afin de tenir compte des effets essentiels de corrélation et disposer de grandeurs comparables entre les deux systèmes examinés une IC 6x6 a été autorisée sur les états fondamentaux à 0° et les singulets couches fermées à 90°. En effet l'influence notable de la corrélation au niveau du fondamental provient essentiellement du mélange important avec la configuration doublement excitée ψ ($\pi^2 \rightarrow \pi^{*2}$) où l'orbitale liante π est remplacée par l'antiliante π^* alors qu'une configuration correspondante n'existe évidemment plus à 90°.

De plus étant donné la position de cette orbitale π dans les deux composés examinés (dernière occupée ou avant dernière occupée) nous avons été amenés à envisager toutes les mono et diexcitations possibles entre les deux dernières orbitales occupées et la première vacante.

3. Analyse des résultats

3.1 *Etats fondamentaux. Structures géométriques, orbitales moléculaires, populations de Mulliken*

3.11 *Structures géométriques*

Pour les deux composés la structure énergétiquement privilégiée à l'état fondamental a été trouvée plane, l'isomère *trans* étant légèrement favorisé par rapport au *cis* dans le cas de HPNH ($\Delta E \simeq 0{,}22$ kcal/mol).

Tous les paramètres géométriques (longueurs et angles) ont été minimisés; les valeurs obtenues ont été reportées dans le tableau 1.

Nous constatons en premier lieu un bon accord d'ensemble

TABLEAU 1. Paramètres géométriques minimisés pour HPNH (*cis* et *trans*) et $HPCH_2$[a]

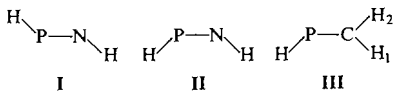

I II III

Paramètre	I	II	III	Exp
P—{N / C	1,5485	1,5402	1,6403	1,670 (1)
P—H	1,4205	1,4391	1,4151	1,420 (1)
N—H	1,0056	1,0021		
C—H_1			1,0743 / 1,0761	1,090[b] (1)
P^N^H_1	112,69	120,09	125,258 / 119,725	HCH 117[b] (1)
N^PH	99,18	104,49	98,29	100 (1)
C				97,5 (2)

[a]Les longueurs sont exprimées en angstroms et les angles en degrés.
[b]Valeurs obtenues pour $H_2C{=}NH$.

entre les données théoriques et celles des structures microondes réalisées pour $HPCH_2$ (12, 13). La deuxième structure qui correspond à une obtention de $HPCH_2$ à partir de $Me_3SiCH_2PH_2$ paraît plus précise mais seules les valeurs de l'angle CPH et du moment dipolaire sont indiquées; leur comparaison avec les résultats de nos calculs est tout à fait satisfaisante.

La liaison P=C (1,64 Å) présente bien un caractère de double liaison puisque trouvée intermédiaire entre une triple liaison (P≡C: 1,54 Å) (16, 17) et une simple liaison (P—C ≃ 1,85 Å) (18*a*).

Il en est de même pour la liaison P=N de 1,55 Å environ nettement plus courte que la simple liaison à 1,72 Å (18*b*) et tout à fait comparable à celle obtenue en rayons X pour $(Me_3Si)_2N$—P=N—SiMe (1,545 Å) (7) et $Me_3Si(tBu)N$—P=N—*t*Bu (1,544 Å) (6).

Par ailleurs, nous remarquons un angle de valence au phosphore du même ordre pour HPNH *trans* et $HPCH_2$ (99°) alors qu'il apparaît pour l'isomère *cis* de 104°.

Cette différence reste toutefois moins grande que celle observée sur l'azote 112°–120°. Ces remarques mettent bien en évidence une certaine rigidité du groupement PH à phosphore dicoordiné.

3.12 *Orbitales moléculaires*

Dans le tableau 2 nous avons reporté les valeurs des énergies obtenues pour les dernières orbitales moléculaires occupées de HPNH (*cis* et *trans*) et de $HPCH_2$ et leurs natures respectives précisées grâce au procédé de localisation de Boys (19) et à un mode d'analyse que nous avons mis au point (20). Nous observons ainsi pour $HPCH_2$ que la dernière orbitale occupée à 9,625 eV correspond à la liaison π_{P-C} avec une nette localisation sur le carbone, l'orbitale à 10,427 eV est associée à la paire σ du phosphore.

Dans le cas de HPNH par contre étant donné la forte interaction entre les paires du phosphore et de l'azote, l'orbitale moléculaire correspondant à la liaison $\pi_{P=N}$ et très fortement localisée sur l'azote à 11,404 eV (isomère *trans*) et 11,468 eV (isomère *cis*) n'est plus la dernière occupée; elle apparaît entre les deux combinaisons des paires σ en opposition de phase et en phase, la première avec un fort poids sur le phosphore et la deuxième sur l'azote. Nous observons également le phénomène bien connu d'une interaction des paires en *trans* nettement plus importante qu'en *cis* respectivement d'environ 4,5 et 2,2 eV.

La première virtuelle pour tous les dérivés correspond à la $\pi^*_{P=X}$ (X = N, C) légèrement plus haute pour $HPCH_2$ que pour HPNH avec une localisation plus importante sur le phosphore particulièrement dans le cas de HPNH.

3.13 *Populations de Mulliken*

Afin de préciser les caractéristiques électroniques des liaisons dans les deux composés HPNH *trans* et $HPCH_2$, nous avons procédé à une analyse de population selon Mulliken et parallèlement à un tracé des orbitales moléculaires essentielles.

Comme il est bien connu que les charges totales sur les atomes et les populations de recouvrement sont des données sensibles au choix de la base sans aucun caractère quantitatif nous les examinons donc en comparatif pour les deux dérivés (figure 1).

En premier lieu, l'examen des charges nettes totales sur les atomes révèle un caractère polaire nettement plus marqué pour P—N que pour P—C avec une accumulation de charge plus grande sur l'azote que sur le carbone reflétant ainsi les électronégativités respectives de ces trois atomes P: 2,1; C: 2,5; N: 3.

Le transfert de charge du groupement PH vers le groupement NH est de 0,45 e^- environ et seulement de 0,19 e^- du groupement PH vers le groupement CH_2.

Bien qu'elle ne soit pas très importante la participation des orbitales *d* au niveau des atomes de phosphore n'est pas négligeable: 0,32 e^- pour HPNH et 0,27 e^- pour $HPCH_2$; dans les deux cas ce sont essentiellement les orbitales *d* de symétrie σ dans le plan de la molécule qui interviennent.

Les populations de recouvrement paraissent voisines pour les deux dérivés aussi bien en total qu'en π légèrement plus faibles pour HPNH que pour $HPCH_2$ mais révèlent dans les deux cas un caractère réel de liaison π.

Le point le plus intéressant concerne la distribution électronique π qui présente toujours en charge nette un caractère asymétrique pour P—N et au contraire une quasi symétrie dans le cas de P—C.

Des conclusions similaires peuvent être déduites de l'examen des contours des orbitales moléculaires π tracés pour les deux dérivés (figures 2 et 3). Dans le cas de HPNH, l'accumulation de charge électronique sur l'azote conduit à une augmentation de l'effet d'écran de la charge nucléaire et en conséquence à une extension de l'orbitale atomique $2p\pi_N$ comparée à celle d'un atome isolé, l'effet inverse intervenant pour le phosphore. Les contours tracés visualisent cet ajustement des orbitales atomiques. Celui réalisé pour $HPCH_2$ bien que du même type met parfaitement en évidence une densité électronique sur le carbone nettement moins importante en π que sur l'azote.

3.14 *Force de liaison π. Etats à 90°*

Pour compléter notre approche nous avons cherché à atteindre pour chaque dérivé un autre "indice" que l'on qualifie habituellement de "force de liaison π".

En effet, en réalisant une rotation de 90° d'une partie de la molécule vis à vis de l'autre la barrière obtenue ΔE_r qui correspond à la rupture de la liaison π est considérée comme représentative de la force de cette liaison puisqu'en première approximation les liaisons σ demeurent inchangées par rotation autour de leur axe $\Delta E_r \simeq \Delta E_\pi$. Il faut donc pour l'évaluation de ΔE_r outre l'état fondamental à 0° déterminer celui à 90° de plus basse énergie.

Des remarques contradictoires (21, 22) ont été faites dans la littérature sur la détermination de cet état à 90° mais deux

Can. J. Chem. Downloaded from www.nrcresearchpress.com by 210.87.254.5 on 09/06/12
For personal use only.

TABLEAU 2. Principales orbitales moléculaires pour HPNH (*cis* et *trans*) et $HPCH_2$

HPNH				
	trans	*cis*	$HPCH_2$	
Orbitale	Energie (eV)	Energie (eV)	Orbitale	Energie (eV)
π^*_{P-N}	2,164	2,144	π^*_{P-C}	2,795
$n_P - n_N$	9,874	10,369	π_{P-C}	9,625
π_{P-N}	11,404	11,468	n_P	10,427
$n_P + n_N$	14,342	12,593	σ_{P-H}, σ_{C-H}	14,021
σ_{P-H}, σ_{N-H}	15,632	17,215	$\sigma_{C\ H\ H}$	16,512
E_{el} (Hartree)	−446,522738	−446,520428		−429,097576
E_t (Hartree)	−395,869101	−395,868812		−379,889229

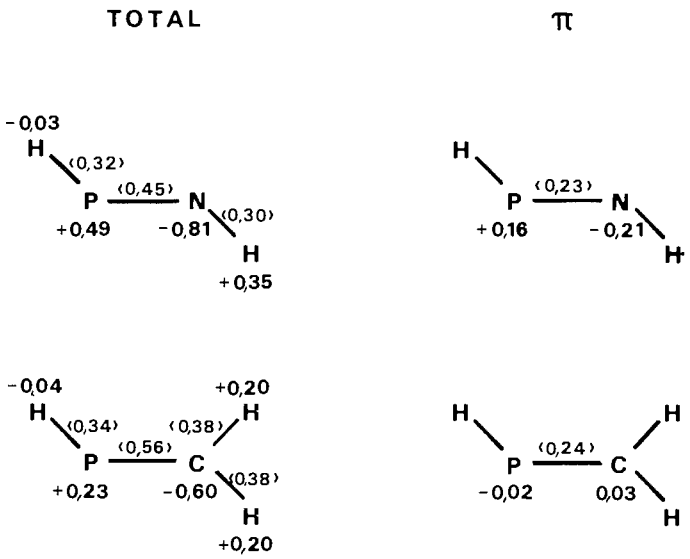

FIG. 1. Analyses de population selon Mulliken pour les états fondamentaux. Charges nettes et populations de recouvrement entre parenthèses.

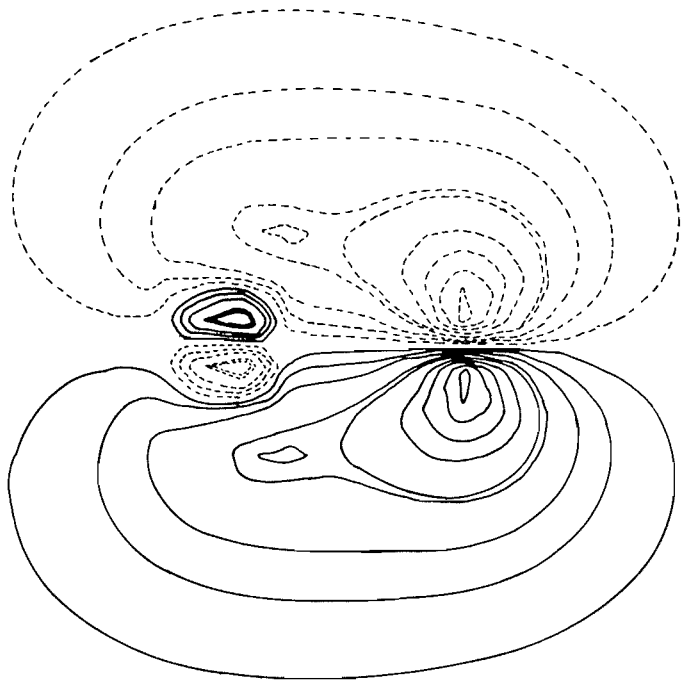

FIG. 2. Contours de l'orbitale $\pi_{P=N}$ dans HPNH *trans*. Les lignes tracées correspondent aux valeurs suivantes de ψ = ±0,02, ±0,05, ±0,08, ±0,13, ±0,14, −0,2, ±0,25, ±0,3, ±0,35.

points semblent bien établis.

D'une part pour une molécule plane du type HXYH avec X = Y, la rotation à 90° conduit à un éclatement de l'orbitale moléculaire doublement occupée à 0° en deux orbitales mono occupées dégénérées. L'état à 90° de plus basse énergie de nature radicalaire (répartition symétrique des électrons de la liaison π sur chaque atome) est atteint par un formalisme couches ouvertes; différents calculs réalisés sur C_2H_4, Si_2H_4 (21, 22) l'ont parfaitement montré.

D'autre part la non identité de X et Y conduit à une levée de dégénérescence d'autant plus importante qu'est grande la différence d'électronégativité entre X et Y; la rotation à 90° conduit alors à un état plus ou moins zwitterionique; on observe en effet une tendance à la localisation des électrons de la liaison π sur l'atome le plus électronégatif et ceci d'autant plus que la liaison π à 0° était polaire. L'état le plus stable à 90° est alors généralement atteint comme l'a remarqué Salem (23) par le calcul du singulet couches fermées; c'est ce que Curtis (22) a également observé dans le cas du silaéthylène H_2CSiH_2.

Pour notre part étant donné l'ambiguïté existant au niveau de $HPCH_2$: X ≠ Y, mais liaison π non polaire à 0°, nous avons, pour être assuré d'obtenir l'état à 90° de plus basse énergie, procédé pour les deux dérivés aux calculs des états couches ouvertes et du singulet couches fermées.

En ce qui concerne les états couches ouvertes un formalisme rigoureux RHF a été utilisé; les paramètres géométriques optimisés à 0° ont été conservés pour le calcul des états à 90°.

S'il nous a été possible d'atteindre sans problème les triplets (tableau 3), il n'en a pas été de même pour les singulets couches ouvertes que nous n'avons pu mener à convergence en dépit de nombreux essais; leur énergie est cependant généralement plus haute que celle du triplet correspondant.

Les énergies obtenues pour les singulets couches fermées ont été reportées dans le tableau 3.

Afin d'obtenir des grandeurs tout à fait comparables pour les deux composés examinés nous avons réalisé comme précisé auparavant une interaction de configurations sur les états fondamentaux et les singulets couches fermées correspondants. Nous sommes ainsi conduits à une évaluation de $\Delta E_r = E_{IC}(\theta = 0°) - E_{IC}(\theta = 90°)$; les valeurs obtenues de 48,1 kcal/mol et 105,4 kcal/mol respectivement pour HPNH et $HPCH_2$ révèlent une liaison π beaucoup plus faible pour HPNH que pour $HPCH_2$.

Can. J. Chem. Downloaded from www.nrcresearchpress.com by 210.87.254.5 on 09/06/12
For personal use only.

Can. J. Chem. Downloaded from www.nrcresearchpress.com by 210.87.254.5 on 09/06/12
For personal use only.

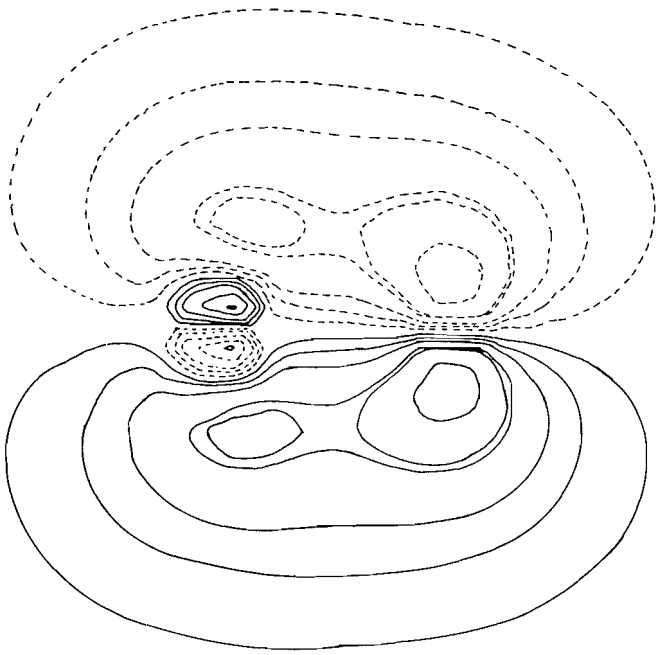

FIG. 3. Contours de l'orbitale $\pi_{P=C}$ dans $HPCH_2$. Les lignes tracées correspondent aux valeurs suivantes de ψ = ±0,02, ±0,05, ±0,08, ±0,13, ±0,14, ±0,2.

Par ailleurs, nous observons conformément aux remarques précédentes une très nette différence énergétique entre le triplet couches ouvertes et le singulet couches fermées dans le cas de HPNH alors que des valeurs énergétiques proches ont été obtenues pour $HPCH_2$.

Nous avons ensuite cherché à mieux cerner les caractéristiques électroniques de l'état à 90° qui correspond à la rupture de la liaison π et qu'il était par la même intéressant d'analyser plus en détail.

L'examen des populations de Mulliken (figure 4) révèle dans le cas de HPNH comme pressenti précédemment une polarité accrue P^+N^- et au contraire dans le cas de $HPCH_2$ un caractère type radicalaire de la liaison P—C dans l'état à 90°.

En analysant de façon plus approfondie les variations de population des diverses orbitales p_y (perpendiculaire au plan moléculaire à 0°) p_x dans le plan moléculaire et p_z selon l'axe de la liaison nous sommes conduits aux remarques suivantes en ce qui concerne la rupture de la liaison π.

Dans le cas de HPNH l'essentiel des mouvements électroniques lors de la rotation réside dans la perte en π du phosphore au profit de l'azote et à l'inverse nous notons un gain léger en σ au niveau du phosphore ce qui correspond au schéma suivant:

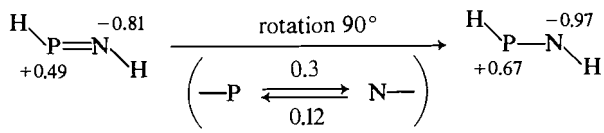

Un comportement tout á fait différent est observé pour $HPCH_2$; un transfert et π très notable du carbone vers le phosphore intervient et conjointement un mouvement apparaît en σ du phosphore vers le carbone ce qui conduit au schéma:

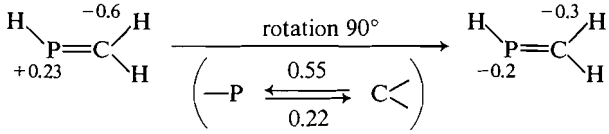

3.15 *Evolution thermique de chaque dérivé sur la nappe du fondamental*

Nous avons également tenté d'examiner l'évolution thermique de chaque dérivé sur la nappe du fondamental par le biais d'une minimisation des états à 90°.

Ceci nous a permis de pressentir qu'un mécanisme de rotation n'était envisageable que dans l'hypothèse d'un changement de multiplicité de la fonction d'onde puisqu'aucun extremum n'a pu être atteint aux environs de 90° pour un état singulet.

Le procédé de minimisation nous amène en effet à envisager sur la nappe du fondamental un processus d'évolution thermique bien différencié pour chaque composé.

Dans le cas de HPNH nous sommes conduits à un extremum plan l'hydrogène porté par l'azote étant situé dans le prolongement de la liaison P—N, le processus mis en jeu est celui de l'inversion de l'azote dans le plan de la molécule, la barrière obtenue étant de l'ordre de 15 kcal/mol environ. Ce comportement est à rapprocher de celui généralement invoqué pour l'isomérisation *cis–trans* aussi bien dans le cas de la formaldoxime (24) que de la diimide (25).

Pour $HPCH_2$, par minimisation, l'état à 90° se transforme rapidement en un intermédiaire 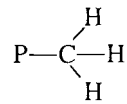 Etant donné la détection expérimentale lors de la pyrolyse de la phosphapropyne P≡CH nous sommes naturellement amenés à envisager une évolution de l'intermédiaire par abstraction d'hydrogène vers P≡CH, la barrière cette fois nettement plus importante se situe aux environs de 75 kcal/mol. Les géométries respectives de ces deux états de transition ont été reportées dans le tableau 4.

3.2 *Réactivité des phospha alkènes et iminophosphanes*

A partir de l'ensemble de ces données nous avons tenté d'interpréter la réactivité de ces deux composés.

A priori la très forte polarisation de la liaison P—N aussi bien en total qu'en π et la faible "force de liaison π" implique que HPNH soit une molécule extrémement réactive. De plus, l'atome de phosphore tout en présentant un caractère électrophile marquée (système π) garde sa nucléophilie: la dernière orbitale moléculaire occupée de ce système étant de type σ nettement localisée sur le phosphore comme le montre le contour de cette orbitale reporté dans la figure 5.

Par contre $HP{=}CH_2$ se caractérise par une force de liaison π nettement plus élevée et une polarité nettement moins marquée particulièrement en π où un caractère radicalaire apparaît.

De plus comme nous l'avons vu l'orbitale moléculaire localisée sur la paire libre du phosphore est énergétiquement plus profonde que dans HP—NH ce qui laisse pressentir une nucléophilie moins marquée.

Cette différence dans la structure électronique reflète bien le comportement chimique de ces molécules.

3.21 *Réaction d'addition*

Une des caractéristiques essentielles de ces deux systèmes est leur facilité de self-addition. Les monomères ne sont

TABLEAU 3. Valeurs énergétiques permettant l'évaluation de la "force de la liaison π"

Etat	Valeurs énergétiques	
	HPNH *trans*	$HPCH_2$
Etat fondamental $\theta = 0°$	−395,866910 H (avant IC)	−379,889229 H (avant IC)
singulet couches fermées	−395,892275 H (après IC)	−379,912664 H (après IC)
Etat $\theta = 90°$	−395,801919 H (avant IC)	−379,743667 H (avant IC)
singulet couches fermées	−395,815542 H (après IC)	−379,744734 H (après IC)
Etat $\theta = 90°$	−395,717929 H	−379,733574 H
triplet couches ouvertes RHF		
ΔE, kcal/mol	48,1	105,4

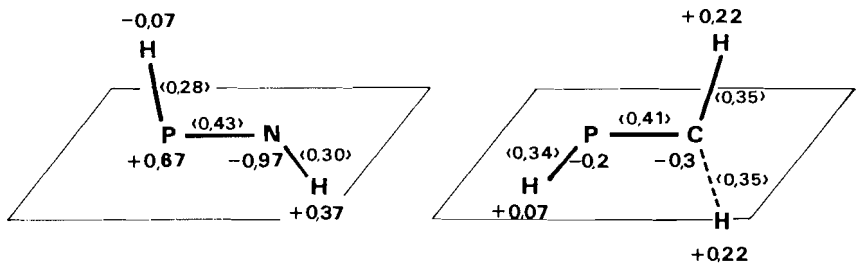

FIG. 4. Analyses de population selon Mulliken pour les états à 90°. Charges nettes et populations de recouvrement entre parenthèses.

TABLEAU 4. Paramètres géométriques optimisés pour les intermédiaires obtenus par minimisation des états à 90°

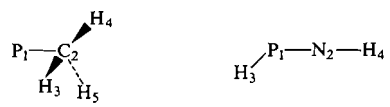

	I	II
P_1—N_2	1,49	1,61
P_1—C_2		
$H_3\hat{P}_1N_2$	105,5	
$P_1\hat{N}_2H_4$	180	
C_2—H_3		1,2
$P_1\hat{C}_2H_3$		70
$P_1\hat{C}_2H_4$		130
$P_1\hat{C}_2H_5$		130

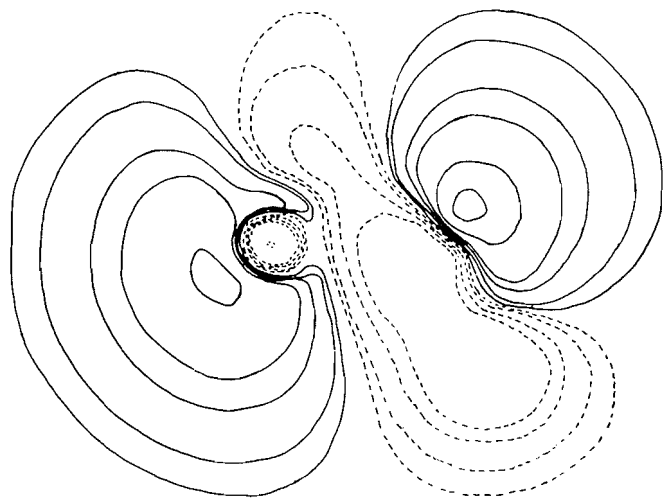

FIG. 5. Contours de la dernière orbitale occupée dans HPNH. Les lignes tracées correspondent aux valeurs suivantes de $\psi = \pm 0{,}01$, $\pm 0{,}02$, $\pm 0{,}05$, $\pm 0{,}08$, $\pm 0{,}18$, $\pm 0{,}3$.

obtenus notamment pour les iminophosphanes que dans des conditions bien particulières l'encombrement sur l'atome de phosphore paraissant un des facteurs importants (7).

Si l'on examine les contours des $\pi^*_{P=X}$ reportés dans les figures 6 et 7, on conçoit que pour une dimérisation (2 + 2) l'étape déterminante correspondra à la formation d'une liaison P—X (recouvrement maximal entre le contour observé sur l'atome X dans l'orbitale π occupée et celui sur P dans l'orbitale π^*) et donc à l'obtention de dimères tête–queue. Il faut toutefois noter que dans le cas de $\pi^*_{P=C}$, la forme de la π^* ne permet pas de rejeter l'hypothèse d'une dimérisation tête–tête fait observé expérimentalement notamment lorsque le carbone porte un substituant donneur (26). Par contre, dans le cas des iminophosphanes si la dimérisation tête–queue est bien observée (27) la réaction de cycloaddition (2 + 1) a été également mise en évidence (28) ce qui s'interprète en effet pour ce motif par une compétition avec l'attaque électrophile sur la paire libre du phosphore qui comme nous l'avons observé a une nette localisation dans la dernière orbitale moléculaire occupée.

Cette réactivité différente est également observée pour l'addition des réactifs polaires. Dans le cas de la double liaison P=C, l'addition 1,2 a été observée pour ROH (29) avec toutefois des conditions drastiques puisque catalysée par le méthylate de sodium.

Cette réaction apparaît également comme compétitive avec celle de substitution sur le phosphore et préservation de la double liaison (30).

Afin de mieux appréhender ce comportement nous avons examiné pour les phospha alkènes l'intermédiaire correspondant à une attaque anionique et pour cela procédé à la minimisation de l'entité $(\overset{HO}{H}\!\!>\!P—CH_2)^-$. Nous avons cependant conservé pour les longueurs C—H et les angles $P\hat{C}H$ les

Can. J. Chem. Downloaded from www.nrcresearchpress.com by 210.87.254.5 on 09/06/12
For personal use only.

Can. J. Chem. Downloaded from www.nrcresearchpress.com by 210.87.254.5 on 09/06/12
For personal use only.

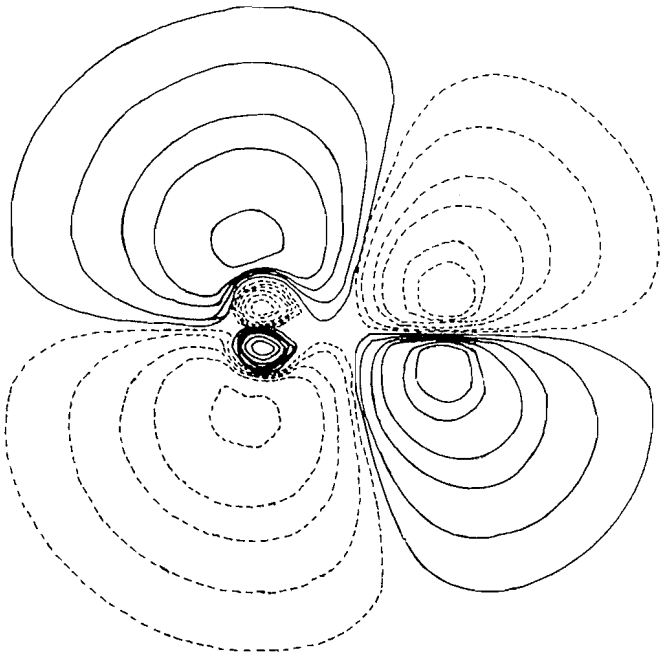

FIG. 6. Contours de l'orbitale $\pi^*_{P=N}$ dans HPNH *trans*. Les lignes tracées correspondent aux valeurs suivantes de ψ = ±0,005, ±0,02, ±0,05, ±0,08, ±0,15, ±0,2.

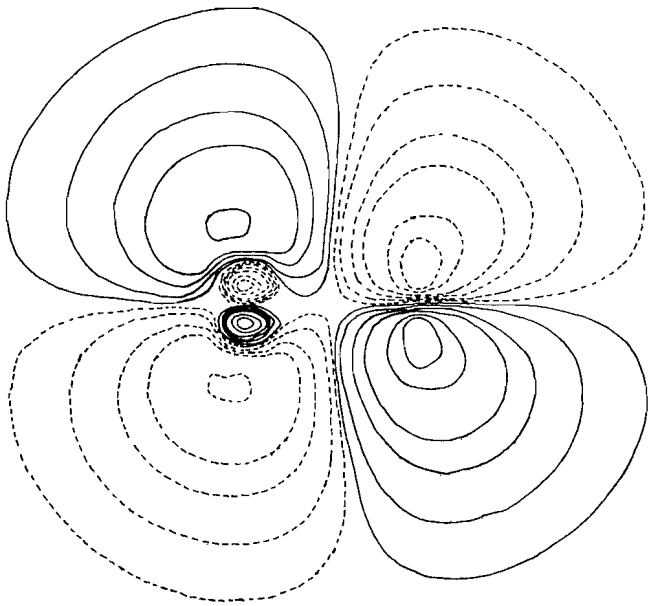

FIG. 7. Contours de l'orbitale $\pi^*_{P=C}$ dans $HPCH_2$. Les lignes tracées correspondent aux valeurs suivantes de ψ = ±0,005, ±0,02, ±0,05, ±0,08, ±0,15, ±0,2.

valeurs obtenues lors de leur minimisation dans $PHCH_2$. Les valeurs optimisées ont été reportées dans le tableau 5.

Nous remarquons tout d'abord une pyramidalisation très nette au niveau de l'atome de phosphore qui s'accompagne d'un allongement de la longueur P—C avec simultanément un très net accroissement de la longueur P—H et une ouverture de l'angle $\widehat{HPC}$.

L'analyse de population selon Mulliken (figure 8) fait

TABLEAU 5. Paramètres géométriques optimisés pour les intermédiaires anioniques

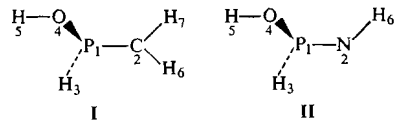

I II

	I	II
P_1—C_2	1,7	1,6
P_1—N_2		
P_1—O_4	1,67	1,67
O_4—H_5	0,95	0,95
P_1—H_3	1,465	1,44
$\widehat{H_3P_1C_2}$	103,6	97
$\widehat{H_3P_1N_2}$		
$\widehat{C_2P_2O_4}$	107,2	105,6
$\widehat{H_3P_1O_4}$	95,4	98,6

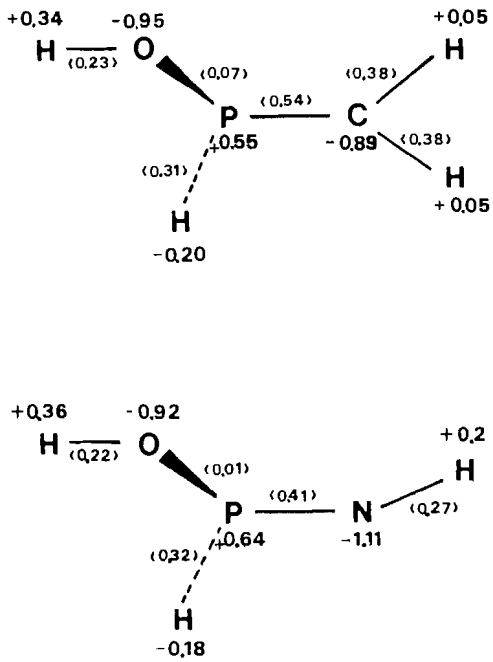

FIG. 8. Analyses de population selon Mulliken pour les intermédiaires anioniques. Charges nettes et populations de recouvrement entre parenthèses.

apparaître une accumulation de charge négative importante sur l'hydrogène porté par le phosphore.

L'observation simultanée d'un allongement de la longueur P—H et d'une forte charge négative sur l'hydrogène traduit bien la possibilité d'une substitution sur le phosphore avec préservation de la double liaison et départ de H^-.

Parallèlement nous notons un caractère fortement négatif du carbone. Vis à vis de $HPCH_2$ nous observons un net accroissement de densité électronique dans la direction perpendiculaire au groupement CH_2 (1,003 dans $HPCH_2$, 1,82 dans $(\begin{smallmatrix}HO\\H\end{smallmatrix}\!>\!P—CH_2)^-$) la dernière orbitale occupée du système de symétrie π présentant une localisation très importante sur l'atome de carbone.

TABLEAU 6. Paramètres géométriques optimisés pour $(HPNH_2)^+$ et $(H_2P—NH)^+$

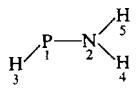

I

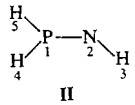

II

	I	II
P—N	1,5818	1,4840
P—H_3	1,42	1,39
P—H_5		1,39
N—H_3	1,01	1,006
N—H_5	1,01	
∧ NPH_3	96,84	127,33
∧ NPH_5		117,48
∧ PNH_3	125,92	130,34
∧ PNH_5	120,65	
E_t (Hartree)	−396,230574	−396,15606
	ΔE = 46,7 kcal/mol	

Ces observations traduisent raisonablement la compétition pour ce système d'une réaction de substitution nucléophile avec préservation de la double liaison et d'une réaction d'addition 1,2.

Dans le cas de la double liaison P=N expérimentalement la seule addition 1,1 a été constatée (27, 31) les conditions opératoires étant toutefois particulièrement douces: il semble que comme pour la dimérisation (2 + 1) il faille invoquer les caractères nucléophile et électrophile de l'atome de phosphore. Nous avons comme précédemment examiné l'intermédiaire résultant d'une attaque anionique par OH^- sur le phosphore.

On constate (tableau 5, figure 8) un comportement légèrement différent puisque l'allongement de la liaison PH et l'accumulation de charge sur l'atome d'hydrogène sont moins importants. De plus, pour cet intermédiaire, la dernière orbitale moléculaire occupée reste une orbitale localisée sur la paire libre du phosphore traduisant ainsi la possibilité pour cet atome d'être le site d'attaque nucléophile et électrophile.

Si donc le caractère nucléophile de l'atome de phosphore dans les iminophosphanes est évident, il nous a semblé utile de compléter notre approche par l'examen du site de protonation sur ce système.

3.22 *Basicité de HP=NH*

Pour définer un site de protonation préférentiel on peut procéder à une détermination de l'énergie d'interaction électrostatique entre une charge ponctuelle (proton) et le potentiel du à la distribution de charge moléculaire; différents travaux ont toutefois mis en évidence la déficience de ce seul mode d'approche (32). En effet, la protonation induit une réorganisation totale des nuages électroniques au voisinage du site concerné et il faut également prendre en compte la relaxation au niveau des structures géométriques. Ceci nécessite la minimisation de tous les paramètres longueurs et angles des différentes espèces protonées possibles.

Pour notre part, en première approche du problème nous avons entrepris la minimisation des deux motifs $(HPNH_2)^+$ et $(H_2PNH)^+$.

Tous les paramètres ont été optimisés à l'exception des longueurs PH et NH, définies a priori à l'aide des résultats d'un travail précédent (33). Les valeurs obtenues ont été reportées dans le tableau 6.

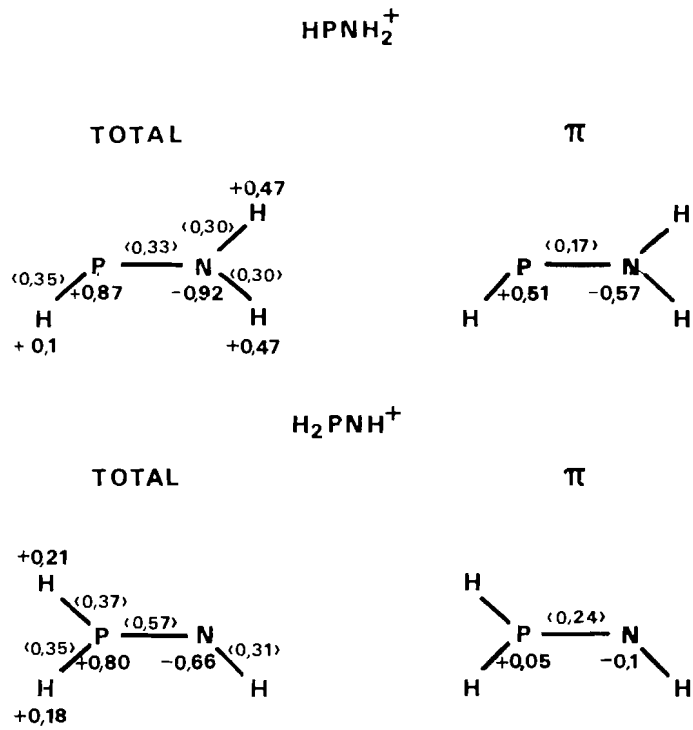

FIG. 9. Analyses de population selon Mulliken pour $HPNH_2^+$ et H_2PNH^+. Charges nettes et populations de recouvrement entre parenthèses.

Par rapport à HPNH nous observons un allongement de la longueur PN dans $(HPNH_2)^+$ et par contre un très net raccourcissement dans $(H_2PNH)^+$.

Il est également intéressant de remarquer la planéité des deux systèmes ainsi que la structure trigonale plan de l'atome protoné.

Si ce résultat pouvait être pressenti en ce qui concerne l'azote on aurait pu penser obtenir une pyramidalisation du phosphore or c'est une structure parfaitement plane qui a été déterminée.

L'examen des énergies obtenus (tableau 6) après une interaction de configurations du même type que celles précédemment réalisées, font apparaître un motif $(HPNH_2)^+$ nettement plus stable que $(H_2PNH)^+$.

Si dans certains cas on peut pressentir une dualité entre le site préférentiel à longue distance et celui réellement favorisé à l'accrochage ceci est peu vraisemblable dans le cas considéré étant donné la forte charge négative de l'azote dans HPNH et l'importante différence énergétique obtenue entre les deux formes protonées (46,7 kcal/mol). Les résultats de l'analyse de population selon Mulliken ont été reportés dans la figure 9 pour les deux composés.

Nous remarquons dans les deux cas une polarité $P^+—N^-$, l'atome de phosphore étant toujours nettement plus positif au total que dans HPNH; par contre, l'atome d'azote dans $(HPNH_2)^+$ apparaît plus négatif que dans HPNH l'inverse étant observé pour $(H_2PNH)^+$.

Un examen plus détaillé nous montre dans le cas de $(HPNH_2)^+$ que l'atome d'azote ayant perdu des électrons au niveau σ en draine en retour fortement en π, ce qui lui confère une charge nette négative importante en π; le phosphore par contre devient fortement positif essentiellement de par le trans-

Can. J. Chem. Downloaded from www.nrcresearchpress.com by 210.87.254.5 on 09/06/12
For personal use only.

fert en π sur l'azote. Nous remarquons également un caractère renforcé de la "paire du phosphore" (accroissement de densité électronique dans la direction correspondante), enfin la population de recouvrement reflète une très forte diminution du caractère de double liaison (0,17 au lieu de 0,23 dans HPNH). Tout ceci révèle nettement dans le cas d'une protonation sur l'azote une structure ion phosphenium $HP^+—NH_2$ (figure 9) et en aucune façon du type $H—P=N^+H_2$ comme on aurait pu l'envisager a priori. Une telle entitée vient d'être récemment mise en évidence (34).

Contrairement à ce qui a été observé précédemment nous ne constatons lors d'une protonation sur le phosphore $(H_2PNH)^+$ qu'un très faible retour en π; par contre, une analyse plus approfondie révèle un transfert type $p \rightarrow d$ dans le plan de la molécule de l'azote vers le phosphore et qui se traduit par l'accroissement notable de l'indice de population total (0,45 dans HPNH → 0,57 dans $(H_2PNH)^+$) cette possibilité de transfert est peut-être l'un des facteurs à l'origine de la planéité observée au niveau du phosphore.

La protonation sur le phosphore ne conduit pas à une structure d'ion nitrenium mais à une entité iminophosphenium $H_2P^+=NH$ avec renforcement de la double liaison vis à vis de HPNH. De telles espèces viennent d'être isolées et caractérisées (35).

4. Conclusion

En conclusion cette étude quantochimique nous a permis de mieux appréhender les caractéristiques des deux motifs P=N et P=C.

Les iminophosphanes sont des molécules très polaires susceptibles de réactions d'addition (2 + 1) ou 1,1, le phosphore présentant pour cette entité une nucléophilie certaine, le site basique étant toutefois l'atome d'azote.

Dans le cas de $HPCH_2$ la force de la liaison π nettement plus grande et la polarité plus atténuée révèlent une molécule plus stable et moins réactive.

Remerciements

Les auteurs remercient les Docteurs R. Wolf et M. Sanchez pour leurs fructueuses discussions au sujet de ce travail.

1. A. F. GRAPOV, L. V. RAZVODOVSKAYA et N. N. MEL'NIKOV. Russ. Chem. Rev. **50**, 324 (1981).
2. R. APPEL, F. KNOLL et I. RUPPERT. Angew. Chem. Int. Ed. Engl. **20**, 731 (1981).
3. Y. CHARBONNEL et J. BARRANS. Tetrahedron, **32**, 2039 (1976).
4. J. P. LEGROS, Y. CHARBONNEL, J. BARRANS et J. GALY. C.R. Acad. Sci. Paris, **286**, 319 (1978).
5. J. P. LEGROS, Y. CHARBONNEL et J. BARRANS. C.R. Acad. Sci. Paris, **291**, 271 (1980).
6. S. POHL. Angew. Chem. Int. Ed. Eng. **15**, 687 (1976).
7. S. POHL. Chem. Ber. **112**, 3159 (1979).
8. E. FLUCK. Topics in phosphorus chemistry. Vol. 10. *Edité par* M. Grayson et E. J. Griffith. Interscience, New York. 1980. p. 193.
9. W. W. SCHOELLER et E. NIECKE. Chem. Commun. **11**, 569 (1982).
10. G. TRINQUIER. J. Am. Chem. Soc. Sous presse.
11. L. E. GUSEL'NIKOV et N. S. NAMETKIN. Chemical Rev. **79**, 529 (1979).
12. M. J. HOPKINSON, H. W. KROTO, J. F. NIXON et N. P. C. SIMMONS. J. Chem. Soc. Chem. Commun. 513 (1976).
13. H. W. KROTO, J. F. NIXON, K. OHNO et N. P. C. SIMMONS. J. Chem. Soc. Chem. Commun. 709 (1980).
14. (*a*) M. PETERSON et R. POIRIER. University of Toronto, Toronto, Ont. Canada; W. C. DAVIDON et L. NAZARETH. Argonne Natl. Lab. Tech. Memos 303, 306. Argonne, Illinois, USA; (*b*) M. J. D. POWELL. Subroutine VA13AD. Atomic Energy Research Establishment (AERE) Subroutine Library, Harwell, Didcot, Berkshire, U.K.; Algorithme decrit par R. Fletcher, Comput. J. **13**, 317 (1970).
15. R. DITCHFIELD, W. J. HEHRE et J. A. POPLE. J. Chem. Phys. **54**, 724 (1971).
16. T. E. GIER. J. Am. Chem. Soc. **83**, 1769 (1961).
17. H. W. KROTO. J. Mol. Spectr. 77, 270 (1979).
18. D. E. C. CORBRIDGE. The structural chemistry of phosphorus. Elsevier Scientific Publishing Company, Amsterdam, London, New York. 1974. (*a*) p. 395; (*b*) p. 289.
19. BOYS. Quantum theory in atoms, molecules and the solid state. *Edité par* P. O. Lowdin. Academic Press, New York. 1966. p. 253.
20. D. GONBEAU, M. LOUDET et G. PFISTER-GUILLOUZO. Tetrahedron, **36**, 381 (1980).
21. R. AHLRICHS et R. HEINZMANN. J. Am. Chem. Soc. **99**, 7452 (1977).
22. M. D. CURTIS. J. Organometal. Chem. **60**, 63 (1973).
23. L. SALEM. J. Am. Chem. Soc. **96**, 3486 (1974).
24. D. LIOTARD, A. DARGELOS et M. CHAILLET. Theoret. Chim. Acta, **31**, 325, (1973).
25. R. AHLRICHS et V. STREMMLER. Chem. Phys. Lett. **37**, 77 (1976); C. A. PARSONS et C. E. DYKSTRA. J. Chem. Phys. **71**, 3025 (1979).
26. G. BECKER. Chemisches Kolloquium Universitat Koln, June 24, 1981.
27. C. LEHOUSSE, M. HADDAD et J. BARRANS. Tetrahedron Lett. 4171 (1982).
28. E. NIECKE, R. RUGER et W. W. SCHOELLER. Angew. Chem. Int. Ed. Engl. **20**, 1034 (1981).
29. TH.C. KLEBACH, R. LOURENS et F. BICKELHAUPT. J. Am. Chem. Soc. 4886 (1978).
30. R. APPEL et V. KUNDGEN. Angew. Chem. Int. Ed. Engl. **21**, 219 (1982).
31. E. NIECKE et W. FLICK. Angew. Chem. Int. Ed. Engl. **12**, 585 (1973).
32. (*a*) A. DARGELOS, S. EL OUADI, D. LIOTARD et M. CHAILLET. Chem. Phys. Lett. **51**, 545 (1977); (*b*) A. PULLMAN et P. BORCHEN. Chem. Phys. Lett. **34**, 7 (1975).
33. D. GONBEAU, D. LIOTARD et G. PFISTER-GUILLOUZO. Nouv. J. Chim. **4**, 227 (1980).
34. O. DAHL. Tetrahedron Lett. 1493 (1982).
35. M. R. MARRE, M. SANCHEZ et R. WOLF. Phosphorus Sulfur. Sous presse.

Can. J. Chem. Downloaded from www.nrcresearchpress.com by 210.87.254.5 on 09/06/12
For personal use only.

Synthesis of Mannich bases from electrochemically generated iminium salts in the presence of silyl enol ethers[1]

ROGER N. RENAUD,[2] DENIS BÉRUBÉ, AND CAMPBELL J. STEPHENS
Division of Chemistry, National Research Council of Canada, Ottawa, Ont., Canada K1A 0R6

Received October 26, 1982

ROGER N. RENAUD, DENIS BÉRUBÉ, and CAMPBELL J. STEPHENS. Can. J. Chem. **61**, 1379 (1983).

The formation of Mannich bases from the reaction of silyl enol ethers with *N*-methyl-*N*-mesitylmethyleniminium salt, generated by the electrochemical oxidation of *N*,*N*-dimethylmesidine, was studied. Important factors influencing the reaction are: (a) the silyl enol ether must be nucleophilic enough to react with the iminium salt and, at the same time, must be more difficult to oxidize than the tertiary amine, (b) the product of the reaction must not be oxidized at the operating potential. Examples are presented in this paper illustrating the successes and limitations of this reaction.

ROGER N. RENAUD, DENIS BÉRUBÉ et CAMPBELL J. STEPHENS. Can. J. Chem. **61**, 1379 (1983).

La formation de bases de Mannich a été étudiée en faisant réagir des éthers silyl énoliques sur le sel *N*-méthyl-*N*-mésitylméthyleniminium préparé par oxydation électrochimique de la *N*,*N*-diméthylmésidine. Les facteurs pouvant influencer la réaction sont: (a) l'éther silyl énolique doit être assez nucléophilique pour réagir avec le sel iminium et, en même temps, doit être plus difficile à oxyder que l'amine tertiaire, (b) le produit de la réaction ne doit être oxydé au potentiel employé. Des exemples montrant le succès et la limitation de cette réaction sont présentés dans cette étude.

Can. J. Chem. Downloaded from www.nrcresearchpress.com by 210.87.254.40 on 09/06/12
For personal use only.

Many methods describing the aminomethylation of ketones are reported in the literature. The classical Mannich reaction is a typical example (1). Recently, aminomethylation was achieved successfully by the nucleophilic attack of silyl enol ethers on *N*,*N*-dimethylmethyleniminium salts (2, 3), chloromethyl methylurethan (4), and aminomethyl ethers (5).

The electrochemical formation of iminium cations from tertiary amines has been extensively studied (6–9). Recently, it was shown that the iminium cation, obtained from the electrochemical oxidation of *N*,*N*-dimethylanilines, gave good yields of addition products with nucleophiles such as diethyl phosphate and dialkylmalonates (7, 8). It seemed to be interesting for us to study the preparation of Mannich bases **4** by the nucleophilic attack of silyl enol ethers **3** on electrochemically prepared iminium cations **2**, according to Scheme 1. Only a selection of silyl enol ethers in the presence of the iminium salt of *N*,*N*-dimethylmesidine **1** are reported in this paper in order to present the scope of the potential of this preparative method.

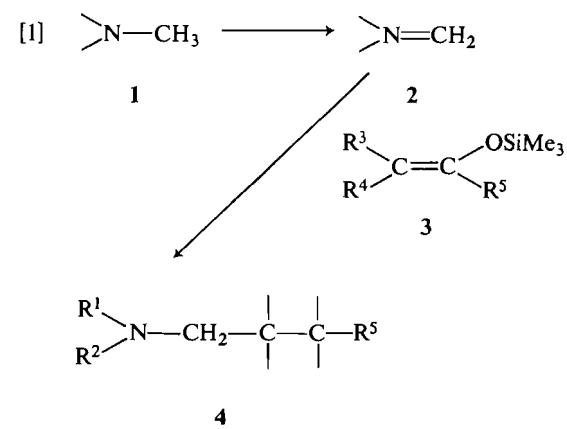

SCHEME 1

Results and discussion

Controlled potential electrolyses were performed at a platinum electrode in acetonitrile containing 0.1 *M* lithium perchlorate. By using a one-compartment cell, a dark solution and an electrode passivation were obtained. The current was reversed for 2 s every minute in order to regenerate the surface of the electrode. A two-compartment cell eliminated these problems and simplified the purification of the products. Nevertheless, the yield of products increased only slightly by using a divided cell. Good yields (Table 1) of **4***a*–**4***d* were obtained[3] for the electrolysis of *N*,*N*-dimethylmesidine in the presence of the silyl enol ethers **3***a*–**3***d*, respectively. However, the Mannich base **4***e* was obtained in low yield from **3***e* while **4***f* was not detected from **3***f*.

Examination of the oxidation potentials of the reactants and the products gave some light on the electrolysis results. The current–potential curve of *N*,*N*-dimethylmesidine in $CH_3CN-LiClO_4$ (0.1 *M*) at a platinum rotating disc electrode showed a half-wave potential ($E_{1/2}$) of 0.55 V. As a result of this experimental condition, the $E_{1/2}$ of the silyl enol ethers and the products have to be considered. Figure 1 illustrates the current–potential curves of the electrochemical oxidation of *N*,*N*-dimethylmesidine, the silyl enol ether **3***a*, and the Mannich base product **4***a*. At 0.45 V, only a small quantity of the product **4***a* is oxidized while the current for the oxidation of *N*,*N*-dimethylmesidine is still reasonable (100–150 mA). Acceptable yields of **4***a*–**4***d* ($E_{1/2} \approx 0.6$ V) were obtained from the silyl enol ethers **3***a*–**3***d* respectively ($E_{1/2} > 1.2$ V) (Table 1). For O-methyl-O-trimethyl silyl isobutylketene acetal (**3***f*) ($E_{1/2} = 0.4$ V), the electrolysis has to be conducted at a potential higher than its own oxidation potential. On the other hand, even if ethyl 3-trimethylsiloxy-2-butenoate (**3***e*) has an oxidation potential ($E_{1/2} = 1.95$ V) high enough, a large quantity of the silyl enol ether **3***e* was recovered and the product **4***e* was obtained in only a very low yield. Further studies are in progress with other silyl enol ethers in order to obtain an explanation for this observation.

[1]NRCC No. 20111.

[2]Author to whom correspondence should be addressed.

[3]No aminomethylated product **4***a* was observed when the electrolysis was conducted in the presence of acetophenone. The formation of the Mannich base ω-[*N*-*tert*-butyl-*N*-methylamino]-propiophenone has been obtained, however, from *N*-methyl-*N*-*tert* methyleniminium perchlorate in the presence of acetophenone in methylene chloride (10).

TABLE 1. Controlled potential electrolysis of *N*,*N*-dimethylmesidine at 0.45 V[a] in the presence of silyl enol ethers

Silyl ether **3**	$E_{1/2}$ (V)	Product[b] **4**	Yield[c] (%)	$E_{1/2}$ (V)	Product[b] **5**	Yield[c] (%)
3*a* 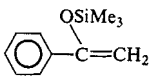	1.30	**4***a* 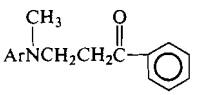	42.7	0.62	—	—
3*b* 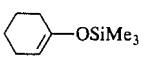	1.25	**4***b* 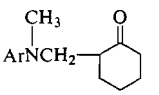	57.9	0.61	**5***b* 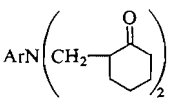	11.5
3*c* 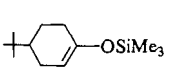	1.35	**4***c* 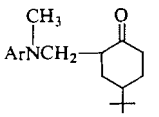	39.4[d]	0.57(ax) 0.68(eq)	—	
3*d* 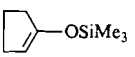	1.22	**4***d* 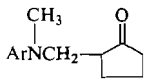	51.1	0.65	**5***d* 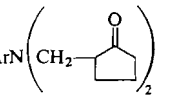	7.3
3*e* 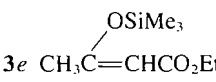	1.95	**4***e* 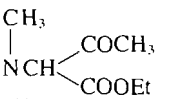	1.3	0.60	—	—
3*f* 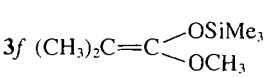	0.4	**4***f* 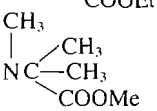	0	—	—	—

[a]The potentials are reported vs. Ag/$AgNO_3$ 10^{-2} *M*.

[b]Ar = 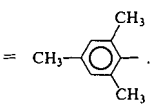 .

[c]Isolated yields and current yields.

[d]A mixture of axial and equatorial stereoisomers in a ratio 1:3 respectively.

Besides the major products **4***b* and **4***d*, some compounds **5***b* and **5***d* were also isolated.[4] These compounds were determined to be the result of the oxidation of **4***b* and **4***d* to give a new iminium cation which reacted with another molecule of silyl enol ether to give **5** (Scheme 2). The same observation was noticed by Shono *et al.* (11) for the oxidation of dimethyl aniline in the presence of methanol as the nucleophile. For **4***a* and **4***c*, the compounds **5***a* and **5***c* are probably formed but could not be obtained pure enough for identification.

The product **4***c* is actually a mixture of two stereoisomers, the axial and the equatorial 2-substituted-4-butyl cyclohexanone in a ratio of 1:3. This ratio was determined by a current–potential curve on the mixture. The axial substituted product has a $E_{1/2}$ of 0.57 V while the equatorial equivalent is at 0.68 V. The stereochemistry was assigned by comparing the wideband proton decoupled, the proton undecoupled, and the spin echo spectra. The methylene carbon at C-2 is adjacent to a nitrogen and most likely appears at 58.05 ppm for the equatorial isomer and at 55.38 ppm for the axial isomer. Also, C-6 for the axial 2-substitution (33.84 ppm) has an upfield shift compared with the equatorial 2-substitution (38.30 ppm). This δ-effect of 4.9 ppm is comparable with the δ-effect of 5 ppm observed for 2-methyl cyclohexane (12). The carbonyl carbon appears at 214.68 ppm and 212.97 ppm for the axial and the equatorial isomers, respectively. Therefore, this downfield shift (208.8 ppm for cyclohexanone and 210.3 ppm for 2-methyl cyclohexanone) is due to the aromatic amino group attached to the methylene group at C-2.

[4]A complete study on the electrochemical oxidation of *N*,*N*-dimethylmesidine in the presence of nucleophiles has been published (7, 8).

Experimental

Reagents

N,*N*-dimethylmesidine was prepared by the Eschweider–Clarke reaction (13). The silyl enol ethers and the O-methyl-O-trimethylsilyl-isobutylketene acetal were obtained by reported methods (14). The acetonitrile was purified as reported in the literature (15).

Analytical methods

Infrared spectra were recorded on a Perkin–Elmer Model 267 spectrophotometer. Proton magnetic resonance spectra were taken in deuteriochloroform on a Varian Associates spectrometer model E.M. 360 and are reported in the δ scale. The ^{13}C magnetic resonance spectra were taken on a Bruker WP-80 apparatus. The mass spectra were obtained from a Finnigan 400 gc–ms spectrometer. The moleculear weight determinations were done on a Mechrolab vapor pressure osmometer model 301A.

Electrochemical instrumentation

All potentials were referred to Ag/0.01 *M* $AgNO_3$ in acetonitrile–$LiClO_4$ (0.1 *M*). Current–potential measurements were obtained using a conventional three-electrode cell equipped with a programmer PAR 175, a potentiostat PAR 173, a coulometer PAR 379, a rotating disc electrode from Tacussel, and a Hewlett–Packard 7045B X–Y recorder. The controlled potential electrolyses for the preparative scale synthesis were carried out in a H-type cell. This cell has a glass frit diaphragm separating the two compartments. The

Can. J. Chem. Downloaded from www.nrcresearchpress.com by 210.87.254.40 on 09/06/12
For personal use only.

Can. J. Chem. Downloaded from www.nrcresearchpress.com by 210.87.254.40 on 09/06/12
For personal use only.

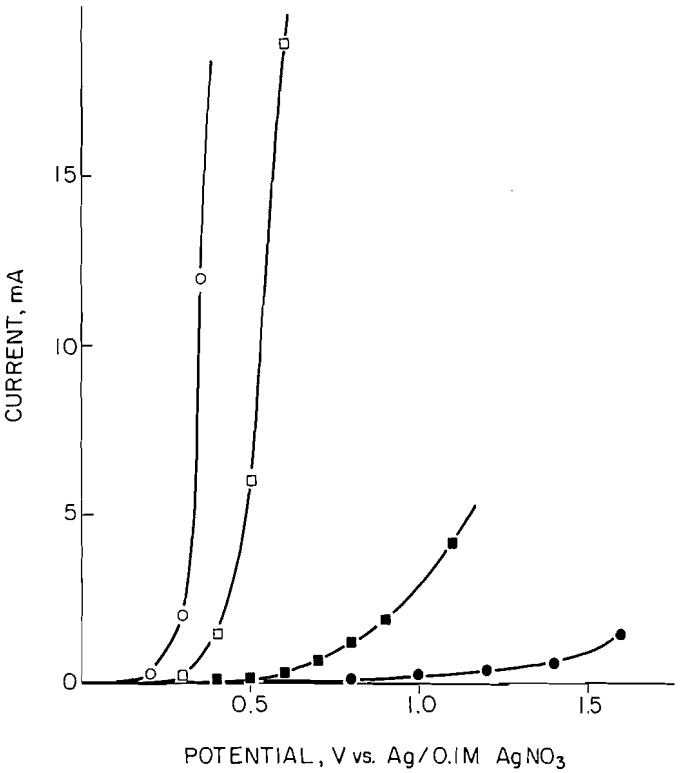

FIG. 1. Current–potential curves. Curve ●: acetonitrile–$LiClO_4$ (0.1 *M*). Curve ■: 1-phenyl-1-trimethylsilyloxyethylene (**3***a*) (0.1 *M*). Curve ○: *N*,*N*-dimethylmesidine (0.1 *M*). Curve □: *N*-methyl-*N*-3-phenylpropanone-3 mesidine **4***a* (0.1 *M*).

anodic compartment (150 mL) contained a semi-circular platinum screen (4 cm × 9 cm). A platinum screen (1 cm × 1 cm) was used as the cathode. The source of energy was obtained from a 300 V Lambda power supply model LB-706-FM, and the potential was controlled manually by means of a high resistance voltmeter.

General procedure

A mixture of $LiClO_4$ (1.34 g), Na_2CO_3 (2.12 g), silyl compound (≈5 mol excess), and *N*,*N*-dimethylmesidine (1.63 g; 0.01 mol) in acetonitrile (125 mL) was placed in the anodic compartment. The cathodic solution was $LiClO_4$ (0.1 *M*) in acetonitrile. The potential of the anodic solution was controlled at ≈0.45 V until 2.0 F/mol has been passed. The anodic solution was filtered and concentrated on a rotary vacuum evaporator. The oily residue was extracted with three 50-mL portions of n-pentane. The pentane was removed on a rotary evaporator. The residue was pumped under a pressure of 10^{-2} Torr for 24 h at room temperature. The volatiles, which were collected in a trap cooled in liquid nitrogen, consisted of unreacted starting materials. The remaining low vapor pressure oil was fractionated by flash chromatography (16) using a column of 2 cm diameter by 40 cm long and the main fraction was further purified by fractional distillation in a bulb-to-bulb apparatus under reduced pressure.

Physical properties of the products

(A) *From 1-phenyl-1-trimethylsilyloxy-ethylene* **3**a

The crude product showed only one important spot on the tlc plate. Purification by flash chromatography using hexane – ethyl acetate (6:1) and by a bulb-to-bulb distillation at 100°C (10^{-2} Torr) gave 1.2 g (42.7%) of a yellow oild (**4***a*) which crystallized on standing (mp 59–60°C); ir ($CHCl_3$): 1680 cm^{-1}; ^1H nmr: 2.18 (s, 9H), 2.61 (s, 3H), 3.22 (q, AB, 4H), 6.72 (s, 2H), 7.42 (m, 3H) 7.78 (m, 2H); ms *m*/*e*: 281 (M^+, 14), 162 ($M^+ - C_8H_7O$, 100). *Anal.* calcd. for $C_{19}H_{23}NO$: C 81.14, H 8.19, N 4.98; found: C 81.18, H 8.26, N 4.84.

(B) *From 1-trimethylsilyloxy-1-cyclohexene* **3**b

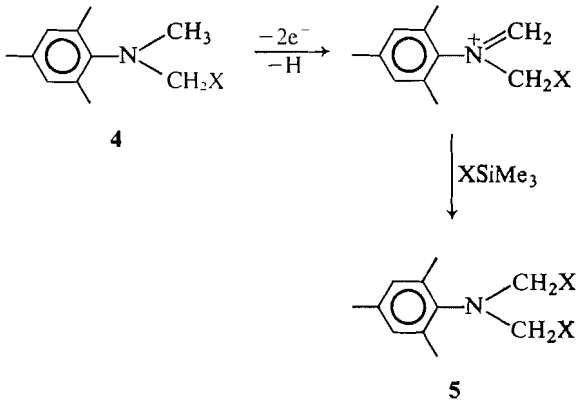

X = the ketonic substituent

SCHEME 2

The residue obtained after removal of the high vapor pressure fraction at 10^{-2} Torr showed two important spots on the tlc plate. The crude product was fractionated by flash chromatography using hexane – ethyl acetate (6:1) as the eluent. Two fractions were obtained. The first one was purified further by bulf-to-bulb distillation at 85°C (10^{-2} Torr) to give 1.5 g (57.9%) of a yellow oil (**4***b*); ir (film): 1710 cm^{-1}; ^1H nmr: 1.9 (broad m, 9H), 2.09 (s, 9H), 2.64 (s, 3H), 3.28 (m, 2H), 6.71 (s, 2H); ms *m*/*e*: 259 (M^+, 7), 162 ($M^+ - C_6H_9O$, 100). *Anal.* calcd. for $C_{17}H_{25}NO$: C 78.76, H 9.65, N 5.41; found: C 78.35, H 9.76, N 5.34. The second fraction amounted to 0.41 g (11.5%) of slightly impure **5***b*; ir (film): 1700 cm^{-1}; ^1H nmr: 1.4–2.6 (broad m including the aromatic CH_3 groups, 29H), 3.2 (m, 4H), 6.80 (s, 2H). Mol. Wt. calcd.: 355; found: 348.

(C) *From 1-trimethylsilyloxy-4-*tert*-butyl-1-cyclohexen* **3**c

The oily product obtained was shown by tlc to contain one major compound and 5 minor ones. The main product **4***c* (1.24 g; 39.4%) was separated by flash chromatography using hexane – ethyl acetate 8:1 as the eluent. A sample of the purified product was distilled in a Späth bulb under a pressure of 10^{-2} Torr at 120°C. A very slight decomposition was noticed at that temperature. Infrared (film): 1703 cm^{-1}; ^1H nmr: 0.89 (s, 9H), 1.68 (m, 8H), 2.28 (broad s, 9H), 2.70 (s, 3H), 3.28 (m, 2H), 6.80 (s, 2H); ms *m*/*e*: 315 (M^+, 6), 162 ($M^+ - C_{10}H_{17}O$, 100). *Anal.* calcd. for $C_{21}H_{33}NO$: C 80.00, H 10.48, N 4.44; found: C 80.06, H 10.37, N 4.40.

(D) *From 1-trimethylsilyloxy-1-cyclopentene* **3**d

The crude mixture contained two important spots on the tlc plate. It was purified by flash chromatography (hexane – ethyl acetate 6:1). The first fraction (**4***d*) was purified further by bulb-to-bulb distillation under a pressure of 10^{-2} Torr at 70°C to give a nearly colorless oil (1.40 g; 57.1%); ir (film): 1725 cm^{-1}; ^1H nmr: 1.92 (m, 7H), 2.24 (s, 9H), 2.72 (s, 3H), 2.90–3.82 (m, 2H), 6.80 (s, 2H); ms *m*/*e*: 245 (M^+, 37), 162 ($M^+ - C_5H_7O$, 100). *Anal.* calcd. for $C_{16}H_{23}NO$: C 78.37, H 9.38, N 5.71; found: C 78.15, H 9.43, N 5.63. The second fraction which corresponded to **5***d* (0.24 g; 7.3%) always contained a slight impurity; ir (film): 1720 cm^{-1}; ^1H nmr: 1.60–2.60 (broad m including the aromatic methyl groups at 2.30, 16H), 2.70–3.70 (m, 4H), 6.80 (s, 2H). Mol. Wt. calcd.: 327; found: 332.

(E) *From ethyl 3-trimethylsilyloxy-2-butenoate* **3**e

A dark brown product was obtained from the electrolytic reaction. The gummy residue, obtained after the removal of the volatile fraction at room temperature under reduced pressure (10^{-2} Torr), was a mixture of at least ten compounds by tlc. After separation by flash chromatography, one of the compounds seemed to correspond to **4***e* (0.02 g; 1.4%) but it was still slightly impure. Infrared (film): 1740 and 1715 cm^{-1}; ^1H nmr: 1.20 (t, 3H), 2.22 (broad s, 12 H), 2.71 (s, 3H) 2.80–3.82 (m, 3H), 4.20 (q, 2H), 6.86 (s, 2H). *Anal.* calcd. for $C_{17}H_{25}NO_3$: C 70.10, H 8.59, N 4.81; found: C 68.64, H 7.82, N 5.07.

(F) *From* O-*methyl*-O-*trimethylsilyl*-*isobutylketene acetal* (**3f**)

The crude product after removal of the volatile fraction at room temperautre (10^{-2} Torr) amounted to only 0.1 g from which no Mannich base could be obtained.

Acknowledgements

We wish to thank Mr. H. Séguin for the elemental analyses and molecular weight determinations, and Mr. M. E. Bednas for the mass spectral determinations.

1. (*a*) F. F. BLICKE. Org. React. **1**, 303 (1942); (*b*) M. TRAMONTINI. Synthesis, 703 (1973).
2. S. DANISHEFSKY, T. KITAHARA, R. MCKEE, and P. F. SCHUDA. J. Am. Chem. Soc. **98**, 6715 (1976).
3. S. MIYATO, H. HOKARI, A. MORI, and H. HASHIMOTO. Chem. Lett. 1213 (1980).
4. S. DANISHEFSKY, A. GUINGANT, and M. PRISBYLLA. Tetrahedron Lett. 2033 (1980).
5. A. HOSOMI, S. IIJIMA, and H. SAKURAI. Tetrahedron Lett. 547 (1982).
6. R. F. NELSON. Technique of electroorganic synthesis. Vol. 5, Part 1. *Edited by* N. L. Weinberg. J. Wiley and Sons, New York. 1974. p. 535.
7. G. BIDAN, M. GENIES, and R. RENAUD. Electrochim. Acta, **26**, 273 (1981).
8. G. BIDAN and M. GENIES. Tetrahedron, **37**, 2297 (1981).
9. V. D. PARKER. Organic electrochemistry. *Edited by* M. M. Baizer. Marcel Dekker, New York. 1973. p. 509.
10. H. VOLZ and H.-H. HILTZ. Justus Liebigs Ann. Chem. **752**, 86 (1971).
11. T. SHONO, Y. MATSUMURA, K. INOUE, H. OHMIZU, and S. KASHIMURA. J. Am. Chem. Soc. **104**, 5753 (1982).
12. J. B. STOTHERS. Carbon-13 NMR spectroscopy. Vol. 24. *Edited by* A. T. Blomquish and H. Wasserman. Academic Press, New York. 1972. p. 404.
13. W. S. EMERSON, F. W. NEWMANN, and T. P. MOUNDRES. J. Am. Chem. Soc. **63**, 972 (1941).
14. (*a*) R. WEST. J. Org. Chem. **23**, 1552 (1958); (*b*) C. AINSWROTH, F. CHEN, and Y-N. KUO. J. Organometal. Chem. **46**, 59 (1972); (*c*) H. O. HOUSE, L. J. CZUBA, M. GALL, and H. D. OLMSTEAD. J. Org. Chem. **34**, 2324 (1969).
15. G. CAUQUIS, H. F. FAHMY, G. PIERRE, and M. H. ELNAGDI. Electrochim. Acta, **24**, 391 (1979).
16. W. C. STILL, M. KAHN, and A. MITRA. J. Org. Chem. **43**, 2923 (1978).

Can. J. Chem. Downloaded from www.nrcresearchpress.com by 210.87.254.40 on 09/06/12
For personal use only.

Syntheses of optically active 2-tetrahydrofuran derivatives

PATRICE C. BÉLANGER AND HAYDN W. R. WILLIAMS
Merck Frosst Canada Inc., P.O. Box 1005, Pointe-Claire/Dorval, Québec, Canada H9R 4P8

Received July 2, 1982[1]

PATRICE C. BÉLANGER and HAYDN W. R. WILLIAMS. Can. J. Chem. **61**, 1383 (1983).

The resolution of 2-tetrahydrofuran-carboxylic acid and assignment of configuration to the enantiomers are reported. New syntheses of the enantiomers of 2-tetrahydrofurancarboxaldehyde are also described.

PATRICE C. BÉLANGER et HAYDN W. R. WILLIAMS. Can. J. Chem. **61**, 1383 (1983).

La résolution de l'acide tétrahydrofuran-2-carboxylique et la détermination de la configuration des énantiomères y sont rapportées. On décrit aussi de nouvelles synthèses des énantiomères de la tétrahydrofuran-2-carboxaldéhyde.

Can. J. Chem. Downloaded from www.nrcresearchpress.com by 210.87.254.6 on 09/06/12
For personal use only.

Introduction

The availabilities of 2-tetrahydrofuranyl derivatives of defined stereochemistry are of current interest because of the introduction of this moiety into compounds with pharmaceutical applications. Thus the 2-tetrahydrofuranylmethyl group has been introduced into saluretics (1), diuretics (2), and more recently into potent analgesics which are claimed to lack some of the undesirable side effects that are observed with the classical opiates (3). Another aspect of the stereochemistry of tetrahydrofuran derivatives which may become important is their use as chiral ligands for metal ions such as lithium (4).

When the tetrahydrofuranylmethyl group can be introduced into a molecule by way of tetrahydrofurfurylamine, this is an attractive approach because of the ease of obtaining both enantiomers from the commercially available racemic amine (2).

Another way that has been used to introduce this functionality is by alkylation of a nucleophilic centre with a 2-tetrahydrofurylmethyl halide (3, 5) or sulphonate (3*b*). This approach is less convenient because of the multistep syntheses of these chiral reagents (some of which are liquids and consequently difficult to obtain optically pure). Furthermore, they are somewhat unreactive alkylating agents (see for example, ref. 6 and ref. 3*b*, p. 1482), and therefore not attractive to use when synthetic strategy dictates the introduction of the group at a late stage in a long sequence.

Accordingly we began a study on the preparations of the enantiomers of 2-tetrahydrofuroic acid, and also investigated more facile preparations of the enantiomers of 2-tetrahydrofurancarboxaldehyde which have been made previously from D-ribose (or D-xylose) and D-lyxose (7). Either of these pairs of chiral tetrahydrofuran derivatives might be convenient alternatives to the reagents mentioned above in an appropriate alkylation procedure.

Results and discussion

The enantiomers of 2-methyltetrahydrofuran-2-carboxylic acid have been described in a German patent (8) but tetrahydrofuran-2-carboxylic acid seems not to have been resolved previously. Thus, treatment of racemic carboxylic acid **1** with half an equivalent of brucine dihydrate in ethyl acetate gave an 81% yield of a salt, which upon recrystallization twice from acetonitrile afforded 51% of the brucine salt of (+)-tetrahydrofuran-2-carboxylic acid **2**. Recovery of (−)-enriched carboxylic acid from the mother liquors and recrystallization of its salt with (+)-ephedrine provided (−)-tetrahydrofuran-2-carboxylic acid **3**. Esterification of the enantiomeric acids with diazomethane gave the corresponding methyl esters and the latter were examined by nmr in the presence of an optical shift reagent to assess their chiral purity. This was greater than or equal to 94% e.e. in the case of

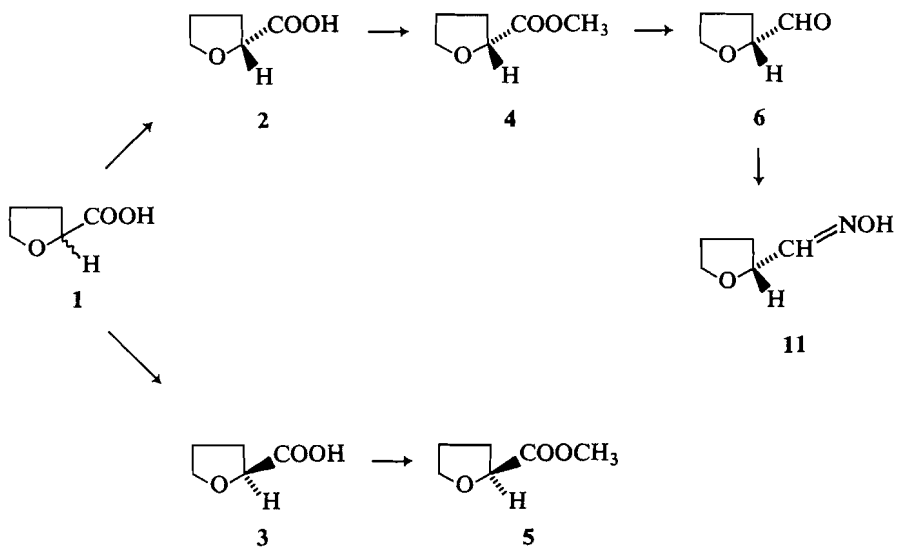

1 **2** **3** **4** **5** **6** **11**

SCHEME 1

[1]Revision received December 29, 1982.

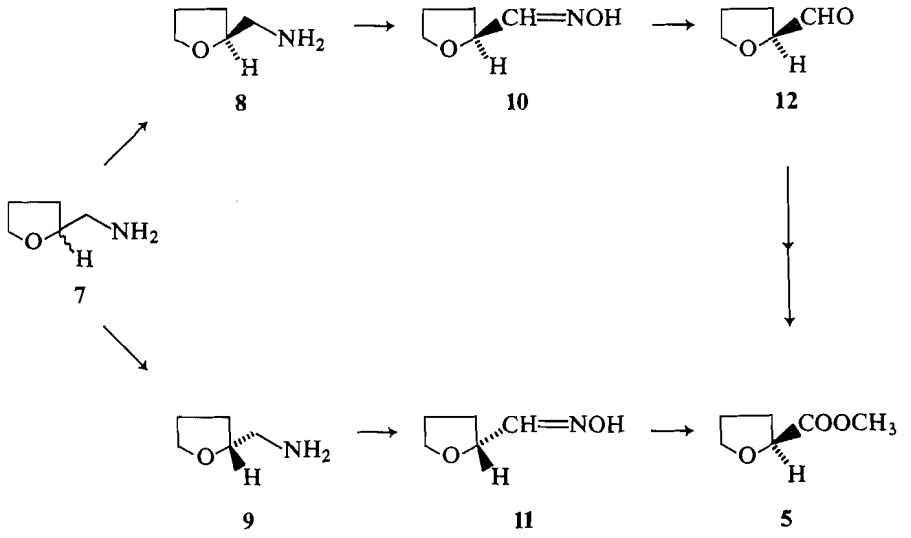

SCHEME 2

(−)-ester **4** derived from (+)-carboxylic acid **2**, and the other ester did not contain a detectable amount of its enantiomer.

The absolute configuration of (+)-tetrahydrofuran-2-carboxylic acid was determined to be *R* by reduction of the corresponding methyl ester with DIBAH to the known *R*-tetrahydrofuran-2-carboxaldehyde **6** (7). However, comparison of the physical properties of **6** prepared in this way with data in the literature (7) was not completely satisfactory. The boiling point was reported to be 75–80°C/2 × 10^{-2} Torr which seemed inordinately high compared to boiling points of 50°C/20 Torr for tetrahydrofurfurylamine and 45°C/2 × 10^{-1} Torr for methyl tetrahydrofuran-2-carboxylate. Our product distilled at 60°C/20 Torr and, by comparing the integration of the aldehydic proton with that for the protons at C-2 and C-5, it was judged to be over 80% monomer (but the spectrum still showed traces of impurity from the reagent). The reported rotation for *R*-tetrahydrofuran-2-carboxaldehyde synthesized from D-ribose (or D-xylose) (7) is −3.4° (*c* 1.2, MeOH). Measurement of the rotation of **6** in methanol gave an initial value of $[\alpha]_D$ −4.3° (*c* = 1.00, MeOH) but this was found to change to −3.3° in about 5 min and to +1.5° in 45 min. After 24 h the reading was +0.9°. A possible explanation of these changes might be a rapid formation of a hemiacetal on dissolving the aldehyde in methanol, followed by a slower formation of acetal and perhaps a much slower concomitant racemization. Measurements of the rotations of these enantiomeric aldehydes in tetrahydrofuran give much higher values than, but of opposite sign to, those determined in methanol, and they correlated well with determinations of optical purity by another method, as will appear later.

The absolute configurations of the tetrahydrofuran-2-carboxylic acid enantiomers do not rest solely on the rather unsatisfactory comparison of the rotation of **6** with the literature value. *S*-Tetrahydrofuran-2-carboxaldehyde **12** was synthesized by another route starting from tetrahydrofurfurylamine, as outlined in Scheme 2.

The latter was resolved by a slight modification of the method of Cragoe (2) which provided both optical isomers by way of their salts with L-tartaric acid, instead of using the more expensive D-tartaric acid for one isomer. The absolute configurations of these amines are known (9). Oxidation of the *S*-isomer with hydrogen peroxide and sodium tungstate (10) afforded the oxime in about 60% yield with little or no racemization as determined by nmr spectrometry in the presence of an optical shift reagent. Unfortunately, reductive hydrolysis of the oxime to the *S*-aldehyde with titanium trichloride (11) afforded the product in only 40% yield, and measurement of the rotation (in THF) suggested that this material had undergone more racemization than the product derived from DIBAH reduction of the ester. However, the optical rotation in solution in tetrahydrofuran showed unequivocally that this aldehyde had the opposite chirality to that obtained from (+)-tetrahydrofuran-2-carboxylic acid and confirmed the assignment of *R* configuration for the latter.

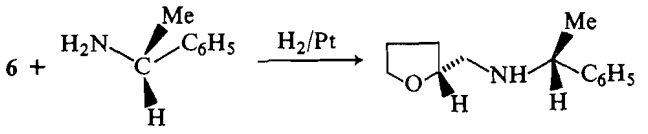

SCHEME 3

Conversion of these aldehydes **6** and **12** to their oximes **10** and **11** provided a means of estimating their optical purity by the nmr method, which was 80% e.e. for **6** and 66% e.e. for **12**.

R-Tetrahydrofuran-2-carboxaldehyde has been used for synthesizing chiral products (5), but it is difficult to assess the optical purity of the aldehyde made from D-ribose compared to that made by the procedure described herein. When **6** was used to alkylate *S*-α-methylbenzylamine by reduction, it gave a mixture of diastereoisomeric secondary amines in a ratio of 9:1 (by hplc analysis), that is, with no significant racemization during the reaction (Scheme 3).

Experimental

Melting points were determined using a Thomas–Hoover melting-point apparatus and are uncorrected. The 90-MHz ^{1}H nmr spectra were recorded with a Varian Associates EM-390 spectrometer using Me_4Si as internal standard. The optically selective nmr shift reagent used was tris [3-(heptafluoropropylhydroxymethylene)-*d*-camphorato] europium(III) derivative. Rotations were recorded with a Perkin–Elmer 241 polarimeter.

R-*Tetrahydrofuran-2-carboxylic acid* **2**

A hot solution of racemic tetrahydrofuran-2-carboxylic acid (51.35 g, 0.443 mol) in ethyl acetate (513 mL) was treated with brucine dihydrate (95.2 g, 0.221 mol) in small portions with stirring. The suspension was allowed to cool and the solid was collected, 97.5 g (81%); mp 192–195°C; $[\alpha]_D$ −6.95° (*c* 1.025, MeOH).

Can. J. Chem. Downloaded from www.nrcresearchpress.com by 210.87.254.6 on 09/06/12
For personal use only.

Can. J. Chem. Downloaded from www.nrcresearchpress.com by 210.87.254.6 on 09/06/12
For personal use only.

The solid was recrystallized twice from acctonitrilc (1.2 L), with evaporation to approximately 500 mL before collecting the product each time; 62.0 g (51%) of the brucine salt of **2**, mp 200.5–201°C; $[\alpha]_D$ −5.8° (*c* 1.00, MeOH) was obtained.

The brucine salt (63.5 g, 0.1165 mol) was treated with *N*-hydrochloric acid (128 mL) and 1:1 ethyl acetate/ether (500 mL). After stirring the mixture for 30 min, sodium chloride (30 g) was added. This resulted in the precipitation of brucine hydrochloride which was filtered off and washed with 1:1 solvent mixture. The aqueous phase was separated and extracted with solvent mixture (5 × 250 mL). After washing the combined extract with saturated sodium chloride solution (500 mL) to which had been added 6 *N* hydrochloric acid (5 mL), the extract was dried (Na_2SO_4) and evaporated. Bulb-to-bulb distillation of the residual oil yielded 13.2 g of **2**, bp approximately 90°C/0.07 Torr; $[\alpha]_D$ +30.4 (*c* 1.01, $CHCl_3$).

S-*Tetrahydrofuran-2-carboxylic acid* ***3***

The mother liquors from the first stage of the resolution were combined and evaporated, and the tetrahydrofuran-2-carboxylic acid enriched in the *S*-isomer was recovered by acidification, extraction, and distillation as described for the *R*-isomer.

A hot solution of the recovered acid (20.2 g, 174 mmol) in ethyl acetate (150 mL) was treated with (+)-ephedrine (28.7 g, 174 mmol) slowly with stirring. The solution was allowed to cool a little and was seeded and cooled to room temperature, giving 28.7 g (59%) of solid, mp 108–112°C; $[\alpha]_D$ +20.0° (*c* 1.00, MeOH).

The solid was recrystallized twice from ethyl acetate (420 mL, then 220 mL) to afford the (+)-ephedrine salt of **10**, 18.8 g (38%); mp 116–116.5°C; $[\alpha]_D$ +13.8° (*c* 1.00, MeOH).

Conversion of this salt to the free acid by the procedure described for **2** gave **3**, $[\alpha]_D$ −30.1° (*c* 1.21, $CHCl_3$).

Methyl R-*tetrahydrofuran-2-carboxylate* ***4***

Treatment of a solution of **2** (2.00 g, 17.2 mmol) in methanol with etheral diazomethane, followed by distillation in a kugelrohr apparatus, provided **4**, 1.96 g (87.7%); oven temperature approximately 50°C/0.1 Torr; $[\alpha]_D$ −8.0° (*c* 0.92, MeOH); nmr δ($CDCl_3$): 4.45 (m, 1H, H at C-1), 3.9 (m, 2H, H at C-4), 3.75 (s, 3H, CH_3), 1.95 (m, 4H, H at C-2 and C-3).

Methyl S-*tetrahydrofuran-2-carboxylate* ***5***

The ester of *S*-chirality was made by esterification of **3** with diazomethane, $[\alpha]_D$ +8.1° (*c* 1.05, MeOH).

In the presence of the optical shift reagent the methyl groups of the two esters can be distinguished, and the relative heights of the two signals can be used as a measure of optical purity. The *S*-ester did not contain a detectable amount of the enantiomer while the *R*-ester had at least 94% e.e. In the latter case the "ringing" of the signal is likely to result in an overestimation of the *S*-methyl ester group which is the upfield signal.

Resolution of tetrahydrofurfurylamine

The procedure supplied by Dr. E. J. Cragoe Jr. (2) and Mr. C. M. Robb was modified slightly to obtain both enatiomers from their salts with L-tartaric acid. The 1:1 salt of tetrahydrofurfurylamine and natural tartaric acid prepared on a molar scale in methanol (1 L) was recrystallized three times from this solvent to give (*R*)-tetrahydrofurfurylammonium hydrogen L-tartrate, 96.9 g, mp 96–97°C dec.; $[\alpha]_D$ −0.56° (*c* 2.00, H_2O).

Crude (*S*)-tetrahydrofurfurylammonium hydrogen L-tartrate (117 g), recovered from the mother liquors of the above recrystallizations, was suspended in boiling ethanol (≈450 mL) and the solid was collected after the suspension had cooled to about 45°C. Repetition of this procedure in hot ethanol (465 mL) gave *S*-tetrahydrofurfurylammonium hydrogen L-tartrate, 96.1 g; mp 126–127°C; $[\alpha]_D$ +36.1° (*c* 2.00, H_2O).

S-*Tetrahydrofuran-2-carboxaldehyde oxime* ***10***

S-Tetrahydrofurfurylamine **8** was liberated from its salt with L-tartrate salt (50.0 g) by treatment with potassium hydroxide (2); 16.25 g (81%); bp 49–52°C/17 Torr; $[\alpha]_D$ + 14.6° (*c* 2.035, MeOH).

A solution of **8** (5.05 g, 50 mmol) in water (50 mL) was treated with sodium tungstate (500 mg), and then at 10–15°C over a period of 3 h with 50% hydrogen peroxide (7.2 mL, 125 mmol). After stirring the mixture a further 30 min, it was saturated with NaCl and extracted with ethyl acetate (5 × 100 mL). The extract was dried ($MgSO_4$) and evaporated to an oil. On distillation, the latter afforded 3.53 g (61%) of pure **10**, bp 100–110°C/0.08 Torr; $[\alpha]_D$ −41.3° (*c* 1.975, MeOH); nmr δ ($CDCl_3$): 7.32 (d, 0.7H, *J* = 7 Hz, *syn* CH=N), 6.84 (d, 0.3H, *J* = 5 Hz, *anti* CH=N), 4.90 (m, 0.3H, H-2 of the *anti*-isomer), 4.33 (m, 0.7H, H-2 of the *syn*-isomer), 3.88 (m, 2H, CH_2O), 1.95 (m, 4H, 2 × CH_2).[2]

R-*Tetrahydrofuran-2-carboxaldehyde oxime* ***11***

The title compound was made from **9**, of rotation $[\alpha]_D$ −14.1 (*c* 2.085, MeOH) by the method described above. The product had bp 85–95°C/0.04 Torr; $[\alpha]_D$ +40.2° (*c* 2.00, MeOH).

The addition of the optical shift reagent to a solution of the racemic oxime in deuterochloroform results in the splitting of the doublet in the nmr spectrum, due to the *syn* CH=N group, into a pair of doublets of almost equal height. The amount of optical shift reagent added is fairly critical because the downfield shift produced on this signal is small relative to the shifts produced on signals upfield of it, and further addition of reagent results in overlap. The doublet of the *R*-isomer is downfield of the *S*-isomer.

The products **10** and **11** above were optically pure within the limits of this procedure.

S-*Tetrahydrofuran-2-carboxaldehyde* ***12***

Method A

The *S*-oxime **10** (2.30 g, 20 mmol) was added to a solution of citric acid monohydrate (6.10 g, 30 mmol) and concentrated ammonium hydroxide (2 mL) in water (40 mL) at −2°C under argon. Titanium trichloride (7.4 g, 48 mmol) was added in small portions. Stirring was continued at room temperature for 2 h and then sodium chloride (6 g) was added before extraction with methylene chloride (10 × 50 mL). The dried (Na_2SO_4) extract was evaporated to yield crude **12**, 795 mg (40%); $[\alpha]_D$ −16.6° (*c* 1.115, THF); nmr δ($CDCl_3$): 9.68 (d, *J* = 1.5 Hz, CHO), 4.25 (m, H at C-2), 3.9 (m, H's at C-5), 1.9 (m, H's at C-3 and C-4). The protons at 9.68 and 4.25 always integrate 1:1 but are low with respect to the other multiplets, probably due to the formation of trioxane or other polymers.

The yield can be increased to about 60% by continuous extraction with methylene chloride but with a slight drop in the specific rotation of the product.

R-*Tetrahydrofuran-2-carboxaldehyde* ***6***

Method B (13)

To a solution of the *R*-ester **4** (464 mg, 4.0 mmol) in a mixture of hexane (20 mL) and ether (8 mL) at −60°C was added 1.0 *M* diisobutylaluminium hydride (10 mL) slowly over 20 min. The mixture was stirred in the cooling bath for 30 min and then it was quenched with saturated NH_4Cl solution. The upper layer was decanted and the lower layer was extracted with methylene chloride (7 × 10 mL). Filtration was necessary to obtain a good separation. The combined extract was dried (Na_2SO_4) and evaporated to give crude **6**, 285 mg (71%); $[\alpha]_D$ +32.7° (*c* 0.995, THF).

The crude product was distilled in a semi-micro climbing-film apparatus (bath temperature ≈60°C/20 Torr) to give a distillate containing about 82% monomeric **6** (by nmr), $[\alpha]_D$ +60.1°C (*c* 0.885, THF). The variation with time of the specific rotation of this product in methanol is described in the discussion.

Examination of the enantiomeric purities of aldehydes ***6*** *and* ***12***

1. *By way of the oximes*

Each of the above aldehydes **6** or **12** (100 mg, 1 mmol) in water (1.5 mL) was treated with sodium acetate trihydrate (136mg) and hydroxylamine hydrochloride (70 mg). The solution was allowed to stand

[2]The ^1H nmr spectrum of the racemic oxime has been described previously (12).

overnight, then sodium chloride (0.5 g) was added and the mixture was extracted several times with ethyl acetate. The product was purified by kugelrohr distillation to afford the oximes in ≈63% yield.

The oxime from **12**, $[\alpha]_D$ −27.3° (*c* 0.97, MeOH), was found to have 66% e.e. by an optical shift nmr method, while that from undistilled **6** had $[\alpha]_D$ +33.3 (*c* 1.675, MeOH) and 80% e.e. by nmr.

In neither of the methods of preparation of the aldehydes were the reaction conditions optimized to reduce racemization, but clearly Method B is the more promising procedure in this regard.

2. *By way of the corresponding ester*

Sodium hydroxide (1 *N*, 2 mL) was added to a solution of silver nitrate (340 mg, 2 mmol) in water (3 mL) and to the stirred suspension of silver oxide was added **12** (100 mg, 1 mmol). The reaction mixture was titrated to pH 6.5 with NaOH and filtered. The filtrate was acidified to pH 6 and extracted several times with ether to provide 2-tetrahydrofurancarboxylic acid (39 mg). The latter was esterified with diazomethane and the ester was purified by chromatography (silica gel, 1:1 ether/hexane) before an nmr optishift study. This showed the ester **5** to have 60% e.e., in fair agreement with the estimated optical purity of the oxime regenerated from this sample of aldehyde, by rotation and nmr. Details of the mr shift reagent results are described in the discussion.

Reductive alkylation of S-α-*methylbenzylamine*[3] *with (2R)-tetrahydrofuran-2-carboxaldehyde*

Crude **6** (265 mg, 2.65 mmol) prepared by DIBAH reduction of ester **4** in methanol (10 mL) was treated with *S*-α-methylbenzylamine (322 mg, 2.65 mmol) and a few drops of acetic acid were added before stirring the mixture at room temperature for 15 min. Platinum oxide (30 mg) was added and the mixture was hydrogenated at room temperature and pressure. The product was purified by column chromatography (Merck silica gel eluted with 0.25:2.5:100 ammonium hydroxide/methanol/chloroform) and the diastereoisomeric products were collected in one fraction, 283 mg; nmr δ($CDCl_3$):7.34 (m, 5H, ArH), 4.1–3.6 (m, 4H, CH_2—O—CH & N—CH), 2.7–2.3 (m, 2H, CH_2N), 2.0–1.5 (m, 4H, CH_2—CH_2), 1.38 (d, 3H, J = 6 Hz, CH_3).

There was no evidence for different shifts for the methyl group in the two diastereoisomers in this product, nor in that made from racemic 2-tetrahydrofurancarboxaldehyde. The latter was made for reference purposes for the estimation of the two diastereoisomeric amines by hplc. Using a μ Bondapak C18 column, 40:60 water/methanol buffered at pH 5.5 with acetic acid/sodium acetate, and flow rate of 1.8 mL/min, the retention time of the (2*R*)-tetrahydrofuran-2-ylmethylamine derivative was 3.1 min and that of the (2*S*)-diastereomer was 2.2 min. By this means the amount of *R*,*S*-diastereoisomer was estimated to be 91.06 ± 0.43% (mean of 5 results). This result is in good agreement with the estimated optical purity of the aldehyde and suggests that no racemization occurred during the reductive alkylation.

[3]1-(−)-α-Methylbenzylamine 99 + % from Aldrich Chemical Co. which has *S* absolute configuration (14).

1. H. HORSTMANN, H. WOLLWEBER, and K. MENG. Brit. Patent No. 1,031,916. Chem. Abstr. **70**, 19915u (1969).
2. E. J. CRAGOE, JR. U.S. Patent No. 3,577,409. Chem. Abstr. **75**, 35739y (1971).
3. (*a*) H. MERZ, K. STOCKHAUS, and H. WICK. J. Med. Chem. **18**, 996 (1975); (*b*) H. MERZ and K. STOCKHAUS. J. Med. Chem. **22**, 1475 (1979).
4. J. K. WHITESELL and B. R. JAW. J. Org. Chem. **46**, 2798 (1981).
5. J. DEFAYE, M. NAUMBERG, and T. REYNERS. J. Heterocycl. Chem. **6**, 229 (1969).
6. G. BARGER, R. ROBINSON, and L. H. SMITH. J. Chem. Soc. 718 (1937).
7. J. DEFAYE. Bull. Soc. Chim. Fr. 2099 (1968).
8. H. MERZ and K. STOCKHAUS. Chem. Abstr. **92**, P198613t (1980).
9. J. W. WESTLEY, R. H. EVANS JR., and J. F. BLOUNT. J. Am. Chem. Soc. **99**, 6057 (1977).
10. U. HANDSCHIN, H. P. SIGG, and CH. TAMM. Helv. Chim. Acta, **51**, 1943 (1968).
11. G. H. TIMMS and E. WILDSMITH. Tetrahedron Lett. 195 (1971).
12. R. D. RIEKE and N. A. MOORE. J. Org. Chem. **37**, 413 (1972).
13. L. I. ZAKHARKIN and I. M. KHORLINA. Tetrahedron Lett. 619 (1962).
14. E. FELDER, D. PITRÈ, and S. BOVERI. Helv. Chim. Acta, **52**, 329 (1969).

Can. J. Chem. Downloaded from www.nrcresearchpress.com by 210.87.254.6 on 09/06/12
For personal use only.

Synthesis and conformational studies of phosphate esters of 1,2-*O*-isopropylidene-α-D-ribo- and xylo- pentofuranoses[1,2]

JEAN-RICHARD NEESER,[3] JEAN M. J. TRONCHET, AND ETIENNE J. CHAROLLAIS

Institut de Chimie Pharmaceutique et Pavillon des Isotopes de l'Université, 30 quai Ernest Ansermet, CH 1211 Genève 4

Received November 22, 1982

JEAN-RICHARD NEESER, JEAN M. J. TRONCHET, and ETIENNE J. CHAROLLAIS. Can. J. Chem. **61**, 1387 (1983).

The synthesis and properties, particularly ^{1}H, ^{31}P, and ^{13}C nmr, of new phosphate esters of 1,2-*O*-isopropylidene-α-D-ribo- and xylo-furanoses are described. For the cyclic phosphates the configuration at the asymmetric phosphorus atom is determined and for all derivatives the preferred conformation of the furanose and dioxaphosphorinane rings and the conformation around the phosphoester bonds are presented. The dependency of $^3J_{POCC}$ coupling constants on factors other than dihedral angles is reported and discussed.

JEAN-RICHARD NEESER, JEAN M. J. TRONCHET et ETIENNE J. CHAROLLAIS. Can. J. Chem. **61**, 1387 (1983).

Nous décrivons la synthèse et les propriétés spectroscopiques (en particulier de rmn ^{1}H, ^{31}P et ^{13}C) de nouveaux esters phosphoriques de *O*-isopropylidène-1,2-α-D-ribo- et xylo-furannoses. Pour les dérivés phosphate cyclique, la configuration au niveau de l'atome de phosphore asymétrique a été attribuée, et pour tous nos composés, la conformation préférentielle des cycles furannosique et dioxaphosphorinanne, ainsi que la conformation autour des liaisons phosphoester, sont déterminées. Nous observons également une variation des constantes de couplage $^3J_{POCC}$ en fonction d'autres facteurs que les angles dièdres et discutons de la signification de tels résultats.

Can. J. Chem. Downloaded from www.nrcresearchpress.com by 210.87.254.5 on 09/06/12
For personal use only.

Considering the importance of pentose phosphates, either by themselves, as structural units of nucleotides, or in metabolic biochemical systems, we were prompted to study derivatives of two important naturally occurring pentoses, namely D-xylose and D-ribose. The observations made on these model compounds might prove useful in the understanding of the conformational properties of biologically important nucleotide derivatives.

Syntheses of derivatives **1** to **12** were carried out from 1,2-*O*-isopropylidene-α-D-xylofuranose (**A**) or 1,2-*O*-isopropylidene-α-D-ribofuranose (**B**), as depicted in Fig. 1.

Results and discussion

1. *Infrared and nuclear magnetic resonance spectroscopy. Configurational assignment of asymmetrical phosphorus atoms in compounds 1 to 4*

As previously reported (6–9), the values of the P=O stretching frequency (around 1300 cm^{-1}) can be used successfully to assign the configuration of phosphorus atoms of a pair of asymmetrical phosphorus-containing epimeric dioxaphosphorinane rings. Such an assignment is dependent on the orientation of the P=O bond, resulting from the conformation of the heterocycles. For example, in compound **1**: ν P=O (equatorial) = 1295 cm^{-1}, and in compound **2**: ν P=O (axial) = 1285 cm^{-1}.

Tables 1–4 summarize the nmr data for compounds **1** to **12**. As previously reported (7–9), ^{31}P chemical shifts of derivatives **1** and **2** show a dependence similar to that of ν P=O, as a function of the orientation of the phosphoryl bond: in compound **1**, δ ^{31}P = +16.80 (P=O equatorial) and in compound **2**, δ ^{31}P = +14.10 (P=O axial). Configurational assignment of the phosphorus atom for **3** was deduced from a comparison of the ^{1}H and ^{13}C nmr spectra of **1** and **3**. The phosphorus atom configuration for **4** was established from the X-ray diffraction data in the crystalline state.

2. *Conformational analysis*

For molecular conformational analysis, nmr coupling constants have been widely used. The most critical aspect of such studies is the choice of vicinal correlations for translating the observed ^3J values into dihedral angles.

As will be discussed in detail later in the text, the $^3J_{HH}$ vs. θ_{HH} and $^3J_{PH}$ vs. θ_{PH} relationships previously proposed by many authors are well-established and widely applicable. On the other hand, the $^3J_{PC}$ vs. θ_{PC} correlation seems less well-documented and poses a more difficult problem for its rationalization. In this study, because of the wide range of nmr data available, it has been possible to translate the observed ^3J coupling constants from the ^{1}H nmr spectra into dihedral angles, using only well-established correlations for conformational assignments, and to use those angles to interpret the $^3J_{PC}$ vs. θ_{PC} relationship derived from the ^3J couplings observed in the ^{13}C nmr spectra.

2.1 *Conformations of furanose rings*

The furanose ring conformations are defined here using the terminology introduced by Altona and Sundaralingam (10). These conformations were determined with the aid of the widely used Karplus relationship (11), modified by Abraham *et al.* (12*a*) for the 1,2-*O*-isopropylidene-furanose bicyclic systems. These authors had proposed the $^3T_2$ conformation for the sugar ring of their molecules, from the following observations: for a *xylo* configuration, for example, $J_{1,2} \simeq J_{3,4}$ (3.5–3.9 Hz) and $J_{2,3} \leq 0.5$ Hz. These facts imply a symmetrical conformation with $\theta_{2,3} \simeq 90°$, and this is compatible only with the $^3T_2$ conformation.

Examination of the data in Tables 2 and 4 warrants some comments: the furanose rings in **1**, **2**, and **3** (α-D-*xylo* configuration) exhibit $J_{2,3} = 0$ in each case. However, $J_{3,4}$ (≃2 Hz) is always smaller than $J_{1,2}$ (≃3.6 Hz). The furanose rings of compounds **4** and **7** to **12** (α-D-*ribo* configuration) are characterized by a similar value for $J_{1,2}$ (3.3–3.6 Hz), and by a large coupling constant $J_{3,4}$ (6.8–9.2 Hz) which suggests an *anti*-orientation of the H—C_3 and H—C_4 bonds.

Using a technique previously developed in our laboratory (12*b*), we have calculated from the coupling constants $J_{1,2}$, $J_{2,3}$, and $J_{3,4}$ the predominant furanose ring conformations for all

[1]Phosphorated sugars: V; for Part IV, see ref. 1; III, ref. 2; II, ref. 3; I, ref. 4.

[2]This work constitutes a part of the Ph.D. Thesis of J.-R.N. (5).

[3]Present address: Research Department, Nestlé Products Technical Assistance Co. Ltd., 1000 Lausanne, Switzerland.

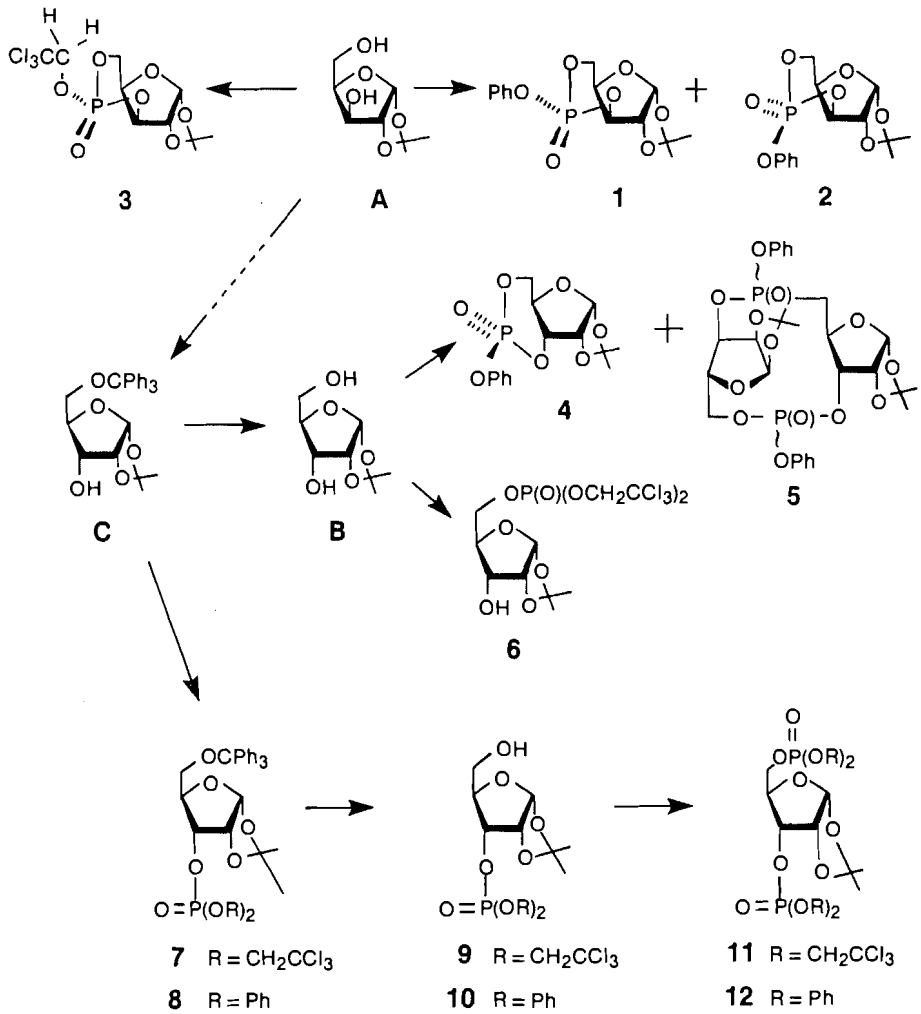

FIG. 1

our compounds. The results of these calculations allow unambiguous assignment of the $^3T_2$ twist form as being the predominant furanose ring conformation for **1**, **2**, and **3**. In the same way, it was found that sugar rings of compounds **7** to **10** adopt the $_2T^3$ twist form; this is very close to the $^3T_2$ conformation and allows equatorial and quasi-equatorial orientations for the substituents on C_3 and C_4 respectively. Due to the complexity of the ^{1}H nmr spectrum of **4** even at 360 MHz, the $^3T_4$ ribofuranose ring conformation for this compound had to be deduced from the X-ray crystal structure determination. This twist form is in accord with that expected for a five-membered sugar ring *trans*-fused to a six-membered phosphate ring (13*a*). Compounds **11** and **12** are characterized by a smaller $J_{3,4}$ value (6.8 and 7.3 Hz respectively) in comparison with the same constant for compounds **7** to **10** (8.6 to 9.2 Hz). Calculations suggest, in both cases, a very unusual $_2T^1$ twist form for the 1,2-*O*-isopropylidene-furanose rings, which probably arises as a result of the particular arrangement between the bulky 3-*O*-phosphoryl and 4-*C*-phosphorylhydroxymethyl groups.

2.2 *Conformational assignment of dioxaphosphorinane rings using $^3J_{HCCH}$ and $^3J_{POCH}$ coupling constants for 1, 2, and 3 and X-ray diffraction data for 4*

In studies of pentose-5-*O*-phosphate derivatives, the $^3J_{HH}$ vs. θ_{HH} correlation proposed by Lee and Sarma (13*a*) (eq. [1]) has been extensively used for determination around the C_4—C_5 bond:

$$[1] \quad {}^3J_{HH} = 10.5 \cos^2 \theta - 1.2 \cos \theta$$

Similarly, a convenient $^3J_{POCH}$ vs. θ_{PH} correlation can be easily deduced from many previous works (13–26), including studies of cyclic phosphates. This relationship has been shown to be susceptible to the coordination number of the phosphorus atom (27), ring-strain, and bond angle distortions (13*b*, 15, 28). However, the $^3J_{POCH}$ vs. θ_{PH} relationship proposed by Lee and Sarma (13*a*) (eq. [2]) has been used extensively and successfully for conformational assignment of various dioxaphosphorinane rings previously studied, including conformationally "free" six-membered rings (19, 20), six-membered phosphate rings fused *cis* to five-membered sugar rings (13*b*, 15), and similar *trans*-fused bicyclic systems (13*a*). The relevant function is:

$$[2] \quad {}^3J_{POCH} = 18.1 \cos^2 \theta - 4.8 \cos \theta$$

In the discussion which follows, we will use both the above relationships together with the well-known dependence of $^4J_{POCCH}$ values on the geometry of the coupling-route bonds (13*a*, 15, 19, 29*a*).

As shown in Table 2, the phosphate rings of **1** and **3** exhibit the following typical constants:

(a) $J_{4,5pro\text{-}R} \simeq J_{4,5pro\text{-}S} \simeq 1.5$–$2$ Hz

(b) small $J_{5pro\text{-}R,P}$ ($\simeq$1.9 Hz) and large $J_{5pro\text{-}S,P}$ (22.3–22.7 Hz) values

Can. J. Chem. Downloaded from www.nrcresearchpress.com by 210.87.254.5 on 09/06/12
For personal use only.

TABLE 1. Chemical shifts (δ) ^1H, ^{31}P, ^{13}C of cyclic phosphates **1** to **4**

Chemical shifts (δ)	Compounds 1	2	3	4
	[a]	[a]	[b]	[c]
H—C_1	6.02	5.79	6.06	5.89
H—C_3	5.08	5.11	5.01	4.26
H—C_5 *pro-R*	4.89	4.86	4.83	?
H—C_2	4.78	4.74	4.76	4.77
H—C_5 *pro-S*	4.69	4.62	4.68	4.32 to 4.41
H—C_4	4.40	4.47	4.39	
H_A \ C—CCl_3 / H_B	—	—	4.80	—
CH_3	1.49 and 1.34	1.45 and 1.31	1.44	1.64 and 1.38
^{31}P	+17.63[d]	+14.93[d]		
			+13.58[e]	+12.44[e]
	+16.80[e]	+14.10[e]		
	[f]	[f]	[f]	[g]
CMe_2	112.66	112.71	112.66	114.79
C_1	105.35	105.53	105.36	105.87
C_2	84.66	85.02	84.65	76.14
C_3	83.76	83.67	83.81	80.17
CH_2—(CCl_3)	—	—	76.97	—
C_4	72.45	73.35	72.25	68.39
C_5	68.84	68.08	68.90	70.07
CH_3	26.70 and 26.27	26.88 and 26.39	26.83 and 26.69	26.16

[a] δ, ^1H, 250 MHz, acetone-d_6.
[b] δ, ^1H, 360 MHz, acetone-d_6.
[c] δ, ^1H, 360 MHz, $CDCl_3$.
[d] δ, ^{31}P, 40.5 MHz, $CDCl_3$ (reference H_3PO_4 10% in acetone-d_6).
[e] δ, ^{31}P, 40.5 MHz, $CDCl_3$ (reference H_3PO_4 85% in D_2O).
[f] δ, ^{13}C, 25.2 MHz, acetone-d_6.
[g] δ, ^{13}C, 90 MHz, $CDCl_3$.

TABLE 2. Coupling constants of cyclic phosphates **1** to **4**

J (Hz)	Compounds 1	2	3	4
$J_{1,2}$	3.6	3.8	3.5	3.5
$J_{2,3}$	0	0	0	4.0
$J_{3,4}$	2.0	2.6	2.0	?
$J_{3,P}$	0	5.1	0	?
$J_{4,5pro\text{-}R}$	<2	2.0	≃1.9	?
$J_{4,5pro\text{-}S}$	≃1.5	1.8	≃1.9	?
$J_{5pro\text{-}R,P}$	<2	3.0	≃1.9	?
$J_{5pro\text{-}S,P}$	22.7	20.3	22.3	?
$J_{5A,5B}$	13.0	12.7	13.2	?
$J_{4,P}$	2.5	2.6	2.0	?
$^3J_{C_2,P}$	10.9	8.0	11.0	7.6
$^2J_{C_3,P}$	7.3	6.2	7.0	5.7
$^3J_{C_4,P}$	7.7	9.0	7.6	5.3
$^2J_{C_5,P}$	7.2	6.2	7.2	9.2
$^2J_{CH_2,P}$ (CCl_3)	—	—	3.9	—

(c) $J_{3,P} = 0$
(d) a long range coupling $^4J_{4,P} = 2$–2.5 Hz.

Inspection of Dreiding models clearly shows the limitations of the conformational mobility of these *cis*-fused bicyclic systems. With respect to the previously assigned $^3T_2$ conformation for the sugar rings in **1** and **3**, the use of the Lee and Sarma relationships (13*a*) (eq. [1] and [2]) immediately shows that criteria (a), (b), and (c) lead to the unambiguous assignment of the chair conformation depicted in Fig. 2 as being the only form adopted by the dioxaphosphorinane rings of **1** and **3**. The bicyclic *cis*-fusion between the six-membered phosphate ring and the five-membered sugar ring implies a chair conformation flattened at the C_4 atom, which is intermediate between the ideally expected $^{C4}C_P$ chair and the $^{O3,O5}F$ form (see Tronchet *et al.* (29*b*)). The specific dihedral angles measured on Dreiding models ($\theta_{P,H5pro\text{-}S} = 175°$; $\theta_{P,H5pro\text{-}R} = 65°$, $\theta_{P,H3} = 75°$) are in complete agreement with the observed values for the coupling constants. It is of interest to note that two routes are responsible for the long range coupling $^4J_{4,P}$, each of them implying three coplanar bonds.

Table 2 shows that most of the constants for compound **2** are of the same order of magnitude as the ones observed for **1** and **3**. On the other hand, the observed $J_{3,P} = 5.1$ Hz coupling constant rules out a single stable form for the six-membered phosphate ring of **2**. A variable temperature nmr study on **2** shows that the $^3J_{3,P}$ value decreases with temperature, suggesting that the flattened chair form ($^{C4}C_P/^{O3,O5}F$) previously described for **1** and **3** is favoured at low temperature. Inspection of a Dreiding model indicates that the dioxaphosphorinane ring of **2** can adopt an intermediate conformation between the twist-boat $^PS_{C5}$ and the boat $^{P,C4}B$ (see Fig. 2). Again using the Lee and Sarma equations, the typical dihedral angles of this form can be translated into coupling constants, and the participation of this new form in the conformational equilibrium of **2** can be

Can. J. Chem. Downloaded from www.nrcresearchpress.com by 210.87.254.5 on 09/06/12
For personal use only.

TABLE 3. Chemical shifts (δ) ^{1}H,[a] ^{31}P,[b] ^{13}C [c] of acyclic phosphates **7** to **12**

Chemical shifts (δ)		Compounds					
		7	**8**	**9**	**10**	**11**	**12**
H—C_1	[a]	5.95	5.90	5.83	5.77	5.84	5.61
H—C_2		4.90	4.81	4.83	4.69	4.86	4.66
H—C_3		4.78	4.89	4.75	4.78	between	4.73
H_A—C—CCl_3		4.66 and 4.53	—	4.77 and 4.69	—	} 4.77 and	—
H_B—C—CCl_3		4.60 and 4.47	—	4.69 and 4.67	—	} 4.62	—
H—C_4		4.23	4.24	4.18	4.11	4.60	4.54
H—C_5 *pro-S*		3.53	3.51	3.99	3.84	4.37	4.27
H—C_5 *pro-R*		3.16	3.15	3.78	3.55	4.32	4.16
OH		—	—	1.89	2.28	—	—
CH_3		1.58 and 1.39	1.54 and 1.33	1.59 and 1.38	1.57 and 1.34	1.59 and 1.38	1.53 and 1.31
^{31}P—OC_3	[b]	+6.80	+13.84	+5.90	+12.77	+6.27	+13.84
^{31}P—OC_5		—	—	—	—	+5.09	+13.07
CMe_2	[c]	113.14	113.06	113.43	113.24	113.72	113.50
C_1		104.04	103.90	103.95	103.71	103.92	103.77
C_3		between } 77.75 and	77.82	77.73	78.00	77.39 to 77.10	77.81
C_4		} 77.26	77.61	78.30	78.40	76.32	76.67
CH_2—(CCl_3)		76.95	—	77.34 and 77.19	—	77.39 to 77.10	—
C_2		75.89	75.96	74.85	74.79	74.90	74.92
C_5		61.68	61.89	59.62	59.42	66.01	65.93
CH_3		26.61	26.60	26.66	26.58	26.63	26.68 and 26.55

[a] δ, ^{1}H, 360 MHz, $CDCl_3$.
[b] δ, ^{31}P, 40.5 MHz, $CDCl_3$ (reference H_3PO_4 10% in acetone-d_6).
[c] δ, ^{13}C, 25.2 MHz, $CDCl_3$: carbons C_2, C_3, and C_4 were assigned from "off-resonance" experiments with selective irradiation of corresponding proton.

TABLE 4. Coupling constants of ayclic phosphates **7** to **12**

J (Hz)	Compounds					
	7	**8**	**9**	**10**	**11**	**12**
$J_{1,2}$	3.6	3.5	3.3	3.5	3.6	3.4
$J_{2,3}$	4.8	4.9	4.7	4.5	4.4	4.6
$J_{3,4}$	9.2	8.6	8.8	8.8	7.3	6.8
$J_{3,P}$	4.8	6.5	6.4	8.0	?	8.5
$J_{4,5pro\text{-}S}$	2.2	2.0	2.1	2.4	2.0	1.8
$J_{4,5pro\text{-}R}$	3.9	4.3	2.7	2.7	11.7	12.0
$J_{5pro\text{-}S,P}$	—	—	—	—	3.0	5.0
$J_{5pro\text{-}R,P}$	—	—	—	—	3.5	3.3
$J_{5A,5B}$	11.0	10.9	12.8	12.8	8.3	5.8
$J_{CH_2,P}$ (CCl_3)	6.0	—	6.4	—	?	—
$^{3}J_{C_2,P_3}$	6.5	5.8	6.0	5.5	5.4	5.7
$^{3}J_{C_4,P_3}$	?	10.3	10.1	8.7	6.3	6.4
$^{3}J_{C_4,P_5}$	—	—	—	—	11.1	10.0
$^{2}J_{C_3,P_3}$	?	0	0	2.9	?	0
$^{2}J_{C_5,P_5}$	—	—	—	—	6.0	5.6
$^{2}J_{CH_2,P}$ (CCl_3)	?	—	3.9	—	3.7	—
$^{3}J_{CCl_3,P}$	11.1	—	11.0	—	11.3	—

finally estimated. The J values deduced from the dihedral angles of this $^{P}S_{C5}/^{P,C4}B$ form ($\theta_{P,H3}$ = 150°; $\theta_{P,H5pro\text{-}R}$ = 110°; $\theta_{P,H5pro\text{-}S}$ = 130°) imply as much as 30% of this conformer in the dioxaphosphorinane equilibrium of **2**. The remaining 70% is attributed to the previously described $^{C4}C_P/^{O3,O5}F$ form.

It is interesting to note that both these conformational assignments for the phosphate rings of epimers **1** and **2** can be correlated with the previous configurational assignments on phosphorus. It is well known (19) that axially oriented alkoxy and aryloxy phosphorus substituents lead to more stable dioxaphosphorinane chair forms than the equatorially oriented ones. In this regard it is not surprising that the phosphoester ring of **1** (axially substituted with a phenoxy group) adopts a pure stable flattened chair form, whereas the same ring in **2** (equatorially substituted) is in equilibrium between two forms in which the chair one is favoured.

Inspection of a Dreiding model clearly shows the rigidity of the *trans*-fused bicyclic system in the case of compound **4**. The X-ray diffraction data of **4** unambiguously show the adoption of a flattened chair form for the phosphorated heterocycle of this compound. The *trans* bicyclic fusion between both the sugar and phosphate rings is responsible for the flattened form, which in fact is intermediate between the $^{P}C_{C4}$ chair and the $F_{C4,O3}$ form (see Fig. 2).

2.3 *Contribution of the coupling constants* $^{3}J_{POCC}$ *to the conformational analysis of dioxaphosphorinane rings of* ***1*** *to* ***4***

Different $^{3}J_{POCC}$ vs. θ_{PC} correlations have already been proposed, but this relationship is dependent on the phosphorus coordination number (30) and, perhaps, on the stereochemistry of the phosphorus atom (31, 32). In addition, studies of different series of compounds suggest different correlation equations. For example, ribonucleotide cyclic phosphate rings give coupling constant values in accord with the relation:

$$[3] \quad ^{3}J_{POCC} = 8-8.6\cos^2\theta \qquad (17, 33-35)$$

However, dioxaphosphorinane ring derivatives of phosphorochloridates or phosphoramidates *cis*-fused to a glucofuranose ring suggest another "Karplus-like" curve (36). More recent

Can. J. Chem. Downloaded from www.nrcresearchpress.com by 210.87.254.5 on 09/06/12
For personal use only.

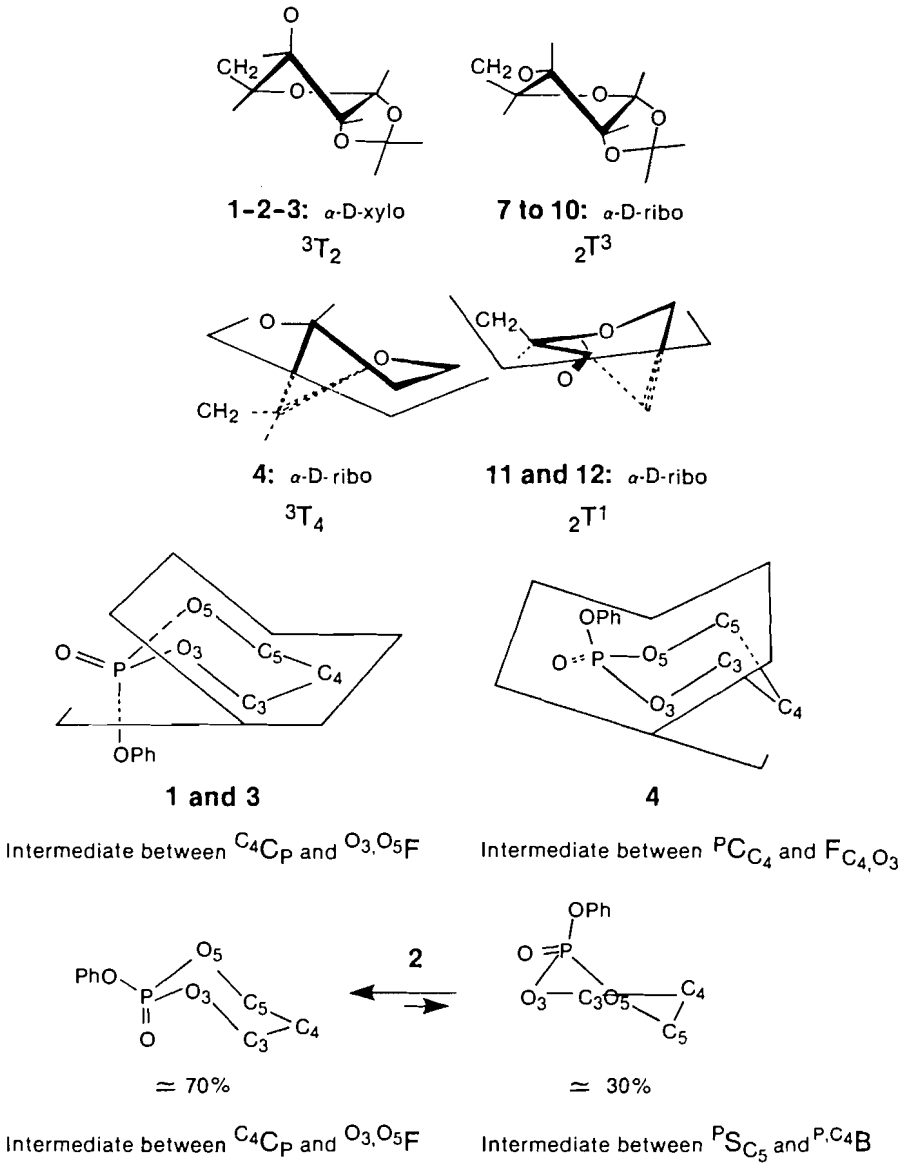

FIG. 2. Conformations of furanose and dioxaphosphorinane rings.

studies of ribonucleotides (37–40) confirm the values of $J_{P,C2'}$ = 8–8.5 Hz ($\theta \simeq 175°$) and $J_{P,C4'}$ = 3–4 Hz ($2 \times \theta = 65°$). On the other hand, studies of cyclic phosphate derivatives of carbohydrate pyranoses led O'Connor *et al.* (41) to propose the use of the extrapolated value of 14 Hz ($\theta = 180°$) to rationalize their assignment of coupling constants of 10.8 to 11.7 Hz, to correspond to dihedral angles ≃ 160°.

The above conformational assignments can be used to study the $^3J_{POCC}$ vs. $\theta_{P,C}$ relationships in our compounds. For this purpose, ^{13}C nmr spectra were recorded in the same solvents as these used for the ^1H measurements. The fact that the conformation of **4** was deduced from its crystal structure requires some careful considerations. Previous studies on similar ribonucleotides (13*a*, 16) have shown in each case the adoption of the same flattened chair, by the ribonucleotides in solution, as that assigned to **4** in the crystalline state. In addition, the rigidity associated with the *trans*-fused bicyclic system of the phosphorated heterocycle of **4** rules out any other conformational contribution in this case. Finally, the axial orientation of the phenoxy substituent on phosphorus is an additional stabilizing factor for the flattened chair in **4**. For all these reasons, we can assume that the observed $^3J_{P,C}$ coupling constants are as significant for the $^PC_{C4}/F_{C4,O3}$ conformation of **4** as they are for the $^{C4}C_P/^{O3,O5}F$ conformation of **1** and **3**.

When a coupling takes place via two routes, the well-established practice is to consider the ^3J correlated value as the sum of both the contributions (17, 33–36); with this assumption, we derive the following correlations (see Table 2).

Compounds **1** and **3**: $\theta_{P,C2} = 160°$ (J = 10.9–11 Hz)
$\theta_{P-O3,C3-C4} = 50°$, $\theta_{P-O5,C5-C4} = 65°$ (J = 7.6–7.7 Hz)

Compound **4**: $\theta_{P,C2} = 174°$ (J = 7.6 Hz)
$\theta_{P-O3,C3-C4} = 59°$, $\theta_{P-O5,C5-C4} = 52°$ (J = 5.3 Hz)

Such values clearly show that the "Karplus-like" approach cannot be used as a unique factor for rationalization of the $^3J_{POCC}$ coupling constants. The $^3J_{P,C2}$ value for **1** and **3** is larger than the one for **4** even though it corresponds to a smaller

Can. J. Chem. Downloaded from www.nrcresearchpress.com by 210.87.254.5 on 09/06/12
For personal use only.

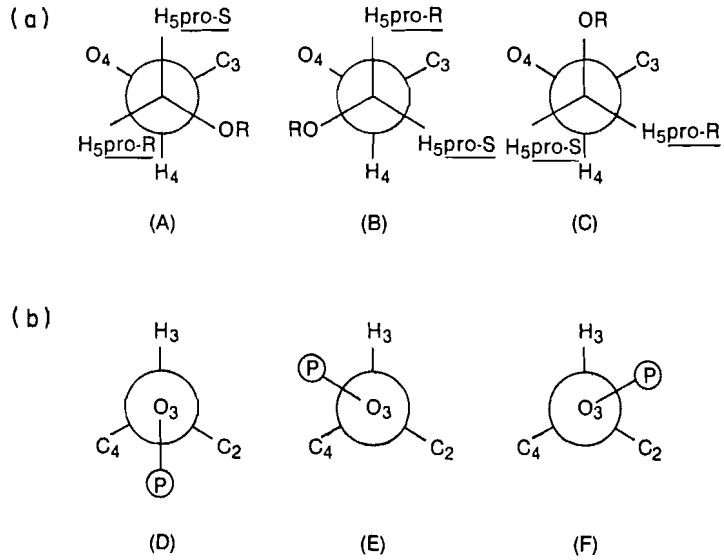

FIG. 3. (a) Possible conformations around C_4—C_5 bond: **7** to **12**, (b) possible conformations around C_3—O_3 bond: **7** to **12**.

dihedral angle. In fact, assuming that the expected $^3J_{POCC}$ vs. $\theta_{P,C}$ relationship has the approximate form:

$$[4] \quad {}^3J_{POCC} = A \cos^2 \theta$$

the observed constants in **1** and **3** lead to the relation:

$$[5] \quad {}^3J_{POCC} = 12.5 \cos^2 \theta$$

whereas those observed for **4** lead to the relation:

$$[6] \quad {}^3J_{POCC} = 8 \cos^2 \theta$$

It is of interest to note that the correlation deduced from **4** (eq. [6]) is in complete agreement with previous results for ribonucleotides (17, 33–35, 37–40). In the same way, the correlation for compounds **1** and **3** (eq. [5]) is in agreement with previous results on different cyclic phosphoesters (41).

The conformational equilibrium previously assigned for the dioxaphosphorinane ring of **2** involves a 30% participation of the $^PS_{C5}/^{P,C4}B$ form, which implies $\theta_{P,C2} = 90°$. The zero value of ^3J generally corresponds to the same dihedral angle and this leads to the conclusion that only 70% (the flattened chair) of the equilibrium contributes to the $^3J_{P,C2}$ in **2** [i.e. 8 Hz $\simeq 0.7 \times 11$ Hz]. This observation suggests a minimal dependence of $^3J_{P,C}$ constants on the stereochemistry of phosphorus. Furthermore, since the phosphoryl P=O and C_3—C_2 bonds are *cis* in compounds **1**, **3**, and **4**, the difference between the relationships (eqs. [5] and [6]) again cannot be attributed to stereochemical factors on phosphorus.

However, two differences between **1** (**3**) and **4** have to be emphasized. First, the fact that both the chair forms are not flattened at the same atom certainly produces important changes in the torsional angles and the ring strain. In this regard, the important differences observed for the $^2J_{POC}$ constants are significant. Secondly, change between the *xylo*- (**1**, **2**, **3**) and the *ribo*-configuration (**4**) produces an inversion in the orientation of the O_3—C_3 bond (the median bond of the coupling route for $^3J_{P,C2}$) with respect to the orientation of the electronegative substituent $-O_2$ on C_2.

In conclusion, *the* $^3J_{POCC}$ *vs.* $\theta_{P,C}$ *"Karplus-like" relationship appears to be drastically more susceptible to ring strain, bond angle distorsions, and epimeric orientation of the electronegative substituents than is the* $^3J_{POCH}$ *vs.* $\theta_{P,H}$ *relationship.*

2.4 *Conformation around the* C_4—C_5 *bond for the acyclic phosphoesters 7 to 12*

In the following analysis we will assume that $^3J_{HCCH}$ constants have values which are the average between *gauche* and *trans*-periplanar ^3J values related to the three possible low-energy rotamers around the C_4—C_5 bond, as shown in Fig. 3. Inspection of Dreiding models precludes (A) from all of the equilibria, for steric reasons. Using the Karplus relationship (11), it immediately appears that in **9** and **10** (where $J_{4,5}$ coupling constants are very small) (C) is the only populated conformation, whereas in **7** and **8** a small participation of (B) in the equilibria has to be considered ($J_{4,5pro\text{-}R}$ = 3.9–4.3 Hz).

The Lee and Sarma relation (13*a*) (eq. [1]) indicates that (B) is the only populated conformation around C_4—C_5 in **11** and **12**. The large couplings ($J_{4,5pro\text{-}R}$ = 11.7–12 Hz) are significant for this *trans*-periplanar orientation of both the protons. Conformation (B) permits a maximum distance between both the phosphoester groups of **11** and **12**.

2.5 *Assignment of conformations around* C_5—O_5 *and* C_3—O_3 *for acyclic phosphoesters 7 to 12, using the* $^3J_{POCH}$ *coupling constants*

Conformational equilibria around the phosphoester bonds C_3—O_3 (compounds **7** to **12**) and C_5—O_5 (**11** and **12**) will be discussed on the basis of previous results (20, 23, 25, 42–45), and assuming that populations of three low-energy rotamers exist in solution. As a result, the observed $^3J_{POCH}$ value will therefore be averaged as follows:

$$[7] \quad {}^3J_{POCH} = (N_1 + N_2)\,{}^3J^g + N_3\,{}^3J^t$$

where N_i is the molar fraction of conformer i and $\sum_i N_i = 1$.

Starting from the successfully used values, $^3J^g_{POCH} = 2.1$ Hz and $^3J^t_{POCH} = 22.9$ Hz (41), study of the conformational equilibrium around the C_5—O_5 bond in **11** and **12** shows unequivocally the large predominance of the rotamer with C_4,P *trans*-periplanar. It is relevant to note that the two $^3J_{5,P}$ constants are small enough to justify such an orientation.

A similar approach to the rotameric composition around the C_3—O_3 bond of **7** to **12** (see Fig. 3) only allows one to min-

Can. J. Chem. Downloaded from www.nrcresearchpress.com by 210.87.254.5 on 09/06/12
For personal use only.

Can. J. Chem. Downloaded from www.nrcresearchpress.com by 210.87.254.5 on 09/06/12
For personal use only.

imize the participation of (D) to the equilibrium around this phosphoester bond ($J_{3,P}$ being relatively small). Further study of the $^3J_{POCC}$ coupling constants is necessary to complete this approach, the phosphorus atom being coupled in this case to one proton and two carbons.

2.6 *Contribution of the coupling constants $^3J_{POCC}$ to the conformational analysis of the phosphoester bonds of acyclic derivatives 7 to 12*

Use of $^3J_{POCC}$ coupling constant values to calculate the rotameric compositions of phosphate groups have already been reported. For the phosphate and the phosphonate derivatives, these constants do not seem susceptible to phosphorus substituents (32, 46). Previous studies (41, 47–52) have generally proposed the value $^3J^g_{POCC} = 2–3$ Hz but are very divergent in the choice of the $^3J^t_{POCC}$ value, which has been assumed by different groups to be 8.5 Hz (47), 10 Hz (48–50), 11 Hz (51), or 14 Hz (41, 52).

In this study, we have had an opportunity to evaluate the effect of the coupled carbon substituents on the $^3J_{POCC}$ values. The compounds available present three very different P—O—CH_2—C phosphoester fragments, namely:

(a) P—O—CH_2—CCl_3 (compounds **7**, **9**, **11**)

(b) P—O—C(5)H_2—C(H)(O)(C) (compounds **11** and **12**)

(c) P—O—CH_2—CH_3 (compounds of refs. 1 and 53)

Again, starting with the $^3J^g_{POCH} = 2.1$ Hz and $^3J^t_{POCH} = 22.9$ Hz values, the rotameric compositions of these fragments can be determined and the $^3J_{P,C}$ values rationalized. The appropriate equations are:

[8] $^3J_{POCH_A} = 22.9\,N_1 + 2.1\,(1 - N_1)$

[9] $^3J_{POCH_B} = 22.9\,N_2 + 2.1\,(1 - N_2)$

[10] $N_3 = 1 - (N_1 + N_2)$

[11] $^3J_{POCC} = {}^3J^t_{POCC}\,N_3 + {}^3J^g_{POCC}\,(1 - N_3)$

Assuming that the possible variaiton of the $^3J^g_{POCC}$ value has to be drastically smaller than the variation of the $^3J^t_{POCC}$ one, the last equation can be solved using the approximate $^3J^g_{POCC} = 2–3$ Hz value. Then from Table 4 we get:

(a) fragment P—O—CH_2—CCl_3
$^3J^t_{POCC} \simeq 17$ Hz (compounds **7** and **9**)

(b) fragment P—O—C(5)H_2—C(4)(O)(C)—H
$^3J^t_{POCC} \simeq 12$ Hz (compounds **11** and **12**)

(c) fragment P—O—CH_2—CH_3
$^3J^t_{POCC} \simeq 8–9$ Hz (compounds of refs. 1 and 53)

These results show unequivocally the very large susceptibility of the $^3J_{POCC}$ constants to the electronegativity of the coupled carbon substituents.

Considering now the C_3—O_3 phosphoester bond of compounds **7** to **12**, similar equation systems lead to a $^3J^t_{POCC}$ value which is not consistent with the values observed for the $^3J_{C4,P3}$ and $^3J_{C2,P3}$ vicinal coupling constants (see Table 4). A variation of 10 to 15 Hz appears in the estimated value of $^3J^t_{POCC}$.

In fact, repulsion between the very bulky substituents in some of these compounds can lead to important variations in bond angles, and changes in furanose ring conformations (see 2.1) can produce important variations in the orientation of the oxygenated electronegative substituents. Again these observations show the large susceptibility of the $^3J_{POCC}$ coupling constants to factors other than dihedral angles. In addition, it is of interest to note that, in studies of 3′-ribonucleotides, the validity of the symmetrical two-state model (which considers that the P—O bond can make two equal angles with the $C_{3'}$—$H_{3'}$ bond) is still under discussion, regarding its applicability to the interpretation of nmr data (50).

Even if a quantitative estimation is not possible, careful inspection of the $^3J_{C4,P3}$ constant (Table 4) seems to show that in **8** to **10**, the (F) conformation depicted in Fig. 3 is predominant for the C_3—O_3 bond, whereas the previously assigned *trans*-periplanar arrangements of both the O_5 and C_3 atoms, and P_5 and C_4 atoms, seem to restore a larger conformational mobility around C_3—O_3 in **11** and **12**.

NOTE ADDED IN PROOF: Since the submission of this work to the journal, an article has appeared (54) on the "Karplus relation" for $^3J_{POCC}$ of nucleotides. Even if the relationship proposed by these authors is not appropriate for most of the compounds of the present study, this report reaches essentially the same conclusions regarding the dependency of $^3J_{POCC}$ on electronegativity of the coupled carbon substituents.

Experimental

Thick and thin layer chromatographic measurements were carried out on HF 254 Merck silica and dry column chromatography on 60F 254 Merck silica. The ir spectra were run on a Perkin–Elmer 357 and uv spectra on a Unicam SP 800 or a Beckman 25 spectrometer. Melting points were determined with a Mettler FP 52 apparatus. The ^{1}H nmr spectra were run at 360 MHz on a Bruker WH 360, at 250 MHz on a Cameca, or at 90 MHz on a Perkin–Elmer R32 instrument; ^{13}C nmr spectra were recorded at 25.2 MHz on a Varian XL 100 and ^{31}P nmr spectra at 40.5 MHz on a Bruker instrument. All chemical shifts (δ) are reported in parts per million. The specific optical rotation $[\alpha]_D$ values were obtained with a Schmidt and Haensch polarimeter and the mass spectra were recorded on a Varian SM-1B at 70 eV (m/z, relative abundance in %).

(S_P)-1,2-O-Isopropylidene-3,5-O-phenoxyphosphoryl-α-D-xylofuranose (1)

Phenylphosphorodichloridate (2.6 mL, 17.3 mmol) was added dropwise to a stirred solution of **A** (2.84 g, 15 mmol) in pyridine (17 mL) at 0°C and the mixture was stirred for 16 h at 20°C. After removing the pyridine, the resultant mixture was dissolved in $CHCl_3$ (50 mL), washed (saturated solution $NaHCO_3$, 2 × 25 mL; H_2O, 4 × 25 mL), dried ($MgSO_4$), and the $CHCl_3$ was removed under reduced pressure. A mixture (4.68 g) of **1** and **2** (21:29, nmr) was obtained and thick layer chromatography with EtOAc/hexane (1:1) as eluant yielded 1.72 g (35%) of **1** and 2.41 g (49%) of **2**. Characterization of **1**: R_f 0.72 (EtOAc/hexane 1:1, 2 developments); mp 101.2–104.3°C; $[\alpha]_D^{22}$ +15.0° (c 0.9, $CHCl_3$); uv (EtOH): 210 nm (ε = 2640); ir (KBr): 1385 and 1375 (CMe_2), 1295 (P=O) cm^{-1}; nmr: see Tables 1 and 2; m/z: 328 (34, M^+), 313 (22, M^+ − Me), 235 (10), 175 (12), 156 (10), 140 (9), 139 (100), 97 (42), 94 (11), 77 (11). *Anal.* calcd. for $C_{14}H_{17}O_7P$: C 51.22, H 5.22, P 9.44; found: C 51.42, H 5.25, P 9.49.

(R_P)-1,2-O-Isopropylidene-3,5-O-phenoxyphosphoryl-α-D-xylofuranose (2)

Obtained as above; R_f 0.40 (EtOAc/hexane 1:1, 2 developments); mp 71.0–72.5°C; $[\alpha]_D^{21}$ +25.6° (c 0.8, $CHCl_3$); uv (EtOH): 208.5 nm (ε = 2210); ir (KBr): 1390 and 1375 (CMe_2), 1285 (P=O) cm^{-1}; nmr: see Tables 1 and 2; m/z: 328 (64, M^+), 313 (77, M^+ − Me), 235 (16), 212 (20), 175 (32), 156 (21), 139 (100), 97 (39), 94 (20), 77 (14). *Anal.* calcd. for $C_{14}H_{17}O_7P$: C 51.22, H 5.22, P 9.44; found: C 51.33, H 5.40, P 9.35.

Can. J. Chem. Downloaded from www.nrcresearchpress.com by 210.87.254.5 on 09/06/12
For personal use only.

*(R_P)-1,2-O-Isopropylidene-3,5-O-(2,2,2-trichloroethoxy)phosphoryl-α-D-xylofuranose (**3**)*

A solution of bis(2,2,2-trichloroethyl)phosphorochloridate (1 g, 2.63 mmol) in pyridine (1.75 mL) was added to a stirred solution of **A** (500 mg, 2.63 mmol) in pyridine (4.25 mL) at 0°C and the mixture was stirred for 2 h at 20°C. After removing the pyridine, the resultant mixture was dissolved in $CHCl_3$ (40 mL), washed (saturated solution $NaHCO_3$, 2 × 20 mL; H_2O, 2 × 20 mL), and the $CHCl_3$ was removed under reduced pressure. The crude compound was crystallized from ether to yield 855 mg of **3** (85%); R_f 0.32 (EtOAc/hexane 1:1); mp 184.9–187.3°C; $[\alpha]_D^{23}$ +8.9° (*c* 1, $CHCl_3$); ir (KBr): 1390 and 1380 (CMe_2), 1300 (P=O) cm^{-1}; nmr: see Tables 1 and 2; *m/z*: 371, 369, and 367 (3, 7, and 7, M^+ − Me), 235 (18), 140 (9), 139 (100), 137 (5), 99 (7), 97 (44), 68 (5), 59 (4), 43 (11). *Anal.* calcd. for $C_{10}H_{14}Cl_3O_7P$: C 31.32, H 3.68, Cl 27.73; found: C 31.52, H 3.89, Cl 27.85.

*(R_P)-1,2-O-Isopropylidene-3,5-O-phenoxyphosphoryl-α-D-ribofuranose (**4**)*

Procedure (a)

Phenylphosphorodichloridate (1.2 mL, 8.04 mmol) was added dropwise to a stirred solution of **B** (1.5 g, 7.95 mmol) in pyridine (30 mL) at 0°C and the mixture was stirred for 16 h at 20°C. After removing the pyridine, the resultant mixture was dissolved in $CHCl_3$ (80 mL), washed (saturated solution $NaHCO_3$, 2 × 40 mL; H_2O, 4 × 40 mL), and concentrated. Thick layer chromatography with EtOAc/hexane (1:1) as eluant (2 developments) yielded 740 mg (28.5%) of **4** and 820 mg (31.5%) of a fraction containing **5**.

Procedure (b)

A suspension of Me_3COK (638 mg, 5.7 mmol) in anhydrous DMSO (11 mL) was prepared in a glove-box under rigourously anhydrous conditions. In the same atmosphere, this suspension was added to a solution of **10** (800 mg, 1.9 mmol) in anhydrous DMSO (9 mL), the resultant mixture was stirred 5 min at 20°C, and a suspension of Dowex 50 pyridinium resin (10 g) in anhydrous pyridine was added. Out of the glove-box, the resultant suspension was filtered, the resin washed with MeOH (10 mL), and the combined filtrates were concentrated under reduced pressure (10^{-2} Torr). Thick layer chromatography with EtOAc/hexane (1:1) as eluant yielded 312 mg (50.3%) of **4**; R_f 0.63 (EtOAc/hexane 1:1, 2 developments); mp 158.6–159.1°C; $[\alpha]_D^{27}$ +36.3° (*c* 1, $CHCl_3$); uv (EtOH): 210 nm (ε = 2300); ir (KBr): 1385 and 1375 (CMe_2), 1300 (P=O) cm^{-1}; ^1H nmr, δ ($CDCl_3$, 360 MHz): 1.38 and 1.64 (2s, 2 × 3H, CMe_2), 4.26 (d × d × d, 1H, H—C_3, $J_{2,3}$ = 4.0), 4.32–4.41 (m, 2H, H—C_4 and H_A—C_5), 4.67 (m, 1H, H_B—C_5), 4.77 (t, 1H, H—C_2, $J_{1,2}$ = 3.5), 5.89 (d, 1H, H—C_1), 7.19–7.39 (m, 5H, Ph); ^{13}C and ^{31}P nmr: see Tables 1 and 2; *m/z*: 328 (42, M^+), 313 (100, M^+ − Me), 177 (12), 175 (52), 149 (21), 117 (10), 97 (10), 94 (15), 77 (21), 57 (12). *Anal.* calcd. for $C_{14}H_{17}O_7P$: C 51.22, H 5.22, P 9.44; found: C 51.26, H 5.48, P 9.25.

*Dimer **5***

Obtained from the above *Procedure (a)*, the fraction of R_f 0.45 yielded, after hplc (EtOAc/hexane 3:2), 495 mg (19%) of **5**: R_f 0.45 (AcOEt/hexane 1:1, 2 developments); mp 190–200°C (dec.); $[\alpha]_D^{26}$ +85.1° (*c* 1, $CHCl_3$); ir (KBr): 1385 and 1375 (CMe_2), 1295 (P=O) cm^{-1}; ^1H nmr δ ($CDCl_3$, 90 MHz): 1.27, 1.33, 1.51 and 1.55 (4s, 4 × 3H, 2 × CMe_2), 4.01–4.80 (m, 10H, 2 × H—C_2, 2 × H—C_3, 2 × H—C_4, 2 × H_2—C_5), 5.70 and 5.81 (2d, 2 × H—C_1, $J_{1,2}$ = 3.6), 7.11–7.44 (m, 10H, 2 × Ph); *m/z*: 641 (19, M^+ − Me), 564 (24), 563 (100), 541 (8), 313 (13), 176 (10), 139 (16), 105 (12), 97 (11), 77 (14), 43 (8). *Anal.* calcd. for $C_{28}H_{34}O_{14}P_2$: C 51.22, H 5.22, P 9.44; found: C 51.17, H 5.32, P 9.36.

*1,2-O-Isopropylidene-5-O-bis(2,2,2-trichloroethoxy)phosphoryl-α-D-ribofuranose (**6**)*

A solution of bis(2,2,2-trichloroethyl)phosphorochloridate (1 g, 2.63 mmol) in pyridine (1.75 mL) was added to a stirred solution of **B** (500 mg, 2.63 mmol) in pyridine (4.25 mL) at 0°C and the mixture was stirred for 2 h at 20°C. After the usual work-up, the reactional mixture yielded 1.07 g (76.5%) of **6**; R_f 0.21 (EtOAc/hexane 1:2); mp 89.8–91.6°C; $[\alpha]_D^{22}$ + 18.4° (*c* 1, $CHCl_3$); ir (KBr): 3470 (OH), 1385 and 1380 (CMe_2), 1290 (P=O) cm^{-1}; ^1H nmr, δ (90 MHz, CD_3OD): 1.35 and 1.54 (2s, 2 × 3H, CMe_2), 3.91 (m, 1H, H_A—C_5, $J_{4,5A}$ = 4.0, $J_{5A,5B}$ = 9.0), 3.99–4.53 (m, 3H, H—C_3, H—C_4, H_B—C_5), 4.58 (d × d, 1H, H—C_2, $J_{1,2}$ = 3.2, $J_{2,3}$ = 4.2), 4.76 (m, 4H, 2 × CH_2CCl_3), 5.77 (d, 1H, H—C_1); *m/z*: 407, 405, 403, and 401 (5, 11, 14, and 7), 367, 365, 363, 361, and 359 (3, 11, 21, 29, and 14), 233, 231, 229 (8, 17, and 18), 139 (100), 129 (75), 100 (66), 99 (61), 97 (80), 85 (37), 59 (78), 43 (57). *Anal.* calcd. for $C_{12}H_{17}Cl_6O_8P$: C 27.04, H 3.22, Cl 39.91; found: C 27.20, H 3.42, Cl 40.10.

*1,2-O-Isopropylidene-3-O-bis(2,2,2-trichloroethoxy)phosphoryl-5-O-trityl-α-D-ribofuranose (**7**)*

A solution of bis(2,2,2-trichloroethyl)phosphorochloridate (7.76 g, 20.4 mmol) in pyridine (40 mL) was added to a stirred solution of **C** (4 g, 9.26 mmol) in pyridine (40 mL) at 0°C and the mixture was stirred for 24 h at 20°C. After the destruction of the excess of reagent with cold water and the usual work-up, dry column chromatography with EtOAc/hexane (1:2) as eluant yielded 6 g (84%) of **7**; R_f 0.81 (EtOAc/hexane 1:2); mp 108.5–109.5°C; $[\alpha]_D^{24}$ +44.7° (*c* 1, $CHCl_3$); uv (EtOH): 211 nm (ε = 14 560); ir (KBr): 1390 and 1380 (CMe_2), 1300 (P=O) cm^{-1}; nmr: see Tables 3 and 4; *m/z*: 521, 519, 517, 515, and 513 (1, 2, 3, 2, and 1), 477, 475, 473, and 471 (3, 5, 7, and 4), 244 (24), 243 (100), 241 (10), 166 (9), 165 (50), 141 (11), 127 (8), 105 (13), 99 (11), 43 (8). *Anal.* calcd. for $C_{31}H_{31}Cl_6O_8P$: C 48.03, H 4.03, Cl 27.44; found: C 48.00, H 4.19, Cl 27.40.

*3-O-Diphenoxyphosphoryl-1,2-O-isopropylidene-5-O-trityl-α-D-ribofuranose (**8**)*

Diphenylphosphorochloridate (3.45 mL, 23.14 mmol) was added dropwise to a stirred solution of **C** (4 g, 9.26 mmol) in pyridine (40 mL) at 0°C and the mixture was stirred for 24 h at 20°C. After the destruction of the excess of reagent with cold water and the usual work-up, dry column chromatography with EtOAc/hexane (1:2) as eluant yielded 5.35 g (87%) of **8**; R_f 0.71 (EtOAc/hexane 1:2); mp 122.0–124.1°C; $[\alpha]_D^{24}$ +57.1° (*c* 1, $CHCl_3$); uv (EtOH): 210.5 nm (ε = 19 820); ir (KBr): 1385 and 1375 (CMe_2), 1295 (P=O) cm^{-1}; nmr: see Tables 3 and 4; *m/z*: 421 (25), 407 (10), 405 (23), 364 (22), 363 (100), 333 (8), 277 (8), 251 (27), 244 (27), 243 (52), 165 (12). *Anal.* calcd. for $C_{39}H_{37}O_8P$: C 70.47, H 5.61; found: C 70.54, H 5.73.

*1,2-O-Isopropylidene-3-O-bis(2,2,2-trichloroethoxy)phosphoryl-α-D-ribofuranose (**9**)*

A suspension of **7** (5.5 g, 7.1 mmol) in aqueous 80% AcOH (750 mL) was heated (45°C) until dissolution (1 h) and the mixture was stirred for 18 h at 20°C. After concentration to 50 mL, addition of water (200 mL), filtration, and again concentration to dryness, dry column chromatography yielded 2.6 g (69%) of **9**; R_f 0.21 (EtOAc/hexane 1:2); mp 96.8–97.6°C; $[\alpha]_D^{23}$ +40.1° (*c* 1, $CHCl_3$); ir (KBr): 1390 and 1385 (CMe_2), 1305 (P=O) cm^{-1}; nmr: see Tables 3 and 4; *m/z*: 523, 521, 519, 517, and 515 (6, 21, 49, 55, and 26, M^+ − Me), 405, 403, and 401 (2, 12, and 12), 369, 367, 365, 363, 361, and 359 (4, 13, 32, 38, 21, and 11), 359, 357, and 355 (6, 17, and 17), 329, 327, and 325 (2, 13, and 17), 233, 231, and 229 (6, 17, and 21), 141 (100), 139 (43), 127 (83), 113 (28), 99 (49), 85 (38). *Anal.* calcd. for $C_{12}H_{17}Cl_6O_8P$: C 27.04, H 3.22, Cl 39.91, P 5.81; found: C 27.24, H 3.24, Cl 39.85, P 5.96.

*3-O-Diphenoxyphosphoryl-1,2-O-isopropylidene-α-D-ribofuranose (**10**)*

The same treatment (see preparation of **9**) from **8** (4.8 g, 7.2 mmol) for 8 1/2 h at 20°C yielded 2.58 g (85%) of **10**; R_f 0.13 (EtOAc/hexane 1:2); mp 90.0–90.8°C; $[\alpha]_D^{23}$ +39.2° (*c* 1, $CHCl_3$); uv (EtOH): 209 nm (ε = 6500); ir (KBr): 1380 and 1370 (CMe_2), 1285 (P=O) cm^{-1}; nmr: see Tables 3 and 4; *m/z*: 271 (56), 252 (13), 251 (100), 250 (12), 175 (27), 142 (24), 141 (26), 113 (29), 94 (40), 85 (11), 69 (11), 43 (15). *Anal.* calcd. for $C_{20}H_{23}O_8P$: C 56.87, H. 5.49; found: C 56.73, H 5.60.

*1,2-O-Isopropylidene-3,5-di-O-[bis(2,2,2-trichloroethoxy)phosphoryl]-α-D-ribofuranose (**11**)*

A solution of bis(2,2,2-trichloroethyl)phosphorochloridate (270 mg, 0.7 mmol) in pyridine (1 mL) was added to a stirred solution of **9** (300 mg, 0.56 mmol) in pyridine (4 mL) at 0°C and the mixture was stirred for 2 h at 20°C. After the usual work-up (see preparation of **6**), the reactional mixture yielded 445 mg (91%) of **11**; R_f 0.48 (EtOAc/hexane 1:2); mp 78.7–79.3°C; $[\alpha]_D^{23}$ +31.1° (*c* 1, $CHCl_3$); ir (KBr): 1385 and 1375 (CMe_2), 1290 (P=O) cm^{-1}; nmr: see Tables 3 and 4; *m/z*: 863, 861, 859, 857, and 855 (1, 1, 2, 2 and 1, M^+ − Me), 763, 761, 759, 757, 755, and 753 (1, 2, 2, 2, 1, and 1), 407, 405, 403, and 401 (1, 1, 2, and 2), 367, 365, 363, 361, and 359 (2, 2, 2, 2, and 1), 341, 339, and 337 (1, 3, and 3), 311, 309, and 307 (1, 2, and 3), 141 (7), 140 (8), 139 (100), 99 (7), 97 (20). *Anal.* calcd. for $C_{16}H_{20}Cl_{12}O_{11}P_2$: C 21.95, H 2.30, Cl 48.58; found: C 22.11, H 2.33, Cl 48.77.

3,5-Di-O-diphenoxyphosphoryl-1,2-O-isopropylidene-α-D-ribofuranose (12)

Reaction of **10** (400 mg, 0.95 mmol) with diphenylphosphorochloridate (0.2 mL, 1.34 mmol), as described in the preparation of **8**, yielded 510 mg (82%) of **12**; R_f 0.29 (EtOAc/hexane 1:2); syrup; $[\alpha]_D^{21}$ +35.2° (*c* 0.9, $CHCl_3$); uv (EtOH): 210.5 nm (ϵ = 9600); ir (film): 1390 and 1380 (CMe_2), 1300 (P=O) cm^{-1}; nmr: see Tables 3 and 4; *m/z*: 564 (7), 563 (29), 562 (100), 503 (5), 408 (14), 390 (4), 254 (15), 252 (23), 251 (7), 139 (14), 137 (8), 97 (4). *Anal.* calcd. for $C_{32}H_{32}O_{11}P_2$: C 58.72, H 4.93, P 9.46; found: C 58.63, H 5.03, P 9.63.

Acknowledgements

This work was supported by the Fonds National Suisse de la Recherche Scientifique (subsides no. 2.781.77 and 2.277.79). The authors would like to thank Professor A. Buchs and Miss O. Clerc for recording the mass spectra, Dr. U. Bürger and Mr. J. P. Saulnier for the 25.2 MHz ^{13}C nmr spectra, Mr. Reutenauer (Centre Grenoblois de Résonance Magnétique, France) for the 250 MHz ^1H nmr spectra, Professor B. Gross, Miss F. Chrétien, and Mr. P. Simon (Université de Nancy, France) for the ^{31}P nmr spectra, Dr. B. Willhalm and Mr. W. Thommen (Firmenich & Co. S.A., Genève) for the 360 MHz ^1H nmr spectra, and Dr. K. Eder for the microanalysis. It is a pleasure to thank Dr. G. Rihs and co-workers (Ciba-Geigy & Co. S.A., Bâle) for the X-ray diffraction study of **4**, and Mrs. C. Baud for technical assistance in the synthesis of some compounds. One of us (J.R.N.) is grateful to Professors R. Barker, L. D. Hall, and G. Pouzard for helpful discussions.

1. J. M. J. TRONCHET, J. R. NEESER, L. GONZALEZ, and E. J. CHAROLLAIS. Helv. Chim. Acta, **62**, 2022 (1979).
2. J. M. J. TRONCHET, A. P. BONENFANT, K. D. PALLIE, and F. HABASHI. Helv. Chim. Acta, **62**, 1622 (1979).
3. J. M. J. TRONCHET, J. R. NEESER, and E. J. CHAROLLAIS. Helv. Chim. Acta, **61**, 1942 (1978).
4. J. M. J. TRONCHET, J. R. NEESER, and E. J. CHAROLLAIS. Helv. Chim. Acta, **60**, 243 (1977).
5. J. R. NEESER. Nouveaux types de sucres phosphorés: synthèse, propriétés spectroscopiques, en particulier RMN-^1H, -^{13}C, -^{31}P. Thèse de doctorat es Sciences No 1999, Université de Genève (1981).
6. K. BERGESEN. Acta Chem. Scand. **24**, 2019 (1970).
7. J. P. MAJORAL and J. NAVECH. Bull. Soc. Chim. Fr. 1331 (1971).
8. J. P. MAJORAL and J. NAVECH. Bull. Soc. Chim. Fr. 2609 (1971).
9. L. D. HALL and R. B. MALCOLM. Can. J. Chem. **50**, 2102 (1972).
10. C. ALTONA and M. SUNDARALINGAM. J. Am. Chem. Soc. **94**, 8205 (1972).
11. M. KARPLUS. J. Chem. Phys. **30**, 11 (1959).
12. (*a*) R. J. ABRAHAM, L. D. HALL, L. HOUGH, and K. A. MCLAUCHLAN. J. Chem. Soc. 3699 (1962); (*b*) T. NGUYEN-XUAN, J. M. J. TRONCHET, and H. BILL. Helv. Chim. Acta, **64**, 1949 (1981).
13. (*a*) C.-H. LEE and R. H. SARMA. J. Am. Chem. Soc. **98**, 3541 (1976); (*b*) M. MACCOSS, C. F. AINSWORTH, G. LEO, F. S. EZRA, and S. S. DANYLUK. J. Am. Chem. Soc. **102**, 7353 (1980).
14. D. B. COOPER, T. D. INCH, and G. J. LEWIS. J. Chem. Soc. Perkin Trans. **1**, 1043 (1974).
15. M. MACCOSS, F. S. EZRA, M. J. ROBINS, and S. S. DANYLUK. Carbohydr. Res. **62**, 203 (1978).
16. B. J. BLACKBURN, R. D. LAPPER, and I. C. P. SMITH. J. Am. Chem. Soc. **95**, 2873 (1973).
17. R. D. LAPPER, H. H. MANTSCH, and I. C. P. SMITH. J. Am. Chem. Soc. **94**, 6243 (1972).
18. M. KAINOSHO and K. AJISAKA. J. Am. Chem. Soc. **97**, 6839 (1975).
19. L. D. HALL and R. B. MALCOLM. Can. J. Chem. **50**, 2092 (1972).
20. B. DONALDSON and L. D. HALL. Can. J. Chem. **50**, 2111 (1972).
21. D. W. WHITE, G. K. MACEVEN, R. D. BERTRAND, and J. G. VERKADE. J. Chem. Soc. Ser. B, 1454 (1971).
22. M. KAINOSHO and T. SHIMOZAWA. Tetrahedron Lett. 865 (1969).
23. M. TSUBOI, F. KURIYAGAWA, K. MATSUO, and Y. KYOGOKU. Bull. Chem. Soc. Jpn. **40**, 1813 (1967).
24. D. W. WHITE and J. G. VERKADE. J. Magn. Reson. **3**, 111 (1970).
25. M. KAINOSHO, A. NAKAMURA, and M. TSUBOI. Bull. Chem. Soc. Jpn. **42**, 1713 (1969).
26. M. MACCOSS, F. S. EZRA, M. J. ROBINS, and S. S. DANYLUK. J. Am. Chem. Soc. **99**, 7495 (1977).
27. M. KAINOSHO and A. NAKAMURA. Tetrahedron, **25**, 4071 (1969).
28. W.-J. KUNG, R. E. MARSH, and M. KAINOSHO. J. Am. Chem. Soc. **99**, 5471 (1977).
29. (*a*) J. S. BRIMACOMBE and A. M. MOFTI. Carbohydr. Res. **16**, 167 (1971); (*b*) J. M. J. TRONCHET, F. BARBALAT-REY, and J. M. CHALET. Carbohydr. Res. **30**, 229 (1973).
30. M. HAEMERS, R. OTTINGER, D. ZIMMERMANN, and J. REISSE. Tetrahedron, **29**, 3539 (1973).
31. A. A. BORISENKO, N. M. SERGEYEV, E. Y. NIFANT'EV, and YU. A. USTYNYUK. J. Chem. Soc. Chem. Commun. 406 (1972).
32. J.-R. LLINAS, E.-J. VINCENT, and G. PEIFFER. Bull. Soc. Chim. Fr. 3209 (1973).
33. R. D. LAPPER, H. H. MANTSCH, and I. C. P. SMITH. J. Am. Chem. Soc. **95**, 2878 (1973).
34. R. D. LAPPER and I. C. P. SMITH. J. Am. Chem. Soc. **95**, 2880 (1973).
35. F. HAYASHI, K. AKASAKA, and H. HATANO. Nucleic Acids Res. Spec. Publ. **2**, s53 (1976).
36. N. K. KOCHETKOV, E. E. NIFANT'EV, M. P. KOROTEEV, Z. K. ZHANE, and A. A. BORISENKO. Carbohydr. Res. **47**, 221 (1976).
37. S. UESUGI and M. IKEHARA. Chem. Pharm. Bull. **26**, 3040 (1978).
38. S. UESUGI, S. TANAKA, and M. IKEHARA. Eur. J. Biochem. **90**, 205 (1978).
39. S. UESUGI, S. TANAKA, and M. IKEHARA. Org. Mag. Reson. **12**, 143 (1979).
40. M. KAINOSHO. Org. Mag. Reson. **12**, 548 (1979).
41. J. V. O'CONNOR, H. A. NUNEZ, and R. BARKER. Biochemistry, **18**, 500 (1979).
42. L. D. HALL and R. B. MALCOLM. Chem. Ind. 92 (1968).
43. M. TSUBOI, S. TAKAHASHI, Y. KYOGOKU, H. HATATSU, T. UKITA, and M. KAINOSHO. Science, **166**, 1504 (1969).
44. M. KAINOSHO. J. Phys. Chem. **74**, 2853 (1970).
45. E. HRUSKA, D. J. WOOD, R. J. MYNOTT, and R. H. SARMA. FEBS Lett. **31**, 153 (1973).
46. G. A. GRAY. J. Am. Chem. Soc. **93**, 2132 (1971).
47. H. H. MANTSCH and I. C. P. SMITH. Biochem. Biophys. Res. Commun. **46**, 808 (1972).

Can. J. Chem. Downloaded from www.nrcresearchpress.com by 210.87.254.5 on 09/06/12
For personal use only.

48. G. GOVIL and I. C. P. SMITH. Biopolymers, **12**, 2589 (1973).
49. Y. WEDMID, C. A. EVANS, and W. J. BAUMANN. J. Org. Chem. **45**, 1582 (1980).
50. W. P. NIEMCZURA and F. E. HRUSKA. Can. J. Chem. **58**, 472 (1980).
51. C.-G. LEE and G.-J. CHANG. J. Carbohydr. Nucleosides Nucleotides, **5**, 343 (1978).
52. T. A. W. KOERNER, R. J. VOLL, L. W. CARRY, and E. S. YOUNATHAN. Biochemistry, **19**, 2795 (1980).
53. J. M. J. TRONCHET, J. R. NEESER, E. J. CHAROLLAIS, and (in part) L. GONZALEZ. J. Carbohydr. Chem. In press.
54. D. B. DAVIES and H. SADIKOT. Org. Magn. Reson. **20**, 180 (1982).

Can. J. Chem. Downloaded from www.nrcresearchpress.com by 210.87.254.5 on 09/06/12
For personal use only.

Synthesis of piperazine-2,5-diones related to bicyclomycin: 1,4-dibenzyl-3-hydroxy-3-[1-(2-methoxyethyl)ethenyl]piperazine-2,5-dione. 2. Route via cyclic intermediates[1]

PETER YATES AND JOHN HAROLD HOARE

Lash Miller Chemical Laboratories, University of Toronto, Toronto, Ont., Canada M5S 1A1

Received November 9, 1982

PETER YATES and JOHN HAROLD HOARE. Can. J. Chem. **61**, 1397 (1983).

1,4-Dibenzyl-3-hydroxy-3-[1-(2-methoxyethyl)ethenyl]piperazine-2,5-dione (**43**), which incorporates several of the structural features of the antibiotic bicyclomycin, has been synthesized via a reaction sequence involving early construction of the piperazine-2,5-dione ring. In model studies 3-isopropylidenepiperazine-2,5-dione was di-*N*-benzylated and epoxidized to give 4,7-dibenzyl-2,2-dimethyl-1-oxa-4,7-diazaspiro[2.5]octane-5,8-dione (**10**). The opening of the epoxide ring of **10** by several reagents was investigated and it was found that treatment with magnesium isopropylcyclohexylamide (MICA) gives 1,4-dibenzyl-3-hydroxy-3-(1-methylethenyl)piperazine-2,5-dione (**23**). Treatment of ethyl 3-(2-methoxyethyl)-3-methylglycidate (**28**) with *p*-toluenesulfonic acid followed by hydrogenation and oxidation gives ethyl 5-methoxy-3-methyl-2-oxopentanoate, which on reaction with chloroacetamide and sulfuric acid followed by treatment of the resulting enamide with ammonia gives (*Z*)- and (*E*)-3-(4-methoxybut-2-ylidene)piperazine-2,5-dione. Di-*N*-benzylation of these followed by epoxidation gives (*Z*)- and (*E*)-4,7-dibenzyl-2-(2-methoxyethyl)-2-methyl-1-oxa-4,7-diazaspiro[2.5]octane-5,8-dione (**41** and **42**). Treatment of **41** with MICA converts it to compound **43**. Chromatography of **43** on silica converts it in part to *N*-benzyl-*N*-(2-benzylamino-2-oxoethyl)-3-(2-methoxyethyl)-2-oxo-3-butenamide, which on treatment with MICA regenerates **43**.

PETER YATES et JOHN HAROLD HOARE. Can. J. Chem. **61**, 1397 (1983).

On a synthétisé la dibenzyl-1,4 hydroxy-3 [(méthoxy-2 éthyl)-1 éthényl]-3 pipérazinedione-2,5 (**43**), qui contient plusieurs des caractéristiques structurales de l'antibiotique bicyclomycine, en faisant appel à une suite de réactions qui font intervenir l'élaboration du cycle pipérazinedione-2,5 dès le début. Dans une étude type on a di-*N*-benzilé l'isopropylidène-3 pipérazinedione-2,5 et on l'a époxydé pour obtenir la dibenzyl-4,7 diméthyl-2,2 oxa-1 diaza-4,7 spiro[2,5] octadione-5,8 (**10**). On a étudié l'ouverture du cycle de l'époxyde du composé **10** par plusieurs réactifs, et on a trouvé que le traitement avec l'isopropylcyclohexylamide de magnésium (ICAM) donne la dibenzyl-1,4 hydroxy-3 (méthyl-1 éthényl)-3 pipérazinedione-2,5 (**23**). Le traitement de la (méthoxy-2 éthyl)-3 méthyl-3 glycidate d'éthyle (**28**) avec l'acide *p*-toluènesulfonique suivi d'une hydrogénation et d'une oxydation donne le méthoxy-5 méthyl-3 oxo-2 pentanoate d'éthyle qui par réaction avec le chloroacétamide et l'acide sulfurique suivie du traitement de l'énamide résultant avec l'ammoniac donne la (méthoxy-4 butylidène-2) pipérazinedione-2,5 (*Z*) et (*E*). La di-*N*-benzylation de ces composés suivie d'une époxydation conduit à la dibenzyl-4,7 (méthoxy-2 éthyl)-2 méthyl-2 oxa-1 diaza-4,7 spiro[2,5] octadione-5,8 (*Z*) et (*E*) (**41** et **42**). Le composé **41** réagit avec le ICAM en donnant le produit **43**. Ce dernier par chromatographie sur de la silice se transforme en partie en *N*-benzyl *N*-(benzylamino-2 oxo-2 éthyl) (méthoxy-2 éthyl)-3 oxo-2 butène-3 amide qui traité avec le ICAM regénère le composé **43**.

[Traduit par le journal]

We have discussed in the previous paper in this series (2) the synthesis of the piperazine-2,5-dione **1** (Bz = benzyl), which is related to the antibiotic bicyclomycin (**2**). This was prepared by a reaction sequence, which we have designated as a route via acyclic intermediates, wherein an intermediate of type **3**

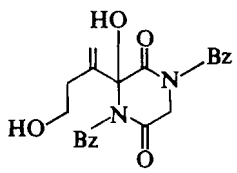

1

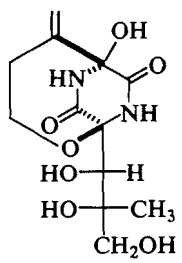

2

was first constructed and then treated with *N*,*N*′-dibenzylglycinamide (**4**) to give a diamide **5**, which was converted to **1** with closure of the piperazine-2,5-dione ring at a late stage in the sequence (Scheme 1). We now describe an alternative synthetic strategy for the synthesis of **1**, which we designate as a route via cyclic intermediates, in which the piperazine-2,5-dione ring is constructed at an early stage of the synthesis in the form of a 3-alkylidene derivative of type **6** which is converted to an epoxide of type **7**, which in turn is manipulated to introduce the desired functionality (Scheme 2).

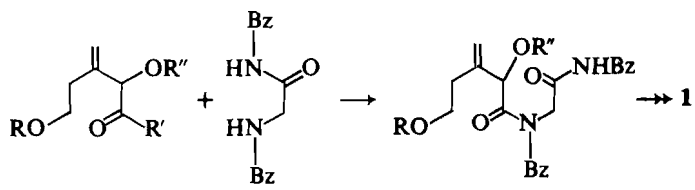

3 **4** **5**

SCHEME 1

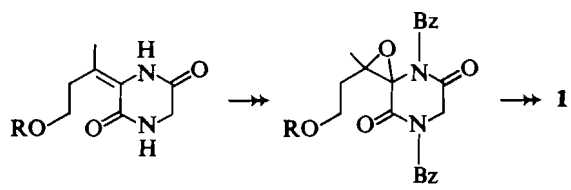

6 **7**

SCHEME 2

Since the preparation of an epoxypiperazine-2,5-dione of type **7** had not been reported previously, we decided to begin

[1]For a preliminary account of part of this work, see ref. 1; for paper 1 in this series, see ref. 2.

Can. J. Chem. Downloaded from www.nrcresearchpress.com by 210.87.254.5 on 09/06/12
For personal use only.

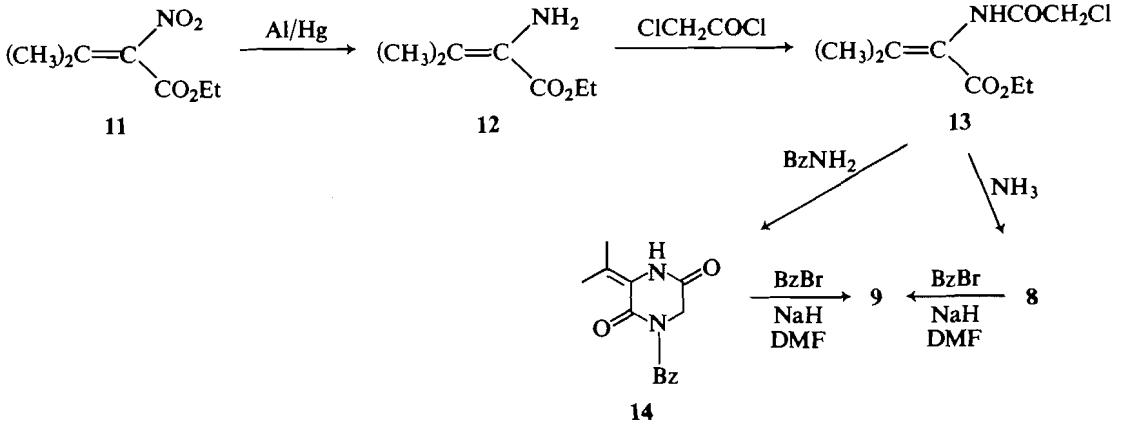

SCHEME 3

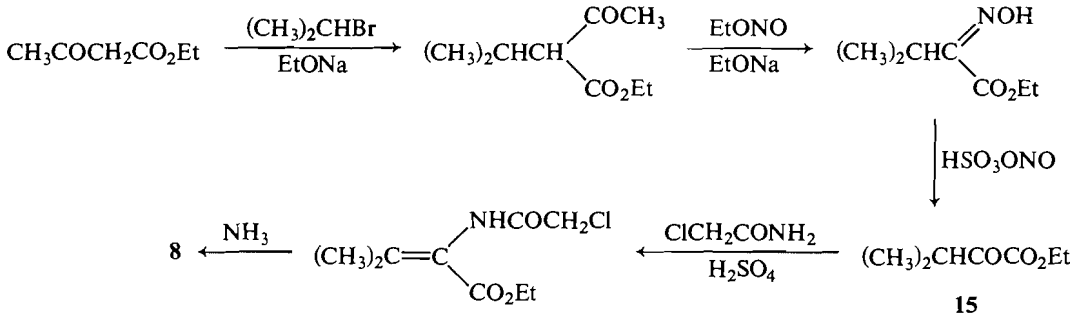

SCHEME 4

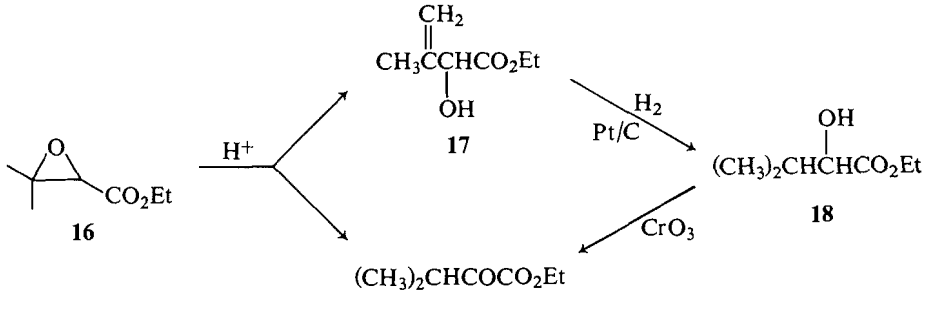

SCHEME 5

our investigation with the preparation of the known 3-isopropylidenepiperazine-2,5-dione (**8**) in order to study its *N*-benzylation to **9** and the epoxidation of this to **10**, and to investigate the reactions of the epoxide.

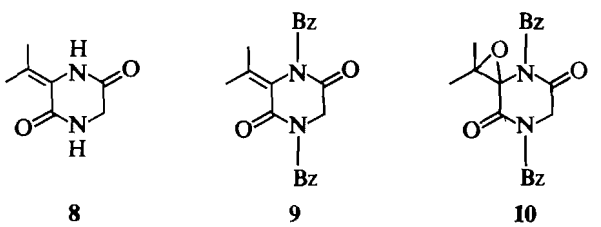

Two routes have been reported for the synthesis of **8**. In the first (3) ethyl 3-methyl-2-nitro-2-butenoate (**11**), prepared by nitration of ethyl 3,3-dimethylacrylate,[2] was reduced with aluminum amalgam to the ene amino ester **12**,[3] which was converted with chloroacetyl chloride to the amide **13**, which in turn was treated with ammonia to give the piperazine-2,5-dione **8** (Scheme 3). On repetition of this reaction sequence we obtained **8**, which was dibenzylated to give **9**. We also investigated the reaction of **13** with benzylamine and found that although it gave the desired mono-*N*-benzyl derivative **14** of **8**, which could be benzylated to give **9**, the yields were low, and **9** is preferably prepared via dibenzylation of **8**.

However, we were unable to improve the poor yield previously reported (3) for the reduction of **11**; furthermore we later encountered difficulties in applying this method to the synthesis of piperazine-2,5-diones of type **6** in the main series

[2]Cf., also, ref. 4.

[3]It is of interest that the α-imino isomer of **12** was not observed to tautomerize to the latter (3).

Can. J. Chem. Downloaded from www.nrcresearchpress.com by 210.87.254.5 on 09/06/12
For personal use only.

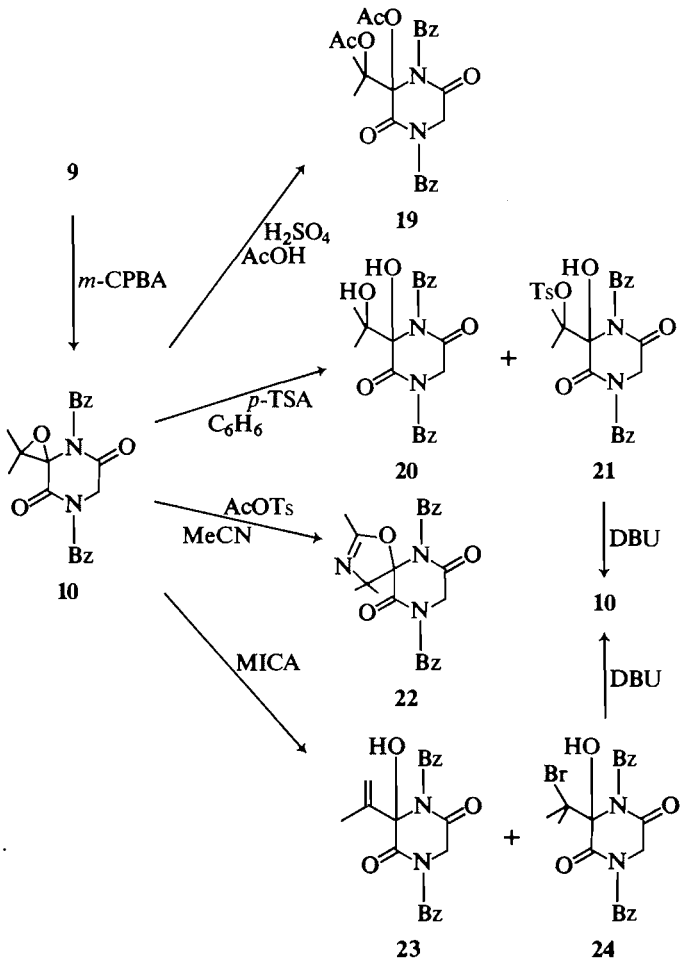

SCHEME 6

(*vide infra*). We therefore turned to the second route (5) for the synthesis of **8**. This involved the synthesis of ethyl α-oxoisovalerate (**15**) by the route shown in Scheme 4 (6) and condensation of this with chloroacetamide in benzene and sulfuric acid[4] to give the amide **13** which, as in the first sequence, was converted to the piperazine-2,5-dione **8** with ammonia.

We considered the synthesis of **15** by this route to be too long and too low yielding to be viable. We therefore investigated the report (8) that **15** could be prepared from the readily available ethyl 3,3-dimethylglycidate (**16**) by treatment with *p*-toluenesulfonic acid in toluene at 80–85°C. The exact details of this work were not available to us, and we carried out the reaction in boiling benzene. Under these conditions we obtained the unsaturated hydroxy ester **17** as the major product and a small amount of **15** (Scheme 5). We were able, however, to utilize this route since hydrogenation of **17** to **18** followed by oxidation gave **15** in good yield. Condensation of this with chloroacetamide and sulfuric acid to give **13** as in Scheme 4 and treatment of this with alcoholic ammonia gave the piperazine-2,5-dione **8** in satisfactory yields and this is undoubtedly the best route to the latter compound. As already noted, this could be dibenzylated to give the desired intermediate **9**.

We next turned our attention to the epoxidation of **9** to **10** (cf., **7**) and the opening of the epoxide ring in the latter. We found that **9** could be converted to **10** by treatment with *m*-chloroperoxybenzoic acid in boiling methylene chloride for 18 hours. It is of interest that in the ^{1}H nmr spectrum of **10** the three sets of methylene proton signals appear as AB systems in contrast with their signals in the spectrum of **9**, where they appear as singlets; this is attributable to the presence of a chiral centre in **10**, but not **9**, which renders diastereotopic each pair of methylene protons. In our initial attempts to open the epoxide ring of **10** we used reagents that we had used successfully previously for the conversion of the epoxide rings of 3-methylglycidic esters to allylic alcohols (ref. 2 and Scheme **5**). However, treatment of the epoxide **10** with acetic anhydride and sulfuric acid gave only the diacetate **19** and none of the desired product **23** (Scheme 6), while treatment with *p*-toluenesulfonic acid in benzene gave a mixture of the diol **20** and the hydroxy tosylate **21**; the latter on reaction with 1,8-diazabicyclo[5.4.0]undec-7-ene (DBU) regenerated the epoxide **10**. Treatment of **10** with acetyl tosylate (9) in acetonitrile gave a product that is considered to be **22** and to arise by intervention of the solvent. During this work Corey *et al.* (10) reported the use of magnesium isopropylcyclohexylamide (MICA) for the opening of epoxide rings and we found that this reagent would bring about the desired cleavage of the epoxide **10** to the allylic alcohol **23**, which was accompanied by the bromohydrin **24**. The preparation of MICA (10) involves treatment of isopropylcyclohexylamine with methylmagnesium bromide; the magnesium bromide produced in this reaction must be responsible for the opening of the epoxide ring of **10** to give **24**. Treatment of the bromohydrin **24** with DBU regenerated the epoxide **10**.

Having carried out these model studies, we returned to the series proper. As mentioned previously, use of an α-nitro α,β-unsaturated ester for the synthesis of the desired 3-alkylidenepiperazine-2,5-dione derivative encountered difficulties. These stemmed from the circumstance that the reaction of 4-methoxy-2-butanone (**25**) (11) with methyl nitroacetate and ammonium acetate gave, instead of the expected α-nitro α,β-unsaturated ester **26**, the saturated nitro keto ester **27**, which must arise via elimination of methanol from **25** followed by Michael addition of methyl nitroacetate (Scheme 7). We therefore adopted a route analogous to that in Scheme 5. In the present case (Scheme 8) treatment of a diastereomeric mixture of the glycidic esters **28**, prepared from the reaction of **25** with ethyl chloroacetate and sodium ethoxide (2), with *p*-toluenesulfonic acid in boiling benzene gave the allylic alcohols **29** and **30** together with a small amount of the α-oxo ester **31**; the desired allylic alcohol **29** was the major reaction product. Catalytic hydrogenation of the product mixture gave a 1:2 mixture of the saturated hydroxy esters **32** and **33**. The latter must result from hydrogenolysis of the CH_3O—C bond, presumably via the allylic ether **30**. Since this was a minor component of the initial mixture, double bond migration must have occurred prior to hydrogenolysis and hydrogenation. Platinum is known to cause less migration of ethylenic double bonds and less hydrogenolysis of allylic alcohols than does palladium (12); we therefore turned to the use of platinum as catalyst, when we obtained a 2:1 mixture of **32** and **33**. This mixture was not separated but was oxidized directly with Jones reagent to give a mixture of the α-oxo esters **31** and **34** which were separated by fractional distillation.

[4]It was originally reported (5) that the best yields for this reaction were obtained by the use of sulfuric acid; however, in later publications from the same laboratory (7) phosphoryl chloride is used exclusively.

Can. J. Chem. Downloaded from www.nrcresearchpress.com by 210.87.254.5 on 09/06/12
For personal use only.

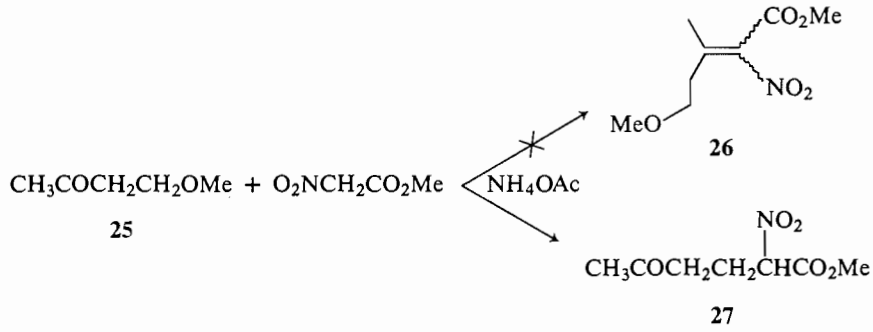

SCHEME 7

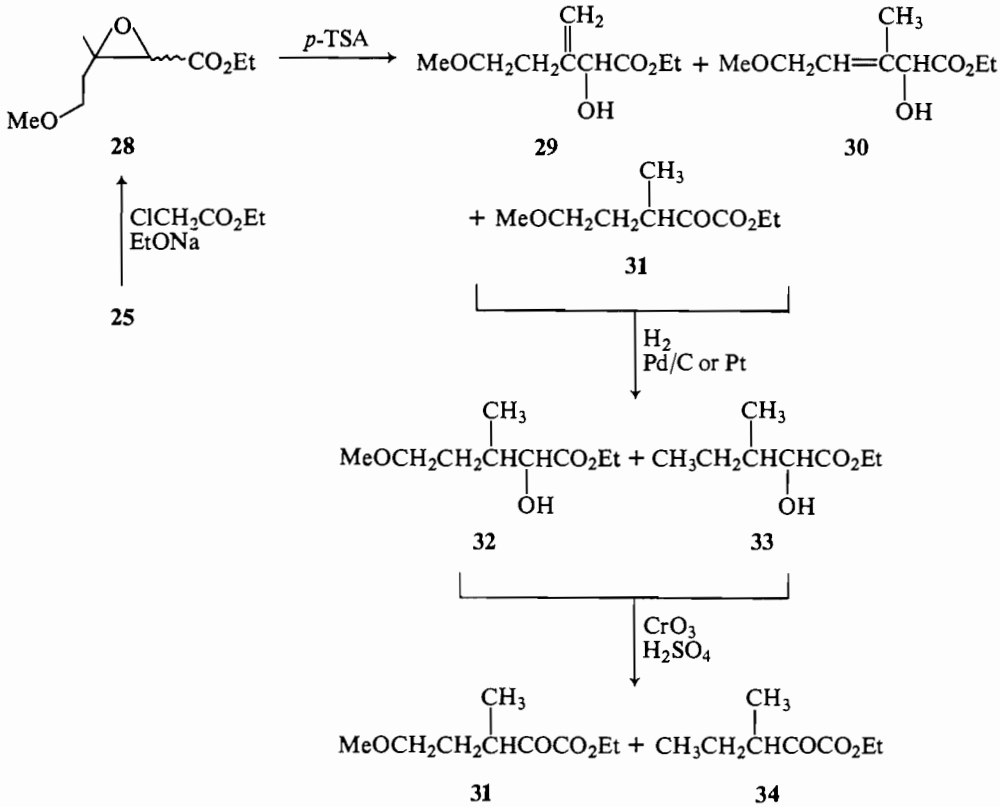

SCHEME 8

Treatment of **31** with chloroacetamide and sulfuric acid in benzene (5) gave a mixture of the *Z* and *E* amides **35** and **36** in a 3:1 ratio (Scheme 9). The configurational assignments to the products were made by the use of ^{1}H nmr spectroscopy, signals at δ 2.05 (s) and 2.37 (t) ppm being assigned to **35** and signals at δ 1.87 (s) and 2.80 (t) ppm to **36**, based on the expected greater deshielding of allylic protons by a carboxylic ester group that bears a *cis* relationship to them (13). This mixture was treated with ethanolic ammonia to give the piperazine-2,5-diones **37** and **38**, also in a 3:1 ratio. This mixture was separated by crystallization and chromatography and the individual stereoisomers were again identified by ^{1}H nmr spectroscopy (**37**: δ 2.27 (s), 1.90 (t) ppm; **38**: δ 1.62 (s), 2.78 (t) ppm), based on the expected similar effect of the carbonyl group of the α,β-unsaturated amide moiety to that of the ester group in **35** and **36** (*cf.* refs 5 and 7). Attempted benzylation of **37** and **38** with two equivalents of benzyl bromide and sodium hydride was unsuccessful, but each isomer could be converted to its *N*,*N*′-dibenzyl derivative, **39** and **40**, respectively, by treatment with silver oxide and benzyl bromide in dimethylformamide, a procedure modeled on a method previously used for the *N*-methylation of piperazine-2,5-dione (14); in each case a mono-*N*-benzylated product was also isolated. Again the dibenzyl isomers could be readily distinguished by ^{1}H nmr spectroscopy: **39**: δ 2.13 (s), 2.48 (t) ppm; **40**: δ 1.80 (t), 2.93 (t) ppm.

Epoxidation of each of **39** and **40** with *m*-chloroperoxybenzoic acid in boiling methylene chloride gave the *Z* and *E* epoxides **41** and **42**, respectively (Scheme 10). It is of interest that differential deshielding effects by the carbonyl group of the α,β-epoxy amide moiety are observable in the ^{1}H nmr spectra of the epoxides that are related to those in the α,β-unsaturated carbonyl compounds discussed above; the effects are smaller (**41**: δ 1.45 (s), 1.80 (m) ppm; **42**: δ 1.35 (s), 1.98 (m) ppm), as expected for the changed spatial relationship of the protons in question and the carbonyl group. As in the model series, the

Can. J. Chem. Downloaded from www.nrcresearchpress.com by 210.87.254.5 on 09/06/12
For personal use only.

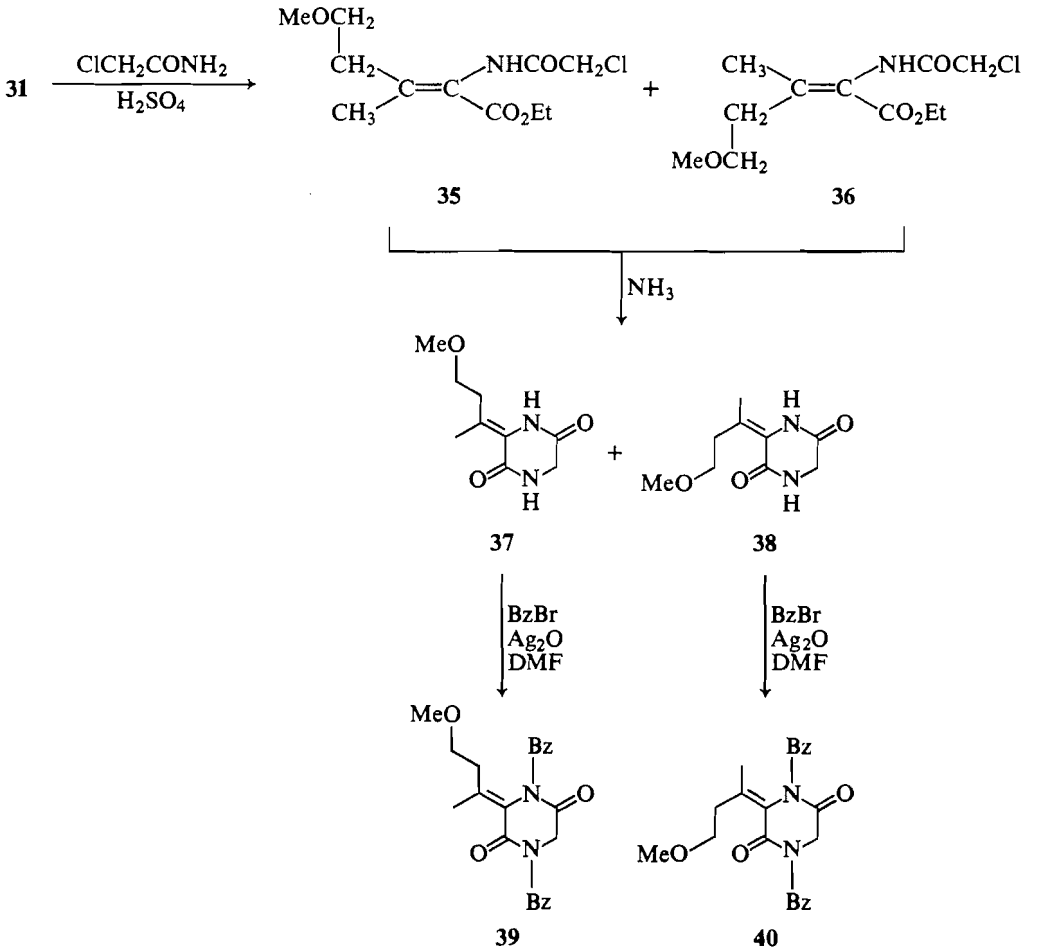

SCHEME 9

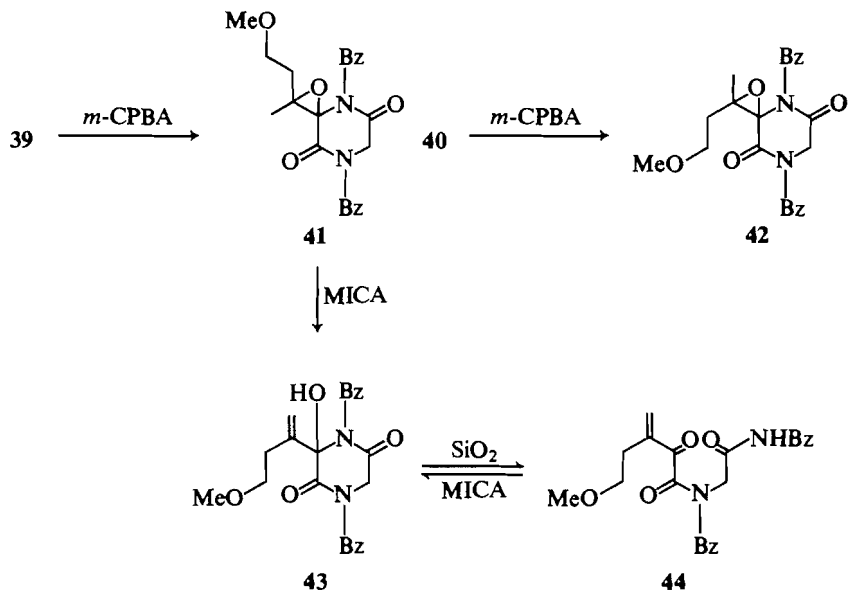

SCHEME 10

introduction of chiral centres in going from **39** and **40** to **41** and **42** resulted in the appearance of the benzylic and ring methylene proton signals in the ^{1}H nmr spectra as AB systems rather than singlets. Treatment of **41** with MICA opened the epoxide ring to give the desired allylic alcohol **43** (this reaction was not investigated with the *E* isomer **42**). Attempted purification of **43** by chromatography on silica returned a 1:1 mixture of **43** and its acyclic isomer **44**, which we had previously indepen-

Can. J. Chem. Downloaded from www.nrcresearchpress.com by 210.87.254.5 on 09/06/12
For personal use only.

Can. J. Chem. Downloaded from www.nrcresearchpress.com by 210.87.254.5 on 09/06/12
For personal use only.

dently synthesized as a key intermediate in our route to **43** via acyclic intermediates (2). The fact that the crude product from the treatment of **41** with MICA was obtained as the cyclic isomer **43** led us to investigate the reaction of MICA with the acyclic isomer **44**. We were happy to find that this reagent brought about efficient closure of **44** to **43**, a transformation that had hitherto eluded us despite the application of a variety of other reagents (2). We consider that the efficacy of MICA relates to the ability of magnesium in the magnesio derivative of **44** to coordinate efficiently with the oxygen atom of the ketonic carbonyl group, thus facilitating attack by nitrogen at the carbon atom of that group.

Of the two routes to the piperazine-2,5-dione **43**, we chose subsequently to use the acyclic route since the MICA reaction with the acyclic intermediate **44** gave a cleaner product than it did with the cyclic epoxide intermediate **42**. We have therefore described our further investigations of piperazine-2,5-diones related to **43** in connection with our discussion of its synthesis by the acyclic route (2).

Experimental

Melting points were determined on a Fisher–Johns apparatus and are uncorrected. Unless otherwise specified, the ir spectra were recorded for $CHCl_3$ solutions and the ^1H and ^{13}C nmr spectra for $CDCl_3$ solutions. Mass spectra were recorded at 70 eV and peak positions (*m/e*) are followed by relative abundances in parentheses. Chromatographic separations were carried out by liquid column chromatography except where otherwise indicated. All R_f values were determined on analytical thin-layer chromatographic silica gel plates. Preparative thin-layer chromatography was carried out on 20 × 20 × 1-mm or 20 × 20 × 2-mm silica gel plates containing a fluorescent indicator. The bands were extracted with methanol and the residue obtained after filtration and evaporation was triturated with chloroform or dichloromethane; filtration and evaporation yielded the product; iodine or uv visualization was employed. Apparatus for the experiments that were carried out under nitrogen was flame dried immediately prior to use under a dry nitrogen flow. All organic extracts were dried over anhydrous $MgSO_4$ and evaporated by means of a rotary evaporator at water aspirator pressure.

*Ethyl 3-methyl-2-oxobutanoate (**15**)*

A solution of *p*-toluenesulfonic acid (prepared from the monohydrate predried in benzene by azeotropic removal of water; 5.4 g, 28 mmol *p*-TSA) and ethyl 3,3-dimethylglycidate (**16**) (2) in benzene (100 mL) was boiled under reflux for 4 h. The benzene solution was washed with water (10 mL), dried, filtered, and concentrated giving an 86% yield of crude ethyl 2-hydroxy-3-methyl-3-butenoate (**17**).

Compound **17** (71.62 g, 0.497 mol) was reduced quantitatively to ethyl 2-hydroxy-3-methylbutanoate (**18**) by catalytic hydrogenation over 5% Pd/C (100 mg) in ethanol at a pressure of 50 psi.

The alcohol **18** (24.0 g, 0.169 mol) in acetone (200 mL) was stirred in an ice bath while Jones reagent (CrO_3 (16.5 g), H_2SO_4 (14 mL), H_2O (40 mL)) was added dropwise with stirring. After addition of the reagent was complete, the ice bath was removed and stirring was continued for 30 min at room temperature. The acetone solution was decanted from the deposited chromium salts, which were washed well with methylene chloride. The combined acetone solution and methylene chloride washings were dried, filtered, and concentrated giving a quantitative yield of **15**.

*4,7-Dibenzyl-2,2-dimethyl-1-oxa-4,7-diazaspiro[2.5]octane-5,8-dione (**10**)*

3-Isopropylidenepiperazine-2,5-dione (**8**) was found to be best prepared by condensation of **15** (7.21 g, 50 mmol) with 2-chlorocetamide (9.35 g, 100 mmol) in benzene (50 mL) containing conc. H_2SO_4 (1 mL) (5). This solution was boiled under reflux for 18 h with azeotropic removal of the water formed. This gave a 70% yield of ethyl 2-[(chloroacetyl)amino]-3-methyl-2-butenoate (**13**), which was cyclized in 90% yield to **8** by treatment with saturated ethanolic ammonia (5).

A solution of **8** (2.00 g, 13 mmol) in dry dimethylformamide (12 mL) was added dropwise with stirring to a suspension of sodium hydride (50% oil dispersion; 1.24 g, 26 mmol) in benzene (15 mL) and benzyl bromide (5.56 g, 32.5 mmol) under nitrogen. The mixture was stirred overnight at room temperature and poured into water (10 mL). The benzene layer was separated and washed with water (3 × 10 mL), dried, filtered, and concentrated. The residue was chromatographed on silica with 1:1 ethyl acetate – hexanes as eluent. The band with R_f = 0.35 was found to give 1,4-dibenzyl-3-isopropylidene-2,5-piperazinedione (**9**) (2.52 g, 58%); ir λ_{max}: 5.90, 6.04 μm; ^1H nmr δ: 6.9–7.4 (m, 10H), 4.72 (s, 2H), 4.55 (s, 2H), 3.72 (s, 2H), 2.15 (s, 3H), 1.90 (s, 3H).

A solution of **9** (1.63 g, 4.87 mmol) and 85% *m*-chloroperoxybenzoic acid (2.00 g, 9.9 mmol) in methylene chloride (90 mL) was boiled under reflux for 20 h. The mixture was washed with aqueous saturated Na_2SO_3 (20 mL) and aqueous 10% $NaHCO_3$ (20 mL) and dried, filtered, and concentrated. The residual oil crystallized on standing and the product was recrystallized from ether to give **10** (1.54 g, 90%) as white feathery crystals, mp 122–123°C; ir λ_{max}: 5.90 μm; ^1H nmr δ: 6.9–7.4 (m, 10H), 4.91 (d, *J* = 15 Hz, 1H), 4.16 (d, *J* = 15 Hz, 1H), 4.71 (d, *J* = 15 Hz, 1H), 4.46 (d, *J* = 15 Hz, 1H), 3.88 (d, *J* = 17 Hz, 1H), 3.75 (d, *J* = 17 Hz, 1H), 1.43 (s, 3H), 1.33 (s, 3H); ^{13}C nmr δ: 166.0 (s), 163.8 (s), 136.9 (s), 135.4 (s), 129.0–127.7 (d), 73.6 (s), 65.3 (s), 50.3 (t), 49.6 (t), 45.0 (t), 19.2 (q), 18.3 (q); *m/e*: 350(6), 259(20), 201(13), 91(100). *Anal.* calcd. for $C_{21}H_{22}N_2O_3$: C 71.98, H 6.33, N 7.99; found: C 71.59, H 6.30, N 8.00.

*Reaction of **10** with acetic anhydride and sulfuric acid. Formation of 3-acetoxy-3-(1-acetoxy-1-methylethyl)-1,4-dibenzylpiperazine-2,5-dione (**19**)*

Compound **10** (253 mg, 0.722 mmol) was dissolved in acetic anhydride (7 mL) and 3 drops of conc. H_2SO_4 were added. The mixture was stirred for 20 min at room temperature and added to benzene (30 mL) and the benzene solution was washed with water (5 × 10 mL). It was then dried, filtered, and concentrated. The residue was dissolved in methylene chloride and hexanes were added dropwise to effect crystallization of **19** (174 mg, 53%); ir λ_{max}: 5.73, 5.95 μm; ^1H nmr δ: 7.13 (m, 10H), 4.00–5.30 (m, 6H), 1.93 (s, 3H), 1.75 (s, 3H), 1.73 (s, 3H), 1.57 (s, 3H).

*Reaction of **10** with p-toluenesulfonic acid. Formation of 1,4-dibenzyl-3-hydroxy-3-(1-hydroxy-1-methylethyl)piperazine-2,5-dione (**20**) and 1,4-dibenzyl-3-hydroxy-3-(1-p-toluenesulfonoxy-1-methylethyl)piperazine-2,5-dione (**21**)*

A solution of *p*-toluenesulfonic acid (prepared from the hydrate, dried in benzene by azeotropic removal of water; 178 mg, 0.936 mmol) and **10** (252 mg, 0.719 mmol) in benzene was stirred at room temperature for 10 min, washed with water (2 mL), dried, filtered, and concentrated. The residue was found to contain a 1:1 mixture of diol **20** and tosylate **21**, as indicated by its ^1H nmr spectrum. It was dissolved in ether and **20** crystallized (60 mg). Concentration of the mother liquor led to the crystallization of **21** (130 mg), leaving a mother liquor containing **21** contaminated with **20**. Diol **20**, mp 182–185°C; ir λ_{max}: 2.98, 5.98 μm; ^{1} nmr δ (acetone-d_6): 7.18 (m, 10H, 3.4–5.1 (m, 6H), 2.07 (m, 2H), 1.33 (s, 3H), 1.27 (s, 3H); *m/e*: 368(6), 310(9), 282(9), 219(8), 149(20), 91(100). Tosylate **21**, mp 174–175°C; ir λ_{max}: 2.93, 2.95 μm; ^1H nmr δ: 7.30 (m, 14H), 5.28 (s, 1H), 4.78 (d, *J* = 15 Hz, 1H), 4.71 (d, *J* = 15 Hz, 1H), 4.42 (d, *J* = 15 Hz, 2H), 3.87 (d, *J* = 18 Hz, 1H), 3.54 (d, *J* = 18 Hz, 1H), 2.40 (s, 3H) 1.70 (s, 3H), 1.60 (s, 3H).

*Reaction of **21** with DBU. Formation of **10***

The tosylate **21** (33 mg, 0.063 mmol) and 1,8-diazabicyclo[5.4.0]-undec-7-ene (DBU) (10 mg, 0.066 mmol) in methylene chloride (5 mL) were stirred at room temperature overnight. The mixture was washed with 3 *M* hydrochloric acid (2 mL), dried, filtered, and concentrated. A quantitative yield of epoxide **10** was obtained.

Can. J. Chem. Downloaded from www.nrcresearchpress.com by 210.87.254.5 on 09/06/12
For personal use only.

*Reaction of **10** with acetyl* p-*toluenesulfonate and acetonitrile. Formation of 6,9-dibenzyl-2,4,4-trimethyl-1-oxa-3,6,9-triazaspiro[4.5]dec-2-ene-7,10-dione (**22**)*

A solution of **10** (223 mg, 0.629 mmol) and acetyl *p*-toluenesulfonate (9) (194 mg, 0.906 mmol) in acetonitrile (5 mL) was stirred at room temperature for 1 h. The mixture was dissolved in methylene chloride (25 mL) and the solution was washed with water (10 mL), aqueous 10% $NaHCO_3$ (10 mL), and saturated aqueous NaCl (10 mL), dried, filtered, and concentrated. The residue was chromatographed on a preparative silica gel plate with 20% ethyl acetate–hexanes (R_f = 0.40) as eluent. This gave 61 mg of an orange oil considered to be crude **22**; ir λ_{max}: 6.00 μm; ^{1}H nmr δ: 7.2–7.3 (m, 10H), 3.6–5.0 (m, 6H), 2.13 (s, 3H), 1.33 (s, 3H), 1.27 (s, 3H); *m/e*: 391, 334(26), 243(40), 91(100).

*1,4-Dibenzyl-3-hydroxy-3-(1-methylethenyl)piperazine-2,5-dione (**23**) and 1,4-dibenzyl-3-(1-bromo-1-methylethyl)-3-hydroxypiperazine-2,5-dione (**24**)*

A solution of magnesium isopropylcyclohexylamide (MICA) (10) was prepared by syringing neat cold methyl bromide into a mixture of magnesium turnings (50 mg, 2.1 mmol) and dry tetrahydrofuran (4 mL) under nitrogen with stirring and mild warming until all of the magnesium was consumed. Additional tetrahydrofuran (7 mL) was added and excess isopropylyclohexylamine (0.5 mL) was syringed into the methylmagnesium bromide – tetrahydrofuran solution with stirring to form MICA after the solution had been stirred at room temperature for 20 min.

A solution of **10** (184 mg, 0.525 mmol) in dry tetrahydrofuran (4 mL) was syringed dropwise with stirring over a period of 1 h into the MICA solution under nitrogen at room temperature. The mixture was stirred overnight at room temperature during which time it assumed a cloudy yellow color. The solution was cooled in an ice bath and 4 *N* hydrochloric acid (3 mL) was added with stirring. The acidified mixture was extracted with methylene chloride (3 × 20 mL). The combined extracts were dried, filtered, and concentrated. The residual gum was dissolved in ether (~5 mL) and **23** crystallized in 40–50% yield. Compound **23** crystallized from chloroform–hexanes as white needles, mp 147–148°C; ir λ_{max}: 2.85, 5.95 μm; ^{1}H nmr δ: 6.9–7.4 (m, 10H), 5.03 (m, 2H), 4.88 (s, 1H), 4.88 (dd, *J* = 15 Hz, 1H), 4.81 (d, *J* = 14 Hz, 1H), 4.34 (d, *J* = 14 Hz, 2H), 3.83 (s, 2H), 1.75 (s, 3H); *m/e*: 350(1), 333(1), 309(2), 281(4), 253(17), 91(100). *Anal.* calcd. for $C_{21}H_{22}N_2O_3$: C 71.98, H 6.33, N 7.99; found: C 71.92, H 6.38, N 8.00.

The mother liquor from the original crystallization of **23** yielded impure **24** as a gum which resisted crystallization; ir λ_{max}: 2.95, 5.93 μm; ^{1}H nmr δ: 7.20 (m, 10H), 3.50–5.23 (m, 7H), 1.88 (s, 6H). This was reconverted to epoxide **10** on treatment with excess DBU (5 equiv.) in methylene chloride.

*Reaction of 4-methoxy-2-butanone (**25**) with methyl nitroacetate. Formation of methyl 2-nitro-5-oxohexanoate (**27**)*

A solution of **25** (11) (2.14 g, 21.0 mol), methyl nitroacetate (15) (2.54 g, 21.3 mmol), and ammonium acetate (1.81 g, 23.5 mmol) in benzene or methanol (75 mL) was boiled under reflux for 2h. In the case of methanol, the methanolic solution was added to methylene chloride (75 mL) and the methylene chloride solution was washed with water (3 × 20 mL), dried, filtered, and concentrated. In the benzene case, the benzene solution was washed with water (3 × 20 mL), dried, filtered, and concentrated. In either case the residue was molecularly distilled at 100°C (0.015 Torr) to give **27** (2.89 g, 73%); ir λ_{max}: 5.53, 5.82 μm; ^{1}H nmr δ: 5.22 (n, 1H), 3.85 (s, 3H), 2.2–2.8 (m, 4H), 2.18 (s, 3H).

*Ethyl 5-methoxy-3-methyl-2-oxopentanoate (**31**)*

A solution of ethyl 3-(2-methoxyethyl)-3-methyglycidate (**28**) (2) (100 g, 0.531 mol) and *p*-toluenesulfonic acid (prepared from the hydrate, dried in benzene by azeotropic removal of water; 3.5 g, 18 mmol) in benzene (100 mL) was boiled under reflux for 5 h, during which time the solution assumed a dark red-brown color. The solution was washed with water (20 mL), dried, filtered, and concentrated and the residue was distilled at 75–85°C (0.025 Torr). The distillate (75 g) contained a 3:1 mixture of ethyl 2-hydroxy-3-(2-methoxyethyl)-3-butenoate (**29**) and ethyl 2-hydroxy-5-methoxy-3-methyl-3-pentenoate (**30**) and a small amount of α-oxo ester **31** as indicated by its ^{1}H nmr spectrum.

This mixture (73 g, 0.39 mol) in ethanol (150 mL) was hydrogenated over PtO_2 (100 mg) in a Parr hydrogenation apparatus at 50 psi pressure of hydrogen. The catalyst was filtered and the filtrate was concentrated to give a 2:1 mixture of ethyl 2-hydroxy-5-methoxy-3-methylpentanoate (**32**) and ethyl 2-hydroxy-3-methylpentanoate (**33**), as indicated by ^{1}H nmr spectroscopy. (The use of 5% Pd/C as catalyst gave a 1:2 mixture of **32** and **33**.) The mixture was used without separation in the next step.

The mixture of **32** and **33** (70 g) in acetone (500 mL) was oxidized with Jones reagent (CrO_3 (29.8 g), conc. H_2SO_4 (25 mL), water (72 mL)) in analogous fashion to the preparation of **15**. The crude product was fractionally distilled through an 8-in. column packed with glass helices. Ethyl methyl-2-oxopentanoate (**34**) (15.8 g) distilled at 0–31°C (0.015 Torr) followed by ethyl 5-methoxy-3-methyl-2-oxopentanoate (**31**) (47.5 g, 68%), bp 55–57°C (0.015 Torr); ir λ_{max}: 5.80 μm; ^{1}H nmr δ: 4.37 (q, *J* = 7 Hz, 2H), 3.40 (m, 2H), 3.23 (s, 3H), 1.87 (m, 3H), 1.33 (t, *J* = 7 Hz, 3H), 1.12 (d, *J* = 7 Hz, 3H); *m/e*: 189, 188, 157(2), 129(8), 115(100), 101(10). *Anal.* calcd. for $C_9H_{16}O_4$: C 57.43, H 8.57; found: C 57.36, H 8.55.

(Z)- *and* (E)-*3-(4-Methoxybut-2-ylidene)piperazine-2,5-dione (**37** and **38**)*

A solution of compound **31** (51.0 g, 0.270 mol) and chloroacetamide (37.0 g, 0.400 mol) in benzene (325 mL) and conc. H_2SO_4 (5.5 mL) was boiled under reflux for 10 h with azeotropic removal of water by means of a Dean–Stark apparatus. The benzene solution was washed well with water, dried, filtered, and concentrated. Unconsumed **31** (19.4 g) was distilled from the residue at 55°C (0.015 Torr) leaving a 3:1 mixture (44.3 g, 62%) of ethyl (*Z*)- and (*E*)-2-[(chloroacetyl)amino]-5-methoxy-3-methyl-2-pentenoate (**35** and **36**) as indicated by its ^{1}H nmr spectrum: δ: 9.17 (br s, 0.7H), 8.00 (br s, 0.3H), 4.13 (m, 4H), 3.53 (m, 5H), 2.80 (t, *J* = 6 Hz, 0.5H), 2.37 (t, *J* = 6 Hz, 1.5H), 2.05 (s, 2H), 1.87 (s, 1H), 1.10 (t, *J* = 7 Hz, 3H).

A solution of this mixture of **35** and **36** (60.0 g, 0.228 mol) in cold saturated alcoholic ammonia (500 mL) was stirred for 2 days at room temperature. The ethanolic solution was concentrated and the residue was dissolved in 2 *N* hydrochloric acid (50 mL). The aqueous solution was extracted several times with methylene chloride (10 × 25 mL). The combined methylene chloride extracts were dried, filtered, and concentrated, leaving a white solid (27.5 g, 61%). The solid was dissolved in chloroform and **38** crystallized as a white solid. The mother liquor contained a mixture of **37** and **38**, which could not be further purified by crystallization. The mixture was chromatographed on silica with 5% methanol – chloroform as eluent. The *Z* isomer **37** (R_f = 0.43) (20.4 g, 45%) was thus separated from the *E* isomer **38** (R_f = 0.24) (3.05 g; total 6.49 g, 14%).

Compound **37** was recrystallized from acetone as white needles, mp 157–158°C; ir λ_{max}: 2.89, 5.91 μm, ^{1}H nmr δ: 8.85 (br s, 1H), 7.23 (br s, 1H), 3.93 (m, 2H), 3.55 (t, *J* = 6 Hz, 2H), 3.37 (s, 3H), 1.90 (t, *J* = 6 Hz, 2H), 2.27 (s, 3H); *m/e*: 198(19), 166(100), 153(24), 138(9), 125(14), 45(65). *Anal.* calcd. for $C_9H_{14}N_2O_3$: C 54.54, H 7.12, N 14.13; found: C 54.72, H 7.16, N 14.10.

Compound **38** was recrystallized from dimethylformamide as white needles, mp 211–212°C; ir λ_{max}: 3.90, 5.91 μm; ^{1}H nmr δ(DMSO-d_6): 9.05 (br s, 1H), 7.80 (br s, 1H), 3.73 (m, 2H), 3.38 (t, *J* = 6 Hz, 2H), 3.20 (s, 3H), 2.78 (t, *J* = 6 Hz, 2H), 1.62 (s, 3H); *m/e*: 198(6), 166(100), 153(20), 138(6), 125(9), 45(35). *Anal.* calcd. for $C_9H_{14}N_2O_3$: C 54.54, H 7.12, N 14.13; found: C 54.51, H 7.18, N 14.16.

*(Z)-1,4-Dibenzyl-3-(4-methoxybut-2-ylidene)piperazine-2,5-dione (**39**)*

A solution of **37** (1.00 g, 5.04 mmol), silver oxide (1.75 g, 7.57 mmol), and benzyl bromide (6.90 g, 40.4 mmol) in dimethyl-

formamide (40 mL) was stirred at room temperature for 8 h. Benzene (100 mL) was added and the solution was filtered through Celite to remove the silver salts. The filtrate was washed with water (3 × 25 mL), dried, filtered, and concentrated. Excess benzyl bromide was removed by molecular distillation at 90°C (0.015 Torr). This residue was chromatographed on silica with 20% ethyl acetate – chloroform as eluent. Compound **39** was eluted (R_f = 0.49) as a yellow gum (578 mg, 30%); ir λ_{max}: 5.78 (sh), 5.96, 6.09 (sh) μm; ^{1}H nmr δ: 7.20 (m, 10H), 4.78 (s, 2H), 4.47 (s, 2H), 3.67 (s, 2H), 3.57 (t, J = 6 Hz, 2H), 3.30 (s, 3H), 2.48 (t, J = 6 Hz, 2H), 2.13 (s, 3H); *m/e*: 378(7), 347(9), 256(33), 91(100). *Acurate Mass* calcd. for $C_{23}H_{26}N_2O_3$: 378.1943; found: 378.1940.

From later chromatographic fractions an *N*-benzyl-3-(4-methoxybut-2-ylidene)piperazine-2,5-dione (R_f = 0.25) (233 mg) was obtained. This was recrystallized from chloroform–hexanes as white needles, mp 88–89°C; ir λ_{max}: 2.91, 5.95 μm; ^{1}H nmr δ: 7.27 (s, 5H), 7.08 (br s, 1H), 5.15 (s, 2H), 4.02 (s, 2H), 3.42 (t, J = 6 Hz, 2H), 3.30 (s, 3H), 2.72 (t, J = 6 Hz, 2H), 2.28 (s, 3H); *m/e*: 288(13), 256(6), 197(35), 165(34), 137(11), 91(100). *Anal.* calcd. for $C_{16}H_{20}N_2O_3$: C 66.55, H 6.99, N 9.71; found: C 66.35, H 6.98, N 9.70.

The above reaction was repeated for 6 h at room temperature. A 39% yield of **39** was obtained after chromatographic separation from uncharacterized polybenzylated products with higher R_f values.

(E)-*1,4-Dibenzyl-3-(4-methoxybut-2-ylidene)piperazine-2,5-dione* (***40***)

A solution of **38** (3.51 g, 17.2 mmol), silver oxide (6.0 g, 26 mmol), and benzyl bromide (24.5 g, 143 mmol) in dimethylformamide (100 mL) was stirred at room temperature for 15 h and worked up as in the preparation of the *Z* isomer **39**. The residue was chromatographed on silica with 20% ethyl acetate – chloroform as eluent. After elution of polybenzylated material of higher R_f, **40** was eluted (R_f = 0.40) as a yellow gum (2.38 g, 37%); ir λ_{max}: 5.93, 6.01 (sh), 6.08 (sh) μm; ^{1}H nmr δ: 7.18 (m, 10H), 4.70 (s, 2H), 4.50 (s, 2H), 3.40 (s, 2H), 3.48 (t, J = 6 Hz, 2H), 3.30 (s, 3H), 2.93 (t, J = 6 Hz, 2H), 1.80 (s, 3H); *m/e*: 378(8), 347(9), 256(31), 91(100). *Accurate Mass* calcd. for $C_{23}H_{26}N_2O_3$: 378.1943; found: 378.1956.

Stripping of the chromatographic column with methanol gave an *N*-benzyl-3-(4-methoxy-2-ylidene)-piperazine-2,5-dione (R_f = 0.08) (248 mg, 5%) as an orange gum which resisted crystallization; ir λ_{max}: 2.93, 5.98 μm; ^{1}H nmr δ: 7.28 (s, 5H), 7.25 (br s, 1H), 5.18 (s, 2H), 4.00 (s, 2H), 3.53 (t, J = 6 Hz, 2H), 3.32 (s, 3H), 3.03 (t, J = 6 Hz, 2H), 2.07 (s, 3H).

(Z)-*4,7-Dibenzyl-2-(2-methoxyethyl)-2-methyl-1-oxa-4,7-diazaspiro[2.5]octane-5,8-dione* (***41***)

A solution of compound **39** (4.76 g, 12.6 mol) and 85% *m*-chloroperoxybenzoic acid (5.25 g, 25.8 mmol) in methylene chloride (225 mL) was boiled under reflux for 18 h. The mixture was washed with saturated aqueous Na_2SO_3(50 mL), water (50 mL), and aqueous 10% $NaHCO_3$ (50 mL), dried, filtered, and concentrated. The residual oil was dissolved in ether and the epoxide **41** crystallized as a white solid (4.49 g, 91%). It was recrystallized from chloroform–cyclohexane as white cubes, mp 148–149°C; ir λ_{max}: 5.91 μm; ^{1}H nmr δ: 7.25 (m, 10H), 3.70–5.02 (3 ABdd, 6H), 3.43 (m, 2H), 3.20 (s, 3H), 1.80 (m, 2H), 1.45 (3, 3H); *m/e*: 394(16), 303(12), 272(6), 219(15), 201(18), 131(12), 91(100). *Anal.* calcd. for $C_{23}H_{26}N_2O_4$: C 70.03, H 6.64, N 7.10; found: C 70.00, H 6.68, N 7.11.

(E)-*4,7-Dibenzyl-2-(2-methoxyethyl)-2-methyl-1-oxa-4,7-diazaspiro[2.5]octane-5,8-dione* (***42***)

The epoxidation of **40** (2.38 g, 6.26 mmol) with 85% *m*-chloroperoxybenzoic acid (3.00 g, 14.8 mmol) in methylene chloride (125 mL) was carried out analogously to the epoxidation of **39**, giving the *E* epoxide **42** (2.05 g, 83%), which was recrystallized from ether as white feathery needles, mp 112–113°C; ir λ_{max}: 5.93 μm; ^{1}H nmr δ: 7.30 (m, 10H), 3.75–5.05 (3 ABdd, 6H), 3.38 (m, 2H), 3.12 (s, 3H), 1.98 (m, 2H), 1.35 (s, 3H); *m/e*: 394(12), 303(5), 272(5), 256(8), 219(11), 201(15), 131(9), 91(100). *Anal.* calcd. for $C_{23}H_{26}N_2O_4$: C 70.03, H 6.64, N 7.10; found: C 69.84, H 6.60, N 7.08.

1,4-Dibenzyl-3-hydroxy-3(1-(2-methoxyethyl)ethenyl)piperazine-2,5-dione (***43***)

A solution of MICA in dry tetrahydrofuran (7 mL) was prepared as in the preparation of **23** from magnesium turnings (0.0296 g, 1.22 mmol), methyl bromide, and isopropylcyclohexylamine (0.30 mL, 1.8 mmol). Epoxide **41** (96 mg, 0.24 mmol) in dry tetrahydrofuran (2 mL) was syringed with stirring into the MICA solution under nitrogen cooled in a Dry Ice – acetone bath. After addition was complete the Dry Ice bath was replaced by an ice bath and the solution was stirred for an additional 2 h. The ice bath was removed and the mixture was stirred overnight at room temperature and poured into 2 *N* hydrochloric acid (2 mL). The acidified solution was extracted with methylene chloride (3 × 20 mL). The combined methylene chloride extracts were dried, filtered, and concentrated giving ~100 mg of crude **43** as a viscous pale yellow gum, with ir and ^{1}H nmr spectra corresponding to those of **43** prepared by treatment of *N*-benzyl-*N*-(2-benzylamino-2-oxoethyl)-3-(2-methylethyl)-2-oxo-3-butenamide (**44**) with MICA (2). It was chromatographed on a preparative silica plate with 20% ethyl acetate – chloroform as eluent. The eluted product (R_f = 0.53) was a 1:1 mixture of **43** and **44** as shown by its ^{1}H nmr spectrum.

Acknowledgement

We thank the Natural Sciences and Engineering Research Council of Canada for support of this work.

1. J. H. HOARE and P. YATES. Chem. Commun. 1126 (1981).
2. P. YATES and J. H. HOARE. Can. J. Chem **61**, 519 (1983).
3. C. SHIN, M. MASAKI, and M. OHTA. Bull. Chem. Soc. Jpn. **44**, 1657 (1971).
4. J. E. BALDWIN, S. B. HABER, C. HOSKINS, and L. I. KRUSE. J. Org. Chem. **42**, 1239 (1977).
5. C. SHIN, M. FUJII, and J. YOSHIMURA. Tetrahedron Lett. 2499 (1971).
6. A. WRETLIND. Acta Chem. Scand. **8**, 1478 (1954).
7. C. SHIN, K. SATO, A. OHTSUKA, K. MIKAMI, and J. YOSHIMURA. Bull. Chem. Soc. Jpn. **46**, 3876 (1973); C. SHIN, M. HAYAKAWA, T. SUZUKI, A. OHTSUKA, and J. YOSHIMURA. Bull. Chem. Soc. Jpn. **51**, 550 (1978).
8. M. A. TALASBAEVA, Z. A. NAVREZOVA, and A. V. SCHELKUNOV. Deposited Doc. VINITI, 244 (1976); Chem. Abstr. **88**, 74008x (1978).
9. M. H. KARGER and Y. MAZUR. J. Org. Chem. **36**, 528 (1971).
10. E. J. COREY, A. MARFAT, J. R. FALCK, and J. O. ALBRIGHT. J. Am. Chem. Soc. **102**, 1433 (1980).
11. D. E. BURKE, J. M. COOK, and P. W. LE QUESNE. J. Am. Chem. Soc. **95**, 546 (1973).
12. R. L. AUGUSTINE. Catalytic hydrogenation. Marcel Dekker Inc., New York. 1965. pp. 68, 137.
13. L. M. JACKMAN and S. STERNHELL. Applications of nuclear magnetic resonance spectroscopy in organic chemistry. 2nd ed. Pergamon Press, Oxford. 1969. p. 171.
14. A. B. MAUGER, R. B. DESAI, I. RITTNER, and W. J. RZESZOTARSKI. J. Chem. Soc. Perkin Trans. **1**, 2146 (1972).
15. S. ZEN. M. KOYAMA, and S. KOTO. Org. Synth. **55**, 77 (1976).

Can. J. Chem. Downloaded from www.nrcresearchpress.com by 210.87.254.5 on 09/06/12
For personal use only.

The monoblocking of symmetrical diketones on insoluble polymer supports[1,2]

ZHANG-HUANG XU,[3] COLIN R. MCARTHUR, AND CLIFFORD C. LEZNOFF
Department of Chemistry, York University, Downsview (Toronto), Ont., Canada M3J 1P3

Received September 1, 1982

ZHANG-HUANG XU, COLIN R. MCARTHUR, and CLIFFORD C. LEZNOFF. Can. J. Chem. **61**, 1405 (1983).

A 1% crosslinked divinylbenzene–styrene copolymer, incorporating vicinal diol groups or their isopropylidene precursors, was used to form the monoacetals of the symmetrical diketones, *p*-diacetylbenzene, 1,2-cyclohexanedione, 1,3-cyclohexanedione, 1,4-cyclohexanedione, and 2,5-hexanedione. The free ketone groups reacted with phenylmagnesium bromide to give, in high yield, after acid hydrolysis from the polymer, the expected products such as 3-phenyl-2-cyclohexen-1-one from 1,3-cyclohexanedione. The ^{13}C nmr spectra of some polymer-bound substrates and simple analogs are described.

ZHANG-HUANG XU, COLIN R. MCARTHUR et CLIFFORD C. LEZNOFF. Can. J. Chem. **61**, 1405 (1983).

On a utilisé un copolymère de divinylbenzène–styrène réticulé à 1%, incorporant un groupe diol vicinal ou son précurseur isopropylidène pour former le monoacétal des dicétones symétriques, *p*-diacétylbenzène, cyclohexanedione-1,2, cyclohexanedione-1,3, cyclohexanedione-1,4 et hexanedione-2,5. Les groupes cétone libres réagissent avec le bromure de phénylmagnésium pour donner avec un fort rendement, les produits attendus tels: la phényl-3 cyclohexen-2 one-1 à partir de la cyclohexanedione-1,3 après clivage de la résine par hydrolyse acide. On décrit les spectres de rmn du ^{13}C de quelques substrats fixés sur le polymère ainsi que ceux des analogues simples.

[Traduit par le journal]

Can. J. Chem. Downloaded from www.nrcresearchpress.com by 210.87.254.5 on 09/06/12
For personal use only.

Acetal formation of ketones represents one of the most common uses of blocking groups in organic synthesis (4). A wide variety of symmetrical diketones have the potential of being used as inexpensive starting materials in the synthesis of complex organic structures, but first it would be necessary to monoprotect *one* of the two identical ketone groups. In fact, the monoprotection of symmetrical diketones has been addressed many times. For example, 1,4-cyclohexanedione ethylene monoacetal (5, 6), other 1,4-dione monoacetals (7), and 1,3-cyclohexanedione ethylene monoacetal (8) have been prepared, but only by circuitous routes or in low yield. Although the most common synthons derived from 1,3-cyclohexanedione are 3-ethoxy-2-cyclohexen-1-one (9, 10) and the 3-halo-2-cyclohexen-1-ones (11, 12), reactions on the former have sometimes proved difficult to perform (13). Monoacetals of *aromatic* 1,2-diketones have been prepared by alkylation procedures (14), but this method cannot be generalized to include all classes of symmetrical diketones.

Insoluble polymer supports (15, 16) can be used to monoblock symmetrical diols (17, 18), aromatic dials (19–21),[4] dihydroxyaromatic compounds (22), diamines (23), and diacid chlorides (24). A solid phase resin incorporating an appropriate functional group can react with a large excess of symmetrical difunctional compound to give the monoprotected derivative, which can be removed from the excess symmetrical difunctional compound by simple filtration. This "fishhook" principle (17, 23, 25) does *not* depend on site-isolation (26) of the polymer-bound functional groups, as these groups are likely to react with only one molecule each of large excesses of the symmetrical difunctional compounds in the solution phase.

In earlier work we have used polymer-bound 1-*O*-benzyl-2,3-*O*-isopropylideneglycerol (**1**) to prepare polymer-bound 3-benzyloxypropan-1,2-diol (**2**). Subsequent use of **2** as a monoacetalization reagent of aromatic dialdehydes has been reported (19–21), but the use of **2** and related polymer-bound 1,3-diols as monoblocking agents for *symmetrical diones* either failed or exhibited low loading capacities for the diones (20).[5] We have recently shown (27) that ^{13}C nmr spectroscopy can be used to characterize polymer-bound substrates and hence we prepared (19) new samples of **1** and **2** for possible use as monoacetalization agents. The ^{13}C nmr of **1** and **2** exhibited the normal broad absorptions due to the aliphatic and aromatic carbons of the cross-linked polystyrene and, for **1**, distinct absorptions for the 2,3-*O*-isopropylideneglyceryl appendage (Table 1). Much to our surprise, the ^{13}C nmr of polymer **2** showed that polymer **2** contained a major amount of polymer **1** resulting from incomplete acid hydrolysis of **1** to **2**. Thus our early work on the use of polymer **2** for the monoacetylation of symmetrical aromatic dials involved the use of a mixture of mostly **1**, admixed with some of **2**, and hence we had done a *transacetalization* as opposed to an *acetalization*.[6] Indeed, reaction of terephthalaldehyde with **1** (instead of **2**) *or* new pure **2**, prepared by hydrolysis of **1** under more vigorous conditions (Experimental), gave us results identical to those previously reported (19). The ^{13}C nmr of pure **2** (Table 1), as prepared herein, did not exhibit the characteristic absorptions of the isopropylidene group in **1**.

The assignments of the ^{13}C absorption peaks in Table 1 are based on coupled and decoupled (Table 1) spectra of **1**, **2**, 1-*O*-benzyl-2,3-*O*-isopropylidene glycerol (**2***a*) (28), and L-1-*O*-benzylglycerol (**2***b*) (Sigma Chem. Co.) (Fig. 1). Polymers **1** and **2** exhibited low intensity peaks for C-1, medium

[1]The use of polymer supports in organic synthesis, Part XXVIII. For parts XXVII to XXV, see refs. 1–3 respectively.

[2]Presented in part at the International Symposium on Polymer Supported Reagents in Organic Chemistry, Lyons, France, June–July, 1982.

[3]Visiting Fellow, Wuhan Teacher's College, Wuhan, China, 1981–1982.

[4]A non-polystyrene based polymer has been used recently (37) in the preparation of monoblocked symmetrical aromatic dialdehydes but extensive double-binding occurred, undoubtedly due to their much higher capacities and the nature of the polymer. This polymer was not used to monoblock symmetrical diketones.

[5]At a recent symposium a report has appeared on using polymer-bound diols as blocking agents of symmetrical diones (38).

[6]Only 5–10 mg of the original samples were still available but 500 mg of sample is required for the ^{13}C nmr of these polymers and hence old polymer **2**, prepared by the old method, yielded **2** containing significant amounts of residual **1** as shown by ^{13}C nmr.

TABLE 1. ^{13}C chemical shifts of some polymer-bound substrates and their monomeric analogs

Compound	Carbon Position[a] 1	2	3[b]	4[b]	5	6, 7	Aromatic
1	73.12	70.62	74.38	66.90	108.8	26.40,25.01	Broad
2	73.56	71.78	70.87	64.21			Broad
2*a*	73.51	71.15	74.78	66.91	109.36	26.79,25.41	138.1 128.4 127.7
2*b*	73.34	71.53	70.95	63.87			137.9 128.4,127.8

[a]Aliphatic carbons numbered from the phenyl group, δ ppm with respect to TMS.
[b]^{13}C chemical shifts of glycerol, δ 62.95 and 72.30 ppm for C-1 and C-2 respectively (DMSO), and 2,3-*O*-isopropylidene glycerol (2,2-dimethyl-1,3-dioxolane-4-methanol), δ 63.11, 76.44, 66.07, 109.41 and 26.74, 26.05 ppm respectively, for the C-1 to C-7 carbons numbered from the alcohol end were used in assigning the absorption peaks.

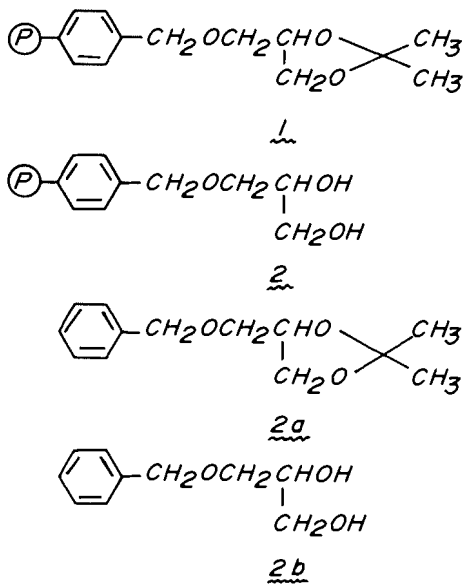

FIG. 1

intensity peaks for C-2, and sharp, high intensity peaks for other carbons, consistent with our earlier observations (27) of reduced mobility of carbons close to the polymer backbone.

Monoprotection of p-*diacetylbenzene (3) and its reaction with Grignard reagent*

Treatment of the polymer-bound isopropylidene derivative (**1**) or the polymer-bound 1,2-diol (**2**) with excess *p*-diacetylbenzene (**3**) gave the polymer-bound *p*-diacetylbenzene monoacetal (**4**) in high yield using *p*-toluenesulfonic acid and triethylorthoformate as a catalyst (29). Standard conditions (30) or the use of the boron trifluoride – ether complex (31) as catalysts afforded **4** in lower yield. The loading capacities of various preparations of **4** were determined by acid hydrolysis of **4** and recovery of the starting dione **3** (Table 2).

The infrared (ir) spectrum of **4** exhibited a characteristic carbonyl absorption at 1690 cm^{-1}. When **4** (prepared from **2**) reacted with phenylmagnesium bromide (**5**) in tetrahydrofuran (THF) polymer **6** was obtained. Polymer **6** no longer exhibited absorptions at 1690 cm^{-1} and a strong O—H absorption at 3400 cm^{-1} indicated that reaction had occurred and was essentially complete. Acid cleavage of **6** liberated 1-(4′-acetylphenyl)-1-phenylethene (**7**), the expected product in 99% yield resulting from the Grignard reaction and dehydration of the labile tertiary benzylic alcohol present in **6** (Scheme 1).

Monoprotection of 1,2-cyclohexanedione (8), 1-3-cyclohexanedione (9), and 1,4-cyclohexanedione (10) and their reactions with phenylmagnesium bromide (5)

Treatment of **1** or **2** with **8**, **9**, or **10** as above yielded the polymer-bound monoblocked acetals **11**, **12**, and **13** respectively. Polymers **11**–**13** exhibited strong absorptions at 1720 cm^{-1} supporting the assigned structures. The ^{13}C nmr spectrum of **12** exhibited a characteristic absorption at 110.7 ppm due to the quaternary carbon of the 5-membered ring acetal. This can be compared to similar absorption peaks for **1** and **2***a* (Table 1). The loading capacities of **11**–**13** prepared under various conditions were determined as for **4** above (Table 2). When the polymer-bound monacetals **12** and **13** were treated with phenylmagnesium bromide (**5**) as before, the polymer-bound tertiary alcohols **14** and **15** were obtained. The ir spectra of **14** and **15** exhibited broad peaks at 3400 cm^{-1}, typical of O—H vibrations, and the carbonyl absorptions had disappeared. Acid hydrolysis of **15** gave the expected 3-phenyl-2-cyclohexen-1-one (**16**) in 90% yield based on the amount of **9** bound to **12**. Similarly, **15** gave a mixture of 4-phenyl-3-cyclohexen-1-one (**17***a*) and 4-phenyl-2-cyclohexen-1-one (**17***b*) in 79% yield. Predictably, the acid cleavage conditions caused elimination of the tertiary alcohol groups and some isomerization to the α,β-unsaturated ketone (**17***b*) (Scheme 2).[7]

Acyclic diketones such as 2,5-hexanedione (**18**) can be monoblocked by the above methods using **2** to give the polymer-bound monacetal (**19**) (Table 2) (Fig. 2). Treatment of other ketones such as 2,3-butanedione (**20**), acetophenone (**21**), and cyclododecanone (**22**) gave the polymer-bound acetals (**23**–**25**) respectively. Only *p*-benzoquinone (**26**) proved unreactive to **2** under the standard conditions.

As shown in Table 2, a used polymer **2** showed no diminution in its capacity to prepare 3-phenyl-2-cyclohexen-1-one (**16**) (32). As mentioned recently, 4-substituted-2-cyclohexen-

[7]The high yields of the Grignard adducts show that double-binding of the symmetrical diones to the polymers is not significant at these capacities.

Can. J. Chem. Downloaded from www.nrcresearchpress.com by 210.87.254.5 on 09/06/12
For personal use only.

TABLE 2. The quantity of ketones attached to polymers **1** or **2**

Polymer	Ketone	Reaction conditions[a]	Product	Amount of bound ketone,[b] mmol/g	Ratio of dione to polymer-bound diol or acetal groups	Unreacted[d] polymer-bound diol groups, mmol/g
1	**3**	A	**4**	0.39	2.1	0.53
1	**3**	B	**4**	0.63	2.4	0.29
1	**3**	C	**4**	0.32	2.5	0.60
2	**3**	A	**4**	0.44	0.7	0.48
2	**3**	B	**4**	0.65	2.5	0.27
2	**3**	C	**4**	0.35	2.7	0.57
2	**8**	A	**11**	0.29	1.5	0.63
2	**9**	A	**12**	0.65[c]	2.3	0.27
2	**9**	A	**12**	0.65	3.1	0.27
1	**10**	B	**13**	0.45	1.9	0.47
2	**10**	A	**13**	0.39	2.5	0.53
2	**18**	A	**19**	0.42	3.5	0.50
2	**20**	A	**23**	0.72	4.7	0.20
2	**21**	A	**24**	0.66	3.1	0.26
2	**22**	A	**25**	0.19	2.3	0.73
2	**26**	A	—	—		

[a]Reaction conditions; A = *p*-toluenesulfonic acid, 80°C, 48 h; B = *p*-toluenesulfonic acid, triethylorthoformate, 80°C, 48 h; C = boron trifluoride – ether complex, room temperature, 24 h.

[b]Determined by liberation from the polymer with 4 *M* HCl at 80°C and purification by preparative tlc.

[c]This value was obtained indirectly from *used* polymer **2**. At least 0.62 mmol/g of **16** was obtained using recycled **2**. This yield is greater than using fresh **2** and hence recycled **2** shows no reduced capacity.

[d]By analysis of residual chloride in **1**, polymers **1** and **2** contain 0.92 mmol/g of vicinal diol moieties and hence the percentage of *reactive* polymer-bound diol groups can be recorded.

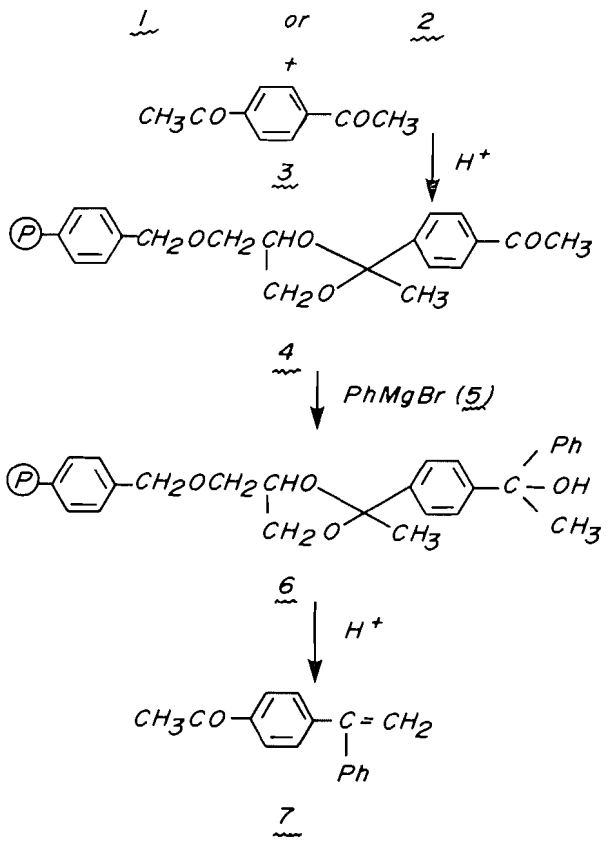

SCHEME 1

1-ones and -3-enones have great synthetic potential (33) and the procedure outlined herein represents the first general method of monoprotecting symmetrical diketones. The free ketone group can be used for synthetic elaboration in multistep synthesis of polycyclic and acyclic compounds.

Experimental

Nuclear magnetic resonance (nmr) spectra for carbon were recorded on a Varian FT-80A spectrometer at 20 MHz using deuterochloroform ($CDCl_3$) as solvent and tetramethylsilane as the internal standard. Parameters used for polymers swollen in $CDCl_3$ were similar to those previously described.[27] Mass spectra (ms) were recorded at 70 eV on a VG Micromass 16F mass spectrometer in the EI mode. Microanalyses were performed by Guelph Chemical Laboratories Ltd., Guelph, Ont. All other instrumentation and general procedures were the same as described previously (34).

Preparation of polymer-bound 1-O-benzyl-2,3-isopropylidene glycerol (1)

A Merrifield resin (Sigma Chemical Col.) containing 1.04 mmol of —CH_2Cl groups per g of resin was treated as previously described (19), except that the mixture was stirred for *48 h instead of 24 h*, to give polymer **1**. A modified Volhard analysis (35) of **1** prepared after 24 h stirring showed 0.33 mmol of residual chloride per g of polymer, while stirring for 48 h or longer resulted in analyses showing only 0.12 mmol of residual chloride. The ^{13}C nmr spectrum of **1** is described in Table 1.

Preparation of polymer-bound 3-benzyloxypropan-1,2-diol (2)

Polymer **1** was treated as previously described (19), except that the mixture of 1.5 *M* aqueous HCl in dioxane (1:1) or 1 *M* H_2SO_4 in dioxane (1:1) was stirred *at 80°C for 72 h* to give polymer **2**. Hydrolysis of the ketal group of **1** was shown to be complete by examination of the ^{13}C nmr of **2** (Table 1).

Polymer-bound p-*diacetylbenzene monoacetal (4)*

As shown in Table 2, the preparation of **4** occurred almost equally as well from polymer **1** as polymer **2** in all three methods, A, B, or C. The procedures are identical using **1** or **2** and hence we describe the preparation of **4** using **1** or **2** as representative.

Method A. Using p-*toluenesulfonic acid*

To 15.91 g of polymer **1** in 100 mL of dry benzene was added 3.07 g of *p*-diacetylbenzene (**3**), 0.20 g of *p*-toluenesulfonic acid, and 9.47 g of anhydrous sodium sulphate. The mixture was heated for 48 h at 80°C. The mixture was filtered, washed twice with pyridine, twice with pyridine–water (1:1), ten times with water, three times

Can. J. Chem. Downloaded from www.nrcresearchpress.com by 210.87.254.5 on 09/06/12
For personal use only.

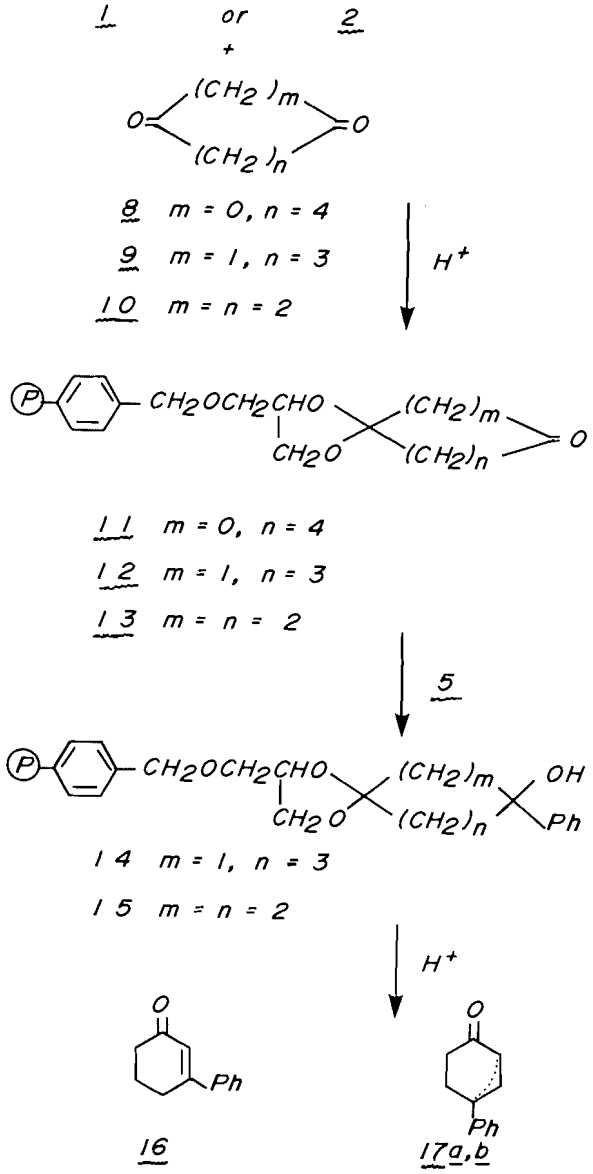

SCHEME 2

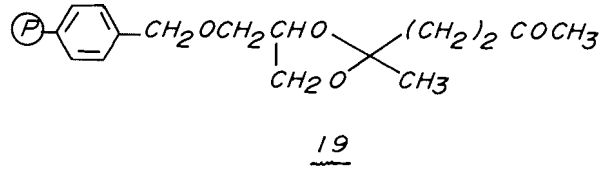

19

FIG. 2

with ethanol, and three times with dry ether, and dried under vacuum to give 16.8 g of polymer (**4**). In general, higher loadings are obtained with greater excesses of symmetrical difunctional compounds (16).

The loading capacity of polymer **4** for **3** was determined as follows. A mixture of 4.50 g of **4** in 10 mL of dioxane and 10 mL of 4 *M* aqueous HCl was stirred at 80°C for at least 48 h. The mixture was filtered and recovered **1** was washed six times with water, once with acetone, three times with ethanol, and three times with ether. The aqueous filtrate was extracted three times with ether. The combined ether extracts were dried over Na_2SO_4, filtered, and evaporated to crude **3**. Purification of **3** by column chromatography or silica yielded 0.176 g of pure **3** in the ether–hexane (1:1) fractions, showing that **4** contained at least 0.39 mmol per g of **3** (Table 2).

Method B. Using p-*toluenesulfonic acid and triethyl orthoformate*

To 2.68 g of polymer **2** in 30 mL of dry benzene was added 1.02 g of **3**, 0.12 g of *p*-toluenesulfonic acid, 0.5 mL of triethyl orthoformate, and 4.1 g of anhydrous sodium sulphate. The mixture was stirred at 80°C for 48 h and worked up as described for method A to give 2.8 g of **4**. The loading capacity (Table 2) of this polymer **4** was determined as for method A.

Method C. Use of boron trifluoride – ether complex

To 2.66 g of **2** in 30 mL of dry benzene was added 1.07 g of **3**, 1.0 mL of boron trifluoride – diethyl ether, and 3.44 g of anhydrous sodium sulphate. The mixture was stirred at room temperature for 24 h and worked up as described for method A to give 2.8 g of **4**. The loading capacity (Table 2) of this polymer **4** was determined as for method A.

The ir spectra of **4** from methods A, B, and C all showed significant C=O stretching vibrations, at 1690 cm^{-1}, of varying intensities depending on the loading capacities (Table 2).

Preparation of the polymer-bound Grignard adduct ***6***

To 6.2 g of **4** (containing 0.39 mmol of **3** per g of **4**) in 70 mL of dry THF was added 0.1 mol of phenylmagnesium bromide (**5**) in 50 mL of dry THF. The mixture was stirred at room temperature for 43 h and at 80°C for 2 h. The mixture was filtered and washed three times each with dry THF, anhydrous ethanol, and dry ether to give 7.0 g of polymer **6**. Polymer **6** showed a broad absorption band at 3400 cm^{-1} and no absorption band at 1690 cm^{-1} in the ir spectrum.

Hydrolysis of ***6*** *to give 1-(4′-acetylphenyl)-1-phenylethene (7)*

A mixture of 5.56 g of **6** in 60 mL of 4 *M* aqueous HCl in dioxane (1:1) was stirred and heated at 80°C for at least 48 h. The mixture was filtered and washed six times with water, twice with hot water, and three times each with acetone, ethanol, and ether. The aqueous filtrate was extracted three times with ether, washed twice with water, and dried over magnesium sulphate. The combined acetone and ether extracts yielded 0.8 g of a yellow oil. Column chromatography on silica gel yielded, in the 1:1 ether–hexane fractions, 0.48 g of 1-(4′-acetylphenyl)-1-phenylethene (**7**) in 99% yield based on the amount of **3** bound to **4**; mp 44–46°C; ir ($CDCl_3$): 1690, 1608, 1275; ^1H nmr δ: 2.61 (s, 3H), 5.52 (s, 2H), 7.42 (s, 5H), 7.7 (A_2B_2, q, 4H); *m/e*: (M^+) 222 (100), ($M^+ - 15$) 207 (100), 176 (82). *Anal.* calcd. for $C_{16}H_{14}O$:C 86.44, H 6.36; found: C 86.53, H 6.40.

*Preparation of polymer-bound aliphatic symmetrical dione monoacetals (****11****–****13****, ****19****, ****23****–****25****)*

The preparations of **11**–**13**, **19**, and **23**–**25** were identical to those described for **4** above by Method A and in one example by Method B (Table 2). All polymer-bound monoacetals showed strong carbonyl absorption at 1710–1730 cm^{-1} in their ir spectra. The loading capacities (Table 2) were determined as above for **4**.

Preparation of the polymer-bound Grignard adducts ***14*** *and* ***15***

Polymer-bound 1,3-cyclohexanedione monoacetal (**12**) (4.8 g), containing 0.65 mmol of **9** per g, reacted with **5** as described for **6** above to give 5.5 g of the polymer-bound adduct **14**.

Similarly, polymer-bound 1,4-cyclohexanedione monoacetal (**13**) (4.8 g), containing 0.39 mmol of **10** per g of **13**, gave 5.5 g of the polymer-bound adduct **15**.

Hydrolysis of ***14*** *to give 3-phenyl-2-cyclohexen-1-one*

A mixture of 4.8 g of **12** was hydrolyzed as described above in the preparation of **7** to give a yellow oil. Chromatography on silica gel using hexane–ether (1:1) gave, in 90% yield, 0.51 g of 3-phenyl-2-cyclohexen-1-one (**16**); mp 62–63°C (lit. (32) mp 64°C); ir: 1668, 1610, 775; ^1H nmr δ: 1.7–2.8 (m, 6H), 6.28 (s, 1H), 7.32 (m, 5H); *m/e*: (M^+) 172 (56), 144 (100), 115 (58).

Hydrolysis of ***15*** *to give a mixture of 4-phenyl-3-cyclohexen-1-one (****17****a) and 4-phenyl-2-cyclohexen-1-one (****17****b)*

A mixture of 4.8 g of **13** was hydrolyzed as above for the preparation of **7** to give a yellow oil. Purification as for **16** gave, in 79% yield, 0.35 g of a mixture of 4-phenyl-3-cyclohexen-1-one (**17***a*) and 4-phenyl-2-cyclohexen-1-one (**17***b*) (36); ir: 1720, 1690. Vapor phase

Can. J. Chem. Downloaded from www.nrcresearchpress.com by 210.87.254.5 on 09/06/12
For personal use only.

chromatography – mass spectroscopy of the mixture of **17***a* and **17***b* exhibited only two peaks in the ratio of 42:58. The mass spectra of the two peaks were consistent with the assigned structures, the first eluting peak showing *m/e* at (M^+) 172 (62), 144 (20), 130 (100), 129 (48), 115 (55) and the latter at (M^+) 172 (65), 130 (100), 129 (66), 115 (45).

Acknowledgements

We thank the Natural Sciences and Engineering Research Council of Canada for financial support of this reasearch. We thank Mr. David J. C. Howarth of York University for providing us with a sample of **2***a*.

1. T. W. HALL, S. GREENBERG, C. R. MCARTHUR, B. KHOUW, and C. C. LEZNOFF. Nouv. J. Chim. **6**, 653 (1982).
2. C. R. MCARTHUR, J.-L. JIANG, and C. C. LEZNOFF. Can. J. Chem. **60**, 2984 (1982).
3. C. R. MCARTHUR, P. WORSTER, J.-L. JIANG, and C. C. LEZNOFF. Can. J. Chem. **60**, 1836 (1982).
4. H. J. E. LOEWENTHAL. *In* Protective groups in organic chemistry. *Edited by* J. F. W. McOmie. Plenum Press, New York. 1973. pp. 373–407; T. W. GREENE. Protective groups in organic synthesis. John Wiley & Sons, New York. 1981. pp. 114–151.
5. M. HASLANGER and R. G. LAWTON. Synth. Commun. **4**, 155 (1974).
6. N. J. LEONARD, L. A. MILLER, and J. W. BERRY. J. Am. Chem. Soc. **79**, 1485 (1957); P. D. GARDNER, G. R. HAMMES, and R. L. BRANDON. J. Org. Chem. **22**, 1206 (1957); D. A. PRINS. Helv. Chim. Acta, **40**, 1621 (1957).
7. J.-L. MOREAU, R. COUFFIGNAL, and R. AROUS-CHTARA. Tetrahedron, **37**, 302 (1981); E. PIERS and B. ABEYSEKERA. Can. J. Chem. **60**, 1114 (1982); A. H. REES. J. Chem. Soc. 3097 (1962).
8. S. JAYARAMAN, R. TARA, K. NARASIMHAN, and S. SWAMINATHAN. Ind. J. Chem. Sect. B, **20**, 800 (1981).
9. W. F. GANNON and H. O. HOUSE. *In* Organic synthesis. Coll. Vol. **V**. Wiley, New York. 1973. p. 539.
10. A. B. SMITH III and P. J. JERRIS. J. Org. Chem. **47**, 1845 (1982).
11. R. D. CLARK and C. H. HEATHCOCK. J. Org. Chem. **38**, 3658 (1973).
12. E. PIERS, K. F. CHENG, and I. NAGAKURA. Can. J. Chem. **60**, 1256 (1982); E. PIERS, J. R. GRIERSON, C. K. LAN, and I. NAGAKURA. Can. J. Chem. **60**, 210 (1982).
13. T. R. HOYE, S. J. MARTIN, and D. R. PECK. J. Org. Chem. **47**, 331 (1982).
14. W. KUESTERS and L. THIL. Chem. Abstr. **88**, 22398e (1978); W. KUESTERS, M. JACOBI, and R. OSTERLOH. Chem. Abstr. **88**, 22399f (1978).
15. N. K. MATHUR, C. K. NARANG, and R. E. WILLIAMS. Polymers as aids in organic chemistry. Academic Press, New York. 1980; J. M. J. FRÉCHET. Tetrahedron, **37**, 663 (1981); A. AKELAH and D. C. SHERRINGTON. Chem. Rev. **81**, 557 (1981).
16. C. C. LEZNOFF. Acc. Chem. Res. **11**, 327 (1978).
17. C. C. LEZNOFF and J. Y. WONG. Can. J. Chem. **50**, 2892 (1972); J. Y. WONG and C. C. LEZNOFF. Can. J. Chem. **51**, 2452 (1973).
18. J. M. J. FRÉCHET and L. J. NUYENS. Can. J. Chem. **54**, 926 (1976); T. M. FYLES and C. C. LEZNOFF. Can. J. Chem. **54**, 935 (1976).
19. C. C. LEZNOFF and J. Y. WONG. Can. J. Chem. **51**, 3756 (1973).
20. C. C. LEZNOFF and S. GREENBERG. Can. J. Chem. **54**, 3824 (1976).
21. C. C. LEZNOFF and W. SYWANYK. J. Org. Chem. **41**, 3203 (1977).
22. C. C. LEZNOFF and D. M. DIXIT. Can. J. Chem. **55**, 3351 (1977).
23. C. C. LEZNOFF and D. M. DIXIT. J. Chem. Soc. Chem. Commun. 798 (1977); D. M. DIXIT and C. C. LEZNOFF. Isr. J. Chem. **17**, 248 (1978).
24. C. C. LEZNOFF and J. M. GOLDWASSER. Tetrahedron Lett. 1875 (1977); J. M. GOLDWASSER and C. C. LEZNOFF. Can. J. Chem. **56**, 1562 (1978).
25. I. T. HARRISON and S. HARRISON. J. Am. Chem. Soc. **89**, 5723 (1967).
26. J. I. CROWLEY and H. RAPOPORT. Acc. Chem. Res. **9**, 135 (1976).
27. A. J. JONES, C. C. LEZNOFF, and P. I. SVIRSKAYA. Org. Magn. Reson. **18**, 236 (1982).
28. B. T. GOLDING and P. V. IOANNOU. Synthesis, 423 (1977).
29. M. DELEPINE. Bull. Soc. Chim. **25**, 580 (1901); A. MARQUET and J. JACQUES. Bull. Soc. Chim. Fr. 1822 (1961); E. VOGEL and M. SCHINZ. Helv. Chim. Acta, **33**, 116 (1950).
30. E. J. SALUI. Chem. Ber. **71**, 1803 (1938).
31. L. F. FIESER and R. STEVENSON. J. Am. Chem. Soc. **76**, 1728 (1954).
32. D. NASIPURI, S. R. R. CHOUDHURY, and A. BHATTACHARYA. J. Chem. Soc. Perkin Trans. **1**, 1451 (1973); F. C. NOVELLO, M. E. CHRISTY, and J. M. SPRAGUE. J. Am. Chem. Soc. **75**, 1330 (1953); S. M. ABDULLAH. J. Indian Chem. Soc. **12**, 62 (1935); W. S. JOHNSON, J. S. BELEW, L. J. CHINN, and R. H. HUNT. J. Am. Chem. Soc. **75**, 4995 (1953).
33. L. A. PAQUETTE and W. A. KINNEY. Tetrahedron Lett. **23**, 131 (1982).
34. V. YEDIDIA and C. C. LEZNOFF. Can. J. Chem. **58**, 1144 (1980).
35. J. M. STEWART and J. D. YOUNG.Solid phase peptide synthesis. W. H. Freeman Ltd., San Francisco. 1969. p. 22.
36. E. D. BERGMANN and J. SZMUSZKOVICZ. J. Am. Chem. Soc. **75**, 3226 (1953).
37. J. M. J. FRÉCHET, E. BALD, and F. ŠVEC. React. Polymers, **1**, 21 (1982).
38. P. HODGE. International Symposium on Polymer Supported Reagents in Organic Chemistry, Lyons, France, June–July, 1982.

Can. J. Chem. Downloaded from www.nrcresearchpress.com by 210.87.254.5 on 09/06/12
For personal use only.

Symmetry in N—H···N bonding, the structure of β-iminoamines and their salts[1]

SYDNEY BROWNSTEIN, ERIC J. GABE, AND LATA PRASAD
Division of Chemistry, National Research Council of Canada, Ottawa, Ont., Canada K1A 0R9

Received November 10, 1982

SYDNEY BROWNSTEIN, ERIC J. GABE, and LATA PRASAD. Can. J. Chem. **61**, 1410 (1983).

Crystals of 2-*N*-phenylamino-4-*N*-phenylimino-2-pentene are orthorhombic, a = 8.7283(6), b = 8.8369(5), c = 18.8798(8) Å, Z = 4, space group $P2_1ab$. It is resolved to R_F = 0.053 for 684 observed reflections. Crystals of 2-*N*-phenylamino-4-*N*-phenylimino-2-pentene hydrochloride are monoclinic, a = 14.6120(9), b = 5.2736(7), c = 20.708(1) Å, β = 102.287(5)°, Z = 4, space group $P2_1/c$. The final residual is 0.054 for 1255 reflections. Crystals of 2-*N*-methylamino-4-*N*-methylimino-2-pentene hydrochloride are trigonal, a = 7.1666(7), c = 15.3299(8) Å, Z = 3, space group $P3_121$. The final residual is 0.044 for 343 observed reflections. The free base exists, in the solid, as the amino-imino form and not as a symmetrical structure. The N—H bond distances in the six-membered ring of the free base are equal as are the N—H bond distances in the infinite chains of the hydrochloride salts. The compounds are fluxional in solution.

SYDNEY BROWNSTEIN, ERIC J. GABE et LATA PRASAD. Can. J. Chem. **61**, 1410 (1983).

Les cristaux de *N*-phénylamino-2 *N*-phénylimino-4 pentène-2 sont orthorhombiques et appartiennent au groupe d'espace $P2_1ab$ avec a = 8,7283(6), b = 8,8369(5), c = 18,8798(8) Å, Z = 4. On a résolu la structure jusqu'à une valeur de R_F = 0,053 pour 684 réflexions observées. Les cristaux du chlorhydrate de *N*-phénylamino-2 *N*-phénylimino-4 pentène-2 sont monocliniques avec a = 14,6120(9), b = 5,2736(7), c = 20,708(1) Å, β = 102,287(5)°, Z = 4, groupe d'espace $P2_1/c$. On obtient une valeur finale de R = 0,054 pour 1255 réflexions. Les cristaux du chlorhydrate de *N*-méthylamino-2 *N*-méthylimino-4 pentène-2 sont trigonaux avec a = 7,1666(7), c = 15,3299(8) Å, Z = 3, groupe d'espace $P3_121$. La valeur résiduelle finale est de 0,044 pour 343 réflexions observées. La base libre existe, dans le solide, sous forme de amino-imino et non comme une structure symétrique. Les longueurs de la liaison N—H des cycles à 6 chaînons de la base libre sont égales comme le sont les longueurs de liaison N—H dans les chaînes sans fin des chlorhydrates. Les composés en solutions sont fluxionnaires.

[Traduit par le journal]

Introduction

It is well known that β-diketones often exist primarily in the enolic form with an intramolecular hydrogen bond. Exchange between the keto and enol forms is sufficiently slow that the relative concentrations and structures of each tautomer can be determined by proton magnetic resonance (1). The chemical shifts of the carbon atoms 2 and 4 in the hydrogen-bonded enolic form are identical. This may arise via rapid exchange between structures **A** and **B** or because the molecule has the symmetrical structure **C** as shown in Scheme 1.

From the variation in chemical shift with changing substituents on carbon atoms 2 and 4, it was concluded that only form **C** is present in solution (2). Direct measurements of such structures in the solid have been made by X-ray and neutron diffraction. The earliest studies reported symmetrical O···H···O bonding as in structure **C** (3, 4). The consensus of more recent studies is that the bonding is asymmetric as in structures **A** and **B** (5–8).

A similar ambiguity exists for β-iminoamines as shown in Scheme 2. Proton resonance spectroscopy shows single lines which cannot distinguish between a rapid averaging of species **D** and **E**, or the existence of structure **F** (9). An X-ray crystal structure determination was undertaken to resolve this ambiguity.

The eneamines are much more basic than the corresponding β-diketones and form salts with mineral acids. The position of protonation in the salts and its effect upon the molecular symmetry and hydrogen bonding are also of interest. The situation is nominally similar to that in 1,8-bis(dimethylamino)-napthalene, a much stronger base than one might expect (10), with a slow rate of proton removal due to the presence of a strong intramolecular hydrogen bond (11).

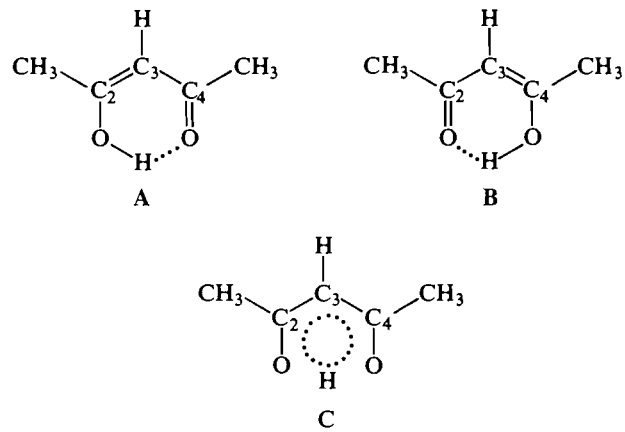

SCHEME 1

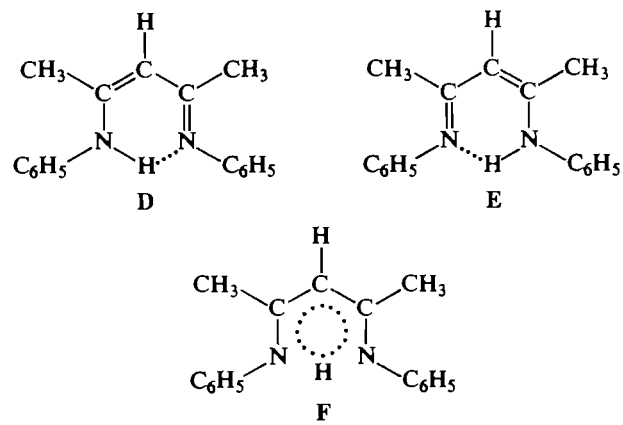

SCHEME 2

[1]NRCC No. 21010.

Can. J. Chem. Downloaded from www.nrcresearchpress.com by 210.87.254.40 on 09/06/12
For personal use only.

TABLE 1. Experimental data

Compound	PPP	PPPH	MMPH
Molecular formula	$C_{17}H_{18}N_2$	$C_{17}H_{19}N_2Cl$	$C_7H_{15}N_2Cl$
Space group	$P2_1ab$	$P2_1/c$	$P3_121$
Z	4	4	3
$F(000)$	536	608	264
Temperature (°C)	23	23	23
a (Å)	8.7283(6)	14.6120(9)	7.1666(7)
b (Å)	8.8369(5)	5.2736(7)	—
c (Å)	18.8798(8)	20.708(1)	15.3299(8)
β (deg)	—	102.287(5)	
V (Å^3)	1456.22	1559.16	681.86
D_c (Mg m^{-3})	1.14	1.22	1.19
No. of reflections in the refinement of cell parameters	68 ($2\theta > 80°$)	27 ($2\theta > 75°$)	22 ($2\theta > 100°$)
μ (cm^{-1}) (λCuKα = 1.5406 Å)	4.87	21.05	32.38
Crystal dimension (mm)	0.35×0.3×0.3	0.30×0.25×0.2	0.4×0.3×0.3
Maximum 2θ°	100	90	110
No. of unique reflns.	824	1255	365
No. of observed reflns. ($I > 2.5\sigma(I)$)	684	773	343
No. of unobserved reflns.	140	482	22
R_F (observed reflns.)	0.053	0.054	0.044
R_{wF} (observed reflns.)	0.034	0.037	0.044
R_F (all reflections)	0.068	0.109	0.046
R_{wF} (all reflections)	0.034	0.038	0.044
$S = [\Sigma\omega(\lvert F_o\rvert - \lvert F_c\rvert)^2/(m-n)]^{1/2}$	5.06	3.31	7.56

TABLE 2. Atomic parameters X, Y, Z, and B_{eq}* for 2-*N*-phenylamino-4-*N*-phenylimino-2-pentene, esd's refer to the last digit printed

Atom	X	Y	Z	B_{eq}
N(1)	0	0.0865(5)	0.17235(18)	4.8(3)
N(2)	0.1837(7)	0.0841(5)	0.28485(18)	5.4(3)
C(1)	0.0142(8)	0.2416(7)	0.17248(20)	4.9(4)
C(2)	0.1040(8)	0.3075(6)	0.22204(20)	4.6(3)
C(3)	0.1847(8)	0.2323(7)	0.27902(19)	5.1(4)
C(4)	−0.0684(8)	0.3413(6)	0.12087(22)	5.6(4)
C(5)	0.2691(8)	0.3332(7)	0.33288(23)	6.1(4)
C(6)	−0.1084(7)	−0.0034(6)	0.13529(22)	4.4(3)
C(7)	−0.1601(7)	0.0214(6)	0.06699(23)	5.0(3)
C(8)	−0.2681(8)	−0.0768(6)	0.03743(21)	5.5(4)
C(9)	−0.3150(9)	−0.2035(7)	0.07428(22)	6.4(4)
C(10)	−0.2593(9)	−0.2321(7)	0.14072(21)	6.2(4)
C(11)	−0.1559(8)	−0.1346(6)	0.17303(22)	4.9(3)
C(12)	0.2552(8)	0.0045(6)	0.34298(23)	5.5(4)
C(13)	0.3768(9)	−0.0897(7)	0.3260 (3)	6.9(4)
C(14)	0.4434(10)	−0.1731(7)	0.3813 (3)	8.7(5)
C(15)	0.3794(9)	−0.1656(7)	0.44802(23)	8.8(5)
C(16)	0.2595(10)	−0.0725(8)	0.46493(23)	9.6(6)
C(17)	0.1928(10)	0.0128(7)	0.41030(24)	7.7(4)

*B_{eq} is the arithmetic mean of the principal axes of the thermal ellipsoid.

TABLE 3. Atomic parameters X, Y, Z, and B_{eq}* for 2-*N*-phenylamino-4-*N*-phenylimino-2-pentene hydrochloride, esd's refer to the last digit printed

Atom	X	Y	Z	B_{eq}
Cl	0.10501(15)	0.1674(5)	0.13614(9)	4.23(13)
N(1)	0.1812 (4)	0.1317(13)	−0.21947(24)	3.3 (4)
N(2)	0.1759 (4)	0.0279(12)	0.0071 (3)	3.2 (4)
C(1)	0.1380 (5)	0.1946(16)	−0.1695 (3)	3.4 (5)
C(2)	0.1735 (5)	0.0869(15)	−0.1073 (3)	2.6 (5)
C(3)	0.1391 (5)	0.1427(16)	−0.0504 (3)	3.0 (4)
C(4)	0.0562 (5)	0.3729(17)	−0.1907 (3)	4.2 (5)
C(5)	0.0596 (5)	0.3144(17)	−0.0460 (3)	4.3 (6)
C(6)	0.2644 (5)	−0.0077(16)	−0.2145 (3)	3.4 (5)
C(7)	0.2626 (5)	−0.2178(17)	−0.2559 (3)	4.2 (5)
C(8)	0.3456 (6)	−0.3516(18)	−0.2562 (3)	5.1 (6)
C(9)	0.4278 (5)	−0.2778(17)	−0.2149 (3)	4.7 (5)
C(10)	0.4290 (5)	−0.0680(17)	−0.1745 (3)	4.2 (5)
C(11)	0.3476 (5)	0.0688(16)	−0.1741 (3)	3.7 (5)
C(12)	0.2549 (5)	−0.1376(16)	0.0231 (3)	3.2 (5)
C(13)	0.3380 (5)	−0.0933(16)	0.0019 (3)	3.7 (5)
C(14)	0.4138 (5)	−0.2584(16)	0.0229 (3)	4.2 (5)
C(15)	0.4071 (5)	−0.4592(17)	0.0650 (4)	5.0 (5)
C(16)	0.3261 (6)	−0.4934(17)	0.0869 (4)	5.0 (6)
C(17)	0.2499 (5)	−0.3341(17)	0.0661 (3)	4.1 (5)

*B_{eq} is the arithmetic mean of the principal axes of the thermal ellipsoid.

Experimental

2-*N*-methylamino-4-*N*-methylimino-2-pentene hydrochloride (MMPH) and the corresponding phenylamino compound (PPPH) were prepared according to the literature procedure and recrystallised from absolute ethanol. The phenylamino compound (PPP) was prepared from the hydrochloride by reaction with triethylamine and was recrystallised from petroleum ether (9).

Intensity data for all the compounds were measured on a Picker 4-circle automatic diffractometer using graphite monochromatised CuKα radiation by θ/2θ scan methods with line profile analysis (12). The unit cell constants were obtained by least-squares refinement of the setting angles of reflections with $2\theta > 75°$ (λCuKα = 1.5406 Å). The relevant experimental details are given in Table 1. The intensities were corrected for Lorentz and polarization effects, using measured values for direct beam polarization (13). Absorption corrections were not considered to be justified because the effects are small and the crystals irregular. For PPP, the space group $P2_1ab$ with equivalent positions (x, y, z; $\frac{1}{2}+x$, $\bar{y}$, $\bar{z}$; $\frac{1}{2}+x$, $\frac{1}{2}-y$, z; x, $\frac{1}{2}+y$, $\bar{z}$), is a non-standard setting of the space group $Pca2_1$. For MMPH the space group $P3_121$ was selected arbitrarily over the enantiomorphic group $P3_221$.

All three structures were solved by the application of MULTAN (14). After several cycles of refinement with isotropic temperature factors, the hydrogen atoms were located in a difference map. The

Can. J. Chem. Downloaded from www.nrcresearchpress.com by 210.87.254.40 on 09/06/12
For personal use only.

Can. J. Chem. Downloaded from www.nrcresearchpress.com by 210.87.254.40 on 09/06/12
For personal use only.

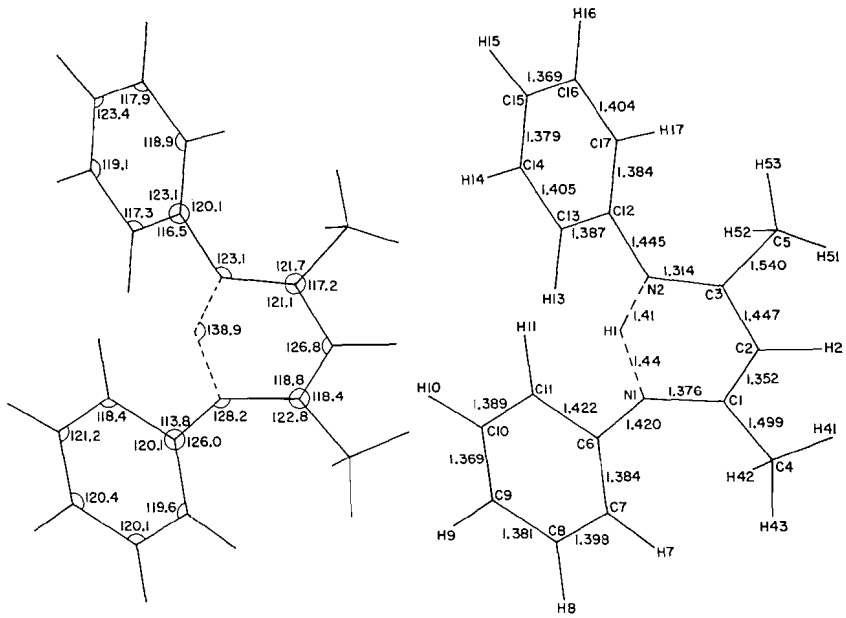

FIG. 1. Atom numbering, bond lengths (σ = 0.008 Å), and bond angles (σ = 0.5°) for PPP.

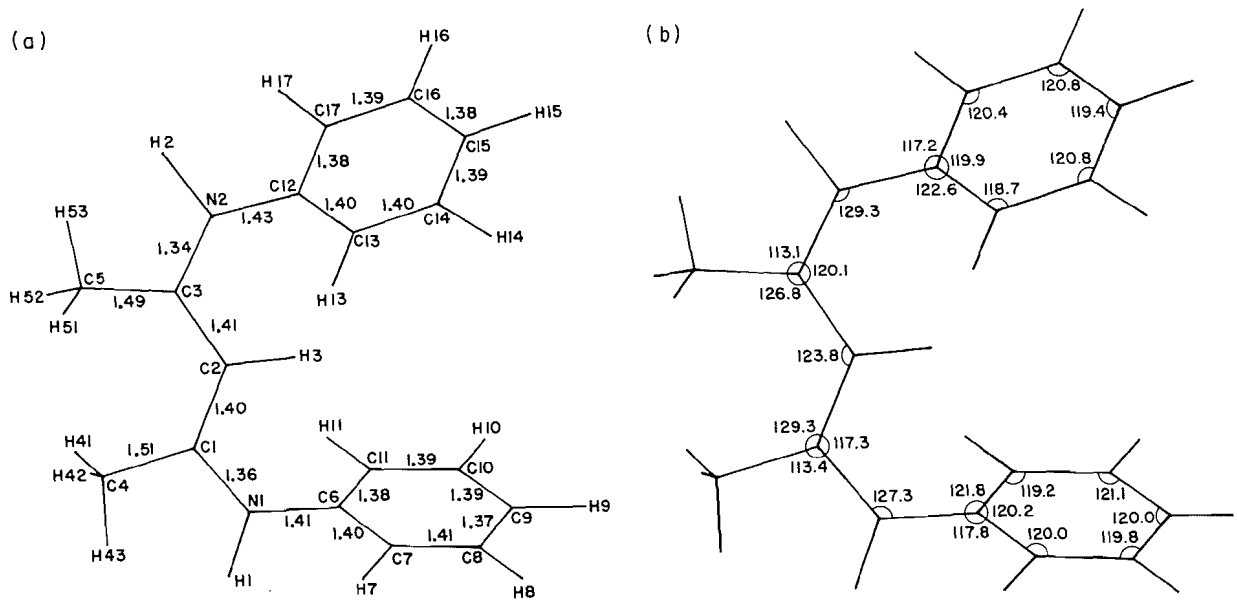

FIG. 2. (*a*) Atom numbering and bond lengths (σ = 0.01 Å) for PPPH; (*b*) bond angles (σ = 0.7°) for PPPH.

structures were refined further by block-diagonal least-squares method with anisotropic temperature factors for the non-hydrogen atoms. Hydrogen atoms were included in all structure factor calculations, but only in PPP were H(1) and H(2) refined with isotropic temperature factors. Counting statistics weights were used throughout ($w = (1/\sigma^2)|F_o|$). The final R-values are given in Table 1. The scattering factors for neutral atoms were taken from International tables for X-ray crystallography (1974). The final positional and equivalent isotropic temperature factors are given in Tables 2, 3, and 4. All calculations were performed using the NRC PDP8-E system of programs (15).

TABLE 4. Atomic parameters X, Y, Z, and B_{eq}* for 2-*N*-methylamino-4-*N*-methylimino-2-pentene hydrochloride, esd's refer to the last digit printed

Atom	X	Y	Z	B_{eq}
Cl	0.2366(3)	0.2366	0	3.55(9)
N	0.3360(8)	0.6557(8)	0.5811(3)	3.0 (3)
C(1)	0.3042(10)	0.4772(10)	0.5415(3)	2.8 (4)
C(2)	0.4762(12)	0.4762	1/2	2.8 (3)
C(3)	0.0748(10)	0.2913(10)	0.5477(3)	3.4 (4)
C(4)	0.5446(11)	0.8518(10)	0.5863(3)	3.7 (4)

*B_{eq} is the arithmetic mean of the principal axes of the thermal ellipsoid.

Discussion

The atom numbering, bond lengths and angles for the three structures are shown in Figs. 1, 2, and 3.

In the structure of PPP there is an intramolecular N—H···N bond (Fig. 1). Within the limits of accuracy of the structure determination, H(1) has refined close to a symmetrical position between N(1) and N(2). The fragment N(1)C(1)C(2)C(3)N(2)

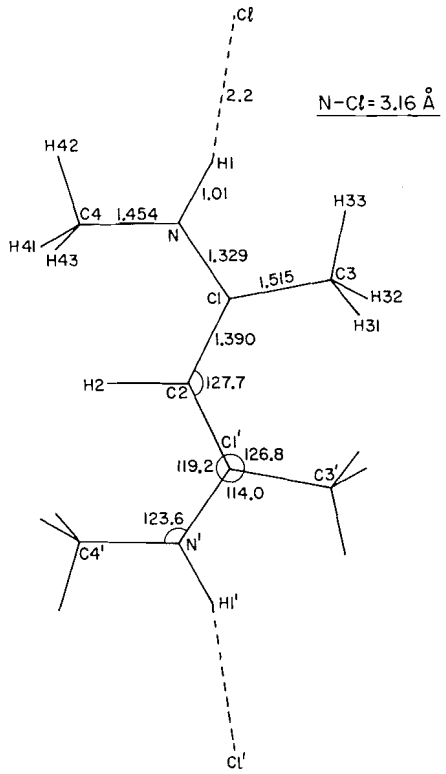

FIG. 3. Atom numbering, bond lengths (σ = 0.008 Å), and bond angles (σ = 0.5°) for MMPH.

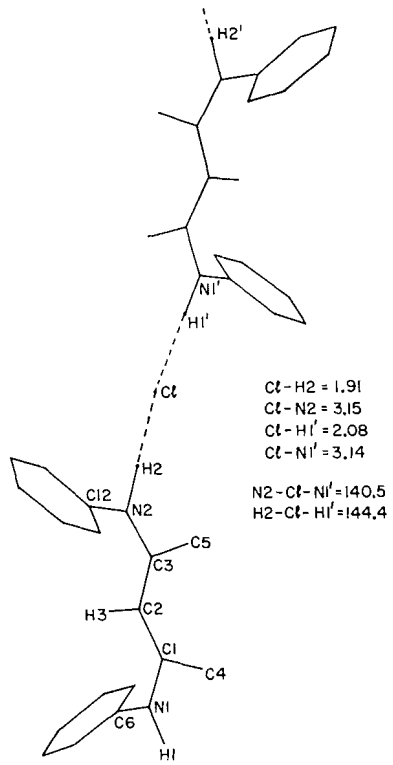

FIG. 4. The relationship between PPPH units.

is not symmetric (Fig. 1) and the molecule does not possess any symmetry as in bisbromobenzoylmethane (3) and bischlorobenzoylmethane (4) where there is a two-fold axis. The only other related structure with an intramolecular N—H···N bond is that of 3,5-dimethyl-1,7-diphenyl-4-(2,4,6-trinitrophenyl)-2,6-diazahepta-2,4-diene in which the N—H···N bond is not symmetric (16). In view of this it seems unlikely that the N—H···N bond in PPP really is symmetric. The molecule may exist in the crystal as a combination of the species **D** and **E**, but the difference in the lengths of the N(1)—C(1) (1.376 Å) and N(2)—C(3) (1.314 Å) bonds strongly suggests that H(1) is really attached to N(1) even though the refined position does not agree with this.

In PPPH, both N(1) and N(2) are protonated. The molecule, though not situated in a position of crystallographic symmetry, appears to possess a plane of symmetry passing through C(2) and perpendicular to the plane C(1)C(2)C(3). The molecules are linked together by N—H···Cl bonds forming zig-zag chains along the (001) direction (Fig. 4).

In MMPH the atoms C(2) and Cl are situated on a crystallographic two-fold axis (Table 3 and Fig. 3). The structure is similar to the phenyl analogue.

Conclusion

Electron density maps suggests that PPP exists in the solid as a combination of the species **D** and **E**, with the convolution of the two H(1) positions producing a diffuse maximum at the symmetrical position. However the N—C bond lengths indicate more strongly that H(1) is attached to N(1). The occurrence of the electron density maximum is probably an artifact of the data and should not be given too much significance.

1. J. L. BURDETT and M. T. ROGERS. J. Am. Chem. Soc. **86**, 2105 (1964).
2. N. N. SHAPETKO, S. S. BERESTOVA, G. M. LUKOVKIN, and YU. S. BOGACHEV. Org. Magn. Reson. **7**, 237 (1975).
3. D. WILLIAMS, R. RUNDLE, and W. DUMKE. Acta Crystallogr. **15**, 627 (1962).
4. G. R. ENGEBRETSON and R. E. RUNDLE. J. Am. Chem. Soc. **86**, 574 (1964).
5. D. E. WILLIAMS. Acta Crystallogr. **21**, 340 (1966).
6. K. KATO. Acta Crystallogr. B**27**, 2028 (1971).
7. F. J. HOLLANDER, D. H. TEMPLETON, and A. ZALKIN. Acta Crystallogr. B**29**, 1552 (1973).
8. R. D. G. JONES. Acta Crystallogr. B**32**, 1807 (1976).
9. J. E. PARKS and R. H. HOLM. Inorg. Chem. **7**, 1408 (1968).
10. R. W. ALDER, P. S. BOWMAN, W. R. S. STEELE, and D. R. WINTERMAN. J. Chem. Soc. Chem. Commun. 723 (1981).
11. A. AWWAL and F. HIBBERT. J. Chem. Soc. Perkin II, 1589 (1977).
12. D. F. GRANT and E. J. GABE. J. Appl. Crystallogr. **11**, 114 (1978).
13. Y. LE PAGE, E. J. GABE, and L. D. CALVERT. J. Appl. Crystallogr. **12**, 25 (1979).
14. G. GERMAIN, P. MAIN, and M. M. WOOLFSON. Acta Crystallogr. A**27**, 368 (1971).
15. A. C. LARSON and E. J. GABE. Computing in crystallography. *Edited by* H. Schenk, R. Olthof-Hazekamp, H. van Koningsveld, and G. C. Bassi. Delft University Press, 1978. p. 81.
16. N. G. FURMANOVA, O. E. KOMPAN, YU. T. STRUCHKOV, I. E. MIKHAILOV, L. P. OLEKHNOVICH, and V. I. MINKIN. Zhur. Struct. Khim. **21**, 98 (1980).

Can. J. Chem. Downloaded from www.nrcresearchpress.com by 210.87.254.40 on 09/06/12
For personal use only.

Partial molal volumes of some halobenzenes in carbon tetrachloride

FEREIDOON SHAHIDI

Department of Chemical Engineering and Applied Chemistry, University of Toronto, Toronto, Ont., Canada M5S 1A4

Received September 17, 1982

FEREIDOON SHAHIDI. Can. J. Chem. **61**, 1414 (1983).

The partial molal volumes at infinite dilution $\bar{V}^0$ for a number of halobenzenes are measured and related to their van der Waals volumes. Results indicate larger volume increments for halogen atoms in halobenzenes than those in alkyl halides. Possible explanations are forwarded. The effect of steric overcrowding in *ortho*-substituted benzenes on the $\bar{V}^0$ values are evaluated.

FEREIDOON SHAHIDI. Can. J. Chem. **61**, 1414 (1983).

On a mesuré les volumes molaires partiels à dilution infinie $\bar{V}^0$ d'un certain nombre d'halobenzènes et on les a rapportés à leurs volumes de van der Waals. Les résultats indiquent que les atomes d'halogènes des halobenzènes subissent une plus forte augmentation de volume que ceux des halogénures d'alkyles. On fournit des explications possibles de ce phénomène. On évalue l'effet d'un encombrement stérique des benzènes substitués en position *ortho* sur les valeurs de $\bar{V}^0$.

[Traduit par le journal]

Introduction

The partial molal volumes, $\bar{V}^0$, of aromatic hydrocarbons and their alkyl derivatives in carbon tetrachloride (1) at 25°C may be calculated using the equation

$$[1] \quad \bar{V}^0 = 11.61 + \sum_1^m n_i I_i - \sum_1^k p_j \delta_j$$

where n_i is the number of groups (methyl, methylene, aromatic $=C<$ or $=C<^{H}$ etc.) of type i and I_i is the volume increment of such a group; δ_j represents the decrement due to the overlap feature j and p_j is the number of such features present in the molecule. The value of 11.61 mL mol^{-1} serves as the covolume factor (2) or the volume of the solvent cavity required to accommodate a point kinetic particle of no intrinsic volume.

In the present paper we test the applicability of eq. [1] to a number of halobenzenes listed in Table 1.

Experimental

The compounds given in Table 1 are commercial products obtained from Aldrich Chemical Co. They were purified by conventional methods of recrystallization and distillation. Carbon tetrachloride was purified as described elsewhere (2).

Densities were measured at 25.00 ± 0.01°C using a Paar digital precision density meter, model DMA 02C, and the apparent molal values were then calculated using eq. [2]

$$[2] \quad \phi_v = \frac{M_2}{W_2}(1/d - W_1/d^0)$$

TABLE 1. Partial molal volumes, $\bar{V}^0$, of halobenzenes in carbon tetrachloride at 25°C

Compound	$\bar{V}^0$/mL mol^{-1} Experimental	$\bar{V}^0$/mL mol^{-1} Calculated	Structural[a] feature
Benzene	90.5±0.3	90.9	—
Fluorobenzene	96.9±0.7	96.5	—
1,2-Difluorobenzene	101.9±0.3	101.7	1×*a*
1,2,4,5-Tetrafluorobenzene	111.3±0.4	112.5	2×*a*
1,2,3,4,5,6-Hexafluorobenzene	122.6±0.3	122.4	6×*a*
Chlorobenzene	101.4±0.1	102.6	—
1,2-Dichlorobenzene	111.6±0.2	113.2	1×*b*
1,3-Dichlorobenzene	114.0±0.4	114.2	—
1,4-Dichlorobenzene	113.7±0.3	114.2	—
1,2,3-Trichlorobenzene	122.3±0.3	123.8	2×*b*
1,3,5-Trichlorobenzene	125.8±0.2	125.8	—
1,2,4,5-Tetrachlorobenzene	135.6±0.1	135.4	2×*b*
1,2,3,4,5-Pentachlorobenzene	145.0±0.2	145.1	4×*b*
1,2,3,4,5,6-Hexachlorobenzene	155.1±0.2	154.8	6×*b*
Bromobenzene	105.0±0.1	105.7	—
1,2-Dibromobenzene	118.1±0.1	118.4	1×*c*
1,4-Dibromobenzene	120.6±0.3	120.6	—
1,3,5-Tribromobenzene	135.6±0.2	135.2	—
2-Bromotoluene	119.8±0.2	120.6	1×*d*
4-Bromotoluene	122.1±0.3	122.4	—
2-Bromomesitylene	153.2±0.2	152.3	2×*d*
Iodobenzene	111.2±0.3	111.6	—
1,4-Diiodobenzene	132.7±0.5	132.2	—

[a]For coding, see Fig. 1.

Can. J. Chem. Downloaded from www.nrcresearchpress.com by 210.87.254.6 on 09/06/12
For personal use only.

Can. J. Chem. Downloaded from www.nrcresearchpress.com by 210.87.254.6 on 09/06/12
For personal use only.

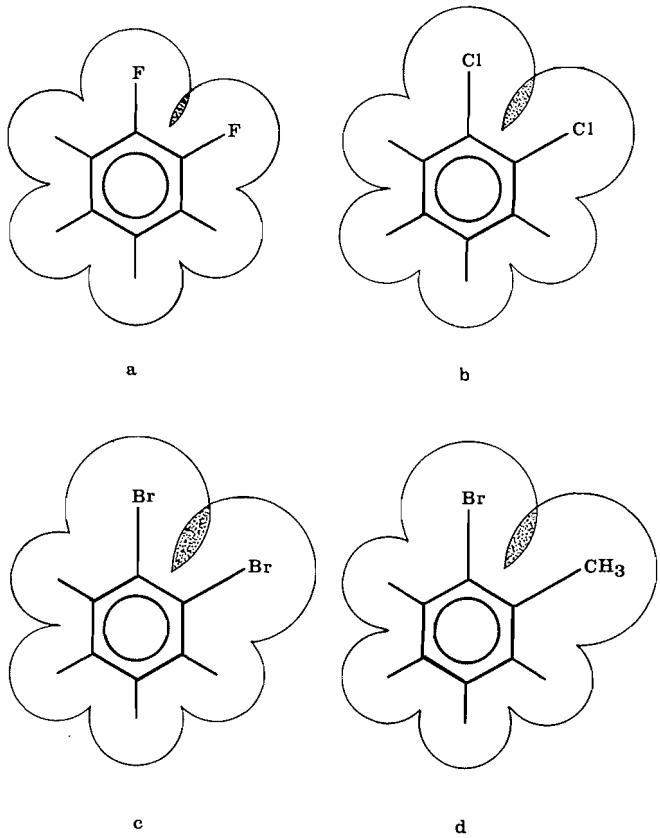

FIG. 1. Scale drawings of *ortho*-disubstituted halobenzene molecules: van der Waals radii of 1.2 Å for hydrogen, 1.47 Å for fluorine, 1.75 Å for chlorine, 1.85 Å for bromine, and 2.0 Å for methyl indicated.

where M_2 is the solute molecular weight, W_2 its weight fraction, W_1 the weight fraction of solvent, and d and d^0 are the densities of the solution and solvent respectively. The partial molal volumes at infinite dilution, $\bar{V}^0$, were then obtained from a least-squares fit of the apparent molal volumes, ϕ_v, to zero concentration. The errors quoted are standard deviations.

Results and discussion

In Table 1, the partial molal volumes, $\bar{V}^0$, obtained experimentally together with those calculated using eq. [1] are tabulated.

Group contributions to the partial molal volumes, I, and volume decrements, δ, caused by steric compression due to the overlap of the van der Waals volumes of *ortho*-substituted groups (features $a-d$ in Fig. 1) are listed in Table 2. The group contributions for the halogen atoms attached to aromatic rings are considerably larger than those obtained for haloalkanes.

The halogen atoms in haloalkanes behaved as if their volumes were smaller than those indicated by their van der Waals volumes V_w (3). The partial molal volume of a solute is made up of V_w plus the void or "empty" volume V^e (4), which depends on the closeness of packing of the solvent molecules about solute molecules. A bromine atom has about the same V_w as a methyl group (5) and if the packing of carbon tetrachloride molecules about it is similar, would be expected to have the same volume increment I.

The volume increment, I, of 24.95 mL mol^{-1} for bromine in benzene bromides is fairly close to that of 26.85 mL mol^{-1} for a methyl group. Furthermore, the *ortho* effect of bromine atoms (feature c) in $\bar{V}^0$ of bromobenzenes is similar to that of a methyl group in methylbenzenes, i.e., 2.20 versus 2.35 mL mol^{-1}. Thus the geometrical size of the groups is reflected in the measured values of $\bar{V}^0$.

The calculated group contributions, I_{calcd}, to the partial molal volumes based on the equation

$$[3] \quad I = V_w + 5.9 \times 10^{-9}A$$

developed elsewhere (5), are much closer to the values obtained experimentally for aryl halides than those found for haloalkanes (3) (see Table 2). It has been shown that the halogen atoms in aryl halides have larger van der Waals volumes than those attached to alkyl chains (4). However, these differences may not fully account for the observed variations in $\bar{V}^0$ values; factors related to the surface area and packing efficiency of solvent molecules about the molecules of solute are important contributors.

Partial molal volumes, $\bar{V}^0$, for cyclohexylbromide (122.6 ± 0.4 mL mol^{-1}) and 1,4-dibromocyclohexane (134.1 ± 0.5 mL mol^{-1}) as well as those for 1- and 2-bromoadamentenes (6) agree well with the calculated $\bar{V}^0$ values using the volume increment of 19.53 mL mol^{-1} for the bromine atom, hence excluding the involvement of conformational effects (7).

In halobenzenes, due to the electron-withdrawing effect of halogen atoms, the π-electron cloud of the benzene rings is made less available towards donor–acceptor complexation (8–11) with the solvent as comapred with unsubstituted aromatic hydrocarbons and their alkyl derivatives. This results in

TABLE 2. Parameters I and δ for calculation of $\bar{V}^0$ using eq. [1]

Group	I/mL mol^{-1} Alkyl	Aryl	Calcd[a]	Structural feature	δ/mL mol^{-1}
F	—	15.72	12.3	*a*	0.29
Cl	17.02	21.80	22.2, 22.7[b]	*b*	0.97
Br	19.53	24.95	26.7, 26.9[b]	*c*	2.20
I	25.45	30.87	34.2, 34.4[b]	*d*	1.68
CH_3	26.85	26.85	26.2		
$=C<^{H}$	—	13.22	—		
$=C<$	—	3.03	—		

[a]Calculated using V_w and A values from ref. 4 in eq. [3].
[b]In aryl halides.

larger $\bar{V}^0$ values than those expected on the basis of the latter two classes of compounds. Since the contributions of aromatic $=C<$ and $=C<^{H}$ are fixed, this "apparent" volume increase will be reflected in the I values for the halogen atoms in aryl halides. Furthermore, the approach of carbon tetrachloride molecules on the π-surfaces of these halobenzenes may be restricted due to unfavorable dipole − induced dipole interactions and this also results in an "apparent" increase in the volume contribution, I, for halogens in these compounds.

Therefore, a combination of the effects considered above may account for the observed differences between the I values of the halogens in aliphatic and aromatic halocompounds. However, these speculations (*vide supra*) must only be considered as "tentative" at this stage.

1. F. SHAHIDI, P. G. FARRELL, J. T. EDWARD, and P. CANONNE. J. Org. Chem. **44**, 950 (1979).
2. J. T. EDWARD, P. G. FARRELL, and F. SHAHIDI. J. Phys. Chem. **82**, 2310 (1978).
3. F. SHAHIDI, P. G. FARRELL, and J. T. EDWARD. J. Phys. Chem. **83**, 419 (1979).
4. A. BONDI. J. Phys. Chem. **68**, 441 (1964).
5. J. T. EDWARD, P. G. FARRELL, and F. SHAHIDI. Can. J. Chem. **57**, 2585 (1979).
6. J. T. EDWARD, P. G. FARRELL, and F. SHAHIDI. Can. J. Chem. **57**, 2892 (1979).
7. K. TANABE and S. SAËKI. J. Mol. Struct. **27**, 79 (1975) and references therein.
8. E. N. GURYANOVA, I. P. GOLDSTEIN, and I. P. ROMM. Donor–acceptor bond. Wiley, New York. 1974. Chapt. 14.
9. F. J. STREITER and D. H. TEPLETON. J. Chem. Phys. **37**, 161 (1962).
10. H. RATAJIZATA. J. Phys. Chem. **76**, 3000 (1972).
11. J. N. SPENCER, J. R. SWEIGART, M. E. BROWN, R. L. BENSING, T. C. HESSINGER, W. KELLY, D. L. HOUSEL, and G. W. REISINGER. J. Phys. Chem. **80**, 811 (1976).

Can. J. Chem. Downloaded from www.nrcresearchpress.com by 210.87.254.6 on 09/06/12
For personal use only.

Nuclear magnetic shielding calculations in the finite perturbation method involving GIAO's at the INDO level and London's approximation. II. Carbon-13 and nitrogen-15

E. C. VAUTHIER

Service de Spectroscopie Moléculaire en Milieu Condensé Laboratoire de Recherches Physiques, associé au CNRS, Université Pierre et Marie Curie, 4, Place Jussieu, Tour 22, 75230, Paris, Cedex 05, France

S. FLISZÁR

Département de Chimie, Université de Montréal, C.P. 6210, Succ. A, Montréal (Qué.), Canada H3C 3V1

F. TONNARD

Département de Physique Cristalline et Chimie Structurale E.R.A. au CNRS No 15, Université de Rennes, Campus de Beaulieu, Av. du Général Leclerc, 3503, Rennes, France

AND

S. ODIOT

Service de Spectroscopie Moléculaire en Milieu Condensé Laboratoire de Recherches Physiques, associé au CNRS, Université Pierre et Marie Curie, 4, Place Jussieu, Tour 22, 75230, Paris, Cedex 05, France

Received November 24, 1982

E. C. VAUTHIER, S. FLISZÁR, F. TONNARD, and S. ODIOT. Can. J. Chem. **61**, 1417 (1983).

Magnetic shielding constants, calculated for C-13 and N-15 nuclei in the finite perturbation method using INDO and London's approximations, are analyzed in terms of mono-, di-, and tricentric contributions, thus permitting an assessment of the relative importance of local vs. nonlocal contributions. For both C-13 and N-15, it appears that the changes in total shielding are almost entirely dictated by those of the local paramagnetic contribution, i.e., $\Delta\sigma_{total} \simeq \Delta\sigma^{P}_{local}$.

E. C. VAUTHIER, S. FLISZÁR, F. TONNARD et S. ODIOT. Can. J. Chem. **61**, 1417 (1983).

Des constantes d'écran magnétique, calculées par la méthode des perturbations finies au niveau INDO avec l'approximation de London pour des noyaux C-13 et N-15, sont analysées en termes de contributions mono-, di- et triatomiques en permettant ainsi une évaluation de l'importance relative des contributions locales et non-locales. Il ressort que les variations totales des constantes d'écran sont pratiquement entièrement dictées par celles de la contribution paramagnétique locale, c.-à-d., $\Delta\sigma_{total} \simeq \Delta\sigma^{P}_{local}$.

Introduction

The rigorous theory of magnetic shielding, which is now clearly described (1), is practically unmanageable for any compound of chemical interest. Reasonable compromises between theoretical rigor and practical feasibility have been offered (2–12) with the result that realistic shielding constants can now be calculated. For a representative collection of carbon-13 shieldings, for example, an average deviation of ~5 ppm between calculated and experimental results covering a range of ~145 ppm is indicative for the sort of precision which can now be obtained (12) and suggests that reasonable confidence can be put in the approximations involved in this type of calculations.

The present study covers carbon-13 and nitrogen-15 nuclei of a diversified group of molecules. Of course, shielding constants are calculated and compared with experimental data. Primarily, however, it appears interesting to gain an insight into the role of electron densities associated (admittedly in a somewhat loose fashion) with the various atoms of a molecule as regards the shielding of any given nucleus. From within the formalism describing the magnetic shielding, this type of insight is offered by numerical analyses of the individual contributing terms and by an evaluation of the relative weights of local vs. nonlocal contributions.

While the results obtained in this manner are obviously not rigorous and should, therefore, not be unduly generalized to other systems without appropriate verifications, it becomes possible to assess the prevailing role of local paramagnetic contributions with a reasonable degree of confidence.

Outline of calculations

The average diamagnetic and paramagnetic contributions, σ^d and σ^p, respectively, to the total average magnetic shielding

$$\sigma = \sigma^d + \sigma^p$$

are calculated using the formalism described earlier (12). This approach is rooted in Pople's finite perturbation theory (3). It involves the INDO approximations (11) on a gauge invariant atomic orbital (GIAO) basis (7) and London's approximation. Moreover, it satisfies the Hermitian requirement for the first-order perturbation matrix reflecting the effect of an applied external magnetic field. The latter condition results in a significant improvement of calculated ^{13}C magnetic shieldings, the average precision being of the order of ~5 ppm (12). The point is that this formalism for σ permits a separation into mono-, di-, and triatomic contributions, thus revealing the relative importance of "local" and "distant" electron densities on the magnetic shielding of a given nucleus. The various contributions making up the total shielding $\sigma(M)$ of nucleus M are: $\sigma^d(M)$ = local diamagnetic shielding, from AO's centered on M; $\sigma^d(K)$ = diamagnetic contribution of all atoms but M, from AO's centered on K; $\sigma^p(M)$ = local paramagnetic shielding, from AO's centered on M; and $\sigma^p(K)$ = paramagnetic contribution of all atoms but M, from AO's centered on K. In addition, we must consider the following sums which have physical meanings although this is not the case for the individual terms, i.e., $\sigma(MK) = \sigma^d(MK) + \sigma^d_0(MK) + \sigma^p_0(MK)$ = total (dia- plus paramagnetic) contribution of all the MK pairs

Can. J. Chem. Downloaded from www.nrcresearchpress.com by 210.87.254.6 on 09/06/12
For personal use only.

Can. J. Chem. Downloaded from www.nrcresearchpress.com by 210.87.254.6 on 09/06/12
For personal use only.

TABLE 1. Shielding constants of C-13 nuclei (ppm)

Molecule (atom*)	σ^d(M)	σ^d(K)	σ^p(M)	σ^p(K)	σ^d(MK)	σ^d_0(MK)	σ^p_0(MK)	σ(M, AB)	σ_{calcd}	$\delta^{calcd}_{CH_4}$	$\delta^{exptl.}_{CH_4}$
C^*H_4	57.81	3.58	−51.51	0	20.89	0.0	0.17	1.82	32.77	0	0
C^*H_3CN	57.58	4.06	−53.33	−0.80	18.71	0.0	−0.37	2.23	28.1	−4.7	−2.4
$C^*H_3CH_2NH_2$	57.85	3.82	−56.30	−0.31	17.63	0.0	0.36	2.25	25.3	−7.5	−19.8
$C^*H_3NH_2$	56.59	4.04	−64.47	−0.56	17.67	0.32	−1.55	2.61	14.6	−18.2	−29.0
$(C^*H_3)_2NH$	56.66	4.04	−68.11	−0.61	17.63	0.05	−0.90	2.28	11.0	−21.8	−37.8
$CH_3C^*H_2NH_2$	56.45	3.97	−63.15	−0.19	14.44	0.72	−2.04	3.60	13.8	−19.0	−38.0
$(C^*H_3)_3N$	56.71	4.06	−71.46	−0.62	17.58	−0.02	−0.45	2.03	7.8	−25.0	−49.6
$CH_2C^*H—CN$	57.54	4.59	−173.88	1.81	17.23	−0.32	−2.05	1.88	−93.2	−126.0	−111.3
HC^*N	56.90	4.91	−183.17	6.66	20.60	0.0	−12.80	0.11	−106.8	−139.6	−113.0
CH_3C^*N	56.72	5.60	−189.41	6.92	18.22	0.35	−13.87	2.26	−113.2	−146.0	−119.3
$CH_2CH—C^*N$	56.75	5.57	−175.79	3.59	18.34	0.0	−12.90	1.58	−102.9	−135.6	−131.1
$C^*H_2CH—CN$	57.68	4.05	−173.64	1.03	19.16	1.29	−5.13	1.75	−93.8	−126.6	−140.0
	58.07	4.32	−174.37	−1.58	16.57	1.58	−3.11	4.00	−94.5	−127.3	−127.1
	57.31	4.74	−180.96	−1.47	16.45	1.72	−6.12	4.76	−103.6	−136.4	−139.1
	56.57	4.69	−196.70	−3.25	16.31	−0.54	−5.71	4.52	−124.1	−156.9	−153.1
	56.98	4.84	−191.28	−4.46	16.34	−0.42	−4.40	3.73	−118.7	−151.5	−149.0
	57.67	4.85	−171.53	−3.27	16.51	1.52	−4.76	4.54	−94.5	−127.3	−130.0
	57.02	4.88	−196.24	−5.18	16.32	1.16	−5.97	4.59	−123.4	−156.2	−155.0
	58.38	4.49	−169.54	−2.48	16.59	0.68	−1.52	3.12	−90.3	−123.1	−125.0
	56.27	5.15	−198.73	−3.91	16.31	1.58	−9.04	1.32	−128.1	−160.9	−160.0
	55.50	5.09	−208.02	−5.73	16.24	0.0	−9.74	4.14	−142.5	−175.3	−162.0

Can. J. Chem. Downloaded from www.nrcresearchpress.com by 210.87.254.6 on 09/06/12
For personal use only.

of atoms involving M, from AO's centered on M and K; $\sigma(M, AB) = \sigma^d(M, AB) + \sigma_0^d(M, AB) + \sigma_0^p(M, AB)$ = contribution of all pairs AB but those involving atom M, from AO's centered on atoms A and B. Finally, the total shielding of atom M is expressed by the sum

$$\sigma = \sigma^d(M) + \sigma^d(K) + \sigma^p(M) + \sigma^p(K) + \sigma(MK) + \sigma(M, AB)$$

which is readily calculated from the appropriate expressions indicated in eq. [9] of ref. 12.

It is clear that the INDO approximations are only there in order to keep the calculations at a manageable level. The quality of the London and INDO approximations involved can be evaluated from the results obtained in this fashion, in comparisons with experimental data. While certainly plagued by occasional lack of precision, the results deduced within the framework of INDO theory still enable a balanced assessment of the major relevant trends governing magnetic shielding.

Results

The calculations were carried out by means of the program NMR C INDO-80[1] which optimizes the Slater exponents in order to account for the molecular environment. Anticipated errors arising from London's approximation are tentatively compensated, at least in part, with the use of the modified INDO parameters $\beta_H^0 = -14.31$ and $\beta_C^0 = -16.57$ eV as determined in an earlier study (12), and $\beta_N^0 = -21.38$ eV. While obviously not free from possible criticisms, namely, as regards the choice of a single β_C^0 parameter for describing all *sp*, sp^2, and sp^3 carbon atoms, the fact remains that this simple parameterization leads to acceptable results considering the large range in shielding which is investigated. Standard geometries were assumed throughout.

The results obtained for carbon nuclei are indicated in Table 1. While there is clearly room for improvements, it appears fair to conclude that the comparison with experimental data supports the general validity of the approximations involved in the present semiempirical approach, namely London's approximation as well as those of INDO theory, including the INDO parameters β^0.

Similarly, Table 2 describes the analysis of the individual contributions to the shielding of nitrogen-15 nuclei. The results are compared with their experimental counterparts and suggest that the approximations involved in these calculations are (under the present conditions) acceptable and justify a reasonable confidence in the individual contributions. The latter are analyzed as follows.

Discussion

To begin with, it appears that the *local* diamagnetic shielding, $\sigma^d(M)$, is virtually constant for a given nucleus, i.e., ~57.1 ± 1.2 ppm for C-13 and ~88.2 ± 1.2 ppm for N-15. This result, which is in line with current views, plays a role in the forthcoming evaluation of the total (dia- and paramagnetic) *local* contributions to the shielding of a nucleus. Moreover, the present calculations illustrate the minor role played by distant atoms on the shielding of heavy nuclei like C-13 and N-15. This point is, indeed, revealed by the contributions of the tricentric integrals, $\sigma(M, AB)$, which are both small and fairly

TABLE 2. Shielding constants of N-15 nuclei (ppm)

Molecule (atom*)	$\sigma^d(M)$	$\sigma^d(K)$	$\sigma^p(M)$	$\sigma^p(K)$	$\sigma^d(MK)$	$\sigma_0^d(MK)$	$\sigma_0^p(MK)$	$\sigma(M, AB)$	σ_{calcd}	$\delta_{NH_3}^{calcd}$	$\delta_{NH_3}^{expt.}$
N^*H_3	89.16	3.08	−146.38	0	14.06	0.0	14.98	1.35	−23.7	0	0
$CH_3N^*H_2$	88.89	3.35	−165.70	0.30	9.95	−3.61	19.38	2.58	−44.9	−21.1	−5.0
$(CH_3)_2N^*H$	88.63	3.58	−181.98	0.93	5.92	−0.27	16.71	3.71	−62.8	−39.0	−12.0
$(CH_3)_3N^*$	88.37	3.78	−194.10	1.85	1.97	−0.43	17.38	4.79	−76.4	−52.6	−18.0
$C_2H_5N^*H_2$	88.95	3.24	−183.52	0.39	9.68	−4.45	22.12	2.35	−61.2	−37.5	−28.0
$NH_2—N^*H_2$	88.16	3.55	−185.21	−0.17	9.88	0.00	13.32	2.46	−68.0	−44.3	−66±20
$CH_3—N^*C$	86.31	7.92	−255.92	0.84	16.43	−0.08	10.70	2.74	−131.0	−107.3	−164
$CH_3—CN^*$	88.37	4.16	−382.71	10.10	12.22	−0.20	9.31	−0.69	−266.4	−242.7	−245
$CH_2CH—CN^*$	88.26	4.24	−414.56	10.12	12.17	−0.04	9.39	−0.71	−291.1	−267.4	−258
HCN^*	87.88	4.22	−386.88	10.35	12.41	0.00	6.33	−0.68	−266.4	−242.6	−297±20
	88.73	4.42	−457.99	−0.88	8.01	−2.17	23.03	3.59	−333.3	−309.6	−300
	88.37	4.31	−466.21	0.31	7.69	0.00	19.19	4.74	−341.6	−317.9	−324
	88.04	4.79	−472.39	−0.65	7.57	0.00	16.86	4.46	−351.3	−327.6	−340
	87.31	4.92	−505.66	−3.82	7.68	0.00	16.12	4.73	−388.7	−365.0	−402

[1]This program can be requested from the first author.

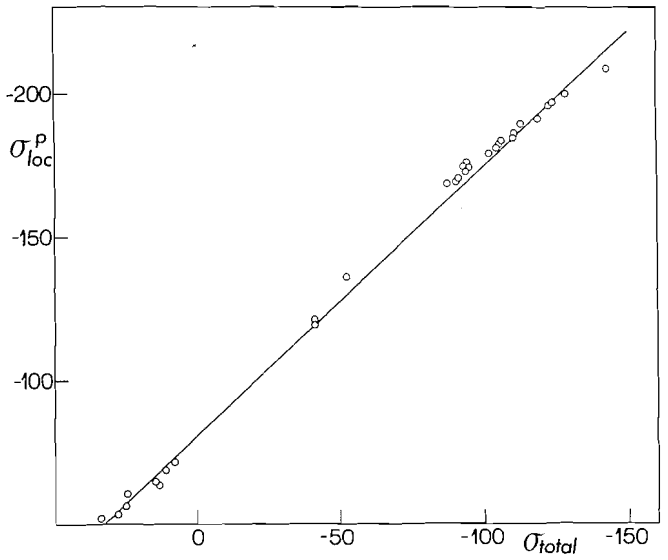

FIG. 1. A comparison of calculated local paramagnetic with total shielding constants of C-13 nuclei (ppm). The results are extracted from Table 1 and ref. 12.

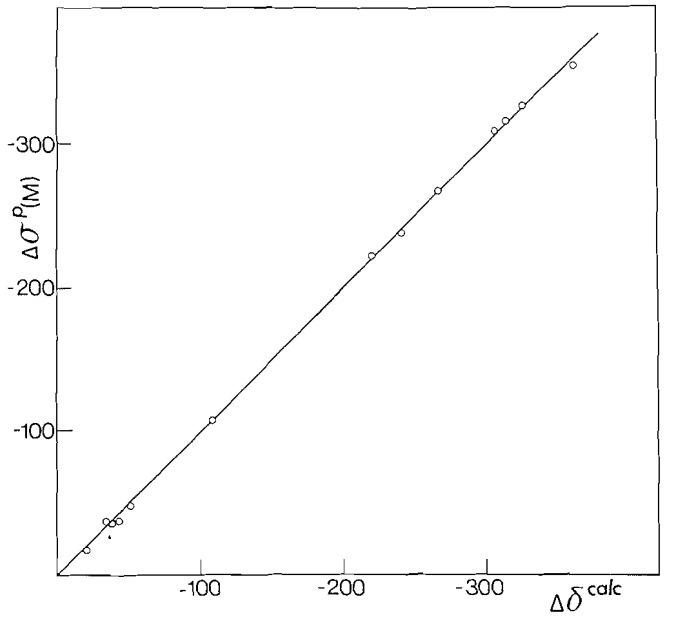

FIG. 2. A comparison between local paramagnetic and total shielding constants (ppm, from Table 2).

constant, particularly in comparison with closely related compound, i.e.,

$$\sigma(M, AB) \simeq 2.8 \pm 2 \text{ ppm (C-13)}$$
$$\simeq 2.5 \pm 3 \text{ ppm (N-15)}$$

The fact that "distant" atoms have only a minor, if any, effect on the shielding of heavy nuclei justifies in part the solvaton model (13) discussed by Jallah-Heravi and Webb (14). For hydrogen, however, the situation is different, as revealed by the relative importance of tricentric integrals in the calculation of σ (12), thus suggesting a possible explanation for solvent effects affecting proton magnetic shielding constants.

On the other hand, the total dia- and paramagnetic contributions of all atoms but M, from AO's centered on K, i.e., $\sigma^{d}(K) + \sigma^{p}(K) + \sigma(MK)$, also appear to be relatively invariant although this is not the case for the individual terms. For N-15 nuclei this sum is 30.6 ± 6 ppm, this average being taken for all the compounds indicated in Table 2. However, the results suggest slightly different values in comparisons involving only atoms of similar nature, namely, 27.9 ± 3 ppm in amines, 35.1 ± 1.5 ppm in nitriles, and 29.3 ± 3 ppm in cyclic compounds. Similarly, the sum $\sigma^{d}(K) + \sigma^{p}(K) + \sigma(MK)$ is ~19.6 ± 4 ppm for the carbon nuclei of the noncyclic molecules and ~13.8 ± 4 ppm for the cyclic molecules indicated in Table 1. Of course, it would be difficult and premature to evaluate how real are the differences between nuclei belonging to different series of compounds; it seems fair, however, to assume that there is some truth in the similarities within a series of closely related molecules.

With these reservations in mind regarding the precise meaning of "constancy" when speaking about the terms examined so far, it appears from the present calculations that the sum of all the contributions other than the local (dia- and paramagnetic) ones is nearly invariant, namely, 20.5 ± 5.5 ppm for C-13 nuclei and 33.1 ± 4 ppm for N-15 nuclei. Of course, this is the result of a number of compensations because the individual terms entering the sum occasionally exhibit significant variations. Turning now to the local paramagnetic term, $\sigma^{p}_{local} = \sigma^{p}(M)$, calculated from AO's centered on M and, moreover, remembering that the local diamagnetic part, $\sigma^{d}(M)$, is virtually constant, it appears that the total variation in shielding, $\Delta\sigma_{total}$, is almost entirely determined by that of the local paramagnetic term, i.e.,

$$\Delta\sigma_{total} \simeq \Delta\sigma^{p}_{local}$$

This result is expressed in Fig. 1 for carbon-13, and in Fig. 2 for nitrogen-15 nuclei.

The results given in Figs. 1 and 2 are self-explanatory. They are significant because they cover an important range of shielding (~160 ppm for ^{13}C and ~400 ppm for ^{15}N) for nuclei belonging to a well diversified group of molecules. Of course, these results are not free from relatively minor uncertainties linked to the necessity of using approximations in order to keep the computations at a manageable level.

Within the precision of the present type of analysis, it seems nonetheless reasonable to retain the essentially local character of the main factors governing the magnetic shielding of heavy nuclei, thus offering a justification for correlations between nmr shifts and atomic charges which, of course, are strictly local properties. Indeed, accurate correlations of this type are occasionally observed in well-defined series of compounds (15), suggesting, in agreement with the present results, that the local charge density determines the major part, by far, of the differences in shielding between nuclei in comparable situations.

Acknowledgements

We express our gratitude to the France–Québec exchange program which made this cooperation possible, and to the National Research Council of Canada for financial assistance.

1. W. H. FLYGARE. Molecular structure and dynamics. Prentice-Hall Inc., Englewood Cliffs, NJ. 1978.
2. R. M. STEVENS, R. M. PITZER, and W. N. LIPSCOMB. J. Chem. Phys. **38**, 550 (1963); W. N. LIPSCOMB. Advances in magnetic resonance. Vol. 2. *Edited by* J. S. Waugh. Academic Press, New York. 1966. p. 137.

Can. J. Chem. Downloaded from www.nrcresearchpress.com by 210.87.254.6 on 09/06/12
For personal use only.

3. J. A. POPLE, J. W. MCIVER, and N. S. OSTLUND. J. Chem. Phys. **49**, 2960 (1968).
4. J. A. POPLE. J. Chem. Phys. **37**, 53 (1962).
5. J. TILLIEU. Ann. Phys. Paris, Vol. 2, **471**, 631 (1957); J. R. DIDRY and J. GUY. C.R. Acad. Sci. **239**, 1203 (1954).
6. W. N. LIPSCOMB. M.T.P. international review of science, physical chemistry. Series 1, Vol. 1. *Edited by* W. B. Brown. Butterworths University Park Press, London. 1972. p. 167.
7. R. DITCHFIELD. Mol. Phys. **27**, 789 (1974).
8. F. RIBAS PRADO, G. GIESSMER-PRETTRE, J. P. DAUDEY, A. PULLMAN, J. F. HINTON, G. YOUND, and D. HARPOL. J. Magn. Res. **37**, 431 (1980).
9. R. DITCHFIELD. Chem. Phys. Lett. **15**, 203 (1972).
10. R. DITCHFIELD, D. P. MILLER, and J. A. POPLE. J. Chem. Phys. **54**, 4186 (1971).
11. P. D. ELLIS, G. E. MACIEL, and J. W. MCIVER. J. Am. Chem. Soc. **94**, 4069 (1978); M. KONDO, I. ANDO, R. CHUJO, and A. NISHIOKA. J. Magn. Reson. **24**, 315 (1976); V. GALASSO. Org. Magn. Reson. **12**, 318 (1979); A. R. GARBER, P. D. ELLIS, K. SEIDMAN, and K. SCHADE. J. Magn. Reson. **34**, 1 (1979).
12. E. VAUTHIER, S. ODIOT, and F. TONNARD. Can. J. Chem. **60**, 957 (1982).
13. A. A. GERMER. Theoret. Chim. Acta, **34**, 245 (1974).
14. M. JALLAH-HERAVI and G. A. WEBB. Org. Magn. Reson. **13**, 116 (1980).
15. S. FLISZÁR, G. CARDINAL, and M.-T. BÉRALDIN. J. Am. Chem. Soc. **104**, 5287 (1982) and references therein.

Can. J. Chem. Downloaded from www.nrcresearchpress.com by 210.87.254.6 on 09/06/12
For personal use only.

The structure and conformation of *cis*-2-phenylcyclobutanecarboxylic acid and *cis*-3-(*p*-fluorophenyl)cyclobutanecarboxylic acid

GEORGE M. REISNER, JAMES D. KORP, IVAN BERNAL, AND RICHARD FUCHS
Department of Chemistry, University of Houston, Houston, TX 77004, U.S.A.

Received October 20, 1982

GEORGE M. REISNER, JAMES D. KORP, IVAN BERNAL, and RICHARD FUCHS. Can. J. Chem. **61**, 1422 (1983).

The structure of *cis*-2-phenylcyclobutanecarboxylic acid (**1**) and *cis*-3-(*p*-fluorophenyl)cyclobutanecarboxylic acid (**2**) have been determined by X-ray diffraction methods. Crystals of **1** are monoclinic, space group $C2/c$ with a = 15.420(8), b = 11.687(6), c = 11.226(5) Å, β = 112.45(4)°, and eight molecules in the unit cell. Crystals of **2** are monoclinic, space group $P2_1/n$, a = 8.038(5), b = 5.405(4), c = 22.69(1) Å, and β = 97.30(4)°, with four molecules in the unit cell. In both compounds the cyclobutane ring is puckered, with dihedral angles of 27° and 31°. The bond joining the substituted ring atoms in **1** is significantly longer (1.581(2) Å) than the other three (average 1.535(2) Å), due to crowding of substituents. In **2** both the carboxyl and phenyl substituents are close to the bisecting geometry, whereas in **1** both substituents deviate from this conformation, the carboxyl more than the phenyl.

GEORGE M. REISNER, JAMES D. KORP, IVAN BERNAL et RICHARD FUCHS. Can. J. Chem. **61**, 1422 (1983).

On a déterminé par diffraction de rayons-X la structure de l'acide phényl-2 cyclobutanecarboxylique *cis* (**1**) et de l'acide (*p*-fluorophényl)-3 cyclobutanecarboxylique *cis* (**2**). Les cristaux du composé **1** sont monocliniques et appartiennent au groupe d'espace $C2/c$ avec a = 15,420(8), b = 11,687(6), c = 11,226(5) Å, β = 112,45(4)° et possèdent 8 molécules par maille. Les cristaux du composé **2** sont monocliniques et appartiennent au groupe d'espace $P2_1/n$ avec a = 8,038(5), b = 5,405(4), c = 22,69(1) Å et β = 97,30(4)° avec 4 molécules par maille. Dans les deux composés le cycle cyclobutane est gauche avec des angles dièdres de 27° et de 31°. La liaison reliant les atomes substitués du cycle dans le composé **1** est nettement plus longue (1,581(2) Å) que celle des trois autres (moyenne: 1,535(2) Å) à cause de l'encombrement des substituants. Les substituants carboxyles et phényle du composé **2** adoptent une conformation qui s'approche d'une géométrie bisectrice tandis que les substituants du composé **1** dévient de cette conformation, le carboxyle déviant d'avantage que le phényle.

[Traduit par le journal]

Recent thermochemical studies of simple cyclobutane derivatives (cyclobutyl cyanide, ethylcyclobutane cyclobutylamine) (1, 2) indicate that all three are stabilized by 2.0 ± 0.4 kcal/mol relative to cyclobutane. This is surprising, because other data (3) demonstrate that these substituents do not stabilize the cyclopropane ring, where substituent-ring π interactions should be more favorable. Also, it is not clear from previous crystal studies (4–8) whether ring bond lengths in cyclobutane derivatives are affected mainly by the electronic properties of substituents (π donors and acceptors, σ donors and acceptors), or by crowding of adjacent substituents. Furthermore, we are unaware of any previous studies on similarly unhindered substituted cyclobutanes which establish whether substituents such as phenyl and carboxyl preferentially assume a ring-bisecting conformation most favorable for π interaction. Since the accuracy of the thermochemical data on cyclobutane (2), and the existence of stabilization in substituted cyclobutanes have been questioned (1), we wished to look for structural evidence of cyclobutane–substituent conjugation. The existence of conjugation (in cyclopropane derivatives, for example ref. 9), is not necessarily reflected in thermochemical stabilization, but stabilization is unlikely in the absence of conjugation.

With this question in mind we have undertaken an X-ray study of two comparably substituted cyclobutane derivatives, *cis*-2-phenylcyclobutanecarboxylic acid (**1**) and *cis*-3-(*p*-fluorophenyl)cyclobutanecarboxylic acid (**2**). As shown in a previous structural determination (9), both the phenyl and the carboxyl group are capable of conjugation with small ring systems.

It is anticipated that the two substituents will be sterically crowded in **1** but not in **2**, and this should permit a distinction to be drawn between steric and electronic effects.

Experimental

Syntheses

cis-2-Phenylcyclobutanecarboxylic acid was synthesized by the method of Burger and Beard (10), and recrystallized from hexane (mp 83.5–85.0°C). A crystal for X-ray study was formed by slow partial evaporation of a hexane solution at room temperature.

cis-3-(*p*-Fluorophenyl)cyclobutanecarboxylic acid (**2**) was synthesized by the low temperature addition of *p*-fluorophenylmagnesium bromide to ethyl 3-ketocyclobutane-1-carboxylate, hydrogenolysis of the resulting hydroxyl group, and ester hydrolysis (11). The material recrystallized from hexane melted at 81.5–83.5°C. A crystal was grown from a heptane solution by partial evaporation at room temperature.

X-ray structure determinations

Data collection methods for the two compounds were similar. Intensity measurements were carried out with an ENRAF-NONIUS CAD-4 computer-controlled diffractometer. A summary of the crystallographically important parameters for data collection and processing is given in Table 1. Accurate cell constants were determined from 25 strong high angle reflections. The intensities were measured using the θ–2θ scan technique, with the scan rate depending on the net count obtained in rapid pre-scans of each reflection. The standard reflections, monitored every 2 h, did not show any significant deviations from the initial measurements. In reducing the data, Lorentz and polarization factors were applied, but no absorption corrections were made.

Both structures were solved using MULTAN (12). All subsequent calculations were carried out using the SHELX-76 (13) system of programs. All the hydrogen atoms were located in difference density Fourier maps. After all shift/esd ratios were less than 1.0, the refinements converged to the agreement factors given in Table 1. No unusually high correlations were noted in either refinement. The atomic scattering factors for C, O, and F were computed from numerical Hartree–Fock wave functions (14); for hydrogen those of Stewart

Can. J. Chem. Downloaded from www.nrcresearchpress.com by 210.87.254.6 on 09/06/12
For personal use only.

TABLE 1. Summary of data collection and processing parameters

Parameter	Value	
	1	**2**
Space group	$C2/c$	$P2_1/n$
Cell constants	a = 15.420(8) Å	a = 8.038(5) Å
	b = 11.687(6)	b = 5.405(4)
	c = 11.226(5)	c = 22.69(1)
	β = 112.45(4)°	β = 97.30(4)°
	V = 1869.7 Å^3	V = 977.9 Å^3
Molecular formula	$C_{11}H_{12}O_2$	$C_{11}H_{11}FO_2$
Molecular weight	176.21	194.21
Molecules per unit cell	8	4
Density (calcd)	1.25 g cm^{-3}	1.32 g cm^{-3}
Absorption coefficient	0.49 cm^{-1}	0.63 cm^{-1}
Wavelength (MoKα)	λ = 0.71073 Å	λ = 0.71073 Å
Data collection range	$4° \leq 2\theta \leq 55°$	$4° \leq 2\theta \leq 55°$
Scan width	$\Delta\theta = (1.05 + 0.35 \tan\theta)°$	$\Delta\theta = (1.05 + 0.35 \tan\theta)°$
Maximum scan time	240 s	240 s
Scan speed range	0.4 to 5° min^{-1}	0.4 to 5° min^{-1}
Total data collected	2341	2622
Data with $I > 3\sigma(I)$	1083	700
Total variables	166	171
$R = \Sigma\|\|F_o\| - \|F_c\|\|/\Sigma\|F_o\|$	0.031	0.037
$R_w = [\Sigma w(\|F_o\| - \|F_c\|)^2 / \Sigma w\|F_o\|^2]^{1/2}$	0.024	0.028
Weights	$w = \sigma(F)^{-2}$	$w = \sigma(F)^{-2}$
Goodness-of-fit	0.68	1.53

TABLE 2. Atomic coordinates and thermal parameters (× 1000) for compound **1**

Atom	X/A	Y/B	Z/C	U_{11}	U_{22}	U_{33}	U_{12}	U_{13}	U_{23}
C1	0.4166(2)	0.5702(2)	0.3479(2)	57(1)	56(1)	49(1)	−1(1)	2(1)	7(1)
C2	0.3890(2)	0.4502(2)	0.2904(3)	56(1)	52(2)	63(2)	11(1)	4(1)	5(1)
C3	0.2873(1)	0.4754(2)	0.2743(2)	58(1)	41(1)	40(1)	0(1)	15(1)	9(1)
C4	0.3136(1)	0.6068(2)	0.2863(2)	55(1)	39(1)	36(1)	3(1)	13(1)	2(1)
C5	0.2864(1)	0.6647(1)	0.1585(2)	47(1)	29(1)	42(1)	0(1)	10(1)	−1(1)
C6	0.2039(1)	0.4290(1)	0.1645(2)	50(1)	33(1)	47(1)	1(1)	16(1)	8(1)
C7	0.2079(2)	0.4011(2)	0.0475(2)	56(1)	72(2)	52(1)	−12(1)	19(1)	−1(1)
C8	0.1295(2)	0.3575(2)	−0.0519(2)	78(2)	75(2)	55(1)	−16(1)	16(1)	−6(1)
C9	0.0472(2)	0.3423(2)	−0.0360(3)	61(2)	54(1)	83(2)	−11(1)	3(1)	0(1)
C10	0.0422(2)	0.3698(2)	0.0797(3)	53(2)	67(2)	106(2)	−4(1)	28(2)	−1(2)
C11	0.1199(2)	0.4123(2)	0.1788(2)	62(2)	54(1)	72(2)	0(1)	31(1)	−2(1)
O1	0.3380(1)	0.6712(1)	0.0982(1)	53(1)	65(1)	50(1)	13(1)	23(1)	18(1)
O2	0.2014(1)	0.7077(1)	0.1158(1)	47(1)	53(1)	53(1)	9(1)	16(1)	14(1)
H11	0.436(1)	0.571(2)	0.445(2)	78(6)					
H12	0.463(1)	0.613(2)	0.327(2)	72(7)					
H21	0.418(1)	0.384(2)	0.348(2)	90(7)					
H22	0.396(1)	0.447(2)	0.206(2)	68(7)					
H3	0.280(1)	0.459(1)	0.357(1)	54(5)					
H4	0.288(1)	0.652(1)	0.340(1)	42(5)					
H7	0.267(1)	0.407(1)	0.037(1)	64(6)					
H8	0.136(1)	0.336(2)	−0.130(2)	83(7)					
H9	−0.008(1)	0.308(2)	−0.104(2)	89(7)					
H10	−0.016(1)	0.357(2)	0.095(2)	94(8)					
H11	0.117(1)	0.431(2)	0.261(2)	71(7)					
H13	0.188(1)	0.748(2)	0.034(2)	136(10)					

et al. (15) were used. Final positional and thermal parameters for compounds **1** and **2** are listed in Tables 2 and 3, respectively. Bond lengths, angles, least-squares planes and torsion angles are given in Tables 4–7.[1]

[1]Tables of observed and calculated structure factors are available, at a nominal charge, from the Depository of Unpublished Data, CISTI, National Research Council of Canada, Ottawa, Ont., Canada K1A 0S2.

Results and discussion

Figures 1 and 2 depict stereoscopically related pairs of compounds **1** and **2**, respectively, and also show the atomic nomenclature used.

In both compounds the cyclobutane ring was found to be puckered, with dihedral angles of about 27° and 31°. These values are typical of non-fused, substituted cyclobutane rings.

Can. J. Chem. Downloaded from www.nrcresearchpress.com by 210.87.254.6 on 09/06/12
For personal use only.

TABLE 3. Atomic coordinates and thermal parameters (× 1000, H × 100) for compound **2**

Atom	X/A	Y/B	Z/C	U_{11}	U_{22}	U_{33}	U_{12}	U_{13}	U_{23}
C1	−0.6903(5)	−0.2807(9)	0.5938(2)	60(3)	68(4)	68(3)	−4(3)	−10(2)	17(3)
C2	−0.6042(6)	−0.1308(12)	0.6463(2)	60(3)	105(5)	47(3)	14(3)	8(3)	10(3)
C3	−0.4362(5)	−0.2523(9)	0.6382(2)	53(3)	63(3)	52(3)	8(3)	−1(2)	6(3)
C4	−0.5143(5)	−0.3055(10)	0.5733(2)	69(3)	71(4)	65(3)	13(3)	−5(2)	−13(3)
C5	−0.8236(6)	−0.1547(11)	0.5529(2)	55(3)	74(4)	68(3)	−2(3)	−4(3)	6(3)
C6	−0.2788(5)	−0.1083(8)	0.6517(2)	54(3)	58(3)	44(2)	13(2)	0(2)	−1(3)
C7	−0.2485(6)	0.1017(10)	0.6196(2)	69(3)	70(4)	71(4)	9(3)	−14(3)	2(3)
C8	−0.1042(6)	0.2438(10)	0.6321(2)	78(3)	68(4)	83(4)	1(3)	1(3)	4(3)
C9	0.0080(6)	0.1688(10)	0.6793(2)	54(3)	78(4)	75(4)	−3(3)	7(3)	−18(3)
C10	−0.0132(6)	−0.0367(10)	0.7122(2)	60(3)	86(4)	52(3)	10(3)	−2(3)	−5(3)
C11	−0.1569(5)	−0.1712(9)	0.6979(2)	62(3)	61(4)	53(3)	5(3)	5(2)	4(3)
O1	−0.7987(3)	0.0479(7)	0.5300(1)	72(2)	88(3)	111(3)	−16(2)	−23(2)	46(2)
O2	−0.9646(4)	−0.2689(6)	0.5437(1)	66(2)	77(2)	108(2)	−12(2)	−24(2)	19(2)
F	0.1505(3)	0.3083(5)	0.6931(1)	78(2)	104(2)	114(2)	−18(2)	4(1)	−17(2)
H1	−0.733(4)	−0.442(6)	0.608(1)	6(1)					
H21	−0.646(4)	−0.152(7)	0.680(1)	7(1)					
H22	−0.601(4)	0.055(7)	0.637(1)	7(2)					
H41	−0.485(4)	−0.455(7)	0.552(1)	7(1)					
H42	−0.485(4)	−0.157(7)	0.541(1)	11(2)					
H3	−0.424(3)	−0.418(6)	0.658(1)	5(1)					
H7	−0.318(4)	0.140(7)	0.585(1)	8(1)					
H8	−0.082(5)	0.393(9)	0.603(2)	13(2)					
H10	0.078(4)	−0.094(7)	0.744(1)	8(1)					
H11	−0.181(3)	−0.321(6)	0.715(1)	3(1)					
H13	−1.061(7)	−0.170(10)	0.526(2)	21(3)					

TABLE 4. Intramolecular bond distances (Å)

Bond	Distance	
	1	**2**
C1—C2	1.536(3)	1.532(5)
C2—C3	1.538(2)	1.533(5)
C3—C4	1.581(2)	1.552(4)
C1—C4	1.532(2)	1.550(5)
C3—C6	1.502(2)	1.484(4)
C6—C7	1.377(2)	1.387(4)
C7—C8	1.392(2)	1.389(5)
C8—C9	1.358(3)	1.371(5)
C9—C10	1.369(3)	1.361(5)
C10—C11	1.379(3)	1.368(5)
C6—C11	1.379(2)	1.384(4)
C1—C5	—	1.490(4)
C4—C5	1.494(2)	—
C5—O1	1.228(2)	1.239(4)
C5—O2	1.311(2)	1.284(4)
C1—H1	—	1.00(3)
C1—H11	1.01(1)	—
C1—H12	0.98(2)	—
C2—H21	0.99(2)	0.89(2)
C2—H22	1.00(1)	1.02(3)
C3—H3	0.99(1)	1.00(2)
C4—H4	0.98(1)	—
C4—H41	—	0.98(3)
C4—H42	—	1.13(3)
C7—H7	0.97(1)	0.93(3)
C8—H8	0.95(1)	1.08(4)
C9—F	—	1.373(4)
C9—H9	0.99(2)	—
C10—H10	0.99(2)	1.01(3)
C11—H11	0.96(2)	0.93(2)
O2—H13	0.98(2)	0.99(5)

TABLE 5. Intramolecular bond angles (deg)

Bonds	Angle	
	1	**2**
C2—C1—C5	—	117.5(4)
C4—C1—C5	—	117.6(3)
C2—C1—C4	89.5(1)	86.5(3)
C1—C2—C3	88.9(2)	89.9(3)
C2—C3—C4	87.7(1)	86.4(3)
C2—C3—C6	122.8(2)	119.4(4)
C4—C3—C6	122.1(1)	121.6(3)
C1—C4—C3	87.5(1)	88.5(3)
C1—C4—C5	115.0(2)	—
C3—C4—C5	112.9(1)	—
O1—C5—O2	122.8(1)	122.9(4)
C1—C5—O1	—	121.6(4)
C1—C5—O2	—	115.6(4)
C4—C5—O1	123.6(2)	—
C4—C5—O2	113.5(2)	—
C3—C6—C7	122.2(2)	121.5(3)
C3—C6—C11	120.2(2)	122.1(4)
C7—C6—C11	117.6(2)	116.4(4)
C6—C7—C8	120.6(2)	122.9(4)
C7—C8—C9	120.8(2)	116.4(4)
C8—C9—C10	119.2(2)	123.6(4)
C9—C10—C11	120.2(2)	117.7(4)
C6—C11—C10	121.6(2)	123.0(4)
C8—C9—F	—	117.6(4)
C10—C9—F	—	118.8(4)

Cotton and Frenz (4) in their review of compounds containing a cyclobutane ring found that the preferred dihedral angle in non-fused systems was 26 ± 3°, unless packing forces required the ring to be planar.

Can. J. Chem. Downloaded from www.nrcresearchpress.com by 210.87.254.6 on 09/06/12
For personal use only.

TABLE 6. Least-squares planes: the first entry is for compound **1**, the second for compound **2**

(*a*) Coefficients of $Ax + By + Cz - D = 0$

	A	*B*	*C*	*D*
Plane *1*; O2, O1, C5, C4 (C1)				
	−0.207	−0.864	−0.459	−8.238
	0.413	−0.471	−0.780	−12.704
Plane *2*; C1, C2, C3				
	0.174	0.367	−0.914	0
	0.267	0.733	−0.625	−11.407
Plane *3*; C2, C3, C4				
	0.120	0.052	−0.991	−2.139
	0.381	0.878	−0.288	−7.374
Plane *4*; C3, C4, C1				
	0.428	−0.026	−0.903	−1.322
	−0.026	0.979	−0.201	−4.359
Plane *5*; C4, C1, C2				
	0.490	0.288	−0.823	1.363
	−0.091	0.840	−0.534	−7.758
Plane *6*; C6, C7, C8, C9, C10, C11				
	−0.169	0.930	−0.328	3.693
	0.547	−0.559	−0.624	−11.071

(*b*) Dihedral angles (deg)

2/4	*3/5*	*1/6*	*1/5*	*6/3*	*1/4*
27.0	27.1	128.2	—	69.3	69.6
31.7	31.0	12.8	90.9	95.9	—

TABLE 7. Torsion angles (deg)

	Torsion angle	
Bonds	**1**	**2**
C3—C4—C5—O1	−89.7	—
C1—C4—C5—O1	8.6	—
C4—C3—C6—C7	84.0	41.4
C2—C3—C6—C7	−26.4	−63.8
C4—C1—C5—O1	—	−49.1
C2—C1—C5—O1	—	52.1

Of the four independent carbon−carbon bonds of the cyclobutane ring in compound **2**, two are significantly longer (1.552(4) and 1.550(5) Å) than the other two (1.532(5) and 1.533(5) Å). This pattern of somewhat unequal bonds occurs in a wide variety of compounds, some of which appear in Cotton's review. Additional examples were recently reported also by Busetti *et al.* (5). The four independent bonds average 1.542(4) Å which is virtually identical to the value of 1.544(3) Å found by Cotton and Frenz (4).

The pattern of the carbon−carbon bonds in the four-membered ring of compound **1** is different. One, C3−C4, is significantly longer (1.581(2) Å) than the other three (1.536(3), 1.538(2), 1.532(2) Å). Carr *et al.* (6) who studied the crystal and molecular structure of *cis*-1,2-dimethoxycarbonyl-1,2-bis(4-nitrophenyl)cyclobutane observed a similar but somewhat larger lengthening of the bond between the two disubstituted atoms (1.606(3) Å). It was suggested that steric hindrance may be responsible for this additional lengthening. Since *cis* substitution of adjacent carbon atoms sometimes results in no significant lengthening of the corresponding ring bond (*cis*-1,2-cyclobutanedicarboxylic acid, C—C = 1.546(3) Å) (7) the possibility that this lengthening may originate in the electron-withdrawing properties of the substituent groups was proposed (6). However, Bock (8) found that in octahydroxycyclobutane, the ring bond lengths are only 1.562(4) and 1.564(2) Å despite the strong electron-withdrawing properties of the hydroxyl groups. But perhaps the σ acceptor quality of the hydroxyl group was in this case balanced by π back donation. In view of the fact that in our case a lengthening of one of the ring bonds occurs only in compound **1** for which the two substituents are in *cis* conformation bonded to adjacent carbons and not for compound **2** which has the same *cis* substituents but on non-adjacent carbons, it seems reasonable to assume that this increase in the C3—C4 bond in compound **1** is mainly due to steric hindrance.

It was found (5) that puckering of the cyclobutane ring decreases the average C—C—C angle from 90° by about 1.6° (4), although values as low as 86.3(2)° and 86(1)° (7, 16) were reported. The angles found for compounds **1** and **2** range between 86.4(3)° and 89.9(3)°.

The six phenyl ring distances average 1.376 Å and 1.377 Å for compounds **1** and **2**, respectively. The variation observed among the individual phenyl bond lengths is probably due to the higher thermal motion of the more distant carbons. The C3—C6 bond of attachment observed for compound **1** (1.502(2) Å) is virtually identical to that of a pure C_{sp^2}—C_{sp^3} bond (1.505 Å) (18), which is indicative of the absence of any conjugation between the phenyl and cyclobutane rings. The somewhat shorter bond of attachment found in compound **2** (1.484(4) Å) might be due to a very slight conjugation between the phenyl and the four-membered ring.

The carboxyl group of compound **2** shows a much smaller difference between the two C—O bond lengths (1.239(4) and 1.284(4) Å) than those observed for compound **1** (1.228(2) and 1.311(2) Å). Also, hydrogen H13 of the OH group has a much

Can. J. Chem. Downloaded from www.nrcresearchpress.com by 210.87.254.6 on 09/06/12
For personal use only.

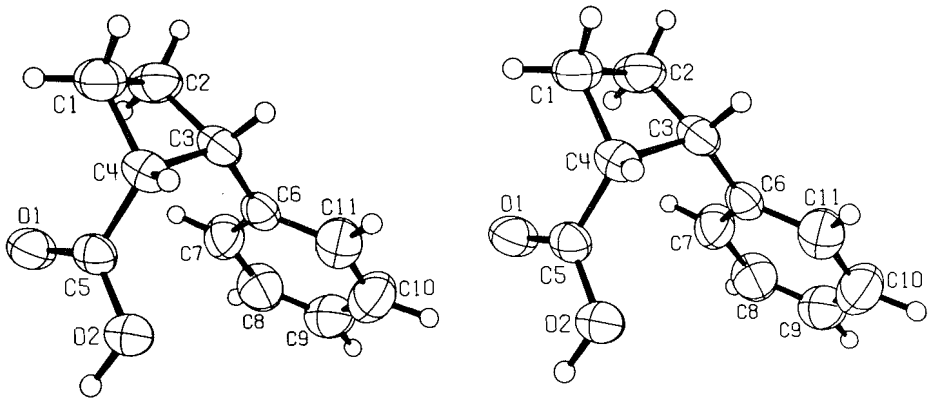

FIG. 1. Stereoscopic view of the atom-labelling scheme for *cis*-2-phenylcyclobutanecarboxylic acid (compound **1**).

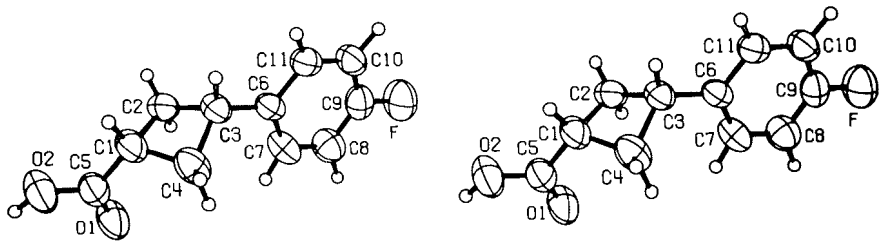

FIG. 2. Stereoscopic view of the atom-labelling scheme for *cis*-3-(*p*-fluorophenyl)cyclobutanecarboxylic acid (compound **2**).

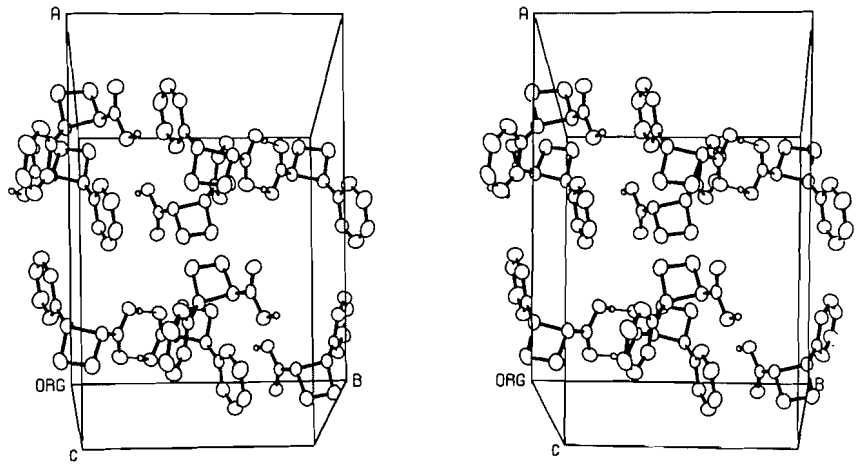

FIG. 3. Stereoscopic view of the molecular packing of **1**. Hydrogens (except H13) are omitted for clarity and the hydrogen bonds between pairs of molecules are included.

higher temperature factor in **2** than in **1**. The bonds of attachment are normal for C_{sp^2}—C_{sp^3} and virtually identical for both compounds (1.494(2) and 1.490(4) Å), again showing no tendency towards conjugation.

The phenyl groups of both compounds are, of course, planar within experimental error. As expected, the carbonyl carbons lie within the plane defined by the three neighboring atoms.

The conformation of the sterically hindered compound **1** differs to a great extent from that observed for compound **2**. Thus, for compound **1** the dihedral angles between the planes of the two substituent groups (phenyl and carboxyl) and the planes defined by those three carbons of the four-membered ring closest to the substituent groups are both about 69°. The dihedral angle between the two substituent groups is 128.2°. In compound **2** the phenyl and carboxyl groups are almost normal to the respective planes of the cyclobutane ring (95.9° and 90.9°). The two substituents are close to being parallel, the dihedral angle between them being 12.8°.

As may be seen from the torsion angles (Table 7) of the unhindered compound **2**, both substituents approach the bisecting conformation with the carbonyl group being somewhat closer to that ideal position than the phenyl. The conformation of the carboxyl group is such that the carboxyl oxygen is nearer to the four-membered ring center with the hydrogen being *syn*-planar positioned. By contrast, the substituents in compound **1** are inhibited by steric problems from achieving the bisecting geometry, the carbonyl group deviating more from the ideal conformation than the phenyl substituent (see torsion

Can. J. Chem. Downloaded from www.nrcresearchpress.com by 210.87.254.6 on 09/06/12
For personal use only.

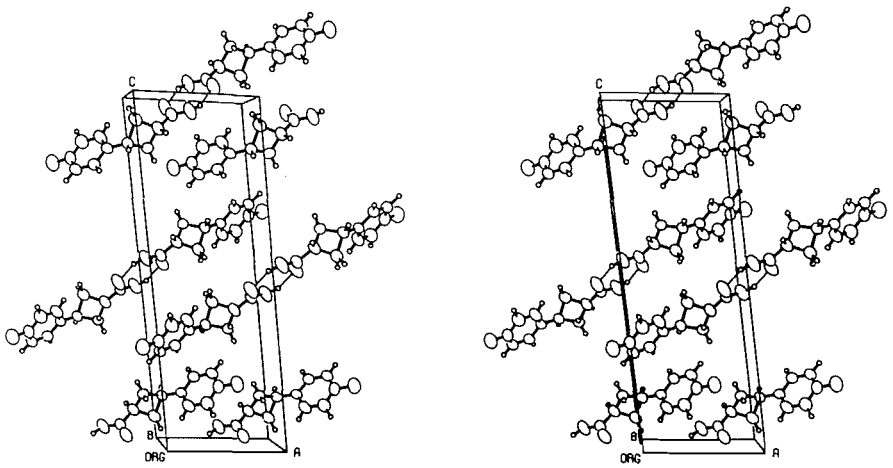

FIG. 4. Stereoscopic view of the molecular packing of **2**. Hydrogen bonds between pairs of molecules are included.

angles, Table 7). The carbonyl oxygen of the carboxyl group is still nearer to the four-membered ring. This situation is in sharp contrast to that recently found by us in *cis*-2(*m*-nitrophenyl)cyclopropanecarboxylic acid (9) where both phenyl and carboxyl groups are far from the bisecting positions with the *phenyl ring* deviating more than the carboxyl group.

The packing of the molecules in the unit cells is shown in Figs. 3 and 4 for compounds **1** and **2**, respectively. Pairs of molecules are mutually hydrogen bonded across crystallographic inversion centers, the bonding being of the "dimer" type found in most carboxylic acids (17). The hydrogen bonding parameters are: **1**: O1...O2 = 2.65(1) Å, H13...O1 = 1.67(2) Å, O2—H13...O1 = 174(2)°; **2**: O1...O2 = 2.65(1) Å, H13...O1 = 1.71(2) Å, O2—H13...O1 = 157(2)°.

Acknowledgements

We thank the U.S. National Science Foundation for providing funds to purchase the diffractometer. We also thank the Robert A. Welch Foundation for research support (IB grant E-594, RF grant E-136) and the Computer Center of the University of Houston for a generous supply of free computing time. Acknowledgement is also made to donors of The Petroleum Research Fund, administered by the American Chemical Society, for partial support of this research.

1. R. FUCHS and J. H. HALLMAN. Can. J. Chem. **61**, 503 (1983).
2. J. B. PEDLEY and J. RYLANCE. Sussex-N.P.L. computer analysed thermochemical data: organic and organometallic compounds. University of Sussex, Brighton, England. 1977.
3. R. FUCHS, J. H. HALLMAN, and M. O. PERLMAN. Can. J. Chem. **60**, 1832 (1982).
4. F. A. COTTON and B. A. FRENZ. Tetrahedron, **30**, 1587 (1974).
5. V. BUSETTI, G. VALLE, G. ZANOTTI, and G. GALLIAZZO. Acta Crystallogr. B**36**, 894 (1980) and references therein.
6. P. CARR, J. L. FINNEY, P. F. LINDLEY, and G. T. DETITTA. Acta Crystallogr. B**33**, 1022 (1977) and references therein.
7. D. VAN DER HELM, I.-N. HSU, and J. M. SIMMS. Acta Crystallogr. B**28**, 3109 (1972).
8. C. M. BOCK. J. Am. Chem. Soc. **90**, 2748 (1968).
9. J. D. KORP, I. BERNAL, and R. FUCHS. Can. J. Chem. **61**, 50 (1983).
10. A. BURGER and C. BEARD. J. Org. Chem. **26**, 2335 (1961).
11. J. A. CAPUTO and R. FUCHS. J. Org. Chem. **33**, 1959 (1968).
12. G. GERMAIN, P. MAIN, and M. M. WOOLFSON. Acta Crystallogr. A**27**, 368 (1971).
13. G. M. SHELDRICK. SHELX-76 Programs for crystal structure determination. University of Cambridge (1976).
14. D. T. CROMER and J. B. MANN. Acta Crystallogr. A**24**, 321 (1968).
15. R. F. STEWART, E. R. DAVIDSON, and W. T. SIMPSON. J. Chem. Phys. **42**, 3175 (1965).
16. I. L. KARLE, J. KARLE, and K. BRITTS. J. Am. Chem. Soc. **88**, 2918 (1966).
17. L. LEISEROWITZ. Acta Crystallogr. B**32**, 775 (1976).
18. L. S. BARTELL and R. A. BONHAM. J. Chem. Phys. **32**, 824 (1960).

Can. J. Chem. Downloaded from www.nrcresearchpress.com by 210.87.254.6 on 09/06/12
For personal use only.

Methylmercury(II) sulfhydryl interactions. Potentiometric determination of the formation constants for complexation of methylmercury(II) by sulfhydryl containing amino acids and related molecules, including glutathione

ALAN P. ARNOLD AND ALLAN J. CANTY[1]

Chemistry Department, University of Tasmania, Hobart, Tasmania, Australia 7001

Received May 5, 1982

ALAN P. ARNOLD and ALLAN J. CANTY. Can. J. Chem. **61**, 1428 (1983).

Formation constants for the interaction of methylmercury(II) with 2-mercaptoethanol, mercaptoacetic acid, *O*-methylmercaptoacetate, 2-mercaptosuccinic acid, L-cysteine, D,L-penicillamine, *N*-acetyl-D,L-penicillamine, glutathione, thiocholine, and 4-mercapto-*N*-methylpiperidine have been determined by potentiometric titration. For the equilibrium $MeHg^+ + RS^{n-} \rightleftharpoons [MeHgSR]^{1-n}$, log β occurs in the range 14.60(1)−17.14(1), with the lowest value obtained for the cationic complex of thiocholine, $MeHgSCH_2CH_2\overset{+}{N}Me_3$. Acid dissociation constants for the ligands are reported. Formation constants for the addition of both one and two equivalents of MeHg(II) to L-cysteine have been determined, giving log *K* ca. 4.1 for the reaction

$$MeHgSCH_2CH(\overset{+}{N}H_3)(CO_2H) + MeHg^+ \rightleftharpoons (MeHg)_2\overset{+}{S}CH_2CH(\overset{+}{N}H_3)(CO_2H)$$

occurring at low pH, and log *K* 8.8 for the reaction

$$MeHgSCH_2CH(NH_2)CO_2^- + MeHg^+ \rightleftharpoons MeHgSCH_2CH(\overset{+}{N}H_2HgMe)CO_2^-$$

occurring at higher pH.

ALAN P. ARNOLD et ALLAN J. CANTY. Can. J. Chem. **61**, 1428 (1983).

On a déterminé par titrage potentiométrique les constantes de formation pour l'interaction du méthylmercure(II) avec le mercapto-2 éthanol, l'acide mercaptoacétique, le *O*-méthylmercaptoacétate, l'acide mercapto-2 succinique, la L-cystéine, la D,L-pénicillamine, la *N*-acétyl-D,L-pénicillamine, la glutathione, la thiocholine et la mercapto-4 *N*-méthylpipéridine. Dans le cas de l'équilibre $MeHg^+ + RS^{n-} \rightleftharpoons [MeHgSR]^{1-n}$, log β est de l'ordre de 14,60(1) à 17,14(1), le complexe cationique de thiocholine, $MeHgSCH_2CH_2\overset{+}{N}Me_3$ donne la plus faible valeur. On rapporte les constantes de dissociation acide des ligands. On a déterminé les constantes de formation dans le cas de l'addition d'un et de deux équivalents de MeHg(II) sur la L-cystéine qui donne log *K* = 4,1 environ pour la réaction

$$MeHgSCH_2CH(\overset{+}{N}H_3)(CO_2H) + MeHg^+ \rightleftharpoons (MeHg)_2\overset{+}{S}CH_2CH(\overset{+}{N}H_3)(CO_2H)$$

se produisant à faible pH et log *K* = 8,8 pour la réaction

$$MeHgSCH_2CH(NH_2)CO_2^- + MeHg^+ \rightleftharpoons MeHgSCH_2CH(\overset{+}{N}H_2HgMe)CO_2^-$$

se produisant à un pH plus élevé.

[Traduit par le journal]

Introduction

The interaction of methylmercury(II) with thiols to form complexes MeHgSR is believed to be important in both the toxicology of MeHg(II) and the use of antidotes containing thiol groups (1). Thus, a fundamental requirement in studying the biological behaviour of MeHg(II) is accurate values of β_{110} for equilibria [1], where RSH are thiols that occur *in vivo*.

[1] $MeHg^+ + RS^- \rightleftharpoons MeHgSR$

[2] $\log \beta_{110} = [MeHgSR]/[MeHg^+][RS^-]$

Early determinations of log β_{110} with mercaptoalbumin (distribution method) (2, 3), cysteine and glutathione (distribution) (3), and 2-mercaptoethanol (potentiometric) (4) gave values in the range 15.7−16.9. Some recent determinations agree well with these values. Thus, Jawaid and Ingman (5) obtained log β_{110} 15.7 ± 0.12 for L-cysteine (potentiometric); and it has been reported that substituted thiophenols form complexes with log β_{110} in the range 10.48−15.60 (potentiometric) (6, 7) to give the relationship log $\beta_{110} = 0.798pK(RSH) + 8.77$, which is also obeyed by the early values (2−4) of log β_{110} within 0.5p*K* units.

However, Hojo *et al.* (8) in a recent potentiometric study obtained values for several thiols, including L-cysteine and glutathione, which are well below the values reported by other workers (log β_{110} 7.19−9.03). Jawaid and Ingman (5), and Reid and Rabenstein (9), have commented on these results and the latter workers have reported log β_{110} for mercaptoacetic acid, mercaptoethanol, mercaptosuccinic acid, cysteine, penicillamine, homocysteine, and *N*-acetylpenicillamine. Reid and Rabenstein obtained values consistent with the early workers and Jawaid and Ingman, but not Hojo *et al.*

The results of Reid and Rabenstein were obtained using novel ^1H nuclear magnetic resonance competition experiments involving determination of K_d for the equilibrium [3], from which β_{110} for MeHgSR can be evaluated from β_{110} for $MeHgSCH_2CO_2^-$ [4] (9).

[3] $MeHgSCH_2CO_2^- + RS^- \rightleftharpoons MeHgSR + {}^-SCH_2CO_2^-$

[4] $$K_d = \frac{[MeHgSR][{}^-SCH_2CO_2^-]}{[MeHgSCH_2CO_2^-][RS^-]} = \frac{\beta_{110} \text{ for MeHgSR}}{\beta_{110} \text{ for } MeHgSCH_2CO_2^-}$$

Swarzenbach and Schellenberg's value of β_{110} for the 2-mercaptoethanol complex was used to calculate β_{110} for $MeHgSCH_2CO_2^-$ after measurement of K_d for mercaptoacetate/2-mercaptoethanol competition.

[1]To whom all correspondence should be addressed.

Can. J. Chem. Downloaded from www.nrcresearchpress.com by 210.87.254.40 on 09/06/12
For personal use only.

Can. J. Chem. Downloaded from www.nrcresearchpress.com by 210.87.254.40 on 09/06/12
For personal use only.

However, discrepancies between reported values for MeHg(II) thiolate formation constants, and reliance of the nmr method on the single determination of β_{110} for 2-mercaptoethanol, indicate that further measurement of β_{110} for a range of thiols is desirable. In addition, MeHg(II) binds to glutathione in red blood cells (10), and thus competitive equilibria between MeHg(II), glutathione, and sulfhydryl containing antidotes for MeHg(II) poisoning (e.g. D-penicillamine (11) and *N*-acetyl-D,L-penicillamine (11, 12)) are important, but the formation constant for interaction of MeHg(II) with glutathione has only been determined in one of the early investigations (distribution method) (3). We report here a potentiometric study of the interaction of MeHg(II) with all of the ligands studied by the nmr method (except for homocysteine), glutathione, *O*-methylmercaptoacetic acid, and the cationic thiols thiocholine and *N*-methyl-4-mercaptopiperidine. Our potentiometric results confirm early values for glutathione and 2-mercaptoethanol, are in complete agreement with constants determined using the nmr method and provide values for the formation constants for addition of a second MeHg(II) group to L-cysteine to form $(MeHg)_2\overset{+}{S}CH_2CH(\overset{+}{N}H_3)(CO_2H)$ and $MeHgSCH_2CH(\overset{+}{N}H_2HgMe)CO_2^-$.

Experimental

Chemicals

The thiols 2-mercaptoethanol (Koch-Light) and mercaptoacetic acid (Aldrich) were fractionally distilled under reduced nitrogen pressure and stored under nitrogen at −20°C. The crystalline thiols L-cysteine, *N*-acetyl-D,L-penicillamine (Koch-Light), D,L-penicillamine (Ega-Chemie), 2-mercaptosuccinic acid (Aldrich), and glutathione (Sigma) were used as received and stored under nitrogen over P_2O_5. Thiocholine perchlorate was a gift from P. Guerney (University of New South Wales). The thiol *O*-methylmercaptoacetic acid was prepared by acid catalysed *O*-alkylation of mercaptoacetic acid in refluxing methanol (bp 46−47.5°C (4 mm), lit. (13) 42−43°C (10 mm)), and 4-mercapto-*N*-methylpiperidine was prepared as described (13) (bp 31−32°C (1 mm), lit. (14) 62°C (0.8 mm)).

A solution of methylmercury(II) hydroxide was obtained by stirring MeHgI (20 mmol, purified as described elsewhere (15, 16)) with freshly prepared silver oxide (ca. 20 mmol) for 12 h under nitrogen in 50 mL of freshly boiled water. The resultant suspension was filtered (Whatman No. 54), in a nitrogen-flushed glovebox, directly into a 1 L volumetric flask containing a slight excess of nitric acid (20 mmol) to give a $MeHg^+/H^+/NO_3^-$ solution with $[MeHg^+]$ and $[H^+]$ nominally 0.02 *M* and 0.005 *M*, respectively. The solution was stored under nitrogen. Values of $[H^+]$ were determined by alkalimetric titration, monitored potentiometrically, after addition of excess KI to remove $MeHg^+$ as insoluble MeHgI. Values of $[MeHg^+]$ were determined as described elsewhere (15, 16), involving titration with thiosulfate in 50% aqueous methanol with Michlers thioketone as an indicator. The composite concentration, $[H^+] + [MeHg^+]$, was also determined by alkalimetric titration in the absence of iodide, and was in agreement with values for $[H^+]$ and $[MeHg^+]$. Concentration of H^+ and $MeHg^+$ remained constant for 15 months.

The 0.1 *M* potassium hydroxide titrant (Merck Titrisol®) was stored in leached borosilicate glass and was protected by Carbasorb®. The alkali was frequently standardised by potentiometric titration against primary standard grade potassium hydrogen phthalate. The equivalent points of these titrations were determined by the program TITRAT, and produced identical titrant concentrations to alternate titrations against borax standardised 0.1 *M* nitric acid in 0.1 *M* potassium nitrate when equivalent points were found by Gran type 1 or type 2 methods (17). These latter titrations also provided estimates of pK_w^c (see below) and indicated the presence of less than 0.1% weakly acidic impurities, e.g. carbonate, silicate.

Water used for preparation of all titration solutions was deionised by mixed bed ion exchange to a specific resistance greater than 4×10^6 ohm cm, then boiled and cooled under nitrogen prior to use.

The ionic strength of potentiometric titration solutions was adjusted to 0.1 *M* with twice recrystallised potassium nitrate or potassium iodide. The latter also serves as a competitive ligand for MeHg(II) in the formation constant titrations (see below).

Potentiometric measurements

All pH measurements were performed in a thermostatted double walled cell based on that of Perrin and Sayce (18), in which the entire assembly was maintained at 25.00 ± 0.02°C to minimise thermal gradients within the electrodes. An Orion Model 7010 digital pH meter was equipped with a standard glass electrode (Philips GA 110) or low resistance glass electrode (Philips GAT 130), together with a glass sleeve double junction saturated calomel reference electrode (Philips R44/2-SD/1) in which the outer bridge solution was 1 *M* potassium nitrate. The inner (reference) half cell of this electrode was vented outside of the titration vessel to preclude contamination by volatile thiols. The electrode pair was standardised before each titration with thermostatted NBS standard solutions (19) (pH 4.008, 6.865, and 10.012).

Solutions for thiol pK determination

Immediately following standardisation of the electrode assembly, 50.0 mL of thiol solution were transferred to the dried purged titration vessel. For thiols containing carboxylic acid groups 0.1 *M* nitric acid was then added to given an initial pH in the range 2.5−3. Titrant (0.1 *M* potassium hydroxide) was delivered by a motorised 5 mL piston burette (Metrohm D535) through a finely drawn glass capillary placed just beneath the solution surface. The solution was purged with high purity nitrogen which has been passed through a column of Carbasorb® (to remove CO_2) and a thermostatted solution of 0.1 *M* potassium nitrate. Magnetic stirring was stopped and nitrogen redirected over the solution surface during pH measurement. The pH readings were recorded when drift was less than 0.001 units per min. Equilibrium was obtained within 1−5 min in at least moderately buffered regions.

Using this procedure 30−60 titration points were collected over periods of 1−3 h. The electrode standardisation was then verified with the pH 6.865 NBS buffer. On the rare occasions that the electrode standardisation had drifted by more than 0.002 pH, the titration was repeated. Early attempts to use combination electrodes, particularly with solutions of some vicinal dithiols, resulted in restandardisation discrepancies of up to 1 pH unit after such titrations, forcing the use of separate glass and reference electrodes.

Solutions for formation constant determination

An aliquot of $MeHg^+/H^+/NO_3^-$ stock solution was added to 50.0 mL of vigorously stirred thiol solution (containing 0.1 *M* potassium iodide) in order to achieve 1:1 or 2:1 $MeHg^+$:thiol stoichiometry. If precipitation of MeHgI was evident during MeHg(II) addition potassium hydroxide titrant was simultaneously added to achieve the minimum pH consistent with a clear solution. The titration procedure was then identical to that for p*K* determinations. It was often convenient to combine the two procedures by titrating the thiol ligand in 0.1 *M* potassium iodide, then adding $MeHg^+/H^+/NO_3^-$ solution and retitrating after readjustment of the ionic strength with potassium nitrate.

Calculation of equilibrium constants

Calibration of the glass electrode in terms of $[H]^+$

The equilibrium constants recorded in this work are concentration constants, requiring that the electrode assembly be calibrated in terms of log $[H^+]$ rather than log $\{H^+\}$. The approach to this problem advocated by Irving *et al.* (20), and expanded by McBryde (21), and Hedwig and Powell (22) was used in this work, where $[H^+]$ is derived from the measured pH by the relationship

$$-\log [H^+] = pH + pH_{cal}$$

where pH_{cal} includes activity coefficient corrections and accounts for

Can. J. Chem. Downloaded from www.nrcresearchpress.com by 210.87.254.40 on 09/06/12
For personal use only.

systematic errors inherent in transferring electrodes from buffers to titration solutions.

Initially pH_{cal} was measured in a series of titrations of strong acid (0.01 *M* HNO_3 in 0.1 *M* KNO_3) with 0.1 *M* potassium hydroxide. However, it is more convenient to treat pH_{cal} as an unknown parameter in the multiparametric curve fitting procedures used to calculate thiol acid dissociation constants or MeHg(II) complex formation constants. In this way pH_{cal} can be estimated from data below pH 4 for the actual titration under study, rather than from separate preliminary titrations. Values of pH_{cal} calculated in this way over many titrations were always in the range −0.08 to −0.05, in agreement with similar values found elsewhere (22, 23) or in this work by separate strong acid – strong base titrations. It should be emphasised that extraction of low p*K*'s (less than 3) from titration data by any calculation or method requires accurate values of $[H^+]$ in this low pH region (20).

For solutions of moderately strong acids in the multimolar level (p*K* less than 3) small errors in $[H^+]$ result in large *systematic* errors in the estimated p*K* value which are not reflected by the usual error estimates produced by least squares procedures.

A related problem is that of accurate values of K_w^c, which equals $[H^+][OH^-]$ in the ionic medium of interest. Estimates of p*K* values greater than 10−11 are highly correlated to errors in K_w^c and to electrode calibration above pH ~ 11, e.g. it can be shown that the uncertainty in pK_w^c produces 10 times this error in the acid dissociation constant of a weak monoprotic acid with pK_w^c approximately 11.5 (20). Values of pK_w^c were obtained from the difference in $E°$ of the electrode assembly in acid and alkaline regions of strong acid/strong base titrations (24), giving $pK_w^c = 13.74 \pm 0.02$ at 25°C in 0.1 *M* potassium nitrate, which agrees favourably with $pK_w^c = 13.784 \pm 0.006$ calculated from the molal value of 0.1 molal KCl at this temperature (25). However, it was found that the thiol p*K* titration data could not be adequately fitted in the region above pH 10 using pK_w^c 13.74. Multiparametric refinement by TITRAT or MINIQUAD 81 (see below) over many titrations produced values of pK_w^c in the range of 13.86 ± 0.04. This value probably includes a small term due to electrode non-linearity above pH 10. It should be noted that there seem to be many reported instances of equilibrium constants calculated at high pH, e.g. thiol p*K*, in which the value of pK_w^c is either not recorded or has been taken from sources using different experimental conditions. Difficulties in this area are reflected by the general lack of agreement between such constants.

Acid dissociation constants of the thiol ligands were obtained together with values of the proton purity of the ligands with the computer program TITRAT. This program is a generalised version of the interactive rigorously weighted non-linear least-squares programs used by Schwartz and Gelb to evaluate two simultaneous acid dissociation constants (26). TITRAT can refine any combination of the parameters applicable to the titration of a polyprotic acid or base mixture by a stock monoprotic acid or base.[2] The running time of the original program was decreased by an order of magnitude by the use of analytical expressions for condition function derivatives, and the convergence properties improved by quadratic optimisation of the parameter shifts during the refinement.

In this work the acid dissociation constants in the concentration form were refined simultaneously with the number of millimoles of ligand and electrode calibration parameters pH_{cal} and pK_w^c.

Protons do not compete effectively in aqueous solutions with MeHg(II) for the thiolate ligands studied here. One means of overcoming this limitation to the use of pH titrations is to reduce the effective MeHg(II) thiolate constant by competition with another ligand. Iodide is particularly well suited in this regard, e.g. solutions of MeHg(II) and 2-mercaptoethanol exhibit buffer regions in the pH range 3−5 in the presence of 0.1 *M* KI, due to the equilibrium

$$MeHgI + HSCH_2CH_2OH \rightleftharpoons MeHgSCH_2CH_2OH + I^- + H^+$$

The formation constant of MeHgI was obtained by pH titration of MeHg(II) in the presence of 0.1 *M* KI, giving log *K* 8.500(1) (lit. 8.60 (ref. 4), 8.7 (ref. 28)). Above pH 8 the equilibrium

$$MeHgI + H_2O \rightleftharpoons MeHgOH + I^- + H^+$$

is established. Similarly, formation constants for MeHgOH and $(MeHg)_2OH^+$ were evaluated by titration in 0.1 *M* KNO_3, giving log β_{10-1} −4.607 (9) (lit. −4.50 (ref. 29), −4.59 (ref. 4), −4.67(3) (ref. 30), −4.70 (ref. 31), −4.40(2) (ref. 32), −4.686(15) (ref. 33)) and log β_{20-1} −2.234 (18) (lit. −2.22 (constant calculated using values of K_w^c recorded in ref. 4), −2.53 (quoted (refs. 32, 33)), −1.725(30) (ref. 33), −2.33 (quoted (refs. 32, 33))).

The ternary MeHg(II)/thiolate/iodide/proton (or hydroxide) systems were treated using a recent version (34) of the program MINIQUAD 75 (35), which allows simultaneous refinement of formation constants and pH calibration parameters pH_{cal} and the analytical proton excess (H_{tot}) for each titration fit. Refinement of H_{tot} simultaneously with the formation constants by MINIQUAD 81 consistently indicated values 1−2 μmol greater than those calculated from anal-

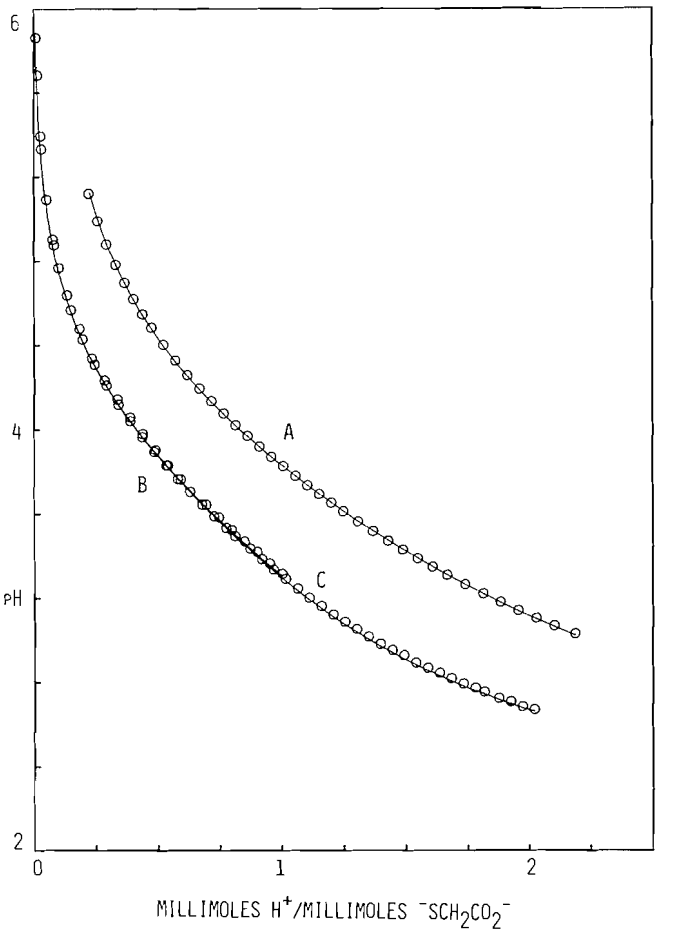

FIG. 1. Titration data for MeHg(II) and mercaptoacetic acid. Data for *A* were obtained with iodide competition, for *B* and *C* without iodide competition. For each titration initial amounts of MeHg(II), $^-SCH_2CO_2^-$, and H^+ are given in mmol followed by molarity of KOH and initial volume; *A*: 0.07703, 0.08244, 0.17977, 0.09947 *M*, 54.97 mL; *B*: 0.1895, 0.1895, 0.1895, 0.09649 *M*, 100.00 mL; *C*: 0.2051, 0.2051, 0.4144, 0.09837 *M*, 102.00 mL. For titration *A* 5.482 mmol of I^- were present.

[2]During this work the programs ACBA (27) and MUPROT (28) were reported. These serve the same purpose as TITRAT, but do not use the statistically rigorous weighting scheme necessary for titrations in which titrant volumes and pH have comparable uncertainties (26). TITRAT is written in OS/8 BASIC for implementation on a Dec PDC/8E minicomputer and uses 12 K core for 60 titration points and up to 6 parameters refined simultaneously. Listings of the program are available on request.

Can. J. Chem. Downloaded from www.nrcresearchpress.com by 210.87.254.40 on 09/06/12
For personal use only.

TABLE 1. Acid dissociation constants for the ligands[a]

Ligand	pK (0.1 M KNO_3 or KI)				Literature values[b]					Reference
2-Mercaptoethanol	*9.58*				9.444				[≈0]	38
					9.72				[≈0]	39
					9.47				[0.3 M $NaClO_4$]	37
Mercaptoacetic acid	3.55	*10.16*			3.60	10.55			[≈0]	40
					3.58	9.78			[0.15 M KNO_3]	41
					3.48	9.92			[0.58 M $NaNO_3$]	42
					3.42	10.20			[0.1 M KCl]	43
					3.35(1)	9.32(2)			[0.3 M KNO_3]	9
O-Methylmercaptoacetate	*7.99*				7.95(2)					44
2-Mercaptosuccinic acid	3.12	4.59	*10.39*		3.64	4.64	10.37		[0.1 M KNO_3]	45
					3.30	4.94	10.64			46
					3.06(1)	4.56(1)	10.39(1)			47
L-Cysteine	1.98(1)	8.23	10.37		1.896(6)	8.178(2)	10.361(1)		[0.1 M KCl]	48
					1.97(1)	8.20(1)	10.87(1)		[0.1 M KNO_3]	49
					1.90	8.12(1)	10.15		[1.0 M $NaNO_3$]	5
						8.48	10.55		[0.15 M KNO_3]	41
						8.13	10.11		[0.1 M KNO_3]	50
D,L-Penicillamine	1.43(8)	8.00	10.59		2.44	7.97	10.46		[0.15 M KNO_3]	51
					1.94	7.93	10.39			52
					1.90(2)	7.932(4)	10.658(3)		[0.1 M KCl]	48
					1.95(1)	7.99(1)	10.56(1)		[0.1 M KNO_3]	53
					2.02(2)	7.92(1)	10.75(1)		[0.1 M KNO_3]	49
						7.88	10.43		[0.1 M KNO_3]	50
N-Acetyl-D,L-penicillamine	3.30	*10.14*			3.18	10.04				54
					3.69(5)	10.01(10)			[0.1 M $NaClO_4$]	55
Glutathione	1.98(2)	3.49	8.75	9.69	2.05	3.40	8.72	9.49	[0.2−0.5 M]	56
					2.09(2)	3.48(1)	8.67(1)	9.54(1)	[0.1 M KNO_3]	49
						3.59	8.75	9.65	[0.15 M KNO_3]	57
							8.74	9.62	[0.16 M KNO_3]	58
Thiocholine	*7.88*					7.7				59
						7.80			[≈0]	60
4-Mercapto-*N*-methylpiperidine	8.33	*10.35*								

[a]Macroscopic concentration constants obtained with TITRAT. Except for the lowest pK values for L-cysteine, D,L-penicillamine, and glutathione, calculated values were to three significant figures, e.g. 2-mercaptoethanol 9.583(2), but are reported to two figures here.

[b]Literature values at 25°C. Mixed constants have been converted to concentration constants by calculation of log γ_{H^+} according to the Davies equation (61).

TABLE 2. Formation constants for methylmercury(II)–thiol complexes

Ligand	Formation constant	This work	Reid and Rabenstein[a]
2-Mercaptoethanol	log β_{110}	16.14(1)	[b]
Mercaptoacetic acid	log β_{110}	16.93(1)	16.92(1)
	log β_{111}	20.69(1)	*20.57(2)*[c]
O-Methylmercaptoacetate	log β_{110}	14.98(2)	
2-Mercaptosuccinic acid	log β_{110}	17.14(1)	17.31(6)
	log β_{111}	21.98(1)	*22.01(8)*[c]
	log β_{122}	25.11(1)	*25.39(11)*[c]
L-Cysteine	log β_{110}	16.46(1)	16.67(1)[d]
	log β_{111}	25.48(1)	*25.32(3)*[c,d]
D,L-Penicillamine	log β_{110}	16.60(1)	16.94(2)
	log β_{111}	25.34(1)	*24.93(3)*[c]
N-Acetyl-D,L-penicillamine	log β_{110}	16.51(1)	
	log β_{111}	19.80(4)	
Glutathione	log β_{110}	15.99(1)	
	log β_{111}	25.24(1)	
	log β_{112}	28.68(2)	
Thiocholine	log β_{110}	14.60(1)	
4-Mercapto-*N*-methylpiperidine	log β_{110}	16.06(3)	
	log β_{111}	25.33(3)	

[a]At 25°C and 0.3 *M* ionic strength. Mixed constants involving protons have been converted to concentration constants using $-\log \gamma_{H^+} = 0.15$ from the Davies equation (61).

[b]Literature value 16.12 at 20°C and 0.1 *M* ionic strength (4).

[c]Values in italics have been derived from measurement of p*K*'s, e.g. for the acid $MeHgSCH_2CO_2H$, log β_{111} = log β_{110} + (p*K* of $MeHgSCH_2CO_2H$).

[d]Jawaid and Ingman obtained log β_{110} 15.70 ± 0.12 and log β_{111} 24.96 ± 0.08 at 25°C and 1 *M* ionic strength (5).

ytical proton concentrations of the thiol and $MeHg^+/H^+/NO_3^-$ solutions. This may reflect the presence of minute quantities of weakly acid silicate or carbonate impurities in the ionic strength adjustment salt or water, or slow leaching of the borosilicate titration vessel, as has been noted elsewhere (36). Such impurities produce slight buffer action for solutions between pH 5 and 8 but do not significantly affect values outside this range. However, neglect of their presence, but not refining H_{tot}, leads to high values of *U* (residual sum of squares, $\sim 10^{-7}$ to 10^{-6}) and *R* (Hamilton *R* factor, ~0.003 to 0.010). Refinement of H_{tot} often improved the degree of fit indicators, e.g. $U \sim 10^{-12}$ to 10^{-9}, $R \sim 0.0003$ to 0.001, and formation constant error estimates, without significantly altering the constants themselves.

Formation constants of the species MeHgI, MeHgOH, and $(MeHg)_2OH^+$ and protonated forms of thiol were fixed in MINIQUAD 81 refinements of MeHg(II) thiolate formation constants. Ternary complexes of the type MeHgI(SR) were rejected by MINIQUAD 81.

A typical example of fit between experimental and calculated titration curves is shown in Fig. 1.

Results and discussion

Acid dissociation and formation constants

Acid dissociation constants (p*K*) for the ligands are given in Table 1, and agree well with previously reported values. Dissociation constants for the thiol groups are given in italics, but since the potentiometric method yields macroscopic constants the two highest values for L-cysteine, D,L-penicillamine, and glutathione are composite macroscopic constants due to simultaneous dissociation of NH_3^+ and SH groups over the same pH region.

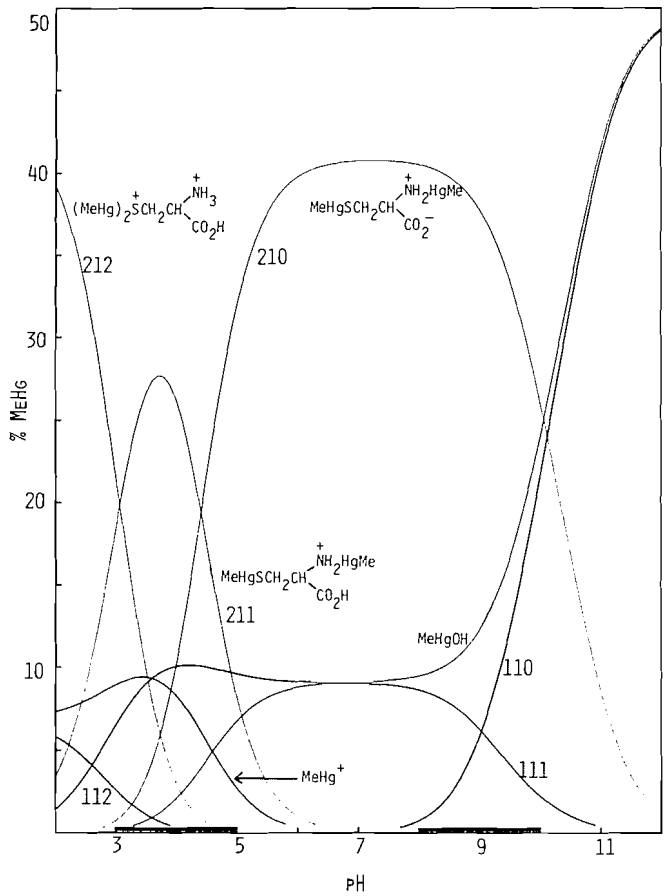

FIG. 2. Species distribution for 0.002 *M* MeHg(II) and 0.001 *M* L-cysteine. The heavy line indicates the pH range of MINIQUAD 81 data. Complex 112: $MeHgSCH_2CH(\overset{+}{N}H_3)(CO_2H)$; 111: $MeHgSCH_2CH(NH_3^+)CO_2^-$; 110: $MeHgSCH_2CH(NH_2)CO_2^-$.

Formation constants for the complexes are given in Table 2, and are in the form log β_{mlh} for equilibria [5], where RS^{n-} represents the fully deprotonated form of the thiol ligand (at pH ca. 12), e.g. 2-mercaptoethanol $^-SCH_2CH_2OH$, L-cysteine $^-SCH_2CH(NH_2)CO_2^-$, and glutathione $^-O_2C(NH_2)CHCH_2CH_2CONHCH(CH_2S^-)CONHCH_2CO_2^-$.

$$[5]\quad m\mathrm{MeHg}^+ + l\mathrm{RS}^{n-} + h\mathrm{H}^+ \rightleftharpoons (\mathrm{MeHg})_m(\mathrm{RS})_l(\mathrm{H})_h^{m+h-nl}$$

$$[6]\quad \beta_{mlh} = \frac{[(\mathrm{MeHg})_m(\mathrm{RS})_l(\mathrm{H})_h^{m+h-nl}]}{[\mathrm{MeHg}^+]^m[\mathrm{RS}^-]^l[\mathrm{H}^+]^h}$$

Thus, the equilibrium constant for equation [1] is described by β_{110}. Dissociation of a proton from a coordinated ligand is usually represented as p*K* of the protonated form of the complex, and may be expressed in terms of β_{mlh}, e.g. for the 2-mercaptoacetic acid complex the dissociation

$$MeHgSCH_2CO_2H \rightleftharpoons MeHgSCH_2CO_2^- + H^+$$

is described by $pK_{111} = \log \beta_{111} - \log \beta_{110}$. Values of log β_{110} are in excellent agreement with the results of Reid and Rabenstein (9), Schwarzenbach and Schellenberg (4), and Jawaid and Ingman (5); and thus support early determinations, involving other biological thiols, by Hughes (2) and Simpson (3).

Sulfhydryl-containing amino acids and peptides

Proton nmr spectroscopic studies indicate that the deprotonated sulfhydryl group of *N*-acetyl-L-cysteine, when coor-

Can. J. Chem. Downloaded from www.nrcresearchpress.com by 210.87.254.40 on 09/06/12
For personal use only.

Can. J. Chem. Downloaded from www.nrcresearchpress.com by 210.87.254.40 on 09/06/12
For personal use only.

dinated to MeHg(II), is able to coordinate to an additional MeHg(II) group (62); and Rabenstein and Fairhurst (63) obtained ^{1}H nmr evidence for similar binding by glutathione in the pH range 0–4. For glutathione at higher pH nmr spectra suggest binding of the second MeHg(II) group to the amine group (63). Several MeHg(II) and PhHg(II) complexes of L-cysteine and D,L-penicillamine with two organomercury groups have been isolated (8, 64, 65) and a MeHg(II) D,L-penicillamine complex isolated from an aqueous solution has been found from an X-ray crystallographic study to have sulfur and amine bound MeHg(II) groups, $MeHgSCMe_2CH(\overset{+}{N}H_2HgMe)CO_2^-$ (64).

Since the ^{1}H nmr and crystallographic results indicate that complexes of 2:1 stoichiometry have structures that differ with pH, evidence was sought for complexes of these stoichiometries with a representative sulfhydryl containing amino acid, L-cysteine, using the potentiometric approach. Solutions containing L-cysteine with more than one equivalent of MeHg(II) were investigated by titration in the absence of iodide. Under these conditions, the sulfur atom may be regarded as "always coordinated", and equilibria were treated assuming a "ligand" of the form $MeHgSCH_2CH(NH_2)CO_2^-$. The data could be satisfactorily refined to give pK_{110} 8.936 (6) (c.f. 9.01 derived from log β_{110} and log β_{111} (Table 2)), pK_{111} 11.60 (2); and for log $\beta'_{ml'h}$ where $l' = MeHgSCH_2CH(NH_2)CO_2^-$ log β'_{110} 8.800 (7), log β'_{111} 13.221 (13), log β'_{112} 15.67 (12), giving derived values of log β_{210} 25.26 (2), log β_{211} 29.69 (3), and log β_{212} 32.13 (13). Thus, for the equilibrium of interest at low pH

$$MeHgSCH_2CH(\overset{+}{N}H_3)(CO_2H) + MeHg^+ \rightleftharpoons (MeHg)_2\overset{+}{S}CH_2CH(\overset{+}{N}H_3)(CO_2H)$$

$$\log K = \log \beta_{212} - \log \beta_{112} \approx 4.1$$

and at higher pH

$$MeHgSCH_2CH(NH_2)CO_2^- + MeHg^+ \rightleftharpoons MeHgSCH_2CH(\overset{+}{N}H_2HgMe)CO_2^-$$

$$\log K = \log \beta_{210} - \log \beta_{110} = 8.8$$

Formation constants for complexes of the type $(MeHg)_2\overset{+}{S}R$ have not been previously reported, but for the proposed equilibrium at higher pH the value of 8.8 compares well with those of 7.88 (ref. 66) and 7.55 (ref. 33) for interaction of MeHg(II) with glycine to form $^-O_2CCH\overset{+}{N}H_2HgMe$. A species distribution diagram (Fig. 2) calculated for a 2:1 ratio of MeHg(II):L-cysteine at 0.002 *M* MeHg(II) illustrates occurrence of these complexes in different pH ranges and, depending on pH, presence of appreciable proportions of the complexes of 1:1 stoichiometry.

Acknowledgements

We thank the National Health and Medical Research Council for financial support, and the Australian Government for a Postgraduate Research Award (to A.P.A.).

1. W. L. HUGHES. Ann. N.Y. Acad. Sci. **65**, 454 (1957); J. T. MCGREGOR and T. W. CLARKSON. Adv. Exptl. Med. Biol. **48**, 64 (1974); A. J. CANTY. Am. Chem. Soc. Symp. Ser. **82**, 327 (1978); A. J. CARTY. Am. Chem. Soc. Symp. Ser. **82**, 339 (1978); D. L. RABENSTEIN. Acc. Chem. Res. **11**, 100 (1978).
2. W. L. HUGHES, JR. Cold Spring Harbour Symp. Quant. Biol. **14**, 79 (1950).
3. R. B. SIMPSON. J. Am. Chem. Soc. **83**, 4711 (1961).
4. G. SCHWARZENBACH and M. SCHELLENBERG. Helv. Chim. Acta, **48**, 28 (1965).
5. M. JAWAID and F. INGMAN. Talanta, **28**, 137 (1981).
6. G. SCHWARZENBACH and U. KARLEN. Unpublished results; H. GROSS. Unpublished results.
7. G. GEIER and I. W. ERNI. Chimia, **27**, 635 (1973).
8. Y. HOJI, Y. SUGIURA, and H. TANAKA. J. Inorg. Nucl. Chem. **38**, 641 (1976).
9. R. S. REID and D. L. RABENSTEIN. Can. J. Chem. **59**, 1505 (1981).
10. D. L. RABENSTEIN, A. A. ISAB, and R. S. REID. Biochim. Biophys. Acta, **720**, 53 (1982).
11. F. BAKIR, S. F. DAMLUJI, L. AMIN-ZAKI, M. MURTADHA, A. KHALIDI, N. Y. AL-RAWI, S. TIKRITI, H. I. DHAHIR, T. W. CLARKSON, J. C. SMITH, and R. A. DOHERTY. Science, **181**, 230 (1973); J. AASETH. Acta Pharmacol. Toxicol. **39**, 289 (1976); T. W. CLARKSON, L. MAGOS, C. COX, M. R. GREENWOOD, L. AMIN-ZAKI, M. A. MAJEED, and S. F. DAMLUJI. J. Pharmacol. Exp. Ther. **218**, 74 (1981).
12. J. AASETH, A. WANNAG, and T. NORSETH. Acta Pharmacol. Toxicol. **39**, 302 (1976).
13. Aldrich Chemical Co. Ltd. Catalog of fine chemicals. 1981–2.
14. H. BARRERA and R. E. LYLE. J. Org. Chem. **27**, 641 (1962).
15. I. W. ERNI. Ph.D. Dissertation, ETH, Zurich. 1977.
16. G. GEIER, I. W. ERNI, and R. STEINER. Helv. Chim. Acta, **60**, 9 (1977).
17. G. GRAN. Acta Chem. Scand. **4**, 559 (1950); Analyst, **77**, 661 (1952); A. JOHANSSON and G. GRAN. Analyst, **105**, 802 (1980); G. GRAN and A. JOHANSSON. Analyst, **106**, 231 (1981); L. PEHRSSON, F. INGMAN, and A. JOHANSSON. Talanta, **23**, 769 (1976).
18. D. D. PERRIN and I. G. SAYCE. Chem. Ind. 661 (1966).
19. Pure Appl. Chem. **51**, 1 (1979).
20. H. M. N. H. IRVING, M. G. MILES, and L. D. PETTIT. Anal. Chim. Acta, **38**, 475 (1967).
21. W. A. E. MCBRYDE. Analyst, **94**, 337 (1969); **96**, 739 (1971).
22. G. R. HEDWIG and H. K. J. POWELL. Anal. Chem. **43**, 1206 (1971).
23. G. NOWOGROCKI, J. CANONNE, and M. WOZNIAK. Bull. Soc. Chim. Fr. **1**, 5 (1976); **1**, 1369 (1976).
24. H. S. ROSOTTI. Talanta, **21**, 809 (1974).
25. F. H. SWEETON, R. E. MESMER, and C. F. BAES. J. Solution Chem. **3**, 191 (1974).
26. L. M. SCHWARTZ and R. I. GELB. Anal. Chem. **50**, 1571 (1978).
27. G. ARENA, E. RIZZARELL, S. SAMMARTANO, and C. RIGANO. Talanta, **26**, 1 (1979).
28. M. WOZNIAK and G. NOWOGROCKI. Talanta, **26**, 1 (1979).
29. T. D. WAUGH, H. F. WALTON, and J. A. LASWICK. J. Phys. Chem. **59**, 395 (1955).
30. P. ZANELLA, G. PLAZZOGNA, and G. TAGLIAVINI. Inorg. Chim. Acta, **2**, 340 (1968).
31. S. LIBICH and D. L. RABENSTEIN. Anal. Chem. **45**, 118 (1973).
32. F. INGMAN and D. H. LIEM. Acta Chem. Scand. **28**A, 947 (1974).
33. M. JAWAID, F. INGMAN, and D. H. LIEM. Acta Chem. Scand. **32**A, 333 (1978).
34. R. N. SYLVA and M. R. DAVIDSON. J. Chem. Soc. Dalton, 465 (1979).
35. P. GANS, A. SABATINI, and A. VACCA. Inorg. Chim. Acta, **18**, 237 (1976).
36. L. CIACATTA. Arkiv. Kemi. **20**, 417 (1963).
37. S. J. BACKS and D. L. RABENSTEIN. Inorg. Chem. **20**, 410 (1981).
38. P. J. ANTIKAINEN and K. TEVANEN. Suomen Kemi. **35**B, 224 (1962).
39. R. J. IRVING, L. NELANDER, and I. WADSÖ. Acta. Chem. Scand. **18**, 769 (1964).
40. D. L. LEUSSING and I. M. KOLTHOFF. J. Am. Chem. Soc. **75**, 3904 (1953).
41. N. C. LI and R. A. MANNING. J. Am. Chem. Soc. **77**, 5225 (1955).

42. D. L. LEUSSING and L. NEWMAN. J. Am. Chem. Soc. **78**, 552 (1956).
43. D. L. LEUSSING. J. Am. Chem. Soc. **80**, 4180 (1958).
44. J. L. KURZ and J. C. HARRIS. J. Org. Chem. **35**, 3086 (1970).
45. G. R. LENZ and A. E. MARTELL. Inorg. Chem. **4**, 378 (1965).
46. G. E. CHENEY, Q. FERNANDO, and H. FREISER. J. Phys. Chem. **63**, 2055 (1959).
47. L. J. PERRIN and D. D. PERRIN. Aust. J. Chem. **22**, 267 (1969).
48. J. H. RITSMA and F. JELLINEK. Rec. Trav. Chim. Pays-Bas, **91**, 923 (1972).
49. L. PILLAI, R. D. BOSS, and M. S. GREENBERG. J. Solution Chem. **8**, 635 (1979).
50. G. R. LENZ and A. E. MARTELL. Biochemistry, **3**, 745 (1969).
51. E. J. KUCHINSKAS and Y. ROSEN. Arch. Biochem. Biophys. **97**, 370 (1962).
52. E. W. WILSON and R. B. MARTIN. Arch. Biochem. Biophys. **142**, 445 (1971).
53. N. KOJIMA, Y. SUGIURA, and H. TANAKA. Bull. Chem. Soc. Jpn. **49**, 445 (1976).
54. D. A. DOORNBOS. Pharm. Weekblad. **102**, 269 (1967).
55. R. L. COATES and M. M. JONES. J. Inorg. Nucl. Chem. **39**, 677 (1976); J. S. CASAS and M. M. JONES. J. Inorg. Nucl. Chem. **42**, 99 (1980).
56. D. L. RABENSTEIN. J. Am. Chem. Soc. **95**, 2797 (1973).
57. N. C. LI, O. GAWRON, and G. BASCUAS. J. Am. Chem. Soc. **76**, 225 (1954).
58. R. B. MARTIN and J. T. EDSALL. Bull. Chem. Soc. Chim. Biol. **40**, 1763 (1958).
59. L. LARSSON and B. HANSEN. Svensk. Kem. Tidskr. **68**, 521 (1956).
60. YA. L. KOSTYUKOVSKII, YU. A. BRUK, A. V. KOKUSHKINA, B. S. MIRKIN, N. M. SLAVACHEVSKAYA, L. M. PAVLOVA, and I. A. BELEN'KAYA. Zh. Obshch. Khim. **42**, 2104 (1972); Chem. Abstr. **78**, 42615*v* (1972).
61. C. W. DAVIES. J. Chem. Soc. 2093 (1938).
62. P. G. SIMPSON, T. E. HOPKINS, and R. HAQUE. J. Phys. Chem. **77**, 2282 (1973).
63. D. L. RABENSTEIN and M. T. FAIRHURST. J. Am. Chem. Soc. **97**, 2086 (1975).
64. Y. S. WONG, A. J. CARTY, and C. CHIEH. J. Chem. Soc. Dalton, 1801 (1977).
65. A. J. CANTY and R. KISHIMOTO. Aust. J. Chem. **30**, 669 (1977).
66. D. L. RABENSTEIN, R. OZUBKO, S. LIBICH, C. A. EVANS, M. T. FAIRHURST, and C. SUVANPRAKORN. J. Coord. Chem. **3**, 263 (1974).

Can. J. Chem. Downloaded from www.nrcresearchpress.com by 210.87.254.40 on 09/06/12
For personal use only.

Etude théorique de la structure et de la réactivité de l'anion du pentazole

MINH-THO NGUYEN
Laboratorium voor Quantum Chemie, Katholieke Universiteit te Leuven, Celestijnenlaan, 200 F, 3030 Heverle, Belgique
MICHEL SANA[1] ET GEORGES LEROY
Université Catholique de Louvain, Laboratoire de Chimie Quantique, Place Louis Pasteur, 1, 1348 Louvain-la-Neuve, Belgique
ET
JOSE ELGUERO[2]
Instituto de Química Médica, CSIC, Juan de la Cierva 3, Madrid-6, Espagne

Reçu le 17 mars, 1982[3]

MINH-THO NGUYEN, MICHEL SANA, GEORGES LEROY et JOSE ELGUERO. Can. J. Chem. **61**, 1435 (1983).

La méthode "*ab initio*" LCAO-SCF-MO avec la base 4-31G a été utilisée pour étudier le supersystème N_5^-. Les trois structures possibles (ion azoture + azote moléculaire, ion pentazène et ion pentazole) et leurs chemins de réaction ont été calculés. L'anion du pentazole est moins stable que les réactifs N_3^- + N_2, mais beaucoup plus stable que l'anion du pentazène; il pourrait constituer un objectif synthétique raisonnable. Les énergies d'activation des différents chemins ont été comparées à celles du supersystème neutre N_5H.

MINH-THO NGUYEN, MICHEL SANA, GEORGES LEROY, and JOSE ELGUERO. Can. J. Chem. **61**, 1435 (1983).

"*Ab initio*" LCAO-SCF-MO calculations using the 4-31G basis set were carried out in order to study the supersystem N_5^-. The three possible stable structures (azide ion + molecular nitrogen, pentazene ion, and pentazole ion) and their reactions paths were calculated. The pentazole anion is less stable than the reagents N_3^- + N_2, but much more stable than the pentazene anion; it could constitute a reasonable synthetic target. The activation energies of the different paths were compared with those of the neutral supersystem N_5H.

Introduction

Au cours de deux précédents travaux nous avons examiné théoriquement le cas de deux molécules aromatiques situées à la frontière de la chimie inorganique et de la chimie organique: le pentazole N_5H **1** (1) et l'héxazine N_6 **2** (2).

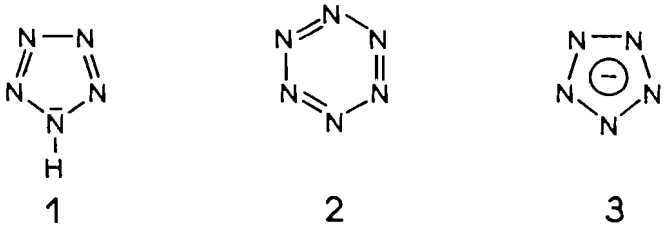

1 2 3

L'objet du présent travail est double: d'une part, étudier théoriquement la structure de l'anion pentazole **3**; d'autre part, examiner sa réactivité en vue de déterminer si l'anion **3** est un objectif synthétique plus réaliste que le pentazole **1**. Parallèlement, nous voulions établir si l'anion pentazole était susceptible d'intervenir dans un mécanisme de fixation de l'azote moléculaire.

Méthode

Tous les calculs ont été effectués par la méthode "*ab initio*" LCAO-SCF-MO. Etant donné le caractère d'ions négatifs des molécules à étudier, la base 4-31G a été choisie (3). Elle permet dans le cas présent d'obtenir des orbitales HOMO d'énergie négative. Les optimisations des géométries ont été effectuées de façon itérative; la précision obtenue est estimée à 0,03 Å sur les distances et 3° sur les angles. Dans ce travail, nous ne tiendrons pas compte des erreurs de superposition dont l'existence est souvent admise dans de tels calculs, en base limitée. En effet, les procédés utilisés pour évaluer ces erreurs de superposition sont sujets à caution lorsque la géométrie du supersystème est fort différente de celle des espèces isolées, ce qui est précisément le cas ici.

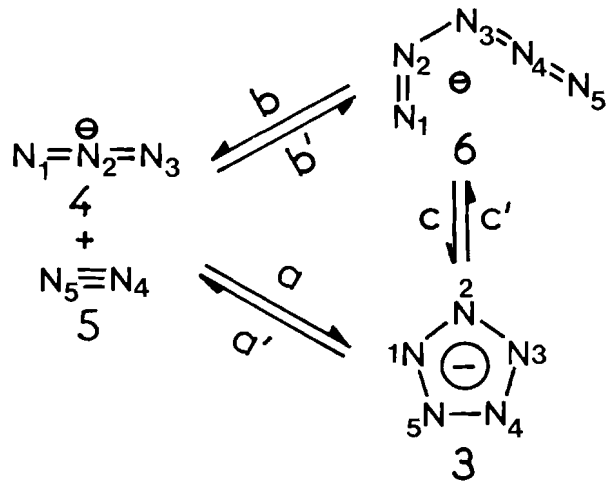

FIG. 1. Isomères de formule N_5^-.

TABLEAU 1. Géométrie de l'ion azoture **4**

Méthode	NN (Å)	NNN (°)	Référence
LCAO-SCF-MO (4-31G)	1,202	180	Ce travail
LCAO-SCF-MO (6-31G)	1,177	180	4
Expérimentale[a]	1,15−1,18	180	5

[a]Valeurs dans les azides ioniques qui dépendent de la nature du cation

[1]Chercheur qualifié du Fonds National Belge de la Recherche Scientifique.
[2]Auteur à qui adresser la correspondance.
[3]Révision reçue le 13 octobre, 1982.

Can. J. Chem. Downloaded from www.nrcresearchpress.com by 210.87.254.6 on 09/06/12
For personal use only.

Can. J. Chem. Downloaded from www.nrcresearchpress.com by 210.87.254.6 on 09/06/12
For personal use only.

TABLEAU 2. Géométries et énergies le long de l'addition ion azoture + azote moléculaire (distances en Å et angles en °)

R^a	τ	β	N_2N_3	N_4N_5	N_1N_5	E (ua)
∞	0	180[b]	1,20[b]	1,10[c]	∞	−271,71103
2,40	0	144	1,24	1,16	2,50	−271,65979
2,10	0	135	1,26	1,20	2,21	−271,63847
1,85*	0	126	1,27	1,24	1,93	−271,63498
1,70	0	122	1,28	1,26	1,78	−271,63938
1,55	0	117	1,30	1,28	1,63	−271,65006
1,26	0	108[d]	1,32[d]	1,32[d]	1,32[d]	−271,69922

[a]Paramètres de structure définis sur la figure 2.
[b]Ion azoture.
[c]Azote moléculaire.
[d]Ion pentazole 3.

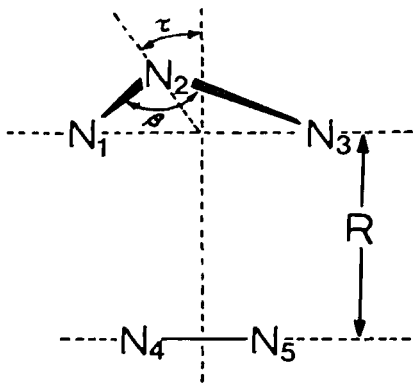

FIG. 2. Paramètres géométriques de l'addition ion azoture + azote moléculaire.

Discussion

1. *Les molécules isolées*

La figure 1 représente les trois formes de la supermolécule N_5^-: ion azoture **4** + azote moléculaire **5**, ion pentazène **6** et ion pentazole **3**.

Le tableau 1 confronte, pour la géométrie de l'ion azoture, les résultats du calcul avec l'expérience. Sa structure électronique est celle d'un dipôle-1,3 de type propargyle, selon la classification d'Huisgen (6). Cependant, les centroïdes de

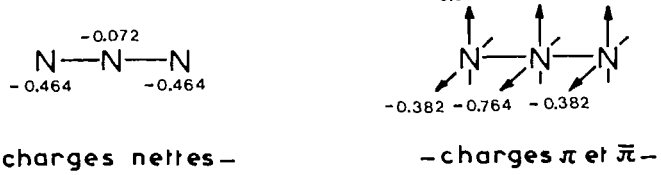

charge (7) indiquent que chaque liaison NN est de nature triple et la formule de structure correspondante suggère l'existence de deux liaisons adjacentes à 6 électrons. En fait, comme certains d'entre nous l'ont démontré (8), une intégration de la densité électronique dans le domaine compris entre deux plans passant par les atomes d'azote terminaux indique la présence de 10 électrons, au lieu de 12, autour de l'atome d'azote central.

La structure de la molécule d'azote **5** a été discutée dans notre travail sur le pentazole (1). Quant à l'anion pentazène **6**, nous donnons ci-dessous sa géométrie optimisée.

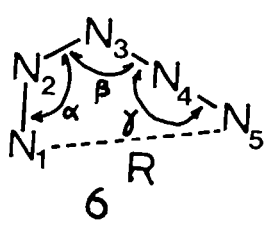

R = 2,87 Å
N_1N_2 = 1,23 Å
N_2N_3 = 1,41 Å
N_3N_4 = 1,25 Å
N_4N_5 = 1,13 Å

α = 110°
β = 107°
γ = 185°

Nous constatons que la liaison N_3N_4 dans l'anion **6** (1,25 Å) a un caractère double plus marqué que dans la pentazène, où elle est quasi simple (1,32 Å (1)); cette différence de structure est due à la délocalisation de la charge négative de l'anion N_5^- sur le squelette moléculaire. Ceci mis à part, la distribution des centroïdes de charge est semblable dans le pentazène et dans son ion négatif.

Finalement, l'anion pentazole **3**, de symétrie D_{5h}, a une distance NN de 1,32 Å et un angle interne de 108° dans sa géométrie d'énergie minimum. Sa structure électronique peut se résumer comme suit :

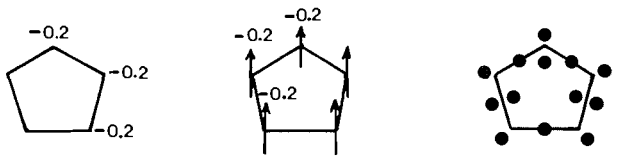

2. *Les chemins réactionnels*

a. Cycloaddition de l'anion azoture sur l'azote moléculaire (**4** + **5** → **3**)

L'ion azoture intervient dans des réactions de cycloaddition dipolaire-1,3 face à des dipolarophiles conventionnels, tels les nitriles (formation de tétrazoles (9)). La réaction avec l'azote moléculaire n'a pas été signalée. Etant donné la parfaite symétrie des réactifs, nous avons imposé la symétrie C_s à la supermolécule. Les paramètres de structure calculés le long du chemin de réaction sont reunis dans le tableau 2.

L'approche des réactifs est coplanaire (τ = 0°) et l'état de transition se situe aux alentours de R = 1,85 Å le long de la coordonnée de réaction comme dans le cas du supersystème neutre "acide hydrazoïque + azote moléculaire" (1). Dans le complèxe activé, le transfert de charge vers le dipolarophile atteint une valeur de 0,38 électrons en base 4-31G. La réaction est endothermique, les réactifs isolés sont plus stables de 15,6 kcal mol^{-1} que l'anion du pentazole. La barrière d'activation est égale à 55,9 kcal mol^{-1} (dans le sens **4** + **5** → **3**). Même si la base 4-31G a tendance à augmenter la barrière d'activation par rapport à celle obtenue en base minimale STO-3G, la valeur trouvée pour le système N_3^- + N_2 est notablement plus haute que celle calculée pour d'autres cycloadditions dipolaires-1,3 (moins de 35 kcal mol^{-1} (10)).

b. Décomposition des dipoles-1,5 : cas de l'anion pentazène (**6** → **4** + **5**)

Cette réaction fait partie d'un vaste ensemble, dans lequel on peut inclure les transpositions de Curtius et de Wolff (11). Sur la figure 3 sont représentés les paramètres de structure retenus dans le calcul du chemin de réaction. Dans le sens inverse *b'* (**4** + **5** → **6**) il correspond à l'addition nucléophile du dipole-1,3 sur la molécule d'azote.

La distance r est choisie comme coordonnée de réaction. Nous n'avons imposé aucune contrainte sur la distance R', en fait, cette distance n'est pas directement optimisée car elle est dépendante des autres paramètres de structure. Pour tous les

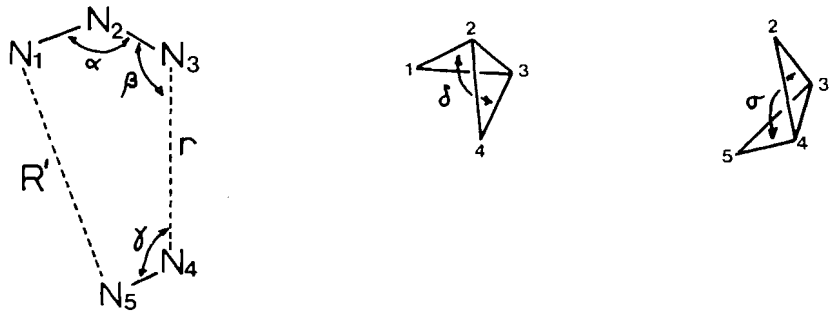

FIG. 3. Paramètres géométriques de l'addition nucléophile.

TABLEAU 3. Paramètres géométriques et énergies totales le long du chemin de l'addition ion azoture + azote moléculaire

r	N_1N_2	N_2N_3	N_4N_5	R'	α	β	γ	E (ua)
∞	1,20[a]	1,20[a]	1,10[b]	∞	180[a]	—	—	−271,72402
1,75	1,23*	1,35	1,13*	3,62	150	100	190	−271,57059
1,60*[d]	1,23*	1,37	1,13*	3,45	135	100	190	−271,56256
1,45	1,23*	1,39	1,13*	3,25	120	103	190	−271,57208
1,30	1,23*	1,41	1,13*	2,95	110	108	185	−271,58042
1,25[c]	1,23[c]	1,41[c]	1,13[c]	2,87[c]	110[c]	107[c]	185[c]	−271,59012

[a]Ion azoture.
[b]Azote moléculaire.
[c]Ion pentazène **6**.
[d]*État de transition ; *non optimisé.

TABLEAU 4. Paramètres géométriques et énergies totales le long du chemin **6** → **3**

R'	N_1N_2	N_2N_3	N_3N_4	N_4N_5	α	β	γ	E (ua)
2,87[a]	1,23	1,41	1,25	1,13	110	107	185	−271,59012
2,52	1,25	1,41	1,26	1,15	110*	107*	170	−271,58541
2,35	1,26	1,41	1,26	1,17	110*	107*	160	−271,58217
2,30*[b]	1,27	1,40	1,26	1,18	110*	107*	150	−271,57806
2,20	1,27	1,39	1,27	1,19	109*	107*	141	−271,58020
1,90	1,29	1,37	1,29	1,24	108*	108*	133	−271,59382
1,61	1,31	1,33	1,32	1,30	108*	108*	120	−271,65503
1,32[c]	1,32	1,32	1,32	1,32	108	108	108	−271,69922

[a]Ion pentazène **6**.
[b]*État de transition ; *non optimisé.
[c]Ion pentazole **3**.

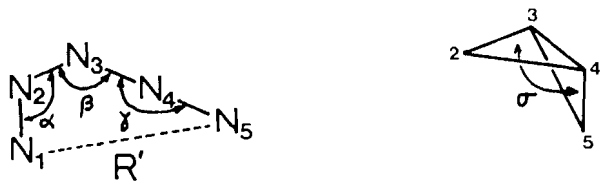

FIG. 4. Paramètres géométriques de la cyclisation de l'anion pentazène en anion pentazole.

points du chemin de réaction, l'optimisation de la géométrie conduit à des valeurs nulles pour les angles δ et σ ; tous les atomes restent dans un même plan. Les résultats obtenus sont reportés dans le tableau 3.

Etant donné la taille importante de la supermolécule, les paramètres du tableau 3 ne sont que partiellement optimisés en base 4-31G. Notons que les angles α et γ diminuent (le dernier restant toujours supérieur à 180°), tandis que l'angle β et les longueurs des liaisons augmentent. Energétiquement, l'anion du pentazène se décompose exothermiquement (~84 kcal mol^{-1}) à une distance r = 1,60 Å avec une barrière d'activation de l'ordre de 17 kcal mol^{-1}. En vue de comparer ce résultat à celui du pentazène (STO-3G : ΔH_R = 43,1 kcal mol^{-1}, $\Delta E^{\neq}$ = 2,5 kcal mol^{-1} (1)), nous avons recalculé en base 4-31G quelques points du chemin de décomposition de ce dernier. Les résultats en base étendue confirment ceux obtenus en base minimale : la barrière à la décomposition du pentazène reste d'environ 1 kcal mol^{-1}. Bien que les chaleurs de décomposition en base 4-31G pour le pentazène et son anion sont proches (−78 et −84 kcal mol^{-1}) en raison de la différence importante entre les deux barrières d'activation nous pouvons admettre que l'anion pentazène est beaucoup plus stable que le composé neutre.

L'analyse des mouvements électroniques en termes de centroïdes de charge est voisine de celle décrite pour la molécule neutre (1). La principale différence est que dans la réaction $HN_3 + N_2 \rightarrow N_5H$, l'analyse de population de Mulliken montre qu'en tout point du chemin de réaction le transfert de

Can. J. Chem. Downloaded from www.nrcresearchpress.com by 210.87.254.6 on 09/06/12
For personal use only.

Can. J. Chem. Downloaded from www.nrcresearchpress.com by 210.87.254.6 on 09/06/12
For personal use only.

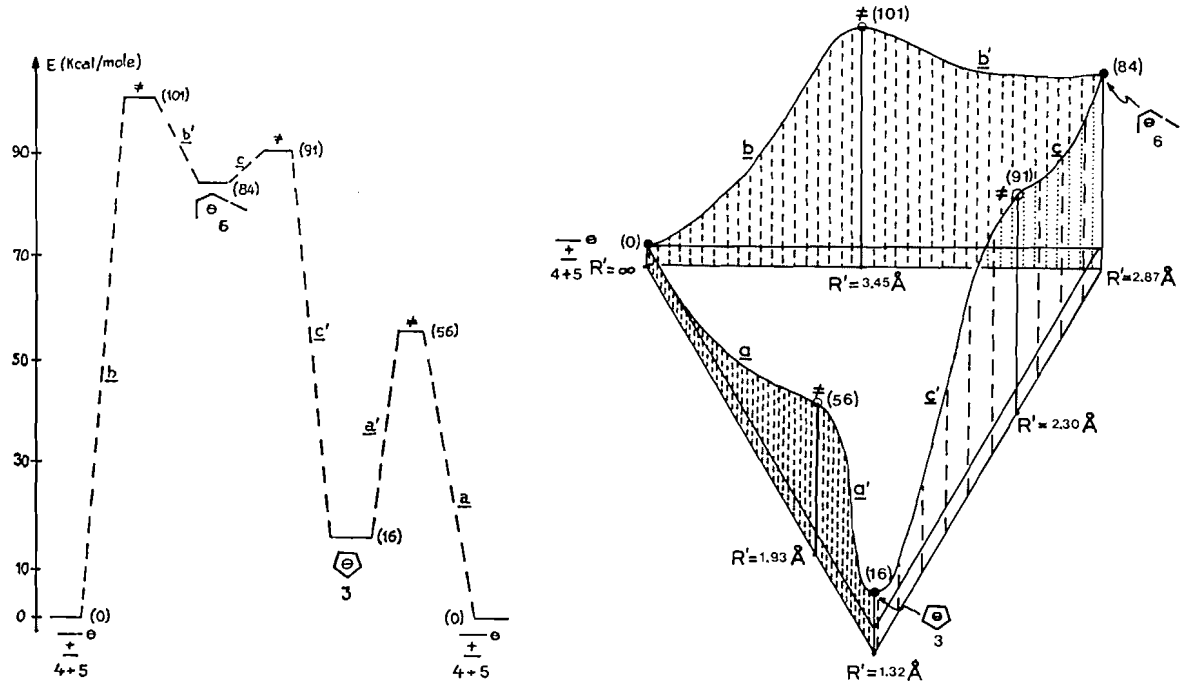

FIG. 5. Energies relatives des points caractéristiques des chemins de réaction du système N_5^- (kcal mol^{-1}, valeurs entre parenthèses).

charge s'effectue de la molécule neutre vers le dipôle-1,3 (le transfert est maximum à l'état de transition, r = 1,34 Å, et vaut, en base 4-31G, 0,15 électrons), tandis que dans le système $N_3^- + N_2 \rightarrow N_5^-$, le transfert de charge se fait de l'anion azoture **4** vers la molécule d'azote **5** et vaut 0,04 électrons à l'état de transition. Cette différence de comportement entre HN_3 et N_3^- est une conséquence de la charge négative de l'ion azoture. En langage chimique usuel, *dans le supersystème neutre, l'entité nucléophile est l'azote moléculaire tandis que dans le supersystème anionique c'est l'ion azoture qui joue ce rôle.*

La différence entre les voies "concertée" *a* et "non concertée" *b* est que dans la première il y a formation de deux liaisons σ distinctes N_1N_5 et N_3N_4 et dans la seconde d'une liaison σ et d'une liaison π entre les deux centres N_3 et N_4.

c. Cyclisation des dipôles-1,5 : cas de l'anion pentazène (**6** → **3**)

Dès les travaux pionniers de Reimlinger en 1970 (12), les cyclisations électrocycliques-1,5 ont reçu une attention considérable comme source d'hétérocycles pentagonaux (13, 14). Dans le cas particulier des anions des dipôles-1,5 on doit citer, par exemple, l'obtention d'anions tétrazoliques par cyclisation d'anions d'azidoimines (15, 16);[4] plusieurs de ces travaux signalent qu'en milieu neutre la forme dipôle-1,5 est stable tandis qu'en milieu basique la forme tétrazole est largement favorisée.

Le chemin de réaction correspondant à la fermeture de l'anion pentazène N_5^- en anion pentazole a été partiellement optimisée en base double 4-31G ; les paramètres de structure et les énergies associées sont reportés dans le tableau 4. Nous avons utilisé le jeu de paramètres défini sur la figure 4. L'optimisation montre que les atomes d'azote restent dans un même plan tout le long du chemin de réaction ($\sigma \cong 0$), le processus d'électrocyclisation est donc planaire.

L'état de transition se situe à R' = 2,30 Å; la barrière d'activation et la chaleur de réaction valent respectivement 7,5 et −68,4 kcal mol^{-1} par rapport à l'ion pentazène. Si nous comparons ces valeurs à celles de la réaction "pentazène → pentazole" calculées en base 4-31G avec la géométrie optimisée en base STO-3G (1): 9,6 kcal mol^{-1} pour $\Delta E^{\neq}$ et −24,8 kcal mol^{-1} pour ΔH_R, nous remarquons que si les barrières d'activation sont du même ordre de grandeur, par contre la différence entre les chaleurs de réaction est énorme. La stabilisation de la forme cyclique par rapport à la forme ouverte est de 43,6 kcal mol^{-1} en passant de la molécule neutre à son anion. Cette stabilisation nous suggère que la délocalisation de la charge négative sur le cycle rend l'anion plus "aromatique" que la molécule neutre.

Au total, ces résultats sont en accord avec l'expérience qui montre que sous forme anionique l'équilibre forme ouverte/forme fermée se déplace vers la forme cyclique (15, 16).[4]

3. *Le bilan énergétique de la supermolécule* N_5^-

Sur la figure 5, nous donnons le profil énergétique de différentes réactions de la supermolécule N_5^- calculée en base double 4-31G.

Les réactifs ($N_3^- + N_2$) restent le système le plus stable, mais la différence d'énergie entre ce dernier en l'anion pentazole **3** n'est que de 16 kcal mol^{-1} au lieu de 54 kcal mol^{-1} dans le système neutre (1). Contrairement au cas du pentazène (1), la décomposition de l'ion pentazène **6** via l'ion pentazole **3** (voie $c-a'$) est favorisé par rapport à sa décomposition directe (voie b'). L'anion pentazole **3** se décompose à son tour en suivant le chemin de cycloreversion a' et la barrière d'activation est nettement plus grande (40 kcal mol^{-1}) que celle de la molécule de pentazole (6 kcal mol^{-1} (1)). Ces résultats nous montrent que l'anion pentazole **3** est plus stable que la molécule neutre, comme il arrive pour d'autres anions cycliques ; ainsi les aza[13] annulènes ont une structure polyènique tandis que l'anion aza[13] annulenyl possède toutes les caractéristiques d'une molécule aromatique (17). Selon nos calculs, il est raisonnable d'admettre que les cycles pentagonaux sont suffisamment grands pour que cette règle soit valable. Signalons

[4]Voir aussi ref. 9, p. 402.

pour terminer que la différence de stabilité entre le pentazole **1** et son anion **3** indique que le premier doit être un composé très acide en solution davantage même que le tétrazole (pK_a = 4,90 (18)).

Conclusion

Les résultats obtenus par le calcul montrent que si l'anion du pentazole **3** n'est pas une entité moléculaire suffisamment stable pour être utilisée pour la fixation de l'azote moléculaire, elle constitue néanmoins un objectif synthétique réaliste. Sa mise en évidence pourrait se faire par échange isotopique, en traitant l'ion azoture marquée à l'azote 15 par un grand excès d'azote moléculaire $^{14}N-^{14}N$ à très haute pression. La formation d'un intermédiaire pentazolique **3** se traduirait par l'échange $^{15}N/^{14}N$ au niveau de l'ion azoture :

$$^{15}N_3^- + {}^{14}N_2 \rightleftharpoons [\mathbf{3}] \rightleftharpoons {}^{14}N_3^- + {}^{15}N_2$$

Ce type d'expériences a été utilisée avec succès par Zollinger (19) pour démontrer l'existence d'un équilibre reversible $PhN_2^+ \rightleftharpoons Ph^+ + N_2$. Une autre possibilité sérait de pieger l'anion **3** sous forme de complèxe π, par exemple, avec du manganèse-tricarbonyle **7** ou avec du fer-cyclopentadienyle **8**. Dans les deux cas, les analogues monoazotés (dérivés de l'anion du pyrrole) sont connus (20).

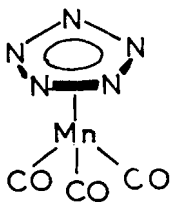

7

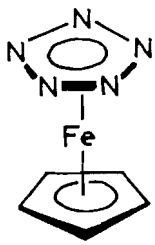

8

1. M. SANA, G. LEROY, M. T. NGUYEN et J. ELGUERO. Nouv. J. Chim. **3**, 607 (1979).
2. T. K. HA, R. CIMIRAGLIA et M. T. NGUYEN. Chem. Phys. Lett. **83**, 317 (1981).
3. W. J. HEHRE, R. DITCHFIELD et J. A. POPLE. J. Chem. Phys. **56**, 2257 (1972).
4. J. LIEVIN, J. BREULET et G. VERHAEGEN. Theoret. Chim. Acta, **52**, 75 (1979).
5. A. TREININ. *Dans* The chemistry of the azido group. *Edité par* S. Patai. Interscience, New York. 1971. p. 14 ; voir aussi : G. A. ASTON, P. E. WILLS et T. P. ZOLKI. J. Am. Chem. Soc. **77**, 3939 (1955).
6. R. HUISGEN. Angew. Chem. Int. Ed. Engl. **2**, 565 (1963) ; **2**, 633 (1963).
7. S. J. BOYS. Rev. Mod. Phys. **32**, 296 (1960) ; J. M. FOSTER et S. J. BOYS. Rev. Mod. Phys. **32**, 300 (1960).
8. G. LEROY, D. PEETERS, A. DEPLUS et M. TIHANGE. Nouv. J. Chim. **3**, 213 (1979).
9. R. N. BUTLER. Recent advances in tetrazole chemistry. *Dans* Advances in heterocyclic chemistry. Vol. 21. *Edité par* A. R. Katritzky et A. J. Boulton. Academic Press, New York. 1977. p. 360.
10. M. SANA, G. LEROY, G. DIVE et M. T. NGUYEN. J. Mol. Struct. **89**, 147 (1982).
11. M. T. NGUYEN. Dissertation de Doctorat, Université Catholique de Louvain, 1980. Voir particulièrement le Chapitre 4.
12. H. REIMLINGER. Chem. Ber. **103**, 1900 (1980).
13. J. ELGUERO. Bull. Soc. Chim. Fr. 1925 (1971).
14. R. HUISGEN. Angew. Chem. Int. Ed. Engl. **19**, 947 (1980).
15. E. ALCALDE, J. DE MENDOZA et J. ELGUERO. Chem. Commun. 411 (1974) ; J. Heterocycl. Chem. **11**, 921 (1974) ; E. ALCALDE et R. M. CLARAMUNT. Tetrahedron Lett. 1523 (1975).
16. S. OLIVELLA et J. VILARRASA. J. Heterocycl. Chem. **16**, 685 (1979).
17. A. G. ANASTASSIOU et R. L. ELLIOT. J. Am. Chem. Soc. **96**, 5257 (1974) ; G. SCHRÖDER, G. FRANK, M. RÖTTELE et J. F. M. OTH. Angew. Chem. Int. Ed. Engl. **13**, 205 (1974).
18. K. SCHOFIELD, M. R. GRIMMETT et B. R. T. KEENE. The azoles. Cambridge University Press, Cambridge. 1976. p. 285.
19. H. ZOLLINGER. Chimia, **35**, 127 (1981); H. B. AMBROZ et T. J. KEMP. Chem. Soc. Rev. **8**, 353 (1979).
20. F. A. COTTON et G. WILKINSON. Advanced inorganic chemistry. Wiley, New York. 1980. p. 1170.

Can. J. Chem. Downloaded from www.nrcresearchpress.com by 210.87.254.6 on 09/06/12
For personal use only.

An investigation of the biphasic kinetics observed during the hydroxide ion-catalyzed hydrolysis of alkyl dithioesters[1]

A. C. STORER

Division of Biological Sciences, National Research Council of Canada, Ottawa, Ont., Canada K1A 0R6

Received October 4, 1982

A. C. STORER. Can. J. Chem. **61**, 1440 (1983).

Kinetic evidence is presented for the establishment of an equilibrium, in dilute aqueous alkaline solutions, between alkyl dithioesters and a species **I**. The species **I** is formed either by the extraction of a proton from, or by the addition of an hydroxide ion to, the dithioester. In the former case **I** would be an anion (probably an enethiolate) formed by the removal of a proton from the α-carbon atom, and in the latter case **I** would be a stabilized tetrahedral intermediate formed by the addition of an hydroxide ion to the thiocarbonyl carbon atom. It has not been possible, using kinetic evidence alone, to distinguish conclusively between these two possibilities. However, using the available evidence, arguments are presented in favor of **I** being an enethiolate anion.

A. C. STORER. Can. J. Chem. **61**, 1440 (1983).

On présente des preuves cinétiques de l'équilibre qui s'établit entre des dithioesters d'alkyle et une espèce **I** en solution alcaline aqueuse diluée. L'espèce **I** se forme soit par élimination d'un proton du dithioester, soit par addition d'un ion hydroxyde sur la dithioester. Dans le premier cas, l'espèce **I** serait un anion (probablement un enethiolate) formé par l'élimination d'un proton de l'atome de carbone en position α et dans le deuxième cas, l'espèce **I** serait un intermédiaire tétraédrique stabilisé formé par l'addition d'un ion hydroxyde sur l'atome de carbone du thiocarbonyle. A partir de cette preuve cinétique uniquement il n'est pas possible d'établir une distinction entre ces deux possibilités. Cependant, à partir des preuves disponibles, on présente des faits qui tendent à prouver que l'espèce **I** est un anion enethiolate.

[Traduit par le journal]

Introduction

In this laboratory extensive studies are underway on the cysteine protease catalysed hydrolysis of thionoesters (1–3). The reaction pathway for these enzymes and substrates involves a dithioacyl enzyme intermediate, the hydrolysis of which can be followed spectrophotometrically (1). In order to compare the hydrolysis of these intermediates with that of the more normal thioacyl enzyme intermediates it is first necessary to compare the base catalysed hydrolysis of simple alkyl dithio- and thiolesters.

Extensive reports have appeared in the literature concerning the base catalysed hydrolysis of esters and thiolesters (e.g. refs. 4–16) and a limited amount of work using thionoesters has been reported (17–20). However, only three reports, none of which contain kinetic analyses, could be found concerning the base catalysed hydrolysis of dithioesters (21–23). According to Sakurada (21), the action of aqueous alkali on ethyl dithioacetate leads to the production of dithioacetic acid, however, two other studies (22, 23) report that thiol acids are produced by dithioester hydrolysis. The conflicting nature of these studies is most probably a reflection of their limited nature and also the high acidity of the α-CH protons of alkyl dithioesters. This acidity is responsible for side reactions at high concentrations of the dithioester (see below).

Nucleophilic displacement reactions involving esters, thiolesters, or thionoesters and hydroxide ions are thought to proceed via the formation of tetrahedral intermediates. However, few examples are available, in the literature, that provide evidence for the existence of such intermediates (13). Concurrent hydrolysis and isotopic oxygen-exchange reactions have been shown to occur in alkaline solutions of esters enriched in carbonyl-^{18}O (10–12, 15), and sulfur–oxygen exchange has been observed during thionoester hydrolysis (17, 18). These observations are consistent with a mechanism involving the formation of a tetrahedral intermediate. Evidence for the existence of such intermediates can also be inferred from the existence of stable salts formed by the addition of sodium methoxide to ethyl trifluoroacetate in di-n-butyl ether (24) and to methyl trifluoroacetate in methanol (25).

The α-CH acidity of the various oxygen and sulfur esters is in the order dithioester > thiolester > ester (26–32). Due to the small amount of information available on the α-CH acidity of thionoesters, they are not included in this comparison (33). The rate constant for the abstraction of an α-hydrogen atom by an hydroxide ion from ethyl thiolacetate has been determined to be 0.0067 $M^{-1} s^{-1}$ and the equivalent rate for methyl acetate has been estimated to be $\simeq 0.0005\ M^{-1} s^{-1}$ (30). Thus, the rate for the thiolester is approximately an order of magnitude greater than that for the oxygen ester. No such measurements have been made for thiono- or dithioesters.

Thiocarbonyl compounds are generally less stable than their oxygen analogues because sulfur does not easily form a double bond to a carbon atom. Stabilization of thiocarbonyls can occur by enethiolization if there is at least one α-hydrogen atom. This mechanism for stabilization is commonly found among simple thiones, e.g. thioketones. In contrast to this, dithioesters at neutral pH are generally quite stable in the thione form, as confirmed by spectroscopic methods (34, 35). However, dithioesters with relatively acidic α-CH protons, i.e. $CH_3CH_2OCOCH_2CSSCH_2CH_3$ (34–37) and CH_3COCH_2-$CSSCH_2CH_3$ which has a pK of 6.85 (28), are readily decolorized by bases and this is thought to be due to the formation of enethiolate anions (36–38).

This communication contains the results of a kinetic study of the reaction of hydroxide ions with several alkyl dithioesters. The results can be explained by the rapid attainment of an equilibrium between the dithioesters and a species (**I**) formed either by the extraction of a proton from, or by the addition of an hydroxide ion to, the dithioester. This equilibration is then followed by a slower hydrolysis of the dithioester and/or the species **I**. The study was facilitated by the fact that dithioesters have a strong absorption peak at around 305 nm and they are sufficiently soluble in aqueous solution.

[1]NRCC No. 21050.

Can. J. Chem. Downloaded from www.nrcresearchpress.com by 210.87.254.42 on 09/06/12
For personal use only.

TABLE 1. The dithioesters used in this study

Compound	Structure
1 Methyl dithioacetate	$CH_3-C(=S)-S-CH_3$
2 Ethyl dithioacetate	$CH_3-C(=S)-S-CH_2CH_3$
3 Methyl dithiopropionate	$CH_3-CH_2-C(=S)-S-CH_3$
4 Ethyl dithio-isobutyrate	$(CH_3)_2CH-C(=S)-S-CH_2CH_3$
5 Ethyl dithiotrimethylacetate	$(CH_3)_3C-C(=S)-S-CH_2CH_3$

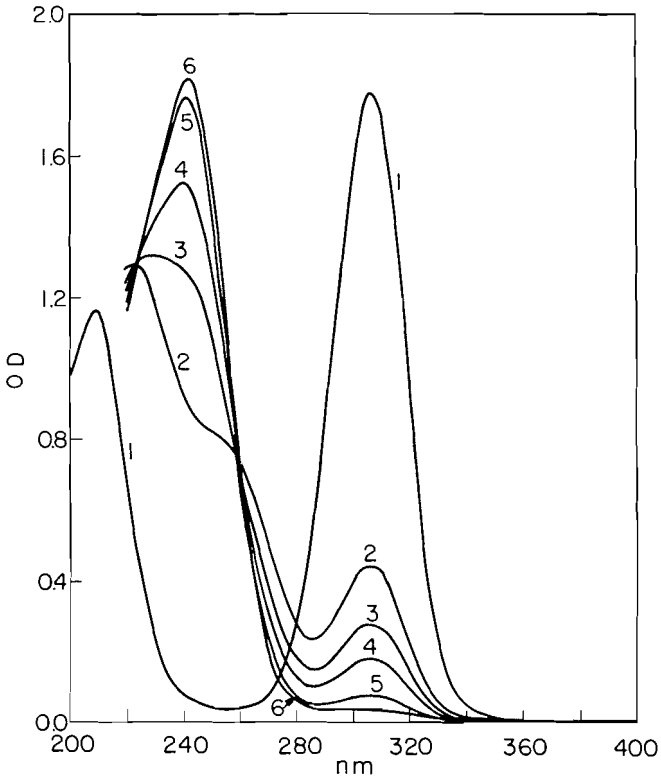

FIG. 1. Absorption spectra of (1) 140 μ*M* ethyl dithioacetate in aqueous solution; and in the presence of 0.1 *M* NaOH at various times after mixing (2) 2 min, (3) 30 min, (4) 60 min, (5) 90 min, and (6) 120 min.

Experimental

The dithioesters listed in Table 1 were synthesized as described by Marvel *et al.* (39) and were obtained as orange-colored oils. The results of elemental analysis agreed with the expected values to within acceptable limits (±0.02 × expected value). All aqueous solutions were prepared using distilled, deionized, boiled water. Base solutions were prepared by diluting the desired quantity of a carbonate-free standard sodium hydroxide solution. Stock solutions of the dithioester were prepared using acetonitrile as solvent such that the final concentration of the nitrile in the reaction mixture was less than 0.5%. Saturated aqueous solutions of dithioester **2** (Table 1) were also used as stock solutions and gave the same results as the acetonitrile solutions, however, the aqueous stock solutions were less stable. The hydrolytic reaction was monitored at 308 nm using a Cary 219 spectrophotometer with the sample compartment thermostated at 20°C.

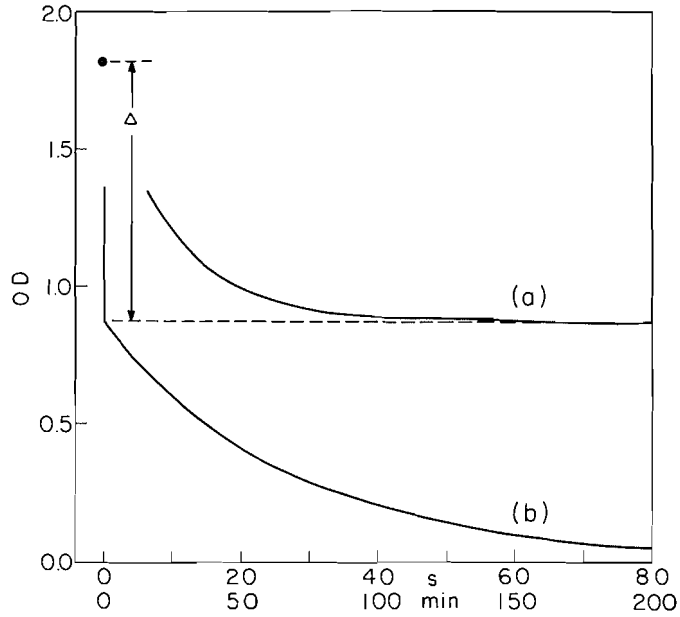

FIG. 2. The variation with the time after mixing of the optical density at 308 nm of an aqueous mixture of 0.032 *M* NaOH and 140 μ*M* ethyl dithioacetate, showing (a) the fast exponential decay and (b) the slow exponential decay.

Due to the small range of hydroxide ion concentrations used, no attempt was made to keep the ionic strength constant as the hydroxide concentration was varied. Papoff and Zambonin (16) have shown that the rates of hydrolysis of methyl and ethyl acetate are not significantly influenced by varying the ionic strength up to 0.5 *M*. The measured rate constants were obtained from plots of log OD against time after correcting for the residual OD after the completion of the reaction. When present, the two kinetic phases were sufficiently separated (Fig. 2) i.e. $k^f_{meas} > 500 \times k^s_{meas}$, that the rate constants were obtained graphically. The straight lines through the data points were obtained by linear least-squares analysis. Acetonitrile (40) and dimethyl sulphoxide (41) were purified before use.

Results

The reactions of the dithioesters with hydroxide ions were carried out at low concentrations of the dithioester, i.e. <1 m*M*. At higher concentrations the reaction mixture became darker in color due to an unwanted side reaction, presumably a Claisen type condensation of the dithioesters (42). On mixing dithioesters **1**, **2**, and **3** with a large excess of sodium hydroxide in aqueous solution a rapid drop is observed in the 308 nm absorption peak of the dithioester (i.e. Figs. 1, 2). This initial drop is complete within two minutes of mixing. The residual absorption at 308 nm then decays away at a much slower rate, being replaced by a product peak at 242 nm. Because of the large difference in the time dependencies of the fast initial drop and the slower decay of the residual absorption peak, both processes can be analysed separately. Rate constants[2] were measured for both the fast decay (k^f_{meas}) and the slow decay (k^s_{meas}) over a range of hydroxide concentrations (e.g. Fig. 3). The constants were obtained from plots of log $(I_t - I_\infty)$ against time (t), where I_t and I_∞ are the OD's, measured at 308 nm, at time t and at the end of the decay, respectively. The plots were linear for more than 90% completion of each process, thus both

[2]The primary pseudo-first-order rate constants, k^f_{meas} and k^s_{meas}, are available, at a nominal charge, from the Depository for Unpublished Data, CISTI, National Research Council of Canada, Ottawa, Ont., Canada K1A 0S2.

Can. J. Chem. Downloaded from www.nrcresearchpress.com by 210.87.254.42 on 09/06/12
For personal use only.

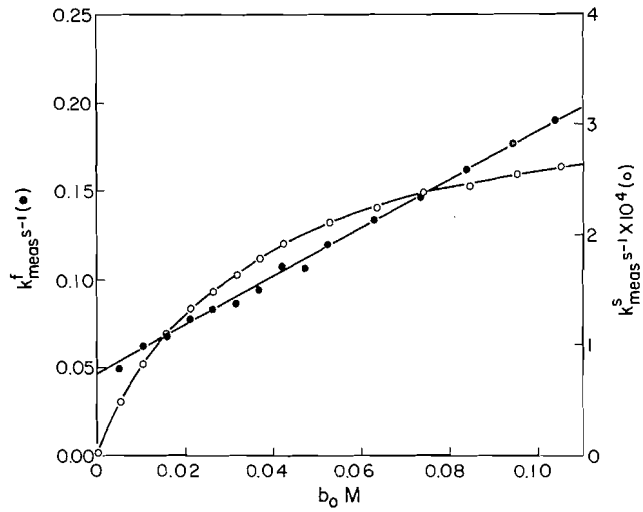

FIG. 3. Plots of k^f_{meas} and k^s_{meas} against the NaOH concentration. The dithioester concentration was 140 μM.

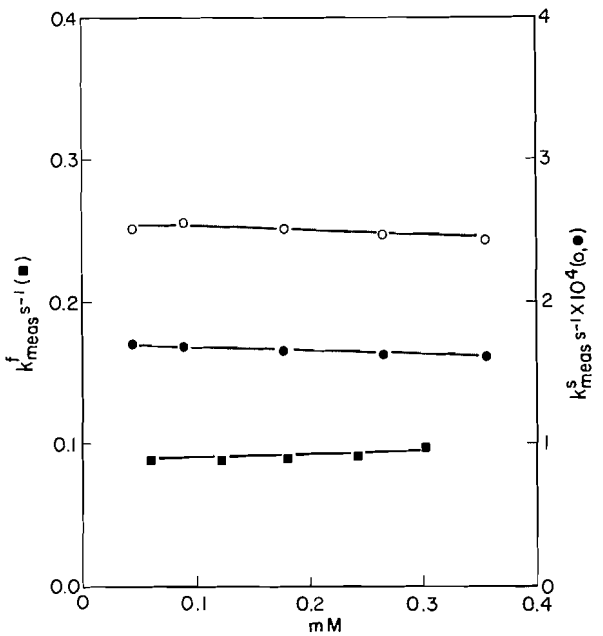

FIG. 4. Plots of (■) k^f_{meas} at 0.032 M NaOH, (•) k^s_{meas} at 0.032 M NaOH, and (○) k^s_{meas} at 0.11 M NaOH as a function of the ethyl dithioacetate concentration.

processes can be defined by single exponential functions. As a check, for some of the reaction mixtures k^s_{meas} values were also obtained by monitoring the appearance of the product peak at 242 nm; in all cases the value of k^s_{meas} obtained was the same as that obtained for the disappearance of the residual dithioester absorption at 308 nm.

From Fig. 3 it can be seen clearly that the magnitude of k^f_{meas} is proportional to the hydroxide ion concentration (b_0) whereas the magnitude of k^s_{meas} is not. At high values of b_0, k^s_{meas} approaches a limiting value that is independent of b_0. Both k^f_{meas} and k^s_{meas} are independent of the dithioester concentration over a modest range (Fig. 4). The reversibility of the first fast step but not of the second slower step can be readily shown by the partial reestablishment of the intensity of the 308 nm absorption peak on neutralization of the base in mixtures of the dithioester and hydroxide ions shortly after mixing (Fig. 5b). The absorption spectra obtained within 2 min of mixing (e.g.

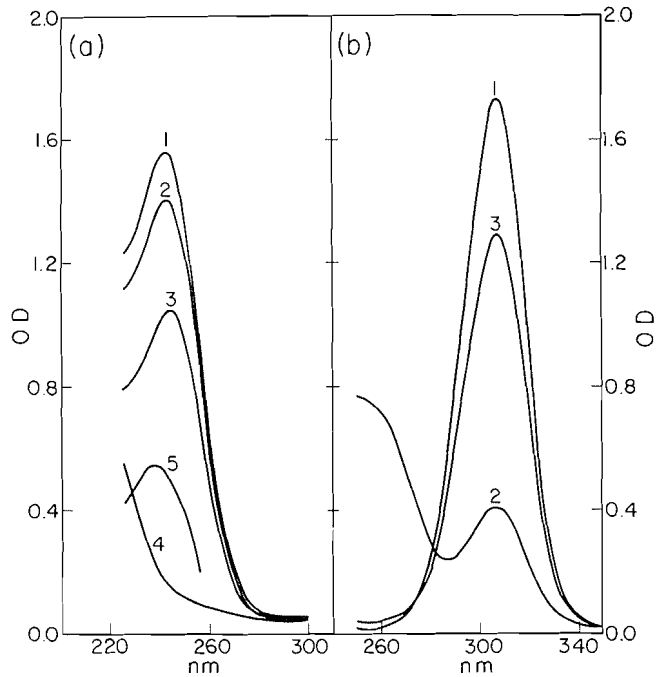

FIG. 5. (a) (1) An absorption spectrum of the products produced in a mixture of 137 μM ethyl dithioacetate and 0.1 M NaOH taken 120 min after mixing; (2) the same spectra after titrating the mixture with concentrated hydrochloric acid to about pH 10, (3) pH 7, and (4) pH 2; (5) the difference spectrum obtained by substracting (3) from (1). (b) (1) The absorption spectrum of a 137 μM aqueous solution of ethyl dithioacetate; (2) the same solution plus 0.1 M NaOH, 2 min after mixing; (3) and after neutralizing the NaOH with hydrochloric acid 10 min after the addition of the NaOH.

Fig. 1) contain mainly features due both to the residual dithioester, i.e. the peak at 308 nm, and to an intermediate, i.e. the peak in Fig. 1 at 223 nm and the shoulder at 258 nm. Because of the slower rate of formation of the final products no significant contributions from them are observed at this time. The peak due to the products at 242 nm is more obvious in spectra obtained at longer times after mixing and is seen to increase in intensity with time. The products were identified as ethyl mercaptan and thiolacetic acid by allowing the reaction to go to completion and then titrating with hydrochloric acid while monitoring the peak at 242 nm (Fig. 5a). At approximately pH 10 there is a drop in the intensity of the products peak and a shift in the λ_{max} to 244 nm. From pH 9 down to pH 4 there is no further change in the absorption spectrum. The peak eventually disappears below pH 4. On subtracting the product spectrum at pH 7 from that obtained prior to any addition of acid, a difference spectrum is obtained (Fig. 5a) which has a λ_{max} at 238 nm. Ethyl mercaptan has a pK of 10.5 (43) and an absorption peak at 238 nm measured for the ionized form, with an extinction coefficient of "approximately 4,000" (44). The predicted absorption at 238 nm for a stoichiometric production of ethyl mercaptide ion from the ethyl dithioacetate in the experiment depicted in Fig. 5a is 0.55; the measured value in the difference spectrum is 0.55. The value of ϵ_{max} for ethyl dithioacetate used in these calculations was $10^{4.1}$ (45). The residual peak at pH 7.0 is very similar to that expected for a stoichiometric production of thiolacetic acid which has a pK of 3.33. The ionized acid has an absorption maximum at 244 nm with an extinct coefficient of $10^{3.9}$. This ϵ_{max} was determined by measuring the OD's of serial dilutions of a stock solution of thiolacetic acid. The predicted optical density at pH 7 in Fig.

Can. J. Chem. Downloaded from www.nrcresearchpress.com by 210.87.254.42 on 09/06/12
For personal use only.

Can. J. Chem. Downloaded from www.nrcresearchpress.com by 210.87.254.42 on 09/06/12
For personal use only.

5a is 1.08 and the measured value is 1.05.

The simplest model consistent with an analysis of the results described above is one in which the initial rapid decrease in absorption at 308 nm is due to the establishment of an equilibrium. This equilibrium would be between the dithioester and another species (**I**) formed by the action of hydroxide ion on the dithioester. The equilibrium is coupled with the slower hydrolysis of the dithioester and/or breakdown of **I**, to give mercaptide and thiolacid anions, i.e.

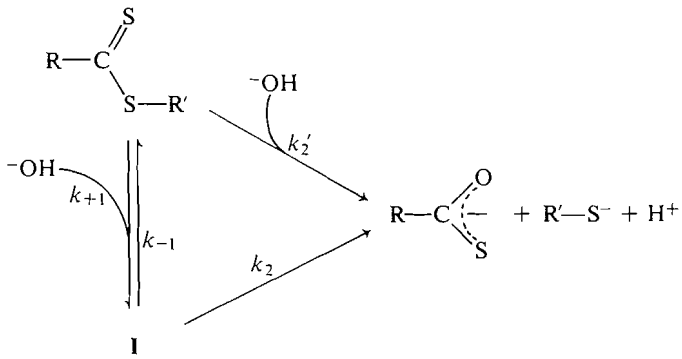

SCHEME 1

The rapid establishment of the equilibrium between the dithioester and **I**, provided that the concentration of hydroxide ion is far in excess of the dithioester and $k^f_{meas} \gg k^s_{meas}$, is given by the equation:

$$[1] \quad \frac{\chi}{\chi_0} = \frac{k_{-1} + k_{+1}b_0 e^{-(k_{-1}+k_{+1}b_0)t}}{k_{-1} + k_{+1}b_0}$$

where χ and χ_0 are the optical densities at 308 nm of the dithioester solution at times t and 0 min respectively, and b_0 is the concentration of hydroxide ions. From eq. [1] the measured rate constant for the fast exponential decay, k^f_{meas}, is given by:

$$[2] \quad k^f_{meas} = (k_{-1} + k_{+1}b_0)$$

Thus Scheme 1 predicts that plots of k^f_{meas} against b_0 for the dithioesters should be linear and yield values for k_{-1} and k_{+1} (Fig. 3, and Tables 2–4). The amplitude of the fast decay, Δ, can be measured directly from the recorder traces (Fig. 2). From eq. [1] it can be shown that:

$$[3] \quad \frac{\chi_0 - \Delta}{\chi_0} = \frac{k_{-1}}{k_{-1} + k_{+1}b_0}$$

Therefore a plot of $(\chi_0 - \Delta)^{-1}$ against b_0 gives a straight line with intercept $1/\chi_0$ and slope K_{eq}/χ_0 where $K_{eq} = k_{+1}/k_{-1}$ (Fig. 6). An equation based on Scheme 1 can also be derived for the rate, k^s_{meas}, of the slow exponential decay. Since the establishment of the equilibrium between the dithioester and **I** is very fast compared with k^s_{meas}, it is not unreasonable to assume that the dithioester and **I** are in equilibrium throughout the course of the slow decay in absorption. This being the case, the desired equation is:

$$[4] \quad \frac{\chi}{\chi_0} = \left\{\exp\left[\frac{-(k_2K_{eq} + k_2')b_0t}{(1 + K_{eq}\cdot b_0)}\right]\right\} \Big/ (1 + K_{eq}\cdot b_0)$$

and k^s_{meas} is therefore given by:

$$[5] \quad k^s_{meas} = \frac{(k_2K_{eq} + k_2')b_0}{(1 + K_{eq}b_0)}$$

The equations show that k^s_{meas} is not expected to be linearly dependent upon b_0 but, as b_0 increases, k^s_{meas} reaches a maximum value that is independent of b_0 (Fig. 3). A plot of b_0/k^s_{meas}

TABLE 2. Aqueous alkaline hydrolysis at 20°C

Dithioester	μM	$[OH^-]$ M	k_{+1} $M^{-1}\,s^{-1}$	k_{-1} s^{-1}	k_2^0 s^{-1}	$k_2^{0\prime}$ $M^{-1}\,s^{-1}$	K_{eq}[a] M^{-1} 1	2	3
$CH_3C(=S)S—CH_3$	155	0.01–0.1	1.51	0.054	0.00037	0.0104	28.0	27.8	—
$CH_3C(=S)S—CH_2CH_3$	140	0.01–0.1	1.36	0.046	0.00034	0.0103	29.3	29.6	30.1
$CH_3CH_2C(=S)S—CH_3$	168	0.002–0.2	0.64	0.0015	—	—	427	422	—

[a] K_{eq} was determined by 3 methods: (1) $K_{eq} = k_{+1}/k_{-1}$; (2) K_{eq} obtained from the amplitude of k^f_{meas}; and (3) K_{eq} obtained from k^s_{meas}; see text for details.

TABLE 3. Alkaline hydrolysis in 60% (v/v) aqueous acetonitrile at 20°C

Dithioester	μM	$[OH^-]$ M	k_{+1} $M^{-1}\,s^{-1}$	k_{-1} s^{-1}	k_2^0 s^{-1}	$k_2^{0\prime}$ $M^{-1}\,s^{-1}$	K_{eq}[a] M^{-1} 1	2	3
$CH_3C(=S)S—CH_2CH_3$	138	0.01–0.1	0.65	0.073	0.000095	0.002	8.9	9.0	—
$(CH_3)_2CHC(=S)S—CH_2CH_3$	40	0.01–0.1	0.0032[b]	0.00013[b]	—	—	24.8	29.4	[b]
$(CH_3)_3CC(=S)S—CH_2CH_3$	30	0.01–0.1	No detectable rate						

[a] see Table 2.
[b] The rate and equilibrium constants for this ester are approximate due to the similarity in the k^f_{meas} and k^s_{meas} rates.

TABLE 4. Alkaline hydrolysis in aqueous DMSO at 20°C

Dithioester	μM	% v/v DMSO	$[OH^-]$ M	k_{+1} $M^{-1}\,s^{-1}$	k_{-1} s^{-1}	k_2^0 s^{-1}	$k_2^{0'}$ $M^{-1}\,s^{-1}$	K_{eq}[a] M^{-1} 1	2	3
$CH_3C(=S)S—CH_2CH_3$	120	0	0.01–0.1	1.36	0.046	0.00034	0.0103	29.3	29.6	30.1
		10	0.02–0.1	2.12	0.044	0.00022	0.0143	48.2	37.1	64.3
		20	0.02–0.1	3.28	0.034	0.00015	0.025	96.5	57.9	595
		30	0.002–0.1	5.15	0.034	0.00008	0.05	151.5	112.1	—
		40	0.002–0.02	9.6	0.023	0.00004	—	371.2	265.4	—
		50	0.002–0.01	19.3	0.008	—	—	1925	950	—
		60	0.002–0.008	52.3	[0.014][b]	[0.000008][b]	[0.44][b]	—	4033	—
		70	0.001–0.003	160	—	—	—	—	20 420	—
$(CH_3)_2CHC(=S)S—CH_2CH_3$	143	60	0.002–0.1	0.358 $M^{-1}\,s^{-1}$[c]						
$(CH_3)_3CC(=S)S—CH_2CH_3$	130	60	0.05–0.5	0.000614 $M^{-1}\,s^{-1}$[c]						

[a] see Table 2.
[b] Values predicted from log–log plots of data at lower [DMSO].
[c] Only a single exponential decay observed.

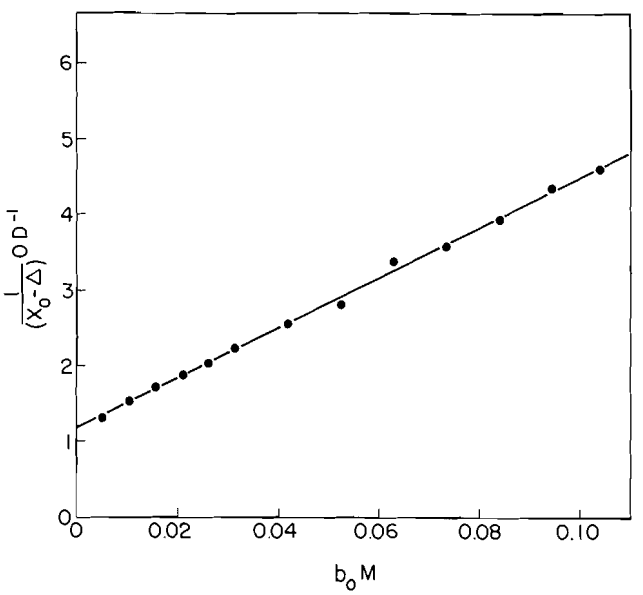

FIG. 6. A plot of $(\chi_0 - \Delta)^{-1}$ against the NaOH concentration. The dithioester concentration was 140 μM.

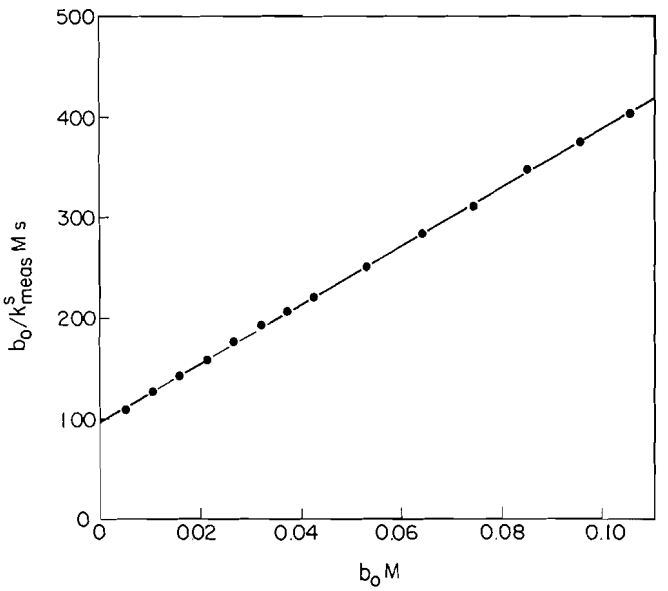

FIG. 7. A plot of b_0/k^s_{meas} against the NaOH concentration. The dithioester concentration was 140 μM.

against b_0 should give a straight line, Fig. 7, from which values for K_{eq} and $(k_2K_{eq} + k_2')$ can be obtained. In order to simplify the discussion of the data only the two limiting cases $k_2 = k_2^0$, $k_2' = 0$ and $k_2 = 0$, $k_2' = k_2^{0'}$ will be considered. Hence the values of k_2^0 and $k_2^{0'}$ given in Tables 2–4 were obtained by alternately applying these assumptions.

Table 2 lists the values of k_{+1}, k_{-1}, k_2^0, $k_2^{0'}$, and K_{eq} obtained in aqueous sodium hydroxide solution for dithioesters **1**, **2**, and **3**. Dithioesters **4** and **5** are insoluble in aqueous solution. A problem arose with measuring k^s_{meas} values for methyl dithioacetate, **1**, in that, due to the high volatility of this dithioester, some is lost from solution by escape from the surface of the liquid, and thus the measured values of k^s_{meas} were too high. To partially overcome this problem and allow for estimates of k_2^0 and $k_2^{0'}$ to be made, an alternative plotting procedure was used to analyse the k^s_{meas} data of **1**. The average of K_{eq} obtained for **1** using k^f_{meas} and Δ (see Table 2) was substituted into eq. [5] and b_0/k^s_{meas} was plotted against $(1 + K_{eq}b_0)$; k_2^0 and $k_2^{0'}$ were then obtained by drawing the asymptote to the plotted line. The amplitude of the fast decay of dithioester **3** was such that in order to determine k_{+1}, k_{-1}, and K_{eq} a lower range of hydroxide ion concentration had to be used. At these lower concentrations of base k^s_{meas} was too slow to be measured accurately, thus no values of k_2^0 and $k_2^{0'}$ were obtained for this dithioester. Table 3 lists the results obtained for dithioesters **2**, **4**, and **5** using a 60% v/v acetonitrile–water mixture in which all three are soluble. For dithioester **4** it was not possible to completely separate k^f_{meas} and k^s_{meas} and so the measured rate constants represent some combination of the two. Immediately after mixing dithioester **4** with base in CH_3CN/H_2O a spectrum similar to that for the intermediate formed from **1** is obtained; however, this is soon lost under a product peak. For dithioester **5** in CH_3CN/H_2O there was no significant decrease in the dithioester absorption over a period of two hours. Table 4 contains the constants obtained for the alkaline hydrolysis of **2** in various DMSO–water mixtures and for **4** and **5** in 60% v/v

Can. J. Chem. Downloaded from www.nrcresearchpress.com by 210.87.254.42 on 09/06/12
For personal use only.

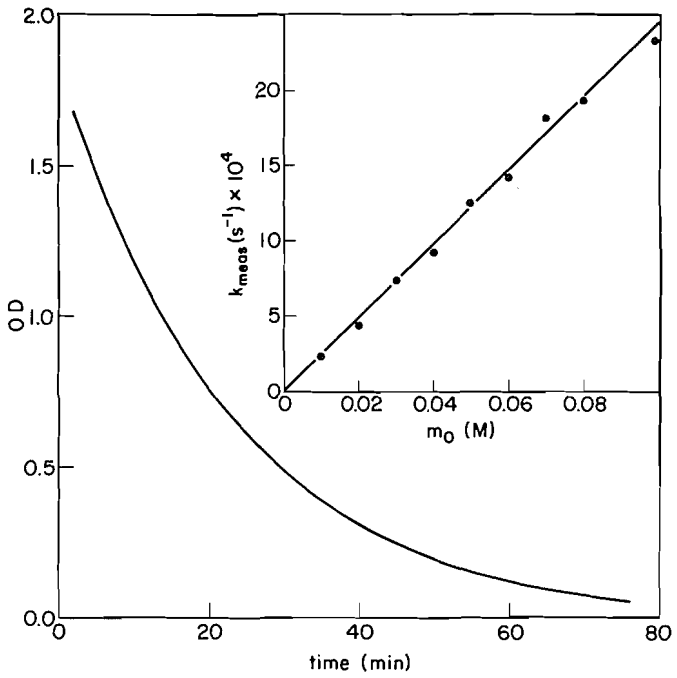

FIG. 8. The variation with the time after mixing of the optical density at 306 nm of a methanolic solution of 0.03 *M* CH_3ONa and 140 μM ethyl dithioacetate. The insert shows a plot of the measured rate constant for this reaction as a function of the methoxide concentration.

DMSO–water. At above 40% v/v DMSO it becomes impossible to measure k^s_{meas} for dithioester **2** because of the increased amplitude of k^f_{meas}. Eventually k^f_{meas} becomes too fast to be measured by the techniques used in this study (i.e. at >70% DMSO). Log–log plots of the kinetic constants for **2** against the % v/v of water give straight lines with slopes −3.96, 1.25, 4.07, and −4.06 for k_{+1}, k_{-1}, k_2^0, and $k_2^{0'}$ respectively. The significance, if any, of these values is unknown; however, using the plots it is possible to predict values for k_{-1}, k_2^0, and $k_2^{0'}$ for dithioester **2**, in 60% v/v DMSO. These values are included in Table 4. For dithioesters **4** and **5** in 60% v/v DMSO, only single exponential processes were involved in the disappearance of their absorbance at 308 nm. The rate constants for these processes are also given in Table 4. For dithioester **2** in H_2O, CH_3CN/H_2O, and $DMSO/H_2O$, it was possible to demonstrate the reversibility of the initial fast phase of the reaction by neutralizing the base with hydrochloric acid. For dithioester **2** in all solvent systems this reversion was rapid. For dithioester **4**, since k^f_{meas} and k^s_{meas} have similar values in CH_3CN/H_2O, only a partial reversion was observed. This reversion was more extensive in $DMSO/H_2O$. However, in both solvent systems the reversion was much slower than for dithioester **2**. In $DMSO/H_2O$, for dithioester **4**, the slow reversion appeared to be independent of excess HCl (up to 0.3 *M*) and had a rate of 0.0024 s^{-1}. The reaction of dithioester **5** with hydroxide ions in $DMSO/H_2O$ was not perceptibly reversed by the addition of HCl. Due to the uv absorbance of DMSO it was not possible to detect any intermediate formation by absorption spectroscopy. However, in CH_3CN/H_2O, features were observed for dithioesters **2** and **4** that correspond to those observed for the intermediates formed from dithioesters **1**, **2**, and **3** in aqueous solution.

The reaction of the dithioesters with sodium methoxide in methanol proceeds with a single exponential decay (Fig. 8) of the dithioester absorption coupled with an increase in absorption of a product peak at 235 nm. For dithioester **2**, after the completion of the reaction the product peak was titrated with aqueous HCl. A partial decrease in intensity of the peak was observed, presumably corresponding to the titration of ethyl thiolate anions. The residual peak which remained even at very low pH had a λ_{max} of 238 nm and corresponded both in position and intensity to that expected for a stoichiometric production of methyl thionoacetate (λ_{max} 238 nm, ϵ_{max} $10^{3.9}$ in CH_3OH). The scheme for the reaction of the dithioesters with methoxide ions in methanol is therefore:

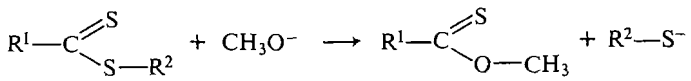

No evidence was obtained for either an intermediate or a reversible step in the reaction. The rate constants obtained for all five dithioesters are given in Table 5. The reaction of **5** with methoxide ions is extremely slow and only an estimate of the upper limit for the rate constant was obtained.

TABLE 5. Reaction with sodium methoxide in methanol at 20°C

Dithioester	μM	$[CH_3O^-]$ *M*	k M^{-1} s^{-1}
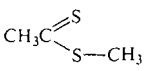	143	0.01–0.1	0.0364
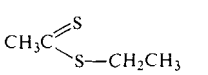	140	0.01–0.1	0.0244
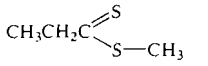	150	0.01–0.1	0.0163
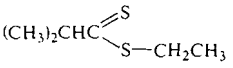	126	0.01–0.1	0.00044
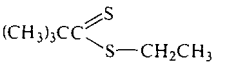	130	0.01–0.1	$<9 \times 10^{-6}$

Discussion

The consistency of the results presented above with those predicted by Scheme 1 and eqs. [1] and [4] provides ample evidence for the existence, in basic solutions, of at least one anionic species in equilibrium with the dithioesters. Rate constants have been obtained for both the formation and breakdown of this anion and values for the equilibrium constant (K_{eq}) for several of the dithioesters have been obtained by different routes. The similarity in the values of K_{eq} and the consistency of the kinetic behaviour with that predicted by Scheme 1 does not exclude the possibility that more than one anion is in equilibrium with the dithioester. However, since no evidence is available for more than one anion, Scheme 1 is the simplest that is fully consistent with the available data.

The kinetic constants (k_2^0 and $k_2^{0'}$) defining the slow exponential decay in Tables 2–4 were obtained by alternately applying limiting conditions to eq. [5], i.e. $k_2 = k_2^0$, $k_2' = 0$ and $k_2 = 0$, $k_2' = k_2^{0'}$. These limiting conditions correspond to two possible explanations for the nature of the anionic species **I**. In the first **I** would be a stabilized tetrahedral intermediate and in the second it would be an enethiolate ion. The two possibilities will be discussed separately.

Can. J. Chem. Downloaded from www.nrcresearchpress.com by 210.87.254.42 on 09/06/12
For personal use only.

Tetrahedral intermediate

By analogy with esters (7, 10–13, 15, 24, 25), thiol esters (14, 15), and thionoesters (17–19) it seems reasonable to assume that dithioesters hydrolyse via a tetrahedral intermediate. The tetrahedral intermediate for esters and thiolesters is generally thought to be a monoanion:

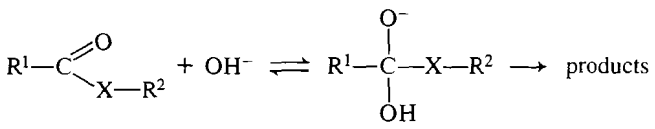

where X = O or S. The base catalysed carbonyl oxygen exchange observed for esters (7, 10–12, 15) and thiol esters (15) is explained by the reversible nature of the addition of the base to the ester coupled with a prototropic shift between the two oxygen atoms. At high concentrations of base it has been proposed that the tetrahedral intermediate formed during ester hydrolysis deprotonates to give a dianion (16):

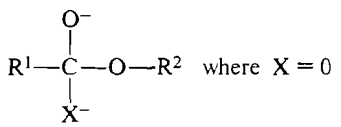

A similar dianion (X = S) has been proposed to account for the pH dependent changes in the O/S exchange observed during the base catalysed hydrolysis of thionoesters (17–19). For ethyl thionobenzoate a value of 12.5 has been proposed for the pK_a for the formation of the dianion from the monoanionic tetrahedral intermediate. It has been pointed out (46) that the assignment of this pK_a value may be in error since it relies on the assumption that the rates of product formation from the monoanion and the dianion are equal. Plots of the product distribution patterns, which depend upon the degree of O/S exchange, for benzoylthionocholine and its dimethylamino analog have midpoints at approximately pH 10 (19). For some thionoesters the extent of O/S exchange is only diminished at the higher pH's (17–19). This is because their alkoxide anions (CH_3CH_2OH, pK 15.9 (18); $(CH_3)_2N\,CH_2CH_2OH$, pK 15 (19)) have similar leaving group abilities to the sulfur dianion (S^{2-}, p$K \simeq 15$). No O/S exchange is observed at high pH for benzoyl thionocholine since the choline anion (pK 13.9) is a better leaving group than the sulfur dianion. It is believed therefore that the lack of any observed O/S exchange for the dithioesters is explained by the formation of a dianionic tetrahedral intermediate in the pH range (>11) used in this study coupled with the leaving group ability of the mercaptide anions (p$K \simeq 10.5$).

Although it is highly probable that the hydrolysis of dithioesters proceeds via a dianionic tetrahedral intermediate, there is some evidence that suggests that **I** is not such a species. This evidence is as follows. For esters, thiolesters, and thionoesters the stability of the tetrahedral intermediates formed, monoanionic or dianionic, is such that no accumulation of this intermediate is possible. Therefore if the anionic species, **I**, that accumulates during the hydroxide ion catalysed hydrolysis of dithioesters is a tetrahedral intermediate, this intermediate must possess some stabilizing property that is unique to the structure:

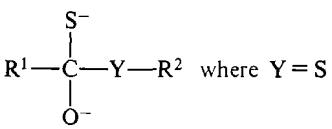

It seems unlikely that this stabilizing property would be absent from the same structure with Y = O. Also if **I** is a tetratrahedral intermediate and if, as seems likely, this intermediate is dianionic for dithioesters, then two equivalents of base would be consumed in the production of **I** and hence plots of k'_{meas} against b_0 should be nonlinear. This is clearly not the case (Fig. 3). The difference in the stability of **I** formed from dithioesters **1** and **3** (Table 2) is difficult to explain if **I** is a tetrahedral intermediate since the change from acetyl to propionyl is only expected to have a small effect on the stability and rates of formation and breakdown of the tetrahedral intermediates formed from these compounds.

Enethiolate ion

The α-CH protons of dithioesters are more acidic than those of the corresponding esters and thiolesters, e.g. the pK_a of $CH_3COCH_2CXYCH_2CH_3$ is 11.0, 9.11, and 6.85 for X = O, Y = O; X = O, Y = S; and X = S, Y = S respectively (28, 32). The contribution of the acetyl group to these pK_a values is quite large, i.e. the pK_a of acetone is ≈20 whereas that of acetylacetone is 9.0 (47). Thus the pK_a of the α-CH protons of simple alkyl dithioesters must be considerably higher than the value of 6.85 given above for $CH_3COCH_2CSSCH_2CH_3$ (28). This latter compound and other relatively acidic dithioesters are readily decolorized by base (34–37), e.g. asymmetric ethyl dithiomalonate is decolorized in sodium acetate solution. The simple alkyl dithioesters studied here are less readily decolorized by base, ie. higher pH's are required to bring about decolorization. However, it is not unreasonable to assume that the mechanism of decolorization is the same for all the dithioesters and that the difference in ease of decolorization is merely a reflection of the differing pK_a's of the dithioesters.

The identification of **I** as an enethiolate anion is supported by the observation that a variation in the nature of the R group in Scheme 1 markedly affects not only the rate but also the extent of production of the enethiolate (Tables 2–4). Substitution of a methyl group for a proton increases the stablility of the double bond and this could account for the increase in the value of the equilibrium constant on going from dithioester **1** to **3**, Table 2. The relative rates of proton abstraction (k_{+1}), normalized for the number of α-CH protons, for dithioesters **1**, **3**, and **4** are 1, 0.64, and 0.02, Tables 2–4 (the value for **4** is an upper limit) and the relative rates for the reverse step (k_{-1}) for dithioesters **1** and **3** are 1.0 and 0.028. The decrease in k_{+1} can possibly be accounted for by an increase in steric hindrance to proton abstraction in the series **1**, **3**, and **4**, whereas the decrease in k_{-1} may be due to an increase in both the steric hindrance and the stability of alkyl substituted double bonds.

Unfortunately the fact that no species **I** was detected for dithioester **5**, which lacks α-CH protons, cannot be used as unequivocal evidence for the identification of **I** as an enethiolate anion. As can be seen from Tables 2–4, as the degree of substitution on the α-C increases, it becomes more difficult to detect **I** because the rate of hydrolysis and the rate of formation of **I** converge. Thus the lack of any detectable species **I** for dithioester **5** could merely be an extension of this convergence to the point where the rate of hydrolysis exceeds the rate of formation of **I**.

From the equilibrium constants in Table 2 it is possible to calculate apparent pK_a's of 12.5 for dithioesters **1** and **2** and of 11.4 for dithioester **3**. These values can be compared with the published value of 6.85 reported for acetyl ethyl dithioacetate (28), the difference of 4.5–5.6 pK units being accounted for by the acetyl group substitution.

Can. J. Chem. Downloaded from www.nrcresearchpress.com by 210.87.254.42 on 09/06/12
For personal use only.

Can. J. Chem. Downloaded from www.nrcresearchpress.com by 210.87.254.42 on 09/06/12
For personal use only.

It was not possible to detect any equilibration process in CH_3O^-/CH_3OH mixtures (Table 5, Fig. 8). If a direct ionization of the dithioester is involved, then it can possibly be expected that an equilibrium should be observed in methanol solution. However, on changing solvent a reversal in the relative rates of hydrolysis and formation of **I** may be occurring such that the equilibration process is not observed. The production of thionoesters from dithioesters by the action of methoxide ions in methanol has been reported previously (31).

Comparison between dithioesters, esters, and thiolesters

From the arguments presented above it seems that the most probable nature of **I** is that of an enethiolate anion. The subsequent comparisons will be made on the assumption that, in Scheme 1, **I** is an enethiolate anion, $k_2 = 0$, and $k_2^{0\prime}$ represents the hydrolysis of the residual dithioester.

The rate of proton abstraction by hydroxide ions from ethyl dithioacetate in aqueous solution (k_{+1}; Table 2) is 1.36 M^{-1} s^{-1} and the comparable rates for ethyl thiolacetate and methyl acetate are 0.0067 M^{-1} s^{-1} and ≃0.0005 M^{-1} s^{-1} respectively (30). The approximately 10-fold difference in the rates for ethyl thiolacetate and methyl acetate is explained by the increased contribution of the resonance form

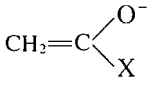

in the carbanions produced from thiolesters (30). It is suggested that the difference in the relative contributions of this resonance form is a result of the greater extent of stabilization of oxygen esters by the resonance form (30).

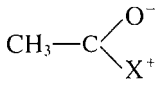

That this resonance form contributes more to the structure of esters than thiolesters can be shown by dipole moment measurements, i.e. oxygen esters have larger dipole moments than their corresponding thiol esters (48). However, similar dipole measurements with dithioesters (48) place their dipole moments between those of the corresponding oxygen and thiolesters. Therefore, although the differences in the rates of proton abstraction from esters, thiolesters, and dithioesters most probably reflects differences in the relative stabilities of the anions formed, no clear correlation can be made to the relative contribution of the form

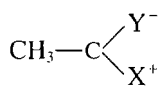

to the structure of the ester, thiolester, or dithioester. It is felt, however, that the greater polarizability of the thiocarbonyl group over the carbonyl group (49) is an important factor in the increased rate of proton abstraction from dithioesters compared to esters and thiolesters.

The rate constants for the alkaline hydrolysis of the dithioesters are given by the $k_2^{0\prime}$ values in Tables 2–4. In aqueous solution only the rates for methyl and ethyl dithioacetates could be obtained and these rates are very similar. The ratio of the corresponding rates for methyl and ethyl acetate is 0.601 (50). If the assumption is made that dithioester **5** cannot form a species **I**, then the measured rate constant for this compound in Table 4 is $k_2^{0\prime}$ (its hydrolytic rate constant). Therefore the ratio of the base catalysed rates of hydrolysis of dithioesters **2** and **5** in 60% aqueous DMSO is 0.0014 and the ratio for the corresponding oxygen esters in 88% aqueous ethanol is 0.0105 (50). The effects of solvent–water mixtures on the rates measured for ethyl dithioacetate (Tables 3 and 4) are those to be expected based on the solvent effects on the hydrolysis of ethyl acetate (41).

The rate constants for the alkaline hydrolysis of ethyl acetate and ethyl thiolacetate, at 20°C in 62% aqueous acetone solution, are very similar, i.e. 0.029 M^{-1} s^{-1} (5) and 0.026 M^{-1} s^{-1} (4) respectively. The thiolacetate study (4) was conducted at several acetone concentrations, thus allowing an extrapolation of the data to 0% acetone to give a rate constant of approximately 0.06 M^{-1} s^{-1} in aqueous solution. This value compares favourably with that of 0.055 M^{-1} s^{-1} (obtained by extrapolation of rates obtained at higher temperatures in ref. 8) for the alkaline hydrolysis of n-butyl thiolacetate in dilute aqueous solution at 20°C. By interpolating data in ref. 41 it has been possible to obtain a value of 0.08 M^{-1} s^{-1} for the alkaline hydrolysis of ethyl acetate in aqueous solution at 20°C. Therefore the comparable rates for the alkaline hydrolysis of ethyl acetate, ethyl thiolacetate, and ethyl dithioacetate in aqueous solution at 20°C are 0.08, 0.06, and 0.0103 M^{-1} s^{-1} respectively. From these data it appears that there is little difference in the rates of alkaline hydrolysis of ethyl acetate and thiol acetate whereas the dithioester is marginally less readily hydrolysed. The alkaline hydrolysis of the ester and thiolester is thought to proceed via a monoanionic tetrahedral intermediate, whereas in the pH range of this study the dithioester hydrolysis is thought to proceed predominantly via a dianionic tetrahedral intermediate, i.e. in this pH range $k_4 \cdot [OH^-] \gg k_5$. The involvement of this dianionic tetrahedral intermediate in dithioester hydrolysis is not inconsistent with a linear dependence of the rate of hydrolysis on the base concentration. It is stated above that **I** cannot be the dianionic tetrahedral intermediate since $k^{f}_{meas} \propto [OH^-]$, not $[OH^-]^2$; however, the formation of **I** is an equilibrium process and, provided $k_4 \gg k_{-3}$ in the scheme above, then $k_{hydrolysis} = [OH^-] \cdot k_3$.

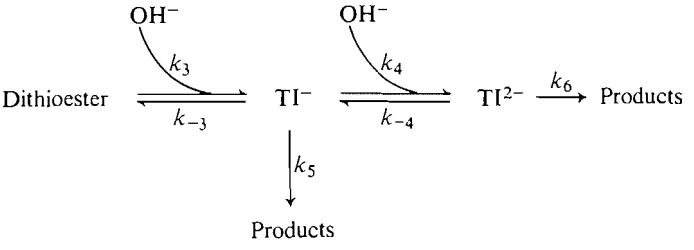

1. A. C. STORER, W. F. MURPHY, and P. R. CAREY. J. Biol. Chem. **254**, 3163 (1979).
2. Y. OZAKI, D. H. PLIURA, P. R. CAREY, and A. C. STORER. Biochemistry, **21**, 3102 (1982).
3. C. P. HUBER, Y. OZAKI, D. H. PLIURA, A. C. STORER, and P. R. CAREY. Biochemistry, **21**, 3109 (1982).
4. J. R. SCHAEFGEN. J. Am. Chem. Soc. **70**, 1308 (1948).
5. P. N. RYLANDER and D. S. TARBELL. J. Am. Chem. Soc. **72**, 3021 (1950).
6. D. S. TARBELL and D. P. HARNISH. Chem. Rev. **49**, 1 (1951).
7. M. L. BENDER. J. Am. Chem. Soc. **73**, 1626 (1951).
8. L. H. NODA, S. A. KUBY, and H. A. LARDY. J. Am. Chem. Soc. **75**, 913 (1953).
9. P. J. HAWKINS and D. S. TARBELL. J. Am. Chem. Soc. **75**, 2982 (1953).
10. M. L. BENDER, R. D. GINGER, and J. P. UNIK. J. Am. Chem. Soc. **80**, 1044 (1958).

11. M. L. BENDER and R. J. THOMAS. J. Am. Chem. Soc. **83**, 4189 (1961).
12. M. L. BENDER, H. MATSUI, R. J. THOMAS, and S. W. TOBEY. J. Am. Chem. Soc. **83**, 4193 (1961).
13. M. L. BENDER. Chem. Rev. **60**, 53 (1962).
14. L. R. FEDOR and T. C. BRUICE. J. Am. Chem. Soc. **87**, 4138 (1965).
15. M. L. BENDER and H. D'A. HECK. J. Am. Chem. Soc. **89**, 1211 (1967).
16. P. PAPOFF and P. G. ZAMBONIN. Talanta, **14**, 581 (1967).
17. S. G. SMITH and M. O'LEARY. J. Org. Chem. **28**, 2825 (1963).
18. S. G. SMITH and R. J. FELDT. J. Org. Chem. **33**, 1022 (1968).
19. P. Y. BRUICE and H. G. MAUTNER. J. Am. Chem. Soc. **95**, 1582 (1973).
20. P. CAMPBELL and B. A. LAPINSKAS. J. Am. Chem. Soc. **99**, 5378 (1977).
21. Y. SAKURADA. Mem. Coll. Sci. Univ. Kyoto Ser. A, **10**, 79 (1926–1927).
22. E. BENARY and A. SCHMIDT. Ber. **57**, 517 (1924).
23. H. JORG. Ber. **60**, 1466 (1927).
24. M. L. BENDER. J. Am. Chem. Soc. **75**, 5986 (1953).
25. J. P. GUTHRIE. Can. J. Chem. **54**, 202 (1976).
26. F. LYNEN. Fed. Proc. Fed. Am. Soc. Exp. Biol. **12**, 683 (1953).
27. M. W. CRONYN, M. P. CHANG, and R. A. WALL. J. Am. Chem. Soc. **77**, 3031 (1955).
28. A. THUILLIER and J. VIALLE. Bull. Soc. Chim. Fr. 2182 (1963).
29. G. E. WILSON. Tetrahedron Lett. 2007 (1967).
30. G. E. LIENHARD and T. C. WANG. J. Am. Chem. Soc. **90**, 3781 (1968).
31. P. VERMEER, J. MEIJER, H. J. T. BOS, and L. BRANDSMA. Recl. Trav. Chim. Pays-Bas, **93**, 51 (1974).
32. B. V. KURGANE, M. T. BRAKMANE, Y. P. STRATYN, and S. A. GILLER. Zh. Organ. Khim. **11**, 926 (1975).
33. J. V. KOSTIR and V. KRAL. Chem. Listy, **41**, 92 (1947).
34. R. MAYER, S. SCHEITHAUER, S. BLEISCH, D. KUNZ, G. BÄHR, and R. RADEGLIA. J. Prakt. Chem. **311**, 472 (1969).
35. R. MAYER. *In* Sulphur in organic and inorganic chemistry. Vol. 3. *Edited by* A. Senning. Marcel Dekker, New York. 1972. Chapt. 27.
36. S. SCHEITHAUER and R. MAYER. Chem. Ber. **100**, 1413 (1967).
37. D. KUNZ, S. SCHEITHAUER, S. BLEICH, and R. MAYER. J. Prakt. Chem. **312**, 426 (1970).
38. J. M. BEINER and A. THUILLIER. C. R. Acad. Sci. Paris Ser. C, **274**, 642 (1972).
39. C. S. MARVEL, P. DE RADZITSKY, and J. J. BRADER. J. Am. Chem. Soc. **77**, 5997 (1955).
40. G. L. LEWIS and C. P. SMITH. J. Chem. Phys. **7**, 1085 (1939).
41. E. TOMMILA and M. L. MURTO. Acta Chem. Scand. **17**, 1947 (1963).
42. S. SCHEITHAUER and R. MAYER. *In* Topics in sulfur chemistry. Vol. 4. *Edited by* A. Senning. Georg Thieme, Stuttgart. 1979. p. 258.
43. J. P. DANEHY and C. J. NOEL. J. Am. Chem. Soc. **82**, 2511 (1960).
44. L. POLGAR. FEBS Lett. **38**, 187 (1974).
45. A. C. STORER, Y. OZAKI, and P. R. CAREY. Can. J. Chem. **60**, 199 (1982).
46. R. HERSHFIELD and G. L. SCHMIR. J. Am. Chem. Soc. **95**, 3994 (1973).
47. M. EIGEN. Angew. Chem. Int. Ed. Engl. **3**, 1 (1964).
48. I. WALLMARK, M. H. KRACKOV, S. H. CHU, and H. G. MAUTNER. J. Am. Chem. Soc. **92**, 4447 (1970).
49. A. MEHLHORN and R. MAYER. Z. Chem. **8**, 321 (1968).
50. C. K. INGOLD. *In* Structure and mechanism in organic chemistry. 2nd ed. Cornell University Press, Ithaca, NY. 1969. p. 1135.

Can. J. Chem. Downloaded from www.nrcresearchpress.com by 210.87.254.42 on 09/06/12
For personal use only.

Infrared spectra of hydrogen-bonded salicylic acid and its derivatives. Methyl salicylate

FOR ERRATA SEE
v.63#6 1985 p.1344

MAREK J. WÓJCIK[1]

Faculty of Chemistry, Jagiellonian University, 30-060 Cracow, Karasia 3, Poland

AND

CZESŁAWA PALUSZKIEWICZ

Regional Laboratory of Physico-Chemical Analyses and Structural Research, 30-060 Cracow, Karasia 3, Poland

Received August 19, 1982

MAREK J. WÓJCIK and CZESŁAWA PALUSZKIEWICZ. Can. J. Chem. **61**, 1449 (1983).

Infrared spectra of hydrogen-bonded methyl salicylate have been studied in the temperature range 173–293 K, in solutions of various concentrations (in CCl_4) and in the gaseous state. Results show that the molecules form monomeric intramolecular hydrogen bonds in the solid, liquid, and gaseous state. Far-infrared spectra were recorded which give the wavenumber of low-frequency O . . . O mode used in theoretical reconstruction of the band connected with the O—H stretching vibration. The position and especially the width of this band are determined to a large extent by the influence of the environment.

MAREK J. WÓJCIK et CZESŁAWA PALUSZKIEWICZ. Can. J. Chem. **61**, 1449 (1983).

On a étudié les spectres infrarouges du salicylate de méthyle comportant des liaisons hydrogènes en solutions de différentes concentrations (dans le CCl_4) et à l'état gazeux dans un intervalle de température allant de 173 à 293 K. Les résultats révèlent que les molécules forment des liaisons hydrogènes intramoléculaires monomères dans l'état solide, liquide et gazeux. On a enregistré les spectres dans l'infrarouge lointain qui donnent la longueur d'un mode O . . . O de faible fréquence utilisé pour la reconstruction théorique de la raie reliée à la vibration d'élongation du O—H. La position et spécialement la largeur de cette raie sont déterminées dans une large mesure par l'influence de l'environnement.

[Traduit par le journal]

1. Introduction

In a previous paper (1) we have studied infrared spectra of hydrogen-bonded crystalline salicylic acid, acetylsalicylic acid, and deuterium-bonded D-salicylic acid. There are common features in the spectra of closely related salicylic and acetylsalicylic acids. The first has both intra- and intermolecular hydrogen bonds (2, 3) whereas in acetylsalicylic acid (aspirin) intramolecular H-bonds are absent and intermolecular are similar to those in salicylic acid (4).

It was tempting to study another compound derived from salicylic acid in which only intramolecular hydrogen bonds can be formed and intermolecular hydrogen bonds are absent. We were interested to find out whether infrared band of this compound, connected with the O—H stretching vibration (ν_s) would be similar to the band located at 3233 cm^{-1} in the infrared spectrum of the crystalline salicylic acid (1).[2]

We have chosen methyl salicylate which has relatively simple infrared ν_s band. Methyl salicylate is liquid at room temperature and its freezing point is 264.6 K.

To make a direct comparison between ν_s bands of methyl salicylate (liquid) and salicylic acid (crystal), it was necessary to look into changes brought by the change of state and temperature variation. We have recorded infrared spectra of methyl salicylate in the temperature range 173–293 K, both in liquid and solid state. The main question was whether these spectra are due to intra-or intermolecular hydrogen bonds or a mixture of them. We were looking for an answer to this question by investigating spectra of solutions of methyl salicylate in CCl_4, changing concentrations, and by recording spectrum of the gaseous methyl salicylate.

Far-infrared spectra were also recorded to determine the wavenumber of a O . . . O mode necessary for theoretical calculation based on the Witkowski–Maréchal model (5, 6).

2. Experimental

Infrared spectra of the liquid and solid methyl salicylate and its solutions in CCl_4 were recorded on a Digilab model 14 Fourier transform spectrophotometer in the Regional Laboratory of Physico-Chemical Analyses and Structural Research in Cracow.

Samples were placed in cells of variable optical path lengths, with the KRS-5 windows for the medium- and high-frequency region and the polyethylene windows for the low-frequency region. Spacers used varied between 0.025 and 3.0 mm. Empty cells or cells with the solvent were used as a reference. Liquid nitrogen was a coolant. Methyl salicylate was cooled slowly below the freezing point down to the liquid nitrogen temperature and then slowly heated. Figure 1 presents the spectra recorded when temperature was increasing.

Infrared spectrum of the gaseous methyl salicylate was recorded on a Perkin–Elmer model 580B spectrophotometer in the Institute of Physics Polish Academy of Sciences in Warsaw by Mr. M. Szcześniak. The length of the cell was 8 cm.

3. Results and discussion

Infrared spectra of methyl salicylate are presented in Fig. I at temperatures varying from 173 to 293 K. The most significant changes in the spectra accompany the temperature interval 264 to 273 K where the phase transition occurs (solid–liquid).

The high-frequency region 2600–3800 cm^{-1} (Fig 1*a*) representing the O—H stretching vibration is more structured on the low-frequency side of the maximum peak (at 3187 cm^{-1} at room temperature) and has a prominent narrow band at

[1]To whom all correspondence should be addressed. Present address: Division of Physical Chemistry, Faculty of Pharmaceutical Sciences, Hongo, Bunkyo-ku, Tokyo 113, Japan.

[2]The band at 3233 cm^{-1} seen in the spectrum of salicylic acid (Fig. 2 of ref. 1) but absent in the spectrum of acetylsalicylic acid (Fig. 1 of ref. 1) was theoretically ascribed to the internal hydrogen bond — compare theoretical lines in both figures.

Can. J. Chem. Downloaded from www.nrcresearchpress.com by 210.87.254.6 on 09/06/12
For personal use only.

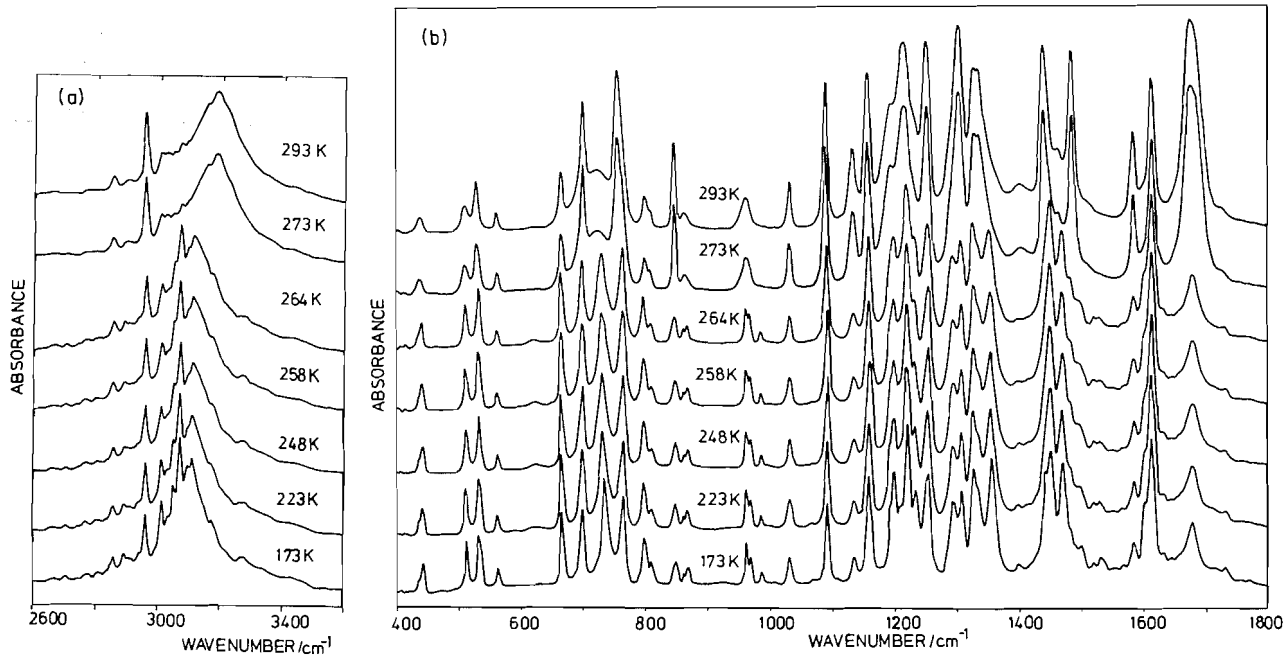

FIG. 1. (*a*) Infrared spectra of methyl salicylate in the region 2600−3800 cm^{-1} at different temperatures; (*b*) infrared spectra of methyl salicylate in the region 400−1800 cm^{-1} at different temperatures.

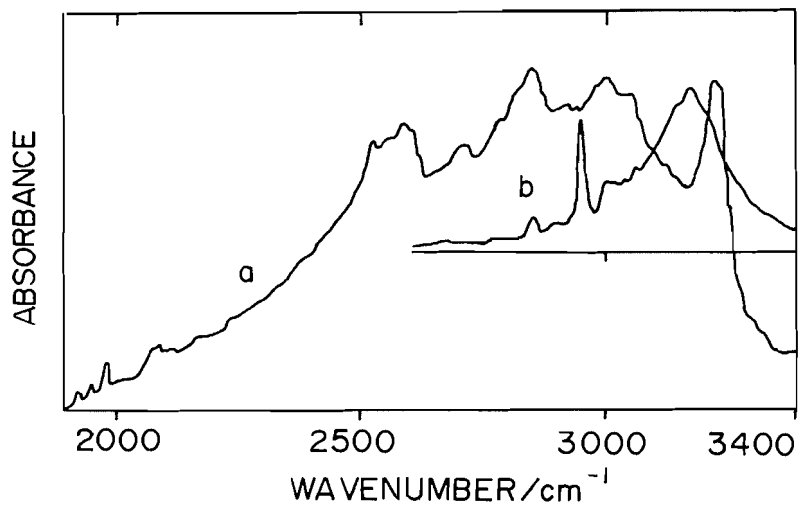

FIG. 2. Infrared spectra of solutions of methyl salicylate in carbon tetrachloride at different concentrations at room temperature. Solid line means the spectrum of the pure methyl salicylate and broken line spectra of solutions.

2955 cm^{-1} due to the CH_3 group. The position of this band remains almost unchanged during the phase transition and variation of temperature though its relative weight becomes smaller when temperature goes down.

The most striking changes accompanying the phase transition are those concerning the position of the central peak. The central peak shifts down to 3111 cm^{-1} and is no longer the most prominent peak. There are two characteristic bands at 3071 and 3012 cm^{-1}, the band at 3071 cm^{-1} being now the strongest with its relative importance increasing with decreasing temperature. These bands are visible in the spectrum of the liquid, in solutions (Fig. 2) and in the gas phase (Fig. 3). Moreover, recently we have observed a prominent peak in this region in the spectrum of O-deuterated salicylaldehyde (7), therefore we think that they are due to C—H vibrations of the benzene ring.

The overall half-width of the ν_s band is not very sensitive to the phase transition nor temperature decrease in the investigated interval (it changes from about 200 cm^{-1} at 293 K to 195 cm^{-1} at 264 K and 170 cm^{-1} at 173 K). It is, however, roughly twice as large as the half-width of the related band in crystalline salicylic acid (the half-width of this band is approximately 90 cm^{-1}). Figure 4 shows the overlay of spectra of salicylic acid and methyl salicylate at room temperature. One observes differences between the ν_s band of methyl salicylate and the band ascribed previously to the internal hydrogen bond both in the position (3187 cm^{-1} and 3233 cm^{-1}) and the width.

The medium-frequency region 400−1800 cm^{-1} (Fig. 1*b*) also shows characteristic changes accompanying the phase transition. The changes below and over the freezing point are not very significant.

Can. J. Chem. Downloaded from www.nrcresearchpress.com by 210.87.254.6 on 09/06/12
For personal use only.

Can. J. Chem. Downloaded from www.nrcresearchpress.com by 210.87.254.6 on 09/06/12
For personal use only.

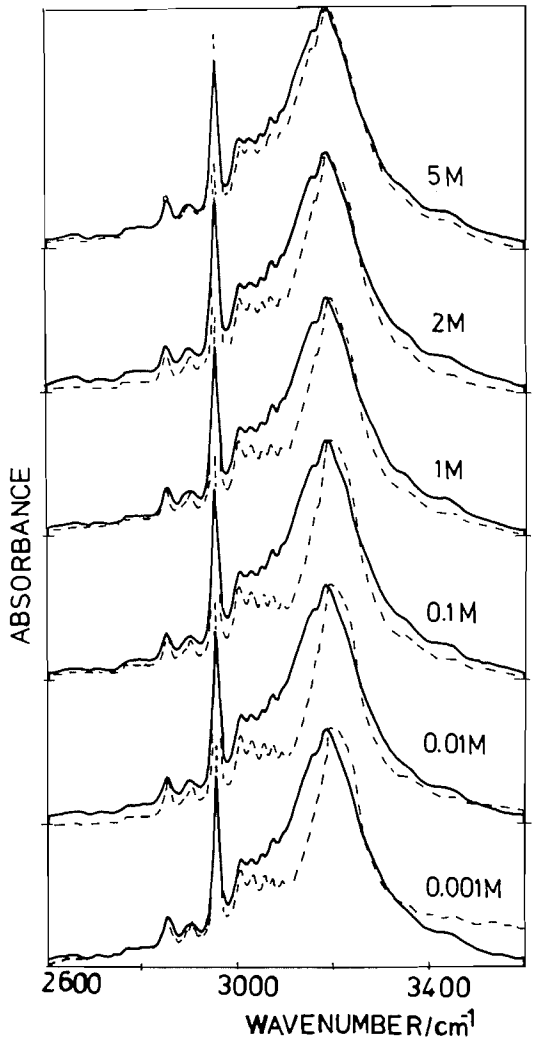

FIG. 3. Infrared spectrum of the gaseous methyl salicylate at 343 K.

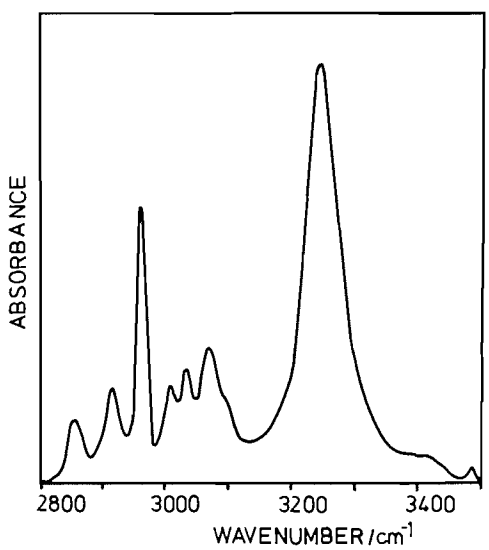

FIG. 4. Comparison between the spectrum of salicylic acid (*a*) and methyl salicylate (*b*) at room temperature.

The experimental facts gathered above show the difference between the ν_s band of methyl salicylate both in the liquid and solid state and the band ascribed to the intramolecular hydrogen bond in salicylic acid. The difference is both in the position and more striking in the width. Also the ν_s band of methyl salicylate seems to be more structured especially in the solid state. The question is whether this band is due to an internal hydrogen bond of a different strength than in salicylic acid or to an intermolecular one, or to a mixture of them.

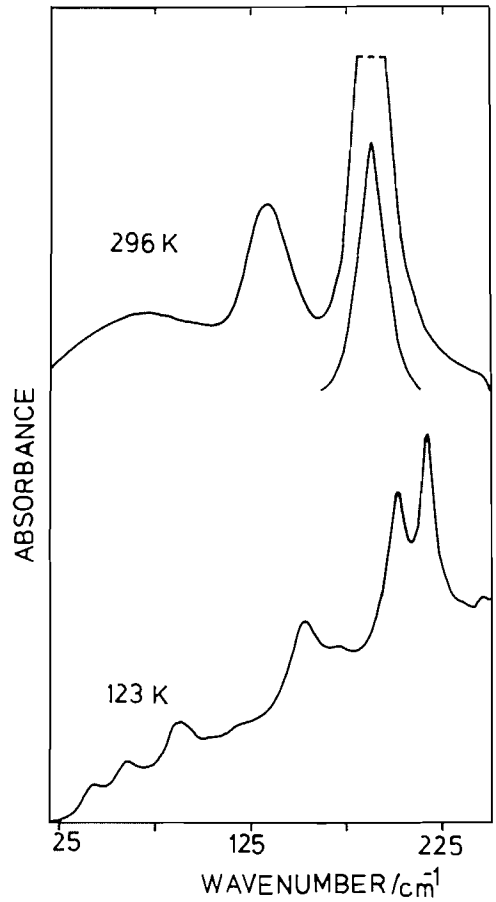

FIG. 5. Far-infrared spectra of methyl salicylate.

To solve this problem we have recorded high-frequency infrared spectra of methyl salicylate in solutions with an inert solvent carbon tetrachloride. Concentrations of methyl salicylate varied from 5 to 0.001 *M*. Results are presented in Fig. 2. One can see that dilution causes narrowing of the ν_s band but does not significantly change positions of the peaks nor the fine structure of the band. The half-width diminishes to 112 cm^{-1} at 0.001 *M*. The structure of the ν_s band of the isolated molecules of methyl salicylate in carbon tetrachloride is essentially the same as the structure of the pure liquid and solid methyl salicylate which indicates that the OH group of this molecule forms an internal hydrogen bond. External perturbations in the liquid (and to smaller extent in the solid) state cause additional broadening of the band.

Figure 3 presents an infrared spectrum of the gaseous methyl salicylate in the region 2800–3500 cm^{-1} at 343 K. The central peak is located at 3255 cm^{-1} and the half-width of the ν_s band is about 60 cm^{-1}. The position of the CH_3 band and secondary features of the spectrum are similar to those observed in the spectra of methyl salicylate in the liquid and solid state and in the solutions. This evidences that molecules of methyl salicylate form intramolecular hydrogen bonds also in the gaseous state.

The position of the ν_s band is now at the higher wavenumber

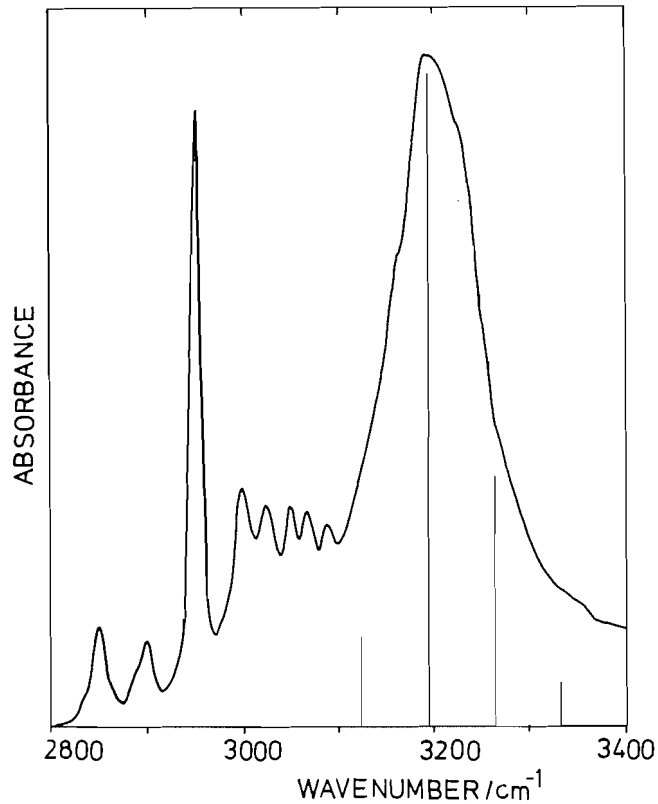

FIG. 6. Comparison between the experimental and calculated infrared spectrum of the 0.001 *M* methyl salicylate in CCl_4 at room temperature. The distortion parameter *b* (6) equals 0.5.

(but not very different) than the position of the ν_s band of the intramolecular hydrogen bond in salicylic acid (3255 cm^{-1} and 3233 cm^{-1}). The half-width is smaller (60 cm^{-1} and 90 cm^{-1}), contrary to the situation in the spectra of the liquid and solid methyl salicylate.[3] The ν_s band in the gaseous state is smooth and is the most similar to the band associated with the intramolecular hydrogen bond in the crystalline salicylic acid.

The experimental facts presented above show that the position of the ν_s band of methyl salicylate and especially its half-width are determined to a large extent by an influence of the environment. We note also that the half-width of this band is much smaller in the gaseous state than in the liquid and solid state which is not always the case (see, e.g., spectra of acetic acid (8, 9) or formic acid (10) in different phases).

[3]But not in solutions with low concentrations of methyl salicylate where the half-width approaches the value found in salicylic acid.

Far-infrared spectra of methyl salicylate in the liquid and solid state in the region 20–250 cm^{-1} are presented in Fig. 5. There are three main peaks in the spectrum at 296 K: 69, 132, and 187 cm^{-1}. These peaks shift upwards to 87, 152, and a doublet 202 and 217 cm^{-1} at 123 K. The value 70 cm^{-1} was used in a theoretical reconstruction of the ν_s band of the 0.001 *M* methyl salicylate in CCl_4 presented in Fig. 6. The calculation was based on the Witkowski–Maréchal model (5, 6) assuming an adiabatic coupling between the O—H stretching vibration and a low-frequency intramolecular O . . . O mode.

The value 70 cm^{-1} is also close to the wavenumber observed in the Raman spectrum of the crystalline salicylic acid (63 cm^{-1}) and used in theoretical reconstruction of infrared spectra of salicylic acid and O-deuterated salicylic acid (65 cm^{-1}) (1). It is probably connected with the low-frequency O . . . O bending vibration in strongly distorted intramolecular hydrogen bond. Two other observed wavenumbers 132 and 187 cm^{-1} were also used in calculations but did not give an agreement with the experimental spectrum.

4. Conclusions

Experimental results reported in this paper evidence that molecules of methyl salicylate form intramolecular hydrogen bonds in the gaseous, liquid, and solid state. Width and position of the ν_s band depend to a large extent on intermolecular interactions. The O—H stretching vibration in methyl salicylate couples with an intramolecular O . . . O mode of the wavenumber close to 70 cm^{-1}, lower than typical values for the O . . . O stretching vibrations in intermolecular hydrogen bonds.

Acknowledgements

The authors would like to thank Mr. M. Szcześniak for recording the infrared spectrum of the gaseous methyl salicylate. They are also indebted to Mr. J. Ściesiński for his help in experimental measurements.

1. M. J. WÓJCIK. Chem. Phys. Lett. **83**, 503 (1981).
2. W. COCHRAN. Acta Crystallogr. **6**, 260 (1953).
3. G. E. BACON and R. J. JUDE. Z. Krist. **138**, 19 (1973).
4. P. J. WHEATLEY. J. Chem. Soc. Suppl. 6036 (1964).
5. A. WITKOWSKI. J. Chem. Phys. 47, 3645 (1967).
6. Y. MARÉCHAL and A. WITKOWSKI. J. Chem. Phys. **48**, 3697 (1968).
7. M. J. WÓJCIK and C. PALUSZKIEWICZ. Unpublished result.
8. M. HAURIE and A. NOVAK. J. Chim. Phys. **62** 146 (1965).
9. A. NOVAK. J. Chim. Phys. **72**, 981 (1975).
10. G. C. PIMENTEL and A. L. MCCLELLAN. The hydrogen bond. Freeman, San Francisco. 1960. p. 104.

Can. J. Chem. Downloaded from www.nrcresearchpress.com by 210.87.254.6 on 09/06/12
For personal use only.

On the positional reactivity order in the sulfuric acid sulfonation of the two naphthalenesulfonic acids[1]

PETER DE WIT AND HANS CERFONTAIN[2]

Laboratory for Organic Chemistry, University of Amsterdam, Nieuwe Achtergracht 129, 1018 WS Amsterdam, The Netherlands

Received November 8, 1982

PETER DE WIT and HANS CERFONTAIN. Can. J. Chem. **61**, 1453 (1983).

The sulfonation in 98.5% H_2SO_4 at 25.0°C of naphthalene-1-sulfonic acid yields 58% 1,5-, 32% 1,6-, and 10% 1,7-disulfonic acids and that of the 2-sulfonic acid 4% 1,3-, 74% 1,6-, 18% 1,7-, and 4% 2,6- + 2,7-disulfonic acids. Further sulfonation of the latter disulfonic acid mixture in 105.2% H_2SO_4 at 25.0°C yields 78% 1,3,6- and 12% 1,3,5- + 1,3,7-trisulfonic acids. Reaction of naphthalene-1,5-disulfonic acid with 105.2% H_2SO_4 at 25°C yields 5-sulfonaphthalene-1-sulfonic anhydride.

Partial rate factors for the sulfonation of naphthalene-1- and -2-sulfonate in highly concentrated aqueous sulfuric acid (where the sulfonating entity is $H_2S_2O_7$) are reported. They are discussed in terms of the difference in the reactivity of the α- and β-positions of the naphthalene skeleton and the electronic and steric effects of the sulfonate substituent already present.

PETER DE WIT et HANS CERFONTAIN. Can. J. Chem. **61**, 1453 (1983).

La sulfonation de l'acide naphtalènesulfonique-1 à 25,0°C dans du H_2SO_4 à 98,5% conduit aux acides disulfoniques-1,5, -1,6 et -1,7 avec des rendements respectifs de 58%, de 32% et de 10%. Dans les mêmes conditions la sulfonation de l'acide naphtalènesulfonique-2 conduit aux acides disulfoniques-1,3 (4%), -1,6 (74%), -1,7 (18%) et à 4% d'acides-2,6 et -2,7. Une sulfonation plus poussée du dernier mélange d'acides à 25,0°C dans du H_2SO_4 à 105,2% donne 78% d'acide trisulfonique-1,3,6 et à 12% d'acide trisulfonique-1,3,5 et -1,3,7. La réaction de l'acide naphtalènedisulfonique-1,5 avec du H_2SO_4 à 105,2% à 25°C conduit à l'anhydride sulfo-5 naphtalènesulfonique-1.

On rapporte les facteurs de vitesse partielle de sulfonations des naphtalènesulfonate-1 et naphtalènesulfonate-2 dans de l'acide sulfurique fortement concentré (ou l'entité sulfonante est $H_2S_2O_7$). On en discute en fonction de la différence de réactivité des positions α et β du squelette naphtalène et des effets électroniques et stériques du substituant sulfonate déjà présent.

[Traduit par le journal]

Can. J. Chem. Downloaded from www.nrcresearchpress.com by 210.87.254.40 on 09/06/12
For personal use only.

The sulfuric acid sulfonation of naphthalene yields a mixture of the 1- and 2-sulfonic acids (1, 2). At room temperature the reaction is kinetically controlled and the 1- and 2-sulfonic acid isomer ratio varies at 25.0°C from 5.9 to 4.3 on increasing the sulfuric acid concentration from 75 to 95% H_2SO_4 (3). At temperatures >150°C the main product of sulfonation is the 2-sulfonic acid which is the thermodynamically more stable product in view of the significant degree of *peri* strain in the 1-sulfonic acid. In fact, there is some steric hindrance for the introduction of a sulfo group *peri* to hydrogen, as appears from the small, but significant, kinetic isotope effect of hydrogen for the sulfonation of the 1-position of naphthalene: for reaction with SO_3 in nitromethane at 0°C, $k_H/k_D = 1.8 \pm 0.1$ (4).

We now report the isomer distribution of disulfonic acids formed in the sulfonation of the two naphthalenesulfonic acids occurring in 98.5% H_2SO_4 at 25.0°C at low substrate concentration (0.25 *M*). The ratio of the disulfonic acid components in the sulfuric acid reaction mixtures was determined after complete substrate conversion by multicomponent ^1H nmr analysis (5) on the basis of the specific absorptions of the disulfonic acid components. As to the sulfonation mixture resulting from the 2-sulfonic acid, the singlet at 9.12 ppm was assigned to the 8-H of the 1,7-disulfonic acid, the triplet at 7.86 ppm to the 3-H of both the 1,6- and 1,7-isomers, and the low intensity absorption in between 7.85 and 7.50 ppm to the 6- and 7-H of the 1,3-isomer. The absorption in between 8.0 and 8.9 ppm not accounted for by these isomers is due to the 2,6- and 2,7-isomers which, as appears from the spectra of authentic samples, do absorb only in between 8.0 and 8.9 ppm. As to the sulfonation mixture of the 1-sulfonic acid, the non-overlapping $\frac{1}{2}$AB absorption at 8.95 and the singlet at 9.14 ppm were assigned to the 4- and 8-H of the 1,5-disulfonic acid and the 8-H of the 1,7-isomer respectively; the remaining absorptions are due to the 1,6-isomer. The absence of absorption below 7.75 ppm sets an upper limit of 2% to the content of the 1,3-isomer of which the 6- and 7-H would absorb in that region.

The isomer distribution for the sulfonation of naphthalene-1-sulfonic acid was thus determined to be 58% 1,5-, 32% 1,6-, and 10% 1,7-disulfonic acids and that of the 2-sulfonic acid 4% 1,3-, 74% 1,6-, 18% 1,7-, and 4% 2,6- + 2,7-disulfonic acids. These data differ significantly from those for the sulfonation at 57°C reported by Spryskov and Karavaev (6) (for the 1-SO_3H with 104% H_2SO_4 75% 1,5-, 15% 1,3- + 1,7-, and 10% 1,6-disulfonic acids and for the 2-SO_3H with 99% H_2SO_4 67% 1,6-, 21% 1,3- + 1,7-, 1% 2,6- and 11% 2,7-disulfonic acids). The present data are preferred in view of the method of analysis (^1H nmr versus derivatization). Moreover, the data of Spryskov and Karavaev for reaction at 57°C may not be strictly thermodynamically controlled, the main high temperature products being the 2,6- and 2,7-disulfonic acids (7). The present data are in line with the observation that the disulfonation of naphthalene with 107% H_2SO_4 at 40°C yields about 70% of the 1,5- and 25% of the 1,6-disulfonic acids (8) and, as to the 2-sulfonic acid, agree with those reported earlier (9).

The sulfonation of aromatic substrates in sulfuric acid in the range of 88−100% sulfuric acid proceeds by a three-step mechanism via σ-complex intermediates in which the electrophilic sulfonating entity is $H_2S_2O_7$ (10). The partial rate factors for that mechanism (determined from the sulfonation rate constants of benzene (11) and the two naphthalenesulfonic acids

[1]Aromatic sulfonation, part 87. Preceding paper: see ref. 25.

[2]Author to whom correspondence may be addressed.

TABLE 1. Partial rate factors for sulfonation with concentrated aqueous sulfuric acid

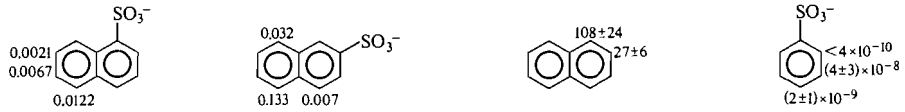

$f_2, f_3, f_4, f_8 < 0.0004$ $f_1, f_3, f_6 < 0.002$

$f_6 + f_7 = 0.007$

TABLE 2. Fractions of mesomeric structures of the various σ-complexes for the sulfonation of the two naphthalenesulfonic acids and benzenesulfonic acid, which are notably destabilized by the positive charge on the sulfur of the sulfo substituent, together with the derived positional reactivity orders

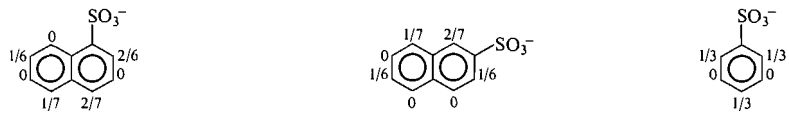

2<4<7<5<3 = 6 = 8 1<3 = 6<8<4 = 5 = 7 2 = 4<3

(3) and the presently reported isomer distribution data) are given in Table 1, together with those of naphthalene (determined from the (extrapolated) rate constant ratio of naphthalene (3) and benzene (11) (=90 ± 20) and the naphthalenesulfonic acid isomer distribution data (3)) and benzenesulfonic acid (12). It should be recalled that the substrate species undergoing electrophilic substitution in concentrated aqueous sulfuric acid is the arenesulfonate anion rather than the uncharged arenesulfonic acid (12, 13).

The partial rate factor order for the sulfonation of an arenesulfonic acid is governed by three factors, viz. (*i*) the differences in the cation localization energies of the positions under scrutiny of the parent arene, (*ii*) the difference in steric hindrance for the introduction of the sulfonic acid group, and (*iii*) the electronic directing effect of the sulfonate substituent already present in the substrate in destabilizing the σ-complexes under comparison (14). An estimate of the substituent effect of the $-SO_3^-$ group in destabilizing the σ-complexes can be obtained by counting the fractions of the mesomeric structures of the various σ-complexes for the introduction of the second sulfo group which are notably destabilized as the result

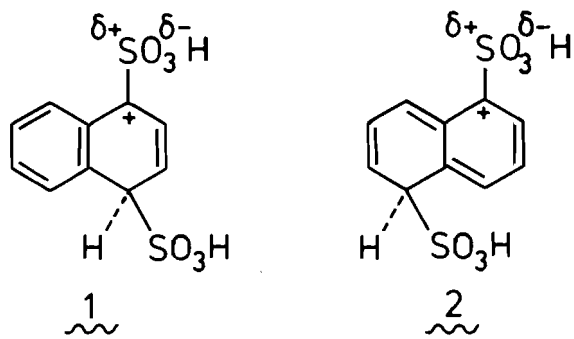

of repulsion between the positive charges on the mutually adjacent aromatic carbon and the S of the sulfonate substituent (sulfur being electropositive relative to oxygen) already present (14, 15). Typical examples of such destabilized mesomeric structures are **1** and **2**. The thus obtained data and the derived positional reactivity orders are given in Table 2.

As to the steric factors, sulfonation *peri* to a sulfonate group is fully impeded (16, 17) and the degree of steric hindrance for sulfonation *ortho* to that substituent is substantial (17, 18). As far as the third factor is concerned, the cation localization energies of benzene and naphthalene (19) predict the positional reactivity order for electrophilic substitution to be: 1-naphthalene > 2-naphthalene > 1-benzene.

Upon introducing a sulfonate substituent, the rate reduction for naphthalene of the positions in the ring containing the sulfonate substituent is $108 : <0.0004 = >3 \times 10^5$ for naphthalene-1-sulfonate and $108 : \leq 0.007 = \geq 2 \times 10^4$ for the 2-isomer, compared with a rate reduction of 4×10^8 for benzenesulfonic acid. The rate reduction in the other ring of the naphthalenesulfonic acids is far less. The observed partial rate factor orders for the sterically accessible α-positions (${}^{2\text{-S}}f_5 > {}^{2\text{-S}}f_8 > {}^{1\text{-S}}f_5 > {}^{2\text{-S}}f_4 > {}^{2\text{-S}}f_1$ and ${}^{1\text{-S}}f_4$) and the β-positions (${}^{2\text{-S}}f_7 \simeq {}^{1\text{-S}}f_6 > {}^{1\text{-S}}f_7 \geq {}^{2\text{-S}}f_6 \simeq {}^{2\text{-S}}f_3 > {}^{1\text{-S}}f_2$ and ${}^{1\text{-S}}f_3$) both compare satisfactorily with the predicted positional reactivity orders (cf. Table 2), except for ${}^{2\text{-S}}f_4$ and ${}^{1\text{-S}}f_3$. The observed values of these two partial rate factors are substantially smaller than predicted on the basis of counting the fraction of mesomeric structures of the σ-complexes which are destabilized as the result of repulsion of the positive charges on the adjacent aromatic C and sulfonate S. This approach unjustly presumes, however, that all the mesomeric structures describing the σ-complex for sulfonation at a given position are equivalent. In fact the structures are of two types, viz. benzenoid and quinoid, of which the latter are higher in energy and thus far less contributing than the former. On the basis of this starting point it can be argued (14) that the positional reactivity orders for the sterically assessible α- and β-positions of naphthalene-1-sulfonic acid will be $4 < 5$ and $3 < 7 < 6$, respectively, and for naphthalene-2-sulfonic acid $4 < 8 < 5$ and $3 \simeq 6 < 7$, respectively, which are in fact the observed positional reactivity orders.[3]

The further reaction of the naphthalenedisulfonic acid mix-

[3]The low values of ${}^{2\text{-S}}f_4$ and ${}^{1\text{-S}}f_3$ may in part be due to the negative inductive effect exerted by the $-SO_3^-$ substituent in addition to the significant $-M$ effect (12, 20).

Can. J. Chem. Downloaded from www.nrcresearchpress.com by 210.87.254.40 on 09/06/12
For personal use only.

tures obtained in 98.5% H_2SO_4 was affected by addition of neat sulfur trioxide so as to raise the sulfuric acid concentration to 105.2% H_2SO_4 at 25.0°C. After 30 h, the reaction mixture starting originally from naphthalene-2-sulfonic acid was found to contain 78% 1,3,6-trisulfonic acid (^{1}H nmr (105% H_2SO_4), δ(ppm): 9.15 (s, 2-H), 8.45 and 8.92 (AB, J = 8−9 Hz, 7- and 8-H), 8.94 and 8.97 (overlapping singlets, 5- and 4-H[4]), 12% 1,3,5- + 1,3,7-isomers (assigned on the basis of the 9.26 singlet to both the 4-H of the 1,3,5- and the 8-H of the 1,3,7-isomer), and 10% unreacted disulfonic acid. Apparently both the 1,3- and the 1,6-disulfonic acids are fully converted into the 1,3,6-trisulfonic acid. The 1,3,5- and 1,3,7-trisulfonic acids thus originate very predominantly from the 1,7-disulfonic acid which, based on the effects of the two sulfo substituents, will be less reactive than the 1,3- and 1,6-disulfonic acids.

Reaction of the disulfonic acid mixture resulting from naphthalene-1-sulfonic acid with 105.2% H_2SO_4 at 25°C led to the formation of a white precipitate which proved to be insoluble in the numerous carefully dried organic solvents tested.[5] The precipitate "dissolved" very slowly in both water and concentrated aqueous sulfuric acid.[6] The ^{1}H nmr and uv spectral data of these two solutions are identical with those of naphthalene-1,5-disulfonic acid. The precipitate is therefore assigned to be the anhydride of two molecules of naphthalene-1,5-disulfonic acid: 5-sulfonaphthalene-1-sulfonic anhydride.[7] In fact the ir spectrum (KBr) shows absorptions at 1406, 1390, and 716 cm^{-1} which are characteristic for the sulfonic anhydride group (22) and at 1180 and 1030 cm^{-1}, which bands are also observed with disodium naphthalene-1,5-disulfonate and are characteristic for the sulfonate group (23).

Experimental

The ^{1}H nmr spectra were recorded with a Varian XL 100 spectrometer. The chemical shifts are relative to neat tetramethylsilane as external reference (concentric capillary). Potassium naphthalene-1- and sodium napthalene-2-sulfonate and the disodium salts of 1,5-, 2,6- and 2,7-disulfonic acids were commercial products which were purified by successive recrystallization from ethanol−water. The sulfonation procedures were as described before (24).

[4]Compare ref. 21.

[5]The turbidity of the reaction mixture of naphthalene with an excess of weak oleum at ≤25°C at the later stages of the reaction was noticed before (8, 21), but it appears that no isolation was attempted.

[6]Naphthalene-1,5-disulfonic acid dissolves rapidly in these two solvents.

[7]Upon shaking in an excess of 105% H_2SO_4, naphthalene-1,5-disulfonate was found to convert slowly into the same white precipitate.

1. C. M. SUTER. The organic chemistry of sulfur. John Wiley and Sons, Inc., New York. 1944. pp. 268−273.
2. H. CERFONTAIN. Mechanistic aspects in aromatic sulfonation and desulfonation. Interscience, New York. 1968. pp. 68−69.
3. H. CERFONTAIN and A. TELDER. Recl. Trav. Chim. Pays-Bas, **86**, 527 (1967).
4. K. LAMMERTSMA and H. CERFONTAIN. J. Chem. Soc. Perkin Trans. 2, 28 (1980).
5. H. CERFONTAIN, A. KOEBERG-TELDER, C. KRUK, and C. RIS. Anal. Chem. **46**, 72 (1974).
6. A. A. SPRYSKOV and B. I. KARAVAEV. Zh. Obshchei Khim. **22**, 1620 (1952); Chem. Abstr. **47**, 8709 (1953).
7. A. A. SPRYSKOV and B. I. KARAVAEV. Zh. Obshchei Khim. **23**, 1712 (1953); Chem. Abstr. **48**, 13667 (1954).
8. H. E. FIERZ-DAVID and A. W. HASSLER. Helv. Chim. Acta, **6**, 1133 (1923).
9. H. E. FIERZ-DAVID and C. RICHTER. Helv. Chim. Acta, **28**, 257 (1945).
10. H. CERFONTAIN and C. W. F. KORT. Int. J. Sulphur Chem. Part C, **6**, 123 (1971).
11. A. W. KAANDORP, H. CERFONTAIN, and F. L. J. SIXMA. Recl. Trav. Chim. Pays-Bas, **81**, 969 (1962).
12. H. CERFONTAIN and Z. R. H. SCHAASBERG-NIENHUIS. J. Chem. Soc. Perkin Trans. 2, 1780 (1976).
13. R. B. MOODIE, K. SCHOFIELD, and T. YOSHIDA. J. Chem. Soc. Perkin Trans. 2, 788 (1975).
14. H. CERFONTAIN. J. Org. Chem. **47**, 4680 (1982).
15. W. C. HERNDON. Tetrahedron, **29**, 3 (1973); J. Am. Chem. Soc. **95**, 2404 (1973); **96**, 7605 (1974); **98**, 887 (1976).
16. K. LAMMERTSMA and H. CERFONTAIN. J. Chem. Soc. Perkin Trans. 2, 673 (1979).
17. H. J. A. LAMBRECHTS and H. CERFONTAIN. Tetrahedron, **38**, 1667 (1982).
18. A. KOEBERG-TELDER and H. CERFONTAIN. J. Chem. Soc. Perkin Trans 2, 633 (1973).
19. C. A. COULSON and A. STREITWIESER, JR. Dictionary of π-electron calculations. Pergamon Press, London. 1965. pp. 35−38.
20. T. A. KORTEKAAS, H. CERFONTAIN, and J. M. GALL. J. Chem. Soc. Perkin Trans. 2, 445 (1978).
21. F. MUTH. *In* Houben-Weyl, Methoden der Organische Chemie. Vol. IX. 4th ed. *Edited by* E. Müller. 1955 p. 477.
22. A. KOEBERG-TELDER, C. RIS, and H. CERFONTAIN. J. Chem. Soc. Perkin Trans. 2, 98 (1974), and cited references.
23. E. REBANE. Acta Chem. Scand. **21**, 657 (1967).
24. K. LAMMERTSMA, C. J. VERLAAN, and H. CERFONTAIN. J. Chem. Soc. Perkin Trans. 2, 719 (1978).
25. H. CERFONTAIN, K. LAALI, and H. J. A. LAMBRECHTS. Recl. Trav. Chim. Pays-Bas. In press.

Can. J. Chem. Downloaded from www.nrcresearchpress.com by 210.87.254.40 on 09/06/12
For personal use only.

Conformation of purine mononucleotides by H{H} and P{H} nuclear Overhauser effects

H. SANTOS AND A. V. XAVIER
Centro de Química Estrutural, U.N.L., 1200 Lisboa, Portugal

AND

C. F. G. C. GERALDES[1]
Chemistry Department, University of Coimbra, 3000 Coimbra, Portugal

Received October 21, 1982

H. SANTOS, A. V. XAVIER, and C. F. G. C. GERALDES. Can. J. Chem. **61**, 1456 (1983).

The proton–proton and phosphorus–proton nuclear Overhauser effect (nOe) of guanosine 5′-monophosphate (5′-GMP) was measured in aqueous solution at different pH values and in the presence of excess La^{III} at acid pH. These data and nOe data from the literature for other mononucleotides were used together with vicinal proton–proton coupling constants to investigate the conformations of mononucleotides in aqueous solution, especially their rotational state about the glycosidic bond. Comparison of observed and calculated enhancements using various conformational models for the glycosidic bond gave predominantly *anti* conformations for 5′-AMP and 5′-GMP and a mixture of *syn* and *anti* conformations for 2′-AMP, 2′-GMP, 3′-AMP, and 3′-GMP. Protonation of 5′-GMP at N-7 of the guanine base alters the amplitude of its torsion angle within the *anti* range. The agreement between the glycosidic nucleotide conformations defined by nOe and by the lanthanide probe method is good but not perfect. As complexation of 5′-GMP with La^{III} through the phosphate group has only a small effect on the conformation of its exocyclic group, a comparison of the two methods is justified.

H. SANTOS, A. V. XAVIER et C. F. G. C. GERALDES. Can. J. Chem. **61**, 1456 (1983).

On a mesuré l'effet Overhauser nucléaire (eOn) proton–proton et phosphore–proton du monophosphate-5′ de guanosine (MPG-5′) en solution aqueuse à différents pH et en présence d'un excès de La^{III} à un pH acide. On a utilisé ces données ainsi que celles de eOn, relevées dans la littérature, conjointement avec les constantes de couplage vicinal proton–proton pour étudier les conformations des mononucléotides en solution aqueuse et plus spécialement leur état rotationnel autour de la liaison glycosidique. La comparaison des exaltations observées et calculées en utilisant divers modèles conformationnelles pour le lien glycosidique a donné de façon prédominante des conformations *anti* pour le MPA-5′ et le MPG-5′ et un mélange de conformations *syn* et *anti* pour le MPA-2′, le MPG-2′, le MPA-3′ et le MPG-3′. La protonation du MPG-5′ au niveau N-7 de la base guanine modifie l'amplitude de son angle de torsion dans le domaine *anti*. L'accord entre la conformation glycosidique du nucléotide définie par le eOn et par la méthode d'essai du lanthane est bon mais non parfait. Une comparaison des deux méthodes se justifie puisque la complexation du MPG-5′ avec La^{III} via le groupe phosphate n'a qu'un effet faible sur la conformation de son groupe exocyclique.

[Traduit par le journal]

Can. J. Chem. Downloaded from www.nrcresearchpress.com by 210.87.254.42 on 09/06/12
For personal use only.

Introduction

Extensive studies of the solution conformation of nucleosides and nucleotides have been carried out with the aim of relating molecular geometry to biological function. The conformation of nucleosides and mononucleotides may be described in terms of the three dihedral angles χ, ψ, and ϕ in the nomenclature of Sundaralingam (1) (Fig. 1) and the pseudorotational state of the furanose ring (2). Nuclear magnetic resonance (nmr) spectroscopy provides a very convenient experimental technique for the solution conformational analysis of nucleosides and mononucleotides in terms of these parameters (3). Torsion about the glycosidic bond may be studied through nuclear Overhauser effect (nOe) methods (4) and the remaining parameters by analysis of measured spin–spin coupling constants (3). The lanthanide probe method (5) has also been widely used in conformational studies of these molecules.

Most of the early applications of homonuclear nOe to the study of the conformations of nucleosides and nucleotides about the glycosidic bond (6–8) have been of a qualitative nature. Quantitative conformational studies, at first restricted to rigid molecules (9), have more recently been applied to flexible molecules using approximate methods (12–15) or the full theory (10, 11, 16, 17). Recently the phosphorus–proton nuclear Overhauser effect has also been used in a conformational study of the sugar–phosphate moiety of various mononucleotides (18).

This study is concerned with a full conformational analysis of guanosine 5′-monophosphate (5′-GMP) in aqueous solution using homonuclear and phosphorus–proton nOe values. The nOe values for other mononucleotides, available in the literature, are also analysed using the same procedure.

Another major aim of this study is the investigation of the effect of La^{III} binding upon the conformation of 5′-GMP in aqueous solution, using nOe and coupling constants data for the 5′-GMP/La^{III} complex, because the possibility of a conformational change induced by probe binding constitutes a major limitation of the lanthanide probe method.

Experimental

The mononucleotides, purchased from Sigma Chemical Company, were lyophilized as frozen solutions in 99.8% D_2O (from Norsk Hydro). The final dry residues were taken up in ~1 mL of 99.8% D_2O and the resultant solutions at pH 7 were passed through columns of Chelex 100 (Bio-Rad Laboratories, Richmond, CA) previously equilibrated with 99.8% D_2O. This procedure frees the nucleotide solutions of cations with charge higher than one. The solutions were then lyophilized at least twice from 99.8% D_2O, and the final solutions were prepared by dissolution in 99.8% D_2O of the required quantity of nucleotide obtained by weighting. pH adjustments were made with DCl or NaOD using a Radiometer PHM63 Digital pH Meter equipped with an Ingold F 3434 electrode. Residual paramagnetic impurities were removed by addition of 1 m*M* EDTA. Residual oxygen was

[1]Author to whom correspondence should be addressed.

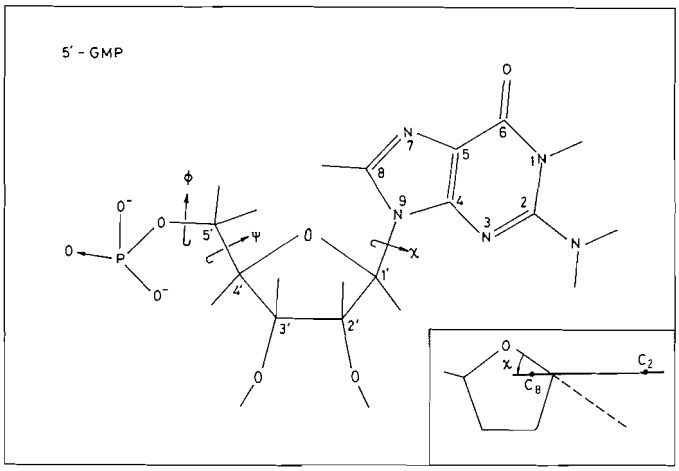

FIG. 1. Chemical structure, torsion angle notation (25), and numbering scheme of 5'-GMP.

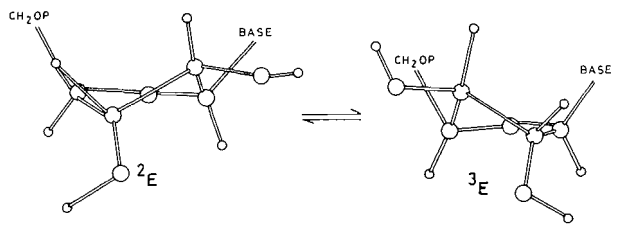

FIG. 2. Diagram of $N(C_{3'}$ *endo*) and $S(C_{2'}$ *endo*) conformations of the furanose ring.

removed by at least four freeze–pump–thaw cycles at less than 10^{-5} Torr.

The lanthanum^{III}/5'-GMP solutions were obtained by dissolution of the nucleotide in a 0.5 *M* lanthanum chloride solution. At pH 1.2 it was not possible to obtain solutions of concentrations higher than 0.015 *M* in 5'-GMP, due to its easy jellification. In these conditions, the percentage of complex formed was about 80%.

The lanthanum chloride solutions were obtained by dissolution in DCl of 99.999% La_2O_3 (from Koch–Light).

All glassware that was to contact the samples, after Chelex treatment, was rinsed with basic EDTA, deionized water, and acetone and then blown dry.

All nmr measurements were made with a JEOL JNM-PF-100 spectrometer, equipped with a JEOL EC100 computer for Fourier transformation. Proton resonance was observed at 100 MHz and phosphorus resonance at 40.49 MHz. Probe temperature was 28°C.

The samples were placed in Wilmad No 507-PP precision tubes and, in the measurements in which benzene was used as standard for area integrations, a 1 mm capillary tube containing benzene was placed concentrically in the main nmr tube.

In order to allow for full relaxation of the observed nuclei, in the proton spectra the time interval between two consecutive pulses was 12 s, and in the ^{31}P spectra a repetition interval of 20 s and a pulse width corresponding to a 45° flip angle were used.

The nOe effects were obtained using a gated decoupling technique which allowed the separation of decoupling and nOe effects (19). An unperturbed spectrum was first collected; then the perturbed spectrum was measured with the proton decoupler at a single frequency (low power) or a broad band of frequencies (high power). Signal areas were measured on expanded spectra via planimetry, and area differences between the perturbed and the unperturbed spectra were recorded as positive or negative nOe's expressed as percentage change. Each value was obtained from at least ten measurements in similar conditions. Experimental precision was 3%. The decoupling power used was the minimum necessary to saturate the spin considered.

Spin-lattice relaxation times were measured by application of a

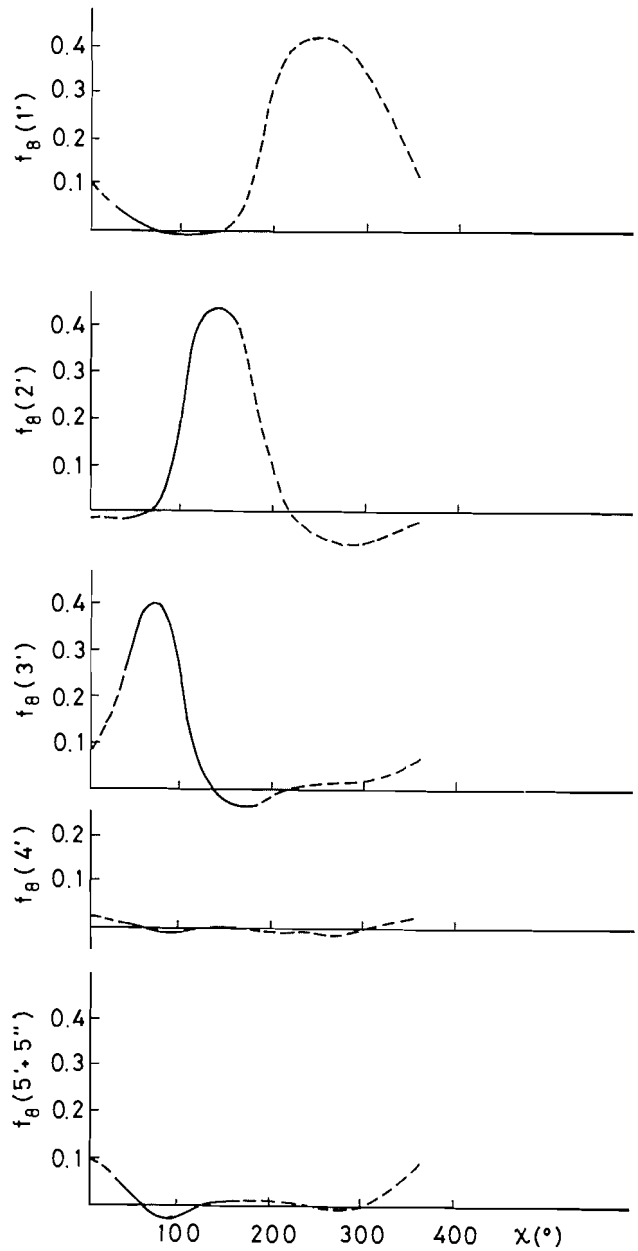

FIG. 3. Plots of various calculated nOe values for H_8 of 5'-GMP vs. glycosidic torsion angle χ, for a $N(C_{3'}$ *endo*) furanose ring conformation and $\psi = 60°$.

180°–τ–90° pulse sequence repeated at time intervals longer than $5T_1$.

The proton spectra of all the nucleotides considered in the present work have been thoroughly studied (20, 21).

The theoretical nOe enhancements $f_8(i)$, for H_8 due to irradiation of the ribose protons, as a function of the torsion angles, were calculated directly from eq. [2], using for this purpose the computer program BURLESK (22) modified to give interproton distances r_{ij} from atom coordinates for various molecular conformations obtained by variation of the ψ and χ angles with increments of 30° and 20° respectively. Two starting conformations were used differing in the geometries adopted for the furanose rings: the $N(C_{3'}$ *endo*) geometry was obtained from the crystal structure coordinates of 5'-GMP (23) and the $S(C_{2'}$ *endo*) geometry was obtained from those coordinates by use of a computer program for model building (Fig. 2). The calculation of the nOe enhancements was carried out in the following way: from the r_{ij} distances, ρ_{ij} values and R_d values were calculated using eqs. [3] and [4]; then $f_8(i)$ values were calculated by a successive approximations

Can. J. Chem. Downloaded from www.nrcresearchpress.com by 210.87.254.42 on 09/06/12
For personal use only.

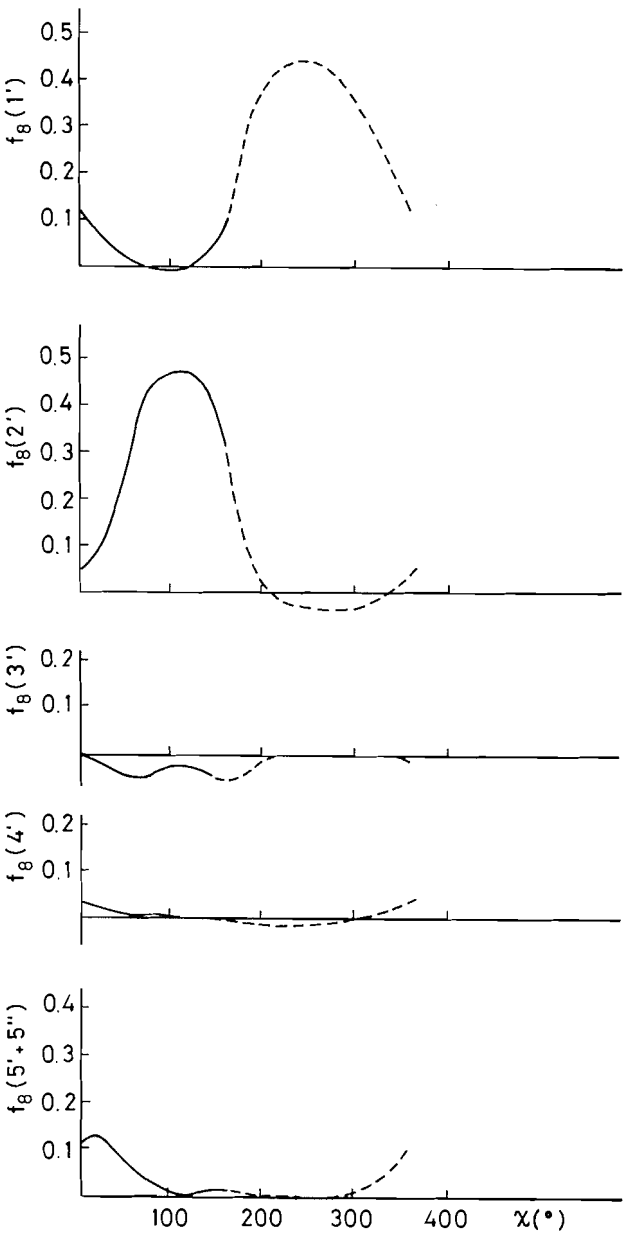

FIG. 4. Plots of various calculated nOe values for H_8 of 5′-GMP vs. glycosidic torsion angle χ, for a $S(C_{2'}$ *endo*) furanose ring conformation and $\psi = 60°$.

method (4) using as a starting point the first term of eq. [2]. A τ_c value of 6×10^{-11}s was used for all i,j pairs, a value calculated for 5′-GMP by Guéron and co-workers (12) using Stokes law. A value of ρ^* of 0.017, estimated for 2′,3′-isopropylideneinosine (10), was used for all protons.

Calculated nOe $f_8(i)$ values vs. glycosidic torsion angle, χ, are represented in Figs. 3 and 4. The full parts of the curves represent the regions where there are no van der Waals contacts between atoms (24).

Results, calculations, and discussion

The nuclear Overhauser effect is defined as the fractional enhancement in the integrated intensity of spin d which occurs upon saturation of spin s as:

$$[1]\quad f_d(s) = \frac{\text{area of } d \text{ when } s \text{ is saturated} - \text{equilibrium area of } d}{\text{equilibrium area of } d}$$

For a given molecular geometry defined by internal variables Ω, subject to certain conditions and approximations (all nuclei are under the extreme narrowing condition, relaxation is exclusively dipole–dipole, cross-correlation effects are negligible, and a single correlation time τ_c can be used for all interaction vectors, $\tau_c(ij)$), which are generally satisfied by small organic systems, it can be shown that (4, 9)

$$[2]\quad f_d(s,\Omega) = \sum_s \frac{\gamma_s \rho_{ds}(\Omega)}{2\gamma_d R_d(\Omega)} - \frac{1}{2\gamma_d R_d(\Omega)} \times \sum_{n \neq d,\, s} \gamma_n \rho_{dn}(\Omega) f_n(s,\Omega)$$

where

$$[3]\quad R_d = \sum_i \rho_{di} + \rho_d^*$$

and

$$[4]\quad \rho_{ij} = \gamma^2_i \gamma^2_j \tau_c / r^6_{ij}$$

where γ_i is the gyromagnetic ratio of nucleus i, r_{ij} is the distance between nucleus i and j, ρ_d^* is the direct relaxation rate of spin i due to "other" relaxation paths, and τ_c is the molecular reorientational correlation time. Because $f_d(s)$ is a function of internuclear distances, comparison of theoretically calculated with observed enhancements can give information about molecular geometry.

H{H}nOe values

The experimental homonuclear nOe's for 5′-GMP and other mononucleotides are given in Table 1. It should be noted that the present nOe data for 5′-GMP are slightly different from previously reported values (12). In the interpretation of these nOe data in terms of conformations of the mononucleotides studied, we will need to use conformer populations derived by an independent method, namely the analysis of vicinal coupling constants. These populations, obtained from the literature, are summarized in Table 3. The most interesting feature of the data is the strong pH dependence of the ribose conformer population in 5′-GMP, which is monitored by the pH dependence of its $J_{2'1'}$ coupling constant (12), see Fig. 5.

Attempts were first made to interpret the observed enhancements in terms of a single torsional conformer about the $C_{1'}$—N bond. Comparison of the theoretical enhancements as a function of χ for each ribose conformation with the observed enhancements led to the conclusion that no single conformer accounts for the observed homonuclear nOe data. Therefore in order to explain the nOe's it is necessary to allow for pseudorotational equilibria in the furanose ring using the $N(C_{3'}$ *endo*) percentage populations of Table 3 and exchange between torsional conformers about the glycosidic bond.

The calculation of theoretical nOe's for molecules with internal motions depends on the exchange conditions as defined by Schirmer *et al.* (10) on the basis of the relative values of the rate constants k for internal motions, the proton relaxation rates $R_d \simeq 1\ s^{-1}$, and the molecular rotational rate $\tau_c^{-1} \equiv \tau_R^{-1} \simeq 2 \times 10^{10}\ s^{-1}$. Ultrasonic relaxation studies (26) and ^1H and ^{13}C spin-lattice relaxation studies (27, 28) allow us to conclude that the rate constants for all internal motions are $k < 10^9\ s^{-1} << \tau_c^{-1}$, so case I (slow, $k << R_d$) or case II (intermediate, $R_d << k << \tau_c^{-1}$) exchange conditions may apply. Although it is extremely improbable that case I conditions prevail, i.e. that $k << 1\ s^{-1}$, in this work the nOe's were calculated for case I exchange conditions, as previous work on

Can. J. Chem. Downloaded from www.nrcresearchpress.com by 210.87.254.42 on 09/06/12
For personal use only.

TABLE 1. Nuclear Overhauser enhancements of the H_8 proton in various mononucleotides upon saturation of the sugar protons

Nucleotide	pH	Concentration (M)	Protons irradiated						Reference
			$H_{1'}$	$H_{2'}$	$H_{3'}$	$H_{5'+5''}$	H_8	$H_{2'+3'}$	
5′-GMP	8.4	0.025	0.11	0.18	0.10	0.03	—		12
	8.0	0.025	0.08	0.22	0.03	0.06	—		*
	8.0	0.05	0.08	0.19	0.02	0.06	—	0.26	*
	2.5	0.05	0.08	0.07	0.05	0.04	—		*
	1.3	0.05	0.08	0.09	0.15	0.08	—	—	12
	1.2	0.05	0.07	0.04	0.06	0.05	0.07†	0.11	*
	1.2	0.025	0.07	0.05	0.07	0.04	—	0.10	*
5′-GMP + La^{3+}	1.2	0.015	0.06	0.05	0.07	0.10	—		*
5′-AMP	7.0	0.05	0.04	0.21	0.09	0.06	—		13
3′-AMP	7.0	0.05	0.20	—	—	0.01	—	0.24	13
3′-GMP	8.9	0.05	0.18	—	—	0.04	—	0.21	12
	1.4	0.05	0.15	—	—	0.05	—	0.13	12
2′-AMP	7.0	0.05	0.16	0.17	0.06	0.03	—	—	13
2′-GMP	8.7	0.05	0.16	0.19	0.10	0.03	—	—	12
	1.2	0.05	0.17	0.08	0.04	0.04	—	—	12

*This work.
†$H_{1'}$ observed.

TABLE 2. Heteronuclear Overhauser $^{31}P\{^1H\}$ enhancements in various mononucleotides

Nucleotide	pH	Concentration (M)	Protons irradiated								References
			$H_{1'}$	$H_{2'}$	$H_{3'}$	$H_{4'}$	$H_{5'+5''}$	$H_{2'}$ + $H_{3'}$	H8	All	
5′-GMP	8.1	0.05	0.16	—	—	0.33	0.50	0.14	0.04	0.60	*
5′-AMP	8.5	0.1	—	—	0.02	0.14	0.47	—	—	1.07	18
ATP†	7.5	0.1	0	—	—	0.46	0.54	0.36	0	0.65	38

*This work.
†The α phosphorus atom.

TABLE 3. Conformer percentage populations for mononucleotides in solution derived from analysis of vicinal coupling constants

Nucleotide	pH	Furanose % N	$C_{4'}$—$C_{5'}$ bond % gg	Reference
5′-GMP	1.2	67	88	*
	7.0	38	72	20
	8.0	32	58	42
5′-GMP + La^{3+}	1.2	67	88	*
5′-AMP	7.0	38	76	20
3′-AMP	7.0	34	80	21
3′-GMP	7.0	41	74	21
2′-AMP	7.0	33	78	21
2′-GMP	7.0	43	69	21
	1.2	54	70	21

*This work.

similar systems has shown that the results of the conformational analysis are essentially the same using case I or case II exchange conditions (17).

In the slow exchange region (case I), the nOe enhancement is described by a generalization of eq. [2] to a discrete set of conformations

$$[5]\quad f_d(s) = \sum_{\Omega} P_\Omega f_d(s, \Omega)$$

where P_Ω is the fraction of molecules in conformation Ω, or to a continuous path described by internal variables Ω

$$[6]\quad f_d(s) = \int f_d(s, \Omega)\, P(\Omega)\, d\Omega$$

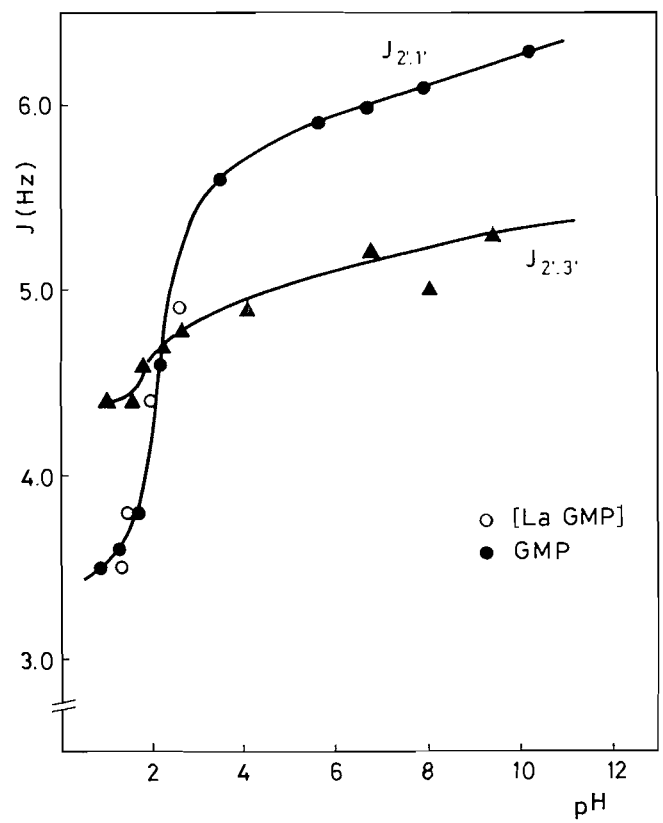

FIG. 5. pH dependence of 5′-GMP proton coupling constants.

Can. J. Chem. Downloaded from www.nrcresearchpress.com by 210.87.254.42 on 09/06/12
For personal use only.

TABLE 4. Best fit calculated $^1H\{^1H\}$ nOe values for purine mononucleotides using a two-site (χ_N, χ_S) distribution

Nucleotide	pH	% *N*	$f_8(i)$ (χ_N, χ_S)	$f_8(1')$	$f_8(2')$	$f_8(3')$	$f_8(5' + 5'')$	*R* factor
5′-GMP	8.0	40	330°, 90°	7	23	2	6	0.01
	1.2	70	0°, 30°	8	3	7	8	0.15
5′-AMP	7.0	40	110°, 30°	3	21	8	11	0.05
3′-AMP	7.0	30	240°, 120°	17	25		0	0.01
3′-GMP	8.9	40	120°, 270°	17	24		0	0.03
	1.4	50	30°, 180°	15	12		7	0.01
2′-AMP	7.0	30	120°, 330°	15	15	4	3	0.02
2′-GMP	8.7	40	100°, 180°	15	16	6	1	0.04
	1.2	50	20°, 180°	17	5	4	7	0.05

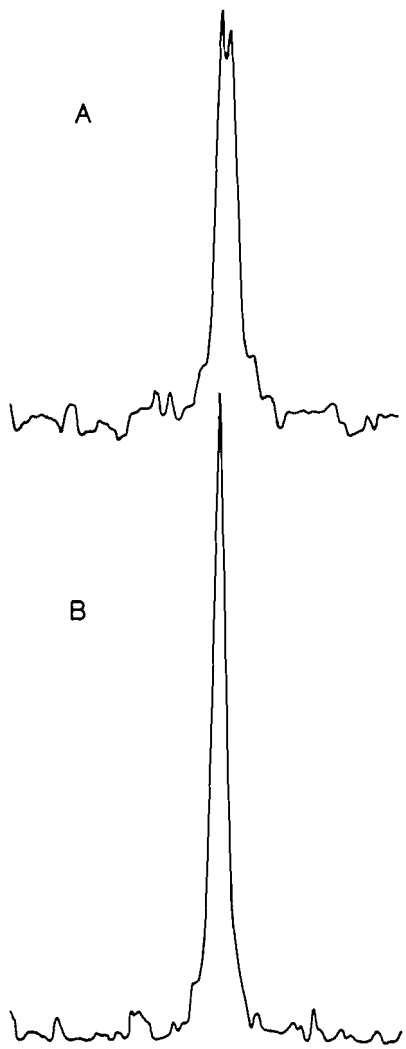

FIG. 6. H_8 resonance in a 5′-GMP 0.05 *M* solution; (A) non-decoupled spectrum showing a $^4J_{1'8} \simeq 0.5$ Hz coupling; (B) decoupled spectrum through $H_{1'}$ irradiation.

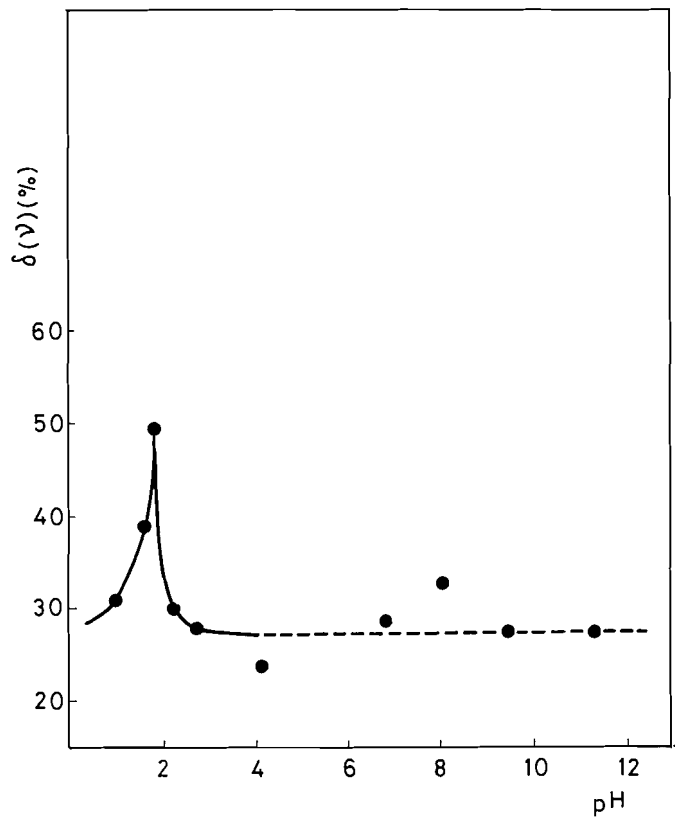

FIG. 7. pH effect on the $^4J_{1'8}$ coupling constant for 5′-GMP; $\delta(\nu) = (\nu - \nu_0)/\nu_0$, where ν is the width at half height of the H_8 resonance in the coupled spectrum and ν_0 is the same width in the decoupled spectrum.

where $P(\Omega)$ is the distribution function for the variable Ω. Therefore two variables are necessary to describe the sugar–base torsion: the allowed angles and the probabilities at these angles. The populations of the *N* and *S* furanose ring conformations used are given in Table 3. The *gauche–gauche* conformation about the $C_{4'}$—$C_{5'}$ bond was chosen as it has been shown to dominate the equilibrium about this bond (Table 3).

Various conformational models for the mononucleotides were used. Calculations were started using discrete two-site χ angle distributions (χ_N, χ_S), where χ_N and χ_S are glycosidic angles associated with the *N* and *S* furanose ring conformations. On the basis of an observed correlation of furanose and base conformations (14), the χ_N and χ_S populations P_N and P_S were assumed to be equal to the populations of the *N* and *S* furanose puckered conformations (Table 3). The (χ_N, χ_S) conformations which give the minimum variance between experimental and calculated homonuclear proton nOe values for various purine mononucleotides, shown in Table 4, indicate that in the case of the adenine mononucleotides, 5′-AMP has an *anti* conformation of the base, but 3′-AMP and 2′-AMP have high populations of both *anti* and *syn* base conformations. The guanine mononucleotides show a pH-dependent conforma-

Can. J. Chem. Downloaded from www.nrcresearchpress.com by 210.87.254.42 on 09/06/12
For personal use only.

TABLE 5. Calculated $^1H\{^1H\}$ nOe values for purine mononucleotides using two-site (χ_N, χ_S) distributions defined by the lanthanide probe method (29, 30)

Nucleotide	pH	% *N*	$F_8(i)$ (χ_N, χ_S)	$f_8(1')$	$f_8(2')$	$f_8(3')$	$f_8(5' + 5'')$
5′-GMP	0.8	70	30°, 40°	4	5	11	15
	7.6	50	120°, 60°	0	33	0	6
5′-AMP	2.0	60	60°, 40°	3	5	21	11
	7.6	50	60°, 40°	2	6	17	12
3′-AMP	7.6	60	20°, 150°	4	15	8	9
2′-AMP	7.6	40	180°, 240°	31	9	−2	0

TABLE 6. Calculated $f_8(i)$ values for different nucleotides obtained from glycosidic angle distributions derived from published potential energy curves

Nucleotide	Distribution	POH. . .N_3†	$O_{5'}H$. . .N_3†	χ angle	Sugar pucker	Reference	$f_8(1')$	$f_8(2')$	$f_8(3')$	$f_8(5' + 5'')$
5′-AMP	1	N	N	*anti*	*N*	37	5	0	28	3
	2	N	N	*anti*	*S*	37	8	8	−1	10
	3:40% 1 + 60% 2	N	N	*anti*	*N/S*	*	7	4	13	6
5′-GMP	4	Y	N	*syn*	*N*	35, 36	13	19	−2	2
	5	Y	N	*syn*	*S*	35, 36	27	12	−4	2
	6	N	N	*anti*	*N*	34	4	−1	16	4
	7	N	N	*anti*	*S*	34	4	8	−2	6
	8:70% 4 + 30% 5	Y	N	*syn*	*N/S*	*	17	17	0	2
	9:70% 6 + 30% 7	N	N	*anti*	*N/S*	*	4	2	11	4
	10:50% 8 + 50% 9	Y/N	N	*syn/anti*	*N/S*	*	11	10	5	3
2′-GMP	11	Y	Y	*syn*	*N*	35	15	12	1	4
	12	Y	N	*anti*	*N*	35	13	−3	9	12
	13	N	Y	*syn*	*N*	35	15	21	−3	1
	14	N	N	*anti*	*N*	35	11	1	16	3
	15	Y	Y	*syn/anti*	*S*	35	6	8	−1	1
	16	Y	N	*syn/anti*	*S*	35	17	21	−1	2
	17	N	Y	*syn*	*S*	35	16	−4	0	0
	18	N	N	*anti*	*S*	35	4	32	−2	5
	19:30% 11 + 70% 15	Y	Y	*syn/anti*	*N/S*	*	9	9	0	2
	20:30% 12 + 70% 16	Y	N	*syn/anti*	*N/S*	*	18	14	2	5
	21:30% 13 + 70% 17	N	Y	*syn*	*N/S*	*	16	4	−1	0
	22:30% 14 + 70% 18	N	N	*anti*	*N/S*	*	6	22	4	5
3′-AMP	23	N	N	*anti*	*N*	34	14	−2	14	6
	24	N	Y	*syn/anti*	*S*	34	17	18	−2	2
	25	N	Y	*syn*	*N/S*	34	42	−6	2	0
	26:30% 23 + 70% 24	N	N	*syn/anti*	*N/S*	*	16	12	3	3
	27:40% 25 + 60% 26	N	Y/N	*syn/anti*	*N/S*	*	26	5	3	2
	28:30% 25 + 70% 26	N	Y/N	*syn/anti*	*N/S*	*	24	7	3	2
3′-GMP	29	N	N	*anti*	*N*	34	12	−2	15	3
	30	N	N	*syn/anti*	*S*	34	19	15	2	2
	31	N	Y	*syn*	*N/S*	34	43	−2	0	0
	32:30% 29 + 70% 30	N	N	*syn/anti*	*N/S*	*	17	10	6	2
	33:40% 31 + 60% 32	N	Y/N	*syn/anti*	*N/S*	*	27	5	4	1
	34:30% 31 + 70% 32	N	Y/N	*syn/anti*	*N/S*	*	25	6	4	1

*This work.
†Y = Yes; N = No.

Can. J. Chem. Downloaded from www.nrcresearchpress.com by 210.87.254.42 on 09/06/12
For personal use only.

tional change of both furanose and base moieties, associated with base protonation at N-7 with a pK_a of 2.7 (31). A similar pH effect is not observed on the conformations of adenine mononucleotides, although adenine is protonated at N-1 with a pK_a of 3.9 (31). 3′-GMP and 2′-GMP at high and low pH have large populations of both *anti* and *syn* base conformations, whereas 5′-GMP has mainly *anti* base conformations, with a larger glycosidic angle amplitude at high pH. Very good fits of experimental nOe's were obtained in all cases using the discrete two-site conformational model, as expressed by *R* factors (41) smaller than 0.05 (see Table 4). The higher value for the 5′-GMP data at pH 1.2 is a consequence of the very small observed nOe's in this case.

The nOe values observed for the La^{III}/5′-GMP complex solutions are very similar to those obtained for the free ligand at the same pH, therefore indicating no significant change of the furanose ring and base conformation induced by the binding of the lanthanide ions. This was confirmed at low pH by identical values obtained for $J_{2'1'}$ coupling constants of the free and La^{III} bound ligand (Fig. 5). A similar observation was found for ribosyl-adenosine 5′,5″-biphosphate (40). The $f_8(5' + 5'')$ value is significantly higher for the La^{III} complex, thus suggesting that, at least in part, the corresponding decreased H_8—$H_{5',5''}$ distance is a consequence of complexation, through an increase of the gt and tg conformer populations about the $C_{4'}$—$C_{5'}$ bond. Of course glycosidic angle values closer to zero for 5′-GMP/La^{III} at pH 1.2 (Table 4) would also decrease the H_8—$H_{5',5''}$ distance and increase $f_8(5' + 5'')$. This conformational change of the exocyclic group of 5′-GMP due to La^{III} complexation was also detected by a decrease of the long-

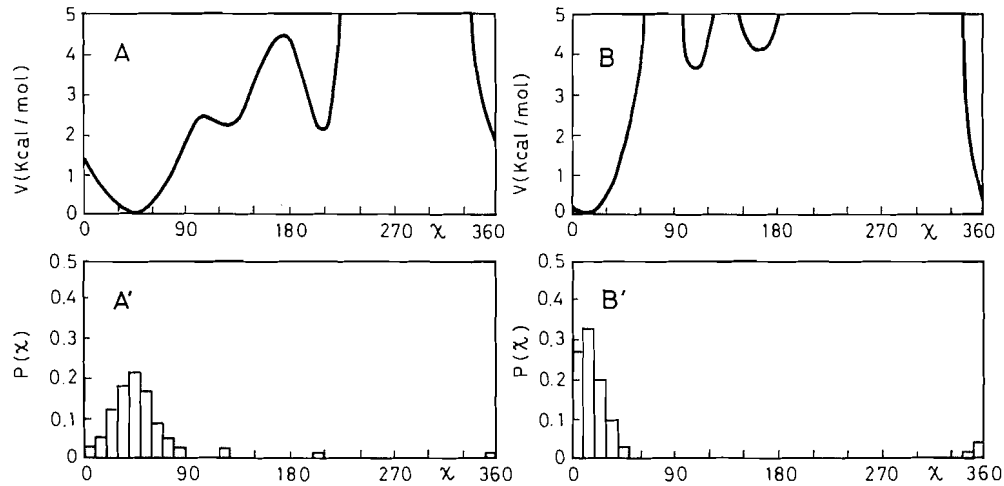

FIG. 8. Calculated potential energy curves for 5′-AMP from the literature (37) (A, B) and χ angle distributions derived from them by Boltzmmans's statistics (A′, B′) (all gg); A, A′ (*N* pucker); B, B′ (*S* pucker).

range $^4J_{PH_{4'}}$ coupling constant in the complex when compared to the value of 1.2 Hz for the free ligand at the same pH (32).

The effect of pH on the base conformation of 5′-GMP was also studied by following the variation with pH of the long range coupling constant between the H_8 base proton and the furanose $H_{1'}$ proton. In a very restricted pH zone, about pH 1.8, a $^4J_{H_8H_{1'}}$ of about 0.5 Hz was observed, as confirmed by $H_{1'}$ irradiation (Fig. 6). A study of the variation of ^4J with pH (Fig. 7) showed that it decreased for pH values lower or higher than about 1.8. Due to its small value, the variation of ^4J was followed through the difference of the half-height width of the H_8 resonance, in the absence and in the presence of $H_{1'}$ irradiation.

Theoretical and experimental studies of $^4J_{HH}$ and $^4J_{PH}$ coupling constants through saturated bonds (32, 33) have shown that they have maximum values for a planar *W* atom arrangement. These studies are applicable to 5′-GMP at low pH (pH < 2) as, when the guanine base is saturated, the bond order C_8—N_9 is about one. The results obtained suggest a variation of the base orientation with pH, through rotation about the glycosidic bond, with a passage through an intermediate position close to a planar arrangement of the bonds involved. As the nOe data point to an *anti* base conformation, this planar–*anti* configuration of the base corresponds to $\chi \simeq 40°$. Comparison with the interpretation of the nOe data (Table 4) suggests that at very low pH (<1.8) χ is smaller than 40°, and base deprotonation at N-7 would cause a base rotation to higher χ values (at least in the *N* furanose conformation). Base protonation at N-7 increases its effective charge from zero to one, changing the electrostatic interactions with other parts of the molecule, namely with the phosphate group. A minimum conformational energy will be obtained for $\chi > 40°$ and for $\chi < 40°$. The $\chi = 40°$ value corresponding to a maximum ^4J value is obtained for an effective charge of the base of about +0.77.

A comparison of the base conformations of the mononucleotides defined, within the discrete two-site conformational model, by nOe and by the lanthanide probe method (29, 30) was carried out through a comparison of the corresponding best fit (χ_N, χ_S) values and of the calculated nOe data for those glycosidic angle values (Tables 4 and 5). In the case of 5′-GMP the two methods agree very well and the best fit (χ_N, χ_S) value obtained by the lanthanide probe method gives calculated nOe data in very good agreement with the experimental nOe data for the 5′-GMP/La^{III} complex. The other mononucleotides do not give such a good agreement of both glycosidic angles and calculated nOe values defined by the two methods.

Another very simple torsional model for mononucleotides was considered, namely the free-rotational model in which all angles have equal probability. According to this model $f_8(1')$ is 0.18 (pure *N*) and 0.19 (pure *S*), $f_8(2')$ is 0.06 (pure *N*) and 0.16 (pure *S*), and $f_8(3')$ is 0.09 (pure *N*) and 0.02 (pure *S*). A comparison of the calculated $f_8(i)$ values for the *N* pucker populations given in Table 3 with the observed values (Table 1) shows that this model is not acceptable.

The experimental data could in principle also be fitted to gaussian distributions (16), but due to theoretical uncertainties (17) such a refinement was not undertaken. This is related to the problem of solution degeneracy: although more complete solutions than those presented in Table 4 exist, they would result in conformational models which in essence do not differ from them.

The nOe values presented in Table 1 were also used to test published potential energy curves for the conformations of mononucleotides about the glycosidic bond (34–37). Angular distributions of χ_N and χ_S values were derived from these potential energy curves by Boltzmann's statistics (Fig. 8) and, with overall weights given by the populations of the furanose *N* and *S* puckers (Table 3), were used to calculate proton nOe's for various combinations of ribose puckers and intramolecular hydrogen bonds (distributions 1 to 34 in Table 6). A comparison of experimental (Table 1) and calculated data (Table 6) indicates that for 5′-AMP the potential energy minimum at $\chi \sim 120°$ is lower than implied by Fig. 8, giving a higher population at $\chi \sim 120°$ and a higher $f_8(2')$ value. The data for 5′-GMP at pH 8.0 suggest that its χ angle conformer population distribution is very similar to 5′-AMP, while at pH 1.2 it is compatible with distribution 9 (Table 6) which assumes no POH...N_3 intramolecular hydrogen bond and consists of χ angles in the *anti* range ($\chi \sim 300°-70°$). The data for 3′-AMP and for 3′-GMP are incompatible with a $O_{5'}H...N_3$ intramolecular hydrogen bond and are best represented respectively by distributions 26 and 32, which consist of χ angles in the mainly *anti* ranges of 220°–320° and 20°–140°.

Can. J. Chem. Downloaded from www.nrcresearchpress.com by 210.87.254.42 on 09/06/12
For personal use only.

Can. J. Chem. Downloaded from www.nrcresearchpress.com by 210.87.254.42 on 09/06/12
For personal use only.

3′-AMP and 3′-GMP at neutral pH have higher populations at $\chi \sim 90°-120°$ than 3′-GMP at acid pH, giving larger $f_8(2' + 3')$ nOe values (Table 1). The data for 2′-AMP and 2′-GMP at neutral pH are very similar and differ considerably from the data for 2′-GMP at acid pH. The 2′-GMP data are incompatible with all theoretical distributions (Table 6) and no 2′-AMP distribution was tested as it is unavailable in the literature. However, the χ angle distributions for 3′-AMP and 3′-GMP should not be very different respectively from 2′-AMP and 2′-GMP at similar pH conditions.

As a whole there is no improvement of the fit of nOe data to the calculated values using distributions derived from potential energy curves when compared to the best fit distributions within the discrete two-state model. Some conclusions about the validity in solution of those potential energy calculations are possible, namely about the details of their shape, the relative depths of their minima, and the existence or not of some intramolecular hydrogen bonds.

P{H} nOe values

Phosphorous–proton nOe data for 5′-GMP and other mononucleotides are recorded in Table 2. A phosphorous spin-lattice relaxation defined entirely by a dipole–dipole interaction would give a phosphorous–proton nOe value of up to 124% (4). The fact that the nOe's are not the theoretical value indicates other modes of relaxation, such as residual impurities or different relaxation mechanisms. The single frequency irradiation nOe's illustrate the potential of P{H} nOe for conformational analysis of mononucleotides (18). Although no quantitative analysis was undertaken, the similar values for irradiation of the $H_{5'} + H_{5''}$ and $H_{4'}$ sugar protons in the three mononucleotides studied (see Table 2) reflect similar joint ψ,ϕ distributions about the $C_{4'}$—$C_{5'}$ and $C_{5'}$—$O_{5'}$ bonds, namely about 0.72 gg, g′g′ (18), in good agreement with $^4J_{PH_{4'}}$ coupling constant values. The low nOe values for $H_{2'}$, $H_{1'}$, and H_8 irradiation in all mononucleotides does not allow any conclusion about the ribose ring and base conformations, as the large internuclear distance renders the P{H} nOe very insensitive to the conformations of these moieties. In particular, a predominant *anti* base conformation, detected by other methods (29, 39), is not precluded as it is entirely compatible with a low $P\{H_8\}$ nOe value.

Conclusions

The present work demonstrates that proton–proton and phosphorus–proton nuclear Overhauser effect measurements are useful methods of nucleotide conformational analysis. Comparison of observed and calculated enhancements allowed a test of various conformational models for these systems to be carried out. For instance, the conformational state about the glycosidic bond cannot be described by any single conformation or by free rotational distributions. The χ angle distributions described by potential energy calculations for the mononucleotides studied give generally good agreement between calculated and experimental nOe's.

Calculations using discrete two-site χ angle distributions (χ_N, χ_S) give predominant *anti* conformations for 5′-AMP and a mixture of *syn* and *anti* conformations for 3′-AMP and 2′-AMP. 3′-GMP and 2′-GMP give a mixture of *syn* and *anti* conformations. In opposition to all these cases, where no pH-dependent conformational change is observed, protonation of 5′-GMP at N-7 of the guanine base induces a conformational change within the *anti* range with a wider glycosidic angle amplitude at high pH. This effect was also monitored by a pH dependence of the $^4J_{H_8H_{1'}}$ coupling constant. La^{III} binding to the phosphate group of 5′-GMP slightly increases the gt + tg conformer populations about the $C_{4'}$—$C_{5'}$ bond in relation to gg, a fact also monitored by a change of the value of the $^4J_{PH_{4'}}$ coupling constant.

The agreement between the glycosidic nucleotide conformations defined by nOe and by the lanthanide probe method (29, 30) is very good for the more rigid mononucleotides 5′-GMP and 5′-AMP and reasonably good for the other mononucleotides studied. The better agreement of the two methods for the more rigid mononucleotides is a consequence of a smaller extent of averaging of very different conformationally dependent geometric functions associated with the two methods.

The use of χ angle distributions described by potential energy calculations for the mononucleotides did not generally improve the fit of the nOe data, but allowed conclusions about their validity in solution. It should be borne in mind that significant nOe may occur from states which do not correspond to minimum energy conformations (15), showing therefore the limitations of earlier approaches (12, 13).

Acknowledgements

This work is a contribution of the Centro de Química Estrutural, IST, Lisbon and of the Centro de Investigação Química (INIC) at the University of Coimbra.The authors thank Dr. C. D. Barry for the execution of the program for model building, and Centro de Cálculo, IST, for alteration of the BURLESK program.

1. M. SUNDARALINGAM. Biopolymers, **7**, 821 (1969).
2. C. ALTONA and M. SUNDARALINGAM. J. Am. Chem. Soc. **94**, 8205 (1972).
3. D. B. DAVIES. Prog. Nucl. Magn. Reson. Spectrosc. **12**, 135 (1978), and references therein.
4. J. H. NOGGLE and R. E. SCHIRMER. The nuclear Overhauser effect: chemical applications. Academic Press, New York. 1971.
5. F. INAGAKI and T. MIYAZAWA. Prog. Nucl. Magn. Reson. Spectrosc. **14**, 67 (1981), and references therein.
6. P. A. HART and J. P. DAVIES. J. Am. Chem. Soc. **91**, 512 (1969).
7. P. A. HART and J. P. DAVIES. Biochem. Biophys. Res. Commun. **34**, 733 (1969).
8. P. A. HART and J. P. DAVIES. J. Am. Chem. Soc. **93**, 753 (1971).
9. R. E. SCHIRMER, J. H. NOGGLE, J. P. DAVIES, and P. A. HART. J. Am. Chem. Soc. **92**, 3266 (1970).
10. R. E. SCHIRMER, J. P. DAVIS, J. H. NOGGLE, and P. A. HART. J. Am. Chem. Soc. **94**, 2561 (1972).
11. P. A. HART and J. P. DAVIS. J. Am. Chem. Soc. **94**, 2572 (1972).
12. T.-D. SON, W. GUSCHLBAUER, and M. GUÉRON. J. Am. Chem. Soc. **94**, 7903 (1972).
13. T.-D. SON and C. CHACHATY. Biochem. Biophys. Acta, **335**, 1 (1973).
14. H.-D. LÜDEMANN, E. WESTHOF, and O. RÖDER. Eur. J. Biochem. **49**, 143 (1974).
15. R. K. NANDA, R. TEWARI, G. GOVIL, and I. C. P. SMITH. Can. J. Chem. **52**, 371 (1974).
16. J. P. DAVIS and P. A. HART. Tetrahedron, **28**, 2883 (1972).
17. W. EGAN, S. FORSÉN, and J. JACOBUS. Biochemistry, **14**, 735 (1975).
18. P. A. HART. Biophys. J. **24**, 833 (1978).
19. R. FREEMAN, H. D. W. HILL, and R. KAPTEIN. J. Magn. Reson. **7**, 327 (1972).
20. D. B. DAVIES and S. S. DANYLUK. Biochemistry, **13**, 4417 (1974).

21. D. B. DAVIES and S. S. DANYLUK. Biochemistry, **14**, 543 (1975).
22. C. D. BARRY, J. A. GLASEL, R. J. P. WILLIAMS, and A. V. XAVIER. J. Mol. Biol. **84**, 471 (1974).
23. W. MURAYAMA, N. NAGASHIMA, and Y. SHIMIZU. Acta Crystallogr. Sect. B, **25**, 2236 (1969).
24. C. D. BARRY, J. A. GLASEL, A. C. T. NORTH, R. J. P. WILLIAMS, and A. V. XAVIER. Biochim. Biophys. Acta, **262**, 101 (1972).
25. M. SUNDARALINGAM, B. PULLMAN, W. SAENGER, V. SASISEKHARAN, and H. R. WILSON. Jerusalem Symp. Quantum Chem. Biochem. **5**, 815 (1973).
26. L. M. RHODES and P. R. SCHIMMEL. Biochemistry, **10**, 4426 (1971).
27. T. IMOTO, K. AKASAKA, and H. HATANO. Chem. Phys. Lett. **32**, 86 (1975).
28. H. PLACH, E. WESTHOF, H.-D. LÜDEMANN, and R. MENGEL. Eur. J. Biochem. **80**, 295 (1977).
29. C. M. DOBSON, C. F. G. C. GERALDES, G. RATCLIFFE, and R. J. P. WILLIAMS. Eur. J. Biochem. **88**, 259 (1978).
30. C. F. G. C. GERALDES. J. Magn. Reson. **36**, 89 (1979).
31. S. S. DANYLUK and F. E. HRUSKA. Biochemistry, **7**, 1038 (1968).
32. L. D. HALL and R. B. MALCOLM. Can. J. Chem. **50**, 2092 (1972).
33. M. BARFIELD. J. Chem. Phys. **41**, 3825 (1964).
34. H. BERTHOD and B. PULLMAN. Biochim. Biophys. Acta, **232**, 595 (1971).
35. H. BERTHOD and B. PULLMAN. FEBS Lett. **30**, 231 (1973).
36. N. YATHINDRA and M. SUNDARALINGAM. Biopolymers, **12**, 297 (1973); **12**, 2075 (1973); **12**, 2261 (1973).
37. R. H. SARMA, C.-H. LEE, F. E. EVANS, N. YATHINDRA, and M. SUNDARALINGAM. J. Am. Chem. Soc. **96**, 7337 (1974).
38. P. A. HART. J. Am. Chem. Soc. **98**, 3735 (1976).
39. P. TANSWELL, J. M. THORNTON, A. V. KORDA, and R. J. P. WILLIAMS. Eur. J. Biochem. **57**, 135 (1975).
40. F. INAGAKI, T. MIYAZAWA, M. MIWA, H. SAITO, and T. SUGIMURA. Biochem. Biophys. Res. Commun. **85**, 415 (1978).
41. M. R. WILLCOTT III, R. E. LENKINSKI, and R. E. DAVIES. J. Am. Chem. Soc. **94**, 1742 (1972).
42. C.-H. LEE, F. E. EVANS, and R. H. SARMA. J. Biol. Chem. **250**, 1290 (1975).

Can. J. Chem. Downloaded from www.nrcresearchpress.com by 210.87.254.42 on 09/06/12
For personal use only.

The structure of psoluthurin A, the major triterpene glycoside of the sea cucumber *Psolus fabricii*[1,2]

FRANÇOIS-XAVIER GARNEAU,[3] JEAN-LUC SIMARD, AND ODETTE HARVEY
Département des sciences fondamentales, Université du Québec à Chicoutimi, Chicoutimi (Qué.), Canada G7H 2B1

AND

JOHN W. APSIMON[3] AND MICHEL GIRARD
Ottawa–Carleton Institute for Research and Graduate Studies in Chemistry, Carleton University, Ottawa, Ont., Canada K1S 5B6

Received November 5, 1982

FRANÇOIS-XAVIER GARNEAU, JEAN-LUC SIMARD, ODETTE HARVEY, JOHN W. APSIMON, and MICHEL GIRARD. Can. J. Chem. **61**, 1465 (1983).

The isolation of the major triterpene glycoside from the sea cucumber *Psolus fabricii* obtained from the north shore of the St. Lawrence estuary is described. Versatile extraction and purification procedures were used and physico-chemical data is presented in support of structure **1** for psoluthurin A.

FRANÇOIS-XAVIER GARNEAU, JEAN-LUC SIMARD, ODETTE HARVEY, JOHN W. APSIMON et MICHEL GIRARD. Can. J. Chem. **61**, 1465 (1983).

L'isolation du triterpène glycoside majeur du concombre de mer *Psolus fabricii* obtenu de la Côte-Nord de l'estuaire du St-Laurent est décrite. Des procédures versatiles d'extraction et de purification ont été utilisées et des données physico-chimiques sont présentées pour appuyer la structure **1** pour la psoluthurine A.

Can. J. Chem. Downloaded from www.nrcresearchpress.com by 210.87.254.6 on 09/06/12
For personal use only.

Introduction

Since Yamanouchi's pioneering studies on sea cucumber saponins (holothurins) (2), several species of various families of this class of echinoderms have been shown to possess these bioactive substances (3). Their molecular structures have been determined to be glycosides of triterpenes of the lanosterol type with a distinctive D-ring fused γ-lactone.

We wish to report the structure of psoluthurin A (**1**), the major triterpene glycoside of *Psolus fabricii* (order Dendrochirota), an arctic–subarctic species collected off the north shore of the St. Lawrence estuary at Les Escoumins, Québec. Our findings constitute the first report of the presence of these holothurins in a species of the family Psolidae. This compound appears to be the first reported example of a saponin of either plant or animal origin containing two sulfate groups. In addition, *P. fabricii* is only the second species so far shown to possess a saponin in which its aglycone is distinguished by a C(16) ketone function; the other species, of a different order, is *Stichopus japonicus* (order Aspidochirota, family Stichopodidae) (3). Isolation and purification procedures are detailed and physico-chemical evidence is presented in support of the assigned structure **1**.

Results and discussion

Isolation and purification procedures

The bright red sea cucumbers, *Psolus fabricii*, were collected slightly downstream from the pilot's wharf close to the village of Les Escoumins on the north coast of the St. Lawrence at a depth of 8–15 m (low tide). Live specimens were kept in low temperature sea water aquaria prior to use.

Preliminary work by our group[4] showed that the use of previously published isolation and purification procedures for a variety of holothurins (4–6) were difficult to apply in our case, as they appear to be tailored to the properties of the particular glycosides. The lack of versatility of these methods led us to develop a more general procedure which is shown in Fig. 1. Soaking the body walls in acetone removed most of the pigments (7) and permitted facile air-drying thereafter. The dried material was ground to a powder and extracted successively with benzene and methanol. An aqueous solution of the crude extract obtained from ethanol (75%) extractions was placed on

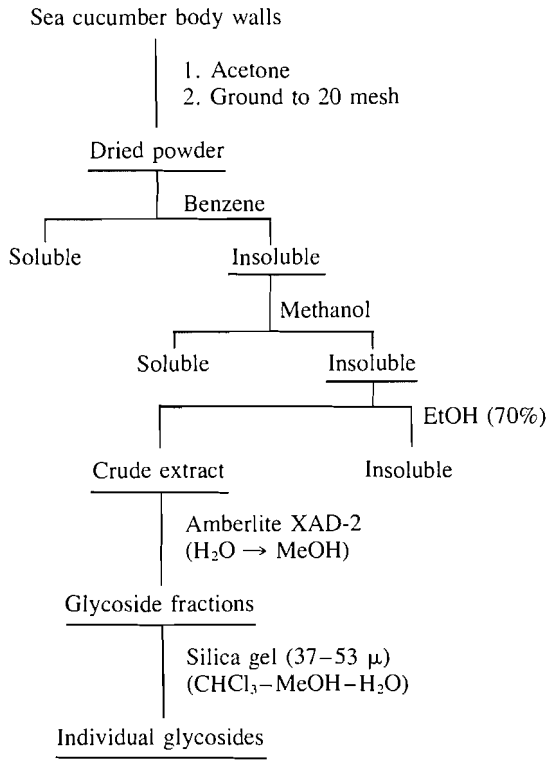

FIG. 1. Isolation and purification procedure for the saponins of *Psolus fabricii*.

[1]Taken in part from the M.Sc. thesis of M. Girard, April 1981, Carleton University, Ottawa.

[2]Part VI in the series Marine Organic Chemistry from Carleton University. For part V see ref. 1.

[3]To whom correspondence may be directed.

[4]F.-X. Garneau and M. Girard. Unpublished results from the Université du Québec à Chicoutimi. 1977.

TABLE 1. ^{13}C nuclear magnetic resonance data[a]

Carbon	25-*O*-Me-stichopogenin A$_4$[b]	PSOL-A[c]	DS-PSOL-A[c]	Carbon	PSOL-A	DS-PSOL-A
1	35.95	36.0	36.5	1′	104.1	105.1
2	27.8	26.8	27.4	2′	82.9	84.5
3	[d]	88.7	89.0	3′	74.9	76.6
4	39.2	39.4(s)[f]	39.9	4′	70.2	70.9
5	52.5	52.7	53.1	5′	65.9	66.9
6	21.8	21.9	22.3			
7	28.2	28.3	28.7	1″	104.7	105.8
8	38.8	38.6	38.9	2″	73.3	73.8
9	151.6	151.9(s)	151.5	3″	86.9	88.3
10	39.7	39.6(s)	40.2	4″	69.3	70.0
11	110.6	111.0	111.2	5″	75.4	78.4
12	32.2	31.9	32.3	6″	67.4	62.3
13	55.6	55.7(s)	55.8			
14	42.0	41.9(s)	42.2	1‴	104.6	105.7
15	51.9	51.9	52.1	2‴	74.7	76.1
16	[e]	213.9	213.1	3‴	75.4	78.1
17	61.6	61.1	61.5	4‴	86.5	87.7
18	175.6	176.4(s)	176.1	5‴	71.3	71.8
19	21.0	20.9	21.3	6‴	17.7	18.4
20	83.3	83.4(s)	83.2			
21	25.1	23.0	22.6	1⁗	105.0	105.8
22	38.5	38.1	38.6	2⁗	74.2	75.2
23	18.5	22.1	22.4	3⁗	86.6	88.1
24	39.9	37.7	38.2	4⁗	69.8	70.7
25	74.4	145.3(s)	145.7	5⁗	76.9	78.5
26	28.3	110.4	110.7	6⁗	67.0	62.4
27	28.4	27.9	28.2	3⁗OMe	60.5	60.9
28	20.8	20.5	20.8			
29	26.9	26.6	26.9			
30	15.7	17.4	16.8			
25-O-Me	51.8					

[a]In ppm downfield from TMS.
[b]In $CDCl_3$.
[c]In pyridine-d_5.
[d]The signal of this carbon is masked by the solvent signals.
[e]Only the 0–200 ppm region was recorded.
[f]Singlets observed in the off-resonance experiments.

a column of Amberlite XAD-2. Washing the column with water removed the inorganic salts and subsequent elution with increasing amounts of methanol resulted in a partial separation of the mixture of glycosides. The polymeric resin XAD-2 of the reversed phase type had been successfully used by Gilgan *et al.* in the isolation of steroid glycosides obtained from starfish (8). Psoluthurin A (**1**) was finally separated from the minor psoluthurins by low-pressure liquid chromatography on silica gel (37–53 μ) using $CHCl_3$–MeOH–H_2O (see experimental) as eluant.

The homogeneity of **1**, a problem frequently encountered with holothurins (9), was verified by reversed-phase thin-layer chromatography (rptlc). The presence of an impurity (<5%) was detected and the physico-chemical data given below were obtained with the slightly impure **1** except for the atomic absorption result. In this latter case, a small amount of the pure substance obtained by reversed-phase hplc was used.

Structural elucidation of psoluthurin A (1)

Psoluthurin A (**1**) was obtained as a white solid, mp 259–263°C (dec.), $[\alpha]_D^{23}$ −32.6° (pyr.), with no uv absorption maximum above 210 nm. The ir spectrum (KBr) showed strong hydroxyl absorption at 3400 cm^{-1} as well as two carbonyl bands at 1765 cm^{-1} and 1745 cm^{-1} indicating a γ-lactone, characteristic of holothurins, and a cyclopentanone respectively. The two bands at 1240 cm^{-1} and 820 cm^{-1} suggest the presence of a sulfate moiety. This latter observation was further substantiated by a positive rhodizonate test (10), the presence of 2.47 atoms of sodium by atomic absorption spectroscopy, and a comparison of ^{13}C nmr data with desulfated psoluthurin A **2** (DS-PSOL-A) (see below). Absorptions at 1650 cm^{-1} (νC=C) and 900 cm^{-1} (νC=CH_2) are indicative of a vinylidene group. The cd spectrum (MeOH), $[\theta]_{235}$ −10 000

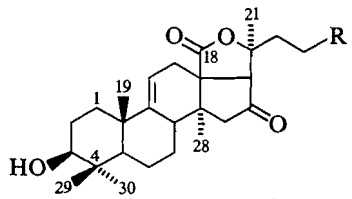

4 (Genin-1) R: CH=

5 (Genin-2) R: CH_2–OH

6 (Genin-3) R: CH_2–OCH_3

and $[\theta]_{300}$ −16 300, confirmed the presence of a γ-lactone (11) and a cyclopentanone (12) respectively.

Can. J. Chem. Downloaded from www.nrcresearchpress.com by 210.87.254.6 on 09/06/12
For personal use only.

Can. J. Chem. Downloaded from www.nrcresearchpress.com by 210.87.254.6 on 09/06/12
For personal use only.

Aqueous acid hydrolysis (2 *N* HCl) of **1** led to the formation of genin-1 (**4**, major) and genin-2 (**5**, minor) as well as the four usual holothurin monosaccharides, xylose, glucose, quinovose, and 3-*O*-methylglucose (identical R_f values by gc with the anomers of the authentic D-sugars). The high resolution mass spectrum of **4**, mp 219–221°C, established the molecular formula of $C_{30}H_{44}O_4$ for the parent ion m/z 468.3239 (calcd.: 468.3241) and the infrared spectrum (CCl_4) showed absorption at 3600 cm^{-1} (OH), 1760 cm^{-1} (γ-lactone), 1740 cm^{-1} (cyclopentanone). Its ultraviolet spectrum in methanol was transparent above 210 nm. The characteristic holothurinogenin mass spectral fragmentation (12) was noted, in particular, a fragment of m/z 423 supports the C(16) ketone function and the m/z 381 ($M^+ - 87$) indicates the C(3)—OH (13). Ions of m/z 109 and 69 are characteristic of side chain fragmentations with a Δ^{24} double bond (11). The physico-chemical data are similar to those reported for stichopogenin-A_2, isolated under identical conditions from holotoxin A (11). Their structural identity was further substantiated by a direct comparison with an authentic sample by tlc.[5] The identification of **5** as stichopogenin-A_4, an aglycone artifact obtained under identical conditions from holotoxin A (14), follows from the similarity of the ir spectra of **5** and **4**, the transparency of the uv spectrum, the lack of formation of **5** under anhydrous methanolysis conditions, and identical tlc behavior when compared with an authentic sample of stichopogenin-A_4.[5] Thus the structure of the triterpene moiety of **1** is identical to that of holotoxin A, as further demonstrated to be the case by the ^{13}C nmr and mass spectral data given below.

Methanolysis of **1** under anhydrous conditions (1% HCl) led to the formation of genin-3 (**6**, major) and **4** (minor) as well as equimolecular quantities of methyl xylopyranoside, methyl quinovopyranoside, methyl glucopyranoside, and methyl 3-*O*-Me-glucopyranoside. The concordance of the behavior of **1** and holotoxin A under identical conditions, the similarity of the ir spectra of **4**, **5**, and **6** and the transparency of the uv spectra, indicate **6** to be 25-methoxystichopogenin-A_4. Confirmation of this structure was obtained by an analysis of its ^{13}C nmr spectrum and a comparison with the spectrum of stichopogenin-A_4 (15*a*) and the spectra of **1** and **2** (Table 1). The signals at 110.6 and 151.6 ppm in the spectrum of **6** indicate the endocyclic double bond to be at 9:11 (14, 16).

Previous studies of holothurins have shown that double bond migration may occur under acidic solvolysis conditions (17, 18). In order to determine the authentic structure of the aglycone of **1**, a ^{13}C nmr spectral study of the latter was carried out (Table 1). The signals at 36.0, 26.8, 88.7, 39.4, 52.7, 26.6, and 17.4 were assigned to carbons C(1), C(2), C(3), C(4), C(5), C(29), and C(30) respectively taking into account the influence of C(3) glycosidation (19). The similar chemical shifts observed for quaternary carbons C(10) and C(14) of **1** and **6** as well as the signals at 151.9 and 111.0 observed in the spectrum of these and other similar substances (14, 16, 18) confirm the 9:11 position for the endocyclic double bond in **1**. The signals at 145.3 and 110.4 were assigned to the side chain double bond at Δ^{25} based on a comparison with the theoretical values (20) showing 145.4 (C(25)) and 109.7 (C(26)) in contrast to 126.3 (C(24)) and 131.5 (C(25)) for Δ^{24}. This then indicates that isomerization of the double bond from Δ^{25} to Δ^{24} occurred on acid hydrolysis of **1** to **4**. The signals at 213.9, 176.5, 83.4, and 55.7 ppm were respectively assigned to the four remaining quarternary carbons C(16), C(18), C(20), and C(13) in agreement with the results reported by Elyakov and co-workers (15). The remaining signals were assigned by comparison with similar compounds (14, 16, 21). These results confirm the structural identity of the triterpene aglycone of **1** with that of holotoxin A and B (14).

TABLE 2. Fast atom bombardment mass spectral data

m/z	Ion
Positive ions	
1327	(Na-K-disulfate) + Na^+ and/or (Na Na disulfate) + K^+
1313	((Na,Na disulfate) + Na^+) + 2
1311	(Na,Na disulfate) + Na^+
1305	(Na,K disulfate) + H^+
1289	(Na,Na disulfate) + H^+
1283	(K,H disulfate) + H^+
1267	(Na,H disulfate) + H^+
1209	(Na monosulfate) + Na^+
1107	(Na sulfate) + Na^+
Negative ions (complementary)	
1281	(Na,K disulfate) − Na^+
1265	(Na,Na disulfate) − Na^+ and/or (Na,K disulfate) − K^+
1163	(Na monosulfate) − Na^+

Information on the oligosaccharide chain of **1** was obtained from the ^{13}C nmr studies. Particularly important was a comparison with the ^{13}C nmr spectrum of **2** (Table 1). The latter was formed by a mild anhydrous acid methanolysis (0.06 *N* HCl – MeOH) at room temperature and gave a negative rhodizonate test as well as a satisfactory elemental analysis. In the case of **1** the chemical shifts of the C(6) carbons of glucose and 3-*O*-Me-glucose as well as that of the methyl carbon of the latter are only very slightly affected by glycosidation sites (22) and hence corresponding signals should be observed in the 60–63 ppm region. However, only two signals appear in this part of the spectrum at 61.1 and 60.5 ppm, assigned to the C(17) of the aglycone and the methyl of 3-*O*-Me-glucose respectively. The signals at 67.0 and 67.4 ppm are indicative of the two C(6) sugar carbons attached to sulfate groups. This is borne out by the disappearance of these two signals in **2** and the appearance of two new signals at 62.3 and 62.4 pm. The deshielding effect observed (≃5 ppm) is in agreement with the results reported by Kitagawa *et al.* (21) for holothurin A and by Archbald *et al.* (23) for monosaccharide sulfates. In addition the ir absorption at 820 cm^{-1} of **1** is characteristic of C(6) sulfates (24).[6] The signals in the range 104–106 ppm assigned to the C(1) carbons of the two psoluthurins are indicative of a β configuration (25). The remaining signals were assigned as shown in Table 1, based partly on relaxation times (T_1), and are in good agreement with previous studies (21, 26). Also in accord with these latter studies were the NT_1 values obtained for the sugars of **2**, 0.20 (xylose), 0.23 (glucose and quinovose), and 0.29 (3-*O*-Me-glucose). These NT_1 values show 3-*O*-Me-glucose to be the terminal sugar (in agreement with the gc–ms and FAB-ms (fast atom bombardment) results presented below) and xylose to be attached to the aglycone. This latter fact was confirmed by the isolation of a xyloside from **2** under mild anhydrous acid (0.25 *N* HCl) methanolysis.

[5]An authentic sample was kindly provided by professor Isao Kitagawa of Osaka University, Japan.

[6]This absorption is absent in the ir spectrum of **2**.

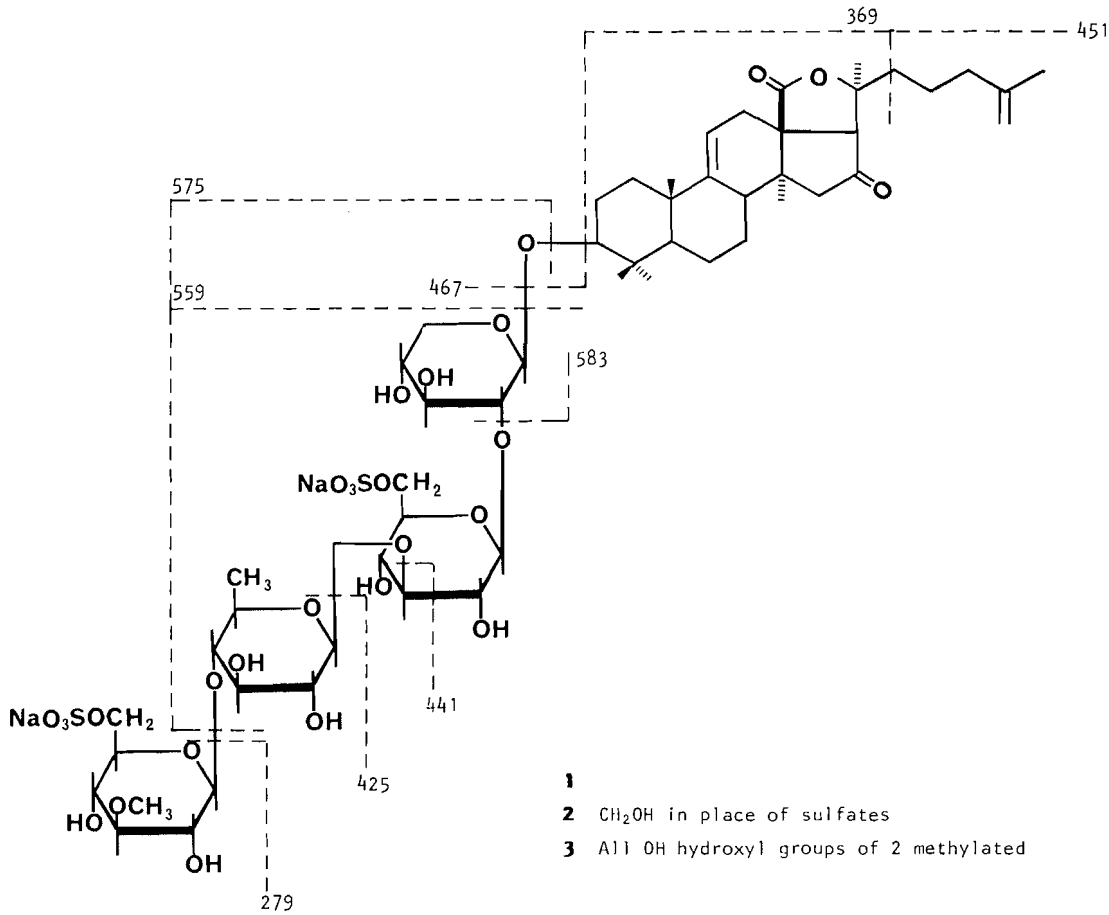

FIG. 2. FAB mass-spectral fragmentation pattern of psoluthurin A (**1**).

The complete sugar sequence as well as further confirmation of the structure of **1** was obtained by FAB mass spectrometry (27, 28). The positive- and negative-ion FAB-mass spectra data for **1** are presented in Table 2 demonstrating the power of FAB-ms for ascertaining the sugar sequence of a glycoside. The structural information this technique provided for **1** is in good agreement with other spectroscopic data. Spectra were recorded on a glycerol support in the positive and negative modes using a ZAB-2f instrument.

Molecular weight information was obtained from the region m/z 1267 through 1327. In particular, the ion m/z 1289 represents the $(M + H)^+$ ion of the di-sodium-disulfate form of the molecule. Other ions are the result of the various combinations possible for the molecular ion, when a trace of potassium salt is present (27, 28). The presence of potassium can be accounted for in two ways: the presence of a potassium-sodium-disulfate analog (m/z 1283, 1305, and 1327) or more simply a trace of an impurity such as KCl or KBr. The former is thought to be more probable due to the presence of a complementary counterpart in the negative spectrum at m/z 1281.

The sequencing of the sugars was also evident from the FAB-mass spectra, as well as the location of the sulfates (Fig. 2). In fact, a peak at m/z 583 indicates that xylose is directly attached to the aglycone moiety and that it does not bear a sulfate group.[7] Peaks at m/z 279 and 575 indicate that 3-*O*-Me-glucose is terminal and that it bears a sulfate moiety. Finally, peaks at m/z 441 and 425 confirmed that quinovose is directly attached to 3-*O*-Me-glucose and that it does not bear a sulfate group.[7] Deduction leaves the glucose unit between quinovose and xylose, and bearing the second sulfate group.

Methylation of **2** resulted in the formation of one major product, permethylated DS-PSOL-A (**3**) (tlc behavior and subsequent methanolysis results). The purified (lplc) permethylated product was methanolysed under anhydrous conditions (2 *N* HCl, 55°C, 3 h) and the following partially methylated monosaccharides of the mixture obtained were identified by gc–ms. Permethylated methyl glucopyranoside (R_f 6.7 (β), 7.4 (α)) gave a mass spectrum identical to that of an authentic sample of the α anomer (R_f 7.4) and was in agreement with the published data (29). The following characteristic ions are of particular note: m/z 187 (A_2;[8] $M^+ - (MeO + MeOH)$), 101 (F_1, G_1), 75 (J_1), and 88 (H_1, base peak). Similarly, methyl-2,3-di-*O*-methylquinovopyranoside (R_f 4.5 (β), 5.0 (α)) gave the same mass spectrum as an authentic sample (R_f 5.0 (α)) and the following ions of particularly important diagnostic value were in accord with the published data (30): m/z 175 (A_1; $M^+ - OMe$), 130 ($B_1 - MeOH$), 88 (H_1, base peak), the very weak 102 ($B_1 - HCO_2Me$), and the absence of 72 (K_1). Further confirmation was obtained from the mass spectrum of methyl-2,3-di-*O*-methyl-4-*O*-trimethylsilylquinovopyranoside[9] showing the following characteristic ions: m/z 247 (A_1; $M^+ -$

[7]These assertions come from the fact that the formation of a *singly charged* ion from the loss of two sulfate groups, or a sulfate +aglycone unit, is not possible.

[8]The symbols used are those found in ref. 29.

[9]Data bank of gc–ms center of INRS-Santé, Montréal.

Can. J. Chem. Downloaded from www.nrcresearchpress.com by 210.87.254.6 on 09/06/12
For personal use only.

Can. J. Chem. Downloaded from www.nrcresearchpress.com by 210.87.254.6 on 09/06/12
For personal use only.

OMe), 159 (F_1), 146 (H_1^1 or H_1^3), 130 (K_1), and 88 (H_1^2; base peak). The following characteristic ions of the mass spectrum of methyl-2,4,6-tri-*O*-methylglucopyranoside were the same as those reported for the β anomer (31) (the relative intensities were also of the same order): *m/z* 173 (A_2; M^+ − (MeO + MeOH)), 102 (r), 101 ($s_1s_3s_4$), 88 (t_1), 87 ($s_2s_5s_6$), 75 (v_2), 74 (t_2t_3), and 71 (base peak). The identification was further confirmed by the following ions of the mass spectrum of methyl-2,4,6-tri-*O*-methyl-3-*O*-trimethylsilylglucopyanoside[9]: *m/z* 245 [M^+ − (MeO + MeOH)], 187 [M^+ − (MeO + Me_3SiOH)], 173 (E_2), 146 (H_1^2; base peak), 131 (H_1 − Me), 102 (K_1), 75 (J_1), 73 (H_2), and the absence of 159 (F_1). The fourth partially methylated monosaccharide, methyl-3,4-di-*O*-methylxylopyranoside, was identified by a comparison of the mass spectrum of its trimethylsilyl derivative with data previously published.[9] The following ions are characteristic of this compound: *m/z* 233 (A_1; M^+ − MeO), 159 (F_1^2; base peak), 146 (H_1^2), 143 [A_2; M^+ − (MeO + Me_3SiOH)], 131 (H_1 − Me), 101 (F_1^1), 88 (H_1), 75 (J_1), and 58 (K_1). These results indicate the following positions of attachment of the four monosaccharides (see Fig. 2): aglycone (C(3)) – xylose (1 → 2) – glucose (1 → 3) – quinovose (1 → 4) – 3-*O*-Me-glucose. The same mass spectra were obtained from the methylated trimethylsilylated monosaccharides from a second methylation–methanolysis experiment of **2**. In this instance the separation was carried out on a SE-30 capillary column (30 m) and the mass spectrum of a disaccharide separated from the mixture showed a signal at *m/z* 363 attributed to the ion MeO^+=CH—CH=CH—O—(2,4,6-tri-*O*-methyl-3-*O*-trimethylsilylglucopyranoside). The presence of this ion, resulting from the characteristic fragmentation of a disaccharide and the presence of fragment ions from the methylated 3-*O*-TMS glucoside as well as the absence of the ion of *m/z* 161 indicates the disaccharide to be composed of 3-*O*-TMS glucose and xylose linked 1–2 (29). This result further confirms the sugar sequence of **2** and accordingly the complete structure of psoluthurin A (**1**) is that proposed in Fig. 2.

Experimental

Melting points were determined on a Fisher–Johns hot stage melting point apparatus or on a Buchi SMP-20 using capillary tubes and are uncorrected. Infrared spectra were recorded on a Perkin–Elmer 237-B grating spectrophotometer. Ultraviolet spectra were recorded on a Perkin–Elmer Coleman 124 "double beam" uv–visible spectrophotometer in 95% ethanol solutions. Optical rotations were measured on a Perkin–Elmer 141 polarimeter using a sodium lamp at a 589 nm wavelength. Carbon-13 nuclear magnetic resonance spectra were recorded on Bruker CXP-300 and WH-400 spectrometers operating at 75.46 MHz and 100.62 MHz respectively or on a CFT-20 spectrometer operating at 25.2 MHz. The spin-lattice relaxation times (T_1) were measured by the inversion recovery method at Université de Montréal. Chemical shifts are expressed in ppm downfield from tetramethylsilane (δ scale). Low resolution mass spectra were obtained on a AEI-MS 12 spectrometer using an ionization energy of 70 eV. Fast atom bombardment mass spectra (FAB-ms) were recorded on a glycerol support in the positive and negative modes using a ZAB-2f instrument (VG Analytical Limited, England). The gc–ms analyses were carried out on a Perkin–Elmer Sigma-3 using columns of 3% OV-17 (2 m) and a SE-30 capillary (30 m) interfaced with a Kratos-AEI M-25 and equipped with a DS-55S (NOVA 3 computer) data processor. Circular dichroism spectra were recorded on a mcd apparatus at Carleton University. Gas–liquid chromatography experiments were accomplished on a Hewlett–Packard 5730-A gas chromatograph equipped with a flame ionization detector. Stainless steel columns (1.8 m long) packed with 3% OV-17 support were used. Thin-layer chromatographic analyses were carried out on precoated silica gel GF-254 (E.M. Reagents) and Kc18 (Whatman) glass plates. Glycoside fractions were developed in the solvent systems $CHCl_3$–MeOH–H_2O 60:42:10 (solvent A) or 65:35:10 (lower layer, solvent B) while the solvent system EtOAc–hexane 50:50 (solvent C) was used for the aglycone fractions. Preparative tlc were performed on precoated silica gel G glass plates (20 × 20 cm, 0.5 mm thickness, E.M. Reagents). Detection was accomplished by spraying a 1% ceric ammonium nitrate in 50% sulfuric acid solution followed by heating at 100–120°C. Low pressure column chromatography separations were carried out on silica gel 60 H (E. Merck, B.D.C.), on Whatman silica gel LPS-1 (13–24 μ), and LPS-2 (37–53 μ). Columns were prepared as a slurry in $CHCl_3$. The hplc separations were carried out on a column (1 × 25 cm) of Spherisorb ODS, 10 μm (C_{18}), using a Waters-244 chromatograph linked to a Kratos SF-770 UV detector. The atomic absorption analysis was carried out on a Perkin–Elmer model 610 using an acetylene–oxygen flame. All solvents used were "reagent grade" and were distilled prior to use.

Isolation and purification of psoluthurin A (1)

The body walls from 177 specimens of the sea cucumber *Psolus fabricii* collected at Les Escoumins, Québec, were treated with 4 L of acetone (residue after evaporation: 99.5 g) and ground to a fine powder (4.21 kg) which was successively extracted several times with benzene and methanol to remove the residual pigments and lipids. The 75% ethanol extracts were combined and evaporated under reduced pressure using a roto-evaporator to give the crude psoluthurin mixture (66.0 g). The mixture was then subjected to an Amberlite XAD-2 resin (Mallinekrodt, 20–50 mesh) column chromatography. In a typical run, a fine suspension of the mixture (3.94 g) in water (50 mL) was placed on a prewashed[10] resin column (4.5 × 54 cm) and eluted with water (1 L), 25% MeOH in water (500 mL), 50% MeOH in water (1.8 L), and methanol (700 mL) to afford a salt-free partially purified glycoside mixture (450 mg). Low pressure column chromatography (silica gel-LPS-2 199 g; 4 × 30 cm; bed volume 390 mL; elution at 12 psi; flow rate 6 mL/min; developing solvent $CHCl_3$–MeOH–H_2O, 60:15:2.1 (525 mL) → 60:20:3.5 (2,750 mL) → 60:25:4.5 (900 mL) of the mixture (228 mg) furnished **1** (167 mg) homogeneous by tlc (solvents A and B), as well as several other glycosides obtained in minute amounts. Psolothurin A (**1**) (2.3 mg) was further purified for the atomic absorption analysis using reversed-phase hplc on a column of Spherisorb ODS eluting with MeOH–H_2O 70:30 followed by recrystallization from 85% aqueous ethanol. The sodium analysis was carried out on an aqueous acidic solution of **1**.

Psoluthurin A (**1**), mp 259–263°C (dec.); $[\alpha]_D^{23}$ −32.6 (*c* 0.45, pyr.); uv λ_{max} (EtOH) (nm): transparent above 210; ir ν_{max} (KBr) (cm^{-1}): 3400 (OH, Br), 1765 (γ-lactone), 1745 (5-memb. ketone), 1240 (S=O), 900 (C=CH_2), 820 (C—O—S); cd (*C* 0.17 *M*, MeOH): $[\theta]_{400}$ 0, $[\theta]_{300}$ −16 000 (neg. max), $[\theta]_{260}$ −1000 (neg. min.), $[\theta]_{235}$ − 10 000, $[\theta]_{220}$ 0, $[\theta]_{210}$ +2000!; FAB-ms: see Table 2; ^{13}C nmr (pyr. $-d_5$): see Table 1; potassium rhodizonate test: positive (yellow coloration); atomic absorption 2.47 ± 0.13 sodium atoms per molecule of **1**.

Aqueous acid hydrolysis of psoluthurin A (1)

1. Carbohydrate constituents

A solution of **1** (50 mg) in 2 *N* HCl (10 mL) was heated under reflux for a period of 4 h. After cooling, the aqueous solution was extracted with $CHCl_3$ (3 × 10 mL) and neutralized with Ag_2CO_3, the AgCl precipitate being removed by filtration on a thin pad of Celite. The solution was then evaporated to dryness under reduced pressure to afford a mixture of carbohydrates (25 mg). The mixture was subjected to trimethylsilylation (32) and the resulting TMS derivatives were analysed by gc (isotherm at 120°C for the initial 4 minutes, then increasing temperature by 1°C/min to 160°C; injection port and detector at 250°C). The retention times of the mixture of sugars were identical to those of the α and β anomers of authentic D-xylose (18.2,

[10]The resin was washed successively with water (300 mL), MeOH (2 L), $CHCl_3$ (2 L), MeOH (2 L), and water (3 L) to eliminate any organic residue present on the resin.

Can. J. Chem. Downloaded from www.nrcresearchpress.com by 210.87.254.6 on 09/06/12
For personal use only.

21.7), D-quinovose (20.2, 23.3), 3-*O*-Me-D-glucose (23.4, 28.3), and D-glucose (31.3, 39.1).

2. Aglycone constituents

The $CHCl_3$ extract were successively washed with $NaHCO_3$ saturated solution (10 mL), NaCl saturated solution (10 mL), and dried over $MgSO_4$. The mixture obtained after evaporation (14 mg) was subjected to preparative tlc (solvent C) to afford **4** (7.2 mg) and **5** (1.0 mg). Genin-1 (**4**) recrystallized from MeOH to give thin white needles, mp 219–221°C; uv λ_{max} (EtOH) (nm): transparent above 210; ir ν_{max} (CCl_4) (cm^{-1}): 3400 (OH), 1760 (γ-lactone), 1740 (5-memb. ketone); ms *m/z* (%): 468.3239 (M^+, calcd. for $C_{30}H_{44}O_4$: 468.3241; 98), 453 ($M^+ - CH_3$; 20), 450 ($M^+ - H_2O$; 9), 435 ($M^+ - CH_3 - H_2O$; 24), 423 (15), 381 (15), 109 (84), 69 (85), 43 (100); R_f (solvent C) 0.37, identical to stichopogenin-A_2 (11). Genin-2 (**5**), mp undetermined; uv λ_{max} (EtOH) (nm): transparent above 210; ir ν_{max} (CCl_4) (cm^{-1}): 3400 (OH), 1750 (γ-lactone and 5-memb. ketone); R_f (solvent C) 0.10, identical to stichopogenin-A_4 (14).

Methanolysis of psoluthurin A (1)

1. Carbohydrate constituents

A solution of **1** (33 mg) in anhydrous 1% HCl – MeOH (10 mL) was refluxed for 3 h. After cooling, the solution was evaporated to dryness and water was added and extracted with $CHCl_3$ (3 × 10 mL). The aqueous solution was treated as before to afford a mixture of methyl glycosides (19 mg) quantitatively analysed by gc (same conditions as in hydrolysis analyses) of the TMS derivatives. (The retention times were identical to those of the authentic methyl D-glycosides of the following sugars: xylose (14.5), quinovose (16.5), 3-*O*-Me-glucose (18.3, 19.5), and glucose (29.5). The relative quantities were determined to be equimolecular by gas-phase chromatography (peak area/mass of TMS derivative).

2. Aglycone constituents

The $CHCl_3$ extracts were treated as before and the residual mixture separated by preparative tlc (solvent C) to give **4** (4 mg), identified by tlc and **6** (6 mg), mp 231–233°C; $[\alpha]_D^{23}$ −113° (*c* 0.11, MeOH), uv λ_{max} (EtOH) (nm): transparent above 210; ir ν_{max} (CCl_4) (cm^{-1}): 3600 (OH), 1745 (γ-lactone and 5-memb. ketone); ^{13}C nmr ($CDCl_3$): see Table 1; R_f (solvent C) 0.28.

Desulfation of psoluthurine A (1)

A solution of **1** (66 mg) in anhydrous 0.08 *M* HCl – MeOH (10 mL) was stirred at room temperature for 24 h. After neutralization with Ag_2CO_3 and evaporation, the residue was subjected to low pressure column chromatography (CH_2Cl_2–MeOH–H_2O, 60:13:2) to afford the desulfated psoluthurin A (**2**, 36 mg), mp 258–259°C (dec.); $[\alpha]_D^{22}$ −80.4° (*c* 1.11, pyridine); uv λ_{max} (EtOH) (nm): transparent above 210; ir ν_{max} (KBr) (cm^{-1}): 3400 (OH), 1745 (5-memb. ketone), 1755 (sh), and 1765 (sh, γ-lactone); ^{13}C nmr (pyr. $-d_5$): see Table 1; potassium rhodizonate test: negative. *Anal.* calcd. for $C_{54}H_{84}O_{22} \cdot 2H_2O$: C 57.84, H 7.9; found: C 57.98, H 7.62.

Methanolysis of desulfated psoluthurin A (2)

A solution of **2** (22 mg) in anhydrous 0.25 *N* HCl – MeOH (5 mL) was stirred at room temperature for 2 h. The mixture of products obtained (presumably prosapogenols by tlc behavior) was partly separated by lplc and afforded a substance (R_f 0.75, CH_2Cl_2–MeOH–H_2O, 60:25:5.4) which was subjected to anhydrous methanolysis (2 *N* HCl – MeOH) at 60°C for 5 h. The solution was evaporated under vacuum and gc analysis (same conditions as the anlysis of the methanolysis of psoluthurin A) of the TMS derivative showed methyl xylopyranoside as the only sugar present.

Permethylation of desulfated psoluthurin A (2)

A solution of the dimsyl carbanion (prepared from NaH (50 mg) and DMSO (1.5 mL) with heating at 65°C for 45 min under N_2) was added to a solution of **2** (14.7 mg) in DMSO (0.5 mL) and stirred for an additional hour. The resulting solution was poured into an ice–water mixture and extracted several times with hexane, washed with water, dried over $MgSO_4$, and evaporated. Low pressure column chromatography (benzene–acetone, 10:1) of the residue afforded the permethylated desulfated psoluthurin A (3.9 mg), as a viscous oil (R_f 0.22, benzene–acetone, 5:1).

Methanolysis of permethylated desulfated psoluthurin A (3)

A solution of **3** (1.4 mg) in anhydrous 2 *N* HCl – MeOH (1.0 mL) was heated under reflux for 3 h. After cooling, the solution was neutralized with Ag_2CO_3, centrifuged, filtered on a 2 μ membrane, evaporated and analysed by gc–ms (3% OV-17: 100 → 180°C, 8°/min; SE-30: 3 min at 80°C then 80 → 180°C, 5°/min); permethylated methyl glucopyranoside: R_f 6.7, 7.5 (3% OV-17); ms *m/z* (%): 187 (2), 176 (2), 131 (3), 111 (4), 102 (6), 101 (45), 88 (100), 75 (52), 73 (21); methyl 2,3-di-*O*-methylquinovopyranoside: R_f 4.5, 5.0 (3% OV-17); ms *m/z* (%): 175 (2), 130 (16), 102 (15), 101 (12), 88 (100); methyl 2,3-di-*O*-methyl-4-*O*-trimethylsilylquinovopyranoside: R_f 15.3, 16.2 (SE-30); ms *m/z* (%): 247 (2), 159 (29), 146 (27), 130 (21), 101 (27), 88 (100), 75 (32), 73 (33); methyl-2,4,6-tri-*O*-methylglucopyranoside: R_f 8.5 (3% OV-17); ms *m/z* (%): 173 (2), 102 (33), 101 (73), 88 (30), 87 (20), 75 (23), 74 (74), 71 (100); methyl-2,4,6-tri-*O*-methyl-3-*O*-trimethylsilylglucopyranoside: R_f 7.8, 8.4 (3% OV-17); ms *m/z* (%): 245 (1), 187 (7), 185 (2), 173 (1), 146 (100), 131 (25), 111 (8), 102 (5), 101 (19), 88 (12), 75 (19), 73 (38); methyl-3,4-di-*O*-methyl-2-*O*-trimethylsilylxylopyranoside: R_f 14.4, 14.5 (SE-30); ms *m/z* (%): 233 (3), 173 (2), 159 (100), 146 (42), 143 (3), 131 (2), 101 (7), 88 (23), 75 (25), 73 (35), 58 (8); methyl-3,4-di-*O*-methyl-2-*O*-(2,4,6-tri-*O*-methyl-3-*O*-trimethylsilyl-glucopyranosyl)-xylopyranoside: R_f 35.0 (SE-30); ms *m/z* (%): 363 (2), 277 (5), 245 (6), 187 (10), 159 (5), 146 (100), 131 (6), 111 (7), 102 (5), 101 (40), 88 (63), 75 (47), 73 (40).

Acknowledgments

We thank the following agencies for financial support of this research: the Natural Sciences and Engineering Research Council of Canada (J.W.A.), the Québec–Ontario exchange projects (J.W.A., F.X.G.), the Government of Québec via the F.C.A.C. program (F.X.G.), and the Fondation de l'Université du Québec à Chicoutimi (F.X.G.). We are grateful to J. R. J. Paré and J. Bélanger (Carleton University) for advice on the FAB/ms interpretation; V.G. Analytical for the FAB/ms spectrum, and I.C.P. Smith of N.R.C. for the ^{13}C nmr (75.46 MHz) spectrum.

1. D. J. BURNELL, J. W. APSIMON, and M. W. GILGAN. Steroids, **39**, 357 (1982).
2. T. YAMANOUCHI. Publ. Seto Mar. Biol. Lab. **4**, 183 (1955).
3. J. BURNELL and J. W. APSIMON. *In* Marine natural products. Chemical and biological perspectives. Vol. V. *Edited by* P. J. Scheuer. Academic Press, New York. In press.
4. J. D. CHANLEY, R. LEDEEN, J. WAX, R. F. NIGRELLI, and H. SOBOTKA. J. Am. Chem. Soc. **81**, 5180 (1959).
5. S. S. N. MURTHY and A. DER MARDEROSIAN. *In* Food-Drugs from the Sea. Proceedings 1973. *Edited by* L. R. Worthen. Marine Technology Soc., Washington, DC. pp. 181–197.
6. G. B. ELYAKOV, T. A. KUZNETSOVA, V. A. STONIK, V. S. LEVIN, and R. ALBORES. Comp. Biochem. Physiol. B, **52**, 413 (1975).
7. E. BULLOCK and C. J. DAWSON. Comp. Biochem. Physiol. **34**, 799 (1970).
8. M. W. GILGAN, R. K. PIKE, and J. W. APSIMON. Comp. Biochem. Physiol. B, **54**, 561 (1976).
9. A. KELECOM, B. TURSCH, and M. VANHAELEN. Bull. Soc. Chim. Belg. **85**, 277 (1976).
10. I. KITAGAWA, M. KOBAYASHI, and T. SUGAWARA. Chem. Pharm. Bull. **26**, 1852 (1978).
11. I. KITAGAWA, T. SUGAWARA, I. YOSIOKA, and K. KURIYAMA. Chem. Pharm. Bull. **24**, 266 (1976).
12. W. L. TAN, C. DJERASSI, J. FAYOS, and J. CLARDY. J. Org. Chem. **40**, 466 (1975).
13. B. TURSCH, I. S. DE SOUZA GUINARAES, B. GILBERT, R. T.

ALPIN, A. M. DUFFIELD, and C. DJERASSI. Tetrahedron, **23**, 761 (1967).
14. I. KITAGAWA, H. YAMANAKA, M. KOBAYASHI, T. NISHINO, I. YOSIOKA, and T. SUGAWARA. Chem. Pharm. Bull. **26**, 3722 (1978).
15. (*a*) A. I. KALINOVSKII, V. F. SHARYPOV, A. K. DZIZENKO, V. A. STONIK, and G. B. ELYAKOV. Bioorg. Khim. **6**, 86 (1980); (*b*) A. I. KALINOVOSKII, V. F. SHARYPOV, V. A. STONIK, and G. B. ELYAKOV. Bioorg. Khim. **6**, 951 (1980).
16. H. BEIERBECK, J. K. SAUNDERS, and J. W. APSIMON. Can. J. Chem. **55**, 2813 (1977).
17. A. KELECOM, D. DALOZE, and B. TURSCH. Tetrahedron, **32**, 2353 (1976).
18. V. A. STONIK, V. F. SHARYPOV, A. I. KALINOVSKII, and G. B. ELYAKOV. Dokl. Akad. Nauk USSR, **245**, 1133 (1979).
19. K. TORI, S. SEO, Y. YOSHIMURA, H. ARITA, and Y. TOMITA. Tetrahedron Lett. 179 (1977).
20. F. W. WEHRLI and T. WHIRLIN. Interpretation of carbon-13 nmr spectra. Heyden, London. 1976. p. 41.
21. I. KITAGAWA, T. NISHINO, and Y. KYOGOKU. Tetrahedron Lett. 1419 (1979).
22. J. B. STOTHERS. *In* Carbon-13 nmr spectroscopy. Academic Press, New York. 1972.
23. P. J. ARCHBALD, M. D. FENN, and A. B. ROY. Carbohydr. Res. **93**, 177 (1981).
24. J. R. TURVEY. Adv. Carbohydr. Chem. **20**, 183 (1965).
25. (*a*) R. U. LEMIEUX and S. KOTO. Tetrahedron, **30**, 1933 (1974); (*b*) R. C. BEIER, B. P. MUNDY, and G. A. STROBEL. Can. J. Chem. **58**, 2800 (1980).
26. A. NESZMELYI, K. TORI, and G. LUKACS. J. Chem. Soc. Chem. Commun. 613 (1977).
27. K. L. RINEHART, JR., M. L. MOORE, and A. N. TYLER. Insight 11. V. G. Analytical Ltd. June 1981.
28. M. BARBER, R. S. BORDOLI, G. J. ELLIOTT, R. D. SEDGWICK, and A. N. TYLER. Anal. Chem. **54**, 645A (1981).
29. N. K. KOCHETKOV and O. S. CHIZOV. Adv. Carbohydr. Chem. **21**, 39 (1966).
30. V. KAVACIK, V. MIHALOV, S. KARACSONYI, and R. TOMAN. Carbohydr. Res. **58**, 203 (1977).
31. K. HEYNS, K. R. SPERLING, and H. F. GRÜTZMACKER. Carbohydr. Res. **9**, 79 (1969).
32. C. C. SWEELEY, R. BENTLEY, M. MAKITA, and W. W. WELLS. J. Am. Chem. Soc. **85**, 2497 (1963).

Can. J. Chem. Downloaded from www.nrcresearchpress.com by 210.87.254.6 on 09/06/12
For personal use only.

Regiochemistry and reactivity in the chlorination of sulfides

JAMES REID HANCOCK, WILLIAM RAYNE HARDSTAFF, PAUL ALAN JOHNS, RICHARD FRANCIS LANGLER,[1] AND WILLIAM STANLEY MANTLE

Department of Chemistry, Mount Allison University, Sackville, N.B., Canada E0A 3C0

Received July 5, 1982[2]

JAMES REID HANCOCK, WILLIAM RAYNE HARDSTAFF, PAUL ALAN JOHNS, RICHARD FRANCIS LANGLER, and WILLIAM STANLEY MANTLE. Can. J. Chem. **61**, 1472 (1983).

Huheey's original method for the calculation of substituent electronegativities is modified so that isomeric groups have different electronegativities. The modified form of Huheey's method is then employed to show that our previously published method for anticipating regiochemistry in asymmetric sulfide chlorinations, i.e., ΔX_P calculations for the α and α′ substituents in the sulfide substrates, is successful in all fifty known cases. A new reactivity function (R_P) is defined, for the sulfenium ion intermediates, which permits one to anticipate when substrates become inert to chlorine in exhaustive chlorinations conducted in aprotic media.

JAMES REID HANCOCK, WILLIAM RAYNE HARDSTAFF, PAUL ALAN JOHNS, RICHARD FRANCIS LANGLER et WILLIAM STANLEY MANTLE. Can. J. Chem. **61**, 1472 (1983).

On a modifié la méthode originale de Huheey relative au calcul de l'électronégativité du substituant de telle sorte que les groupes isomères ont des électronégativités différentes. On a alors utilisé la forme modifiée de la méthode de Huheey pour montrer que notre méthode, de prévision de la régiochimie des chlorations asymétriques des sulfures i.e. les calculs de ΔX_P pour les substituants en positions α et α′ des sulfures, publiée antérieurement s'applique parfaitement à tous les 50 cas connus. On définit une nouvelle fonction de réactivité (R_P), pour les ions sulfenium intermédiaires, qui permet de prévoir le moment où les substrats ne réagissent plus avec le chlore dans les chlorations exhaustives réalisées en milieu aprotique.

[Traduit par le journal]

Introduction

As part of our continuing studies on the chlorinolyses of organosulfur compounds, we have reported a study of regiochemistry in asymmetric sulfide chlorinations (1). The currently accepted mechanism for these reactions (*vide* Scheme 1) is due to Wilson and Huang (2).

Our previous discussion (1) considered the nature of the CSπ bonding in the intermediate sulfenium ions[3] (**A**, Scheme 1). The old view that CSπ bonding in sulfenium ions is inferior to the corresponding COπ bonding due to "the more diffused nature of the sulfur orbital" (4) is inconsistent with recent MO computations (5). We have learned of a much earlier suggestion (6) that CSπ bonding in related systems is superior to CNπ bonding.

As a result of our bonding arguments, we have suggested that the preferred sulfenium ion will be the one which has the most electronegative substituents on the sp^2 carbon (1). To determine which side chain will be preferentially chlorinated, (*i*) sum the electronegativities of the substituents on the α carbon of the starting sulfide and (*ii*) subtract the sum of the substituent electronegativities for the α′ carbon, i.e. for **1**:

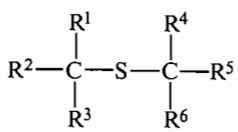

1

$$[1] \quad \Delta X_P = [X_P(R^1) + X_P(R^2) + X_P(R^3)] - [X_P(R^4) + X_P(R^5) + X_P(R^6)]$$

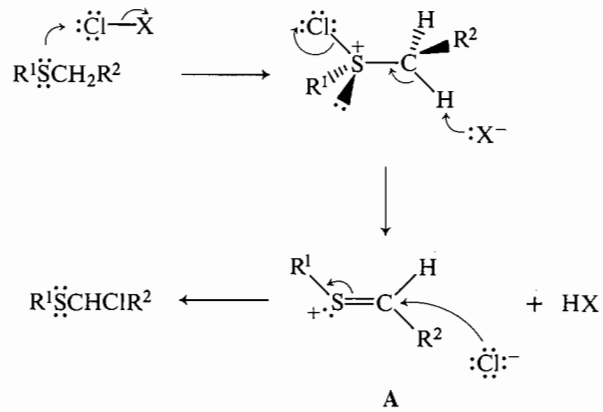

SCHEME 1

If $\Delta X_P < 0$, then reaction goes preferentially into the side chain bearing R^4, R^5, and R^6 but if $X_P > 0$, then reaction goes preferentially into the side chain bearing R^1, R^2, and R^3. A semiquantitative correlation was found between the yield of major regioisomer and ΔX_P for the thirty known asymmetric sulfide chlorinations (1, 7) with essential regiospecificity observed for all cases where $\Delta X_P \geq 0.20$.

Substituent electronegativities were determined using Huheey's method and the parameters which he provided (8, 9). Since that time, we have completed a study comparing net group charges obtained by Huheey's group electronegativity method with those obtained by *ab initio* and semi-empirical molecular orbital calculations (10). One of the conclusions of this study was that Huheey's parameters for the phenyl group ($a = 8.03$, $b = 1.21$, and $X_P = 2.49$) (9) required revision to those parameters shown in Table 1. Revision of the phenyl parameters requires the revision of electronegativity parameters for the phenyl substituted groups shown as entries 2–4 in Table 1. These new parameters furnish new values for some of our previously tabulated ΔX_P's. The cases affected are presented in Table 2. These revisions produce no net change in

[1]Author to whom correspondence should be addressed at: Department of Chemistry and Chemical Engineering, Florida Institute of Technology, 150 West University Boulevard, Melbourne, FL 32901, U.S.A.

[2]Revision received January 14, 1983.

[3]These ions have also been called sulfonium ions (1) and thionium ions (3).

Can. J. Chem. Downloaded from www.nrcresearchpress.com by 210.87.254.40 on 09/06/12
For personal use only.

TABLE 1. Revised group electronegativity parameters

Group	a	b	X_P	Reference cited for unrevised parameters
1. Ph-	7.81	26.67	2.41	1,9
2. $PhSO_2$-	12.84	4.25	4.10	1,9
3. $PhCH_2$-	7.47	3.71	2.30	11
4. PhCO-	10.80	6.11	3.42	—
5. $ClCH_2CH_2$-	7.55	1.81	2.33	—
6. CH_3CHCl-	8.00	1.81	2.48	1
7. $PhCH_2CH_2$-	7.43	2.00	2.29	—
8. CH_3CHPh-	7.54	2.00	2.32	—
9. $CH_3SO_2CH_2CH_2$-	7.84	1.02	2.42	11
10. $CH_3CH(SO_2CH_3)$-	9.06	1.02	2.83	—
11. $PhSO_2CH_2CH_2$-	8.10	1.43	2.51	11
12. $CH_3CH(SO_2Ph)$-	10.58	1.43	3.34	—

TABLE 2. Revised ΔX_P values for asymmetric sulfides

Compound	Revised ΔX_P	Previous ΔX_P	Reference
1. $PhCH_2SCH_3$	0.21	0.29	1
2. p-$ClC_6H_4CH_2SCH_2Ph$	0.14	0.07	1
3. $ClCH_2SCH_2Ph$	0.53	0.45	1
4. $NCCH_2SCH_2Ph$	1.43	1.35	1
5. $PhSO_2CH_2SCH_2Ph$	1.69	0.41	1
6. $CH_3SO_2CH_2SCH_2Ph$	0.69	0.61	1
7. $CH_3SO_2CHClSCH_2Ph$	1.43	1.35	1
8. $PhCH_2SCH(CH_3)_2$	0.07	0.15	1
9. $PhCH_2CH_2SCH_3$	0.10	0.24	11

TABLE 3. Regioisomeric chlorosulfides: ΔX_P predictions using Huheey's unmodified method

Sulfide substrate ($R^1CH_2SCH_2R^2$)	Chlorosulfide product		ΔX_P	
	Major (% yield)	Minor (% yield)	($X_{R^1} - X_{R^2}$)	Reference
Reagent: SO_2Cl_2				
1. $ClCH_2SCH_3$	Cl_2CHSCH_3 (100)	—	0.74	1
2. $ClCH_2CH_2SCH_3$	$ClCH_2CHClSCH_3$ (100)	—	0.27	—
3. $ClCH_2CH_2CH_2SCH_3$	$ClCH_2CH_2CHClSCH_3$ (85)	$ClCH_2CH_2CH_2SCH_2Cl$ (15)	0.19	—
4. $CH_3CHClCH_2SCH_3$	$CH_3CHClCHClSCH_3$ (100)	—	0.19	—
5. $CH_3CH_2CH_2SCH_3$	$CH_3CH_2CHClSCH_3$ (72)	$CH_3CH_2CH_2SCH_2Cl$ (28)	0.08	—

the performance of our approach to the prediction of regiochemistry in asymmetric sulfide chlorinations.

Results and discussion

Our first concern in the present study was that isomeric groups may not have the same directing ability in these reactions. Should that be the case, then Huheey's original method, for which "isomeric groups will yield identical electronegativities" (8), has an inherent feature that constitutes a limitation for our approach to regiochemical predictions in asymmetric sulfide chlorinations.

Fundamental to Huheey's original approach to the calculation of group electronegativities (8) is the assumption that all atoms in a group equalize their electronegativities. Thus, two substituents in the same group will have the same electronegativity whether they are remote from or immediately adjacent to each other. Since inductive effects fall off rapidly with distance and are generally thought to be exhausted within three bonds, this assumption is clearly untenable for remote substituents. Such sets of isomeric groups require more than one set of electronegativity parameters. The series of sulfide chlorinations shown in Table 3 presents the problem as it applies to ΔX_P calculations and regiochemistry. With the shift of chlorine ($\alpha \rightarrow \beta \rightarrow \gamma$) in cases $1 \rightarrow 3$, regioselectivity declines, as expected, on the basis of diminishing ΔX_P. However, previous experience (1) suggests that a ΔX_P value of 0.19 (case 3) should indicate essential regiospecificity. Indeed, case 4, for which ΔX_P is 0.19, is regiospecific.

We suggest that (*i*) Huheey's original X_P of 2.39 for chloroethyl groups is best viewed as intermediate between the values appropriate for the 1-chloroethyl and the 2-chloroethyl groups, (*ii*) the 1-chloroethyl group is unlikely to have a X_P value

Can. J. Chem. Downloaded from www.nrcresearchpress.com by 210.87.254.40 on 09/06/12
For personal use only.

Can. J. Chem. Downloaded from www.nrcresearchpress.com by 210.87.254.40 on 09/06/12
For personal use only.

significantly different from that for the chloromethyl group (X_P = 2.47), and (*iii*) the 2-chloroethyl group should have a X_P value much closer to that for the ethyl group (X_P = 2.29). The preceding points are compatible with Huheey's earlier suggestion that the origin of the problem of obtaining different X_P values for different isomeric groups is the failure of his original approach to account for the "dilution of polar effects" (8).

Given that asymmetric sulfide chlorinations have been found to exhibit regioselectivities which correlate with substituent ΔX_P values, the chlorinations (cases 3 and 4, Table 3) permit one to obtain reasonable estimates for the two X_P values in question, i.e., $ClCH_2CH_2$, 2.33 and CH_3CHCl, 2.45. Assuming that (*i*) it is satisfactory for all isomeric groups in the same set to have the same "*b*" values, (*ii*) each group has a X_P value intermediate between the X_P values for its component groups e.g., for $ClCH_2CH_2$, X_P should fall between 2.29 (X_P for CH_2) and 2.47 (X_P for $ClCH_2$), and (*iii*) the X_P value for the central atom directly attached to the group of interest is weighted more heavily than its nearest central atom and so on, the following formula may be obtained for group electronegativity which varies with isomeric structure *and* furnishes the appropriate values for the isomeric chloroethyl groups.

$$[2] \quad a_1 = \frac{3^{n-1}a_1 + 3^{n-2}a_2 + 3^{n-3}a_3 + \ldots + 3^{n-n}a_n}{3^{n-1} + 3^{n-2} + 3^{n-3} + \ldots + 3^{n-n}}$$

Thus a_1 is the Mulliken electronegativity[4] for an isomeric group where a_1, a_2 ..... a_n are the Mulliken electronegativities for each component group containing one central atom. Equation [2] will also afford unique answers for chains which have side chains capable of existing in isomeric form. All component groups which are equidistant from the point of contact must have equal weights. Thus a unique electronegativity for **8** can be obtained readily as shown in eq. [3].

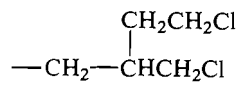

8

$$[3] \quad a_8 = \frac{3^3a_{CH_2} + 3^2a_{CH} + 3^1a_{CH_2Cl} + 3^1a_{CH_2} + 3^0a_{CH_2Cl}}{3^3 + 3^2 + 3^1 + 3^1 + 3^0}$$

Table 1 (entries 5–12) presents revised electronegativity parameters for some isomeric ethyl groups. Table 4 presents the results of reactions between a selection of asymmetric sulfides and molecular chlorine or sulfuryl chloride. The ΔX_P values tabulated reflect our modifications to Huheey's electronegativity parameters. As was the case previously (1), the substituent electronegativity difference (ΔX_P) correctly anticipates the observed regioselectivity in every case.

Two previous proposals for the prediction of regiochemistry in these reactions had been advanced i.e. (*i*) reaction will go into the side chain bearing the most acidic α-H atoms (13) and (*ii*) reaction will go into the side chain which is best able to support positive charge (14). We have argued (1) that the first proposal is inconsistent with the reaction shown in eq. [5] and the second proposal is inconsistent with the results shown in eq. [6].

[4]In keeping with Huheey's approach, we use Mulliken electronegativities ($X_M \equiv a$) to carry out calculations. The relationship between Mulliken and Pauling electronegativities is X_P = 0.336 (X_M − 0.615).

[5] 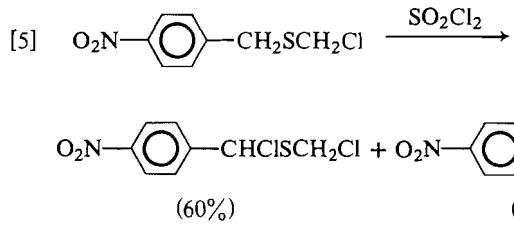

(60%) (40%)

[6] $PhCH_2SCH_2Cl \xrightarrow{SO_2Cl_2} PhCH_2SCHCl_2$ (100%)

We wished to find a single substrate which would have a common regiochemical outcome predicted by both previous approaches and a different outcome predicted by our approach based on ΔX_P. 4-Chloro-1-phenyl-2-thiabutane **9** is such a system. The α-phenyl group would be expected to (*i*) acidify the α-protons substantially more than an α-chloromethyl group and (*ii*) stabilize an incipient carbonium ion substantially more than an α-chloromethyl group. Thus both of these views lead to the conclusion that chlorination should occur nearly exclusively at the benzylic carbon. However, a consideration of the ΔX_P value for this system (X_P $ClCH_2$, 2.47 (11); X_P Ph, 2.41 (Table 1)) leads to the conclusion that reaction should produce similar amounts of both regioisomers with a modest predominance of the dichloroethyl benzyl sulfide. Equation [7] presents the results of this chlorination:

[7] $ClCH_2CH_2SCH_2Ph \xrightarrow[CCl_4]{SO_2Cl_2}$

9

$ClCH_2CHClSCH_2Ph$ (65%) + $ClCH_2CH_2SCHClPh$ (35%)

The reaction in eq. [7] along with those in Table 4 and our previous results (1) bring the total to fifty asymmetric sulfide chlorinations for which ΔX_P predictions of regioselectivity are successful.

Our initial report (1) failed to discuss only one asymmetric sulfide chlorinolysis known at that time. Paquette (15) had reported the chlorinolysis of the novel dibenzothiepins shown in Scheme 2.

These results provide a contrast to the chlorinolysis of dibenzyl sulfide which affords the α,α-dichlorosulfide cleanly. Paquette has suggested that formation of the cross-chlorinated systems **3** and **6** is due to steric compression between the second chlorine and the nearest R group in **4** and **7**. We would like to suggest that the origin of **3** and **6** more likely lies with bimolecular elimination (*vide* Scheme 1) occurring from chlorosulfonium cation conformations which have the initial α-chlorine in a pseudoaxial position, thereby forcing reaction into the opposite side.[5] Such a proposal has been frequently advanced to rationalize the regiochemistry of thiane-1-oxide chlorinations (7). Formation of cross-chlorinated sulfides might well be a hallmark of chlorinolyses of medium-ring sulfides.

In our previous study (1), virtually all of the substituents affecting the regiochemical outcome of sulfide chlorinations were situated on a carbon attached to sulfur. We hoped, for this

[5]This proposal presupposes that the elimination step requires a transdiaxial relationship between α-H and Cl, a possibility suggested earlier (16).

TABLE 4. Regioisomeric chlorosulfides from sulfide chlorinations (revised parameters)

Sulfide substrate ($R^1CH_2SCH_2R^2$)	Chlorosulfide product: Major (% yield)	Chlorosulfide product: Minor (% yield)	ΔX_P[a] ($X_{R^1} - X_{R^2}$)	Reference
Reagent: Cl_2				
1. $CH_3SO_2CH_2SCH_2CH_3$	$CH_3SO_2CHClSCH_2CH_3$ (100)	—	0.83	1
2. $CH_3SO_2CHClSCH_2CH_3$	$CH_3SO_2CCl_2SCH_2CH_3$ (100)	—	1.57	1
3. $CH_3SO_2CH_2SCHClCH_3$	$CH_3SO_2CHClSCHClCH_3$ (100)	—	0.10	1
4. $CH_3SO_2CHClSCHClCH_3$	$CH_3SO_2CCl_2SCHClCH_3$ (100)	—	0.84	1
5. $ClCH_2SCH_2CH_3$	$Cl_2CHSCH_2CH_3$ (100)	—	0.67	—
6. $NCCH_2SCH_3$	$NCCHClSCH_3$ (100)	—	1.64	—
7. $NCCHClSCH_3$	$NCCCl_2SCH_3$ (100)	—	2.38	—
8. $NCCHClSCH_2CN$	$NCCCl_2SCH_2CN$ (100)	—	0.74	—
Reagent: SO_2Cl_2				
9. $PhSO_2CHClSCH_2Ph$	$PhSO_2CCl_2SCH_2Ph$ (100)	—	2.43	14
10. $ClCH_2SCH_3$	Cl_2CHSCH_3 (100)	—	0.74	1[b]
11. $ClCH_2CH_2SCH_3$	$ClCH_2CHClSCH_3$ (100)	—	0.27	—
12. $ClCH_2CH_2CH_2SCH_3$	$ClCH_2CH_2CHClSCH_3$ (85)	$ClCH_2CH_2CH_2SCH_2Cl$ (15)	0.13	—
13. $CH_3CHClCH_2SCH_3$	$CH_3CHClCHClSCH_3$ (100)	—	0.28	—
14. $CH_3CH_2CH_2SCH_3$	$CH_3CH_2CHClSCH_3$ (72)	$CH_3CH_2CH_2SCH_2Cl$ (28)	0.08	—
15. $CH_3C(O)CH_2SCH_2Ph$	$CH_3C(O)CHClSCH_2Ph$ (100)	—	0.28	—
16. $CH_3C(O)CH_2SCH_2Ph$*p*Br	$CH_3(O)CHClSCH_2Ph$*p*Br (100)	—	0.16	—
17. $PhCH_2CH_2CH_2SCH_3$[c]	$PhCH_2CH_2CHClSCH_3$ (79)	$PhCH_2CH_2CH_2SCH_2Cl$ (21)	0.09	—
18. $ClCH_2CH_2SCH_2CH_3$	$ClCH_2CHClSCH_2CH_3$ (100)	—	0.20	—
19. $CH_3OC(O)CH_2SCH_2CH_3$	$CH_3OC(O)CHClSCH_2CH_3$ (100)	—	0.67	—
20. $NCCH_2SCH_2(O)COCH_3$	$NCCHClSCH_2(O)COCH_3$ (100)	—	0.90	—

[a]The new electronegativity parameters presented in Table 1 were used to calculate ΔX_P's.
[b]This case has been tabulated previously (1) and is included here for convenient comparison with similar systems which follow it in the table.
[c]The preparation of this compound involved an apparently unprecedented Grignard reaction (see Experimental).

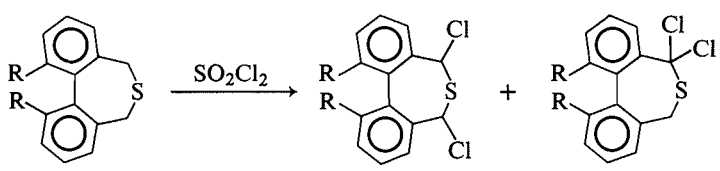

2 R = H
5 R = CH_3

3 R = H (2.9%)
6 R = CH_3 (9.6%)

4 R = H (33%)
7 R = CH_3 (34%)

SCHEME 2

study, to obtain useful results from the chlorination of systems in which the functional group under consideration was β to sulfur. Toward that objective, we have prepared the sulfides **10***a*, **10***b*, and **10***c*.

Can. J. Chem. Downloaded from www.nrcresearchpress.com by 210.87.254.40 on 09/06/12
For personal use only.

TABLE 5. ^{1}H nuclear magnetic resonance parameters for 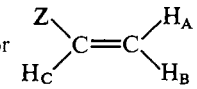

Z	H	δ	J_{AB}(Hz)	J_{AC}(Hz)	J_{BC}(Hz)	Reference
CH_3SO_2—						—
	H_C	6.90	—	~15	~8	
	H_B	6.18	~0	—	~9	
	H_A	6.60	~0	~15	—	
CH_3S—						
	H_C	—	—	16.4	10.3	18
	H_B	—	−0.3	—	10.3	
	H_A	—	−0.3	16.4	—	
$CH_3SO_2CH_2S$						
	H_C	6.5	—	~16	~10	1
	H_B	5.6	~−1	—	~10	
	H_A	5.4	~−1	~16	—	

TABLE 6. Products from $PhCH_2SCH_2CN + SO_2Cl_2$

			Products (% yield)	
Δt (min)	Temperature (°C)	Solvent	$PhCH_2SCH_2CN$	$PhCH_2S\underset{\displaystyle Cl}{\underset{\vert}{C}}HCN$
30	40	CH_2Cl_2	24	76
30	62	$CHCl_3$	53	47
30	76	CCl_4	81	19

TABLE 7. Extent of sulfide chlorinations[a]

Sulfide	ΣX_P	Products (% yield)	
1. CH_3SCH_3	13.20	CH_3SCH_3(0)	$ClCH_2SCH_3$(100)
2. $PhCH_2SCH_3$[b]	13.41	$PhCH_2SCH_3$(0)	$PhCHClSCH_3$(100)
3. $CH_3SO_2CH_2SCH_2Ph$[b]	14.31	$CH_3SO_2CH_2SCH_2Ph$(25)	$CH_3SO_2CHClSCH_2Ph$(75)
4. CH_3SCH_2CN	14.84	CH_3SCH_2CN(20)	$CH_3SCHClCN$(80)
5. $NCCH_2SCH_2CO_2CH_3$	15.58	$NCCH_2SCH_2CO_2CH_3$(61)	$NCCHClSCH_2CO_2CH_3$(39)

[a]Chlorinations were carried out with sulfuryl chloride in carbon tetrachloride at room temperature.
[b]ΣX_P for this sytem was calculated using the phenyl parameters shown in Table 1.

$ZCH_2CH_2SCH_3$

10*a* Z = CH_3O_2C—
10*b* Z = $PhCH_2SO_2$—
10*c* Z = CH_3SO_2—

Our approach to the synthesis of these systems goes through the corresponding β-chloro intermediate (—SCH_3 is introduced in the last step). Base-catalyzed elimination of HCl produces the corresponding vinyl systems which have a pronounced tendency to polymerize. We have, consequently, telescoped the procedure so that the vinyl systems are prepared *in situ* and the Michael addition of the appropriate mercaptan carried out without isolation of the vinyl intermediates (see, for example, ref. 17).

Chlorination of the substrates **10***a* → **10***c* furnished crude products in which the dominant product(s) was/were not the simple regioisomeric α-chlorosulfide(s). We have chosen to investigate the chlorination of **10***c* in more detail. Column chromatography of the crude product afforded a moderate yield of a colorless oil whose spectra were consistent with a vinyl sulfone-sulfide structure. In the nmr, the vinyl protons appeared as a pair of doublets (δ 7.70 and 6.15, J_{AC} ~ 15 Hz). Table 5 presents some appropriate spectral parameters which clearly implicate the *trans* structure for **11** as shown in eq. [8].

[8] $CH_3SO_2CH_2CH_2SCH_3 \xrightarrow[CHCl_3]{SO_2Cl_2}$

10*c*

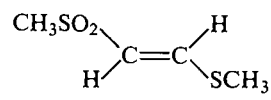

11

Thus, an assessment of the directing ability of substituents situated on β-carbons in asymmetric sulfide chlorinations is only possible when those substituents have a relatively weak acidifying effect on the protons attached to the β-carbon (see eq. [7] for an example).

No results have been published indicating that any feature of these reactions is sensitive to the polarity of the aprotic solvent employed. In particular, we have been unable to find any examples of a shift in regioselectivity attributable to a change in solvent polarity. Table 6 presents results which indicate that these reactions proceed more rapidly in polar aprotic solvents than in nonpolar aprotic solvents. Since these reactions were all

Can. J. Chem. Downloaded from www.nrcresearchpress.com by 210.87.254.40 on 09/06/12
For personal use only.

Can. J. Chem. Downloaded from www.nrcresearchpress.com by 210.87.254.40 on 09/06/12
For personal use only.

conducted at reflux in the appropriate chlorocarbon solvent, the salutory effect of higher polarity (lower boiling) methylene chloride is firmly established. These results are consistent with the ionic mechanism established for these reactions (see Scheme 1).

In our previous paper (1), we suggested that reactivity for sulfides in these reactions is dependent upon (*i*) the sum of the electronegativities of the substituents (ΣX_P) on the α and α′ carbon atoms and (*ii*) the substituent electronegativity difference (ΔX_P). From the reactions considered at that time, it was clear that ΣX_P is the more important factor. The results shown in Table 7 show that ΣX_P alone can be a useful guide to reactivity for some sulfide chlorinations. We have found that systems for which $\Sigma X_P \leq 14.91$ will monochlorinate readily.

For systems where $\Sigma X_P > 14.91$, the substitution pattern becomes important and ΣX_P alone is not a reliable guide to reactivity. We have been unable to find a correlation between reactivity and any function with ΣX_P and ΔX_P as variables. This difficulty is not surprising, in that these parameters are applicable to the ground state sulfide which is clearly a poor representation of the transition state giving rise to the key sulfenium ion intermediate. In fact, the correlation between ΔX_P and observed regiochemistry in asymmetric sulfide chlorinations must be fortuitous since it also represents an extrapolation of ground state properties to transition state properties. We have found that a useful reactivity function can be obtained using electronegativity parameters for sulfenium ion substituents, i.e., X_P is obtained for R^1R^2C— and $R^3R^4R^5C$— in **12** and the resultant values summed to furnish ΣX_P^*. When chlorination proceeds

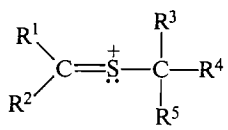

12

into the disfavored side chain, as indicated by ΔX_P, then ΣX_P^* correlates with the gross reactivity of the system in question; viz. ΣX_P^* will indicate whether or not the substrate is inert to Cl_2. Since ΔX_P loses its definition for sulfenium ions, we have accounted for the enhanced reactivity of molecules which can chlorinate in the favored side chain by reducing ΣX_P^* by 1. Thus a systematic approach to anticipating gross reactivity of sulfide substrates for which $\Sigma X_P > 14.91$ is now available: (*i*) determine ΔX_P for reaction into the side chain under consideration; for reaction into the favored side $r = -1$; for reaction into the disfavored side $r = 0$, (*ii*) determine ΣX_P^* for the requisite sulfenium ion intermediate, and (*iii*) evaluate R_P', which is defined in eq. [9].

$$[9] \quad R_P' = \Sigma X_P^* + r$$

A more convenient scale of values is obtained with R_P which is defined in eq. [10].

$$[10] \quad R_P = R_P' - 5.22$$

The final form of our reactivity function (R_P) gives values <0 for molecules which are still able to react with Cl_2 at a useful rate and values >0 for molecules which are inert.[6] Since R_P does not account for a number of important factors, notably the nature of the solvent, these numbers should not be taken to indicate relative reactivities, but simply to indicate whether further reaction is likely (e.g., it is futile to attempt to obtain 1,1,1,3,3-pentachloro-2-thiapropane by chlorinating 1,1,1,3-tetrachloro-2-thiapropane (entry 5, Table 8)). When the fifty sulfide chlorinations of regiochemical interest are supplemented with those substrates for which the regiochemistry is trivial, there are some sixty-seven sulfide chlorinations to which R_P calculations potentially apply. For thirty-seven of these reactions $\Sigma X_P \leq 14.91$. R_P values for the remaining thirty cases are presented in Table 8.

In attempting to apply ΔX_P and R_P predictions to the outcome of sulfide chlorinations, one should bear in mind that α-chlorination is *not* expected to occur when (*i*) one of the substituents on sulfur is unusually susceptible to external nucleophilic attack (S_N1 or S_N2) which will lead to the cleavage af a CS bond (7), (*ii*) a β-carbon bears a strongly acidifying group, and (*iii*) the substrate contains a substituent capable of neighboring group participation (12).

In conclusion, we have (*i*) further modified Huheey's method for the calculation of group electronegativity parameters, (*ii*) extended the number of asymmetric sulfide chlorinations for which ΔX_P correctly anticipates the regiochemical outcome, and (*iii*) defined a new function R_P which permits an assessment of the gross reactivity of sulfide substrates in reactions with Cl_2.

Experimental

General

Details have been provided previously (1).

Chlorinations with sulfuryl chloride

The following procedure was employed for the chlorination of those new substrates listed under "*Reagent*: SO_2Cl_2" in Table 4. The desired sulfide (0.5 g) was dissolved in carbon tetrachloride (10 mL) and a solution of sulfuryl chloride (1 equivalent) in carbon tetrachloride (10 mL) added dropwise over 5 minutes. The reaction mixture was stirred at ambient temperature for 0.5 h and the solvent evaporated. The product mixture in most cases was analyzed by integrated nmr. The outcome of the following cases could not be determined by nmr alone.

Chlorination of 2-oxo-5-phenyl-4-thiapentane

$PhCH_2SCH_2C(O)CH_3$ (entry 15, Table 4) which had ir ($CHCl_3$) 1701 cm^{-1} was subjected to the procedure outlined under "Chlorinations with sulfuryl chloride". The homogeneous product, $PhCH_2SCHClC(O)CH_3$, had ir[7] ($CHCl_3$): 1740 cm^{-1}; nmr ($CDCl_3$) δ: 2.33 (3H, s), 4.00 (2H, s), 5.30 (1H, 2), and 7.4 (5H, s).

Chlorination of 2-oxo-5-p-bromophenyl-4-thiapentane

p-$BrPhCH_2SCH_2C(O)CH_3$ (entry 16, Table 4) which had ir ($CHCl_3$) 1710 cm^{-1} was subjected to the procedure outlined under "Chlorination with sulfuryl chloride". The homogeneous product, *p*-$BrPhCH_2SCHClC(O)CH_3$, had ir[7] ($CHCl_3$): 1738 cm^{-1}; nmr ($CDCl_3$) δ: 2.33 (3H, s), 3.90 (2H, s), 5.33 (1H, s), 7.26 (2H, d), and 7.53 (2H, d).

Chlorination of methyl 4-cyano-3-thiabutyrate

$NCCH_2SCH_2CO_2CH_3$ (entry 20, Table 4) which had ir (CCl_4) 1748 cm^{-1} was subjected to the procedure outlined under "Chlorinations with sulfuryl chloride". Since reaction was incomplete, the reaction was repeated on the crude product. The homogeneous product, $NCCHClSCH_2CO_2CH_3$, had ir (CCl_4): 1750 cm^{-1}; nmr ($CDCl_3$) δ: 3.86 (5H, m) and 5.96 (1H, s).

[6]By "inert" we mean that there is no observable formation of the α-chlorosulfide (by nmr) after chlorination of 0.5 g for 4 h at ambient temperature.

[7]A shift to higher νCO is associated with a field effect for α-halocarbonyl compounds (20).

Can. J. Chem. Downloaded from www.nrcresearchpress.com by 210.87.254.40 on 09/06/12
For personal use only.

TABLE 8. Sulfide reactivity parameters[a,b]

Sulfide	r	ΣX_P	R_P	Experimental result	Reference
1. p-$O_2NPhCHClSCH_2Cl$	−1	5.43	−0.79	Reactive	13
2. $Cl_2CHSCH_2Ph$$p$$NO_2$	−1	5.72	−0.50	Reactive	13
3. Cl_2CHSCH_2Cl	−1	5.35	−0.87	Reactive	1
4. Cl_3CSCH_3	0	5.21	−0.01	Reactive	1
5. Cl_3CSCH_2Cl	0	5.47	0.25	Unreactive	1
6. $ClCH_2CCl_2SCH_3$	0	4.96	−0.26	Reactive	—
7. $Cl_3CSCH_2CH_3$	0	5.17	−0.05	Reactive	—
8. $ClCH_2CCl_2SCH_2Cl$	0	5.24	0.02	Unreactive	—
9. $Cl_3CSCHClCH_3$	0	5.30	0.08	Unreactive	—
10. $NCCH_2SCH_2Ph$	−1	5.41	−0.81	Reactive	12
11. $NCCHClSCH_2Ph$	−1	5.60	−0.62	Reactive	12
12. $PhSO_2CH_2SCH_2Ph$	−1	5.76	−0.46	Reactive	12
13. $PhSO_2CHClSCH_2Ph$	−1	5.89	−0.33	Reactive	12
14. $CH_3SO_2CHClSCH_2Ph$	−1	5.34	−0.88	Reactive	1
15. $NCCH_2SCH_2CH_3$	−1	5.39	−0.83	Reactive	14
16. $NCCHClSCH_3$	−1	5.57	−0.65	Reactive	—
17. $NCCCl_2SCH_3$	0	5.53	0.31	Unreactive	—
18. $NCCHClSCH_2CN$	−1	6.15	−0.07	Reactive	—
19. $NCCCl_2SCH_2CN$	0	6.27	1.05	Unreactive	—
20. $NCCH_2SCH_2C(O)OCH_3$	−1	5.84	−0.38	Reactive	—
21. $CH_3SO_2CHClSCH_2CH_3$	−1	5.32	−0.90	Reactive	1
22. $CH_3SO_2CH_2SCHClCH_3$	−1	5.35	−0.87	Reactive	1
23. $CH_3SO_2CCl_2SCH_2CH_3$	0	5.33	0.11	Unreactive	1
24. $CH_3SO_2CHClSCHClCH_3$	−1	5.43	−0.79	Reactive	1
25. $CH_3SO_2CCl_2SCHClCH_3$	0	5.46	0.24	Unreactive	1
26. p-$ClPhC(O)CCl_2SCH_3$	0	5.10	−0.12	Reactive	12
27. p-$ClPhC(O)CCl_2SCH_2Cl$	0	5.36	0.14	Unchecked	12
28. $PhSCHCl_2$	−1	5.29	−0.93	Reactive	19
29. $CH_3CH_2OC(O)CCl_2SCH_3$	0	5.12	−0.10	Reactive	12
30. $CH_3CH_2OC(O)CCl_2SCH_2Cl$	0	5.38	0.16	Unchecked	12

[a] $R_P > 0$ implies sulfide is inert to Cl_2 and $R_P < 0$ implies sulfide will react with Cl_2.
[b] New chlorinations were carried out with Cl_2.

Chlorinations with Cl_2

The following procedure was employed for the chlorination of the new substrates listed in Table 8. The desired sulfide (0.5 g) was dissolved in carbon tetrachloride[8] (5 mL) and Cl_2 bubbled (ca. 200 mL/min) into the solution. The chlorinations were interrupted after 5, 15, and 50 min and the crude product checked by nmr at each stage. When two nmr's were the same, chlorination was carried out for a further 4 h and the final product checked by nmr.

Preparation of 1-chloro-2-thiabutane

Ethanethiol (4.993 g) and p-formaldehyde (2.466 g) were added to methylene chloride (25 mL) and the mixture cooled with an ice/water bath. HCl (ca. 200 mL/min) was bubbled into the reaction mixture for 50 min. Methylene chloride (100 mL) was added and the resultant solution dried ($MgSO_4$) and concentrated. The residue was rectified at ambient pressure affording clean chlorosulfide (5.225 g, bp 128−131°C). The product had ir (CCl_4): 2950 and 1250 cm^{-1}; nmr ($CDCl_3$) δ: 1.36 (3H, t), 2.86 (2H, q), and 4.86 (2H, s).

Preparation of 1-cyano-2-thiapropane

Four preparative runs were carried out as described below and the crude products from each run combined. Sodium cyanide (5.077 g) was dissolved in dry DMSO (200 mL) and 1-chloro-2-thiapropane (10.008 g) added dropwise over 5 min. The reaction mixture was stirred at ambient temperature for 1 h. Water (300 mL) was added and the resultant solution washed with diethyl ether (three 200-mL portions). The combined organic layers were washed with 5% HCl (two 200-mL aliquots) and water (200 mL). The organic layer was dried ($MgSO_4$) and concentrated. The combined material from four runs was distilled at reduced pressure affording impure cyanosulfide (4.528 g, bp 100−120°C/100 Torr). The distilled cyanosulfide was chromatographed on silica gel (400 g) employing chloroform elution (100 mL fractions). Fractions 12−19 were combined and distilled affording clean cyanosulfide (2.190 g, bp 98−100°C/100 Torr). The cyanosulfide had ir ($CHCl_3$): 2245 cm^{-1}; nmr ($CDCl_3$) δ: 2.33 (3H, s) and 3.33 (2H, s); ms m/e: 87 (M^+, 70%), 61 (80%), and 47 (100%).

Preparation of 1,3-dicyano-2-thiapropane

Sodium sulfide nonahydrate (8.67 g) was added to 95% ethanol (50 mL) and the mixture brought to gentle reflux. Chloroacetonitrile (5.02 g) in 95% ethanol (50 mL) was added dropwise over 50 min. Upon completion of the addition the reaction mixture was refluxed for an additional 0.5 h. Norite (ca. 5 g) was added and the resultant hot mixture filtered through Celite. Water (100 mL) was added and the resultant mixture washed with chloroform (three 100-mL aliquots). The combined chloroform layers were concentrated, affording a black oil. The crude oil was chromatographed on silica gel (100 g) employing chloroform elution (100 mL fractions). Fractions 4−6 were combined and concentrated affording a yellow solid. The chromatographed product was recrystallized (2×) from 95% ethanol affording clean dicyanosulfide (0.702 g, mp 39−41°C). The dicyanosulfide had ir ($CHCl_3$): 2290 cm^{-1}; nmr ($CDCl_3$) δ: 3.60 (s); ms m/e: 112 (M^+, 37.5%), 72 (40.6%), 45 (59.3%), and 41 (100%).

Preparation of 4-chloro-2-thiabutane

The preparation and properties of 4-chloro-2-thiabutane have been detailed previously (17).

Preparation of 5-chloro-2-thiapentane

The preparation and properties of 5-chloro-2-thiapentane have been detailed previously (11).

[8] For cases where the sulfide was not soluble in CCl_4, chloroform was used.

Preparation of 2-thia-4-pentanone

Sodium metal (3.803 g) was dissolved in methanol (250 mL) and the solution cooled with an ice/water bath. Methanethiol (25 mL) was slowly bubbled into the solution. Chloroacetone (14.999 g) in methanol (50 mL) was added dropwise over 10 min and the reaction mixture stirred at ambient temperature overnight. Water (250 mL) was added and the resultant mixture washed with methylene chloride (four 100-mL portions). The combined organic layers were dried ($MgSO_4$) and concentrated. The residue was rectified at reduced pressure affording the ketosulfide (12.730 g, bp 90−92°C/100 Torr). The ketosulfide had ir ($CHCl_3$): 1705 cm^{-1}; nmr ($CDCl_3$) δ: 2.10 (3H, s), 2.30 (3H, s), and 3.23 (2H, s): ms *m/e*: 104 ($M^{+\cdot}$, 38.7%), 61 (80.0%), and 43 (100%).

Preparation of 2-thia-4-pentanol

Lithium aluminum hydride (4.792 g) was covered with dry diethyl ether (300 mL) and the mixture refluxed 0.5 h. The mixture was cooled to room temperature and a solution of 2-thia-4-pentanone (12.70 g) in diethyl ether (100 mL) added dropwise over 1 h. The reaction mixture was refluxed for 1 h. Ethyl acetate (25 mL) was added dropwise. 1% HCl (100 mL) was added slowly. Water (300 mL) was added and the layers separated. The aqueous layer was washed with methylene chloride (five 100-mL aliquots). The organic layers were combined and concentrated. The residue was rectified at reduced pressure affording the sulfide-alcohol (9.059 g, bp 103−105°C/100 Torr). The sulfide-alcohol had ir ($CHCl_3$): 3475 cm^{-1}; nmr ($CDCl_3$) δ: 1.26 (3H, d), 2.16 (3H, s), 2.70 (3H, m), and 3.93 (1H, m); ms *m/e*: 106 ($M^{+\cdot}$, 55%), 62 (100%), and 45 (68%).

Preparation of 4-chloro-2-thiapentane

A solution of 2-thia-4-pentanol (9.059 g) in chloroform (30 mL) was brought to gentle reflux. A solution of thionyl chloride (10.116 g) in chloroform (15 mL) was added dropwise over 10 min. The reaction mixture was refluxed for 6 h and the solvent evaporated. The residue was distilled twice at reduced pressure yielding clean chlorosulfide (3.503 g, bp 82−84°C/100 Torr). The chlorosulfide had ir ($CHCl_3$): 3000 cm^{-1}; nmr ($CDCl_3$) δ: 1.63 (3H, d), 2.20 (3H, s), 2.86 (2H, m) and 4.10 (1H, m); ms *m/e*: 126 (8.7%), 124 ($M^{+\cdot}$, 26.2%), and 61 (100%).

Preparation of 1-phenyl-2-thia-4-pentanone

Sodium metal (3.781 g) was dissolved in absolute ethanol (250 mL) and benzylthiol (20 mL) added. Chloroacetone (14.800 g) was added and the reaction mixture stirred at ambient temperature for 48 h. Water (250 mL) was added and the resultant mixture washed with chloroform (five 100-mL aliquots). The combined organic layers were dried ($MgSO_4$) and concentrated. The residue was distilled at reduced pressure yielding the ketosulfide (23.857 g, bp 138−140°C/1.4 Torr). The product had ir ($CHCl_3$): 1701 cm^{-1}; nmr ($CDCl_3$) δ: 2.16 (3H, s), 3.06 (2H, s), 3.63 (2H, s), and 7.26 (5H, s); ms *m/e*: 180 ($M^{+\cdot}$, 14.2%), 123 (37.8%), and 91 (100%).

Preparation of p-*bromobenzyl chloride*

p-Bromobenzyl alcohol (50 g) was dissolved in chloroform (100 mL) and the solution brought to gentle reflux. A solution of thionyl chloride (32 g) in chloroform (30 mL) was added dropwise over 20 min. The reflux was continued for four hours and the solvent evaporated. The crude product was rectified at reduced pressure affording the bromochloride (32.69 g, bp 115°C/6 Torr). The product had ir ($CHCl_3$): 1600 and 1590 cm^{-1}; nmr ($CDCl_3$) δ: 4.53 (2H, s), 7.23 (2H, d), and 7.50 (2H, d); ms *m/e*: 208 (7.4%), 206 (29.7%), 204 ($M^{+\cdot}$, 23.4%), 171 (97.8%), and 169 (100%).

Preparation of p-*bromobenzyl thiol*

A solution of *p*-bromobenzyl chloride (32.70 g) and thiourea (12.11 g) in 95% ethanol (80 mL) was refluxed for 26 h. Water (95 mL) and sodium hydroxide (9.6 g) were added and the resultant solution refluxed for 2 h. Water (100 mL) was added and the resultant mixture washed with methylene chloride (four 100-mL aliquots). The combined organic layers were dried ($MgSO_4$) and concentrated. The residue was distilled at reduced pressure affording *p*-bromobenzylthiol (22.96 g, bp 115−117°C/2.8 Torr). The mercaptan had ir ($CHCl_3$): 1595 cm^{-1}; nmr ($CDCl_3$) δ: 1.73 (1H, t), 3.63 (2H, d), 7.06 (2H, d), and 7.36 (2H, d); ms *m/e*: 204 (30.6%), 202 ($M^{+\cdot}$, 29.7%), 171 (100%), and 169 (100%).

*Preparation of 1-*p*-bromophenyl-2-thia-4-pentanone*

Sodium metal (0.566 g) was dissolved in methanol (100 mL) and *p*-bromobenzylthiol (5.000 g) added. Chloroacetone (2.277 g) was added dropwise and the reaction mixture stirred at ambient temperatre for 24 h. Water (100 mL) was added and the resultant mixture washed with methylene chloride (four 100-mL aliquots). The combined organic layers were dried ($MgSO_4$) and concentrated. The residue was chromatographed on silica gel (400 g) employing chloroform elution (100-mL fractions). Fractions 10−20 were combined and concentrated. The chromatographed product was dissolved in hot 95% ethanol and treated with charcoal. After concentration and drying the ketosulfide was obtained as a colorless waxy solid (0.770 g). The product had ir ($CHCl_3$): 1710 cm^{-1}; nmr ($CDCl_3$) δ: 2.16 (3H, s), 3.06 (2H, s), 3.60 (2H, s), 7.18 (2H, d), and 7.46 (2H, d); ms *m/e*: 260 (11%), 258 ($M^{+\cdot}$, 11%), 171 (78%), 169 (80%), and 43 (100%).

Preparation of 5-phenyl-2-thiapentane

A mixture of magnesium metal (2.016 g) and benzylchloride (10.293 g) in diethyl ether (300 mL) was refluxed for 3 h. A solution of 4-chloro-2-thiabutane (3.008 g) (17) in diethyl ether (60 mL) was added dropwise over 10 min and reflux continued for 1.5 h.

The cooled reaction mixture was poured into saturated aqueous ammonium chloride (500 mL) and the layers separated. The aqueous layer was washed with diethyl ether (two 200-mL aliquots). The combined organic layers were dried ($MgSO_4$) and concentrated. The crude residue was applied to five preparative tlc plates which were developed with carbon tetrachloride. The middle bands (R_f, ca. 0.7) were scraped, combined, and washed with chloroform. Upon concentration and distillation of the residue, 5-phenyl-2-thiabutane (0.185 g, bp 97°C/1.4 Torr) was obtained. The sulfide had ir ($CHCl_3$): 2940 and 1610 cm^{-1}; nmr ($CDCl_3$) δ: 1.87 (2H, m), 2.07 (3H, s), 2.54 (4H, m), and 7.24 (5H, s); ms *m/e*: 166 ($M^{+\cdot}$, 63.3%), 118 (100%), 117 (70%), and 91 (56.6%). This sample was identical in all respects with one obtained by the base-catalyzed reaction of methanethiol with the tosylate derived from 3-phenyl-1-propanol.

Preparation of 1-chloro-3-thiapentane

The preparation and properties of 1-chloro-3-thiapentane have been detailed previously (17).

Preparation of methyl 3-thiapentanoate

The preparation and properties of methyl 3-thiapentanoate have been detailed previously (11).

Preparation of methyl 4-chloro-2-thiabutanoate

The methyl ester of thioglycolic acid (4.925 g) and paraformaldehyde (1.418 g) were added to methylene chloride (25 mL) and the mixture cooled with an ice/water bath. HCl was bubbled (ca. 200 mL/min) into the reaction mixture for 1 h. The reaction mixture was diluted to 100 mL with methylene chloride, dried ($MgSO_4$), and concentrated. The residue was rectified at reduced pressure affording the sulfide-ester (3.846 g, bp 89−91°C/6 Torr). The sulfide-ester had ir ($CHCl_3$): 1740 cm^{-1}; nmr ($CDCl_3$) δ: 3.56 (2H, s), 3.86 (3H, s), and 4.93 (2H, s); ms *m/e*: 156 (8.3%), 154 ($M^{+\cdot}$, 23.3%), 97 (13.3%), 95 (41.6%), and 74 (100%).

Preparation of methyl 4-cyano-2-thiabutanoate

Sodium cyanide (1.580 g) was added to anhydrous DMSO (200 mL). Methyl 4-chloro-2-thiabutanoate (5.025 g) was added dropwise to the reaction mixture. Upon completion of the addition the reaction was stirred at ambient temperature for 1 h. Water (300 mL) was added and the resultant solution washed with diethyl ether (three 200-mL aliquots). The combined ether layers were washed with 5% HCl (two 200-mL portions) and water (200 mL). The organic layer was dried ($MgSO_4$) and concentrated. The crude residue was distilled at reduced pressure affording clean cyanosulfide-ester (1.200 g, bp 138−140°C/5 Torr). The cyanosulfide-ester had ir (CCl_4): 2250 (very

Can. J. Chem. Downloaded from www.nrcresearchpress.com by 210.87.254.40 on 09/06/12
For personal use only.

weak) and 1750 cm^{-1}; nmr ($CDCl_3$) δ: 3.56 (2H, s), 3.63 (2H, s), and 3.86 (3H, s); ms *m/e*: 145 ($M^{+\cdot}$, 43.1%), 86 (75%), and 74 (100%).

Preparation of ***9***

The preparation and properties of 4-chloro-1-phenyl-2-thiabutane have been reported previously (17).

Preparation of ***10***a

The preparation and properties of methyl 2-thiapentanoate have been reported previously (11).

Preparation of ***10***b

Sodium (0.632 g) was dissolved in absolute ethanol (100 mL). 2-Chloroethyl benzyl sulfone (3.000 g) (17) was added and the reaction mixture stirred at ambient temperature for 15 min. Methanethiol (5 mL) was slowly bubbled into the solution and the reaction mixture refluxed for 1 h. Water (100 mL) was added and the resultant mixture washed with chloroform (three 100-mL aliquots). The combined chloroform layers were dried ($MgSO_4$) and concentrated. The residue was recrystallized from 95% ethanol yielding colorless flakes of ***10b*** (1.840 g, mp 106.5–109°C). The sulfone-sulfide had ir ($CHCl_3$): 1320 and 1120 cm^{-1}; nmr ($CDCl_3$) δ: 2.10 (3H, s), 3.04 (4H, m), 4.30 (2H, s), and 7.44 (5H, s); ms *m/e*: 230 ($M^{+\cdot}$, 1.8%), 91 (100%), 75 (32.7%), and 74 (29.0%). *Anal.* calcd. for $C_{10}H_{14}O_2S_2$: C 52.10, H 6.10; found: C 52.35, H 6.14.

Preparation of ***10***c

2-Chloroethyl methyl sulfone (4.999 g) (17) was added to a solution of pyridine (60 mL) and triethylamine (7.083 g) and the reaction stirred at ambient temperature for 5 min. The reaction mixture was cooled with an ice/water bath and methanethiol (5 mL) slowly distilled into the reaction mixture. The reaction mixture was stirred at ambient temperature overnight. Chloroform (150 mL) was added and the resultant solution washed with 5% HCl (50-mL portions) until the aqueous pH remained acidic. The organic phase was dried ($MgSO_4$) and concentrated. The residue was rectified at reduced pressure affording a crystalline distillate (1.602 g, bp 114°C/0.3 Torr, mp 31–34°C). The sulfone-sulfide had ir ($CHCl_3$): 1325 and 1150 cm^{-1}; nmr ($CDCl_3$) δ: 2.16 (3H, s), 3.00 (5H, s and m), and 3.30 (2H, m); ^{13}C nmr ($CDCl_3$)[9] δ: 14.74, 25.52, 40.47, and 53.58; ms *m/e*: 154 ($M^{+\cdot}$, 25%), 75 (89.5%), and 74 (100%).

Chlorinolysis of ***10***c

The sulfone-sulfide ***10c*** (0.437 g) was chlorinated as described under "Chlorinations with sulfuryl chloride". The crude was chromatographed on silica gel (50 g) employing chloroform elution (50-mL aliquots). Fractions 6 and 7 were combined affording clean vinylogous thiosulfonate **11** (0.245 g) as a colorless oil. The vinylogous thiolsulfonate had ir ($CHCl_3$): 1315 and 1130 cm^{-1}; nmr ($CDCl_3$) δ: 2.35 (3H, s), 3.00 (3H, s), 6.15 (1H, d, $J \sim 15$ Hz), and 7.70 (1H, d, $J \sim 15$ Hz).

[9]Spectrum was decoupled.

Acknowledgements

The authors are indebted to Mr. C. Roderique for technical assistance. We thank Dr. J. H. Kim for running the mass spectra. We are grateful to Dalhousie University and Mount Allison University for financial support in the form of grants from their respective Research Development Funds.

1. T. P. AHERN, D. G. KAY, and R. F. LANGLER. Can. J. Chem. **56**, 2422 (1978), and references therein.
2. G. E. WILSON, JR. and M. G. HUANG. J. Org. Chem. **35**, 3002 (1970).
3. B. M. TROST, M. VAULTIER, and M. L. SANTIAGO. J. Am. Chem. Soc. **102**, 7929 (1980).
4. W. TAGAKI. *In* Organic chemistry of sulfur. *Edited by* S. Oae. Plenum Press, New York. 1977. p. 254.
5. F. BERNARDI, I. G. CSIZMADIA, H. B. SCHLEGEL, and S. WOLFE. Can. J. Chem. **53**, 114 (1975).
6. P. HAAKE and W. B. MILLER. J. Am. Chem. Soc. **85**, 4044 (1963).
7. W. R. HARDSTAFF and R. F. LANGLER. *In* Sulfur in organic and inorganic chemistry. Vol. 4. *Edited by* A. Senning. M. Dekker, Inc., New York. 1982. pp. 193–243.
8. J. E. HUHEEY. J. Phys. Chem. **69**, 3284 (1965).
9. (*a*) J. E. HUHEEY. J. Phys. Chem. **70**, 2086 (1966); (*b*) J. Org. Chem. **31**, 2365 (1966).
10. W. K. JARDINE, R. F. LANGLER, and J. A. MACGREGOR. Can. J. Chem. **60**, 2069 (1982).
11. R. F. LANGLER, Z. A. MARINI, and E. S. SPALDING. Can. J. Chem. **57**, 3193 (1979).
12. W. G. PHILLIPS and K. W. RATTS. J. Org. Chem. **36**, 3145 (1971).
13. L. A. PAQUETTE, L. S. WITTENBROOK, and K. SCHREIBER. J. Org. Chem. **33**, 1080 (1968).
14. D. L. TULEEN and T. B. STEPHENS. J. Org. Chem. **34**, 31 (1969).
15. L. A. PAQUETTE. J. Am. Chem. Soc. **86**, 4089 (1964).
16. G. E. WILSON, JR. and R. ALBERT. J. Org. Chem. **38**, 2160 (1973).
17. H. O. FONG, W. R. HARDSTAFF, D. G. KAY, R. F. LANGLER, R. H. MORSE, and D. N. SANDOVAL. Can. J. Chem. **57**, 1206 (1979).
18. F. A. BOVEY. Nuclear magnetic resonance spectroscopy, Academic Press, New York, 1969. p. 358.
19. J. M. LAVANISH. Tetrahedron Lett. 3847 (1973).
20. L. J. BELLAMY. Advances in infrared group frequencies. Methuen, London. 1968. p. 141.

Can. J. Chem. Downloaded from www.nrcresearchpress.com by 210.87.254.40 on 09/06/12
For personal use only.

Hydrogen fluoride laser induced multiphoton decomposition of 2,2,2-trifluoroethanol[1]

ROBERT D. MCALPINE, D. K. EVANS, AND J. W. GOODALE

Physical Chemistry Branch, Atomic Energy of Canada Limited, Research Company, Chalk River Nuclear Laboratories, Chalk River, Ont., Canada K0J 1J0

Received November 9, 1982

ROBERT D. MCALPINE, D. K. EVANS, and J. W. GOODALE. Can. J. Chem. **61**, 1481 (1983).

The HF laser-induced multiphoton decomposition (MPD) of 2,2,2-trifluoroethanol (TFE) was studied for two different "dog-bone" irradiation geometries using TFE pressures from 0.134 to 3.82 kPa. The depletion kinetics of TFE are first order in TFE pressure and the formation kinetics for several of the large number of products display pseudo-first order kinetics with pressure dependent stoichiometric ratios.

Three different theoretical models for decomposition probability versus fluence were tested. All were integrated over a complex irradiation geometry and were found to predict equally well the number of decomposed TFE molecules to within a factor of 3 or 4 of the experimental result.

ROBERT D. MCALPINE, D. K. EVANS et J. W. GOODALE. Can. J. Chem. **61**, 1481 (1983).

On a étudié la décomposition par multiphotons (DMP) du trifluoro-2,2,2 éthanol (TFE) induite par un laser au HF en utilisant deux géométries différentes d'irradiation du type "dog-bone" à des pressions de TFE allant de 0,134 à 3,82 kPa. La cinétique de la diminution du TFE est d'ordre un dans l'échelle de pression du TFE et la cinétique de la formation de plusieurs des nombreux produits est de pseudo ordre un lorsque la pression dépend des rapports stoechiométriques.

On a vérifié trois différents modèles théoriques de probabilité de décomposition en fonction de la fluence. On les a tous intégrés dans une géométrie d'irradiation complexe et on a trouvé qu'ils prédisent bien et de façon égale le nombre de molécules de TFE décomposées à un facteur qui représente de 3 ou 4 fois les résultats expérimentaux.

[Traduit par le journal]

1. Introduction

Comparison studies (1, 2) of pulsed HF laser-induced multiphoton absorption (MPA) and decomposition (MPD) of hydroxyl-containing molecules have demonstrated the relative ease of MPA and MPD for molecules having the onset of the "quasi-continuum" (3) occurring for excitation of one or two photons. This onset occurs earlier for "large" molecules, such as 2,2,2-trifluoroethanol (TFE) than for "small" molecules. Consequently, at low pressures, HF laser-induced MPA and MPD for TFE are considerably easier than for the "small" molecule methanol. For methanol, excitation to the "quasi-continuum" requires absorption of 4−5 HF laser photons (1, 2). This, and the large anharmonicity of the mode initially pumped, is what distinguishes "large" from "small" molecules (1, 2).

For the preliminary studies of the HF laser-induced MPD of TFE reported in ref. 2, kinetics were obscured by the pressure dependence of the stoichiometric ratios (the number of product molecules per TFE decomposed). This variation has now been clarified and consistent kinetic results are reported.

In ref. 2 the probability of decomposition as a function of laser fluence, $f(E)$, was measured and an exponential form first suggested by Fuss (4) was fitted to the results. Two other functional forms for $f(E)$ have been suggested: a Cumulative Log-Normal Distribution Function (CLNDF), which arises from the energy grained master equation description of collisionless MPD (5−7), and an empirical form which was used to describe the MPD yields of CDF_3 (8). To further the understanding of MPD, it is important to develop and test predictive descriptions for MPD yields. Two focussed beam (dog-bone type (9)) geometries were chosen and the data for $f(E)$ from ref. 2 were used to predict the decomposition yields for the two irradiation geometries for each of the three models. We have done the appropriate decomposition experiments in the two geometries to allow the comparison of the predictions of these models with experimental results.

[1]Issued as AECL contribution number 8012.

2. Experimental

2.1 *Irradiation source and geometry*

The P_1 (7) line ($\bar{\nu}$ = 3644.16 cm^{-1} (10); radiant energy, E = 170 ± 20 mJ; divergence, θ = 0.5 mrad, pulse width (FWHM) 270 ns) of a Lumonics Model 212A pulsed HF laser, equipped with an unstable resonator front optic, was used for all irradiations. A cylindrical cell of length 7.5 cm, outside diameter 2.5 cm, and volume 39.9 cm^3 was fitted with sapphire windows. The centre of the focal region was located 4.25 cm behind the front window.

Two irradiation geometries (see Fig. 1) were obtained by use of two different focal length (F) lenses. A germanium lens, antireflection coated for 2.6−3.1 μm of F = 20 cm, was used for Geometry A and an uncoated CaF_2 lens, F = 122 cm, was used for Geometry B.

2.2 *Analytical procedures*

Products not condensable at −196°C (H_2, CO, and CH_4) were analyzed by mass spectrometry as previously described (11, 12). Condensable products were analyzed with a Hewlett−Packard model 5700 A gas chromatograph using dual 3.05 m long, 3.18 mm od stainless steel columns packed with 80−100 mesh Poropak-Q. Quantitative analysis was obtained by comparison of peak area with calibration curves obtained from samples for each of the pure compounds: CF_2=CF_2, CF_2=CH_2, CF_2=CHF, and TFE. If H_2O or HF are products, they would not be detected by this system.

A Finnigan model 1020B computerized gas chromatograph/mass spectrometer was used to identify the following additional products: CO_2, C_2F_6, CHF_3, $CF_3CF_2CF_3$, CF_3CF_2H, CHF=CHF (*trans*), CF_2HCl (impurity), CF_2=CH—CF_3, and CF_3CF_2CHO. There are at least eight additional minor products which were detected but not identified.

3. Results and discussion

3.1 *MPD Kinetics and pressure dependence*

For Geometry A, the amount of TFE consumed and of products obtained were measured as a function of both the number of laser pulses, m, and the TFE initial pressure, P. These results are given in Table 1, and their fit to a single first order rate law (2), for the decomposition of TFE with $k_1(A)$ = (4.8 ± 1.3) × 10^{-5} $(pulse)^{-1}$, is shown in Fig. 2. A similar, though less extensive, study for Geometry B (Table 1) also follows a

Can. J. Chem. Downloaded from www.nrcresearchpress.com by 210.87.254.40 on 09/06/12
For personal use only.

Can. J. Chem. Downloaded from www.nrcresearchpress.com by 210.87.254.40 on 09/06/12
For personal use only.

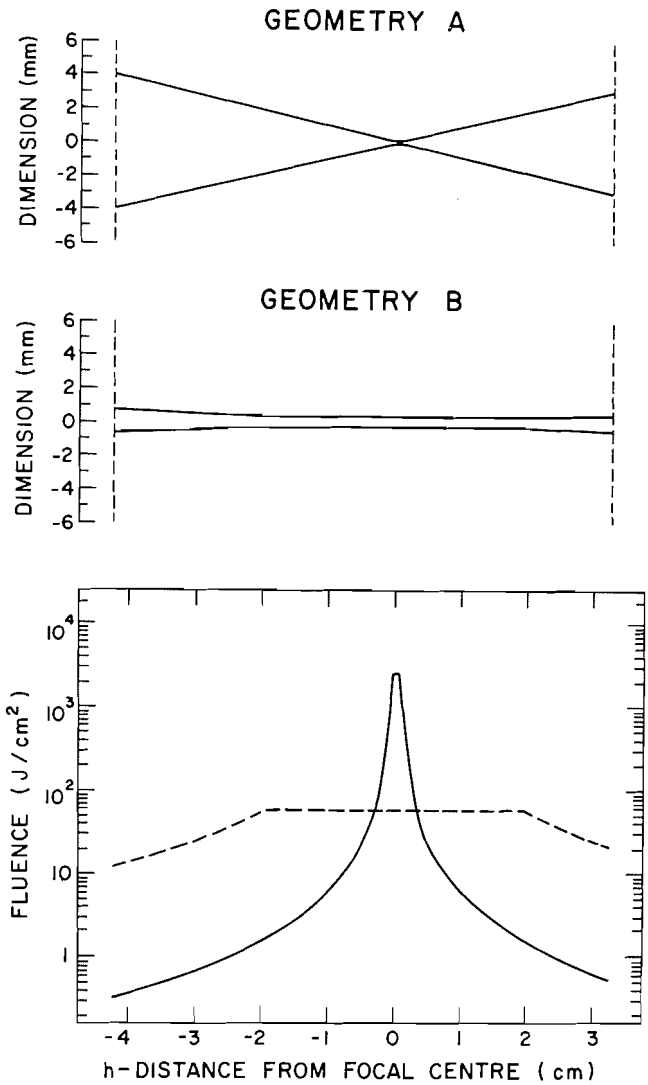

FIG. 1. The irradiation geometries used in this study, and the corresponding spatial dependence of fluence (bottom graph). The solid line (——) corresponds to Geometry A and the dashed line (----) to Geometry B.

first order rate law, with $k_1(B) = (2 \pm 1) \times 10^{-4}$ pulse^{-1}. The difference between $k_1(A)$ and $k_1(B)$ reflects the fact that both a different fraction of the TFE molecules is in the photolysis zone in each case, and, because of the different distribution of E, different fractions of the "illuminated" molecules decompose.

MPD of TFE to give various products can be represented by eq. [1].

$$[1] \quad q_0\, CF_3CH_2OH \rightarrow q_1\, CO + q_2\, C_2F_4 + q_3\, H_2 + q_4\, CF_2CH_2 + q_5\, CF_2CHF + q_6\, CH_4 + \ldots$$

The stoichiometric ratio of each product, η_i, which may be pressure dependent (2), is defined by [2].

$$[2] \quad \eta_i = q_i/q_o$$

The array of products which was observed indicates a complex decomposition chemistry. The major products observed do not account for all the atoms from the measured decomposition of TFE (see Table 1). The discrepancy can largely be accounted for by assuming H_2O and HF are products which would not be detected by our analytical technique. As the pressure or the number of pulses increases, the products observed tend to account for most of the C and F atoms from the decomposed TFE. Quite possibly, as product concentrations build up, they react with primary products from later pulses to give the observed molecules. We must still assume H_2O is a product to get an atom balance for the high pressure, long irradiation experiments. In such a complex system it is unlikely that product formation (except for primary products) would be simple first order. The formation of products such as C_2F_4 and the pressure dependence of some of the stoichiometric ratios (2) in the MPD and TFE demonstrate that the chemistry is complex in this system. We have tested to what extent first order (or more correctly, pseudo-first order) kinetics can fit the dependence of the amount of various products on the number of laser pulses.

In Fig. 3 is shown a fit of the data to a pseudo-first order form of the type given in eq. [3].

$$[3] \quad M^i_m/N_o = \eta_i[1 - \exp(-k_1 m)]$$

where N_o is the number of TFE molecules before photolysis and M^i_m is the number of the i'th product molecules present after m laser pulses. Values of η_i, the slopes from Fig. 3, are given in Table 2. These confirm that the stoichiometric ratios are, indeed, pressure dependent. Further, these results show that, for a fixed pressure, and for up to 50% TFE conversion, pseudo-first order forms provide a reasonable approximation of the quantities of products formed in the MPD of TFE.

The stoichiometry results for the products CO and H_2 differ from those reported earlier (2) by ~2-fold. The earlier results (2) were obtained using cylindrical rather than dog-bone geometry. For the former geometry, cell windows terminate the photolysis zone, and this suggests that wall effects (which are unlikely for Geometry A) in the formation of H_2 and CO may be responsible for the ~2-fold difference in the stoichiometric ratios.

From the photolysis results reported above, we are not able to elucidate the primary photochemical decomposition mechanism. The products observed are typical of a complex, free-radical scheme.

3.2 *Comparisons of theories and experiments*

The decomposition probability of TFE as a function of average fluence, $f(E)$, was previously measured for a cylindrical excitation geometry (2). Several models (4–8) have appeared which allow us to predict the total number of TFE molecules decomposed per pulse (D) for complex geometries such as the "dog-bone" shape (9), if $f(E)$ is known. We have used the data from ref. 2 in these models to calculate D for each of Geometries A and B. These are compared with the results of MPD experiments for these geometries.

For the "dog-bone" Geometries A or B, the differential decomposition of TFE is given by eq. [4]

$$[4] \quad \frac{dD}{dh} = f_i(E) N \frac{dV}{dh}$$

where h is the longitudinal distance (as in Fig. 1) from focal center, N is the TFE number density, and $V(h)$ describes the "dog-bone" photolysis geometry. Integration of [4], which depends on the choice of $f_i(E)$, will give the decomposition yield, D.

The three different models used for $f_i(E)$ are given by eqs.

TABLE 1. The number of TFE molecules decomposed and of several product molecules formed after m HF laser pulses. N_0 and N_m are respectively the number of TFE molecules in the cell before and after m pulses

10^{-2} m Pulses	10^{-18} N_0 Molecules	10^{-18} N_m Molecules	10^{-17} (CO) Molecules	10^{-17} (CF_2CF_2) Molecules	10^{-17} (H_2) Molecules	10^{-17} (CF_2CH_2) Molecules	10^{-17} (CF_2CHF) Molecules	10^{-16} (CH_4) Molecules
				Geometry A. Initial TFE pressure = 0.134 kPa				
5	1.37	1.27	0.051	0.081	0.013	0.028	0.021	0.012
10	1.33	1.14	0.17	0.14	0.031	0.043	0.032	0.011
25	1.32	1.07	—	0.38	—	0.13	0.12	—
25	1.32	1.10	0.48	0.39	0.11	0.10	0.078	0.026
50	1.31	1.12	—	1.3	—	0.13	0.25	—
50	1.31	1.10	—	0.68	—	0.19	0.24	—
50	1.33	0.94	0.96	0.75	0.18	0.27	0.22	0.066
75	1.35	0.83	1.3	0.92	0.23	0.34	0.27	0.081
100	1.32	0.89	1.8	1.1	0.28	0.29	0.35	0.091
100	1.33	0.83	1.8	1.1	0.31	0.46	0.38	0.11
150	1.33	0.58	2.4	1.3	0.37	0.55	0.46	0.13
				Geometry A. Initial TFE pressure = 0.823 kPa				
1	8.07	7.93	0.15	0.21	0.066	0.073	0.037	0.016
5	8.05	7.75	0.86	0.91	0.43	0.40	0.18	0.11
10	8.13	7.75	—	1.7	—	0.91	0.38	—
20	8.06	7.18	2.7	2.8	1.2	0.99	0.64	0.30
50	8.11	6.42	9.6	6.1	4.2	3.4	1.5	1.0
75	8.12	5.77	12.0	6.9	4.9	3.7	2.1	1.2
75	8.11	6.01	11.0	8.6	4.5	3.2	2.2	1.1
100	8.12	6.00	14.0	11.0	4.9	5.8	2.7	1.4
150	8.11	4.96	17.0	13.0	6.6	6.8	3.4	1.6
150	—	—	16.0	—	5.5	—	—	1.6
150	8.11	4.68	—	12.0	—	7.0	3.5	—
				Geometry A. Initial TFE pressure = 1.34 kPa				
2	13.6	13.6	0.75	0.78	0.38	0.26	0.16	0.088
5	13.5	—	1.7	1.6	0.89	0.75	0.30	0.19
10	13.6	12.8	3.8	3.2	2.2	1.7	0.66	0.47
10	13.4	12.7	3.6	3.5	1.9	1.4	0.72	0.43
25	13.5	—	13.0	8.1	5.6	4.1	1.6	1.4
50	13.5	11.3	15.0	12.0	6.4	6.6	2.6	1.7
75	13.5	9.11	22.0	12.0	9.0	9.5	3.9	2.3
100	13.4	8.84	27.0	25.0	11.0	13.0	5.8	2.6
150	13.6	7.38	38.0	28.0	15.0	17.0	7.1	3.6
				Geometry B				
20	1.36	1.01	0.97	0.78	0.15	0.30	0.23	0.040
10	8.11	7.20	4.0	3.6	2.1	1.9	0.84	0.50
5	15.9	15.0	5.0	4.2	2.7	2.2	0.93	0.59
2.5	39.2	36.5	14.0	9.6	6.4	4.8	1.7	1.3

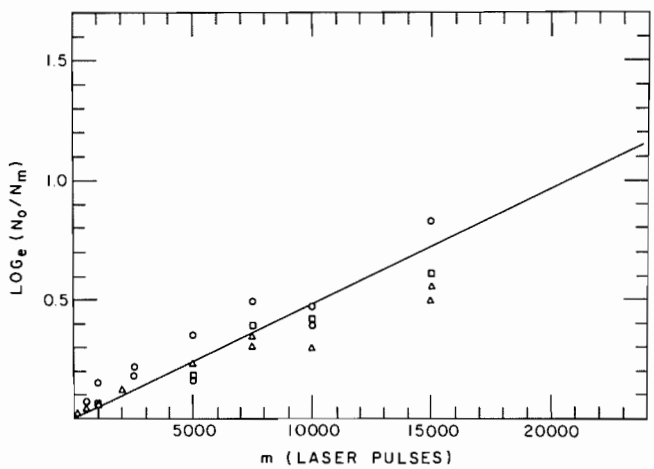

FIG. 2. First order kinetic plot for the HF laser induced MPD of TFE. Initial TFE pressures are represented by the following symbols: (○) 0.134 kPa; (△) 0.823 kPa; (□) 1.34 kPa.

TABLE 2. Stoichiometric ratios for several products of the HF laser MPD of TFE for different initial TFE pressures. These results were obtained by least-squares fits to eq. [3]. The 95% error intervals are given

Product	Initial pressure 0.134 kPa	Initial pressure 0.823 kPa	Initial pressure 1.34 kPa
CO	0.35±0.01	0.43±0.04	0.52±0.04
$CF_2{=}CF_2$	0.23±0.04	0.30±0.02	0.40±0.05
H_2	0.057±0.003	0.17±0.02	0.21±0.02
$CF_2{=}CH_2$	0.077±0.010	0.16±0.01	0.24±0.01
$CF_2{=}CHF$	0.072±0.005	0.082±0.002	0.099±0.006
CH_4	0.0020±0.0001	0.0042±0.0005	0.0052±0.0005

[5] to [7]

$$[5]\quad f_1(E) = \exp\,[-90/E]$$

$$[6]\quad f_2(E) = \int_{-\infty}^{(\log_e E-4.7)/0.7} (2\pi)^{-1/2} \exp\,(-t^2/2)\mathrm{d}t$$

Can. J. Chem. Downloaded from www.nrcresearchpress.com by 210.87.254.40 on 09/06/12
For personal use only.

Can. J. Chem. Downloaded from www.nrcresearchpress.com by 210.87.254.40 on 09/06/12
For personal use only.

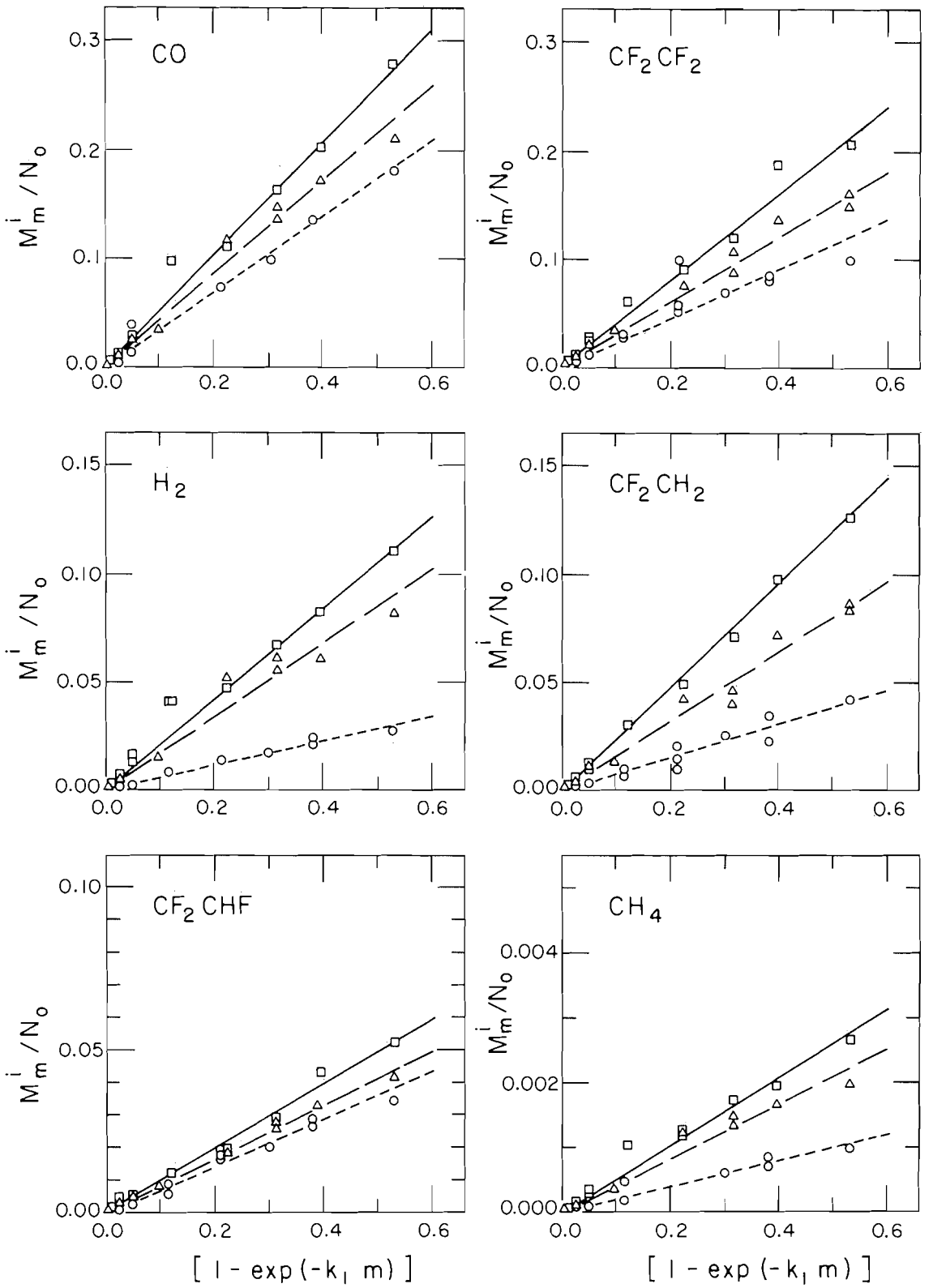

FIG. 3. A fit of various products indicated to pseudo-first order kinetics (see ref. 2) for three initial TFE pressures. The initial TFE pressures are represented as follows: (○), (....) 0.134 kPa; (△), (----) 0.823 kPa; (□) (——) 1.34 kPa. The slopes of the lines give the stoichiometric ratios, η_i.

[7] $f_3(E) = (E/125)^3$, $E < 125$ J/cm^2

$= 1 \qquad E \geq 125$ J/cm^2

The first form, $f_1(E)$ was discussed by Fuss (4). The second form is the CLNDF (5–7) and the parameters, $\mu = 4.7$ and $\sigma = 0.7$ (the standard deviation), were obtained by plotting the measured values of f versus $\log_e E$ as is described in refs. 5–7. The third form was used to describe the MPD of CDF_3 (8).

Plots of the form of $f_i(E)$ for these models are shown in Fig.

TABLE 3. A comparison of measured and calculated values of the total number of TFE molecules decomposed (D) for two different geometries. The TFE pressure was 1.33 kPa

	Measured	Calculated Model 1	Calculated Model 2	Calculated Model 3
Geometry A	$(6.3\pm1.7) \times 10^{14}$	1.4×10^{14}	1.4×10^{14}	1.3×10^{14}
Geometry B	$(2.6\pm1.3) \times 10^{15}$	1.1×10^{15}	8.9×10^{14}	5.0×10^{14}

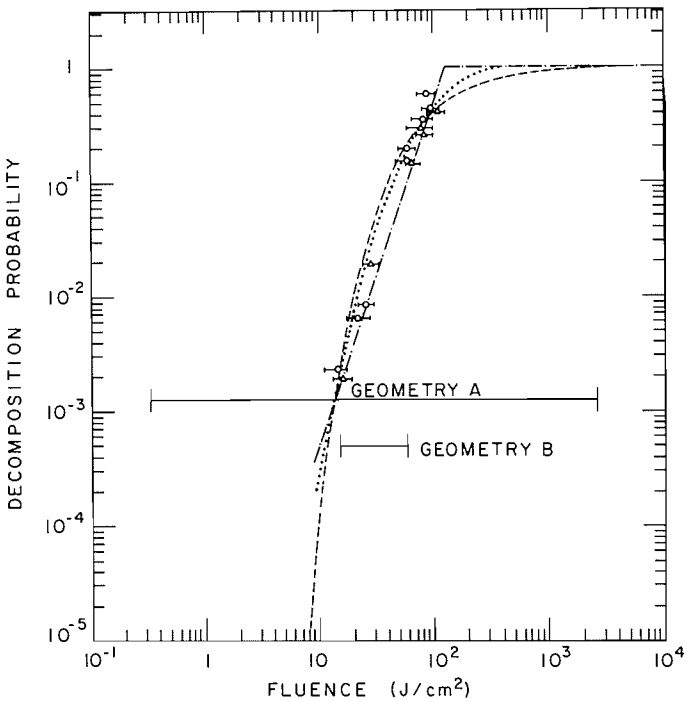

FIG. 4. Plots of $f_i(E)$ versus fluence for the MPD of TFE according to the three models discussed in the text. The various models, eqs. [5] to [7] respectively, are shown as follows: (----). Model 1; (....), Model 2; (-·-·-), Model 3. Also shown are the experimental points from ref. 2 for the following TFE initial pressures: (○), 1.00 kPa; (△), 1.33 kPa. The solid horizontal lines show the range of fluences for each of Geometries A and B.

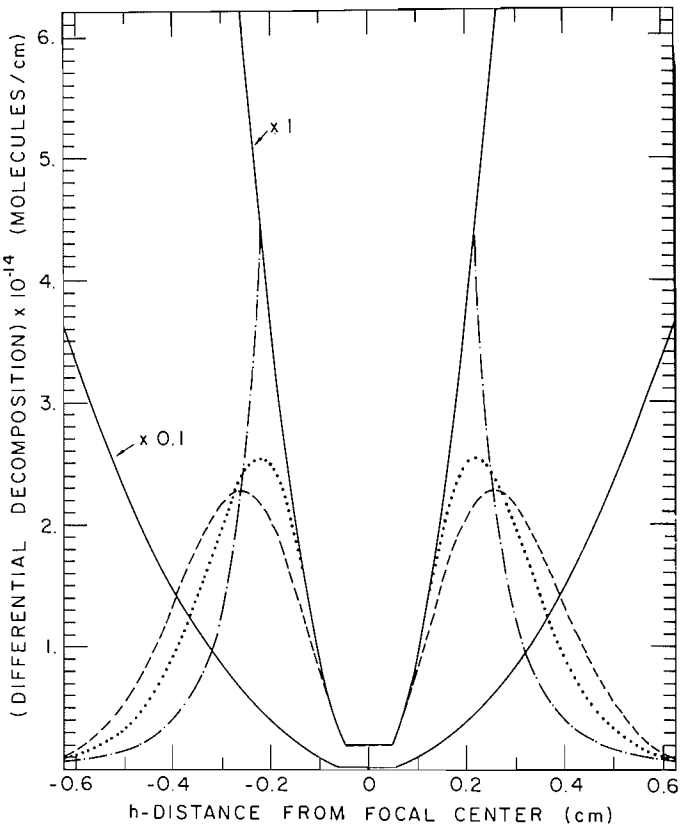

FIG. 5. Plots of the differential decomposition (eq. [4]) (TFE pressure = 1.33 kPa) versus h for Geometry A acording to the three models discussed in the text. The various models are shown as follows: (----), Model 1; (....), Model 2; (-·-·-), Model 3. The solid line shows the differential decomposition as it would appear if all of the irradiated molecules decomposed (that is $f_i \equiv 1$). A second solid line shows the first one reduced by a factor of 10 and is included since the first line goes off scale.

4 along with the data of ref. 2. All three models provide a reasonable fit to these data, and it is not possible to choose one over the others.

Plots of the differential decomposition (eq. [4]) for the three models are given in Fig. 5 for Geometry A. All three models demonstrate clearly that MPD occurs in the region within 6 mm of focal centre and well away from the cell walls. For Geometry B a similar plot shows the MPD is confined mainly to the region within about 3 cm of focal centre. Cell walls and windows would not play a significant role in either of these geometries according to all the models.

A numerical evaluation of the values of D for each model (TFE pressure 1.33 kPa) is given in Table 3, with experimental results for comparison. Models 1 and 2 agree very closely with each other and all the models correctly predict decomposition to within a factor of 3 or 4 for each geometry. This agreement is, perhaps, as good as can be expected considering the experimental uncertainties (the errors in k_1, the wider range of irradiation fluences than was used to determine the parameters for each model, and the errors associated with measuring f) encountered in these types of experiments. All three of these models provide a crude prediction of D, and currently, one cannot be judged as yielding results superior to the others.

4. Conclusions

The previously reported (2) pressure dependence of the H_2 and CO yields for TFE was complicated by the effect of pressure dependent stoichiometric ratios. This effect has now been measured and the depletion kinetics for the HF laser-induced MPD of TFE (an example of a large OH-containing molecule) are shown to follow first order behavior.

The three models for decomposition probability versus fluence predicted decomposition yields equally well for the complex geometries used in these experiments to within a factor of 3 or 4 of experimental results.

The products of the MPD of TFE are a complex array typical of free-radical reactions with possibly more than one primary decomposition channel. A selection of these products was shown to follow pseudo-first order kinetics even to the point at

Can. J. Chem. Downloaded from www.nrcresearchpress.com by 210.87.254.40 on 09/06/12
For personal use only.

which almost half of the available TFE had been decomposed. The results of this study did not allow the primary decomposition channels to be identified.

Acknowledgement

The authors are grateful to Dr. M. Gauthier of the Laser Chemistry Group, Division of Chemistry, National Research Council of Canada for obtaining the gc/ms results.

1. R. D. McAlpine, D. K. Evans, and F. K. McClusky. J. Chem. Phys. **73**, 1153 (1980).
2. D. Anderson, R. D. McAlpine, D. K. Evans, and H. M. Adams. Chem. Phys. Lett. **79**, 337 (1981).
3. N. Bloembergen. Opt. Commun. **15**, 416 (1975).
4. W. Fuss. Chem. Phys. **36**, 135 (1979).
5. J. R. Barker. J. Chem. Phys. **72**, 3686 (1980).
6. A. C. Baldwin and J. R. Barker. J. Chem. Phys. **74**, 3813 (1981).
7. A. C. Baldwin and J. R. Barker. J. Chem. Phys. **74**, 3823 (1981).
8. J. B. Marling, I. P. Herman, and S. J. Thomas. J. Chem. Phys. **72**, 5603 (1980).
9. R. S. Hallsworth and N. R. Isenor. Chem. Phys. Lett. **22**, 283 (1973).
10. T. F. Deutsch. Appl. Phys. Lett. **10**, 234 (1967).
11. D. K. Evans, R. D. McAlpine, and F. K. McClusky. Chem. Phys. **32**, 81 (1978).
12. R. D. McAlpine, D. K. Evans, and F. K. McClusky. Chem. Phys. **39**, 263 (1979).

Can. J. Chem. Downloaded from www.nrcresearchpress.com by 210.87.254.40 on 09/06/12
For personal use only.

Hétérobicycles sulfurés dérivés de l'α-thioglycérol. Synthèse d'alkyl-2,8-dioxa-6-thiabicyclo[3.2.1]octanes[1]

JACQUES GELAS ET MARC TEPPAZ-MISSON

Université de Clermont-Ferrand, École Nationale Supérieure de Chimie, Ensemble Scientifique des Cézeaux, Boite Postale 45, 63170 Aubière, France

Reçu le 25 octobre, 1982

JACQUES GELAS et MARC TEPPAZ-MISSON. Can. J. Chem. **61**, 1487 (1983).

La synthèse de 2,8-dioxa-6-thiabicyclo[3.2.1]octanes, substitués en position 1, 4 ou 7 par des groupements alkyle ou phényle, est décrite. Quatre méthodes de préparation sont comparées: (*i*) action du sulfure de sodium sur les 2,4-dichloroalkyl-1,3-dioxolannes; (*ii*) action du sulfure de sodium sur les ditosylates de 2,4-di(hydroxyalkyl)-1,3-dioxolannes; (*iii*) action des cétones α-halogénées sur l'α-thioglycérol; (*iv*) action des cétones α-hydroxylées sur l'α-thioglycérol. Les structures des dioxathiabicyclooctanes ont été établies par spectrographie de rmn ^{1}H (les spectres de masse ont été décrits par ailleurs) et confirmée chimiquement par désulfuration par le nickel Raney.

JACQUES GELAS and MARC TEPPAZ-MISSON. Can. J. Chem. **61**, 1487 (1983).

The synthesis of 2,8-dioxa-6-thiobicyclo[3.2.1]octanes, substituted by alkyl or phenyl groups in positions 1, 4, or 7, is described. Four synthetic routes are compared: (*i*) action of sodium sulfide on 2,4-dichloro-1,3-dialkyldioxolanes; (*ii*) action of sodium sulfide on the ditosylates of 2,4-dihydroxyalkyl-1,3-dioxolanes; (*iii*) action of α-haloketones on α-thioglycerol; and (*iv*) action of α-hydroxyketones on α-thioglycerol. The structures of the dioxathiabicyclooctanes have been established by proton nmr (mass spectra have already been described) and chemically confirmed by desulfurization by Raney Nickel.

[Journal translation]

Can. J. Chem. Downloaded from www.nrcresearchpress.com by 210.87.254.6 on 09/06/12
For personal use only.

Un grand intérêt est porté depuis longtemps vers l'étude d'analogues oxygénés, azotés et sulfurés du système bicyclo-[3.2.1]octane en raison notamment des éventuelles applications biologiques ou pharmacologiques de tels composés. Nous avons dans ce but mis au point diverses voies d'accès à des hétérobicycles obtenus à partir d'un acétal cyclique fonctionnalisé du type 1,3-dioxolanne (voir publications citées dans la référence 1). Le présent mémoire décrit une série de (±)-alkyl-2,8-dioxa-6-thiabicyclo[3.2.1]octanes.[2]

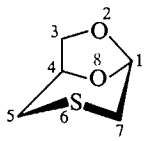

De tels bicycles présentent en particulier l'intérêt de se prêter à une étude de leur fragmentation sous impact électronique (2) susceptible d'être comparée à celle de ses homologues oxygénés (3); ils permettent également l'accès aux sulfoxydes et sulfones correspondants (4) ainsi qu'à des 1,4-oxathiannes fonctionnalisés par un groupement hydroxyméthyle obtenus par hydrogénolyse des bicycles (4, 5).

A notre connaissance, la première mention dans la littérature du dioxathiabicyclooctane date de 1965 et est due à Foster et coll. (6) qui avaient obtenu le 1(*R*),4(*R*)-dioxathiabicyclooctane à partir du 1,6-anhydro-β-D-glucopyranose; l'hydrolyse de la fonction acétal permettait alors l'accès à une classe nouvelle de "sucres" contenant un hétéroatome supplémentaire (dérivé du 2-hydroxy-1,4-oxathianne). Nous comparons ici quatre voies d'accès possibles aux alkyl-dioxathiabicyclooctanes.

[1]Recherches dans la série des acétals cycliques: Partie XXV; Partie XXIV: voir réf.1.

[2]Nous indiquerons simplement "dioxathiabicyclooctane" dans la suite du mémoire.

Synthèse des dioxathiabicyclo[3.2.1]octanes

Action du sulfure de sodium sur les 2,4-dichloroalkyl-1,3-dioxolannes (Méthode A)

La cyclisation de composés dihalogénés sous l'action du sulfure de sodium est une méthode connue pour permettre l'accès à des cycles sulfurés. Citons simplement la synthèse du thiophanne dans le diméthylsulfoxyde (7) et celle du dioxathiabicyclooctane dans le méthanol en présence d'iodure de potassium (8). Dans notre cas cette méthode présente l'inconvénient du point de vue de son rendement de n'utiliser que le seul stéréoisomère *cis* (Schéma 1) du mélange *cis*−*trans* des dioxolannes obtenus par acétalisation classique d'une chlorhydrine avec une cétone halogénée (9). L'isomère *trans* reste inattaqué ou subit des dégradations sans intérêt ici.

Le rendement ne dépasse guère de ce fait 30 à 35% et est sujet à des variations inattendues.

Dans le cas du bicycle **3** les deux diastéréoisomères **3**a (Me-7 axial) et **3**e (Me-7 équatorial) sont obtenus dans la proportion 75:25.

Action du sulfure de sodium sur les ditosylates de dioxolannes-diols (Méthode B)

Les 2,4-di(hydroxyalkyl)-1,3-dioxolannes ont été préparés (10) par action de cétones α-hydroxylées sur le glycérol (reflux dans le benzène en présence d'acide et dans un appareil de Dean−Stark). Les diols sont ensuite traités de façon classique par le chlorure de *para*-toluènesulfonyle et immédiatement soumis à l'action du sulfure de sodium (Schéma 2). Cette méthode présente, comme la précédente, l'inconvénient de ne faire intervenir que les dioxolannes *cis*. Elle est de plus inapplicable à la synthèse d'un dérivé disubsitué en 5 ou en 7 qui nécessiterait la préparation d'un tosylate d'alcool tertiaire.

Action des cétones α-halogénées sur l'α-thioglycérol (Méthode C)

Dans une note (11) l'un d'entre nous avait décrit l'obtention *directe* du bicycle 2 par action de la chloropropanone sur l'α-thioglycérol (Schéma 3). Dans ce cas la totalité des réactifs est utilisée. On opère au sein de pyridine et de benzène: la

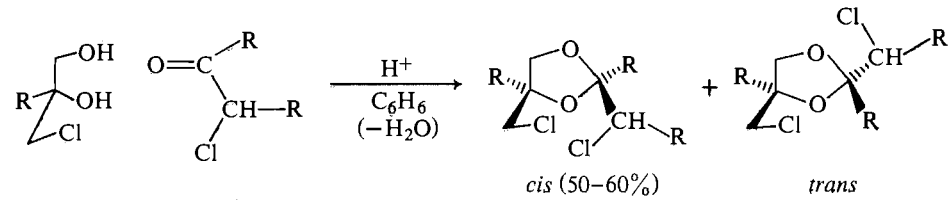

Composé	R-1	R-4	R-7
1	H	H	H
2	Me	H	H
3	Me	H	Me
4	Me	Me	H

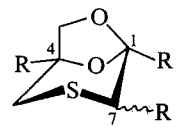

SCHÉMA 1. Méthode A.

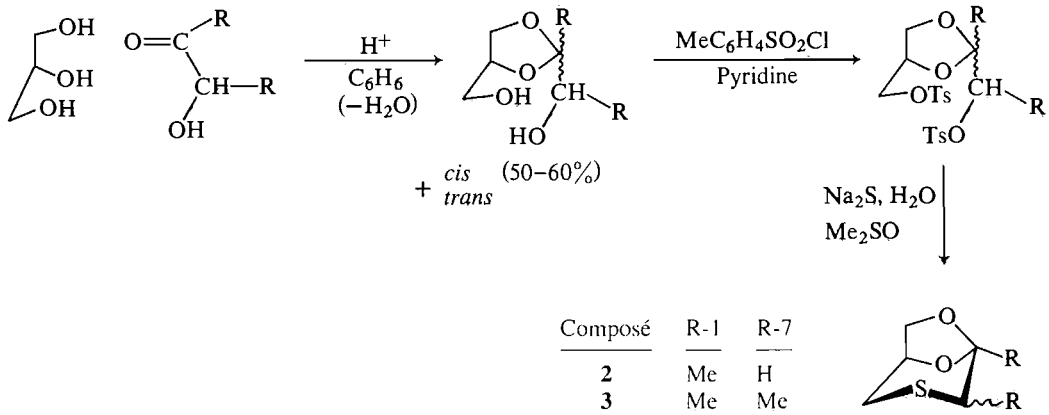

Composé	R-1	R-7
2	Me	H
3	Me	Me

SCHÉMA 2. Méthode B.

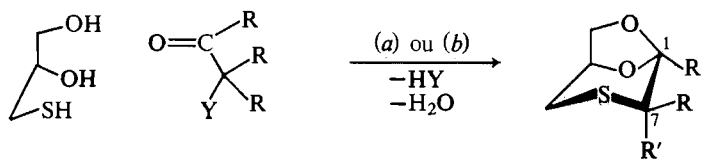

(*a*) Pyridine, benzène
Y = Cl
(*b*) Xylène, H+
Y = OH

Méthode C

Méthode C′

Composé	R-1	R-7	R′-7	Méthode
2	Me	H	H	(*a*) (*b*)
3	Me	Me ou H		(*a*) (*b*)
5	Ph	H	H	(*a*) (*b*)
6	Me	Me	Me	(*b*)

SCHÉMA 3. Méthodes C et C′.

réaction d'acétalisation est catalysée par le chlorure de pyridinium formé par l'élimination d'acide chlorhydrique (lequel se dégage spontanément en l'absence de pyridine dès que l'on mélange les réactifs); le benzène permet (piège de Dean–Stark) d'éliminer l'eau au fur et à mesure de sa formation. Nous montrons ici par la synthèse des dérivés **3** (mélange de stéréoisomères) et **5** avec un excellent rendement que la méthode semble généralisable à toute cétone α-halogénée.

Il n'en reste pas moins que la formation d'acide chlorhydrique (même "neutralisé" presqu'instantanément par la pyridine) peut être préjudiciable à l'utilisation de composés carbonylés très fragiles. De plus, les cétones α-chlorés tertiaires ne sont pas très courantes. C'est pourquoi nous avons pensé compléter cette méthode par une réaction similaire mais utilisant des cétones α-hydroxylées entraînant uniquement l'élimination d'eau.

Action des cétones α-hydroxylées sur l'α-thioglycérol (Méthode C′)

Dans ce cas les dioxathiabicyclooctanes sont obtenus direc-

Can. J. Chem. Downloaded from www.nrcresearchpress.com by 210.87.254.6 on 09/06/12
For personal use only.

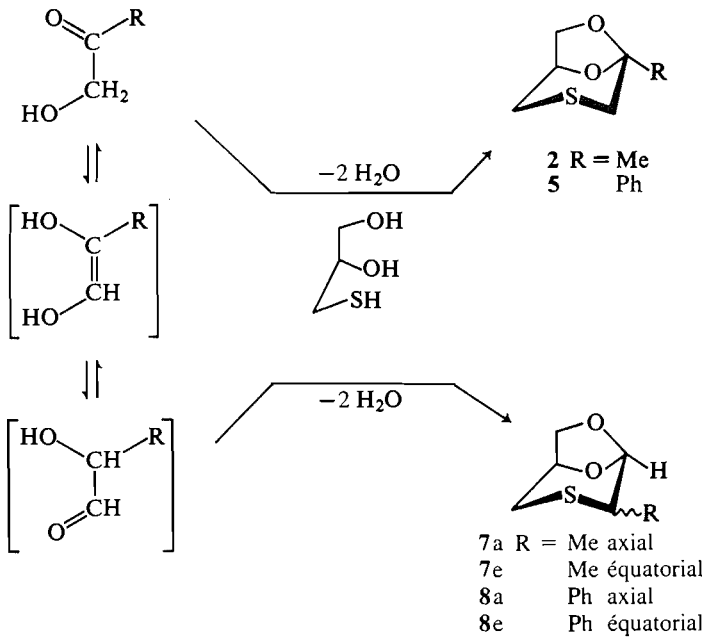

SCHÉMA 4. Isomérisation acétol ⇌ aldéhyde lactique et hydroxyméthylphénylcétone ⇌ phényl-2 hydroxy-2 éthanal.

TABLEAU 1. Spectres de rmn ^1H des dioxathiabicyclooctanes[a]

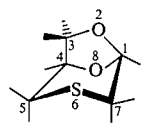

Composés	R-1	H-3 *endo*	H-3 *exo*	R-4	H-5 ax	H-5 éq	R-7 ax	R-7 éq
1	m 5,56 (1)	d 4,35 (1)	dd 3,85 (1)	m 4,66 (1)	m 3,25 (1)	m 2,24 (1)	m 2,97 (1)	m 2,13 (1)
2	s 1,38 (3)	d 4,27 (1)	dd 3,87 (1)	m 4,63 (1)	m 3,12 (1)	m 2,20 (1)	d 2,87 (1)	m 2,03 (1)
3e	s 1,34 (3)	d 4,20 (1)	dd 3,89 (1)	m 4,63 (1)	m 3,21 (1)	dd 2,13 (1)	q 3,05 (1)	d 1,03 (3)
3a	s 1,30 (3)	d 4,13 (1)	dd 3,78 (1)	m 4,53 (1)	m 3,13 (1)	m 1,92 (1)	d 1,40 (3)	m 2,93 (1)
4	s 1,40 (3)	d 4,27 (1)	dd 3,43 (1)	s 1,35 (3)	m 2,86 (1)	m 2,23 (1)	d 2,76 (1)	m 2,02 (1)
5	m 7,50 (5)	d 4,50 (1)	dd 4,03 (1)	m 4,83 (1)	m 3,27 (1)	m 2,10 (1)	d 3,10 (1)	m 2,45 (1)
6	s 1,46 (3)	d 4,10 (1)	dd 3,80 (1)	m 4,56 (1)	m 3,20 (1)	m 2,07 (1)	s 1,26 (3)	s 1,10 (3)
7e	m 5,28 (1)	d 4,29 (1)	dd 3,90 (1)	m 4,73 (1)	m 3,26 (1)	m 2,17 (1)	m 3,13 (1)	d 1,06 (3)
7a	m 5,32 (1)	d 4,39 (1)	dd 3,87 (1)	m 4,66 (1)	m 3,36 (1)	m 2,09 (1)	d 1,44 (3)	m 2,55 (1)
8e[b]	m 5,42 (1)	d 4,43 (1)	dd 3,93 (1)	m 4,68 (1)	m 3,46 (1)	m 2,18 (1)	s 4,20 (1)	m 7,33 (5)

Couplages géminés			Couplages vicinaux					Couplage à longue distance
$^2J_{3,3}$	$^2J_{5,5}$	$^2J_{7,7}$	$^3J_{3endo,4}$	$^3J_{3exo,4}$	$^3J_{5ax,4}$	$^3J_{5éq,4}$	$^3J_{1,7éq\ ou\ ax}$	$^4J_{3exo,5ax}$
6,4−6,6	12,8−13,0	12,4−12,6	0−1,0	5,8−6,0	2,0−2,4	2,4−2,6	0,8	1,0−1,4

[a]Solvant: tétrachlorure de carbone sauf pour les composés **7** et **8** (chloroforme). Les déplacements chimiques sont indiqués en ppm par rapport au tétraméthylsilane (multiplicité: s, singulet; d, doublet; q, quadruplet; m, multiplet). Les constantes de couplage indiquées en valeur absolue sont les espacements de signaux mesurés sur les agrandissements et sont exprimées en Hz.

[b]Le spectre du composé **8**a, en mélange avec son isomère **8**e, est nettement caractérisé seulement par la présence de deux singulets larges à 5,58 (H-1) et à 3,61 (H-7éq).

tement par chauffage des matières premières (reflux dans le xylène) en présence d'acide *para*-toluènesulfonique et dans un appareil de Dean−Stark (Schéma 3). Il est nécessaire d'ajouter lentement le composé carbonylé dans le milieu afin d'éviter de provoquer une réaction de dimérisation des α-cétols suivis d'une cyclodéshydratation en trioxabicyclo[2.2.1]heptanes (12). Le rendement est excellent au départ des cétols secondaires (obtention de **3**a (Me-7-axial) et **3**e (Me-7 équatorial) dans la proportion 25:75 inverse de celle observée pour la méthode A) et tertiaire (obtention de **6**), mais reste médiocre pour les cétols primaires (obtention de **2** et **5**). Par ailleurs, pour ces derniers (action de l'hydroxypropanone et action de l'hydroxyméthylphénylcétone) on observe (Schéma 4) la formation secondaire des deux stéréoisomères des bicycles **7** et **8**. Celle-ci résulte vraisemblablement d'une isomérisation partielle des cétoalcools respectivement en aldéhyde lactique et phényl-2 hydroxy-2 éthanal. Une telle isomérisation est tout à fait comparable à la transformation de Lobry de Bruyn et Alberda van Ekenstein, classique en série glucidique (13) et possible aussi bien en milieu acide que basique. On peut donc

Can. J. Chem. Downloaded from www.nrcresearchpress.com by 210.87.254.6 on 09/06/12
For personal use only.

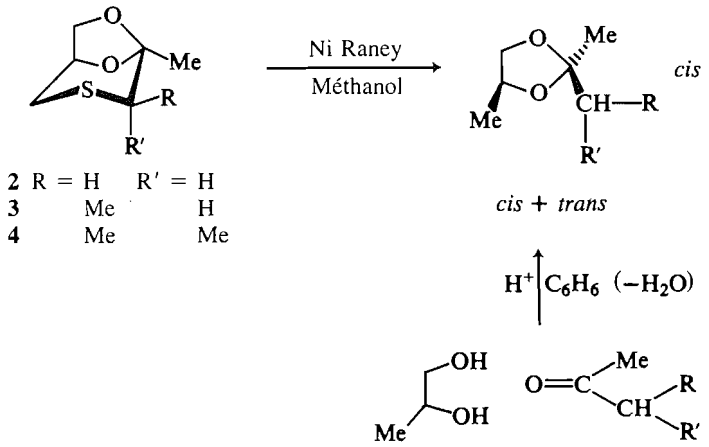

2 R = H R′ = H
3 Me H
4 Me Me

SCHÉMA 5. Désulfuration des dioxathiabicyclooctanes.

invoquer (13) le passage par la forme *ènediol* des produits de départ (Schéma 4). On peut rapprocher cette observation de l'interprétation qui avait été proposée (14) pour expliquer la présence de 2,6-diméthylpyrazine au sein de la 2,5-diméthylpyrazine préparée par pyrolyse du glycérol en présence de sels d'ammonium: dégradation du glycérol en hydroxypropanone que s'isomérise partiellement en aldéhyde lactique avant l'intervention de l'ammoniac. Il est à noter enfin que la présence d'eau dans le thioglycérol de départ accroît la faible tendance à former les bicycles résultant d'une transposition de la cétone hydroxylée.

Identification des dioxathiabicyclooctanes

Elle repose essentiellement sur l'étude de leurs spectres de rmn (Tableau 1). Leurs spectres de masse ont été étudiés par ailleurs (2).

Lorsqu'on compare les trioxabicyclooctanes (1) (homologues uniquement oxygénés) aux dioxathiabicyclooctanes, on constate que l'introduction d'un atome de soufre entraîne un déplacement très important du signal des protons équatoriaux vers les champs forts. Cet effet, beaucoup moins marqué pour les protons axiaux a pour conséquence: (*i*) d'étaler assez largement en fréquence les spectres pour permettre d'approcher une analyse au premier ordre correcte; (*ii*) de différencier nettement les protons en α de l'atome de soufre selon leur stéréochimie. L'ordre proton axial−proton équatorial respectivement à *champ faible* et *champ fort* est l'inverse de celui observé pour un cyclohexane ou un tétrahydropyranne (15). Il est à noter que la différence $\delta_{Hax} - \delta_{Héq}$ est de l'ordre de 0,6 à 1,2 ppm et est donc nettement plus élevée que celle qui est observée pour le thiacyclohexane (15) ($\Delta\delta \simeq 0{,}2$ ppm) ou pour les oxathiannes (16) ($\Delta\delta \simeq 0{,}1$ à 0,7 ppm). Ceci peut vraisemblablement être attribué à l'anisotropie du pont méthylènoxy dans les dioxathiabicyclooctanes. L'attribution des différents signaux à tel ou tel proton a été confirmée par double-irradiation des protons en cause. L'intensité de la constante de couplage pour les protons géminés H-3 *exo* et H-3 *endo* est du même ordre de grandeur que celle déterminée pour les protons en même position dans les trioxabicyclooctanes (1) et conforme à celle attendue pour un cycle oxygéné à cinq maillons (17). En revanche, pour les protons géminés en α de l'atome de soufre la constante est sensiblement plus élevée (de 1 à 2 Hz) que celle observée dans les homologues oxygénés (pour une discussion des effets d'un hétéroatome sur les constantes J_{gem} voir la mise au point de Cahill *et al.* (17)).

Compte-tenu du recouvrement des valeurs du couplage vicinal $J_{4,5}$ que H-5 soit axial ou équatorial, il serait dangereux d'attribuer la stéréochimie de H-5 sur la seule indication d'un couplage ax−éq plus élevé que le couplage éq−éq. Une attribution plus sûre de cette stéréochimie repose sur l'observation d'un couplage à longue distance mettant en jeu H-5 axial et H-3 *endo* selon un chemin de couplage en *W*. On peut constater que l'existence de ce couplage (de valeur peu différente de celle relevée pour les trioxabicyclooctanes (1)) est en faveur d'une conformation chaise peu déformée pour le cycle 1,4-oxathianne des dioxathiabicyclooctanes. L'absence d'une déformation importante paraît confirmée par le faible (sinon nul) couplage vicinal entre H-3 *endo* et H-4 qui de ce fait forment dans l'espace un angle dièdre proche de 90°. Le couplage ^4J observé ici est le seul qui soit facilement et nettement attribué; cependant, une analyse plus fine permettrait vraisemblablement de mettre en évidence d'autres types de couplages (notamment $^4J_{1,4}$ et $^5J_{1,5éq}$) décelés précédemment dans les trioxabicyclooctanes (1, 18).

Ainsi que nous le discutons dans le paragraphe suivant, le problème de la localisation de l'atome de soufre dans la molécule bicyclique s'est posé pour les composés obtenus directement à partir du thioglycérol et des dérivés carbonylés. Il a été résolu par l'analyse spectrographique (rmn); le résultat a été confirmé chimiquement:

(*i*) Le déplacement à champ fort des protons en α de l'atome de soufre permet une attribution aisée de ces protons sur le spectre. Lorsqu'il s'agit d'un groupement méthylène on constate que la constante de couplage géminé (12−13 Hz) est celle attendue pour un cycle à six chaînons (1,4-oxathianne) et non celle (6−7 Hz) qui serait observée (17) pour un cycle à cinq chaînons (1,3-oxathiolanne). Ceci est confirmé par la valeur de la constante de couplage (6−7 Hz) pour les protons géminés situés à champ plus faible (CH_2 en α de O-2).

(*ii*) La structure des composés est confirmée par la réaction de désulfuration par le nickel Raney (19) effectuée sur un certain nombre d'entre eux (Schéma 5). La position de l'atome de soufre dans les dioxathiabicyclooctanes est attribuée grâce à l'identification aisée des alkyl-1,3-dioxolannes obtenus par comparaison (rmn) avec les couples de diastéréoisomères authentiques préparés par acétalisation du 1,2-propanediol et parfaitement identifiés par Eliel et coll. (8).

Mécanisme de formation

L'acétalisation de l'α-thioglycérol par une cétone

Can. J. Chem. Downloaded from www.nrcresearchpress.com by 210.87.254.6 on 09/06/12
For personal use only.

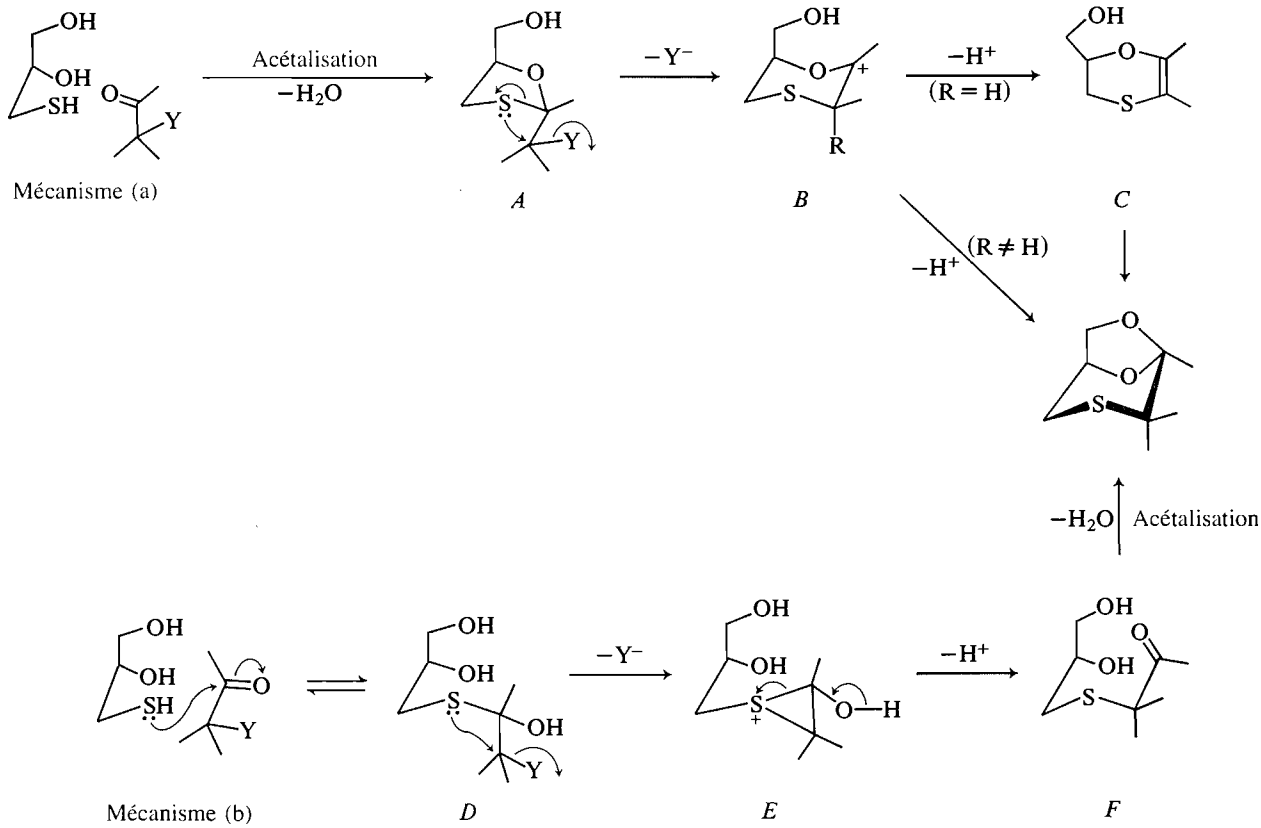

SCHÉMA 6. Mécanisme de formation des dioxathiabicyclooctanes.

α-halogénée ou α-hydroxylée peut théoriquement conduire à trois types d'hétérocycles: 1,3-dioxolanne, 1,3-oxathiolanne et 1,3-oxathianne. En fait, pour des raisons d'interaction *syn*-axiales existant dans le cycle à six chaînons (20) la formation du dernier type d'hétérocycle peut être écartée (contrôle thermodynamique en milieu acide). Pour des cétones aliphatiques il est connu (21) que l'acétalisation de l'α-thioglycérol conduit exclusivement à des 1,3-oxathiolannes (confirmant ainsi la plus grande réactivité de la fonction thiol vis à vis du groupement carbonyle comparée à celle de la fonction alcool). Compte-tenu de la structure des bicycles que nous obtenons (1,3-dioxolannes pontés) nous pouvons proposer: (*i*) soit l'évolution très rapide d'un 1,3-oxathiolanne du type *A* (Schéma 6, mécanisme (a)), produit cinétique de la réaction; (*ii*) soit la formation du bicycle sans passage par un oxathiolanne (mécanisme (b)).

Une transformation comparable avait été proposée par Parham *et al.* (22) pour expliquer la formation d'oxathiène (type *C*) à partir de l'oxathiolanne formé par la réaction du thioglycol et du chloracétaldéhyde diméthylacétal.

L'évolution des intermédiaires *A* ou *D* peut se produire selon le mécanisme de type S_N2 suggéré sur le schéma 6 ou par un autre processus; il n'est pas exclu qu'un carbocation puisse intervenir, particulièrement lorsque l'atome de carbone porteur de Y est quaternaire. La formation des bicycles par addition de la fonction alcool sur la double-liaison de l'oxathiène *C* paraît en revanche peu vraisemblable pour au moins deux raisons: (*i*) le bicycle **6** (R = R′ = Me) ne peut donner un tel intermédiaire *D*; (*ii*) pour des réactions proches (action de cétones α-halogénées ou α-hydroxylées sur le 1,2-dithioglycérol) nous avons isolé (23)[3] des dithiènes (composés du type *D* où l'atome d'oxygène est remplacé par un second atome de soufre) qui ne subissent pas de cyclisation dans les conditions de la réaction. Il n'en reste pas moins que plusieurs mécanismes peuvent entrer en concurrence. Le caractère de meilleur groupe partant de l'atome d'halogène par rapport à la fonction alcool peut favoriser un mécanisme prévoyant l'expulsion rapide d'hydracide préalablement à toute autre réaction. Lorsque la réaction des cétones halogénées est menée en l'absence de pyridine c'est effectivement ce que l'on constate expérimentalement.

Cette étude est actuellement étendue aux séries des 1,2- et 1,3-dithioglycérols ainsi qu'à celle du trithioglycérol. Les résultats ainsi obtenus dans ces séries modèles sont également appliqués en série glucidique pour leur intérêt synthétique et biologique.

Partie expérimentale

Les analyses par chromatographie en phase gazeuse ont été réalisées sur un appareil Hewlett–Packard 5750 équipé d'une colonne Carbowax 20 M. Les séparations d'échantillons par chromatographie en phase gazeuse ont été effectuées sur un appareil Varian–Aerograph 750 N (colonne Carbowax 20 M, 9 mm × 6 m). Les spectres de rmn ^1H ont été réalisées sur un appareil Varian T 60. Les analyses centésimales ont été faites au Service Central de Microanalyse du CNRS.

Synthèse des dioxathiabicyclooctanes

Méthode A: Action du sulfure de sodium sur les 2,4-dichloroalkyl-1,3-dioxolannes

Une solution de sulfure de sodium nonahydrate (48 g, 0.2 mol) dans 100 mL de méthanol est additionnée de 0.1 mol d'un dichloroalkyldioxolanne (cf. Schéma 1) préparé selon les réfs. 9 et 24 et de 2 g d'iodure de potassium. On porte à reflux durant quatre à cinq jours. Après refroidissement on ajoute 250 mL d'eau, extrait au dichlorométhane, sèche (sulfate de sodium) et évapore le solvant sous vide. Le résidu est distillé. Le dioxathiabicyclooctane correspondant

[3]J. Gelas et M. Teppaz-Misson, résultats inédits.

Can. J. Chem. Downloaded from www.nrcresearchpress.com by 210.87.254.6 on 09/06/12
For personal use only.

Can. J. Chem. Downloaded from www.nrcresearchpress.com by 210.87.254.6 on 09/06/12
For personal use only.

distille en tête (rendement 30 à 35%), suivi du dichloroalkyldioxolanne *trans* inattaqué (le rendement calculé en tenant compte de la réaction du seul dérivé *cis* est de 45 à 50%).

De nombreux autres composés minoritaires sont détectés par chromatographie en phase gazeuse. Un rendement légèrement supérieur est obtenu en remplaçant le méthanol par le diméthylsulfoxyde et en portant le mélange réactionnel vers 100°C durant environ trois jours.

Méthode B: Action du sulfure de sodium sur les ditosylates de 2,4-dihydroxyalkyl-1,3-dioxolannes

Une solution de 0.1 mol d'un dihydroxyalkyldioxolanne (cf. Schéma 2), préparé selon la réf. 10, dans 100 mL de pyridine anhydre est refroidie à 0°C. On ajoute par petites portions du chlorure de *para*-toluènesulfonyle (41.8 g, 0.22 mol) sous une forte agitation. On laisse revenir à température ambiante et on maintient l'agitation durant 24 h. On verse sur un mélange de glace et de carbonate de sodium, extrait au dichloromethane. L'extrait est lavé plusieurs fois par une solution aqueuse saturée de bicarbonate de potassium. On sèche et évapore les solvants sous vide. On reprend par 20 mL de toluène anhydre et chasse le solvant sous vide, l'opération étant répétée trois fois afin d'éliminer totalement la pyridine. Le résidu (le plus souvent amorphe) est immédiatement placé en solution dans 100 mL de diméthylsulfoxyde. On ajoute 0.2 mol de sulfure de sodium nonahydrate et porte à 80−100°C durant 24 h. Après refroidissement, on ajoute 200 mL d'eau et extrait au dichlorométhane. L'extrait est lavé plusieurs fois par 50 mL d'eau. On sèche, évapore le solvant et distille rapidement hors du résidu le dioxathiabicyclooctane qui peut ensuite être rectifié (rendement environ 40%, 60% si l'on tient compte du fait que seul le dérivé *cis* réagit).

Méthode C: Action des cétones α-halogénées sur l'α-thioglycérol

Une solution de 3-mercapto-1,2-propanediol (α-thioglycérol, 21.6 g, 0.2 mol) dans un mélange de 400 mL de benzène et de 400 mL de pyridine est placée dans un ballon bicol de 1 L surmonté d'une boule à brome et d'un piège de Dean−Stark. On ajoute à température ambiante par la boule à brome, 0.22 mol de cétone α-chlorée (cf. Schéma 3, composés commerciaux) et on porte à reflux de benzène qui élimine progressivement l'eau formée au cours de la réaction.

Lorsque 3 à 4 mL d'eau (0.2 mol environ) ont été recueillis, le ballon est refroidi et les solvants sont évaporés sous vide. Le résidu est dissous dans du dichlorométhane qui est lavé à l'eau, séché et évaporé. Le dioxathiabicyclooctane formé est distillé (rendement 80 à 85%).

Méthode C': Action des cétones α-hydroxylées sur l'α-thioglycérol

Un mélange de xylène (700 mL environ), d'α-thioglycérol (21.6 g, 0.2 mol) et d'acide *para*-toluènesulfonique (2 g) est vigoureusement agité dans un Erlenmeyer de 1 L placé sur un agitateur magnétique chauffant et surmonté d'une dérivation munie d'une part d'un piège de Dean−Stark et d'autre part d'une boule à brome. On porte à reflux et on ajoute goutte à goutte l'α-hydroxycétone choisie (cf. Schéma 3, composés commerciaux). La réaction est arrêtée lorsque deux équivalents d'eau ont été recueillis (environ 0.4 mol, 7 à 8 mL). On ajoute environ 5 g de carbonate de sodium et on agite durant une heure. On filtre et évapore le xylène sous pression réduite. On distille le résidu sous vide. Dans le cas du composé **5** (et parfois également pour le composé **6**) le résidu cristallise; le dioxabicyclooctane est alors recristallisé directement (dans le méthanol pour **5** et un mélange méthanol − éther de pétrole 40−65°C pour **6**) (rendements respectifs: composés **2** et **5**: 20−25%; composé **3**: 85%; composé **6**: 90%).

Dans le cas de la préparation des composés **2** et **5** à partir de cétols primaires, on isole par chromatographie en phase gazeuse préparative respectivement les composés **7**a et **7**e séparément (rendement: 5%) et les composés **8**a et **8**e en mélange (rendement 8%).

Désulfuration des dioxathiabicyclooctanes

Une suspension de nickel Raney fraîchement préparée selon la réf. 25 (10 mL de suspension agitée et lavée plusieurs fois par du méthanol anhydre) est additionnée d'une solution du dioxathiabicyclooctane (cf. Schéma 5) dans l'éthanol (5 mL d'éthanol pour 1 mmol de substrat). On ajoute une solution de soude (40 mg, 1 mmol) dans l'éthanol (2 mL) et on porte à reflux jusqu'à ce que tout le bicycle de départ ait disparu (contrôle par chromatographie, durée 15 à 30 min).

On filtre et distille l'éthanol avec précaution (les dioxolannes obtenus sont volatils); le résidu est repris par du tétrachlorure de carbone et analysé par chromatographie en phase gazeuse et par rmn ^{1}H. L'identification est confirmée par comparaison avec des échantillons authentiques préparés par acétalation classique du 1,2-propanediol avec respectivement l'acétone (cas du dérivé **2**), la méthyléthylcétone (cas de **3**) et la méthylisopropylcétone (cas de **4**). Dans les deux derniers exemples, l'acétalation conduit au mélange des deux isomères *cis* et *trans*, alors que le seul isomère *cis* est obtenu par désulfuration.

Constantes physiques et analyses des dioxathiabicyclooctanes

1: Eb 104−106°C/12 Torr (lit. (6*b*) Eb 47−49°C/0.1 Torr). *Anal.* calc. pour $C_5H_8O_2S$: C 45,45, H 6,06, O et S 24,24; tr.: C 45,41, H 6,02, O 24,20, S 24,13.

2: Eb 96−98°C/13 Torr, pf 51−52°C. *Anal.* calc. pour $C_6H_{10}O_2S$: C 49,32, H 6,85, O et S 21,92; tr.: C 49,31, H 6,84, O 21,98, S 21,79.

3: Eb 90−95°C/12 Torr, mélange des isomères **3**a et **3**e séparés par chromatographie en phase gazeuse préparative. *Anal.* calc. pour $C_7H_{12}O_2S$: C 52,50, H 7,50, O et S 20,00; tr.: C 52,61, H 7,56, O 19,84, S 20,21.

4: Eb 84−85°C/11 Torr, pf 50−51°C. *Anal.* calc. pour $C_7H_{12}O_2S$: cf. composé **3**; tr.: C 52,44, H 7,40, O 20,31, S 20,05.

5: pf 92−93°C. *Anal.* calc. pour $C_{11}H_{12}O_2S$: C 63,46, H 5,77, O et S 15,38; tr.: 63,42, H 5,87, O 15,66, S 15,20.

6: Eb 94−96°C/11 Torr. *Anal.* calc. pour $C_8H_{14}O_2S$: C 55,17, H 8,05, O et S 18,39; tr.: C 55,15, H 7,99, O 18,52, S 18,17.

7: Mélange des isomères **7**a et **7**e isolés et séparés par chromatographie en phase gazeuse préparative. *Anal.* calc. pour $C_6H_{10}O_2S$: cf, composé **2**; tr.: C 49,29, H 6,82, O 22,03, S 21,81.

8: Mélange des isomères **8**a et **8**e isolés par chromatographie en phase gazeuse préparative. *Anal.* calc. pour $C_{11}H_{12}O_2S$: cf. composé **5**; tr.: C 63,44, H 5,75,O 15,43, S 15,27.

1. P. CALINAUD et J. GELAS. Can. J. Chem. **56**, 2292 (1978).
2. P. CALINAUD, J. GELAS, D. HORTON et J. D. WANDER. Org. Mass Spectrom. **13**, 438 (1978).
3. (*a*) P. CALINAUD, J. GELAS, D. HORTON et J. D. WANDER. J. Chem. Soc. Perkin Trans. 2, 1145 (1974); (*b*) Org. Mass Spectrom. **11**, 1037 (1976).
4. P. CALINAUD. Thèse d'Etat, Clermont-Ferrand no E248, Sept. 1977.
5. J. GELAS et S. VEYSSIÈRES-RAMBAUD. Carbohydr. Res. **37**, 303 (1974).
6. (*a*) K. W. BUCK, A. B. FOSTER, A. R. PERRY, M. H. QADIR et J. M. WEBBER. Chem. Commun. 433 (1965); (*b*) K. W. BUCK, F. A. FAHIM, A. B. FOSTER, A. R. PERRY, M. H. QADIR et J. M. WEBBER. Carbohydr. Res. **2**, 14 (1966).
7. R. LETT, S. BORY, B. MOREAU et A. MARQUET. Bull. Soc. Chim. Fr. 2299 (1972).
8. W. E. WILLY, G. BINSCH et E. L. ELIEL. J. Am. Chem. Soc. **72**, 5394 (1970).
9. (*a*) J. GELAS. Bull. Soc. Chim. Fr. 2341 (1970); (*b*) 2349 (1970), et références citées.
10. J. GELAS et M. TEPPAZ-MISSON. C. R. Acad. Sci. (C), **271**, 218 (1970).
11. J. GELAS. Tetrahedron Lett. 509 (1971).
12. P. CALINAUD, J. GELAS et S. VEYSSIÈRES-RAMBAUD. Bull. Soc. Chim. Fr. 2769 (1973).
13. (*a*) C. A. LOBRY DE BRUYN et W. ALBERDA VAN EKENSTEIN. Recl. Trav. Chim. Pays-Bas, **14**, 156 (1895); (*b*) W. PIGMAN et E. F. L. ANET. *Dans* The carbohydrates. Vol IA. *Edité par* W. Pigman et D. Horton. Academic Press, New York. 1972. p. 165.

14. J. GELAS et R. RAMBAUD. Bull. Soc. Chim. Fr. 2393 (1970).
15. J. B. LAMBERT et S. I. FEATHERMAN. Chem. Rev. **75**, 611 (1975).
16. A. B. FOSTER, T. D. INCH, M. H. QADIR et J. M. WEBBER. Chem. Commun. 1086 (1968).
17. R. CAHILL, R. C. COOKSON et T. A. CRABB. Tetrahedron, **25**, 4681 (1969).
18. J. GELAS, D. HORTON et J. D. WANDER. J. Org. Chem. **39**, 1946 (1974).
19. W. A. BONNER et R. A. GRIMM. *Dans* The chemistry of organic sulfur compounds. Vol. 2. *Edité par* N. Kharasch et C. Y. Meyers. Pergamon Press, New York. 1966. p. 35, et références citées.
20. (*a*) H. C. BROWN, J. H. BREWSTER et H. SHECHTER. J. Am. Chem. Soc. **76**, 467 (1954); (*b*) J. GELAS. Bull. Soc. Chim. Fr. 2341 (1970), et références citées.
21. R. BOEHM et H. HANNING. Pharmazie, **24**, 526 (1969).
22. W. E. PARHAM, J. HEBERLING et H. WYNBERG. J. Am. Chem. Soc. **77**, 1169 (1955).
23. S. VEYSSIÈRES-RAMBAUD. Thèse de 3ème Cycle, Clermont-Ferrand no 344, 1973.
24. P. CALINAUD et J. GELAS. Bull. Soc. Chim. Fr. 1228 (1975).
25. H. R. BILLICA et H. ADKINS. Org. Synth. **29**, 24 (1949).

Can. J. Chem. Downloaded from www.nrcresearchpress.com by 210.87.254.6 on 09/06/12
For personal use only.

Diffusion with hydrolysis equilibria: transport coefficients of aqueous SO_2, NH_3, and Na_2CO_3 [1]

D. G. LEAIST[2]

Division of Chemistry, National Research Council of Canada, Ottawa, Ont., Canada K1A 0R9

Received June 4, 1982

D. G. LEAIST. Can. J. Chem. **61**, 1494 (1983).

Practical equations are derived for estimating diffusion coefficients and Onsager transport coefficients of aqueous solutes subject to hydrolysis. The derivation is based on the Nernst–Hartley method which is extended to include chemical reaction of solute with solvent. The derived equations and existing mobility data are used to estimate transport coefficients of aqueous SO_2 (20°C), NH_3 (15°C), and Na_2CO_3 (25°C). In dilute solution where hydrolysis is extensive, rates of diffusion of SO_2 and NH_3 are increased by about 50% and 25%, respectively, relative to unhydrolyzed solute. Because of the carbonate–bicarbonate equilibrium, diffusion in aqueous Na_2CO_3 is a ternary process characterized by coupled transport of NaOH. In dilute solution the NaOH flux may exceed the flux of Na_2CO_3.

D. G. LEAIST. Can. J. Chem. **61**, 1494 (1983).

On a dérivé des équations pratiques pour évaluer les coefficients de diffusion et les coefficients de transport de Onsager des solutés aqueux soumis à l'hydrolyse. La dérivation se base sur la méthode de Nernst–Hartley que l'on a élargie afin d'inclure la réaction chimique du soluté avec le solvant. On a utilisé l'équation dérivée ainsi que les données de mobilité existantes pour évaluer les coefficients de transport des solutions aqueuses de SO_2 (20°C), de NH_3 (15°C) et de Na_2CO_3 (25°C). En solution diluée où l'hydrolyse est importante, les vitesses de diffusion du SO_2 et du NH_3 augmentent d'environ de 50% et de 25% respectivement par rapport au soluté non hydrolysé. A cause de l'équilibre carbonate–bicarbonate, la diffusion dans du Na_2CO_3 aqueux est un processus ternaire caractérisé par un transport couplé de NaOH. En solution diluée le flux de NaOH doit excéder celui du Na_2CO_3.

[Traduit par le journal]

Can. J. Chem. Downloaded from www.nrcresearchpress.com by 210.87.254.6 on 09/06/12
For personal use only.

1. Introduction

Our objective in this paper is to determine the effects of hydrolysis on the diffusional properties of aqueous solutes. Because highly mobile hydrogen or hydroxide ions are produced, such effects require careful attention in cases of extensive hydrolysis.

Ammonia, carbon dioxide, chlorine, and sulfur dioxide are important examples of molecular solutes which hydrolyze. Among hydrolyzing electrolytes are those which contain carbonate, phosphate, sulfide, and cyanide as well as iron, zinc, aluminum, uranium, and numerous other metal ions (1). Diffusion of these solutes in aqueous media occurs in a variety of technological and biological processes; particular applications involve gas absorption, transport of corrosion products, and migration of minerals in groundwater.

By extending the well-known Nernst–Hartley (2, 3) method (thoroughly discussed by Robinson and Stokes in ref. 4) to include chemical reaction of solute with solvent, we develop practical equations for predicting transport coefficients of hydrolyzing solutes. Molecular solutes are considered first, followed by treatment of electrolytes. To illustrate the main points we discuss diffusion in dilute aqueous SO_2, NH_3, and Na_2CO_3. We confine our attention to isothermal, isobaric systems free of externally applied forces. Furthermore, the rate of hydrolysis is assumed to be rapid compared to diffusion so that local chemical equilibrium exists (refs. 5, 22; ref. 28, p. 296).[3]

2. Molecular solutes

Theory

Consider molecular solute M in aqueous solution with equilibria

$$M + H_2O \overset{K_h}{\rightleftharpoons} M\cdot H_2O \overset{K_1}{\rightleftharpoons} H^+ + (MOH)^-$$

The diffusional flux of solute comprises four chemical species numbered as follows: 1, unhydrated molecular M; 2, the hydrate $M\cdot H_2O$; 3, $(MOH)^-$; and 4, H^+. Because diffusion is characterized by zero flow of electric current, fluxes of $(MOH)^-$ and H^+ are equal. Local chemical equilibrium of the above reactions places two additional constraints on the fluxes of species. Therefore, diffusion of aqueous M is a binary process.

Fick's equation

$$[1] \quad J = -D\nabla c$$

and the Onsager equation

$$[2] \quad J = -L\nabla\mu$$

relate the total molar flux of solute to gradients in solute concentration and chemical potential (6, 7). Flow equations for the chemical species may also be written (8)

$$[3] \quad \hat{j}_i = -\sum_{k=1}^{4} \hat{l}_{ik}\nabla\hat{\mu}_k \qquad i = 1, 2, 3, 4$$

where molar fluxes, transport coefficients, and gradients in electrochemical potentials of the species are denoted by $\hat{j}_i$, $\hat{l}_{ik}$, and $\nabla\hat{\mu}_k$, respectively. The constraints imposed on the species fluxes by zero flow of electric current and by chemical equilibrium are expressed as

$$[4] \quad \hat{j}_3 = \hat{j}_4$$

---

[1]NRCC No. 21164.

[2]Present address: Department of Chemistry, University of Western Ontario, London, Ont., Canada N6A 5B7.

[3]Although rapid hydrolysis is usually an accurate approximation, the slow hydrolysis of carbon dioxide is a notable exception to this rule: the formation of carbonic acid $CO_2 + H_2O \rightarrow H_2CO_3$ is the rate-limiting step.

Can. J. Chem. Downloaded from www.nrcresearchpress.com by 210.87.254.6 on 09/06/12
For personal use only.

[5][4] $\nabla\hat{\mu}_1 = \nabla\hat{\mu}_2$

[6] $\nabla\hat{\mu}_2 = \nabla\hat{\mu}_3 + \nabla\hat{\mu}_4$

Equations [2] and [3] are closely related. For example, the total solute flux equals the sum of fluxes of M, $M\cdot H_2O$, and $(MOH)^-$ species and is expressed as

[7] $J = \hat{j}_1 + \hat{j}_2 + \hat{j}_3$

Also, the solute chemical potential gradient equals the sum of the electrochemical potential gradients of the ions.[3]

[8] $\nabla\mu = \nabla\hat{\mu}_3 + \nabla\hat{\mu}_4$

To estimate the transport coefficients, we make the dilute solution approximations, as others (2–4, 8, 9–17) have done, that (*i*) all off-diagonal $\hat{l}_{ik}$ coefficients are zero

[9] $-\hat{j}_i = \hat{l}_{ii}\nabla\hat{\mu}_i$

and that (*ii*) the mobility of each species is constant.

[10] $\hat{l}_{ii} = \hat{c}_i\hat{u}_i = \hat{c}_i\hat{D}_i/RT$

$\hat{c}_i$, $\hat{u}_i$, and $\hat{D}_i$ denote the concentration (in moles per unit volume), mobility, and diffusivity of the *i*th species.

Substituting eqs. [3]–[10] into eq. [2], we obtain after some algebra (17) the following expression for the Onsager coefficient

[11] $$L = \frac{c}{RT}\left[(1-\beta)\frac{\hat{D}_1 + K_h\hat{D}_2}{1+K_h} + \beta\frac{\hat{D}_3\hat{D}_4}{\hat{D}_3+\hat{D}_4}\right]$$

The apparent degree of hydrolysis defined by

[12] $$\beta = \frac{[(MOH)^-]}{[M] + [M\cdot H_2O] + [MOH^-]} = \frac{\hat{c}_3}{c}$$

is obtained[4] from the formula

[13] $$K_a = \frac{\beta^2 c}{1-\beta}\frac{y_\pm^2}{y}$$

where K_a is the apparent hydrolysis constant (measured by conductivity or by electromotive force cells), $y_\pm$ $(= (\hat{y}_3\hat{y}_4)^{1/2})$ and y are activity coefficients, and c is the formal concentration of solute. The term $(\hat{D}_1 + K_h\hat{D}_2)/(1 + K_h)RT$ in eq. [11] is interpreted as the number-average mobility of molecular species M and $M\cdot H_2O$; $\hat{D}_3\hat{D}_4/(\hat{D}_3 + \hat{D}_4)RT$ represents the mobility of fully ionized $M\cdot H_2O$. In practice, $\hat{D}_i$ values are obtained from binary data, and, for charged species, from molar ionic conductivities by use of the relation $\hat{D}_i = RT\hat{\lambda}_i/F^2\hat{z}_i^2$.

The derivative of the solute chemical potential with respect to concentration is required to obtain the expression for D (6, 7)

[14] $D = L\partial\mu/\partial c$

Following the usual hydrate convention (18, 19), we have

[15] $\mu = \mu^0 + RT\ln[(1-\beta)cy]$

Differentiation of eqs. [13] and [15] gives

[16] $$\frac{\partial\mu}{\partial c} = \frac{RT}{c}\left[1 + \frac{\beta}{2-\beta}\left(1 + \frac{\mathrm{d}\ln(y_\pm^2/y)}{\mathrm{d}\ln c}\right) + \frac{\mathrm{d}\ln y}{\mathrm{d}\ln c}\right]$$

In the limiting cases of no hydrolysis ($\beta = 0$) and complete hydrolysis ($\beta = 1$), $\partial\mu/\partial c$ is approximately RT/c and $2RT/c$, respectively. Thus for a given concentration gradient, hydrolysis increases the chemical potential gradient (the virtual force driving the diffusional process).

Equations [11] and [16] are combined to give

[17] $$D = \left[(1-\beta)D_0 + \beta D_\pm/2\right] \times \left[1 + \frac{\beta}{2-\beta}\left(1 + \frac{\mathrm{d}\ln(y_\pm^2/y)}{\mathrm{d}\ln c}\right) + \frac{\mathrm{d}\ln y}{\mathrm{d}\ln c}\right]$$

The term $D_0 = (\hat{D}_1 + K_h\hat{D}_2)/(1 + K_h)$ represents the number-average diffusivity of molecular species M and $M\cdot H_2O$. $D_\pm = 2\hat{D}_3\hat{D}_4/(\hat{D}_3 + \hat{D}_4)$ is the Nernst diffusion coefficient for fully ionized $M\cdot H_2O$.

Omission of activity coefficient terms in eq. [17] may lead to larger errors in the estimated value of D than errors arising from approximations by eqs. [9]–[10] (4). If the activity coefficient terms are neglected, however, the expression for D simplifies considerably to

[18] $D = 2[(1-\beta)D_0 + \beta D_\pm/2]/(2-\beta)$

which emphasizes that D is not a simple number-weighted average of the diffusivities of molecular and ionized forms of solute.

It is often convenient to define diffusional fluxes of solute relative to the solvent component (6, 7). Strictly speaking, the equations derived here refer to solute fluxes relative to *unreacted* solvent. Since the flux of hydrolyzing solute is accompanied by a flux equal to $[(1-\beta)K_h + \beta]J$ of reacted solvent (as $M\cdot H_2O$, $(MOH)^-$, and H^+), diffusion coefficients in the true solvent-fixed frame are smaller by a factor of $1 - [(1-\beta)K_h + \beta]c/c_0$ where c_0 is the concentration of the solvent. In most cases, however, this distinction is negligible because of the high concentration of solvent relative to solute.

In the preceding discussion, hydrolysis of the solute was presumed to liberate H^+. By interchanging H^+ and OH^- the same analysis can of course be applied to alkaline hydrolysis reactions such as $M + H_2O \rightleftarrows (HM)^+ + OH^-$.

To illustrate the magnitude of effect of hydrolysis on diffusion of molecular solutes we shall use the equations which were developed together with experimental mobility data to estimate the transport coefficients of dilute aqueous SO_2 and NH_3.

SO_2–H_2O (20°C)

Sulfur dioxide hydrolyzes rapidly (20) to give bisulfite and hydrogen ions (21, 23)

$$SO_2 + H_2O \rightleftarrows H^+ + HSO_3^-$$

$$K_a = 0.0146 \text{ mol dm}^{-3}$$

The hydrate H_2SO_3 is also present, but in negligible proportion ($K_h \approx 0$) (24–26). Diffusivities of the ions in dilute solution are accurately known from their conductivities (ref. 4, Appendix 6.2; refs. 21, 22): $\hat{D}_3(HSO_3^-) = 1.21 \times 10^{-9}$ and $\hat{D}_4(H^+) = 8.45 \times 10^{-9}$ m^2 s^{-1}. While the diffusivity of molecular SO_2 is more uncertain, both self-diffusion data (25) and extensive gas absorption studies (27–31) suggest $\hat{D}_1(SO_2) = 1.45$ $(\pm 0.05) \times 10^{-9}$ m^2 s^{-1} as a reasonable value. Based on these data, calculated values of the degree of hydrolysis, mobility (L/c), and diffusion coefficient of aqueous SO_2 at various concentrations are listed in Table 1. In the calculations the activity coefficient of molecular SO_2 was set equal to unity

[4]It is tacitly assumed that the solution is dilute enough so that the activity of water is very nearly unity.

TABLE 1. Transport coefficients of dilute aqueous SO_2 (20°C)

$10^3 \times c$ (mol dm^{-3})	β	$10^{12} \times L/c$ (mol m s^{-1} N^{-1})	$10^9 \times D$ (m^2 s^{-1})
0.01	1.00	0.43	2.12
0.1	0.99	0.43	2.10
1.0	0.94	0.44	2.02
5.0	0.81	0.47	1.86
10.0	0.71	0.48	1.78
50.0	0.46	0.52	1.62
100.0	0.37	0.54	1.57

(23). For the charged species, the semi-empirical relation (ref. 20, Chapt. 23; ref. 32)

$$[19] \quad \hat{y}_i = \exp\left[-A\hat{z}_i^2 I^{1/2}/(1 + I^{1/2})\right]$$

was used with A (20°C) = 1.17. For this system, the ionic strength I equals βc.

Although hydrolysis of SO_2 produces highly mobile H^+, we see in Table 1 that complete hydrolysis actually reduces the mobility of the solute relative to unhydrolyzed solute by about 25% — motion of molecular SO_2 together with its hydrolysis products through the solvent experiences more frictional resistance than in the absence of hydrolysis. On the other hand, hydrolysis increases the diffusivity by about 50%, primarily as a result of the increased free energy gradient.

At extremely low concentrations (less than about 10^{-5} mol dm^{-3}) both dissociation of bisulfite to form sulfite ions ($pK_a = 6.9$) (1, 25) and production of OH^- by self-ionization of water (15, 33) must be taken into account. We shall neglect these complications here.

NH_3–H_2O (15°C)

Hydrolysis products of ammonia include ammonium and hydroxide ions (34, 35)

$$NH_3 + H_2O \rightleftarrows NH_4^+ + OH^-$$

$$K_a = 1.64 \times 10^{-5} \text{ mol dm}^{-3}$$

Significant amounts of the hydrate NH_4OH are also present (36, 37). The ionic diffusivities (ref. 4, Appendix 6.2) are: $\hat{D}_3(NH_4^+) = 1.54 \times 10^{-9}$ and $\hat{D}_4(OH)^- = 4.09 \times 10^{-9}$ m^2 s^{-1}. For the number-average diffusivity of hydrated and unhydrated ammonia, $D_0 = (\hat{D}_1(NH_3) + K_h\hat{D}_2(NH_4OH))/(1 + K_h)$, we use the experimental value (38–41) 1.77 ($\pm$0.10) $\times 10^{-9}$ m^2 s^{-1} determined for the binary diffusion coefficient of aqueous ammonia at concentrations large compared to K_a where the degree of hydrolysis is negligible. It is worth emphasizing that because NH_3 and NH_4OH species are present in constant proportion (9, 36, 37) $[NH_4OH]/[NH_3] = K_h$, separate values of their diffusivities are not required for our purposes.

Calculated transport coefficients of aqueous ammonia are listed in Table 2. Equation [19] was used to compute ionic activity coefficients with A (15°C) = 1.16 (ref. 20, chapt. 23, 32). Again, the activity coefficients of the molecular species were set equal to unity. The results suggest that hydrolysis reduces the mobility of the solute by about 35% while increasing its diffusivity by about 25%. Because the hydrolysis constant is relatively small, hydrolysis has an appreciable effect on the diffusional properties of ammonia solutions only at very low concentrations.

TABLE 2. Transport coefficients of dilute aqueous NH_3 (15°C)

$10^3 \times c$ (mol dm^{-3})	β	$10^{12} \times L/c$ (mol m s^{-1} N^{-1})	$10^9 \times D$ (m^2 s^{-1})
0.01	0.70	0.56	2.02
0.05	0.43	0.63	1.90
0.1	0.33	0.66	1.86
0.5	0.17	0.70	1.81
1.0	0.12	0.72	1.80
10.0	0.04	0.74	1.78
100.0	0.01	0.75	1.77

3. Electrolytes

Theory

Compared to hydrolyzing molecular solutes, the diffusional behaviour of hydrolyzing electrolytes is more complex. Consider aqueous electrolyte $C_{\nu_c}A_{\nu_a}$. Let anion A^{z_a} hydrolyze as follows

$$A^{z_a} + H_2O \rightleftarrows (HA)^{z_a+1} + OH^-$$

Relative to undissociated solvent, four chemical species diffuse: C^{z_c}, A^{z_a}, $(HA)^{z_a+1}$, and OH^-. Because fluxes of species are constrained by local chemical equilibrium of the hydrolysis reaction and by zero flow of electric current, two diffusional fluxes are linearly independent. Diffusion of the electrolyte is a *ternary* process.

That aqueous $C_{\nu_c}A_{\nu_a}$ is a binary system for equilibrium thermodynamic properties yet its diffusional properties are ternary is interpreted as follows. At thermodynamic equilibrium the requirements of electroneutrality, equilibrium of the hydrolysis reaction, and stoichiometry serve to fix the concentrations of all species for a given concentration of electrolyte. Along an electrolyte concentration gradient, however, there are non-equilibrium fluxes of ions. Because more than two ions are present, they diffuse at different rates. In particular, highly mobile OH^- diffuses more rapidly than $(HA)^{z_a+1}$. Hence the stoichiometry requirement $[(HA)^{z_a+1}] = [OH^-]$ valid at thermodynamic equilibrium does not apply to the diffusing electrolyte. It follows that diffusion cannot be described by a flux of $C_{\nu_c}A_{\nu_a}$ alone — a second flux, say of electrolyte $C(OH)_{\nu_{OH}}$, must also be specified.

In the event of further hydrolysis reactions such as

$$(HA)^{z_a+1} + H_2O \rightleftarrows (H_2A)^{z_a+2} + OH^-$$

diffusion of the electrolyte would remain a ternary process: although each additional reaction produces one additional chemical species, there is also one additional chemical equilibrium to be satisfied and therefore no additional independent fluxes.

How does hydrolysis influence the rate of diffusion of the electrolyte? As mentioned earlier, there are opposing tendencies to increase the free energy gradient of the electrolyte and to decrease its mobility. Furthermore, so that zero flow of electric current is maintained, the flux of rapidly diffusing OH^- tends to increase the flux of C^{z_c} counterions at the expense of reduced fluxes of coions $(HA)^{z_a+1}$ and A^{z_a}. To illustrate these points in greater detail, we shall consider diffusion in aqueous sodium carbonate. A specific example is chosen rather than the general case for the sake of clarity.

Na_2CO_3–H_2O (25°C)

Hydrolysis of the carbonate ion in aqueous Na_2CO_3 produces bicarbonate and hydroxide ions (20, 42)

Can. J. Chem. Downloaded from www.nrcresearchpress.com by 210.87.254.6 on 09/06/12
For personal use only.

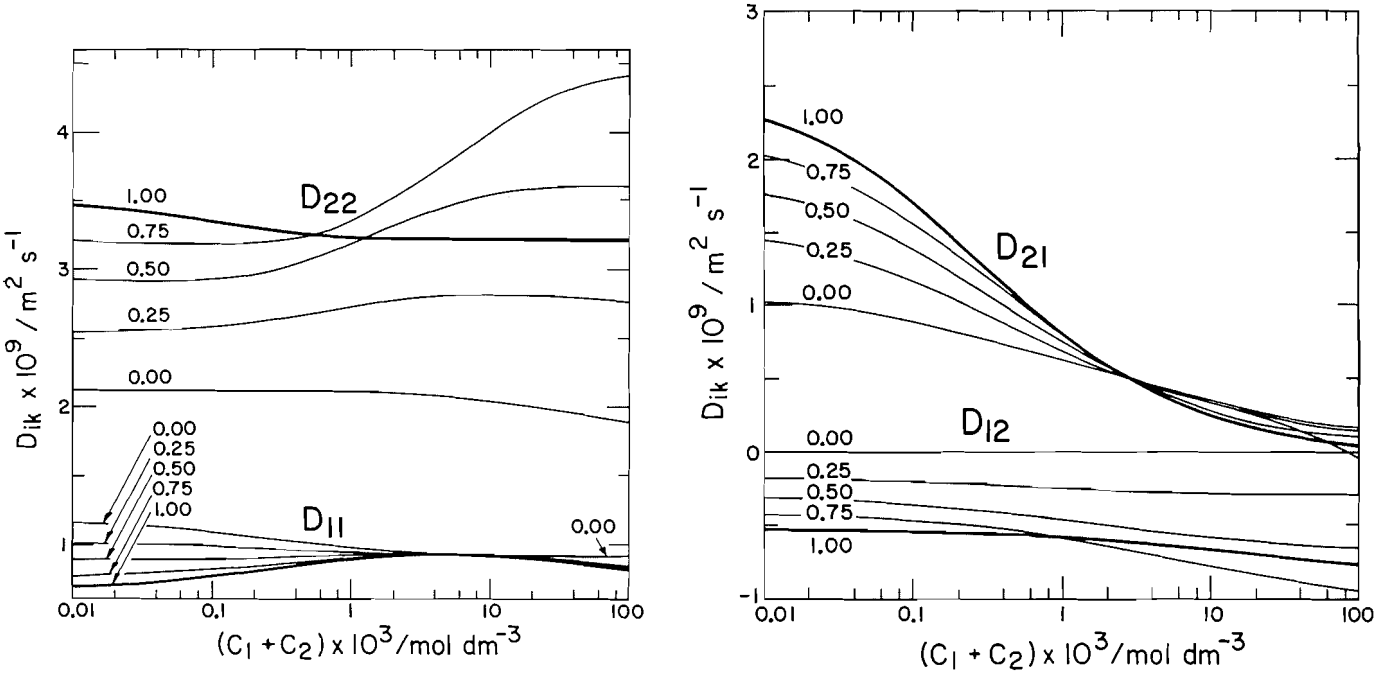

FIG. 1. Calculated diffusion coefficients of $Na_2CO_3(c_1)$–$NaOH(c_2)$–H_2O (25°C) plotted against the total electrolyte concentration $c_1 + c_2$ for different values of $c_1/(c_1 + c_2)$. The heavy curves labelled "1.00" refer to aqueous Na_2CO_3 without added NaOH.

[20] $CO_3^{2-} + H_2O \rightleftarrows HCO_3^- + OH^-$

$K_a = 2.15 \times 10^{-4}$ mol dm^{-3}

Ternary diffusion of the salt is conveniently described (6, 7) in terms of molar fluxes of the neutral components 1, Na_2CO_3 (both hydrolyzed and unhydrolyzed forms); and 2, NaOH.

$$[21]\quad -J_i = \sum_{k=1}^{2} L_{ik}\nabla\mu_k \qquad i = 1, 2$$

$$[22]\quad -J_i = \sum_{k=1}^{2} D_{ik}\nabla c_k \qquad i = 1, 2$$

This representation has the advantage that one of the fluxes (J_1 here) accounts for the entire flux of carbonate and bicarbonate ions. We number the various species as follows: 1, CO_3^{2-}; 2, OH^-; 3, Na^+; and 4, HCO_3^-. Flow equations for the species are identical to eq. [3]. Constraints imposed on the species fluxes by zero flow of electric current and by chemical equilibrium are expressed as

$$[23]\quad \hat{j}_3 = 2\hat{j}_1 + \hat{j}_2 + \hat{j}_4$$

$$[24]^4\quad \nabla\hat{\mu}_1 = \nabla\hat{\mu}_2 + \nabla\hat{\mu}_4$$

Equations [21] and [3] for electrolyte and species fluxes are related as follows: the flux of Na_2CO_3 component equals the sum of CO_3^{2-} and HCO_3^- fluxes;

$$[25]\quad J_1 = \hat{j}_1 + \hat{j}_4$$

the flux of NaOH component equals the flux of OH^- in excess of HCO_3^-;

$$[26]\quad J_2 = \hat{j}_2 - \hat{j}_4$$

and the electrolyte chemical potential gradients equal the sum of the electrochemical potential gradients of the constituent ions

$$[27]\quad \nabla\mu_1 = \nabla\hat{\mu}_1 + 2\nabla\hat{\mu}_3$$

$$[28]\quad \nabla\mu_2 = \nabla\hat{\mu}_2 + \nabla\hat{\mu}_3$$

Proceeding as in Section 2, we obtain (17)

$$[29]\quad L_{11} = \frac{\hat{l}_{11}(\hat{l}_{22} + \hat{l}_{33} + \hat{l}_{44}) + \hat{l}_{44}(\hat{l}_{22} + \hat{l}_{33})}{4\hat{l}_{11} + \hat{l}_{22} + \hat{l}_{33} + \hat{l}_{44}}$$

$$[30]\quad L_{12} = L_{21} = -\frac{\hat{l}_{33}\hat{l}_{44} + 2(\hat{l}_{11}\hat{l}_{22} + \hat{l}_{11}\hat{l}_{44} + \hat{l}_{22}\hat{l}_{44})}{4\hat{l}_{11} + \hat{l}_{22} + \hat{l}_{33} + \hat{l}_{44}}$$

$$[31]\quad L_{22} = \frac{\hat{l}_{33}(\hat{l}_{22} + \hat{l}_{44}) + 4(\hat{l}_{11}\hat{l}_{22} + \hat{l}_{11}\hat{l}_{44} + \hat{l}_{22}\hat{l}_{44})}{4\hat{l}_{11} + \hat{l}_{22} + \hat{l}_{33} + \hat{l}_{44}}$$

with $\hat{l}_{ii} = \hat{c}_i\hat{D}_i/RT$. Diffusivities of the ions in dilute solution are accurately known from conductivity data (ref. 4, Appendix 6.2): $\hat{D}_1(CO_3^{2-}) = 0.92 \times 10^{-9}$; $\hat{D}_2(OH^-) = 5.28 \times 10^{-9}$; $\hat{D}_3(Na^+) = 1.33 \times 10^{-9}$; and $\hat{D}_4(HCO_3^-) = 1.18 \times 10^{-9}$ m^2 s^{-1}.

Solute chemical potentials are expressed as

$$[32]\quad \mu_1 = \mu_1^0 + RT \ln [(2c_1 + c_2)^2(1 - \beta)c_1\hat{y}_1\hat{y}_3^2]$$

$$[33]\quad \mu_2 = \mu_2^0 + RT \ln [(2c_1 + c_2)(\beta c_1 + c_2)\hat{y}_2\hat{y}_3]$$

Concentrations of Na_2CO_3 and NaOH components are denoted by c_1 and c_2, respectively. The degree of hydrolysis of Na_2CO_3 defined by

$$[34]\quad \beta = \frac{[HCO_3^-]}{[CO_3^{2-}] + [HCO_3^-]}$$

is obtained[4] from the formula

$$[35]\quad K_a = \frac{\beta c_1(\beta c_1 + c_2)}{(1 - \beta)c_1}\frac{\hat{y}_2\hat{y}_4}{\hat{y}_1}$$

Following differentiation of eqs. [32], [33], and [35], expressions for the diffusion coefficients are obtained by use of the relation (6, 7)

Can. J. Chem. Downloaded from www.nrcresearchpress.com by 210.87.254.6 on 09/06/12
For personal use only.

Can. J. Chem. Downloaded from www.nrcresearchpress.com by 210.87.254.6 on 09/06/12
For personal use only.

$$[36]\quad D_{ik} = \sum_{m=1}^{2} L_{im}\partial\mu_m/\partial c_k$$

In Fig. 1, calculated values of the four diffusion coefficients of $Na_2CO_3(c_1)-NaOH(c_2)-H_2O$ (25°C) are plotted against the total solute concentration $c_1 + c_2$ for several values of the ratio $c_1/(c_1 + c_2)$. Activity coefficients were computed using eq. [9] with A (25°C) = 1.18 (ref. 20, chapt. 23; ref. 32). First we shall discuss diffusion coefficients of aqueous Na_2CO_3 without added NaOH ($c_2 = 0$, heavy lines labelled "1.00").

D_{11} determines the flux of Na_2CO_3 produced per unit concentration gradient in that component. At concentrations large compared to K_a so that the degree of hydrolysis is negligible, yet dilute enough so that the Nernst–Hartley approximations are accurate, the expression for D_{11} simplifies to

$$[37]\quad D_{11}(\beta = 0) = \frac{3\hat{D}_{CO_3^{2-}}\hat{D}_{Na^+}}{\hat{D}_{CO_3^{2-}} + 2\hat{D}_{Na^+}}\left(1 + \frac{d\ln y_{\pm 1}}{d\ln c_1}\right)$$

where $y_{\pm 1} = (\hat{y}_1\hat{y}_3^2)^{1/3}$. At lower concentrations hydrolysis increases the proportion of HCO_3^- relative to CO_3^{2-}. In the limit of infinite dilution hydrolysis is complete and we have

$$[38]\quad D_{11}(\beta = 1) = \frac{4\hat{D}_{Na^+}\hat{D}_{HCO_3^-}}{\hat{D}_{OH^-} + 2\hat{D}_{Na^+} + \hat{D}_{HCO_3^-}} = 0.69 \times 10^{-9}\ m^2\ s^{-1}$$

In ternary diffusion studies it is usually taken for granted that solute 1 is unable to produce coupled flow of solute 2 in solutions free of solute 2: $D_{21} \rightarrow 0$ as $c_2/c_1 \rightarrow 0$ (10, 16, 43, 44). It is remarkable that in aqueous Na_2CO_3 without added NaOH the cross-diffusion coefficient D_{21} (which determines the flux of NaOH produced per unit Na_2CO_3 gradient) is very large and positive. In fact, D_{21} is more than three times as large as D_{11} at high dilution (refer to the curve for D_{21} labelled "1.00"). This means that the Na_2CO_3 gradient produces an initial flux of NaOH more than three times larger than the Na_2CO_3 flux, even though the solution is free of added NaOH! In effect, as OH^- diffuses more rapidly than either CO_3^{2-} or HCO_3^-, the Na_2CO_3 gradient generates "its own" NaOH flux. In the limit of infinite dilution the expression for D_{21} simplifies to

$$[39]\quad D_{21}(\beta = 1) = \frac{4\hat{D}_{Na^+}(\hat{D}_{OH^-} - \hat{D}_{HCO_3^-})}{\hat{D}_{OH^-} + 2\hat{D}_{Na^+} + \hat{D}_{HCO_3^-}} = 2.39 \times 10^{-9}\ m^2\ s^{-1}$$

That the limiting value of D_{21} is proportional to the difference in diffusivity between hydrolysis products OH^- and HCO_3^- is noteworthy; this difference is the source of the multicomponent nature of the diffusional properties of aqueous Na_2CO_3.

The cross-diffusion coefficient D_{12} measures the ability of the NaOH flux to produce coupled flow of Na_2CO_3. As mentioned earlier, the flux of rapidly diffusing OH^- reduces the flux of coions CO_3^{2-} and HCO_3^-. This accounts for both the negative sign of D_{12} as well as the reduction in the main diffusion coefficient of Na_2CO_3 by hydrolysis.

The curve for D_{22} labelled "1.00" gives the diffusion coefficient of trace amounts of NaOH in aqueous Na_2CO_3 as a function of Na_2CO_3 concentration. In dilute mixtures of strong electrolytes (10, 43, 44) (NaCl–NaOH–H_2O for example) its value is approximately equal to the diffusivity of OH^-, about $5.3 \times 10^{-9}\ m^2\ s^{-1}$. In aqueous Na_2CO_3, however, its value is considerably lower: 3.2 to $3.5 \times 10^{-9}\ m^2\ s^{-1}$. This discrepancy arises because in aqueous Na_2CO_3, not all hydroxide is transported as the OH^- species. Instead, some hydroxide reacts with bicarbonate (eq. [20]) and is transported as CO_3^{2-} plus H_2O with countercurrent flux of HCO_3^-.

$Na_2CO_3(c_1)-NaOH(c_2)-H_2O$ (25°C)

Also plotted in Fig. 1 are ternary diffusion coefficients of aqueous Na_2CO_3 with added NaOH. These curves are plotted against the total electrolyte concentration $c_1 + c_2$ for values of $c_1/(c_1 + c_2)$ equal to 0.00, 0.25, 0.50, and 0.75. The curve for D_{22} labelled "0.00", for example, gives the binary diffusion coefficient of aqueous NaOH as a function of concentration.

To first approximation, multicomponent diffusion coefficients in dilute mixtures of strong electrolytes are constant for fixed electrolyte ratios. This behaviour is primarily a result of electrostatic nature of the coupling between ionic fluxes (10, 43, 44). Because there are chemical as well as electrostatic interactions between the fluxes, the diffusion coefficients plotted in Fig. 1 for fixed ratios of Na_2CO_3 to NaOH do not follow this simple pattern. The diffusion coefficient for trace amounts of Na_2CO_3 in aqueous NaOH (curve for D_{11} labelled "0.00") illustrates this point nicely. Neglecting minor activity coefficient terms, we have

$$[40]\quad D_{11}(c_1/c_2 = 0) = (1 - \beta)\hat{D}_{CO_3^{2-}} + \beta\hat{D}_{HCO_3^-}$$

At very low NaOH concentrations where hydrolysis of CO_3^{2-} is essentially complete, trace amounts of Na_2CO_3 diffuse as HCO_3^-, while at higher NaOH concentrations the carbonate–bicarbonate equilibrium is shifted in favor of CO_3^{2-} and transport as CO_3^{2-} predominates.

$Na_2CO_3(c_1')-NaHCO_3(c_2')-H_2O$

Although convenient, the description of diffusion of aqueous Na_2CO_3 in terms of fluxes J_1 and J_2 of components Na_2CO_3 and NaOH is not unique. Another description would be in terms of fluxes J_1' and J_2' of Na_2CO_3 and $NaHCO_3$. Since $J_1 = J_1' + J_2'$, $J_2 = -J_2'$; $c_1 = c_1' + c_2'$; and $c_2 = -c_2'$, eq. [22] may be transformed from the Na_2CO_3–NaOH representation into the Na_2CO_3–$NaHCO_3$ representation. The two sets of diffusion coefficients are related by $D_{11}' = D_{11} + D_{21}$, $D_{12}' = D_{11} + D_{12} - D_{21} - D_{22}$, $D_{21}' = D_{21}$, and $D_{22}' = D_{22} - D_{21}$.

4. Conclusions

A procedure based on the Nernst–Hartley method has been developed to estimate diffusion coefficients of aqueous solutes which hydrolyze.[5] The procedure allows detailed interpretation of the concentration dependence of the diffusion coefficients in terms of (*i*) changes in the solute free energy gradient caused by hydrolysis and (*ii*) changes in the mobility of the solute arising from changes in the proportion of unhydrolyzed solute and hydrolysis products. At low concentrations where the procedure may be used with confidence, diffusion coefficients have been estimated for several systems. Typically, hydrolysis may either increase or decrease the rate of diffusion by several tens of per cent. The diffusion coefficients are most sensitive to concentration at solute concentrations of the same order of magnitude as the hydrolysis constant where similar amounts of unhydrolyzed solute and hydrolysis products are present in solution. In the case of a hydrolyzing salt, diffusion is a ternary process (four diffusion coefficients must be specified) pro-

[5]Although we have dealt only with estimating diffusion coefficients of hydrolyzing solutes, the same procedure is applicable to diffusion with solvolysis in nonaqueous solvents.

ducing coupled fluxes of acid or hydroxide hydrolysis products which may exceed the flux of salt itself.

Acknowledgment

The author was very fortunate to have numerous helpful comments from J. R. Farnand.

1. J. A. DEAN (*Editor*). Lange's handbook of chemistry. 12th ed. McGraw Hill, New York. 1978. pp. 5–14.
2. W. NERNST. Z. Phys. Chem. **2**, 613 (1888).
3. G. S. HARTLEY. Phil Mag. **12**, 473 (1931).
4. R. A. ROBINSON and R. H. STOKES. Electrolyte solutions. 2nd ed. Academic Press, New York. 1959. Chapt. 11.
5. W. H. STOCKMAYER. J. Chem. Phys. **33**, 1291 (1960).
6. D. D. FITTS. Nonequilibrium thermodynamics. McGraw Hill, New York. 1962.
7. S. R. DE GROOT and P. MAZUR. Non-equilibrium thermodynamics. Interscience Publishers, New York. 1962.
8. R. P. WENDT. J. Phys. Chem. **69**, 1227 (1965).
9. H. S. HARNED and R. M. HUDSON. J. Am. Chem. Soc. **73**, 3781 (1951); **73**, 5880 (1951).
10. L. J. GOSTING. *In* Advances in protein chemistry. Vol. 11. Academic Press, New York. 1956.
11. G. T. A. MÜLLER and R. H. STOKES. Trans. Faraday Soc. **53**, 642 (1957).
12. J. M. CREETH and R. H. STOKES. J. Phys. Chem. **64**, 946 (1960).
13. C. W. GARLAND, S. TONG, and W. H. STOCKMAYER. J. Phys. Chem. **69**, 1718 (1965).
14. R. P. WENDT. J. Chem. Educ. **51**, 646 (1974).
15. P. PASSINIEMI, S. LIUKKONEN, and Z. NOSZTICZIUS. J. Chem. Soc. Faraday Trans. 1, **76**, 2552 (1980).
16. D. G. LEAIST and P. A. LYONS. J. Phys. Chem. **85**, 1756 (1981).
17. D. G. LEAIST. J. Chem. Soc. Faraday Trans. 1. **78**, 3069 (1982).
18. G. N. LEWIS and M. RANDALL. Thermodynamics. 2nd ed. (revised). McGraw Hill, New York. 1961. p. 272.
19. K. DENBIGH. The principles of chemical equilibrium. 3rd ed. Cambridge University Press. 1971. p. 296.
20. M. EIGEN, K. KUSTIN, and G. MAASS. Z. Phys. Chem. N.F. **30**, 130 (1961).
21. W. B. CAMPBELL and O. MAASS. Can. J. Res. **2**, 42 (1930).
22. O. M. MORGAN and O. MAASS. Can. J. Res. **5**, 162 (1931).
23. H. F. JOHNSTONE and P. W. LEPPLA. J. Am. Chem. Soc. **56**, 2233 (1934).
24. M. FALK and A. P. GIGUÉRE. Can. J. Chem. **36**, 1124 (1958).
25. T. ERIKSEN. Chem. Eng. Sci. **22**, 727 (1967).
26. F. A. COTTON and G. WILKINSON. Advanced inorganic chemistry. 3rd ed. Interscience Publishers. 1972. p. 296.
27. R. P. WHITNEY and J. E. VIVIAN. Chem. Eng. Progr. **45**, 323 (1949).
28. H. GROOTHIUS and H. KRAMERS. Chem. Eng. Sci. **4**, 17 (1955).
29. S. LYNN, J. R. STRAATEMEIER, and H. KRAMERS. Chem. Eng. Sci. **4**, 49 (1955).
30. H. L. TOOR and S. H. CHIANG. A. I. Ch. E. J. **5**, 339 (1959).
31. P. V. DANCKWERTS. Chem. Eng. Sci. **23**, 1045 (1968).
32. E. A. GUGGENHEIM and J. C. TURGEON. Trans. Faraday Soc. **51**, 747 (1955).
33. L. A. WOOLF. J. Phys. Chem. **76**, 1166 (1972).
34. R. G. BATES and G. D. PINCHING. J. Am. Chem. Soc. **72**, 1393 (1950).
35. M. EIGEN. *In* Progress in reaction kinetics. Vol. 2. Pergamon Press, Oxford. 1965. p. 285.
36. D. BERG and A. PATTERSON, JR. J. Am. Chem. Soc. **75**, 5731 (1953).
37. E. ARNOLD, H. FREITAG, and A. PATTERSON, JR. *In* The structure of electrolytic solutions. Wiley, New York. 1959. Chapt. 18.
38. S. ARRHENIUS. Z. Phys. Chem. **10**, 51 (1892).
39. R. ABEGG. Z. Phys. Chem. **11**, 248 (1893).
40. E. W. WASHBURN (*Editor*). International critical tables. Vol. 5. McGraw Hill, New York. 1926. p. 64.
41. D. M. HIMMELBAU. Chem. Rev. **64**, 527 (1964).
42. H. S. HARNED and S. R. SCHOLES. J. Am. Chem. Soc. **63**, 1706 (1941).
43. I. J. O'DONNELL and L. J. GOSTING. *In* The structure of electrolytic solutions. Wiley, New York. 1959. Chapt. 11.
44. D. G. LEAIST and P. A. LYONS. Aust. J. Chem. **33**, 1869 (1980).

Can. J. Chem. Downloaded from www.nrcresearchpress.com by 210.87.254.6 on 09/06/12
For personal use only.

Investigation of the possible pathways for magnetic exchange interactions in homobinuclear chelates of naphthazarin

CONSTANTINOS A. TSIPIS AND MICHAEL P. SIGALAS
Laboratory of Inorganic Chemistry, University of Thessaloniki, Thessaloniki, Greece

AND

VASILIOS P. PAPAGEORGIOU AND MARIA N. BAKOLA-CHRISTIANOPOULOU[1]
Department of Chemical Engineering, College of Engineering, University of Thessaloniki, Thessaloniki, Greece

Received March 15, 1982

CONSTANTINOS A. TSIPIS, MICHAEL P. SIGALAS, VASILIOS P. PAPAGEORGIOU, and MARIA N. BAKOLA-CHRISTIANOPOULOU. Can. J. Chem. **61**, 1500 (1983).

Homobinuclear complexes of the binucleating naphthazarinato ligand of the general formula $[M_2(C_{10}H_4O_4)(C_{10}H_8N_2)_2]^{2+}$-$(PF_6^-)_2$, where M = Cu, Ni, and Zn, $C_{10}H_4O_4$ = naphthazarinato ligand, and $C_{10}H_8N_2$ = 2,2′-bipyridyl, have been prepared and studied. In these complexes the naphthazarinato ligand, acting as a bridging unit between the two metal centers, supports the propagation of magnetic exchange interactions through its extensive π-electron system. The spectroscopic and magnetic data of the compounds showed that each metal ion is surrounded by two oxygen and two nitrogen donor atoms in a nearly tetrahedral configuration (C_{2v} point group) with the naphthazarinato ligand adopting a centrosymmetrical structure of C_{2h} symmetry. The room-temperature magnetic data of the copper(II) and nickel(II) homobinuclear chelates (1.32 and 1.73 BM per metal ion at 8000 G, respectively), as well as the slight decrease of the magnetic moments as the magnetic field strength decreases are indicative of the operation of antiferromagnetism in these chelates. Quantum mechanical calculations of the Hückel LCAO-MO type improved by ω-technique have been used to provide a qualitative guide to the possible pathways for the superexchange processes observed in the tetrahedral copper(II) and nickel(II) chelates, as well as to explain qualitatively why there is no antiferromagnetic interactions propagated by the bridging naphthazarinato ligand in analogous homobinuclear chelates with other coordination geometries such as square planar, square-pyramidal, trigonal bipyramidal, and octahedral.

CONSTANTINOS A. TSIPIS, MICHAEL P. SIGALAS, VASILIOS P. PAPAGEORGIOU et MARIA N. BAKOLA-CHRISTIANOPOULOU. Can. J. Chem. **61**, 1500 (1983).

On a préparé et étudié les complexes homobinucléaires du ligand naphthazarinato binucléant de formule générale $[M_2(C_{10}H_4O_4)(C_{10}H_8N_2)_2]^{2+}(PF_6^-)_2$ où M = Cu, Ni et Zn, $C_{10}H_4O_4$ = ligand naphthazarinato et $C_{10}H_8N_2$ = bipyridyl-2,2′. Dans ces complexes le ligand naphthazarinato agit comme unité de pont entre les deux centres métalliques et est responsable, au moyen de son système accentué d'électrons π, de la propagation des interactions d'échange magnétique. Les données spectroscopiques et magnétiques relatives à ces composés révèlent que chaque ion métallique est entouré de deux atomes donneurs d'oxygène et d'azote dans une configuration quasi tétraédrique (point de group C_{2v}) avec le ligand naphthazarinato adoptant une structure centrosymétrique de symétrie C_{2h}. Les données magnétiques à la température ambiante se rapportant aux chélates homobinucléaires du cuivre(II) et du nickel(II) (1,32 et 1,73 BM) par ion métallique à 8000 G respectivement) aussi bien que la légère diminution des moments magnétiques avec la force du champ magnétique sont une indication de la présence d'un antiferromagnétisme dans ces chélates. On a utilisé les calculs de mécanique quantique du type Hückel LCAO-MC améliorés par la technique-ω pour obtenir un guide qualitatif des schémas possibles des processus de superéchange observés dans les chélates tétraédriques du cuivre(II) et du nickel(II) aussi bien pour expliquer qualitativement l'absence d'interactions antiferromagnétiques propagées par le ligand naphthazarinato en position de pont dans les chélates homobinucléaires analogues avec d'autres géométries de coordination tel le carré plan, la pyramide carrée, la bipyramide trigonale et octaédrique.

[Traduit par le journal]

Introduction

The dianion of 5,8-dihydroxy-1,4-naphthoquinone (commonly knwon as naphthazarin) is a potential binucleating ligand, which forms stable polynuclear or binuclear chelates with bivalent metal ions (1, 2). Due to its extensive π-electron system, the naphthazarinato binucleating ligand would be expected to support the propagation of magnetic exchange interactions (superexchange interactions) between two paramagnetic metal ions. However, in a recent study of the magnetic exchange interactions in some five- and six-coordinated binuclear complexes of copper(II) and nickel(II) containing a bridging naphthazarinato ligand no antiferromagnetic exchange interactions were detected (2). This is not surprising, since it is now well-established (2–5) that the strength and mechanism of such magnetic exchange interactions are primarily depended upon the symmetry and energy of the orbitals of both the metal ions and the binucleating ligand. In other words, the coordination geometry about the central paramagnetic metal ions, as well as the structure of the bridging unit are the most important factors determining the operation of magnetic exchange interactions. In this regard it will be important the study of the ability of the naphthazarinato binucleating ligand to support magnetic exchange interactions in binuclear complexes with other coordination geometries about the central paramagnetic metal ions.

In the present paper we report on our results concerning: (*i*) the synthesis and characterization of some new four-coordinated homobinuclear chelates of the binucleating naphthazarinato ligand of the general formula $[M_2(C_{10}H_4O_4)$-$(C_{10}H_8N_2)_2]^{2+}$ $(PF_6^-)_2$, where M = Cu, Ni, and Zn, $C_{10}H_4O_4$ = naphthazarinato ligand, and $C_{10}H_8N_2$ = 2,2′-bipyridyl; (*ii*) the study of their structural and magnetic properties; and (*iii*) the theoretical prediction, on the basis of HMO quantum chemical calculations improved by ω-technique, of the possible pathways for the superexchange processes observed in the copper(II) and nickel(II) chelates. The quantum chemical calculations

[1]To whom all correspondence should be addressed.

Can. J. Chem. Downloaded from www.nrcresearchpress.com by 210.87.254.6 on 09/06/12
For personal use only.

Can. J. Chem. Downloaded from www.nrcresearchpress.com by 210.87.254.6 on 09/06/12
For personal use only.

also have been used to confirm the structure of the naphthazarinato ligand, as well as to interpret the electronic spectra of the new compounds.

Experimental

Physical measurements

Infrared spectra were recorded, in the region of 4000–250 cm^{-1}, on a Perkin-Elmer 467 spectrophotometer using KBr discs or Nujol mulls. Electronic spectra were obtained on a Perkin-Elmer Hitachi 200 spectrophotometer and on a Cary 17D spectrophotometer, using freshly prepared solutions in DMF. Magnetic susceptibility measurements were done by the Faraday technique at different magnetic field strengths using $Hg[Co(SCN)_4]$ as the calibrant. Diamagnetic corrections were made using Pascal's constants. Conductivity measurements were done in a Wheatstone bridge Model RC 216 B_2 using 10^{-3} *M* solutions in DMF. Carbon, hydrogen, and nitrogen were determined using a Perkin-Elmer 240 Elemental Analyzer.

Starting materials

All solvents were of reagent grade and were used without further purification in synthetic work. All the other reagents were obtained commercially.

Preparation of the chelates

The investigated homobinuclear chelates were of the general formula $[M_2(C_{10}H_4O_4)(C_{10}H_8N_2)_2](PF_6^-)_2$ (where M = Cu, Ni, and Zn, and $C_{10}H_8N_2$ = 2,2′-bipyridyl). The 2,2′-bipyridyl ligand was selected as the nonbridging ligand because it prevents the formation of polynuclear chelates. The new chelates were prepared according to the following general method:

Into a three-necked flask equipped with a magnetic stirrer, a reflux condenser, and a separatory funnel, were charged 0.475 g (2.4 mmol) of naphthazarin and 100 cm^3 of methylene chloride as a solvent. To the resulting solution, a solution containing 5.0 mmol of the metal acetate, 0.78 g (5.0 mmol) of 2,2′-bipyridyl, and 2.00 g (12.3 mmol) of NH_4PF_6 in 100 cm^3 of ethanol was added slowly under continuous magnetic stirring. The reaction mixture was left for 1 h at room temperature and then was refluxed for 4 h. After cooling, the mixture was filtered and the precipitate was washed several times with small portions of water, ethanol, and methylene chloride and dried under vacuum over P_2O_5. The isolated chelates are soluble in DMF and DMSO, but insoluble in water and in all common organic solvents. The yields of the reactions were almost quantitative (more than 80%). All the chelates are deep blue in color and do not melt up to 300°C. Their analytical data are as follows: *Anal.* calcd. for $[Cu_2(C_{10}H_4O_4)(C_{10}H_8N_2)_2](PF_6)_2$: C 39.27, H 2.19, N 6.10; found: C 39.54, H 2.29, N 6.15; *Anal.* calcd. for $[Ni_2(C_{10}H_4O_4)(C_{10}H_8N_2)_2](PF_6)_2$: C 39.69, H 2.22, N 6.17; found: C 40.01, H 2.16, N 5.98; *Anal.* calcd. for $[Zn_2(C_{10}H_4O_4)(C_{10}H_8N_2)_2](PF_6)_2$: C 39.11, H 2.18, N 6.08; found: C 39.41, H 2.28, N 6.18.

Calculations

Quantum chemical calculations were performed using the Hückel LCAO-MO method improved by ω-technique (6, 7). In the course of the HMO calculations the following parameters were adopted: for the quinonic oxygen atoms $h = 1.00$ and $k = 1.20$ and for the phenolic oxygen atoms $h = 1.50$ and $k = 0.70$. The value of ω was chosen as 0.9. The self-consistent charge (SCC) process was applied simultaneously to both the quinonic and phenolic oxygen atoms. The 14 × 14 secular determinants were factorized by taking advantage of the symmetry of the molecules and standard methods of group theory.

Results and discussion

The structure of naphthazarin has been a matter of considerable controversy in a number of papers published up to date (8–15). The following three different possible structures have been proposed:

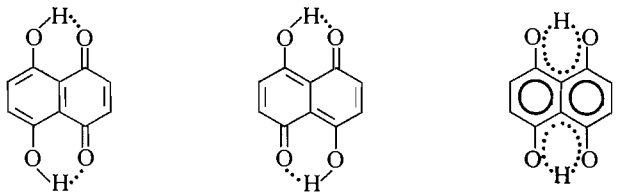

I **II** **III**

Schmand and Boldt (13) showed, by spectroscopic studies, that the naphthazarin molecule exists in solution as 5,8-dihydroxy-1,4-naphthoquinone (structure **I**, C_{2v} point group), which according to the authors must be more stable than the centrosymmetrical 1,5-quinoid structure (structure **II**, C_{2h} point group). On the contrary, very recently Bratan and Strohbusch (15) showed, by ir and ^1H nmr spectroscopy, that the molecular structure of naphthazarin in solution is that of a centrosymmetrical structure with highly mobile protons in intramolecular hydrogen bonds. The fast tunnelling of the two protons interconvert the two equivalent centrosymmetrical 1,5-quinoid structures giving their average structure **III** which belongs to the D_{2h} point group. According to these authors the 1,5-quinoid structure must be more stable than the 1,4-quinoid structure. The crystal structure determination of the free naphthazarin (12) showed a nearly D_{2h} symmetry for the molecule. Strictly speaking, the symmetry of the naphthazarin molecule refering in this paper is C_{2h}, since the shortest C···O bonds were those at 1- and 5-positions. Thus the X-ray structure determination of the naphthazarin molecule supports the idea of Bratan and Strohbusch that the 1,5-quinoid structure is the more stable one.

An analogous situation exists also in the case of naphthazarin diacetate, where some studies showed that the 1,5-quinoid structure is the more stable one (11) in solution, while the X-ray structure determination (14) showed that in solid state naphthazarin diacetate exists as 5,8-diacetoxy-1,4-naphthoquinone.

With the foregoing ambiguous aspects about the structure of naphthazarin in mind and the fact that the knowledge of its structure is of crucial importance in our attempts to gain an insight on the possible pathways for the magnetic exchange interactions, we calculated by the HMO method and the total π-electron energies for all the three possible structures of naphthazarin. According to the HMO calculations, the electron configurations of the three possible structures of naphthazarin in their ground states are written:

structure **I**: $1b_1^2, 1a_2^2, 2b_1^2, 2a_2^2, 3b_1^2, 4b_1^2, 5b_1^2$

structure **II**: $1a_u^2, 1b_g^2, 2b_g^2, 2a_u^2, 3a_u^2, 3b_g^2, 4a_u^2$

structure **III**: $1b_{3u}^2, 1b_{2g}^2, 1b_{1g}^2, 1a_u^2, 2b_{3u}^2, 2b_{1g}^2, 3b_{3u}^2$

For these electron configurations one could easily obtain the following total π-electron energies:

$$E_\pi(C_{2v}) = 14\alpha + 24.486\beta$$

$$E_\pi(C_{2h}) = 14\alpha + 24.814\beta$$

and

$$E_\pi(D_{2h}) = 14\alpha + 24.566\beta$$

These values of the π-electron energies clearly indicate that structure **II** is the more stable one for the naphthazarin molecule. The energy difference between structures **I** and **II** is equal

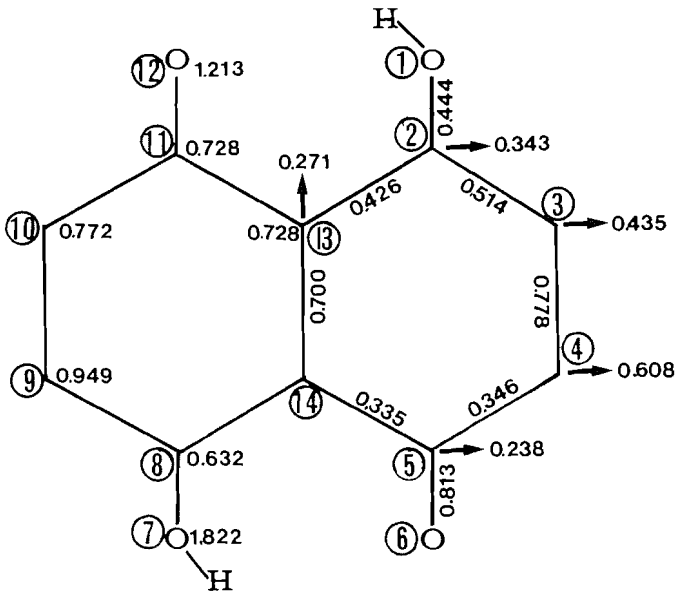

FIG. 1. Homobinuclear chelates of naphthazarin.

to 0.328β which corresponds to about 5.576 kcal. The present quantum chemical results justify both the assumption made by Bratan and Strohbusch (15) that the 1,4-quinoid structure must have a higher energy than the 1,5-quinoid structure and the results of the X-ray structure determination (12). The calculated bond orders (Fig. 1) for the more stable C_{2h} structure of naphthazarin are in accordance with the bond lengths calculated by X-ray structure determination (12). Also in Fig. 1 are shown the charge densities q_i on each atom i and the free valence number F_i. Both HOMO and LUMO in the centrosymmetrical 1,5-quinoid structure are localized on the benzenoid system of the molecule.

The D_{2h} structure of naphthazarin is an average of two equivalent centrosymmetrical C_{2h} structures which are interconverted by fast tunneling of the two protons (15). However, since the tunneling rates decrease exponentially with increasing mass of the tunneling particle, the D_{2h} structure could not be adopted in metal chelates where the hydrogen atoms of naphthazarin are substituted from the heavier metal ions. Thus in metal chelates we would expect structure **II** to predominate over the other structures. In fact, this assumption was justified by the examination of the electronic and ir spectra of the chelates under investigation.

In Table 1 the obtained singlet electronic transition energies for the 1,5-quinoid structure are compared with the experimental ones. A brief description of the MO's involved in the reported transitions and their symmetry and polarization are given. It must be noted that for the metal chelates only the intraligand transitions are reported in Table 1. From the results presented in Table 1 it is evident that the electronic spectra of naphthazarin and those of its metal chelates are well interpreted in terms of the C_{2h} symmetry for the naphthazarinato moiety. Although we did not take into consideration configuration interaction, a good agreement is found between theoretical and experimental data.

The C_{2h} structure of the naphthazarinato ligand in its metal chelates was further supported from the examination of the ir spectra. The most relevant absorption bands in the ir spectra of the investigated chelates together with their tentative assignments are listed in Table 2. All the chelates showed a number of intense bands in the region of 1200–1700 cm^{-1}. In naphthazarin the stretching frequency of the carbonyl groups occurs at 1621 cm^{-1}, while that of the coordinated carbonyl groups in the metal chelates is shifted to lower wavenumbers. The shifts amount to some 65 cm^{-1}. The $\nu(C\cdots O)_1$ band in naphthazarin is broader than in the metal chelates, a fact which can be ascribed to a superposition of two absorptions at almost the same frequency for the naphthazarin molecule (15). The bands which are superimposed were the expected B_{1u} and B_{2u} normal modes of the carbonyl groups for a D_{2h} structure of naphthazarin. On the other hand, the narrow $\nu(C\cdots O)_1$ band of the studied chelates is indicative of a C_{2h} structure for the naphthazarinato ligand, since only one band of B_{1u} symmetry is expected for a C_{2h} structure. Of considerable importance are also the bands which occur in the region of about 1280 cm^{-1}. These bands were attributed to the $\nu(C\cdots O)_2$ stretching frequencies (16–18) and show the same pattern as the $\nu(C\cdots O)_1$ bands. These bands are thus again narrow and sharp in the case of the metal chelates, indicative for the C_{2h} structure of the naphthazarinato ligand. The position of the $\nu(C\cdots O)_2$ bands indicates that the C—O bond has a significant fractional double bond character as would be expected from the extension of the π-electron system of the ligand. Finally, in the ir spectra of the chelates studied were observed all the bands, which are characteristic of the 2,2′-bipyridyl ligand (19–21) and the PF_6^- anion (22), as well as of the MO_2N_2 moiety (23, 24).

Conductivity measurements in the case of the copper(II) chelate in DMF solutions gave Λ_μ = 159 mho cm^2 mol^{-1}, a value which is in the range of the values observed for 1:2 electrolytes in the same solvent (25). Unfortunately, the low solubility of the nickel(II) and zinc(II) chelates in DMF prevented the conductivity measurements for these chelates, although very dilute solutions showed that these compounds are also electrolytes. The above data clearly show that the investigated chelates are homobinuclear dicationic compounds containing the binucleating naphthazarinato ligand as a bridging unit with the C_{2h} structure. The excess positive charge is balanced by PF_6^-. It must be noted that the X-ray structure determination on an analogous five-coordinated dicopper complex (2) showed that the bridging naphthazarinato unit adopts the C_{2h} symmetry. This fact further supports our results on the structure of the bridging naphthazarinato ligand in the four-coordinated homobinuclear chelates under investigation.

We have next attempted to explore the possible pathways for the magnetic exchange interactions observed in the investigated homobinuclear chelates of copper(II) and nickel(II), in terms of pairwise interactions of dimeric molecular orbitals. For this purpose we need to know, apart from the symmetry properties of the π-molecular orbitals of the naphthazarinato ligand, the symmetry properties of the orbitals of the metal ions which are occupied by the unpaired electron(s) as well. Therefore, we must first know the structure and symmetry of the MO_2N_2 moiety contained in these chelates. The magnetic data of the investigated chelates can be used for this purpose. Unfortunately, the crystal-field bands in the electronic spectra of the studied chelates correlated to their structures was impossible to be observed, since they are masked from the very intense intraligand and charge transfer transitions.

For the diamagnetic zinc(II) chelate, each metal ion is surrounded by two oxygen and two nitrogen donor atoms in a nearly tetrahedral geometry with C_{2v} symmetry, since it is well known that zinc(II) four-coordinated complexes adopt the tetrahedral structure. The paramagnetic nature of the four-

Can. J. Chem. Downloaded from www.nrcresearchpress.com by 210.87.254.6 on 09/06/12
For personal use only.

TABLE 1. Theoretical and experimental electronic transitions of the studied compounds

Nature	Symmetry*	Naphthazarin (C_{2h}) Calcd. (kK)	Naphthazarin (C_{2h}) Exp. (kK)	Zinc(II) chelate exp. (kK)	Nickel(II) chelate exp. (kK)	Copper(II) chelate exp. (kK)
$4a_u \rightarrow 4b_g$	B_u	9.30	—	—	—	—
$3a_u \rightarrow 4b_g$	B_u	16.34	16.34 18.01	16.53 17.79	16.00 16.83	16.53 17.92
$4a_u \rightarrow 5b_g$	B_u	19.73	19.42 20.61	19.04 20.20	18.52 20.41	19.34
$3a_u \rightarrow 5b_g$	B_u	26.76	28.98	26.72	27.30	27.02
$2a_u \rightarrow 4b_g$	B_u	30.18	—	—	—	—
$2a_u \rightarrow 5b_g$	B_u	40.60	37.45	38.01	37.81	36.40
$4a_u \rightarrow 6b_g$	B_u	43.80	—	—	—	—

*The electronic transitions are all xy-polarized.

TABLE 2. The most relevant ir frequencies (cm^{-1}) of the investigated compounds and their assignments

Compound	$\nu(C\cdots O)_1$	$\nu(C\cdots O)_2$
$C_{10}H_6O_4$	1621 vs	1232 vs
$[Cu_2(C_{10}H_4O_4)(C_{10}H_8N_2)_2](PF_6)_2$	1555 vs	1282 vs
$[Ni_2(C_{10}H_4O_4)(C_{10}H_8N_2)_2](PF_6)_2$	1556 vs	1278 m
$[Zn_2(C_{10}H_4O_4)(C_{10}H_8N_2)_2](PF_6)_2$	1560 vs	1271 m

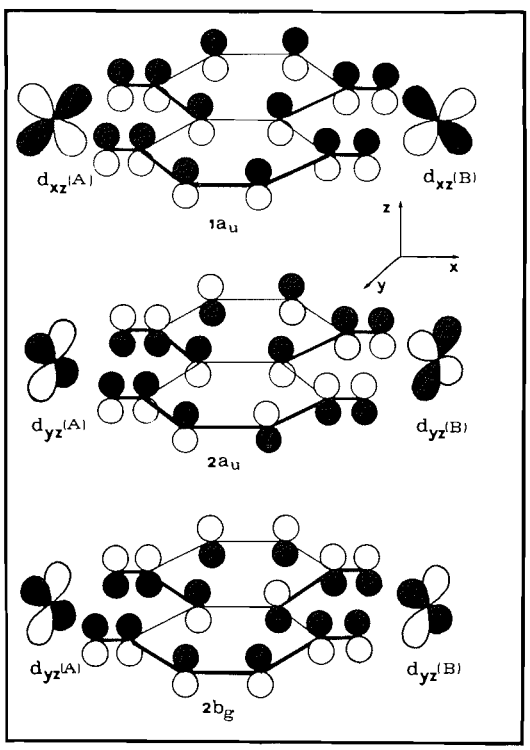

FIG. 2. Schematic representation of the possible interactions between dimeric MO's of the metal centers and π-MO's of the bridging unit supporting superexchange processes.

coordinated nickel(II) chelate (μ_{eff} = 1.69 BM, 1.73 BM, and 1.73 BM at 4000 G, 8000 G, and 11700 G, respectively) excludes the square-planar configuration and hence we can also accept the tetrahedral structure around the central atoms with C_{2v} symmetry for this chelate. For the copper(II) chelate the room temperature magnetic moment (μ_{eff} = 0.91 BM, 1.32 BM, and 1.29 BM at 4000 G, 8000 G, and 11700 G, respectively) does not give us any strong support for the square-planar or tetrahedral geometry, although in analogy with the other two chelates we have reason to believe that the copper(II) chelate probably also adopts the tetrahedral structure around the central atoms with C_{2v} symmetry. Nevertheless, as we shall see later, the magnetic exchange interactions observed exclude the square-planar structure for the copper(II) chelate. According to the above aspects all the homobinuclear chelates under investigation must have a centrosymmetric structure of C_{2h} symmetry with tetrahedral coordination geometry of the central atoms.

The room temperature magnetic data of the copper(II) and nickel(II) homobinuclear chelates reflect a considerable spin–spin interaction between the unpaired electrons on the two metal centers. The low magnetic moments observed both at low and high field strengths are indicative of the operation of antiferromagnetism in these compounds. Also the slight decrease of the magnetic moments as the magnetic field strength decreases is indicative of the operation of antiferromagnetism. These observations show that our binuclear d^9–d^9 system displays the singlet (antiferromagnetism) ground state. The same happens also in the binuclear d^8–d^8 system.

For the copper(II) binuclear chelate (d^9–d^9 system), if we assume the tetrahedral structure about the central atoms with local C_{2v} symmetry the unpaired electron at each copper(II) center will be located in one of the d_{xy}, d_{xz}, and d_{yz} atomic orbitals. All these three AO's are nondegenerate in the C_{2v} point group and belong to the A_2, B_1, and B_2 irreducible representations, respectively. Depending on the type of the AO in which the unpaired electron(s) reside, the magnitude of the magnetic exchange interactions will be gauged by the energy separation between the bonding and antibonding dimeric MO's, whose nature and symmetry in C_{2h} point group are:

$$\varphi_1 \sim d_{xy}(A) + d_{xy}(B) \qquad B_u$$
$$\varphi_2 \sim d_{xy}(A) - d_{xy}(B) \qquad A_g$$
$$\varphi_3 \sim d_{xz}(A) + d_{xz}(B) \qquad A_u$$
$$\varphi_4 \sim d_{xz}(A) - d_{xz}(B) \qquad B_g$$
$$\varphi_5 \sim d_{yz}(A) + d_{yz}(B) \qquad B_g$$
$$\varphi_6 \sim d_{yz}(A) - d_{yz}(B) \qquad A_u$$

Can. J. Chem. Downloaded from www.nrcresearchpress.com by 210.87.254.6 on 09/06/12
For personal use only.

Can. J. Chem. Downloaded from www.nrcresearchpress.com by 210.87.254.6 on 09/06/12
For personal use only.

On the bridging naphthazarinato unit there are π-molecular orbitals which belong to A_u and B_g irreducible representations. Hence, only the symmetry adapted combinations φ_3,φ_4 and φ_5,φ_6 resulting from the d_{xz} and d_{yz} AO's, respectively, can interact with the a_u and b_g π MO's of the ligand. The symmetry adapted combination $\varphi_3(a_u)$ can be combined with the $1a_u$, $3a_u$, and $6a_u$ π MO's of the ligand and the $\varphi_4(b_g)$ with the $1b_g$, $4b_g$, and $7b_g$ π MO's. On the other hand, the symmetry adapted combination $\varphi_5(b_g)$ can be combined with the $2b_g$, $3b_g$, and $5b_g$ π MO's and the $\varphi_6(a_u)$ with the $2a_u$, $5a_u$, and $7a_u$ π MO's. However, among the a_u and b_g π MO's of the ligand only those which do not contain any nodal plane between the two copper(II) centers will be able to support the propagation of the magnetic exchange interactions. Thus, only the $1a_u$, $2a_u$, and $2b_g$ π MO's of the ligand combined with the φ_3, φ_6, and φ_5 symmetry adapted combinations, respectively, will support the observed magnetic exchange processes. These possible combinations are depicted schematically in Fig. 2. The same situation is also expected to exist in the case of the nickel(II) chelate (d^8–d^8 system) where the two unpaired electrons on each nickel(II) center occupy the d_{xz} and d_{yz} AO's.

If now we assume for the copper(II) chelate the square-planar configuration (point group C_{2v}) the unpaired electron will be located in the $d_{x^2-y^2}$ AO which belongs to A_1 irreducible representation in the C_{2v} point group. In this case the magnetic exchange interactions will be gauged by the energy separation of the following bonding φ_1 and antibonding φ_2 MO's:

$$\varphi_1 \sim d_{x^2-y^2}(A) + d_{x^2-y^2}(B) \qquad A_g$$

$$\varphi_2 \sim d_{x^2-y^2}(A) - d_{x^2-y^2}(B) \qquad B_u$$

Since in the bridging naphthazarinato unit there are no π MO's of A_g and B_u symmetry any magnetic exchange interaction will not be allowed in this case. Hence, the observed magnetic exchange interactions in the copper(II) chelate is in support of the tetrahedral structure adopted also from this chelate as in the case of the nickel(II) and zinc(II) chelates.

In the previous discussion on the possible pathways for the magnetic exchange interactions supported by the π-electron system of the bridging naphthazarinato ligand we ignored its σ-electron system. CNDO/2 calculations on the naphthazarinato ligand in its C_{2h} structure showed (2) that there are σ-MO's pertaining to a_g and b_u symmetry species. Hence one would expect these MO's to interact with the φ_1 and φ_2 dimeric MO's in the case of the tetrahedral and square-planar homobinuclear chelates discussed above, since they pertain to the same symmetry species. However, the energies and the overlap characteristics of these MO's do not allow such interactions and therefore could not be possible pathways for magnetic exchange interactions (2). It is obvious then that the magnetic exchange interactions observed in our complexes are mainly supported by the π-electron system of the bridging naphthazarinato unit.

Finally, it is worthwhile to note that previous studies of the magnetic exchange interactions in analogous five- and six-coordinated homobinuclear complexes of copper(II) and nickel(II) showed that the naphthazarinato bridging unit does not have the ability to support such interactions (2). This is not surprising, since according to our results the ability of the bridging naphthazarinato ligand (C_{2h} symmetry) to support superexchange interactions through its extensive π-electron system depends on the coordination geometry about the central atoms which determines the nature of the d AO's where the unpaired electron(s) reside. Thus, for the five-coordinated dicopper complex, $[Cu_2(dien)_2(DHNQ)](BPh_4)_2$, the unpaired electron resides on the $d_{x^2-y^2}$ AO whose bonding and antibonding combinations pertain to a_g and b_u symmetry species, respectively. However, in the bridging naphthazarinato unit there are no π MO's of a_g and b_u symmetry and therefore no magnetic exchange interactions will expected for this complex. For the six-coordinated dinickel complex, $[Ni_2(tren)_2(DHNQ)](BPh_4)_2$, the two unpaired electrons will be located on the $d_{x^2-y^2}$ and d_{z^2} AO's whose bonding and antibonding combinations pertain to a_g and b_u symmetry species, respectively. It is obvious then that no magnetic interactions will be expected for this complex because of the lack of the suitable symmetry molecular orbitals in the bridging unit. Any magnetic exchange interaction supported by the σ MO's of the bridging ligand pertaining to a_g and b_u symmetry species is excluded on the basis of their energy and overlap characteristics (2).

We can conclude from our results that the naphthazarinato binucleating ligand in its C_{2h} structure could support magnetic superexchange interactions through its extensive π-electron system only in the case of four-coordinated homobinuclear chelates of copper(II) and nickel(II) with tetrahedral geometry. For other geometries, such as square-planar, square-pyramidal, trigonal bipyramidal, and octahedral naphthazarinato bridging unit could not support such phenomena, because of the lack of any possible pairwise orbital interaction between dimeric molecular orbitals in such coordination geometries.

1. H. F. HOLTZCLAW, JR. and H. D. COBLE. J. Inorg. Nucl. Chem. **36**, 1049 (1974).
2. C. G. PIERPONT, L. C. FRANCESCONI, and D. N. HENDRICKSON. Inorg. Chem. **17**, 3470 (1978).
3. E. F. HASTY, T. J. CORBURN, and D. N. HENDRICKSON. Inorg. Chem. **17**, 2636 (1978); earlier papers are referenced.
4. P. J. JAY, J. C. THIBEAULT, and R. HOFFMANN. J. Am. Chem. Soc. **97**, 4884 (1975).
5. J. A. BERTRAND, J. H. SMITH, and P. G. ELLER. Inorg. Chem. **13**, 1649 (1974).
6. G. W. WHELAND and D. E. MANN. J. Chem. Phys. **17**, 264 (1949).
7. A. STREITWIESER. J. Am. Chem. Soc. **82**, 4123 (1960).
8. M. L. JOSIEN, N. FUSON, J. M. LEBAS, and T. M. GREGORY. J. Chem. Phys. **21**, 331 (1953).
9. D. HADZI and N. SHEPPARD. Trans. Faraday Soc. **50**, 911 (1954).
10. E. MERIAN. Chimia, **13**, 181 (1959).
11. S. ALVARADO, F. FARINA, and J. L. MARTIN. Tetrahedron Lett. 3377 (1970).
12. P. D. CRADWICK and H. HALL. Acta Crystallogr. B**27**, 1990 (1971).
13. (*a*) H. L. K. SCHMANDT and P. BOLDT. J. Am. Chem. Soc. **97**, 447 (1975); (*b*) H. L. K. SCHMANDT, H. KRATZIN, and P. BOLDT. Liebigs Ann. Chem. 1560 (1976).
14. J. G. RODRIGUEZ, F. H. CANO, and S. GARCIA-BLANCO. Acta Crystallogr. B**33**, 491 (1977).
15. S. BRATAN and F. STROHBUSCH. J. Mol. Struct. **61**, 409 (1980).
16. R. M. ISSA, Y. Z. AHMED, and A. H. ZEWAIL. Egypt. J. Chem. **15**, 1 (1972).
17. M. ST. C. FLETT. J. Chem. Soc. 1441 (1948).
18. D. HADZI and N. E. SHEPPARED. J. Am. Chem. Soc. **73**, 5460 (1950).
19. S. P. SINHA. Spectrochim. Acta, **20**, 879 (1964).
20. S. P. SINHA. Spectrochim. Acta, **22**, 57 (1966).
21. R. G. INSKEEP. J. Inorg. Nucl. Chem. **24**, 763 (1962).
22. R. BELLAMY. The infrared spectra of complex molecules. Methuen, London. 1958.
23. K. KRISHNAN and R. PLANE. Inorg. Chem. **5**, 852 (1966).
24. M. MIKAMI, L. NAKAGAWA, and T. SHIMANOUCHI. Spectrochim. Acta, **23**A, 1037 (1967).
25. W. J. GEARY. Coord. Chem. Rev. **7**, 81 (1971).

Comparison of Mn^{2+}, Co^{2+}, and Cu^{2+} binding to fulvic acid as measured by fluorescence quenching

DAVID K. RYAN,[1] CARL P. THOMPSON, AND JAMES H. WEBER[2]
Department of Chemistry, University of New Hampshire, Durham, NH 03824, U.S.A.

Received July 28, 1982

DAVID K. RYAN, CARL P. THOMPSON, and JAMES H. WEBER. Can. J. Chem. **61**, 1505 (1983).

The binding of Cu^{2+} to soil-derived fulvic acid (SFA) measured by fluorescence quenching titration is much stronger than Co^{2+} and Mn^{2+} which are similar. The conditional stability constants from curve fitting at pH 6 are 1.1×10^5 for Cu^{2+}, 5.1×10^3 for Co^{2+}, and 4.2×10^3 for Mn^{2+}. The slight advantage in strength for Co^{2+} over Mn^{2+} is also demonstrated by the binding curves at pH 6 and 7. These two metal ions not only tend to bind more weakly but also bind to fewer sites, giving complexing capacity values of about 1.5×10^{-6} *M* compared to 2.0×10^{-5} for Cu^{2+} at pH 6. This lower binding capacity may be due to outer sphere complexation that does not allow access to some sites complexed by inner sphere binding Cu^{2+}. Scattering experiments demonstrate that Cu^{2+} is more effective at precipitating and aggregating SFA than Co^{2+} and Mn^{2+}. Cu^{2+} probably neutralizes the negative charges on SFA molecules allowing larger hydrophobic aggregates to form and precipitate.

DAVID K. RYAN, CARL P. THOMPSON et JAMES H. WEBER. Can. J. Chem. **61**, 1505 (1983).

La liaison du Cu^{2+} à l'acide fulvique provenant de la terre (AFT) mesurée par titration d'extinction de la fluorescence est plus forte que celle du Co^{2+} et du Mn^{2+} qui sont très semblables. Les constantes de stabilité conditionnelle tirées des courbes d'ajustement à un pH de 6 sont de $1{,}1 \times 10^5$ pour le Cu^{2+}, de $5{,}1 \times 10^3$ pour le Co^{2+} et de $4{,}2 \times 10^3$ pour le Mn^{2+}. On démontre également le léger avantage, du point de vue de la force, du Co^{2+} sur le Mn^{2+} à l'aide des courbes de liaison à des pH de 6 et 7. Ces deux ions métalliques non seulement tendent à se lier plus faiblement mais également se lient à un plus petit nombre de sites en donnant des valeurs de capacité de complexation d'environ $1{,}5 \times 10^{-6}$ *M* comparé à $2{,}0 \times 10^{-5}$ pour le Cu^{2+} à un pH de 6. Cette faible capacité de liaison peut être due à une complexation hors sphère qui ne permet pas l'accès à quelques sites complexés par la liaison du Cu^{2+} à l'intérieure de la sphère. Des expériences de dispersion démontrent que le Cu^{2+} est plus efficace pour précipiter et agglutiner le AFT que le Co^{2+} et le Mn^{2+}. Le Cu^{2+} neutralise probablement les charges négatives des molécules de AFT permettant ainsi à des agrégats hydrophobes plus volumineux de se former et de précipiter.

[Traduit par le journal]

Introduction

The transport, toxicity, and removal of trace metal ions in aquatic systems is intimately related to their speciation (1, 2). Under certain conditions naturally occurring humic and fulvic acids can play a major role in determining the forms of certain trace elements present in natural waters (3, 4). The ability to predict speciation of various metal ions in a given system relies heavily on the stability of metal complexes of organic matter and inorganic ligands. Only the latter complexes are relatively well understood. In order to obtain reliable information on the extremely complex trace metal – humic material interactions, existing data must be supported and confirmed using alternate methods. This is especially true for the challenging analytical problems that natural systems provide.

In this study the natural fluorescence of soil-derived fulvic acid (SFA) is used as a probe to compare the complexation of Mn^{2+}, Co^{2+}, and Cu^{2+} and to demonstrate the effect of pH. Binding of these paramagnetic metal ions to natural organic matter results in quenching of its fluorescence (5–9), and we have related this effect to the fraction of this natural ligand that is bound (5). This type of information is completely analogous to Scatchard's (10) $\bar{\nu}$ ([bound metal ion]/[total ligand]) which is usually calculated from free and total metal ion concentrations (7, 11, 12). However, fluorescence measures free ligand concentration and provides data that is complementary to ion-selective electrode (ISE) experiments or other methods that measure free metal ion in equilibrium with fulvic acid (7).

Our results have implications for the nature and strength of binding of Mn^{2+}, Co^{2+}, and Cu^{2+} to humic matter in natural waters. In addition, Rayleigh scattering experiments conducted simultaneously with fluorescence give valuable solubility information about SFA – metal ion complexes. We use scattering polarization measurements to determine whether or not aggregation of precipitate particles is significant.

Experimental

The apparatus and procedures used for fluorescence quenching titrations have been described in detail elsewhere (5, 6). All solutions used in this study were 10 mg/L SFA in 0.1 *M* KNO_3 and filtered through 0.4 nm filters. In all experiments the SFA solutions were titrated at constant pH with 1000 mg/L Mn^{2+}, Co^{2+}, or Cu^{2+} atomic absorption standards (Fisher, 50-M-81, 50-C-193, and 50-C-194). The fluorescence excitation wavelength was 350 nm with emission measured at 445 nm. Rayleigh scattering measurements were made with both excitation and emission monochromators set at 500 nm. Scattering polarization experiments were done at 400 nm with a SLM Instruments model 8000/8000S spectrofluorometer with data aquisition system. No wavelength filters were used between the sample and detector.

Results and discussion

Titrating a solution of SFA with a paramagnetic metal ion causes its fluorescence to be quenched (5, 7). The degree of quenching is related to two factors; the quenching ability of the metal ion and the extent of complexation. Figure 1 shows the decrease in fluorescence intensity of 10 mg/L SFA in 0.1 *M* KNO_3 as Mn^{2+} is added at pH 5, 6, 7, and 8. At least duplicate titrations were conducted for each pH and the reproducibility is fairly good. A trend of increased fluorescence quenching with increasing pH is clearly evident. This same trend is demonstrated for Co^{2+} in Fig. 2. These results are directly comparable to our previous work with Cu^{2+} (5) done under identical conditions and analogous to initial studies with these systems (7).

[1]Present address: Harold E. Edgerton Research Laboratory, New England Aquarium, Boston, MA 02110, U.S.A.

[2]To whom all correspondence should be addressed.

Can. J. Chem. Downloaded from www.nrcresearchpress.com by 210.87.254.42 on 09/06/12
For personal use only.

Can. J. Chem. Downloaded from www.nrcresearchpress.com by 210.87.254.42 on 09/06/12
For personal use only.

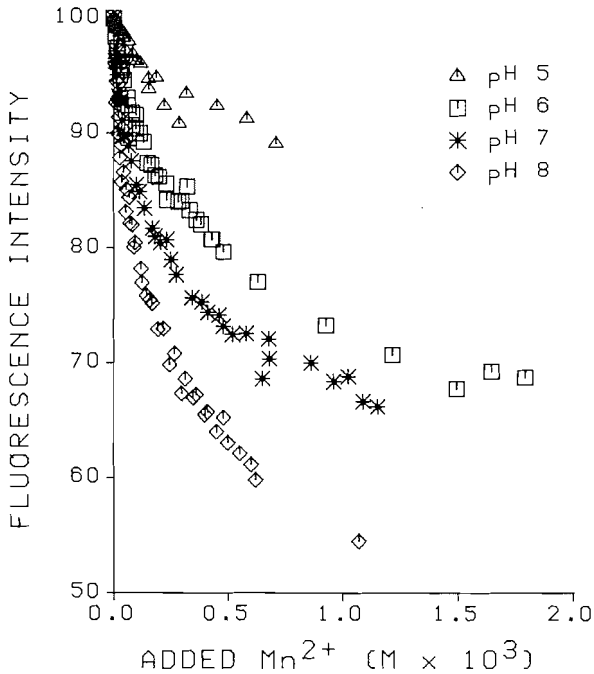

FIG. 1. Fluorescence quenching curves for 10 mg/L soil fulvic acid (SFA) with Mn^{2+} in 0.1 *M* KNO_3 at four pH values. Duplicate titrations are shown for pH 5 and 8, triplicates for pH 6 and 7.

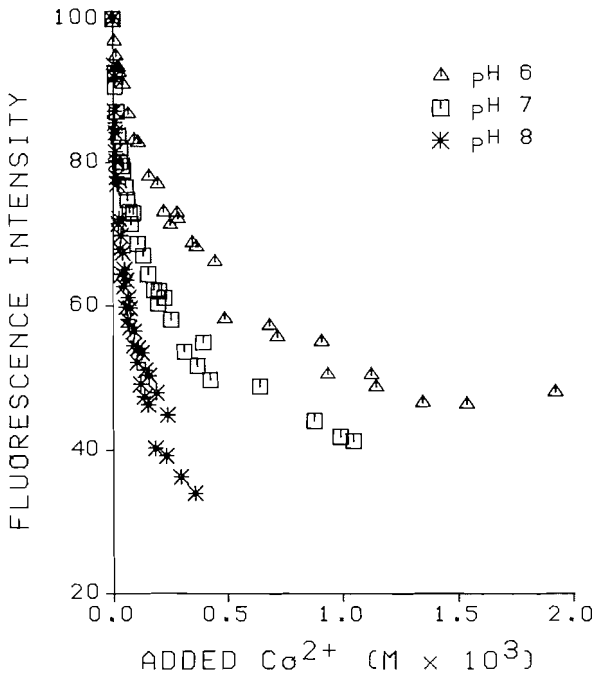

FIG. 2. Fluorescence quenching curves with Co^{2+} under the same conditions as in Fig. 1. Duplicate titrations are shown for pH 8, triplicates for pH 6 and 7.

We explain these data by noting that as pH increases conditional stability constants for weak acid ligands increase (13). At higher pH there is less competition from protons for potential metal ion binding sites. For a fixed ratio of total metal ion concentration (C_M) to total ligand concentration (C_L) the fraction of the ligand complexed will be greater at higher pH. The quenching ability of a given metal ion is assumed to be constant as pH is varied and the overall quenching effect is related to the extent of complexation. Changes in SFA fluorescence with pH

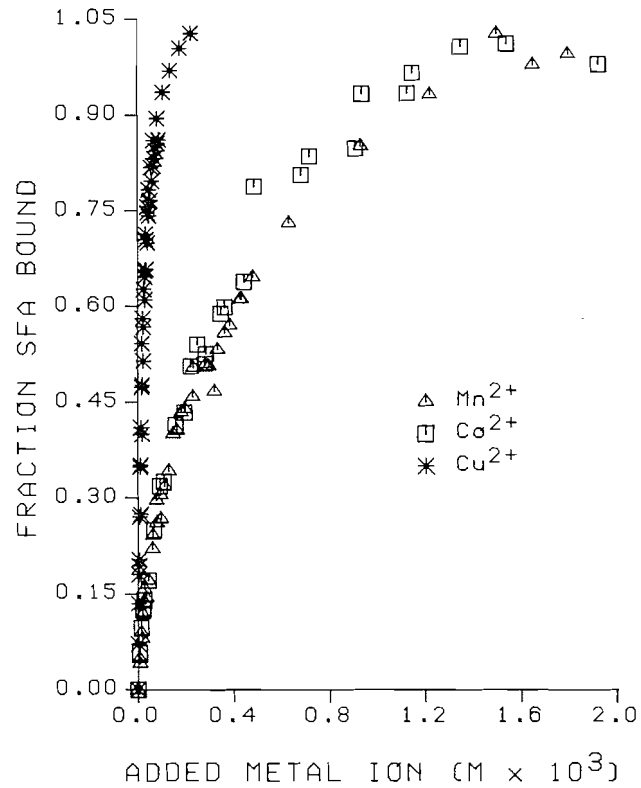

FIG. 3. Binding curves of total added metal ion concentration vs. fraction of soil fulvic acid bound ($[ML]/C_L$) for Mn^{2+}, Co^{2+}, and Cu^{2+} at pH 6. Results for Co^{2+} and Mn^{2+} and experimental conditions are the same as in Figs. 1 and 2. Dashed line indicates theoretical maximum where all SFA is bound.

in the absence of metal ion have been shown to be small in the pH range of these experiments (7). Therefore the trends observed in Figs. 1 and 2 show the effect of pH on the conditional stability constant.

We did not correct the data for metal ion hydrolysis. The general effect of hydrolysis is to reduce the amount of metal ion available to complex with SFA and quench its fluorescence. The fraction of the free metal ion hydrolyzed is constant at constant pH and is therefore easily accounted for. A more quantitative treatment has been given previously (6).

The relationship between the measured fluorescence intensity and complexation can be described mathematically by eq. [1].

$$[1] \quad [ML]/C_L = (I_L - I)/(I_L - I_{ML})$$

C_L is the total concentration of binding sites for the ligand, [ML] is the concentration of complex regardless of stoichiometry, and $[ML]/C_L$ is the fraction of ligand bound to the metal ion. The fluorescence intensity I is the measured value at any point in the titration and I_L and I_{ML} are the limiting intensities when all the ligand is free and bound, respectively. For convenience in making comparisons I_L is set to 100% in Figs. 1 and 2. The right side of eq. [1] describes fluorescence quenching as the ratio of the decrease in the initial fluorescence intensity observed at any point in the titration to the difference between the maximum and minimum values.

Equation [1] allows construction of binding curves (total added metal ion vs. fraction of SFA bound) from fluorescence titration data. Figures 3 (pH 6) and 4 (pH 7) show comparisons of this type for Mn^{2+}, Co^{2+}, and Cu^{2+}. Triplicate curves for

Can. J. Chem. Downloaded from www.nrcresearchpress.com by 210.87.254.42 on 09/06/12
For personal use only.

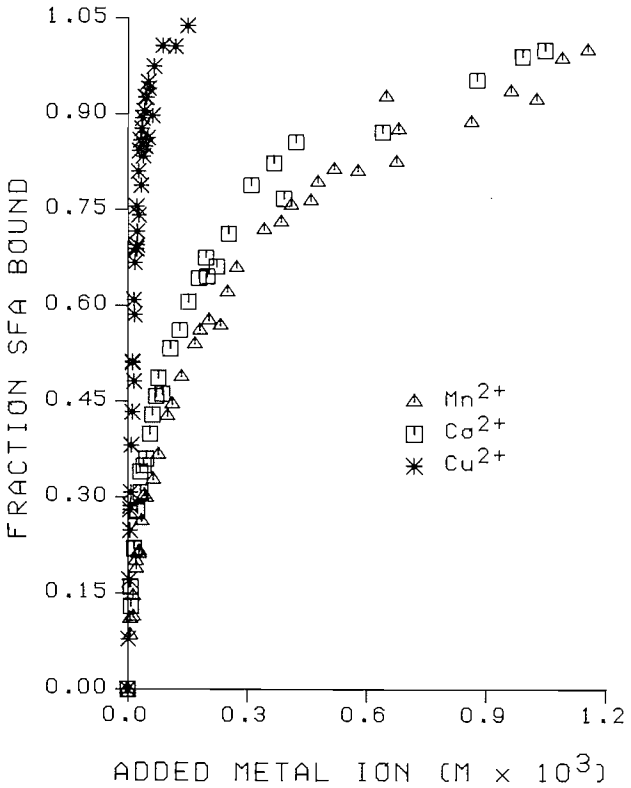

FIG. 4. Binding curve for pH 7, all other conditions are the same as in Fig. 3.

each metal ion are given at both pH values. Cu^{2+} binds very strongly at both pH's, and is at or near complete saturation of the ligand at about 1×10^{-4} *M* Cu^{2+} added. The curves for Mn^{2+} and Co^{2+} are quite similar to each other, but show much weaker binding than Cu^{2+}. In both Figs. 3 and 4 the curves for Mn^{2+} fall just below that for Co^{2+}, indicating that the conditional stability constant (K) for Mn^{2+}–SFA is slightly lower. Curve fitting analysis described previously (5, 6) substantiates this to some extent. Pooled replicate experiments at pH 6 gave conditional K values of 4.2×10^3 for Mn^{2+} and 5.1×10^3 for Co^{2+}. The C_L values were 1.5×10^{-6} *M* for both metal ions. These values compare with a K of 1.1×10^5 and C_L of 2.0×10^{-5} for Cu^{2+} at pH 6 (5). Experiments with Co^{2+} and Mn^{2+} at pH 7 did not converge on meaningful results for the constants; the fitted C_L values were negative. The most likely reason for this is that the pH 7 experiments were not carried far enough for curve fitting to be effective. From Fig. 4 it is evident that the Mn^{2+} and Co^{2+} curves do not quite level off at the end as they did for pH 6 (Fig. 3).

Various K values for complexation of these metal ions with different organic ligands also indicate that Cu^{2+} binds much more strongly than Co^{2+} and Mn^{2+}, whose binding strengths are similar. For example salicylic acid, a reasonable model ligand for fulvic acid, forms complexes of these metal ions with log K values of 5.9 for Mn^{2+}, 6.7 for Co^{2+}, and 10.6 for Cu^{2+} at 25°C and 0.1 *M* ionic strength (14). This trend is predominantly rationalized on the basis of "effective nuclear charge" (15). In addition Co^{2+} should have a slight advantage in binding strength over Mn^{2+} due to ligand field stabilization energy upon complex formation. The binding of Cu^{2+}, Co^{2+}, and Mn^{2+} to fulvic acid follows the relationships expected from inorganic considerations. In the large amount of literature on Cu^{2+} – fulvic acid complexation it is accepted that Cu^{2+} is among the strongest binding of the divalent cations (16). Co^{2+} and Mn^{2+} are generally considered to be much weaker than Cu^{2+} and often indistinguishable in binding strength.

To distinguish the type of binding of Mn^{2+} and Cu^{2+} to SFA Deczky and Langford (17) used nmr. Their results indicate that Mn^{2+} binds to SFA with its hydration shell intact. This outer sphere binding is opposite to the behavior of Cu^{2+} which loses its associated water molecules and shows inner sphere behavior. Although their work was done at pH 2 and 4, the interpretation can probably be extended to the higher pH values used in this study due to the very low hydrolysis constant of $10^{-10.5}$ for Mn^{2+} (18). Because of the outer sphere binding in Mn^{2+}–SFA, and by analogy in Co^{2+}–SFA, the attraction may be primarily electrostatic in nature, resulting in weaker binding.

The strength of metal ion – SFA binding can also affect the shapes of the relatively large molecules of SFA. Strong inner sphere complexation may cause conformational changes to make available binding sites that weaker outer sphere complexation of Mn^{2+} cannot induce. In the absence of metal ion the shapes of SFA molecules are probably mainly controlled by hydrogen bonding and electrostatic forces. In the pH 5 to 8 range of these studies the carboxyl groups are predominantly ionized and phenolic groups are partially ionized or essentially unionized. The repulsion between ionized carboxyls and possible hydrogen bonding between ionized carboxylate and unionized phenolic groups probably controls the shape of SFA molecules. A flat molecule may be folded over and held in a particular configuration in this way.

The same functional groups that determine conformation are also involved in binding metal ions. An ion such as Mn^{2+} that binds weakly is not effective at competing with protons for weakly acidic phenolic sites. It can therefore only bind to certain carboxyls. In addition many sites may be occluded in a microenvironment internal to a folded molecule of SFA. The strong binding of Cu^{2+}, however, can probably break up the majority of the existing hydrogen bonds by forming a very stable coordination complex with several sites. Bresnahan *et al.* (19) previously observed a large increase in Cu^{2+}–SFA binding between pH 5 and 6. The Cu^{2+} binding may alter the shape of the molecule and give it a new configuration. This new conformation is controlled by the Cu^{2+} ion and could consist of the molecule being fully or partially wrapped around one or more metal ion center. This type of conformational change may expose sites that were internal to the molecule, thus making them available for binding to additional Cu^{2+} ions. Mn^{2+} cannot induce the conformational changes so the internal sites remain unavailable, giving lower binding capacities for this metal ion.

The discussion of the type of binding of Mn^{2+} and Cu^{2+} to SFA may have implications for their fluorescence quenching ability. In the absence of conclusive structural and spectral information concerning the binding sites and fluorophors of fulvic acid it is impossible to determine the exact mechanism of quenching (20). However, any process will probably contribute to the quenching to a greater or lesser extent, depending on the distance of the metal ion center from the binding site. Mn^{2+} is insulated from the binding site by its hydration sphere. Thus it is probably farther from the fluorophore and may not perturb the orbitals of SFA to such a large degree. Therefore its quenching ability as well as its binding ability may be impaired. Co^{2+} may behave like Mn^{2+} as evidenced by similar binding ability.

TABLE 1. I_{ML} values at various pH values

	I_{ML}		
M^{2+}	pH 5	pH 6	pH 7
Mn^{2+}	—	68.6	66.2
Co^{2+}	—	46.9	41.2
Cu^{2+} [a]	40.2[b]	22.4	20.7

[a]Determined by curve fitting.
[b]Less reliable value (see ref. 5).

A direct comparison of the relative fluorescence quenching effects of Mn^{2+}, Co^{2+}, and Cu^{2+} on SFA can be made using I_{ML} values. Table 1 lists the experimentally determined values for Co^{2+} and Mn^{2+} from this work, and those determined from curve fitting for Cu^{2+} (5). These values represent the limit of quenching ability since they are the residual fluorescence, reported as percent of total, when $[ML]/C_L$ (eq. [1]) is unity. Some generalizations can be made from these data. Copper ion quenches to the greatest extent. For example, at pH 6 and 7 Cu^{2+} quenches nearly 80% of SFA fluorescence, Co^{2+} is less than half as effective, and Mn^{2+} is the poorest quencher by far. Cu^{2+} binds to many more sites than either Mn^{2+} or Co^{2+} and this is the reason for its greater quenching ability. However, these other ions are not capable of binding to the extent that Cu^{2+} does and therefore cannot quench as much. It is also evident from Table 1 that I_{ML} values decrease with increasing pH. The additional value for Cu^{2+} at pH 5 also supports this. The reason for the observed trend may be related to the variation of SFA fluorescence with pH (7). It must be noted that the values in Table 1 are reported as percentage of the maximum value at that pH. All fluorescence intensities in the absence of metal ion are normalized to 100% as discussed above.

Another marked difference was noted for Co^{2+} and Mn^{2+} compared with Cu^{2+} in titrations of SFA. Previous studies have shown that Cu^{2+} causes an increase in solution scattering and eventually effects the precipitation of fulvic acid (5, 12, 21) and natural water organic matter (6) while Co^{2+} and Mn^{2+} do not. In these titrations the maximum Co^{2+} and Mn^{2+} concentration attained was about five to ten times that of Cu^{2+}. We observed no scattering increase for Mn^{2+}, a relatively small increase for Co^{2+}, and a large increase for Cu^{2+}. Sholkovitz and Copeland (22) obtained similar results for the coagulation of river organic matter by Cu^{2+}, Co^{2+}, and Mn^{2+}. They found Co^{2+} gave no measurable precipitation and Mn^{2+} very little, while Cu^{2+} and Fe^{3+} were extremely effective. Their conclusion is that cation-induced coagulation is less for Mn^{2+} and Co^{2+} because of their weaker association to humic materials. In this study, since Co^{2+} and Mn^{2+} did not cause a great deal of scattering, it was possible to conduct the titrations well into the region where fluorescence leveled off. This allowed direct experimental determination of I_{ML} values which was not possible for Cu^{2+} (5).

We previously proposed (5, 23) that Cu^{2+} induces aggregation of SFA as well as precipitation. Figure 5 curve *A* is a Rayleigh scattering titration curve for 10 ppm SFA in 0.1 *M* KNO_3 with Cu^{2+} at pH 7. As Cu^{2+} is added, the number of precipitate particles formed increases and scattering increases. Of particular interest in Fig. 5 is the region of curve *A* near 1.5×10^{-4} *M* added Cu^{2+} where the slope decreases defining a break in the curve. Our previous work using centrifugation as well as scattering showed that precipitation did not cease in this region and we concluded that aggregation may be taking place

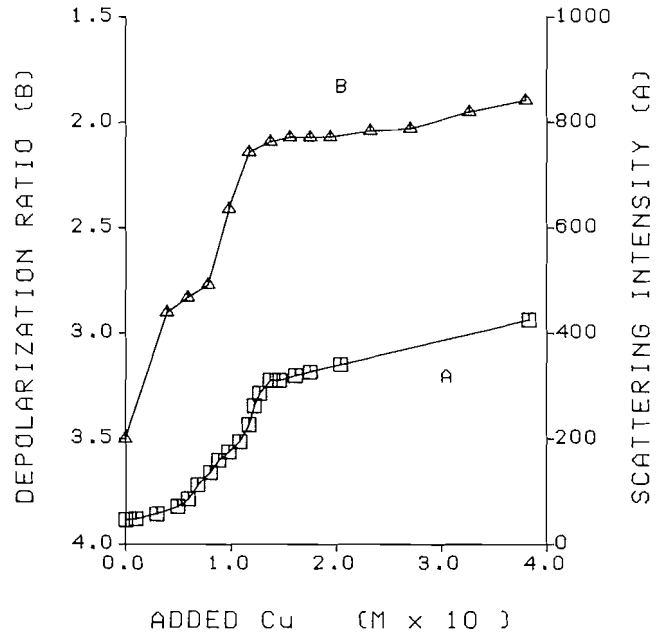

FIG. 5. Total added Cu^{2+} concentration vs. Rayleigh scattering intensity (arbitrary units) measured at 500 nm (curve A, right axis) and depolarization ratio ($I_\perp/I_\parallel$) measured at 400 nm (curve B, left axis) at pH 7. All other conditions are the same as in Figs. 1–4.

(5). The formation of large aggregates may explain why precipitation occurs with a simultaneous loss in sensitivity of scattering. The larger aggregates are less efficient at scattering light of a given wavelength than smaller particles (24). Thus, once aggregation becomes significant above 1.5×10^{-4} *M* Cu^{2+} the rate at which scattering increases is less.

To support this conclusion we conducted a scattering polarization experiment. Using a plane-polarized source, allowed measurement of the intensity of Rayleigh scattering for both parallel ($I_\parallel$) and perpendicular ($I_\perp$) components. The scattering polarization of a Cu^{2+}–SFA solution also changes as Cu^{2+} is added and binds to SFA. From Fig. 5 (curve *B*) it is evident that the depolarization ratio ($p = I_\perp/I_\parallel$) decreases rapidly at first and then seems to level off, decreasing slowly after that. This behavior is inversely related to the Rayleigh scattering in curve *A*.

The decrease in the depolarization ratio indicates that the scattering particles are becoming more isotropic (25). That is to say the initial Cu^{2+}–SFA particles formed are probably somewhat anisotropic (possibly pancake shaped (26)), but may become more isotropic due to aggregate formation. The aggregates may more closely approach a spherical shape giving rise to isotropic scattering and lower depolarization ratios. Although the evidence presented does not conclusively prove the proposed theory of aggregate formation, it is presented as a possible explanation. This phenomenon also explains why the Rayleigh scattering curve undergoes a "break" or drastic change in slope at the same total Cu^{2+} concentrations as the depolarization curve. The scattering intensity of unpolarized light measured at 90° may have some extra components of polarization due to anisotropy (25). As aggregates form and the scattering particles become more isotropic, the added component due to anisotropic scattering becomes less. Thus the scattering does not increase as rapidly once the polarization has leveled off. The effect of anisotropy on scattering can be written

Can. J. Chem. Downloaded from www.nrcresearchpress.com by 210.87.254.42 on 09/06/12
For personal use only.

[2] $I_s = I_R + I_a$

where I_s is the measured scattering intensity, I_R the Rayleigh component, and I_a the anisotropic component. This effect may be rather large due to the size of p. An equation has been derived to calculate the additional scattering due to anisotropy (I_a) from polarization data (25). For SFA with no Cu^{2+} added this is 1.08. At the end of the titration it is 1.03. Thus corrections of scattering intensity for anisotropy may be important for SFA and have bearing on molecular weight calculated from light scattering (21).

Acknowledgement

This work was supported in part by grant OCE79-10571 from the National Science Foundation.

1. G. SPOSITO. Environ. Sci. Technol. **15**, 396 (1981).
2. W. B. NEELEY. Chemicals in the environment–distribution, transport, fate, analyses. Marcel Dekker, New York. 1980.
3. T. M. FLORENCE and G. E. BATLEY. CRC Crit. Rev. Anal. Chem. **9**, 219 (1980).
4. R. F. C. MANTOURA and J. P. RILEY. Anal. Chim. Acta, **76**, 97 (1975).
5. D. K. RYAN and J. H. WEBER. Anal. Chem. **54**, 986 (1982).
6. D. K. RYAN and J. H. WEBER. Environ. Sci. Technol. **16**, 866 (1982).
7. R. A. SAAR and J. H. WEBER. Anal. Chem. **52**, 2095 (1980).
8. M. SCHNITZER and K. GHOSH. Soil Soc. Am. J. **45**, 25 (1981).
9. J. T. CLINE and J. F. HOLLAND. Fluorometric evidence for the reaction of heavy metals with pore water organics. ERDA Symp. Series **42**, 1977. pp. 264–279.
10. G. SCATCHARD. Ann. N.Y. Acad. Sci. **51**, 660 (1949).
11. R. A. SAAR and J. H. WEBER. Environ. Sci. Technol. **14**, 877 (1980).
12. R. A. SAAR and J. H. WEBER. Geochim. Cosmochim. Acta, **44**, 1381 (1980).
13. A. RINGBOM and E. WÄNNINEN. *In* Treatise on analytical chemistry. Part 1. Vol. 2. *Edited by* I. M. Kolthoff and P. J. Elving. Interscience, New York. 1979.
14. A. E. MARTELL and R. M. SMITH. Critical stability constants. Vol. 3: Other organic ligands. Plenum Press, New York. 1977. p. 186.
15. J. E. HUHEEY. Inorganic chemistry principles of structure and reactivity. 2nd ed. Harper and Row, New York. 1978.
16. R. F. C. MANTOURA, A. DICKSON, and J. P. RILEY. Estuarine Coastal Mar. Sci. **6**, 387 (1978).
17. K. DECZKY and C. H. LANGFORD. Can. J. Chem. **56**, 1947 (1978).
18. C. F. BAES and R. E. MESMER. The hydrolysis of cations. Wiley-Interscience, New York. 1976. pp. 267–274.
19. W. T. BRESNAHAN, C. L. GRANT, and J. H. WEBER. Anal. Chem. **50**, 1675 (1978).
20. C. A. PARKER. Photoluminescence of solutions with applications to photochemistry and analytical chemistry. Elsevier, New York. 1968.
21. A. W. UNDERDOWN, C. H. LANGFORD, and D. S. GAMBLE. Anal. Chem. **53**, 2134 (1981).
22. E. R. SHOLKOVITZ and D. COPELAND. Geochim. Cosmochim. Acta, **45**, 181 (1981).
23. D. P. RAINVILLE and J. H. WEBER. Can. J. Chem. **60**, 1 (1982).
24. E. D. OLSEN. Modern optical methods of analysis. McGraw-Hill, New York. 1975.
25. H. GUTFREUND. *In* MPT international review of science. Biochemistry series one. Vol. 1. Butterworth's University Press, Woburn, MA. 1974. p. 359.
26. A. LAPEN and W. R. SEITZ. Anal. Chim. Acta, **134**, 31 (1982).

Can. J. Chem. Downloaded from www.nrcresearchpress.com by 210.87.254.42 on 09/06/12
For personal use only.

Photoisomerization of gaseous tetramethylethylene in the far ultraviolet

GUY J. COLLIN[1] AND HÉLÈNE DESLAURIERS

Département des Sciences Fondamentales, Université du Québec à Chicoutimi, Chicoutimi (Qué.), Canada G7H 2B1

Received November 12, 1982

GUY J. COLLIN and HÉLÈNE DESLAURIERS. Can. J. Chem. **61**, 1510 (1983).

We have studied the gaseous photoisomerization of tetramethylethylene at 184.9 nm in the presence of various quenchers. The quantum yield of isomers is a function of the pressure, such that $[\Phi(\text{isomer})]^{-1} = a + b[P]^{-1}$. It is shown that the isomerization efficiency of a quencher M correlates with the intermolecular well depth between the photoexcited molecule A* and the quencher M, $\epsilon_{A^*,M}$. The log of the efficiency of isomerization is a linear function of this well depth.

Moreover, molecular oxygen, nitric oxide, and temperature have distinctive effects on the photoisomerization quantum yield measured at 213.8 nm: oxygen has a reverse effect, whereas nitric oxide induces a very strong isomerization.

GUY J. COLLIN et HÉLÈNE DESLAURIERS. Can. J. Chem. **61**, 1510 (1983).

La photoisomérisation du tétraméthyléthylène gazeux a été systématiquement étudiée à 184.9 nm en présence de plusieurs intercepteurs. L'inverse du rendement quantique des isomères croît linéairement avec l'inverse de la pression du stabilisant. Les efficacités du stabilisant semble corréler l'importance du puits de potentiel, $\epsilon_{A^*,M}$, entre la molécule excitée et la molécule ou l'atome stabilisant, de telle sorte que le log de l'efficacité de l'isomérisation est une fonction linéaire de ce puits de potentiel.

En outre l'oxygène moléculaire, l'oxyde nitrique et la température ont un effet très particulier sur la photoisomérisation à 213,8 nm: l'oxyde nitrique induit une très forte isomérisation tandis que l'oxygène a un effet contraire.

Introduction

In a recent paper, we reported the photolytic study of tetramethylethylene (TME) at 184.9 nm and in the region very close to the absorption threshold, i.e. at 213.8 and 228.8 nm. At low pressure, between 1 and 30 Torr, two families of products have been observed. In the first one, there are products such as 3-methyl-1,2-butadiene, 2,3-dimethyl-1,3-butadiene, 2-butyne, and isoprene. They are formed in the fragmentation processes of the photoexcited molecule; their quantum yield decreases with an increase in the pressure of the reaction chamber. Isomers are products of the second one: they are 2,3-dimethyl-1-butene (2,3-DM-1-B), 3,3-dimethyl-1-butene (3,3-DM-1-B), and 1,1,2-trimethylcyclopropane (1,1,2-TMCP). The quantum yield of these compounds increases with an increase in the total pressure (1).

In this report we intend to focus our attention on the isomerization processes in order to improve, if possible, the knowledge of the relationship between these processes and the nature of the available excited electronic states formed in the photoabsorption process.

Experimental

The experimental methods and details have already been described (1). Tetramethylethylene and cyclohexane are API products (impurity 0.08 ± 0.2 and 0.007 ± 0.004 mol%, respectively). All other additives are from Matheson of Canada. They have a purity stated as being more than 99.99%, except CH_3Cl (99.5%), n-C_4H_{10} (99.9%), and NO (99.0%). They are used as received. All these materials and the photolytic mixtures were analyzed by gas-chromatography using a squalane column and a double flame ionization detector (1).

In the temperature effect study at 213.8 nm, the reaction chamber was built with a double wall containing a water circulating system. Thus, the inside wall of the reaction chamber has the desired temperature, except for the quartz window, which is at room temperature. The shape and volume of the reaction chamber are similar to those of the already described photolytic cell (1).

Results

The results are shown in tables and graphs. They are presented as quantum yields. At this point, a correction to the previous quantum yields reported at 184.9 nm should be made. In the data processing, a factor of 2.0 was forgotten, so that all the previous quantum yields reported in ref. 1 must be divided by this factor.

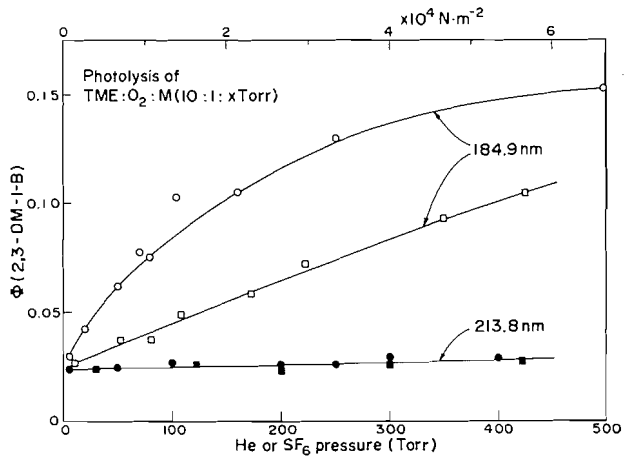

FIG. 1. Photolysis of TME:O_2:M (10:1:x Torr) mixtures at 213.8 (●, ■) and 184.9 nm (○, □). M = SF_6 (○, ●) or He (□, ■).

TABLE 1. 213.8 nm photoisomerization of TME temperature effects[a]

	Φ		
T(°C)	2,3-DM-1-B	3,3-DM-1-B	1,1,2-TMCP
10	0.026	0.014	0.018
20	0.027	0.015	0.019
40	0.030	0.013	0.022
62	0.034	0.016	0.022
72	0.039	0.018	0.024

[a]Starting mixture TME:O_2:SF_6 (10:1:200 Torr); $\Delta\Phi/\Phi \simeq 10\%$. The variation of pressure resulting from the temperature changes has a negligible effect on the quantum yields.

(a) At 213.8 nm

(*1*) The isomerization of the starting material is much less pronounced than observed at 184.9 nm: Fig. 1.

(*2*) An increase of the temperature from 10 to 72°C has a

[1]To whom all correspondence should be addressed.

Can. J. Chem. Downloaded from www.nrcresearchpress.com by 210.87.254.6 on 09/06/12
For personal use only.

Can. J. Chem. Downloaded from www.nrcresearchpress.com by 210.87.254.6 on 09/06/12
For personal use only.

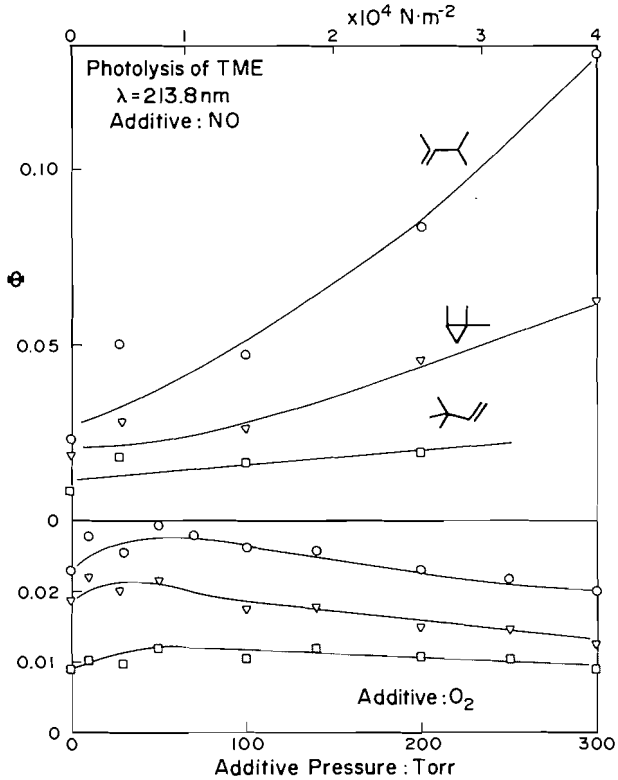

FIG. 2. Photolysis of TME (10 Torr) at 213.8 nm in the presence of either NO (upper part) or O_2 (lower part).

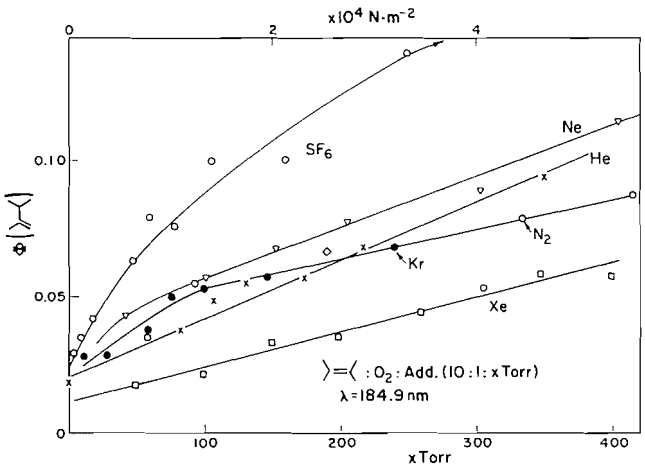

FIG. 3. Photolysis of TME:O_2:M (10:1:x Torr) mixtures at 184.9 nm: the quantum yield of 2,3-DM-1-B versus the pressure of quencher, x.

rather small effect on the 3,3-DM-1-B and 1,1,2-TMCP quantum yields and a more pronounced one on that of 2,3-DM-1-B: Table 1.

(*3*) The addition of NO results in a very strong increase of the isomer quantum yields: compare the effects of NO and SF_6 in Figs. 1 and 2.

(*4*) The addition of O_2 has a reverse effect on the isomer quantum yields: a small increase may be observed at low oxygen content ($P \leq 50$ Torr). At higher oxygen pressure, the three isomer quantum yields decrease: Fig. 2.

(b) At 184.9 nm

(*1*) Figures 3–5 show the general increase in the quantum

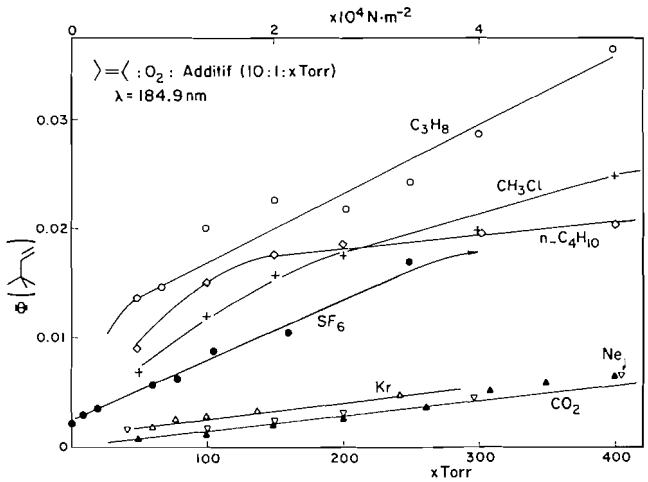

FIG. 4. Photolysis of TME:O_2:M (10:1:x Torr) mixtures at 184.9 nm: the quantum yield of 3,3-DM-1-B versus the pressure of quencher, x.

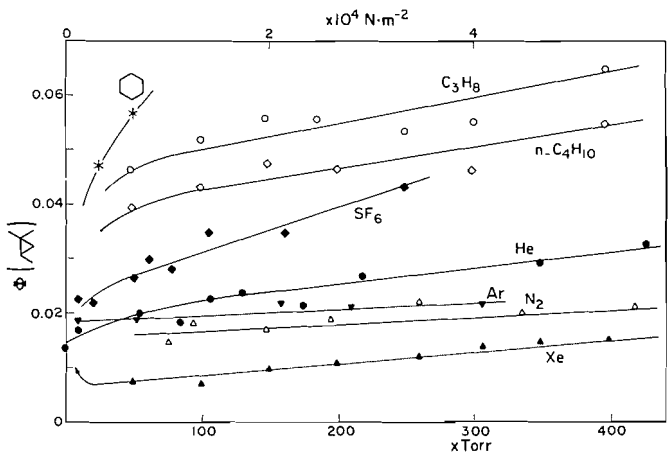

FIG. 5. Photolysis of TME:O_2:M (10:1:x Torr) mixtures at 184.9 nm: the quantum yield of 1,1,2-TMCP versus the pressure of quencher, x.

yield of each of the three isomers with an increase in the pressure of the chosen additive. At first glance, it can be stated that an increase in the pressure results in an increase of the isomerization. However, a comment must be made for the xenon and CO_2 cases. Although they follow the above stated rule, the addition of a few Torr of one of them decreases the isomer quantum yields. At high pressures, they are among the worst additive as far as efficiency in isomerization is concerned.

(*2*) The addition of 10 or 100 Torr of NO to 10 Torr of TME does not change the 1,1,2-TMCP quantum yield and multiplies by ca. 4.0 the 2,3-DM-1-B quantum yield: $\Phi_{NO}(1,1,2\text{-TMCP}) = 0.02$ and $\Phi_{NO}(2,3\text{-DM-1-B}) = 0.08_5$.

Discussion

(a) At 184.9 nm

In the previous paper from this laboratory, a mechanism was proposed in order to explain such an isomerization (1);

[1] TME + $h\nu \rightarrow$ TME* ($I\phi^*$)

[2] TME* $\rightarrow$ TME (+ $h\nu_0$ or I.C.)

[3] TME* + TME $\rightarrow$ 2 TME

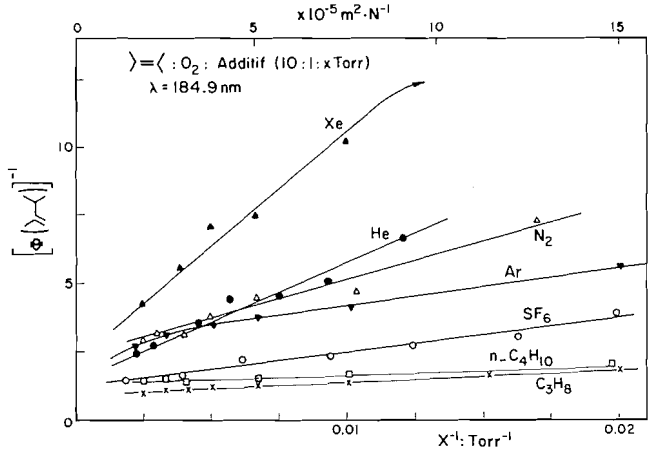

FIG. 6. The reverse of Φ(2,3-DM-1-B) versus the reverse of the additive pressure.

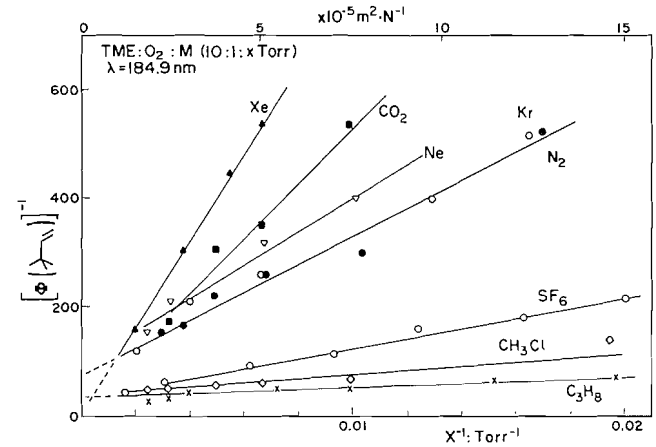

FIG. 7. The reverse of Φ(3,3-DM-1-B) versus the reverse of the additive pressure.

[4] $TME^* + TME \rightarrow P^* + TME$ (→ isomer P)

[5] $TME^* + M \rightarrow TME + M$

[6] $TME^* + M \rightarrow P^* + M$ (→ isomer P)

Process [2] contains very low fluorescence: $\Phi(h\nu_0) \simeq 2 \times 10^{-5}$ (2) and also fragmentation processes at low pressure following the internal conversion of the electronic energy of the photoexcited molecule. Processes [3] and [5] are deactivation processes brought about by physical collisions and processes [4] and [6] are of the induced preisomerization kind. A simple kinetic treatment of this mechanism leads to the following expression:

$$[A] \quad \frac{\phi^*}{\Phi(P)} = \frac{k_2 + [TME](k_3 + k_4) + [M](k_5 + k_6)}{k_4[TME] + k_6[M]}$$

Two interesting limiting cases are obvious. If [M] = 0, [A] becomes

$$[A'] \quad \frac{1}{\Phi(P)} = \frac{k_2}{k_4[TME]\phi^*} + \frac{k_3 + k_4}{k_4\phi^*}$$

and if [M] ≫ TME, it becomes

$$[A''] \quad \frac{1}{\Phi(P)} = \frac{k_2}{k_6[M]\phi^*} + \frac{k_5 + k_6}{k_6\phi^*}$$

Thus, in both cases, the inverse of the isomer quantum yields is a linear function of the inverse of the pressure either of TME (1) or M. Figures 6 and 7 are examples of this behavior. Table 2 gives a systematic report for expressions [A'] or [A'']. It includes all data measured at M pressure above 100 Torr: [M] ≥ 10[TME]: and $[\Phi(\text{isomer})]^{-1} = a + b[M]^{-1}$. The a value, taken at $[M]^{-1} = 0$, is the inverse of the quantum yield of the pertinent isomer formed in the presence of a very high amount of the additive M. Table 3 shows these quantum yields at "infinite" pressure. Thus additives are more or less efficient as far as isomerization is concerned. The rare monoatomic gasses are among the least efficient. On the other hand, CH_3Cl and propane are very good.

At this "infinite" pressure all processes included in process [2] may be ignored in a first approximation: $\phi^* = 1.0$. In any case, fluorescence has a very low quantum yield and the fragmentation processes are negligible at 100 Torr and higher pressures. Thus, in the presence of TME alone, the total efficiency for isomerization is 0.29, and the deactivation process [3] accounts for 71% of the TME* + TME colliding process. It can likewise be assumed that the ratio $k_3/(k_3 + k_4)$ for propane is 0.33_8 and, of course, $k_4/(k_3 + k_4)$ is 0.66_2 or less. Thus, one third of the TME* + C_3H_8 efficient collisions lead to isomerization.

At this point, it is relevant to come back to the expression [A'']. By using helium as a reference, the following expression may be deduced.

$$[B] \quad \frac{b(He)}{b(M)} = \frac{k_2}{\phi^* k_{6,He}} \times \frac{\phi^* k_{6,M}}{k_2}$$

or

$$\frac{b(He)}{b(M)} = \frac{k_{6,M}}{k_{6,He}}$$

where b(He) and b(M) are the slope of the plot $[\Phi(\text{isomer})]^{-1}$ versus $[M]^{-1}$ (Table 2), and $k_{6,M}$ and $k_{6,He}$ are the second order rate constants for the M or He induced preisomerization processes. By correcting each k value by the square of the collision diameter and by the reduced mass of the colliding partners, such that

$$k_{x,y} = A_{x,y}(\sigma_x + \sigma_y)^2 \mu_{x,y}^{-1/2}$$

one may calculate the $A_{6,M}/A_{6,He}$ ratios (Table 4). The same kind of calculations may be done with the zero intercepts, ($[M]^{-1} = 0$) of the same plots.

$$[C] \quad \frac{a(He)}{a(M)} = \frac{k_{5,He} + k_{6,He}}{\phi^* k_{6,He}} \times \frac{k_{6,M}\phi^*}{k_{5,M} + k_{6,M}}$$

or

$$\frac{a(M)}{a(He)} \times \frac{A_{6,M}}{A_{6,He}} = \frac{A_{5,M} + A_{6,M}}{A_{5,He} + A_{6,He}}$$

The results are shown in Table 5. Thus, both Tables 4 and 5 indicate the relative efficiencies of processes [5] and processes [5] + [6] for each quencher and isomer. Lin *et al.* (3) have developed a relationship "to correlate the rate constants k_M or cross-sections σ_M for a series of added gasses M which collisionally induce a state formation A* → B" (3). The relation is

$$[D] \quad \ln k_M = \ln C + \beta(\epsilon_{MM}/k)^{1/2}$$

Can. J. Chem. Downloaded from www.nrcresearchpress.com by 210.87.254.6 on 09/06/12
For personal use only.

TABLE 2. Photoisomerization of TME at 184.9 nm[a], experimental values for $[\Phi(\text{isomer})]^{-1} = a + b[M]^{-1}$

M	2,3-DM-1-B			3,3-DM-1-B			1,1,2-TMCP		
	r^2 [d]	a[c]	b[f]	r^2	a	b	r^2	a	b
He	0.86	9.1	1 040	0.98	33.7	41 400	0.63	29.2	1 880
Ne	0.91	21.6	470	0.90	105	32 000	—	42	—
Ar	0.88	19.8	730	0.98	—	75 000	0.69	35	2 720
Kr	0.93	9.8	920	0.98	100	23 000	0.82	43	1 490
N_2	0.96	8.2	1 060	0.97	60	26 000	0.80	40.4	1 700
CH_4	0.98	6.6	405	0.99	42	8 300	0.94	23.4	820
SF_6	0.93	5.7	480	0.98	30	9 200	0.86	21.6	740
SF_6[b]	0.97	6.4	520	0.99	22	11 500	0.91	25	600
Xe	0.98	6.8	4 000	0.86	94	58 000	0.91	44.4	10 000
C_3H_8	0.90	4.1	150	0.93	28	2 400	0.70	16.6	250
n-C_4H_{10}	0.98	5.1	140	0.96	35	3 600	0.74	19.4	310
CO_2	—	n.m.	n.m.	0.99	30	48 000	0.94	56	7 400
CH_3Cl	0.94	4.5	290	0.99	27	5 800	0.89	19.2	440
C_6H_{12}[e]	0.99	4.4	350	0.93	29	5 600	0.97	26.6	260

[a]Starting mixtures: TME:O_2:M (10:1:x Torr) with $x \geq 100$ Torr.
[b]See ref. 1
[c]See ref. 1, TME.
[d]Correlation coefficient of the linear regression.
[e]In units of $[\Phi]^{-1}$.
[f]In units of $[\Phi]^{-1}$ [Torr].

TABLE 3. Photoisomerization of TME at 184.9 nm, quantum yields of isomers at "infinite" pressure

M	Quantum yield			
	2,3-DM-1-B	3,3-DM-1-B	1,1,2-TMCP	Σ[b]
He	0.110	0.03_0	0.03_4	0.17_4
Ne	0.093	0.01_0	0.02_4	0.12_7
Ar	0.102	0.00_6	0.03_0	0.13_8
Kr	0.102	0.01_0	0.02_3	0.13_5
N_2	0.113	0.01_4	0.02_5	0.15_2
CH_4	0.152	0.02_4	0.04_3	0.21_9
SF_6	0.176	0.03_4	0.04_6	0.25_6
SF_6[a]	0.165	0.04_5	0.04_0	0.25_0
Xe	0.14_0	0.01_1	0.02_3	0.17_4
C_3H_8	0.24_3	0.03_5	0.06_0	0.33_8
n-C_4H_{10}	0.19_6	0.03_0	0.05_1	0.27_1
CO_2	n.m.[c]	0.02_7	0.01_6	$>0.04_3$
CH_3Cl	0.21_2	0.03_5	0.05_0	0.29_7
C_6H_{12}[a]	0.22_5	0.03_5	0.03_7	0.29_0

[a]See ref. 1.
[b]Sum of the isomer quantum yields.
[c]Not measured.

where C and β are constants and ϵ_{MM} is the well depth between pairs of M molecules. Figures 8 and 9 are the plots of ln $A_{6,M}$ and ln $(A_{5,M} + A_{6,M})$ versus $(\epsilon_{MM}/k)^{1/2}$ and show such correlations. In Fig. 8, the three lines represent the best sets of data points ($r^2 = 0.93$). In the 2,3-DM-1-B case, the Ne, Xe, C_3H_8, and n-C_4H_{10} data have not been included. It is obvious that neon gives a very high efficiency; the same seems also true for the two alkanes, whereas Xe has very low efficiency. In the 3,3-DM-1-B and 1,1,2-TMCP cases, the same set of data has been included in the linear regressions. Again, Ne and Xe have been ignored as well as CO_2 and Ar, but now propane and n-butane are included. Figure 9 shows a much less obvious interpretation. The 3,3-DM-1-B line gives a good correlation coefficient provided that the Ne, CH_3Cl, Xe, and CO_2 cases are discarded. The 2,3-BM-1-B case gives two possible answers: either the He and CH_3Cl points or the C_3H_8 and n-C_4H_{10} points are included ($r^2 = 0.90$); Ne, Ar, and Xe are obviously discarded. Finally, the 1,1,2-TMCP coefficient of determination is poor: $r^2 = 0.88$. At this point, it should be recalled that the (ϵ_{MM}/k) values may be derived through several methods giving rise to various results. Thus, uncertainties are associated with these values (3, 4). However, it is obvious that CO_2 and Xe have very low efficiency. As noted by Lin *et al.*, there are several exceptions and many quenchers present a large deviation from the correlation. For example, Ne was noted as a "special case", and the "heavy atom effect of Xe" is well known (3). From the ratio given in Fig. 9, it appears that if xenon reacts with TME* at a rate higher or much higher than does helium, it gives rise to products different from those formed in the processes [5] and [6]. Resonance specific to some M partners may be present, and their data do not fit in with the above correlations. This may be the case for TME itself, where the agreement is not good (Fig. 9). However, it is beyond the scope of this paper to speculate deeply on these exceptions.

(b) At 213.8 nm

As has been said above the isomerization quantum yields are lower at this wavelength compared to what they are at 184.9 nm. In order to avoid absorption of light by O_2 at 184.9 nm, the effect of this quencher was made at 213.8 nm. Although there is a small increase of the isomer quantum yields at low pressure, these quantum yields decrease smoothly with high oxygen content: the pressure effect is the reverse. Thus, oxygen does not promote the isomerization; it reacts slowly with the photoexcited molecule; when it does so, isomers are not among the products. The effect of molecular oxygen in a photochemical system is rather complex (5). Some electronic S_1-T mixings may be present in this system.

On the other hand, the nitric oxide effect is rather important. Although the well depth for SF_6 is greater than the NO one by a factor of 1.33 (3), NO has a much higher efficiency as far as isomerization is concerned. Again, the effect of nitric oxide in a photochemical system may be complex (6), and possible

Can. J. Chem. Downloaded from www.nrcresearchpress.com by 210.87.254.6 on 09/06/12
For personal use only.

TABLE 4. Photolysis of TME at 184.9 nm, relative efficiencies of isomerization[a]

M	M (g)	σ_M (Å)[d]	Relative efficiency 2,3-DM-1-B	3,3-DM-1-B	1,1,2-TMCP
He	4	2.2	1.0	1.0	1.0
Ne	20	2.8	3.9	2.3	—
Ar	40	3.4	2.9	1.1	1.4
Kr	84	3.6	2.7	4.3	3.1
N_2	28	3.7	1.6	2.7	1.9
CH_4	16	3.82	3.4	6.5	3.0
SF_6	146	5.51	4.1	8.5	4.8
SF_6[b]	—	—	3.8	6.8	5.9
Xe	131	4.1	0.63	1.73	0.45
C_3H_8	44	4.8	9.5	23.7	10.3
n-C_4H_{10}	58	5.0	12.4	19.2	10.1
CO_2	44	4.5	—	1.46	0.43
CH_3Cl	50	3.6	7.5	14.9	8.9
C_6H_{12}[c]	84	6.0	4.6	11.4	11.2

[a]Arbitrary units: $A_{6,M}/A_{6,He}$.
[b]See ref. 1.
[c]TME; in that case: $A_{4,M}/A_{6,He}$.
[d]See ref. 11.

TABLE 5. Photolysis of TME at 184.9 nm, total relative efficiencies[a]

M	$(\epsilon_{MM}/k)^{1/2}$[d]	Total relative efficiency 2,3-DM-1-B	3,3-DM-1-B	1,1,2-TMCP
He	3.2	1.0	1.0	1.0
Ne	5.9	9.4	7.2	—
Ar	11.0	6.3	—	1.7
Kr	13.1	2.9	12.9	4.5
N_2	9.7	1.5	4.7	2.6
CH_4	12.1	2.4	8.1	2.4
SF_6	14.2	2.6	7.6	3.6
SF_6[b]	—	2.7	4.5	5.1
Xe	14.9	0.47	4.8	0.68
C_3H_8	15.3	4.3	19.7	5.7
n-C_4H_{10}	17.5	6.9	19.9	6.7
CO_2	14.0	—	1.3	0.82
CH_3Cl	19.8	3.7	11.9	5.7
C_6H_{12}[c]	19.5	2.2	9.9	10.2

[a]Arbitrary units: $(A_{5,M} + A_{6,M})/(A_{5,He} + A_{6,He})$.
[b]See ref. 1.
[c]TME; $\epsilon_{MM}/k = 1.15T_b$.
[d]These values are from ref. 3, except in TME case. The sources include Lennard–Jones 12-6 values determined from virial coefficients, Stockmayer values, and estimates from boiling points.

intersystem crossing channels are open in the presence of NO.

In a recent study of the trimethylamine photolysis, Obi *et al.* observed that O_2 and NO quenched quite efficiently the fluorescence of trimethylamine (7). They suggested that the quenching effect of O_2 may be attributed to a charge transfer process occurring from the photoexcited molecule. In the present case, the process would be

[7] $\quad TME + O_2 \rightarrow [TME^+ \ldots O_2^-]^*$

Obviously, the NO quenching process and the O_2 one do not produce the same products.

At this wavelength the pressure of the additive was insufficient to be very far from the "infinite" limit. At this point, it is worthwhile to recall the relative yield of isomers measured in the neat liquid TME (8). Although in this report there was no indication of the incident wavelength used, it is likely that a continuum photolyzed the liquid sample from the cut-off of the quartz cell to the absorption threshold of TME. With these conditions, Kropp *et al.* found similar quantities of 2,3-DM-1-B and 3,3-DM-1-B and smaller quantities of TMCP (Table 6). These observations seem to suggest a strong wavelength dependence of the products as it was noted in the gas phase (1): Table 6. Moreover, it is interesting to note that the temperature effect was more pronounced on the 2,3-DM-I-B quantum yield than the one observed with the two other isomers.

Finally, it is worthwhile to recall some interesting observations made at 184.9 nm (Table 6). The 2,3-DM-1-B quantum yield is proportional to the total pressure: $\Phi(2,3\text{-DM-1-B}) = \alpha P$. The 3,3-DM-1-B and 1,1,2-TMCP quantum yields are such that $\Phi(x) = \delta + \lambda P$. Moreover, the ratio $\Phi(1,1,2\text{-TMCP})/\Phi(3,3\text{-DM-I-B})$ is closed to 4. Thus these last two products may be formed from the same intermediate, which is different from the one involved in the 2,3-DM-1-B

Can. J. Chem. Downloaded from www.nrcresearchpress.com by 210.87.254.6 on 09/06/12
For personal use only.

TABLE 6. Photoisomerization of TME, wave length effects

λ (nm)	TME[a]	O_2[a]	Φ 2,3-DM-1-B	Φ 3,3-DM-1-B	Φ 1,1,2-TMCP
184.9	32	3	0.07_6	0.00_7	0.03_2
213.8	50	5	0.017	0.009	0.013
228.8	105	10	0.27	0.58	1.0
≥200[b]	Liquid	—	18	17	4

[a]Pressure units: Torr (1 Torr = 133 Nm^{-2}).
[b]From ref. 8.

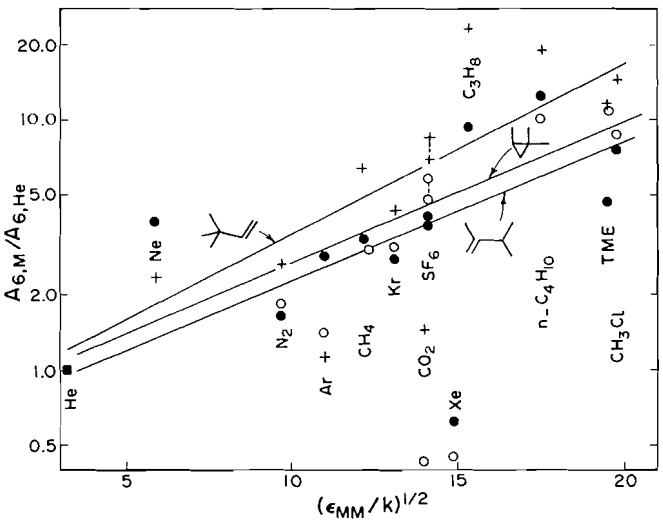

FIG. 8. The ln $(A_{6,M}/A_{6,He})$ versus $(\epsilon_{MM}/k)^{1/2}$ plot relative to 2,3-DM-1-B: ●, 3,3-DM-1-B: +, and 1,1,2-TMCP: ○. The lines correspond to the best correlations: see text. For (ϵ_{MM}/k) values, see footnote *d*, Table 5.

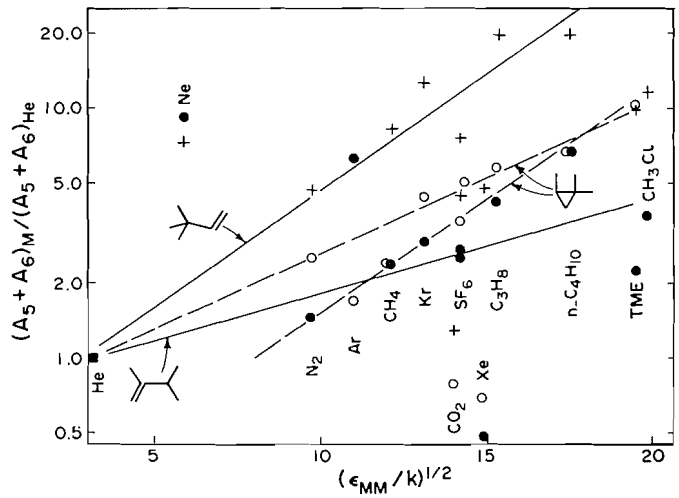

FIG. 9. The ln $|(A_5 + A_6)_M/(A_5 + A_6)_{He}|$ versus $(\epsilon_{MM}/k)^{1/2}$ plot relative to 2,3-DM-1-B: ●, 3,3-DM-1-B: +, and 1,1,2-TMCP: ○. The lines correspond to the best correlations: see text. For (ϵ_{MM}/k) values, see footnote *d*, Table 5.

formation. These observations are also in agreement with the observations made in the direct irradiation of TME in hydroxylic media (9).

[8] TME + $h\nu \rightarrow S_1 \rightarrow (TME)^{Ry}$

[9] TME + $h\nu \rightarrow \ldots \rightarrow (TME)^{?}$

[10] $(TME)^{Ry} \rightarrow (M)^{\cdot\cdot}$

[11*a*] $\longrightarrow$ 1,1,2-TMCP

[11*b*] $\longrightarrow$ 3,3-DM-1-B

[12] $(TME)^{?} \rightarrow$ 2,3-DM-1-B

where $(TME)^{Ry}$ is the Rydberg excited state; $(TME)^{?}$ is an unspecified excited state, but it may be the π,σ^* one since the π,π^* excited state is generally associated with the *cis–trans* isomerization. $(M)^{\cdot\cdot}$ has a carbene structure probably formed as a result of a 1,2-alkyl shift (10).

Acknowledgements

We would like to express our gratitude to NSERC and the "FONDS FCAC" for generous help. We are also indebted to Dr. P. Roberge (Laval University) for many helpful discussions.

1. G. J. COLLIN, H. DESLAURIERS, and A. WIĘCKOWSKI. J. Phys. Chem. **85**, 944 (1981).
2. F. HIRAYAMA and S. LIPSKY. J. Chem. Phys. **62**, 576 (1975).
3. H.-M. LIN, M. SEAVER, K. Y. TANG, A. W. W. KNIGH, and C. PARMENTER. J. Chem. Phys. **70**, 5442 (1979).
4. R. C. IRETON and B. S. RABINOVITCH. J. Phys. Chem. **78**, 1979 (1974).
5. N. J. TURRO. *In* Modern molecular photochemistry. The Benjamin/Cummings Publ. Co., Inc., Menlo Park, CA. 1978.
6. J. A. BARLTROP and J. C. DOYLE. *In* Principles of photochemistry. J. Wiley and Sons, New York, NY. 1978. p. 117.
7. K. OBI and Y. MATSUMI. Chem. Phys. **49**, 95 (1980).
8. P. J. KROPP, H. G. FRAVEL, JR., and T. R. FIELDS. J. Am. Chem. Soc. **98**, 840 (1976).
9. P. J. KROPP, E. J. REARDON, JR., Z. L. F. GAIBEL, K. F. WILLIARD, and J. H. HATTAWAY, JR. J. Am. Chem. Soc. **95**, 7058 (1973).
10. P. J. KROPP. US ARO Report, ARO-12810-2. 1978.
11. J. HAGEGE, P. C. ROBERGE, and C. VERMEIL. Trans. Faraday Soc. **64**, 3288 (1968).

Can. J. Chem. Downloaded from www.nrcresearchpress.com by 210.87.254.6 on 09/06/12
For personal use only.

A preparative and multinuclear nuclear magnetic resonance spectroscopic study of $As(SPh)_x(SePh)_{3-x}$ ($x = 0-3$), $Sb(SPh)_x(SePh)_{3-x}$ ($x = 0-3$), $Bi(SPh)_3$, $Bi(SePh)_3$, $[Sn(SPh)_x(SePh)_{3-x}]^-$ ($x = 0-3$), $Pb(SePh)_3^-$, and $Pb(SPh)_3^-$ and some related thiolatoplumbates(II)

J. J. Ivan Arsenault and Philip A. W. Dean[1]

Department of Chemistry, University of Western Ontario, London, Ont., Canada N6A 5B7

Received November 12, 1982

J. J. Ivan Arsenault and Philip A. W. Dean. Can. J. Chem. **61**, 1516 (1983).

The phenyl selenolates of tin(II), lead(II), arsenic(III), antimony(III), and bismuth(III), $M(SePh)_n$ (M = Sn(II) or Pb(II), $n = 2$; M = As(III), Sb(III), or Bi(III), $n = 3$), have been synthesized by acid–base reaction of the appropriate metal acetate (for M = Sn(II) or Pb(II)) or thiophenolate (for all five elements) with PhSeH, and characterized by elemental analysis and, for the Group V elements, ^{77}Se and ^{13}C nmr spectroscopy.

$M(SPh)_2$ and $M(SePh)_2$ (M = Sn(II) or Pb(II)) are poorly soluble in MeOH but dissolve in the presence of an equimolar or greater amount of PhS^- or $PhSe^-$. The soluble stannate(II) complexes are triligated as shown by the slow exchange ^{119}Sn and, where appropriate, ^{77}Se nmr spectra of the series $[Sn(SPh)_x(SePh)_{3-x}]^-$ ($x = 0-3$) measured for the supernatant liquor of mixtures in which $\{Sn(EPh)_2\}_{total}/PhE^-_{total} > 1$. The corresponding plumbate(II) complexes are probably triligated also, but are labile on the nmr timescale; the parent complexes $Pb(EPh)_3^-$ have been characterized in solution by ^{207}Pb and ^{13}C (E = S and Se) and ^{77}Se (E = Se) nmr spectroscopy. For both Pb(II) and Sn(II), the order of chemical shifts in the metal nmr spectra is $\delta(MSe_3) > \delta(MS_3)$. The metal nmr spectra of the mixtures $M(SePh)_2:PhSe^-:PhS^- \approx 1:2:4$ (M = Sn(II) or Pb(II)) show that the coordination of $PhSe^-$ occurs in preference to coordination of PhS^- for both tin(II) and lead(II).

Thiolatoplumbates(II) might be formed during some antidotal treatments for lead poisoning, so "fingerprint" ^{207}Pb nmr spectra have been measured for a range of model soluble species formed in $Pb(SR)_2$–(excess)RS^- mixtures in MeOH, including some mixtures containing newly synthesized and characterized lead thiolates derived from dithiolate anions. For RS^- = MeS^-, EtS^-, PhS^-, $C_6H_{11}S^-$ (for which "$Pb(SR)_2$" has been shown to be $Pb(SC_6H_{11})(OAc)$), $^-S(CH_2)_2S^-/2$, $^-SCH_2CHS^-Me/2$, and $^-SCH_2CHS^-CH_2OH^2$, δ_{Pb} (from $PbMe_4$ in toluene as reference) falls in the comparatively short range 2518–2999 ppm.

The redistribution of ligands between $M(SPh)_3$ and $M(SePh)_3$ in chloroform to give equilibrium mixtures of $M(SPh)_x(SePh)_{3-x}$ occurs slowly on the preparative timescale for M = As, rapidly on the preparative timescale but slowly on the ^{13}C and ^{77}Se nmr timescales for M = Sb, and rapidly on the ^{13}C and ^{77}Se nmr timescales for M = Bi. Thus ^{13}C and, where appropriate, ^{77}Se nmr data are reported for $M(SPh)_x(SePh)_{3-x}$ (M = As or Sb) and $Bi(EPh)_3$ (E = S or Se). In addition, it has been possible, using ^{13}C nmr assessment of species distribution in the systems $Sb(SPh)_3$–$As(SePh)_3$ and $Bi(SPh)_3$–$As(SePh)_3$, to deduce that for the trivalent Group V elements the order of preference for $PhSe^-$ over PhS^- as ligands is Bi > Sb > As.

Trends in the ^{13}C nmr data for $M(SPh)_x(SePh)_{3-x}$ (M = As or Sb) and ^{77}Se nmr data for a range of metal complexes of $PhSe^-$ have been discussed. The selenium chemical shifts are influenced primarily by the acceptor atom and are in the order Cd(II) < Zn(II) < Pb(II) < Sn(II) < As(III) < Bi(III) < Sb(III).

J. J. Ivan Arsenault et Philip A. W. Dean. Can. J. Chem. **61**, 1516 (1983).

On a synthétisé les sélénolates de phénylétain(II), arsenic(III), antimoine(III) et bismuth(III), $M(SePh)_n$ (M = Sn(II) ou Pb(II), $n = 2$; M = As(III), Sb(III) ou Bi(III), $n = 3$) en utilisant une réaction acide–base de l'acétate métallique approprié (pour M = Sn(II) ou Pb(II) ou du thiophénolate (de tous les 5 éléments) avec le PhSeH et on les a caractérisés par l'analyse élémentaire et, dans le cas des éléments du groupe V, par le spectroscopie de rmn du ^{77}Se et du ^{13}C.

Le $M(SPh)_2$ et le $M(SePh)_2$ (M = Sn(II) ou Pb(II) sont faiblement solubles dans le MeOH mais ils se disolvent en présence d'une quantité équimolaire ou plus de PhS^- ou de $PhSe^-$. Les complexes de stannate(II) solubles sont tricoordonnés comme le montrent les spectres rmn d'échange lent du ^{119}Sn et lorsque le cas se présente, ceux du ^{77}Se des séries $[Sn(SPh)_x(SePh)_{3-x}]^-$ ($x = 0-3$), des mélanges de liqueur surnageante dans lesquelles le rapport $[Sn(EPh)_2]_{total}/PhE^-_{total} > 1$. Les complexes correspondants de plumbate(II) sont probablement tricoordonnés également, mais ils sont labiles dans l'échelle de temps de la rmn. On a caractérisé les complexes apparentés de $Ph(EPh)_3^-$ en solution par la spectroscopie de rmn du ^{207}Pb et du ^{13}C (E = S et Se) et du ^{77}Se (E = Se). L'ordre de grandeur des déplacements chimiques dans les spectres rmn du métal est de: $\delta(MSe_3) > \delta(MS_3)$ pour le Pb(II) et le Sn(II). Les spectres de rmn du métal des mélanges de $M(SePh)_2:PhSe^-:PhS^-$ 1:2:4 (M = Sn(II) ou Pb(II)) montrent que la coordination du $PhSe^-$ est privilégiée par rapport à celle du PhS^- dans le cas de l'étain(II) et du plomb(II).

Les thiolatoplombates(II) peuvent se former lorsqu'on utilise certains antidotes contre l'empoisonnement par le plomb. Ainsi on mesure les spectres de rmn du ^{207}Pb "empreintes digitales" d'un certain nombre d'espèces solubles modèles formées dans les mélanges de $Pb(SR)_2$–RS(excès) dans le méthanol incluant quelques mélanges contenant les nouveaux thiolates de plomb, dérivés des anions dithiolates, que l'on a synthétisés et caractérisés. Dans le cas où RS^- = MeS^-, EtS^-, PhS^-, $C_6H_{11}S^-$ (pour lesquels on a montré que le "$Pb(SR)_2$" est du $Pb(SC_6H_{11})(AcO)$), $^-S(CH_2)_2S^-/2$, $^-SCH_2CHS^-Me/2$ et $^-SCH_2CHS^-CH_2OH^2$, le δ_{Pb} (à partir du $PbMe_4$ dans le toluène comme référence) tombe dans l'intervalle comparativement courte de 2518–2999 ppm.

La redistribution des ligands entre $M(SPh)_3$ et $M(SePh)_3$ dans le chloroforme pour donner des mélanges à l'équilibre de $M(SPh)_x(SePh)_{3-x}$ se fait lentement à l'échelle préparative pour M = As, rapidement à l'échelle préparative mais lentement dans les échelles de temps de la rmn du ^{13}C et du ^{77}Se pour M = Sb, et rapidement dans l'échelle de temps de la rmn du ^{13}C

[1]To whom all correspondence should be addressed.

Can. J. Chem. Downloaded from www.nrcresearchpress.com by 210.87.254.6 on 09/06/12
For personal use only.

et du Se pour M = Br. Ainsi on rapporte les données de la rmn du ^{13}C et de la rmn du ^{77}Se, lorsque le cas se présente, relatives au complexe $M(SPh)_x(SePh)_{3-x}$ (M = As ou Sb) et $Bi(EPh)_3$ (E = S ou Se). De plus en utilisant les estimations, en rmn du ^{13}C, de la distribution des espèces dans les systèmes $Sb(SPh)_3-As(SePh)_3$ et $Bi(SPh)_3-As(SePh)_3$, il est possible de conclure que dans le cas des éléments trivalents du groupe V l'ordre de préférence pour $PhSe^-$ par rapport à PhS^- comme ligands est Bi > Sb > As.

On discute des tendances des données de la rmn du ^{13}C relatives au $M(SPh)_x(SePh)_{3-x}$ (M = As ou Sb et des données de la rmn du ^{77}Se se rapportant à un certain nombre de complexes métalliques du $PhSe^-$. Les déplacements chimiques du sélénium sont influencés en premier lieu par l'atome accepteur et sont dans l'ordre: Cd(II) < Zn(II) < Pb(II) < Sn(II) < As(III) < Bi(III) < Sb(III).

[Traduit par le journal]

Introduction

Recent publications from this laboratory have reported multinuclear nmr data for thiolato- and selenolato-zincates, -cadmates, and -mercurates(II) (1, 2). In addition, combined ^{113}Cd and ^{31}P nmr spectroscopic scrutiny of cadmium complexes of phosphine oxides, sulfides, and selenides (3–5) has shown these to be useful models for the ^{113}Cd nmr chemical shifts of the CdE_4 (E = O, S, or Se) kernels, among others. More lately, a ^{31}P and metal nmr investigation has been made of complexes of tin(II) and lead(II) with $EP(chx)_3$[2] (E = O, S, or Se), or mixtures of the sulfide and selenide, as ligands, and ^{119}Sn and ^{207}Pb chemical shift data (as appropriate) measured for the MO_3, MS_3, MSe_3, and MS_xSe_{3-x} (M = ^{119}Sn or ^{207}Pb) kernels (6). The last-mentioned results were intended to provide a basis for the metal nmr component of the multinuclear nmr study of thiolato- and selenolato-stannates(II) and -plumbates(II), which we now describe. As our work on the tin(II) and lead(II) species progressed, it became evident that a knowledge of the chemical and ^{77}Se and ^{13}C nmr spectroscopic behaviour of $M(SPh)_3$, $M(SePh)_3$ and, if possible, $M(SPh)_x(SePh)_{3-x}$ (M = As, Sb, or Bi), would be a useful complement, and details of our study of these species are provided here too.

Lead(II) thiolates, $Pb(SR)_2$, generally of poor solubility, have been extensively investigated (e.g. refs. 7–10), and in recent years their tin(II) analogs, which have similar solubility properties, have been a subject of interest also (e.g. refs. 9–12). We could find no previous mention of dissolution of these thiolates in the presence of excess thiolate ion or of characterization of the soluble species so formed.

The phenylthiolates of trivalent arsenic, antimony, and bismuth are known compounds (e.g. refs. 7, 9, 13, 14). In contrast the phenylselenolates of these elements have received little attention; as part of a brief study of $As(SePh)_3$ (prepared from $AsCl_3$ and $Me_3SiSePh$), ^1H nmr and low frequency infrared and Raman data but not analytical data were presented (15), and attempts to prepare $M(SePh)_3$ (M = As or Sb) from MCl_3 and NaSePh yielded only PhSeSePh (13). The arsenic–selenium bond is of particular interest because arsenic and selenium compounds may interact *in vivo* (e.g. refs. 16–19).

A vicinal dithiol, sodium 2,3-dimercaptopropane-1-sulfonate (DMPS), is now being used as a therapeutic chelator in cases of lead poisoning (20), and it seems possible soluble thiolatoplumbates might be formed during treatment. Therefore we have looked at a wider range of thiolate complexes in the case of lead(II) than in the cases of the other elements, for which only phenylthiolate has been used as a model thiolate ligand.

[2]Abbreviations used: chx = cyclohexyl (C_6H_{11}); BAL = $HSCH_2CH(SH)CH_2OH$; DMPS = $HSCH_2CH(SH)CH_2SO_3^-Na^+$.

Experimental

Materials

Reagent grade arsenic trichloride and lead methanethiolate and certified grade antimony trichloride, bismuth(III) and tin(II) oxides, and lead acetate, all from Fisher Scientific Co. Ltd., were used as received.

Proton nmr revealed no significant impurities in ethanethiol, cyclohexylthiol, ethanedithiol, 1,3-propanedithiol, 2,3-dimercapto-1-propanol (BAL), sodium 2,3-dimercapto-1-propanesulfonate (DMPS), bis(2-mercaptoethyl) ether or sulfide (all from Aldrich Chemical Co.), 1-mercapto-2-propanol (from K & K), 2-mercaptoethanol (from Eastman Kodak Co.), 1,2-propanedithiol, 1,2- or 1,4-butanedithiol or 1,5-pentanedithiol (all from Chemical Procurement Labs. Inc.), while ^{13}C nmr showed phenylthiol (Eastman Kodak Co.) and phenylselenol (Strem Chemicals, Inc.) to be satisfactorily pure; all these compounds were used without further purification.

The literature routes to bismuth(III) acetate (21), tin(II) acetate (22), $Pb(SPh)_2$ and $Pb(SEt)_2$ (8), $Bi(SPh)_3$ (9), and $As(SPh)_3$ and $Sb(SPh)_3$ (13) were used, except that $Sb(SPh)_3$ was prepared in ethanol, not benzene.

General manipulative procedure

All preparations and other manipulations involving thiols or phenylselenol or their anions were carried out using deoxygenated solvents under nitrogen or argon. All solid products were dried under vacuum. Solids known or suspected to be air-sensitive ($Sn(OAc)_2$, $Sn(SPh)_2$, and the Group IV and V phenylselenolates) were stored and weighed in a nitrogen-filled glovebox.

Preparation of lead(II) thiolates

Shaw and Woods (8) reported the synthesis of a range of compounds $Pb(SR)_2$ from simple monothiolates by addition of a stoichiometric amount of the thiol in ethanol to a solution of lead(II) acetate in aqueous ethanol. No dithiols were studied in this earlier work. We have investigated the applicability of the method of Shaw and Woods as a route to 1:1 compounds of Pb(II) with a variety of dithiolates, and have prepared in pure form[3] the compounds containing the dithiolates of ethanedithiol, propane-1,2- and -1,3-dithiols, butane-1,2- and -1,4-dithiols, pentane-1,5-dithiol, BAL, DMPS, and bis(2-mercaptoethyl) ether and sulfide, by combination of stoichiometric amounts of the dithiol in ethanol (or aqueous ethanol for DMPS) and lead acetate in aqueous ethanol at approximately 65°C. (The exact stoichiometry does not seem to be critical: 1:1, 2:1, and 1:2 mixtures of $Pb(OAc)_2$ and $HS(CH_2)_2SH$ all yielded the 1:1 product.) For comparison with the BAL complex, the compounds $Pb(SR)_2$ derived from 2-mercaptoethanol and 1-mercapto-2-propanol have also been made. Earlier, the 1:1 compound of lead(II) and the 2,3-dimercapto-1-propanesulfonate trianion has been synthesized from PbO and the parent acid of DMPS in water (25). Also, a compound $(\overline{S.Pb.S.CH_2.CHCH_2SO_3})_2Pb$ is said to be formed from $Pb(OAc)_2$ and DMPS (26).

In the earlier work (8), $Pb(OAc)_2$ and chxSH gave a product that could not be obtained analytically pure but which contained only about

[3]Several lead dithiolates have been prepared for use as synthetic intermediates in a route to cyclic disulfides (23, 24), but no evidence of purity was reported.

Can. J. Chem. Downloaded from www.nrcresearchpress.com by 210.87.254.6 on 09/06/12
For personal use only.

TABLE 1. Analytical data for some lead(II) thiolates, $Pb(SR)_2$

$(SR)_2$ in $Pb(SR)_2$	Formula	Colour	Analysis (%) Theoretical C	H	S	Found C	H	S
$S(CH_2)_2S$	$C_2H_4PbS_2$	Pale yellow	8.03	1.35	21.39	8.14	1.46	19.18
						8.18	1.44	21.85
SCH_2CHMeS	$C_3H_6PbS_2$	Bright yellow	11.49	1.93	20.43	11.56	2.10	20.35
SCH_2CHEtS	$C_4H_8PbS_2$	Bright yellow	14.68	2.46	19.55	14.67	2.41	20.17
$SCH_2CH(S)CH_2OH$	$C_3H_6OPbS_2$	Yellow	10.94	1.84	19.43	11.56	2.05	20.13
$SCH_2CH(S)CH_2SO_3^-Na^+$	$C_3H_5NaO_3PbS_3$	Yellow	8.68	1.21	23.12	8.68	1.30	22.85
$S(CH_2)_3S$	$C_3H_6PbS_2$	Bright yellow	11.49	1.93	20.43	11.42	1.97	21.08
$S(CH_2)_4S$	$C_4H_8PbS_2$	Bright yellow	14.68	2.46	19.55	14.71	2.44	18.51
$S(CH_2)_5S$	$C_5H_{10}PbS_2$	Bright yellow	17.59	2.95	18.75	17.67	3.22	18.65
$S(CH_2)_2S(CH_2)_2S$	$C_4H_8PbS_3$	Yellow	13.27	2.24	26.72	13.55	2.31	26.49
$S(CH_2)_2O(CH_2)_2S$	$C_4H_8OPbS_2$	Yellow	13.99	2.35		14.18	2.34	
$(S(CH_2)_2OH)_2$	$C_4H_{10}O_2PbS_2$	Off-white	13.30	2.79		13.97	2.58	
$(SCH_2CH(OH)Me)_2$	$C_6H_{14}O_2PbS_2$	Off-white	18.51	3.62		17.62	3.16	
$(SC_6H_{11})(OAc)$	$C_8H_{14}O_2PbS$	Yellow	25.19	3.70		25.34	3.73	
						26.32	4.48	

TABLE 2. Analytical data for some metal phenylselenolates

Compound	Formula	Colour	Analysis (%) Theoretical C	H	Found C	H
$Sn(SePh)_2$	$C_{12}H_{10}Se_2Sn$	Yellow	33.45	2.34	33.37	2.26
$Pb(SePh)_2$	$C_{12}H_{10}PbSe_2$	Orange	27.75	1.94	27.82	1.90
$As(SePh)_3$	$AsC_{18}H_{15}Se_3$	Pale yellow	39.80	2.78	39.89	2.82
$Sb(SePh)_3$	$C_{18}H_{15}SbSe_3$	Bright yellow	36.65	2.56	36.63	2.60
$Bi(SePh)_3$	$BiC_{18}H_{15}Se_3$	Deep red	31.92	2.23	31.74	2.20

half of the theoretical amount of sulfur. We find this compound to be Pb(Schx)(OAc).

Our results demonstrate that the method of Shaw and Woods (8) is of wide applicability. Analytical data for new lead thiolates, and those which have not been obtained previously from $Pb(OAc)_2$, are given in Table 1.

Preparation of $Sn(SPh)_2$ from $Sn(OAc)_2$

$Sn(SPh)_2$ was made from $Sn(OAc)_2$ and PhSH in essentially the same manner used for $Pb(SPh)_2$ (8): the stoichiometric amount of PhSH in ethanol was added to a well-stirred slurry of $Sn(OAc)_2$ in aqueous ethanol at 50°C, forming pale yellow insoluble $Sn(SPh)_2$. (Higher temperatures caused decomposition of the $Sn(OAc)_2$.) *Anal.* calcd. for $C_{12}H_{10}S_2Sn$: C 42.78, H 2.99; found: C 42.96, H 2.86.

As noted above, $Sn(SPh)_2$ has been prepared previously by a variety of routes (9–12) but not, apparently, by the one used here.

Preparation of $Sn(SePh)_2$ and $Pb(SePh)_2$

In a straightforward extension of the method used to prepare the phenylthiolates (ref. 8 and see above), the phenylselenolates formed when the stoichiometric amount of PhSeH in ethanol was added to a well stirred slurry of the appropriate metal(II) acetate in aqueous ethanol at room temperature. In both cases, stirring was continued for ca. 30 min before filtering off the product, which was yellow for tin(II) and orange for lead(II). Analytical data for the new compounds are given in Table 2.

These compounds could also be prepared by addition of a stoichiometric amount of PhSeH to a stirred slurry of the appropriate $M(SPh)_2$ at room temperature. The colours of the (insoluble) phenylselenolates are immediately apparent. If a slight excess of $M(SPh)_2$ is used, the supernatant liquor after 30 min stirring shows only PhSH by ^{13}C nmr, demonstrating the completeness of the selenol–thiol exchange.

Preparation of $As(SePh)_3$, $Sb(SePh)_3$, and $Bi(SePh)_3$

Preliminary ^{13}C nmr experiments showed that $M(SPh)_3$ (M = As, Sb, or Bi) in $CDCl_3$ underwent complete selenol–thiol exchange with PhSeH at a rate that was fast on the preparative timescale for Sb and Bi but slow for As. The synthesis of the metal(III) phenylselenolates took advantage of this behaviour. To a solution ($As(SPh)_3$) or slurry ($Sb(SPh)_3$ and $Bi(SPh)_3$) of the metal(III) phenylthiolate (5 mmol) in $CHCl_3$ at room temperature, PhSeH (slight excess over 15 mmol) was added. This addition resulted in a colour change (colourless to yellow) in the case of As(III), and a colour change (pale yellow to bright yellow for Sb(III); orange to deep red for Bi(III)) and solubilization for the other two elements. After stirring for an appropriate time (ca. 1 h for Bi or Sb; ca. 12 h for As) the solvent was removed *in vacuo*. The solids which remained were triturated with several aliquots of degassed methanol to remove possible contaminants (PhSH, PhSeH, or PhSeSePh), and finally dried *in vacuo*, to yield pale and bright yellow powders for $As(SePh)_3$ and $Sb(SePh)_3$, respectively, and dark red needles for $Bi(SePh)_3$. Analytical data for the new compounds are given in Table 2.

Nuclear magnetic resonance sample preparation

Solutions of $PhSe^-$ or PhS^- or other thiolates in methanol or CD_3OD were produced by stoichiometric acid–base reaction with $CH_3O^-Na^+$ or $CD_3O^-Na^+$, itself formed *in situ* from metallic sodium.

$M(SPh)_2$–$M(SePh)_2$–(PhS^- or $PhSe^-$) and $M(SPh)_2$–PhSeH mix-

Can. J. Chem. Downloaded from www.nrcresearchpress.com by 210.87.254.6 on 09/06/12
For personal use only.

Can. J. Chem. Downloaded from www.nrcresearchpress.com by 210.87.254.6 on 09/06/12
For personal use only.

tures for M = Sn or Pb were shaken or stirred for several minutes at room temperature, and then filtered into the nmr tube through a 10 mm fine sinter if necessary (as it was, for instance, in cases where excess $M(SPh)_2$ or $M(SePh)_2$ was used). The stoichiometry was chosen to ensure that in solution $[M]_{total} \approx 0.25$ *M*. Solutions were prepared from other $Pb(SR)_2-RS^-$ mixtures in the same manner.

$M(SPh)_3-PhSeH$ (M = As, Sb, or Bi), $M(SPh)_3-M(SePh)_3$ (M = As, Sb, or Bi), and $M(SPh)_3-M'(SePh)_3$ (M = Sb, M′ = As; M = Bi, M′ = As or Sb) mixtures, and samples of $M(SPh)_3$ and $M(SePh)_3$ alone, in $CHCl_3$ or $CDCl_3$, were made up from appropriate masses (volume for PhSeH) of the components, and filtered into the nmr tube through a 10 F sinter if necessary. Normally $[M]_{total}$ was kept at 0.25 *M*. However, a saturated solution of relatively poorly soluble $Bi(SPh)_3$ was used. Thorough flushing of nmr tubes, sinters, pipettes, etc. with N_2 or argon was *essential* for the preparation of stable solutions containing the phenylselenolates.

Nuclear magnetic resonance spectra were measured on freshly prepared samples if possible; if this was not possible, the samples were flame-sealed and stored in liquid nitrogen until the spectra could be obtained.

Nuclear magnetic resonance samples to be used for metal and ^{77}Se nmr studies of the stannous and plumbous complexes on the WH-400 were made up in flame-sealed 9 mm od hand made nmr tubes that were a sliding fit in standard 10 mm nmr tubes. For ^{77}Se nmr studies of $M(SePh)_3$ and $M(SePh)_3-M(SPh)_3$ mixtures on the WH-400, samples were kept in capped argon-filled standard 10 mm nmr tubes; similarly, samples for ^{13}C nmr scrutiny using the XL-200 were kept in capped, argon-filled standard 5 mm nmr tubes. Flame-sealed hand made 10 mm od nmr tubes were used to hold samples for preliminary ^{13}C and ^{207}Pb nmr study on the XL-100.

Nuclear magnetic resonance spectra

Preliminary ^{13}C and ^{207}Pb nmr spectra (with and without proton decoupling, respectively) were measured on spinning samples using a Varian XL-100-12 spectrometer system operating at 25.2 and 20.9 MHz, respectively. The 10 mm od sample tubes were held coaxially in a standard 12 mm od tube, and D_2O (at 308 K) or, for variable temperature, $(CD_3)_2CO$, in the outer annulus provided a ^2D lock, as described previously (e.g. ref. 1). The ^{207}Pb nmr spectra were referenced by sample interchange with 1.0 *M* $Pb(NO_3)_2$, for which δ_{Pb}(1.0 *M* $Pb(NO_3)_2$(aq)) = $\delta_{Pb}(PbMe_4$(toluene)) + 2961 ppm (27). The ^{13}C nmr spectra were referenced to external dioxane in D_2O for 308 K measurements or the CD_3 signal of external $(CD_3)_2CO$ for reduced temperature measurements; at 308 K δ_C(external dioxane in D_2O) $\approx \delta_C$(internal TMS) − 67.8 ppm while δ_C(external $(CD_3)_2CO$) $\approx \delta_C$(internal TMS) − 29.4 ppm but is slightly temperature sensitive. Typically, satisfactory ^{207}Pb nmr spectra of 0.25 *M* solutions required aequisition of several thousand transients using a 12.5 kHz spectral window, a 45° (40 μs) pulse width, a 1 s acquisition time, and a 4.3 s cycle time. On the XL-100 the 20.9 MHz region contains many "glitches" so that comparison with spectra of samples containing no lead is an essential. Carbon-13 nmr spectra were obtained using conditions reported previously (1). Proton-decoupled 50.3 MHz ^{13}C nmr spectra were measured with a Varian XL-200 spectrometer system, using spinning samples, a ^2D lock and, typically, a 10 kHz spectral window, 3 μs (45°) pulse width, a 1.6 s acquisition time, and a 2 s cycle time. Samples with $[Ph]_{total} \approx 0.75$ *M* gave acceptable spectra in several hundred to several thousand transients depending whether they contained one or several species. The solvent signal was used as internal reference and converted to the TMS scale using δ_C(TMS, int) = $\delta_C(CDCl_3$, int) + 77.05 = $\delta_C(CD_3OD$, int) + 49.00 ppm.

A Bruker WH-400 spectrometer system was used to obtain 295 K and variable temperature ^{77}Se, ^{119}Sn, and ^{207}Pb nmr spectra at 76.4, 149.2, and 83.4 MHz, respectively (the last after preliminary measurement at 20.9 MHz as described above). The primary references, used externally, were saturated H_2SeO_3(aq), neat $SnMe_4$, and 1.0 *M* $Pb(NO_3)_2$(aq), respectively. The ^{77}Se data were converted to neat Me_2Se as reference using $\delta_{Se}(Me_2Se$(neat)) = $\delta_{Se}(H_2SeO_3$(aq)) + 1326 ppm; the ^{207}Pb data were converted to $PbMe_4$ (in toluene) as reference as indicated above. In obtaining these spectra, neither proton decoupling nor a ^2D lock was normally used, and only those samples in standard 10 mm tubes were spun (i.e. only the samples containing Group V elements); samples in 9 mm od nmr tubes would not always spin satisfactorily, so for consistency all were kept stationary. After initial location of the signals using a 50 kHz spectral window, smaller spectral windows were normally used. Typical operating conditions were: for ^{77}Se, 10 kHz spectral window, 38 μs (90°) pulse width and 0.8 s acquisition and 1.8 s cycle time; for ^{119}Sn, 20 kHz spectral window, 25 μs (60°) pulse width, 0.4 s acquisition and cycle time; for ^{207}Pb, 10 kHz spectral window, 38 μs (90°) pulse width and 0.8 s acquisition and cycle time. (The larger spectral window was used for ^{119}Sn to accommodate the spectra of mixtures where several signals were present (see below).)

Elemental microanalyses

Analyses were performed by Guelph Chemical Laboratories Ltd.

Results and discussion

Tin(II) complexes

Tin(II) thiophenolate, $Sn(SPh)_2$, is poorly soluble in MeOH at room temperature, but becomes completely soluble in the presence of an equimolar or greater amount of SPh^- or $SePh^-$. The corresponding tin(II) selenophenolate, $Sn(SePh)_2$, exhibits the same behaviour. Evidently, soluble stannate(II) complexes are formed in solution, and we have characterized these by a combination of ^{119}Sn, ^{77}Se, and ^{13}C nmr.

A solution in which $Sn(SPh)_2/SPh^- = 1/2$ gives, at 295 K, a single ^{119}Sn nmr line, with $\delta_{Sn} = 136$ ppm, essentially the same chemical shift found for the supernatant liquor from a mixture in which $Sn(SPh)_2/SPh^- > 1$ (Table 3). These two results show that only a single tin(II) complex exists in the $Sn(SPh)_2-SPh^-$ system. Similarly, the system $Sn(SePh)_2-SePh^-$ gives a single ^{119}Sn nmr signal with a shift quite insensitive to composition, showing that only a single soluble phenylselenolate complex is formed in this system. At 295 K neither the ^{119}Sn resonance of the mother liquor from $Sn(SePh)_2/SePh^- > 1$ nor the ^{119}Sn resonance from the solution with $Sn(SePh)_2/SePh^- < 1$ shows satellites from those isotopomers containing ^{77}Se (natural abundance 7.6%, spin $I = 1/2$). At reduced temperature the spectrum of the solution containing excess $PhSe^-$ still shows no ^{77}Se satellites, but if $Sn(SePh)_2/PhSe^- > 1$ the expected one bond $^{77}Se—^{119}Sn$ coupling can be observed, and is 710 Hz at 198 K, similar in magnitude to the 570 Hz found for $Sn(SeP(chx)_3)_3^{2+}$ at 213 K (6). The presence of excess free $PhSe^-$ must induce rapid free−bound ligand exchange, a conclusion supported by the observation of only a single phenyl pattern in the reduced temperature 50.3 MHz ^{13}C nmr spectra of mixtures with $Sn(SePh)_2/SePh^- < 1$. As rapid ligand exchange requires excess free ligand, the exchange process at the tin(II) centre must be associative, a conclusion also reached from nmr data for $Sn(SeP(chx)_3)_3^{2+}-SeP(chx)_3$ mixtures in SO_2 (6). It is not possible to tell from the ^{119}Sn nmr spectra of $Sn(SPh)_2-SPh^-$ mixtures whether free−bound ligand exchange is rapid. However, partial resolution of free and bound PhS^- resonances occurs at temperatures below ca. 223 K in the 50.3 MHz ^{13}C nmr spectra (though not the 25.2 MHz ^{13}C nmr spectra) of mixtures with $Sn(SPh)_2/SPh^- < 1$, so it seems that the rate of associative ligand exchange on tin(II) is less for PhS^- than for $PhSe^-$.

The triligated nature of the soluble stannate(II) complexes was confirmed by the ^{119}Sn and ^{77}Se nmr spectra of mixed ligand systems prepared from appropriate combinations of

TABLE 3. Metal, selenium-77, and carbon-13 spectra of some species with phenylthiolate and/or phenylselenolate as ligands

Species	Solvent	δ_M[a] (ppm) (Approx. $\nu_{1/2}$ (Hz))	δ_{Se}[b] (ppm) (Approx. $\nu_{1/2}$ (Hz))	E in PhE	δ_C[c] (ppm) C_1	$C_{2,6}$	$C_{3,5}$	C_4
$Sn(SPh)_3^-$[d]	CD_3OD	123(120);[e] 140(8)[f,g,h]		S	145.23	135.41	128.57	123.08
$Sn(SPh_2)_2(SePh)^-$[d]	CD_3OD	150(120)[e]	191(300)[i]		[j]			
$Sn(SPh)(SePh)_2^-$[d]	CD_3OD	170(120)[e]	179(300)[i]		[j]			
$Sn(SePh)_3^-$[d]	CD_3OD	185(120);[e] 207(130)[f,k,l]	164(200)[i]	Se	133.87	135.95	129.01	124.98
$Pb(SPh)_3^-$[d,m]	CD_3OD	2818(70)[f]		S	139.15	132.92	129.21	124.94
$Pb(SePh)_3^-$[d,m]	CD_3OD	3105(25);[i,n] 3188(50)[f,n]	127(500)[i]	Se	135.89	132.54	129.15	125.43
$As(SPh)_3$	$CDCl_3$			S	132.51	134.81	129.16	128.37
$As(SPh)_2(SePh)$	$CDCl_3$		288(75)[f]	S	133.31	134.57	129.15	128.29
				Se	127.58	136.11	129.29	128.42
$As(SPh)(SePh)_2$	$CDCl_3$		278(75)[f]	S	134.10	134.36	129.12	128.25
				Se	128.56	135.88	129.26	128.37
$As(SePh)_3$	$CDCl_3$		266(75)[f]	Se	129.40	135.71	129.25	128.32
$Sb(SPh)_3$	$CDCl_3$			S	132.00	135.18	129.19	127.91
$Sb(SPh)_2(SePh)$	$CDCl_3$		414(90)[f]	S	132.87	134.90	129.12	127.82
				Se	125.74	136.59	129.32	128.11
$Sb(SPh)(SePh)_2$	$CDCl_3$		406(90)[f]	S	133.64	134.74	129.09	127.76
				Se	126.67	136.41	129.28	128.06
$Sb(SePh)_3$	$CDCl_3$		397(90)[f]	Se	127.46	136.22	129.22	127.97
$Bi(SPh)_3$[m]	$CDCl_3$			S	132.46	136.12	128.50	128.40
$Bi(SePh)_3$[m]	$CDCl_3$		311(110)[f]	Se	126.36	137.42	128.57	128.52

[a]For the tin complexes M = ^{119}Sn; chemical shifts were measured relative to external neat $SnMe_4$ at 295 K. For the lead complexes M = ^{207}Pb; chemical shifts are given relative to $PbMe_4$ in toluene after measurement relative to external 1 *M* $Pb(NO_3)_2$(aq) at 295 K and conversion using $\delta_{Pb(NO_3)_2} = \delta_{PbMe_4} + 2961$ ppm (27). Estimated error for both δ_{Sn} and δ_{Pb} is ±1 ppm.

[b]Relative to external neat Me_2Se; measured initially relative to external saturated H_2SeO_3(aq) at 295 K and converted using $\delta_{Me_2Se} = \delta_{H_2SeO_3} + 1326$ ppm. Estimated error ±1 ppm.

[c]Relative to TMS, at 294 K; measured initially relative to the solvent ^{13}C signal and converted using $\delta_{TMS} = \delta_{CD_3OD} + 49.00 = \delta_{CDCl_3} + 77.05$ ppm; estimated error ±0.02 ppm.

[d]In the supernatant liquid from mixtures where $\{M(EPh)_2\}_{total}/EPh^-_{total} > 1$ (see text).

[e]At 198 K in mixtures of $[Sn(SPh)_x(SePh)_{3-x}]^-$.

[f]At 295 K.

[g]For the supernatant from $Sn(SPh)_2/SPh^- > 1$.

[h]At 195 K, $\delta_{Sn} = 125$ ppm, $\nu_{1/2} \approx 30$ Hz.

[i]At 213 K.

[j]Separate ^{13}C spectra of mixed ligand species could not be observed at reduced temperature (see text).

[k]For the supernatant from $Sn(SePh)_2/SePh^- > 1$.

[l]At 195 K, $\delta_{Sn} = 184$ ppm, $\nu_{1/2} \approx 50$ Hz, $^1J(^{77}Se—^{119}Sn) = 710 \pm 10$ Hz.

[m]Ligand exchange is fast on the nmr timescale at all accessible temperatures; separate spectra from mixed ligand species could not be observed.

[n]No ^{77}Se satellites observed.

$Sn(EPh)_2$ and PhE^- (E = S, Se) such that $\{Sn(EPh)_2\}_{total}/PhE^-_{total} > 1$ (to reduce the free−bound ligand exchange rate). The 198 K ^{119}Sn nmr spectra show, as the S/Se ratio of the mixture is changed, a total of four resonances which can readily be attributed to $[Sn(SPh)_x(SePh)_{3-x}]^-$ with chemical shifts covering the ^{119}Sn chemical shift range from 123 ($x = 3$) to 185 ppm ($x = 0$) and increasing monotonically but not linearly with x (Table 3).[4] These ^{119}Sn nmr chemical shifts and their span are quite similar to those found for $[Sn(SP(chx)_3)_x(SeP(chx)_3)_{3-x}]^{2+}$ for which δ_{Sn} (from $SnMe_4$) ≈ 181, 161, 133, and 94 ppm for $x = 0$, 1, 2, and 3, respectively (6). Of the three $PhSe^-$-containing species, only for $Sn(SePh)_3^-$ could the ^{77}Se satellites be observed with certainty in the 198 K spectra; they should be most intense for this species. (Statistically, the Sn $^{77}SeSe_2$ kernel should be 19.4% of all $SnSe_3$.) As noted above, these satellites are absent at 295 K showing that intermolecular $PhSe^-$ exchange is rapid at this temperature. Consistent with intermediate-to-fast ligand exchange, at 295 K a single very broad resonance with composition-dependent chemical shift, is observed for mixtures of various $[Sn(SPh)_x(SePh)_{3-x}]^-$. A single much sharper ^{119}Sn resonance is found when mixtures with $Sn(EPh)_2/EPh^- < 1$ are studied at 295 K, and this behaviour allows an assessment of the preference of Sn(II) for SPh^- or $SePh^-$ in these systems. A mixture of composition $Sn(SePh)_2/SePh^-/SPh^- \approx 1/2/4$ gave a resonance with a ^{119}Sn nmr chemical shift of 194 ppm, much closer to that of $Sn(SePh)_3^-$ (205 ppm when $Sn(SePh)_2/SePh^- \approx 1/2$) than to that of $Sn(SPh)_3^-$ (136 ppm when $Sn(SPh)_2/SPh^- \approx 1/2$). Hence we conclude that tin(II) has marked, though perhaps not complete, preference for $PhSe^-$ over PhS^-.

In agreement with the ^{119}Sn nmr results, a total of three ^{77}Se resonances are found for the supernatant liquor from

[4]The incremental chemical shifts from $\delta(Sn(SPh)_3^-)$ can be accommodated in terms of pairwise additivity parameters (28), $\Delta\delta_{S-Se}$ and $\Delta\delta_{Se-Se}$ are approximately 14 and 18 ppm for $[Sn(SPh)_x(SePh)_{3-x}]^-$; the corresponding values for $[Sn(SP(chx)_3)_x(SeP(chx)_3)_{3-x}]^{2+}$ are 19 and 29 ppm (6).

Can. J. Chem. Downloaded from www.nrcresearchpress.com by 210.87.254.6 on 09/06/12
For personal use only.

Can. J. Chem. Downloaded from www.nrcresearchpress.com by 210.87.254.6 on 09/06/12
For personal use only.

$Sn(EPh)_2-PhE^-$ mixtures with $\{Sn(EPh)_2\}_{total}/PhE^-_{total} > 1$. By following intensity variation as a function of $(S/Se)_{bound}$, these resonances can be assigned to $[Sn(SPh)_x(SePh)_{3-x}]^-$ ($x = 0-2$), as shown in Table 3.

In the reduced temperature 50.3 MHz ^{13}C nmr spectra of solutions which gave slow exchange ^{119}Sn and/or ^{77}Se nmr spectra we were unable to resolve separate signals for the various species $[Sn(SPh)_x(SePh)_{3-x}]^-$ that were known to be present. There is no inconsistency here, for the signal separations in the 76.4 MHz ^{77}Se nmr spectra are 920 Hz minimum, and those in the 149.2 MHz ^{119}Sn nmr spectra are 360 Hz minimum (i.e. $^1J(^{77}Se—^{119}Sn)/2$), whereas by comparison with the ^{13}C nmr data for the isoelectronic species $Sb(SPh)_x(SePh)_{3-x}$ (see below), signal separations of 50 Hz or less could be expected for the various resonances in the 50.3 MHz ^{13}C spectra. The linewidths in the reduced temperature ^{77}Se and ^{119}Sn nmr spectra are quite large (Table 3) and almost certainly contain a contribution from lifetime broadening; i.e. these are slow-exchange but not limiting spectra. The exchange rate which only broadens the ^{77}Se and ^{119}Sn lines is, apparently, sufficient to collapse the ^{13}C nmr spectra with their smaller chemical shift differences. In short, exchange seems to be slow (but existent) on the 76.4 MHz ^{77}Se and 149.2 MHz ^{119}Sn nmr timescales but fast on the 50.3 MHz ^{13}C nmr timescale.

Lead complexes

Like their stannous analogs, $Pb(SPh)_2$ and $Pb(SePh)_2$ are poorly soluble in MeOH but dissolve in the presence of equimolar or greater amounts of PhS^- or $PhSe^-$. The soluble components of $Pb(SPh)_2-PhS^-$ or $Pb(SePh)_2-PhSe^-$ mixtures give, at 295 K, ^{207}Pb nmr chemical shifts that are barely dependent on the $Pb(EPh)_2/PhE^-$ ratio, e.g. at 295 K for solutions in which $Pb(EPh)_2/EPh^- \approx 1/2$, $\delta_{Pb} = 2808$ and 3173 ppm for E = S and Se respectively, close to the values found for the corresponding mixtures with $Pb(EPh)_2/EPh^- > 1$ (Table 3). Thus each of the systems $Pb(EPh)_2-EPh^-$ contains only a single species $Pb(EPh)_x^{(x-2)-}$. The value of x could not be determined from our ^{207}Pb, ^{77}Se, or ^{13}C nmr studies of $Pb(SPh)_x^{(x-2)-}:Pb(SePh)_x^{(x-2)-}$ mixtures because no slow exchange spectra could be obtained. Thus, for instance, the supernatant liquor from a mixture with $Pb(SePh)_2/PhS^- \approx 1.1$ gave a single broad ^{207}Pb nmr resonance ($\delta_{Pb} \approx 3036$ ppm; $\nu_{1/2} \approx 600$ Hz) at 295 K but at 213 K no observable signal in the range 2690–3289 ppm. The exchange rate must be in the intermediate region relative to frequency separation of the expected lines in the 83.4 MHz ^{207}Pb nmr spectrum at 213 K, and in the intermediate-to-fast region at 295 K. Also, for the solution component of $Pb(SePh)_2/SePh^- > 1$ at reduced temperature, we could observe neither ^{77}Se satellites in the ^{207}Pb nmr spectrum nor ^{207}Pb (natural abundance 22.6%; spin $I = 1/2$) satellites in the ^{77}Se nmr spectrum, showing that the rate of intermolecular ligand exchange is fast relative to the (unknown) magnitude of $^1J(^{77}Se—^{207}Pb(II))$.

The chemical behaviour of the plumbous systems mirrors that of the stannous systems discussed above, and this suggests that x is three. The 295 K ^{207}Pb nmr chemical shifts of $Pb(SPh)_3^-$ and $Pb(SePh)_3^-$ (Table 3) are reasonably close to those found for $Pb(SP(chx)_3)_3^{2+}$ and $Pb(SeP(chx)_3)_3^{2+}$ (approximately 2457 and 3011 ppm, respectively, in SO_2 at 213 K (6)), allowing for the existence of sizeable solvent and temperature effects in ^{207}Pb nmr spectra. Indeed a prior knowledge of the ^{207}Pb nmr chemical shifts of the $EP(chx)_3$ complexes shortened considerably the time needed to find the ^{207}Pb resonances of the PhE^- complexes.

To compare the competitiveness of $PhSe^-$ and PhS^- for coordination to lead(II), the ^{207}Pb nmr spectrum of a solution of composition $Pb(SePh)_2/PhSe^-/PhS^- \approx 1/2/4$ was examined at 295 K. The single quite sharp ($\nu_{1/2} \approx 30$ Hz) exchange averaged resonance had a chemical shift of 3151 ppm, much closer to the shift of $Ph(SePh)_3^-$ than to that of $Pb(SPh)_3^-$ (Table 3). It can be concluded that coordination of $PhSe^-$ to lead(II) is strongly preferred over coordination of PhS^-.

As discussed in the Introduction, thiolatoplumbates may be formed during treatment with thiol-containing therapeutic chelators in cases of lead intoxication. Therefore we thought it desirable to establish the range of ^{207}Pb chemical shifts for lead(II) complexes with a wider selection of thiolates as ligands. The dissolution of $Pb(SR)_2$ in MeOH in the presence of excess SR^- appears to be fairly general: of the thiolates examined only the 1:1 lead(II) thiolates with $^-S(CH_2)_2S^-$ and $^-SCH_2CHS^-CH_2SO_3^-Na^+$ were poorly soluble in the presence of excess of the corresponding thiolate. In methanol solutions containing $Pb(SR)_2/RS^- \approx 1/6$ ($Pb(SR)(OAc)/RS^- \approx 1/5$ for R = chx), δ_{Pb} was found to be 2999, 2941, 2814, 2965, 2518, and 2551 ppm for RS^- = MeS^- (at 295 K), EtS^- (at 295 K; $\delta_{Pb} = 2772$ ppm in water at 305 K), $chxS^-$ (at 305 K), $^-S(CH_2)_3S^-/2$ (at 305 K), $^-SCH_2CHS^-Me/2$ (at 305 K), and $^-SCH_2CHS^-CH_2OH/2$ (at 305 K). From this preliminary screening we conclude that the ^{207}Pb chemical shifts of thiolatoplumbates(II) fall into a comparatively narrow region of the total ^{207}Pb nmr chemical shift range so that ^{207}Pb nmr may be a useful technique in detecting the presence of this type of complex. A possible complication is the lability of these complexes, which can cause extensive line broadening if intermediate-to-fast exchange between multiple sites can occur. It is interesting that a cyclohexylthiolato complex, probably $Pb(Schx)_3^-$ from the ^{207}Pb nmr chemical shift, is formed even though $Pb(Schx)_2$ could not be synthesized via $Pb(OAc)_2$ (see Experimental section). Also noteworthy are the somewhat different values of δ_{Pb} found for the two vicinal dithiolates studied. Because of the lability of the complexes we were unable to establish with certainty that chelation occurs in these cases, though this seems probable. The stoichiometries of the lead(II) thiolates with the dianion of BAL, $^-S(CH_2)_2OH$, and $^-SCH_2CHOHMe$, 1:1 with the dithiolate and 2:1 with the monothiolates (see Experimental section), argues against involvement of the hydroxy group of BAL in coordination to lead.

Arsenic, antimony, and bismuth complexes

We have studied the chemical and ^{77}Se and ^{13}C nmr spectroscopic behaviour of $M(SPh)_3$, $M(SePh)_3$, and $M(SPh)_x(SePh)_{3-x}$ (M = As, Sb, or Bi) for comparison with the tin(II) and lead(II) complexes described above. Details of the ^{77}Se and ^{13}C nmr spectra obtained are included in Table 3.

In $CDCl_3$ as solvent, a redistribution of ligands between $As(SPh)_3$ and $As(SePh)_3$ occurs over a period of several hours at room temperature, as indicated by the time dependence of the ^{13}C nmr spectra. By variation of the $As(SPh)_3/As(SePh)_3$ ratio, equilibrium mixtures of various species $As(SPh)_x(SePh)_{3-x}$ can be formed, as expected for an apparently near statistical redistribution, and their separate ^{77}Se and ^{13}C spectra measured. The behaviour of $Sb(SPh)_3-Sb(SePh)_3$ mixtures is similar except that the ligand redistribution is fast on the chemical timescale though not on the nmr timescale. In this case, the redistribution is complete within approximately the time

Can. J. Chem. Downloaded from www.nrcresearchpress.com by 210.87.254.6 on 09/06/12
For personal use only.

needed to mix the components: no time dependence of the ^{13}C nmr spectra was noted. At ambient probe temperature, separate ^{13}C and, when expected, ^{77}Se nmr spectra are observed for $Sb(SPh)_x(SePh)_{3-x}$.

In contrast to the nmr spectral behaviour of the arsenic- or antimony-containing systems, ^{13}C and ^{77}Se nmr spectra characteristic of fast intermolecular exchange are found at all accessible temperatures for $Bi(SPh)_3-Bi(SePh)_3$ mixtures. There is no doubt, however, that mixed ligand systems do form, for both the ^{77}Se and the ^{13}C nmr chemical shifts vary as the $Bi(SPh)_3/Bi(SePh)_3$ ratio is changed, and in addition there are obvious colour changes in the mixtures. Because of the lability of $Bi(SPh)_x(SePh)_{3-x}$, only data for $Bi(SPh)_3$ and $Bi(SePh)_3$ are included in Table 3. Overall, the trend in the lability of the Group V species, i.e. lability increasing with atomic number, is the same as found for the analogous Group IV complexes (see above).

The occurrence of slow exchange nmr spectra for the arsenic and antimony complexes allowed a study of the distribution of SPh^- and $SePh^-$ competitively between pairs of the Group V elements. Accordingly, we measured the ^{13}C nmr spectra of equilibrated mixtures $M(SPh)_3-M'(SePh)_3$ where M = Sb and M′ = As, and where M = Bi and M′ = As or Sb. The As–Sb mixtures gave slow exchange ^{13}C spectra for both $As(SPh)_x(SePh)_{3-x}$ and $Sb(SPh)_x(SePh)_{3-x}$, and from the overall stoichiometry and the distribution of the various species it was apparent that the preference for $PhSe^-$ over PhS^- was Sb > As. Similarly the As–Bi mixtures gave slow exchange spectra for $As(SPh)_x(SePh)_{3-x}$ along with fast exchange spectra for $Bi(SPh)_x(SePh)_{3-x}$, and it was possible to conclude that the preference for $PhSe^-$ over PhS^- was Bi $\gg$ As. The order of preference Bi > Sb could not be confirmed directly because Sb–Bi mixtures gave fast exchange ^{13}C nmr spectra at 294 K and slow exchange spectra could not be obtained even for $Sb(SPh)_x(SePh)_{3-x}$ by reducing the temperature. Nevertheless, it is evident that within the series of Group V elements the overall order of preference for $PhSe^-$ over PhS^- is Bi > Sb > As. We could not measure the preference of individual elements for $PhSe^-$ vs. PhS^-, but our results for the isoelectronic species $Sn(EPh)_3^-$ and $Pb(EPh)_3^-$ (see above) suggest that it should be $PhSe^- > PhS^-$ for Sb and Bi at least.

A number of empirical correlations are evident from the data in Table 3. In the ^{77}Se nmr spectra of both $As(SPh)_x(SePh)_{3-x}$ and $Sb(SPh)_x(SePh)_{3-x}$ there is a linear or near-linear increase in shielding as x increases. The trend to increasing shielding with increasing x is found for the ^{13}C resonances of C_2, C_3, and C_4 of both PhS^- and $PhSe^-$ bound to As or Sb also, albeit on a much smaller scale and not always linearly, while the corresponding C_1 resonances show a near-linear decrease in shielding with increase in x. In the case of δ_{C_4} the changes observed appear to reflect slight shifting of electrons throughout the molecules as sulfur is replaced by less electronegative selenium: considering one —SPh or —SePh, change of the attached group from $(PhS)_2M-$ to $(PhSe)_2M-$ should result in electron release into the phenyl ring of interest and this is known to cause increased shielding (29), as is observed. The same effect can account for the observed changes in δ_{C_3}; however, δ_{C_1} and δ_{C_2} are known to be sensitive to other factors as well, because of their closer proximity to the atom which is being varied, and similarly the factors affecting δ_{Se} may include through-space as well as through-bond effects.

The data in Table 3 and elsewhere (2*a*, 30) show that the biggest influence on δ_{Se} of $PhSe^-$ is the atom to which the selenium is attached. The known variation of δ_{Se} with metal atom is Cd(II) < Zn(II) < Pb(II) < Sn(II) < As(III) < Bi(III) < Sb(III). Because of its sensitivity to acceptor atom, δ_{Se} should prove a useful probe for specific metal–selenolate bonds once a sufficient library of model data is available.

Acknowledgments

This work was made possible by an Operating Grant (to P.A.W.D.) and a Strategic Grant in Environmental Toxicology (to P.A.W.D. jointly with Drs. M. J. Stillman and G. M. Cherian of the Departments of Chemistry and Pathology, respectively, U.W.O.), both from the Natural Sciences and Engineering Research Council of Canada (N.S.E.R.C.). N.S.E.R.C. also provided a Major Installation Grant to the Southwestern Ontario NMR Centre where the high field ^{77}Se, ^{119}Sn, and ^{207}Pb nmr spectra were obtained with the expert technical help of Mr. Bruce MacDonald. Dr. J. B. Stothers and Mrs. V. Richardson of this Department measured the high field ^{13}C nmr spectra, while Mrs. H. M. Schroeder, previously of this Department, ably assisted in obtaining initial low field ^{13}C and ^{207}Pb nmr spectra.

1. G. K. CARSON, P. A. W. DEAN, and M. J. STILLMAN. Inorg. Chim. Acta, **56**, 59 (1981).
2. G. K. CARSON and P. A. W. DEAN. Inorg. Chim. Acta, (*a*) **66**, 37 (1982); (*b*) **66**, 157 (1982).
3. P. A. W. DEAN and M. K. HUGHES. Can. J. Chem. **58**, 180 (1980).
4. P. A. W. DEAN and L. POLENSEK. Can. J. Chem. **58**, 1627 (1980).
5. P. A. W. DEAN. Can. J. Chem. **59**, 3221 (1981).
6. P. A. W. DEAN. Can. J. Chem. **60**, 2921 (1982).
7. E. EMMET REID. Organic chemistry of bivalent sulfur. Vol. 1. Chemical Publishing Co., New York. 1958. Chapt. 2, and references therein.
8. R. A. SHAW and M. WOODS. J. Chem. Soc. A, 1561 (1971).
9. M. E. PEACH. J. Inorg. Nucl. Chem. **41**, 1390 (1979).
10. J. L. HENCHER, M. KHAN, F. F. SAID, R. SIELER, and D. G. TUCK. Inorg. Chem. **21**, 2787 (1982).
11. P. G. HARRISON and S. R. STOBART. Inorg. Chim. Acta, **7**, 306 (1973).
12. W. D. HONNICK and J. J. ZUCKERMAN. Inorg. Chem. **17**, 501 (1978).
13. T. B. BRILL and N. C. CAMPBELL. Inorg. Chem. **12**, 1884 (1973).
14. YU. V. BARABASH, YU. G. SKRYPNIK, I. A. SHEVCHUK, and Z. G. KOROTKOVA. J. Anal. Chem. **34**, 1163 (1979).
15. J. E. DRAKE and R. T. HEMMINGS. J. Chem. Soc. Dalton, 1730 (1976).
16. R. E. HOLMBERG, JR. and V. H. FERM. Arch. Environ. Health, **18**, 873 (1969).
17. J. PARIZEK. *In* Effects and dose–response relationship of toxic metals. *Edited by* G. F. Nordberg. Elsevier Scientific Publishing Co., Amsterdam. 1976. Chapt. C2, p. 498 and references therein.
18. E. J. UNDERWOOD. Trace elements in human and animal nutrition. 4th ed. Academic Press, New York. 1977. Chapt. 12 and references therein.
19. G. N. SCHRAUZER, D. A. WHITE, J. E. MCGINNESS, C. J. SCHNEIDER, and L. J. BELL. Bioinorg. Chem. **9**, 245 (1978).
20. G. M. CHERIAN. Personal communication.
21. W. RIGBY. J. Chem. Soc. 794 (1951).
22. J. D. DONALDSON, W. MOSER, and W. B. SIMPSON. J. Chem. Soc. 5942 (1964).
23. L. FIELD and R. B. BARBEE. J. Org. Chem. **34**, 36 (1969).

24. R. H. CRAGG and A. F. WESTON. Tetrahedron Lett. 655 (1973).
25. V. E. PETRUN'KIN. Ukrain. Khim. Zhur. **22**, 787 (1956); Chem. Abstr. **51**, 14537*h* (1957).
26. V. E. PETRUN'KIN. Ukrain Khim. Zhur. **22**, 603 (1956); Chem. Abstr. **51**, 5692*h* (1957).
27. R. K. HARRIS, J. D. KENNEDY, and W. MCFARLANE. NMR and the periodic table. *Edited by* R. K. Harris and B. E. Mann. Academic Press, London. 1978. Chapt. 10 and references therein.
28. E. R. MALINOWSKI. J. Am. Chem. Soc. **91**, 4701 (1969), and references therein.
29. J. B. STOTHERS. Carbon-13 NMR spectroscopy. Academic Press, New York. 1972. Chapt. 5, Sect. IV, and references therein.
30. G. K. CARSON and P. A. W. DEAN. Unpublished data.

Can. J. Chem. Downloaded from www.nrcresearchpress.com by 210.87.254.6 on 09/06/12
For personal use only.

Second sphere coordination of phenols, anilines, and benzoic acids to the hexacyanocobaltate(III) anion

DONALD R. EATON,[1] RICHARD J. BUIST, AND CAROL V. ROGERSON
Department of Chemistry, McMaster University, Hamilton, Ont., Canada L8S 4M1

Received July 19, 1982

DONALD R. EATON, RICHARD J. BUIST, and CAROL V. ROGERSON. Can. J. Chem. **61**, 1524 (1983).

Complexing between the hexacyanocobaltate(III) anion and ten substituted phenols, eight substituted anilines, and eight substituted benzoic acids has been studied in dimethyl sulfoxide solutions by means of ^{59}Co nmr. For the phenols substantial changes in the chemical shifts and in the line widths are observed and are attributed to hydrogen bonding interactions. Effective equilibrium constants and chemical shifts for the hydrogen bonded species have been calculated. The equilibrium constants vary with the phenol substituent, being largest for electron withdrawing substituents and smallest for electron donating substituents. The chemical shifts are virtually independent of substituent. The data show that the lifetimes of the hydrogen bonded complexes are long compared to the rotational correlation time. The complex with *para*-nitrophenol has also been studied by measuring ^{1}H and ^{13}C spin–lattice relaxation times. These measurements allow the separation of the increase in ^{59}Co line width due to increase in correlation time and that due to increase in quadrupole coupling constant. From the ^{13}C measurements a value of the correlation time for the complex of 2.8 10^{-10} s is obtained together with a ^{59}Co quadrupole coupling constant of 8.34 MHz. The equilibrium constants for complex formation with the anilines are small and only the products of the equilibrium constant and the chemical shift of the hydrogen bonded complex can be derived from the experimental data. The benzoic acids show evidence of dimerization in solution and this again prevents the calculation of absolute equilibrium constants. The data, however, do indicate that the ability to form hydrogen bond complexes does not vary dramatically with the acid strength of the hydrogen donor. With phenols and benzoic acids there is considerable line broadening on complex formation but with anilines only a small line broadening is observed. This is consistent with very short hydrogen bond lifetimes for the aniline complexes.

DONALD R. EATON, RICHARD J. BUIST et CAROL V. ROGERSON. Can. J. Chem. **61**, 1524 (1983).

Faisant appel à la rmn du ^{59}Co, on a étudié la complexation de l'anion hexacyano cobaltate(III) avec dix phénols substitués, huit anilines substituées et huit acides benzoïques substituées dans des solutions de diméthylsulfoxide. Dans le cas des phénols on observe des changements importants dans les déplacements chimiques et dans la largeur des raies et on les attribue à des interactions de liaison hydrogène. On a calculé les constantes effectives d'équilibre et les déplacements chimiques des espèces liées par des liaisons hydrogènes. Les constantes d'équilibre varient avec le substituant du phénol, cette constante est plus élevée dans le cas des substituants électro-attracteurs et plus faible dans le cas des substituants électro-donneurs. Les déplacements chimiques sont virtuellement indépendants du substituant. Les données montrent que les temps de vie des complexes liés par des liaisons hydrogènes sont longs par rapport au temps de corrélation rotationnelle. On a également étudié le complexe avec le *para*-nitrophénol en mesurant les temps de relaxation spin réseau du ^{1}H et du ^{13}C. Ces mesures permettent de séparer l'augmentation de largeur de la raie du ^{59}Co due à l'augmentation du temps de corrélation et celle due à l'augmentation de la constante de couplage quadrupolaire. A partir des mesures de ^{13}C on obtient une valeur de 2,8 × 10^{-10} pour le temps de relaxation du complexe ainsi qu'une valeur de constante de couplage quadrupolaire du ^{59}Co de 8,34 MHz. Les constantes d'équilibre de formation du complexe avec les anilines sont faibles et on ne peut déduire que les produits de la constante d'équilibre et du déplacement chimique, du complexe lié par des liaisons hydrogènes, à partir des données expérimentales. Les acides benzoïques se dimérisent en solution et ceci empêche de calculer les constantes absolues d'équilibre. Les données cependant indiquent que la capacité des complexes à former des liaisons hydrogènes ne varient pas de façon marquée avec l'acidité du donneur d'hydrogène. Dans le cas des phénols et des acides benzoïques il y a un élargissement considérable de la raie lors de la formation des complexes mais dans le cas des anilines on observe qu'un faible élargissement de la raie. Ces résultats sont en accord avec des temps de vie très courts des liaisons hydrogènes des complexes de l'aniline.
[Traduit par le journal]

Introduction

Ligands held in the second coordination sphere of metal complexes potentially play an important role as intermediates in a variety of reactions. Ligand exchange (1), electron transfer (2), and catalytic mechanisms (3) involving second sphere intermediates have all been discussed. A major barrier to the evaluation of the importance of these ideas is the lack of quantitative information on the stabilities and labilities of second sphere complexes. It is essential to be able to estimate the equilibrium constant for complex formation and the lifetime of the intermediate to adequately assess its possible role in a given mechanism. This information is often difficult to obtain. Hydrogen bonding is probably one of the more important interactions responsible for the binding of second sphere ligands. There have been a number of studies (4–6) leading to equilibrium constant information on such complexes but very little rate data is available. The present paper reports the results of a study of hydrogen bonding interactions between the hexacyanocobaltate(III) anion and phenols, anilines, and benzoic acids.

^{59}Co nmr provides an attractive approach to the study of second coordination sphere equilibria and kinetics (7). The chemical shifts are very large and therefore provide a sensitive probe for second sphere interactions. Chemical shift data can be used to obtain equilibrium constants for the formation of second sphere complexes. We have reported previously (8) that there is also considerable broadening of the lines on hydrogen bond formation. The extent of this broadening varies considerably with the nature of the hydrogen donor. The broadening results from a decrease in the relaxation time of the ^{59}Co nucleus. The details depend on the relative values of the lifetime of

[1]To whom all correspondence should be addressed.

Can. J. Chem. Downloaded from www.nrcresearchpress.com by 210.87.254.42 on 09/06/12
For personal use only.

Can. J. Chem. Downloaded from www.nrcresearchpress.com by 210.87.254.42 on 09/06/12
For personal use only.

the hydrogen bonded complex and the rotational correlation time of the molecule. On the basis of nmr (8) and infrared studies (9) it has been deduced that for strong hydrogen bonds the former is greater and for weak hydrogen bonds the latter is greater. The line width studies therefore have the potential to provide information on the hydrogen bond lifetimes. The ^{59}Co relaxation times depend on both a correlation time and a quadrupole coupling constant. The ^{59}Co studies by themselves do not provide sufficient information to separate changes in relaxation time produced by changes in correlation time and changes produced by increased quadrupole coupling. The ^{59}Co nmr studies have therefore been supplemented by measurements of ^{1}H and ^{13}C relaxation times of complexing phenols. The strategy for the analysis of the phenol data is therefore to use ^{59}Co chemical shifts to obtain second sphere equilibrium constants. The way these equilibrium constants vary with the substituent on the phenyl ring is of particular interest. Proton T_1 measurements on the phenol provide additional information of the relative values of the hydrogen bond lifetime and the rotational correlation time and indicate the relative importance of changes in correlation time and quadrupolar coupling. Calculation of the ^{59}Co relaxation times for the second sphere complexes is accomplished by combining the equilibrium data from the chemical shifts with the line broadening data. Finally ^{13}C T_1 measurements on the phenol lead to the calculation of a correlation time for the complex and hence to effective ^{59}Co quadrupole coupling constants for the hydrogen bonded molecules. The range of acidities covered by the phenols is limited. The study has therefore been extended by considering substituted benzoic acids and anilines. Benzoic acids are considerably stronger acids than phenols — the pK_a of benzoic acid is 4.19 and that of phenol 9.89. Anilines show primarily basic properties. The NH_2 protons are only very weakly acidic so that the three series of benzoic acids, phenols, and anilines span a very wide range of acidities.

Experimental

^{59}Co nmr spectra were obtained using a Bruker WH90 FT NMR spectrometer at a frequency of 21.36 MHz. Proton and ^{13}C spectra were obtained using a Bruker WP80 FT spectrometer. Spin–lattice relaxation times (T_1) were measured by the inversion recovery technique (180–τ–90 pulse sequence). Deuterated dimethyl sulphoxide (Norrell Chem. Co.) was used as a solvent throughout. This avoids competition from the solvent for hydrogen bonding sites on the cobalticyanide ion. The solubility of potassium cobalticyanide in dimethyl sulfoxide is limited. The addition of cyclohexyl-18-crown-6-ether increases the solubility by complexing the potassium ions allowing a concentration of 0.05 *M* to be obtained easily. This concentration was used throughout. We have shown previously (8) that the crown ether does not affect the chemical shifts or line widths of the ^{59}Co resonances. It does, however, effect the T_1's of the phenol as described below. ^{59}Co line widths are reported as the full width at half intensity. The chemical shifts are reported relative to $K_3Co(CN)_6$ in Me_2SO_4-d_6. This resonance occurs at a chemical shift of +283 ppm from the usual reference of $K_3Co(CN)_6$ in water. All phenols were of analytical quality and used without further purification. The temperature of the nmr probe was 25 ± 0.5°C for both instruments. The deuterated solvent was used to provide a deuterium lock. Equilibrium constant calculations were carried out on an Osborne 1 microcomputer using BASIC programming.

The ^{59}Co line widths are sensitive to small amounts of water in the Me_2SO_4-d_6. The amount of water tends to vary a little from sample to sample. It was shown that this variation does not affect the increase in line width caused by the addition of the organic compound and that errors in the reported parameters from this source are negligible.

Results

A. ^{59}Co chemical shifts and line widths — phenols

It has been shown previously (7, 8) that the cobalticyanide ion will form hydrogen bonds with suitable proton donating molecules and this leads to a high field shift in the ^{59}Co nmr resonance. This is consistent with an increased ligand field strength for the hydrogen bonded CN^- ion resulting from additional π backbonding placing additional negative charge on the nitrogen adjacent to the electropositive hydrogen. Such hydrogen bonding is not likely to occur with dimethyl sulfoxide and hence its choice as a solvent. Phenols possess an acidic hydroxyl group well suited to hydrogen bond formation. It has been well documented (10–12) that phenols hydrogen bond to dimethylsulfoxide and hence the observed ^{59}Co shifts will be the outcome of a competition between the solvent and the cobalticyanide for the phenolic hydrogen bond. The choice of a range of phenols with both electron withdrawing and electron donating substituents allows a systematic study of this competition. It is also anticipated that hydrogen bond formation will lead to an electric field gradient at the Co nucleus leading to more rapid quadrupolar relaxation and hence an increase in line width.

Tables of the chemical shifts and line widths at different phenol concentrations are available from the Depository of Unpublished Data.[2] Ten substituted phenols have been examined with substituents ranging from the electron withdrawing nitro group to the electron donating amino and methoxy groups. Changes of around 100 ppm in chemical shift and up to more than 1 kHz in line width are observed. They range from a chemical shift of 50.0 ppm and a line width increase of 544 Hz for 1.249 *M* *p*-aminophenol to a chemical shift of 128.9 ppm and a linewidth increase of 1185 Hz for 1.103 *M* *p*-nitrophenol.

B. Relaxation measurements

The ^{59}Co line widths reported above depend upon the relaxation times of both hydrogen bonded and non-hydrogen bonded species. The nature of this dependence is a function of the relationship between the lifetime of the hydrogen bonded complex and its rotational correlation time. Rotational correlation times for metal complexes are usually $\sim 10^{-11}$ s. Less is known of hydrogen bond lifetimes but for amine–water hydrogen bonds Emerson *et al.* (13) have derived values in the range 10^{-10}–10^{-12} s, i.e., comparable to the rotational correlation times. In previous studies (8, 9) we have deduced that for the cobalticyanide ion the hydrogen bond lifetimes can be either longer or shorter than the correlation time depending on the strength of the hydrogen bond. The theory of nmr relaxation under conditions of very rapid chemical exchange has been reviewed by Laszlo (14) who has designated studies in this area "dynamic NMR II". Anderson and Fryer (15) have shown that although the general formulation is complex there are two simple limiting cases. If the chemical exchange lifetime is $\gg \tau_2$ (the rotational correlation time) relaxation rates are averaged, i.e.,

$$[1] \quad \frac{1}{T_2} = \frac{P_A}{T_{2A}} + \frac{P_B}{T_{2B}}$$

[2]Complete set of data is available upon request, at a nominal charge, from the Depository of Unpublished Data, CISTI, National Research Council of Canada, Ottawa, Ont., Canada K1A 0S2.

Can. J. Chem. Downloaded from www.nrcresearchpress.com by 210.87.254.42 on 09/06/12
For personal use only.

TABLE 1. Proton spin lattice relaxation times of *para*-nitrophenol[a]

PNO_2phenol (M)	Crown ether (M)	KCl (M)	Cobalticyanide $K_3Co(CN)_6$ (M)	T_1 (s)[b]		
				7.7 ppm[c]	6.6 ppm[d]	OH
0.044	—	—	—	3.37	2.53	—
0.538	—	—	—	2.71	1.58	0.97
1.37	—	—	—	2.02	1.13	0.63
2.00	—	—	—	1.79	1.07	0.68
0.050	0.229	0.148	—	2.59	2.15	—
0.462	0.164	0.15	—	3.26	2.28	—
1.32	0.145	0.13	—	1.15	0.63	0.40
2.23	0.168	0	—	1.43	0.74	0.41
0.047	0.167	—	0.060	1.96	1.00	—
0.470	0.163	—	0.050	2.42	1.57	—
1.27	0.124	—	0.041	1.84	1.38	—
2.19	0.165	—	0.050	0.67	0.38	0.48

[a]Solvent DMSO-d_6.
[b]Errors in T_1 ±0.1 s.
[c]7.7 ppm resonance assigned to proton *ortho* to NO_2.
[d]6.6 ppm resonance assigned to proton *ortho* to OH.

TABLE 2. ^{13}C spin lattice relaxation times of *para*-nitrophenol[a]

Crown ether (M)	KCl (M)	$K_3Co(CN)_6$ (M)	PNO_2phenol (M)	T_1 (s)	
				129 ppm	119 ppm
—	—	—	2.55	1.01±0.09	1.11±0.05
0.166	—	0.035	0.40	1.04±0.02	1.04±0.02
0.123	—	—	0.462	2.52±0.09	2.20±0.11
0.130	—	0.052	0.475	1.17±0.02	1.09±0.02
0.126	0.135	—	0.450	1.93±0.02	1.94±0.04

[a]Solvent DMSO-d_6.

TABLE 3. Equilibrium constants, chemical shifts, and line widths of second sphere complexes with phenols

Substituent	K_{app}[a]	$\Delta\nu$ (ppm)[a]	Correlation coefficient	Line width (Hz)[a]
p-NO_2	2.726	164	0.990	2408
H	0.584	168	0.998	2453
m-NO_2	1.252	159	0.999	2331
p-NH_2	0.231	228	0.962	3327
m-NH_2	1.208	126	0.999	1841
p-F	0.970	167	0.999	2441
p-CN	2.176	163	0.999	2385
p-OCH_3	0.596	181	0.996	2648
p-C_6H_5	1.014	155	0.994	2273
p-COOH	1.626	145	0.980	2129

[a]Statistical error 1%.

If the converse is true relaxation times are averaged, i.e.,

$$[2] \quad T_2 = P_A T_{2A} + P_B T_{2B}$$

In both bases P_A and P_B are the fractional populations of the two chemically distinct sites which can be obtained from the ^{59}Co chemical shifts. In the extreme narrowing case ($\omega^2\tau^2 \ll 1$) $T_1 = T_2$ and the above equations are equally applicable to T_1. The ^{59}Co line widths can be used to determine which (if either) of these limiting conditions is applicable. This information has been supplemented with ^1H and ^{13}C T_1 measurements on *para*-nitrophenol in the presence and absence of cobalticyanide ions. The results of these measurements are reported in Tables 1 and 2. If T_1, T_{1A}, P_A, and P_B are known T_{1B} can be calculated using either eq. [1] or [2]. The use of the correct equation should lead to constant values for T_{1B} at all concentrations of phenol and cobalticyanide. It is apparent from the data in Tables 1 and 2 that the T_1's are also dependent on the concentrations of *para*-nitrophenol and of crown ether. Comparisons between relaxation times with and without cobalticyanide must therefore be made at constant *p*-nitrophenol and crown ether concentrations. In the presence of potassium cobalticyanide the crown ether is present as a potassium complex. The measurements in the absence of cobalticyanide were therefore carried out with the addition of an equivalent amount of potassium chloride to complex the crown ether. The line broadening mechanism for the ^{59}Co is not completely certain (we have recently demonstrated substantial field dependences of line widths for Co complexes which are not anticipated for quadrupolar broadening). We have previously shown (8) that both T_1 and T_2 are decreased on hydrogen bond formation eliminating "chemical exchange" as a line broadening mechanism. There remains the problem of separating the effect due to a change in quadrupole coupling constant (or chemical shift anisotropy if this is important) and that due to a change in correlation time. This difficulty is not present in the ^1H and ^{13}C T_1 measurements. In both cases dipolar relaxation is dominant and the change in T_1 on hydrogen bond formation can be ascribed to a change in correlation time. In the case of the aromatic carbons bonded to hydrogen dipolar relaxation due to the directly bonded hydrogen is expected to dominate. This is confirmed by measurement of the nuclear Overhausser enhancement (16). A value of 1.83 ±

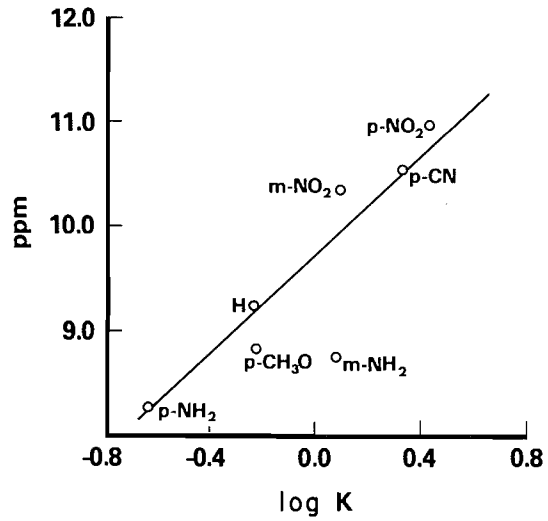

FIG. 1. Correlation of equilibrium constants with hydroxyl proton chemical shifts (ref. 12).

0.20 was obtained comparable with the theoretical value of 2.0 for complete intramolecular dipolar relaxation. From the ^{13}C measurements we can therefore calculate an absolute value of the correlation time of the hydrogen bonded complex and use this to obtain an effective quadrupole coupling constant.

C. Chemical shifts and line widths — anilines and benzoic acids

^{59}Co chemical shifts and line widths for $Co(CN)_6^{3-}$ in the presence of various anilines and benzoic acids are available from the Depository of Unpublished Data. The changes in chemical shift and the increases in line width for anilines are both considerably smaller than the corresponding changes for phenols. A similar set of measurements using *N,N*-dimethyl aniline showed no shifts or line broadening confirming the necessary presence of an NH_2 group for second sphere bonding. Thus 0.862 *M p*-anisidine produces a chemical shift of 5.7 ppm and an additional broadening of only 11 Hz. At the other extreme 1.219 *M p*-nitroaniline gives a chemical shift of 43.1 ppm and a broadening of 84 Hz. Both the chemical shifts and increases in line widths for the benzoic acids are greater than for corresponding anilines, but in spite of the greater pK_a's are smaller than those for the phenols. Thus 1.057 *M p*-aminobenzoic acid gives a shift of 44.6 ppm and a broadening of 692 Hz whereas 0.632 *M p*-nitrobenzoic acid produces a shift of 54.3 ppm and a broadening of 1429 Hz.

Discussion

A. Chemical shifts of phenols

The initial objective of the present study is to determine how the equilibrium constants for the formation of hydrogen bonded second sphere complexes and the chemical shifts of these complexes vary with phenol substituent. The chemical shift is a measure of the change in the electronic properties of the cyanide ligand and hence of the strength of the hydrogen bond formed. The simplest model is to assume the formation of a 1:1 complex between the cobalticyanide and the phenol, i.e.,

$$Co(CN)_6^{3-} + P \rightleftarrows Co(CN)_6^{3-}P$$

It is implied that both the "free" phenol and the cobalticyanide are solvated by the dimethylsulfoxide. It may be readily shown that the concentration of free phenol (P) and the observed chemical shift ($\Delta\nu$) are related by the equation:

$$[3] \quad \frac{P}{\Delta\nu} = \frac{1}{K\Delta\nu_\infty} + \frac{P}{\Delta\nu_\infty}$$

where K is the equilibrium constant for the above reaction and $\Delta\nu_\infty$ is the chemical shift of the hydrogen bonded adduct. A plot of $P/\Delta\nu$ versus P should therefore be linear with a slope of $1/\Delta\nu_\infty$ and an intercept of $1/K\Delta\nu_\infty$. This equation is readily solved by successive approximation with the initial assumption that the concentration of free phenol equals the total phenol concentration. Table 3 gives the values of K and $\Delta\nu_\infty$ obtained on the assumption of a 1:1 complex. The correlation coefficients for the final fit to eq. [3] are also given. They are generally greater than 0.99, indicating that this model gives a satisfactory fit to the data. The degree of association of the cobalticyanide for a given concentration of phenol is readily obtained as $\Delta\nu/\Delta\nu_\infty$. Plots of this function versus the observed line width are also satisfactorily linear and give the line widths of the cobalticyanide/phenol complexes shown in Table 3.

The above model is overly simplified in two respects. It neglects possible association of the phenol molecules in solution and it neglects the formation of second sphere complexes of stoichiometries other than 1:1. Covington *et al.* (17–19) and more recently Kitaigorodskii, Nakipelov, and Zamaraev (20) have derived expressions for the equilibria which remove these limitations. Tsuno *et al.* (11) and Fujio *et al.* (12) have demonstrated that the self association of phenols in dimethyl sulfoxide is negligible at concentrations below 0.5 *M*. Presumably the strength of the hydrogen bond formed with the solvent is greater than that formed by a phenol dimer. The linearity of the fit to eq. [3] indicates that self-association is not important. This fit does not, however, prove that only a 1:1 complex is formed. We have carried out calculations assuming other stoichiometries and obtain equally good fits. These calculations assumed that the equilibrium constant for binding the second phenol was equal to that for the first phenol. From previous mixed solvent studies it is clear that the equilibrium constants for successive addition of second sphere ligands become progressively smaller. The analysis of Kitaigorodski *et al.* (20) demonstrates that data of the type reported in the present paper cannot be unambiguously fitted to a unique set of equilibrium constants. However, these authors concluded that the equilibrium constant K_{eff} found by assuming a 1:1 complex provides a true measure of the stability of the outer sphere complex. Numerical analysis showed that the values of K_1, the true equilibrium constant, were only slightly larger than K_{eff}, the value obtained by neglecting complexes of higher stoichiometries. We take therefore the K_{eff} values of Table 3 as a measure of the stability of the hydrogen bonded complexes. Errors in this equilibrium constant will of course lead to errors of a similar magnitude in the chemical shift and line width parameters of Table 3.

An alternative method of analysing this data is provided by the Scratchard Plot (21):

$$\Delta\nu/P = K\Delta\nu_\infty - K\Delta\nu$$

which is eq. [3] cast in a different form. A number of data sets have been analysed in this manner. The values of K and $\Delta\nu_\infty$ obtained are very similar to those given in Table 3. The Scratchard Plot is useful in enzyme studies to distinguish different complexing sites but it does not appear suitable for deciding the stoichiometry in a case with several identical complexing sites.

Can. J. Chem. Downloaded from www.nrcresearchpress.com by 210.87.254.42 on 09/06/12
For personal use only.

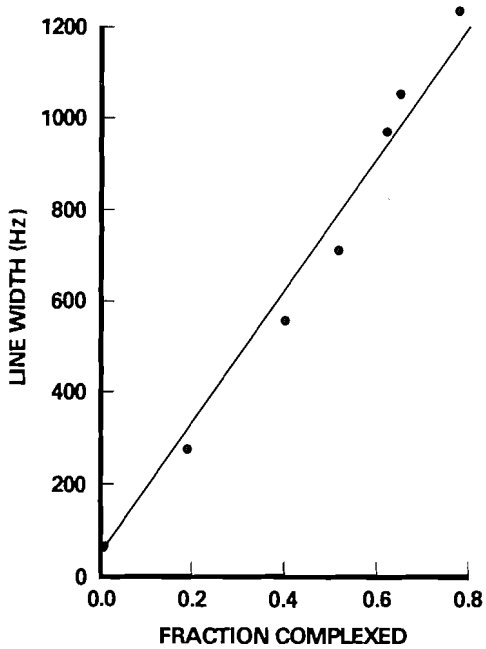

FIG. 2. Variation of line width with degree of association for *para*-nitrophenol.

The most notable feature of the results of Table 3 is that the differences in the effects of the different phenols arise almost entirely from differences in equilibrium constants. With the exception of the amino phenols, the chemical shifts and line widths of the hydrogen bonded complexes are almost independent of substituent. The amino phenols can hydrogen bond either through the OH group or the NH_2 group and this is a likely source of their anomalous behaviour. The equilibrium constants are largest for the most electron withdrawing substituents and smallest for the most electron donating substituents. They can be correlated with a variety of other measures of electron withdrawing ability such as pK_a's and Hammett and other forms of substituent parameters. Shown in Fig. 1 is a plot of ln K_{eff} versus the chemical shift of the hydroxyl proton in DMSO. Fujio *et al.* (12) have used these proton chemical shifts to derive substituent parameters and have discussed their relationship to the electronic structure of the phenols in some detail. Eymen and Drago (10) have related the proton chemical shifts to hydrogen bond strengths. The values of K_{eff} can be equally well correlated with any of these parameters.

B. Relaxation times of phenol complexes

The increases in line width of the ^{59}Co resonance on addition of phenol reflect a decrease in T_2. It is usually considered that the dominant relaxation mechanism for ^{59}Co is quadrupolar. In this case:

$$\frac{1}{T_2} = \frac{3}{40}\frac{2I+3}{I^2(2I-1)}\left(\frac{e^2Qq}{h}\right)^2\left(1+\frac{\eta^2}{3}\right)\tau_2$$

A decrease in T_2 can be the result of either an increase in the quadrupole coupling constant e^2Qq or an increase in the correlation time τ_2 or both. It is not possible to separate these two effects on the basis of ^{59}Co data alone. The proton and ^{13}C relaxation data of Tables 1 and 2 have been used for this purpose. It is assumed that the T_1's for the protons and carbons result entirely from dipolar relaxation which is unaffected by complexation so that any change in relaxation time reflects a change in correlation time.

The observed relaxation times are an average of the relaxation properties of the complexed and uncomplexed molecules which are in rapid chemical exchange and it is first necessary to decide how to carry out the averaging. As pointed out above, depending on whether the chemical exchange lifetime is long or short relative to the correlation time, either the relaxation rates or the relaxation times should be averaged. In the former case a plot of line width versus degree of association (obtained from the chemical shift data) should be linear. In the latter case a plot of 1/line width versus degree of association should be linear. Figure 2 shows the plot versus line width for *para*-nitrophenol. It is clearly linear, showing that the exchange lifetimes are greater than the correlation times. The line widths of Table 3 have been evaluated on this basis.

The proton T_1's of Table 1 confirm this conclusion and allow us to estimate the contribution of the change in correlation time to the line width increase. We note first that the T_1's are dependent on the concentration of the phenol. This most probably reflects viscosity changes. There is also a decrease on adding crown ether. Complexing between crown ether and *para*-nitrophenol has indeed been reported by Virtanen and Viirret (22) in carbon tetrachloride. A weaker complex would be expected in dimethyl sulphoxide but significant interaction is obviously occurring. It is therefore necessary to compare the T_1's at equal concentrations of both phenol and crown ether in the presence and absence of cobalticyanide. The data of Table 2 shows decreases of from 50–100% on the addition of cobalticyanide. This analysis neglects the change in viscosity resulting from the relatively low concentration (0.05 *M*) of cobalticyanide.

These changes are much smaller than the changes in the ^{59}Co line width produced by similar concentrations of *para*-nitrophenol — more than an order of magnitude increase is observed. We deduce that the major contribution to the increased line widths of the ^{59}Co is the electric field gradient induced by the hydrogen bond leading to a greatly increased quadrupole coupling constant. The proton T_1's can also be used to check the form of the averaging of the relaxation. Values of T_1 complexed can be calculated based on either of eqs. [1] and [2]. Averaging of the relaxation times leads to negative values for T_1 complexed which is clearly inadmissible. Averaging of the relaxation rates gives reasonably consistent values of T_1 complexed as shown by the data in Table 4.

The ^{13}C relaxation times in Table 2 allow us to carry this analysis a little further. Qualitatively, the ^{13}C T_1's behave quite similarly to the ^1H T_1's. They decrease with increasing *para*-nitrophenol concentration, with increasing crown ether concentration, and with the addition of cobalticyanide. It is assumed that the ^{13}C relaxation of the aromatic carbons directly bonded to hydrogen is determined by dipole–dipole interaction with the neighbouring hydrogen, i.e. (24),

$$\frac{1}{T_1} = \frac{\mu_0^2\gamma_H^2\gamma_C^2h^2}{12\pi^2}\frac{I(I+1)}{r^6}\tau_2$$

This assumption is confirmed by the Overhauser effect measurement and is consistent with results reported for nitrobenzene and other aromatic molecules (16). Using the equilibrium constant of Table 3 and assuming averaging of the free phenol and complexed phenol relaxation rates, we obtain values of T_1 for the complex of 0.16 s and 0.14 s from the two aromatic carbons bearing protons. Using an average value of 0.15 s this leads to a correlation time of 2.8×10^{-10} s for the *para*-nitrophenol complex. The corresponding value for "free"

Can. J. Chem. Downloaded from www.nrcresearchpress.com by 210.87.254.42 on 09/06/12
For personal use only.

TABLE 4. Calculated ^{1}H relaxation times of second sphere complex[a]

			7.7 ppm				6.6 ppm			
					T_{1e}				T_{1e}	
PNO_2phenol[c]	$K_3Co(CN)_6$[c]	α[b]	T_1(obs)	T_{1f}	Fast exchange	Slow exchange	T_1(obs)	T_{1f}	Fast exchange	Slow exchange
0.047	0.060	0.1273	1.96 ±0.14	2.59 ±0.08	<0	0.74 ±0.25	1.00 ±0.12	2.15 ±0.07	<0	0.21 ±0.05
0.470	0.050	0.0579	2.42 ±0.03	3.26 ±0.19	<0	0.47 ±0.10	1.57 ±0.10	2.28 ±0.14	<0	0.26 ±0.10
2.19	0.050	0.0195	0.67 ±0.02	1.43 ±0.13	<0	0.024 ±0.004	0.38 ±0.01	0.74 ±0.02	<0	0.015 ±0.001

[a]T_{1f} is T_1 "free" of phenol; T_{1e} is T_1 of complex.
[b]Degree of association calculated assuming a 1:1 complex. This is a poor assumption for the 2.19 *M* solution.
[c]Concentration in mol/L.

TABLE 5. $K\Delta\nu$ values for phenols, benzoic acids, and anilines

Substituent	Aniline[a]	Benzoic acid[b]	Phenol[c]	r^1 [d]
H	9	69	98	0.9921
m-NO_2	21		199	0.9975
p-NO_2	36	135	447	0.9962
p-Cl	14	91		0.9992
p-F		98	162	
m-NH_2		90	152	
p-NH_2		43	53	
p-OH		208		
m-OH				
o-Cl		108		
p-CN			355	
p-OCH_3	9			0.9978
p-C_6H_5			157	
p-COOH			236	
p-Br	16			0.9942

[a]From slopes of $\Delta\nu$ versus concentration plots.
[b]From intercepts — see text.
[c]From data in Table 3.
[d]Correlation coefficients for aniline plots.

para-nitrophenol is 2.2×10^{-11} s. Ader and Loewenstein (23) have reported a correlation time of 1.8×10^{-11} s for "free" cobalticyanide ion. This was obtained by combining the ^{14}N line width with the ^{14}N quadrupole coupling constant from solid state data. The complexed cobalticyanide should have the same correlation time as the complexed *para*-nitrophenol since both refer to the same molecule. The correlation time is proportional to the cube of the molecular radius. The radius for $Co(CN)_6^{3-}$ is given as 3.9 Å. The increase of correlation time from 1.8×10^{-11} s to 2.8×10^{-10} s requires an increase of the radius to 9.75 Å. A model assuming normal bond lengths and a phenolic hydrogen bond with an H—O—C angle of 105° gives a separation between the Co atom and the average position of the oxygen atoms of the nitro group of 9.8 Å. This indicates that the correlation time obtained from the ^{13}C results is reasonable for a hydrogen bonded adduct between $Co(CN)_6^{3-}$ and *para*-nitrophenol. This correlation time can now be used to obtain an effective ^{59}Co quadrupole coupling constant for the adduct. Using the line width from Table 3 (2408 Hz) gives a quadrupole coupling constant of 8.34 MHz. This is fairly small compared with the quadrupole coupling constants of complexes with different first sphere ligands but not unreasonable for a second sphere effect.

C. *Complexing with anilines and benzoic acids*

Analysis of the chemical shift data for anilines and benzoic acids is more restricted than that for phenols. Equation [3] may be rewritten:

$$\Delta\nu = \frac{K[\mathrm{An}]}{1 + K[\mathrm{An}]}\Delta\nu_\infty$$

If $K[\mathrm{An}] \ll 1$, a linear relationship between $\Delta\nu$ and [An] is anticipated. The slope of such a plot gives the product $K\Delta\nu_\infty$ but it is not possible to obtain K and $\Delta\nu_\infty$ independently. This is the case for the present data for anilines. Table 5 gives the slopes, and correlation coefficients for these plots. The correlation coefficients are generally greater than 0.99, indicating a satisfactory fit.

The behaviour of the benzoic acids is somewhat different. Plots of eq. [3] are not linear. Figure 3 shows two examples of such plots for benzoic acids. They show a pronounced upward curvature. The probable explanation involves the formation of benzoic acid dimers. Dimers of carboxylic acids have been extensively studied in many solvents (25–27). It would be anticipated that the monomer would be favoured in a solvent such as dimethylsulphoxide, which is capable of forming hydrogen bonds, compared to nonpolar solvents such as benzene. The formation of dimers in dimethylsulphoxide is demonstrated by the observation that the proton resonance of the carboxylic acid hydrogen shows a concentration dependence of its chemical shift and line width. It differs in this respect from the hydroxyl resonance of phenols (11, 12). The effect of dimer formation on the ^{59}Co chemical shifts will be to cause a smaller shift at high concentrations of acid, since less monomer is available to complex with the $Co(CN)_6^{3-}$. The curvature of Fig. 3 is consistent with this interpretation. K and $\Delta\nu_\infty$ cannot therefore be obtained independently from the slope and intercept. However, the intercept at zero concentration can be estimated fairly reliably and according to eq. [3] this provides a value of $K\Delta\nu_\infty$ at extreme dilution, i.e. under conditions where the effects of dimerization are minimal. These values are also given in Table 5. This table also contains the corresponding quantities for the phenols for the purpose of comparison. The variation of $K\Delta\nu_\infty$ with substituent is similar for all three sets of data as is illustrated for anilines and phenols in Fig. 4. In all cases electron withdrawing substituents produce the larger shifts and electron donating substituents the smaller shifts. In the case of phenols it was shown that the equilibrium constants rather than the chemical shifts of the hydrogen bonded complex provided

Can. J. Chem. Downloaded from www.nrcresearchpress.com by 210.87.254.42 on 09/06/12
For personal use only.

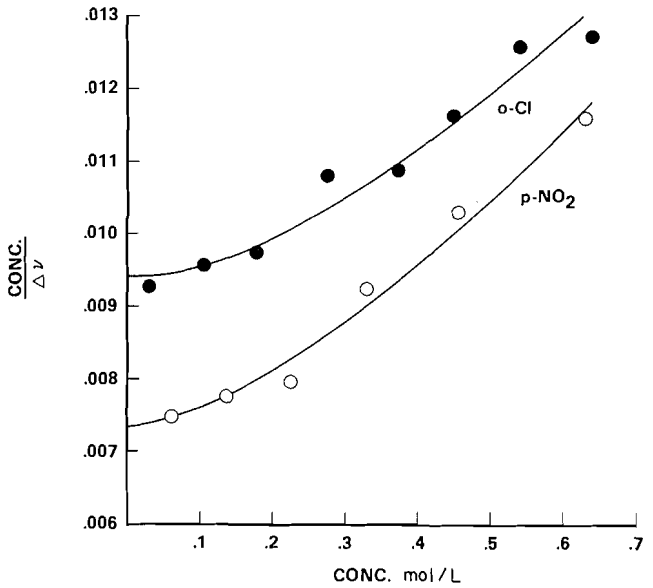

FIG. 3. Plots of $[B]/\Delta\nu$ versus [B] for benzoic acids.

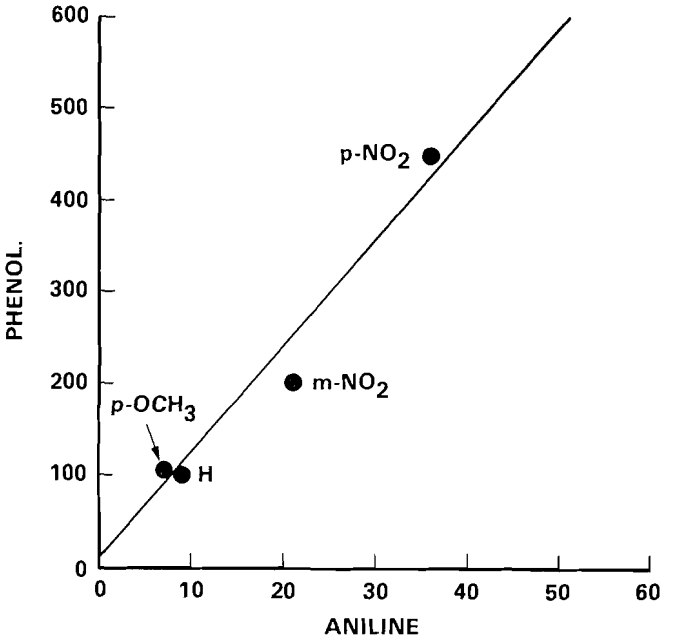

FIG. 4. Correlation of $K\Delta\nu_\infty$ for phenols and anilines.

the major sources of variation. In fact, the chemical shifts for a wide range of hydrogen bonded complexes are remarkably constant. They range (8) from ~350 ppm for the fully hydrogen bonded complex in formic acid, to 280 ppm in pure water, 200 ppm in methanol, and around 150 ppm estimated for the 1:1 complex with phenols. If this trend is followed it seems reasonable that the shift for an aniline complex would be rather less than that for a phenol complex and certainly not greater. This leads to the conclusion that the equilibrium constants for the anilines are no more than one order of magnitude smaller than those for the phenols since the products $K\Delta\nu_\infty$ are smaller by this amount.

A similar estimate for the benzoic acids can be obtained. It can be argued that the values of $\Delta\nu_\infty$ for the benzoic acids will be not less than those for the phenols and probably somewhat larger. It follows that the equilibrium constants are less than those of the phenols by a factor of no more than 2 or 3.

The most notable feature of these results is the relatively modest variation in hydrogen bonding ability over a very wide range of pK_a's. This most probably reflects the competitive nature of the hydrogen bonding process. If a molecule will form stronger hydrogen bonds with the cobalticyanide it will also form stronger hydrogen bonds with the solvent dimethylsulfoxide so that the fraction hydrogen bonded to the metal complex is relatively insensitive to hydrogen bonding ability. For the carboxylic acids hydrogen bonding leading to dimerization also becomes competitive and the net result is a smaller fraction of molecules bonded to the cobalticyanide than in the case of the weaker phenolic acids. The implication of this result is that second sphere hydrogen bonded complexes could be of importance as reaction intermediates for a wide range of acid strengths.

D. The lifetimes of the hydrogen bonds

It has been noted above that if the hydrogen bonds have long lifetimes ($\gg$ the correlation time) and relaxation rates are averaged and if they have short lifetimes ($<$ the correlation time) the relaxation times are averaged (14). The choice of averaging conditions has a large effect on the extent of line broadening. This point may be illustrated with a numerical example. If there is rapid exchange between two species one with a line width of 100 Hz and one with a line width of 1 Hz and 50% of each is present, the resulting line will have a width of 50.5 Hz if the line widths are averaged. Averaging of relaxation times gives a line width of 1.98 Hz, i.e., in one case there is an increase in line width of a factor of 50 on complex formation and in the other case of a factor of 2 for the same degree of complex formation.

In the case of the phenols it is clear that the rates are averaged, indicating that the lifetime is greater than 10^{-10} s. An upper limit of 10^{-6} s can be inferred from the lack of chemical shift broadening ($T_1 = T_2$) in spite of the 150 ppm (equivalent to 3200 Hz at the field of the present experiments) chemical shift difference of the complexed and free forms. In the case of the anilines and benzoic acids we cannot obtain absolute values for the dependence of line width on complex concentration since the absolute values of the equilibrium constants are not known. Relative values can, however, be obtained. The fraction of cobalticyanide complexed is proportional to the chemical shift. The line widths should therefore be proportional to chemical shifts if relaxation rates rather than relaxation times are averaged.

In the converse case a plot of line width versus the reciprocal of chemical shift would be appropriate. For the phenols and benzoic acids plots of line widths versus chemical shifts are linear with correlation coefficients always greater than 0.98 and in most cases greater than 0.99. The slopes of such plots are given in Table 6. The increases in line widths for the anilines are very small. In fact with the exception of the *p*-nitroaniline they are comparable to the increases which would be anticipated from the larger viscosities of the more concentrated solutions. The rate of increase in line width with increase in chemical shift is much smaller than observed for the phenols and benzoic acids as shown by the data in Table 6. The correlation of line width with chemical shift for the anilines is poor. It should be noted that the figures in the three columns of Table 6 are only directly comparable if the chemical shifts for the aniline, phenol, and benzoic acid complexes were identical. If, as anticipated, the aniline shifts are rather smaller than the phenol shifts and the benzoic acid shifts rather larger, the

Can. J. Chem. Downloaded from www.nrcresearchpress.com by 210.87.254.42 on 09/06/12
For personal use only.

TABLE 6. Dependence of line widths on chemical shifts[a]

Substituent	Aniline	Phenol	Benzoic acid
p-NO_2	2.0	9.3	25.4
m-NO_2	0.2	11.5	
p-CN		8.9	
p-C_6H_5		11.4	
p-Cl	1.6		24.5
o-Cl			16.5
p-Br	1.1		
p-F		5.9	18.8
H	0.8	6.0	16.1
p-OCH_3	1.2	7.5	
m-OCH_3	1.8		
p-OH			14.6
p-NH_2		9.9	14.3
m-NH_2		7.4	16.5

[a]Increase in line width/chemical shift Hz/ppm.

differences between the three sets of data would be more pronounced. The implication of these data is that the stronger hydrogen bond formed by the benzoic acid produces a larger electric field gradient at the Co and hence a large quadrupole coupling constant and a broader line. These data also indicate that p-hydroxybenzoic acid and p-aminobenzoic acid interact primarily through the carboxylic acid group and p-aminophenol primarily through the phenolic hydroxide. The very small broadening and its poor correlation with chemical shift caused by the anilines is consistent with the hypothesis that weak hydrogen bonds have lifetimes less than the rotational correlation time of the complexes. Unfortunately the very small broadening and the consequent large percentage errors in the line width increases prevent a quantitative test of this possibility. If, however, this is the case, it is the lifetime of the complex, rather than the equilibrium constant, which limits the mechanistic importance of second sphere hydrogen bonded complexes.

Acknowledgement

We are indebted to the Natural Science and Engineering Research Council of Canada for financial support of this research.

1. S. BEHRENDT, C. H. LANGFORD, and L. S. FRANKEL. J. Am. Chem. Soc. **91**, 3945 (1969).
2. V. GUTMANN, G. GRITZNER, and K. DANKSAGMULLER. Inorg. Chem. Acta, **17**, 81 (1976).
3. A. R. BOATE and D. R. EATON. Can. J. Chem. **55**, 2432 (1977).
4. L. S. FRANKEL, C. H. LANGFORD, and T. R. STENGLE. J. Phys. Chem. **74**, 1376 (1970).
5. K. L. CRAIGHEAD, P. JONES, and R. G. BRYANT. J. Phys. Chem. **79**, 1868 (1975).
6. D. R. EATON, H. O. OHORODNYK, and L. SEVILLE. Can. J. Chem. **49**, 1218 (1971).
7. P. LASZLO and A. STOCKIS. J. Am. Chem. Soc. **102**, 7818 (1980).
8. D. R. EATON, C. V. ROGERSON, and A. C. SANDERCOCK. J. Phys. Chem. **86**, 1365 (1982).
9. D. R. EATON and A. C. SANDERCOCK. J. Phys. Chem. **86**, 1371 (1982).
10. D. P. EYMAN and R. S. DRAGO. J. Am. Chem. Soc. **88**, 1617 (1966).
11. Y. TSUNO, M. FUJIO, Y. TAKAI, and Y. YUKAWA. Bull. Chem. Soc. Jpn. **45**, 1519 (1972).
12. M. FUJIO, M. MISHIMA, Y. TSUNO, T. YUKAWA, and Y. TAKAI. Bull. Chem. Soc. Jpn. **48**, 2127 (1975).
13. M. T. EMERSON, E. GRUNWALD, M. L. KAPLAN, and R. A. KROMHOUT. J. Am. Chem. Soc. **82**, 6307 (1960).
14. P. LASZLO. Prog. Nucl. Magn. Reson. Spectrosc. **13**, 257 (1980).
15. J. E. ANDERSON and P. A. FRYER. J. Chem. Phys. **50**, 3784 (1969).
16. J. R. LYERLAN and G. C. LEVY. Topics in carbon-13 NMR spectroscopy. Vol. 1. *Edited by* G. C. Levy. Wiley, New York. 1974. p. 114.
17. A. K. COVINGTON, T. H. LILLEY, K. E. NEWMAN, and G. A. PORTERHOUSE. J. Chem. Soc. Faraday Trans. 1, **69**, 963 (1973).
18. A. K. COVINGTON, I. R. LANTZKE, and J. M. THAIN. J. Chem. Soc. Faraday Trans. 1, **70**, 1869 (1974).
19. A. K. COVINGTON and J. M. THAIN. J. Chem. Soc. Faraday Trans. 1, **70**, 1879 (1974).
20. A. N. KITAIGORODSKII, V. M. NEKIPELOV, and K. I. ZEMAREV. Zh. Struckt. Khim. **19**, 686 (1979).
21. D. A. DERANLEAU. J. Am. Chem. Soc. **91**, 4044, (1960); **91**, 4050 (1960).
22. P. O. I. VIRTANEN and J. VIIRRET. Finnish. Chem. Lett. 142 (1978).
23. R. ADER and A. LOEWENSTEIN. J. Magn. Reson. **5**, 248 (1971).
24. M. L. MARTIN, G. J. MARTIN, and J. DELPUECK. Practical NMR spectroscopy. Heyden, London 1980. p. 18.
25. N. MULLER and P. I. ROSE. J. Phys. Chem. **69**, 2564 (1965).
26. N. MULLER and O. R. HUGHES. J. Phys. Chem. **70**, 3975 (1966).
27. Y. H. YOON, S. T. LEE, D. J. SHIEH, and H. EYRING. Chem. Phys. Lett. **38**, 24 (1976).

Can. J. Chem. Downloaded from www.nrcresearchpress.com by 210.87.254.42 on 09/06/12
For personal use only.

Molecular rearrangements. Part XX.[1] Thermolysis of carboxylic acid esters[2]

M. M. ALY, M. Z. A. BADR, A. M. FAHMY, AND S. A. MAHGOUB
Chemistry Department, Faculty of Science, Assiut University, Assiut, Egypt, A.R.E.

Received November 25, 1982

M. M. ALY, M. Z. A. BADR, A. M. FAHMY, and S. A. MAHGOUB. Can. J. Chem. **61**, 1532 (1983).

Thermolysis of phenyl benzoate on heating under reflux for ca. 10 days in a nitrogen atmosphere gives phenol, *o*- and *p*-hydroxybiphenyl, biphenyl, and carbon monoxide. Phenyl phenylacetate under the same conditions gives toluene, bibenzyl, stilbene, phenol, *o*- and *p*-benzylphenol, 9-phenylxanthene, water, and carbon monoxide. Thermolysis of benzyl benzoate is accompanied by decarboxylation and the formation of toluene, diphenylmethane, bibenzyl, stilbene, and biphenyl. Thermolysis of benzyl phenylacetate proceeds smoothly, affording carbon dioxide, toluene, bibenzyl, and stilbene. It was concluded that thermolyses of esters proceeds through a free radical mechanism involving homolytic fission of either the O—CO or O–alkyl bond with subsequent decomposition of the radicals so formed.

M. M. ALY, M. Z. A. BADR, A. M. FAHMY et S. A. MAHGOUB. Can. J. Chem. **61**, 1532 (1983).

Le benzoate de phényle chauffé au reflux sous atmosphère d'azote pendant 10 jours environ donne le phénol, les *o*- et *p*-hydroxybiphényle, le biphényle et le monoxyde de carbone. Dans les mêmes conditions la thermolyse du phénylacétate de phényle donne le toluène, le bibenzyle, le stilbène, le phénol, les *o*- et *p*-benzylphénol, le phényl-9 xanthène, l'eau et le monoxyde de carbone. La thermolyse du benzoate de benzyle s'accompagne d'une décarboxylation avec formation de toluène, de diphénylméthane, de bibenzyle, de stilbène et de biphényle. La thermolyse du phénylacétate de benzyle donne le bioxyde de carbone, le toluène, le bibenzyle et le stilbène. On conclut que la thermolyse des esters se fait selon un mécanisme de radical libre qui implique la fission homolytique de la liaison O—CO ou O–alkyle suivie de la décomposition des radicaux formés.
[Traduit par le journal]

The isomeric change of phenolic esters to hydroxyketones under the influence of Lewis acid catalysts, known as the Fries rearrangement, has long been used for its synthetic value (1).

Recently, the photo-Fries rearrangement has been a subject of extensive study (2) and it is now well established that the process involves fragmentation into free radicals which undergo extensive geminate recombinations.

Similarly the noncatalysed thermal rearrangement of esters became of increasingly great importance, since esters can be used as additives for lube oils (3) although the mechanism is still subjudice that it may involve ketene formation or homolysis of the ester molecule at different sites, according to the stability of the radicals so formed.

The present work describes the behaviour of some carboxylic acid esters when heated at their reflux temperatures, ca. 320°C.

Thermolysis of phenyl benzoate was found to give rise to phenol, *o*- and *p*-hydroxybenzophenone, *o*- and *p*-hydroxybiphenyl, biphenyl, and carbon monoxide. Such results can be accounted for in terms of a free radical mechanism involving benzoyl–oxygen bond homolysis (route (*a*)) forming phenoxyl and benzoyl radical pairs that can undergo C—C coupling, forming the isomeric *o*- and *p*-hydroxybenzophenones. Moreover, the benzoyl radicals may undergo decarbonylation forming phenyl radicals that subsequently attack the phenol molecule to give *o*- and *p*-hydroxybiphenyl or dimerize into biphenyl (cf. Scheme 1).

However, it may be assumed that biphenyl can be obtained from dimerization of phenyl radicals formed through homolysis of the O—Ph bond of the ester (route (*b*)), yet such a suggestion was ruled out by the absence of benzoic acid or carbon dioxide, even in trace amounts. Furthermore, on pyrolysis of *p*-cresylbenzoate, no methyl-substituted biphenyls were detected among the pyrolysates.

The absence of the carbon–oxygen dimer of the phenoxyl radicals, namely, *o*- and *p*-phenoxyphenols (as proved by glc), emphasizes the results obtained from spin resonance work (4) where it is possible to deduce that ca. 80% of the unpaired spin density resides on the *ortho* and *para*-ring carbon atoms.

Moreover, the oxygen–oxygen dimer, namely, diphenylperoxide, would probably be unstable under such conditions and need not be considered (5).

Replacement of the phenyl with the benzyl group in the acid moiety of phenyl benzoate resulted in extensive decarbonylation. Thus, thermolysis of phenyl phenylacetate leads to the formation of toluene, bibenzyl, stilbene, 9-phenylxanthene, and water as neutral products together with carbon monoxide, phenol, and *o*- and *p*-benzylphenol. The formation of these products necessitates the homolysis of the CO—O bond as for phenyl benzoate, forming phenoxyl and phenylacetyl radical pairs. The phenylacetyl free radicals eventually decarbonylate to give benzyl free radicals which participate in the formation of toluene, bibenzyl, and stilbene as mentioned in previous work (6). The normal fate of phenoxyl radicals is to form phenol, through H abstraction, and isomeric *o*- and *p*-benzylphenols, through coupling with benzyl radicals. The formation of 9-phenylxanthene can be rationalized as proceeding by the mechanism suggested by Hickinbottom and El-Kobaisi (7*a*), cf. Scheme 2.

It may be assumed that the phenylacetyl free radicals may give rise to phenyl ketene (8). However, this suggestion was ruled out by the absence of phenylacetic acid among the products. Moreover, no significant amounts of *o*- and/or *p*-hydroxyphenylacetophenone were detected in such ester pyrolysis which would be exptected if the phenylacetyl free radicals survived long enough to couple with phenoxyl radicals.

On the other hand, replacement of the phenyl with the benzyl group in the phenolic moiety of phenyl benzoate gave a quite different result, where the thermolysis of benzyl benzoate gives rise to toluene, diphenylmethane, bibenzyl, stilbene, biphenyl, tetraphenylethane, and carbon dioxide. Such results imply the preliminary homolysis of the benzyl–O bond (a) rather than the benzyl–O bond (b) into benzyl and benzoate radical pairs. The

[1]For Part XIX, see ref. 22.

[2]Presented in part at the International Symposium on Organic Free Radicals, Freiburg i. Br., West Germany, Aug. 31 – Sept. 4 (1981), p. 288 of abstract.

Can. J. Chem. Downloaded from www.nrcresearchpress.com by 210.87.254.105 on 09/06/12
For personal use only.

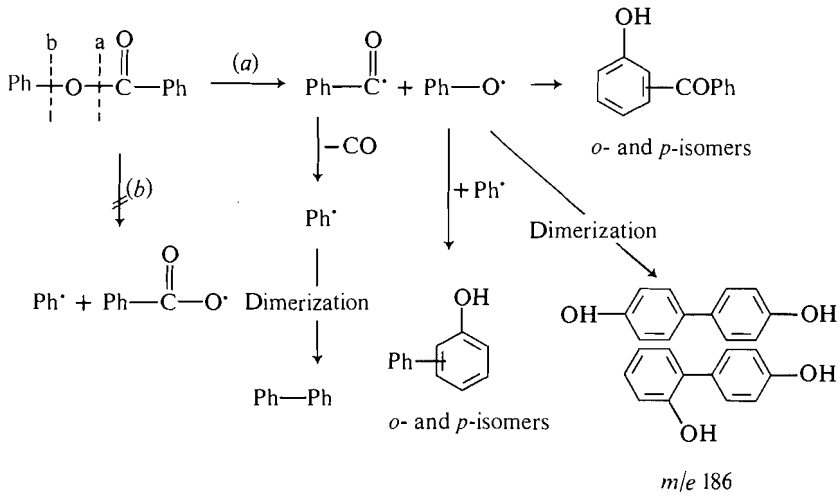

SCHEME 1

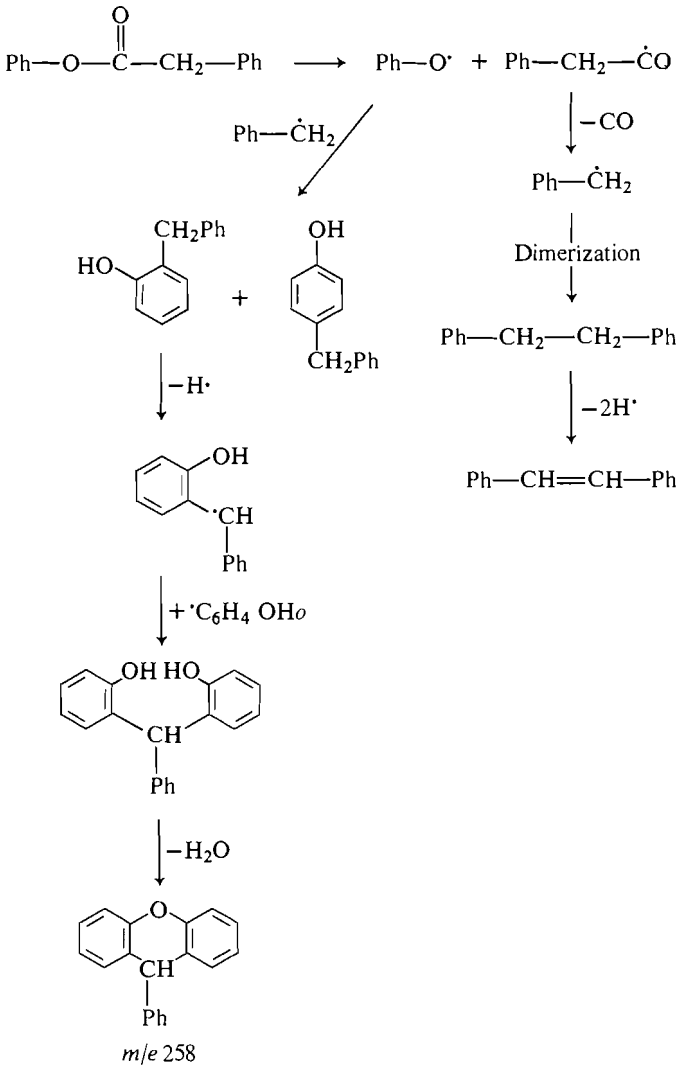

SCHEME 2

ease of rupture parallels the decrease in bond dissociation energy values, being 83 and 69 kcal mol^{-1} for (b) and (a) bonds, respectively (9). The normal fate of benzyl radicals is to form toluene, bibenzyl, and stilbene, whereas the benzoate radicals decarboxylate into carbon dioxide and phenyl radicals. Coupling of benzyl and phenyl radicals leads to the formation of diphenylmethane, while addition of phenyl radicals to the olefinic double bond of stilbene leads to the formation of tetraphenylethane (cf. Scheme 3).

The secondary attack of the free radicals on some undecomposed ester molecules need not be considered since the bulk of the products is reasonably explained on the basis of the suggested mechanism.

Homolysis of benzylic hydrogen in benzyl benzoate and phenyl phenylacetate needs higher bond dissociation energy (98.3–100.2 kcal mol^{-1}) (9) as compared with that required for the CO—O bond.

Benzyl phenylacetate undergoes facile decomposition on heating, evolving CO_2 and furnishing mainly toluene, bibenzyl, and stilbene together with an unidentified resinous material.

Experimental

All melting points are uncorrected. The ir spectroscopic analyses were carried out on a Pye–Unicam ir spectrophotometer, Model SP 200 G. The glc measurements were carried out on a Pye–Unicam gas chromatograph, "Series 104", equipped with a dual flame ionization detector, Model 24. The columns used were 4 ft × 5 mm packed with 20% SE on Chromosorb W (35–80 mesh) or 10% SE 30 on Celite (60–80 mesh). Thin-layer chromatography was carried out on glass plates covered with silica gel (25–40 mesh) and eluted with benzene–cyclohexane (3:1 v/v) or ether – petroleum ether (40–60°) (1:7 v/v). Molecular weight determinations of some reaction products were carried out by mass spectrophotometer, Model A.E.I. M.S. 902.

General procedure

The appropriate ester (20 g) was pyrolyzed by reflux under a nitrogen atmosphere for ca. 10 days (except for benzyl phenylacetate where pyrolysis was complete after 20 h reflux). The carbon monoxide formed was detected by platinum chloride test paper and absorbed in a trap containing ammoniacal cuprous chloride, whereas carbon dioxide was detected by lime water or baryta solution. The products were separated as indicated in previous work (10) and identified by tlc, glc, ir, or mixture melting point with authentic samples whenever possible. The results are shown in Tables 1 and 2.

Preparation of reference compounds

o-Hydroxybenzophenone (11): crystallized from ethanol, mp 37–39°C; bp 171–173°C/12 Torr; oxime mp 143°C.

p-Hydroxybenzophenone (12): crystallized from ethanol, mp 132–135.5°C; oxime mp 152°C.

o-Hydroxybiphenyl (13): needles from petroleum ether (40–60°C),

Can. J. Chem. Downloaded from www.nrcresearchpress.com by 210.87.254.105 on 09/06/12
For personal use only.

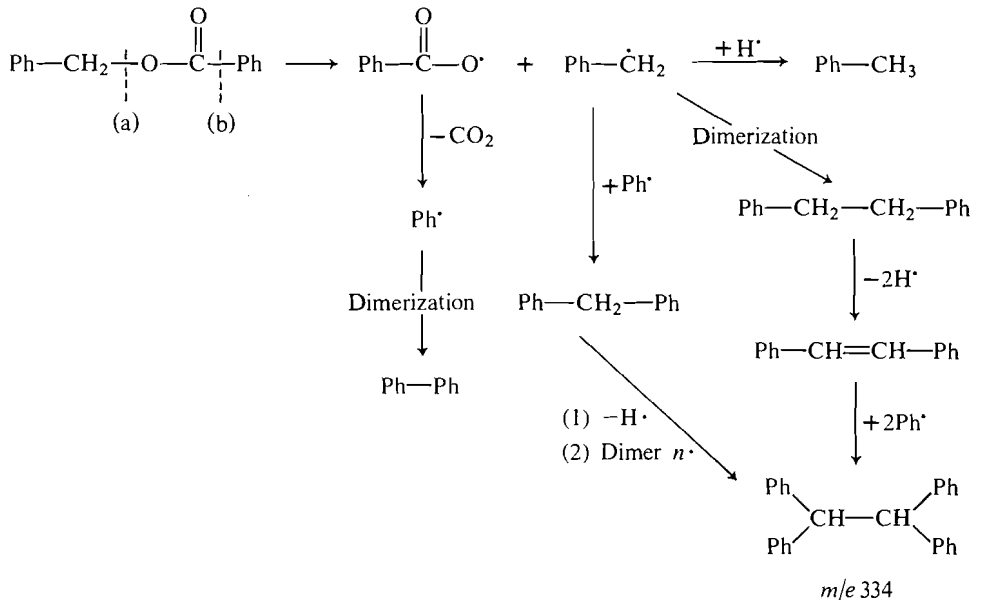

SCHEME 3

TABLE 1. Pyrolysis products of phenyl benzoate and phenyl phenylacetate

Ester used (g)	Product	Yield g (%)	Boiling point °C/10 Torr
Phenyl benzoate (20)	Carbon monoxide	Evolved	
	Phenol	5.23 (26.5)	80–82
	o-Hydroxybiphenyl	1.35 (6.15)	130–135
	p-Hydroxybiphenyl	1.03 (5.15)	142–148
	o-Hydroxybenzophenone	1.47 (7.35)	168–172
	2,4′-Dihydroxybiphenyl	0.46 (2.3)	205–210
	4,4′-Dihydroxybiphenyl	1.87 (9.35)	230–235
	p-Hydroxybenzophenone	1.06 (5.3)	340–345
	Biphenyl	1.83 (9.15)	125–128
	Residue	1.25	—
Phenyl phenylacetate (20)	Carbon monoxide	Evolved	
	Phenol	2.30 (11.5)	80–82
	o-Benzylphenol	2.20 (11.0)	170–172
	p-Benzylphenol	1.60 (8.0)	177–180
	Toluene	0.62 (3.1)	65–70
	Trans-stilbene	2.80 (14.0)	160–162
	Bibenzyl	3.62 (18.1)	145–155
	9-Phenylxanthene	2.43 (12.15)	132–137
	Residue	1.20	—

TABLE 2. Pyrolysis products of benzyl benzoate and benzyl phenylacetate

Product	Boiling point °C	Yield, g (%) From benzyl benzoate[a]	Yield, g (%) From benzyl phenylacetate[a]
Carbon dioxide	—	Evolved	
Toluene	65–70	0.53 (2.65)	2.5 (12.5)
Biphenyl	125–128	1.30 (6.5)	—
Bibenzyl	145–155	4.20 (21)	8.5 (42.5)
Stilbene	160–162	1.85 (9.25)	4.0 (20)
Other products	—	4 (20)[b]	—
Residue	—	0.53	3.2

[a]Starting amount of ester was 20 g in each case.
[b]1,1,2,2-Tetraphenylethane, bp 250–256°C, crystallized from ethanol; mp and mmp 210–212°C.

Can. J. Chem. Downloaded from www.nrcresearchpress.com by 210.87.254.105 on 09/06/12
For personal use only.

mp 56°C; bp 145°C/14 Torr: acetyl derivative mp 62–63°C.

p-Hydroxybiphenyl (14): needles from ethanol, mp 164–165°C; acetyl derivative mp 88–89°C.

2,4′-Dihydroxybiphenyl (15): prisms from ethanol, mp 162–163°C; diacetyl derivative mp 94°C.

4,4′-Dihydroxybiphenyl (16): needles from ethanol, mp 274–275°C; diacetyl derivative mp 160–161°C.

2,2′-Dihydroxybiphenyl (17): prisms from toluene, mp 109°C; diacetate derivative mp 95°C.

o-Benzylphenol (18): crystallized from petroleum ether (40–60°C), mp 52°C; bp 180–190°C/17 Torr; phenylurethane derivative, mp 117°C.

p-Benzylphenol (18): crystallized from petroleum ether (40–60°C), mp 84°C; benzoate derivative mp 87°C.

1,1,2,2,-Tetraphenylethane (7): crystallized from ethanol, mp 210–212°C.

9-Phenylxanthene (7*a*): crystallized from ethanol, mp 145°C.

Phenyl benzoate (19): crystallized from ethanol, mp 67–68°C.

Phenyl phenylacetate (20): crystallized from petroleum ether (40–60°C), mp 42°C; bp 168–170°C/10 Torr.

Benzyl phenylacetate (21): colourless liquid, bp 180–182°C/10 Torr; n_D^{20} 1.0941.

1. A. H. BLATT. Chem. Rev. **27**, 413 (1940), and references therein.
2. V. I. STENBERG. Organic photochemistry. Vol. 1. O. L. Chapman, New York, NY. 1967. p. 127.
3. D. C. BYFORD. Chem. Ind. 1082 (1971).
4. W. T. DIXON and R. O. C. NORMAN. J. Chem. Soc. 4857 (1964).
5. C. WALLING. Free radicals in solution. J. Wiley & Sons, New York. 1957. p. 466.
6. M. Z. A. BADR and M. M. ALY. Tetrahedron, **28**, 3401 (1972).
7. (*a*) W. J. HICKINBOTTOM and F. M. EL-KOBAISI. J. Chem. Soc. 1286 (1960); (*b*) J. F. NORRIS, R. THOMAS, and B. M. BROWN. Ber. **43**, 2940 (1910).
8. S. B. NORFOLK and R. TAYLOR. J. Chem. Soc. 280 (1976).
9. S. W. BENSON and H. E. O'NEAL. Kinetic data on gas phase unimolecular reactions. National Bureau of Standards, Washington, DC. NSRDSNBS 21 (1970); R. C. Weast (*Editor*).CRC handbook of chemistry and physics. 62nd ed. CRC Press, Boca Raton. FL. F L93 (1981–1982).
10. M. Z. A. BADR, M. M. ALY, and S. S. SALEM. Tetrahedron, **33**, 3155 (1977); M. Z. A. BADR, M. M. ALY, and F. F. ABDEL-LATIF. J. Org. Chem. **44**, 324 (1979).
11. E. P. KOHLER and W. F. BRUCE. J. Am. Chem. Soc. **53**, 1569 (1931).
12. F. F. BLICKE and O. J. WEINKAUFF. J. Am. Chem. Soc. **54**, 1446 (1932).
13. R. C. HUSTON. J. Am. Chem. Soc. **46**, 2775 (1924).
14. L. C. RAIFORD and J. C. COLBERT. J. Am. Chem. Soc. **47**, 1454 (1925).
15. C. FINZI and A. MANGINI. Gazz. Chim. Ital. **62**, 1193 (1933).
16. R. HIRSCH. Ber. **22**, 335 (1889).
17. W. BORSCHE and B. G. B. SCHOLTEN. Ber. **50**, 596 (1917).
18. R. C. HUSTON. J. Am. Chem. Soc. **46**, 2775 (1924).
19. J. W. MEYER and G. S. HAMMOND. J. Am. Chem. Soc. **94**, 2219 (1972).
20. W. AUTENREITH and G. THOMAE. Ber. **57**, 423 (1924).
21. M. GOMBERG and C. C. BUCHLER. J. Am. Chem. Soc. **42**, 2065 (1920).
22. M. Z. A. BADR, M. M. ALY, and A. M. FAHMY. J. Org. Chem. **46**, 4784 (1981).

Can. J. Chem. Downloaded from www.nrcresearchpress.com by 210.87.254.105 on 09/06/12
For personal use only.

Crystal structures of two methylmercury complexes with 1-methylimidazoline-2-thione

ALBERT R. NORRIS,[1] SPENCER E. TAYLOR, AND ERWIN BUNCEL
Department of Chemistry, Queen's University, Kingston, Ont., Canada K7L 3N6

AND

FRANCINE BÉLANGER-GARIÉPY AND ANDRÉ L. BEAUCHAMP[1]
Département de Chimie, Université de Montréal, C.P. 6210, Succ. A, Montréal (Qué.), Canada H3C 3V1

Received October 12, 1982

ALBERT R. NORRIS, SPENCER E. TAYLOR, ERWIN BUNCEL, FRANCINE BÉLANGER-GARIÉPY, and ANDRÉ L. BEAUCHAMP. Can. J. Chem. **61**, 1536 (1983).

$[CH_3Hg(C_4H_6N_2S)]NO_3$ belongs to space group $P\bar{1}$, $a = 7.146(2)$, $b = 7.783(3)$, $c = 10.184(5)$ Å, $\alpha = 72.95(3)$, $\beta = 71.09(3)$, $\gamma = 81.83(2)°$, and $Z = 2$. The structure was refined to $R = 0.039$ (1850 nonzero reflections). The crystal contains complex cations in which the CH_3Hg^+ ion is bonded to the exocyclic sulfur atom by a Hg—S bond of 2.382(2) Å. The nitrate ions form secondary bonds to mercury and hydrogen bonds to the acidic proton attached to N(3). $[CH_3Hg(C_4H_5N_2S)]$ is monoclinic, space group Cc, $a = 7.734(1)$, $b = 17.125(3)$, $c = 6.061(3)$ Å, $\beta = 99.66(3)°$, and $Z = 4$. Refinement converged to $R = 0.039$ (678 nonzero reflections). The crystal consists of individual monomeric molecules in which the CH_3Hg^+ ion forms a Hg—S bond of 2.338(7) Å. The molecular packing is considered as unusual, since Hg forms no intermolecular secondary bonds in the equatorial plane, even though N(3) has an available lone pair. This lone pair on N(3) is completely free, owing to the absence of H-bond donors in the structure. The applicability of HSAB theory to the present results (S- versus N-binding) is considered.

ALBERT R. NORRIS, SPENCER E. TAYLOR, ERWIN BUNCEL, FRANCINE BÉLANGER-GARIÉPY et ANDRÉ L. BEAUCHAMP. Can. J. Chem. **61**, 1536 (1983).

Le $[CH_3Hg(C_4H_6N_2S)]NO_3$ appartient au groupe d'espace $P\bar{1}$ avec $a = 7,146(2)$, $b = 7,783(3)$, $c = 10,184(5)$ Å, $\alpha = 72,95(3)$, $\beta = 71,09(3)$, $\gamma = 81,23(2)°$ et $Z = 2$. On a affiné la structure jusqu'à une valeur de $R = 0,039$ (1850 réflexions observées). Le cristal contient des cations complexes dans lesquels l'ion CH_3Hg^+ est lié à l'atome de soufre exocyclique par une liaison Hg—S de 2,382(2) Å. Les ions nitrates forment des liaisons secondaires avec le mercure et des liaisons hydrogène avec le proton acide attaché à N(3). Le $[CH_3Hg(C_4H_5N_2S)]$ est monoclinique et appartient au groupe d'espace Cc avec $a = 7,734(1)$, $b = 17,125(3)$, $c = 6,061(3)$ Å, $\beta = 99,66(3)°$ et $Z = 4$. On a affiné la structure jusqu'à une valeur de $R = 0,039$ (678 réflexions observées). Les cristaux sont des molécules monomères individuelles dans lesquelles l'ion CH_3Hg^+ forme une liaison Hg—S de 2,338(7) Å. L'empilement moléculaire est inhabituel puisque le Hg ne forme pas de liaisons secondaires intramoléculaires dans le plan équatorial bien que le N(3) ait un doublet libre disponible. Ce doublet libre sur N(3) est complètement libre à cause de l'absence de donneurs de liaison hydrogène dans la structure. On discute des résultats en relation avec la théorie HSAB.

[Traduit par le journal]

Introduction

Structural studies of the interaction of metal ions with 1-methylimidazoline-2-thione (**1**), hereafter referred to by its trivial name methimazole, are of interest, in part because of the possible application of the resulting complexes as antitumour drugs (1). Complexes of **1** with Pt(II), Pd(II) (2), as well as Co(II) and Zn(II) (3), have been structurally characterized. It

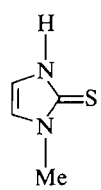

1

has also been reported (4) that the use of methimazole (and other sulfur-containing thyroid hormone inhibitors) affords a significant degree of protection against the effects of dimethylmercury and diphenylmercury intoxication in laboratory animals. An investigation of the complexes formed by methimazole with $CH_3Hg(II)$ hence appeared to be of interest, as an extension of our studies dealing with interactions of $CH_3Hg(II)$ with imidazole derivatives (5) and various nucleic bases (6–12).

Structural identification of metal ion complexes in the imidazole and methimazole series has in the past relied heavily on spectroscopic methods such as ir and nmr and it is only recently that X-ray crystallographic studies have been used for this purpose. In this regard, the crystal structure of the free ligand is not known, but the 1,3-dimethyl analog has been studied by Ansell (13) and a number of derivatives with sugar groups as substituents have been examined by Marquez and co-workers (14, 15). Some of the molecules investigated by the latter group are analogs of 1-methylimidazoline-2-thione, since only one of the ring nitrogen atoms is blocked by an alkyl or aryl group (15). Thus, these compounds also raise the problem concerning the position of the acidic proton. This was not explicitly discussed by the authors, who assumed that the proton was attached to N(3) rather than to the exocyclic sulfur atom. We are inclined to consider this assumption as correct, because if N(3) were free (16), the C(2)—N(3)—C(4) angle should be appreciably smaller than C(2)—N(1)—C(5), which is not the case.

Complexes of 1,3-dimethylimidazoline-2-thione with $AsCl_3$ (17) and with Co(II) (18) were studied by X-ray diffraction. As expected, the metal atoms interact with sulfur, which is the only available donor atom. Blocking the sulfur atom, as in 1-methyl-2-(methylthio)imidazole results in binding to N(3), which bears no proton in this ligand (19). The problem is not so simple with 1-methylimidazoline-2-thione (methimazole), because the proton on N(3) is not an efficient blocking group.

[1]Correspondence may be addressed to either of these authors.

Can. J. Chem. Downloaded from www.nrcresearchpress.com by 210.87.254.6 on 09/06/12
For personal use only.

Can. J. Chem. Downloaded from www.nrcresearchpress.com by 210.87.254.6 on 09/06/12
For personal use only.

Coordination may take place at sulfur leaving the hydrogen on N(3), but the opposite distribution cannot be ruled out. The former pattern had been found in the 2:1 adduct with $CdCl_2$ (20), and while this work was in progress, two crystallographic studies showed the same type of binding in 4:1 compounds with $Co(ClO_4)_2$ (21) and $Zn(NO_3)_2$ (22).

The two crystal structures reported here were determined in connection with preparative and solution work (8) aimed at establishing the mode of interaction of the heavy CH_3Hg^+ ion with methimazole. The ^1H nmr results favored CH_3Hg^+ binding to the exocyclic sulfur atom of these compounds in DMSO solution. However, infrared bands used by other workers to determine the binding site pointed to the opposite conclusion. Therefore, unambiguous structural information from X-ray diffraction appeared desirable.

Experimental section

$[CH_3Hg(C_4H_6N_2S)]NO_3$

$C_5H_9HgN_3O_3S$ fw = 391.80

Triclinic, space group $P\bar{1}$, a = 7.146(2), b = 7.783(3), c = 10.184(5) Å, α = 72.95(3), β = 71.09(3), γ = 81.83(2)°, V = 511.6 Å^3, D_o = 2.52 g cm^{-3} (flotation in bromoform – ethylene dichloride), D_c = 2.543 g cm^{-3}, Z = 2 formula units per cell, μ(CuKα) = 307.7 cm^{-1}, λ(CuK$\bar{\alpha}$) = 1.54178 Å, t = 23°C.

Crystals suitable for X-ray diffraction work were obtained as described elsewhere (8). The specimen used for data collection had the following distances between the indicated pairs of faces: 0.24 mm (001 and 00$\bar{1}$), 0.043 mm (100 and $\bar{1}$00), and 0.063 mm (010 and 0$\bar{1}$0).

Triclinic Laue symmetry (space groups $P1$ or $P\bar{1}$) was deduced from a set of precession and cone axis photographs. The reduced cell obtained from the films was confirmed by the autoindexing procedure carried out on 25 reflections found by the SEARCH routine and centered on an Enraf-Nonius CAD4 diffractometer. The Niggli parameters clearly indicated that the crystal could not be described in a space group of higher symmetry. The final cell parameters were obtained by least-squares refinement on the setting angles of the 25 reflections.

The intensity data were collected in the $\omega/2\theta$ scan mode. A fixed slit of 4.0 mm was used and the scan range (ω) was (1.00 + 0.14 tan θ)° extended 25% on each side for background measurements. Prescans at 10° min^{-1} were done and all weak reflections ($I < \sigma(I)$) were not remeasured at low speed. Their F_o and $\sigma(F_o)$ values were taken from the prescan counts. For stronger reflections, scan speed S between 10 and 1° min^{-1} was selected to make the $I/\sigma(I)$ ratio = 100, but a maximum scan time of 90 s was imposed. Three standard reflections were monitored every hour. They showed random fluctuations of $<\pm 4\%$ about their respective means. Crystal orientation was checked every 100 reflections by recentering three reflections. Misorientation was always <0.1° and no crystal recentering was done during data collection.

A set of 2274 independent reflections (hkl, $h\bar{k}l$, $hk\bar{l}$, and $h\bar{k}\bar{l}$, $2\theta \leq 140°$) was measured. The net intensity I was obtained from $I = (P - B/0.50)S$, where P is the total scan count and B is the total background count measured during one half of the scanning time. The standard deviation was calculated from $\sigma^2(I) = (P + B/0.25)S^2 + (0.02I)^2$. A total of 1850 reflections with $I > 2.5\sigma(I)$ was retained for structure determination. An absorption correction was applied at a later stage in the refinement (Gaussian integration, grid 10 × 10 × 10, transmission coefficient = 0.030–0.180). The data were finally corrected for the Lorentz and polarization effects.

The structure was solved by the heavy-atom method and refined by full-matrix least-squares. The centrosymmetric $P\bar{1}$ space group was assumed first. Mercury was positioned from a three-dimensional Patterson synthesis and all nonhydrogen atoms were located from a subsequent difference Fourier synthesis (ΔF) phased on Hg. Isotropic refinement led to the R index $\Sigma||F_o| - |F_c||/\Sigma|F_o| = 0.132$. Anisotropic refinement reduced R to 0.069. At this point, the absorption correction was applied and the R factor reduced to 0.039. The hydrogens attached to C(4), C(5), and N(3) were fixed at their ideal positions (C—H = 0.95, N—H = 0.85 Å, B_{iso} = 6.0 Å^2). Their parameters were not refined, but their coordinates were recalculated after each cycle of refinement. The hydrogens of the methyl groups could not be clearly distinguished from the general background in the ΔF map. Individual weights based on counting statistics were applied in the last least-squares cycles. Anisotropic refinement converged to R = 0.039 and $R_w = [\Sigma_w(|F_o| - |F_c|)^2/\Sigma_w|F_o|^2]^{1/2} = 0.055$. The goodness-of-fit ratio was 2.41 (118 parameters varied). There were no indications in the final ΔF map that the space group could be $P1$ instead of $P\bar{1}$. The map contained a few peaks of 1.0–1.5 e/Å^3 within 1.4 Å from Hg and the general background was $<\pm 0.66$ e/Å^3.

TABLE 1. Refined fractional coordinates

(*a*) $[CH_3Hg(C_4H_6N_2S)]NO_3$ (× 10^4, Hg × 10^5, H × 10^3)

Atom	X	Y	Z	U_{eq}[a]
Hg	21897(4)	40578(4)	9710(3)	548(2)
S	1047(4)	7133(3)	691(2)	61(1)
O(1)	5492(11)	5165(11)	1957(8)	78(3)
O(2)	7767(12)	3214(12)	2452(10)	89(4)
O(3)	5075(18)	3493(30)	3995(13)	225(12)
N(1)	−995(10)	8013(9)	3187(8)	58(3)
N(3)	1845(11)	6759(10)	3213(8)	62(3)
N(10)	6154(10)	3917(12)	2796(8)	67(3)
C(1)	−2764(15)	8774(15)	2719(13)	74(4)
C(2)	604(12)	7269(10)	2443(8)	52(3)
C(4)	1015(19)	7180(17)	4503(13)	79(5)
C(5)	−741(16)	8047(16)	4482(11)	74(4)
C(6)	3138(20)	1335(14)	1367(15)	82(5)
H(3)	299	625	295	76
H(4)	158	691	527	76
H(5)	−163	857	520	76

(*b*) $[CH_3Hg(C_4H_5N_2S)$ (× 10^3, Hg × 10^5, S × 10^4)

Atom	X	Y	Z	U_{eq}[b]
Hg	25000	7251(4)	50000	610(3)
S	4991(9)	674(3)	3288(12)	57(2)
N(1)	529(2)	162(1)	−22(2)	6(1)
N(3)	284(3)	177(2)	115(4)	9(1)
C(1)	704(2)	134(1)	−49(4)	7(1)
C(2)	428(2)	139(1)	128(3)	5(1)
C(4)	284(6)	233(2)	−50(6)	13(2)
C(5)	429(4)	220(1)	−151(4)	9(1)
C(6)	22(12)	75(3)	630(15)	20(4)
H(4)	199	273	−87	8
H(5)	455	245	−281	8

[a] U_{eq} × 10^3, Hg × 10^4.
[b] U_{eq} × 10^2, Hg × 10^3, S × 10^3.

$[CH_3Hg(C_4H_5N_2S)]$

$C_5H_8HgN_2S$ fw = 328.79

Monoclinic, Cc, a = 7.734(1), b = 17.125(3), c = 6.061(3) Å, β = 99.66(3)°, Z = 4, D_o = 2.74(2) g cm^{-3}, D_c = 2.759 g cm^{-3}, λ(MoK$\bar{\alpha}$) = 0.71069 (graphite monochromator), μ(MoKα) = 196.1 cm^{-1}, t = 23°C.

The specimen used had the following dimensions: 0.068 mm (1$\bar{1}$0 and $\bar{1}$10) × 0.112 mm (110 and $\bar{1}\bar{1}$0) × 0.48 mm (001 and 00$\bar{1}$). Space group Cc or $C2/c$ were deduced from a set of precession and cone axis photographs (systematic absences: hkl, $h + k \neq 2n$; $h0l$, $l \neq 2n$). The data were collected as described above, with a scan range of ω = (1.0 + 0.35 tan θ)°. A set of 908 independent hkl and $hk\bar{l}$ reflections was collected ($2\theta \leq 55°$), of which 678 had an $I/\sigma(I)$ ratio >3.0. An absorption correction was applied (transmission factor = 0.08–0.35).

Can. J. Chem. Downloaded from www.nrcresearchpress.com by 210.87.254.6 on 09/06/12
For personal use only.

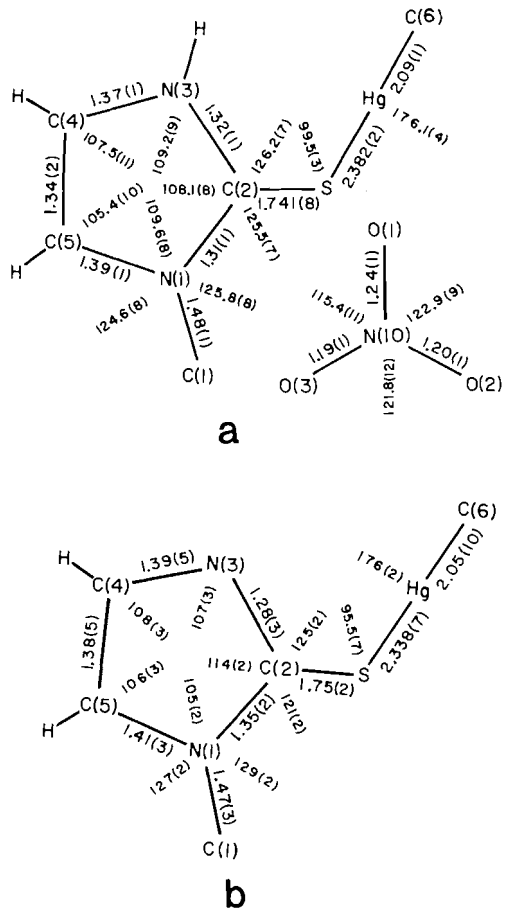

FIG. 1. Numbering scheme and intramolecular interatomic distances and bond angles. *a* = $[CH_3Hg(C_4H_6N_2S)]NO_3$; *b* = $[CH_3Hg(C_4H_5N_2S)]$.

In space group $C2/c$ (general equipoint of order 8), the molecule would have to sit on a symmetry element. The Patterson map showed no peaks that could be assigned to vectors between Hg atoms occupying equipoints $4a$ to $4d$. Equipoint $4e$ (two-fold axis) could not be ruled out at this stage. However, the four S atoms would have to lie on a symmetry element as well. This would introduce specialization in the Hg—S vectors (u and w = 0, 1/4 or 1/2). No peaks corresponding to such vectors could be found, even though their heights should have been just below those of the Hg—Hg vectors. These considerations, as well as the fact that a structure in which Hg would lie on a two-fold axis appeared unlikely, led us to solve the structure in space group Cc. The Hg atom was positioned on a general equipoint. Its y coordinate was determined from the Patterson map, whereas the x and z coordinates were arbitrarily chosen to fix the origin. Since the Hg atoms defined a centrosymmetric set, the resulting ΔF map was expected to contain a pair of overlapping images related by the pseudo-inversion center. The pair of strong peaks corresponding to the S atoms in these images was easily recognized in the map. One of them was arbitrarily used to fix the enantiomorph. A ΔF map phased on Hg and S revealed the positions of the atoms in the five-membered ring.

Isotropic refinement led to R = 0.089. Anisotropic refinement of all nonhydrogen atoms (H(4) and H(5) fixed with B = 6.0 Å^2 and methyl hydrogens not found) converged to R = 0.039 and R_w = 0.043. The goodness-of-fit ratio was 1.31 (78 parameters varied). The final ΔF map had a general background $<\pm 0.35$ e/Å^3, with some peaks of 0.9–1.2 e/Å^3 near Hg.

A few extra cycles of refinement were calculated after changing the signs of all coordinates, in order to determine whether anomalous dispersion could distinguish between the two enantiomorphic structures. The parameters changed by $\leq 0.8\sigma$ and the R factor remained the same. This is not surprising, since the Hg atoms, which are the only significant contributors to anomalous dispersion (f'_{Hg} = −2.7, f''_{Hg} = 9.3, f'_S = 0.13, f''_S = 0.16), define a centrosymmetric arrangement.

The refined coordinates for both structures are listed in Table 1. Lists of structure factors and thermal parameters are available upon request.[2] The scattering curves were those of Cromer and Waber (23) except for hydrogen (24). Anomalous dispersion terms f' and f'' for Hg and S were taken from Cromer (25).

Description of the structure and discussion

The structures are schematically represented in Fig. 1, with interatomic distances and bond angles.

$[CH_3Hg(C_4H_6N_2S)]NO_3$

The ligand in the $[CH_3Hg(C_4H_6N_2S)]^+$ cation behaves as observed in the Cd(II) (20), Co(II) (21), and Zn(II) complexes (22): the acidic hydrogen is bound to N(3) and the metal is attached to sulfur. Mercury exhibits its common linear coordination (S—Hg—C(6) = 176.1(4)°). It forms a Hg—C bond of normal length (2.09(1) Å) (26) and the bond to the exocyclic sulfur atom (Hg—S = 2.382(2) Å) is typical of two-coordinated mercury forming a number of extra secondary bonds (27). The metal–sulfur bond is not coplanar with the ring (Hg—S—C(2)—N(1) = −134°) and the angle at sulfur is ~100°.

Crystal structures on seven imidazoline-2-thione moieties having a free thione group give an average value of 1.691 Å for the C(2)=S bond length (see supplementary material). This bond is lengthened to 1.741(8) Å upon CH_3Hg^+ coordination and a similar lengthening was observed in the $AsCl_3$ complex with the dimethyl derivative (17). Metal coordination, as well as methylation, to sulfur is likely to reduce the double bond character of C(2)=S and it appears to be reasonable that the C—S distances in the complexes approach the value found in the S-methylated compound (1.74 Å) (19). It is not clear, however, why the lighter elements seem to affect the C(2)=S bond to a much smaller extent: Zn (21), 1.708 Å; Co (22), 1.717 Å; Co (18), 1.696 Å.

Within the experimental error of the present study, the geometry of the five-membered ring is not significantly modified by complexation to sulfur (21). The ring, including the N(1)-methyl group, is planar within 2.5σ (0.028 Å), but the sulfur-to-plane distance is large (0.130(2) Å). The almost identical internal C—N—C angles at N(1) and N(3) confirm the presence of a hydrogen atom attached to N(3), since an angle 4–5° smaller is expected for a free lone pair on nitrogen (16).

The nitrate ion shows the expected trigonal structure and it is planar within 0.5σ (0.005 Å).

As is usually the case in the solid state, two-coordinate mercury expands its coordination number by forming weak bonds in the equatorial plane (assuming C—Hg—S as the axial direction) (Table 2). Oxygens O(1) of two nitrate ions bridge a pair of mercury atoms (Fig. 2), thus leading to a centrosymmetric dimeric unit. Each of these oxygens is much more strongly bonded to one mercury (2.833 Å) than to the other (3.153 Å). On the same side as the weaker contact, O(1)

[2]Tables of observed and calculated structure factor amplitudes, anisotropic temperature factors, and least-squares plane calculations are available, at a nominal charge, from the Depository of Unpublished Data, CISTI, National Research Council of Canada, Ottawa, Ontario, Canada K1A 0S2.

TABLE 2. Environment of mercury in $[CH_3Hg(C_4H_6N_2S)]NO_3$

Bond	Distance (Å)	Bond	Distance (Å)
Hg—C(6)	2.09(1)	Hg—O(1)	3.153(8)
Hg—S	2.382(2)	Hg—O(1)^a	2.833(8)
		Hg—O(2)^b	3.101(9)

Bonds	Angle (deg)	Bonds	Angle (deg)
C(6)—Hg—O(1)	93.9(4)	O(1)—Hg—O(1)^a	93.0(2)
C(6)—Hg—O(1)^a	93.1(4)	O(1)—Hg—O(2)^b	134.1(2)
C(6)—Hg—O(2)^b	93.1(4)	O(1)^a—Hg—O(2)^b	131.8(2)
C(6)—Hg—S	176.1(4)	Hg—O(1)—Hg^a	87.0(2)
S—Hg—O(1)	84.7(2)	Hg—O(1)—N(10)	114.3(6)
S—Hg—O(1)^a	90.6(2)	Hg—O(1)—N(3)	70.9(3)
S—Hg—O(2)^b	85.5(2)	Hg^a—O(1)—N(10)	116.1(6)
		Hg^a—O(1)—N(3)	128.8(3)
		N(3)—O(1)—N(10)	115.1(6)

$^a 1 - x, 1 - y, -z.$
$^b x - 1, y, z.$

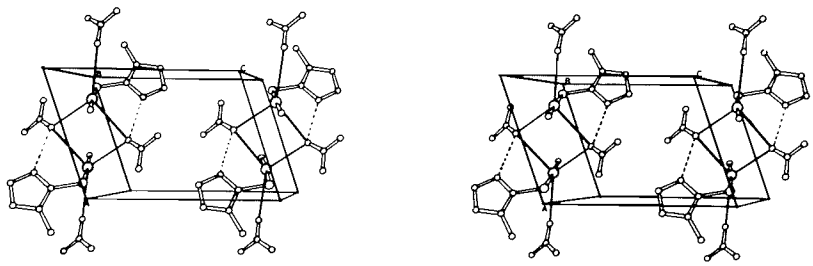

FIG. 2. Stereo view of the unit cell of $[CH_3Hg(C_4H_6N_2S)]O_3$ down the b^* axis. The origin is at the top left corner of the cell, a and c are in the plane of the figure (a down, c to the right). Mercury is shown as a larger sphere and O(1) is the bridging oxygen of the nitrate ions. The remaining atoms can be identified by reference to Fig. 1. Hydrogens are omitted.

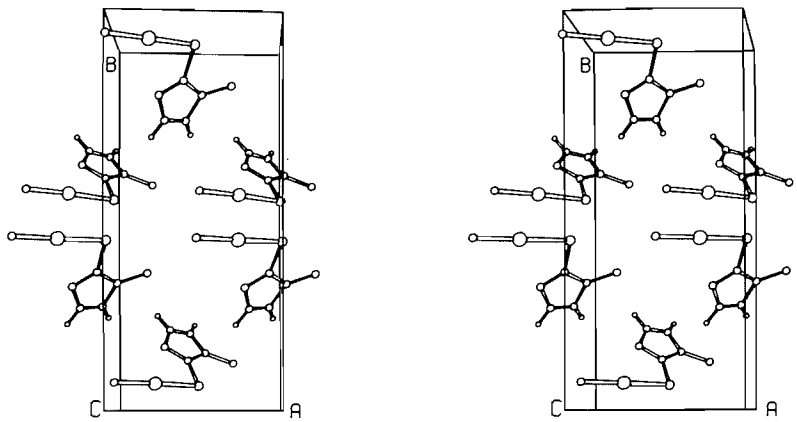

FIG. 3. Stereo view of the unit cell of $[CH_3Hg(C_4H_5N_2S)]$. Mercury is shown as a larger sphere and hydrogens are omitted. The atoms can be identified by reference to Fig. 1.

acts as the acceptor in a strong H-bond involving N(3)—H(3): N(3)—O(1) = 2.79(1) Å, C(2)—N(3)—O(1) = 116.9(6)°, C(4)—N(3)—O(1) = 133.9(8)°, N(10)—O(1)—N(3) = 115.1(6)°. Each Hg atom completes a (2+3)-coordination by interacting weakly with O(2) of a nitrate ion belonging to another dimer (Hg...O(2) = 3.10 Å).

$[CH_3Hg(C_4H_5N_2S)]$

The structure consists of individual monomeric molecules in which the CH_3Hg^+ ion is coordinated to the sulfur atom of the ligand in its anionic form (Fig. 1*b*). Mercury is linearly coordinated as usual and the Hg—CH_3 bond length is normal. The angle at sulfur (95.5(7)°), although smaller than in the previous compound, is still in the normal range. The lengthening of the C2=S bond, discussed above, is again observed but in this case, the large standard deviations make the effect barely significant. The CH_3Hg^+ lies in the plane of the ring, with a

Can. J. Chem. Downloaded from www.nrcresearchpress.com by 210.87.254.6 on 09/06/12
For personal use only.

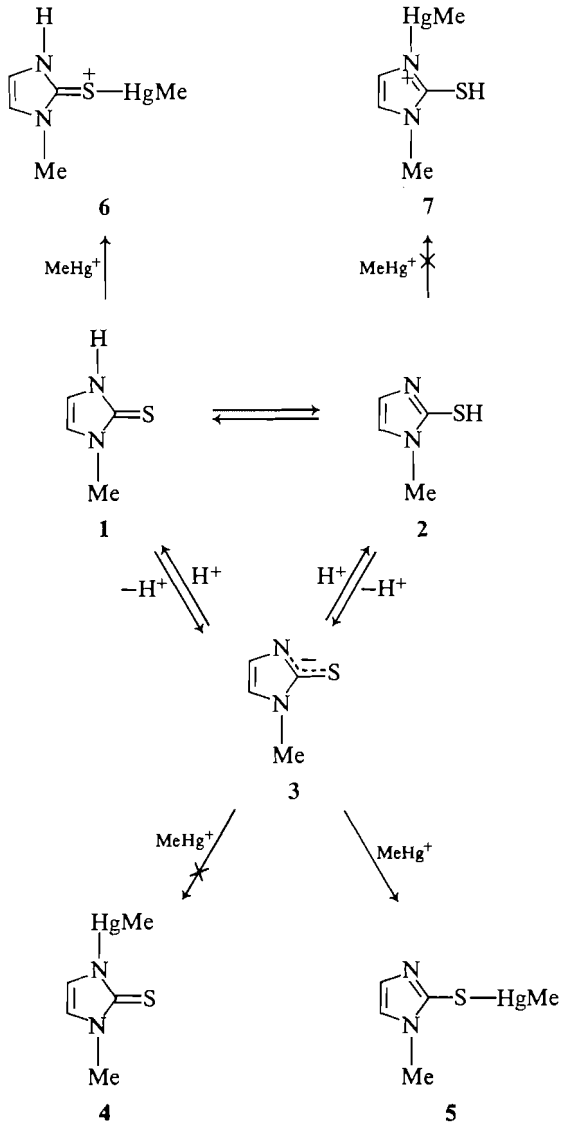

SCHEME 1

Hg—S—C(2)—N(1) torsion angle of 182(2)°. It is noteworthy that the Hg—S bond (2.338(7) Å) is significantly shorter than in the cationic complex (2.382(2) Å). As shown in the packing diagram in Fig. 3, mercury does not form the usual intermolecular contacts with donor atoms on adjacent molecules, in spite of the fact that lone pairs are available on N(3) and S. The absence of such intermolecular contacts may provide the explanation for the reduction in the Hg—S bond length.

The light-atom coordinates have high esd's and the large resulting errors on the geometry of the ring preclude any comparisons with other structures.

Discussion

In both of these compounds, the CH_3Hg^+ ion exhibits its usual behavior, forming only one additional short bond and showing linear two-coordination. The absence of any secondary bonds by intermolecular contacts with N(3) or S in $[CH_3Hg(C_4H_5N_2S)]$ is somewhat surprising, however.

The lengthening of the C=S bond observed upon coordination suggests that it is close to a single bond in the complexes. As further support for this assumption, one can point out that the metal–sulfur bond is not forced into a particular orientation with respect to the ring: the CH_3Hg^+ group lies in the plane of the ring in $[CH_3Hg(C_4H_5N_2S)]$, but it makes an angle of −134° in $[CH_3Hg(C_4H_6N_2S)]NO_3$. A wide range of orientations has also been found in other complexes (15, 21, 22). Thus, it seems that the metal—S—C(2)—N(3) torsion angle is not imposed by electronic effects, but by crystal packing. It is likely that the CH_3Hg^+ group can rotate unhindered in the free molecule.

Since the X-ray crystallographic studies here reported have confirmed our previous conclusions based on chemical and spectroscopic studies (8), some observations can be made as to the applicability of HSAB theory (28, 29) concerning reactivity in these systems.

The neutral complex $[CH_3Hg(C_4H_5N_2S)]$ (**5**) is derived by the action of CH_3Hg^+ on the deprotonated species **3**, in aqueous solution under basic conditions. Interestingly, the tautomeric equilibrium between **1** and **2** (Scheme 1) has been found to favor predominantly **1** in several solvents (8) (see, however, ref. 6). These results, i.e. coordination of CH_3Hg^+ to the sulfur atom of **3** while H^+ coordinates to the nitrogen, are readily accommodated on the basis of HSAB theory. Thus the soft Hg atom prefers the soft sulfur site, the harder N3 atom being used to accept the hard H^+ cation.

Formation of the cationic complex $[CH_3Hg(C_4H_6N_2S)]NO_3$ (**6**) can also be discussed on the basis of Scheme 1, which considers coordination of CH_3Hg^+ to either of the neutral tautomeric species **1** or **2**. That **6** is favored exclusively over **7** is again in complete accord with expectations on the basis of HSAB theory.

1. H. SIGEL (*Editor*). Metal ions in biological systems. Vol. 11. Metal complexes as anticancer agents. Marcel Dekker, New York. 1980.
2. J. DEHAND and J. JORDANOV. Inorg. Chim. Acta, **17**, 37 (1976).
3. E. S. RAPER and J. L. BROOKES. J. Inorg. Nucl. Chem. **39**, 2163 (1977).
4. S. SZABO, P. KOURONAKIS, K. KOVACS, B. TUCHWEBER, and B. D. GARG. Toxicol. Appl. Pharmacol. **30**, 175 (1974).
5. A. R. NORRIS, E. BUNCEL, and S. E. TAYLOR. J. Inorg. Biochem. **16**, 279 (1982).
6. E. BUNCEL, A. R. NORRIS, W. J. RACZ, and S. E. TAYLOR. J. Chem. Soc. Chem. Commun. 562 (1979); Inorg. Chem. **20**, 98 (1981).
7. S. E. TAYLOR, E. BUNCEL, and A. R. NORRIS. J. Inorg. Biochem. **15**, 131 (1981).
8. E. BUNCEL, A. R. NORRIS, S. E. TAYLOR, and W. J. RACZ. Can. J. Chem. **60**, 3033 (1982).
9. L. PRIZANT, R. RIVEST, and A. L. BEAUCHAMP. Can. J. Chem. **59**, 2290 (1981).
10. L. PRIZANT, M. J. OLIVIER, R. RIVEST, and A. L. BEAUCHAMP. Can. J. Chem. **59**, 1311 (1981); R. SAVOIE, J. J. JUTIER, L. PRIZANT, and A. L. BEAUCHAMP. Spectrochim. Acta, **38A**, 561 (1982); R. SAVOIE, D. POIRIER, L. PRIZANT, and A. L. BEAUCHAMP. J. Raman Spectrosc. **11**, 481 (1981); L. PRIZANT, M. J. OLIVIER, R. RIVEST, and A. L. BEAUCHAMP. J. Am. Chem. Soc. **101**, 2765 (1979).
11. M. AUTHIER-MARTIN, J. HUBERT, R. RIVEST, and A. L. BEAUCHAMP. Acta Crystallogr. B**34**, 273 (1978).
12. F. GUAY and A. L. BEAUCHAMP. Inorg. Chim. Acta, **66**, 57 (1982).
13. G. B. ANSELL. J. Chem. Soc. Perkin **2**, 841 (1972).
14. R. JIMENEZ-GARAY, A. LOPEZ-CASTRO, and R. MARQUEZ. Acta Crystallogr. B**32**, 1367 (1976); I. BARRAGAN, A. LOPEZ-CASTRO, and R. MARQUEZ. Acta Crystallogr. B**34**, 295 (1978); B**33**, 2244 (1977); A. CONDE, E. MORENO, and R. MARQUEZ.

Can. J. Chem. Downloaded from www.nrcresearchpress.com by 210.87.254.6 on 09/06/12
For personal use only.

Acta Crystallogr. B**33**, 794 (1977); S. PEREZ-GARRIDO, A. LOPEZ-CASTRO, and A. MARQUEZ. An. R. Soc. Esp. Fis. Quim. A**69**, 179 (1973).
15. S. PEREZ-GARRIDO, A. CONDE, and R. MARQUEZ. Acta Crystallogr. B**30**, 2348 (1974); A. CONDE, E. MORENO, and R. MARQUEZ. Acta Crystallogr. B**31**, 648 (1975).
16. A. C. WANG and B. M. CRAVEN. Acta Crystallogr. B**35**, 510 (1979).
17. D. J. WILLIAMS, C. O. QUICKSALL, and K. J. WYNNE. Inorg. Chem. **17**, 2071 (1978).
18. N. KHEDDAR, J. PROTAS, M. LEBACCON, R. GUGLIELMETTI, and J. E. GUERCHAIS. Bull. Soc. Chim. Fr. 803 (1976).
19. A. LAIDOUDI, N. KHEDDAR, and M. C. BRIANSO. Acta Crystallogr. B**34**, 778 (1978); B**34**, 782 (1978).
20. L. CAVALCA, P. DOMIANO, A. MUSATTI, and P. SGARABOTTO. J. Chem. Soc. Chem. Commun. 1136 (1968).
21. I. W. NOWELL, A. G. COX, and E. S. RAPER. Acta Crystallogr. B**35**, 3047 (1979).
22. E. W. RAPER and I. W. NOWELL. Acta Crystallogr. B**35**, 1600 (1979).
23. D. T. CROMER and J. T. WABER. Acta Crystallogr. **18**, 104 (1965).
24. R. F. STEWART, E. R. DAVIDSON, and W. T. SIMPSON. J. Chem. Phys. **42**, 3175 (1965).
25. D. T. CROMER. Acta Crystallogr. **18**, 17 (1965).
26. J. HUBERT and A. L. BEAUCHAMP. Acta Crystallogr. B**36**, 2613 (1980).
27. A. L. BEAUCHAMP and D. GOUTIER. Can. J. Chem. **50**, 977 (1972) and references therein.
28. S. AHRLAND, J. CHATT, and N. R. DAVIES. Q. Rev. Chem. Soc. **11**, 265 (1958).
29. R. G. PEARSON. J. Am. Chem. Soc. **85**, 3533 (1963); J. Chem. Educ. **45**, 581 (1968).

Can. J. Chem. Downloaded from www.nrcresearchpress.com by 210.87.254.6 on 09/06/12
For personal use only.

Motional behavior of 2,3:5,6-di-*O*-isopropylidene-α-D-mannofuranose in solution. A ^{13}C spin-lattice relaxation study

PHOTIS DAIS AND ARTHUR S. PERLIN
Department of Chemistry, McGill University, Montreal (Que.), Canada H3C 3G1

Received December 1, 1982

PHOTIS DAIS and ARTHUR S. PERLIN. Can. J. Chem. **61**, 1542 (1983).

^{13}C nuclear magnetic resonance spin-lattice relaxation times (T_1) have been used to probe the motional behavior of 2,3:5,6-di-*O*-isopropylidene-α-D-mannofuranose (**1**) in dimethyl sulfoxide solution. This system offers structural features well suited to the study of a variety of internal motions, i.e., ring oscillation, ring puckering interconversion, and methyl internal rotation, all of which are superimposed on an isotropic overall reorientation. Among various models examined to evaluate internal rotations, a two-sites jump model was found satisfactory for interpreting the oscillation and puckering motions of the flexible 5,6-*O*-isopropylidene ring, whereas a diffusional model described hindered rotation of the geminal methyl groups of the rigid 2,3-*O*-isopropylidene ring from 15° to 80°C. The activation energy associated with the temperature dependence of the rate of overall molecular tumbling was found to agree with the hydrodynamical prediction of 4.57 kcal/mol associated with the temperature dependence of the ratio (η/T). In addition, an explicit treatment of the relaxation data vs. solution viscosities, as a function of temperature, indicated that **1** reorients under the "slip" boundary conditions.

PHOTIS DAIS et ARTHUR S. PERLIN. Can. J. Chem. **61**, 1542 (1983).

On a fait appel aux temps de relaxation spin réseau (T_1) en rmn du ^{13}C pour étudier le mouvement du di-*O* isopropylidène 2,3:5,6-α-D mannofurannose (**1**) en solution dans le diméthylsulfoxyde. Ce système présente des caractéristiques structurales qui conviennent parfaitement à l'étude de divers mouvements internes, i.e. l'oscillation du cycle, l'interconversion gauche du cycle et la rotation interne du méthyle, qui se superposent tous à une réorientation globale isotropique. Parmi les divers modèles étudiés pour évaluer les rotations internes, on a trouvé un modèle discontinu à deux sites satisfaisant pour interpréter les mouvements d'oscillation et de gauchissement du cycle flexible de *O*-isopropylidène-5,6 tandis qu'un modèle de diffusion décrit la rotation des groupes méthyles géminés du cycle rigide de *O*-isopropylidène-2,3 entre 15° et 80°C. On a trouvé que l'énergie d'activation associée à l'influence de la température sur la vitesse du mouvement moléculaire global s'accorde avec la prédiction hydrodynamique de 4,5 kcal/mol associée à l'influence de la température sur le rapport (η/T). De plus un traitement explicite des données de relaxation versus la viscosité de la solution, en fonction de la température indique que le composé **1** se réoriente dans des conditions limites de "glissement".

[Traduit par le journal]

Introduction

Measurements of ^{13}C nmr spin-lattice relaxation provide (1–5) valuable information about the molecular dynamics of compounds in solution. Relaxation data are utilized in the present study to describe the motional behaviour of a carbohydrate acetal derivative, namely 2,3:5,6-di-*O*-isopropylidene-α-D-mannofuranose (**1**). Some conformational properties of **1** were described recently (6), in particular, the favoured orientation of its anomeric hydroxyl group in methylsulfoxide. More generally, however, compound **1** is a useful model for the examination of multiple internal rotations of differing angular amplitudes. Here, attention is focused on motional features of the two *O*-isopropylidene substituents of the molecule, i.e., internal barriers to rotation of the *C*-methyl groups, librational motions of the rings, and interconversions between their puckered conformations.

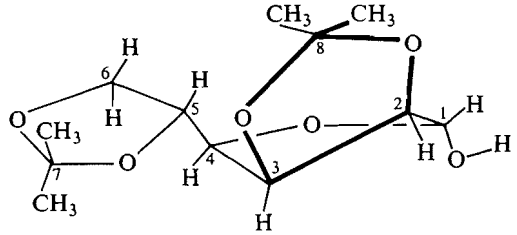

1

Precise details about the dynamics of such a molecule as **1** are not likely to be readily accessible (7, 8), since several degrees of freedom exist for contributions to the relaxation of C—H vectors within its flexible segments, as well as because of difficulty in partitioning observed relaxation times (or rates) into individual contributions from different origins. However, the examination of **1** was facilitated by the fact that one or more of the motional components proved to influence the relaxation of some nuclei but not others, and that **1** exhibits (6) overall isotropic molecular tumbling. Moreover, a relatively broad approach was taken, through the application of different motional models that allow for both internal motion and overall isotropic diffusion. As will be shown, interpretations of the relaxation measurements carried out with **1** over the temperature range 15–80°C are strongly dependent on the models adopted. Also, internal jump models suggested by theoretical calculations proved to be the most satisfactory in accounting for the effects of temperature on the spin-lattice relaxation of ^{13}C nuclei of the *O*-isopropylidene substituents. Finally, viscosity as well as nmr data suggest that **1** reorients according to the "slip" hydrodynamic model.

Experimental

^{13}C nuclear magnetic resonance relaxation experiments were conducted at 50.3 MHz under conditions of full ^1H-noise decoupling with a Varian XL-200 spectrometer, equipped with a variable temperature probe. The temperature was controlled to within ±0.3°C by the computer of the spectrometer, by means of a precalibrated copper–constantan thermocouple in the probe insert. The spin-lattice relaxation times were measured by the standard two-pulse inversion recovery technique. The pulse duration for a 180° flip angle, checked periodically by producing a null in the amplitude of the fid, was 28 μs, whereas the acquisition time was 1.023 s with an 8 kHz spectral window and 16 384 data points. The waiting time between sequences was 5× the estimated value of the longest T_1 at each temperature and

Can. J. Chem. Downloaded from www.nrcresearchpress.com by 210.87.254.5 on 09/06/12
For personal use only.

TABLE 1. ^{13}C spin-lattice relaxation times (in seconds)[a] and nOe factors[b] for 2,3:5,6-di-*O*-isopropylidene-α-D-mannose[c] as a function of temperature

Temperature (°C)	Relaxation times (s)									
	C-1	C-2	C-3	C-4	C-5	C-6	CH_3(*exo*)[d]	CH_3(*endo*)[d]	CH_3(*exo*)[e]	CH_3(*endo*)[e]
15	0.37	0.37	0.38	0.39	0.41	0.27	0.39	0.54	0.59	0.52
	(2.96)	(2.90)	(2.94)	(2.94)	(2.90)	(3.03)	(3.00)	(2.89)	(3.06)	(2.95)
25	0.44	0.45	0.44	0.47	0.51	0.34	0.45	0.65	0.74	0.62
	(2.96)	(2.94)	(2.96)	(2.86)	(2.99)	(2.93)	(3.05)	(2.93)	(2.95)	(2.88)
30	0.57	0.61	0.61	0.63	0.67	0.45	0.57	0.75	0.89	0.75
	(3.00)	(2.94)	(3.08)	(2.98)	(2.86)	(3.17)	(3.09)	(3.01)	(2.78)	(3.19)
35	0.66	0.68	0.67	0.74	0.78	0.51	0.66	0.89	0.99	0.88
40	0.72	0.75	0.75	0.81	0.86	0.55	0.73	1.00	1.14	1.00
	(2.89)	(3.13)	(3.19)	(2.94)	(2.98)	(2.90)	(2.80)	(2.96)	(3.12)	(3.03)
45	0.80	0.90	0.88	0.93	0.99	0.64	0.82	1.09	1.21	1.12
50	0.92	1.00	0.97	0.95	1.11	0.70	0.90	1.23	1.32	1.23
	(3.06)	(2.84)	(3.04)	(2.99)	(2.95)	(3.00)	(3.14)	(2.92)	(2.74)	(2.93)
55	1.10	1.08	1.11	1.15	1.26	0.78	1.00	1.33	1.43	1.32
60	1.18	1.24	1.20	1.23	1.36	0.88	1.08	1.40	1.56	1.41
65	1.24	1.27	1.25	1.29	1.47	0.92	1.14	1.56	1.69	1.50
	(3.13)	(3.01)	(3.10)	(3.00)	(2.96)	(2.92)	(2.82)	(2.88)	(3.03)	(3.19)
70	1.47	1.49	1.47	1.45	1.69	1.11	1.29	1.70	1.85	1.72
75	1.57	1.59	1.59	1.60	1.84	1.22	1.40	1.80	2.00	1.77
	(3.08)	(3.03)	(2.99)	(2.93)	(2.95)	(2.99)	(3.14)	(2.96)	(2.99)	(3.19)
80	1.78	1.80	1.81	1.86	2.10	1.33	1.55	1.96	2.29	2.04

[a] Probable error better than ±5%; reproducibility ±5% to ±10%.
[b] The values in parentheses; the accuracy, based on the error of the integrated intensities, was generally ±5%, and always better than ±10%.
[c] Solutions, 1.0 *M* in DMSO-d_6.
[d] Attached to the fused 2,3-*O*-isopropylidene ring.
[e] Attached to the flexible 5,6-*O*-isopropylidene ring.

TABLE 2. Calculated and experimental T_1 values for C-6 carbon nucleus[a]

(°C)	η (cP)	$T_{1,R(S)}$	τ_R (ps)	T_1, C_6(exptl.)	T_1, C_6(calcd.)[b,c]	T_1, C_6(calcd.)[c,d]	T_1, C_6(calcd.)[e]	T_1, C_6(calcd.)[f]
15	—	0.38	123.9	0.27	0.27 (20°)	0.27 (21°)	0.27	0.24
25	4.05	0.45	104.7	0.34	0.34 (21°)	0.34 (23°)	0.33	0.29
30	3.53	0.60	78.5	0.45	0.44 (21°)	0.45 (23°)	0.44	0.38
35	—	0.69	68.3	0.51	0.50 (20°)	0.51 (22°)	0.48	0.42
40	2.80	0.76	62.0	0.55	0.55 (20°)	0.56 (22°)	0.53	0.46
45	—	0.88	53.5	0.64	0.63 (20°)	0.64 (22°)	0.61	0.52
50	2.33	0.96	49.0	0.70	0.69 (20°)	0.70 (22°)	0.67	0.57
55	—	1.11	42.4	0.78	0.80 (20°)	0.79 (21°)	0.77	0.65
60	1.95	1.21	38.9	0.88	0.87 (20°)	0.88 (22°)	0.83	0.70
65	—	1.26	37.4	0.92	0.92 (21°)	0.92 (22°)	0.86	0.73
70	1.67	1.47	32.0	1.11	1.10 (21°)	1.11 (23°)	1.04	0.85
75	1.54	1.59	29.6	1.22	1.21 (21°)	1.22 (24°)	1.11	0.91
80	1.43	1.81	26.0	1.33	1.35 (21°)	1.32 (22°)	1.26	1.02

[a] By employing the two states puckering model as expressed by eq. [2].
[b] $\tau_A = \tau_B = 10^{-12}$ s.
[c] The values within parentheses are the angles θ which reproduce the experimental data.
[d] $\tau_A = 10^{-12}$ s, $\tau_B = 2 \times 10^{-12}$ s.
[e] $\tau_A = \tau_B = 10^{-11}$ s and θ equal the values in the 6th column; see footnote (*b*).
[f] $\tau_A = \tau_B = 10^{-10}$ s and θ values as in footnote (*e*).

a total of 100 scans was accumulated for each spectrum. Typically, 15–20 equispaced τ values were used, covering approximately a 2.0 s T_1 range, and the τ values were "arrayed" in each run by utilizing the XL-200 program. To minimize systematic errors, and factor out time as a variable in long experiments, the interleaving procedure available with the spectrometer was used. Values of T_1 were determined by a two-parameter fit using an equilibrium magnetization value (M_0) that was the average of at least four separate determinations. The probable error in the two-parameter fit in the T_1 calculations was ±5% or better at each temperature whereas, in general, the reproducibility was 5–10%, the upper limit pertaining at high temperatures. Samples of 1.0 *M* of **1** in DMSO-d_6 were degassed by three freeze–pump–thaw cycles before use. The ^{13}C nOe measurements were carried out on the same spectrometer by "gated decoupling" (9), three experiments being performed for each nOe value. Delays of at least 10× the longest T_1 were used between the 90° pulses.

Viscosity measurements were performed with a precalibrated Ubbelohde viscometer immersed in a silicone bath, at temperatures varying by not more than ±0.1°. Density measurements were made with a bicapillary pycnometer at the same temperatures in the same bath. Solutions of 1.0 *M* 2,3:5,6-di-*O*-isopropylidene-α-D-mannofuranose in DMSO-d_6 were employed for all of the measurements.

Can. J. Chem. Downloaded from www.nrcresearchpress.com by 210.87.254.5 on 09/06/12
For personal use only.

Can. J. Chem. Downloaded from www.nrcresearchpress.com by 210.87.254.5 on 09/06/12
For personal use only.

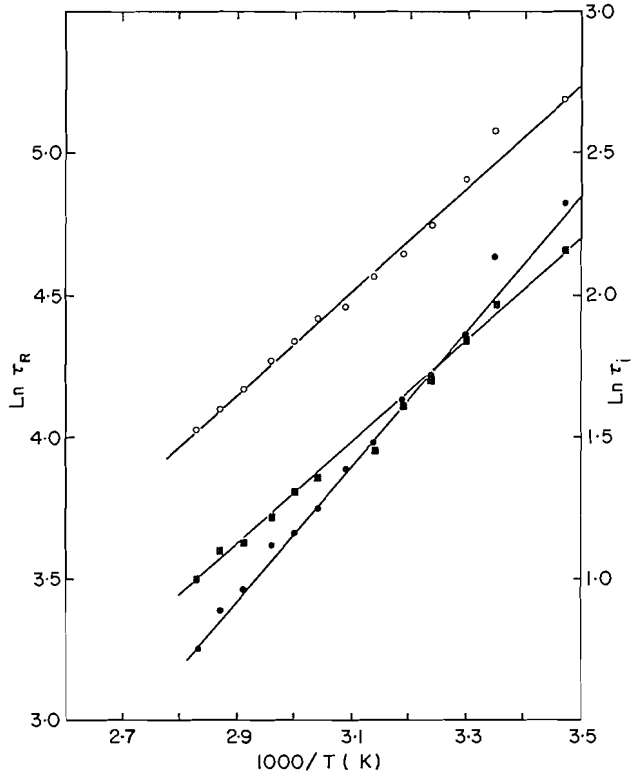

FIG. 1. Temperature dependence of the overall (τ_R) and methyl internal rotation rates (τ_i) of **1** in DMSO-d_6 solution. (●) Overall molecular motion; (○) *exo* methyl group; (■) *endo* methyl group.

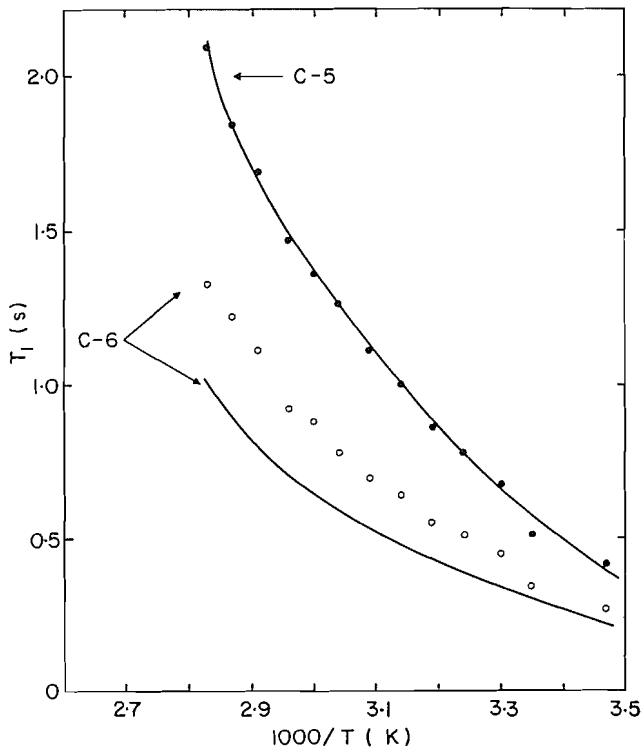

FIG. 2. Simulation of $1/T$ dependence of T_1 of C-5 and C-6 of **1**. The theoretical curves (solid lines) have been calculated with τ_R values from Table 2, taking $\tau_G = 0.8 \times 10^{-14}$ s, $E_G = 6.41$ kcal/mol.

Results and approximate analysis

Overall molecular motion

Carbon-13 T_1 values obtained from 15°C to 80°C for the protonated carbons of **1** are summarized in Table 1. The nOe factors for several sets of measurements (Table 1) indicate that the protonated carbons of **1** relax at all temperatures predominantly via the dipole–dipole interaction. T_1 values of carbons 1 to 4 of the mannose ring increase with increasing temperature in accord with the dipole relaxation theory (3, 4) and as these values are equal within experimental error at each temperature, it is clear that **1** reorients isotropically as a whole. Table 2 lists the numerical average of the T_1 values ($T_{1,R}$) for each temperature or, better, the average of the correlation times, (τ_R) calculated by means of eq. [1], which reflects the rate of the overall orientation of the molecule about its center of mass

$$[1] \quad \frac{1}{T_1} = \frac{N\gamma_H^2\gamma_C^2\hbar}{r_{C-H}^6}\tau_R$$

Equation [1] holds for isotropic motion and in the extreme narrowing approximation of a dipolar process, which is met in the present study as confirmed by the maximum values of the nOe factors (Table 1). γ_H and γ_C are the gyromagnetic ratios of ^1H and ^{13}C nuclei respectively, $2\pi\hbar$ is Planck's constant, N is the number of protons directly attached to the carbon of interest, and r_{C-H} is the C—H bond length (equal to 1.08 Å).

An Arrhenius plot of τ_R on a logarithmic scale vs. reciprocal temperature (K^{-1}) (Fig. 1) yields an activation energy of 4.88 ± 0.64 kcal/mol with a pre-exponential factor $\tau_R = 2.5 \pm 1.5 \times 10^{-14}$ s.

5,6-O-Isopropylidene ring

As seen in Table 1, the relaxation times of carbon-5 and, particularly, carbon-6 of the flexible 5,6-*O*-isopropylidene ring are longer than predicted by eq. [1] assuming that these carbons relax only via the overall motion of the molecule. This lack of agreement suggests that additional degrees of freedom influence the relaxation of the C-5—H-5 and C-6—H-6, C-6—H-6′ vectors.

Stereochemical models suggest that rotation of the ring about the C-4—C-5 axis is severely hindered mainly by nonbonded interactions involving the methyl groups. Therefore, the motion of the ring about this axis may be regarded as an oscillation with a certain angular amplitude. In attempting to simulate the experimental T_1 data in terms of molecular motional characteristics, possible models were evaluated. Some theoretical expressions (10–14) describe internal motion as a jump between several stable conformations. According to these models, the rates of jumping or, equivalently, the lifetimes of the various conformations, determine the relaxation rates. However, the fact that low-amplitude diffusion is ineffective (12, 13) in causing relaxation suggests that a jump model involving relatively few conformations should be generally suitable for describing relaxation. Consequently, a model consisting of two alternate conformational states is taken to be an appropriate description of oscillation in the flexible 5,6-*O*-propylidene ring of **1**. This leads to an evaluation of T_1 in terms of the overall diffusion rate, the internal diffusion rates (or, equivalently, the lifetimes of the two states), the angle between a particular C—H vector and the axis about which it rotates due to the jump, and the range through which the C—H vector jumps. When τ_R is the molecular correlation time for overall isotropic motion, τ_A and τ_B are the life times of the two stable states, the angle β is defined by the relaxation vector and the axis about which the vector jumps, and θ is one-half of the jump range (i.e., the jumps in between $-\theta$ and $+\theta$), the spin-lattice relaxation time is given by (12, 13)

Can. J. Chem. Downloaded from www.nrcresearchpress.com by 210.87.254.5 on 09/06/12
For personal use only.

$$[2]\quad \frac{1}{T_1} = \frac{N\gamma_H^2\gamma_C^2\hbar^2}{r_{C-H}^6}\left[(1-C)\frac{\tau_R}{1+\omega^2\tau_R^2} + C\frac{\tau_N}{1+\omega^2\tau_N^2}\right]$$

where

$$[3]\quad \tau_N^{-1} = \tau_R^{-1} + \tau_C^{-1},\ \tau_C^{-1} = \tau_A^{-1} + \tau_B^{-1}$$

and

$$[4]\quad C = \frac{3\tau_A\cdot\tau_B}{(\tau_A+\tau_B)^2}[\sin^2\beta(1-\cos 2\theta)][2-\sin^2\beta(1-\cos 2\theta)]$$

In a model corresponding to the limit $\tau_A = \tau_B$, which was derived by Ghesquiere *et al.* (11) to interpret the dynamic behaviour of the pyridyl ring in poly(4-vinyl pyridine), which is adopted here, the relation obtained for the dipolar relaxation rate of ^{13}C is given (11) by

$$[5]\quad \frac{1}{T_1} = \frac{3}{80}\frac{N\gamma_H^2\gamma_C^2\hbar^2}{r_{C-H}^6}\left\{A_1\left[\frac{\tau_R}{1+(\omega_H-\omega_C)^2\tau_R^2} + \frac{3\tau_R}{1+\omega_C^2\tau_R^2} + \frac{6\tau_t}{1+(\omega_H+\omega_C)^2\tau_R^2}\right] + A_2\left[\frac{\tau_t}{1+(\omega_H-\omega_C)^2\tau_t} + \frac{3\tau_t}{1+\omega_C^2\tau_t^2} + \frac{6\tau_t}{1+(\omega_H+\omega_C)^2\tau_t^2}\right]\right\}$$

where

$$[6]\quad A_1 = \frac{2}{3}(1-3\cos^2\beta)^2 + \sin^2 2\beta(1+\cos\theta) + \sin^4\beta(1+\cos 2\theta)$$

$$A_2 = \sin^2 2\beta(1-\cos\theta) + \sin^4\beta(1-\cos 2\theta)$$

τ_t is the correlation time defined as

$$[7]\quad \tau_t^{-1} = \tau_R^{-1} + \tau_G^{-1}$$

τ_G being the correlation time of the oscillation. The other parameters in eqs. [5] and [6] have their usual meaning, as before. In the limit $\tau_A = \tau_B = \tau_G$ eqs [2] and [5] become identical, with coefficients $C = 3/8\,A_1$ and $(1-C) = 3/8\,A_2$.

In molecular system **1**, the fixed axis of the oscillation is the C-4—C-5 axis, $\beta = 111.5°$, and $\omega_H = 5.65\times10^8$ rad/s and $\omega_C = 1.42\times10^8$ rad/s, for the 200.1 and 50.3 MHz observed frequencies of ^1H- and ^{13}C-nuclei, respectively. When eq. [5] is used for fitting the theoretical $T_1 = f(1/T)$ curves to experimental data for C-5 and C-6, therefore, the other parameters needed are θ, τ_R, $\tau_G°$, E_G the pre-exponential factor, and the activation energy of the oscillation. Parameter τ_R for the isotropic motion of **1** for each temperature is given in Table 2. Therefore, the best fit of the T_1 vs. $1/T$ curve was obtained by choosing the smallest possible value of θ corresponding to the experimental T_1 for each value of τ_G, the procedure being repeated to obtain optimal agreement over the whole temperature range. Figure 2 shows the simulation of the $1/T$ dependence of T_1 for C-5, obtained by taking $\tau_G° = 0.80\times10^{-14}$ s, $E_G = 6.41$ kcal/mol, and an oscillation amplitude varying from 30° – 70° and increasing with temperature between 15°C and 80°C. It was then found that the application of eq. [2] with the condition that $\tau_A = \tau_B = \tau_G = 10^{-10}$ s, led to the same conclusion for C-5 as far as the angular amplitude of oscillation is concerned. Hence the 5,6-*O*-isopropylidene ring

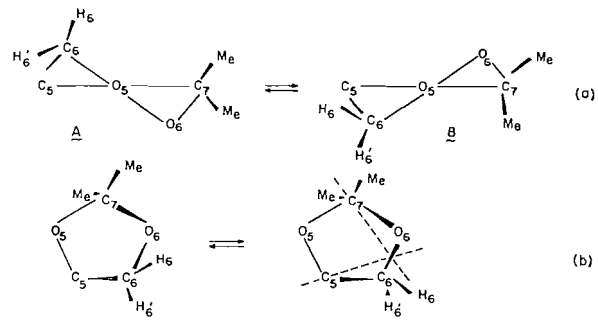

FIG. 3. Dynamic models for the flexible 5,6-*O*-isopropylidene ring in **1**. (a) Interconversion between two antisymmetric C_2 forms; (b) Same, as viewed perpendicular to the C_5—O_5—C_7 plane. The two effective internal jump axes are indicated by dotted lines.

oscillates between two stable states with a rather high activation energy. Also, the slow internal correlation times relative to the correlation time of the overall motion indicate that ring oscillation does not significantly affect the relaxation of C-5, despite the increase in the oscillation amplitude with increasing temperature.

It may be noted that several sets of parameters fit the relaxation data in both models. At a given temperature, a combination of low 2θ amplitudes (10° – 15°) and fast jump rate (10^{-11} – 10^{-12} s) leads to the same experimental T_1 value as a larger amplitude and slow jump rate. However, the number of possible solutions is drastically reduced by reference to coupling constants (6). Hence, $^3J_{H\text{-}4,H\text{-}5}$ coupling (6.38 Hz) indicates that the equilibrium orientation of the C-5—H-5 vector with respect to the C-4—H-4 vector is intermediate between *gauche* and *trans*; i.e., the ring performs an oscillational motion with an amplitude of about 60°.

A final result worth noting is related to the different stabilities of the two states characterized by the τ_A and τ_B lifetimes. If, for instance, $\tau_A \gg \tau_B$, then no relaxation effect would be observed even if $\tau_A \ll \tau_R$. However, this is not true for the present system, as indicated by the relaxation data, at high temperatures especially, where T_1, C-5 > $T_{1,R}$ (Tables 1 and 2). Calculations of T_1 performed using $\tau_A = 10^{-10}$ s, $\tau_B = 2\times10^{-10}$ s and $\tau_A = 10^{-10}$ s, $\tau_B = 3\times10^{-10}$ s resulted in small increases (2° – 3°) in the values of θ. Although the resulting range of motion does not change appreciably, it is not unreasonable that the lifetimes of the states could differ by a factor of 2 or 3. The set of parameters used to evaluate T_1 of C-5 does not also fit for T_1 of C-6 (Fig. 2). This discrepancy, which increases with temperature, is a consequence of the different β angles formed by the C-6—H-6 (−58°) and C-6—H-6′ (43°) vectors with respect to the oscillation axis, and results in an average T_1 value for C-6. However, a second source of the large deviation observed between theoretical and experimental T_1's (Fig. 2) may be found in the puckering motion of the flexible *O*-isopropylidene ring. Not only can this motion be justified by the relaxation data but also from C—H and H—H coupling constants, which demonstrated (6) the existence of a conformational equilibrium between two sites characterized by the *gauche* or *trans* orientation of O-6 with respect to H-5. Puckering motion of this kind has been treated quantitatively for other systems, particularly for the tetrahydropyrrole ring of proline, either when the amino acid was free or was incorporated into various peptides (12).

From the foregoing discussion it is seen that the C-6—H-6, H-6′ vectors relax via three types of motion: (1) librational

Can. J. Chem. Downloaded from www.nrcresearchpress.com by 210.87.254.5 on 09/06/12
For personal use only.

reorientation of the isopropylidene ring about the C-4—C-5 axis, (2) puckering motion of the ring, and (3) isotropic overall reorientation. However, the derivation of a theoretical expression of relaxation time that partitions these three motional components is not straightforward, even if these motions are considered to be independent.

A comparison between the relaxation times of C-5 and $T_{1,R}$ (Tables 1 and 2) shows only a small difference, which ranges from 8% at 15°C to 16% at 80°C. Consequently, the terms containing the τ_G correlation time in the general equation may be omitted, and the equation simplified to eq. [5] or to the more general eq. [2]. Now τ_A and τ_B represent the lifetimes of the isopropylidene ring in the two stable states A and B, defined in Fig. 3a, which depicts the interconversion between two antisymmetric twisted forms. This model assumes that atoms C-5—O-5—C-7 are nearly coplanar, and that C-6 occupies an *endo* or *exo* position relative to the C-4—C-5 axis. Angle β is formed by the C-6—H-6, H-6′ vectors and the two effective internal jump axes (12), represented by dotted lines in Fig. 3b, where the ring is viewed perpendicular to the C-5—O-5—C-7 plane; 2θ is the total range through which the C-6—H-6 and/or C-6—H-6′ vectors move from $-\theta$ to $+\theta$. A value of 77.7° for angle β was calculated by taking bond lengths of C-5—C-6 = 1.55 Å, C-5—O-5 = C-6—O-6 = C-7—O-7 = 1.43 Å, and bond angles for O-5—C-5—C-6 = O-5—C-6—O-6 = O-5—C-7—O-6 = 104°, and C-7—O-5—C-5 = C-7—O-6—C-6 = 108°. This geometry of the isopropylidene ring was based on several crystallographic data for *O*-isopropylidene aldofuranose derivatives (ref. 26 in ref. 8). T_1 values calculated for C-6 using different τ_A and τ_B lifetimes are summarized in Table 2 for comparison with experimental data. The best fit was obtained with $\tau_A = 10^{-12}$ s and $\tau_B = 2 \times 10^{-12}$ s and a range of $2\theta = 40° - 48°$. Good results also were obtained by the use of $\tau_A = \tau_B = 10^{-12}$ s, although these lifetimes resulted in small decreases in the values of 2θ, i.e., 40° – 42°. Overall, the range through which the C-6—H-6, H-6′ vectors move is within the range of motion found (12, 13) for most proline derivatives studied. The calculated ratios of NT_1, C-6/NT_1, C-5 fall significantly below 2, suggesting that the stabilities of the two twisted forms of the isopropylidene ring (Fig. 3a) may differ. This is also consistent with the indication (6) from coupling constants that conformation B is preponderant. Therefore, the lifetimes of the two conformations may differ by a factor of 2 to 3.

The experimental data can be reproduced as well by using $\tau_A = \tau_B = 10^{-11}$ s and $\tau_A = \tau_B = 10^{-10}$ s, together with a substantial increase in the range of motion, i.e., $2\theta \sim 60°$ and 80°, respectively. However, as this alternative corresponds to a slow puckering motion approximating the low rate of oscillation of the ring and, therefore, should have little influence on the relaxation of C-6, it is not in agreement with the experimental data.

Methyl groups

Two pairs of geminal *C*-methyl groups are attached to the molecular frame of **1**. That the internal rotation of these groups is hindered can be verified by the negligible contribution of the spin-rotation mechanism to the relaxation of the four symmetric tops at all temperatures (Table 1). Furthermore, the maximum values of the nOe factors (Table 1) suggest an explicit relationship between the dipolar T_1's and the methyl barrier to rotation, which reflects the magnitude of steric interference experienced by the methyl tops. The internal reorientation rate of a methyl group rotation can be expressed by eq.

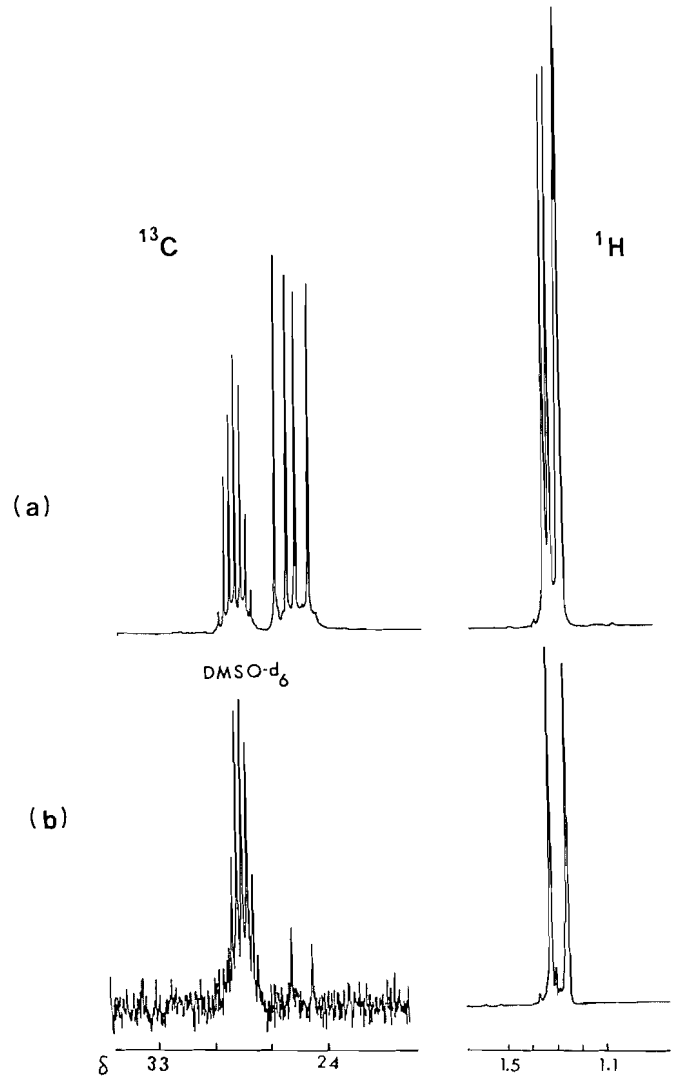

FIG. 4. Partial ^{13}C and ^{1}H nmr spectra of the methyl groups of **1** in acetone-d_6. (a) Nondeuterated compound; (b) deuterated compound.

[8], which represents the stochastic diffusion model (15)

$$[8] \quad \frac{1}{T_{1,\,CH_3}} = \frac{3\gamma_H^2\gamma_H^2\hbar^2}{r_{C-H}^6}\tau_R\left[A + B\frac{6\tau_i}{6\tau_i + \tau_R} + C\frac{3\tau_i}{3\tau_i + 2\tau_R}\right]$$

where τ_i is the correlation time for the internal motion, τ_R is the correlation time for the overall isotropic reorientation, and *A*, *B*, *C* are geometric terms defined previously (15). If jumps between three equivalent positions separated by 120° are assumed, the last term becomes $C(6\tau_i/6\tau_i + \tau_R)$ (15).

The pair of methyl groups of the 5,6-*O*-isopropylidene ring of **1** is not amenable to a rigorous quantitative treatment in terms of internal motion about C—CH_3, due to the multiple internal motions of the ring itself. However, this limitation does not apply to the geminal methyl groups of the 2,3-*O*-isopropylidene ring. Being fused to the mannofuranose moiety, this ring is clearly far more rigid, as can be verified from the analysis of ^{1}H—^{1}H couplings and ^{1}H-relaxation data for **1** (6). Before proceeding with an analysis of the internal rotation of these latter methyl groups, it is necessary to identify their signals in the ^{13}C nmr spectrum of **1**.

The four methyl groups absorb at δ 26.97, 26.17, 25.57, 24.65 and δ 1.36, 1.33, 1.27, 1.26 in ^{13}C and ^{1}H nmr spectra, respectively, in acetone-d_6 solution (Fig. 4a). To distinguish

Can. J. Chem. Downloaded from www.nrcresearchpress.com by 210.87.254.5 on 09/06/12
For personal use only.

between the two geminal pairs we selectively deuterated the methyls of the 5,6-*O*-isopropylidene ring. That is, acid-catalysed exchange between **1** and the acetone-d_6 solvent resulted in the elimination of two of the methyl resonances in either the ^{13}C or ^{1}H nmr spectrum (Fig. 4b). Because of the marked lability of the 5,6-*O*-isopropylidene substituent relative to that at C-2—C-3, the peaks remaining at δ 26.17, 24.65 and 1.35, 1.25 must have been due to the geminal pair of the 2,3-*O*-isopropylidene substituent. A further distinction within each pair of methyls was based on ^{1}H-nOe measurements. Irradiation of the methyl proton resonating at δ 1.25 caused a strong enhancement of the spatially proximate H-2 (7.8 ± 1.2%) and H-3 (10.0 ± 2.3%) of the mannose ring. Therefore, the peak at δ 1.26 (and corresponding ^{13}C peak at 24.65) is assigned to the *exo* methyl group of the fused ring, whereas the *endo* methyl group of the same ring accounts for the signals at δ 1.36 and 26.17. Analogously, irradiation of the methyl proton resonating at δ 1.27 led to enhancement of the H-5 resonance by 5.5 ± 0.8%. This result confirms the assignment of the signals at δ 1.27 and 25.57 to the *endo* methyl group of the 5,6-*O*-isopropylidene substituent, whereas those of the *exo* group are assigned by difference.

The motional characteristics of the methyl rotors attached to the rigid 2,3-*O*-isopropylidene ring can be described either by diffusion or jump models, although a diffusion process (jumps < 10°) may be anticipated in the DMSO used as solvent, due to its relatively high viscosity. An appropriate test as to whether or not reorientation is diffusional, is to compare the correlation times, τ_i, with the mean period of the free rotor (χ-test) (16).

If τ_i is much larger than τ_f (the time the free rotor takes to reorient through one rad), i.e. when $x = \tau_i/\tau_f \gg 1$, then the process is diffusional. Accordingly, the experimental T_1's lead to χ-values of 163.9 (15°C) and 57.2 (80°C) for the *exo* methyl group, and 64.3 (15°C) and 24.4 (80°C) for the *endo* methyl. These values, which are far greater than unity, indicate that the diffusion limit offers a good approximation for describing the motion of the methyl groups. Figure 1 shows the temperature dependence of the calculated relaxation rates, τ_i, for the two methyl groups, assuming C—C—H angles of 109.47°. From these plots, the activation energies for methyl group rotation were found to be 3.7 ± 0.6 and 3.3 ± 0.7 kcal/mol for the *exo* and *endo* methyls, respectively. Blunt and Stothers (17) have shown that in systems characterized by moderate steric interference for the methyl group, average C—C—H angles of 112° to 113° may reasonably be expected, and that these values should be considered for calculations using eq. [8]. By using a C—C—H angle of 112°, the respective activation energies were found to be 3.8 ± 0.6 (*exo*) and 3.4 ± 0.6 (*endo*) kcal/mol. However, the effect of angle on the calculated energies depends on the ratio $T_{1,CH_3}/T_{1,R}$ and is more important the larger this ratio becomes. The limit of rapid rotation for an angle of 109.47° is $T_{1,CH_3}/T_{1,R} = 3$, whereas that for an angle of 112° is $T_{1,CH_3}/T_{1,R} = 4$. In the present study, the relaxation time ratios range from 1.03 (15°C) to 0.86 (80°C) for the *exo* methyl group, and 1.55 (15°C) to 1.26 (80°C) for the *endo* methyl. Nevertheless, as already shown, the higher values of these ratios for the *endo* group do not also correspond to a greater increase in activation energy relative to the *exo* group, when the C—C—H angle is increased. In summary, the calculated τ_i and E_α values are fairly insensitive to variations in the C—C—H angle, due to the small increase of the $T_{1,CH_3}/T_{1,R}$ ratio with temperature.

It is of interest to assess possible sources of the hindrance to methyl group rotation. Assuming that viscosity effects on internal motion are of the same magnitude for both the *exo* and *endo* methyl groups of the fused 2,3-*O*-isopropylidene ring, then any difference observed in activation energies should reflect a difference between the two groups in nonbonded interactions they experience in the molecular frame. In this event, a simple expression of the activation energy would be an energy barrier separating two rotamers, one with minimum and the other with maximum interactions between the appropriate groups. Because the CH_3—C—CH_3 bond angle in fused *O*-isopropylidene rings of systems analogous to **1** is close to 113.7° (see ref. 26 in ref. 8), significantly higher than the idealized value of 109.47°, methyl–methyl interactions in the eclipsed conformations are probably not so important. Similarly, the O-2—C-8—O-3 angle is reduced to 106° from 109.47°, which does not favor interactions within the isopropylidene skeleton. In this respect, it is worth noting that the barriers to internal rotation of geminal methyl groups in camphor derivatives are lower than those in adamantanes (18) due, undoubtedly, to the smaller C-1—C-7—C-4 angle (significantly less than 109.47°) in the former molecules.

Molecular models indicate that the energy differences between the staggered and eclipsed conformations of the methyl groups are accounted for mainly by interactions with H-2, H-3, and H-5. Owing to the twist conformation ($^2T_3$) of the mannose ring (6) and the associated distortion of the *O*-isopropylidene ring, there are nonequivalent interactions between the *exo* methyl and H-2 and H-3 (principally H-2), thereby inducing a preferred conformation for this group and increasing its activation energy relative to the *endo* methyl. The energy barrier to internal rotation of the latter must be due mainly to interactions with H-5 since all other protons of the mannose moiety are too remote (>4.8 Å). However, because of the librational motion of the C-5—H-5 vector described previously, the methyl H-5 interactions are relaxed somewhat when the C-5—H-5 vector is in the extreme opposite site with respect to the *endo* methyl group. This situation is reflected in the lower activation energy of the *endo* relative to the *exo* methyl group.

The hydrodynamic behavior of ***1***

Simple hydrodynamic theory (19, 20) shows that the reorientation of a solute particle in a viscous medium can be described by the equation

$$[9] \quad \tau_R = C(\eta/T)$$

where η is the shear viscosity of the solution, T the absolute temperature of the liquid, and C a parameter which depends on the molecular shape, the solvent, the concentration, and the specific solute–solvent interactions. In a process activated by rotational diffusion the activation energy of the overall molecular motion, as calculated earlier from the nmr data, can be equated with the activation energy associated with the ratio η/T. This prediction is upheld by measurements of the solution viscosity (Table 2) as a function of temperature. These data, when plotted as ln (η/T) vs. $1/T$, gave a very good straight line (correlation coefficient = 0.9994) with a slope corresponding to an E_α = 4.57 kcal/mol, i.e., very close to the value of 4.88 kcal/mol derived from the nmr data.

Although the activation energy of the overall molecular reorientation is related to the viscous properties of the solution, molecular geometry and the specific nature of solute–solvent interactions also play an important role in rotational relaxation. Short range interactions or intermolecular collisions between

molecules of the solute and solvent create torques which alter the angular momentum, and hence the reorientational properties, of the probe molecule. In other words, the molecular reorientation may be hydrodynamic, depending on the nature of the coupling of the probe solute molecule to the solvent. One way to account for hydrodynamic effects on rotational relaxation in an explicit form is by the use of eq. [9], according to the Debye–Stokes–Einstein hydrodynamic model (19)

$$[10] \quad \tau_R = \frac{V_S}{k}\frac{\eta}{T}$$

where V_S is the volume of the solute and k is Boltzmann's constant. This equation holds for spherical solute molecules which are much larger than those of the solvent, and when the latter rotate at the surface of the solute particles (with the particle), i.e., under the "stick boundary condition". Equations [9] and [10] predict that a plot of τ_R vs. η/T should be a straight line,[1] with slope $C = V_S/k$, which proved to be true for the present experimental data (correlation coefficient = 0.9934). The experimental slope was found to be 7.8 (deg.ns/cP), which is far smaller than the calculated slope of 1593 (deg.ns/cP) given by eq. [10], assuming the stick boundary conditions. A volume (V_S) of 219.9 Å^3 was calculated from van der Waals' increments (21), which agrees well with volumes estimated from molecular models.

Hu and Zwanzig (22) have considered a rotating spheroid under the "slip boundary conditions", where the rotating particle displaces the surrounding fluid, which, in contrast to the stick case, exerts no drag force on the particle. Under slip boundary conditions, C_{slip} is zero for a sphere, and approaches unity for increasingly nonspherical spheroids.

To fit the experimental slope using the slip boundary conditions, one must assume that molecule **1** is a prolate ellipsoid with a ratio of ~0.92 for the lengths of the shorter and longer axes, that is, an almost spherical molecule. This result is in good agreement with the nmr data, which are clearly consistent with a nearly spherical particle reorienting isotropically. However, the "slip" model predicts (20, 22, 23) that the overall reorientation of a spherical molecule must be viscosity independent provided that the molecule reorients within its "own volume". This behavior may be excluded for the present system, particularly as the value of activation energy of the overall motion is about 5 kcal/mol. The viscosity dependence of the overall motion of **1** may be explained by a relatively weak coupling of translational and rotational motion, promoted by association of DMSO molecules with the OH group and possibly also with various ring oxygens of **1** (24). Despite their extremely short lifetimes, these possible dipole complexes may significantly influence the reorientational motion, because even these relatively weak interactions could reduce the coefficient C in eq. [8] decisively (20, 25).

[1]It is often convenient to express eq. [9] by $\tau_R = C(\eta/T) + \tau_R^\circ$ where τ_R° is an experimentally determined parameter, which appears to be of the order of the free-rotor correlation time (20). However, our data are not precise enough to determine such small additive terms. Equations [9] and [10] seem adequate for an analysis of our data.

Acknowledgments

The authors express their gratitude to Dr. Françoise Sauriol for kind assistance, and to McGill University and the Natural Sciences and Engineering Research Council of Canada for generous support. Viscosity measurements were carried out by Alison Burgess and Dr. R. Brown.

1. J. R. LYERLA, JR. and D. M. GRANT. Int. Rev. Sci. Phys. Chem. Series. Vol. 4. Butterworth, London. 1972. Chapt. 5.
2. J. R. LYERLA, JR. and G. C. LEVY. Topics in carbon-13 nmr spectroscopy. Vol. 1. *Edited by* G. C. Levy. Wiley–Interscience, New York. 1974. Chapt. 3.
3. E. BREITMAIER, K. SPOHN, and S. BERGER. Angew. Chem. Int. Ed. Engl. **14**, 144 (1975).
4. S. BERGER. Prog. Phys. Org. Chem. **16**, 239 (1978).
5. D. A. WRIGHT and D. E. AXELSON. Topics in carbon-13 nmr spectroscopy. Vol. 3. *Edited by* G. C. Levy. Wiley–Interscience, New York. 1979. Chapt. 2.
6. P. DAIS and A. S PERLIN. Can. J. Chem. **60**, 1648 (1982).
7. W. T. HUNTRESS, JR. J. Phys. Chem. **73**, 103 (1969).
8. P. DAIS. Ph.D. Thesis, University of Toronto (1980).
9. R. FREEMAN, H. D. W. HILL, and R. KAPTEIN. J. Magn. Reson. **7**, 327 (1972).
10. M. BALDO, K. J. IRGOLIC, and G. C. PAPPALARDO. Mol. Phys. **38**, 1467 (1979).
11. D. GHESQUIERE, B. BAN, and C. CHACHATY. Macromolecules, **10**, 743 (1977).
12. R. E. LONDON. J. Am. Chem. Soc. **100**, 2678 (1978).
13. R. E. LONDON. Magnetic resonance in biology. Vol. 1. *Edited by* J. S. Cohen. Wiley–Interscience, New York. 1980. Chapt. 1, and references therein.
14. B. BAN. J. Magn. Reson. **45**, 118 (1981).
15. (*a*) D. E. WOESSNER. J. Chem. Phys. **37**, 647 (1962); (*b*) A. ALLERHAND, D. DODDRELL, and R. KOMOROSKI. J. Chem. Phys. **55**, 189 (1971); (*c*) D. E. WOESSNER and B. S. SNOWDEN. Adv. Mol. Relaxation Processes, **3**, 181 (1972).
16. W. T. HUNTRESS, JR. J. Chem. Phys. **48**, 3524 (1968).
17. J. W. BLUNT and J. B. STOTHERS. J. Magn. Reson. **27**, 515 (1976).
18. H. BEIRBECK, R. MARTINO, and J. K. SAUNDERS. Can. J. Chem. **58**, 102 (1980).
19. A. EINSTEIN. Investigations on the theory of the Brownian movement. Dover, New York, NY. 1956. pp. 19–34.
20. D. R. BAUER, J. I. BRAUMAN, and R. PECORA. J. Am. Chem. Soc. **96**, 6840 (1974).
21. J. T. EDWARD. J. Chem. Educ. **47**, 261 (1970).
22. C. M. HU and R. ZWANZIG. J. Chem. Phys. **60**, 4354 (1974).
23. D. R. BAUER, G. R. ALMS, J. I. BRAUMAN, and R. PECORA. J. Chem. Phys. **61**, 2255 (1974).
24. W. MACKIE and A. S. PERLIN. Can. J. Chem. **44**, 2039 (1966); O. L. CHAPMAN and R. W. KING. J. Am. Chem. Soc. **86**, 1256 (1964).
25. K. L. OETTME, G. RUDAKOFF, and R. RADEGLIA. Adv. Mol. Relaxation Interaction Processes, **12**, 87 (1978).

Can. J. Chem. Downloaded from www.nrcresearchpress.com by 210.87.254.5 on 09/06/12
For personal use only.

Open-chain nitrogen compounds. Part IV.[1] Synthesis of 5-hydroxy-1,2,3-triazoles from 1-aryl-3-(ethoxycarbonylmethyl)triazenes: a new route to α-diazo-*N*-arylacetamides

KIM. M. BAINES AND KEITH VAUGHAN[2]
Department of Chemistry, Saint Mary's University, Halifax, N.S., Canada B3H 3C3

AND

DONALD L. HOOPER AND LORNE F. LEVECK
Department of Chemistry, Dalhousie University, Halifax, N.S., Canada B3H 4J3

Received November 1, 1982

KIM M. BAINES, KEITH VAUGHAN, DONALD L. HOOPER, and LORNE F. LEVECK. Can. J. Chem. **61**, 1549 (1983).

A series of triazenes of type ArN=N—NH—CH_2CO_2Et, *N*-arylazoglycine ethyl esters, have been prepared by coupling the arene diazonium salt, $ArN_2^+ \cdot X^-$, with ethyl glycinate, $NH_2CH_2CO_2Et$; an electron-withdrawing substituent, e.g. NO_2, CN, CO_2R, and Cl, in the *ortho* or *para* position of the aryl group is essential for efficient coupling. The *p*-substituted arylazoglycine ethyl esters cyclize when treated with alcoholic potassium hydroxide to afford the potassium salts of the 1-aryl-5-hydroxy-1,2,3-triazoles, which can be obtained free by acidification of the potassium salt solution with acetic acid. Reaction of the potassium salts with acetic anhydride yields the 1-aryl-5-acetoxy-1,2,3-triazoles. The 5-hydroxytriazoles, when heated in ethanol, rearrange to α-diazoacetanilides, $ArNH \cdot COCHN_2$. The diazoamides can be obtained in low yield directly from the triazenes by prolonged refluxing in ethanol. *o*-Substituted aryltriazenes do not cyclize under the same conditions but fragment to the arylamine.

KIM M. BAINES, KEITH VAUGHAN, DONALD L. HOOPER et LORNE F. LEVECK. Can. J. Chem. **61**, 1549 (1983).

On a préparé une série de triazènes du type ArN=N—NH—CH_2CO_2Et, esters *N*-arylazoglycinate d'éthyle, en couplant le sel diazionium de l'arène $ArN_2^+ \cdot X^-$ avec le glycinate d'éthyle, $NH_2CH_2CO_2Et$. Un substituant électro-attracteur, par exemple: NO_2, CN, CO_2R et Cl, en position *ortho* ou *para* du groupe aryle est essentiel pour un couplage efficace. L'ester arylazoglycinate d'éthyle substitué en position *para* se cyclise dans l'hydroxyde de potassium alcoolique en donnant les sels de potassium des aryl-1 hydroxy-5 triazoles-1,2,3 que l'on peut obtenir à l'état libre en acidifiant la solution de sel de potassium avec l'acide acétique. La réaction du sel de potassium avec l'anhydride acétique conduit aux aryl-1 acétoxy-5 triazoles-1,3,5. Par chauffage dans l'éthanol les hydroxy-5 triazoles se transposent en α-diazoacétanilides, $ArNH \cdot COCHN_2$. On peut obtenir les diazoamides avec un faible rendement en partant directement des triazènes que l'on porte longuement au reflux dans l'éthanol. Dans les mêmes conditions les aryltriazènes substitués en position *ortho* ne se cyclisent pas mais se fragmentent pour donner des arylamines.

[Traduit par le journal]

In Part III (1) of this series, the synthesis and characterization of a number of α-substituted 1-aryl-3-alkyltriazenes (ArN=N·NH·CH_2Y, e.g. Y = CN and CO_2R) was described. In a further study (2), the α-cyanomethyl triazenes were found to undergo cyclization to afford 5-amino-1-aryl-1,2,3-triazoles (**1**) which in turn undergo rearrangement in

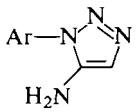

1

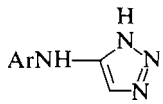

2

protic media to give the isomeric 5-(arylamino)-1,2,3-triazoles (**2**). The results reported in this paper originate from the logical extension of the amino-triazole synthesis to the synthesis of the 5-hydroxy-1,2,3-triazole system (**4**) via the analogous 1-aryl-3-(ethoxycarbonylmethyl)triazenes (**3**). Triazenes of type **3** do indeed give rise to 5-hydroxytriazoles (**4**), which show a facility to undergo rearrangement to the α-diazoacetamides (**5**). This study describes (a) the general reaction conditions required to achieve the synthesis of the 5-hydroxytriazoles, (b) the optimal conditions for a general synthesis of the α-diazoacetamides (**5**), (c) the characterization of a series of compounds of both types **4** and **5**. In addition, the spectroscopic properties of the triazenes of type **3** are explored in order to explain their degradation in solution.

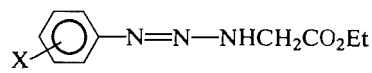

3	X
a	*p*-NO_2
b	*p*-CN
c	*p*-Cl
d	*p*-EtO_2C
e	*p*-MeO_2C
f	*o*-NO_2
g	*o*-Ac

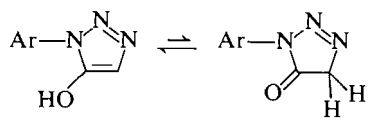

4 **6**

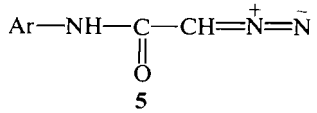

5

5-Hydroxytriazoles are available through a limited number of routes, the most general being the reaction between an organic azide and an activated methylene compound (e.g. malonic ester) (3). Open-chain triazene intermediates in these reactions have been postulated (4, 5), but the hypothesis has not been experimentally verified. Indeed, the potential use of triazenes of type **3** as triazole synthons has been largely ignored; a close analogy is the recently reported synthesis of

[1]For Part III, see ref. 1.

[2]Author to whom all correspondence should be addressed.

Can. J. Chem. Downloaded from www.nrcresearchpress.com by 210.87.254.5 on 09/06/12
For personal use only.

Can. J. Chem. Downloaded from www.nrcresearchpress.com by 210.87.254.5 on 09/06/12
For personal use only.

TABLE 1. 1-Aryl-3-(ethoxycarbonylmethyl)triazenes (**3**)

Compound	X	Yield (%)	Melting point (°C)	Solvent	Infrared (cm^{-1})	Nuclear magnetic resonance ($CDCl_3$)				
						NH	CH_2N	CH_2CH_3	X	Aromatic
3*a*	*p*-NO_2[a]	80	98–99 (yellow needles)	Hexane/benzene	3300, 1710 1510, 1340	9.3 (br, s)	4.5 (s)	4.3 (q) 1.3 (t) (J = 7.1 Hz)	—	7.4 (br, d) 8.13 (d) (J = 8.9 Hz)
3*b*	*p*-CN	75	78.5–80 (pale green plates)	Benzene/ petroleum ether	3195, 3170 2220, 1727	—	4.44 (s)	4.27 (q) 1.31 (t) (J = 7.2 Hz)	—	7.62 (d) 7.39 (br, d) (J = 8.6 Hz)
3*c*	*p*-Cl	77	76–76.5 (colourless needles)	Hexane	3395, 1734	7.37 (br, s)	4.36 (s)	4.25 (q) 1.29 (t) (J = 7.1 Hz)	—	7.31 (s)
3*d*	*p*-EtO_2C	71	74–75 (white needles)	Hexane { white / yellow }	3321, 1720 / 3230, 1749 1685	9.5 (br, s)	4.40 (s)	4.33 (q) 1.33 (t) (J = 7.2 Hz)	4.21 (q) 1.22 (t) (J = 7.2 Hz)	7.34 (d) 8.0 (d) (J = 8.0 Hz)
3*e*	*p*-MeO_2C[a]	88	70–71	Naphtha/ pet. ether	3320, 1730 1715	9.4 (br, s)	4.5 (s)	4.3 (q) 1.3 (t) (J = 7.0 Hz)	3.9 (s) (*O*-Me)	8.06 (d) 7.4 (br, d) (J = 8.5 Hz)
3*f*	*o*-NO_2	53	Oil[b]	—	—	—	4.30 (s)	4.23 (q) 1.24 (t) (J = 7.1 Hz)	—	7.3–7.8 (m)
3*g*	*o*-CH_3CO	73	115–117	—	1750, 1680	8.9 (br, s)	5.55 (s)	4.1 (q) 1.1 (t) (J = 7.0 Hz)	2.65 (s) (MeCO)	7.2–8.0 (m)

[a]Reference 1.
[b]Separated from reaction mixture by extraction with diethylether and washing ether extracts with aqueous $NaHCO_3$ and water, before drying and evaporation.

TABLE 2. 1-Aryl-5-hydroxy-1,2,3-triazoles (**4**)

Compound	X	Yield (%)	Melting point (°C)	Infrared (cm^{-1})	Nuclear magnetic resonance (DMSO-d_6)[a]
4*a*	*p*-NO_2	69	125–130	3119 (w) 2390 (br) 1600 (m) 1520 1380 858	8.43 (d, 2H, J = 9.2 Hz) 8.12 (d, 2H, J = 9.2 Hz) 7.15 (s, 1H)
4*b*	*p*-CN	78	110–112	3150 (w) 2370 (br) 2236 (sh) 1595 842	8.04 (s, 4H) 7.73 (s, 1H) 7.14 (s, 1H)
4*c*	*p*-Cl	99	118.5–122	3100 (m) 2600 (br) 1605 (s)	7.82 (d, 2H, J = 8.8 Hz) 7.62 (d, 2H, J = 8.8 Hz) 7.12 (s, 1H)
4*d*	*p*-EtO_2C	80	181–189	3167 (w) 2630 (br) 1719 (s) 1604	8.17 (d, 2H, J = 8.8 Hz) 7.97 (d, 2H, J = 8.8 Hz) 7.16 (s, 1H) 4.46 (q, 2H, J = 7.2 Hz) 1.36 (t, 3H, J = 7.2 Hz)

[a]The *p*-substituted aromatic patterns are nearly first order AA'BB' systems. Apparent chemical shifts and coupling constants are reported.

5-ethoxy-1*H*-1,2,3-triazoles by coupling of alkenediazonium salts with primary alkylamines (6). Previous studies of triazenes of type **3**, otherwise named *N*-arylazoglycine ethyl esters, have been directed at their degradation to α-diazocarboxylic esters (eq. [1]):

[1] $ArN{=}N{-}NH{-}CH_2CO_2Et \rightarrow ArNH_2 + N_2CHCO_2Et$

Conversion of *N*-(*p*-nitrophenylazo)-glycine ethyl ester (**3***a*) to *p*-nitroaniline and ethyl diazoacetate proceeds smoothly in a two-phase system of methylene chloride and 6% aqueous acetic acid (7). The diazoacetate can be formed quantitatively, without isolation of the intermediate triazene (**3***a*), by coupling the *p*-nitrobenzenediazonium salt and ethyl glycinate in dry dimethylformamide with a slight molar excess of triethylamine (8). Clearly, the tendency of triazenes of type **3** towards degradation necessitates careful control of reaction conditions to achieve cyclization.

Experimental

Melting points were determined with a Kofler hot stage apparatus and are uncorrected. Infrared spectra were recorded with liquid paraffin mulls on a Perkin–Elmer model 299 spectrophotometer. The uv spectra were recorded on a Varian/Cary 219 spectrophotometer. The ^1H nmr spectra were recorded on Varian Em-360 and CFT-20 spectrometers and the ^{13}C nmr spectra were obtained on the CFT-20 spectrometer. Microanalyses were carried out by the Canadian Microanalytical Laboratory, Vancouver, B.C.

1-Aryl-3-(ethoxycarbonylmethyl)triazenes (3)

General procedure

The arylamine ($ArNH_2$) (0.013 mol) was dissolved in 2 *M* hydrochloric acid (30 mL), diluted with water (40 mL), and diazotized at 0°C over a period of 1–2 h with sodium nitrite (0.013 mol) dissolved in water (10 mL). The diazonium salt solution was filtered and the clear filtrate treated with a solution of glycine ethyl ester hydrochloride (0.013 mol). After stirring the cold mixture for 15 min, a ten-fold molar excess of sodium acetate trihydrate (20 g) was added and the triazene precipitated slowly (over 2 h) from the reaction mixture. The product was filtered, dried, and recrystallized from a suitable solvent. The yields and physical data of the triazenes are given in Table 1.

The *p*-nitro- (**3***a*) and *p*-chloro- (**3***c*) phenyl triazenes recrystallize from nonpolar aprotic solvents without complication. However, heating the *p*-cyano- (**3***b*) or *p*-ethoxycarbonyl- (**3***d*) phenyltriazenes in a similar solvent results in the formation of oils. In the case of the *p*-cyano derivative (**3***b*) the oil was removed by charcoal treatment of the hot solution, but in the recrystallization of **3***d* from hexane the oil persists even after several charcoal treatments and two solid forms of **3***d* were obtained. A yellow amorphous solid forms when the oil cools; a different form of **3***d* crystallizes from the solution as fine white needles. The yellow and white forms of **3***d* have the same melting points and give identical elemental analyses. Solutions of the two forms of **3***d* give identical ir, uv, and nmr spectra, whereas ir spectra of the solids in Nujol mulls are substantially different.

The uv spectra of the two forms of **3***d* in ethanol or hexane have identical absorption maxima; λ_{max} (EtOH): 223(16 000), 310(19 050) nm; λ_{max} (hexane): 221(9950), 289(19 250) nm. The ^1H and ^{13}C nmr spectra in deuteriochloroform are identical. In the ^{13}C spectra of freshly prepared solutions, both yellow and white forms show two methyl signals at 13.9 and 14.07 ppm, two methylene carbons at 60.5 and 61.2 ppm, coincident aromatic peaks at 130.5 ppm, and a broad signal at 118 ppm representing the carbons *ortho* to the tautomeric system $-N{=}N{-}NH- \rightleftharpoons -NH{-}N{=}N-$. The unprotonated carbons of the aromatic ring were not resolved from the noise before decomposition of the triazene became the dominant phenomenon. The methylene carbon between N and carbonyl groups in the glycine moiety was not observed; this is common for rapid tautomerism in triazene systems (9).

The ir spectra of the yellow and white forms of **3***d* as Nujol mulls are strikingly different. The white form has a single broad carbonyl band at 1720 cm^{-1}, presumably the overlapping bands of the ester carbonyl groups, and NH absorption at 3320 cm^{-1}; the yellow form has two carbonyl bands well separated at 1750 and 1685 cm^{-1} and NH absorption at 3230 cm^{-1}. Chloroform solution ir spectra of the yellow and white forms are identical, showing carbonyl bands at 1740 and 1710 cm^{-1} and NH bands at 3430 and 3330 cm^{-1}.

Can. J. Chem. Downloaded from www.nrcresearchpress.com by 210.87.254.5 on 09/06/12
For personal use only.

TABLE 3. 1-Aryl-5-acetoxy-1,2,3-triazoles (**8**)

Compound	X	Yield (%)	Melting point (°C)	Solvent	Infrared (cm^{-1})	Nuclear magnetic resonance ($CDCl_3$)[a]
8*a*	*p*-NO_2	65	142–143 (yellow prisms)	Benzene	3160 (w) 1810	8.5 (d, 2H, J = 8 Hz) 7.93 (d, 2H, J = 8 Hz) 7.87 (s, 1H) 2.39 (s, 3H)
8*b*	CN	83	113–115 (pale yellow needles)	Hexane/ benzene	3160 (w) 2240 1800	7.85 (s, 5H) 2.32 (s, 3H)
8*c*	Cl	92	81–82 (white needles)	Hexane	3170 (w) 1810 1780	7.80 (s, 1H) 7.54 (s, 4H) 2.32 (s, 3H)
8*d*	CO_2Et	73	94–95 (pale yellow needles)	Hexane	3165 (w) 1800 1775 1715	8.3 (d, 2H, J = 8 Hz) 7.83 (s, 1H) 7.77 (d, 2H, J = 8 Hz) 4.43 (q, 2H, J = 7 Hz) 2.34 (s, 3H) 1.42 (t, 3H, J = 7 Hz)

[a]See note *a*, Table 2.

TABLE 4. Carbon-13 nuclear magnetic resonance chemical shifts of the 1-aryl-5-acetoxy-1,2,3-triazoles (**8**)

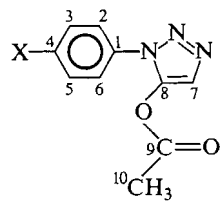

	X			
C	Cl[a]	NO_2[b]	C≡N[b]	$CO_2C_2H_5$[b]
1	—	142.75	142.59	142.51
2, 6	123.70	123.26	123.12	122.51
3, 5	128.62	124.98	133.31	130.61
4	—	147.42	112.67	130.21
7	121.26	122.34	122.07	121.99
8	137.53	139.59	137.98	137.98
9	172.06	163.85	163.85	164.08
10	21.07	20.49	20.36	21.17
			117.35 (*C*≡N)	165.06 (*C*=O)
				61.09 (—*C*H_2)
				15.01 (—CH_2—*C*H_3)

[a]Solvent DMSO-d_6.
[b]Solvent $CDCl_3$.

*1-Aryl-5-hydroxy-1,2,3-triazoles (**4**)*

An alcoholic solution of potassium hydroxide (1.0 g, 0.018 mol) was added dropwise with continuous stirring to a solution of the appropriate triazene (0.009 mol) (**3**) in absolute ethanol (25–100 mL). The resulting deep red solution was stirred at room temperature and the reaction followed by tlc to completion. The time required varied with the substituent in the aryl group as follows: *p*-nitro-, 1h; *p*-cyano-, 1.5 h; *p*-chloro-, 10 min; *p*-ethoxycarbonyl-, 40 min. In the case of the *p*-cyanophenyltriazene (**3***b*), a precipitate formed during the reaction and was removed by filtration before continuing. The ethanolic solution was evaporated to dryness under vacuum and the residue dissolved in the minimum volume of distilled water (20–50 m). In the case of *p*-nitrophenyltriazene (**3***a*), a water-insoluble product was removed by filtration and identified (mp and ir spectrum) as *p*-nitroaniline (yield 18%). The aqueous solution was acidified with glacial acetic acid (~5 mL), whereupon the hydroxytriazole (**4**) precipitated from solution and was filtered, washed with distilled water, and dried. Owing to the solubility characteristics of the hydroxytriazoles, appropriate solvents for recrystallization could not be found. When a suitable solvent was found, e.g. nitromethane, the triazoles invariably were found to undergo the rearrangement to the diazoacetamide spontaneously in the hot solvent. Purification of each triazole was achieved as follows.

4*a* (*p*-Nitrophenyl-), the yellow triazole, resisted all attempts at purification by recrystallization or chromatography but was ob-

Can. J. Chem. Downloaded from www.nrcresearchpress.com by 210.87.254.5 on 09/06/12
For personal use only.

TABLE 5. *N*-Aryl-α-diazoacetamides (**5**)

Compound	X	Method	Yield (%)	Melting point (°C)	Solvent	Infrared (cm^{-1})	Nuclear magnetic resonance (DMSO-d_6)[a]
5*a*	NO_2	A B	93 5	171–175 (dec.) (burnt orange needles)	CH_3NO_2	3105 (w) 2115 (s) 1655	10.41 (br, s) 8.2 (d, 2H) 7.76 (d, 2H) 5.62 (s, 1H)
5*b*	CN	A	98	163–165 (dec.)	CH_3NO_2	3100 (w) 2224 (m) 2115 (s) 1655 (m)	10.16 (br s) 7.72 (s, 4H) 5.57 (s, 1H)
5*c*	Cl	A	99	136–137.5 (dec.) (yellow amorphous)	CH_3NO_2	3098 (w) 2104 (s) 1630 (m)	9.85 (br s) 7.57 (d, 2H) 7.31 (d, 2H) 5.50 (s, 1H)
5*e*	CO_2Me	B	4	158–161 (yellow amorphous)	Benzene	3100 (w) 2100 (s) 1715 (s) 1650 (m)	10.1 (br s) 7.9 (d, 2H) 7.65 (d, 2H) 5.6 (s, 1H) 3.8 (s, 3H)
5*d*[b]	CO_2Et	A	92	225 (dec.)	—	3300 (w) 2100 (s) 1705 1675 (s)	10.12 (br s) 8.0 (m, 4H) 5.04 (s, 1H) 4.34 (q, 2H) 1.36 (t, 3H)

[a]See note *a*, Table 2.
[b]Physical/spectral data based on crude product, which resisted attempts at purification.

tained as a single component (tlc analysis) by two successive acetone triturations.

4*b* (*p*-Cyanophenyl-) was obtained as a single yellow component (tlc analysis) after two triturations with chloroform.

4*c* (*p*-Chlorophenyl-) (pale orange) was of sufficient purity for analysis without further treatment.

4*d* (*p*-Ethoxycarbonylphenyl-) (pale yellow) was the major component of a two-compound mixture (tlc analysis) obtained from the crude product by two triturations with acetone, followed by trituration with benzene. The second component was unidentified. Physical data of the triazoles are detailed in Table 2.

Potassium salts of **4**a *and* **4**b

(a) The potassium salt of 1-(*p*-nitrophenyl)-5-hydroxy-1,2,3-triazole (**4***a*) was isolated from the red alcoholic solution by slow evaporation of the solvent; long lustrous brown needles of the salt resulted, mp > 300°C, yield 86%; ir (Nujol): 3380 (very broad), 1670 (weak), and 1600 cm^{-1}; nmr (DMSO-d_6): 8.48, 8.18 (AA′BB′ pattern, 4H), and 6.1 (s, 1H, =CH) ppm).

(b) Similarly, the potassium salt of **4***b* precipitated in the basic alcoholic solution of the triazene (**3***b*). The salt had mp 286–289°C, yield 27%; ir (Nujol): 3550 (sharp), 3270 (broad), 2225 (sharp), 1664 (w), and 1610 cm^{-1}; nmr (DMSO-d_6): 8.33, 7.69 (AA′BB′ pattern, 4H), and 6.08 (s, 1H, =CH) ppm.

1-Aryl-5-acetoxy-1,2,3-triazoles (8)

The potassium salt of the 5-hydroxytriazole was prepared as described above by reaction of the appropriate triazene (**3**) (0.004 mol) with alcoholic potassium hydroxide (0.008 mol). The potassium salt was dissolved in water (50 mL), mixed with ice (~10 g), and treated with acetic anhydride (0.75 g) with vigorous stirring. The red colour of the potassium salt disappeared within 5 minutes and a yellow or white precipitate of the acetoxytriazole was formed. The solid was filtered, washed, dried, and recrystallized from hexane or benzene to afford the acetoxytriazoles (**8**). Physical data are given in Tables 3 and 4.

N-*Aryl-α-diazoacetamides (5)*

General procedure

Method A

The 1-aryl-5-hydroxytriazole (**4**) (0.005 mol) was dissolved in absolute ethanol (~50 mL) and refluxed for 1.5–2 h. The solvent was removed under vacuum and the residue purified by recrystallization to afford the diazoacetamides (**5***a*, *b*, *c*, and *d*).

Method B

The 1-aryl-3-(ethoxycarbonylmethyl)triazene (**3**) (0.008 mol) was dissolved in absolute ethanol (125 mL) and the mixture refluxed for several hours. The progress of the reaction was followed by tlc until successive chromatograms showed no change in the composition of the mixture; in none of the examples followed by this method could a single component be obtained. The reaction time varied from 2–6.5 h. The solvent was removed under vacuum to afford a gummy residue which was purified by successive triturations and recrystallizations to yield the diazoacetamides (**5***a* and *e*). Analogous reaction with the *p*-chlorophenyl- (**3***c*) and *p*-ethoxycarbonylphenyl- (**3***d*) triazenes gave mixtures of products with the spectroscopic properties expected of the diazoacetamide, but the pure material could not be isolated.

Table 5 gives the yields obtained by methods A and B and the physical data of the diazoacetamides.

*Degradation of 1-(*p*-nitrophenyl)-3-(ethoxycarbonylmethyl)triazene (3*a*)*

(a) Triazene **3***a* (0.30 g) was dissolved in absolute ethanol (20 mL) and mixed with triethylamine (13.9 mL, 0.1 mol). The solution, which changed colour to bright orange immediately, was refluxed for 1 h. The solvent was removed under vacuum and the residue washed with water and filtered to yield crude *p*-nitroaniline (0.150 g, 90%), which was identified by comparison of the ir spectrum with an authentic sample.

(b) Triazene **3***a* (0.30 g) was dissolved in absolute ethanol (20 mL) and mixed with concentrated hydrochloric acid (4.0 mL, 0.05 mol).

Can. J. Chem. Downloaded from www.nrcresearchpress.com by 210.87.254.5 on 09/06/12
For personal use only.

Can. J. Chem. Downloaded from www.nrcresearchpress.com by 210.87.254.5 on 09/06/12
For personal use only.

The mixture was left at ambient temperature for 36 h and the solvent removed under vacuum. The residue was washed with water and filtered to yield *p*-nitroaniline (0.1 g, 60%).

(c) Triazene (**3***a*) (0.30 g) was dissolved in absolute ethanol (20 mL), then mixed with acetic acid (20 mL) and the mixture refluxed for 1 h. The solvent mixture was removed under vacuum to yield a gummy residue; the presence of *p*-nitroaniline in the residue was confirmed by tlc.

(d) A small quantity (~50 mg) of triazene **3***a* was dissolved in chloroform and left to stand. Small aliquots of the solution were examined by tlc over a period of several days. After 24 h at room temperature, there was detectable degradation of the triazene into two products, in addition to the spot of unchanged triazene on the tlc. One of the products has identical R_f to *p*-nitroaniline. Spectroscopic analysis of the residue in the chloroform solution shows that the second product is ethyl diazoacetate (see eq. [1]). The solution ir spectrum in chloroform shows absorption at 2100 cm^{-1} and the structure is confirmed by the ^1H nmr spectrum in $CdCl_3$: 4.72 (singlet, N_2CH). 4.22 (quartet, J = 7.1 Hz, O—CH_2), and 1.27 (triplet, J = 7.1 Hz, CH_3) ppm.

*Reaction of 1-(o-nitrophenyl)-3-ethoxycarbonylmethyltriazene (**3**f) with potassium hydroxide*

The *o*-nitrophenyltriazene (**3***f*) (3.2 g) and potassium hydroxide (0.76 g) were dissolved in a minimum volume of ethanol and the solution left to stir for 4 hours. The solvent was removed under vacuum and the residue treated with water. The insoluble fraction was removed by filtration and identified, by ir spectroscopy and tlc, as *o*-nitroaniline (1.0 g, 42%). The filtrate was divided into two equal portions. The first portion was acidified with glacial acetic acid (2 mL) and stirred for several hours; no precipitation was evident. The second portion was treated with acetic anhydride and stirred for several hours, but again no reaction occurred.

Discussion

The method (1) of preparation of 1-aryl-3-(ethoxycarbonylmethyl)triazenes (**3**) by reaction of the arenediazonium salt with ethyl glycinate has been extended to include several new examples. Each of the compounds **3***a*–*e* includes an electron-withdrawing substituent in the aryl moiety. The presence of such a substituent in the arenediazonium ion appears essential to efficient diazo-coupling with ethyl glycinate. Attempted reaction with benzenediazonium ion gave an intractable mixture, while the triazene product from *p*-toluene diazonium ion showed the spectroscopic properties expected, but could not be isolated.

Compounds **3***a*–*e* were obtained in high yield, could be recrystallized from nonpolar solvents, and were stable for reasonable storage periods. Compound **3***c*, the *p*-chloro derivative, was noticeably less stable than others, completely decomposing to a black tar after 2 months at room temperature. Compound **3***d*, the *p*-ethoxycarbonyl derivative, is unique in this series in that recrystallization leads to two different solid forms, which become identical in solution. The reasonable explanation of this result is that these forms differ only in arrangement of molecules in the solid.

By analogy with the easy cyclization of 3-cyanomethyltriazenes (2), the 3-ethoxycarbonylmethyltriazenes might be expected to be readily converted to the hydroxytriazoles (**4**) on refluxing in ethanol. When this was attempted, thin-layer chromatography indicated that reaction did occur, but not a single reaction. When the solvent was removed from each such reaction mixture, the residue showed intense infrared absorption at 2100 cm^{-1}. After several careful triturations and successive recrystallizations small yields (<5%) of the α-diazoacetamides **5***a* and **5***e* were obtained. These compounds show the 2100 cm^{-1} absorption as a dominant feature of their infrared spectra.

Hence we may conclude that the reaction **3** → **5** is one of the reactions of the triazenes **3** in hot ethanol; presumably **4** is an intermediate that rearranges to the α-diazoacetamide in the protic solvent. The poor yields of the diazoamides led us to investigate other reactions of the triazenes **3** in order to improve yields and to isolate the hydroxytriazoles **4**. Ethanolic triethylamine, ethanolic acetic acid, and ethanolic hydrochloric acid each result in decomposition of the triazene as evidenced by high yields of the corresponding aniline. No such decomposition occurs when the triazenes are allowed to react with alcoholic potassium hydroxide at room temperature.

With alcoholic KOH a single product, the potassium triazolate (**7**) is formed in high yield within 1 hour. The reaction is general for all triazenes (**3***a*–*d*) treated in this way; the potassium salts of the *p*-nitrophenyl (**4***a*) and *p*-cyanophenyl (**4***b*) triazoles were isolated in crystalline form and characterized spectroscopically. Acidification of aqueous solutions of the salts with acetic acid precipitates the hydroxytriazoles (**4***a*–*d*) in high yield. Only the *p*-nitrophenyltriazene **3***a* showed any decomposition to the aniline in this reaction.

The *p*-chlorophenyltriazole **4***c* precipitated with glacial acetic acid was pure enough for analysis. The other three triazoles were particularly resistant to purification, rearranging to the diazoacetamide when recrystallization was attempted, and decomposing when subjected to either column or preparative thin-layer chromatography. Trituration with appropriate solvents yielded sufficiently pure material for spectroscopic study.

The most distinctive feature of the infrared spectra of the hydroxytriazoles is the broad band in the region 2300–2600 cm^{-1}, a region where absorption of a strongly hydrogen-bonded enolic hydroxyl group might be expected. The enol structure **4** is evidently the preferred tautomer of the triazoles, rather than a keto-form such as **6**; the ir spectra are blank in the region of carbonyl absorption. The ^1H nmr shows the singlet absorption of the CH of the aromatic triazole ring at 7.1 ppm. In the potassium salt (**7**) this peak is shifted to 6.1 ppm, most likely as a result of the resonance **7′** ↔ **7″**. The OH signal is

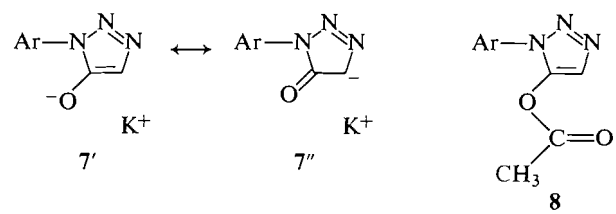

7′ **7″** **8**

clearly distinguished from the aromatic protons at 7.73 ppm in the spectrum of the *p*-cyanophenyl triazole (**4***b*).

Further unequivocal characterisation of the hydroxytriazoles was provided by reaction of the potassium salts (**7**), in aqueous solution, with acetic anhydride to afford the 5-acetoxytriazoles (**8**) in high yield. Unlike the hydroxytriazoles, the acetate derivatives recrystallized without change from nonpolar solvents so that analytically pure materials were obtained. The acetates show strong absorption in the ir at 1800–1810 cm^{-1}, which is unusually high frequency for an ester carbonyl group and may indicate that the triazole moiety is strongly electron withdrawing. The ^1H nmr spectra exhibit an acetyl Me resonance at ~2.4 ppm and an aromatic, one-proton singlet at 7.8–7.9 ppm, assigned to the hydrogen attached to C-4 of the triazole ring; the latter is shifted significantly downfield compared to the corresponding resonance in the hydroxytriazole.

TABLE 6. ^{13}C nuclear magnetic resonance assignments of **4***d*

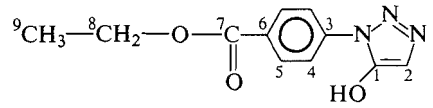

Carbon	Chemical shift (ppm)
1	115.54
2	130.61
3	130.01
4	121.39
5	130.78
6	150.82
7	166.75
8	61.12
9	14.24

TABLE 7. ^{13}C nuclear magnetic resonance assignments of **5***a*

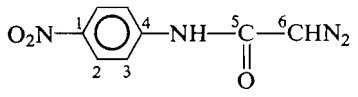

Carbon	Chemical shift (ppm)
1	145.9
2	125.1
3	118.2
4	141.7
5	164.5
6	49.1

TABLE 8. ^{13}C nuclear magnetic resonance assignments of **7***a*

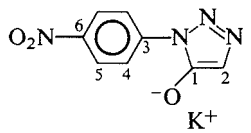

Carbon	Chemical shift (ppm)
1	161.05
2	112.69
3	142.53
4	117.03
5	124.76
6	144.67

Although 1-*p*-chlorophenyl-5-acetoxy-1,2,3-triazole (**8***c*) survives recrystallization without degradation or rearrangement, it, like the triazene (**3***c*), has quite a short shelf life at room temperature. After only a few weeks of storage, samples of **8***c* were found to contain acetic acid, which was definitely not present when the samples were fresh. Further investigation showed that **8***c* had undergone hydrolysis to the hydroxytriazole (**4***c*), presumably by nucleophilic acyl substitution following absorption of ambient moisture. The other acetates (**8***a*, *b*, and *d*) have not shown any tendency to decompose.[3]

[3]NOTE ADDED IN PROOF: Acetate **8***d* also shows signs of decomposition after storage for 8–10 months.

Degradation of the *p*-chlorophenyl-5-acetoxytriazole (**8***c*) was also observed when attempts were made to record its ^{13}C nmr spectrum in DMSO-d_6. Many of the signals in the spectrum of **8***c* were doubled, suggesting that hydrolysis to the hydroxytriazole in the nmr tube had occurred during the 10–12 hours required to record a spectrum. Decomposition may also explain why the signals from the quaternary aromatic carbons, C-1 and C-4, were not detected. The other acetoxytriazoles were sufficiently soluble in deuteriochloroform to give full ^{13}C spectra, which are summarized in Table 4. All carbons in compounds **8***a*, **8***b*, and **8***d* were detected and assigned to their respective signals, so that the structure of these acetates have been unequivocally confirmed by the ^{13}C nmr data, thus removing any doubt that might exist regarding the structure-proof of the parent 5-hydroxytriazoles (**4**).

The *N*-aryl-α-diazoacetemides (**5**) were obtained in high yield by refluxing the triazoles (**4**) for short periods in absolute ethanol. The products obtained in this way were much purer than the mixtures obtained by refluxing the triazenes. All of **5***a*–*d* were satisfactorily recrystallized, albeit in some cases only with extreme care, from nitromethane. The spectroscopic properties of these compounds include the distinctive 2100 cm^{-1} infrared absorption and, in the ^1H nmr, the NH signals between 9.8 and 10.4 ppm, with the diazo CH at 5.6 ppm.

The ^{13}C nmr spectra of one triazole, one triazolate, and one diazoacetamide were obtained to help verify the structure assigned. In the fully decoupled spectrum of 1-(*p*-ethoxycarbonylphenyl)-5-hydroxy-1,2,3-triazole (**4***d*) eight signals are apparent. The assignments of these signals are listed in Table 6. The ^{13}C spectrum of *N*-(*p*-nitrophenyl)-α-diazoacetamide (**5***a*) also confirmed the structure proposed; the signals are assigned in Table 7. The chemical shift of the CH in the diazo group is much smaller than initially expected; however, Albright and Freeman have observed (10) that the diazo carbon is shielded by an extraordinary amount, compared with normal sp^2 hybridized carbons. The ^{13}C spectrum of **7***a* (Table 8) is consistent with the resonance, **7′** ↔ **7″**; the chemical shift of the oxygen-bearing carbon in the triazole ring at 161.05 ppm accords with the carbonyl character of this group.

The application of this synthesis to *ortho*-substituted phenyl triazoles of type **4** was unsuccessful. Coupling *o*-nitrobenzene diazonium ion with ethyl glycinate gave a moderate yield of the triazene (**3***f*), which was obtained as an oil and characterized by ^1H nmr (Table 1). This triazene decomposes on storage; a crystalline material growing in the oil was identified from its ir spectrum as *o*-nitroaniline and the presence of ethyl diazoacetate (eq. [1]) in the residual oil was evident from the band at 2100 cm^{-1}. Degradation of **3***f* to *o*-nitroaniline was also observed in reaction with alcoholic KOH; there was no evidence of cyclization of **3***f* to a triazole in the KOH-catalysed reaction or when **3***f* was refluxed in ethanol.

Although *p*-acetylbenzenediazonium salt does not couple readily with primary alkylamines, the isomeric *o*-acetylbenzenediazonium ion couples with ethyl glycinate, neutralized with sodium acetate, to give a good yield of the *o*-acetylphenyltriazene (**3***g*). Compound **3***g* is a bright, orange solid with spectroscopic features mostly consistent with the triazene structure. The nmr spectrum shows all the expected ^1H signals and the ir spectrum has carbonyl absorption at 1750 (ester) and 1680 (ketone) cm^{-1}. The only inconsistent feature is the non-observation of NH ir absorption. Triazene **3***g* does not recrystallize unchanged from ethanol or benzene; a complex mixture of products results when **3***g* is heated in ethanol but

Can. J. Chem. Downloaded from www.nrcresearchpress.com by 210.87.254.5 on 09/06/12
For personal use only.

TABLE 9. Analytical data of reported compounds

Compound	Formula	Calculated			Found		
		C	H	N	C	H	N
3*a*	$C_{10}H_{12}N_4O_4$	47.62	4.80	22.21	47.47	4.73	22.18
3*b*	$C_{11}H_{12}N_4O_2$	57.18	5.42	24.11	56.9	5.17	24.14
3*c*	$C_{10}H_{12}N_3O_2Cl$	49.72	5.26	17.34	49.69	4.97	17.39
3*d*	$C_{13}H_{17}N_3O_4$	55.91	6.09	15.05	55.82	6.02	15.00
4*a*	$C_8H_6N_4O_3$	46.61	2.93	27.18	46.82	2.31	26.38
4*b*	$C_9H_6N_4O$	58.06	3.25	30.09	58.05	2.72	29.07
4*c*	$C_8H_6N_3OCl$	49.16	3.07	21.49	49.09	2.78	21.37
8*a*	$C_{10}H_8N_4O_4$	48.39	3.25	22.57	49.14	2.85	22.48
8*b*	$C_{11}H_8N_4O_2$	57.89	3.53	24.55	58.48	3.22	24.58
8*c*	$C_{10}H_8N_3O_2Cl$	50.56	3.37	17.68	50.21	2.96	17.61
8*d*	$C_{13}H_{13}N_3O_4$	56.73	4.76	15.27	56.44	4.49	15.13
5*a*	$C_8H_6N_4O_3$	46.61	2.93	27.18	46.38	2.51	26.80
5*b*	$C_9H_6N_4O$	58.06	3.25	30.09	57.79	2.82	29.49
5*c*	$C_8H_6N_3OCl$	49.12	3.07	21.49	49.17	2.63	21.09
5*d*	$C_{10}H_9N_3O_3$	54.80	4.14	19.17	55.82	3.94	—

conversion to a diazomide is not evident.

In conclusion, the results reported here describe a convenient and unequivocal route to the 1-aryl-5-hydroxytriazole system without substituents at the 4-position of triazole ring. Other general methods of synthesis, e.g. the reaction of azides with reactive methylene compounds (3), afford triazoles substituted at C-4. This paper also describes conditions for the rearrangement of the hydroxytriazoles to α-diazoacetamides, which are not readily available by other routes. These results confirm the predictions made by Olsen (5), who postulated that 5-hydroxytriazoles should rearrange to the diazoacetamide. Whereas Olsen suggested the rearrangement might be reversible, the equilibrium **4** $\rightleftharpoons$ **5** appears to lie in favour of the diazoamide under the conditions used here. This ring-opening reaction is very similar to the Dimroth rearrangement of aminotriazoles via an α-diazoacetamidine intermediate (11), which is the imino-analogue of the α-diazoacetanilide. Whereas the diazoacetamidines are unstable and recyclize spontaneously, the diazoamides cannot follow the Dimroth pathway any further and, as we have shown here, are sufficiently stable to permit isolation.

Analytical data for the reported compounds are given in Table 9.

1. T. A. DANIELS, S. SIDI, and K. VAUGHAN. Can. J. Chem. **55**, 3751 (1977).
2. K. M. BAINES, T. W. ROURKE, K. VAUGHAN, and D. L. HOOPER. J. Org. Chem. **46**, 856 (1981).
3. O. DIMROTH. Justus Liebigs Ann. Chem. **373**, 336 (1910).
4. M. BEGTRUP and C. PEDERSEN. Acta Chem. Scand. **18**, 1333 (1964).
5. C. E. OLSEN. Acta Chem. Scand. **27**, 2989 (1973).
6. R. W. SAALFRANK and E. ACKERMAN. Justus Liebigs Ann. Chem. 7 (1981); 3456 (1981).
7. R. J. BAUMGARTEN. J. Org. Chem. **32**, 484 (1967).
8. J. F. MCGARRITY. J. Chem. Soc. Chem. Commun. 558 (1974).
9. D. L. HOOPER and K. VAUGHAN. J. Chem. Soc. Perkin Trans. 2, 1161 (1981).
10. T. A. ALBRIGHT and W. J. FREEMAN. Org. Magn. Reson. **9**, 75 (1977).
11. T. L. GILCHRIST and G. E. GYMER. Adv. Heterocycl. Chem. **16**, 79 (1974).

Can. J. Chem. Downloaded from www.nrcresearchpress.com by 210.87.254.5 on 09/06/12
For personal use only.

Electrical and thermal properties of Na_2SO_4 doped with $NaVO_3$, $Ln_2(SO_4)_3$ (Ln = Eu, Pr)

NOBUHITO IMANAKA, GIN-YA ADACHI,[1] AND JIRO SHIOKAWA

Department of Applied Chemistry, Faculty of Engineering, Osaka University, Yamadaoka Suita, Osaka, 565, Japan

Received July 7, 1982[2]

NOBUHITO IMANAKA, GIN-YA ADACHI, and JIRO SHIOKAWA. Can. J. Chem. **61**, 1557 (1983).

In order to develop useful solid electrolytes for SO_2 detectors, Na_2SO_4, Na_2SO_4–$Eu_2(SO_4)_3$, Na_2SO_4–$NaVO_3$, and Na_2SO_4–$NaVO_3$–$Ln_2(SO_4)_3$ (Ln = Eu, Pr) systems have been prepared, and their electrical and thermal properties have been measured. By doping Na_2SO_4 with $Eu_2(SO_4)_3$, the electrical conductivity increases and the apparent activation energy of the Na_2SO_4–$Eu_2(SO_4)_3$ system shows a value between those of Na_2SO_4-III and Na_2SO_4-I. Addition of $NaVO_3$ and $Ln_2(SO_4)_3$ (Ln = Eu, Pr) to Na_2SO_4 suppressed the phase transformation, by stabilizing the structure of the Na_2SO_4-I phase even at a relatively low temperature.

NOBUHITO IMANAKA, GIN-YA ADACHI et JIRO SHIOKAWA. Can. J. Chem. **61**, 1557 (1983).

Dans le but de mettre au point des électrolytes solides utiles pour les détecteurs au SO_2, on a préparé des systèmes de Na_2SO_4, Na_2SO_4–$Eu_2(SO_4)_3$, Na_2SO_4–$NaVO_3$ et Na_2SO_4–$NaVO_3$–$Ln_2(SO_4)_3$ (Ln = Eu, Pr) et on a mesuré leurs propriétés électriques et thermiques. En dopant le Na_2SO_4 avec du $Eu_2(SO_4)_3$, la conductivité électrique augmente et l'énergie d'activation apparente du système Na_2SO_4–$Eu_2(SO_4)_3$ atteint une valeur qui se situe entre celles du Na_2SO_4-III et du Na_2SO_4-I. L'addition de $NaVO_3$ et de $Ln(SO_4)_3$ (Ln = Eu, Pr) à du Na_2SO_4 supprime la transformation de phase en stabilisant la structure de la phase Na_2SO_4-I même à une température relativement faible.

[Traduit par le journal]

Introduction

Polymorphism and electrical conductivity of Na_2SO_4 have been studied by many investigators (1–18). It has been known that Na_2SO_4 has five polymorphisms and that it exhibits Na^+ ion conduction at an elevated temperature. Sodium sulfate exhibits the Na_2SO_4-V phase at room temperature. On heating, the Na_2SO_4-V phase transforms firstly to a metastable phase, Na_2SO_4-III, and then to Na_2SO_4-I, a high temperature phase. On the other hand, the Na_2SO_4-I phase transforms to Na_2SO_4-III, a low temperature phase, which takes several months before its transformation to the Na_2SO_4-V phase. The existence of phase IV is still questioned.

Recently, attempts have been made to utilize $(Na, K)_2SO_4$ as molten (19, 20) or solid electrolytes (21–23) for detecting SO_2 or SO_3 in gases. However, a disadvantage in using Na_2SO_4 or K_2SO_4 (24) as a solid electrolyte is the presence of a phase transformation and the lack of sufficient electrical conductivity at low temperatures. Furthermore, it is difficult to establish the SO_2–SO_3 equilibrium rapidly at the surface of solid electrolytes. Attempts have often been made to increase the electrical conductivity of Na_2SO_4 by doping with divalent or trivalent cations (25–30). However, phase transformations still remain. In this paper, $Ln_2(SO_4)_3$ (Ln = Eu, Pr) is used as a dopant to increase the electrical conductivity and $NaVO_3$ is added to establish the SO_2–SO_3 equilibrium quickly.

Experimental

Anhydrous Na_2SO_4 and $NaVO_3$ were purchased from Wako pure Chemical Industries Ltd. $Eu_2(SO_4)_3$ and $Pr_2(SO_4)_3$ were prepared by adding concentrated sulfuric acid to Eu_2O_3 and Pr_6O_{11}, respectively. Two-component systems, Na_2SO_4–$Eu_2(SO_4)_3$ and Na_2SO_4–$NaVO_3$, and three-component systems, Na_2SO_4–$NaVO_3$–$Ln_2(SO_4)_3$ (Ln = Eu, Pr) were prepared, firstly by mixing the appropriate amount of Na_2SO_4, $NaVO_3$, and $Ln_2(SO_4)_3$ (Ln = Eu, Pr) and then by sintering the mixtures for 3 h at 1073 K.

Electrical conductivities were measured by means of the complex impedance method (30, 31) with a Hewlett Packard vector impedance meter 4800A using the apparatus shown in Fig. 1. Reproducibility of the results, log (σT), was within $\pm 0.3\ \Omega^{-1}\ cm^{-1}\ K$. σ and T represent electrical conductivity and absolute temperature, respectively. A Chromel–Alumel thermocouple was used to measure temperature. X-ray diffraction analyses were performed by using a Rigaku Rotaflex diffractometer with CuKα radiation. DTA measurements were done with a Rigaku Thermoflex.

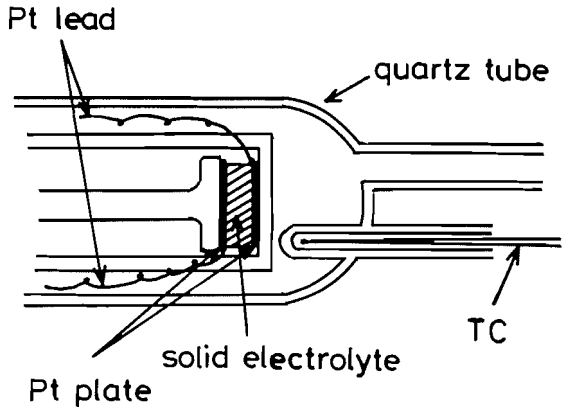

FIG. 1. Apparatus for electrical conductivity measurements.

Results and discussion

The two-component systems

The Na_2SO_4–$Eu_2(SO_4)_3$ system

In the Na_2SO_4–$Eu_2(SO_4)_3$ system, samples of Na_2SO_4 doped with 0.7 mol% $Eu_2(SO_4)_3$, 4.1 mol% $Eu_2(SO_4)_3$, and 8.2 mol% $Eu_2(SO_4)_3$ were prepared. Temperature dependences of Na_2SO_4 and their electrical conductivities are shown in Fig. 2. Na_2SO_4 and Na_2SO_4 doped with 0.7 mol% $Eu_2(SO_4)_3$ exhibited a discontinuity due to the phase transformation of Na_2SO_4-III to Na_2SO_4-I. On the other hand, the samples doped with more than 0.7 mol% $Eu_2(SO_4)_3$ exhibited no change in slope. By doping $Eu_2(SO_4)_3$ into Na_2SO_4, cation vacancies were produced to increase the electrical conductivity and described as $(Na_{(2-3x)/2}Eu_{x/2}\square_x)_2SO_4$, where $\square$ is a cation vacancy. In the

[1]Author to whom all correspondence should be addressed.

[2]Revision received January 20, 1983.

Can. J. Chem. Downloaded from www.nrcresearchpress.com by 210.87.254.105 on 09/06/12
For personal use only.

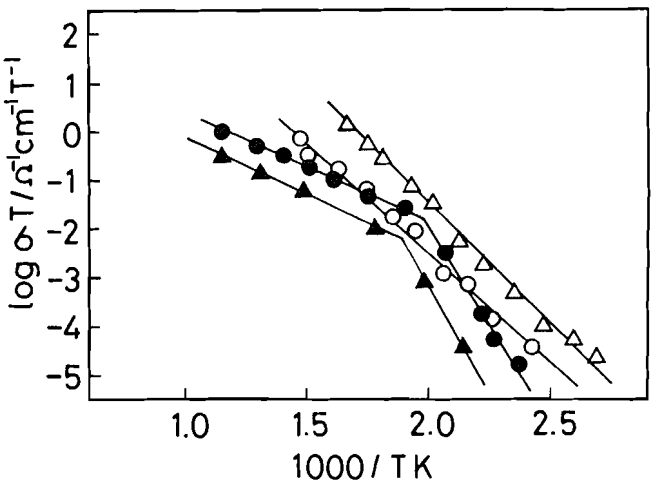

FIG. 2. Temperature dependences of electrical conductivities for the $Na_2SO_4-Eu_2(SO_4)_3$ system. -○- $Na_2SO_4-Eu_2(SO_4)_3$ = 91.8:8.2; -△- $Na_2SO_4-Eu_2(SO_4)_3$ = 95.9:4.1; -●- $Na_2SO_4-Eu_2(SO_4)_3$ = 99.3:0.7; -▲- Na_2SO_4.

TABLE 1. The phases and thermal properties of the $Na_2SO_4-Eu_2(SO_4)_3$ system

Na_2SO_4 (mol%)	$Eu_2(SO_4)_3$ (mol%)	Phases[a]	DTA peaks[b] (K)
99.3	0.7	α + Na_2SO_4-V	493
95.9	4.1	γ + Na_2SO_4-V	553
91.8	8.2	γ + Na_2SO_4-V	563, 573, 818, 1003

[a]The α phase is similar to the Na_2SO_4-III phase (15, 16); the γ phase is different from any Na_2SO_4 phase; Na_2SO_4-V is the initial raw material. X-ray analyses were done at room temperature.
[b]Reproducibility of DTA temperature is within 2 K.

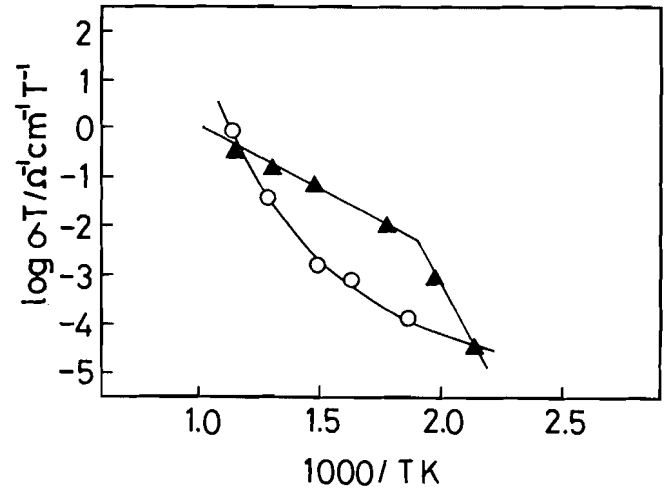

FIG. 3. Temperature dependences of electrical conductivities for $Na_2SO_4-NaVO_3$ = 95:5. -○- $Na_2SO_4-NaVO_3$ = 95:5; -▲- Na_2SO_4.

cases of Na_2SO_4 doped with 4.1 mol% $Eu_2(SO_4)_3$ and 8.2 mol% $Eu_2(SO_4)_3$, $(Na_{0.89}Eu_{0.04}\square_{0.08})_2SO_4$ and $(Na_{0.79}Eu_{0.07}\square_{0.14})_2SO_4$ were formed. In the $Na_2SO_4-Eu_2(SO_4)_3$ system, Na_2SO_4 doped with 4.1 mol% $Eu_2(SO_4)_3$ exhibited the highest electrical conductivity. By doping 8.2 mol% $Eu_2(SO_4)_3$ into Na_2SO_4, its electrical conductivity is about one-tenth that for Na_2SO_4 doped with 4.1 mol% $Eu_2(SO_4)_3$. The reason why Na_2SO_4 doped with 4.1 mol% $Eu_2(SO_4)_3$ exhibited the highest electrical conductivity in the $Na_2SO_4-Eu_2(SO_4)_3$ system may be attributed to the fact that the vacancies produced by doping of Eu^{3+} have a tendency to make clusters when $Eu_2(SO_4)_3$ is dissolved to more than 4.1 mol%.

TABLE 2. The phases and thermal properties of the $Na_2SO_4-NaVO_3$ system

Na_2SO_4 (mol%)	$NaVO_3$ (mol%)	Phases[a]	DTA peaks[b] (K)
98	2	α + Na_2SO_4-V	533, 888
95	5	α + Na_2SO_4-V + trace $NaVO_3$	528, 888
93	7	α + trace Na_2SO_4-V + trace $NaVO_3$	528, 878
90	10	α + trace Na_2SO_4-V + trace $NaVO_3$	523, 873

[a]The α phase is similar to Na_2SO_4-III (15, 16); Na_2SO_4-V and $NaVO_3$ are the initial raw materials. X-ray analyses were done at room temperature.
[b]Reproducibility of DTA temperature is within 5 K.

The apparent activation energies for Na_2SO_4-III and Na_2SO_4-I calculated from the logarithm of electrical conductivity multiplied by absolute temperature vs. the reciprocal absolute temperature curve are 73 kJ/mol and 20 kJ/mol, respectively. The apparent activation energy for Na_2SO_4 doped with 4.1 mol% $Eu_2(SO_4)_3$, 40 kJ/mol, is between 73 kJ/mol for Na_2SO_4-III and 20 kJ/mol for Na_2SO_4-I.

The phases and thermal properties of the $Na_2SO_4-Eu_2(SO_4)_3$ system are summarized in Table 1. From X-ray analysis, some of the original Na_2SO_4-V still remained in all samples. Formation of a $Na_2SO_4-Eu_2(SO_4)_3$ solid solution does not seem to be a facile process. By a DTA measurement, some peaks are detected with no weight change, hence phase transformations were considered to occur. Therefore the two component system, $Na_2SO_4-Eu_2(SO_4)_3$, is not suitable for solid electrolytes.

The $Na_2SO_4-NaVO_3$ system

In the $Na_2SO_4-NaVO_3$ system, Na_2SO_4 doped with 2 mol% $NaVO_3$, 5 mol% $NaVO_3$, 7 mol% $NaVO_3$, and 10 mol% $NaVO_3$, where these mol% are initial concentrations of the dopant, were prepared. In all samples of Na_2SO_4 doped with $NaVO_3$, electrical conductivities are greatly lowered by the doping. A representative behavior is shown in Fig. 3. The structure of Na_2SO_4 is partially destroyed by doping of $NaVO_3$ because the volume of the VO_3^- anion is larger than that of SO_4^{2-}. Doping by $NaVO_3$ does not affect the electrical charge balance. The phases and thermal properties of $Na_2SO_4-NaVO_3$ are summarized in Table 2. From X-ray analysis, Na_2SO_4-V still remained in all samples and $NaVO_3$ remained in most samples except Na_2SO_4 doped with 2 mol% $NaVO_3$. These results are probably due to the low solubility of $NaVO_3$ in solid Na_2SO_4. By a DTA measurement, some peaks due to phase transformations are observed in all samples listed in Table 2. Electrical conductivities of the two-component system $Na_2SO_4-NaVO_3$ are very low. Doping of a third component to the $Na_2SO_4-NaVO_3$ system is necessary in order to improve electrical conductivities.

The three-component systems

The $Na_2SO_4-NaVO_3-Eu_2(SO_4)_3$ system

In the $Na_2SO_4-NaVO_3-Eu_2(SO_4)_3$ system, samples of Na_2SO_4 doped with 0.9 mol% $NaVO_3$ and 1.0 mol% $Eu_2(SO_4)_3$, 1.7 mol% $NaVO_3$ and 2.0 mol% $Eu_2(SO_4)_3$, 2.4 mol% $NaVO_3$

Can. J. Chem. Downloaded from www.nrcresearchpress.com by 210.87.254.105 on 09/06/12
For personal use only.

TABLE 3. The phases and thermal properties of the Na_2SO_4–$NaVO_3$–$Eu_2(SO_4)_3$ system

Na_2SO_4 (mol%)	$NaVO_3$ (mol%)	$Eu_2(SO_4)_3$ (mol%)	Phases[a]	DTA peaks[b] (K)
98.1	0.9	1.0	α	493
96.3	1.7	2.0	α	398, 458
94.6	2.4	3.0	β	573 (small)
93.2	2.8	4.0	β	—
91.0	4.0	5.0	β	—

[a] The α and β phases are similar to the Na_2SO_4-III and Na_2SO_4-I phases, respectively (15, 16). X-ray analyses were done at room temperature.
[b] Reproducibility of DTA temperature is within 5 K.

TABLE 4. The phases and thermal properties of the Na_2SO_4–$NaVO_3$–$Pr_2(SO_4)_3$ system

Na_2SO_4 (mol%)	$NaVO_3$ (mol%)	$Pr_2(SO_4)_3$ (mol%)	Phases[a]	DTA peaks[b] (K)
98.0	1.0	1.0	α	493
96.0	2.0	2.0	α	413
94.4	2.6	3.0	β	—
92.8	3.2	4.0	β	—
91.1	3.9	5.0	β	583 (very small)

[a] The α and β phases are similar to the Na_2SO_4-III and Na_2SO_4-I phases, respectively (15, 16). X-ray analyses were done at room temperature.
[b] Reproducibility of DTA temperature is within 8 K.

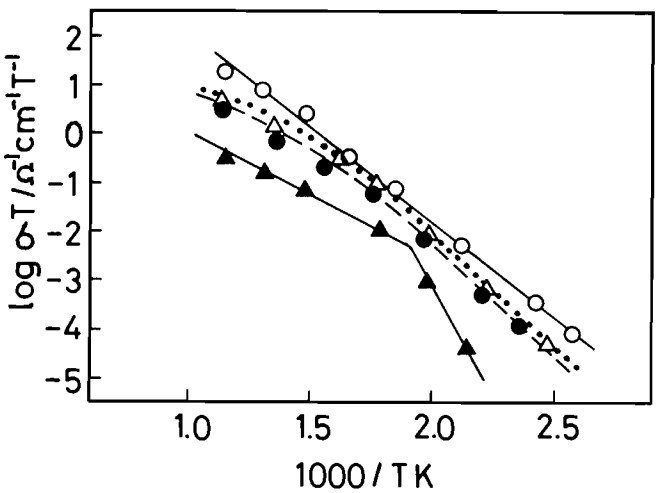

FIG. 4. Temperature dependences of electrical conductivities for the Na_2SO_4–$NaVO_3$–$Eu_2(SO_4)_3$ system which exhibit the β phase. –○– Na_2SO_4–$NaVO_3$–$Eu_2(SO_4)_3$ = 91.0:4.0:5.0; ·△· Na_2SO_4–$NaVO_3$–$Eu_2(SO_4)_3$ = 93.2:2.8:4.0; –●– Na_2SO_4–$NaVO_3$–$Eu_2(SO_4)_3$ = 94.6:2.4:3.0; –▲– Na_2SO_4.

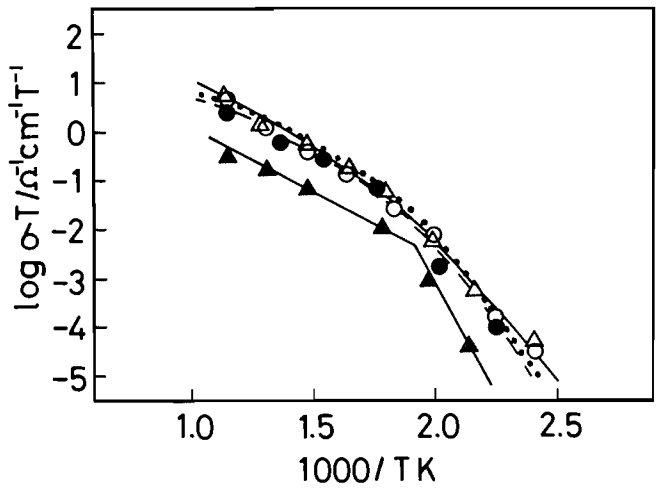

FIG. 5. Temperature dependences of electrical conductivities for the Na_2SO_4–$NaVO_3$–$Pr_2(SO_4)_3$ system which exhibit the β phase. –○– Na_2SO_4–$NaVO_3$–$Pr_2(SO_4)_3$ = 91.1:3.9:5.0; ·△· Na_2SO_4–$NaVO_3$–$Pr_2(SO_4)_3$ = 92.8:3.2:4.0; –●– Na_2SO_4–$NaVO_3$–$Pr_2(SO_4)_3$ = 94.4:2.6:3.0; –▲– Na_2SO_4.

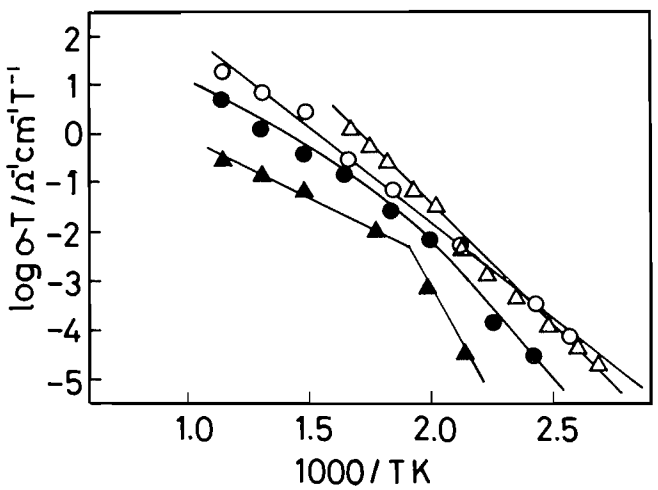

FIG. 6. Temperature dependences of electrical conductivities for Na_2SO_4, Na_2SO_4–$Eu_2(SO_4)_3$, and Na_2SO_4–$NaVO_3$–$Ln_2(SO_4)_3$ (Ln = Eu, Pr). –○– Na_2SO_4–$NaVO_3$–$Eu_2(SO_4)_3$ = 91.0:4.0:5.0; –●– Na_2SO_4–$NaVO_3$–$Pr_2(SO_4)_3$ = 91.1:3.9:5.0; –△– Na_2SO_4–$Eu_2(SO_4)_3$ = 95.9:4.1; –▲– Na_2SO_4.

and 3.0 mol% $Eu_2(SO_4)_3$, 2.8 mol% $NaVO_3$ and 4.0 mol% $Eu_2(SO_4)_3$, and 4.0 mol% $NaVO_3$ and 5.0 mol% $Eu_2(SO_4)_3$ were prepared. The phases and thermal properties are summarized in Table 3. From X-ray analysis, peaks due to the raw materials, $NaVO_3$ and $Eu_2(SO_4)_3$, have disappeared in all samples. The samples that showed the α phase are Na_2SO_4 doped with 0.9 mol% $NaVO_3$ and 1.0 mol% $Eu_2(SO_4)_3$, and 1.7 mol% $NaVO_3$ and 2.0 mol% $Eu_2(SO_4)_3$. The samples that exhibited the β phase are Na_2SO_4 doped with 2.4 mol% $NaVO_3$ and 3.0 mol% $Eu_2(SO_4)_3$, 2.8 mol% $NaVO_3$ and 4.0 mol% $Eu_2(SO_4)_3$, and 4.0 mol% $NaVO_3$ and 5.0 mol% $Eu_2(SO_4)_3$. The α and β phases are similar to the Na_2SO_4-III phase (15, 16) (a low temperature phase) and the Na_2SO_4-I phase (15, 16) (a high temperature phase), respectively. In a DTA measurement, the samples that exhibited the α phase show some endothermal peaks, due to phase transformations. On the other hand, the samples that exhibited the β phase show no endothermal peak, which means no phase transformation occurred. Therefore, the samples that exhibited the β phase in the Na_2SO_4–$NaVO_3$–$Eu_2(SO_4)_3$ system have potential as solid electrolytes for a SO_2 detector concentration cell. Electrical conductivities of the Na_2SO_4–$NaVO_3$–$Eu_2(SO_4)_3$ samples which exhibit the β phase are shown in Fig. 4. Compared with Na_2SO_4, the electrical conductivities increased about 1.0–2.0 orders of magnitude and the break in the log (σT) vs. $10^3/T$ relation disappeared. Electrical conductivities increased with increasing concentration of the dopants $NaVO_3$ and $Eu_2(SO_4)_3$, that is, the doping of $NaVO_3$ hardly influences the conductivity of the samples. The samples of Na_2SO_4–$NaVO_3$–$Eu_2(SO_4)_3$ which exhibited the β phase maintain the structure of the Na_2SO_4-I phase even at a relatively low temperature. Therefore, the electrical conductivities of this system at a low temperature are

Can. J. Chem. Downloaded from www.nrcresearchpress.com by 210.87.254.105 on 09/06/12
For personal use only.

Can. J. Chem. Downloaded from www.nrcresearchpress.com by 210.87.254.105 on 09/06/12
For personal use only.

much greater than those of Na_2SO_4.

The apparent activation energy for a sample of Na_2SO_4 doped with 4.0 mol% $NaVO_3$ and 5.0 mol% $Eu_2(SO_4)_3$, which is expected to be the best one of the five samples considered because its conductivity curve is almost linear without discontinuities, is 32 kJ/mol. This apparent activation energy, 32 kJ/mol, is smaller than 40 kJ/mol for Na_2SO_4 doped with 4.1 mol% $Eu_2(SO_4)_3$. The sample of Na_2SO_4 doped with 4.0 mol% $NaVO_3$ and 5.0 mol% $Eu_2(SO_4)_3$ having the Na_2SO_4-I (a high temperature phase) structure and a low apparent activation energy is considered to be a good solid electrolyte for a SO_2 detector concentration cell.

The Na_2SO_4–$NaVO_3$–$Pr_2(SO_4)_3$ system

In the system Na_2SO_4–$NaVO_3$–$Pr_2(SO_4)_3$, Na_2SO_4 doped with 1.0 mol% $NaVO_3$ and 1.0 mol% $Pr_2(SO_4)_3$, 2.0 mol% $NaVO_3$ and 2.0 mol% $Pr_2(SO_4)_3$, 2.6 mol% $NaVO_3$ and 3.0 mol% $Pr_2(SO_4)_3$, 3.2 mol% $NaVO_3$ and 4.0 mol% $Pr_2(SO_4)_3$, and 3.9 mol% $NaVO_3$ and 5.0 mol% $Pr_2(SO_4)_3$ were prepared. The phases and thermal properties are summarized in Table 4. From X-ray analysis, the raw materials $NaVO_3$ and $Pr_2(SO_4)_3$ were not detected in all samples. The samples doped with 1.0 mol% $NaVO_3$ and 1.0 mol% $Pr_2(SO_4)_3$, and 2.0 mol% $NaVO_3$ and 2.0 mol% $Pr_2(SO_4)_3$ showed the α phase. On the other hand, the samples doped with 2.6 mol% $NaVO_3$ and 3.0 mol% $Pr_2(SO_4)_3$, 3.2 mol% $NaVO_3$ and 4.0 mol% $Pr_2(SO_4)_3$, and 3.9 mol% $NaVO_3$ and 5.0 mol% $Pr_2(SO_4)_3$ exhibited the β phase. In a DTA measurement, the samples that exhibited the β phase show no endothermal peak (the sample Na_2SO_4 doped with 3.9 mol% $NaVO_3$ and 5.0 mol% $Pr_2(SO_4)_3$ shows a peak at 587 K, but very small), due to the fact that no phase transformation occurred. Therefore, the samples that exhibited the β phase in Na_2SO_4–$NaVO_3$–$Pr_2(SO_4)_3$ are also good ones for solid electrolytes. The electrical conductivities of Na_2SO_4–$NaVO_3$–$Pr_2(SO_4)_3$ samples which exhibit the β phase are shown in Fig. 5. Electrical conductivities increase about 1.5 orders of magnitude in comparison with Na_2SO_4 and there is no break in the conductivity curve. Cation vacancies increase by doping more $Pr_2(SO_4)_3$. On the other hand, electrical conductivities decrease by doping more $NaVO_3$. These effects cancel each other, the electrical conductivities having almost the same curve in these three samples. The samples of Na_2SO_4–$NaVO_3$–$Pr_2(SO_4)_3$ which exhibit the β phase also keep the structure of the Na_2SO_4-I phase even at a relatively low temperature. Therefore, the electrical conductivities at low temperature are much higher than those of Na_2SO_4.

The apparent activation energy for the sample of Na_2SO_4 doped with 3.9 mol% $NaVO_3$ and 5.0 mol% $Pr_2(SO_4)_3$ is 34 kJ/mol; this sample is considered to be the best one of the five considered, because its electrical conductivity curve is almost linear without discontinuities over the temperature range between 445 K and 769 K. The apparent activation energy, 34 kJ/mol, is smaller than 40 kJ/mol for Na_2SO_4 doped with 4.1 mol% $Eu_2(SO_4)_3$.

Electrical conductivities of Na_2SO_4–$NaVO_3$–$Ln_2(SO_4)_3$ (Ln = Eu, Pr) compared with Na_2SO_4–$Eu_2(SO_4)_3$ and Na_2SO_4 are shown in Fig. 6. By doping Na_2SO_4 with $Eu_2(SO_4)_3$, or $NaVO_3$ with $Ln_2(SO_4)_3$ (Ln = Eu, Pr) the log (σT) vs. $10^3/T$ plot shows an almost linear relationship although phase transformations still occur in the Na_2SO_4–$Eu_2(SO_4)_3$ system. Doping Na_2SO_4 prevents Na_2SO_4 from forming the Na_2SO_4-I phase because the volume of the VO_3^- anion is greater than that of SO_4^{2-}. On the other hand, by adding $Ln_2(SO_4)_3$ (Ln = Eu, Pr) to the Na_2SO_4–$NaVO_3$ system, the disadvantage that the volume of the VO_3^- anion is larger than that of the SO_4^{2-} is cancelled because the Ln^{3+} cation (Ln = Eu, Pr) radius is greater than that of the Na^+. As a result, the Na_2SO_4–$NaVO_3$–$Ln_2(SO_4)_3$ (Ln = Eu, Pr) system easily forms the high temperature Na_2SO_4-I phase. Lattice defects are increased by doping with Ln^{3+} (Ln = Eu, Pr). Therefore the electrical conductivities of Na_2SO_4–$NaVO_3$–$Ln_2(SO_4)_3$ (Ln = Eu, Pr) at relatively low temperatures increase compared with those of Na_2SO_4 and Na_2SO_4–$Eu_2(SO_4)_3$.

In the three-component systems, the apparent activation energy of Na_2SO_4 doped with 4.0 mol% $NaVO_3$ and 5.0 mol% $Eu_2(SO_4)_3$, $(Na_{0.86}Eu_{0.05}\square_{0.09})_2SO_4$ – 0.04 $NaVO_3$, 32 kJ/mol, is slightly smaller than that of Na_2SO_4 doped with 3.9 mol% $NaVO_3$ and 5.0 mol% $Pr_2(SO_4)_3$, $(Na_{0.86}Pr_{0.05}\square_{0.09})_2SO_4$ – 0.04 $NaVO_3$, 34 kJ/mol. Electrical conductivities of Na_2SO_4–$NaVO_3$–$Eu_2(SO_4)_3$ are higher than those of Na_2SO_4–$NaVO_3$–$Pr_2(SO_4)_3$. In both three-component systems, the concentration of cation vacancies is 0.09 and very close to 0.08 for Na_2SO_4 doped with 4.1 mol% $Eu_2(SO_4)_3$, which means that most of cation vacancies are able to act as sites for Na^+ ion migration. Therefore the concentration of cation vacancies is not a main factor for the difference in electrical properties. One reason for the difference in electrical conductivities and apparent activation energies for Na_2SO_4–$NaVO_3$–$Eu_2(SO_4)_3$ and Na_2SO_4–$NaVO_3$–$Pr_2(SO_4)_3$ comes from the difference of ionic radius between Eu^{3+} (0.126 nm) (32) and Pr^{3+} (0.132 nm) (32). Because the ionic radius of Na^+ (0.126 nm) (32) is closer to that of Eu^{3+} (0.126 nm) (32) rather than to that of Pr^{3+} (0.132 nm) (32), the Na_2SO_4–$NaVO_3$–$Eu_2(SO_4)_3$ system maintains the structure of the Na_2SO_4-I phase better than the Na_2SO_4–$NaVO_3$–$Pr_2(SO_4)_3$ system.

In the three-component systems, electrical conductivities are the highest and the apparent activation energies are the lowest of the present systems. The three-component systems of Na_2SO_4–$NaVO_3$–$Ln_2(SO_4)_3$ (Ln = Eu, Pr) are considered to be good solid electrolytes as a SO_2 detector concentration cell, especially at relatively low temperatures.

1. B. N. MEHROTRA, TH. HAHN, H. ARNOLD, and W. EYSEL. Acta Crystallogr. Sect. A, **31**, S79 (1975).
2. V. AMIRTHALINGAM, M. D. KARKHANAVALA, and U. R. K. RAO. Acta Crystallogr. Sect. A, **33**, 522 (1977).
3. H. FISCHMEISTER. Acta Crystallogr. Sect. A, **7**, 776 (1954).
4. A. G. NORD. Acta Crystallogr. Sect. A, **31**, S79 (1975).
5. F. C. KRACEK. J. Phys. Chem. **33**, 1281 (1929).
6. F. C. KRACEK and R. E. GIBSON. J. Phys. Chem. **33**, 1304 (1929).
7. F. C. KRACEK and R. E. GIBSON. J. Phys. Chem. **34**, 188 (1930).
8. F. C. KRACEK and C. L. KSANDA. J. Phys. Chem. **34**, 1741 (1930).
9. G. E. BRODALE and W. F. GIAUQUE. J. Phys. Chem. **76**, 737 (1972).
10. K. S. PITZER and L. V. COULTER. J. Am. Chem. Soc. **60**, 1310 (1938).
11. G. BRODALE and W. F. GIAUQUE. J. Am. Chem. Soc. **80**, 2042 (1958).
12. Q. R. GOYAL, V. V. DESHPANDE, and M. D. KARKHANAVALA. Indian J. Chem. **9**, 1006 (1971).
13. J. E. D. DAVIES and W. F. SANDFORD. J. Chem. Soc. Dalton Trans. 1912 (1975).
14. C. A. CODY, L. DICARLO, and R. K. DARLINGTON. J. Inorg. Nucl. Chem. **43**, 398 (1981).
15. E. L. KREIDL and I. SIMON. Nature, **181**, 1529 (1958).
16. Y. SAITO, K. KOBAYASHI, and T. MARUYAMA. Solid State Ionics, 393 (1981).

17. K. KOBAYASHI and Y. SAITO. Thermochim. Acta, **53**, 299 (1982).
18. R. M. MURRAY and E. A. SECCO. Can. J. Chem. **56**, 2616 (1978).
19. F. J. SALZANO and L. NEWMAN. J. Electrochem. Soc. **119**, 1273 (1972).
20. L. G. BOXALL and K. E. JOHNSON. J. Electrochem. Soc. **118**, 885 (1971).
21. K. T. JACOB and D. BHOGESWARA RAO. J. Electrochem. Soc. **126**, 1842 (1979).
22. M. GAUTHIER and A. CHAMBERLAND. J. Electrochem. Soc. **124**, 1579 (1977).
23. M. GAUTHIER, A. CHAMBERLAND, A. BÉLANGER, and M. POIRIER. J. Electrochem. Soc. **124**, 1584 (1977).
24. H. ARNOLD, W. KURTZ, A. RICHTER-ZINNIUS, J. BETHKE, and G. HEGER. Acta Crystallogr. Sect. B, **37**, 1643 (1981).
25. M. NATARAJAN and E. A. SECCO. Can. J. Chem. **53**, 1542 (1975).
26. H. H. HÖFER, W. EYSEL, and U. v. ALPEN. Mater. Res. Bull. **13**, 265 (1978).
27. H. H. HÖFER, W. EYSEL, and U. v. ALPEN. J. Solid State Chem. **36**, 365 (1981).
28. H. H. HÖFER, U. v. ALPEN, and W. EYSEL. Acta Crystallogr. Sect. A, **34**, S358 (1978).
29. K. L. KREESTER, W. EYSEL, and TH. HAHN. Acta Crystallogr. Sect. A, **31**, S79 (1975).
30. Y. SUZUKI, T. TAKAHASHI, and T. KOIZUMI. Nihon-Kagaku-Kaishi, 1701 (1975).
31. J. E. BAUERLE. J. Phys. Chem. Solids, **30**, 2657 (1969).
32. R. D. SHANNON. Acta Crystallogr. Sect. A, **32**, 751 (1976).

Can. J. Chem. Downloaded from www.nrcresearchpress.com by 210.87.254.105 on 09/06/12
For personal use only.

The crystal and molecular structures of 1,2,7,9-tetrathia-3,6,8,10-tetra-aza-cyclohept(*e*)indene, a novel tricyclic carbon–sulphur–nitrogen ring system

PENELOPE W. CODDING, HANS KOENIG, AND RICHARD T. OAKLEY[1]

Department of Chemistry, University of Calgary, Calgary, Alta., Canada T2N 1N4

Received October 25, 1982

PENELOPE W. CODDING, HANS KOENIG, and RICHARD T. OAKLEY. Can. J. Chem. **61**, 1562 (1983).

The crystal and molecular structures of 1,2,7,9-tetrathia-3,6,8,10-tetra-aza-cyclophept(*e*)indene, a novel carbon–sulphur–nitrogen heterocycle based on the phenazulene ring system, are reported. Crystals of the compound are orthorhombic, space group *Pbca*, a = 7.1334(8), b = 14.761(2), c = 16.677(2) Å, V = 1756.0(3) Å^3, Z = 8. The structure was solved by direct methods and refined by full-matrix least-squares procedures to a final R = 0.044 and R_w = 0.027. Molecules of the title compound consist of a five-membered C—S—S—N—C ring and a seven-membered C—N—S—N—S—N—C ring fused to a benzene ring. Internal structural parameters and the cell packing pattern suggest a dipolar charge distribution. The molecules are stacked in parallel planes in a head-to-tail fashion; the interplanar separation is 3.39 Å and the angle between the molecular planes and the *a* axis is 18°. The electronic spectrum of the molecule is discussed in relation to the perimeter model.

PENELOPE W. CODDING, HANS KOENIG et RICHARD T. OAKLEY. Can. J. Chem. **61**, 1562 (1983).

On rapporte la structure moléculaire et la structure cristalline du tétrathia-1,2,7,9 tétra-aza-3,6,8,10 cyclohept(*e*)indène, un nouvel hétérocycle, contenant le carbone, le soufre et l'azote, basé sur le système cyclique phénazulène. Les cristaux de ce composé sont orthorhombiques et appartiennent au groupe d'espace *Pbca* avec a = 7,1334(8), b = 14,761(2), c = 16,677(2) Å, V = 1756,0(3) Å^3, Z = 8. On a résolu la structure par les méthodes directes et on l'a affinée par la méthode des moindres carrés jusqu'à des valeurs de R = 0,044 et de R_w = 0,027. Les molécules du composé mentionné dans le titre comprennent un cycle à cinq chainons C—S—S—N—C et un cycle à sept chainons C—N—S—N—S—N—C condensés sur le cycle benzène. Les paramètres structuraux internes et le dessin de l'entassement moléculaire suggèrent une distribution de charge bipolaire. Les molécules sont entassées dans des plans parallèles en positions tête contre queue; la séparation des plans est de 3,39 Å et l'angle entre les plans moléculaires et l'axe *a* est de 18°. On discute du spectre électronique de la molécule en fonction du modèle du périmètre.

[Traduit par le journal]

Introduction

The unique electrical properties of $(CH)_x$ and $(SN)_x$ polymers (1) have demonstrated the potential applications of nonmetallic chemistry in the development of new conducting materials. The design and preparation of polymers and macrocycles featuring a combination of carbon–carbon and sulphur–nitrogen linkages thus represent an appealing challenge to synthetic chemists. Recently several such systems have been reported (2–6). In the course of our own work on the construction of heterocycles containing conjugated sulphur–nitrogen bonds (7) we have discovered the novel tricyclic molecule 1,2,7,9-tetrathia-3,6,8,10-tetra-aza-cyclohept(*e*)indene **1**, an inorganic analogue of the recently reported phenazulene ring system **2** (8). In the present paper we describe the crystal and molecular structures of **1**.

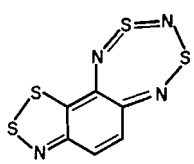

1

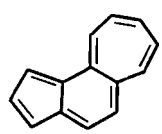

2

Experimental

Starting materials and general procedures

The bifunctional sulphur diimide $Me_3SiNSN(C_6H_4)NSNSiMe_3$ was prepared as recently described (4). Sulphur dichloride (Fisher) was distilled from phosphorus trichloride prior to use. Ultraviolet–visible spectra were recorded on a Cary 219 spectrophotometer. Chemical analyses were performed by MHW laboratories, Phoenix, Arizona.

[1]Author to whom correspondence may be addressed.

TABLE 1. Crystal data

Formula	$C_6H_2N_4S_4$
FW	258.37
Space group	*Pbca*
a (Å)	7.1334(8)
b (Å)	14.7610(19)
c (Å)	16.6770(16)
V (Å^3)	1756.0(3)
Z	8
D_c (g cm^{-3})	1.95
Crystal dimensions (mm)	0.29 × 0.09 × 0.09
Radiation	MoKα = 0.71069 Å graphite monochromator
Maximum θ (°)	25.0
Scan range (°)	$\Delta w = 1.5(0.6 + 0.347 \tan \theta)$
Unique reflections	1548
No. with $I > 3\sigma(I)$	775
μ (cm^{-1})	9.98

Preparation of $C_6H_2S_4N_4$, 1

A solution of $Me_3SiNSN(C_6H_4)NSNSiMe_3$ (1.00 g, 2.9 mmol) in 200 mL of methylene chloride was added dropwise over a 5 h period to a stirred solution of sulphur dichloride (0.30 g, 2.9 mmol) in 1200 mL of methylene chloride. After 24 h the mixture was filtered and the filtrate concentrated on a rotary evaporator to ~50 mL. This dark green/blue solution was eluted through a short 50-mm plug of silica and the dark blue solution so obtained evaporated to dryness. The bronze coloured residue was recrystallized from hot toluene to give metallic golden needles of $C_6H_2S_4N_4$, **1** (12 mg, 0.4 mmol, 1%), mp 254–257°C. Ultraviolet–visible (CH_2Cl_2) λ_{max} (log ε): 625(4.0), 582(4.0), 366(4.0), 342(4.0). *Anal.* calcd. for $C_6H_2S_4N_4$: C 27.91, H 0.78, N 21.71, S 49.61; found: C 28.13, H 1.06, N 21.43, S 49.36. *Mol. wt.* calcd. for $C_6H_2S_4N_4$: 257.9162; found: 257.9159.

Can. J. Chem. Downloaded from www.nrcresearchpress.com by 210.87.254.42 on 09/06/12
For personal use only.

Can. J. Chem. Downloaded from www.nrcresearchpress.com by 210.87.254.42 on 09/06/12
For personal use only.

TABLE 2. Atomic coordinates ($\times 10^4$), $U_{equivalent}$ ($\times 10^3$) for sulphur, nitrogen, and carbon atoms, and U_{iso} ($\times 10^3$) for the hydrogen atoms. $U_{equivalent}$ is $1/3 \sum_i U_{ii}$ of the diagonalized U_{ij} matrix

Atom	x/a	y/b	z/c	U_{eq}
S1	10005(2)	2773(1)	3828(1)	35
S2	9089(2)	1391(1)	5000(1)	36
S3	9396(2)	1793(1)	1416(1)	32
S4	8714(2)	866(1)	539(1)	38
N1	9568(7)	2171(3)	3090(2)	31
N2	9751(7)	2389(3)	4705(2)	35
N3	8591(7)	654(3)	4351(2)	31
N4	8152(7)	32(3)	1116(2)	36
C1	8273(8)	174(4)	1892(3)	26
C2	8865(8)	1052(3)	2170(3)	25
C3	9016(8)	1287(3)	2983(3)	23
C4	8580(8)	598(4)	3564(3)	24
C5	7980(8)	−275(4)	3256(3)	32
C6	7812(8)	−488(3)	2487(4)	31
H5*	7655	−744	3644	39
H6*	7397	−1081	2324	38

*The hydrogen atom parameters were not refined. U_{iso} was set to 1.2 × the U_{iso} of the atom to which they are bonded.

X-ray analysis

A needle shaped crystal of **1** was used for data collection on an Enraf Nonius CAD4F diffractometer. The crystallographic data are summarized in Table 1. After alignment of the crystal, 25 reflections were centered and indexed using the automatic routines of the instrument. The cell was identified as orthorhombic; this lattice assignment was confirmed and the space group determined by examination of the intensities measured during the data collection. Systematic absences of $(0kl)$, $k = 2n + 1$, $(h0l)$, $l = 2n + 1$, and $(hk0)$, $k = 2n + 1$ identified the space group as *Pbca*. Data were collected at room temperature using an $\omega/2\theta$ scan of 96 steps, of which the central 64 steps were taken as the peak, P, and the first and last 16 steps were taken as backgrounds, $B1$ and $B2$ so that $I = [P - 2(B1 + B2)]Q$, where Q was the scan rate. Lorentz and polarization corrections were applied and E values were calculated by applying a K-curve. No absorption correction was made.

Initial coordinates for all the sulphur, carbon, and nitrogen atoms of the molecule were obtained by direct methods (MULTAN 78 (9)) and refined by full-matrix least-squares techniques using isotropic thermal parameters to give residual indices of $R = \Sigma(||F_o| - |F_c||)/\Sigma|F_o| = 0.082$ and $R_w = (\Sigma w(|F_o| - |F_c|)^2/\Sigma wF_o^2)^{1/2} = 0.087$. After a refinement of anisotropic thermal parameters and coordinates, a difference Fourier synthesis revealed the positions of the two unique hydrogen atoms. They were included in the model at idealized positions (d(C—H) = 0.95 Å) with thermal parameters 20% greater than the isotropic thermal parameters of the C atoms to which they were bonded. The hydrogen atom parameters were not refined. The reflections included in the final refinement were observed reflections plus those unobserved data with I_c values greater than $3\sigma(I_o)$, i.e. a total of 1203 data. After convergence of the least-squares refinement with a maximum shift/error = 0.004, the residual indices for the 1203 reflections and the 127 variables were $R = 0.044$ and $R_w = 0.027$. The weights were defined as $(\sigma^2(F))^{-1}$ and the standard deviation of an observation of unit weight was 0.90. Atomic coordinates for the structure are given in Table 2. Table 3 provides intramolecular bond length and intervalence angle information.[2] All computations were done using the XRAY 76 system of programs (10) implemented on a Honeywell computer with a Multics operating system. Scattering factors were those of Cromer and Mann (11).

[2]The anisotropic thermal parameters (Table 4) and the table of observed and calculated structure amplitudes (Table 5) are available at a nominal charge from the Depository of Unpublished Data, CISTI, National Research Council of Canada, Ottawa, Ont., Canada K1A 0S2.

TABLE 3. Bond distances (Å) and angles (°). The estimated standard deviation in the last digit is in parenthesis

Atom	Distance	Atom	Angle
S1—N1	1.550(4)	N1—S1—N2	120.4(2)
S1—N2	1.579(4)		
S2—N2	1.624(4)	N2—S2—N3	119.0(2)
S2—N3	1.575(4)		
S3—S4	2.061(2)	C2—S3—S4	92.6(2)
S3—C2	1.708(5)		
S4—N4	1.614(5)	S3—S4—N4	98.1(2)
N1—C3	1.375(7)	C3—N1—S1	134.9(3)
		S1—N2—S2	129.8(3)
N3—C4	1.315(6)	S2—N3—C4	136.9(4)
N4—C1	1.315(7)	S4—N4—C1	116.7(4)
C1—C2	1.439(8)	N4—C1—C2	118.7(5)
C1—C6	1.431(8)	N4—C1—C6	123.9(5)
		C2—C1—C6	117.3(5)
C2—C3	1.403(7)	S3—C2—C1	113.9(4)
		S3—C2—C3	122.4(4)
		C1—C2—C3	123.7(5)
C3—C4	1.439(7)	N1—C3—C2	112.5(4)
		N1—C3—C4	130.1(4)
		C2—C3—C4	117.4(5)
C4—C5	1.452(8)	N3—C4—C3	128.9(5)
		N3—C4—C5	114.2(5)
		C3—C4—C5	116.8(4)
C5—C6	1.326(8)	C4—C5—C6	125.4(5)
		C5—C6—C1	119.2(5)

Results and discussion

Preparation of $C_6H_2S_4N_4$, 1

We have recently reported the reaction between *N*-phenyl-*N'*-trimethylsilyl sulphur diimide $PhNSNSiMe_3$ and sulphur dichloride, which yields the novel anti-aromatic 12π-electron heterocycle **3** (eq. [1]) (7). As a continuation of this work we have explored the reaction of the bifunctional *p*-phenylene derivative $Me_3SiNSN(C_6H_4)NSNSiMe_3$, **4**, with sulphur di-

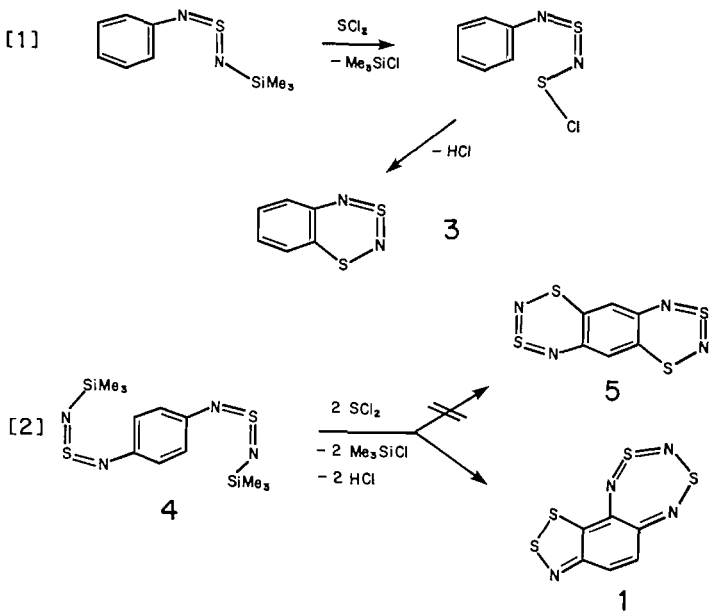

Can. J. Chem. Downloaded from www.nrcresearchpress.com by 210.87.254.42 on 09/06/12
For personal use only.

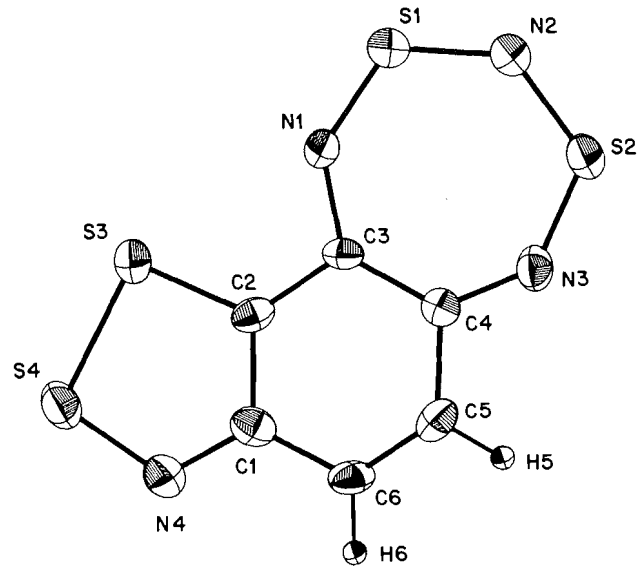

FIG. 1. An ORTEP drawing (50% probability ellipsoids) of the molecule, showing the atom numbering scheme. The hydrogen atoms are drawn as an arbitrary spheroid of 0.1 Å radius.

chloride (eq. [2]) with the intent of producing the tricyclic anthracene-like molecule **5**. It has already been shown that the principal product of this reaction (albeit with a different stoichiometry) is the polymer $(—SNSNC_6H_4NSN—)_x$ (4), but small amounts of a tractable compound are also formed. Chromatography of the reaction mixture reveals an intense blue component which, upon subsequent separation and crystallization, can be isolated as metallic gold needles with the empirical formula $C_6H_2S_4N_4$. Although this analysis is consistent with the anticipated product **5**, an X-ray crystal structure determination of the compound has revealed the novel phenazulene-like framework **1**. We have no immediate explanation for the formation of **1** rather than **5**; further studies on related electrophilic annelations may provide an answer.

Crystal, molecular, and electronic structures of 1

An ORTEP drawing of the molecule indicating the atom numbering scheme is shown in Fig. 1. As a whole the molecule is essentially planar (σ = 0.001 Å), the two largest deviations from the mean molecular plane occurring at S3(0.030 Å) and N1(0.027 Å). The slight buckling of the perimeter at these two sites probably reflects the rather short nonbonded contact S3---N1 (2.850(4) Å), which is considerably shorter than the sum of the van der Waals' radii for sulphur and nitrogen (3.35 Å) (12). The structural parameters within the rings (Table 3) point to a delocalized π-system whose ground state cannot be adequately represented by a single valence bond structure such as **1**. Other likely resonance contributors are **6** and **7**. Indeed the dipolar formulation **8** provides perhaps the most useful basis for describing the principal features of the molecular and crystal structures.

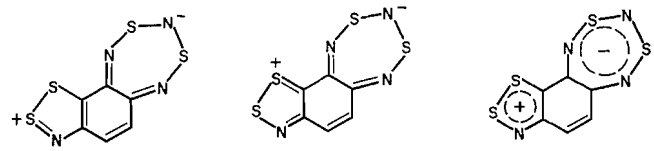

6 **7** **8**

According to **8** the molecule consists of a cyclic 5-atom

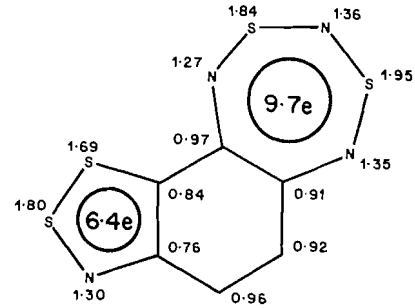

FIG. 2. Extended Hückel π-charge densities. Circled numbers represent total π-charge densities in the different rings.

6π-electron dithiazolium cation fused to a cyclic 7-atom 10π-electron $C_2S_2N_3^-$ anion by means of the C2—C3 bond. The strongly localized nature of the C5—C6 π-bond is reflected by its shortness (1.326 Å) relative to the other C—C bonds (range 1.403−1.425 Å) and the C—C distance in benzene (1.39 Å) (13). While the 5-membered C_2S_2N ring can be considered as a simple hybrid of the better-known dithiadiazolium **9** (14) and dithiolium **10** (15) cations, the latter 7-membered $C_2S_2N_3$ ring represents a novel structural unit in SN heterocyclic chemistry. If treated in isolation, e.g. **11**, the π-system of this anion can be viewed as isoelectronic with the thiotrithiazyl cation **12** (16). Consistently the mean SN distances in the $C_2S_2N_3$ ring of **1** closely resemble those found in $S_4N_3^+$ salts (17).

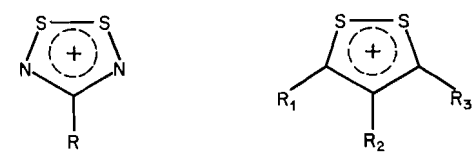

9 **10**

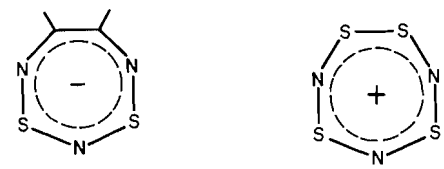

11 **12**

Extended Hückel (EH) molecular orbital calculations on a planar projection of **1** refine the valence bond picture and substantiate the charge distribution suggested by **8**. Thus, a summation of the EH π-charge densities over the nine occupied π-orbitals (Fig. 2) reveals a total π-charge density on the C_2S_2N and $C_2S_2N_3$ rings of 6.4 and 9.7 π-electrons respectively, i.e. there is a net π-charge transfer of about 0.6 electrons from the small to the large ring.

The arrangement of the molecules in the unit cell provides further evidence in favour of the dipolar representations **6**, **7**, and **8**. The molecules form stacks in the *a* direction, the packing being such that the five-membered C_2S_2N ring of one molecule lies approximately over the seven-membered ring of the molecule below it (see Fig. 3). This pattern repeats itself throughout the stack, producing an alternating sequence of molecules, i.e. the positively charged end of one molecule is

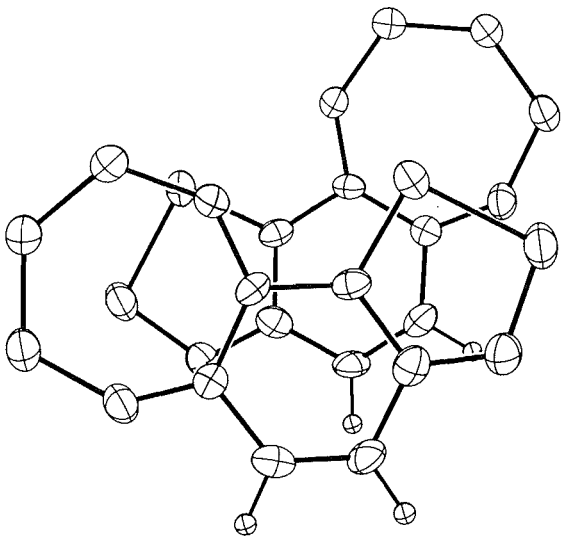

FIG. 3. Heat-to-tail packing of two molecules, viewed from a direction perpendicular to their mean planes.

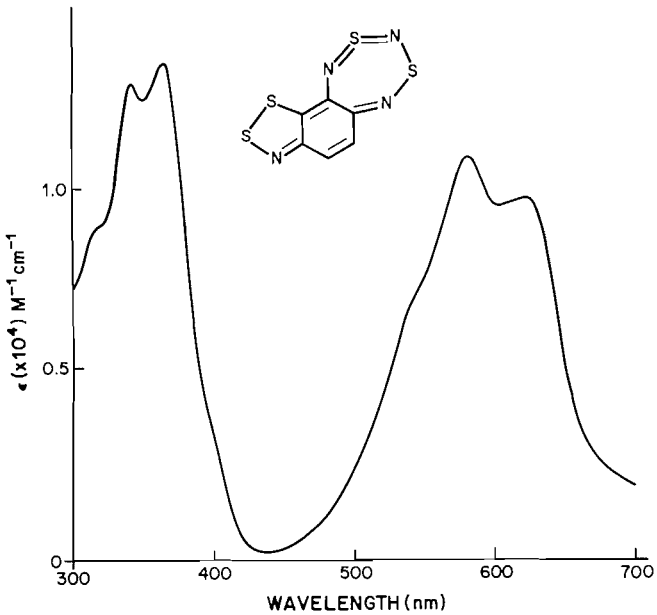

FIG. 4. Ultraviolet–visible spectrum of $C_6H_2S_4N_4$ (in CH_2Cl_2).

sandwiched between the negative ends of its two nearest neighbours, and vice versa. This head-to-tail mode of packing is typical of many $\pi-\pi^*$ donor–acceptor complexes (18); in the present case the structure represents a novel example of a self-complexing molecule (18, 19). The planes of consecutive molecules in the stack are parallel and make an angle of 18° with the *a* axis. The interplanar separation is uniformly 3.39 Å, i.e. there is no pairing of the molecules. The observed spacing is reminiscent of that found in naptho[1,8-*cd*:4,5-*c'd'*]bis-[1,2,6]thiadiazine (3.40 Å) (2*a*) and graphite (3.35–3.37 Å) (20).

While the structural evidence points to the possibility of intermolecular charge transfer interactions in the solid state, there are no indications of such phenomena in dilute solution. The colour of the compound in solution (deep blue) differs markedly from that in the solid state (metallic bronze), and the visible spectrum shows no deviations from the Beer–Lambert law. Indeed the appearance of the spectrum (Fig. 4) finds an appealing explanation through the use of the perimeter model (21, 22). Within the confines of this approximation, those cyclic π-electron systems which possess $4n + 2$ electrons inside their perimeters (regardless of cross-links or heteroatoms) will be characterized by four electronic transitions, generally referred to as L_1, L_2, B_1, and B_2 in order of increasing energy. In essence the four bands correspond to excitations from the two highest occupied π-levels of the perimeter to the two lowest unoccupied orbitals. In phenazulene, which is a 14π-electron perimeter, there appears to be a reasonable correlation between theory (23) and experiment (8). In the present case, where we have an 18π-electron system with low symmetry, all four transitions are expected to be allowed. It is therefore tempting to assign the observed bands to these four transitions. The absorptions visible as shoulders on the main bands may be evidence of vibronic coupling or second order excitations not dealt with by the simple theory. Detailed analysis of the MCD spectrum of the molecule would undoubtedly clarify the assignments.

Acknowledgments

We thank the Natural Sciences and Engineering Research Council of Canada, the Research Corporation, and the Alberta Heritage Foundation for Medical Research for financial support in the form of operating grants, a NSERC University Research Fellowship (to R.T.O.), an AHFMR Scholarship (to P.W.C.), and a NSERC Summer Undergraduate Scholarship (to H.K.).

1. M. M. LABES, P. LOVE, and L. F. NICHOLS. Chem. Rev. **79**, 1 (1979).
2. (*a*) R. C. HADDON, M. L. KAPLAN, and J. H. MARSHALL. J. Am. Chem. Soc. **100**, 1235 (1978); (*b*) A. GIEREN, V. LAMM, R. C. HADDON, and M. L. KAPLAN. J. Am. Chem. Soc. **101**, 7277 (1979); (*c*) J. P. BOUTIQUE, J. RIGA, J. J. VERBIST, J. DELHALLE, J. G. FRIPIAT, J. M. ANDRE, R. C. HADDON, and M. L. KAPLAN. J. Am. Chem. Soc. **104**, 2691 (1982).
3. (*a*) F. WUDL and E. T. ZELLERS. J. Am. Chem. Soc. **102**, 4284 (1980); (*b*) F. WUDL, E. T. ZELLERS, and D. NALEWAJEK. J. Org. Chem. **45**, 3211 (1980).
4. O. J. SCHERER, G. WOLMERSHAÜSER, and R. JOTTER. Z. Naturforsch. Teil B, **37**, 432 (1982).
5. I. ERNEST, W. HOLICK, G. RIHS, D. SCHOMBURG, G. SHOHAM, D. WENKERT, and R. B. WOODWARD. J. Am. Chem. Soc. **103**, 1540 (1981).
6. A. VEGAS, A. PEREZ-SALAZAR, A. J. BANISTER, and R. G. HEY. J. Chem. Soc. Dalton Trans. 1812 (1980).
7. J. KOENIG and R. T. OAKLEY. J. Chem. Soc. Chem. Commun. 73 (1983).
8. H. PRINZBACH, H. BINGMANN, A. BECK, D. HUNKLER, H. SAULER, and E. HÄDICKE. Chem. Ber. **114**, 1697 (1981).
9. P. MAIN, S. E. HULL, L. LESSINGER, M. M. WOLFSON, G. GERMAIN, and J.-P. DECLERCQ. MULTAN 78. A system of computer programs for the automatic solution of crystal structure from X-ray diffraction data. Universities of York, England and Louvain, Belgium. 1978.
10. J. M. STEWART. The X-ray system of crystallographic programs. Computer Science Center, University of Maryland, College Park, MD. 1976.
11. D. T. CROMER and J. B. MANN. Acta Crystallogr. Sect. A, **24**, 321 (1968).
12. L. PAULING. The nature of the chemical bond. 3rd ed. Cornell University Press, New York. 1960. p. 260.
13. E. G. COX, D. W. CRUICKSHANK, and J. A. S. SMITH. Proc. R. Soc. London, Ser. A., **247**, 1 (1958).
14. O. ANDREASEN, A. C. HAZELL, and R. G. HAZELL. Acta Crystallogr. Sect. B, **33**, 1109 (1977).

Can. J. Chem. Downloaded from www.nrcresearchpress.com by 210.87.254.42 on 09/06/12
For personal use only.

15. C. TH. PEDERSEN. Sulphur Rep. **1**, 1 (1980).
16. J. W. WALUK and J. MICHL. Inorg. Chem. **21**, 556 (1982).
17. (*a*) J. WEISS. Z. Anorg. Allg. Chem. **333**, 314 (1964); (*b*) A. W. CORDES, R. F. KRUH, and E. R. GORDON. Inorg. Chem. **4**, 681 (1965); (*c*) G. MOSS, T. N. GURU ROW, and P. COPPENS. Inorg. Chem. **19**, 2396 (1980); (*d*) J. J. MAYERLE, G. WOLMERSHAÜSER, and G. B. STREET. Inorg. Chem. **18**, 1161 (1979).
18. F. H. HERBSTEIN. Perspect. Struct. Chem. **4**, 166 (1971).
19. C. K. PROUT and E. E. CASTELLANO. J. Chem. Soc. A, 2775 (1970).
20. (*a*) P. L. WALKER and G. IMPERIAL. Nature, **180**, 1184 (1957); (*b*) J. B. NELSON and D. P. RILEY. Proc. Phys. Soc. London, **57**, 477 (1945).
21. J. R. PLATT. J. Chem. Phys. **17**, 484 (1949).
22. J. MICHL. J. Am. Chem. Soc. **100**, 6812 (1978), and following papers.
23. R. ZAHRADNIK, J. MICHL, and J. KOPECKY. Collect. Czech. Chem. Commun. **31**, 640 (1966).

Can. J. Chem. Downloaded from www.nrcresearchpress.com by 210.87.254.42 on 09/06/12
For personal use only.

Nonadditive effects of polysubstitution in CH_4 and CH_3: a test of *ab initio* and semiempirical MO methods

N. COLIN BAIRD

Department of Chemistry, University of Western Ontario, London, Ont., Canada N6A 5B7

Received November 18, 1982

N. COLIN BAIRD. Can. J. Chem. **61**, 1567 (1983).

The effects to the bond lengths and molecular energy of making multiple substitutions at the same carbon atom in methane and the methyl free radical are studied using various molecular orbital methods. All *ab initio* calculations were based upon the Hartree–Fock formalism (unrestricted in the case of free radicals) and employed the STO-3G (with *d* orbitals on chlorine), 3-21G, and 4-31G bases, the last both with and without a set of Gaussian *d* orbitals on the carbon. The semiempirical methods used were the MINDO/3 and MNDO methods of Dewar and co-workers; computations for polysubstituted ethanes by these two methods also are reported. The *ab inito* methods which use a split valence shell basis set account very well for the trends in bond lengths and heats of formation, at least when the polysubstituent is fluorine or hydroxyl. In contrast, the semiempirical calculations and the *ab initio* STO-3G results gave very poor results. Finally, the role of interactions between the AH bonds in a variety of hydrides AH_n is illustrated using experimental energetics.

N. COLIN BAIRD. Can. J. Chem. **61**, 1567 (1983).

Faisant appel à différentes méthodes de calcul d'orbitales moléculaires, on a étudié les effets des substitutions multiples au niveau du même atome de carbone du méthane et du radical libre méthyle, sur les longueurs de liaison et sur l'énergie moléculaire. Les calculs *ab initio* reposent tous sur le formalisme de Hartree–Fock (sans restriction dans le cas des radicaux libres) et utilisent les bases: STO-3G (avec les orbitales *d* du chlore), 3-21G et 4-31G. Les deux dernières sont utilisées avec ou sans l'ensemble d'orbitales *d* de gauss du carbone. On a utilisé les méthodes semi-empiriques telles le MINDO/3 et le MNDO de Dewar et de ses collaborateurs. On rapporte également les calculs effectués par ces deux méthodes sur les éthanes polysubstitués. Les méthodes *ab inito* qui impliquent l'ensemble de base de la couche de valence dédoublée rendent très bien compte des tendances des longueurs de liaison et des chaleurs de formation lorsque le polysubstituant est au moins le fluor ou l'hydroxyle. Les calculs semi-empiriques et les résultats *ab initio* du STO-3G donnent au contraire de très faibles résultats. Finalement on illustre le rôle des interactions entre les liaisons AH de divers hydrures AH_n en utilisant l'énergétique expérimentale.

[Traduit par le journal]

Can. J. Chem. Downloaded from www.nrcresearchpress.com by 210.87.254.42 on 09/06/12
For personal use only.

Introduction

For many purposes, polyatomic molecules can be profitably considered to be systems containing noninteracting two-centre bonds. However, the interaction between bonds, especially if they are equivalent, can have important ramifications to physical properties (e.g. the stability and geometry of conjugated hydrocarbons) and to chemical behavior (e.g. in reactions subject to orbital symmetry control).

The rather peculiar behavior of hydrocarbons which contain multiple substitution at the same carbon by highly-electronegative substituents has been long recognized. The most famous examples are the various fluorinated methanes, whose unusual characteristics have traditionally been attributed to resonance among valence-bond structures involving doubly-bonded fluorine; e.g.

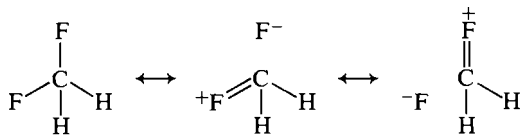

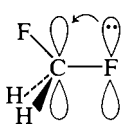

From an analysis using molecular oribtal theory (1) of disubstituted molecules XCH_2Y, it has been suggested that one of the principal stabilizing interactions in such systems is back-bonding from fluorine to carbon via donation of electron density from a p_π lone pair on one fluorine into the antibonding σ^*_{CF} orbital associated with the second fluorine and which lies in the same plane as the lone pair. The other stabilizing factor, which evidently is more important with weak π donors and strong σ acceptors such as fluorine, is the bond strengthening which results from a depletion of electron density about the carbon.

Our interest in the present report is not so much to investigate the origin of the polysubstitution effects; rather it is to survey common calculational procedures in order to discover which are reliable in quantitatively reproducing the nonadditive energetic and geometric effects associated with multiple substitution. For the *ab initio* methods, we wish to determine whether these effects lie within the Hartree–Fock framework, and if so what is the minimum size of basis set that should be used. Some testing of *ab initio* MO methods in their handling of the energetic effects of polysubstitution has been reported by Pople and by Radom and their co-workers (1*a*–*d*). Here we extend and generalize their analysis, making use of published and archival results (1) as well as some new calculations. Similarly Dewar and co-workers have already made some comments regarding the behavior of the MNDO and MINDO/3 methods in reproducing nonadditive effects in the fluoromethanes (2), and here we incorporate and extend their analysis.

Method of calculation

All new *ab initio* MO calculations reported herein were obtained using the GAUSSIAN-76 program (3) on a CDC Cyber 73 computer. The basis sets for the *s* and *p* orbitals correspond to the expansions of Pople and co-workers and use their standard molecular scaling factors (4*a*, *b*, *c*). In some of the 4-31G calculations (as noted in text) a set of six Gaussian *d* orbitals, each of exponent 0.80 (4*d*), was added to the central

TABLE 1. CF bond lengths (Å) in fluoromethanes (relative to CH_3F)

Species	Experimental[a]	*Ab initio* calculation[b] via STO-3G	3-21G	4-31G	4-31G*(C)	Semi-empirical calculations MNDO	MINDO/3
CF_4	−0.060	−0.018	−0.079	-0.06_3	-0.06_7	0.000	−0.070
CHF_3	−0.051	−0.013	−0.058	-0.04_8	-0.05_3	+0.006	−0.060
CH_2F_2	−0.026	−0.007	−0.031	-0.02_5	-0.03_0	+0.003	−0.037
CH_3F	0	0	0	0	0	0	0

[a]Experimental values of r_{CF} are 1.383 Å for CH_3F from ref. 13, 1.357 Å for CH_2F_2 from ref. 14, 1.332 Å for CHF_3 from ref. 15, and 1.323 Å for CF_4 from ref. 16.

[b]The STO-3G and 3-21G results all are based upon calculations reported in ref. 1*e*; the 4-31G and 4-31G*(C) results are based upon new optimizations. The bond angles used in the calculations with *d* orbitals are those found to be optimum without any *d*. Details of the results are given in Table D-1.

TABLE 2. MNDO bond lengths (Å) in fluoroethanes

Molecule A—B	CF length In Group A	CF length In Group B	CC length
CF_3—CF_3	1.345	1.345	1.683
—CHF_2	1.350	1.344	1.659
—CH_2F	1.354	1.344	1.623
—CH_3	1.358	—	1.588
CHF_2—CF_3	1.344	1.350	1.659
—CHF_2	1.349	1.349	1.642
—CH_2F	1.353	1.349	1.605
—CH_3	1.357	—	1.572
CH_2F—CF_3	1.344	1.354	1.623
—CHF_2	1.349	1.353	1.605
—CH_2F	1.350	1.350	1.578
—CH_3	1.353	—	1.550
CH_3—CF_3	—	1.358	1.588
—CHF_2	—	1.357	1.571
—CH_2F	—	1.353	1.550
—CH_3	—	—	1.521

carbon atom; this basis set is denoted in the text as 4-31G*(C). The STO-3G* basis for chlorine employs five *d* orbitals,[1] with standard exponent (3*c*). All results were obtained using the Hartree–Fock procedure, unrestricted in the case of open shell species. The conformations assumed in $CH_2(OH)_2$ and $CH(OH)_3$ were the idealizations found optimum in previous calculations for these molecules (1*b*, *c*). Fuller details concerning the results of the calculations reported here for the first time are given in Tables D-1 to D-5.[2]

All new MINDO/3 (5*a*) and MNDO calculations were obtained using the MINDO/3 (5*a*) and MNDOC (5*b*) computer programs on a CDC Cyber 170-835 computer.

Results and discussion

One striking effect of multiple fluorine substitution at the same carbon is the progressive contraction of the CF bond lengths. Each substitution of F for H in methane shortens all the carbon–fluorine bonds. The overall effect amounts to 0.06 Å in going from CH_3F to CF_4, i.e. about one-third the difference between single and double bonds formed by carbon with other elements of the same row.

The changes in the CF bond lengths in the polyfluoromethanes, relative to that computed for CH_3F, are given in Table 1 for *ab initio* calculations by the STO-3G, 3-21G, 4-31G, and 4-31G*(C) (i.e., with *d* orbitals on carbon) basis sets, for semiempirical MO calculations by the MNDO and MINDO/3 methods (2, 6) as are experimental values.

All *ab initio* calculations predict the correct qualitative trend, i.e. that CF distances progressively decrease with each additional substitution of fluorine for hydrogen, from CH_3F to CF_4. However, the STO-3G basis greatly underestimates the magnitude of the contractions, the overall decrease being only 0.018 Å compared to the observed 0.06 Å. The split valence-shell orbital bases, with or without *d* orbitals on carbon, account very well for the contractions, the overall decreases being 0.079 Å, 0.06_3 Å, and 0.06_7 Å by 3-21G, 4-31G, and 4-31G*(C), respectively. (The effect of the *d* orbitals is to contract all the CF lengths by about the same amount, $0.03_5 \pm 0.00_3$ Å.)

The MINDO/3 method also reproduces very well the experimental trend in CF bond lengths. However, the MNDO method fails completely in this regard, since it predicts small *increases* in CF length from CH_3F to CH_2F_2 and to CHF_3. (Both results were noted by Dewar and co-workers (2).) To investigate the generality of these trends, we have obtained optimum MNDO and MINDO/3 geometries for the various polyfluoroethane series, i.e. $CH_3CH_{3-n}F_n$, $CH_2FCH_{3-n}F_n$, $CHF_2CH_{3-n}F_n$, and $CF_3CH_{3-n}F_n$. For the CH_2F—R units, a decrease of 0.004 Å is predicted to occur whenever the number of F atoms within the R group is increased by one. Similar, though somewhat less constant, increases occur within the CHF_2—R and CF_3—R groups (see Table 2). Clearly, then, the MNDO method predicts that CF lengths undergo some contraction due to changes in the inductive effect of the groups bonded to the carbon. However, if the results in Table 2 are reconsidered from the viewpoint of variations in R_{CF} due to a change in the number of fluorine atoms bonded to that same carbon, virtually no changes (within ±0.002) occur. This experience is consistent with the behavior of the fluoromethane series. Experimentally, few results are available but it is clear that large contractions, of the order of 0.06–0.07 Å do occur in going from CH_2FCH_2F to CF_3CH_3 and CF_3CF_3 respectively (2), in contrast to the small MNDO predicted changes of −0.002 Å and 0.010 Å, respectively.

Interestingly, the MNDO calculations predict large changes in the CC bond length in the polyfluoromethanes as the number

[1]As a referee has pointed out, such a basis for chlorine is unsaturated with respect to *s* and *p* orbitals, and the *d* orbitals will not act exclusively as polarization functions. However Pople and co-workers have successfully used this basis (3*c*).

[2]Complete set of data is available at a nominal charge, upon request, from the Depository of Unpublished Data, CISTI, National Research Council of Canada, Ottawa, Ont., Canada K1A 0S2.

Can. J. Chem. Downloaded from www.nrcresearchpress.com by 210.87.254.42 on 09/06/12
For personal use only.

TABLE 3. CF bond lengths (Å) in fluoromethyl radicals (relative to CH_2F)

Species	Experimental	STO-3G[a]	3-21G[a]	4-31G[b]	4-31G*[(C)]	MNDO	MINDO/3
CF_3	—	+0.002	−0.038	−0.042	−0.030	$+0.00_8$	-0.02_4
CHF_2	—	0.000	—	−0.023	-0.01_6	$+0.00_5$	-0.02_5
CH_2F	0	0	0	0	0	0	0

[a]From ref. 1c.
[b]From ref. 17.

TABLE 4. Relative CCl bond lengths (Å) in chloromethanes and chloromethyl radicals

Species	Experimental[a]	STO-3G[b]	3-21G[b]	4-31G	STO-3G*[(C)]	MNDO	MINDO/3
CCl_4	−0.016	+0.013	−0.060	-0.3_0	—	-0.01_3	$+0.00_8$
$CHCl_3$	−0.018	+0.003	−0.057	-0.02_5	—	-0.01_3	-0.00_1
CH_2Cl_2	−0.004	−0.001	−0.039	-0.01_4	$+0.00_2$	-0.00_0	-0.00_3
CH_3Cl	0	0	0	0	0	0	0
CCl_3	—	—	—	—	—	-0.00_6	$+0.02_7$
$CHCl_2$	—	—	—	$+0.00_3$	-0.00_8	-0.00_7	$+0.01_7$
CH_2Cl	—	0	0	0	0	0	0

[a]See Table III of M. J. S. Dewar and H. S. Rzepa, to be published.
[b]From ref. 1e.

of fluorines is varied (Table 2). Elongations of about 0.03, 0.03, 0.02, and 0.02 Å within the CF_3—R, CHF_2—R, CH_2F—R, and CH_3—R series, respectively, occur for each substitution of H by F within the R group. Overall, from CH_3CH_3 to CF_3CF_3, a total elongation of 0.16 Å is predicted; experimentally (2) the increase is much smaller ($\sim 0.02_4$ Å). Presumably the increase is due to increasing population of the C—C antibonding MO by electron donation from the fluorines.

Comparisons of bond lengths predicted by MINDO/3 were hampered by the tendency, previously noted by Dewar *et al.* (2) for the method to predict (incorrectly) π-complexes of F_2 with ethylenes for polyfluorinated ethanes. In the present case, this occurred for staggered conformations of CF_3CH_2F, CF_3CHF_2, and CHF_2CHF_2. In the only remaining complete series, i.e. $CH_3CH_{3-n}F_n$, decreases of 0.03_1 Å and 0.02_7 Å are predicted by going from $n = 1-2$, and $n = 2-3$, respectively.

The CF bond is predicted by all split valence-shell *ab initio* calculations to undergo contraction in the fluoromethyl free radical series (Table 3). Again the minimal STO-3G basis set predicts essentially no effect, as does the semiempirical MNDO method. The MINDO/3 results predict a contraction from CH_2F to CHF_2, but no change from the latter to CF_3.

A contraction in the carbon−chlorine bond lengths is found experimentally to occur in going from CH_3Cl to CH_2Cl_2 and again from CH_2Cl_2 to $CHCl_3$; these changes, however, are much smaller than those in the corresponding fluorocarbons. Again contractions in the carbon−halogen distance are not predicted by STO-3G calculations, even with the addition of *d* orbitals on chlorine (Table 4). However, the 4-31G basis set calculations again reproduces the changes very well, whereas 3-21G predicts as large values as are obtained for the fluoromethanes. Experimentally, the C—Cl length does not change significantly from $CHCl_3$ to CCl_4 (see Table 4); this is correctly predicted by the split valence shell calculations. Curiously the MNDO method, which failed completely for fluoromethanes, does very well in accounting for the C—Cl bond length changes in the chloromethanes (Table 4). It also predicts a contraction of −0.008 (−0.022 Å experimental) in going from CH_3CH_2Cl to CH_3CHCl_2, and −0.003 (+0.005 Å) from the latter to CH_3CCl_3. The bond length changes predicted for the chloromethyl radicals are small (Table 4).

The carbon−oxygen and oxygen−hydrogen bond lengths, and the COH angles, in methanol and in methanediol also were optimized using the 4-31G basis with *d* orbitals on carbon. A contraction in R_{CO} of 0.01_6 Å is predicted from CH_3OH to $CH_2(OH)_2$, which is somewhat less than the decrease of 0.021 Å obtained in 4-31G calculations (7).

The nonadditive energetic effects of multiple substitution have traditionally been gleaned from experimental thermochemical heats of formation, ΔH_f, of a series of molecules, e.g. CH_4, CH_3X, ... CX_4. If the bond energies in such molecules remain exactly constant from one member to another, the increment $\Delta\Delta H_f$ in the heat of formation upon substitution of H by X will be a constant. Conversely, any changes $\Delta\Delta\Delta H_f$ to the increment are a direct measure of the nonadditivity of bond energies. The same information can be obtained from $\Delta\Delta E$, the change to the increment in total energy E computed for a molecule.

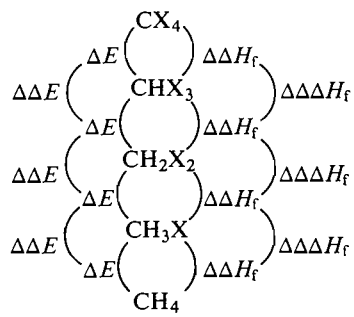

We have computed $\Delta\Delta\Delta H_f$ and $\Delta\Delta E$ values for the fluorinated, chlorinated, and hydroxylated methanes and for the fluorinated and chlorinated methyl radicals from experimental heats of formation (where available), calculated ΔH_f's for the MNDO and MINDO/3 methods, and calculated *ab initio* E's for the various basis sets; the results are listed in Table 5. To save space, the $\Delta\Delta\Delta H_f$ or $\Delta\Delta E$ value is listed for the common member of the two series concerned; e.g. the $\Delta\Delta\Delta H_f$ calcu-

Can. J. Chem. Downloaded from www.nrcresearchpress.com by 210.87.254.42 on 09/06/12
For personal use only.

TABLE 5. Nonadditive energetics[a] (in kcal mol^{-1}) for substituted methanes and methyl radicals

		$\Delta\Delta E$ calculated via					
CH_nX_{m-n}	$\Delta\Delta\Delta H_f$[b]	STO-3G	3-21G	4-31G	4-31G*(C)	MNDO	MINDO/3
CH_3F	14.1	22.9	13.9	9.8	12.7	1.8	9.9
CH_2F_2	6.7	8.8	9.7	5.5	8.2	1.4	5.0
CHF_3	−2.5	5.2	1.2	−3.0	−0.8	−1.8	−2.7
CH_2F	9.6[c]	6.9	—	7.2	10.2	−4.1	19.4
CHF_2	1.4[c]	4.8	—	1.5	3.7	−7.3	2.1
CH_3OH	15.4[d][13.1]	11.2	17.4	—	16.1	5.5	0.7
$CH_2(OH)_2$	−[7.8]	—	—	—	4.4	0.8	−0.8[f]
$CH(OH)_3$	−[1.4]	—	—	—	—	3.1	−12.6
CH_3Cl	1.5[e]	−3.8 −0.7 (d_{Cl})	−7.2	−5.4	—	−5.2	−2.0
CH_2Cl_2	−1.3[e]	−3.3	−4.7	−4.6	—	−4.5	−3.6
$CHCl_3$	−4.2[e]	−3.0	−3.7	−4.3	—	−4.5	−4.9
CH_2Cl	+0.3	−0.8	−4.7	—	—	7.6	−1.3
$CHCl_2$	0.0	—	—	—	—	−7.2	0.5

[a]The $\Delta\Delta E$ value for a species CH_nX_{m-n} is the ΔE for the reaction

$$2\ CH_nX_{m-n} \rightarrow CH_{n+1}X_{m-n-1} + CH_{n-1}X_{m-n+1}$$

where $m = 4$ for closed-shells and $m = 3$ for free radicals. The $\Delta\Delta\Delta H_f$ value for a species CH_nX_{m-n} is $-\Delta H°$ (at 298 K) for the same reaction.

[b]Calculated from data in ref. 9 unless indicated otherwise.

[c]Calculated from data in ref. 11.

[d]Calculated from data in ref. 8; see also Discussion in text.

[e]Calculated using ΔH_f of −19.6 and −22.8 kcal for CH_3Cl and CH_2Cl_2 respectively from ref. 8, and of −24.7 and −22.4 for $CHCl_3$ and CCl_4 respectively both from ref. 18.

[f]Calculated using non-optimized geometry for $CH(OH)_3$; see Table D-3 for details.

lated from the $\Delta\Delta H_f$ values for CH_2X_2 and CH_3X and for CH_3X and CH_4 is listed as the entry for CH_3X. For this particular case, our $\Delta\Delta E$ parameter is identical to the bond separation energy term defined by Pople and co-workers (1).

In each of the series of substituted methanes and methyl radicals, the experimental $\Delta\Delta\Delta H_f$ values are positive for CH_3X or CH_2X and decrease continuously with successive substitution for X = F or OH. This behavior implies that although the interaction of such C—X bonds with each other is more stabilizing than those of C—H bonds with each other, the magnitude of each bond−bond interaction decreases with increasing substitution. Qualitatively, this behavior is reproduced by *ab initio* calculations using any of the basis sets. Those computed using STO-3G, however, clearly are unreliable (Table 5). The results from the 3-21G and 4-31G basis sets are very good for the fluoromethanes, and give some hope that with minor improvement essentially quantitative results can be obtained. It was for this reason that we tried adding *d* orbitals to the central carbon with the 4-31G basis. These results, labelled 4-31G*(C) for the fluoromethanes, the fluoromethyl radicals, and for the hydroxymethanes (where available) agree almost exactly with experiment (rms error = 1.6 kcal). From these results it can be concluded that changes in correlation energy must make only negligible contributions to energy nonadditivity in such molecules.

Since the $\Delta\Delta E$ values using the 4-31G*(C) basis appear reliable, they can be combined with experimental heats of formation for lesser-substituted compounds to obtain ΔH_f values for more highly-substituted members of the same series. Thus the $\Delta\Delta E$ of +16.1 kcal can be combined with the known heats of formation of −17.9 and −48.1 for methane and methanol to yield an extrapolated ΔH_f of −94.4 kcal for methanediol, in good agreement with the estimate (?) of −93.5 given by Benson (8). Similarly the ΔH_f of methanetriol is estimated to be −145.1 kcal mol^{-1}. Interestingly, the $\Delta\Delta H_f$ values (9) for the $CH_n(OCH_3)_{4-n}$ series are 13.1, 7.8, and −1.4 kcal mol^{-1}. If the $\Delta\Delta E$ value for $CH(OH)_3$ is indeed approximately +2 kcal, the extrapolated ΔH_f for $C(OH)_4$ is about −198 kcal.

The $\Delta\Delta E$ (and $\Delta\Delta\Delta H_f$) values can be combined to yield the total stabilization energy due to all bond interactions and the energy per bond−bond interaction. For CH_2F_2, CHF_3, and CF_4 the totals are 12.7 (14.2), 33.6 (34.4), and 53.7 (53.6) kcal mol^{-1} respectively from the 413-G*(C) (and experimental) results; the energy per interaction decreases along the series, from 12.7 (14.2) to 11.2 (11.5) to 8.9 (8.9) kcal. The 4-31G*(C) interaction per bond pair decreases from 16.1 in $CH_2(OH)_2$ to 12.2 kcal in $CH(OH)_3$. A decrease in the effectiveness of each interaction as the number of participating substituents increases is expected to the extent that hyperconjugation and simple delocalization contribute significantly to the overall change.

In the case of the methane molecule, multiple substitution of hydrogen by chlorine is predicted to involve nonadditive energy effects which are slightly destabilizing, rather than stabilizing as in the case for multiple F or OH substitution; the effect amounts to about 5 kcal per substitution. In other words, the interaction of C—H bonds with C—Cl and with other C—Hs is predicted to be slightly more powerful than of C—Cl bonds with each other. Experimentally the destabilizing effects of multiple substitution are observed in the transition from CH_2Cl_2 to $CHCl_3$ to CCl_4, but not earlier in the series (see $\Delta\Delta\Delta H_f$ values in Table 5). If the $\Delta\Delta E$ values for the chloromethanes behave as do those for the fluoromethanes and fluoromethyl radicals, addition of *d* orbitals to the carbon atom will make the 4-31G results less negative by approximately 2.5 kcal each. Even so, the theoretical calculations predict some destabilization upon each multiple chlorine substitution. In-

Can. J. Chem. Downloaded from www.nrcresearchpress.com by 210.87.254.42 on 09/06/12
For personal use only.

TABLE 6. Relative bond dissociation energies in substituted methanes

Bond	Dissociation energy (in kcal mole^{-1}) via				
	Experimental[a]	STO-3G[b]	3-21G	4-31G	4-31G*[(C)]
H—CH_3	(0)	(0)	(0)	(0)	(0)
H—CH_2F	−3	−9.8	−3.2[d]	−1.7	−2.4
H—CHF_2	−3	−16.1	—	−0.7	−2.4
H—CF_3	+2	−19.1	—	+4.3	+2.1
H—CH_2Cl	−3	−8.4	—	0.0	—
H—$CHCl_2$	−5	−16.6	—	−0.8	—
H—CH_2OH	−10, −8[c]	−10.5[d]	−5.5[d]	−6.2[c]	—
H—CH_2NH_2	−9, −10[c]	−9.8[d]	−9.8[d]	−8.9[c]	—
H—CH_2CH_3	−6	−4.2[d]	−2.5[d]	−3.3[c]	—
F—CH_3	(0)	(0)	(0)	(0)	(0)
F—CH_2F	+10	+0.3	+10.8[d]	+8.2	+10.2
F—CHF_2	+17	+2.8	—	+14.6	+18.4
F—CF_3	+22	+5.1	—	+16.6	+22.1

[a]Unless indicated otherwise, from ref. 11.
[b]With *d* orbitals on chlorine (i.e. STO-3G*) for H—CH_2Cl and H—$CHCl_2$.
[c]From ref. 19.
[d]Deduced from data given in ref. 1*e* and 12.
[e]From ref. 12*a*; the 4-31G energy was evaluated at the geometry optimum for the STO-3G basis set.

spection of the 4-31G Mulliken population analysis for the *ab initio* calculations for the mono- and disubstituted methanes indicates that the rather significant π bonding between carbon and halogen which occurs in difluoromethane (via back donation of electron density from F to C (1*a*) occurs to a much lesser extent (about one-third as much) in dichloromethane as measured by the increase in CX bond overlap population. Interestingly, the electron transfer from halogen is almost as large with chlorine as with fluorine (0.018 e versus 0.023 e) but the effect is less, reflecting perhaps the usual inability of atoms in the chlorine row to form π bonds as well as do atoms in the fluorine row of the Periodic Table. The total CX bond overlap populations increase continuously from CH_3F to CH_4 whereas they decrease continuously from CH_3Cl to CCl_4.

Experimental thermochemistry for other chlorinated hydrocarbons supports the contention that the interaction of C—Cl bonds with C—H bonds is slightly less stabilizing than that of C—H bonds with each other, and is greater than that of C—Cl bonds with each other. In particular, the isomerization of 1,1-dichloroethane to the 1,2 isomer is a thermoneutral process (10). Further, the change in ΔH_f upon symmetrical chlorination of ethane is 10.5 kcal for the first pair of chlorines, 5.2 for the second, and −1.4 for the third, i.e. the $\Delta\Delta\Delta H_f$ values become *less* negative as the extent of substitution increases (10).

For the various chloroethane series, i.e. CH_3—R, CH_2Cl—R, $CHCl_2$—R, and CCl_3—R where R varies from CH_3 to CCl_3, the MNDO and MINDO/3 methods predict $\Delta\Delta E$ values all of which are negative and in the range from −3.7 to −6.0 kcal (MNDO) and −2.5 to −6.1 kcal (MINDO/3). Very little variation in the CCl or CC bond lengths is observed. (Detailed values are available from Tables D-4 and D-5.)

As with fluoroethanes, the MNDO method predicts that some lengthening of the carbon−carbon bond occurs for each substitution of chlorine for hydrogen; however, the total elongation from ethane to hexachloroethane amounts to only 0.05 Å. The MINDO/3 results for chloroethanes also predict elongation with substitution, but only to about half the extent predicted by MNDO.

It is well known that MO theory, even at the Hartree−Fock limit, yields very inaccurate results for the dissociation energies for individual bonds and for all bonds in a molecule, since the change in correlation energy upon dissociation is often of the same order of magnitude as the change in Hartree−Fock energy. Thus for example, the present 4-31G*[(C)] calculations predict the CH_3—H bond dissociation energy to be 86.4 kcal mol^{-1} (uncorrected for vibrational effects) compared to the experimental value of 105 ± 1 kcal mol^{-1}, and the $CH_4 \rightarrow C + 4H$ energy to be 324.6 kcal mol^{-1}, compared to 397.2 experimentally. However, much of chemistry is concerned not simply with the magnitude of the dissociation energy of a particular bond AB in polyatomic molecules XX′X″ABYY′Y″ but rather with the effect on this quantity of varying the groups X and Y bonded to atoms A and B respectively. One could imagine that the change in correlation energy upon AB bond scission is small compared to the change in Hartree−Fock energy when the substituted groups X and Y are varied. The present results offer some hope in this regard. In Table 6 we have listed the C—H bond dissociation energies, relative to that in methane, for XX′X″CH molecules, where the groups X are drawn from hydrogen, fluorine, chlorine, hydroxyl, amino, and methyl (results for the latter three groups being obtained, where available, from the literature). In general, the STO-3G basis overestimates the effect of the groups X in lowering the C—H bond dissociation energies, at least when the effect experimentally is small or of opposite sign. In contrast, the 4-31G basis generally underestimates the stabilization. The 4-31G basis with *d* orbitals on carbon does quite well, successfully predicting that the H—CH_2F and H—CHF_2 dissociation energies are equal and a few kilocalories below that for H—CH_3, and that the energy for H—CF_3 *exceeds* the value for methane.

The total energies for the fluoromethanes and fluoromethyl radicals can be combined to obtain C—F bond dissociation energies; these are listed in Table 6 relative to the values for CH_3—F. Each substitution of hydrogen by fluorine raises substantially the C—F energy, and this trend is reproduced very well by the 4-31G calculations when *d* orbitals are included.

Can. J. Chem. Downloaded from www.nrcresearchpress.com by 210.87.254.42 on 09/06/12
For personal use only.

TABLE 7. Average bond energies (kcal mol^{-1}) in hydrides[a]

Hydride formula	Bond energy			
	B	C	N	O
AH	80.7	80.6	75±4	102.3
AH_2	—	91.8	85.6	110.8
AH_3	89.0[b]	97.5[c]	93.4	—
AH_4	—	99.4	—	—

Hydride formula	Bond energy			
	Al	Si	P	S
AH	68	71.3	73.5[b]	82±3
AH_2	—	—	75.3	87.6
AH_3	—	71.4	77.9[b]	—
AH_4	—	77.1[b]	—	—

[a]Calculated from data in ref. 11 unless indicated otherwise.
[b]Calculated from data in ref. 8.
[c]Calculated from data in ref. 20.

The effects are underestimated grossly by the STO-3G basis set, and to some extent by 4-31G.

The C—F bond energies in the fluoromethanes vary significantly, but the C—H energies do not, because the favourable interactions between the different carbon–fluorine bonds occur to almost equal extents in the radical and molecule which have equal numbers of fluorines. Removal of a fluorine eliminates the interaction of this C—F bond with all remaining C—F linkages; thus D(C—F) increases with the number of fluorines in the free radical left behind.

It is not generally realized that interaction among bonds greatly stabilizes polyatomic molecules. The clearest evidence of this effect is provided by the progression in the average A—H bond energy in a series of hydrides AH_n as n increases from unity. The available experimental data on these trends is summarized in Table 7. For each series in which data are available, i.e. A = boron, carbon, nitrogen, oxygen, silicon, phosphorus, and sulphur, the average A—H bond energy invariably increases with n. Usually the biggest increase occurs from AH to AH_2, the succeeding increases decreasing with n (see especially the carbon hydrides). The simplest interpretation of this data is that interaction of C—H bonds with each other, i.e. delocalization of the MOs over as many equivalent hydrogen nuclei as possible, is greatly stabilizing. The total stabilization of all four bonds in CH_4 amounts to 75 kcal mol^{-1}, of the three bonds in NH_3 and PH_3 amounts to ~55 and ~13, and of the two bonds in H_2O and H_2S amounts to 17 and 11 respectively. The total stabilization of the two bonds in AH_2 species is approximately constant at ~19 ± 2 kcal in C, N, O and that of the three in AH_3 amounts to ~53 kcal. The corresponding stabilization energies all are considerably smaller in the hydrides of silicon, phosphorus, and sulphur.

It would be of interest also to display average bond energy terms in other AX_n molecules as a function of n for other atoms and groups X. In most cases, however, π bonding between X and unused atomic orbitals of the central atom A in molecules where n has not reached its normal maximum complicates the analysis (not to mention a scarcity of experimental data).

Acknowledgements

The author is grateful to the Natural Sciences and Engineering Research Council of Canada for financial support, and to Joseph F. Megyesi and L. Gail Parkhill for assistance with the calculations.

1. (*a*) L. RADOM, W. J. HEHRE, and J. A. POPLE. J. Am. Chem. Soc. **93**, 289 (1981); (*b*) W. A. LATHAN, L. RADOM, W. J. HEHRE, and J. A. POPLE. J. Am. Chem. Soc. **95**, 699 (1973); (*c*) G. A. JEFFREY, J. A. POPLE, and L. RADOM. Carbohydr. Res. **25**, 117 (1972); (*d*) A. PROSS and L. RADOM. J. Computational Chem. **1**, 295 (1980); (*e*) R. A. WHITESIDE, M. J. FRISCH, J. S. BINKLEY, D. J. DEFREES, H. B. SCHLEGEL, K. RAGHAVACHARI, and J. A. POPLE. Carnegie-Mellon quantum chemistry archive. 2nd ed. Carnegie-Mellon University, Pittsburgh, PA. 1981.
2. (*a*) R. C. BINGHAM, M. J. S. DEWAR, and D. LO. J. Am. Chem. Soc. **97**, 1307 (1975); (*b*) M. J. S. DEWAR and H. S. RZEPA. J. Am. Chem. Soc. **100**, 58 (1978).
3. J. S. BINKLEY, R. A. WHITEHEAD, P. C. HARIHARAN, R. SEEGER, J. A. POPLE, W. J. HEHRE, and M. D. NEWTON. Quantum Chemistry Program Exchange 11, 368 (1978).
4. (*a*) W. J. HEHRE, R. F. STEWART, and J. A. POPLE. J. Chem. Phys. **51**, 2657 (1969); (*b*) R. DITCHFIELD, W. J. HEHRE, and J. A. POPLE. J. Chem. Phys. **54**, 724 (1971); (*c*) J. B. COLLINS, P. VON RAGUE SCHLEYER, J. S. BINKLEY, and J. A. POPLE. J. Chem. Phys. **64**, 5142 (1976); (*d*) N. C. BAIRD and K. F. TAYLOR. Chem. Phys. Lett. **80**, 83 (1981).
5. (*a*) M. J. S. DEWAR, H. METIU, P. J. STUDENT, A. BROWN, R. C. BINGHAM, D. H. LO, C. A. RAMSDEN, H. KOLLMAR, P. WEINER, and P. K. BISCHOF. Quantum Chemistry Program Exchange Program 279 (1977); (*b*) W. THIEL. Quantum Chemistry Program Exchange Program 438 (1982).
6. (*a*) R. C. BINGHAM, M. J. S. DEWAR, and D. LO. J. Am. Chem. Soc. **97**, 1285 (1975); (*b*) M. J. S. DEWAR and W. THIEL. J. Am. Chem. Soc. **99**, 4899 (1977); **99**, 4907 (1977).
7. S. VISHVESHWARA. Chem. Phys. Lett. **59**, 30 (1978).
8. S. W. BENSON. Thermochemical kinetics. 2nd ed. Wiley, New York. 1976.
9. J. B. PEDLEY and J. RYLANCE. Sussex-N.P.L. computer analysed thermochemical data: organic and organometallic compounds. University of Sussex, England. 1977.
10. J. D. COX and G. PULCHER. Thermochemistry of organic and organometallic compounds. Academic Press. 1970.
11. R. C. WEAST (*Editor*). Handbook of chemistry and physics. 60th ed. The Chemical Rubber Co., Cleveland, OH. 1979–80.
12. (*a*) W. A. LATHAN, L. A. CURTISS, W. J. HEHRE, J. B. LISLE, and J. A. POPLE. Prog. Phys. Org. Chem. **11**, 175 (1974). (*b*) M. D. NEWTON, W. A. LATHAN, W. J. HEHRE, and J. A. POPLE. J. Chem. Phys. **52**, 4064 (1970).
13. D. J. DEFREES, B. A. LEVI, S. K. POLLACK, W. J. HEHRE, J. S. BINKLEY, and J. A. POPLE. J. Am. Chem. Soc. **101**, 4085 (1979).
14. E. HIROTA, T. TANAKA, A. SAKAKIBARA, Y. OHASHI, and Y. MORINO. J. Mol. Spectr. **34**, 222 (1970).
15. J. N. GHOSH, R. TRAMBARULO, and W. GORDY. J. Chem. Phys. **20**, 605 (1952).
16. C. G. THORNTON. Diss. Abstr. **14**, 604 (1954).
17. F. BERNARDI, W. CHERRY, S. SHAIK, and N. D. EPIOTIS. J. Am. Chem. Soc. **100**, 1352 (1978).
18. G. D. MENDENHALL, D. M. GOLDEN, and S. W. BENSON. J. Phys. Chem. **77**, 2707 (1973).
19. D. GRILLER and F. P. LOSSING. J. Am. Chem. Soc. **103**, 1587 (1981).
20. M. H. BAGHAL-VAYJOOEE, A. J. COLUSSI, and S. W. BENSON. Int. J. Chem. Kinet. **11**, 147 (1979).

Can. J. Chem. Downloaded from www.nrcresearchpress.com by 210.87.254.42 on 09/06/12
For personal use only.

The nature of bonding in hexahalothorates and hexahalouranates(IV)

ALAN D. WESTLAND AND M. T. H. TARAFDER
Department of Chemistry, University of Ottawa, Ottawa, Ont., Canada K1N 9B4

Received September 30, 1982

ALAN D. WESTLAND and M. T. H. TARAFDER. Can. J. Chem. **61**, 1573 (1983).

Enthalpies of reaction have been determined by solution calorimetry for the process $2AX(c) + ThX_4(c) = A_2ThX_6(c)$ where A = K, Cs and X = Cl, Br. The measurements afforded the following values of standard enthalpies of formation ΔH_f^0 (298 K), in kJ mol^{-1}: K_2ThCl_6, −2108; Cs_2ThCl_6, −2151; K_2ThBr_6, −1774; Cs_2ThBr_6, −1826. The standard enthalpies of formation of $ThCl_6^{2-}$ (g), $ThBr_6^{2-}$ (g), UCl_6^{2-} (g), and UBr_6^{2-} (g) and the two-halide ion affinities of $ThCl_4$, $ThBr_4$, UCl_4, and UBr_4 were compared by assuming semi-empirical (Kapustinskii) values of the lattice energies of the complexes. Homolytic and heterolytic bond energies were also calculated.

ALAN D. WESTLAND et M. T. H. TARAFDER. Can. J. Chem. **61**, 1573 (1983).

On a déterminé par calorimétrie de solution, les enthalpies de réaction du processus: $2AX(c) = ThX_4(c) = A_2ThX_6(c)$ où A = K, Cs et X = Cl, Br. Les mesures fournissent les valeurs suivantes des enthalpies normales de formation ΔH_f^0 (298 K) en kJ mol^{-1}: K_2ThCl_6, −2108; Cs_2ThCl_6, −2151; K_2ThBr_6, −1774; Cs_2ThBr_6, −1826. On a comparé les enthalpies normales de formation du $ThCl_6^{2-}$ (g), du $ThBr_6^{2-}$ (g), du UCl_6^{2-} (g), du UBr_6^{2-} (g) et les affinités de deux ions halogénures du $ThCl_4$, du $ThBr_4$, du UCl_4 et du UBr_4 en se servant des valeurs semi-empiriques (Kapustinskii) des énergies de réseau des complexes. On a également calculé les énergies de liaison homolytique et hétérolytique.

[Traduit par le journal]

Introduction

There have been no reports of thermochemical measurements on ternary salts of thorium tetrabromide. An early calorimetric investigation of A_2ThCl_6 salts (1) shows a lack of internal consistency and the value, −62.3 kJ, obtained for the process $2CsCl + ThCl_4 = Cs_2ThCl_6$ disagrees with the value −73.6 kJ obtained by Fuger and Brown (2). In the earlier work, the ternary salts were prepared by fusing a mixture of the component chlorides, while the later workers obtained Cs_2ThCl_6 by crystallization from ethanolic hydrochloric acid. In a previous research (3), one of us found that Cs_2NbCl_6 prepared by crystallization from solution provided an enthalpy of solution which was several kJ mol^{-1} less negative than that of a sample prepared in the dry way. A redetermination of the heats of solution of complexes prepared in the dry way appeared to be desirable as well as the study of bromothorates.

Vdovenko *et al.* (4, 5) have studied the thermochemistry of the A_2UCl_6 and A_2UBr_6 salts. Also, Fuger and Brown determined the enthalpy of formation of Cs_2UCl_6 and obtained a result in fairly good agreement with that in ref. 4.

Results and discussion

Enthalpies of reaction [1] were determined by measuring the heats of solution of each of the substances participating in the reaction:

$$[1] \quad 2AX(c) + ThX_4(c) \overset{\Delta H_1}{=} A_2ThX_6(c)$$

The combination of reaction enthalpies, $2\Delta H_2 + \Delta H_3 - \Delta H_4$, which is derived from processes [2] to [4], is very nearly equivalent to ΔH_1. This has been shown previously for analogous systems (6, 7). The braces denote solutions of

$$[2] \quad AX(c) + \{HCl, ThX_4\} \overset{\Delta H_2}{=} \text{solution}$$

$$[3] \quad ThX_4(c) + \{HCl, AX\} \overset{\Delta H_3}{=} \text{solution}$$

$$[4] \quad A_2ThX_6(c) + \{HCl\} \overset{\Delta H_4}{=} \text{solution}$$

4.0 molar hydrochloric acid containing the appropriate quantities of the solutes indicated. It was assumed that the thorium compounds are labile and that the complexes therefore gave the same dissolved species as were formed when AX and ThX_4 were dissolved separately. At any rate, the complex, Cs_2ThCl_6, may be crystallized from a solution of the component chlorides in concentrated acid (2).

TABLE 1. Enthalphy of solution, ΔH_2, for alkali halides in 4.02 molar hydrochloric acid. Values taken from ref. 6 and 7

Compound	ΔH_2 (kJ mol^{-1})
KCl	18.39±0.11
CsCl	13.70±0.24
KBr	19.87±0.04
CsBr	23.25±0.15

Acid was used in the calorimeter in order to suppress in part the hydrolysis of dissolved thorium compounds. When water was used in the calorimeter, as in Chauvenet's work (1), hydrolysis caused undue evolution of heat, and the calculation of enthalpies of complex formation involved taking differences of large numbers.

The heats of solution, ΔH_2, ΔH_3, and ΔH_4, are recorded in Tables 1 to 3, respectively. In our work with the tetrahalides of various elements, the measured enthalpies were essentially independent of sample size. Thus, the solutes behaved as though they were at infinite dilution. We believe this condition to have obtained in the present study as well.

The heats of solutions of the alkali halides at infinite dilution in 4 *M* hydrochloric acid are not measurably influenced by the presence of small quantities of the solutes, MX_4. Therefore, values of ΔH_2 obtained in previous researches (6, 7) were used in the present work. Equivalent amounts of alkali halide were added to the calorimeter liquid when the enthalpies of solution of $ThCl_4$ and $ThBr_4$ were measured, although there was no evidence that such additions had any influence on the measurements.

As a check on the purity of the $ThCl_4$, we obtained the value

Can. J. Chem. Downloaded from www.nrcresearchpress.com by 210.87.254.40 on 09/06/12
For personal use only.

Can. J. Chem. Downloaded from www.nrcresearchpress.com by 210.87.254.40 on 09/06/12
For personal use only.

TABLE 2. Enthalpy of solution of thorium halides, ΔH_3, in 4.02 molar hydrochloric acid containing alkali halide

Compound	Sample weight (g)	ΔH_3 (kJ mol^{-1})	Mean
$ThCl_4$	1.7835	−213.2	
	1.3514	−215.4	
	1.2694	−213.9	
	1.2495	−213.3	
	1.6085	−213.0	−213.8±1.0
$ThBr_4$	2.1541	−263.5	
	1.7000	−264.5	
	1.8065	−260.0	
	1.7778	−265.7	
	2.1062	−260.8	−262.9±2.4

TABLE 3. Enthalpy of solution of alkali-metal hexahalometallates, ΔH_4, in 4.02 molar hydrochloric acid

Compound	Sample weight (g)	ΔH_4 (kJ mol^{-1})	Mean
K_2ThCl_6	2.1941	−124.8	
	1.1760	−125.0	
	0.9671	−126.2	
	1.9890	−127.5	
	1.3559	−128.1	−126.3±1.5
Cs_2ThCl_6	3.4708	−104.5	
	2.9195	−104.3	
	3.0215	−107.0	
	2.5034	−105.3	−105.3±1.2
K_2ThBr_6	1.2039	−198.4	
	1.4558	−202.6	
	1.3083	−200.5	
	1.5305	−199.5	−200.2±1.8
Cs_2ThBr_6	2.0607	−144.5	
	2.1315	−142.5	
	1.9867	−144.2	
	2.4398	−143.0	
	2.3357	−142.8	−143.3±1.0

−186.2 kJ mol^{-1} for the enthalpy of solution in 6.0 *M* hydrochloric acid. This compares well with the value −185.3 kJ mol^{-1} obtained by Eyring and Westrum (8).

The uncertainty limits given in Tables 1−3 are the standard deviations of the measurements. These limits do not include an estimate of accuracy as influenced by purity of materials, etc. An additional uncertainty pertains to the potassium complexes. It has been the practice in this laboratory to investigate two or three alkali salts of a given haloanion in order to examine the results for self-consistency. In the case of the alkali halothorates, however, the phase diagrams of the ACl−$ThCl_4$ systems reveal that the salts of Na, K, and Rb melt incongruently (9, 10). There is some disagreement about this, as other groups of workers claim that K_2ThCl_6 melts congruently (11, 12), but an examination of the various phase diagrams leads us to believe that a too-rapid cooling of the melt produced the compound in some cases by a nonequilibrium process. We therefore sought to obtain the potassium salt by rapid air-cooling of a melt of the stoichiometric composition. Also, melts with the compositions $KThCl_5$ and K_3ThCl_7 were cooled in a similar way to produce these reported compounds. Debye−Scherrer patterns of each of the three solids so obtained were distinct from one another. The potassium salts, K_2ThCl_6 and K_2ThBr_6, gave patterns which were indexed as tetragonal while the caesium salts were trigonal (13).

TABLE 4. Enthalpy of complexing, ΔH_1, of the alkali-metal hexahalothorates

Compound	ΔH_1 (kJ mol^{-1})
K_2ThCl_6	−50.66±2
Cs_2ThCl_6	−81.1 ±2
K_2ThBr_6	−23.3 ±3
Cs_2ThBr_6	−73.1 ±3

A line with $\sin^2\theta = 0.0149$ appeared strongly in the patterns of $KThCl_5$ and K_3ThCl_7 and weakly in the pattern of K_2ThCl_6. It is therefore likely that a small quantity of the 1:1 and/or the 3:1 compound occurred in the preparation of K_2ThCl_6. The heat of solution of an equimolar mixture of $KThCl_5$ and K_3ThCl_7 would differ from the heat of solution of $2K_2ThCl_6$ by the enthalpy of the process [5]:

$$[5] \quad 2K_2ThCl_6 = KThCl_5 + K_3ThCl_7$$

This may be a small quantity as in the case of the analogous process: $3CaB_2O_4 = CaB_4O_7 + Ca_2B_2O_5$ for which $\Delta H_{reaction}$ is −2.1 kJ (14). If the K_2ThCl_6 contained as much as 10 mole percent impurities and the enthalpy of reaction [5] were as much as ±20 kJ, the error in the measured value of ΔH_4 would be only ±1 kJ mol^{-1}. The thermal data for the potassium salts are thus the subject of some uncertainty in this way, but it will be seen below that the data for the various salts are reasonably self-consistent.

The enthalpies of formation of the complexes relative to the component halides are listed in Table 4 and the standard enthalpies of formation from the elements are given in Table 5. The enthalpies of formation of the gaseous ions, ThX_6^{2-} and UX_6^{2-}, are also presented. The values for the gaseous anions depend upon a calculation of lattice energies of the ternary salts. These calculations followed the method of Kapustinskii and Yatsimirskii (15) and the ancillary data used are also included in Table 5. In addition, the following enthalpies of formation were used (all values in kJ mol^{-1}): KCl(c), −436.7 (16); CsCl(c), −442.8 (16); KBr(c), −393.8 (16); CsBr(c), −394.5 (17); $ThCl_4$(c), −1184.4 (18); $ThBr_4$(c), −963.4 (18); UCl_4(c), −1018.4 (4); UBr_4(c), −802.5 (18). Enthalpies of formation of Cs_2UCl_6 and K_2UBr_6 from the component halides have been reported as −100.8 and −43.5 kJ mol^{-1}, respectively (4, 5).

The lattice energies calculated by the Kapustinskii−Yatsimirskii method are not accurate because the anionic groups are treated as mere point charges. A superior approach is that of Jenkins and Pratt but their procedure requires a knowledge of the metal−halogen distances and the partial charges on the atoms (19). The cruder calculations are presented here in the belief that they lead to valid qualitative comparisons between closely related compounds.

Scheme 1 embodies the cycles from which the relations [6]

$$\begin{array}{ccc} 2A^+(g) + 2X^-(g) + MX_4(g) & \xrightarrow{\overline{\Delta H}_s(g)} & 2A^+(g) + [MX_6]^{2-}(g) \\ \uparrow U_{AX} \quad \uparrow \Delta H_{subl.} & & \uparrow U_{A_2MX_6} \\ 2AX(c) + MX_4(c) & \xrightarrow{\Delta H_1} & A_2[MX_6](c) \end{array}$$

SCHEME 1

TABLE 5. Calculated enthalpies of formation at 298 K

Compound	Symmetry	Lattice constant (Å)	r(Å)*	U (kJ mol^{-1})	$\Delta H_f(A_2MX_{6,c})$ (kJ mol^{-1})	$\Delta H_f^0(MX_6^{2-},g)$ (kJ mol^{-1})	Mean $\Delta H_f^0(MX_6^{2-},g)$
K_2ThCl_6	Tetragonal	a 10.36 c 9.32	4.37	1582	−2108	−1555	
Cs_2ThCl_6	Trigonal	a 7.629 c 6.050	4.670	1492	−2151	−1563	−1559
K_2ThBr_6	Tetragonal	a 11.478 c 7.94	4.478	1561	−1774	−1241	
Cs_2ThBr_6	Trigonal	a 9.537 c 8.10	4.74	1473	−1826	−1257	−1249
Cs_2UCl_6	Trigonal	a 7.507 c 6.050	4.620	1507	−2005	−1403	
K_2UBr_6	Tetragonal	a 10.94 c 10.67	4.742	1473	−1634	−1190	

*r is the effective cation−anion distance as given by Yatsimirskii's method (15).

TABLE 6

(a) Double halide-ion affinities, $\overline{\Delta H_x}(g)$, for the process $MX_4(g) + 2X^-(g) = MX_6^{2-}(g)$. Values in kJ mol^{-1}

Condensed phase reaction product	$\overline{\Delta H_x}(g)$	Mean
K_2ThCl_6	−147.5	
Cs_2ThCl_6	−155.8	−151.6
K_2ThBr_6	−15.0	
Cs_2ThBr_6	−31.0	−23.0
Cs_2UCl_6	−99.8	
K_2UBr_6	−108.7	

(b) Double halide-ion affinities for related systems, kJ mol^{-1}

	Cl	Br
Zr	−26	−9, −1
Hf	−37	−46
Sn	+39	+46
Nb	+3	+5
Ta	−35	+38

and [7] may be derived (ss = standard state).

[6] $\Delta H_f^0(A_2MX_6,c) = \Delta H_1 + 2\Delta H_f^0(AX,c) + \Delta H_f^0(MX_4,c)$

[7] $\Delta H_f^0(MX_6^{2-},g) = U(A_2MX_6) - 2\Delta H_f^0(A^+,g) + \Delta H_f^0(A_2MX_6,c)$

ΔH_f^0 for $K^+(g)$ and $Cs^+(g)$ were taken to be 514.2 and 452.3 kJ mol^{-1} respectively (16).

The two-halide ion affinities, $\Delta H_x(g)$ are of interest as they refer to the process of forming the complex anion in the gas phase in which the effects of crystal forces do not play a role. The values of $\overline{\Delta H_x}(g)$ are given by [8]:

[8] $\overline{\Delta H_x}(g) = \Delta H_f^0(MX_6^{2-},g) - 2\Delta H_f^0(X^-,g) - \Delta H_f^0(MX_4,g)$

The energy of reorganizing sp^3 hydridization of the MX_4 molecule to sp^3d^2 hybrids is involved in $\underline{\Delta H_x}(g)$ but it is difficult to evaluate this factor. Values of $\overline{\Delta H_x}(g)$ are listed in Table 6(a).

As expected for a class a type ion such as Th^{4+}, the chloride ion affinity of $ThCl_4(g)$ is very much more negative than the bromide ion affinity of $ThBr_4(g)$. However, the situation is reversed for $UCl_4(g)$ and $UBr_4(g)$. This reversal of the expected result was found also with hafnium chloride and bromide (6, 7). It can be concluded that U^{IV} has incipient class b character, or in Pearson's terminology, U^{IV} is a softer acid than Th^{IV}. We believe that the tendency toward class b character shown by certain high-valent elements may be attributed to their power to polarize atoms bonded to them. Indeed, U^{IV} has a greater effective nuclear charge than has Th^{IV} owing to the poor shielding of the $5f$ electrons. Uranium would thus be better able to accept the charge density inherent in $p_\pi \rightarrow d_\pi$ bonding. The argument should apply to both MX_6^{2-} and the tetrahalides, but π-bonding is presumably weaker for the latter because of their tetrahedral geometry. Strong π-bonding should therefore favour the anions.

By referring to Table 6(b), the two-halide ion affinities of MX_4 (M = Th, U) may be compared with those of MX_4 (M = Zr, Hf, Nb, Ta, Sn), a group of compounds studied previously in this laboratory.

The chloride ion affinity of $ThCl_4(g)$ and the bromide ion affinity of $UBr_4(g)$ are the greatest of all the values listed. This is remarkable in view of the large size of the actinide ions for which $M^{4+} - X^-$ coulombic interaction is not strong. However, $X^- - X^-$ repulsions in the MX_6^{2-} groups would be smaller for the actinide ions also. The order of the acceptor strength towards Cl^- is $ThCl_4 > UCl_4 > HfCl_4 > TaCl_4 > ZrCl_4 > NbCl_4 > SnCl_4$. The order of bromide affinities is similar except that the thorium compound follows that of hafnium.

Jenkins and Pratt have shown that the chloride ion affinities of various other transition element tetrachlorides follow the same trend of diminishing in magnitude toward the right in a period (20, 21). They found the same to be true for the homolytic M—Cl bond energies as well. Rather paradoxically, Brown *et al.* found that the stretching force constant increases in the series $HfCl_6^{2-}$ through $PtCl_6^{2-}$ and they related this to trends in σ- and π-bonding and optical electronegativities (22).

However, the two-halide ion affinities represent differences between the thermodynamic states of reactants and products and, therefore, may not relate in a simple fashion to bond order and force constants of product species alone.

The calculations that led to the foregoing results made use of data taken from the literature. The enthalpies of sublimation at the indicated temperatures were (values in kJ mol^{-1}): $ThCl_4$

Can. J. Chem. Downloaded from www.nrcresearchpress.com by 210.87.254.40 on 09/06/12
For personal use only.

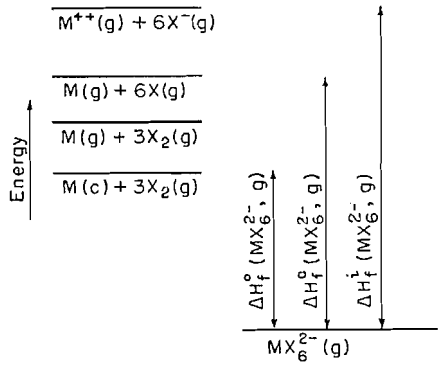

FIG. 1

(1131 K), 247.0 (23); $ThBr_4$ (1088 K), 184.0 (23); UCl_4 (863 K), 193.7 (17); UBr_4 (792 K), 175.3 (17). Use of the heat capacities (14, 24) gave the following room temperature values: 269.0; 204.8; 207.4; 189.5 kJ mol^{-1} respectively. The standard enthalpies of formation of $Cl^-(g)$ and $Br^-(g)$ were taken to be −246.0 and −233.9 kJ mol^{-1} respectively (25).

Jenkins and Pratt have defined bond energies in two ways (20) that involve the quantities shown in Fig. 1. One definition refers to the process [9]:

$$[9] \quad MX_6^{2-}(g) \xrightarrow{\Delta H_f^a} M(g) + 6X(g) + 2e$$

in which case the average (homolytic) bond energy, $E(M—X)_{hom}$, is defined as

$$[10] \quad E(M—X)_{hom} = -\frac{1}{6}\Delta H_f^a(MX_6^{2-},g)$$

Alternatively, by referring to the heterolytic fission of the bond [11]:

$$[11] \quad MX_6^{2-}(g) \xrightarrow{\Delta H_f^i} M^{4+}(g) + 6X^-(g)$$

the average (heterolytic) bond energy, $E(M—X)_{het}$ is given as:

$$[12] \quad E(M—X)_{het} = -\frac{1}{6}\Delta H_f^i(MX_6^{2-},g)$$

Pearson and Mawby (26) have maintained that the heterolytic bond energy represents the coordinate bond energy and is more informative. From Fig. 1 it is evident that

$$[13] \quad -\Delta H_f^a(MX_6^{2-},g) = \Delta H_f^0(M,g) + 6\Delta H_f^0(X,g) - \Delta H_f^0(MX_6^{2-},g)$$

and

$$[14] \quad -\Delta H_f^i(MX_6^{2-},g) = \Delta H_f^0(M^{4+},g) + 6\Delta H_f^0(X^-,g) - \Delta H_f^0(MX_6^{2-},g)$$

We used the following data from the sources cited:

Data		Reference
$\Delta H_f^0(Th,g)$	= 598.3 kJ mol^{-1}	27
Ionization potential, $\sum_1^4 I$, Th	= 6.0 + 11.5 + 20 + 28.7 = 66 eV	28–31
$\Delta H_f^0(U,g)$	= 527.2 kJ mol^{-1}	5, 32
Ionization potential, $\sum_1^4 I$, U	= 68.0 eV	33
$\Delta H_{dissoc}^0(Cl_2)$	= 242.0 kJ mol^{-1}	16
$\Delta H_{dissoc}^0(Br_2)$	= 192.9 kJ mol^{-1}	16
1eV	= 96.49 kJ mol^{-1}	

TABLE 7. Homolytic, $E(M—X)_{hom}$, and heterolytic, $E(M—X)_{het}$, bond energies in $MX_6^{2-}(g)$ ions. Values in kJ mol^{-1}

Compound	$E(M—X)_{hom}$	Mean	$E(M—X)_{het}$	Mean
K_2ThCl_6	480		1182	
Cs_2ThCl_6	481	481	1183	1183
K_2ThBr_6	403		1142	
Cs_2ThBr_6	406	404	1144	1143
Cs_2UCl_6	443		1173	
K_2UBr_6	383		1150	

TABLE 8. Raman spectral data of ThX_4 and $(Alk)_2ThX_6$

Compound	Th—X Stretching frequency (cm^{-1})
$ThCl_4$	300 s
K_2ThCl_6	282 vs*
Cs_2ThCl_6	310 s
$ThBr_4$	195 s
K_2ThBr_6	175 s
Cs_2ThBr_6	198 vs

*s = strong; vs = very strong.

Bond energy data (Table 7) indicate that the energy of the Th—X bond is essentially the same in K_2ThX_6 and Cs_2ThX_6 despite the differences in structure and the attendant uncertainties in the calculation of lattice energies. The agreement affords some assurance about the validity of the methodology. Thus when we compare M—Cl and M—Br bonds, the difference, significant although not large, is presumed to be meaningful. Also, the Th—X and U—X bonds have almost the same heterolytic energy within experimental error. The slight differences that are discernable are responsible for the class *a* and class *b* distinctions referred to earlier. Thus, small differences in bond energies can be quite significant when there are as many as six bonds in the molecule.

The homolytic bond energies for the Th—X bonds are significantly greater than those for the U—X bonds. The difference for the chlorides, 38 kJ per bond, agrees well with the difference, 39 kJ per bond, between the values quoted by Jenkins and Pratt (34). The absolute values given by these authors differ from ours because of the different method of calculating lattice energies.

Solid state Raman spectra of $ThCl_4$, $ThBr_4$, and the alkali complexes were recorded from 800 to 100 cm^{-1} (Table 8). The very strong band at 300 cm^{-1} for $ThCl_4$ is assigned to the totally symmetric Th—Cl stretch (35–37). This is shifted to 282 cm^{-1} and 310 cm^{-1} in K_2ThCl_6 and Cs_2ThCl_6, respectively. The corresponding mode gives a band at 195 cm^{-1} in the spectrum of $ThBr_4$ (36) and this also is seen to be shifted upon complexation. Woodward and Ware obtained spectra for $ThCl_6^{2-}$ and UCl_6^{2-} in methyl cyanide solution and derived the stretching force constants (a_{1g} mode), 1.51 and 1.40 mdyn/Å, respectively (38). These values conform to the relative bond energies. Unfortunately, the vibrational spectra of the solid compounds do not reveal the various modes required for a force field calculation.

Experimental

Preparation of compounds

Thorium tetrachloride was obtained by passing CCl_4 vapour, entrained in a stream of dry nitrogen, over ThO_2 at 600°C. The product

Can. J. Chem. Downloaded from www.nrcresearchpress.com by 210.87.254.40 on 09/06/12
For personal use only.

Can. J. Chem. Downloaded from www.nrcresearchpress.com by 210.87.254.40 on 09/06/12
For personal use only.

so obtained was purified by repeated vacuum sublimation in a platinum tube heated to 760°C. The final product was handled in a dry nitrogen atmosphere and was stored in sealed ampoules. *Anal.* calcd. for $ThCl_4$: Cl 37.93; found: Cl 37.84%.

Thorium tetrabromide was prepared by a published method (39) with little modification. Bromine (25 mL) was added dropwise to thorium powder (4.18 g, Alpha Ventron, purity 99.9%) in 5 mL of methyl cyanide. The mixture was refluxed under N_2 for 12 h. The solid product was heated for 4 h at 180°C and was subsequently sublimed under vacuum in a platinum tube heated to 550°C. The product was handled in a dry nitrogen atmosphere and was stored in sealed ampoules. *Anal.* calcd. for $ThBr_4$: Br 57.93; found: Br 57.70%.

Preparation of ternary salts

The preparation of K_2ThCl_6 is typical. Potassium chloride was dried at 500°C *in vacuo* and mixed with the stoichiometric amount of $ThCl_4$. The mixture, with a weight of about 7 g, was sealed *in vacuo* in a quartz tube and this was heated in a tube furnace. Once a clear liquid had been formed, the tube was agitated to bring about thorough mixing. The melt was quenched in air and the solidified mass was ground in a dry nitrogen atmosphere.

X-ray diffraction patterns were obtained by the Debye–Scherrer technique. Line spacings were determined by the Straumanis technique and the lattice constants were obtained from extrapolated Nelson–Riley plots.

Calorimetric measurements

The calorimeter and its calibration have been described previously (3). In the present study, it contained 300 cm^3 of 4.02 molar hydrochloric acid and was operated at 25°C. The compound under study was contained in a thin-walled glass bulb which was crushed under the acid at the appropriate moment. Dissolution was complete in 4 min or less. The calorimeter was calibrated electrically before and after each sample run and the mean of the two calibrations was used. The temperature of the calorimeter liquid was restored to 25°C after each series of readings by means of allowing a few drops of liquid nitrogen to evaporate in a well which extended down into the calorimeter liquid. The temperature data were treated by the numerical method described by Kubaschewski *et al.* in order to correct for heat loss or gain (14).

Spectra

Raman spectra of the solids were obtained with a Control Laser Model 552A argon laser (5145 Å) operated at 2.0 watts. The finely ground samples were held in sealed Pyrex capillary tubes.

Acknowledgement

The authors are grateful to the Canadian Commonwealth Scholarship and Fellowship Committee for the grant of a scholarship to M.T.H.T.

1. E. CHAUVENET. Ann. Chim. Phys. **23**, 425 (1911).
2. J. FUGER and D. BROWN. J. Chem. Soc. (A), 841 (1971).
3. D. LAL and A. D. WESTLAND. J. Chem. Soc. Dalton Trans. 2505 (1974).
4. V. M. VDOVENKO, V. A. VALKOV, and I. G. SUGLOBOVA. Radiokhimiya, **16**, 363 (1974).
5. V. M. VDOVENKO, I. G. SUGLOBOVA, and D. E. CHIRKST. Radiokhimiya, **16**, 203 (1974).
6. P. GELBMAN and A. D. WESTLAND. J. Chem. Soc. Dalton Trans. 1598 (1975).
7. R. MAKHIJA and A. D. WESTLAND. J. Chem. Soc. Dalton Trans. 1707 (1977).
8. L. EYRING and E. F. WESTRUM, JR. J. Am. Chem. Soc. **72**, 5555 (1950).
9. R. OYAMADA. Denki Kagaku, **39**, 2 (1971).
10. V. I. IONOV, B. G. KORSHUNOV, V. V. KOKORIEV, and I. S. MOROZOV. Tsvetn. Metall. 102 (1960 (3)).
11. V. N. DIESYATNIK, V. A. DUBININ, I. F. NITCHKOV, and S. P. RASPOPIN. Tsvetn. Metall. 87 (1966 (4)).
12. A. N. VOKHMYAKOV, V. N. DESYATNIK, and N. N. KURBATOV. Sov. At. Energy, **35**, 424 (1973).
13. S. SIEGEL. Acta Crystallogr. **9**, 827 (1956).
14. O. KUBASCHEWSKI, E. LL. EVANS, and C. B. ALCOCK. *In* Metallurgical thermochemistry. 4th ed. Pergamon Press, Oxford. 1967.
15. K. B. YATSIMIRSKII. Russ. J. Inorg. Chem. **6**, 518 (1961).
16. D. A. STULL (*Editor*). JANAF Thermochemical Tables. Dow Chemical Co., Midland, Michigan. 1960–1966.
17. F. ROSSINI (*Editor*). Selected values of chemical thermodynamic properties. National Bur. Standards, Washington, Circular 500, 1952.
18. J. FUGER and D. BROWN. J. Chem. Soc. Dalton Trans. 428 (1973).
19. H. D. B. JENKINS and K. F. PRATT. Proc. R. Soc. London, Ser. A, **356**, 115 (1977).
20. H. D. B. JENKINS and K. F. PRATT. Adv. Inorg. Chem. Radiochem. **22**, 1 (1979).
21. H. D. B. JENKINS and K. F. PRATT. Prog. Solid State Chem. **12**, 125 (1979).
22. T. L. BROWN, W. G. MCDOUGLE, and L. G. KENT. J. Am. Chem. Soc. **92**, 3645 (1970).
23. W. FISCHER, R. GEWEHR, and M. WINGCHEN. Z. anorg. allgem. Chem. **242**, 182 (1939).
24. I. BARIN, O. KNACKE, and O. KUBASCHEWSKI. *In* Thermochemical properties of inorganic substances. Springer Verlag, New York. 1973.
25. J. D. COX (*Editor*). CATCH Tables, Computer analysis of thermochemical data. University of Sussex. 1974.
26. R. G. PEARSON and R. J. MAWBY. Halogen Chem. **3**, 55 (1967).
27. P. D. ZAVITSANOS. U. S. Natl. Tech. Inform. Serv., AD Rep. No. 762917 and No. 773197/9GA. 1973.
28. D. L. HILDENBRAND and E. MURAD. J. Chem. Phys. **61**, 5466 (1974).
29. J. SUGAR. J. Chem. Phys. **59**, 788 (1973); **60**, 4103 (1974).
30. E. G. RAUH and R. J. ACKERMAN. J. Chem. Phys. **60**, 1396 (1974).
31. G. V. SAMSONOV. *In* Handbook of the physicochemical properties of the elements. Plenum Press, New York. 1968.
32. A. PATTORET, J. DROWART, and S. SMOES. *In* Thermodynamics of nuclear materials. Symposium proceedings. Vienna. 1968. p. 613.
33. L. A. MAIJ. Latv. PSR Zinat. Akad. Vestis, Kim. Ser. **51**, 337 (1976).
34. H. D. B. JENKINS and K. F. PRATT. Inorg. Chim. Acta, **32**, 25 (1979).
35. E. W. BOHRES, W. KRASSER, H. J. SCHENK, and K. SCHWOCHAU. J. Inorg. Nucl. Chem. **36**, 812 (1974).
36. J. GOFFART, J. FUGER, B. GILBERT, L. HOCKS, and G. DUYCKAERTS. Inorg. Nucl. Chem. Lett. **11**, 581 (1975).
37. R. OYAMADA and S. YOSHIDA. J. Phys. Soc. Jpn. **38**, 1786 (1975).
38. L. A. WOODWARD and M. J. WARE. Spectrochim. Acta, Part A, **24**, 924 (1968).
39. Z. M. S. AL-KAZZAZ and R. A. LOUIS. Z. anorg. allgem. Chem. **440**, 286 (1978).

The radiolysis at room temperature and 118°C of aqueous solutions containing sodium nitrate and either sodium formate or 2-propanol

ALLEN JOHN ELLIOT AND FREDERICK CHARLES SOPCHYSHYN

Atomic Energy of Canada Limited Research Company, Chalk River Nuclear Laboratories, Physical Chemistry Branch, Chalk River, Ont., Canada K0J 1J0

Received November 19, 1982

ALLEN JOHN ELLIOT and FREDERICK CHARLES SOPCHYSHYN. Can. J. Chem. **61**, 1578 (1983).

Deoxygenated sodium nitrate solutions ($\leq 2.5 \times 10^{-2}$ *M*) containing sodium formate (≤ 0.5 *M*) have been irradiated at room temperature and 118°C. With formate concentrations $\leq 5 \times 10^{-2}$ *M*, $G(NO_2^-)$ increased ~25% over the temperature range. Calculations suggest part of this increase in $G(NO_2^-)$ may arise from an increase in the overall solvated electron yield. With 0.5 *M* sodium formate solutions containing 2.5×10^{-2} *M* sodium nitrate, $G(NO_2^-)$ rose from 3.6 at room temperature to ~14 at 118°C, suggesting the occurrence of a chain reaction at higher formate concentrations. $G(H_2O_2)$ and $G(H_2)$ were not functions of temperature for all the above solutions.

The pH dependence of $G(NO_2^-)$ was determined at room temperature for sodium nitrate solutions containing either sodium formate or 2-propanol. The $G(NO_2^-)$ as a function of pH could only be modelled satisfactorily with rate constants from the literature in the sodium formate case.

It is concluded that the solvated electron yield in irradiated aqueous solutions at elevated temperatures cannot be confidently deduced from measurements made with nitrate as an electron scavenger in the presence of formate ions or alcohols.

ALLEN JOHN ELLIOT et FREDERICK CHARLES SOPCHYSHYN. Can. J. Chem. **61**, 1578 (1983).

On a irradié des solutions désoxygénées de nitrate de sodium ($\leq 2{,}5 \times 10^{-2}$ *M*) contenant du formiate de sodium ($\leq 0{,}5$ *M*) à la température de la pièce et à 118°C. Dans cet intervalle de température et pour des concentrations en formiate $\leq 5 \times 10^{-2}$ *M*, $G(NO_2^-)$ augmente de 25% environ. Les calculs suggèrent qu'une partie de cette augmentation de $G(NO_2^-)$ peut être due à l'augmentation du rendement global en électrons solvatés. Pour des solutions de formiate de sodium 0,5 *M* contenant du nitrate de sodium à une concentration de $2{,}5 \times 10^{-2}$ *M*, $G(NO_2^-)$ passe de 3,6 à la température de la pièce à 14 environ à 118°C ce qui suggère la présence de réaction en chaîne lorsque les concentrations en formiate sont élevées. Dans toutes les solutions étudiées $G(H_2O_2)$ et $G(H_2)$ ne dépendent pas de la température.

On a déterminé l'influence du pH sur $G(NO_2^-)$ pour des solutions de nitrate de sodium contenant soit du formiate de sodium, soit du propanol-2 à la température de la pièce. Les constantes de vitesse relevées dans la littérature, dans le cas du formiate de sodium, permettent d'établir un modèle satisfaisant uniquement pour $G(NO_2^-)$ en fonction du pH.

On conclut donc qu'on ne peut déduire avec exactitude le rendement en électron solvaté dans les solutions aqueuses irradiées à des températures élevées à partir des mesures prises avec les nitrates comme pièges à électrons en présence d'ions formiates ou d'alcools.

[Traduit par le journal]

Introduction

In nuclear reactors, water, which can be used as a moderator (70–120°C) or a heat transfer medium (~300°C), is subjected to intense fields of ionizing radiation. While the radiation chemistry of aqueous solutions at room temperature is, in general, well understood (1), the very little data published (2–4) on water-radiolysis at higher temperatures is often confusing. As an example, Freeman and co-workers (3) report that the *G*-value (number of species formed per 100 eV of radiation energy absorbed) of the solvated electron, e^-_{aq}, increases from 2.7 at room temperatures to 4.8 at 300°C yet Burns and Marsh (4) report a $G(e^-_{aq})$ of 0.4 at 400°C.

The yields of e^-_{aq}, hydroxyl radicals, hydrogen atoms, molecular hydrogen, and hydrogen peroxide in radiolysed water are measured by adding chemical scavengers and analyzing for products (1–4). The measured yield is dependent on the reactivity (R) of the scavenger (5) present, where R is defined in eq. [1],

$$[1] \quad R = k_{X+S}[S]$$

and k_{X+S} is the rate constant for reaction of a primary radical (X = e^-_{aq}, $\dot{O}H$, $\dot{H}$) with the scavenger (5). For small values of R ($<10^7$ s^{-1}), only those primary radicals which escape the spur will be scavenged but as R increases, primary radicals will be scavenged from the spur itself (1, 5). Draganić and Draganić (5) have systematically documented this effect at room temperature. The effect of a moderate rise in temperature (<150°C) will reflect the change in k_{X+S} relative to geminate recombination and diffusion out of the spur for the primary species plus any increase or decrease in overall radical yield.

Interpretation of scavenger experiments require an understanding of the underlying chemistry. In this paper we report results obtained from the radiolysis of solutions at room temperature and 118°C which contain the nitrate ion, which is often used as an electron scavenger, and the formate ion or 2-propanol molecule, both of which are used as hydroxyl radical scavengers.

Experimental

The solute chemicals (purchased from Fisher Scientific Ltd. or Anachem Chemicals Ltd.) were used as supplied. The water was triply distilled. In experiments where the yields at room temperature were compared to those at 118°C, the solutions were irradiated in cylindrical Pyrex cells. The samples were degassed, and ~10 mL of solution transferred to the ~13 mL cell which was then sealed with a flame. The samples were irradiated in a thermostated oil bath in an AECL Gammacell, the dose rate of which was $\sim 2 \times 10^{19}$ eV kg^{-1} s^{-1}. Samples irradiated at 118 ± 3°C were rapidly cooled immediately after irradiation to room temperature (25 ± 3°C). In other room temperature experiments, solutions were irradiated in syringes after being saturated with the appropriate UHP gas. Nitrous oxide (Matheson) was first passed through a RIDOX (Fisher) column to remove oxygen.

The nitrite ion concentration was determined by the diazo-method (6) using an extinction coefficient at 540 nm of 52 860 M^{-1} cm^{-1}. Hydrogen peroxide yields were assayed by the tri-iodide ion method

Can. J. Chem. Downloaded from www.nrcresearchpress.com by 210.87.254.42 on 09/06/12
For personal use only.

Can. J. Chem. Downloaded from www.nrcresearchpress.com by 210.87.254.42 on 09/06/12
For personal use only.

(7) utilizing an extinction coefficient at 350 nm of 25 500 M^{-1} cm $^{-1}$. A McLeod gauge was used to measure the gas yields volumetrically and the fraction of the gas in the sample was determined on a CEC-21-610 mass spectrometer.

Since hydrogen peroxide was to be assayed from solutions irradiated at 118°C, the thermal stability of $\sim 2 \times 10^{-4}$ M hydrogen peroxide solutions was followed at 25, 70, 100, and 118°C. These samples which were prepared from a 30% hydrogen peroxide solution (unstabilized) were degassed and sealed in Pyrex cells as used for the irradiations. The hydrogen peroxide and oxygen concentrations were followed with time. The peroxide decomposed at measurable rates only at 100°C and 118°C and here the half-lives were 5–6 h and 0.75–1 h, respectively. The sum of the peroxide concentration plus twice the oxygen concentration equalled the initial peroxide concentration. As no irradiation was longer than 60 s and since the solutions were cooled immediately, the thermal decomposition of peroxide will not be a source of error in the experiments at 118°C.

Results

The G-values of nitrite, hydrogen peroxide, and hydrogen are summarized in Figs. 1 and 2 and Table 1 for degassed sodium nitrate solutions containing sodium formate irradiated at room temperature and 118°C. The hydrogen peroxide and hydrogen concentrations were linearly dependent on the dose received; the G-values given in Table 1 are the mean of at least five determinations and the errors are one standard deviation.

As can be seen in Fig. 1, $G(NO_2^-)$ decreased with increased dose and when extrapolated to zero dose, $G(NO_2^-)$ obtained at room temperature agreed with those previously reported by Draganić and Draganić (5) whose results are given by the triangles in this figure. At 118°C, $G(NO_2^-)$ was always greater than the room temperature results; however, for 0.5 M sodium formate solutions, $G(NO_2^-)$ (Fig. 2) was higher than expected (see later) so a number of further experiments were carried out. Firstly, to see if ionic strength was a factor, a 2.5×10^{-3} M sodium nitrate, 5×10^{-3} M sodium formate solution was irradiated with and without 0.2 M sodium sulphate present. At best, $G(NO_2^-)$ was marginally higher for the solution containing the sodium sulphate as can be seen in Fig. 1 for both irradiation temperatures. Secondly, to see if a stable end-product formed during the irradiation was capable of reducing nitrate ions to nitrite at 118°C, solutions containing sodium nitrate and 0.5 M sodium formate were first irradiated at room temperature and then heated at 118°C for longer than 10 min. There was always a small increase in $G(NO_2^-)$, as shown by the diamond symbols in Fig. 2, but the increases were probably within experimental error and therefore not considered to be significant.

Solutions of sodium nitrate with the 0.5 M sodium formate replaced by 0.5 M 2-propanol were also irradiated. For a nitrate concentration of 2.5×10^{-2} M $G(NO_2^-)$ was 3.0 and 3.4 at room temperature and 118°C respectively, while for a nitrate concentration of 2.5×10^{-3} M, the corresponding $G(NO_2^-)$ were 2.6 and 2.8. As with the formate samples, the $G(NO_2^-)$ decreased with increasing dose so the quoted values are those extrapolated to zero dose.

No nitrite was detectable in an unirradiated sodium nitrate solution containing either formate or 2-propanol which had been preheated to 118°C. However, care had to be taken in sealing the cells during sample preparation to ensure no nitrate was left in the constriction as this thermally decomposed to form nitrite.

The effect of pH on $G(NO_2^-)$ is shown in Fig. 3*a* for N_2-saturated 5.0×10^{-2} M sodium formate solutions containing

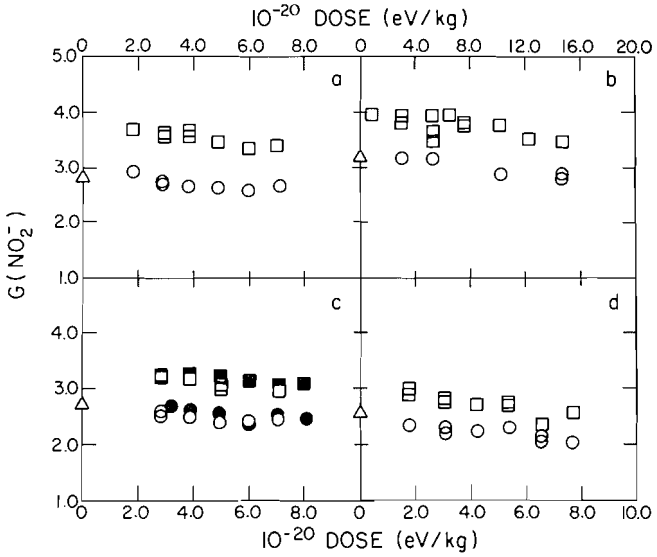

FIG. 1. The yield of nitrite at room temperature (○) and 118°C (□) as a function of dose from degassed solutions containing: (*a*) 2.5×10^{-3} M sodium nitrate and 5.0×10^{-2} M sodium formate; (*b*) 2.5×10^{-2} M sodium nitrate and 5.0×10^{-2} M sodium formate; (*c*) 2.5×10^{-3} M sodium nitrate and 5.0×10^{-3} M sodium formate (open points), containing 0.2 M sodium sulphate (solid points); (*d*) 2.9×10^{-4} M sodium nitrate and 5×10^{-2} M sodium formate. The triangles (△) are the room temperature values from ref. 5.

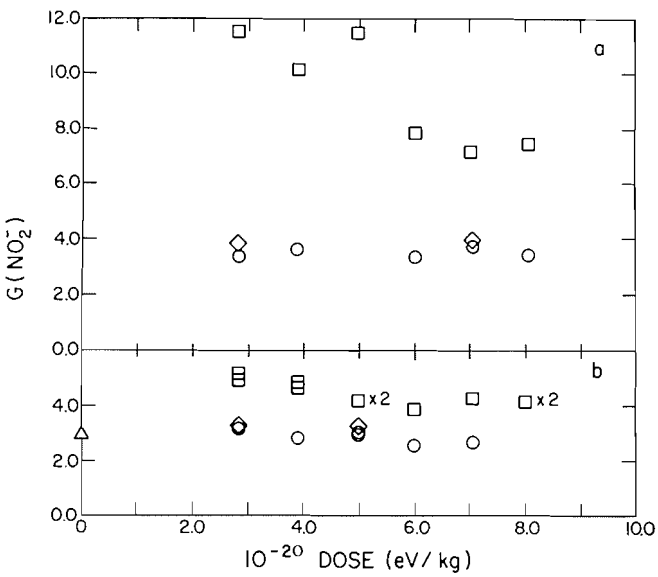

FIG. 2. The yield of nitrite at room temperature (○) and 118°C (□) as a function of dose from degassed solutions containing: (*a*) 2.5×10^{-2} M sodium nitrate and 5.0×10^{-1} M sodium formate; (*b*) 2.5×10^{-3} M sodium nitrate and 5.0×10^{-1} M sodium formate. The diamond (◇) symbols are for solutions irradiated at room temperature and heated to 118°C before analysis. The triangle (△) symbol is the room temperature result from ref. 5.

either 2.5×10^{-3} M or 2.5×10^{-2} M sodium nitrate irradiated at room temperature. Shown in Fig. 3*b* are the results when the formate was replaced by 5×10^{-2} M 2-propanol.

To investigate the decrease of $G(NO_2^-)$ with dose for both formate ion and 2-propanol solutions, the reactions of $CO_2^{\cdot-}$ and $(CH_3)_2\dot{C}OH$ with nitrite ions were followed at room temperature. Firstly, nitrous oxide saturated solutions containing

TABLE 1. $G[H_2O_2]$ and $G[H_2]$ from irradiated solutions containing sodium formate on sodium nitrate

		$G(H_2O_2)$		$G(H_2)$	
$[NaNO_3]/M$	[Na formate]/M	25°C	118°C	25°C	118°C
2.9×10^{-4}	5×10^{-2}	0.43 ±0.05	0.43 ±0.05	1.15 ±0.27	1.28 ±0.23
2.5×10^{-3}	5×10^{-2}	0.54 ±0.06	0.47 ±0.06		
2.5×10^{-2}	5×10^{-2}	0.65 ±0.05	0.60 ±0.05	0.70 ±0.16	0.92 ±0.17
2.5×10^{-3}	5×10^{-3}	0.53 ±0.09	0.56 ±0.05	0.75 ±0.13	0.86 ±0.16
2.5×10^{-3}*	5×10^{-3}*	0.40 ±0.09	0.42 ±0.02	0.66 ±0.04	0.72 ±0.04
2.5×10^{-3}	5×10^{-1}	0.27 ±0.07	0.22 ±0.06	0.72 ±0.05	0.85 ±0.06
2.5×10^{-2}	5×10^{-1}	0.32 ±0.10	0.31 ±0.05	0.70 ±0.08	0.85 ±0.05

*Also contains 0.2 M Na_2SO_4.

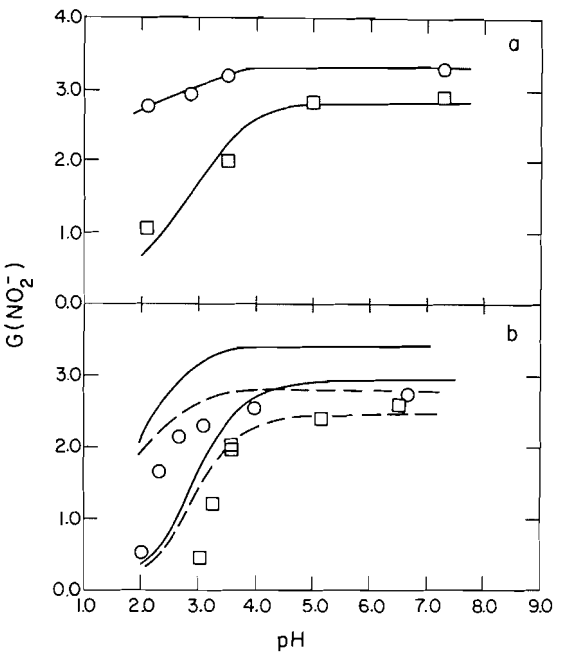

FIG. 3. The yield of nitrite as a function of pH at room temperature from 2.5×10^{-3} M sodium nitrate (○) and 2.5×10^{-2} M sodium nitrate (□) solutions containing: (*a*) 5.0×10^{-2} M sodium formate; (*b*) 5.0×10^{-2} M 2-propanol. The solid and dashed lines are computer calculated yields (see text).

0.5 M sodium formate and $3-20\times10^{-5}$ M sodium nitrite and, secondly, nitrogen saturated solution containing 0.26 M acetone, 0.26 M 2-propanol, and $3-20\times10^{-5}$ M sodium nitrite were irradiated in syringes. In both cases $G(NO_2^-$ loss) was ~1.9.

Discussion

One of the most widely used methods to determine the scavengable yield of e^-_{aq} has been to measure $G(NO_2^-)$ in deoxygenated solutions containing nitrate ions as an electron scavenger and either formate (5, 9, 10), 2-propanol (5, 11–13), ethanol (5, 8, 14), or methanol (13) as a hydroxyl radical scavenger.

Reaction [2] indicates the species present in irradiated neutral water.

[2] $H_2O \rightsquigarrow e^-_{aq}, \dot{O}H, \dot{H}, H_2O_2, H_2$

When nitrate ions and one of the above hydroxyl radical scavengers are present, the generally accepted mechanism is reactions [3] and [4] followed by [9]–[11] in the case of formate and [17]–[19] for 2-propanol (5, 9–13) (see Table 2). The other alcohols react in a manner similar to 2-propanol. Provided the formate or 2-propanol concentration is twice the nitrate concentration so that reaction [10] or [18] scavenges greater than 95% of the hydrogen atoms in competition with [4] then $G(NO_2^-)$ can be equated to $G(e^-_{aq})$ scavenged. However, for this last relationship to hold it must be assumed that reactions [11] and [19] are sufficiently fast so that no nitrogen dioxide is converted to nitrite via reactions [5]–[7].

The pH dependence of $G(NO_2^-)$ at room temperature

In the present study, $G(NO_2^-)$ was used as a measure of $G(e^-_{aq})$ scavenged for irradiations at room temperature and 118°C. The choice of which hydroxyl radical scavenger, formate or 2-propanol, was based on how well the pH dependence, at room temperature, of $G(NO_2^-)$ (Fig. 3) could be modelled since the only rate constants not known are [11] and [10] (Table 2).

By comparing Fig. 3*a* to 3*b*, it is obvious that for similar reactivity (eq. [1]) of solutes, $G(NO_2^-)$ for the 2-propanol solutions was lower than that of the corresponding formate solutions for pH > 5.5 where reaction [8] does not compete significantly. In fact, this is generally true of all nitrate solutions where alcohols are used as a hydroxyl scavenger (5, 9–14). This suggests that [19] is either too slow to compete with [5]–[7] and [20] or that reaction of the alcohol-radicals with nitrogen dioxide does not form nitrite exclusively. A possible reaction could be [21].

[21] $(CH_3)_2COH + \dot{N}O_2 \rightarrow (CH_3)_2C(NO_2)(OH)$

The pH dependence of $G(NO_2^-)$ for nitrate–formate solutions can be satisfactorily modelled (using the computer program MACKSIMA CHEMIST (22)) with the reactions and rate

Can. J. Chem. Downloaded from www.nrcresearchpress.com by 210.87.254.42 on 09/06/12
For personal use only.

TABLE 2. Reactions with rate constants for irradiated nitrate solutions

No.	Reaction	Rate constant	Reference
[3]	$NO_3^- + e_{aq}^- \xrightarrow{H^+} \dot{N}O_2 + OH^-$	$1.05\times10^{10}\ M^{-1}\ s^{-1}$	15
[4]	$NO_3^- + \dot{H} \rightarrow \dot{N}O_2 + OH^-$	$1.2\times10^{7}\ M^{-1}\ s^{-1}$	16
[5]	$\dot{N}O_2 + \dot{N}O_2 \rightarrow N_2O_4$	$2k = 9.0\times10^{8}\ M^{-1}\ s^{-1}$	18
[6]	$N_2O_4 \rightarrow \dot{N}O_2 + \dot{N}O_2$	$6.9\times10^{3}\ s^{-1}$	18
[7]	$N_2O_4 + H_2O \rightarrow NO_3^- + NO_2^- + 2H^+$	$1.8\times10^{1}\ M^{-1}\ s^{-1}$	17
[8]	$H^+ + e_{aq}^- \rightarrow \dot{H}$	$2.0\times10^{10}\ M^{-1}\ s^{-1}$	15
[9]	$HCOO^- + \dot{O}H \rightarrow CO_2^{\cdot-} + H_2O$	$2.5\times10^{9}\ M^{-1}\ s^{-1}$	17
[10]	$HCOO^- + \dot{H} \rightarrow CO_2^{\cdot-} + H_2$	$2.5\times10^{8}\ M^{-1}\ s^{-1}$	16
[11]	$\dot{N}O_2 + CO_2^{\cdot-} \rightarrow NO_2^- + CO_2$	$\geq6\times10^{9}\ M^{-1}\ s^{-1}$	See text
[12]	$CO_2^{\cdot-} + CO_2^{\cdot-} \rightarrow (CO_2^-)_2$	$2k = 2.0\times10^{9}\ M^{-1}\ s^{-1}$	19
[13]	$HCOOH \rightarrow HCOO^- + H^+$	$8.6\times10^{6}\ s^{-1}$	20
[14]	$HCOO^- + H^+ \rightarrow HCOOH$	$5.0\times10^{10}\ s^{-1}$	20
[15]	$HCOOH + \dot{O}H \rightarrow CO_2^{\cdot-} + H_2O + H^+$	$1.5\times10^{8}\ M^{-1}\ s^{-1}$	17
[16]	$HCOOH + \dot{H} \rightarrow CO_2^{\cdot-} + H_2 + H^+$	$1.2\times10^{6}\ M^{-1}\ s^{-1}$	16
[17]	$(CH_3)CHOH + \dot{O}H \rightarrow (CH_3)_2\dot{C}OH + H_2O$	$2.9\times10^{9}\ M^{-1}\ s^{-1}$	17
[18]	$(CH_3)_2CHOH + \dot{H} \rightarrow (CH_3)_2\dot{C}OH + H_2$	$8.0\times10^{7}\ M^{-1}\ s^{-1}$	16
[19]	$\dot{N}O_2 + (CH_3)_2\dot{C}OH \rightarrow NO_2^- + (CH_3)_2C{=}O$	$6\times10^{9}\ M^{-1}\ s^{-1}$	See text
[20]	$(CH_3)_2\dot{C}OH + (CH_3)_2\dot{C}OH \rightarrow (CH_3)_2C{=}O + (CH_3)_2CHOH$ or $(CH_3)_2C(OH){-}C(OH)(CH_3)_2$	$2k = 1.4\times10^{9}\ M^{-1}\ s^{-1}$	21

constants in Table 2 provided the rate constant k_{11} was equal to or greater than $6 \times 10^9 M^{-1} s^{-1}$. This value of k_{11} is greater than $(2k_5 \times 2k_{12})^{1/2}$ as would be expected for a redox reaction (23). The initial G-values for the species formed in reaction [2] were taken from the reactivity plots in ref. 5. Although both reactions [3] and [8] are ionic strength dependent, the actual magnitude of the dependence is ambiguous from the literature (24–27). The values used (Table 2) were a conservative attempt to correct for ionic strength and the calculated results are given by the solid lines in Fig. 3*a*.

The pH dependences of $G(NO_2^-)$ for the nitrate–2-propanol solutions (Fig. 3*b*) are similar to those reported by Sawai (11). As noted earlier, $G(NO_2^-)$ for this system is lower than that for the corresponding formate solution of the same reactivity. A fit between the experimental results and those calculated using the rate constants in Table 2 could not be obtained using G-values for the products in [2] calculated from reactivities (5) (solid line – Fig. 3*b*). An attempt to fit the data with the scavenged $G(e^-_{aq})$ equated to $G(NO_2^-)$ for pH > 5.5 (and the G-values for the other species formed in [6] scaled down to ensure a mass balance) was also unsuccessful as shown by the dashed lines in Fig. 3*b*. The rate constant k_{19} was fixed at $6 \times 10^9 M^{-1} s^{-1}$ for these calculations. From this it was apparent that the chemistry in irradiated nitrate–2-propanol is not well understood, so for the majority of the high temperature studies the nitrate–formate system was used.

Comparison of the radiolyses of nitrate solutions at room temperature and 118°C

At room temperature, the results for $G(NO_2^-)$ when extrapolated to zero dose agree reasonably with those of Draganić and Draganić (5) (Fig. 1); however, the decrease of $G(NO_2^-)$ with dose cannot be due to depletion of the initial solutes. Since it was found that both $CO_2^{\cdot-}$ and $(CH_3)_2\dot{C}OH$ could react with nitrite ions in sodium nitrite solutions, the same reaction [22]

[22] $NO_2^- + CO_2^{\cdot-}$ or $(CH_3)_2\dot{C}OH \rightarrow$ products

might be occurring in the nitrate solutions in competition with [11] or [19] as the nitrite concentration builds up during the irradiation.

When the nitrate–formate solutions were irradiated at 118°C, $G(NO_2^-)$ was always greater than that at room temperature (Fig. 1). For formate concentrations of $5 \times 10^{-3} M$ and $5 \times 10^{-2} M$, the increase in $G(NO_2^-)$ of 25% over the room temperature value is compatible with most of the published $G(e^-_{aq})$ data. Freeman and co-workers (3) used sulphur hexafluoride (SF_6) and nitrous oxide (N_2O) as electron scavengers and found for SF_6 over the temperature range 23°C to 106°C a 20% increase in $G(F^-/6)$ while for N_2O, $G(N_2)$ increased 19% over the range 23°C to 80°C. Kalecinski (8) who irradiated deoxygenated 0.1 M potassium nitrate and 0.1 M ethanol solutions found $G(NO_2^-)$ increased 16% over the temperature range 20°C to 130°C. However, above 130°C, Kalecinski found $G(NO_2^-)$ decreased to zero by ~195°C.

When the formate was replaced by 0.5 M 2-propanol (which has ÒH reactivity similar to the formate) in our experiments, the increases in $G(NO_2^-)$ were 8% and 15% for the 2.5×10^{-3} M and $2.5 \times 10^{-2} M$ sodium nitrate respectively. Again these results are consistent with earlier published results (3, 8) and the present results with formate concentrations less than 0.5 M. However, with the 0.5 M formate solutions, when extrapolated to zero dose, the increase in $G(NO_2^-)$ of 55% and 280% for $G(NO_2^-)$ from $2.5 \times 10^{-3} M$ and $2.5 \times 10^{-2} M$ nitrate concentrations respectively appears high when compared to the above results.

Figure 1*c* shows that raising the ionic strength from $7.5 \times 10^{-3} M$ to $3 \times 10^{-1} M$ with 0.2 M Na_2SO_4 did not affect $G(NO_2^-)$ significantly. The hydrogen and hydrogen peroxide yields for all the nitrate–formate solutions were temperature independent within experimental error (Table 1). Heating to 118°C, solutions previously irradiated at room temperature did not affect $G(NO_2^-)$ (Fig. 2). Taking these results in total indicates that for the 0.5 M formate solutions, nitrate is not being reduced to nitrite by a stable end product of the radiation at 118°C, and it is not high ionic strength giving rise to the increase in $G(NO_2^-)$. The results suggest that the high nitrite

Can. J. Chem. Downloaded from www.nrcresearchpress.com by 210.87.254.42 on 09/06/12
For personal use only.

yields in 0.5 *M* formate solutions arise from a chain reaction, possibly initiated by the direct action of the radiation on the formate ion, which reduces nitrate to nitrite.

Calculation of $G(e^-_{aq})$ *from* $G(NO_2^-)$ *at 118°C*

Leaving aside the 0.5 *M* formate solutions, the question arises as to whether the increase of 25% in $G(NO_2^-)$ found for the solutions with lower formate concentrations reflects a real increase in the overall e^-_{aq} yield; an increase in the reactivity of the nitrate; or simply a chain reaction as postulated in the 0.5 *M* formate case. Based on an activation energy of 2–4 kcal/mol for reaction [3] (24), the reactivity of the nitrate ion will increase by a factor of two to five. Presumably the reactivity of formate (reaction [9]) will increase by a similar amount. This should lead to an increase in e^-_{aq} scavenged for the low solute concentrations and, hence, an increased $G(NO_2^-)$ (5).

One approach to determine whether, in addition to the increased reactivity of the solutions at 118°C, there is an increase in the overall $G(e^-_{aq})$ is the following. With the nitrate – 5×10^{-2} *M* formate solution, assume in going from 25°C to 118°C that: the yield of the products in [6] do not change; the reactivity plots in ref. 5 are still valid; and the rate constants for [3] and [9] increase a factor of five. The predicted increases in $G(NO_2^-)$ for 2.9×10^{-4} *M*, 2.5×10^{-3} *M*, and 2.5×10^{-2} *M* nitrate solutions are 10%, 17%, and 20%, respectively. The corresponding calculated decreases in $G(H_2O_2)$ are 19%, 17%, and 14%. However, $G(H_2O_2)$ is not a function of temperature in the current experiments (Table 1). The predicted decrease in $G(H_2)$ of ~10% is within the experimental error of our experiments (Table 1). Furthermore, the predicted increases in $G(NO_2^-)$ do not account for the observed 25% increase observed at *all* nitrate concentrations. This indicates that reactivity alone under these conditions cannot account for the results. However, if the reactivity increase is coupled with an increase in the yield of the products of reaction [6] at 118°C then this may account for the results.

The constancy of the 25% increase in $G(NO_2^-)$ for all solutions with formate less than 0.5 *M* suggests that the processes occurring in the 0.5 *M* formate solutions are not occurring in the dilute solutions. In the 0.5 *M* formate case the percentage increase in $G(NO_2^-)$ was nitrate concentration dependent (Fig. 2).

Conclusions

The use of nitrate as an electron scavenger in the presence of formate or 2-propanol is not a good method to use in evaluating $G(e^-_{aq})$ at temperatures above room temperature. The chemistry of the solutions is complex and not completely understood. The weakness of the scheme lies, in part, in expecting 100% efficiency from reactions [11] and [19]. In principle, the best scavengers are those which are converted by the e^-_{aq} (or $\dot{O}H$) directly into a stable product or to an intermediate which decays by a first order process to a stable product. Studies towards this end are under way in these laboratories now.

Acknowledgements

The authors wish to thank Dr. J. W. Fletcher for valuable discussions during the course of this work. The technical support of E. B. Selkirk is also greatly appreciated.

1. (*a*) J. W. T. SPINKS and R. J. WOODS. An introduction to radiation chemistry. Wiley-Interscience, New York. 1976; (*b*) I. G. DRAGANIĆ and Z. D. DRAGANIĆ. The radiation chemistry of water. Academic Press, New York and London. 1971.
2. (*a*) R. W. MATTHEWS. AAEC/TM537, Lucas Heights, Australia. 1970; (*b*) C. J. HOCHANADEL and J. A. GHORMLEY. Radiat. Res. **16**, 653 (1962); (*c*) H. KUBOTA. J. Inorg. Nucl. Chem. **28**, 3053 (1966); (*d*) D. R. MCCRACKEN and G. V. BUXTON. Nature, **292**, 439 (1981).
3. K. N. JHU, T. G. RYAN, and G. R. FREEMAN. J. Phys. Chem. **79**, 868 (1975).
4. W. G. BURNS and W. R. MARSH. J. Chem. Soc. Faraday Trans. **77**, 197 (1981).
5. Z. D. DRAGANIĆ and I. G. DRAGANIĆ. J. Phys. Chem. **77**, 765 (1973).
6. A. O. ALLEN, C. J. HOCHANADEL, J. A. GHORMLEY, and T. W. DAVIS. J. Phys. Chem. **56**, 575 (1952).
7. W. A. SEDDON. Thesis, University of Edinburgh. 1962.
8. J. KALECINSKI. Bull. Acad. Polanaise, Sci. Chim. **21**, 209 (1973).
9. B. HICKEL. CEA-R-4046 Saclay, France. 1970.
10. E. HAYON. Trans. Faraday Soc. **61**, 735 (1964).
11. T. SAWAI. Bull. Chem. Soc. Jpn. **39**, 955 (1966).
12. A. APPLEBY, G. SCHOLES, and M. SIMIC. J. Am. Chem. Soc. **85**, 3891 (1963).
13. J. T. ALLEN. J. Phys. Chem. **68**, 2697 (1964).
14. C. BAQUEL, J. C. ROUX, and J. SUTTON. J. Phys. Chem. **74**, 4210 (1970).
15. M. ANBAR, M. BAMBENEK, and A. B. ROSS. Natl. Stand. Ref. Data Ser. 43 (U.S. Natl. Bur. Stand.), 1973.
16. M. ANBAR, FARHATAZIZ, and A. B. ROSS. Natl. Stand. Ref. Data Ser. **51** (U.S. Natl. Bur. Stand.), 1975.
17. FARHATAZIZ and A. B. ROSS. Natl. Stand. Ref. Data Ser. **59**, (U.S. Natl. Bur. Stand.), 1977.
18. M. GRATZEL, A. HENGLEIN, J. LILIE, and G. BECK. Ber. Bungenges Physik. Chem. **73**, 646 (1969).
19. G. V. BUXTON and R. M. SELLERS. Trans. Faraday Soc. **69**, 555 (1973).
20. M. EIGEN, W. KRUSE, G. MAASS, and L. DEMAEYER. Prog. Reaction Kinet. **2**, 287 (1964).
21. M. SIMIC, P. NETA, and E. HAYON. J. Phys. Chem. **73**, 3794 (1969).
22. A. W. BOYD, M. B. CARVER, and R. J. DIXON. Radiat. Phys. Chem. **15**, 177 (1980).
23. W. A. PRYOR. Free radicals. McGraw-Hill, New York. 1966.
24. B. CERCEK. Int. J. Radiat. Phys. Chem. **3**, 231 (1971).
25. J. E. ALDRICH, M. J. BRONSKILL, R. M. WOLFF, and J. W. HUNT. J. Chem. Phys. **55**, 530 (1971).
26. G. CZAPSKI and H. A. SCHWARZ. J. Phys. Chem. **66**, 471 (1962).
27. E. PELED and G. CZAPSKI. J. Phys. Chem. **74**, 2903 (1970).

Can. J. Chem. Downloaded from www.nrcresearchpress.com by 210.87.254.42 on 09/06/12
For personal use only.

Organic sulfur mechanisms. 24. Preparation and reactions of 2-hydroxyethanesulfonyl chloride, the first hydroxyalkanesulfonyl chloride[1]

JAMES FREDERICK KING AND JOHN HENRY HILLHOUSE
Department of Chemistry, University of Western Ontario, London, Ont., Canada N6A 5B7

Received December 21, 1982

JAMES FREDERICK KING and JOHN HENRY HILLHOUSE. Can. J. Chem. **61**, 1583 (1983).

2-Hydroxyethanesulfonyl chloride (**1***a*) is readily made by reaction of an aqueous solution of 2-mercaptoethanol (**4***a*) with chlorine. This is the first clearly proved preparation of a compound which is both an alcohol and a sulfonyl chloride. Reactions of **1***a* with water and alcohols evidently proceed largely by intramolecular cyclization to the transient β-sultone (**2***a*), which then undergoes nucleophilic ring opening to form the products. In the presence of tertiary amines a minor but significant part of the reaction is shown by deuterium labelling to proceed via hydroxymethylsulfene (**14**), the principal reaction of which is simply to add the alcohol or water; only a small part, if any, of the sulfene (**14**) loses the hydroxyl group to give the ethenesulfonate derivatives (**13** or **22**). Aqueous chlorination of 3-mercapto-1-propanol gave 3-chloro-1-propanesulfonyl chloride (**5***a*) and 1,3-propane sultone (**2***b*) with no sign of any 3-hydroxy-1-propanesulfonyl chloride (**1***b*). A mechanism for the aqueous chlorination process invoking a cyclic chlorooxasulfoxonium ion (**27**) is discussed.

JAMES FREDERICK KING et JOHN HENRY HILLHOUSE. Can. J. Chem. **61**, 1583 (1983).

On prépare facilement le chlorure d'hydroxy-2 éthanesulfonyle (**1***a*) en faisant réagir une solution aqueuse de mercapto-2 éthanol (**4***a*) avec le chlore. C'est la première fois qu'on prépare un composé qui est à la fois un alcool et un chlorure de sulfonyle. Le composé **1***a* réagit avec l'eau et l'alcool principalement par cyclisation intramoléculaire en donnant le β-sultone (**2***a*) qui par ouverture nucléophile du cycle conduit aux produits désirés. Le marquage au deutérium permet d'établir qu'en présence d'amines tertiaires il se produit une réaction secondaire importante par l'intermédiaire d'un hydroxyméthylsulfène (**14**) qui s'additionne principalement sur l'eau ou l'alcool; seule une faible partie, s'il y en a, du sulfène (**14**) perd le groupe hydroxyle pour donner les dérivés éthènesulfonates (**13** ou **22**). La chloration aqueuse du mercapto-3 propanol-1 donne le chlorure de chloro-3 propane-1 sulfonyle (**5***a*) et le propane-1,3 sultone (**2***b*) sans aucune trace de chlorure d'hydroxy-3 propane-1 sulfonyle (**1***b*). On discute un mécanisme de chloration aqueuse qui fait intervenir un ion chlorooxasulfoxonium cyclique (**27**).

[Traduit par le journal]

Introduction

In connection with our study of the pyridine-promoted hydrolysis of ethenesulfonyl chloride (1), the question arose as to whether 2-hydroxyethanesulfonyl chloride (**1***a*) – or indeed any compound with both alcohol and sulfonyl chloride groups – was capable of being prepared in pure form. An alcohol, of course, normally reacts with a sulfonyl chloride to give the

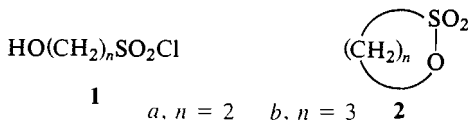

1 *a*, $n = 2$ *b*, $n = 3$ **2**

sulfonic ester as the initial product, but the reaction in the absence of catalysis is not, in fact, particularly fast at room temperature. Geiseler and Laue's estimate for the rate of reaction of 1-propanesulfonyl chloride in 1-butanol at 25°C corresponds to a half reaction time of 27 hours (2). Scott and Lutz, presumably to obtain a conveniently rapid rate for kinetic studies, used as their medium refluxing ethanol, in which 1-octanesulfonyl chloride showed a half-life of 8 min (3). These bimolecular reactions give, of course, only a rough lower limit to the rate of reaction of the analogous bifunctional species (**1**), since **1** is capable of cyclization to form **2**, and for certain ring sizes this will be much faster than the corresponding bimolecular process. Such a reaction of **1***a*, however, would lead to the four-membered ring sultone **2***a*, and the formation of four-membered sulfur-containing rings is typically not much faster than the bimolecular reaction at ordinary concentrations (4, 5). In addition, the electron-withdrawing influence of the nearby chlorosulfonyl group might be expected to lower the nucleophilicity of the hydroxyl function, thereby enhancing the stability of **1***a*.

Preparation of compounds with both chlorosulfonyl and *phenolic* hydroxyl groups has been reported on occasion (6–10), the first being the synthesis of **3***b* seventy-five years ago (6). Although the presence of the two substituents *ortho*

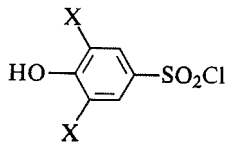

3
a X = H
b X = Br

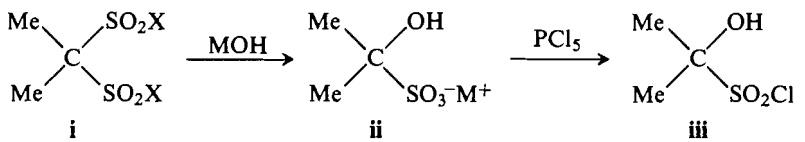

i **ii** **iii**

S = OPh or NMePh (M = Na or Ba/2)

FIG. 1.

[1]Part 23: see ref. 64.

Can. J. Chem. Downloaded from www.nrcresearchpress.com by 210.87.254.42 on 09/06/12
For personal use only.

Can. J. Chem. Downloaded from www.nrcresearchpress.com by 210.87.254.42 on 09/06/12
For personal use only.

to the hydroxyl in **3***b* appears to lead to easier preparation and lower reactivity, the simplest member of the series (**3***a*) has been obtained in crystalline form and is not especially fragile (9). The hydroxyl group of an alcohol is more nucleophilic than that of a phenol, however, and we were not surprised that a search of the chemical literature turned up no properly authenticated examples of a compound with both an alcoholic hydroxyl and a chlorosulfonyl function.[2]

The most frequently used routes to alkanesulfonyl chlorides involve either (*i*) reactions of the sulfonic acid (or salt) with an inorganic acid chloride like thionyl chloride or phosphorus pentachloride, or else (*ii*) aqueous chlorination of a thiol or like material with the sulfur at a low oxidation level (17). Obviously the inorganic acid chloride route is a poor candidate for the synthesis of **1** since any reagent likely to convert a sulfo group to a chlorosulfonyl might also be expected to transform an alcohol to the chloride, and, in fact, the reaction of sodium 2-hydroxyethanesulfonate ("isethionate") with either $POCl_3$–PCl_5 or $SOCl_2$–dimethylformamide is a good preparative route to 2-chloroethanesulfonyl chloride (**5***a*) (18).

More surprising, perhaps, are the reports that chlorination of mercaptoalkanols also proceeds with replacement of the hydroxyl by chlorine according to the general equation **4** → **5**.

$$HO(CH_2)_nSH \xrightarrow{Cl_2/H_2O} Cl(CH_2)_nSO_2Cl$$

4 **5**

a, *n* = 2 *d*, *n* = 5
b, *n* = 3 *e*, *n* = 6
c, *n* = 4

Gilbert, for example, describes a procedure involving chlorination followed by careful addition of water in which **5***a* is prepared from **4***a* in 94% yield (19). Goethals and Verzele (20) report that chlorination of aqueous suspensions of **4***b*, **4***c*, **4***d*, or **4***e* yields the corresponding ω-chloro-1-alkanesulfonyl chloride (**5**) as the major, or only, identified product.

Although these results were obviously not directly encouraging, they were indirectly helpful. Upon consideration of possible mechanisms for these processes (which are discussed in detail in the Results and discussion section), we were led to try simple chlorination of an aqueous solution of **4***a*, and found that the major isolated product was, indeed, **1***a*, along with a smaller amount of **5***a*. This preparation, together with the proof of structure and the reactions of **1***a* with water and alcohols, make up the substance of this paper. To our knowledge, **1***a* is the first characterized compound which is both an alcohol and an alkanesulfonyl chloride. It is also probably the simplest such compound capable of isolation at room temperature.[3] Part of this work has been described in preliminary form (24).

Results and discussion

*Preparation and proof of structure of 2-hydroxyethanesulfonyl chloride (**1**a)*

In our hands best preparative yields (~30%) of **1***a* were obtained by very rapid chlorination of an ice-cooled solution of **4***a*, followed by rapid work-up. The latter involved extraction of the reaction mixture first with benzene, then with methylene chloride, and then saturation of the aqueous layer with sodium chloride followed by further extraction with methylene chloride. The benzene extracts contained all of the 2-chloroethanesulfonyl chloride (**5***a*) (10% yield) mixed with some **1***a* (7%), the methylene chloride extracts on removal of solvent gave essentially clean 2-hydroxyethanesulfonyl chloride (**1***a*) in 28% yield, as a slightly syrupy liquid which gave appropriate elemental analyses and showed peaks characteristic of the hydroxyl and chlorosulfonyl groups at 3590, 3460, 1375, 1168, and 1058 cm^{-1} in the infrared. The ^{13}Cmr spectrum, which showed only peaks at 56.9 and 67.6 ppm, and the ^{1}Hmr spectrum with two perturbed triplets centred at 3.98 and 4.28 and a singlet at 2.8 ppm are clearly in excellent agreement with the assigned structure.[4] A solution of **1***a* in $CDCl_3$ (0.1 *M*) was stable for at least six months at room temperature, whereas the neat compound, though stable at −20°C, was approximately half decomposed after three weeks at room temperature.

A number of runs on a preparative scale (i.e. 10 to 30 g of **4***a*) carried out more or less as described above gave yields of **1***a* varying from about 10 to 35%. We have not systematically attempted to maximize the yield but we can offer a few pointers. (*i*) A large excess of chlorine seems to be necessary; smaller amounts lead to incompletely oxidized products characterized by a bad smell and relatively high-field peaks in the ^{1}Hmr spectrum. (*ii*) Rapid work-up appears to help minimize hydrolysis of **1***a*. (*iii*) Most of the **5***a* can be removed from a mixture of **1***a* and **5***a* by washing the neat liquid with cyclohexane; the work-up described above, however, is preferable when a sample of **1***a* without any **5***a* is desired.

These reactions, together with a number of transformations carried out to provide further evidence for the assigned structure (**1***a*), are summarized in Scheme 1. Reaction of **1a** with acetyl chloride gave a good yield of 2-acetoxyethanesulfonyl

[2]A hydroxyalkanesulfonyl chloride structure (**iii**), had, in fact, been suggested by Schroeter and Sulzbacher in 1928 (11) for a material obtained by reaction of PCl_5 with a substance assigned structure (**ii**), which in turn had been made by the action of strong base on **i**. In 1918, when Schroeter first proposed (12) structure **ii** for the product from **i**, the then accepted structure for the adduct of acetone and bisulfite was not **ii** but rather the α-hydroxysulfite formulation, $Me_2C(OH)OSO_2^-$ (Fig. 1). In 1926 Raschig and Prahl (13, 14) presented a formidable case for the α-hydroxy-sulfonate structure for aldehyde- and ketone-bisulfite adducts, and Schroeter and Sulzbacher attempted to refute the Raschig and Prahl revision by the following argument: they felt they had proved **ii** to be the structure of the product from **i**, this product was different from the acetone-bisulfite adduct, and therefore the acetone-bisulfite adduct could not have structure **ii**. Subsequent extensive work including two X-ray crystallographic structure determinations (15, 16, and references cited) has fully confirmed the α-hydroxy-sulfonate structure for the bisulfite adducts, however, and hence the compound from **i** cannot have structure **ii**, and there is thus no basis for assigning stucture **iii** to the product of its reaction with PCl_5. To the best of our knowledge neither of these materials has been studied since 1928, and their chemical natures are unknown.

[3]The simplest number of the series is, of course, hydroxymethanesulfonyl chloride, but it seems unlikely that this, or any other geminal hydroxy-sulfonyl chloride (including **iii** in footnote 2), can be isolated at room temperature. As we have noted (21), it is difficult to prepare and keep any compound of the general structure RSO_2Z when Z is a good nucleofuge and R a group capable of forming a reasonably stable cation, R^+; see also refs. 22 and 23. Except under the mildest conditions, any reaction capable of giving $HOCH_2SO_2Cl$ would thus be expected to give CH_2O, SO_2, and HCl, or products of their further reaction.

[4]NOTE ADDED IN PROOF: Very recent experiments by Mr. K. C. Khemani in this laboratory have (a) led to improved yields of **1***a* (>80% on a 25 mmol scale), and (b) enabled unambiguous assignment of the 56.9 ppm peak to C-2 and that at 67.6 ppm to C-1.

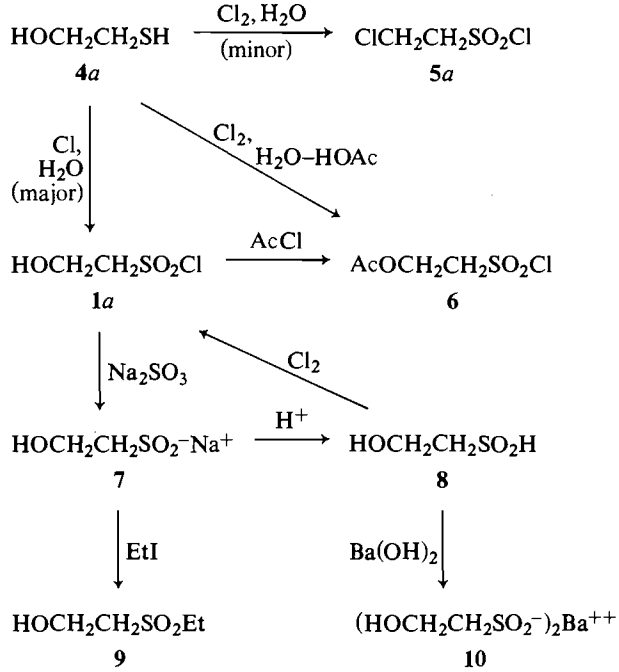

SCHEME 1

chloride (**6**), identical with a specimen prepared by Anschütz' method (7); the acetoxysulfonyl chloride (**6**) was also obtained as the product of chlorination of 2-mercaptoethanol (**4***a*) in a 1:1 mixture of water and acetic acid. Reduction of **1***a* with sodium sulfite gave the sodium sulfinate (**7**); the sulfinic acid **8** was obtained by acidification and continuous extraction of a solution of **7**, and was readily converted back to **1***a* by brief chlorination. Reaction of the sodium sulfinate **7** with ethyl iodide gave a modest yield of ethyl 2-hydroxyethyl sulfone (**9**), identical to a sample prepared from sodium ethanesulfinate and ethylene chlorohydrin (25). These observations clearly establish the structure **1***a* beyond reasonable doubt.

The barium sulfinate (**10**) in Scheme 1 is of interest in connection with the report by Hesse *et al.* (26) that this compound is the chief product of the reaction of ethylene sulfone with barium hydroxide. As our first route to the synthesis of **1***a* we had, in fact, attempted to make **10**, expecting that it would be easily converted to **1***a*. As we shall describe in detail in a separate paper, in our hands the major product of the reaction of ethylene sulfone with barium hydroxide was, in fact, the ethanesulfonate salt. After preparing authentic **10** as shown in Scheme 1 we were able to show that the product obtained from ethylene sulfone contained less than 5% of **10**.

Hydrolysis of 2-hydroxyethanesulfonyl chloride (1a)

Our original interest in preparing **1***a* stemmed from its possible use as a source of hydroxymethylsulfene (**14**), the chemistry of which we wished to examine to determine if it played any part in the hydrolysis of ethenesulfonyl chloride. Since sulfenes are most commonly generated from an alkanesulfonyl chloride by the action of a tertiary amine, we have accordingly looked at the reaction of **1***a* with tertiary amines and water. Prior to discussing the hydrolysis in the presence of amines, however, it is appropriate to look at the reaction with water alone.

Hydrolysis of **1***a* at pH 4.0 (in the pH-stat apparatus using sodium hydroxide as the titrant to maintain constant pH) gave, in addition to (*i*) the expected sodium 2-hydroxyethanesulfonate (**11**), (*ii*) a small amount of sodium 2-chloroethanesulfonate (12), and (*iii*) an unidentified product in what appears to be a somewhat larger amount (see Table 1 and the top line of Scheme 2). At pH 11.0 the same products plus a trace of sodium ethenesulfonate (**13**) were observed. As indicated in Table 1, addition of potassium chloride increased the yield of **12**. Compounds **11** and **12**, along with a trace of **13**, were found also in the product of reaction in D_2O (apparent pH 3.0 and 11.0); the spectra showed no sign of any deuterium incorporation.[5]

In the presence of pyridine, the reaction in D_2O (at apparent pH 6.0) showed two changes as indicated in the bottom line of Scheme 2: (*i*) the betaine **16** was formed as the major product, and (*ii*) about half of the 2-hydroxyethanesulfonate salt was the monodeuterated material (**15**). As indicated in Scheme 2, the latter product presumably arises from trapping of the sulfene (**14**) which is formed as a minor intermediate (ca. 15 to 20%) in the reaction of **1***a* with pyridine. Even this minor proportion of hydroxymethylsulfene (**14**) formation serves, however, to answer the question which prompted this study in the first place, viz. how does hydroxymethylsulfene (**14**) react in aqueous pyridine? The yield of the monodeuterated 2-hydroxyethanesulfonate (**15**), compared with the very small yield of ethenesulfonate (**13**), shows clearly that virtually all of the sulfene (**14**) goes to 2-hydroxyethanesulfonate and little, if any, loses OH^- to form the ethenesulfonate (**13**).

The sulfene (**14**) is, of course, but a minor contributor in the reactions of 2-hydroxyethanesulfonyl in water and all or most of the other products that we have identified may be easily explained by postulating that they are formed by way of β-sultone (**2***a*) (see Scheme 2, dotted lines radiating from **2***a*). The unsubstituted β-sultone (**2***a*) has never been isolated, though it has been postulated as an intermediate (27) and a number of substituted analogues have been prepared, either by cycloaddition of sulfur trioxide onto alkenes (28–32) or by the reaction of perhalogenated aldehydes or ketones with alkanesulfonyl chlorides and tertiary amines (33–37). β-Sultones lacking halogen substituents react readily with such nucleophiles as water, methanol, pyridine, and aniline to give the products derived from substitution with C—O cleavage (28, 38), and it is therefore reasonable to propose, as in Scheme 2, that the betaine (**16**) and the 2-chloroethanesulfonate (**12**) arise from the sultone (**2***a*). Clearly, with aqueous 0.54 *M* KCl at pH 4.0 (see Table 1), this means that at least half of the product is formed from **2***a*, and one may make a reasonable case that most, and perhaps all, of the **11** also comes from **2***a*. To do this we make use of the Swain–Scott equation, $\log k/k_0 = sn$, which is known to work reasonably well for alkyl transfer processes (39). Taking $n = 3.04$ for chloride ion (39) and assigning $s = 0.65$ as a typical value for a primary alkyl sulfonate ester,[6] we then obtain $\log k_{Cl}/k_0 = 2$, or $k_{Cl}/k_0 = 100$, where k_{Cl} and k_0 are the second-order rate constants for the reaction of **2***a* with chloride ion and water, respectively. If **12** and **11** are formed only from **2***a*, the product ratio will therefore be given by $k_{Cl}[Cl^-]/k_0[H_2O]$. Hence for a reaction in which the initial value of $[Cl^-]$ is 0.54 *M* and $[H_2O] = 55$ *M*, the

[5] For simplicity in this discussion we ignore the deuteration of the hydroxyl hydrogen, which will, of course, have roughly the deuterium content of the active hydrogen of the particular medium.

[6] Cf. Ethyl tosylate, $s = 0.66$ (39), ethyl mesylate, $s = 0.64$, butyl mesylate, $s = 0.65$, etc. (40).

Can. J. Chem. Downloaded from www.nrcresearchpress.com by 210.87.254.42 on 09/06/12
For personal use only.

TABLE 1. Products of the hydrolysis of 2-hydroxyethanesulfonyl chloride at 25°C[a]

pH	Concentration of added KCl (*M*)	Relative percentage yields of products[b] $HOCH_2CH_2SO_3^-Na^+$ (**11**)	$ClCH_2CH_2SO_3^-Na^+$ (**12**)
4.0	(None)	90[c]	3[c]
4.0	0.1	79[c]	19[c]
4.0	0.54	52[d]	48[d]
11.0	(None)	85[c,d]	2[c,d]
11.0	0.1	80[c]	17[c]
"3.0"[e]	(None)	89[f]	11[f]
"11.0"[e]	(None)	95[d,f]	58[d]

[a]pH-stat apparatus; initial concentration of **1***a*, 4×10^{-3} to 2.4×10^{-2} *M*.
[b]Estimated by integration of ^{1}Hmr spectra (D_2O) of the crude reaction products.
[c]The ^{1}Hmr spectrum showed the presence of a further, unidentified product.
[d]Peaks due to $CH_2{=}CHSO_3^-$ (up to 2%) were observed.
[e]In D_2O; pH "3.0" and "11.0" refer to pH-meter readings.
[f]No deuterium was incorporated into the methylene positions.

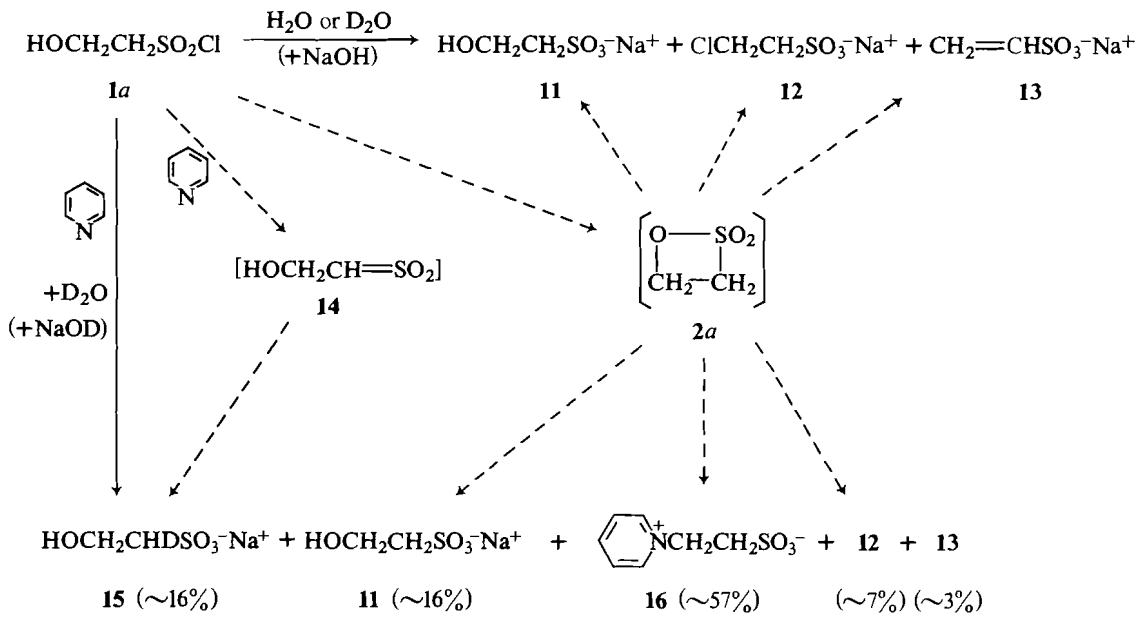

SCHEME 2

product ratio, **12**/**11**, would be predicted to be ~1, which is, within experimental error, that found under these conditions (0.9 ± 0.1, see Table 1). Similarly the hydrolysis in 0.1 *M* KCl is predicted to give a product ratio around 0.2; the observed value is 0.24 ± 0.07. The assignment of $s = 0.65$ for **2***a* is, of course, only a guess for illustrative purposes, but it should perhaps be noted that a value significantly smaller than 0.65 would predict a smaller yield of **12**, i.e. would make it impossible for Scheme 2 to account for the amount of **12** actually formed. On the other hand, a value much larger than 0.65 would imply that **2***a* is distinctly more selective than ethyl tosylate or ethyl or butyl mesylate. We find it difficult to quantify the effects of (a) the presence of the sulfonyl group β to the reacting carbon, and (b) the release of ring strain in this reaction, but if, as seems quite possible, these two effects are opposed then the combined effect may well be small and hence *s* may, in fact, be close to 0.65. This line of reasoning would indicate that most, and perhaps all, of the **11** and **12** formed in the simple hydrolyses at pH 4.0 and 11.0 and similarly most of the product not derived from the sulfene (**14**) in the pyridine-promoted reaction, are formed by way of β-sultone.[7] It is clear, however, that the point is by no means proved, and, recalling that some of these hydrolyses give a material as yet unidentified, further experiments are required to give a clear picture of the hydrolysis of **1***a*.

The very small amount of **13** produced in these reactions warrants brief mention. Of the various ways in which it might arise, perhaps the simplest is by hydrolysis of a small amount of **5***a* present as impurity in the **1***a*; **13** is the exclusive (>98%) product of hydrolysis of **5***a* at pH 6.0, and, in fact, the yield of **13** places an upper limit on the amount of **5***a* present in these samples of **1***a*. Formation of the "dimer", $HOCH_2CH_2SO_2$-

[7]Safety note: Since 1,3-propane sultone (**2***b*) has been identified as a strong carcinogen (Org. Synth. **58**, 168 (1978)) it would seem prudent to suspect β-sultone (**2***a*) also. We therefore recommend that until future experiments show this to be unnecessary, such likely sources of β-sultone as 2-hydroxyethanesulfonyl chloride (**1***a*) be handled with all precautions appropriate to a potentially highly hazardous material.

Can. J. Chem. Downloaded from www.nrcresearchpress.com by 210.87.254.42 on 09/06/12
For personal use only.

Can. J. Chem. Downloaded from www.nrcresearchpress.com by 210.87.254.42 on 09/06/12
For personal use only.

$OCH_2CH_2SO_2Cl$, by the conventional reaction of the alcohol and chlorosulfonyl groups of two molecules of **1***a*, could also lead to **13** since, by analogy with **5***a*, hydrolysis of the "dimer" might well give equivalent quantities of **13** and **11**. Finally, for the pyridine-promoted reaction, some of the **13** could arise from the sulfene by loss of hydroxide on trapping, as mentioned above.

Reactions of 2-hydroxyethanesulfonyl chloride with an alcohol and a tertiary amine

Although carried out under somewhat different conditions, the reactions of **1***a* with alcohols and tertiary amines in methylene chloride are quite similar to the pyridine-promoted hydrolysis. The most prominent products are the ester (**17**), the betaine (**19**), and the 2-chlorosulfonate salt (**20**) (See Table 2 and Scheme 3). Except for a brief, century-old paper describing the formation in very low yield of ethyl 2-hydroxyethanesulfonate by a silver salt procedure (41*a*),[8] alkyl hydroxyalkanesulfonates were to our knowledge previously unknown compounds and rigorous evidence for these structures (**17***a* and **17***b*) was therefore required. The neopentyl ester (**17***b*) gave correct elemental analyses and showed appropriate infrared and ^{1}Hmr spectra (see Experimental). The butyl ester (**17***a*) was identical to a fully characterized specimen prepared by a substrate–reagent ion-pair (SRIP) reaction of butyl [2]betylate 2-hydroxyethanesulfonate (**23**), a procedure developed simultaneously in this laboratory as part of our work on the chemistry of betylates (42, 43). In addition, acetylation of **17***a* gave butyl 2-acetoxyethanesulfonate (**24**), characterized by elemental analyses and spectra, and by the observation of identical ^{1}Hmr peaks in the spectrum of the product from the reaction of 2-acetoxyethanesulfonyl chloride (**6**) with 1-butanol and triethylamine; this spectrum also showed the presence of an almost equivalent amount of butyl ethenesulfonate (**22**, R = Bu).

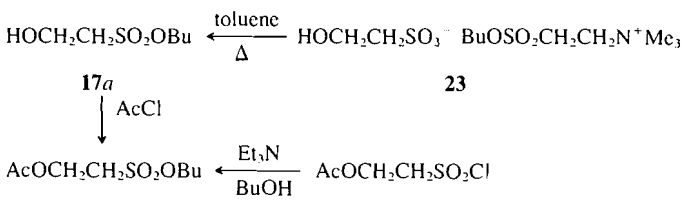

The mechanism of formation of the ester (**17**) follows from the reaction with 1-butanol-*d* which gives mostly the monodeuterated ester (**18**), clearly pointing to the intermediacy of the sulfene (**14**) as indicated in Scheme 3. The other major products, **19** and **20**, and probably at least some of 2-hydroxyethanesulfonate salt (**21**) very likely come from β-sultone (**2***a*) by reaction with the amine, chloride ion, and adventitious water, respectively. It is possible that a little of the 2-hydroxysulfonate salt (**21**) is formed from the ester (**17***a*) by transfer of the butyl group to the amine or some other nucleophile, but the lack of deuterium in the salt (**21**) formed in the presence of butanol-*d* shows this reaction to be unimportant. Such a pathway also does not account for the **21** formed in the reactions with neopentyl alcohol, since control experiments show the neopentyl ester to be completely stable to these conditions. The ethenesulfonate esters (**22**) could arise (a) from small amounts of 2-chloroethanesulfonyl chloride (**5***a*) present

TABLE 2. Tertiary-amine promoted reactions of 2-hydroxyethanesulfonyl chloride (**1***a*) with alcohols[a]

		Percentage yields of products[b]				
Alcohol (R′OH)	Amine (R_3N)	$HOCH_2CH_2SO_2OR'$ (**17**) (or $HOCH_2CHDSO_2OR'$ (**18**))	$R_3\overset{+}{N}CH_2CH_2SO_3^-$ (**19**)	$ClCH_2CH_2SO_3^-$ $R_3\overset{+}{N}H$ (**20**)	$HOCH_2CH_2SO_3^-$ $R_3\overset{+}{N}H$ (**21**)	$CH_2{=}CHSO_2OR$ (**22**)
1-Butanol	Pyridine	7	57	28	<1	3
1-Butanol	Trimethylamine	33	38	20	7	3
1-Butanol-*d*[c]	Trimethylamine	40[c]	40[c]	14[c]	3[c]	3[c]
1-Butanol	Triethylamine	27	22	43	<1	3
1-Butanol	Quinuclidine	30	29	21	10	<1
Neopentyl alcohol	Pyridine	8	35	40	8	2
Neopentyl alcohol	Trimethylamine	25	51	5	10	6

[a]In CH_2Cl_2 at room temperature with excess amine (1.5 to 10 equiv.) and alcohol (~10 equiv.).
[b]The product was analyzed by a combination of extraction and ion exchange procedures with the relative composition of binary mixtures (e.g. **17** and **22**) obtained from ^{1}Hmr spectra (see Experimental).
[c]The 2-hydroxyethanesulfonic ester from the reaction with 1-butanol-*d* was estimated from its ^{1}Hmr spectrum to consist of >80% of **18** and <20% of **17**. The other products from this reaction showed no sign of deuterium incorporation.

[8] Cf. Reference 41*b* and also ref. 41*c*.

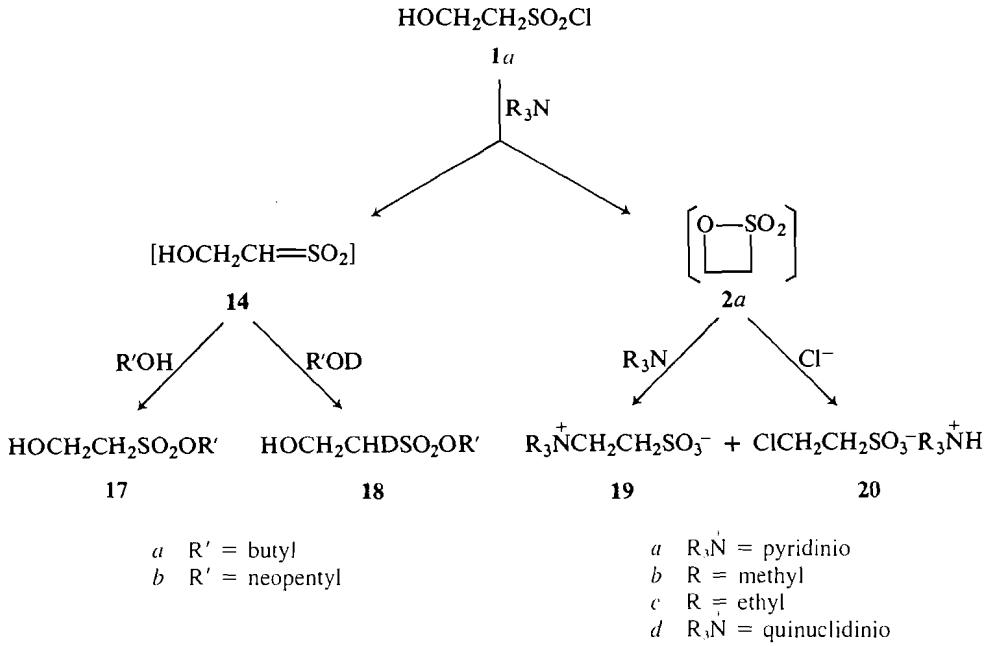

SCHEME 3

as impurity in the starting material, or (b) as secondary products from the trapping of the sulfene (**14**). The comparatively small amount of ethenesulfonate salt (**13**) already noted in the hydrolysis experiments (Table 1) indicates that the amount of **5***a* in these samples of **1***a* does not exceed 1%, and hence that at least some of the **22** comes by way of the sulfene (**14**). This latter reaction is perhaps most simply visualized in a generalized form as follows:

$$XCH_2CH_2{=}SO_2 \xrightarrow{HZ} [XCH_2\bar{C}HSO_2Z] \begin{cases} \xrightarrow{H^+} XCH_2CH_2SO_2Z \\ \rightarrow CH_2{=}CHSO_2Z + X^- \end{cases}$$

(Somewhat more complex schemes involving, for example, concerted addition to different conformers of the sulfene, are not, however, rigorously excluded.) A specific example of the above general scheme has been proposed (44) to account for the formation of both ethenesulfonate and betylate esters from the sulfene $R_3N^+CH_2CH{=}SO_2$. In addition, the observation of both **24** and **22** (R = butyl) from the acetoxysulfonyl chloride (**6**) (see above) also points to the operation of such a pathway. The small proportion of ethenesulfonate ester when X = OH, as compared to $X = R_3N^+$ or OAc, is in good agreement with the relatively poor, but not totally neglible, leaving group reactivity, or nucleofugality (45), of the hydroxyl group.

It should be noted that the reaction with 1-butanol-*d* provides evidence not only for the sulfene route to the hydroxy-ester (**17**), but also, since all of the other products lack deuterium, specifically against the intermediacy of the sulfene (**14**) in the formation of **19** and **20**. This means that if **19** and **20** arise from β-sultone (**2***a*), it cannot have been formed from the sulfene (**14**). This is not very surprising since such a cyclization is in Baldwin's terminology a 4-*endo-trig* process, which, with first-row elements at least, is strongly "disfavoured" (46). β-Sultone formation is, in our view, most probably a general-base assisted direct cyclization of **1***a*, a respectable 4-*exo-tet* reaction.

One feature apparent from Table 2 is the difference in the yield of the hydroxy-ester (**17**) with different amines. The saturated tertiary amines give 25–40% of **17** whereas pyridine leads to <10% of **17** and correspondingly larger amounts of the products formed from β-sultone (**2***a*). This recalls earlier observations in this laboratory (47) on the reaction of methanesulfonyl chloride with *p*-toluidine-d_2 and a tertiary amine; the predominant product with triethylamine (after work-up) was the monodeuterated amide, $CH_2DSO_2NHC_6H_4CH_3$, but with pyridine was the undeuterated amide $CH_3SO_2NHC_6H_4CH_3$. Also related are the recent findings of Farng and Kice (48) in the reactions of 1-butanesulfonyl chloride with piperidine-*d* and morpholine-*d*; the piperidide and morpholide were α-monodeuterated to the extent of 72% and 15% respectively. These results are consistent with competing elimination–addition (sulfene) and direct substitution mechanisms in which the elimination is more sensitive to change in base strength than the substitution (48), a picture that is in itself consistent with the high sensitivity to base change shown by the rate of sulfene formation from methanesulfonyl chloride (49).

The mechanism of the aqueous chlorination of mercaptoalkanols

As the final point of discussion we turn to the possible mechanisms of conversion of **4** into **1** and **5** by the action of chlorine and water. In the top line of Scheme 4 we show a simple pathway from **4** to **5**. We have not specified the route from **4** to **25**, but of the numerous possible (and perhaps parallel) paths the sequence **4** → $HO(CH_2)_nSCl$ → $HO(CH_2)_nSCl_3$ → **25** has the advantage that there is precedent for each step, though under somewhat different conditions, in reactions reported by Douglass *et al.* (50). Two other valuable observations reported by Douglass in his pioneering studies (51) are also relevant to the proposed scheme. The first, that alcohols react very quickly with a sulfinyl chloride, fits with the proposed conversion of **25** to **26**; this cyclization must be quick to compete with the hydrolysis of the sulfinyl chloride (**25** → **28**) which is known in the general case also to be rapid. The second point from Douglass' work (51) is his observation that chlorination of methyl methanesulfinate gives methanesulfonyl chloride and methyl chloride; this is the simplest possible

Can. J. Chem. Downloaded from www.nrcresearchpress.com by 210.87.254.42 on 09/06/12
For personal use only.

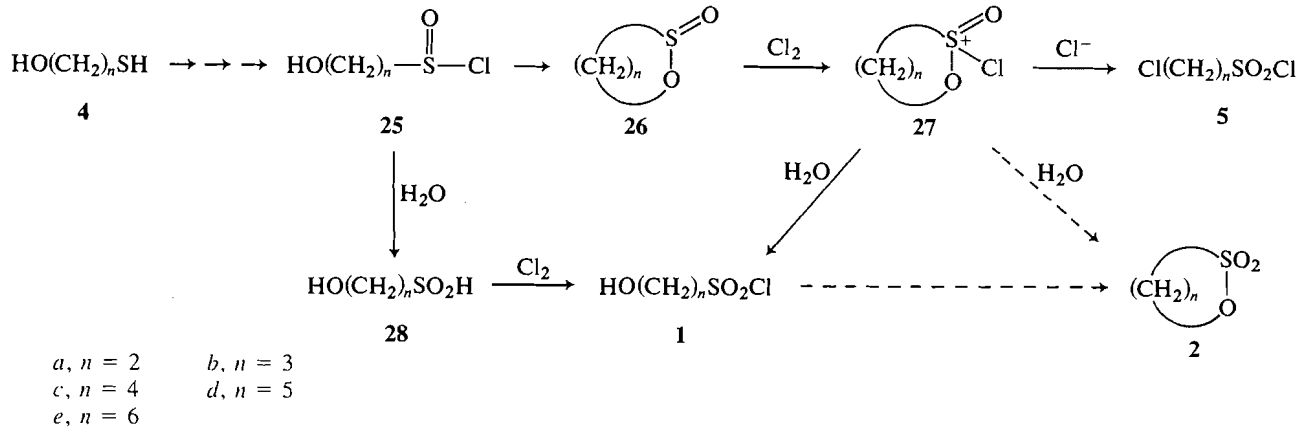

SCHEME 4

precedent for the proposed reaction **26** → **5**. We have noted (52) a closely related process,

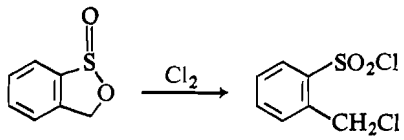

and it seemed likely at the time that a chlorooxasulfoxonium ion (like **27**) was an intermediate in this conversion (53). This view has since been strengthened by reports of (a) the isolation of stable aryloxysulfoxonium salts (54), and (b) the observation of products readily derivable from other closely related sulfoxonium intermediates (55–58). A further point in support of the mechanism in Scheme 4 is the comment by Goethals and Verzele (20) that their sample of **5***c* "contains 5% butane sultone" (**2***c*), a by-product nicely consistent with the intermediacy of **27***c*.

For the formation of the hydroxysulfonyl chloride (**1**) Scheme 4 shows two possible paths, one by way of the open-chain sulfinic acid (**28**), the other via the sulfoxonium ion (**27**); a third possibility in which **26** is hydrolyzed to **28**, which then gives **1**, is probably not significant owing to the comparative slowness of the acid-catalyzed hydrolysis of sulfinic esters (59). The sequence **25** → **28** → **1** is well-precedented but, lest it be too quickly favoured over the other route, we should point out that if **5** is indeed formed from **27** then it is highly likely that at least some **1** is, too. As has already been mentioned above in our discussion of the role of β-sultone in the hydrolysis of **1***a*, a 0.5 *M* aqueous solution of chloride ion in reaction with an electrophile with a Swain–Scott *s*-value of 0.65 should give about equal amounts of the products of reaction with chloride ion and water, respectively. If, as seems reasonable to us, the selectivity of **27** is no higher than that of **2**, then in the early stages of the reaction at least, in which $[Cl^-] < 1$ or 2 *M*, a significant fraction of **27** must give **1**. It should be noted, however, that reaction of one equivalent of **4** with excess chlorine generates four to six equivalents of chloride ion, and, as a result, the chloride ion concentration jumps abruptly during the reaction, and less **1***a* would be formed from **27***a* as the final concentration of chloride ion is reached.

In the course of this study we have also had a brief look at chlorination of 3-mercapto-1-propanol (**4***b*) under our conditions. We found no sign of the hydroxysulfonyl chloride (**1***b*), the organic-soluble product being a mixture of 3-chloropropane-1-sulfonyl chloride (**5***b*) and the propane sultone (**2***b*), each in about 25% yield. To check to see if the γ-sultine (**26***b*) could be an intermediate in the reaction of **4***b*, we chlorinated a sample of **26***b* and indeed obtained both the sultone (**2***b*) and the sulfonyl chloride (**5***b*); the yields (77% and 13%, respectively) were different from those obtained from **4***b*, though this is probably due to the much lower concentration of chloride ion present in the reaction of the sultine (**26***b*). It is possible that no **1***b* was formed at all in this reaction, but it seems to us more likely that it was, in fact, formed and was all rapidly converted to **2***b*. The correct explanation of this and a number of other points of mechanism raised in this paper, however, must await futher experiments, which we hope to be able to describe in due course.

Experimental

Melting points were obtained with a Gallenkamp melting point apparatus and are uncorrected. Refractive indices were determined on a thermostatically controlled Bausch and Lomb Abbé refractometer. Infrared (ir) spectra were recorded on Perkin–Elmer 621 or Beckman 4250 spectrometers; spectra were calibrated using a polystryrene film. The ^{1}Hmr spectra were obtained with Varian T-60 or XL-100 instruments, with all reported δ values from spectra run on the latter instrument; peak positions are in ppm downfield from tetramethylsilane (TMS) except for D_2O solutions for which either sodium 3-(trimethylsilyl)propionate (TSP) or sodium 3-(trimethylsilyl)propanesulfonate (DSS) was the reference compound. The pH-stat apparatus consisted of a Radiometer Model 25 pH meter equipped with a Radiometer Titrator 11 automatic titrator, a Radiometer GK2401B electrode, and an Aminco automatic burette with a 3 mL syringe reservoir. The reaction vessel was a Radiometer V520 vessel equipped with a V525 thermostatting jacket. The temperature was maintained constant by a Haake FJ constant temperature circulating apparatus.

Unless otherwise indicated, solvents and regular reagents were reagent grade and used as supplied. 2-Mercaptoethanol, 1,3-propanedithiol, 1,3-propane sultone, 3-mercapto-1-propanol, neopentyl alcohol, sodium 2-chloroethanesulfonate, and quinuclidine were supplied by Aldrich Chemical Col. and sodium 2-hydroxyethanesulfonate (as "isethionic acid, sodium salt") by Eastman Kodak. Authentic samples for spectroscopic identification of reaction products were obtained and (or) purified as follows: (*i*) sodium 2-chloroethanesulfonate (**12**) by recrystallization of the commercial material from absolute ethanol; (*ii*) 2-chloroethanesulfonyl chloride (**5***a*) by the method of Le Berre *et al.* (18); (*iii*) sodium ethenesulfonate (**13**) by hydrolysis of **5***a* at pH 11.0 followed by recrystallization from absolute ethanol (mp >385°C); (*iv*) butyl and neopentyl ethenesulfonates (**22***a* and **22***b*) (**22***a* by Dr. M. Aslam) from reaction of the alcohol with **5***a* and trimethylamine (43); (*v*) pyridine betaine (**16** and **19***a*) as described by Le Berre *et al.* (60); (*vi*) the trimethyl betaine (**19***b*) by the method of Blumbergs *et al.* (61); (*vii*) 3-chloro-1-propanesulfonyl chloride (**5***b*) from J. D. Lock (43); (*viii*) 2-chlorethanesulfonic and

Can. J. Chem. Downloaded from www.nrcresearchpress.com by 210.87.254.42 on 09/06/12
For personal use only.

Can. J. Chem. Downloaded from www.nrcresearchpress.com by 210.87.254.42 on 09/06/12
For personal use only.

2-hydroxyethanesulfonic acids by passing an aqueous solution of the sodium salt down a column of Rexyn 101 (H^+) resin (Fisher), eluting with water until the eluant was not acidic, and evaporation of the water under reduced pressure.

In the normal work-up of a reaction mixture all organic-layer extracts were dried over magnesium sulfate, filtered, and the solvent evaporated under reduced pressure with a rotary evaporator.

*2-Hydroxyethanesulfonyl chloride (**1**a)*[7]

Chlorine was bubbled very rapidly into a solution of 2-mercaptoethanol (**4***a*) (30 mL, 0.43 mol) in water (100 mL) cooled in an ice bath; the temperature of the solution changed rapidly from ~4°C to ~40°C. The reaction mixture was then extracted with (a) benzene (4 × 50 mL), (b) methylene chloride (5 × 50 mL), and then, after saturation with NaCl, the mixture was finally extracted with (c) methylene chloride, first with four 50-mL portions and then in a continuous extractor for 3 h. The ^{1}Hmr spectra of the three sets of extracts (after work-up) showed: (a) benzene extract (oil, 11.3 g), a singlet at 4.0 ppm appropriate to 2-chloroethanesulfonyl chloride (**5***a*) surrounded by a characteristic symmetrical multiplet in the range 3.5–4.5 ppm, judged by integration to correspond to a 57:43 mixture of **5***a* and **1***a* (or respective yields of 10% and 7%); (b) the first CH_2Cl_2 extract (yellowish slightly viscous liquid, 8.8 g); and (c) second CH_2Cl_2 extract (colorless liquid, 8.4 g); both showed only the multiplet pattern with no sign of the singlet due to **5***a* (28% combined yield of **1***a* from extracts (b) and (c)). The purest specimens of **1***a* obtained in this way (extract (c)) were colorless, slightly viscous liquids with the following properties: n_D^{25} 1.4902; ir (CH_2Cl_2) ν_{max}: 3590 (s), 3460 (br,w), 3060 (w), 2925 (w), 2890 (w), 1375 (vs), 1168 (vs), 1058 (vs), 1015 (m), 840 (w), 592 (s), 550 (br s) cm^{-1}; ^{1}Hmr ($CDCl_3$) δ: 2.82 (s, 1H, disappeared on addition of D_2O), and a characteristic pattern of two "triplets" (at 100 MHz) (each 2H) centred at 3.98 and 4.28 ppm; ^{13}Cmr ($CDCl_3$) δ: 56.9, 67.6. *Anal.* calcd. for $C_2H_5ClO_3S$: C 16.61, H, 3.49, S 22.18, Cl 24.52; found: C 16.88, H 3.63, S 22.23, Cl 24.30. A reasonably pure specimen of **1***a* could also be obtained by extraction of the aqueous solution with methylene chloride, and then triturating the mixture of sulfonyl chlorides isolated in this manner repeatedly with cyclohexane to remove **5***a*, leaving **1***a* behind as a colorless liquid.

If the rate of addition of chlorine was not fast or if the period of chlorination was less than 10 min, then the isolated material stank of reduced sulfur compounds and the ^{1}Hmr spectrum showed extra peaks around 2.6–3.0 and 3.5–3.9 ppm. The addition of ice during the chlorination period (final temperature ~30°C) or the use of methylene chloride instead of benzene for the initial extractions had little effect on the overall yield of **1***a* obtained.

A series of ^{1}Hmr spectra of a sample of neat **1***a* kept at −20°C, and of a $CDCl_3$ solution (6 mg in 0.5 mL) kept at room temperature, showed no change over a 3 month interval, but that of a neat sample kept at room temperature over the same period showed a gradual decrease in intensity and loss of detail in the 3.5 to 4.5 ppm region, with an estimated half-life of roughly 3 weeks. The products of the decomposition were not apparent from the spectra; there was no sign of either ethenesulfonyl chloride or 2-chlorethanesulfonyl chloride (**5***a*). In an experiment to determine how efficiently it may be recovered from aqueous solution, 1.50 g of the sulfonyl chloride (**1***a*) was dissolved in a saturated solution of sodium chloride in water (50 mL) at room temperature. After standing for 2–3 min the solution was extracted with methylene chloride (3 × 50 mL). The organic extracts were combined, dried, filtered, and evaporated to yield 1.32 g (88%) of **1***a*.

*Reaction of 2-hydroxyethanesulfonyl chloride (**1**a) with acetyl chloride*

2-Hydroxyethanesulfonyl chloride (**1***a*) (1.5 g, 10 mmol) was combined with acetyl chloride (5.0 mL, 70 mmol). After 72 h at room temperature the excess acetyl chloride was evaporated and the oily residue distilled under reduced pressure (bath temperature 110°C, 2.5 Torr) in a cold finger apparatus to yield a clear colorless oil (1.6 g, 83%). The refractive index, ir, and ^{1}Hmr spectra of this material were identical to those of an authentic specimen of 2-acetoxyethanesulfonyl chloride (**6**), prepared from sodium 2-acetoxyethanesulfonate and phosphorus pentachloride as described by Anschütz (7). The pure compound was obtained by distillation of the crude product under reduced pressure (bp 72–73°C, 0.1 Torr); n_D^{25} 1.4639 (lit. (7) n_D^{25} 1.4633); ir (neat) ν_{max}: 2995 (w), 2935 (w), 1745 (vs), 1370 (vs), 1230 (vs), 1160 (vs), 1070 (s), 1035 (s), 705 (s), 535 (s) cm^{-1}; ^{1}Hmr ($CDCl_3$) δ: 2.13 (s, 3H), 4.07 (t, 2H), 4.65 (t, 2H).

*Chlorination of 2-mercaptoethanol (**4**a) in aqueous acetic acid*

2-Mercaptoethanol (**4***a*) (20 mL, 0.29 mol) was dissolved in a 1:1 mixture (100 mL) of water and acetic acid, and the solution cooled in an ice bath. Chlorine was bubbled into this solution with vigorous magnetic stirring for 30 min. The yellow solution was extracted with methylene chloride (4 × 30 mL), the extracts on work-up followed by azeotroping with toluene gave a crude product (37 g) which was then distilled under reduced pressure (bp 70–72°C, 0.1 Torr) to yield a colorless oil (15 g, 30%); the ^{1}Hmr and ir spectra were identical to those of an authentic specimen of 2-acetoxyethanesulfonyl chloride (**6**).

*2-Hydroxyethanesulfinic acid (**8**)*

A solution of sodium sulfite (3 g, 24 mmol) in water (15 mL) was added to 2-hydroxyethanesulfonyl chloride (**1***a*) (1.0 g, 6.9 mmol). The resulting solution was allowed to stand at room temperature for 2 h, then extracted twice with methylene chloride. The aqueous layer was acidified to pH 1.0 with 2 *M* sulfuric acid, and continuously extracted with ether for 72 h. The organic extract yielded a pale yellow oil (0.55 g, 75%), n_D^{25} 1.4235; ir (neat) ν_{max}: 3360 (b), 1058 (s), 813 (m) cm^{-1}; ^{1}Hmr (D_2O) δ: 3.04 (t, 2H), 4.01 (t, 2H).

A mixture of barium hydroxide octahydrate (387 mg, 1.23 mmol) in water (20 mL) was combined with 2-hydroxyethanesulfinic acid (**8**) (270 mg, 2.45 mmol) at room temperature. After stirring for 75 min, the solvent was evaporated under reduced pressure (water bath temperature 35°C) to yield **10** as an off-white solid (0.430 g, 50%) which decomposed above 350°C; ir (Nujol) ν_{max}: 1060 (m), 1010 (sh), 985 (s), 950 (m) cm^{-1}; ^{1}Hmr (D_2O) δ: 2.60 (t, 2H), 3.92 (t, 2H); *Anal.* calcd. for $BaC_4H_{10}O_6S_2$: C 13.51, H 2.83; found: C 13.22, H 3.09. 2-Hydroxyethanesulfinic acid (**8**) (750 mg, 6.8 mmol) was dissolved in water (10 mL) and the pH adjusted to 6.0 with 1.0 *M* sodium hydroxide solution. After standing for 10 min at room temperature the solvent was evaporated to yield **7** as a gummy residue which crystallized upon standing (0.83 g, 92%), mp 81–83°C; ^{1}Hmr (D_2O) δ: 2.58 (t, 2H), 3.91 (t, 2H). The salt (**7**) was used without further purification in the following reaction.

*Reaction of sodium 2-hydroxyethanesulfinate (**7**) with ethyl iodide*

The sodium sulfinate (**7**) (0.75 g, 5.7 mmol) was dissolved in absolute alcohol (25 mL) containing ethyl iodide (9.75 g, 62.5 mmol), and the solution refluxed for 22 h and then evaporated under reduced pressure to yield a red solid. This residue was triturated with chloroform (3 × 25 mL), the extracts were combined and dried, and the solvent was removed to yield a red oil (0.45 g). The oil was dissolved in water (10 mL) and the solution maintained at pH 10–11 with 1.0 *M* NaOH solution for 2 h. Extraction with chloroform gave a light yellow oil (100 mg, 15%). Recrystallization of this material from benzene gave colorless needles (17 mg) whose mp and ^{1}Hmr and ir spectra were identical to those of an authentic sample of ethyl 2-hydroxyethylsulfone (**9**) prepared as described below.

Utilizing a slight modification of the literature (25) procedure, freshly recrystallized sodium ethanesulfinate (see below) (3.0 g, 25.9 mmol) was dissolved in a mixture of ethanol (30 mL) and water (20 mL) and 2-chloroethanol (2.1 g, 26.2 mmol) added. The solution was heated on a steam bath for 50 h. Evaporation of the solvent under reduced pressure gave a white solid which was dissolved in water and continuously extracted with chloroform for 72 h. Work-up of the organic layer gave a yellow oil (1.0 g) which yielded **9** as colorless needles (0.175 g, 5%) from benzene; mp 40.5–42°C; ir ($CHCl_3$) ν_{max}:

Can. J. Chem. Downloaded from www.nrcresearchpress.com by 210.87.254.42 on 09/06/12
For personal use only.

3350 (br w), 3028 (m), 2945 (w), 1460 (w), 1410 (w), 1315 (vs), 1280 (w), 1235 (w), 1128 (vs), 1063 (m) cm^{-1}; ^{1}Hmr ($CDCl_3$) δ: 1.42 (t, 3H), 2.36 (s, 1H), 3.00–3.29 (m, 4H), 4.14 (m, 2H). The sodium ethanesulfinate used in this preparation was obtained by reduction of ethanesulfonyl chloride with sodium sulfite using the method described for the preparation of **7**; recrystallization from 95% ethanol gave crystals with a decomposition point >200°C and the following spectra: ir (Nujol) ν_{max}: 1185 (br w), 1040 (s), 1010 (s), 979 (s), 665 (s) cm^{-1}; ^{1}Hmr (D_2O) δ: 1.09 (t, 3H), 2.35 (q, 2H).

*Chlorination of 2-hydroxyethanesulfinic acid (**8**) in deuterium oxide*

2-Hydroxyethanesulfinic acid (**8**) (0.050 g, 0.45 mmol) was dissolved in D_2O (0.5 mL) and placed in an nmr tube. Chlorine was bubbled into this solution for 10 min at room temperature. After this time the ^{1}Hmr spectrum indicated the presence of 2-hydroxyethanesulfonyl chloride (**1***a*), with a trace (~5%) of 2-hydroxyethanesulfonic acid.

*Hydrolysis of 2-hydroxyethanesulfonyl chloride (**1**a)*

The general procedure is illustrated by the reaction at pH 4.0. The sulfonyl chloride (**1***a*) (147 mg, 1.02 mmol) was dissolved in dry 1,2-dimethoxyethane (DME) (1.0 mL). This solution was injected with stirring into water (50 mL) maintained at 25.0°C and pH 4.0 using the pH-stat apparatus with 0.1 *M* sodium hydroxide titrant. After 90 min the pH was adjusted to 7.0 and the solvent evaporated to yield a colorless solid. The ^{1}Hmr spectrum (D_2O) of this material showed absorptions only in the 2.9–4.0 ppm region, corresponding to sodium 2-hydroxyethanesulfonate (**11**), sodium 2-chloroethanesulfonate (**12**), and an unidentified material; the identity of **11** and **12** was shown by comparison with ^{1}Hmr spectra of authentic specimens. Integration of these peaks in the ^{1}Hmr spectrum gave the relative proportions of **11**, **12**, and the unidentified material as 90, 3, and 6%, respectively. These results and those from related reactions are listed in Table 1.

As a control experiment, a solution of sodium 2-hydroxyethanesulfonate (**11**) (100 mg, 0.68 mmol) and sodium 2-chloroethanesulfonate (**12**) (90 mg, 0.54 mmol) (molar percentages: 56% **11** and 44% **12**) in water (100 mL) containing KCl (800 mg, 13 mmol) was divided into equal parts. With the first the pH was adjusted to 4.0 with 1.0 *M* HCl and held at 25.0°C for 2 h; on evaporation of the water and dissolution in D_2O the ^{1}Hmr spectrum showed peaks due to **11** and **12** (only) in the ratio 56 to 44. The second part was treated with 0.1 NaOH to give pH 10.5 and the solution maintained at 20°C for 35 min; the pH was lowered to 7.0 with 1.0 *M* HCl and the water evaporated. Integration of the ^{1}Hmr spectrum showed the presence of only **11** (61%) and **12** (39%).

*Reaction of 2-hydroxyethanesulfonyl chloride (**1**a) with pyridine in deuterium oxide*

The sulfonyl chloride (**1***a*) (0.330 g, 7.27 mmol) was added to a stirred solution of pyridine (2.0 mL, 24.9 mmol) in D_2O (50 mL) maintained at 25°C and apparent pH 6.0 with 2.2 *M* sodium deuteroxide titrant (prepared from sodium and D_2O). After 30 min the pH was adjusted to 7.5 and the solution extracted with ether (4 × 30 mL). The aqueous layer was evaporated under reduced pressure to yield a colorless solid, the ^{1}Hmr spectrum (D_2O) of which showed peaks at 3.0–4.0, 5.0, 5.8–7.0, and 8.0–9.0 ppm, indicating the presence of pyridine betaine (**17**), sodium 2-chloroethanesulfonate (**12**), sodium 2-hydroxyethanesulfonate, and sodium ethenesulfonate (**13**) in the relative proportions (as estimated by integration) of 57%, 7%, 33%, and 3% respectively. No deuterium was evident in any of the products except sodium 2-hydroxyethanesulfonate, which was estimated (by integration of the absorptions at 3.12 and 3.90 ppm) to be half monodeuterated at the α carbon, i.e. 50% **15** and 50% **11**.

In a control experiment a mixture of **11** (110 mg, 0.74 mmol), **12** (38 mg, 0.23 mmol), and **17** (75 mg, 0.4 mmol) was dissolved in D_2O (30 mL); the relative amounts were confirmed by the ^{1}Hmr spectrum and then adjusted to pH 6.0 with DCl in D_2O. After 30 min at room temperature the pH was raised to 7.0 with 0.1 *M* NaOD, the solution extracted with ether, and the residual aqueous layer evaporated; the ^{1}Hmr spectrum showed the presence of **11**, **12**, and **13** in the original proportions, with no deuterium incorporation or other materials in evidence.

*Reaction of 2-hydroxyethanesulfonyl chloride (**1**a) with tertiary amines and primary alcohols in methylene chloride*

In a series of experiments 2-hydroxyethanesulfonyl chloride (**1***a*) (~0.5 g, 3.5 mmol) was dissolved in methylene chloride (~40 mL) containing either 1-butanol or neopentyl alcohol (10 equiv.). The tertiary amine (in excess) was then injected with stirring into the solution at room temperature. With pyridine or trimethylamine a precipitate was observed within the first 5 min of the reaction. Washing with water (1 × 40 mL) and work-up of the methylene chloride layer yielded an oil whose composition was determined by ^{1}Hmr spectroscopy. In all experiments, the oil consisted of the 2-hydroxyethanesulfonate and ethenesulfonate esters (**17** and **22**), as shown by comparison with ^{1}Hmr spectra of authentic specimens. In one reaction a sample of authentic neopentyl ethenesulfonate (**22***b*) was added to a nmr tube containing the crude reaction mixture of esters; the peaks attributed to the **22***b* were increased accordingly.

The aqueous extract was evaporated under reduced pressure, and the residue dissolved in water (1–2 mL). This solution was added to a short column of Rexyn 101 (H^+), and the column eluted with water until the eluant was no longer acidic towards pH paper. The eluant was then evaporated, and the residue triturated repeatedly with anhydrous ether (5 × 30 mL). These ether extracts were combined and evaporated to give an oil. The ^{1}Hmr spectrum (D_2O) showed absorptions in the 3.0–4.0 ppm region indicating the presence of 2-hydroxyethanesulfonic acid and 2-chloroethanesulfonic acid (identified by comparison with ^{1}Hmr spectra of authentic specimens of the acids). The amounts of the two acids (estimated by integration) are reported in Table 2 as overall percentage yields of the salts **20** and **21**. The ether-insoluble residue was weighed and identified as the betaine (**19**) corresponding to the amine employed, by comparison of its ^{1}Hmr spectrum with that of the authentic material.

*Butyl 2-hydroxyethanesulfonate (**17**a)*

The crude reaction mixture containing butyl ethenesulfonate (**22***a*) and butyl 2-hydroxyethanesulfonate (**17***a*) (obtained from reaction of **1***a* with trimethylamine and 1-butanol) was triturated repeatedly with hexanes. The ^{1}Hmr and ir spectra of the residue insoluble in hexanes were identical with those of an authentic specimen of **18***a* prepared by the betylate route (43); ^{1}Hmr ($CDCl_3$) δ: 0.96 (t, 3H), 1.24–1.93 (m, 4H), 2.56 (s, 1H), 3.35 (t, 2H), 4.08 (t, 2H), 4.28 (t, 2H).

*Neopentyl 2-hydroxyethanesulfonate (**17**b)*

The ester (**17***b*) was isolated as a colorless oil by cold finger distillation under reduced pressure (0.002 Torr, oil bath temperature 90°C) of the mixture obtained from a reaction of 2-hydroxyethanesulfonyl chloride (**1***a*) with trimethylamine and neopentyl alcohol; ir (CH_2Cl_2) ν_{max}: 3610 (w), 2970 (m), 1353 (s), 1160 (s), 1058 (m), 900 (vs), 937 (s) cm^{-1}; ^{1}Hmr ($CDCl_3$) δ: 1.01 (s, 9H), 2.78 (br s, 1H), 3.37 (t, 2H), 3.93 (s, 2H), 4.09 (t, 2H). *Anal.* calcd. for $C_7H_{16}O_4S$: C 42.68, H 8.24, S 16.30; found: C 42.84, H 8.22, S 16.34.

*Butyl 2-acetoxyethanesulfonate (**24**)*

Butyl 2-hydroxyethanesulfonate (**17***a*) (0.100 g, 0.55 mmol) was dissolved in $CDCl_3$ (0.5 mL). Acetyl chloride (0.5 mL, 7.0 mmol) was added and the solution left overnight. Evaporation of the solvent gave an oil which was distilled in a cold finger apparatus under reduced pressure (0.5 Torr, bath temperature 120°C). The distillate was dissolved in methylene chloride (~1 mL) and run down a short column of silica gel (BDH, 35–70 mesh) using methylene chloride. Evaporation of the solvent gave **24** as a colorless oil (70 mg, 53%); ir (CH_2Cl_2) ν_{max}: 3060 (w), 2965 (m), 2935 (m), 1750 (s), 1360 (s), 1235 (s), 1165 (s), 1050 (m), 1038 (m), 938 (s), 910 (m), 888 (m) cm^{-1}; ^{1}Hmr ($CDCl_3$) δ: 0.96 (t, 3H), 1.20–1.90 (m, 4H), 2.10 (s, 3H), 3.44 (t, 2H), 4.27 (t, 2H), 4.49 (t, 2H). *Anal.* calcd. for

Can. J. Chem. Downloaded from www.nrcresearchpress.com by 210.87.254.42 on 09/06/12
For personal use only.

$C_8H_{16}O_5S$: C 42.84, H 7.19, S 14.30; found: C 42.78, H 7.02, S 14.38.

*2-(*N-N,N-*Triethylammonio)ethanesulfonate (triethyl betaine,* **19***c)*

Triethylamine (1.4 mL, 0.01 mol) was injected into a solution of sodium 2-bromoethanesulfonate (**61**) (2.0 g, 9.5 mmol) in water (40 mL) and the solution allowed to stand at room temperature for 11 days. Evaporation of the solvent gave a white solid which was dissolved in water (~2 mL), added to a short column of Rexyn 300 (H-OH) resin, and eluted with water. Evaporation of the solvent gave a colorless crystalline solid (0.075 g, 35%), which decomposed above 280°C; ir (Nujol) ν_{max}: 1270 (w), 1238 (m), 1213 (s), 1195 (s), 1155 (w), 1040 (s) cm^{-1}; ^{1}Hmr (D_2O) δ: 1.32 (t, 9H), 3.43 (m, 10H). *Anal.* calcd. for $C_8H_{19}NO_3S$: C 45.91, H 9.15, N 6.69, S 15.32; found: C 46.03, H 9.31, N 6.81, S 15.36.

2-(Quinuclidinio)ethanesulfonate (quinuclidine betaine, **19***d)*

The crude betaine (**19***d*) formed in a reaction of the sulfonyl chloride (**1***a*) with quinuclidine and 1-butanol was separated by filtration and recrystallized from absolute alcohol to yield a colorless solid, dec. >390°C; ir (Nujol) ν_{max}: 1277 (m), 1187 (s), 1112 (m), 1040 (s), 792 (m) cm^{-1}; ^{1}Hmr (D_2O) δ: 1.82–2.33 (m, 7H), 3.20–3.68 (m, 10H). *Anal.* calcd. for $C_9H_{17}NO_3S$: C 49.29, H 7.81, N 6.39, S 14.62; found: C 49.29, H 7.89, N 6.44, S 14.71.

*Reaction of 2-hydroxyethanesulfonyl chloride (*1a*) with 1-butanol-*d *and trimethylamine in methylene chloride*

The sulfonyl chloride (**1***a*) (500 mg, 3.45 mmol) was treated with trimethylamine (~0.5 mL, 6 mmol) and 1-butanol-*d* (Merck Sharp and Dohme Canada Ltd., 99 at.% D) (2.65 g, 35 mmol) in dry methylene chloride (40 mL) following the above general procedure. After 1 h at room temperature, the reaction was worked up and the reaction products were observed to be butyl 2-hydroxyethanesulfonate (40%), butyl ethenesulfonate (**22**, R = Bu) (3%), 2-chloroethanesulfonic acid (14%), trimethyl betaine (**19***a*) (40%), and 2-hydroxyethanesulfonic acid (3%). Only the 2-hydroxyethanesulfonate ester was observed to have incorporated deuterium, and was estimated (by integration of the methylene absorptions at 4.27 and 3.34 ppm) to be >80% **18***a*.

Control experiments to determine the effect of reaction conditions and work-up on product ratios

(a) A solution of trimethylammonium 2-chloroethanesulfonate (**20***b*) (130 mg, 0.64 mmol, prepared as described below), the trimethyl betaine (**19***b*) (113 mg, 0.68 mmol), $Me_3NH^+Cl^-$ (210 mg, 0.33 mmol), and 1-butanol (1 mL, 10 mmol) in water (50 mL) was evaporated under reduced pressure. This material was then dissolved in water and run through an ion exchange resin and the products separated by trituration with ether, as described above for the work-up of the aqueous extract from the reaction of **1***a* with a primary alcohol and a tertiary amine. The ether-insoluble residue (90 mg) was shown to be entirely the betaine (**19***b*) (100% recovery) and the ether-soluble material (90 mg) exclusively 2-chloroethanesulfonic acid (98% recovery).

(b) A mixture of the pyridine betaine (**19***a*) (52 mg, 0.28 mmol), neopentyl alcohol (600 mg, 0.68 mmol), pyridinium chloride (140 mg, 1.2 mmol), **12** (180 mg, 1.08 mmol), and **11** (190 mg, 1.28 mmol) was dissolved in water (40 mL), the water evaporated, and the residue treated with Rexyn 101 (H^+) followed by ether trituration as above. The presence of **11**, **12**, and **19***a* was shown by the ^{1}Hmr spectra which, with the weights of the recovered materials, indicated recovery to be 109%, 94%, and 81%, respectively.

(c) Trimethylamine (~0.5 mL, 6 mmol) was added to a solution of butyl 2-hydroxyethanesulfonate (**17***a*) (77 mg, 0.43 mmol) and 1-butanol (320 mg, 4.3 mmol) in methylene chloride (30 mL) and the mixture allowed to stand at room temperature for 1 h. Work-up as before gave **17***a* (61 mg, 79%) and a mixture of 2-hydroxyethanesulfonic acid and the trimethyl betaine (**19***b*) corresponding to 16% and 2% respective yields.

(d) Triethylamine (0.10 mL, 0.72 mmol) was added to a solution of neopentyl 2-hydroxyethanesulfonate (**17***b*) (90 mg, 0.46 mmol) and neopentyl alcohol (350 mg, 4.0 mmol) in methylene chloride (300 mL) and the mixture allowed to stand for 1 h at room temperature. Work-up gave back **17***b* (75 mg) as a pale yellow oil, the ^{1}Hmr spectrum of which showed no sign of neopentyl ethenesulfonate (**22***b*).

(e) Triethylamine (0.20 mL, 1.5 mmol) was added to a solution of neopentyl ethenesulfonate (**22***b*) (88 mg), triethylammonium chloride (60 mg), and neopentyl alcohol (50 mg) in $CDCl_3$ (1.0 mL). The ^{1}Hmr spectrum after 24 h showed no observable reaction.

*Aqueous chlorination of 3-mercapto-1-propanol (*4b*)*

3-Mercapto-1-propanol (**4***b*) (1.3 g, 14 mmol, prepared according to the method of Djerassi and Gorman (62) from 3-mercaptopropionic acid) was dissolved in water (50 mL) and cooled in an ice bath. Chlorine was bubbled into this solution for 10 min with magnetic stirring. The solution was extracted several times with methylene chloride; the extracts on work-up gave a colorless oil (1.0 g) which, by comparison of its ^{1}Hmr spectrum with those of authentic samples, was shown to be an equimolar mixture of 3-chloro-1-propanesulfonyl chloride (**5***b*) and 1,3-propane sultone (**2***b*) (yield of each, 24%). Similar chlorination of 1,3-propane sultine (**26***b*) (0.45 g, 4.2 mmol, prepared from 1,3-propanedithiol by the method of Harpp *et al.* (63)), gave a colorless oil (0.50 mg) shown by ^{1}Hmr to be **2***b* (77%) and **5***b* (13% yield).

Acknowledgements

We thank Professor J. B. Stothers for the ^{13}Cmr spectrum, Dr. M. Aslam and Mr. J. D. Lock for comparison specimens, and the Natural Sciences and Engineering Research Council of Canada for financial support of this work.

1. J. F. KING and J. H. HILLHOUSE. J. Chem. Soc. Chem. Commun. 454 (1979).
2. G. GEISELER and P. LAUE. Chem. Ber. **95**, 867 (1962).
3. R. B. SCOTT, JR. and R. E. LUTZ. J. Org. Chem. **19**, 830 (1954).
4. F. G. BORDWELL and W. T. BRANNEN, JR. J. Am. Chem. Soc. **86**, 4645 (1965).
5. E. L. ELIEL, W. H. PEARSON, L. M. JEWELL, and A. G. ABATJOGLOU. Tetrahedron Lett. 331 (1980).
6. T. ZINCKE and W. GLAHN. Ber. **40**, 3039 (1907).
7. R. ANSCHÜTZ. Justus Liebigs Ann. Chem. **415**, 64 (1918).
8. W. L. HALL. J. Org. Chem. **31**, 2672 (1966).
9. R. W. CAMPBELL and H. W. HILL, JR. J. Org. Chem. **38**, 1047 (1973).
10. R. J. CREMLYN and T. CRONJE. Phosphorus Sulfur **6**, 413 (1979).
11. G. SCHROETER and M. SULZBACHER. Ber. **61**, 1616 (1928).
12. G. SCHROETER. Justus Liebigs. Ann. Chem. **418**, 161 (1918).
13. F. RASCHIG. Ber. **59**, 859 (1926).
14. F. RASCHIG and W. PRAHL. Justus Liebigs. Ann. Chem. **448**, 265 (1926).
15. T. KURODA, T. ASHIDA, Y. SASADA, and M. KAKUDO. Bull. Chem. Soc. Jpn. **40**, 1377 (1967).
16. T. S. CAMERON and W. J. CHUTE. Acta Crystallogr. Sect. B, **35**, 325 (1979).
17. M. QUAEDVLIEG. *In* Methoden der organischen Chemie (Houben-Weyl). Vol. 9. George Thieme Verlag, Stuttgart. 1955. p. 343.
18. A. LE BERRE, A. ÉTIENNE, and B. DUMAITRE. Bull. Soc. Chim. Fr. 946 (1970).
19. E. E. GILBERT. Synthesis, 3 (1969).
20. E. J. GOETHALS and M. VERZELE. Bull. Soc. Chim. Belg. **74**, 21 (1965).
21. J. F. KING and M. ASLAM. Can. J. Chem. **57**, 3278 (1979).
22. S. P. MCMANUS, M. R. SMITH, F. T. HERRMANN, and R. A. ABRAMOVITCH. J. Org. Chem. **43**, 647 (1978).
23. H. O. FONG, W. R. HARDSTAFF, D. G. KAY, R. F. LANGLER, R. H. MORSE, and D. N. SANDOVAL. Can. J. Chem. **57**, 1206 (1979).

24. J. F. KING and J. H. HILLHOUSE. J. Chem. Soc. Chem. Commun. 295 (1981).
25. J. VON BRAUN, E. ANTON, and K. WEISBACH. Ber. **63**, 2847 (1930).
26. G. HESSE, E. REICHOLD, and S. MAJMUDAR. Chem. Ber. **90**, 2106 (1957).
27. G. A. SOKOLSKII, M. A. BELAVENTSEV, and I. L. KNUNYANTS. Izv. Akad. Nauk SSSR. Ser. Khim. 625 (1970).
28. F. G. BORDWELL, M. L. PETERSON, and C. S. RONDESTVEDT, JR. J. Am. Chem. Soc. **76**, 3945 (1954).
29. I. L. KNUNYANTS and G. A. SOKOLSKII. Angew. Chem. Int. Ed. Engl. **11**, 583 (1972).
30. L. L. MULLER and J. HAMER. 1,2-Cycloaddition reactions. Interscience, New York. 1967. pp. 276–286.
31. E. E. GILBERT. Sulfonation and related reactions. Interscience, New York. 1965. pp. 42–55.
32. M. NAGAYAMA, O. OKUMURA, S. NODA, H. MANDAI, and A. MORI. Bull. Chem. Soc. Jpn. **47**, 2158 (1974).
33. D. BORRMANN and R. WEGLER. Chem. Ber. **99**, 1245 (1966).
34. F. I. LUKNITSKII and B. A. VOVSI. Dokl. Akad. Nauk SSSR, **172**, 1327 (1967).
35. F. I. LUKNITSKII and B. A. VOVSI. Zh. Org. Khim. **3**, 1499 (1967); **3**, 2139 (1967).
36. W. E. TRUCE and L. K. LIU. Chem. Ind. (London), 457 (1969).
37. J. R. NORELL. Chem. Commun. 1291 (1970).
38. F. G. BORDWELL and M. L. PETERSON. J. Am. Chem. Soc. **76**, 3952 (1954); **76**, 3957 (1954).
39. C. G. SWAIN and C. B. SCOTT. J. Am. Chem. Soc. **75**, 141 (1953).
40. S. OSTERMAN-GOLKAR, L. EHRENBERG, and C. A. WACHTMEISTER. Radiat. Bot. **10**, 303 (1970).
41. (*a*) N. STEMPNEWSKY. Zh. Russ. Fiz-Khim. Ova. **14**, 95 (1882); (*b*) Ber. **15**, 947 (1882); (*c*) C. M. SUTER. The organic chemistry of sulfur. John Wiley and Sons, New York. 1944. p. 133.
42. J. F. KING and M. ASLAM. Tetrahedron Lett. **22**, 3573 (1981).
43. J. F. KING, S. M. LOOSMORE, M. ASLAM, J. D. LOCK, and M. J. MCGARRITY. J. Am. Chem. Soc. **104**, 7108 (1982).
44. J. F. KING and S. M. LOOSMORE. J. Chem. Soc. Chem. Commun. 1011 (1976).
45. C. J. M. STIRLING. Acc. Chem. Res. **12**, 198 (1979).
46. J. E. BALDWIN. J. Chem. Soc. Chem. Commun. 734 (1976).
47. J. F. KING and Y. I. KANG. J. Chem. Soc. Chem. Commun. 52 (1975).
48. L. O. FARNG and J. L. KICE. J. Am. Chem. Soc. **103**, 1137 (1981).
49. E. A. LUINSTRA. Ph.D. Thesis. University of Western Ontario, 1971. pp. 59–73.
50. I. B. DOUGLASS, B. S. FARAH, and E. G. THOMAS. J. Org. Chem. **26**, 1996 (1961).
51. I. B. DOUGLASS. J. Org. Chem. **30**, 633 (1965).
52. J. F. KING, A. HAWSON, B. L. HUSTON, L. J. DANKS, and J. KOMERY. Can. J. Chem. **49**, 943 (1971).
53. J. A. KOMERY. M.Sc. Thesis. University of Western Ontario, 1969. p. 20.
54. G. R. CHALKLEY, D. J. SNODIN, G. STEVENS, and M. C. WHITING. J. Chem. Soc. (C), 682 (1970).
55. T. DURST and K. C. TIN. Can. J. Chem. **49**, 2374 (1971).
56. F. JUNG and T. DURST. J. Chem. Soc. Chem. Commun. 4 (1973).
57. F. JUNG, N. K. SHARMA, and T. DURST. J. Am. Chem. Soc. **95**, 3420 (1973).
58. E. U. JONSSON, C. C. BACON, and C. R. JOHNSON. J. Am. Chem. Soc. **93**, 5306 (1971).
59. M. KOBAYASHI, R. NISHI, and H. MINATO. Bull. Chem. Soc. Jpn. **47**, 888 (1974).
60. A. LE BERRE, A. ÉTIENNE, and B. DUMAITRE. Bull. Soc. Chim. Fr. 954 (1970).
61. P. BLUMBERGS, A. B. ASH, F. A. DANIHER, C. L. STEVENS, H. O. MICHEL, B. E. HACKLEY, JR., and J. EPSTEIN. J. Org. Chem. **34**, 4065 (1969).
62. C. DJERASSI and M. GORMAN. J. Am. Chem. Soc. **75**, 3704 (1953).
63. D. N. HARPP, J. G. GLEASON, and D. K. ASH. J. Org. Chem. **36**, 322 (1971).
64. J. F. KING and T. M.-L. LEE. Can. J. Chem. **59**, 362 (1981).

Can. J. Chem. Downloaded from www.nrcresearchpress.com by 210.87.254.42 on 09/06/12
For personal use only.

Rate enhancements for the nickel(II)−PADA complexation in mixed anionic micelles

PAUL D. I. FLETCHER
Chemical Laboratory, University of Kent at Canterbury, Canterbury, Kent, United Kingdom CT2 7NH

AND

JOANNE R. HICKS AND VINCENT C. REINSBOROUGH
Chemistry Department, Mount Allison University, Sackville, N.B., Canada E0A 3C0

Received August 3, 1982[1]

PAUL D. I. FLETCHER, JOANNE R. HICKS, and VINCENT C. REINSBOROUGH. Can. J. Chem. **61**, 1594 (1983).

Rate enhancements for the Ni^{2+}_{aq} and pyridine-2-azo-*p*-dimethylaniline (PADA) reaction have been obtained in four simple equimolar binary micellar systems: sodium dodecylsulfate − sodium decylsulfate, sodium dodecylsulfate − sodium octylsulfate, sodium octylsulfate − sodium hexylsulfate, and sodium octylsulfate − sodium octanesulfonate. The rate enhancement curves were similar to those obtained for pure surfactants and were consistent with a 1:1 mixed micelle except for the third system where the micelle was richer in sodium octylsulfate. The kinetic analysis revealed no dramatic changes in hydrophobic or electrostatic forces on forming the mixed micelles

PAUL D. I. FLETCHER, JOANNE R. HICKS et VINCENT C. REINSBOROUGH. Can. J. Chem. **61**, 1594 (1983).

On a obtenu les accroissement de vitesse de la réaction du Ni^{2+}_{aq} et de la pyridine-azo-2 *p*-diméthylaniline (PADA) dans quatre systèmes micellaires binaires simples: dodécylsulfate de sodium − décylsulfate de sodium, dodécylsulfate de sodium − octylsulfate de sodium, octylsulfate de sodium − hexylsulfate de sodium et octylsulfate de sodium − octanesulfonate de sodium. Les courbes d'accroissement de vitesse ressemblent beaucoup à celles obtenues pour les surfactants purs et sont en accord avec une micelle mixte 1:1 à l'exception du troisième système où la micelle est plus riche en octylsulfate de sodium. L'analyse cinétique ne révèle pas de changements importants dans les forces hydrophobes ou électrostatiques lors de la formation des micelles mixtes.

[Traduit par le journal]

Introduction

Surfactants in nature and in industry occur as mixtures of homologs or similar compounds, in which case multicomponent, rather than one-component, micelles are likely responsible for the distinctive properties of the surfactant solutions. Apart from some thermodynamic work relating the critical micelle concentration (cmc) to mole fraction (1,2), little else of a fundamental nature has been done on mixed micellar aqueous systems of this type. Stenius *et al.* recently reported that in the sodium abietate + sodium oleate system, a model system for surfactants in wood, mixed micelles were formed in which larger amounts of additive could be solubilized than in either pure abietate or oleate micelles (3). Such a synergistic effect is of interest because it may explain nature's choice of particular surfactant combinations. Once the principles governing this enhancement in properties are discovered, applications should be possible in medicine and industry.

In this paper, some simple binary anionic surfactant solutions are investigated for variation in micellar form and for any evidence of synergism. The probe that is used is the kinetics of the metal−ligand substitution reaction between Ni^{2+}_{aq} and pyridine-2-azo-*p*-dimethylaniline (PADA). Complexation is strongly accelerated in the presence of anionic micelles since the reagents are preferentially adsorbed into the surface region of the micelles, Ni^{2+}_{aq} by coulombic forces and PADA by hydrophobic attraction. The extent of reaction can be predicted from the distribution coefficients for each reagent partitioning between the bulk water and the micelle surface region and some knowledge of the volume in which the reaction occurs on the micelles (4−7).

Changes in hydrophobicity and electrostatic forces within the micelle are directly reflected in changes in the partitioning constants as shown in our recent study relating the kinetics of this probe reaction to solubilizate sites in pure micelles (8). It should be possible to use this same probe to detect major increases in either of these forces, i.e. to look for evidence of synergism, and to gain insight into the micellar constitution when anionic surfactants are mixed.

Experimental

The experimental procedure and the stopped-flow instrumentation have been described elsewhere (8−10). Essentially, the probe reaction was carried out at 298.2 K with pH fixed at 7.6−7.9 with phosphate buffering. Pseudo-first order conditions prevailed with $[Ni^{2+}] = 1.0 \times 10^{-3}$ or 5.0×10^{-4} mol dm^{-3} and $[PADA] = 1.0 \times 10^{-5}$ mol dm^{-3}. The kinetic rate constants (k_{obs}) were obtained from exponential decay curves in the normal fashion.

A dye-laser photochemical relaxation method was used to measure the faster times (the dead time of the stopped-flow spectrometer was 2−3 milliseconds) and to provide a second measure of the slower times by a different technique for the equimolar SLS−SDS system. A description of the dye-laser photolysis method has been given by Robinson and White (11). The stopped-flow and the photolysis values of k_{obs} were in reasonable agreement in the overlap regions.

The surfactants were obtained from Eastman Kodak, PADA from Sigma, and $Ni(NO_3)_2 \cdot 6H_2O$, the source of Ni^{2+}_{aq}, from Fisher Scientific.

Results and discussion

In this study, four simple, binary, anionic micellar systems were investigated kinetically by means of the probe reaction. The first two were mixes of sodium alkylsulfates where the difference in chain length was two carbon atoms: sodium dodecylsulfate (SLS) − sodium decylsulfate (SDS) and sodium octylsulfate (SOS) − sodium hexylsulfate (SHS). The third system was SLS−SOS with four carbon atoms being the difference in chain length. In the fourth system, the chain lengths of the two surfactants were the same at eight carbons but the head group was modified from sulfate to sulfonate: sodium octyl-

[1]Revision received February 2, 1983.

Can. J. Chem. Downloaded from www.nrcresearchpress.com by 210.87.254.42 on 09/06/12
For personal use only.

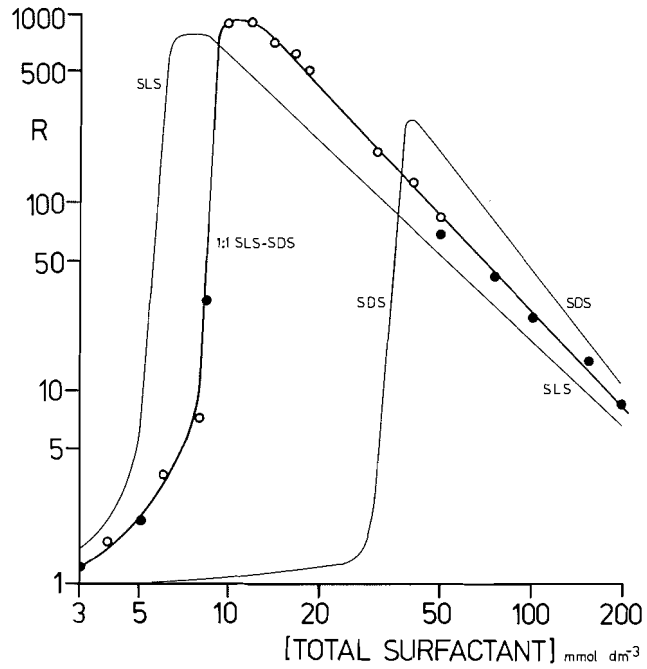

FIG. 1. Rate enhancements for the Ni^{2+}–PADA reaction in the system SLS–SDS. Open circles are laser photolysis data points while closed circles are stopped-flow experimental points.

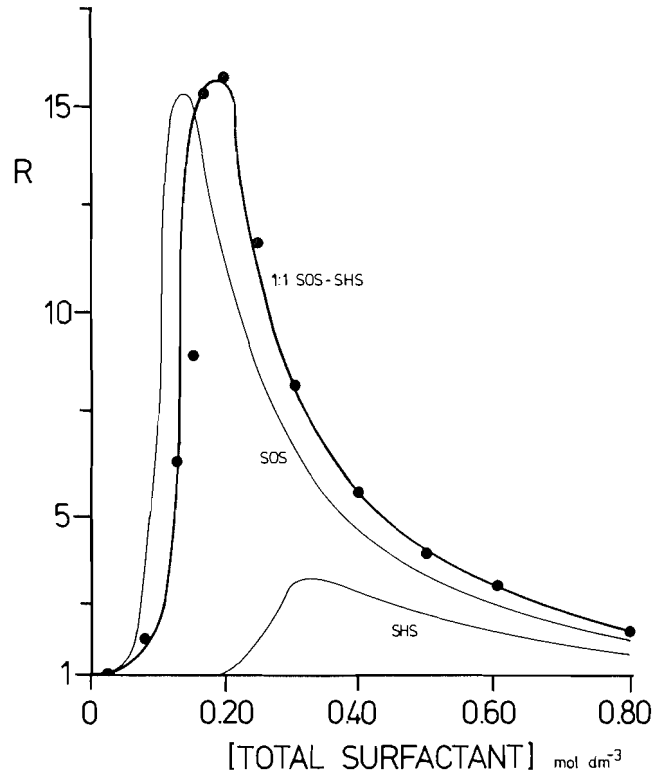

FIG. 2. Rate enhancements for the Ni^{2+}–PADA reaction in the system SOS–SHS.

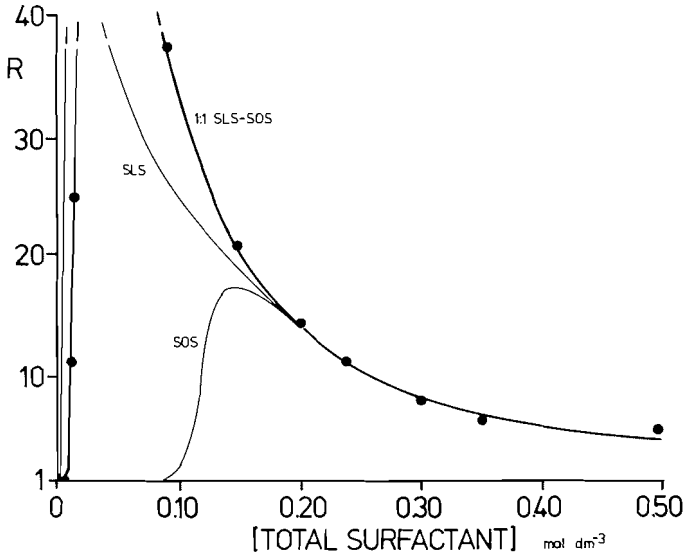

FIG. 3. Rate enhancements for the Ni^{2+}–PADA reaction in the system SLS–SOS.

sulfate (SOS) – sodium octanesulfonate (SOSO).

The kinetic equation relating the observed rate constants (k_{obs}) to the partitioning constants when the reaction occurs on both the micelle surface and in the bulk aqueous solution is (6, 7)

$$[1] \quad k_{obs} = k_1^{m}[Ni^{2+}]/(CV_s\{1 + (CK_{Ni})^{-1}\}\{1 + (CK_{PADA})^{-1}\}) + k^{m}_{-1}$$

where k_1^{m} and k_{-1}^{m} are the forward and backward kinetic rate constants for the reaction on the micelle surface; C, the concentration in mol dm^{-3} of micellar surfactant, i.e. the total surfactant concentration less the cmc; V_s, the reaction volume per mole of surfactant; K_{Ni} and K_{PADA}, the partitioning constants for each reagent between the bulk water and micellar pseudophase.

The partitioning constants are defined as

$$[2] \quad K_{species} = [Species]_m/C[Species]_{aq}$$

K_{Ni} and K_{PADA} are measured independently through the murexide technique (12, 13) and solubility studies (6, 10) respectively. The value of V_s is found by computer-fitting the k_{obs} data to eq. [1].

In eq. [1], it is reasonable to assume that $k_1^{m} = k_1^{aq}$ and $k_{-1}^{m} = k_{-1}^{aq}$ since the rate-determining step in the complex formation is the ejection of water. The k_{obs} values are more meaningfully plotted as rate enhancement R given by the ratio k_1^{app}/k_1^{aq} where k_1^{app} is the coefficient of $[Ni^{2+}]$ in eq. [1] or the apparent forward rate constant.

First of all, it must be noted that the rate enhancement curves in the four mixed micellar systems resemble in every respect R behaviour in pure surfactant systems (Figs. 1–4). In very dilute solutions no rate enhancement can be detected but, in the region of presumably the cmc of the mixed micelle, there is a sharp increase in R to a maximum over a narrow concentration range and then a more gradual decrease in more concentrated surfactant solution to just a few times the rate in water. No kinks, bumps, or unusual behaviour of any sort can be detected as might be expected if more than one type of micelle can be formed at different concentrations. When cmc values of the pure surfactants are widely separated, there seems to be no "memory" in the R value in the neighbourhood of the larger cmc. All of this argues for a single type of micelle being formed in each mixed surfactant system from the cmc to higher concentrations and implies that in this micelle the two surfactants do not act independently.

Can. J. Chem. Downloaded from www.nrcresearchpress.com by 210.87.254.42 on 09/06/12
For personal use only.

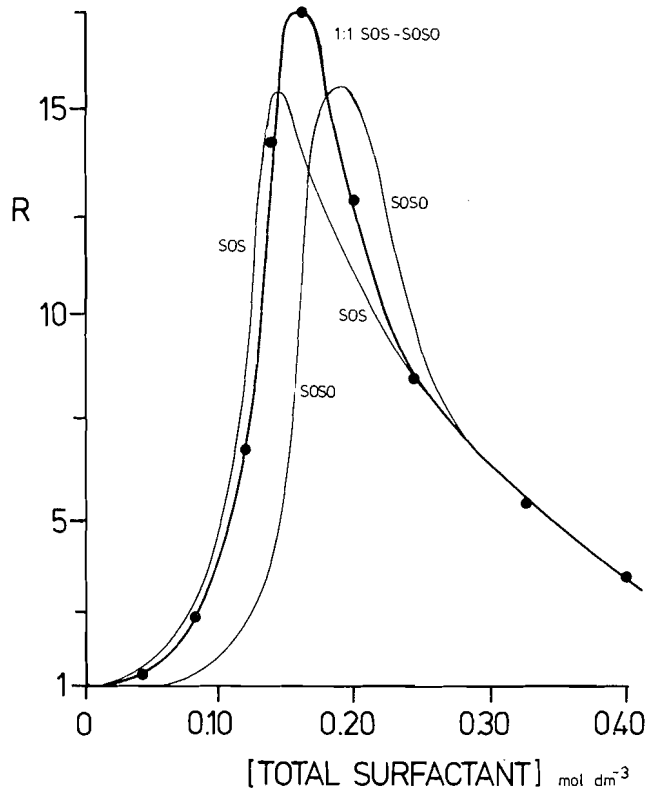

FIG. 4. Rate enhancements for the Ni^{2+}–PADA reaction in the system SOS–SOSO.

Figure 1 compares the R values for the equimolar SLS–SDS system with those of the pure surfactants. The sum of the concentrations of the two surfactants is taken as the surfactant concentration in the mixed system. This manner of plotting the concentration presupposes that the surfactants in the mixed system are both actively involved in micellization and not that one in the presence of the other is merely being solubilized.

The cmc can be estimated from the surfactant concentration at which R is a maximum (C_{max}) from the relationship (10):

$$C_{max} = \text{cmc} + (K_{Ni}\, K_{PADA})^{-1/2}$$

The cmc for the 1:1 mole ratio SLS–SDS system with 10^{-3} mol dm^{-1} Ni^{2+} present is thus 6×10^{-3} mol dm^{-3} in total surfactant. This value is intermediate between the cmc values of the pure surfactant but is closer to the cmc of the longer chained homolog as found by other investigators (14, 15). Table 1 compares the cmc values obtained by this technique for the pure and mixed surfactant systems examined in this study.

R curves were also obtained for the 1:2 and 2:1 mole ratio SLS–SDS systems but are not reproduced here since they were intermediate in predictably proportional fashion between the curves for the pure surfactants. These observations are consistent with a mixed micelle in which the monomers of each surfactant are present roughly in the same ratio in which they are in solution. This is reasonable since the incorporation of either a decylsulfate or dodecylsulfate into the micellar state cannot be much different energetically.

The second system investigated, equimolar SOS–SHS, is again a situation where the surfactant homologs differ by 2 carbon atoms but the chains are shorter and only just sufficiently long to produce micellization.

A complete concentration scan for k_{obs} was possible for this system by the stopped-flow technique since the rate enhancements were not nearly as pronounced (Fig. 2). The R curve resembles that for pure SOS except that, when the sum [SOS] + [SHS] is used to express concentration, the curve was displaced slightly to higher concentration. The cmc for the mixed micelle is slightly greater than for pure SOS.

It is sometimes found that in the presence of a longer chained surfactant another surfactant does not form micelles, but acts simply as a solubilized amphiphilic solute (2). SHS forms micelles only weakly (16) and in the presence of SOS is probably not totally available as "surfactant", i.e. micellar component. If the concentration unit were chosen as [SOS] + 0.5[SHS], then the R curve for the equimolar system would more nearly coincide with the pure surfactant values. In other words, the distribution of SHS to SDS monomers in the mixed micelle formed from equimolar solutions was probably closer to 1:2 than 1:1.

The third system examined was the equimolar SLS–SOS system where the carbon chain difference is four carbon atoms. The pure surfactants have markedly different cmc values: 4×10^{-3} mol dm^{-3} for SLS and 0.115 mol dm^{-3} for SOS, both in 10^{-3} mol dm^{-3} Ni^{2+} (6), and the cmc for the mixed system in the same concentration of Ni^{2+} is 8×10^{-3} mol dm^{-3} from the C_{max} value. When R values are plotted against the total surfactant concentration, in the region above the cmc for pure SOS, the three curves for SLS, SOS, and equimolar SLS–SOS are indistinguishable (Fig. 3). From the previous discussion for the SLS–SDS system, a 1:1 micelle is probably being formed in the SLS–SOS system also.

In the fourth system studied, equimolar SOS–SOSO, mixing the two surfactants brings about only a change in headgroup, sulfonate or sulfate. In Fig. 4 are shown the R curves for the equimolar SOS–SOSO system with the pure surfactant curves included. As with the SLS–SDS and SLS–SOS systems, the rate enhancement behaviour over the entire mixed micellar range for this system is consistent with a random mixing of SOS and SOSO monomers in the micellar unit. This system displayed the most ideal behaviour of the systems investigated.

Complete kinetic analyses were performed on the equimolar SLS–SDS, SLS–SOS, and SOS–SOSO systems where the R curve behaviour points to 1:1 mole ratio micelles. The values of K_{PADA} found through solubility measurements, K_{Ni} through the murexide technique, and V_s through computer-fitting eq. [1] are listed in Table 1 along with the corresponding values for the pure surfactants.

The partitioning constants in Table 1 give no indication that any major changes in hydrophobic attraction or surface potential are occurring in the formation of these mixed micelles. The reaction volumes are similarly uninteresting although V_s for the equimolar SLS–SOS system is, within experimental error (roughly 10% in V_s), identical to that for pure SLS. The longer chained surfactant may essentially define the size of the mixed micelle when the head group of both surfactants is the same.

Thus, the only hint at synergistic effects in these simple mixed micellar systems is a slight increase in the maximum in the rate enhancement for the probe reaction over either of the R_{max} values for the pure surfactants. It is difficult to know what this means since this is a problematic micellar concentration region (5). However, in the mixed micelles investigated in this work the differences in the surfactants are only slight so that more dramatic differences may lead to greater increases in rate enhancement maxima.

Can. J. Chem. Downloaded from www.nrcresearchpress.com by 210.87.254.42 on 09/06/12
For personal use only.

TABLE 1. Critical micelle concentration rate enhancement parameters for mixed equimolar surfactants. (Corresponding values for the pure surfactants[a] are given in brackets.)

System	Critical micelle concentration mmol dm^{-3}	K_{PADA} dm^3 mol^{-1}	K_{N_1} dm^3 mol^{-1}	V_s dm^3 mol^{-1}
SLS−SDS	6 (4−40)	1000 (2800−1050)	300 (650−90)	0.43 (0.29−0.45)
SLS−SOS	8 (4−115)	700 (2800−300)	45 (100−25)	0.30 (0.29−0.70)
SOS−SOSO	120 (115−150)	200 (300−85)	30 (25−22)	0.67 (0.70−0.71)

[a]References 6, 7.

Acknowledgements

We are grateful to the Natural Sciences and Engineering Research Council of Canada and the Science and Engineering Research Council (U.K.) for financial assistance.

1. C. TANFORD. The hydrophobic effect: formation of micelles and biological membranes. 2nd ed. Wiley−Interscience, New York. 1980. p. 95.
2. K. SHINODA, T. NAKAGAWA, B. TAMAMUSHI, and T. ISEMURA. Colloidal surfactants. Academic Press, New York. 1963. pp. 63−67.
3. P. STENIUS, H. PALONEN, G. STROM, and L. ODBERG. *In* Surfactants in solution. *Edited by* K. L. Mittal and B. Lindman. Plenum Press, New York. In press.
4. A. D. JAMES and B. H. ROBINSON. J. Chem. Soc. Faraday Trans. 1, **74**, 10 (1978).
5. J. HOLZWARTH, W. KNOCHE, and B. H. ROBINSON. Ber. Bunsenges. Phys. Chem. **82**, 1001 (1978).
6. P. D. I. FLETCHER and V. C. REINSBOROUGH. Can. J. Chem. **59**, 1361 (1981).
7. J. R. HICKS and V. C. REINSBOROUGH. Aust. J. Chem. **35**, 15 (1982).
8. J. R. HICKS and V. C. REINSBOROUGH. *In* Surfactants in solution. *Edited by* K. L. Mittal and B. Lindman. Plenum Press, New York. In press.
9. B. H. ROBINSON, N. C. WHITE, and C. MATEO. Adv. Mol. Relaxation Processes,**7**, 321 (1975).
10. V. C. REINSBOROUGH and B. H. ROBINSON. J. Chem. Soc. Faraday Trans. 1, **75**, 2395 (1979).
11. B. H. ROBINSON and N. C. WHITE. J. Chem. Soc. Faraday Trans. 1, **74**, 2625 (1978).
12. M. FISCHER, W. KNOCHE, B. H. ROBINSON, and J. WEDDERBURN. J. Chem. Soc. Faraday Trans. 1, **75**, 119 (1979).
13. M. FISCHER, W. KNOCHE, P. D. I. FLETCHER, B. H. ROBINSON, and N. C. WHITE. Colloid Polym. Sci. **258**, 733 (1980).
14. K. J. MYSELS and R. J. OTTER. J. Colloid Sci. **16**, 462 (1961).
15. L. SHEDLOVSKY, C. W. JACOB, and M. B. EPSTEIN. J. Phys. Chem. **67**, 2075 (1963).
16. D. A. W. ADAIR, V. C. REINSBOROUGH, and S. J. ZAMORA. Adv. Mol. Relaxation Processes, **11**, 63 (1977).

Can. J. Chem. Downloaded from www.nrcresearchpress.com by 210.87.254.42 on 09/06/12
For personal use only.

Dynamic stereochemistry of 2,3,12,13-tetrathia- and -tetraselena[4,4]metacyclophanes[1]

KEITH R. DIXON AND REGINALD H. MITCHELL[2]
Department of Chemistry, University of Victoria, Victoria, B.C., Canada V8W 2Y2

Received August 24, 1981[3]

KEITH R. DIXON and REGINALD H. MITCHELL. Can. J. Chem. **61**, 1598 (1983).

2,3,12,13-Tetrathia- and -tetraselena[4,4]metacyclophanes exhibit temperature dependent ^{1}H nmr spectra in which the methylene resonances change from AB spectra in the low temperature limit to singlets at higher temperatures. Coalescence temperatures are 256 and 208 K, respectively, and a complete line-shape analysis yields $\Delta G^{0\ddagger}_{298}$ (thia) = 53.2 kJ mol^{-1} and $\Delta G^{0\ddagger}_{298}$ (selena) = 46.5 kJ mol^{-1}. The spectra and thermodynamic data are interpreted in terms of a mechanism involving interconversion of *syn* conformers with little or no involvement of the *anti* conformers previously assumed to dominate in this type of molecule.

KEITH R. DIXON et REGINALD H. MITCHELL. Can. J. Chem. **61**, 1598 (1983).

Les spectres de rmn du ^{1}H des tétrathia-2,3,12,13 et des tétraséléna[4,4]métacyclophanes dépendent de la température. Dans ces spectres la résonance du méthylène qui donne un spectre du type AB à basse température devient un singulet à température plus élevée. Les températures de coalescence sont respectivement de 256 et de 208 K et une analyse complète de la forme des raies donne $\Delta G^{0\ddagger}_{298}$ (thia) = 53,2 kJ mol^{-1} et $\Delta G^{0\ddagger}_{298}$ (selena) = 46,5 kJ mol^{-1}. On interprète les spectres et les données thermodynamiques en fonction d'un mécanisme qui fait intervenir une interconversion des conformères *syn* avec peu ou pas du tout de participation des conformères *anti* qui présumément dominent dans ce type de molécule.

[Traduit par le journal]

Introduction

The static and dynamic stereochemistry of cyclophanes has been of particular synthetic and theoretical interest for more than 20 years, and has been extensively reviewed (1).

Stereochemical assignments in the larger [*m*,*n*]cyclophanes are not trivial and one cannot necessarily assume that the *anti* conformer is the most stable, as it appears to be for [2,2]metacyclophane, **1** (2). For example, relatively recent papers have shown that **2** is coplanar and isomerizes via a stepped *anti* conformer (3) and that both the thiacyclophane **3** (4) and the selena analogue **4** (5) are *syn* (**3***a*, **4***a*) in the solid state as well as in solution. In these latter cases there appears to be little evidence for participation of the *anti* conformers **3***b*, **4***b*. Newkome and Kawato (3) have pointed out that whenever the metacyclophane bridges possess functionality that restricts the rotational freedom, e.g. CH_2—X—X—CH_2, deviations from the *anti* stepped mode might occur. Moreover very recently the trithia-bridged compound **5** has also been reported to be *syn* (6).

It thus seemed pertinent to examine the bis(disulphide) **6** and the bis(diselenide) **7** in light of this data, and at the same time to undertake a study of the mechanisms and thermodynamics of the dynamic processes occurring in these molecules. Such a study is of additional interest since the literature does not appear to contain any previous comparisons between thia- and selena-cyclophanes.

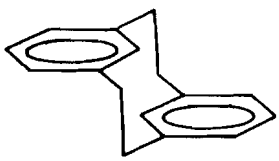

1

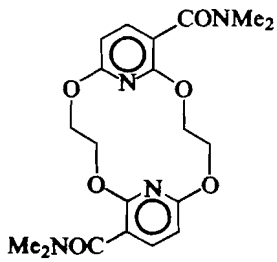

2

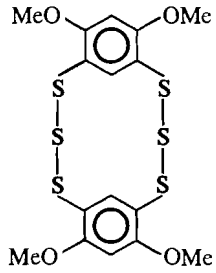

5

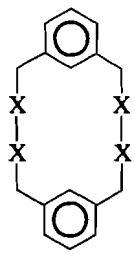

6 X = S
7 X = Se

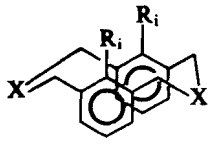

3*a* X = S, R = H
4*a* X = Se, R = H
8 X = S, R = CH_3

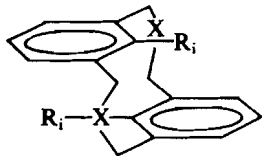

3*b* X = S, R = H
4*b* X = Se, R = H
9 X = S, R = CH_3
10 X = S, R = H, NH_2

Results

The tetraselenide, **7**, was prepared as previously described (7). The ^{1}H nmr spectra at 180 K show the methylene protons as an "AB" pattern (with J_{AB} typical of a geminal coupling) and as temperature is increased, the pattern coalesces to a single peak. Our spectra show no significant differences from those published (7) and hence are not reproduced again here. However, these results were previously thought to be produced by a rapid interchange between *syn* and *anti* conformers, with restricted rotation of the methylene bridges, whereas the more detailed analysis of the present paper suggests a new interpretation of the dynamic stereochemistry (see Discussion). Our line-shape analysis also provides full thermodynamic parame-

[1]For the nomenclature system used in these compounds, see ref. 23.
[2]Author to whom correspondence may be addressed.
[3]Revision received January 20, 1983.

Can. J. Chem. Downloaded from www.nrcresearchpress.com by 210.87.254.40 on 09/06/12
For personal use only.

Can. J. Chem. Downloaded from www.nrcresearchpress.com by 210.87.254.40 on 09/06/12
For personal use only.

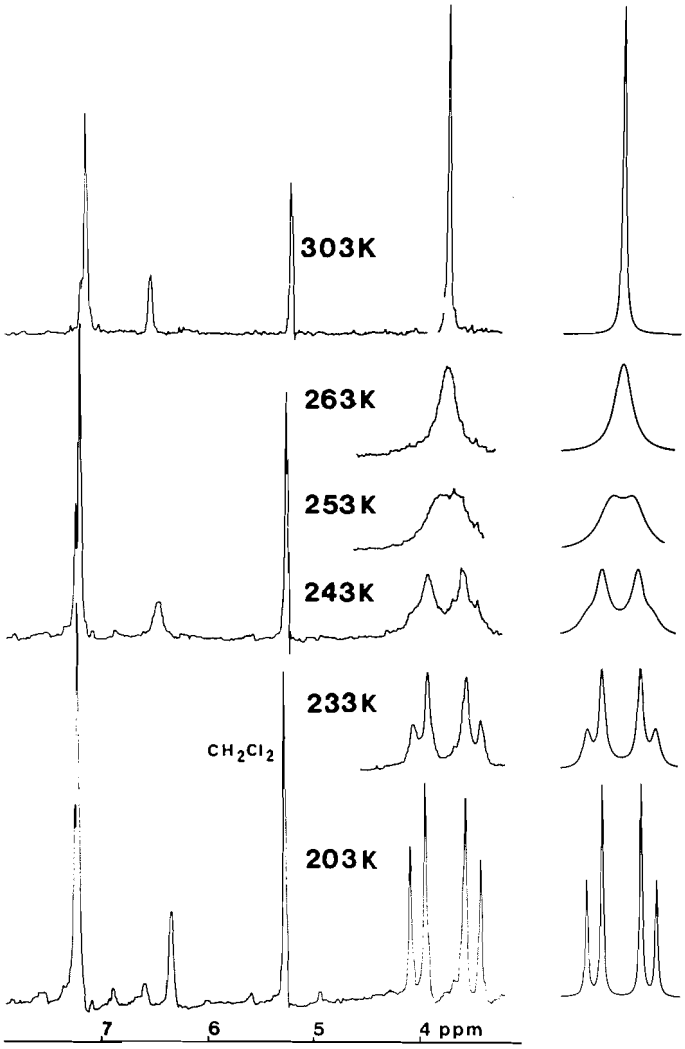

FIG. 1. Temperature variation of the ^{1}H nmr spectrum for **6** in $CDCl_3$–CD_2Cl_2 (1:2) solution. Computer-simulated line shapes for the methylene resonances are shown on the right.

ters where the previous work included only an estimate of $\Delta G^{\ddagger}$ (42.6 kJ mol^{-1}) obtained from measurement of the coalescence temperature (208 K).

The tetrasulphide, **6**, was prepared by the method of Chan and co-workers (8) and had identical properties to those reported previously (2, 9). Sato *et al.* (2) made no mention of temperature dependence of the ^{1}H nmr spectra, but we have found a variation of the methylene proton patterns similar to that described above for the tetraselenide, **7**. Moreover, the resonances due to the internal and external aromatic protons remain essentially unchanged[4] during the changes in the methylene resonances, a clear indication that *syn* $\rightleftharpoons$ *anti* interchange is not occurring. The methylene proton spectra are shown in Fig. 1, together with simulated spectra obtained from the DNMR3 computer programme (10).

Preliminary simulations of spectra in the low temperature ranges established the following parameters:

6: J_{AB} = 12.9 Hz; ν_{AB} = 44.0 Hz; T_2 = 0.13 s
7: J_{AB} = 11.0 Hz; ν_{AB} = 37.4 Hz; T_2 = 0.08 s

[4]Except for a slight broadening of the internal proton resonance at intermediate temperatures, an effect treated in detail in the Discussion.

TABLE 1. Rate constants determined by line-shape analysis at various temperatures for **6** and **7**

6		**7**	
Temperature (K)	Rate (s^{-1})	Temperature (K)	Rate (s^{-1})
203	0.4	183	4
223	4	187	7
233	15	191	12
238	23	195	22
243	40	199	32
245.5	50	203	44
248	60	205	56
250.5	80	207	65
253	95	209	83
255.5	115	213	120
258	140	218	200
263	220	223	300
273	500		
303	4000		

Also, these preliminary results indicated that ν_{AB} does not vary significantly with temperature. The correct choice of ν_{AB} is of course well-defined by the spectra until near the coalescence point, but at higher temperatures the choice of ν_{AB} and rate constant (k) become critically interrelated and the necessity to assume that ν_{AB} is constant places limitations on the ultimate reliability of the rate data. The other important parameter is the choice of transverse relaxation time ($T_2 = 1/(\pi w)$ where w = width at half-height of peaks not broadened by exchange). This parameter choice has a critical effect in the low temperature region, where resolution of J_{AB} is collapsing but the A and B regions are still resolved, but in this region the correct choice is fairly clearly indicated by the low temperature limit spectra. Line width probably decreases as temperature is increased, possibly due to the viscosity broadening at the lower temperatures, but fortunately once A and B begin to coalesce, the choice of T_2 is not critical. Consequently, this probably does not represent a significant limitation on the reliability of the data. Once the preliminary parameters were established, careful matching of observed and calculated spectra for both **6** and **7** yielded the rate constants given in Table 1, and Eyring plots of ln (k/T) against $1/T$ (Fig. 2). produced the following least-squares straight lines:

6: $\ln (k/T) = -(5438)(1/T) + 20.52$
correlation coefficient, R_c = 0.9992
7: $\ln (k/T) = -(4139)(1/T) + 18.89$
correlation coefficient, R_c = 0.9973

Comparison of these equations with the standard transition-state theory equation (11):

$$\ln (k/T) = \frac{-\Delta H^{0\ddagger}}{R} (1/T) + \frac{\Delta S^{0\ddagger}}{R} + \ln (k/h)$$

then enabled $\Delta H^{\ddagger}$, $\Delta S^{\ddagger}$, and hence $\Delta G^{\ddagger}$ to be calculated, and these parameters are summarized in Table 2. This table also includes Arrhenius activation energies, E_a, which were derived from the slopes of Arrhenius plots (ln k against $1/T$) assuming:

$$\ln k = -E_a/R\ (1/T) + \ln A$$

Few line-shape analyses (12) have been made on thiacyclophanes; the simpler $\Delta\nu$, T_c method (13) to obtain $\Delta G^{\ddagger}$ at the coalescence temperature is usually resorted to (see, for

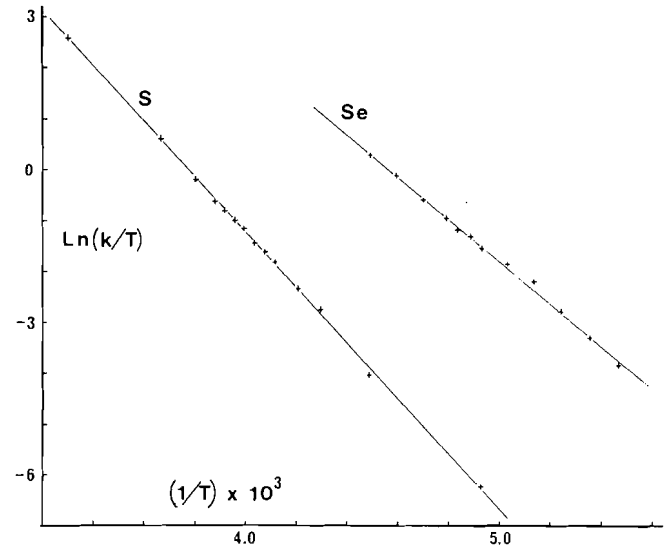

FIG. 2. Plots of ln (k/T) against $1/T$ for **6** (lower plot labelled S) and **7** (upper plot labelled Se).

TABLE 2. Thermodynamic parameters for **6** and **7**

Parameter	**6**	**7**
E_a (kJ mol^{-1})	47.3	36.1
$\Delta H^{0\ddagger}$ (kJ mol^{-1})	45.2	34.4
$\Delta S^{0\ddagger}$ (J K^{-1})	−26.9	−40.5
$\Delta G^{0\ddagger}_{298}$ (kJ mol^{-1})	53.2	46.5

TABLE 3. Comparison of line-shape analysis and T_c method of determining $\Delta G^{\ddagger}_{T_c}$ for **6** and **7**

	6	**7**
$\Delta\nu$ (Hz)	44.0	37.4
T_c (K)	256.0	209.0
$\Delta G^{\ddagger}_{T_c}$ (calcd. as ref. 13) (kJ mol^{-1})	50.6	41.3
$\Delta G^{\ddagger}_{T_c}$ (calcd. from data in Table 2) (kJ mol^{-1})	52.1	42.9

example, ref. 14). The simple method is strictly valid only for coalescing singlets but in the present "AB" case good agreement with line-shape analysis is found (Table 3) even though the coupling constant is relatively large compared to the chemical shift ($\nu_{AB}/J_{AB} \sim 4$).

Discussion

The chemical shifts of the internal aryl hydrogens, H_i, of **6** and **7** are very similar to those found in the known *syn* conformers, **3** and **4**, and are quite different from that in the *anti* conformer, **10** (see Table 4). Also, in the known *anti*-**9**, the outer aryl hydrogens appear as a multiplet, whereas in **3**, **4**, **6**, **7**, and **8** the corresponding resonances are all singlets. This suggests that, of the possible conformers illustrated in Fig. 3, the stable forms of **6** and **7** are more likely to by *syn* conformers such as A–E than *anti* conformers F and G. An *anti*-coplanar conformer H (similar to **2**) could also yield a chemical shift for H_i in the region normally associated with *syn* conformers, since the internal aryl protons are well removed from the shielding region of the other aromatic ring, just as they are in *syn* conformers. However, inspection of models shows that conformer H is unlikely for **6** and **7** because in these molecules (unlike **2**) H_i would strongly interact with the chalcogenide bridges, causing distortion towards the stepped *anti* conformers F and G, moving H_i into the shielding region of the other aromatic ring and towards a more typically "*anti*" chemical shift. Also, we have been unable to differentiate H_A and H_B in **6** (see H) even at 250 MHz, whereas this was possible in a derivative of **2** (3).

Other important considerations are: (a) the preferred C—S—S—C dihedral angle of about 90° (15), which means that conformers such as C probably need not be considered further, and (B) the fact that the low temperature limit spectra for **6** and **7** show only two types of methylene protons, which probably excludes conformers D, E, and G.

Of the remaining possibilities, A and B, the latter seems more likely because of the chemical shift similarity between **3** and **4** and **6** and **7**. In the solid state **3** and **4** both have conformations similar to B in which the heteroatoms are as distant as possible from H_i (4, 5), and in A the surrounding of H_i by the four heteroatoms would be expected to cause a substantial chemical shift (5). Additional support for these conclusions has now been obtained by X-ray crystallography. The subsequent paper (16) reports that in the solid state **6** is indeed basically the *syn* conformer represented by B, except that the aromatic rings are inclined to each other at a dihedral angle of 101° rather than being exactly parallel. The conformation found by X-ray is shown in structure **11**.

The dynamic process now needs to be explained, with B as the preferred conformer. As the temperature is raised, the non-equivalent protons of B (see structure **11**) are rendered equivalent. In order for this to happen (*i*) the aromatic rings must fold outward by rotation of the aromatic–methylene carbon bonds, passing through a coplanar state, and (*ii*) rotation about the X—X bridges must occur to invert these. Whilst these processes could occur together to give a planar intermediate such as H as a "transition state", a less energetic process would seem to be sequential. This might also explain the behaviour of the internal proton resonances (see Fig. 1): for **6**, the H_i singlet is at δ 6.38 at the low temperature limit, broadens slightly at intermediate temperatures, and then sharpens again at the high temperature limit, these changes being accompanied by a slight downfield shift to δ 6.63. This is expected for the above mechanism, with the broadening due to relatively slow rates involving more than one intermediate conformer with approximately coplanar rings. A minor amount of another conformer could also be involved, where signals are lost in the spectrum noise. The evidence is, however, completely convincing that a *syn* ⇌ *anti* exchange is not occurring. Thus the presence of *syn* and *anti* conformers at low temperature, exchanging rapidly at higher temperatures, would require two H_i resonances in the low temperature limit, and a low temperature *syn* form ex-

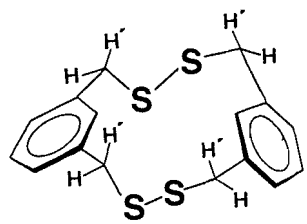

11

Can. J. Chem. Downloaded from www.nrcresearchpress.com by 210.87.254.40 on 09/06/12
For personal use only.

TABLE 4. Comparison of ^{1}H nmr spectra (δ) of **3**, **4**, **5**, **7**, **8**, **9**, and **10** (90 MHz, $CDCl_3$)

	Compound						
	syn-**3**	*syn*-**4**	**6**	**7**	*syn*-**8**	*anti*-**9**	*anti*-**10**
H-aryl	6.91	7.04	7.23	7.17	6.66	7.4–7.0	7.5–6.7
H_i	6.82	6.46	6.63	6.67	—	—	. 5.0
—CH_2—(bridge)	3.71	3.78	3.79	4.00	3.90	3.68	4.1–3.2
—CH_3	—	—	—	—	2.54	1.30	—
Reference	4	5, 20	This work	This work	21	21	22

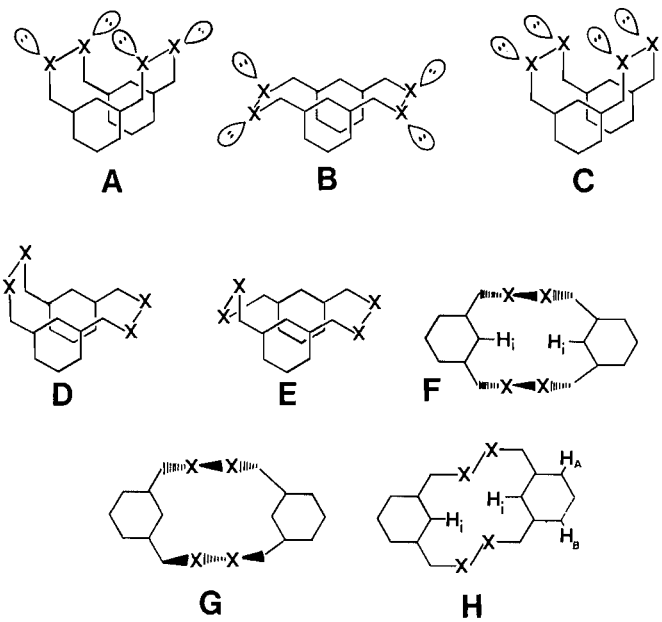

FIG. 3. Probable major conformations of **6** and **7**.

changing with a new *anti* conformer at high temperature would require an upfield shift of H_i towards the typical *anti* value of δ 5.0 (see Table 4).

While it is well known (17) that there are pitfalls in determination of $\Delta H^{\ddagger}$ and $\Delta S^{\ddagger}$ by line-shape analysis, we believe the differences observed (Table 2) for **6** and **7** are worthy of some comment. Examination of molecular models suggests no particular strain barriers to any of the above processes, but the various bond rotation processes are expected to occur more easily for the selenaphane relative to the thiaphane because the longer bonds to selenium (18) will result in a general reduction in steric interactions. One particular consequence is that the internal hydrogens will pass each other more easily as the aromatic rings become coplanar in the selenaphane. Thus, the higher enthalpy of activation (Table 2) for **6** relative to **7** is to be expected on this mechanism. The more negative entropy of activation in the selenaphane, **7**, is more difficult to interpret, but it probably also results from the greater "floppiness" produced by the longer bonds, necessitating more molecular ordering to achieve the transition state.

It is also of interest to consider why the analogous compounds **3** and **4**, with monochalcogenide bridges, both show singlet methylene bridge resonances down to <180 K. While this could be due simply to accidental chemical shift equivalence, it seems more likely to us that a dynamic process similar to that described above is operating, but at a faster rate in **3** and **4**. Bushweller *et al.* (19) have pointed out that the presence of adjacent atoms possessing lone pairs leads to substantial enhancement of the barrier to ring inversion in 6-membered rings, including the tetrathiacyclohexane, **12**. Thus, rotation about the X—X bonds in **6** and **7** may represent a significant barrier due to lone pair interactions and rates would be faster in the monochalcogenide bridged species, **3** and **4**. Additionally, the more complex sequences of bond rotations occurring in the dichalcogenide bridge species, **6** and **7**, probably have a statistically lower probability ("pre-exponential effect") and hence the rates are slower. The diselenide bridge compound, **7**, would be faster than the disulphide bridges, **6**, because of the longer Se—Se bond.

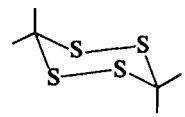

12

In conclusion, in these bis(dihetero) [4,4] bridged cyclophanes, *syn* conformers are the more stable low temperature forms. At higher temperatures the methylene bridge protons are rendered equivalent by a dynamic process which probably involves intermediates with approximately coplanar aromatic rings. The *anti* conformers which have usually been described for simple metacyclophanes are not involved to any significant extent.

Experimental

The complexes **6** and **7** were prepared as previously described (7, 8). The ^{1}H nmr spectra were recorded at 90 MHz on a Perkin–Elmer R32B spectrometer. Samples were dissolved in 1:2 $CDCl_3$–CD_2Cl_2 and CH_2Cl_2 was added as internal reference.

Simulated line shapes were calcualted by the DNMR3 computer programme (10) on an IBM 3031 computer and plotted on a Tektronic 4013 graphics screen for preliminary work or a Calcomp 1039 drum-plotter for final data.

1. (*a*) D. J. CRAM. Rec. Chem. Prog. **20**, 71 (1959); (*b*) B. H. SMITH. Bridged aromatic compounds. Academic Press, New York. 1964; (*c*) D. J. CRAM and J. M. CRAM. Acc. Chem. Res. **4**, 204 (1971); (*d*) F. VÖGTLE and P. NEUMANN. Angew. Chem. Int. Ed. Engl. **11**, 73 (1972); Synthesis, 85 (1973); (*e*) S. MISUMI and T. OTSUBO. Acc. Chem. Res. **11**, 251 (1978); (*f*) F. VÖGTLE and G. HÖHNER. Top. Curr. Chem. **74**, 1 (1978).
2. T. SATO, M. WAKABAYASHI, K. HATA, and M. KAINOSHO. Tetrahedron, 2737 (1971).
3. G. R. NEWKOME and T. KAWATO. J. Am. Chem. Soc. **101**, 7088 (1979).
4. W. ANKER, G. W. BUSHNELL, and R. H. MITCHELL. Can. J. Chem. **57**, 3080 (1979).
5. G. W. BUSHNELL and R. H. MITCHELL. Can. J. Chem. **60**, 362 (1982).
6. F. BOTTINO, S. FOTI, and S. PAPPALARDO. Tetrahedron Lett. 1171 (1979); F. BOTTINO and S. PAPPALARDO. J. Chem. Soc. Perkin Trans. 1, 718 (1981).

Can. J. Chem. Downloaded from www.nrcresearchpress.com by 210.87.254.40 on 09/06/12
For personal use only.

7. R. H. MITCHELL. Can. J. Chem. **54**, 238 (1976).
8. T. F. TAM, P. C. WONG, T. W. SIU, and T. L. CHAN. J. Org. Chem. **41**, 1289 (1976).
9. V. BOEKELHEIDE and J. L. MONDT. Tetrahedron Lett. 1203 (1970).
10. D. A. KLEIER and D. BINSCH. Programme 165, Quantum Chemistry Programme Exchange. Indiana University. 1969.
11. I. AMDUR and G. G. HAMMES. Chemical kinetics. McGraw Hill, New York. 1966. pp. 55, 56.
12. H. M. HUTTON, W. E. HIEBERT, and V. MARK. Can. J. Chem. **56**, 1261 (1978); G. HUNTER, R. F. JAMESON, and M. SHIRALIAN. J. Chem. Soc. Perkin Trans. 2, 712 (1978); D. J. BRICKWOOD, W. D. OLLIS, J. S. STEPHANATOU, and J. F. STODDART. J. Chem. Soc. Perkin Trans. 1, 1398 (1978); L. M. JACKMAN and F. A. COTTON (*Editors*). Dynamic nuclear magnetic resonance spectroscopy. Academic Press, New York. 1975.
13. I. C. CALDER and P. J. GARRATT. J. Chem. Soc. B, 660 (1967); M. S. GUTOWSKI and C. H. HOLM. J. Chem. Phys. **25**, 1228 (1956); S. GLASSTONE, K. J. LAIDLER, and H. EYRING. The theory of rate processes. McGraw–Hill Book Co., Inc., London. 1941. Chapt. 1.
14. F. VÖGTLE and L. SCHUNDER. Chem. Ber. **102**, 2677 (1969); F. VÖGTLE and P. NEUMANN. Tetrahedron, **26**, 5299 (1970); Tetrahedron Lett. 115 (1970); H. FÖRSTER and F. VÖGTLE. Angew. Chem. Int. Ed. Engl. **16**, 429 (1977); K. BÖCKMANN and F. VÖGTLE. Chem. Ber. **114**, 1048 (1981).
15. S. J. ABRAHAMS. Q. Rev. **10**, 407 (1956).
16. G. W. BUSHNELL and R. H. MITCHELL. Can. J. Chem. **61**, 1603 (1983).
17. G. BINSCH and H. KESSLER. Angew. Chem. Int. Ed. Engl. **19**, 411 (1980); I. O. SUTHERLAND. *In* Annual reports of NMR spectroscopy. *Edited by* F. Mooney. Academic Press, London. 1971. pp. 71–235.
18. I. L. KARLE and J. KARLE. *In* Organic selenium compounds: their chemistry and biology. *Edited by* D. L. Klayman and W. H. H. Gunther. Wiley–Interscience, New York, NY. 1973. Chapt. XV.
19. C. H. BUSHWELLER, J. GOLINI, G. U. RAO, and J. W. O'NEIL. J. Am. Chem. Soc. **92**, 3055 (1970).
20. R. H. MITCHELL. Can. J. Chem. **58**, 1398 (1980).
21. R. H. MITCHELL and V. BOEKELHEIDE. J. Am. Chem. Soc. **96**, 1547 (1974).
22. R. VÖGTLE, W. WIEDER, and H. FÖRSTER. Tetrahedron Lett. 4361 (1974).
23. F. VÖGTLE and P. NEUMANN. Tetrahedron, **26**, 5847 (1970).

Can. J. Chem. Downloaded from www.nrcresearchpress.com by 210.87.254.40 on 09/06/12
For personal use only.

The crystal and molecular structure of 2,3,12,13-tetrathia[4,4]metacyclophane[1]

KATHY A. BEVERIDGE, GORDON W. BUSHNELL, AND REGINALD H. MITCHELL[2]
Department of Chemistry, University of Victoria, Victoria, B.C., Canada V8W 2Y2

Received January 24, 1983

KATHY A. BEVERIDGE, GORDON W. BUSHNELL, and REGINALD H. MITCHELL. Can. J. Chem. **61**, 1603 (1983).

Conformations in a variety of cyclophane structures are discussed, as determined by X-ray diffraction in crystals and by ^{1}Hmr in solution. Established nomenclature is brought forward (*syn*/*anti* and *synclinal*/*anticlinal*) and used to deal with an intermediate case which has been examined by both techniques. The crystal and molecular structure of the title compound, $C_{16}H_{16}S_4$, is determined and refined to $R = 0.0497$. The crystal is orthorhombic, space group *Pbca*, $a = 16.593(2)$, $b = 10.018(2)$, $c = 19.407(3)$ Å at 25(2)°C, $Z = 8$, $D_{calc} = 1.386$ g cm^{-3}. The molecular conformation in the crystal is *anticlinal* with a dihedral angle between the benzene rings of 101°. The benzene rings are displaced laterally by 0.727 Å and the sequence of torsion angles is similar in the two bridging chains.

KATHY A. BEVERIDGE, GORDON W. BUSHNELL et REGINALD H. MITCHELL. Can. J. Chem. **61**, 1603 (1983).

On discute des conformations des diverses structures du cyclophane, telles que déterminées par diffraction de rayons-X et par la rmn du ^{1}H en solution. On reprend la nomenclature établie (*syn*/*anti* et *synclinal*/*anticlinal*) et on l'utilise pour traiter un cas intermédiaire que l'on a étudié à l'aide des deux techniques. On a déterminé la structure du crystal et la structure moléculaire du composé mentionné dans le titre, $C_{16}H_{16}S_4$, et on les a affinées jusqu'à une valeur de $R = 0{,}0497$. Le cristal est orthorombique et appartient au groupe d'espace *Pbca*, avec $a = 16{,}593(2)$, $b = 10{,}018(2)$, $c = 19{,}407(3)$ Å à 25°C(2), $Z = 8$, $D_{calc} = 1{,}386$ g cm^{-3}. Dans le cristal, la conformation moléculaire est *anticlinale* avec un angle dièdre de 101° entre les noyaux de benzène. Les noyaux benzéniques sont déplacés latéralement de 0,727 Å et l'ensemble des angles de torsion est identique dans les deux chaînes pontées.

[Traduit par le journal]

Introduction

The preceding paper (1) discusses the variable temperature ^{1}Hmr spectra of the bis-disulphide **1** in comparison to related cyclophanes, in terms of the dynamics of the possible conformational processes occurring in solution in the molecule. This paper reports the structure of **1** in the solid state as determined by X-ray diffraction. This is also of special interest since no crystal structure of a [4,4]metacyclophane appears to have been reported in the literature. Indeed, the literature on crystal structures of the higher cyclophanes is fairly scant; related examples worthy of comment are the octasulphide (paracyclophane) **2** (2) and the tetrasulphide (paracyclophane) metal complex **3** (3), as well as the [4,2]cyclophane **4** (4) and [3,3]cyclophanes **5** (4) and **6** (5).

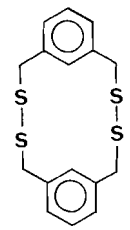

1

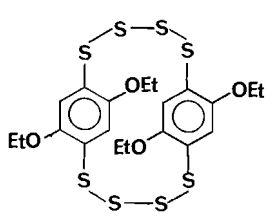

2

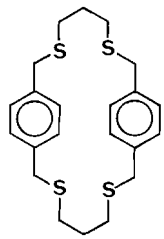

3

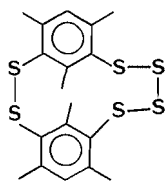

4

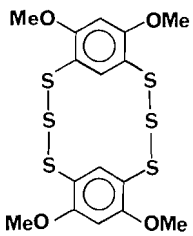

5

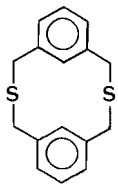

6

Of necessity the benzene rings of the two paracyclophanes **2** and **3** are *syn*, however, metacyclophanes can exist in *syn* or *anti* conformers. In some cases, e.g., **7** and **8**, both conformers are capable of independent existence and can be isolated (6). In the case of **6** only one state, probably a rapidly averaging mixture of conformers, is found in solution, while in the solid state **6** is found as the *syn* conformer (5). Likewise **5** was found in the solid state to be *syn* (4), whereas the [4,2]cyclophane **4** was found to be *anti* (4). While no crystal structure data is available on the oxa[4,4]cyclophane **9**, solution ^{1}Hmr spectroscopic data indicate the *anti*-coplanar structure to be pre-

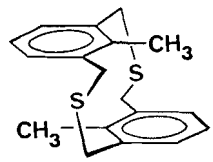

7

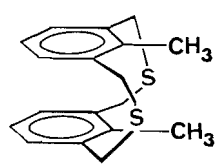

8

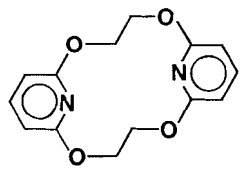

9

[1]*Chemical Abstract* name: 3,4,12,13-tetrathiatricyclo[13,3,1,1^{6,10}]-eicosa-1(19),6,8,10(20),15,17-hexaene.

[2]Author to whom reprint requests should be addressed.

Can. J. Chem. Downloaded from www.nrcresearchpress.com by 210.87.254.6 on 09/06/12
For personal use only.

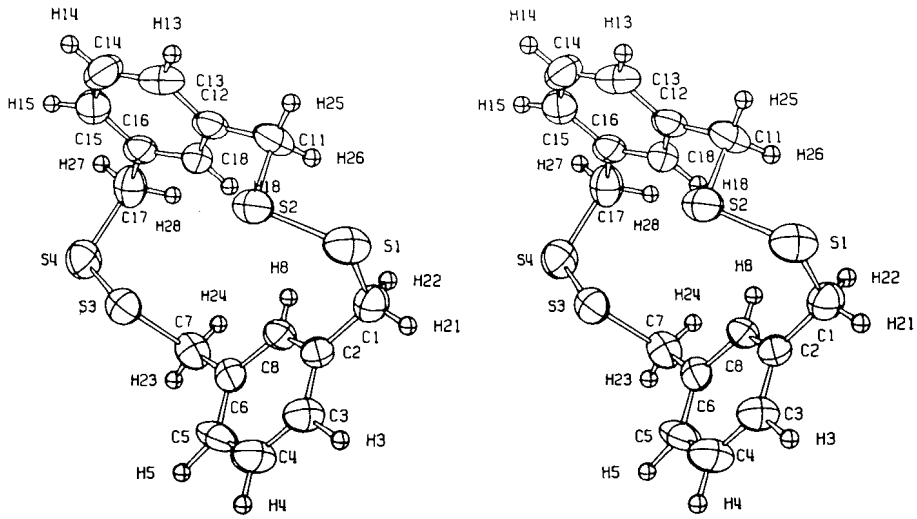

FIG. 1. An ORTEP drawing of tetrasulphide **1**. The hydrogen atoms are drawn as small spheres for clarity.

TABLE 1. Fractional atomic coordinates and temperature parameters*

Atom	x/a	y/b	z/c	U_{eq}
S(1)	34309(9)	48946(19)	−3824(8)	636(7)
S(2)	37207(9)	34912(17)	3302(8)	579(6)
S(3)	20289(9)	22214(16)	21522(8)	556(6)
S(4)	23588(10)	19608(18)	31490(8)	660(7)
C(1)	2624(4)	5854(7)	17(4)	59(3)
C(7)	1450(4)	3766(7)	2103(3)	54(3)
C(11)	4377(4)	4333(8)	956(4)	60(3)
C(17)	3280(4)	2971(8)	3239(4)	62(3)
C(2)	1958(3)	5049(6)	323(3)	45(2)
C(3)	1331(4)	4519(7)	−67(3)	58(3)
C(4)	739(4)	3783(7)	252(4)	66(3)
C(5)	749(4)	3539(7)	956(4)	60(3)
C(6)	1374(4)	4044(6)	1348(3)	45(2)
C(8)	1962(4)	4804(6)	1025(3)	45(3)
C(12)	4424(4)	3430(7)	1565(3)	49(3)
C(13)	4959(4)	2365(8)	1597(4)	61(3)
C(14)	4944(4)	1497(8)	2140(4)	66(3)
C(15)	4414(4)	1675(7)	2678(4)	55(3)
C(16)	3881(4)	2747(7)	2667(3)	47(2)
C(18)	3895(4)	3600(7)	2105(3)	46(2)
H(21)	245(3)	635(5)	−33(3)	54(20)
H(22)	281(3)	648(5)	35(3)	53(20)
H(23)	100(3)	358(5)	235(3)	52(19)
H(24)	172(4)	448(6)	233(3)	68(22)
H(25)	486(3)	448(5)	75(2)	31(15)
H(26)	414(4)	526(7)	106(3)	89(25)
H(27)	348(3)	256(5)	364(3)	61(19)
H(28)	315(3)	396(6)	326(2)	60(19)
H(3)	123(2)	479(4)	−66(2)	13(10)
H(4)	28(3)	340(5)	−4(3)	73(20)
H(5)	24(3)	299(5)	116(2)	57(16)
H(8)	236(3)	513(5)	125(2)	31(16)
H(13)	534(3)	225(5)	117(3)	56(17)
H(14)	527(3)	79(6)	219(3)	68(23)
H(15)	436(2)	105(4)	312(2)	13(11)
H(18)	354(3)	436(6)	212(3)	59(19)

*Estimated standard deviations are given in parentheses. Coordinates × 10^n where n = 5,4,3 for S,C,H. Temperature parameters × 10^n where n = 4,3,3, for S,C,H. U_{eq} = the equivalent isotropic temperature parameter for the non-hydrogen atoms. $U_{eq} = 1/3\sum_i\sum_j U_{ij}a_i^*a_j^*(a_i\cdot a_j)$. $T = \exp -(8\pi^2 U_{iso}\sin^2\theta/\lambda^2)$.

TABLE 2. Interatomic distances (Å)*

Atoms	Distance	Atoms	Distance
(a) Bonds to sulfur			
S(2)—S(1)	2.030(2)	S(4)—S(3)	2.027(2)
C(1)—S(1)	1.821(7)	C(11)—S(2)	1.836(6)
C(7)—S(3)	1.824(7)	C(17)—S(4)	1.841(7)
(b) Exocyclic bonds			
C(2)—C(1)	1.491(8)	C(12)—C(11)	1.491(9)
C(6)—C(7)	1.497(8)	C(16)—C(17)	1.509(9)
(c) Aromatic ring bonds			
C(3)—C(2)	1.393(8)	C(13)—C(12)	1.389(9)
C(4)—C(3)	1.375(8)	C(14)—C(13)	1.368(9)
C(5)—C(4)	1.388(8)	C(15)—C(14)	1.376(9)
C(6)—C(5)	1.383(8)	C(16)—C(15)	1.391(8)
C(8)—C(6)	1.387(8)	C(18)—C(16)	1.385(8)
C(8)—C(2)	1.385(8)	C(18)—C(12)	1.378(8)

*Estimated standard deviations are given in parentheses.

ferred (7). As discussed in the preceding paper, [1]Hmr did not clearly distinguish between a *syn* or an *anti* relatively-extended conformer for **1**. This information was thus sought for **1** by determination of the crystal structure.

syn, *anti* Nomenclature in phanes

Despite the fact that the nomenclature of phanes has been described in detail (8) and the stereochemistry of phanes has been reviewed (9), almost nothing has been said about the use of *syn* and *anti* to describe (6) compounds such as **8** and **7**. Indeed, in these particular cases the use of the terms *syn* and *anti* referring to the relative orientations of the benzene rings is quite clear and leads to no confusion. Although the original assignments of structure of, for example, **7** and **8**, were made by [1]Hmr (6, 10), subsequent X-ray crystal studies have borne them out (11). A problem arises, however, with higher cyclophanes which can adopt conformations in between these two extremes. Consider the three conformers depicted by **A**, **B** and

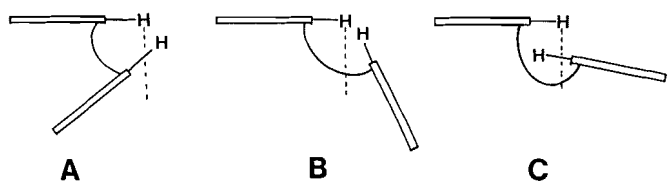

Can. J. Chem. Downloaded from www.nrcresearchpress.com by 210.87.254.6 on 09/06/12
For personal use only.

TABLE 3. Bond angles (°)*

Atoms	Angle	Atoms	Angle
	(a) Angles at sulfur		
C(1)—S(1)—S(2)	104.5(3)	C(17)—S(4)—S(3)	104.1(2)
C(7)—S(3)—S(4)	107.5(2)	C(11)—S(2)—S(1)	105.8(3)
	(b) Methylene angles		
C(2)—C(1)—S(1)	115.4(5)	C(16)—C(17)—S(4)	113.4(5)
C(6)—C(7)—S(3)	104.7(4)	C(12)—C(11)—S(2)	106.1(5)
	(c) Angles external to the benzene rings		
C(3)—C(2)—C(1)	122.8(6)	C(13)—C(12)—C(11)	122.3(7)
C(5)—C(6)—C(7)	122.3(6)	C(15)—C(16)—C(17)	121.6(6)
C(8)—C(2)—C(1)	119.0(6)	C(18)—C(12)—C(11)	119.7(7)
C(8)—C(6)—C(7)	119.0(6)	C(18)—C(16)—C(17)	119.8(6)
	(d) Aromatic ring angles		
C(8)—C(2)—C(3)	118.1(6)	C(18)—C(12)—C(13)	117.9(7)
C(4)—C(3)—C(2)	119.5(6)	C(14)—C(13)—C(12)	120.7(7)
C(5)—C(4)—C(3)	122.0(6)	C(15)—C(14)—C(13)	120.9(7)
C(6)—C(5)—C(4)	119.0(7)	C(16)—C(15)—C(14)	119.6(7)
C(8)—C(6)—C(5)	118.8(6)	C(18)—C(16)—C(15)	118.5(6)
C(6)—C(8)—C(2)	122.5(6)	C(16)—C(18)—C(12)	122.2(6)

*Estimated standard deviations are given in parentheses.

C. Assignment of structure by ^{1}Hmr would lead to both **A** and **B** being referred to as *syn* conformers, since in either case the internal protons would not be exceptionally shielded by the opposite benzene ring, i.e., would appear at δ 6.2–7.2. Only when the angle between the planes of the benzene rings is sufficiently obtuse and the two substituents have passed each other is it that the substituent of one ring extends into the strongly shielded region (12) of the opposite ring (δ 4.0–5.5). Only in this case would the conformer likely be regarded as *anti*. Clearly the angle required to achieve this will vary for various substituents and is somewhat subjective depending upon how shielded the author feels the internal substituents are. For example, in the previous paper we have concluded that **1** is a *syn* conformer on the basis of ^{1}H nmr data coupled with the X-ray data determined below. In fact, the solid state **1** corresponds most closely to conformer **B** and thus from a crystallographer's viewpoint would be considered an *anti*-cyclophane. We thus here propose a solution to this dilemma, which might be useful in future studies of the higher cyclophanes, and makes use of the terms *synclinal* (*sc*) and *anticlinal* (*ac*) already established in organic stereochemistry nomenclature (13).

If the dihedral angle between the two benzene ring planes of the phane is $0 < \theta \leq 90°$, we suggest the conformer be known as *synclinal*, **D**, and if $90 < \theta < 180°$, the conformer be known

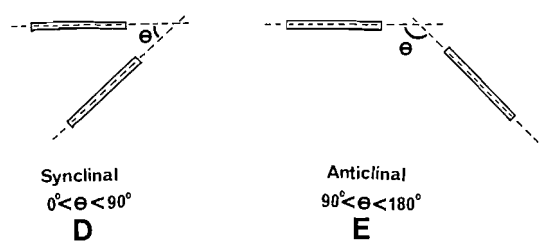

as *anticlinal*, **E**. As will be seen below, **1** then becomes an *anticlinal* conformer.

Experimental

X-ray measurements

A small colourless block-shaped crystal (0.18 × 0.28 × 0.21 mm) was mounted along the *b*-axis on a glass fibre and subjected to Weissenberg and precession photography using CuK_α radiation. The crystal was then transferred to a Picker 4-circle diffractometer using Zr-filtered MoK_α radiation and automated with a PDP-11/10 computer. The unit cell was refined by least squares from the 2θ values of 8 pairs of reflections in the range 19–35°. The crystal data are:

$C_{16}H_{16}S_4$ Mol. Wt. 336.54

Orthorhombic, space group *Pbca* (No. 61), a = 16.593(2), b = 10.018(2), c = 19.407(3) Å, V_{cell} = 3226(1) Å^3, T = 25(2)°C, Z = 8 molecules per cell, D_{meas} = 1.385 g cm^{-3}, D_{calc} = 1.386 g cm^{-3} (flotation in CCl_4/*m*-xylene), μ = 5.38 cm^{-1} (λ = 0.71069 Å), crystal shape by face indices and perpendicular distances to a central origin: ±(101), 0.090 mm; ±(10$\bar{1}$), 0.1005 mm; ±(010), 0.141 mm. Intensity measurements were by a step scan of 200 steps of 0.01° in 2θ, counting for 0.25 s per step, with a background counting time of 25 s at each end of the scan. One octant of the reciprocal space sphere was measured out to 2θ = 40°. Three standard reflections, 400, 020, 006, preceded each batch of 50 measurements and were used in the scaling of the data. The stability of the standard counts was excellent. Lorentz and polarization corrections were applied to 1759 measurements and those for which $I < \sigma(I)$ were rejected leaving 1229 reflections in the file. Absorption corrections were not necessary, and were not applied.

Structure determination

The crystallographic program SHELX-76 kindly supplied by Dr G. Sheldrick was used for this work (14). Atomic scattering factors were for the neutral atoms (15), and the correction for anomalous dispersion was included (16). The structure was solved by direct methods and refined by the method of least squares minimizing $\sum w\Delta^2$ where $\Delta = ||F_o| - |F_c||$, and $w = 1/(\sigma^2(F) + 0.001F^2)$. The refinement proceeded normally and all atoms including the hydrogen atoms were found. The thermal vibration was treated isotropically for hydrogen and anisotropically for the heavier atoms. 245 parameters were determined from 1229 measurements. The convergence was satisfactory with a maximum shift/esd of 0.20 and the final residuals were R =

Can. J. Chem. Downloaded from www.nrcresearchpress.com by 210.87.254.6 on 09/06/12
For personal use only.

TABLE 4. Mean planes and torsion angles

(a) Plane definition

Plane	Atoms	Description
1	C(2)—C(6), C(8)	Benzene ring 1
2	C(12)—C(16), C(18)	Benzene ring 2
3	C(4), C(8), C(14), C(18)	The central plane
4	S(1)—S(4)	The sulphur atoms
5	C(2)—C(6), C(12)—C(16), C(8), C(18)	Both benzene rings

(b) Coefficients of $Ax + By + Cz = D$ (Å)*

Plane	A	B	C	D	χ^{2}†
1	0.5334	−0.8312	−0.1569	−2.5700	4.2
2	−0.6719	−0.5719	−0.4707	−8.3307	4.8
3	0.5407	0.3047	−0.7841	1.5255	1319
4	−0.1299	−0.8975	−0.4216	−4.5004	137 157
5	−0.0765	−0.9150	−0.3961	−4.6639	94 740

(c) Perpendicular distance of atoms from the plane (Å)

Plane	Atoms and distances
1	C(1), 0.013(8), C(7), 0.076(7); S(1), 1.647(2); S(3), 1.860(2)
2	C(17), 0.014(8); C(11), 0.096(8); S(4), 1.701(2); S(2), 1.881(2)
3	C(4), −0.090(7); C(8), 0.141(6); C(14), 0.110(8); C(18), −0.136(6)
4	S(1), −0.327(2); S(2), 0.290(2); S(3), 0.305(2); S(4), −0.347(2)

(d) Angles between normals to planes (°)

Planes	Angle	Planes	Angle
1–2	79.0	4–5	3.5
1–5	38.6	1–4	42.0
2–5	40.4	2–4	37.0
3–5	90.6	3–4	90.8
1–3	80.9	2–3	99.7

(e) Torsion angles (°)

Atoms	Angle	Atoms	Angle
C(8)—C(2)—C(1)—S(1)	98.3(7)	C(18)—C(16)—C(17)—S(4)	95.8(7)
C(2)—C(1)—S(1)—S(2)	48.6(6)	C(16)—C(17)—S(4)—S(3)	47.6(5)
C(1)—S(1)—S(2)—C(11)	80.4(4)	C(17)—S(4)—S(3)—C(7)	83.9(4)
S(1)—S(2)—C(11)—C(12)	166.1(4)	S(4)—S(3)—C(7)—C(6)	168.7(4)
S(2)—C(11)—C(12)—C(18)	93.1(7)	S(3)—C(7)—C(6)—C(8)	89.7(6)

*An orthogonal axis system is used with x along the a-axis, y in the (a, b) plane, and z along c^{*}.
†$\chi^{2} = \sum_{i} p_i^{2}/\sigma^{2}(p_i)$ summing over all atoms, i, in the plane.

0.0497, $R_w = \sum\sqrt{w}\Delta/\sum\sqrt{w}F_o = 0.0456$, $R_g = \sqrt{(\sum w\Delta^{2}/\sum wF_o^{2})} = 0.0506$. The final difference map had a maximum of 0.25 e Å^{-3} and a minimum of −0.33 e Å^{-3}. The structure factor tables have been deposited together with the temperature parameters, the bond lengths and angles involving the hydrogen atoms, and selected intermolecular distances.[3]

Discussion

The fractional atomic coordinates and isotropic temperature parameters are given in Table 1. Figure 1 is an ORTEP drawing of the molecule. Table 2 contains the bond lengths, all of which are quite normal. The S—S bond lengths are accurate enough to make comparison with other literature values interesting and for **1** are very similar to those of S1—S2 of **2** (2) and are approximately 0.03 Å shorter than those of the more strained examples **4** and **5** (4). The C—S bonds in the disulphide bridges of **1** are only marginally longer than those of **6** (5) or **8** (11), and are similar to other C—S values (17).

Bond angles are given in Table 3, and here we begin to see in the sulphur angles an approximate symmetry in the bridging chains, with the relationships being S(1) to S(4) and S(2) to S(3). The angles at methylene carbon atoms C(1) and C(17) are

[3]Copies may be obtained, at a nominal charge, from the Depository of Unpublished Data, CISTI, National Research Council of Canada, Ottawa, Ont., Canada K1A 0S2.

Can. J. Chem. Downloaded from www.nrcresearchpress.com by 210.87.254.6 on 09/06/12
For personal use only.

similar as are those of C(7) and C(11). The angles in Table 3(c) show that a distinction can be made between those external to the 14-ring having a mean value of 122.3(3)° and those in the 14-ring with a mean value of 119.4(3)°. In Table 3(d) the benzene ring angles are just above 120° (mean = 121.9(3)°) at the central carbon atoms C(8), C(18), C(4), C(14) and a little less at sides (mean 119.0(2)°). This small effect has been noted in other metacyclophanes (5, 11).

The results of the mean plane and torsion angle calculations are given in Table 4. The benzene rings are planar to within the accuracy of this structure determination. The angle between the normals to the planes is 79°, and θ in **E** is thus 101°. Since this angle is >90°, the conformer is best regarded as *anticlinal*, despite the fact that from a ^{1}Hmr viewpoint (as discussed above) it might be regarded as *syn*. In contrast, the angle θ for **6** is 20.6° and for **8** is 10.3°, clearly both are *syn* or *synclinal* conformers.

It is interesting that planes 4 and 5 are nearly coincident (see constants $A-D$, and the dihedral angle of 3.5°) and very close to being at 90° to plane 3. This suggests a convenient reference system for the molecule, without implying coplanar sets of atoms. In the case of plane 3 the displacements of the atoms from the mean plane given in Table 4(c) are quite small, and considering that the atoms defining this plane are widely spaced, this suggests only small angular rotations about axes perpendicular to the planes of the benzene rings. The bridging chains restrict such rotation. The perpendicular line segment between the skew lines C(4)—C(8) and C(14)—C(18) was calculated to be 0.727 Å, and this is a reasonable indication of the lateral displacement of one benzene ring relative to the other. The displacements of the methylene carbon atoms from the benzene ring planes are toward the same side as the sulphur atoms. The perpendicular distances are asymmetric across each benzene ring individually, and show an approximate symmetry relating C(1) to C(17) and C(7) to C(11). The torsion angles along the bridging chains are arranged in Table 4(e) to show the approximate symmetry. The C—C—C—S torsion angles are 90–98°, close to a right angle. The S—S lone pair repulsion forces the C—S—S—C torsion angle to be 80–84°, consistent with the range 74–110° found (18) for other disulphides. The S—S—C—C angles are 11–14° below the idealized values of 60° and 180°.

Conclusions

In the solid state, **1** exists as an *anticlinal*-conformer, with the angle θ of **E** (between the benzene ring planes) being 101°. This is sufficiently far from 180° to make the interpretation of solution ^{1}Hmr data more difficult, in that the internal hydrogen atoms are not shielded as in most *anti*-conformers of small bridge metacyclophanes. The terms *synclinal* and *anticlinal* are proposed to describe metacyclophane conformations.

Acknowledgements

We thank the University of Victoria and the Natural Sciences and Engineering Research Council of Canada for operating grants, and Mr. K. Hartman for illustrative photography.

1. K. R. DIXON and R. H. MITCHELL. Can. J. Chem. **61**, 1598 (1983).
2. J. S. RICCI and I. BERNAL. Chem. Commun. 1453 (1969).
3. B. K. BALBACH, A. R. KORAY, A. OKUR, P. WÜLKNITZ, and M. L. ZIEGLER. J. Organomet. Chem. **212**, 77 (1981).
4. N. BRESCIANI-PAHOR, M. CALLIGARIS, and L. RANDACCIO. Acta Crystallogr. Sect. B, **36**, 632 (1980).
5. W. ANKER, G. W. BUSHNELL, and R. H. MITCHELL. Can. J. Chem. **57**, 3080 (1979).
6. R. H. MITCHELL and V. BOEKELHEIDE. J. Am. Chem. Soc. **96**, 1547 (1974).
7. G. R. NEWKOME and T. KAWATO. J. Am. Chem. Soc. **101**, 7088 (1979).
8. F. VÖGTLE and P. NEUMANN. Tetrahedron Lett. 5329 (1964); Tetrahedron, **26**, 5847 (1970).
9. F. VÖGTLE and P. NEUMANN. Angew. Chem. Int. Ed. Engl. **11**, 73 (1972); F. VÖGTLE and G. HOHNER. Topics Curr. Chem. **74**, 1 (1978).
10. R. H. MITCHELL and V. BOEKELHEIDE. Tetrahedron Lett. 1197 (1970).
11. B. R. DAVIS and I. BERNAL. J. Chem. Soc. B, 2307 (1971).
12. C. E. JOHNSON and F. A. BOVEY. J. Chem. Phys. **29**, 1012 (1958); J. W. EMSLEY, F. FEENEY, and L. H. SUTCLIFFE. *In* High resolution nuclear magnetic resonance spectroscopy. Pergammon Press, Oxford. 1965. p. 595.
13. IUPAC Rules, Section E, J. Org. Chem. **35**, 2849 (1970).
14. G. SHELDRICK. SHELX-76, a program for crystal structure determination. Anorganisch-Chemisches Institut der Universität Göttingen. 1976.
15. D. T. CROMER and J. T. WABER. International tables for X-ray crystallography. Vol. IV. Kynoch Press, Birmingham, England. 1974. Table 2.2B. p. 99.
16. D. T. CROMER. International tables for X-ray crystallography. Vol. IV. Kynoch Press, Birmingham, England. 1974. Table 2.3.1. p. 148.
17. J. RICCI and I. BERNAL. J. Chem. Soc. B, 806 (1970); J. Am. Chem. Soc. **91**, 4078 (1969).
18. S. C. ABRAHAMS. Q. Rev. **10**, 407 (1956).

Can. J. Chem. Downloaded from www.nrcresearchpress.com by 210.87.254.6 on 09/06/12
For personal use only.

Crystalline conformation and structure of lichenan and barley β-glucan

I. TVAROSKA,[1] K. OGAWA,[2] Y. DESLANDES,[3] AND R. H. MARCHESSAULT[3,4]

Department of Chemistry, Université de Montréal, Montréal (Qué.), Canada H3C 3J7

Received November 22, 1982

I. TVAROSKA, K. OGAWA, Y. DESLANDES, and R. H. MARCHESSAULT. Can. J. Chem. **61**, 1608 (1983).

An investigation based on X-ray fiber diffraction and conformational analysis methods has provided a proposed chain conformation and crystalline structure for lichenan, a poly β(1→3) cellotriose. The analysis of the fiber diagram of the hydrated form of lichenan led to a trigonal unit cell of dimension $a = b = 9.92$ Å and c (fiber axis) = 42.03 Å, with cellotriose as the asymmetric unit and six cellotriose residues per unit cell. A unit cell of the dry form is also trigonal with $a = b = 9.36$ Å and $c = 42.03$ Å. A right-handed threefold helix made up of three cellotriose residues was derived from a comparison of experimental helical parameters with isoenenergy conformational maps made by plotting dihedral angles (ϕ, ψ) at the β(1→3) linkage. A virtual bond approach was also used to arrive at the proposed conformation which is stabilized by intramolecular hydrogen bonds between all carbohydrate units. The refinement of geometrical and packing parameters produced results consistent with an antiparallel arrangement of the two chains corresponding to a space group symmetry of $P3_1$. The naturally occurring copolysaccharides known as mixed (1→3) and (1→4) β-glucans from the cell walls of barley endosperm have been shown to crystallize in the same fashion as lichenan.

I. TVAROSKA, K. OGAWA, Y. DESLANDES et R. H. MARCHESSAULT. Can. J. Chem. **61**, 1608 (1983).

Une étude basée sur la diffraction de rayons-X de la fibre et sur les méthodes d'analyse conformationnelle permet de proposer une conformation de la chaîne et de la structure cristalline du lichénane, un poly β cellotriose (1→3). L'analyse du diagramme de fibre de la forme hydratée du lichénane conduit à une maille élémentaire trigonale de dimension $a = b = 9{,}92$ Å et c (axe de la fibre) = 42,03 Å avec le cellotriose comme unité asymétrique et 6 unités cellotriose par maille élémentaire. Une maille élémentaire de la forme non hydratée est également trigonale avec $a = b = 9.36$ Å et $c = 42{,}03$ Å. On a déduit une hélice ternaire droite comprenant trois unités cellotriose à partir d'une comparaison des paramètres hélicoidaux expérimentaux avec les cartes conformationnelles d'isoénergie obtenues en traçant les angles dièdres (ϕ, ψ) au niveau du lien β(1→3). On a également utilisé une approche de liaison virtuelle pour arriver à la conformation proposée que se stabilise par des liaisons hydrogènes intramoléculaires entre toutes les unités de carbohydrate. L'amélioration des paramètres géométriques et des paramètres d'entassement donne des résultats qui s'accordent avec un arrangement anti-parallèle des deux chaînes correspondant au groupe d'espace de symétrie $P3_1$. On montre que les copolysaccharides naturels, connus comme étant des mélanges de β glucanes (1→3) et (1→4) provenant des parois des cellules de l'endosperme de l'orge, cristallisent comme le lichénane.

[Traduit par le journal]

Introduction

The crystalline structure and microfibrillar morphology of cellulose has been extensively investgated. While this β(1→4) linked glucan is universally acknowledged as the dominant skeletal material of the plant world, it is now obvious that other glycans have important structural roles in the biological world (1). In algal (2) and fungal cell walls (3) the β(1→3) linkage is associated with a helical structure capable of wide variations in flexibility (4). The ultimate in structural rigidity of β(1→3) linked glycans is a triple helical structure (2, 5–7). It is of considerable interest, therefore, to examine a regular copolysaccharide containing both the β(1→4) and β(1→3) linkage such as found in lichenan (Fig. 1). Structural studies (8) on the product from Iceland Moss have established an ideal structure for lichenan as a poly β(1→3) cellotriose. It is to be noted that this strutural perturbation of cellulose leads to a drastically modified solubility, e.g. lichenan is soluble in water and dimethyl sulfoxide (DMSO).

Although it is sometimes referred to as a white amorphous powder, there is a published record (9) of X-ray diffraction from lichenan as early as 1930. At that time it was recorded as a powder pattern and interpretated as similar to β-cellulose, an early terminology for regenerated cellulose (10). As will be seen below, the analogy between lichenan and regenerated cellulose was valid although it would have been more precise to refer to "water" cellulose, the rare hydrate of cellulose which is found in freshly regenerated material (11). A fiber diagram would have revealed that the two equatorial reflections of "water" cellulose, as found in lichenan fibers, are on the first layer line rather than the equator. This observation had an important influence in establishing the structure which we will propose.

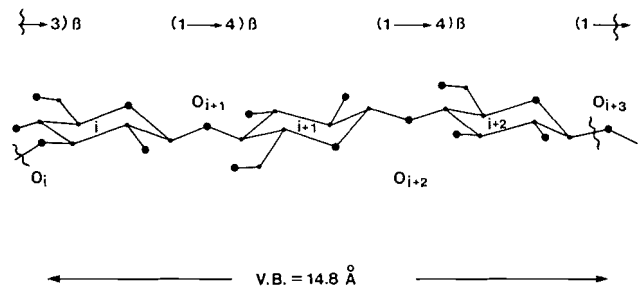

FIG. 1. A schematic representation of the lichenan repeating unit; the virtual bond length (V.B. = 14.8 Å) corresponding to the distance between O_{i+3} and O_i is indicated.

Although the ideal structure (12) for lichenan is a poly β(1→3) cellotriose the material is considered different from the general category of mixed (1→3) ,and (1→4) β-glucans which generally are thought to have a statistical distribution of linkages with predominance of the (1→4) linkage. Thus β-glucans are substitutionally perturbed cellulose structures with a ratio of

[1]Present address: Institute of Chemistry, Slovak Academy of Sciences, 80933 Bratislava, Czechoslovakia.

[2]Present address: Radiation Center of Osaka Prefecture, Shinke-Cho, Sakai, Osaka 593, Japan.

[3]Present address: Xerox Research Centre of Canada, 2480 Dunwin Drive, Mississauga, Ont., Canada L5L 1J9.

[4]Author to whom correspondence may be addressed.

Can. J. Chem. Downloaded from www.nrcresearchpress.com by 210.87.254.40 on 09/06/12
For personal use only.

Can. J. Chem. Downloaded from www.nrcresearchpress.com by 210.87.254.40 on 09/06/12
For personal use only.

(1→3) to (1→4) linkages of about 1:2.5. Accordingly, in this study, the crystallization properties deduced for lichenan were compared to those of a typical barley glucan.

Experimental

Samples

The starting material was Iceland Moss (*Cetraria islandica*) purchased from Pennick Co., New York; the purification procedure followed was that of Perlin and Suzuki (8). The samples were characterized by ^1H and ^{13}C nmr which showed that the sample corresponded to a regular copolysaccharide of cellotriose units linked by β(1→3) linkages (12) (Fig. 1).

A second sample of lichenan was prepared according to the same procedure at a later date. This sample was purchased from Sigma Chemical (Prod. No. L-6133) and the ratio of (1→4) to (1→3) linkages was 1.5 to 1.6 as measured by Professor M. Takagi (Osaka Prefecture University) using methylation analysis and the alkaline OPD method (13).

A sample of barley glucan from Biocon (Australia) Pty. Ltd., batch NO. 80147, was kindly provided by Prof. B. A. Stone of La Trobe University. This sample was reported to have a molecular weight in the range (14) of 150 000. Enzymatic degradation (14) methods provided a measure of the (1→4) to (1→3) ratio which was 2.33, and analysis of the enzymatically derived sequence information supports the concept of a statistical structure (14). This sample was studied by X-ray diffraction methods in the same way as lichenan.

Film preparation and orientation

An attempt to prepare a film by evaporation of a 6% aqueous solution of lichenan on a clean glass plate yielded a noncontinuous film. A continuous film was prepared by evaporation (vacuum oven at 50°C, 3 h) of a 10% DMSO solution which gave a brown-colored, flexible film.

The DMSO cast film was stretched in 80% (vol.%) isopropanol − H_2O at room temperature by loading the film with an appropriate weight. The stretched film (2.25 times), was subsequently air-dried under tension. Then the film kept under tension was annealed in 75% methanol − H_2O at 173°C in a sealed bomb. After this treatment the film was washed in methanol and air-dried.

Efforts to increase crystallinity by mild hydrolysis treatment (H_2O or aqueous 0.001 to 0.1 *N* HCl was painted on the film at room temperature) were of no avail. These studies, however, allowed us to establish that there was no isopropanol or methanol trapped in the films.

All X-ray data on an oriented annealed film were recorded after the film was conditioned at least 24 hours at 98% relative humidity. Density of such films was measured by flotation in a toluene − carbon tetrachloride density gradient column. X-ray studies on the dry polymorph were performed by drying the oriented film in vacuum over P_2O_5 for at least 24 hours.

Method of conformational analysis

The coordinates of the various atoms in the cellotriose unit (henceforth the "residue") which is our repeating unit (8, 12) (Fig. 1), have been calculated by using the bond distances and bond and torsional angles from the crystal structure of cellobiose (15). The coordinates of the residue were obtained by covalently joining two cellobiose units "head-to-tail" with all glycosidic torsional angles (ϕ_i ψ_i) being made identical. The ultimate reducing end glucose was then discarded, leaving only the coordinates of a cellotriose starting residue with end-to-end distance or virtual bond (V. B.), $O_i(3)\cdots O_{i+3}$ (3), of 14.8 Å. This value is about 2.5% lower than the maximum conformationally allowed end-to-end distance, which would be 15.2 Å. Another, more extended model of cellotriose with a β(1→4) glycosidic angle $\tau = 120°$ and an end-to-end distance of 15.05 Å has been considered also. The structure of the residue was kept constant in the conformational analysis part of the calculations, including an intramolecular hydrogen bond between O(3) and O(5) of contiguous residues. However, during the crystal structure refinement the program (cf. below) allowed adjustment of the residue geometry.

The unpublished proposal of the IUPAC−IUB Subcommission on Polysaccharide Nomenclature[5] has been used for the notation of the atoms and conventions of torsional angles in this paper.

For the two-dimensional conformational energy map the glycosidic torsional angles are $\phi = \theta[H_{i+2}(1), C_{i+2}(1), O_{i+3}(3)]$ and $\psi = \theta[C_{i+2}(1) O_{i+3}(3), O_{i+3}(3), C_{i+3}(3), H_{i+3}(3)]$; the potential energy has been computed by taking into account the following contributions; van der Waals E_{nb}, torsional E_{tors}, hydrogen bond E_{hb}, and glycosidic valence angle, $\tau_L = \tau(C_{i+2}(1), O_{i+3}(3), C_{i+3}(3)]$, deformation E_{def}. The total potential energy E_{tot} of a given conformation is expressed as a sum of these contributions.

$$E_{tot} = E_{nb} + E_{tors} + E_{hb} + E_{def}$$

The van der Waals interactions between nonbonded atoms were evaluated using Lennard−Jones (6−12) potential functions, with the parameters proposed by Scott and Scheraga (17, 18). Threefold intrinsic torsional potential expressions were used for rotations around the $C_{i+2}(1)$—$O_{i+3}(3)$ and $O_{i+3}(3)$—$C_{i+3}(3)$ bonds, with barriers of 0.899 and 2.7 kcal mol^{-1} respectively (19, 20). Hydrogen bond energies were calculated by an empirical (21) inverse third power expression $E_{hb} = -55.0/R^3$ where R is the distance between oxygen atoms and should lie between 2.6 Å and 3.2 Å. The energy term for valence angle deformation at the glycosidic angle has been taken as harmonic in the displacement from a reference (strain-free) value τ_0.

$$E_{def}(\tau_L) = \tfrac{1}{2} k_\tau (\tau_L - \tau_0)^2$$

Both τ_0 and the force constant k_τ has been treated as constant throughout the calculation with values 109.28 deg and 0.0487 kcal mol^{-1} deg^{-2}, respectively.

Models of lichenan having left or right chirality, the appropriate helix symmetry, n, and advance per residue, h, with the above defined geometry were generated from a virtual bond analysis (22). The virtual bond method has allowed us to examine possible relative orientations of contiguous residues with the required helical parameters imposed by the chosen n and h. The virtual bond in this case is defined as the vector joining bridge-atoms at the ends of a cellotriose unit (Fig. 1). Different conformations were generated by a rotation (δ) about the virtual bond. The starting position ($\delta = 0°$) has been chosen so as to place the atom C(1) in the xy plane. The step interval for δ rotation was 1°.

For determining the position of the chains in the unit cell we have tested suitable models for the crystal structure of lichenan by a packing analysis approach. Each model was packed into the unit cell while minimizing the function (23, 24).

$$Y = \sum_{i=1}^{I} \frac{r_i - r_{0i}^{\,2}}{SD_i^{r}} + \sum_{j=1}^{J} \frac{\theta_j - \theta_{0j}^{\,2}}{SD_j^{\theta}} + \sum_{k=1}^{K} \frac{\Phi_k - \Phi_{0k}^{\,2}}{SD_k^{\Phi}} + \frac{1}{W^2} \sum_{\substack{l=1 \\ m=2}}^{L,M} \omega_{lm} (d_{lm} - d_{0lm})^2$$

where r_i are bond lengths, θ_i bond angles, Φ_k conformational angles, and d_{lm} nonbonded distances for the i, j, k, l, m corresponding variables in the monomer residue, while r_{0i}, θ_{0j}, Φ_{0k} and SD_i^r, SD_j^θ, SD_k^Φ are their standard values and standard deviations, respectively, obtained from the known crystal structure of cellobiose (15) and ω_{lm} are scaling factors (24). The d_{0lm} were previously determined by Zugenmaier and Sarko from packing of known crystal structures of carbohydrates (24).

Results

X-Ray diffraction

High humidity was required in order to get the best fiber

[5]Abbreviations and symbols for description of polysaccharide conformation follow ref. 16.

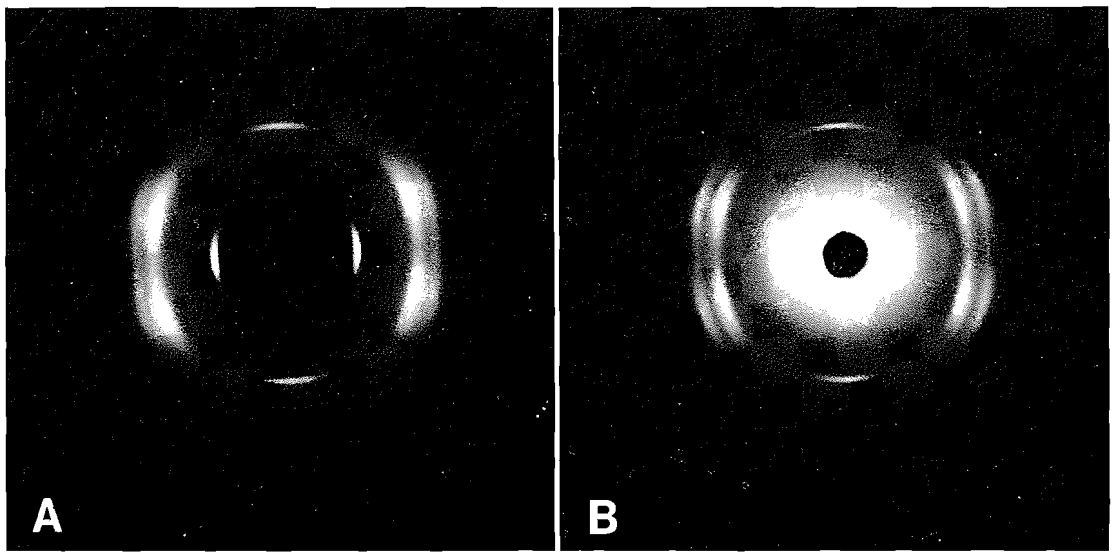

FIG. 2. Fiber diagrams; (A) "dry" recorded in vacuum; (B) "hydrate" recorded at 97.5% R.H.

TABLE 1. The variation of the d_{100} spacing with relative humidity

% Relative humidity	d_{100} (Å)
In vacuum	8.12
10	8.28
50	8.30
92	8.49
87	8.59

TABLE 2. Calculated and observed d-spacings for lichenan unit cells. For the hydrate form, $a = b = 9.92$ Å, $c = 42.03$ Å, and $\gamma = 120°$. For the dry form, $a = b = 9.36$ Å, $c = 42.03$ Å, and $\gamma = 120°$.

Miller index			Hydrate form		Dry form	
h	k	l	$d_{calc.}$	$d_{obs.}$	$d_{calc.}$	$d_{obs.}$
0	0	3	14.01	—	14.01	14.01
1	0	0	8.59	8.60	8.11	8.12
0	0	9	4.67	4.69	4.67	4.71
1	1	3	4.66	4.64	4.43	4.44
1	1	5	4.27	4.33	3.78	—
2	0	4	3.97	3.99	3.78	3.87
1	1	10	3.77	3.76	3.73	3.75
0	0	12	3.50	3.49	3.50	3.49
2	1	0	3.25	3.22	3.06	—
1	1	10	3.20	3.15	3.12	3.10
1	1	12	2.86	2.86	2.80	—

patterns of the hydrate form, e.g. the same sample at 10% relative humidity (R.H.) compared to 98% was less oriented and slightly less crystalline. There was evidence of the influence of H_2O on the pattern (or hydration of the "continuous" type) since the base plane of the unit cell increases steadily with relative humidity. Table 1 shows the variation of the strongest equatorial spacing (d_{100}) with relative humidity.

The diffraction pattern (Fig. 2) shows a strong meridional reflection with a spacing of 4.67 Å, which we have chosen to interpret as the average advance per glucose, hence 14.01 Å per cellotriose in the chain. The single strong equatorial reflection present had a spacing of 8.59 Å, which is similar to the strongest equatorial spacing in the "water" cellulose unit cells described by Warwicker and Wright (11). The fiber diagram was indexed (cf. Table 2) on the basis of a trigonal unit cell with $a = b = 9.92$ Å and c (fiber axis) = 42.03 Å. The measured density of 1.48 g/cm^3 is consistent with a unit cell containing six cellotriose residues and eighteen molecules of water, i.e. about one water molecule per glucose unit.

One very weak reflection on the equator (d-spacing = 5.76 Å) could not be indexed with the trigonal unit cell; it required an orthorhombic unit cell, obtained by enlarging the trigonal cell to twice its volume. This very weak reflection was ignored in the study.

Additional studies on oriented film samples subsequent to the above analysis have confirmed and amplified the above experimental data. For example, an annealed lichenan film of the second sample (Sigma) gave similar diffraction patterns to those observed with the first sample. But when the film was X-rayed in vacuum, it clearly showed additional meridional reflections, (003) and (006), with spacings of 14.0 and 7.0 Å, respectively. A reflection at 8.5 Å may possibly be a (005) or a (105) reflection. This confirms the use of the cellotriose unit as asymmetric residue in this analysis. The unit cell of the dry form is trigonal with $a = b = 9.36$ Å and $c = 42.03$ Å.

The following structure refinement is based on the experimental data from Fig. 2*a*. At this point it should be mentioned that barley glucan yielded the same kind of X-ray fiber diffraction pattern as lichenan. In general a lower degree of lateral order was present.

Energy contour maps

To obtain information on the conformational space accessible for different τ_L, energy contour maps for these angles were calculated. The maps were obtained by fixing τ_L at different values: 110.0°, 115.8°, 117.5°, and 122.0°, respectively. The energy was computed over 10° intervals (in proximity of the minima over 3° intervals) of ϕ and ψ. For simplicity, the energy contours have been drawn only for the energy values 3.0, 6.0, 9.0, and 12.0 kcal/mol above the absolute minimum energy. The helical parameters n and h were also calculated and contours of *iso-n* (for $n = 2.5$, 3, 4, and 5) and *iso-h* (for $h = \pm 13.0$, ± 13.5, ± 14.0, and ± 14.5 Å) were superposed on energy contour maps. Conformational energy maps for poly

Can. J. Chem. Downloaded from www.nrcresearchpress.com by 210.87.254.40 on 09/06/12
For personal use only.

Can. J. Chem. Downloaded from www.nrcresearchpress.com by 210.87.254.40 on 09/06/12
For personal use only.

β(1→3) cellotriose are shown in Figs. 3–5. While the overall features of the maps for different τ_L are similar, differences in detail are found. Only a small percentage of the conformational space lies within the 6 kcal/mol relative energy contour. The maps demonstrate how this area increases with glycosidic angle τ_L. In all cases, this area can be divided into three regions surrounding the individual minimum energy conformation. The lowest energy regions are always in the neighborhood of the conformations (38.0, 163.0), (38.0, −7.0), and (168.0, 13.0). An interesting finding from these maps is that for $\tau_L = 110.0°$ these regions are separated by a surface with relative energy higher than 12 kcal/mol. However, for $\tau = 115.8°$ two minima, and for $\tau_L > 117.5$ all three minima are connected by a 9 kcal/mol contour, which means that the transition barrier between these minima is lower than 9 kcal/mol. The maps also show that the enlargement of the angle τ_L causes a significant change in the position of the absolute minimum energy conformation (marked by X). This is a reflection of the flexibility introduced by the β(1→3) linkage into the cellulose backbone.

The influence of the value of the glycosidic angle on the magnitude of the individual terms in the total energy and number of contacts for the above described three conformations is shown in Table 3. Increasing τ_L from 110.0 to 122.0° increases the contribution of the valence angle deformation energy term from 0.01 kcal/mol to 7.68 kcal/mol which is one of the reasons for a different value of the total energy within the same conformation.

For a given τ_L one of the most important factors for a stabilization of the conformation is the presence of intramolecular hydrogen bonds. Five types of intramolecular hydrogen bonds between contiguous residues were possible: $O_{i+2}(5)\cdots O_{i+3}(2)$; $O_{i+2}(5)\cdots O_{i+3}(4)$; $O_{i+2}(2)\cdots O_{i+3}(4)$; $O_{i+2}(6)\cdots O_{i+3}(2)$; and $O_{i+2}(6)\cdots O_{i+3}(4)$, respectively. The influence of this energy term on the total energy can be seen in Table 3.

The detailed analysis of all contributions to the nonbonding energy term shows, as one could expect, that the most important ones are from interactions between the i+2 and the i+3 glucose unit, i.e. across the β(1→3) linkage. We can, therefore, compare our results with published data for laminaribiose (β(1→3) glucan) (25, 26), and indeed the shape of the preferred area for poly(β(1→3) cellotriose) is in general agreement with the map obtained by Sathyanarayan and Rao (25) although a preferred area at (38.0°, 163.0°) was not present in their map. These authors also considered only four types of intramolecular hydrogen bonds. However, from our calculation, it follows that the geometrical arrangement for the oxygen atom $O_{i+2}(6)$ in some conformations allows hydrogen atoms of $O_{i+3}(2)$ or $O_{i+3}(4)$ hydroxyls to form a hydrogen bond with the $O_{i+2}(6)$ atom. The crystal and molecular structure of laminaribiose proposed by Takeda *et al.* (26) shows that its conformation can be described as (27.9, −37.5°) with a glycosidic angle of 118.2°. The conformation lies in the low energy region (Figs. 3–5 and Table 3) and is stabilized by an intramolecular hydrogen bond between the O(4′) and O(5) atoms with a distance of 2.78 Å between oxygens.

Helical parameter maps superposed on the conformational energy contours show that a right-handed helix is preferred and conformations corresponding to helical structures of this chirality are mostly in proximity to one (38.0, −7.0) of the three minimum energy conformations in Figs. 3, 4 and 5. For instance, for a glycosidic angle $\tau_L = 115.8°$ (Fig. 4), the 3_1 helix corresponds to two points in φ, ψ conformational space: (69.0,

TABLE 3. Influence of glycosidic angle, τ_L, on magnitude of energy terms

φ, ψ	τ_L	Number of short contacts	E_{tot}	E_{def}	E_{tors}	E_{nb}	E_{nb}(tot)	Hydrogen bond energies				
								$O_{i+2}(5)\cdots O_{i+3}(2)$	$O_{i+2}(6)\cdots O_{i+3}(2)$	$O_{i+2}(5)\cdots O_{i+3}(4)$	$O_{i+2}(6)\cdots O_{i+3}(4)$	$O_{i+3}(2)\cdots O_{i+3}(4)$
(168.0, 13.0)	110.0	4	−0.8778	0.0104	2.4850	1.1151	−4.4884	—	−2.0388	—	—	−2.4496
	115.8*	3	−5.5054	1.9226	2.4850	−2.7611	−7.1520	−3.0736	−1.7553	—	—	−2.3231
	122.0	0	1.3148	7.6814	2.4850	−3.9730	−4.8786	−2.6631	—	—	—	−2.2155
(38.0, −7.0)	110.0*	1	−2.8109	0.0104	2.8770	−1.0857	−4.6126	—	—	−2.8499	−1.7626	—
	115.8	0	−0.3.778	1.9226	2.8770	−2.6524	−2.5250	—	—	−2.5250	—	—
	122.0	0	5.2476	7.6814	2.8770	−3.0666	−2.2442	—	—	−2.2442	—	—
(38.0, 163,0)	110.0	3	−1.8963	0.0104	0.7671	−0.0930	−2.5808	—	−2.5808	—	—	—
	115.8	2	−2.6891	1.9226	0.7671	−3.1968	−2.1820	—	−2.1820	—	—	—
	122.0*	2	−0.3509	7.6814	0.7671	−4.0860	−4.7134	−2.8731	−1.8403	—	—	—

*Minimum energy conformation for given τ_L.

Can. J. Chem. Downloaded from www.nrcresearchpress.com by 210.87.254.40 on 09/06/12
For personal use only.

TABLE 4. Coordinates of the cellotriose unit

Atom	x	y	z
O1	−1.6475	2.0708	4.8021
O2	−1.7924	0.7750	2.3763
O3	−1.3720	2.3764	0.0
O4	0.2371	4.7126	0.4213
O5	−0.9342	3.9966	3.8217
O6	−0.0476	6.4559	4.4037
C1	−0.9188	2.5752	3.7220
C2	−1.6152	2.1787	2.4241
C3	−0.8070	2.7313	1.2612
C4	−0.6727	4.2522	1.4087
C5	−0.1458	4.6245	2.7985
C6	−0.2772	6.1177	3.0474
HC1	0.1128	2.1964	3.7395
HC2	−2.6070	2.6518	2.4091
HC3	0.2004	2.2971	1.3143
HC4	−1.6540	4.7236	1.2507
HC5	0.9064	4.3191	2.8947
HC61	−1.2823	6.4523	2.7505
HC62	0.4344	6.6604	2.4079
O11	−1.0027	1.4813	10.1754
O21	−1.9877	3.9889	9.1325
O31	−1.1956	4.4855	6.5328
O51	−0.7357	0.7211	8.0612
O61	−0.7770	1.6697	6.4375
C11	−1.4623	1.6454	8.8848
C21	−1.1936	3.0567	8.4085
C31	−1.5901	3.1980	6.9483
C41	−0.9798	2.0910	6.0843
C51	−1.1771	0.7039	6.6946
C61	−0.3870	−0.3711	6.0086
HC11	−2.5394	1.4291	8.8376
HC21	−0.1274	3.2972	8.5322
HC31	−2.6851	3.1307	6.8788
HC41	0.0936	2.2830	5.9402
HC51	−2.2454	0.4436	6.6631
HC61	−0.5219	−0.2879	4.9200
HC621	0.6844	−0.2242	6.2097
O12	−1.3720	−2.3764	14.0100
O22	0.3545	−2.8297	11.9128
O32	−0.1027	−1.1021	9.6020
O52	−2.1764	−0.4800	13.0431
O62	−3.8151	1.5882	13.5008
C12	−1.0256	−1.3093	13.1771
C22	−0.6632	−1.8523	11.7985
C32	−0.2851	−0.6794	10.9084
C42	−1.4497	0.3175	10.8540
C52	−1.9133	0.6976	12.2640
C62	−3.2308	1.4532	12.2175
HC12	−0.1861	−0.7420	13.6030
CH22	−1.5560	−2.3325	11.3739
HC32	0.5730	−0.1707	11.3676
HC42	−2.2888	−0.1295	10.3005
HC52	−1.1459	1.3110	12.7583
H612	−3.9304	0.9305	11.5487
H622	−3.0671	2.4498	11.7817

3.0) and (125.0, −59.0). Only the first of them, however, lies in the low energy region. The absence of the *iso-n* contour corresponding to a twofold helix shows that there is no such conformation for poly(β(1→3) cellotriose) allowed within the present geometry of the residue and angular interval $110° \leq \tau_L \leq 122°$.

Virtual bond method

From the meridional reflection (d = 4.67 Å) it follows that helix repeat distances equal to the following values: 28.02 Å, 70.05 Å, 42.03 Å, 98.07 Å, and 64.04 Å correspond, respectively, to helices: $\pm 2_1$, $\pm 5_2$, $\pm 3_1$, $\pm 7_2$, and $\pm 4_1$. All these helices have been analyzed by the virtual bond method. The results show that the existence of the lichenan chain in a twofold helix with repeat distance 28.02 Å was possible only for a glycosidic angle $\tau_L \geq 136°$. If another, more extended, type of geometry for the cellotriose unit in lichenan is used (with virtual bond length equal to 15.04 Å), the condition for a 2_1 helix is achieved when τ_L is 128.0° or greater. This limitation justifies elimination of the twofold helix conformation with repeat distance 28.02 Å from further consideration. The $\pm 5_2$, $\pm 7_2$, and $\pm 4_1$ helices were also eliminated based on energy calculations. For a right-handed threefold helix the allowed conformations of the chain with τ_L in the range 110°−122° are found for a rotation about the virtual bond in the degree interval $194° \leq \delta \leq 356°$ and correspond respectively to the conformational subspace with $-62° \leq \phi \leq 125°$ and $-62° \leq \psi \leq 62°$. From these conformations, however, only a few in the range $301° \leq \delta \leq 342°$ are possible because of energy considerations. The more stable 3_1 helix (right-handed) of lichenan is at $\delta = 328°$ which corresponds to $\tau_L = 115.8°$, $\phi = 72.5°$, and $\psi = 1.5°$ with helix energy $E_{hel} = -1.6$ kcal/mol. In this conformation the 3_1 helix is stabilized by an intramolecular hydrogen bond: $O_{i+2}(5) \cdots O_{i+3}(4)$. The distance between these oxygen atoms is 2.74 Å and the corresponding hydrogen bond energy is 2.26 kcal/mol. The coordinates of the asymmetric unit (cellotriose) are reported in Table 4.

Crystal structure refinement of lichenan

From the X-ray diffraction pattern and the conformational analysis it follows that lichenan has two right-handed threefold helical chains in its trigonal unit cell. The X-ray data are consistent with six trigonal space groups: $P3_1$, $P3_121$, $P3_2$, $P3_221$, $P3_112$, and $P3_212$. Two of the possibilities, $P3_212$ and $P3_112$, may be rejected for stereochemical reasons as they would require antiparallel (coaxial) double helices, which is not sterically possible. From the virtual bond analysis it follows that left-handed helices can be eliminated and therefore two other space groups, $P3_2$ and $P3_221$, can be rejected also. The final choice of space group is between $P3_1$ and $P3_121$. In both remaining space groups, $P3_1$ and $P3_121$, the two lichenan chains are located with helix axis coaxial with the threefold screw axis parallel to c at ($x_f = 1/3$, $y_f = 2/3$) and ($x_f = 2/3$, $y_f = 1/3$). In respect to this, three different models of the crystal structure are possible: in the $P3_1$ space group two different models with two independent parallel or antiparallel chains, in the $P3_121$ case two antiparallel chains with a twofold screw axis relating them along the short diagonal of the unit cell. From conformational and X-ray data it is impossible to distinguish between these three choices, hence each model was studied separately by varying the usual packing parameters (the relative axial rotation and translation of both chains) to find the most probable model based on energy considerations.

The foregoing conformational analysis has provided the most probable single chain conformation and this has been used as a starting point in the refinement of the crystal structure. At first, only rotation and translation for parallel and antiparallel chain models of the lichenan structure were considered. Once the minimum packing energy for these variables was found, other variables (e.g. ϕ, ψ, τ, side group rotation, glycosidic bond length) connected with the residue geometry were taken

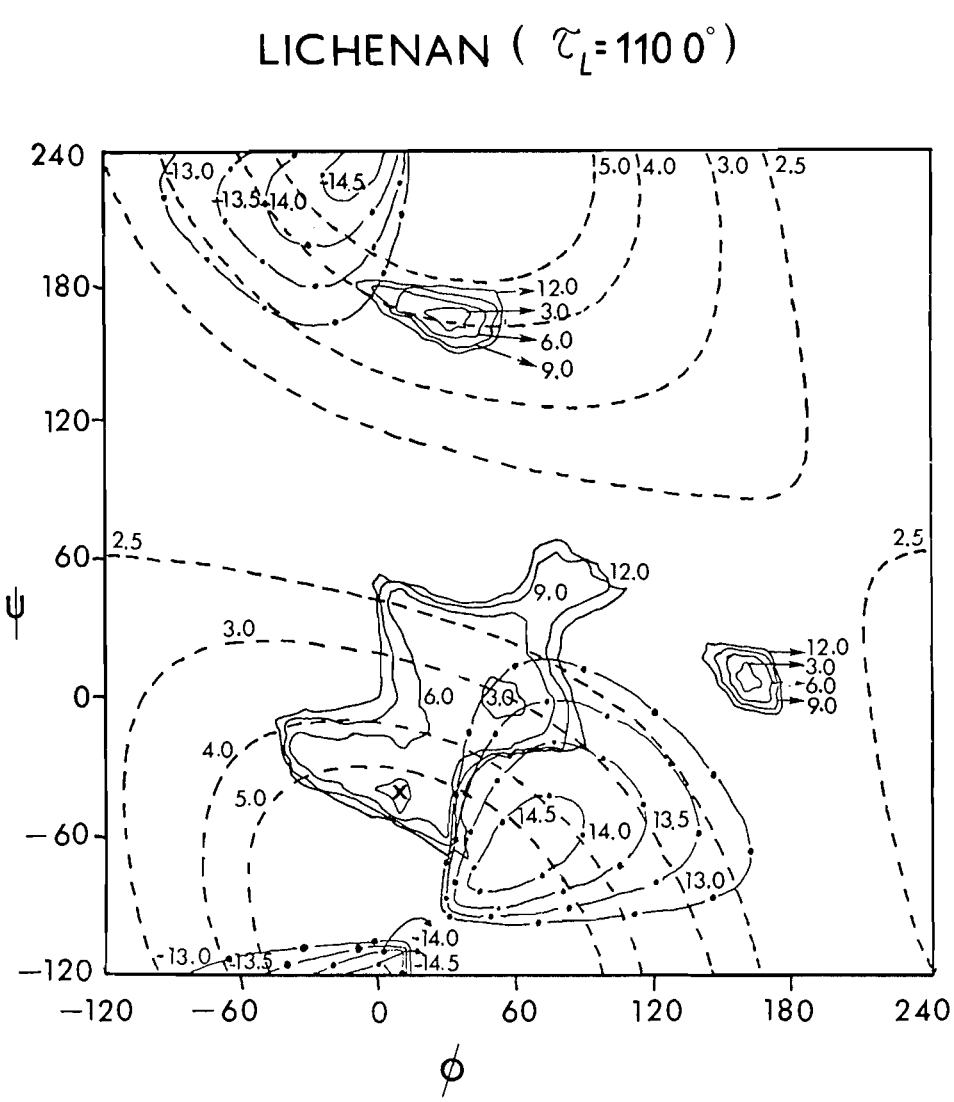

FIG. 3. A ϕ, ψ conformational energy map for $\beta(1\rightarrow3)$ cellotriose. The isoenergy contours are in kcal/mol over the lowest energy conformation (denoted by X); the curves of *iso-h* (-·-·-·) and *iso-n* (---) are superposed on energy contours. Left handed helices are indicated by $-h$. Glycosidic angle τ_L = 110.0°.

into consideration.

For the model with two antiparallel chains related by a two-fold screw symmetry operation (space group $P3_121$) we always found some unacceptably short intermolecular contacts. The removal of this restriction during the refinement always resulted in a change of position for one of the chains and yielded an energetically more acceptable packing arrangement. The energy based preference of antiparallel chains for the less symmetrical space group, $P3_1$, in comparison to the more symmetrical $P3_121$ led to the conclusion that the most probable space group is $P3_1$. The final values of the geometrical parameters which developed in refinement of the two most probable models of the crystal structures of lichenan, one for antiparallel and one for parallel chains, are shown in Table 5 together with values of the starting model of the chain. Both models have no short contacts between different chains and their interchain energy factors are very similar, 3.65 and 5.86, respectively. However, there is a large difference in the internal helical stability of the models. The helix energies (E_{hel}) are, respectively, −1.48 kcal/mol and 16.69 kcal/mol, thus the antiparallel model is considerably favored. The antiparallel model has two types of intramolecular hydrogen bonds: two between individual glucose units in the cellotriose residue [$O_i(5)\cdots O_{i+1}(3)$; $O_{i+1}(5)\cdots O_{i+2}(3)$] and one between the cellotriose residues across the $\beta(1\rightarrow3)$ linkage [$O_{i+2}(5)\cdots O_{i+3}(4)$]. Very weak intermolecular hydrogen bonds, $O_i(6)\cdots O_i(6)$ (r = 3.5 Å), between different chains were detected.

Since only the base plane of the unit cell underwent change as a function of relative humidity (Table 1) and c (fiber axis) is the same in both unit cells, it is suggested that the molecular conformation is not affected by water and we assume that water molecules are located between the lichenan chains in the corners of the unit cell as in hydrate cellulose (11) and $\beta(1\rightarrow4)$ xylan (27).

The proposed model of the lichenan crystal structure has been determined by refinement of only 17 variables describing the geometry of the helical chain and position of the chain in the unit cell. A full refinement would have required consideration of 162 variables and positioning 330 atoms not counting the water molecules. If the latter were included, it would be 226 variables and 348 atoms. This would probably have

Can. J. Chem. Downloaded from www.nrcresearchpress.com by 210.87.254.40 on 09/06/12
For personal use only.

Can. J. Chem. Downloaded from www.nrcresearchpress.com by 210.87.254.40 on 09/06/12
For personal use only.

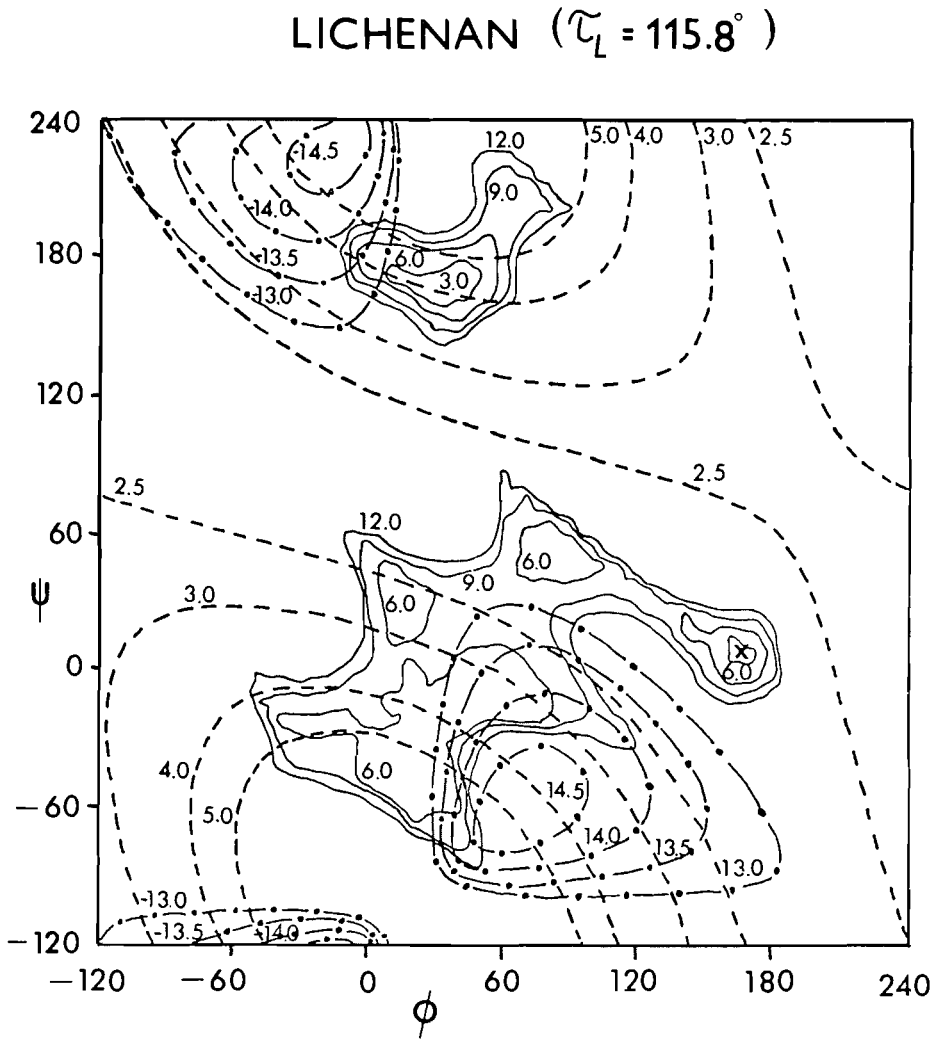

FIG. 4. The same as for Fig. 3 except for τ_L = 115.8°.

TABLE 5. Values of geometrical parameters for the lichenan helix: isolated chain, antiparallel packing, parallel packing

Parameter (Å, degrees, or no units)	Starting model (best single helix)	Antiparallel chain packing	Parallel chain packing
t; w_1; w_2		7.92; −79.1; 75.9	−4.57; 23.0; 44.8
τ_L; ϕ_L; ψ_L	115.8; 72.5; 1.5	114.4; 74.7; 0.4	110.0; 90.7; −9.8
r $O_{i+2}(5)\cdots O_{i+3}(4)$	2.74	2.82	2.57
τ_i; ϕ_i; ψ_i	116.1; 44.6; −13.7	116.4; 48.2; −4.6	116.3; 43.6; −15.5
τ_{i+1}; ϕ_{i+1}; ψ_{i+1}	116.1; 44.6; −13.7	115.3; 36.3; −16.3	117.8; 46.9; −14.0
r $C_i(1)$, $O_i(1)$	1.397	1.382	1.385
r $O_{i+1}(1)$, $C_{i+1}(4)$	1.445	1.402	1.417
r $C_{i+1}(1)$, $O_{i+1}(1)$	1.379	1.393	1.391
r $O_{i+1}(1)$, $C_{i+2}(4)$	1.419	1.413	1.432
$\chi_i(5)$	48.7	63.5	63.5
$\chi_{i+1}(5)$	70.5	57.8	57.8
$\chi_{i+2}(5)$	48.7	63.5	63.1
r $O_{i-1}(5)\cdots O_{i+1}(3)$	2.68	2.94	2.72
r $O_{i+1}(5)\cdots O_{i+2}(3)$	2.68	2.62	2.55
Packing energy		3.65	5.86
E_{Hel} (kcal/mol)	−1.63	−1.48	16.69

yielded a lower helix energy; however, without better X-ray diffraction data the excessive computer time involved was not justified.

Discussion

Lichenan is an example of a homoglucan which could be classified as a substitutional copolymer. By a periodic change

Can. J. Chem. Downloaded from www.nrcresearchpress.com by 210.87.254.40 on 09/06/12
For personal use only.

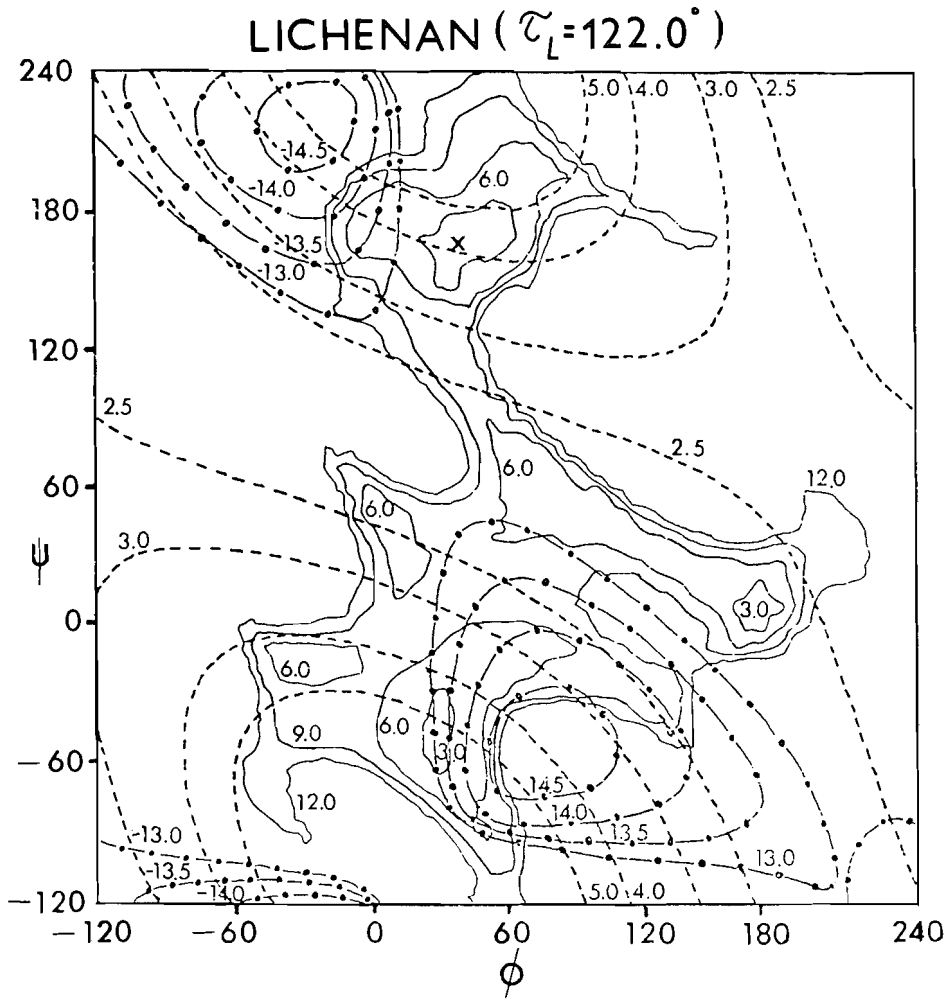

FIG. 5. The same as for Fig. 3 except for τ_L = 122.0°.

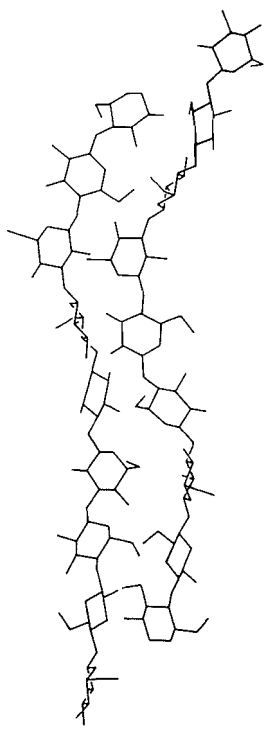

FIG. 6. The projection of lichenan unit cell onto (110) plane. The chains have antiparallel polarity.

in every third glycoside bond a considerable change in its physical properties is achieved compared to those of cellulose. The crystal structure still bears resemblance to cellulose but it is a regenerated cellulose hydrate rather than the familiar native cellulose structure. The packing, as shown in Fig. 6, gives rise to a compact structure wherein, at any level of the *c* axis, the inclined cellotriose moieties mesh with their neighbors to form long sheets of close-packed units. Because of the threefold axis along each chain, the same picture is obtained on viewing along different directions of the unit cell. Since intermolecular forces are weak, judging from interchain distances, the actual structure is perhaps paracyrystalline or sheet-like rather than truly three-dimensional. The cellulose II structure, which lichenan resembles, has strong intermolecular hydrogen bonds of slightly unequal strength in two nearly perpendicular directions. Since both β(1→3) and β(1→4) glucans are used as cell wall skeletal materials in fungi and plants respectively, it is not surprising to find this hybrid molecule in a cell wall role. Clearly, the structural requirements of a moss are minimal compared to shrubs and trees, so the lesser tendency in lichenan than in cellulose to organize and crysallize probably has a functional basis.

Of considerable interest was the fact that barley glucan, with a greater predominance of (1→4) linkages, crystallized in exactly the same fashion as lichenan. Indeed the patterns displayed less lateral order, i.e. greater line broadening. This suggests that the overall degree of crystallinity of the barley

glucan is less than for the chemically more regular lichenan. Two explanations can be proposed: the straightforward one is that the X-ray pattern of barley glucan corresponds only to the regular poly(cellotriose) segments. The other is based on structural accommodation similar to the isomorphous replacement concept. This concept would imply that the crystal structure is able to accommodate statistically occurring β(1→3) linkages because the extended chain cellulose segments produce a sheet-like packing of hydrate cellulose domains.

Barley glucan derives intermolecular cohesiveness from this cellulose hydrate packing but the low perfection and hydratability preserve the needed cell wall permeability characteristics. Thus, by adjusting the ratio of (1→4) to (1→3) linkages and their regularity, a change in a cell wall functional property, e.g. permeability, or strength, or deformability, can be achieved.

Acknowledgements

The authors wish to thank M. Vincendon of the CERMAV, Grenoble, France, and A. S. Perlin of the Pulp and Paper Research Institute of Canada, for preparing and chemically characterizing some of the samples used in this study. Helpful discussions were held with P. R. Sundararajan and T. L. Bluhm of the Xerox Research Centre of Canada, Mississauga, Ontario and A. Sarko, of the College of Forestry, Syracuse, N.Y. One of us (I.T.) gratefully acknowledges financial assistance from the National Research Council of Canada. Stimulating discussions with Prof. Bruce Stone led to the inclusion of barley glucan in this study.

1. R. D. PRESTON. The physical biology of plant cell walls. Chapman and Hall, London. 1974.
2. E. D. T. ATKINS and K. D. PARKER. J. Polymer Sci. Part C. **28**, 69 (1969).
3. J. JELSMA and D. R. KREGER. Carbohydr. Res. **43**, 200 (1975).
4. D. A. REES and W. E. SCOTT. J. Chem. Soc. (B), 469 (1971).
5. T. L. BLUHM and A. SARKO. Can. J. Chem. **55**, 293 (1977).
6. R. H. MARCHESSAULT, Y. DESLANDES, K. OGAWA, and P. R. SUNDARARAJAN. Can. J. Chem. **55**, 300 (1977).
7. Y. DESLANDES, R. H. MARCHESSAULT, and A. SARKO. Macromolecules. **13**, 1466 (1980).
8. A. S. PERLIN and S. SUZUKI. Can. J. Chem. **40**, 50 (1957).
9. K. WARD. *In* Cellulose and cellulose derivatives. *Edited by* E. Ott. Interscience Publishers Inc., New York, 1943. p. 23.
10. P. H. HERMANS. The physics and chemistry of cellulose. Elsevier Publishing Co., New York. 1949.
11. J. O. WARWICKER and A. C.WRIGHT. J. Appl. Polymer Sci. **11**, 659 (1967).
12. D. GAGNAIRE, R. H. MARCHESSAULT, and M. VINCEDON. Tetrahedron Lett. 3953 (1975).
13. N. MORITA, K. HAYASHI, M. TAKAGI, and K. MIYANO. Agric. Biol. Chem. Jpn. Submitted.
14. J. R. WOODWARD, D. R. PHILLIPS, and G. B. FINCHER. Carbohydrate Polymers. In press; J. R. WOODWARD, G. B. FINCHER, and B. A. STONE. Carbohydrate Polymers. In press.
15. S. S. C. CHU and G. A. JEFFREY. Acta Crysallogr. Sect. B. **24**, 830 (1968).
16. Draft S.C.B.N./PS/7 IUPAC–IUB Subcommission on Biochemical Nomenclature. R. H. Marchessault, Chairman (1975).
17. R. A. SCOTT and H. A. SCHERAGA. J. Chem. Phys. **44**, 3054 (1966).
18. R. A. SCOTT and H. A. SCHERAGA. J. Chem. Phys. **45**, 2091 (1966).
19. I. TVAROSKA and T. BLEHA. Tetrahedron Lett. 249 (1975).
20. I. TVAROSKA and T. BLEHA. J. Mol. Struc. **24**, 249 (1975).
21. J. BLACKWELL, A. SARKO, and R. H. MARCHESSAULT. J. Mol. Biol. **42**, 379 (1969).
22. P. R. SUNDARARAJAN and R. H. MARCHESSAULT. Can. J. Chem. **53**, 3562 (1975).
23. P. ZUGENMAIER and A. SARKO. Biopolymers, **15**, 2121 (1976).
24. P. ZUGENMAIER and A. SARKO, Acta Crystallogr. Sect. B. **28**, 3158 (1972).
25. B. K. SANTHYANARAYAN and V. S. R. RAO. Biopolymers, **11**, 1379 (1972).
26. H. TAKEDA, N. YASUOKA, and N. KASAI. Carbohydr. Res. **53**, 137 (1977).
27. I. NIEDUSZINSKI and R. H. MARCHESSAULT. Nature **232**, 45 (1971).

Can. J. Chem. Downloaded from www.nrcresearchpress.com by 210.87.254.40 on 09/06/12
For personal use only.

Reaction of methanethiol with species produced in a microwave discharge through water vapor

C. H. CHANG, P. L. GOODFRIEND,[1] M. D. BENTLEY, and R. J. ANDEREGG
Department of Chemistry, University of Maine at Orono, Orono, ME 04469, U.S.A.

Received August 4, 1982[2]

C. H. CHANG, P. L. GOODFRIEND, M. D. BENTLEY, and R. J. ANDEREGG. Can. J. Chem. **61**, 1617 (1983).

The products of reaction of methanethiol with species produced by passage of water vapor through a microwave discharge were studied. Mass spectrometric analysis demonstrated the presence of SO_2, CH_3SSCH_3, CH_3SSSCH_3, $CH_3SSSSCH_3$, $CH_3SSCH_2SCH_3$, $CH_3SCH_2SCH_3$, and S_8. These products are consistent with a mechanism involving abstraction of hydrogen from CH_3SH by OH and other radicals as the important primary process.

C. H. CHANG, P. L. GOODFRIEND, M. D. BENTLEY et R. J. ANDEREGG. Can. J. Chem. **61**, 1617 (1983).

On étudie les produits de la réaction du méthanethiol avec les espèces produites par le passage de la vapeur d'eau à travers une décharge de microondes. L'analyse par spectroscopie de masse démontre la présence du SO_2, du CH_3SSCH_3, du CH_3SSSCH_3, du $CH_3SSSSCH_3$, du $CH_3SSCH_2SCH_3$, du $CH_3SCH_2SCH_3$ et du S_8. Ces produits sont en accord avec un mécanisme qui implique comme processus primaire important l'enlèvement d'hydrogène à partir du CH_3SH par le groupe OH et par d'autres radicaux.

[Traduit par le journal]

Can. J. Chem. Downloaded from www.nrcresearchpress.com by 210.87.254.40 on 09/06/12
For personal use only.

Introduction

Problems resulting from emission of organic sulfur compounds into the atmosphere from biogenic sources, industrial plants, and sewage treatment plants (1) have stimulated intense interest in the detailed chemistry of these compounds in the atmosphere. In particular, the oxidation of organic sulfur compounds is a major contributor to acid rain. It is believed that the sequence of reactions in which sulfur compounds are degraded is initiated primarily by reaction with OH radicals (2) although reaction with O atoms may also play a role to a lesser extent (3).

Clearly, it is important to know the identity of the products of the elementary reactions involved both in determining the fate of the sulfur compounds and in elucidating reaction mechanisms. In spite of this fact, there is very little published information about the reaction products, with most recent studies having dealt with the kinetics of the reactions (2–5).

The object of the investigation reported here has been to identify the products of the reaction of OH radicals with methanethiol, CH_3SH. Because the generation of OH radicals in sufficient concentration to produce enough product for analysis necessarily generates other free radicals as well, it was necessary to run a series of control experiments to attempt to unravel the reactions of CH_3SH with other species.

Product analysis of the reaction of photolytically produced OH radicals with CH_3CH_2F was carried out by Singleton *et al.* (6). These experiments were possible since there was no interference from the photolysis of the CH_3CH_2F. Cvetanovic *et al.* (7) studied the products of gas phase reactions of CH_3SH, C_2H_5SH, CH_3SSCH_3, and CH_3SCH_3 with O atoms produced by the mercury sensitized photodecomposition of N_2O. The OH plus CH_3SH system does not lend itself to this approach, either by continuous or flash photolysis.

The production of OH radicals by an electrical discharge through water vapor was pioneered by Oldenberg (8) who was able to monitor OH concentration for as long as 1/8 of a second after the discharge. In a critical study of OH concentrations produced in discharges through water vapor, Kaufman and DelGreco (9, 10) found that the concentration of H atoms is much higher than the concentrations of OH radicals, but that OH is continuously regenerated throughout the flow system. They presented a method of producing OH radicals in higher initial concentrations by reaction of H atoms with NO_2:

[1] $H + NO_2 \rightarrow OH + NO$

The presence of NO_2 and NO complicates the interpretation of the reaction products. Consequently, the choice was made to use a microwave discharge in water vapor as the source of OH radicals. Unlike the situation in a kinetics experiment in which the rate is followed by monitoring OH concentration as a function of time, continuous generation of OH along the flow is helpful in the product analysis experiment. It is necessary, however, to examine separately the products of reactions with H atoms alone, etc. The work was therefore broadened to include control experiments as well. The investigation included product analyses of the following systems.

1. Argon alone was passed through the microwave discharge and mixed with CH_3SH.
2. H_2 gas dissociated to atoms in a microwave discharge was allowed to react with CH_3SH.
3. Water vapor, both alone and with argon carrier gas, was passed through a microwave discharge and the resulting products allowed to react with CH_3SH downstream from the discharge.
4. The same as 3 above with ^{18}O enriched water.
5. Ar, with and without H_2, was passed through the microwave cavity, mixed with NO_2, and allowed to react with CH_3SH.

The results of these experiments are described in the present paper.

Experimental

Radicals were produced by passing the gases to be dissociated through an Evenson microwave cavity powered by an HV15A Scintillonics Inc. power supply [2450 MC]. Except in a few control experiments, an argon carrier gas was used. The argon was supplied by Liquid Carbonics Co. and had a stated purity of 99.998 percent.

The system reaction chamber was constructed from quartz tubing (2.5 cm od). In each experiment, the whole system was first evacuated to a pressure of less than 200 μm, and was pumped continuously during the reaction. Water vapor or H_2 was premixed with argon

[1]Author to whom correspondence should be addressed.
[2]Revision received February 9, 1983.

Can. J. Chem. Downloaded from www.nrcresearchpress.com by 210.87.254.40 on 09/06/12
For personal use only.

before passing through the microwave discharge region, and methanethiol was added 6 cm downstream from the position of the microwave discharge.

When argon was used as a carrier gas, the flow was adjusted to maintain the discharge in the region of the microwave cavity without excessive "channeling". Although the flow rate was not measured and presumably varied somewhat from run to run, twenty-two replications of the Ar − H_2O experiment, and seventeen of the Ar − H_2 experiment gave uniformly reproducible results. Flows of H_2 were adjusted so as to give the discharge the characteristic red color of the Balmer α line. Distilled water was placed in a storage trap and degassed gradually. $H_2{}^{18}O$, which was transferred from the ampoule to a storage trap, was also degassed. Water vapor was entrained in the flow of gas at its vapor pressure at room temperature. When water alone (without argon) was used, it was allowed to boil off at room temperaure at the reduced pressure of the system. The $H_2{}^{18}O$ was supplied by the Isotopes Division of KOR Inc. and had a quoted isotopic purity of 97 percent.

The methanethiol used in the experiments was purified by trap to trap distillation on a vacuum line, and its purity shown to be greater than 99.9 percent by capillary gas chromatography. Prior to introduction into the vacuum chamber, CH_3SH was distilled into the reservoir under vacuum and condensed at liquid nitrogen temperature. It was allowed to come to room temperature, and its introduction into the mixing region was controlled by its vapor pressure.

After mixing in the reaction region, the gases were passed through cold traps at liquid nitrogen temperature where products were accumulated.

Quartz windows on the reaction chamber allowed observation of intense emission of the 3064 Å band of the OH radical when the flow was adjusted so that the discharge was moved into the reaction chamber. The detector was a Jarrell Ash plane grating spectrograph. Although Kaufman and DelGreco (9) showed that discharges in water are far less efficient in generating OH radical concentrations than reactions of H atoms with NO_2, our attempts to use the H + NO_2 reactions led to complex mixtures of complicated products with or without the H atoms present. It was therefore discarded as a technique for the purposes of this investigation. In spite of the fact that the focus of Kaufman and DelGreco's argument was to dismiss the water discharge as a source of OH, their results show OH present and reformed in the flow system in concentrations sufficient to yield observable products in our experiments. Because of the sensitivity of the gc−ms system and the fact that products were accumulated over an extended period of time, the low concentration of OH radicals was less of a limitation.

For analysis of the products, the trap was allowed to warm to room temperature, removed from the line, and a septum inserted. The gas phase was sampled at room temperature using a gas syringe and injected directly into the gas chromatograph of the gc−ms system. For analysis of the less volatile materials, tetrahydrofuran (20 μL) was injected into the trap at room temperature. A portion of the resulting solution of products was injected into the gc−ms for analysis. A yellow solid residue remained in water experiments. Samples of this material were removed from the trap and introduced into the mass spectrometer directly.

Analysis of products was performed using a Hewlett−Packard 5985B gas chromatograph/mass spectrometer system. The gas chromatograph was fitted with a 30 m × 0.32 mm fused silica capillary column, wall coated with Durabond DB-1 (J and W Scientific). The entire effluent of the gas chromatograph was directed into the source of the mass spectrometer which was maintained at 200°C. Helium was used as carrier gas at a flow of 1−2 mL/min. Both the splitless injector and the interface transfer line were maintained at or above 250°C. The column temperature was held at 60°C for five minutes and then linearly programmed at 8°/min to 280°C. For very volatile materials, such as SO_2, the gc oven temperature was held constant at 30°C.

Results

In many of the experiments with dissociated water vapor, a blue chemiluminescent glow was observed in the mixing region, but was not studied spectroscopically.

Interesting phenomena were observed in the traps at liquid nitrogen temperature. In both the hydrogen and water vapor experiments, a band of pink material was observed which disappeared on warming. On several occasions, traps in water vapor experiments have exploded. Thus intermediates from the reactions are apparently trapped at low temperature. Wet chemical tests with iodide on the material in the traps showed no indications of peroxides or other strong oxidizers.

In the control experiments in which argon alone was passed through the microwave discharge and interacted with methanethiol, no evidence of chemical reaction was observed and no reaction products were found. In all of the other types of experiments, reaction products were observed. Reaction products were identified by mass spectrometry. The molecular formulae were verified by analysis of the isotope ratios of the molecular ion and its isotope peaks. The mass spectra of all identified products are in agreement with published spectra. The abbreviated mass spectra (2 most abundant peaks in each 14 amu) were as follows.

CH_3—S—S—CH_3 *m/z* (%): 42 (40), 45 (66), 48 (9), 61 (15.6), 71 (24), 72 (23.5), 79 (80), 81 (6.2), 94 (100), 96 (9.2) (published spectrum in ref. 11).

CH_3—S—S—S—CH_3 *m/z* (%): 45 (13), 47 (9.6), 49 (2), 61 (5.2), 64 (11.3), 72 (1.9), 79 (35), 80 (11.2), 94 (2.6), 96 (0.8), 111 (16.5), 113 (2.3), 126 (100), 128 (13.8) (published spectrum in ref. 11).

CH_3—S—CH_2—S—CH_3 *m/z* (%): 45 (29.7), 46 (10.6), 59 (4.4), 61 (100), 62 (3.7), 63 (5.1), 76 (1.1), 78 (1.7), 92 (0.7), 93 (1.6), 108 (49), 110 (4.2) (published spectrum in ref. 12).

CH_3—S—CH_2—S—S—CH_3 *m/z* (%): 48 (3.7), 61 (100), 63 (7.7), 64 (6.6), 78 (3.6), 79 (8.1), 93 (3.9), 94 (2.6), 140 (8.3), 142 (1.1) (published spectrum in ref. 13).

CH_3—S—S—S—S—CH_3 *m/z* (%): 45 (41), 47 (26), 49 (7.3), 61 (17), 64 (43), 72 (13), 79 (100), 80 (11), 91 (5.6), 94 (30.4), 111 (11.2), 112 (3), 126 (9), 128 (1.8), 140 (1.3), 158 (68.8), 159 (3.9), 160 (12.5) (published spectrum in ref. 14).

It should be noted, however, that some possible low molecular weight products, such as methane, would not have been separated and detected under the chromatographic conditions used.

The results of the experiments are presented in Table 1. With argon alone, no reaction products were observed. Hydrogen experiments produced CH_3—S—S—CH_3 as the only identifiable species. Dimethyl disulfide, dimethyl trisulfide (CH_3—S—S—S—CH_3), dimethyl tetrasulfide

TABLE 1. Products obtained in this study

Products	Molecular weight	Source of radicals			
		$H_2{}^{16}O$	$H_2{}^{18}O$	NO_2*	H_2
SO_2	64	X	X	X	
CH_3SSCH_3	94	X	X	X	X
$CH_3SCH_2SCH_3$	108	X	X		
CH_3SSSCH_3	126	X	X		
$CH_3SCH_2SSCH_3$	140	X	X		
$CH_3SSSSCH_3$	158	X	X		
S_8	256	X	X		
		X denotes compounds present			

*Reaction of CH_3SH with radicals generated from NO_2 yielded complex mixtures of products which were not analyzed. See text.

(CH_3—S—S—S—S—CH_3), and SO_2 were identified as major products in the water experiments. Minor products CH_3—S—CH—S—CH_3 and CH_3—S—CH_2—S—S—CH_3 and a deposit of S_8 in the trap were also found in the water experiments. In the $H_2{}^{18}O$ experiments, the only observed species to contain ^{18}O was $S^{18}O_2$. When NO_2 was used, with or without H atoms, complex mixtures of products were formed, but not analyzed.

Discussion

Clearly, with the experimental arrangement used for these studies, reaction of CH_3SH with excited argon atoms was not a factor. No reaction products were observed in the Ar experiments, and Ar did not affect the results of the H_2O experiments. The only major product from the H-atom experiments was CH_3SSCH_3, which can be simply explained by the following reactions:

[2] $H + CH_3SH \rightarrow CH_3S + H_2$

[3] $2CH_3S \rightarrow CH_3SSCH_3$

The product mixture resulting from the experiments with water vapor also had CH_3SSCH_3 as a major component, but also contained SO_2, S_8, CH_3SSSCH_3, $CH_3SSSSCH_3$, and small amounts of $CH_3SCH_2SSCH_3$ and $CH_3SCH_2SCH_3$. It is significant that no oxygen-containing species other than SO_2 and certainly H_2O (although it was not determined) were observed. The possibility that some of the sulfur-containing species were actually oxygen-containing species was ruled out by both S isotope ratio calculations in mass spectra and the $H_2{}^{18}O$ labeling experiments.

Because no oxygenated sulfur species, other than SO_2, were observed in this investigation, we feel a mechanism involving abstraction as a primary step is reasonable, although attack on sulfur could also be postulated. Attack at sulfur has been observed in the reaction of OH and CH_3—S—CH_3 (15), as well as in the attack of O atoms on CH_3—SH (7), and the reaction of H atoms on CH_3—S—CH_3 and CH_3—S—S—CH_3 (16). In any case, the oxygen in our experiments is found only in SO_2 and not in more complex molecular species.

Finally, it should be noted that the rate of reaction of either O or OH with CH_3—S—S—CH_3 is much higher than the rate of reaction with CH_3—SH (2, 3). If substantial quantities of CH_3—S—S—CH_3 were built up, subsequent products could be a result of further reaction of CH_3—S—S—CH_3 with radicals generated in our discharge.

Acknowledgements

We wish to thank Dr. John Toth for running mass spectrometric analyses on the reaction products.

1. T. E. GRAEDEL. Rev. Geophys. Space Phys. **15**, 421 (1977).
2. P. H. WINE, N. M. KRUETTER, C. A. GUMP, and A. R. RAVISHANDARA. J. Phys. Chem. **85**, 2660 (1981).
3. W. S. NIP, D. L. SINGLETON, and R. J. CVETANOVIC. J. Am. Chem. Soc. **103**, 3526 (1981).
4. J. H. LEE, I. N. TANG, and R. B. KLEMM. J. Chem. Phys. **72**, 1793 (1980).
5. MING-TAUN LEU and R. H. SMITH. J. Phys. Chem. **85**, 2570 (181).
6. D. L. SINGLETON, G. PARASKEVOPOULOS, and R. S. IRWIN. J. Phys. Chem. **84**, 2339 (1980).
7. R. J. CVETANOVIC, D. L. SINGLETON, and R. S. IRWIN. J. Am. Chem. Soc. **103**, 3530 (1981).
8. O. OLDENBERG. J. Chem. Phys. **3**, 266 (1935).
9. F. KAUFMAN and F. P. DELGRECO. J. Chem. Phys. **35**, 1895 (1961).
10. F. P. DELGRECO and F. KAUFMAN. Discuss. Faraday Soc. **33**, 128 (1962).
11. S. R. HELLER and G. W. A. MILNE (*Editors*). EPA/NIH Mass spectral data base. U.S. Dept. of Commerce, # NSRDS- NBS 63, 1978.
12. R. N. HASZELDINE, B. HIGGENBOTTOM, R. B. RIGBY, and A. E. TIPPING. J. Chem. Soc. Perkin Trans. 1, 155 (1972).
13. R. G. BUTTERY, D. G. GUADAGNI, L. C. LING, R. M. SEIFERT, and W. LIPTON. J. Agric. Food Chem. **24**, 829 (1976).
14. M. BOELENS, P. J. DE VALOIS, H. J. WOBBEN, and A. VAN DER GEN. J. Agric. Food Chem. **19**, 984 (1971).
15. S. HATAKEYAMA, M. OKUDA, and H. AKIMOTO. Geophys. Res. Lett. **9**, 583 (1982).
16. T. YOKOTA and O. P., STRAUSZ. J. Phys. Chem. **83**, 3196 (1979).

Can. J. Chem. Downloaded from www.nrcresearchpress.com by 210.87.254.40 on 09/06/12
For personal use only.

Alkylammonium hexachlorostannates(IV), $(R_nNH_{4-n})_2SnCl_6$: crystal structure, infrared spectrum, and hydrogen bonding[1]

OSVALD KNOP, T. STANLEY CAMERON, AND MARGARET ANN JAMES

Department of Chemistry, Dalhousie University, Halifax, N.S., Canada B3H 4J3

AND

MICHAEL FALK

Atlantic Research Laboratory, National Research Council of Canada, Halifax, N.S., Canada B3H 3Z1

FOR ERRATA SEE V.62 #6 1984 P. 1227

OSVALD KNOP, T. STANLEY CAMERON, MARGARET ANN JAMES, and MICHAEL FALK. Can. J. Chem. **61**, 1620 (1983).

In an effort to advance our understanding of the principles governing the structures of and the hydrogen bonding in alkylammonium hexachlorostannates(IV), $(R_nNH_{4-n})_2SnCl_6$, we have determined the room-temperature crystal structures of $(Me_2NH_2)_2SnCl_6$ and $(Me_3NH)_2SnCl_6$ (variants of the antifluorite structure); $(EtNH_3)_2SnCl_6$ and $(n\text{-}PrNH_3)_2SnCl_6$ (*anti*-CdI_2 type, with orientational disorder in the Et compound); and $(n\text{-}Pr_3NH)_2SnCl_6$. We have also studied the infrared spectra in the regions of the NH and ND stretching fundamentals, between 10 and 293 K, of these five compounds and of $(MeNH_3)_2SnCl_6$, $(Me_3NH)_2SnBr_6$, $(Et_2NH_2)_2SnCl_6$, $(n\text{-}Bu_3NH)_2SnCl_6$ and, in less detail, the mixed-anion salt $(n\text{-}Pr_2NH_2)_3(SnCl_6)Cl$. The spectra are often complicated by Fermi resonance involving absorptions diagnostically critical for the strength and type of N—H···Cl bonding and for the site symmetry at the N atom. In this respect they are less useful than the corresponding spectra of the unsubstituted ammonium compounds reported previously. Several of the spectra provide striking examples of temperature-tuned Fermi resonance of NH and ND vibrations. The N—H···Cl bonds are invariably trifurcated, bifurcated, or at least highly bent; these characteristics give rise to anomalous temperature dependence of the frequencies of the NH and ND stretching fundamentals. Temperature-induced transitions were detected in $(Me_2NH_2)_2SnCl_6$ ($T_{tr} \sim 100$ K), $EtNH_3)_2SnCl_6$ ($T_{tr} \sim 125$ K), and $(Et_2NH_2)_2SnCl_6$ ($T_{tr} \sim 330$ K). The specific results for the ten compounds studied are discussed in detail. The discussion also includes the limits of usefulness of the isotopic dilution technique; symmetry aspects of the cation–anion packing in alkylammonium hexahalometallates(IV); symmetries of the arrangements of the $SnCl_6$ octahedra; the geometry of hydrogen bonding in $(R_nNH_{4-n})_2SnCl_6$; and the possibility of detection of the presence of hydrogen bonding from molecular volume trends.

OSVALD KNOP, T. STANLEY CAMERON, MARGARET ANN JAMES et MICHAEL FALK. Can. J. Chem. **61**, 1620 (1983).

Pour mieux comprendre les principes régissant les structures et la liaison hydrogène des hexachlorostannates(IV) d'alkylammonium $(R_nNH_{4-n})_2SnCl_6$, nous avons déterminé, à la température de la pièce, les structures cristallines du $(Me_2NH_2)_2SnCl_6$ et du $(Me_3NH)_2SnCl_6$ (des variantes de la structure antifluorine); du $(EtNH_3)_2SnCl_6$ et du $(n\text{-}PrNH_3)_2SnCl_6$ (de type CdI_2 *anti* avec un désordre rotationnel dans le composé Et); et du $(n\text{-}Pr_3NH)_2SnCl_6$. Nous avons également étudié les spectres infrarouges dans les régions d'élongation fondamentale du NH et du ND entre 10 et 293 K, de ces cinq composés et des composés suivants: $(MeNH_3)_2SnCl_6$, $(Me_3NH)_2SnBr_6$, $(Et_2NH_2)_2SnCl_6$, $(n\text{-}Bu_3NH)_2SnCl_6$ et, avec moins de détail, ceux du sel à l'anion mixte, $(n\text{-}Pr_2NH_2)_3(SnCl_6)Cl$. Les spectres sont souvent compliqués par la résonance de Fermi qui implique les absorptions caractéristiques important pour la force et le type de liaison N—H···Cl et pour la symétrie de site de l'atome N. A cet égard ils sont moins utiles que les spectres correspondants des composés ammonium non substitués rapportés antérieurement. Plusieurs spectres fournissent des exemples frappants de résonance de Fermi des vibrations du NH et du ND contrôlée par la température. Les liaisons N—H···Cl sont invariablement trifurquées, bifurquées ou au moins fortement déformées; ces caractéristiques donnent lieu à une influence anormale de la température sur les fréquences des élongations fondamentales du NH et du ND. On a décelé des transitions induites par la température dans le $(Me_2NH_2)_2SnCl_6$ ($T_{tr} \sim 100$ K), dans le $(EtNH_3)_2SnCl_6$ ($T_{tr} \sim 125$ K) et dans le $(Et_2NH_2)_2SnCl_6$ ($T_{tr} \sim 330$ K). On discute en détail des résultats spécifiques obtenus pour les dix composés étudiés. La discussion porte également sur les limites de l'utilité de la technique de dilution isotopique; sur les aspects de la symétrie de l'entassement cation-anion dans les hexahalométallates(IV) d'alkylammonium; sur les symétries des arrangements du $SnCl_6$ octaédrique; sur la géométrie de la liaison hydrogène dans le $(R_nNH_{4-n})_2SnCl_6$ et sur la possibilité de détecter la présence d'une liaison hydrogène à partir des tendances du volume moléculaire.

[Traduit par le journal]

The ratio of the N-hydrogen to the chlorine atoms in the alkylammonium hexachlorostannates(IV), $(R_nNH_{4-n})_2SnCl_6$, varies from $\frac{1}{3}$ (for $n = 0$) to zero (for $n = 4$). This provides for the formation of N—H···Cl hydrogen bonds of a variety of types. In the specific case of $n = 3$, the implications of the existence of the unique N-hydrogen for the ir manifestations of the hydrogen bonding have been discussed earlier (1), with particular reference to $(Et_3NH)_2SnCl_6$.

We have now extended that investigation to other alkylammonium hexachlorostannates, with a view to obtaining a clearer understanding of the effect of the alkyl substitution on the crystal architecture of modified alkylammonium hexahalometallates(IV) in general and on the hydrogen bonding in such compounds in particular. To assist in the interpretation of the newly obtained ir spectra of the compounds marked * below, we have determined, or redetermined, the crystal structures of five additional compounds (marked †), so that structural *and* spectroscopic comparisons are now possible in three unbroken series: $(NH_4)_2SnCl_6$ (2–4), *$(MeNH_3)_2SnCl_6$ (1MHS) (5, 6), *†$(Me_2NH_2)_2SnCl_6$ (2MHS) (7, 8), *†$(Me_3NH)_2SnCl_6$ (3MHS) (9), $(Me_4N)_2SnCl_6$ (4MHS) (2, 9), *†$(EtNH_3)_2SnCl_6$ (1EHS) (10), *$(Et_2NH_2)_2SnCl_6$ (2EHS), $(Et_3NH)_2SnCl_6$ (3EHS) (1), $(Et_4N)_2SnCl_6$ (4EHS) (11), *†(n-$PrNH_3)_2SnCl_6$ (1PHS), *(n-$Pr_2NH_2)_2SnCl_6$ (2PHS),[2] *†(n-$Pr_3NH)_2SnCl_6$ (3PHS), *(n-$BuNH_3)_2SnCl_6$ (1BHS) (plus *$(Me_3NH)_2SnBr_6$). The results, which are reported and discussed in the following, include several striking examples of temperature-scanned Fermi resonance (FR) of NH and ND vibrations.

[1]NRCC No. 21040.

[2]Concerning the identity of this compound see Infrared spectra and Experimental sections.

Can. J. Chem. Downloaded from www.nrcresearchpress.com by 210.87.254.105 on 09/06/12
For personal use only.

TABLE 1. Crystallographic data of $(Me_2NH_2)_2SnCl_6$ (2MHS), $(Me_3NH)_2SnCl_6$ (3MHS), $(EtNH_3)_2SnCl_6$ (1EHS), $(n\text{-}PrNH_3)_2SnCl_6$ (1PHS), and $(n\text{-}Pr_3NH)_2SnCl_6$ (3PHS)[a]

Datum	2MHS		3MHS	1EHS	1PHS	3PHS
	This work	Ref. 8				
Formula weight	423.59		451.65	423.59	451.65	619.97
a, Å	14.422(3)[b]	14.446(3)	12.210(3)[c]	7.265(1)[d]	10.050(3)	31.771(7)
b, Å	7.332(1)[b]	7.340(2)			7.198(4)	10.404(5)
c, Å	7.200(2)[b]	7.220(1)		8.410(1)[d]	11.923(3)	19.965(7)
β, deg					104.83(3)	114.79(2)
V, Å^3	761.3(3)	765.6(3)	1820.3(4)	384.4(2)	833.8(3)	5991(8)
Z	2		4	1	2	8
$\bar{a}$, Å	7.247	7.261	7.692	7.271	7.470	9.081
d_{obs}, g/cm^3	1.850[e]	1.83(5)	1.654,[e] 1.652[f]	1.830[e]	1.808[e]	1.362
d_{calcd}, g/cm^3	1.848	1.837	1.648	1.829	1.799	1.375
Space group	*Pnnm* (No. 58)		*Pa*3 (No. 205)	$P\bar{3}m1$ (No. 164)	$P2_1$ (No. 4)	$C2/c$ (No. 15)
F(000)	412		888	206	444	2544
Reflections						
Total counted	791	2661	1820	781	1676	4288
Unique, total	713		542	287	1590	2773
Unique, used[g]	618	1207	375	282	1263	765
$100R$; $100R_w$	4.2; 4.0	4.6; 4.8	2.3; 2.2[h]	5.3; 4.6[i]	2.8; 2.8	6.3; 6.7[i]

[a]Radiation, Mo $K\alpha_1$, λ = 0.70926 Å; μ_{Mo} = 22–25 cm^{-1}; θ range, 2–25°.
[b]14.28, 7.38, 7.26 Å (7).
[c]12.19 Å (9).
[d]7.24, 8.41 Å (10).
[e]Reference 12.
[f]Reference 14.
[g]Used in the refinement. In the present work, $I > 1\sigma(I)$.
[h]The reflections 111, 002, and 004 suffered from extinction and were omitted in the refinement.
[i]Without alkyl hydrogens.

Unless stated otherwise, R will denote a normal alkyl.

Crystal structures

Crystal data of the compounds studied in this work are listed in Table 1. Details of the structure refinements will be found under Experimental.

$(Me_2NH_2)_2SnCl_6$

2MHS, which was measured by Ries (12) and described as orthorhombic pseudotetragonal (D_{2h}, axial ratio 1.0158:1:1.9661), corresponds to the denser of the two forms of $(Me_2NH_2)_2PtCl_6$, both reported as having point-group symmetry D_{2h} (cf. ref. 12 and literature cited therein). We have found no mention of polymorphism of 2MHS in the literature and no evidence of it in our own work.

The essential features of the 2MHS structure were established by Corey and Wyckoff (7). However, on repeating the structure determination we discovered that the systematic absences were compatible with the space group *Pmnn* but not with the $Pmn2_1$ claimed in ref. 7. Inspection of Table 2 shows that Corey and Wyckoff's choice of the positional parameters effectively corresponds to solving the structure in *Pmnn*, the centrosymmetric supergroup of index 2 of $Pmn2_1$ (with *Pmnn* in standard setting, $P2_1nm \subset Pnnm$). *Pmnn* would thus have been the natural choice in ref. 7, had it not been for the presence of a few reflections indicative of $Pmn2_1$ which eventually turned out to be spurious. For comparison, we refined the structure both in *Pnnm* and $P2_1nm$ (Tables 2 and 3[3]). The N—H and C—H bond lengths were constrained and the Me groups were refined as rigid bodies. The $R(P2_1nm)$ and $R_w(P2_1nm)$, 0.046 and 0.043, respectively, were both slightly higher than those for the refinement in *Pnnm* (Table 1). Predictably, the positional and thermal parameters of atoms like C(1) and C(2) etc. in $P2_1nm$, related by $4(g)(Pnnm) \rightarrow [2(a) + 2(a)](P2_1nm)$ and $8(h)(Pnnm) \rightarrow [4(b) + 4(b)](P2_1nm)$, were highly correlated.

Table 2 also shows the results of a recent structure determination of 2MHS in *Pnnm* by Ben Ghozlen *et al.* (8), which came to our attention only when our own refinements were completed. Apart from the difference arising from the different treatment of the H atoms (unconstrained refinement leading to the expectedly short but chemically unreasonable N—H bond lengths in ref. 8), the two sets of positional parameters agree to within one esd in each individual value; the esd's of ref. 8 are roughly half as large as ours owing to about twice the volume of data.

The structure consists of sheets of almost regular $SnCl_6$ octahedra held together by hydrogen bonds in such a way that each Me_2NH_2 group is symmetrically hydrogen-bonded to two $SnCl_6$, and each $SnCl_6$ is the recipient of hydrogen bonds from four Me_2NH_2 (Fig. 1). The hydrogen bonds (Table 4) may be described as asymmetrically trifurcated or perhaps closer to out-of-plane bifurcated. The $[(Me_2NH_2)_2SnCl_6]^0_\infty$ sheets are fitted together by sheets of the Me(2) groups, whilst the H(11) hydrogens of Me(1) groups reach into spaces between the octahedra in an $SnCl_6$ sheet.

$(Me_3NH)_2SnCl_6$

The gross features of the 3MHS structure were determined as early as 1929 by Wyckoff and Corey (9), who described it as a lower-symmetry ($Pa3$) variant of the antifluorite ($Fm3m$)

[3]This table has been deposited. Copies are available upon request, at a nominal charge, from the Depository of Unpublished Data, CISTI, National Research Council of Canada, Ottawa, Ont., Canada K1A 0S2.

Can. J. Chem. Downloaded from www.nrcresearchpress.com by 210.87.254.105 on 09/06/12
For personal use only.

TABLE 2. $(Me_2NH_2)_2SnCl_6$: positional parameters ($\times 10^4$)[a]

Atom		*Pnnm* x	*Pnnm* y	*Pnnm* z	Atom		$P2_1nn$[b] x	$P2_1nn$[b] y	$P2_1nn$[b] z
Sn(1)	2(*a*)	0	0	0	Sn(1)	2(*a*)	0	0	0
Cl(1)	4(*g*)	1420(2)	8219(4)	0	Cl(1)	2(*a*)	−1415(16)	−8190(35)	0
		1429(1)	8215(2)	0	Cl(2)		1421(16)	8247(34)	0
Cl(2)	8(*h*)	0637(1)	1926(2)	2411(2)	Cl(3)	4(*b*)	0640(10)	1928(17)	2447(18)
		0638(1)	1924(1)	2412(1)	Cl(4)		−0633(13)	−1931(20)	2371(20)
N(1)	4(*g*)	3634(6)	3117(13)	0	N(1)	2(*a*)	−3641(25)	−3078(49)	0
		3626(3)	3123(6)	0	N(2)		3626(24)	3146(50)	0
H(1)	8(*h*)	406(6)	374(13)	095(11)	H(N1)	4(*b*)	297(3)	365(5)	122
		398(3)	348(4)	086(6)	H(N2)		595(3)	652(5)	122
C(1)	4(*g*)	3632(12)	1143(17)	0	C(1)	2(*a*)	−3506(52)	−1249(70)	0
		3637(6)	1137(8)	0	C(2)		3718(36)	0983(96)	0
C(2)	4(*g*)	2725(8)	3988(24)	0	C(3)	2(*a*)	−2748(48)	−4100(127)	0
		2728(4)	3996(11)	0	C(4)		2661(56)	3751(158)	0
*H(11) [H(4)]	4(*g*)	4344(12)	0635(17)	0	H(C2,1)	2(*a*)	443(4)	052(10)	0
		437(5)	042(9)	0	H(C1,1)		420(5)	−071(7)	0
*H(12) [H(5)]	8(*h*)	3270(12)	0661(17)	1225	H(C2,2)	4(*b*)	337(4)	048(10)	1225
		331(3)	073(7)	099(8)	H(C1,2)		−314(5)	−078(7)	1225
*H(21) [H(2)]	4(*g*)	2816(8)	5451(24)	0	H(C4,1)	2(*a*)	264(6)	522(16)	0
		281(5)	483(8)	0	H(C3,1)		290(5)	−554(13)	0
*H(22) [H(3)]	8(*h*)	2339(8)	3584(24)	1225	H(C4,2)	4(*b*)	231(6)	324(16)	1225
		246(4)	347(5)	118(7)	H(C3,2)		−235(5)	−376(13)	1225

[a]The parameters of the H atoms (except those marked *) have been multiplied by 10^3. The uncertainties are single esd's in units of the last digit. Second entry under *Pnnm* is from ref. 8. Transformations: $abc(Pnnm) \rightarrow \bar{b}ca(Pmn2_1$, ref. 7), $abc(Pnnm) \rightarrow cba(Pmnn$, ref. 8); $xyz(Pnnm) \rightarrow \bar{y} + y(Sn), z, x$ ($Pmn2_1$, ref. 7); $xyz(Pnnm) \rightarrow zyx(Pmnn$, ref. 8); $y(Sn) = 0.2502$.

[b]Parameters from ref. 7: Cl(2) = −Cl(1), 0.140, 0.820, 0; Cl(3) = −Cl(4), 0.065, 0.190, 0; N(2) = −N(1), 0.370, 0.310, 0; C(2) = −C(1), 0.355, 0.125, 0; C(4) = −C(3), 0.280, 0.375, 0.

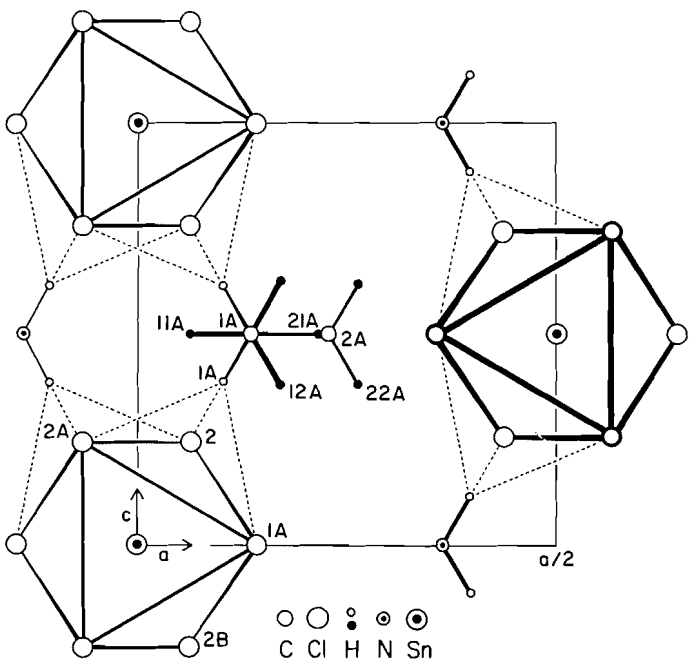

FIG. 1. Hydrogen bonding in 2MHS. Projection on 010. The N(1) atom is eclipsed by C(1A). For distances and angles see Table 4.

4MHS arrangement, noting a slight displacement of the $SnCl_6$ octahedra by rotation about their respective threefold axes.

The intensities were collected in orthorhombic symmetry ($Pbca \subset Pa3$) and the structure was refined in both *Pbca* and $Pa3$. The N—H and C—H bond lengths were constrained and the Me groups were refined as rigid bodies. The refinement in *Pbca* gave slightly higher *R*'s than for $Pa3$ (Table 1), but otherwise the positional parameters were very close to those obtained in the refinement in $Pa3$, presumed to be the correct space group.

The results of the refinement in $Pa3$ (Table 5) confirm the previous (9) partial determination. There was no indication of disorder in the structure. The bond distances and interatomic contacts (Table 6 and Fig. 2*A*) are unexceptional. The $SnCl_6$ octahedra are practically regular, with the Sn—Cl bonds rotated away from the unit-cell edges. The N—H vectors are in the threefold axes, with the H atoms engaged in symmetrically trifurcated N—H···Cl bonds. Unlike in $(NH_4)_2SnCl_6$ (2–4), the N—H vectors are directed at the Sn atoms; the Me groups point, asymmetrically, away from the Sn atoms. Each $SnCl_6$ octahedron is associated with two Me_3NH groups to form centrosymmetric $Me_3NH\cdots Cl_3SnCl_3\cdots HNMe_3$ units. The H···H separation across the Sn atom is ca. 6.5 Å. Other H_N neighbours of an H_N atom are also ca. 6.5 Å away; their respective N—H vectors are at tetrahedral angles to the reference N—H bond. The H···Cl contacts of the Me groups are shown in Fig. 2*B*. The shortest of these, 2.87 Å, is between H(11) and Cl(1A) (in Fig. 2*B*, H(21) and Cl(1B)), the corresponding C—H(11)—Cl(1A) angle being ca. 138°.

$(EtNH_3)_2SnCl_6$

This salt and the corresponding chloroplatinate were reported many years ago by Wyckoff (10) as hexagonal ($P\bar{3}m1$, $Z = 1$) and described as layer structures resembling that of the trigonal form of $(NH_4)_2SiF_6$. Only the metal and Cl positions were established. The N positions were inferred, and the Et groups were considered "rotating".

Can. J. Chem. Downloaded from www.nrcresearchpress.com by 210.87.254.105 on 09/06/12
For personal use only.

TABLE 4. $(Me_2NH_2)_2SnCl_6$: interatomic distance (Å) and bond angles (deg)[a]

Atoms	Distance		Bonds	Angle	
	This work	Ref. 8		This work	Ref. 8
Sn(1)—Cl(1A)	2.429(3)	2.434(1)	Cl(1A)—Sn(1)—Cl(2)	89.6(1)	90.37(3)
Sn(1)—Cl(2)	2.419(2)	2.424(1)	Cl(1A)—Sn(1)—Cl(2A)	90.4(1)	89.63(3)
N(1)—C(1)	1.447(15)	1.458(7)	Cl(2)—Sn(1)—Cl(2A)	88.3(1)	88.14(3)
N(1)—C(2)	1.458(16)	1.447(7)	Cl(2)—Sn(1)—Cl(2B)	91.7(1)	91.86(3)
N(1)—H(1)	[1.02][b]	0.85(4)	C(1)—N(1)—C(2)	115.9(12)	116.9(5)
C(1)—H(11)		1.18(8)	C(1)—N(1)—H(1)	117(6)	108(2)
C(1)—H(12)	[1.08][b]	0.91(5)	C(2)—N(1)—H(1)	111(7)	114(2)
C(2)—H(21)		0.87(6)	H(1A)—N(1A)—H(1B)	84(12)	94(4)
C(2)—H(22)		1.01(5)	N(1A)—H(1A)—Cl(1A)	117(8)	126
Cl(1A)···Cl(2)	3.417(4)	3.424	N(1A)—H(1A)—Cl(2)	143(12)	135(3)
Cl(1A)···Cl(2A)	3.439(4)	3.447	N(1A)—H(1A)—Cl(2A)	138(12)	147(3)
Cl(2)···Cl(2A)	3.369(3)	3.373			
Cl(2)···Cl(2B)	3.472(3)	3.483	Coordinate transformations:		
N(1A)···Cl(1A)	3.602(10)	3.611	N(1A), C(1A), C(2A), H(11A), H(21A):	$\frac{1}{2}-x, y-\frac{1}{2}, \frac{1}{2}$	
N(1A)···Cl(2)	3.518(10)	3.522(4)	H(1A), H(12A), H(22A):	$\frac{1}{2}-x, y-\frac{1}{2}, \frac{1}{2}-z$	
N(1A)···Cl(2A)	3.438(10)	3.455(3)	H(1B):	$\frac{1}{2}-x, y-\frac{1}{2}, \frac{1}{2}+z$	
H(1A)···Cl(1A)	3.02(11)	3.05	Cl(1A):	$x, y-1, 0$	
H(1A)···Cl(2)	2.65(13)	2.87(3)	Cl(2A):	$\bar{x}, \bar{y}, z$	
H(1A)···Cl(2A)	2.61(13)	2.72(4)	Cl(2B):	$x, y, \bar{z}$	

[a]See Fig. 1.
[b]Constrained in refinement.

TABLE 5. $(Me_3NH)_2SnCl_6$: positional and thermal parameters ($\times 10^4$)[a]

Atom	Equipoint	x y z	U_{11} U_{22} U_{33}	U_{12} U_{13} U_{23}
Sn	4(*a*)	{0}	{389(3)}	{−31(1)}
Cl(1)	24(*d*)	−0264(1)	604(6)	−39(4)
		1943(1)	393(5)	1(5)
		0332(1)	570(6)	−1(5)
N(1)	8(*c*)	{2034(3)}	{485(14)}	{−62(15)}
H(1)	8(*c*)	{1552(3)}	949(309)[b]	
C(1)	24(*d*)	3121(4)	640(30)	−106(31)
		1505(6)	931(43)	−152(27)
		2098(5)	776(35)	188(27)
H(11)	24(*d*)	3623(4)		
		2035(6)	867(162)[b]	
		2597(5)		
H(12)	24(*d*)	3533(4)		
		1344(6)	1267(255)[b]	
		1332(5)		
H(13)	24(*d*)	2984(4)		
		0742(6)	1009(207)[b]	
		2524(5)		

[a]Braces: $x = y = z$, $U_{11} = U_{22} = U_{33}$, $U_{12} = U_{13} = U_{23}$.
[b]Isotropic temperature factor.

The present structure determination (Table 7) has confirmed these findings. With the N—C(1) bond placed on a threefold axis, and constraining the N—H, N—C, and C—C bond lengths and the CNH and NCC angles, the C(1)—C(2) bond was found to be orientationally disordered with respect to the threefold axis. The thermal parameters of C(1) were about twice, and those of C(2) about three times, those of the N atom. A difference Fourier section at the height of C(1) with this atom and all the hydrogens omitted from F_c shows a slight triangularity of the inner contours of the local maximum centred on the threefold axis (Fig. 3, top). A corresponding section at the height of C(2) with this atom and all the hydrogens omitted displays clearly a threefold maximum (Fig. 3, bottom). The shortest possible distance between C(2) sites is only 1.96 Å (Fig. 4), hence the instantaneous distribution of the C(1)—C(2) orientations in the crystal must be governed by the necessity to avoid simultaneous occupation of sites at this distance. Because of the disorder no attempt was made to refine the alkyl hydrogens. For comparison, the structures of the corresponding *iso*-propyl and *tert*-butyl salts are being examined.

Each N-hydrogen engages in a nearly symmetrically trifurcated N—H···3Cl bond. The H···Cl distances (Table 8) are comparable to that in $(NH_4)_2SnCl_6$, 2.79 Å (13). The nature of the disorder is commented upon later in this paper.

(n-PrNH$_3$)$_2$SnCl$_6$

The structure of this compound has not been determined previously, but from optical measurements (12) the crystal was concluded to belong to the C_{2h} point group.

The systematic absences indicated space groups $P2_1/m$ or $P2_1$, $Z = 2$. Refinement in $P2_1$, with constraints on N—H, C—H, N—C, C—C, and the HNH and HNC angles, and with anisotropic temperature factors on all atoms except the hydrogens, resulted in $R = 0.028$. However, the y coordinates of several of the nonhydrogen atoms were close to $\frac{1}{4}$ and the $SnCl_6$ octahedron appeared to be practically mirror-symmetric (Table 9), so the refinement was repeated in $P2_1/m$ with these atoms in 2(*e*), and again in $P2_1/m$ with these atoms having the same coordinates as in the $P2_1$ refinement but in a twofold disorder with respect to reflection in the $y = \frac{1}{4}$ plane. The R values for these two refinements (anisotropic but H not included) were 0.048 and 0.041 respectively, with esd's of the carbon U_{ii} 3–4 times as large as in the $P2_1$ refinement. Thus while the structure in its gross features is pseudo-$P2_1/m$, the true space-group symmetry is $P2_1$. The proximity to $P2_1/m$ caused the inverse matrix in the $P2_1$ refinement to be ill-conditioned. Con-

Can. J. Chem. Downloaded from www.nrcresearchpress.com by 210.87.254.105 on 09/06/12
For personal use only.

Can. J. Chem. Downloaded from www.nrcresearchpress.com by 210.87.254.105 on 09/06/12
For personal use only.

TABLE 6. $(Me_3NH)_2SnCl_6$: interatomic distances (Å) and bond angles (deg)

Atoms	Distance	Atoms	Bond angle
Sn—Cl(1)	2.429(1)	Cl(1)—Sn—Cl(2)	89.4(1)
N—H(1)	[1.02][a]	N—H(1)—Cl(1)	133(1)
H(1)···Cl(1), Cl(2), Cl(3)	2.71(1)	C—N—C	111.6(4)
N—C	1.478(6)	H(1)—N—C	107.2(4)
C(1)—H(11), H(12), H(13)	[1.08][a]		
C(1)···C(2), C(3)	2.445(7)	Coordinate transformations:	
Cl(1)···Cl(2), Cl(3)	3.415(3)	Cl(1) = −Cl(4)	x y z
Cl(1)···Cl(5), Cl(6)	3.454(3)	Cl(2) = −Cl(5)	z x y
H(11)···Cl(1A)	2.87(1)	Cl(3) = −Cl(6)	y z x
H(11)···Cl(2A)	3.54(1)	Cl(1A)	$1+x$ y $\frac{1}{2}-z$
H(11)···Cl(1B)	3.63(1)	Cl(2A)	$\frac{1}{2}+z$ x $\frac{1}{2}-y$
H(11)···Cl(6A)	3.96(1)	Cl(6A)	$\frac{1}{2}-y$ $\bar{z}$ $\frac{1}{2}+x$
H(11)···Cl(3)	4.55(1)	Cl(1B)	$\frac{1}{2}-z$ $\frac{1}{2}+x$ y
H(12)···Cl(3)	3.02(1)	Cl(2B)	$\frac{1}{2}-y$ $\frac{1}{2}+z$ x
H(12)···Cl(6B)	3.26(1)	Cl(6B)	$\frac{1}{2}+x$ $\frac{1}{2}-y$ $\bar{z}$
H(12)···Cl(2A)	3.62(1)	Cl(1C)	y $\frac{1}{2}-z$ $\frac{1}{2}+x$
H(12)···Cl(1B)	4.43(1)	Cl(3C)	x $\frac{1}{2}-y$ $\frac{1}{2}+z$
H(13)···Cl(6A)	3.00(1)	Cl(6C)	$\bar{z}$ $\frac{1}{2}+x$ $\frac{1}{2}-y$
H(13)···Cl(2A)	3.19(1)	H(11)	x y z
H(13)···Cl(2)	3.54(1)	H(21)	z x y
H(13)···Cl(3)	3.67(1)	H(31)	y z x
H(13)···Cl(1A)	3.69(1)		

[a]Constrained in refinement.

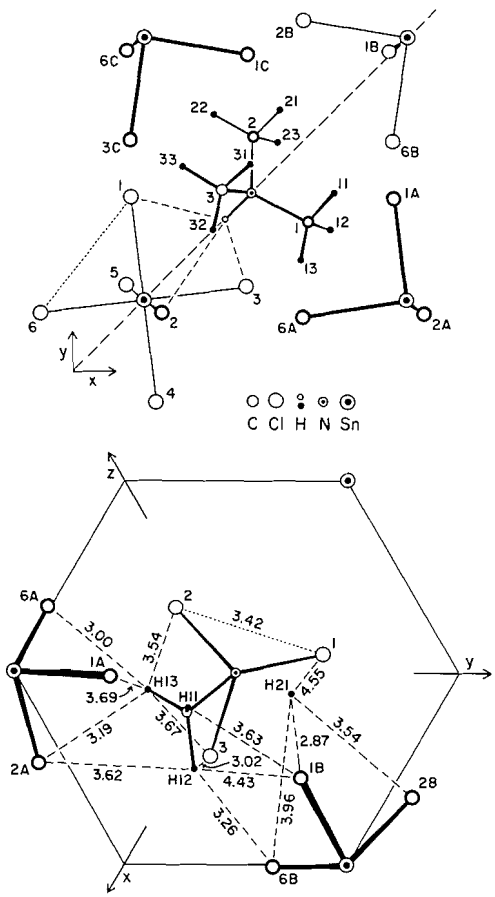

FIG. 2. Essential features of the 3MHS structure (*A*) (top) Projection on 001. (*B*) (bottom) Projection down [111] showing the H···Cl contacts of the methyl groups.

sequently, the esd's quoted in Tables 9–11, which were generated by freeing the $P2_1$ refinement from the bond-length constraints, must be viewed with great caution.

TABLE 7. $(EtNH_3)_2SnCl_6$: positional and thermal parameters[a,b]

Atom	Equipoint	x y z	U_{11} U_{22} U_{33}	U_{12} U_{13} U_{23}
Sn	1(*a*)	0	235(3)	0
		0	235(3)	0
		0	709(9)	0
Cl	6(*i*)	1592(2)	558(21)	167(22)
		−1592(2)	451(11)	−50(28)
		1623(4)	947(17)	199(12)
N	2(*d*)	2/3	503(25)	0
		1/3	503(25)	0
		1667(13)	603(28)	0
C(1)	2(*d*)	2/3	1234(30)	0
		1/3	1234(30)	0
		3425(13)	1113(30)	0
C(2)[c]	6(*i*)	5582(29)	1844(30)	450(30)
		−5582(29)	1844(30)	−128(30)
		4264(26)	1809(30)	128(30)
H(N)	6(*i*)	7428(22)		
		−7428(22)	736(30)[d]	
		1251(22)		

[a]All nonspecial parameter values have been multiplied by 10^4.
[b]$x(Cl) = 0.16$, $z(Cl) = 0.17$, $z(N) \sim 0.184$ (10).
[c]Threefold orientational disorder, see text.
[d]Isotropic temperature factor.

The structure may be regarded as a monoclinically distorted *anti*-CdI_2-type packing of the composite ions (Fig. 5*A*). There are two types of cation in the unit cell. Each N-hydrogen forms highly-bent, bi- or trifurcated N—H···Cl bonds, the strongest having d(H···Cl) ~ 2.44 Å and NHCl ~ 156° (Table 11 and Fig. 5*B*). The terminal carbons C(13) and C(23) must be vibrationally highly mobile, as seen from their large thermal

TABLE 8. $(EtNH_3)_2SnCl_6$: interatomic distances (Å) and bond angles (deg)

Atoms	Distance	Atoms	Angle
Sn—Cl	2.424(2)	Cl(z)—Sn—Cl(z)	91.4(1)
N···Cl	3.634(2) (2×) 3.529(2) (1×)	Cl(z)—Sn—Cl($\bar{z}$)	88.6(1)
		N—H—Cl	134(3) (2×) 138(4) (1×)
H(N)···Cl	2.85(1) (2×) 2.71(2) (1×)		
Cl(z)···Cl(z)	3.470(2)		
Cl(z)···Cl($\bar{z}$)	3.386(5)		

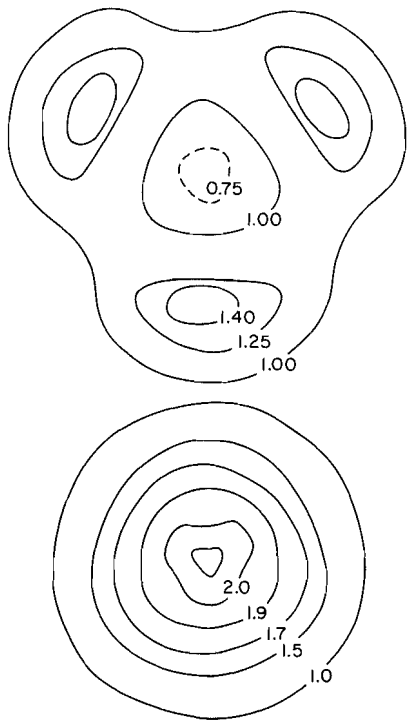

FIG. 3. Difference electron density maps of 1EHS displaying the orientational disorder of the ethyl group. (Top) Section parallel to 0001 at $z = 0.34$ with C(1) removed. (Bottom) Section parallel to 0001 at $z = 0.44$ with C(2) removed. The contour scale is in e/Å^3.

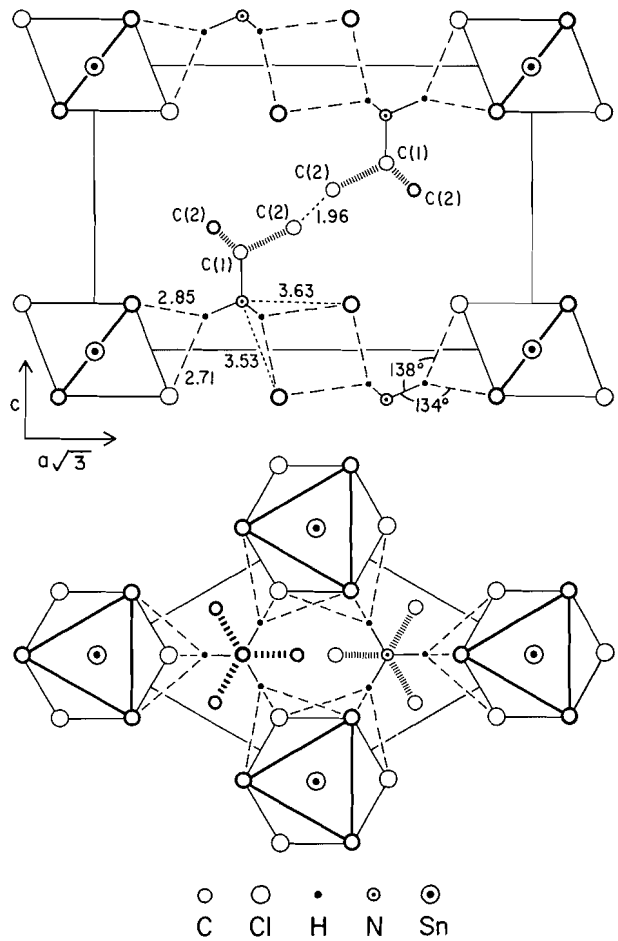

FIG. 4. Hydrogen bonding in 1EHS. (*A*) (top) Projection on $11\bar{2}0$. (*B*) (bottom) Projection on 0001. The C—C bonds corresponding to the three alternative positions of the terminal C atoms are indicated by "shaded" lines.

parameters (Table 10).[3] The Sn—Cl distances in the noncentrosymmetric $SnCl_6$ octahedron range from 2.41 to 2.45 Å, and the acute ClSnCl angles of vicinal Cl atoms from 87.6 to 90.0°.

(n-$Pr_3NH)_2SnCl_6$

No crystallographic information appears to be available on 3PHS in the literature. For the corresponding chloroplatinate two forms were reported by Ries (12), one triclinic (from MeOH) and another, less dense, of D_{2h} symmetry (from aqueous solution above 30°C). The 3PHS structure described below would seem to correspond to the triclinic form.

3PHS has a large monoclinic cell, with all atoms in general positions. In the refinement the N—H, N—C, C—C bond lengths and the NCC and CCC angles were constrained. With the alkyl hydrogens not included the structure refined to $R = 0.063$ (anisotropic temperature factors on Sn and Cl, isotropic on all the other atoms). The refinement was not continued beyond this stage (see below). The positional parameters are listed in Table 12, the thermal parameters in Table 13,[3] and interatomic distances and bond angles in Table 14.

The $SnCl_6$ octahedra are noncentrosymmetric but not severely distorted. The Cl···Cl edge distances range from 3.35 to 3.48 Å and the ClSnCl angles subtending the edges, from 88.3 to 91.4°. The cations have umbrella-like, pseudotrigonal conformations: the midpoints of the N—C and C—C bonds in the three extended N—C—C—C zig–zag chains in each of the two nonequivalent cations are approximately coplanar (Fig. 6). This implies that the *n*-Pr_3NH dipoles effectively coincide with the N—H bonds.

The structure may be regarded as consisting of two interpenetrating systems of centrosymmetric pairs of *n*-Pr_3NH groups (Fig. 7). The cations are hydrogen-bonded to the $SnCl_6$ octahedra by strongly bent N—H···Cl bonds, which indicates

Can. J. Chem. Downloaded from www.nrcresearchpress.com by 210.87.254.105 on 09/06/12
For personal use only.

Can. J. Chem. Downloaded from www.nrcresearchpress.com by 210.87.254.105 on 09/06/12
For personal use only.

TABLE 9. $(n\text{-}PrNH_3)_2SnCl_6$: positional parameters[a]

Atom	x	y	z	Atom	x	y	z
Sn	−0711	¼	7283	H(11)	1663	2069	3874
Cl(1)	0639	0136	6625	H(12)	1718	3637	4917
Cl(2)	0628	4927	6637	H(13)	1819	1376	5234
Cl(3)	0974	2543	9172	H(111)	3952	1659	4343
Cl(4)	−1951	4941	7963	H(112)	3864	3692	4872
Cl(5)	−2329	2493	5386	H(121)	5047	1045	6264
Cl(6)	−1997	0098	7955	H(122)	3613	0546	6114
N(1)	2082	2382	4724	H(131)	5089	3897	7816
C(11)	3597	2476	4955	H(132)	3849	3370	7424
C(12)	4265	1646	6157	H(133)	4364	4478	6814
C(13)	4248	2965	7126	H(21)	−0832	1808	10238
N(2)	−1247	2418	10845	H(22)	−0797	2288	11713
C(21)	−2734	2095	10518	H(23)	−1325	3830	10863
C(22)	−3506	3030	11280	H(211)	−3186	1744	9836
C(23)	−5037	2586	10920	H(212)	−2967	1069	10727
				H(221)	−3038	2834	12247
				H(222)	−3451	4475	11172
				H(231)	−5319	3202	11590
				H(232)	−5206	1162	10927
				H(233)	−5417	3044	10054

[a]All nonspecial parameter values have been multiplied by 10^4. The esd's were <0.0001 for Sn, 0.0001–0.0006 for Cl, 0.0004–0.0008 for N and C, and 0.0008 for H (but see section under Crystal structures, $(n\text{-}PrNH_3)_2SnCl_6$).

TABLE 11. $(n\text{-}PrNH_3)_2SnCl_6$: N···Cl and H···Cl distances (Å) and NHCl bond angles (deg)

Atom			Distance		
N	H	Cl[a]	N···Cl[b]	H···Cl[c]	Angle[d]
1	11	2′D	*3.303	2.708	117.3
		4′D	*3.627	2.748	144.5
		1′	3.427	3.143	97.4
		6′	*3.727	3.162	116.2
		5′D	3.533	3.431	87.3
1	12	2	*3.521	2.724	134.1
		1′	*3.427	2.815	119.0
		5′	*3.692	2.885	136.5
1	13	1	*3.397	2.441	155.8
		5′D	*3.533	2.969	115.7
		2′D	3.303	3.050	95.2
2	21	3	*3.354	2.524	138.2
		6	*3.728	2.943	134.3
		3′C	*3.520	3.161	102.2
2	22	2′C	*3.415	2.572	139.8
		1′B	*3.515	2.827	125.2
		6′B	3.743	3.401	101.7
2	23	3′B	*3.700	2.698	167.0
		1′B	*3.515	3.045	109.1
		6′B	3.743	3.400	101.7
		4	3.790	3.446	102.0

[a]Primed atoms: $(\bar{x}, \frac{1}{2} + y, 1 - z)$ + A(0, 1, 0), B(0, 0, 1), C(0, $\bar{1}$, 1), D(0, $\bar{1}$, 0).
[b]esd = 0.009 Å; *, considered hydrogen-bonded.
[c]esd = 0.02 Å.
[d]esd = 3°.

that hydrogen bonding in this crystal is not an important structure-determining factor and that its optimization in the circumstances produces at best an inefficient hydrogen-bonding geometry (Fig. 6). Although the N(1′)—H(1′)—Cl(1) angle is ca. 136°, there is no other suitable Cl acceptor within a reasonable bonding distance,[4] and the H(1′)···Cl(1) distance is ~2.89 Å. The N(2)—H(2)—Cl(3) angle is larger, ca. 150°, and the H(2)···Cl(3) separation is ~2.38 Å. In addition, there is a Cl(5) atom ca. 3.17 Å away from H(2), but the N(2)—H(2)—Cl(5) angle, ~128°, is too small for the N(2)—H(2)···Cl bond to be considered effectively bifurcated. The two nonequivalent $n\text{-}Pr_3NH$ units are *cis* to the $SnCl_6$ octahedron, in contrast to the *trans* configurations found in 3MHS and 3EHS and in fact in all the alkylammonium hexachlorostannates so far studied (see section on Structural principles).

The Sn(1)—Cl(1)—H(1′) angle corresponding to the H(1′)···Cl(1) distance of ~2.89 Å is ~126° and thus quite small if the N(1′)—H(1′)···Cl(1) bond is considered as highly bent but not bifurcated. A small MC1H angle in alkylammonium compounds is, however, not without precedent: the Cd—H(1)—Cl(2′) angle in the orthorhombic phase of $(Me_3NH)CdCl_3$ is only 105(3)° (Fig. 1 of ref. 15), and the Cl(2′)···H(1)—N bond is normal, not appreciably bent.

Examination of the CNC angles (Table 14) reveals a considerable departure from the tetrahedral angle and a considerable variation at each N atom, particularly at N(1), 91–136°. These deviations from the expected values are large and difficult to account for in view of the realistic constraints on the N—C and C—C bond lengths in the refinements. Refinement of the structure both with additional constraints and without any constraints did not improve the cation geometry. The unusually large thermal parameters of some of the C atoms (and the esd's in general) suggest that the cations at room temperature possess appreciable flexibility and that this may be the reason preventing the proposed — otherwise chemically reasonable — structure from being refined further. It is also possible that the crystal contains a certain degree of disorder of an undetermined nature.

[4]Cl(4E), at ~5.36 Å from H(1′), is at an N(1′)—H(1′)—Cl(4E) angle of ~138° (Table 14).

Can. J. Chem. Downloaded from www.nrcresearchpress.com by 210.87.254.105 on 09/06/12
For personal use only.

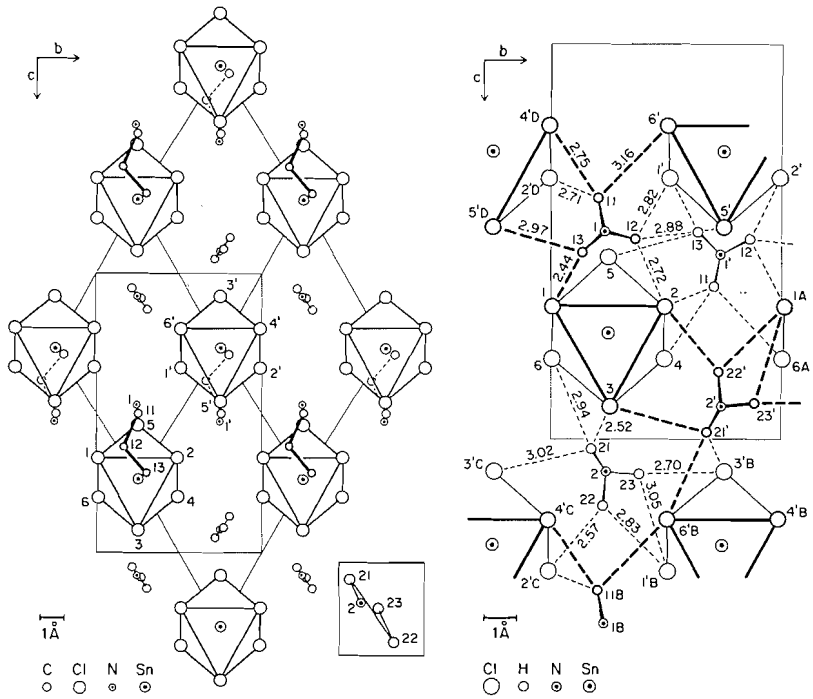

FIG. 5. Essential features of the 1PHS structure. (*A*) (left) Projection along *a* on 100 displaying the basic similarity with the *anti*-CdI_2-type packing. The centres of the Sn atoms form a puckered layer only 1.4 Å thick. An enlargement of cation 2 is shown for clarity. (*B*) (right) Hydrogen bonding scheme. For additional H···Cl distances, NHCl angles and symmetry code see Table 11.

TABLE 12. $(n\text{-}Pr_3NH)_2SnCl_6$: positional parameters ($\times 10^4$)

Atom	*x*	*y*	*z*
Sn(1)	1363(1)	4911(3)	2239(1)
Cl(1)	1954(4)	3346(10)	2908(7)
Cl(2)	0781(5)	6465(14)	1573(8)
Cl(3)	0783(4)	3717(12)	2491(6)
Cl(4)	1909(4)	6157(10)	1954(6)
Cl(5)	1563(4)	6134(11)	3370(5)
Cl(6)	1165(5)	3635(12)	1152(6)
N(1)	1723(16)	9938(53)	2376(22)
H(1)	1951(16)	10663(53)	2525(22)
C(111)	1951(17)	9932(99)	1865(28)
C(112)	1595(16)	10345(99)	1097(25)
C(113)	1850(22)	10473(74)	0592(29)
C(121)	2089(19)	9105(50)	2902(21)
C(122)	2184(17)	9532(49)	3689(21)
C(123)	2605(17)	8785(54)	4237(23)
C(131)	1288(21)	10519(43)	2339(45)
C(132)	1009(22)	9476(48)	2519(50)
C(133)	0584(24)	10119(76)	2562(51)
N(2)	0789(12)	4287(36)	4119(21)
H(2)	0850(12)	4364(36)	3675(21)
C(211)	1248(13)	3999(41)	4727(19)
C(212)	1467(13)	2888(35)	4474(22)
C(213)	1987(13)	2836(60)	4992(31)
C(221)	0646(28)	5519(41)	4331(26)
C(222)	0553(27)	6505(43)	3713(26)
C(223)	0474(28)	7830(40)	3984(39)
C(231)	0429(18)	3279(46)	3933(19)
C(232)	0338(18)	3016(48)	4620(23)
C(233)	0083(22)	1720(49)	4503(31)

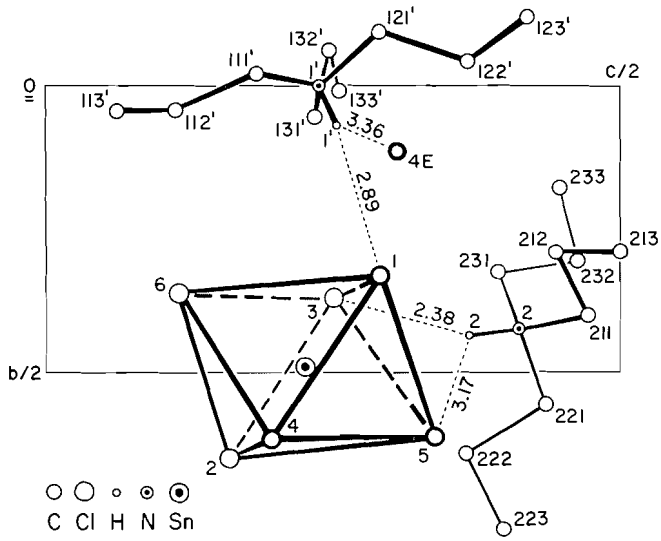

FIG. 6. An asymmetric unit of the 3PHS structure showing the N—H···Cl bonding. Projection along *a* on 100.

Infrared spectra

Survey spectra in the range of 4000–200 cm^{-1}, at room temperature and 10 K, were recorded for all the compounds listed in the Introduction. Since our interest is mainly in hydrogen bonding, we are reporting only the spectra in the region of NH and ND stretching fundamentals of the alkylammonium ions. Different levels of deuteration were employed to suit particular purposes; the D contents stated refer to replacement of the N-hydrogens by D. Spectra of the trialkylammonium salts will be dealt with first, partly because they are an extension of the previous work on 3EHS (1), but also because they illustrate most clearly temperature-tuned FR, a feature common, to a varying extent, to all the spectra.

Trialkylammonium salts

$(Me_3NH)_2SnCl_6$ and $(Me_3NH)_2SnBr_6$

Expectation from crystal structure. The gross features of the

Can. J. Chem. Downloaded from www.nrcresearchpress.com by 210.87.254.105 on 09/06/12
For personal use only.

TABLE 14. $(n\text{-}Pr_3NH)_2SnCl_6$: N···Cl and H···Cl distances (Å) and NHCl bond angles (deg)[a]

Atoms	Distance	Atoms	Angle
Sn(1)—Cl(1)	2.420(10)	Cl(1)—Sn(1)—Cl(3)	91.3(4)
Sn(1)—Cl(2)	2.396(13)	Cl(1)—Sn(1)—Cl(4)	91.3(4)
Sn(1)—Cl(3)	2.443(13)	Cl(1)—Sn(1)—Cl(5)	89.9(4)
Sn(1)—Cl(4)	2.417(14)	Cl(1)—Sn(1)—Cl(6)	88.6(4)
Sn(1)—Cl(5)	2.433(11)	Cl(2)—Sn(1)—Cl(3)	89.1(5)
Sn(1)—Cl(6)	2.392(12)	Cl(2)—Sn(1)—Cl(4)	88.3(5)
Cl(1)···Cl(3)	3.476(20)	Cl(2)—Sn(1)—Cl(5)	90.2(4)
Cl(1)···Cl(4)	3.460(19)	Cl(2)—Sn(1)—Cl(6)	91.3(5)
Cl(1)···Cl(5)	3.431(22)	Cl(3)—Sn(1)—Cl(5)	90.1(4)
Cl(1)···Cl(6)	3.361(21)	Cl(3)—Sn(1)—Cl(6)	88.4(5)
Cl(2)···Cl(3)	3.395(22)	Cl(4)—Sn(1)—Cl(5)	90.2(4)
Cl(2)···Cl(4)	3.352(22)	Cl(4)—Sn(1)—Cl(6)	91.4(5)
Cl(2)···Cl(5)	3.419(22)	C(111)—N(1)—C(121)	91(5)
Cl(2)···Cl(6)	3.424(27)	C(111)—N(1)—C(131)	133(5)
Cl(3)···Cl(5)	3.449(25)	C(121)—N(1)—C(131)	136(6)
Cl(3)···Cl(6)	3.369(14)	C(211)—N(2)—C(221)	105(4)
Cl(4)···Cl(5)	3.436(13)	C(211)—N(2)—C(231)	117(4)
Cl(4)···Cl(6)	3.444(25)	C(221)—N(2)—C(231)	113(5)
N(1′)···Cl(1)	3.69(7)	N(1′)—H(1′)—Cl(1)	136(5)
N(1′)···Cl(4E)	4.17(6)	N(1′)—H(1′)—Cl(4E)	138(7)
N(2)···Cl(3)	3.30(3)	N(2)—H(2)—Cl(3)	150(9)
N(2)···Cl(5)	3.88(6)	N(2)—H(2)—Cl(5)	128(9)
H(1′)···Cl(1)	2.89(6)	Sn(1)—Cl(1)—H(1′)	126(5)
H(1′)···Cl(4E)	3.36(6)		
H(2)···Cl(3)	2.38(4)		
H(2)···Cl(5)	3.17(6)		

[a]Primed atoms: $x, y-1, z$; Cl(4E), $\frac{1}{2}-x, y-\frac{1}{2}, \frac{1}{2}-z$.

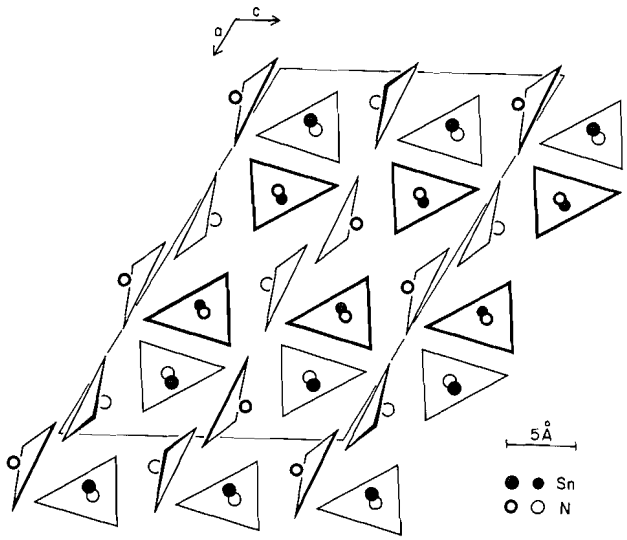

FIG. 7. Schematic presentation of the organization of the 3PHS structure (see text). Projection on 010. Each triangle represents a n-Pr_3NH group; the vertices correspond to the positions of the three terminal carbons. Only the Sn atoms of the $SnCl_6$ octahedra are shown.

3MHS structure are the same as those of $(NH_4)_2SnCl_6$ (see section on Structural principles), and the N—H···3Cl bond is in both cases symmetrically trifurcated. The difference is in the N—H···Cl distance, which in 3MHS is shorter than in the ammonium compound, 2.71 Å as against 2.79 Å, and in the direction of the N—H vectors, which in 3MHS point at, but in $(NH_4)_2SnCl_6$ away from the Sn atoms. As a result, in 3MHS the single N—H bond per cation participates in the formation of discrete hydrogen-bonded $[Me_3NH]^+\cdots{}^-[Cl_3SnCl_3]^-\cdots{}^+[HNMe_3]$ groupings, so that the crystal may be formally regarded as a pseudomolecular crystal consisting of electroneutral $[A^+B^{2-}A^+]$ units arranged and oriented in a way resembling the molecules in a CO_2 crystal. This is quite different from the tetrahedrally uniform and coincident charge- *and* hydrogen-bonding interactions between nearest-neighbour NH_4^+ and $SnCl_6^{2-}$ in the typically ionic ammonium salt. The effect of lattice compression on the NH and ND frequencies (cf. ref. 13) should thus be expected to be significantly less pronounced. The direction of change in the NH and ND stretching frequencies in 3MHS relative to the ammonium salt is difficult to predict, as it depends not only on the crystal-determined features but also on the difference in the intrinsic hydrogen-bond *donor* strength of NH_4^+ and Me_3NH^+.

Spectrum of 3MHS. The band shapes in the NH and ND stretching regions were virtually independent of the degrees of deuteration (Fig. 8), indicating a near absence of vibrational coupling between NH (or ND) vibrations of neighbouring Me_3NH^+ ions. Spectra at any convenient H/D ratio may therefore be used for correlation of spectral and crystallographic features.

At 10 K the ND stretching fundamental ν(ND) was a very narrow ($\Delta\nu_{1/2} = 2.1$ cm^{-1} for the best mull, cf. Fig. 8) singlet at 2370.3(2) cm^{-1} (Fig. 9*A*). The adjacent small peaks correspond to overtone and combination levels of Me_3ND^+. They appear to borrow some, possibly most, of their intensity from ν(ND) through moderately weak FR. Since Me_3ND^+ has 36 fundamental internal vibrations and hence 666 binary overtone and combination levels, in principle all of them distinct, matching of minor spectral features with specific band assignments seemed subject to considerable ambiguity and was not

Can. J. Chem. Downloaded from www.nrcresearchpress.com by 210.87.254.105 on 09/06/12
For personal use only.

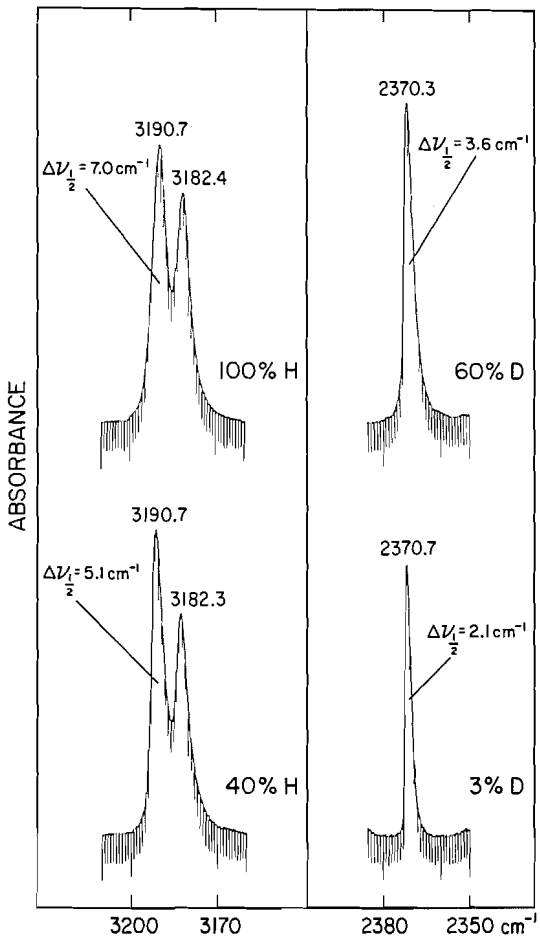

FIG. 8. Effect of isotopic dilution on the spectrum of 3MHS at 10 K, in the region of the NH (left) and ND (right) stretching fundamentals.

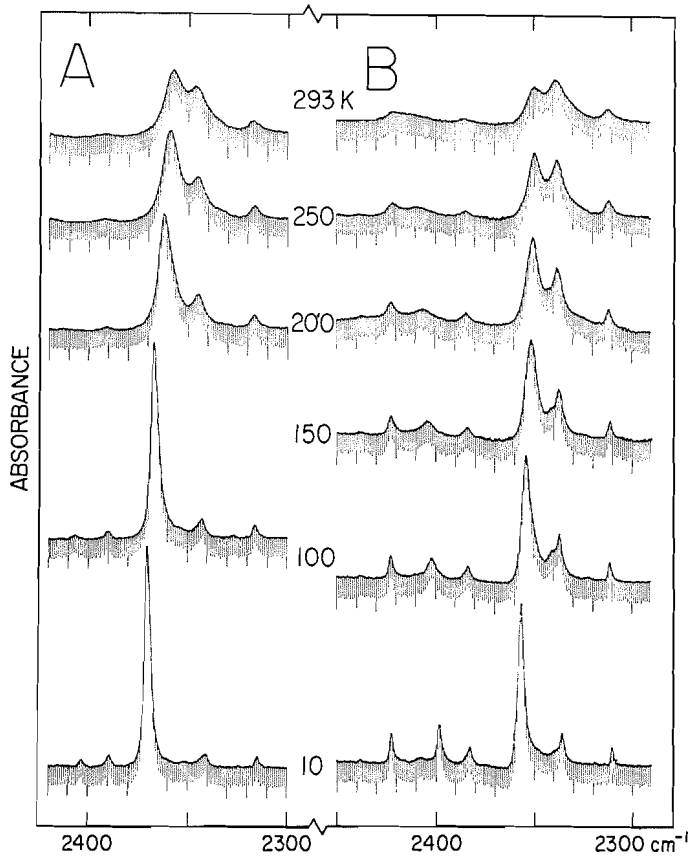

FIG. 9. The ND stretching fundamental of (*A*) $(Me_3NH)_2SnCl_6$ (3% D) and (*B*) $(Me_3NH)_2SnBr_6$ (18% D) at different temperatures.

attempted.

With increasing temperature ν(ND) gradually shifted to lower wavenumbers, while the small companion bands shifted, more slowly, to higher wavenumbers (Fig. 9*A*). As a result of this differential movement the overtone bands on the high-wavenumber side of ν(ND) kept losing intensity while those on the low-wavenumber side were growing. By the time room temperature was reached the now much broader ν(ND) was in close resonance with its nearest overtone neighbour on the low-wavenumber side, producing a doublet, at 2357.6(5) and 2347.7(6) cm^{-1}, with a 57:43 intensity ratio. The unperturbed position ν^0(ND) of the fundamental was calculated (see Experimental) to be 2353.3(9) cm^{-1}, with a FR constant $2W$ of 9.8 cm^{-1}. The position of the unperturbed ν(ND) had therefore shifted by −17.0(9) cm^{-1} on going from 10 to 293 K.

The NH stretching fundamental ν(NH) (Fig. 10*A*) started off at 10 K as a FR doublet, at 3190.7(2) and 3182.3(2) cm^{-1}, with an intensity ratio of 58:42. This corresponds to ν^0(NH) = 3186.5(3) cm^{-1} and $2W$ = 8.3 cm^{-1}. With increasing temperature ν(NH) gradually moved out of resonance. Between 80 and 200 K it was a singlet, in weak resonance with the neighbouring overtone levels. Above 200 K it began to approach closely the overtone on the low-wavenumber side and move steadily into close FR. The doublet observed at room temperature was at 3163(2) and 3157(2) cm^{-1}, with an intensity ratio of 51:49, corresponding to $2W$ = 6(2) cm^{-1}, ν^0(NH) = 3160(3) cm^{-1}, and a shift of −26(3) cm^{-1} on warming the sample from 10 K to room temperature.

$(Me_3NH)_2SnBr_6$ was examined mainly to see if its spectrum supported our interpretation of the 3MHS spectrum. This was found to be the case. The behaviour of the NH and ND stretching fundamentals was, except for details of FR, basically the same as in 3MHS, so even though the structure of the bromo compound has not been determined, it is reasonable to conclude that $(Me_3NH)_2SnBr_6$ is isostructural with 3MHS. As in the 3MHS case, the stretching bands were practically independent of the degree of deuteration.

The ν(ND) fundamental, which at 10 K was a narrow ($\Delta\nu_{1/2}$ = 3.5 cm^{-1}) singlet at 2356.8(2) cm^{-1} (Fig. 9*B*), with increasing temperature gradually entered into resonance with an overtone at about 2336 cm^{-1}, to become a close doublet near room temperature. The components of this resonance doublet at 293 K were at 2349.2(6) and 2338.2(6) cm^{-1}, with an intensity ratio of 45:55. From this we deduced ν^0(ND) = 2343.1(9) cm^{-1} and $2W$ = 11 cm^{-1} at 10 K; the temperature shift $\Delta\nu^0$(ND) from 10 to 293 K was −13.7(9) cm^{-1}.

The triplet observed in the NH stretching region at 10 K (Fig. 10*B*) consisted of a central ν(NH) peak at 3162.1(2) cm^{-1} and side peaks at 3177 and 3155 cm^{-1}, the latter two being overtones in moderately weak FR with ν(NH). On increasing the temperature ν(NH) shifted to lower wavenumbers and the intensity of the 3177 cm^{-1} peak gradually vanished, while that of the 3155 cm^{-1} peak increased. By ca. 220 K a 1:1 doublet (in full resonance, $2W$ = 9.5 cm^{-1}) was observed. At still higher temperatures the relative intensity of the low-wavenumber component increased, indicating that ν(NH) has now shifted past the position of the overtone and that the resonance was now decreasing. At room temperature the band was a broad

Can. J. Chem. Downloaded from www.nrcresearchpress.com by 210.87.254.105 on 09/06/12
For personal use only.

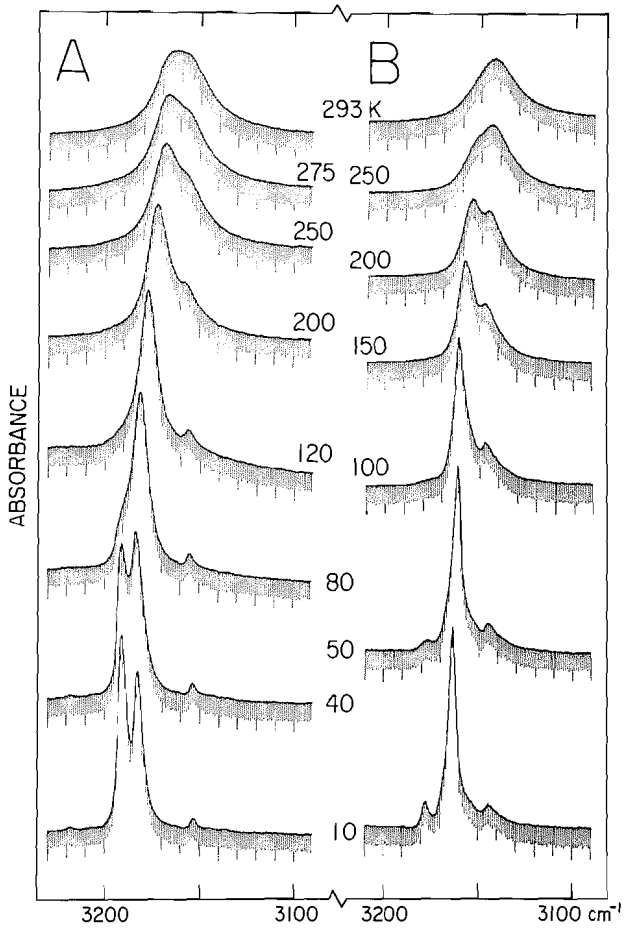

FIG. 10. The NH stretching fundamental of (*A*) $(Me_3NH)_2SnCl_6$ (0% D) and (*B*) $(Me_3NH)_2SnBr_6$ (0% D) at different temperatures.

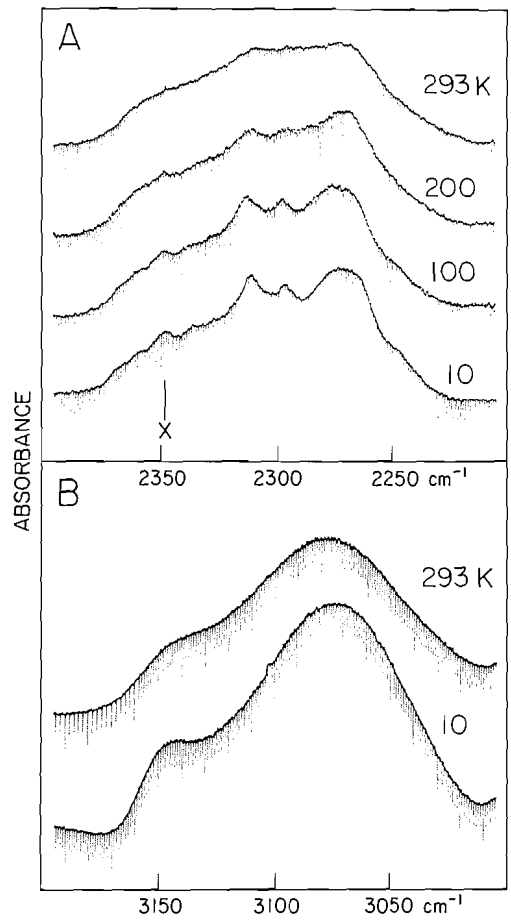

FIG. 11. The NH stretching fundamental of 3PHS (0% D) (*B*) and the ND stretching fundamental of 3PHS (68% D) (*A*) at different temperatures. The band marked X is present in the spectrum of the undeuterated compound.

singlet centred at 3142.0(8) cm^{-1}, hence the full temperature shift was $-20.1(8)$ cm^{-1}.

$(Et_3NH)_2SnCl_6$

Although the spectrum of 3EHS has already been reported (1), we return to it here in order to examine details of the FR. In this salt, too, coupling of the NH (or ND) stretching vibrations is virtually absent: ν(NH) was a singlet at all temperatures between 10 and 293 K. It shifted from 3117.8 at 10 K to 3109.7 cm^{-1} at 293 K, a total of $-8.1(5)$ cm^{-1}. The ND stretch was a Fermi doublet, with $2W = 24.2$ cm^{-1} and ν^0(ND) = 2317.0 and 2311.3 cm^{-1} at 10 and 293 K respectively. The total shift of $-5.3(7)$ cm^{-1} matches well the corresponding shift for ν(NH) derived directly from the spectra.

(n-$Pr_3NH)_2SnCl_6$

In this crystal the two nonequivalent N atoms at sites of C_1 symmetry ideally should give rise to two NH (or ND) stretching absorptions.

At 10 K the ND stretching fundamental consisted of three broad bands, centred at 2312(1), 2297(1), and 2273(2) cm^{-1} (Fig. 11*A*). The first two appeared to be the components of a Fermi doublet with an intensity ratio of 53:47. On this assumption $2W = 15$ cm^{-1} and ν^0(ND) = 2305(1) cm^{-1}. The band at 2273 cm^{-1} was much broader and positioned much lower than most of the ND fundamentals we have encountered in this work. It would thus appear to originate in a more strongly hydrogen-bonded ND group than that giving rise to the doublet; the only candidate is the highly asymmetrically bifurcated N(2)—H(2)···Cl(3) grouping, with H···Cl ~ 2.38 Å and NHCl ~ 150°. Increasing temperature gradually broadened all three bands, with only very small wavenumber shifts. At 293 K the resonance doublet had peak maxima at 2309(2) and 2295(2) cm^{-1} and an intensity ratio close to unity, yielding ν^0(ND) = 2302(2) cm^{-1} and an overall temperature shift of $-3(2)$ cm^{-1}. The corresponding position of the low-lying band was 2272(2) cm^{-1}, with a temperature shift of $-1(2)$ cm^{-1}.

The ν(NH) fundamental contained only two resolved features (Fig. 11*B*). The broad and intense band at 3074 cm^{-1} clearly is the counterpart of the 2273 cm^{-1} ND band (the isotopic ratio is 3074/2273 = 1.352). The 2312 cm^{-1} component of the ND doublet appears to have its counterpart in the NH band at ca. 3142 cm^{-1} at 10 K, the position of this band shifting slightly to lower wavenumbers with increasing temperature, ca. 3138 cm^{-1} at 293 K. The additional intensity between the bands at 3074 and 3142 cm^{-1} may correspond to the second component of the ND doublet. The NH bands were broader than the corresponding ND bands, and this resulted in a more severe overlap of the features in the NH stretching region and precluded a more accurate description of these features.

(n-$Bu_3NH)_2SnCl_6$

The crystal structure of 3BHS has not been determined. A preliminary survey of the spectra showed broad NH and ND bands strongly resembling those of 3PHS. The ND stretching fundamental at 10 K was centred at 2295(3) cm^{-1} and shifted

Can. J. Chem. Downloaded from www.nrcresearchpress.com by 210.87.254.105 on 09/06/12
For personal use only.

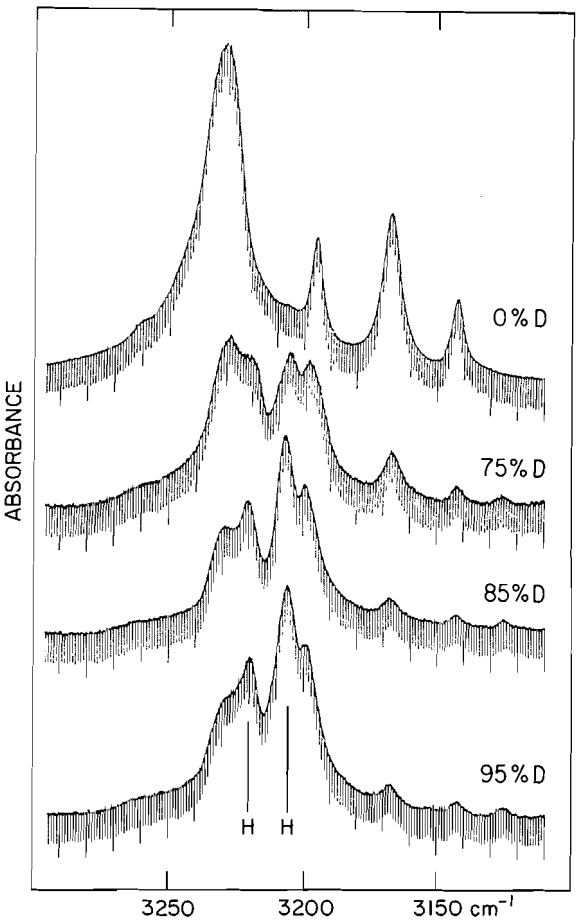

FIG. 12. Effect of isotopic dilution on the spectrum of 1MHS at 10 K, in the region of the NH stretching fundamental. The bands marked H are due to the $MeNHD_2^+$ probe ion.

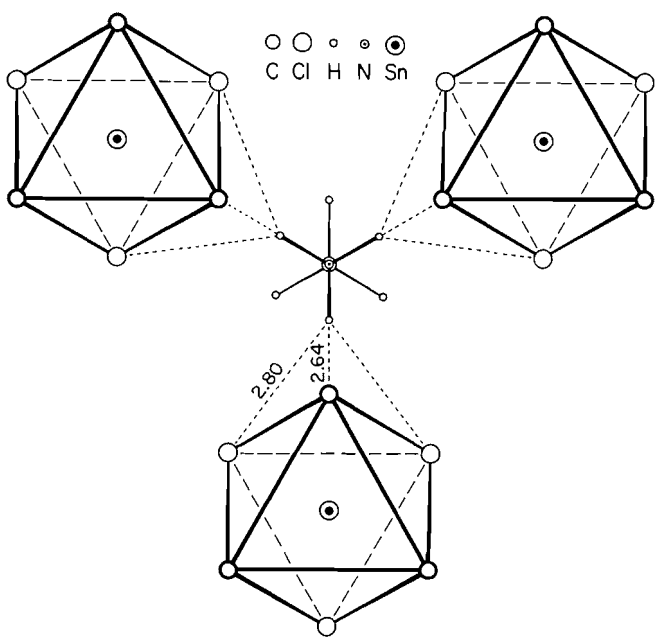

FIG. 13. Hydrogen bonding in 1MHS (after ref. 6). Projection on 0001 of the hexagonal unit cell. The C atom is eclipsed by the N atom.

by $-3(7)$ cm^{-1} to 2292(7) cm^{-1} at 293 K. The ν(NH) fundamental centred at 3082(2) cm^{-1} at 10 K and 3073(3) cm^{-1} at

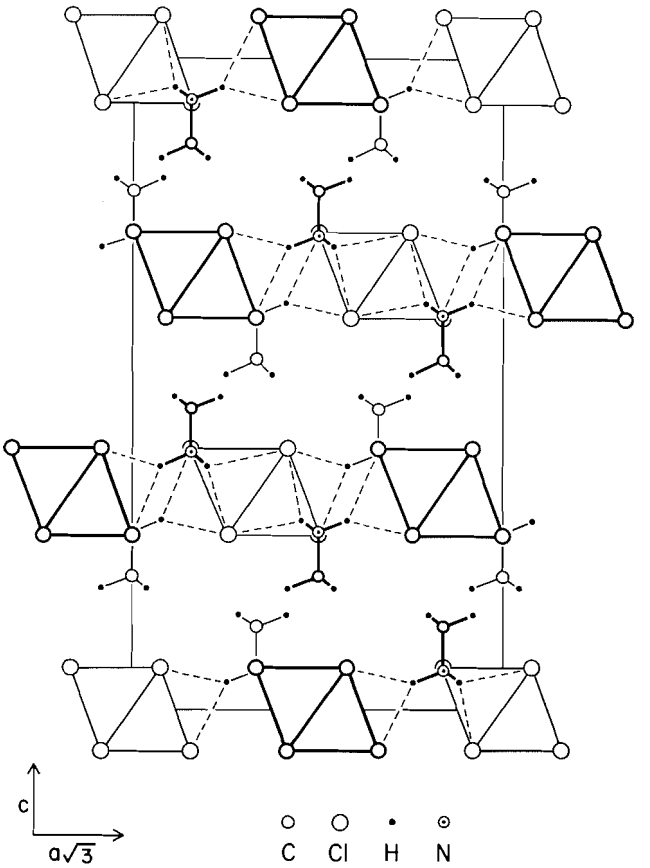

FIG. 14. Two-dimensional hydrogen-bonding networks in the $MeNH_3\cdots Cl_3SnCl_3\cdots H_3NMe$ layers of the 1MHS structure (based on ref. 6). Projection on $11\bar{2}0$.

293 K, which yields an overall shift of $-9(4)$ cm^{-1}.

Monoalkylammonium salts

The band shapes of the NH and ND stretching fundamentals of 1RHS were highly dependent on the degree of deuteration (Fig. 12). This is largely due to the coupling of H (or D) motions *within* the cations: the spectrum in the NH region is derived from the NH groups of the RNH_3^+, RNH_2D^+, and $RNHD_2^+$ ions, and that in the ND region contains contributions from the ND groups of the RND_3^+, $RNHD_2^+$, and RNH_2D^+ ions, the relative intensities of the individual absorptions varying with the D content of the sample. Isotopic dilution was thus required to obtain structurally useful information on individual hydrogens.

$(MeNH_3)_2SnCl_6$

In this crystal ($R\bar{3}m$, single type of $MeNH_3^+$), the site symmetry at the N atom is C_{3v} both at room temperature and at 120 K (i.e. below the temperature of the only transition detected between 20 and 300 K, 154.3 K) (6, 16–18). The H atoms could not be located in the difference Fourier maps, but the three equivalent N$\cdots$Cl distances of 3.46 Å and the six equivalent N$\cdots$C distances of 3.59 Å (all at room temperature), together with the assumption of staggered cation conformation and of tetrahedral CNH angles, lead to the supposition (6) that the three hydrogens engage in trifurcated N—H$\cdots$3Cl bonds (Figs. 13 and 14). These bonds are nearly symmetric, H$\cdots$Cl = 2.64 Å (1×) and 2.80 Å (2×), NHCl = 136° (1×) and 133° (2×) if d(N—H) is taken to be 1.02 Å. The spectroscopic expectation for the $MeNH_2D^+$ probe ion would thus be a single

Can. J. Chem. Downloaded from www.nrcresearchpress.com by 210.87.254.105 on 09/06/12
For personal use only.

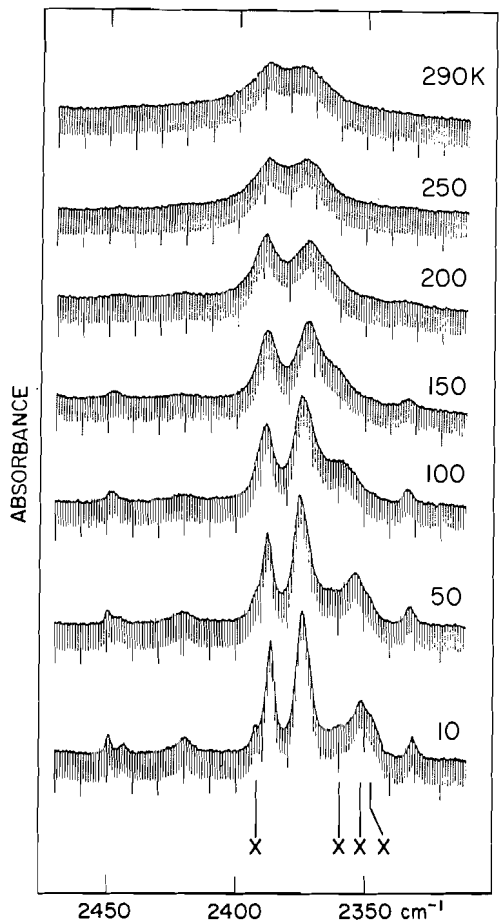

FIG. 15. The ND stretching fundamental of 1MHS (2% D) at different temperatures. Bands marked X occur also in the spectrum of the undeuterated compound.

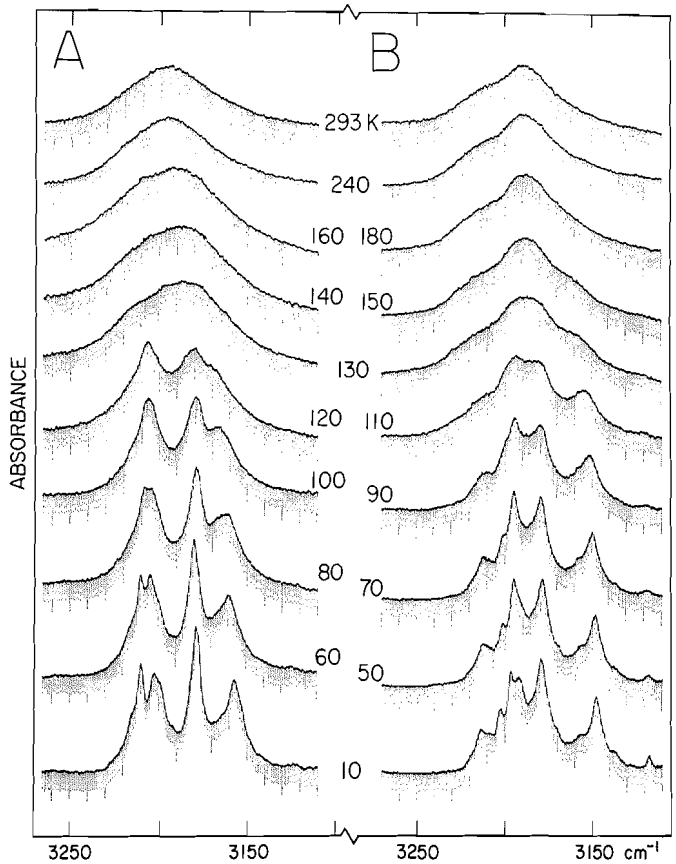

FIG. 16. The NH stretching fundamentals of (*A*) 1EHS (90% D) and (*B*) 1PHS (90% D) at different temperatures.

ND stretching absorption. Its frequency should decrease with increasing temperature, but perhaps not in the same way as in 3MHS and $(NH_4)_2SnCl_6$ because of the different librational mobility of the $MeNH_3^+$ ion and the possible torsional–oscillatory interaction of the NH_3 and CH_3 groups (cf., for example, ref. 19).

The spectrum of $MeNH_2D^+$ in 1MHS (2% D) at 10 K (Fig. 15) contained in the ND stretching region a doublet at 2386.7(2) and 2374.6(3) cm^{-1}, with an intensity ratio of 31:69. Assuming that the doublet is due to FR, $\nu^0(ND)$ = 2378(1) cm^{-1}, $2W$ = 11.2 cm^{-1}.[5] The four small peaks nearby (at 2449.5, 2443.3, 2419.5, and 2331.0 cm^{-1}) are clearly due to overtone and combination levels in much weaker resonance with ν(ND). Temperature increase had only a minor effect on the spectral features: $\nu^0(ND)$ at 293 K is 2381(2) cm^{-1}, which yields 3(2) cm^{-1} for the total shift between 10 and 293 K, an uncertain but apparently positive value. There was no indication in the spectra of any phase transition.

The NH stretching fundamental of the $MeNHD_2^+$ probe ion at high D levels also was a doublet (Fig. 12), with components at 3220.3(2) and 3206.0(2) cm^{-1} and an intensity ratio of 40:60 at 10 K. Assuming it to be a Fermi doublet, $\nu^0(NH)$ = 3211.5(8) cm^{-1} and $2W$ = 13.4 cm^{-1}. Increasing temperature brought only a gradual broadening of the bands, with almost no change in the positions or intensities of the doublet components.

$(EtNH_3)_2SnCl_6$

The space group $P\bar{3}m1$ of 1EHS at room temperature is only statistical. The local symmetry at a N atom in the orientationally disordered structure is effectively no higher than C_s (with H—N—C(1)—C(2) in the mirror plane) and strictly only C_1. The expected NH (or ND) stretching absorption of the $EtNHD_2^+$ (or $EtNH_2D^+$) probe ion will depend on how strongly the CH_3 group affects the NH stretching vibration. In principle the stretching band is expected to be a 2:1 doublet, unresolved if the effect of the CH_3 on the equivalence of the three N-hydrogens is small, resolved (though probably closely spaced) if the effect is appreciable.

At 10 K the ν(NH) fundamental of $EtNHD_2^+$ consisted of four well-separated peaks at 3210.2(2), 3202.3(4), 3178.6(2), and 3157.1(4) cm^{-1}, plus at least two other, partially resolved, features (Fig. 16*A*). This multiplet is probably too wide and too complex to be the result of only one stretching fundamental in resonance with a number of overtone or combination levels. The distribution of ir absorption intensity is consistent with at least three and probably six distinct NH fundamentals, possibly with minor complications from FR. The changes in the band shapes from 10 to 125 K were gradual. Several of the features of the 10 K spectrum broadened and eventually coalesced, and the 3202 and 3211 cm^{-1} bands underwent a thermal collapse analogous to that observed recently in the spectra of $(NH_4)_2Cr_2O_7$ (22).

[5]For the presumably isostructural $(MeNH_3)_2PtCl_6$ the corresponding $\nu^0(ND)$ estimate is 2375 cm^{-1} (20). References 20 and 21 contain further spectroscopic results on the $MeNH_3^+$ ion, including a normal-coordinate analysis in C_{3v} symmetry.

Can. J. Chem. Downloaded from www.nrcresearchpress.com by 210.87.254.105 on 09/06/12
For personal use only.

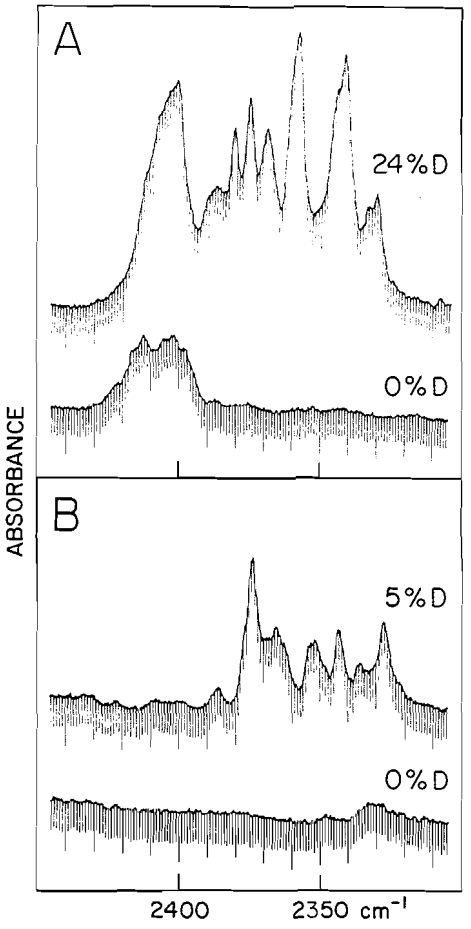

FIG. 17. The ND stretching fundamentals of (*A*) 1EHS (24% D) and (*B*) 1PHS (5% D) at 10 K, with their respective 0% D baselines.

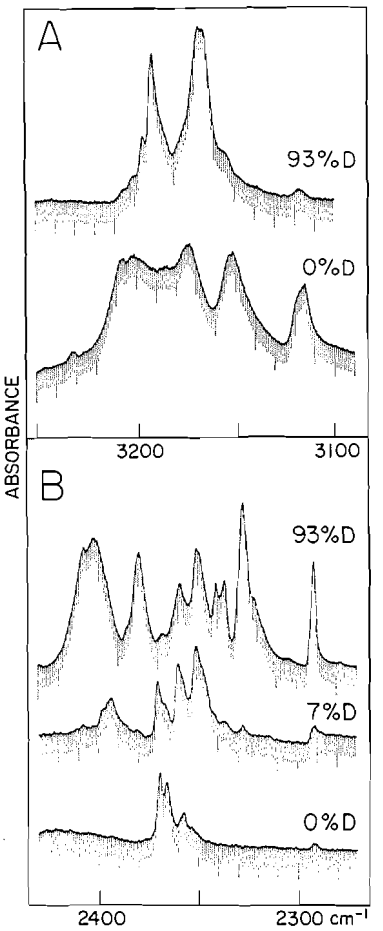

FIG. 18. Effect of isotopic dilution on the spectrum of 2MHS at 10 K in the region of the NH (*A*) and ND (*B*) stretching fundamentals.

At 125(5) K the ν(NH) multiplet changed sharply into a symmetric singlet ($\Delta\nu_{1/2}$ = 50 cm^{-1}). This change appears to correspond to a transition to a high-temperature phase in which the three N-hydrogens of a cation, nonequivalent at low temperatures, are statistically equivalent. The ν(NH) singlet in the high-temperature phase shifted from 3186(2) cm^{-1} at 130 K to 3196(2) cm^{-1} at 293 K.

The corresponding ND stretching region in the spectrum of the $EtNH_2D^+$ probe ion (Fig. 17*A*) is complicated by the strong background absorption of the undeuterated species as well as by FR.

(n-PrNH$_3$)$_2$SnCl$_6$

The hydrogens of the two nonequivalent N atoms (each of symmetry C_1) all engage in bifurcated or trifurcated N—H···Cl bonds, with H···Cl distances ranging from 2.44 to 3.16 Å (Table 11). The ν(ND) stretching fundamental of the *n*-$PrNH_2D^+$ probe ion would therefore be expected to consist of six components, with frequencies of the same order as that of $\nu_1(NH_3D^+)$ in $(NH_4)_2SnCl_6$, ~2375 cm^{-1}.

The spectrum of the *n*-$PrNH_2D^+$ ion at low D concentration at 10 K contained a complex absorption in the ND stretching region, with at least ten peak ranging from 2386 to 2327 cm^{-1} (Fig. 17*B*). As in the case of 1EHS, we seem to be dealing here with six ND fundamentals plus complications from FR and baseline absorption. However, in contrast to 1EHS, the spectral features — largely broadening and coalescence of most bands — changed with increasing temperature gradually, with no evidence of a phase transition below room temperature.

The 10 K spectrum of the *n*-$PrNHD_2^+$ ion at high D concentration corresponded, in the NH stretching region, more closely to the expected six components. The peak centres ranged from 3213.5(7) to 3147.6(3) cm^{-1} (Fig. 16*B*). As the the temperature increased, these features broadened and some partially coalesced, but at least two distinct features remained even at room temperature. There was no evidence of any sharp spectral change that might indicate a phase transition.

Dialkylammonium salts

As in the case of 1RHS, the band shapes of the NH and ND stretching fundamentals of the dialkyl salts were found to depend strongly on the degree of deuteration of the sample (Fig. 18) and isotopic dilution had to be resorted to.

(Me$_2$NH$_2$)$_2$SnCl$_6$

The C_s site symmetry of the N atoms and the equivalence of the two bifurcated N—H···2Cl bonds in the room-temperature structure lead to the expectation, ideally, of single NH and ND absorptions with frequencies which will decrease with increasing temperature.

The NH stretching fundamental of the Me_2NHD^+ probe ion at 10 K consisted of a doublet at 3191.1(2) and 3167.6(4) cm^{-1} (Fig. 19*A*). An additional feature, at 3165.8(6) cm^{-1}, was present at 10 K but disappeared by 50 K. Increasing temperature gradually reduced the doublet spacing until at 100 K only a singlet, at 3185.2(8) cm^{-1}, was observed. Above that temperature, which appears to correspond to a transition, the singlet gradually moved to lower wavenumbers and at 293 K ended up at 3181.7(8) cm^{-1}.

Can. J. Chem. Downloaded from www.nrcresearchpress.com by 210.87.254.105 on 09/06/12
For personal use only.

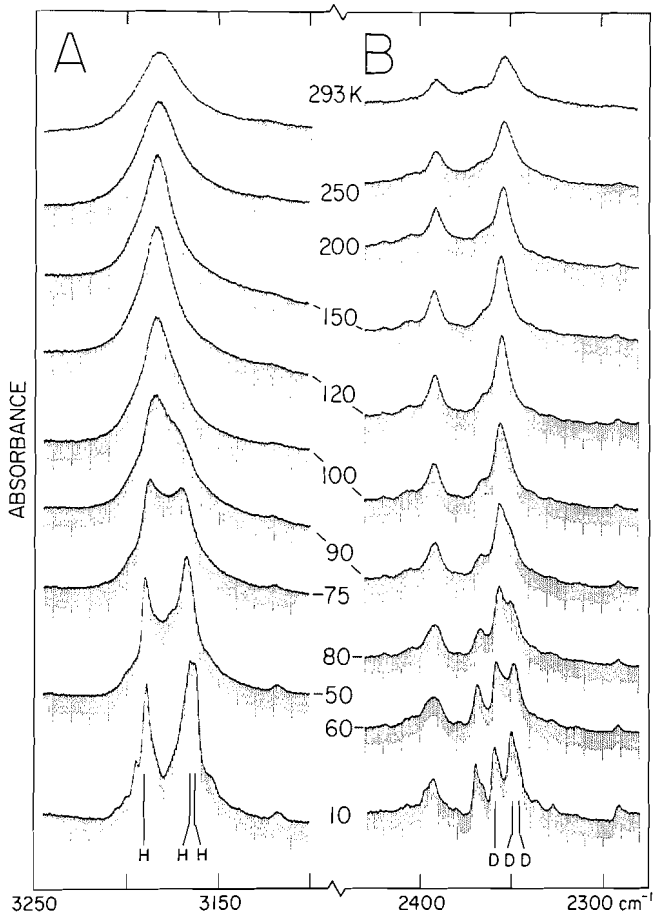

FIG. 19. The NH stretching fundamental of 2MHS (93% D) (*A*) and the ND stretching fundamental of 2MHS (9% D) (*B*) at different temperatures. Only the bands marked H and D are due to the Me_2NHD^+ probe ion.

The corresponding ND stretching fundamental also was essentially a doublet at low temperatures, with main components at 2359.2(3) and 2350.0(3) cm^{-1} (Fig. 18*B*). The additional small ND feature, at 2347.4(8) cm^{-1} at 10 K, was absent above 40 K. Bands at 2370 and 2366 cm^{-1} belong to the main isotopic species $Me_2NH_2^+$, while those at 2398, 2393, 2337, and 2327 cm^{-1} probably originated in a small amount of the $Me_2ND_2^+$ species. With increasing temperature the doublet collapsed, at first gradually and then sharply, to a singlet at 2355.7(4) cm^{-1} at 100 K. This singlet then slowly shifted to 2352.6(10) cm^{-1} at 293 K (Fig. 19*B*). These changes are entirely analogous to those in ν(NH).

The evolution with temperature (Fig. 20) seems to indicate that below 100 K two types of N-hydrogens are present, with different environments. The gradual collapse of the doublet below this temperature is remarkably similar to that observed for $(NH_4)_2SnBr_6$ (Fig. 10 of ref. 23). The sharp emergence of a singlet at ca. 100 K then corresponds to a transition in which the two hydrogens become equivalent.

The cause of the additional doubling of the lower-wavenumber component between 10 and 40 K is either FR or — more likely, as it occurs for both ν(NH) and ν(ND) — the nonequivalence of two types of $Me_2NH_2^+$ ions.

$(Et_2NH_2)_2SnCl_6$

The crystal structure of 2EHS (C_{2h}, ref. 24) has not yet been determined. The NH and ND stretching fundamentals of the Et_2NHD^+ probe ion at 10 K (Fig. 21) showed a marked resemblance to the corresponding spectra of 2MHS: ν(NH) consisted mainly of a doublet at 3146.9(3) and 3117.4(3) cm^{-1}, with two weaker bands at lower wavenumbers, possibly due to overtone levels enhanced by FR. The corresponding ND stretching fundamental (Fig. 21*B*) also was a doublet, at 2325.5(3) and 2313.5(3) cm^{-1}, the additional bands being mostly accounted for as due to $Et_2NH_2^+$ and small amounts of $Et_2ND_2^+$. Some minor extra features may be due to Et_2NHD^+ through FR.

As in the case of 2MHS, the doublets seem to correspond to a loss of equivalence of the NH_2 hydrogens, but the reason for the greater intensity of the high-wavenumber component is not clear.

Both doublets underwent a gradual collapse as the temperature was raised (Fig. 20). Unlike for 2MHS, however, this process was continuous up to room temperature. The evolution with temperature points to the existence of a transition in the vicinity of 330 K.

(n-$Pr_2NH_2)_2SnCl_6$

The crystal structure of 2PHS is not yet known. Ries (12) reported the crystal symmetry of the chloroplatinate and the bromoplatinate (dimorphic) to be C_{2h}.

The spectrum of our preparation was unusual. The undeuterated material had bands at 3220 and 3100 cm^{-1} which match similar doublets in the spectra of 2MHS and 2EHS and are due to the antisymmetric and symmetric stretching of NH_2 groups. However, in addition to this absorption in the accustomed region the spectrum also exhibited an intense absorption (*Y* in Fig. 22) with the main peak at 2780 cm^{-1}. This is 300–400 cm^{-1} below the NH stretching fundamentals of the other hexachlorostannates examined, the spectra of the latter showing in this region only weak bands due to binary combinations of CH deformation modes.

On deuteration the intensity of band *Y* and that of the "regular" NH stretching absorptions decreased (Fig. 22). This reduction of intensity was accompanied by the appearance of one group of bands in the 2360–2200 cm^{-1} region (corresponding to "regular" ND stretching) and another, equally intense, in the 2160–2020 cm^{-1} region (*Z* in Fig. 22). The latter group is clearly the ND stretching analog of the *Y* bands. The changes produced by deuteration indicate that *Y* and *Z* owe their intensities to NH and ND stretching, respectively. Their frequencies are comparable to those of the NH and ND stretching modes in Et_3NHCl, in which the unique, straight N—H···Cl bond is much shorter than the N—H···Cl bonds in the alkylammonium hexachlorostannates (results to be published and ref. 25; unpublished work by R. C. Lord quoted in ref. 26; ref. 27).

These spectral features were sufficiently unexpected to warrant a closer look at the identity of our presumed 2PHS preparation (see Experimental). A crystal-structure determination, intially not contemplated at this stage, revealed the product to be not 2PHS but the "adduct" of 2PHS and *n*-Pr_2NH_2Cl, $(n\text{-}Pr_2NH_2)_3(SnCl_6)Cl$. The implications of this finding will be reported elsewhere.

Discussion

Infrared spectra

Low-temperature transitions

The existence of low-temperature transitions in 2MHS (T_{tr} ~ 100 K), 2EHS (T_{tr} ~ 330 K), and 1EHS (T_{tr} ~ 125 K) is recognizable from a clear change in the appearance of the NH

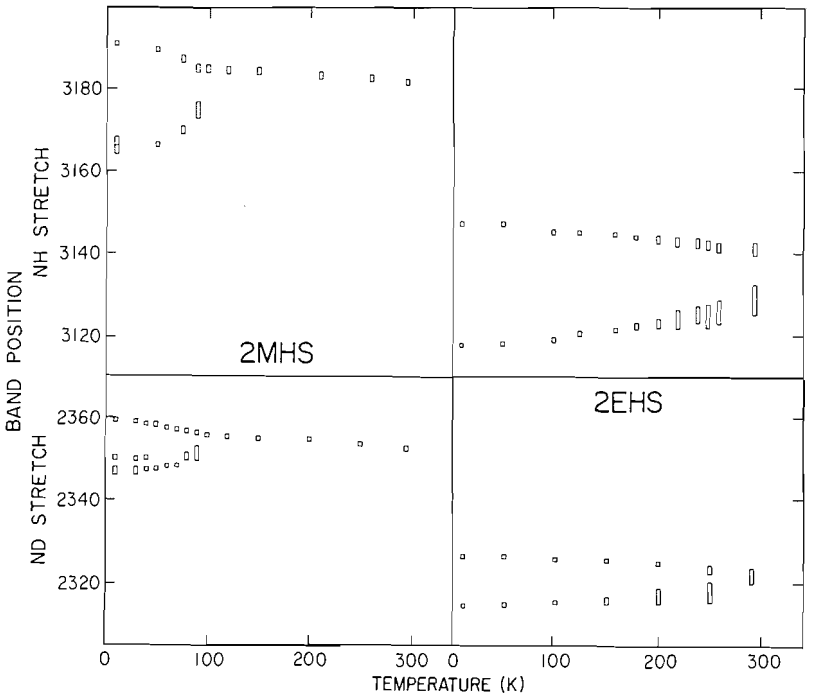

FIG. 20. Positions of the absorption maxima vs. temperature for 2MHS (from Fig. 19) and 2EHS (from Fig. 21).

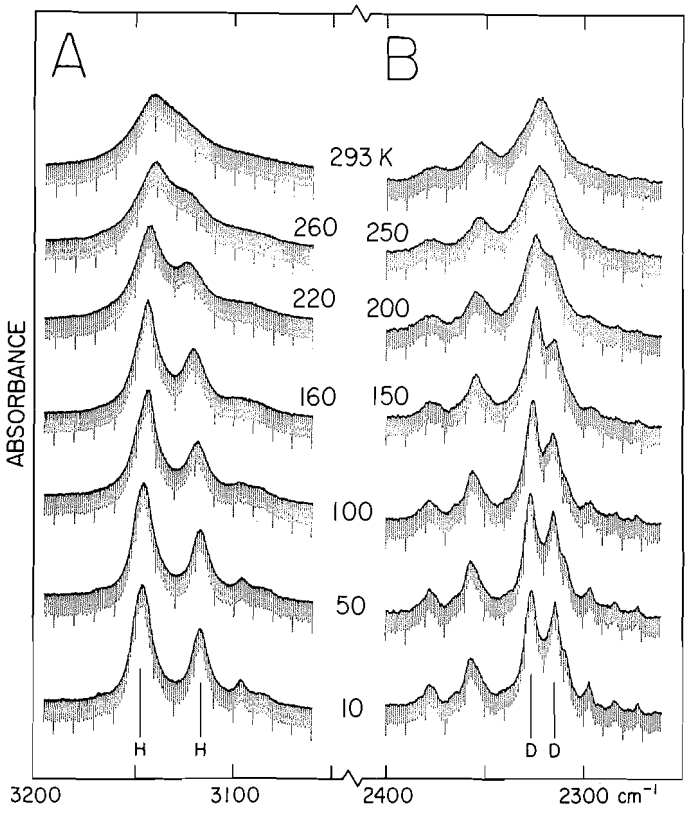

FIG. 21. The NH and ND stretching fundamentals of 2EHS at different temperatures. (*A*) 2EHS (95% D); (*B*) 2EHS (11% D). Only the features marked H and D are due to the Et_2NHD^+ probe ion.

and ND absorptions in each of the spectra (Figs. 16*A*, 17, and 20).[6] None of these transitions seems to have been reported previously. No indication of low-temperature transitions between 10 and 293 K was discernible in the spectra of 1MHS, 1PHS, and 3MHS. The spectra of 2PHS and 2BHS were inconclusive in this respect.

1MHS. It is not surprising that the transition at 154.3 K detected in 1MHS by ^{35}Cl nqr (16) and by calorimetric and ir (18) as well as crystallographic (6) measurements was not observed in our NH and ND stretching spectra.[7] This transition is of a subtle and unusual nature: it occurs between phases of the same space-group symmetry, without doubling of the unit cell, and manifests itself crystallographically by a discontinuity in the temperature variation of c (Fig. 23). At the same time the Cl spin–lattice relaxation time decreases sharply as T_{tr} is approached from either side, but the proton relaxation time and its second moment remain practically unaffected (28). Only one ^{35}Cl resonance was present on either side of T_{tr}, hence all Cl atoms are crystallographically equivalent in both phases (16). The total ΔS_{tr}, $1.60(18)R$, is large enough for a transition of the order–disorder type, and the critical properties also are consistent with an order–disorder mechanism (18). It is suggested (18) that the reorientational motion of the $CH_3NH_3^+$ ion changes at T_{tr} from a weakly-hindered rotation at $T > T_{tr}$ to a more restricted motion at $T < T_{tr}$, but beyond this the nature and cause of the transition remain unexplained.

1EHS. The transition in this compound is almost certainly associated with orientational ordering of the Et groups. In that case the orientational disorder at $T > T_{tr}$ must be dynamic rather than frozen-in static, as cooling would be unlikely to produce an ordered arrangement from a disorder which already is frozen in at room temperature.

2RHS. The transitions in 2MHS and 2EHS appear to be of the same type (Fig. 20). The doublet produced from the single stretching absorption in 2MHS on cooling consists of a high-frequency component only slightly above the singlet absorp-

[6]Spectroscopic evidence of a transition at ~180 K in $(n\text{-}Pr_2NH_2)_3(SnCl_6)Cl$ will be discussed elsewhere.

[7]Similarly, no changes attributable to the transition in the vicinity of 125 K (16) were observed in the spectra of $(MeNH_3)_2PtCl_6$ (20).

Can. J. Chem. Downloaded from www.nrcresearchpress.com by 210.87.254.105 on 09/06/12
For personal use only.

Can. J. Chem. Downloaded from www.nrcresearchpress.com by 210.87.254.105 on 09/06/12
For personal use only.

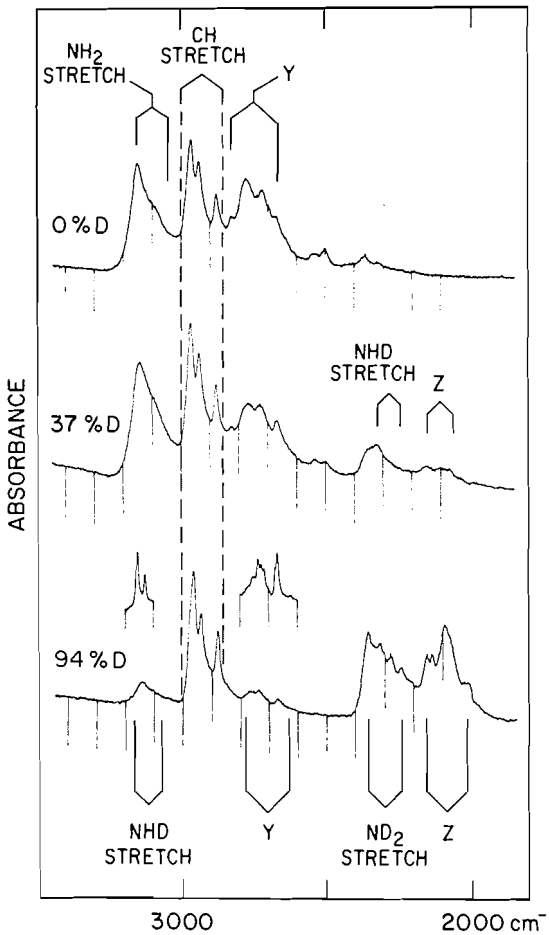

FIG. 22. Spectra of "2PHS" (= $(n\text{-}Pr_2NH_2)_3(SnCl_6)Cl$) in the region of NH and ND stretching fundamentals (fluorocarbon mulls at room temperature). For bands marked *Y* and *Z* see text. The two inserts refer to the 94% D sample at 10 K.

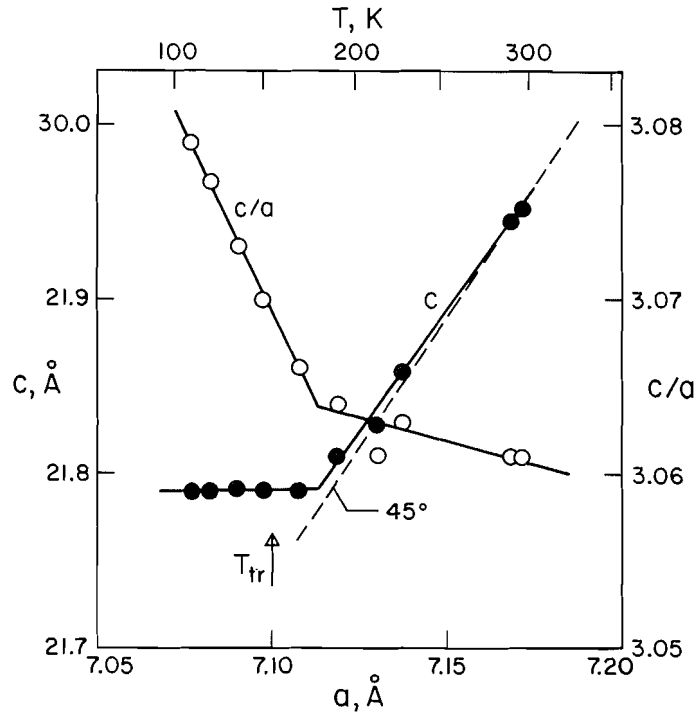

FIG. 23. Variation of the unit-cell dimensions and the axial ratio of 1MHS with temperature (data taken from ref. 6).

tion, and a low-frequency component noticeably below the original singlet. In 2EHS the transition does not take place within the temperature interval studied, but otherwise the evolution of ν with T is similar. In 2MHS, where the room-temperature structure is well established, the transition appears to destroy the equivalence of the N-hydrogens. This could be achieved either by reducing the C_s symmetry of the cation in the upper phase to C_1, or by splitting the original set of $Me_2NH_2^+$ ions into two subsets (both with site symmetry C_s or C_2, or one with C_s and the other with C_2), but in any event cooling through T_{tr} results in a strengthening of some (probably half) of the N—H···Cl bonds, all of which are undifferentiated at $T > T_{tr}$. An analogous situation may exist in 2EHS, except that the strengthening must be present already in the room-temperature structure. The spectrum of this salt will be discussed further when we have completed the crystal-structure determination now in progress.

Hydrogen bonding

The variation, with composition, of the isolated (and Fermi-unperturbed) ND stretching frequency at 10 K is shown in Fig. 24; the NH stretching frequency varies in an analogous manner. The complications due to FR, to the existence of low-temperature transitions and to the presence of extraneous features in the NH and ND stretching regions preclude clear-cut general statements about the effect of alkyl substitution in the ammonium ion on the strength of hydrogen bonding. In fact, almost all the information which can be extracted from the ND spectra of Fig. 24 could have been obtained by inspection from the NH stretching fundamentals of the undeuterated samples. This is an important — and not advantageous — difference from the situation in ammonium compounds, where isotopic dilution in most cases is essential.

The range of the ν(ND) fundamental in compounds investigated[8] is about 2380–2270 cm^{-1}, i.e. not above $\nu_1(NH_3D^+)$ of $(NH_4)_2SnCl_6$ (4). Insofar as one can speak of discernible trends in this group of spectra, the least ambiguous indication of a trend is present in the 3RHS series. Both ν(NH) and ν(ND) decrease with the increasing mean linear unit-cell dimension $\bar{a} = (V/Z)^{1/3}$ (Fig. 25). The decrease is steep from Me to Et but levels off after Et and seems to tend to a steady value in the vicinity of 2300 cm^{-1} for ν(ND) and 3080 cm^{-1} for ν(NH). This steady value for ν(ND) is in the general region of the extrapolated "free-ion" $\nu_1(NH_3D^+)$ value in ammonium halides (13).

The variation of ν(NH) and ν(ND) of 3RHS with temperature merits attention. For NH_4 compounds containing symmetrically trifurcated hydrogen bonds a plot of the difference $\Delta\nu_1(NH_3D^+) = \nu_1(10\text{ K}) - \nu_1(293\text{ K})$ vs. d(H···X) (Fig. 8 of ref. 4) revealed a quasiexponential correlation: the shorter the trifurcated H···X distance in this common-cation, variable-anion series, the larger $\Delta\nu_1(NH_3D^+)$, i.e. the more pronounced the decrease of ν(ND) with increasing temperature. A corresponding plot for the variable-cation, common-anion 3RHS series cannot be produced because of the ambiguity in choosing the appropriate d(H···X) when the trifurcation is asymmetric or the hydrogen-bonding geometry even more dissimilar. Furthermore, d(H···X) spans a much narrower range in the 3RHS

[8]Disregarding the lower-frequency group of ND absorptions in $(n\text{-}Pr_2NH_2)_3(SnCl_6)Cl$ (initially taken for 2PHS). This group originates in H···Cl^- interactions.

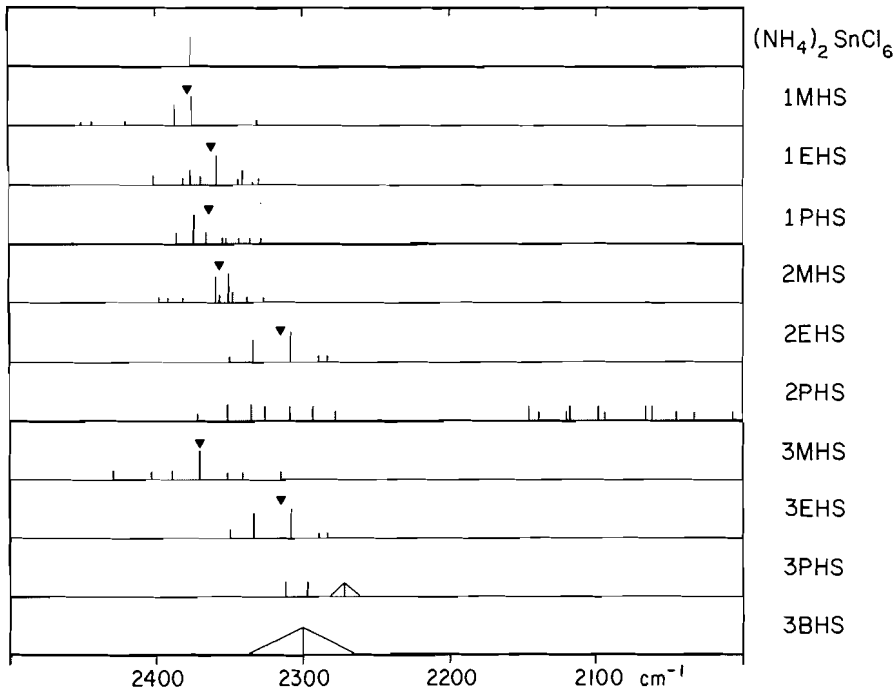

FIG. 24. Synoptic presentation of the ND stretching absorptions at 10 K. Triangles indicate the calculated positions of ND stretching fundamentals unperturbed by Fermi resonance. 2PHS in reality refers to $(n\text{-}Pr_2NH_2)_3(SnCl_6)Cl$ (see text).

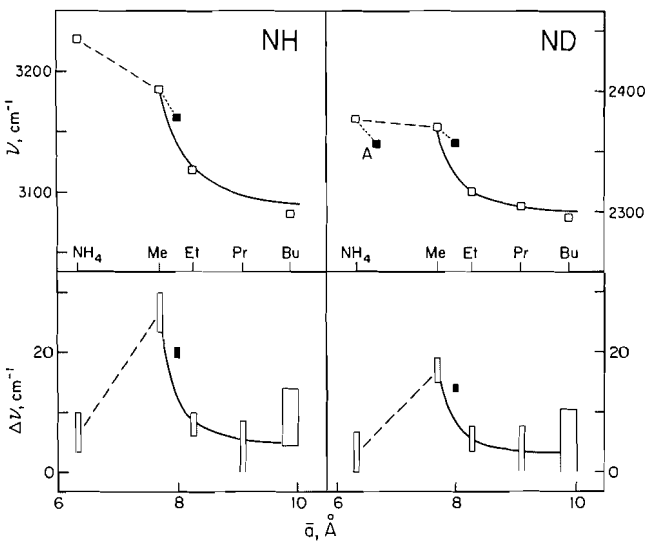

FIG. 25. Variation of ν(NH) and ν(ND) (top) and $\Delta\nu = \nu(10\text{ K}) - \nu(293\text{ K})$ (NH and ND) (bottom) of 3RHS with the mean linear unit-cell dimension $\bar{a}$. Open rectangles, 3RHS; full rectangles, $(Me_3NH)_2SnBr_6$; *A*, $(NH_4)_2SnBr_6$. The $\bar{a}$(3BHS) value is estimated.

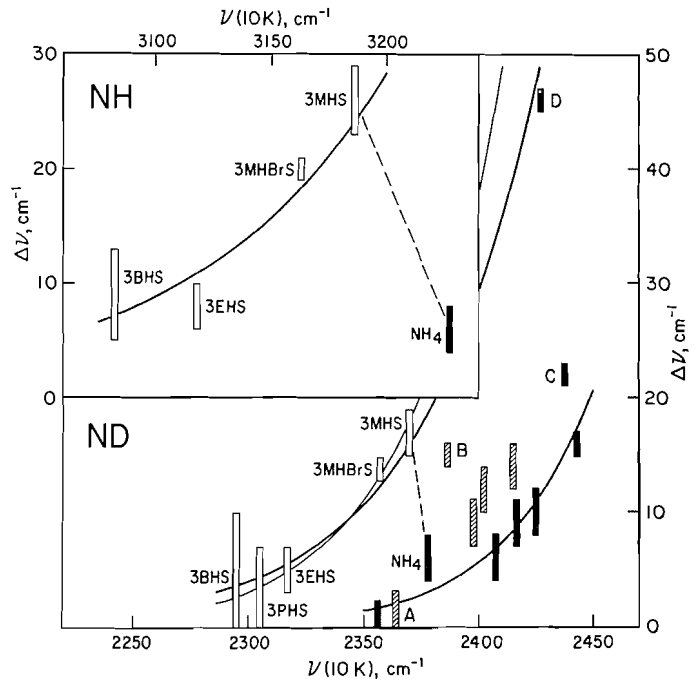

FIG. 26. Variation of $\Delta\nu = \nu(10\text{ K}) - \nu(293\text{ K})$ (NH and ND) of 3RHS (open rectangles) with ν(NH) and ν(ND). Ammonium compounds containing symmetrically (full rectangles) and asymmetrically (shaded rectangles) trifurcated N—H···X bonds are included for comparison. *A*, NH_4BPh_4 (58); *B*, bifurcated N—H···2O bond in taurine (29); *C*, NH_4CuSO_3 (4); *D*, NH_4SnF_3 (4); 3MHBrS = $(Me_3NH)_2SnBr_6$. A reliable ν(NH) value for 3PHS could not be established.

than in the NH_4 series (2.2–2.9 Å) and a local variation due to causes specific to a particular 3RHS structure might, in a narrow d(H···X) range, be mistaken for a general trend. However, a $\Delta\nu$ vs. $\bar{a}$ plot (Fig. 25) shows a trend similar to that for ν vs. $\bar{a}$, i.e. indicative of an overall volume effect, with a monotonic variation for 3RHS but a strikingly different behaviour for $(NH_4)_2SnCl_6$.

The similarity of the variation of $\Delta\nu$ and that of ν with $\bar{a}$ suggests that the intermediary of the external dimensional parameter can be eliminated by relating the quantities derived from the spectra alone, viz. by plotting $\Delta\nu$ against ν. In this plot (Fig. 26) $(NH_4)_2SnCl_6$ again occupies a special position, but the ν(ND) points for 3RHS show a clear trend in that $\Delta\nu$ increases with ν. $(Me_3NH)_2SnBr_6$ fits in this series in spite of the difference in anion. For ν(NH) the trend is less convincing because of the absence of a point for 3PHS (see above) in

Can. J. Chem. Downloaded from www.nrcresearchpress.com by 210.87.254.105 on 09/06/12
For personal use only.

Can. J. Chem. Downloaded from www.nrcresearchpress.com by 210.87.254.105 on 09/06/12
For personal use only.

conjunction with the large uncertainty in $\Delta\nu$(3BHS). However, the existence of the trend is supported by the features of the corresponding $\Delta\nu$ vs. ν plot for ammonium compounds included for comparison in Fig. 26. This plot contains all the NH_4 compounds involving symmetrically trifurcated N—H···X bonds for which the isotopically isolated $\nu_1(NH_3D^+)$ (i.e. ν(ND)) frequency is known, plus a few instances of N—H···X bonds which are trifurcated but not symmetrically, and also the asymmetrically bifurcated N—H···2O bond in taurine. In spite of the variety of anions the same trend as in the 3RHS series is observed — a clear increase of $\Delta\nu$(ND) with ν(ND). Since the ν(ND) values of the NH_4 compounds fall in a higher wavenumber region, the point for $(NH_4)_2SnCl_6$ occupies its natural place in this series.

These observations can be summarized as follows: ν increases with decreasing $\bar{a}$ both for 3RHS and NH_4 compounds, and $\Delta\nu$ increases with ν in both groups. The explanation of the increase of ν with decreasing $\bar{a}$ in these ionic crystals is to be looked for in the effect on ν of the dominance of the Coulombic lattice compression and economy of packing over that of an increase in the acceptor strength of X, the two effects working in opposite directions. The existence of this overcompensation is well documented for cubic $(NH_4)_2MX_6$, all of which contain symmetrically trifurcated N—H···3X bonds (13, 29). In 3MHS and 3EHS hydrogen bonds connect each anion with two cations to form quasi-electroneutral units, thus giving rise to a "molecular" $[R_3NH\cdots Cl_3SnCl_3\cdots HNR_3]$ crystal. In such crystals one might expect the H···X distance to be governed more closely by the X acceptor than in the corresponding NH_4 compounds, where the structure is spatially more homogeneous, and consequently ν to decrease with the increasing acceptor strength of X. This appears, however, not to be the case, for on replacing Cl in 3MHS by Br (to form the presumably isostructural analog) ν decreases. Thus even here the variation in the spacing of the ionic charges in the crystal is the decisive factor determining the trend in ν: the minimum separation of the centroids of negative charge (as measured by the shortest Sn···Sn distances at room temperature) is 7.10 Å in $(NH_4)_2SnCl_6$, 7.49 Å in $(NH_4)_2SnBr_6$, 8.63 Å in 3MHS, 8.95 Å in $(Me_3NH)_2SnBr_6$ (estimated from densities), and 8.54 and 9.58 Å in 3EHS (mean, 9.06 Å).

The increase in the temperature shift $\Delta\nu$ with ν (Fig. 26) is tentatively accounted for by the variation of the H···X distance with the angular displacement α of the NH vector pivoting about N (Fig. 27). At very low temperatures this vector is in a quasi-static equilibrium position with respect to the X atoms of a trifurcated N—H···3X bond. With increasing temperature the H atom undergoes momentary displacements toward one of the acceptor atoms at a time, as a result of a bending motion of the NH bond and a librational motion of the cation as a whole (4, 13, 29). The relative importance of each motion depends on details of the hydrogen bonding and on the librational mobility of the cation.

Fitting the ν(ND) points for the symmetrically trifurcated N—H···3X bonds in cubic $(NH_4)_2MX_6$ (MX = SiF, SnCl, SnBr) and trigonal $(NH_4)_2MF_6$ (M = Ge, Sn, Ti) in Fig. 26 to an exponential function gives $\Delta\nu(ND) = 1.47 \times 10^{-28} \exp 0.02741\nu(ND)$, $r^2 = 0.834$, which suggests the existence of a correlation. If, in a first approximation, it is assumed that a certain increase in temperature, e.g. from 10 to 293 K, produces in these crystals a comparable increase in the angular amplitude α by which the NH vector is displaced pivoting about the stationary N atom toward X at a constant N—H bond

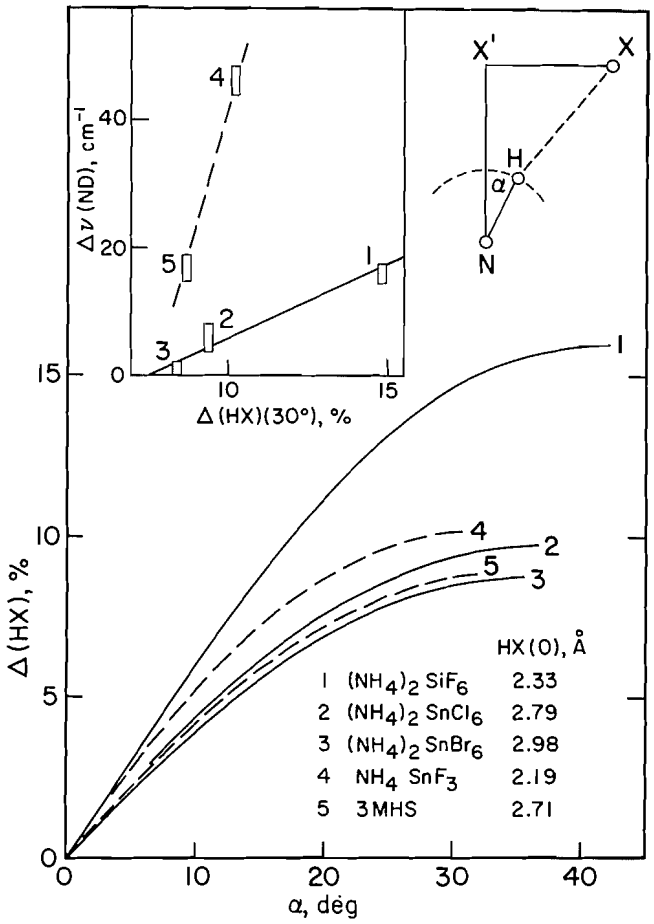

FIG. 27. Variation of $\Delta(HX) = -100[HX(\alpha) - HX(0)]/HX(0)$ of the H···X distance in a symmetrically trifurcated N—H···X bond with the angular displacement α of the NH vector of constant length pivoting about N. In NH_4SnF_3 and 3MHS there is an Sn atom on the NX′ trigyre above X′; in $(NH_4)_2SiF_6$, $(NH_4)_2SnCl_6$, and $(NH_4)_2SnBr_6$ this atom is absent. $X\cdots X' = d(X\cdots X)/\sqrt{3}$. Inset: plot of $\Delta\nu$(ND) against Δ(HX) (30°).

length, then the percentage decrease in the instantaneous H···X distance is larger for X = F than for X = Cl or Br (Fig. 27) and the difference grows with α, i.e. with temperature. Thus for $\alpha = 10°$ the ratio of the percentage decrease in H···X in $(NH_4)_2SiF_6$ to that in $(NH_4)_2SnCl_6$ is ~1.40, for $\alpha = 20°$ it is ~1.62, and for $\alpha = 30°$, ~1.74. Since a shortening of the H···X distance results in a stronger H···X bond, ν(NH) and ν(ND) must decrease with increasing α, and the ν observed at a particular temperature is a measure of this amplitude for a particular X (for $\alpha = 30°$ see inset of Fig. 27).

In the 3RHS series the hydrogen bond is symmetrically trifurcated in only two of the five compounds, viz. 3MHS and the presumably isostructural $(Me_3NH)_2SnBr_6$. However, *all five* $\Delta\nu$(ND) vs. ν(ND) points appear to form a coherent set (Fig. 26). Fitting them to an exponential function yields $\Delta\nu(ND) = 3.397 \times 10^{-25} \exp 0.02499\nu(ND)$, $r^2 = 0.984$; and similarly, $\Delta\nu(NH) = 2.675 \times 10^{-15} \exp 0.01153\nu(NH)$, $r^2 = 0.844$. Since the HX(0) (i.e. $d(H\cdots X)$ at $\alpha = 0°$) distances and the Δ(HX) vs. α curves for 3MHS and $(NH_4)_2SnCl_6$ are not greatly different (Fig. 27), the reason for the much larger $\Delta\nu$(ND) and $\Delta\nu$(NH) in 3MHS cannot be sought in the H···X distance and its variation alone. The structures of 3MHS and $(NH_4)_2SnCl_6$ differ in two important respects: the librational mobility of the cation in 3MHS is reduced because of the bulk and mass of the

Can. J. Chem. Downloaded from www.nrcresearchpress.com by 210.87.254.105 on 09/06/12
For personal use only.

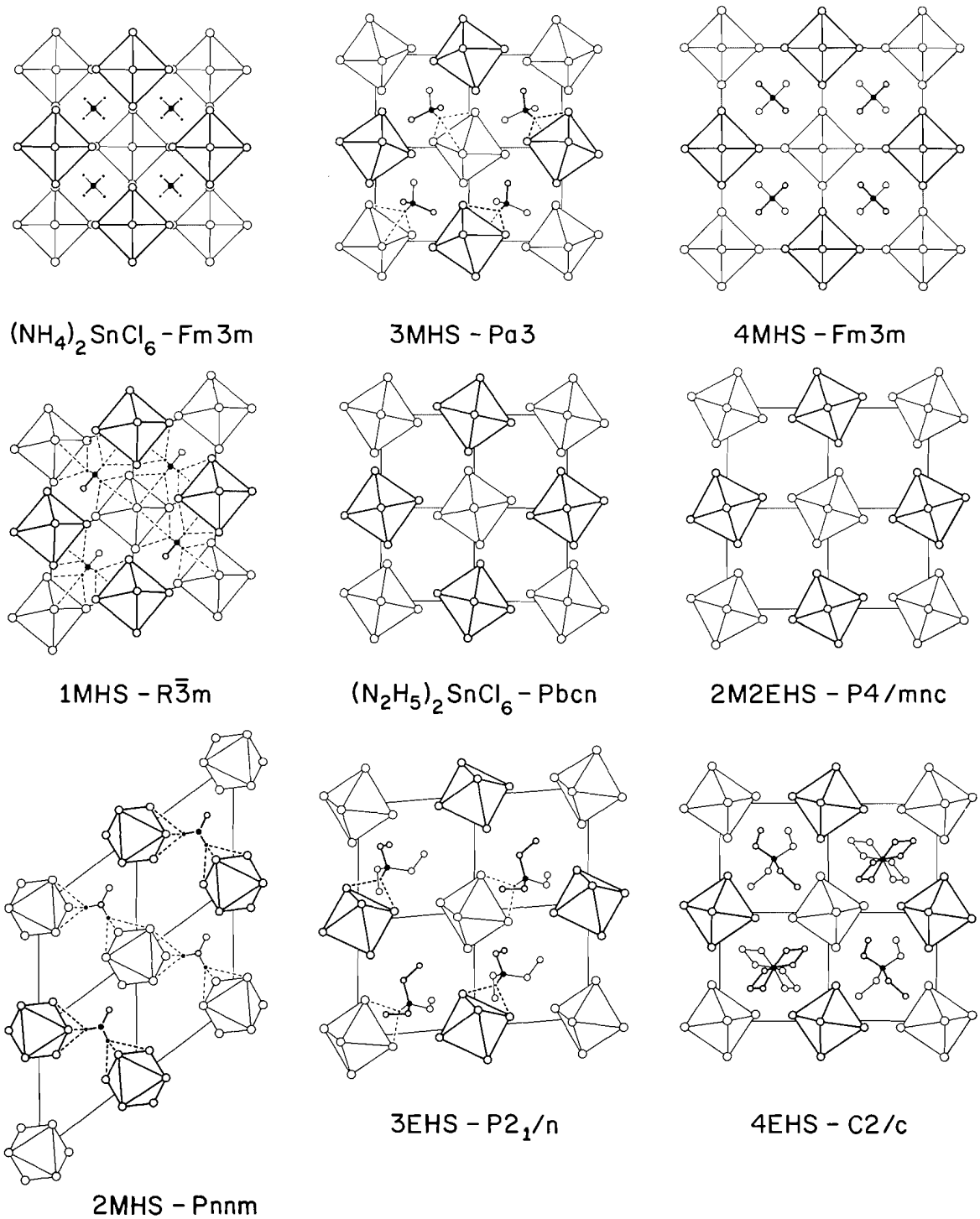

FIG. 28. $(R_nNH_{4-n})_2SnCl_6$ structures deriving from the *Fm*3*m* antifluorite structure. The projected lower half of the unit cell in each case is made to correspond to the lower four octants of the $(NH_4)_2SnCl_6$ antifluorite unit cell. The top half (not shown) is related by a symmetry operation appropriate to the respective space group. References: 2MHS, 3MHS, see text; $(NH_4)_2SnCl_6$, 2, 3; 1MHS, 6; 4MHS, 2; 3EHS, 1; 4EHS, 11; 2M2EHS, 44; $(N_2H_5)_2SnCl_6$, 43. The structure determinations of the two last-named compounds are incomplete and only the $SnCl_6$ octahedra are shown. In the 2MHS projection carbons C(1) coincide with the nitrogens. Alkyl hydrogens are not shown.

CH_3 groups, and the NH vector points at the Sn atom in 3MHS (H···Sn = 3.28 Å) but away from it in $(NH_4)_2SnCl_6$. In this 3MHS resembles NH_4SnF_3 (4), in which the NH_4^+ ion is anchored by three strong equivalent N—H···F bonds to different anions, while the NH vector, on a threefold axis, points at an Sn atom, H···Sn = 2.87 Å (*D* in Fig. 26); $\Delta\nu$(ND) in this fluoride is the largest reported to date, ~46 cm^{-1}. Indeed, the five 3RHS points *and D* can be fitted to an exponential function just as satisfactorily ($r^2 = 0.982$, $\Delta\nu(ND) = 5.21 \times 10^{-22} \exp 0.02183\nu(ND)$) as the 3RHS points alone. Whether this is fortuitous or indicative of a general trend we cannot say at present.

Fermi resonance and the limits of usefulness of the isotopic dilution technique

Temperature-tuned FR has been found to occur, to a greater or lesser extent, in the spectra of all the alkylammonium hexa-

Can. J. Chem. Downloaded from www.nrcresearchpress.com by 210.87.254.105 on 09/06/12
For personal use only.

halostannates(IV) we have examined to date, but in 3MHS and its bromo analog the phenomenon is particularly striking. This is because (*1*) several overtone levels are involved; (*2*) the fundamental *and* the overtone absorptions are sharp, at least at low temperatures; and (*3*) temperature shifts of the absorption frequencies are large relative to level spacings and bandwidths.

While in unsubstituted ammonium compounds use of the isotopic dilution technique (4, 13, 29) has resulted in avoiding, in the ND stretching region of the NH_3D^+ probe ion, complications from FR, this should probably be regarded as a felicitous collusion of circumstances rather than a rule. The likelihood that eligible overtones or combination bands of fundamentals of NH_4^+ or small inorganic anions will fall between 2450 and 2200 cm^{-1} is not great, but if such an encroachment does occur the complication can usually be dealt with. If necessary, the NH stretching absorption of the NHD_3^+ probe ion in a very highly deuterated crystal can be examined instead. Spectra of the alkylammonium salts of composite anions are different in this respect. The NH or ND stretching region or both are as a rule invaded by absorptions due to overtones or combination bands of the cation, of symmetry species suitable for FR interaction. When the FR is temperature-tuned, recognition of its presence is facilitated and the resonance can, in favourable cases, be analyzed and the position of the unperturbed ND or NH stretching fundamental extracted, as with 1MHS and the three 3RHS discussed above. Failing this, a complete deuteration of the alkyl part of the cation may lead to removal of the objectionable FR.[9] Unfortunately, increasing complexity of the alkyl may render the spectral regions of interest intractable and their analysis resistant to remedies which would be successful in the simple cases. The difficulty becomes serious when the ND stretching absorptions fall below 2300 cm^{-1}, i.e. when the hydrogen bonding is in a range ordinarily considered as medium strong, and was found prohibitive in our attempts to analyze the isotopically isolated NH and ND spectra of ω-aminoalkanesulfonic acids (G. Keresztury, O. Knop, and M. Falk, unpublished results).

Structural principles

Dimensions of the $SnCl_6$ octahedra

The $SnCl_6$ octahedra in $(R_nNH_{4-n})_2SnCl_6$ are on the whole quite regular. The weighted mean of the Sn—Cl distances in ten structures of recent vintage is 2.425(12) Å (a total of 72 occurrences corresponding to 28 different values; conventional refinement). Correction for thermal motion would increase the individual d(Sn—Cl) values to a different extent, depending on the structure and on the model assumed. For example, in $(NH_4)_2SnCl_6$ the uncorrected value of 2.421 Å is raised to 2.428–2.430 Å on the riding model (2, 3) and to 2.445 Å on the independent-motion model (2). In 4MHS, however, the uncorrected value, 2.402 Å, is increased to 2.446 Å (riding model) and 2.489 Å (independent motion) (2), i.e. an increase of 1.8% and 3.6% respectively compared with 0.3% and 1.0% for $(NH_4)_2SnCl_6$. For other compounds the corrected d(Sn—Cl) values are not available.

Cation–anion packing: antifluorite type

The alkylammonium hexachlorostannates(IV) differ, structurally, from simple ionic $A^+{}_2B^{2-}$ crystals mainly in that both A and B are composite ions. The most symmetric, though not the densest, packing of A^+ and B^{2-} in simple ionic crystals is realized in the cubic ($Fm3m$) antifluorite arrangement characterized by A···4B and B···8A coordinations (30). This type of packing, with or without distortion, is widely represented among $[A]_2[MX_6]$ compounds (A, alkali or other univalent cation; X, halogen).

In the hexachlorostannates (Fig. 28), the antifluorite structure may be visualized as based on a fcc cell in which the corners and face centres are occupied by regular $SnCl_6$ octahedra with orientations consistent with the $Fm3m$ symmetry. When this unit cell is divided into eight equivalent cubic subcells, the octahedra occupy alternate corners of these small cubes and each of the subcells contains one cation. This highly symmetric structure is exemplified by $(NH_4)_2SnCl_6$ (2, 3) and 4MHS (2, 9), in which the site symmetry at the centres of the subcells is the same as the symmetry of the free cation, T_d.[10] With Et_4N^+, even though the ion could realize an effective T_d symmetry in the crystal *dynamically* or by static orientational disorder (a possibility which might exist above room temperature), a higher packing density can be achieved by a conformation of lower symmetry. The cation symmetry observed in 4EHS is in fact only C_2 (11). The antifluorite lattice is preserved but it is distorted to monoclinic. In addition, the carbons closest to N in one of the two nonequivalent Et_4N^+ ions can occupy alternative positions, which results in a disorder on that nitrogen sublattice (Fig. 28). As the alkyl chain in R_4N^+ lengthens, the possibility of existence of structural alternatives increases. This is illustrated by the following pairs of dimorphs (the densest form is listed first):

$(Et_4N)_2MCl_6$	M = Sn	C_{2h} (39); cubic ? (24)
	M = Pt	C_{2h} (12); cubic ? (39)
$(n\text{-}Pr_4N)_2MCl_6$	M = Sn	C_i (24); D_{2h} (24)[11]
	M = Pt	C_i (12); D_{2h} (39)
$(n\text{-}Pr_4N)_2MBr_6$	M = Sn	D_{4h} (39); ? (39)
	M = Pt	C_{2v} (39); monoclinic (39)
$(i\text{-}Bu_4N)_2PtCl_6$ (39)		C_{2h}; ?

The possibility cannot be excluded that even for 4MHS the true unit cell is larger than the $Fm3m$ ($Z = 4$) cell derived from $(NH_4)_2SnCl_6$, and that the structure may in fact have a more complicated arrangement of the $SnCl_6$ octahedra. The symmetry of $(Me_4N)_2TeBr_6$ has been reported (40) as $Fd3c$ ($Z =$

[9]In the case of 1MHS this did not result in a useful simplification. The spectrum of $(CD_3NH_3)_2SnCl_6$ in the NH stretching region was essentially identical with that of the undeuterated compound, and that in the ND stretching region was even more complex than for $(CH_3NH_3)_2SnCl_6$.

[10]The same symmetry has been reported for $(Me_4N)_2CeCl_6$ (31), $(Me_4N)_2PtF_6$ (32), and, with reservations, for $(Me_4N)_2PtCl_6$ (33). However, for $(Me_4N)_2SiF_6$ at room temperature the structure appears to be of symmetry $I4/m \subset Fm3m$, with the SiF_6 octahedra in a "ferro" arrangement (34). The $Fm3m$ symmetry also appears to occur in a number of $(Me_4N)_2MX_6$ chlorides and bromides where M is a 5*f* element (Th, Pa, U, Pu) and in the high-temperature form of $(Et_4N)_2PuCl_6$ (35–37), while the corresponding $(Et_4N)_2MCl_6$ and $(Et_4N)_2PaBr_6$ at room temperature crystallize in $Fmmm \subset Fm3m$ (36, 37). $(Et_4N)_2PaF_6$ is dimorphic, fcc and tetragonal, the latter form (isostructural with the U compound) probably related to $Fm3m$; $(Et_4N)_2PaOCl_5$ is stated to be monoclinic, $C2/c$ or Cc, and related to $(Et_4N)_2PaCl_6$ (38).

[11]The difference between the densities quoted for the two forms of 4PHS in ref. 24, 1.548 and 1.314 g/cm^3, is so large that the possibility of a misprint (1.548 instead of 1.348?) is not excluded, especially as a density of 1.548 g/cm^3 is significantly higher than that of either form of the corresponding chloroplatinate.

Can. J. Chem. Downloaded from www.nrcresearchpress.com by 210.87.254.105 on 09/06/12
For personal use only.

32) and that of $(Me_4N)_2ReBr_6$ as $I4_1/acd \subset Fd3c$ (11). The observation, in $(Me_4N)_2PtCl_6$, of extra reflections not indexable on $Fm3m$ ($Z = 4$) suggests (33, 40) that the symmetry of this structure, too, may be $Fd3c$ ($Z = 32$), and there are indications (2, 40) that this might also be the case for 4MHS.

When the maximum symmetry of the free cation is no longer T_d, the $Fm3m$ symmetry of the crystal is lowered and the cubic subcells may become cuboids. At the same time the $SnCl_6$ octahedra will undergo distortion and rotational displacements about the Sn atom, but they remain centrosymmetric. This is observed for $MeNH_3^+$ and Me_3NH^+. Both cations have trigonal symmetry, and one might expect the overall cubic symmetry to be maintained if the cations were to align themselves in such a way that their threefold axes coincided with the threefold axes of a cubic unit cell of $Fm3m$ subgroup symmetry. However, while the trigonal symmetry of the cation is prominent in both the 1MHS and 3MHS structures, in 1MHS the overall symmetry is reduced to $R\bar{3}m$ (a noncubic subgroup of $Fm3m$),[12] whereas in 3MHS the trigonal cation does take advantage of the possibility of alignment along the trigyres of a cubic unit cell, but in a space group ($Pa3$) which is not a subgroup of $Fm3m$. A lowering of the crystal symmetry is not observed in the cubic 1M3EHS (9); however, the structure has not yet been determined and it is likely that the $MeEt_3N^+$ ions (C_{3v} in their highest-symmetry conformation) in this crystal are orientationally disordered.[13]

Cation–anion packing: other types

The effect of an additional lowering of the cation symmetry will depend also on the shape of the cation. With small alkyls (Me, Et) the space-group symmetry may be unrelated to $Fm3m$ but the antifluorite arrangement will be preserved, as in 2MHS, 3EHS, and even $(N_2H_5)_2SnCl_6$ (43) and probably 2M2EHS (44).[14] However, the cation shape begins to compete with the cation symmetry: Et_3NH^+ in its most symmetric conformation is trigonal but 3EHS is monoclinic (1). On the other hand, cation shape or size or both appear to be the structure and symmetry determining factors when the alkyl contains three or more C atoms. Thus the structure of 3PHS not only is monoclinic, but it no longer is based on the antifluorite arrangement: the zig-zag *n*-propyl chains are "linearly" extended (cf. Figs. 6 and 7),[15] resulting in a cation shape which appears to match poorly the shape of the $SnCl_6$ octahedra and leads to a different type of anion lattice. Moreover, the octahedra are not centrosymmetric.

An arrangement different from the antifluorite is also observed in the trigonal 1EHS (ref. 10, this work). This compound (and the monoclinically distorted 1PHS) has a layer structure of the *anti*-CdI_2 type, similar to that observed in the room-temperature form of the trigonal $(NH_4)_2SiF_6$ and in $(MeNH_3)_2TeCl_6$ (46). Interestingly, the last-named crystal transforms on cooling into an antifluorite $R\bar{3}m$ phase, presumably isostructural with 1MHS (46).[12] The corresponding $(MeNH_3)_2MCl_6$ (M = Pd, Pt, Sn, Se, Pb), $(MeNH_3)_2MBr_6$ (M = Pd, Pt, Sn, Se), and $(MeNH_3)_2PtI_6$ at room temperature are all of the antifluorite ($R\bar{3}m$) type and all undergo low-temperature transitions (47).

Orientation of the $SnCl_6$ octahedra

In recent years much attention has been paid to the nature and mechanism of solid-state transitions in antifluorite A_2MX_6 halides (cf. for example, refs. 48 and 49). Many, probably most, of these transitions are characterized by cooperative rotational displacements of the MX_6 octahedra from their orientation in the $Fm3m$ phase (e.g. in K_2SnCl_6, ref. 50), with the attendant formation of "ferro" (in-phase rotations) or "antiferro" (anti-phase rotations) arrangements of the MX_6 orientations on the original M lattice complex $Fm3m$. Consideration of such arrangements is relevant also for the alkylammonium hexachlorostannates.

Of the nine antifluorite-type room-temperature structures listed in Table 15 and schematized in Fig. 28, five (2MHS, 2M2EHS, 3EHS, 4EHS, and $(N_2H_5)_2SnCl_6$) have antiferro arrangements of the $SnCl_6$ octahedra, but their space groups are not "zellengleiche" subgroups (and in two cases *no* subgroups) of $Fm3m$. This raises the question of whether these room-temperature structures should be regarded as low-temperature variants of structures of higher symmetry presumed to exist above room temperature. Nothing is known at present about transitions above room temperature in these crystals, but if they do occur, what is the relationship of the two structures involved in a transition?

Clearly the highest possible symmetry would be $Fm3m$, as actually observed for $(NH_4)_2SnCl_6$[16] and 4MHS (but see above). Since in considering the arrangement of the $SnCl_6$ rotational orientations only the anion sublattices are involved, the problem is one of determining (*a*) the lattice complex LC formed by the Sn atoms; (*b*) the equivalence of the $SnCl_6$ orientations on the LC imposed by the space group SG; and (*c*) the formal relationship of the SG symmetry to that of the LC. When the antiferro order involves only two orientations, the LC|SG relationship defines a dichromatic (black-white, Shubnikov) space group of type IV (51) based on a dichromatic Bravais lattice. The chromatic translation of this lattice, together with the site symmetry at Sn, then describes the geometry of the antiphase rotations, the colour change corresponding to the change of sense of the rotational displacement. Thus if a transition exists, between room temperature and the melting or decomposition temperature of the crystal, and if it is of the antiferro to "*para*" type, the SG symmetry of the high phase would be expected to be that of the appropriate LC as specified in the LC|SG column of Table 15.

In $(NH_4)_2MX_6$ the cation is known not to be the causative factor in $Fm3m \rightarrow$ antiferro transitions, as such transitions for a given MX_6 occur equally in A_2MX_6 with A a structureless alkali ion. To what extent an alkylammonium ion participates, through hydrogen bonding, in the antiferro–*para* rearrangements on the anion lattice is not known.

The $SnCl_6$ orientation in $(NH_4)_2SnCl_6$, 1MHS ($R\bar{3}m \subset$

[12]The $R\bar{3}m$ the structure of 1MHS and other methylammonium hexahalometallates(IV) may be described as of the *anti*-$CdCl_2$ (C 19) type. The relationship of the *anti*-$CdCl_2$ to the antifluorite structure is discussed in ref. 41.

[13]The structure of 3MEHS also is of the fcc type (42).

[14]The tetragonal ($P4/mnc$) partial structure proposed for 2M2EHS contains an antifluorite $SnCl_6$ lattice (44). However, it requires that the cation be of D_2 symmetry, which the ion clearly does not possess. The structure would thus have to be orientationally disordered, but for a complete disorder one would expect the two dimensions of the pseudocubic cell ($C4/mcn$, $a_{cub} = a_{tetra}\sqrt{2} = 12.82$ Å, $c_{cub} = c_{tetra} = 14.12$ Å) to be more closely similar.

[15]Full extension of *n*-propyl chains is also encountered in (*n*-Pr_4N)Br, where the *n*-Pr_4N^+ ion has S_4 symmetry (45).

[16]Cubic $(NH_4)_2SnCl_6$ is known not to undergo a transition on cooling to 10 K (4, 49, 61).

TABLE 15. Space groups (SG) of the antifluorite-type $(R_nNH_{4-n})_2SnCl_6$ and the corresponding site symmetries (SS) at the Sn atoms and the Sn lattice complexes (LC)

Compound	SG	SS	LC[a]	LC|SG[b]
$(NH_4)_2SnCl_6$	$Fm3m$	$m3m$	$Fm3m$	
1MHS	$R\bar{3}m$[c]	$\bar{3}m$	$R\bar{3}m$	
2MHS	$Pnnm$[d]	$2/m$	$Immm$	$P_Inmm-Immm\|Pnnm$
3MHS	$Pa3$[d]	$\bar{3}$	$Fm3m$	
4MHS	$Fm3m$	$m3m$	$Fm3m$	
2M2EHS	$P4/mnc$[c]	$4/m$	$I4/mmm$	$P_I4/mnc-I4/mmm\|P4/mnc$
3EHS	$P2_1/n$[d]	$\bar{1}$	$C2/m$	$P_A2_1/c-A2/m\|P2_1/c$
4EHS	$C2/c$[d]	$\bar{1}$	$C2/m$	$C_c2/c-2C2/m\|C2/c$
$(N_2H_5)_2SnCl_6$	$Pbcn$[c]	2	$Cmcm$[f]	$C_Amcm-Fmmm\|Cmcm$[f]

[a]All the LC's are either $Fm3m$ or subgroups of $Fm3m$. They are all invariant except $Cmcm$ which has one degree of freedom. See also *f*.

[b]Shubnikov group indicating the chromatic Bravais translation.

[c]Subgroup of $Fm3m$.

[d]Not a subgroup of $Fm3m$.

[e]Not a "zellengleiche" subgroup of $Fm3m$.

[f]$Fmmm$ if $y[Pbcn, 4(c)] = \frac{1}{4}$; $Fmmm \subset Fm3m$. Otherwise $P_Cbcn-Cmcm|Pbcn$ and $C_Amcm-Fmmm|Cmcm$.

$Fm3m$) and 4MHS are to be regarded in this context as of the *para*, or "neutral", type. Although the LC in 3MHS is $Fm3m$, the Bravais lattice is not dichromatic, as it involves more than one chromatic translation, and the arrangement of the $SnCl_6$ orientations is to be viewed as *multiply* antiferro.

Geometry of the hydrogen bonding

On the principle that all N-hydrogens and Cl atoms in $(R_nNH_{4-n})_2SnCl_6$ will participate in hydrogen bonding to the maximum possible extent the type and connectivity of the hydrogen bonds would be expected to be determined primarily by the $H_N:Cl = (4 - n)/3$ ratio and by the tendency of all the Cl atoms to participate in the hydrogen bonding equitably. The cation:anion ratio being constant regardless of n, the existence of $[R_nNH_{4-n}\cdots Cl_3SnCl_3\cdots H_{4-n}NR_n]$ groupings containing the maximum possible number of *intra* but forming no *inter* hydrogen bonds would seem possible. Such groupings indeed occur in 3MHS and 3EHS, where they are centrosymmetric and the hydrogen bonds are respectively trifurcated and bifurcated. Similar groupings occur also in 3PHS, but their geometry in this crystal is highly distorted. However, they do not occur in the other compounds.

In 1MHS and 1EHS each RNH_3 engages in three trifurcated N—H···Cl bonds, each to a *different* $SnCl_6$, to form infinite two-dimensional hydrogen-bond networks (Figs. 4, 13, 14). Each $RNH_3\cdots Cl_3SnCl_3\cdots H_3NR$ sandwich thus contains two layers of equivalent H_N atoms, one layer on each side of the Sn layer. The difference between 1MHS and 1EHS is only in the size of R (i.e. in the vertical separation of the Sn layers) and in the orientational disorder of the Et groups in 1EHS at room temperature. The shape and size of R probably also determine the type of cation/anion packing, viz. *anti*-$CdCl_2$-type in 1MHS and *anti*-CdI_2 type in 1EHS (see above and ref. 41). In 1PHS the packing also is of the *anti*-CdI_2 type, though less recognizably so than in 1EHS: the existence of two types of cations, each occurring in two vertical orientations, results in a pseudohexagonal unit cell with a base four times that of the simple "*anti*-CdI_2" cell (Fig. 5*A*); some of the hydrogen bonds are asymmetrically bifurcated rather than trifurcated (Fig. 5*B*).

Similarly, in 2MHS only trifurcated hydrogen bonds are observed, this time connecting the $SnCl_6$ octahedra to infinite linear chains (Figs. 1 and 28). Given the observed propensity for trifurcated or bifurcated bonds, the facts known to date may be summarized by saying that a cation in an alkylammonium hexachlorostannate may be expected to form $4 - n$ trifurcated (or bifurcated) N—H···X bonds. The connectivity of the resulting hydrogen-bond system may then be described as three-dimensional ($n = 0$, $(NH_4)_2SnCl_6$), two-dimensional ($n = 1$, 1RHS), one-dimensional ($n = 2$, 2MHS), or "zero-dimensional" ($n = 3$, isolated groupings as in 3RHS). Work is in progress to determine whether situations of mixed dimensionality exist.

Is the presence of hydrogen bonding evident in molecular volume trends?

Where a reliable structure determination of an alkylammonium hexachlorostannate is not available, some idea of the general effect of the cation geometry on packing density can be obtained from a scrutiny of the volume per formula unit V_1. The densities of many compounds of this class were measured, with these considerations in mind, with considerable accuracy long before the advent of X-ray diffraction (12, 14, 24, 39). The set for the hexachloroplatinates is more extensive than that for the hexachlorostannates, and since in practically all the known cases the hexachloroplatinate is isomorphic with the corresponding hexachlorostannate, conclusions from the platinates will be taken as valid also for the stannates. Irregularities in the expected trends in V_1 would be thought to be indicative of the effect of hydrogen bonding.

The V_1 values calculated from the densities given in refs. 12, 14, 24, and 39 agree, with few exceptions, surprisingly well with the unit-cell volumes per formula unit $V/Z = \bar{a}^3$ where the latter are known. The differences amount to less than 1% for 7 of the 10 stannates for which the comparison can be made. For 1MHS and 2MHS they are larger, 1.7 and 1.3% respectively, but still acceptable; for M3EHS the difference of 2.8% does not rule out the possibility that the density and the X-ray determination may have been carried out on different polymorphs of this salt. For the platinates the comparison can be made for only four compounds and the overall accuracy is more difficult to assess.[17]

The V_1 are displayed in different ways in Figs. 29–32.

[17]Curiously, the poorest agreement in the platinate series, 4.8%, obtains for $MeNH_3^+$, the same cation that shows a significant discrepancy in the stannate series.

Can. J. Chem. Downloaded from www.nrcresearchpress.com by 210.87.254.105 on 09/06/12
For personal use only.

Can. J. Chem. Downloaded from www.nrcresearchpress.com by 210.87.254.105 on 09/06/12
For personal use only.

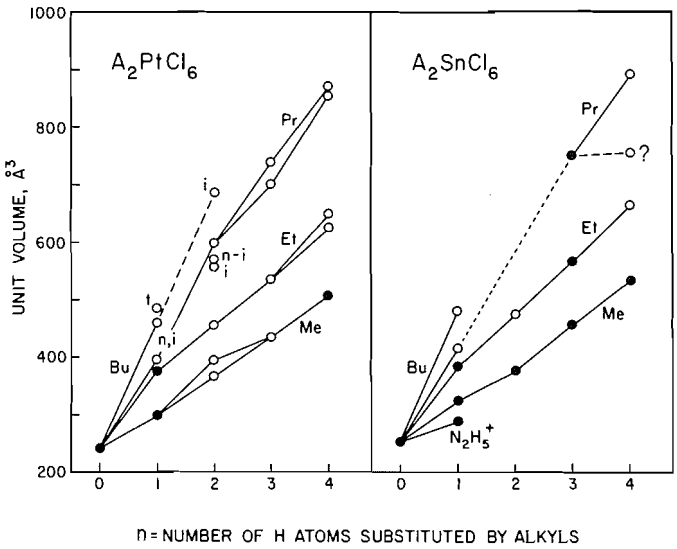

FIG. 29. A_2MCl_6 (A = R_nNH_{4-n} or N_2H_5; R = Me, Et, Pr, Bu; M = Pt, Sn): effect of progressive alkyl substitution on the volume per formula unit V_1. Full circles, V_1 calculated from unit-cell dimensions; open circles, V_1 calculated from density. Note the existence of polymorphs.

Progressive replacement of the ammonium hydrogens by the same alkyl results in a steady increase in V_1 (Fig. 29); the trends in the Pt and Sn series are closely parallel. Inspection of the Me_nNH_{4-n} and Et_nNH_{4-n} series shows that the introduction of the first alkyl perturbs the $(NH_4)_2MCl_6$ structure more for Et than for Me, but the additional alkyl groups increase V_1 almost linearly, although to different extents: the V_1 increments per CH_2 are ~35 Å^3 for the Me, ~23 Å^3 for the Et, and ~28 Å^3 for the *n*-Pr series. They all are much larger than the estimate of 17 Å^3 for the CH_2 volume increment in *purely molecular*, single-constituent crystals of organic compounds forming homologous series (52). The reason for these large increments is undoubtedly to be looked for in the tendency of the ionic structures to adopt packings distinguished by minimizing electrostatic interactions between ionic charges at the cost of reducing the maximum *geometrically* achievable packing density. This may be likened to the effect — acting in the opposite direction — of hydrogen bonding which is responsible for the open structures of NH_4F and ice.

The effect on V_1 of X in $(R_3NX)_2MCl_6$ (X = H, Me, Et, *n*-Pr, *n*-Bu, *n*-Am; M = Pt, Sn) (Fig. 31) does not lend itself to a straightforward interpretation. However, it appears that when at least one of the three R groups in the cation is *n*-Pr, the V_1 trend becomes indifferent to X to the extent that it is quasi-linear, or at least non-decreasing, relative to the increasing number of C atoms in X. This indicates that X = H does not produce an anomalous packing density, which in turn implies that hydrogen bonding in the individual R_3NH compounds is unimportant as a structure-affecting factor and probably very weak and of unfavourable geometry. In the Me_3NX series it is difficult to decide whether the initial steep increase from X = H to X = Me and Et reflects primarily the contracting effect of H or an unusually large increment due to the inability of the small alkyl, Me or Et, to assume a "folded" conformation and thus reduce its space requirements, always remembering that the Coulombic interaction will tend to make V_1 as small as possible in the circumstances. The same tendency is observed in the Me_2EtNX, $MeEt_2NX$, and Et_3NX series.

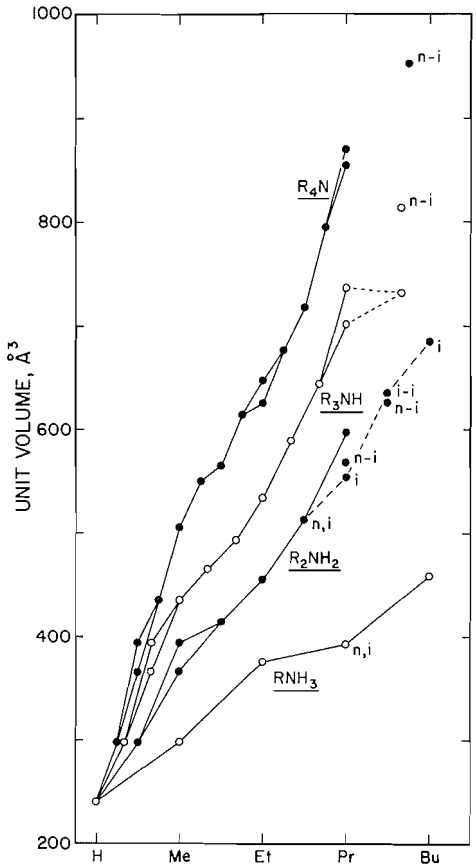

FIG. 30. A_2PtCl_6: effect of alkyl substitution on V_1. A = RNH_3, R_2NH_2, R_3NH, R_4N; binary combinations of neighbouring alkyls (H–Me, Me–Et, Et–Pr, Pr–Bu) are included. The alkyls are normal (*n*) unless indicated otherwise (*i*, *iso*). Note the existence of polymorphs.

In any event, when looking for an indication of significant hydrogen bonding in V_1 comparisons, one must have a clear *a priori* notion of what ought to be the magnitude of the V_1 increment that would be indicative of the presence of such bonding. Figure 32 brings to light three important factors. First, if every H_N formed a hydrogen bond, and if the formation of the bond resulted in a significant volume contraction, one would expect that, in a group of *cation-isomeric* A_2PtCl_6, V_1 would be smallest for A richest in H_N and largest for a fully alkylated cation. However, Fig. 32 shows that $V_1(Me_2NH_2) > V_1(EtNH_3)$, $V_1[Et(n\text{-}Pr)NH_2] > V_1(MeEt_2NH)$, and the V_1 of $n\text{-}Pr_2NH_2$, $(i\text{-}Pr)(i\text{-}Bu)NH_2$, $i\text{-}Bu_2NH_2$, $n\text{-}Pr_3NH$, and $Et(i\text{-}Bu)_2NH$ are all larger than the V_1 of the respective fully alkylated isomers with the same number of C atoms.

Secondly, since polymorphs occur, one cannot be certain that, in cases where only one form has been described, another form does not exist which might have a lower V_1 and thus possibly invalidate a conclusion reached for a group of isomeric A_2MCl_6 in ignorance of this polymorph.

Thirdly, the V_1 differences *between polymorphs* of a particular compound may be larger than those *between isomers* in a group, regardless of whether or not hydrogen bonding is present. This point is illustrated in Fig. 32 and Table 16. It is seen that the V_1 differences between polymorphs can amount to as much as 7–8% and that even for fully alkylated cations for which hydrogen bonding is not possible. For comparison, for the cubic/trigonal $(NH_4)_2SiF_6$, ΔV_1 = 6.5%, whereas for the

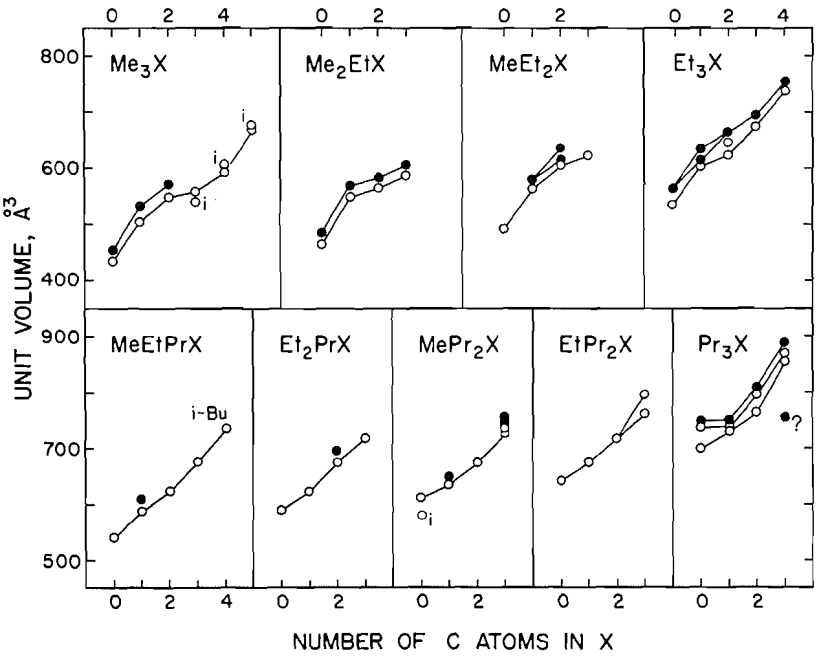

FIG. 31. $(R_3NX)_2MCl_6$ (M = Pt, Sn): effect of substitution (X = H, Me, Et, Pr, Bu, Am) on V_1. Full circles, Sn; open circles, Pt. With the exception of X = H all the compounds are quaternary salts with no possibility of hydrogen bonding.

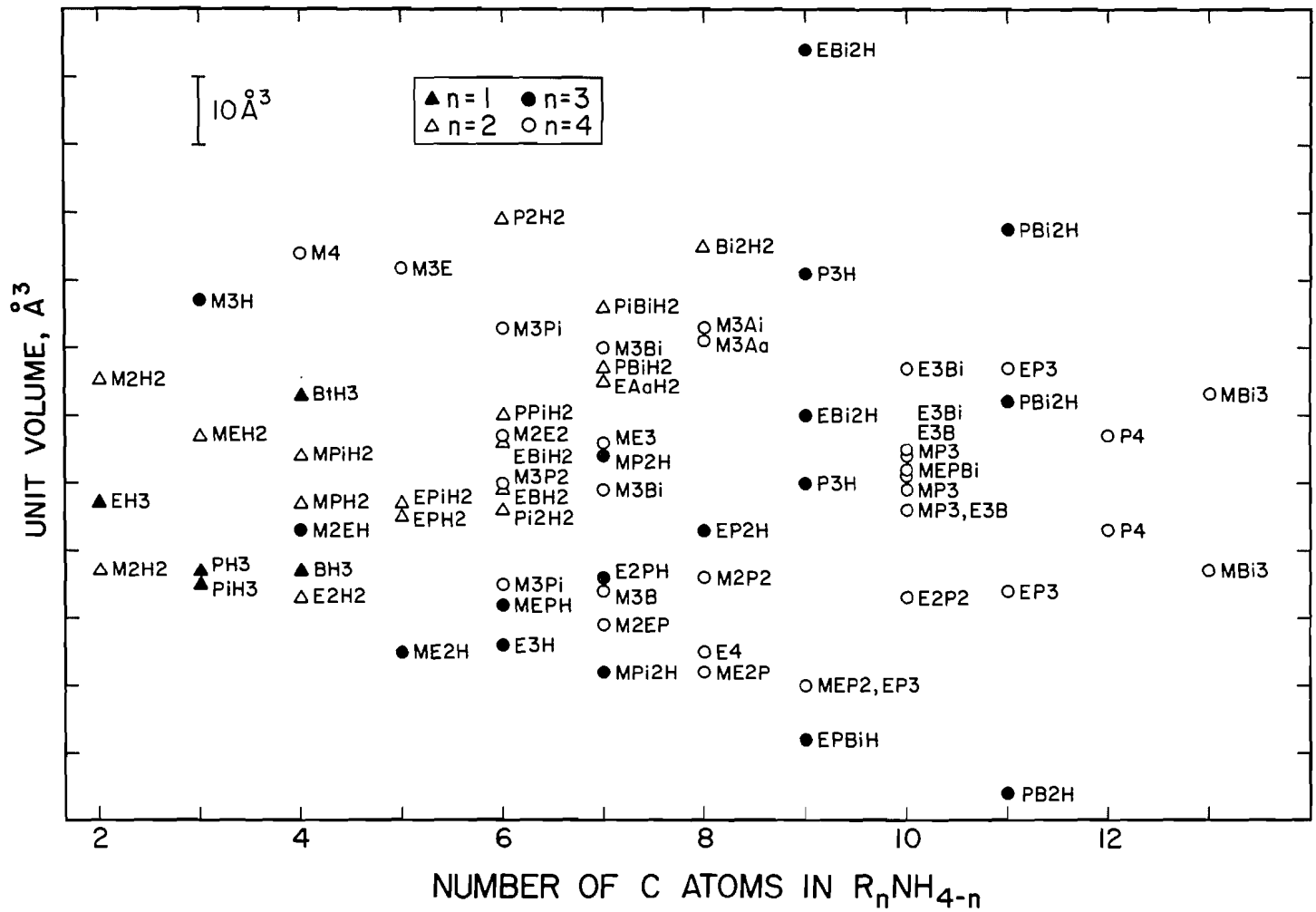

FIG. 32. Effect of isomerism on the V_1 of $(R_nNH_{4-n})_2PtCl_6$. M = Me, E = Et, P = *n*-Pr, B = *n*-Bu, A = *n*-Am, i = iso, a = active; EBi2H stands for Et(*i*-Bu_2)NH etc. The origin of the V_1 scale varies from compound to compound; comparisons are to be made only within a column.

Can. J. Chem. Downloaded from www.nrcresearchpress.com by 210.87.254.105 on 09/06/12
For personal use only.

TABLE 16. Difference in the volume per formula unit V_1 (Å^3) for A_2PtCl_6 dimorphs[a]

A	ΔV_1	$100\Delta V_1/V_1$
Me_2NH_2	27.7	7.6
$Me_3(i\text{-Pr})N$	40.9	7.5
$Me_3(i\text{-Bu})N$	21.1	3.5
$n\text{-Pr}_3NH$	36.2	5.2
$Et(i\text{-Bu})_2NH$	53.6	7.5
$Et_3(n\text{-Bu})N$	8.1	1.1
$Et_3(i\text{-Bu})N$	12.0	1.6
$Me(n\text{-Pr})_3N$	5.5	0.8
$(n\text{-Pr})(i\text{-Bu})_2N$	23.1	2.9
$Et(n\text{-Pr})_3N$	33.0	4.3
$n\text{-Pr}_4N$	14.3	1.7
$Me(i\text{-Bu})_3N$	25.9	3.3

[a]Calculated from densities (12, 14, 24, 39). Cations arranged by increasing number of C atoms in A. V_1 refers to the denser form.

cubic/trigonal $(NH_4)_2SnF_6$, $\Delta V_1 = -4.2\%$ (cf. ref. 29). In purely molecular crystals (52) the differences are, for example, 2.4–4.0% for the acridine polymorphs, 3.9% for phenazine, 0.6% for p-$C_6H_4Cl_2$; and about the same when hydrogen bonding is present, e.g. ca. 3.9% for resorcinol, 2.7% for oxalic acid, and 1.3–1.7% for the glycine polymorphs, always relative to the densest form. The claim cannot thus be made that the presence and extent of hydrogen bonding are recognizable from V_1 trends and comparisons.

This conclusion is implicit in the belief that the primary structure-determining factor is the maximization of the overall packing density consistent with a minimization of the Coulombic energy, even if the result is a poor hydrogen-bonding geometry, as exemplified by the structure of 3PHS.

Experimental

Preparation

The salts were prepared by combining a solution of the amine in 95% EtOH with an equivalent amount of an aqueous solution of H_2SnCl_6 (or H_2SnBr_6) containing a small excess of HCl (or HBr) to counteract possible hydrolysis. The crystals obtained by slow evaporation at room temperature were recrystallized from 50% EtOH acidified with HCl or HBr. Deuteration was achieved by similar recrystallization from D-containing solutions.

Surprisingly, the ir spectrum of the product intended to be 2PHS was of a type different from all the other spectra, in that it contained NH and ND stretching frequencies far lower than any previously encountered in an alkylammonium hexachlorostannate (see above) and, in fact, lower than the NH and ND stretching frequencies of n-$PrNH_3Cl$. The starting material was verified by ^{13}C nmr to be n-Pr_2NH of high purity, but the elemental analysis of the product indicated a considerably higher C content than required for 2PHS, with smaller discrepancies in the H, N, and Cl contents. To resolve the difficulty we determined only quite recently the crystal structure of the product, with the result (details to appear shortly) that the compound studied turned out unexpectedly to be $(n\text{-}Pr_2NH_2)_3SnCl_7 = (n\text{-}Pr_2NH_2)_3(SnCl_6)Cl$, analogous with $(NH_4)_3(SiF_6)F$ (53) and $K_3(SiF_6)F$ (54), in satisfactory agreement with the elemental analysis. It is interesting that none of the other hexachlorostannates showed, under comparable conditions of preparation, any tendency to form a chloride adduct, and that three different preparations designed to yield 2PHS, each followed by one or more recrystallizations, resulted in the adduct. Efforts to prepare authentic 2PHS are under way.

Structure determination

A CAD-4 four-circle diffractometer was used in the determination of the unit-cell dimensions and in the intensity collection. The intensities were reduced by routine procedures (55). Lorentz and polarization corrections were applied but no absorption or extinction corrections. The scattering factors for neutral atoms were taken from ref. 56. The structures were solved using the SHELX system (57).

In each case the Sn atoms were located from the E-map and all other nonhydrogen atoms were found on a subequent Fourier map. Full-matrix least-squares ($w\Delta F^2$ = minimum) refinement was carried out with isotropic temperature factors on heavy atoms until R was reduced to a reasonably low value. After locating the hydrogens (from a difference Fourier map or from structural considerations), refinement was continued with anisotropic temperature factors on the nonhydrogen atoms and isotropic factors on the hydrogens, unless stated otherwise. The anisotropic temperature factor is defined as

$$T = \exp[-2\pi^2(U_{11}h^2a^{*2} + U_{22}k^2b^{*2} + U_{33}l^2c^{*2} + 2U_{23}klb^*c^* + 2U_{13}hla^*c^* + 2U_{12}hka^*b^*)]$$

Where a refinement was carried out with constraints on bond lengths, the distances were assigned at 1.02 Å for N—H, 1.08 Å for C—H, 1.48 Å for N—C, and 1.54 Å for C—C, within limits appropriate to each case (57). To constrain HNH angles to tetrahedral, appropriate H···H distances (1.66 Å) were assigned.

Lists of structure factors (Tables 17–21) have been deposited.[3]

Infrared spectra

Spectra were recorded on a Perkin-Elmer model 180 spectrophotometer fitted with a closed-cycle He refrigerator. Suitable samples were obtained by mulling finely ground crystals with fluorocarbon or hydrocarbon oil. The mulls were sandwiched between KBr or CaF_2 plates. KBr pellets were used for survey spectra in the 4000 to 200 cm^{-1} region.

Analysis of Fermi resonance

In the spectra complicated by FR the position of the unperturbed NH or ND stretching fundamental was derived from the positions and relative intensities of the FR multiplet as follows. The observed wavenumber separation, $D = \nu_1 - \nu_2$, of a pair of vibrational levels undergoing FR is given by

$$[1] \quad D^2 = d^2 + 4W^2$$

where $d = \nu^0_1 - \nu^0_2$ is the separation of the unperturbed levels in the absence of resonance and W is the FR constant (59, 60). The separation that would be observed if the two unperturbed levels coincided (i.e. $d = 0$) is $2W$. When a fundamental at ν^0_1 and of inherent intensity I^0 is perturbed by an overtone level at ν^0_2, of negligible inherent intensity, the intensity ratio of the perturbed doublet is, from first-order perturbation theory,

$$[2] \quad I_2/I_1 = (D - d)/(D + d)$$

where $I_1 + I_2 = I^0$, $I_1 \geq I_2$. The two transitions are shifted equally and in opposite directions, so that

$$[3] \quad \nu^0_1 + \nu^0_2 = \nu_1 + \nu_2 = 2\bar{\nu}$$

From eqs. [1]–[3],

$$[4] \quad W = [(I_1I_2)^{1/2}/(I_1 + I_2)]D$$

$$[5] \quad \nu^0_1 = (I_1\nu_1 + I_2\nu_2)/(I_1 + I_2)$$

i.e. the position of the unperturbed fundamental is simply the weighted mean of the observed Fermi doublet. This can be generalized to Fermi multiplets, so long as the participating overtone levels have negligible intensities compared to the intensity of the fundamental.

POSTSCRIPT. A redetermination of the crystal structure of 4MHS at 160 and at 295 K has in fact shown (62) that 4MHS above its T_{tr} = 149(7) K has a unit cell of $Fd3c$ symmetry, corresponding to an octuple $Fm3m$ cell, with the $SnCl_6$ octahedra rotated with respect to the cubic translation axes. In this respect 4MHS thus resembles $(Me_4N)_2TeBr_6$. Structure determination below T_{tr}, at 115 K, seems to indicate that the symmetry of the low-temperature phase of 4MHS is not higher than tetragonal.

Can. J. Chem. Downloaded from www.nrcresearchpress.com by 210.87.254.105 on 09/06/12
For personal use only.

Can. J. Chem. Downloaded from www.nrcresearchpress.com by 210.87.254.105 on 09/06/12
For personal use only.

Acknowledgments

We thank Mr. Klaus Jochem for assistance with some of the computations. This investigation was carried out with financial support from the Natural Sciences and Engineering Research Council of Canada through grants to the two first-named authors.

1. O. KNOP, T. S. CAMERON, M. A. JAMES, and M. FALK. Can. J. Chem. **59**, 2550 (1981).
2. T. R. BRILL, R. C. GEARHART, and W. A. WELSH. J. Magn. Reson. **13**, 27 (1974).
3. J. A. LERBSCHER and J. TROTTER. Acta Crystallogr. B, **32**, 2671 (1976).
4. O. KNOP, W. J. WESTERHAUS, and M. FALK. Can. J. Chem. **58**, 270 (1980).
5. R. W. G. WYCKOFF. Am. J. Sci. **16**, 349 (1928).
6. K. KITAHAMA, H. KIRIYAMA, and Y. BABA. Bull. Chem. Soc. Jpn. **52**, 324 (1979).
7. R. B. COREY and R. W. G. WYCKOFF. Z. Kristallogr. **89**, 469 (1934).
8. M. H. BEN GHOZLEN, A. DAOUD, and J. W. BATS. Acta Crystallogr. B, **37**, 1415 (1981).
9. R. W. G. WYCKOFF and R. B. COREY. Am. J. Sci. **18**, 437 (1929).
10. R. W. G. WYCKOFF. Z. Kristallogr. **68**, 231 (1928).
11. H. SOWA, U. DRÜCK, and A. KUTOGLU. Cryst. Struct. Commun. **10**, 699 (1981).
12. A. RIES. Z. Kristallogr. **36**, 321 (1902).
13. O. KNOP, I. A. OXTON, and M. FALK. Can. J. Chem. **57**, 404 (1979); **57**, 2003 (1979).
14. K. WENDEKAMM. Z. Kristallogr. **85**, 35 (1933).
15. G. CHAPUIS and F. J. ZUNIGA. Acta Crystallogr. B, **36**, 807 (1980).
16. Y. KUME, R. IKEDA, and D. NAKAMURA. J. Magn. Reson. **20**, 276 (1975).
17. Y. FURUKAWA, H. KIRIYAMA, and R. IKEDA. Bull Chem. Soc. Jpn. **50**, 1927 (1977).
18. T. MATSUO, M. UEDA, and H. SUGA. Chem. Phys. Lett. **82**, 577 (1981).
19. C. J. LUDMAN, C. I. RATCLIFFE, and T. C. WADDINGTON. J. Chem. Soc. Faraday 2, **72**, 1759 (1976).
20. I. A. OXTON, O. KNOP, and J. L. DUNCAN. J. Mol. Struct. **38**, 25 (1977).
21. I. A. OXTON and O. KNOP. J. Mol. Struct. **37**, 59 (1977).
22. G. KERESZTURY, O. KNOP, and M. FALK. Can. J. Chem. **60**, 1972 (1982).
23. O. KNOP, I. A. OXTON, W. J. WESTERHAUS, and M. FALK. J. Chem. Soc. Faraday 2, **77**, 811 (1981).
24. A. RIES. Z. Kristallogr. **39**, 49 (1904).
25. F. GENET. Bull. Soc. Fr. Miner. Crist. **88**, 463 (1965).
26. G. C. PIMENTEL and A. L. MCCLELLAN. The hydrogen bond. W. H. Freeman and Co., San Francisco. 1960. Fig. 3–21, p. 107.
27. R. S. MCDOWELL. Doctoral thesis. Massachusetts Institute of Technology, Cambridge, MA. 1960.
28. R. IKEDA, Y. KUME, D. NAKAMURA, Y. FURUKAWA, and H. KIRIYAMA. J. Magn. Reson. **24**, 9 (1976).
29. O. KNOP, W. J. WESTERHAUS, and M. FALK. Can. J. Chem. **58**, 867 (1980).
30. C. GARNI. Das allgemeine Fachwörterbuch der Sauerkrautwissenschaft. 27th ed. E. Wiener-Verlag, Frankfurt. 1979.
31. D. T. CROMER and R. J. KLINE. J. Am. Chem. Soc. **76**, 5282 (1954).
32. YU. I. MIRONOV, S. V. ZEMSKOV, G. I. ZHARKOVA, B. I. OBMOIN, and YU. I. NIKONOROV. Izv. Sib. Otd. AN SSSR, ser. khim. nauk, 95 (1976); Chem. Abstr. **86**, 10959*j* (1977).
33. R. W. BERG and I. SØTOFTE. Acta Chem. Scand. B, **33**, 157 (1979).
34. R. B. COREY. Z. Kristallogr. **89**, 10 (1934).
35. E. STARITZKY and J. SINGER. Acta Crystallogr. **5**, 536 (1952).
36. D. BROWN and P. J. JONES. J. Chem. Soc. A, 243 (1967).
37. D. BROWN, B. WHITTAKER, and N. EDELSTEIN. Inorg. Chem. **13**, 1805 (1974).
38. D. BROWN, C. T. REYNOLDS, and P. T. MOSELEY. J. Chem. Soc. Dalton, 857 (1972).
39. A. RIES. Z. Kristallogr. **49**, 513 (1911).
40. R. W. BERG and K. NIELSEN. Acta Chem. Scand. A, **33**, 157 (1979).
41. O. KNOP. J. Solid State Chem. **45**, 223 (1982).
42. R. W. G. WYCKOFF and R. B. COREY. Am. J. Sci. **17**, 239 (1929).
43. W. SCHAFFER. Acta Crystallogr. **7**, 242 (1954).
44. R. W. G. WYCKOFF and R. B. COREY. Am. J. Sci. **18**, 138 (1929).
45. A. ZALKIN. Acta Crystallogr. **10**, 557 (1957).
46. K. KITAHAMA and H. KIRIYAMA. Acta Crystallogr. A, **34**, S302 (1978).
47. Y. KUME, R. IKEDA, and D. NAKAMURA. J. Magn. Reson. **33**, 331 (1979).
48. R. L. ARMSTRONG and H. M. VAN DRIEL. *In* Advances in nuclear quadrupole resonance. Vol. 2. *Edited by* J. A. S. Smith. Heyden and Son, London. 1975. p. 179.
49. K. RÖSSLER and J. WINTER. Chem. Phys. Lett. **46**, 566 (1977).
50. H. BOYSEN and A. W. HEWAT. Acta Crystallogr. B, **34**, 1412 (1978).
51. C. J. BRADLEY and A. P. CRACKNELL. The mathematical theory of symmetry in solids. Clarendon Press, Oxford. 1972.
52. A. I. KITAIGORODSKY. Molecular crystals and molecules. Academic Press, New York and London. 1973.
53. J. L. HOARD and M. B. WILLIAMS. J. Am. Chem. Soc. **64**, 633 (1942).
54. D. L. DEADMORE and W. F. BRADLEY. Acta Crystallogr. **15**, 186 (1962).
55. T. S. CAMERON and R. E. CORDES. Acta Crystallogr. B, **35**, 748 (1979).
56. International tables for X-ray crystallography. Vol. IV. The Kynoch Press, Birmingham, England. 1974.
57. G. SHELDRICK. SHELX system report. University Chemical Laboratories, Lensfield Road, Cambridge, England. 1976.
58. W. J. WESTERHAUS, O. KNOP, and M. FALK. Can. J. Chem. **58**, 1355 (1980).
59. G. HERZBERG. Molecular spectra and molecular structure. Vol. 2. Van Nostrand, New York. 1945. pp. 215*ff*.
60. J. R. SCHERER. *In* Advances in infrared and Raman spectroscopy. Vol. 5. *Edited by* R. J. H. Clark and R. E. Hester. Heyden and Son, London. 1978. pp. 149*ff*.
61. R. J. C. BROWN and S. L. SEGEL. J. Magn. Reson. **45**, 284 (1981).
62. K. NIELSEN and R. W. BERG. Acta Chem. Scand. A, **34**, 153 (1980).

A systematic study on volumetric interactions of cyclohexanone with various aliphatic hydrocarbons

B. CHAWLA,[1,2] RAM PARKASH, AND S. K. SURI

Department of Chemistry, Indian Institute of Technology, Hauz Khas, New Delhi-110 016, India

Received June 14, 1982

B. CHAWLA, RAM PARKASH, and S. K. SURI. Can. J. Chem. **61**, 1647 (1983).

Excess volumes of mixing, V^E, for binary mixtures of cyclohexanone with *n*-hexane, *n*-heptane, *n*-octane, *n*-nonane, *n*-decane, *n*-dodecane, *n*-tetradecane, and *n*-hexadecane at 25°C were determined from the precise and accurate experimental density data. The sign and magnitude of V^E were discussed in terms of the strength of the unlike interactions present in the binary mixtures.

Excess volumes of mixing of equimolar concentration ($V^E_{0.5}$) were also obtained. Attempts were made to interpret $V^E_{0.5}$ in terms of the size and polarity of the constituent molecule. The two effects could not be separated, but a good linear relation between $V^E_{0.5}$ and the solubility parameter was found.

B. CHAWLA, RAM PARKASH et S. K. SURI. Can. J. Chem. **61**, 1647 (1983).

Utilisant des données précises de densité expérimentales on a déterminé les volumes en excès de mélange V^E des mélanges binaires de cyclohexanone avec le *n*-hexane, le *n*-heptane, le *n*-nonane, le *n*-décane, le *n*-dodécane, le *n*-tétradécane et le *n*-hexadécane à 25°C. On discute du signe et de l'ordre de grandeur de V^E en fonction de la force des interactions contraires présentes dans les mélanges binaires.

On a également obtenu les volumes en excès de mélange de concentration équimolaire ($V^E_{0.5}$). On a essayé d'interpréter le ($V^E_{0.5}$) en fonction de la dimension et de la polarité de la molécule fondamentale. On ne peut pas séparer les deux effets, mais on a trouvé une bonne corrélation linéaire entre $V^E_{0.5}$ et la paramètre de solubilité.

[Traduit par le journal]

1. Introduction

Since the excess volume, V^E, of a binary mixture of a polar solute in a nonaqueous solvent is the result of unlike/like interactions (between the two molecules) governed by the combined contributions (such as size and polarity of the constituents), the V^E data do not show any obvious relationship with the properties of the constituents (1–4). In order to compare the experimental V^E values with the properties of the constituents, one must break V^E values into two major contributions such as, $V^E_{(size)}$ and $V^E_{(polarity)}$, which require V^E data from systematic studies on volume changes of binary mixtures. However, only a few such studies (but not exhaustive) have been reported in the literature (5, 6). Therefore, with a view to understand the factors determining the unlike interactions between the molecules of mixtures, we report in this paper the excess volumes of mixing of cyclohexanone with *n*-hexane, *n*-heptane, *n*-octane, *n*-nonane, *n*-decane, *n*-dodecane, *n*-tetradecane, and *n*-hexadecane at 25°C.

2. Experimental

Materials

Commercially available cyclohexanone, *n*-hexane, *n*-heptane, *n*-octane, *n*-nonane, *n*-decane, and *n*-dodecane of stated purity more than 99% were purified before their use according to established procedures (7). *n*-Tetradecane and *n*-hexadecane, samples of highest purity, were obtained from Koch-Light Lab. and Sigma Chemical Co., respectively, and were used without further purification. The purified reagents were stored under a dry nitrogen atmosphere during their use. The boiling points, densities, and refractive indices of the reagents agreed closely with the accepted literature values (7, 8). The amount of water present in each of these reagents was determined by a Karl Fischer Titrator, Model Aquatest IV (Photovolt Corporation, New York) and was found to be less than 0.01%. The reagents which were found to have more than 0.01% water were dried over activated 4A molecular sieves.

Apparatus and procedure

The values of V^E at 25°C were calculated from the experimental densities which were measured with a Vibrating-Tube Digital Density Meter (9) Model DMA 602/DMA-60 from Anton Paar, Austria. Water from a constant temperature bath was circulated through the metal block of the density meter at a flow rate of 3 $dm^3\ min^{-1}$. The thermal stability of the bath was better than $\pm 1 \times 10^{-3}$°C and was maintained by a Tronac PTC-40 proportional temperature controller. The density meter was calibrated with water and dry air every day. The density of water at 25°C was taken as 0.9970429 g cm^{-3} from Wagenbreth and Blanke (10).

Since differential measurements were performed, it was ensured that equal volumes of both the sample and the reference liquid were used by carefully completely filling the measuring cell (U-tube). It was ensured that there was no microbubble of air left inside the U-tube. The ports were finally plugged with small Teflon stoppers, which prevented any loss of liquid by vaporization. After the measurements, the sample was removed and the U-tube was then flushed with an appropriate cleaning solvent (e.g. acetone, alcohol, etc.), followed by air-drying with the help of the built-in pump. The reproducibility of the measurements was generally better than 3×10^{-5} g cm^{-3}. The details of the experimental technique for the preparation of solutions have been described earlier (11). The maximum uncertainty in the excess volumes of mixing data is expected to be less than ± 0.008 $cm^3\ mol^{-1}$.

3. Results and discussion

The excess volumes of mixing, V^E, for the binary mixtures as a function of solution composition at 25°C are recorded in Table 1 and plotted as a function of composition of cyclohexanone in Fig. 1. Along with experimental excess volumes, V^E_{exptl}, the calculated excess volumes, V^E_{calcd}, and δV^E ($V^E_{exptl} - V^E_{calcd}$) are also reported in Table 1 for all the systems at all solution compositions. The V^E_{calcd} are based on eq. [1]

$$[1]\quad V^E = X_1(1 - X_1)[A + B(2X_1 - 1) + C(2X_1 - 1)^2 + D(2X_1 - 1)^3 + E(2X_1 - 1)^4]$$

where X_1 is the mole fraction of cyclohexanone and A, B, C, D, and E are constants. The values of constants A, B, C, D, and

[1]To whom all correspondence should be addressed.

[2]Present address: Department of Chemistry, Paul M. Gross Chemical Laboratory, Duke University, Durham, NC 27706, U.S.A.

Can. J. Chem. Downloaded from www.nrcresearchpress.com by 210.87.254.5 on 09/06/12
For personal use only.

TABLE 1. Excess volumes of mixing, V^E, for the binary mixtures of cyclohexanone with various hydrocarbons at 25°C

Mole fraction of $C_6H_{10}O$	V^E (cm^3 mol^{-1}) Experimental	Calculated	δV^E	Mole fraction of $C_6H_{10}O$	V^E (cm^3 mol^{-1}) Experimental	Calculated	δV^E
	$C_6H_{10}O + C_6H_{14}$				$C_6H_{10}O + C_{10}H_{22}$		
0.0654	−0.054	−0.052	−0.002	0.0955	0.203	0.205	−0.002
0.1308	−0.136	−0.143	0.007	0.1672	0.298	0.292	0.006
0.1475	−0.173	−0.168	−0.005	0.3168	0.410	0.414	−0.004
0.2345	−0.298	−0.300	0.002	0.4332	0.451	0.455	−0.004
0.3395	−0.432	−0.428	−0.004	0.5519	0.431	0.432	−0.001
0.4678	−0.511	−0.508	−0.003	0.7441	0.326	0.314	0.012
0.7793	−0.369	−0.372	0.003	0.8815	0.215	0.223	−0.008
0.8413	−0.281	−0.293	0.012	0.9566	0.121	0.119	0.002
0.9259	−0.173	−0.155	−0.018		$C_6H_{10}O + C_{12}H_{26}$		
0.9575	−0.086	−0.093	0.007	0.0938	0.186	0.187	−0.001
	$C_6H_{10}O + C_7H_{16}$			0.2287	0.472	0.464	0.008
0.0677	0.038	0.035	0.003	0.3588	0.621	0.632	−0.011
0.1290	0.024	0.033	−0.009	0.6002	0.601	0.605	−0.004
0.2482	0.004	−0.001	0.005	0.6858	0.556	0.536	0.020
0.4248	−0.037	−0.047	0.010	0.7792	0.440	0.451	−0.011
0.4880	−0.061	−0.061	0.000	0.8367	0.388	0.389	−0.001
0.6322	−0.101	−0.087	−0.014	0.9751	0.099	0.099	0.000
0.7406	−0.101	−0.095	−0.006		$C_6H_{10}O + C_{14}H_{30}$		
0.7659	−0.088	−0.093	0.005	0.1302	0.418	0.417	0.001
0.8508	−0.067	−0.075	0.008	0.2378	0.579	0.583	−0.004
0.9274	−0.043	−0.040	−0.003	0.3564	0.739	0.733	0.006
	$C_6H_{10}O + C_8H_{18}$			0.6317	0.773	0.782	−0.009
0.1025	0.095	0.091	0.004	0.7069	0.698	0.699	−0.001
0.1357	0.100	0.107	−0.007	0.8023	0.577	0.556	0.021
0.2811	0.163	0.156	0.007	0.8594	0.432	0.450	−0.018
0.4356	0.173	0.179	−0.006	0.9114	0.334	0.330	0.004
0.6177	0.130	0.129	0.001		$C_6H_{10}O + C_{16}H_{34}$		
0.6928	0.095	0.094	0.001	0.1639	0.499	0.499	0.000
0.8747	0.037	0.037	0.000	0.2527	0.689	0.689	0.000
0.9682	0.018	0.018	0.000	0.3481	0.807	0.813	−0.006
	$C_6H_{10}O + C_9H_{20}$			0.3956	0.846	0.851	−0.005
0.2472	0.284	0.284	0.000	0.4541	0.899	0.883	0.016
0.3358	0.349	0.350	−0.001	0.6247	0.895	0.897	−0.002
0.5305	0.319	0.320	−0.001	0.7428	0.794	0.803	−0.009
0.6793	0.259	0.252	0.007	0.8784	0.502	0.494	0.008
0.7141	0.223	0.233	−0.010	0.9384	0.270	0.272	−0.002
0.7794	0.196	0.190	0.006				
0.8355	0.148	0.143	0.005				
0.8394	0.132	0.139	−0.007				
0.9646	0.018	0.018	0.000				

TABLE 2. Parameters of eq. [1] and standard deviation, $\sigma(V^E)$, in cm^3 mol^{-1} at 25°C for binary mixtures of cyclohexanone with various hydrocarbons

System (1) + (2)	A	B	C	D	E	$\sigma(V^E)$
$C_6H_{10}O + C_6H_{14}$	−2.0569	−0.2443	0.4129	−0.7425	0.3290	±0.009
$C_6H_{10}O + C_7H_{16}$	−0.2525	−0.4098	−0.1753	−0.3468	0.6470	±0.007
$C_6H_{10}O + C_8H_{18}$	0.6859	−0.4286	−0.7359	0.0618	1.1570	±0.005
$C_6H_{10}O + C_9H_{20}$	1.3292	−0.7705	0.6027	1.4606	−2.3947	±0.006
$C_6H_{10}O + C_{10}H_{22}$	1.8002	−0.4658	−0.4696	0.6586	1.9937	±0.006
$C_6H_{10}O + C_{12}H_{26}$	2.6385	−0.6026	−0.2847	1.9529	0.7078	±0.010
$C_6H_{10}O + C_{14}H_{30}$	3.3268	0.3300	−0.8212	−0.4775	2.8665	±0.011
$C_6H_{10}O + C_{16}H_{34}$	3.5922	0.4914	1.7789	0.3598	−1.5567	±0.008

E were evaluated by fitting experimental values of V^E and X_1 to eq. [1] by a least-square computer programme and are given in Table 2. The standard deviations, $\sigma(V^E)$ (defined in the usual way), of the V^E values are given in Table 2. These constants can be taken to represent the experimental results because the standard deviations for all the systems are observed to be comparable with the estimated uncertainties in the experimental determinations of V^E.

Can. J. Chem. Downloaded from www.nrcresearchpress.com by 210.87.254.5 on 09/06/12
For personal use only.

Can. J. Chem. Downloaded from www.nrcresearchpress.com by 210.87.254.5 on 09/06/12
For personal use only.

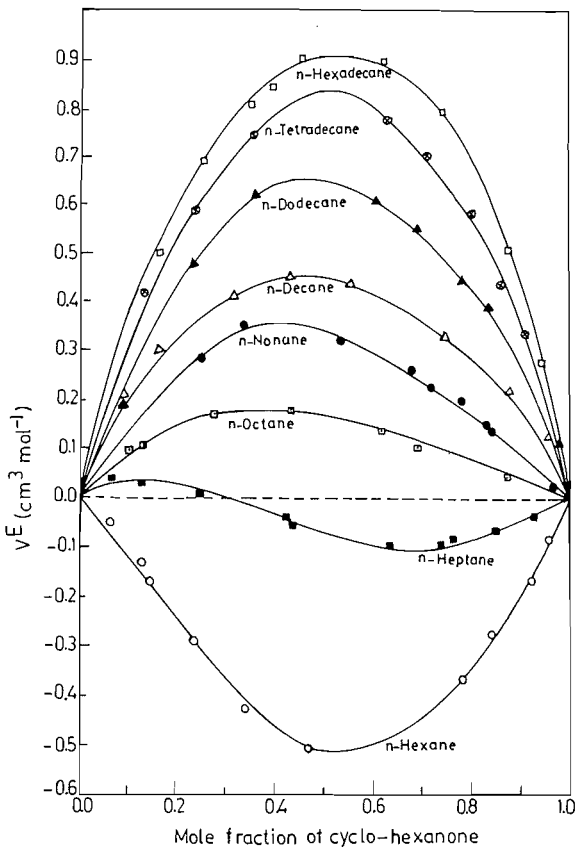

FIG. 1. Excess volumes of mixing, V^E, as a function of the composition for binary mixtures of cyclohexanone with various aliphatic hydrocarbons at 25°C.

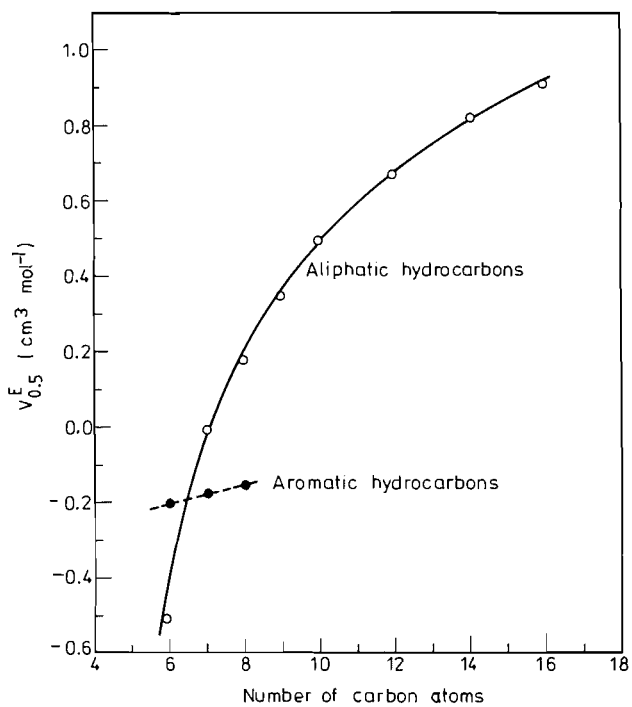

FIG. 2. Excess volumes at equimolar concentration, $V^E_{0.5}$, versus the number of carbon atoms in hydrocarbons.

It is observed from Fig. 1 that V^E varies almost symmetrically with the mole fraction of cyclohexanone and shows a maximum somewhere around equimolar concentration for each of the binary mixtures studied except for that of cyclohexanone and *n*-heptane. The excess volumes of mixing for mixtures of *n*-octane, *n*-nonane, *n*-decane, *n*-dodecane, *n*-tetradecane, and *n*-hexadecane with cyclohexanone are positive over the entire composition range. The positive V^E values

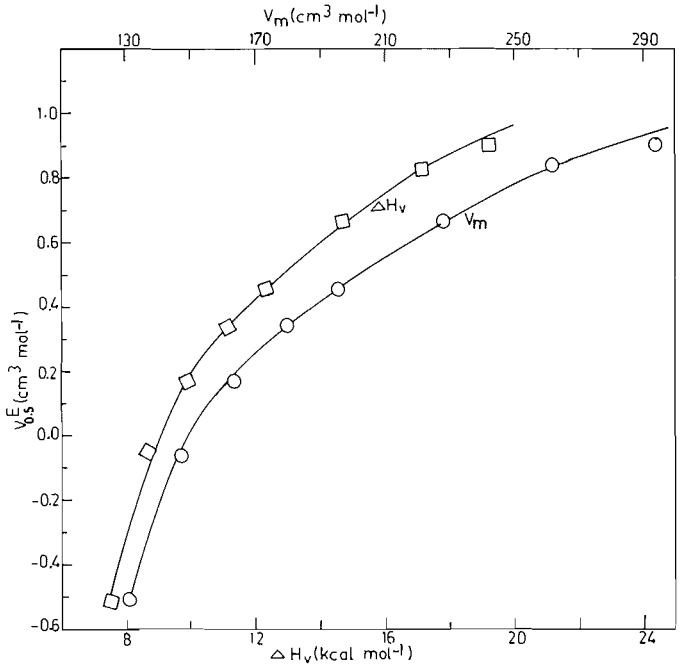

FIG. 3. Excess volumes at equimolar concentration, $V^E_{0.5}$, versus heats of vaporization and molar volumes of hydrocarbons at 25°C.

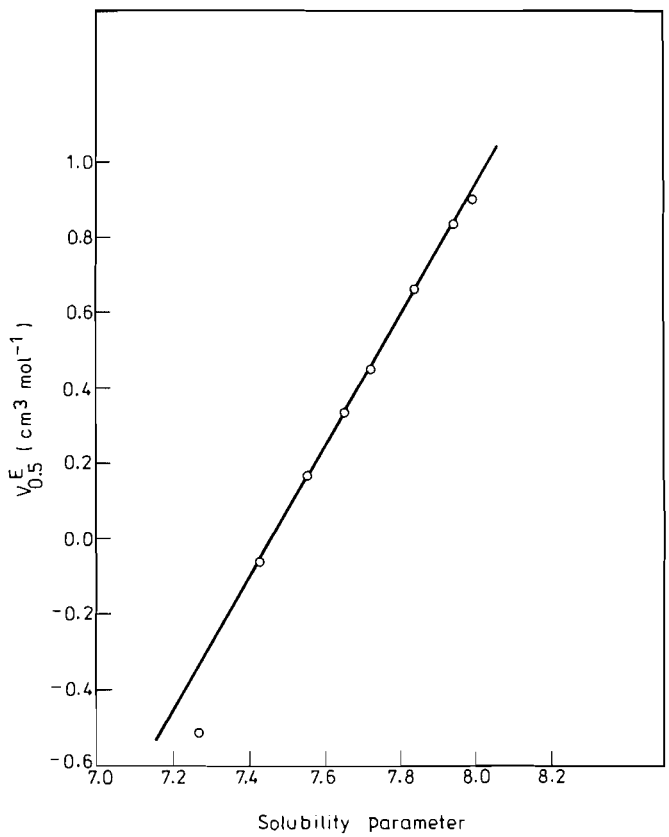

FIG. 4. Excess volumes at equimolar concentration, $V^E_{0.5}$, versus solubility parameters of hydrocarbons at 25°C.

TABLE 3. Molar volumes, V_m, heats of vaporization, ΔH_v, solubility parameter, $[(\Delta H_v - RT)/V_m]^{1/2}$, of various hydrocarbons and excess volumes at equimolar concentration, $V^E_{0.5}$, of $C_6H_{10}O$ + hydrocarbon systems at 25°C

Hydrocarbon	V_m ($cm^3\ mol^{-1}$)	ΔH_v[a] (kcal mol^{-1})	$[(\Delta H_v - RT)/V_m]^{1/2}$ (cal $cm^{-3})^{1/2}$	$V^E_{0.5}$ ($cm^3\ mol^{-1}$)
n-Hexane	131.61	7.54	7.27	−0.514
n-Heptane	147.47	8.74	7.43	−0.063
n-Octane	163.54	9.92	7.55	0.171
n-Nonane	179.68	11.10	7.65	0.342
n-Decane	195.92	12.28	7.72	0.450
n-Dodecane	228.60	14.64	7.84	0.660
n-Tetradecane	261.40	17.10[b]	7.95	0.831
n-Hexadecane	294.11	19.22	7.96	0.898

[a]Reference 12.
[b]Reference 13.

indicate that the unlike interactions present in these systems are weak. Furthermore, the increase in the value of V^E with the increasing size of the hydrocarbon (from *n*-octane to *n*-hexadecane) is taken to be an indication of a decrease in the strength of unlike interactions. On the other hand, the negative values of V^E for the cyclohexanone + *n*-hexane system is suggestive of the presence of stronger unlike intermolecular interactions as compared to those of other higher hydrocarbon systems under investigation. However, the positive V^E at lower concentrations and negative afterwards (see Fig. 1) for cyclohexanone + *n*-heptane system is suggestive of its intermediate behaviour.

To the best of our knowledge, there are no data available in the reported literature for the excess volumes of mixing of any of binary mixtures under investigation to compare with our results.

From Fig. 1, it is clear that V^E values at equimolar concentration ($V^E_{0.5}$) for the binary mixtures of cyclohexanone with various hydrocarbons are the best representations of the intermolecular interactions present in these mixtures. Therefore, the $V^E_{0.5}$ values obtained are compared with the molar volumes, the heats of vaporization, and the solubility parameters of the hydrocarbons in Table 3.

The increase in the value of $V^E_{0.5}$ with increasing size of hydrocarbon as shown in Fig. 2 ($V^E_{0.5}$ versus number of carbon atoms of hydrocarbon) is not linear. The increase in $V^E_{0.5}$ is sharp from C_6 to C_7 and it slows down with further increase in the carbon atoms. Recently, similar behaviour has been observed for tetrahydrofuran + hydrocarbon and triethylamine + hydrocarbon systems by Suri (2, 3). For the sake of comparison, we have also plotted in Fig. 2 the $V^E_{0.5}$ for cyclohexanone + aromatic hydrocarbons (4), and it is observed that the change in $V^E_{0.5}$ with the increase in carbon atoms is very small as compared to those of the aliphatic hydrocarbon systems.

The linear increase in molar volume and heat of vaporization of hydrocarbons with the increase in number of their carbon atoms reveals that neither of the two major causes (V^E_{inter} or V^E_{geom}) is alone responsible for the non-linear increase in $V^E_{0.5}$ with increasing size of hydrocarbons (Fig. 2). This was further supported with the observed non-linear behaviour of $V^E_{0.5}$ versus heats of vaporization and molar volumes of hydrocarbons (Fig. 3). The linear relation between $V^E_{0.5}$ and the solubility parameter (Fig. 4) suggests that the dipoles present in these mixtures are responsible for the nonlinear increase of $V^E_{0.5}$ observed therein. Therefore, separation and quantification of the contribution due to the increasing size of the hydrocarbon to $V^E_{0.5}$ is not possible from these sets of data alone. Further attempts in this direction are in progress and will be discussed somewhere else.

Acknowledgement

We are very thankful to Professor J. C. Ahluwalia, I.I.T., Delhi, for the use of the Digital Density Meter in his laboratory.

1. S. K. SURI and B. CHAWLA. J. Chem. Eng. Data, **26**, 268 (1981).
2. S. K. SURI. Can. J. Chem. **59**, 2839 (1981).
3. S. K. SURI. J. Chem. Eng. Data, **25**, 390 (1980).
4. B. CHAWLA, S. K. MEHTA, R. V. JASRA, and S. K. SURI. Can. J. Chem. To be published.
5. Y. P. HANDA and G. C. BENSON. Fluid Phase Equilibria, **3**, 185 (1979).
6. R. BATTINO. Chem. Rev. **71**, 5 (1971).
7. J. A. RIDDICK and W. B. BUNGER (*Editors*). Techniques of organic chemistry. Vol. II. Organic solvents. Wiley-Interscience, New York. 1970.
8. J. TIMMERMANS. Physico-chemical constants. Vol. II. Elsevier, Amsterdam. 1965.
9. A. K. MISHRA. Ph.D. Thesis. I.I.T., New Delhi, India. 1981.
10. (*a*) H. WAGENBRETH and H. BLANKE. PTB-Mitt. **6**, 412 (1971); (*b*) C. H. W. HIRS and S. N. TIMASHEFF (*Editors*). Methods of Enzymology. Academic Press, New York. 1979.
11. R. C. MAHESHWARI, S. K. SURI, and U. S. TIWARI. J. Chem. Eng. Data, **24**, 237 (1979).
12. J. D. COX and G. PILCHER. Thermochemistry of organic and organometallic compounds. Academic Press Inc., London. 1970.
13. R. R. DREISBACH. Physical properties of chemical compounds. Am. Chem. Soc. Publication, Vol. II. 1955.

Can. J. Chem. Downloaded from www.nrcresearchpress.com by 210.87.254.5 on 09/06/12
For personal use only.

3-Methylpyridine complexes of cobalt(II) and nickel(II) hexafluorophosphate and hexafluoroarsenate. Crystal and molecular structure of $Ni(H_2O)_2(3\text{-}CH_3C_5H_4N)_6(PF_6)_2$

RAYMOND M. MORRISON, ROBERT C. THOMPSON, AND JAMES TROTTER

Department of Chemistry, University of British Columbia, 2036 Main Mall, Vancouver, B.C., Canada V6T 1Y6

Received October 21, 1982

RAYMOND M. MORRISON, ROBERT C. THOMPSON, and JAMES TROTTER. Can. J. Chem. **61**, 1651 (1983).

Reaction of aqueous solutions containing Co^{2+} or Ni^{2+} and PF_6^- or AsF_6^- with excess 3-methylpyridine yields crystals of compounds of composition $M(H_2O)_2(3mpy)_6(EF_6)_2$. Blue crystals of diaquohexakis(3-methylpyridine)nickel(II) hexafluorophosphate, $C_{36}H_{46}F_{12}NiN_6O_2P_2$, are monoclinic, a = 10.497(1), b = 20.074(3), c = 21.836(5) Å, β = 103.93(2)°, Z = 4, space group Cc. The structure was determined with Mo$K\alpha$ CAD4 diffractometer data by direct methods, and refined by full-matrix least-squares procedures to R = 0.048 for 2723 reflections with $I \geq 3\sigma(I)$. The structure consists of $\{Ni(3mpy)_4[(OH_2)(3mpy)]_2\}^{2+}$ cations and PF_6^- anions. The cation contains a NiN_4O_2 chromophore with water molecules occupying *trans* positions of a distorted octahedron about nickel. One additional 3-methylpyridine molecule is H-bonded to each of the water molecules with O—H...N distances of 2.717(11) and 2.719(11) Å. Weak interaction of each water molecule via its second hydrogen atom with a PF_6^- ion is indicated by the positioning of the anions. The O—H...F distances are 2.958(11) and 2.959(11) Å. Two other complexes of this type, where M is Ni and E is As and where M is Co and E is P, are reported here and on the basis of spectroscopic and magnetic studies are assigned structures similar to the Ni/P complex.

Decomposition of the *aquo* complexes under mild conditions yields compounds of composition $M(3mpy)_4(EF_6)_2$. $Ni(3mpy)_4(PF_6)_2$ is assigned a square planar structure with weakly interacting PF_6^- anions in axial positions. Both $Co(3mpy)_4(EF_6)_2$ complexes, where E is P or As, have tetrahedral $[Co(3mpy)_4]^{2+}$ cations and non-coordinated anions.

RAYMOND M. MORRISON, ROBERT C. THOMPSON et JAMES TROTTER. Can. J. Chem. **61**, 1651 (1983).

Les solutions aqueuses contenant du Co^{2+} ou du Ni^{2+} et du PF_6^- ou du AsF_6^- réagissent avec un excès de méthyl-3 pyridine en donnant un composé cristallin le $M(H_2O)_2(3mpy)_6(EF_6)_2$. Les cristaux bleus d'hexafluorophosphate de diaquohexakis (méthyl-3 pyridine) nickel(II) $C_{36}H_{46}F_{12}NiN_6O_2P_2$ sont monocliniques et appartiennent au groupe d'espace Cc avec a = 10,497(1), b = 20,074(3), c = 21,836(5) Å, β = 103,93(2)°, Z = 4. On a déterminé la structure par des méthodes directes en utilisant un diffractomètre de type Mo$K\alpha$ CAD4 et on l'a affinée par la méthode des moindres carrés (matrice entière) jusqu'à une valeur de R = 0,048 pour 2723 réflexions avec $I \geq 3\sigma(I)$. La structure comprend des cations de $\{Ni(3mpy)_4[(OH_2)(3mpy)]_2\}^{2+}$ et des anions PF_6^-. Le cation contient un chromophore NiN_4O_2 avec les molécules d'eau en positions *trans* dans un octaèdre déformé autour du nickel. De plus la méthyl-3 pyridine est liée par des liaisons hydrogène à chaque molécule d'eau avec des distances O—H...N de 2,717(11) et de 2,719(11) Å. La position des anions témoigne d'une faible interaction de chaque molécule d'eau avec l'ion PF_6^- par l'intermédiaire de son second atome d'hydrogène. Les distances O—H...F sont de 2,958(11) et de 2,959(11) Å. On rapporte deux autres complexes de ce type où M = Ni et E = As et où M = Co et E = P, et en se basant sur les études spectroscopiques et magnétiques on leur attribue une structure semblable à celle du complexe Ni/P.

La décomposition des complexes *aqueux* dans des conditions douces conduit à des produits de composition $M(3mpy)_4(EF_6)_2$. On attribue une structure plan-carrée au complexe $Ni(3mpy)_4(PF_6)_2$ avec une faible interaction des anions en positions axiales. Les deux complexes de $Co(3mpy)_4(EF_6)_2$ où E = P ou As ont des cations $[Co(3mpy)_4]^{2+}$ tétraédriques et des anions non coordonnées.

[Traduit par le journal]

Introduction

Earlier communications on synthesis, structure, and bonding in cobalt(II) and nickel(II) complexes containing PF_6^- and AsF_6^- have been concerned with pyridine (py) and 4-methylpyridine (4mpy) derivatives (1–4). PF_6^- and AsF_6^- complexes of the type $Co(py)_4A_2$ and $Ni(py)_4A_2$ contain non-coordinated anions (2, 4); in contrast, the anions are co-ordinated in the corresponding perchlorates (5, 6) leading to the conclusion that the EF_6^- ions should be assigned weaker ligating abilities than ClO_4^-. Consistent with this is the observation that, although species such as $[Co(py)_6]^{2+}$ and $[Ni(py)_6]^{2+}$ are not obtainable in the solid state with ClO_4^- as the counter anion, these species are found in the solid state in combination with PF_6^- and AsF_6^- (2, 4).

The work with 4-methylpyridine complexes yielded crystalline materials suitable for X-ray studies (3, 4, 7) and led to some interesting comparisons with the pyridine derivatives (and in turn prompted the present extension of the work). Whereas reaction of excess pyridine with aqueous solutions containing cobalt(II) or nickel(II) and the EF_6^- anions gives six-coordinate complexes of the type $[M(py)_6](EF_6)_2$ (2), reactions involving 4-methylpyridine under similar conditions form compounds of composition $[M(H_2O)_2(4mpy)_8](EF_6)_2$. Structurally related to the perchlorate complex, $[Ni(H_2O)_2(4mpy)_4](ClO_4)_2$ (8), these compounds are six-coordinate and have *trans* coordinated water molecules each of which is strongly H-bonded to two additional 4-methylpyridine ligands (3). Another interesting comparison concerns $[Ni(py)_4](AsF_6)_2$ and $[Ni(4mpy)_4](AsF_6)_2$. The pyridine complex has been found to undergo a structural change at low temperatures to a form which contains coordinated AsF_6^-, while no such phenomenon is observed for the 4-methylpyridine analogue (4). Finally, comparisons of the electronic spectra of related 4-methylpyridine and pyridine complexes showed that whereas the greater basicity of 4-methylpyridine (pK_a of 6.02 compared to 5.17 for pyridine (9)) appears to result in a significant increase in energy in the electronic absorption bands of $Cu(4mpy)_4(EF_6)_2$ complexes over the pyridine analogues (10), it has no detectable effect on the electronic spectra of analogous cobalt and nickel compounds (3).

To investigate the effect of varying neutral ligand basicity further and to explore the possible effects of steric crowding in the neutral ligands, we studied other methylpyridine complexes of cobalt and nickel. We were unable to isolate stable

Can. J. Chem. Downloaded from www.nrcresearchpress.com by 210.87.254.5 on 09/06/12
For personal use only.

TABLE 1. Analytical data

Compound	Calculated %			Found %		
	C	H	N	C	H	N
$Co(H_2O)_2(C_6H_7N)_6(PF_6)_2$	45.8	4.91	8.91	45.5	5.15	8.90
$Ni(H_2O)_2(C_6H_7N)_6(PF_6)_2$	45.8	4.91	8.91	45.8	4.77	8.99
$Ni(H_2O)_2(C_6H_7N)_6(AsF_6)_2$	41.9	4.50	8.15	41.9	4.49	8.12
$Co(C_6H_7N)_4(PF_6)_2$	40.0	3.91	7.77	40.0	4.00	7.79
$Co(C_6H_7N)_4(AsF_6)_2$	35.6	3.49	6.92	35.7	3.51	6.98
$Ni(C_6H_7N)_4(AsF_6)_2$	35.6	3.49	6.93	35.4	3.50	6.74

2-methylpyridine analogues (where steric crowding effects are presumably too great, leading to instability); however, several 3-methylpyridine (3mpy; pK_a = 5.68 (9)) complexes were isolated and characterized.

Experimental

Materials

3-Methylpyridine was refluxed over barium oxide for 24 h then distilled at atmospheric pressure. Other materials were reagent grade and used as received.

All products were found to be unstable in air. All manipulations were performed in an inert atmosphere box filled with dry nitrogen.

Preparations

Diaquohexakis(3-methylpyridine)cobalt(II) and nickel(II) hexafluorophosphate and hexafluoroarsenate, $M(H_2O)_2(3mpy)_6(EF_6)_2$

These compounds were obtained by the method described previously for the preparation of the 4-methylpyridine complexes of composition $M(H_2O)_2(4mpy)_8A_2$ (3). In the present work, however, instead of using a 2:1 ratio of NH_4PF_6 (or $KAsF_6$) to metal nitrate, the ratio employed was about 2.5:1. The addition of excess salt was found to improve the crystallization which took place within about a week. The crystals (orange–red for cobalt and blue for nickel) were washed with a solution of 5 mL 3-methylpyridine in 50 mL water. Since they tended to lose 3-methylpyridine on prolonged exposure to the atmosphere or to a vacuum, the crystals were stored in sealed vials while still "wet" with the washing liquid. Just prior to further use the crystals were dried for about 15 min *in vacuo* at room temperature. Subsequent decomposition under these "dry" conditions was sufficiently slow for all but one of the compounds that reliable elemental analysis, spectral and magnetic data could be obtained.

$Co(H_2O)_2(3mpy)_6(AsF_6)_2$ was, however, so unstable as a "dry" solid that it could not be properly characterized. Its composition is not known for certain but is assumed to be as indicated by analogy with the other complexes prepared in the same manner. The ultimate product of its decomposition under vacuum is, as described below, $Co(3mpy)_4(AsF_6)_2$.

Tetrakis(3-methylpyridine)cobalt(II) hexafluoroarsenate and hexafluorophosphate, $Co(3mpy)_4(EF_6)_2$

These compounds were obtained as violet powders from the corresponding dried $Co(H_2O)_2(3mpy)_6(EF_6)_2$ complexes by grinding to a fine powder in the inert atmosphere box followed by pumping *in vacuo* for 24 h. No heating was required. The compounds are extremely hygroscopic.

Tetrakis (3-methylpyridine)nickel(II) hexafluoroarsenate, $Ni(3mpy)_4(AsF_6)_2$

$Ni(H_2O)_2(3mpy)_6(AsF_6)_2$ was ground to a fine powder in the inert atmosphere box and then dried under vacuum and at room temperature for 24 h. The light blue–yellow powder was then transferred to the dry-box where it was placed in a flask containing a large excess of chloroform. Upon stirring, the suspended material changed to an orange–yellow powder which was filtered, washed with chloroform, and dried *in vacuo*.

Analyses

C, H, and N analyses were obtained by P. Borda of the Department of Chemistry, The University of British Columbia. Analytical data are given in Table 1.

Spectroscopic and magnetic susceptibility measurements

Infrared spectra, electronic spectra, and magnetic susceptibility data were obtained using equipment and methods described previously (3).

X-ray crystal analysis

Crystals of $Ni(H_2O)_2(3mpy)_6(PF_6)_2$ are unstable in air and were sealed in 0.3 mm diameter Lindemann capillaries for study. The initial Weissenberg and precession photographs indicated a monoclinic space group and the systematic absences (*hkl*: $h + k = 2n + 1$; *h*0*l*: $l = 2n + 1$ ($h = 2n + 1$); 0*k*0: ($k = 2n + 1$)) gave the space group as Cc (C_s^4, No. 9) or $C2/c$ (C_{2h}^6, No. 15). Intensity statistics were ambiguous, but observation of significant intensity differences between *hk*0 Friedel pairs indicated space group Cc.

The crystal chosen for data collection was mounted in a random orientation on the Enraf-Nonius CAD4 computer-controlled diffractometer equipped with monochromated Mo$K\alpha$ (λ = 0.71069 Å) X-ray source; 25 reflections were found automatically in reciprocal space and indexed to a triclinic unit cell. A simple transformation of the unit cell was needed to give the *C*-centered monoclinic cell indicated by the preliminary photographs. The crystal data are:

$C_{36}H_{46}F_{12}N_6NiO_2P_2$ fw = 943.5

monoclinic, space group Cc, a = 10.497(1), b = 20.074(3), c = 21.836(5) Å, β = 103.93(2)°, V = 4466 Å^3, Z = 4, ρ_{calcd} = 1.41, μ(Mo$K\alpha$) = 11.9 cm^{-1}.

The reflection intensities were collected in the range $2 \leq 2\theta \leq 50°$ with an ω scan, scan angle (1.10 + 0.35 tan θ)°, extended 25% on both sides to provide background counts, with a horizontal aperature of (1.75 + tan θ) mm. Three orientation control reflections were measured every 100 reflections and the orientation matrix recalculated if the scattering vector was greater than 0.1° from the calculated position. Three intensity control reflections were measured every 3600 seconds of X-ray exposure time; during the data collection, the mean of their intensities varied randomly ±1.3%. In the data reduction, Lorentz-polarization (LP) corrections were applied and an estimated standard deviation was assigned: $\sigma^2(I) = S + 4(B_1 + B_2) + (dI)^2$, where S = scan count and B_1 and B_2 = background counts; d was adjusted during the refinement, with a final value of 0.076. Of the 4054 reflection data collected (including *hk*0 Friedel pairs), 2723 (67%) had $I \geq 3\sigma(I)$.

The structure was solved by direct methods applied in space group $C2/c$. The largest peak on the *E*-map, at 1/2, 1/8, 1/4, apparently corresponded to the Ni atom on a special (*e*) position of C_2 symmetry; two further peaks of about one-quarter the height of the Ni atom could be interpreted as two independent half-phosphorus atoms separated by only 2.8 Å. This would represent a disordered structure and a more reasonable interpretation in terms of Cc was confirmed by further analysis. C, N, O, and F atom positions were determined from electron-density maps phased on Ni and 2P, and the structure was refined by full-matrix least-squares procedures, with scattering factors from ref. 11, and anomalous dispersion corrections for Ni and P (choice of the correct axial directions gave good agreement between F_o and F_c for the *hk*0 Friedel pairs; reversed choice of axis gave

Can. J. Chem. Downloaded from www.nrcresearchpress.com by 210.87.254.5 on 09/06/12
For personal use only.

TABLE 2. Final positional (fractional × 10^4, Ni and P × 10^5) and isotropic thermal parameters ($U \times 10^3$ Å^2) with estimated standard deviations in parentheses

Atom	x	y	z	U_{eq}
Ni	50000	12491(6)	25000	40
P(1)	19682(31)	−5959(17)	8868(14)	64
P(2)	35809(31)	30943(16)	41131(14)	64
O(1)	5169(6)	2213(3)	2888(3)	50
O(2)	4779(6)	285(3)	2113(3)	53
N(1)	3872(7)	935(4)	3134(3)	43
C(11)	2794(9)	563(5)	2925(5)	49
C(12)	2050(9)	302(5)	3304(5)	57
C(13)	2432(12)	432(6)	3948(6)	70
C(14)	3515(12)	831(8)	4174(5)	69
C(15)	4256(10)	1078(5)	3758(5)	55
C(16)	865(12)	−123(6)	3027(7)	83
N(2)	3225(8)	1567(4)	1865(4)	46
C(21)	2364(9)	1939(5)	2074(5)	49
C(22)	1251(9)	2194(5)	1701(5)	57
C(23)	981(11)	2059(6)	1050(6)	71
C(24)	1850(12)	1663(7)	823(6)	68
C(25)	2986(10)	1428(5)	1240(5)	58
C(26)	337(12)	2625(6)	1976(8)	87
N(3)	6111(8)	1542(4)	1855(4)	50
C(31)	6953(10)	1109(5)	1693(5)	59
C(32)	7591(12)	1227(6)	1220(6)	68
C(33)	7341(12)	1832(7)	903(6)	69
C(34)	6480(11)	2293(6)	1070(5)	65
C(35)	5901(10)	2129(5)	1543(4)	53
C(36)	8535(19)	713(8)	1067(9)	127
N(4)	6756(8)	961(4)	3146(4)	47
C(41)	7758(10)	1390(5)	3307(5)	57
C(42)	8871(10)	1272(6)	3778(6)	67
C(43)	8952(11)	671(7)	4104(6)	70
C(44)	7911(12)	208(6)	3926(6)	65
C(45)	6852(11)	367(5)	3452(4)	54
C(46)	9951(14)	1791(8)	3939(9)	114
N(5)	7184(8)	3101(5)	3137(5)	66
C(51)	7617(12)	3227(7)	3757(7)	75
C(52)	8709(12)	3642(6)	4002(6)	69
C(53)	9349(12)	3893(6)	3563(7)	78
C(54)	8899(13)	3765(6)	2938(6)	74
C(55)	7780(13)	3368(6)	2726(7)	75
C(56)	9129(19)	3762(11)	4688(7)	121
N(6)	6544(9)	−603(4)	1865(5)	68
C(61)	6371(12)	−735(7)	1240(6)	74
C(62)	7212(13)	−1140(6)	1009(6)	71
C(63)	8267(12)	−1400(6)	1430(7)	74
C(64)	8471(13)	−1272(6)	2074(6)	75
C(65)	7556(12)	−866(6)	2268(6)	72
C(66)	6938(20)	−1255(11)	305(7)	124
F(11)	3081(13)	−1034(6)	1299(5)	146
F(12)	1889(11)	−1091(5)	326(4)	121
F(13)	2073(10)	−90(5)	1449(4)	117
F(14)	3080(12)	−186(6)	692(6)	152
F(15)	989(15)	−1024(7)	1117(8)	189
F(16)	953(16)	−150(7)	471(7)	205
F(21)	4887(10)	2688(5)	4305(6)	148
F(22)	2359(11)	3513(7)	3879(9)	193
F(23)	2964(20)	2649(7)	4524(7)	208
F(24)	3128(10)	2582(5)	3554(4)	120
F(25)	4066(11)	3599(5)	4671(4)	122
F(26)	4293(13)	3520(6)	3694(5)	143

distinctly poorer agreement, within Friedel pair differences in the wrong sense for most reflections). The weights were taken as $w = 1/\sigma^2(F)$, and final R and R_w were 0.048 and 0.061, respectively, for the 2723 reflections with $I > 3\sigma(I)$ (0.051 and 0.063, respectively, for opposite sense of a and c axis). For all 4054 reflections, $R = 0.091$. A final difference map had maximum fluctuations of +0.4 and −0.2 e Å^{-3}. The final positional and thermal parameters are given in Tables 2 and 3,[1] respectively. The observed and calculated structure factors have been placed in the Depository of Unpublished Data.[1]

Results and discussion

Syntheses

The reaction of aqueous solutions containing Co^{2+} or Ni^{2+} and PF_6^- or AsF_6^- with excess 3-methylpyridine results in the crystallization, over a period of about one week, of complexes of composition $M(H_2O)_2(3mpy)_6(EF_6)_2$. These materials lose 3-methylpyridine on prolonged exposure, at room temperature, to the atmosphere or to a vacuum. The cobalt(II) complexes are particularly unstable; the hexafluoroarsenate decomposed so readily at ordinary temperatures that its characterization was not possible and both it and the hexafluorophosphate derivative readily gave the $Co(3mpy)_4(EF_6)_2$ complexes when subjected to a dynamic vacuum at room temperature. By comparison (3), the related 4mpy complexes, $Co(H_2O)_2(4mpy)_8(EF_6)_2$ require elevated temperatures for complete conversion to $Co(4mpy)_4(EF_6)_2$. The nickel complexes, $Ni(H_2O)_2(3mpy)_6(EF_6)_2$, are slightly more stable than the cobalt analogues; on exposure to a dynamic vacuum for 24 h at room temperature they yield mixtures of starting material and $Ni(3mpy)_4(EF_6)_2$ product. Complete conversion of the hexafluoroarsenate to $Ni(3mpy)_4(AsF_6)_2$ was obtained here by stirring a sample of the mixtures in chloroform, a procedure not unlike that used to prepare the corresponding pyridine derivative (4).

Crystal structure analysis

The question of whether the materials of composition $M(H_2O)_2(3mpy)_6(EF_6)_2$ contain MN_6 chromophores or MN_4O_2 chromophores with non-coordinated 3-methylpyridine ligands was resolved through a single crystal X-ray diffraction study of $Ni(H_2O)_2(3mpy)_6(PF_6)_2$. The stucture consists of $\{Ni(3mpy)_4[(OH_2)(3mpy)]_2\}^{2+}$ cations and PF_6^- anions. The cation (Fig. 1) contains a NiN_4O_2 chromophore with water molecules occupying *trans* positions of a distorted octahedron about nickel. Four of the 3-methylpyridine ligands are bonded to nickel and the other two are connected, through hydrogen bonds, one to each of the coordinated water molecules. The O—H.....N distances of 2.719(11) and 2.717(11) Å (Table 4) are shorter than the value 2.812 Å found in $Ni(NCS)_2(qn)_4(H_2O)_2$, a complex containing similarly bonded quinoline molecules (12). The 3-methylpyridine moieties are all planar, within experimental error, and the bond distances and angles in the rings are similar to those found in a microwave study of pyridine (13). The Ni—N distances (Table 4) are 2.114–2.135(8), mean 2.122 Å, and Ni—O are 2.103(6) and 2.102(8) Å. These distances compare with Ni—N = 2.18 Å and Ni—O = 2.13 Å in the quinoline complex (12). The *trans* bonds show slight deviations from linearity (178.2, 178.5, 178.7°), but overall the distortion of the chromophore is not very great and the symmetry of the ligand field about nickel may be reasonably described as D_{4h}.

Close examination of the structure provides evidence for significant cation–anion interaction in this complex (Fig. 1).

[1]Anisotropic thermal parameters (Table 3), full listing of bond lengths and angles, and structure factors are available, at a nominal charge, from the Depository of Unpublished Data, CISTI, National Research Council of Canada, Ottawa, Ont., Canada K1A 0S2.

Can. J. Chem. Downloaded from www.nrcresearchpress.com by 210.87.254.5 on 09/06/12
For personal use only.

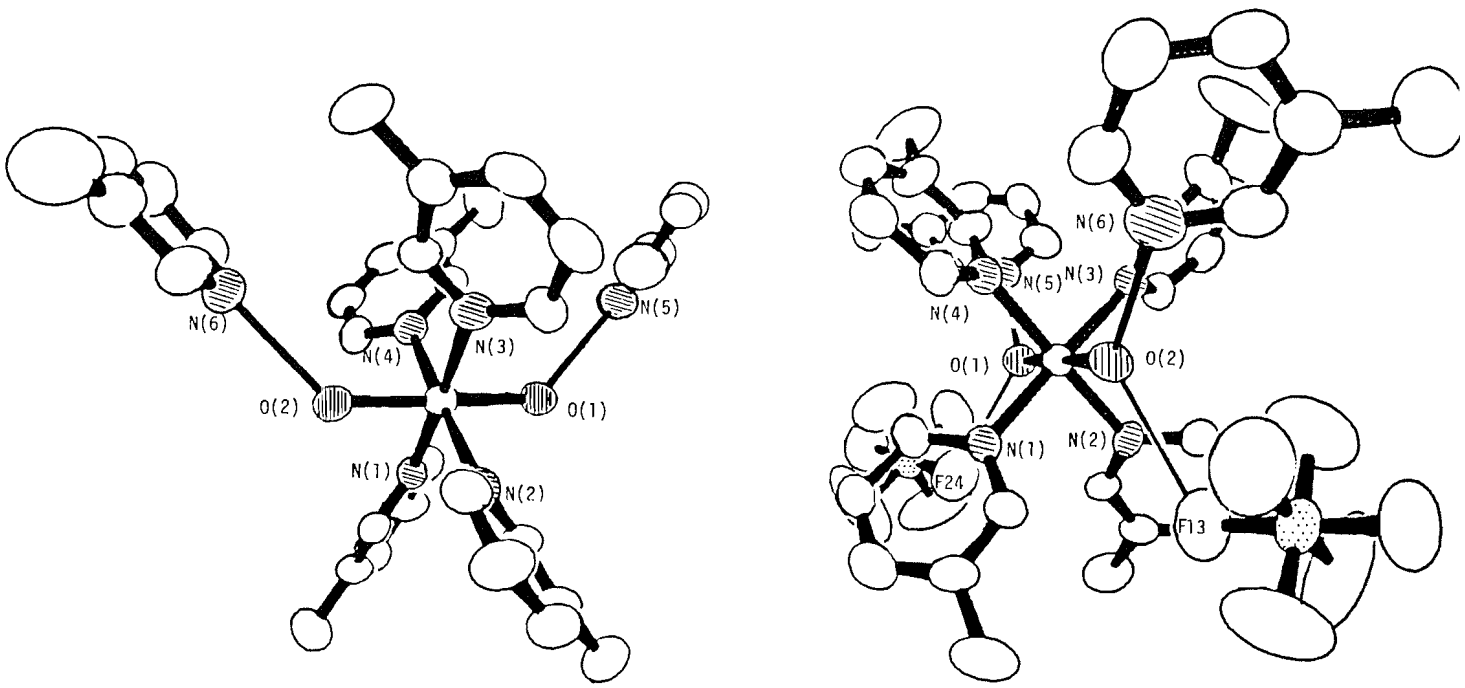

FIG. 1. Two views of $[Ni(H_2O)_2(3mpy)_6]^{2+}$; the right-hand view includes the PF_6 groups. All atoms drawn with 50% probability thermal ellipsoids.

Each water molecule is clearly hydrogen bonded to a 3-methylpyridine ligand through one of its hydrogen atoms. Interaction of each water molecule via its second hydrogen atom with a PF_6^- ion is indicated by the positioning of the anions. The hydrogen bonding involved here, however, must be considered very weak. The O—H...F distances of 2.958(11) and 2.959(11) Å observed in this complex are significantly longer, for example, than the values 2.38 Å, 2.44 Å, and 2.41–2.49 Å observed in $KH_2PO_3.HF$ (14), $KF.(CH_2CO_2H)_2$ (15), and $KF.CH_2(CO_2H)_2$ (15), respectively, and are just outside the range of 2.56 to 2.86 Å observed in a number of metal fluoride hydrates (16).

The ligands are oriented so that the $Ni(3mpy)_4O_2$ grouping has approximate D_2 symmetry; inclusion of the hydrogen-bonded 3mpy molecules and the PF_6^- ions gives roughly C_2 symmetry for the whole complex of one cation and two anions (Fig. 1), although there is no required crystallographic symmetry (C_1). The complex are further linked together in the crystal only by van der Waals forces.

The geometries at the O atoms are not far from planar, with mean angles Ni—O...N = 132.0(3), Ni—O...F = 115.5(3), N...O...F = 110.4(3), sum = 358°.

The PF_6^- ions exhibit typical large thermal motion. The thermal parameters are smallest for the F atoms involved in the interactions with the water molecules, F(13) and F(24), and the atoms *trans* to these in the octahedral anion, F(12) and F(25); for these atoms the U(isotropic) values (Table 2) are all about 0.12 Å^2 (corresponding to rms displacements of about 0.35 Å), while for the other four atoms of each PF_6^- ion, U(isotropic) = 0.14–0.21 Å, with individual U_{ij} values (Table 3) as high as 0.37 Å (rms displacement 0.6 Å). The weak O—H...F interactions therefore appear to be strong enough to anchor the PF_6^- ions, with the main thermal motion being librations (or rotations) about the F(13)...F(12) and F(24)...F(25) axes. The P—F(13) and P—F(24) bonds are the longest among the P—F bonds at 1.576(8) and 1.581(8) Å respectively; however, the differences from the other P—F bonds are not statistically significant, and all these P—F distances are probably affected by libration errors. The P—F...O angles are 115.1(5)°.

Although we do not have X-ray data for the other two aquo-complexes studied here, the magnetic properties and electronic and vibrational spectra of both of them (to be discussed below) are consistent with their having the same basic structure as $Ni(H_2O)_2(3mpy)_6(PF_6)_2$.

Electronic spectra and magnetism

The assignment of electronic spectra and calculation of ligand field and magnetic parameters (Table 5) were performed as described previously (3). The three $M(H_2O)_2(3mpy)_6(EF_6)_2$ complexes exhibit electronic spectra which may be assigned assuming O_h symmetry about the metal. Although the X-ray studies on the nickel hexafluorophosphate derivative show clearly that the chomophore involved is of the MO_4N_2 type, the symmetry lowering is not sufficient to give rise to detectable band splitting. The calculated Dq values for all three of these complexes are significantly greater than the values for the corresponding $M(py)_6(EF_6)_2$ compounds (2). This is consistent with our earlier studies on 4-methylpyridine complexes where we found that the MN_4O_2 complexes had higher Dq values than those with MN_6 chromophores, and supports our earlier contention (3) that greater steric crowding associated with having six heterocyclic ligands bonded directly to the metal as in the pyridine complexes leads to longer and therefore weaker metal–ligand bonds. A comparison of analogous six-coordinate 3mpy and 4mpy complexes shows that in spite of the similarity in chromophores (MN_4O_2) the Dq values are not simply related to ligand base strength. The 3mpy complexes consistently have higher Dq values in spite of the fact that 4mpy is a stronger base (9). Clearly differences in the axial ligand groups and small differences in bond lengths, bond angles and, possibly, the pitch of the heterocyclic ligands, which affects the extent of π-electron delocalization (10), dom-

Can. J. Chem. Downloaded from www.nrcresearchpress.com by 210.87.254.5 on 09/06/12
For personal use only.

TABLE 4. Summary of bond lengths (Å) and angles (deg) with standard deviations in parentheses

(*a*) Nickel coordination

Bond	Length	Bonds	Angle
Ni—N(1)	2.123(7)	N(1)—Ni—N(2)	88.6(3)
N(2)	2.135(8)	N(3)	178.7(3)
N(3)	2.116(8)	N(4)	91.0(3)
N(4)	2.114(8)	N(2)—Ni—N(3)	91.1(3)
O(1)	2.103(6)	N(4)	178.2(3)
O(2)	2.102(7)	N(3)—Ni—N(4)	89.3(3)
		O(1)—Ni—O(2)	178.5(3)
		O(1)—Ni—N(1)	90.9(3)
		N(2)	87.8(3)
		N(3)	90.4(3)
		N(4)	90.5(3)
		O(2)—Ni—N(1)	88.0(3)
		N(2)	91.1(3)
		N(3)	90.7(3)
		N(4)	90.6(3)

(*b*) Pyridine groups

Bond	Length	Mean	Bonds	Angle	Mean
N—C(1)	1.34–1.36(1)	1.34	Ni—N—C	120–122(1)	121
N—C(5)	1.32–1.36(1)	1.34	C(1)—N—C(5)	118–120(1)	119
C(1)—C(2)	1.35–1.41(2)	1.38	N—C(1)—C(2)	123–124(1)	124
C(2)—C(3)	1.36–1.41(2)	1.39	C(1)—C(2)—C(3)	116–118(1)	117
C(3)—C(4)	1.36–1.42(2)	1.39	C(1)—C(2)—C(6)	119–121(1)	120
C(4)—C(5)	1.36–1.42(2)	1.39	C(3)—C(2)—C(6)	121–124(1)	122
C(2)—C(6)	1.48–1.52(2)	1.51	C(2)—C(3)—C(4)	119–121(1)	120
			C(3)—C(4)—C(5)	118–120(1)	119
			C(4)—C(5)—N	120–123(1)	121

(*c*) Anions

Bond	Length	Mean	Bonds	Angle	
P—F	1.515–1.581(10)	1.552	F—P—F	86.0–94.5	174.9–178.7(9)

(*d*) Hydrogen bonds

Bond	Length	Bond	Length
O(1)—H...N(5)	2.719(11)	O(2)—H...N(6)	2.717(11)
O(1)—H...F(24)	2.958(11)	O(2)—H...F(13)	2.959(11)

Can. J. Chem. Downloaded from www.nrcresearchpress.com by 210.87.254.5 on 09/06/12
For personal use only.

inate here.

The magnetic properties of the $M(H_2O)_2(3mpy)_6(EF_6)_2$ compounds (Table 5) are generally consistent with spin-free six-coordinate complexes. In the case of $Co(H_2O)_2(3mpy)_6(PF_6)_2$ the temperature dependence of the magnetic moment (Table 6) provides a measure of the distortion of the ligand environment from regular octahedral stereochemistry. There is excellent agreement between measured magnetic moments and those calculated using the four parameter approach of Figgis *et al.* (17) for spin-free cobalt(II) in an axially compressed tetragonal environment. The parameter values (Table 6) are the same to within experimental error as those calculated for the structurally similar $Co(H_2O)_2(4mpy)_8(EF_6)_2$ complexes (3).

$Ni(3mpy)_4(AsF_6)_2$ is yellow, diamagnetic (over the range 300 to 80 K), and shows a single absorption band in the visible region (Table 5) with a maximum close in energy to that observed for the 4mpy analogue. The complex clearly involves square planar $[Ni(3mpy)_4]^{2+}$ cations and non-coordinated anions. While the corresponding $Ni(py)_4(AsF_6)_2$ has been shown to undergo a structure change at low temperature to a paramagnetic form involving coordinated anions (4) this 3mpy complex, like its 4mpy analogue, undergoes no such change.

The magnetic properties and electronic spectra of the $Co(3mpy)_4(EF_6)_2$ compounds (Table 5) are consistent with spin-free tetrahedral cobalt(II). The differences in Dq and B values between these complexes and analogous pyridine (2) and 4-methylpyridine (3) complexes cannot be considered significant. This shows that in spite of the greater basicity of the methylpyridine ligands and in spite of the potential for greater steric crowding in the 3-methylpyridine complexes, the coordinating properties of these three ligands are not sufficiently different to produce a measurable effect in the electronic spec-

Can. J. Chem. Downloaded from www.nrcresearchpress.com by 210.87.254.5 on 09/06/12
For personal use only.

TABLE 5. Electronic spectral data and magnetic properties

Compound	Energies of band maxima (kK)[a,b] (a)	(b)	(c)		Assignments[c]	Dq (cm^{-1})[d]	B (cm^{-1})[d]	μ_{eff}[d]	θ
$Ni(H_2O)_2(3mpy)_6(PF_6)_2$	26.8 s 16.7 s	27.1 s 17.0 s 10.8 m			$^3A_{2g}(F) \rightarrow {}^3T_{1g}(P)$ $\rightarrow {}^3T_{1g}(F)$ $\rightarrow {}^3T_{2g}(F)$	1080	780	3.17	−6.0
$Ni(H_2O)_2(3mpy)_6(AsF_6)_2$	26.8 s 16.7 s	27.1 s 17.0 s 10.8 m			$^3A_{2g}(F) \rightarrow {}^3T_{1g}(P)$ $\rightarrow {}^3T_{1g}(F)$ $\rightarrow {}^3T_{2g}(F)$	1080	780	3.16	−15.0
$Co(H_2O)_2(3mpy)_6(PF_6)_2$		22.8 — 9.17			$^4T_{1g}(F) \rightarrow {}^4T_{1g}(P)$ $\rightarrow {}^4A_{2g}(F)$ $\rightarrow {}^4T_{2g}(F)$	1040	860	4.93	—
$Ni(3mpy)_4(AsF_6)_2$	22.5 s	23.3 s	22.3(85)					Diamagnetic	
$Co(3mpy)_4(PF_6)_2$	25.6 w 22.7 w 18.9 sh 17.7 s	25.6 w 22.7 w 19.6 sh 17.5 s 9.30 m 5.21 w	18.86 sh 17.78 8.51	(490) (79)	$^4A_2(F) \rightarrow {}^4T_1(P)$ $\rightarrow {}^4T_1(F)$ $\rightarrow {}^4T_2(F)$	550	730	4.28	+1.0
$Co(3mpy)_4(AsF_6)_2$	26.0 w 22.7 w 19.2 sh 17.7 s	23.3 w 19.0 sh 17.4 s 9.30 m 5.26 w	18.6 sh 17.86 8.70 —	(233) (77)	$^4A_2(F) \rightarrow {}^4T_1(P)$ $\rightarrow {}^4T_1(F)$ $\rightarrow {}^4T_2(F)$	550	730	4.42	+2.0

[a] s = strong, m = medium, w = weak, sh = shoulder.

[b] (a) Diffuse reflectance, (b) Nujol mull, (c) solution (dichloromethane for nickel complex and equal volume mixture of dichloromethane and chloroform for cobalt complexes); molar extinction coefficients in parentheses.

[c] Approximate assignments assuming O_h or T_d symmetry. Unassigned weak bands and shoulders probably due to spin-forbidden transitions.

[d] Calculated as described in ref. 3.

TABLE 6. Cryomagnetic data for $Co(H_2O)_2(3mpy)_6(PF_6)_2$

Temperature (K)	μ_{eff} (BM)[a] (a)	(b)
296	4.93	4.92
273	4.88	4.90
251	4.82	4.90
227	4.85	4.88
203	4.83	4.85
178	4.78	4.82
150	4.70	4.75
140	4.72	4.73
104	4.64	4.61
85	4.52	4.50

[a](a) experimental, (b) theoretical values from ref. 17 for $A = 1.40$, $k = 0.95$, $\nu = 3$, and $\lambda = -155$ cm^{-1}.

TABLE 7. Infrared spectra,[a] anion bands

Compound	Assignments (O_h symmetry)[a] $\nu_1(A_{1g})$	$\nu_2(E_g)$	$\nu_3(F_{1u})$	$\nu_4(F_{1u})$
$Co(H_2O)_2(3mpy)_6(PF_6)_2$	741 w	[b]	839 vs	555 s
$Ni(H_2O)_2(3mpy)_6(PF_6)_2$	740 w	[b]	830 vs	555 s
$Ni(H_2O)_2(3mpy)_6(AsF_6)_2$	[c]	568 w	700 vs	395 s
$Co(3mpy)_4(PF_6)_2$	[b]	[b]	840 vs	555 s
$Co(3mpy)_4(AsF_6)_2$	[c]	[b]	690 vs	395 s
$Ni(3mpy)_4(AsF_6)_2$	665 m	555 m	700 vs	392 s

[a]In cm^{-1}. Abbreviations: s = strong, m = medium, w = weak, v = very. Samples as Nujol mulls.
[b]Not observed.
[c]Possibly obscured by ν_3 of AsF_6^-.

tra of these tetrahedral species. It is interesting to note that in complexes of the type $ML_4(EF_6)_2$ (where M is Co, Ni, or Cu, L is py, 3mpy, or 4mpy, and E is P or As), only in the case of the $CuL_4(EF_6)_2$ series has it been possible to relate changes in electronic spectra to the relative coordinating strengths of the pyridine-type ligands (10). Changing the neutral ligand alters the tetragonality of the copper complex and although the change is very small in this case, the dependence of the energy of the maximum in the electronic spectra on tetragonality is clearly sufficiently great for the effect to be seen.

Infrared spectra

Bands arising primarily from anion vibrations and those due to vibrations associated with the 3mpy ligands are relatively easy to distinguish. The anion bands, assigned on the basis of O_h symmetry, are listed in Table 7. The criteria for non-coordinated EF_6^- anions, given previously (3), are met for all complexes with the possible exception of $Ni(3mpy)_4(AsF_6)_2$. As we found for analogous py and 4mpy complexes, the ν_1 and ν_2 vibrations of the nickel complex appear with medium intensity, indicative of weak cation–anion interaction (10).

The infrared spectra of the aquo complexes in the OH stretching region are particularly interesting. All three complexes exhibited a strong very broad OH stretching absorption with a maximum centred around 2850 cm^{-1} and a sharper intense band around 3570 cm^{-1} (Fig. 2). This is consistent with the presence of two types of OH bonds, one involving relatively strong H-bonding to 3-methylpyridine and resulting in the band at 2850 cm^{-1} and the other involving weak H-bonding to PF_6^- and giving the 3570 cm^{-1} band. In comparison, the 4-methylpyridine complexes of composition $M(H_2O)_2(4mpy)_8(EF_6)_2$ have structures in which the axial water molecules have both protons strongly H-bonded to 4-methylpyridine groups (3) and these compounds (Fig. 2) exhibit only one broad band, presumably comprising both the symmetric and the asymmetric HOH stretching, centred around 3000 cm^{-1}. An example of a related complex in which none of the protons of the water molecules are H-bonded to a strong base is $Ni(H_2O)_2(4mpy)_4(ClO_4)_2$. This complex exhibits a strong band at 3420 cm^{-1} with a shoulder at 3280 cm^{-1} assignable to HOH asymmetric and symmetric stretches respectively (8).

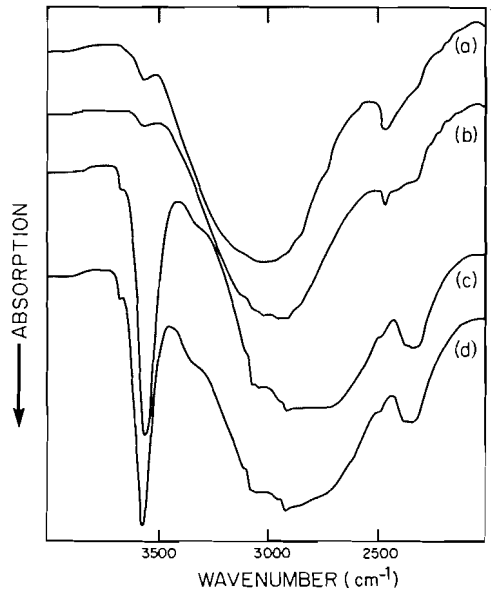

FIG. 2. Infrared spectra, 4000 to 2000 cm^{-1} region, hexachlorobutadiene mull: (a) $Ni(H_2O)_2(4mpy)_8(PF_6)_2$, (b) $Co(H_2O)_2(4mpy)_8(PF_6)_2$, (c) $Co(H_2O)_2(3mpy)_6(PF_6)_2$, (d) $Ni(H_2O)_2(3mpy)_6(PF_6)_2$.

Acknowledgements

We thank the Natural Sciences and Engineering Research Council of Canada for financial support and the University of British Columbia Computing Centre for assistance.

1. H. G. MAYFIELD, JR. and W. E. BULL. J. Chem. Soc. A, 2279 (1971).
2. R. M. MORRISON and R. C. THOMPSON. Inorg. Nucl. Chem. Lett. **12**, 937 (1976).
3. R. M. MORRISON and R. C. THOMPSON. Can. J. Chem. **56**, 985 (1978).
4. R. M. MORRISON, R. C. THOMPSON, and J. TROTTER. Can. J. Chem. **58**, 238 (1980).
5. D. W. HERLOCKER and M. R. ROSENTHAL. Inorg. Chim. Acta, **4**, 501 (1970).
6. D. A. ROWLEY and R. S. DRAGO. Inorg. Chem. **7**, 795 (1968).
7. R. M. MORRISON, R. C. THOMPSON, and J. TROTTER. Can. J. Chem. **57**, 135 (1979).
8. M. S. SUN and D. G. BREWER. Can. J. Chem. **49**, 1502 (1971).
9. H. C. BROWN and X. R. MIHM. J. Am. Chem. Soc. **77**, 1723 (1955).
10. R. M. MORRISON and R. C. THOMPSON. Can. J. Chem. **60**, 1048 (1982).
11. International tables for X-ray crystallography. Volume IV. Kynoch Press, Birmingham. 1974.

Can. J. Chem. Downloaded from www.nrcresearchpress.com by 210.87.254.5 on 09/06/12
For personal use only.

12. E. ĎURČANSKÁ, J. GARAJ, and M. DUNAJ-JURČO. Inorg. Chim. Acta, **29**, 149 (1978).
13. B. BAK, L. HANSEN, and J. RASTRUP-ANDERSON. J. Chem. Phys. **22**, 2013 (1954).
14. H. ALTENBURG and D. MOOTZ. Acta Crystallogr. B **27**, 1982 (1971).
15. J. EMSLEY, D. J. JONES, and R. S. OSBORN. J. Chem. Soc. Chem. Commun. 703 (1980); J. EMSLEY, D. J. JONES, and R. KURODA. J. Chem. Soc. Dalton Trans. 1179 (1982).
16. V. I. SIMONOV and B. V. BUTVESKY. Acta Crystallogr. B**34**, 355 (1978).
17. B. N. FIGGIS, M. GERLOCK, J. LEWIS, F. E. MABBS, and G. WEBB. J. Chem. Soc. A, 2086 (1968).

Can. J. Chem. Downloaded from www.nrcresearchpress.com by 210.87.254.5 on 09/06/12
For personal use only.

A quadruply bonded dimolybdenum compound containing a novel bridging and chelating hexadentate ligand

KENNETH R. BREAKELL, STEVEN J. RETTIG, ALAN STORR, AND JAMES TROTTER

Department of Chemistry, University of British Columbia, 2036 Main Mall, Vancouver, B.C., Canada V6T 1Y6

Received December 7, 1982

KENNETH R. BREAKELL, STEVEN J. RETTIG, ALAN STORR, and JAMES TROTTER. Can. J. Chem. **61**, 1659 (1983).

The synthesis, physical properties, and molecular structure of $(N_2C_3H_5)^+[Mo_2(\mu\text{-}CH_3CO_2)[CH_3Ga(N_2C_3H_3)O]_4]^- \cdot 2(C_4H_8O)$ are reported. Crystals of pyrazolium (μ-acetato)[1,3,5,7-tetramethyl-1,3,5,7-tetrakis(pyrazol-1-yl)cyclotetragalloxanato(4−)]dimolybdate(II)-bis(tetrahydrofuran) are orthorhombic, a = 10.638(2), b = 32.779(4), c = 12.617(1) Å, Z = 4, space group *Cmcm*. The structure was solved by Patterson and Fourier syntheses and was refined by full-matrix least-squares procedures to R = 0.032 and R_w = 0.041 for 1957 reflections with $I \geq 3\sigma(I)$. The structure consists of THF molecules and $(N_2C_3H_5)^+[Mo_2(\mu\text{-}CH_3CO_2)[CH_3Ga(N_2C_3H_3)O]_4]^-$ ion-pair units, the latter displaying exact C_{2v} symmetry. The pyrazolium cation is joined to the complex anion by a pair of strong N—H···O hydrogen bonds (H···O = 1.49(6) Å). The Mo_2^{4+} unit is bridged by a single acetato group, the remaining coordination sites being occupied by the hexadentate bridging and chelating $[CH_3Ga(N_2C_3H_3)O]_4^{4-}$ ligand. Bond lengths are: Mo—Mo = 2.127(1), Mo—N = 2.151(3), Mo—O = 2.090(4) and 2.115(4), Ga—O = 1.853(2) and 1.861(2), Ga—N = 1.961(3), and Ga—C = 1.950(6) Å.

KENNETH R. BREAKELL, STEVEN J. RETTIG, ALAN STORR et JAMES TROTTER. Can. J. Chem. **61**, 1659 (1983).

On rapporte la synthèse, les propriétés physiques et la structure moléculaire du $(N_2C_3H_5)^+[Mo_2(\mu\text{-}CH_3CO_2)[CH_3Ga(N_2C_3H_3)O]_4]^- \cdot 2(C_4H_8O)$. Les cristaux de (μ-acéto)[tétraméthyl-1,3,5,7 tétrakis-1,3,5,7 (pyrazol-1) cyclotétragalloxanato-(4−)] dymolybdate(II) bis (tétrahydrofuranne) de pyrazolium sont orthorhombiques et appartiennent au groupe d'espace *Cmcm* avec a = 10,638(2), b = 32,779(4), c = 12,617(1) Å, Z = 4. On a résolu la structure par les synthèses de Patterson et de Fourier et on la affinée par la méthode des moindres carrés (matrice entière) jusqu'à des valeurs de R = 0,032 et de R_w = 0,041 pour 1957 réflexions avec $I \geq 3\sigma(I)$. La structure comprend des molécules de THF et la paire d'ions $(N_2C_3H_5)^+(Mo_2(\mu\text{-}CH_3CO_2)[CH_3Ga(N_2C_3H_3)O]_4]^-$. La paire d'ion exhibant une symétrie exacte C_{2v}. Le cation pyrazolium est lié à l'anion complexe par deux fortes liaisons hydrogène du type N—H···O (H···O = 1,49(6) Å). Un groupe simple acétato forme un pont avec l'ion Mo^{4+}, les autres sites de coordination étant occupés par le ligand hexadendate $[CH_3Ga(N_2C_3H_3)O]_4^{4-}$ qui forme un pont et qui chélate également. Les longueurs de liaison sont de: Mo—Mo = 2,127(1), Mo—N = 2,151(3), Mo—O = 2,090(4) et 2,115(4), Ga—O = 1,853(2) et 1,861(2) Ga—N = 1,961(3) et Ga—C = 1,950(6) Å.

[Traduit par le journal]

Can. J. Chem. Downloaded from www.nrcresearchpress.com by 210.87.254.105 on 09/06/12
For personal use only.

Introduction

A recent report has highlighted the growing importance of the field of metal–metal bonded species and in particular has illuminated the special place of the Cr triad in its development (1). Multiply bonded dimolybdenum species have been particularly amenable to study and of these, compounds having a quadruple bond between the two metal atoms have received a great deal of attention. This paper describes the synthesis and structure of a dimolybdenum complex having a Mo≡Mo quadruple bond, a bridging acetato group, and an unusual bridging and chelating hexadentate ligand.

Experimental

Starting materials

Air-sensitive materials were handled in a glove box under an atmosphere of oxygen-free, dry nitrogen, or in a nitrogen-blanketed apparatus. Tetrahydrofuran (THF) was dried by refluxing over lithium aluminum hydride and was used immediately following distillation. Dimolybdenum tetraacetate was prepared by a standard route (2) and the $Na^+[CH_3Ga(N_2C_3H_3)_3]^-$ ligand was prepared as a THF solution as detailed elsewhere (3).

Reaction of $Mo_2(CH_3CO_2)_4$ with $Na[CH_3Ga(N_2C_3H_3)_3]$

A slurry of $Mo_2(CH_3CO_2)_4$ (0.753 g, 1.76 mmol) in THF was reacted with a 50.0 mL aliquot of ligand solution $Na^+[CH_3Ga(N_2C_3H_3)_3]^-$ (1.09 g, 3.53 mmol). After stirring for several minutes the reaction mixture, initially orange, became a dark wine-red color. Slow evaporation of THF solvent from the filtrate from this reaction yielded a tacky purple solid and numerous orange crystals (approximately 30% yield). The latter were found to be suitable for X-ray diffraction studies providing precautions were taken to prevent air-exposure. Selected crystals were mounted in glass capillaries which were then sealed off under an atmosphere of nitrogen gas. The results of the structure determination are reported below. From more sporting physical methods the following information was obtained: *Anal.* Calcd. for $(N_2C_3H_5)^+[Mo_2(\mu\text{-}CH_3CO_2)[CH_3Ga(N_2C_3H_3)O]_4]^- \cdot 2(C_4H_8O)$: C 30.7, H 4.3, N 12.3; found: C 30.5, H 4.3, N 12.1.

Mass spectrum (Varian MAT CH4 spectrometer)

With a probe temperature of approximately 220°C and at 70 eV signals due to the parent ion (M^+ where M = $(N_2C_3H_5)^+[Mo_2(\mu\text{-}CH_3CO_2)[CH_3Ga(N_2C_3H_3)O]_4]^-$) and the $(M - Me)^+$ ion could be clearly seen even though multi-line signals (23 peaks over 25 mass units) arise from all the possible isotopic combinations of four Ga and two Mo atoms.

Nuclear magnetic resonance (Varian XL 100 FT spectrometer)

The ^1H nmr spectrum of the complex showed clearly the presence of pyrazolyl (2.35 d, 2.61 d, 3.94 t), acetato methyl (8.86 s), and gallium methyl (9.96 s) moieties in addition to signals due to the THF molecules (8.58 m, 6.43 m). (τ values realtive to $\tau_{C_6H_6}$ = 2.84; $J_{HCCH} \approx 2$ Hz for pyrazolyl protons.)

X-ray crystallographic analysis of $(N_2C_3H_5)^+[Mo_2(\mu\text{-}CH_3CO_2)\text{-}[CH_3Ga(N_2C_3H_3)O]_4]^- \cdot 2(C_4H_8O)$

A crystal bounded by the six faces (followed by their distances in mm from a common origin): (0 1 2), 0.150, (0 −1 2), 0.213, ±(2 −6 1), 0.252, ±(2 6 −1), 0.200 was mounted in a general orientation. Unit-cell parameters were refined by least-squares on 2 sin θ/λ values for 25 reflections (2θ = 40–46°) measured on a diffractometer with MoKα$_1$ radiation (λ = 0.70930 Å). Crystal data at 22°C are:

$C_{29}H_{48}Ga_4Mo_2N_{10}O_8$ fw = 1135.52

Orthorhombic, a = 10.638(2), b = 32.779(4), c = 12.617(1) Å, V = 4399.7 Å^3, Z = 4, ρ_c = 1.714 g cm^{-3}, $F(000)$ = 2256, μ(MoKα) = 29.99 cm^{-1}. Absent reflections: hkl, $h + k$ odd, and $h0l$, l odd. Space group *Cmcm* (D_{2h}^{17}, No. 63) from structure analysis.

Can. J. Chem. Downloaded from www.nrcresearchpress.com by 210.87.254.105 on 09/06/12
For personal use only.

Intensities were measured with graphite-monochromated MoKα radiation (λ = 0.71073 Å) on an Enraf-Nonius CAD4-F diffractometer. An ω–0.33θ scan at 1.01–6.71° min^{-1} over a range of (0.60 + 0.35 tan θ) degrees in ω (extended by 25% on both sides for background measurement) was employed. Data were measured to 2θ = 60°. The intensities of three check reflections, measured every 3600 s throughout the data collection, remained constant to within 2.5%. After data reduction,[1] an absorption correction was applied using the Gaussian integration method (4, 5). Transmission factors ranged from 0.412 to 0.751 for 268 integration points. Of the 3489 independent reflections measured, 1957 (56.1%) had intensities greater than $3\sigma(I)$ above background where $\sigma^2(I) = S + 2B + (0.04(S - B))^2$ with S = scan count and B = normalized background count.

The centrosymmetric space group *Cmcm* was indicated by the *E*-statistics and by the Patterson function, from which the heavy-atom coordinates were determined. Coordinates of all atoms except those associated with the solvent molecules were easily located from subsequent difference maps. These atoms were refined (H isotropic, other anisotropic) to $R = 0.051$, at which point the location of the two solvent molecules could be deduced. The THF molecules occupy two independent sites (A and B) in the lattice, each of which lies at the intersection of two mirror planes. Site A lies halfway between two mirror-related complex molecules roughly along the Mo—Mo axis and is centered at approximately 1/2, 0.18, 1/4. The A site is at least fourfold disordered with one THF molecule having its mean plane approximately in the *bc* plane while the second molecule has two carbon atoms (C(A2)) in common with the first and is oriented roughly at a right angle to the first molecule (in the *ab* plane). The B site lies along the twofold axis of the complex beyond the acetato methyl group (the protons of which are also, and necessarily, twofold disordered) and has its centre at approximately 0, 0.44, 1/4. At the B site there are three different orientations, two of which have O(B1) and C(B1) in common, the third containing O(B2), C(B3), and O(B1) (the latter position occupied by both C and O). The relative site occupancy factors for all THF atoms were estimated from relative heights on the difference map and were not refined; their appropriateness may be judged by the magnitudes of the final isotropic thermal parameters. The eleven independent atoms comprising the two solvent molecules were included in subsequent cycles of refinement. The scattering factors of ref. 6 were used for non-hydrogen atoms and those of ref. 7 for hydrogen atoms. Anomalous scattering factors from ref. 8 were used for the Mo and Ga atoms. The weighting scheme, $w = 1/\sigma^2(F)$ where $\sigma^2(F)$ is derived from the previously defined $\sigma^2(I)$ gave uniform average values of $w(|F_o| - |F_c|)^2$ over ranges of both $|F_o|$ and sin θ/λ and was employed in the final stages of refinement. Convergence was reached at $R = 0.032$ and $R_w = 0.041$ for 1957 reflections with $I \geq 3\sigma(I)$. For all 3489 reflections $R = 0.088$. The function minimized was $\Sigma w(|F_o| - |F_c|)^2$, $R = \Sigma||F_o| - |F_c||/\Sigma|F_o|$ and $R_w = (\Sigma w(|F_o| - |F_c|)^2/\Sigma w|F_o|^2)^{1/2}$.

On the final cycle of refinement the mean and maximum parameter shifts corresponded to 0.04 and 0.44σ respectively. The maximum parameter shift was associated with the x coordinate of C(A3). The mean error in an observation of unit weight was 1.100. A final difference map revealed a peak of 0.77 e $Å^{-3}$ near Mo and a peak of 0.74 e $Å^{-3}$ near the C(A3) position, the remainder of the map being essentially featureless. The final positional and thermal parameters appear in Tables 1 and 2[2] respectively. Measured and calculated structure factors have been placed in the Depository of Unpublished Data.[2]

[1]The computer programs used include locally written programs for data processing and locally modified versions of the following: ORFLS, full-matrix least-squares, and ORFFE, function and errors, by W. R. Busing, K. O. Martin, and H. A. Levy; FORDAP, Patterson and Fourier syntheses, by A. Zalkin; ORTEP II, illustrations, by C. K. Johnson.

[2]The structure factor table, Table 2 (anisotropic thermal parameters) and other material mentioned in the text are available, at a nominal charge, from the Depository of Unpublished Data, CISTI, National Research Council of Canada, Ottawa, Ont., Canada K1A OS2.

TABLE 1. Final positional (fractional × 10^5, H and solvent C and O × 10^4) and isotropic thermal parameters ($U \times 10^3$ $Å^2$) with estimated standard deviations in parentheses

Atom	x	y	z	U_{eq}/U_{iso}
Mo[1]	9996(4)	17881(1)	25000	38
Ga	15799(5)	9078(1)	12084(4)	51
O(1)[1]	15566(36)	11767(11)	25000	44
O(2)[1]	10440(36)	24333(11)	25000	49
O(3)[1]	0	6756(12)	10126(31)	50
N(1)	14103(30)	17684(10)	8316(26)	45
N(2)	16399(35)	14044(11)	3428(25)	54
N(3)[1]	0	−501(16)	19638(38)	58
C(1)	15564(46)	20588(15)	1006(39)	61
C(2)	18972(61)	18876(19)	−8535(42)	82
C(3)	19297(55)	14751(17)	−6753(37)	71
C(4)[2]	0	26209(26)	25000	52
C(5)[2]	0	30807(33)	25000	87
C(6)[1]	0	−4419(23)	16422(59)	68
C(7)[2]	0	−6955(30)	25000	73
C(8)	29346(75)	5220(23)	9271(64)	91
H(N)[1]	0	266(20)	1526(54)	83(22)
H(1)	1197(44)	2336(17)	245(45)	95(18)
H(2)	2130(56)	2054(15)	−1415(40)	92(18)
H(3)	1705(53)	1232(18)	−1189(43)	109(21)
H(5a)[2]	793(91)	3186(30)	2500	25(24)
H(5b)[1]	512(73)	3138(22)	1671(54)	43(22)
H(6)[1]	0	−514(27)	862(86)	143(38)
H(7)[2]	0	−1032(28)	2500	71(29)
H(8a)	2560(83)	294(23)	1262(58)	156(36)
H(8b)	3759(53)	653(20)	950(54)	112(24)
H(8c)	2781(99)	400(27)	183(85)	246(49)
O(A1)[3]	3631(23)	1949(8)	2500	88(7)
O(A2)[3]	4844(100)	1463(12)	2500	231(24)
C(A1)[2]	4575(37)	1858(11)	1399(28)	139(14)
C(A2)[1]	4400(21)	2140(6)	1932(18)	201(11)
C(A3)[2]	4582(33)	1653(9)	1752(26)	115(12)
O(B1)[2]	944(20)	4139(7)	2500	177(8)
O(B2)[3]	0	4716(10)	2500	196(13)
C(B1)[2]	292(34)	4188(8)	1613(21)	112(10)
C(B2)[4]	0	4588(11)	1666(29)	137(11)
C(B3)[2]	1236(24)	4504(8)	2500	116(8)
C(B4)[4]	1078(36)	4406(11)	1923(30)	83(9)

[1-4] refer to site occupancies of 0.5, 0.25, 0.125, and 0.1875 respectively. The O(B1) position is 50% O and 50% C.

TABLE 3. Bond lengths (Å) with estimated standard deviations in parentheses

Bond	Length (Å)	Bond	Length (Å)
Mo —O(1)	2.090(4)	N(1)—N(2)	1.365(4)
Mo —O(2)	2.115(4)	N(1)—C(1)	1.335(5)
Mo —N(1)	2.151(3)	N(2)—C(3)	1.341(5)
Mo —Mo′	2.1267(9)	N(3)—C(6)	1.347(8)
Mo —N(1)″	2.151(3)	N(3)—N(3)″	1.353(9)
Ga —O(1)	1.853(2)	C(1)—C(2)	1.377(7)
Ga —O(3)	1.861(2)	C(2)—C(3)	1.371(8)
Ga —N(2)	1.961(3)	C(4)—C(5)	1.507(13)
Ga —C(8)	1.950(6)	C(6)—C(7)	1.365(9)
O(2)—C(4)	1.296(5)		

Bond lengths and angles not involving hydrogen atoms appear in Tables 3 and 4 respectively. Intra-annular torsion angles defining ring conformations are listed in Table 5. Distances and angles involving hydrogen and a complete list of torsion angles (Tables 6–8) are included as supplementary material.

TABLE 4. Bond angles (deg) with estimated standard deviations in parentheses*

Bonds	Angle (deg)	Bonds	Angle (deg)
O(1)—Mo —O(2)	162.3(2)	Ga —O(1)—Ga″	123.2(2)
O(1)—Mo —N(1)	85.04(9)	Mo —O(2)—C(4)	117.7(4)
O(1)—Mo —Mo′	106.47(10)	Ga —O(3)—Ga′	129.1(2)
O(1)—Mo —N(1)″	85.04(9)	Mo —N(1)—N(2)	120.3(2)
O(2)—Mo —N(1)	91.47(9)	Mo —N(1)—C(1)	132.7(3)
O(2)—Mo —Mo′	91.28(11)	N(2)—N(1)—C(1)	106.9(3)
O(2)—Mo —N(1)″	91.47(9)	Ga —N(2)—N(1)	117.9(2)
N(1)—Mo —Mo′	101.72(9)	Ga —N(2)—C(3)	133.2(3)
N(1)—Mo —N(1)″	156.3(2)	N(1)—N(2)—C(3)	108.8(4)
Mo′—Mo —N(1)″	101.72(9)	C(6)—N(3)—N(3)″	107.5(4)
O(1)—Ga —O(3)	107.4(2)	N(1)—C(1)—C(2)	110.1(5)
O(1)—Ga —N(2)	95.47(14)	C(1)—C(2)—C(3)	105.4(5)
O(1)—Ga —C(8)	118.6(3)	N(2)—C(3)—C(2)	108.8(4)
O(3)—Ga —N(2)	107.1(2)	O(2)—C(4)—C(5)	119.0(4)
O(3)—Ga —C(8)	112.2(3)	O(2)—C(4)—O(2)′	122.1(8)
N(2)—Ga —C(8)	114.4(3)	C(5)—C(4)—O(2)′	119.0(4)
Mo —O(1)—Ga	117.39(10)	N(3)—C(6)—C(7)	110.0(7)
Mo —O(1)—Ga″	117.39(10)	C(6)—C(7)—C(6)″	104.9(9)

*Here and elsewhere in this report primed and double-primed atoms have coordinates related to those in Table 1 by the symmetry operations $-x, y, z$ and $x, y, 1/2 - z$ respectively.

TABLE 5. Intra-annular torsion angles (deg) with standard deviations in parentheses

Atoms	Value (deg)
N(1)—Mo —O(1)—Ga	−18.7(2)
N(2)—Ga —O(1)—Mo	20.0(2)
O(1)—Ga —N(2)—N(1)	−12.1(3)
Mo —N(1)—N(2)—Ga	0.1(4)
O(1)—Mo —N(1)—N(2)	10.6(3)
O(3)—Ga —O(1)—Ga″	73.3(3)
O(1)—Ga —O(3)—Ga′	46.3(3)

Results and discussion

Earlier reports (3, 9, 10) have described the synthesis and coordination chemistry of the tridentate anionic methyl(tris-pyrazolyl)gallate ligand, $CH_3Ga(N_2C_3H_3)_3^-$. In the present study this anion was reacted with dimolybdenum tetraacetate in an attempt to replace two of the bridging acetato groups in that molecule with the gallate ligands according to the stoichiometric equation:

$$Mo_2(CH_3CO_2)_4 + 2Na^+[CH_3Ga(N_2C_3H_3)_3]^- \rightarrow [CH_3Ga(N_2C_3H_3)_3]_2Mo_2(CH_3CO_2)_2 + 2Na^+CH_3CO_2^-$$

It was then hoped to study in detail the coordination geometry of the gallate ligand and in particular to investigate any possible axial interactions at the molybdenum centres. In an earlier report a similar reaction was probed using the tris-pyrazolyl borate anion, $HB(N_2C_3H_3)_3^-$, as reactant (11). In that investigation the desired reaction proceeded smoothly to replace two bridging acetato groups by borate ligands. The latter acted as bidentate chelating ligands at each Mo atom with the third pyrazolyl group of one of the ligands being weakly interacting with one of the metal atoms in an axial position. Since there were no steric requirements to prevent such an interaction at both molybdenum atoms it was proposed at that time that, for electronic reasons, quadruply bonded pairs of Mo atoms have little tendency to bind electron donors in coaxial positions. The weak interaction found at one Mo centre was argued to arise from conformational necessity rather than from any desire of the metal atom to enter into an axial bonding arrangement. The present study was initiated to probe further this reluctance of such dimolybdenum units to bind axially positioned ligands. The gallate ligand employed here, whilst similar to the $HB(N_2C_3H_3)_3^-$ ligand in many respects, has been shown to exhibit somewhat different behavior in related complexes, primarily due to the disparity between the Ga—N and B—N bond lengths (3, 9, 10, 12). It was hoped, therefore, that these differences might manifest themselves in some small but subtle changes in any resulting dimolybdenum species prepared via the above reaction. However, it became rapidly obvious from early spectral measurements that the desired reaction had not been accomplished. Indeed it required the crystal structure determination to enable us to rationalize this collection of data. The structure which materialized from the X-ray work was, to say the least, surprising and totally unique in the field of quadruply bonded dimolybdenum units. The initial molecule has retained but one bridging acetato group with the remaining six coordination positions being taken up by oxygen and nitrogen atoms from, in effect, a hexadentate chelating and bridging methyl gallium pyrazolyl oxo ligand (see below). The origin of this ligand is not known but could have arisen because of traces of water in the THF solvent. The overall transformation would involve loss of two pyrazole molecules and a tetramerization of the resultant oxo species.

$$[CH_3Ga(N_2C_3H_3)_3]^- + H_2O \rightarrow [CH_3Ga(N_2C_3H_3)O]^- + 2N_2C_3H_4$$

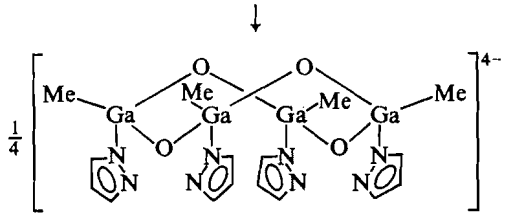

The formation of such an eight-membered $(Ga—O)_4$ ring is not without precedent and indeed the structure of the tetramer $[(CH_3)_2Ga(OH)]_4$ is well documented (13). In the present scheme the formally Mo(II) centres are thus neutralized by the 4− charge on the hexadentate ligand. The bridging acetato

Can. J. Chem. Downloaded from www.nrcresearchpress.com by 210.87.254.105 on 09/06/12
For personal use only.

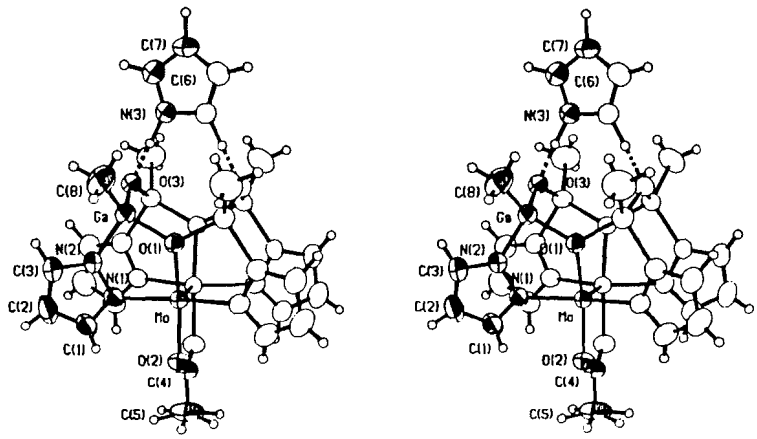

FIG. 1. Stereoscopic view of the ion-pair unit $(N_2C_3H_5)^+[Mo_2(\mu\text{-}CH_3CO_2)[CH_3Ga(N_2C_3H_3)O]_4]^-$, 50% probability thermal ellipsoids shown for the non-hydrogen atoms. Hydrogen atoms have been assigned artificially small thermal parameters for the sake of clarity.

ligand is then formally counterbalanced by a positive pyrazolium ion $N_2C_3H_5^+$ which is strongly hydrogen-bonded to the two oxygens of the $(Ga—O)_4$ ring which are not coordinated to Mo atoms. The origin of the oxo species is not known with any certainty but previous examples of "adventious" water creeping uninvited into similar reactions have been documented. Thus the 3,5-dimethylpyrazolyl based ligand $[CH_3Ga(N_2C_5H_7)_3]^-$ was very prone to conversion to the hydroxy species $[CH_3Ga(N_2C_5H_7)_2(OH)]^-$ in sterically demanding situations even when rigorous attempts to eliminate water had been made (14). More recently the reaction of $Mo_2(CH_3CO_2)_4$ with $Na^+(C_2H_5)_2B(N_2C_3H_3)_2^-$ has been reported to result in the incorporation of $[(C_2H_5)_2B(N_2C_3H_3)(OH)]^-$ ligands in the dimolybdenum product, a purely unexpected result attributed to adventious water entry into the reaction medium (15).

Crystal structure of $(N_2C_3H_5)^+[Mo_2(\mu\text{-}CH_3CO_2)\text{-}[CH_3Ga(N_2C_3H_3)O]_4]^-\cdot 2(C_4H_8O)$

The crystal structure consists of ion-pair units $(N_2C_3H_5)^+[Mo_2(\mu\text{-}CH_3CO_2)[CH_3Ga(N_2C_3H_3)O]_4]^-$ (Fig. 1) and THF molecules. The pyrazolium cation is linked by a pair of strong N—H···O hydrogen bonds to the two uncoordinated oxygen atoms of the $(Ga—O)_4$ ring (N(3)—H(N)···O(3), H···O = 1.49(6), N···O = 2.665(6) Å, N—H···O = 178(5)°). Each ion-pair unit is associated with two others through a system of weak C—H···O interactions across adjacent centres of symmetry, resulting in an infinite linear arrangement extending along the crystallographic *a* axis (C(6)—H(6)···O(3) $(-x, -y, -z)$, H···O = 2.42(10), C···O = 3.436(8) Å, C—H···O = 179(7)°). One of the partially occupied site A THF oxygen atoms is involved in a very weak axial interaction with the Mo_2^{4+} system: Mo—O(A1) = 2.85(2) Å, Mo′—Mo—O(A1) = 169.3(5)°. All other nonbonded distances correspond to normal van der Waals interactions.

The ion-pair complex possesses exact $m2m$ (C_{2v}) symmetry, the conformation about the Mo—Mo axis being exactly eclipsed. One mirror plane contains the two Mo atoms, the non-hydrogen atoms of the acetato group, and the O(1) atoms of the $(Ga—O)_4$ ring while the second mirror plane bisects the metal–metal bond and contains the pyrazolium cation and the O(3) atoms of the $(Ga—O)_4$ ring. At each Mo atom a pair of fused five-membered MoOGaNN chelate rings is formed (each having an O-envelope conformation). These chelate rings are linked to those associated with the other Mo atom by single-atom bridges between Ga atoms and by three-atom bridges between O atoms.

The Mo—Mo distance of 2.127(1) Å lies near the middle of the range of known Mo≣Mo quadruple bond lengths (from 2.037(2) Å in $Mo_2[(C_5H_4N)NC(O)CH_3]_4$ (16) to 2.183(2) Å in $Mo_2(allyl)_4$ (17)). The Mo—Mo distance reported here is equal (within experimental error) to the value of 2.129(1) Å reported for the complex $Mo_2(CH_3CO_2)_2[(C_2H_5)_2B(N_2C_3H_3)_2]_2$ (18), in which each Mo atom has an N_2O_2 donor set comprising the basal plane. Several factors influencing the length of Mo≣Mo quadruple bonds have been noted. Substitution of two μ-RCO_2 groups of $Mo_2(\mu\text{-}RCO_2)_4$ (Mo—Mo = 2.091(2), 2.090(4), and 2.093(2) Å respectively for R = H (19), CH_3 (20), and CF_3 (21)) by chelating ligands (L) leads to an increase of about 0.036 Å in the Mo—Mo bond length (22) for compounds of the type $Mo_2(\mu\text{-}CH_3CO_2)_2L_2$ (Mo—Mo = 2.129(1), 2.129(1), and 2.131(1) Å respectively for L = $(C_2H_5)_2B(N_2C_3H_3)_2$ (18), $C_5H_7O_2$ (23), and $C_6H_5NC(CH_3)C(H)C(CH_3)O$ (24)). Further lengthening of the metal–metal bond is known to result (16) from substitution of all bridging RCO_2 ligands (for example: Mo—Mo = 2.156(1) Å in $Mo_2[(C_2H_5)_2B(N_2C_3H_3)_2]_2$-$[(C_2H_5)_2B(N_2C_3H_3)(OH)]_2$ (15)), or in cases where a significant axial interaction is present (the weak axial interaction in the present structure is not expected to have any significant effect). In spite of what is known about the dimolybdenum system, predictions of Mo—Mo bond lengths, especially in cases where new types of ligands are involved, still cannot be made (16).

The Mo—N(pyrazolyl), Mo—O(μ-acetato), and Mo—O(1) distances of 2.151(3), 2.115(4), and 2.090(4) Å are similar to those reported for related structures (15, 16–24). It is interesting to note that the Mo—O bond to the $[CH_3Ga(N_2C_3H_3)O]_4^{4-}$ ligand is significantly shorter than that to the acetato group, the near planarity at O(1) suggesting the possibility of π-interactions with both the dimolybdenum system and with the gallium atoms. In fact both Ga—O distances (Ga—O(1) = 1.853(2) and Ga—O(3) = 1.861(2) Å) are considerably shorter than the mean Ga—O distance of 1.96 Å reported for $[(CH_3)_2Ga(OH)]_4$ (13). The Ga—N (1.961(3) Å), Ga—C (1.950(6) Å), and all other bond lengths and angles are as expected.

The pyrazolium cation lies in a mirror plane and is thus exactly planar while the pyrazolyl ring is planar within experi-

Can. J. Chem. Downloaded from www.nrcresearchpress.com by 210.87.254.105 on 09/06/12
For personal use only.

mental error ($\chi^2 = 2.6$ for N_2C_3, mean deviation from the plane = 0.0035 Å).

Acknowledgments

We thank the Natural Sciences and Engineering Research Council of Canada for financial support and the University of British Columbia Computing Centre for assistance.

1. F. A. COTTON and M. H. CHISHOLM. Chem. Eng. News, 40 (1982).
2. T. A. STEPHENSON, E. BANNISTER, and G. WILKINSON. J. Chem. Soc. Sect. A, 2538 (1964).
3. K. R. BREAKELL, S. J. RETTIG, D. L. SINGBEIL, A. STORR, and J. TROTTER. Can. J. Chem. **56**, 2099 (1978).
4. P. COPPENS, L. LEISEROWITZ, and D. RABINOVICH. Acta Crystallogr. **18**, 1035 (1965).
5. W. R. BUSING and H. A. LEVY. Acta Crystallogr. **22**, 457 (1967).
6. D. T. CROMER and J. B. MANN. Acta Crystallogr. Sect. A, **24**, 321 (1968).
7. R. F. STEWART, E. R. DAVIDSON, and W. T. SIMPSON. J. Chem. Phys. **42**, 3175 (1965).
8. D. T. CROMER and D. LIBERMAN. J. Chem. Phys. **53**, 1891 (1970).
9. S. J. RETTIG, A. STORR, and J. TROTTER. Can. J. Chem. **57**, 1823 (1979).
10. K. S. CHONG, S. J. RETTIG, A. STORR, and J. TROTTER. Can. J. Chem. **57**, 3107 (1979).
11. D. M. COLLINS, F. A. COTTON, and C. A. MURILLO. Inorg. Chem. **15**, 1861 (1976).
12. F. G. HERRING, D. J. PATMORE, and A. STORR. J. Chem. Soc. Dalton Trans. 711 (1975).
13. G. S. SMITH and J. L. HOARD. J. Am. Chem. Soc. **81**, 3907 (1959).
14. K. R. BREAKELL, S. J. RETTIG, A. STORR, and J. TROTTER. Can. J. Chem. **57**, 139 (1979).
15. F. A. COTTON, B. W. S. KOLTHAMMER, and G. N. MOTT. Inorg. Chem. **20**, 3890 (1981).
16. F. A. COTTON, W. H. ILSLEY, and W. H. KAIM. Inorg. Chem. **18**, 2717 (1979).
17. F. A. COTTON and J. R. PIPAL. J. Am. Chem. Soc. **93**, 5441 (1971).
18. F. A. COTTON, P. LAHUERTA, and B. R. STULTS. Inorg. Chem. **15**, 1866 (1976).
19. F. A. COTTON, J. G. NORMAN, JR., B. R. STULTS, and T. R. WEBB. J. Coord. Chem. **5**, 217 (1976).
20. F. A. COTTON, Z. C. MESTER, and T. R. WEBB. Acta Crystallogr. Sect. B, **30**, 2768 (1974).
21. F. A. COTTON and J. G. NORMAN, JR. J. Coord. Chem. **1**, 161 (1971).
22. D. M. COLLINS, F. A. COTTON, and C. A. MURILLO. Inorg. Chem. **15**, 1861 (1976).
23. C. D. GARNER, S. PARKES, I. B. WALTON, and W. CLEGG. Inorg. Chim. Acta, **31**, L451 (1978).
24. F. A. COTTON, W. H. ILSLEY, and W. H. KAIM. Inorg. Chim. Acta, **37**, 267 (1979).

Can. J. Chem. Downloaded from www.nrcresearchpress.com by 210.87.254.105 on 09/06/12
For personal use only.

Electron and ion transport in gaseous methanol and water: density and temperature effects[1]

NORMAN GEE AND GORDON R. FREEMAN
Department of Chemistry, University of Alberta, Edmonton, Alta., Canada T6G 2G2

Received September 30, 1982

NORMAN GEE and GORDON R. FREEMAN. Can. J. Chem. **61**, 1664 (1983).

Electron and cation mobilities in methanol and water vapor measured at $293 \leq T$ (K) ≤ 617 were used to estimate the corresponding momentum transfer cross sections. The electron cross sections correlate with the square of the dipole moment. Unlike the nonpolar gases, where the average cross section for electrons $\sigma_{ave,e}$ is only 0.01–0.1 times that for cations $\sigma_{ave,+}$, methanol has $\sigma_{ave,e} \approx 0.5\sigma_{ave,+}$ and water has $\sigma_{ave,e} \approx \sigma_{ave,+}$. The thermal electrons exchange energy with the molecules mainly through molecular rotational modes, as opposed to elastic modes.

The onset of electron quasilocalization in the saturated vapor occurs at $n_{ql} \approx 5 \times 10^{25}$ molecules/m^3 ($n_{ql}/n_c \approx 0.010$) in methanol and 3×10^{25} ($n_{ql}/n_c \approx 0.003$) in water. These are about 10-fold lower densities than in hydrocarbons, where $n_{ql}/n_c \approx 0.1$. The Ioffe–Regel limit for quasifree states gives $n_{ql} \approx 0.36 \times (Tn\mu_e)_{ql}$, which holds quite well when the gas molecules are relatively rigid. However, for flexible molecules such as the *n*-alkanes larger than propane, the Ioffe–Regal limit predicts too large values for n_{ql}.

The density normalized mobility of cations $n\mu_+$ in saturated methanol vapor is constant at 1.02×10^{21} molecules/m V s up to 67×10^{25} molecules/m^3 (25 Amagats). In saturated water vapor $n\mu_+ = 1.87 \times 10^{21}$ molecules/m V s up to 30×10^{25} molecules/m^3 (11 Amagats).

NORMAN GEE et GORDON R. FREEMAN. Can. J. Chem. **61**, 1664 (1983).

On a mesuré les mobilités du cation et de l'électron dans des vapeurs de méthanol et d'eau à des températures comprises entre 293 et 617 K dans le but d'évaluer les sections droites de transfert du moment correspondant. Les sections droites de l'électron sont en accord avec le carré du moment dipolaire. Contrairement aux gaz non polaires, où la section droite moyenne de l'électron $\sigma_{ave,e}$ est seulement de 0,01 à 0,1 fois celle des cations $\sigma_{ave,+}$, le méthanol a une section droite de $\sigma_{ave,e} \approx 0{,}5\sigma_{ave,+}$ et l'eau une section droite de $\sigma_{ave,e} \approx \sigma_{ave,+}$. Les électrons thermiques échangent principalement de l'énergie avec les molécules à travers les modes de rotation moléculaires, par opposition aux modes élastiques.

Le début de la quasi localisation de l'électron dans la vapeur saturée se situe à $n_{ql} \approx 5 \times 10^{25}$ molécules/m^3 ($n_{ql}/n_c \approx 0{,}010$) dans le méthanol et à 3×10^{25} ($n_{ql}/n_c \approx 0{,}003$) dans l'eau. Ces valeurs représentent des densités 10 fois inférieures à celles des hydrocarbures où $n_{ql}/n_c \approx 0{,}1$. La limite de Ioffe–Regel des états quasi libres donne $n_{ql} \approx 0{,}36$ $(Tn\mu_e)_{ql}$ qui est très valable quand les molécules gazeuses sont relativement rigides. Cependant, dans le cas des molécules flexibles tels les *n*-alcanes, homologues supérieurs du propane, la limite de Ioffe–Regel prédit de trop fortes valeurs de n_{ql}.

La densité normalisée de mobilité des cations $n\mu_+$ dans la vapeur saturée de méthanol est constante à 1,02 $\times 10^{21}$ molecules/m V s jusqu'à 67×10^{25} molecules/m^3 (25 Amagats). Dans la vapeur d'eau saturée $n\mu_+ = 1{,}87 \times 10^{21}$ molecules/m V s jusqu'à 30×10^{25} molecules/m^3 (11 Amagats).

[Traduit par le journal]

Introduction

The contribution of the molecular electric dipole moment D to the net interaction of electrons and ions with organic fluids has recently been assessed in the series propane, propene, and dimethyl ether (1). Each of these molecules has an anisotropic polarizability that makes a major contribution to the net charge – induced dipole interaction. The permanent dipole affects the magnitude but not the nature of the overall charge–molecule interaction. It had similarly been concluded from conductance, scavenging, and spectroscopic studies that the behavior of extra electrons in nonspherelike, nonpolar molecular liquids differs in degree but not in kind from that in polar liquids (2–6).

In liquid hydrocarbons that have gas phase dipole moments up to 0.5 D (debye) the effect of polarity is masked by the effect of the physical shape (degree of sphericity) of the molecule (7). The shape correlates with the depth of the solvation potential well. The well is deeper with molecules that are less spherelike, because such molecules tend to have more anisotropic polarizabilities and their rotation in the liquid phase is more hindered. In the low density gas phase the effect of molecular shape on electron scattering is the opposite of that in the dense liquid. Electrons with energies <0.10 eV are more strongly scattered by more spherelike molecules (8).

When the molecular dipole moment is greater than about 1.0 D, as in dimethyl ether, electron behavior in both the low and high density fluids begins to be dominated by the dipole moment (1). In alcohols and water the strongly polar OH group dominates the electron behavior. The relative effects of different groups are evidenced by decreasing electron mobilities and increasing optical absorption energies of solvated electrons as one proceeds through the series alkanes, ethers, alcohols (1, 2, 4–6, 9–12). The ability of OH groups to cluster together may be responsible for the observed electron (13) and ion (14) behavior in saturated water vapor. Clustering effects, and their sensitivity to temperature, appear to be greater in water vapor (13, 14) than in organic vapors (1, 7, 15).

To obtain more information about the effect of the OH group, the previous series (1) has been extended from dimethyl ether (H_3COCH_3) to methanol (H_3COH) and water (HOH). Earlier studies of ion and electron mobilities in these vapors (13, 14, 16–24) were over more limited ranges of temperature and density than those in the present work, except a study of electrons in water vapor which reached a higher density but had a smaller temperature range (13).

Experimental

Water was fractionally distilled in sequence from acidic dichro-

[1]Assisted financially by the Natural Sciences and Engineering Research Council of Canada.

Can. J. Chem. Downloaded from www.nrcresearchpress.com by 210.87.254.6 on 09/06/12
For personal use only.

Can. J. Chem. Downloaded from www.nrcresearchpress.com by 210.87.254.6 on 09/06/12
For personal use only.

mate, basic permanganate, and from no reagent. About 300 cm^3 of the triply distilled water was poured into an electrolysis cell (6 cm^2 plate electrodes separated by 3 cm) that formed part of a grease-free vacuum line. The cell contained 5 g of methyl viologen hydrate crystals (Aldrich Chemical Co.). After sealing the filling tube with a flame, the sample was degassed by evacuation and stirring for 45 min (25), electrolysed at 0.5 V for two days, then distilled under vacuum into a trap containing 3 g of potassium hydroxide (BDH Analar grade). The potassium hydroxide had been melted under vacuum and sputtered to degas it. The aqueous hydroxide solution was further degassed by stirring under vacuum. When water samples were needed they were distilled from the hydroxide solution into the irradiation cell.

Methanol (Aldrich Gold Label, spectrophotometric grade) was deaerated by bubbling about 100 cm^3 of it with UHP argon (Matheson) for about 30 min at the rate of ~3 dm^3/min through a sintered glass frit. The half-life of solvated electrons in the liquid was 3.0 μs at 298 K (pulse dose 6×10^{16} eV/g). The methanol was stored under UHP argon at a pressure slightly greater than atmospheric. To prepare a sample, methanol was transferred without contact with the atmosphere, into a previously evacuated vacuum line and degassed by several trap-to-trap distillations, the receiver at 77 K being continually open to high vacuum.

The radiolysis conductance cell, temperature control, and pulse conductance measuring systems have been described previously (9, 26–28). A 30, 100, or 300 ns pulse of 1.7 MeV X rays delivered a dose of 0.3, 1, or 3×10^{11} eV/g, respectively, to the sample. The electron flight times were about 100-fold smaller than those of the ions. The former were measured with the aid of an amplifier that had a 0–97% rise time of 60 ns (27); the latter were measured with a slower, more sensitive amplifier (15, 26).

The mobilities were determined with both positive and negative applied voltages to check for effects of adventitious fields. No voltage polarity effect was identified. The value of the thermal electron mobility at a given (n, T) is typically the average of fourteen measurements covering a ≳10-fold range of voltage. Each ion mobility is the average of about ten measurements over a ≳5-fold voltage range. The mean deviation of electron mobilities from the mean is 2%, and of ion mobilities is 4%.

The physical properties of gaseous water and methanol were taken from ref. 29. No gas densities were given for methanol at T <333 K. However, at 333 K < T <373 K tabulated densities were an average of 8% higher than those calculated from the vapor pressures and the ideal gas equation. So at 293 K < T <333 K densities were taken to be 8% higher than those calculated from the vapor pressure and the ideal gas equation.

Results

Electron mobilities μ_e in water and methanol vapors at various densities are plotted against inverse temperature in Fig. 1. The saturated vapor density increases with increasing temperature, so the mobilities decrease sharply (triangles in Fig. 1). In a constant density vapor the electron mobility increases gently with increasing temperature, for both water and methanol.

Cation mobilities μ_+ in the vapors (Fig. 2) are two orders of magnitude lower than those of electrons, but the temperature coefficients are similar (compare Figs. 1 and 2).

The mobilities in Figs. 1 and 2 were measured at electric field strengths E/n < 10 Td (Td = 10^{-21} V m^2/molecule), where they are independent of field strength (Fig. 3). Electron mobilities increase at E/n > 12 Td in methanol vapor and at >24 Td in water vapor (Fig. 3).

The density normalized mobilities of electrons in a given vapor at room temperature agree with those reported earlier (16, 17, 20, 22, 23), within 10%.

The density normalized electron mobilities in the saturated

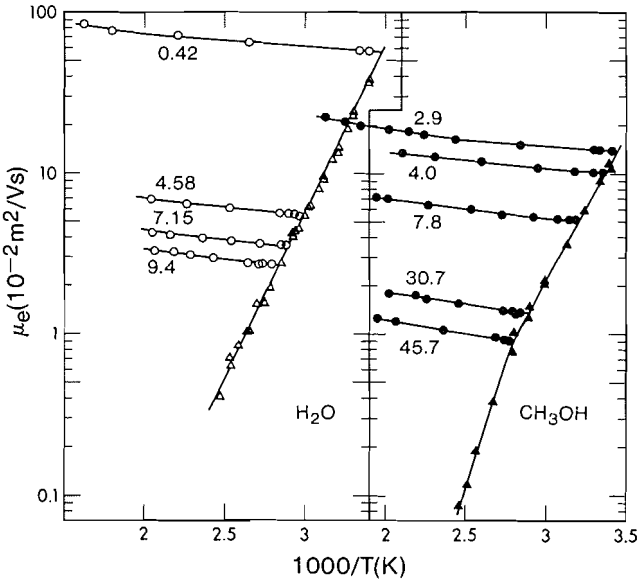

FIG. 1. Arrhenius plots of electron mobilities at different gas densities. ○, ●, nonsaturated vapor at the density indicated ($n/10^{24}$ molecule m^{-3}). △, ▲, coexistence vapor, density increases with increasing T.

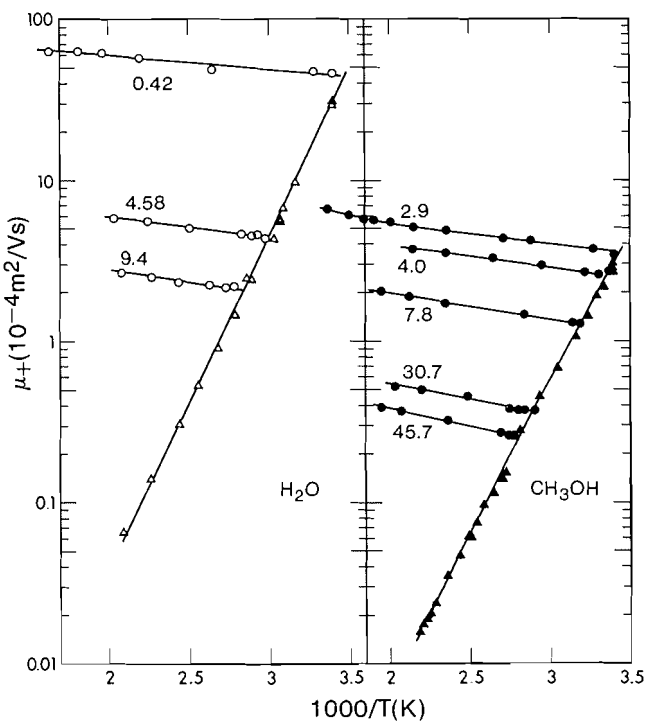

FIG. 2. Arrhenius plots of cation mobilities. The symbols mean the same as in Fig. 1.

vapors are nearly constant at $n < 5 \times 10^{25}$ molecules/m^3 in methanol and $<3 \times 10^{25}$ molecules /m^3 in water. At higher densities $n\mu_e$ decreases (Fig. 4). At 396 K and $n = 4.1 \times 10^{25}$ molecules/m^3 the electrons in water vapor were partially consumed by reaction, with a first half-life of 1.0 μs measured at both 700 and 3000 V/cm. The time τ required for the electron current to fall to zero was therefore less than the flight time t_d over the distance l between the electrodes. The value of τ decreased less rapidly than E^{-1}. "Apparent" values of the mobility were estimated from $l^2/V\tau$, plotted against V^{-1} and

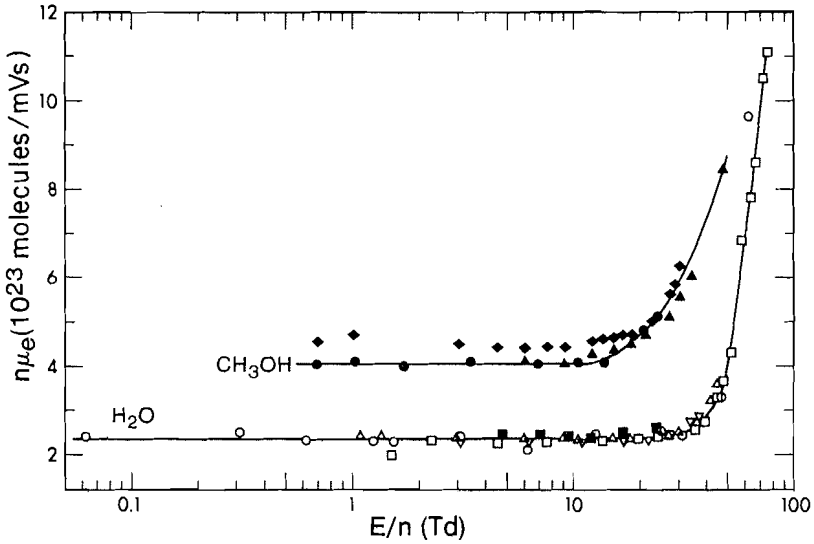

FIG. 3. Electric field dependence of electron mobilities, normalized for gas density n. Td = 10^{-21} V m^2/molecules. The following data represent (ref., T/K, $n/10^{24}$ m^{-3}). Methanol: ● (this work, 294, 2.9), ▲ (22, 293, 0.06–0.8), ◆ (23, 300, <4.6). Water: ■ (this work, 294, 0.4), ○ (16, 300, 0.04–0.8), △ (17, 293, 0.06–0.5), □ (20, 298, 0.02–0.1), ▽ (23, 300, <0.9). The results are for nonsaturated vapors at 297 ± 4 K.

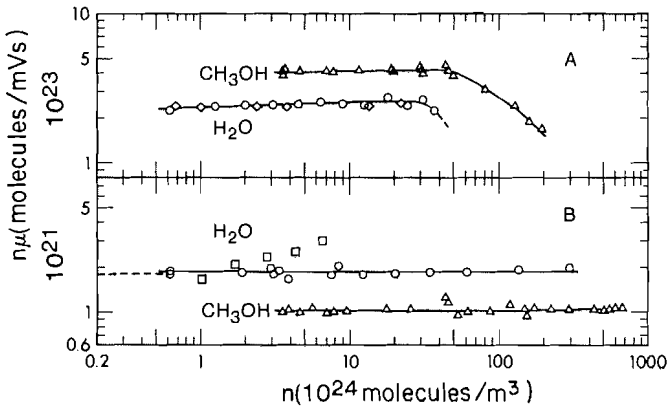

FIG. 4. Density dependence of density normalized mobilities in the saturated vapors. A, electrons: △, ○, this work; ◇, water, ref. 13; B, ions: △, ○, this work; □, water, ref. 14. ---, nonsaturated water vapor, 293 K, ref. 17.

extrapolated to $V^{-1} = 0$. The results indicated that $n\mu_e$ decreases rapidly at $n > 4.0 \times 10^{25}$ molecules/m^3. The normalized cation mobilities $n\mu_+$ are constant up to the highest densities studied, which were 30×10^{25} molecules/m^3 for water and 67×10^{25} molecules/m^3 for methanol. In the context of the density of the critical fluid n_c (1), the maximum densities just mentioned correspond to only $n/n_c = 0.028$ and 0.13, respectively.

Discussion

1. Low density gases

(a) Field dependence threshold and the contribution of inelastic scattering. The electron mobilities increase at high fields (Fig. 3). The threshold $(E/n)_e^{thr}$ for field dependence is ~12 Td in methanol and ~24 Td in water vapor. The ratio of the threshold drift velocity, $v_d^{thr} = \mu E^{thr}$, to the speed of sound c_0 in the gas reflects the relative contribution of inelastic components to the electron scattering (27, 30–33). For low density gases (34),

[1] $$c_0 = (\gamma kT/M)^{1/2}$$

where γ is the heat capacity ratio (35), k is Boltzmann's constant, and M is the molecular mass. The threshold fields in the low density gases are listed in Table 1 for water, methanol, dimethyl ether, propene, and propane. Although the molecular electric dipole moments in this series vary by a factor of 22 (36), the density normalized mobilities $n\mu_e$ by a factor of 71, and the threshold fields $(E/n)_e^{thr}$ by a factor of 100, the threshold drift velocities v_d^{thr} vary by only a factor of 2 (Table 1). The effect of a larger dipole moment is to increase the electron scattering cross section and to decrease $n\mu_e$ (37), so that a higher E/n is needed to reach the threshold electron drift velocity.

The ratio v_d^{thr}/c_0 is similar in each of the gases of the series (Table 1). The values 10–16 are much greater than unity and indicate that the energy gained by the electrons through acceleration in the electric field is removed mainly by inelastic collisions with the molecules at $T \gtrsim 300$ K. At thermal energies (~0.02 eV) the inelastic molecular mode is rotational excitation.

Threshold drift velocities for field dependence of ion mobilities are similar to those for electrons (15, 27, 33). The threshold field $(E/n)_+^{thr}$ for ions can be estimated using eq. [2] (33):

[2] $$(E/n)_+^{thr} \approx (3kT/M)^{1/2}/n\mu_+$$

The factor $(3kT/M)^{1/2}$ in eq. [2] is the root-mean-square velocity of the molecules. It is ~60% greater than the speed of sound in polyatomic molecular gases. The present data for 297 K yield $(E/n)_+^{thr} \approx 640/1.88 \times 10^{21} = 340 \times 10^{-21}$ V m^2/molecule = 340 Td in water vapor and $480/1.02 \times 10^{21} = 470$ Td in methanol vapor. These fields are higher than the maxima used in the present or earlier work (17, 19, 21), and explains the observed field independence of the ion mobilities.

(b) Temperature dependence and scattering cross sections. The temperature dependence of the mobility at low fields reflects the energy dependence of the momentum transfer cross sections σ_m (16, 38–40). The electron mobility may be approximately represented by eq. [3] (39):

Can. J. Chem. Downloaded from www.nrcresearchpress.com by 210.87.254.6 on 09/06/12
For personal use only.

TABLE 1. Molecular properties and threshold fields for electron heating at 297 ± 2 K

Compound	D^a (D)	γ^b	c_0^c (m/s)	$n\mu_e^d$ (10^{23} molecule/m V s)	$(E/n)_e^{thr}$ (Td)	$v_d^{thr,e}$ (m/s)	$\frac{v_d^{thr}}{c_0}$
HOH	1.84	1.12	392	2.35	24	5600	14
CH_3OH	1.69	1.23	308	4.05	12	4900	16
CH_3OCH_3	1.30	1.13	246	6.3[f]	4[f]	2500	10
CH_3CHCH_2	0.36	1.13	258	57.[g]	0.48[g]	2700	11
$CH_3CH_2CH_3$	0.084	1.11	249	167.[g]	0.22[g]	3700	15

[a]Permanent dipole moment. $D = 1 \times 10^{-18}$ esu cm $= 3.34 \times 10^{-30}$ C m, ref. 36.
[b]Heat capacity ratio, ref. 35.
[c]Speed of sound, eq. [1].
[d]Values at low fields.
[e]Threshold drift velocity $= (n\mu_e)(E/n)_e^{thr}$.
[f]Reference 1.
[g]Reference 7.

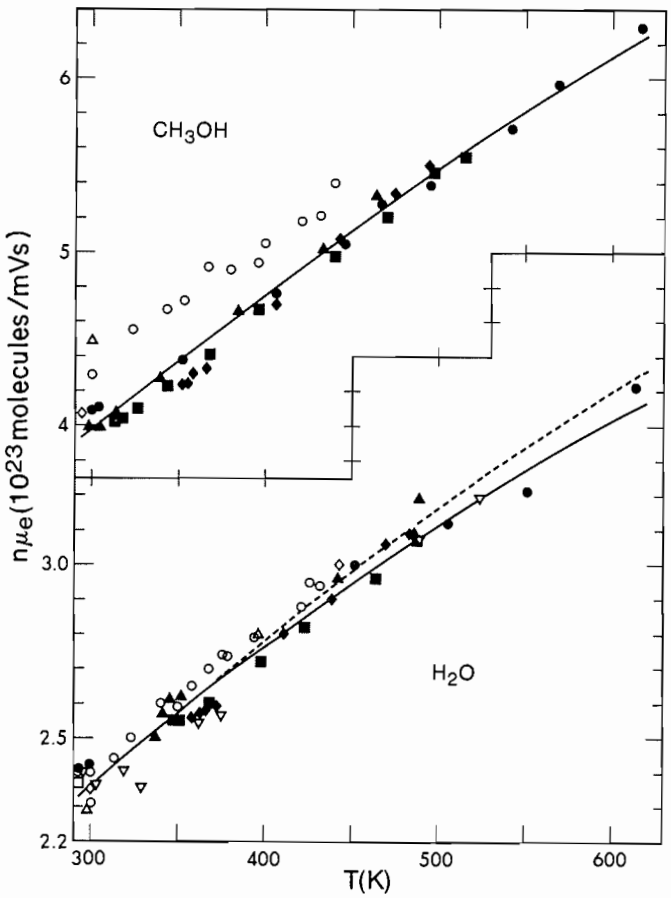

FIG. 5. Temperature dependence of density normalized mobilities of electrons in nonsaturated vapors. The lines were calculated from eq. [4] or [7], using the corresponding cross sections in Fig. 6. The following numbers represent (ref., $n/10^{24}$ molecule m^{-3}): CH_3OH: ◇ (22, 0.06−0.8), △ (23, <4.6), ○ (24, <4.6), ● (this work, 2.9), ▲ (this work, 4.0), ■ (this work, 7.8), ◆ (this work, 30.7). Average deviation of present results from line, 1.3%. H_2O: ▽ (13, <40), ◇ (16, 0.04−0.8), □ (17, 0.06−0.5), △ (20, 0.02−0.1), ◊ (23, <0.9), ○ (24, <0.9), ● (this work, 0.42), ▲ (this work, 4.58), ◆ (this work, 9.4). Average deviation of present results from solid line, 1.5%.

$$[3] \quad n\mu_e = \frac{-4\pi e}{3m}\int_0^\infty \frac{v^2}{\sigma_{m,e}}\frac{df_0}{dv}dv$$

where e and m are the electron charge and mass, v is the electron velocity relative to that of the molecules, $\sigma_{m,e}$ is the

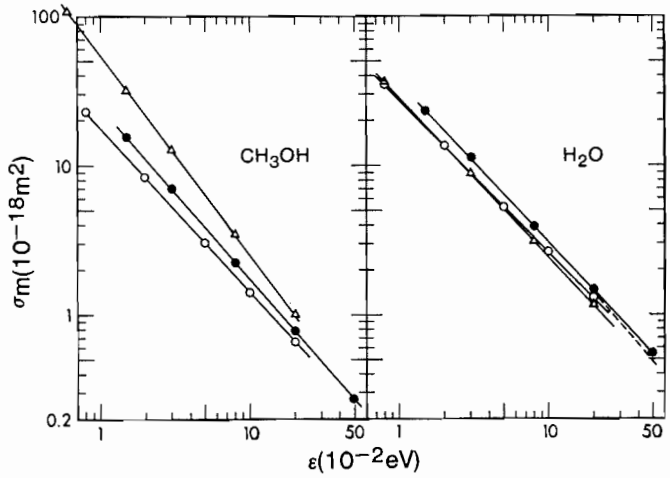

FIG. 6. Energy dependence of electron (○, ●) and cation (△) momentum transfer cross sections. ●, estimated from equation [4]; ○, △, from [7]. ----, H_2O from ref. 16 increased 1.08-fold.

electron momentum transfer cross section of the molecule, and f_0 is the isotropic term in the velocity distribution. For a Maxwellian distribution $f = (m/2\pi kT)^{3/2}\exp(-mv^2/2kT)$ and one obtains:

$$[4] \quad n\mu_e = \frac{8\pi e^2}{3m}\left(\frac{m}{2\pi kT}\right)^{5/2}\int_0^\infty \frac{v^3}{\sigma_{m,e}}\exp\left(-\frac{mv^2}{2kT}\right)dv$$

The present low density $n\mu_e$ data are plotted against temperature in Fig. 5. The values for water agree with those reported earlier (13, 16, 17, 20, 23, 24) within about ±3%. The values for methanol agree with those in ref. 22, but are ~9% lower than those in refs. 23 and 24. Equation [4] was fitted to the data in Fig. 5 by numerical manipulation (1, 7) to obtain $\sigma_{m,e}$ as a function of v, or of energy $\epsilon = \frac{1}{2}mv^2$, for water and methanol molecules. The cross sections are plotted in Fig. 6 (closed circles). The reliability of the cross sections depends on the sensitivity of the integral in eq. [4] to a change in $\sigma_{m,e}$. At 455 K, near the middle of the temperature range, the integral for methanol reaches 2% of its final value at $\epsilon = 0.02$ eV, and 97% at 0.3 eV. For water at 455 K the integral goes from 2 to 98% of its final value between $\epsilon = 0.02$ and 0.3 eV. The electron scattering cross sections are relatively unreliable outside this energy zone.

Scattering by point dipoles would give $\sigma_{m,e} \propto \epsilon^{-1}$ (37). The actual energy dependence is a bit steeper:

Can. J. Chem. Downloaded from www.nrcresearchpress.com by 210.87.254.6 on 09/06/12
For personal use only.

TABLE 2. Cross sections for scattering neutral molecules, electrons, and cations

Compound	$\bar{\alpha}^a$ (10^{-30} m^3)	$\sigma_\alpha{}^b$ (10^{-20} m^2)	$n\mu_e{}^c$ (10^{23} molecule/m V s)	$\sigma_{ave,e}{}^c$ (10^{-20} m^2)	$n\mu_+{}^d$ (10^{21} molecule/m V s)	$\sigma_{ave,+}{}^d$ (10^{-20} m^2)
HOH	1.5	17	2.35	590	1.88	510
CH_3OH	3.2	27	4.05	340	1.02	710
CH_3OCH_3	5.2	38	6.3[e]	220	1.0[e]	580
CH_3CHCH_2	6.0	42	57.[e]	24	1.7[f]	380
$CH_3CH_2CH_3$	6.2	42	167.[e]	8.3	1.9[f]	330

[a]Mean polarizability, ref. 36, sect. 14207.
[b]Neutral molecule scattering cross section, $\sigma_\alpha \approx 4\pi\alpha^{2/3}$.
[c]297 ± 2 K, eq. [13].
[d]298 K, eq. [15], assuming $M_r = M/2$.
[e]References 1 and 7.
[f]Reference 15.

methanol

[5] $\sigma_{m,e}(10^{-19}\ \text{m}^2) = 1.20\epsilon^{-1.15}$

water

[6] $\sigma_{m,e}(10^{-19}\ \text{m}^2) = 2.6\epsilon^{-1.07}$

where $0.02 \leq \epsilon \leq 0.3$ eV. The mobilities calculated from these cross sections are shown as lines in Fig. 5. Cross sections for water in ref. 16 gave $n\mu_e$ values about 8% higher than those obtained in the present work. The cross sections from ref. 16 were increased by 8% and plotted in Fig. 6 for comparison; the corresponding values of $n\mu_e$ are shown as the dashed curve in Fig. 5.

The equation relating the ion mobility $n\mu_+$ to momentum transfer cross sections $\sigma_{m,+}$ is [7] (38, 40):

$$[7] \quad n\mu_+ = \frac{3e\sqrt{\pi}}{8M_r}\left(\frac{2kT}{M_r}\right)^{5/2} \Big/ \int_0^\infty v^5\sigma_{m,+}\exp\left(-\frac{M_r v^2}{2kT}\right)dv$$

where M_r is the ion–molecule reduced mass. The ion mobilities are plotted against temperature in Fig. 7. Fitting eq. [7] to the mobilities by numerical integration over progressively adjusted $\sigma_{m,+}$ distributions (1, 7) resulted in the cross sections shown in Fig. 6 (triangles). The ion mass was taken equal to the molecular mass M, although it was probably greater than that due to clustering, $ROH_2^+(ROH)_n$. The true value of M_r was therefore between M and $M/2$. The sensitive energy range for the $\sigma_{m,+}$ fitting procedure was about 0.008 to 0.2 eV, which is somewhat lower than the sensitive range for the electron cross sections:

methanol

[8] $\sigma_{m,+}(10^{-19}\ \text{m}^2) = 1.10\epsilon^{-1.34}$

water

[9] $\sigma_{m,+}(10^{-19}\ \text{m}^2) = 2.06\epsilon^{-1.07}$

Curiously, for water the electron momentum transfer cross section is 26% larger than the ion scattering cross section at the same energy (Fig. 6). For nonpolar molecules electron momentum transfer cross sections (7, 16, 22, 27, 28, 30, 31) are usually 1–2 orders of magnitude smaller than ion momentum transfer cross sections at the same energy (15). For polar gases the electron cross sections are usually similar to but smaller than the ion cross sections at the same energy (1, 13, 16, 22–24). Cross sections for scattering ions are greater than those for scattering neutral molecules (Table 2 and ref. 41). To elucidate the unusual case of electron and ion scattering by

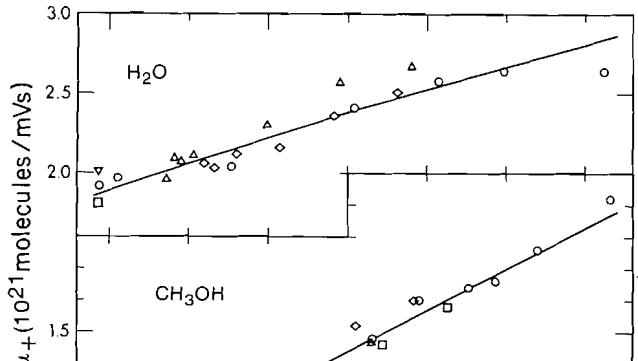

FIG. 7. Temperature dependence of density normalized mobilities of ions in nonsaturated vapors. The lines were calculated from eq. [7] using the corresponding cross sections in Fig. 6. The following numbers represent (ref., $n/10^{24}$ molecule m^{-3}): CH_3OH: ○ (this work, 2.9), △ (this work, 4.0), □ (this work, 7.8), ◇ (this work, 30.7). Average deviation from line, 2.6%. H_2O: □ (17, 0.03–0.50), ▽ (19, 0.53), ○ (this work, 0.42), △ (this work, 4.58), ◇ (this work, 9.4). Average deviation from line, 3.1%.

water, two points should be considered. (*i*) The cations are probably clustered to some extent (21, 42), which would increase the reduced mass and decrease the estimated values of $\sigma_{m,+}$. This would increase the unusual inverted difference between the estimated electron and ion cross sections. Although there is no direct evidence that electrons are clustered by molecules under the present conditions, the formation of transient anions as in [10] would increase the time-averaged mass of the negative charge, and thereby increase the effective cross section estimated on the basis of the electron mass:

[10] $e^- + (ROH)_n \rightleftharpoons (ROH)_n^-$

where $n = 1, 2, \cdots$. The large cross section of water is mainly attributable to the large dipole moment (see next section), but [10] might make some contribution that causes the water points in Fig. 8 to fall below the line. (*ii*) The ion and electron cross sections were calculated from different equations, respectively [4] and [7], involving different approximations. The same set of ($n\mu$, T) data generates somewhat larger values of σ_m from eq. [4] than from [7]. It has been suggested (43, 44) that when

Can. J. Chem. Downloaded from www.nrcresearchpress.com by 210.87.254.6 on 09/06/12
For personal use only.

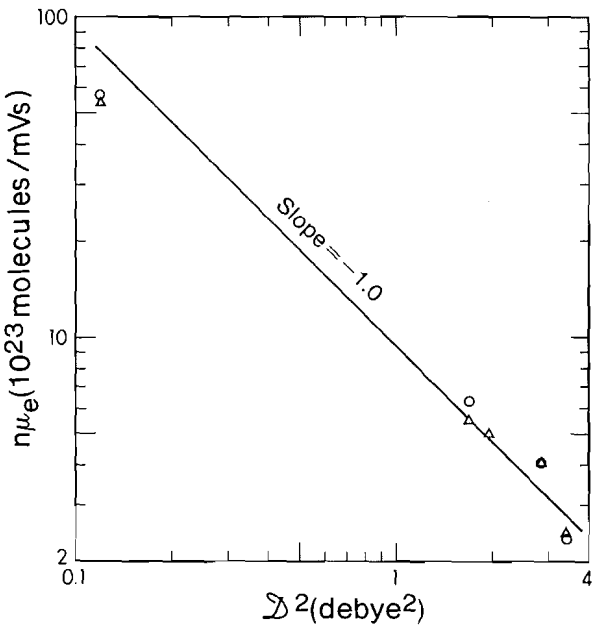

FIG. 8. Correlation of density normalized electron mobility with the square of the molecular dipole moment D^2. ○, low density gases at 297 ± 2 K (Table 1); △, low density saturated vapors at the middle of the experimental low density range. The gases reported from left to right are propene (46), dimethyl ether (1), ammonia (45), methanol, and water.

inelastic processes make a major contribution to electron scattering, as they do in the present systems, eq. [7] is more appropriate than [4]. Values of $\sigma_{m,e}$ obtained from [7] are accordingly shown in Fig. 6 for comparison. The corresponding equations are, for $0.008 \leq \epsilon \leq 0.2$ eV:

methanol

$$[11] \quad \sigma_{m,e}(10^{-19}\ \mathrm{m}^2) = 1.12\epsilon^{-1.10}$$

water

$$[12] \quad \sigma_{m,e}(10^{-19}\ \mathrm{m}^2) = 2.5\epsilon^{-1.02}$$

These cross sections used in [7] give the same mobilities as do [5] and [6] in [4], respectively, within <0.5%.

The above points can be summarized by rewriting [4] and [7] in terms of average velocities $\langle v \rangle$ and average cross sections σ_{ave} (15, 30):

$$[13] \quad n\mu_e = \left(\frac{8}{3\pi}\right)\left(\frac{e}{m}\right)\frac{1}{\langle v \rangle}\frac{1}{\sigma_{ave,e}}$$

where

$$[14] \quad \sigma_{ave,e} = \langle v \rangle / \langle v/\sigma_{m,e} \rangle$$

and

$$[15] \quad n\mu_+ = \left(\frac{3}{4}\right)\left(\frac{e}{M_r}\right)\frac{1}{\langle v \rangle}\frac{1}{\alpha_{ave,+}}$$

where

$$[16] \quad \sigma_{ave,+} = \langle v^3\sigma_{m,+} \rangle / \langle v^3 \rangle$$

and

$$[17] \quad \langle v \rangle = (8kT/\pi M_r)^{1/2}$$

For electron scattering, M_r in [17] equals m. The numerical coefficients in eqs. [13] and [15] have a ratio $(8/3\pi)/(3/4) = 1.13$, so a given set of $n\mu$, M_r, and $\langle v \rangle$ values would give σ_{ave} from [13] 1.13 times larger than that from [15]. Actually, the different averaging procedures inherent in [4] and [7] lead to slightly different apparent energy dependences of σ_m, so the difference between cross sections at a given energy obtained from a set of ($n\mu$, T) data can be somewhat greater than 13%.

(c) Dipole moment dependence. The value of $n\mu_e$ in polar gases varies approximately as the inverse square of the molecular dipole moment D^{-2} (37). This is shown for water, methanol, ammonia (45), dimethyl ether (1), and propene (46) in Fig. 8, for both nonsaturated (at 297 K) and saturated vapors.

2. Density dependence

In the low density saturated vapors of methanol and water, that is, at low temperatures, the value of $n\mu_e$ is approximately independent of n (Fig. 4). The same is true in many substances (1, 7, 27, 30, 31, 45). The slight increase of $n\mu_e$ with n (Fig. 4) is due to the concomitantly increasing temperature.

In methanol at $n > 5 \times 10^{25}$ molecules/m^3 the value of $n\mu_e$ decreases (Fig. 4). This signals the onset of quasilocalization of the electrons. Ioffe and Regel (47) pointed out that the electron cannot be considered to be quasifree when the mean free path L is smaller than the de Broglie wavelength λ of the particle. The threshold density n_{ql} for quasilocalization can therefore be compared with the Ioffe–Regel limit through the equation

$$[18] \quad L \approx \lambda$$

or

$$[19] \quad (n_{ql}\sigma_{ave,e})^{-1} \approx h/m\langle v \rangle$$

whence

$$[20] \quad n_{ql} \approx m\langle v \rangle / h\sigma_{ave,e}$$

where h is Planck's constant. From eqs. [13], [17], and [20] one obtains

$$[21] \quad n_{ql} \approx 0.36(Tn\mu_e)_{ql}$$

Mott and Davis (48) misquote (or discretely correct?) the Ioffe–Regel limit as $L \approx \lambda\!\!\!^{-} = \lambda/2\pi$, which would predict n_{ql} values 2π times larger than those of eq. [21]. It is difficult to choose between the forms so we kept the original, as did other workers (13).

A plot of n_{ql} against $(Tn\mu_e)_{ql}$ for a number of polar and nonpolar saturated vapors is shown in Fig. 9. The points that fall near the line for eq. [21] correspond to relatively rigid molecules, whether they are polar or nonpolar: water, methanol, dimethyl ether (1), propene (46), propane (46), ethane (49), methane (30), and xenon (27). The points for flexible molecules such as *n*-butane (7), *n*-pentane (31), and *n*-hexane (50) have values of n_{ql} about an order of magnitude lower than those predicted by the Ioffe–Regel limit.

It should be noted that the Ioffe–Regel criterion depends only on the average density and the temperature. It does not take into account the density fluctuations that occur in the vapors near the vapor–liquid coexistence curve, and which are largely responsible for quasilocalization in nonpolar gases such as xenon (27), methane (30), and ethane (49). Heating the nonpolar vapor to remove it from the vapor–liquid coexistence region reduces the extent of quasilocalization (27), and increases the value of n_{ql} by an amount that has not been measured yet.

Heating the strongly polar vapors water (13) and ammonia (45) in the unsaturated region apparently increases n_{ql} by

Can. J. Chem. Downloaded from www.nrcresearchpress.com by 210.87.254.6 on 09/06/12
For personal use only.

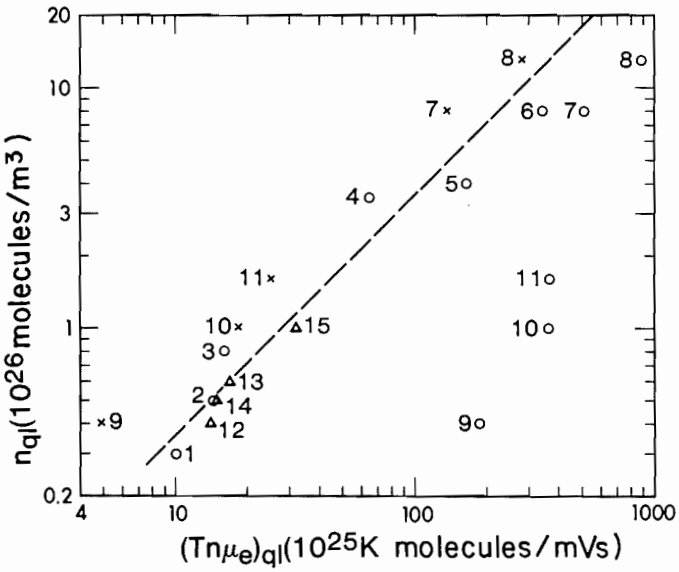

FIG. 9. Correlation between threshold density for quasilocalization n_{ql} and $(Tn\mu_e)_{ql}$ in saturated vapors (○). *1*, water, 387 K; *2*, methanol, 360 K; *3*, dimethyl ether, 292 K (1); *4*, xenon, 215 K (27); *5*, propene, 303 K (46); *6*, methane, 156 K (30); *7*, propane, 338 K (46); *8*, ethane, 284 K (49). The dashed line represents eq. [21]. Also included are: *9*, *n*-hexane 362 K (50); *10*, *n*-pentane, 360 K (31); *11*, *n*-butane, 332 K (7). Unsaturated vapors (△): *12* and *13*, water, 463 and 523 K (13); *14* and *15*, ammonia, 300 and 460 K (45). ×, $(n_{ql}/n_c)(Tn\mu_e)_{ql}$ for the C_2-C_6 *n*-alkanes.

amounts that conform to the Ioffe–Regel criterion (Fig. 9). The large scattering cross sections of the polar molecules seem to minimize the effect of clusters in the quasilocalization process.

For the C_2 to C_6 *n*-hydrocarbons the deficit of n_{ql} below that predicted by eq. [21] increases as the carbon chain length increases. The values of n_{ql} in ethane to *n*-hexane vary as $\bar{\alpha}^{-3}$, rather than as $\bar{\alpha}^{-2}$ which might have been expected for clustering due to induced dipole – induced dipole interactions. Although the reason is unclear, multiplying the ethane to *n*-hexane $(Tn\mu_e)_{ql}$ values by n_{ql}/n_c shifts the values to just above the Ioffe–Regel line (Fig. 9).

Acknowledgement

We thank B. L. Henson for tabulated values of μ_+ in water vapor from ref. 14. The assistance of the staff of the Radiation Research Center is gratefully acknowledged.

1. N. GEE and G. R. FREEMAN. Can. J. Chem. **60**, 1034 (1982).
2. G. R. FREEMAN and J. M. FAYADH. J. Chem. Phys. **43**, 86 (1965).
3. J. C. RUSSELL and G. R. FREEMAN. J. Chem. Phys. **48**, 90 (1968).
4. G. R. FREEMAN. J. Phys. Chem. **77**, 7 (1973).
5. F.-Y. JOU and G. R. FREEMAN. J. Phys. Chem. **80**, 909 (1977).
6. F.-Y. JOU AND G. R. FREEMAN. Can. J. Chem. **57**, 591 (1979).
7. N. GEE and G. R. FREEMAN. J. Chem. Phys. **78**, 1951 (1983) and references therein.
8. G. R. FREEMAN, I. GYÖRGY, and S. S.-S. HUANG. Can. J. Chem. **57**, 2626 (1979).
9. J.-P. DODELET and G. R. FREEMAN. Can. J. Chem. **53**, 1263 (1975).
10. J. H. BAXENDALE. Can. J. Chem. **55**, 1996 (1977).
11. H. A. GILLIS, N. V. KLASSEN, G. G. TEATHER, and K. H. LOKAN. Chem. Phys. Lett. **10**, 48 (1971).
12. J. H. BAXENDALE, C. BELL, and P. WARDMAN. Chem. Phys. Lett. **12**, 347 (1971).
13. V. GIRAUD and P. KREBS. Chem. Phys. Lett. **86**, 85 (1982).
14. B. L. HENSON. J. Phys. D**11**, 1405 (1978); J. Phys. D**12**, L65 (1979).
15. N. GEE and G. R. FREEMAN. Can. J. Chem. **59**, 2988 (1981).
16. J. L. PACK, R. E. VOSHALL, and A. V. PHELPS. Phys. Rev. **127**, 2084 (1962).
17. J. J. LOWKE and J. A. REES. Aust. J. Phys. **16**, 447 (1963).
18. R. W. CROMPTON, J. A. REES, and R. L. JORY. Aust. J. Phys. **18**, 541 (1965).
19. H. RYZKO. Proc. Phys. Soc. London, **85**, 1283 (1965).
20. J. F. WILSON, F. J. DAVIS, D. R. NELSON, R. N. COMPTON, and O. H. CRAWFORD. J. Chem. Phys. **62**, 4204 (1975).
21. F. D. LANGE. Int. J. Mass Spectrom. Ion Phys. **37**, 341 (1981).
22. T. L. COTTRELL, W. J. POLLOCK, and I. C. WALKER. Trans. Faraday Soc. **64**, 2260 (1968).
23. L. G. CHRISTOPHOROU and A. A. CHRISTODOULIDES. J. Phys. B**2**, 71 (1969).
24. L. G. CHRISTOPHOROU and D. PITTMAN. J. Phys. B**3**, 1252 (1970).
25. R. BATTINO, M. BANZOFF, M. BOGAN, and E. WILHELM. Anal. Chem. **43**, 806 (1971).
26. J.-P. DODELET and G. R. FREEMAN. Can. J. Chem. **55**, 2264 (1977).
27. S. S.-S. HUANG and G. R. FREEMAN. J. Chem. Phys. **68**, 1355 (1978).
28. T. WADA and G. R. FREEMAN. Phys. Rev. A**24**, 1066 (1981).
29. N. B. VARGAFTIK. Tables on the thermophysical properties of liquids and gases. 2nd ed. J. Wiley, Halsted Press. 1975.
30. N. GEE and G. R. FREEMAN. Phys. Rev. A**20**, 1152 (1979).
31. I. GYÖRGY and G. R. FREEMAN. J. Chem. Phys. **70**, 4769 (1979).
32. B. V. PARANJAPE. Phys. Rev. A**21**, 405 (1980).
33. R. E. ROBSON and E. A. MASON. Phys. Rev. A**25**, 2411 (1982).
34. E. HAUSMANN and E. P. SLACK. Physics. Van Nostrand, New York. 1944. p. 412.
35. R. C. WEAST (*Editor*). Handbook of chemistry and physics, 57th ed. CRC Press, Cleveland OH. 1976. P.D-162.
36. H. STUART. Landolt-Bornstein Zahlenwerte und Funktion, I. band, 3 teil. *Edited by* A. Eucken and K. H. Hellwege. Springer-Verlag, Berlin. 1951. sect 14206.
37. S. ALTSHULER. Phys. Rev. **107**, 114 (1957).
38. F. W. MORRISON, G. R. AKRIDGE, H. W. ELLIS, R. Y. PAI, E. W. MCDANIEL, L. A. VIEHLAND, and E. A. MASON. J. Chem. Phys. **63**, 2238 (1975).
39. (*a*) J. L. PACK and A. V. PHELPS. Phys. Rev. **121**, 798 (1961); (*b*) G.H. HUXLEY and R. W. CROMPTON. The diffusion and drift of electrons. Wiley, New York. 1974. Chapt. 3.
40. E. W. MCDANIEL and E. A. MASON. The mobility and diffusion of ions in gases. Wiley and Sons, New York. 1973. Chapt. 5.
41. N. GEE, S. S.-S. HUANG, T. WADA, and G. R. FREEMAN. J. Chem. Phys. **77**, 1411 (1982).
42. C. E. YOUNG and W. E. FALCONER. J. Chem. Phys. **57**, 918 (1972).
43. O. H. CRAWFORD, M. DALGARNO, and P. B. HAYS. Mol. Phys. **13**, 181 (1967).
44. W. R. GARRETT. Mol. Phys. **24**, 465 (1972).
45. P. KREBS, K. BUKOWSKI, V. GIRAUD, and M. HEINTZE. Ber. Bunsenges. Phys. Chem. **86**, 879 (1982).
46. N. GEE and G. R. FREEMAN. Rad. Phys. Chem. **15**, 267 (1980).
47. A. F. IOFFE and A. R. REGEL. Prog. Semicond. **4**, 237 (1960).
48. N. F. MOTT and E. A. DAVIS. Electronic processes in non-crystalline materials. Clarendon Press, Oxford. 1971. pp. 3, 8.
49. N. GEE and G. R. FREEMAN. Phys. Rev. A**22**, 301 (1980).
50. S. S.-S. HUANG and G. R. FREEMAN. Can. J. Chem. **56**, 2388 (1978).

Can. J. Chem. Downloaded from www.nrcresearchpress.com by 210.87.254.6 on 09/06/12
For personal use only.

Potentiometric analysis of humic substances and other colloids

PAUL A. ARP

Department of Forest Resources, University of New Brunswick, Fredericton, N.B., Canada E3B 6C2

Received November 16, 1982

PAUL A. ARP. Can. J. Chem. **61**, 1671 (1983).

The acid–base behaviour of colloidal suspensions of γ-Al_2O_3, TiO_2 (rutile), high surface-charge latex, and humic substances in water is reexamined by using a Nernst-like model and two electrostatic models to simulate the proton-affecting surface potential. The Nernst-like model is based on the assumption that the proton-affecting surface potential is proportional to the Nernst potential. The other models are based on conventional double-layer assumptions. All models yield numerically consistent information about (*i*) number of chemically discernible functional groups (or collections of funetional groups), (*ii*) their dissociation constants and concentrations, (*iii*) the free H^+- (or OH^--) concentrations in the suspending medium, (*iv*) surface area of colloidal substance, and (*v*) surface potential (and charge) as function of p*h*. Potentiometric analyses are performed on documented titration curves by employing a modified version of the ACBA (acid–base) program developed by Arena *et al*. The goodness-of-fit information provided by this program suggests that the Nernst-like model is particularly useful for generating and verifying estimates for surface capacities as function of p*h*.

PAUL A. ARP. Can. J. Chem. **61**, 1671 (1983).

On a étudié de nouveau le comportement acide–base des suspensions colloïdales de γ-Al_2O_3, de TiO_2 (rutile), d'un latex à grande charge de surface, et des substances humiques dans l'eau, en utilisant un modèle de type Nernst et deux modèles électrostatiques pour simuler le potentiel de surface influencé par le proton. Le modèle de type Nernst se base sur la supposition que le potentiel de surface influencé par le proton est proportionnel au potentiel de Nernst. Les autres modèles se basent sur l'hypothèse conventionnelle de la couche double. Tous les modèles fournissent des informations numériques importants au sujet: (*i*) du nombre de groupes fonctionnels que l'on peut distinguer chimiquement (ou d'un ensemble de groupes fonctionnels), (*ii*) de leurs constantes de dissociation et de leurs concentrations, (*iii*) des concentrations en H^+ (ou OH^-) libres dans la suspension, (*iv*) de la surface du colloide et (*v*) du potentiel de surface (et de la charge) en fonction du pH. On a effectué des analyses potentiométriques sur les courbes de titration connus en utilisant un version modifiée du programme ACBA (acide–base) mis au point par Arena et ses collaborateurs. L'information adéquate fournie par ce programme suggère que le modèle de type Nernst est particulièrement utile pour engendrer et vérifier les évaluations des capacités de surface en fonction du pH.

[Traduit par le journal]

Can. J. Chem. Downloaded from www.nrcresearchpress.com by 210.87.254.6 on 09/06/12
For personal use only.

Introduction

The acid–base behaviour of colloidal materials such as oxide suspensions, humic substances, and polyelectrolytes in general may be influenced by (*i*) association–dissociation equilibria of proton-carrying functional groups, (*ii*) electrostatic attraction or repulsion due to charges located on the molecules, (*iii*) intra- and intermolecular hydrogen bonding, (*iv*) burial of acidic groups in hydrophobic environments (Veis (1)). The objective of this paper is to show that the acid–base behaviour of substances with rigid or near-rigid microstructure (i.e. restricted molecular motion relative to nearest neighbour interactions among the various H^+-ion adsorption/desorption sites) appears to be controlled by chemical equilibria, with electrostatic contributions becoming effective at high surface charge density. The analysis is based on a reinterpretation of published titration curves using the ACBA-program developed by Arena *et al*. (2) specifically modified to take acid–base affecting surface potentials into account. The modified version is verified by comparison with the chemical modelling exercise described by Westall and Hohl (3) using γ-Al_2O_3- and TiO_2-titration curves as case studies. The analysis is then applied to the reexamination of a monofunctional latex surface and several humic substances.

Theory

(a) General

The proton dissociation–association behaviour of rigid or near-rigid colloidal substances subjected to titration is perhaps best understood once the proton association constant

$$[1] \quad K_i = K_{0i} \exp(-F\Psi^s/RT)$$

of each chemically discernible functional group ($i = 1, 2, \ldots N_L$) is determined. Here, each K_{0i} represents the intrinsic proton-association constant of a particular group and Ψ^s is the proton-affecting surface potential. In the following, two electrostatic models and one non-electrostatic model are described by which Ψ^s, K_{0i}, and K_i may be obtained in a numerically consistent way by potentiometric analysis.

(b) The diffuse double layer

The electrostatic potential near a charged interface — according to the Gouy–Chapman theory for flat surfaces — is given by

$$[2] \quad \Psi = \frac{2RT}{F} \ln \frac{\coth(F\Psi^s/4RT) + \exp(-\kappa x)}{\coth(F\Psi^s/4RT) - \exp(-\kappa x)}$$

where x is distance from the surface and

$$[3] \quad 1/\kappa = (\epsilon\epsilon_0 RT/2000I)^{1/2}/F$$

is the "characteristic" thickness (Debye length in m) of the diffuse ion–layer at the interface. Also, R is the universal gas constant (= 8.31 J/mol deg K); F is Faraday's constant (= 96 487 C/mol), T is absolute temperature (K), ϵ is the dielectric constant of the suspending medium ($\approx$ 80 for water at 25°C), ϵ_0 is the permittivity of free space (= 8.85×10^{-12} F/m), and I is the ionic strength of the suspending medium (mol/L). The interfacial charge density — as predicted by the same theory — is given by

$$[4] \quad \sigma = -\epsilon\epsilon_0[d\Psi/dx]_{x=0}$$
$$= (1/\lambda)(8000\epsilon\epsilon_0 RTI)^{1/2} \sinh(F\Psi^s/2RT) + \sigma_R$$

Can. J. Chem. Downloaded from www.nrcresearchpress.com by 210.87.254.6 on 09/06/12
For personal use only.

The charge density, in addition, may also be obtained from the titration relationship

$$[5]\quad \sigma(\text{exp}) = \frac{T_\sigma F}{SC} = \left[\frac{v \cdot C_h^T + V_0(C_h^0 + \sum C_{Ai}^{0+})}{v + V_0} - h + \frac{K_W}{h}\right]\frac{F}{SC}$$

and from the principles of mass action (i.e., eq. [1]) and charge conservation, i.e.

$$[6]\quad \sigma(\text{calcd}) = \frac{F}{SC^0}\left[\sum_{i=1}^{N_L}\frac{K_{0i}C_{Ai}^0 h}{K_{0i}h + \exp(F\Psi^s/RT)} - \sum C_{Ai}^{0-}\right]$$

where T_σ is the analytical interfacial acid (base) concentration (equiv./L), σ_R is the surface charge density at an appropriate reference potential Ψ_R^s, h is the free H^+-ion concentration of the suspending medium, K_W is the ionic product of water, v is the volume of titrant added to titrand (also to be denoted as $v(\text{exp})$), V_0 is the initial volume of titrand, C_h^T is the analytical acid concentration of the titrant, C_h^0 is the initial analytical acid concentration of the titrand, $\sum C_{Ai}^{0+(-)}$ is the initial sum concentration of all functional groups that may assume positive (negative) charges (for reasons of simplicity only one positive or negative charge per group is allowed), S is surface area of colloidal substance (m^2/g), and

$$[7]\quad C = C^0/(1 + v/V_0)$$

is the colloidal concentration (g/L). The surface potential, therefore, can be obtained from eqs. [4] and [5], with a check provided by eq. [6] to assess the quality of the assumed $\sigma - \Psi^s$ relationship for each tritration point. The λ-parameter of eq. [4] may be considered as an adjustable constant signifying (*i*) that the proton-adsorbing surface may not be flat (or smooth) and (*ii*) that the adsorbed H^+- and OH^--ions have finite size, with diameters similar to that of water molecules or H_3O^+-ions ($\simeq$3 Å). More specifically, the empirical relationship

$$[8]\quad \sigma = (8000\epsilon\epsilon_0 RTI)^{1/2} \times \left(\frac{1}{1 + a\kappa}\sinh\frac{F\Psi^s}{2RT} + \frac{2}{b\kappa}\tanh\frac{F\Psi^s}{4RT}\right) + \sigma_R$$

derived from Loeb *et al.* (4) for spherical particles surrounded by an ionic double layer may be used instead of eq. [4] to calculate Ψ^s. Here, a is the width of the surface-fixed solvent- (water-) layer, and b is the average particle radius, or — more generally — the radius of the effective curvature for irregularly shaped particles or rough surfaces. For small potentials, i.e. $F\Psi^s/4RT \ll 1$, eq. [8] reduces to eq. [4] with

$$1/\lambda = \left(\frac{1}{b\kappa} + \frac{1}{1 + a\kappa}\right)$$

Combining eqs. [4], [5], and [7] yields

$$[9]\quad \Psi^s = (2RT/F)\sinh^{-1}[f(T_\sigma - T_\sigma^R)(1 + v/V_0)]$$

with

$$[10]\quad f = \lambda F(8000\epsilon\epsilon_0 RTI)^{-1/2}/SC^0$$

as an adjustable parameter, and $T_\sigma^R = T_\sigma$ when $\Psi^s = 0$.

(c) The constant capacitance model

The constant capacitance model is in all respects identical to the diffuse double layer model except that $\sinh(F\Psi^s/2RT)$ is linearized so that

$$[11]\quad \Psi^s = (2RT/F)[f(T_\sigma - T_\sigma^R)(1 + v/V_0)]$$

(d) The pseudo-Nernst model

The law of mass action involving all proton-adsorbing surface groups is given by

$$[12]\quad K = K_1^{a_1}K_2^{a_2}K_3^{a_3}\ldots = K_{01}^{a_1}K_{02}^{a_2}K_{03}^{a_3}\ldots \times \exp[-(a_1 + a_2 + a_3\ldots)F\Psi^s/RT] = \left(\frac{1 - \alpha_1}{\alpha_1}\right)^{a_1}\left(\frac{1 - \alpha_2}{\alpha_2}\right)^{a_2}\left(\frac{1 - \alpha_3}{\alpha_3}\right)^{a_3}\ldots h^{(-a_1 - a_2 - a_3\ldots)}$$

where α_i denotes the h-dependent degree of dissociation for each functional group, and

$$a_i = C_{Ai}/C_{A1} \text{ with } C_{Ai} = C_{Ai}^0 V_0/(v + V_0)$$

Equation [14], therefore, yields yet another way for expressing the surface potential, i.e.

$$[13]\quad \frac{F\Psi^s}{RT} = \ln\frac{h}{h^0} + \sum_{i=1}^{N_L} C_{Ai}^0 \ln\frac{1 - \alpha_i}{\alpha_i}\Big/\sum_{i=1}^{N_L} C_{Ai}^0$$

with

$$[14]\quad \ln h^0 = -\sum_{i=1}^{N_L} C_{Ai}^0 \ln K_{0i}/\sum_{i=1}^{N_L} C_{Ai}^0$$

It appears from [13] that the potential-determining H^+- (or OH^--) ions produce a surface potential different from the expected particle (Nernst) potential given by

$$[15]\quad F\Psi^p/RT = \ln h/h^0$$

To illustrate, set $N_L = 1$ in [13] and obtain

$$[16]\quad F\Psi^s/RT = \ln h/h^0 - \ln(1 - \alpha_1)/\alpha_1 = F\Psi^p/RT - \ln(1 - \alpha_1)/\alpha_1$$

with $h_0 = 1/K_{0i}$. For $N_L = 2$ and $C_{A1} = C_{A2}$, it follows that

$$[17]\quad \frac{F\Psi^s}{RT} = \ln\frac{h}{h^0} - \frac{1}{2}\ln\frac{1 - \alpha_1}{\alpha_1}\frac{1 - \alpha_2}{\alpha_2}$$

with $h^0 = (K_{01}K_{02})^{-1/2}$. Furthermore, h^0 coincides with the point of zero potential (or zero charge) when the two groups involved assume equal but opposite charges.

Equation [16] has found extensive and successful use in analyzing the acid–base behaviour of many monofunctional surfaces, especially micelles and monolayers (5–7), and certain globular proteins (1, 8). Less successful is the application of eq. [16] to polyfunctional surfaces encountered, e.g., with oxide suspensions, most biopolymers, and humic substances because several degrees of dissociation are involved. Oxide surfaces tend to be bifunctional (amphoteric) yielding a "pseudo-Nernst" potential near $h \simeq h^0$ (de Hek *et al.* (9); Healy and White (10)) approximately given by

$$[18]\quad \Psi^s \simeq \mu^*(RT/F)\ln h/h^0$$

with

$$\mu^* = \mu/(1 + \mu)$$

and

TABLE 1. Formulae for charge and differential capacitance for the constant-capacitance (cc), diffuse double layer (dl), and pseudo-Nernst (pn) surface models*

Type of model	σ	$C = d\sigma/d\Psi^s$
cc	Eq. [11]	A/λ
d	Eq. [4]	$(A/\lambda)\cosh(F\Psi^s/2RT)$
pn, general	$\frac{F}{SC^0}\left[\sum_{i=1}^{N_L} C_{Ai}/B - \sum C_{Ai}^{0-}\right]$	$\left(\frac{F}{SC^0}\right)\left(\frac{F}{RT}\right)\sum_{i=1}^{N_L} C_{Ai}\exp(F\Psi^s/\mu RT)/(B^2K_{ai}h^0)$
pn, monofunctional surface	$\sigma_m[1 + \exp(F\Psi^s/\mu RT)] = \sigma_m/[1 + (h/h^0)^{1-\mu}]$	$(A/\lambda)[\cosh(F\Psi^s/\mu RT)]^{-2}$
pn, amphoteric surface	$\frac{2\sigma_m \sinh(F\Psi^s/\mu RT)}{\beta + 2\cosh(F\Psi^s/\mu RT)}$	$(A/\lambda)(\beta + 2)\frac{2 + \beta\cosh(F\Psi^s/\mu RT)}{[\beta + 2\cosh(F\Psi^s/\mu RT)]^2}$

*$A = (F/2RT)(8000\epsilon\epsilon_0 RTI)^{1/2}$; $B = 1 + \exp(-F\Psi^s/\mu RT)/(K_{0i}h^0)$; $\sigma_m = FC_{A1}/SC^0$; $\beta = \sqrt{K_{01}/K_{02}} + \sqrt{K_{02}/K_{01}}$.

$$\mu = 4fC_{A1}^0 h^0 K_{01}(1 + h^0K_{01})^{-2}$$
$$= 4fC_{A2}^0 h^0 K_{02}(1 + h^0K_{02})^{-2}$$

obtained from eqs. [4] and [6] by Taylor expansion of $F\Psi^s/RT$ with respect to $\Delta \ln h = \ln h/h^0$. Equation [18] thus provides a charge-independent way for assessing Ψ^s of amphoteric surfaces near the point of zero charge. The same equation, in a general sense, may also be viewed as a "pseudo-Nernst" surface model to yield Ψ^s by considering $\mu^* = \mu/(1 + \mu)$ as an adjustable parameter, with μ given by

$$\mu = 2fh^0\sum_{i=1}^{N_L} K_{0i}C_{Ai}/(1 + h^0K_{0i})^2$$

and h^0 by eq. [14].

(e) Model-by-model comparison

Each model produces a different $\sigma-\Psi^s$ relationship, yet all three models converge to the same form when $\Psi^sF/RT \ll 1$, i.e.

$$[19]\quad \left(\frac{2RT}{F}\right)\frac{\sigma_{exp} - \sigma_R}{(8000\epsilon\epsilon_0 RTI)^{1/2}} = \frac{\Psi^s_{cc}}{\lambda_{cc}} = \frac{\Psi^s_{dl}}{\lambda_{dl}} = \frac{\Psi^s_{pn}}{\lambda_{pn}}$$

with cc, dl, and pn denoting the possibility that each model may produce a different λ-value. The following major differences exist between the three models.

(*i*) The dl-model limits Ψ^s to

$$[20]\quad (F\Psi^s_{dl}/RT)_{max,\ min} = \pm 2\sinh^{-1}\{f_{dl}[\sum C_{Ai}^{0+(-)} + T_\sigma^R(1 + \nu/V_0)]\}$$

on the low and high side of ph^0, respectively. The cc-model also curbs the surface potential but the pn-model does not.

(*ii*) The differential surface capacitance $C = d\sigma/d\Psi^s$ predicted by the dl-model (see Table 1 and Fig. 1) passes through a single minimum at $\Psi^s_{dl} = 0$ with no inflection points locatable on either side of this minimum. The pn-model, in contrast, predicts a maximum or minimum for C_{pn} at $\Psi^s_{pn} = 0$. For example, the pn-capacitance for amphoteric surfaces passes through a maximum at $\Psi^s_{pn} = 0$ provided $\beta \leq 4$. Otherwise C_{pn} (max) is found at

$$(F\Psi^s_{pn}/RT)_{max} = \pm\mu_{pn}\cosh^{-1}(\beta/2 - 4/\beta)$$

with

$$C_{pn}(max) = A\beta^2/[8\lambda_{pn}(\beta - 2)]$$

(*iii*) The differential capacitance associated with the dl-model approaches a limiting value with increasing absolute surface potential. The pn-model, in contrast, predicts that the surface capacitance vanishes at high and low surface potentials.

(f) Parametric estimation

Any Ψ^s-generating model may be used to predict the behaviour of each K_i-value once accurate estimates for h, K_{0i}, C_h^T, C_h^0, C_{Ai}^0, K_W, and f are secured. Such estimates may be obtained by employing a non-linear least-squares method to interpret a titration curve associated with a particular colloidal substance for its parametric information content. The least-squares method — according to Arena *et al.* (2) — may be based on minimizing the error-square sum of the difference between actual and calculated added titrant volumes, i.e., minimize

$$U = \sum_{k=1}^{N_T}[v_k(exp) - v_k(calcd)]^2$$

where N_T denotes the total number of titration steps. An explicit expression for v_k(calcd), i.e.

$$[21]\quad v_k(calcd) = -\frac{V_0}{h_k - K_W/h_k - C_h^T}\left\{h_k - K_W/h_k - C_h^0 + \sum_{i=1}^{N_L}\left[\frac{C_{Ai}^0K_{0i}h_k}{h_kK_{0i} + \exp(F\Psi^s_k/RT)} - C_{Ai}^0np_i^0\right]\right\}$$

is obtained from the titration relationships

$$A_{ik} = a_{ik} + h_ka_{ik}K_{0i}\exp(-F\Psi^s_k/RT)$$
$$= V_0\cdot C_{Ai}^0/(v_k + V_0)$$

and

$$H_k = h_k - K_W/h_k + h_k\sum_{i=1}^{N_L} a_{ik}K_{0i}\exp(-F\Psi^s_k/RT)$$
$$= [v_k\cdot C_h^T + V_0\cdot(C_h^0 + np_i^0\cdot C_{Ai}^0)]/(v_k + V_0)$$

Here np_i^0 is the number of protons bound per functional group (limited to one for reasons of simplicity), and A_{ik} and a_{ik}, respectively, are the analytical and free (i.e., unprotonated) concentrations of each functional group at the kth titration point; H_k represents the corresponding analytical concentration for the total acidity of the titrant. The free H^+-ion concentration, i.e., h_k, may be obtained potentiometrically by employing the equation

Can. J. Chem. Downloaded from www.nrcresearchpress.com by 210.87.254.6 on 09/06/12
For personal use only.

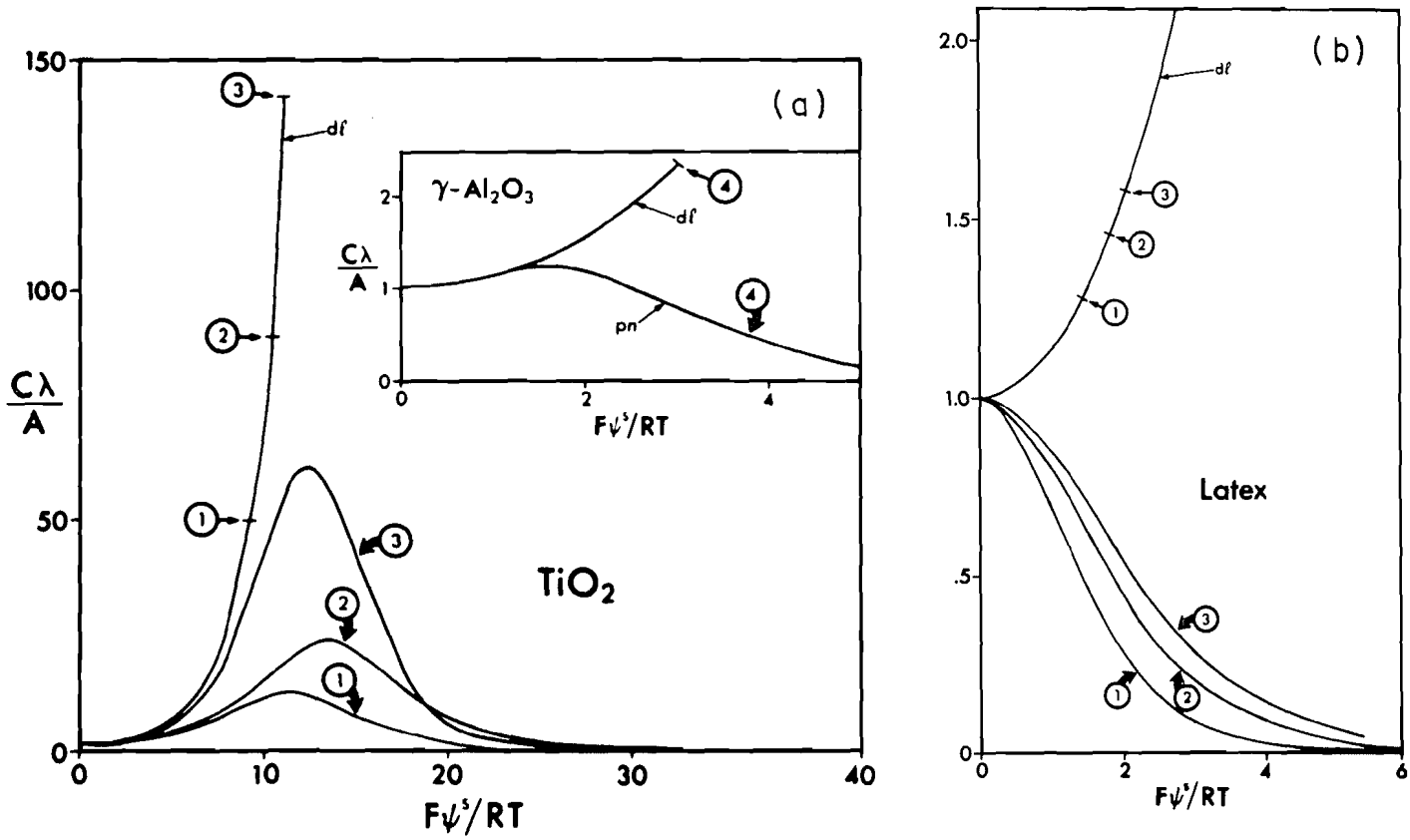

FIG. 1. Plot of $C\lambda/A$ versus $F\Psi^s/RT$ for TiO_2 and γ-Al_2O_3 (part *a*) and for a monofunctional latex surface (part *b*) according to the dl-model (upper curve) and pn-model (lower curves) when $I = 0.1$, 0.01, and 0.001. Each case for I is denoted here by ① (or ④), ②, and ③, respectively. Also, each curve is calculated by using the appropriate equation and information provided by Tables 1 and 3. Dashes through the dl-lines identify $(C_{dl}\lambda/A)_{max}$ and $(F\Psi^s_{dl}/RT)_{max}$ for each value of I.

$$E_k = E_0 + s_L \ln h_k + j_A h_k$$

where E_k is the electromotive force measured (e.g.) with glass and calomel electrodes, and E_0, s_L, and j_A represent additional parameters also requiring least-squares refinement.

The acid–base (ACBA) computer program in ref. 2 minimizes U when $\Psi^s = 0$. Only slight adjustments to the basic algorithm, however, need to be made to minimize U when $\Psi^s \neq 0$ and employing models based on the double layer theory or the modified Nernst equation (i.e., eq. [18]). These methods, as seen below, produce nearly identical results for the characterization of surface acidity although the pseudo-Nernst model may be preferred because of its ability to fit the experimental data particularly well. Furthermore, the optimal f-values, in principle, may be used to determine S and b provided that (*i*) the H^+-ions are the only surface-potential generating ions in the suspending medium, (*ii*) there are no permanent, p*h*-independent charges associated with the surface, and (*iii*) the substance of interest is not subjected to extensive shrinking and swelling due to the uncoiling of polymeric microstructure during the course of the titration. Both S and b may be found from experimental f-versus-I data using the relationship

$$[22] \quad \frac{\kappa}{1 + a\kappa} = -\frac{1}{b} + \frac{1}{S}\frac{F\kappa}{f(8000\epsilon\epsilon_0 RTI)^{1/2}C^0} = -\frac{1}{b} + \frac{1}{S}g$$

and plotting (or regressing) $\kappa/(1 + a\kappa)$ versus g with slope and intercept yielding the surface area (m^2/l) and the effective surface curvature of the colloid–solution interface, respectively.

Procedure

A number of published titration curves (Table 2) providing sufficient information for rigorous analysis were selected, magnified (approximately 3×), and digitized with a TRS-80 digitizer yielding a precision of approximately ±0.05 mm per $x-y$ coordinate measurement. Between 25 to 60 well-spaced titration points per curve were obtained and submitted to the modified ACBA-program for analysis. Optimal values for f and μ^* corresponding to minimal U-values were found by scanning either f (for cc- and dl-calculations) or μ^* (for pn-calculations) through a range of feasible values while simultaneously refining all other titration parameters of interest. Also analyzed were the surface charge – p*h* isotherms (Figs. 3 and 4 in ref. 10) for the monofunctional, high-charge carboxylic acid latex studied by Ottewill and Yates (11).

Discussion

(a) Amphoteric surface

Shown in Table 3 is a model-by-model comparison between reported and refined titration parameters for γ-Al_2O_3 and TiO_2. It appears that the general agreement among the various numerical estimates for K_{01}, K_{02}, C_h^0, and ph^0 is satisfactory, but that there are major discrepancies for f, μ, λ, and μ^*. A substantial portion of these differences, however, can be traced to model-dependent differences in $1/\lambda$. To check this algebraically and numerically, set

Can. J. Chem. Downloaded from www.nrcresearchpress.com by 210.87.254.6 on 09/06/12
For personal use only.

TABLE 2. Titration parameters of selected colloids

Type of colloid	Reference	Temperature (°C)	Supporting electrolyte	V_0 (mL)	Titrant	Colloid concentration g/L	Colloid concentration mequiv./L
γ-Al_2O_3	Fig. 4 in (3)	25	0.1 *M* $NaClO_4$	100?	0.1 *M* KOH?	8.174	0.128
TiO_2	Fig. 5 in (3)	25	0.001 *M* KNO_3	100?	0.1 *M* KOH?	12.07	0.4825
			0.010 *M* KNO_3	100?			
			0.100 *M* KNO_3	100?			
Fulvic acid	Fig. 2 in (15)	25	0.1 *M* KCl	100	0.1 *M* KOH	1.0	7.723
Fulvic acid fraction I	Fig. 3 in (16)	20	0.1 *M* NaOH & 0.1 *M* HCl	4	0.1 *M* NaOH	5.0	12.65
						2.5	6.48
Fulvic acid fraction II	Fig. 3 in (16)	20	0.1 *M* NaOH & 0.1 *M* HCl	4	0.1 *M* NaOH	2.0	16.33
						1.0	8.13
Humic acid	Fig. 2 in (23)	25?	0.1 *M* KNO_3	60	0.3346 *M* KOH	1.7	8.33
Humic acid	Fig. 1 in (24)	25	0.001 *M* KCl	50	0.1 *M* KOH?	2.0	3.00
			0.005 *M* KCl				
			0.010 *M* KCl				
			0.025 *M* KCl				
			0.050 *M* KCl				
			0.075 *M* KCl				
			0.100 *M* KCl				
			0.200 *M* KCl				

$$\frac{\kappa}{1+a\kappa} = -\frac{1}{b_{dl}} + \frac{1}{S}g_{dl}$$

$$= -\frac{1}{b_{pn}} + \frac{1}{S}g_{pn} = -\frac{1}{b_{pn}} + \frac{1}{S}g_{dl} + \Delta\left(\frac{1}{b}\right)_{pn}$$

$$= -\frac{1}{b_{cc}} + \frac{1}{S}g_{cc} = -\frac{1}{b_{cc}} + \frac{1}{S}g_{dl} + \Delta\left(\frac{1}{b}\right)_{cc}$$

and calculate

$$\Delta\left(\frac{1}{b}\right)_{pn} = \frac{1}{b_{pn}} - \frac{1}{b_{dl}}$$

and

$$\Delta\left(\frac{1}{b}\right)_{cc} = \frac{1}{b_{cc}} - \frac{1}{b_{dl}}$$

from

$$\Delta\left(\frac{1}{b}\right)_m = \kappa\Delta\left(\frac{1}{\lambda}\right)_m = \frac{F^2}{2\epsilon\epsilon_0 RTSC^0}\Delta\left(\frac{1}{f}\right)_m$$

$$= \frac{2F^2C_{A1}}{\epsilon\epsilon_0 RTSC^0}\Delta\left(\frac{\sqrt{K_{01}/K_{02}}}{\mu}\right)_m$$

$$= \frac{2F^2C_{A1}}{\epsilon\epsilon_0 RTSC^0}\Delta\left[\sqrt{K_{01}/K_{02}}\left(\frac{1}{\mu^*} - 1\right)\right]_m$$

by using the appropriate values for each parameter from Table 3. Inspection of the results will show that $\Delta(1/b)_m$ for either m = pn or m = cc remains nearly constant for the three ionic strengths considered (see also Fig. 2). The refined titration parameters are therefore internally consistent. It is thus possible to convert the parametric results peculiar to one model to those of another model by knowing the precise values for $\Delta(1/b)_m$ and h_m^0 (3).

Each model produces an acceptable fit between the actual and calculated titration volumes, as indicted by the standard deviation values

$$SD_U = \sqrt{U/(N_T - N_V)}$$

shown in Table 3 ($N_V \equiv$ number of refined titration parameters). In particular, note that

$$SD_U^{pn} < SD_U^{cc} < SD_U^{dl}$$

The pseudo-Nernst model, in fact, is capable of producing a nearly random residual for v(calcd) − v(exp). Furthermore, a good U-fit, according to eqs. [5], [6], and [21], also implies a good σ-fit, i.e.

$$SD_\sigma = \sqrt{[\sigma(\text{exp}) - \sigma(\text{calcd})]^2/(N_T - N_V)}$$

$$\simeq SD_U(C_h^T - h + K_w/h)(F/SC^0V_0)$$

The pn-model, therefore, yields an experimentally acceptable $\sigma-\Psi^s$ relationship, thereby implying that (*i*) the proton-affecting surface potential is not limited to a constant value at high and low p*h*-values, and (*ii*) that the surface capacitance of the oxide surfaces is expected to vanish at high and low surface potentials (recall Fig. 1). Surface potential and capacitances obtained by ζ-potential measurements, however, may still be limited to constant, non-zero values at high and low p*h*-values because (*i*) such measurements probe the diffuse ion-layer potential at the plane of shear (i.e., at $x \simeq 20$ Å), but not at the $x = 0$ plane where proton adsorption and desorption takes place, (*ii*) the approximate ζ-potential predicted by each model via eq. [20] is remarkably insensitive to the type of surface model employed (see Table 3), (*iii*) the exact potential–distance relationship at $x = 0$ is generally unknown, but can be expected to depend on the physical and chemical properties of the underlying surface, the surrounding solution, and type of ions nearby in addition to the electrostatic conditions imposed on the surface by the surrounding ion-layers.

The model-dependent $\kappa/(1 + a\kappa)$-versus-g plots for TiO_2 appear to yield straight, parallel lines (Fig. 2), with a slope corresponding to a surface area of 20 m^2/g in exact agreement with crystallographic and tritium exchange determinations

Can. J. Chem. Downloaded from www.nrcresearchpress.com by 210.87.254.6 on 09/06/12
For personal use only.

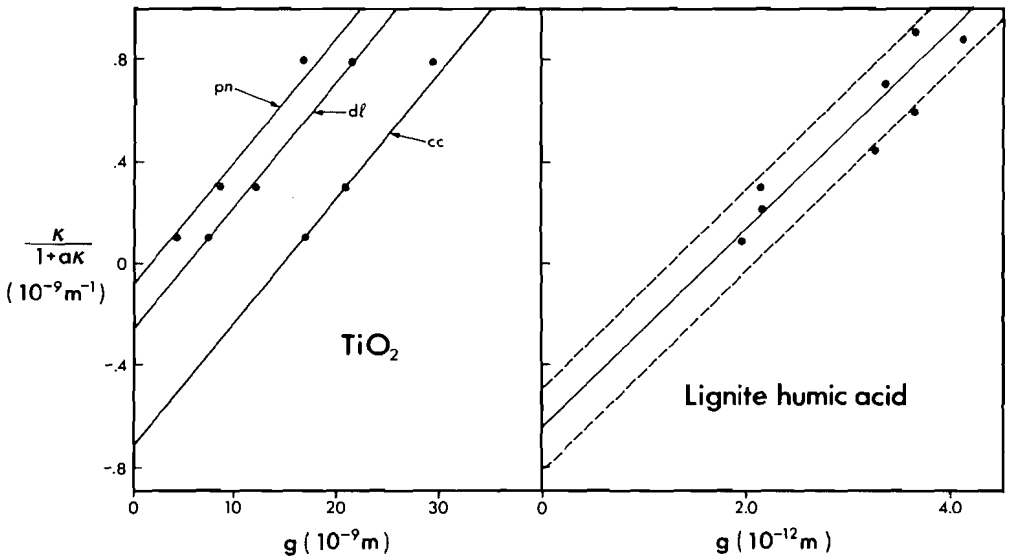

FIG. 2. Plots of $\kappa/(1 + a\kappa)$ versus g for TiO_2 (3) and lignite humic acid (23). The latter plot (pn-model only) is generated by assuming that the functional group concentrations C_{A3}, C_{A4}, and C_{A5} are given by 74, 80, and 60 mequiv./100 g, respectively (see Table 6). Also, $C_h^0 = 39$ mequiv./100 g.

done for the same suspension as reported in ref. 3. Each model, however, produces a different intercept and therefore a different effective radius for surface curvature, i.e.

$$b^s_{cc} = 1.4 \text{ Å} < b^s_{dl} = 37 \text{ Å} < b^s_{pn} = 100 \text{ Å} < b^s_{geom} = 352 \text{ Å}$$

where b^s_{geom} is the geometric radius assuming a spherical particle shape and a particle density of 4.26 g/cm^3 (12). Rutile particles, however, are strongly acicular (13) so that the λ-parameter appearing in eq. [9] should actually be interpreted by the electrostatic expression

$$[23] \quad \lambda = b\kappa\left[\frac{K_0(a'\kappa)}{a'\kappa K_1(a'\kappa)} + \ln\left(\frac{a'}{b}\right)\right]$$

with $a' = b + a$ and $K_0(a'\kappa)$ and $K_1(a'\kappa)$ as modified Bessel functions of the second kind (8). Solving eq. [23] for b (now the effective radius of the rod-shaped particles to be denoted b^R_m) by numerical analysis yields the following values in Å-units:

$$I = 0.1 \qquad b^R_{cc} = 3.0 < b^R_{dl} = 16 < b^R_{pn} = 112$$
$$I = 0.01 \qquad b^R_{cc} = 3.1 < b^R_{dl} = 13 < b^R_{pn} = 33$$
$$I = 0.001 \qquad b^R_{cc} = 3.3 < b^R_{dl} = 12 < b^R_{pn} = 33$$

The geometric rod-radius is given by $b^R_{geom} = 235$ Å. Both electrostatic interpretations of the best-fitted λ-values thus yield particle radii substantially below geometric expectations, thereby suggesting that the acid–base affecting surface potential (or surface capacitance, see Table 3) may not be purely electrostatic, at least not in a straightforward sense. The similarity between the various b-values for a specific model, however, provides an important guide to the analysis of potentiometric titration curves of colloidal substances as shown above. The only inconsistency relevant to this concept occurs with the pn-model at $I = 0.1$, but numerical analysis reveals a strong dependence of b on λ near $\lambda = 1.24$ such that (e.g.) $b^R_{pn} = 160$ Å at $\lambda = 1.26$ and $b^R_{pn} = 35$ Å at $\lambda = 1.12$.

The surface area and effective surface curvature for γ-Al_2O_3, unfortunately, cannot be obtained from the single $I = 0.1$ titration, but the acid–base association behaviour of this colloid appears to be well established with all three models producing effectively the same numbers.

General experience in applying the three models to the γ-Al_2O_3 and TiO_2-titration curves indicated that the dl-model seems to have the best convergence behaviour, yielding unambiguous optimal f-values in most cases. The other two models are prone to produce "false" minima as illustrated in Table 3 for TiO_2 ($I = 0.1$) with and without C^0_h as an additional refinable parameter. The inclusion of C_{A1} ($= C_{A2}$) as refinable parameter did not affect the convergence behaviour of any model, in each case yielding the same surface site concentrations as specified in Table 3.

(b) Monofunctional surface

The σ–ph data in ref. 11 for a monofunctional latex surface can be related to the pn-relationship

$$\log(\sigma_m/\sigma - 1) = -(1 - \mu^*)\text{p}h + (1 - \mu^*)\text{p}h^0$$

as shown in Fig. 3. The agreement between the experimental points and the best-fitted straight lines is excellent except when σ is small. The slope and (or) intercept of each line may therefore be used to determine μ* and other parameters (see Table 4).

The choice of locating the $\Psi^s_R = 0$ reference potential at $\sigma = \sigma_m/2$ is perhaps unusual although consistent with eq. [16]. The reference potential normally associated with the $\sigma = 0$ conditions is such that $\Psi^{s'}$ in

$$[24] \quad K = K'_0 \exp(-F\Psi^{s'}/RT)$$

may reflect the "true" electrostatic potential of the surface, with K'_0 as the intrinsic proton association constant when the degree of dissociation given by $\alpha = \sigma/\sigma_m$ is equal to zero. By invoking a constant capacitance model, i.e.

$$\sigma = (1/\lambda)(8000\epsilon\epsilon_0 RTI)^{1/2} F\Psi^{s'}/2RT$$

it follows that

Can. J. Chem. Downloaded from www.nrcresearchpress.com by 210.87.254.6 on 09/06/12
For personal use only.

Can. J. Chem. Downloaded from www.nrcresearchpress.com by 210.87.254.6 on 09/06/12
For personal use only.

TABLE 3. Titration parameters for γ-Al_2O_3 and TiO_2 (rutile) according to the constant capacitance (cc) double layer (dl), and pseudo-Nernst (pn) models for colloid-solution interfaces

Type of colloid	Ionic strength (equiv./L)	Type of model	log K_{01}	log K_{02}	ph^0	C_b^0 (mequiv./L)	SD_u (mL)	f (L/equiv.)	μ*	μ	λ	$\Psi^s_{dl(max)}$ (mV)	C‡ (μF/cm^2)
γ-Al_2O_3*	0.1	cc§	7.40	9.24	8.32	—	—	—	—	—	—	—	—
		cc	7.54	9.15	8.35	—	0.029	1 850	0.492	0.968	—	±74.6	—
		dl§	7.66	8.98	8.32	—	—	—	—	—	—	—	—
		dl	7.29	8.94	8.12	—	0.040	1 950	0.482	0.929	—	±75.3	—
		pn	7.50	9.18	8.34	—	0.023	1 890	0.490	0.961	—	±76.3	—
TiO_2†	0.1	cc§	3.45	8.05	5.75	—	—	—	—	—	—	—	—
		cc	2.70	7.34	5.02	4.77	0.041	10 000	0.477	0.911	0.938	±234.9	77.8
		cc	3.40	8.22	5.81	4.72	0.096	7 500	0.359	0.561	0.703		103.8
		dl	3.48	8.07	5.78	4.72	0.121	10 300	0.500	1.000	0.966	±236.5	75.6
		pn	3.28	7.07	5.18	4.76	0.022	14 800	0.780	3.55	1.392	±256.8	52.6
		pn	3.80	7.82	5.81	4.72	0.042	13 200	0.710	2.45	1.24	±248.2	59.0
	0.01	cc§	3.11	8.66	5.89	—	—	—	—	—	—	—	—
		cc	2.96	8.66	5.81	4.73	0.050	10 500	0.222	0.285	0.311	±238.4	74.1
		dl	3.38	8.52	5.95	4.72	0.096	18 500	0.489	0.957	0.548	±266.5	42.1
		pn	3.39	7.93	5.66	4.73	0.026	25 050	0.720	2.57	0.743	±282.1	31.1
	0.001	cc§	2.71	9.31	6.01	—	—	—	—	—	—	—	—
		cc	2.48	9.45	5.97	4.73	0.050	13 000	0.075	0.082	0.122	±248.4	60.0
		dl	1.84	9.04	5.94	4.73	0.065	29 500	0.312	0.454	0.177	±290.2	26.4
		pn	3.10	8.43	5.72	4.73	0.024	51 200	0.680	2.13	0.480	±318.6	15.2

*$C^0_{A1} = C^0_{A1} = 1.05$ mequiv./L for dl-model (= 1.12 for cc- and pn-models); $S = 129$ m^2/g (3).
†$C^0_{A1} = C^0_{A2} = 4.83$ mequiv./L for all models; $S = 20$ m^2/g.
‡Differential surface capacitance at $\Psi^s = 0$.
§Taken from ref. 3.

TABLE 4. Titration parameters and relevant information describing the electrostatic behaviour of a monofunctional latex colloid according to the pn-model

I	μ*	μ	λ**	$C_{pn}(\Psi^s=0)$ (μF/cm^2)	$(\Psi^s_{dl})_m$† (mV)	maximum ζ potential¶ (−) (mV)	
0.1 N	0.433*	0.795	0.407	178‖	75†	8.1‡	—
0.05 N	—	—	—	—	80§	16‡	≃18–30¶
0.01 N	0.510*	1.04	0.168	137‖	92†	40‡	≃33–55¶
0.001 N	0.548*	1.21	0.062	117‖	105§	77‡	—
0.0005 N	—	—	—	—	110†	85‡	≃60–83¶

*From the slopes of the appropriate plots in Fig. 3.
†$(\Psi^s_{dl})_m = \Psi^s_{dl}$ (max) − Ψ^s_{dl} (min), see eq. [20].
‡Estimated double layer potential at x = 20 Å.
§From interpolation of the Ψ^s_m-versus-log I plot based on the remaining points (see †).
‖$C_{pn}(\Psi^s = 0) = A/\lambda_{pn}$, see Table 1.
¶Experimental values according to ref. 10.
**$\lambda = (2\mu/\sigma_m)\,(8000\epsilon\epsilon_0 RTI)^{1/2}$; $\sigma_m = -14.6\mu$C/cm^2.

TABLE 5. Proton-association constants for a monofunctional latex colloid and for TiO_2 particles as function of ionic strength according to the pn-model

	Latex			TiO_2			
I	log K_0*	log K_0'†	log K_0^0‡	log K_{01}*	log K_{01}^0‡	log K_{02}*	log K_{02}^0‡
0.1 N	5.92	5.23	6.31	3.80	2.88	7.82	8.34
0.01 N	6.73	5.78	6.22	3.39	3.03	7.93	8.15
0.001 N	7.30	6.25	6.40	3.10	2.97	8.43	8.51

*pn-model prediction.
†Adjusted K_0-values by invoking cc-model.
‡Activity-coefficient adjusted K_0'- or K_{0i}-values (i = 1, 2).

$$\log K = \log K_0' + 1.737\mu\alpha$$

and therefore

$$\log K_0 = \log K_0' + 0.869\mu$$

The resulting values for log K_0' — see Table 4 — appear to be less dependent on I than log K_0. In fact, the remaining differences could possibly be due to the expected ionic strength effect on activity coefficients γ_{sh}, γ_s, and γ_h (see Table 5), suggesting that the equilibrium constant

$$[25]\quad K_0^0 = K_0'\gamma_{sh}/\gamma_s\gamma_h = a_{sh}/a_s a_h$$

can now be determined by an experimental procedure. Further evidence supporting this possibility comes from examining the pn-model predictions for K_{01} and K_{02} associated with the rutile–water interface as shown in Table 5, with K_{02}^0 given as above, and K_{01}^0 given by

$$[26]\quad K_{01}^0 = K_{01}\gamma_{sh2}/\gamma_{sh}\gamma_h = a_{sh2}/a_{sh}a_h$$

To produce nearly constant values for K_0^0, K_{01}^0, and K_{02}^0 it is assumed (tentatively) that γ_s and γ_{sh} follow the ionic-strength dependent trend associated with trivalent anions and cations. Other factors also accounting for at least part of the variation in log K_0' may be due to (*i*) surface complexation of counterions (especially at high ionic strength), and (*ii*) chemisorption of other surface-potential generating ions present in the supporting electrolyte either as impurities or as intended constituents (see Davis *et al.* (14)).

The general applicability of the pn-model for assessing the surface potential behaviour of a latex surface is also substantiated by the fact that the predicted maximum $\Psi^{s'}$-values for the equivalent dl-model agree well with measured ζ potentials of latex colloids with similar site density (Table 4 and ref. 10). The maximum surface potential, in this case, is given by

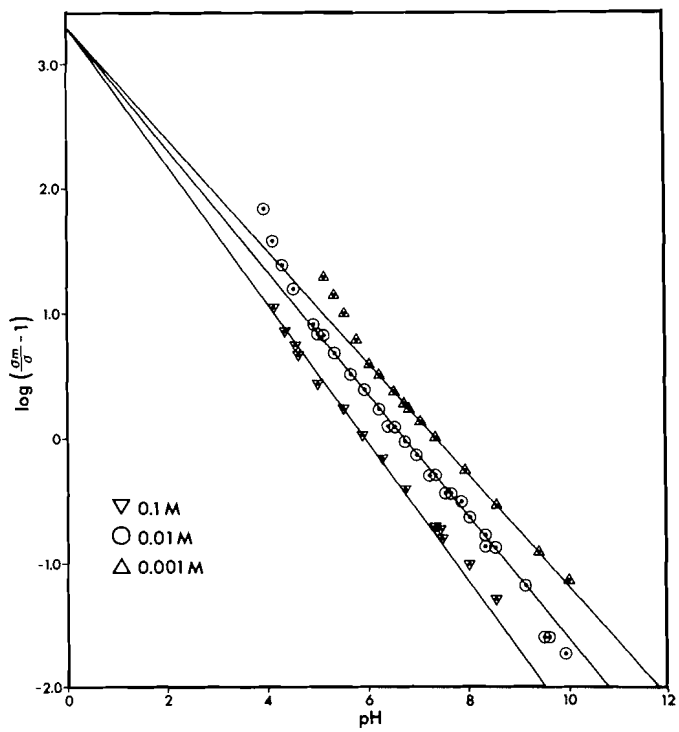

FIG. 3. Plot of log $(\sigma_m/\sigma - 1)$ versus ph for the latex colloid analyzed by Ottewill and Yates (11). Superimposed on the experimental points are the best-fitted straight lines with a common intercept at ph = 0.

Can. J. Chem. Downloaded from www.nrcresearchpress.com by 210.87.254.6 on 09/06/12
For personal use only.

Can. J. Chem. Downloaded from www.nrcresearchpress.com by 210.87.254.6 on 09/06/12
For personal use only.

$$\Psi_m^{\wedge} = \Psi_{dl}^{\wedge}(\max) - \Psi_{dl}^{\wedge}(\min) = 4RT/F \sinh^{-1} \mu$$

The resulting $\Psi_m^{\wedge}$-values, in turn, are adjusted to the corresponding ζ-potentials by using eq. [2] and setting $x = 20$ Å.

(c) Humic substances

Quantitative information regarding the acid–base behaviour of humic substances following pn-model analysis of the corresponding titration curves (Table 2) is collected in Table 6. Analyses via the dl- and cc-models lead to similar (but not identical) results analogous to the pattern described above for oxide suspensions. The results in Table 6 are arranged into eight groups depending on the value of each K_0-constant to facilitate comparison among the various substances examined.

Optimal parametric precision in terms of asymptotic standard deviations calculated for each refined parameter is in most cases better than 20% as long as the titration curve in question is not "overspecified". Overspecification may occur when the estimates of some of the parameters to be refined are strongly correlated with one another. Estimates for K_{0i} and C_{Ai} in general tend to be weakly correlated, but a sudden lack of resolution for some of these parameters appears whenever N_L — the postulated number of chemically discernible groups — exceeds a critical value $N_{L_{max}}$. Evaluation of $N_{L_{max}}$ is carried out by examining each titration curve with the modified ACBA-program using incremental N_L-values (one at a time) from $N_L = 1$ to $N_L = N_{L_{max}} + 1$. By so doing it is found that $N_{L_{max}}$ appears to depend on (*i*) the type of humic substance analyzed, and (*ii*) the p*h*-range considered.

The fact that individual functional groups can be resolved with excellent precision (provided $N_L \leq N_{L_{max}}$) is surprising. Each distinct section of a titration curve of humic matter is likely to represent not one functional group but a collection of groups with a range of overlapping K_0-values (15). The following suggestions are offered to guide proper interpretation of Table 6. (*i*) Each K_{0i}-value may be taken to represent an average K_0-value for each chemically discernible collection of functional groups thereby identified. (*ii*) Quantitative information regarding the range of K_0-values per collection of groups cannot be obtained by the approach outlined above. It is suspected, however, that this range depends on N_L, and should be minimal when $N_L = N_{L_{max}}$. For example, decreasing N_L progressively from $N_{L_{max}}$ to 1 must lead to an increased effect of $\Psi^{\wedge}$ on K_i (see below), thereby broadening the K_i-range for each collection of groups considered.

In the subsequent discussion the term "group" may be freely interchanged with the term "collection of groups" with the understanding that the quantitative evaluation of the actual range of groups per collection remains, as yet, unresolved. It should also be remembered that each group within a particular collection is assumed to dissociate or associate at most one H^+-ion as expressed by eqs. [6], [12], [13], and [14].

Podsolic fulvic acid

Gamble's titration curve (15) yields at most four chemically discernible groups (or collections of groups) over the experimental p*h*-range from 2.9 to 11.4. Restricting evaluation to 3, 2, and 1 groups increases the implied *f*-value (i.e., $\Psi^{\wedge}$-potential) with only a slight loss in overall goodness-of-fit. A model with just one group operating, therefore, appears to fit the titration data nearly as well as the almost purely chemical model with four groups. A one-group model, however, implies that the log *K*-versus-α relationship given by

TABLE 6. Refined titration parameters for various humic substances

Reference	*f* (equiv./L)	Fraction	$-pK_{01}$	$-pK_{02}$	$-pK_{03}$	$-pK_{04}$	$-pK_{05}$	$-pK_{06}$	$-pK_{07}$	$-pK_{08}$	C_{A1}	C_{A2}[a]	C_{A3}[a]	C_{A4}[a]	C_{A5}[a]	C_{A6}[a]	C_{A7}[a]	C_{A8}[a]	C_k^0	pK_w	μ	*f* L/equiv.	E_0 mV	SD_w mL
Gamble (1970), Fig. 2.	0.1	—	—	3.01	4.71	—	6.34	8.35	—	—	—	363	239	—	94	80	—	—	0	13.62	0.155	134	427	0.048
	0.1	—	—	3.10	4.33	—	6.34	—	—	—	—	263	415	—	116	—	—	—	0	13.53	0.54	488	420	0.050
	0.1	—	—	—	4.26	—	6.23	—	—	—	—	—	703	—	120	—	—	—	0	13.57	0.67	634	422	0.053
	0.1	—	—	—	3.88	—	—	—	—	—	—	—	773	—	—	—	—	—	0	13.49	0.73	700	419	0.080
Van Dijk (1971), Fig. 2.	0.1	—	—	—	3.94	5.45	—	7.38	9.37	—	—	—	62	204	—	84	105	—	0	13.8	0.10	134	—	0.080
	0.1	—	—	—	—	5.88	—	7.69	9.42	11.55	—	—	—	229	—	85	78	594	0	13.8	0.16	209	—	0.096
Stevenson (1976), Fig. 1.	0.001	—	—	—	3.41	5.09	6.64	—	—	—	—	—	55	88	62	—	—	—	28	13.8	0.26	332	—	0.056
	0.005	—	—	—	3.59	5.48	6.94	—	—	—	—	—	83	99	71	—	—	—	75	13.8	0.24	302	—	0.072
	0.010	—	—	—	4.28	5.61	6.89	—	—	—	—	—	60	83	60	—	—	—	32	13.8	0.24	302	—	0.060
	0.025	—	—	—	3.76	5.01	6.21	—	—	—	—	—	85	79	61	—	—	—	56	13.8	0.27	319	—	0.050
	0.050	—	—	—	4.39	5.64	7.27	—	—	—	—	—	77	81	74	—	—	—	27	13.8	0.24	368	—	0.053
	0.075	—	—	—	4.42	5.59	6.92	—	—	—	—	—	75	69	55	—	—	—	15	13.8	0.24	324	—	0.060
	0.100	—	—	—	3.47	5.05	6.50	—	—	—	—	—	118	83	59	—	—	—	42	13.8	0.24	329	—	0.038
	0.200	—	—	—	3.87	5.08	6.46	—	—	—	—	—	88	73	60	—	—	—	41	13.8	0.24	304	—	0.039
Davis & Mott (1981), Fig. 3.	0.1	I, forward	—	—	—	—	6.27	7.96	9.22	—	—	—	—	—	30	57	172	—	6	13.68	0.08	47	—	0.016
	0.1	I, backward	—	—	—	—	6.45	8.32	9.55	—	—	—	46	—	44	86	102	—	304	13.79	0.00	0	—	0.017
	0.1	2 × I, forward	—	—	—	—	5.71	7.74	9.15	—	—	—	—	—	31	54	182	—	12	13.64	0.12	41	—	0.027
	0.1	2 × I, backward	—	—	4.34	—	6.35	8.08	9.13	—	—	—	54	—	41	52	119	—	284	13.78	0.10	78	—	0.020
	0.1	II, forward	1.83	—	3.92	5.45	—	7.61	—	—	1339	—	274	98	—	145	—	—	1006	13.60	0.30	155	—	0.017
	0.1	II, backward	2.05	—	4.28	6.08	—	8.33	—	—	1925	—	286	125	—	126	—	—	1591	13.71	0.32	178	—	0.022
	0.1	2 × II, forward	1.86	—	3.88	5.32	—	7.75	—	—	938	—	293	129	—	170	—	—	632	13.47	0.32	144	—	0.034
	0.1	2 × II, backward	1.70	—	3.81	5.40	—	8.06	—	—	863	—	244	103	—	123	—	—	1445	13.71	0.20	94	—	0.051

[a]Mequiv./100 g.

Can. J. Chem. Downloaded from www.nrcresearchpress.com by 210.87.254.6 on 09/06/12
For personal use only.

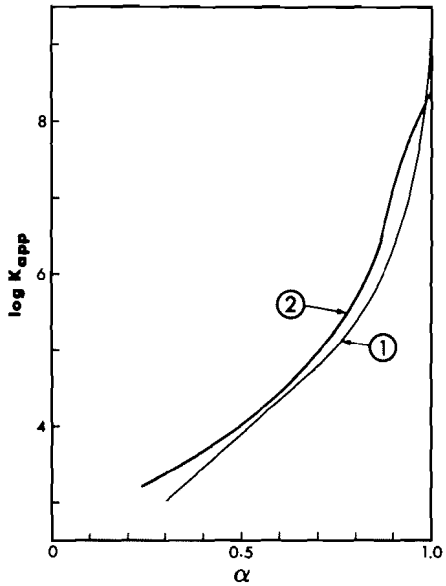

FIG. 4. Plots of log K_{app} versus α for soil fulvic acid (15) when represented by one (lower curve) and four (upper curve) chemically discernible collections of functional groups. Similar plots for two and three chemically discernible collections of groups fall between the two curves shown.

$$\log K = \log K_0' + 2fC_{Al}\alpha$$

$$= \log K_0' + \frac{0.869\lambda F C_{Al}}{SC^0(8000\epsilon\epsilon_0 RTI)^{1/2}}\alpha$$

should be linear. Yet actual plots of "apparent" pK (i.e., ph + log $(1 - \alpha)/\alpha$) versus calculated, N_L-dependent α-values are invariably curved (16, 17) and in general agreement with the multigroup prediction ($N_{L_{max}} = 4$) shown in Fig. 4. Furthermore, the shape of these curves does not seem to depend on ionic strength (18) thereby suggesting that (*i*) electrostatic effects on proton adsorption (desorption) are weak and (*ii*) that the nearest neighbour interactions among the various proton adsorption sites should not be affected by macrostructural rearrangements of each humic molecule as caused by changes in surface potential and ionic strength. Large changes in nearest neighbour interactions, however, are expected to occur on flexible polymer electrolytes during the uncoiling of such substances in aqueous solutions at low ionic strength. In fact, the accompanying pK_{app}-versus-α plots tend to be convex rather than concave (19–21). The uncoiling of humic substances at low ionic strength (and at high ph-values, see Ghosh and Schnitzer (22)) is therefore probably limited to the uncoiling of macromolecular structure, leaving the Ψ^s-determining core(s) of the basically aromatic humic molecule intact.

Soil humic acid

Van Dijk's titration curve (23) yields at most five chemically discernible groups (or collections of groups) over the ph-range from 3.2 to 11.2. The humic substance involved appears to be less acidic than the fulvic acid above, but tends to be more complex in the upper ph-range, with each of the three K_0-values indicating strong phenolic and enolic group characteristics. This titration curve was analyzed twice, each time over a differently restricted ph-range (i.e., 3.2 to 10 and 4.7 to 11.2) to illustrate that the deletion or inclusion of certain groups is affected by the ph-range considered once the total number of refinable K_0- and C_A-values is fixed. The K_0-values and concentrations of the common groups, however, remain numerically consistent with respect to one another.

Lignite humic acid

The potentiometric behaviour of a humic acid extracted from surface-weathered lignite was documented by Stevenson (24) over an ionic strength range from 0.001 to 0.2 N and a restricted ph-range from 3.7 to 8.0. Three proton-yielding groups are identifiable within this range as shown in Table 6, all three groups being similar to corresponding groups in Van Dijk's soil extract. All K_0-values, concentrations, and f-values are unexpectedly consistent over the I-range considered. Refining the K_0-values by keeping all concentrations fixed, however, leads to I-dependent f-values such that the plot of $\kappa/(1 + a\kappa)$ versus g (Fig. 2) yields a sloping scattergram with a best-fitted slope of 0.39×10^{-3} g/m^2. The surface-area estimate for lignite humic acid is therefore $\simeq$ 2600 m^2/g. The scatter observed in this plot probably relates to the procedures employed in generating and digitizing the underlying titration curves. For example, each titration curve was constructed from the ph-readings of ten specially prepared solutions. At least twice as many points were taken from each such curve to allow potentiometric analysis via the modified ACBA-program. Rigorous interpretation of these data beyond the comments above is therefore not possible.

Soil fulvic acid fractions

Davis and Mott (16) fractionated a soil fulvic acid extract into a polysaccharide and non-polysaccharide fraction. They also titrated these fractions forward (with 0.1 N NaOH) and backward (with 0.1 N HCl) thereby generating four types of titration curves, each of which was further repeated for low and high organic-matter concentrations. The following points may be noted from Table 6: (*i*) Individual K_0-values are not much affected by forward or backward titration, or by colloid concentrations. They are, however, affected by type of fraction. (*ii*) The polysaccharide fraction gained a new group at log $K_0 \simeq 4.3$ in exchange of an equivalent loss of concentration associated with its log $K_0 \simeq 9.2$ group on backward titration. (*iii*) Reduced resolution for the log $K_0 \simeq 1.9$ group in the non-polysaccharide fraction leads to overestimates of C_{Al} and initial free base content (i.e., C_h^0) associated with the corresponding titrand solutions.

It was proposed (16) that Fraction I should experience OH^--induced oxidation when subjected to ph-values exceeding 8, possibly leading to formation of saccharinic acid. Fraction II with an ash content of 9.9% (by oven-dried weight) was also observed to consume additional OH^--ions when left standing at ph-values in excess of 7.0, but the humic substance involved appeared to remain unchanged. The results of Table 6 evidently substantiate these claims.

In summary, it is suggested that the acid–base behaviour of humic matter appears to be controlled by a number of identifiable collections of functional groups. Electrostatic forces are also present, but their effects on proton adsorption in terms of refined f-values, surface charge densities, and maximum dl-model potentials appear to be consistently small in comparison with similar values for oxide surfaces (see Table 7). Humic colloids, perhaps, distinguish themselves from other polymers on account of microstructural rigidity and irregularity thereby implying I- and ph-independent (or nearly independent) and presumably unchanging nearest neighbour interactions among the various proton adsorption/desorption sites. Davis and Mott

TABLE 7. Summary for surface charge, potential, and area data (I = 0.1)

Substance	S (m^2/g)	C^0 (g/L)	T_σ^m (mequiv./100 g)	T_σ^m (mequiv./L)	σ_m‡ ($\mu C/cm^2$)	f (L/equiv.)	Ψ_{dl}^m‡ (mV)
γ-Al_2O_3	129	8.174	±13.7	±1.12	±10.2	1890	±77
TiO_2	20	12.07	±40.0	±4.83	±193	13200	±249
Lignite HA	2600	2.0	−200	4.40	−8.2	329	−60
Soil HA	6900*	1.7	−430†	7.31	−6.0	134	−45
Soil FA	6300*	1.0	−780	7.80	−11.9	134	−47
Latex	—	—	—	—	−14.6	—	−75

*Estimated from viscosimetric data (22).
†Does not include C_{AS} from Table 6.
‡Maximum values for σ, T_σ, and Ψ_{dl}^s. In particular, $\sigma_m = T_\sigma^m F/SC^0$ and $\Psi_{dl}^m = (2RT/F)\sinh^{-1}(fT_\sigma^m)$.

(16), Young *et al.* (17), Burch *et al.* (25), Wilson and Kenney (26), and Gamble (15, 27) have also discussed the acid–base behaviour of humic substances in terms of electrostatic and chemical models. Their interpretations, however, are largely based on restricting modelling to at most two chemically discernible collections of groups, with basic information obtained from potentiometric titration curves by way of Gran-plot procedures or some other technique for end-point detection. No such restriction, in principle, is encountered in the modified ACBA-procedure employed above, thereby facilitating a quantitatively rigorous presentation of many chemical and electrostatic features affecting humic substances.

Concluding remarks

Application of the modified ACBA program to the interpretation of potentiometric titration curves of colloidal substances with rigid or near-rigid macrostructure and/or microstructure may lead to an improved understanding of the acid–base behaviour of such substances. The success of the pn-model to fit titration data as published in the literature is particularly noteworthy in view of its general performance and similarity to the Nernst equation. It is possible that this model may form an important conceptual link between "particle" potentials accessible by electrochemical measurement and "surface" potentials made available by ζ-potential measurement and double layer theory. For example, one may represent the electrochemical potential ($\tilde{\mu}$) for the H^+-ion equilibrium within a particle (p), at the colloid surface (s) and throughout the surrounding solution far removed from the surface (l) as follows:

$$\tilde{\mu}_p = \mu_p + F\Psi^p = \tilde{\mu}_s = \mu_s + F\Psi^s = \tilde{\mu}_l = \mu_l + F\Psi^l$$

with $\mu_m = \mu_m^0 + RT \ln a_m$ as the chemical potential for H^+ at m = p, s, and l. Setting $a_p = 1$ (i.e., unit activity for H^+-ions in particle medium) and $\Psi^l = 0$ (by convention), it follows that

$$\Psi^s = (RT/F) \ln a_l/a_s + \text{constant}$$

and

$$\Psi^p = (RT/F) \ln a_l/a_p + \text{constant}$$

$$= \frac{RT}{F}\int_{a_l^0}^{a_l} \frac{d\Psi^p}{d \ln a_l} = \frac{RT}{F} \ln a_l/a_l^0 \simeq \frac{RT}{F} \ln h/h^0$$

The particle potential Ψ^p (or Nernst potential) is therefore not identical with the surface potential Ψ^s. Moreover, Ψ^s may not be purely electrostatic, because the electrochemical expression

[27] $\tilde{\mu} = \mu + F\Psi$

involves a customary but non-thermodynamic assumption (28). Also, surface potentials according to diffuse double-layer models are based on electrostatic assumptions, whereas the pn-model assumes that

[28] $\Psi^s = \mu^* \Psi^p$

The pn-model, therefore, imparts a non-electrostatic component to Ψ^s which reduces to a constant when $F\Psi^s/RT \ll 1$, i.e., when the cc-, dl-, and pn-models merge (see eq. [19]). Perhaps it is of interest to further explore the pn-model by reinterpreting some of the many published surface capacitance – surface charge (or surface potential) relationships, and among these especially those with "humps" (29). One example offered to facilitate reinterpretation of electrochemical data is obtained by invoking the constant surface capacitance assumption in connection with eq. [18]. This yields

[29] $\sigma \simeq k \ln h/h^0$

with

$$k = 2(FC_{Al}/SC^0)(1 - \mu^*)/(2 + \beta)$$
$$= (8000\epsilon\epsilon_0 RTI)^{1/2}/\lambda$$

valid for amphoteric surfaces. This equation applies reasonably well to data derived from potentiometric titrations of aged oxide suspensions at high ionic strength (9). Equation [29], in turn, provides a simple way for calculating the degree of dissociation $\alpha = 1 - \alpha_1 - \alpha_2$ for amphoteric surfaces (10) at any ph near ph^0, i.e.

$$\alpha \simeq \frac{1 - \mu^*}{1 + \beta/2} \ln \frac{h}{h^0}$$

Slightly more complicated expressions may be obtained for σ and α when applying the diffuse double-layer model to eq. [18]. In addition, similar expressions apply to amphoteric surfaces and substances affected by potential-generating ions other than H^+. Finally, cation-exchange reactions of the type

$$SH + M^+ = SM + H^+$$

may also be examined by empirically generalizing eq. [18] to

[30] $F\Psi^s/RT = \mu^* \ln [(h + K_{MH}M)/h^0]$

with M as cation concentration and $K_{MH} = [H][SM]/[M][SH]$ as cation exchange constant (30). The approach suggested here is therefore general, and may be used as a basis for further analysis of a great variety of electrochemical systems.

Can. J. Chem. Downloaded from www.nrcresearchpress.com by 210.87.254.6 on 09/06/12
For personal use only.

Acknowledgements

Special thanks are due to the authors of the various papers cited, especially Arena *et al.* (2), Westall and Hohl (3), and Healy and White (10). Financial support of this work was received from the National Science and Engineeering Council of Canada (Grant #A7803) and from the Canadian Forestry Service Subvention Fund.

1. A. VEIS. Biological polyelectrolytes. Marcel Dekker, NY. 1970. p. 291.
2. G. ARENA, E. RIZZARELLI, and S. SAMMARTANO. Talanta, **26**, 1 (1979).
3. J. WESTALL and H. HOHL. Adv. Colloid Interface Sci. **12**, 265 (1980).
4. A. L. LOEB, J. TH. G. OVERBEEK, and P. H. WIERSEMAN. The electrical double layer around a spherical colloid particle. MIT Press, Cambridge, MA. 1961.
5. S. H. YALKOWSKI and G. ZOGRAFI. J. Colloid Interface Sci. **34**, 525 (1970).
6. F. TOKIWA. Adv. Colloid Interface Sci. **3**, 389 (1972).
7. E. D. GODDARD. Adv. Colloid Interface Sci. **4**, 45 (1974).
8. C. TANFORD. Physical chemistry of macromolecules. John Wiley and Sons. 1961. p. 710.
9. H. DE HEK, R. J. STOL, and P. L. DE BRUYN. J. Colloid Interface Sci. **64**, 72 (1978).
10. T. W. HEALY and L. R. WHITE. Adv. Colloid Interface Sci. **9**, 303 (1978).
11. R. H. OTTEWILL and D. E. YATES. NATO Advanced Study Institute, Polymer Colloids. University of Trondheim, Norway. 1975.
12. R. C. WEAST. Handbook of chemistry and physics. 49 ed. The Chemical Rubber Co. 1968.
13. Y. G. BÉRUBÉ and P. L. DE BRUYN. J. Colloid Interface Sci. **27**, 305 (1968).
14. J. A. DAVIS, R. O. JAMES, and J. O. LECKIE. J. Colloid Interface Sci. **63**, 480 (1978).
15. D. S. GAMBLE. Can. J. Chem. **48**, 2662 (1970).
16. H. DAVIS and C. J. B. MOTT. J. Soil Sci. **32**, 379 (1981).
17. S. D. YOUNG, B. W. BACHE, D. WELCH, and A. ANDERSON. J. Soil Sci. **32**, 579 (1981).
18. A. M. POSNER. *In* Proceedings 8th International Congress of Soil Science III, 161 (1964).
19. P. L. DUBIN and U. P. STRAUSS. J. Phys. Chem. **74**, 2842 (1970).
20. T. KURUCSEV and D. E. JOYCE. Polymer, **21**, 1457 (1980).
21. A. MINAKATA, K. MATSUMURA, S. SASAKI, and H. OHNUMA. Macromolecules, **13**, 1549 (1980).
22. K. GHOSH and M. SCHNITZER. Soil Sci. **129**, 266 (1980).
23. H. VAN DIJK. Geoderma. **5**, 53 (1971).
24. F. J. STEVENSON. Soil Sci. Soc. Am. J. **40**, 665 (1976).
25. R. D. BURCH, C. H. LANGFORD, and D. S. GAMBLE. Can. J. Chem. **56**, 1196 (1978).
26. D. E. WILSON and P. KENNEY. Limno. Oceanogr. **22**, 281 (1977).
27. D. S. GAMBLE. Can. J. Chem. **50**, 2680 (1972).
28. J. LYKLEMA. *In* Physical chemistry: enriching topics from colloid and surface science. *Edited by* H. van Olphen and K. J. Mysels. Theorex, La Jolla, CA. 1975. p. 281.
29. M. J. SPARNAAY. The electrical double layer. Pergamon. 1972. p. 415.
30. G. EISENMAN. Glass electrodes for hydrogen and other cations. Marcel Dekker, NY. 1967. p. 582.

Can. J. Chem. Downloaded from www.nrcresearchpress.com by 210.87.254.6 on 09/06/12
For personal use only.

An experimental study of the influence of hydration on the reactivity of the hydroxide anion in the gas phase at room temperature

ASIT B. RAKSIT and DIETHARD K. BOHME

Department of Chemistry and Centre for Research in Experimental Space Science, York University, Downsview, Ont., Canada M3J 1P3

Received November 15, 1982

Can. J. Chem. Downloaded from www.nrcresearchpress.com by 210.87.254.40 on 09/06/12
For personal use only.

ASIT B. RAKSIT and DIETHARD K. BOHME. Can. J. Chem. **61**, 1683 (1983).

Flowing afterglow measurements of rate constants and ionic products are reported which explore the influence of step-wise hydration on the reactivity of the hydroxide anion in the gas phase at 296 ± 2 K. Rate constants have been measured for the reactions of $OH^-.(H_2O)_n$ and/or $OD^-.(D_2O)_n$ with CO_2, SO_2, CH_3OH, C_2H_5OH, C_2H_2, CH_3COCH_3, CH_3NO_2, and HCN, in most instances for values of n from 0 to 3. The reactions with CO_2 and SO_2 involve ligand addition or exchange and the results of their study corroborate earlier measurements. The remaining reactions proceed by proton transfer. For these reactions the results establish trends in reactivity as a function of step-wise hydration when relative acidity is preserved and when a reversal occurs in the relative acidity upon hydration. The fast hydrated acid–base reactions were observed to establish interesting hydrated product ions many of which underwent secondary reactions involving the exchange of H_2O or D_2O for the reagent molecule.

ASIT B. RAKSIT et DIETHARD K. BOHME. Can. J. Chem. **61**, 1683 (1983).

On rapporte les mesures de phosphorescence d'écoulement des constantes de vitesse et des produits ioniques. Ces mesures permettent d'étudier l'influence d'une hydratation par étape sur la réactivité de l'anion hydroxyde en phase gazeuse à 296 ± 2 K. On a mesuré les constantes de vitesse des réactions de $OH^-.(H_2O)_n$ et/ou de $OD^-.(D_2O)_n$ avec les molécules suivantes: CO_2, SO_2, CH_3OH, C_2H_5OH, C_2H_2, CH_3COCH_3, CH_3NO_2 et HCN et ceci pour des valeurs de n allant de 0 à 3 dans la plupart des cas. Les réactions avec CO_2 et SO_2 impliquent l'addition ou l'échange de ligand et les résultats de leur étude corroborent les mesures antérieures. Les réactions avec les autres substances se font par transfert de proton. Dans le cas de ces réactions, les résultats établissent la tendance de la réactivité en fonction de l'hydratation par étape lorsqu'on protège l'acidité relative et lorsqu'il se produit une inversion de l'acidité relative durant l'hydratation. On a observé des réactions rapides acide–base hydraté afin d'identifier les ions hydratés intéressants dont plusieurs subissent des réactions secondaires qui impliquent, dans le cas du réactif, un échange de H_2O ou de D_2O.

[Traduit par le journal]

Introduction

The hydroxide ion is an important base in solution chemistry and has become so as well in gas-phase ion chemistry. In the gas phase the bare hydroxide ion has a high basicity and a high reactivity which are now both well established (1) and much is known of the reactivity of the hydrated species in solution. In this study we explore the influence of step-wise hydration on the intrinsic reactivity of the hydroxide ion in the gas phase, primarily with measurements of the specific rates and ionic products of reactions of type [1]

$$[1] \quad OH^-.(H_2O)_n + AH \rightarrow A^-.(H_2O)_m + (n - m + 1)H_2O$$

for values of n = 1 to 3. The measurements were carried out using a flowing plasma mass spectrometer (flowing afterglow) system (2, 3) which allows the hydrated species to be produced in an inert atmosphere in thermalized and controlled amounts and to be identified and monitored with a mass spectrometer. The reagent acids, AH, were chosen to span a range in overall energetics sufficient to establish the pattern of reactivity which emerged from these studies. The observed trends in reactivity begin to bridge the gap between the gas phase and solution. For a number of acids reaction [1] was observed to be followed by further ion chemistry which exhibits a clear tendency of the solvent aggregate of the solvated ions to evolve to a state of maximum stability by solvent exchange and solvent addition reactions.

Experimental

The experiments were carried out in a flowing plasma mass spectrometer (flowing afterglow) system. Details of the instrument together with the method of operation and data analysis have been reported elsewhere (2, 3). The hydrated hydroxide ions were established by introducing water vapour, either H_2O or D_2O, past the electron gun in either a flowing helium or hydrogen plasma. Ions were hydrated upstream by reactions of type [2] at total pressures of ca.

$$[2] \quad OH^-.(H_2O)_n + H_2O + He(H_2) \rightarrow OH^-.(H_2O)_{n+1} + He(H_2)$$

0.4 Torr and thermalized by collisions with the buffer gas molecules prior to the reaction region. The reacting mixture was sampled through a small orifice mounted at the tip of a nose cone situated at the end of the reaction region and mass analysed with a quadrupole mass spectrometer. The observed variations of the reactant ion signals as a function of neutral reagent addition provided the raw data from which the rate constants were derived.

The partial pressure of the added water vapour was varied from ca. 0.005 to 2 mTorr in order to achieve a wide range in the initial relative population of the hydrated hydroxide ions. The hydroxide ion was observed to add up to three water molecules at the operating conditions of the experiments reported here. In deriving rate constants from the observed decays of $OH^-.(H_2O)_n$ account was taken of the initial decay which could arise due to the depletion of the precursor ion $OH^-.(H_2O)_{n-1}$. The magnitude of the depletion could be assessed in those studies in which the daughter ion $OH^-.(H_2O)_n$ did not react with the added neutral reagent. In many experiments D_2O was used in place of H_2O to avoid overlap of ion signals, particularly of $OH^-.(H_2O)_n$ and $Cl^-.(H_2O)_{n-1}$ and of $OH^-.(H_2)_2$ and $CN^-.HCN$.

Results

The results of the measurements are summarized in Tables 1 and 2. The sources of uncertainty associated with the determination of the rate constants have been described previously (2, 3). The following section describes the measurements in

TABLE 1. Rate constants[a] measured for binary reactions of $OH^-.(H_2O)_n$ with CO_2 and SO_2 at 296 ± 2 K

n	CO_2	SO_2[b]
1	≥0.4	1.0±0.3 (≥0.5)
2	0.54±0.22	1.2±0.3 (≥0.5)
3	0.56±0.22	1.2±0.4 (1.2±0.5)
2, 3, 4[c]	0.6	2

[a]In units of 10^{-9} cm^3 $molecule^{-1}$ s^{-1}.
[b]Values in parentheses apply to $OD^-.(D_2O)_n$.
[c]Reference 4.

more detail. They are presented in order of increasing acidity of the reagent acids. The reactions with CO_2 and SO_2 were investigated in part to assess the performance of the instrument. Previous flowing afterglow measurements for these two reactions carried out primarily in O_2 buffer gas were available for comparison (4).

CO_2, SO_2

The unsolvated hydroxide ion rapidly associates with CO_2 and SO_2 in the gas phase to form the anions of carbonic and sulphurous acid, respectively, via reactions [3] and [4] where M is a third body.

[3] $OH^- + CO_2 + M \rightarrow HCO_3^- + M$

[4] $OH^- + SO_2 + M \rightarrow HSO_3^- + M$

Reaction [3] was investigated in H_2 buffer gas at total pressures in the range 0.276 to 0.582 Torr while reaction [4] was studied in a He buffer with OH^- between 0.320 and 0.447 Torr and with OD^- between 0.317 and 0.567 Torr. Figure 1 displays the observed pressure dependencies for the apparent binary rate constants which were measured. The slopes of these plots provide ternary rate constants of (1.0 ± 0.3) and (4.2 ± 1.3) × 10^{-27} cm^6 $molecule^{-2}$ s^{-1} for reactions [3] and [4], respectively. A comparison with the previously reported measurements indicates the H_2 to be slightly more effective as a stabilizing third body for HCO_3^- than O_2 which in turn is more effective than He: rate constants of 7.6 and 2.5 × 10^{-28} cm^6 $molecule^{-2}$ s^{-1}, respectively, have been reported for the latter two buffer gases (4). Our results also indicate that the relative effectiveness of O_2 and He in stabilizing HCO_3^- is approximately the same as that in stabilizing HSO_3^-: a rate constant of 1.0 × 10^{-26} cm^6 $molecule^{-2}$ s^{-1} has been reported for reaction [4] with M = O_2 (4).

The hydrated hydroxide ions were observed to undergo the binary ligand exchange reactions [5] and [6] reported

[5] $OH^-.(H_2O)_n + CO_2 \rightarrow HCO_3^-.(H_2O)_m + (n - m)H_2O$

[6] $OH^-.(H_2O)_n + SO_2 \rightarrow HSO_3^-.(H_2O)_m + (n - m)H_2O$

previously by Fehsenfeld and Ferguson (4). In writing these reactions allowance has been made for the excess energy in these exothermic reactions to cause some of the H_2O to be "boiled-off" and so permit m to take on values from 0 to $n - 1$. In the present experiments in which the flowing plasma contained a mixture of $OH^-.(H_2O)_n$ ions with n = 0 to 3, product ions were observed for m = 0, 1, and 2 but the latter in only relatively trace amounts. The rate constants determined from these experiments are summarized in Table 1. They compare favourably with the values obtained previously by Fehsenfeld and Ferguson (4).

CH_3OH

We have reported previously that the bare hydroxide ion rapidly removes a proton from methanol in the gas phase, k = (2.2 ± 0.6) × 10^{-9} cm^3 $molecule^{-1}$ s^{-1} (5). Also hydration of the OH^- was observed to promote the reverse of reaction [7]. Measurements of the equilibrium constant for reaction [7]

[7] $OH^-.(H_2O)_n + CH_3OH \rightleftharpoons CH_3O^-.(H_2O)_n + H_2O$

for n = 1, 2, and 3 provided insight into the shift of the position of equilibrium for this reaction with hydration (6). Reaction [7] is rapid, $k > 10^{-9}$ cm^3 $molecule^{-1}$ s^{-1}, for n = 0 to 3 and the product ions quickly undergo secondary reactions with CH_3OH which displace H_2O in the solvation shell as is indicated by reaction [8]. In this study the measurements were repeated with

[8] $CH_3O^-.(H_2O)_n + CH_3OH \rightleftharpoons CH_3O^-.(H_2O)_{n-1}.CH_3OH + H_2O$

$OD^-.(D_2O)_n$ ions derived from heavy water and a very similar behaviour was observed. The semi-logarithmic decays recorded for these solvated ions and the formations of product ions were indicative of fast reactions of type [9] for n = 0 to 4. Increased curvature was apparent in the decays of

[9] $OD^-.(D_2O)_n + CH_3OH \rightarrow CH_3O^-.(D_2O)_n + HOD$

$OD^-.(D_2O)_n$ with increasing values of n which may be attributed to reverse reactions with the source gas D_2O which was present in the reaction tube in large excess to the HOD generated by reaction [9], viz to reactions of type [10]. Plots of the ion

[10] $CH_3O^-.(D_2O)_n + D_2O \rightarrow OD^-.(D_2O)_n + CH_3OD$

concentration ratios $[CH_3O^-.(D_2O)_n]/[OD^-.(D_2O)_n]$ against flow of CH_3OH exhibited linearity at higher flows of CH_3OH. Normally such linearity would be indicative of equilibrium but in this case the linearity is a consequence of the rate equalities [11] rather than the equilibrium equalities [12], and thus pro-

[11] $k_9[OD^-.(D_2O)_n][CH_3OH] = k_{10}[CH_3O^-.(D_2O)_n][D_2O]$

[12] $k_9[OD^-.(D_2O)_n][CH_3OH] = k_{-9}[CH_3O^-.(D_2O)_n][HOD]$

vides a measure of k_9/k_{10} rather than k_9/k_{-9}. Values for k_9/k_{10} of ≥ 5.3 × 10^2, ≥1.7 × 10^2, 22, and 10 were obtained for n = 1, 2, 3, and 4, respectively. These are close to the values of ≥1.3 × 10^3, 1.5 × 10^2, and 25 for n = 1, 2, and 3 which were obtained previously for k_7/k_{-7} and are thus indicative of a negligible isotope effect.

The product ions of reaction [9] were observed to rise and then fall at higher additions of methanol concomitant with the production of ions with masses corresponding to the cluster ions $CH_3O^-.(D_2O)_{n-1}.CH_3OH$ with n = 1, 2, and 3. These observations can be attributed to rapid solvent exchange reactions of type [13] and indicate a preference for methanol over heavy water in the solvation of CH_3O^-.

[13] $CH_3O^-.(D_2O)_n + CH_3OH \rightarrow CH_3O^-.(D_2O)_{n-1}.CH_3OH + D_2O$

CH_2CCH_2, $C_6H_5CH_3$

Allene and toluene have equal acidities in the gas phase (7). We have reported previously that the bare hydroxide ion will abstract a proton from these two acids with essentially unit efficiency and that hydration of the bare ion with just one molecule of water lowers this efficiency by more than a factor of 10^3 (7).

Can. J. Chem. Downloaded from www.nrcresearchpress.com by 210.87.254.40 on 09/06/12
For personal use only.

TABLE 2. Rate constants[a] measured for binary reactions of $OH^-.(H_2O)_n$ and $OD^-.(D_2O)_n$ with acids, AH, at 296 ± 2 K

AH	Rate constant $n=0$	$n=1$	$n=2$	$n=3$
CH_3OH	2.2±0.6	2.1±0.5		
	[2.7±0.8]	[2.3±0.7]		
CH_2CCH_2	1.7±0.4	≤0.001	≤0.001	≤0.001
$C_6H_5CH_3$	2.6±0.6	≤0.001		
C_2H_5OH	2.2±0.7	2.0±0.7	1.0±0.6	0.7±0.5
	[2.1±0.6]	[1.9±0.6]	[0.9±0.4]	[0.7±0.4]
C_2H_2	2.2±0.4	≥1	≤0.01	≤0.01
	[1.9±0.4]	[≥1]	[≤0.001]	[≤0.001]
CH_3COCH_3	3.8±0.8	3.4±0.9	≥1	≤0.01
	[3.9±0.8]	[3.2±0.8]	[≥1]	[≤0.01]
CH_3NO_2	3.5±0.7	2.8±0.7	2.2±0.6	2.0±0.6
	[3.4±0.7]	[2.5±0.6]	[2.4±0.6]	[2.2±0.6]
HCN	3.5±0.7	3±1		3±1
	[3.4±0.7]	[3.1±0.8]	[3.0±0.8]	[2.9±0.7]

[a]Rate constants and their estimated accuracies are given in units of 10^{-9} cm^3 molecule^{-1} s^{-1}. The numbers in brackets refer to reactions with $OD^-.(D_2O)_n$.

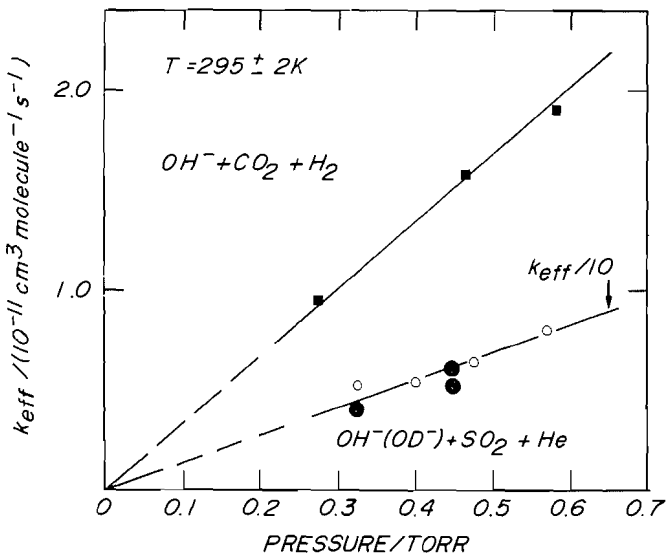

FIG. 1. Observed dependence of the effective two-body rate constant on the total pressure for the association of $OH^-(OD^-)$ with CO_2 and SO_2 at 295 ± 2 K. The open circles refer to measurements made with OD^-.

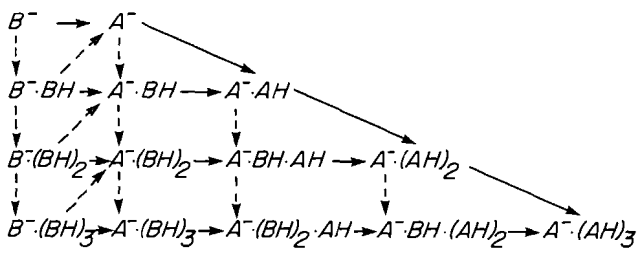

FIG. 2. A general scheme representative of the possible solvated ion chemistry proceeding under flowing afterglow conditions for the acid–base reactions investigated in this study. The solid horizontal arrows represent solvated acid–base or solvent exchange reactions with AH. The dashed vertical arrows represent possible solvent addition reactions with BH. The dashed diagonal arrows represent possible solvated acid–base reactions with a concomitant "boiling-off" of solvent BH.

C_2H_5OH

The reactivities of $OH^-.(H_2O)_n$ and $OD^-.(D_2O)_n$ observed for their reactions with ethanol were similar to those observed for methanol. Rapid proton transfer reactions of type [14] were indicated for $n = 1$ to 3. The measured rate constants are listed

[14] $OD^-.(D_2O)_n + C_2H_5OH \rightarrow C_2H_5O^-.(D_2O)_n + HOD$

in Table 2. Also the hydrated ethoxide ions were observed to react further by solvent exchange reactions of type [15]. At

[15] $C_2H_5O^-.(D_2O)_n + C_2H_5OH \rightarrow C_2H_5O^-.(D_2O)_{n-1}.C_2H_5OH + D_2O$

still higher flows of ethanol, ion signals were observed to rise at $m/e = 137$ and 157 and finally at $m/e = 183$. This behaviour is consistent with still further displacement of D_2O by C_2H_5OH to ultimately establish ethoxide ions solvated exclusively by ethanol as is indicated by the general scheme shown in Fig. 2. All of the ions indicated in this scheme were observed for BH = D_2O and AH = C_2H_5OH.

C_2H_2

We have reported previously that OH^- rapidly abstracts a proton from acetylene to produce C_2H^- (8). The results of the present study indicate that this reactivity is extremely sensitive to the degree of hydration. As is evident from the observations recorded in Fig. 3, the reactivity remains high with the addition of one molecule of water to OH^- but the addition of a second molecule of hydration leads to an abrupt drop in reactivity by more than two orders of magnitude. For reactions of type [16] and the heavy water analogues, our observations indicate that

[16] $OH^-.(H_2O)_n + C_2H_2 \rightarrow C_2H^-.(H_2O)_n + H_2O$

$k \geq 1 \times 10^{-9}$ cm^3 molecule^{-1} s^{-1} for $n = 0$ and 1 but $k \leq 1 \times 10^{-11}$ cm^3 molecule^{-1} s^{-1} for $n = 2$ and 3. An ion with a mass corresponding to the product of reaction [17] was clearly identified. The curvature in the decay of $OD^-.D_2O$ in Fig. 3 is

[17] $OD^-.D_2O + C_2H_2 \rightarrow C_2H^-.D_2O + HOD$

caused by the rapid occurrence of the reverse reaction [18] with D_2O which is in large excess over the HOD produced by

[18] $C_2H^-.D_2O + D_2O \rightarrow OD^-.D_2O + C_2HD$

Can. J. Chem. Downloaded from www.nrcresearchpress.com by 210.87.254.40 on 09/06/12
For personal use only.

Can. J. Chem. Downloaded from www.nrcresearchpress.com by 210.87.254.40 on 09/06/12
For personal use only.

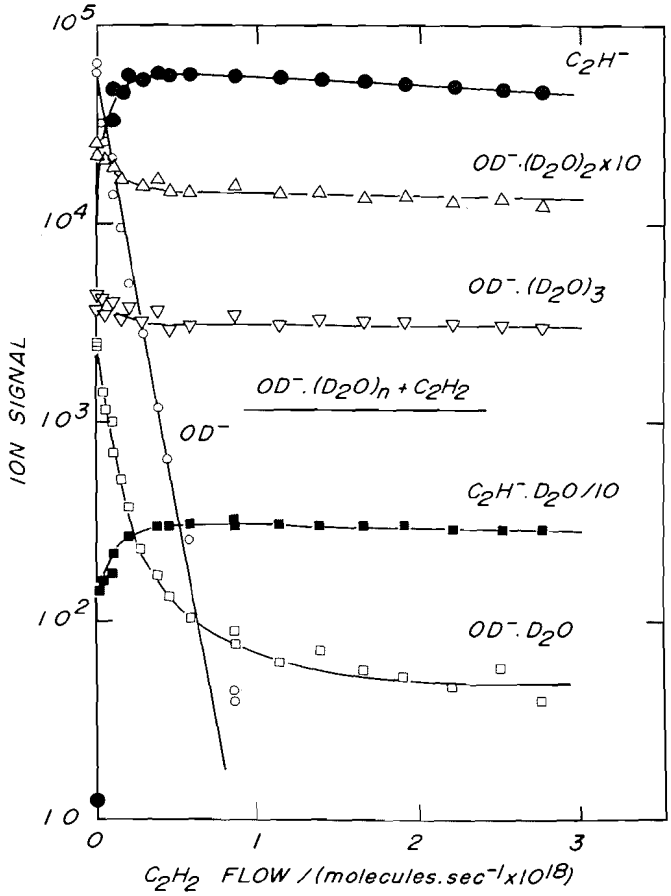

FIG. 3. Observations recorded for the reactions of $OD^-.(D_2O)_n$ with acetylene in a He buffer. T = 296 K, P = 0.331 Torr, $\bar{v}$ = 8.1 × 10^3 cm s^{-1}, L = 46 cm, and the flow of D_2O is approximately 2 × 10^{19} molecules s^{-1}.

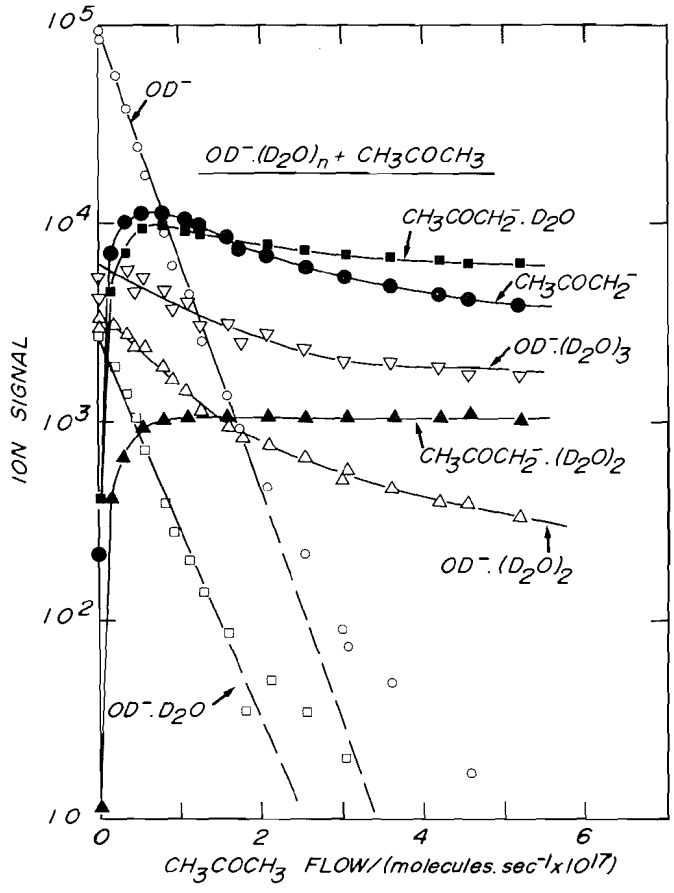

FIG. 4. Observations recorded for the reactions of $OD^-.(D_2O)_n$ with acetone in a He buffer. T = 295 K, P = 0.316 Torr, $\bar{v}$ = 8.0 × 10^3 cm s^{-1}, L = 46 cm, and the flow of D_2O is approximately 2 × 10^{19} molecules s^{-1}.

reaction [17]. A fit to this curvature provided lower limits for k_{17}/k_{18} of 8 × 10^2 and for k_{17} of 1 × 10^{-9} cm^3 $molecule^{-1}$ s^{-1}. The slight decays observed initially in the profiles for $OD^-.(D_2O)_2$ and $OD^-.(D_2O)_3$ are attributable to the depletion in the reaction region of their precursor ions, $OD^-.D_2O$ and $OD^-.(D_2O)_2$, respectively. The $C_2H^-.D_2O$ did not react further to exchange D_2O for C_2H_2.

CH_3COCH_3

Figure 4 illustrates the reactivities of $OD^-.(D_2O)_n$ towards acetone. OD^- and $OD^-.D_2O$ are seen to react rapidly with acetone with a concomitant rise in the $CH_3COCH_2^-$ and $CH_3COCH_2^-.D_2O$ ion signals. The rate constants for both of these reactions were measured to be ≥ 3 × 10^{-9} cm^3 $molecule^{-1}$ s^{-1} (see Table 2). Reaction [19] and the analogous reactions [20] and [21] with D_2O appeared to

[19] $OH^-.(H_2O)_2 + CH_3COCH_3 \rightleftharpoons CH_3COCH_2^-.(H_2O)_2 + H_2O$

[20] $OD^-.(D_2O)_2 + CH_3COCH_3 \rightarrow CH_3COCH_2^-.(D_2O)_2 + HOD$

[21] $CH_3COCH_2^-.(D_2O)_2 + D_2O \rightarrow OD^-.(D_2O)_2 + CH_3COCH_2D$

achieve equilibrium under the conditions employed in these experiments. The corresponding ion ratio plots were linear and provided values for k_{19}/k_{-19} = 3 × 10^2 and for k_{20}/k_{21} = 4 × 10^2. The situation for the reaction of $OD^-.(D_2O)_3$ is somewhat uncertain. There is a slight decay in the $OD^-.(D_2O)_3$ signal initially but it appears to level off at moderate flows of acetone. This behaviour was interpreted to reflect the removal of the $OD^-.(D_2O)_2$ percursor ion in the reaction region and a low reactivity for the $OD^-.(D_2O)_3$, $k \leq 1 \times 10^{-11}$ cm^3 $molecule^{-1}$ s^{-1}. The product ion $CH_3COCH_2^-.(D_2O)_3$ did not appear to be produced. An alternative interpretation would involve a reverse reaction of the $CH_3COCH_2^-.(D_2O)_3$ with D_2O which strongly favours a net production of $OD^-.(D_2O)_3$. At the flows of D_2O and acetone employed this would still imply an equilibrium constant for reaction [22] or the analogous reactions with D_2O

[22] $OH^-.(H_2O)_3 + CH_3COCH_3 \rightleftharpoons CH_3COCH_2^-.(H_2O)_3 + H_2O$

of less than unity.

CH_3NO_2

The ions $OH^-.(H_2O)_n$ and $OD^-.(D_2O)_n$ with n = 0 to 3 all were observed to react rapidly with nitromethane in the manner indicated by reaction [23].

[23] $OH^-.(H_2O)_n + CH_3NO_2 \rightarrow CH_2NO_2^-.(H_2O)_m + (n - m + 1)H_2O$

All of the corresponding product ions, viz. $CH_2NO_2^-.(H_2O)_n$ and $CH_2NO_2^-.(D_2O)_n$ with n = 0 to 3, were observed to be produced but product distributions for the individual hydrated ions could not be ascertained. The rate constants measured for the disappearance of the reactant ions are given in Table 2. Exchange of H_2O or D_2O for CH_3NO_2 was observed at higher flows of CH_3NO_2 in secondary switching reactions such as reactions [24] and [25] but no attempt was made to follow the

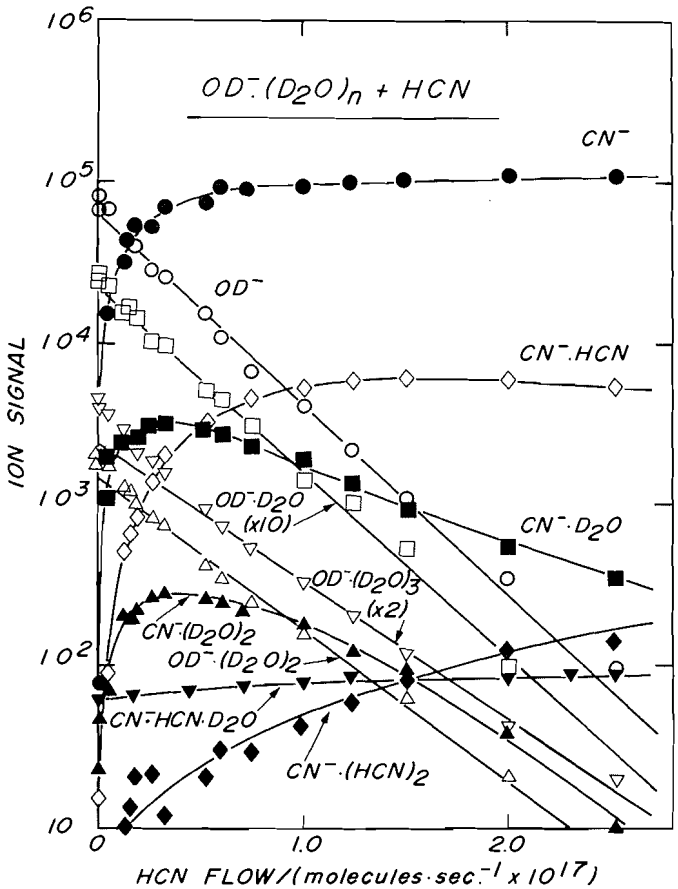

FIG. 5. Observations recorded for the reactions of $OD^-.(D_2O)_n$ with HCN in a He buffer. T = 298 K, P = 0.337 Torr, $\bar{v}$ = 7.3 cm s^{-1}, L = 46 cm, and the flow of D_2O is approximately 3 × 10^{19} molecules s^{-1}.

[24] $CH_2NO_2^-.D_2O + CH_3NO_2 \rightarrow CH_2NO_2^-.CH_3NO_2 + D_2O$

[25] $CH_2NO_2^-.(D_2O)_2 + CH_3NO_2 \rightarrow CH_2NO_2^-.D_2O.CH_3NO_2 + D_2O$

kinetics of these processes in detail.

HCN

Figure 5 shows the influence of hydration on the reaction of the hydroxide ion with HCN observed under flowing afterglow conditions. The primary reactions which were observed may be interpreted in terms of eq. [26]. The ions $OD^-.(D_2O)_n$ were all observed to react very rapidly with HCN with rate constants

[26] $OD^-.(D_2O)_n + HCN \rightarrow CN^-.(D_2O)_m + (n - m)D_2O + HOD$

$\geq 3 \times 10^{-9}$ cm^3 $molecule^{-1}$ s^{-1}. Similar results were obtained with $OH^-.(H_2O)_n$ except for n = 2 in which case the decay of the ion was obscured by the rise in the secondary product ion $CN^-.HCN$. Product ions for reaction [26] were observed for m = 0, 1, and 2. There was no evidence for the formation of $CN^-.(D_2O)_3$ to match the initial $OD^-.(D_2O)_3$ signal. Apparently the fast reaction of this latter ion leads to the "boil-off" of at least one molecule of D_2O.

Both $CN^-.D_2O$ and $CN^-.(D_2O)_2$ were observed to undergo rapid secondary reactions involving the exchange of D_2O for HCN as indicated in reactions [27] to [29].

[27] $CN^-.D_2O + HCN \rightarrow CN^-.HCN + D_2O$

[28] $CN^-.(D_2O)_2 + HCN \rightarrow CN^-.D_2O.HCN + D_2O$

[29] $CN^-.D_2O.HCN + HCN \rightarrow CN^-.(HCN)_2 + D_2O$

Discussion

Previous measurements carried out in our laboratory have clearly established the intrinsic reactivity of the bare hydroxide ion in the gas phase towards a variety of oxygen and carbon acids (5). Here we have scrutinized changes in this reactivity as a function of step-wise hydration. The bare hydroxide ion is allowed to build up a hydration shell by successive additions of water molecules upstream in a flowing He or H_2 buffer gas at low total pressures (ca. 0.3 Torr). The resulting $OH^-.(H_2O)_n$ ions then participate in hydrated ion–molecule reactions with the added neutral as they enter the reaction region downstream. The hydrated product ions have an opportunity to establish solvated ions of higher stability by solvent exchange or solvent addition reactions. The overall reaction scheme initiated by acid–base reactions is summarized in Fig. 2.

The mode of reaction of OH^- with CO_2 and SO_2 was observed to change upon hydration from three-body association to a binary switching reaction. Both three-body association reactions are relatively fast as in both instances ions of high stability are formed: the reaction with CO_2 is likely to yield the covalently bonded bicarbonate ion, $OCO(OH)^-$, and the bisulfite ion, $OSO(OH)^-$, is likely to be formed in the reaction with SO_2. The binary switching or ligand exchange reactions with the hydrated hydroxide ions proceed close to the collision limit. The higher rate constants for SO_2 can be attributed to its permanent dipole moment and also SO_2 has a slightly higher polarizability than CO_2. Application of the average-dipole-orientation (ADO) theory (9, 10) to the collisions of $OH^-.(H_2O)_n$ with SO_2 and the Langevine theory (11) to the collisions of $OH^-.(H_2O)_n$ with CO_2 yields ratios of collision rate constants for SO_2 to CO_2 which are approximately equal to 2 for n = 1, 2, and 3. These ratios are in accord with the ratios of the reaction rate constants determined in this study.

The product distributions associated with each specific degree of hydration were not resolved in this study, but, as in the earlier results reported by Fehsenfeld and Ferguson (4), the recorded product spectra indicated a strong bias towards formation of unsolvated HCO_3^- and HSO_3^-, and more so in the latter case. The same reactions have recently been investigated in tandem mass spectrometry studies at collision energies less than 1 eV (CM) in which the ions with a specific degree of solvation were selected with a mass spectrometer before they were allowed to react (12). The results of these studies also indicated very little retention in the product ions of the water of hydration of the reactant ions. With the exception of the reaction of $OH^-.(H_2O)_3$ with CO_2 which produced primarily $HCO_3^-.H_2O$, the reactions of $OH^-.(H_2O)_{1,2,3}$ with CO_2 and SO_2 were observed to produce predominantly the unhydrated product ions HCO_3^- and HSO_3^-, respectively. It has been suggested that the excess energy available in these reactions is sufficient to cause the water of hydration to be "boiled-off" in the course of the reaction (4).

The reaction of hydroxide ions with CO_2 makes a significant contribution to the total rate of disappearance of CO_2 in aqueous solution at pH values above about 7.5, and above pH 10 it predominates (13). The analogous reaction with SO_2 apparently does not compete to a measurable degree with the normal hydration of SO_2 by H_2O which is 100 million times as rapid as that of CO_2 (14). Reaction [30] has a reported rate constant in aqueous solution at 25°C of 6.0 × 10^3 M^{-1} s^{-1} or 1.0 × 10^{-17}

[30] $OH^-(aq) + CO_2(aq) \rightarrow HCO_3^-(aq)$

Can. J. Chem. Downloaded from www.nrcresearchpress.com by 210.87.254.40 on 09/06/12
For personal use only.

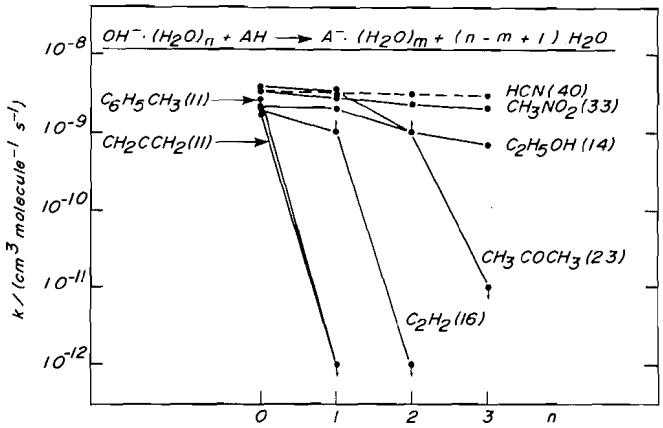

FIG. 6. Observed trends in the rate constants for reactions of hydrated hydroxide ions with acids, AH, as a function of step-wise hydration. The values indicated in parentheses correspond to the relative intrinsic acidities of the acids AH and H_2O, i.e. $-\Delta G^0$ (in kcal mol^{-1}) for the unhydrated reactions at 298 K.

cm^3 $molecule^{-1}$ s^{-1} with an apparent Arrhenius activation energy of 13.25 kcal mol^{-1} (15). This is in contrast with the observations for reaction [5] between hydrated hydroxide ions, $OH^-.(H_2O)_n$, and CO_2 in the gas phase which indicate reaction on essentially every collision.

The rate constants measured in this study for the reactions of hydrated hydroxide ions with acids, AH, are presented graphically in Fig. 6. As this figure clearly illustrates, hydration of the highly reactive bare hydroxide ion results in either a slight or a precipitous reduction in the specific rate of reaction, the latter occurring after the addition of three, two, or even just one molecule of water. The following examination of the overall energetics of these reactions suggests that these trends in reactivity with degree of hydration are thermodynamically rather than kinetically controlled.

The intrinsic exoergicities of the acid–base reactions investigated in this study span a range from 11 to 40 kcal mol^{-1}. The differences in gas-phase acidity indicated in Fig. 6 represent average values derived from the absolute gas-phase acidities based on pulsed-ICR (16) and flowing afterglow measurements (7, 17, 18). Hydration of the hydroxide ion acts to decrease the reaction exoergicity and can render the reaction endoergic unless it is offset by the hydration energy of the conjugate base that is produced (and the hydration energy of possible hydrated neutral products). The standard enthalpies and free energies of hydration for $OH^-.(H_2O)_n$ are available from gas-phase measurements (they are reported here as positive quantities and so refer to the removal of water molecule from the hydrated ion): they are 25, 16.4, 15 and 19, 10, and 7.5 kcal mol^{-1}, for n = 1, 2, and 3, respectively (19). In contrast, the hydration energies of the conjugate bases produced in the reactions which were investigated are generally not known. Values of 13.8 and 7.9 kcal mol^{-1} are available for the standard enthalpy and free energy of hydration of CN^- with one water molecule (19). Also a calculated value of 18 kcal mol^{-1} is available for the binding energy (ΔE) of $C_2H^-.H_2O$ (20) which allows us to estimate the overall energetics for the reaction of $OH^-.H_2O$ with C_2H_2. But because of the sparsity of energies of hydration, we can only surmise the thermodynamic situation for the majority of the reactions investigated.

Allene and toluene are the acids closest in intrinsic acidity to that of water. The carbanions produced by their deprotonation appear to have energies of hydration insufficient to compensate for the high hydration energy of OH^- in spite of the intrinsic exoergicity of 11 kcal mol^{-1}. The weak hydration of carbanions is not unexpected (21). Our results suggest a standard free energy of hydration for $C_6H_5CH_2^-$ and $C_3H_3^-$ of less than 8 kcal mol^{-1}. The sharp drop by more than three orders of magnitude in the specific rate for deprotonation observed with the addition of just one molecule of water is therefore a manifestation of an immediate reversal in the relative acidity of these two carbon acids and water.

A similar reversal in relative acidity is apparent with acetylene but in this case two molecules of water are required to drive the proton transfer endoergic. The unhydrated reaction is exoergic by 16 kcal mol^{-1} which alone is almost enough to compensate for the free energy of hydration of OH^- and thus to render exoergic the formation of unhydrated C_2H^-. Transformation of the calculated energy of hydration, ΔE = 18 kcal mol^{-1}, into an enthalpy of hydration (20) and correction for the entropy change for the association of H_2O to C_2H^- estimated to be -20 cal mol^{-1} deg^{-1} (19) yields an estimated standard free energy of hydration for C_2H^- of 9 kcal mol^{-1}. Reaction [31] is thus estimated to be exoergic by 6 kcal mol^{-1}. This is in

[31] $OH^-.H_2O + C_2H_2 \rightleftharpoons C_2H^-.H_2O + H_2O$

reasonable accord with the value of 4 kcal mol^{-1} which may be derived from the measured ratio of rate constants of 8×10^2 obtained in this study for the similar reaction with heavy water and neglecting isotope effects. An average value of 5 kcal mol^{-1} for the exoergicity of reaction [31] yields an upper limit of 5 kcal mol^{-1} for the standard free energy for removal of H_2O from $C_2H^-.(H_2O)_2$ if the failure to observe a reaction between $OH^-.(H_2O)_2$ and C_2H_2 is attributed to endoergicity.

Figure 6 suggests that a reversal in relative acidity also occurs with acetone, delayed in this case until the addition of at least three water molecules to OH^-. This result is consistent with the early observations of a relative acidity for acetone and water in the gas-phase which is reverse to that observed in aqueous solution (22), and with a rate constant of only 4.5×10^{-22} cm^3 $molecule^{-1}$ s^{-1} reported for the reaction of hydroxide ions with acetone in aqueous solution (23).

No reversals in relative acidity were observed with ethanol, nitromethane, and hydrogen cyanide. Ethanol is an oxygen acid whose conjugate base is expected to be strongly hydrated. This accounts for the continued high reactivity of the hydrated hydroxide ions towards ethanol in contrast to the falloff in reactivity observed for the reactions with acetylene and acetone which are intrinsically more exoergic. Nitromethane and hydrogen cyanide are intrinsically the strongest of the acids investigated. The intrinsic exoergicities of the proton-transfer reactions with these two acids are extremely high allowing for almost total "boil-off" of the water of hydration up to n = 3: reaction [23] is exoergic for m down to $n - 2$ and reaction [26] is exoergic for m = 0, viz. no retention of water. Thus, while the order of acidity between H_2O and ethanol is preserved primarily by the strong hydration of $C_2H_5O^-$, the order between H_2O and both HCN and CH_3NO_2, whose conjugate bases are expected to be more weakly hydrated, is preserved largely as a result of the much higher intrinsic exoergicities. Again these results are consistent with rate measurements made in solution and with known solution acidities. For example, the reaction between hydroxide ions and HCN is extremely rapid in aqueous solution proceeding at close to the diffusion limit, $k = 6 \times 10^{-12}$ cm^3 $molecule^{-1}$ s^{-1} (23).

We have recently reported a parallel study of the gas-phase

Can. J. Chem. Downloaded from www.nrcresearchpress.com by 210.87.254.40 on 09/06/12
For personal use only.

reactivity of methoxide ions solvated with methanol towards the same acids used in the present experiments (7). There is good correlation with the observations and interpretations reported here and, taken together, the studies of these two systems have provided new insight into the transition in the kinetics of acid–base reactions between the gas-phase and solution (24).

Acknowledgement

We thank the Natural Sciences and Engineering Research Council of Canada for financial support.

1. S. D. TANNER, G. I. MACKAY, and D. K. BOHME. Can. J. Chem. **59**, 1615 (1981).
2. D. K. BOHME, R. S. HEMSWORTH, H. W. RUNDLE, and H. I. SCHIFF. J. Chem. Phys. **58**, 3504 (1973).
3. G. I. MACKAY, R. S. HEMSWORTH, and D. K. BOHME. Can. J. Chem. **54**, 1624 (1976).
4. F. C. FEHSENFELD and E. E. FERGUSON. J. Chem. Phys. **61**, 3181 (1974).
5. S. D. TANNER, G. I. MACKAY, and D. K. BOHME. Can. J. Chem. **59**, 1615 (1981).
6. G. I. MACKAY and D. K. BOHME. J. Am. Chem. Soc. **100**, 327 (1978).
7. G. I. MACKAY, A. B. RAKSHIT, and D. K. BOHME. Can. J. Chem. **60**, 2394 (1982).
8. D. K. BOHME, G. I. MACKAY, H. I. SCHIFF, and R. S. HEMSWORTH. J. Chem. Phys. **61**, 2175 (1974).
9. L. BASS, T. SU, W. J. CHESNAVICH, and M. T. BOWERS. Chem. Phys. Lett. **34**, 119 (1975).
10. T. SU, E. C. F. SU, and M. T. BOWERS. J. Chem. Phys. **69**, 2243 (1978).
11. G. GIOUMOUSIS and D. P. STEVENSON. J. Chem. Phys. **29**, 294 (1958).
12. P. M. HIERL, M. J. HENCHMAN, and J. F. PAULSON. Paper presented at the 29th Annual Conference on Mass Spectrom. and Allied Topics, Minneapolis, MN, May 24–29 (1981).
13. Y. POCKER and D. W. BJORKQUIST. J. Am. Chem. Soc. **99**, 6537 (1977).
14. M. EIGEN, K. KUSTIN, and G. MAASS. Z. Physik. Chem. (N.F.) **30**, 130 (1961).
15. J. A. SIRS. Trans. Faraday Soc. **54**, 201 (1958).
16. J. E. BARTMESS, J. A. SCOTT, and R. T. MCIVER. J. Am. Chem. Soc. **101**, 6046 (1979).
17. G. I. MACKAY and D. K. BOHME. Int. J. Mass Spectrom. Ion Phys. **26**, 327 (1978).
18. D. BETOWSKI, G. MACKAY, J. PAYZANT, and D. BOHME. Can. J. Chem. **53**, 2365 (1975).
19. P. KEBARLE. Ann. Rev. Phys. Chem. **28**, 445 (1977).
20. R. R. SQUIRES. Private communication.
21. R. B. MCMAHON and P. KEBARLE. J. Am. Chem. Soc. **96**, 5940 (1974).
22. D. K. BOHME, E. LEE-RUFF, and L. B. YOUNG. J. Am. Chem. Soc. **94**, 5153 (1972).
23. M. EIGEN. Angew. Chem., Int. Ed. Eugl. **3**, 1 (1964).
24. D. K. BOHME, A. B. RAKSHIT, and G. I. MACKAY. J. Am. Chem. Soc. **104**, 1100 (1982).

Can. J. Chem. Downloaded from www.nrcresearchpress.com by 210.87.254.40 on 09/06/12
For personal use only.

COMMUNICATION

The ambident reactivity of aromatic amines in their reactions with *N*-2-(2,4,6-trinitrophenyl)-4,6-dinitrobenzotriazole-1-oxide, a new heterocyclic super-electrophile

ERWIN BUNCEL AND RICHARD A. RENFROW
Department of Chemistry, Queen's University, Kingston, Ont., Canada K7L 3N6

AND

MICHAEL J. STRAUSS
Department of Chemistry, University of Vermont, Burlington, VT 05405, U.S.A.

Received January 11, 1983

ERWIN BUNCEL, RICHARD A. RENFROW, and MICHAEL J. STRAUSS. Can. J. Chem. **61**, 1690 (1983).

Reaction between the title compound **2** and 2,6-dimethylaniline, or *N*,*N*-dimethylaniline, gives rise to spectrally observable Meisenheimer type σ-complexes in which bonding has occurred between the *para* carbon of the aromatic amine and the benzotriazole moiety of **2**; however, aniline reacts at the picryl moiety to give the product of displacement **5**, via the aniline nitrogen as the nucleophilic atom.

ERWIN BUNCEL, RICHARD A. RENFROW et MICHAEL J. STRAUSS. Can. J. Chem. **61**, 1690 (1983).

La réaction du composé **2** avec la diméthyl-2,6 aniline ou la *N*,*N*-diméthylaniline conduit à des complexes σ du type Meisenheimer que l'on peut observer par spectroscopie et dans lesquels la liaison s'établit entre le carbone en position *para* de l'amine aromatique et la portion benzotriazole du composé **2**. Cependant, l'aniline réagit au niveau de la portion picryle en donnant le produit de déplacement **5** par l'intermédiaire de l'azote de l'aniline qui joue le rôle de nucléophile.

[Traduit par le journal]

Electron-deficient nitroaromatics such as 1,3,5-trinitrobenzene (TNB) are known to interreact with a variety of nucleophilic reagents to give Meisenheimer type σ-complexes, a number of which have been fully characterized (1). Extension of the studies to heterocyclic systems such as the nitrobenzofuroxan derivatives has been of interest in part because of the known antileukemic and immunosuppressive activities of these compounds, which have been considered to result from σ-complex formation by intracellular thiol and amino functions of aminoacids and proteins (2). Recent studies have shown that the nitrobenzofuroxans form highly stable σ-complexes with a number of nucleophiles (3) and 4,6-dinitrobenzofuroxan (**1**) has thus been termed a super-electrophile.

1

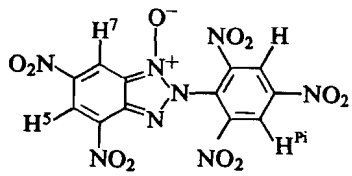

2

We have recently prepared the title compound **2** with a view of examining its reactivity towards nucleophiles, in comparison with 4,6-dinitrobenzofuroxan as well as conventional electrophiles such as TNB. Interestingly, we found (4) that attack by several nucleophiles occurs at both the benzotriazole and the picryl ring moieties, the former process giving rise to spectrally observable σ-complexes **3**, the latter to displacement products (PicNu) via the intermediate adducts **4**.

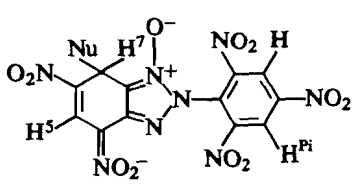

3

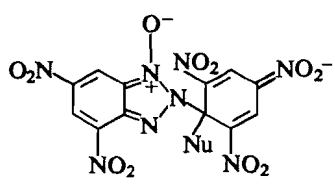

4

We have now extended the study to aromatic amines and have observed both these modes of reactivity. However, an unexpected regioselectivity has been observed in the reaction of aniline as compared to 2,6-dimethylaniline or *N*,*N*-dimethylaniline, the former undergoing attack only at the picryl ring and the latter two only at the benzotriazole moiety. Moreover, the σ-complexes formed with the latter two amines are not nitrogen-bound but are the carbon-bound species. The ambident behaviour of aromatic amines observed in this system is reminiscent of the first report on ambident reactivity in σ-complex formation, in the reaction of phenoxide ion with TNB (5).

Reaction of **2** with one equivalent of aniline in $(CD_3)_2SO$ as followed by ^1H nmr spectroscopy was found to result in the rapid disappearance of the resonances due to **2** (δ: 9.78 (s, 2H, H^{Pi}), 9.72 (d, 1H, J = 2.5 Hz, H^5), 9.36 (d, 1H, J = 2.5 Hz, H^7)) and the appearance of signals characteristic of the substitution product **5** (Nu = PhNH) (δ: 9.20 (s, 2H, H^{Pi}), 7.40 (m, 5H, ArH)), as well as **6***a* or **6***b* (δ: 9.36 (d, 1H, J = 2.5 Hz, H^5), 9.15 (d, 1H, J = 2.5 Hz, H^7)), as formed according to the equation:

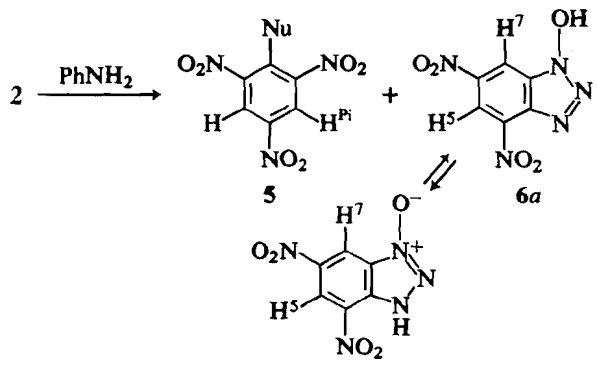

5 **6***a* **6***b*

Can. J. Chem. Downloaded from www.nrcresearchpress.com by 210.87.254.5 on 09/06/12
For personal use only.

Can. J. Chem. Downloaded from www.nrcresearchpress.com by 210.87.254.5 on 09/06/12
For personal use only.

Use of two equivalents of aniline gave rise to **5** and the anion of **6** (δ: 9.13 (d, 1H, J = 2.5 Hz, H^5), 9.05 (d, 1H, J = 2.5 Hz, H^7)). The anion is converted into its protonated form on addition of trifluoroacetic acid.

The observed overall preference for attack by aniline at the picryl moiety over the benzotriazole moiety is presumably the result of a combination of a facile formation of adduct **4** (Nu = PhNH) and its subsequent rapid irreversible decomposition. In comparison, nucleophilic addition at the benzotriazole moiety to give **3** could be expected to be kinetically and thermodynamically disfavored, judging by the results of our previous work on the interaction of aniline with TNB (6).

It seemed possible that attack at the picryl centre of **2** could be disfavored through structural modification in the aromatic amine, leading to unfavorable steric interactions in the process. A plausible candidate in this context appeared to be 2,6-dimethylaniline, since with this amine the transition state in formation of **4** would experience severe buttressing interactions between the methyl groups and the *ortho* nitro groups of the picryl moiety as well as the NO_2 group at C4 of the benzotriazole moiety. This expectation was borne out, at least in part, by the results.

Thus the addition of one equivalent of 2,6-dimethylaniline to a solution of **2** in $(CD_3)_2SO$ gave rise to a strongly coloured solution indicative of the formation of a σ-complex. However, the nmr characteristics of the species produced show that bonding has occurred not via nitrogen but via the *para* carbon of the aniline moiety. Thus the disappearance of the resonances due to **2** on addition of the amine corresponded to the appearance of signals characteristic of **7**, i.e. δ: 9.49 (s, 2H, H^{Pi}), 9.00 (s, 1H, H^5), 5.59 (s, 1H, H^7), 7.23 (s, 2H, ArH), 2.35 (s, 6H, CH_3). The conversion to **7** was rapid and complete.

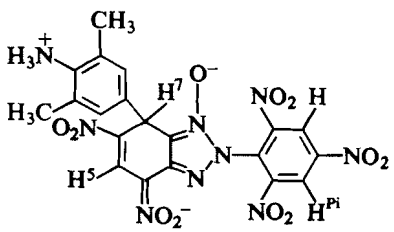

7

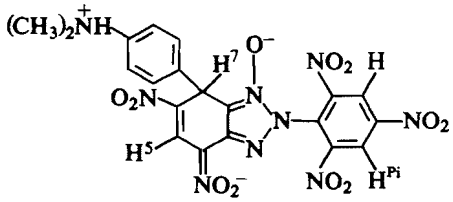

8

The facile formation of the carbon-bonded adduct **7** suggested the possibility that *N*,*N*-dimethylaniline might react likewise to yield **8** and the results showed this to be the case. The identity of **8** was shown by the following nmr characteristics of the species as formed in $(CD_3)_2SO$ solution: δ: 9.48 (s, 2H, H^{Pi}), 9.00 (s, 1H, H^5), 5.70 (s, 1H, H^7), 7.61 (s, 4H, ArH), 3.19 (s, 6H, CH_3). The formation of **8** as a spectrally observable species represents the first recorded case of a Meisenheimer complex formed by the tertiary amine and is also, to our knowledge, one of very few examples of the formation of zwitterionic Meisenheimer complexes.

Thus the present work has revealed a marked contrast in the reactivity of the title compound **2** versus the reactivity of TNB as the standard electrophile in Meisenheimer complex formation. TNB does not react with *N*,*N*-dimethylaniline at all and it interacts with aniline so weakly that there is a requirement for catalysis by a tertiary amine which serves to deprotonate the initially formed zwitterionic N-bound adduct, thereby stabilizing the anionic anilide σ-complex (7). Formation of the stable zwitterionic carbon-bound σ-complexes **7** and **8** from the interaction of the aromatic amines with **2** is definitive of the powerful electrophilic properties of this novel heterocyclic system.

Acknowledgements

Support of this research by grants from the National Research Council of Canada (E.B.) and the Naval Surface Weapons Center at Silver Spring, MD (M.J.S.) is gratefully acknowledged.

1. (*a*) M. R. CRAMPTON. Adv. Phys. Org. Chem. **7**, 211 (1969); (*b*) M. J. STRAUSS. Chem. Rev. **70**, 667 (1970); (*c*) C. A. FYFE. The chemistry of the hydroxyl group, Part 1. *Edited by* S. Patai. Wiley, London. 1971; (*d*) J. H. FENDLER, W. L. HINZE, and L. J. LIU. J. Chem. Soc. Perkin Trans. 2, 1768 (1975); (*e*) C. F. BERNASCONI. Chimia, **34**, 1 (1980); (*f*) F. TERRIER. Chem. Rev. **82**, 77 (1982); (*g*) G. A. ARTAMKINA, M. P. EGOROV, and I. P. BELETSKAYA. Chem. Rev. **82**, 427 (1982); (*h*) E. Buncel. The chemistry of amino, nitro and nitroso compounds, Supplement F. *Edited by* S. Patai. Wiley, London. 1982.
2. (*a*) P. B. GHOSH and M. W. WHITEHOUSE. J. Med. Chem. **11**, 305 (1968); **12**, 158 (1969); (*b*) P. B. GHOSH, B. TERNAI, and M. W. WHITEHOUSE. J. Med. Chem. **15**, 225 (1972); (*c*) Med. Res. Rev. **1**, 159 (1981).
3. (*a*) W. P. NORRIS and J. OSMUNDSEN. J. Org. Chem. **30**, 2407 (1965); (*b*) L. DINUNNO, S. FLORIO, and P. E. TODESCO. J. Chem. Soc. Perkin Trans. 2, 1469 (1975); (*c*) F. TERRIER, F. MILLOT, and W. P. NORRIS. J. Am. Chem. Soc. **98**, 5883 (1976); (*d*) E. BUNCEL, N. CHUAQUI-OFFERMANNS, and A. R. NORRIS. J. Chem. Soc. Perkin Trans. 1, 415 (1977); (*e*) E. BUNCEL, N. CHUAQUI-OFFERMANNS, R. Y. MOIR, and A. R. NORRIS. Can. J. Chem. **57**, 494 (1979).
4. R. A. RENFROW, M. J. STRAUSS, S. COHEN, and E. BUNCEL. Submitted for publication.
5. (*a*) E. BUNCEL and J. G. K. WEBB. J. Am. Chem. Soc. **95**, 8470 (1973); (*b*) E. BUNCEL, A. JONCZYK, and J. G. K. WEBB. Can. J. Chem. **53**, 3761 (1975); (*c*) E. BUNCEL and W. EGGIMANN. Can. J. Chem. **54**, 2436 (1976).
6. E. BUNCEL and W. EGGIMANN. J. Am. Chem. Soc. **99**, 5958 (1977).
7. (*a*) E. BUNCEL and H. W. LEUNG. J. Chem. Soc. Chem. Commun. 19 (1975); (*b*) E. BUNCEL, W. EGGIMANN, and H. W. LEUNG. J. Chem. Soc. Chem. Commun. 55 (1977); (*c*) E. BUNCEL and W. EGGIMANN. J. Chem. Soc. Perkin Trans. 2, 673 (1978).

Energy transfer by an exchange mechanism in fluid solutions. A generalized treatment

J. M. G. MARTINHO AND J. C. CONTE

Centro de Química-Física Molecular, Complexo I, Instituto Superior Técnico, Av. Rovisco Pais, 1000 Lisboa, Portugal

Received August 16, 1982[1]

J. M. G. MARTINHO and J. C. CONTE. Can. J. Chem. **61**, 1693 (1983).

Energy transfer in solution by an exchange mechanism has been analysed. The diffusion equation with an added sink term describing the energy transfer process was solved for steady-state conditions using the radiation boundary condition. The transfer rate constant so obtained takes into account the possibility that the reaction does not occur during an encounter. In the limit the equations contain the cases of totally absorbing and totally reflecting barriers. The short range effects were analysed and their influence was introduced under new boundary conditions.

J. M. G. MARTINHO et J. C. CONTE. Can. J. Chem. **61**, 1693 (1983).

On a analysé le transfert d'énergie en solution selon un mécanisme d'échange. En utilisant la condition limite de radiation, on a résolu l'équation de diffusion qui décrit le transfert d'énergie dans l'état stationnaire en incluant dans cette équation un terme d'affaiblissement. La constante de vitesse ainsi obtenue tient compte de la possibilité de non réaction lors de la rencontre. A la limite l'équation contient les cas de barrières totalement absorbées et totalement réfléchies. On a analysé les effets à courte distance et on a introduit leur influence en deça des conditions de frontière nouvelle.

[Traduit par le journal]

Can. J. Chem. Downloaded from www.nrcresearchpress.com by 210.87.254.42 on 09/06/12
For personal use only.

1. Introduction

The transfer of electronic energy between an energy donor (D) and an energy acceptor (A) takes place essentially by one of the two mechanisms: Coulomb interaction (1, 2) and exchange interaction (2). When the electronic transitions of the donor and acceptor are allowed (e.g. singlet–singlet transfer) the transfer is usually of the first type. For spin forbidden transitions (e.g. triplet–triplet transfer) the mechanism of transfer is of the exchange type. In this case, discussed by Dexter (2), the transfer probability per unit time, $w(r)$, depends exponentially on the relative distance between the donor and the acceptor. The same exponential dependence on distance is found in the study of electron transfer reactions (3).

Formerly studied in rigid systems (4), this transfer has also been the subject of study in solutions (5, 6). It has been shown that the transfer rate constant depends on the energy difference between the donor and the acceptor triplet states. For energy transfer processes, where this difference is lower than 5 kcal mol^{-1}, the back transfer process must also be considered (7).

However, even for the cases where the back transfer is unimportant, the values obtained for the transfer rate constant in fluid solutions are lower than those predicted by the theory of diffusion controlled reactions (8). Wagner and Kochevar (9) have shown that the diffusion controlled limit is only reached for viscosities greater than 3 cP. There is evidence (10, 11) that for high viscosities the rate constant is greater than the diffusion limit.

In this paper the diffusion equation for steady state conditions is solved with a sink term describing the energy transfer processes. We use adequate boundary conditions that take into account short range effects and also the possibility that the reaction does not occur during an encounter.

2. Energy transfer in solution

Let us assume, following Dexter (2), that the probability of transfer per unit time between an energy donor and an acceptor at a distance r is given by

$$[1] \quad w(r) = A \exp\left(-\frac{2r}{L}\right)$$

where A (s^{-1}) is a constant depending on the properties of the donor–acceptor pair and L is the mean effective Bohr radius of the pair.

Following the excitation of the solution with a δ-pulse of electromagnetic radiation, the excited donor molecules (concentration c_D^*) are able to transfer their energy to the acceptor molecules (concentration c_A) with probability $w(r)$. Using a statistical analysis developed by Waite (12) for the study of partially diffusion controlled reactions, Gösele and co-workers (13, 14) obtained, for the normalized distribution function of the pairs D_i–A_j, the following equation

$$[2] \quad \frac{\partial}{\partial t} U_{ij} = D \Delta U_{ij} - w(r) U_{ij}$$

where D is the sum of the diffusion coefficients of the donor and the acceptor. For a process with spherical symmetry, the rate constant for the energy transfer process is given by

$$[3] \quad k(t) = 4\pi D R_c^2 \left(\frac{\partial U_{ij}}{\partial r}\right)_{r=R_c} + \int_{r=R_c}^{\infty} w(r) U_{ij} 4\pi r^2 \, dr$$

where the first term gives the component of the transfer at the encounter distance R_c, and the second term gives the component of the transfer due to exchange interactions for distances greater than R_c.

In this approach the short-range caging effects are not considered. These effects were studied by Northrup and Hynes (15), for the partially diffusion controlled reactions under steady-state conditions. These authors considered that the diffusion equation should be modified to include the effect of the mean potential $u(r)$ of a pair of reacting molecules and also the dependence of the diffusion coefficient on the separation of reacting molecules which is due to dynamical correlations.

We will consider first the standard diffusion eq. [2] and we will return to this problem later.

For excitation by means of radiation from a conventional source it is reasonable to assume a uniform distribution of donor and acceptor molecules. Then all U_{ij} are identical and we have the boundary condition

$$[4] \quad U(r, t = 0) = 1 \qquad r > R_c$$

We need another boundary condition at the encounter distance. The so-called Smoluchowski's boundary condition (16)

[1]Revision received February 8, 1983.

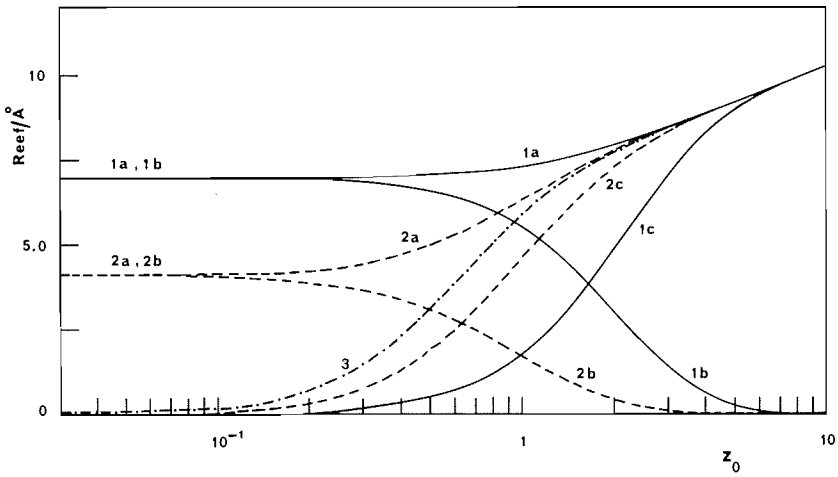

FIG. 1. Variation of the transfer effective distance, R_{eef} with z_0, for L = 1.5 Å, R_c = 7.0 Å, and different values of β: 1, β = 1.0 × 10^{15} cm^{-1}; 2, β = 2.0 × 10^7 cm^{-1}; 3, β = 0 cm^{-1}; a, R_{eef} according to eq. [15]; b, R''_{eef} according to eq. [16]; c, R'_{eef} according to eq. [17].

[5] $U(r = R_c, t) = 0$

has been used quite often, implying that the probability of reaction at the encounter distance, R_c, is unity. However, this probability, γ, depends on the rate constant for the reaction at the encounter, k_{te}, and on the rate constant for the dissociation of the pair, k_{-D}, according to the relationship

[6] $$\gamma = \frac{k_{te}}{k_{te} + k_{-D}}$$

For solvents of low viscosity (η ≈ 1 cP) k_{-D} is of the order of 10^{11} s^{-1} and k_{te} is usually lower. Then γ is less than one and so it is necessary to reconsider the use of boundary conditions (5). If we assume that the probability of reaction of the pairs at the encounter distance is proportional to the probability that they lie in a thin spherical shell of thickness ΔR, we obtain the so-called radiation boundary condition (12, 17, 18)

[7] $$4\pi D(R_c + \Delta R)^2 \left(\frac{\partial U}{\partial r}\right)_{r = R_c + \Delta R} = k_c U(R_c, t),\ \Delta R \to 0$$

where $k_c = 4\pi R_c^2\, \Delta R\, K$ represents a specific rate constant for the pair disappearance in the spherical shell due to a collision process with rate constant K (s^{-1}).

Equation [2] with conditions [4] and [7] has no analytical solution. However, it is possible to obtain a solution for long times, where the steady-state approximation ($\partial U/\partial t = 0$) is valid. If we make the substitutions

[8] $v = Ur$

[9] $$z^2 = \frac{AL^2}{D} \exp\left(-\frac{2r}{L}\right)$$

we obtain from [2] the Bessel equation

[10] $$z^2 \frac{d^2v}{dz^2} + z \frac{dv}{dz} - z^2 v = 0$$

which gives, under conditions [4], [7], and $U(r \to \infty, t) = 1$

[11] $$U(z) = \frac{L}{r}\left\{K_0(z) - \frac{L(1 + \beta R_c)K_0(z_0) - z_0 R_c K_1(z_0)}{L(1 + \beta R_c)I_0(z_0) + z_0 R_c I_1(z_0)} I_0(z)\right\}$$

where

[12] $$z_0^2 = \frac{AL^2}{D} \exp\left(-2\frac{R_c}{L}\right)$$

is the value of z for the encounter distance R_c, $K_\nu(z)$ and $I_\nu(z)$ are the modified Bessel functions of second and first kind, respectively, of order ν and argument z, and

[13] $$\beta = \frac{k_c}{4\pi D R_c^2}$$

is a parameter which takes into account the fact that the probability of reactions at the encounter may be less than one.

The rate constant can be obtained by substitution of eq. [11] into eq. [3]. However, we can obtain a more adequate form for $k(t)$ applying Gauss's theorem to eq. [3], and then

[14] $$k(t) = 4\pi D \lim_{r \to \infty}\left(r^2 \frac{\partial U}{\partial r}\right) - \int_{R_c}^{\infty} \frac{\partial U}{\partial t} 4\pi r^2\, dr$$

from which we get the rate constant for long times

[15] $$k_\infty = k(t \to \infty) = 4\pi D R_c \left\{1 + \frac{L}{R_c}\left[E + \ln\left(\frac{z_0}{2}\right) + \frac{L(1 + \beta R_c)K_0(z_0) - z_0 R_c K_1(z_0)}{L(1 + \beta R_c)I_0(z_0) + z_0 R_c I_1(z_0)}\right]\right\}$$

where E is Euler's constant (E = 0.57721 . . .).

The rate constant k_∞ is the sum of two terms (see eq. [3]). The first, k_D, is the component for the encounter distance and, due to the boundary condition used (see eq. [7]), is given by

[16] $$k_D = k_c U(z_0) = 4\pi D R_c \frac{L\beta R_c}{L(1 + \beta R_c)I_0(z_0) + z_0 R_c I_1(z_0)}$$

The second, k_E, takes into account the transfer processes for distances greater than R_c, and is given by

[17] $$k_E = 4\pi D R_c \left\{1 + \frac{L}{R_c}\left[E + \ln\left(\frac{z_0}{2}\right) + \frac{L(1 + \beta R_c)K_0(z_0) - z_0 R_c K_1(z_0) - \beta R_c^2}{L(1 + \beta R_c)I_0(z_0) + z_0 R_c I_1(z_0)}\right]\right\}$$

Figure 1 shows the values of the effective distance for the transfer

$$R_{eef} = \frac{k_\infty}{4\pi D}$$

Can. J. Chem. Downloaded from www.nrcresearchpress.com by 210.87.254.42 on 09/06/12
For personal use only.

Can. J. Chem. Downloaded from www.nrcresearchpress.com by 210.87.254.42 on 09/06/12
For personal use only.

as a function of z_0 for different values of β and $R_c = 7$ Å. The contributions for the encounter distance R_{ecf}^{D} and greater distances R_{ecf}^{k} are also presented in the figure. Three different regions can be seen: for high values of the diffusion coefficient ($z_0 < 0.1$), all the transfer processes take place at the encounter and the rate constant is given by

$$[18] \quad k_\infty \simeq 4\pi D R_c \frac{\beta R_c}{1 + \beta R_c}$$

Then, taking eq. [13] into account one obtains

$$[19] \quad \frac{1}{k_\infty} = \frac{1}{k_c} + \frac{1}{4\pi D R_c}$$

It is thus possible to obtain k_c as well as the encounter distance R_c. The value of k_c is the value of the rate constant for very large diffusion coefficients and so it will approach the value obtained in the vapour phase.

For small values of the diffusion coefficients ($z_0 > 5$), almost all of the transfer processes occur at distances greater than R_c and

$$[20] \quad k_\infty = 2\pi D L \left[2E + \ln\left(\frac{AL^2}{4D}\right)\right]$$

For intermediate values of $z_0 (0.1 < z_0 < 5)$ both transfer processes are important and k_∞ must be evaluated from eq. [15].

The present analysis shows that, as indicated in the introduction, R_{ecf} values depend on the diffusion coefficient and may be greater or less than R_c. For an instantaneous reaction at the encounter and large diffusion coefficients ($z_0 \ll 1$) the effective distance is given by R_c.

Some results published by André *et al.* (10) show that the effective distance can be greater than R_c, as with the quenching of POPOP by CBr_4 in mixtures of cyclohexane and cyclohexanol. In other systems (19), however, the authors found for the effective distance the actual R_c value. This difference was interpreted (19) as being due to short range effects which are analysed below.

2.1. *The effect of transient terms*

The relationships considered so far are valid for times large enough so that the steady-state approximation can be considered a reasonable approximation. Butler *et al.* (20) have shown that the steady state is reached for $t_\infty \gg R_{ecf}^2/\pi D$. For shorter times, a time dependent equation of the form

$$[21] \quad k(t) = 4\pi D R_{ecf}\left[1 + \frac{R_{ecf}}{\sqrt{\pi D t}}\right]$$

already obtained in the study of diffusion controlled reactions, must be a good approximation. Butler *et al.* (20) have shown, from numerical integration of eq. [2] with Smoluchowski's boundary condition, that this is true for values of $t > 10L^2/4D$. For short times, $t < L^2/4D$, they have shown that material diffusion can be neglected and then the theoretical treatment developed by Inokuti and Hirayama (21) should be adequate. Recently Allinger and Blumen (22) have studied the effect of material diffusion on the energy transfer by an exchange mechanism and obtained for the decay function a complex equation that certainly is a good approximation for values of $t < 10L^2/4D$.

The theoretical equations presented in the literature cover all times following excitation. Now there is a need for experimental decay studies to test these theoretical results.

2.2. *Influence of short range effects*

In the preceding sections we neglected the presence of short range effects. These effects, which must include cage effects, orientational and steric effects, are important but very complex to treat, mainly because our knowledge of the structure of liquids is limited. Then, to take these effects into account, we use a simplified model that was proposed by André *et al.* (23) to treat the partially diffusion controlled reactions. We assume that short range effects can be isolated in a spherical shell of thickness $\Delta R = R' - R_c$, where there is no diffusion and the transfer occurs with a rate constant K' (s^{-1}) independent of distance. In the outer region ($r > R'$) the system is well described by eq. [2]. Then we must use the boundary condition (23)

$$[22] \quad 4\pi D R'^2 \left(\frac{\partial U}{\partial r}\right)_{r=R'} = K' V_1 U(R', t) + V_1 \left(\frac{\partial U}{\partial t}\right)_{r=R'}$$

where $V_1 = 4/3\ \pi (R'^3 - R_c^3)$ is the volume of the spherical shell.

The rate constant is given by

$$[23] \quad k(t) = \int_{R_c}^{R'} K'\ U(R', t)\ 4\pi r^2\, dr + \int_{R'}^{\infty} w(r)\ U(r, t)\ 4\pi r^2\, dr$$

$$= 4\pi D R'^2 \left(\frac{\partial U}{\partial r}\right)_{r=R'} - V_1 \left(\frac{\partial U}{\partial t}\right)_{r=R'} + \int_{R'}^{\infty} w(r)\ U(r, t)\ 4\pi r^2\, dr$$

which can be put in the form

$$[24] \quad k(t) = 4\pi D \lim_{r\to\infty}\left(r^2 \frac{\partial U}{\partial r}\right) - V_1 \left|\frac{\partial U}{\partial t}\right|_{r=R'} - \int_{R'}^{\infty} \frac{\partial U}{\partial t} 4\pi r^2\, dr$$

For steady-state conditions, the last two terms in eq. [24] are zero and then we obtain, by solving eq. [2], the rate constant

$$[25] \quad k'_\infty = 4\pi D R' \left\{1 + \frac{L}{R'}\left[E + \ln\left(\frac{z'_0}{2}\right) + \frac{L(1 + \beta' R') k_0(z'_0) - z'_0 R' k_1(z'_0)}{L(1 + \beta' R') I_0(z'_0) - z'_0 R' I_1(z'_0)}\right]\right\}$$

which is identical to eq. [15], if we replace R_c by R', z_0 by z'_0 (which is the value of z for R'), and β by $\beta' = K' V_1/4\pi D R'^2$.

For high viscosities ($z'_0 \gg 1$) this equation reduces to eq. [20] that predicts a linear variation of R_{ecf} with $(-\ln D)$. For low viscosities ($z'_0 \ll 1$) we get an equation similar to eq. [19] with $|k_c| = K' V_1$ and a value R' in place of R_c. This is in accordance with the results presented by Butler and Pilling (11) and André *et al.* (10).

2.3. *Theoretical decay curves and quantum yields*

The decay curves of the donor in the presence of the acceptor must contain three terms: a term describing the decay due to radiative and non-radiative processes of the donor in the absence of the acceptor, a second term due to the "static" energy transfer process in the shell, and a dynamic term describing the energy transfer process in the outer region ($r > R'$). Due to the static term the concentration of donor molecules at $t = 0$ is given by $c_D^*(0) \exp(-N V'_1 c_A)$, where $c_D^*(0)$ is the concentration

Can. J. Chem. Downloaded from www.nrcresearchpress.com by 210.87.254.42 on 09/06/12
For personal use only.

of the initially excited molecules, N is Avogadro's number, and V_1' is a reacting volume which is related to the volume of the shell and also to the rate constant k_c'. If there is an instantaneous reaction in the shell ($k_c' \rightarrow \infty$) then V_1' is reduced (23, 24) to the shell volume V_1. The dynamic process is described for sufficiently long times by the rate constant

$$[26] \quad k(t) = 4\pi DNR_{ref}\left[1 + \frac{R_{ref}}{\sqrt{\pi Dt}}\right]$$

The decay function, after a δ-pulse of excitation, is then given by

$$[27] \quad c_D^*(t) = c_D^*(0)\exp(-NV_1'c_A)\exp\left[-\frac{t}{\tau_0} - k_0c_At\left(1 + \frac{2R_{ref}}{\sqrt{\pi Dt}}\right)\right]$$

with $k_0 = 4\pi DN\,R_{ref}$, and τ_0 the decay time of the donor in the absence of the acceptor. The quantum yield is given by (23)

$$[28] \quad \Phi_D \simeq \Phi_D^0 \times \frac{I(\lambda)\exp(-NV_1'c_A)}{1 + k_0\tau_0c_A}$$

where Φ_D^0 is the quantum yield of the donor in the absence of the acceptor and

$$[29] \quad \lambda = \frac{2}{\pi^{1/2}}\frac{k_0\tau_0c_A}{(1 + k_0\tau_0c_A)^{1/2}}\frac{R_{ref}}{(D\tau_0)^{1/2}}$$

with

$$[30] \quad I(\lambda) = 1 - \frac{1}{2}\lambda\pi^{1/2}\exp\left(\frac{\lambda^2}{4}\right)\operatorname{erfc}\left(\frac{\lambda}{2}\right)$$

From the experimental decay curves we can obtain the effective distance R_{ref}, and the diffusion coefficient D. The effective distance can be compared with the theoretical values predicted by eqs. [15] and [25] and hence it is possible to obtain some information about the presence or absence of short range effects. From the quantum yields we can confirm the results obtained from the decay curves and also obtain the reacting volume V_1'.

3. Conclusions

The present work is a general treatment for the energy transfer processes in solution by an exchange mechanism, which incorporates as particular cases some other treatments.

In the continuous limit eq. [15] is reduced for large values of β ($\beta R_c \gg 1$) to the case of a totally absorbing barrier, which is the result already obtained by Pilling and Rice (25), i.e.,

$$[31] \quad k_\infty = 4\pi DR_c\left\{1 + \frac{L}{R_c}\left[E + \ln\left(\frac{z_0}{2}\right) + \frac{k_0(z_0)}{I_0(z_0)}\right]\right\}$$

For fast diffusing, the rate constant obtained by Allinger and Blumen (22)

$$[32] \quad k_\infty = \int_{R_c}^{\infty} 4\pi r^2 A\exp\left(-\frac{2r}{L}\right)dr = \pi AL\exp\left(-\frac{2R_c}{L}\right)[2R_c^2 + 2LR_c + L^2]$$

is easily obtained from eq. [15] if we let $z_0 \rightarrow 0$ (large values of D) for the case of a totally reflecting barrier ($\beta = 0$).

From eq. [25] we can obtain, if we neglect the energy transfer processes for $r > R'$, the results obtained by André *et al.* (23) for steady-state conditions.

The treatment developed does not take into account the possibility of back transfer. This transfer is important for low exothermic processes and complicates the analysis. A theoretical treatment recently presented by Balzani *et al.* (26) explains reasonably well the known experimental results obtained in fluid solutions.

Acknowledgements

The authors would like to thank one of the referees for some useful comments. Financial support from the I.N.I.C. (Lisbon) is gratefully acknowledged.

1. TH. FÖRSTER. Ann. Phys. **2**, 55 (1948).
2. D. L. DEXTER. J. Chem. Phys. **21**, 836 (1953).
3. R. K. HUDDLESTON and J. R. MILLER. J. Phys. Chem. **86**, 200 (1982).
4. A. N. TERENIN and V. L. ERMOLAEV. Dokl. Akad. Nauk SSSR, **85**, 547 (1952).
5. H. L. J. BÄCKSTRÖM and K. SANDROS. Acta Chem. Scand. **12**, 823 (1958); **14**, 48 (1960).
6. G. PORTER and F. WILKINSON. Proc. R. Soc. Ser. A, **264**, 1 (1961).
7. S. NORDIN and R. L. STRONG. Chem. Phys. Lett. **2**, 429 (1968).
8. T. TAKEMURA, M. AIKAWA, and H. BABA. Bull. Chem. Soc. Jpn. **47**, 2476 (1974).
9. P. J. WAGNER and I. KOCHEVAR. J. Am. Chem. Soc. **90**, 2232 (1968).
10. J. C. ANDRÉ, M. BOUCHY, and W. R. WARE. Chem. Phys. **37**, 119 (1979).
11. P. R. BUTLER and M. J. PILLING. Chem. Phys. **39**, 33 (1979).
12. T. R. WAITE. Phys. Rev. **107**, 463 (1957).
13. U. GÖSELE, M. HAUSER, U. K. A. KLEIN, and R. FREY. Chem. Phys. Lett. **34**, 519 (1975).
14. U. K. A. KLEIN, R. FREY, M. HAUSER, and U. GÖSELE. Chem. Phys. Lett. **41**, 139 (1976).
15. S. H. NORTHRUP and J. T. HYNES. J. Chem. Phys. **71**, 871 (1979).
16. M. VON SMOLUCHOWSKI. Z. Physik. Chem. **92**, 192 (1917).
17. F. C. COLLINS and G. E. KIMBALL. J. Colloid Sci. **4**, 425 (1949).
18. G. WILEMSKI and M. FIXMAN. J. Chem. Phys. **58**, 4009 (1973).
19. M. L. VIRIOT, J. C. ANDRÉ, and W. R. WARE. J. Photochem. **14**, 133 (1980).
20. P. R. BUTLER, M. J. PILLING, S. A. RICE, and T. J. STONE. Can. J. Chem. **55**, 2124 (1977).
21. M. INOKUTI and F. HIRAYAMA. J. Chem. Phys. **43**, 1978 (1965).
22. K. ALLINGER and A. BLUMEN. J. Chem. Phys. **75**, 2762 (1981).
23. J. C. ANDRÉ, M. BOUCHY, and W. R. WARE. Chem. Phys. **37**, 103 (1979).
24. J. C. ANDRÉ, M. NICLAUSE, and W. R. WARE. Chem. Phys. **28**, 371 (1978).
25. M. J. PILLING and S. A. RICE. J. Chem. Soc. Faraday Trans. 2, **72**, 792 (1976).
26. V. BALZANI, F. BOLLETTA, and F. SCANDOLA. J. Am. Chem. Soc. **102**, 2152 (1980).

Protecting groups for the pyrrole nitrogen atom. The 2-chloroethyl, 2-phenylsulfonylethyl, and related moieties[1]

CARLOS GONZALEZ, ROBERT GREENHOUSE,[2] AND RAMON TALLABS
Syntex, S. A., División de Investigación, Apartado Postal 10-820, México 10, D.F., México

AND

JOSEPH M. MUCHOWSKI[2]
Syntex Research, Institute of Organic Chemistry, 3401 Hillview Avenue, Palo Alto, CA 94304, U.S.A.

Received October 20, 1982

CARLOS GONZALEZ, ROBERT GREENHOUSE, RAMON TALLABS, and JOSEPH M. MUCHOWSKI. Can. J. Chem. **61**, 1697 (1983).

The 2-chloroethyl and 2-phenylsulfonylethyl moieties are versatile protecting groups for the pyrrole nitrogen atom. The 2-chloroethyl group is easily attached under phase transfer conditions using 1,2-dichloroethane. The 2-phenylsulfonylethyl moiety is readily appended under both phase transfer and homogeneous solution conditions using 2-phenylsulfonylethyl chloride **5**. Deprotection of the *N*-(2-chloroethyl)pyrroles is accomplished by means of efficient three-step, one-pot sequences via the *N*-vinyl compounds **3** and subsequent degradation of the *N*-(1-hydroxyethyl) compounds **4** or the acetoxymercuration derivatives **5** obtained therefrom. The 2-phenylsulfonylethyl group is excised by a reverse Michael reaction using sodium hydride or DBN as the base.

The utility of the 2-chloroethyl protecting group is exemplified in a synthesis of benzyl cyclopenta[*b*]pyrrole-5-carboxylate **13** from 1-(2-chloroethyl)-4-oxotetrahydroindole **2***d*.

CARLOS GONZALEZ, ROBERT GREENHOUSE, RAMON TALLABS et JOSEPH M. MUCHOWSKI. Can. J. Chem. **61**, 1697 (1983).

Les unités chloro-2 ethyle et phénylsulfonyl-2 éthyle sont des groupes protecteurs versatiles pour l'atome d'azote du pyrrole. On attache facilement le groupe chloro-2 éthyle, dans des conditions de transfert de phase, en utilisant de dichloro-1,2 éthane. On fixe rapidement le groupe phénylsulfonyl-2 éthyle dans des conditions de transfert de phase et en solution homogène en utilisant le chlorure de phénylsulfonyl-2 éthyle **5**. On réalise la déprotection des *N*-(chloro-2 éthyle)pyrroles en trois étapes efficaces dans un seul récipient par l'intermédiaire des composés *N*-vinyliques **3** et de la dégradation subséquente des composés *N*-(hydroxy-1 éthyl) **4** ou des dérivés d'acétoxymercuriation du composé **5**. On élimine le groupe phénylsulfonyl-2 éthyle au moyen d'une réaction de Michael inverse en utilisant l'hydrure de sodium ou le DBN comme base.

On démontre l'utilité du groupe protecteur chloro-2 éthyle en synthétisant, pour les besoins du laboratoire, le carboxylate-5 de benzyleyclopenta[*b*]pyrrole **13** à partir du (chloro-2 éthyle)-1 oxo-4 tétrahydroindole **2***d*.

[Traduit par le journal]

In connection with synthetic studies in progress in these laboratories, it became necessary to develop general methodology for the protection of the pyrrole nitrogen atom. This need arose because the protecting groups currently in use are either of limited applicability or the general utility thereof is unknown. For example, the benzyl group has been used as a pyrrole N-protector on several occasions (1) but sodium in liquid ammonia is required to remove it and many functional groups would not survive these conditions. The 3,4-dimethoxybenzyl moiety, scission of which is effected with 5% sulfuric acid in trifluoroacetic acid containing excess anisole, is reported (2) to be useful for the N-protection of certain polysubstituted pyrroles, but no further examples of the application of this group have been published. The benzyloxymethyl moiety (3) has considerable potential for pyrrole N-protection. It is easily attached (benzyl chloromethyl ether/NaH) and removed (hydrogenolysis, then aqueous base), however, its applicability has only been demonstrated for diethyl pyrrole-3,4-dicarboxylate.[3] The β-(methoxyethoxy)-methyl group is said (1*c*) to serve as an N-protector, but the removal thereof has not been described. Various acyl residues, such as acetyl (1*b*), benzoyl (1*b*), and benzenesulfonyl (1*b*, 4) have been employed to block position-1 in pyrroles, however, these electron-withdrawing entities drastically alter the nucleophilic character of the heterocyclic ring system. Finally, it has recently been shown (5) that the readily removable (chromous acetate) *N*,*N*-dimethylamino) group functions as a useful pyrrole N-blocking moiety. Unfortunately, each pyrrole derivative thus protected must be synthesized *de novo*.

The ideal pyrrole N-protector should be inexpensive and easy to put on and take off in the presence of a wide variety of functional groups. It should itself be inert to a broad spectrum of reactions and should not significantly reduce the nucleophilicity of the pyrrole system. In a previous publication from these laboratories, an instance of the use of the 2-chloroethyl moiety as a pyrrole nitrogen protecting group was described (6). The present work reports on the optimized conditions for the attachment and removal of that moiety as well as the 2-phenylsulfonylethyl group. In addition, a brief account of the 2-phenylsulfinylethyl unit as a potential pyrrole N-blocking group is given. Of the three groups, the 2-chloroethyl moiety comes the closest to fulfilling the requirements stipulated above.

The 2-chloroethyl unit was readily appended, in high yields (see Table 1) to the nitrogen atom of various pyrrole derivatives **1** under phase transfer conditions using 1,2-dichloroethane as the organic phase and reactant, with tetra-n-butylammonium iodide as the phase transfer agent. One technique which was devised for the cleavage of the blocking group from **2** was based on the previous observations (6) that **2** could be dehydrochlorinated to **3** and the *N*-vinyl group could be removed therefrom in a two-step sequence via the carbinolamine der-

[1]Contribution No. 628 from the Syntex Institute of Organic Chemistry.

[2]Authors to whom correspondence should be addressed.

[3]An example has been encountered of the saturation of the pyrrole nucleus prior to the hydrogenolysis of the benzyl moiety of the protecting group (R. Greenhouse and R. Tallabs, unpublished observation).

Can. J. Chem. Downloaded from www.nrcresearchpress.com by 210.87.254.40 on 09/06/12
For personal use only.

TABLE 1. Reaction times, yields, physical constants of *N*-protected pyrroles

Compound no.	R^1	R^2	Reaction time (h)	Yield (%)	Melting point (°C)	Analysis: Calcd. C	Calcd. H	Calcd. N	Found C	Found H	Found N
2*a*	CHO	H	1	94	Oil	53.34	5.12[a]		53.57	5.17	
2*b*	COC_6H_5	H	1	89	54.5[b]	66.81	5.17	5.99	66.85	5.16	5.89
2*c*	SCH_3	H	8	93	Oil	47.85	5.74	7.97	47.39	5.75	7.78[c]
2*d*	$-(CH_2)_3CO-$		2	85	Oil	60.76	6.12	7.09	60.92	6.24	6.78
6*a*	CHO	H	6[d]	84	87–88	59.30	4.98	5.32	59.18	4.90	5.33
6*b*	COC_6H_5	H	2	87	96.5–97	67.23	5.05	4.13	67.18	5.34	4.06
6*c*	SCH_3	H	3[d]	80	82–83	55.49	5.37	4.98	55.66	5.32	4.97
6*d*	$-(CH_2)_3CO-$		16[d]	91	102–103	63.34	5.65	4.62	63.15	5.59	4.57
8			24	86	Oil	70.53	5.30	4.33	70.27	5.34	4.04
9			2	88	Oil	74.24	5.57	4.56	74.01	5.64	4.53

[a]Not analysed for nitrogen.
[b]This and all the other solid compounds were crystallized from dichloromethane–hexane.
[c]*m/e* 175.0222; 177.0193 (calcd. for $C_7H_{10}{}^{35}ClNS$, 175.0221; $C_7H_{10}{}^{37}ClNS$, 177.0190).
[d]Prepared from **5** and the sodium salt of the pyrrole. See experimental section.

ivative **4**. Thus, reaction of the chloroethyl compounds with sodium hydride, in DMF or acetonitrile at room temperature, produced the *N*-vinylpyrroles which on hydration with aqueous hydrochloric acid[4] in acetonitrile provided the 1-hydroxyethyl compounds **4**. These substances were converted into the deprotected pyrroles on heating with sodium acetate in aqueous acetonitrile.[5] Although intermediates **3** and **4** could be isolated,[6] it was not necessary to do so. The yields in each step were in excess of 90% and therefore the entire reaction sequence was routinely carried out in one pot. By this procedure the *N*-(2-chloroethyl)pyrroles **2***a* and **2***b* were transformed into pyrrole-2 carboxaldehyde and 2-benzoylpyrrole **1***a* and **1***b* in 71% and 85% yield, respectively.

For pyrroles which did not bear a nuclear deactivating substituent, the acidic conditions required to convert the *N*-vinyl compound **3** into the carbinolamine **4** were too vigorous to permit the survival of the pyrrole moiety. In these cases **3** was reacted with excess mercuric acetate and the supposed acetoxy mercury compound **5** was cleaved, in the same pot, with sodium borohydride. It was not determined if the borohydride reagent was, in fact, a necessary ingredient in this deprotection sequence, i.e. **5** itself is expected to be cleaved under alkaline conditions. A specific example of the utilization of this modification of the deblocking process is described at the end of this section (see Scheme 4). Further study of the process is clearly in order.

The 1-(2-phenylsulfonylethyl)pyrroles **6** were prepared from 2-phenylsulfonylethyl chloride and the pyrroles by the phase

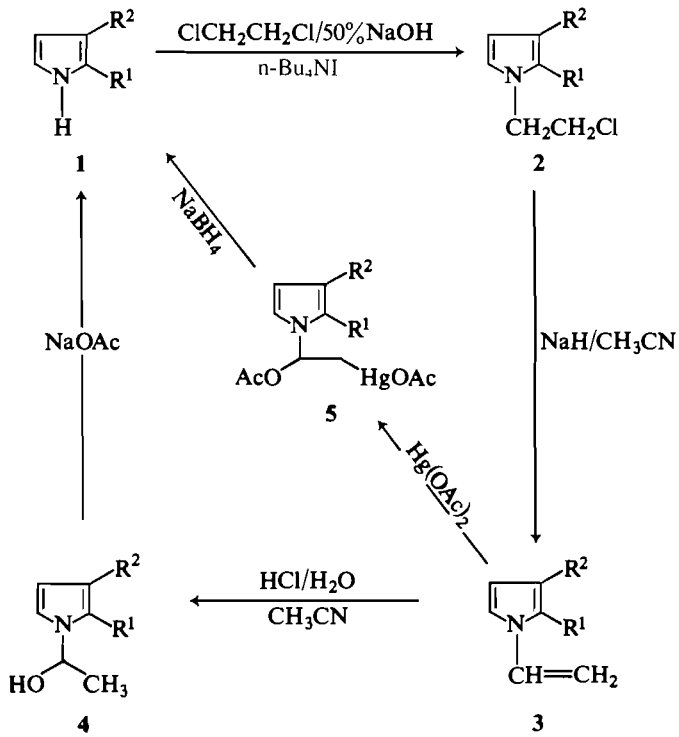

SCHEME 1

transfer technique, or from 2-phenylsulfonylethyl chloride and the sodium salts of the pyrroles in DMF solution (see Table 1). The removal of this blocking group was effected with sodium hydride or DBN (1,5-diazabicyclo[4.3.0]-non-5-ene) in DMF solution at room temperature. Thus, pyrrole-2-carboxaldehyde and 2-benzoylpyrrole were obtained from **6***a* and **6***b* in 75% and 84% yield, respectively, using the sodium hydride process.[7]

A brief study was made of the use of the 2-phenylsulfinylethyl unit as a pyrrole N-blocking group. For example, 1-(2-phenylsulfinylethyl)-2-benzoylpyrrole **8** could be pre-

[4]*N*-vinylindoles have similar acid sensitivity (7).
[5]Silver benzoate was used for the previously reported example (6).
[6]For example, **3***b* and **4***b* were isolated as oils in greater than 95% yields and were characterized by ir and nmr spectroscopy. Thus, the *N*-vinyl compound **3***b* had ir (chloroform) absorptions at 1645 (C=C) and 1630 (C=O) cm^{-1}, and nmr (deuteriochloroform) resonances for the olefinic hydrogens at δ 5.11 (dd, 2H, J_{gem} = 0 Hz, J_{cis} = 9 Hz, J_{trans} = 16 Hz) and 7.90 (dd, 1H, J_{cis} = 9 hz, J_{trans} = 16 Hz, partially obscured by C_6H_5 multiplet). The hydroxyethyl derivative **4***b* showed ir (chloroform) bands at 3480 (OH), 3400 (OH), and 1605 (C=O) cm^{-1}, and nmr (deuteriochloroform) absorptions at δ 1.75 (d, 3H, *J* = 6 Hz, CH_3) and ~ 6.3 (m, 2H, CHOH). Analogous compounds were isolated and rigorously characterized in the above mentioned publication (6).

[7]The 2-phenylsulfonylethyl group has recently been used for the protection of the 3′-phosphodiester function in oligodeoxyribonucleotide synthesis (8).

Can. J. Chem. Downloaded from www.nrcresearchpress.com by 210.87.254.40 on 09/06/12
For personal use only.

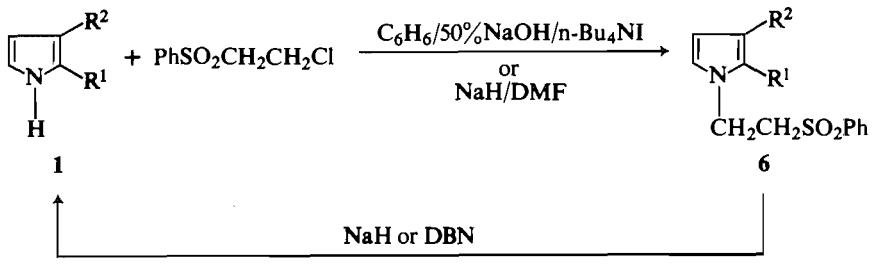

SCHEME 2

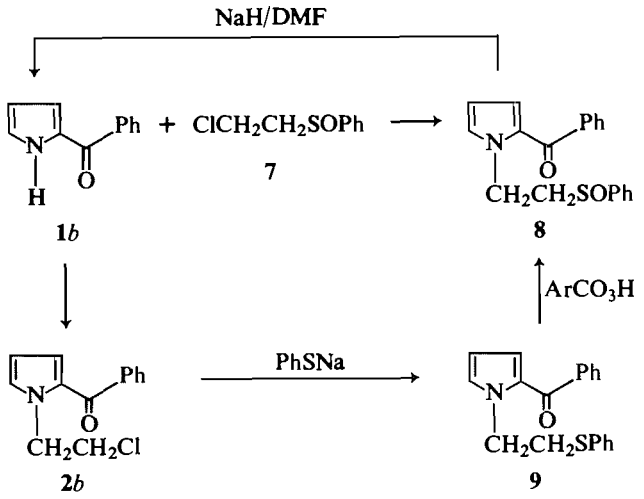

SCHEME 3

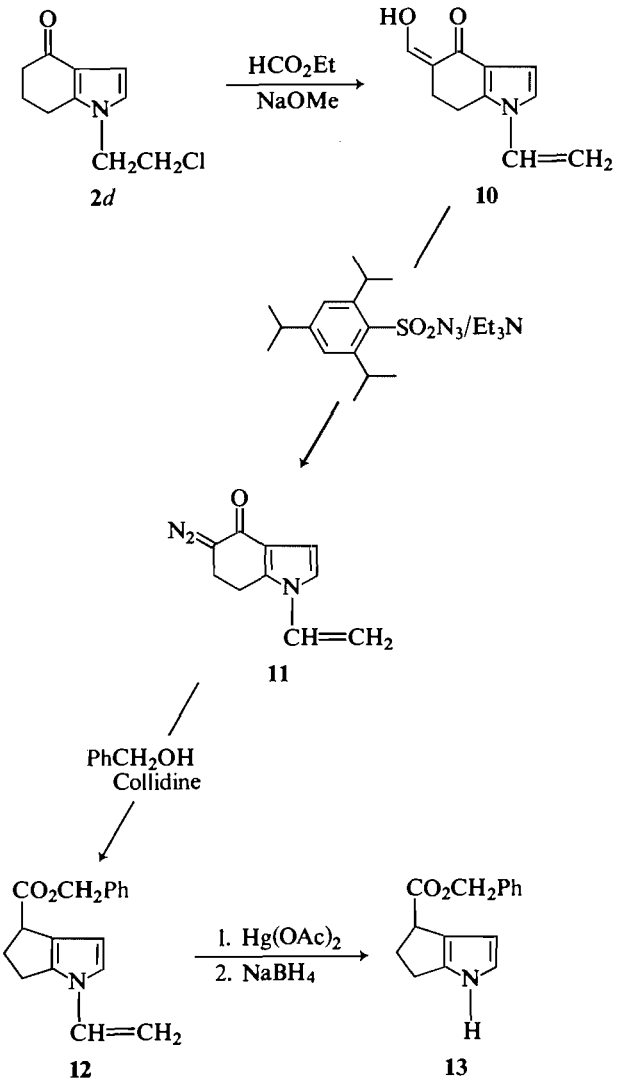

SCHEME 4

pared directly from 2-benzoylpyrrole and 2-phenylsulfinylethyl chloride **7**, or by *m*-chloroperbenzoic acid oxidation of the sulfide **9**. Although the sulfoxide **8** was converted into the *N*-vinyl compound **3***b* on heating in xylene containing excess pyridine, the removal of the *N*-2-phenylsulfinylethyl group was best effected under reverse Michael conditions using sodium hydride as the base. Thus, the use of the 2-phenylsulfinylethyl moiety as a means of protecting the 1-position of pyrroles is at least feasible.

Except for their sensitivity to strong bases and powerful nucleophiles, the susceptibility of *N*-(2-chloroethyl)pyrroles to various reaction conditions parallels that of the corresponding *N*-alkylpyrroles. Thus, those N-protected pyrroles not bearing a deactivating substituent can be acylated (e.g. with ethyloxalyl chloride (9)), and 2-acylpyrroles can be methoxymethylated at C-4 in strongly acidic media (e.g., dimethoxymethane/hydrochloric acid (1 *N*) in acetic acid – benzene/reflux (9)), or reduced with sodium borohydride in methanol solution ($\leq$ 0°C) to the alcohol without affecting the protecting group.[8] As implied by the latter reaction, the 2-chloroethyl group is relatively stable to methanolic sodium hydroxide but more vigorous conditions (sodium methoxide in tetrahydrofuran/room temperature (see below)) cause dehydrohalogenation to the *N*-vinyl compounds, which are, however, resistant to further degradation under these conditions. Indeed, provided that the reaction medium is basic, the *N*-vinyl moiety is also a useful protecting group (see below). The chloro group can be displaced by powerful nucleophiles. Of particular interest is the conversion of *N*-(2-chloroethyl)-2-benzoylpyrrole **2***b* into the sulfide **9** with sodium thiophenolate. The *N*-(2-phenylsulfenylethyl) moiety is itself a useful blocking group which has the added advantage that it is not susceptible to degradation by bases. It can be removed after oxidation to the sulfoxide (see above) or the sulfone.

The synthesis of benzyl cyclopenta[*b*]pyrrole-5-carboxylate **13** in five steps from 1-(2-chloroethyl)-4-oxotetrahydroindole **2***d* is illustrative of the utility of the 2-chloroethyl protecting group. Thus, the sodium methoxide promoted reaction of **2***d* with ethyl formate, in tetrahydrofuran solution at room temperature, caused both formylation at C-6 and dehydrohalogenation of the chloroethyl moiety. The generation of the *N*-vinyl group at this early stage in the reaction sequence

[8]E. Velarde and R. Salas, unpublished observations.

Can. J. Chem. Downloaded from www.nrcresearchpress.com by 210.87.254.40 on 09/06/12
For personal use only.

Can. J. Chem. Downloaded from www.nrcresearchpress.com by 210.87.254.40 on 09/06/12
For personal use only.

was not problematical because the subsequent steps, prior to deprotection, were effected under basic conditions. The *N*-vinyl hydroxymethylene ketone **10** was converted into the α-diazoketone **14** with 2,4,6-triisopropylbenzenesulfonyl azide in the presence of triethylamine and the diazo compound was transformed into the ring-contracted benzyl ester **12** in hot (175°C) collidine containing benzyl alcohol. Cleavage of the vinyl group from **12** by prior hydration to the carbinolamine was not possible because of the sensitivity of this pyrrole, and presumably other non-inductively stabilized pyrroles, to degradation under acidic conditions. The acetoxymercuration procedure, though not optimized, obviated this difficulty. It is noteworthy that the synthesis of **13** could not be accomplished without blocking the pyrrole nitrogen atom of **1***d*.

Experimental

The melting points were determined in a Mel-Temp apparatus and are corrected. The infrared spectra were measured in chloroform solution with a Perkin–Elmer model 237 grating infrared spectrophotometer. The ultraviolet spectra were recorded in methanol with a Perkin–Elmer model 402 ultraviolet visible spectrometer. The nmr spectra were obtained with a Varian T-60 spectrometer in deuteriochloroform solution. The chemical shifts are expressed as ppm (δ) from internal tetramethylsilane. The high resolution mass spectrum was obtained with a Varian MAT 311A spectrometer.

Starting materials

Pyrrole-2-carboxaldehyde was purchased from the Aldrich Chemical Co. Literature procedures were followed to prepare 2-benzoylpyrrole (10), 2-methylthiopyrrole (11), 4-oxo-4,5,6,7-tetrahydroindole (12), 2-phenylsulfenylethyl chloride (13), 2-phenylsulfinylethyl chloride (14), and 2-phenylsulfonylethyl chloride (15).

*Synthesis of 1-(2-chloroethyl)pyrroles. 1-(2-Chloroethyl)pyrrole-2-carboxaldehyde, 2*a

The synthesis of compound **2***a* was typical. Fifty percent aqueous sodium hydroxide (5 mL) was added, at 0°C, to a stirred solution of pyrrole-2-carboxaldehyde (0.500 g, 5.26 mmol) and tetrabutylammonium iodide (1.89 g, 1 equiv.) in 1,2-dichloroethane (10 mL). For all cases except **2***c* (see below), the mixture was then heated to reflux temperature, with vigorous stirring, where it was maintained for 1 h. For **2***c* the reaction mixture was kept at room temperature for 8 h. The cooled mixture was diluted with water and extracted with dichloromethane. The organic phase was washed successively with 2 *N* hydrochloric acid and water and then it was dried over sodium sulfate and evaporated *in vacuo*. The residue was percolated through a short column of silica gel using hexane – ethyl acetate (85:15) as the percolating solvent. The product was obtained as a colorless oil (0.780 g, 94%) homogeneous by tlc; uv: 207 (2400), 258 (7410), 288 (14 500) nm; ir: 1660 cm $^{-1}$; nmr δ: 3.75 (t, 2H, J = 7 Hz), 4.60 (t, 2H, J = 7 Hz), 6.10 (dd, 1H, $J_{3,4}$ = 4.0 Hz, $J_{4,5}$ = 2.5 Hz), 7.06 (m, 2H), 9.40 (s, 1H). The physical data for this and all the other compounds are found in Table 1.

Synthesis of 1-(2-phenylsulfonylethyl)pyrroles

A. *Phase transfer technique. 1-(2-Phenylsulfonylethyl)-2-benzoylpyrrole* **6**b

The general procedure is exemplified by that used for the title compound. The process utilized was identical to that described for the synthesis of compound **2***a* except that 2-phenylsulfonylethyl chloride (3 equiv.) in benzene solution was used. The product was purified by percolation through silica gel using hexane – ethyl acetate (3:2) as the percolating solvent; uv: 221 (12 600), 251 (8510), 265 sh (6370), 273 (6170), 305 (13 800) nm; ir: 1625 cm $^{-1}$; nmr δ: 3.43 (t, 3H, J = 7 Hz), 4.60 (t, 3H, J = 7 Hz), 6.16 (dd, 1H, $J_{3,4}$ = 4.0 Hz, $J_{4,5}$ = 3.0 Hz), 6.73 (dd, 1H, $J_{3,4}$ = 4.0 Hz, $J_{3,5}$ = 1.6 Hz), 6.97 (t, $J_{4,5}$ = 3.0 Hz, $J_{3,5}$ = 1.6 Hz), 7.17–7.93 (m, 10H).

B. *From the sodium salt of the pyrrole in DMF solution. 1-(2-Phenylsulfonylethyl)-4-oxo-4,5,6,7-tetrahydroindole* **6**d

The oxo compound **1***d* (0.500 g, 3.7 mmol) was added to a stirred suspension of 50% sodium hydride (in mineral oil, 0.098 g, 1.1 equiv.) in anhydrous DMF (5 mL) maintained in a nitrogen atmosphere at room temperature. When gas evolution had ceased, 2-phenylsulfonylethyl chloride (1.51 g, 2 equiv.) was added and stirring was continued for 16 h. The solvent was removed *in vacuo* (for compounds **6***a* and **6***c*, the mixture was diluted with ether (60 mL) and washed with water) and ethyl acetate was added to the residue. The mixture was filtered, and the filtrate was dried over sodium sulfate and evaporated *in vacuo*. The residue was subjected to tlc on silica gel using hexane – ethyl acetate (3:7) as the developing solvent. The tlc pure solid was obtained in 91% yield; uv: 219 (15 500), 250 (10 500), 266 (8510), 272 (8510) nm; ir: 1660 cm $^{-1}$; nmr δ: 1.93–2.97 (m, 6H), 3.15 (t, 2H, J = 7.5 Hz), 4.34 (t, 2H, J = 7.5 Hz), 6.53 (s, 2H), 7.54–8.02 (m, 5H).

1-(2-Phenylsulfinylethyl)-2-benzoylpyrrole 8

A. *Phase transfer technique*

The synthesis of **8** was carried out as described for **6***b* except that the alkylation was effected with 2-phenylsulfinylethyl chloride (1.1 equiv.) at room temperature (benzene) for 24 h. The crude product was subjected to column chromatography on silica gel using hexane – ethyl acetate (3:2) as the developing solvent to give the sulfoxide **8** in 86% yield; uv: 212 (12 600), 248 (9550), 305 (10 700) nm; ir: 1620 cm^{-1}; nmr δ: 3.34 (m, 2H, J = 6.6, 14 Hz), 4.74 (t, 2H, J = 6.6 Hz), 6.13 (dd, 1H, $J_{3,4}$ = 3.9 Hz, $J_{4,5}$ = 2.6 Hz), 6.70 (dd, 1H, $J_{3,4}$ = 3.9 Hz, $J_{3,5}$ = 1.8 Hz), 7.05 (t, 1H, $J_{4,5}$ = 2.6 Hz, $J_{3,5}$ = 1.8 Hz), 7.28–7.75 (m, 10H).

B. m-*Chloroperbenzoic acid oxidation of* **9**

m-Chloroperbenzoic acid (85%, 0.217 g, 1.07 mmol) was added portionwise to a stirred solution of the sulfide **9** (0.330 g, 0.98 mmol) in anhydrous dichloromethane (50 mL) cooled in an ice-bath. One hour following the completion of the addition an additional quantity of the oxidant (0.040 g) was added to consume a small amount of starting material shown to be present by tlc. After a further 20 min the solution was washed with saturated sodium bicarbonate solution, and the organic phase was combined with a dichloromethane extract of the aqueous phase and dried over sodium sulfate. The solvent was removed *in vacuo* leaving an oil (0.277 g, 88%) which was spectroscopically identical to the sulfoxide **8** prepared by method A.

1-(2-Phenylsulfenylethyl)-2-benzoylpyrrole 9

Sodium hydride in mineral oil (50%, 0.239 g, 4.98 mmol) was added to a stirred solution of thiophenol (0.500 g, 4.55 mmol) in anhydrous DMF (10 mL) maintained in a nitrogen atmosphere. After 1 h, 1-(2-chloroethyl)-2-benzoylpyrrole (1.166 g, 4.79 mmol) was added all at once and stirring was continued for 2 h. The solution was diluted with ether and then washed well with water. The organic phase was dried over sodium sulfate and evaporated *in vacuo*. The residue was subjected to tlc on silica gel using hexane – ethyl acetate as the eluting solvent. The product (1.24 g, 88%) was obtained as an oil; uv: 213 (17 400), 253 (15 500), 306 (13 800) nm; ir: 1628, 1578, 1525 cm^{-1}; nmr δ: 3.42 (t, 2H, J = 6.7 Hz), 4.61 (t, 2H, J = 6.7 Hz), 6.17 (dd, 1H, $J_{3,4}$ = 4.0 Hz, $J_{4,5}$ = 3.0 Hz), 6.75 (dd, 1H, $J_{3,4}$ = 4.0 Hz, $J_{3,5}$ = 1.6 Hz), 6.79 (t, 1H), 7.17–7.87 (m, 10H).

Deprotection of the N-*(2-chloroethyl)pyrroles*

A. *Conversion of* N-*(2-chloroethyl)pyrrole-2-carboxaldehyde* **2**a *into pyrrole-2-carboxaldehyde* **1**a

Sodium hydride (60%, 0.139 g, 3.48 mmol) was added to a stirred solution of the chloro compound (0.500 g, 3.18 mmol) in dry acetonitrile (15 mL) maintained in a nitrogen atmosphere. The solution was heated at 50°C for 2 h, cooled to room temperature, and 6 *M* hydrochloric acid (5.3 mL, 31.8 mmol) was added dropwise. After 6 h at room temperature, a solution of sodium acetate (2.9 g, 35.4 mmol) in water (5 mL) was added and the solution was heated at reflux temperature for 0.5 h. The solution was diluted with water and then extracted with ether. The extract was washed with water, dried over

Can. J. Chem. Downloaded from www.nrcresearchpress.com by 210.87.254.40 on 09/06/12
For personal use only.

sodium sulfate, and evaporated *in vacuo*. The crude product was subjected to tlc on silica gel using hexane – ethyl acetate (9:1) as the developing solvent. The product (0.182 g, 71%, tlc homogeneous) was crystallized from dichloromethane–hexane to give the aldehyde (0.166 g) with mp 42–43°C.

B. *Conversion of* N-*(2-chloroethyl)-2-benzoylpyrrole* **2**b *into 2-benzoylpyrrole* **1**b

Sodium hydride in mineral oil (60%, 0.038 g, 0.95 mmol) was added, at 50°C, to a stirred solution of the chloro compound (0.200 g, 0.86 mmol) in dry acetonitrile (15 mL) maintained in a nitrogen atmosphere. After 0.5 h at this temperature, 50% hydrochloric acid (3 mL, 18 mmol) was added. After an additional 0.5 h, a solution of sodium acetate (1.91 g, 23 mmol) in water (2.5 mL) was added and the solution was heated at reflux temperature for 0.25 h. The cooled solution was extracted with dichloromethane, and the extract was dried over sodium sulfate and evaporated *in vacuo* to give 2-benzoylpyrrole (0.124 g, 85%) with mp 76–77°C.

Deprotection of the N-*(2-phenylsulfonylethyl)pyrroles*

A. *Sodium hydride*

Sodium hydride in mineral oil (60%, 1.1 equiv.) was added to a stirred solution of the phenylsulfonyl compound (1 equiv.) in anhydrous dimethylformamide (7 mL/mmol) at room temperature (nitrogen atmosphere). After 2.5 h the solution was diluted with ether, the mixture was washed with water, and the organic phase was dried over sodium sulfate and evaporated *in vacuo*. The crude product was purified by crystallization (dichloromethane–hexane for 2-benzoylpyrrole) or column chromatography on silica gel (hexane – ethyl acetate (4:1); 2-formylpyrrole) followed by crystallization (ether–hexane; 2-formylpyrrole).

B. *Diazabicyclo[4.3.0]non-5-ene*

The procedure was identical to that described above except that diazabicyclo[4.3.0]non-5-ene (5–7 equiv.) and diethylamine (10 equiv.) were used instead of sodium hydride. In this way, 2-benzoylpyrrole was obtained in 83% yield, after tlc on silica gel using hexane – ethyl acetate (4:1) as the eluting solvent followed by crystallization as above.

Conversion of N-*(2-phenylsulfinylethyl)-2-benzoylpyrrole* **8** *into 2-benzoylpyrrole*

A solution of the sulfoxide **8** (0.600 g, 1.86 mmol) in anhydrous DMF (5 mL) was added to a stirred suspension of 60% sodium hydride (in mineral oil, 0.082 g, 2.05 mmol) in dry DMF (10 mL) maintained in an atmosphere of nitrogen. After 4 h at room temperature, water was added and the product was extracted into ethyl acetate. The aqueous phase was saturated with sodium chloride and extracted with benzene. The combined extracts were dried over sodium sulfate and evaporated *in vacuo*. The residue was purified by tlc on silica gel using hexane–ether (2:3) as the developing solvent. This process yielded 2-benzoyl pyrrole (0.290 g, 91%) with mp 78°C.

1-Vinyl-4-oxo-4,5,6,7-tetrahydroindole-4-carboxaldehyde **10**

A solution of the chloro compound **2***d* (14.2 g, 71.8 mmol) in dry tetrahydrofuran (40 mL) was added to a stirred suspension of sodium methoxide (15.5 g, 290 mmol) in anhydrous tetrahydrofuran (100 mL) containing anhydrous ethyl formate (21.5 g, 290 mmol). After 2 h at room temperature, water was added and the solution was acidified to pH 4 with 1 *M* hydrochloric acid. The product was extracted into ethyl acetate, and the extract was dried over sodium sulfate and evaporated *in vacuo*. The solid which remained was crystallized from ethyl acetate – hexane to give material (12.7 g, 93%) with mp 98.5–100°C; uv: 239 (14 500), 274 (12 600), 322 sh (5010) nm; ir: 1641, 1585 cm^{-1}; nmr δ: 2.72 (m, 4H), 4.95 (d, 1H, J_{cis} = 9.0 Hz), 5.28 (d, 1H, J_{trans} = 15.4 Hz), 6.68 (d, 1H, $J_{2,3}$ = 3.1 Hz), 6.86–7.25 (m, 1H), 7.06 (d, 1H, $J_{2,3}$ = 3.1 Hz), 7.32 (s, 1H). *Anal.* calcd. for $C_{11}H_{11}NO_2$: C 69.83, H 5.86, N 7.40; found: C 69.56, H 5.94, N 7.47.

1-Vinyl-4-oxo-5-diazo-4,5,6,7-tetrahydroindole **11**

A suspension of 2,4,6-triisopropylbenzenesulfonyl azide (15) (22.8 g, 73.8 mmol) in anhydrous dichloromethane (40 mL) was added to a stirred solution of **10** (12.7 g, 67.1 mmol) in dry dichloromethane (100 mL) containing triethylamine (14.1 g, 141 mmol) at 0°C. The mixture was stirred at room temperature for 20 h, water was added, and the organic phase was dried and evaporated *in vacuo*. The residue was subjected to column chromatography on neutral alumina (500 g, Fluka, Act II) and the product (9.5 g, 76%) was eluted with ethyl acetate – hexane (1:1). On crystallization from ethyl acetate – hexane, a bright yellow solid was obtained with mp 84–86°C; uv: 206 (6150), 241 (9190), 269 sh (6150), 326 (8820) nm; ir: 2055, 1650, 1615 cm^{-1}; nmr δ: 3.01 (m, 4H), 4.93 (dd, 1H, J_{gem} = 1.1 Hz, J_{cis} = 9.0 Hz), 5.26 (dd, 1H, J_{gem} = 1.1 Hz, J_{trans} = 15.6 Hz), 6.67 (d, 1H, $J_{2,3}$ = 3.1 Hz), 6.81–7.07 (m, 1H), 6.99 (d, 1H, $J_{2,3}$ = 3.1 Hz). *Exact Mass* (high resolution mass spectrum) calcd. for $C_{10}H_9N_3O$: 187.0746; found (ms): 187.0749.

Benzyl 1-vinylcyclopenta[b]pyrrole-5-carboxylate **12**

A solution of the diazo compound (3.47 g, 17.6 mmol) in collidine (15 mL) containing benzyl alcohol (6 mL) was heated in an oil bath maintained at 175°C for 20 min. The cooled solution was diluted with ether, washed with 1 *N* hydrochloric acid, dried, and evaporated *in vacuo*. The residue was subjected to column chromatography on silica gel using hexane – ethyl acetate (7:3) to elute the oily, somewhat unstable product (1.93 g, 41%); uv: 217 (13 700), 248 (14 600) nm; ir: 1734, 1651 cm^{-1}; nmr δ: 2.79–3.07 (m, 2H), 3.90 (m, 1H), 4.62 (dd, 1H, J_{gem} = 1.3 Hz, J_{cis} = 9.7 Hz), 5.03 (dd, 1H, J_{gem} = 1.3 Hz, J_{trans} = 15.3 Hz), 5.21 (s, 2H), 6.14 (d, 1H, $J_{2,3}$ = 3.0 Hz), 6.76 (dd, 2H, J_{cis} = 9.7 Hz, J_{trans} = 15.3 Hz), 6.85 (d, 1H, $J_{2,3}$ = 3.0 Hz), 7.43 (s, 5H); mass spectrum *m/e* 267 (M^+). *Anal.* calcd. for $C_{17}H_{17}NO_2$: C 76.38, H 6.41, N 5.24; found: C 75.92, H 6.53, N 5.11.

Benzyl cyclopenta[b]pyrrole-5-carboxylate **13**

A solution of the *N*-vinyl compound **12** (1.00 g, 37.5 mmol) in acetonitrile (25 mL) was added to a solution of mercuric acetate (3.7 g, 106 mmol) in 10% aqueous acetonitrile (25 mL) and the solution was stirred at room temperature until the reaction was complete by tlc (0.5 h). Sodium borohydride (0.57 g) was then added in portions and, when the vigorous reaction had subsided, the mixture was filtered through Celite. The filtrate was diluted with saturated sodium chloride solution and extracted with ethyl acetate. The extract was dried, the solvent was removed *in vacuo*, and the residue was percolated through a short column of silica gel using hexane – ethyl acetate as the percolating solvent mixture. The product (0.593 g, 66%) was obtained as an oil; uv: 217 (8910), 241 (5750), 266 (457), 268 (309) nm; ir: 3515, 3420, 1733 cm^{-1}; nmr δ: 2.78 (m, 4H), 3.77–4.09 (m, 1H), 5.18 (s, 2H), 6.06 (d (after D_2O exchange), 1H, J = 2.8 Hz), 6.69 (d (after D_2O exchange), 1H, J = 2.8 Hz), 7.41 (s, 5H). *Anal.* calcd. for $C_{15}H_{15}NO_2$: C 74.67, H 6.27, N 5.81; found: C 74.99, H 6.36, N 5.67.

1. (*a*) S. Baroni, R. Stradi, and M. J. Saccarello. J. Heterocycl. Chem. **17**, 1221 (1980); (*b*) W. A. Remers, R. H. Roth, G. J. Gibbs, and M. J. Weiss. J. Org. Chem. **36**, 1232 (1971); **36**, 1241 (1971); (*c*) D. P. Schumacher and S. S. Hall. J. Org. Chem. **46**, 5060 (1981).
2. M. I. Jones, C. Froussois, and D. A. Evans. J. Chem. Soc. Chem. Commun. 472 (1976).
3. H. J. Anderson and J. K. Groves. Tetrahedron Lett. 3165 (1971).
4. R. X. Xu, H. J. Anderson, N. J. Gogan, C. E. Loader, and R. McDonald. Tetrahedron Lett. **22**, 4899 (1981); J. Rokach, P. Hamel, M. Kakushima, and G. M. Smith. Tetrahedron Lett. **22**, 4901 (1981).
5. G. R. Martinez, P. A. Grieco, and C. V. Srinivasan. J. Org. Chem. **46**, 3760 (1981).
6. J. Ackrell, F. Franco, R. Greenhouse, A. Guzmán, and J. M. Muchowski. J. Hetereocycl. Chem. **17**, 1081 (1980).
7. E. S. Domina, N. P. Glazkova, G. G. Skvortsova, and M. F. Shostakovskii. Khim. Atsetilena, 203 (1968); Chem Abstr. **71**, 61120b (1969).
8. M. Balgobin, S. Josephson, and J. B. Chattopadhyaya. Tet-

rahedron Lett. **22**, 1915 (1981).
9. H. CARPIO, E. GALEAZZI, R. GREENHOUSE, A. GUZMÁN, E. VELARDE, Y. ANTONIO, A. LEON, V. PÉREZ, R. SALAS, D. VALDES, J. ACKRELL, D. CHO, P. GALLEGRA, O. HALPERN, R. KOEHLER, M. L. MADDOX, J. M. MUCHOWSKI, A. PRINCE, D. TEGG, T. C. THURBER, A. R. VAN HORN, and D. WREN. Can. J. Chem. **60**, 2295 (1982).
10. J. WHITE and G. MCGILLIVRAY. J. Org. Chem. **42**, 4248 (1977).
11. F. FRANCO, R. GREENHOUSE, and J. M. MUCHOWSKI. J. Org. Chem. **47**, 1682 (1982).
12. J. M. BOBBIT, C. L. KULKARNI, C. P. DUTTA, H. KOFOD, and K. M. CHIONG. J. Org. Chem. **43**, 3541 (1978).
13. A. H. FORD-MOORE, R. A. PETERS, and R. W. WAKELIN. J. Chem. Soc. 1754 (1949).
14. F. G. BORDWELL and W. T. BRANNEN. J. Am. Chem. Soc. **86**, 4645 (1964).
15. R. E. HARMON, G. WELLMAN, and S. K. GUPTA. J. Org. Chem. **38**, 11 (1973).

Can. J. Chem. Downloaded from www.nrcresearchpress.com by 210.87.254.40 on 09/06/12
For personal use only.

Sulphurous negative ions in a fuel-rich, CH_4-O_2 flame with OCS additive

JOHN M. GOODINGS, KAMAL ELGUINDI, AND DIETHARD K. BOHME
Department of Chemistry, York University, 4700 Keele Street, Downsview, Ont., Canada M3J 1P3

Received December 15, 1982

JOHN M. GOODINGS, KAMAL ELGUINDI, and DIETHARD K. BOHME. Can. J. Chem. **61**, 1703 (1983).

Sulphurous negative ions S^-, SH^-, SO^-, SO_2^-/S_2^-, SO_3^-, HSO_3^-, SO_4^-, and HSO_4^- were observed when 0.2% of carbonyl sulphide (OCS) was added to a conical, laminar, premixed, fuel-rich (equivalence ratio $\phi = 2.15$) CH_4-O_2 flame burning at atmospheric pressure. Profiles were obtained of ion concentration vs. distance along the flame axis by sampling the flame through a pinhole into a quadrupole mass spectrometer. Some of the ion signals observed in the flame reaction zone are very large, particularly that for HSO_4^-. None of the sulphurous ions detected contain carbon. Of those listed above, only S^-, SH^-, SO^-, and SO_2^- persist downstream through the burnt gas. The sulphurous ions are formed by chemical ionization processes of neutral sulphurous intermediates reacting with the naturally-occurring ions present in any hydrocarbon flame. The ion chemistry is discussed, as is the underlying neutral chemistry of sulphur relevant to the flame environment. The ion profiles show the rapidity with which OCS is oxidized through SH and SO to SO_2 even within the reaction zone of this fuel-rich flame. No evidence was obtained for the presence of sulphuric or sulphurous acids, and the presence of S_2 was not confirmed.

JOHN M. GOODINGS, KAMAL ELGUINDI et DIETHARD K. BOHME. Can. J. Chem. **61**, 1703 (1983).

On a observé des ions sulfureux négatifs: S^-, SH^-, SO^-, SO_2^-/S_2^-, SO_3^-, HSO_3^-, SO_4^- et HSO_4^- lorsqu'on ajoute 0,2% de sulfure de carbonyle (OCS) à la flamme de CH_4-O_2, conique, laminaire, prémélangée et enrichie (rapport d'équivalence $\phi = 2,15$) brûlant à la pression atmosphérique. On a obtenu les profils de la concentration en ions en fonction de la distance le long de l'axe de la flamme en injectant des échantillons de flamme à travers un trou d'épingle dans un spectromètre de masse quadrupolaire. Quelques uns des signaux observés dans la zone de réaction de flamme sont très intenses, particulièrement ceux du HSO_4^-. Les ions sulfureux détectés ne contiennent pas de carbone. Parmi ceux mentionnés, seuls S^-, SH^-, SO^- et SO_2^- existent encore dans le courant gazeux qui brûle. Les ions sulfureux se forment par ionisation chimique des intermédiaires sulfureux neutres qui réagissent avec les ions que l'on trouve habituellement dans n'importe quelle flamme d'hydrocarbure. On discute de la chimie de l'ion en tant que chimie neutre sous-jacente du soufre se rapportant à l'environnement de la flamme. Les profils de l'ion révèlent la rapidité avec laquelle le OCS est oxydé par l'intermédiaire du SH et du SO en SO_2 même à l'intérieur de la zone de réaction de cette flamme riche en combustible. On n'a pas de preuve de la présence d'acides sulfuriques ou sulfureux, et on n'a pas pu confirmer la présence de S_2.

[Traduit par le journal]

Introduction

The release of sulphur compounds into the troposphere through the use of sulphur-bearing fossil fuels for industrial and domestic heating, power generation, and transportation constitutes the major man-made sources of air contaminants. The effects on human health and vegetation have long been recognized. Besides being phytotoxic with the obvious damage to plants through acid rain, high levels of sulphur compounds have been linked to a variety of environmental and health problems (1). For example, SO_2 is a severe irritant to the eyes, mucous membranes, and skin, the irritant effects being caused by the rapidity with which SO_2 forms sulphurous acid on contact with moist surfaces. Present measures to combat SO_x emissions from combustion operations through the selection of low-sulphur fuels or by sulphur removal from the exhaust are costly. The inevitable need to use high-sulphur coal in the future points to the desirability of controlling sulphur emissions at the source.

This work attempts to trace the early chemistry of formation of sulphur compounds in a hydrocarbon flame. Sulphur ions resulting from the reaction of naturally-occurring flame ions with sulphurous neutral species are detected by sampling the flame at atmospheric pressure into a mass spectrometer. These ions, produced from fast ion–molecule reactions, can be used as an in-situ probe of the underlying neutral chemistry of combustion. The objective of this phase of the study is to explore the formation and disappearance of negative sulphurous ions in, and downstream of, the reaction zone of a fuel-rich, CH_4-O_2 flame doped with 0.2% of carbonyl sulphide (OCS). Pairs of ion concentration profiles are measured along the axis of conical flames with and without OCS additive to reveal the presence of sulphurous ions. Both the neutral chemistry and the ion chemistry of sulphur relevant to the flame are discussed.

Experimental

All of the ion concentration measurements were performed on the same CH_4-O_2 flame of fuel-rich composition (equivalence ratio $\phi = 2.15$) whose ion chemistry we have studied extensively in the past (2, 3). It was of the laminar premixed type with a conical luminous reaction zone (height $\approx$ 5 mm, base diameter $\approx$ 3 mm, thickness $\approx$ 0.3 mm) to facilitate ionic sampling along the flame axis into a mass spectrometer. The flame has an adiabatic flame temperature of 2460 K and a burnt gas velocity of approximately 1 m s^{-1}. It was stabilized at atmospheric pressure on a simple, tubular, quartz burner (2.3 mm id) surrounded by a flowing argon shield to minimize the entrainment of atmospheric air. For this work, provision was made to add 0.22 mol% of OCS to the premixed gas; it could be added or removed without altering the flame. All gases were used straight from the cylinders without further purification ($CH_4 > 99.0\%$, $O_2 > 99.6\%$, Ar $> 99.9\%$, OCS $> 97.5\%$). The burner was mounted on a motor-driven carriage with accurate axial alignment and calibrated drive providing spatial resolution of ± 0.02 mm along the flame axis (designated z) for ion profile measurements.

The flame – ion mass spectrometer has been described previously in detail (2). The flame burned against a 60°, conical, chromium, sampling nozzle of orifice diameter ca. 0.1 mm mounted in a water-cooled flange of the type described by Hayhurst and Telford (4). The sampled ions pass through two stages of differential pumping into a quadrupole mass filter. The mass-analyzed ions are detected with a parallel-plate Faraday cage connected to a vibrating reed electrometer having a grid-leak resistance of 10^{11} ohms. The ion signal magnitudes in the figures are quoted in volts based on the detected ion current passing through 10^{11} ohms. We have adopted a normalization technique different from that used previously. The profiles shown in the figures include a correction for mass discrimination in the filter against

Can. J. Chem. Downloaded from www.nrcresearchpress.com by 210.87.254.6 on 09/06/12
For personal use only.

Can. J. Chem. Downloaded from www.nrcresearchpress.com by 210.87.254.6 on 09/06/12
For personal use only.

ions of high m/e measured at high resolving power (unit resolution); the mass discrimination increases with increasing resolving power. The groups of negative sulphurous ions are sufficiently well spaced such that each group could be measured at very low resolving power as a broad single "peak". The individual m/e's within a group measured at high resolving power are normalized to the signal magnitude of the "peak" at low resolving power. The $H_xSO_4^-$ group yields the largest negative ion signal we have ever observed. The dynamic range of sensitivity of the apparatus is five orders of magnitude. A method has been described (2, 5) for locating a reproducible origin ($z = 0$) in the *flame* (not referred to the burner) corresponding to the downstream edge of the luminous reaction zone on the flame axis. In this way, a family of ion profiles at different mass numbers m/e can be accurately overlaid on the distance scale z.

It should be pointed out that some ion signals are subject to distortion during sampling by the mass spectrometer. The flame gas is cooled in passing through the thermal boundary layer surrounding the sampling orifice, and again during the expansion to supersonic velocity which proceeds for a few orifice diameters just inside the sampling nozzle. This can affect the signal ratio of two ions participating in a fast ion–molecule reaction having a reaction time (relaxation time) comparable to, or less than, the sampling time (of order 1 μs). In these circumstances, the ratio will change to some extent during sampling in favour of the product ion in the exothermic direction of the reaction. An extreme case is the production of hydrate ions, since a large water concentration in the flame produces a high rate of hydration. In the present study where some of the sulphurous ions of relatively high molecular weight may result from clustering reactions with sulphur dioxide, their signals may be enhanced by cooling during sampling. However, such enhancements are not expected to affect the interpretation of the sulphurous flame chemistry. These sampling effects for flames have been discussed in a series of papers by Hayhurst *et al.* of which refs. 6–8 are particularly relevant.

Neutral sulphur chemistry in hydrocarbon flames

A complete review of the reactions of neutral sulphurous species will not be attempted here. However, relevant reactions studied by a number of workers are listed in Table 1; where the temperature dependence is known, the rate constants have been calculated at 2000 K. The reactions are drawn from Westley's table of recommended rate constants for chemical reactions occurring in combustion (9). The sulphur chemistry is summarized in the reaction flow diagram given in Fig. 1.

Initially, the OCS additive is attacked by O and H atoms to form SO and SH, respectively (reactions [1] and [2]), whose rates may be nearly equal in our flame. In any case, SH is rapidly attacked by O in reaction [4*a*] to yield the same SO product. In turn, SO can react with O_2 or O (reactions [5*a*] and [6]) to give the major product SO_2. The back reaction [5*b*] can regenerate SO from SO_2, but should be very slow early in the reaction zone. The reaction of H with SO_2 does not regenerate SO, but adds rather slowly [7] to form HSO_2. This completes what might be regarded as the main-line sulphur chemistry; namely,

$$OCS \rightarrow (SH) \rightarrow SO \rightarrow SO_2$$

Sulphur is further involved in minor side-line chemistry. Sulphur atoms can be produced by H and O radical attack on both SO and SH (reactions [8*c*], [9*a*], [10*a*], and [4*b*]). However, SO is regenerated by reaction of S atoms with O_2 by [9*b*] or with OH by [8*a*]. The regeneration rate of SH by reaction [10*b*] involving S with H_2 may be comparable downstream despite its small rate constant due to the high concentration of H_2 (0.4 mole fraction) in the fuel-rich burnt gas (2).

As a second side-line, diatomic sulphur S_2 can be formed by reaction [11*a*] of S with SH, but is destroyed by the reverse reaction [11*b*] with H atoms. A further sink for S_2 is its reaction [12*b*] with O atoms to form SO; the reverse reaction [12*a*] as a source of S_2 can be disregarded. Reaction [3] of OCS with S is a significant source of S_2 only if the concentration of S becomes appreciable before OCS is exhausted. Thus, S_2 feeds back rapidly into the main-line sulphur chemistry, and its steady-state concentration in the fuel-rich flame is expected to be low.

A third side-line concerns H_2S. The only reaction listed by Westley (9) for its production is [13] involving the reaction of the SH radical with itself. However, several sink reactions are known for the destruction of H_2S by H, OH, and CH_3 radicals (reactions [14], [15], and [16], respectively). As an aside, we do have evidence for the presence of H_2S in the flame from the positive ion chemistry where we detect H_3S^+, presumably arising from proton transfer to H_2S. Under the fuel-rich flame conditions, it is possible that the reverse of reaction [14] constitutes the major source of H_2S since the concentration of H_2 is high in the burnt gas.

An obvious question is the degree to which the reactions are balanced in different parts of the flame linking the pairs of species SH/H_2S, SH/S, S_2/S, SO/S, and SO/SO_2. An indication is given by some of the ion profiles below which show a similar tailing out downstream in the burnt gas. It will be noted that Table 1 and Fig. 1 do not mention any sulphurous species containing carbon. Their inclusion is not thought to be warranted because, in general, the rates of reactions listed in Westley (9) of C, CH, CH_2, etc. with sulphurous species are low due to the small steady-state concentrations of the hydrocarbon neutrals. Also, addition reactions similar to [7] are known from the chemistry of the stratosphere near 220 K for the formation of HSO_3 from OH + SO_2 + M, and SO_3 from O + SO_2 + M (13, 14); the SO_3 so formed combines with water to form sulphuric acid. However, we do not have any evidence for these processes occurring at flame temperatures.

Results

Figure 2 shows total positive and total negative ion profiles with, and without, the injection of 0.2% of OCS into the premixed flame gas. In these and subsequent ion profile data, the conical flame is sampled into the mass spectrometer along its axis (distance z in mm); the flame reaction zone near the tip of the cone occupies the region from approximately $z = -0.3$ to 0 mm. The total positive ion profile shows little change in magnitude or peak shape with OCS injection. However, the total negative ion profile shows a dramatic increase in magnitude of the upstream peak (4. 5 ×) with the addition of 0.2% of OCS and a much greater persistance of the downstream peak into the burnt gas region of the flame.

Figures 3–7 inclusive present profiles for sulphurous negative ion species at individual m/e. Each figure gives data for a group of similar ions; the groups are ordered according to increasing mass. Figure 3 shows profiles for the H_xS^- group ($x = 0, 1$). In the absence of OCS, the profile at 32 amu is due to O_2^-, and shows a single peak upstream. With OCS injection, the profile becomes double-peaked. The upstream peak falls to a magnitude of one-third and shifts slightly in the downstream direction; evidently O_2^- acts as a source or reagent ion for the production of sulphurous negative ions by ion–molecule reactions. In addition, a new peak due to S^- appears downstream and tails out into the burnt gas. It is apparent from this and other profiles which show similar tailing behaviour that some of the sulphurous negative ions involve species of relatively high

TABLE 1. Neutral reactions involving sulphurous species relevant to the fuel-rich hydrocarbon flame doped with OCS

No.	Reactions	Rate constant[a]	T (K)[d]	Reference
[1]	$O + OCS \rightarrow SO + CO$	[d]4.1×10^{-12}	1 200	10
[2]	$H + OCS \rightarrow SH + CO$	[c]2.2×10^{-14}	298	10
[3]	$S + OCS \rightarrow S_2 + CO$	[c]1.0×10^{-12}	2 000	10
[4a]	$SH + O \rightarrow SO + H$	4.7×10^{-11}	2 000	11
[4b]	$\rightarrow S + OH$	1.4×10^{-13}	2 000	11
[5a]	$SO + O_2 \rightarrow SO_2 + O$	[c]1.5×10^{-13}	2 000	10
[5b]	$SO_2 + O \rightarrow SO + O_2$	[c]3.3×10^{-14}	2 000	10
[6]	$SO + O + M \rightarrow SO_2 + M$	[c]1.8×10^{-31}	298	10
[7]	$H + SO_2 + M \rightarrow HSO_2 + M$	[d]1.4×10^{-32}	2 000	10
[8a]	$S + OH \rightarrow SO + H$	4.7×10^{-11}	2 000	11
[8b]	$\rightarrow SH + O$	1.7×10^{-13}	2 000	11
[8c]	$SO + H \rightarrow S + OH$	1.1×10^{-12}	2 000	11
[9a]	$SO + O \rightarrow S + O_2$	3.7×10^{-12}	2 000	11
[9b]	$S + O_2 \rightarrow SO + O$	[c]2.3×10^{-12}	250–450	10
[10a]	$SH + H \rightarrow S + H_2$	[d]2.5×10^{-11}	298	10
[10b]	$S + H_2 \rightarrow SH + H$	[d]2.0×10^{-13}	2 000	10
[11a]	$S + SH \rightarrow S_2 + H$	4.7×10^{-11}	2 000	11
[11b]	$S_2 + H \rightarrow S + SH$	9.0×10^{-12}	2 000	11
[12a]	$S + SO \rightarrow S_2 + O$	1.5×10^{-13}	2 000	11
[12b]	$S_2 + O \rightarrow S + SO$	4.7×10^{-11}	2 000	11
[13]	$SH + SH \rightarrow H_2S + S$	[d]1.3×10^{-11}	295	10
[14]	$H_2S + H \rightarrow SH + H_2$	[d]2.1×10^{-12}	470	10
[15]	$H_2S + OH \rightarrow SH + H_2O$	[c]8.4×10^{-12}	900	10
[16]	$H_2S + CH_3 \rightarrow SH + CH_4$	1.1×10^{-14}	600	12

[a]Rate constants are given in units of cm^3 molecule^{-1} s^{-1}, or cm^6 molecule^{-2} s^{-1} where appropriate.
[b]Each rate constant has been calculated at a temperature as close to 2 000 K as the available data permit.
[c]Approximate uncertainty ≃ ±30%.
[d]Approximate uncertainty ≃ ±50%.
[e]Approximate uncertainty ≃ ±70%.

Can. J. Chem. Downloaded from www.nrcresearchpress.com by 210.87.254.6 on 09/06/12
For personal use only.

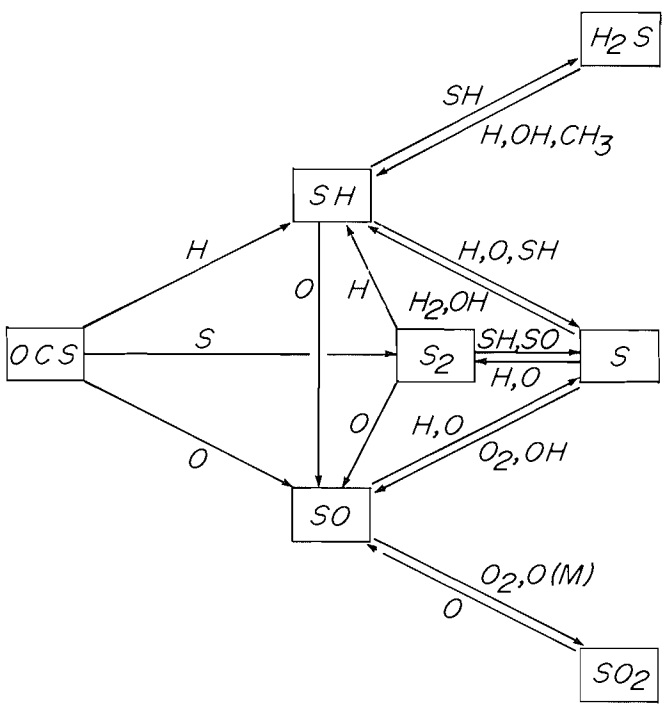

FIG. 1. Reaction scheme for sulphur chemistry in a fuel-rich, hydrocarbon flame.

electron affinity (EA) which can better withstand collisional electron detachment at the high temperature of the burnt gas.

In the absence of OCS, a small single peak is observed at 33 amu in the reaction zone due to HO_2^-. With OCS injection, the much larger double-peaked profile shown in Fig. 3 arises due to SH^- with a small contribution from $^{33}S^-$. Recall that sulphur has four stable isotopes; namely, ^{32}S (natural abundance = 95.0%), ^{33}S (0.76%), ^{34}S (4.22%), and ^{36}S (0.014%). Other isotopic species of sufficient natural abundance to make significant contributions to some of these profiles include deuterium D (0.015%), ^{17}O (0.037%), and ^{18}O (0.0204%). For example, the double-peaked profile at 34 amu can be derived from $^{32}SD^-$, $^{34}S^-$, and $^{33}SH^-$; these sulphurous species will account for all of the downstream portion, whereas the upstream peak is further complicated by a small and unknown contribution from the $O^-.H_2O$ hydrate. Similar considerations will apply to the profile at 35 amu, but in this case the profile magnitude indicates contributions from $OH^-.H_2O$ and also $^{35}Cl^-$ present as an impurity. The mass assignments including isotopic contributions for all of the negative sulphurous ion profiles measured are summarized by groups in Table 2.

Consider now the small, double-peaked profiles at 48 amu shown in Fig. 4. In the absence of OCS, the upstream and downstream peaks are attributed to O_3^- and C_4^-, respectively. With OCS injection, the decrease and shift of the upstream peak presumably indicates the involvement of O_3^- as a source of sulphurous negative ions, as noted above for O_2^-. The increase in the downstream peak may be indicative of SO^-. However, the clear evidence for SO^- is the tail of the profile which persists far downstream into the burnt gas. Corroborative evidence from $^{34}SO^-$ at 50 amu is obscured by the presence of $O_2^-.H_2O$.

With reference to Fig. 5, in the absence of OCS, the signal detected at 64 amu is negligible and that at 66 amu is very small. With OCS injection, the fairly large profile at 64 amu

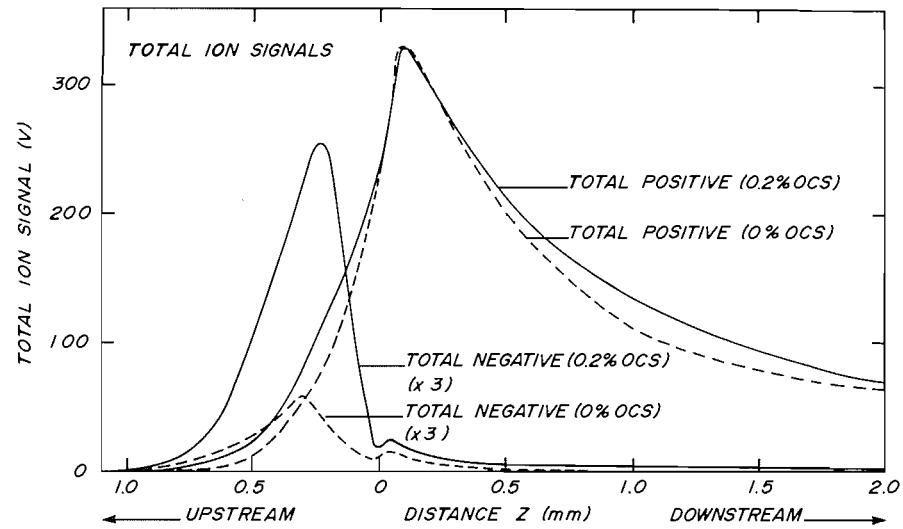

FIG. 2. Total positive and negative ion profiles with, and without, 0.2% OCS additive.

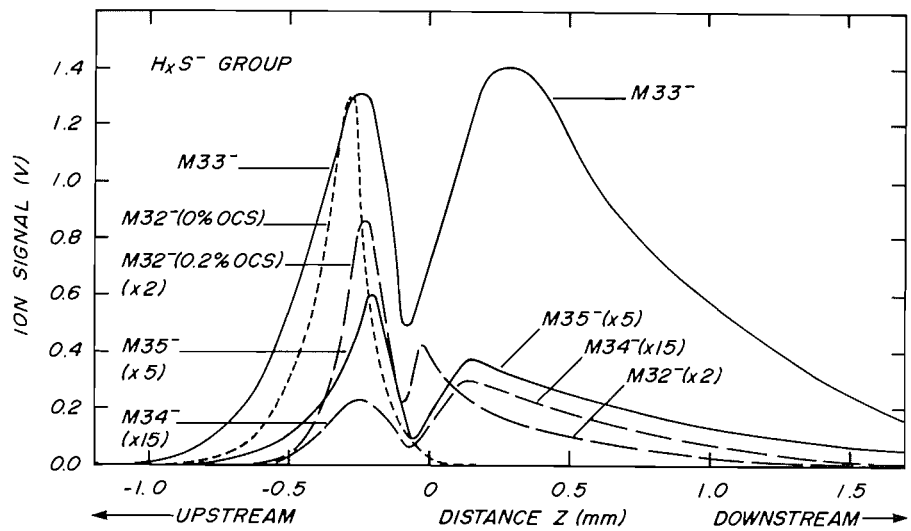

FIG. 3. Negative sulphurous ion profiles: isotopic species of S⁻ and SH⁻. All profiles are taken with the addition of 0.2% of OCS except for one profile at −32 amu as indicated.

could be attributed to SO_2^- or S_2^-. However, the relative size and similar shape of the profile at 66 amu identifies both peaks as being almost entirely due to SO_2^- and not S_2^-; this serves as an excellent example of the utility of isotopes for species identification.

The $H_xSO_3^-$ group ($x = 0, 1$) of ions is shown in Fig. 6. When OCS is not present, the signals at 80–83 amu are all negligibly small. When 0.2% of OCS is added, large profiles are observed. The single-peaked pair at 80 and 82 amu are attributed to $^{32}SO_3^-$ and $^{34}SO_3^-$, respectively; the latter contains minor contributions from other isotopic species as well. The double-peaked pair of profiles at 81 and 83 amu are identified mainly as $H^{32}SO_3^-$ and $H^{34}SO_3^-$, respectively, although other isotopic species will contribute. As a clue to the ion chemistry dicussed in the next section, it is noteworthy that the profile observed for O^- at 16 amu (not shown here) is single-peaked, while that for OH^- at 17 amu (also not shown) is double-peaked (15). Thus, it is credible that the ions observed in this group are the cluster ions $O^-.SO_2$ and $OH^-.SO_2$.

Similarly for the $H_xSO_4^-$ group ($x = 0, 1$) of ions shown in Fig. 7, the signals at 96–99 amu with OCS absent were negligibly small. With OCS injection, sulphurous negative ion profiles were observed, all single-peaked and one of them very large. They derive, in order of increasing mass 96–99 amu, from $^{32}SO_4^-$, $H^{32}SO_4^-$, $^{34}SO_4^-$, and $H^{34}SO_4^-$ with a number of other isotopic contributions indicated in Table 2. In fact, the peak for HSO_4^- at 97 amu is the largest negative ion signal we have ever observed. In the absence of OCS, the profile for O_2^- at 32 amu (Fig. 3) and the very small one for HO_2^- at 33 amu (not shown) are both single-peaked (15). In keeping with the cluster ion interpretation mentioned in the previous paragraph, the $H_xSO_4^-$ ions might conceivably arise as $O_2^-.SO_2$ and $HO_2^-.SO_2$ clusters.

In summary, the parent negative ions for which profiles were obtained include S^-, SH^-, SO^-, $SO_2^-(S_2^-)$, SO_3^-, HSO_3^-, SO_4^-, and HSO_4^-. Somewhat surprisingly, we were unable to obtain any evidence for sulphurous negative ions containing carbon in the fuel-rich flame.

Discussion of the sulphurous negative ion chemistry

It remains to discuss the probable ion–molecule reactions which are relevant to the sulphurous negative ions observed.

Can. J. Chem. Downloaded from www.nrcresearchpress.com by 210.87.254.6 on 09/06/12
For personal use only.

Can. J. Chem. Downloaded from www.nrcresearchpress.com by 210.87.254.6 on 09/06/12
For personal use only.

TABLE 2. Relative isotopic contributions of sulphurous negative ion groups above mass number M amu

Parent ion	M		$M + 1$		$M + 2$		$M + 3$	
H_xS^- group: M = *32*								
S^-	$^{32}S^-$	[a](1)	$^{33}S^-$	[b](0.0080)	$^{34}S^-$	(0.0444)		
SH^-			$^{32}SH^-$	(1)	$^{33}SH^-$	(0.0080)	$^{34}SH^-$	(0.0444)
Other ions	O_2^-		HO_2^-		$O^-.H_2O$		$OH^-.H_2O$; $^{35}Cl^-$	
SO^- group: M = *48*								
SO^-	$^{32}S^{16}O^-$	(1)			$^{34}S^{16}O^-$	(0.0444)		
					$^{32}S^{18}O^-$	(0.0020)		
Other ions	O_3^-; C_4^-				$O_2^-.H_2O$; $C_4H_2^-$			
SO_2^-/S_2^- group: M = *64*								
SO_2^-	$^{32}S^{16}O_2^-$	(1)			$^{34}S^{16}O_2^-$	(0.0444)		
					$^{32}S^{18}O^{16}O^-$	(0.0041)		
S_2^-	$^{32}S_2^-$	(1)			$^{34}S^{32}S^-$	(0.0888)		
$H_xSO_3^-$ group: M = *80*								
SO_3^-	$^{32}S^{16}O_3^-$	(1)	$^{33}S^{16}O_3^-$	(0.0080)	$^{34}S^{16}O_3^-$	(0.0444)		
			$^{32}S^{17}O^{16}O_2^-$	(0.0011)	$^{32}S^{18}O^{16}O_2^-$	(0.0061)		
HSO_3^-			$H^{32}S^{16}O_3^-$	(1)	$H^{33}S^{16}O_3^-$	(0.0080)	$H^{34}S^{16}O_3^-$	(0.0444)
					$H^{32}S^{17}O^{16}O_2^-$	(0.0011)	$H^{32}S^{18}O^{16}O_2^-$	(0.0061)
Other ions							$SO_2^-.H_2O$	
$H_xSO_4^-$ group: M = *96*								
SO_4^-	$^{32}S^{16}O_4^-$	(1)	$^{33}S^{16}O_4^-$	(0.0080)	$^{34}S^{16}O_4^-$	(0.0444)		
			$^{32}S^{17}O^{16}O_3^-$	(0.0015)	$^{32}S^{18}O^{16}O_3^-$	(0.0082)		
HSO_4^-			$H^{32}S^{16}O_4^-$	(1)	$H^{33}S^{16}O_4^-$	(0.0080)	$H^{34}S^{16}O_4^-$	(0.0444)
					$H^{32}S^{17}O^{16}O_3^-$	(0.0015)	$H^{32}S^{18}O^{16}O_3^-$	(0.0082)
Other ions	$S^-.SO_2$; S_3^-		$SH^-.SO_2$; $SH^-.S_2$		$SO_3^-.H_2O$		$HSO_3^-.H_2O$	

[a]The parent ion composed of the most probable isotopes is designated unity (1).
[b]Relative contributions of less probable isotopic species are included which contribute >0.1% of unity (1).

Can. J. Chem. Downloaded from www.nrcresearchpress.com by 210.87.254.6 on 09/06/12
For personal use only.

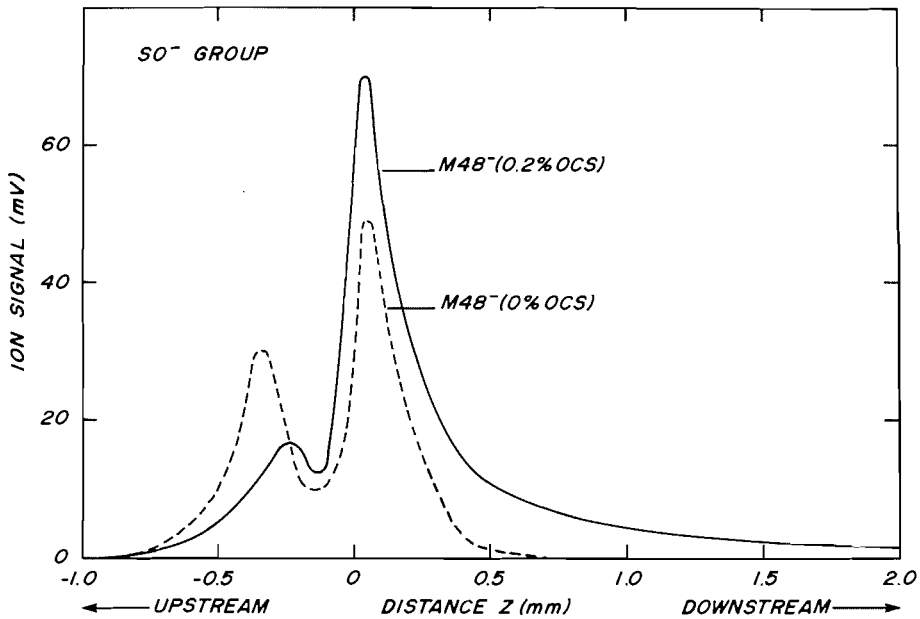

FIG. 4. Negative sulphurous ion profiles: SO⁻.

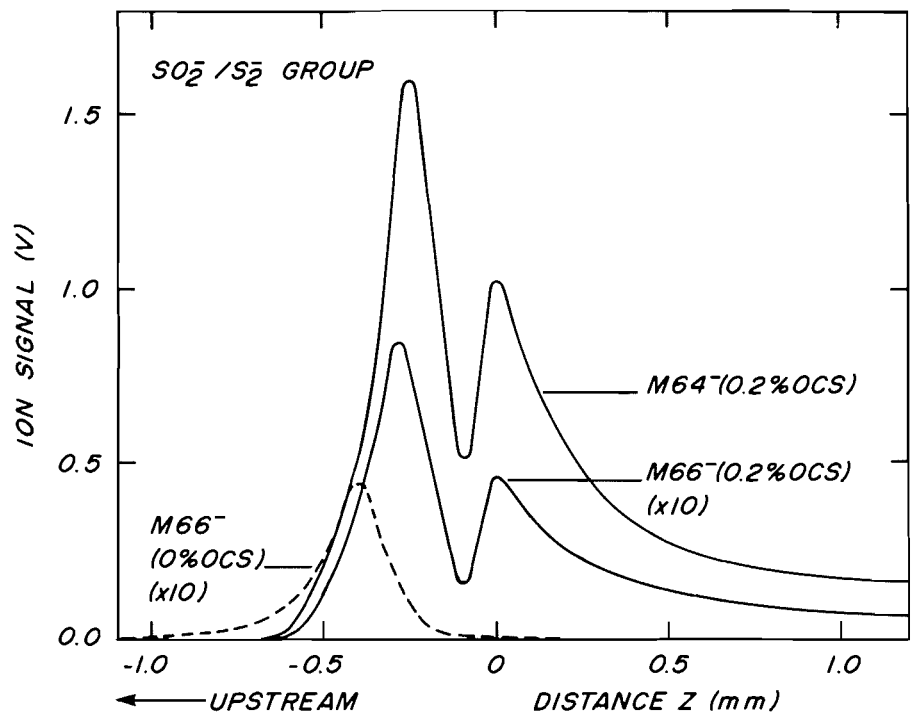

FIG. 5. Negative sulphurous ion profiles: isotopic species of SO_2^- (S_2^-). Also shown is the signal at −66 amu in the absence of OCS additive.

Those which have been studied previously by other workers, usually at room temperature, are listed in Table 3. Many are drawn from the compilation by Albritton (16). The discussion of the ion chemistry reveals the sulphurous neutral species expected to be present in the flame as intermediates and products.

There is general agreement that the main primary source of ions in a hydrocarbon flame is the chemi-ionization reaction (27, 28)

[17] $CH + O \rightarrow HCO^+ + e^-$

The negative ion chemistry commences upstream with three-body attachment of the electrons released in reaction [17] to O_2 molecules (3)

[18] $e^- + O_2 + M \rightarrow O_2^- + M$

In this study, one might expect sulphurous negative ions to arise initially by dissociative electron attachment to OCS. There are five plausible reaction channels to form O^-, C^-, S^-, SO^-, and CS^-; for example

[19] $e^- + OCS \rightarrow S^- + CO$

Although some of them have been observed at relatively high energies using electron beams (29, 30), all will be endothermic

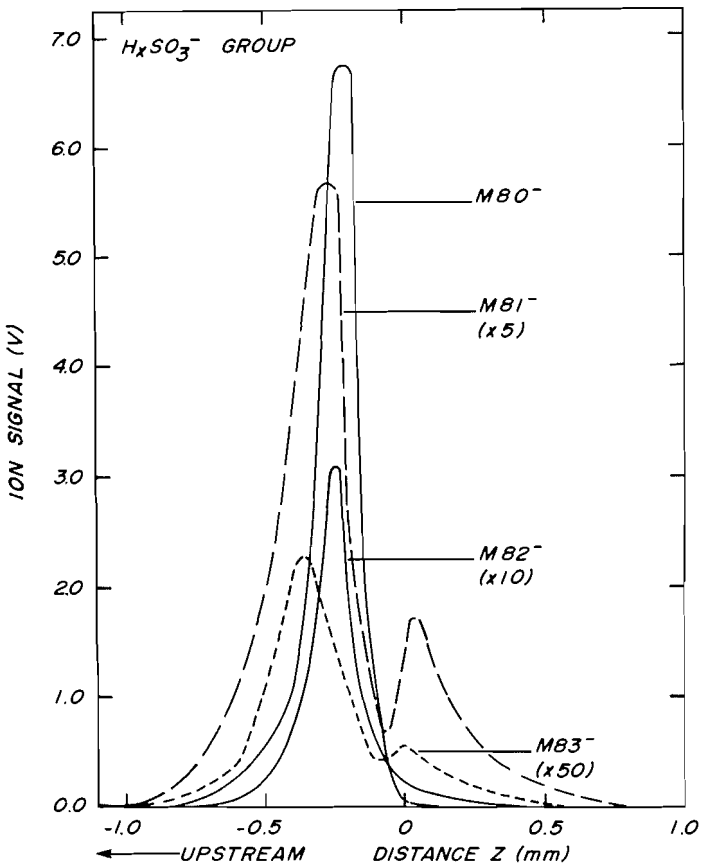

FIG. 6. Negative sulphurous ion profiles: isotopic species of SO_3^- and HSO_3^-. All profiles are taken with the addition of 0.2% of OCS.

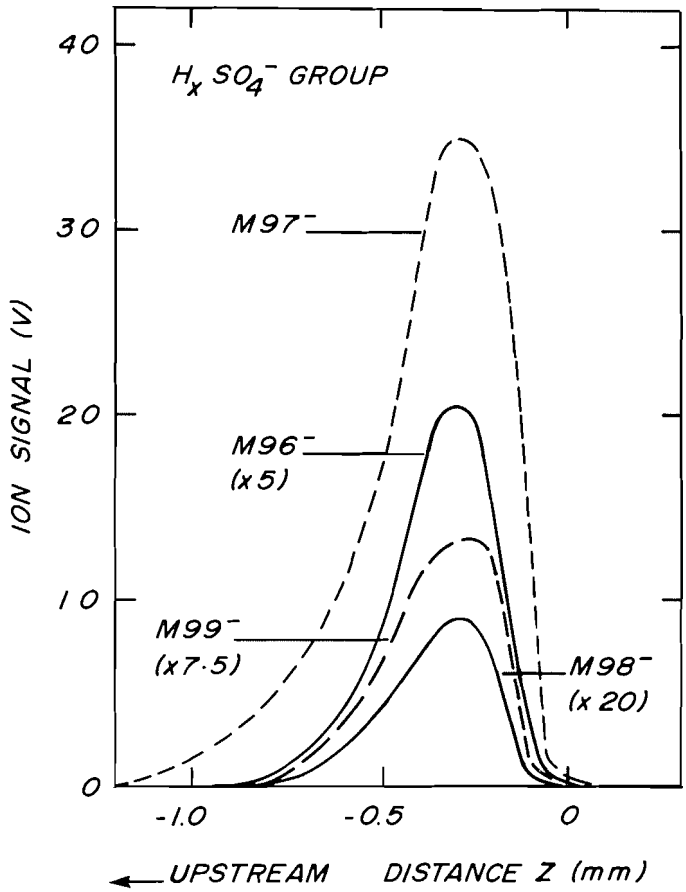

FIG. 7. Negative sulphurous ion profiles: isotopic species of SO_4^- and HSO_4^-. All profiles are taken with the addition of 0.2% of OCS.

at normal flame temperatures. Of the five, reaction [19] is the most favourable with an endothermicity of approximately 25 kcal mol^{-1}.

However, several of the sulphurous neutrals invoked in Fig. 1 have electron affinities (EA) greater than that of O_2, and can give rise to some of the observed sulphurous ions by charge transfer reactions

$$[20]\quad O_2^- + SH \rightarrow SH^- + O_2 \qquad EA(SH) = 2.319\ eV \qquad (31)$$

$$[21]\quad + SO \rightarrow SO^- + O_2 \qquad EA(SO) = 1.09\ eV \qquad (32)$$

$$[22]\quad + SO_2 \rightarrow SO_2^- + O_2 \qquad EA(SO_2) = 1.097\ eV \qquad (33)$$

$$[23]\quad + S \rightarrow S^- + O_2 \qquad EA(S) = 2.077\ eV \qquad (34)$$

Reaction [22] has a high rate constant measured at 300 K given in Table 3. It is perhaps significant that SH^- (Fig. 3) and SO^- (Fig. 4) originate farther upstream than do SO_2^- (Fig. 5) and S^- (Fig. 6) in keeping with the sequence of neutral reactions presented in Fig. 1. Also, SH^- could logically be formed by proton transfer from H_2S to a strong base such as OH^-

$$[24]\quad OH^- + H_2S \rightarrow SH^- + H_2O$$

It is not possible to differentiate between SH^- formed by proton transfer from H_2S or by charge transfer to SH. In addition, SO_2^- and SO^- could be formed by atom transfer reactions

$$[25]\quad O_2^- + OCS \rightarrow SO_2^- + CO$$

$$[26]\quad \rightarrow SO^- + CO_2$$

Both are exothermic, although reaction [26] involves a good deal of chemical rearrangement.

As was mentioned in presenting the Results for the $H_xSO_3^-$ and $H_xSO_4^-$ groups, some of the remaining sulphurous ions can be formed in clustering reactions with SO_2

$$[27]\quad OH^- + SO_2 + M \rightarrow HSO_3^- + M$$

$$[28]\quad HO_2^- + SO_2 + M \rightarrow HSO_4^- + M \qquad EA(HSO_4) > 4.5\ eV \qquad (21)$$

Reaction [27] has the very high rate constant measured at 296 K given in Table 3. Viggiano *et al.*'s determination (21) of a lower limit for $EA(HSO_4)$ based on Benson's somewhat uncertain value (35) for the bond dissociation energy of sulphuric acid $D(H—HSO_4) = 4.5$ eV means that dissociative electron attachment to H_2SO_4

$$[29]\quad e^- + H_2SO_4 \rightarrow HSO_4^- + H$$

would be exothermic, certainly near room temperature. The fact that the HSO_4^- profile (Fig. 7) does not persist downstream is strong evidence that sulphuric acid is not a major product in the burnt gas of the flame. The very large signals obtained for HSO_4^- in the reaction zone are not surprising in view of the very high values of $EA(HSO_4)$; once HSO_4^- forms by SO_2 clustering according to reaction [28], it will be very stable against loss by charge transfer to SH, SO, SO_2, etc. Also, if HSO_4^- is formed in the reaction zone by proton abstraction from H_2SO_4 by the strong base OH^-

$$[30]\quad OH^- + H_2SO_4 \rightarrow HSO_4^- + H_2O$$

the HSO_4^- profile ought to be double-peaked like that for OH^-

Can. J. Chem. Downloaded from www.nrcresearchpress.com by 210.87.254.6 on 09/06/12
For personal use only.

TABLE 3. Ion–molecule reactions involving sulphurous species relevant to the fuel-rich flame doped with OCS

No.	Reactions	[a]Rate constant	Temperature or energy	Reference
[22]	$O_2^- + SO_2 \rightarrow SO_2^- + O_2$	[b]1.9×10^{-9}	303 K	17
		3.9×10^{-9}	0.13 eV	18
[27]	$OH^- + SO_2 + O_2 \rightarrow HSO_3^- + O_2$	[b]1.0×10^{-26}	296 K	19
[31]	$CO_3^- + SO_2 \rightarrow SO_3^- + CO_2$	[b]4.0×10^{-10}	0.04–1.9 eV	20
		[b]3.5×10^{-10}	185–605 K	20
[32]	$HCO_3^- + SO_2 \rightarrow HSO_3^- + CO_2$	[b]1.7×10^{-9}	296 K	19
[33]	$O_3^- + SO_2 \rightarrow SO_3^- + O_2$	[b]1.7×10^{-9}	0.04–1.8 eV	20
		[b]1.7×10^{-9}	185–605 K	20
[34]	$O_2^-.H_2O + SO_2 \rightarrow SO_4^- + H_2O$	[b]1.8×10^{-9}	303–304 K	17
[35]	$O^- + H_2SO_4 \rightarrow HSO_4^- + OH$	[d]1.54×10^{-9}	343 K	21
[36]	$SO_2^- + O_2 + O_2 \rightarrow SO_4^-* + O_2$	[c]Observed	296 K	19
[37a]	$SO_4^-* + H \rightarrow HO_2^- + SO_2$	[c]1.6×10^{-10}	296 K	22
[37b]	$\rightarrow SO_2^- + HO_2$	SO_2^- was the major product ion		
[38]	$S^- + CO \rightarrow e^- + OCS$	[b]3.1×10^{-10}	300 K	23
[39]	$S^- + O_2 \rightarrow e^- + SO_2$	[b]3×10^{-11}	300 K	24
	$S^- + H_2 \rightarrow e^- + H_2S$	$<1 \times 10^{-15}$	300 K	24
[40]	$SH^- + H \rightarrow e^- + H_2S$	[d]1.3×10^{-9}	296 K	25
[41a]	$O^- + SO_2 \rightarrow e^- + SO_3$	$2.0–0.8 \times 10^{-9}$	0.05–0.28 eV	18
[41a]	$O^- + SO_2 \rightarrow e^- + SO_3$	2.1×10^{-9}	0.04–2.0 eV	26
[41b]	$\rightarrow SO_2^- + O$	Major channel at higher energies		

[a]Rate constants are given in units of cm^3 molecule^{-1} s^{-1}, or cm^6 molecule^{-2} s^{-1} where appropriate.
[b]The measurement uncertainty is ±30%.
[c]The measurement uncertainty is ±40%.
[d]The measurement uncertainty is +100%, −50%.
[e]SO_4^-* designates the less stable isomer of SO_4^-.

or HSO_3^-. Presumably HSO_4^- is lost near the end of the reaction zone because the flame attains maximum temperature and the H atom concentration rises (2, 36), both of which favour associative detachment of electrons by the reverse (endothermic) direction of reaction [29]. All things considered, the large signal detected for HSO_4^- does not provide evidence for the presence of sulphuric acid in the flame. It probably forms, however, in the cool, wet, gaseous envelope surrounding the flame proper.

Other ion–molecule reactions listed in Table 3 have been measured which can form ions of the $H_xSO_3^-$ and $H_xSO_4^-$ groups. Some of these might be regarded as switching reactions or anion transfer

[31] $CO_3^-(O^-.CO_2) + SO_2 \rightarrow SO_3^-(O^-.SO_2) + CO_2$

[32] $HCO_3^-(OH^-.CO_2) + SO_2 \rightarrow HSO_3^-(OH^-.SO_2) + CO_2$

[33] $O_3^-(O^-.O_2) + SO_2 \rightarrow SO_3^-(O^-.SO_2) + O_2$

[34] $O_2^-.H_2O + SO_2 \rightarrow SO_4^-(O_2^-.SO_2) + H_2O$

Certainly all of the reagent ions in reactions [31]–[34] have been observed in the fuel-rich flame with OCS absent (3, 15). In addition, a fast proton transfer reaction akin to [30] involving O^- as the proton acceptor has been measured (21)

[35] $O^- + H_2SO_4 \rightarrow HSO_4^- + OH$

Also, SO_4^- can be produced by a clustering reaction of SO_2^- with O_2

[36] $SO_2^- + O_2 + O_2 \rightarrow SO_4^-* + O_2$

although the less stable isomer of SO_4^- is formed, designated SO_4^-* (19). Its reaction with H atoms has been observed to produce two channels (22)

[37a] $SO_4^-* + H \rightarrow HO_2^- + SO_2$

[37b] $\rightarrow SO_2^- + HO_2$ major channel at 296 K

Many other reactions involving the $H_xSO_3^-$ and $H_xSO_4^-$ ions undoubtedly exist, but have not been measured to date.

Several examples involving the loss of sulphurous species by associative electron detachment have been measured

[38] $S^- + CO \rightarrow e^- + OCS$

[39] $S^- + O_2 \rightarrow e^- + SO_2$

[40] $SH^- + H \rightarrow e^- + H_2S$

[41a] $O^- + SO_2 \rightarrow e^- + SO_3$

[41b] $\rightarrow SO_2^- + O$ major channel at high energy

Reactions [38]–[40] have been measured at room temperature. The behaviour of reaction [41] as a function of energy or temperature may by typical and significant for flames. Although associative detachment may dominate at room temperature, a different ion–molecule reaction channel may become the major one at high temperature; e.g. charge transfer in the case of reaction [41]. In general, most of the sulphurous negative ions observed are logical candidates for associative detachment reactions with prominent flame neutrals such as H, O, OH, H_2, CO, etc. It is difficult to imagine that such reactions have large rate constants at flame temperatures in view of the large signals obtained for most of the sulphurous negative ions observed.

With regard to the burnt gas region downstream, the HSO_3^- profile (Fig. 6) persists to some extent in keeping with the interpretation of its formation as a cluster ion of OH^- with SO_2 by reaction [27]. The similarity to the OH^- profile was mentioned near the end of the section on Results. However, four of

Can. J. Chem. Downloaded from www.nrcresearchpress.com by 210.87.254.6 on 09/06/12
For personal use only.

the ion profiles (S^- and SH^- in Fig. 3, SO^- in Fig. 4 and SO_2^- in Fig. 5) persist far downstream through the burnt gas where no negative ions are detected in the same flame with OCS absent. From the electron affinities given beside reactions [20]–[23], a mechanism can be envisaged involving formation by three-body electron attachment primarily to SO_2, with subsequent charge transfer to SH, S, and SO, balanced by loss processes involving associative electron detachment with H, O, and CO, and collisional detachment. Such a network of reactions is reasonable to account for the persistent steady-state profiles observed for these four ionic species. It is consistent with the presence throughout the burnt gas of the sulphurous neutral species, SH, SO, SO_2, and S.

Conclusions

A number of conclusions may be drawn from this work pertaining to both the ion chemistry and the neutral chemistry of sulphur in flames.

Ion chemistry

(*1*) Most of the sulphurous negative ion chemistry seems to be understandable in terms of the relatively few ion–molecule reactions involving sulphurous species measured to date near room temperature.

(*2*) Negative ion clustering and switching (or anion transfer) reactions with SO_2 appear to be prominent.

(*3*) None of the sulphurous negative ions detected contain carbon, even under fuel-rich conditions.

(*4*) For analytical purposes concerned with the mass-spectrometric monitoring of sulphur in flames, very large signals of HSO_4^- were detected around the flame reaction zone. Persisting downstream through the burnt gas, SH^- and SO_2^- are the logical candidates.

Neutral chemistry

(*5*) The profiles show that all of the expected sulphur compounds — $SH(H_2S)$, SO, $SO_2(S_2)$, S — are present *early in the flame reaction zone*. The rates of the chemical reactions summarized in Fig. 1 which interconvert these species must be fast in the flame environment, since OCS is rapidly oxidized to SO_2 even under fuel-rich conditions.

(*6*) The main-line neutral sulphur chemistry in the flame appears to follow the sequence OCS → (SH) → SO → SO_2. The species S, S_2, and H_2S are involved in chemical side-lines. No direct evidence was obtained for S_2, however.

(*7*) No evidence was obtained for H_2SO_4 or H_2SO_3 in the flames proper, although they will undoubtedly form in the cooler, wet region adjacent to the combustion envelope.

1. A. G. COOPER. Sulphur oxides and other sulphur compounds, a bibliography with abstracts. U.S. Dept. of Health Education and Welfare, Washington, DC. 1965.
2. J. M. GOODINGS, D. K. BOHME, and C.-W. NG. Combust. Flame, **36**, 27 (1979).
3. J. M. GOODINGS, D. K. BOHME, and C.-W. NG. Combust. Flame, **36**, 45 (1979).
4. A. N. HAYHURST and N. R. TELFORD. Combust. Flame, **28**, 67 (1977).
5. D. K. BOHME, J. M. GOODINGS, and C.-W. NG. Int. J. Mass Spectrom. Ion Phys. **24**, 335 (1977).
6. A. N. HAYHURST and D. B. KITTELSON. Combust. Flame, **28**, 137 (1977).
7. N. A. BURDETT and A. N. HAYHURST. J. Chem. Soc. Faraday Trans. I, **78**, 2997 (1982).
8. A. N. HAYHURST and N. R. TELFORD. Proc. R. Soc. London A, **322**, 483 (1971).
9. F. WESTLEY. Table of recommended rate constants for chemical reactions occurring in combustion. NSRDS-NBS 67, U.S. Government Printing Office, Washington, DC. 1980.
10. D. L. BAULCH, D. D. DRYSDALE, J. DUXBURY, and S. J. GRANT. Evaluated kinetic data for high temperature reactions. Vol. 3: Homogeneous gas phase reactions of the O_2–O_3 system, the CO–O_2–H_2 system, and of sulphur containing species. Butterworths, London. 1976.
11. S. W. BENSON, D. M. GOLDEN, R. W. LAWRENCE, R. SHAW, and R. W. WOOLFOLK. Estimating the kinetics of combustion including reactions involving oxides of nitrogen and sulphur. U.S. Environmental Protection Agency Report No. EPA-600/2-2-75-019. August, 1975.
12. J. A. KERR and M. J. PARSONAGE. Evaluated kinetic data on gas phase hydrogen transfer reactions of methyl radicals. Butterworths, London. 1976.
13. R. P. TURCO, P. HAMILL, O. B. TOON, R. C. WHITTEN, and C. S. KIANG. J. Atmospher. Sci. **86**, 699 (1979).
14. C. K. MOORTGAT and C. E. JUNGE. Pure Appl. Geophys. **115**, 759 (1977).
15. S. D. TANNER. Ph.D. Thesis, York University, Downsview, Ont., Canada M3J 1P3. 1980.
16. D. L. ALBRITTON. Ion–neutral reaction rate constants measured in flow reactions through 1977. Atomic Data and Nuclear Data Tables, **22**, No. 1. July, 1978.
17. D. W. FAHEY, H. BOHRINGER, F. C. FEHSENFELD, and E. E. FERGUSON. J. Chem. Phys. **76**, 1799 (1982).
18. V. K. LAKDAWALA and J. L. MORUZZI. J. Phys. D: Appl. Phys. **14**, 2015 (1981).
19. F. C. FEHSENFELD and E. E. FERGUSON. J. Chem. Phys. **61**, 3181 (1974).
20. D. L. ALBRITTON, I. DOTAN, G. E. STREIT, F. C. FEHSENFELD, and E. E. FERGUSON. Planet. Space Sci. To be published.
21. A. A. VIGGIANO, R. A. PERRY, D. L. ALBRITTON, E. E. FERGUSON, and F. C. FEHSENFELD. J. Geophys. Res. **85**, 4551 (1980).
22. F. C. FEHSENFELD. J. Chem. Phys. **63**, 1686 (1975).
23. E. E. FERGUSON. Acc. Chem. Res. **3**, 402 (1970).
24. F. C. FEHSENFELD and E. E. FERGUSON. J. Chem. Phys. **51**, 3512 (1969).
25. F. C. FEHSENFELD, C. J. HOWARD, and E. E. FERGUSON. J. Chem. Phys. **58**, 5841 (1973).
26. W. LINDINGER, D. L. ALBRITTON, F. C. FEHSENFELD, and E. E. FERGUSON. J. Chem. Phys. **63**, 3238 (1975).
27. H. F. CALCOTE. Eighth Symposium (International) on Combustion. Williams & Wilkins, Baltimore, MD. 1962. p. 184.
28. K. N. BASCOMB, J. A. GREEN, and T. M. SUGDEN. Adv. Mass Spectrom. **2**, 66 (1962).
29. K. A. G. MACNEIL and J. C. J. THYNNE. J. Phys. Chem. **73**, 2960 (1969).
30. J. G. DILLARD and J. L. FRANKLIN. J. Chem. Phys. **48**, 2353 (1968).
31. L. M. BRANSCOMB. Phys. Rev. **148**, 11 (1966).
32. D. FELDMAN. Z. Naturforsch. A**25**, 621 (1970).
33. R. J. CELOTTA, R. A. BENNETT, and J. L. HALL. J. Chem. Phys. **60**, 1740 (1974).
34. H. HOTOP and W. C. LINEBERGER. J. Phys. Chem. Ref. Data, **4**, 539 (1975).
35. S. W. BENSON. Chem. Rev. **78**, 23 (1978).
36. J. W. HASTIE. Combust. Flame, **21**, 187 (1973).

Can. J. Chem. Downloaded from www.nrcresearchpress.com by 210.87.254.6 on 09/06/12
For personal use only.

The thermal decomposition of azobenzene

DONALD BARTON, MICHAEL HODGETT, PAUL SKIRVING, MICHAEL WHELTON, KEITH WINTER, AND CATHY VARDY
Department of Chemistry, Memorial University of Newfoundland, St. John's, Nfld., Canada A1B 3X7

Received March 17, 1982[1]

DONALD BARTON, MICHAEL HODGETT, PAUL SKIRVING, MICHAEL WHELTON, KEITH WINTER, and CATHY VARDY. Can. J. Chem. **61**, 1712 (1983).

The rate of nitrogen formation during the thermal decomposition of azobenzene in static and stirred-flow systems was measured over the temperature range of 368.9°C to 437.4°C. The first order rate constant was found to be given by the expression

$$k = 10^{16.6\pm0.5} \exp(-278{,}000 \pm 7000/8.314T)\ s^{-1}$$

A consideration of the equilibrium constant between *cis*-azobenzene and *trans*-azobenzene, and the rate of attainment of equilibrium, leads to the conclusion that a small concentration of *cis*-azobenzene is always present, at equilibrium with the *trans* isomer. Since the *cis* isomer is likely to be more reactive than the *trans* isomer the rate constant cannot be ascribed to the *trans* isomer alone. No effect of variation of surface-to-volume ratio could be detected. Some preliminary experiments in which toluene and ethylene were employed as additives indicated that these did not affect the rate of formation of nitrogen. Nevertheless, because of a certain amount of scatter in the results, a small effect could not be excluded. There were at least nine products, in addition to nitrogen.

DONALD BARTON, MICHAEL HODGETT, PAUL SKIRVING, MICHAEL WHELTON, KEITH WINTER et CATHY VARDY. Can. J. Chem. **61**, 1712 (1983).

On a mesuré la vitesse de formation de l'azote lors de la décomposition thermique de l'azobenzène dans des systèmes à écoulement statique et à écoulement perturbé dans un intervalle de température allant de 368,9°C à 437,4°C. On a trouvé que l'expression suivante donne la constante de vitesse d'ordre un:

$$k = 10^{16.6\pm0.5} \exp(-278{,}000 \pm 7000/8{,}314T)\ s^{-1}$$

En tenant compte de la constante d'équilibre entre l'azobenzène *cis* et l'azobenzène *trans*, et de la vitesse à laquelle cet équilibre est atteint, on conclut qu'une faible concentration d'azobenzène *cis* est toujours présente en équilibre avec l'isomère *trans*. Puisque l'isomère *cis* est ordinairement plus réactive que l'isomère *trans*, on ne peut attribuer la constante de vitesse à l'isomère *trans* uniquement. On ne peut pas déceler l'effet d'une variation de surface sur le rapport du volume. Quelques expériences préliminaires dans lesquelles on a utilisé le toluène et l'éthylène comme additifs indiquent que ces additifs n'affectent pas la vitesse de formation de l'azote. Néanmoins, on ne peut pas exclure un léger effet à cause d'une certaine dispersion dans les résultats. Il y a au moins neuf produits en plus de l'azote.

[Traduit par le journal]

Introduction

Even though azobenzene should occupy the position of the prototype substance in gas-phase reactions of aromatic azo compounds, as does azomethane for aliphatic azo compounds, little attention has been given to its gas-phase reactions. This situation appears to have arisen from the fact that M. J. Jaquiss and M. Szwarc were unable to detect any reaction in flow systems with toluene, up to, apparently, 700°C (1). Subsequently the supposition of extreme unreactivity appeared a number of times in the literature, reinforcing this belief. Several years ago, while preparing for an investigation of azobenzene in the gas phase, we found the report by Inokawa *et al.* (2), in which the discovery of accelerated thermal decomposition of 1,2-dichloroethane by azobenzene in the temperature range of 400°C to 500°C was described. We selected 400°C for our first experiment and found that nitrogen was evolved at a rate which was convenient for study using an ordinary static system. Since that time the reactivity of azobenzene has been clearly confirmed by Leiba and Oref, who pyrolyzed it in sealed glass tubes (3). Another reference to its reactivity appeared in Engel's review (4) of aliphatic azo compounds which cited the work of Louw and Rothuizen (5) who had studied the gas-phase phenylation of arenes using, among other substances, azobenzene as a source of phenyl radicals at 500°C. In retrospect we can see that its reactivity had been well established. Of course, because of the size of the azobenzene molecule, it did not attract interest in connection with energy transfer processes, as did azomethane; moreover, the low volatility of such substances tends to discourage their investigation in the gas phase.

The original reason for starting this investigation was to determine the usefulness of azobenzene as a source of phenyl radicals, although it soon became apparent that the reaction would be inherently interesting and that comparison with reactions of other azo compounds would be important.

Experimental

Both static and stirred-flow systems were used. The experiments which were carried out on the static system are classified as either preliminary or regular experiments, for reasons which will be explained.

Materials

For the preliminary experiments zone-refined azobenzene, obtained from the Aldrich Chemical Company, was used without treatment. For all other reported experiments azobenzene, obtained from British Drug Houses, catalogue number B15005-30, was first crystallized from methanol, then zone refined, then sublimed, and finally zone refined again. This method of purification is essentially that of Cammenga *et al.* (6), except that zone refining was carried out in air rather than in argon. No impurities were detected using thin-layer chromatography. Phillips research grade of ethylene was used without treatment, as was toluene-d_8, obtained from Merck Sharp and Dohme Canada Limited.

[1]Revision received February 28, 1983.

Can. J. Chem. Downloaded from www.nrcresearchpress.com by 210.87.254.42 on 09/06/12
For personal use only.

TABLE 1. Order and rate constants for benzene formation

Temperature, °C	Number of runs	Order	ln k*
386.0±0.2	7	0.89±0.07	−15.52±0.21
413.4±0.3	22		−13.01±0.31
423.5±0.2	17	0.86±0.07	−11.91±0.17

*k is defined as $k = (-[C_6H_6]/t)/[C_{12}H_{10}N_2]_i$. Errors here and in the other tables are standard deviations.

Static system

The experiments which were carried out on the static system employed two spherical Pyrex reaction vessels which were almost identical except that one contained Pyrex tubes. Those parts of the vacuum system which were exposed to azobenzene or condensable products were contained in an air bath which was thermostatted at 155°C to 160°C. Capacitance manometers were used for measuring pressure and calibrated Chromel–Alumel thermocouples were used for measuring temperature (7). Nitrogen was collected in a gas burette and sometimes removed for analysis by mass spectrometer. The benzene, in a number of experiments, was swept from a trap to a gas chromatograph, and the accumulated solid products were examined by thin-layer chromatography.

Preliminary experiments are so designated because greased stopcocks were used and a slight uptake of azobenzene by grease was observed during some of these experiments. The regular experiments are those in which metal valves with polyimide seats and gaskets were used in appropriate places. Arrhenius parameters for nitrogen formation were derived from results of regular experiments.

Flow system

The reaction vessel, similar to that described by Mulcahy and Williams (8) for stirred-flow systems, was made of quartz, with a volume of 1316 cm^3. The flow sequence was so designed that no valves or stopcocks were used on the upstream side of the reaction vessel, and valves with Viton diaphragms were used in suitable places on the downstream side. Appropriate parts were contained in an air bath. Temperature and pressure measurements and collection of nitrogen were carried out as described for the static system. Collection periods were usually in the range of 30 to 60 minutes.

Results

Products

All of the reported products are those obtained from experiments in which the extent of reaction was quite low. On the flow system the ratio of yield of nitrogen to the number of moles of azobenzene passing through the reaction vessel varied from 0.003 to 0.03. On the static system the corresponding ratio was generally in the range from 0.01 to 0.05. The fraction of azobenzene reacted is likely greater than these ratios suggest since various products containing nitrogen are observed.

Products passing through a liquid nitrogen trap

Molecular nitrogen is plentiful, as is usual in pyrolysis of azo compounds. A number of samples of this fraction from the static system were examined by mass spectrometer. Hydrogen was always found although the concentration was not very reproducible. At 413.4°C the mean concentration of hydrogen in nitrogen, from 18 experiments, was 0.64% and, at 423.5°C, 1.6% from 24 experiments. No other products could be found in this fraction.

Products passing through a trap at 0°C

The accumulated products, a small drop, from all of the reported experiments on the flow system were subjected to mass spectrometric and proton magnetic resonance analysis. The spectra were consistent with the presence of aniline and benzene. Small amounts of other products or impurities could also be detected. The yield of benzene relative to nitrogen increased over an extended time.

It is worth mentioning at this point that much effort was wasted by using B.D.H. azobenzene, without further purification, on the flow system. Not only did the composition of the products seem somewhat different than that from the purified azobenzene but, also,the rate of nitrogen formation was different. In fact, the rate of nitrogen formation could be increased by increasing the flow rate at low extent of reaction. This observation is consistent with the presence of an impurity which reacts almost to completion, producing nitrogen. Untreated azobenzene had been used because the flow system consumed so much material that a sufficient supply of purified azobenzene for numerous runs could not be maintained.

The remaining fraction

Most of this fraction could be easily distilled or sublimed with the exception of a small amount of black material, which nevertheless was volatile enough to find its way from reaction vessel to trap. The 1005 cm^3 reaction vessel on the static system remained clean, indicating that little or no breakdown to carbon took place.

Qualitative analysis of this fraction was started, but by no means completed, using thin-layer chromatography followed by mass spectrometric examination of the fractions. Six products were evident although more may eventually be found. One has the mass spectrum reported in the literature for carbazole and another that reported for diphenylamine (9). A third and fourth have mass spectra which one would expect of phenylazobenzene and of triphenylamine. The other two have not been identified. Biphenyl was not found but the possibility still exists that it may have been missed.

Rate of reaction

All data on rate of reaction were obtained from experiments in which the extent of reaction was small, as described above.

Benzene

The results are shown in Table 1, in which $[C_{12}H_{10}N_2]_i$ is the initial concentration of azobenzene.

Nitrogen

The results from the static system which were used to obtain the Arrhenius parameters for nitrogen formation were treated in the following way. Yield of nitrogen as a function of time was obtained for various initial concentrations of azobenzene and the slopes of the yield vs. time plots were obtained by linear regression analysis. Because small negative intercepts were often observed, the lines were not forced to pass through the origin. Reaction orders at three temperatures were obtained by means of ln−ln plots using the slopes of the yield vs. time plots and the initial concentrations of azobenzene. Rate constants which are obtained from such ln−ln plots are extremely sensitive to the order. Therefore the data were treated in a

Can. J. Chem. Downloaded from www.nrcresearchpress.com by 210.87.254.42 on 09/06/12
For personal use only.

TABLE 2. Order and rate constants* for nitrogen formation

Temperature, °C	Number of runs	Order	k, s^{-1}
423.5±0.2	43s†	0.96±0.06	(6.81±0.46) × 10^{-5}
413.4±0.3	45s	1.03±0.10	(3.07±0.30) × 10^{-5}
386.0±0.2	19s	1.08±0.01	(4.43±0.15) × 10^{-6}
368.9±0.3	10s	—	(9.40±2.12) × 10^{-7}
437.4±0.1	5f	—	(1.39±0.05) × 10^{-4}
423.1±0.4	3f	—	(6.11±0.47) × 10^{-5}
402.5±0.0	3f	—	(1.47±0.10) × 10^{-5}

*The origin of each rate constant is explained in the text
†Abbreviations: s, static system; f, flow system.

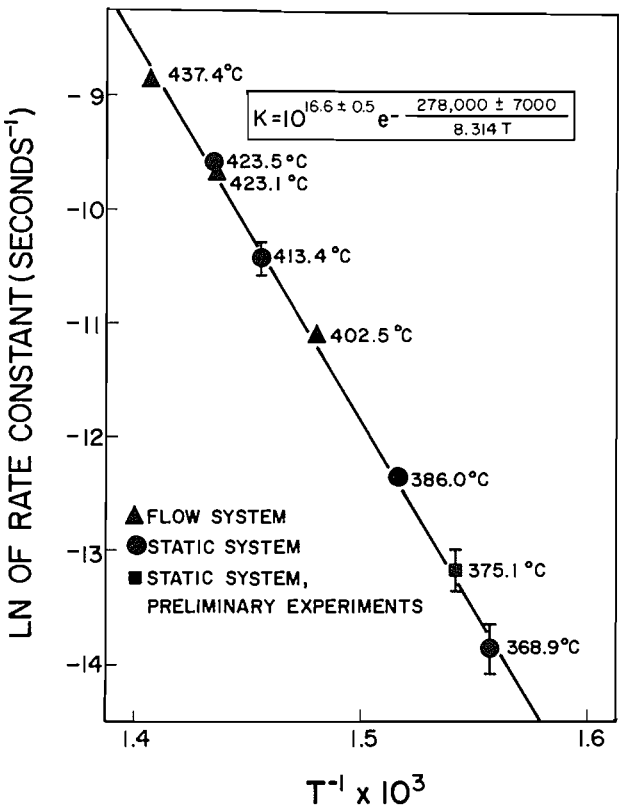

FIG. 1. Arrhenius plot for nitrogen formation. The results of preliminary experiments were not used to determine the Arrhenius parameters. The bars represent standard deviations of rate constants. If none are shown they are smaller than the data symbols.

self-consistent way by defining the rate constant as $k = S/[C_{12}H_{10}N_2]_i$ s^{-1}, in which S represents the slope of the yield–time line. The data are thus forced to fit a first order rate expression. The mean rate constant from several concentrations of azobenzene, at each temperature, was then calculated. Because yield vs. time data were not available from the flow system, the rate constants were defined as $k = ([N_2]/t)/[C_{12}H_{10}N_2]$ s^{-1}. $[C_{12}H_{10}N_2]$ is calculated from the total pressure in the reaction vessel. The data for nitrogen are summarized in Table 2 and the Arrhenius plot is shown in Fig. 1.

Effect of variation of surface-to-volume ratio

The number of experiments carried out in the packed vessel was too small to allow treatment of data by the yield vs. time method. Therefore the rate constants were defined by the expression $k = ([N_2]/t)/[C_{12}H_{10}N_2]_i$. In order to facilitate comparison of the results with those found using the unpacked vessel, the results from the unpacked vessel were treated in the same way, using only those experiments in which the initial pressures were equal to or greater than those in the packed vessel. Reaction times of experiments in both vessels were sufficiently long to avoid appreciable effects of the apparent induction period. The results are shown in Table 3. No effect of surface is evident.

TABLE 3. Effect of surface-to-volume ratio on rate of formation of nitrogen

Area, cm^2	Volume, cm^3	Temperature, °C	Number of runs	ln k*
1147	980	369.0±0.2	6	−13.97±0.30
550	1005	368.9±0.3	11	−14.02±0.21
1147	980	423.5±0.1	8	−9.70±0.04
550	1005	423.5±0.2	47	−9.65±0.21

*k is defined in the text.

TABLE 4. Effect of toluene and ethylene on rate of formation of nitrogen

Mole fraction of toluene or ethylene	Temperature, °C	Number of runs	ln k*
0	375.1±0.2	32	−13.18±0.18
0.90 C_2H_4	375.6±0.3	10	−13.27±0.11
0.93 C_7D_8	375.6±0.3	4	−13.02±0.09

*k is defined in the text.

Effect of toluene and ethylene

We wish to emphasize that these results were obtained from the preliminary experiments, that is, those in which greased stopcocks were used, and some error in concentration of azobenzene is possible due to dissolution in the grease. Nevertheless, the mean rate constant in the absence of additives is almost identical to that found from the Arrhenius plot of the data from the regular experiments in which polyimide seated and gasketted valves were used, as can be seen in Fig. 1. This correspondence allows confidence to be placed in the results of the preliminary experiments. With due consideration to the errors, as seen in Table 4, no effect is apparent. A small effect, such as that observed for ethylene on azomethane (11) would be obscured by these errors. The rate constants are defined as in the previous section.

Comments on the results of Leiba and Oref

The Arrhenius parameters which were reported by Leiba and

Can. J. Chem. Downloaded from www.nrcresearchpress.com by 210.87.254.42 on 09/06/12
For personal use only.

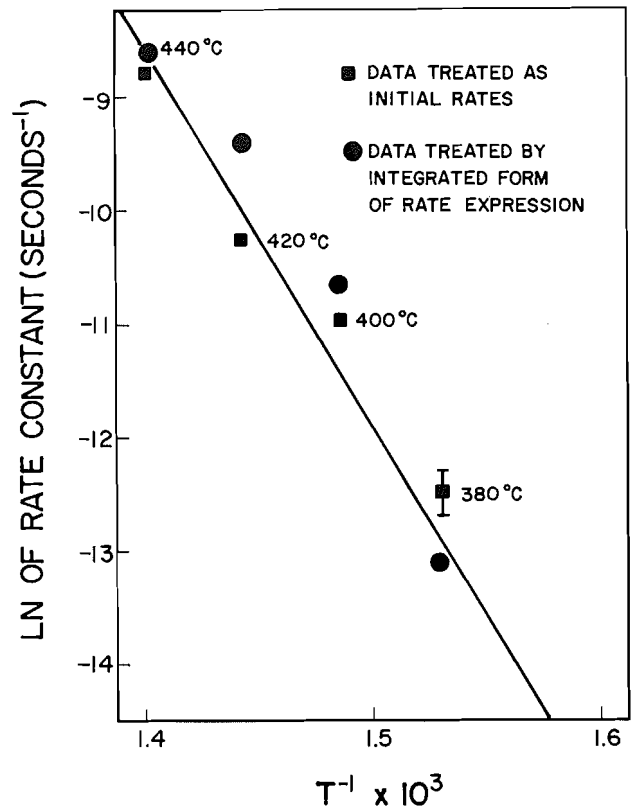

FIG. 2. The results of Leiba and Oref treated as initial rate data. The error at 380°C is standard deviation. Their reported rate constants are also shown. The line is *our* Arrhenius plot.

Oref (3) are not the same as ours. There are, however, certain problems connected with their data, and the treatment of their data, which led us to the conclusion that their Arrhenius parameters are suspect. Leiba and Oref reported the results of twenty-one experiments in which weighed samples of azobenzene were heated in sealed glass ampoules. After being heated for various lengths of time, the ampoules were cooled and the yields of nitrogen were determined. The results were fitted to the integrated form of the first order rate expression by assuming, implicitly, that the number of moles of nitrogen was equal to the number of moles of azobenzene which had reacted. Leiba and Oref, who postulated the existence of involatile nitrogen-containing products, did not, apparently, consider this problem of stoichiometry when treating their data. There is also a possibility that the stoichiometry is a function of time, because reactive intermediates such as amines and azo compounds are likely to be present. Therefore, the integrated form of the rate expression may not be applicable.

Other reasons for avoiding the integrated form of the rate expression become apparent when their data for the ratio $[N_2]/[C_{12}H_{10}N_2]_i$ are plotted as a function of time. Even though the initial pressures differ among the various runs this would be a legitimate plot of first order data, which should be concave with respect to the time axis. An examination of the data obtained at 380°C reveals that the extent of reaction, as measured by the yield of nitrogen, is small, $[N_2]/[C_{12}H_{10}N_2]_i$ being less than 0.03. Due to errors of measurement or other factors, a definite increase in yield as time progresses is not apparent. The use of an integrated form of the rate expression under these circumstances should not be expected to produce a significant rate constant. In order to compare their results with ours, the yields of nitrogen were treated as initial rate measurements. The mean of six rate constants at 380°C is plotted in Fig. 2, in which the solid line represents the Arrhenius plot of our results. Their result, using the integrated form, is also shown and is seen to be similar to that using initial rates, and is also very close to our Arrhenius plot, which is surprising when the scatter and small extent of reaction are considered.

An examination of the data obtained at 400°C and at 420°C reveals additional problems. At 400°C the rate is essentially the same for all points, and at 420°C the rate clearly increases as time progresses and then becomes constant, so in neither case can information be obtained from the integrated form. If, however, the first two data at 400°C, and the first at 420°C, are treated as initial rates, the two rate constants straddle our Arrhenius plot, as can be seen in Fig. 2. At 440°C the extent of reaction is large and the rate clearly decreases as time progresses, so that if the problem of stoichiometry is ignored, an integrated rate expression may be applied. There are too few data, however, to definitely establish the order in this way. Nevertheless, the rate constant which was calculated by Leiba and Oref from the measurements at 440°C coincides precisely with our Arrhenius plot. In addition, the first point, when treated as an initial rate, yields a rate constant which is also very close to our Arrhenius plot. In summary, therefore, the treatment of these data by means of the integrated form of the first order rate expression cannot be expected to produce results of any significance except, possibly, at 440°C. On the other hand, estimates of the initial rates produce rate constants which are self-consistent and also in reasonable agreement with ours.

Discussion

Products

The following reactions account for the products which have been identified so far.

Although hydrazines have been observed among the products of decomposition of azoalkanes, they may be too reactive to be observed here because the temperature is rather high. For

$$C_6H_5N{=}NC_6H_5 \rightarrow 2C_6H_5\bullet + N_2$$
$$C_6H_5\bullet + C_6H_5N{=}NC_6H_5 \rightarrow C_6H_6 + C_6H_5N{=}NC_6H_4\bullet$$
$$C_6H_5 + C_6H_5N{=}NC_6H_4\bullet \rightarrow C_6H_5N{=}NC_{12}H_9$$
$$C_6H_5\bullet + C_6H_5N{=}NC_6H_5 \rightarrow (C_6H_5)_2N{-}\dot{N}C_6H_5$$
$$(C_6H_5)_2N{-}\dot{N}C_6H_5 + C_6H_5N{=}NC_6H_5 \rightarrow (C_6H_5)_2N{-}NH(C_6H_5) + C_6H_5N{=}NC_6H_4\bullet$$
$$(C_6H_5)_2N{-}NH(C_6H_5) \rightarrow (C_6H_5)_2N\bullet + (C_6H_5)HN\bullet$$
$$(C_6H_5)_2N\bullet + C_6H_5N{=}NC_6H_5 \rightarrow (C_6H_5)_2NH + C_6H_5N{=}NC_6H_4\bullet$$
$$(C_6H_5)HN\bullet + C_6H_5N{=}NC_6H_5 \rightarrow C_6H_5NH_2 + C_6H_5N{=}NC_6H_4\bullet$$
$$(C_6H_5)_2N\bullet + C_6H_5\bullet \rightarrow (C_6H_5)_3N$$

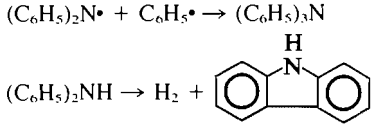

Can. J. Chem. Downloaded from www.nrcresearchpress.com by 210.87.254.42 on 09/06/12
For personal use only.

Can. J. Chem. Downloaded from www.nrcresearchpress.com by 210.87.254.42 on 09/06/12
For personal use only.

example, the rate constant for decomposition of phenylhydrazine is $k = 10^{15.5} \exp(-214000/8.314T)$ s^{-1} (10), as measured by the toluene carrier technique, so that the concentration of hydrazines of similar reactivity would remain low. One possible source of hydrogen, the reaction of diphenylamine to produce carbazole, is shown. This reaction might take place at the surface, the rate being very erratic.

The ratio of benzene to nitrogen increases as the extent of reaction increases, Such behaviour may be ascribed to decomposition of products, producing benzene, or to an increased rate of hydrogen abstraction by phenyl radicals, relative to addition, as products accumulate. Benzene formation has a very strong temperature dependence as would be consistent with competitive addition and abstraction reactions, the abstraction reactions having the greater activation energy. Because of the probable difficulty in recovery of benzene, it is best not to give too much quantitative significance to the benzene data.

Nitrogen

As a basis for discussion we assume that nitrogen, at low extent of reaction, arises directly from azobenzene, and that any contribution of chain reactions is negligible. The results of experiments in which ethylene or toluene was present support this assumption, although a small effect of additives cannot be excluded.

Equilibrium constant for isomerization

Although the equilibrium constant for isomerization in the gas phase is unknown, a good estimate can be made. Cammenga *et al.* (6) found $\Delta H^{\ominus}$ (298.15 K) of the reaction *trans*-$C_{12}H_{10}N_2$(g) → *cis*-$C_{12}H_{10}N_2$(g) to be +47.8 kJ mol^{-1}. If $\Delta S^{\ominus}$ and $\Delta C_p^{\ominus}$ are small, as may be true for such reactions (e.g. see the properties of some alkenes, ref. 12), then $K_p \simeq \exp(-47800/8.314T)$. The estimated equilibrium constants at the upper and lower limits of temperature achieved in this study are listed in Table 5. Even if allowance were made for small values of $\Delta S^{\ominus}$ and $\Delta C_p^{\ominus}$, the *trans* isomer would clearly predominate.

Relaxation time for isomerization

Although the *trans* isomer is predominant at equilibrium, both in the air bath and reaction vessel, the question of the rate of attainment of equilibrium, following introduction into the reaction vessel, is an important one. Rates of isomerization have been measured in organic solvents but not in the gas phase. Since the rate constants are not very dependent upon the nature of the solvent, the assumption has been made that they are applicable to the gas phase. The rate constant for isomerization from the *cis* to the *trans* forms in benzene, for example, is $k = 2.10 \times 10^{11} \exp(-97490/8.314T)$ s^{-1} (13). This rate constant, along with the estimated equilibrium constants, allows estimates to be made of the rate constants in both directions and the relaxation times, as listed in Table 5. Therefore, when azobenzene is introduced into the reaction vessel from the air bath, relaxation is likely to be rapid. It was considered possible that the apparent induction period might be connected in some way to isomerization,[2] but the relaxation time is too short for this to be so. Of course, if our estimate of the relaxation time is much too low, the argument is invalid.

Rate of decomposition of the two isomers

Engel described two limiting kinds of azo compounds, classified according to their rates of isomerization and decomposition (4). One kind has a low activation energy for isomerization, relative to decomposition, and the other, a high activation energy for isomerization relative to decomposition. Azobenzene is evidently an example of the former. Measurement of the separate rate constants for decomposition of this kind appears to be impossible because of the rapid rate of interconversion of the isomers. If the assumption is made, as Engel did for the azoalkanes, that the transition states for decomposition are identical, an enthalpy − activation energy − entropy diagram may be constructed as in Fig. 3. Then by using the transition state formulation of the rate constant, $k = (ekT/h) \exp \Delta S^{\ddagger}/R \exp(-E/RT)$, for each isomer along with $K_p = \exp \Delta S^{\ominus}/R \exp(-\Delta H^{\ominus}/RT)$ and $E_c + \Delta H^{\ominus} = E_t$ and $\Delta S_c^{\ddagger} + \Delta S^{\ominus} = \Delta S_t^{\ddagger}$, where *c* and *t* represent *cis* and *trans* isomers, it is easily shown that one-half of the nitrogen arises from the *cis* isomer and one-half from the *trans* isomer.[3] The rate constant for decomposition of the *trans* isomer would therefore be equal to one-half of the observed rate constant, $k_t = 2.06 \times 10^{16} \exp(-278000/8.314T)$ s^{-1}. In order to estimate k_c an accurate expression for K_p is needed. Nevertheless, the estimate already made may be used to give $k_c \simeq 2.06 \times 10^{16} \exp(230000/8.314T)$ s^{-1}. It is clear that the observed rate constant may not be simply ascribed to the *trans* isomer, even though the concentration of the *cis* isomer is very small over the entire temperature range.

TABLE 5. Estimated values of rate constants and equilibrium constants for the isomerization reaction *trans*-$C_{12}H_{10}N_2$(g) ⇄ *cis*-$C_{12}H_{10}N_2$(g)

Parameter	Value at 368.9°C	Value at 437.4°C
K_p	1.29×10^{-4}	3.06×10^{-4}
k(*cis* → *trans*)	2.46×10^{3} s^{-1}	1.43×10^{4} s^{-1}
k(*trans* → *cis*)	3.15×10^{-1} s^{-1}	4.38 s^{-1}
Relaxation time	4.06×10^{-4} s	6.99×10^{-5} s

π-Bond energy of nitrogen

It is interesting to calculate the second π-bond energy of nitrogen by using data from studies of thermal decomposition of several azo compounds. This is done using the sequence of reactions

[1] $C_6H_5N{=}NC_6H_5 \rightarrow C_6H_5N{=}N\cdot + C_6H_5\cdot$

[2] We are grateful to Dr. Robert Back for emphasizing this point.

[3] The mechanism of nitrogen formation is assumed to be

$$trans\text{-}C_{12}H_{10}N_2 \underset{k_b}{\overset{k_f}{\rightleftharpoons}} cis\text{-}C_{12}H_{10}N_2$$

$$trans\text{-}C_{12}H_{10}N_2 \xrightarrow{k_t} N_2 + 2C_6H_5\cdot$$

$$cis\text{-}C_{12}H_{10}N_2 \xrightarrow{k_c} N_2 + 2C_6H_5\cdot$$

A complete solution of this mechanism has been reported by Seeman and Farone (15). If equilibrium is maintained between the two isomers, the rate expression has the simple form

$$d[N_2]/dt = \{(k_t + k_c K_p)/(K_p + 1)\}[C_{12}H_{10}N_2]$$

The sum of the concentrations of the two isomers is $[C_{12}H_{10}N_2]$ and $K_p = k_f/k_b$. If, in addition, $K_p \ll 1$, $d[N_2]/dt = (k_t + k_c K_p) \times [C_{12}H_{10}N_2]$, and $[C_{12}H_{10}N_2]$ becomes essentially the concentration of the *trans* isomer. In the transition state formulation $k_t = k_c K_p$ if the transition states are identical, and the rates of formation of nitrogen from the two isomers become equal.

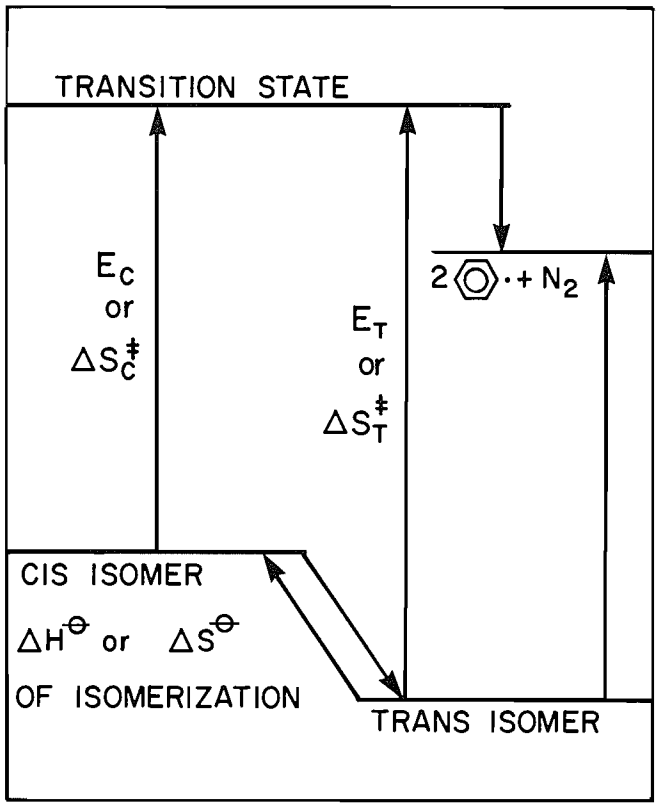

FIG. 3. Path diagram for decomposition of the two isomers following Engel's argument. Symbols are defined in the text.

[2] $C_6H_5N{=}N\cdot \rightarrow C_6H_5\cdot + \cdot N{=}N\cdot$

[3] $\cdot N{=}N\cdot \rightarrow N_2$

Reactions [2] and [3] are usually written as a single reaction but are now written as two in order to emphasize what is meant by the π-bond energy, $-\Delta H_3^{\ominus}$ (14). The enthalpy change of reaction [4]

[4] $C_6H_5N{=}NC_6H_5 \rightarrow 2C_6H_5\cdot + N_2$

is equal to the sum of the others, and if $\Delta H_1^{\ominus} \simeq \Delta H_2^{\ominus} = E$, where E is the Arrhenius activation energy, $\Delta H_3^{\ominus} = \Delta H_4^{\ominus} - 2E$. Benson had calculated $-\Delta H_3^{\ominus}$ using data for azomethane and obtained a value of the π-bond energy which he thought to be a reasonable upper limit, 338 kJ mol^{-1} (see ref. 10, p. 32). If two-bond rupture occurs, the effect is expected to be a lowering of E, since reactions [2] and [3] together are exothermic, signifying that $\Delta H_1^{\ominus} > E$ and therefore that $-\Delta H_3^{\ominus} > 338$ kJ, which was thought to be unreasonably high. Subsequently the enthalpy of formation of a number of azoalkanes was found from combustion studies and, as a result, a better estimate of the enthalpy of formation of azomethane was made (16). Only the enthalpy of formation of azoisopropane was available to Benson, and even that has been appreciably revised (17). In the meantime, Engel and Bishop obtained a lower value of $-\Delta H_3^{\ominus}$ or E_π, using different values of E and enthalpy of formation of azomethane (18).

The resulting estimates of the second π-bond energy, at the median temperature of each study, are listed in Table 6.

It is astonishing to find that values of $\Delta H_3^{\ominus}$ which are calculated from independent data, arising from such different substances as azobenzene and azomethane, are practically identical, and that such different values of E and $\Delta H_4^{\ominus}$ generate values of $\Delta H_3^{\ominus}$ which are so close to one another. If the π-bond energy is actually that found from azomethane and azobenzene data, we conclude, using this model, that there is an appreciable contribution of two-bond rupture in the decomposition of azoisopropane and azoethane.

TABLE 6. Second π-bond energy of N_2,* kJ mol^{-1}

	T	$\Delta H_4^{\ominus}$	E	$\Delta H_3^{\ominus}$
Azoisopropane	573 K	120±9	197±3	−273±10
Azoethane	573 K	128±9	205±2	−282±9
Azomethane	552 K	142±11	232±3	−322±12
Azobenzene	675 K	241±9	278±7	−315±16

*Data and references may be obtained from the Depository or the authors.

Such a conclusion should be treated cautiously for at least two reasons. It is very difficult to be certain that Arrhenius parameters of elementary reactions have been observed. For example, even azomethane, the most thoroughly studied of all, may well have a lower activation energy than that found in the presence of nitric oxide (for a comment on this possibility see ref. 19). For azobenzene, only preliminary evidence as to the effect of additives is available. In addition, an entirely different interpretation of the decomposition of three azoalkanes was considered by Gowenlock *et al.* (20). They concluded, from appearance potentials of radicals, that E is greater than $\Delta H_1^{\ominus}$. Besides, the radical $\cdot N{=}N\cdot$ was considered to be like the $A\,^3\Sigma_u^+$ spectroscopic state with energy E^*, and that if a radical such as $C_6H_5N{=}N\cdot$ is formed, E should be equal to $\frac{1}{2}(E^* + \Delta H_4)$, much greater than observed values.

Acknowledgements

We are greatly indebted to several members of the Department of Chemistry for their advice and encouragement and in particular to Dr. Peter Golding for his continuing interest and assistance. We thank the Department of Chemistry and the Division of Junior Studies of Memorial University for financial support.

1. M. J. JAQUISS and M. SZWARC. Nature (London), **170**, 312 (1952).
2. S. INOKAWA, R. GOTO, H. ARIOKA, and M. KUSE. Kogyo Kagaku Zasshi **67**, 1540 (1964).
3. A. LEIBA and I. OREF. J. Chem. Soc. Faraday Trans. **75**, 2694 (1979).
4. P. S. ENGEL. Chem. Rev. **80**, 99 (1980).
5. R. LOUW and J. W. ROTHUIZEN. Tetrahedron Lett. 3807 (1967).
6. H. K. CAMMENGA, E. BEHRENS, and E. WOLF. *In* Proc. of the 8th Int. Symp. on the Reactivity of Solids. *Edited by* J. Wood, O. Lindqvist, C. Helgesson, and N. G. Vannerberg. Plenum Press, New York. 1977. p. 481.
7. R. P. BENEDICT. Fundamentals of temperature, pressure, and flow measurements. 2nd ed. Wiley, New York. 1977.
8. M. F. R. MULCAHY and D. J. WILLIAMS. Aust. J. Chem. **14**, 534 (1961).
9. A. CORNU and R. MASSOT. Compilation of mass spectral data. 2nd ed. Heyden, London. 1975.
10. S. W. BENSON and H. E. O'NEAL. Kinetic data on gas phase unimolecular reactions. National Bureau of Standards (United States), 1970. p. 445.
11. W. FORST and O. K. RICE. Can. J. Chem. **41**, 562 (1963).
12. D. R. STULL, E. F. WESTRUM, JR., and G. C. SINKE. The chemical thermodynamics of organic compounds. Wiley, New York. 1969.
13. J. HALPERN, G. W. BRADY, and C. A. WINKLER. Can. J. Res. (B)**28**, 140 (1950).

Can. J. Chem. Downloaded from www.nrcresearchpress.com by 210.87.254.42 on 09/06/12
For personal use only.

14. S. W. BENSON. Thermochemical kinetics. 2nd ed. Wiley, New York. 1976, p. 64.
15. J. I. SEEMAN and W. A. FARONE. J. Org. Chem. **43**, 1854 (1978).
16. R. L. MONTGOMERY and F. D. ROSSINI. J. Phys. Chem. **82**, 575 (1978).
17. P. S. ENGEL, J. L. WOOD, J. A. SWEET, and J. L. MARGRAVE. J. Am. Chem. Soc. **96**, 2381 (1974).
18. P. S. ENGEL and D. J. BISHOP. J. Am. Chem. Soc. **97**, 6754 (1975).
19. D.-R. CHANG and O. K. RICE. Int. J. Chem. Kinet. **1**, 171 (1969).
20. B. G. GOWENLOCK, J. R. MAJER, and D. R. SNELLING. Trans. Faraday Soc. **58**, 670 (1962).

Can. J. Chem. Downloaded from www.nrcresearchpress.com by 210.87.254.42 on 09/06/12
For personal use only.

Donor numbers: ^{27}Al quadrupole relaxation as a measure of solvent donicity towards the sodium ion

MARION C. DAY,[1] JAMES H. MEDLEY, AND NASEER AHMAD
Department of Chemistry, Louisiana State University, Baton Rouge, LA 70803, U.S.A.

Received November 4, 1982

MARION C. DAY, JAMES H. MEDLEY, and NASEER AHMAD. Can. J. Chem. **61**, 1719 (1983).

A new method is presented for the determination of solvent donicity towards the sodium ion that avoids solvent–solvent interactions. Using the system

$NaAlEt_4$–benzene–donor

the response of the ^{27}Al quadrupole relaxation to anion symmetry as a function of donor:Na^+ ratio is monitored by both ^{27}Al line widths and methylene ^{1}H absorptions. The assumption is made that anion symmetry is dependent on the cation–anion interaction which is dependent on the stability of the donor–Na^+ solvates. The ordering of donors is found to differ from the generally accepted listing. A ranking of seventeen donors is given.

MARION C. DAY, JAMES H. MEDLEY et NASEER AHMAD. Can. J. Chem. **61**, 1719 (1983).

On présente une nouvelle méthode de détermination du caractère donneur du solvant envers l'ion sodium, qui élimine les interactions solvant–solvant. Utilisant le système

$NaAlEt_4$–benzène–donneur

on a enregistré la réponse de relaxation quadrupolaire du ^{27}Al à la symétrie de l'anion en fonction du rapport donneur: Na^+ en faisant appel à la fois à la largeur de la raie du ^{27}Al et aux absorptions du ^{1}H du méthylène. On pense que la symétrie de l'anion dépend de l'interaction cation–anion qui est fonction de la stabilité des produits de solvation du système donneur–Na^+. On trouve que l'arrangement des donneurs diffère du schéma généralement accepté. On présente une classification comprenant dix-sept donneurs.

[Traduit par le journal]

Introduction

The importance of solvent donicity to the study of ionic solutions in nonaqueous media is certainly well accepted today with the Gutmann donor numbers being the most commonly used representation (1). This is simply ΔH of the reaction

[1] $D + SbCl_5 \rightarrow SbCl_5D$

Obviously ΔH of this reaction does not give a complete measure of the complexing ability of the donor, D. Nevertheless, it does seem to give a reasonable measure of the desired quantity. Extensions of the Gutmann scale have been made using a variety of techniques (2), but Gutmann distinguishes between donor numbers determined by eq. [1], and values obtained by alternative methods (2). The extended Gutmann scale is now generally used regardless of the Lewis acid. But one cannot help but question the general applicability of the scale, particularly towards small cations such as Li^+, Na^+, and K^+, where the ion–solvent interaction may be more reasonably considered as ion–dipole.

This question appeared to be resolved as a result of the ^{23}Na nmr chemical shift studies of Erlich, Roach, and Popov (3). They observed the ^{23}Na chemical shifts of sodium tetraphenylborate in eleven different solvents and noted a linear relationship between the chemical shifts and the Gutmann donor numbers. This was later extended to sixteen different donors (4). However, a complication arose when Greenberg and Popov later found that pyridine (py) appeared to be a much weaker donor than either dimethylsulfoxide (DMSO) or tetramethylurea (TMU) (5). Both of these have lower donor numbers than pyridine, yet in the mixed solvent systems of DMSO–py and TMU–py, the Na^+ ion was preferentially solvated in each case by the supposed weaker donor. Greenberg and Popov rationalized these results by means of solvent structure arguments (5). It was later reported from this laboratory that py is, in fact, a relatively poor donor towards the Na^+ ion (6) and this was supported by Popov (7).

In our studies of the sodium ion, we have noted a number of donors that seem to be out of line with those listed in the extended Gutmann scale. And, although we find many that do agree with those of Gutmann as well as with the ^{23}Na chemical shift study of Popov and co-workers, our observations indicate that the extended Gutmann donor numbers are not generally applicable to the sodium ion. This is unfortunate in light of the strong interest in solution studies of the sodium ion.

We have taken advantage of the unique behavior of the system

$NaAlEt_4$–benzene–donor

to determine donicities toward the sodium ion. In this study we are observing the line widths at half height of the ^{27}Al nmr band as a function of donor:Na^+ ratio. Because of the ^{27}Al quadrupole ($I = 5/2$), the relaxation rate is strongly dependent on the symmetry of the $AlEt_4^-$ ion, and this is dependent on the cation–anion interactions. If the cation is totally solvated, the anion will assume t_d symmetry (8), but if a site is available on the cation, the resultant ion–ion interaction will lead to an electric field gradient and a corresponding line broadening of the ^{27}Al signal.

The ^{27}Al quadrupole relaxation is also reflected in the ^{1}H nmr spectra, and this offers an additional probe of the symmetry of the $AlEt_4^-$ ion (8*b*). In samples containing anions with cubic symmetry, the methylene absorption appears as a well defined nine-line pattern representing the fortuitous overlapping of resonances resulting from essentially equal spin–spin interactions of methylene protons with both the neighboring methyl protons and the aluminum nucleus. Conversely, in samples containing

[1]To whom all correspondence should be addressed.

Can. J. Chem. Downloaded from www.nrcresearchpress.com by 210.87.254.42 on 09/06/12
For personal use only.

TABLE 1. Relative donicities towards the sodium ion

Donor	4:1 D:Na^+ $W_{1/2}$[d]	4:1 D:Na^+ Concentration (M)	4:1 D:Na^+ 9-line pattern	6:1 D:Na^+ $W_{1/2}$[d]	6:1 D:Na^+ Concentration (M)	6:1 D:Na^+ 9-line pattern	D as solvent $W_{1/2}$[d]	D as solvent Concentration (M)	D as solvent 9-line pattern	Gutmann DN
HMPA	3.0	0.36	S	2.0	0.3	S	3.0	0.3	S	38.8
DMSO	10	2.14	M^-	4.5	1.25	S	3.0	0.3	S	29.8
DMF	4.5	0.38	M^+	4.5	0.3	S	6.0	0.3	S	26.6
DMA	4.5	0.53	M	3.5	0.3	S	2.0	0.3	S	27.8
1M-2PY	6.0	0.48	W^+	3.5	0.3	M^+	4.5	0.3	S	27.3
TMP	7.0	0.60	W^+	4.0	0.3	M^+	4.5	0.3	S	23
TMU	8.0	0.40	W	3.5	0.3	S	3.0	0.3	S	28.9[b]
PC	17	0.51	—	8.0	0.52	M	4.0	0.3	S	15.1
1,3PDA[a]	39	0.60	—	8.0	0.6	W	4.5	0.3	S	—[c]
DME[a]	41	0.60	—	7.0	0.6	W	2.0	0.3	S	24[b]
AN	30	0.30	—	18	0.3	—	6.5	0.3	S	14.1
THF	41	0.30	—	21	0.3	—	6.0	0.3	S	20
py	49	0.30	—	28	0.3	—	4.5	0.3	S	33.1
DMC	52	0.30	—	36	0.3	—	11	0.3	M	—[c]
DEE	88	0.30	—	86	0.3	—	68	0.3	—	19.2
TEA	170	0.30	—	166	0.3	—	136	0.3	—	61[b]
QN	250	0.30	—	250	0.3	—	330	0.3	—	—[c]

[a]Bidentate.
[b]Based on ^{23}Na chemical shifts.
[c]Not determined.
[d]In units of Hz.

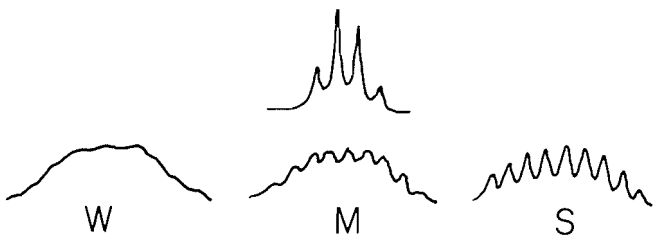

FIG. 1. Methylene resonances representing various degrees of symmetry in the $AlEt_4^-$ ion.

highly distorted anions, the $^{27}Al-{}^1H$ spin–spin interactions are not observed in the ^1H nmr spectra. Rather, the resonance collapses to a 1,3,3,1 quartet resulting from the remaining $^1H-{}^1H$ spin interaction. The two extremes, a nine-line pattern representing anionic t_d symmetry and a quartet corresponding to the highly distorted anion, as would occur in the presence of a strong donor and a weak donor respectively, are logically related to solvent-separated and contact ion-pairs (8).

Experimental procedures

The preparation of $NaAlEt_4$, benzene, and the samples is described elsewhere (9). Propylene carbonate (PC) and dimethylcarbonate (DMC) were distilled over molecular sieves. The other solvating agents[2] were distilled over CaH_2 and handled as described earlier (6, 9). ^1H noise decoupled ^{27}Al nmr spectra were obtained on a Bruker WP-200 FTNMR Spectrometer with a broad band tunable probe. The spectra were acquired using 2 K data points over a spectral window of 500 Hz for a digital resolution of 0.5 Hz. Spectra with very broad resonances were acquired using a 1000 Hz spectral window. The ^1H spectra were obtained on a Varian A60A spectrometer. In most instances the salt concentrations were 0.30 M. However, solutions of strong donors in these systems tend to form two liquid phases in benzene at certain D:Na^+ ratios. Consequently, where two phasing is restrictive, the concentration will vary, except for the DMSO systems, ranging up to a maximum of 0.60 M. For the DMSO systems, much higher concentrations occur (4:1 D:Na^+ = 2.14 M and 6:1 D:Na^+ = 1.25 M). No corrections have been made for solution viscosity. Except for the DMSO systems, it is felt that viscosity does not significantly affect the interpretation of the data. The viscosities of those systems tested were of the order of 1 cp at both the 4:1 and 6:1 ratios of D:Na^+. For DMSO, the viscosity was approximately 10 cp at the 4:1 ratio and 2 cp at the 6:1 ratio.

[2]Hexamethylphosphoramide (HMPA); dimethylsulfoxide (DMSO); dimethylformamide (DMF); dimethylacetamide (DMA); 1-methyl-2-pyrolidone (1M-2PY); trimethylphosphate (TMP); tetramethylurea (TMU); 1,3-propanediamine (1,3PDA); dimethoxyethane (DME); acetonitrile (AN); tetrahydrofuran (THF); pyridine (py); diethylether (DEE); triethylamine (TEA); quinuclidine (QN).

Results and discussion

In Table 1, the ^{27}Al line widths at half height are given at donor:Na^+ ratios of (*a*) 4:1, (*b*) 6:1, and (*c*) with donor as solvent. The nine-line pattern characteristic of solvent separated ion-pairs is also presented. The symbolism for the nine-line pattern is shown in Fig. 1. The well-defined pattern symbolized by S represents a highly symmetrical $AlEt_4^-$ ion. For those designated as M and W, a high degree of symmetry is also assumed. In contrast, the quartet shows the methylene resonance in a highly distorted $AlEt_4^-$ ion. By considering both the ^{27}Al line widths and the methylene proton resonances (nine-line pattern), we propose the order of donicities towards the sodium ion listed in Table 1. The only donor whose position is clearly questionable is DMSO. The data indicate it should be placed below DMA or perhaps TMU. However, considering the affects of viscosity on the spectra, there seems to be no basis for changing its position from that in the Gutmann scale at this time.

We have chosen the data based on the 4:1 D:Na^+ ratio for our primary evaluation. Whether the solvation number of the Na^+ ion is 4 or 6 with a given donor, the four-coordinated species is capable of forming a predominantly solvent-separated ion-pair (6*b*). This point is supported by a con-

Can. J. Chem. Downloaded from www.nrcresearchpress.com by 210.87.254.42 on 09/06/12
For personal use only.

sideration of the ^1H nmr spectra of the DMF, DMA, and TMU solvates. In this series, the 4:1 solvate with TMU should clearly form a more sterically hindered cation toward the anion than either DMF or DMA. Yet we observe that both the ^{27}Al line widths and the appearance of the nine-line pattern indicate that TMU is the weakest donor of the three. This logically can be attributed to equilibria of the type

$$Na^+ \cdot 4D \leftrightharpoons Na^+ \cdot 3D + D$$
$$Na^+ \cdot 3D + AlEt_4^- \leftrightharpoons [Na^+ \cdot 3D/AlEt_4^-]^0$$

There several particularly interesting points to note. First one can see that the listing can be divided into four general groups. (*1*) Strong donors: HMPA–TMU; (*2*) intermediate donors: PC; 1,3PDA; and DME; (*3*) moderate donors: AN–DMC; (*4*) weak donors: DEE–QN. It seems reasonable to conclude that any of the donors from DMC to HMPA will form predominately solvent-separated ion-pairs in the respective pure solvent. One may then expect that differences in ionic behavior in these pure solvents could more reasonably be attributed to solvent dielectric constant than to specific ion–solvent interaction.

It should also be noted that nitrogen donors are especially poor donors towards the sodium ion. On the extended Gutmann DN scale, TEA and py are considered to be very strong donors, and they may be towards $SbCl_5$. But this is not the case towards the sodium ion. We reported the poor donor ability of TEA towards the sodium ion in 1968 (10), and it is confirmed in this study. In an earlier study, Garst and co-workers, using the ketyl spectra of sodium benzophenone ketyl in a variety of solvents, also observed that both py and TEA are poor donors towards the sodium ion (11). Popov *et al.* have attributed the poor donicity of py to a sodium ion (hard) – nitrogen (soft) hard–soft acid–base behavior (7).

Among those we have studied, there are five donors that show quite different relative solvating ability towards the sodium ion than expected from the extended Gutmann donor number scale. These are TMU, AN, py, PC, and TEA. The most striking is TEA which has the highest DN on the extended Gutmann scale, 61. Yet it is among the poorest donors towards the sodium ion.

Finally, it is tempting to use the ^{27}Al line widths to imply solvation numbers for the sodium ion. It may well be that for the strong donors this is possible. However, it is far from certain. We are presently extending this study in combination with ^{23}Na nmr measurements with the intent of determining solvation numbers and are also applying this technique to the determination of a donor scale towards the lithium ion.

Acknowledgements

The authors wish to express their appreciation for the support of this work by the National Science Foundation through NSF grant CHE-8004473 and to the Ethyl Corporation for the aluminum alkyls.

1. (*a*) C. REICHARDT. Solvent effects in organic chemistry. Verlag Chemie, New York. 1979. p. 17; (*b*) T. R. GRIFFITHS and D. C. PUGH. Coord. Chem. Rev. **29**, 129 (1979).
2. V. GUTMANN. The donor acceptor approach to molecular interactions. Plenum Press, New York. 1978.
3. R. H. ERLICH, E. ROACH, and A. I. POPOV. J. Am. Chem. Soc. **92**, 4989 (1970).
4. A. I. POPOV. Pure Appl. Chem. **41**, 275 (1975).
5. M. S. GREENBERG and A. I. POPOV. Spectrochim. Acta, **31**A, 697 (1975).
6. (*a*) M. C. DAY and N. AHMAD. Vth Int. Conf. on Nonaq. Solns., Leeds, England. July 1976; (*b*) N. AHMAD and M. C. DAY. J. Am. Chem. Soc. **99**, 941 (1977).
7. A. HOURDAKIS and A. I. POPOV. J. Soln. Chem. **6**, 299 (1977).
8. (*a*) E. S. GORE and H. S. GUTOWSKY. J. Phys. Chem. **73**, 2515 (1969); (*b*) T. D. WESTMORELAND, N. S. BHACCA, J. D. WANDER, and M. C. DAY. J. Organomet. Chem. **38**, 1 (1972).
9. (*a*) E. G. HÖHN, J. A. OLANDER, and M. C. DAY. J. Phys. Chem. **73**, 3880 (1969); (*b*) F. W. FREY and P. KOBETZ. J. Org. Chem. **26**, 2950 (1961).
10. E. SCHASCHEL and M. C. DAY. J. Am. Chem. Soc. **90**, 503 (1968).
11. J. GARST, D. WALMSLEY, C. HEWITT, W. RICHARDS, and E. ZABOLOTNY. J. Am. Chem. Soc. **86**, 412 (1964).

Can. J. Chem. Downloaded from www.nrcresearchpress.com by 210.87.254.42 on 09/06/12
For personal use only.

Ionized ethylidene ketene and its homologue methylene ketene

JOHAN K. TERLOUW[1]
Analytical Chemistry Laboratory, University of Utrecht, Croesestraat, 77A, 3522 AD, Utrecht, The Netherlands
AND
JOHN L. HOLMES[1] AND F. P. LOSSING
Chemistry Department, University of Ottawa, Ottawa, Ont., Canada K1N 9B4

Received December 16, 1982

JOHAN K. TERLOUW, JOHN L. HOLMES, and F. P. LOSSING. Can. J. Chem. **61**, 1722 (1983).

The gas phase pyrolyses of crotonic and acrylic-trifluoroacetic anhydrides were shown to yield ethylidene ketene [$CH_3CH{=}C{=}C{=}O$] and methylene ketene [$CH_2{=}C{=}C{=}O$], respectively. The former was identified via the collisional activation mass spectrum of its molecular ion. The ionization energies of the two ketenes, 8.68 and 9.12 ± 0.05 eV respectively, measured using energy selected electrons, lead to 215 and 233 kcal mol^{-1} for their ionic heats of formation.

JOHAN K. TERLOUW, JOHN L. HOLMES et F. P. LOSSING. Can. J. Chem. **61**, 1722 (1983).

La pyrolyse en phase gazeuse de l'anhydride crotonique et de l'anhydride acrylic-trifluoroacétique donne respectivement le cétène éthylidène [$CH_3CH{=}C{=}C{=}O$] et le cétène méthylène [$CH_2{=}C{=}C{=}O$]. On a identifié le premier par l'intermédiaire du spectre de masse d'activation collisionnelle de son ion moléculaire. Les énergies d'ionisation des deux cétènes, 8,68 et 9,12 ± 0,05 eV respectivement, mesurées en utilisant des électrons d'énergie convenable, conduisent à des chaleurs ionique de formation de 215 et de 233 kcal mol^{-1}.

[Traduit par le journal]

Can. J. Chem. Downloaded from www.nrcresearchpress.com by 210.87.254.6 on 09/06/12
For personal use only.

Introduction

In a recent publication (1) on the characterization and properties of isomeric $[C_4H_4O]^{+\cdot}$ ions, it was proposed that the low pressure, short contact-time pyrolysis of the mixed anhydride of crotonic and trifluoroacetic acids should yield ethylidene ketene (*a*), buta-1,2-dienone, $CH_3CH{=}C{=}C{=}O$. The gas-phase ion chemistry of its isomer vinyl ketene, (*b*), had been

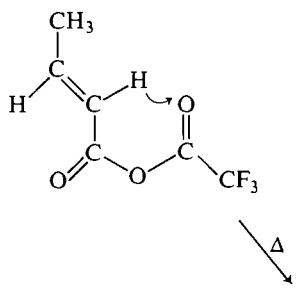

$$CH_3CH{=}C{=}C{=}O + CF_3COOH$$

described earlier (2). In these experiments (1) the pyrolysis oven was attached to the electron monochromator and associated quadrupole mass spectrometer apparatus (3) used to measure ionization (IE) and appearance energies (AE); $\Delta H_f[CH_3CH{=}C{=}C{=}O]^{+\cdot}$ was reported to be 202 kcal mol^{-1}, IE = 8.07 eV.

Since the completion of our study (1), Bock and co-workers (4) have published the pyrolytic formation of vinyl and ethylidene ketenes by means of photoelectron spectroscopy (PES). Ethylidene ketene was only observed using the short contact time, low pressure pyrolysis (760 K) of an ethylidene malonate (5-ethylidene-2,2-dimethyl-1,3-dioxane-4,6-dione). At longer contact times, vinyl ketene, the thermodynamically more stable product, predominated. The vertical IE of (*a*) was given as 8.9 eV; the presence of (*b*) (vertical IE = 8.4 eV) and/or other pyrolysis products made uncertain the identification of the vertical band for (*a*) but its satisfactory assignment was aided by MNDO calculations. MNDO calculations were also used to estimate $\Delta H_f[CH_3CH{=}C{=}C{=}O]$ = 12 kcal mol^{-1}; this together with the above IE gives $\Delta H_f[CH_3CHC{=}C{=}O]^{+\cdot}$ = 217 kcal mol^{-1}.

However, both our and Bock's pyrolytic methods lack a detection system which can establish the structural identity of ionized pyrolysis products. Because of this shortcoming of our equipment and in view of the disagreement between the above two IE values, a pyrolysis inlet system of similar design to that used for the thermochemical measurements (3) was built and attached to the ion source of the Utrecht VG ZAB-2F mass spectrometer. Collisional activation (CA) mass spectra could now be used to examine ions of m/z = 68 and having the molecular formula $[C_4H_4O]^{+\cdot}$.

We report here the solution of the above problem together with thermochemical data for ionized methylene ketene, $[CH_2{=}C{=}C{=}O]^{+\cdot}$, a small molecule of potential interest in interstellar chemistry. Neutral methylene ketene has been made by Blackman *et al.* (5) in a series of microwave spectroscopic studies of substituted ketenes. The flash vacuum pyrolyses of diphenylmethyl propiolate, 2′,2′-dimethylspiro[bicyclo[2,2,1]hept-5-ene-2,5′-[1,3]dioxan]-4′,6′-dione and acrylic anhydride all yielded the desired product. The latter was the best source, being efficiently (albeit incompletely) pyrolyzed at 680–730 K and 0.2–0.5 Torr. Pyrolysis conditions are clearly important in such work; Bock and co-workers (4) could not observe methylene ketene for this pyrolysis in their apparatus, obtaining instead the ketene's decomposition products, acetylene and carbon monoxide, together with acrylic acid.

Although deemed unsuitable for post-pyrolysis trapping experiments (6), we find the mixed anhydrides to be particularly satisfactory for mass spectrometric investigations because of their relatively high volatility and the absence of interference from the cogenerated unsaturated acid.

Results and discussion

Production and identification of ethylidene ketene

Table 1 shows the effect of pyrolysis temperature on relative

[1]Authors to whom correspondence may be addressed.

Can. J. Chem. Downloaded from www.nrcresearchpress.com by 210.87.254.6 on 09/06/12
For personal use only.

TABLE 1. Partial mass spectra[a] of crotonic-trifluoroacetic anhydride and its pyrolysis products

	Pyrolysis temperature, K				
m/z	300	720	920	1020	Ion
69	280	105	70	20	$[CF_3]^+$, $[C_4H_5O]^+$ [b]
68	20	65	100	25	$[C_4H_4O]^{+\cdot}$
53	2	15	55	10	$[C_3HO]^+$
45	110	350	220	220	$[CO_2H]^+$
41	310	155	65	60	$[C_3H_5]^+$
40	80	95	190	320	$[C_3H_4]$
39	180	155	220	290	$[C_3H_3]^+$

[a]Quadrupole mass spectrometer; ionizing electron energy 25 V (3). Partial mass spectra only, for semi-quantitative comparison.
[b]$[C_4H_5O]^+$ only present at 300 K, observation from VG ZAB-2F mass spectrometer.

ion product yields, measured using the apparatus described in ref. 3. 920 K was the optimum temperature for maximum pyrolytic yield of C_4H_4O. At higher temperatures the yield fell and C_3H_4, the probable decomposition product (loss of CO), increased. Note that *m/z* 68 and *m/z* 53 are only minor peaks in the normal (room temperature) mass spectrum. Experiments performed using the ZAB-2F mass spectrometer's pyrolytic inlet system gave similar product distributions as the temperature was raised. Pyrolysis temperatures were not directly comparable because of differences in thermocouple positions in the two ovens. As can be seen from Table 2, the CA mass spectrum of *m/z* 68 ions produced at optimum pyrolysis conditions is dominated by peaks at *m/z* 39, 40, and 53. The latter peak, loss of $CH_3^{\cdot}$, is also prominent in the corresponding normal mass spectrum (Table 1). This CA mass spectrum, which is very different from all those reported previously (1), is deemed to be that of ionized ethylidene ketene; the peak at *m/z* 53 is certainly highly structure diagnostic. Only $[CH_3COC{\equiv}CH]^{+\cdot}$ displayed an intense *m/z* 53 ion in its normal and CA mass spectra (1) to yield the same fragment ion by simple bond cleavage:

$$[CH_3COC{\equiv}CH]^{+\cdot} \rightarrow CH_3^{\cdot} + HC{\equiv}C{-}\overset{+}{C}{=}O$$
$$[CH_3CH{=}C{=}C{=}O]^{+\cdot} \rightarrow CH_3^{\cdot} + HC{\equiv}C{-}\overset{+}{C}{=}O$$

These new observations render invalid our earlier proposal (1) that the CA mass spectrum of $[C_4H_4O]^{+\cdot}$ ions produced from the dissociative ionization of itaconic and citraconic anhydrides and the methyl ester of allene carboxylic acid have the ethylidene ketene structure.

Essentially no ethylidene ketene was generated at temperatures ca. 250 K above optimum (see Table 2). This was concluded from the normal mass spectrum where, although *m/z* 68 was still present, *m/z* 53 had vanished. Also present were new peaks (e.g. *m/z* 44, 66) arising from complex pyrolyses. The CA mass spectrum of these *m/z* 68 ions resembles that of vinyl ketene more closely than that of any of the other fourteen $[C_4H_4O]^{+\cdot}$ ions reported previously (1). The imperfect match between the relative abundances of *m/z* 42 and 40, both of which arise from unimolecular as well as collisionally induced fragmentations, may well be due to internal energy effects, to which the former are always sensitive. The possible coproduction of other $[C_4H_4O]$ isomers cannot, however, entirely be ruled out. Note that Bock and co-workers (4) observed that at long contact times ethylidene ketene was also replaced by vinyl ketene.

Thermochemistry of ionized ethylidene ketene and methylene ketene

The ionisation energy (IE) of $[CH_3CH{=}C{=}C{=}O]$ was measured using energy selected electrons (3) at the optimal condition for its production (Table 1); IE = 8.68 ± 0.05 eV. $\Delta H_f[CH_3CH{=}C{=}C{=}O]$ = +15.1 kcal mol^{-1}, by additivity (7) and using a $(CO)_d$ term = −17.7 kcal mol^{-1}, a revised value because of a change in $\Delta H_f[CH_2CO]$ from −14.6 (8) to −11.4 kcal mol^{-1} (9). Whence, $\Delta H_f[CH_3CH{=}C{=}C{=}O]^{+\cdot}$ = 215 kcal mol^{-1}. The above IE is to be compared with the *vertical* IE of Bock and co-workers (4), 8.9 eV. They chose a MNDO calculation to obtain ΔH_f for the neutral ketene = +12 kcal mol^{-1}; these results give $\Delta H_f[CH_3CH{=}C{=}C{=}O]^{+\cdot}$ = 217 kcal mol^{-1}.

The AE of *m/z* 53, $[HC{\equiv}C{-}\overset{+}{C}{=}O]$, was also measured, 11.02 ± 0.05 eV; $\Delta H_f[HC{\equiv}C{-}C{=}O]$ = 234 kcal mol^{-1} ($\Delta H_f[CH_3^{\cdot}]$ = 34 kcal mol^{-1} (8)), a result which compares favorably with that obtained from the AE of *m/z* 53 from $CH_3COC{\equiv}CH$ (1), 230 kcal mol^{-1}.

The pyrolysis of acrylic-trifluoroacetic anhydride was used to generate methylene ketene at an optimum temperature of 1020 K. The base peak in the normal mass spectrum of the anhydride is *m/z* 55 and *m/z* 54 is absent. At the optimum pyrolysis temperature, *m/z* 55 and *m/z* 54 display similar abundances, indicating that the pyrolysis is incomplete. However, at higher temperatures the $CH_2{=}C{=}C{=}O$ yield falls as a result of its decomposition to C_2H_2 and CO. $\Delta H_f[CH_2{=}C{=}C{=}O]^{+\cdot}$ = 233 kcal mol^{-1} from IE = 9.12 ± 0.05 eV and $\Delta H_f[CH_2{=}C{=}C{=}O]$ = 22.8 kcal mol^{-1}, again from additivity (ref. 7 and see above).

The effect of methyl substitution in ionized methylene ketene is to reduce $\Delta H_f[ion]^{+\cdot}$ by 18 kcal mol^{-1}, substantially less than the same replacement on ketene itself, 25 kcal mol^{-1} ($\Delta H_f[CH_2{=}C{=}O]^{+\cdot}$ = 210 kcal mol^{-1} (8, 9); $\Delta H_f[CH_3CH{=}C{=}O]^{+\cdot}$ = 185 kcal mol^{-1} (IE = 8.95 eV (12); $\Delta H_f[CH_3CH{=}C{=}O]$ = −21.5 kcal mol^{-1} (ref. 7, and see above)). The effect on ketene is typical of the methyl substitution – ion size relationship discussed elsewhere (13), but the effect on methylene ketene is lower than expected by ca. 7 kcal mol^{-1}. This discrepancy could arise from an inadequacy in the additivity terms for such molecules or from the charge distribution being different from that obtaining in the simple ketenes.

It is useful also to compare $\Delta H_f[CH_2{=}C{=}C{=}O]^{+\cdot}$ and $\Delta H_f[CH_2{=}C{=}O]^{+\cdot}$ with those of the isoelectronic ions $[CH_2{=}C{=}CH_2]^{+\cdot}$, ΔH_f = 269 kcal mol^{-1} (8) and $[CH_2{=}C{=}C{=}CH_2]^{+\cdot}$, ΔH_f = 293 kcal mol^{-1} (IE = 9.2 ± 0.05 eV (10, 11), $\Delta H_f[CH_2{=}C{=}C{=}CH_2]$ = 81 kcal mol^{-1} (7)). Thus $\Delta(\Delta H_f)$ for the oxy-ions, 23 kcal mol^{-1}, is within experimental error the same as that for the isoelectronic hydrocarbon ions, 24 kcal mol^{-1}.

Experimental

The pyrolysis oven, electron monochromator, and associated apparatus for measuring IE and AE values has been described (3). The CA mass spectra were obtained using a VG ZAB-2F mass spectrometer by conventional means (14). The pyrolysis oven for the ZAB instrument was constructed of silica, electrically heated, and with a high temperature zone of ca. 2.5 cm length. The exit from the oven into the ion source was situated ca. 3.5 cm from the ionizing electron beam in a

TABLE 2. Partial collisonal activation mass spectra of ionized C_4H_4O. Pyrolysis product from crotonic-trifluoroacetic anhydride compared with vinyl ketene (3)

	Mass spectra, *m/z*											
Pyrolysis	67	54	53	52	51	50	42	41	40	39	38	37
Optimum (see text)	46	1.5	94	6	4	6.5	9.5	4	100	94	42	28
Optimum + 250 K	11	5.5	5	1	2.5	5	24	8	71	100	27	20
(Vinyl ketene)	6	4	3.5	1	2.5	5.5	18	7	36	100	33	22

standard electron-impact ion source. Compounds were introduced via a 100 lusec sintered glass leak from a heated gold plated vapour reservoir of volume ca. 0.12 L. The anhydrides were synthesized from the appropriate acid chloride and sodium trifluoroacetate by a standard procedure (15).

1. P. C. BURGERS, J. L. HOLMES, F. P. LOSSING, A. A. MOMMERS, F. R. POVEL, and J. K. TERLOUW. Can. J. Chem. **60**, 2246 (1982).
2. J. K. TERLOUW, P. C. BURGERS, and J. L. HOLMES. J. Am. Chem. Soc. **101**, 225 (1979).
3. K. MAEDA, G. P. SEMELUK, and F. P. LOSSING. Int. J. Mass Spectrom. Ion Phys. **1**, 395 (1968); F. P. LOSSING and J. C. TRAEGER. Int. J. Mass Spectrom. Ion Phys. **19**, 9 (1976).
4. S. MOHMAND, T. HIRABAYASHI, and H. BOCK. Chem. Ber. **114**, 2609 (1981).
5. G. L. BLACKMAN, R. D. BROWN, R. F. C. BROWN, F. W. EASTWOOD, G. L. MCMULLEN, and M. L. ROBERTSON. Aust. J. Chem. **31**, 209 (1978).
6. R. D. BROWN, R. F. C. BROWN, F. W. EASTWOOD, P. O. GODFREY, and D. MCNAUGHTON. J. Am. Chem. Soc. **101**, 4705 (1979).
7. S. W. BENSON, F. R. CRUICKSHANK, D. M. GOLDEN, G. R. HAUGEN, H. E. O'NEAL, A. S. RODGERS, R. SHAW, and R. WALSH. Chem. Rev. **69**, 279 (1969).
8. H. M. ROSENSTOCK, K. DRAXL, B. W. STEINER, and J. T. HERRON. J. Phys. Chem. Ref. Data Suppl. **6**, 1 (1977).
9. J. B. PEDLEY and J. RYLANCE. Computer analysed thermochemical data; organic and organometallic compounds. University of Sussex. 1977.
10. H. M. ROSENSTOCK, K. E. MCCULLOH, and F. P. LOSSING. Int. J. Mass Spectrom. Ion Phys. **25**, 327 (1977).
11. F. BROGLI, E. HEILBRONNER, E. KLOSTER-JENSEN, A. SCHMELZER, A. S. MANOCHA, J. A. POPLE, and L. RADOM. Chem. Phys. **4**, 107 (1974).
12. H. BOCK, T. HIRABAYASHI, S. MOHMAND, and B. SOLOUKI. Angew. Chem. **89**, 106 (1977).
13. J. L. HOLMES and F. P. LOSSING. Can. J. Chem. **60**, 2365 (1982).
14. J. K. TERLOUW, P. C. BURGERS, and H. HOMMES. Org. Mass Spectrom. **14**, 387 (1979).
15. A. I. VOGEL. Textbook of practical organic chemistry. Longmans, Green and Co., New York. 1978.

Can. J. Chem. Downloaded from www.nrcresearchpress.com by 210.87.254.6 on 09/06/12
For personal use only.

An iterative technique for calculating surface tensions of non-electrolyte solutions

DOUGLAS E. GOLDSACK AND BRIAN R. WHITE
Department of Chemistry, Laurentian University, Sudbury, Ont., Canada P3E 2C6

Received July 8, 1982[1]

DOUGLAS E. GOLDSACK and BRIAN R. WHITE. Can. J. Chem. **61**, 1725 (1983).

The surface tension of mixtures of organic non-electrolytes of high polarity difference has been shown to be calculable to within a 1% average error using a Newton–Raphson iterative technique to solve the implicit Butler equations for the surface concentrations combined with a better approximation to the surface density of the pure components through an anisotropic surface model. Application of these same techniques to aqueous systems was attempted with some success. However, significant deviations between observed and calculated surface tensions for some binary aqueous systems still remain. It is suggested that these deviations could be accounted for by the inclusion of non-ideal behaviour in the surface and bulk phases.

DOUGLAS E. GOLDSACK et BRIAN R. WHITE. Can. J. Chem. **61**, 1725 (1983).

On montre que l'on peut calculer la tension de surface des mélanges de non électrolytes organiques ayant une grande différence de polarité, avec une marge d'erreur de 1%. On utilise la technique itérative de Newton–Raphson pour résoudre les équations implicites de Butler relatives aux concentrations de surface combinées avec une meilleure approximation en ce qui a trait à la densité de surface des composés purs dans un modèle de surface anisotropique. On a essayé, avec un certain succès, d'appliquer ces mêmes techniques aux systèmes aqueux. Cependant on a encore observé des écarts importants entre les tensions de surface observées et calculées de quelques systèmes aqueux binaires. On suggère que ces écarts sont dûs à l'inclusion d'un comportement non idéal dans la surface et dans les phases encombrées.

[Traduit par le journal]

Can. J. Chem. Downloaded from www.nrcresearchpress.com by 210.87.254.5 on 09/06/12
For personal use only.

Introduction

An earlier study (1) has shown that the surface tension, σ, of binary mixtures of organic non-electrolytes could be calculated with an explicit equation to within 1–3% error for most systems. This equation consists of a linear component and a first and second order deviation term given by:

$$[1] \quad \sigma = \sigma_1 X_1 + \sigma_2 X_2 + RTX_1X_2\Delta\left[\frac{(A_2A_1)}{A_1A_2}\right] - \frac{RT}{2}X_1X_2\Delta^2\left[\frac{A_1X_1 + A_2X_2}{A_1A_2}\right]$$

where σ_1 and σ_2 are the surface tensions, A_1 and A_2 are the molar surface areas, and X_1 and X_2 are the bulk liquid mole fractions of components 1 and 2 respectively, R is the gas constant and T is the absolute temperature. The term Δ is a dimensionless parameter defined by:

$$[2] \quad \Delta = \frac{(\sigma_2 - \sigma_1)A_1A_2}{(A_1X_1 + A_2X_2)RT}$$

This equation assumes a monolayer model for the surface of the liquid, as well as ideal solution behaviour in both the surface and bulk liquid phases. Furthermore, when volume fraction statistics were substituted for mole fraction statistics, no significant improvement in predicting the surface tension of these binary mixtures was noted (1).

Equation [1] was found to be generally useful only for non-polar–non-polar and polar–non-polar binary systems for which $(\sigma_2 - \sigma_1) < 10$ ergs/cm^2. For polar–non-polar systems where $(\sigma_2 - \sigma_1) > 20$, eq. [1] was found to be inapplicable because the mathematical approximations used in deriving eq. [1] are not valid. For these types of systems, only implicit equations in σ are valid, and these equations are intractible.

Since there is a great deal of interest in aqueous systems of non-electrolytes, particularly for biological applications, and since such systems generally have $(\sigma_2 - \sigma_1)$ values much greater than 20 ergs/cm^2 as well as large differences in molar volumes, it would be useful to find a general mathematical approach for determining the surface tension of such mixtures. The purpose of this paper is to outline such a mathematical approach, and to show to what extent the ideal solution approximation for both the surface and bulk phases can be applied to these extremely polar–non-polar mixtures. It will also be shown that the use of surface volumes, as determined from the anisotropic surface model (2) rather than bulk liquid volumes, for calculating the molar surface area values, A_i, results in a substantial improvement in the calculated surface tensions of such systems.

Theory

If it is assumed that the surface layer can be treated as a separate phase, and if it is further assumed that the bulk liquid and surface phases are ideal, then the surface tension of a binary liquid mixture is given by:

$$[3] \quad \sigma = \sigma_1 + \frac{RT}{A_1}\ln\frac{X_{1S}}{X_{1B}}$$

$$[4] \quad \sigma = \sigma_2 + \frac{RT}{A_2}\ln\frac{X_{2S}}{X_{2B}}$$

where X_{1S}, X_{2S} and X_{1B}, X_{2B} are the mole fractions of component 1 and 2 respectively in the surface and bulk phases. These equations are known as the Butler equations (3). If eqs. [3] and [4] are multiplied by X_{1B} and X_{2B} respectively and added, the resulting surface tension equation then consists of a linear term containing known bulk liquid concentrations and non-linear terms due to the free energy of mixing.

$$[5] \quad \sigma = (\sigma_1X_{1B} + \sigma_2X_{2B}) + X_{1B}\frac{RT}{A_1}\ln\frac{X_{1S}}{X_{1B}} + X_{2B}\frac{RT}{A_2}\ln\frac{X_{2S}}{X_{2B}}$$

If a method existed for measuring or calculating the surface concentrations X_{1S} or X_{2S}, then it would be possible to predict directly the surface tension of any binary liquid system. It has been shown previously (1) that the introduction of a dimensionless parameter, Δ, which was first used by Prigogine *et al.*

[1]Revision received February 18, 1983.

(4), led to an explicit equation for σ in terms of bulk concentrations given by the following relation:

$$[6] \quad \sigma = \sigma_1 X_1 + \sigma_2 X_2 + \frac{X_1 RT}{A_1} \ln (1 + X_2\Delta) + \frac{X_2 RT}{A_2} \ln (1 - X_1\Delta)$$

where

$$[7] \quad \Delta = \frac{(\sigma_2 - \sigma_1)A_1 A_2}{(A_1 X_1 + A_2 X_2)RT}$$

and X_1, X_2 without the subscripts refer to bulk liquid concentrations only. The use of the parameter Δ is restricted to solutions where $X_1\Delta$ and $X_2\Delta$ are significantly smaller than unity. Under these conditions eq. [6] can be expanded to yield:

$$[8] \quad \sigma = (\sigma_1 X_1 + \sigma_2 X_2) + RTX_1X_2\Delta\left[\frac{(A_2 - A_1)}{A_1A_2}\right] - RTX_1X_2\Delta^2\left[\frac{A_1X_1 + A_2X_2}{A_1A_2}\right]$$

For most non-electrolyte organic systems, the parameter Δ is less than unity for $(\sigma_2 - \sigma_1) < 10$ ergs/cm^2, and eq. [8] is found to predict the surface tension of binary mixtures of such systems to within 1 to 3% error. However, for systems with $(\sigma_2 - \sigma_1) > 20$ ergs/cm^2, particularly aqueous systems, the Δ approach cannot be used since the approximations $X_1\Delta$ and $X_2\Delta < 1$ do not apply. Attempts at using implicit equations with linear first approximations to σ for such systems failed. Therefore a more direct method of solving the implicit functions of σ must be used for these type of systems. Such an approach is outlined as follows.

Since for a binary system,

$$[9] \quad X_{1S} + X_{2S} = 1$$

the Butler equations [3] and [4] can be equated and rearranged as follows by defining a molar surface area ratio $r = A_1/A_2$:

$$[10] \quad \left(\frac{X_{2S}}{X_{2B}}\right)^r \left(\frac{X_{1B}}{X_{1S}}\right) = \exp\left[\frac{(\sigma_1 - \sigma_2)A_1}{RT}\right] = K_1$$

If eq. [10] can be solved for the mole fraction of one surface component, then the surface tension of a binary system can be predicted using eq. [5] and this known surface mole fraction.

It has been previously shown (1) that the molar surface areas, A_i, can be calculated from bulk molar volumes, V_{iB}, by the following relation:

$$[11] \quad A_i = 1.021 \times 10^8 V_{iB}^{2/3}$$

where A_i is given in units of cm^2/mol. This relation assumes that the molar volume of the surface layer, V_S, is equal to that of the bulk liquid molar volume, V_B, for each component. However, it has been shown that a better approximation for the surface molar volume is given by an equation derived from an anisotropic surface model (2):

$$[12] \quad V_S = V_C^{3/5} V_B^{2/5}$$

where V_C is the critical molar volume of the substance. For this improved model of the surface molar volume, the molar surface area would be related to the bulk liquid molar volume by:

$$[13] \quad A_i = 1.021 \times 10^8 V_{iC}^{6/15} V_{iB}^{4/15}$$

Both estimates for calculating these molar area values have been tested in this study. The values of V_C for all the systems studied were taken from Reid *et al.* (5) except for sulfolane which was estimated using Lydersen's method as outlined by Reid *et al.*

For many organic systems the ratio of the molar surface areas, r, is approximately unity. For these cases, assuming r is unity, eq. [10] can be solved explicitly for the surface mole fraction of any component, and yields:

$$[14] \quad X_{1S} = \frac{X_{1B}}{X_{1B} + X_{2B}K_1}$$

$$[15] \quad X_{2S} = \frac{X_{2B}}{X_{2B} + \frac{X_{1B}}{K_1}}$$

With these approximations for X_{1S} and X_{2S}, eq. [5] for the surface tension of a binary system can now be written in explicit form as:

$$[16] \quad \sigma = (\sigma_1 X_1 + \sigma_2 X_2) - \frac{RT}{A}\left[X_1 \ln (X_1 + X_2K_1) + X_2 \ln \left(X_2 + \frac{X_1}{K_1}\right)\right]$$

Equation [16] reveals a negative deviation from the linear surface tension term similar to that of the Δ parameter approach given in eq. [8]. Calculations of the surface tensions of binary organic systems has shown that eq. [16] with $A_2 = A_1 = A$ yields the same surface tension values as the Szyszkowski equation (1).

For those systems where r cannot be approximated by unity, the surface mole fraction can still be obtained from eq. [10] by use of the Newton–Raphson iterative technique (6). This technique is particularly useful for calculating the surface tension of aqueous systems. For most aqueous nonelectrolyte mixtures not only is the r factor significantly different from unity, but also the surface tension differences are much larger than 10 ergs/cm^2 which limits the usefulness of the Δ parameter approach.

To make use of the Newton–Raphson iterative technique, eq. [10] is first rearranged in terms of the known quantities K_1, X_{1B}, X_{2B}. The unknown quantity X_{1S} is then calculated through a difference function $f(X_{1S})$:

$$[17] \quad f(X_{1S}) = \frac{X_{1S}}{(1 - X_{1S})^r} - C$$

where C is a known quantity for any solution given by:

$$[18] \quad C = \frac{X_{1B}}{X_{2B}^r K_1}$$

This difference function will have an exact value of zero when the quantity X_{1S} has been determined exactly.

The Newton–Raphson technique then allows the mole fraction of component 1 in the surface phase, X_{1S}, to be obtained from a first approximation estimate, given as X_{1S}^0 and a deviation term:

$$[19] \quad X_{1S} = X_{1S}^0 - \frac{f(X_{1S}^0)}{f'(X_{1S}^0)}$$

where

$$[20] \quad f'(X_{1S}^0) = \frac{1 + (r - 1)X_{1S}^0}{(1 - X_{1S}^0)^{r+1}}$$

Can. J. Chem. Downloaded from www.nrcresearchpress.com by 210.87.254.5 on 09/06/12
For personal use only.

TABLE 1. Average percent error using the DEL and Newton–Raphson approaches for predicting the surface tension of binary liquid mixtures*

System	T (°C)	Ref.	$\sigma_1 - \sigma_2$	σ_L	Δ approach σ_B	Δ approach σ_S	Newton–Raphson σ_B	Newton–Raphson σ_S
$CCl_4 + C_6H_{12}$	20	7	1.71	0.67	0.51	0.49	0.51	0.49
$C_6H_{12} + C_6H_5CH_3$	20	7	−3.25	1.72	1.37	1.22	1.36	1.22
$C_6H_6 + C_6H_{12}$	30	8	3.70	1.46	0.82	0.66	0.82	0.65
$CCl_4 + CS_2$	25	9	−5.90	3.68	2.06	1.70	2.05	1.68
CH_3CN + EtOH	20	13	6.73	2.40	2.09	2.04	2.04	1.96
$C_6H_{12} + C_6H_5Cl$	20	7	−8.22	2.83	0.98	0.50	0.99	0.30
Dioxane + C_6H_{12}	30	8	8.35	3.08	0.64	0.34	0.64	0.37
C_6H_6 + 2,2,4(Me)$_3$-pentane	30	12	9.64	8.18	1.51	0.98	1.67	0.45
n-$C_6H_{14} + C_6H_6$	20	11	−9.92	6.07	1.60	1.31	1.72	0.48
$C_6H_5NO_2 + C_6H_{12}$	30	8	18.35	13.44	5.00	3.27	5.15	2.22
Sulpholane + EtOH	30	10	28.10	14.79	5.30	5.43	5.47	1.87
Glycerol + EtOH	25	14	40.50	25.54	8.60	17.40	6.23	1.15

*$\sigma_L = \sigma_1 X_1 + \sigma_2 X_2$; σ_B = surface tensions calculated with eq. [11] for molar surface areas A_i; σ_S = surface tensions calculated with eq. [13] for molar surface areas.

TABLE 2. Comparison of the calculated surface tensions from the DEL approach and the Newton–Raphson technique using bulk and surface molar areas

X_1	σ_{obs}	σ_L	DEL approach σ_B	DEL approach σ_S	Newton–Raphson technique σ_B	Newton–Raphson technique σ_S
Glycerol + Ethanol at 25°C: $\sigma_1 - \sigma_2$ = 4.050 Dynes/cm						
1.0000	62.50	62.50	62.50	62.50	62.50	62.50
0.8183	38.90	55.14	48.20	44.44	45.13	39.46
0.6668	32.70	49.00	38.42	32.49	37.76	33.40
0.5386	29.60	43.81	31.75	24.81	33.34	30.06
0.4287	27.70	39.36	27.28	20.16	30.31	27.85
0.3334	26.10	35.50	24.38	17.68	28.06	26.24
0.2501	25.40	32.13	22.62	16.79	26.32	25.01
0.1765	24.20	29.15	21.69	17.05	24.93	24.03
0.1112	23.90	26.50	21.38	18.14	23.78	23.23
0.0527	22.90	24.13	21.52	19.84	22.82	22.57
0.0000	22.00	22.00	22.00	22.00	22.00	22.00
Ave. % error		25.54	8.60	17.40	6.23	1.15
Stand. dev.		6.35	3.82	4.51	2.24	0.42
Sulpholane + Ethanol at 30°C: $\sigma_1 - \sigma_2$ = 28.10 Dynes/cm						
1.0000	49.5	49.50	49.50	49.50	49.50	49.50
0.8172	39.2	44.36	41.76	40.00	40.89	37.79
0.6797	32.6	40.50	36.55	33.82	35.96	32.88
0.5649	28.7	37.27	32.65	29.40	32.58	29.93
0.4663	26.9	34.50	29.68	26.21	30.08	27.89
0.3719	25.6	31.85	27.18	23.76	27.96	26.23
0.2852	24.7	29.41	25.22	22.08	26.20	24.90
0.2083	24.0	27.25	23.77	21.11	24.78	23.84
0.1303	23.3	25.06	22.60	20.69	23.44	22.86
0.0634	22.6	23.18	21.86	20.81	22.36	22.08
0.0000	21.4	21.40	21.40	21.40	21.40	21.40
Ave. % error		14.79	5.30	5.43	5.47	1.87
Stand. dev.		3.24	1.80	1.52	1.50	0.74

Bringing together eqs. [17] through [20] then yields for X_{1S} the final relation:

$$[21] \quad X_{1S} = X^0_{1S} + \left[\frac{C(1 - X^0_{1S})^{r+1} - X^0_{1S}(1 - X^0_{1S})}{1 + (r - 1)X^0_{1S}}\right]$$

The value of X_{1S} obtained from the first iteration is then used to replace X^0_{1S} and the calculation is repeated until no further change in the value of X_{1S} occurs. Generally this requires three or four iterations.

It may be noted that the Newton–Raphson technique as applied to the determination of the surface mole fraction is parallel to and an improvement on the first order approximation used by Prigogine *et al.* (4). In their approximation, the surface mole fraction X_{1S} was given by:

$$[22] \quad X_{1S} = X_{1B} + X_{1B}X_{2B}\Delta$$

Similarly the Newton–Raphson approach can be written as:

$$[23] \quad X_{1S} = X_{1B} - \frac{f(X_{1B})}{f'(X_{1B})}$$

where the bulk mole fraction X_{1B} has been used as a first approximation for X^0_{1S} in eqs. [19] and [20].

Equation [21] combined with eq. [5] was applied to a variety of aqueous and non-aqueous systems using both estimates of the molar surface areas given by eqs. [11] and [13]. These data are presented in Tables 1 through 3 and displayed as deviations from the linear surface tension dependence in Figs. 1 and 2.

Discussion

As a check on the validity of the iterative technique for calculating the surface tension of binary systems, several organic systems with $(\sigma_1 - \sigma_2) < 10$ ergs/cm^2 were tested using both the Δ approach (eq. [8]) and the Newton–Raphson technique (eqs. [5] and [21]). The results of these calculations are given in Table 1. No significant difference is found between either of these techniques. However for both approaches, use of the anisotropic formula for the molar surface area in most cases generates a slight improvement in the surface tension values between observed and calculated over those predicted using bulk liquid molar area values.

Can. J. Chem. Downloaded from www.nrcresearchpress.com by 210.87.254.5 on 09/06/12
For personal use only.

TABLE 3. Average percent error using the DEL and Newton–Raphson approaches for predicting the surface tension of binary aqueous mixtures*

Systems	T (°C)	Ref.	$\sigma_1 - \sigma_2$	σ_L	Δ approach		Newton–Raphson	
					σ_B	σ_S	σ_B	σ_S
Water + glycerol	25	14	9.50	2.85	1.09	1.06	0.90	0.71
Water + ethylene glycol	30	19	24.91	8.77	3.34	2.68	2.33	0.36
Water + dioxane	26	18	39.31	29.18	9.68	10.59	7.51	3.60
Water + methanol	30	15	49.99	36.34	11.31	13.06	8.04	1.99
Water + acetone	20	17	49.50	55.38	19.72	22.38	12.75	5.59
Water + ethanol	25	16	50.17	57.30	21.55	21.73	18.11	9.95

*Refer to Table 1 for the meaning of σ_L, σ_B, and σ_S.

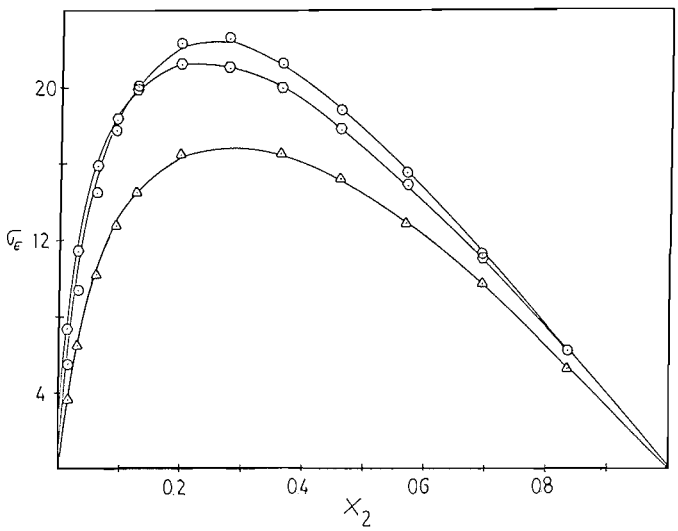

FIG. 1. Excess surface tension of water + methanol at 30°C. △, excess surface tension calculated with eq. [11] to approximate the molar surface area; ⊙, excess surface tension calculated with eq. [13] for the molar area; ⊙, represents the experimental excess surface tension defined as $\sigma_E = X_1\sigma_1 + X_2\sigma_2 - \sigma_{exp}$.

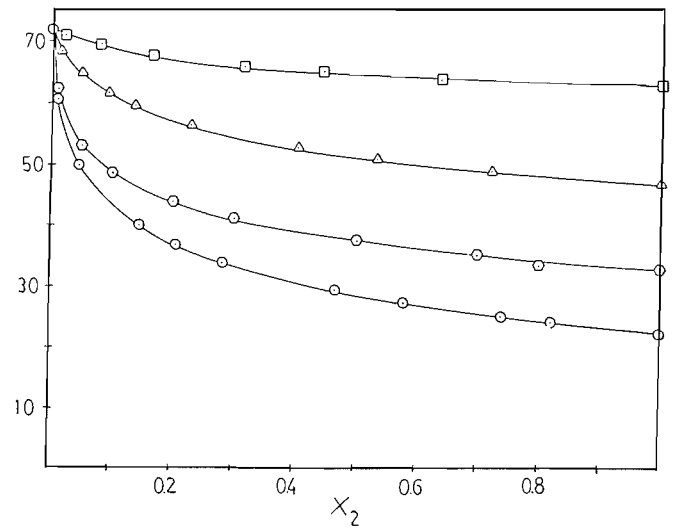

FIG. 2. Plot contrasting the magnitude of the drop in surface tension, for four binary non-electrolyte systems of varying surface tension differences. ⊡, water + glycerol; △, water + ethylene glycol; ⊙, water + dioxane; ⊙, water + ethanol.

As the surface tension difference ($\sigma_1 - \sigma_2$) increases and the r factor deviates more significantly from unity, the improvement between observed and calculated values is more noticeable when surface molar area values are employed. For example with the benzene–isooctane system at 30°C, $(\sigma_1 - \sigma_2) = 9.64$ and $r = 0.662$. Using the Δ approach, the average percent error between observed and calculated surface tensions decreases from 1.51% to 0.98% on changing from bulk to surface volumes for calculation of the molar surface areas. The comparable errors using the iterative technique are 1.67% and 0.45%.

For values of $\sigma_1 - \sigma_2$ much larger than 20 ergs/cm^2 the iterative technique showed much better agreement between observed and calculated surface tensions. For instance, the glycerol–ethanol system, with a $\sigma_1 - \sigma_2$ value of 40.5 ergs/cm^2, was detailed in ref. 1 and a poor fit was shown to occur with the Δ approach, whereas the iterative approach yields an average error of about 1% particularly when surface molar area values are calculated via the anisotropic surface model. Similar statements can be made about the sulfolane–ethanol system with a $\sigma_1 - \sigma_2$ value of 28.1 ergs/cm^2. Table 2 gives more details of the concentration dependence of the surface tension of these two systems in terms of the above mentioned calculations. These tests indicated that the iterative technique could be applied generally and, in particular, should be applicable to a series of aqueous systems with large $\sigma_1 - \sigma_2$ values.

Table 3 gives a more detailed comparison of the Δ and iterative approach for six aqueous systems. Since $\sigma_1 - \sigma_2$ for these systems is much greater than 20 ergs/cm^2, the mathematical approximations used in deriving eq. [8] are not valid for these systems. However, it is useful to contrast this explicit Δ equation with the iterative equation to indicate the order of magnitude of improvement to be expected with a mathematically exact (though more complex) relation for σ for these systems.

For all aqueous systems the iterative approach yields a better calculated value of the surface tensions than does the Δ method by at least a twofold decrease in average % error. Furthermore, the use of molar surface volumes for calculating the molar surface areas again shows that a significant decrease occurs in the difference between observed and calculated surface tension values over those calculated using the bulk molar liquid volume approximation. These points are more clearly illustrated in Fig. 1 where the deviation from the linear surface tension terms for observed and calculated surface tensions for the aqueous methanol system is plotted.

Figure 2 illustrates the most interesting characteristic of aqueous surface tension plots, i.e. the rapid drop in surface tension at very low mole fractions of solute for a wide variety of organic solutes. This rapid drop has been a source of consternation for some time since no simple obvious explanation could

Can. J. Chem. Downloaded from www.nrcresearchpress.com by 210.87.254.5 on 09/06/12
For personal use only.

account for this effect.

In fact, it seems that this effect is due to two factors: all aqueous non-electrolyte systems have r values very much different than unity, ca. 0.35 to 0.6 in these cases, as well as a very large difference in $\sigma_1 - \sigma_2$ values (ca. 50 ergs/cm^2). The combination of these two factors results in this rapid drop in surface tension at low mole fractions of solute for aqueous systems.

This can be seen clearly from Fig. 2 which contrasts the surface tension curves for several aqueous non-electrolyte systems. This point can also be shown mathematically from eq. [8]. The rapid drop in surface tension is proportional to the slope of the $\sigma - X_2$ curve, i.e., to $d\sigma/dX_2$. From eq. [8], $d\sigma/dX_2$ is given by:

$$[24] \quad \frac{\partial \sigma}{\partial X_2} = (\sigma_2 - \sigma_1) \times \left\{1 + \left[\frac{(1 - 2X_2)(rX_1 + X_2) - X_1X_2(1 - r)}{(rX_1 + X_2)^2}\right] \times \left[(1 - r) - \frac{(\sigma_2 - \sigma_1)A_1}{2RT}\right]\right\}$$

For the systems illustrated in Fig. 2, at a fixed mole fraction, it is found that the dominant term governing this slope is $(\sigma_2 - \sigma_1)$. Hence the rapid drop in aqueous non-electrolyte systems is primarily due to the magnitude of the surface tension difference between the two components of the system.

It is noted that there is still a substantial error remaining in the calculated values of the surface tension of some aqueous systems. It must be remembered, however, that the equations used for calculating the surface tensions of these mixtures are based on the assumption that the bulk and surface phases are ideal; that is, the heat of mixing of these systems is zero and hence the activity coefficient effects are negligible. It is probable that this assumption is not valid for these aqueous systems, e.g., water–ethanol, water–acetone.

Conclusions

The iterative technique for calculating surface tensions of systems of high polarity difference (large $\sigma_1 - \sigma_2$ values) is an improvement over the explicit Δ function approach first utilized by Prigogine *et al.* (4) and more completely expanded upon (1). Furthermore, the anisotropic surface model (2) for calculating molar surface areas improves the agreement between observed and calculated surface tensions for a large variety of systems. There is no significant difference between the iterative technique or the Δ function approach for calculating the surface tensions of mixtures of systems with low polarity differences, e.g. $(\sigma_1 - \sigma_2) < 10$ ergs/cm^2. However, for organic liquid systems with large polarity differences, e.g. $\sigma_1 - \sigma_2 > 20$ ergs/cm^2, the iterative technique combined with the anisotropic molar surface area equation, is able to account for the surface tensions of such mixtures to within 1–2% error.

For aqueous non-electrolyte systems, where the $\sigma_1 - \sigma_2$ values are significantly greater than 20 ergs/cm^2, even the combination of the iterative technique along with the better estimated molar surface area values is unable to account totally for the surface tension concentration curves. Hence, further work needs to be done on the temperature dependence of aqueous non-electrolyte systems with a view to elucidating the effects of surface orientation and/or heat of mixing on the activity coefficients of such solutions in the surface and bulk liquid phases.

1. D. E. GOLDSACK and C. D. SARVAS. Can. J. Chem. **59**, 2968 (1981).
2. L. J. PAQUETTE. M.Sc. Thesis, Laurentian University. 1982.
3. J. A. V. BUTLER. Proc. R. Soc. A, 135 (1932); 348 (1932).
4. R. DEFAY, I. PRIGOGINE, A. BELLEMANS, and D. H. EVERETT. Surface tension and adsorption. John Wiley and Sons, New York. 1966.
5. R. C. REID, J. M. PRAUSNITZ, and T. K. SHERWOOD. The properties of gases and liquid. 3rd ed. McGraw Hill Book Co., New York. 1977.
6. I. S. SOKOLNIKOFF and R. M. REDHEFFER. Mathematics of physics and modern engineering. McGraw-Hill Book Co. Inc., New York. 1958.
7. M. SISKOVA and V. SECOVA. Coll. Czech. Chem. Com. **35**, 2702 (1970).
8. S. K. SURI and V. RAMAKRISHNA. J. Phys. Chem. **72**, 3073 (1968).
9. W. E. SHIPP. J. Chem. Eng. Data, **15**, 308 (1970).
10. E. TOMMILA, E. LINDELL, M.VIRTALAINE, and R. LAAKSO. Suom. Kemistil. **42**, 95 (1969).
11. K. RIDGWAY and P. A. BUTLER. J. Chem. Eng. Data, **12**, 509 (1967).
12. H. B. EVANS, JR. and H. L. CLEVER. J. Phys. Chem. **68**, 3433 (1964).
13. V. AMNA-LUISE VIERK. Z. Anorcan. Allgem. Chem. **261**, 283 (1950).
14. R. C. ERNST, C. H. WATKINS, and H. H. RUWE. J. Phys. Chem. **40**, 627 (1936).
15. J. LIVINGSTON, R. MORGAN, and M. NEIDLE. J. Am. Chem. Soc. **35**, 1856 (1913).
16. L. L. BIRCUMSHAW. J. Chem. Soc. 887 (1922).
17. K. S. HOWARD and R. A. MCALLISTER. J. A.I. Ch.E. **3**, 325 (1957).
18. J. W. BREITENBACK and H. EDELHAUSER. Monat. Chem. **84**, 385 (1953).
19. K. NAKANISHI, T. MATSUMOTO, and M. HAYATSU. J. Chem. Eng. Data, **16**(1), 44 (1971).

Can. J. Chem. Downloaded from www.nrcresearchpress.com by 210.87.254.5 on 09/06/12
For personal use only.

β-Lactams. XI. Synthesis of *N*-phosphorylated mono- and bicyclic β-lactams[1]

GEORGE JUST, DENISE DUGAT, AND WHI-YU LIU
Department of Chemistry, McGill University, Montreal, P.Q., Canada H3A 2K6

Received November 8, 1982

GEORGE JUST, DENISE DUGAT, and WHI-YU LIU. Can. J. Chem. **61**, 1730 (1983).

Starting from appropriately substituted monocyclic β-lactam, *N*-phosphorylated mono- and bicyclic β-lactams have been synthesized.

GEORGE JUST, DENISE DUGAT et WHI-YU LIU. Can. J. Chem. **61**, 1730 (1983).

Des β-lactames mono- et bicycliques *N*-phosphorylés ont été synthétisés à partir de β-lactames monocycliques.

Can. J. Chem. Downloaded from www.nrcresearchpress.com by 210.87.254.40 on 09/06/12
For personal use only.

Some time ago (2, 3), we postulated that the ring strain of penicillins and cephalosporins, which seems to be responsible for the high frequency of β-lactam ir absorption and hence also for their chemical and biological reactivity, may be replaced by electronic activation, and that properly activated monocyclic β-lactams should possess antibacterial activity. As part of this continuing program, we described the synthesis of bicyclic β-lactam **5**, in which the β-lactam nitrogen is directly attached to a phosphate. Because of the importance of the recently described *N*-sulfated monobactams (4), we also describe the synthesis of *N*-phosphorylated monobactams **21***b* and **24***b* using methodology developed for the preparation of **5**.

Phenyl cyclophosphoramidate **1***a* was treated with ethyl malonyl chloride (5) to give **2***a* in excellent yield (6). Amide **2***a* underwent base catalyzed diazo exchange with *p*-toluenesulfonyl azide (7) to afford **3***a*. We next attempted to form the β-lactam **4***a* by a carbene insertion reaction, a method pioneered by Corey and Felix (8) and extensively applied by Lowe and co-workers (9) to the synthesis of a variety of bicyclic β-lactams. Irradiation of the α-diazo-amide **3***a* at 0°C in carbon tetrachloride using a Rayonet photochemical reactor, with maximum output at 350 mμ, led to a complicated reaction mixture. The infrared spectrum did not show any diazo or β-lactam absorptions at 2200 or ~1750 cm^{-1}, respectively. Using flash chromatography, one of the less polar spots isolated proved to be phenol. Since phenol absorbs in the ultraviolet spectrum at 210 mμ and 270 mμ, we suspected that it might interfere with the carbene insertion reaction under the photolysis condition. We therefore decided to replace the phenoxy moiety by a trichloroethyl group. This protecting group can be removed in the presence of a β-lactam (10), and should not absorb light.

Addition of 3-amino-1-propanol and triethylamine to trichloroethyl dichlorophosphate, prepared *in situ* by reaction of trichloroethyl alcohol and triethylamine with phosphorus oxychloride, afforded the cyclophosphoramidate **1***b*, in 93% yield, after flash chromatography. It was coupled, as before, with ethyl malonyl chloride to give amide **2***b*. The diazo compound **3***b* was obtained in a manner analogous to that of its corresponding phenyl derivative **3***a*.

Irradiation as described before, or treatment with copper in toluene or rhodium acetate in methylene chloride (11), gave a mixture of products which were not identified.

In a second, more successful series of reactions, alcohol **7***a* (12) was transformed to its tetrahydropyranyl ether **7***b* (13). Reaction of **7***b* with *n*-butyllithium at −78°C in dry tetrahydrofuran, followed by addition of diphenylchlorophosphate, gave the reactive diphenylphosphoramidate **9** in 80% yield. Deprotection with pyridinium *p*-toluenesulfonate (13) gave alcohol **11**, clearly characterized by its nmr spectrum.

Reaction of diphenylphosphoramidate **11** with anhydrous cesium fluoride[2] in *tert*-butanol gave the cyclized β-lactam **5**, in 20% yield, along with phenol and β-lactam **13**, as the sole side products that could be isolated. Attempts to improve the yield of the reaction and to eliminate the side product **13** were

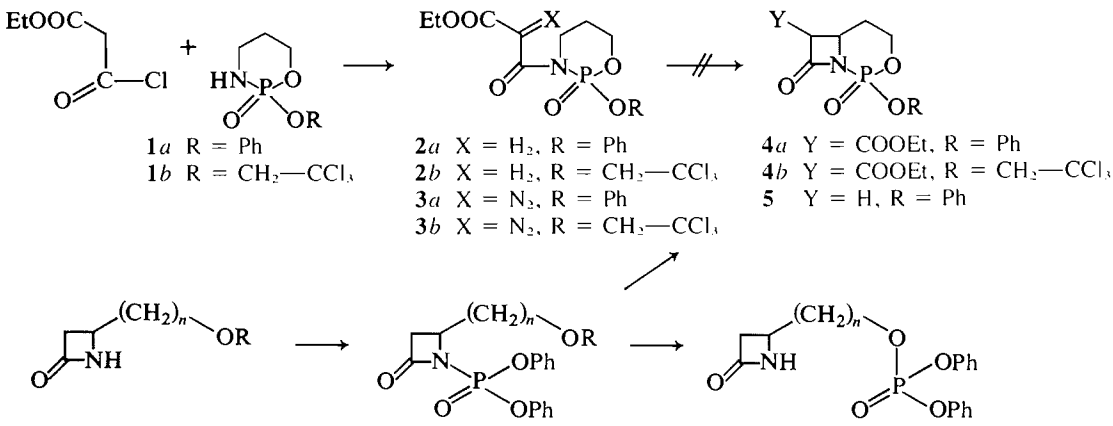

1*a* R = Ph
1*b* R = CH_2—CCl_3

2*a* X = H_2, R = Ph
2*b* X = H_2, R = CH_2—CCl_3
3*a* X = N_2, R = Ph
3*b* X = N_2, R = CH_2—CCl_3

4*a* Y = COOEt, R = Ph
4*b* Y = COOEt, R = CH_2—CCl_3
5 Y = H, R = Ph

6 *n* = 1, *a* R = H, *b* R = THP
7 *n* = 2, *a* R = H, *b* R = THP

8 *n* = 1, R = THP
9 *n* = 2, R = THP
10 *n* = 1, R = H
11 *n* = 2, R = H

12 *n* = 1
13 *n* = 2

[1]Abstracted in part from ref. 1.
[2]Reference 14; also unpublished results of Dr. Ogilvie's laboratory, McGill University.

Can. J. Chem. Downloaded from www.nrcresearchpress.com by 210.87.254.40 on 09/06/12
For personal use only.

in vain. This suggested that perhaps the β-lactam nitrogen was in part acting as the leaving group, during treatment with CsF, instead of the phenoxide anion.

Both structures **5** and **13** were proven by 200 MHz ^{1}H nmr spectra and by mass spectrometry, which showed *m/e*'s due to loss of ketone. In addition, monocyclic β-lactam **13** was prepared by reaction of alcohol **7***a* with diphenylchlorophosphate. Attempts to hydrolyze this material to the free phosphoric acid failed.

When this sequence was repeated using alcohol **6***a* (**6***a* → **6***b* → **8** → **10** → **11** → **12**), obtained by sodium borohydride reduction of 4-carbobenzyloxyazetidinone kindly provided by Dr. Christensen, Merck Laboratories, no bicyclic lower homolog corresponding to **5** was obtained, and only monocyclic diphenylphosphate **12** was isolated. The latter was identical to **12**, prepared from alcohol **6***a* and diphenylchlorophosphate.

The formation of monocyclic β-lactam, although conceptually simple, was fraught with experimental difficulties due to the acid-lability of the N—P bond. β-Lactam **16**, prepared by adaptation of known procedures (15) via the sequence **14** → **15** → **16**, was phosphorylated with dibenzylchlorophosphate in a manner similar to that described before. Catalytic hydrogenolysis of dibenzylphosphate **17***a* in methanol over Pd/C at 1 atm gave after 1 h the phosphoric acid **17***b* which was characterized by conversion to its dimethylester **17***c* using diazomethane. Deblocking of the *t*-BOC group of **17***a* under a variety of acidic conditions did not lead to the expected amine **18**. Instead, either N—P bond cleavage (trifluoroacetic acid (16)), or opening of the β-lactam ring (*p*-toluenesulfonic acid, ethyl acetate (17)) was observed.

Therefore, **16** was hydrolyzed in trifluoroacetic acid (16) at 0°C to the ammonium salt **19**. Reaction of **19** with phenylacetyl chloride (18) gave β-lactam amide **20**. Formation of a mono anion by means of butyllithium at −78°C, followed by addition of dibenzylchlorophosphate, gave phosphorylated β-lactam **21***a*. Catalytic debenzylation using 10% Pd/C in methanol gave the phosphoric acid **21***b* which could be characterized, as was acid **17***b*, by conversion to its methyl ester **21***c*.

Similarly, compound **19** was transformed in phosphoric acid **25***b* in the following manner. First, reaction of **19** with the

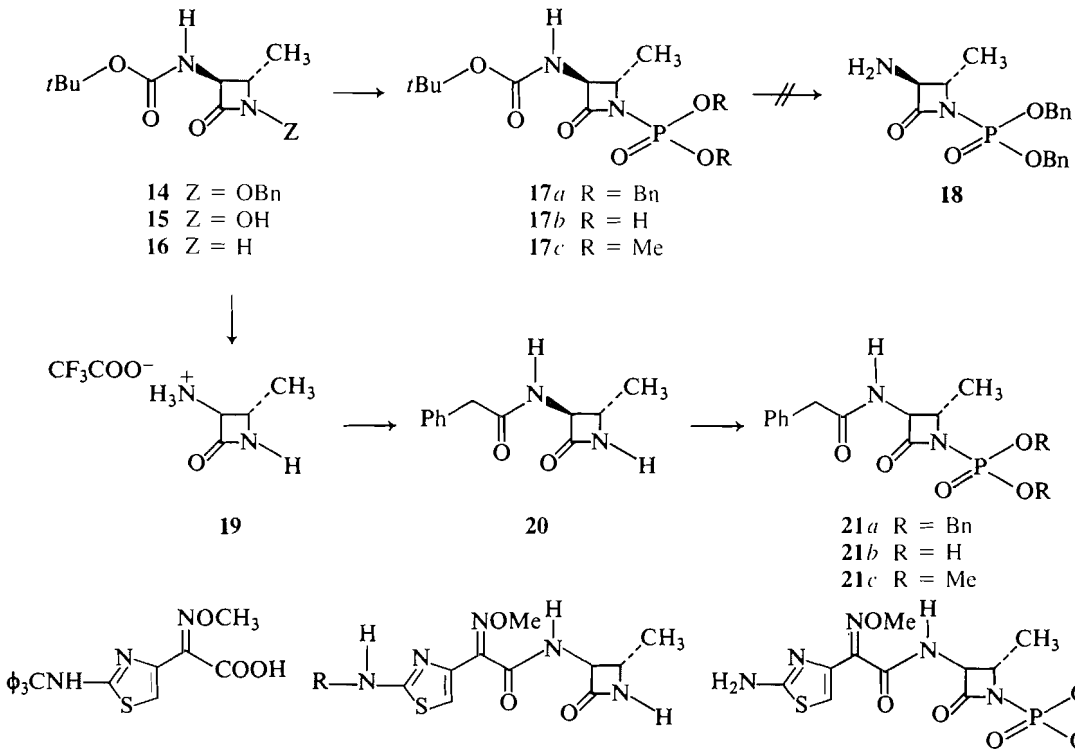

appropriate acid **22** (19) was carried out in THF/CH_2Cl_2, using *N*-ethoxycarbonyl-2-ethoxy-1,2-dihydroquinoline (EEDQ) (20) as coupling agent. Deblocking of the trityl group by formic acid in a methanolic solution led, after 1 h refluxing, to β-lactam **24** in 83% yield. The dibenzylphosphate **25***a*, isolated by phosphorylation of **24** as described before, was hydrogenolyzed under two different conditions, both requiring long reaction times. Thus, under the first set of conditions, previously used (10% Pd/C, hydrogen at 1 atm, methanol), debenzylation gave, after 10 h, the phosphoric acid **25***b* which could be isolated as free acid or as its triethylamine salt **25***d*. Under the second set of conditions (hydrogen at 1 atm, 1 equiv. of $KHCO_3$ in THF−ethanol−water (ref. 21)), hydrogenolysis provided after 6 h the corresponding monopotassium salt **25***e*.

All compounds reported gave good, interpretable nmr and mass spectra except for **25***a*, **25***b*, and **25***c*, where mass spectra could not be interpreted.

None of the *N*-phosphates tested had notable antibacterial activity when compared to Squibb's monobactam SQ 26.776 or piperacillin.

In view of the extensive work of the Squibb group on phosphorylated monobactams (monophosphams) recently described

(22), we do not plan to do any further work in the monophospham area.

Experimental

Thin-layer chromatography was performed on Merck Silica Gel 60 aluminum-backed plates. Flash chromatography was done with Woelm Silica (32–63 μ) using predistilled solvents. Melting points were determined on a Gallenkamp block and are uncorrected. Optical rotations were measured in a 1 dm cell on a Perkin–Elmer 141 polarimeter. Nuclear magnetic resonance spectra were recorded on Varian T-60, T-60A, and XL-200 spectrometers. Infrared (ir) spectra were run on a Perkin–Elmer 297 spectrophotometer. Mass spectra were taken on HP5984A or LKB 9000 spectrometers.

Phenyl cyclophosphoramidate **1**a

To 3-amino-1-propanol (1 g, 13.3 mmol) in dry methylene chloride (20 mL) was added pyridine (3.16 g, 40 mmol) and phenyldichlorophosphate (2.8 g, 13.3 mmol) at 0°C. The mixture was stirred at room temperature for 18 h. The solution was washed with water (2 × 15 mL), dried ($MgSO_4$), and evaporated. The residue was purified by flash chromatography (ethyl acetate) to afford 2.24 g (79%) of **1***a* as a colorless oil. Infrared (film) ν_{max}: 3250 (NH, amide), 1590, 1485, 1260, 1210 cm^{-1}; ^{1}Hmr ($CDCl_3$) δ: 1.2–2.4 (m, 2H, CH_2), 2.8–3.7 (m, 2H, CH_2N), 4.1–4.7 (m, 3H, NH, CH_2O), 7.32 (s, 5H, C_6H_5); ms (70 eV, 69°C), *m/e* (‰): 213 (643, $M^{+\cdot}$), 120 (382, $M^{+\cdot} - C_6H_5O^{\cdot}$).

Amide **2**a

To a solution of **1***a* (1.44 g, 6.76 mmol) in THF (10 mL), ethyl malonyl chloride (1.02 g, 6.78 mmol) in THF (5 mL) was added. The reaction was followed by means of tlc. When starting material disappeared (~15 h), the solvent was evaporated. The residue was introduced into a flash chromatography column to afford 1.85 g (84%) of **2***a* as a colorless oil. Infrared (film) ν_{max}: 1740 (C=O, ester), 1690 (C=O, amide) cm^{-1}; ^{1}Hmr ($CDCl_3$) δ: 1.24 (t, 3H, CH_3), 1.6–2.5 (m, 2H, $NCH_2CH_2CH_2O$), 3.0–3.6 (m, 1H, CHN), 3.83, 3.90 (2s, 2H, CH_2CO), 4.11 (q, 2H, CH_3CH_2), 4.1–4.9 (m, 3H, CH_2O, CHN), 7.30 (s, 5H, C_6H_5); ms (20 eV, 20°C), *m/e* (‰): 327 (20, $M^{+\cdot}$), 234 (1000, $M^{+\cdot} - C_6H_5O^{\cdot}$).

Diazo-amide **3**a

To a solution of **2***a* (1.85 g, 5.66 mmol) in acetonitrile (20 mL) containing triethylamine (0.63 g, 6.24 mmol) was added *p*-toluenesulfonyl azide (1.18 g, 5.98 mmol) at 0°C. The mixture was stirred for 40 h at room temperature. The solvent was evaporated below 30°C and replaced by methylene chloride (40 mL). After being washed with 0.4 *N* potassium hydroxide, water, dried ($MgSO_4$), and evaporated, the residue was purified by flash chromatography (petroleum ether – ethyl acetate, 1:1) to afford 1.70 g (85%) of **3***a* as a yellow oil. Infrared (film) ν_{max}: 2135 (N_2), 1730 (C=O, ester), 1690, 1650, 1590, 1490 cm^{-1}; ^{1}Hmr ($CDCl_3$) δ: 1.30 (t, 3H, CH_3), 1.6–2.5 (m, 2H, CH_2), 3.2–3.8 (m, 1H, NCH), 4.30 (q, 2H, CH_3CH_2), 4.0–4.7 (m, 3H, NCH, $NCH_2CH_2CH_2O$), 7.23 (s, 5H, C_6H_5); ms (20 eV, 60°C), *m/e* (‰): 353 (32, $M^{+\cdot}$), 325 (245, $M^{+\cdot} - N_2$), 260 (77, $M^{+\cdot} - C_6H_5O^{\cdot}$), 253 (341), 94 (1000).

Trichloroethyl cyclophosphoramidate **1**a

A solution of 2,2,2-trichloroethyl alcohol (0.49 g, 3.28 mmol) and triethylamine (0.33 g, 3.27 mmol) in anhydrous tetrahydrofuran (3 mL) was added dropwise at −78°C into phosphorus oxychloride (0.5 g, 3.27 mmol) in THF (5 mL) under nitrogen atmosphere. After stirring 0.5 h, the temperature slowly increased to room temperature within 1 h and the mixture was cooled again to −78°C. To the cooled mixture, a solution of 3-amino-1-propanol (0.245 g, 3.26 mmol) and triethylamine (0.693 g, 6.86 mmol) in THF (3 mL) was added. The mixture was allowed to warm to room temperature and stirred for another 4 h. The tetrahydrofuran was evaporated. The residue was added to methylene chloride (50 mL) and water (40 mL). The organic layer was washed with 1% HCl (30 mL), dried ($MgSO_4$), and evaporated. The crude product was purifed by flash chromatography (ethyl acetate) to obtain 0.81 g (93%) of **1***b* as a light yellow oil. Infrared (film) ν_{max}: 3250 (NH), 1420, 1335, 1260, 1100 cm^{-1}; ^{1}Hmr ($CDCl_3$) δ: 1.5–2.5 (m, 2H, $NCH_2CH_2CH_2O$), 3.0–3.7 (m, 2H, NCH_2), 4.1–4.8 (m, 3H, $NHOCH_2$), 4.50 (d, 2H, CH_2CCl_3, J = 7 Hz); ms (70 eV, 20°C), *m/e* (‰): 273 (4, $M^{+\cdot}$ + 6, Cl_3^{37}), 271 (18, $M^{+\cdot}$ + 4, $Cl_1^{35}Cl_2^{37}$), 269 (55, $M^{+\cdot}$ + 2, $Cl_2^{35}Cl_1^{37}$), 267 (57, $M^{+\cdot}$, Cl_3^{35}), 120 (1000, $M^{+\cdot} - OCH_2CCl_3^{\cdot}$).

Amide **2**b

This compound was obtained from **1***b* via the procedure for the preparation of **2***a*, in 90% yield after flash chromatography (petroleum ether – EtOAc, 1.5:1). Infrared (film) ν_{max}: 1735 (C=O, ester), 1690 (C=O, amide), 1330, 1300 cm^{-1}; ^{1}Hmr ($CDCl_3$) δ: 1.30 (t, 3H, CH_3), 1.7–2.3 (m, 2H, $NCH_2CH_2CH_2O$), 3.1–3.7 (m, 1H, NCH), 3.8–4.8 (mb, 3H, OCH_2, NCH), 3.90, 4.04 (2s, 2H, CH_2), 4.20 (q, 2H, CH_3CH_2), 4.70 (d, 2H, OCH_2CCl_3, J = 7 Hz); ms (70 eV, 37°C), *m/e* (‰): 385 (15, $M^{+\cdot}$ + 4, $Cl_1^{35}Cl_2^{37}$), 383 (36, $M^{+\cdot}$ + 2, $Cl_2^{35}Cl_1^{37}$), 381 (38, $M^{+\cdot}$, Cl_3^{35}), 234 (194, $M^{+\cdot} - OCH_2CCl_3^{\cdot}$).

Diazo-amide **3**b

Compound **3***b* was obtained from **2***b* via the procedure for the preparation of **3***a*, in 80% yield after flash chromatography (petroleum ether – EtOAc, 1.5:1). Infrared (film) ν_{max}: 2115 (N_2), 1720 (C=O, ester), 1650 (C=O, amide, 1330 cm^{-1}; ^{1}Hmr ($CDCl_3$) δ: 1.30 (t, 3H, CH_3), 1.6–2.3 (m, 2H, $NCH_2CH_2CH_2O$), 3.1–3.8 (m, 1H, NCH), 3.8–4.8 (m, 5H, NCH, CH_2O, OCH_2CH_3), 4.80 (d, 2H, OCH_2CCl_3, J = 7 Hz); ms (70 eV, 51°C), *m/e* (‰): 272 (14, $M^{+\cdot} - EtOOCCN_2CO^{\cdot}$ + 6, Cl_3^{37}), 270 (44, $M^{+\cdot} - EtOOCCN_2CO^{\cdot}$ + 4, $Cl_1^{35}Cl_2^{37}$), 268 (81, $M^{+\cdot} - EtOOCCN_2CO^{\cdot}$ + 2, $Cl_2^{35}Cl_2^{37}$), 266 (14, $M^{+\cdot} - EtOOCCN_2CO^{\cdot}$, Cl_3^{35}).

β-*Lactam* **7**b

A solution of β-lactam **7***a* (4.39 mg, 3.82 mmol) and dihydropyran (482 mg, 5.73 mmol) in dry methylene chloride (10 mL) containing pyridinium *p*-toluenesulfonate (PPTS) (96 mg, 0.382 mmol) was stirred for 8 h at room temperature. The solution was diluted with ether and washed with half-saturated brine to remove the catalyst. After drying and evaporation of the solvent, flash chromatography (ethyl acetate) gave 410 mg (54%) THP ether **7***b*. Infrared (film) ν_{max}: 3300 (NH), 1760 (C=O) cm^{-1}; ^{1}Hmr ($CDCl_3$) δ: 1.4–2.1 (m, 8H, CH_2CH_2O, $CHCH_2CH_2CH_2$), 2.49 (ddd, 1H, CHHCO, J_{gem} = 13 Hz, J_{trans} = 2.2 Hz, J_{NH} = 1.1 Hz), 3.10 (ddd, 1H, CHHCO, J_{gem} = 13 Hz, J_{cis} = 4.2 Hz, J_{NH} = 1.1 Hz), 3.3–4.1 (m, 5H, CHNH, $2CH_2O$), 4.6 (bm, 1H, $CH_2OCHOCH_2$), 6.3–6.7 (bs, 1H, NH); ms (70 eV, 20°C), *m/e* (‰): 199 (99, $M^{+\cdot}$), 99 (103, $M^{+\cdot} - HOCH(CH_2)_4O$), 85 (1000, THP^+).

β-*Lactam* **9**

Under a nitrogen atmosphere, a solution of β-lactam **7***b* (253 mg, 1.27 mmol) in dry THF (5 mL) was cooled to −78°C and treated with n-BuLi (1 equiv.) in THF. After being stirred for 10 min, diphenyl chlorophosphate (342 mg, 1.27 mmol) was added dropwise, and stirring, at −78°C, was continued for a period of 30 min. The reaction mixture was warmed to room temperature by itself. After adding methylene chloride (20 mL), the organic layer was washed with water (2 × 15 mL), dried ($MgSO_4$), and evaporated. The residue was purified by flash chromatography (petroleum ether – ethyl acetate; 1:1.5) to afford 438 mg of β-lactam **9** in 80% yield. Infrared (film) ν_{max}: 1790 (C=O, β-lactam) cm^{-1}; ^{1}Hmr ($CDCl_3$) δ: 1.2–2.1 (m, 8H, CH_2CH_2O, $CH_2CH_2CH_2$), 2.6–3.0 (m, 2H, CH_2CO), 3.1–4.0 (m, 5H, CHN, CH_2O, CH_2O), 4.2 (b, 1H, CH), 7.00 (s, 10H, $2C_6H_5$).

β-*Lactam* **6**b

Compound **6***b* was obtained from β-lactam **6***a*, via the procedure for the preparation of **7***b*, in 80% yield after flash chromatography (EtOAc). Infrared (film) ν_{max}: 3280 (NH), 1750 (C=O, β-lactam) cm^{-1}; ^{1}Hmr ($CDCl_3$) δ: 1.2–2.0 (m, 6H, $OCH(CH_2)_3$), 2.51 (app.bd, 1H, COCHH, J_{gem} = 14 Hz), 2.96 (2ddd, 1H, COCHH, J_{gem} = 14, J_{cis} = 4 Hz, J_{NH} = 1.5 z), 3.2–4.0 (m, 4H, OCH_2, OCH_2), 4.48 (bs, 1H, OCH), 6.7–7.0 (bs, 1H, NH); ms (70 eV, 19°C), *m/e* (‰): 185 (21 $M^{+\cdot}$), 85 (1000, THP^+).

Can. J. Chem. Downloaded from www.nrcresearchpress.com by 210.87.254.40 on 09/06/12
For personal use only.

Can. J. Chem. Downloaded from www.nrcresearchpress.com by 210.87.254.40 on 09/06/12
For personal use only.

β-*Lactam* ***8***

This compound was obtained from **6***b*, via the same procedure as for the preparation of **9**, in 85% yield used for the next reaction without purification. Infrared (film) ν_{max}: 1795 (β-lactam), 1595, 1490 (aromatic C=C), 1290 (P=O) cm $^{-1}$; ^{1}Hmr ($CDCl_3$) δ: 1.1−2.0 (m, 6H, $CH_2CH_2CH_2$), 2.9−3.2 (m, 2H, CH_2CO), 3.2−4.0 (m, 5H, $2OCH_2$, NCH), 4.2−4.5 (m, 1H, OCH), 7.12 (s, 10H, $2C_6H_5$); ms (70 eV, 76°C), *m/e* (‰): 417 (54, $M^{+\cdot}$), 333 (47, $M^{+\cdot}$ − DHP), 275 (287 ($M^{+\cdot}$ − $CH_2CHCH_2OTHP^{\cdot}$), 94 (936, $C_6H_5OH^{+\cdot}$), 77 (1000).

β-*Lactam* ***10***

Compound **10** was obtained from **8** via the procedure for the preparation of **11**, in 60% yield after flash chromatography (petroleum ether − EtOAc, 1:2.5). Infrared (film) ν_{max}: 3600−3200 (OH), 1790 (C=O, β-lactam), 1590, 1485 (aromatic C=C), 1280 (P=O) cm $^{-1}$; ^{1}Hmr ($CDCl_3$) δ: 2.5−3.4 (m, 2H, CH_2CO), 3.2−3.5 (b, 1H, OH, exchangeable with D_2O), 3.5−3.7 (m, 2H, CH_2OH), 4.0−4.1 (m, 1H, CHN), 7.27 (s, 10H, $2C_6H_5$); ms (70 eV, 26°C), *m/e* (‰): 333 (165, $M^{+\cdot}$), 275 (820, $M^{+\cdot}$ − CH_2CHCH_2OH), 233 (280 $(O)P(OC_6H_5)_2^+$), 94 (664, $C_6H_5OH^{+\cdot}$), 77 (1000).

β-*Lactam* ***11***

A solution of THP ether **9** (180 mg, 0.42 mmol) and pyridinium *p*-toluenesulfonate (PPTS) (20 mg, 0.08 mmol) in absolute ethanol (5 mL) was stirred at 55°C (oil bath temperature) for 5 h. The solvent was evaporated *in vacuo*, and the residue was chromatographed (EtOAc − petroleum ether, 2:1) to afford 124 mg (85%) of β-lactam **11**. Infrared (film) ν_{max}: 3450 (OH), 1790 (C=O, β-lactam) cm $^{-1}$; ^{1}Hmr 200 MHz ($CDCl_3$ and D_2O) δ: 1.6−2.0 (m, 2H, CH_2CH_2OH), 2.79 (ddd, 1H, COC*H*H, J_{gem} = 16 Hz, $J_{cis} = J_{PH} \simeq 3$ Hz), 3.22 (ddd, 1H, COC*H*H, J_{gem} = 16 Hz, $J_{trans} = J_{PH} \simeq 6$ Hz), 3.4−3.8 (m, 2H, CH_2OH), 4.0−4.2 (m, 1H, NCH), 7.38 (m, 10H, $2C_6H_5$); ms (70 eV, 56°C), *m/e* (‰): 347 (101, $M^{+\cdot}$), 276 (961, $M^{+\cdot}$ − CH_2=CH−$(CH_2)_2OH$ + 1), 254 (117, $M^{+\cdot}$ − $OC_6H_5^{\cdot}$), 77 (1000).

Bicyclic β-*lactam* ***5***

To a solution of **11** (150 mg, 0.43 mmol) in *t*-BuOH (2 mL) was added CsF (66 mg, 0.43 mmol). After stirring at room temperature for 2 h, the solvent was evaporated. Ethyl acetate was added. The mixture was washed with brine, dried, and evaporated to afford 22 mg (20%) of β-lactam **5**, after flash chromatography (petroleum ether − EtOAc, 1:2); mp 103°C; ir (CH_2Cl_2) ν_{max}: 1760 (C=O, β-lactam), 1590, 1490, 1190 cm $^{-1}$; ^{1}Hmr (acetone-d_6) δ: 1.8−2.2 (m, 2H, CH_2), 2.90 (app.dd, 2H, CH_2CO), 3.8−5.0 (m, 3H, CH, CH_2O), 6.9−7.5 (m, 5H, C_6H_5); ^{1}Hmr 200 MHz (acetone-d_6 and D_2O) δ: 1.8−2.2 (m, 2H, CH_2), 2.8−3.0 (m, 2H, CH_2O), 3.9−4.1 (m, 1H, CH), 4.3−4.7 (m, 2H, CH_2O), 6.9−7.5 (m, 5H, C_6H_5); ms (70 eV, 82°C), *m/e* (‰): 254 (372, $M^{+\cdot}$ + 1), 212 (1000, $M^{+\cdot}$ − CH_2=C=O).

β-*Lactam* ***13***

To a solution of alcohol **7***a* (150 mg, 1.3 mmol) and pyridine (162 mg, 1.43 mmol) in CH_2Cl_2 (10 mL) was added dropwise diphenyl chlorophosphate (349 g, 1.3 mmol). After stirring for 2 h the solution was washed with water (3 × 5 mL) and brine (8 mL), dried ($MgSO_4$), and evaporated to give 392 mg (87%) of β-lactam **13** after flash chromatography. Infrared (film) ν_{max}: 1765 (C=O, β-lactam), 1590, 1490 (C=C, aromatic) cm $^{-1}$; ^{1}Hmr 200 MHz ($CDCl_3$) δ: 1.8−2.2 (m, 2H, CH_2), 2.60 (ddd, 1H, COC*H*H, J_{gem} = 15 Hz, J_{trans} = 2 Hz), 3.05 (ddd, 1H, COCH*H*, J_{gem} = 15 Hz, J_{cis} = 5 Hz, J_{NH} = 2 Hz), 3.6−3.8 (m, 1H, CH), 4.2−4.6 (m, 2H, CH_2O), 6.3 (bs, 1H, NH), 7.1−7.5 (m, 10H, $2C_6H_5$); ms (70 eV, 55°C), *m/e* (‰): 347 (46, $M^{+\cdot}$), 305 (437, $M^{+\cdot}$ − CH_2=C=O), 304 (203, $M^{+\cdot}$ − OCNH).

Alcohol ***6***a

To a solution of 4-carbobenzyloxyazetidinone (0.205 g, 1 mmol) in methanol (10 mL) was added sodium borohydride (114 mg, 3 mmol) in portions. After stirring at room temperature for 18 h, concentrated HCl was added dropwise to neutralize to pH 5. The precipitate was filtered off and the filtrate was evaporated to dryness. The residue was purified by flash chromatography (EtOAc − methanol, 10:1) to afford 0.05 g (50%) of alcohol **6***a*. Infrared (film) ν_{max}: 3400−3000 (NH, OH), 1730 (C=O, β-lactam) cm $^{-1}$; ^{1}Hmr (acetone-d_6) δ: 2.6 (dd, 1H, COC*H*H, J_{gem} = 15 Hz, J_{trans} = 2Hz), 2.9 (m, 1H, COCH*H*, J_{gem} = 15 Hz, J_{cis} = 5 Hz, J_{NH} = 1.5 Hz), 3.5−3.9 (m, 3H, CH_2O, CH), 4.2 (bs, 1H, OH), 7.3 (bs, 1H, NH); gc−ms (TMS derivative), *m/e* (‰): 245 (24, $M^{+\cdot}$, di-TMS derivative).

β-*Lactam* ***12***

Diphenyl chlorophosphate (0.31 mL, 1.48 mmol) was added dropwise to a solution of alcohol **6***a* (149 mg, 1.48 mmol) and triethylamine (0.21 mL) in anhydrous tetrahydrofuran (5 mL). After stirring for 0.5 h methylene chloride (20 mL) was added to the reaction mixture. The organic layer was washed with water (2 × 15 mL), dried ($MgSO_4$), and evaporated to dryness. The residue was purified by flash chromatography (EtOAc) to afford 438 mg (89%) of β-lactam **12**. Infrared (film) ν_{max}: 3260 (NH), 1780 (C=O, β-lactam), 1590, 1490 (aromatic C=C), 1290 (P=O) cm $^{-1}$; ^{1}Hmr ($CDCl_3$) δ: 2.51 (ddd, 1H, C*H*HCO, J_{gem} = 15 Hz, J_{trans} = 3 Hz, J_{NH} = 1.5 Hz), 2.83 (ddd, 1H, C*H*HCO, J_{gem} = 15 Hz, J_{cis} = 4 Hz, J_{NH} = 1.5 Hz), 3.5−3.8 (m, 1H, CHN), 3.9−4.3 (m, 2H, CH_2O), 6.6 (bs, 1H, NH), 7.00 (s, 10H, $2C_6H_5$); ms (70 eV, 55°C), *m/e* (‰): 333 (34, $M^{+\cdot}$), 291 (1000, $M^{+\cdot}$ − CH_2=C=O), 94 (861, $C_6H_5OH^{+\cdot}$), 77 (820, $C_6H_5^{+\cdot}$).

*4-Methyl-3-[(*tert*-butoxycarbonyl)amino]-1-hydroxyazetidinone* ***15*** (ref. 15*b*)

Compound **14** (1.53 g, 5 mmol) was dissolved in 140 mL of methanol and hydrogenated at 1 atm of H_2 in the presence of 10% Pd/C (140 mg); filtration and evaporation gave **15** as a white solid; mp 143−145°C (recrystallized from ether−hexanes); $[\alpha]_D^{20}$ −30.8° (*c* 1.05, CH_3OH); ir (Nujol) ν_{max}: 3350 (NH), 1775 (CO, β-lactam), 1685 (CO, *t*-BOC) cm $^{-1}$; ^{1}Hmr (CD_3OD) δ: 1.4 (d, 3H, CH_3, *J* = 6.5 Hz), 1.46 (s, 9H, *t*-Bu), 3.76 (9d, 1H, CHMe, *J* = 6.5, 1.5 Hz), 4.0 (br m, 1H, C*H*NH), 4.8 (br s, 2H).

*4-Methyl-3-[(*tert*-butoxycarbonyl)amino]azetidinone* ***16*** (ref. 15*b*)

Compound **15** (1.92 g, 8.9 mmol) was dissolved in 18 mL of CH_3OH and added to 73 mL of H_2O at pH 7. While the mixture was stirred under N_2 and the pH maintained at 7 by dropwise addition of 3 *N* NaOH solution, 36 mL (4 equiv.) of a 15% aqueous solution of $TiCl_3$ (BDH) was added dropwise. After the addition was completed, stirring was continued for 3 h. The aqueous mixture was then adjusted to pH 8 and extracted with three 30-mL portions of ethyl acetate. The combined ethyl acetate was washed with brine, dried over $MgSO_4$, filtered, and evaporated. The residue was recrystallized from ethyl acetate − hexanes to give 0.77 g (3.85 mmol, 43%) of **16**; mp 123−125°C; $[\alpha]_D^{20}$ −60.5° (*c* 1.1, CH_3OH); ir ($CHCl_3$) ν_{max}: 3440 and 3320 (NH), 1760 (CO β-lactam), 1710 (CO, *t*-BOC) cm $^{-1}$; ^{1}Hmr ($CDCl_3$) δ: 1.4 (d, 3H, CH_3, *J* = 6.5 Hz), 1.45 (s, 9H, *t*-Bu), 3.68 (qd, 1H, C*H*Me, *J* = 6.5, 1.5 Hz), 4.16 (dd, 1H, C*H*NH, *J* = 7.0, 1.5 Hz), 5.85 (d, 1H, NH amide, *J* = 7.0 Hz), 7.0 (br s, 1H, NH β-lactam).

*4-Methyl-3-[(*tert*-butoxycarbonyl)amino]-1-dibenzylphosphoryl-2-azetidinone* ***17***a

Under a nitrogen atmosphere, a solution of β-lactam **16** (150 mg, 0.75 mmol) in dry THF (15 mL) was cooled at −78°C and treated with n-BuLi (1.1 equiv.). The reaction mixture was stirred for 20 min and a solution of dibenzyl chlorophosphate (266 mg, 0.9 mmol) in THF (2 mL) was added dropwise; stirring at −78°C was continued for 1 h. The solution was allowed to warm up to −10°C. The solvent was removed and, after adding ethyl acetate, the organic layer was washed twice with brine, dried on $MgSO_4$, and evaporated. The residue was purified by flash chromatography (ethyl acetate − hexanes, 45:55) to afford 208 mg of β-lactam **17***a* in 60% yield; $[\alpha]_D^{20}$ −3.9° (*c* 1.35, CH_3OH); ir ($CDCl_3$) ν_{max}: 3300 (NH), 1785 (CO β-lactam), 1710 (CO *t*-BOC), 1270 (P=O) cm $^{-1}$; ^{1}Hmr ($CDCl_3$) δ: 1.33−1.43 (s + d, 12H, *t*-Bu + CH_3), 3.70−4.20 (m, 3H, CH—CH, NH), 5.0−5.2 (2d, 4H, $2CH_2$, J_{P-OCH_2} = 9 Hz), 7.3 (s, 10H, $2C_6H_5$); ms (70 eV, 80°C), *m/e* (‰), 304 (110, $M^{+\cdot}$ − *t*-BOCNHCHCO + 1,

Can. J. Chem. Downloaded from www.nrcresearchpress.com by 210.87.254.40 on 09/06/12
For personal use only.

$M^{+\cdot}$ − *t*-BOCNHCHCHCH$_3$ + 1), 157 (70, *t*-BOCNHCHCO$^+$, *t*-BOCNHCHCHCH$_3^+$), 107 (40, $C_6H_5CH_2O^+$), 101 (350, *t*-BuOCO$^+$), 91 (880, $C_6H_5CH_2^+$), 57 (1000, *t*-Bu$^+$, $\overline{CH_2—CO—NH}^{+\cdot}$, $\overline{CH_2—CHMe—NH}^{+\cdot}$).

*4-Methyl-3-[(*tert*-butoxycarbonyl)amino]-1-phosphoryl-2-azetidinone* **17**b

Dibenzylphosphoramidate **17***a* (40 mg, 0.087 mmol) was dissolved in methanol (5 mL) and hydrogenated for 1 h at 1 atm of H_2 in the presence of 10% Pd/C (5 mg). After filtration and evaporation, the residue was washed with chloroform (3 × 1 mL) to afford 22 mg of amidophosphoric acid **17***b* in 90% yield; pH (CH_3OH solution) 2.5−3; ir ($CHCl_3$) ν_{max}: 3450−2600 (OH), 3350 (NH), 1760 (CO β-lactam), 1705 (CO *t*-BOC), 1250 (P=O) cm^{-1}; ^{1}Hmr 200 MHz (D_2O) δ: 1.33 (s, 9H, *t*-Bu), 1.43 (d, 3H, CH_3, J = 6.5 Hz), 3.7−5.0 (m, 5H); ms (70 eV), *m/e* (‰): 497 (120, $M^{+\cdot}$ + 1 + 3TMS), 397 (120), 395 (740, $M^{+\cdot}$ − *t*-BuOCO + 3TMS), 340 (370, $M^{+\cdot}$ − *t*-BOCNHCHCO + 1 + 3TMS, $M^{+\cdot}$ − *t*-BOCNHCHCHCH$_3$ + 1 + 3TMS), 323 (150, $M^{+\cdot}$ − *t*-BuO + 3TMS), 101 (20, *t*-BuOCO$^+$), 73 (1000, *t*-BuO$^+$), 57 (340, *t*-Bu$^+$, $\overline{CH_2—CO—NH}^{+\cdot}$, $\overline{CH_2—CHMe—NH}^{+\cdot}$).

*4-Methyl-3-(*tert*-butoxycarbonyl)amino]-1-dimethylphosphoryl-2-azetidinone* **17**c

To a suspension of β-lactam phosphoric acid **17***c* (8.5 mg, 0.03 mmol) in CH_2Cl_2 (1 mL) was added dropwise at 0°C a solution of diazomethane (2.5 equiv.) in ether. The reaction mixture was warmed to room temperature by itself. After evaporation of the solvent 10 mg of dimethylphosphoramidate **17***c* were obtained in a quantitative yield; ir ($CHCl_3$) ν_{max}: 3450 (NH), 1780 (CO β-lactam), 1715 (CO *t*-BOC), 1270−1180 (P=O) cm^{-1}; ^{1}Hmr ($CDCl_3$) δ: 1.3−1.45 (s + d, 12H, *t*-Bu + CH_3), 3.6−4.4 (m, 2H, CH—CH), 3.8−4.0 (2d, 4H, 2 OCH_3, $J_{P—OCH_3}$ = 12 Hz), 5.2 (br d, 1H, NH); ms (70 eV), *m/e* (‰): 235 (60 $M^{+\cdot}$ − *t*-BuO), 157 (20, *t*-BOCNHCHCO$^+$, *t*-BOCNHCHCHCH$_3^+$), 152 (460, $M^{+\cdot}$ − *t*-BOCNHCHCO + 1, $M^{+\cdot}$ − *t*-BOCNHCHCHCH$_3$ + 1), 109 (80, $\overline{PO(OMe)_2}^{+\cdot}$), 101 (245, *t*-BuOCO$^+$), 57 (1000, *t*-Bu$^+$, $\overline{CH_2—CO—NH}^{+\cdot}$, $\overline{CH_2—CHMe—NH}^{+\cdot}$).

β-*Lactam* **19**

β-Lactam **16** (200 mg, 1 mmol) was dissolved in trifluoroacetic acid (1 mL) at 0°C. After stirring for 10 min, the acid was removed by evaporation and the residue washed with carbon tetrachloride (3 × 1 mL); ir (film) ν_{max}: 3450−2680 (NH, OH), 1770 (CO β-lactam), 1670 (CO) cm^{-1}; ^{1}Hmr (CD_3COCD_3) δ: 1.5 (d, 3H, CH_3, J = 6.5 Hz), 3.8−4.4 (m, 3H, C*H*Me, NH_2), 5.05 (d, 1H, C*H*NH, J = 1.5 Hz).

4-Methyl-3-phenylacetamido-2-azetidinone **20**

To a solution of β-lactam **19** (214 mg, 1 mmol) and pyridine (237 mg, 3 mmol) in dry methylene chloride (20 mL) was added, dropwise under nitrogen, phenylacetyl chloride (232 mg, 1.5 mmol) in 5 mL methylene chloride. After the addition was complete the solution was stirred for 3 h, washed with pH 4.5 buffer (KH_2PO_4) and water, dried ($MgSO_4$), and evaporated. The crude product was purified by flash chromatography (ethyl acetate) to afford a colorless solid (50 mg) in 23% yield; mp 138−140°C; $[\alpha]_D^{20}$ −36.0° (*c* 0.65, CH_3OH); ir ($CHCl_3$) ν_{max}: 3420 and 3300 (NH), 1760 (C=O β-lactam), 1670 (C=O amide), 1600 (C=C) cm^{-1}; ^{1}Hmr ($CDCl_3$) δ: 1.5 (d, 1H, CH_3, J = 6.5 Hz), 3.4−3.7 (m, 3H, CH_2, C*H*Me), 4.5 (dd, 1H, C*H*NH, J = 6.0, 2.0 Hz), 6.5 (br s, 1H, NH β-lactam), 6.8 (d, 1H, NH amide, J = 6.0 Hz), 7.3 (s, 5H, C_6H_5); ms (70 eV), *m/e* (‰): 175 (380, $C_6H_5CH_2CONHCHCO^+$, $\underline{C_6H_5CH_2CONHCHCHMe^+}$), 91 (670, $C_6H_5CH_2^+$), 57 (1000, $\overline{CH_2—CO—NH}^{+\cdot}$, $\overline{CH_2—CHMe—NH}^{+\cdot}$).

4-Methyl-3-phenylacetamido-1-dibenzylphosphoryl-2-azetidinone **21**a was prepared from β-lactam **20** as described for **17***a*, in 30% yield after flash chromatography (EtOAc−hexanes, 60:40); ir ($CHCl_3$) ν_{max}: 3400 (NH), 1780 (CO β-lactam), 1670 (CO amide), 1270−1180 (P=O) cm^{-1}; ^{1}Hmr ($CDCl_3$) δ: 1.5 (d, 3H, CH_3, J = 6.5 Hz), 3.65 (s, 2H, CH_2), 3.75−4.1 (m, 1H, C*H*Me), 4.2−4.4 (dd, 1H, C*H*NH, J = 7.0, 2.0 Hz), 5.1−5.3 (2d, 4H, $2CH_2$, J = 9 Hz), 6.1 (d, 1H, NH, J = 7.0 Hz), 7.4 (s, 15H, $3C_6H_5$); ms (70 eV), *m/e* (‰): 478 (150, $M^{+\cdot}$), 304 (140, $M^{+\cdot}$ − $C_6H_5CH_2CONHCHCO$ + 1, $M^{+\cdot}$ − $C_6H_5CONHCHCHMe$ + 1), 281 (490), 175 (490, $C_6H_5CH_2CONHCO^+$, $\underline{C_6H_5CH_2CONHCHCHMe^+}$), 91 (1000, $C_6H_5CH_2^+$), 57 (170, $\overline{CH_2—CONH}^{+\cdot}$, $\overline{CH_2CHMe—NH}^{+\cdot}$).

4-Methyl-3-phenylacetamido-1-phosphoryl-2-azetidinone **21**b was prepared from β-lactam **21***a* as described for **17***b*. Yield: 85%; pH (CH_3OH solution) 3.5; ir (Nujol) ν_{max}: 3450−3000 (OH, NH), 1750 (C=O β-lactam), 1650 (C=O amide), 1200 (P=O) cm^{-1}; ^{1}Hmr (CD_3OD) δ: 1.5 (d, 3H, CH_3, J = 6.5 Hz), 3.6 (s, 2H, CH_2), 3.7−4.6 (m, 3H, CH—CH, NH), 7.3 (s, 5H, C_6H_5).

4-Methyl-3-phenylacetamido-1-dimethylphosphoryl-2-azetidinone **21**c was prepared from β-lactam **21***b* as described for **17***c*; ms (70 eV), *m/e* (‰): 327 (5, $M^{+\cdot}$ + 1), 175 (10, $C_6H_5CH_2CONHCHCO^+$, $C_6H_5CH_2CONHCHCHMe^+$), 152 (1000, $M^{+\cdot}$ − $C_6H_5CH_2CONHCHCO$ + 1, $M^{+\cdot}$ − $C_6H_5CH_2CONHCHCHMe$ + 1), 109 (20, $\overline{PO(OCH_3)_2}^+$), 91 (380, $C_6H_5CH_2^+$), 57 (70, $\overline{CH_2CONH}^{+\cdot}$, $\overline{CH_2—CHMe—NH}^{+\cdot}$).

β-*Lactam* **23**

To a solution of β-lactam **19** (1.07 g, 5 mmol) in 150 mL of dry THF−CH_2Cl_2 (1:2) was added triethylamine (0.60 g, 6 mmol) at 0°C and under nitrogen. The reaction mixture was stirred for 1 h and allowed to warm to room temperature. Then two solutions, trityl acid **22** (2.66 g, 6 mmol) in 30 mL dry CH_2Cl_2 and EEDQ (1.48, 6 mmol) in 20 mL dry CH_2Cl_2, were successively added dropwise. After stirring for a period of 15 h, the solvent was removed and ethyl acetate added. The organic layer was washed with a 4% $NaHCO_3$ solution (2 × 20 mL) and brine, dried ($MgSO_4$), and evaporated. The crude material was purified by flash chromatography (EtOAc−hexanes 75:25) to afford 0.98 g of β-lactam **23** in 38% yield; mp 135−140°C; $[\alpha]_D^{20}$ −31.4° (*c* 1.35, CH_3OH); ir ($CHCl_3$) ν_{max}: 3420 and 3360 (NH), 1765 (CO β-lactam), 1680 (CO amide) cm^{-1}; ^{1}Hmr ($CDCl_3$) δ: 1.5 (d, 3H, CH_3, J = 6.5 Hz), 4.0 (s, 3H, OCH_3), 3.5−4.0 (qd, 1H, C*H*Me, J = 6.5, 2.0 Hz), 4.4−4.6 (dd, 1H, C*H*NH, J = 6.0, 2.0 Hz), 6.2 (s, 1H, NH β-lactam), 6.6 (s, 1H, CH=), 7.1 (d, 1H, NH amide), 7.3 (s, 15H, $3C_6H_5$).

β-*Lactam* **24**

Trityl β-lactam **23** (485 mg, 0.92 mmol) in 75 mL of methanol − formic acid (4:1) was refluxed for 1 h. After evaporation of the solvent, the crude material was washed with carbon tetrachloride to give 227 mg (0.80 mmol, 86%) of amino β-lactam **24**; mp 125−130°C (dec.); $[\alpha]_D^{20}$ −70.5° (*c* 2.47, CH_3OH); ir ($CHCl_3$) ν_{max}: 3480, 3410, 3300 (NH), 1760 (CO β-lactam), 1670 (CO amide), 1600 (C=C) cm^{-1}; ^{1}Hmr (CD_3COCD_3) δ: 1.4 (d, 3H, CH_3, J = 6.5 Hz), 3.6−4.0 (m, 4H, OCH_3, C*H*Me), 4.5−4.7 (dd, 1H, CHNH, J = 8.0, 2.0 Hz), 6.72 (s, 1H, CH=), 6.92 (br s, 2H, NH_2), 7.5 (s, 1H, NH β-lactam), 8.4 (d, 1H, NH amide); ms (70 eV), *m/e* (‰): 283 (80, $M^{+\cdot}$), 252 (100, $M^{+\cdot}$ − OCH_3), 240 (150, $M^{+\cdot}$ − CONH, $M^{+\cdot}$ − MeCHNH), 126 (1000), 125 ($H_2N—C=N—C—C\equiv N$, 99 (S—CH)), 83 (300), 57 (250).

N-*dibenzylphosphoryl* β-*lactam* **25**a was prepared from compound **24** (227 mg, 0.8 mmol) following the procedure described for **17***a*. However, in the present case, the organic layer was washed with a 4% $NaHCO_3$ solution and brine. The crude compound was purified by flash chromatography (EtOAc) to afford 150 mg of β-lactam **25***a* in 35% yield; $[\alpha]_D^{20}$ −18.4° (*c* 1.05, CH_3OH); ir ($CHCl_3$) ν_{max}: 3480, 3380 (NH), 1780 (CO β-lactam), 1670 (CO amide), 1600 (C=C), 1190 (P=O) cm^{-1}; ^{1}Hmr 200 MHz ($CDCl_3$) δ: 1.43 (d, 3H, CH_3, J = 6 Hz), 3.89 (s, 3H, OCH_3), 4.15 (qd, 1H, C*H*Me, J = 6.0, 2.0 Hz), 4.62 (dd, 1H, C*H*NH, J = 7.0, 2.0 Hz), 5.11−5.17 (2d, 4H, $2CH_2$, $J_{P—OCH_2}$ = 8 Hz), 5.76 (s, 2H, NH_2), 6.66 (s, 1H, CH=), 7.22 (m, 10H, $2C_6H_5$), 8.11 (br d, 1H, NH, J = 7 Hz); ms (70 eV), *m/e* (‰): 187 (180), 167 (110), 149 (370), 107 (170), 100 (830), 97

(160), 91 (1000, $C_6H_5CH_2^+$), 83 (103), 79 (100), 69 (680), 57 (760), 55 (610), 45 (250).

N-*phosphoryl* β-*lactam* **25**b was prepared from **25***a* (47 mg, 0.086 mmol) according to the method given for **17***b*. After 10 h of reaction, filtration, and evaporation, the crude material was recrystallized in MeOH−EtOAc (1:3) to give phosphoric acid **25***b* in 80% yield; pH (MeOH solution) 5.5; $[\alpha]_D^{20}$ 26.3° (*c* 0.18, CH_3OH); ir (KBr) ν_{max}: 3600−2900 (NH, OH), 1745 (CO β-lactam), 1665 (CO amide), 1210 (P=O) cm^{-1}; ^{1}Hmr 200 MHz (CD_3OD) δ: 1.47 (d, 3H, CH_3, J = 6.5 Hz), 3.93 (s, 3H, OCH_3), 3.47−3.77 (m, 1H, C*H*Me), 4.2−4.4 (m, 1H, C*H*NH), 6.8 (s, 1H, CH=), 7.22−7.47 (m, 5H, NH_2, NH, 2OH); ms (70 eV), *m/e* (‰): 368 (40), 97 (110), 91 (200), 83 (180), 69 (370), 57 (450), 55 (410), 44 (1000).

N-*dimethyl phosphoryl* β-*lactam* **25**c was prepared from compound **25***b* as described for **17***c*; ms (70 eV), *m/e* (‰): 279 (60), 167 (120), 149 (280), 130 (120), 121 (110), 97 (160), 95 (120), 91 (110), 85 (150), 83 (220), 81 (250), 73 (360), 71 (330), 69 (655), 57 (780), 55 (680), 43 (1000).

Triethylamine salt **25**d was obtained by addition of triethylamine (5 mg, 0.05 mmol) to a solution of acid **25***b* (9 mg, 0.025 mmol) in 1 mL MeOH. After stirring for 5 min, the solvent was removed to afford 13 mg of β-lactam **25***d* in 92% yield; ir (KBr) ν_{max}: 3550−3300 (NH), 1745 (CO β-lactam), 1660 (CO amide), 1610 (C=C), 1245, 1205 (P=O) cm^{-1}; ^{1}Hmr (CD_3OD) δ: 1.3−1.5 (t + d, 9H, $2CH_2$—CH_3, CH_3, J = 7.5, 6.5 Hz), 3.1 (q, 4H, $2CH_2$—Me, J = 7.5 Hz), 3.5−4.6 (m, 5H, C*H*Me, C*H*NH, OCH_3), 6.85 (s, 1H, CH=), 7.3 (m, 5H, 3NH, NH_2).

Monopotassium salt **25**e

Dibenzylphosphoramidate **25***a* (5.4 mg, 0.01 mmol) was dissolved in 2 mL THF−EtOH (1:1) and 12 μL of a 1 *M* aqueous solution of $KHCO_3$ (0.012 mmol) was added. The mixture was hydrogenated for 6 h in the presence of 20% Pd(OH)/C (3 mg). After filtration and evaporation, the residue was washed with ethyl acetate to afford 3.8 mg (95%) of potassium salt **25***e*; ir (KBr) ν_{max}: 3600−2900 (OH, NH), 1745 (CO β-lactam), 1655 (CO amide), 1595 (C=C), 1250 (P=O) cm^{-1}.

Acknowledgements

We wish to thank the Natural Sciences and Engineering Research Council of Canada and Lederle Laboratories for financial support, Dr. Françoise Saulnier for taking the 200 MHz ^{1}H nmr spectra, Dr. Orval Mamer and associates of the Biomedical Mass Spectrometry Unit, McGill University for the mass spectral data, Ms. Nida Kuck, Lederle Laboratories, for biological tests, and Dr. S. Lang for providing a sample of acid **22**.

1. W.-Y. Liu. Ph.D. Thesis, McGill University, 1982.
2. G. Just and T. J. Liak. Can. J. Chem. **56**, 211 (1978).
3. G. Just and R. Zamboni. Can. J. Chem. **56**, 2720 (1978).
4. A. Imada, K. Kitano, K. Kintaka, M. Muroi, and M. Asai. Nature, **289**, 590 (1981); R. B. Sykes, C. M. Cimarusti, D. P. Bonner, K. Bush, D. M. Floyd, N. H. Georgopapadakou, W. H. Koster, W. C. Liu, W. L. Parker, P. A. Principe, M. L. Rathnum, W. A. Slusarchyk, W. H. Trejo, and J. S. Wells. Nature, **291**, 489 (1981).
5. D. S. Breslow, E. Baumgarten, and C. R. Hauser. J. Am. Chem. Soc. **66**, 1286 (1944).
6. K. Pankiewicz, R. Kinas, W. J. Stec, A. B. Foster, M. Jarman, and J. M. S. Van Maanen. J. Am. Chem. Soc. **101**, 7712 (1979).
7. W. V. E. Doering and C. H. Depuy. J. Am. Chem Soc. **75**, 5955 (1953); M. Regitz. Angew. Chem. Int. Ed. Engl. **6**, 733 (1967).
8. E. J. Corey and A. M. Felix. J. Am. Chem. Soc. **87**, 2518 (1965).
9. D. M. Brunwin and G. Lowe. J. Chem. Soc. Perkin Trans. 1, 1321 (1973); J. Chem. Soc. (C), 3756 (1971); J. Parker and G. Lowe. Chem. Commun. 577 (1971); 865 (1971); D. M. Brunwin and G. Lowe. Chem. Commun. 589 (1972); M. V. J. Ramsay and G. Lowe. J. Chem. Soc. Perkin Trans. 1, 479 (1973).
10. R. B. Woodward, K. Heusler, J. Gosteli, P. Naegeli, W. Oppolzer, R. Ramage, S. Ranganathan, and H. Vorbrüggen. J. Am. Chem. Soc. **88**, 852 (1966); R. B. Woodward. Science, **153**, 487 (1966).
11. R. J. Ponsford and R. Southgate. J. Chem. Soc. Chem. Commun. 846 (1979).
12. D. B. R. Johnston, S. M. Schmitt, F. A. Bouffard, and B. G. Christensen. J. Am. Chem. Soc. **100**, 313 (1978); F. A. Bouffard, D. B. R. Johnston, and B. G. Christensen. J. Org. Chem. **45**, 1130 (1980).
13. M. Miyashita, A. Yoshikoshi, and P. A. Grieco. J. Org. Chem. **42**, 3772 (1977).
14. K. K. Ogilvie, S. L. Beaucage, N. Theriault, and D. M. Entwistle. J. Am. Chem. Soc. **99**, 1277 (1977).
15. (*a*) M. J. Miller, P. G. Mattingly, M. A. Morrison, and J. F. Kerwin. J. Am. Chem. Soc. **102**, 7026 (1980); (*b*) P. G. Mattingly and M. J. Miller. J. Org. Chem. **45**, 410 (1980).
16. L. D. Cama and B. G. Christensen. Tetrahedron Lett. 4233 (1978).
17. P. G. Mattingly and M. J. Miller. J. Org. Chem. **46**, 1557 (1981).
18. G. Just and T. J. Liak. Can. J. Chem. **56**, 211 (1978).
19. R. Bucourt, R. Heymès, A. Lutz, L. Pénasse, and J. Perronnet. C. R. Acad. Sci. Paris, Ser. D, **284**, 1847 (1977).
20. B. Belleau and G. Malek. J. Am. Chem. Soc. **90**, 1651 (1968); G. H. Hakimelahi and G. Just. Can. J. Chem. **57**, 1932 (1979).
21. J. V. Heck, M. J. Szymonifka, and B. G. Christensen. Tetrahedron Lett. **23**, 1519 (1982).
22. W. H. Koster, R. Zahler, D. P. Bonner, H. W. Chang, C. M. Cimarusti, G. A. Jacobs, and M. Perri. Monophosphams: monocyclic β-lactam antibiotics activated by N-1 phosphonic (-inic) acids. A comparative study to monobactams (2-oxoazetidine-1-sulfonic acids). Abstract 674, XXII Interscience Conference on Antimicrobial Agents and Chemotherapy Poster Session − New Monobactams. October 5, 1982.

Can. J. Chem. Downloaded from www.nrcresearchpress.com by 210.87.254.40 on 09/06/12
For personal use only.

Infrared spectra of crystalline *n*-alkanes. Changes observed during the phase I → phase II transition[1]

HECTOR L. CASAL, DAVID G. CAMERON, AND HENRY H. MANTSCH
Division of Chemistry, National Research Council of Canada, Ottawa, Ont., Canada K1A 0R6

Received August 6, 1982[2]

HECTOR L. CASAL, DAVID G. CAMERON, and HENRY H. MANTSCH. Can. J. Chem. **61**, 1736 (1983).

Detailed measurements of the changes in the infrared spectra of *n*-nonadecane and *n*-heneicosane on transition from the orthorhombic to the so-called "hexagonal" or "rotator" phase are reported.

HECTOR L. CASAL, DAVID G. CAMERON et HENRY H. MANTSCH. Can. J. Chem. **61**, 1736 (1983).

On rapporte les mesures détaillées des changements observés dans les spectres infrarouges du *n*-nonadécane et du *n*-hénéicosane lors de la transition de la phase orthorhombique à la soi-disant phase "hexagonale" ou "rotateur".

[Traduit par le journal]

Can. J. Chem. Downloaded from www.nrcresearchpress.com by 210.87.254.42 on 09/06/12
For personal use only.

Introduction

The normal alkanes undergo a variety of solid–solid phase transitions (1, 2). In particular, odd-numbered *n*-alkanes undergo a transition from a low temperature orthorhombic crystal form (phase I) to a high temperature form (phase II), sometimes referred to as the "rotator" or "hexagonal" phase.

In this paper we report on the changes induced in the infrared spectra of *n*-nonadecane (n-$C_{19}H_{40}$) and *n*-heneicosane (n-$C_{21}H_{44}$) by the phase I to phase II transition. The nature of this transition is relevant to two general areas of study.

Firstly, the properties of phase II are of intrinsic interest. Studies have shown that the chains undergo hindered rotation (1, 3, 4), that *gauche* bonds are present (5–7), and that there exists interchain vibrational coupling (8). All these effects are both chain length and temperature dependent. Secondly, the transition is relevant to studies of the properties of model biomembranes. The hydrated diacylphosphatidylcholines exhibit a "pretransition" some 2–10°C below the temperature of the gel to liquid-crystal transition. A variety of changes can be monitored in the infrared spectra of these lipids and, to a first approximation, parallel those observed at the phase I to phase II transition of *n*-alkanes, and as the temperature is raised in phase II (9, 10).

Experimental

n-Nonadecane and *n*-heneicosane were gifts from R. G. Snyder. The preparation and purification have been described (11); their purity was determined by gas–liquid chromatography to be higher than 99.7%. The sample of n-1,1,1,17,17,17-hexadeuteroheptadecane (n-$C_{17}H_{30}D_6$) was a gift from L. C. Leitch; its purity was higher than 99.5%.

Temperature regulation was achieved with a thermostated cell mount (12). Spectra of thin (2–10 μm) films between KBr windows were recorded on a Digilab FTS-15 Fourier transform infrared spectrometer equipped with a wide range mercury cadmium telluride detector (Infrared Associates, New Brunswick, NJ). Six hundred scans, recorded with a maximum optical path difference of 1 cm, were co-added, triangularly apodized, zero-filled once, and Fourier transformed to yield a resolution of 1 cm^{-1} and an encoding interval of 0.5 cm^{-1}.

Frequencies and full-width at half-height (FWHH) were determined by the methods previously described, using three data points for the centre of gravity computation (13).

[1]NRCC No. 20700.

[2]Revision received March 3, 1983.

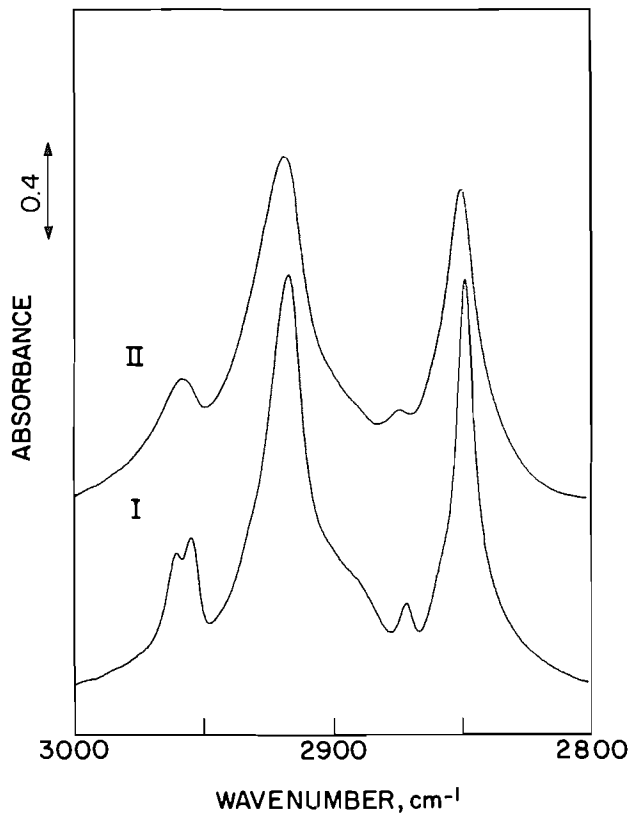

FIG. 1. C—H stretching region of the infrared spectrum of n-$C_{21}H_{44}$ in phase I (lower trace, 1°C) and phase II (upper trace, 36°C).

Results

In Table 1 we list the frequencies and assignments (14, 15) of the infrared spectra of phase I and phase II *n*-nonadecane and *n*-heneicosane.

The temperature dependence of the spectra is discussed below; as the thermotropic behaviour of the two *n*-alkanes is essentially the same, detailed data are only presented for n-$C_{21}H_{44}$.

C—H stretching

The C—H stretching region of the infrared spectrum of solid n-$C_{21}H_{44}$ is shown in Fig. 1; the bottom trace is the spectrum of phase I (1°C) and the top trace is that of phase II (36°C).

Figure 2 shows the temperature dependence of the intensities, frequencies, and widths of the antisymmetric and

TABLE 1. Frequencies (cm $^{-1}$) of the bands in the infrared spectra of n-$C_{19}H_{40}$ and n-$C_{21}H_{44}$ in phase I and phase II[a]

n-$C_{19}H_{40}$			n-$C_{21}H_{44}$		
Assignment[b]	Phase I (1°C)	Phase II (26°C)	Assignment[b]	Phase I (1°C)	Phase II (36°C)
r_a	2960.0 s	2956.0 s	r_a	2959.5 s	2956.0 s
r_b	2954.0 s	2956.0 s	r_b	2954.0 s	2956.0 s
d	2917.3 s	2917.5 s	d	2917.2 s	2917.4 s
d^+	2849.2 s	2849.5 s	d^+	2849.5 s	2849.7 s
δ	1473.6 s 1461.8 s	1468.5 s	δ	1473.6 s 1462.6 s	1468.5 s
α	1465.3 s		α	1465.3 s	
α+δ	1459.8 sh 1446.0 m	1459.8 sh	α+δ	1456.7 sh 1446.0 m	1458.3 sh
U+W	1374.5 m	1377.2 m	U+W	1384.2 m 1375.0 m	1384.9 sh 1379.4 m
W_1	1196.5 vw	1198.6 vw	W_1	1196.0 w	1199.2 vw
W_2	1207.5 w	1209.5 w	W_2	1204.6 w	1207.0 w
W_3	1228.7 w	1230.4 w	W_3	1222.0 w	1224.6 w
W_4	1245.5 w	1246.9 w	W_4	1238.0 vw	—
W_5	1262.8 vw	1264.2 vw	W_5	1254.2 w	1256.4 w
W_6	1280.0 vw	1281.0 vw	W_6	1268.0 vw	1270.0 vw
W_7	1298.5 w	1299.2 w	W_7	1286.3 w	1288.4 w
W_8	1317.0 vw	—	W_8	1305.0 vw	—
W_9	1330.0 vw	—	W_9	1317.0 w	1319.6 w
			W_{11}	1342.0 w	1343.0 w
			W_{12}	1362 vw	1362 vw sh
P_1	719.2 s 729.6 s	719.5 s	P_1	719.8 s 730.8 s	721.2 s
P_7	743.8 m 749.5 m	744.9 m	P_7	743.0 m	740.0 sh
P_9	783.5 m 781.9 m	782.2 w	P_9	762.4 m 766.3 m	764.3 w
P_{11}	841.5 s	839.2 m	P_{11}	808.5 m	808.3 m
P_{13}	905.6 w 908.0 w	904.9 w	P_{13}	862 w, sh 865 m	864.3 m
P_{15}	969.8 w 973.8 w	970 w	P_{15}	923.8 w 927.9 m	924.7 m
P_{17}	1029 vw	1030 vw	P_{17}	980 w[c] 986 w[c]	— —
β	891.8 m 889	888.8 m	β	892.4 m	890.2 m
			T_{14}	1270 vw[d]	1275 w
			T_{17}	1190 w	—
T_{16}	1286 vw	1286 vw	T_{19}	1178 vw	—
T_{17}	1180.8 w	1180.8 vw	T_{20}	1172 vw	1175 vw
T_{18}	1171.6 w	1172 vw			
R_1	1134.2 m	1132.6 m	R_1	1134.8 m	1133.5 m
R_2	1121 vw	1119 vw	R_2	1124.1 m	1123.0 m
R_3	1088.5 m	1087.3 m	R_3	1094.5 m	1094.0 m
R_{14}	1057 vw	—	R_4	1067.0 w	1066.4 w
R_{13}	1054 vw, sh	1055 w	R_{13}	1046 w	1045 vw
R_{12}	1044 vw	1044 vw	R_{12}	1034 sh	1035 vw
R_{11}	1037 vw	1038 vw	R_5	1028 w	1028 w
R_{10}	1024 vw	1026 vw	R_{11}	1023 w, sh	—
R_9	1000 vw 997 vw	998 vw	$R_{10,6}$	998 vw	—
			R_9	986 vw	—
R_6	998 vw	—	R_7	975 vw	—
R_8	984 vw	—			

[a]The symbols s, m, w, sh, and v represent: strong, medium, weak, shoulder, and very respectively.

[b]The abbreviations used for labelling bands are the same as those of refs. 14 and 15; they are: r_a, methyl asymmetric C—H stretch (in-skeletal plane); r_b, methyl asymmetric C—H stretch (out-of-skeletal plane); d, methylene antisymmetric C—H stretch; d^+, methylene symmetric C—H stretch; δ, methylene HCH bend; α, methyl asymmetric bending; U, methyl symmetric bending; W, methylene wagging (W, is the ith component of the band progression); T, methylene twisting (T, is the ith component of the band progression) P, methylene rocking (P, is the ith component of the band progression); R, C—C stretch (R, is the ith component of the band progression).

[c]Overlap with C—C stretching.

[d]Overlap with CH_2 wagging.

Can. J. Chem. Downloaded from www.nrcresearchpress.com by 210.87.254.42 on 09/06/12
For personal use only.

Can. J. Chem. Downloaded from www.nrcresearchpress.com by 210.87.254.42 on 09/06/12
For personal use only.

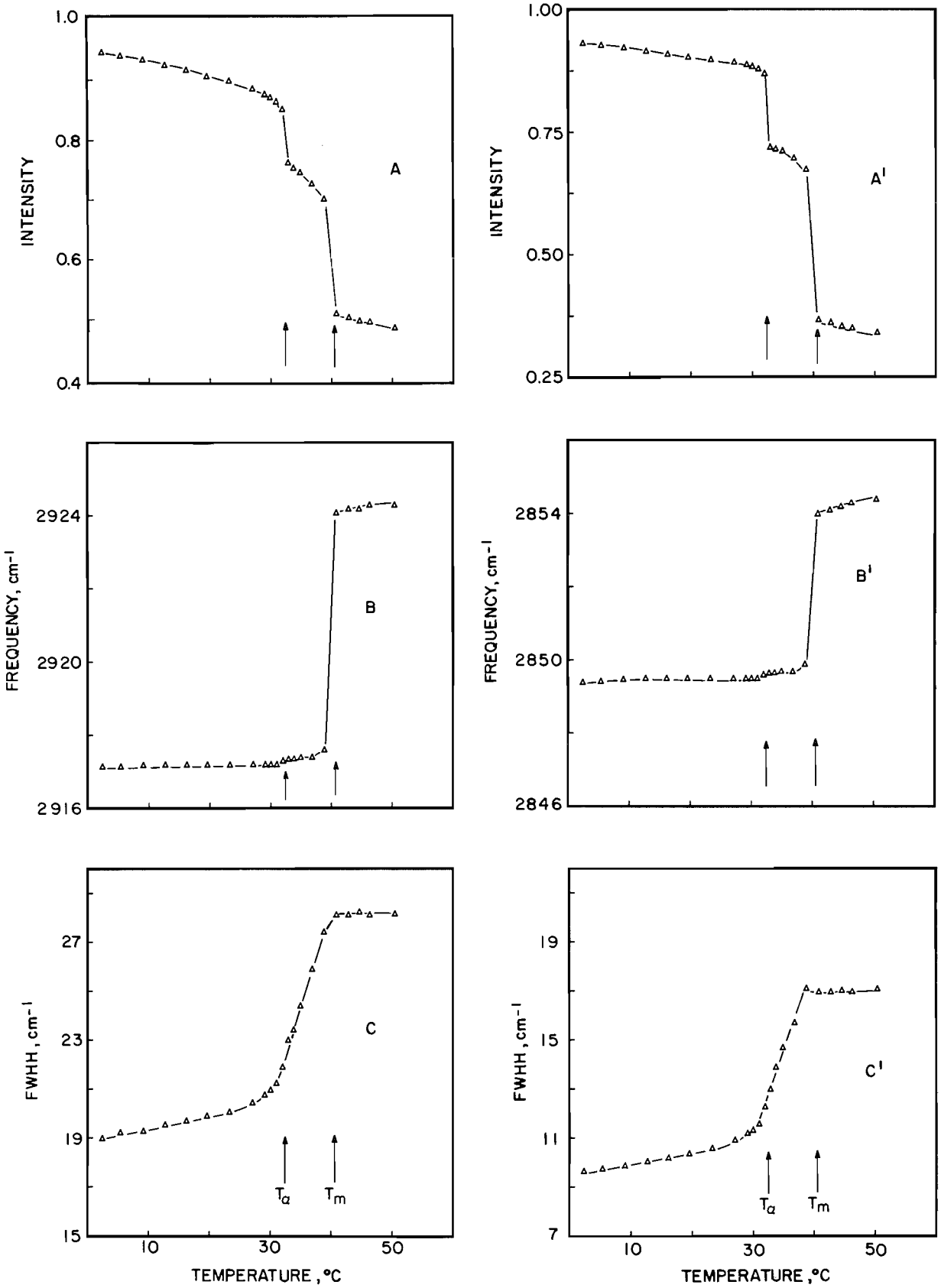

FIG. 2. Temperature dependence of the antisymmetric CH_2 (A, B, C) and symmetric CH_2 (A', B', C') stretching bands in the spectrum of n-$C_{21}H_{44}$: A and A', integrated intensity (baselines from 2947 to 2878 cm^{-1} (A), and 2866 to 2806 cm^{-1} (A')); B and B', frequency; C and C', full width at half height (FWHH) (baseline from 3000 to 2800 cm^{-1}). In this and all other plots T_α indicates the temperature of the phase I $\rightarrow$ phase II transition, and T_m indicates the melting point. Note that the intensity scales are arbitrary, and only meant to convey information on the change of integrated intensity for a given band. Comparisons of absolute values between different figures cannot be made.

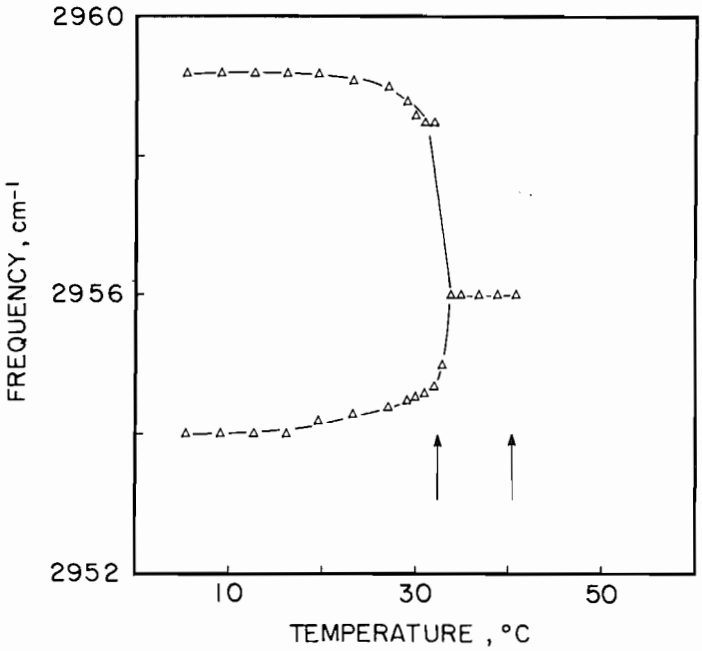

FIG. 3. Temperature dependence of the frequency of the components of the methyl antisymmetric stretching mode in the spectrum of n-$C_{21}H_{44}$.

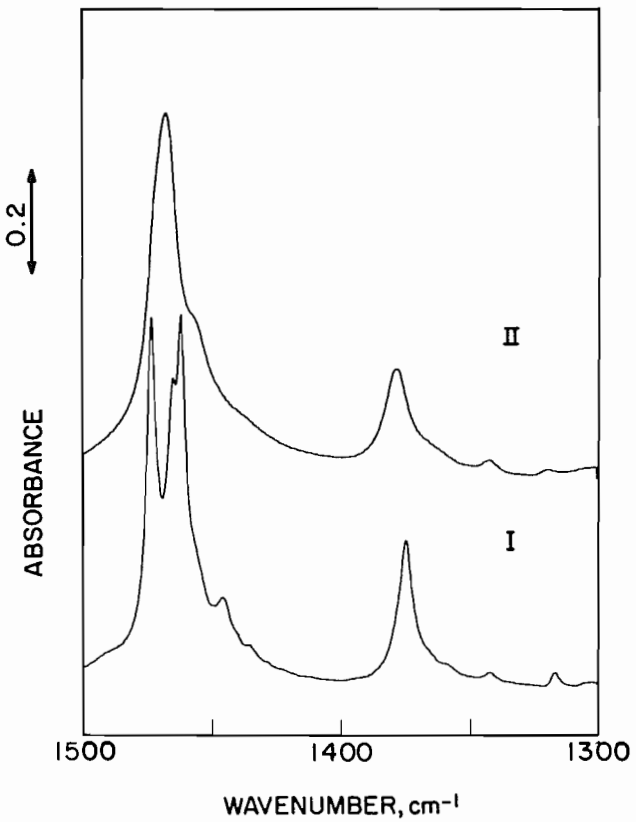

FIG. 4. 1500–1300 cm^{-1} region of the spectrum of n-$C_{21}H_{44}$ in phase I (1°C) and phase II (36°C).

symmetric CH_2 stretching bands. Quite dissimilar behaviour is observed for these parameters. The intensities decrease steadily as the temperature is raised in phase I and phase II, and there is an abrupt change at 32.5°C, the transition temperature (T_α). In contrast, the frequencies are almost the same in phase I and phase II, the shifts at 32.5°C being small (0.2 cm^{-1}).

The values of the FWHH also vary steadily in both phases. However, in contrast to the discontinuities in the intensity and frequency plots at T_α, there is merely a change in the gradient of the bandwidth plot.

The frequencies of the in-plane and out-of-plane components of the methyl asymmetric stretching mode versus temperature are plotted in Fig. 3. The separation between the two components starts to decrease at ~25°C, and at T_α the two components collapse into one band.

CH_2 scissoring and CH_3 bending

The HCH scissoring and CH_3 bending bands are observed in the 1500–1300 cm^{-1} region, shown in Fig. 4 for n-$C_{21}H_{44}$. The principal results of transition from phase I to phase II are a major reduction in the degree of crystal field splitting of the HCH scissoring mode (8) and a slight increase in intensity at 1450 cm^{-1}. Parallel changes are observed in the CH_2 rocking bands (see below) and have been reported in detail in ref. 8.

Figure 5 shows the temperature dependence of the integrated intensity of the 1520–1420 cm^{-1} region. The intensity includes a contribution from the asymmetric methyl bending at 1465 cm^{-1}. However, a similar increase in integrated intensity at T_α was observed in the spectra of n-$C_{17}H_{30}D_6$, hence the data of Fig. 5 can be taken as representative of the HCH scissoring bands.

CH_2 wagging

The methylene wagging band progression is observed in the 1380 to 1180 cm^{-1} region, as shown in Fig. 6 for n-$C_{21}H_{44}$. The transition to phase II results in changes in the intensities, widths, and frequencies of all components of the progression. Excepting for W_{11} (1342 cm^{-1}), the intensities decrease. The apparent increase in the intensity of this band is due to the occurrence in phase II of a band (~1343 cm^{-1}) due to the wagging of CH_2 groups adjacent to *gauche* defects (16). Other bands present only in phase II and associated with *gauche* defects (16) are observed at 1300 and 1275 cm^{-1}. We also note that the apparent absence of T_{17} (1190 cm^{-1}) in phase II is due to overlap of T_{17} with W_1 (1196 cm^{-1}) in this phase.

Figure 7 shows plots of temperature versus the integrated intensity, frequency, and width of the W_2 band in the spectrum of n-$C_{21}H_{44}$, its thermal behaviour being representative of the CH_2 wagging bands. The transition to phase II results in an abrupt shift to higher frequency of about 2 cm^{-1}, broadening (~25%), and a major reduction in intensity (~40%). A feature evident in this figure is that both the frequency and FWHH start changing well below the temperature of transition, paralleling the early onset of changes in the methyl stretching bands (Fig. 3).

CH_2 rocking and twisting

The methylene rocking band progression extends from 1170 to 720 cm^{-1}; this region of the spectrum of n-$C_{21}H_{44}$ in phase I and phase II is shown in Fig. 8. Transition to phase II results in greatly reduced splitting of the progression bands and decreased integrated intensities.

The spectrum of phase II contains additional bands characteristic of nonplanar conformers, which are not present in the spectrum of phase I. They appear at 875 and 958 cm^{-1} (CH_3 rock, C—C stretch); 1078 cm^{-1} (CH_2 wag, C—C stretch); 1162 cm^{-1} (CH_2 rock, CH_3 rock), and at 755, 783, and 832 cm^{-1} (CH_2 rock). The subject of nonplanar conformers in phase II n-alkanes is discussed in ref. 6.

Can. J. Chem. Downloaded from www.nrcresearchpress.com by 210.87.254.42 on 09/06/12
For personal use only.

Can. J. Chem. Downloaded from www.nrcresearchpress.com by 210.87.254.42 on 09/06/12
For personal use only.

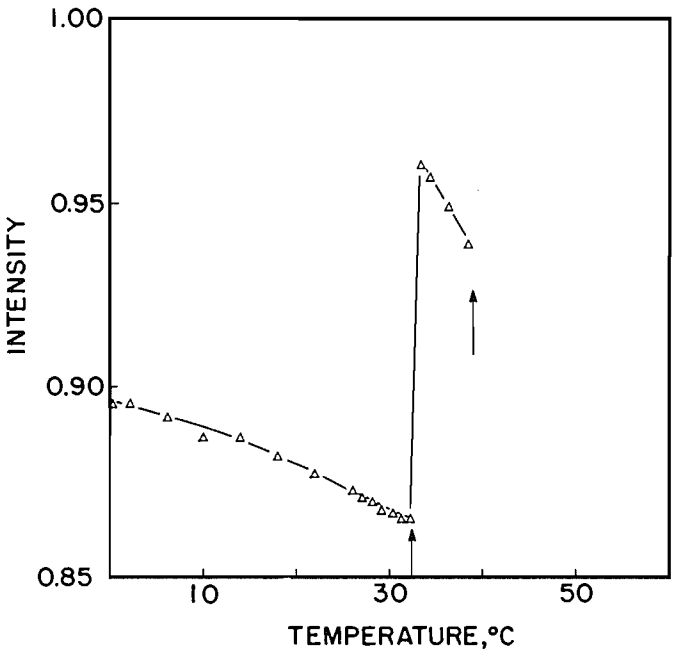

FIG. 5. Temperature dependence of the intensity of the 1470 cm^{-1} region of the spectrum of n-$C_{21}H_{44}$. The intensity was measured using a baseline from 1520 to 1420 cm^{-1} (see note on Fig. 2 caption).

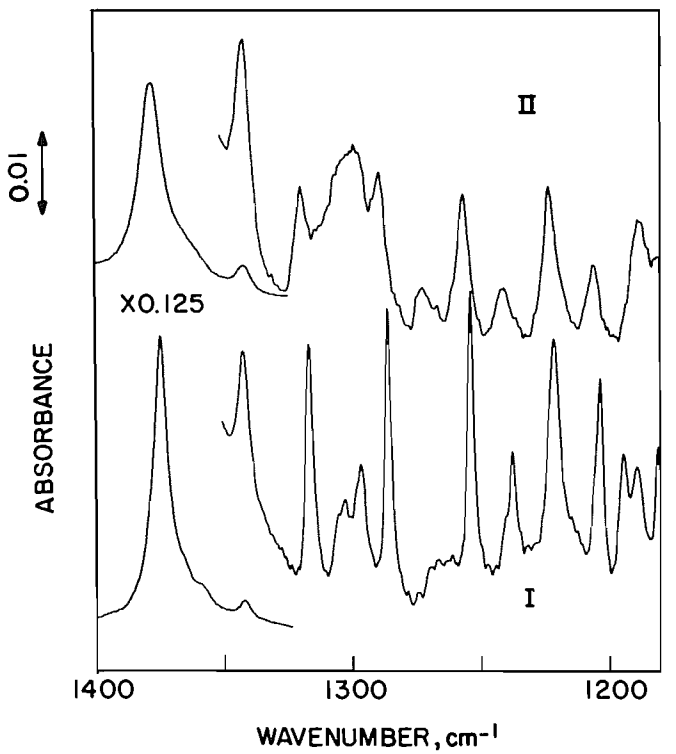

FIG. 6. Methylene wagging band progression, 1400–1180 cm^{-1} region of the spectrum of n-$C_{21}H_{44}$ in phase I (1°C) and phase II (36°).

Plots of temperature versus the integrated intensity of the P_{11} component of the CH_2 rocking progression, and of the methyl symmetric in-plane rocking band of n-$C_{21}H_{44}$ are shown in Fig. 9. As for the CH_2 stretching, scissoring, and wagging modes, the intensity of the methyl rocking mode (Fig. 9*B*) is not constant in phase I, but decreases with increasing temperature. In contrast, the intensity of the CH_2 rocking band (Fig. 9*A*) is

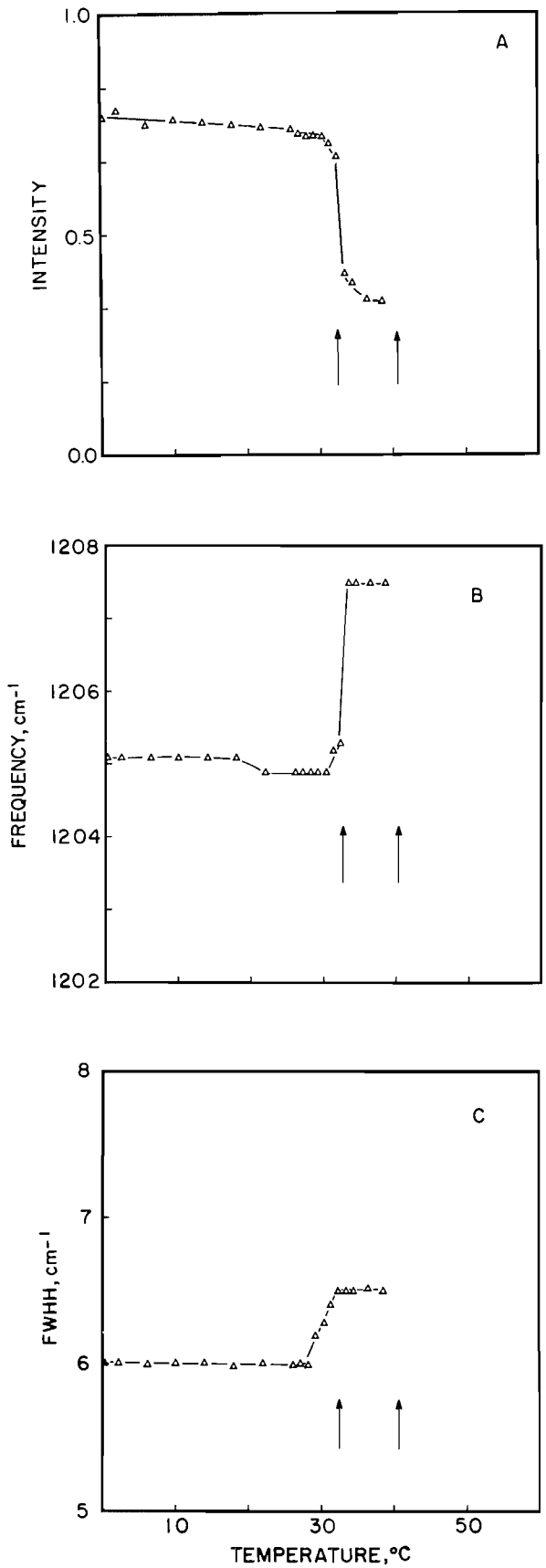

FIG. 7. Temperature dependence of the W_2 component of the CH_2 wagging band progression of n-$C_{21}H_{44}$: *A*, intensity (see note on Fig. 2 caption); *B*, frequency; *C*, FWHH (baseline from 1216 to 1200 cm^{-1}).

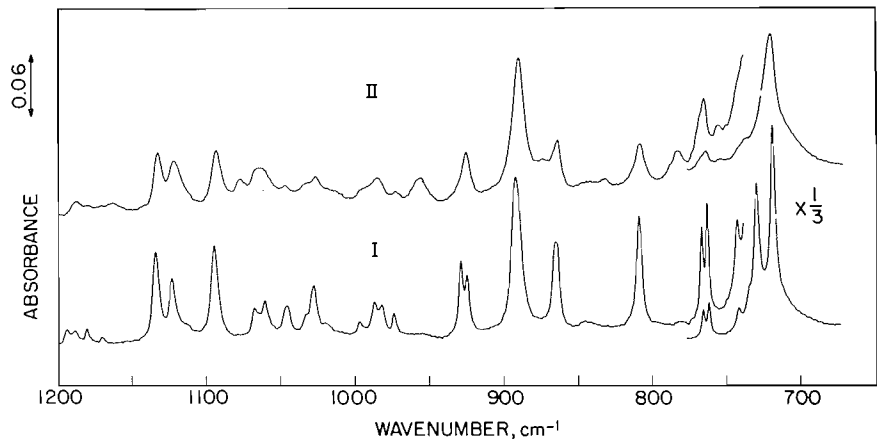

FIG. 8. Methylene rocking band progression, 1200–700 cm^{-1} region of the spectrum of n-$C_{21}H_{44}$ in phase I (1°C) and phase II (36°).

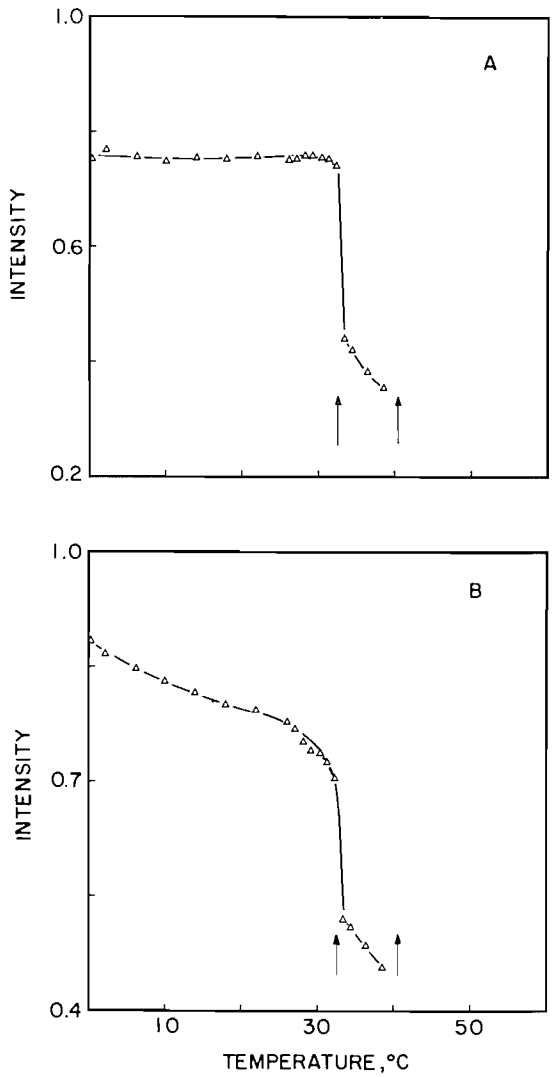

FIG. 9. Temperature dependencies of the intensities of A, the P_{11} component of the methylene rocking progression (baseline from 820 to 800 cm^{-1}) and B, the methyl symmetric in-plane rocking band of n-$C_{21}H_{44}$ (baseline from 906 to 880 cm^{-1}) (see note on Fig. 2 caption).

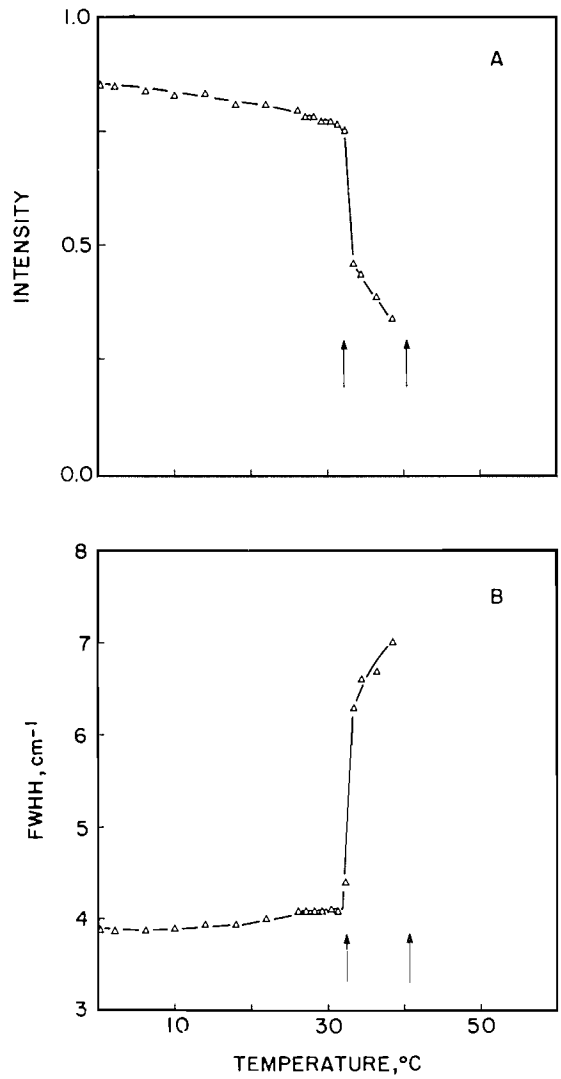

FIG. 10. Temperature dependence of the R_3 component of the C—C stretching band progression of n-$C_{21}H_{44}$: A, intensity (see note on Fig. 2 caption); B, FWHH (baseline from 1108 to 1085 cm^{-1}).

constant in phase I. The transition to phase II is marked by a large, abrupt decrease in intensity with a further decrease within phase II. In Fig. 9B we also note that, as with other methyl bands (Figs. 3 and 7), the gradient of the plot changes at about 25°C, well below the phase transition temperature.

The CH_2 twisting band progression (1300–1170 cm^{-1}) is very weak and overlapped by the methylene wagging band

Can. J. Chem. Downloaded from www.nrcresearchpress.com by 210.87.254.42 on 09/06/12
For personal use only.

TABLE 2. Changes in integrated intensity and density of n-$C_{21}H_{44}$ at T_α, and in phases I and II, with increasing temperature

	% Change at T_α	Rate of change, % °C^{-1}	
		Phase I	Phase II
Band[a]			
d and d'	−12	−0.3	−1.2
W_2	−40	−0.3	−3.0
P_{11}	−30	−0.2	−4.0
β	−24	−0.5	−2.0
Density[b]	−4.5	−0.1	−0.3

[a]The abbreviations are the same as those in Table 1.
[b]Calculated from changes in the unit cell volume (17).

progression (Fig. 6). In general, the transition results in a decrease in intensity, and little change in frequency (Table 1).

C—C stretching

The C—C stretching band progression is observed in the 1150–950 cm^{-1} region, shown in Fig. 8.

The temperature dependencies of the intensity and width of the R_3 component of the progression of n-$C_{21}H_{44}$ are shown in Fig. 10. The data are similar in form to those observed for the CH_2 wagging bands, except that at T_α the frequency decreases rather than increases (Table 1). The possibility that the temperature dependence of the band is affected by coupling with the methyl symmetric in-plane rocking mode (11) was eliminated by the observation of similar behaviour by the R_3 band in the spectrum of n-$C_{17}H_{30}D_6$.

Discussion

These data demonstrate that the transition from phase I to phase II results in changes in all bands in the infrared spectrum. Compared to the spectral changes resulting from melting of the alkanes, these are relatively minor. The only generalized major trend is a reduction in integrated intensity on transition to phase II. In this regard the overall increase in intensity in the 1520–1420 cm^{-1} region reflects the increased intensity near 1450 cm^{-1}; examination of difference spectra shows that the bands near 1470 cm^{-1} decrease in integrated intensity.

In general, the overall changes result from the reduction in intermolecular interactions on transition, and the increased mobility and slight conformational disorder in this phase. As indicated in the Introduction, the detailed structure of phase II is dependent on both chain length and temperature, and requires further elucidation. However, there are several trends evident in these data which point to potential areas of study.

Firstly, the rates of change of density and of the integrated intensities of several bands in phases I and II, and during the transition, are summarized in Table 2. In general, the integrated intensity changes much more rapidly than the density. There is no readily available explanation for this behaviour, particularly in phase I where there is no perturbation by *gauche* rotamers, and the chain mobility is minimal.

Secondly, at least three of the plots (Figs. 3, 7*C*, and 9*B*) show the onset of change several degrees below the transition temperature.

Thirdly, some bandwidth plots do not show an abrupt discontinuity; rather, the width increases over a range of a few degrees. The extreme case of this is observed in the plots (Figs. 2*C* and 2*C'*) derived from the CH_2 stretching bands, where the transition is only marked by a change in gradient.

Finally, there are major reductions in the intensities, and shifts in the frequencies of the components of the CH_2 wagging progression as a result of transition to phase II. It has been suggested that the intensities of these bands provide a suitable monitor of the number of *gauche* bonds in a primarily *trans* chain (18). However, in these systems the introduction of an average population of one *gauche* bond per chain (6) is simultaneous with a 40% reduction in the integrated intensities of the CH_2 wagging bands (Fig. 7 and Table 2). Consequently, a simple, direct correlation between wagging intensity and population of *gauche* bonds cannot be made.

Acknowledgement

We thank J. Doucet for providing us with the values of the unit cell volumes of n-$C_{19}H_{40}$ and n-$C_{21}H_{44}$.

1. A. MÜLLER. Proc. R. Soc. London, Ser. A. **138**, 514 (1932).
2. M. G. BROADHURST. J. Res. Nat. Bur. Stand. Section A, **66**, 241 (1962).
3. J. D. HOFFMAN. J. Chem. Phys. **20**, 541 (1952).
4. T. ISHINABE. J. Chem. Phys. **72**, 353 (1980).
5. B. EWEN, G. R. STROBL, and D. RICHTER. Faraday Discuss. **69**, 19 (1980).
6. R. G. SNYDER, M. MARONCELLI, S. P. QI, and H. L. STRAUSS. Science, **214**, 188 (1981).
7. G. ZERBI, R. MAGNI, M. GUSSONI, K. H. MORITZ, A. BIGOTTO, and S. DIRLIKOV. J. Chem. Phys. **75**, 3175 (1981).
8. H. L. CASAL, H. H. MANTSCH, D. G. CAMERON, and R. G. SNYDER. J. Chem. Phys. **77**, 2825 (1982).
9. D. G. CAMERON, H. L. CASAL, and H. H. MANTSCH. Biochemistry, **19**, 3665 (1980).
10. D. G. CAMERON, E. F. GUDGIN, and H. H. MANTSCH. Biochemistry, **20**, 4496 (1981).
11. A. A. SCHAERER, C. J. BUSSO, A. E. SMITH, and L. B. SKINNER. J. Am. Chem. Soc. **77**, 2017 (1955).
12. D. G. CAMERON and R. N. JONES. Appl. Spectrosc. **35**, 448 (1981); D. G. CAMERON and G. M. CHARETTE. Appl. Spectrosc. **35**, 224 (1981).
13. D. G. CAMERON, J. K. KAUPPINEN, D. J. MOFFATT, and H. H. MANTSCH. Appl. Spectrosc. **36**, 245 (1982).
14. R. G. SNYDER and J. H. SCHACHTSCHNEIDER. Spectrochim. Acta, **19**, 85 (1963).
15. R. G. SNYDER, S. L. HSU, and S. KRIMM. Spectrochim. Acta, **34A**, 395 (1978).
16. R. G. SNYDER. J. Chem. Phys. **47**, 1316 (1967).
17. J. DOUCET, I. DENICOLO, and A. CRAIEVICH. J. Chem. Phys. **75**, 1523 (1981).
18. U. P. FRINGELI. Biophys. J. **34**, 173 (1981).

Can. J. Chem. Downloaded from www.nrcresearchpress.com by 210.87.254.42 on 09/06/12
For personal use only.

Selenoketone spectroscopy: vibronic analysis of the $\tilde{A}^1A_2 \leftarrow \tilde{X}^1A_1$ and $\tilde{a}^3A_2 \leftarrow \tilde{X}^1A_1$ $n \rightarrow \pi^*$ electronic transitions in F_2CSe [1]

M. Y. BÖLÜK AND D. C. MOULE

Department of Chemistry, Brock University, St. Catharines, Ont., Canada L2S 3A1

AND

D. J. CLOUTHIER

Herzberg Institute of Astrophysics, National Research Council of Canada, Ottawa, Ont., Canada K1A 0R6

Received November 16, 1982

M. Y. BÖLÜK, D. C. MOULE, and D. J. CLOUTHIER. Can. J Can. J. Chem. **61**, 1743 (1983).

The spectrum of F_2CSe has been surveyed over the 700–200 nm wavelength region and three distinct absorptions identified. These are the spin-allowed $\tilde{A}^1A_2 \leftarrow \tilde{X}^1A_1$ and spin-forbidden $\tilde{a}^3A_2 \leftarrow \tilde{X}^1A_1$ overlapping $n \rightarrow \pi^*$ transitions, λ_{max} = 434 nm, and the orbitally-allowed $\tilde{B}^1A_1 \leftarrow \tilde{X}^1A_1$ $\pi \rightarrow \pi^*$ transition, λ_{max} = 236 nm. Vibrational assignments for the band systems have been made and the out-of-plane energy levels analyzed in terms of a quadratric-Lorentzian double minimum potential. The barriers to inversion for the $\tilde{A}^1A_2/\tilde{a}^3A_2$ states were found to be 2483/2923 cm^{-1} and the out-of-plane angles 30.1/31.4 deg. The singlet–triplet separation was $E(\tilde{A}^1A_2) - E(\tilde{a}^3A_2)$ = 671 cm^{-1}. The $\tilde{B}^1A_1$ system displays continuous structure and was not subject to a vibrational analysis.

M. Y. BÖLÜK, D. C. MOULE et D. J. CLOUTHIER. Can. J Can. J. Chem. **61**, 1743 (1983).

On a étudié le spectre du F_2CSe dans l'intervalle de longueur d'onde allant de 700 à 200 nm et on identifié trois absorptions distinctes. Ce sont: les absorption de spin permis le spin $\tilde{A}^1A_2 \leftarrow \tilde{X}^1A_1$, et de spin interdit $\tilde{a}^3A_2 \leftarrow \tilde{X}^1A_1$, les transitions de recouvrement $n \rightarrow \pi^*$, λ_{max} = 434 nm, et la transition permise orbitalement $\tilde{B}^1A_1 \leftarrow \tilde{X}^1A_1$ $\pi \rightarrow \pi^*$, λ_{max} = 236 nm. On a identifié les vibrations et on a analysé les niveaux d'énergie hors du plan en fonction du potentiel minimum double du type quadratique-Lorentzien. On a trouvé que les barrières à l'inversion des états $\tilde{A}^1A_2/\tilde{a}^3A_2$ sont de 2483/2923 cm^{-1} et les angles hors du plan sont de 30.1/31.4 degrés. La séparation singulet triplet est: $E(\tilde{A}^1A_2) - E(\tilde{a}^3A_2)$ = 671 cm^{-1}. Le système $\tilde{B}^1A_1$ montre une structure continue et n'est pas sujette à une analyse vibrationnelle.

[Traduit par le journal]

Introduction

The electronic structures of molecules containing the carbonyl or thiocarbonyl chromophores have been the subject of extensive research (*1*, 2). While techniques such as inelastic electron scattering and photoelectron spectroscopy have been employed for this purpose, much of the information about the electronic states has come from optical absorption and emission spectroscopy.

The visible and ultraviolet spectra of thiocarbonyl molecules are characterized by two absorptions. In the region 700–400 nm, the thiocarbonyl halides display a weak absorption, $f \simeq 10^{-4}$, which is attributed to the promotion of an electron from the nonbonding sulphur n orbital to an antibonding π^* orbital localized in the C=S bond. A second much stronger absorption, $f \simeq 10^{-1}$, is found in these molecules at 280–240 nm. The strength of this absorption and its position in the spectrum has led to its assignment, $\pi \rightarrow \pi^*$.

The addition of an electron to the π^* orbital increases the electron density at the carbon atom with the result that the $n\pi^*$ and $\pi\pi^*$ states are usually nonplanar. The potential function which describes the out-of-plane distortion in these states contains a set of minima at the equilibrium position which are separated by a potential barrier at the planar configuration. It is the heights of these barriers to molecular inversion which has been the subject of some interest. The creation of a partially filled π^* orbital results in a destabilization of the double bond, with the nominal bond order of 2 for the $\tilde{X}$ ground state falling to 1.5 for the $\tilde{A}$ and $\tilde{a}$ $n\pi^*$ states and to 1.0 for the $\pi\pi^*$ state. The changes in vibrational frequency on electronic excitation are a reflection of the differences in structure in the combining states. The correlation of the frequencies among the carbonyl and thiocarbonyl molecules can be used to elucidate their structural and dynamical differences.

The purpose of the present work was to extend the literature which exists on the spectroscopy of the carbonyl and thiocarbonyl compounds to the selenocarbonyl series of molecules. Selenocarbonyl difluoride, F_2CSe, is the only known tetratomic in this class of molecules (3). The ground state structure (4) and vibrational frequencies (5) have been investigated but no information is available on the electronic spectroscopy. It was hoped that a study of the visible and uv spectra could lead to information about the structure and bonding in the lower electronic excited states of the C=Se group.

Experimental

Selenocarbonyl difluoride was prepared by the pyrolysis of $(F_2CSe)_2$ dimer in a spiral tube at 200°C. The polymeric material $(F_2CSe)_x$ was warmed to 150°C to form the dimer. The preparation of this material has been described by Haas (3). The monomer and the cyclic dimer were separated by trap-to-trap distillation immediately before the spectra were recorded.

Survey spectra of F_2CSe were recorded over the 700–200 nm region with a Cary 14 spectrophotometer. The structured bands of the transition centered at 434 nm were clearly observed with a 10 cm cell at a pressure of 22 Torr, while only 1 Torr was needed to record the spectrum at 236 nm.

Medium resolution spectra of the lower region were photographed with a 6 meter Ebert spectrograph (6) at a reciprocal linear dispersion of 1.30 nm/cm. The path length of the cell was 90 cm, and at room temperature 70 and 12 Torr pressures were used which are equivalent to 8.3×10^{-2} and 1.4×10^{-2} m-atm path length × pressure respectively. Spectra were also recorded at −78°C at 6.0×10^{-3} m-atm. A 450 W Xe arc was used as a continuous source of radiation, and lines from a Fe–Ne hollow cathode lamp for calibration. Profiles of the absorption bands were obtained from the negatives with a single beam microdensitometer. The frequencies (in cm^{-1}) of the bands

[1]NRCC No. 21197.

Can. J. Chem. Downloaded from www.nrcresearchpress.com by 210.87.254.5 on 09/06/12
For personal use only.

Can. J. Chem. Downloaded from www.nrcresearchpress.com by 210.87.254.5 on 09/06/12
For personal use only.

which were assigned in this study are shown in Table 1. This listing represents about 80% of the bands observed in the 527–540 nm region.

Results and assignments

Electronic assignment

Figures 1 and 2 show the survey spectra of F_2CSe which were recorded with the Cary-14 spectrophotometer. These absorption bands appear in the uv–visible region and can be classified by their intensity, frequency, and structure. The first absorption occurs in the visible region, and it consists of an extensive series of vibronic bands which extend from 500 to 350 nm. The maximum oscillator strength for this system is $f = 3.5 \times 10^{-4}$. At higher energies a second system is observed which is completely free from vibrational structure. This strong system, $f = 2.5 \times 10^{-2}$, is centered at 240 nm. The oscillator strengths were calculated from the observed gas pressures in the cell. It was assumed that the sample was pure, and that the cyclic dimer did not introduce a measurable partial pressure. A third system was observed as the onset of an absorption at 200 nm.

The low energy absorption has the characteristics of a transition which is not allowed by electric dipole selection rules. The ground state with filled electronic shells has A_1 symmetry, and an electronically forbidden transition would terminate only on an A_2 upper state. The first observed system is assigned to the spin forbidden and spin allowed transitions $\tilde{a}^3A_2 \leftarrow \tilde{X}^1A_1$ and $\tilde{A}^1A_2 \leftarrow \tilde{X}^1A_1$ respectively. The singlet and triplet states arise from the promotion of an electron from the nonbonding n orbital on the selenium to the antibonding π^* orbital. The assignment of the second system comes from an analogy to the thiocarbonyl halide molecules. This group of molecules displays an intense absorption system in the 270 nm region. The assignment of these bands to the z polarized $\pi \rightarrow \pi^*$ $\tilde{B}^1A_1 \leftarrow \tilde{X}^1A_1$ transition is now well established (2). This is the assignment which is given to the $\lambda_{max} = 240$ nm band shown in Fig. 2. Our assignment of the third system is more tentative. While MO calculations are not available for this molecule, simple considerations would place the $n \rightarrow 3s$ Rydberg promotion as the third transition in the spectrum.

Vibrational analysis of the $\tilde{a}^3A_2 \leftarrow \tilde{X}^1A_1$ *electronic transition*

The starting point for the vibrational analysis of the first absorption spectrum was the recognition of two major factors. The first of these relates to the higher atomic number of selenium $z = 34$ compared to sulphur $z = 16$. The greater electron density at the Se atom relaxes the $\Delta S = 0$ selection rule with the result that the singlet–triplet transition is expected to contribute to the intensity of the low energy end of the spectrum. The other major assumption which was used in the initial assignment is that the molecule is nonplanar in the excited singlet and triplet states and the spectrum displays the characteristics of inversion doubling. Moreover, the combination of a planar ground state and a nonplanar excited state should give rise to strong activity to the Q_4 mode leading to progressions in ν_4' and ν_4''. Transitions from quanta of ν_4'' would appear weakly in the spectrum as hot bands. A comparison of the spectrum observed at room temperatures and that recorded at dry ice temperature revealed the hot band intervals which are collected together in Table 2. From the selection rules for the singlet–triplet transition, the hot band interval is given as 0_0^0–$4_1^1 = \nu_4'' - \Delta$. The difference between the observed intervals and ν_4'' is a measure of the inversion doubling splitting Δ. For example, 4_0^6–$4_1^7 =$ 565 cm^{-1}, and as $\nu_4'' = 575$ cm^{-1} then $\Delta = 10$ cm^{-1}. This is a relatively small value of the inversion doubling splitting and indicates a substantial barrier in the $\tilde{a}$ state.

TABLE 1. Band frequencies and assignments for the $\tilde{a}^3A_2 \leftarrow \tilde{X}^1A_1$ and $\tilde{A}^1A_2 \leftarrow \tilde{X}^1A_1$ transitions in F_2CSe

Assignment	Type	(cm^{-1})	Assignment	Type	(cm^{-1})
4_1^3	S–T	18986	$1_0^1 4_0^1$	S–S	20818
0_0^0	S–T	19018	$2_0^1 4_0^3$	S–S	20886
3_0^1	S–T	19415	$3_0^2 4_0^4$	S–T	20891
4_0^2	S–T	19561	$2_0^2 4_0^2$	S–T	20896
4_1^2	S–S	19653	$3_0^2 4_0^3$	S–S	20995
2_0^1	S–T	19689	$2_0^2 4_0^1$	S–S	21007
4_0^1	S–S	19689	$3_0^1 4_0^6$	S–T	21034
3_0^2	S–T	19805	4_0^8	S–T	21128
$3_0^1 4_0^2$	S–T	19953	$3_0^1 4_0^5$	S–S	21150
4_1^7	S–T	20068	$1_0^1 2_0^1 3_0^1$	S–T	21201
4_0^4	S–T	20103	$1_0^1 4_0^4$	S–T	21231
4_1^4	S–S	20187	4_0^7	S–S	21284
$2_0^1 4_1^5$	S–T	20198	$1_0^1 4_0^3$	S–S	21357
$2_0^1 4_0^2$	S–T	20228	$2_0^2 3_0^1 4_0^1$	S–S	21393
4_0^3	S–S	20228	$2_0^1 4_0^5$	S–S	21427
$3_0^2 4_0^2$	S–T	20345	$1_0^1 3_0^2 4_0^2$	S–T	21490
$2_0^1 4_0^1$	S–S	20351	$3_0^2 4_0^5$	S–S	21526
$3_0^1 4_0^4$	S–T	20495	$2_0^2 4_0^3$	S–S	21545
$1_0^1 3_0^1$	S–T	20545	$1_0^1 2_0^1 3_0^2$	S–T	21597
$3_0^1 4_0^3$	S–S	20616	$2_0^3 4_0^1$	S–S	21662
4_0^6	S–T	20633	$3_0^1 4_0^7$	S–S	21668
4_1^6	S–S	20683	$1_0^1 2_0^1 3_0^2 4_0^1$	S–S	21718
$1_0^1 4_0^2$	S–T	20717	4_0^9	S–S	21800
4_0^5	S–S	20764	$2_0^2 3_0^1 4_0^3$	S–S	21926
$2_0^1 4_0^4$	S–T	20770	$2_0^2 4_0^5$	S–S	22082
			$2_0^3 4_0^3$	S–S	22200

The assignment of the out-of-plane mode for the upper electronic state, ν_4', began at the low energy end of the absorption. It is here that the spectrum is expected to consist of bands from the $\tilde{a}^3A_2 \leftarrow \tilde{X}^1A_1$ transition. In this region, the band pattern was complex and many combinations of intervals were possible candidates for a vibrational assignment. However, it was observed that the bands appeared to consist of two distinct types, a set of sharp double-headed features and a set of more diffuse single-headed bands. A successful set of frequency differences was obtained by combining the wavenumbers of pairs of bands with similar rotational contours. An interval of 540 ± 5 cm^{-1} was found which was common to 21 frequency differences. These intervals could be grouped into smooth progressions of up to five members. The strength of these progressions and their lengths in the spectrum allow us to make an assignment to ν_4'. The drop in the frequency from 575 to 540 cm^{-1} is to be anticipated for a system which undergoes a loss of molecular planarity on electronic excitation. Frequency differences between various vibrational levels of the upper state are given in Table 3. A clear progression of five members in an interval of 543 cm^{-1} was found to lock onto a pair of features at 19018 and 18990 cm^{-1}. This was the first band that was observed in the long path length experiments and was assigned to the 0_0^0 origin band. Other bands of the $\tilde{a}^3A_2 \leftarrow \tilde{X}^1A_1$ system appeared as

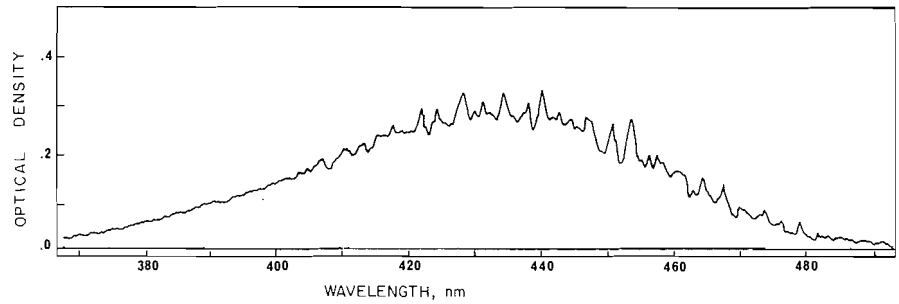

FIG. 1. The visible spectrum of F_2CSe recorded with a Cary 14 spectrophotometer. The pressure of the gas was 22 mm Hg and the path length 10 cm.

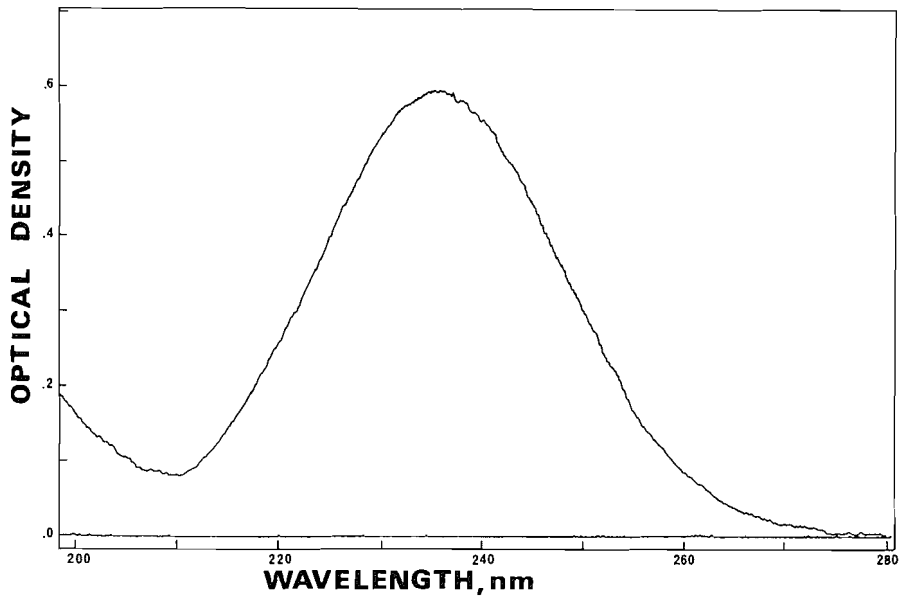

FIG. 2. The near ultraviolet spectrum of F_2CSe recorded with a Cary 14 spectrophotometer. The pressure of the gas was 1 mm Hg, the path length was 10 cm.

TABLE 2. Frequency differences isolating ν_4''

$\tilde{A}^1A_2 \leftarrow \tilde{X}^1A_1$		$\tilde{a}^3A_2 \leftarrow \tilde{X}^1A_1$	
Attached difference	cm^{-1}	Attached difference	cm^{-1}
$4_0^1-4_1^0$	—	$0_0^0-4_1^1$	—
$4_0^3-4_1^2$	575	$4_0^2-4_1^3$	575
$4_0^5-4_1^4$	577	$4_0^4-4_1^5$	—
$4_0^7-4_1^6$	601	$4_0^6-4_1^7$	565
		$2_0^14_0^4-2_0^14_1^5$	572

doublets in the spectrum with a peak separation of about 30 cm^{-1}. This behaviour is similar to what has been observed in the corresponding transition in F_2CS (7).

In the $n \rightarrow \pi^*$ electronic transition, the promoted electron is placed into the π^* antibonding orbital. The result is a destabilization of the structure in which the selenocarbonyl group is reduced from a bond order of 2 to 1.5. It would be anticipated that ν_1 would decrease in value from its ground state of 1287 cm^{-1} and display well characterized intervals of about 1000 cm^{-1}. One such interval was located in the spectrum with a frequency of 1156 cm^{-1} in combination with other excited state levels.

Higher members were not observed because the weaker singlet–triplet bands merge into the stronger bands of the singlet–singlet transition. The modes ν_5 and ν_6 of b_2 vibrational species would not be expected to be present in the spectrum, and are not observed.

Vibrational analysis of the $\tilde{A}^1A_2 \leftarrow \tilde{X}^1A_1$ *electronic transition*

The $\tilde{A}$ and $\tilde{a}$ states have a common electronic configuration and differ only in the spins of the n and π^* electrons. The orbitals occupied by these electrons occupy different regions of space and consequently their interaction is small. The result is that the exchange energy required to elevate the molecule from the $\tilde{a}$ system to the $\tilde{A}$ system is small, less than 1000 cm^{-1}. The molecular structure and the force constants in the two states should be similar. As a consequence, it was possible to use the vibrational intervals and the intensity patterns of the $\tilde{a} \leftarrow \tilde{X}$ system as a template for the assignment of the $\tilde{A} \leftarrow \tilde{X}$ system. A major difference is that the hot band intervals are larger than the ground state frequency, ν_4'', by the inversion doubling splitting, $4_0^1-4_1^0 = \nu_4'' + \Delta$. Hot band intervals are tabulated in Table 2. The progressions in ν_4' extending back to the vibronic suborigins are given in Table 3. The spectrum could be followed out to 2500 cm^{-1} of vibrational excitation. At that point the bands become too diffuse for further analysis. The observed frequencies for the $\tilde{A}$ state are close to those of the $\tilde{a}$ state. For example, in the $\tilde{a}/\tilde{A}$ states, ν_1 = (1156/1129), ν_2 = (671/662), ν_3 = (397/388), and ν_4 = (543/539).

Can. J. Chem. Downloaded from www.nrcresearchpress.com by 210.87.254.5 on 09/06/12
For personal use only.

TABLE 3. Frequency differences between various vibrational levels

(*a*) From the 0_0^0 level of the $\tilde{a}^3A_2$ excited state (cm^{-1})

		2_0^1	2_0^2	3_0^1	3_0^2	1_0^1	$1_0^1 3_0^1$	$1_0^1 3_0^2$	$1_0^1 2_0^1 3_0^1$	$1_0^1 2_0^1 3_0^2$
0_0^0	0	671	—	397	787	—	1527	—	2183	2579
4_0^2	543	1210	1878	935	1327	1699		2472		
4_0^4	1085	1752		1477	1873	2213				
4_0^6	1615			2016						
4_0^8	2110									

(*b*) From the 4_0^1 level of the $\tilde{A}^1A_2$ excited state (cm^{-1})

		2_0^1	2_0^2	2_0^3	3_0^1	3_0^2	1_0^1	$2_0^2 3_0^1$	$1_0^1 2_0^1 3_0^2$
4_0^1	0	662	1318	1973	—	—	1129	1704	2029
4_0^3	539	1197	1856	2511	927	1306	1668	2237	
4_0^5	1075	1738	2393	—	1461	1837			
4_0^7	1595				1979				
4_0^9	2111								

TABLE 4. The energy levels of the out-of-plane mode ν_4' of F_2CSe (cm^{-1})

	$^1A_2$			$^3A_2$		
ν_4'	Obsd	Calcd	Res.	Obsd	Calcd	Res.
0	0	0.0	0.0	0	0.0	0.0
1	0	0.0	0.0	0	0.0	0.0
2	539	540.1	−1.1	543	548.7	−5.7
3	539	540.6	−1.6	543	548.7	−5.7
4	1073	1067.8	5.2	1085	1088.8	−3.8
5	1075	1072.4	2.9	1088	1090.1	−1.1
6	1569	1570.2	−1.2	1615	1615.5	0.5
7	1595	1594.7	0.3	1625	1622.4	2.6
8	—	2021.9	—	2110	2109.9	0.1
9	2111	2114.0	−3.0	—	2147.2	—

TABLE 5. Inversion barriers for the substituted tetraatomic carbonyl, thiocarbonyl, and selenocarbonyl molecules (cm^{-1})

	C=O	C=S	Se
	$\tilde{A}^1A_2$		
H	316[a]	0[d]	—
Cl	3170[b]	598[e]	—
F	8200[c]	3076[f]	2483
	$\tilde{a}^3A_2$		
H	762[a]	7[d]	—
Cl	—	726[e]	—
F	—	3100[g]	2923

[a] From ref. 11.
[b] From ref. 12.
[c] From ref. 13.
[d] From ref. 14.
[e] From ref. 15.
[f] From ref. 16.
[g] From ref. 7.

Potential energy functions for the inversion mode

The vibrational levels of the ν_4' in the $\tilde{a}^3A_2$ and $\tilde{A}^1A_2$ states are presented in Table 4. The potential for the out-of-plane problem can be treated as a one-dimensional function which implies that the interactions of this mode with the remaining vibrational modes can be neglected. In this study, three different functions were used in the fit of the calculated set of levels to the observed levels. The initial calculation employed a model function which was constructed from an harmonic oscillator term perturbed by a Gaussian barrier. This potential has been used to describe the inversion modes of a number of pyramidal molecules (1). In this case, the model function was unsuitable in that it yielded a set of energy levels which were highly anharmonic for all values of the adjustable parameters. In a second calculation, a quartic oscillator term was added to the potential to reduce the vibrational energies at higher values of the vibrational quantum number. This procedure was found to be ineffective even for very large contributions from the quartic oscillator term. In the third trial function, a satisfactory fit to the observed levels was obtained. The potential function in this case consisted of the harmonic oscillator perturbed by a Lorentzian barrier

$$V(z) = AZ^2 + B/(C + Z^2)$$

where Z is the reduced coordinate defined by Chan and Stelman (8). The best fit to the $\tilde{A}^1A_2/\tilde{a}^3A_2$ data came from the parameters $A = 81.4/81.7$, $B = 24500/29000$, $C = 5.0/5.2$. Observed and calculated energy manifolds of ν_4' are shown in Table 4. The systematic increase in the residuals (obsd − calcd) with the vibrational quantum number of the earlier calculations has been eliminated. The barriers in the double well functions of the $\tilde{A}^1A_1$ and $\tilde{a}^3A_2$ states were 2483 and 2923 cm^{-1} respectively, while the corresponding values for Z_m, the minima in the functions, were 3.514 and 3.692. The relationship between the mass adjusted coordinate, z, and the normal coordinate is $Q = (h/4\pi\nu_0)^{1/2}z$ which leads to values of Q_m at the potential minima of 1.304×10^{-20} and 1.0806×10^{-20} $g^{1/2}$ cm, respectively. The out-of-plane coordinate Q_4 is related to the angle displacement θ through the reduced mass relationship:

$$Q_4(\theta) = \int_0^{\theta}[\mu(\theta)]^{1/2}\, r\,d\theta$$

where the reduced mass is that of Jones and Coon (9). In this model calculation, it is assumed that Q_4 is derived from the internal coordinate, θ, which is defined, and the angle between

Can. J. Chem. Downloaded from www.nrcresearchpress.com by 210.87.254.5 on 09/06/12
For personal use only.

TABLE 6. Vibrational frequencies (cm $^{-1}$) of F_2CSe, F_2CS, and F_2CO in the ground and first excited states

	F_2CSe			F_2CS^b			F_2CO^c	
	$\tilde{X}^a$	$\tilde{A}$	$\tilde{a}$	$\tilde{X}$	$\tilde{A}$	$\tilde{a}$	$\tilde{X}$	$\tilde{A}$
$\nu_1(a_1)$	1287	1129	1156	1365.2	1100.6	1186	1929.9	1030
$\nu_2(a_1)$	705	662	671	789.3	736.3	729	965.6	830
$\nu_3(a_1)$	432	388	397	526.2	385.8	391	582.9	465
$\nu_4(b_1)$	575	539	543	623.2	557.9	566	767.4	670
$\nu_5(b_2)$	1207	—	—	1200	—	—	1243.7	1216
$\nu_6(b_2)$	351	—	—	418	—	—	619.9	—

[a] From ref. 5.
[b] From ref. 7.
[c] From ref. 13.

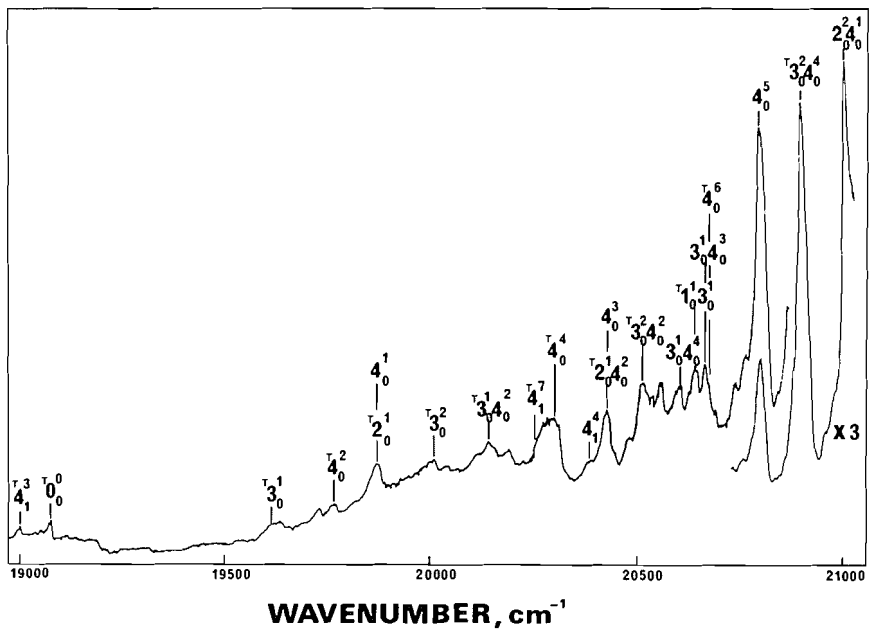

FIG. 3. Microdensitometer tracing of the visible absorption spectrum of F_2CSe. The bands of the singlet–triplet transition are labelled with a T.

the CSe bond and the line meeting the FCF angle. The geometric parameters used in the reduced mass were those of the ground state structure (4). For the states $\tilde{A}^1A_2/\tilde{a}^3A_2$, θ_m = 30.1/31.4 deg.

Discussion

Table 5 presents values for the barrier heights of the tetra-atomic carbonyl and thiocarbonyl compounds along with those of selenocarbonyl difluoride. There are large variations in the barriers for this group of molecules and it is apparent that the heights are sensitive to the nature of the attached group. It is possible to extend Walsh's rules (10) to these groups of molecules. The principle on which his correlation is based is that the MO energy of the system decreases (more stable) when electron density flows from a p type AO to an s type AO. The variation in the heights of the barriers should parallel the $2p_\pi$ and $2s$ density changes at the carbon atom. The substitution of the electronegative halogen group for hydrogen stabilizes the σ MO and leaves the π MO relatively unaffected. This perfluoro effect has been observed in the photoelectron spectrum of H_2CO and F_2CO (17). The σ MO's in these compounds belong to the a_1 and b_2 representations while the π and π^* MO's are of b_1 species. When the molecule is distorted from the planar C_{2v} symmetry to the nonplanar form, the a_1 and b_1 representations correlate with a' and a_2 and b_2 with a'' of the C_s point group. In a nonplanar system, the $\sigma-\pi$ distinction is no longer valid and the electron density is pulled from the O, S, and Se atoms to the C atom by the electronegative substituent. The result is that there is a net charge flow from the $2p_\pi$ to the $2s$ carbon AO and from the viewpoint of the Walsh postulate a change in electron density in this direction would result in a nonplanar distortion at the carbon centre. The electronegativity of the H/Cl/F groups in $H_2CO/Cl_2CO/F_2CO$ parallel the barrier heights 316/3170/8200. The barrier height decrease from S/Se of 3076/2483 is not unexpected. This is a consequence of the larger and more diffuse orbitals of Se relative to S which are capable of accommodating π^* density which would normally flow to the C centre.

The excited state vibrational frequencies

The F_2CSe frequencies in the $\tilde{X}$, $\tilde{A}$, and $\tilde{a}$ states are given in Table 6 along with the frequencies of F_2CS and F_2CO. The behaviour of the ν_1(C=X) stretching mode can be explained in terms of the ratios of the frequency drop on excitation $\tilde{A}/\tilde{X}$.

Can. J. Chem. Downloaded from www.nrcresearchpress.com by 210.87.254.5 on 09/06/12
For personal use only.

They are: F_2CO 1030/1929.9, F_2CS 1100.6/1365.2, F_2CSe 1129/1287. That is, the reduction in frequency is greater for carbonyl compounds followed by the thio and selenocarbonyl compounds. If ν_1 is assumed to be a valence vibration in the $\tilde{X}$ and $\tilde{A}$ states, it is possible to predict the change in bond length on excitation through the use of the empirical rule $\omega r^3 =$ constant (18). For the C=O/C=S/C=Se groups, the bond length extensions are 0.272/0.118/0.077 Å. The C=X bond lengths can be considered in terms of a two-step process, removal of an electron from the n orbital and the addition of the electron to the π^* orbital. Information about the first process comes from the photoelectron spectrum. In the PES of F_2CO (17), the ionization of the n electron leads to a reduction in ν_1(C=O), $\tilde{A}/\tilde{X}$ of 1550/1929.9 cm^{-1} whereas in F_2CS (19), the ν_1(C=S) frequency changes very little (1370/1365.2). The conclusion follows that the n orbital in F_2CS is nonbonding while in F_2CO it is bonding. The shift in ν_1(C=X) frequency on $n \rightarrow \pi^*$ electronic excitation reflects the antibonding nature of the π^* orbital in F_2CS and both the bonding nature of the n orbital and antibonding character of the π^* orbital in F_2CO.

Singlet–triplet interval

The correlation of the singlet–triplet intervals among the carbonyl, thiocarbonyl, and selenocarbonyl molecules is of interest (Fig. 3). In the series $H_2CO/H_2CS/Cl_2CS/F_2CS/F_2CSe$ (1, 20, 15, 7), the singlet–triplet intervals are respectively 3000/ 1887/1224/1286/671 cm^{-1}. The intervals can be approximated as twice the exchange integral, and depend on the repulsions between the unpaired n and π^* electrons. The larger and diffuse orbitals of Se relative to S and O provide additional space for the unpaired electrons which lowers the repulsion and decreases the singlet–triplet gap.

Acknowledgement

The authors wish to thank Dr. A. Haas of the Ruhr Universität, West Germany for the generous gift of a sample of F_2CSe polymer.

1. D. C. Moule and A. D. Walsh. Chem. Rev. **75**, 67 (1975).
2. R. P. Steer. Rev. Chem. Intermed. **4**, 1 (1981).
3. A. Haas, B. Koch, and W. Welcman. Z. Anorg. Allg. Chem. **427**, 114 (1976).
4. D. Christen, M. Oberhammer, W. Zeil, A. Haas, and A. Darmadi. J. Mol. Struct. **66**, 203 (1980).
5. A. Haas, H. Willner, H. Burger, and G. Pamelke. Spectrochim. Acta, **33A**, 937 (1977).
6. D. C. Moule, P. D. Foo, and A. Biernacki. J. Phys. E. **4**, 449 (1971).
7. D. C. Moule. Can. J. Chem. **48**, 2623 (1970).
8. S. L. Chan and D. Stelman. J. Mol. Spectrosc. **10**, 278 (1963).
9. V. T. Jones and J. B. Coon. J. Mol. Spectrosc. **31**, 137 (1969).
10. A. D. Walsh. J. Chem. Soc. 2260 (1953).
11. P. Jensen and P. R. Bunker. J. Mol. Spectrosc. **94**, 114 (1982).
12. D. C. Moule and P. D. Foo. J. Chem. Phys. **55**, 1262 (1971).
13. R. H. Judge and D. C. Moule. J. Chem. Phys. In press.
14. P. Jensen and P. R. Bunker. J. Mol. Spectrosc. In press.
15. D. C. Moule and C. R. Subramaniam. J. Mol. Spectrosc. **53**, 443 (1974).
16. D. C. Moule and A. K. Mehra. J. Mol. Spectrosc. **35**, 137 (1970).
17. C. R. Brundle, M. B. Robin, N. A. Kuebler, and H. Basch. J. Am. Chem. Soc. **94**, 1451 (1972).
18. G. Herzberg. Spectra of diatomic molecules. Van Nostrand, New York. 1950. p. 457.
19. D. Chadwick. Can. J. Chem. **50**, 737 (1972).
20. R. H. Judge, D. C. Moule, and G. W. King. J. Mol. Spectrosc. **81**, 37 (1980).

Can. J. Chem. Downloaded from www.nrcresearchpress.com by 210.87.254.5 on 09/06/12
For personal use only.

Relaxation pathway analysis by ^{1}H spin-lattice relaxation and nuclear Overhauser effect difference measurements. Application to a reassignment of the ^{1}H nmr spectrum of strychnine and to the determination of the structure and stereochemistry of some strychnine sulfonic acids

WALTER J. CHAZIN AND LAWRENCE D. COLEBROK[1]

Department of Chemistry, Concordia University, 1455 de Maisonneuve Blvd., W., Montreal, P.Q., Canada H3G 1M8

AND

JOHN T. EDWARD

Department of Chemistry, McGill University, 801 Sherbrooke St., W., Montreal, P.Q., Canada H3A 2K6

Received December 28, 1982

WALTER J. CHAZIN, LAWRENCE D. COLEBROOK, and JOHN T. EDWARD. Can. J. Chem. **61**, 1749 (1983).

The ^{1}H relaxation pathway analysis of strychnine and some strychnine sulfonic acids has been carried out by spin-lattice relaxation and nuclear Overhauser effect difference measurements. Some previously reported ^{1}H chemical shifts and coupling constants for strychnine are shown to be in error. New assignments for positions 15, 17, 18, and 20 have been made. Proposed sites of substitution of the sulfonic acids have been verified, and the previously undetermined stereochemistry of one of the acids has been established.

WALTER J. CHAZIN, LAWRENCE D. COLEBROOK et JOHN T. EDWARD. Can. J. Chem. **61**, 1749 (1983).

Faisant appel aux mesures de relaxation spin-réseau et de différence d'effet Overhauser nucléaire, on a mesuré le processus de relaxation du ^{1}H de la strychnine et de quelques acides sulfoniques dérivés de la strychnine. On montre que quelques-uns des déplacements chimiques et des constantes de couplage du ^{1}H de la strychnine rapportés antérieurement sont erronés. On a fait de nouvelles attributions pour les positions 15, 17, 18 et 20. On a vérifié les sites de substitution proposés pour les acides sulfoniques et on a établi la stéréochimie de l'un des acides que l'on n'avait pas encore établie.

[Traduit par le journal]

Introduction

In 1908–1909, Leuchs and Schneider (1) obtained three mono sulfonic acids (designated SSA-I, -II, and -III) on work-up of the solution obtained by bubbling sulfur dioxide through a warm aqueous solution of strychnine (I)[2] containing suspended manganese dioxide. Although Leuchs and his collaborators continued to study these sulfonic acids for more than 30 years (2), little became known of their structures, other than that SSA-I was not sulfonated on the aromatic ring or at the 11-position, until further studies were undertaken by one of us (J.T.E.) (3).

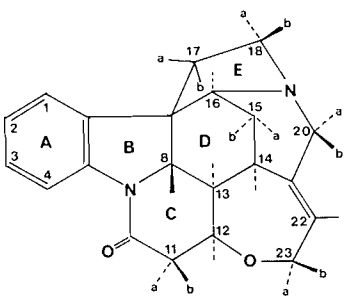

On repeating Leuchs' procedures, the same three strychnine sulfonic acids were isolated. X-ray crystallographic analysis of a sample of SSA-I obtained at this time showed it to have the sulfonic acid group located at the allylic 14-position (4).

On the basis of pH measurements, ^{13}C nmr spectra, and chemical arguments, the locations of the sulfonic acid groups in SSA-II and SSA-III were assigned as the vinylic 22-position and the allylic 20-position, respectively (3). The stereochemistry of substitution at position 20 in SSA-III was not established.

We have recently undertaken an evaluation of the potential of ^{1}H spin-lattice relaxation rate (R_1) measurements for the determination of the structure and stereochemistry of organic molecules (5, 6), and decided that this technique would be useful in the analysis of the structure of the strychnine sulfonic acids. Such measurements are used to analyze dipolar relaxation pathways, which are directly related to the three-dimensional structure of the molecule. When necessary, specific relaxation pathways can be identified by nuclear Overhauser effect (nOe) enhancements (7).

Initially, chemical shift assignments were made by comparison with published data on strychnine (8). However, as the analysis of the ^{1}H R_1 data was being refined, some anomalies in the published assignments became apparent.[3] As a result, it was decided that a re-evaluation of the ^{1}H nmr spectrum of strychnine was necessary, before completing the structure determinations of the strychnine sulfonic acids. These studies are reported in a separate section, below.

Relaxation pathway analysis

In dilute solution (typically 0.1 M, or less) in a nonviscous, deuterated solvent, the spin-lattice relaxation of protons in organic molecules of mol. wt. < 1000 is dominated by dipole–dipole interactions with the other protons in the molecule. The rate equation for dipolar relaxation of a proton j is given by:

$$[1] \quad R_{1_j} = K[\sum_i (1/r_{ij})^6 \tau_{c_{ij}}] \qquad i \neq j$$

where K is the product of a number of constants, the r_{ij}'s are

[1]Author to whom correspondence may be addressed.

[2]The conventional structure used here for strychnine represents the entantiomer of the natural material.

[3]Tavernier *et al.* (9) reported that the geminal coupling constant for the C-17 protons had been incorrectly assigned in the literature (8).

Can. J. Chem. Downloaded from www.nrcresearchpress.com by 210.87.254.40 on 09/06/12
For personal use only.

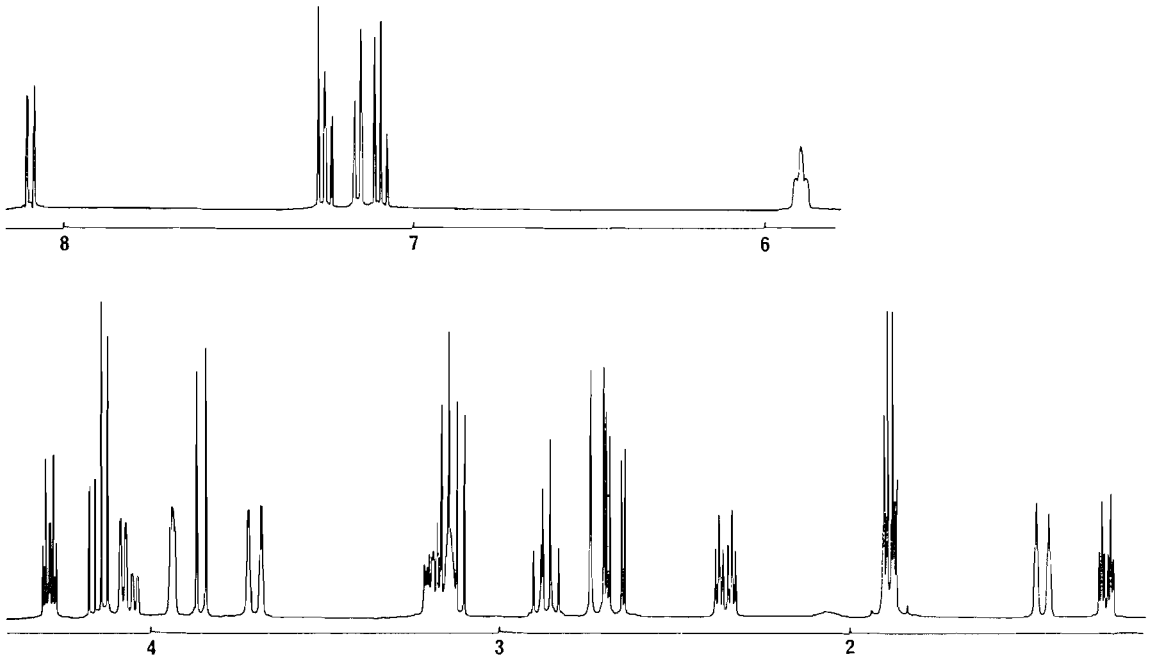

FIG. 1. Resolution enhanced 400 MHz ^{1}H spectrum of strychnine, 0.1 *M* in $CDCl_3$. Upper trace, low field region; lower trace, high field region.

the internuclear distances between the proton j under consideration and the other protons in the molecule, and the $\tau_{c_{ij}}$'s are the rotational correlation times for the r_{ij} internuclear vectors. Each term in this expression constitutes a specific dipolar relaxation pathway.

For rigid, isotropically tumbling molecules all of the relaxation vectors will have the same τ_c, so that the ratio of R_1 values for any protons in the molecule depends only on inter-proton distances:

$$[2]\quad \frac{R_{1_j}}{R_{1_k}} = \frac{\sum_i (1/r_{ij})^6}{\sum_i (1/r_{ik})^6} \qquad \begin{matrix} i \neq j \\ i \neq k \end{matrix}$$

The inverse sixth power dependence on internuclear distance implies that relaxation contributions are significant only for the nearest neighbors of a particular proton. In consequence, R_1 values and nOe enhancement factors are extremely sensitive to *local* structure and stereochemistry. Due to the unique location of each proton in the molecule, there is a unique set of relaxation pathways which characterize each proton. In many instances the various relaxation pathways to and from a particular proton can be found, through the use of nOe and R_1 experiments, thereby establishing its identity.

Relaxation pathways may be evaluated semi-quantitatively for these molecules, assuming that the molecules tumble isotropically, and by measuring internuclear distances on Dreiding molecular models. Relative R_1 values can be calculated directly from [2], while relative nOe enhancements can be predicted from an evaluation of each $(1/r_{ij})^6$ term.

These calculations serve as an invaluable aid in the interpretation of the experimental data, but their limitations in terms of quantitative comparative analysis are obvious. Interpretation of the experimental data is not based upon a single measurement but on trends seen in several measurements. The use of several observations to obtain information on a single site compensates for inaccuracies associated with calculations based on a model and for experimental errors.

Results and discussion

A re-evaluation of the ^{1}H nmr assignments of strychnine

The previous assignments of the ^{1}H nmr spectrum of strychnine (8) were made at 250 MHz using a combination of aromatic-solvent-induced chemical shift changes, selective deuteration, double resonance techniques, and computer simulation of spectra. Interpretation of the ^{1}H spectrum of strychnine (Fig. 1) in the present study was based on relaxation pathway analysis and was facilitated by the greater chemical shift dispersion at 400 MHz. In agreement with the preliminary analysis of the ^{1}H R_1 values of the strychnine sulfonic acids, a comparison of the experimental and calculated ^{1}H R_1 values of strychnine suggested that the stereochemical assignments of the geminal proton pairs at positions 15, 18, and 20 should be reversed.

Relaxation pathway analysis was carried out in order to establish characteristic relaxation pathways for each proton of interest. Although both ^{1}H R_1 and nOe difference (nOed) (10, 11) experiments were used, the nOe data proved more definitive. The following discussion, therefore, centres on the nOe experiments. The measured enhancements were analyzed with the aid of calculated enhancements although, in fact, most of the nOe factors could be interpreted by simple inspection of molecular models. At least one key enhancement could be identified for all protons irradiated except H-12 (Table 1). A key enhancement is defined as (1) an nOe enhancement which serves to identify either the transitions irradiated or the transitions enhanced, or (2) an nOe enhancement which identifies a unique relaxation pathway having implications concerning the overall molecular structure. The final assignments were checked by computer simulation of portions of the spectrum.

The signals due to the isolated C-20 methylene group, adjacent to nitrogen, were originally assigned (8) as the simple AB pattern (with some long range coupling) at 3.70 and 2.72 ppm. The C-15 proton signals (1.46 and 2.36 ppm) were assigned by comparison with the spectrum of 11a,11b,16-d_3-strychnine (8). These assignments have recently been confirmed by 2D hetero-

Can. J. Chem. Downloaded from www.nrcresearchpress.com by 210.87.254.40 on 09/06/12
For personal use only.

TABLE 1. Nuclear Overhauser effect enhancements determined for strychnine by the difference technique[a]

Proton irradiated	Key enhancement	Other enhancements	Negative enhancements[b,c]
1	16,17a[d],2[d]		
12		13,11b,11a,14	
13	15b	8,12,14	15a
14	20a	13,15a,15b,12,22	23a
15a	20a	15b,16,14	13
15b	13	15a,16,14	20a,8
16	1	15a,15b,17a[d]	2
17a[e]	1	17b,[d]16,18a	
17b[e]	8	17a,[d]18b	
18a	16	18b,17a[d]	8
18b	8,22,20b	18a,17b[d]	
20a	15a[c]	20b	15b,22
20b	22,18b[d]	20a	
22	20b,23b,18b[c]	8[c]	20a
23a	14,12	23b,22	
23b	22	23a	

[a]Spectra were determined at 400 MHz at ambient temperature (about 20°C) on non-degassed 0.1 *M* solutions in $CDCl_3$ and DMSO-d_6. Except for cases where overlap of signals in one solvent (e.g. H-17a and H-17b in $CDCl_3$) prevented individual measurements, nOe enhancements were observed for both solvents.

[b]Negative enhancements arise from the three-spin effect (17), and depend on the choice of experimental conditions.

[c]$CDCl_3$ only.

[d]DMSO-d_6 only.

[e]In $CDCl_3$ solution there is a small chemical shift difference between H-17a and H-17b. Since their transitions could not be irradiated separately, a single experiment measuring the enhancements from both protons was carried out. The enhancements could be measured separately for a DMSO-d_6 solution, since the chemical shift dispersion is greater.

and homo-correlation methods.[4]

Although there is no question as to the assignment of these four signals to the C-20 and C-15 protons, respectively, the problem of the stereochemistry of the assignments was not satisfactorily resolved.

The key relaxation pathways among the protons at C-15, 18, 20, 22, and 23 are indicated on the partial structure (Fig. 2). Irradiation of the downfield (3.70 ppm) H-20 signal produced an nOe enhancement of the downfield (2.36 ppm) H-15 signal (Fig. 3). Based on calculated nOe values, it is clear that the only significant relaxation pathway for one of the C-20 protons with one of the C-15 protons is between H-20a and H-15a. Irradiation at 2.36 ppm gave the expected enhancement to the signal at 3.70 ppm, further corroborating the assignment. For additional proof, the other C-20 proton, H-20b, was identified by key nOe enhancements to and from H-18b (2.87 ppm) and the vinylic proton, H-22. Since the assignment of H-22 is unambiguous, the above experiments verify the assignments of both H-18b and H-20b. In addition, H-15b (1.46 ppm) was characterized by enhancements to and from H-13 (unambiguously identified previously (ref. 8 and footnote 4)).

The nuclear Overhauser effects to and from H-20b and H-18b served as an entry into the ABMX system of protons 17a, 17b, 18a, and 18b. This spin system was initially analyzed from spectra of a DMSO-d_6 solution because, in this solvent, the four signals were more clearly separated and the C-17 protons were less tightly coupled than in $CDCl_3$ solution. Calculations predicted that these protons could be differentiated by their nOe enhancements. Experimental results (Table 1) verify that H-18b has effective relaxation pathways to H-8, H-22, and H-20b, whereas H-18a has an effective pathway to H-16. The C-17 protons were also distinguished by large key enhancements between H-17a and H-1, and between H-17b and H-8 (Table 1).[5]

Attempted computer simulation, using the program LAOCOON III (12), of the DMSO-d_6 ABMX spectrum, with an H-17a,17b geminal coupling constant at the previously reported (8) value of 0.2 Hz, failed to produce a reasonable fit. When the simulation was repeated starting from a more normal value (13*a*) of −13 Hz for the geminal coupling constant, the calculation converged rapidly to an excellent fit to the experimental spectrum.

The information obtained from the DMSO-d_6 spectrum was then correlated with the $CDCl_3$ spectrum. The relative ^1H R_1 values and the nOe enhancements for the C-18 geminal protons were measured; analysis of these data led to assignment of the signals. A LAOCOON III simulation yielded an excellent fit to the experimental spectrum. The set of corrected assignments

[4]S. Wehrli. Personal communication.

[5]The existence of an efficient inter-ring relaxation pathway between the aromatic ring proton, H-1, and H-17a provides structural information about the strychnine molecular framework. The close proximity of H-17a on a bridging ring is partially responsible for the observation that H-1, on the apparently isolated aromatic system, relaxes much faster than the corresponding proton at position 4, and even faster than H-2 and H-3, which have more close neighbouring protons on the aromatic ring. There is also an efficient inter-ring relaxation pathway between H-1 and H-16. It should be noted that the usual two-dimensional representation [1] of the strychnine structure gives a misleading impression of the relative placement of H-1 with respect to H-16 and H-17a.

Can. J. Chem. Downloaded from www.nrcresearchpress.com by 210.87.254.40 on 09/06/12
For personal use only.

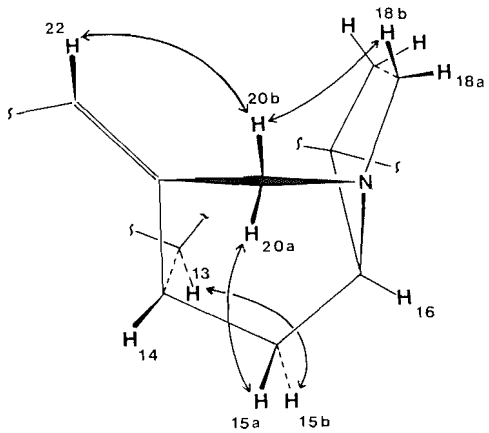

FIG. 2. View of the strychnine molecule in the vicinity of C-20. Important relaxation pathways are indicated by arrows. The site of substitution of SSA-I is 14, SSA-II is 22, and SSA-III is 20a.

and coupling constants obtained by this analysis is given in Table 2.

A final point of interest concerns the coupling (0.9 Hz, see Table 2) between the vinylic proton, H-22, and the C-20 proton with a signal at 3.70 ppm, originally assigned to H-20b (8). The dihedral angle between H-20b and the plane of the double bond is very close to 0°. The presence of any measurable coupling between H-22 and H-20b would, therefore, be unusual (13*b*). When the stereochemistry of the original assignments at C-20 was reversed, this coupling constant no longer appeared to be anomalous. The dihedral angle between H-20a and the plane of the double bond is about 100°, so a small (<3 Hz), but significant, coupling is to be expected (13*b*).

The nOe enhancements discussed above were critical in determining that the assignments of the chemical shifts of the geminal proton pairs at positions 15, 18, and 20 should be reversed, and that the coupling constant assignments for the geminal protons at C-17 should be revised. The power of the nOed technique to determine selected details of structure and stereochemistry has been clearly demonstrated.

Strychnine sulfonic acids

SSA-I was used in the present study as a model compound to evaluate the viability of the relaxation pathway analysis technique, since its structure has been unambiguously established by X-ray crystallography (4). Using only ^{1}H R_1 data, it was possible to verify the previously assigned (3) sites of substitution of SSA-II and SSA-III, and to establish the stereochemistry of the sulfonic acid group of SSA-III. This stereochemical assignment has been verified by nOed experiments.

Proton chemical shifts assignments for the acids were made initially by comparing the 400 MHz ^{1}H spectra with the spectrum of strychnine in DMSO-d_6 and $CDCl_3$. NOed experiments and computer simulations were employed to analyze the spectrum of SSA III. Verification of the structural assignments was achieved by comparing experimental (Table 3) and calculated R_1 values of protons in the immediate vicinity of the sites of substitution, as outlined above.

Since replacement of a hydrogen atom by a sulfonic acid group changes the moments of inertia of the molecule, there are corresponding differences in correlation times for tumbling (τ_c) which affect the measured R_1 values. For this reason, normalization (6) of the R_1 values is necessary before intercomparisons may be made. The normalizing proton is chosen

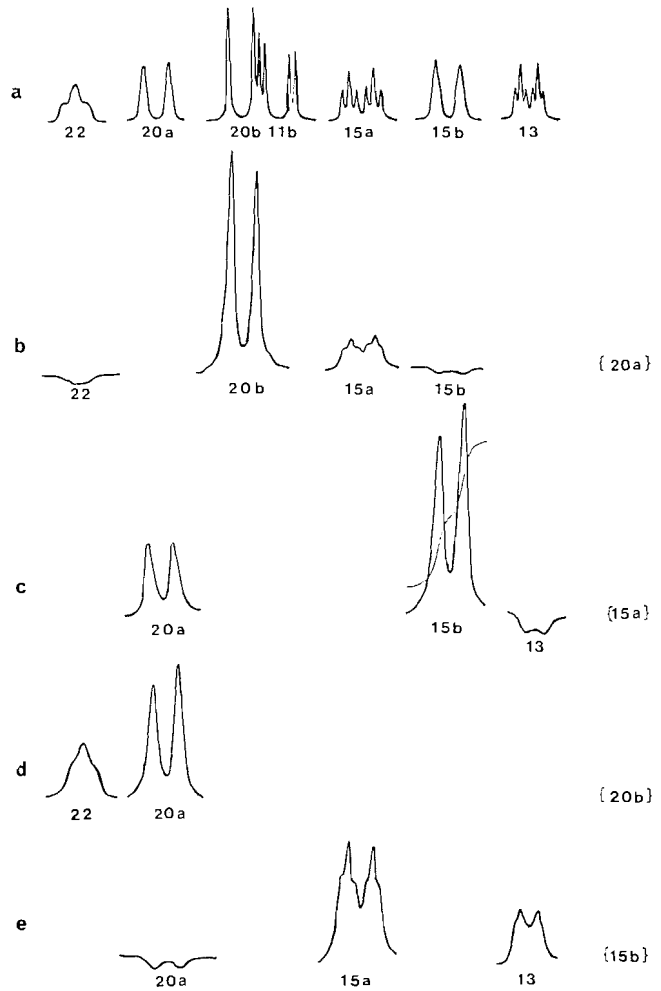

FIG. 3. Selected nOed measurements used to establish assignments of H-15a, H-15b, H-20a, and H-20b: (a) normal spectrum, 0.1 *M* in $CDCl_3$, (b)–(e) nOed measurements on same sample with proton irradiated indicated at right {}.

to be at a position remote from the site(s) of substitution, so that its intrinsic R_1 will not be directly influenced by the substituent. This procedure will also compensate for differences in experimental conditions (e.g. temperature) in different sets of measurements. Inter-comparisons between the R_1 values of strychnine and the sulfonic acids were avoided because strychnine is insufficiently soluble in the common solvent, D_2O, chosen for the sulfonic acids.

Since SSA-I and SSA-II were sparingly soluble in D_2O, it proved necessary to add a drop of NaOD solution to improve their solubility. This created a complication in that the hydrogen atoms at position 11 are acidic, and were replaced by deuterium. Reductions in the R_1 values of H-8 (16%), H-12 (19%), and H-13 (5%) of these compounds were expected, because deuterium has only about 6.3% of the relaxation efficiency of protium. These factors were easily accounted for in the calculations.

Strychnine sulfonic acid I

The site of substitution (C-14) of SSA-I may be inferred from the disappearance of the ^{1}H signal (3.14 ppm) attributed to H-14 in strychnine,[6] and the resulting change in the appearance of multiplets arising from protons coupled to H-14 (i.e.

[6]In DMSO-d_6 solution containing one drop of 40% DCl/D_2O.

Can. J. Chem. Downloaded from www.nrcresearchpress.com by 210.87.254.40 on 09/06/12
For personal use only.

TABLE 2. Revised ^{1}H chemical shifts and coupling constants for strychnine[a]

Proton	^{1}H chemical shifts[b]	Coupling constants, J (Hz)[c]
15a	2.36	15a,15b = −14.5 15a,16 = 4.9 15a,14 = 4.0
15b	1.46	15b,16 = 2.0 15b,14 = 1.0
17a	1.88	17a,17b = −15.5 17a,18a = 8.4 17a,18b = 11.7
17b	1.89	17b,18a = 0.1 17b,18b = 6.9
18a	3.19	18a,18b = −10.1
18b	2.87	
20a	3.70	20a,20b = −14.7 20a,22 = 0.9
20b	2.72	

[a]The remaining assignments were in agreement with those in ref. 8. Chemical shifts and coupling constants for the 17 and 18 protons were determined by spectral simulation, using the program LAOCOON III (12). The other values were measured directly from the spectra.
[b]In ppm from TMS, $CDCl_3$ solutions.
[c]Negative signs were assumed for geminal coupling constants.

H-13, H-15a, H-15b). Calculation of the effect of replacement of H-14 on the R_1 values of neighboring protons predicted reductions in the R_1 values of H-12 (11%), H-13 (20%), H-15a (10%) and H-15b (7%). A significant effect on the R_1 value of H-23a (10%) was also predicted, but was not measurable for experimental reasons.[7] Analysis of the R_1 value of H-12 is complicated by the effect of deuteration of 11a and 11b, but the magnitude of this influence could be established by comparing the H-12 R_1 values (Table 3) of SSA-II (deuterated) and SSA-III (nondeuterated). The difference in H-12 R_1 values of SSA-II and SSA-I could then be attributed to the effect of substitution at position 14. On comparing the other R_1 values of SSA-I with those of SSA-II, the reductions predicted by the calculations were apparent. A large decrease in the R_1 value of H-13 and smaller decreases in the R_1 values of H-15a and H-15b were observed. This unique combination of effects on measured R_1 values is in complete agreement with the assignment of position 14 as the site of substitution.

Strychine sulfonic acid II

Initial verification of the site of substitution in SSA-II was provided by the disappearance of the characterisic H-22 vinyl proton signal (5.90 ppm) of strychnine,[6] accompanied by only minor changes in the appearance of other signals. The only R_1 value showing a significant reduction was that of H-20b (Table 3). Calculations identified H-20a (65%), H-18b (16%), and H-22 (16%) as the major contributors to the relaxation of H-20b, thereby establishing three possible sites of substitution. H-22 was the logical choice because substitution at 20a would reduce the R_1 of H-20b to a much greater extent than had been observed, and substitution at 18b would cause substantial R_1 effects on other protons, in particular H-18a and H-8. Calculation of the effect on other protons from replacement of H-22 predicted significant decreases in R_1 values *only* for H-20b and H-23b. For practical reasons,[7] an R_1 value for H-23b could not be measured, but there was agreement between the calculated and observed influences on H-20b. Hence, for this molecule, the R_1 evidence clearly indicated that substitution has occurred at position 22.

TABLE 3. Normalized R_1 values[a] of the strychnine sulfonic acids[b]

Proton	Strychnine sulfonic acid I	II	III
1	0.63	0.70	0.70
2	0.48	0.53	0.53
3	0.50	0.55	0.52
4	0.33	0.34	0.38
8	0.78[d]	0.82[d]	0.89
11a	[c]	[c]	1.7
11b	[c]	[c]	1.7
12	0.64[d]	0.89[d]	1.3
13	0.76	1.1	1.1
14	[e]	1.2	1.1
15a	2.3	2.6	2.0
15b	2.2	2.6	2.4
16	1.0 (1.88)	1.0 (1.98)	1.0 (1.98)
17a	2.1	2.0	1.9
17b	2.2	2.1	2.2
18a	2.0	2.0	1.8
18b	2.4	2.4	2.0
20a	2.1	2.0	[e]
20b	2.2	1.8	0.58
22	0.90	[e]	0.91
23a	[f]	2.1	2.0
23b	1.7	[f]	1.7

[a]R_1 values normalized to the R_1 value of H-16. The absolute R_1 value (s^{-1}) of H-16 in each isomer is noted (in parentheses).
[b]Non-degassed 0.1 *M* solutions in D_2O. One drop of NaOD solution was added to solubilize SSA-I and SSA-II.
[c]Proton substituted by deuterium.
[d]R_1 value reduced as a result of deuteration at position 11.
[e]Site of substitution.
[f]R_1 value not measurable (see footnote 7).

Strychnine sulfonic acid III

The site of substitution (C-20) of SSA-III could be inferred from the ^{1}H spectrum, the only two substantial differences with respect to the spectrum of strychnine being the loss of the AB pattern of the H-20 signals (3.70 and 2.72 ppm),[6] and the appearance of a sharp singlet, shifted significantly downfield (6.0 ppm). The loss of two signals from the spectrum without

[7]In SSA-I, the H-23a signal is in close proximity to the residual HOD signal of the solvent, and a reliable R_1 value could not be obtained. The spread of saturation power from solvent suppression has the effect of reducing the intensity of the H-23a signal and making the apparent R_1 value larger. The same problem also arises for the H-23b signal of SSA-II.

Can. J. Chem. Downloaded from www.nrcresearchpress.com by 210.87.254.40 on 09/06/12
For personal use only.

Can. J. Chem. Downloaded from www.nrcresearchpress.com by 210.87.254.40 on 09/06/12
For personal use only.

significant effects on coupling constants directly implied that substitution had occurred at position 20, since this is the only site with magnetically isolated (i.e. with no vicinal coupling constants) geminal protons. The large downfield shift of the remaining proton signal is consistent with a geminal relationship with the sulfonic acid substituent. The assignment was in agreement with the previous studies on SSA-III (3).

A powerful and efficient means of determining the stereochemistry at C-20 is to evaluate the relaxation pathways of the remaining proton. Figure 2 summarizes the most important pathways (arrows) available to H-20a and H-20b. Calculation of the effects on the R_1 values of neighboring protons for substitution at 20a indicated significant reductions in the R_1 values of H-20b (65%) and H-15a (16%). The corresponding calculation for substitution at 20b indicated significant reductions in the R_1 values of H-20a (74%), H-18b (14%), and H-22 (41%). A clear distinction between the possibilities should, therefore, be possible.

Close inspection of the spectrum of SSA-III indicated that changes in the magnitudes of the coupling constants of the 17 and 18 protons are induced by substitution, implying a change in the geometry of ring E, and possible changes in the efficiencies of the relaxation pathways for H-18b. Together with an observed reduction in the normalized R_1 value of H-18b, there were corresponding changes in the relative R_1 values of H-17a, H-17b, and H-18a. This complication led to uncertainty in the prediction of the relaxation contribution from H-20b, so that the R_1 value of H-18b could not be used as a basis of the assignment. Since there was no spectral evidence of a conformational change affecting any other protons, a distinction between the two sites of substitution, 20a and 20b, was made based on the R_1 values of H-15a and H-22.

Comparison of the R_1 values (Table 3) of SSA-III with SSA-I and SSA-II showed that the R_1 value of H-22 was not affected, but that of H-15a was reduced. The reduction in the R_1 value of H-15a relative to that of its geminal neighbor, H-15b, is a good indication that H-15a has been substantially affected. Consistency in the R_1 values of H-14 and H-16 suggested that there was no significant change in ring geometry affecting H-15a and H-15b. It is clear, therefore, that the site of substitution in SSA-III is 20a.

To substantiate this assignment, the nOed spectrum was measured for irradiation of the remaining H-20 resonance. This experiment was ideal from a practical standpoint, since the signal was completely isolated from the rest of the spectrum, and from a theoretical standpoint since the specific relaxation pathways of this proton could be characterized. A large enhancement was seen for H-22, and a small enhancement for H-18b. These nuclear Overhauser enhancements clearly establish that the irradiated resonance arises from a proton located at 20b (Fig. 2), thus confirming that the site of substitution in SSA-III is 20a.

Conclusions

The ^{1}H nmr spectrum of strychnine has been reassigned and the structures and stereochemistry of the three strychnine sulfonic acids are now clearly established. This study illustrates the ability of relaxation pathway analysis, used in conjunction with a simple mathematical model which enables the prediction of relative relaxation rates, to provide structural and stereochemical information on complex organic molecules. The experiments may be carried out easily and rapidly, using a modern, high field spectrometer. Degassing is unnecessary if qualitative information is to be obtained. In the first level of analysis (R_1 measurements) there is a high information content in that the relaxation rates of all protons in a molecule are obtained in a single experiment. If necessary, specific information on relaxation pathways (i.e. on relationships to near neighbors of a particular proton) may then be obtained by the more time-consuming, but more selective and sensitive, nOed experiment.

Experimental

Strychnine was obtained from commercial sources (Sigma Chemical Co.). The preparation and isolation of the three strychnine sulfonic acids have been described elsewhere (3). The compounds were dried overnight under reduced pressure at 120°C over P_2O_5. Nondegassed, 0.1 *M* solutions in $CDCl_3$, D_2O, and DMSO-d_6 were used for the nmr experiments. The solutions were not degassed because the intramolecular relaxation contribution from dissolved oxygen, which is expected to be equivalent for all protons in the molecules (6), should not affect qualitative results. In a molecule of the size and rigidity of strychnine, intramolecular ^{1}H dipolar relaxation is very efficient, so the effects of dissolved oxygen are small.

All spectra were measured at 400 MHz at ambient temperature (about 20°C), using a Bruker WH-400 spectrometer (Montreal Regional High Field NMR Laboratory). Free induction decays (fids) were accumulated into 16K (nOe experiments) or 32K (normal spectra, R_1 data sets) word data blocks with frequency windows of 4000 Hz, quadrature detection, and phase cycling. R_1 values were determined by the null point method (6), using the inversion–recovery pulse sequence (14, 15) with simultaneous suppression of the residual solvent peak when necessary. The absolute accuracy of R_1 measurements is typically ±10%, but, within a single experiment, the relative R_1 values can be determined to a precision of better than ±5%. Calculations to determine nOe and relative R_1 values were carried out on a Hewlett–Packard 1000 computer, using inter-proton distances measured from Dreiding molecular models.

Steady-state nOe difference spectra were obtained using a slightly modified version of the method of Hall and Sanders (10), who acquired nOe spectra for four chemical shifts with a single control. Our method is designed for efficient qualitative studies, emphasizing acquisition of an entire set of nOed spectra for the molecule under study. Difference spectra were obtained for up to eight different chemical shifts (on-resonance acquisitions), using only a single control (off-resonance acquisition). The acquisition of eight fids rather than four (10) after the equilibration period further improves efficiency by reducing the number of these equilibration periods by half. With these modifications and computer control of the decoupler, a complete set of nOe spectra could be obtained in a single overnight run (about 10 hours). It should be noted that this method requires that drift be kept to a minimum for clean subtraction, so that the high stability of a superconducting magnet is necessary. Irradiation times were about 5 $\times T_1$, although accurate data can be acquired with significantly shorter irradiation periods.

The nOe difference spectra were then produced by subtraction of the reference free induction decay from the decay containing the nOe information. Both data sets were subjected to exponential multiplication corresponding to line broadening of 0.8–1.5 Hz, before Fourier transformation. Substantial line broadening optimized the quality of the difference spectra, particularly for tall, narrow lines. The resultant nulling of unenhanced signal was very satisfactory, as had been reported previously by Hall and Sanders (10). These workers also suggested the use of subsaturating power levels to achieve frequency selectivity. This proved to be satisfactory for most experiments. When complete selectivity could not be achieved, the approach taken was to acquire additional experiments in which changes in the decoupler power or frequency were made (16). By correlating the effects on enhancements to the changes in experimental conditions, specific relaxation pathways could usually be determined. Occasionally, the presence of negative nOe enhancements (see Fig. 3)

arising from three-spin effects (17) was also helpful in establishing specific relaxation pathways.

Acknowledgments

This work was supported by operating grants from the Natural Sciences and Engineering Research Council of Canada, which also provided funding towards the purchase of the 400 MHz spectrometer. One of us (W.J.C.) wishes to thank the Ministry of Education, Province of Quebec, for a Fellowship. We are indebted to Dr. S. Wehrli, Bruker Instruments, Inc., for copies of the 2D correlation spectra of strychnine. We wish to thank Dr. C. Rodger for helpful discussions and Bruker Spectrospin (Canada) Ltd. for the use of facilities to carry out corroborative experiments.

1. H. LEUCHS and W. SCHNEIDER. Ber. **41**, 4393 (1908); **42**, 2681 (1909).
2. H. LEUCHS and H. G. BOIT. Ber. **73**, 855 (1940), and earlier papers referenced therein.
3. J. T. EDWARD, P. G. FARRELL, S. A. SAMAD, R. WOJTOWSKI, and S. C. WONG. Can. J. Chem. **58**, 2380 (1980).
4. D. S. SAKE GOUDA, L. CARTZ, and S. NATARAJAN. Acta Crystallogr. Sect. B, **29**, 2760 (1973).
5. J-M. NAVARRE, L. D. COLEBROOK, and L. D. HALL. Org. Magn. Reson. **14**, 410 (1980); M. A. KHADIM, L. D. COLEBROOK, and L. D. HALL. J. Heterocycl. Chem. **17**, 651 (1980).
6. L. D. COLEBROOK and L. D. HALL. Can. J. Chem. **58**, 2016 (1980).
7. J. H. NOGGLE and R. E. SCHIRMER. The nuclear Overhauser effect. Academic Press, New York. 1971.
8. J. C. CARTER, G. W. LUTHER, and T. C. LONG. J. Magn. Reson. **15**, 122 (1974).
9. D. TAVERNIER, M. J. O. ANTEUNIS, M. J. G. TITS, and L. J. G. ANGENOT. Bull. Soc. Chim. Belg. **87**:**9**, 595 (1978).
10. L. D. HALL and J. K. M. SANDERS. J. Am. Chem. Soc. **102**, 5703 (1980).
11. G. KOTOVYCH and G. H. M. AARTS. Org. Magn. Reson. **18**, 77 (1982), and references therein.
12. S. CASTELLANO and A. A. BOTHNER-BY. J. Chem. Phys. **41**, 3863 (1964).
13. L. M. JACKMAN and S. STERNHELL. Applications of nuclear magnetic resonance spectroscopy. 2nd ed. Pergamon Press, London. 1969. (*a*) pp. 270–277; (*b*) p. 316.
14. R. L. VOLD, J. S. WAUGH, M. P. KLEIN, and D. E. PHELPS. J. Chem. Phys. **48**, 3831 (1976).
15. M. L. MARTIN, G. J. MARTIN, and J.-J. DELPUECH. Practical nmr spectroscopy. Heyden, London. 1980. pp. 254–259.
16. J. K. M. SANDERS, J. C. WATERTON, and I. S. J. DENNISS. J. Chem. Soc. P1, 1150 (1978).
17. J. MERSH and J. K. M. SANDERS. Org. Magn. Reson. **18**, 122 (1982).

Can. J. Chem. Downloaded from www.nrcresearchpress.com by 210.87.254.40 on 09/06/12
For personal use only.

A new type of crown ether. III.[1] Triethylene glycolic diester of naphthalene dithioglycolic acid

LIDIA PRAJER-JANCZEWSKA, KRYSTYNA RUDOLF, AND TADEUSZ LIS
Institute of Chemistry, University of Wrocław, 50-383 Wrocław, Poland

AND

MARIAN JANCZEWSKI AND JANINA BISKUP
Institute of Chemistry, University of Lublin, 20-614 Lublin, Poland

Received August 9, 1982[2]

LIDIA PRAJER-JANCZEWSKA, KRYSTYNA RUDOLF, TADEUSZ LIS, MARIAN JANCZEWSKI, and JANINA BISKUP. Can. J. Chem. **61**, 1756 (1983).

The structure of 2,7-(11,22-diono-12,15,18,21-tetraoxa-9,24-dithia)-hexadecylene-naphthalene was investigated by ^{1}H and ^{13}C nmr and mass spectrometry. An X-ray structural investigation indicated the dissymmetric ansa structure of this compound in the crystalline state.

LIDIA PRAJER-JANCZEWSKA, KRYSTYNA RUDOLF, TADEUSZ LIS, MARIAN JANCZEWSKI et JANINA BISKUP. Can. J. Chem. **61**, 1756 (1983).

Faisant appel à la spectrométrie de masse et à la rmn du ^{1}H et du ^{13}C, on a étudié la structure du (diono-11,22 tetraoxa-12,15,18,21 dithia-9,24)-2,7 hexadécylène-naphtalène. Une étude par cristallographie de rayons-X indique que ce composé à l'état cristallin présente une structure de type ansa disymétrique.

[Traduit par le journal]

Introduction

The title macrolide (Fig. 1) was obtained with ca. 10% yield from the precursor, 2,7-naphthalene dithioglycolic acid dichloride (1).

The possibility of the arrangement of some related poly-oxathia-alkylene dionic chains over the plane of the naphthalene ring offers an interesting problem in the projected series of compounds, especially in the case in which the chains are bonded to two rings of the naphthalene moiety. This will, of course, be the reason for the ability of these compounds to complex with different types of substances and to act as inclusion systems in certain reactions, especially in those characteristic of natural compounds (e.g. in cyclodextrins (2) or in the antibiotic rifamycin B (3)) and for synthetic (4) multidentates.

Experimental

The nmr spectra were recorded on a Bruker 90 MHz spectrometer. Mass spectra were taken on a WSM-2 mass spectrometer; samples were introduced into the instrument via the direct insertion probe at room temperature; ion accelerating voltage: 3.0 kV, source temperature 160°C, pressure 5×10^{-7} Torr. The spectra were run at 70 eV and also at lower energy. From the mass spectrum the molecular ion was found to be at m/z 422, corresponding to $C_{20}H_{22}O_6S_2$. The main peak was at m/z 274.

A crystal suitable for single X-ray study was obtained from a saturated solution in DMF. For intensity measurements a specimen 0.8 × 0.8 × 0.7 mm was cut from a large crystal. Data were collected on a Syntex $P2_1$ four-circle diffractometer with Cu K_α radiation and graphite monochromator. The density of a few crystals was determined by flotation in a mixture of *n*-hexane/carbon tetrachloride, whose density was subsequently determined with a pycnometer. The crystal data were:

$C_{20}H_{22}O_6S_2$ $M = 422.52$

Monoclinic, $a = 5.831(3)$, $b = 37.49(2)$, $c = 9.234(4)$ Å, $\beta = 100.00(4)°$, $U = 1987.9$ Å^3, $Z = 4$, $D_c = 1.41$ g cm^{-3}, $D_{obs} = 1.42$ g cm^{-3}, Cu K_α radiation, $\lambda = 1.5418$ Å, μ(Cu K_α) = 2.65 mm^{-1}, space group $P2_1/c$.

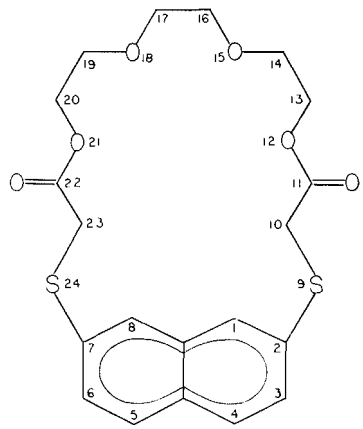

FIG. 1. The title compound. The numbering corresponds to that in Tables 1 and 2.

2672 Reflections were measured within the limits $2\theta < 115°$, 2540 with $I > 1.96\sigma(I)$ were used for the structure determination. One standard reflection was monitored after every 100 reflections; no significant change in intensity was observed. A $2\theta-\omega$ scan technique was employed. The intensities were corrected for Lorentz and polarization effects and an absorption correction was made from the φ-scan data. The scattering factors for neutral atoms employed in the calculations were those given (5). All the calculations were performed on a NOVA 1200 minicomputer with programs supplied by Syntex (6).

The crystal structure was solved by use of MULTAN (7). The solution was based on 165 reflections with $E > 1.8$. The E map corresponding to the solution with the best figure of merit revealed the positions of 21 non-hydrogen atoms. The remaining non-hydrogen atoms were located from several Fourier and difference-Fourier syntheses. Full-matrix least-squares refinement, first with isotropic, then with anisotropic thermal parameters gave $R = 0.113$ and 0.074, respectively. All H-atoms were included in geometrically calculated positions with d(C—H) = 1.0 Å and with isotropic thermal parameters of 4.5 Å^2, but were not permitted to refine. Their positions were, however, updated with respect to the subsequent refined positions of their attached carbon atoms. The function minimized was $\Sigma w(|F_o| - |F_c|)^2$ with $w = [(\sigma^2(F) + 0.0001F_o^2]^{-1}$. The final refinement results gave a conventional R value,

[1]For part II see ref. 1.

[2]Revision received February 17, 1983.

Can. J. Chem. Downloaded from www.nrcresearchpress.com by 210.87.254.6 on 09/06/12
For personal use only.

TABLE 1. ^{1}H nuclear magnetic resonance values of the respective protons (in $CDCl_3$)

Carbon atoms adjacent to the respective protons in Fig. 1	Number of protons and type of signal	δ ppm (relative to TMS)	J (Hz)
C-10, C-23	4H, s, —$COCH_2S$—	3.24	
C-14, C-19	4H, m, —$COOCH_2CH_2O$—	3.45–3.54	
C-16, C-17	4H, s, central methylene	3.73	
C-13, C-20	4H, m, —$COOCH_2$—	4.20–4.29	
C-3, C-6	2H, dd	ca. 7.45	*ortho*($C_{3,4}$): 8.25
C-4, C-5	2H, d	ca. 7.72	
C-1, C-8	2H, d	ca. 7.825	*meta*($C_{1,3}$): 1.57

TABLE 2. ^{13}C nuclear magnetic resonance values of the respective carbon atoms (in $CDCl_3$)

Aliphatic carbon atoms (compare Fig. 1)	δ ppm (relative to TMS)	δ ppm of the aromatic carbon atoms
10, 23	36.21	125.13
11, 22	169.53	128.06
13, 20	64.81	128.25
14, 19	69.1	131.44
16, 17	70.46	133,45
		134.34

$\Sigma||F_o| - |F_c||/\Sigma|F_o|$, of 0.042 and a weighted R value, $[\Sigma w(|F_o| - |F_c|)^2/\Sigma w|F_o|^2]^{\frac{1}{2}}$ of 0.059 for all non-zero reflections. The goodness-of-fit, $[\Sigma w\Delta F^2/(m - s)]^{\frac{1}{2}}$, where m is the number of reflections used and s is the number of parameters refined, is 7.72. There were no significantly large positive or negative electron density peaks in a final difference Fourier synthesis; the largest positive region was 0.4 e Å^{-3} and the largest negative region was 0.3 e Å^{-3}. The final atomic positional parameters are given in Table 3, the bond lengths and angles in Tables 4 and 5, respectively.[3]

Description of the structure and discussion

The ^{1}H nmr spectrum of the compound shows that this diester is nonplanar. The structure of the diester in $CDCl_3$ solution either is symmetric or rapid conformational changes cause the protons to appear in the symmetrical positions. The CH_2 groups are influenced by the paramagnetic field resulting from the ring current of the naphthalene system. The conformation of the protons bonded with C(16) and C(17) (Fig. 1) located in the range of paramagnetic influence of the ring current may dominate. The reason for this is shown by the chemical shifts of these protons in a slightly lower field than would be present if they were located above the naphthalene ring plane (Table 1). The magnetic equivalence of chemically equivalent protons in solution implies a range of conformations whose interconversion is rapid on the nmr time-scale.

The ^{13}C nmr measurements characterize the individual C atoms (Table 2).

In the mass spectrogram the most abundant peak (m/z 274) indicates the easy splitting of ester C—O bonds.

The crystal structure of the title racemic compound is composed of discrete molecules with conformations of probably lower energy than those in the $CDCl_3$ solution (Table 1). One of the enantiomers was considered (Fig. 2). The naphthalene ring was planar to within 0.01 Å. The bond lengths were similar to those of some β-substituted (8) and 2,7-disubstituted

[3]Tables of temperature factors are available, at a nominal charge, from the Depository of Unpublished Data, CISTI, National Research Council of Canada, Ottawa, Canada K1A 0S2.

TABLE 3. Final atomic parameters*

	x	y	z	B_{eq}
S(1)	0.5216(2)	0.31236(2)	0.1240(1)	3.31
S(2)	1.2444(2)	0.44923(2)	0.6806(1)	2.92
O(1)	1.1218(4)	0.28349(6)	0.3280(3)	3.62
O(2)	1.0765(5)	0.30089(7)	0.6237(3)	4.74
O(3)	0.9046(5)	0.36298(6)	0.8782(3)	4.17
O(4)	0.9834(4)	0.43545(5)	0.9358(3)	3.88
O(5)	0.7848(4)	0.25618(6)	0.3455(3)	4.33
O(6)	0.7624(5)	0.48311(6)	0.8634(3)	4.20
C(1)	0.8109(6)	0.29466(8)	0.1415(3)	3.15
C(2)	1.1462(6)	0.47988(8)	0.8075(4)	3.25
C(3)	0.8977(6)	0.27587(7)	0.2841(4)	2.96
C(4)	0.9407(6)	0.46682(7)	0.8703(3)	2.78
C(5)	1.2466(6)	0.26611(9)	0.4580(4)	4.14
C(6)	1.2930(6)	0.29164(11)	0.5810(4)	4.80
C(7)	1.1048(7)	0.32476(9)	0.7425(4)	4.36
C(8)	0.8692(7)	0.33717(9)	0.7635(4)	4.08
C(9)	0.7166(7)	0.38711(9)	0.8709(4)	4.16
C(10)	0.7896(6)	0.41635(9)	0.9792(4)	4.05
C(11)	0.7537(6)	0.36201(7)	0.3196(3)	2.91
C(12)	0.5631(6)	0.35338(7)	0.2196(3)	2.92
C(13)	0.3799(6)	0.37824(8)	0.1798(4)	3.40
C(14)	0.3963(6)	0.41110(8)	0.2434(4)	3.50
C(15)	0.5915(5)	0.42127(7)	0.3482(3)	2.73
C(16)	0.6164(6)	0.45522(8)	0.4144(4)	3.12
C(17)	0.8069(6)	0.46399(7)	0.5150(4)	2.98
C(18)	0.9865(5)	0.43899(7)	0.5561(3)	2.59
C(19)	0.9698(6)	0.40593(7)	0.4925(3)	2.64
C(20)	0.7747(5)	0.39601(7)	0.3873(3)	2.56
H(1)	0.919	0.3149	0.132	4.5
H(111)	0.813	0.2772	0.060	4.5
H(2)	1.102	0.5028	0.755	4.5
H(22)	1.278	0.4841	0.891	4.5
H(5)	1.397	0.2567	0.437	4.5
H(55)	1.149	0.2460	0.485	4.5
H(6)	1.368	0.3135	0.549	4.5
H(66)	1.398	0.2803	0.666	4.5
H(7)	1.200	0.3456	0.721	4.5
H(77)	1.184	0.3123	0.834	4.5
H(8)	0.777	0.3166	0.792	4.5
H(88)	0.786	0.3482	0.670	4.5
H(9)	0.578	0.3745	0.896	4.5
H(99)	0.678	0.3974	0.770	4.5
H(10)	0.840	0.4059	1.080	4.5
H(01)	0.657	0.4332	0.981	4.5
H(11)	0.881	0.3441	0.346	4.5
H(13)	0.240	0.3717	0.106	4.5
H(14)	0.267	0.4286	0.215	4.5
H(16)	0.491	0.4733	0.386	4.5
H(17)	0.820	0.4884	0.560	4.5
H(19)	1.099	0.3883	0.522	4.5

*$B_{eq} = \frac{1}{3}(B_{11} + B_{22} + B_{33})$.

Can. J. Chem. Downloaded from www.nrcresearchpress.com by 210.87.254.6 on 09/06/12
For personal use only.

TABLE 4. Interatomic distances (Å) and angles (°)

(a) Distances

Atoms	Distance	Atoms	Distance
S(1)—C(1)	1.794(3)	S(2)—C(2)	1.804(3)
S(1)—C(12)	1.769(3)	S(2)—C(18)	1.770(3)
C(1)—C(3)	1.502(4)	C(2)—C(4)	1.501(4)
C(3)—O(1)	1.331(4)	C(4)—O(4)	1.326(3)
C(3)—O(5)	1.195(4)	C(4)—O(6)	1.198(4)
O(1)—C(5)	1.446(4)	O(4)—C(10)	1.452(4)
C(5)—C(6)	1.474(5)	C(10)—C(9)	1.495(5)
C(6)—O(2)	1.430(4)	C(9)—O(3)	1.414(4)
O(2)—C(7)	1.403(4)	O(3)—C(8)	1.422(4)
C(7)—C(8)	1.495(5)	C(15)—C(20)	1.426(4)
C(12)—C(11)	1.355(4)	C(18)—C(19)	1.368(4)
C(11)—C(20)	1.415(4)	C(19)—C(20)	1.412(4)
C(12)—C(13)	1.417(4)	C(18)—C(17)	1.408(4)
C(13)—C(14)	1.361(4)	C(17)—C(16)	1.359(4)
C(14)—C(15)	1.412(4)	C(16)—C(15)	1.408(4)

(b) Angles*

Bonds	Angle	Bonds	Angle
C(1)—S(1)—C(12)	103.4	C(2)—S(2)—C(18)	103.3
S(1)—C(1)—C(3)	114.9	S(2)—C(2)—C(4)	114.1
C(1)—C(3)—O(1)	109.3	C(2)—C(4)—O(4)	111.5
C(1)—C(3)—O(5)	125.2	C(2)—C(4)—O(6)	123.8
O(1)—C(3)—O(5)	125.5	O(4)—C(4)—O(6)	124.7
C(3)—O(1)—C(5)	118.8	C(4)—O(4)—C(10)	118.0
O(1)—C(5)—C(6)	110.2	O(4)—C(10)—C(9)	108.8
C(5)—C(6)—O(2)	108.5	C(10)—C(9)—O(3)	108.0
C(6)—O(2)—C(7)	112.4	C(9)—O(3)—C(8)	112.9
O(2)—C(7)—C(8)	108.3	O(3)—C(8)—C(7)	106.9
S(1)—C(12)—C(11)	124.9	S(2)—C(18)—C(19)	117.7
S(1)—C(12)—C(13)	114.3	S(2)—C(18)—C(17)	122.6
C(13)—C(12)—C(11)	120.8	C(17)—C(18)—C(19)	119.6
C(12)—C(11)—C(20)	120.9	C(18)—C(19)—C(20)	121.5
C(11)—C(20)—C(15)	118.9	C(19)—C(20)—C(15)	118.5
C(11)—C(20)—C(19)	122.6	C(14)—C(15)—C(16)	123.5
C(14)—C(15)—C(20)	118.3	C(16)—C(15)—C(20)	118.3
C(15)—C(14)—C(13)	121.9	C(15)—C(16)—C(17)	121.7
C(14)—C(13)—C(12)	119.3	C(16)—C(17)—C(18)	120.3

*Estimated standard deviations are about 0.3°.

(9) naphthalenes.

The S—C_{sp^2} bond lengths are somewhat smaller (ca. 1.770(3) Å) than those of the S—C_{sp^3} bonds (ca. 1.799(3) Å) and both kinds are in the range of the known S—C lengths: 1.770(3) – 1.843(2) Å (10) for C_{sp^3} and, e.g., 1.705–1.748 Å (11), and typically 1.77 Å (12) for C_{sp^2}. The ester alkoxy C—O bonds (average 1.329(4) Å), as well as the carbonyl bonds (1.197(4) Å), are in the same expected range (ca. 1.325(2) and 1.202(2) Å, respectively) as in 2,6-diketo-18-crown-6 (13). The etheric alkoxy C—O bonds (ca. 1.449(4) Å) are of the same order of length as analogous bonds in the same crown (1.459 Å). In the ether portion the C—C bond lengths (ca. 1.485(5) Å) and the C—O distances (etheric: 1.42(1) Å) are similar to those of the mentioned crown compound (1.494(2) and 1.416(4) Å, respectively (13)).

The large distance between the 2- and 7-positions in the substituted naphthalene (Fig. 1) suggested that the two S atoms are coplanar with the naphthalene ring, similar to the methyl substituents, −0.03(1) and −0.02(1) Å, in the much more overcrowded 1,8-dibenzoyl-2,7-dimethylnaphthalene (9). Meanwhile these S atoms are displaced from the plane of the naphthalene by about 0.06 Å in the direction opposite to the main part of the chain. The angles formed by attachment of these S atoms to the *ortho* carbons are unequal, 124.9(3)° and 114.3(3)° at C(12), and 117.7(3)° and 122.6(3)° at C(18) (Fig. 2, Table 4(b)). This is further reflected in the torsional angles about the S—C bonds (Table 5, Fig. 2). Further, in the thia-oxa-alicyclic bow the angles formed by the S atoms have the usual value, ca. 103.3(2)°. The apical angles of the C(3) through C(10) atoms, e.g. C(1)—C(3)—O(1), C(2)—C(4)—O(4), and so on (Fig. 2, Table 4) are formed normally, 106.9(3)–110.2(3)°, and only those formed by the C(1) and C(2) are a little larger (ca. 114.5(3)°), similar to those of the compared (13) crown ether, ca. 113°.

The torsion angles O—C—C—O in both the alkoxide parts are of the usual synclinal value, 68.2(7)° and 63.3(7)°; compare ±70.6° (9) and ca. 60° (14). The S(2)—C(2)—C(4)—O(4) angle, 56.1(3)°, is similar; however, in contrast to this value, that of the second torsion angle S(1)—C(2)—C(3)—O(1) is −141.3(6)°, which shows the anticlinal conformation of this set of atoms. Moreover, the angle O(2)—C(7)—C(8)—O(3) of the other portion, being −176.3(7)°, corresponds to the

Can. J. Chem. Downloaded from www.nrcresearchpress.com by 210.87.254.6 on 09/06/12
For personal use only.

Can. J. Chem. Downloaded from www.nrcresearchpress.com by 210.87.254.6 on 09/06/12
For personal use only.

TABLE 5. Analysis of the configuration of the compound

(a) Conformational angles (°)

Bonds	Angle
C(11)—C(12)—S(1)—C(1)	−19.2(6)
C(19)—C(18)—S(2)—C(2)	−149.4(7)
C(13)—C(12)—S(1)—C(1)	158.7(5)
C(17)—C(18)—S(2)—C(2)	34.1(8)
C(12)—S(1)—C(1)—C(3)	82.0(5)
C(18)—S(2)—C(2)—C(4)	51.0(7)
S(1)—C(1)—C(3)—O(5)	41.2(7)
S(2)—C(2)—C(4)—O(6)	−124.8(9)
S(1)—C(1)—C(3)—O(1)	−141.3(6)
S(2)—C(2)—C(4)—O(4)	56.1(8)
O(5)—C(3)—O(1)—C(5)	2.1(9)
O(6)—C(4)—O(4)—C(10)	11.6(9)
C(1)—C(3)—O(1)—C(5)	−175.5(7)
C(2)—C(4)—O(4)—C(10)	−169.4(8)
C(3)—O(1)—C(5)—C(6)	−107.5(6)
C(4)—O(4)—C(10)—C(9)	102.8(8)
O(1)—C(5)—C(6)—O(2)	68.2(7)
O(4)—C(10)—C(9)—O(3)	63.3(7)
C(5)—C(6)—O(2)—C(7)	179.0(8)
C(10)—C(9)—O(3)—C(8)	−170.4(7)
C(6)—O(2)—C(7)—C(8)	171.2(7)
C(9)—O(3)—C(8)—C(7)	155.6(7)
O(2)—C(7)—C(8)—O(3)	−176.3(7)

(b) Distances (Å) from plane through naphthalene moiety (atoms used to define the plane are indicated by an asterisk)

Atom	Distance	Atom	Distance
C(11)*	0.008(3)	C(12)*	0.005(3)
C(13)*	−0.002(3)	C(14)*	−0.009(4)
C(15)*	−0.007(3)	C(16)*	0.009(3)
C(17)*	0.009(3)	C(18)*	−0.008(3)
C(19)*	−0.005(3)	C(20)*	0.000(3)
S(1)	0.064(1)	S(2)	0.060(1)
O(1)	0.200(3)	O(4)	−2.953(3)
O(2)	−1.983(3)	O(3)	−3.713(3)
O(5)	−1.438(3)	O(6)	−2.549(3)
C(1)	0.696(3)	C(2)	−0.850(3)
C(3)	−0.332(3)	C(4)	−2.200(3)
C(5)	−0.584(4)	C(10)	−4.193(4)
C(6)	−1.034(4)	C(9)	−3.993(4)
C(7)	−2.484(3)	C(8)	−3.293(4)

antiperiplanar conformation. The other torsion angles fit the main shape of the chiral skew ansa-multidentate (Table 5, Fig. 2). The bow shows the different positions of C(1) and C(2) atoms in comparison with the plane of the naphthalene ring, which is characterized by the torsion angles C(1)—S(1)—C(12)—C(11), −19.2(6)°, semiperiplanar, and C(2)—S(2)—C(18)—C(19), −149.4(7)°, quasi-antiperiplanar (Fig. 2, Table 4).

Deviations from the best least-squares plane calculated for the four ring O atoms in Å: O(1), 0.110(3); O(2), −0.293(3); O(3), 0.227(3); O(4), −0.066(3) indicate that these atoms form a quasi-plane. The S(2) atom is placed near to such a plane, −0.78 Å, but the S(1) atom is displaced much more,

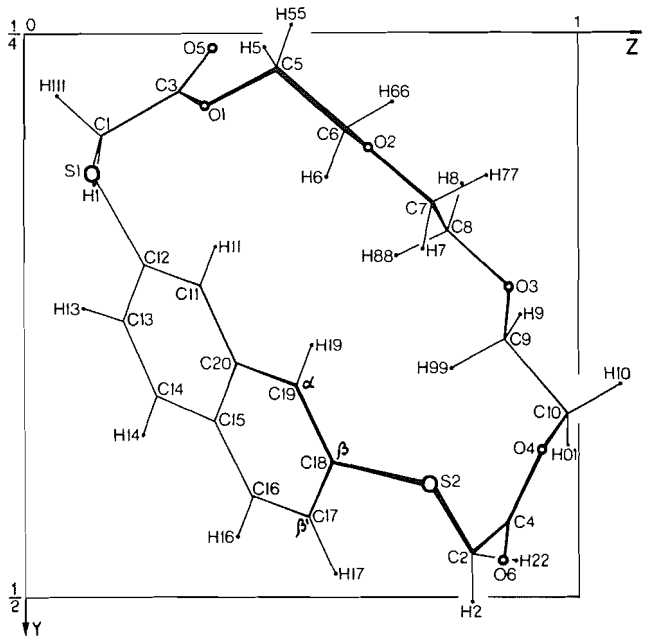

FIG. 2. The crystal structure projected on the (100) plane. The numbering corresponds to that in Tables 3, 4, and 5.

3.85 Å, to the other side of this plane. The C(1), C(3), O(5), O(1) and C(2), C(4), O(6), O(4) sets of atoms are planar, but are differently stretched, ca. 100° and ca. 60° respectively, in relation to the quasi-plane of the four ring O atoms.

1. L. PRAJER-JANCZEWSKA, M. JANCZEWSKI, and J. BISKUP. Pol. J. Chem. In press.
2. L. M. BENDER and M. KOMIYAMA. Cyclodextrin chemistry. Springer Verlag, New York. 1977.
3. P. SENSI, P. MARGALITH, and M. T. TIMBAL. Farmaco Ed. Sci. **14**, 146 (1959).
4. G. A. MELSON (*Editor*). Coordination chemistry of macrocyclic compounds. Plenum Press, New York, London. 1977.
5. International Tables for X-Ray Crystallography. Vol. 4. Kynoch Press, Birmingham. 1974.
6. XTL Structure Determination System Operation Manual, Syntex Analytical Instruments Inc., 10040 Bubb Road, Cupertino, CA 95014 U.S.A.
7. G. GERMAIN, P. MAIN, and M. M. WOOLFSON. Acta Crystallogr. Sect. A, **27**, 368 (1971).
8. J. E. JØRGENSON and A. B. HANSEN. Acta Crystallogr. Sect. B, **38**, 991 (1982).
9. P. H. GORE and K. HENRICK. Acta Crystallogr. Sect. B, **36**, 2462 (1980).
10. W. DOBROWOLSKA and M. BUKOWSKA-STRZYŻEWSKA. Acta Crystallogr. Sect. B. **36**, 317 (1980), and references cited.
11. M. BUKOWSKA-STRZYŻEWSKA and B. PNIEWSKA. Acta Crystallogr. Sect. B, **35**, 633 (1979).
12. G. ARGAY, A. KÁIMÁN, Á. NAHLOWSKI, and B. RIBÁR. Acta Crystallogr. Sect. B, **31**, 1956 (1975).
13. N. K. DALLEY and S. B. LARSON. Acta Crystallogr. Sect. B, **35**, 1901 (1979).
14. N. K. DALLEY. Synthetic multidentate macrocyclic compounds. *Edited by* R. M. Izatt. J. J. Christensen, New York. 1978. Chapt. 4. pp. 207–243.

A study of Br/NO_2 substitution reactions and nuclear magnetic resonance of 2,2-diaryl-1-picrylhydrazines

PATRICIA F. CURRIE, J. WILSON QUAIL,[1] ANN C. M. RUSK, AND JOHN A. WEIL[1]
Department of Chemistry, University of Saskatchewan, Saskatoon, Sask., Canada S7N 0W0

Received December 1, 1982

PATRICIA F. CURRIE, J. WILSON QUAIL, ANN C. M. RUSK, and JOHN A. WEIL. Can. J. Chem. **61**, 1760 (1983).

A series of compounds of type 2-M_a-2-M_b-1-picrylhydrazine with M_a, M_b = phenyl, *p*-bromophenyl, and *p*-nitrophenyl has been investigated. Conversion of *p*-bromophenyl into *p*-nitrophenyl caused by reaction with NO_2 has been observed in compounds of the above series. Parameters of the ^1H and ^{13}C nmr spectra for the members of the series are reported. The new compound 2-(*p*-bromophenyl)-2-(*p*-nitrophenyl)-1-picrylhydrazine has been prepared and characterized using mass spectrometry, nuclear magnetic resonance, electron paramagnetic resonance, thin-layer chromatography, and elemental analysis.

PATRICIA F. CURRIE, J. WILSON QUAIL, ANN C. M. RUSK et JOHN A. WEIL. Can. J. Chem. **61**, 1760 (1983).

On a étudié une série de composés du type M_a-2-M_b-2 picryl-1 hydrazine avec M_a, M_b = phényle, *p*-bromophényle et *p*-nitrophényle. Dans les composés de cette série, on a observé la transformation du *p*-bromophényle en *p*-nitrophényle par suite de la réaction avec le NO_2. On rapporte les paramètres des spectres de rmn du ^1H et du ^{13}C de ces composés. On a préparé le nouveau composé (*p*-bromophényle)-2 (*p*-nitrophényle)-2 picryl-1 hydrazine et on l'a caractérisé en faisant appel à la spectrométrie de masse, à la rmn, à la rpe, à la chromatrographie en couche mince et à l'analyse élémentaire.

[Traduit par le journal]

Introduction

A series of compounds of type 2-M_a-2-M_b-1-picrylhydrazine with M_a, M_b = phenyl, *p*-bromophenyl, and *p*-nitrophenyl has been investigated. These various different molecular species will be denoted by DM_aM_b—H. The work reported here is a continuation of a project studying the reaction products resulting from reaction of bromine with the free radical 2,2-diphenyl-1-picrylhydrazyl (denoted as DH_2) (1). At ice temperatures, fast addition of bromine to DH_2 or to the corresponding hydrazine DH_2—H in solution gives the expected products DHBr—H or DBr_2—H, with bromine substitution into the *para* position(s) of the phenyl ring(s). However, substantial yields of 2-(*p*-nitrophenyl)-2-phenyl-1-picrylhydrazine ($DH(NO_2)$—H) were found at somewhat higher temperatures (60°C) and with slow addition of bromine. It was postulated that this compound was formed by reaction of DH_2 with NO_2, displaced from nitro groups in the picryl ring of DH_2 by bromine. The picryl-substituted products 2-(*p*-nitrophenyl)-2-phenyl-1-(2-bromo-4,6-dinitrophenyl)hydrazine and 2-(*p*-bromophenyl)-2-phenyl-1-(2-bromo-4,6-dinitrophenyl)-hydrazine were subsequently identified by proton nmr studies. The preparation of mono- and dinitrated diphenylpicrylhydrazines through reaction of DH_2 and NO_2 had previously been described (2). Thus a series of compounds DHBr—H, $DH(NO_2)$—H, DBr_2—H, $D(NO_2)_2$—H, and D'H(NO_2)—H, D'HBr—H (with D' denoting Br substitution for NO_2 in the *o*-position of the picryl ring) is available for study.

In the present project, replacement of Br by NO_2 was found to occur and has been investigated. No ^{13}C nmr study of the molecules listed above has yet appeared in the literature. To characterize chemical and physical variations within this series more completely and to assign unambiguously all of the peaks in the carbon nmr spectra of the compounds, it proved useful also to prepare the previously unreported compound $DBr(NO_2)$—H in which the two phenyl rings contain Br and NO_2, respectively, at the *para* positions. This hydrazine also was utilized in studying replacement of Br by NO_2 in phenyl groups.

[1]Authors to whom correspondence should be addressed.

Experimental

A. *Starting material*

1. 2-(*p*-Bromophenyl)-2-phenyl-1-picrylhydrazine (DHBr—H) was prepared by rapid addition of bromine to DH_2—H in $CHCl_3$ solution at ice temperature, as described in ref. 1. Separation from the reaction mixture was achieved by elution with chloroform from an Alcoa F-20 alumina column. Red-orange crystals, mp 182–184°C, were obtained after recrystallization from chloroform/petroleum ether.

2. $DH(NO_2)$—H was prepared as described in ref. 2. The product was separated from impurities on an alumina column using ethanol as the elutant and by recrystallization from ethanol/acetic acid.

3. The hydrazyl $DH(NO_2)$ was prepared by oxidizing $DH(NO_2)$—H with PbO_2 in chloroform (2).

B. *$DBr(NO_2)$—H synthesis*

Matheson 98% min purity NO_2 was slowly bubbled through a stirred solution of 0.5 g DHBr—H in 50 mL of chloroform cooled to 0–2°C. The reaction was monitored at two-minute intervals for formation of phenyl-nitrated product: the samples taken were spotted on Brinkmann 5538 silica gel tlc sheets with toluene developer, and the NO_2 flow was stopped (usually within 10 minutes) when samples taken indicated formation of a nitrated-phenyl species located at $R_f \sim 0.23$ (1).

The resulting solution was intensely brown in color, indicating oxidation of the hydrazine species to hydrazyls by excess NO_2. Reduction to the typical orange color of the hydrazines was effected by shaking the reaction mixture with ~0.2 g of solid sodium dithionite and 1–2 mL of 3% H_2O_2. This step simplified the product separation, done by adsorption chromatography on Alcoa alumina F-20 using 85:15 (v/v) chloroform/ethanol eluant. This first bands eluted contained low yields of unidentified brominated material. The dark red (wine-colored) band at the top of the column moved slowly, and eventually split into three sections which eluted $DH(NO_2)$—H, $DBr(NO_2)$—H, and then $D(NO_2)_2$—H, in that order.

The desired compound $DBr(NO_2)$—H could be recrystallized from a variety of solvents, including acetone, ethanol, chloroform, and acetic acid. Diarylpicrylhydrazines exhibit tenacious retention of solvent (1), so that attempts to obtain solvent-free crystals by heating at 120°C in vacuum for 24 h were unsuccessful. Elemental analyses obtained for the product recrystallized from various solvents gave the results in Table 1.

Mass spectra were recorded on an AEI MS-12 mass spectrometer operated at 70 eV. Diarylpicrylhydrazines under electron bombardment fragment via N—N bond fission, to give diarylamine ions con-

TABLE 1. Elemental analysis and properties of $DBr(NO_2)$—H:nZ crystallized from various solvents Z

	nZ							
	1 Acetone		1 Ethanol		1 Chloroform		1 Acetic acid + 1 ethanol	
Parameter	found	calc'd	found	calc'd	found	calc'd	found	calc'd
C, %	45.1	45.4	43.5	42.5	36.6	35.7	43.0	42.2
N, %	14.4	14.5	14.6	14.9	12.2	13.2	13.2	13.4
H, %	3.1	3.0	3.0	3.0	2.1	1.9	3.4	3.4
Color	Orange		Orange		Red-brown		Orange	
T_{melt}, °C	90–94		118–122		93–95		116–120	

TABLE 2(a). Chemical shifts of the N—H and *m*-picryl protons in the 2,2-diaryl-1-picrylhydrazines*

	δ(N—H)	δ_a(picryl)	δ_b(picryl)
DH_2—H	10.13	8.54	9.20
DHBr—H	10.08	8.55	9.21
$DH(NO_2)$—H	10.21	8.61	9.22
DBr_2—H	10.05	8.55	9.22
$DBr(NO_2)$—H	10.19	8.62	9.25
$D(NO_2)_2$—H	10.40	8.51	9.24

*In dichloromethane-d_2 solvent at ca. 295 K, with chemical shifts in ppm measured relative to the internal TMS peak taken to be at δ = 0.

TABLE 2(b). ^{1}H nmr data for the aryl groups in the 2,2-diaryl-1-picrylhydrazines*

	Phenyl			*p*-Bromophenyl			*p*-Nitrophenyl		
Compound	δ(*o*)	δ(*m*)	δ(*p*)	δ(*o*)	δ(*m*)	N_J (Hz)	δ(*o*)	δ(*m*)	N_J (Hz)
DH_2—H	7.130	7.357	7.207	—	—	—	—	—	—
DHBr—H	7.140	7.375	7.245	7.008	7.460	9.2	—	—	—
$DH(NO_2)$—H	7.240	7.452	7.366	—	—	—	7.171	8.171	9.5
$D(NO_2)_2$—H	—	—	—	—	—	—	7.339	8.247	9.2
$DBr(NO_2)$—H	—	—	—	7.136	7.575	8.9	7.172	8.170	9.6
DBr_2—H	—	—	—	7.015	7.480	9.1	—	—	—

*Conditions as given in Table 2(a).

taining amine protons presumably originating from the N-picryl fragments (1). The expected doublet at m/z 292–294 ascribed to the *p*-bromophenyl-*p*-nitrophenylamine +1 ion was observed; loss of bromine (plus pick-up of a phenyl proton) led to a prominent peak at m/z 214, i.e., to the phenyl-*p*-nitrophenylamine +1 ion (1).

Oxidation with lead dioxide in benzene gives the hydrazyl $DBr(NO_2)$ which is intensely brown in solution. The hydrazyl was shown to be paramagnetic by observation of its electron paramagnetic resonance (epr) spectrum. The stability of the free radical in solution was demonstrated by the lack of change in the epr spectrum of a sealed degassed sample after standing six weeks.

Other methods of preparation of $DBr(NO_2)$—H were examined as well. A sample of $DH(NO_2)$—H prepared as described in ref. 2 was dissolved in benzene at room temperature. A 3% Br_2 (v/v) in chloroform solution was added, to attain a 2:1 mole ratio $DH(NO_2)$—H/Br_2. The precipitate recovered was substantially unreacted $DH(NO_2)$—H. Use of the hydrazyl $DH(NO_2)$ instead of the hydrazine resulted in a more complicated reaction mixture. The yield of $DBr(NO_2)$—H in these attempts was much lower than that obtained by the above method of nitrating DHBr—H with NO_2.

C. *Magnetic resonance*

Proton (^{1}H) nmr spectra were recorded on a Bruker WH-400 spectrometer at ambient temperature (ca. 295 K) and on a Bruker WP-60 at low temperatures. Chemical shifts (Tables 2a, b) were measured in ppm relative to the peak of internal tetramethylsilane (TMS) taken to be at δ = 0, and are deemed accurate to ±0.01 ppm.

Ambient (303 K) and low temperature ^{13}C nmr spectra were recorded at 15.08 MHz on a Bruker WP-60 spectrometer. Acetone-d_6 and dichloromethane-d_2 were used as solvents. Here chemical shifts (Tables 3, 4) were measured relative to the internal ^{13}C TMS peak taken to be at δ = 0, and are accurate to ±0.1 ppm.

The epr spectra of the hydrazyl free radicals obtained by oxidation of the above hydrazines are well known (2, 3), with the exception of the new radical $DBr(NO_2)$. Dilute deoxygenated solutions of this species in benzene were studied at room temperature, using our Bruker B-ER 418S epr spectrometer operating at ca. 9.4 GHz.

Results and discussion

$DBr(NO_2)$—H was reacted with NO_2 under the same conditions as in the synthesis of $DBr(NO_2)$—H. A 95% yield of $D(NO_2)_2$—H was obtained. The identity of the latter was confirmed by proton nmr. A similar experiment performed with DBr_2—H and NO_2 produced substantial yields of $D(NO_2)_2$—H, as well as some $DBr(NO_2)$—H. During initial attempts to synthesize $DBr(NO_2)$—H from DHBr—H, overnitration by NO_2 also was found to result in formation of the dinitro compound. In the DBr_2—H reaction with NO_2 the for-

TABLE 3. Chemical shifts of the ^{13}C peaks of the 2,2-diaryl-1-picrylhydrazines*

Carbon	DH_2—H	DHBr—H	$DH(NO_2)$—H	DBr_2—H	$DBr(NO_2)$—H	$D(NO_2)_2$—H
1	143.0	142.8	143.1	142.6	143.4	141.6
2	134.7	135.0	135.5	135.0	136.0	135.5
3	127.2	127.2	127.4	127.2	127.5	127.5
4	136.8	136.8	137.5	137.2	137.3	137.9
5	125.6	125.6	125.8	125.5	126.0	125.7
6	140.3	140.2	140.3	140.1	139.8	139.8
7	146.6	146.1	144.5			
8	121.1	122.3	125.3			
9	129.8	130.1	130.6			
10	125.6	126.4	128.5			
11		146.1		145.5	143.7	
12		122.0		123.2	127.1	
13		132.4		132.7	133.6	
14		117.0		118.1	120.9	
15			152.7		152.3	150.1
16			117.1		117.5	121.3
17			125.3		125.5	125.7
18			142.3		142.4	145.0

*In acetone-d_6 solvent at ca. 250 K, with chemical shifts in ppm measured relative to the internal TMS peak taken to be at $\delta = 0$.

TABLE 4. Chemical shifts of the ^{13}C peaks of the 2,2-diaryl-1-picrylhydrazines*

Carbon	DH_2—H	DHBr—H	$DH(NO_2)$—H	DBr_2—H	$DBr(NO_2)$—H	$D(NO_2)_2$—H
1	142.9	142.8	143.9	142.5	144.3	142.2
2, 6†	—	—	—	—	—	—
3, 5	126.4	126.7	126.7	126.4	126.6	126.6
4	137.3	137.7	138.2	137.6	138.3	138.3
7	147.2	146.5	145.2			
8	121.4	122.5	125.4			
9	129.9	130.2	130.9			
10	125.9	126.7	128.7			
11		146.5		145.8	144.3	
12		122.5		123.4	126.9	
13		132.6		132.8	133.8	
14		117.5		118.4	121.2	
15			153.1		152.4	150.4
16			117.7		118.2	121.5
17			125.4		125.5	125.7
18			142.5		142.2	145.5

*Conditions as given in Table 3, except that $T \sim 304$ K.
†Broad, near C-4 lines.

mation of some $D'(NO_2)_2$—H, in which Br substitution for NO_2 in the *o*-position of the picryl ring had occurred, was confirmed by proton nmr and mass spectroscopy. This compound is analogous to $D'H(NO_2)$—H and D'HBr—H identified in our first report (1).

Thus, from the reactions studied it is clear that a bromine atom in the *p*-position of a phenyl group can be replaced by a nitro group through reaction with NO_2, in inert organic solvents. An extensive review of the reactions of NO_2 with organic compounds has been published by Riebsomer (4); however, no specific mention of such replacements was made. Another early review (5) of "anomalous" nitrations catalogues studies in which halogens, alkyl, alkoxyl, acyl, carboxyl, and sulfonic groups have been replaced by one or more nitro groups. Use of NO_2 (N_2O_4) is not cited. More modern treatises (6, 7) on the subject also do not discuss NO_2 nitration reactions of aromatic molecules in inert solvents. It thus appears that this type of nitration, as reported herein, is not well-known in organic chemistry. On the other hand, there is a growing awareness of the existence of reactions in which radicals replace other radicals in aromatic compounds; for example, see the recent review of ipso substitution (8). The reactions observed by us seem to be of this type. Detailed rate and mechanism studies now are feasible and desirable.

Characterization of $DBr(NO_2)$—H

Since unsolvated $DBr(NO_2)$—H could not be prepared, proton nmr was used to confirm the identity of this compound crystallized from various solvents (see Table 1). Despite drying the product in a vacuum oven at temperatures up to 120°C, peaks due to the solvent were always observable in the nmr spectra.

Two separate proton A_2X_2 subspectra were observed for $DBr(NO_2)$—H. One A_2X_2 subspectrum occurred with multiplets at $\delta = 7.14$ and 7.58 ppm and with a magnitude for $N_J = J_{AX} + J_{AX'}$ of 8.9 Hz. These numbers are very similar (Table 2b) to corresponding values found for the *p*-bromophenyl protons in DHBr—H and in DBr_2—H. The other subspectrum has

multiplets at $\delta = 7.17$ and 8.17 ppm with a value for N_J of 9.6 Hz. These values are almost identical (Table 2b) to the corresponding ones observed for $DH(NO_2)$—H, but somewhat displaced upfield from the values observed for $D(NO_2)_2$—H.

In addition to indicating the *p*-bromophenyl and *p*-nitrophenyl groups, the proton nmr spectrum of $DBr(NO_2)$—H also established the presence of the N—H proton and of two nonequivalent *m* protons on the picryl ring. For the latter, the low temperature observation of the AB multiplet with $J = 2.6$ Hz, resolving from the room temperature broad picryl resonances, verifies that a picryl group is indeed present (9). Thus the proton nmr spectrum confirms all the structural components of $DBr(NO_2)$—H.

Analysis of the ^{14}N hyperfine structure in the epr spectrum of $DBr(NO_2)$ was carried out as described in ref. 3 using Gaussian lineshape functions with width $\Delta = 4.97$ G. The resulting coupling parameters, $A(N_2) = 6.70(5)$ G and $A(N_1) = 10.50(5)$ G, are consistent with the similar parameters reported in ref. 3, i.e., with the known *para*-substituent effects of Br and NO_2.

^1H nuclear magnetic resonance assignments

Samples of DH_2—H, DHBr—H, $DH(NO_2)$—H, DBr_2—H, $DBr(NO_2)$—H, and $D(NO_2)_2$—H in dichloromethane-d_2 at room temperature all exhibited a broad peak at $\delta \sim 10$ ppm due to the N—H protons and two very broad peaks ($\delta_a \sim 8.6$ and $\delta_b \sim 9.2$) due to the *meta* protons on the picryl rings. Samples of DH_2—H, DHBr—H, and $DH(NO_2)$—H all showed similar patterns of three multiplets arising from the *o*, *m*, and *p* protons of the phenyl groups. DHBr—H, $DH(NO_2)$—H, DBr_2—H, $DBr(NO_2)$—H, and $D(NO_2)_2$—H all exhibited symmetric pairs of multiplets assignable as A_2X_2 spectra resulting from *para*-substituted phenyl groups. As discussed, $DBr(NO_2)$—H showed two separate symmetric A_2X_2 spectra from its *p*-bromophenyl and its *p*-nitrophenyl groups, respectively. Some 60 MHz ^1H nmr spectra of the above set of compounds were obtained at 250 K. In all cases the picryl proton peaks resolved into an AB spectrum with $J = 2.6 \pm 0.1$ Hz.

^{13}C nuclear magnetic resonance assignments

The ^{13}C nmr spectra taken of the 2,2-diaryl-1-picrylhydrazines dissolved in dichloromethane-d_2 at ca. 300 K could not be uniquely assigned due to the broadness of some lines, the averaging of the *m*-picryl carbons, the averaging of the *o*-picryl carbons, and accidental degeneracies. However, at 248.5 K, using acetone-d_6 and dichloromethane-d_2 as solvents, all carbons of all molecules in the series could be observed. The effect of lowering the temperature can be seen in the ^{13}C nmr spectrum of $DH(NO_2)$—H (Fig. 1).

In order to compare the ^{13}C nmr spectra of the six molecules, it was helpful to utilize a special numbering system (see Fig. 1). The picryl carbons were numbered 1 to 6 by the normal convention. The phenyl, *p*-bromophenyl, and *p*-nitrophenyl groups each show four carbon resonances, consistent with the proton spectra of these molecules and with free rotation about their carbon—hydrazine nitrogen (N-2) bond. The four carbon *types* for each ring have been numbered starting at the carbon attached to the hydrazine unit, followed by the carbons *ortho*, *meta*, and *para* to this unit. Thus the carbons of phenyl groups are numbered 7 to 10, the carbons of *p*-bromophenyl groups are numbered 11 to 14, and the carbons of *p*-nitrophenyl groups are numbered 15 to 18.

In the case of DBr_2—H, ^{13}C nmr spectra were obtained at 5° intervals between 275 K and 315 K, using dichloromethane-d_2 as solvent. At 275 K, the *ortho* carbons of the picryl group are

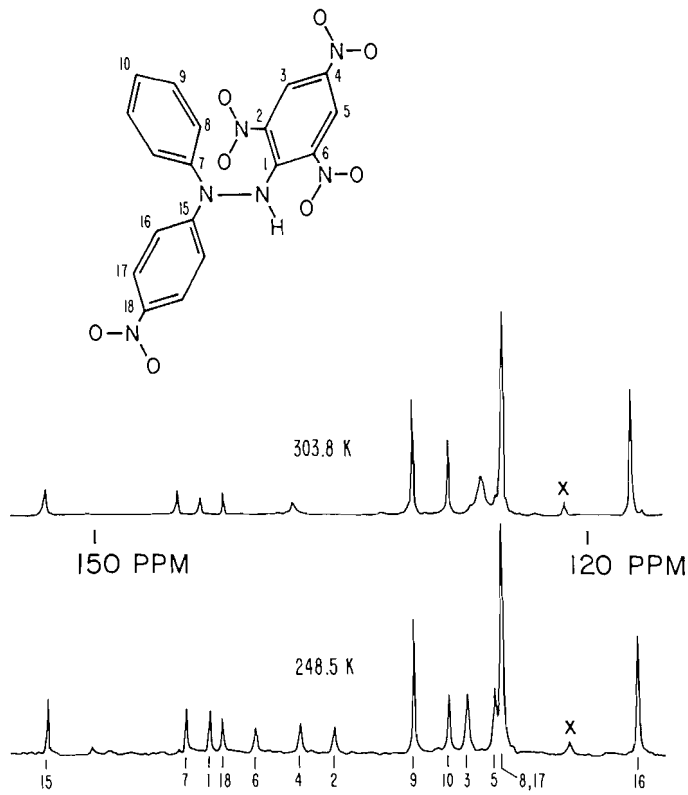

FIG. 1. The ^{13}C nmr spectra of $DH(NO_2)$—H in acetone-d_6, at temperatures 303.8 and 248.5 K. The peak labelled X arises from an impurity.

nonequivalent, as are the *meta* carbons of the picryl group. The collapse of the *meta* carbon resonances to one line and the collapse of the *ortho* carbon resonances to one line could be followed as the temperature was increased. These spectral changes are consistent with the collapse of the *meta* picryl proton resonances of DH_2—H in dichloromethane as the temperature is increased from 213 K to 309 K (9). At low temperatures there is restricted rotation of the picryl ring about the (N-1)—(C-1) bond and the two *ortho* nitro groups are inequivalent (9, 10), causing nonequivalence of the carbon atoms C-2,6 and also of C-3,5. As the temperature is increased the pairs of atoms become effectively equivalent, on our nmr time scale, due to faster rotation.

Specific proton decoupling experiments were carried out by us on the picryl protons in DHBr—H and $D(NO_2)_2$—H. In both cases the *meta* proton with its resonance at higher field was found to be attached to the (*meta*) carbon with its resonance at lower field.

Broad-band decoupled and gated decoupled spectra of all six compounds of our series in acetone-d_6 were obtained, both at ambient temperature and at 248.5 K. The splitting patterns and the coupling constants helped to decide some of the assignments. The assigned chemical shifts for all carbons in the six molecules at 248.5 K are given in Table 3. The assignments of the peaks observed at ambient temperature are given in Table 4.

The chemical shifts of the picryl carbon atoms are insensitive to the *p*-aryl substituents on the remainder of the molecule. The chemical shift for each of the six carbons on the picryl group falls into a narrow range for all six molecules. The assignments of the *ortho* pair (C-2, C-6) and the *meta* pair (C-3, C-5) require some further explanation.

TABLE 5. The splitting patterns and $^{13}C—^{1}H$ coupling constants (in Hz) of the 2,2-diaryl-1-picrylhydrazines*

		$DH_2—H$		DHBr—H		$DH(NO_2)—H$		$DBr_2—H$		$DBr(NO_2)—H$		$D(NO_2)_2—H$	
Carbon	Multiplicity†	^{1}J	^{3}J	^{1}J	^{3}J	^{1}J	^{3}J	^{1}J	^{3}J	^{1}J	^{3}J	^{1}J	^{3}J
3	dd	174.5	5.6	174.5	5.6			173.6	5.6			175.4	5.6
5	dd	174.5	5.6	176.4	5.1	175.5	5.6	175.4	4.6				
8	dm	160.6		161.									
9	dm	161.1		163.4									
10	dm	164.3		~155									
12	dd			164.3	4.6			164.3	5.2	165.0	4.6		
13	dd			167.2	5.6			168.0	5.6	168.6	5.6		
16	dd					167.5	5.1			166.8	5.6	168.0	5.6
17	dd									168.7	4.7	170.8	4.6

*Conditions as given in Table 3.
†Abbreviations: dd, doublet of doublets; dm, doublet of multiplets.

In general, an electron-attracting substituent, such as nitro, on a phenyl ring deshields the substituted carbon, shields the carbon adjacent to the substituted carbon, and deshields the protons on the carbons adjacent to the substituent (11, 12). From a table of substituent effects on phenyl rings (11), it can be seen that the larger the carbon deshielding at the substituted position, the greater the shielding at the carbons adjacent to the substituted position.

It is believed that, because of steric interference of the diphenylamine group, one picryl nitro group *ortho* to the amine linkage is twisted out of the plane of the picryl ring (1, 9). By definition, this is the nitro group on C-2. The hydrazine proton presumably strengthens the asymmetric structure by H-bonding to an oxygen of the nitro group on C-6. The nitro group on C-2 should have less mesomeric interaction with the picryl ring and thus have a smaller electron-withdrawing effect. Thus, one would expect chemical shifts in the order

$$\delta_{C(2)}<\delta_{C(6)},\ \delta_{C(3)}>\delta_{C(5)},\ \delta_{H(3)}<\delta_{H(5)}$$

The assignments were made on this basis. The phenyl groups on N-2 could contribute either shielding or deshielding to the nearest atoms of the picryl ring, depending on the average positions of the phenyl rings. We are unable to evaluate this possibility because of the lack of structural information about the subject molecules. Solvent interactions with the nitro groups are also expected to be appreciable. The nonequivalence of the *meta* hydrogens is observed without the presence of phenyl groups, for example in various N-substituted picrylanilines (9, 13).

Turning now to the chemical shifts of the phenyl carbons, it can be seen from Tables 3 and 4 that a *p*-bromo substituent in one phenyl ring has very little effect on the other phenyl ring, whereas a *p*-nitro substituent on one ring has a substantial effect on the other. In the latter case, the *o*- and *p*-positions in the second ring are deshielded and the position of attachment to the hydrazine moiety is shielded. Only the *m*-position escapes the effect of the nitro substituent in the other ring. These long-range substituent effects imply interaction between the two phenyl groups through the joining nitrogen, probably involving the lone pair of electrons on the nitrogen.

Presumably the *p*-nitrophenyl group withdraws electron density from the remainder of the molecule, in particular from the adjacent phenyl (or *p*-bromophenyl) group, resulting in enhanced shielding of the *p*-nitrophenyl group protons. In the case of $D(NO_2)_2—H$, the two *p*-nitro groups are in opposition to each other, preventing such increased shielding of these protons.

The splitting patterns and coupling constants for the carbons with attached hydrogen atoms are tabulated in Table 5. The "doublet of doublets" splitting pattern is characteristic of carbons 3, 5, 12, 13, 16, and 17, where there is a large one-bond C—H coupling and a small three-bond coupling. The two-bond couplings are too small to be resolved. Peaks of the phenyl group carbons (C-8,9,10) are all proton-split doublets of multiplets which could not be further resolved. The one-bond coupling constants for the *meta* picryl carbons (C-3, C-5) are distinctly large ($^{1}J_{C—H} \sim 175$ Hz). At the other extreme, C-8 and C-9 have one-bond couplings in the range 160.6 to 163.4 Hz. C-12 consistently has $^{1}J_{C—H}$ of about 164.5 Hz. Carbons 13, 16, and 17 have one-bond coupling constants in the range of 166.8 to 170.8 Hz. The three-bond coupling constants included in Table 5 are seen to be insensitive to the structural variations in our molecules.

The coupling constants and splitting patterns were used to distinguish between C-8 and C-12 for DHBr—H, for which the chemical shifts are very similar. In gated decoupled spectra, the carbons (C-7, C-11, C-15) attached to N-2 of the hydrazine moiety all appear as 1:2:1 triplets with comparable splittings (7.5, 8.4, and 8.7 Hz, respectively), due to coupling through three bonds to the *meta* hydrogens. Unexpectedly, C-1 exhibits a 1:3:3:1 quartet with a splitting of ~7 Hz. As there are only two hydrogen atoms on the picryl ring, C-1 must be coupled appreciably with the N—H hydrogen. Nucleus C-14 exhibits a triplet of triplets ($^{3}J_{C—H} \sim 10$ Hz, $^{2}J_{C—H} \sim 3$ Hz). Here the attached bromine atom induces larger C—H coupling constants over two and three bonds.

In summary, the ^{13}C nmr parameters of the 2,2-diaryl-1-hydrazines are now available, and will allow future detailed study of the hindered rotations and other dynamic effects in these molecules.

Acknowledgements

This work was carried out under the auspices of the Natural Sciences and Engineering Research Council of Canada. Our thanks also go to Mrs. A. Booth and Mr. R. Teed for providing mass-spectral and elemental analysis results. We are most grateful to the University of Alberta Chemistry Department for allowing access to its high-field nmr facility.

1. P. F. CURRIE, J. W. QUAIL, and J. A. WEIL. Can. J. Chem. **58**, 723 (1980).
2. J. A. WEIL, K. V. SANE, and J. M. KINKADE JR. J. Phys. Chem. **65**, 710 (1961).

3. M. M. CHEN, K. V. SANE, R. I. WALTER, and J. A. WEIL. J. Phys. Chem. **65**, 713 (1961).
4. J. L. RIEBSOMER. Chem. Rev. **36**, 157 (1945).
5. D. V. NIGHTINGALE. Chem. Rev. **40**, 117 (1948).
6. J. G. HOGGETT, R. B. MOODIE, J. R. PENTON, and K. SCHOFIELD. Nitration and aromatic reactivity. Cambridge University Press. 1971.
7. K. SCHOFIELD. Aromatic nitration. Cambridge University Press. 1980.
8. M. TIE [illegible]. Acc. Chem. Res. **13**, 51 (1980).
9. J. HEIDBERG, J. A. WEIL, G. A. JANUSONIS, and J. K. ANDERSON. J. Chem. Phys. **41**, 1033 (1964).
10. J. A. WEIL, A. BLUM, A. H. HEISS, and J. K. KINNAIRD. J. Chem. Phys. **46**, 3132 (1967).
11. F. W. WEHRLI and T. WIRTHLIN. Interpretation of carbon-13 nmr spectra. Heyden and Son, New York. 1976. p. 47.
12. J. W. EMSLEY, J. FEENEY, and L. H. SUTCLIFFE. High resolution nuclear magnetic resonance spectroscopy. Vol. 1. Pergamon Press, London. 1965. p. 149.
13. J. VON JOUANNE and J. HEIDBERG. Ber. Bunsenges. Phys. Chem. **75**, 261 (1971).

Biosynthesis of antifungal stress metabolites from potato: observation of hydride shifts via the "β-hop" from incorporation of [2-$^2H_3$,2-^{13}C]acetate and ^{13}Cmr[1,2]

ALBERT STOESSL AND J. B. STOTHERS

London Research Centre, Agriculture Canada and the Chemistry Department, University of Western Ontario, London, Ont., Canada N6A 5B7

Received December 21, 1982

ALBERT STOESSL and J. B. STOTHERS. Can. J. Chem. **61**, 1766 (1983).

The proposed migration of hydrogen from C-5 to C-4 in the biosynthesis of the potato phytoalexins lubimin (**2**), rishitin (**5**), and 3-hydroxylubimin (**6**) has been studied by incorporation of [2-$^2H_3$,2-^{13}C]acetate. Direct observation of the predicted β-shift of the C-5 signal produced by ^{2}H at C-4 provided conclusive confirmation of the hydride (deuteride) shift. Results of some [4,4-$^2H_2$]mevalonate incorporation experiments followed by ^{2}Hmr are also described.

ALBERT STOESSL et J. B. STOTHERS. Can. J. Chem. **61**, 1766 (1983).

On a étudié la migration d'hydrogène du carbone en position 5 vers le carbone en position 4 lors de la biosynthèse de la phytoalexine de la pomme de terre la lubimine (**2**), de la rishitine (**5**) et de l'hydroxy-3 lubimine (**6**) en incorporant l'acétate [$^2H_3$-2, ^{13}C-2]. Les observations directes du glissement β du signal du C-5 produit par ^{2}H au niveau C-4 confirment le glissement d'hydrure (deutérure). On décrit également les résultats des expériences d'incorporation du mévalonate [$^2H_2$-4,4] que l'on a suivies en rmn du ^{2}H.

[Traduit par le journal]

Many of the sesquiterpenoid stress compounds produced by members of the *Solanaceae* (1−3) can be regarded as rearranged eudesmanoids, at least in a formal sense (4−6). Although the pathways of their biosynthesis are not always as straightforward as originally envisaged (6), there is now firm experimental evidence for postulated methyl and methylene migrations in several instances (7−10). In addition to these carbon-to-carbon migrations, some rearrangements were postulated to proceed with 1,2-hydride shifts from C-5 to C-4 of the eudesmane skeleton. The reality of such a shift was demonstrated recently for the biosynthesis of capsidiol (**1**) from sweet pepper, through direct observation with ^{2}Hmr of deuterium derived from [4,4-$^2H_2$]mevalonic acid (MVA) at C-4 in **1** (11). Despite the probable common eudesmanoid origins, **1** exhibits structural and biosynthetic features which set it apart from the vetispiranes, such as lubimin (**2**), which are the most frequently encountered stress products of the *Solanaceae*. It was therefore important to verify the proposed hydride shift in the formation of these compounds as well. We wish to describe the results of experiments which establish the existence of such shifts.

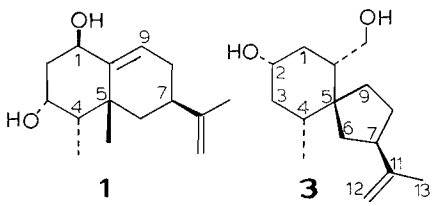

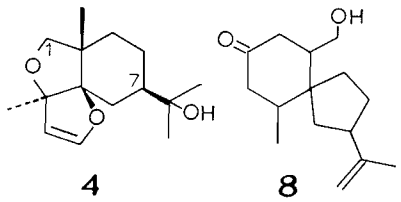

Potato tubers, which produce several compounds of interest in this context, were supplemented with [4,4-$^2H_2$]MVA after inoculation with *Alternaria solani*. This fungus was chosen as stress inducer because it converts much of the lubimin (**2**) which is formed initially into the easily crystallized 15-dihydrolubimin (**3**) (12), thus facilitating purification and, probably, also leading to increased yields. After the usual incubation period, labelled 15-dihydrolubimin (**3**), phytuberol (**4**), and rishitin (**5**) were isolated. These three compounds arise from three different major biosynthetic pathways available to stressed *Solanaceae*. The ^{2}Hmr spectrum of **4**-d_x contained two, approximately equally intense signals at 1.5 and 3.5 ppm, indicating the presence of deuterium at C-7 and -1, respectively. This is completely consistent with our biosynthetic sequence proposed previously (5, 6, 9), according to which deuterium from the third MVA unit is lost from C-5 of a hypothetical eudesmanoid intermediate.

For **3**, the ^{2}Hmr spectrum had two absorption bands in the ratio of ca. 2:1. This is consistent with incorporation of one deuterium from each of the three MVA units involved in the biosynthesis, with two nearly equivalent ^{2}H nuclei giving rise to the more intense band near 1.35 ppm. This is the region in which the 4- and axial 1-protons are known to absorb, while the second band, 2.25 ppm, coincides with the shielding expected for deuterium on C-7. These results, therefore, are compatible with the sequence outlined in Scheme 1, including a 5,4-hydride shift, but cannot confirm its validity.

In the case of **5**, the ^{2}Hmr spectrum consisted of a single broad absorption centred at 2.1 ppm showing the presence of deuterium at any or all of the three expected positions, C-1, -4, and -7. A comparison of the relative intensity of this band with respect to the natural abundance signal for the solvent ($CHCl_3$), the weight of which was accurately known, indicated an incorporation level of ca. 3%. This was comparable to the observed level for **3**, obtained in the same manner. Thus, these results appear to favor the presence of three different deuterium atoms but, as for **3**, do not confirm it. Clearly, a new approach was required.

Substitution of a proton by deuterium at a given carbon atom produces a small but readily detectable shift for the resonance signal of an immediately neighboring ^{13}C nucleus. This two-

[1]Part 104 of ^{13}Cmr studies; for Part 103 see ref. 19; for Part 102 see ref. 20; for Part 101 see ref. 21; for Part 100 see ref. 22.

[2]Part 44 of the series "Postinfectional inhibitors from plants"; for Part 43 see ref. 23; for Part 42 see ref. 15.

Can. J. Chem. Downloaded from www.nrcresearchpress.com by 210.87.254.6 on 09/06/12
For personal use only.

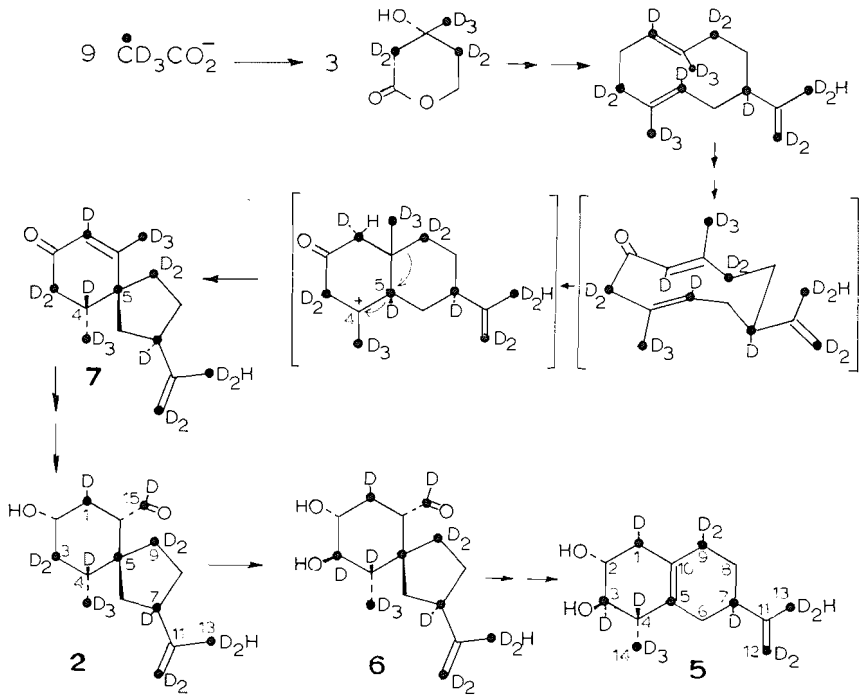

SCHEME 1

bond, isotope effect may be termed a β-shift and, for saturated systems, is ca. 0.1 ppm (13). With high ^2H incorporation, these effects are easily observed but with low ^2H incorporation the shifts may not be observable unless ^2H and β-^{13}C substitution occur simultaneously with significant probability. In practice, for biosynthetic experiments, this condition will be met only if both ^2H and ^{13}C atoms are incorporated from the same precursor molecule, for example by the intact incorporation of $^2H_3{}^{12}C\cdot{}^{13}CO_2H$ (14). It occurred to us that the condition will also be met if a "—$^2H^{13}C$—" unit is incorporated with subsequent migration of the ^2H nucleus to a contiguous carbon atom. For example, with $^2H_3{}^{13}C\cdot CO_2H$ as the precursor, migration of the deuterium either to C-1 of the same acetate residue or to another carbon which becomes attached to C-2 of this unit, will satisfy the requirement for ready detection of the β-shift. We have proposed the term "β-hop"[3] for this technique (15).

For the purpose of the present study, sodium [2-$^2H_3$,2-^{13}C]-acetate was applied to potato tubers, inoculated with *Monilinia fructicola*.[4] After the usual incubation period, lubimin (**2**) hydroxylubimin (**6**), and rishitin (**5**) were isolated and each was found to exhibit the expected β-shift for C-5 in the ^{13}Cmr spectrum. This is illustrated for **5** in Fig. 1; this spectrum contains fourteen prominent singlets whose shieldings (see Table 1) agree precisely with those previously reported for **5** (9). One at δ_C 129.0, arising from C-5, is accompanied by a singlet of comparable intensity at slightly (0.045 ppm) higher field as shown in the inset. The latter is the isotope-shifted component produced by the presence of deuterium at C-4, the deuterium having been originally bonded to C-5 at an earlier stage in the biosynthetic sequence. It is readily apparent that the intensity of the absorption at δ_C 129 is much greater than that for either of the signals at δ_C 124.9 and 148.9 (C-10 and -11, respectively) although each of the three is due to non-protonated carbons; this establishes that C-5 is ^{13}C-enriched. The singlets for C-2, -4, -6, and -8 exhibited integrated intensities significantly smaller than those for the seven remaining protonated carbons, revealing the seven additional sites of ^{13}C incorporation. In addition, these more intense singlets are each accompanied by absorption produced by the presence of directly bonded deuterium. One-bond isotope shifts are generally in the range, 0.3−0.6 ppm, towards higher field, and since $J_{CD} \sim 20$ Hz for saturated carbon, the presence of one directly bonded deuterium atom gives rise to a triplet ^{13}C pattern as is discernible for C-1, -3, and -7. More complex ^2H-coupled patterns appear with the signals for C-9, -12, -13, and -14. The methyl carbons, of course, may have from 0−3 deuterium atoms directly bonded and the absorptions for —CH_3, —CH_2D, and —CHD_2 were observable for C-13 as shown in Fig. 2. The triplet and quintet patterns for the mono- and dideuteriated carbons, respectively, are indicated in Fig. 2a and were confirmed by recording the INEPT spectrum (16) in which the phase of the CH_3 and —CHD_2 signals is opposite that for the CH_2D absorption (see Fig. 2b). In any event, the spectrum readily reveals the sites of ^{13}C and ^2H incorporation and establishes the existence of a hydride (deuteride) shift from C-5 to C-4 in the biosynthetic sequence.

Analogous results were obtained for **2** and **6**. In their ^{13}C spectra, the signal for C-5 at δ_C 46.9 and 48.3, respectively, was accompanied by a singlet of comparable intensity at higher field; in each case the isotope shift was found to be 0.085 ppm. To confirm the result for **2**, the sample was reduced to crystalline **3** with borohydride and the ^{13}C spectrum of the product exhibited a closely spaced pair of singlets for C-5 at δ_C 46.7 with an isotope shift of 0.080 ppm. The spectra for **2**, **3**, and **6** contained signals for eight carbons having somewhat enhanced singlets together with the characteristic ^2H-coupled patterns. Thus, the $^{13}C/^2H$ labelled centres were readily identified.

As may be seen in Fig. 1 for **5**, there is variation in the relative intensity of the ^2H-coupled patterns and their accom-

[3]We thank Phyllis Stoessl for suggesting this term.

[4]This fungus was used as inducer in the only partially fulfilled expectation that it would favor rishitin formation.

Can. J. Chem. Downloaded from www.nrcresearchpress.com by 210.87.254.6 on 09/06/12
For personal use only.

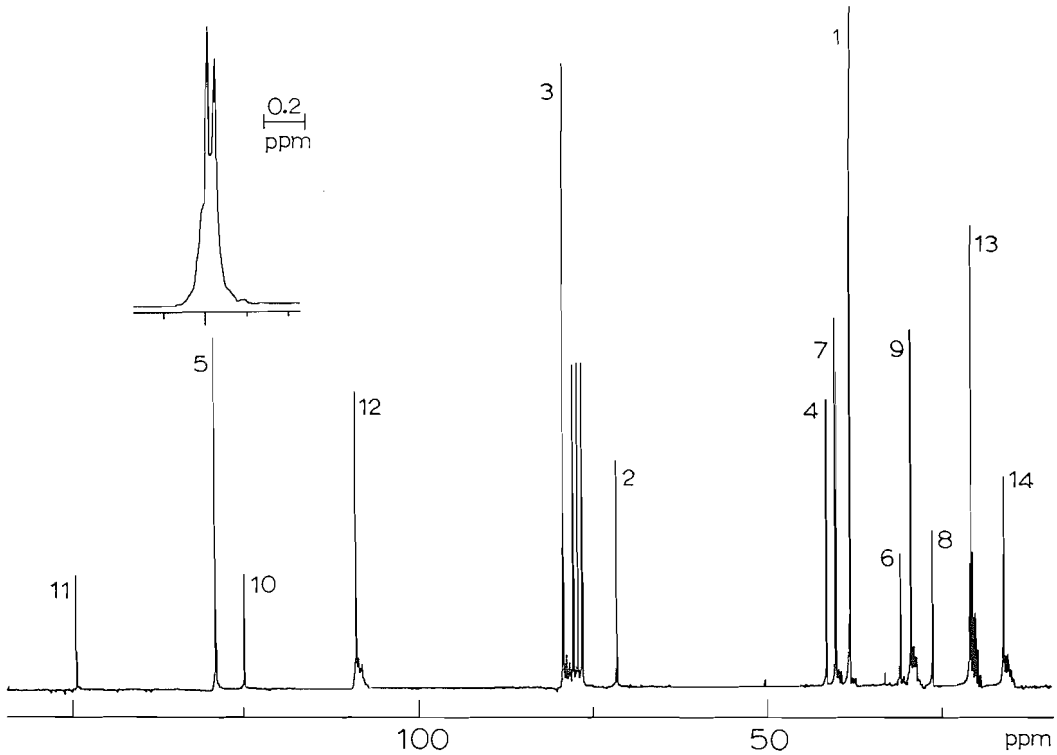

FIG. 1. The ^{13}Cmr spectrum of rishitin-$^{2}H_n$,$^{13}C_n$ (**5**) from incorporation experiments with [2-$^{2}H_3$-2-^{13}C]acetate. Inset is an expansion of the C-5 absorption showing the isotope shift produced by deuterium on C-4 (see text).

TABLE 1. ^{13}C shieldings[a] for **2**, **3**, **5**, and **6**

Compound	C-1	C-2	C-3	C-4	C-5	C-6	C-7	C-8	C-9	C-10	C-11	C-12	C-13	C-14	C-15
2	33.3	69.3	40.3	41.0	46.9	41.8	47.4	32.6	25.9	58.4	147.3	108.8	21.2	16.4	205.0
3	36.7	69.9	40.8	41.2	46.7	40.6	47.4	32.7	25.4	48.5	148.1	108.2	21.5	16.7	64.1
5	38.4	71.5	79.2	41.7	129.1	31.2	40.5	26.6	29.7	124.9	148.9	109.0	21.1	16.5	
6	30.5	74.1	76.8	47.1	48.3	42.2	47.3	32.7	26.8	57.6	147.0	109.0	21.2	11.2	204.3

[a]Data obtained for $CDCl_3$ solutions in ppm from internal TMS.

panying singlets for the various labelled centres other than the methyl carbons. For example, the singlets for C-1 and -3 in **5** (Fig. 1) are significantly enhanced; this is indicative of some deuterium loss during the biosynthesis. Similar behavior was found in the spectra of **2**, **3**, and **6** for each of which the most intense signal appeared near 33 ppm. In earlier work (9), this signal had been assigned to C-6 while a signal near 42 ppm was attributed to C-1. The present results require that these assignments be reversed; the revised shieldings are listed in Table 1.

The labelling patterns which have been identified as discussed above for **2**, **3**, **5**, and **6** are consistent with the incorporation of $^{2}H_3{}^{13}CCOO^{-}Na^{+}$ as outlined in Scheme 1. This sequence incorporates the recent results of Murai and coworkers (10) which demonstrated that solavetivone (**7**) is an intermediate in the sequential biosynthesis of **2**, **6**, and **5**, while our earlier proposals (5, 6, 9) suggested possible separate pathways to **2**, **5**, and **7**. The intervention of **7** and related intermediates, either before or after its generation,[5] provides an opportunity for hydrogen exchange at C-1 and -3 which could account for somewhat lower levels of deuterium at these centres and the apparent enhancement of the C-1 signal in **2**, **5**, and **6** noted above. The C-3 signal for **2** was not significantly enhanced relative to the remaining enriched centres, presumably because this carbon can be dideuterated in the initial farnesyl pyrophosphate precursor while C-1 is monodeuterated. Qualitatively, the deuterium content at C-1 is similar in **2**, **5**, and **6**, which implies that this centre is not involved in the **6** → **5** rearrangement. It must be emphasized that, in fact, a number of differently labelled MVA species will be involved because the labelled acetate precursor undoubtedly undergoes $^{1}H/^{2}H$ exchange in the acetate pool. In addition, one can expect that kinetic isotope effects may tend to disfavor incorporation of the more heavily deuterated species into MVA. As a consequence, some deuterium loss can be anticipated to occur during the sequence. Nevertheless in each case the absorption for C-5 was a pair of closely spaced singlets, one coinciding precisely with the signal found for natural abundance material and the second at slightly higher field, 0.05−0.09 ppm, clearly establishing the presence of deuterium at the neighboring C-4 centre. Deuterium originally bonded to C-5 has, therefore, migrated via a 1,2-hydride (deuteride) shift. This intramolecular migration, or "β-hop", is clearly revealed by these incorporation results.

This "β-hop" technique should prove useful as a general and unambiguous method for the detection of 1,2-hydride mi-

[5]It has been suggested, but not confirmed, that an isolubimin (**8**) is an intermediate between **7** and **2** (17).

Can. J. Chem. Downloaded from www.nrcresearchpress.com by 210.87.254.6 on 09/06/12
For personal use only.

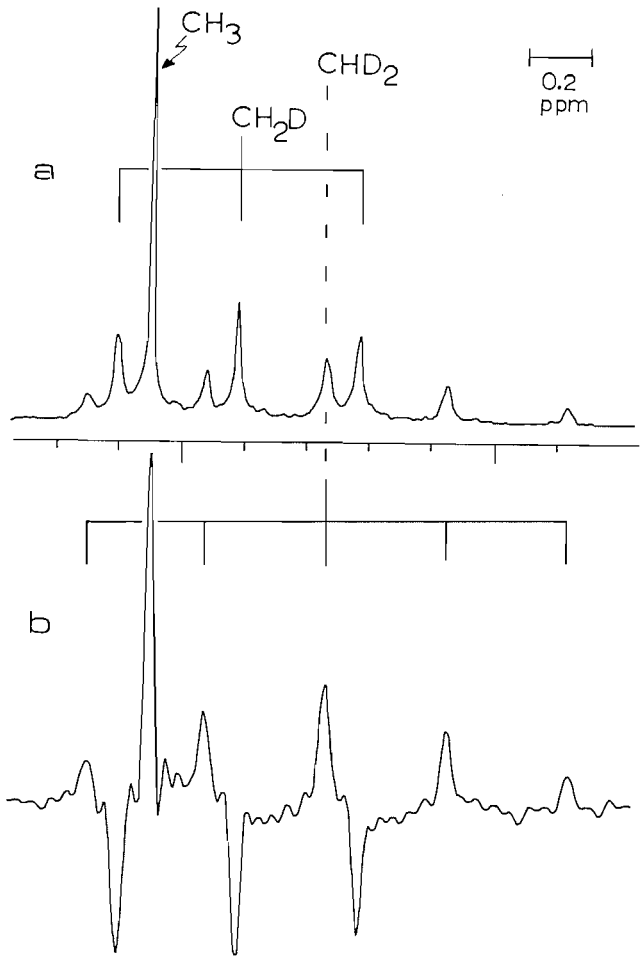

FIG. 2. The ^{13}Cmr absorption for C-13 (δ_C 21.1) in rishitin-$^2H_1$,$^{13}C_1$: (a) normal ^{1}H-decoupled spectrum, (b) the INEPT spectrum.

grations both in biosynthetic and mechanistic studies. Its applicability is by no means restricted to the incorporation of acetate; migration of deuterium from any —^{2}H^{13}C— unit to a contiguous carbon will give rise to the β-shift.

Experimental

General laboratory procedures were those described in earlier reports (9, 11, 12). The nmr spectra were obtained using a Varian XL-200 spectrometer operating at 30.7 (^{2}H) and 50.3 MHz (^{13}C) in the Fourier transform mode with 5 mm sample tubes containing 0.5 mL of solution in the solvents indicated.

Incorporation of [4,4-$^2H_2$]MVA into potato metabolites

Potatoes (25 kg; *cv.* Kennebec, aged 4 months at 4°C after harvest) were inoculated with a mycelial suspension (1.9 L) of *Alternaria solani* ATCC 44204 as described previously (9), incubated in the dark at room temperature for 24 h, and then treated with a solution (248 mL) containing (±)-[4,4-$^2H_2$]MVA (332 mg) available from an earlier study (11). After another 24 h, diffusates and loose necrotic tissue were collected and extracted with Et_2O (3 × half volume). Chromatography of the evaporated extract (330 mg) over SiO_2 (Camag DF5; 300 g) in MeOH/$CHCl_3$ (5:95 and 1:9) yielded the following compounds, identified by tlc behavior and nmr spectra.

Phytuberol (**4**), 3.9 mg after chromatography in Et_2O; ^{2}Hmr (C_6H_6): 1.5, 3.5 ppm.

Rishitin (**5**), 61 mg, before rechromatography in *i*-PrOH/EtOAc (5:95); ^{2}Hmr ($CHCl_3$): 2.15 ppm; ^{13}Cmr ($CDCl_3$): see Table 1.

15-Dihydrolubimin (**3**), 38.7 mg crude, 20.0 mg after recrystallization from Et_2O, mp 127–129°C; ^{2}Hmr ($CHCl_3$): 1.35; 2.25 ppm; ^{13}Cmr ($CDCl_3$): see Table 1.

Incorporation of [2-$^2H_3$,2-$^{13}C_1$]acetate into potato metabolites

In a similar experiment, potatoes (20 kg; *cv.* Sebago, stored at 4°C for 3 months after purchase in local market ca. 4 months after harvest) were inoculated with a spore suspension of *Monilinia fructicola* (2×10^5 spores/mL; ca. 800 mL), sodium [2-$^2H_3$-2-$^{13}C_1$]acetate (Merck Sharp & Dohme, Montreal, 98 at.% ^{2}H, 90 at.% ^{13}C-2; 413.5 mg (4.81 mmol) in H_2O (960 mL)) being added after 1 day. Incubation for a further day, extraction, and chromatography as before gave the following products.

Lubimin (**2**), 3.9 mg after rechromatography in MeOH/Et_2O (5:95); after determination of the ^{13}Cmr spectrum (see Table 1) this slightly impure sample was reduced with sodium borohydride (18) to the dihydro derivative **3**, mp 123–127°C, 1.3 mg after recrystallization from CCl_4; ^{13}Cmr ($CDCl_3$): see Table 1.

Rishitin (**5**), 20.6 mg after rechromatography in MeOH/Et_2O (5:95); ^{13}Cmr ($CDCl_3$): see Table 1.

3-Hydroxylubimin (**6**), 5.9 mg after rechromatography in *i*-PrOH/EtOAc 5:95. This product could not be crystallized but appeared chromatographically and spectroscopically pure; ^{13}Cmr ($CDCl_3$): see Table 1.

Acknowledgements

We wish to thank the Natural Sciences and Engineering Research Council of Canada for financial support.

1. T. MASAMUNE, A. MURAI, and N. KATSUI. Kagaku to Seibutsu **16**, 648 (1978).
2. J. KUĆ. *In* Phytoalexins. *Edited by* J. A. Bailey and J. W. Mansfield. Blackie and Sons, Glasgow. 1982. pp. 81–105.
3. A. STOESSL, J. B. STOTHERS, and E. W. B. WARD. Phytochemistry, **15**, 885 (1976).
4. A. STOESSL, E. W. B. WARD, and J. B. STOTHERS. *In* Host plant resistance to pests. ACS Symposium Series, No. 62. *Edited by* P. A. Hedin. American Chemical Society, Washington, DC. 1977. pp. 61–77.
5. J. B. STOTHERS. Pure Appl. Chem. **53**, 1241 (1981).
6. A. STOESSL. *In* Phytoalexins. *Edited by* J. A. Bailey and J. W. Mansfield. Blackie and Sons, Glasgow. 1982. pp. 133–180.
7. F. C. BAKER and C. J. W. BROOKS. Phytochemistry, **15**, 689 (1976).
8. G. I. BIRNBAUM, C. P. HUBER, M. L. POST, J. B. STOTHERS, J. R. ROBINSON, A. STOESSL, and E. W. B. WARD. J. Chem. Soc. Chem. Commun. 330 (1976).
9. A. STOESSL, J. B. STOTHERS, and E. W. B. WARD. Can. J. Chem. **56**, 645 (1978).
10. A. MURAI, S. SATO, A. OSADA, N. KATSUI, and T. MASAMUNE. J. Chem. Soc. Chem. Commun. 32 (1982).
11. Y. HOYANO, A. STOESSL, and J. B. STOTHERS. Can. J. Chem. **58**, 1894 (1980).
12. A. STOESSL. Physiol. Plant Pathol. **20**, 263 (1982).
13. J. L. JURLINA and J. B. STOTHERS. J. Am. Chem. Soc. **104**, 4677 (1982), and references cited therein.
14. C. ABELL and J. STAUNTON. J. Chem. Soc. Chem. Commun. 856 (1981).
15. A. STOESSL and J. B. STOTHERS. J. Chem. Soc. Chem. Commun. 880 (1982).
16. G. A. MORRIS and R. FREEMAN. J. Am. Chem. Soc. **101**, 760 (1979).
17. E. B. KALAN and S. F. OSMAN. Phytochemistry, **15**, 775 (1976).
18. A. STOESSL, J. B. STOTHERS, and E. W. B. WARD. Can. J. Chem. **53**, 3351 (1975).
19. B. A. DAWSON, J. L. JURLINA, A. K. GHOSH, and J. B. STOTHERS. J. Chem. Soc. Chem. Commun. 204 (1983).
20. B. A. DAWSON and J. B. STOTHERS. Org. Magn. Reson. **21**, 217 (1983).

Can. J. Chem. Downloaded from www.nrcresearchpress.com by 210.87.254.6 on 09/06/12
For personal use only.

21. M. J. McGARRITY, J. F. KING, and J. B. STOTHERS. Tetrahedron Lett. **23**, 4465 (1982).
22. A. STOESSL, C. H. UNWIN, and J. B. STOTHERS. Can. J. Chem. **61**, 372 (1983).
23. A. DOUX-GAYAT, G. DÉFAGO, H. KERN, A. STOESSL, and J. B. STOTHERS. J. Chem. Soc. Chem. Commun. 157 (1983).

Can. J. Chem. Downloaded from www.nrcresearchpress.com by 210.87.254.6 on 09/06/12
For personal use only.

Comparative nitrosation of etintidine and cimetidine

THOMAS A. MONTZKA,[1] PETER F. JUBY, JOHN D. MATISKELLA, HENRY M. HOLAVA, AND R. R. CRENSHAW

Pharmaceutical Research and Development Division, Bristol-Myers Company, Syracuse, NY 13221–4755, U.S.A.

Received December 16, 1982

THOMAS A. MONTZKA, PETER F. JUBY, JOHN D. MATISKELLA, HENRY M. HOLAVA, and R. R. CRENSHAW. Can. J. Chem. **61**, 1771 (1983).

Etintidine (**4**), a new histamine H_2-receptor antagonist, was compared with cimetidine (**1**) for susceptibility to in vitro nitrosation at pH 1 and pH 3. Each agent formed two mono-*N*-nitrosoguanidine derivatives: *N*-cyano-*N'*-{2-[(5-methyl-1*H*-imidazol-4-yl)methylthio]ethyl}-*N''*-nitroso-*N''*-(2-propynyl)guanidine (**5**) and *N*-cyano-*N'*-{2-[(5-methyl-1*H*-imidazol-4-yl)methylthio]ethyl}-*N'*-nitroso-*N''*-(2-propynyl)guanidine (**6**) from etintidine and *N*-cyano-*N'*-methyl-*N''*-{2-[(5-methyl-1*H*-imidazol-4-yl)methylthio]ethyl}-*N'*-nitrosoguanidine (**2**) and *N*-cyano-*N'*-methyl-*N''*-{2-[(5-methyl-1*H*-imidazol-4-yl)methylthio]ethyl}-*N''*-nitrosoguanidine (**11**) from cimetidine. The *N*-nitroso derivative **5** from etintidine cyclized to 2-cyanoimino-3-{2-[(5-methyl-1*H*-imidazol-4-yl)methylthio]ethyl}-4-methylene-1-nitroso-imidazoline (**7**) at neutral or basic pH's. Both agents were nitrosated less at pH 3 than at pH 1, and at both pH's nitrosation of etintidine was considerably less than that of cimetidine. At pH 1, with a nitrite concentration about 150–500 times that expected in fasting human gastric juice, formation of **5** and **6** from etintidine was barely detectable (each <0.5%). Comments are made on the standard WHO conditions for investigating nitrosation of drugs.

THOMAS A. MONTZKA, PETER F. JUBY, JOHN D. MATISKELLA, HENRY M. HOLAVA et R. R. CRENSHAW. Can. J. Chem. **61**, 1771 (1983).

On compare l'étintidine (**4**), un nouvel antagoniste récepteur de H_2 de l'histamine, avec la cimétidine (**1**) du point de vue de la sensibilité à la nitrosation in vitro à des pH de 1 et de 3. Chaque agent donne deux dérivés de mono-*N*-nitrosoguanidine: la *N*-cyano-*N'*{[(méthyl-5 imidazol 1*H*-yl-4)méthylthio]-2 éthyl}-*N''*-nitroso-*N''* (propynyl-2) guanidine (**5**) et la *N*-cyano-*N'*{[(méthyl-5 imidazol 1*H*-yl-4)méthylthio]-2 éthyl}-*N'*-nitroso-*N''* (propynyl-2) guanidine (**6**) à partir de l'étintidine et la *N*-cyano-*N'*-méthyl-*N''* {[(méthyl-5 imidazol 1*H*-yl-4)méthylthio]-2 éthyl}-*N'*-nitrosoguanidine (**2**) et la *N*-cyano-*N'*-méthyl-*N''*{[(méthyl-5 imidazol 1*H*-yl-4)méthylthio]-2 éthyl}-*N''*-nitrosoguanidine (**11**) à partir de la cimétidine. Les dérivés nitroso **5** provenant de l'étintidine se cyclisent en cyanoimino-2{[(méthyl-5 imidazol 1*H*-yl-4)méthylthio]-2 éthyl}-3 méthylène-4 nitroso-1 imidazoline (**7**) à pH neutre ou basique. La nitrosation des deux agents est plus faible à un pH de 3 qu'à un pH de 1 et aux deux pH la nitrosation de l'étintidine est beaucoup plus faible que celle de la cimétidine. On décèle rarement la formation des produits **5** et **6** (chacun <0,5%) à partir de l'étintidine pH de 1 et pour une concentration en nitrite d'environ 150 à 500 fois plus grande que celle du suc gastrique humain à jeûn. On formule des commentaires sur les conditions normales WHO d'étude de la nitrosation des médicaments.

[Traduit par le journal]

Can. J. Chem. Downloaded from www.nrcresearchpress.com by 210.87.254.105 on 09/06/12
For personal use only.

The question has arisen as to whether long-term treatment of disorders of the esophagus, stomach, and duodenum with cimetidine (**1**) might lead to the eventual development of gastric cancer (1). At the root of this concern are a number of factors which include the susceptibility of cimetidine to *N*-nitrosation in vitro (2, 3), the mutagenicity of *N*-nitrosocimetidine (4), the carcinogenic properties of many *N*-nitroso compounds in animals (5), the structural similarities between *N*-nitrosocimetidine (**2**) and the known animal carcinogen *N*-methyl-*N'*-nitro-*N*-nitrosoguanidine (MNNG, **3**) (1, 2), the presence of nitrosating species in the stomach (6), and the possibility for levels of nitrosating species and total extractable gastric *N*-nitroso compounds to rise under conditions of lowered gastric acidity (7, 8). Speculation continues in spite of the findings that long-term studies of cimetidine in rats and dogs have revealed no signs of carcinogenesis (9), in vivo formation of *N*-nitrosocimetidine has not been reported, and there is no direct evidence to associate the development of cancer in man with exposure to *N*-nitroso compounds (6).

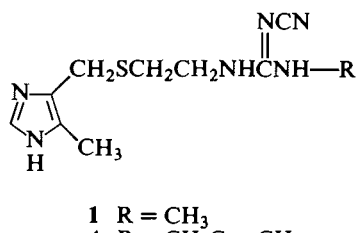

1 R = CH_3
4 R = $CH_2C{\equiv}CH$

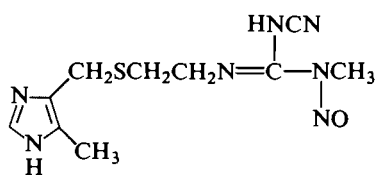

2

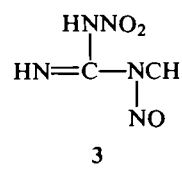

3

A new histamine H_2-receptor antagonist etintidine (BL-5641, **4**), with a potency approximately twice that of cimetidine, was recently reported from these laboratories (10). Because of the structural similarity between cimetidine (**1**) and etintidine (**4**), and because of a regulatory concern in the nitrosation issue, we have compared etintidine with cimetidine for their susceptibilities to *N*-nitrosation in vitro. This paper describes the results and our conclusions from this study.

Chemistry

The nitrosation of etintidine with excess sodium nitrite (4–10 equivalents) in 2 *N* hydrochloric acid gave three products (**5**, **6**, **7**) after neutralization and extraction as outlined in Scheme 1. The three products were separated and purified by

[1]Author to whom inquiries may be addressed.

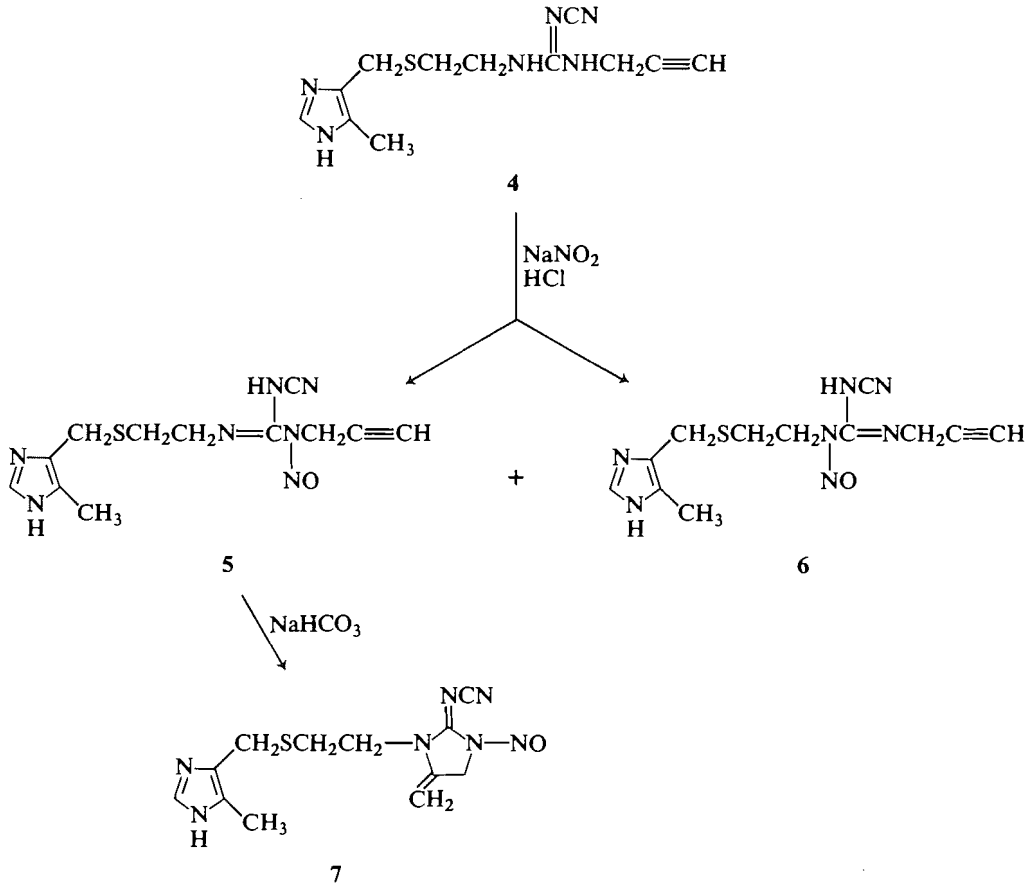

SCHEME 1. Nitrosation of etintidine

semipreparative hplc. The N^b-nitroso[2] compound **5** could not be obtained free from the imidazoline **7** except in acidic solution owing to its facile cyclization to **7** at neutral or basic pH.

The structural assignment for **6** is supported by elemental analysis, weak maxima in the 380–420 nm region of the uv spectrum (N—NO, $n \rightarrow \pi^*$) (11, 12), and consistent ^1H and ^{13}C nmr spectral data. In the ^1H nmr spectrum (see Table 1), the chemical shifts of the protons of both methylene groups adjacent to the guanidine nitrogens are shifted downfield compared to etintidine, with the methylene protons next to the N^a-NO (CH_2^a in Table 1) shifting further (0.73 ppm) than the propynyl methylene protons (CH_2^b in Table 1) (0.41 ppm). The propynyl methylene protons show as a sharp doublet resulting from coupling to the acetylenic hydrogen. No evidence of coupling to an N—H is seen, therefore we have assigned the tautomer as indicated by **6**. In the case of etintidine, both the CH_2^a and CH_2^b methylenes are coupled to adjacent NH's supporting the tautomer designated in **4**.

[2]For consistency and ease of specifying related products, we have labeled the nitrogens N, N^a, N^b as indicated below:

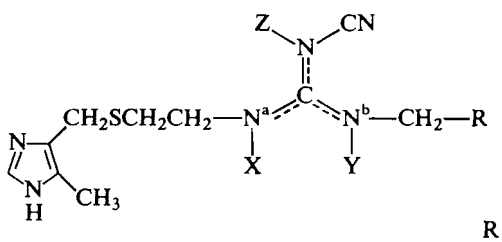

R = H, —C≡CH
X,Y,Z, see Table 1

TABLE 1. ^1H nmr chemical shifts

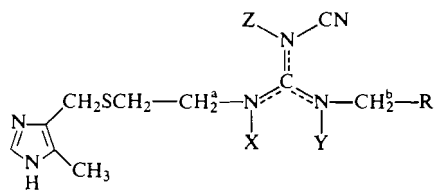

	R	X	Y	Z	^1H nmr chemical shifts[a] CH_2^a	CH_2^b
4 (Etintidine)	C≡CH	H	H	—	3.36	4.00
5	C≡CH	—	NO	H	3.84	4.65
6	C≡CH	NO	—	H	4.09	4.41
1 (Cimetidine)	H	H	H	—	3.32	2.76
2	H	—	NO	H	3.72	3.25
11	H	NO	—	H	3.99	3.17

[a]The nmr spectra were run in DMSO-d_6. Chemical shifts are recorded in ppm relative to Me_4Si.

The structural assignment of **7** is based on ^1H nmr data (discussed below), elemental analysis, and ^{13}C nmr and uv spectra. The structure of **5** is supported by ^1H nmr data (see below) on a mixture of **5** and **7**, and by the ease of conversion of **5** to **7**. The ^1H nmr (360 MHz) spectrum of **7** in DMSO-d_6 shows the absence of the acetylenic proton (3.3–3.5 ppm region) and the presence of two exocylic olefinic protons at 4.82 ppm (1H) and 4.56 ppm (1H). On scale expansion these

Can. J. Chem. Downloaded from www.nrcresearchpress.com by 210.87.254.105 on 09/06/12
For personal use only.

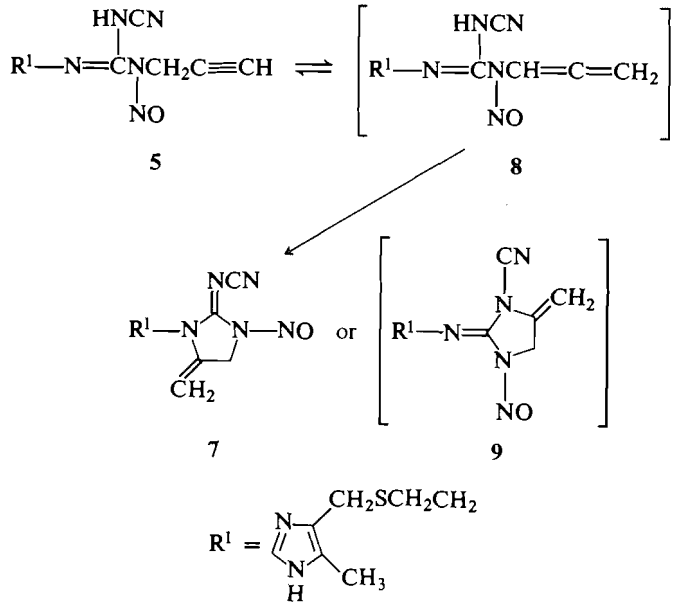

SCHEME 2

appear as narrow multiplets with small couplings to each other and very small long-range coupling to the endocyclic methylene protons. The endocyclic methylene protons appear as a singlet at 4.54 ppm (2H) which on scale expansion show as a very narrow multiplet due to long-range coupling to the olefinic protons. In the ^{1}H nmr spectrum of the mixture of **5** and **7**, the protons of both methylene groups adjacent to the guanidine group in **5** are shifted downfield compared to etintidine (see Table 1) with the methylene protons next to the N^b-NO (CH_2^b in Table 1) shifting further (0.65 ppm) than the methylene protons on the N^a-nitrogen (0.48 ppm).

The cyclization of **5** to **7** was demonstrated by hplc isolation and spiking experiments. A pure fraction of **5** in solution was obtained from reverse phase hplc using an acetonitrile–water–phosphate buffered (pH 4.0) mobile phase. In this solution (pH 4) no evidence of cyclization of **5** to **7** was observed (up to 1.5 hours). When this solution was treated with sodium bicarbonate, the conversion of **5** to **7** was complete in less than one hour. This cyclization may occur via the allene **8** (Scheme 2) (13). The nitrosation of the N^b-guanidine nitrogen activates the propynyl methylene protons so that under neutral or basic conditions the reversible isomerization of **5** to **8** occurs. Cyclization of **8** to **7** follows. Although we have indicated the cyclization to have occurred on the N^a-nitrogen (**7**), our data do not rule out the possibility of cyclization on the N—CN nitrogen to give **9**. We have not observed an analogous cyclization of either etintidine or **6**.

Previously, only one mono-*N*-nitrosated product of cimetidine, an N^b-nitroso derivative, appears to have been isolated and characterized (2, 3). This was indicated to have the tautomeric structure **10** (2). Because the nitrosation of etintidine

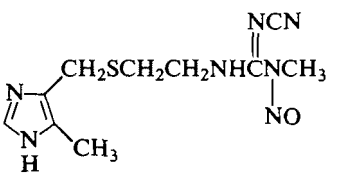

10

gave two mono-*N*-nitroso derivatives, we reexamined the nitrosation of cimetidine.

When cimetidine was nitrosated under similar conditions used for etintidine, two mono-*N*-nitroso products were isolated as indicated in Scheme 3. These products **2** and **11** were isolated in approximately 7:1 ratio with the major product apparently the same as the previously described N^b-nitrosated compound **10** (2). Compound **10** has been shown to be a methylating agent, as would be expected if nitrosation had occurred on the N^b-nitrogen (2). The ^{1}H nmr spectra of both **2** and **11** show a downfield shift for the protons of the methyl and methylene groups attached to the cyanoguanidine nitrogens compared to cimetidine (see Table 1). In the case of the N^b-nitroso compound **2**, the methyl protons are shifted further (0.49 ppm) than the N^a-methylene protons (CH_2^a in Table 1) (0.40 ppm), and in the N^a-nitroso compound **11** the methylene protons (CH_2^a in Table 1) are shifted further (0.67 ppm) than the methyl protons (0.41 ppm) relative to cimetidine. Again, our tautomeric assignments are based on ^{1}H nmr. In **2** the CH_2^a is a sharp triplet not coupled to an NH and in **11** the N^b-methyl is a singlet. In the ^{1}H nmr of cimetidine, both the CH_2^a and the N^b-CH_3 are coupled to NH's, which is consistent with the tautomeric structure indicated by **1**.

We have not seen any evidence of a dinitrosated product, although recently a dinitrosated product has been reported when approximately 25 equivalents of $NaNO_2$ were used (14).

Comparative nitrosation of cimetidine and etintidine

It has been reported (3) that cimetidine was nitrosated <0.5% at pH 4 and 6% at pH 3 under the experimental conditions recommended (15) by a WHO study group for comparing nitrosatable drugs (10 mmol/L compound; 40 mmol $NaNO_2$; pH 3–4; 37°C; one and 4 hour reaction times). When the nitrosation was carried out at pH 1, 39–43% nitrosation occurred (3).

Our initial comparative nitrosation experiments were done in open reaction vessels at pH 1 using WHO recommended concentrations and temperature. The products were analyzed by hplc using a variable wavelength detector set at 220 nm (see Table 2). We found cimetidine was nitrosated rapidly, with peak nitrosation occurring in less than one hour (38% at 1/2 hour). Analysis of the reaction at 4 hours showed a significant loss of the nitrosated cimetidines (4% compared to 38% at 1/2 hour) and a corresponding increase in cimetidine (96% compared to 62% at 1/2 hour). Apparently the nitrosation of cimetidine is a reversible reaction, reversal occurring as nitrosation species are lost to the atmosphere from an open vessel (16). Consequently all subsequent comparative nitrosations were carried out in closed vials.

The nitrosation of cimetidine and etintidine was compared in closed vials, first using WHO recommended concentrations (10 mmol/L drug, 40 mmol/L $NaNO_2$), temperature, and time intervals at both pH 1 and pH 3. The results are summarized in Tables 3 and 4.

At pH 1 cimetidine was nitrosated 51–54% (Table 3) to give both N-nitrosated products **2** and **11** with the N^b-nitroso compound **2** predominant by a factor of 12 at one hour and 6 after 4 hours. Etintidine at pH 1 was nitrosated 6–13% (Table 3) to give both **5** and **6**. About equal amounts of **5** and **6** were present after 4 hours. None of the cyclic material **7** was observed at this pH. The major difference was the amount of the N^b-nitrosoetintidine **5** formed (4–8%) as opposed to the amount of N^b-nitrosocimetidine **2** formed (45–48%). The N^a-nitrosated

Can. J. Chem. Downloaded from www.nrcresearchpress.com by 210.87.254.105 on 09/06/12
For personal use only.

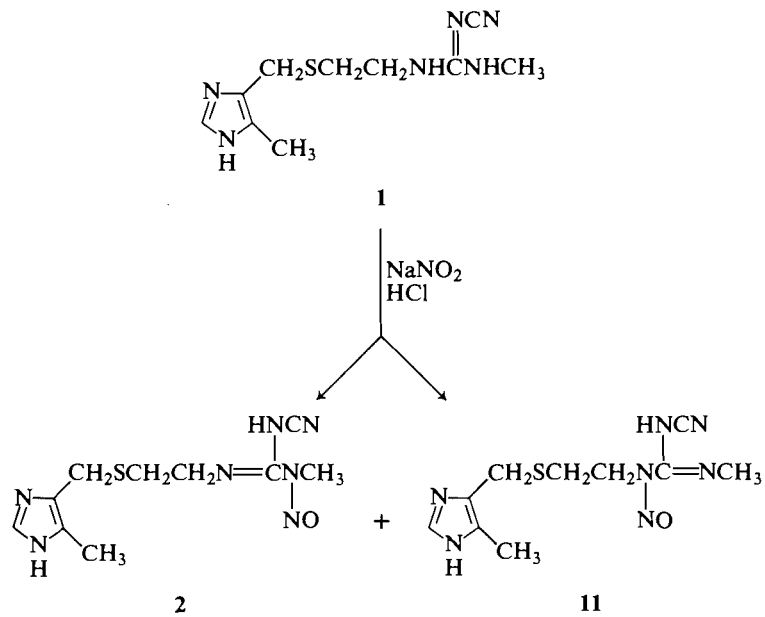

SCHEME 3. Nitrosation of cimetidine

TABLE 2. Nitrosation of cimetidine at pH 1 and 37–38°C (open reaction vessel)[a]

Time, h	% Cimetidine unreacted[c]	Analysis of reaction[b]		
		% **1**	% **2**	% **11**
0	100	100	—	—
0.5	65	62	34	4
1	71	70	26	4
4	94	96	2.4	1.5

[a]10 mmol/L cimetidine; 40 mmol/L $NaNO_2$.
[b]Relative percentage of products in reaction mixture.
[c]Compared to peak height of zero time hplc.

derivatives (**6**, **11**) appeared to form about equally though again etintidine may possibly form less N^a-nitroso product.

At pH 3 (Table 4) both cimetidine and etintidine were nitrosated considerably less than at pH 1. Only 4% of the major nitrosation product **2** of cimetidine was formed while the minor isomer **11** was barely detectable (0.6%) at 4 hours. Both *N*-nitroso products of etintidine were barely detectable (<0.5%).

When, however, the concentration of nitrite at pH 1 was reduced to 2 mmol/L and that of cimetidine or etintidine to 0.5 mmol/L, thus retaining the recommended 4:1 drug/nitrite molar ratio, the mononitroso products **2** and **11** of cimetidine were formed in only 4.5 and 0.9% yields, respectively (Table 3). The mononitroso products **5** and **6** of etintidine were barely detectable (each <0.5%, Table 3) at this lower concentration.

Discussion and conclusions

At pH 1 and 3 etintidine and cimetidine each formed two mono-*N*-nitrosoguanidine derivatives in vitro. Our results confirm that nitrosation of cimetidine decreases as the pH is raised (3) and show a similar effect of pH on nitrosation of etintidine.

At both pH 1 and 3 etintidine was nitrosated considerably less than cimetidine, and the extent of nitrosation of both compounds was dependent on the concentration of nitrite. Thus at pH 1, with the WHO recommended concentration of nitrite (40 mmol/L), nitrosation of etintidine was 6–13% compared to 51–54% for cimetidine. This nitrite concentration, however, is approximately 3 000–10 000 times that to be expected in fasting normal human gastric juice (17, 18) and about 140 times that after a nitrite rich meal (17). Reducing the nitrite concentration at pH 1 to a more reasonable level of 2 mmol/L, which is still about 150–500 times that to be expected in fasting normal human gastric juice (17, 18) and about 7 times that after a nitrite rich meal (17), total nitrosation of etintidine was less than 1% (barely detectable) compared to 5% for cimetidine. At pH 3 with 40 mmol/L nitrite, total nitrosation of etintidine was less than 1% compared to 1–5% cimetidine. Clearly, the extent of in vitro nitrosation of etintidine at both pH 1 and 3 under normal physiological nitrite concentrations would be small indeed and beyond our present limits of detection.

At pH 1 and 3 both etintidine and cimetidine were nitrosated on the N^a-cyanoguanidine nitrogen to a similar (small) extent, as might be predicted based on the similarity of environment. Etintidine was nitrosated on the N^b-cyanoguanidine nitrogen considerably less than cimetidine, probably the result of the greater electronic withdrawing and steric hindrance properties of the propynyl compared to the methyl group.

Standard WHO conditions for comparing nitrosatable drugs in vitro include a recommended pH range of 3–4, which, it is suggested, is optimal for most nitrosation reactions (15). This may be the case for secondary amines, but is not the case for cimetidine and etintidine, and may well not be the case for other amide, urea, or cyanoguanidine type compounds (6, 12). The pH range for testing should be extended down to 1, the lower limit being within the pH range of the human stomach (19).

Since N-nitrosation can be a readily reversible reaction (6) as has been shown for cimetidine, standardization (or statement) of reaction vessel conditions (open or closed) is important. Judging from the reasonably comparable percentage conversions of cimetidine to *N*-nitrosocimetidine attained by Bavin *et al.* (3) and ourselves, the former workers' experiments presumably were conducted in closed vessels/cells. Finally, perhaps the difficulties which have apparently been experienced in

Can. J. Chem. Downloaded from www.nrcresearchpress.com by 210.87.254.105 on 09/06/12
For personal use only.

TABLE 3. Comparative nitrosation at pH 1 and 37–38°C

Compound	Time, h	N^b-NO product	%	N^a-NO product	%
40 mmol/L $NaNO_2$					
Cimetidine (10 mmol/L)	1	**2**	47.5	**11**	4
	4	**2**	45.3	**11**	8
Etintidine (10 mmol/L)	1	**5**	6(4–8)	**6**	2
	4	**5**	6(4–8)	**6**	5
2 mmol/L $NaNO_2$					
Cimetidine (0.5 mmol/L)	1	**2**	5.0	**11**	~0.7
	4	**2**	4.5	**11**	~0.9
Etintidine (0.5 mmol/L)	1	**5**	<0.5	**6**	<0.5
	4	**5**	<0.5	**6**	<0.5

TABLE 4. Comparative nitrosation at pH 3 and 37–38°C

Compound	Time, h	N^b-NO product	%	N^a-NO product	%
40 mmol/L $NaNO_2$					
Cimetidine (10 mmol/L)	1	**2**	1.3	**11**	<0.5
	4	**2**	4.2	**11**	<0.6
Etintidine (10 mmol/L)	1	**5**	<0.5	**6**	<0.5
	4	**5**	<0.5	**6**	<0.5

attempts to isolate or identify *N*-nitrosocimetidine from the gastric juices of subjects receiving cimetidine (20) may have been compounded by this reversibility potential.

Experimental

Melting points were determined on a Fisher–Johns melting point apparatus and are uncorrected. Ultraviolet spectra were recorded on a Varian–Cary model 219 spectrophotometer over the range of 350–450 nm using 95% EtOH as solvent. The ^1H and ^{13}C nmr spectra were recorded on a Varian XL100 instrument or, when indicated, on a Bruker 360 MHz instrument. Chemical shifts were recorded in parts per million (δ) relative to Me_4Si as internal standard.

High pressure liquid chromatography (hplc) was performed using a Waters Associates M6000 pump and U6K loop injector and a LDC variable wavelength uv detector. The following columns, mobile phases, and wavelengths were used: (A) Alltech RSil $C_{18}HL$ (10 μ) (250 × 4.6 mm), 3:2 H_2O–MeCN, 220 nm; (B) Whatman Mag 9 Partisil-10 silica gel (500 × 9 mm), 20:1 MeCN – 95% EtOH, 254 nm; (C) Alltech RSil $C_{18}HL$ (10 μ) (250 × 4.6 mm), 2:1 H_2O–MeCN, 0.01 molar in H_3PO_4 adjusted to pH 4.0 with 20% NaOH, 220 nm; (D) Waters μ-Porasil silica gel (300 × 3.9 mm), 200:10:1 CH_2Cl_2 – 95% EtOH – conc. NH_4OH, 235 nm; (E) Waters μ-Bondapak C_{18} (10 μ) (300 × 3.9 mm), 8:1 H_2O–MeCN, 0.01 molar in H_3PO_4 adjusted to pH 4.0 with 20% NaOH, 220 nm.

For the comparative nitrosation studies, the solutions were analyzed by hplc (5.0–10.0 μL injections) using peak height comparisons to known mixtures of starting materials and products. The data in Tables 3 and 4 are the average of 3 or more hplc determinations. Because the N^b-nitrosoetintidine (**5**) was not obtained pure, the value for **5** was determined assuming a similar uv response (220 nm) for **5** and **6** and this accounts for the ranges (estimated) given in Table 3.

*Nitrosation of etintidine (BL-5641) (**4**)*

A solution of **4** (1.6 g, 5.8 mmol) in 50 mL H_2O and 10 mL concentrated HCl was treated in portions with $NaNO_2$ (3.5 g, 50 mmol) over a period of 10 min. This solution was stirred 30 min at 20°C and then added to a stirred mixture of EtOAc (100 mL), $NaHCO_3$ (15 g), and H_2O (60 mL). The two layers were separated and the aqueous layer extracted further with EtOAc (2 × 75 mL). The dried (Na_2SO_4) extracts were concentrated to leave an amorphous foam (1.8 g). The hplc (A) analysis of this material indicated three products, **5** (*k'* 4.3), **6** (*k'* 2.7), **7** (*k'* 3.6), and starting material **4** (*k'* 2.6). These materials were separated by semi-preparative hplc (B) and characterized as indicated below.

*N-Cyano-N'-{2-[(5-methyl-1H-imidazol-4-yl)methylthio]ethyl}-N'-nitroso-N''-(2-propynyl)guanidine (**6**)*

The first material off the hplc was identified as **6** and was obtained as a viscous oil containing MeCN (0.25 mol): uv λ: 390 nm (shoulder), λ_{max}: 402 (ε 155), λ 420 (shoulder); ^1H nmr (Me_2SO-d_6) δ: 7.57 (s, 1H, imidazole H), 4.41 (d, 2H, N—CH_2—C≡), 4.09 (t, 2H, CH_2—CH_2—NNO), 3.73 (s, 2H, imidazole CH_2—S), 3.44 (t, 1H, ≡CH), 2.60 (appears to be triplet for S—CH_2—CH_2 under Me_2SO peaks), 2.24 (s, 3H, imidazole CH_3), 2.17 (s, 0.75 H, CH_3CN); ^{13}C nmr (Me_2SO-d_6) δ: 155.5 (N—C(=N)—N), 133.2 (C-2 imidazole), 129.3 and 124.8 (C-4 and C-5 imidazole), 113.7 (C≡N), 78.7 (CH_2—C≡C), 74.8 (C≡CH), 42.2 (imidazole CH_2—S), 32.0, 26.8, 25.9 (N—CH_2CH_2S and N—CH_2—C≡), 9.6 (imidazole CH_3). *Anal.* calcd. for $C_{12}H_{15}N_7OS \cdot 0.25(C_2H_3N)$: C 47.46, H 5.03, N 32.18; found: C 47.13, H 5.40, N 31.89.

*N-Cyano-N'-{2-[(5-methyl-1H-imidazol-4-yl)methylthio]ethyl}-N''-nitroso-N''-(2-propynyl)guanidine (**5**)*

The second material off the hplc was identified as **5**. Very careful fraction cutting was required to separate **5** from the starting material **4** which came off the hplc immediately after **5**. Material **5** was obtained free of starting material, but was not obtained free from **7** since concentration of the hplc fractions of **5** always resulted in partial cyclization of **5** to **7** (see below); ^1H nmr (on mixture of **5** and **7**) (Me_2SO-d_6) δ: 7.47 (s, imidazole H (**5** and **7**)), 4.83 (m, one of =CH_2 (**7**)), 4.65 (d, N(NO)CH_2C≡ (**5**)), 4.55 (d, other =CH_2 and endocyclic CH_2 (**7**)), 3.84 (2 overlapping t, CH_2—CH_2—N (**5** and **7**)), 3.75 (s, imidazole CH_2—S (**7**)), 3.76 (s, imidazole CH_2S (**5**)), 3.32 (t, ≡CH (**5**)), 2.81 and 2.73 (2 overlapping t, S—CH_2—CH_2 (**5** and **7**)), 2.18 and 2.19 (ss, imidazole CH_3 (**5** and **7**)).

*2-Cyanoimino-3-{2-[(5-methyl-1H-imidazol-4-yl)methylthio]ethyl}-4-methylene-1-nitrosoimidazoline (**7**)*

The fourth material isolated from the semi-preparative hplc was an amorphous solid identified as **7**; uv λ_{max}: 400 nm (ε 252), λ_{max}: 418 (ε 178); ^1H nmr (pyridine-d_5) δ: 7.88 (s, 1H, imidazole H), 5.02 (q, 1H, one of =CH_2), 4.59 (d, 3H, other =CH_2 and endocyclic CH_2),

Can. J. Chem. Downloaded from www.nrcresearchpress.com by 210.87.254.105 on 09/06/12
For personal use only.

Can. J. Chem. Downloaded from www.nrcresearchpress.com by 210.87.254.105 on 09/06/12
For personal use only.

4.06 (s) and 4.02 (t) (4H, imidazole CH_2—S and CH_2CH_2-N), 2.98 (t, 2H, S—CH_2—CH_2), 2.38 (s, 3H, imidazole CH_3); ^{1}H nmr (Bruker; Me_2SO-d_6) δ: 7.52 (s, 1H, imidazole H), 4.82 (m, 1H, one of =CH_2), 4.56 (m, 1H, other =CH_2), 4.54 (s, 2H (narrow multiplet on scale expansion), endocyclic CH_2), 3.85 (t, 2H, CH_2CH_2N), 3.74 (s, 2H, imidazole CH_2S), 2.72 (t, 2H, S—CH_2—CH_2), 2.18 (s, 3H, imidazole CH_3); ^{13}C nmr (Bruker; Me_2SO-d_6) δ: 151.7 (s, N—C(=N)—N), 136.1 (s, N—C(=CH_2)—), 133.2 (d, C-2 imidazole), 129.7 and 126.0 (ss, C-4 and C-5 imidazole), 113.0 (C≡N), 88.0 (t, C=CH_2), 47.0 (t, endocyclic CH_2), 41.5 (t, imidazole CH_2—S), 26.7 (tt, S—CH_2CH_2—N), 9.76 (q, CH_3). *Anal.* calcd. for $C_{12}H_{15}N_7OS$: C 47.20, H 4.95, N 32.11; found: C 46.84, H 4.90, N 32.34.

Cyclization of ***5*** *and* ***7*** (analytical hplc detection)

A. The mixture of **5** and **7** from above was dissolved in Me_2SO + MeCN and treated with 2 drops of dilute $NaHCO_3$. The reaction was followed by hplc (C). The hplc indicated complete conversion of the **5** to **7** within 1 h.

B. A pure fraction (in solution) of **5** was isolated from the analytical hplc (C). Reanalysis of a portion of this solution both immediately and after 1.5 h showed only **5**. Treatment of this pure fraction with a few drops of dilute $NaHCO_3$ converted **5** completely to **7** within 1 h (identity by hplc spiking).

*Nitrosation of cimetidine (**1**)*

A solution of **1** (1.26 g, 5 mmol) in water (50 mL) and concentrated HCl (10 mL) was treated in portions with $NaNO_2$ (3.5 g, 50 mmol) over 10 min. The reaction was stirred for 0.5 h at room temperature (20°C). The reaction was diluted with water (60 mL), layered with EtOAc (100 mL), and neutralized with $NaHCO_3$ (15 g). The layers were separated and the aqueous layer was extracted with additional EtOAc (2 × 75 mL). The EtOAc extracts were dried (Na_2SO_4) and concentrated to a yellow gum (1.3 g). The hplc (D) analysis indicated two products (**2** (k' 1.0) and **11** (k' 1.43); 7:1 ratio) and some starting material (k' 3.43). These products were separated by preparative hplc (Waters Associates Prep LC 500A; one PrepPAK-500/silica column; elution with 200:2:1 CH_2Cl_2 – 95% EtOH – conc. NH_4OH; 200 mL/minute) and characterized as indicated below.

N-*Cyano*-N′-*methyl*-N″-*{2-[(5-methyl-1*H*-imidazol-4-yl)methylthio]-ethyl}*-N′-*nitrosoguanidine* (***2***)

The first material eluted was the major product, identified as **2**, mp 112–114°C dec. (from MeCN) (lit. (2) mp 112–113°C); uv λ: 385 nm (shoulder), λ_{max}: 397 (ε 200), λ: 414 (shoulder). ^{1}H nmr (Me_2SO-d_6) δ: 7.42 (s, 1H, imidazole H), 3.72 (s and t, 4H, imidazole CH_2—S and CH_2CH_2N), 3.25 (s, 3H, N—CH_3), 2.78 (t, 2H, S—CH_2—CH_2), 2.14 (s, 3H, imidazole CH_3); ^{13}C nmr (Me_2SO-d_6) δ: 156.1 (N—C(=N)—N), 133.2 (C-2 imidazole), 129.4 and 125.0 (C-4 and C-5 imidazole), 114.2 (C≡N), 42.3 (imidazole CH_2—S), 31.0 (N—CH_3), 29.7 and 26.3 (S—CH_2CH_2—N), 9.7 (imidazole CH_3). *Anal.* calcd. for $C_{10}H_{15}N_7OS$: C 42.69, H 5.37, N 34.85; found: C 42.68, H 5.36, N 34.73.

N-*Cyano*-N′-*methyl*-N″-*{2-[(5-methyl-1*H*-imidazol-4-yl)methylthio]-ethyl}*-N″-*nitrosoguanidine* (***11***)

The second material eluted was the minor product, identified as **11**, mp 128–131°C dec. (from MeCN); uv λ: 385 nm (shoulder), λ_{max}: 402 (ε 163), λ: 418 (shoulder); ^{1}H nmr (Me_2SO-d_6) δ: 7.60 (s, 1H, imidazole H), 3.99 (t, 2H, CH_2CH_2—NNO), 3.68 (s, 2H, imidazole CH_2—S), 3.17 (s, 3H, N—CH_3), 2.5 (appears to be triplet for S—CH_2—CH_2 under Me_2SO peaks), 2.18 (s, 3H, imidazole CH_3); ^{13}C nmr (Me_2SO-d_6) δ: 155.9 (N—C(=N)N), 133.2 (C-2 imidazole), 129.2 and 124.8 (C-4 and C-5 imidazole), 114.2 (C≡N), 41.9 (imidazole CH_2—S), 29.4 (N—CH_3), 26.9 and 26.0 (S—CH_2CH_2—N), 9.7 (imidazole CH_3). *Anal.* calcd. for $C_{10}H_{15}N_7OS$: C 42.69, H 5.37, N 34.85; found: C 42.86, H 5.08, N 34.95.

Nitrosation of cimetidine at pH 1 (open reaction vessel)

A suspension of **1** (139 mg, 0.55 mmol) in 50 mL H_2O was adjusted to pH 1.0 with concentrated HCl. The final volume was adjusted to 55 mL with H_2O. This solution was warmed to 36°C and 5.0 mL withdrawn for reference hplc sample. The remaining solution was treated with $NaNO_2$ (138 mg, 2.0 mmol). The temperature was held constant at 36–37°C. The pH fell to 0.93 during the first hour of reaction and was readjusted to 1.0 with 20% NaOH. No further adjustment was needed (pH range 0.98–1.0). The reaction was analyzed by hplc (E) at 0.5 h, 1 h, and 4 h (5.0 mL reaction solution diluted to 50.0 mL with H_2O for analysis). The results are summarized in Table 2.

Comparative nitrosation of etintidine and cimetidine at pH 1

*Etintidine (**4**) (40 mmol/L $NaNO_2$)*

A solution of **4** hydrochloride (172 mg, 0.55 mmol) in 50 mL H_2O was adjusted to pH 1.0 with 3 *N* HCl (about 4.5 mL required). Additional H_2O was added to obtain a volume of 55 mL. This solution was warmed to 35°C and 5.6 mL was withdrawn for reference hplc samples.[3] The remaining solution was treated with $NaNO_2$ (138 mg, 2.0 mmol). The pH remained at 1.0 so that no adjustment was necessary. Two sample vials were filled, sealed, and heated in an oil bath maintained at 37–38°C. At 1 h, 2.6 mL of one of the vials was diluted to 25.0 mL with H_2O and analyzed by hplc (C). At 4 h, 2.6 mL of the other vial was diluted to 25.0 mL with H_2O and analyzed by hplc. The results are summarized in Table 3.

*Cimetidine (**1**) (40 mmol/L $NaNO_2$)*

A suspension of **1** (141 mg, 0.55 mmol) in 50 mL H_2O was adjusted to pH 1.0 with 3 *N* HCl (about 5 mL required). This solution was warmed to 35°C and 5.6 mL was withdrawn for reference hplc samples.[3] The remaining solution was treated with $NaNO_2$ (139 mg, 2.0 mmol). The pH remained at 1.0 so that no adjustment was required. Two sample vials were filled, sealed, and heated in an oil bath maintained at 37–38°C. At 1 h, 2.6 mL of one vial was diluted to 25.0 mL with H_2O and analyzed by hplc (E). At 4 h, 2.6 mL of the other vial was diluted to 25.0 mL and analyzed by hplc. The results are summarized in Table 3.

*Etintidine (**4**) (2 mmol/L $NaNO_2$)*

A solution of **4** hydrochloride (156 mg, 0.5 mmol) in 990 mL H_2O was adjusted to pH 1.0 with concentrated HCl.[3] To this solution was added $NaNO_2$ (138 mg, 2.0 mmol). The pH remained at 1.0. Two sample vials were filled, sealed, and heated in an oil bath maintained at 37–38°C. At 1 h, the solution in one of the vials was analyzed by hplc (C). At 4 h, the solution in the other vial was analyzed by hplc. The results are summarized in Table 3.

*Cimetidine (**1**) (2 mmol/L $NaNO_2$)*

A suspension of **1** (126 mg, 0.5 mmol) in 990 mL H_2O was adjusted to pH 1.0 with concentrated HCl.[3] To this solution was added $NaNO_2$ (138 mg, 2.0 mmol). The pH remained at 1.0. Two sample vials were filled, sealed, and heated in an oil bath maintained at 37–38°C. At 1 h, the solution in one of the vials was analyzed by hplc (E). At 4 h, the solution in the other vial was analyzed. The results are summarized in Table 3.

Comparative nitrosation of etintidine and cimetidine at pH 3

*Etintidine (**4**)*

A solution of **4** hydrochloride (174 mg, 0.56 mmol) and NaCl (128 mg, 2.19 mmol) in 55 mL 0.05 *M* H_3PO_4 was adjusted to pH 3.0 with 20% NaOH. This solution was warmed to 35°C and 5.6 mL was withdrawn for reference hplc samples.[3] The remaining solution was treated with $NaNO_2$ (140 mg, 2.0 mmol). The pH was readjusted to 3.0 with 40% H_3PO_4. Two sample vials were filled, sealed, and heated in a oil bath maintained at 37–38°C. At 1 h, 2.6 mL of one of the vials was diluted to 25.0 mL with H_2O and analyzed by hplc (C). At 4 h, 2.6 mL of the other vial was diluted to 25.0 mL with H_2O and analyzed by hplc. The results are summarized in Table 4.

*Cimetidine (**1**)*

A solution of **1** (140 mg, 0.55 mmol) and NaCl (164 mg, 2.8 mmol)

[3]In all cases the starting solution was analyzed at zero time and after heating in a sealed vial at 37°C for 4 h. Cimetidine was stable at both pH 1 and pH 3. Etintidine was stable at pH 3 but decomposed slightly (~5%) after 4 h at pH 1 and 37°C.

in 55 mL 0.05 *M* H_3PO_4 was adjusted to pH 3.0 with 20% NaOH. This solution was warmed to 35°C and 5.6 mL was withdrawn for reference hplc samples.[3] The remaining solution was treated with $NaNO_2$ (140 mg, 2.0 mmol). The pH was readjusted to 3.0 with 40% H_3PO_4. Two sample vials were filled, sealed, and heated in an oil bath maintained at 37–38°C. At 1 h, 2.6 mL of one of the vials was diluted to 25.0 mL with H_2O and analyzed by hplc (E). At 4 h, 2.6 mL of the other vial was diluted to 25.0 mL with H_2O and analyzed by hplc. The results are summarized in Table 4.

Acknowledgments

We thank the Analytical Research Department for their services and Dr. A. A. Algieri for valuable discussions concerning structure **7**.

1. J. B. ELDER, P. C. GANGULI, and I. E. GILLESPIE. Lancet, **1**, 1005 (1979).
2. A. B. FOSTER, M. JARMAN, D. MANSON, and H.-R. SCHULTEN. Cancer Lett. **9**, 47 (1980).
3. P. M. G. BAVIN, G. J. DURANT, P. D. MILES, R. C. MITCHELL, and E. S. PEPPER. J. Chem. Res. 212 (1980).
4. B. L. POOL, G. EISENBRAND, and D. SCHMÄHL. Toxicology, **15**, 69 (1979).
5. W. LIJINSKY. *In* N-Nitrosamines. *Edited by* J.-P. Anseline. ACS Symposium Series No. 101, ACS, Washington, DC. 1979. pp. 165–173.
6. G. A. DIGENIS and C. H. ISSIDORIDES. Bioorg. Chem. **8**, 97 (1979).
7. P. I. REED, K. HAINES, P. L. R. SMITH, F. R. HOUSE, and C. L. WALTERS. Lancet, **2**, 553 (1981), and references cited therein.
8. R. BRIMBLECOMBE. Lancet, **2**, 686 (1981).
9. G. P. CREAN, G. B. LESLIE, and F. J. C. ROE. Lancet, **2**, 797 (1979).
10. R. L. CAVANAGH, J. J. USAKEWICZ, and J. P. BUYNISKI. Fed. Proc. Fed. Am. Soc. Exp. Biol. **39**, 768 (1980).
11. C. N. R. RAO and K. R. BHASKAR. *In* The chemistry of the nitro and nitroso groups. Pt. 1. *Edited by* H. Feuer. Interscience Publishers, New York. 1969. pp. 137–163.
12. S. J. MIRVISH. Toxicol. Appl. Pharmacol. **31**, 325 (1975).
13. M. C. CASERIO. *In* Selective organic transformations. Vol. I. *Edited by* B. S. Thyagarajan. Wiley Interscience, New York. 1970. pp. 239–299.
14. D. ICHINOTSUBO, E. A. MACKINNON, C. LIU, S. RICE, and H. F. MOWER. Carcinogenesis, **2**, 261 (1981).
15. WHO Drug Information, **2** (April–June), 4 (1978).
16. T. A. TURNEY and G. A. WRIGHT. Chem. Rev. **59**, 497 (1959).
17. C. L. WALTERS, C. S. DYKE, M. J. SAXBY, and R. WALKER. IARC Sci. Publ. 187 (1976).
18. S. DEFLORA and A. PICCIOTTO. Carcinogenesis, **1**, 925 (1980).
19. F. W. SUNDERMAN and F. BOENER. *In* Normal values in clinical medicine. W. B. Landers Company, Philadelphia. 1950. p. 230.
20. Minutes, FDA Advisory Committee on Gastrointestinal Drugs. Vol. I. Rockville, Maryland. June 2, 1980.

Can. J. Chem. Downloaded from www.nrcresearchpress.com by 210.87.254.105 on 09/06/12
For personal use only.

Electronic spectral study of amino-acid complexes of Nd(III)

ASHOK KOTHARI AND SUDHINDRA N. MISRA
Department of Chemistry, University of Jodhpur, Jodhpur-342001, India

Received April 6, 1982[1]

ASHOK KOTHARI and SUDHINDRA N. MISRA. Can. J. Chem. **61**, 1778 (1983).

Neodymium(III) complexes with histidine and diols (ethanediol, prop-1,2-diol, but-2,3-diol, 2-butene-1,4-diol, pent-1,5-diol, and hex-1,6-diol) of the type MAB, MA_2B, and MAB_2 have been synthesized and characterised. The values of Slater–Condon (F_k), Lande' (ζ_{4f}) spin orbital interactions, oscillator strength (P), and Judd–Ofelt (T_λ) intensity parameters have been calculated. Using these parameters, energies and intensities of ten levels in all the complexes in the region 360–920 nm have been computed. The agreement between the computed and experimental values is good. Using F_2 values, the nephelauxetic ratio β, and bonding parameter $b^{1/2}$ have been calculated, these infer the incidence of some covalent character in these complexes.

ASHOK KOTHARI et SUDHINDRA N. MISRA. Can. J. Chem. **61**, 1778 (1983).

On a synthétisé et caractérisé des complexes du néodyme(III) avec l'histidine et des diols (éthanediol, propanediol-1,2, butanediol-2,3, butène-2 diol-1,4, pentadiol-1,5 et hexadiol-1,6). Ces complexes sont du type MAB, MA_2B et MAB_2. On a calculé les valeurs de Slater–Condon (F_k), les interactions d'orbitale de spin (ζ_{4f}) de Lande, la force de l'oscillateur (P) et les paramètres d'intensité de Judd–Ofelt (T_λ). A partir de ces paramètres on a calculé les énergies et les intensités de 10 niveaux pour tous les complexes dans la région de 360–920 nm. Il existe un bon accord entre les valeurs calculées et expérimentales. En utilisant les valeurs de F_2 on a calculé le rapport néphélauxétique β et le paramètre de liaison $b^{1/2}$ qui impliquent l'incidence d'un certain caractère covalent dans ces complexes.

[Traduit par le journal]

Introduction

The absorption spectra of complexed rare earth ions in the $f \leftrightarrow f$ transition region have been studied by various workers to give information regarding the structure and composition of the complexes (1–11). The present investigation was undertaken with a view to make the comparative study of various energy and intensity parameters for different energy levels of Nd(III) ternary complexes containing both oxygen and nitrogen donor ligands. Histidine, a functional amino acid, is well known as a proton donor, proton acceptor, and a nucleophilic reagent.

The values of various electronic spectral parameters like Slater–Condon (F_k), Lande' (ζ_{4f}), oscillator strength (P), Judd–Ofelt (T_λ), nephelauxetic ratio (β), and bonding ($b^{1/2}$), which give useful information regarding interelectronic repulsion, spin–orbit interaction, nephelauxetic effect, and bonding in the complexes, have been computed by using a partial multiple regression method (12).

Experimental

L-Histidine monohydrochloride and diols (ethanediol, prop-1,2-diol, but-1,3-diol, 2-butene-1,4-diol, pent-1,5-diol, and hex-1,6-diol) were obtained from Fluka A. G. and B.D.H. Ltd., and neodymium chloride (99.9%) from Indian Rare Earths Ltd.. The complexes have been synthesized in the molar ratio 1:1:1, 1:2:1, and 1:1:2 by a reported method (13) and were characterized by elemental and infrared spectral analysis.[2]

The absorption spectra of the complexes were recorded on Carl-Zeiss Spectrophotometer in the 360–920 nm region in methanol. The recorded spectra was photographically expanded to locate the energies of the transition using glass prism. The energies recorded in wavelength have been reported in wave numbers.

Results and discussion

(i) Energy parameters

The energy levels of various transitions were obtained experimentally as well as computed by using the following relationship:

$$[1]\quad E_j(F_k, \zeta_{4f}) = E_{oj}(F_k^0, \zeta_{4f}^0) + \sum_{k=2,4,6}\left(\frac{\partial E_j}{\partial F_k}\right)\Delta F_k + \left(\frac{\partial E_j}{\partial \zeta_{4f}}\right)\Delta\zeta_{4f}$$

where E_{0j} is the zero-order energy (14) of the jth level putting the observed energy value E_j and zero-order energy value and the partial derivatives for the free ion, F_2, F_4, F_6, and ζ_{4f} have been computed by using the partial multiple regression method (12).

In most of the cases of the parameters F_k and ζ_{4f} of Nd(III) complexes exhibit a decrease from the corresponding values of the Nd(III) free ion. The decrease in the interelectronic repulsion and spin–orbit interaction indicates the expansion of the central metal ion orbital on complexation and is in accordance with the theory for the origin and the intensity of $f \leftrightarrow f$ transitions reported earlier.

The average value of F_4/F_2 for Nd(III) complexes ($\simeq$ 0.152) is larger than those calculated by using the Hartree Fock method ($\simeq$ 0.13) but they are nearer to the values for the free ion (0.1531). The same trend has been observed for the ratio F_6/F_2.

A comparison of the observed and calculated values of the energy levels (Tables 6–8) shows that the rms deviation between ±45.32 to ±71.04 indicates good results even though the radial eigenfunctions have been assumed to be hydrogenic and also best fit for the partial multiple regression method. Red shift of all the energy levels from that of the free ion supports complexation.

In Table 1 the Nd(III) complexes have been arranged in the decreasing order of nephelauxetic ratio (β) and increasing order of bonding parameter ($b^{1/2}$), with the exception in case of Nd(hist)$_2$2-butene-1,4-diol. The very low value of β and very high value of $b^{1/2}$ in the series is due to the presence of π-bonding in case of 2-butene-1,4-diol which might be responsible for the greater complexation (12). The positive val-

[1]Revision received January 14, 1983.

[2]Data available on request from the authors.

Can. J. Chem. Downloaded from www.nrcresearchpress.com by 210.87.254.6 on 09/06/12
For personal use only.

Can. J. Chem. Downloaded from www.nrcresearchpress.com by 210.87.254.6 on 09/06/12
For personal use only.

TABLE 1. Computed values of various spectroscopic parameters (F_2, ζ_{4f}, β, $b^{1/2}$, %δ, $\%^rF_2$, $\%^r\zeta_{4f}$) of Nd(III) complexes with histidine and diole

Parameters / complexes	F_2 (in cm^{-1})	F_4 (in cm^{-1})	F_6 (in cm^{-1})	ζ_{4f} (in cm^{-1})	F_4/F_2	F_6/F_2	β	$b^{1/2}$	%δ	$\%^rF_2$	$\%^r\zeta_{4f}$
Nd^{3+} (free ion)	331.160	50.714	5.154	884.00	0.15314	0.01556	—	—	—	—	—
Nd(hist)(ethanediol)	330.327	50.380	5.241	863.93	0.15251	0.01586	0.9974	0.0360	0.2606	0.2515	2.27
Nd(hist)(prop-diol)	329.805	50.874	5.201	852.31	0.15425	0.01577	0.9959	0.0452	0.4116	0.4091	3.61
Nd(hist)(but-diol)	329.163	51.068	5.194	847.78	0.15514	0.01578	0.9927	0.0604	0.7353	0.6030	4.09
Nd(hist)(butene-diol)	328.378	51.059	5.192	856.02	0.15548	0.01581	0.9916	0.0648	0.8471	0.8400	3.16
Nd(hist)(pent-diol)	329.509	50.509	5.234	863.57	0.15328	0.01588	0.9937	0.0561	0.6339	0.4985	2.31
Nd(hist)(hex-diol)	329.512	50.670	5.211	858.93	0.15377	0.01581	0.9950	0.0500	0.5025	0.4976	2.84
Nd(hist)$_2$(ethanediol)	330.469	50.196	5.245	865.82	0.15189	0.01587	0.9979	0.0324	0.2104	0.2086	2.06
Nd(hist)$_2$(prop-diol)	330.198	50.620	5.242	859.19	0.15330	0.01587	0.9970	0.0387	0.3009	0.3028	2.81
Nd(hist)$_2$(but-diol)	330.068	50.670	5.227	859.72	0.15351	0.01583	0.9967	0.0406	0.3310	0.3297	2.74
Nd(hist)$_2$(butene-diol)	326.555	51.646	5.188	861.17	0.15815	0.01588	0.9860	0.0836	1.4198	1.3905	2.58
Nd(hist)$_2$(pent-diol)	330.131	50.280	5.227	863.01	0.15230	0.01583	0.9968	0.0400	0.3210	0.3107	2.37
Nd(hist)$_2$(hex-diol)	329.973	50.478	5.203	859.50	0.15768	0.01576	0.9964	0.0426	0.3613	0.3584	2.77
Nd(hist)(ethanediol)$_2$	330.725	50.094	5.274	863.71	0.15146	0.01594	0.9986	0.0264	0.1402	0.1313	2.30
Nd(hist)(prop-diol)$_2$	330.543	50.110	5.263	867.80	0.15160	0.01592	0.9981	0.0308	0.1903	0.1863	1.83
Nd(hist)(but-diol)$_2$	330.257	50.793	5.248	852.54	0.15379	0.01589	0.9972	0.0374	0.2807	0.2726	3.56
Nd(hist)(butene-diol)$_2$	327.884	51.581	5.183	848.90	0.15731	0.01580	0.9901	0.0703	0.9998	0.9892	3.97
Nd(hist)(pent-diol)$_2$	329.218	50.365	5.249	866.04	0.15298	0.01594	0.9941	0.0543	0.5935	0.5864	2.03
Nd(hist)(hex-diol)$_2$	329.846	51.009	5.229	853.00	0.15464	0.01585	0.9961	0.0441	0.3915	0.3967	3.51

TABLE 2. Computed values of T_λ-parameters of Nd(III) complexes with histidine and diols

Complexes	$T_2\times10^{10}$	$T_4\times10^{10}$	$T_6\times10^{10}$	T_4/T_6
Nd^{3+}(aquo ion)*	2.9700	4.3200	4.1800	1.0330
Nd(hist)(ethanediol)	6.5144	6.1554	8.7314	0.7049
Nd(hist)(prop-diol)	6.1412	8.0134	9.3327	0.8586
Nd(hist)(but-diol)	6.4750	8.1658	9.1197	0.8950
Nd(hist)(butene-diol)	8.4824	6.7880	9.5474	0.7109
Nd(hist)(pent-diol)	6.4600	8.9826	9.1597	0.9806
Nd(hist)(hex-diol)	6.5521	9.1499	9.5545	0.9576
Nd(hist)$_2$(ethanediol)	7.0761	9.3399	10.9810	0.8505
Nd(hist)$_2$(prop-diol)	7.8693	7.3242	10.0160	0.7312
Nd(hist)$_2$(but-diol)	7.3413	9.9231	11.3980	0.8706
Nd(hist)$_2$(butene-diol)	7.5931	9.6208	11.3610	0.8468
Nd(hist)$_2$(pent-diol)	8.1770	6.2718	10.7130	0.5854
Nd(hist)$_2$(hex-diol)	7.7979	8.7038	11.6460	0.7473
Nd(hist)(ethanediol)$_2$	5.9419	7.6705	8.9498	0.8570
Nd(hist)(prop-diol)$_2$	6.1231	7.5910	9.1184	0.8324
Nd(hist)(but-diol)$_2$	6.9479	7.5745	9.8982	0.7652
Nd(hist)(butene-diol)$_2$	6.9627	9.4309	10.5230	0.8962
Nd(hist)(pent-diol)$_2$	7.0832	8.1623	9.9388	0.8212
Nd(hist)(hex-diol)$_2$	7.0220	8.4426	10.3650	0.8145

ues of $b^{1/2}$ indicate covalent bonding in the complexes. The small value of $b^{1/2}$ and small variation of it suggests that the 4*f*-orbitals are very slightly involved in the bonding of lanthanide complexes.

Spectral intensities

The experimental value of oscillator strength is obtained from:

$$[2]\quad P_{expt} = 4.318 \times 10^{-9} \int \epsilon(\nu)d\nu$$

where $\epsilon(\nu)$ is the molar extinction coefficient corresponding to energy ν in wave number. Theoretically the oscillator strength, P_{cal}, of the induced-dipole transition of energy ν (cm^{-1}) in accordance with Judd–Ofelt relation [1] can be expressed as:

$$[3]\quad P_{cal} = \sum_{\lambda=2,4,6} T_\lambda \nu (f^n\psi|U^{(\lambda)}|f^n\psi' J)^2$$

It has been found that, in general, the oscillator strength for Nd^{3+} complexes can be expressed in terms of T_4 and T_6 parameters only. But it is important to note that the effect of solvent or ligand on the intensity of a hypersensitive transition can be explained by T_2 parameters only.

The values of T_λ-parameters have been computed from the Judd–Ofelt expression by using the partial multiple regression method where the values of reduced matrix elements have been taken from Carnall *et al.* (2). For Nd(III) complexes the Judd–Ofelt relation is applicable in the present form:

$$[4]\quad P_{obs} = [U^{(2)}]^2\nu \times T_2 + [U^{(4)}]^2\nu \times T_4 + [U^{(6)}]^2\nu \times T_6$$

The nephelauxetic ratio (β) and bonding parameter ($b^{1/2}$), along with the ratios F_4/F_2, F_6/F_2, $\%^rF_2$, and $\%^r\zeta_{4f}$ which infer some covalency due to complexation have also been reported (Table 1).

The ratio of T_4/T_6 parameter is nearly constant for these complexes indicating the same symmetry of the complexes in solution (Table 2). It is important to note that the hypersensitive transition (which is sensitive to environmental changes), $^4G_{5/2} \leftarrow {}^4I_{9/2}$ exhibits the increase in the intensity with the increase in covalency of the complexes. The hypersensitivity has been found to be proportional to the nephelauxetic ratio (β).

Can. J. Chem. Downloaded from www.nrcresearchpress.com by 210.87.254.6 on 09/06/12
For personal use only.

TABLE 3. Computed values of oscillator-strength of the bands observed for Nd(III) complexes with histidine and diols (type MAB)

	Nd(hist)(ethanediol)		Nd(hist)(prop-diol)		Nd(hist)(but-diol)		Nd(hist)(butene-diol)		Nd(hist)(pent-diol)		Nd(hist)(hex-diol)	
Levels	$P_{expt}\times10^6$	$P_{cal}\times10^6$	$P_{expt}\times10^6$	$P_{cal}\times10^6$	$P_{expt}\times10^6$	$P_{cal}\times10^6$	$P_{expt}\times10^6$	$P_{cal}\times10^6$	$P_{expt}\times10^6$	$P_{cal}\times10^6$	$P_{expt}\times10^6$	$P_{cal}\times10^6$
$^2P_{1/2}$	0.5353	0.5416	0.5805	0.7043	0.1608	0.7168	0.2585	0.5959	0.3734	0.7894	0.3792	0.8037
$^4G_{11/2}$	0.1959	0.2218	0.1277	0.2532	0.3179	0.2509	0.2138	0.2432	0.6575	0.2616	0.5712	0.2698
$^4G_{9/2}$	1.8534	1.6029	1.9254	1.3560	2.0136	1.8905	2.1583	1.7733	1.9351	2.0028	1.9879	2.0579
$^2G_{9/2}$	0.2882	0.4185	0.3736	0.4852	0.2373	0.4836	0.7431	0.4610	0.3339	0.5080	0.3102	0.5229
$^4G_{7/2}$	3.8750	3.4060	4.0631	4.0425	4.6029	4.0935	4.6734	3.9285	4.7553	4.3415	4.1503	4.4515
$^4G_{5/2}$	15.3740	14.9220	16.1780	15.7180	16.2100	16.3290	18.6520	18.4550	16.6320	16.8260	16.9300	17.1390
$^4F_{9/2}$	1.8787	0.5848	0.5444	0.6422	0.4532	0.6320	0.2342	0.6394	0.4113	0.6476	0.2413	0.6726
$^4F_{7/2}$	6.3863	5.2509	5.5100	5.6986	5.4685	5.5657	6.3242	5.7240	5.4004	5.6333	5.9424	5.8869
$^4F_{5/2}$	6.7119	6.1217	7.2787	6.9631	6.9243	6.9595	6.4471	6.7039	7.2194	7.1622	7.5402	7.3971
$^4F_{3/2}$	2.3099	2.1705	2.4429	2.6980	2.3647	2.7218	2.6776	2.3829	2.4814	2.5660	2.5766	3.0116
r.m.s. deviation (σ)	$\pm0.6193\times10^{-6}$		$\pm0.2808\times10^{-6}$		$\pm0.2886\times10^{-6}$		$\pm0.4016\times10^{-6}$		$\pm0.2994\times10^{-6}$		$\pm0.2923\times10^{-6}$	

TABLE 4. Computed values of oscillator-strength of the bands observed for Nd(III) complexes with histidine and diols (type MA_2B)

	Nd(hist)$_2$(ethanediol)		Nd(hist)$_2$(prop-diol)		Nd(hist)$_2$(but-diol)		Nd(hist)$_2$(butene-diol)		Nd(hist)$_2$(pent-diol)		Nd(hist)$_2$(hex-diol)	
Levels	$P_{expt}\times10^6$	$P_{cal}\times10^6$	$P_{expt}\times10^6$	$P_{cal}\times10^6$	$P_{expt}\times10^6$	$P_{cal}\times10^6$	$P_{expt}\times10^6$	$P_{cal}\times10^6$	$P_{expt}\times10^6$	$P_{cal}\times10^6$	$P_{expt}\times10^6$	$P_{cal}\times10^6$
$^2P_{1/2}$	0.3206	0.8218	0.1434	0.6444	0.2988	0.8731	0.3849	0.8436	0.1719	0.5512	0.1246	0.7645
$^4G_{11/2}$	0.4253	0.2973	0.5019	0.2569	0.1432	0.3112	0.9492	0.3064	0.2829	0.2571	0.2191	0.3008
$^4G_{9/2}$	2.1729	2.2108	2.3825	1.8757	2.3481	2.3241	2.3092	2.2797	2.2870	1.8019	2.1400	2.1895
$^2G_{9/2}$	0.5099	0.5693	0.4120	0.4883	0.2731	0.5973	0.2217	0.5871	0.2876	0.4767	0.5059	0.5704
$^4G_{7/2}$	4.4428	4.7048	4.5809	4.0854	4.5043	4.9613	4.7116	4.8790	4.4452	3.8745	4.6003	4.6595
$^4G_{5/2}$	17.8870	18.2000	18.4430	17.9310	18.6590	19.0470	18.9480	19.1880	18.6750	17.7070	18.4920	18.8760
$^4F_{9/2}$	0.2602	0.7553	0.3649	0.6746	0.2961	0.7877	0.6249	0.7812	0.3484	0.6997	0.2654	0.7851
$^4F_{7/2}$	6.3543	6.6999	6.4870	6.0426	6.5481	6.9578	6.6232	6.9024	6.6077	6.3719	6.4587	7.0207
$^4F_{5/2}$	8.1732	8.2379	8.7627	7.0912	8.4909	8.5438	8.4572	8.4267	8.3791	7.1358	8.2452	8.3091
$^4F_{3/2}$	2.6849	3.1476	2.7537	2.5563	2.8342	3.3311	2.8543	3.2416	2.7242	2.3227	2.4709	3.0252
r.m.s. deviation (σ)	$\pm0.3326\times10^{-6}$		$\pm0.6456\times10^{-6}$		$\pm0.3849\times10^{-6}$		$\pm0.2191\times10^{-6}$		$\pm0.5970\times10^{-6}$		$\pm0.3836\times10^{-6}$	

Can. J. Chem. Downloaded from www.nrcresearchpress.com by 210.87.254.6 on 09/06/12
For personal use only.

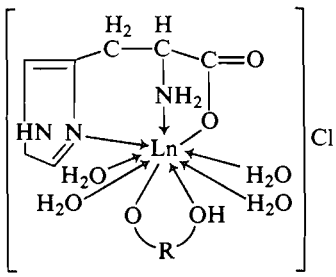

1:1:1
(MAB)

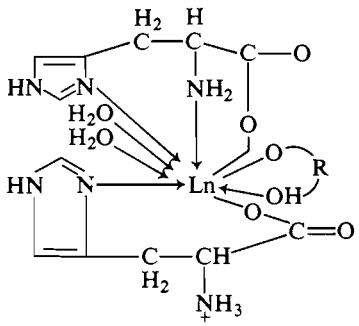

1:2:1
(MA_2B)

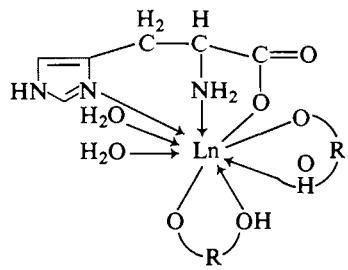

1:1:2
(MAB_2)

Choppin *et al.* (15, 16) have suggested the strong inner sphere complexation in glycinate complexes. According to them, during the formation of these complexes the hydration sphere around lanthanides is disrupted completely by the amino acid moiety. Choppin and Henrie (8) at the same time believed that increase in the degree of innersphere complexation contributes towards the enhancement of intensity of intra $f \leftrightarrow f$ transitions. Contrary to this the observed intensities of these ternary complexes are very low ($P \sim 14.922 \times 10^{-6}$ to 19.188×10^{-6}) (Tables 3–5). No doubt amino acids are expected to form inner sphere complexes by forming an ionic linkage with carboxylic oxygen and an additional linkage due to the amino group. The infrared spectra in the solid state of these compounds also indicate inner sphere complexation but on dissolution it appears that amino group participation is delinked by the solvent effect and the amino acid binds itself with the metal ion as a zwitterion (17). The proton from the carboxylic group migrates towards the amino group and the oxygen of the carboxylic group links to the metal ion while the remaining amino acid molecule hangs in space. The classical zwitterion resonance form of the acid is promoted by the highly charged lanthanide ion. This in fact contributes a significant amount of electrondensity to the lanthanide ion. This might be one of the reasons why low intensities of these bands are observed in these complexes. In spite of significant contribution from inner

TABLE 5. Computed values of oscillator-strength of the bands observed for Nd(III) complexes with histidine and diols (type MAB_2)

	Nd(hist)(ethanediol)$_2$		Nd(hist)(prop-diol)$_2$		Nd(hist)(but-diol)$_2$		Nd(hist)(butene-diol)$_2$		Nd(hist)(pent-diol)$_2$		Nd(hist)(hex-diol)$_2$	
Levels	$P_{expt}\times10^6$	$P_{cal}\times10^6$	$P_{expt}\times10^6$	$P_{cal}\times10^6$	$P_{expt}\times10^6$	$P_{cal}\times10^6$	$P_{expt}\times10^6$	$P_{cal}\times10^6$	$P_{expt}\times10^6$	$P_{cal}\times10^6$	$P_{expt}\times10^6$	$P_{cal}\times10^6$
$^2P_{1/2}$	0.3624	0.6749	0.1503	0.6679	0.1871	0.6664	0.1242	0.1151	0.1738	0.7165	0.2347	0.7428
$^4G_{11/2}$	0.3802	0.2432	0.2640	0.2449	0.3945	0.2577	0.3276	0.2897	0.2291	0.2651	0.4116	0.2765
$^4G_{9/2}$	1.8053	1.8091	1.7484	1.8170	2.0485	1.8877	2.1789	2.1821	2.1766	1.9701	2.0810	2.0446
$^2G_{9/2}$	0.4933	0.4646	0.2418	0.4676	0.8031	0.4895	0.2679	0.5583	0.3110	0.5064	0.4495	0.5283
$^4G_{7/2}$	3.5530	3.8631	3.7228	3.8834	4.1129	4.0433	4.6394	4.6723	4.3092	4.2342	4.3350	4.3681
$^4G_{5/2}$	14.9720	15.1190	15.1420	15.3260	16.6340	16.6620	17.6950	17.9990	17.1100	17.2720	17.2530	17.4480
$^4F_{9/2}$	0.3889	0.6157	0.5468	0.6261	0.7200	0.6678	0.1995	0.7276	0.4899	0.6785	0.5032	0.7088
$^4F_{7/2}$	5.2779	5.4496	5.3111	5.5473	5.8787	5.6610	6.2420	6.4135	5.7673	6.0090	5.9766	6.3040
$^4F_{5/2}$	6.7024	6.6651	6.7839	6.7334	7.4511	7.1144	7.7845	7.9573	7.4093	7.2979	7.7447	7.6142
$^4F_{3/2}$	2.3749	2.5771	2.2698	2.5732	2.5780	2.6148	2.7830	3.1392	2.3684	2.7754	2.4315	2.8778
r.m.s. deviation (σ)		$\pm0.1894\times10^{-6}$		$\pm0.2325\times10^{-6}$		$\pm0.2330\times10^{-6}$		$\pm0.2539\times10^{-6}$		$\pm0.2609\times10^{-6}$		$\pm0.2592\times10^{-6}$

Can. J. Chem. Downloaded from www.nrcresearchpress.com by 210.87.254.6 on 09/06/12
For personal use only.

TABLE 6. Computed values of energies in cm^{-1} of the band of Nd(III) complexes of the type MAB

Energy levels	Nd(hist)ethanediol		Nd(hist)prop-diol		Nd(hist)but-diol		Nd(hist)butene-diol		Nd(hist)pent-diol		Nd(hist)hex-diol	
	E_{expt}	E_{cal}	E_{expt}	E_{cal}	E_{expt}	E_{cal}	E_{expt}	E_{cal}	E_{expt}	E_{cal}	E_{expt}	E_{cal}
$^2P_{1/2}$	23094.68	23084.94	23068.05	23058.42	23041.47	23031.70	23041.47	23026.40	23068.05	23059.21	23054.75	23052.75
$^4G_{11/2}$	21645.02	21512.97	21621.62	21483.05	21590.01	21440.01	21645.02	21453.45	21645.02	21484.16	21598.27	21486.68
$^4G_{9/2}$	21052.63	21065.91	21030.50	21038.68	21008.40	21014.06	21052.63	21052.37	21052.63	21055.97	21041.55	21050.53
$^2G_{9/2}$	19569.47	19515.37	19531.25	19506.51	19493.17	19401.09	19531.25	19486.33	19512.19	19495.21	19493.17	19502.17
$^4G_{7/2}$	19175.45	19153.22	19193.85	19158.75	19157.08	19137.06	19120.45	19111.18	19157.08	19135.30	19193.85	19146.61
$^4G_{5/2}$	17211.70	17247.51	17241.38	17275.21	17241.38	17252.91	17211.70	17221.33	17182.13	17219.79	17211.70	17244.51
$^4F_{9/2}$	14684.28	14703.56	14641.28	14674.05	14619.88	14646.65	14619.88	14667.57	14622.75	14692.23	14673.51	14683.36
$^4F_{7/2}$	13210.04	13285.16	13227.51	13263.36	13175.23	13248.82	13157.89	13248.55	13175.23	13265.24	13227.51	13270.52
$^4F_{5/2}$	12422.36	12462.46	12422.36	12459.57	12406.94	12437.41	12406.94	12431.85	12422.36	12442.93	12406.94	12451.72
$^4F_{3/2}$	11467.89	11446.79	11467.89	11459.95	11454.75	11444.30	11441.64	11426.22	11454.75	11427.18	11467.89	11442.19
r.m.s. deviation	±55.20		±51.14		±62.34		±71.04		±64.89		±45.32	

TABLE 7. Computed values of energies in cm^{-1} of the bands of Nd(III) complexes of the type MA_2B

Level	$Nd(hist)_2$(ethanediol)		$Nd(hist)_2$(prop-diol)		$Nd(hist)_2$(but-diol)		$Nd(hist)_2$(butene-diol)		$Nd(hist)_2$(pent-diol)		$Nd(hist)_2$(hex-diol)	
	E_{expt}	E_{cal}	E_{expt}	E_{cal}	E_{expt}	E_{cal}	E_{expt}	E_{cal}	E_{expt}	E_{cal}	E_{expt}	E_{cal}
$^2P_{1/2}$	23094.68	23081.41	23094.68	23085.79	23094.68	23082.87	23014.96	23020.89	23068.05	23061.01	23054.75	23054.75
$^4G_{11/2}$	21645.02	21516.51	21598.27	21491.29	21645.02	21504.66	21598.27	21437.57	21621.62	21503.67	21598.27	21508.33
$^4G_{9/2}$	21052.63	21059.05	21043.77	21059.15	21052.63	21067.90	21008.40	21117.74	21030.50	21043.96	21019.44	21044.18
$^2G_{9/2}$	19569.47	19512.43	19569.47	19506.57	19569.47	19517.88	19531.25	19489.38	19531.25	19504.24	19569.47	19513.66
$^4G_{7/2}$	19157.08	19146.23	19175.45	19152.57	19193.85	19162.85	19138.75	19145.44	19175.45	19140.50	19157.08	19153.69
$^4G_{5/2}$	17241.38	17242.79	17226.51	17248.81	17241.38	17259.94	17211.70	17169.25	17226.53	17244.00	17211.70	17266.24
$^4F_{9/2}$	14662.75	14705.23	14673.51	14690.73	14673.51	14696.35	14662.75	14675.74	14684.28	14693.30	14673.30	14691.28
$^4F_{7/2}$	13227.51	13286.68	13218.77	13274.78	13210.04	13282.30	13175.23	13228.25	13210.04	13280.18	13192.61	13285.37
$^4F_{5/2}$	12422.36	12462.82	12406.94	12454.89	12422.36	12462.58	12406.94	12407.75	12422.36	12458.62	12422.36	12466.61
$^4F_{3/2}$	11454.75	11444.47	11454.75	11446.53	11467.89	11453.00	11441.64	11392.38	11454.75	11443.76	11467.89	11456.08
r.m.s. deviation	±52.10		±47.47		±56.23		±68.42		±47.79		±50.81	

Can. J. Chem. Downloaded from www.nrcresearchpress.com by 210.87.254.6 on 09/06/12
For personal use only.

TABLE 8. Computed values of energies in cm^{-1} of the band of Nd(III) complexes of the type MAB_2

Energy level	Nd(hist)(ethanediol)$_2$		Nd(hist)(prop-diol)$_2$		Nd(hist)(but-diol)$_2$		Nd(hist)(butene-diol)$_2$		Nd(hist)(pent-diol)$_2$		Nd(hist)(hex-diol)$_2$	
	E_{expt}	E_{cal}	E_{expt}	E_{cal}	E_{expt}	E_{cal}	E_{expt}	E_{cal}	E_{expt}	E_{cal}	E_{expt}	E_{cal}
$^2P_{1/2}$	23094.68	23081.71	23094.68	23087.69	23094.68	23081.82	23041.47	23026.75	23041.47	23045.67	23094.68	23083.83
$^4G_{11/2}$	21668.47	21481.66	21645.02	21509.54	21598.27	21457.44	21598.27	21426.94	21598.27	21460.27	21621.62	21475.26
$^4G_{9/2}$	21030.50	21030.79	21052.63	21060.39	21030.50	21032.20	21052.63	21056.41	21052.63	21046.80	21052.63	21058.20
$^2G_{9/2}$	19512.19	19482.64	19531.25	19504.53	19531.25	19485.40	19531.25	19481.61	19493.17	19471.32	19569.47	19505.51
$^4G_{7/2}$	19120.45	19119.86	19157.08	19137.07	19138.75	19140.74	19157.08	19146.90	19120.45	19109.05	19157.08	19161.63
$^4G_{5/2}$	17211.70	17219.02	17182.13	17225.39	17211.70	17247.78	17182.13	17227.11	17196.90	17180.47	17241.38	17261.54
$^4F_{9/2}$	14641.28	14684.83	14684.28	14705.16	14619.88	14665.15	14598.54	14649.71	14619.88	14678.69	14641.28	14677.19
$^4F_{7/2}$	13192.61	13267.16	13210.04	13280.83	13210.04	13258.41	13157.89	13235.23	13140.60	13247.80	13192.61	13267.89
$^4F_{5/2}$	12406.94	12443.98	12422.36	12455.22	12422.36	12442.50	12406.94	12422.92	12406.94	12423.57	12422.36	12452.03
$^4F_{3/2}$	11441.64	11430.25	11467.89	11434.64	11454.75	11444.74	71441.64	11426.97	11467.89	11403.58	11467.89	11452.52
r.m.s. deviation	±67.02		±53.92		±53.20		±65.76		±62.72		±58.44	

sphere complexation, it has been argued earlier (18) that the increase in the intensity of the hypersensitive transition is due to the lowering of the coordination number of the lanthanide. Infrared spectral patterns and analytical data indicate the presence of a varying number of water molecules in these complexes (1:1:1 = 4, 1:2:1 = 2, and 1:1:2 = 2).

The terdentate attachment of histidine and monofunctional bidentate attachment of the diol moiety along with a varying number of coordinated water molecules yield nona-coordinated environment around neodymium. The intensities of the transitions in complexes of different series are not varied to a great extent and can be interpreted in terms of the same coordination number of neodymium.

A slightly higher value for the intensities of bands was observed in MA_2B complexes containing a larger number of nitrogen coordinating sites. The MA_2B complexes also showed the comparatively higher magnitude of the nephelauxetic effect ($1 - \beta$) yielding higher magnitude for mixing coefficients (b).

A plot of νb^2 against P has given a linear correlation with a positive slope which suggests that the increase in the incidence of covalent character brings about the intensification of the bands.

1. S. MISUMI, S. KIDA, T. ISOBE, and A. INAZUMI. Bull. Chem. Soc. Jpn. **41**, 25 (1968).
2. W. T. CARNALL, P. R. FIELDS, and B. G. WYBOURNE. J. Chem. Phys. **42**, 3797 (1965).
3. D. E. HENRIE and G. R. CHOPPIN. J. Chem. Phys. **49**, 477 (1968).
4. P. C. MEHTA and S. P. TANDON. J. Chem. Phys. **52**, 4313 (1970).
5. D. G. KARRAKER. J. Inorg. Nucl. Chem. **33**, 3713 (1971).
6. R. D. PEACOCK. Structure and bonding. Vo. 22, Springer-Verlag, Berlin. 1975. p. 88.
7. W. T. CARNALL, P. R. FIELDS, and K. RAJNAK. J. Chem. Phys. **49**, 4412 (1968); **49**, 4424 (1968); **49**, 4443 (1968); **49**, 4447 (1968); **49**, 4450 (1968).
8. D. E. HENRIE. Coord. Chem. Rev. **18**, 199 (1976).
9. K. B. YATSIMIRSKII and N. D. DAVIDENKO. Coord. Chem. Rev. **27**, 223 (1979).
10. S. S. L. SURANA, M. SINGH, and S. N. MISRA. J. Inorg. Nucl. Chem. **42**, 61 (1980).
11. G. K. JOSHI, M. P. BHUTRA, and SUDHINDRA N. MISRA. J. Inorg. Nucl. Chem. **43**, 525 (1981).
12. C. H. GOULDEN. Method of statistical analysis. Asia Publishing House, Bombay, Calcutta, Delhi, Madras, New York. 1964. Chapt. 8. p. 134.
13. A. KOTHARI, R. K. JAIN, A. AHMED, and S. N. MISRA. J. Inorg. Nucl. Chem. **43**, 2905 (1981).
14. E. Y. WONG. J. Chem. Phys. **35**, 544 (1961).
15. G. R. CHOPPIN and A. J. GRAFFEO. Inorg. Chem. **4**, 1254 (1965).
16. G. R. CHOPPIN and S. P. TANNER. Inorg. Chem. **7**, 2046 (1968).
17. K. F. BELYAEVA, M. A. P. KOSHITS, T. I. MALINOVSKII, *et al.* Zh. Strukt. Khim. **10**, 470 (1969); **10**, 557 (1969).
18. S. N. MISRA. J. Sci. Ind. Res. In press.

Model compounds for biodegradation studies on hydrocarbon-type dielectric fluids

WILLEM HENDRIK BAARSCHERS AND MARIA ANGELA LI

Department of Chemistry, Lakehead University, Oliver Road, Thunder Bay, Ont., Canada P7B 5E1

Received November 9, 1982

WILLEM HENDRIK BAARSCHERS and MARIA ANGELA LI. Can. J. Chem. **61**, 1784 (1983).

The hydrocarbons 7-methylpentadecane (**1**, $n = 0$) and 7-methyl-9-*n*-hexyl heptadecane (**1**, $n = 1$) have been synthesized. These compounds are suitable as model compounds for biodegradation studies on mixtures of oligomers of 1-octene and related compounds which have been proposed as dielectric fluids for the replacement of PCB's. The synthesis confirms the feasibility of isotope labelling for such biodegradation studies.

WILLEM HENDRIK BAARSCHERS et MARIA ANGELA LI. Can. J. Chem. **61**, 1784 (1983).

On a synthétisé le méthyl-7 pentadécane (**1**, $n = 0$) et le méthyl-7 *n*-hexyl-9 heptadécane (**1**, $n = 1$). Ces composés constituent des modèles convenables pour étudier la biodégradation des mélanges d'oligomères de l'octène-1 et des composés apparentés que l'on propose comme fluides diélectriques en remplacement du BPC. La synthèse confirme la possibilité de marquage isotopique dans les études de biodégradation.

[Traduit par le journal]

Introduction

A mixture of oligomers of 1-octene with average molecular weight 850 and general structure **1** ($n \approx 5.5$) has been described (1) and patented (2) as a dielectric fluid. This material, PAO-20E (Uniroyal Canada Ltd) is recommended as a suitable replacement for polychlorinated biphenyls. No study on the biodegradability of this material could be found in the literature to date. It was decided to approach such a study by means of model compounds such as the dimer (**1**, $n = 0$) and trimer

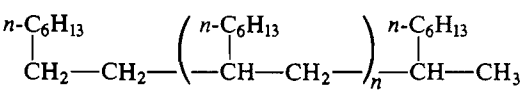

1

(**1**, $n = 1$) of 1-octene. Such an approach has some specific advantages.

Firstly, although many branched chain hydrocarbons are readily biodegradable (3), the sheer molecular size of products like PAO-20E (average $C_{60}H_{122}$) may well prevent biodegradation by microorganisms. Use of model compounds could not only determine if biodegradation of hydrocarbons with this particular branching pattern does take place, but also establish a possible limiting size in the homologous series **1**.

Secondly, the absence of functional groups prevents use of spectroscopic methods for the analysis of unchanged hydrocarbons in culture extracts and gas chromatography of compounds with this high a molecular weight is not feasible (4). The use of lower homologues **1**, which are expected to be readily eluted from conventional gas chromatography columns, would circumvent this difficulty.

Thirdly, metabolites of these branched hydrocarbons are expected to be aliphatic acids, alcohols, and esters (5), which would be difficult to distinguish from similar compounds produced by the natural metabolism of microorganisms (6). A synthetic method for model compounds **1** ($n = 0$ and $n = 1$) could be used for carbon isotope labelling, which in turn would allow for subsequent identification of metabolites by liquid scintillation counting or carbon-13 nuclear magnetic resonance.

The synthesis of compounds **1** ($n = 0$ and $n = 1$), some aspects of the characterization of compounds of this kind, and the feasibility of isotope labelling are discussed in this report.

The hydrocarbons 7-methyl-pentadecane (**1**, $n = 0$, also **5***f* in Scheme 1) and 7-methyl-9-*n*-hexyl-heptadecane (**1**, $n = 1$, also **7***d* in Scheme 1) were synthesized by repeated application of the malonic ester synthesis (7) and manipulation of functional groups as described below and summarized in Scheme 1.

Experimental

A Perkin–Elmer model 3920B dual column gas chromatograph with flame ionization detectors was used. Nitrogen was the carrier gas (25–35 mL/min) in glass columns (1.8 m, 2 mm id) packed with SE-30 silicone rubber gum (5%) or EGSS-X (10%) on Gaschrom Q, at temperatures from 120–240°C. (All column materials were from Chromatographic Specialties Ltd., Brockville, Ontario.)

Proton nmr spectra were recorded on a Bruker WP-80 spectrometer with deuterochloroform solutions containing tetramethylsilane as an internal standard at $\delta = 10$.

1-Bromohexane, 1-bromooctane, and cyclohexyl methanol (**8***a*) were used as supplied (Aldrich Chemical Co.) and diethyl malonate (**2**) was redistilled before use. Compounds **4** and **5** with R′ = *n*-C_4H_9 and **8***a* and *b* were prepared by methods similar to those used in the sequence **2** → **7***d* which is described for R′ = *n*-C_6H_{13} below.

Diethyl hexylmalonate **3**

Diethyl malonate (**2**, 16.11 g) was added to a solution of Na (2.29 g) in EtOH (50 mL) and 1-bromohexane was added to the clear solution. The mixture was refluxed (2.5 h), most of the solvent distilled off, and the residue dispersed in H_2O (40 mL). Extraction (CH_2Cl_2) and removal of the solvent gave a residue which was distilled at 16 Torr. Diethyl hexylmalonate (**3**, 20.12 g, 82%) was obtained as a colourless oil (bp 134–138°C) which was homogeneous on tlc and gc; ir: 1765 (ester) cm^{-1}; ms *m/e*: 244(M^+).

Diethyl hexyl-octylmalonate **4**a

Diethyl hexylmalonate (**3**, 17.9 g) in a solution of Na (2.93 g) in EtOH (50 mL) and 1-bromooctane (12.9 g) were allowed to react and the product was isolated as above. Diethyl hexyl-octylmalonate (**4***a*, 19.17 g, 80.6%) was obtained as a colourless oil with bp 182–186°C (12 Torr) which was homogeneous on tlc and gc; ir: 1760 cm^{-1}; ms *m/e*: 356(M^+).

Hexyl-octylmalonic acid **4**b

The diester (**4***a*, 19.17 g) was added to KOH (11.6 g) in H_2O (20 mL) and the mixture heated (90°C) for 5 h, cooled, acidified, and extracted with Et_2O. Removal of the solvent gave the diacid (**4***b*, 14.33 g, 88.4%) as white crystals, mp 73–85°C, which were characterized as the dianilide, mp 119.5°C; ir: 3495, 1700, 1540 cm^{-1}; ms *m/e*: 450(M^+). *Anal.* calcd. for $C_{29}H_{42}N_2O_2$: C 77.29, H 9.39, N 6.22; found: C 77.19, H 9.10, N 5.95.

Can. J. Chem. Downloaded from www.nrcresearchpress.com by 210.87.254.105 on 09/06/12
For personal use only.

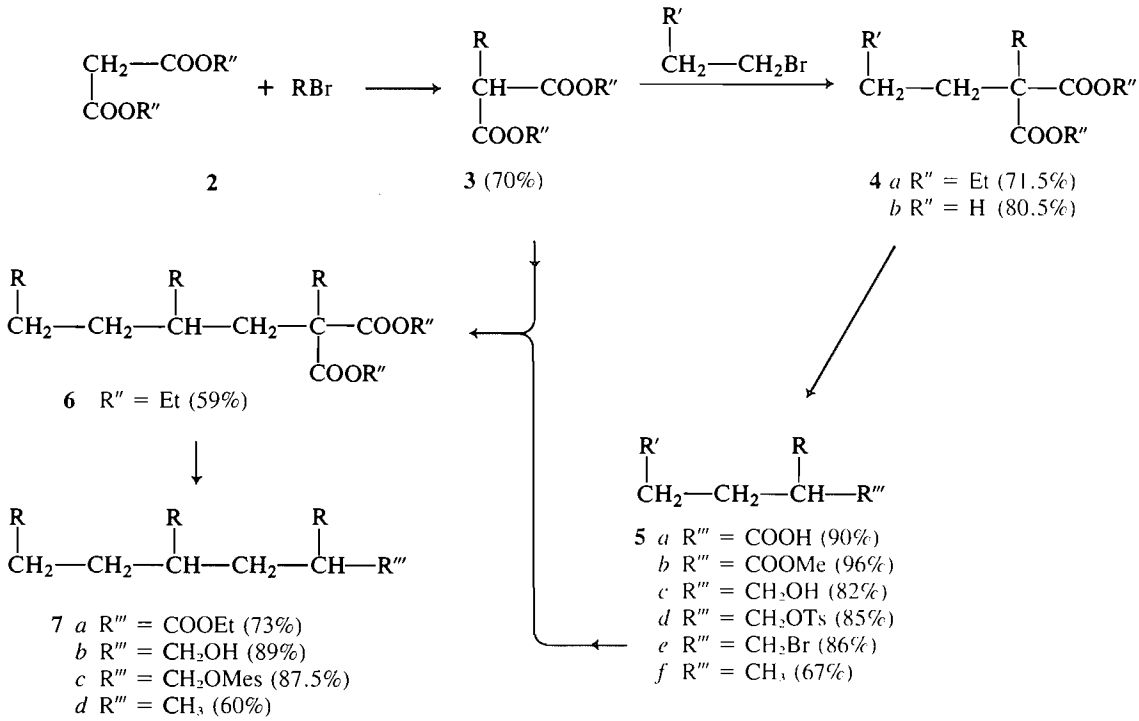

SCHEME 1. Syntheses of 7-methyl pentadecane (**5***f*) and 7-methyl-9-hexyl heptadecane (**7***d*). R = *n*-C_6H_{13}; R′ = *n*-C_6H_{13} or *n*-C_4H_9 (see discussion). Percentages in parentheses are averages of yields obtained in several trials in each reaction.

2-Hexyl-decanoic acid **5**a

The dicarboxylic acid (**4***b*) was decarboxylated in small portions by mixing 2.01 g with glass powder (1.72 g) and heating the mixture at 145°C for 3.5 h in N_2. Extraction (Et_2O) and removal of the solvent gave 2-hexyl-decanoic acid (**5***a*, 1.62 g, 95%) as a colourless oil, which was homogeneous on tlc and gc. The anilide had mp 78.0–78.5°C; ms *m/e*: 331(M^+). *Anal.* calcd. for $C_{22}H_{37}NO$: C 79.70, H 11.25, N 4.22; found: C 79.69, H 11.29, N 4.11.

Methyl 2-hexyldecanoate **5**b

Excess diazomethane in Et_2O was added to 2-hexyldecanoic acid (**5***a*, 10.8 g) in Et_2O and the mixture was stirred briefly. Evaporation of solvent and excess reagent left a residue which was filtered, in Et_2O, through silica gel to give the monoester **5***b* (9.6 g, 95%) which was homogeneous on tlc and gc; ir: 1750 cm^{-1}; ms *m/e*: 270(M^+).

2-Hexyl-1-decanol **5**c

Methyl 2-hexyldecanoate (11.44 g), dissolved in dry THF (20 mL) was added to LAH (1.36 g) in THF (30 mL), and the mixture was refluxed, with stirring, for 3 h. A saturated aqueous solution of Na_2SO_4 was added with cooling, and the resulting mixture was extracted with Et_2O. Removal of the solvent and filtration of the residue in Et_2O, through silica gel, gave 2-hexyl-1-decanol (**5***c*, 8.36 g, 82%) as a colourless oil, which was homogeneous on tlc and gc; ir: 3650 cm^{-1}; ^{1}Hmr δ: 3.55 (s, 1H) ppm; ms *m/e*: 224(M^+ − 18).

7-Methylpentadecane **5**f

To the alcohol (**5***c*, 5.30 g), in dry pyridine (30 mL), was added *p*-toluene sulfonyl chloride (5.10 g). The clear solution was kept at 0°C for 2 h and H_2O (30 mL) was added. The mixture was extracted with $CHCl_3$, the extracts washed (dilute H_2SO_4, H_2O, aqueous Na_2HCO_3, and H_2O), and the solvent removed. The residue, after filtration in $CHCl_3$ through silica gel, gave the tosyl ester **5***d* (7.34 g, 85%) as a colourless, homogeneous (tlc, gc) liquid; ir: 1190, 1200 cm^{-1}; ^{1}Hmr δ: 3.96 (s, 1H); ms *m/e*: 224(M^+ − HOTs). *Anal.* calcd. for $C_{23}H_{40}SO_3$: C 69.70, H 10.1; found: C 70.07, H 9.79. The tosylate (5.04 g) in DMSO (5 mL) was added to $NaBH_4$ (1.65 g) in DMSO (20 mL), the mixture refluxed for 2 h with stirring, diluted with H_2O, and extracted with Et_2O (3 × 25 mL). The combined extracts, after removal of the solvent, gave a residue which was chromatographed on silica gel. Elution with petroleum ether gave pure (tlc, gc) 7-methylpentadecane (1.96 g, 68.1%) as a colourless oil; ms *m/e*: 226(M^+). *Anal.* calcd. for $C_{16}H_{34}$: C 84.96, H 15.04; found: C 84.48, H 14.60.

7-(Bromomethyl)-pentadecane **5**e

2-Hexyl-1-decanol (5.07 g) was mixed with aqueous HBr (48%, 3.42 g) and the mixture was refluxed (4 h) while HBr gas was bubbled through. The mixture was extracted with benzene and the extract concentrated and filtered through silica gel. Removal of the solvent gave 7-(bromomethyl)-pentadecane (**5***e*, 6.11 g, 95.7%) as a yellow homogeneous (tlc, gc) oil; ^{1}Hmr δ: 3.39 (s, 1H) ppm; ms *m/e*: 306, 304(M^+).

Diethyl hexyl-(2-hexyldecyl)malonate **6**

Diethyl hexylmalonate (**3**, 5.49 g) was alkylated with 7-(bromomethyl)-pentadecane (6.67 g) as above. The crude product was chromatographed on silica gel. Elution with $C_6H_{12}/CHCl_3$ (1:1) gave the diester (**6**, 6.04 g, 59%) which was homogeneous on tlc and gc; ms *m/e*: 468(M^+).

Ethyl 2,4-dihexyldodecanoate **7**a

A mixture of the diester (**6**, 1.03 g), LiCl (0.18 g), DMSO (3.6 mL), and H_2O (0.4 mL) was refluxed for 4 h, poured into cold H_2O (15 mL), and extracted with hexane (8 × 25 mL). Removal of the solvent gave a residue which was chromatographed on silica gel, using $C_6H_{12}/CHCl_3$ (1:1) as eluent to give pure (tlc, gc) ethyl 2,4-dihexyldodecanoate (**7***a*, 0.63 g, 73%); ms *m/e*: 396(M^+).

2,4-Dihexyldodecanol **7**b

LAH reduction of the monoester **7***a* and work-up as described above for the ester **5***b* gave the alcohol **7***b* in 89% yield; ir: 3650 cm^{-1}; ^{1}Hmr δ: 3.50 (s, 1H) ppm; ms *m/e*: 336(M^+ − 18).

7-Methyl-9-hexyl-heptadecane **7**d

To 2,4-dihexyldodecanol (**7***b*, 0.5 g) in CH_2Cl_2 (7 mL) and trimethylamine (0.21 g) was added methanesulfonyl chloride (0.18 g) at −10°C, and the mixture stirred for 15 min. The mixture was washed successively with H_2O, cold 10% HCl, saturated Na_2CO_3 solution,

Can. J. Chem. Downloaded from www.nrcresearchpress.com by 210.87.254.105 on 09/06/12
For personal use only.

TABLE 1. Proton magnetic resonance data for key derivatives

Compound	δ Values (ppm) X = OH	X = OTs	X = Br
	3.47	4.25	3.32
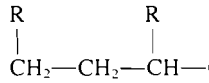	3.55	3.96	3.39
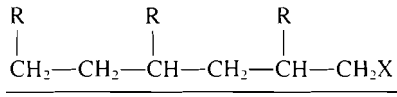	3.50	3.88	—

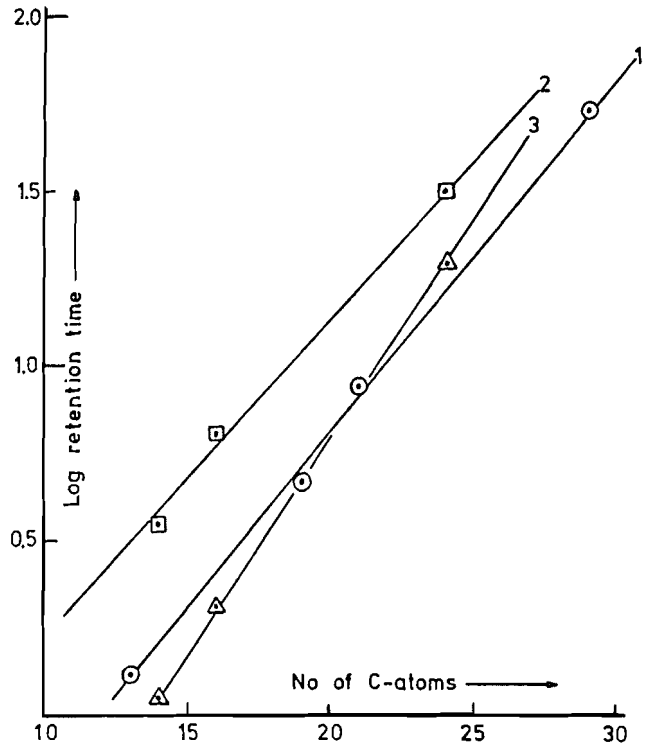

FIG. 1. Examples of straight line plots of no. of carbon atoms/molecule vs. log retention time. 1, Diethyl esters **3**, **4**, and **6** (SE 30, 210°C). 2, Alcohols **5***c* (R′ = *n*-C_6H_{13} and R′ = *n*-C_4H_9) and **7***b* (EGSS-X, 170°C). 3, Hydrocarbons **5***f* (R′ = *n*-C_6H_{13} and R′ = *n*-C_4H_9) and **7***d* (SE 30, 190°C).

and H_2O. The organic layer was dried, the solvent removed, and the residue, in CH_2Cl_2, filtered through silica gel to give the mesylate **7***c* (0.53 g); ir: 1180, 1350 cm^{-1}. The mesylate **7***c* was reduced with LAH, as above, to give the hydrocarbon **7***d* (60%) as a colourless, homogeneous (tlc, gc) oil; ms *m/e*: 338(M^+).

8 *a* R‴ = CH_2OH
b R‴ = CH_2OTs
c R‴ = CH_2Br

The other compounds discussed (i.e. the series **5** with R′ = *n*-C_4H_9 and compounds **8***b* and *c*) were prepared and characterized by methods described above. Characteristic ^{1}Hmr data are summarized in Table 1 and gc retention characteristics are summarized in Fig. 1.

Results and discussion

7-Methyl-pentadecane (**1**, *n* = 0, also **5***f* in Scheme 1) has been described in the literature in discussions of insect chemistry (8) and photochemistry (9). An earlier synthesis (10) of this compound was based on the reaction of a Grignard compound with a ketone or a fatty acid ester. The malonic ester synthesis (11) would allow for the sequential synthesis of compounds **1** with increasing values of *n*, and is particularly attractive because of the ready availability of starting materials in view of future plans for the synthesis of isotope-labelled versions of **1**.

The manipulation of the various functional groups was achieved with standard reactions, described in the literature, with minor modifications. Thus, the three-step sequence (hydrolysis, decarboxylation, esterification) usually employed with substituted malonic esters gave good yields in the dimer series (**4***a* → **5***b*), but was unsatisfactory in the trimer series, where the conversion of **6** → **7***a* by decarbethoxylation (11) was superior. Similarly, the tosylate (**5***d*) could be prepared (12) and reduced to the dimer (**5***f*) in acceptable yields, but the use of the mesylate **7** (13) gave better yields in the trimer series.

All intermediate and final products were purified until they were homogeneous on thin-layer chromatography and on two different gas chromatography columns.

Characterization of some of the compounds had to be carried out indirectly. Traces of trapped solvent in samples too small for purification by distillation gave rise to unsatisfactory combustion analysis results. Also, the presence of a single functional group in large molecules with a predominantly hydrocarbon character greatly limited the usefulness of spectroscopic methods. While in some cases infrared spectra provided useful information (e.g. the conversion of the alcohols **5***c* and **7***b* (ν_{max} 3630 cm^{-1}) into the corresponding sulfonate esters (ν_{max} 1180, 1350, 1370 cm^{-1})), full characterization of most compounds was achieved by a combination of proton magnetic resonance spectroscopy and gas chromatography. The chemical shift of the single methine proton adjacent to the functional groups R‴ in compounds **5**, **7**, and the additional model compounds **8** is sufficiently sensitive to the nature of R‴. The δ-values, summarized in Table 1, leave no doubt to the identity of the alcohols (**5***c*, **7***b*, and **8***a*) and their conversions into the sulfonate esters (**5***d*, **7***c*, and **8***b*), which causes a downfield shift of 0.3–0.8 ppm, or conversion to the bromides (**5***e* and **8***c*) which

Can. J. Chem. Downloaded from www.nrcresearchpress.com by 210.87.254.105 on 09/06/12
For personal use only.

causes an upfield shift of 0.15 ppm.

Additional evidence for characterization was obtained by preparing the compounds **4** and **5** with R′ = n-C_4H_9, which made available a sufficient number of compounds to utilize the linear relationship of the number of carbon atoms with the log of the gas chromatographic retention times (14). Together with the other spectroscopic evidence, the almost perfect straight-line fit of these relationships (see Fig. 1) provides for unambiguous characterization of all compounds.

Finally, with respect to planned biodegradation studies, this synthesis shows that the preparation of compounds labelled with carbon isotopes is quite feasible. From the yields obtained (see Scheme 1) it may be calculated that, starting with some 5 g of diethyl malonate, moderately enriched with either carbon-13 or carbon-14, a final yield of 0.9 g of labelled dimer (**5***f*) or 0.5 g of labelled trimer (**7***d*) may be expected. An additional 1.5 g of labelled diethyl malonate would be required for producing the trimer labelled at both tertiary carbons. Such quantities would be sufficient for conducting biodegradation studies with microorganisms so that isolated metabolites could be readily detected with liquid scintillation methods or to give significant signal enhancement in carbon-13 nuclear magnetic resonance spectra.

Preliminary biodegradation studies of unlabelled dimer **5***f* and trimer **7***d* with known hydrocarbon degraders such as *Saccharomycopsis lipolitica* (15), and carbon-13 nmr studies with some of the present compounds are in progress.

Acknowledgement

The authors appreciate the generous financial support of Environment Canada, Inland Waters Directorate.

1. D. H. ANTONSEN, P. S. HOFFMAN, and R. S. STEARNS. Ind. Eng. Chem. Prod. Res. Dev. **2**, 224 (1963).
2. F. C. LOVELESS. U.S. Pat. No. 4,041,098 (1977).
3. G. S. FONKEN and R. A. JOHNSON. Chemical oxidations with microorganisms. Marcel Dekker Inc., New York. 1972. p. 41.
4. D. LUI and P. T. S. Wong. *In* Proc. 3rd Intern. Biodegrad. Symp. *Edited by* J. M. Sharply and A. M. Kaplan. Barking, G.B. 1976. p. 175.
5. R. M. ATLAS and R. BARTHA. Residue Rev. **49**, 49 (1973).
6. M. J. KLUG and A. J. MARKOVETZ. J. Bacteriol. **93**, 1847 (1967).
7. R. T. MORRISON and R. N. BOYD. Organic chemistry. 3rd ed., Allyn and Bacon, Inc., Boston. 1973. p. 847.
8. T. IKESHOJI, I. ICHIMOTO, T. OHO, Y. NAOSHIMA, and H. UEDA. Appl. Entomol. Zool. **12**, 265 (1977).
9. P. KOURIM. Int. J. Radiat. Phys. Chem. **1**, 345 (1969).
10. J. P. WIBAUT and H. BRAND. Recl. Trav. Chim. Pays-Bas, **80**, 97 (1961).
11. A. P. KRAPCHO, J. F. WEIMASTER, J. M. ELDRIDGE, E. G. E. JAHNGEN, A. J. LOVEY, and W. P. STEPHENS. J. Org. Chem. **43**, 138 (1978).
12. R. S. TIPSON. J. Org. Chem. **9**, 235 (1944).
13. R. K. CROSSLAND and K. L. SERVIS. J. Org. Chem. **35**, 3195 (1970).
14. A. T. JAMES and A. J. P. MARTIN. J. Appl. Chem. **6**, 105 (1956).
15. E. J. NYNS, J. P. AUQUIERE, and A. L. WIAUX. Zeitschr. Allgem. Mikrobiol. **9**, 373 (1969).

Can. J. Chem. Downloaded from www.nrcresearchpress.com by 210.87.254.105 on 09/06/12
For personal use only.

Heteroanthracyclines. 1. 4-Demethoxyxanthodaunomycinone (6,7,9,11-tetrahydroxy-9-acetyl-7,8,9,10-tetrahydrobenzo(*B*)xanthen-12-one)[1]

CHIU-MING WONG,[2] WASIMUL HAQUE, HING-YAT LAM,[3] KIRK MARAT, AND E. BOCK
Department of Chemistry, University of Manitoba, Winnipeg, Man., Canada R3T 2N2

AND

AI-QIAO MI
Chengdu Institute of Organic Chemistry, Chinese Academy of Sciences, Chengdu, People's Republic of China

Received November 30, 1982

CHIU-MING WONG, WASIMUL HAQUE, HING-YAT LAM, KIRK MARAT, E. BOCK, and AI-QIAO MI. Can. J. Chem. **61**, 1788 (1983).

Two heteroanthracyclinones, namely 4-demethoxyxanthodaunomycinone (**29**) and its epimer 4-demethoxy-7-epixanthodaunomycinone (**30**), were synthesized using 2-acetyl-5,8-dimethoxytetralin (**12**) as starting material. Condensation of **12** with 2-methoxybenzoic acid followed by hydrolysis and oxidative cyclization gave xanthones **17** and **18** which were converted to **19** and **20** for the purpose of separation and structure assignment by dipole moment. Hydrolysis of **19** followed by alkylation with chloromethyl methyl ether and oxidation with molecular oxygen gave **26** and **27**, which on acid hydrolysis gave 4-demethoxyxanthodaunomycinone (**29**) and 4-demethoxy-7-epixanthodaunomycinone (**30**). Preliminary biological assays with MCF-7, a human breast cancer cell line, showed that both **29** and **30** were weakly active while daunomycinone, the aglycone of **2**, showed no activity under similar conditions.

CHIU-MING WONG, WASIMUL HAQUE, HING-YAT LAM, KIRK MARAT, E. BOCK et AI-QIAO MI. Can. J. Chem. **61**, 1788 (1983).

On a synthétisé deux hétéroanthracyclinones: la déméthoxy-4 xanthodaumycinone (**29**) et son épimère la déméthoxy-4 épi-7 xanthodaumycinone (**30**) en partant de l'acétyl-2 diméthoxy-5,8 tétraline (**12**). La condensation du composé **12** sur l'acide méthoxy-2 benzoïque, suivie d'une hydrolyse et d'une cyclisation oxydante conduit aux xanthones **17** et **18** que l'on transforme en composés **19** et **20** pour les besoins de séparation et d'identification de structure par le moment dipolaire. L'hydrolyse du composé **19** suivie de l'alkylation avec l'éther chlorométhyle méthyle et de l'oxydation subséquente du produit obtenu avec l'oxygène moléculaire donne les composés **26** et **27** qui par hydrolyse acide donnent accès à la déméthoxy-4 xanthodaunomycinone (**29**) et à la déméthoxy-4 épi-7 xanthodaunomycinone (**29**) et à la déméthoxy-4 épi-7 xanthodaunomycinone (**30**). Un essaie biologique préliminaire avec le MCF-7, une des cellules du cancer du sein, montre que les deux composés **29** et **30** sont faiblement actifs tandis que la daunomycinone, l'aglycone du composé **2** dans les mêmes conditions n'a aucune activité.

[Traduit par le journal]

Introduction

The rewarding results of clinical application of some antitumor anthracyclines such as adriamycin (**1**), daunomycin (**2**), and carminomycin (**3**) and their simple derivatives are well documented (1). Efforts to improve the potency and efficacy of these first generation anthracycline antitumor drugs also met with encouraging results. Synthetic analogues such as 4-demethoxydaunomycin (**4**), 4-demethoxy-4′-deoxyadriamycin (**5**), and 4-demethoxy-11-deoxydaunomycin (**6**) are much more potent than the first generation natural anthracyclines (2, 3). However, both the synthetic and natural products are cardiotoxic and prolonged administration invariably leads to congestive heart failure (3).

Adriamycin and daunomycin bind strongly to chromosomal DNA (4), inhibiting its template function and mitotic process, causing the degeneration and destruction of cells. X-ray crystallography indicated that daunomycin molecules sit in the major groove of the DNA double helix intercalating successive base-pairs. The basic nitrogen atom of daunosamine together with the chromophore of the aglycone are involved in intercalation (5). The C-9 hydroxy and the acetyl groups are implicated to help stabilize the intercalation, possibly through hydrogen bonding, and inversion at C-7 prevents intercalation (6).

It was proposed that adriamycin stimulated the generation of superoxide in the heart cells, which have low superoxide dismutase activity. Accumulation of the highly toxic superoxide and hydrogen peroxide is responsible for the cardiotoxicity (7).

A reasonable suggestion linking the adriamycin molecule with the superoxide formation is that the quinone moiety of adriamycin may function as an electron acceptor, taking electrons from a specific site of the NADH dehydrogenase. The resulting semiquinone **7** then participates in a nonenzymatic redox reaction with molecular oxygen leading to superoxide and subsequent hydrogen peroxide formation (8). In addition, it is also possible that **7** may become an active precursor of the quinone methide (**8**) which is less likely to form when the quinone is strongly hydrogen-bonded with the C-6 phenolic function. Quinone methides are powerful alkylating and cytotoxic agents (9).

It is therefore reasonable to speculate that cardiotoxicity and intercalating and alkylating properties are three different characters of antitumor anthracycline antibiotics. Recently, adriamycin was found to exert its cytotoxic action by interaction with cell membrane (10). The mechanism of interaction is not known. Lipid peroxidation triggered by the formation of **7**, as suggested by Bachur (11), Hochstein (12), and Myres (13), could be responsible for the membrane damage. In this case, the quinone chromophore becomes responsible for the superoxide formation which in turn becomes responsible for both

[1]Presented at the 63rd CIC Conference, Ottawa, June 1980.
[2]Author to whom all correspondence should be addressed.
[3]American Leukemia Society Scholar, Department of Medicine, University of Manitoba, Winnipeg, Manitoba.

Can. J. Chem. Downloaded from www.nrcresearchpress.com by 210.87.254.105 on 09/06/12
For personal use only.

Can. J. Chem. Downloaded from www.nrcresearchpress.com by 210.87.254.105 on 09/06/12
For personal use only.

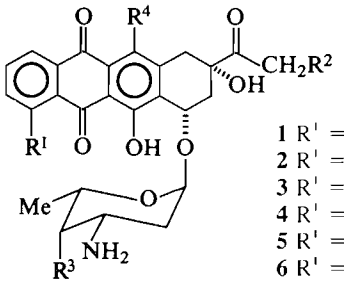

1 $R^1 = OCH_3$, $R^2 = R^3 = R^4 = OH$
2 $R^1 = OCH_3$, $R^2 = H$, $R^3 = R^4 = OH$
3 $R^1 = R^3 = R^4 = OH$, $R^2 = H$
4 $R^1 = R^2 = H$, $R^3 = R^4 = OH$
5 $R^1 = R^3 = H$, $R^2 = R^4 = OH$
6 $R^1 = R^2 = R^4 = H$, $R^3 = OH$

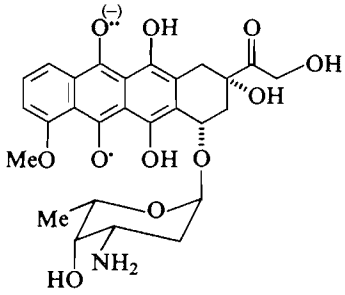

7

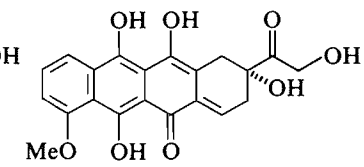

8

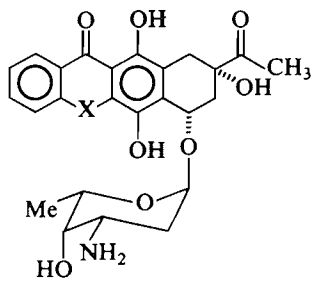

9 X = O
10 X = S
11 X = SO

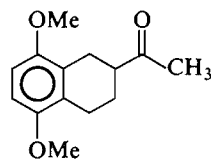

12

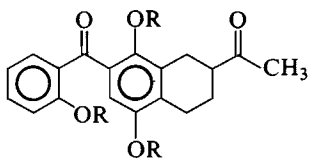

13 R = CH_3
15 R = H

cytoxicity and cardiotoxicity. Making heteroanthracyclines, such as 4-demethoxyxanthodaunomycin (**9**), 4-demethoxythioxanthodaunomycin (**10**), and 4-demethoxy-5-sulfoxodaunomycin (**11**), available could help clarify the origin of cardiotoxicity and cytotoxicity of anthracyclines.

Results and discussion

The tetracyclic xanthone skeleton of **9** was constructed using the versatile 2-acetyl-5,8-dimethoxy tetralin (**12**) (14) as starting compound. Condensation of the tetralin (**12**) with 2-methoxybenzoic acid in trifluoroacetic acid solution gave a mixture of two isomers **13** and **14**. The reaction temperature was maintained at 20–24°C. Below 15°C, the reaction was very slow and at 40°C, trifluoroacetylation of the tetralin (**12**) was a major reaction. The two isomers were separated by high performance liquid chromatography on silica and were characterized by ir, ^{1}Hmr, and ms. However, separation at this stage for preparative purposes is not practical. The isomeric mixture (**13** and **14**) was hydrolysed by aluminium chloride to the

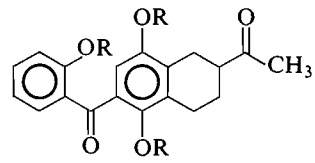

14 R = CH_3
16 R = H

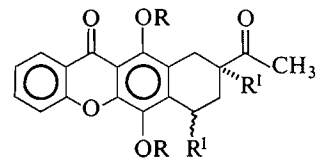

17 R = R' = H
19 R = CH_2—Ph, R' = H
21 R = CH_2—Ph, R' = OH
25 R = CH_2—OCH_3, R' = H

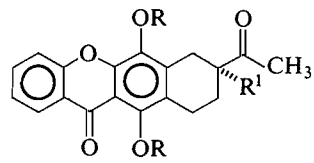

18 R = R' = H
20 R = CH_2Ph, R' = H
24 R = CH_2Ph, R' = OH

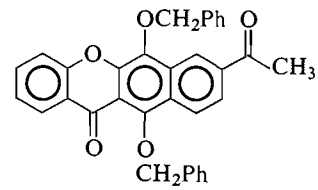

22

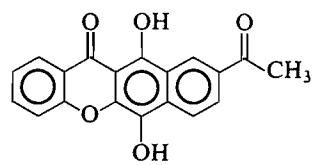

23

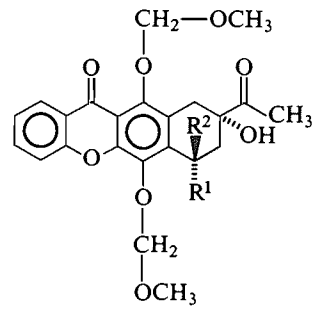

26 R' = OH, R^2 = H
27 R' = H, R^2 = OH

phenols **15** and **16**; hydrolysis by trimethyl chlorosilane (15) or potassium cyanide in dimethylsulfoxide (16) gave only a mixture of partially demethylated products.

Oxidative cyclization of **15** and **16** by lead tetracetate gave the tetracyclic xanthones **17** and **18** in excellent yield. Large scale separation of **17** and **18** was accomplished easily by column chromatography of their corresponding dibenzyl ethers **19** and **20** on silica, followed by acid hydrolysis. Structure assignment to **19** and **20** based on spectroscopic data was inconclusive. However, the first isomer collected had a dipole moment of 3.5 D and was assigned structure **20**, the calculated value of which was 3.48 D. The second isomer collected from the column had a dipole moment of 4.1 D and was assigned structure **19**, the calculated value of which was 4.9 D. Dipole moments of **19** and **20** were calculated using the reported dipole moment of xanthone, 3.14 D (17), and published values for benzene solution group moments (18).

Oxidation of **19** by molecular oxygen in the presence of potassium *tert*-butoxide in *N*,*N*-dimethylformamide solution gave a good yield of the dihydroxyxanthone **21** (19). Attempts to form an isopropylidene derivative of, or to debenzylate **21** invariably led to aromatization of ring D (**23**). Oxidation of isomer **20** under similar conditions yielded the monohydroxylated xanthone (**24**) or the aromatized product (**22**) depending on the length of the oxidation process. However, methoxymethylation of **17** with chloromethyl methyl ether under proper conditions gave an excellent yield of **25** which, under similar oxidation conditions, gave **26** as the major product and **27** as the minor product. The *cis*-geometry of the C-7

Can. J. Chem. Downloaded from www.nrcresearchpress.com by 210.87.254.105 on 09/06/12
For personal use only.

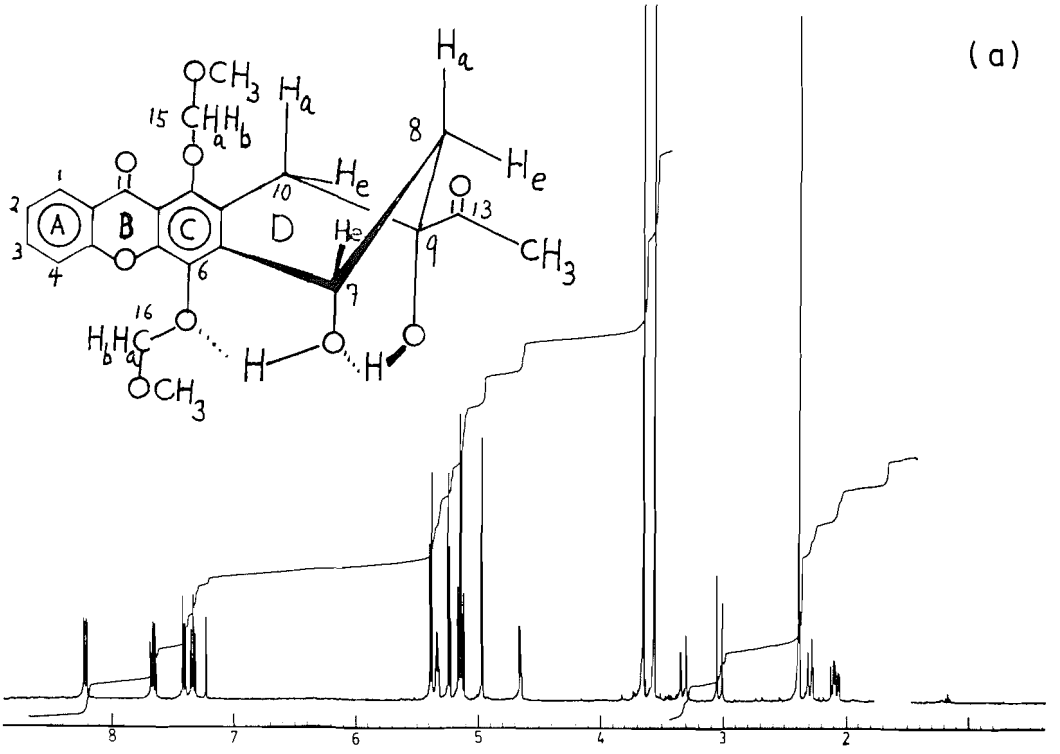

FIG. 1. (a)–(d) Bruker WH-400 ^{1}Hmr spectrum of **26** and the first order analysis of C_{15}, C_{16}, and D-ring protons. (a) Complete spectrum of **26** in $CDCl_3$.

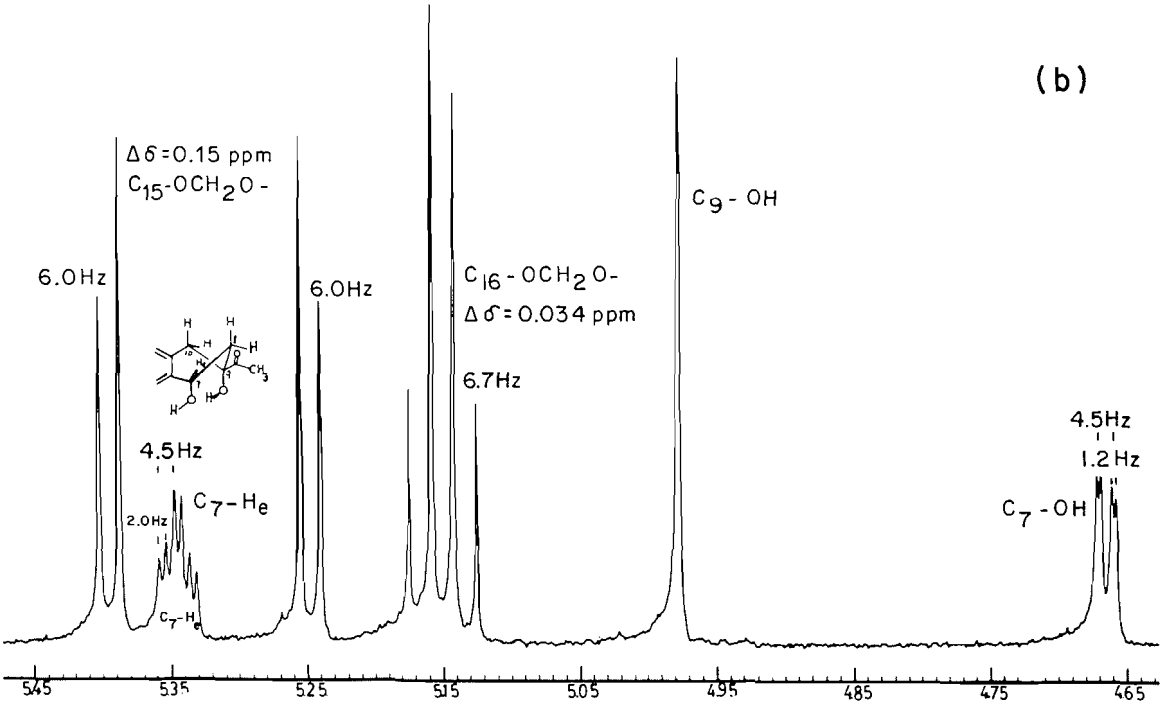

FIG. 1. (b) Expanded area between 4.65–5.45 ppm corresponding to C_7—H_e, C_7—OH, C_{15}—OCH_2O—, and C_{16}—OCH_2O—.

and C-9 hydroxy functions of **26** was established by detailed analysis of the high field ^{1}Hmr spectrum and computer simulated ^{1}Hmr spectrum of the D-ring of **26** (Figs. 1(a)–1(d) and 2).

The C_7—H_e appears as doublets of a triplet at 5.343 ppm. Its quasi-equatorial position is locked by the hydrogen-bond formation between the C_7—OH proton and the C_6-phenolic oxygen and revealed by the coupling constants. The $J_{7e,8a} = 4.5$ Hz corresponds to a dihedral angle of 45° and $J_{7e,8e} = 2.1$ Hz corresponds to a dihedral angle of 60°. The $J_{7e,7OH} = 4.6$ Hz corresponds to a dihedral angle of 40°, which agrees well with the H—O—C_7—H angle when the hydroxy proton hydrogen-bonds the C_6 oxygen. The C_7—OH appears as a quartet at 4.665 ppm due to coupling with C_7—H_e ($J_{7e,7OH} = 4.6$ Hz) and

Can. J. Chem. Downloaded from www.nrcresearchpress.com by 210.87.254.105 on 09/06/12
For personal use only.

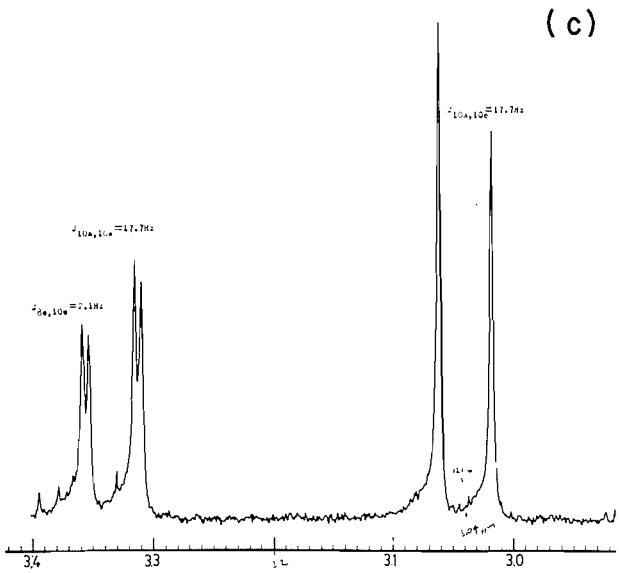

FIG. 1. (c) Expanded area between 3.0–3.4 ppm corresponding to C_{10}—H_aH_e.

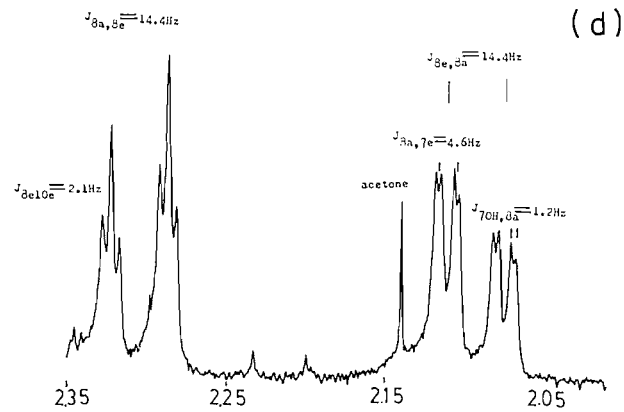

FIG. 1. (d) Expanded area between 2.05–2.35 ppm corresponding to C_8—H_aH_e.

C_8—H_a ($J_{7OH,8a}$ = 1.2 Hz). The latter is a four-bond coupling which is discernible only if the C_7—OH is locked by hydrogen bonding as suggested. The C_8—H_e appears as triplets of a doublet at 2.305. Its geminal coupling is $J_{8a,8e}$ = 14.4 Hz and its vicinal coupling is $J_{8e,7e}$ = 4.5 Hz and its four-bond coupling is $J_{8e,10e}$ = 2.1 Hz. The C_8—H_a appears at 2.092 as doublets of a quartet due to couplings with C_8—H_e ($J_{8a,8e}$ = 14.4 Hz), C_7—H_e ($J_{8a,7e}$ = 4.5 Hz), and C_7—OH ($J_{8a,7OH}$ = 1.2 Hz). The C_{10}—H_e appearing at 3.335 ppm as a quartet couples with C_{10}—H_a ($J_{10e,10a}$ = 17.7 Hz) and C_8—H_e ($J_{10e,8e}$ = 2.1 Hz). The C_{10}—H_a at 3.04 ppm appearing as a doublet couples to C_{10}—H_e only ($J_{10a,10e}$ = 17.7 Hz). Figures 1 and Fig. 2 show the ^{1}Hmr spectrum, including the conformation of the D-ring, and the computer simulated spectrum of the D-ring of **26**, respectively. The complete analysis of the ^{1}Hmr spectrum of **27** is difficult due to the presence of a slow equilibrium between **27** and **28**. The infrared spectrum shows a weak absorption at 1715 cm^{-1}; two methyl peaks at 2.39 ppm and 1.36 ppm integrated for 3 protons correspond to the C_{13}—CH_3 of **27** and **28**; two peaks at 3.60 ppm and 3.66 ppm integrated for 3 protons are tentatively assigned to C_{16}—O—CH_3 and two peaks at 3.703 and 3.708 ppm integrated for 3 protons are tentatively assigned to C_{15}—O—CH_3 of **27** and **28**; a quartet at

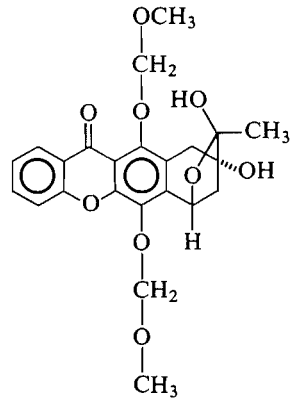

28

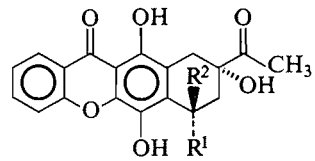

29 R^1 = OH, R^2 = H
30 R^1 = H, R^2 = OH

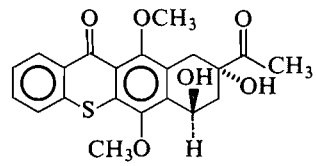

31

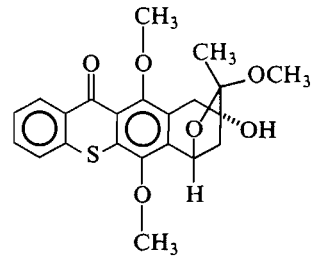

32

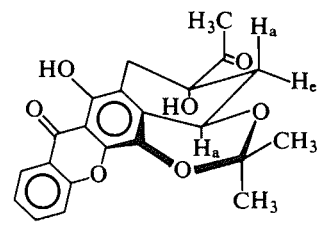

33

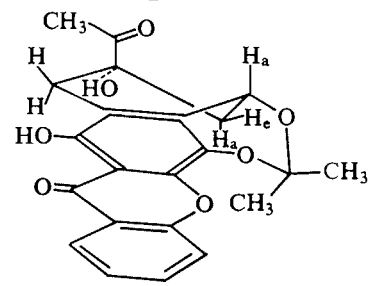

34

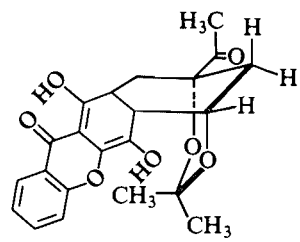

35

5.324 ppm ($J_{15a,15b}$ = 6.1 Hz, $\Delta\delta_{Ha,Hb}$ = 0.152 ppm) and a singlet at 5.211 ppm, together integrated for 2 protons, are assigned to the C_{15}—H_2 of **27** and **28**, respectively; a quartet at 5.159 ppm ($J_{16a,16b}$ = 6.2 Hz, $\Delta\delta_{Ha,Hb}$ = 0.034 ppm) and a singlet at 5.169 ppm, together integrated for 2 protons, are assigned to the C_{16}—H_2; a doublet at 5.475 ppm ($J_{7OH,7H}$ = 5.8 Hz) and a singlet at 4.16 ppm, together integrated for one proton, are assigned to the C_7—OH of **27** and **28**; a broad doublet of a triplet at 5.432 ppm integrated for one proton is assigned to the C_7—H which is spin–spin coupled to C_7—OH ($J_{7H,7OH}$ = 5.8 Hz), C_8—H_a ($J_{7H,8a}$ = 6.3 Hz), and C_8—H_e ($J_{7H,8e}$ = 2.0 Hz). The C_9—OH appears as two singlets at 3.0 and 3.10 ppm, integrated for one proton. Similar equilibrium also exists in the thioxanthodaunomycinone derivative (**31**) which reacts with excess 2,2-dimethoxypropane in the pres-

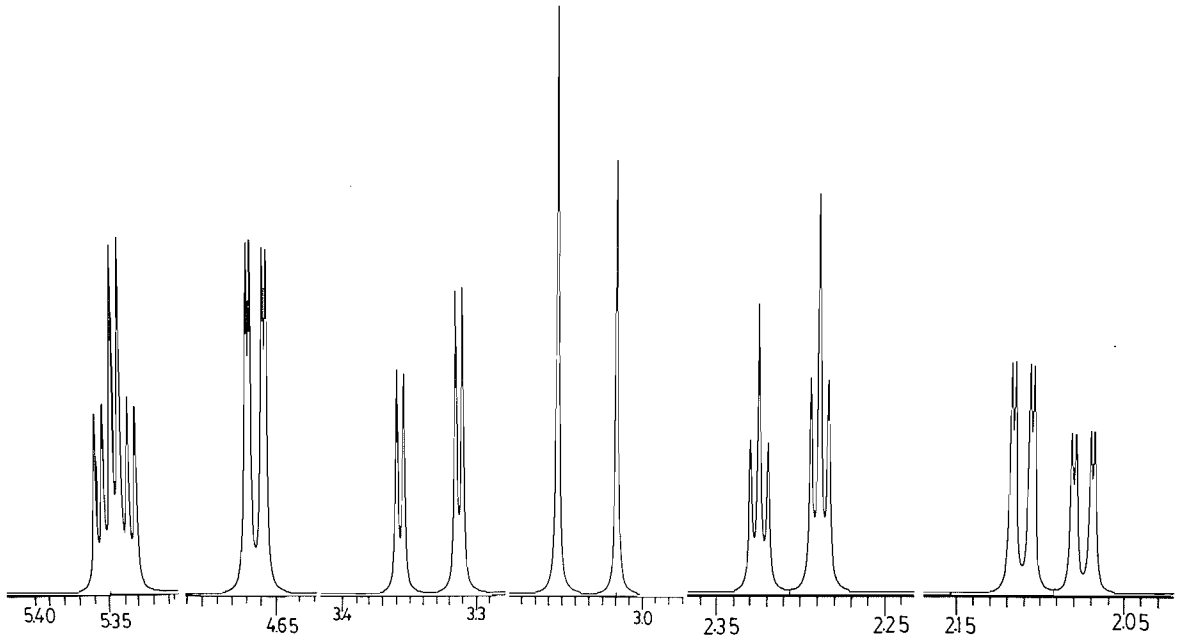

FIG. 2. Computer simulated spectrum of C_7—H_e, C_7—OH, C_8—H_aH_e, and C_{10}—H_aH_e.

ence of anhydrous *p*-toluenesulfonic acid to give exclusively **32**.[4]

Hydrolysis of **26** in dilute hydrochloric acid – acetone solution gave **29**, while **27** under similar conditions gave **30**. Both **26** and **27**, upon dissolving in trifluoroacetic acid followed by the addition of water, could be converted to a mixture of **29** and **30**. Reaction of **29** or **30** with dimethoxypropane in the presence of *p*-toluene sulfonic acid gave two isopropylidene derivatives, **33** and **34**, instead of **35**. This conclusion was arrived at solely on the basis of the coupling constants of the C_7—H of **33** and **34**. A Dreiding model of **33** shows that the H_7—C_7—C_8—H_{8a} extends a dihedral angle of about 180° and H_7—C_7—C_8—H_{8e} extends a dihedral angle of 60°, while **34** has the two corresponding dihedral angles of 160° and 40°. Thus, it is possible to come to a conclusion, according to the Karplus approximation, that the C_7—H spin–spin coupling constants of **33** and **34** will not differ greatly. However, in the case of **35**, the H_7—C_7—C_8—H_{8a} and H_7—C_7—C_8—H_{8e} can each extend a dihedral angle of about 60° and the C_7—H is likely to appear as a triplet (J = 2 Hz approximately) rather than as a quartet, in the case of **33** at 4.88 ppm ($J_{7a,8a}$ = 11 Hz, $J_{7a,8e}$ = 5.5 Hz) and in the case of **34** at 5.26 ppm ($J_{7a,8e}$ = 7 Hz). The isopropylidene methyl groups of **33** seem to be equivalent and appear as a 6-proton singlet while the isopropylidene methyl groups of **34** are nonequivalent. One methyl group appears at 1.72 ppm and the other is moved upfield to 1.63 ppm due to the shielding effect of the C-ring.

Preliminary in vitro cytotoxicity assays done in our laboratory using tumor cells MCF-7, a human breast cancer cell line, as indicator showed that both 34-demethoxyxanthodaunomycinone (**29**) and 4-demethoxy-7-epixanthodaunomycinone (**30**) were weakly cytotoxic. Daunomycinone, the aglycone of daunomycin (**2**), showed no cytotoxicity under similar conditions.

A more detailed study of the biological properties of 4-demethoxyxanthodaunomycin (**9**), 4-demethoxythioxanthodaunomycin (**10**), and 4-demethoxy-5-sulfoxodaunomycin (**11**) will be reported in later communications.

[4]Unpublished work by the authors; see also ref. 19*b*.

Experimental

All melting points were recorded on a Fischer–Johns apparatus and were uncorrected. Nuclear magnetic resonance spectra were recorded on a Varian spectrometer A56/60A or a HA 100, Bruker WH-90, or Bruker WH-400 spectrometer, using tetramethylsilane as internal standard unless otherwise specified. Infrared spectra were recorded on a Perkin–Elmer 710 infracord and dipole moments were taken on a DM01 Kahl dipolometer. Mass spectra were recorded on a Finnigan 1015 or a A.E.I. MS-50. Elemental analyses were performed by C. Daessle or Geller Laboratories.

*Preparation of 2-acetyl-5,8-dimethoxy-7-(2-methoxybenzoyl)tetralin (**13**) and 2-acetyl-5,8-dimethoxy-6-(2-methoxybenzoyl)tetralin (**14**)*

To a solution of trifluoracetic anhydride (38 mL) and 2-methoxybenzoic acid (40 g) was added 2-acetyl-5,8-dimethoxytetralin (12 g) followed by trifluoracetic acid (5 mL), keeping the temperature of the solution at 18–20°C. A second portion of trifluoroacetic acid (10 mL) was added after the solution was stirred for 1 h and stirring was continued for a total of 9 h. The trifluoroacetic acid was removed under reduced pressure and the residue was dissolved in chloroform (300 mL). The chloroform solution, washed with water, saturated sodium bicarbonate solution (3 × 100 mL), and dried over magnesium sulfate, was evaporated under reduced pressure to give a tinted clear residue (23 g); ir (cm^{-1}): 1710 ($COCH_3$), 1660 (phenone); ^{1}Hmr (δ): 7.6–7.35 (m, 2H, aromatic), 7.15–6.83 (m, 2H, aromatic), 6.90 (s, 1H, aromatic), 3.77 (s, 3H, —OCH_3), 3.70 (s, 3H, OCH_3), 3.46 (s, 3H, OCH_3), 2.22 (s, 3H, $COCH_3$); ms: 368 (M^+), 353, 325. *Mol. Wt.* (high resolution ms) calcd. for $C_{22}H_{24}O_5$: 368.1624; found: 368.1630.

*2-acetyl-5,8-dihydroxy-7-(2-hydroxybenzoyl)tetralin (**15**) and 2-acetyl-5,8-dihydroxy-6-(2-hydroxybenzoyl)tetralin (**16**)*

Aluminium chloride (40 g) was added to a chloroform solution (400 mL) of **13** and **14** (13 g) and stirred mechanically at room temperature for 25 h. The excess of aluminium chloride was decomposed by water and the chloroform solution washed with saturated oxalic acid solu-

Can. J. Chem. Downloaded from www.nrcresearchpress.com by 210.87.254.105 on 09/06/12
For personal use only.

Can. J. Chem. Downloaded from www.nrcresearchpress.com by 210.87.254.105 on 09/06/12
For personal use only.

tion, water, and saturated sodium bicarbonate solution and dried over magnesium sulfate, then evaporated under reduced pressure. The residue was dissolved in methylene chloride (20 mL) and ether (20 mL) from which a yellow crystalline product (3 g) was collected. The mother liquor was subjected to column chromatography on silica and an additional amount of yellow crystalline product (1.5 g) was isolated. Isomer **15** could be isolated after tedious recrystallizations (5×) from acetone, mp 224–227°C; ir(cm^{-1}): 3570 (phenol —OH), 3600–2900 (chelated phenolic H), 1705 (—$COCH_3$), 1620 (phenone), 1600, 1580 (aromatic); ^{1}Hmr (δ): 11.5 (chelated OH), 9.60 (br s, chelated OH), 8.05 (br s, nonchelated OH), 7.7–7.3 (m, 2H, aromatic), 7.15–7.85 (m, 3H, aromatic), 2.24 (s, 3H, $COCH_3$), ms: 326 (M^+), 309, 279, 232. *Mol. Wt.* (high resolution ms) calcd. for $C_{19}H_{18}O_5$: 326.1153; found: 326.1154. *Anal.* calcd. for $C_{19}H_{18}O_5$: C 69.93, H 5.52; found: C 70.11, H 5.44. The combined mother liquor was evaporated to dryness and some of the solid residue was subjected to high pressure liquid chromatographic separation on a silica column. The first isomer (**16**) collected was recrystallized from acetone, mp 208–211°C. Spectroscopic properties are similar to those of **15**. Structures were established by comparing the oxidative cyclization products with those obtained from the hydrolysis of **19** and **20** (*vide infra*).

7,8,9,10-Tetrahydro-6,11-dihydroxy-9-acetylxanthen-12-one (17) and 7,8,9,10-tetrahydro-6,11-dihydroxy-9-acetylxanthen-5-one (18)

The isomeric mixture of **15** and **16** (3 g) together with lead tetraacetate (4.4 g) in glacial acetic acid (8 mL) was ground in a mortar for 20 min at ambient temperature. The acidic slurry was washed into a separatory funnel and extracted with ethyl acetate (4 × 200 mL). The combined ethyl acetate solution was stirred with sodium thiosulfate solution (10%, 100 mL) for 2 h at room temperature, washed with water, and dried over magnesium sulfate. Evaporation of the solvent to dryness gave a yellow solid residue (2.6 g) which was purified by recrystallization from acetone, mp 219–225°C; separation could be done easily via the dibenzyl derivatives **19** and **20**.

Separation of 17 and 18

The isomeric mixture of **17** and **18** (4 g), benzyl bromide (8 mL), and pulverized anhydrous potassium carbonate (20 g) in acetone (300 mL) was heated under reflux for 14 h in a nitrogen atmosphere. The acetone solution was cooled, filtered, and evaporated to give an oily residue which was subjected to further evacuation and heating to remove the excess benzyl bromide and acetone dimer. The residue, which could be easily crystallized from ether on standing, was separated by column chromatography on silica (DSF-256 Merck) into its components (**19** and **20**) using toluene as eluent. Isomer **20** (2.6 g) was recrystallized from methylene chloride – ether, mp 119–120°C; ir (cm^{-1}): 1710 ($COCH_3$), 1660 (phenone), 1600 (aromatic); ^{1}Hmr (δ): 8.35 (dd, 1H, C_1—H, $J_{1,2}$ = 7 Hz, $J_{1,3}$ = 2 Hz, aromatic), 7.78–7.33 (m, 14H, aromatic), 5.17 (s, 2H, C_6—O—CH_2Ph), 5.09 (q, 2H, C_{12}—O—CH_2Ph, J_{gem} = 10 Hz, Δδ = 0.14 ppm), 2.18 (s, 3H, $COCH_3$); ms: 504, 413, 323. *Mol. Wt.* (high resolution ms) calcd. for $C_{33}H_{28}O_5$: 504.1937; found 504.1942; dipole moment estimated for **20**: 3.5 D; found: 3.48 D.

Heating **20** (2.2 g) in an acidic methanolic solution (concentrated hydrochloric acid 25 mL, methanol 50 mL) under reflux for 16 h gave the xanthone **18** (1.4 g) which was purified by recrystallization from acetone, mp 239–242°C; ir (cm^{-1}): 3650 (OH), 3400–2900 (chelated phenolic H), 1705 ($COCH_3$), 1650, 1630 (phenone), 1610 (aromatic); ^{1}Hmr (δ): 12.10 (s, 1H, chelated, OH), 8.26 (d,d 1H, $J_{3,4}$ = 7 Hz, $J_{2,4}$ = 1.8 Hz, aromatic), 7.30–7.80 (m, 3H, aromatic), 5.25 (br s, 1H, —OH), 2.31 (s, 3H, $COCH_3$); ms: 324 (M^+), 309, 281. *Mol. Wt.* (high resolution ms) calcd. for $C_{19}H_{16}O_5$: 324.0998; found: 324.1002.

Isomer **19** (2 g) was recrystallized from methylene chloride – ether, mp 138–140°C; estimated dipole moment for **19**: 4.9 D, found: 4.19 D. Spectroscopic data are similar ro those of **20** above. *Anal.* calcd. for $C_{33}H_{28}O_5$: C 78.57, H 5.56; found: C 78.47, H 5.65. Debenzylation as in the case of **20** gave **17** (1.2 g), which was also purified by recrystallization from acetone, mp 264–267°C; spectroscopic data are similar to those of **18**.

7,8,9,10-Tetrahydro-9-acetyl-6,11-dimethoxymethylenoxyxanthen-12-one (25)

Chloromethyl methyl ether (5 mL), freshly prepared by passing distilled chloromethyl methyl ether through an alumina column (G-1, neutral), was added dropwise under a nitrogen atmosphere to an anhydrous acetone solution (200 mL) containing freshly baked pulverized potassium carbonate (20 g) and **17** (1.2 g). The solution was heated under reflux for 4 h, cooled, filtered, and concentrated. Methylene chloride was added to the residue and the solution was filtered to remove the potassium carbonate, evaporated under reduced pressure, and finally subjected to further evacuation and heating to remove the acetone dimer. The clear residue (1.48 g), upon addition of ether, crystallized and was recrystallized from methylene chloride – ether, mp 152–154°C; ir (cm^{-1}): 1710 ($COCH_3$), 1660 (phenone), 1605 (aromatic); ^{1}Hmr (δ): 8.27 (dd, 1H, $J_{1,2}$ = 8 Hz, $J_{1,3}$ = 2 Hz, C_1—H), 8.0–7.33 (m, 3H, aromatic), 5.22 (s, 2H, —O—CH_2—O—), 5.20 (s, 2H, —OCH_2—O—), 3.70 (s, 3H, —OCH_3), 3.66 (s, 3H, OCH_3), 2.28 (s, 3H, $COCH_3$); ms: 412 (M^+), 381, 367, 337. *Mol. Wt.* (high resolution ms) calcd. for $C_{23}H_{24}O_7$: 412.1515; found: 412.1519.

*4-Demethoxy-bis-*O*-methoxymethylxanthodaunomycinone (26) and 4-demethoxy-bis-*O*-methoxymethyl-7-epixanthodaunomycinone (27)*

Potassium *tert*-butoxide (850 mg) was added to a solution of anhydrous dimethylformamide (150 mL) and *tert*-butyl alcohol (20 mL). The solution was stirred with occasional warming until the solid material was completely dissolved and then cooled in a −25°C cold bath. Trimethyl phosphite (2.7 mL) was added, followed by the xanthone (**25**) (900 mg). Dry oxygen was introduced into the solution through a gas-dispersion tube, keeping the cold bath between −25°C and −15°C for 1.5 h. Cold dilute hydrochloric acid (0.1 *M*) was added to the solution, with vigorous stirring, until the pH = 8.

Water (300 mL) was added to the solution which was exhaustively extracted with chloroform (3 × 200 mL). The combined chloroform extracts, washed with water and dried over magnesium sulfate, were concentrated under reduced pressure to give a residue which was subjected to further heating under vacuum until it was free of dimethyl formamide. The semi-solid residue was subjected to preparative thin-layer chromatographic separation and **26** (420 mg) was isolated and recrystallized from acetone–ether, mp 162–164°C; ir (cm^{-1}): 3430 (OH), 1715 ($COCH_3$), 1660 (phenone), 1605 (aromatic); ^{1}Hmr (δ): 8.236 (dd, C_1—H, $J_{1,2}$ = 7.8 Hz, $J_{1,3}$ = 2.0 Hz), 7.70–7.33 (m, 3H, aromatic), 5.324 (q, 2H, J_{gem} = 6.1 Hz, Δδ = 0.148 ppm, C_{11}—O—CH_2—O—), 5.345 (dt, 1H, C_7—He, $J_{7e,7OH}$ = 4.6 He, $J_{7e,8a}$ = 4.5 Hz, $J_{7e,8e}$ = 2.1 Hz), 5.151 (q, 2H, C_6—OCH_2O—, J_{gem} = 6.7 Hz, Δδ = 0.034 ppm), 4.98 (s, 1H, C_9—OH), 4.665 (q, 1H, C_7—OH, $J_{7e,OH}$ = 4.6 Hz, $J_{7OH,8a}$ = 1.2 Hz), 3.66 (s, 3H, OCH_3), 3.57 (s, 3H, OCH_3) 3.335 (q, 1H, C_{10}—H_e, $J_{10a,10e}$ = 17.7 Hz, $J_{10e,8e}$ = 2.1 Hz), 3.04 (d, 1H, C_{10}—H_a, $J_{10a,10e}$ = 17.7 Hz), 2.38 (s, 3H, $COCH_3$), 2.305 (td, 1H, C_8—H_e, $J_{8a,8e}$ = 14.4 Hz, $J_{8e,7e}$ = 2.1 Hz, $J_{8e,10e}$ = 2.1 Hz), 2.092 (dq, 1H, C_8—H_a, $J_{8a,8e}$ = 14.4 Hz, $J_{8a,7e}$ = 4.5 Hz, $J_{8a,7OH}$ = 1.2 Hz) (Fig. 1); ms: 444 (M^+), 414, 426, 382. *Mol. Wt.* (high resolution ms) calcd. for $C_{23}H_{24}O_9$: 444.1413; found: 444.1411.

The minor isomeric product (**27**) (140 mg) was isolated and purified by recrystallization from acetone–ether, mp. 156–158°C; ir (cm^{-1}): 3560 (OH), 3470 (OH), 1715 ($COCH_2$, weak), 1660 (phenone), 1605 (aromatic); ms: 444 (M^+), 414, 382; ^{1}Hmr: the presence of a slow equilibrium between **27** and **28** makes the complete analysis of the ^{1}Hmr spectrum difficult. Reaction of **26** and **27** with trifluoroacetic acid followed by water led to the formation of both **29** and **30** in the same ratio.

4-Demethoxyxanthodaunomycinone (29) and 4-demethoxy-7-epixanthodaunomycinone (30)

To a stirred solution of acetone (20 mL) containing **26** (180 mg) was added dropwise concentrated hydrochloric acid (1/2 mL) at room temperature and the stirring was continued for 6 h. The solution, diluted with water (50 mL), was extracted with ethyl acetate (3 × 100 mL). The combined extracts, washed with saturated sodium bicar-

Can. J. Chem. Downloaded from www.nrcresearchpress.com by 210.87.254.105 on 09/06/12
For personal use only.

bonate solution and dried over magnesium sulfate, were evaporated to dryness to give the yellow crystalline 4-demethoxyxanthodaunomycinone **29** (130 mg) which was purified by recrystallization from acetone, mp 216–218°C; ir (cm^{-1}): 3550–2900 (OH), 1710 ($COCH_3$), 1660 (weak), 1635 (strong) (hydrogen-bonded phenone), 1615, 1600 (aromatic); ^{1}Hmr (δ) (DMSO-d_6): 12.17 (s, 1H, hydrogen-bonded C_{11}—OH), 9.24 (br s, 1H, C_6—OH), 8.20 (dd 1H, C_1—H, $J_{1,2}$ = 8 Hz, $J_{1,3}$ = 1.5 Hz), 8.02–7.41 (m, 3H, aromatic), 5.97 (s, 1H, C_9—OH), 5.63 (br s, 1H, C_7—OH), 5.13 (br t, 1H, C_7—H, J = 5 Hz), 2.87 (q, 2H, C_{10}—H_aH_e, J_{gem} = 8 Hz, Δδ = 0.12 ppm), 2.26 (s, 3H, $COCH_3$), 2.12 (br d, 2H, C_8—H_aH_e, J_{gem} = 5 Hz); ms: 356 (M^+), 338, 320, 305, 295. *Anal.* calcd. for $C_{19}H_{16}O_7$: C 64.05, H 4.53; found: C 64.09, H 4.51.

Hydrolysis of **27** to 4-demethoxy-7-epixanthodaunomycinone (**30**) was done similarly; mp 199–202°C. *Mol. Wt.* (high resolution ms) calcd. for $C_{19}H_{16}O_7$: 356.0891; found: 356.0893.

*Isopropylidenes **33** and **34***

The xanthone **30** (15 mg) was added to an anhydrous benzene solution (20 mL) containing toluenesulfonic acid (10 mg) and freshly distilled 2,2-dimethoxypropane (0.1 mL). The solution was stirred for 5 h at room temperature, washed with saturated sodium bicarbonate solution, dried over magnesium sulfate, and evaporated to dryness under reduced pressure. Two crystalline products **33** (3 mg) and **34** (4 mg) in addition to two other minor compounds were isolated by tlc on silica. The isopropylidene (**33**) was recrystallized from methylene chloride and ether, mp 204–206°C; ir (cm^{-1}): 3550 (C_6—OH), 3550–2900 (C_{11}—OH), 1710 ($COCH_3$), 1650 (weak), 1630 (strong) (phenone), 1610, 1600 (aromatic); ^{1}Hmr (δ): 12.39 (s, 1H, C_{11}—OH), 8.28 (dd, 1H, C_1—H, $J_{1,2}$ = 8 Hz, $J_{1,3}$ = 2 Hz), 7.86–7.30 (m, 3H, aromatic), 5.25 (dd, 1H, C_7—H, $J_{7e,8e}$ = 11 Hz, $J_{7e,8a}$ = 6 Hz), 4.28 (s, 1H, C_6—OH), 3.01 (q, 2H, C_{10}—H_eH_a, $J_{10e,10a}$ = 18 Hz, Δδ = 0.55 ppm), 2.26 (s, 3H, $COCH_3$), 2.12 (dq, 2H, $J_{7e,8e}$ = 11 HZ, $J_{7e,8a}$ = 6 HZ, $J_{8a,8e}$ = 18 Hz, Δδ = 0.33 ppm), 1.71 (s, 6H, CH_3—C—CH_3); ms: 396 (M^+), 338, 320, 277. *Mol. Wt.* (high resolution ms) calcd. for $C_{22}H_{20}O_7$: 396.1203; found: 396.1208.

The isopropylidene **34** was recrystallized from methylene chloride – ether, mp 193–195°C; ir (cm^{-1}): 3480 (C_9—OH), 3500–2900 (C_{11}—OH), 1710 ($COCH_3$), 1650, 1630 (hydrogen-bonded phenone), 1610, 1600 (aromatic); ^{1}Hmr (δ): 12.42 (s, 1H, C_{11}—OH), 8.29 (dd, 1H, C_1—H, $J_{1,2}$ = 8 Hz, $J_{1,3}$ = 2 Hz), 7.88–7.31 (m, 3H, aromatic), 4.88 (dd, 1H, C_7—H, $J_{7e,8e}$ = 10 Hz, $J_{7e,8a}$ = 7 Hz), 3.01 (s, 1H, C_9—OH), 2.93 (q, 2H, C_{10}—H_aH_e, $J_{10a,10e}$ = 16 Hz, Δδ = 0.50 ppm), 2.41 (s, 3H, $COCH_3$), 2.27 (dq, 2H, C_8—H_aH_e, $J_{7e,8a}$ = 7 Hz, $J_{7e,8e}$ = 10 Hz, $J_{8e,8a}$ = 15 Hz, Δδ = 1.0 ppm), 1.70 (s, 3H, C—CH_3), 1.61 (s, 3H, C—CH_3); ms: 396 (M^+), 338, 320, 295, 277. *Mol. Wt.* (high resolution ms) calcd. for $C_{22}H_{20}O_7$: 396.1203: found, 396.1206.

Acknowledgements

Financial and material support from Farmatalia Carlo Erba of Italy and from NSERC are greatly appreciated.

1. (*a*) S. K. CARTER, A. DIMARCO, M. GHIONE, I. H. KRAKOFF, and G. MATHE. International Symposium on Adriamycin. Springer Verlag, 1972; (*b*) EORTC International Symposium Adriamycin Review. European Press Medikon, 1975.
2. (*a*) K. TATSUTA and T. TAKEUCHI. J. Antibiot. **33**, 1581 (1980); (*b*) H. UMEZAUN, Y. TAKAHASHI, M. KINOSHITA, and M. NAGANAWA. J. Antiobiot. **33**, 1581 (1980).
3. F. ARCAMONE. Doxorubicin anticancer antibiotics. Medicinal chemistry. Vol. 17. Academic Press, New York. 1981. p. 31.
4. A. DIMARCO, M. GAETANI, P. ONEZZI, B. M. SCARPINATO, R. SILVERTRINI, M. SOLDATI, T. DASDATI, T. DASDIA, and L. VALENTINI. Nature, **201**, 706 (1964).
5. W. J. PIGRAM, W. FALBER, and L. D. HAMILTON. Nature New Biology, **235**, 17 (1972).
6. T. W. PLUMBRIDGE and J. R. BROWN. Biochim. Biophys. Acta, **563**, 181 (1979).
7. N. R. BACHUR, S. L. GORDON, M. V. GEE, and H. KON. Proc. Natl. Acad. Sci. U.S.A., **76**, 954 (1979).
8. V. BERLIN and W. A. HASELTINE. J. Biol. Chem. **256**, 4747 (1981).
9. (*a*) A. C. SARTORELLI. Cancer chemotherapy. ACS Symposium Series 30, A.C.S., Washington, DC. 1976. pp. 71–86; (*b*) H. W. Moore. Science, **197**, 527 (1977).
10. T. R. TRITTON and G. YEE. Science, **217**, 248 (1982).
11. N. R. BACHUR. Cancer Res. **38**, 1945 (1978).
12. P. HOCHSTEIN. Biochem. Biophys. Res. Commun. **77**, 797 (1977).
13. A. MYRES. Cancer Chemother. Rep. **60**, 961 (1976).
14. (*a*) C. M. WONG, R. SCHWENK, D. POPIEN, and T. L. HO. Can. J. Chem. 466 (1973); (*b*) C. M. WONG, H. Y. P. LAM, W. HAQUE, A. Q. MI, and G. S. YANG. Can. J. Chem. **61**, 562 (1983).
15. T. MORITA, Y. OKAMOTO, and H. SAKURAI. J. Chem. Soc. Chem. Commun. 874 (1978).
16. J. R. MCCARTHY, J. L. MOORE, and R. J. CREGGE. Tetrahedron Lett. 5183 (1978).
17. C. G. LEFEVRE and R. J. W. LEFEVRE. J. Chem. Soc. 196 (1937).
18. V. I. MINKIN, O. A. OSIPOV, and Y. A. ZHDANOV. Dipole moment in organic chemistry. Plenum Press, New York. 1970. p. 91.
19. (*a*) C. E. COBURN, D. K. ANDERSON, and J. S. SWENTON. J. Chem. Soc. Chem. Commun. 987 (1982); (*b*) C. M. WONG, A. Q. MI, W. HAQUE, and H. Y. LAM. Synth. Commun. **13**, 15 (1983).

The metal nuclear magnetic resonance spectra of some tin(II) and lead(II) complexes with polydentate phosphines

PHILIP A. W. DEAN

Department of Chemistry, University of Western Ontario, London, Ont., Canada N6A 5B7

Received July 9, 1982[1]

PHILIP A. W. DEAN. Can. J. Chem. **61**, 1795 (1983).

The previously reported 1:1 complexes formed in $MeNO_2$ between $M(SbF_6)_2$ (M = Sn or Pb) and $Ph_2P(CH_2)_2PPh_2$, $PhP[(CH_2)_2PPh_2]_2$, $MeC(CH_2PPh_2)_3$, $P[(CH_2)_2PPh_2]_3$, and $[Ph_2P(CH_2)_2]_2P(CH_2)_2\overset{+}{P}HPh_2$ have been studied by metal (^{119}Sn or ^{207}Pb) nmr. The metal chemical shifts span the comparatively narrow range of −586 to −792 ppm and 60 to −269 ppm, relative to the resonance of MMe_4, for ^{119}Sn and ^{207}Pb nmr, respectively. The implications of these data regarding the denticity of the ligand in $M(P[(CH_2)_2PPh_2]_3)^{2+}$ are discussed, and a comparison with the metal nmr spectra of related stannous and plumbous complexes is made.

PHILIP A. W. DEAN. Can. J. Chem. **61**, 1795 (1983).

Faisant appel à la rmn du métal (^{119}Sn ou ^{207}Pb), on a étudié les complexes du type 1:1, formés dans le $MeNO_2$, entre le $M(SbF_6)_2$ (M = Sn ou Pb) et le $Ph_2P(CH_2)PPh_2$, le $PhP[(CH_2)_2PPh_2]_2$, le $MeC(CH_2PPh_2)_3$, le $P[(CH_2)_2PPh_2]_3$, et le $[Ph_2P(CH_2)_2]_2P(CH_2)_2\overset{+}{P}HPh_2$. Les déplacements chimiques du métal s'étendent sur l'intervalle comparativement étroit de −586 à −792 ppm et de 60 à −269 ppm par rapport à la résonance du MMe_4 pour le ^{119}Sn et le ^{207}Pb respectivement. On discute des implications de ces données en fonction du caractère donneur du ligand dans le $M(P[(CH_2)_2PPh_2]_3)^{2+}$ et on les comparées avec les spectres du métal des complexes stanneux et plombeux apparentés.

[Traduit par le journal]

Introduction

In recent work from this laboratory the ^{31}P nmr spectra of some new stannous and plumbous complexes with a variety of polydentate phosphines were presented (1), the complexes being prepared *in situ* from $M(SbF_6)_2$ (M = Sn or Pb) and the appropriate ligand in $MeNO_2$. For both metals, the observation of one bond metal–phosphorus couplings showed that these spectra were recorded under conditions where intermolecular ligand exchange was slow on the nmr timescale. However, the spectra of the complexes thought to be $M(PP_3)^{2+}$ (PP_3 = $P(CH_2CH_2PPh_2)_3$)[2] showed, in addition to unremarkable values for metal coupling to the unique phosphorus atom ($^1J(M—P_B)$ = 1482 and 2136 Hz for M = ^{119}Sn and ^{207}Pb, respectively), peculiarly small couplings to the nmr-equivalent terminal phosphorus atoms, P_A: 705 Hz for coupling to ^{119}Sn, compared with 1279–1665 Hz for other values of $^1J(^{119}Sn–^{31}P)$ observed; 476 Hz for coupling to ^{207}Pb, compared with 1714–2136 Hz for other values of $^1J(^{207}Pb–^{31}P)$ observed. Two possible explanations for these "anomalies" were considered: firstly the PP_3 complexes could contain the unusual (compared with the other complexes examined) MP_4 kernel, or, secondly, there could occur in these complexes one or more rapid intramolecular "end-on, end-off" exchange processes such as

[1]

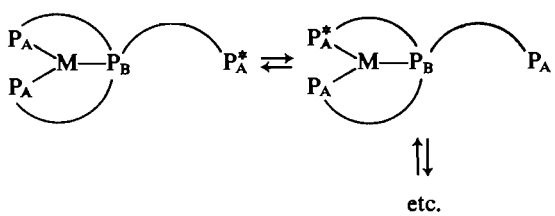

which would lead to values of $^1J(M—^{31}P)$ below those expected for a static M—P bond.

If the unusual ^{31}P nmr spectra of the $M(PP_3)^{2+}$ complexes is a manifestation of an unusual coordination kernel, it seems reasonable that the metal nmr chemical shifts of the PP_3 complexes should show significant differences from the corresponding shifts of species with "normal" ^{31}P nmr spectra. To allow the necessary comparison, metal nmr spectra have now been obtained for most of the phosphine complexes reported earlier, and are described and discussed in the present paper. Quite apart from any structural implications, these data are of some intrinsic interest, as this is one of a very limited number of instances where metal nmr spectra have been reported for analogous complexes of divalent tin and lead (2).

Experimental

Preparation of samples for metal nmr

Samples with metal concentration 0.22 *m* (≡ 2.5×10^{-4} mol/mL $MeNO_2$, approximately the same concentration used for our earlier ^{31}P nmr study (1)) were prepared by the procedure reported earlier (1): under dry nitrogen, the appropriate molar ratio (M:L ≈ 1:0.8 for all of the phosphine complexes except $M(PP_2(PH))^{3+}$ for which, for best results (cleanest spectra), M:L ≈ 1:0.45) of solid $M(SbF_6)_2$ and ligand were combined in a baked out (140°C) nmr tube hand made of 8 mm od standard wall Pyrex tubing in the earlier part of this work and 9 mm od tubing in the later part; next, outside the glove box, freshly distilled $MeNO_2$ was added by standard N_2-vacuum techniques and the sample was cooled then flame sealed under vacuum, allowed to warm to room temperature and homogenized by shaking briefly (a few minutes). Thereafter the samples were stored in liquid nitrogen until used. Samples produced and stored in this way give reproducible ^{31}P and metal nmr spectra when fresh.

Phosphorus-31 nmr spectra

Prior to measurement of the metal nmr spectra, the 260 K 40.5 MHz $^{31}P-\{^1H\}$ nmr spectra were obtained to confirm the presence of the desired phosphine complexes. For ^{31}P nmr spectroscopy, 8 mm sample tubes were held concentrically in a 12 mm od nmr tube using a Teflon spacer, while the 9 mm tubes were a tight sliding fit in a conventional thin-walled 10 mm nmr tube which was held concentrically in the 12 mm nmr tube, but otherwise the spectra were recorded exactly as already described, using $(CD_3)_2CO/OP(OMe)_3$ (for reduced temperature) or $D_2O/OP(OMe)_3$ (for ambient probe tem-

---

[1]Revision received February 25, 1983.

[2]Abbreviations used in this paper: $Ph_2P(CH_2)_2PPh_2$ = dppe; $[Ph_2P(CH_2)_2]_2PPh$ = etp; $[Ph_2P(CH_2)_2]_3P$ = PP_3; $[Ph_2P(CH_2)_2]_2P(CH_2)_2\overset{+}{P}HPh_2$ = $PP_2(PH)^+$; $MeC(CH_2PPh_2)_3$ = tripod.

TABLE 1. Tin-119 nmr data for some tin(II) complexes with polydentate phosphines at 295 K in nitromethane

Complex[a]	δ_{Sn}[b] (ppm)	$^1J(^{119}Sn—^{31}P)$[c] (Hz) P_A[d]	P_B[d]	Description[e]
$Sn(O_2NMe)_x^{2+}$	−1540[f]			s
$Sn(dppe)^{2+}$	−586	~1740[g]		t
$Sn(etp)^{2+}$	−686	1593	1381	t of d
$Sn(tripod)^{2+}$	−792	1285		q
$Sn(PP_3)^{2+}$ [h]	−756	702	1478	q of d
$Sn(PP_2(PH))^{3+}$	−702	1574	1414	t of d

[a]For abbreviations used see footnote 2.

[b]Relative to the resonance of external $SnMe_4$ in $CDCl_3$; shifts were measured initially from the signal of $Sn(O_2NMe)_x^{2+}$ by sample interchange and converted to $SnMe_4$ as reference using $\delta_{(SnMe_4(CDCl_3))} = \delta_{(Sn(O_2NMe)_x^{2+}(MeNO_2))} - 1540$ ppm; shifts to higher frequency than the reference are taken as positive; estimated error in spectral measurement ≤ 1 ppm; linewidths of multiplet components were ≲ 25 Hz except where noted.

[c]Estimated error ±4 Hz, except where noted otherwise.

[d]P_A = —PPh_2; P_B = >PPh or >P—

[e]s = singlet; d = doublet; t = triplet; q = quartet; the splitting due to P_A is given first.

[f]$\nu_{1/2} \approx 3800$ Hz.

[g]$\nu_{1/2} \approx 550$ Hz.

[h]Values quoted for a solution in which $Sn/PP_3 = 1.12$ and the tin concentration is 0.22 *m* (see text).

perature) in the outer annulus as a deuterium lock/reference material (1).[3]

Metal nmr spectra

The 260 K and 295 K ^{119}Sn and ^{207}Pb nmr spectra were obtained using a Bruker WH-400 spectrometer operating at 149.21 and 83.71 MHz, respectively (at the resonance of the appropriate metal(IV) tetramethyl which was used as a reference),[3] without lock or proton-decoupling, with the stationary 8 mm or 9 mm od nmr tubes held in a 10 mm nmr tube by a Teflon spacer for the smaller tube and by the close fit of the two tubes for the larger tube. (The pulsed high power decoupler of this high field instrument was not used because it induces non-uniform temperature effects which, combined with the large temperature dependences of ^{119}Sn and ^{207}Pb nmr chemical shifts (see ref. 2 and later), causes unwanted line broadening. Not all of the home-made sealed tubes would spin satisfactorily, so for consistency all samples were measured stationary; with the linewidths measured here the reduction in resolution should be insignificant.) Typically, after initially locating the resonance(s) with a larger spectral window, satisfactory ^{119}Sn nmr spectra of the phosphine complexes in the 0.22 *m* solutions were obtained in several hundred transients using 65° (25 μs) pulses applied at 42 min^{-1} with a spectral window of 20 kHz and an acquisition time of 0.41 s. (In one case a sample with $Sn(SbF_6)_2:PP_3 \approx 1.6:1$, containing, initially, $Sn(PP_2(PH))^{3+}$ and $Sn(PP_3)^{2+}$, was run overnight (26000 transients) with a spectral window of 25 kHz; the spectra of decomposition products were then evident in the spectrum (see later).) Satisfactory ^{207}Pb nmr spectra were obtained in a similar length of time with similar operating conditions except that a 45° (19 μs) pulse was used.

In the interests of economy of instrument time, no attempt was made to locate any resonance from the generally small excess of metal ions that must be present in these solutions. However, such signals are clearly not in the chemical shift range of the phosphine complexes and almost certainly more shielded than this (Tables 1 and 2). The observation of one-bond metal phosphorus couplings in the ^{31}P and metal nmr spectra precludes a significant rate of intermolecular ligand exchange.

[3]Chemical shifts to higher frequency than the reference are taken as positive.

Results and discussion

Details of the 295 K ^{119}Sn nmr spectra of the various tin(II)–phosphine complexes found in fresh[4] nitromethane solutions are given in Table 1, and those of the 295 K ^{207}Pb nmr spectra of the corresponding lead(II)–phosphine complexes in Table 2. In general the linewidths of the ^{119}Sn nmr signals of the various stannous complexes were quite small (≲25 Hz), and the spectra observed for the dppe, etp, tripod, and $PP_2(PH)^+$ complexes were just the simple symmetrical splitting patterns (from $^1J(^{119}Sn-^{31}P)$) expected if the polydentate phosphines behave in a chelating (as opposed to bridging) manner, as has been deduced from the previously reported ^{31}P nmr spectra (1).[5] A representative ^{119}Sn nmr spectrum, that of $Sn(etp)^{2+}$, is shown in Fig. 1*a*. Similarly the ^{207}Pb nmr spectra of the analogous plumbous complexes were exactly as expected from the chelated structures proposed (1) on the basis of their ^{31}P nmr spectra,[5] allowing for the fact that the linewidths of the ^{207}Pb signals generally exceeded those found in the ^{119}Sn spectra of the analogous tin(II) species. In these spectra the broader lines mean that small signal separations were not resolved as can be seen, for example, in the ^{207}Pb nmr spectra of $Pb(etp)^{2+}$ (Fig. 1*b*) which is typical of those obtained in this work. The PP_3 complexes of tin(II) and lead(II) give a doublet of quartets in their respective metal nmr spectra (Tables 1 and 2), consistent with the real or time-averaged C_3 ligand symmetry implied by the published ^{31}P nmr data (1). As discussed below, the interpretation of the nmr spectra of these PP_3 complexes is not straightforward.

[4]As noted in ref. 1, both tin- and lead-containing solutions deteriorate over a period of hours at 308 K. This decomposition has not been studied in detail, and with one exception no evidence for decomposition was found in the time taken to measure the metal nmr spectra at 295 K. In one case a sample with $Sn(SbF_6)_2:PP_3 \approx 1.6:1$ was run overnight and showed not only ^{119}Sn nmr spectra from $Sn(PP_3)^{2+}$ and $Sn(PP_2(PH))^{3+}$ but also two other multiplets: one at $\delta_{Sn} = -707$ ppm with a triplet splitting of 1562 Hz and a doublet splitting of 1425 Hz, the other at $\delta_{Sn} = -734$ ppm with a triplet splitting of 956 Hz and a doublet splitting of 1654 Hz. These are evidently tin(II)–phosphine species; the origin of the first is not clear, but the 956 Hz coupling is associated with a doublet–doublet ($\delta_P = 9.4$ ppm, $J = 10$ and 38 Hz) found in the 308 K ^{31}P nmr spectrum of $Sn(PP_3)^{2+}$-containing solutions which have been allowed to stand at room temperature for ca. 12 h.

[5]In ref. 1, the small magnitude of $^3J(P—P)$ was cited in support of chelating behaviour. In addition, several conceivable bridged structures can be discarded on the basis of the symmetry implied by the slow-exchange ^{31}P spectra reported in ref. 1. For the lead complexes, the absence in the ^{31}P or metal nmr spectra of any evidence for isotopomers such as $^{207}PbPb$, $^{207}Pb_2$ etc. (expected to have significant abundance because of the relatively high natural abundance of ^{207}Pb (21.11%)) seems to rule out all other possible ligand-bridged structures. For example, the ^{207}Pb satellites in the ^{31}P nmr spectrum of the 1:1 Pb^{2+}:dppe complex are sharp singlets consistent with the occurrence of chelating dppe and show no evidence for the P—P coupling expected in the X(^{31}P) part of the AXX′X″X‴ spin system of the dimer $^{207}Pb(dppe)_2Pb$. (P—P coupling can be sizeable for bridging dppe; see, for example, ref. 3.) By extension, the close similarity between the ^{31}P and metal nmr spectra of the tin(II) and lead(II) complexes implies chelated and not ligand-bridged structures for the stannous complexes too. Also, though the natural abundances of ^{119}Sn (8.68%) and ^{117}Sn (7.67%) are too low to allow unequivocal confirmation of the absence of isotopomers in the ^{31}P spectra of tin(II)–phosphine complexes, the linewidths in the ^{119}Sn spectra are much smaller than in the ^{207}Pb spectra so that second order coupling to ^{31}P should be easier to see.

TABLE 2. Lead-207 nmr data for some lead(II) complexes with polydentate phosphines at 295 K in nitromethane

Complex[a]	δ_{Pb}[b] (ppm)	Approximate $\nu_{1/2}$ of multiplet components (Hz)	$^1J(^{207}Pb—^{31}P)$[c] (Hz)		Description[e]
			P_A[d]	P_B[d]	
$Pb(O_2NMe)_x^{2+}$	−3342	70			s
$Pb(dppe)^{2+}$	60*f*	250	~1704		t
$Pb(etp)^{2+}$	56	65	~1843	~1843	Apparent q (unresolved t of d)
$Pb(tripod)^{2+}$	−190	50	1780		q
$Pb(PP_3)^{2+}$[g]	−269	120	487	2148	q of d
$Pb(PP_2PH))^{3+}$	−2	110	~1814	~1814	Apparent q (unresolved t of d)

[a] See footnote *a* Table 1.
[b] Relative to the resonance of external $PbMe_4$ in toluene; shifts were measured initially relative to the signal of 1.0 *M* $Pb(NO_3)_2$(aq) by sample interchange and converted to $PbMe_4$ as reference using $\delta_{(PbMe_4(toluene))} = \delta_{(1.0\ M\ Pb(NO_3)_2(aq))} - 2961$ ppm (7); shifts to higher frequency than the reference are taken as positive; estimated error in spectral measurement ±1 ppm.
[c] See footnote *c*, Table 1.
[d] See footnote *d*, Table 1.
[e] See footnote *e*, Table 1.
[f] At 260 K; this resonance could not be observed with certainty at 295 K.
[g] Values quoted are for a solution in which $Pb/PP_3 = 1.19$ and the lead concentration is 0.22 *m* (see text).

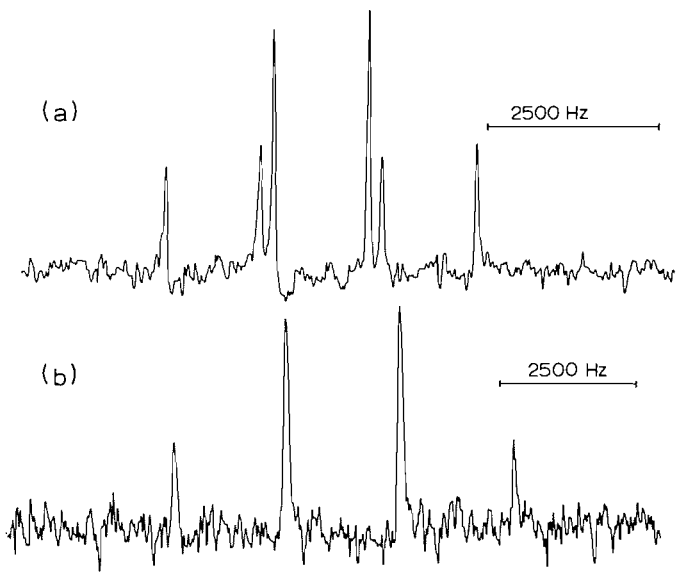

FIG. 1. (*a*) 149.2 MHz ^{119}Sn nmr spectrum of $Sn(etp)^{2+}$ at 206 K in a nitromethane solution containing $Sn(SbF_6)_2$:etp = 1.3:1 with a total tin concentration of 0.22 *m*. (Obtained using 69 90° (35 μs) pulses, acquisition and cycle times of 0.41 s and 1.41 s, respectively, and 20 kHz spectral window. 25 Hz of line broadening has been applied.) (*b*) 83.7 MHz ^{207}Pb nmr spectrum of $Pb(etp)^{2+}$ at 295 K in a nitromethane solution containing $Pb(SbF_6)_2$:etp = 1.3:1 with a total lead concentration of 0.22 *m*. (Obtained using 485 45° (19 μs) pulses, acquisition and cycle times of 0.16 s and 1.16 s, respectively, and 50 kHz spectral window. 20 Hz of line broadening has been applied.) Notes: *1*. etp = $[Ph_2P(CH_2)_2]_2PPh$; *2*. the horizonal scales in (*a*) and (*b*) are different.

It is noteworthy that, under identical conditions, the ^{119}Sn resonances of $Sn(dppe)^{2+}$ are very broad compared with those of the other tin complexes, and the analogous lead complex, in contrast to the other lead complexes, seems to give an unobservably broad resonance at 295 K. However, it is probably significant that the dppe complexes (which give ^{31}P spectra with sharp metal satellite spectra (ref. 1 and see footnote 5)) have fewer bound phosphorus atoms than species giving sharper lines, so that one site at least on the metal ion is presumably occupied by another donor (e.g. the solvent) or equilibrium mixture of donors (e.g. solvent and SbF_6^-). Some kinetic process at this site, occurring at an appropriate rate on the metal nmr timescale, might account for the observed broadening.

With the exception of $Pb(dppe)^{2+}$ (above), the splitting patterns found in the ^{119}Sn and ^{207}Pb nmr spectra of the various species are unaffected by reduction in temperature to 260 K, showing that there are no kinetic processes which can be slowed in the range 295–260 K. The most significant change is an increase in the metal nuclear shielding as the temperature is lowered, e.g. for ^{119}Sn, $\delta_{295} - \delta_{260}$, is 11, and 5 ppm for $Sn(O_2NMe)_x^{2+}$ and $Sn(etp)^{2+}$, respectively; for ^{207}Pb, $\delta_{295} - \delta_{260}$ is 17 and 39 ppm for $Pb(O_2NMe)_x^{2+}$ and $Pb(etp)^{2+}$, respectively. Such increasing shielding with decreasing temperature is normally found for temperature-dependent chemical shifts (see, for example, ref. 4); the generally larger temperature dependence of δ_{Pb} is consistent with the larger range of chemical shifts found for the lead complexes.

Dissolution of $M(SbF_6)_2$ (M = Sn or Pb) in $MeNO_2$ probably produces the solvated cations $M(O_2NMe)_x^{2+}$. On formation of the phosphine complexes from the parent cations, nmr complexation shifts of 750 to 950 ppm occur for the ^{119}Sn complexes (Table 1) and 3070 to 3400 ppm for the ^{207}Pb complexes (Table 2). For analogous compounds of lead and tin, the range of ^{207}Pb nmr chemical shifts to the range of ^{119}Sn chemical shifts has been found in earlier work to be about three or greater (e.g. refs. 2 and 5). Also, ^{119}Sn nmr complexation shifts to higher frequency have been found on formation of various $R_3P.SnCl_2$ from $(THF)_xSnCl_2$, the exact magnitude of the complexation shift being very dependent on the nature of R (6).

Compared with the magnitudes of the complexation shifts found for the various phosphine complexes examined here, the

range of ^{119}Sn or ^{207}Pb nmr chemical shifts within the series of phosphine complexes examined is quite small. Thus for the stannous complexes studied $\delta_{^{119}Sn}$ appears to be more sensitive to the presence of coordinated phosphorus atoms than to the number of phosphorus atoms coordinated. For example, the ^{119}Sn resonance of $Sn(dppe)^{2+}$ is deshielded by 100 ppm from the resonance of $Sn(etp)^{2+}$, there being a change from two to three coordinated phosphorus atoms between these species. If the effect of substituting phosphorus atoms into $Sn(O_2NMe)_4^{2+}$ approached additivity, the signal from $Sn(dppe)^{2+}$ should be shielded by ca. 300 ppm from that of $Sn(etp)^{2+}$. A similar situation holds for the analogous plumbous complexes, even allowing for the slight ambiguity introduced by an inability to observe the ^{207}Pb nmr spectrum of $Pb(dppe)^{2+}$ at 295 K coupled with the appreciable temperature sensitivity of δ_{Pb} (see above).

Within the comparatively small ^{119}Sn and ^{207}Pb nmr chemical shift ranges observed for the metal(II)–phosphine complexes (Tables 1 and 2) there is clearly some dependence on the nature of the ligand, as shown by the divergent chemical shifts of $M(etp)^{2+}$ and $M(tripod)^{2+}$, both of which contain tridentate phosphorus donor ligands. What is not evident is whether the difference reflects different geometries in the MP_3 kernel, the higher basicity of the central phosphorus atom of etp, the different number and/or size of the chelate rings, or some combination of these features. To resolve these questions study of complexes with a much wider range of ligands would be needed.

The metal chemical shifts of $M(etp)^{2+}$ and $M(PP_2(PH))^{3+}$ are close together for both M = ^{119}Sn and M = ^{207}Pb, as expected for species with essentially the same skeleton in the coordinated ligand, much closer than the metal chemical shifts of $M(etp)^{2+}$ and $M(PP_3)^{2+}$ which would also be expected to be similar if the PP_3 behaved in an etp-like manner as in [1]. In fact, the resonances of the discrete $M(PP_3)^{2+}$ complexes are probably slightly more shielded than the data given in Tables 1 and 2 suggest. It now appears that the ^{31}P nmr spectra earlier attributed to a single 1:1 complex of M^{2+} and PP_3 (1) must be a weighted average spectrum of at least two complexes, for from the wider range of ^{31}P nmr spectra now available it is evident that the ^{31}P nmr spectral parameters are sensitive to M/L in the solutions used, which contain excess M^{2+}.[6] For instance, in the 260 K ^{31}P nmr spectrum of the lead "complex", δ_{P_A}, $\nu_{1/2}(P_A)$, $^1J(^{207}Pb—P_A)$, δ_{P_B}, $^1J(^{207}Pb—P_B)$ and $^3J(P_A—P_B)$ change smoothly from 24.6 ppm, ~6 Hz, 429 Hz, 79.4 ppm, 2150 Hz, and 46 Hz when $Pb/PP_3 = 1.19 \pm 0.05/1$, to 29.3 ppm, ~60 Hz, ~504 Hz, 80.5 ppm, 2127 Hz, and 43 Hz when $Pb/PP_3 = 1.49 \pm 0.06/1$. (The P_B signal remains sharp as L/M is changed (see, for example, Fig. 1*c* of ref. 1).) The behaviour of the $Sn^{2+}–PP_3$ system is qualitatively similar. Evidently, the real $M(PP_3)^{2+}$ complex, regardless of whether it contains an MP_4 or an MP_3 kernel, is in equilibrium with a form containing $M(PP_3)^{2+}$ complexed by excess M^{2+}. Quantification of the spectral changes is complicated by the formation of $M(PP_2(PH))^{3+}$ as M/L is increased, but the occurrence of one or perhaps both, of equilibria [2] and [3] seem most likely:

[2] $M^*(PP_3) + M \rightleftarrows$ 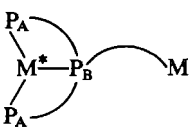

2

[3] $M^*(PP_3) + M \rightleftarrows$ 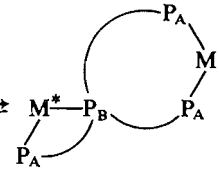

3

To be consistent with the ^{31}P nmr data P_B must remain anchored to M*, as $^1J(M^*—P_B)$ is observed and of the normal magnitude for static one-bond couplings of this type (1), the equilibria must be labile, as the nmr spectra require rapid averaging of P_A environments, and probably, the equilibrium or equilibria must lie close to the right.

The illustrative data given above for "$Pb(PP_3)^{2+}$" show that $^1J(M—P_A)$ *increases* as M/L is increased. This means that the values of $^1J(M—P_A)$ reported previously (1) *exaggerate* the magnitude of this coupling, so that the already anomalously low value should, in reality, be even lower (e.g. a value of approximately 390 Hz for $^1J(^{207}Pb—P_A)$ gives a fair fit of the exchange-average data for $Pb(PP_3)^{2+}$). Similarly the metal chemical shifts given for $Sn(PP_3)^{2+}$ and $Pb(PP_3)^{2+}$ in Tables 1 and 2, respectively (which correspond to the shifts of M* in [2] and [3] above) must be approximately the population-weighted averages of the shifts of $M(PP_3)^{2+}$ and **2** and/or **3**. Now in **2**, M* is expected to have a chemical shift similar to $M(PP_2)(PH))^{3+}$, while in **3** the chemical shift will probably be close to that of $M(dppe)^{2+}$. Thus from the shifts given in Tables 1 and 2 and the stoichiometries of the solutions from which the data were obtained we can estimate that the true $Sn(PP_3)^{2+}$ and $Pb(PP_3)^{2+}$ complexes should have metal chemical shifts of approximately −780 and approximately −340 ppm, respectively.

For both ^{119}Sn and ^{207}Pb, the difference between the shifts just estimated for the discrete $M(PP_3)^{2+}$ complexes and the shifts of the corresponding etp and $PP_2(PH)^+$ complexes appear, when combined with the anomalies found in the ^{31}P nmr spectra (especially the small values of $^1J(M—P_A)$ (ref. 1 and see above)), to favour an MP_4 kernel for the $M(PP_3)^{2+}$ complexes. More definitive evidence seems to require a study of the $M(PP_3)^{2+}$ complexes in the solid state or frozen solution by techniques not available in this laboratory, for example, solid state ^{31}P nmr, or, for M = ^{119}Sn, ^{119}Sn Mössbauer spectroscopy.

Tin-119 nmr data are now available for several stannous complexes of the type SnX_3 (this work and refs. 2 and 7); nuclear shielding varies with donor atom in the sequence O > P > Cl > S > Se. Similarly, nuclear shielding of ^{207}Pb in $Pb^{II}X_3$ varies as O > P > S > Se (this work and ref. 2).

[6] I am grateful to a referee for stressing this point.

Acknowledgements

This work was made possible by an Operating Grant from the Natural Sciences and Engineering Reseach Council of Canada. The high field metal nmr spectra were obtained at the Southwestern Ontario NMR Centre, funded by a Major Installation Grant from NSERC, with the expert technical assistance of Mr. Bruce MacDonald.

1. P. A. W. Dean, D. D. Phillips, and L. Polensek. Can. J. Chem. **59**, 50 (1981).
2. P. A. W. Dean. Can. J. Chem. **60**, 2921 (1982).
3. R. L. Keiter, S. L. Kaiser, N. P. Hansen, J. W. Brodack, and L. W. Cary. Inorg. Chem. **20**, 283 (1981).
4. P. J. Burke, R. W. Matthews, I. D. Cresshill, and D. G.

GILLIES. J. Chem. Soc. Dalton, 132 (1981) and references therein.
5. J. D. KENNEDY, W. MCFARLANE, and G. S. PYNE. J. Chem. Soc. Dalton, 2332 (1977).
6. W.-W. DU MONT and H.-J. KROTH. Z. Naturforsch. **35**b, 700 (1980).
7. R. K. HARRIS, J. D. KENNEDY, and W. MCFARLANE. NMR and the Periodic Table. *Edited by* R. K. Harris and B. E. Mann. Academic Press, London. 1978. Chapt. 10.

A phosphorus-31 nuclear magnetic resonance spectroscopic study of complexes of zinc with some phosphine oxides, sulfides, and selenides[1]

PHILIP A. W. DEAN[2] AND GEETHA K. CARSON

Department of Chemistry, University of Western Ontario, London, Ont., Canada N6A 5B7

Received December 20, 1982

PHILIP A. W. DEAN and GEETHA K. CARSON. Can. J. Chem. **61**, 1800 (1983).

$Zn(SbF_6)_2$ in liquid SO_2 has been shown to act as an acceptor towards a variety of phosphine oxides, sulfides, and selenides, forming complexes which have been characterized in solution using ^{31}P nmr. Slow-exchange ^{31}P nmr spectra are reported for the complexes ZnL_n^{2+} (n = 6, L_2 = $Ph_2P(O)CH_2P(O)Ph_2$ or L_3 = $(Ph_2P(O)(CH_2)_2)_2P(O)Ph$; n = 4, L_2 = $Ph_2P(E)CH_2P(E)Ph_2$ (E = O, S, or Se) or *bidentate* $(Ph_2P(E)CH_2)_3CMe$ (E = S or Se), or L = $(C_6H_{11})_3PE$ (E = O, S, or Se) or R_3PE (E = S or Se, R = Ph or *o*-C_6H_4Me); n = 3, L_3 = $(Ph_2P(E)(CH_2)_2)_2P(E)Ph$ (E = S or Se) or L = R_3PE (E = S or Se, R = C_6H_{11}, Ph, or *o*-C_6H_4Me); n = 2, L = R_3PE (E = S or Se, R = *o*-C_6H_4Me or, perhaps, C_6H_{11}); n = 1 (possibly), L = (*o*-$C_6H_4Me)_3PS$), and partial spectra for $[Zn(ScP(C_6H_{11})_3)_x(SP(C_6H_{11})_3)_{n-x}]^{2+}$ (n = 3 or 4). No evidence was found for the mixed oxide-chalcogenide species $[Zn(EP(C_6H_{11})_3)_x(OP(C_6H_{11})_3)_{4-x}]^{2+}$. In most cases the ^{31}P nmr spectra are very similar to those reported earlier for the corresponding cadmium complexes. However, in most instances where comparison could be made it was found that the rate of intermolecular ligand exchange was less for the zinc complexes than for their cadmium counterparts. (Complexes with $(Ph_2P(O)(CH_2)_2)_2P(O)Ph$ and $Ph_2P(O)(CH_2)_2P(O)Ph_2$ are exceptional in being more labile for zinc than cadmium.)

PHILIP A. W. DEAN et GEETHA K. CARSON. Can. J. Chem. **61**, 1800 (1983).

On montre que le $Zn(SbF_6)_2$ dans du SO_2 liquide agit comme un accepteur envers divers oxydes de phosphine, de sulfure et de séléniure, en formant des complexes que l'on a caractérisés en solution par la rmn du ^{31}P. On rapporte les spectres de rmn du ^{31}P d'échange lent des complexes de ZnL_n^{2+} (n = 6, L_2 = $Ph_2P(O)CH_2P(O)Ph_2$ ou L_3 = $(Ph_2P(O)(CH_2)_2)_2P(O)Ph$; n = 4, L_2 = $Ph_2P(E)CH_2P(E)Ph_2$ (E = O, S ou Se) ou *bidentate*. $(Ph_2P(E)CH_2)_3CMe$ (E = S ou Se), ou L = $(C_6H_{11})_3PE$ (E = O, S ou Se) ou R_3PE (E = S ou Se, R = Ph ou *o*-C_6H_4Me); n = 3, L_3 = $(Ph_2P(E)(CH_2)_2)_2P(E)Ph$ (E = S ou Se) ou L = R_3PE (E = S ou Se, R = C_6H_{11}, Ph ou *o*-C_6H_4Me); n = 2, L = R_3PE (E = S ou Se, R = *o*-C_6H_4Me ou peut être C_6H_{11}); n = 1 (possiblement), L = (*o*-$C_6H_4Me)_3PS$) et les spectres partiels de $[Zn(ScP(C_6H_{11})_3)_x(SP(C_6H_{11})_3)_{n-x}]^{2+}$ (n = 3 ou 4). On n'a pas pu prouver l'existence d'espèces mixtes du type oxyde-chalcogéniure: $[Zn(EP(C_6H_{11})_3)_x(OP(C_6H_{11})_3)_{4-x}]^{2+}$. Dans la plupart des cas les spectres de rmn du ^{31}P sont très semblables à ceux rapportés antérieurement pour les complexes correspondants du cadmium. Cependant dans la plupart des cas, où il est possible d'établir une comparaison, on trouve que la vitesse d'échange intermoléculaire de ligand est plus faible dans le cas du zinc que dans le cas des complexes correspondants du cadmium. (Les complexes avec $(Ph_2P(O)(CH_2)_2)_2P(O)Ph$ et $Ph_2P(O)(CH_2)_2P(O)Ph_2$ sont exceptionnels en ce sens qu'ils sont plus labiles dans le cas du zinc que dans le cas du cadmium.)

[Traduit par le journal]

Introduction

In earlier work from this laboratory (1, 2), it was shown that a wide variety of new complexes of cadmium with phosphine oxides, sulfides, and selenides could be prepared from $Cd(MF_6)_2$ (M = As or Sb) with the appropriate ligand in liquid SO_2. The MF_6^- anions and the solvent SO_2 are very weak donors so that coordination by the ligand(s) of interest is facilitated in these systems. Phosphorus-31 nmr proved a useful tool to characterize the complexes, a selection of which then provided the basis for a ^{113}Cd nmr study of species containing these model Group VIA donor ligands (3). A helpful feature of both the ^{31}P and the ^{113}Cd nmr spectra of the cadmium complexes is the occurrence of two-bond $^{113}Cd—E—^{31}P$ (E = O, S, or Se) nuclear spin–spin coupling which is readily observable for E = S or Se (1, 2) and observable with ^{113}Cd enrichment for E = O (3). The splitting patterns observed in the ^{113}Cd nmr spectra both allow unambiguous assignment of these and confirm the interpretation of the ^{31}P nmr spectra.

With the ^{31}P and metal nmr spectra of the cadmium complexes in hand, we felt it would be instructive to measure analogous spectra of some related zinc complexes for comparison. As the first part of our study we have measured ^{31}P nmr spectra for a range of the title complexes, and report them here. Zinc-67 (4.1% natural abundance, spin I = 5/2) is a quadrupolar nucleus and so the ^{31}P nmr spectra of the zinc complexes contain no observable $^{67}Zn—E—^{31}P$ spin coupling. In themselves they are thus not as informative as those of their cadmium analogs. However, with a prior knowledge of the spectra of the cadmium complexes the spectra of the zinc complexes can be assigned with some confidence, as we show.

To our knowledge, there have been no previous ^{31}P nmr studies of complexes of zinc with phosphine sulfides or selenides, perhaps because of the difficulty of interpreting an isolated spectrum (see above). However, zinc complexes with phosphine selenides and, particularly, phosphine sulfides are well-established. Most involve zinc halides and are of the type $ZnX_2 . L_2$ where L represents a donor with one P=S (or Se) donor site or L_2 a donor with two such sites (eg. refs. 4–10). The complexes $2ZnX_2 . Ph_3PSe$ (X = Cl or Br) have also been reported (11), as have the species $[ZnL_4](ClO_4)_2$ (L = $SePMe_3$ (6) or L_2 = $dppmS_2$ (12)), which demonstrate the importance of the nature of the anion in maximizing the number of ligands that can be bound.[3]

Zinc complexes with phosphine oxides and related phosphoryl donor ligands have been a topic of extensive interest, though relatively few ^{31}P nmr investigations have been reported

[1]No reprints available.

[2]Address correspondence to this author.

[3]Abbreviations used in this paper: Cy = *c*-C_6H_{11}; *o*-tol = *o*-C_6H_4Me; $dppmE_2$ = $Ph_2P(E)CH_2P(E)Ph_2$; $dppeO_2$ = $Ph_2P(O)(CH_2)_2P(O)Ph_2$; $tripodE_3$ = $MeC(CH_2P(E)Ph_2)_3$; $triphosE_3$ = $PhP(E)((CH_2)_2P(E)Ph_2)_2$; TTA = thenoyltrifluoroacetonate (1−).

Can. J. Chem. Downloaded from www.nrcresearchpress.com by 210.87.254.5 on 09/06/12
For personal use only.

Can. J. Chem. Downloaded from www.nrcresearchpress.com by 210.87.254.5 on 09/06/12
For personal use only.

(see below). The most important types of complexes known are: ZnL_2X_2 (L = ligand with one P=O donor site or L_2 = ligand with two P=O donor sites, X = coordinating anion) (e.g. refs. 13–17), $[ZnL_4]X_2$ (L = ligand with one P=O donor site or L_2 = ligand with two P=O donor sites; X = weakly coordinating anion) (e.g. refs. 13–15, 17–20), $[ZnL_5]X_2$ (L = ligand with one P=O donor site; X = weakly coordinating anion) (e.g. refs. 19, 21, 22), and $[ZnL_6]X_2$ (L = $(HOCH_2)_3P{=}O$, X = ClO_4^- (23); L_2 = ligand with two P=O donor sites, X = weakly coordinating anion (e.g. refs. 14, 24); L_3 = ligand with three P=O donor sites; X = weakly coordinating anion (e.g. ref. 25)).

A few ^{31}P nmr data are available for zinc complexes of phosphine oxides. In an early application of ^{31}P nmr, Walker and Li (26) used ^{31}P nmr to determine the formation constant (10 L mol^{-1}) of the (isolable) 1:1 complex $Zn(TTA)_2 \cdot OP(n\text{-}C_8H_{17})_3$ in CCl_4 at 299 K. More recently, ligand exchange with excess free ligand was found to be fast on the ^{31}P nmr timescale at ambient probe temperature for both $Zn(OPBu^n{}_3)_4^{2+}$ in DMSO and $Zn(dppmO_2)Cl_2$ in CH_2Cl_2 (15); from the position of the single exchange-averaged resonance observed in these cases, it was deduced that ligand dissociation is significant for the former system, but not for the latter. Lincoln and co-workers were able to reach the slow exchange region of the reduced temperature ^{31}P nmr spectrum for $Zn(OP(NMe_2)_3)_4^{2+}$—$OP(NMe_2)_3$ (19) and $Zn(OPPh_3)_4^{2+}$—$OPPh_3$ (20) mixtures in CD_2Cl_2, but not for ZnL_5^{2+}—L (L = $OP(OMe)_3$ or $OPMe(OMe)_2$) mixtures in the same solvent (19). In all these previous ^{31}P nmr studies of phosphoryl donor ligands sizeable positive values of the complexation shift, $\Delta\delta_P$ (= $\delta_{P,\ complex} - \delta_{P,\ free\ ligand}$) were found.

Experimental

Materials

Zinc hexafluoroantimonate, $Zn(SbF_6)_2$, was synthesized by the literature method (27). The ligands were prepared, and sulfur dioxide dried, as reported earlier (1–3, 28).

Manipulations

All transfers of the extremely moisture-sensitive $Zn(SbF_6)_2$ were carried out in a dry-nitrogen filled glovebox in which the atmosphere was maintained by circulation through liquid nitrogen cooled traps. Similarly all weighings were carried out in the glovebox. Sulfur dioxide was added to the nmr samples outside the box from a calibrated glass and Teflon vacuum line.

Phosphorus-31 nmr spectra

Nuclear magnetic resonance samples were prepared in flame-sealed hand made 10 mm od nmr tubes, and 40.54 MHz ^{31}P—{^1H} nmr spectra measured using an XL-100-12 spectrometer system, as described before (1, 2, 28). The ^{31}P nmr chemical shifts are given relative to external $OP(OMe)_3$ in $(CD_3)_2CO$, used as a reference/lock substance, in the annulus between the 10 mm tubes and a standard 12 mm od nmr tube; approximate conversion to H_3PO_4 (at 308 K) as reference is $\delta_{OP(OMe)_3(ext)} \approx \delta_{H_3PO_4(ext)} - 1.7$ ppm. Shifts to higher frequency than the reference are taken as positive. We estimate that δ_P and values of $^1J(^{31}P—^{77}Se)$ have maximum errors of ±0.1 ppm and ±2 Hz, respectively, as in ref. 2.

Results and discussion

Complexes of phosphine oxides

Samples containing $Zn(SbF_6)_2$ and $OPCy_3$ show two ^{31}P nmr resonances at ambient or reduced temperature when $OPCy_3/Zn > 4$. The more shielded of these is from excess free ligand and by studying the mixtures as a function of L/Zn the other can be attributed to $Zn(OPCy_3)_4^{2+}$. The ^{31}P chemical shift of this complex, and hence its complexation shift, both given in Table 1, are very similar to the 62.4 ppm (6.9 ppm) found for the cadmium analog (3). Evidently $Zn(OPCy_3)_4^{2+}$, like $Cd(OPCy_3)_4^{2+}$ (3), but unlike other $Zn(OPR_3)_4^{2+}$ (R = Bu" (15), NMe_2 (19), or Ph (20)), undergoes slow ligand exchange with excess free ligand at ambient probe temperature. A chemical dissimilarity between Zn^{2+}—$OPCy_3$ and Cd^{2+}—$OPCy_3$ mixtures concerns the formation of poorly soluble $M(OPCy_3)_3(SbF_6)_2$. This is formed in cadmium-rich mixtures but not in zinc-rich mixtures; in the latter case Zn^{2+} (solv.) and $Zn(OPCy_3)_4^{2+}$ seem to coexist in solution.

TABLE 1. ^{31}P nmr spectral parameters of some zinc complexes with phosphine oxides

Complex[a]	T (K)	δ_P[b] (ppm)	$\Delta\delta_P$[c] (ppm)
$Zn(OPCy_3)_4^{2+}$	209[d]	62.2	~1.8[e]
	308[d]	62.1	~4.9[e]
$Zn(dppmO_2)_3^{2+}$	209[d,f]	34.1	6.6
	308[d,f]	32.9	6.9
$Zn(dppmO_2)_2^{2+}$	209[f]	41.7	14.2
	308[f]	41.5	15.4
$Zn(triphosO_3)_2^{2+}$	204[g]	46.0(A)[h]	−1.0
		37.5(B)[h]	0.4
		35.6(C)[h]	−1.5

[a]Cy = c-C_6H_{11}; $dppmO_2$ = $Ph_2P(O)CH_2P(O)Ph_2$; $triphosO_3$ = $PhP(O)((CH_2)_2P(O)Ph_2)_2$.

[b]Measured relative to external $OP(OMe)_3$ in $(CD_3)_2CO$; $\delta_{OP(OMe)_3(ext)} \approx \delta_{H_3PO_4(ext)} - 1.7$ ppm; positive chemical shifts are to higher frequency than the reference; estimated error in measurement ±0.1 ppm or less.

[c]$\Delta\delta_P = \delta_P(complex) - \delta_P(free\ ligand)$.

[d]Slow exchange with excess free ligand at 209 and 308 K.

[e]δ_P and $\nu_{1/2}$ for free $OPCy_3$ depend markedly on temperature and solute concentration.

[f]Slow ligand exchange between 3:1 and 2:1 complexes at 209 and 308 K.

[g]Slow exchange with excess free ligand at 204 K, intermediate exchange at 308 K; the resonances B and C appear to be collapsing (intramolecular exchange) before intermolecular exchange becomes rapid (cf. ref. 1).

[h]A = non-terminal phosphorus atom, B and C = terminal phosphorus atom; $J(AB) \approx 7$ Hz; $J(AC)$ and $J(BC)$ are not observed.

Slow exchange ^{31}P nmr spectra are found at 308 K or below for $Zn(SbF_6)_2$–$dppmO_2$ mixtures over a range of L/Zn.[4] When L/Zn > 3 the spectra show two lines. The more shielded signal, attributable to excess free ligand, disappears at L/Zn ≈ 3 so that the highest complex formed is $Zn(dppmO_2)_3^{2+}$ which, by analogy with $Zn(triphosO_3)_2^{2+}$ (see below), probably contains an octahedral ZnO_6 core. When L/Zn < 3 a second species is formed which does not exchange ligands with the 3:1 complex at an nmr-detectable rate; its ^{31}P resonance is deshielded from that of $Zn(dppmO_2)_3^{2+}$ and becomes predominant at L/Zn ≈ 2. Hence the second zinc complex is $Zn(dppmO_2)_2^{2+}$. Details of the ^{31}P nmr spectra of the $dppmO_2$ complexes are included in Table 1. The ^{31}P chemical shift of the 3:1 complex is similar to that of $Cd(dppmO_2)_3^{2+}$ (34.5 ppm) which also exchanges slowly on the nmr timescale with excess free ligand at ambient probe temperature (1). However, the ^{31}P nmr chemical shift (and complexation shift) of $Zn(dppmO_2)_2^{2+}$ are significantly larger than found for

[4]The slow exchange ^{31}P nmr spectra observed for complexes of $Zn(SbF_6)_2$ and $dppmO_2$ in SO_2 at ambient probe temperature contrasts with the fast exchange spectra observed for $ZnCl_2 \cdot dppmO_2$–$dppmO_2$ mixtures in CH_2Cl_2 (15). This behaviour is consistent with the order of Lewis acidity $Zn(SbF_6)_2 > ZnCl_2$.

Can. J. Chem. Downloaded from www.nrcresearchpress.com by 210.87.254.5 on 09/06/12
For personal use only.

$Cd(dppmO_2)_2^{2+}$ (36.8 ppm (9.6 ppm) at 220 K (1)). In addition, ligand exchange in $Cd(dppmO_2)_2^{2+} - Cd(dppmO_2)_3^{2+}$ mixtures is fast at ambient probe temperature unlike the behaviour found here for the zinc complexes. A plausible explanation for these differences lies in the larger size of the cadmium ion: this should favour solvent and/or anion coordination to $Cd(dppmO_2)_2^{2+}$ (albeit short-lived to be consistent with the ^{31}P nmr spectra) and lead to a lower Lewis acidity at Cd and hence, probably, a smaller $\Delta\delta_P$; it should also favour what appears to be an S_E2 exchange process between the 2:1 and 3:1 complexes.

At 204 K, samples containing $triphosO_3/Zn > 2$ give a slow exchange ^{31}P nmr spectrum consisting of the partly superimposed spectra of excess free $triphosO_3$ and a 2:1 complex, $Zn(triphosO_3)_2^{2+}$. The spectrum of the 2:1 complex consists of three equally intense regions of resonance labelled A, B, and C in Table 1. As the temperature is raised, B and C begin collapsing together but intermolecular exchange with free ligand starts to occur before this process is complete and results in a broadened spectrum at 308 K. Nevertheless B and C can be assigned to the coordinated —$Ph_2P(O)$ groups and hence C to the coordinated —PhP(O)— group of a complexed $triphosO_3$. Overall this spectrum resembles that of $Cd(triphosO_3)_2^{2+}$ for which an *s-fac* structure has been suggested (1),[5] and so we tentatively assign the zinc complex the same structure. In these species the inequivalence of the terminal phosphoryl sites is thought to arise from the particular ligand conformation frozen out at low temperature (1). The lability of the zinc complex at ambient probe temperature is in contrast to the slow intermolecular exchange found for $Cd(triphosO_3)_2^{2+} - triphosO_3$ mixtures under the same conditions (1). The same order of lability, Zn > Cd, holds for complexes of $Ph_2P(O)(CH_2)_2P(O)Ph_2$; we could not obtain slow exchange ^{31}P nmr spectra of any $Zn^{2+} - dppeO_2$ mixtures at any accessible temperature (though $\Delta\delta_P$(ave) was significant), whereas slow exchange spectra have been measured for $Cd^{2+} - dppeO_2$ mixtures at reduced temperature (1). Possibly the bite of the seven-membered chelate ring gives a worse fit on Zn^{2+} than on the larger Cd^{2+}, resulting in labilization of the zinc complexes relative to the cadmium complexes.

Complexes with phosphine sulfides

At 199 K the ^{31}P nmr spectra of SO_2 solutions in which $dppmS_2/Zn(SbF_6)_2 > 2$ exhibit two signals. The more shielded of these is due to excess free $dppmS_2$ and variation of the L/M ratio shows that the less shielded arises from the 2:1 complex $Zn(dppmS_2)_2^{2+}$. This species has been isolated previously (12) and is now shown to exist in undissociated form in solution under the conditions of our experiment. The nmr spectral parameters of the complex are given in Table 2. As the temperature is increased from 199 K the signals from samples containing $Zn(dppmS_2)_2^{2+}$ and excess $dppmS_2$ broaden and eventually, close to ambient probe temperature, collapse to a single exchange-averaged signal. Clearly ligand exchange between free and bound $dppmS_2$ is rapid on the nmr timescale at or near 308 K. Overall, however, the zinc complex is less labile than its cadmium analog for which slow exchange ^{31}P nmr spectra could not be obtained under any conditions (1).

[5]An *s-fac* structure is also favoured for the complex $Zn(L\ L\ L)_2^{2+}$ of the tridentate phosphoryl donor ligand $(Me_2N)_2P(O)NMeP(O)(NMe_2)NMeP(O)(NMe_2)_2$ (25); this is the only other related species we are aware of.

TABLE 2. ^{31}P nmr spectral parameters of some zinc – phosphine sulfide complexes, $Zn(SPR_3)_n^{2+}$, in liquid SO_2 at 209 K

SPR_3[a]	n in $Zn(SPR_3)_n^{2+}$	δ_P[b] (ppm)	$\Delta\delta_P$[c] (ppm)
$SPPh_3$	4[d,e]	39.4	−1.8
$SPPh_3$	3[e]	40.8	0.4
$SP(o\text{-tol})_3$	4[d,f]	43.7	5.7
$SP(o\text{-tol})_3$	3[f,g]	41.4	3.4
$SP(o\text{-tol})_3$	2[g,h]	41.0	2.9
$SP(o\text{-tol})_3$	1(?)[h]	40.7	2.6
$SPCy_3$	4[d,i]	64.4	−0.4
$SPCy_3$	3[i]	65.9	1.2
$SPCy_3$	2(?)	67.0	2.2
$dppmS_2/2$[j]	4	37.7	4.6

[a]o-tol = $o\text{-}C_6H_4Me$; Cy = $c\text{-}C_6H_{11}$; $dppmS_2 = Ph_2P(S)CH_2P(S)Ph_2$.

[b]Measured relative to external $OP(OMe)_3$ in $(CD_3)_2CO$; $\delta_{OP(OMe)_3(ext)} \approx \delta_{H_3PO_4(ext)} - 1.7$ ppm; positive chemical shifts are to higher frequency than the reference; estimated error in measurement ±0.1 ppm or less.

[c]$\Delta\delta_P = \delta_P$(complex) − δ_P(free ligand).

[d]Slow exchange with excess free ligand at 209 K, intermediate exchange at 308 K.

[e]Slow ligand exchange between 4:1 and 3:1 complexes at 209 K, fast exchange at 308 K.

[f]Slow ligand exchange between 4:1 and 3:1 complexes at 209 K, intermediate exchange at 308 K.

[g]Slow ligand exchange between 3:1 and 2:1 complexes at 209 K, fast exchange at 308 K.

[h]Slow ligand exchange in mixtures of 3:1, 2:1, and 1:1(?) complexes at 209 K, fast exchange at 308 K.

[i]Intermediate ligand exchange in mixtures of 4:1 and 3:1 complexes at 308 K.

[j]At 199 K; free-bound ligand exchange is slow at this temperature but fast at 308 K.

Solutions in which $SPR_3/Zn(SbF_6)_2 > 4$ (R = Ph, *o*-tol, or Cy) are readily shown by reduced temperature ^{31}P nmr spectroscopy to contain $Zn(SPR_3)_4^{2+}$, with, presumably, a tetrahedral ZnS_4 kernel. Phosphorus-31 nmr data for these complexes are included in Table 2; the values of $\Delta\delta_p$ are similar to those found for the related cadmium complexes (1, 2). Each of the zinc complexes, like $Zn(dppmS_2)_2^{2+}$ (above) is less labile than the corresponding cadmium complex, for free and bound ligand signals are incompletely collapsed at 308 K for the zinc complexes, but completely exchange-averaged for the cadmium complexes (1, 2). When SPR_3/Zn is reduced below 4, the pale yellow colour of excess SPR_3 in SO_2 disappears and the free ligand line in the reduced temperature ^{31}P nmr spectra is no longer seen. Instead, in each case a second signal attributable to bound SPR_3 is evident. From the variation of resonance intensity as a function of L/M it is clear that $Zn(SPR_3)_3^{2+}$ is formed. The ^{31}P nmr spectra of the 1:3 complexes are outlined in Table 2; again they resemble those of their cadmium analogs. As has been noted for the corresponding cadmium complexes (2), the extent of solvent or anion coordination in these $M(SPR_3)_3^{2+}$ species is not known, so it is unclear whether they contain the expectedly planar MS_3 core. When SPR_3/Zn is reduced below three, an additional signal was observed for R = Cy; this had intensity that varied as expected for $Zn(SPCy_3)_2^{2+}$ and a tentative assignment has been made accordingly (Table 2). (No evidence for $Cd(SPCy_3)_2^{2+}$ was found in earlier work (2).) Similarly, two additional signals were observed for R = *o*-tol, with an order of appearance and intensity variation suggesting the formation of first $Zn(SP(o\text{-tol})_3)_2^{2+}$ and then $Zn(SP(o\text{-tol})_3)^{2+}$. No additional signals were observed for R = Ph. However, we cannot preclude the possi-

TABLE 3. ^{31}P nmr spectral parameters of some zinc – phosphine selenide complexes, $Zn(ScPR_3)_n^{2+}$, in liquid SO_2 at 209 K

$ScPR_3$[a]	n in $Zn(ScPR_3)_n^{2+}$	δ_P[b] (ppm)	$\Delta\delta_P$[c] (ppm)	$\lvert^1J(^{31}P—^{77}Se)\rvert$[d] (Hz)	$\Delta^1J(^{31}P—^{77}Se)$[e] (Hz)
$ScPPh_3$	4[f,g]	29.5	−3.7	582	−71
$ScPPh_3$	3[g]	31.6	−1.5	537	−116
$ScP(o\text{-tol})_3$	4[f,g]	30.0	3.0	587	−42
$ScP(o\text{-tol})_3$	3[g,h]	28.1	1.1	530	−89
$ScP(o\text{-tol})_3$	2(?)[h]	30.2	3.2	~508	~−121
$ScPCy_3$	4[f,i]	61.1	−1.2	551	−26
$ScPCy_3$	3[h,i]	64.0	1.7	504	−73
$ScPCy_3$	2[h]	65.1	2.8	474	−103
$dppmSe_2$/2[f]	4[f]	27.8	5.0	574[k]	−112

[a] o-tol = o-C_6H_4Me; Cy = c-C_6H_{11}; $dppmSe_2$ = $Ph_2P(Se)CH_2P(Se)Ph_2$.
[b] Measured relative to external $OP(OMe)_3$ in $(CD_3)_2CO$; $\delta_{OP(OMe)_3(ext)} \approx \delta_{H_3PO_4(ext)} + 1.7$ ppm; positive chemical shifts are to higher frequency than the reference; estimated error in measurement ±0.1 ppm or less.
[c] $\Delta\delta_P = \delta_P$(complex) − δ_P(free ligand).
[d] Estimated error ±2 Hz, except where noted.
[e] $\Delta J = J$(complex) − J(free ligand).
[f] Slow exchange with excess free ligand at the temperature of measurement but fast exchange at 308 K.
[g] Fast ligand exchange between 4:1 and 3:1 complexes at 308 K.
[h] Fast ligand exchange between 3:1 and 2:1 complexes at 308 K.
[i] Intermediate exchange between 4:1 and 3:1 complexes at 308 K.
[j] At 194 K.
[k] ±5 Hz.

bility that a 1:2 complex is formed in this case but gives a signal coincident with that of the 1:3 complex, as was found for $Cd(SP(o\text{-tol})_3)_{2\text{ or }3}^{2+}$ (2).

The 209 K ^{31}P nmr spectrum of an SO_2 solution in which triphosS_3/Zn = 1 showed an AMX spectrum which was assigned straightforwardly and is characterized by the parameters given in Table 4. This pattern is very similar to that observed for $Cd(triphosS_3)^{2+}$ (1), in which case it was interpreted in terms of the monomeric structure **I** (with a rigid conformation at reduced temperature causing inequivalence of the two —$P(E)Ph_2$ groups) or dimeric structure **II**, a prejudice being

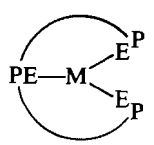

I

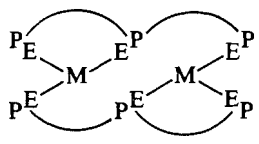

II

expressed for **I**. The same interpretation can clearly be made here. At 209 K, mixtures in which L/M > 1 give broad ^{31}P nmr resonances indicating ligand exchange at an intermediate rate between the species present. (Although the comparative broadness of the nmr signals made assignment impossible, the spectra seem more complicated than expected for a simple mixture of $Zn(triphosS_3)^{2+}$ and excess triphosS_3.) In contrast, a fast exchange averaged AX_2 spectrum is found under the same conditions for cadmium (1).

TripodS_3, like triphosS_3, is a potentially tridentate ligand. However, the ligand has been shown to behave in a bidentate manner in $Cd(tripodS_3)_2^{2+}$ (1) and similar behaviour is found using zinc as an acceptor here. Only a 1:2 species, $Zn(tripodS_3)_2^{2+}$, could be identified with certainty in $Zn(SbF_6)_2$–tripodS_3 mixtures using ^{31}P nmr. At 308 K this complex, which, in contrast to $Cd(tripodS_3)_2^{2+}$, shows no nmr-detectable exchange with free ligand, has a ^{31}P nmr spectrum (Table 4) comprised of three equally intense lines. This is just the spectrum expected for

$$[Zn(((S)Ph_2PCH_2)_2\overset{Me}{C}CH_2PPh_2(S))_2]^{2+}$$

of time-averaged C_2 symmetry, and therefore we assign $Zn(tripodS_3)_2^{2+}$ the bis(bidentate) structure. On lowering the temperature, slight changes in chemical shift occur but the most marked change is the splitting of the least shielded resonance into two equally intense components. Similar but more extensive splitting in the resonances of the bound —$PPh_2(S)$ groups has been found for $Cd(tripodS_3)_2^{2+}$ and attributed to destruction of the C_2 symmetry by conformational effects (1). In the spectrum of the cadmium complex the resonances of the bound groups are readily apparent because of the $^{113/111}Cd$—^{31}P satellites (1). The ^{31}P nmr spectrum of $Zn(tripodS_3)_2^{2+}$ (Table 4) is assigned by analogy with that of $Cd(tripodS_3)_2^{2+}$

Complexes with phosphine selenides

Coordination is easier to show unambiguously for phosphine selenides than for phosphine sulfides because for the selenides it leads not only to a complexation shift $\Delta\delta_P$ normally, but also to a reduction in the magnitude of the $^1J(^{31}P—^{77}Se)$ satellite splitting (from ^{77}Se, 7.58% natural abundance, spin $I = 1/2$) (e.g. refs. 1, 2, 28–33).

In the system $Zn(SbF_6)_2$–$dppmSe_2$ in SO_2, the complex $Zn(dppmSe_2)_2^{2+}$ is readily detected by reduced temperature ^{31}P nmr of solutions in which L/M > 2. Details of the spectrum of this presumably tetrahedral complex are given in Table 3; both $\Delta\delta_P$ and $\Delta^1J(^{31}P—^{77}Se)$ are very similar to those found for $Cd(dppmSe_2)_2^{2+}$ (1). The major difference between the zinc and cadmium complexes is in their lability on the nmr timescale: whereas separate ^{31}P nmr signals from $Zn(dppmSe_2)_2^{2+}$ and free $dppmSe_2$ can be observed at 194 K, only an exchange-averaged spectrum is observed at this temperature for $Cd(dppmSe_2)_2^{2+}$–$dppmSe_2$ mixtures (1). At 308 K rapid exchange of free and bound ligand occurs for $Zn(dppmSe_2)_2^{2+}$–$dppmSe_2$ mixtures; the behaviour at intermediate temperatures is approximately the same as for $Zn(dppmS_2)_2^{2+}$–$dppmS_2$ mixtures (see above).

Complex formation between $Zn(SbF_6)_2$ and representative

Can. J. Chem. Downloaded from www.nrcresearchpress.com by 210.87.254.5 on 09/06/12
For personal use only.

TABLE 4. ^{31}P nmr spectral parameters of $Zn(triphosE_3)^{2+}$ and $Zn(tripodE_3)_2^{2+}$ (E = S or Se) in liquid SO_2 at 209 K[a]

Complex	Phosphorus[b]	δ_P[c] (ppm)	$\Delta\delta_P$[d] (ppm)	$\lvert^1J(^{31}P—^{77}Se)\rvert$[e] (Hz)	$\Delta^1J(^{31}P—^{77}Se)$[f] (Hz)	$J(PP)$[g] (Hz)
$Zn(triphosS_3)^{2+}$	A[h]	60.3	8.7			$^3J(AB) = 27$
	B[i]	49.5	5.6			$^3J(AC) = 68$
	C[i]	45.5	1.6			$^5J(BC) \approx 0$
$Zn(triphosSe_3)^{2+}$	A[h]	49.5	6.1	[j]		$^3J(AB) = 23$
	B[i]	42.1	6.7	[j]		$^3J(AC) = 66$
	C[i]	34.6	−0.8	~535	~−133	$^5J(BC) \approx 0$
$Zn(tripodS_3)_2^{2+}$[k]	A[l]	30.8	−2.7			
	B[l]	32.2[5]	−1.2			$^4J(PP)$ (not obs.)
		32.3[9]	−1.1			
	C[l]	30.8	−2.7			
$Zn(tripodSe_3)_2^{2+}$[k]	A[m]	19.9	−2.2	672	+12	
	B[m]	18.2[5]	−3.8	540	−120	$^4J(PP)$ (not obs.)
		18.4[7]	−3.6	546	−114	
	C[m]	16.3	−5.8	550±5	−110	

[a]$triphosE_3$ = $PhP(E)((CH_2)_2P(E)Ph_2)_2$; $tripodE_3$ = $MeC(CH_2P(E)Ph_2)_3$.

[b]Resonances are labelled as for the corresponding cadmium complexes (1).

[c]Measured relative to external $OP(OMe)_3$ in $(CD_3)_2CO$; $\delta_{OP(OMe)_3(ext)} \approx \delta_{H_3PO_4(ext)} - 1.7$ ppm; positive chemical shifts are to higher frequency than the reference; estimated error in measurement ±0.1 ppm or less.

[d]$\Delta\delta_P = \delta_P$(complex) − δ_P(free ligand).

[e]Estimated error ±2 Hz except where noted otherwise.

[f]$\Delta J = J$(complex) − J(free ligand).

[g]Estimated error ±1 Hz.

[h]Terminal phosphorus atom.

[i]Non-terminal phosphorus atom.

[j]Could not be observed with certainty.

[k]This spectrum consists of three resonances at 308 K.

[l]At 308 K, $\delta_P(\Delta\delta_P)$ = 31.0 (−2.3), 33.1 (−0.2), and 31.5 ppm (−1.8 ppm), for P_A, P_B, and P_C respectively; by analogy with results for $Cd[(SPPh_2CH_2)_2MeCH_2PPh_2S]_2^{2+}$ (1) P_A is assigned to the unbound $\rangle$PS group.

[m]At 308 K, $\delta_P(\Delta\delta_P)$ and ^1J(P—Se) are 20.0 (−1.9) and 702, 18.9 (−3.0), and ~545, and 17.0 ppm (−4.9 ppm) and ~550 Hz for P_A, P_B, and P_C, respectively; exchange with excess free ligand is slow at both 209 and 308 K; P_A is assigned to the unbound $\rangle$PSe group.

monophosphine selenides, R_3PSe, is indicated visually by blanching of the yellow colour of the ligand−SO_2 solutions (due to $R_3PSe \cdot SO_2$ (28)). At reduced temperature, ^{31}P nmr spectra attributable to the complexes $Zn(SePR_3)_4^{2+}$ (R = Ph, *o*-tol, or Cy) can be observed; details of the spectra are given in Table 3. At 209 K intermolecular ligand exchange between the 1:4 complexes and the corresponding free R_3PSe is slow on the nmr timescale but the rate of exchange becomes rapid by 308 K. In a comparison of the ^{31}P nmr spectra of $Zn(SePR_3)_4^{2+}$ (Table 3) and $Cd(SePR_3)_4^{2+}$ (1, 2) the most striking similarity is in the values of $^1J(^{31}P—^{77}Se)$ (and hence $\Delta J(^{31}P—^{77}Se)$) which are identical within experimental error.

As R_3PSe/Zn (R = Ph, Cy, or *o*-tol) is reduced in the appropriate solutions, the complexes $Zn(SePR_3)_3^{2+}$ are formed; the ^{31}P nmr spectra of these species (Table 3) show sufficient similarity to those of their cadmium analogs (2) to support these assignments. When R = *o*-tol or Cy, entities of even lower ligation number are formed when $L/M \lesssim 2$. The ^{31}P nmr spectra of these (Table 3) have smaller ^{77}Se satellite splittings than the corresponding 1:3 complexes, and, in addition, the value of $^1J(^{31}P—^{77}Se)$ found when R = *o*-tol is close to that observed for $Cd(SeP(o\text{-tol})_3)_2^{2+}$ (504 Hz (2)). Hence it is probable that the complexes formed are $Zn(SePR_3)_2^{2+}$ (R = *o*-tol or Cy). It seems certain that $Zn(SePPh_3)_2^{2+}$ is not formed because its smaller ^{77}Se satellite splitting should have been evident even if there was no significant ^{31}P nmr chemical shift difference between the 1:3 and 1:2 complexes.

When $triphosSe_3/Zn(SbF_6)_2$ = 1, a 1:1 complex is formed giving, at 209 K, a slow-exchange ^{31}P nmr spectrum of the AMX type, an easily recognizable and interpretable pattern; the spectral parameters are given in Table 4. However, in many attempts we could not produce $Zn(triphosSe_3)^{2+}$ as cleanly as $Zn(triphosS_3)^{2+}$ (see above): the nmr spectrum invariably contained other lines varying in intensity from attempt to attempt. We can offer no simple explanation for this behaviour, but because of it, and because of overlap with the AMX centre band, not all of the ^{77}Se satellites of the spectrum of $Zn(triphosSe_3)^{2+}$ could be observed. In comparison with $Cd(triphosSe_3)^{2+}$, which undergoes rapid intermolecular ligand exchange with free $triphosSe_3$ at all temperatures (1), the zinc complex undergoes slower ligand exchange. As for the corresponding trisulfide (see above), broad ^{31}P nmr lines are found for $Zn(triphosSe_3)^{2+}$−$triphosSe_3$ mixtures at 209 K. Either of structures **I** and **II** is consistent with the slow-exchange spectrum of $Zn(triphosSe_3)^{2+}$.

A 1:2 complex, $Zn(tripodSe_3)_2^{2+}$, is formed with Zn^{2+} and $tripodSe_3$ in SO_2. At 308 K the ^{31}P nmr spectrum of this complex consists of three equally intense resonances and is not noticeably changed in the presence of excess $tripodSe_3$. The least shielded resonance (P_A in Table 4) has a ^{77}Se satellite splitting *larger* than that of uncomplexed $tripodSe_3$, while the other two resonances have smaller values of $^1J(^{31}P-^{77}Se)$ than the free ligand. Clearly only two of the three PSe groups of the ligand are coordinated, and $Zn(tripodSe_3)_2^{2+}$, like $Zn(tripodS_3)_2^{2+}$ (see above), should be formulated as a bis-(bidentate) complex of time-averaged C_2 symmetry. At re-

Can. J. Chem. Downloaded from www.nrcresearchpress.com by 210.87.254.5 on 09/06/12
For personal use only.

duced temperatures this symmetry is apparently reduced, P_B being split (Table 4). Again we attribute this loss of symmetry to conformational effects. Both the chemical shifts and the values of $^1J(^{31}P—^{77}Se)$ found for $Zn(tripodSe_3)_2^{2+}$ (Table 4) are remarkably similar to those found earlier for $Cd(tripodSe_3)_2^{2+}$ (1). Chemically the major difference between $Zn(tripodSe_3)_2^{2+}$ and $Cd(tripodSe_3)_2^{2+}$ is in the lability of the bound ligand: whereas the zinc complex is non-labile on the nmr timescale at 308 K with or without excess $tripodSe_3$, $Cd(tripodSe_3)_2^{2+}$ undergoes intermolecular exchange at an intermediate rate under the same conditions (1).

Complexes of mixed ligands

To further strengthen our assignments for the 1:3 and 1:4 complexes with R_3PS and R_3PSe, we investigated the low temperature ^{31}P nmr spectra of solutions containing mixtures of $SPCy_3$ and $SePCy_3$ at different (total L)/Zn and $SPCy_3/SePCy_3$ ratios.

When (total L)/Zn $\gtrsim$ 4, a total of four signals was observed for coordinated $SPCy_3$ when the S/Se ratio was varied, as expected for the formation of $|Zn(SePCy_3)_x(SPCy_3)_{4-x}|^{2+}$. (At the same time we found that the sulfide and selenide compete approximately equally for coordination to the zinc.) For a typical sample at 209 K, the values of $\delta_P(SPCy_3(coord))$ were 64.4_6, 64.3_4, 64.1_9, and 64.0_2 ppm for $x = 0$, 1, 2, and 3 respectively, assignments being made from variation of the spectrum with change in S/Se ratio. Unfortunately we could not obtain the complementary information from the $SePCy_3$ region: the total variation of chemical shift and $^1J(^{31}P—^{77}Se)$ were insufficient to allow satisfactory resolution of the different centreband and ^{77}Se satellite resonances anticipated for the selenide in the various mixed ligand complexes. Nevertheless the existence of the four-coordinate complexes is confirmed.

Using (total L)/Zn < 3 (to avoid complications in the spectra from the co-existence of the four-coordinate species) a total of three signals from bound Cy_3PSe was observed in the expected region, in agreement with prediction for $|Zn(SePCy_3)_x(SPCy_3)_{3-x}|^{2+}$. Assignments were made by studying intensity as a function of the S/Se ratio, and in a typical sample $\delta_P(SePCy_3$ (coord)) and $^1J(^{31}P—^{77}Se)$ were 63.8_7 and 502, 64.0_1 and 503, and 64.1_9 ppm and 504 Hz for $x = 1$, 2, and 3, respectively. In this series the separate resonances expected for $SPCy_3$ bound in the different complexes could not be observed, but again the stoichiometry, 1:3 in these complexes, is confirmed despite this lack.

Attempts to produce species with mixtures of $SPCy_3$ and $OPCy_3$ or $SePCy_3$ and $OPCy_3$ as ligands were unsuccessful. At (total L)/Zn $\approx$ 4 (excess $OPCy_3$ displaces $EPCy_3$ (E = S or Se) completely) the major species present were identified as $Zn(EPCy_3)_4^{2+}$ (E = S or Se) and $Zn(OPCy_3)_4^{2+}$ by their reduced temperature ^{31}P nmr spectra. This is the same "antisymbiotic" (34) behaviour found earlier for divalent cadmium (3), tin (33), and lead (33) as acceptors.

Acknowledgments

We thank the Natural Sciences and Engineering Research Council of Canada for financial support in the form of an Operating Grant to P.A.W.D., and Mrs. Heather Schroeder, until recently of this Department, for expert technical assistance in obtaining some of the nmr spectra.

1. P. A. W. DEAN and M. K. HUGHES. Can. J. Chem. **58**, 180 (1980).
2. P. A. W. DEAN and L. POLENSEK. Can. J. Chem. **58**, 1627 (1980).
3. P. A. W. DEAN. Can. J. Chem. **59**, 3221 (1981).
4. D. W. MEEK and P. NICPON. J. Am. Chem. Soc. **87**, 4951 (1965).
5. M. A. A. BEG and K. S. HUSSEIN. Chem. Ind. 1181 (1966).
6. A. M. BRODIE, G. A. RODLEY, and C. J. WILKINS. J. Chem. Soc. (A), 2927 (1969).
7. K. C. MALHOTRA. Indian J. Chem. **12**, 823 (1974).
8. G. P. MCQUILLAN and I. A. OXTON. Inorg. Chim. Acta, **29**, 69 (1978); J. Chem. Soc. Dalton, 895 (1979).
9. A. J. BLAKE, G. P. MCQUILLAN, and I. A. OXTON. Spectrochim. Acta, **36**A, 501 (1980).
10. T. S. LOBANA, S. S. SANDHU, and T. R. GUPTA. J. Indian Chem. Soc. **58**, 80 (1981).
11. K. C. MALHOTRA, G. MEHROTA, and S. C. CHAUDRY. Indian J. Chem. **16**A, 905 (1978).
12. E. W. AINSCOUGH, H. E. BERGEN, A. M. BRODIE, and K. A. BROWN. J. Chem. Soc. Dalton, 1649 (1976).
13. H. R. HAYS and D. J. PETERS. *In* Organic phosphorus compounds. Vol. 3. *Edited by* G. M. Kosolapoff and L. Maier. Wiley-Interscience, New York. 1972. Chapt. 6, and refs. therein.
14. M. W. G. DE BOLSTER and W. GROENEVELD. *In* Topics in phosphorus chemistry. Vol. 8. *Edited by* E.J. Griffith and M. Grayson. Interscience, New York. 1976. Chapt. 5, and refs. therein.
15. S. O. GRIM and L. C. SATEK. J. Coord. Chem. **6**, 39 (1976).
16. J. C. DEQUEIROZ, C. AIROLDI, and A. P. CHAGAS. J. Inorg. Nucl. Chem. **43**, 1207 (1981).
17. C. A. KOSKY, J.-P. GAYDA, J. F. GIBSON, S. F. JONES, and D. J. WILLIAMS. Inorg. Chem. **21**, 3173 (1982).
18. M. W. G. DE BOLSTER, C. BOUTKAN, T. A. VAN DER KNAAP, L. VAN ZWEEDEN, I. E. KORTRAM, and W. L. GROENEVELD. Z. anorg. chem. **443**, 269 (1978).
19. M. N. TKACZUK and S. F. LINCOLN. Aust. J. Chem. **33**, 3621 (1980).
20. S. F. LINCOLN, D. L. PISANIELLO, T. M. SPOTSWOOD, and M. N. TKACZUK. Aust. J. Chem. **34**, 283 (1981).
21. N. M. KARAYANNIS, E. E. BRADSHAW, L. L. PYTLEWSKI, and M. M. LABES. J. Inorg. Nucl. Chem. **32**. 1079 (1970).
22. N. M. KARAYANNIS, C. M. MIKULSKI, M. J. STROCKO, and L. L. PYTLEWSKI. Inorg. Chim. Acta, **8**, 91 (1974).
23. C. M. MIKULSKI, J. S. SKRYANTZ, N. M. KARAYANNIS, L. L. PYTLEWSKI, and L. S. GELFAND. Inorg. Chim. Acta, **27**, 69 (1978).
24. C. R. WHITE and M. D. JOESTEN. J. Inorg. Nucl. Chem. **38**, 2173 (1976).
25. M. W. G. DE BOLSTER, J. DEN HEIJER, and W. L. GROENEVELD. Z. Naturforsch. **27**B, 1324 (1972).
26. W. R. WALKER and N. C. LI. J. Inorg. Nucl. Chem. **27**, 411 (1965).
27. L. C. DAMUDE and P. A. W. DEAN. J. Organomet. Chem. **168**, 123 (1979).
28. P. A. W. DEAN. Can. J. Chem. **57**, 754 (1979).
29. W. J. STEC, A. OKRUSZEK, B. UZNANSKI, and J. MICHALSKI. Phosphorus, **2**, 97 (1972).
30. C. GLIDEWELL and E. J. LESLIE. J. Chem. Soc. Dalton, 527 (1977).
31. S. O. GRIM, E. D. WALTON, and L. C. SATEK. Inorg. Chim. Acta, **27**, L115 (1978); Can. J. Chem. **58**, 1476 (1980).
32. I. J. COLQUHOUN and W. MCFARLANE. J. Chem. Soc. Dalton, 658 (1981).
33. P. A. W. DEAN. Can. J. Chem. **60**, 2921 (1982).
34. C. K. JØRGENSEN. Inorg. Chem. **3**, 1201 (1964).

Can. J. Chem. Downloaded from www.nrcresearchpress.com by 210.87.254.5 on 09/06/12
For personal use only.

Régiosélectivité d'additions de nucléophiles sur des dialkoxycarbonyle quinoxalinotropones

ALAIN TURCK, ROLAND BOUTTE ET GUY QUÉGUINER[1]

Université de Rouen, Institut National Supérieur de Chimie Industrielle de Rouen, Laboratoire de Chimie Organique Hétérocyclique, F-76130 Mont Saint Aignan, France

Reçu le 25 novembre 1982

ALAIN TURCK, ROLAND BOUTTE et GUY QUÉGUINER. Can. J. Chem. **61**, 1806 (1983).

Nous avons étudié la régiosélectivité d'additions de type Michaël sur des tropones accolées à la quinoxaline: les dialkoxycarbonyle quinoxalinotropones. Nous avons utilisé des nucléophiles carbonés (malonate d'éthyle et malononitrile), oxygénés (méthylate de sodium), soufrés (méthyl et benzyl mercaptans), azotés (méthyl, phénylhydrazine et aniline). Nous avons pu montrer que ces additions conduisaient en général à des monoadditions de type 1,4 (par référence aux α énones) ou à des produits pontés provenant d'une bis-addition de type 1,4 (αα′ diénone). Nous avons pu élucider les structures complexes obtenues par référence aux travaux de B. Föhlisch et coll. en série homoaromatique. Dans le cas des hydrazines substituées nous avons pu apporter un élement de réponse au mécanisme du réarrangement proposé par ces mêmes auteurs.

ALAIN TURCK, ROLAND BOUTTE, and GUY QUÉGUINER. Can. J. Chem. **61**, 1806 (1983).

We have studied the regioselectivity of Michael type additions on tropones attached to quinoxalines, i.e. dialkoxycarbonyl quinoxalinotropones. We used carbon nucleophiles (ethyl malonate and malononitrile), oxygen nucleophiles (sodium methoxide), sulphur nucleophiles (methyl and benzyl mercaptans), and nitrogen nucleophiles (methyl and phenylhydrazine, aniline). We have shown that, in general, these reactions lead to 1,4-monoadditions or to bridged products arising from a bis-1,4-addition process. We have determined the structures of the complexes obtained by comparison to the work of Fohlisch *et al.* in the homoaromatic series. For the case of substituted hydrazines, we present some evidence on the rearrangement mechanisms proposed by these authors. [Journal translation]

L'intérêt chimique et biologique des dérivés troponiques suscite depuis quelques années de nombreuses publications. En particulier plusieurs dérivés comportant un cycle aromatique accolé au cycle troponique ont été synthétisés (1−10). Après avoir étudié la réduction par divers borohydrures alcalins de tropones de la quinoxaline **1**, nous avons entrepris une étude de

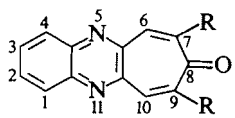

1

1*a* R = COOR′
1*b* R = phényl

la régiosélectivité d'additions de type Michaël de nucléophiles carbonés, oxygénés, soufrés, azotés sur un cycle troponique accolé à un cycle aromatique. Cette étude sur les dialkoxycarbonyl-7,9 oxo-8 (8*H*) cyclohepta[*b*]quinoxalines **1***a* s'appuie sur les résultats obtenus par B. Föhlisch et coll. à partir des benzotropones (1, 11, 12, 15).

Une structure telle que **1***a* présente trois sites électrophiles principaux 6, 8, 10. Les agents nucléophiles peuvent donc conduire à des composés résultants (*i*) d'une simple attaque en 6, 10, ou 8; (*ii*) d'une double attaque 6,8 ou 6,10 avec un nucléophile monofonctionnel; une attaque de type 6,10 sur une diénone a été observée par Foster et Payne (13); (*iii*) d'une double attaque 6,8 ou 6,10 avec un nucléophile polyfonctionnel conduisant éventuellement à un produit ponté. House *et al.* (14) ont donné un exemple d'une telle attaque de type 6,8 sur une α énone;[2] (*iv*) d'une triple attaque 6,8,10 comme indiquée par Thiele et Hädicke (15) avec des hydrazines.

Il faut souligner l'intérêt de ces réactions conduisant en particulier à des analogues d'antiparkinsoniens tels que la benzotropine et à des analogues hétérocycliques de précurseurs de la tropanone et de l'atropine (parasympatholytiques) (16).

I. Addition de nucléophiles carbonés

1. *Addition de Michaël avec l'acétone dicarboxylate d'éthyle-1,3*

Nous avons obtenu les produits de bis-addition 6,10 **4***a* et **4***b* par action des acétones dicarboxylate de méthyle et d'éthyle **2***a* et **2***b* sur le composé **1***a*.

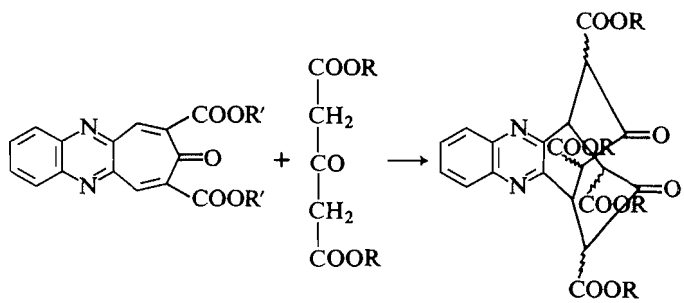

1*aa* R′ = CH_3 **2***a* R = CH_3 **4***a* R = CH_3
1*ab* R′ = C_2H_5 **2***b* R = C_2H_5 **4***b* R = C_2H_5

Remarquons que lors de la synthèse de la dicarbethoxy-7,9 oxo-8 (*H*) cyclohepta[*b*]quinoxaline **1***ab* nous avions constaté la formation du même produit d'addition **4***b* au cours de la réaction de l'acétone dicarboxylate d'éthyle **2***b* sur la diformyl quinoxaline **3**.

Le composé **4***b* présente un spectre de rmn complexe qui ne correspond pas à la formule développée d'un composé dicétonique. La comparaison du spectre de rmn de **4***b* avec celui du composé analogue en série benzénique dont la structure a été démontrée par Föhlisch (1) montre que le composé **4***b* est sous la forme du bisénol **6**.

Nous observons un singulet à 13,28 ppm correspondant à deux protons échangeables par D_2O. Ce signal doit correspon-

[1]Auteur à qui adresser la correspondance.

[2]On pourrait aussi envisager des réactions intermoléculaires pouvant conduire à des polymères.

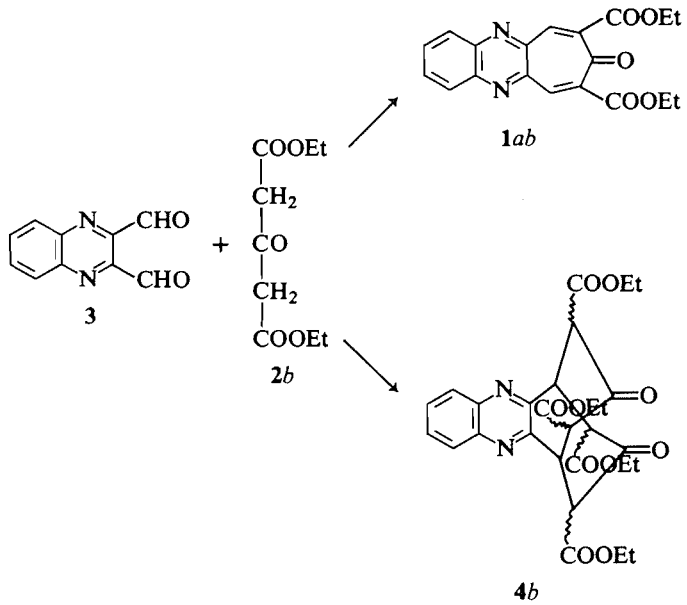

3 2b 1ab 4b

dre à des protons d'énols chélatés avec des fonctions ester voisines. Le déplacement chimique supérieur à ceux observés

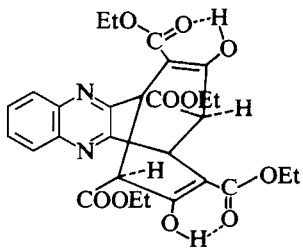

6

par Rhoads (17) pour la forme énol de carbethoxy-2 cyclanones **5** indique une très forte liaison hydrogène.

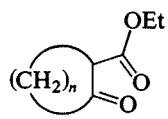

5

La présence de protons de type énol est confirmée par le spectre infrarouge qui montre une bande d'absorption large vers 1650 cm^{-1} et une plus étroite vers 1615 cm^{-1}; ces bandes sont caractéristiques (18) d'un groupe C=O chélaté de l'ester d'une part et du groupe C=C de l'énol d'autre part. De même le spectre ultraviolet montre une absorption dont la longueur d'onde et le coefficient d'extinction (λ = 255 nm, log ϵ 4,12) sont typiques d'une forme énol chélatée (19).

La synthèse de composés analogues a été signalée par quelques auteurs: (*i*) D. J. Bertelli (20) lors de la synthèse du composé homologue dans la série de l'indane:

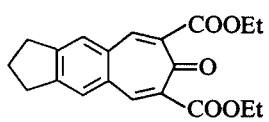

7

(*ii*) D. Letouzé (8) dans notre laboratoire, en série pyridinique:

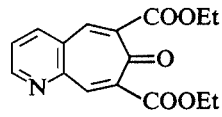

8

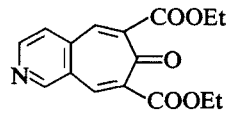

9

La dernier auteur a montré que la forme préférentielle en solution était de type **6**.

Synthèse du tétrahydro-6,7,9,10 époxy-8,13 propano-6,10 (8H) cyclohepta[b]quinoxaline diol-8,13 **11**

Le tétraester **6** présente deux fois l'élément de structure d'un β-oxoester énolisé et peut donc s'hydrolyser et se décarboxyler facilement. Nous l'avons traité par un mélange d'acides chlorhydrique et acétique et avons obtenu la dicétone **10**.

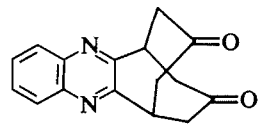

10

Ce type de composé est susceptible par des attaques nucléophiles de conduire à une cyclisation intramoléculaire (1). Par chauffage de **10** dans l'eau on obtient **11** dont la structure est confirmée par infrarouge et rmn.

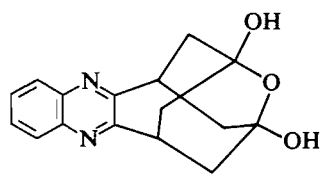

11

2. *Addition de Michaël avec des composés présentant un seul méthylène actif*

Nous envisageons ensuite la réaction de nucléophiles carbonés ne présentant qu'un site nucléophile pour déterminer si nous obtiendrons un produit résultant de l'addition d'une mole de nucléophile sur un site 6 ou 8 ou sur deux sites (pontage) 6,8 ou 6,10 ou de deux moles de nucléophiles sur deux sites 6,8 ou 6,10.

Nous étudions la réaction avec le malonate d'éthyle et le malononitrile.

(a) *Malonate de méthyle*

Si la réaction est conduite à 20°C dans le méthanol en présence de triéthylamine on obtient le produit de monoaddition en 6, **12**.

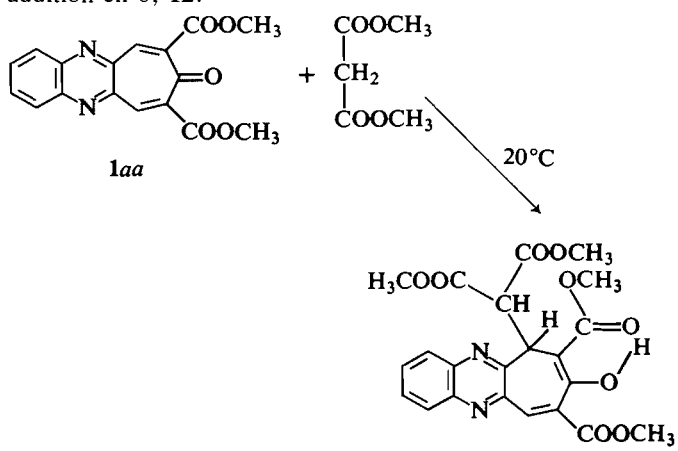

1aa 12

12

A 60°C l'action du malonate de méthyl sur **1***aa* conduit au composé de diaddition pontée 6,10, **13**.

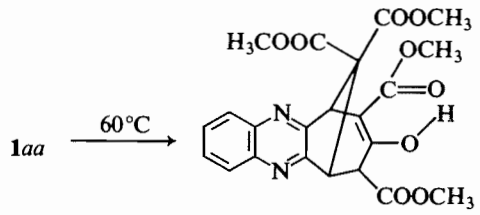

13

Le produit **13** peut présenter deux isomères **14***a* et **15***a* suivant que le substituant carbométhoxylé en C(9) se trouve en position axiale ou équatoriale.

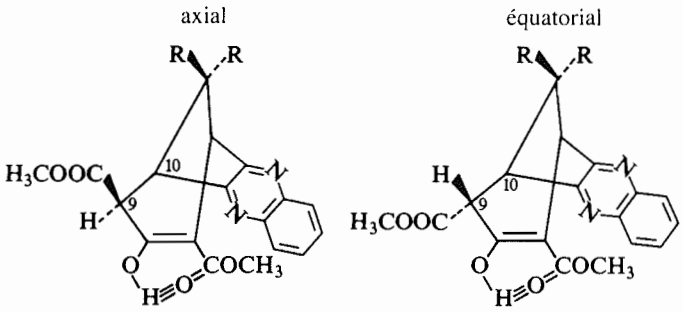

14*a* R = $COOCH_3$
b R = CN

15*a* R = $COOCH_3$
b R = CN

Le composé **13** présente une constante de couplage J_{9-10} = 6 Hz qui est très proche de celle trouvée par Föhlisch sur son homologue en série benzénique $J_{8,9}$ = 5.6 Hz pour un composé sous la forme équatoriale ($J_{8,9} \leq 2$ Hz pour la forme axiale) ce qui indique comme celui-ci l'a démontré (12) que **13** est sous la forme équatoriale **15***a*.

(b) *Action du malononitrile*

Nous n'avons jamais pu isoler de composé de monoaddition. Dans le méthanol, en présence de triéthylamine, on obtient directement la dicarbométhoxy-7,9 dicyano-12,12 hydroxy-8 dihydro-9,10 méthano-6,10 (6*H*) cyclohepta[*b*]quinoxaline **16** (produit d'addition ponté en 6,10).

Notons que Föhlisch (11) a synthétisé des composés analogues à partir du dicarbométhoxy-6,8 oxo-7 (7*H*) benzocycloheptène, il n'observe qu'un isomère équatorial alors que nous avons mis en évidence la présence des 2 isomères axiaux et équatoriaux.

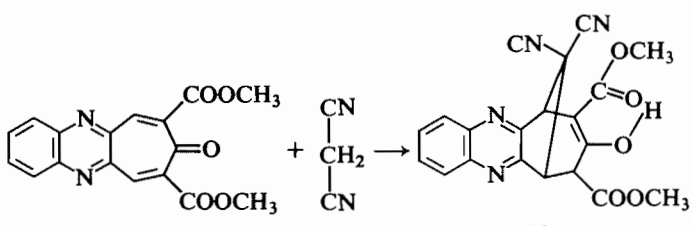

1*aa* **16**

Le composé **16** dont la structure est proche de celle du tétraester **13** présente un spectre de résonance magnétique nucléaire nettement différent. Nous avons en particulier constaté la présence de deux singulets correspondant à des protons de type énol (δ = 12,63 et δ = 12,4 ppm). Il y a donc un mélange de deux isomères. Nous pouvons écarter les isomères correspondant à une monoaddition. En effet de tels composés donneraient en rmn un massif fortement déblindé correspondant à cinq protons (quatre protons du cycle benzénique et le proton H(10)). Ceci se traduirait, dans le mélange, par une intégration excédentaire dans la zone des protons aromatiques, or celle-ci indique exactement quatre protons. Ce spectre ne peut donc s'expliquer que par un mélange de deux isomères **14***b* et **15***b* où les groupes carbométhoxyles en C(9) se trouvent respectivement en position axiale ou équatoriale, ce dernier composé étant majoritaire (75%).

L'encombrement stérique du groupe $-C\equiv N$, plus faible que celui d'une fonction ester, explique que l'on observe la formation de 25% de composé axial dans le cas du composé **13**.

L'action des nucléophiles carbonés envisagés conduit soit à des monoadditions en 6 soit à des adduits pontés en 6,10. Ces résultats concordent avec ceux de Britten Kelly et Willis (21) dans le cas d'une αα′diénone. Dans le cas des additions avec pontage on constate la formation prépondérante du dérivé possédant une fonction ester en position équatoriale sur (C9).

Notons qu'avec les nucléophiles carbonés utilisés nous n'avons pas observé de produits résultants d'une attaque nucléophile sur le carbone C(8) (C=O) ni de bis-addition de deux moles de nucléophile à la fois en 6 et 10 ou 6 et 8 alors que House *et al.* (14) ont obtenu une addition de type 6,8 avec la cyclohéxène-2 one.

II. Nucléophiles oxygénés et soufrés

1. *Nucléophile oxygéné*

Par action du méthylate de sodium sur **1***aa* nous obtenons la dicarbométhoxy-7,9 hydroxy-8 méthoxy-6 (6*H*) cyclohepta[*b*]quinoxaline **17**.

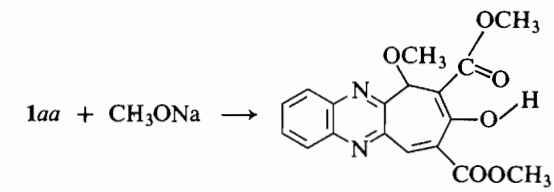

17

Nous constatons sans ambiguité d'après le spectre rmn une monoaddition.

Foster et Payne (13) ont isolé au cours d'une réaction analogue sur la diméthoxy-4,4′ cyclohexadiène-2,5 one **18** la tétraméthoxy-3,4,4′5′ cyclohexanone-2,5 **19** avec un rendement de 17%.

18 **19**

Dans le but d'obtenir une bis-addition nous avons fait réagir deux équivalents de méthylate de sodium sur **1***aa*; nous avons obtenu le même composé de monoaddition **17**.

2. *Nucléophiles soufrés*

Nous avons fait réagir dans le méthanol à chaud les méthyl et benzylmercaptans. Nous avons obtenu avec de bons rendements les composés d'addition **20** et **21**.

En faisant agir CH_3SH sur le composé **18**, Foster et Payne

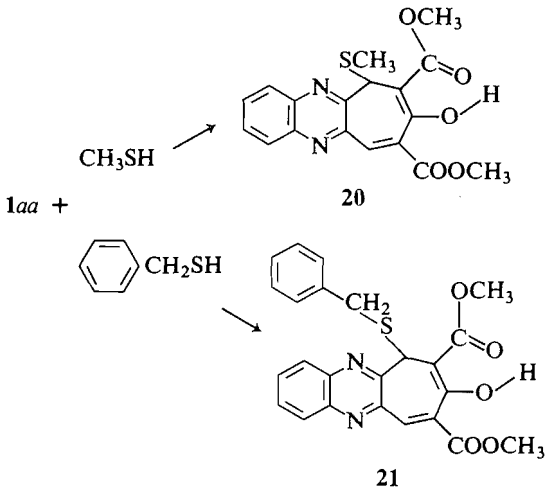

(13) ont obtenu une bis-addition avec un excellent rendement.

Dans le cas des nucléophiles oxygénés et soufrés utilisés

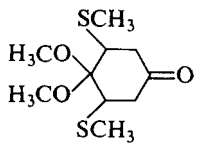

19bis

nous n'avons pas rencontré de bis-addition de deux moles de nucléophile en 6 et 10 ou 6 et 8, ni d'addition en C(8).

III. Nucléophiles azotés

Les nucléophiles azotés tels que les méthyl, phénylhydrazines et l'aniline sont susceptibles comme les nucléophiles carbonés de donner lieu à des pontages.

Les méthyl et phénylhydrazines conduisent aux composés **22** et **23**.

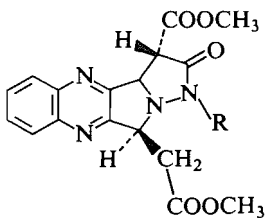

22 R = CH_3
23 R = phényl

Les produits **22** et **23** ont été identifiés grâce à leur spectre de rmn par analogie avec celui du carbométhoxy-3 oxo-2 tétrahydro-2,3,3a,8 (1H) pyrazolo[5,1-*a*]isoindole **24** dont Föhlisch et coll. (15) ont démontré la structure par RX.

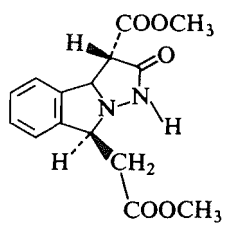

24

La formation de ce type de composé peut s'expliquer à partir du monoadduit **25** par deux mécanismes différents proposés par Föhlisch et coll. (15).

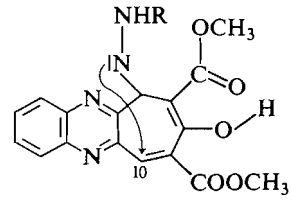

25

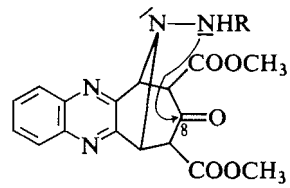

26

(a) Attaque nucléophile sur C(10) conduisant à un produit ponté **25** puis attaque de l'azote libre sur (C8) (carbonyle) suivie d'une ouverture du cycle en (C7)—C(8). Remarquons que l'attaque du C(8) est favorisée par la proximité géométrique de l'azote.

(b) Attaque de l'azote substitué sur le carbonyle puis attaque en (C10) après ouverture du cycle en C(8).

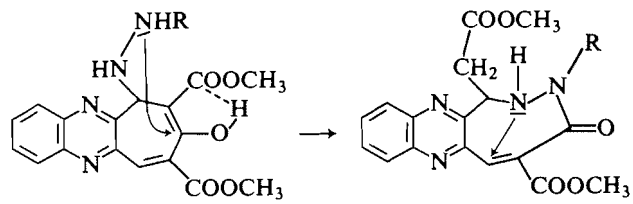

27

Pour essayer de mettre en évidence la formation d'un des intermédiaires **26** ou **27** nous avons tenté de suivre cette réaction en rmn. Nous avons fait agir à température ambiante la phénylhydrazine sur le diester **1***aa* dans le méthanol deutérié CH_3OD.[3] Nous avons observé directement l'apparition du composé deutérié **28** caractérisé par les signaux des protons H(10) et H(11).

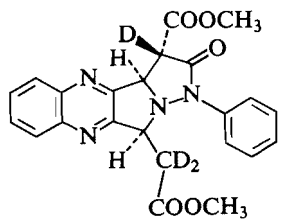

28

Nous avons pu synthétiser **29**, un analogue de l'intermédiaire **26** par l'action de l'aniline sur le composé **1***ab*. La

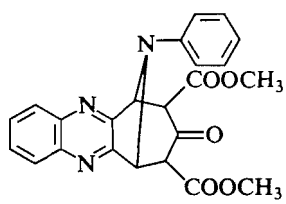

29

[3]L'utilisation de CH_3OD permet une simplification du spectre de rmn de **28** et donc une meilleure possibilité d'analyse du mélange réactionnel susceptible de contenir **28** et les espèces intermédiaires recherchées.

synthèse de **29** prouve la possibilité d'existence d'un intermédiaire de réaction ponté de type **26**. De plus, nous n'avons jamais rencontré avec les nucléophiles utilisés une attaque nucléophile directe sur le sommet 8. Tout ceci nous permet de proposer le premier des deux mécanismes envisagés par Föhlisch et coll. (15).

Conclusions

Les différentes réactions d'additions nucléophiles réalisées sur la 8*H* cyclohepta[*b*]quinoxaline dicarboxylate de méthyle-7,9 **1***a* conduisent exclusivement à des monoadditions de type I et à des produits pontés de bis-addition 6,10 de type II ou II′. Nous n'avons jamais obtenu d'addition provenant d'une

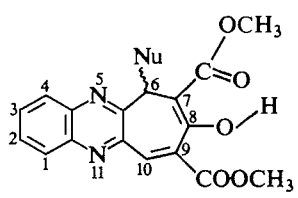

I

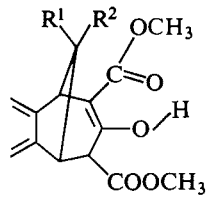

II

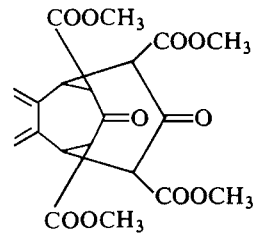

II′

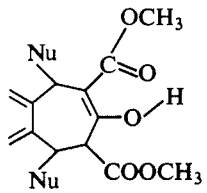

III

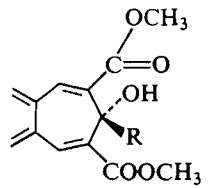

IV

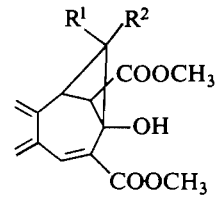

V

attaque nucléophile initiale en C(8) conduisant à une structure de type IV, de produits non pontés de bis-addition en 6 et 10 de type III ni de produits provenant d'un pontage en 6,8 de type V comme dans le cas d'une α énone (14).

Nous avons rencontré une triple attaque 6,10 puis 8 lors de l'action de dérivés de l'hydrazine. L'attaque en 8 conduit à une réarrangement complexe et nous avons pu apporter un élément au mécanisme de ce réarrangement.

Les additions de Michaël ainsi que les additions nucléophiles sur les cétones sont connues pour être réversibles. Föhlisch et coll. ont montré que pour la benzotropone le pontage 6,10 était aussi réversible dans les conditions de la réaction. Ce sont donc des réactions sous contrôle thermodynamique et le facteur déterminant est la stabilité des produits finals.

De l'étude de nos résultats il ressort que les produits de structure III, IV et V sont moins stables que ceux de structure I, II ou II′. Les structures IV et V ne possèdent plus la stabilisation apportée par la liaison hydrogène forte de l'H énolique avec l'oxygène de l'ester en α qui existe dans toutes les autres structures.

Nous n'avons pas d'hypothèse satisfaisante pour expliquer la plus faible stabilité des produits de structure III par rapport à ceux de structure I et II ou II′.

La réaction avec le malonate de méthyle montre la plus grande stabilité de la structure pontée II par rapport à la structure I.

Par action d'un nucléophile polyfonctionnel: acétone dicarboxylate de méthyl-1,3 nous observons une structure pontée de type II′ et non de type II. La structure II′ présente deux liaisons hydrogènes intramoléculaires alors que la structure II n'en présente qu'une, de plus cette forme II′ a des tensions de cycle plus faibles.

En outre ce travail nous a permis d'accéder à de nombreux composés polycycliques complexes dont nous avons pu préciser les structures.

Partie expérimentale

Les points de fusion ont été déterminés sur un banc de Kofler et n'ont pas été corrigés.

Les microanalyses ont été réalisées sur un appareil Technicon.

Les spectres ir ont été enregistrés soit avec un spectrographe Perkin–Elmer 237 soit avec un spectrographe Beckman IR 4250.

Les spectres de rmn ont été enregistrés dans le deutériochloroforme avec le TMS comme référence interne ou dans le DMSO avec le HMDS comme référence interne avec un appareil Varian T 60. Les déplacements chimiques sont exprimés en ppm par rapport au TMS.

*Dihydroxy-8,13 dihydro-9,10 propéno-10,6 (6*H*) cyclohepta(*b*)-quinoxaline tétracarboxylate d'éthyle-7,9,12,14* **4**b

Méthode (a)

Ce produit a d'abord été obtenu lors de la synthèse de la diméthoxycarbonyl-7,9 oxo-8 (8*H*) cyclohepta(*b*)quinoxaline. Après filtration du milieu réactionnel, on ajoute dans le filtrat de l'éther de pétrole jusqu'à éclaircissement de la solution. On filtre, puis on évapore à sec. Le résidu ainsi obtenu est extrait à l'éther sulfurique à chaud.

Méthode (b)

500 mg (2,69 mmol) de quinoxaline dicarboxyaldéhyde-2,3 **3** sont dissous dans 50 cm^3 de méthanol. On ajoute 1,09 g (5,4 mmol) d'acétone dicarboxylate d'éthyle-1,3 et trois gouttes de triéthylamine. On agite une heure à température ambiante. Un précipité apparait. Après filtration et lavage à l'éther on obtient 870 mg (55%) de produit d'addition. Recristallisation dans l'éthanol.

Méthode (c)

500 mg (1,42 mmol) de diéthoxycarbonyl-7,9 oxo-8 (8*H*) cyclohepta(*b*)quinoxaline **1***ab* sont mis en suspension dans 50 cm^3 de méthanol. On ajoute 290 mg (1,42 mmol) d'acétone dicarboxylate d'éthyle-1,3 et trois gouttes de triéthylamine. On agite à froid pendant une heure. Un précipité blanc apparaît. On filtre, lave à l'éther. On obtient 630 mg (80%) de composé d'addition. Recristallisation dans l'éthanol, *F*: étalé à partir de 210°C; ir (KBr, cm^{-1}): 3000, 2950 (CH), 1730, 1650 (C=O), 1615 (C=C); ^{1}H rmn ($CDCl_3$) δ: 0,76 (t, 6H, J = 7 Hz, CH_3), 1.46 (t, 6H, CH_3), 3.76 (q, 4H, CH_2), 3,90 (d, 2H, J_{9-10} = 4,5 Hz, H(9) et H(14), 4,36 (q, 4H, CH_2), 5,05 (d, 2H,

J_{6-14} = 4,5 Hz, H(6) et H(10), 7,83 (m, 4H, H(1), H(2), H(3), H(4)), 13,28 (s, 2H, H énol). *Anal.* calc. pour $C_{28}H_{28}N_2H_{10}$: C 60,86, H 5,11, N 5,07; trouvé: C 60,92, H 4,85, N 5,42.

*Dihydroxy-8,13 dihydro-9,10 propano-10,6 (6*H*) cyclohepta(*b*)-quinoxaline tétracarboxylate de méthyle-7,9,12,14* **4**a

Ce composé peut être synthétisé par l'une ou l'autre des méthodes (b) et (c); *F*: étalé à partir de 208°C; ir (KBr, cm^{-1}): 3000, 2960 (CH), 1735, 1650 (C=O), 1615 (C=C); ^{1}H rmn (CDCl3) δ: 3,33 (s, 6H, CH_3), 3,94 (s, 6H, CH_3), 3,96 (d, 2H, J_{9-10} = 4,5 Hz, H(9) et H(14)), 5,08 (d, 2H, J_{6-14} = 4,5 Hz, H(6) et H(10)), 7,85 (m, 4H, H(1), H(2), H(3), H(4)), 13,28 (s, 2H, H énol). *Anal.* calc. pour $C_{24}H_{20}N_2O_{10}$: C 58,07, H 4,06, N 5,64; trouvé: C 58,43, H 3,87, N 5,33.

*Tétrahydro-6,7,9,10 propano-6,10 (8*H*) cyclohepta(*b*)quinoxaline dione-8,13* **10**

500 mg (1,0 mmol) de dihydroxy-8,13 dihydro-9,10 propano-6,10 (6*H*) cyclohepta(*b*)quinoxaline tétracarboxylate de méthyle-7,9,12,14 **4**a sont dissous dans un mélange de 10 cm^3 d'acide acétique concentré et 2,5 cm^3 d'acide chlorhydrique concentré. On laisse à reflux 16 h. On évapore à sec. On reprend le résidu solide à chaud dans 20 cm^3 d'éther. On refroidit, on filtre. On obtient 230 mg (85%) de produit; *F* > 250°C; ir (KBr, cm^{-1}): 3040, 3000, 2920 (CH), 1690, (C=O); ^{1}H rmn (DMSO) δ: 2,87 (m, 8H, H(7), H'(7), H(9), H'(9), H(11), H'(11), H(13), H'(13)), 3,68 (m, 2H, H(6) et H(10)), 7,93 (m, 4H, H(1), H(2), H(3), H(4)). *Anal.* calc. pour $C_{16}H_{14}N_2O_2$: C 72,17, H 5,30, N 10,52; trouvé: 72,31 H 5,43, N 10,24.

*Tétrahydro-7,8,9,10 epoxy-8,13 diol-8,13 propano-6,10 (6*H*) cyclohepta(*b*)quinoxaline* **11**

200 mg (0,75 mmol) de tétrahydro-6,7,9,10 dione-8,13 propano-6,10 (8*H*) cyclohepta(*b*)quinoxaline **10** sont recristallisés dans 20 mL d'eau. Après filtration le produit est séché sur chlorure de calcium sous vide. On obtient 110 mg (55%) de dialcool; *F* > 250°C; ir (KBr, cm^{-1}): 3310(OH), 2960, 2915, 2560 (CH), 1635 (C=C); ^{1}H rmn (DMSO) δ: 1,82 (m, 8H, H(7), H'(7), H(9), H'(9), H(11), H'(11), H(12), H'(12)), 3,59 (m, 2H, H(6) et H(10)), 6,24 (s, 2H, OH), 7,81 (s, 4H, H(1), H(2), H(3), H(4)). *Anal.* calc. pour $C_{16}H_{16}N_2O_3$: C 67,59, H 5,67, N 9,85; trouvé: C 67,85, H 5,48, N 9,73.

*Hydroxy-8 [bis(methoxycarbonyl)methyl]-6 (6*H*) cyclohepta(*b*)-quinoxaline dicarboxylate de méthyle-7,9* **12**

200 mg (0,62 mmol) de diméthoxycarbonyl-7,9 oxo-8-(8*H*) cyclohepta(*b*)quinoxaline sont mis en suspension dans 10 cm^3 de méthanol. On ajoute 81 mg (0,61 mmol) de malonate de méthyle et une goutte de triéthylamine. On agite 12 heures à froid. Un précipité apparaît. Après filtration et rinçage avec deux fois 5 cm^3 d'éther, on obtient 150 mg (55%) d'un produit blanc; *F* = 185°C; ir (KBr, cm^{-1}): 3000 (OH), 2950, 2840 (CH), 1725 (C=O), 1645 (C=C); ^{1}H rmn ($CDCl_3$) δ: 3,30 (s, 3H, CH_3), 3,75 (s, 3H, CH_3), 3,97 (s, 6H, CH_3), 3,98 (d, 1H, H(11)), 5,53 (s, 1H, H(6)), 7,96 (m, 4H, H(1), H(2), H(3), H(4)), 8,2 (s, 1H, H(10)), 12,88 (s, 1H, H énol). *Anal.* calc. pour $C_{22}H_{20}N_2O_9$: C 57,90, H 4,42, N 6,14; trouvé: C 57,63, H 4,65, N 6,08.

*Hydroxy-8 dihydro-9,10 methano-6,10 (6*H*)cyclohepta(*b*)quinoxaline tétracarboxylate de méthyle-7,9,11* **13**

200 mg (0,62 mmol) de diméthoxycarbonyl-7,9 oxo-8-(8*H*) cyclohepta(*b*)quinoxaline sont mis en suspension dans 10 cm^3 de méthanol. On chauffe à environ 50°C. On ajoute trois gouttes de triéthylamine et une solution de 99 mg (0,745 mmol) de malonate de méthyle dans 10 cm^3 de méthanol jusqu'à dissolution complète du diester de départ. On agite une demi-heure à 50°C, puis on refroidit la solution. Le précipité apparu est filtré, lavé avec un peu d'éther. On obtient 190 mg (65%) d'un composé blanc. *F* = 205°C; ir (KBr, cm^{-1}): 3000 (OH), 2955, 2905, 2840 (CH), 1740, 1720 (C=O), 1640, 1615 (C=C); ^{1}H rmn ($CDCl_3$) δ: 3,58 (s, 6H, CH_3), 3,78 (s, 3H, CH_3), 3,93 (s, 3H, CH_3), 4,42 (s, 2H, H(9) et H(10)), 4,92 (s, 1H, H(6)), 7,80 (m, 4H, H(1), H(2), H(3), H(4)), 12,08 (s, 1H, H énol). *Anal.* calc. pour $C_{22}N_{20}N_2O_9$: C 57,90, H 4,42, N 6,14; trouvé C 58,13, H 4,28, N 6,39.

*Dicyano-11,11 hydroxy-8 dihydro-9,10 methano (6*H*) cyclohepta(*b*)-quinoxaline dicarboxylate de méthyle-7,9* **16**

200 mg (6,17 mmol) de diméthoxycarbonyl-7,9 oxo-8(8*H*) cyclohepta(*b*)quinoxaline sont dissous dans 5 cm^3 de méthanol. On ajoute trois gouttes de triéthylamine et du malononitrile par petites quantités jusqu'à dissolution complète du diester. On agite à température ambiante pendant une heure. On évapore à sec. On dissout dans 100 mL de chloroforme et on lave la solution obtenue avec une solution de 2,5 cm^3 d'acide chlorhydrique concentré dans 90 cm^3 d'eau. Après séparation la phase chloroformée est séchée sur sulfate de magnésium, puis évaporée à sec. Recristallisation méthanol/éther. On obtient 160 mg (65%) d'un solide jaune; F = 194°C; ir (KBr, cm^{-1}): 3000 (OH), 2960 (CH), 2255 (C≡N), 1745 (C=O), 1665, 1620, 1610 (C=C); ^{1}H rmn ($CDCl_3$) **14***b* δ: 3,96 (s, 6H, CH_3), 4,80 (d, 1H, J_{6-9} = 1,5 Hz, H(9)), 4,96 (d, 1H, H(6)), 7,95 (m, 4H, H(1), H(2), H(3), H(4)), 12,63 (s, 1H, H énol), H(10) indéterminé; ^{1}H rmn ($CDCl_3$) **15***b* δ: 3,67 (s, 3H, CH_3), 3,96 (s, 3H, CH_3), 4,28 (d, 1H, J_{9-10} = 5,5 Hz, J_{6-9} = 1,5 Hz, H(9)), 4,46 (q, 1H, H(10)), 4,96 (d, 1H, H(6)), 7,95 (m, 4H, H(1), H(2), H(3), H(4)), 12,40 (s, 1H, H énol). *Anal.* calc. pour $C_{20}H_{14}N_4O_5$: C 61,54 H 3,62, N 14,35; trouvé: C 61,78 H, 3,92, N 14,95.

*Méthoxy-6 hydroxy-8 (6*H*) cyclohepta(*b*)quinoxaline dicarboxylate de méthyle-7,9* **17**

100 mg (0,31 mmol) de diméthoxycarbonyl-7,9 oxo-8-(8*H*) cyclohepta(*b*)quinoxaline sont mis en suspension dans 10 mL de méthanol. On ajoute 30 mg de sodium et on agite pendant 20 minutes à la température de reflux. On refroidit et on filtre le précipité formé. Après rinçage avec 5 mL d'éther sulfurique et séchage sous vide on obtient 80 mg (72%) d'un solide jaune pâle; F = 222°C; ir (KBr, cm^{-1}): 3440 (OH), 3060, 3000, 2860, 2820 (CH), 1740, 1735 (C=O), 1650 (C=C); ^{1}H rmn ($CDCl_3$) δ: 3,16 (s, 3H, CH_3), 3,93 (s, 6H, CH_3), 5,88 (s, 1H, H(6)), 7,96 (m, 5H, H(1), H(2), H(3), H(4), H(10)), 13,07 (s, 1H, H énol). *Anal.* calc. pour $C_{18}H_{16}N_2O_6$: C 60,67, H 4,53, N 7,86; trouvé: C 60,89, H 4,67, N 7,95.

*Méthylthio-6 hydroxy-8 (6*H*) cyclohepta(*b*)quinoxaline dicarboxylate de méthyle-7,9* **20**

100 mg (0,31 mmol) de diméthoxycarbonyl-7,9 oxo-8-(8*H*) cyclohepta(*b*)quinoxaline sont dissous dans 5 mL de méthanol saturé en méthylthiol. On ajoute 3 gouttes de triéthylamine et on agite 10 heures à température ambiante. Le précipité formé est filtré, lavé à l'éther, séché sous vide. On obtient 70 mg (60%) d'un solide jaune; *F* = décomposition à partir de 220°C; ir (KBr, cm^{-1}): 3420 (OH), 3040, 2960, 2950, 2920, 2840 (CH), 1730 (C=O), 1645 (C=C); ^{1}H rmn ($CDCl_3$) δ: 1,90 (s, 3H, SCH_3), 3,97 (s, 3H, OCH_3), 5,65 (s, 1H, H(6)), 7,98 (m, 5H, H(1), H(2), H(3), H(4), H(10)), 13,05 (s, 1H, H énol). *Anal.* calc. pour $C_{18}H_{16}N_2O_5S$: C 58,06, H 4,33, N 7,52; trouvé: C 58,35, H 4,09, N 7,28.

*Benzylthio-6 hydroxy-8 (6*H*) cyclohepta(*b*)quinoxaline dicarboxylate de méthyle-7,9* **21**

100 mg (0,31 mmol) de diméthoxycarbonyl-7,9 oxo-8-(8*H*) cyclohepta(*b*)quinoxaline sont mis en suspension dans 20 mL de méthanol. On ajoute 3 gouttes de triéthylamine et 80 mg (0,65 mmol) de benzylthiol. On agite 2 heures à température ambiante. On filtre le précipité apparu; on le lave avec 10 mL d'éther puis on le sèche sous vide. On obtient 80 mg (55%) d'un solide jaune; *F* = décomposition à partir de 240°C; ir (KBr, cm^{-1}): 3010 (OH), 2960, 2940 (CH), 1725 (C=O), 1650, 1640 (C=C); ^{1}H rmn ($CDCl_3$) δ: 3,54 (s, 2H, CH_2), 3,77 (s, 3H, CH_3), 3,94 (s, 3H, CH_3), 5,68 (s, 1H, H(6)), 7,13 (m, 5H, H phényl), 7,93 (m, 5H, H(1), H(2), H(3), H(4), H(10)), 12,9 (s, 1H, H énol). *Anal.* calc. pour $C_{24}H_{20}N_2O_5S$: C 64,27, H 4,49, N 6,25; trouvé: C 64,57, H 4,71, N 6,22.

*Carbométhoxyméthyl-11 méthoxycarbonyl-7 tétrahydro-6,7,8,10 oxo-8 phenyl-9(9)pyrazolo(5,1-*a*)pyrrolo(3,4-*b*)quinoxaline* **23**

100 mg (0,31 mmol) de diméthoxycarbonyl-7,9 oxo-8-(8*H*) cyclo-

hepta(*b*)quinoxaline sont mis en suspension dans 5 mL de méthanol. On ajoute 65 mg de phénylhydrazine. On chauffe à reflux une demi-heure. Un précipité apparait après refroidissement. Après filtration, on reprend le solide dans 5 mL d'éther à chaud et on filtre à nouveau après refroidissement. On obtient 80 mg (60%) d'un solide blanc; F = 154°C; ir (KBr, cm^{-1}): 3050, 2940 (CH), 1720, 1700 (C=O), 1585 (C=C); ^1H rmn ($CDCl_3$) δ: 2,81 (m, 2H, $J_{12-12'}$ = 16,5 Hz, H(12) et H'(12)), 3,46 (s, 3H, CH_3), 3,9 (s, 3H, CH_3), 4,22 (d, 1H, H(7)), 5,32 (m, 1H, $J_{11-12} = J_{11-12'}$ = 5,5 Hz, H(11)), 5,88 (d, 1H, H(6b)), 7,7 (m, 9H, H(2), H(3), H(4), H(5), H'(2), H'(3), H'(4), H'(5), H'(6)). *Anal.* calc. pour $C_{23}H_{20}N_4O_5$: C 63,88, H 12,96, N 4,66; trouvé: C 63,42, H 12,91, N 4,61.

Même mode opératoire que précédemment mais en utilisant CD_3OD comme solvant: on obtient le composé trideutérié en C(12) et C(7) **28**; ^1H rmn ($CDCl_3$) δ: 3,45 (s, 3H, CH_3), 3,93 (s, 3H, CH_3), 5,35 (s, 1H, H(11)), 5,89 (s, 1H, H(6b)), 7,81 (m, 9H, H(2), H(3), H(4), H(5), H'(2), H'(3), H'(4), H'(5), H'(6).

Carbométhoxyméthyl-11 tétrahydro-6b,7,8,10 méthyl-9 méthoxycarbonyl-7 oxo-8 (9H) pyrazolo(5,1-a)pyrrolo(3,4-b)-quinoxaline
22

Même mode opératoire que précédemment avec 100 mg (0,31 mmol) de diméthoxycarbonyl-7,9 oxo-8 (8*H*) cyclohepta(*b*)-quinoxaline et 30 mg (0,65 mmol) de méthylhydrazine. On obtient 65 mg (55%) d'un solide blanc; *F* = 219°C; ir (KBr, cm^{-1}): 2940 (CH), 1735, 1720 (C=O), 1680 (C=C); ^1H rmn ($CDCl_3$) δ: 2,89 (d, 2H, $J_{12-11} = J_{12'-11}$ = 6 Hz, H(12) et H'(12)), 3,2 (s, 3H, CH_3), 3,67 (s, 3H, CH_3), 3,92 (s, 3H, CH_3), 3,95 (d, 1H, J_{7-6b} = 11 Hz, H(7)), 5,3 (t, 1H, H(11)), 5,74 (d, 1H, H(6b)), 7,95 (m, 4H, H(2), H(3), H(4), H(5)). *Anal.* calc. pour $C_{18}H_{18}N_4O_5$: C 58,37, H 4,90, N 15,13; trouvé: C 58,14, H 4,63, N 14,96.

Phénylamino-6,10 dihydro-9,10 hydroxy-8 (6H) cyclohepta(b)-quinoxaline dicarboxylate de méthyle-7,9 **29**

100 mg (0,31 mmol) de diméthoxycarbonyl-7,9 oxo-8-(8*H*) cyclohepta(*b*)quinoxaline dicarboxylate de méthyle sont mis en suspension dans 20 mL de méthanol. On ajoute 75 mg (0,69 mmol) d'aniline et 3 gouttes de triéthylamine. On porte à reflux pendant trois heures, puis on refroidit à −20°C. Un précipité apparait. Après filtration et rinçage avec 5 mL d'éther, on obtient 70 mg (50%) d'un solide jaune pâle; *F* = 173°C; ir (KBr, cm^{-1}): 3070, 3040, 3000, 2950 (CH), 1725 (C=O), 1645, 1640, 1590 (C=C); ^1H rmn ($CDCl_3$) δ: 3,65 (s, 3H, CH_3), 3,98 (s, 3H, CH_3), 4,14 (d, 1H, J_{9-10} = 5,5 Hz, H(9)), 5,58 (d, 1H, H(10)), 5,82 (s, 1H, H(6)), 7,14 (m, 5H, H'(2), H'(3), H'(4), H'(5), H'(6)), 7,88 (m, 4H, H(1), H(2), H(3), H(4)). *Anal.* calc. pour $C_{23}H_{19}N_3O_5$:C 66,18, H 4,59, N 10,07; trouvé: C 65,97, H 4,31, N 10,38.

1. B. FÖHLISCH. Justus Liebigs Ann. Chem. 1839 (1973).
2. M. S. Cook et E. J. FORBES. Tetrahedron, **24**, 4501 (1968).
3. R. GUILLARD et P. FOURNARI. Bull. Soc. Chim. **4**, 1436 (1971).
4. W. RIED et H. BODERN. Ber. **89**, 708 (1956).
5. C. V. GRECO et M. PESCE. J. Org. Chem. **37**, 676 (1972).
6. T. GAUMANN, R.W. SCHMIDT et E. HEILBRONNER. Helv. Chim. Acta, **39**, 1985 (1956).
7. D. J. BERTELLI, T. G. ANDREWS et JR. P. O. CREWS. J. Am. Chem. Soc. **91**, 5286 (1969).
8. D. LETOUZÉ. Thèse de 3ème cycle, Université de Rouen (1975).
9. J. DUFLOS. Thèse de 3ème cycle, Université de Rouen (1975).
10. G. DUPAS. Thèse de Docteur Ingénieur, Université de Rouen (1980).
11. B. FÖLISCH. Justus Liebigs Ann. Chem. 1851 (1973).
12. B. FÖLISCH. Justus Liebigs Ann. Chem. 1861 (1973).
13. C. H. FOSTER et D. A. PAYNE. J. Am. Chem. Soc. **100**, 2834 (1978).
14. H. O. HOUSE, M. B. DETAR, R. F. SIELOFF et D. V. DERVEER. J. Org. Chem. **45**, 3545 (1980).
15. U. THIELE, E. HÄDICKE, B. NOVOTNY et B. FÖHLISCH. Justus Liebigs Ann. Chem. 1148 (1975).
16. H. C. BEYERMAN, C. M. SIEGMANN, F. L. J. SIXMA et J. H. WISSE. Recl. Trav. Chim. Pays-Bas, **75**, 1445 (1956).
17. S. J. RHOADS. J. Org. Chem. **31**, 171 (1966).
18. M. J. LEONARD, H. S. GUTOWSKY, W. J. MIDDLETON et E. M. PETERSON. J. Am. Chem. Soc. **74**, 4070 (1952).
19. S. J. RHOADS et C. PRYDE. J. Org. Chem. **30**, 3212 (1965).
20. D. J. BERTELLI. J. Org. Chem. **29**, 3032 (1962).
21. M. BRITTEN KELLY et B. J. WILLIS. Synthesis, **1**, 27 (1980).

Platinum(II) and magnesium(II) nucleotide complexes. Synthesis, FT-ir spectra, and structural properties

H. A. TAJMIR-RIAHI AND T. THEOPHANIDES
Département de Chimie, Université de Montréal, Montréal (P.Q.), Canada H3C 3V1

Received November 29, 1982

H. A. TAJMIR-RIAHI and T. THEOPHANIDES. Can. J. Chem. **61**, 1813 (1983).

Guanosine-5′-monophosphate (5′-GMP) reacts with Pt(II) and Mg(II) metal ions to give complexes of the type $Pt(5'\text{-GMP})_n Cl_2.xH_2O$, *cis*- and *trans*-$[Pt(NH_3)_2(5'\text{-GMP})_2]Cl_2.xH_2O$ and $Mg(5'\text{-GMP}).xH_2O$, where $n = 1, 2, 3, 4$ and $x = 4-10$.

Spectroscopic and chemical evidence showed marked similarities with those of the structurally known N_7-bonded 5′-GMP complexes of Mn(II), Co(II), Ni(II), Cu(II), and Cd(II) metal ions. Therefore, Pt(II) and Mg(II) are also found to be N_7-bonded in these series of nucleotide complexes.

The direct phosphate coordination was observed in Mg(II) nucleotide complexes obtained from acidic solution, whereas Mg(II) complexes prepared from neutral solution showed no direct phosphate–Mg(II) interaction. Pt(II) complexes exhibited no direct phosphate metal bonding, while the possibility of an indirect Pt(II)–phosphate interaction through a hydrogen-bonded water molecule can be proposed here.

H. A. TAJMIR-RIAHI et T. THEOPHANIDES. Can. J. Chem. **61**, 1813 (1983).

La guanosine monophosphate-5′ (GMP-5′) réagit avec les ions métalliques du Pt(II) et du Mg(II) en donnant des complexes de $Pt(GMP\text{-}5')_n Cl_2.xH_2O$, de $[Pt(NH_3)_2(GMP\text{-}5')_2]Cl_2.xH_2O$ *cis* et *trans* et de $Mg(GMP\text{-}5').xH_2O$, où $n = 1, 2, 3, 4$ et $x = 4-10$.

Les preuves spectroscopiques et chimiques font apparaître des similitudes prononcées avec les complexes de GMP-5′, liés par l'azote en position 7, des ions métalliques du Mn(II), du Co(II), du Ni(II), du Cu(II) et du Cd(II) dont la structure est connue. Cependant, on a également trouvé du Pt(II) et du Mg(II) liés par l'azote en position 7 dans cette série de complexes de nucléotide.

On a observé la coordination directe du phosphate dans les complexes de nucléotide du Mg(II) obtenues à partir d'une solution acide, tandis que les complexes du Mg(II) préparés à partir d'une solution neutre n'ont aucune interation directe phosphate–Mg(II). Les complexes de Pt(II) n'ont aucune liaison phosphate–métal directe, cependant on propose l'existence possible d'une interaction indirecte Pt(II)–phosphate par l'intermédiaire de la liaison hydrogène de la molécule d'eau.

[Traduit par le journal]

Can. J. Chem. Downloaded from www.nrcresearchpress.com by 210.87.254.5 on 09/06/12
For personal use only.

Introduction

Nucleotides react with alkali, alkaline earth, transition and non-transition metal ions (1–3) to give complexes of the type $M_2L.nH_2O$ and $M'L.nH_2O$, where M = Na^+, K^+, Ag^+, Hg^{2+}, M′ = Zn(II), Cd(II), Pb(II), Ca(II), Ba(II), Mn(II), Fe(II), Ni(II), Co(II), Cu(II), Al(III), n = 2–8 and L = adenosine-5′-monophosphate (5′-AMP), guanosine-5′-monophosphate (5′-GMP), inosine-5′-monophosphate (5′-IMP), uridine-5′-monophosphate (5′-UMP), citydine-5′-monophosphate (5′-CMP), and 2-deoxyguanosine-5′-monophosphate (5′-DGMP). The solid state complexes of all the said metal cations have been obtained and characterized by elemental analysis, ir and nmr spectroscopy (1–3).

Interaction of nucleotides and polynucleotides with Mg(II) and Pt(II) in solution has been the subject of numerous studies (4–11). Nuclear magnetic resonance and Raman spectroscopy were widely used to characterize the nature of the metal–ligand bonding and the coordination sites, which were used by the ligand upon complex formation.

So far, X-ray crystallographic evidence available on Pt(II) nucleotide complexes is as follows: (*a*) *cis*-$Pt(NH_3)_2(IMP)_2^{2-}$ (12) with N_7-coordination site used by IMP and (*b*) $Pt(en)(CMP)_2^{2-}$ (13), where the Pt(II) is bound to N_3 and the phosphate oxygen atom directly. Recently, the crystal structures of $Pt(tn)(IMP)_2^{2-}$ (14) and Pt(tn)(Me-5′-GMP)$_2$ (15) showed also N_7-coordination. Rich *et al.* (16) recently have determined the structure of *Z* and *B* DNA in a polymerization process in the presence of Mg(II) ions, where it has been found that GMP residues are coordinated to Mg(II) through N_7 with an indirect phosphate oxygen coordination via a water molecule. The remaining coordination sites of Mg(II) are occupied with five water molecules.

In the present work several complexes of Pt(II) and Mg(II) with 5′-GMP have been synthesized and characterized by elemental analysis, molar conductivity and FT-ir spectroscopy not reported so far. We have also prepared a series of structurally known nucleotide metal complexes (16–27), in order to compare and correlate the spectroscopic results obtained here with the corresponding known compounds, to obtain information about the coordination site and structural properties of the new Mg(II) and Pt(II) complexes studied here. The structurally known complexes with their coordination sites are given in Table I.

X-ray powder photographs were also used to find out any similarities between those of the structurally known compounds and the newly synthesized Mg(II) complexes.

Experimental

Materials

All the chemicals were reagent grade and were used without further purification. K_2PtCl_4 was purchased from Johnson Matthey and Mallory Ltd. The nucleotides in acid and sodium salt forms were purchased from Sigma Chemical Company.

Preparation of Mg(II) complexes

Magnesium(II) complexes were synthesized at two different pH ranges, namely 4–6 and 7–9. 5′-GMP (1 mmol) was dissolved in 30 mL of H_2O and added to the solution of $MgCl_2.6H_2O$ (1 mmol) in 20 mL of H_2O. The pH of the solution was adjusted at the pH values mentioned above with 0.1 *N* HNO_3 or 0.1 *N* NaOH and was heated at 60°C for 30 min. After cooling down at room temperature, a white precipitate appeared; this was filtered off and washed with cold water

TABLE 1. Structurally known nucleotide complexes of some metal ions

Compound	Coordination site	Reference
$Cu_3(GMP)_3.8H_2O$	N_7 and O atom of PO_3^{2-} and $2H_2O$	17
$Ni(GMP).8H_2O$	N_7 and 5 H_2O	18
$Co(GMP).8H_2O$	N_7 and 5 H_2O	19
$Mn(GMP).8H_2O$	N_7 and 5 H_2O	20
$Cd(GMP).8H_2O$	N_6 and 5 H_2O	21
$Co_2(UMP)_2.4H_2O$	O atoms of H_2O and PO_3^{2-}	22
$Cd(IMP).3H_2O$	N_7, O atoms of OH groups and PO_3^{2-}	23
$Ni(AMP).6H_2O$	N_7 and 5 H_2O	24
$Zn(IMP).3H_2O$	N_7 and O atoms of PO_3^{2-}	25
$Cu(IMP).3H_2O$	N_7 and O atoms of PO_3^{2-}	26
$Cd(CMP).H_2O$	N_3 and O atoms of PO_3^{2-}	27
$Co(CMP).H_2O$	N_3 and O atoms of PO_3^{2-}	27
$Pt(tn)(Me\text{-}5'\text{-}GMP)_2$	N_7 of the purine ring only	15
$Pt(IMP)_2(NH_3)_2^{2-}$	N_7 of the purine ring only	12
$Pt(IMP)_2(tn)^{2-}$	N_7 of the purine ring only	14
$Pt(CMP)_2(en)^{2-}$	N_3 and O atoms of PO_3^{2-}	13

TABLE 2. Analytical data and millimolar conductance of Pt(II) and Mg(II)–GMP complexes

Compound		M^{2+}	C	H	N	Cl^-	Colour	Conductivity (Ω^{-1} cm^2 mol^{-1})
1. $K[Pt(GMP)Cl_3].4H_2O$	Found	24.00	14.92	2.75	7.51	12.60	Yellow	220
	Calcd	23.55	14.50	2.42	8.45	12.86		
2. $K[Pt(GMP)Cl_3].C_2H_5OH$		24.55	16.68	3.67	9.76	12.90	Yellow	210
		24.34	18.00	2.25	8.85	13.30		
3. $Pt(GMP)_2Cl_2.6H_2O$		16.50	20.14	4.07	11.02	5.90	Pale yellow	260
		16.20	19.93	3.00	11.62	5.90		
4. $Pt(GMP)_3Cl_2.6H_2O$		11.85	22.50	3.00	11.95	4.15	White	300
		12.03	22.22	2.35	12.35	4.30		
5. $Pt(GMP)_4Cl_2$		9.90	25.50	3.10	14.25	3.70	White	320
		10.12	24.95	2.50	14.53	3.68		
6. *cis*-$[Pt(NH_3)_2(GMP)_2]Cl_2.6H_2O$		15.95	19.76	4.41	13.57	5.40	White	200
		15.75	19.38	3.40	13.57	5.73		
7. *trans*-$[Pt(NH_3)_2(GMP)_2]Cl_2.6H_2O$		15.35	19.50	3.90	13.30	5.50	White	240
		15.75	19.38	3.40	13.57	5.73		
8. $Mg(GMP).10H_2O$		4.10	21.49	5.26	11.15	—	White	160
		4.26	20.91	5.57	12.19	—		
9. $Mg(GMP).6H_2O$		4.55	23.20	4.90	13.10	—	White	150
		4.88	23.94	4.78	13.95	—		

and air dried. Mg(II) complexes of the nucleotides are soluble in hot water and slightly in hot alcohol, and they can be recrystallized from 0.1 *N* HCl or HNO_3 solution. The complexes show a conductivity value of 120–180 Ω^{-1} cm^2 mol^{-1}, corresponding to 1:1 electrolytes. The analytical data and millimolar conductances are given in Table 2.

Synthesis of Pt(II) complexes

The Pt(II) complexes of 5′-GMP were prepared by addition of the stoichiometric amount of K_2PtCl_4 or *cis*- and *trans*-$Pt(NH_3)_2Cl_2$ to the solution of the nucleotides in 200 mL of water in the presence of appropriate amount of NaCl at room temperature. The solutions were kept in the dark for one week and then the amount of water was reduced to 40 mL under low pressure at 50°C. The mixture of ethanol–ether (50 mL) was then used to bring down the precipitate. The precipitate (yellowish white) was redissolved in a small amount of water and reprecipitated by the addition of ethanol–ether, then dried in a desiccator over $CaCl_2$ and analyzed to give the empirical formula of $Pt(5'\text{-}GMP)_nCl_2.xH_2O$, where $n = 1, 2, 3, 4$ and $x = 4–6$. The complexes are soluble in H_2O and acidic solution only and not in the common organic solvents. Their colour varies from yellow for the 1:1 to white for the 4:1 complexes. They show high values of molar conductivity and this is mainly due to the presence of Na^+ ions associated with 5′-GMP molecule in these Pt(II)–GMP complexes. The analysis and millimolar conductances are shown in Table 2. The structurally known complexes were prepared by routine methods (1–4) and were analyzed for metal ion.

Physical measurements

FT-ir have been recorded on a DIGILAB FTS-15/C Fourier Transform Michelson infrared interferometer equipped with a high-sensitivity HgCdTe detector and a KBr beam splitter with a spectral resolution of 2 to 4 cm^{-1}.

Conductance measurements were carried out on a conductoscope, E365B METROHM.

X-ray powder pattern photographs were taken by using a powder camera (Philips, Debye-Scherre) with Copper K_α-radiation and nickel filters.

Elemental analysis

Pt(II) content has been analyzed by atomic absorption. Mg(II) content was determined complexometrically. C, H, N were analyzed at Schwarzkops Microanalytical Laboratory (U.S.A.). Halide was determined as silver halide.

Can. J. Chem. Downloaded from www.nrcresearchpress.com by 210.87.254.5 on 09/06/12
For personal use only.

Can. J. Chem. Downloaded from www.nrcresearchpress.com by 210.87.254.5 on 09/06/12
For personal use only.

Results and discussion

Raman and nmr techniques have been widely used to distinguish between complexation sites in nucleotides (4, 5, 7–11); with nucleotides reliable correlation between structures and spectral information is still missing. Infrared spectroscopy has been the least used technique to demonstrate the coordination mode of the nucleotide–metal complexes in solid state.

Since we had unambiguous X-ray structural information on a series of transition and non-transition metal nucleotide complexes (6, 17–27), we carefully examined their FT-ir spectra hoping to detect characteristic features for each structural type of the complexes synthesized in this work for Mg(II) and Pt(II) nucleotide complexes and to establish a correlation between the spectral changes and the N_7-coordination site in nucleotides.

It should be noted that our ir spectra for 5′-GMP are in good agreement with the vibrational studies previously reported by Lord and Thomas (28), Lautie and Novak (29), and Chinsky *et al.* (30) and our discussion is largely based on the normal coordinate analysis carried out by Tsuboi *et al.* (31–33).

5′-GMP complexes

X-ray analysis shows that Cu(II) is directly bonded to N_7 of the base and to the oxygen atom of the phosphate group as well as to water molecules in the $Cu_3(GMP)_3(H_2O)_8$ compound (17), whereas the divalent metals Mn, Co, Ni, and Cd are bonded to N_7 and to the oxygen atom of H_2O (which are hydrogen-bonded to PO_3^{2-} group in the corresponding 5′-GMP complexes (18–21). Here the FT-ir spectra of these two types of complexes are analyzed and compared with those of Mg(II) and Pt(II) complexes. The main features of the spectra will be discussed in two different parts, namely, 4000–2700 cm^{-1} and 1800–400 cm^{-1}. The 5′-$GMPNa_2$ molecule with numbering of the atoms is illustrated in **1**.

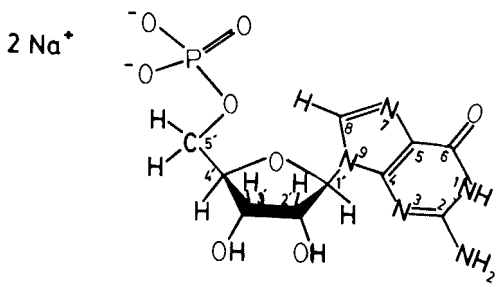

1

4000–2700 cm^{-1}. In this region, due to the presence of the strong intramolecular hydrogen-bonding of the free 5′-GMP (34) and its metal derivatives (21), very little information can be obtained on the nature of metal–ligand interaction, since there have not been considerable changes in the position of hydrogen-bonded NH_2, NH, and OH vibration frequencies of the free 5′-GMP upon complexation. A small shift of the bands at about 3500–3300 cm^{-1} in the spectra of the free base related to the asymmetric and symmetric stretching vibrations of NH_2, NH, and OH to higher frequencies in the spectra of the metal complexes would be due to the general weakening and the rearrangement of the strong hydrogen-bonding network of the ligand on complexation.

1800–400 cm^{-1}. In this region, the ir spectra of 5′-GMP showed considerable changes upon complexation. Spectral changes observed in this region will be discussed below: (*a*) The pyrimidine and purine vibration frequencies (1800–1180 cm^{-1}) and (*b*) the PO_3^{2-} stretching vibration frequencies (1180–900 cm^{-1}). Structurally known N_7-coordinated complexes of Co, Ni, and Cu (17–20) showed marked similarities in the pyrimidine and purine region of the spectra (Fig. 1), meanwhile Cu showed marked differences in the PO_3^{2-} region of the spectra, and this is mainly due to the direct Cu–phosphate bonding compared to the indirect metal–phosphate interaction of the Co and Ni cations (Fig. 1). *cis*-, *trans*-$Pt(NH_3)_2(GMP)_2Cl_2$ and other K_2PtCl_4 complexes of 5′-GMP showed similarities with those of the structurally known complexes mentioned above in both regions of the spectra (Fig. 2), whereas Mg(II) complexes show marked similarities with the structurally known N_7-bonded Cd(II) compound (21) (Fig. 3). The ir spectra of the structurally known compounds and those of Pt(II) and Mg(II) are shown in Figs. 1, 2, and 3. The possible assignments are given in Table 3.

(a) The pyrimidine and purine vibration frequencies (1800–1180 cm^{-1}). In the spectrum of the free 5′-GMP there are five absorption bands at 1692 cm^{-1} (bs), 1662 cm^{-1} (sh), 1597 cm^{-1} (s), 1575 cm^{-1} (sh), and 1535 cm^{-1} (m) assignable mainly to the stretching of $C_6{=}O$, the scissoring mode of NH_2, $C_4{-}N_3$, $C_4{-}C_5$, and the $C_4{-}N_9$ stretching vibrations, respectively (28–33). These absorption bands showed considerable changes upon N_7-coordination in the structurally known metal complexes (Fig. 1 and Table 3). The $C_6{=}O$ stretching vibration of the free base at 1692 cm^{-1} lost intensity, but did not show any considerable displacement ($\Delta\nu = \pm 6$ cm^{-1}), and this would be mainly due to the participation of the O_6 atom of 5′-GMP in hydrogen bonding upon complexation. In the free 5′-GMP acid (34) the O_6 atom is not hydrogen bonded, whereas in the metal complexes (20, 21) the O_6 is hydrogen bonded to a water molecule coordinated to the metal ion. The crystal structure of Pt(tn)(Me-5′-$GMP)_2$ showed a strong hydrogen bonding of the O_6 atom via a water molecule connected to a phosphate oxygen atom (P—O···H—O—H···O_6) (15). This hydrogen-bonding network causes the broadening of the $C_6{=}O$ stretching which shifts to a lower frequency. The bending (scissoring) motion of NH_2 of the free ligand at 1662 cm^{-1} gained intensity, and in some cases split into two components in the spectra of metal complexes (Fig. 1). The crystal structure of 5′-GMP acid (34) shows strong O···H—N—H···O hydrogen-bonding to the phosphate group, whereas such a hydrogen-bonding system would be weakened in the crystal structures of the metal complexes (17–20). Releasing or weakening of the NH_2 group from hydrogen-bonding causes the sharpening and shifting of the NH_2 stretching vibration at 3400 cm^{-1} to a higher frequency, and the bending mode of NH_2 group at 1662 cm^{-1} to a lower frequency. It should be noted that metalation or deprotonation of the NH_2 group brings considerable changes to the said absorption frequencies. The band at 1597 cm^{-1} in the spectrum of 5′-GMP mainly due to the skeletal vibrations, gained intensity, and shifted to 1600–1610 cm^{-1}. This shift is due to the inductive effect of the metal ion electrophile bound to N_7, which causes less electron delocalization, and finally less contribution to the skeletal vibrations of the ring system. Similar effects were observed in the spectra of Mg(II) and Pt(II) complexes.

A band with medium intensity at 1479 cm^{-1} of the free base, assignable to the vibration involving primarily the five-

Can. J. Chem. Downloaded from www.nrcresearchpress.com by 210.87.254.5 on 09/06/12
For personal use only.

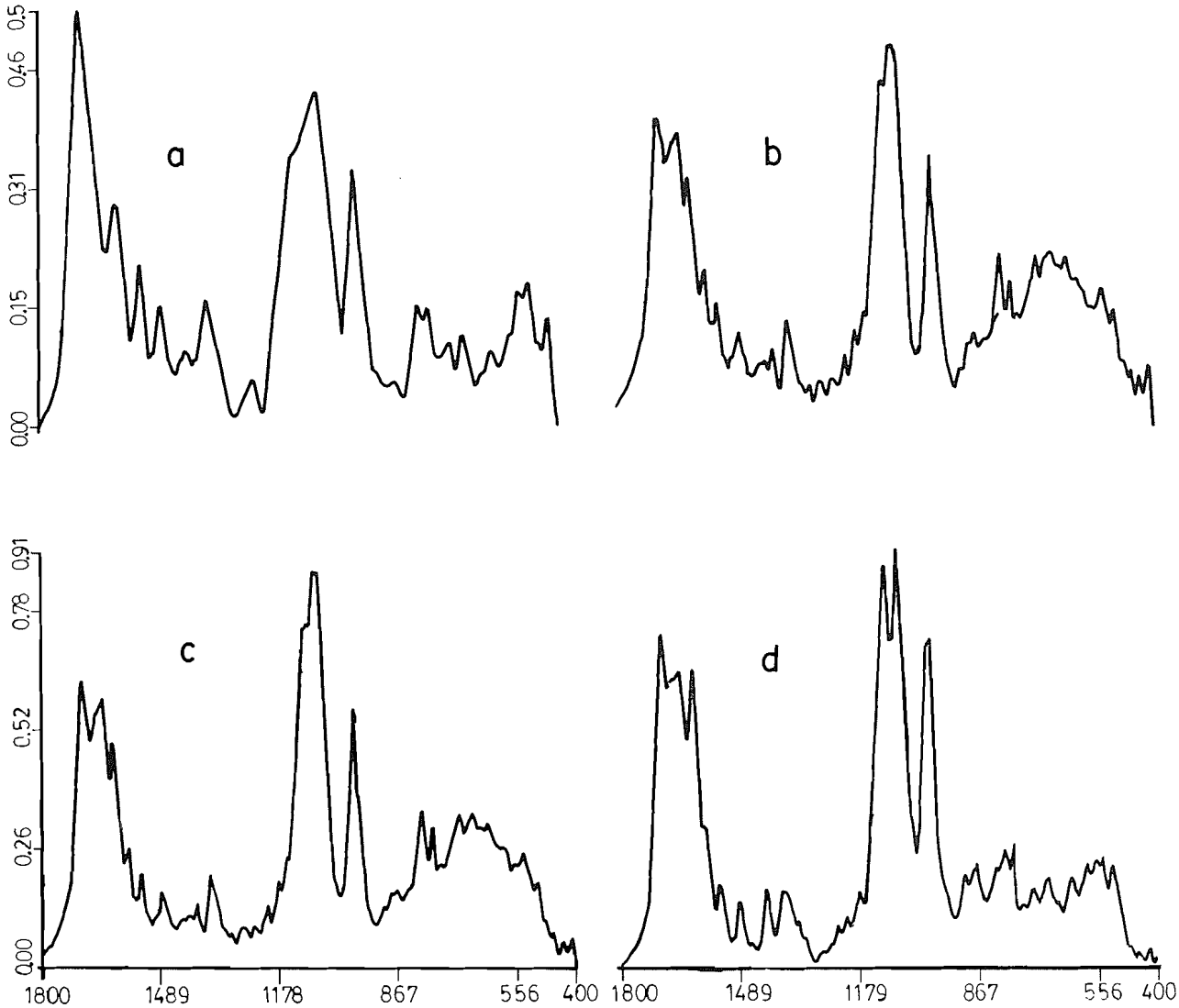

FIG. 1. FT-ir spectra of 5′-GMP and its structurally known N_7-bonded metal complexes in the region 1800–400 cm^{-1} for *a*, 5′-$GMPNa_2$; *b*, $CoGMP.8H_2O$; *c*, $NiGMP.8H_2O$; and *d*, $Cu_3(GMP)_3.8H_2O$.

membered ring C_8—H bending and the N_7—C_8 stretching frequencies (35), split into two absorption bands at 1476 cm^{-1} (m) and 1465 cm^{-1} (sh) in the spectra of N_7–metal complexes. The said absorption band also shifted to 1500 cm^{-1} in the spectra of Pt(II) complexes (Fig. 2 and Table 3). It has been found (35) that the Raman line corresponding to the said absorption at 1480 cm^{-1} disappeared upon protonation and methylation and it shifted on deuteration of H_8, whereas heavy metalation and particularly platination do not affect the Raman line of the said absorption to the same extent (9, 11, 36). It has been experimentally found (37) that the $C{=}N^+$ groups have in general higher frequencies than the parent C=N groups; therefore protonation (38) or metalation (39) could bring an increase to the infrared absorption and of the C=N stretching frequency of the purine ring system in these series of metal nucleotide complexes.

Three absorption bands with medium intensities at 1333, 1254, and 1204 cm^{-1} in the spectrum of 5′-GMP were mainly assigned to N_7—C_8, C_8—N_9, and N_7—C_5 stretching frequencies (30–33), each one appeared as a doublet at about *1350–1290 cm^{-1}*, *1280–1240 cm^{-1}*, and *1205–1210 cm^{-1}* in the spectra of the structurally known N_7–GMP complexes, respectively. A medium absorption band at 1180 cm^{-1} in the spectrum of the free base related to N_7–C_8 (31) showed intensity changes in the spectra of the said metal complexes. These observed shifts upon N_7-coordination can be explained by a distortion of the imidazol ring, where the vibrations are mostly localized and therefore N_7-metalation could change the electron distribution in the ring system. The shift of each component of the N_7—C_8 stretching vibration to a higher frequency upon N_7 metal bonding was explained above.

The shoulder absorption band at 1125 cm^{-1} in the infrared spectrum of 5′-GMP was attributed to the C—O stretching vibration of the sugar ring (35) shifted to lower frequency (1110 cm^{-1}) in the spectra of metal complexes. This shift would be either due to the rearrangement of the strong intramolecular hydrogen-bonding of O_2'—H···N_3 and O_3'—H···O_4' system found in the crystal structure of the free ligand (34), or to the conformational changes around the phosphate–ribose bond upon indirect (via H_2O) or direct coordination of the phosphate group in these series of metal–GMP complexes.

Cd–GMP complexes

The Cd(II) ion forms two complexes with the 5′-GMP mol-

Can. J. Chem. Downloaded from www.nrcresearchpress.com by 210.87.254.5 on 09/06/12
For personal use only.

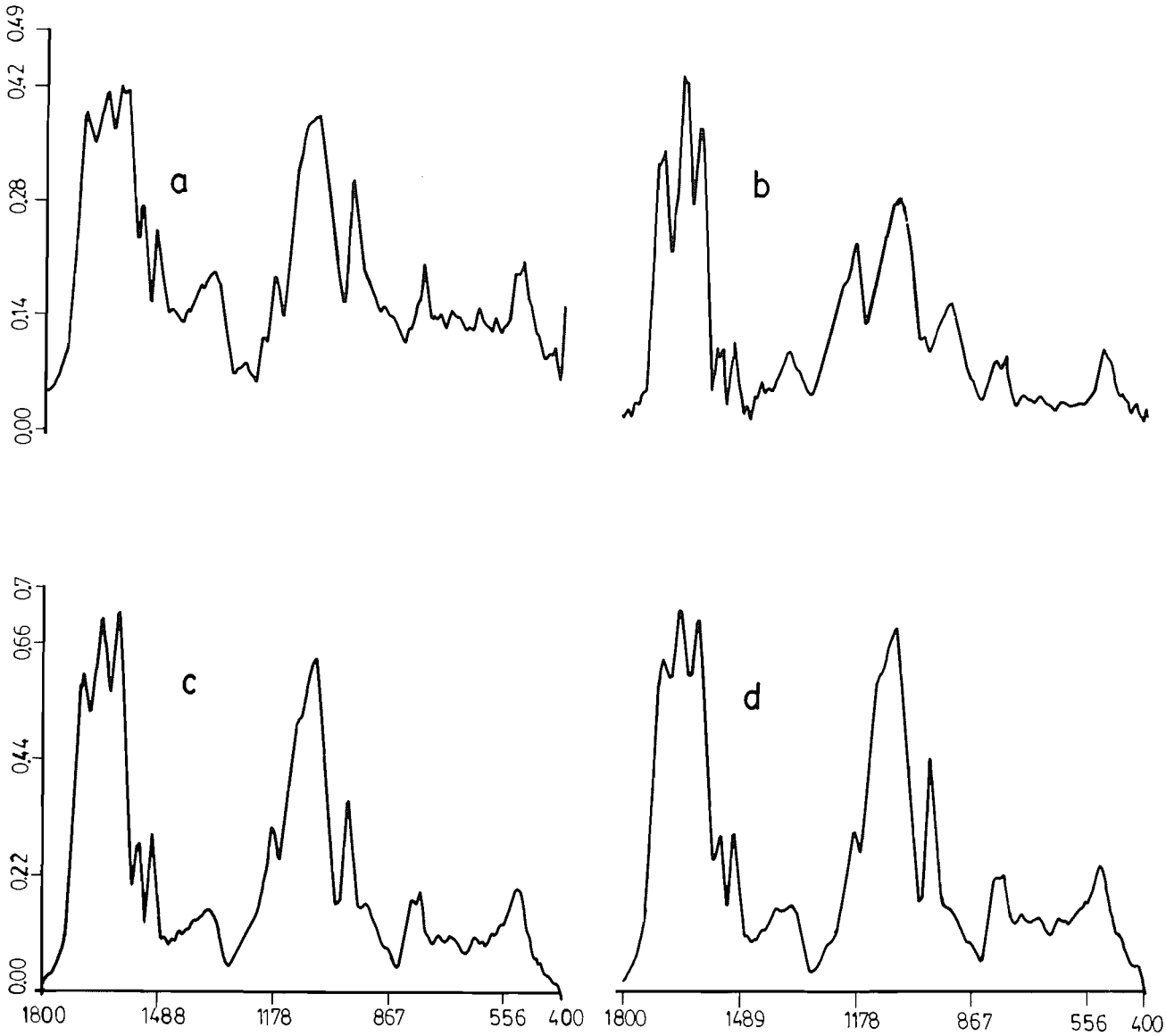

FIG. 2. FT-ir spectra of Pt(II)–GMP complexes in the region 1800–400 cm^{-1} for *a*, $[Pt(GMP)_4]Cl_2$; *b*, $K[Pt(GMP)Cl_3].4H_2O$; *c*, *cis*-$[Pt(GMP)_2(NH_3)_2]Cl_2.6H_2O$; and *d*, *trans*-$Pt(GMP)_2(NH_3)_2]Cl_2.6H_2O$.

ecule, one was obtained at pH = 6–7 which shows similarity with those of the structurally known N_7-bonded transition metal complexes (Figs. 1 and 3) and the other was recrystallized at pH = 4–5, which is structurally known (21) to be N_7-bonded and showed dissimilarities with those of the corresponding transition metal complexes in the region 1700–1600 cm^{-1} (Figs. 1 and 3). The dissimilarities observed in this region of the spectra are reflected in the crystal structures of these complexes. The Cd(II) ion is bonded to the N_7-atom of the 5′-GMP molecule as well as to five water molecules and shows indirect Cd–carbonyl interaction via a hydrogen-bonded water molecule containing also a hydrogen-bonded NH_2 group. In the corresponding copper complexes the Cu(II) ion is N_7-bonded and exhibits direct Cu–OPO_3 interaction as well as coordination to two water molecules (17), but it contains no indirect Cu–carbonyl interaction via a hydrogen-bonded water molecule. In addition, it does not show any strong hydrogen-bonded NH_2 group. Therefore, the dissimilarities observed in the region 1700–1600 cm^{-1} are due to the different hydrogen-bonding networks of carbonyl and NH_2 groups in these cadmium complexes.

It is worth noting that the ir spectra of Mg(II) complexes synthesized in this work showed marked similarities to the structurally known cadmium compound (Fig. 3). Therefore, these complexes are structurally related in terms of N_7-bonding and the possibility of the indirect Mg–carbonyl interaction through a hydrogen-bonded water molecule can not be ruled out.

(b) The phosphate vibrations of mononucleotides (1100–900 cm^{-1}). The mononucleotides, 5′-GMP, 5′-AMP, 5′-IMP, 5′-UMP, and 5′-CMP have a phosphate group at C-5′ of the ribose ring. The disodium salts of these bases contain a phosphate group capable of acting as a polydentate ligand or hydrogen-bonding agent.

The Raman spectra of the phosphate group in mononucleotides, polynucleotides, and DNA have been extensively studied (40–43). There are also some calculations on the normal vibrational modes of the phosphate group and the ribose in DNA (41, 43), but the ir spectra of the nucleotide phosphate group has not yet been fully investigated (33, 42).

Can. J. Chem. Downloaded from www.nrcresearchpress.com by 210.87.254.5 on 09/06/12
For personal use only.

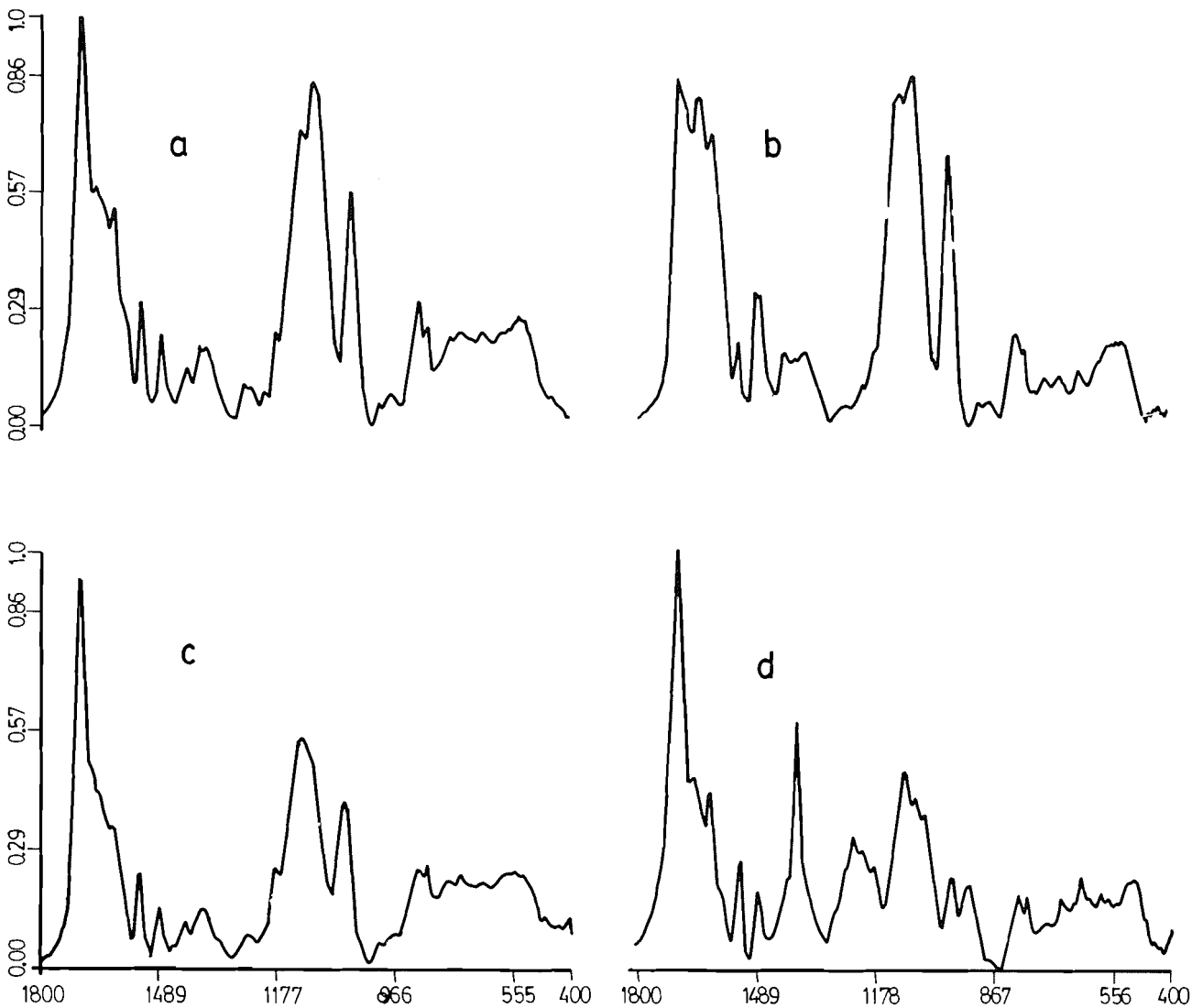

FIG. 3. FT-ir spectra of Mg(II) and Cd(II)–GMP complexes in the region 1800–400 cm^{-1} for *a*, $CdGMP.8H_2O$ (pH = 4–5); *b*, $CdGMP.8H_2O$ (pH = 5–6); *c*, $MgGMP.10H_2O$ (pH = 7); and *d*, $MgGMP.6H_2O$ (pH = 4).

The monoalkyl phosphate anion (CH_3—OPO_3^{2-}) shows infrared absorption bands in the region 1115–750 cm^{-1} (42), which can be compared with those of the already mentioned mononucleotides in this region of the spectra, and the results are given in Table 4. There are also two other absorption bands with medium intensities in the ir spectra of the PO_3^{2-} group (42) at 600–400 cm^{-1}, which are assigned to the PO_3^{2-} symmetric deformation (550 cm^{-1}) and the PO_3^{2-} degenerate deformation (460 cm^{-1}) (Table 4). Six fundamental frequencies are expected for the PO_3^{2-} ion of C_{3v} symmetry, three of these belong to the symmetric vibrations of A_1 type and the other three are related to the doubly degenerate vibrations of the *E* type. The CH_3–OPO_3^{2-} no longer has C_{3v} symmetry due to the lack of a C_3 axis and possesses a lower C_s symmetry. Therefore, the degeneracy of the absorption at 1100 cm^{-1} has been removed and split into a doublet at 1115 and 1090 cm^{-1} (Table 4). In the FT-ir spectra of the solid mononucleotides studied here such splitting has not been observed (see Table 4), but most likely it was overlapped by the strong and broad absorption at 1090 cm^{-1}. Upon coordination of the PO_3^{2-} group the degeneracy of the vibration frequencies is removed (in CH_3—OPO_3^{2-} it has been partially removed) and the three of the six vibrational modes are split, each one into a doublet due to the lowering of the symmetry (Table 3).

The Raman spectra of mononucleotides (40) containing PO_3^{2-}, such as 5′-AMP and 5′-GMP, showed lines at 850, 882, and 980 cm^{-1} assignable to the PO_3^{2-} symmetric stretchings and at 1123 and 1170 cm^{-1} related to asymmetric stretchings. Protonation and metalation caused large perturbation in the intensity of the said frequency changes (44). The Cu(II) ion is coordinated directly to the phosphate group, as well as to the N_7-atom in $Cu(GMP)_3.8H_2O$ (17), whereas the corresponding complexes of Co(II), Ni(II), Mn(II), and Cd(II) ions are indirectly bonded to the phosphate group via two hydrogen-bonded water molecules, in addition to the linkage through the N_7-atom of the base (18–21). The crystal structure of the 5′-GMP acid shows (34) that PO_3^{2-} is involved in a strong intramolecular hydrogen-bonding, as well as the protonation of N_7 in a zwitterionic type, but the crystal structure of 5′-$GMPNa_2$ salt has not yet been determined. Comparing the ir spectra of 5′-GMP with the corresponding Mn(II), Co(II), Ni(II), Cu(II), and Cd(II) complexes in the region of 1070–970 cm^{-1} and the absorption band at 805 cm^{-1}, the spectra of the free ligand shows drastic changes in the Cu(II) complex, upon phosphate

Can. J. Chem. Downloaded from www.nrcresearchpress.com by 210.87.254.5 on 09/06/12
For personal use only.

TABLE 3. FT-ir bands (cm^{-1}) and possible assignments for 5′-GMP complexes of structurally known N_7-bonded Mn^{2+}, Co^{2+}, Ni^{2+}, Cu^{2+}, and Cd^{2+} in comparison with those of the corresponding Pt^{2+} and Mg^{2+} in *a* and *b* regions

5′-GMP-Na_2	Mn(GMP).$8H_2O$	Co(GMP).$8H_2O$	Ni(GMP).$8H_2O$	Cu_3(GMP)$_3$.$8H_2O$	Cd(GMP).$8H_2O$	*cis*-[$PtNH_3)_2$-(GMP)$_2$]Cl_2.$6H_2O$	Pt(GMP)$_2$ Cl_2.$6H_2O$	Mg(GMP).$10H_2O$	Mg(GMP).$6H_2O$	Possible assignments
a										
1692 bs	1690 vs	1690 vs	1690 vs	1694 vs	1694 vs	1694 vs	1693 s	1697 bs	1695 s	$\nu C_6{=}O > \nu C_6{=}C_5$ (31–33)
1662 sh	1655 sh	1656 sh	1656 sh	1663 sh	1656 s	1653 sh	1655 sh	1660 sh	1655 sh	$\delta NH_2 > \nu C_2{-}N_2$ (31–33)
	1645 s	1640 s	1640 s	1648 s	1643 sh	1643 s	1643 vs	1645 w	1638 w	
1597 s	1611 s	1611 s	1611 s	1611 s	1610 s	1599 s	1597 vs	1611 m	1616 sh	$\nu C_4{-}N_3 > \nu C_4{-}C_5 > \nu C_5{-}N_7$ (28, 31)
1575 sh	1570 m	1570 m	1560 m	1551 sh	1550 sh	1550 w	1543 sh	1550 sh	1560 sh	$\nu C_5{-}C_4 > \delta N_1{-}H > \nu C_6{-}N_1$ (31)
1535 m	1533 m	1535 m	1535 m	1539 m	1533 m	1543 m	1537 m	1536 m	1535 m	$\nu C_4{-}N_9 > \nu C_6{=}O > \nu C_2{-}N_1$ (31)
1479 m	1476 m	1478 m	1479 m	1489 sh	1479 m	1503 m	1501 s	1483 m	1483 m	$\delta C_8{-}H > \nu C_8{-}N_7$ (35)
	1465 sh	1465 sh	1466 sh	1450 w	—	—	—	—	1466 sh	
1415 m	1425 w	1423 vw	1423 vw	1416 m	1420 sh	1423 w	1422 vw	—	1420 w	$\delta CH + \delta CH_2$ (33, 35)
1410 sh	1410 vw	1412 vw	1412 vw	—	1412 m	1412 vw	1410 vw	1414 w	1410 sh	
1358 s	1389 m	1391 w	1391 m	1374 m	1379 m	1383 m	1385 vw	1383 m	1375 w	ν(pyrimidine ring) (29)
1333 sh	1352 m	1352 m	1354 m	1350 sh	1358 m	1348 m	1350 m	1357 m	1367 m	$\nu C_8{-}N_9 > \nu C_8{-}N_7 > \delta N_1{-}H > \nu C_2{-}N_2$ (30, 31)
	1290 vw	1300 w	1300 w	1300 w	1300 sh	1300 sh	1310 sh	1330 sh	1330 sh	
1254 sh	1280 w	1280 w	1290 w	1290 w	1290 w	1290 vw	1250 sh	—	—	$\nu C_6{-}N_1 > \nu C_5{-}N_7$ (31)
	1260 w	1260 w	1260 w	1260 vw	1265 m	1270 vw	—	1254 m	1250 m	
1234 s	1236 m	1235 m	1236 m	1240 m	1236 m	—	—	—	—	—
1204 m	1216 sh	1215 sh	1216 sh	—	1216 sh	1218 w	1215 sh	1220 sh	—	$\delta C_8{-}H > \nu C_8{-}N_7$ (31)
	1205 s	1206 s	1208 s	1208 m	1204 m	1205 s	1205 m	1206 m	1208 m	
1180 m	1177 m	1177 m	1175 m	1178 m	1175 m	1175 w	1177 w	1175 sh	1182 sh	$\nu C_8{-}N_7 > \nu N_9$—sugar $> \nu C_4{-}N_3$ (31)
	1155 m	1153 m	1155 m	—	1150 m	—	—	—	—	
b										
1125 sh	1109 sh	1107 sh	1109 sh	1111 vs	1112 sh	1109 vs	1110 sh	1107 bs	1102 bs	νC—O of the sugar ring (33, 35)
—	—	—	—	1040 sh	—	—	—	—	—	
1070 bs	1084 vs	1080 vs	1080 vs	1076 vs	1080 bs	1084 s	1069 bs	1080 sh	1076 sh	νPO_3^{2-} deg. (33, 42)
—	—	—	—	1001 sh	—	—	—	—	1052 s	
972 s	981 s	982 s	980 s	991 vs	979 vs	974 s	976 s	993 s	976 s	νPO_3^{2-} sym. (33, 42)
—	—	—	—	975 sh	—	—	—	—	940 s	
805 s	802 s	802 s	802 s	815 s	802 s	800 s	800 m	792 m	802 m	νP—O (33, 42)
—	—	—	—	790 w	—	—	—	—	—	

*s, strong; m, medium; b, broad; sh, shoulder; w, weak; v, very; ν, stretching; δ, bending.

TABLE 4. FT-ir absorption bands (cm^{-1}) of the nucleotide phosphate group in the region of 1120–450 cm^{-1}, compared with those of the corresponding absorption bnads of $CH_3OPO_3^{2-}$ *

5′-CMPNa$_2$	5′-UMPNa$_2$	5′-IMPNa$_2$	5′-AMPNa$_2$	5′-GMPNa$_2$	CH_3—OPO_3^{2-}
—	—	—	—	—	1115 PO_3^{2-} deg. (*A′*)
1080 bs	1086 bs	1092 bs	1091 bs	1070 bs	1090 PO_3^{2-} deg. (*A″*)
—	—	1072	—	—	—
—	—	—	—	—	1056 C—O str. (*A″*)
984 vs	979 vs	976 vs	976 vs	972 s	983 PO_3^{2-} sym. str.
820 s	816 s	825 m	797 s	805 m	750 P—O str. (*A′*)
580 m	565 m	527 m	540 m	540 m	PO_3^{2-} sym. def. (*A*)
—	—	—	—	—	—
470 w	460 w	480 w	470 m	460 m	PO_3^{2-} deg. def. (*E*)
—	—	—	—	—	—

*s, strong; b, broad; m, medium; w, weak; v, very.

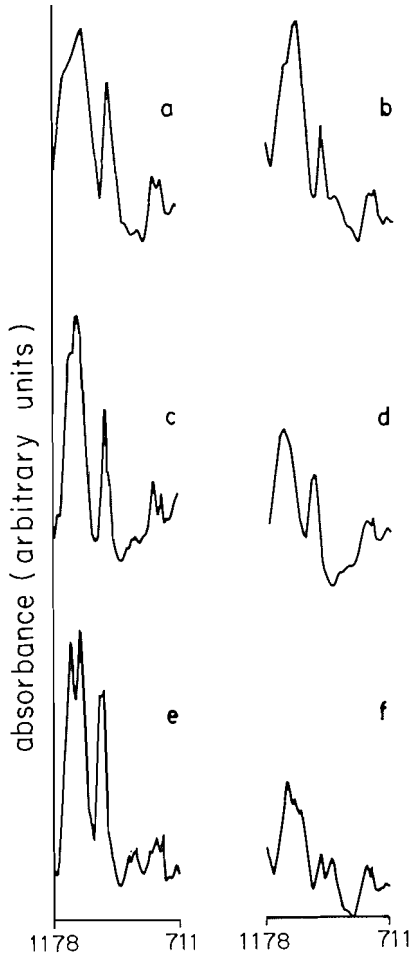

FIG. 4. FT-ir spectra of 5′-GMPNa$_2$ and its metal complexes in the phosphate region 1178–711 cm^{-1} for *a*, 5′-GMPNa$_2$; *b*, *cis*-[Pt(GMP)$_2$(NH$_3$)$_2$]Cl$_2$.6H$_2$O; *c*, NiGMP.8H$_2$O; *d*, MgGMP.10H$_2$O (pH = 7); *e*, Cu$_3$(GMP)$_3$.8H$_2$O; and *f*, MgGMP.6H$_2$O (pH = 4).

coordination (Fig. 4). The bands at 1070, 972, and 805 cm^{-1} split each one into two components, whereas in the analogous Mn(II), Ni(II), Co(II), and Cd(II) complexes, where the phosphate is not directly bound to these metal cations (18–21), there has been no significant changes in this region of the spectra (Fig. 4 and Table 3).

Cu(II) and Zn(II) are also directly bonded to the PO_3^{2-} group of the 5′-IMP molecule (25, 26), as well as to the N_7 of the purine base residue, whereas in the corresponding Ni(II) and Co(II) complexes the phosphate group is not directly bonded to these metal ions (45). On comparing the ir spectra of these nucleotide complexes, the absorption bands at 1092 and 976 cm^{-1} in the spectra of the free 5′-IMPNa$_2$ showed splitting and shifting in the Cu(II) and Zn(II) complexes, whereas the corresponding Co(II) and Ni(II) complexes did not show appreciable changes in this region of the spectra.

The Co(II) ion is coordinated to the phosphate group of the 5′-UMPNa$_2$ molecule only in Co$_2$(UMP)$_2$.4H$_2$O (22). On comparing the ir spectra of free 5′-UMPNa$_2$ with that of Co(II) complexes, each of the bands at 1086, 979, and 816 cm^{-1} has been split into a doublet in the spectrum of Co$_2$(UMP)$_2$.4H$_2$O.

Co(II) and Cd(II) are directly bonded to the phosphate group of the 5′-CMP molecule, as well as to the N_3 of the pyrimidine base residue (27). The ir spectra of the Co(II) and Cd(II) complexes showed splitting of the bands at 1080, 984, and 812 cm^{-1} by comparison with that of the free ligand in the same region of the spectra.

In NiAMP.6H$_2$O, the only crystal structure known (24) for the 5′-AMP nucleotide, the Ni(II) ion is bonded to N_7 of the base moiety and to five water molecules (two of these water molecules are hydrogen-bonded to a phosphate group). The ir spectrum of 5′-AMP in the phosphate absorption region showed no considerable changes upon complexation in the NiAMP.6H$_2$O complex.

It could be conlcuded from the observations made on the ir spectra of all the structurally known (17–27) examples discussed here that (*a*) the absorption bands at about 1100, 970, and 800 cm^{-1} in the spectra of mononucleotides are certainly due to the PO_3^{2-} vibrational frequencies, as assigned in Table 4. They show large perturbations upon phosphate coordination. Due to the skeletal and the breathing modes of the pyrimidine and purine vibrational frequencies together with the NH_2 out-of-plane wagging (30) vibrations in the region 700–400 cm^{-1} of the spectra of the nucleotide complexes, it is very difficult to distinguish any changes which occurred for the sym. def. (*A*) and the deg. def. (*E*) (Table 4), upon metal coordination or hydrogen-bonding. The ir spectra of the Pt(II) and the Mg(II) complexes of the 5′-GMP molecule studied here show great similarities with those of the corresponding hydrogen-bonded phosphate group (indirect coodination through water molecules) in the Ni(II) complex (Fig. 4 and Table 3), and no marked similarities with the directly coordinated PO_3^{2-} group as in the Cu–GMP complex (due to the lack of splitting or considerable changes in the region 1100–900 cm^{-1}). Therefore, it can be suggested that the phosphate group of 5′-GMP is indirectly linked to Pt(II) and Mg(II) via hydrogen-bonded water mole-

Can. J. Chem. Downloaded from www.nrcresearchpress.com by 210.87.254.5 on 09/06/12
For personal use only.

Can. J. Chem. Downloaded from www.nrcresearchpress.com by 210.87.254.5 on 09/06/12
For personal use only.

cules, similar to those of the known Co(II), Ni(II), Cd(II), and Mn(II) 5′-GMP complexes. It should be noted that the ir spectra of the Mg(GMP).$6H_2O$ compound synthesized at pH = 4 showed a direct phosphate–Mg interaction by exhibiting the splitting and shifting of the absorption bands at 1070, 972, and 805 cm^{-1} which are related to the phosphate vibrational frequencies upon metal coordination, whereas the spectra of the Mg(GMP).$10H_2O$ complex obtained at pH = 7–9 showed marked similarities with that of Ni(GMP).$8H_2O$ compound containing hydrogen-bonded phosphate groups (Fig. 4).

Sugar ribose stretching vibrations and other vibrational frequencies

The ribose vibrational frequencies appear almost as sharp bands (28) with medium intensities in the region of 1400–400 cm^{-1} of the spectra. Most of these absorptions are obscured by the strong and broad absorptions of the phosphate group in the region of 1100–800 cm^{-1} and the base vibrational frequencies in the other regions of the spectra. The phosphate–ribose stretching vibration shows two weak absorption bands at 870 and 777 cm^{-1} in the spectra of the 5′-GMP molecule. The one at 870 cm^{-1} shows considerable changes upon direct or indirect metal–phosphate coordination in the spectra of structurally known metal complexes (Fig. 1). These changes can be explained by the inductive effect of the PO_3^{2-} electron distribution on the ribose–phosphate bond or by conformational changes about the phosphodiester bond upon PO_3^{2-} complexation (9). The other ribose ring vibrational frequencies at about 900, 770, and 710 cm^{-1}, which are very weak in the spectra of the free ligand, do not show changes in the spectra of the metal complexes (Fig. 1).

The ring breathing mode at 680 cm^{-1} (31) in the spectra of 5′-GMP shifted to 700 cm^{-1} in the spectra of the N_7–metal complexes (Fig. 1). The bending vibration and the out-of-plane deformation modes of NH_2 and NH (28, 31) at 700–500 cm^{-1} in the ligand spectra do not shift considerably upon N_7-complex formation.

The metal–nitrogen stretching vibrations of all the 5′-GMP complexes studied here occurred in the lower region (400–200 cm^{-1}) of the spectra and will be reported elsewhere.

Conclusions

On the basis of spectroscopic studies of some structurally known metal complexes compared to the unknown Pt(II) and Mg(II) complexes synthesized here, the following conclusions can be drawn.

Metalation at the N_7-site of 5′-GMP brings drastic spectral changes which are often difficult to be rationalized, mainly due to the vibrations of the purine ring system which are strongly coupled. Coordination can also change the electron distribution within the ring system and further complicates the vibrational problem. However, some of the most meaningful and common changes observed in the vibrational spectra of 5′-GMP on complexation with different metal cations are summarized below.

The characteristic features of the N_7-bonding of guanine are: (*1*) modification of the band at 1480 cm^{-1}; (*2*) splitting of the bands at 1333, 1254, and 1204 cm^{-1}, and (*3*) shift of the band at 680 cm^{-1}, assigned to breathing mode of the ring system, to 700 cm^{-1} in the spectra of metal–GMP complexes.

The characteristic features of metal–phosphate bonding are: (*1*) splitting and shifting of the broad and strong absorption bands at 1090 and 970 cm^{-1}, upon direct metal–phosphate bonding and (*2*) the lack of splitting indicative of an indirect phosphate–metal bonding via a hydrogen-bonded water molecule.

It is interesting that the reaction between the Mg(II) ion and 5′-GMP at pH = 9–6 produces complexes with no direct Mg–OPO_3 interaction, whereas at pH = 5 and lower the direct phosphate–Mg bonding is prevailing.

The Pt(II) ion is N_7-bonded in all the GMP synthesized complexes and exhibits no direct Pt–OPO_3 interaction. Due to the lack of crystallographic evidence and the absence of any considerable infrared absorption band changes at 1690 cm^{-1} (C_6=O stretching), the possibility of direct or indirect Pt–carbonyl interaction does not occur for these solid state Pt(II) complexes studied here.

Acknowledgements

We wish to acknowledge the financial assistance of the Natural Sciences and Engineering Research Council of Canada and the loan of platinum salts from Johnson Matthey and Mallory Ltd.

1. M OGAWA and T. SAKAGUCHI. Yakugaku Zasshi, **91**, 750 (1971); **92**, 1166 (1972).
2. M. OGAWA. Yakugaku Zasshi, **91**, 618 (1971) and references therein.
3. M. OGAWA and T. SAKAGUCHI. Chem. Pharm. Bull. **19**, 1650 (1971).
4. M. POLISSIOU, M. T. PHAN. VIET, M. ST-JACQUES, and T. THEOPHANIDES. Can. J. Chem. **59**, 3297 (1981) and references therein.
5. A. T. MARCELIS, C. G. VAN KRALINGEN, and J. REEDIJK. J. Inorg. Biochem. **13**, 213 (1980) and references therein.
6. G. M. CLORE and A. M. GRONENBORN. J. Am. Chem. Soc. **104**, 1369 (1982).
7. A. LANIR and N. T. YU. J. Biol. Chem. **254**, 5882 (1979).
8. M. POLISSIOU and T. THEOPHANIDES. Inorg. Chim. Acta, **56**, L_1–L_3 (1981).
9. T. THEOPHANIDES, G. MAKRIGIANNIS, and P. PAPAGIANNAKOPOULOS. Inorg. Chim. Acta, **46**, 263 (1980).
10. T. THEOPHANIDES and M. POLISSIOU. Conversation in the discipline biomolecular stereodynamics. Vol. II. Adenine Press. 1981. p. 487.
11. G. Y. H. CHU, S. MANSY, R. E. DUNKAN, and R. S. TOBIAS. J. Am. Chem. Soc. **100**, 593 (1978); **100**, 607 (1978).
12. D. M. L. GOODGAME, I. JEEVES, F. L. PHILLIPS, and A. C. SKAPSKI. Biochim. Biophys. Acta, **378**, 153 (1975); T. J. KISLENMACKER, C. C. CHIANG, P. CHALLIPOYIL, and L. G. MARZILLI. J. Am. Chem. Soc. **101**, 1143 (1979).
13. S. LOUIE and R. BAU. J. Am. Chem. Soc. **99**, 3874 (1977).
14. T. J. KISTENMACHER, C. C. CHIANG, P. CHALILPOYIL, and L. G. MARZILLI. Biochem. Biophys. Res. Commun. **84**, 70 (1978).
15. L. G. MARZILLI, P. CHALIPOIL, C. C. CHIANG, and T. J. KISTENMACHER. J. Am. Chem. Soc. **102**, 2480 (1980).
16. A. H. J. WANG, G. J. QUIGLEY, F. J. KOLPAK, G. V. D. MAREL, J. H. VAN BOOM, and A. RICH. Science, **211**, 171 (1981).
17. K. AOKI, G. R. CLARK, and J. D. ORBELL. Biochim. Biophys. Acta, **425**, 369 (1976).
18. P. DE MEESTER, D. M. L. GOODGAME, A. C. SKAPSKI, and B. T. SMITH. Biochim. Biophys. Acta, **340**, 113 (1974).
19. P. DE MEESTER, D. M. L. GOODGAME, T. J. JONES, and A. C. SKAPSKI. C. R. Acad. Sci. Paris, **279**, 667 (1974).
20. P. DE MEESTER, D. M. L. GOODGAME, T. J. JONES, and A. C. SKAPSKI. Biochem. J. **139**, 791 (1974).
21. K. AOKI. Acta Crystallogr. B**32**, 1454 (1976).
22. B. A. CARTWRIGHT, D. M. L. GOODGAME, I. JEEVES, and A. C. SKAPSKI. Biochim. Biophys. Acta, **477**, 195 (1977).
23. D. M. L. GOODGAME, I. JEEVES, C. D. REYNOLDS, and A. C. SKAPSKI. Nucl. Acid Res. **2**, 1375 (1975).

24. A. D. COLLINS, P. DE MEESTER, D. M. L. GOODGAME, and A. C. SKAPSKI. Biochim. Biophys. Acta, **402**, 1 (1975).
25. P. DE MEESTER, D. M. L. GOODGAME, T. J. JONES, and A. C. SKAPSKI. Biochim. Biophy. Acta, **353**, 392 (1974).
26. K. AOKI. J. Chem. Commun. 600 (1977).
27. G. R. CLARK and J. D. ORBELL. Chem. Commun. 697 (1975).
28. R. C. LORD and G. J. THOMAS. Spectrochim. Acta, **23**A, 2551 (1967).
29. A. LAUTIE and A. NOVAK. J. Chim. Phys. **71**, 415 (1974).
30. L. CHINSKY, P. Y. TURPIN, M. DUQUESENE, and J. BRAHMS. Biopolymers, **17**, 1347 (1978).
31. M. TSUBOI, S. TOKAHOSHI, and I. HORADA. Physicochemical properties of nucleic acid. Vol. 2 *Edited by* J. Duchense. Academic Press, New York. 1973. p. 91.
32. M. TSUBOI and Y. NISHIMURA. Raman spectroscopy linear and non-linear. *Edited by* G. Laseombe. Wiley Hyden. 1982. pp. 683, 703.
33. M. TSUBOI. Infrared and Raman spectroscopy in basic principles in nucleic acid chemistry. Vol. 1. Academic Press. 1974. p. 407.
34. J. EMERSON and M. SUNDARALINGAM. Acta Crystallogr. B**36**, 1510 (1980).
35. M. J. LANA and G. J. THOMAS, JR. Biochemistry, **18**, 3839 (1979); S. MANSY and W. L. PETICOLAS. Biochemistry, **15**, 2650 (1976).
36. T. THEOPHANIDES. Interaction of metal ions with nucleic acids. *In* Infrared and Raman spectroscopy of biological molecules. *Edited by* T. Theophanides. R. Reidel Publsihing Co. Dordrecht, Holland. 1979. p. 205.
37. C. SANDORFY. The chemistry of the carbon–nitrogen double bond. *Edited by* S. Patai. John Wiley, New York. 1970. p. 42.
38. M. F. C. LADD, D. C. POVEY, J. I. BULLOCK, and H. A. TAJMIR-RIAHI. Acta Crystallogr. B**35**, 2013 (1979).
39. F. A. HART, M. UL-HUQUE, and C. N. CAUGHLAN. Chem. Commun. **1240** (1970); F. A. HART and D. A. DURHAM. J. Inorg. Nucl. Chem. **31**, 145 (1969).
40. L. RIMAI, T. COLE, J. L. PARSONS, J. T. HECHMONTT, and E. B. CAREW. Biophys. J. **9**, 320 (1969).
41. E. B. BROWN and W. L. PETICOLAS. Biopolymers, **14**, 1259 (1975).
42. M. TSUBOI, T. SHIMANOUCHI, and T. KYOGOKU. Adv. Chem. Phys. **7**, 435 (1964).
43. K. C. LU, E. W. PROHOFSKY, and L. L. VANZNDT. Biopolymers, **16**, 2491 (1977).
44. S. MANSY and R. S. TOBIAS. J. Am. Chem. Soc. **96**, 6874 (1974).
45. K. AOKI. Bull. Chem. Soc. Jpn. **48**, 1260 (1975).

Can. J. Chem. Downloaded from www.nrcresearchpress.com by 210.87.254.5 on 09/06/12
For personal use only.

Synthesis and crystal structure analysis of trichloro(dimethylformamide)bis(dimethylsulfoxide)rhodium(III)

F. D. ROCHON, P. C. KONG, AND R. MELANSON

Département de chimie, Université du Québec à Montréal, C.P. 8888, Succ. A, Montréal (Qué.), Canada H3C 3P8

Received August 16, 1982[1]

F. D. ROCHON, P. C. KONG, and R. MELANSON. Can. J. Chem. **61**, 1823 (1983).

mer-[Rh(DMSO)$_2$(DMF)Cl$_3$] was prepared by dissolving [Rh(DMSO)$_3$Cl$_3$] in dimethylformamide (DMF). It forms monoclinic crystals, a = 11.530(3), b = 8.971(2), c = 15.912(3) Å, β = 107.88(2)°, Z = 4, and space group $P2_1/c$. The structure was refined by full-matrix least-squares analysis to a conventional R factor of 0.038 (3495 observed reflections).

The coordination around the Rh atom is octahedral. The compound is the peripheral or the 1,2,6-isomer. The DMF molecule is in *trans* position to a DMSO ligand and bonded to rhodium through the oxygen atom. The two molecules of DMSO are bonded to rhodium through sulfur. The Rh—Cl(1) bond (2.366(1) Å) *trans* to a DMSO molecule seems slightly longer than the two Rh—Cl bonds *trans* to each other (2.329(1) and 2.343(1) Å).

F. D. ROCHON, P. C. KONG et R. MELANSON. Can. J. Chem. **61**, 1823 (1983).

mer-[Rh(DMSO)$_2$(DMF)Cl$_3$] a été synthétisé en dissolvant [Rh(DMSO)$_3$Cl$_3$] dans le diméthylformamide (DMF). Le composé cristallise dans le système monoclinique, a = 11,530(3), b = 8,971(2), c = 15,912(3) Å, β = 107,88(2)°, Z = 4 et le groupe d'espace $P2_1/c$. La structure a été affinée par moindres-carrés à matrice entière jusqu'à un facteur R = 0,038 (3495 réflexions observées).

La coordination autour de l'atome de rhodium est octaédrique. Le composé est l'isomère 1,2,6. La molécule de DMF est en position *trans* d'un ligand DMSO et liée au rhodium par l'atome d'oxygène. Les deux molécules de DMSO sont liées au rhodium par le soufre. Le lien Rh—Cl(1) (2,366(1) Å) en position *trans* d'un ligand DMSO, semble légèrement plus long que les deux liens Rh—Cl en *trans* de chacun d'eux (2,329(1) et 2,343(1) Å).

Can. J. Chem. Downloaded from www.nrcresearchpress.com by 210.87.254.40 on 09/06/12
For personal use only.

In the early 1970's, interest in rhodium compounds was greatly enhanced when their potential as anticancer agents was discovered (1). Chemotherapeutic studies on rhodium compounds are encouraged by the fact that contrary to *cis*-[Pt(NH$_3$)$_2$Cl$_2$] and other antitumor agents, they produce only slight chromosome damage in treated cells (2). We have been studying platinum compounds for many years, partly with a view of synthesizing better antitumor agents than *cis*-[Pt(NH$_3$)$_2$Cl$_2$]. Recently, we have decided to study a few rhodium compounds to compare their chemical behavior with platinum compounds.

Many years ago, Kukushkin and Rubtsova (3) synthesized [Rh(DMSO)$_3$Cl$_3$]. The authors suggested that two molecules of DMSO were bonded to Rh through the sulfur atoms, while the third molecule was coordinated through the oxygen atom. The latter is more labile and more easily displaced by other nucleophiles, even by the weak chloro ligand, to form [Rh(DMSO)$_2$Cl$_4$]$^-$. One chloro ligand in [Rh(DMSO)$_2$Cl$_4$]$^-$ can be easily displaced by NH$_3$ or pyridine (py) to form [Rh(DMSO)$_2$(NH$_3$)Cl$_3$] or [Rh(DMSO)$_2$(py)Cl$_3$]. These reactions show that the oxygen-coordinated DMSO is a weaker ligand than NH$_3$ or pyridine (4).

When [Rh(DMSO)$_3$Cl$_3$] was dissolved in dimethylformamide (DMF) and recrystallized in the presence of a small quantity of ether, bright orange crystals were isolated. Infrared spectroscopy showed that the product contained some DMF. Since then, no Rd−DMF compound has yet been reported in the literature, we therefore decided to determine the crystal structure of the orange compound. The results of the structure analysis have shown that the oxygen-bonded DMSO had been replaced by DMF during the recrystallization process. The compound was identified as [Rh(DMSO)$_2$(DMF)Cl$_3$].

DMF is an oxygen-coordinated ligand and cannot displace chloro ligands from K[Pt(py)Cl$_3$] (5). We have done a comparative study of the two oxygen-coordinated ligands (DMF and DMSO) in the following reaction

$$[Rh(DMSO)_3Cl_3] \rightleftarrows [Rh(DMSO)_2(DMF)Cl_3]$$

This reaction will be briefly discussed in this paper.

Experimental

[Rh(DMSO)$_3$Cl$_3$] was synthesized by the method described by Kukushkin and Rubtsova (4). The compound was dissolved in dimethylformamide. A small quantity of diethylether was added to the solution which was set aside. Bright orange crystals were slowly formed which were later found to be [Rh(DMSO)$_2$(DMF)Cl$_3$].

A set of precession photographs indicated the monoclinic $P2_1/c$ space group. The cell parameters were calculated by least-squares refinement of the setting angles of 15 independent peaks centered on a Syntex P$\bar{1}$ diffractometer using graphite monochromatized MoKα radiation.

Crystal data

$RhCl_3C_7H_{19}NS_2O_3$ mw = 438.63

Monoclinic, $P2_1/c$, a = 11.530(3), b = 8.971(2), c = 15.912(3) Å, β = 107.88(2)°, Z = 4, V = 1566.3(6) Å^3, D_x = 1.859 g cm^{-3}, D_m = 1.86(2) g cm^{-3} (flotation), λMoKα = 0.71069 Å, μMoKα = 18.17 mm^{-1}, and T = 22°C.

The intensity data were collected from a crystal having 9 faces with approximate dimensions of 0.23 × 0.25 × 0.48 mm. A total of 4621 independent reflections were measured in the region of $2\theta < 60°$ by the $2\theta/\theta$ scan technique using MoKα radiation. During the data collection, three standard reflections were measured after every 47 reflections. Their variations were less than 3% from their respective means. The reflections (3495) for which the intensity was greater than $2.5\sigma(I)$ were considered as observed. The standard deviation $\sigma(I)$ was calculated as already described (6). An absorption correction based on the equations of the crystal faces was applied to all the reflections. The transmission factors varied from 0.659 to 0.697. The data were then corrected for the Lorentz and polarization effects. The scattering factors of Cromer and Waber (7) were used for rhodium, chlorine, sulphur, oxygen, nitrogen, and carbon, those of Stewart, Davidson, and Simpson (8) were used for hydrogen. The anomalous dispersion terms (9) of rhodium, chlorine, and sulphur were included in the calculations.

[1]Revision received March 9, 1983.

Can. J. Chem. Downloaded from www.nrcresearchpress.com by 210.87.254.40 on 09/06/12
For personal use only.

The position of the rhodium atom was easily located from the three-dimensional Patterson map. The positions of all the other atoms, except the hydrogen atoms, were obtained by structure factor and Fourier map calculations. The refinement of the parameters was done by full-matrix least-squares calculations. In the early stages of refinement, unit weight was assigned to all the reflections. Later individual weights $w = 1/\sigma^2(F)$ were applied. The hydrogen atom in the DMF molecule was fixed at the calculated position, assuming a sp^2 hybridization of the C atom and a C—H distance of 0.95 Å. It was assigned an isotropic thermal parameter of 6.0 Å^2. The hydrogen atoms on the $-CH_3$ groups could not be located. The refinement of the scale factor, the coordinates and anisotropic temperature factors of all the non-hydrogen atoms converged to $R = \Sigma||F_o| - |F_c||/\Sigma|F_o| = 0.038$ and $R_w = [\Sigma w(|F_o| - |F_c|)^2/\Sigma w|F_o|^2]^{1/2} = 0.050$. The final difference Fourier map did not show peaks higher than ± 0.4 e Å^{-3}.

The calculations were carried out with a Cyber 73 computer and the programs used have already been described (6). A table of observed and calculated structure factors is available from the Depository of Unpublished Data.[2]

Results and discussion

The refined atomic parameters are listed in Table 1. A list of the anisotropic temperature factors is available.[2] A labelled diagram of the molecule is shown in Fig. 1. The bond lengths and the bond angles are shown in Table 2.

The coordination around the Rh atom is octahedral. The angles are close to the expected 90 and 180°, but there are some slight distorsions from the ideal octahedron (Table 2). These deviations are probably caused by the smaller size of the oxygen atom compared to chlorine or sulfur atoms.

The compound $[Rh(DMSO)_2(DMF)Cl_3]$ is the peripheral or the 1,2,6-isomer. The three chlorine atoms are meridional. The two DMSO molecules are in *cis* position and the DMF ligand is *trans* to one of the DMSO molecule. The crystal structure of $[Rh(DMSO)_3Cl_3]$ has been determined by Sokol and Porai-Koshits (10) and Sokol, Rubtsova, Gribenyuk, and Porai-Koshits (11) with low accuracy ($R = 0.125$ and 0.14 respectively). The results have shown that $[Rh(DMSO)_3Cl_3]$ is also the peripheral isomer. Two DMSO ligands (in *cis* positions) are bonded to Rh through the sulfur atom, while the third one, which is in *trans* position to a DMSO, is bonded to Rh through the oxygen atom. In our compound *mer*-$[Rh(DMSO)_2(DMF)Cl_3]$ the DMSO bonded to Rh through the O atom in $[Rh(DMSO)_3Cl_3]$ has been replaced by a DMF molecule, also bonded through O.

The Rh—Cl bond distances are 2.329(1), 2.343(1), and 2.366(1). The latter bond in *trans* position to a DMSO molecule seems significantly longer than the two Rh—Cl bonds *trans* to each other. In $[Rh(DMSO)_3Cl_3]$ the Rh—Cl bonds are 2.33 to 2.34 Å. In *trans*-$Na[Rh(DMSO)_2Cl_4]$, the Rh—Cl bonds range from 2.32 to 2.34 Å (12). In $[RhCl_3(DMSO)(py)_2]$ in which two Cl atoms are *trans* to each other and the third one *trans* to a pyridine ligand, the six Rh—Cl bonds range from 2.314 to 2.348 Å (13). Pt—Cl bonds in *trans* position to DMSO are also longer (~0.02 Å) than normal bonds (14–16).

The Rh—S distances are 2.242(1) and 2.290(1) Å. The bond in the position *trans* to DMF is shorter than the bond *trans* to Cl(1). In $[RhCl_3(DMSO)(py)_2]$ the Rh—S bond is 2.28 Å. The DMSO ligands in $[Rh(DMSO)_2(DMF)Cl_3]$ have approximate tetrahedral geometry about S, the angles ranging from 102 to 116°. The S—O distances are 1.461(4) and 1.467(4) Å and the S—C distances vary from 1.774(5) to 1.800(6) Å. The structure of the coordinated DMSO molecules is very similar to the structure of free DMSO (17, 18) and to the structure of coordinated DMSO in the Rh and Pt complexes mentioned above.

DMF is bonded to Rh through the O atom as in *trans*-$[Pt(DMF)(2,6\text{-lutidine})Cl_2]$ (19). The Rh—O bond of 2.112(3) Å is probably normal. To our knowledge, this study is the first structure determination of a rhodium–DMF complex. In the above Pt compound, the Pt—O distance is 2.051(6) Å. Rhodium, like platinum, being a soft metal, does not usually form bonds with the oxygen atom. DMF exists as a resonance structure of the two mesomeric forms $(CH_3)_2NCHO$ and $(CH_3)_2N^+CHO^-$. Because of the ionic form, rhodium will form bonds more easily with the oxygen atom than with the nitrogen atom. The decrease in multiplicity of the C—O bond and the increased multiplicity of the C—N bond resulting from the ionic resonance structure have been observed in all published crystal structures involving DMF molecules (19). It is inter-

TABLE 1. Final positional structure parameters, estimated standard deviations ($\times 10^4$) and temperature factors

Atom	x	y	z	U_{eq} (Å^2)*
Rh	7583.3(3)	7741.5(4)	1598.3(2)	209
Cl(1)	7931(1)	5149(1)	1548(1)	381
Cl(2)	6664(1)	7737(1)	74(1)	404
Cl(3)	8641(1)	7787(1)	3112(1)	340
S(1)	5744(1)	7372(1)	1765(1)	259
S(2)	7392(1)	10255(1)	1768(1)	256
O(1)	4886(3)	8601(4)	1462(3)	432
O(2)	6951(3)	10709(4)	2502(2)	396
O(3)	9267(3)	8176(4)	1378(2)	337
N	10740(3)	7616(4)	777(3)	341
C(1)	5011(5)	5715(7)	1214(4)	603
C(2)	5874(5)	6965(7)	2882(3)	483
C(3)	8844(4)	11102(5)	1909(4)	403
C(4)	6486(4)	11145(6)	785(3)	362
C(5)	9691(4)	7381(5)	906(3)	363
C(6)	11493(6)	8866(8)	1169(5)	778
C(7)	11217(5)	6552(7)	247(4)	602

*$U_{eq} = \frac{1}{3}(U_{11} + U_{22} + U_{33} + 2U_{13}\cos\beta)$.

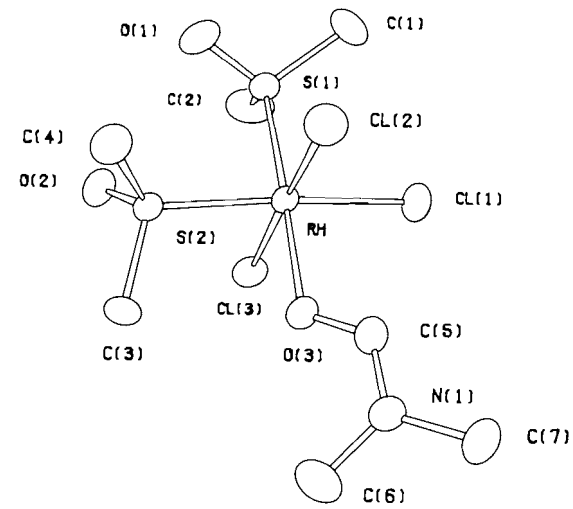

FIG. 1. Labelled diagram of the molecule $[Rh(DMSO)_2(DMF)Cl_3]$.

[2]Lists of structure factors and anisotropic thermal parameters are available, at a nominal charge, from the Depository of Unpublished Data, CISTI, National Research Council of Canada, Ottawa, Ont., Canada K1A 0S2.

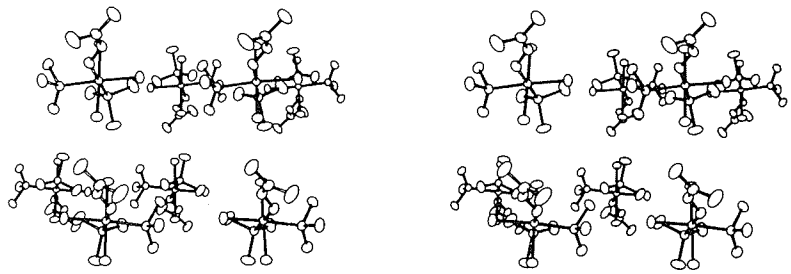

FIG. 2. Stereoscopic diagram of the packing in the crystal $[Rh(DMSO)_2(DMF)Cl_3]$. ***b*** and ***c*** are parallel to the bottom and side of the page respectively, and the view is down ***a****.

TABLE 2. Bond distances (Å) and bond angles (deg)

Bond	Distance	Bonds	Angle
Rh—Cl(1)	2.366(1)	Cl(1)—Rh—Cl(2)	89.46(4)
Rh—Cl(2)	2.329(1)	Cl(1)—Rh—Cl(3)	90.69(4)
Rh—Cl(3)	2.343(1)	Cl(1)—Rh—S(1)	91.99(4)
Rh—S(1)	2.242(1)	Cl(1)—Rh—S(2)	174.68(4)
Rh—S(2)	2.290(1)	Cl(1)—Rh—O(3)	90.1(1)
Rh—O(3)	2.112(3)	Cl(2)—Rh—Cl(3)	175.84(4)
S(1)—O(1)	1.461(4)	Cl(2)—Rh—S(1)	88.78(4)
S(2)—O(2)	1.467(4)	Cl(2)—Rh—S(2)	95.44(4)
S(1)—C(1)	1.800(6)	Cl(2)—Rh—O(3)	88.6(1)
S(1)—C(2)	1.774(5)	Cl(3)—Rh—S(1)	95.37(4)
S(2)—C(3)	1.788(5)	Cl(3)—Rh—S(2)	84.27(4)
S(2)—C(4)	1.781(5)	Cl(3)—Rh—O(3)	87.3(1)
O(3)—C(5)	1.241(6)	S(1)—Rh—S(2)	90.18(4)
C(5)—N	1.304(6)	S(1)—Rh—O(3)	176.6(1)
N—C(6)	1.438(8)	S(2)—Rh—O(3)	87.9(1)
N—C(7)	1.488(7)	Rh—S(1)—O(1)	114.7(2)
		Rh—S(1)—C(1)	112.6(2)
		Rh—S(1)—C(2)	110.9(2)
		Rh—S(2)—O(2)	115.9(1)
		Rh—S(2)—C(3)	108.3(2)
		Rh—S(2)—C(4)	113.0(2)
		Rh—O(3)—C(5)	123.2(3)
		O(1)—S(1)—C(1)	107.1(3)
		O(1)—S(1)—C(2)	109.1(2)
		C(1)—S(1)—C(2)	101.5(3)
		O(2)—S(2)—C(3)	108.7(2)
		O(2)—S(2)—C(4)	108.7(2)
		C(3)—S(2)—C(4)	101.2(2)
		O(3)—C(5)—N	124.0(5)
		C(5)—N—C(6)	121.6(5)
		C(5)—N—C(7)	120.5(4)
		C(6)—N—C(7)	117.9(5)

esting to observe that DMF has the same structure, whether it is free (20), coordinated to a metal, or uncomplexed as a molecule of crystallization (19). In our Rh compound, the C—O bond is 1.241(6) Å and the C—N bond is 1.304(6) Å. In *trans*-[Pt(DMF)(2,6-lutidine)Cl_2], the C—O bond was 1.253 Å and the C—N bond 1.326 Å. All the published structures containing DMF have shown that DMF is planar. In $[Rh(DMSO)_2(DMF)Cl_2]$ the DMF ligand is also planar. The angles around the N atom are close to 120° and the angle at the carbonyl C is 124°.

The packing of the molecules in the crystal is shown in Fig. 2. There is no hydrogen bonding. It appears that the normal van der Waals attractions are the only packing forces in the crystal.

The infrared spectrum of $[Rh(DMSO)_2(DMF)Cl_3]$ in a Nujol mull showed that the carbonyl stretching of DMF is lowered by 38 cm^{-1} (from 1668 cm^{-1} in free DMF to 1630 cm^{-1} in $[Rd(DMSO)_2(DMF)Cl_3]$ indicating that the oxygen atom is the donor atom. The far infrared spectrum of the complex showed bands at 438(sh), 426(sh), 412(m), 379(s), 355(s), 328(s), and at 295(vw) cm^{-1}. The nmr spectrum of the rhodium compound in chloroform was also measured. The aldehyde proton is shifted downfield upon coordination by 0.23 ppm (from 8.10 (δ) to 8.33 ppm) while the CH_3—N protons are shifted by about 0.2 ppm (DMF: 2.87 and 2.95 ppm; $[Rd(DMSO)_2(DMF)Cl_3]$: 3.08 and 3.11 ppm). There are two peaks for the methyl protons of the DMSO molecules indicating two different environments of the methyl groups (3.44 and 3.64 ppm).

$[Rh(DMSO)_2(DMF)Cl_2]$ was prepared by dissolving $[Rh(DMSO)_3Cl_3]$ in DMF. In $[Rh(DMSO)_3Cl_3]$ two DMSO ligands are bonded to Rh through the S atom. These bonds are quite strong. The third DMSO molecule is bonded to Rh through the O atom. This bond should be quite weak and this DMSO ligand can be easily replaced by other ligands like DMF.

$$[Rh(DMSO)_3Cl_3] \underset{\text{DMSO}}{\overset{\text{DMF}}{\rightleftharpoons}} [Rh(DMSO)_2(DMF)Cl_3]$$

When $[Rh(DMSO)_2(DMF)Cl_3]$ is dissolved in DMSO and some ether is added to the solution, crystals of $[Rh(DMSO)_3Cl_3]$ can be isolated. Therefore the above reaction is reversible.

Acknowledgments

The authors are grateful to the Natural Sciences and Engineering Research Council of Canada, the Ministère de l'Education du Québec, and the National Cancer Institute of Canada for financial support.

1. M. J. CLEARE. Coord. Chem. Rev. **12**, 349 (1974) and references therein.
2. P. N. RAO, M. L. SMITH, S. PATHAK, R. A. HOWARD, and J. L. BEAR. J. Natl. Cancer Inst. **64**, 905 (1980) and references therein.
3. YU. N. KUKUSHKIN and N. D. RUBTSOVA. Russ. J. Inorg. Chem. **14**, 980 (1969).
4. YU. N. KUKUSHKIN and N. D. RUBTSOVA. Russ. J. Inorg. Chem. **14**, 1113 (1969).
5. P. C. KONG and F. D. ROCHON. Can. J. Chem. **56**, 441 (1978).
6. R. MELANSON and F. D. ROCHON. Can. J. Chem. **53**, 2371 (1975).
7. D. T. CROMER and J. T. WABER. Acta Crystallogr. **18**, 104 (1965).
8. R. F. STEWART, E. R. DAVIDSON, and W. T. SIMPSON. J. Chem. Phys. **42**, 3175 (1965).
9. D. T. CROMER. Acta Crystallogr. **18**, 17 (1965).
10. V. I. SOKOL and M. A. PORAI-KOSHITS. Koord. Khim. **1**(4), 577 (1975).

Can. J. Chem. Downloaded from www.nrcresearchpress.com by 210.87.254.40 on 09/06/12
For personal use only.

11. V. I. SOKOL, N. D. RUBTSOVA, A. YU. GRIBENYUK, and M. A. PORAI-KOSHITS. Zh. Strukt. Khim. **15**(4), 716 (1974).
12. V. I. SOKOL, N. D. RUBTSOVA, and A. YU. GRIBENYUK. Zh. Strukt. Khim. **15**(2), 319 (1974).
13. P. COLAMARINO and P. ORIOLI. J. Chem. Soc. Dalton Trans. 845 (1976).
14. R. MELANSON, J. HUBERT, and F. D. ROCHON. Acta Crystallogr. B**32**, 1914 (1976).
15. R. MELANSON and F. D. ROCHON. Acta. Crystallogr. B**33**, 3571 (1977).
16. R. MELANSON and F. D. ROCHON. Acta Crystallogr. B**34**, 941 (1978).
17. M. A. VISWAMITRA and K. K. KANNAN. Nature, **209**, 1016 (1966).
18. R. THOMAS, C. B. SHOEMAKER, and K. ERIKS. Acta Crystallogr. **21**, 12 (1966).
19. F. D. ROCHON, P. C. KONG, and R. MELANSON. Can. J. Chem. **58**, 97 (1980).
20. L. V. VILKOV, P. A. AKISHIN, and J. PRESNYAKOVA. J. Struct. Chem. **3**, 5 (1962).

Can. J. Chem. Downloaded from www.nrcresearchpress.com by 210.87.254.40 on 09/06/12
For personal use only.

Constituents from *Adina cordifolia*

SANTOSH K. SRIVASTAVA
Department of Chemistry, University of Sagar, Sagar (M.P.) 470003 India

Received May 22, 1981[1]

SANTOSH K. SRIVASTAVA. Can. J. Chem. **61**, 1827 (1983).

Four compounds isolated from the stem of *Adina cordifolia* were identified as stigmasta-5,22-diene-3β-*O*-α-L-rhamnopyranosyl-(1→4)-β-D-xylopyranoside, α-amyrin, octacosanol, and naringenin-7-methylether-4′-*O*-α-L-rhamnopyranoside on the basis of spectral and chemical evidence.

SANTOSH K. SRIVASTAVA. Can. J. Chem. **61**, 1827 (1983).

En se basant sur les preuves spectrales et chimiques, on a identifié quatre composés provenant de la tige de l'*Adina cordifolia*. Ce sont: le stigmastadiène-5,22 3β-*O*-α-L-rhamnopyranosyl β-D xylopyranoside(1→4), l'α-amyrine, l'octacosanol et l'éther-méthyl-7 *O*-α-L-rhamnopyranoside-4 de la naringénine.

[Traduit par le journal]

Can. J. Chem. Downloaded from www.nrcresearchpress.com by 210.87.254.6 on 09/06/12
For personal use only.

Introduction

The plant *Adina cordifolia* has been used in oriental medicine since ancient times as a very important component of various prescriptions acting as antiseptic and febrifuge (1). This communication records the isolation and structure of two known compounds, α-amyrin and octacosanol, and two new compounds, stigmasta-5,22-diene-3β-*O*-α-L-rhamnopyranosyl-(1→4)-β-D-xylopyranoside (**1**) and naringenin-7-methylether-4′-*O*-α-L-rhamnopyranoside (**2**), which are reported for the first time in nature. Previous chemical investigations by Srivastava *et al.* (2, 3) show that the stem of *A. cordifolia* yields a number of flavonoids.

Results and discussion

Four compounds were isolated from the stem of *A. cordifolia* (for details see Experimental) which were designated as compound A (stigmasta-5,22-diene-3β-*O*-α-L-rhamnopyranosyl-(1→4)-β-D-xylopyranoside) (**1**), B (α-amyrin), C (octacosanol), and D (naringenin-7-methylether-4′-*O*-α-L-rhamnopyranoside) (**2**). The known compounds B and C were identified as α-amyrin and octacosanol by the agreement of their mp, mmp, ir, ms, derivatives, and chromatographies with authentic samples. The isolation and identification of two new compounds A and D are described in detail.

Compound A

Repeated column chromatography of the petroleum ether (bp 40−60°C) soluble part of the rectified spirit extract of the stem of *A. cordifolia* on an Al_2O_3 column (C_6H_6−MeOH, 1:9) and crystallization yielded a pure brown amorphous substance, $C_{40}H_{66}O_9$ (M^+ at *m/z* 690), mp 130°C (dec.); $[\alpha]_D^{30}$ +58.5° ($CHCl_3$). It gave characteristic saponin reactions, copious lather with H_2O, and haemolysed red blood cells. Acid hydrolysis (7% H_2SO_4) of the saponin afforded a genin, L-rhamnose, and D-xylose (identical paper chromatographies and glc (alditol acetates)) (4) as the sugar components. The genin had mp 155−157°C; $[\alpha]_D^{25}$ −48° ($CHCl_3$); and molecular formula $C_{29}H_{48}O$ (M^+ at *m/z* 412) by mass spectrometry. From the detailed study of the ir, ^1H nmr, ms spectra, acetate derivative, oxidation (5), reduction (H_2−Pt), Oppenhauer oxidation ($(Me_3CO)_3Al$ + C_6H_{12} + Ph·Me under reflux) (6, 7), and ozonolysis (8) the genin was shown to be stigmasta-5,22-diene-3β-ol (poriferasterol or the C_{24} epimer of stigmasterol) which was confirmed by co-chromatography with an authentic sample (9, 10). When A was subjected to periodate oxidation (11), it consumed 3.00 moles of periodate and liberated 2.00 moles of HCO_2H per 1 mole of the saponin, thus indicating the presence of two units of monosaccharide in the pyranose form. Quantitative estimation of the genin (gravimetric) and the sugars by the Dubois method (12) showed that the genin, L-rhamnose, and D-xylose were present in the molar ratio of 1:1:1. A glc analysis of the alditol acetates of the sugars obtained from the acid hydrolysate (freed from the genin) further showed the presence of L-rhamnose and D-xylose in the ratio 1:1. When saponin A was methylated (13), then subjected to acid hydrolysis, it afforded an aglycone poriferasterol (mp, mmp, and co-thin-layer chromatography) and two methylated sugars 2,3-di-*O*-methyl-D-xylose and 2,3,4-tri-*O*-methyl-L-rhamnose (paper chromatrographies and glc of alditol acetates). The sequence of the sugars in the saponin was established as follows. Partial acid hydrolysis of A resulted in the formation of L-rhamnose (co-paper chromatography, as an end sugar) and prosaponin (**3**). This prosaponin, on complete acid hydrolysis, yielded D-xylose (co-paper chromatography) and an aglycone, poriferasterol (mp, mmp, and co-thin layer chromatography). Hence the structure of the saponin can be represented as stigmasta-5,22-diene-3β-*O*-α-L-rhamnopyranosyl-(1→4)-β-D-xylopyranoside. The configurations of the anomeric carbon atoms of the sugars in the methylated saponin were deduced by the application of Klyne's rule of molecular rotation (14, 15) and were found to be α for L-rhamnose and β for D-xylose. Thus the structure of saponin A was assigned as **1**.

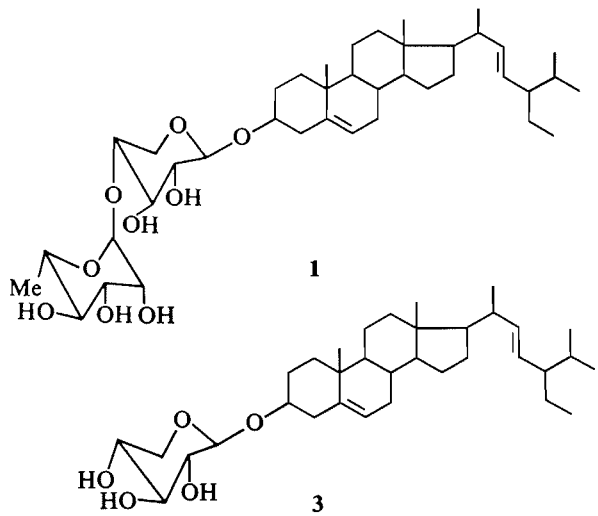

1

3

[1]Revision received February 18, 1983.

Can. J. Chem. Downloaded from www.nrcresearchpress.com by 210.87.254.6 on 09/06/12
For personal use only.

Compound D

This compound was purified over a magnesol column (EtOH) and crystallized as pale yellow needles from EtOAc – petroleum ether (1:9), mp 80–84°C, $C_{22}H_{24}O_9$ (M^+ at m/z 432). It gave characteristic flavanone colour reactions: purplish brown with $FeCl_3$, yellow with NaOH, reddish colour with Mg–HCl, Na–Hg/HCl, and 2,4-DNP. Acid hydrolysis of glycoside D gave an aglycone, mp 152–154°C, $[\alpha]_D^{30}$ +30° (MeOH), which was identical with an authentic sample of naringenin-7-methylether (16) (sakuranetin) (mp, mmp, uv, ir, ^{1}H nmr; and co-thin-layer chromatography). In the hydrolysate, freed from the aglycone, L-rhamnose was detected by thin-layer, paper, and co-chromatographies and also with glc (alditol acetate). When D was subjected to periodate oxidation, the glycoside consumed 2.00 moles of periodate with the liberation of 1.00 mole of HCO_2H per 1 mole of the glycoside, thus indicating that the monosaccharide is in pyranose form. KOH degradation (17) of glycoside D yielded phloroglucinol monomethylether, mp 74°C (lit. (16) mp 75°C), and co-thin-layer chromatography suggested that the site of rhamnosidation is the C-4′ OH. Glycoside D was permethylated (13), then subjected to acid hydrolysis, affording naringenin-5,7-dimethylether (18) (mp, mmp, uv, ir, ^{1}H nmr, and co-thin layer chromatography) and 2,3,4,-tri-*O*-methyl-L-rhamnose (R_G value and glc of alditol acetate). This provides further confirmation that the rhamnosidation occurs at C-4′. The nature of the sugar linkage was deduced by Klyne's generalization rule (14) and was found to be α. Thus it may be concluded that compound D was naringenin-7-methylether-4′-*O*-α-L-rhamnopyranoside (**2**).

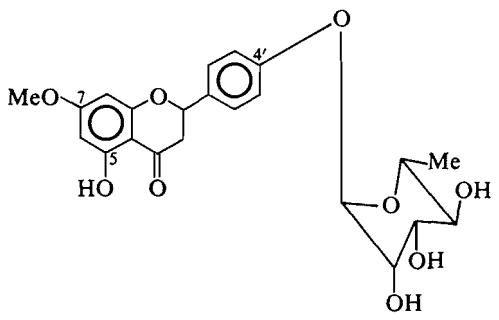

2

Experimental

Melting points are uncorrected; column, thin-layer, and paper chromatographic analyses were performed at room temperature. Sugars were characterized spectrophotometrically by the PhOH–H_2SO_4 method (12), using a Klett–Summerson photoelectric colorimeter and also by Whatmann filter paper No. 1, descending paper chromatography technique, using *n*-butanol – acetic acid – water (4:1:5) as a developing solvent and aniline hydrogen phthalate for revealing the spot.

Plant material

The stem was obtained from the local city Sagar, and was identified by the Botanical Survey of India, Allahabad.

Isolation and purification

The air-dried and powdered stem of *A. cordifolia* (2 kg) was extracted with triple-distilled ethanol under reflux. The total ethanolic extract (1.5 L) was concentrated (100 mL) and shaken separately with petroleum ether and absolute EtOH (99.5%). The petroleum ether extract (500 mL) gave a mixture of three compounds (thin layer chromatographic examination) which were separated on Al_2O_3 using different gradients of C_6H_6–MeOH to yield compounds A (2 g, C_6H_6–MeOH, 1:9); B (200 mg, C_6H_6–MeOH, 3:7), and C (220 mg, C_6H_6–MeOH, 5:5). The absolute EtOH extract deposited a single compound, D (thin-layer chromatographic examination) (800 mg).

Compound A (stigmasta-5,22-diene-3β-O-α-L-rhamnopyranosyl-(1→4)-β-D-xylopyranoside

Melting point 130°C (dec.); $[\alpha]_D^{30}$ +58.5° ($CHCl_3$); $C_{40}H_{66}O_9$ (M^+ at m/z 690); thin-layer chromatography (Si gel): R_f 0.40 ($CHCl_3$–MeOH, 8:2). *Anal.* calcd. for $C_{40}H_{66}O_9$: C 69.56, H 9.56; found: C 69.57, H 9.55%.

Acid hydrolysis of the saponin

The saponin (1 g) was dissolved in a minimum amount of absolute alcohol (99.5%) (25 mL) and was refluxed with 7% H_2SO_4 (100 mL) for 6 hours, concentrated, diluted with H_2O (100 mL), and cooled to yield genin as a white amorphous solid which was crystallized as microcrystalline colourless needles ($CHCl_3$–MeOH), mp 156–157°C; $[\alpha]_D^{30}$ −49.00 ($CHCl_3$); $C_{29}H_{48}O$ (M^+ at m/z 412). *Anal.* calcd. for $C_{29}H_{48}O$: C 84.46, H 11.65; found C 84.48, H 11.65%. Monoacetate (100 mg of the genin + 8 mL C_5H_5N + 5 mL Ac_2O): mp 145–146°C; $[\alpha]_D^{30}$ −53.00° ($CHCl_3$). *Anal.* calcd. for $C_{31}H_{50}O_2$: C 81.93, H 11.01; found: C 81.90, H 11.00%. The aqueous solution after neutralization ($BaCO_3$) gave D-xylose and L-rhamnose (R_f 0.28 and 0.37, respectively, in the solvent *n*-butanol – acetic acid – water, 4:1:5, finally confirmed with co-paper chromatographies).

Reduction of the genin

The genin (100 mg) and Pt catalyst (100 mg) in the glacial acetic acid (20 mL) were shaken with H_2 for 10 hours, worked up as usual, and crystallized (Et_2O), mp 142–144°C; $[\alpha]_D^{30}$ +25.00° ($CHCl_3$). *Anal.* calcd. for $C_{29}H_{52}O$: C 83.63, H 12.50; found: C 83.62, H 12.50%. The reduced product did not give the tests for unsaturation (tetranitromethane and Br_2 water test).

Oppenhauer oxidation of the genin

The genin (100 mg) in dry C_6H_{12} (5 mL) was mixed with $(Me_2CHO)_3Al$ (120 mg) in Ph·Me (10 mL) and refluxed for 23 h. The reaction mixture was washed in turn with 2 *N* H_2SO_4, H_2O, and aqueous $NaHCO_3$. The product was crystallized as colourless needles (MeOH), mp 75–80°C; $[\alpha]_D^{30}$ +58.5° ($CHCl_3$). *Anal.* calcd. for $C_{29}H_{46}O$: C 84.87, H 11.21; found: C 84.88, H 11.20%. It was identical with poriferast-5,22-diene-3-one (poriferastadienone) (mp, mmp, and co-thin-layer chromatography).

Ozonolysis of the genin

The genin (100 mg) in glacial acetic acid (10 mL) was ozonized for 2 hours at an O_3 concentration of about 2%, the exit gases being led through 20 mL H_2O. The reaction mixture passed through a Si column. The distillate (20 mL) was collected, a solution of 100 mg crystallized *p*-NO_2—Ph—NH—NH_2 in 10 mL glacial acetic acid was gradually added, and hydrazone crystallized out immediately (MeOH), mp 85–88°C (dec.), identical with α-ethylisovaleraldehyde (co-thin-layer chromatography). *Anal.* calcd. for $C_{13}H_{20}N_3O_2$: C 62.40, H 8.00, N 16.80; found: C 62.40, H 8.00, N 16.82%.

Catalytic hydrogenation of the genin acetate

The genin acetate (100 mg) was treated with PtO_2 (100 mg) in glacial acetic acid (15 mL) and worked up usual. The product was crystallized (MeOH–Me_2CO) and identified as poriferastanyl acetate *Anal.* calcd. for $C_{31}H_{54}O_2$: C 84.22, H 11.83; found: C 84.23, H 11.84%.

Quantitative estimation of the sugars of the saponin by gas–liquid chromatography

The saponin (100 mg) was hydrolysed with acid as was done earlier. The filtrate was neutralized with $BaCO_3$ and filtered. The filtrate containing the sugar mixtures was evaporated to dryness *in vacuo*. This was then dissolved in H_2O (20 mL) and reduced with $NaBH_4$ (750 mg) for 4 hours. The reduced product was treated with Dowex 50 (H^+) and the solution was concentrated. The H_3BO_3 was removed by co-distillation with MeOH and the product was acetylated with Ac_2O–Py (5:5) at 100°C for 40 min, diluted with H_2O, evaporated to dryness, dissolved in $CHCl_3$, and glc was performed. From the areas

Can. J. Chem. Downloaded from www.nrcresearchpress.com by 210.87.254.6 on 09/06/12
For personal use only.

of peaks corresponding to alditol acetates, D-xylose and L-rhamnose were found in 1:1 molar ratio.

Permethylation and hydrolysis of the saponin

Permethylation of the saponin was carried out by Hakomori's method (13) (15% NaH dispersed in oil (180 mg) with DMSO (20 mL) kept on an oil bath at 80°C for 1 hour). A solution of the saponin (100 mg) in DMSO (4 mL) was added dropwise to the contents of the same oil bath with constant stirring and the mixture was kept again at 80°C for 3 hours until the olive-green colour appeared. The olive-green solution was cooled in ice and MeI (2.5 mL) was slowly added with shaking. It was then left overnight at room temperature. The fully methylated product was isolated in the usual way (syrup) (120 mg) and showed no absorption band for hydroxyl group in the ir spectrum. The fully methylated product was hydrolysed with $N-H_2SO_4$ under reflux for 5 hours. The hydrolysate was neutralized with $BaCO_3$, filtered, deionized, and evaporated to a syrup (80 mg).

Identification of the methylated sugars by paper chromatography and gas–liquid chromatography

The syrup (obtained as above) was divided into two portions. The first portion was examined by paper chromatography with the solvent system butanol–ethanol–water (5:1:4) (upper layer). Two spots were observed with R_G values 0.74 and 1.01, corresponding to 2,3-di-*O*-methyl-D-xylose and 2,3,4-tri-*O*-methyl-L-rhamnose (19–21), respectively.

The second portion was reduced with $NaBH_4$ and acetylated as described earlier. The partially methylated alditol acetates were identified by glc from their relative retention times (22) with respect to 2,3,4,6-tetra-*O*-methyl-D-glucitol diacetate. Two peaks were observed with relative retention times 0.94 and 2.20, which corresponded to 2,3-di-*O*-methyl-D-xylitol triacetate and 2,3,4-tri-*O*-methyl-L-rhamnitol diacetate, respectively.

Periodate oxidation of the saponin

A solution of the saponin (30 mg) in ethanol (20 mL) was treated with an equal volume of 0.1 *M* $NaIO_4$. After 48 h the uptake of periodate and liberated HCO_2H were estimated by the standard titration method as corresponding to 3.00 and 2.00 moles, respectively.

Partial hydrolysis of the saponin

The saponin (200 mg) was dissolved in ethanol (20 mL) and hydrolysed with 7% H_2SO_4 (50 mL) at 90°C for 20 min and worked up in the usual way. Prosaponin (**3**) was separated out and the aqueous hydrolysate yielded only L-rhamnose (co-paper chromotagraphy) as an end sugar. The prosaponin (**3**) on further acid hydrolysis (4 hours) gave poriferasterol (mp, mmp, and co-thin-layer chromatography) and D-xylose (which was attached to the genin part) by co-paper chromatography.

Compound B (α-amyrin)

This compound was purified over the column of Al_2O_3 (C_6H_6–MeOH, 3:7) as a white amorphous solid which crystallized as white needles (ethanol), mp 185–186°C (lit. (16, 23) mp 186°C); $[\alpha]_D^{25}$ +83.00° ($CHCl_3$); molecular formula $C_{30}H_{50}O$ (M^+ at *m/z* 426); thin-layer chromatography (Si gel): R_f 0.52 ($CHCl_3$–MeOH, 8:2) and 0.68 (butanol – acetic acid – water, 4:1:5); ir ν_{max} (KBr) cm^{-1}: 3350 (br, OH), 3000, 2950, 2895, 1649, 1425, 1382, 1210, 1060, 1028, 880, and 725; ms: 426 (M^+), 411 (M^+-Me), 408 (M^+-H_2O), 393 ($M^+-(Me + H_2O)$), 189, 187, 149, and 147. *Anal.* calcd. for $C_{30}H_{50}O$: C 84.50, H 11.73; found: C 84.51, H 11.72%. Acetate (50 mg of the compound + 5 mL C_5H_5N + 4 mL Ac_2O): mp 220–223°C; $C_{32}H_{52}O_2$ (M^+ at *m/z* 468). *Anal.* calcd. for $C_{32}H_{52}O_2$: C 79.91, H 11.11; found: C 80.00, H 11.10%. Benzoate (50 mg of the compound + 5 mL C_5H_5N + 5 mL $PhCO\cdot Cl$): mp 190–191°C; $C_{37}H_{54}O_2$ (M^+ at *m/z* 530). *Anal.* calcd. for $C_{37}H_{54}O_2$: C 83.77, H 10.18; found: C 83.75, H 10.20%.

Compound C (octacosanol)

This compound was purified over the column of Al_2O_3 (C_6H_6–MeOH, 5:5) as a white amorphous compound, mp 82–85°C (lit. (16, 24) mp 83.2–83.4°C); $C_{28}H_{58}O$ (M^+ at *m/z* 410); thin-layer chromatography (Si gel): R_f 0.72 ($CHCl_3$–MeOH, 8.2); ir ν_{max} (KBr) cm^{-1}: 3345 (br, OH), 2920, 2840, 1460, 1410, 1378, 1366, 1330, 1174, 730–725. Acetate (Ac_2O/Py): mp 66–67°C; $C_{30}H_{60}O_2$ (M^+ at *m/z* 452). *Anal.* calcd. for $C_{30}H_{60}O_2$: C 79.64, H 13.27; found: C 79.65, H 13.25%. Iodide: mp 64°C.

Compound D (naringenin-7-methylether-4′-O-α-L-rhamnopyranoside

This compound was purified over the column of magnesol (EtOH) and crystallized (EtOAc – petroleum ether mixture, 1:9), mp 80–84°C; $C_{22}H_{24}O_9$ (M^+ at *m/z* 432); thin-layer chromatography (Si gel): R_f 0.63 ($CHCl_3$–MeOH, 7:3) and paper chromatography (Whatmann No. 1 filter paper, descending technique): R_f 0.92 (butanol – acetic acid – water, 4:1:5) and 0.28 (15% glacial acetic acid); uv λ_{max} (MeOH) nm: 290, 330 (sh); +$AlCl_3$: 315, 335 (sh); +NaOAc: 290, 332 (sh); ir ν_{max} (KBr) cm^{-1}: 3400 (br, OH), 2930, 2870, 1680, 1600, 1480, 1400, 1365, 1210, 1175, 1160, 825, 810, and 720; ^1H nmr (DMSO-d_6, TMS, 90 MHz), δ: 7.20 (d, 2H, *J* = 8.5 Hz, H-2′ and H-6′), 6.80 (d, 2H, *J* = 8.5 Hz, H-3′ and H-5′), 6.45 (d, 2H, *J* = 2.5 Hz, H-6 and H-8), 3.78 (s, 3H, 1 × MeO), 5.40 (1H, H-2), 2.80 (2H, H-3), 1.32 (d, 3H, *J* = 12 Hz, rhamnose Me), 5.00–4.00 (m, sugar protons). *Anal.* calcd. for $C_{22}H_{24}O_9$: C 61.11, H 5.55; found: C 61.12, H 5.53%. The glycoside (500 mg) was dissolved in ethanol (25 mL) and to it 40 mL of 7% H_2SO_4 was added. The mixture was refluxed on a water bath for 4 hours and worked up as usual, which gave naringenin-7-methylether (mp, mmp, uv, ir, ^1H nmr, and co-thin-layer chromatography) and L-rhamnose (co-paper chromatography and alditol acetates). Methylation followd by acid hydrolysis afforded naringenin-5,7-dimethylether (mp, mmp, uv, ir, ^1H nmr, and co-thin-layer chromatography) and 2,3,4,-tri-*O*-methyl-L-rhamnose (R_G 1.01 in butanol–ethanol–water, 5:1:5 and alditol acetates).

Acknowledgements

The author expresses his gratitude to the Director, CIBA Research Centre, Bombay (India) for spectral data and microanalyses and to Dr. (Mrs.) Savitri Devi Srivastava for her valuable suggestions.

1. R. N. CHOPRA, S. L. NAYAR, and I. C. CHOPRA. Glossary of Indian medicinal plants. CSIR publication. Delhi, India. 1956. p. 7.
2. S. K. SRIVASTAVA, R. K. GUPTA, and S. D. SRIVASTAVA. Indian J. Chem. **20**, 833 (1981).
3. S. K. SRIVASTAVA and S. D. SRIVASTAVA. Paper accepted for presentation at the 13th international symposium on the chemistry of natural products. Pretoria, S. Africa. 1982. Paper No. A-2.
4. H. BJORNDAL, B. LINDBERG, and S. SVENSSON. Acta Chem. Scand. **21**, 1801 (1967).
5. D. H. R. BARTON and P. DEMAYO. J. Chem. Soc. 887 (1954).
6. A. M. LYON and W. BERGMANN. J. Org. Chem. **7**, 428 (1942).
7. E. R. H. JONES, P. A. WILKINSON, and R. H. KERLOGUE. J. Chem. Soc. 391 (1942).
8. F. R. VALENTINE, JR., and W. BERGMANN. J. Org. Chem. **6**, 452 (1941).
9. N. P. S. BISHT and R. SINGH. J. Indian Chem. Soc. **45**, 707 (1978).
10. S. ELSEVIER. Encyclopaedia of organic chemistry. Vol. 14. Series III. Elsevier Publishing Company, London. 1954. p. 1838.
11. E. L. HIRST, L. HOUGH, and J. K. N. JONES. J. Chem. Soc. 928 (1949).
12. M. DUBOIS, K. A. GILLES, J. K. HAMILTON, P. A. REBERS, and F. SMITH. Anal. Chem. **28**, 350 (1956).
13. S. HAKOMORI. J. Biochem. Tokyo, **55**, 205 (1964).
14. W. KLYNE. Biochem. J. **47**, 41 (1950).
15. V. HARIHARAN and S. RANGASWAMI. Phytochemistry, **9**, 409 (1970).
16. I. HEILBRON and H. M. BUNBURY. Dictionary of organic compounds. Eyre and Spottiswoode, London. 1953.

17. L. H. BRIGGS and R. H. LOCKER. Chem. Soc. 2157 (1949).
18. K. P. TIWARI, S. D. SRIVASTAVA, and S. K. SRIVASTAVA. Chem. Scr. **13**, 191 (1978–79).
19. F. SMITH and R. MONTGOMERY. The chemistry of plant gums and mucilages and some related polysaccharides. Reinhold, New York. 1959. p. 225.
20. K. BUTLER, P. F. LLOYD, and M. STACEY. J. Chem. Soc. 1531 (1955).
21. E. LEDERER and M. LEDERER. Chromatography. Elsevier Publishing Company, London. 1957. pp. 250–251.
22. O. LARM, B. LINDBERG, and S. SVENSSON. Carbohydrate Res. **31**, 120 (1973).
23. F. S. SPRING and T. VICKERSTAFF. J. Chem. Soc. 249 (1937).
24. J. S. CHAUHAN, S. K. SRIVASTAVA, and S. D. SRIVASTAVA. Planta Med. **36**, 183 (1979).

Can. J. Chem. Downloaded from www.nrcresearchpress.com by 210.87.254.6 on 09/06/12
For personal use only.

The stationary-state approximation in the photolysis of acetone

A. J. C. NICHOLSON
CSIRO Division of Chemical Physics, P.O. Box 160, Clayton, Victoria, Australia 3168

Received October 25, 1982

A. J. C. NICHOLSON. Can. J. Chem. **61**, 1831 (1983).

A mechanism has been written for the photolysis of acetone at 313 nm and 253.7 nm and the differential equations involved solved rigorously. Testing this mechanism has revealed inconsistencies between different sets of experiments that were not previously obvious. The stationary-state approximation is valid up to ca. 0.5% decomposition but its practical usefulness is minimal. Graphs are given showing the variation of all significant quantum yields with temperature, pressure, and light intensity.

A. J. C. NICHOLSON. Can. J. Chem. **61**, 1831 (1983).

On propose un mécanisme pour la photolyse de l'acétone à 313 et 253,7 nm et on a résolu de façon rigoureuse les équations différentielles qui y sont impliquées. La vérification de ce mécanisme révèle, entre les différents groupes d'expérience, des contradictions qui n'étaient pas évidentes. L'approximation de l'état stationnaire est valable jusqu'à une décomposition de 0,5% envirion mais son utilité pratique est très faible. On présente des graphiques qui illustrent la variation de tous les rendements quantiques appréciables en fonction de la température, de la pression et de l'intensité de la lumière.
[Traduit par le journal]

Can. J. Chem. Downloaded from www.nrcresearchpress.com by 210.87.254.42 on 09/06/12
For personal use only.

In 1913 Bodenstein (1) first postulated that the very low concentrations of intermediates present in photolytic reactions could be taken as constant in the early stages of reaction. This "stationary-state approximation" can be used to convert the series of coupled differential equations describing the reactions occurring, into an equivalent series of simultaneous equations. These can sometimes be solved but more often require further approximations to obtain relationships between experimental conditions and final products in which the concentrations of intermediates have been eliminated. Recently developed mathematical techniques (2) for computer solution of such differential equations have made the approximation unnecessary. Farrow and Edelson (3) have shown that the approximation can give erroneous results in some circumstances and recommend that it should be abandoned or at least never used without checking whether it is applicable to a particular case.

The photolysis of acetone has probably been studied as extensively as that of any single molecule. The present paper is an attempt to write a complete mechanism for the acetone photolysis, to solve the differential equations rigorously, and to determine the limits of validity of the stationary-state approximation. A common mechanism could not be found to cover two different sets of experimental results that appeared, at first glance, to be "in good agreement". This reveals where further experimental work is required.

Selection of experimental data

(A) Quantum yield of carbon monoxide production, Φ_{CO}

All workers agree that Φ_{CO} tends to one with increase in temperature. Calvert and Pitts (4) recommend acetone as an actinometer stating that $\Phi_{CO} = 1$ for all wavelengths and intensities at pressures <50 Torr and temperatures >125°C. The experimental evidence on which this is based is surprisingly limited and there is disagreement over the value of the temperature at which $\Phi_{CO} = 1$. Leermakers (5) places this temperature between 148°C and 163°C, while Herr and Noyes (6) place it around 115°C. Pitts, Margerum, Taylor, and Brim (7) give a measurement at 125°C as "1 within experimental error" although their figures would suggest 0.95 ± 0.05. Shaw and Toby (8) give 0.86 at 122°C and 1 at 210°C, and state that Φ_{CO} is independent of pressure over the range 3–219 Torr: Cundall and Davies, CD (9), assume $\Phi_{CO} = 1$ at 135°C and 50 Torr: Pearson (10) chooses 131°C and 145 Torr. Caldwell and Hoare (11) at 120°C, and Boyd, Carter, and Kutschke (12) at 145°C, are in agreement that Φ_{CO} is constant to within 2% over the pressure range from 60–130 Torr. Yet any mechanism involving collisional deactivation of excited states would suggest Φ_{CO} should decrease with increasing pressure at temperatures where the concentration of acetyl radicals is small. No data on this pressure effect are available in the crucial temperature range between 75°C and 100°C.

In view of these uncertainties, an author's quantum yields were only used uncorrected when light intensities were measured directly. When acetone was used as an actinometer and Φ_{CO} assumed to be one at a stated temperature, the value of Φ_{CO} at this temperature was calculated by the mechanism given below and used to correct the quoted intensities and quantum yields of other products. This correction only amounted to a few percent. It will be suggested that there is a small variation in Φ_{CO} with pressure and light intensity.

(B) Quantum yields of ethane and methane

A wider range of experimental data is available on the rates of formation of ethane, $R_{C_2H_6}$, and methane, R_{CH_4}. The results of different experimenters are easier to compare than those on carbon monoxide formation because of the relationship discovered by Dorfman and Noyes (13) that $R_{CH_4}/[A]R_{C_2H_6}^{1/2} =$ constant, where [A] is the concentration of acetone. This relationship has been extensively checked for acetone (14, 15); its particular merit is that the constant is independent of pressure, light wavelength, and light intensity. Results from seven experimental papers are used in Fig. 1 to establish a very reliable value of this constant and of its variation with temperature.

(C) Quantum yields of other products

Few quantitative measurements have been made on products other than the above. Estimates have frequently been made from the conditions for material balance.

Mechanism

The reactions chosen to describe the photolysis are set out in Table 1. This mechanism is an expanded version of the schemes given by Heicklen and Noyes (16) and by CD (9). The former authors showed from fluorescence and phosphor-

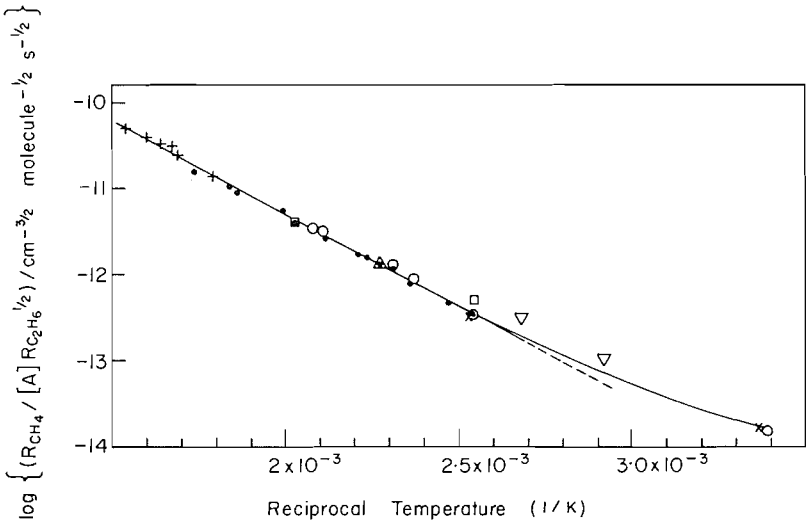

FIG. 1. Plot of $R_{CH_4}/[A]R_{C_2H_6}^{1/2}$ vs. $1/T$. R represents rate of formation and [A] is the concentration of acetone. □ ref. 8, ▽ ref. 10, × ref. 13, ● ref. 16, ○ ref. 15, + ref. 17, △ ref. 18.

TABLE 1. Reactions and rate constants (λ = 313 nm)

	Reaction	A'/s^{-1} or cm^3 molecule^{-1} s^{-1}	E/kJ	Reference
[1]	$A + h\nu \rightarrow {}^1A_m$	I/[A]		
[2]	${}^1A_m \rightarrow CH_3 + CH_3CO$	2.5×10^{16}	66	a
[3]	${}^1A_m + A \rightarrow {}^1A_0 + A$	2×10^{-12}		a
[4]	${}^1A_0 + A \rightarrow 2A$	2×10^{-12}		a
[5]	${}^1A_0 \rightarrow {}^3A_n$	4×10^{8}		b
[6]	${}^3A_n \rightarrow CH_3 + CH_3CO$	1.25×10^{10}	24	a
[7]	${}^3A_n + A \rightarrow {}^3A_0 + A$	4×10^{-12}		a
[8]	${}^3A_0 + A \rightarrow 2A$	2×10^{-12}		a
[9]	$CH_3CO + A \rightarrow CH_3 + CO + A$	5×10^{-10}	50	c
[10]	$CH_3 + A \rightarrow CH_4 + CH_2COCH_3$	5×10^{-13}	40.6	d
[11]	$2CH_3 \rightarrow C_2H_6$	4×10^{-11}		e
[12]	$CH_3 + CH_3CO \rightarrow A$	10^{-11}		f
[13]	$2CH_3CO \rightarrow (CH_3CO)_2$	5×10^{-12}		f
[14]	$CH_3CO \xrightarrow{wall} (1/2)\,(CH_3CO)_2$	4.5×10^{18}/[A]		g
[15]	$2CH_2COCH_3 \rightarrow (CH_2COCH_3)_2$	5×10^{-12}		f
[16]	$CH_3 + CH_2COCH_3 \rightarrow C_2H_5COCH_3$	10^{-11}		f
[17]	$CH_3CO + CH_2COCH_3 \rightarrow CH_3COCH_2COCH_3$	10^{-11}		f
[18]	$CH_3 + CH_3CO \rightarrow CH_4 + CH_2CO$	10^{-12}		d
[19]	$2CH_3CO \rightarrow CH_3CHO + CH_2CO$	5×10^{-13}		h
[20]	$CH_3CO + A \rightarrow CH_3CHO + CH_2COCH_3$	10^{-13}	45	h

escence measurements and the latter, from measurements of the *cis–trans* isomerization of olefins in the presence of photolysing acetone, that both singlet and triplet excited states are involved in the photolysis. The transitions giving fluorescence and phosphorescence have a total quantum yield of 0.02 only (9) at 50°C and have not been included in the mechanism. The reaction producing ethylene which occurs above 200°C (17) has also been ignored.

A represents the acetone molecule in its ground state, ${}^1A_m$ and ${}^1A_0$ the first excited singlet of acetone in its mth and zeroth levels, ${}^3A_n$ and ${}^3A_0$ levels of the lowest triplet state; concentrations, in molecules cm^{-3}, are indicated by square brackets; pressure, p, is in Torr; the intensity, I, is the rate of light absorption in quanta (q) cm^{-3} s^{-1}. Rate constants, k, are in the form $k = A' \exp(-E/RT)$ with A' in s^{-1} or cm^3 molecule^{-1} s^{-1}; activation energy, E, in J mol^{-1}, T, the temperature in K and R = 8.314 J K^{-1} mol^{-1}.

(*a*) For reasons given below under Results, k_2 and k_6 were fitted to the Φ_{CO} values of Pearson (10) rather than those of CD (9). A'_3, A'_4, A'_7, A'_8 are the estimates of CD.

(*b*) This value for k_5 is that of Shortridge, Yang, and Lee (22). The reaction is believed to be first-order (9).

(*c*) Values of k_9 cover a range of thousands! The latest was measured by Watkins and Word (23) who give a unimolecular value $k_{9\infty} = 2.5 \times 10^{13} \exp(-72\,000/RT)$ and calculate a correction factor for pressures between 1 and 1000 Torr. The half pressure between uni- and bimolecular rates is at around 500 Torr at 0°C. The bimolecular constant chosen here gives the same value of rate constant at 25°C and 50 Torr as that given by Watkins and Word. Φ_{CO} is not sensitive to the value chosen.

(*d*) Figure 1 gives a plot of $\log R_{CH_4}/[A]R_{C_2H_6}^{1/2}$ vs. $1/T$ from many experimenters (8, 10, 13–15, 17, 18). Where this is a straight line it is taken that reactions [10] and [11] are the only

Can. J. Chem. Downloaded from www.nrcresearchpress.com by 210.87.254.42 on 09/06/12
For personal use only.

Can. J. Chem. Downloaded from www.nrcresearchpress.com by 210.87.254.42 on 09/06/12
For personal use only.

ones producing CH_4 and C_2H_6 respectively; hence this line gives $k_{10}/k_{11}^{1/2}$. Ausloos and Steacie (19) showed that the low temperature deviation from the straight line can be partially accounted for by reaction [18]. This is arbitrarily assigned a rate constant one tenth of that of reaction [12]. This gives the curved portion of Fig. 1 in reasonable agreement with experiment. Johnston (34) has suggested that this curvature can be accounted for by quantum mechanical tunnelling but this possibility is not considered in the mechanism given here.

(*e*) The value for k_{11} is very reliable (20) for pressures above 50 Torr. For lower pressures (18, 21) the reaction moves towards the region of 3rd order kinetics.

(*f*) Reactions [12], [13], [15], [16], [17]. Few quantitative rate constants are available. Reactions of CH_3CO are not important except at low temperatures. For the most important, reaction [13], $k = 5 \times 10^{-12}$ is chosen intermediate between the estimates of Avery, Hayes, and Phillips (24), 1.32×10^{-11}, and Szirovica and Walsh (25), 4.15×10^{-13}. The same value is chosen for k_{15}. Reactions of CH_2COCH_3 are important whenever CH_4 is formed but not enough experimental data are available to test this estimate.

(*g*) It seems necessary to postulate that biacetyl can be formed both by homogeneous (26) and heterogeneous (27) combination of acetyl radicals. The latter is covered by reaction [14]. This can only be a very approximate representation since its rate will be sensitive both to the nature of the walls and the distance of the light beam from the walls. It can be regarded as an arbitrary parameter to reproduce the experimental observation that Φ_{CO} increases with increasing pressure at low temperatures; reaction [9] alone is not fast enough to provide such a result.

(*h*) Reactions [19] and [20] are relatively unimportant. One or both may account for the formation of acetaldehyde at low temperatures.

Results

The reactions and rate constants of Table 1 were used in a computer program devised by Davies (28). For a nominated acetone concentration, light intensity, and temperature the program calculates the concentrations of all intermediates and products as a function of time. Quantum yields are calculated from these as required.

For Φ_{CO} and its variation with temperature CD (9) (their Fig. 1) consider their results "agree closely" with those of Pearson (10). This is not so when allowance is made for the different pressures at which Φ_{CO} was measured. CD measured rates at two temperatures to give $k_2 = 2.5 \times 10^{16} \exp(-70\,700/RT)$ and $k_6 = 2.5 \times 10^{10} \exp(-26\,800/RT)$ and get a good fit to their data using reactions [1]–[8]. If the additional reactions of CH_3CO are included, reactions [9], [12], [13], [14], [17], [18], [19], and [20], a best fit is obtained with $k_2 = 1.8 \times 10^{16} \exp(-71\,000/RT)$ and $k_6 = 1.25 \times 10^{10} \exp(-24\,000/RT)$. However, the rate constants used by CD result in a sharp decrease in Φ_{CO} with acetone pressure such that calculation for the experimental conditions of Pearson give values of both Φ_{CO} and $\Phi_{C_2H_6}$ that are 50% too low. Accordingly the value of $k_2 = 2.5 \times 10^{16} \exp(-66\,000/RT)$ was used which gives a best fit to Pearson's value of Φ_{CO} as shown in Fig. 2 and also a fair fit to his $\Phi_{C_2H_6}$ and Φ_{CH_4} values.

A difficulty arises in applying this mechanism to CD's results because these authors only specify their intensities as between 10^{12} and 5×10^{12} q cm^{-3} s^{-1}. Figure 3 shows that for both intensities the calculated curves lie appreciably above the

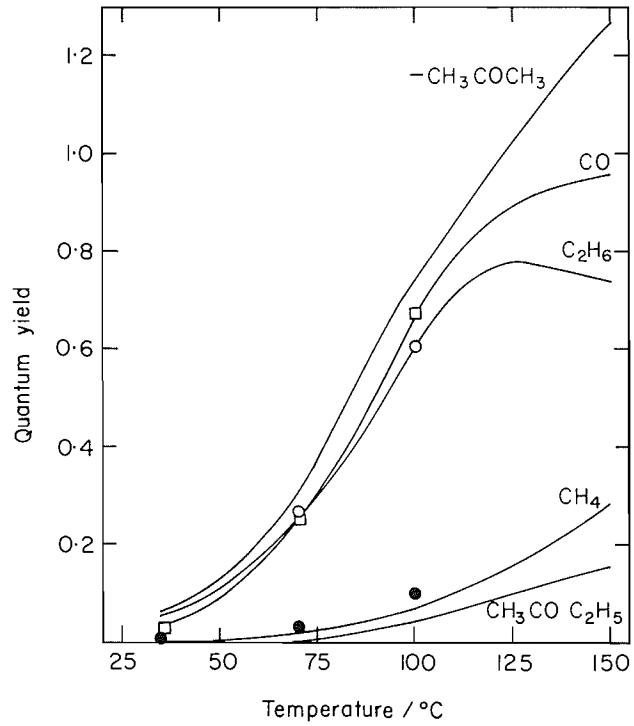

FIG. 2. Calculated quantum yields as a function of temperature at $\lambda = 313$ nm, $I = 7.17 \times 10^{13}$ q cm^{-3} s^{-1}, $p = 145$ Torr. Experimental points from Pearson (10), CO □, C_2H_6 ○, CH_4 ●.

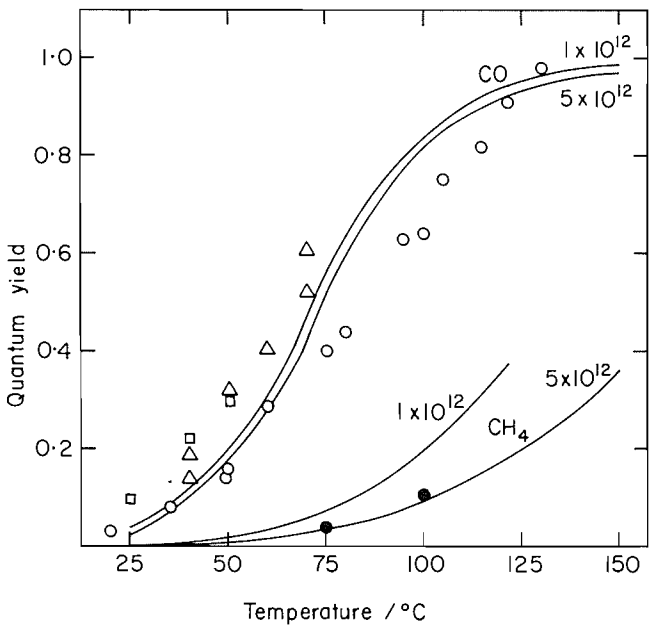

FIG. 3. Calculated quantum yields as a function of temperature at $\lambda = 313$ nm, $I = 10^{12}$ and 5×10^{12} q cm^{-3} s^{-1}, $p = 50$ Torr CO, ○ CD (9), □ Herr and Noyes (6), △ Heicklen and Noyes (16). CH_4, ● CD (9).

experimental values obtained by CD at 50 Torr. It seems more plausible that CD's results are low rather than that Pearson's are high. In Fig. 3 the results of Heicklen and Noyes (16) and the low temperature results of Herr and Noyes (6) are included. Both support high values of Φ_{CO}. The measurements of Heicklen and Noyes were made at very low conversions and they showed that, as products accumulate, biacetyl reduces Φ_{CO} by reacting with the triplet acetone. The results of Herr and

Can. J. Chem. Downloaded from www.nrcresearchpress.com by 210.87.254.42 on 09/06/12
For personal use only.

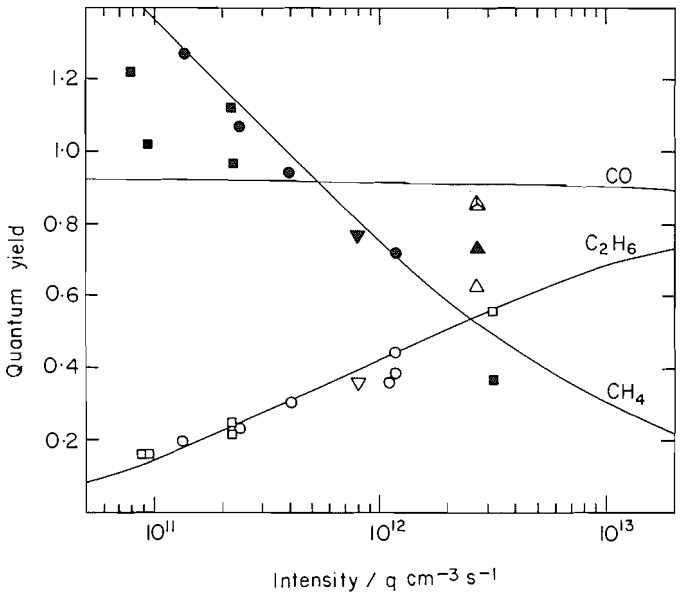

FIG. 4. Calculated quantum yields as a function of intensity. λ = 313 nm, T = 122°C, p = 125 Torr; □ ref 13, ○ ref. 15, △ ref. 8, ▽ ref. 18. C_2H_6 open symbols, CH_4 filled, CO ◬.

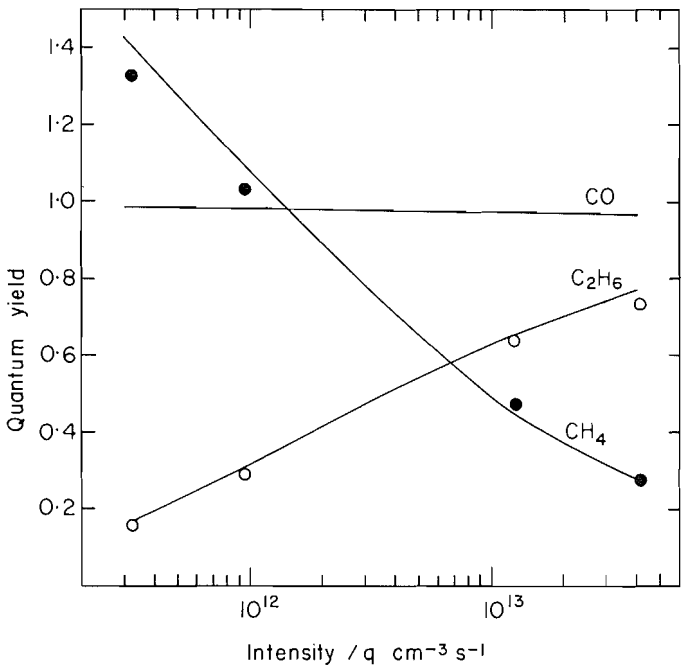

FIG. 5. Calculated quantum yields as a function of intensity. λ = 313 nm, T = 150°C, p = 100 Torr; ref. 15; C_2H_6 open symbols, CH_4 filled.

Noyes at high temperatures have been omitted because they failed to detect methane in conditions where it is now known that it should have been found.

The rate constant ratio, $k_{10}/k_{11}^{1/2}$, was deduced from the data in Fig. 1 which are independent of intensity and pressure. Accordingly, a sensitive test of this value is obtained by seeing how the individual values of $\Phi_{C_2H_6}$ and Φ_{CH_4} vary with intensity and pressure. Figures 4 and 5 for intensity and Fig. 6 for pressure illustrate this; the temperature, pressure, and intensities have been chosen to cover conditions where a reasonable number of measurements by different experimenters are available.

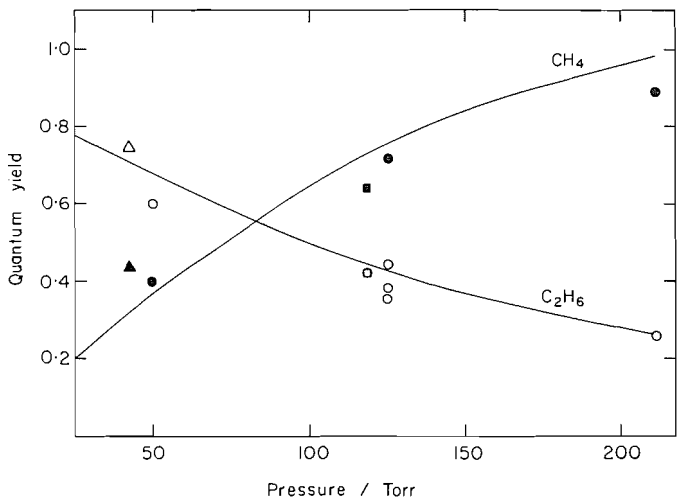

FIG. 6. Calculated quantum yields as a function of pressure; λ = 313 nm, T = 122°C, I = 10^{12} q cm^{-3} s^{-1}; △ ref. 8, □ ref. 13, ○ ref. 15. C_2H_6 open symbols, CH_4 filled.

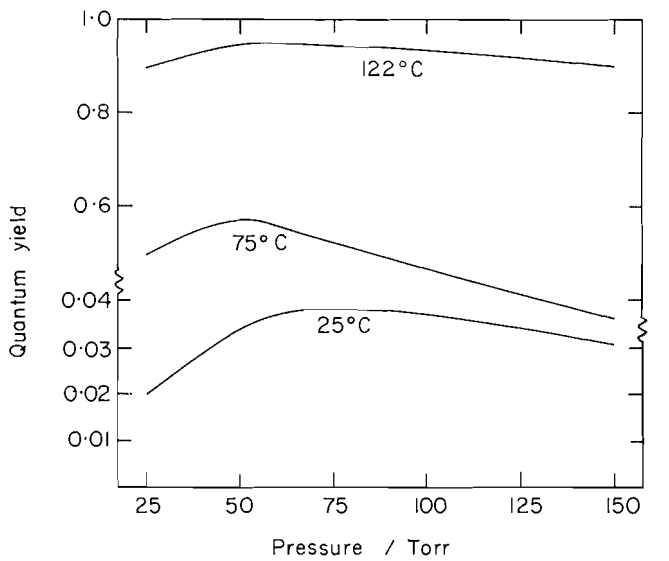

FIG. 7. Calculated quantum yield of CO as a function of pressure at 25°C, 75°C, and 122°C. I = 10^{12} q cm^{-3} s^{-1}, λ = 313 nm.

Figure 7 gives a plot of the variation of Φ_{CO} with pressure at I = 10^{12} q cm^{-3} s^{-1} for three temperatures. At 25°C, Φ_{CO} increases with pressure up to about 100 Torr in agreement with experiment (6, 30) although the absolute values given in these early papers are about three times those given in more recent papers (9, 10). The gentle curvature of the calculated values at 122°C would explain why measurements at this temperature have been taken to indicate that Φ_{CO} does not vary with pressure.

Over the range of conditions covered by Figs. 2–6 agreement between experiment and calculation is sufficiently good to suggest that the mechanism should have a reasonable predictive value for conditions where no experimental data exist. Figures 8, 9, and 10 cover such regions; with Fig. 2 they provide a latin square for I = 2 × 10^{10} and 7.17 × 10^{13} q cm^{-3} s^{-1} and p = 50 and 145 Torr all at λ = 313 nm.

Only a few experiments are available for λ = 253.7 nm. CD showed that at this wavelength the maximum value of Φ_{CO} for decomposition via the triplet is about 0.09, i.e., decomposition

Can. J. Chem. Downloaded from www.nrcresearchpress.com by 210.87.254.42 on 09/06/12
For personal use only.

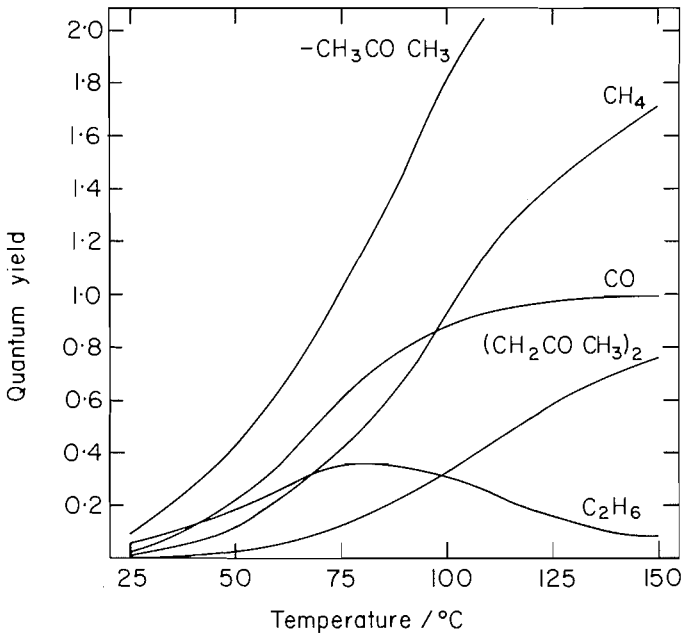

FIG. 8. Calculated quantum yields as a function of temperature. λ = 313 nm, p = 50 Torr, $I = 2 \times 10^{10}$ q cm^{-3} s^{-1}.

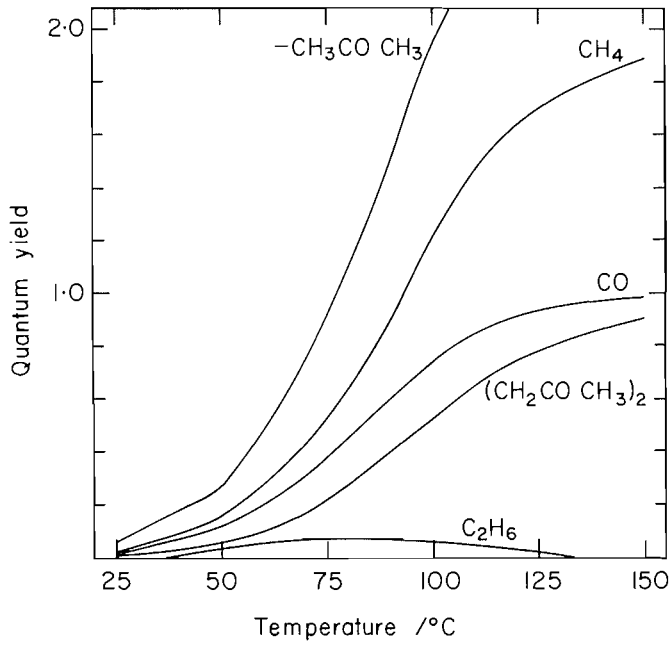

FIG. 10. Calculated quantum yields as a function of temperature. λ = 313 nm, p = 145 Torr, $I = 2 \times 10^{10}$ q cm^{-3} s^{-1}.

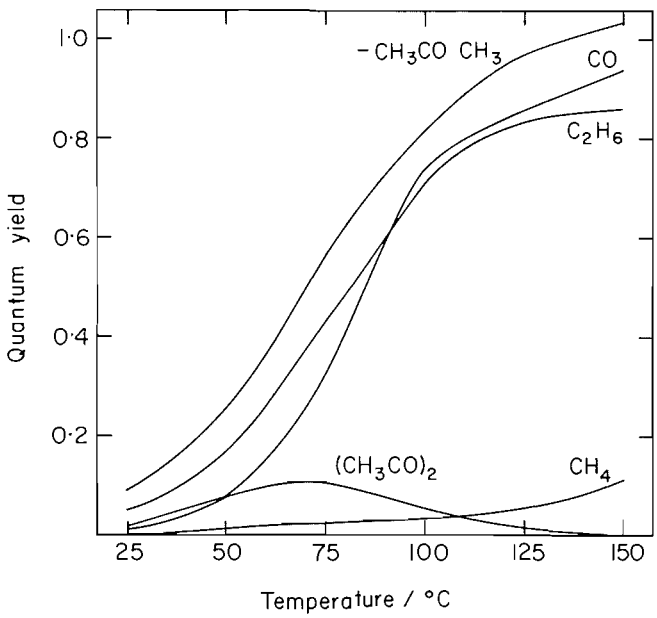

FIG. 9. Calculated quantum yields as a function of temperature. λ = 313 nm, p = 50 Torr, $I = 7.17 \times 10^{13}$ q cm^{-3} s^{-1}.

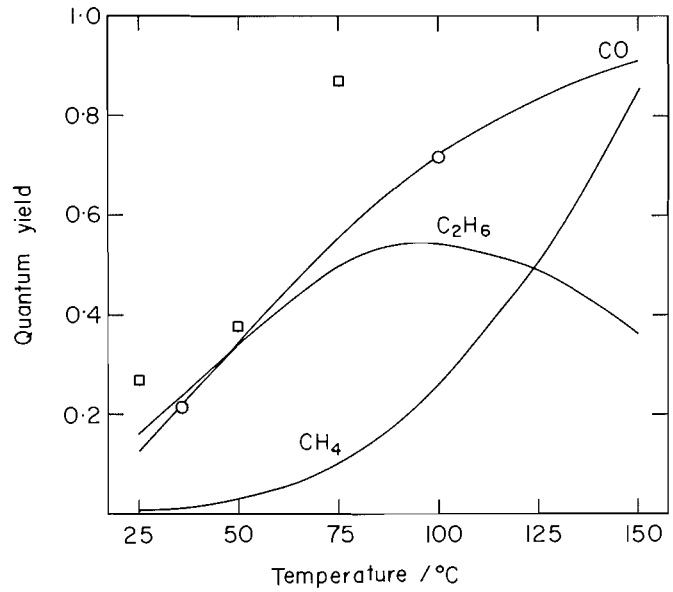

FIG. 11. Calculated quantum yields as a function of temperature. λ = 253.7 nm, p = 145 Torr, $I = 4 \times 10^{12}$ q cm^{-3} s^{-1}. ○, Pearson (10), □ Herr and Noyes (6) for CO.

is largely via the singlet state which is excited to higher vibrational levels by the more energetic quantum. It was found that the single change of k_2 to $1.5 \times 10^{10} \exp(-21\,500/RT)$ gave a fit to Pearson's measurements as shown in Fig. 11. The calculated triplet contribution to Φ_{CO} is 0.016 at 25°C and 0.086 at 150°C. The variation of $\Phi_{C_2H_6}$ and Φ_{CH_4} with intensity for this λ = 253.7 nm mechanism is given in Fig. 12 and compared with experimental values. Figure 12 for λ = 253.7 nm is almost but not quite the same as Fig. 5 for λ = 313 nm.

Minor products

Quantum yields of minor products are shown in Figs. 2, 8, 9, and 10 when they are greater than 0.01. Biacetonyl ranks as a major product at high temperatures and low intensities. The quantum yield of acetone disappearance can be calculated from any of the equations derived from the conditions for material balance — the most convenient is

$$-\Phi_{CH_3COCH_3} = \Phi_{CO} + \Phi_{CH_4} + \Phi_{(CH_3CO)_2} + 2\Phi_{CH_3CHO} + \Phi_{CH_3COCH_2COCH_3}$$

for which the last three terms are negligible except at low temperatures.

Figure 13 shows that for this photolysis the steady-state approximation is an excellent one. For a representative set of conditions, λ = 313 nm, p = 100 Torr, T = 100°C, and $I = 10^{12}$ q cm^{-3} s^{-1} all three free radicals have reached a steady state after 1 s reaction time. This is maintained for 10^4 s at

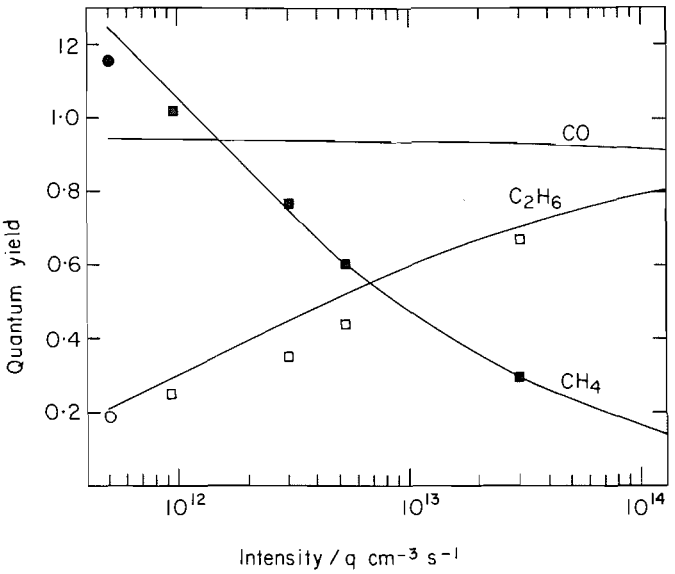

FIG. 12. Calculated quantum yields as a function of intensity. λ = 253.7 nm, T = 150°C, p = 100 Torr, □ ref. 14, ○ ref. 15, C_2H_6 open symbols, CH_4 filled.

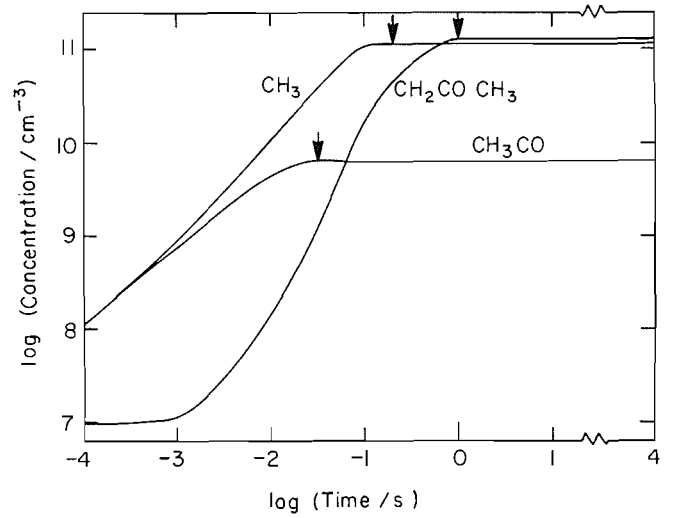

FIG. 13. Log–log plot of concentration of free radicals vs. time. p = 100 Torr, T = 100°C, $I = 10^{12}$ q cm^{-3} s^{-1}.

which time the concentrations begin to drop. The decrease is not visible on the scale of the diagram but amounts to a fall of 0.3% from the maximum. The concentrations of the excited states, $^1A_n = 5 \times 10^4$ cm^{-3}, $^3A_0 = 3 \times 10^4$ cm^{-3}, $^3A_m = 1.5 \times 10^4$ cm^{-3}, and $^1A_0 = 2.5 \times 10^3$ cm^{-3} have reached steady states in less than 10^{-4} s and also remain constant to 10^4 s. The time at which departure from the steady state is noticeable to this extent corresponds to about 0.5% of acetone decomposed. For other conditions of temperature and intensity the same limit of 0.5% decomposition holds.

Discussion

At p = 100 Torr and T = 100°C (Fig. 13), the lifetimes of the excited states range from 10^{-8} to 2×10^{-7} s while those of the free radicals lie between 0.2 and 0.7 s. At times between 1 s and 10^4 s which correspond to 5×10^{-5} and 0.5% decomposition the steady-state approximation is an excellent one.

For practical use the equations derived from the steady-state approximation usually require further approximation by elimination of reactions judged to be unimportant. For example, CD ignore reactions [12]–[20] in order to obtain an equation linear in [CH_3CO] and calculate

$$[i] \quad \Phi_{CO} = \frac{k_2}{k_2 + k_3[A]} + \frac{k_3[A]}{k_2 + k_3[A]} \cdot \frac{k_5}{k_5 + k_4[A]} \cdot \frac{k_6}{k_6 + k_7[A]}$$

They also assume $k_5/(k_5 + k_4[A]) \sim 1$. This effectively gives a 4-parameter (E_2, E_6, A'_2/A'_3, and A'_6/A'_7) equation which gives a reasonable fit to their experimental results. It may be noted that their equation is independent of the value of k_9. However, a dilemma arises when eq. [i] is used: k_2 and k_6 are the only constants which vary with temperature and the S-shaped curve of Φ_{CO} vs. T results from competition between them and the deactivation reactions [3] and [7]; yet such a scheme must give a Φ_{CO} which decreases with increasing pressure. This does not seem to be in agreement with the limited experimental evidence available and as outlined above, Fig. 3, makes the experiments of CD and Pearson difficult to reconcile. The difficulty can be overcome by introducing reaction [14] when the steady-state solution becomes

$$[ii] \quad \Phi_{CO} = \Phi_{CO}[i] \times k_9[A]^2/(k_9[A]^2 + k_{14})$$

By suitable choice of k_9 and k_{14} this gives a Φ_{CO} that increases with pressure at low temperatures and only decreases slowly at high temperatures, Fig. 7. Values of both k_9 and k_{14} are uncertain as is knowledge of the experimental variation of Φ_{CO} with pressure. The values chosen here give Φ_{CO} at 25°C increasing with pressure (25–100 Torr) at 313 nm as required by the experiments of Herr and Noyes (6) and Howland and Noyes (29).

At 25°C, p = 50 Torr and $I = 2 \times 10^{10}$ q cm^{-3} s^{-1} it can be calculated from the mechanism of the present paper that the reactions omitted by CD only contribute 1.5% to the removal of acetyl radicals: Φ_{CO} calculated by the steady-state approximation [ii] is 95% of the value obtained from the full calculation. On the other hand, at 36°C, p = 145 Torr, and $I = 7.17 \times 10^{13}$ q cm^{-3} s^{-1} these reactions contribute 40% and Φ_{CO} calculated by [ii] is 170% of the value obtained from the full calculation.

For calculation of any other quantum yields the steady-state equations for [CH_3], and [CH_2COCH_3] are complex under all conditions. Thus although the steady-state approximation is true for appreciable times in the acetone photolysis its usefulness is minimal.

As is always the case it is impossible to prove that a complex mechanism that fits the known facts is unique. More detailed mechanism involving further vibrational states of ^1A and ^3A could undoubtedly be written that would fit the experiments as adequately as the one given here. Nevertheless this mechanism is claimed as the most comprehensive available and it is suggested that the graphs of Figs. 2, 3, 7, 8, 9, 10, 11 could well replace those given by Herr and Noyes (6). These latter have been republished in so many monographs (30, 31) and reviews (32, 33) that they have gained an authority never claimed by the authors (who suggested their quantum yields were accurate to ±10%). Only Fig. 9 of this paper looks like the figures obtained by Herr and Noyes. It is understandable from their Figs. 3, 4, and 7 that they believed $\Phi_{CO} = \Phi_{C_2H_6} = -\Phi_{CH_3COCH_3} = 1$ above 75°C. In reality, the temperature at which Φ_{CO} tends

Can. J. Chem. Downloaded from www.nrcresearchpress.com by 210.87.254.42 on 09/06/12
For personal use only.

to 1 is much higher than 75°C, Φ_{CH_4} tends to 2, $\Phi_{C_2H_6} + \Phi_{(CH_2COCH_3)_2} + \Phi_{C_2H_5COCH_3}$ tends to 1, and $-\Phi_{CH_3COCH_3}$ tends to 3. The mechanism given here predicts that Φ_{CO} is not truly independent of pressure and intensity and that while Φ_{CO} (253.7) is $>\Phi_{CO}$ (313) at low temperatures, at higher temperatures the reverse holds.

It would particularly test this mechanism if the variation of Φ_{CO} with pressure were measured at around 75–100°C. More accurate measurements of Φ_{CO} at low temperatures and with minimal percentage decompositions are also needed.

1. M. BODENSTEIN. Z. f. physicalische Chem. **85**, 329 (1913).
2. C. W. GEAR. Numerical initial value problems in ordinary differential equations. Prentice-Hall, Englewood Cliffs, NJ. 1971. Chapt. 11.
3. L. A. FARROW and D. EDELSON. Int. J. Chem. Kinet. **6**, 787 (1974).
4. J. G. CALVERT and J. N. PITTS, JR. Photochemistry. Wiley and Sons, New York. 1966. p. 782.
5. J. A. LEERMAKERS. J. Am. Chem. Soc. **56**, 1899 (1934).
6. D. S. HERR and W. A. NOYES, JR. J. Am. Chem. Soc. **62**, 2052 (1940).
7. J. N. PITTS, JR., J. D. MARGERUM, R. P. TAYLOR, and W. BRIM. J. Am. Chem. Soc. **77**, 5499 (1955).
8. H. SHAW and S. TOBY. J. Phys. Chem. **72**, 2337 (1968).
9. R. B. CUNDALL and A. S. DAVIES. Proc. R. Soc. London. Ser. A, **290**, 563 (1966).
10. G. S. PEARSON. J. Phys. Chem. **67**, 1686 (1963).
11. J. CALDWELL and D. E. HOARE. J. Am. Chem. Soc. **84**, 3987 (1962).
12. R. K. BOYD, G. B. CARTER, and K. O. KUTSCHKE. Can. J. Chem. **46**, 175 (1968).
13. L. M. DORFMAN and W. A. NOYES, JR. J. Chem. Phys. **16**, 557 (1948).
14. A. F. TROTMAN-DICKENSON and E. W. R. STEACIE. J. Chem. Phys. **18**, 1097 (1950).
15. A. J. C. NICHOLSON. J. Am. Chem. Soc. **73**, 3981 (1951).
16. J. HEICKLEN and W. A. NOYES, JR. J. Am. Chem. Soc. **81**, 3858 (1959).
17. L. MANDELCORN and E. W. R. STEACIE. Can. J. Chem. **32**, 331 (1954).
18. R. H. LINNELL and W. A. NOYES, JR. J. Am. Chem. Soc. **73**, 3986 (1951).
19. P. AUSLOOS and E. W. R. STEACIE. Can. J. Chem. **33**, 47 (1955).
20. D. L. BAULCH and J. DUXBURY. Combust. Flame, **37**, 313 (1980).
21. R. E. DODD and E. W. R. STEACIE. Proc. R. Soc. London, Ser. A, **223**, 283 (1954).
22. R. G. SHORTRIDGE, W. YANG, and E. K. C. LEE. J. Am. Chem. Soc. **77**, 1936 (1973).
23. K. W. WATKINS and W. WORD. Int. J. Chem. Kinet. **6**, 855 (1974).
24. H. H. Avery, D. M. Hayes, and L. PHILLIPS. J. Phys. Chem. **73**, 3498 (1969).
25. L. SZIROVICA and R. WALSH. J. Chem. Soc. Faraday Trans. 1, **70**, 33 (1974).
26. H. W. ANDERSON and G. K. ROLLEFSON. J. Am. Chem. Soc. **63**, 816 (1941).
27. S. Y. HO, R. A. GORSE, and W. A. NOYES, JR. J. Phys. Chem. **79**, 1632 (1975).
28. H. L. DAVIES and M. Y. SMITH. Proc. Eighth Australian Computer Conference, Australian Computer Society Inc. Canberra, 1978.
29. J. J. HOWLAND and W. A. NOYES, JR. J. Am. Chem. Soc. **66**, 974 (1944).
30. W. A. NOYES, JR. and P. A. LEIGHTON. The photochemistry of gases. Reinhold, New York. 1941.
31. E. W. R. STEACIE. Atomic and free radical reactions. 2nd ed. Reinhold, New York. 1954.
32. W. DAVIS, JR. Chem. Rev. **40**, 201 (1947).
33. W. A. NOYES, JR., G. B. PORTER, and J. E. JOLLEY. Chem. Rev. **56**, 49 (1956).
34. H. S. JOHNSTON. Advances in chemical physics. *Edited by* I. Prigogine. Interscience, New York. 1961.

Can. J. Chem. Downloaded from www.nrcresearchpress.com by 210.87.254.42 on 09/06/12
For personal use only.

The solvolysis of tri-*p*-tolyl[2-^{13}C]vinyl bromide in 70% HOAc − 30% H_2O

CHOI CHUCK LEE, ERIC C. F. KO, CRAIG A. OBAFEMI, AND J. WILSON QUAIL
Department of Chemistry, University of Saskatchewan, Saskatoon, Sask., Canada S7N 0W0

Received January 6, 1983

CHOI CHUCK LEE, ERIC C. F. KO, CRAIG A. OBAFEMI, and J. WILSON QUAIL. Can. J. Chem. **61**, 1838 (1983).

Tri-*p*-tolyl[2-^{13}C]vinyl bromide (**3**-Br-2-^{13}C) was solvolyzed in 70% HOAc − 30% H_2O and the scrambling of the label from C-2 to C-1 in the reaction product was found to decrease with increasing concentrations of added NaOAc. For example, the 18.5% scrambling found for the solvolysis of **3**-Br-2-^{13}C in 70% HOAc in the absence of any NaOAc was decreased to 7.7% when the reaction was carried out in the presence of 4770 m*M* NaOAc. Common-ion rate depression as well as isotopic exchange between [^{82}Br]Et_4NBr and the organic substrate, **3**-Br, were observed, indicating the formation of the dissociated tri-*p*-tolylvinyl cation. Apparently, the tri-*p*-tolylvinyl cation, similar to the trianisylvinyl cation, is of sufficient stability to allow it to discriminate between different nucleophiles.Thus the presence of increasing concentrations of the acetate ion would favor the product-forming capture of the tri-*p*-tolylvinyl cation at the expense of the 1,2-shift process, resulting in a decrease in the extent of scrambling. From the observed scrambling data, selectivity ratios such as k_{OAc}/k_{SOH} and $k_{OAc}/k_{t(Tol)}$ were calculated.

CHOI CHUCK LEE, ERIC C. F. KO, CRAIG A. OBAFEMI et J. WILSON QUAIL. Can. J. Chem. **61**, 1838 (1983).

On a effectué la solvolyse du bromure (Br-**3**-^{13}C-2) de tri-*p*-tolyl[^{13}C-2]vinyle dans une solution de HAcO−H_2O à 70:30 en pourcentage et on a trouvé que, dans les produits de la réaction, le taux de mélange de C-2 à C-1 diminue lorsqu'on augmente la concentration en NaAcO ajouté. Par exemple, le taux de mélange de 18,5% trouvé dans la solvolyse du Br-**3**-^{13}C-2 dans du HAcO à 70% en l'absence de NaAcO tombe à 7,7% en présence de NaAcO à 4770 m*M*. On a observé la diminution de la vitesse de l'ion commun aussi bien que l'échange isotopique entre le [^{82}Br]Et_4NBr et le substrat organique, Br-**3**, ce qui indique la formation du cation tri-*p*-tolylvinyle dissocié. Apparemment, le cation tri-*p*-tolylvinyle, identique au cation trianisylvinyle, est suffisamment stable pour permettre de distinguer les différents nucléophiles. Ainsi la présence d'une concentration croissante de l'ion acétate favorise le produit de capture du cation tri-*p*-tolylvinyle aux dépens du glissement 1−2 résultant d'une diminution du taux de mélange. A partir des données de mélange observées, on a calculé les rapports de sélectivité tels que: k_{AcO}/k_{SOH} et $k_{AcO}/k_{t(Tol)}$.

[Traduit par le journal]

Since the first demonstration by Grob and Cseh (1) of the involvement of vinyl cations in the solvolysis of α-bromostyrenes, much work has been done and a book was published in 1979 on vinyl cations (2). More recently, Apeloig *et al.* (3) have reported on the experimental and computational evidence for the formation of α-arylvinyl cations in the gas phase, and numerous references on vinyl cations were cited by these authors (3). Our studies in this area chiefly involved investigations on degenerate rearrangements arising from 1,2-aryl shifts in isotopically labeled triarylvinyl cations, and a review on such degenerate rearrangements appeared in 1980 (4). Among the interesting findings from the degenerate rearrangement studies was the observation that in the solvolysis of triphenyl[2-^{14}C]vinyl bromide (**1**-Br-2-^{14}C) in 70% HOAc − 30% H_2O (to be designated as 70% HOAc, which was used as solvent since the solvolysis of **1**-Br in pure HOAc was too slow), the extent of scrambling of the isotopic label from C-2 to C-1 in the reaction product showed no significant variations when the reaction was carried out in the presence of up to 30 molar equivalents of added NaOAc (5). On the other hand, in the solvolysis of trianisyl[2-^{14}C]vinyl bromide (**2**-Br-2-^{14}C) in 70% HOAc, the scrambling of the label in the product was found to decrease with increasing amounts of added NaOAc (5).

In an attempt to explain the different effects of NaOAc on the solvolysis of **1**-Br-2-^{14}C and **2**-Br-2-^{14}C, the possibility was considered that in the solvolysis of **2**-Br-2-^{14}C, the dissociated "free" trianisylvinyl cation was formed and the extent of scrambling arising from 1,2-anisyl shifts in the trianisylvinyl cation would be decreased by the presence of the more nucleophilic acetate ion, while in the solvolysis of **1**-Br-2-^{14}C, ionization might have proceeded only to the ion-pair stage and the degenerate rearrangement resulting from 1,2-phenyl shifts in the ion-pair could be insensitive to externally added nucleophiles (5, 6). However, recent work in this laboratory has shown that in the solvolysis of **1**-Br or **2**-Br in 70% HOAc, a common-ion rate depression was observed for the reaction of either **1**-Br or **2**-Br carried out in the presence of added Et_4NBr and that there was incorporation of ^{82}Br into the **1**-Br or **2**-Br due to exchange with added ^{82}Br-labeled bromide ion (7). Since both common-ion rate depression and ^{82}Br exchange would be diagnostic for the formation of dissociated ions (8), it was concluded that the solvolysis of **1**-Br and **2**-Br in 70% HOAc both would proceed to the dissociated ion, and the insensitivity of the extent of scrambling towards added NaOAc in the solvolysis of **1**-Br-2-^{14}C could be attributed to a lack of ability of the less stable triphenylvinyl cation to discriminate between different nucleophiles (7). Since the stability of the tri-*p*-tolylvinyl cation is intermediate between the stabilities of the triphenylvinyl and trianisylvinyl cations, it would be of interest to ascertain whether the tri-*p*-tolylvinyl cation could discriminate between different nucleophiles in the reaction medium. Thus, in the present work, the effect of added NaOAc on the extent of scrambling in the solvolysis of tri-*p*-tolyl[2-^{13}C]vinyl bromide (**3**-Br-2-^{13}C) in 70% HOAc was investigated. ^{13}C instead of ^{14}C was used as the label so that the necessity of oxidative degradations required in the determination of ^{14}C scrambling may be avoided, since such oxidations would also oxidize the *p*-methyl substituent of the *p*-tolyl group. In conjunction with the isotopic scrambling work, common-ion rate depression and ^{82}Br exchange were also studied.

Tri-*p*-tolyl[2-^{13}C]vinyl bromide (**3**-Br-2-^{13}C) has been synthesized and its acetolysis in the presence of AgOAc resulted in 13−14% scrambling of the ^{13}C-label from C-2 to C-1 in the reaction product (9). This scrambling was attributed to 1,2-tolyl shifts in the tri-*p*-tolylvinyl cation and was determined

Can. J. Chem. Downloaded from www.nrcresearchpress.com by 178.218.224.3 on 09/06/12
For personal use only.

TABLE 1. Data from the solvolysis of tri-*p*-tolyl[2-^{13}C]vinyl bromide (**3**-Br-2-^{13}C) in 70% HOAc − 30% H_2O in the presence of added NaOAc at 150 ± 1°C

Expt.	[**3**-Br-2-^{13}C] (m*M*)	[NaOAc] (m*M*)	Reaction time (min)	% Reaction[a]	Scrambling in product (%)	Mean[b]	k_{SOH}/k_{nTolH}	k_{OAc}/k_{SOH} (M^{-1})	k_{OAc}/k_{nTolH}[c] (M^{-1})
1[e]	47	—	50	48; 48	17.7; 18.6				
2[e]	47	—	90	74; 75	19.3; 18.1				
3[e]	47	—	240	94; 95	19.0; 18.7				
4	6.0	—	240	100	18.1	18.5±0.8	6.8		
5	5.9	59	240	100	16.8	16.8	7.9	2.7	18.4
6	5.9	176	240	100	15.9	15.9	8.6	1.5	10.2
7	47	488	50	52	14.4				
8	47	488	90	67	14.6				
9	47	488	240	99	14.9	14.6±0.3	9.7	0.9	6.1
10	47	1430	50	27	11.1				
11	47	1430	90	48	11.5				
12	47	1430	240	99	11.5				
13	6.0	1430	240	100	11.6	11.4±0.3	13.5	0.7	4.8
14	6.0	2500	240	100	9.9	9.9	16.2	0.6	4.1
15	47	4660[f]	240	51	7.7	7.7	22.0	0.3	2.0

[a]From titration of the liberated Br^- ion.

[b]Mean %scrambling ± maximum deviation from the mean for a given set of experiments with identical [NaOAc]. For Expts. 5, 6, 14, and 15, the data were derived from single experiments.

[c]$k_{SOH} = k_{HOAc}[HOAc] + k_{H_2O}[H_2O] + k_{OAc}[OAc^-]$; $k_{SOH} = k_{HOAc}[HOAc] + k_{H_2O}[H_2O]$. For Expts. 1–4 with no added OAc^-, $k_{SOH}/k_{nTolH} = k_{SOH}/k_{nTolH} = 6.8$.

[d]From $(k_{OAc}/k_{SOH}) \times 6.8$.

[e]From ref. 10; the scrambling in the recovered reactant from Expts. 1 and 2 was found to be negligibly small (10).

[f]Saturated solution of NaOAc at room temperature; during the reaction the **3**-Br-2-^{13}C was not completely dissolved and two phases existed.

by the conversion of the reaction product, tri-*p*-tolyl[1,2-^{13}C]vinyl acetate (**3**-OAc-1,2-^{13}C), to 1,2,2-tri-*p*-tolyl-[1,2-^{13}C]ethanol (**4**-1, 2-^{13}C) followed by ^{13}C nmr analysis of the ^{13}C distribution in the C-1 and C-2 positions of **4**-1,2-^{13}C (9). In conjunction with a study on the migratory aptitudes of some aryl groups in triarylvinyl cations, **3**-Br-2-^{13}C has also been solvolyzed in 70% HOAc without the presence of any added salt and about 18.5% scrambling of the label was observed in the product, tri-*p*-tolyl[1,2-^{13}C]ethanone (**5**-1,2-^{13}C) (10). In the present work, **3**-Br-2-^{13}C was solvolyzed in 70% HOAc in the presence of various amounts of added NaOAc. The product was found to be **5**-1,2-^{13}C, any **3**-OAc-1,2-^{13}C that might have been formed apparently was hydrolyzed under the conditions of the reaction. The **5**-1,2-^{13}C product was reduced to 1,2,2,-tri-*p*-tolyl[1,2-^{13}C]ethanol (**4**-1,2-^{13}C) and then analyzed by ^{13}C nmr to give the scrambling results summarized in Table 1. As an illustration of the 1,2-shift mechanism for the scrambling of the ^{14}C- or ^{13}C-label in the triarylvinyl cation, given in Scheme 1 are the processes leading to the formation of isotopically unrearranged and rearranged triarylethanones obtained after complete reaction from the solvolysis of **1**-Br-2-^{14}C, **2**-Br-2-^{14}C, or **3**-Br-2-^{13}C in 70% HOAc.

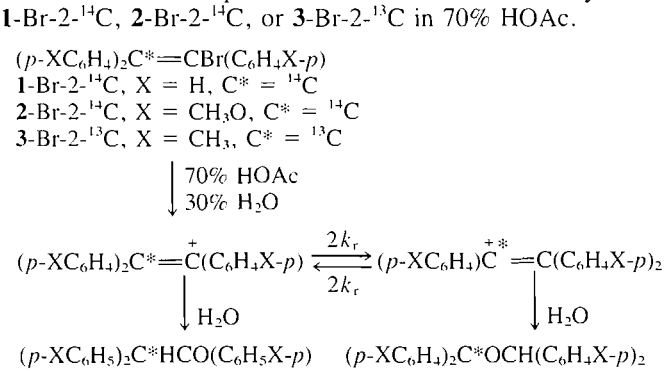

SCHEME 1

In the studies on ^{82}Br exchange, ordinary **3**-Br was solvolyzed in 70% HOAc in the presence of 1, 10, or 30 molar equivalents of added [^{82}Br]Et_4NBr and the incorporation of ^{82}Br into the recovered unconsumed **3**-Br was determined. Assuming that 100% exchange would correspond to a complete mixing of the ^{82}Br in the added Et_4NBr and in the substrate **3**-Br, from the observed incorporation of ^{82}Br in the recovered **3**-Br, the % exchange could be calculated, an illustration of the calculation being given in the Experimental section. The results, given in Table 2, definitely showed the occurrence of exchange between the added Br^- ion and the substrate, **3**-Br. Moreover, as might be expected, the further the reaction has proceeded, the greater extent of exchange was observed in the recovered **3**-Br. From Table 2, it might also be pointed out that the single point measurements of % reaction would indicate that the rate of solvolysis of **3**-Br in 70% HOAc was lowered with an increase in the concentration of the added Br^- ion. This common-ion rate depression was confirmed as the rate of solvolysis of 20 m*M* **3**-Br in 70% HOAc in the presence of 0, 60, or 180 m*M* Et_4NBr at 150 ± 0.2°C was found to be 2.17×10^{-4}, 1.90×10^{-4}, or 1.20×10^{-4} s^{-1}, respectively.

The observed ^{82}Br exchange and common-ion rate depression in the solvolysis of **3**-Br in 70% HOAc are similar in behavior to triphenylvinyl bromide (**1**-Br) and trianisylvinyl bromide (**2**-Br) (7), and are indicative of the formation of the dissociated tri-*p*-tolylvinyl cation. As already discussed previously (5, 7), the generalized mechanism involving 1,2-shifts to give rise to isotopic scrambling may be depicted by Scheme 2, where R^+ and R'^+ are the isotopically unrearranged and rearranged tri-*p*-tolyl[2-^{13}C]vinyl and tri-*p*-tolyl[1-^{13}C]vinyl cations, respectively. The effect of added NaOAc, as recorded in Table 1, showed that the scrambling in the product was decreased with an increase in the concentration of added OAc^- ion, a behavior similar to that found for **2**-Br-2-^{14}C (5) but different from that observed for **1**-Br-2-^{14}C, the scrambling in

Can. J. Chem. Downloaded from www.nrcresearchpress.com by 178.218.224.3 on 09/06/12
For personal use only.

TABLE 2. Data from exchange reactions between 47 m*M* tri-*p*-tolylvinyl bromide (**3**-Br) and [^{82}Br]Et$_4$NBr in 70% HOAc −30% H_2O at 150 ± 1°C

Expt.	[^{82}Br]Et$_4$NBr (m*M*)	Reaction time (min)	% Reaction[a]	^{82}Br incorporated in recovered **3**-Br (%)	Extent of ^{82}Br exchange in recovered **3**-Br (%)[b]
1	47	50	46	6.8	25
2	47	90	68	6.4	40
3	470	50	20	0.36	5
4	470	90	35	0.92	16
5	1410	50	13	0.15	5
6	1410	90	24	0.33	13

[a]From titration of the liberated Br^- ion in parallel control experiments.
[b]Complete mixing of the ^{82}Br in the Et$_4$NBr and **3**-Br corresponds to 100% exchange.

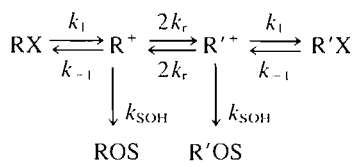

SCHEME 2

the solvolysis with **1**-Br-2-^{14}C being unaffected by NaOAc (5). Apparently the tri-*p*-tolylvinyl cation, like the trianisylvinyl cation, is of sufficient stability and with a sufficiently long lifetime to allow for the discrimination between different nucleophiles in the product-forming capture of the cation by the different nucleophiles (7). With the presence of increasing concentrations of the more nucleophilic OAc^- ion, formation of the unrearranged product is favored at the expense of the 1,2-shift process, thus giving rise to a decrease in the extent of scrambling.

It may be noted from Table 1 that, for a series of experiments with a given concentration of added NaOAc, the scrambling observed was independent of the concentration of the substrate and independent of the extent of reaction. This behavior is also similar to that observed for **2**-Br-2-^{14}C (5). For the scrambling processes as depicted in Scheme 2, it has been shown that, at complete reaction, eq. [1] holds (5, 10, 11). Since eq. [1]

[1] $[ROS]/[R'OS] = 1 + (k_{SOH}/2k_r)$

does not involve the concentration of the substrate, the extent of scrambling would be independent of substrate concentration, as was observed (cf., for example, Expts. 3 and 4, and Expts. 12 and 13, Table 1). Again as discussed in the treatment of the scrambling data from **2**-Br-2-^{14}C (5), the independence of the extent of scrambling with changes in the extent of reaction is consistent with the finding that in Expts. 1 and 2, Table 1, recovered unconsumed reactant showed essentially no scrambling (negligibly small amount of R'X in Scheme 2) (10). The observations of ^{82}Br exchange and the lack of any significant amount of scrambling in the recovered substrate are again similar to the behaviour of **1**-Br-2-^{14}C and **2**-Br-2-^{14}C in their solvolysis in 70% HOAc, suggesting that the capture of the triarylvinyl cation to return to RX is much faster than the internal rearrangement in the cation through 1,2-shifts (7).

From the effects of added NaOAc on the extent of scrambling, a number of selectivity ratios have been calculated for the solvolysis of **2**-Br-2-^{14}C in 70% HOAc (5). Similar treatments of the data can be made using the scrambling results in Table 1. For the product-forming processes as depicted in Scheme 2, k_{SOH} is the pseudo first order rate constant for the bimolecular capture of the cation by all the nucleophiles present. To separate the effects of added OAc^- ion, k_{SOH} and $k_{SOH'}$ for the product-forming processes in 70% HOAc − 30% H_2O with no added NaOAc and with added NaOAc, respectively, may be defined by eqs. [2] and [3]

[2] $k_{SOH} = k_{HOAc}[HOAc] + k_{H_2O}[H_2O]$

[3] $k_{SOH'} = k_{OAc}[OAc^-] + k_{HOAc}[HOAc] + k_{H_2O}[H_2O]$
$= k_{OAc}[OAc^-] + k_{SOH}$

Using eq. [4], which is a modification of eq. [1], and the mean scrambling values in Table 1, $k_{SOH'}/k_{r(Tol)}$ can be calculated and the results are included in Table 1. It is seen that

[4] $(100 - \%\text{scrambling}/\%\text{scrambling})$
$= 1 + (k_{SOH'}/2k_{r(Tol)})$

$k_{SOH'}/k_{r(Tol)}$ increases with increasing concentrations of added OAc^- ion, as is expected, since the addition of OAc^- ion favors product formation, the $k_{SOH'}$ process, at the expense of scrambling, the $k_{r(Tol)}$ process.

For Expts. 1−4, Table 1, with a mean scrambling of 18.5%, $k_{SOH'}/k_{r(Tol)}$ was calculated to be 6.8. Since no NaOAc was present in these experiments, $k_{SOH'}$ would be the same as k_{SOH}, thus giving rise to eq. [5]

[5] $k_{SOH}/k_{r(Tol)} = 6.8$

For Expt. 5, Table 1, with 59 m*M* added NaOAc and a scrambling of 16.8%, eq. [6] can be written:

[6] $k_{SOH'}/k_{r(Tol)} = (0.059\ k_{OAc} + k_{SOH})/k_{r(Tol)} = 7.9$

From eqs. [5] and [6], the selectivity ratios, k_{OAc}/k_{SOH} and $k_{OAc}/k_{r(Tol)}$ for Expt. 5 can be obtained:

[7] (From [6]/[5]) $k_{OAc}/k_{SOH} = 2.7\ M^{-1}$

[8] (From [7] × [5]) $k_{OAc}/k_{r(Tol)} = 2.7 \times 6.8 = 18.4\ M^{-1}$

The ratios k_{OAc}/k_{SOH} and $k_{OAc}/k_{r(Tol)}$ have a unit of M^{-1} because k_{SOH} is a pseudo first order rate constant and no composite concentration for the HOAc − H_2O solvent system was used in the calculations. These selectivity ratios, calculated for the various mean scrambling values, are also included in Table 1. It may be noted that these ratios as recorded in Table 1 are not constant, and their magnitude decreases as the concentration of the added NaOAc increases. A major factor that may be responsible for this trend could be due to the use of concentrations in the calculations. Since the activities of the acetate

Can. J. Chem. Downloaded from www.nrcresearchpress.com by 178.218.224.3 on 09/06/12
For personal use only.

ion rather than its concentrations are involved in the rates of reaction and corrections for such effects would be more drastic at higher concentrations, there should be a decrease in the calculated selectivity ratios with increasing concentrations of added NaOAc, as was obtained. In Expts. 5 and 6, Table 1, with relatively lower concentrations of added acetate ion and thus involving less drastic corrections, the observed k_{OAc}/k_{SOH} were greater than unity, indicating that the capture of the tri-*p*-tolylvinyl cation was indeed faster for the acetate ion than for 70% HOAc.

Experimental

Solvolysis reactions

The synthesis of **3**-Br-2-^{13}C, its solvolysis in 70% HOAc, and the ^{13}C nmr analysis of the extent of scrambling in the reaction product have already been described in the literature (9, 10). In the present work, the solvolyses were carried out in the presence of various concentrations of added NaOAc as given in Table 1. In Expts. 7, 8, or 9, Table 1, for example, a solution of 712 mg (1.9 mmol) of **3**-Br-2-^{13}C and 1600 mg (19.5 mmol) of NaOAc in 40 mL of 70% HOAc was placed in a sealed tube and heated in an oil bath at 150 ± 1°C for 50, 90, or 240 min. The reaction mixture was then worked up as described previously (10) to give 1,2,2-tri-*p*-tolyl-[1,2-^{13}C) ethanol for ^{13}C nmr analysis, again according to procedures already described (9).

^{82}Br exchange reactions

The procedure used for the study of exchange between ^{82}Br-labeled bromide and **3**-Br is similar to that employed in analogous exchange studies with **1**-Br and **2**-Br (7). The individual experiments as given in Table 2 were carried out in sealed tubes. After the desired reaction time, each tube was cooled in an ice bath before it was opened and, if necessary, an appropriate amount of **3**-Br was added as carrier. The mixture was then extracted with $CHCl_3$ and from the extract the unconsumed **3**-Br was recovered and purified by passage through an alumina column. The ^{82}Br activity incorporated into the recovered **3**-Br was then measured using a γ-ray counter. The added [^{82}Br]Et_4NBr and the recovered **3**-Br were counted as solutions in 70% HOAc. A sample containing a known amount of ^{82}Br was used as a reference standard and the standard was counted immediately before and after the counting of a sample to provide the correction for the decay of the ^{82}Br.

As an illustration of the experimental data, the details for Expt. 1, Table 2, are described. In this experiment, a solution of 712 mg (1.9 mmol) of **3**-Br and 399 mg (1.9 mmol) of [^{82}Br]Et_4NBr in 40 mL of 70% HOAc in a sealed tube was heated at 150 ± 1°C for 50 min. Upon work-up of the reaction mixture, and without the use of any additional **3**-Br carrier, 95.6 mg of **3**-Br was recovered.

From a parallel experiment under the same conditions, except that ordinary Et_4NBr without the label was utilized, titration of the liberated bromide ion showed that the extent of reaction was 46%. Thus, after the reaction, the original substrate remaining was $0.54 \times 712 = 384$ mg. The ^{82}Br activity in the 95.6 mg of recovered **3**-Br was 9.05×10^5 dpm. The total ^{82}Br activity in the unconsumed **3**-Br would be $(384/95.6) \times 9.05 \times 10^5 = 3.64 \times 10^6$ dpm. The total ^{82}Br activity introduced as [^{82}Br]Et_4NBr was 5.36×10^7 dpm. Therefore, the incorporation of ^{82}Br into the recovered unconsumed reactant was $[3.64 \times 10^6)/(5.36 \times 10^7)] \times 100 = 6.8\%$.

For 100% exchange, there would be a complete mixing of 100% of the ^{82}Br in the 1.9 mmol of substrate and 1.9 mmol of Et_4NBr, and the ^{82}Br incorporation in the recovered reactant would be $100/(1.9 + 1.9) = 26.3\%$ ^{82}Br/mmol **3**-Br. The observed incorporation in the recovered reactant was 6.8% of the ^{82}Br in (0.54×1.9) mmol of **3**-Br, or $6.8/(0.54 \times 1.9) = 6.6\%$ ^{82}Br/mmol **3**-Br. Therefore, the extent of exchange in the recovered reactant was $(6.6/26.3) \times 100 = 25\%$.

Acknowledgment

The financial support given by the Natural Sciences and Engineering Research Council of Canada is sincerely acknowledged.

1. C. A. GROB and G. CSEH. Helv. Chim. Acta, **47**, 194 (1964).
2. P. J. STANG, Z. RAPPOPORT, M. HANACK, and L. R. SUBRAMANIAN. Vinyl cations. Academic Press, New York. 1979.
3. Y. APELOIG, W. FRANKE, Z. RAPPOPORT, H. SCHWARZ, and D. STAHL. J. Am. Chem. Soc. **103**, 2770 (1981).
4. C. C. LEE. *In* Isotopes in organic chemistry. Vol. 5. Isotopes in cationic reactions. *Edited by* E. Buncel and C. C. Lee. Elsevier Scientific Publishing Co., Amsterdam. 1980. Chapt. 1.
5. C. C. LEE, E. C. F. KO, and Z. RAPPOPORT. Can. J. Chem. **58**, 2369 (1980).
6. C . C. LEE and E. C. F. KO. Can. J. Chem. **56**, 2459 (1978).
7. C. C. LEE, C. A. OBAFEMI, and Z. RAPPOPORT. Can. J. Chem. **60**, 3019 (1982).
8. D. J. RABER, J. M. HARRIS, and P. v. R. SCHLEYER. *In* Ions and ion pairs in organic reactions. Vol. 2. *Edited by* M. Szwarc. John Wiley and Sons, New York. 1974. Chapt. 3.
9. C. C. LEE, A. J. PAINE, and E. C. F. KO. Can. J. Chem. **55**, 2310 (1977).
10. C. C. LEE, E. C. F. KO, and Z. RAPPOPORT. Can. J. Chem. **58**, 884 (1980).
11. Y. HOUMINER, E. NOY, and Z. RAPPOPORT. J. Am. Chem. Soc. **98**, 5632 (1976).

Can. J. Chem. Downloaded from www.nrcresearchpress.com by 178.218.224.3 on 09/06/12
For personal use only.

Kinetics and thermodynamics of dissociation of nickel(II)–isoquinoline complexes in tetrahydrofuran. Effect of trace water on ligand substitution kinetics

P. K. CHATTOPADHYAY[1] AND B. KRATOCHVIL[2]

Department of Chemistry, University of Alberta, Edmonton, Alta., Canada T6G 2G2

Received November 5, 1982

P. K. CHATTOPADHYAY and B. KRATOCHVIL. Can. J. Chem. **61**, 1842 (1983).

Rate constants and associated activation parameters for the dissociation of $(solv)_5Ni(isoquin)^{2+}$ (solv = solvent, isoquin = isoquinoline) were determined in tetrahydrofuran (THF) over the range 15 to 35°C by stopped-flow spectrophotometry. Comparison of the enthalpy of activation $\Delta H_b^{\ddagger}$ for the dissociation of $(solv)_5Ni(isoquin)^{2+}$ in THF with previous results in other solvents reveals that the linear relation between $\Delta H_b^{\ddagger}$ for the dissociation of this ion in the various solvents and the Gutmann donicity can be extended to THF. From this relation the donor number of THF is found to be 18.8 ± 0.5, in agreement with the value 19.3 reported from other methods. Dissociation of $(solv)_5Ni(isoquin)^{2+}$ in THF is controlled by an I_d-type mechanism, as was previously observed in other protic and aprotic solvents. The rate of dissociation in THF is strongly affected by the free-water concentration in the medium.

P. K. CHATTOPADHYAY et B. KRATOCHVIL. Can. J. Chem. **61**, 1842 (1983).

Faisant appel à la spectrophotométrie du flux stoppé, on a déterminé les constantes de vitesse et les paramètres d'activation de la dissociation du $(solv)_5Ni(isoquin)^{2+}$ avec (solv = solvant, isoquin = isoquinoléine) dans le tétrahydrofuranne (THF) dans un intervalle de température allant de 15 à 35°C. La comparaison de l'enthalpie d'activation $\Delta H_b^{\ddagger}$ de la dissociation du $(solv)_5Ni(isoquin)^{2+}$ dans le THF avec les résultats antérieurs obtenus pour d'autres solvants, révèle qu'on peut étendre au THF, la relation linéaire entre $\Delta H_b^{\ddagger}$ de la dissociation de cet ion dans divers solvants et le caractère donneur de Gutmann. A partir de cette relation on trouve que le nombre donneur du THF est de 18,8 ± 0,5 en accord avec la valeur de 19,3 rapportée à partir d'autres méthodes. La dissociation du $(solv)_5Ni(isoquin)^{2+}$ dans le THF est contrôlée par un mécanisme de type I_d tel qu'observé antérieurement dans d'autres solvants protiques et aprotiques. La vitesse de dissociation dans le THF est fortement affectée par la concentration en eau libre du milieu.

[Traduit par le journal]

Introduction

The Lewis basicity of solvents toward metal ions as Lewis acids is an important parameter in the intrinsic solvating capacities of the solvents. Values for the donicities of alcohols relative to nickel(II) as a Lewis acid can be obtained by extrapolating the linear relation between the enthalpy of activation $\Delta H_b^{\ddagger}$ for the dissociation of $(solv)_5Ni(isoquin)^{2+}$ (solv = solvent, isoquin = isoquinoline) or $(solv)_5Ni(SCN)^+$ and the Gutmann donor number for solvents to the corresponding values of $\Delta H_b^{\ddagger}$ in alcohols as solvents. These donicities have been observed to be unexpectedly low for methanol, ethanol, and *n*-propanol (1). The significance of these low values is unclear. A similarly low value for the donor number of methanol has also been reported from nmr studies (2). Accordingly, it was of interest to see whether the relation holds for additional solvents whose donor numbers can be estimated independently.

Tetrahydrofuran (THF) is frequently employed as a reaction medium for organic synthesis. It is stable to powerful reductants and can be prepared very dry. The donor number of THF has been determined coulometrically with $SbCl_5$ as a reference Lewis acid (3). THF is of interest also because it is a convenient solvent for the study of the effect of trace water on the rate of dissociation of metal–ligand complexes.

The Lewis basicity of most organic solvents, especially dipolar aprotic solvents, is sharply affected when even traces of water are present. The effect of water on solvent basicity is generally linear up to a concentration of a few millimolar and then levels off gradually as the concentration is further increased. It is not yet possible to define unambiguously the state of aggregation of water in many organic solvents. Since in ligand-substitution kinetics the microscopic molecular properties of the medium, especially in the immediate vicinity of the dissociating ion, are more important than the macroscopic characteristics of the bulk solvent (4), the effect of trace water on the dissociation of $(solv)_5Ni(isoquin)^{2+}$ should be significant in a solvent of low dielectric constant such as THF, and investigation of the magnitude of this effect should provide useful information on the water distribution.

Experimental

Chemicals

THF (J. T. Baker, ACS grade) was distilled fractionally under nitrogen. The middle fraction was refluxed with $LiAlH_4$ (Alpha Ventron) powder for 2 days in an atmosphere of dry nitrogen. This portion was then distilled fractionally over nitrogen under reduced pressure. The middle fraction was collected in a glass-stoppered bottle and stored in the dark in an atmosphere of dry nitrogen in a dry box (Kewaunee Scientific). All THF was used within 6 to 12 h of the final distillation. Deionized water was distilled twice from alkaline $KMnO_4$ in a closed all-glass distillation apparatus.

Nickel(II) was introduced as either hexakisacetonitrile nickel(II) perchlorate or monohydrated nickel(II) perchlorate. Both salts gave the same results. Methods of preparation of the salts were as previously reported (5, 6). The analytical procedure for determining the concentrations of the nickel(II) solutions (1) and the method for purification of isoquinoline (7) (Aldrich, mp 26 to 28°C, bp 242°C) have also been described previously. $LiAlH_4$ and perchloric acid (70 to 72%, Fisher Chemical Co., analytical grade) were used as obtained.

Instrumentation and experimental procedure

All solutions were prepared with oven-dried glassware in a dry box filled with dry nitrogen gas. Standard procedures for handling nonaqueous solutions so as to minimize water contamination were followed. In order to observe the effect of acid and nickel(II) concentrations on the rate of dissociation of $(solv)_5Ni(isoquin)^{2+}$, a series of solutions were prepared in which the nickel(II) concentration was varied from 1.25×10^{-3} *M* to 5.0×10^{-3} *M* in four increments while

[1]Present address: Department of Chemistry, University of Pittsburgh, Pittsburgh, PA 15260, U.S.A.

[2]To whom all correspondence should be addressed.

Can. J. Chem. Downloaded from www.nrcresearchpress.com by 210.87.254.5 on 09/06/12
For personal use only.

Can. J. Chem. Downloaded from www.nrcresearchpress.com by 210.87.254.5 on 09/06/12
For personal use only.

the ligand concentration was held constant at 7.0×10^{-5} *M*. This procedure ensured the formation of only the 1 : 1 complex in all solutions (4, 8). Acid solutions were prepared by adding weighed quantities of 70 to 72% perchloric acid to measured volumes of solvent and calculating the molar concentrations of acid from the weights. The concentrations ranged from 0.0576 to 0.0125 *M*. For measurement of the thermodynamic parameters associated with the dissociation of the complex, solutions of $(solv)_5Ni(isoquin)^{2+}$ were prepared in which the concentration of nickel(II) was held at 5.0×10^{-4} *M* and that of isoquinoline at 5.0×10^{-5} *M*, while the acid solutions were varied from 4.27×10^{-3} *M* to 36.2×10^{-3} *M*. All concentrations refer to final values after mixing during the kinetic experiments.

The first-order rate constant for the dissociation of $(solv)_5Ni(isoquin)^{2+}$ was determined from the rate of formation of protonated isoquinoline (H^+isoquin). This rate was measured by monitoring the absorbance at 332 nm with time after mixing equal volumes of $(solv)_5Ni(isoquin)^{2+}$ and acid solutions. In all experiments the concentration of acid was at least 100 times that of $(solv)_5Ni(isoquin)^{2+}$ to ensure that the observed first-order dissociation rate constant would be independent of acid concentration. Kinetic measurements were made on a stopped-flow spectrophotometer (Durrum Instrument Co., Model D-110). A description of the instrument, including modifications for better temperature control, has been given (8, 9). The temperature of the thermostated waterbath and cell was controlled within ±0.3°C, the value being measured with a calibrated quartz thermometer (Hewlett Packard, Model 2801A). Changes in absorbance with time were recorded on a storage oscilloscope (Tektronix, Model R 564B) and an oscilloscope Polaroid Land camera (Tektronix, Model C-12). All measurements were repeated several times with different batches of solvent and reagents; all results agreed within at least ±1 to 2%.

Results and discussion

Results of the kinetic measurements are displayed in Table 1. The major conclusions are the following.

(*a*) The rate of dissociation of the complex is independent of nickel(II) concentration when the concentrations of acid (H_3O^+), free water (H_2O^*), and ligand are all held constant. During these measurements the concentration of nickel(II) was 15 to 70 times higher than that of the ligand, and the concentration of acid about 10 times higher than that of the nickel(II) (Table 1, Set A). From this result we conclude that the dissociation of $(solv)_5Ni(isoquin)^{2+}$ in THF produced by addition of H_3O^+ can be represented by relations similar to those observed in other solvents (1, 6):

$$[1] \quad (solv)_5Ni(isoquin)^{2+} \underset{k_f}{\overset{k_b}{\rightleftharpoons}} (solv)_5Ni(solv)^{2+} + isoquin$$

$$[2] \quad isoquin + H_3O^+ \overset{k_1}{\rightleftharpoons} (H_3O^+isoquin)$$

From eqs. [1] and [2] it can be shown that, when $[H_3O^+] \gg$ [isoquin], as in this work, the experimentally determined pseudo-first-order rate constant k_{obs} is given by

$$[3] \quad k_{obs} = \frac{k_b k_1 [H_3O^+]}{k_1[H_3O^+] + k_f[Ni(solv)_6]^{2+}}$$

If $k_1[H_3O^+] \gg k_f[Ni(solv)_6]^{2+}$, $k_{obs} = k_b$. Previous work in water and alcohols (1) showed that, when $[Ni]^{2+}$ is 10 to 100 times higher than the ligand concentration, and $[H_3O^+] \geq [Ni]^{2+}$, k_{obs} is the true dissociation constant of $(solv)_5Ni(isoquin)^{2+}$. The independence of k_{obs} of nickel(II) concentrations suggests a dissociation process corresponding to eqs. [1], [2], and [3]. The value of k_b can be taken to be the true value of the dissociation rate constant in THF if the small amount of water introduced into the dry THF by the perchloric acid dihydrate is assumed not to change the true dissociation constant of $(solv)_5Ni(isoquin)^{2+}$ in the rate-determining step of the dissociation process.

TABLE 1. Dissociation rate constants (k_b) of $(solv)_5Ni(isoquin)^{2+}$ in tetrahydrofuran at 25°C at various concentrations of nickel(II), acid, and free water[a,b]

Concentration of acid, *M* ($C_{H_3O^+}$)	Concentration of free water, *M* ($C_{H_2O^*}$)	Concentration of Nickel(II), *M* ($C_{Ni^{2+}}$)	k_b, s^{-1}
Set A			
2.82×10^{-2}	2.82×10^{-2}	1.25×10^{-3}	9.49
2.82×10^{-2}	2.82×10^{-2}	2.50×10^{-3}	9.49
3.12×10^{-2}	3.12×10^{-2}	3.75×10^{-3}	9.24
3.12×10^{-2}	3.12×10^{-2}	5.00×10^{-3}	9.24
Set B			
0.86×10^{-2}	0.86×10^{-2}	1.25×10^{-3}	7.37
1.73×10^{-2}	1.73×10^{-2}	1.25×10^{-3}	8.25
3.62×10^{-2}	3.62×10^{-2}	1.25×10^{-3}	9.90
5.45×10^{-2}	5.45×10^{-2}	1.25×10^{-3}	10.7
Set C			
0.93×10^{-2}	10.56×10^{-2}	1.25×10^{-3}	14.9
3.87×10^{-2}	10.56×10^{-2}	1.25×10^{-3}	14.4
5.76×10^{-2}	10.56×10^{-2}	1.25×10^{-3}	13.5

[a](solv) = solvent, (isoquin) = isoquinoline.
[b]Isoquinoline concentration held constant throughout at 7.0×10^{-5} *M*.

(*b*) k_{obs} increases when both $[H_3O^+]$ and $[H_2O^*]$ are increased at a constant concentration of $(solv)_5Ni(isoquin)^{2+}$ (Table 1, Set B). However, k_{obs} decreases with an increase in acid concentration when both the complex and H_2O^* concentrations are held constant along with the nickel(II) and ligand concentrations (Table 1, Set C).

The study of temperature effects summarized in Table 2 shows that k_{obs} increases when $[H_3O^+]$ and $[H_2O^*]$ are increased at a constant concentration of the complex over the range 15 to 35°C.

All the results in Tables 1 and 2 can be explained by the dissociation process represented by eqs. [1] and [2] through consideration of the following points: (*1*) trace amounts of water in THF influence the rate-determining step in the dissociation process and increase k_b; (*2*) acid has no direct influence on k_b until $k_1[H_3O^+] \gg k_f[Ni(solv_6)]^{2+}$. As $[H_3O^+]$ and $[H_2O^*]$ are simultaneously increased, however, the effective concentration of H_2O^* in the medium, and accordingly its effect on k_b, is decreased. Consequently, as $[H_3O^+]$ increases at a fixed concentration of free water, k_{obs} decreases. This effect may be explained as follows.

When trace levels of perchloric acid dihydrate (commercial 72% material) are added to anhydrous THF, a solvent of low dielectric constant, the proton is likely present principally as the $H(H_2O)_2^+$ species. As the concentration of perchloric acid dihydrate is increased, aggregation of the solvated hydronium ions into clusters containing $[H^+(H_2O)_2]_2$ and higher species may result in concentrations of free water that are lower than the calculated values. Under these conditions a plot of k_{obs} against theoretical free-water concentration would give a curve of the same type as that observed experimentally in Fig. 1. The true first-order dissociation rate constant can be evaluated by extrapolating the curve to zero free-water concentration. True rate constants for the dissociation of $(solv)_5Ni(isoquin)^{2+}$ in THF evaluated in this way at different temperatures are given

TABLE 2. Dissociation rate constants (k_b) of $(solv)_5Ni(isoquin)^{2+}$ in tetrahydrofuran at several temperatures with various concentrations of acid $[H_3O^+]$ and free water $[H_2O^*]$ in the medium[a]

		k_b				
$[H_3O^+]$, M	$[H_2O^*]$, M	15°C	20°C	25°C	30°C	35°C
4.27×10^{-3}	4.27×10^{-3}	2.64				
8.80×10^{-3}	8.80×10^{-3}	3.10				
21.5×10^{-3}	21.5×10^{-3}	3.49				
35.8×10^{-3}	35.8×10^{-3}	3.64				
4.40×10^{-3}	4.40×10^{-3}		3.75			
8.70×10^{-3}	8.70×10^{-3}		4.41			
18.3×10^{-3}	18.3×10^{-3}		5.05			
26.3×10^{-3}	26.3×10^{-3}		5.50			
5.00×10^{-3}	5.00×10^{-3}			6.25		
8.90×10^{-3}	8.90×10^{-3}			7.26		
17.9×10^{-3}	17.9×10^{-3}			8.64		
30.5×10^{-3}	30.5×10^{-3}			9.70		
4.50×10^{-3}	4.50×10^{-3}				9.36	
9.20×10^{-3}	9.20×10^{-3}				10.9	
21.6×10^{-3}	21.6×10^{-3}				13.9	
36.2×10^{-3}	36.2×10^{-3}				15.2	
4.60×10^{-3}	4.6×10^{-3}					14.0
8.10×10^{-3}	8.1×10^{-3}					15.5
18.6×10^{-3}	18.6×10^{-3}					20.1
27.8×10^{-3}	27.8×10^{-3}					23.0
I[b]	0	1.80	2.90	4.75	7.60	12.1

[a]Concentrations of nickel(II) and isoquinoline held constant at 5.0×10^{-4} M and 5.0×10^{-5} M.

[b]I represents concentration of acid in molarity satisfying $I \geq 4.0\times10^{-3}$ M. Values of k_b at $[H_2O^*] = 0$ at different temperatures were calculated from Fig. 1 (see text). Using the temperature coefficient of k_b at $[H_2O^*] = 0$ (k_b being independent of $C_{H_3O^+}$, $C_{Ni^{2+}}$, and C_{ligand}), $\Delta H^{\ddagger}$ and $\Delta S^{\ddagger}$ for dissociation of $(solv)_5Ni(isoquin)^{2+}$ in THF were calculated to be $16.2_6 \pm 0.1$ kcal and -1.1 ± 0.4 eu.

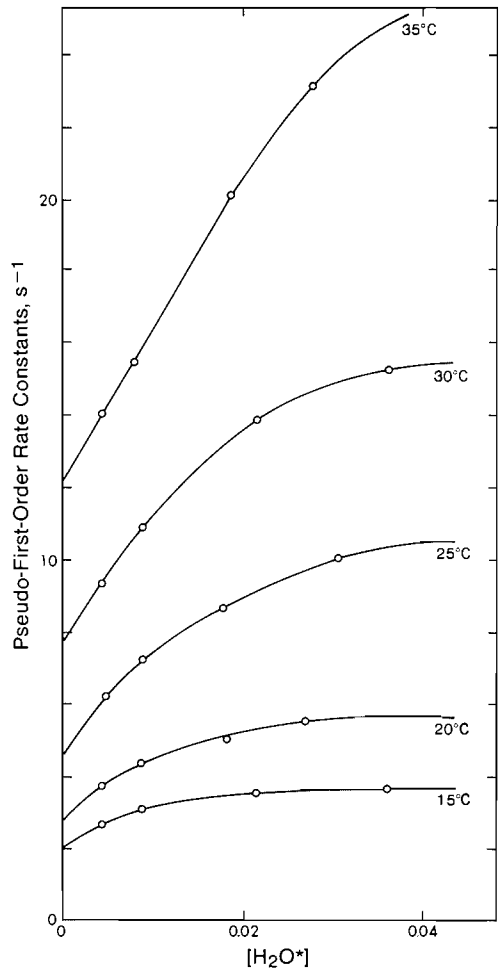

FIG. 1. Pseudo-first-order rate constants for the dissociation of the monocomplex of nickel(II) with isoquinoline in THF as a function of the calculated concentration of free water present.

in Table 2. As the temperature of the solution is increased, $[H_3O^+]$ will decrease and $[H_2O^*]$ will increase and approach the theoretical value. Therefore, k_{obs} will be linear with respect to the theoretically calculated free-water concentration in the medium. This observation explains why the deviations from linearity for plots of k_{obs} against $[H_2O^*]$ are least at 35°C and greatest at 15°C (Fig. 1).

Trace water clearly has a profound effect on the rates of many reactions in aprotic organic solvents, especially of low dielectric constant. The effect generally levels off with increasing water concentration. Whether the water molecules are uniformly distributed throughout the organic medium or are present as hydrogen-bonded clusters or aggregates is uncertain. In contrast to the behavior of hydrogen-bonding solvents of high dielectric constant such as the lower alcohols, THF may facilitate the formation of water clusters by intensifying dipole–dipole and induced ion – dipole interactions among the water molecules. Both the number and size of such clusters would likely decrease with increasing temperature.

The mechanistic pathways for the dissociation of $(solv)_5Ni(isoquin)^{2+}$ induced by H_3O^+ in THF fit an I_d-type mechanism similar to that observed for other systems (10). The pathways can be represented by

[8] $(isoquin)Ni(solv)_5^{2+} + (solv) \underset{k_b}{\rightleftarrows} (isoquin)Ni(solv)_5^{2+}, (solv)$

[9] $(isoquin)Ni(solv)_5^{2+}, (solv) \underset{k_f}{\rightleftharpoons} (solv)Ni(solv)_5^{2+}, (isoquin)$

Any condition that influences the rate-controlling step, represented by eq. [9], will affect k_b. When a small amount of water is added to anhydrous THF, at least one of the THF solvent molecules in $(solv)_5Ni(isoquin)^{2+}$ is likely replaced by a water molecule. The stronger interaction of H_2O^* with Ni^{2+} and isoquinoline thereby increases the value of k_b. Contrary to previous results in alcoholic solvents, the addition of even a small amount of water to anhydrous THF influences the rate-controlling step by changing the structure of the dissociating $(solv)_5Ni(isoquin)^{2+}$ ion to $(solv)_4(H_2O^*)Ni(isoquin)^{2+}$ ion. The H_2O^* in the latter ion is attached to Ni^{2+} by a coordinate bond, the strength of which depends on the intrinsic properties of H_2O^* relative to Ni^{2+}, and by ion–dipole interaction forces. In THF this interaction between Ni^{2+} and H_2O^* will be higher than the corresponding values in alcohols, owing to the lower dielectric constant of THF. Consequently, less water is required to form $(solv)_4(H_2O^*)Ni(isoquin)^{2+}$ from $(solv)_5Ni(isoquin)^{2+}$ in THF than in alcohols. This fact may explain why, contrary to the observation of this study, a small amount of water introduced into dry alcoholic solvents along with H_3O^+ has no effect on the dissociation of $(solv)_5Ni(isoquin)^{2+}$ at a particular temperature, whereas an equivalent amount of water in dry THF increases the dissociation rate constant at the same temperature. Also, the difference in size and polarity of water relative to the lower alcohols is small compared to the difference between water and THF.

Can. J. Chem. Downloaded from www.nrcresearchpress.com by 210.87.254.5 on 09/06/12
For personal use only.

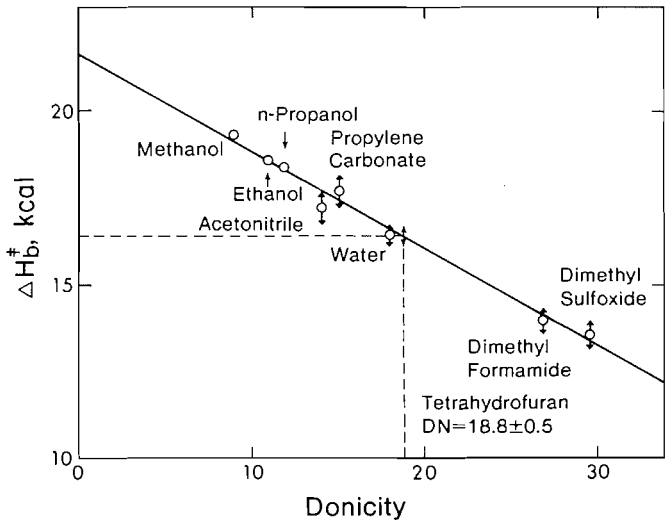

FIG. 2. Relation between the enthalpy of activation for the dissociation of the monocomplex of nickel(II) with isoquinoline against solvent donicity. From the plot the donicity of THF is predicted to be 18.8 ± 0.5.

Enthalpies and entropies of activation associated with the dissociation of $(solv)_5Ni(isoquin)^{2+}$ in THF were calculated from the true dissociation rate constants at different temperatures with the standard thermodynamic equations (Table 2). Plotting $\Delta H_b^{\ddagger}$ for the dissociation of $(solv)_5Ni(isoquin)^{2+}$ in different solvents against the Gutmann donor numbers for those solvents (1) gives a value for THF on the Gutmann donicity scale of 18.8 ± 0.5 (Fig. 2). Gutmann reported 19.3 for the donor number of THF (3), in agreement with the value reported in this work. Thus the linear relation between $\Delta H_b^{\ddagger}$ in different solvents and the donor numbers of the solvents for the dissociation of $(solv)_5Ni(isoquin)^{2+}$ can be extended to anhydrous THF.

It would be useful to extend the relation between $\Delta H_b^{\ddagger}$ and Gutmann donor numbers for the dissociation of $(solv)_5Ni(isoquin)^{2+}$ to other solvents, protic as well as dipolar aprotic. Also, Lewis acids other than nickel(II) and differently charged ionic as well as neutral ligands other than isoquinoline should be investigated to assess the generality of the approach.

In summary, dissociation of $(solv)_5Ni(isoquin)^{2+}$ in THF induced by H_3O^+ is controlled by the same I_d-type mechanism as observed for this and similar nickel complexes in many solvents, and the linear relation between $\Delta H_b^{\ddagger}$ and the Gutmann donor number of various solvents can be extended to THF. The existence of solvated hydronium ions associated with clusters of water molecules is postulated in THF containing trace concentrations of water at low temperature. Low concentrations of free water in anhydrous THF increase appreciably the true dissociation rate constant of $(solv)_5Ni(isoquin)^{2+}$, especially at 35°C. From kinetic measurements of the dissociation constant of the complex at 35°C, the presence of water in dry THF can be detected at concentrations as low as 1 ppm.

Acknowledgements

Financial support by the Natural Sciences and Engineering Research Council of Canada and the University of Alberta is gratefully acknowledged. The authors thank Mr. J. F. Merz, President, and Mr. L. Reckner, Vice President, of Scott Environmental Technology, Inc., Plumsteadville, PA 18949, for providing facilities to P.K.C. during the preparation of this manuscript.

1. P. K. CHATTOPADHYAY and B. KRATOCHVIL. Inorg. Chem. **15**, 3104 (1976); **19**, 2953 (1979).
2. (*a*) A. I. POPOV. Paper presented at 172nd National Meeting, American Chemical Society, San Francisco, September, 1976; (*b*) M. TANAKA. Private communication; (*c*) R. S. DRAGO and B. B. WAYLAND. J. Am. Chem. Soc. **87**, 357 (1965); (*d*) R. S. DRAGO, G. C. VOGEL, and T. E. NEEDHAM. J. Am. Chem. Soc. **93**, 6014 (1971).
3. V. GUTMANN. Fortschr. Chem. Forsch. **27**, 59 (1972).
4. P. K. CHATTOPADHYAY and J. F. COETZEE. Anal. Chem. **46**, 2014 (1974).
5. B. KRATOCHVIL, D. A. ZATKO, and R. MARKUZEWSKI. Anal. Chem. **38**, 770 (1966).
6. P. K. CHATTOPADHYAY and B. KRATOCHVIL. Can. J. Chem. **55**, 1609 (1977).
7. P. K. CHATTOPADHYAY and B. KRATOCHVIL. Can. J. Chem. **54**, 2540 (1976).
8. P. K. CHATTOPADHYAY and J. F. COETZEE. Inorg. Chem. **12**, 113 (1973).
9. P. K. CHATTOPADHYAY and J. F. COETZEE. Anal. Chem. **44**, 2117 (1977).
10. C. H. LANGFORD and H. B. GRAY. Ligand substitution processes. W. A. Benjamin, New York. 1965.

Can. J. Chem. Downloaded from www.nrcresearchpress.com by 210.87.254.5 on 09/06/12
For personal use only.

Intramolecular participation by the thiol group in amide hydrolysis: the general acid-catalyzed pathway[1]

ROBERT S. MCDONALD,[2] PATRICIA PATTERSON,[3] AND ANN STEVENS-WHALLEY[3]
Department of Chemistry, Mount Saint Vincent University, Halifax, N.S., Canada B3M 2J6

Received March 31, 1982[4]

ROBERT S. MCDONALD, PATRICIA PATTERSON, and ANN STEVENS-WHALLEY. Can. J. Chem. **61**, 1846 (1983).

The hydrolysis of *N*-n-propyl-2-mercaptomethylbenzamide has been investigated in HCl and a series of buffers over the pH region 0–8.5 at 40.0°C, μ = 1.0. Nucleophilic participation by the thiol group during amide hydrolysis produces 2-thiophthalide as the stable product. The second-order rate constant for the acid-catalyzed reaction is 10^7 times greater than that for the hydrolysis of *N*-propylbenzamide.

The pH–rate profile and buffer catalysis data are indicative of a change in rate-determining step near pH 3–3.5 from the uncatalyzed formation of neutral tetrahedral intermediate at low pH to its general acid-catalyzed breakdown (or a kinetic equivalent) at high pH. The Brønsted catalysis plot for this latter process is most consistent with rate-determining general base-catalyzed breakdown of the cationic tetrahedral intermediate directly to product.

ROBERT S. MCDONALD, PATRICIA PATTERSON et ANN STEVENS-WHALLEY. Can. J. Chem. **61**, 1846 (1983).

On a étudié l'hydrolyse du *N*-n-propylmercapto-2 méthylbenzamide dans du HCl et dans diverses solutions tampon dans l'intervalle de pH allant de 0 à 8,5 à 40,0°C, μ = 1,0. La participation nucléophile du groupe thiol à l'hydrolyse de l'amide conduit au thio-2 phtalide comme produit stable. La constante de vitesse d'ordre deux de la réaction catalysée par un acide est de 10^7 fois supérieure à celle de l'hydrolyse du *N*-propylbenzamide. La courbe de la vitesse en fonction du pH et les données de la catalyse par les solutions tampon indiquent un changement dans l'étape déterminante à un pH voisin de 3 à 3,5 à partir de la formation non catalysée de l'intermédiaire tétraédrique neutre à faible pH jusquà sa rupture générale catalysée par un acide (ou un équivalent cinétique) à fort pH. La courbe de catalyse de Brønsted de ce dernier processus s'accorde d'avantage avec une étape déterminante de rupture générale, catalysée par une base, de l'intermédiaire tétraédrique cationique donnant directement le produit.

[Traduit par le journal]

A thiol group has been implicated in the catalytic activity of a number of enzymes either through the coenzyme (1, 2)[5] or as an integral part of the enzyme active site (3–6). Members of the family of cysteine proteases possess a thiol group which has been assigned a nucleophilic role during peptide (amide) hydrolysis (4–6).

Considerable information may be gained on the mechanism of enzyme-catalyzed reactions by the study of appropriate model compounds which react by an intramolecular pathway (7). However, a survey of recent reviews (8, 9) reveals that reports of the thiolysis of an amide (either intermolecular or intramolecular) are conspicuous by their absence (see, however, refs. 10 and 11).

In order to obtain direct evidence for thiol group participation during amide hydrolysis, the *N*-alkyl-2-mercaptomethylbenzamides (**1**) were synthesized and their hydrolytic behaviour studied in buffered aqueous solution over a range of pH. Nucleophilic participation by sulfur would lead to 2-thiophthalide (**2**), or its basic hydrolysis product, and amine.

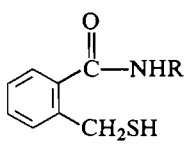

1

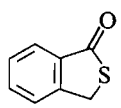

2

a, R = —$CH_2CH_2CH_3$
b, R = —$CH_2CH_2OCH_3$

Experimental

General

Melting points were taken on a Gallenkamp apparatus and are uncorrected. An Orion 601A pH meter with a research grade combination electrode was used for all pH measurements. The meter was calibrated with two Fisher-certified buffers selected to bracket the pH of the solutions. Nuclear magnetic resonance (nmr) spectra were recorded at 60 MHz or 80 MHz on either a Varian EM360A or a Bruker WP-80 spectrometer. Chemical shifts are given in ppm (δ) relative to internal TMS in $CDCl_3$ solution. Infrared (ir) spectra were recorded on a Beckman Acculab 6 spectrometer; solid samples were run in KBr pellets, the liquids as thin films between NaCl plates. Peak positions are quoted in cm^{-1}.

Ultraviolet (uv) spectra were recorded on a Beckman 24 spectrophotometer equipped with a dedicated 10-inch flat bed recorder, four-position manual sample changer, electronic temperature controller, and temperature readout accessory. This machine was also used to monitor the kinetic runs. Microanalyses were performed by Mr. P. Borda, Microanalytical Laboratory, Department of Chemistry, University of British Columbia.

Materials

Liquid amines were dried overnight over KOH pellets, distilled from zinc dust at atmospheric pressure, and stored under N_2 until ready to use. Imidazole was recrystallized from benzene using decolorizing charcoal until colorless crystals were obtained; mp, after drying *in vacuo*, 89–90.5°C (lit. (12) mp 90–91°C). All other buffer components were reagent grade and used without further purification. The purification of water and dioxane and the preparation of buffer solutions has been described (13).

2-Thiophthalide, **2** (14), was prepared by a modification of literature procedures. The 2-(benzylmercaptomethyl)benzoic acid was obtained in 66% yield by the method described by Storm and Koshland (15). The cyclization–debenzylation was accomplished with refluxing trifluoroacetic anhydride according to Lumma *et al.* (16). Crude **2**, produced in 86% yield, was purified initially by chromatography on silica gel (80–200 mesh). Elution with pentane gave a trace of dibenzyl disulfide and considerable benzyl trifluoroacetate in the early

[1]Presented in part at the International Symposium on Physical Organic Chemistry, Toronto, Ontario, August, 1979.
[2]Author to whom correspondence should be addressed.
[3]Summer research assistant.
[4]Revision received March 4, 1983.
[5]See also ref. 1, pp. 175–177 and ref. 2*b*, pp. 178–180.

Can. J. Chem. Downloaded from www.nrcresearchpress.com by 210.87.254.5 on 09/06/12
For personal use only.

Can. J. Chem. Downloaded from www.nrcresearchpress.com by 210.87.254.5 on 09/06/12
For personal use only.

fractions. Pentane–ether (15:1) eluted **2** as a pale yellow solid, mp 53–55°C. Repeated recrystallization from pentane–ether afforded colorless needles, mp 58.5–60°C (lit. (14) mp 58–60°C). Spectroscopic data are as follows: ir: 1685 (γ-thiolactone carbonyl); uv (H_2O) λ_{max} (log ε): 213 (4.02), 243 (4.04), 269 (3.92); nmr δ: 4.48[6] (s, 2H), 7.2–8.0 (m, 4H). *Anal.* calcd. for C_8H_6OS: C 63.97, H 4.03, S 21.35; found: C 64.02, H 4.00, S 21.30.

The *N*-alkyl-2-mercaptomethylbenzamides (**1**) proved to be remarkably sensitive to aerial oxidation during prepration and isolation, and special precautions had to be taken to minimize disulfide formation during the kinetic runs. This instability presumably results from the method of preparation which is outlined below.

Thiolactone **2** (20–250 mg) was dissolved in large excess (2–3 mL) of neat liquid amine and sealed off with Parafilm under N_2 in a small round-bottom flask. Reaction was allowed to proceed at room temperature in the dark until nmr revealed less than 5% of **2** remained. This required 20–30 min for the n-propylamine and 10 h for the 2-methoxyethylamine (prolonged reaction times are to be avoided). No ring opening of **2** could be detected after treatment with isopropylamine for 24 h or with *tert*-butylamine for 8 months. Excess amine was then removed under reduced pressure at 30–35°C and the residual colorless liquid used without further purification. All attempts to isolate analytically pure **1** resulted in contamination with **2** or disulfide. However, the following spectral data are consistent with the proposed structure for **1***a*: ir: 2530 (v w, SH), 1626 (amide I), 1551 (amide II), 1315 (amide III); uv (H_2O) no λ_{max} above 215 nm; nmr,[7] δ: 0.98 (t, 3H), 1.2–1.8 (m, 2H), 3.39 (q, 2H), 3.88 (s, 2H), 6.5–8 (v broad s, 1H), 7.2–7.5 (m, 4H). Further evidence to support the structure for **1***a* comes from spectral and microanalytical data collected for the disulfide which must have **1***a* as its precursor.

The disulfide separated out in 95% yield when **2** and a 3-fold excess of n-propylamine were refluxed together in ether solution for one hour. The colorless solid was purified by crystallization from dioxane–water and after drying *in vacuo* had mp 175–176°C; nmr, δ: 0.97 (t, 6H), 1.35–1.85 (m, 4H), 3.37 (q, 4H), 3.87 (s, 4H), 6.3–6.6 (v broad s, 2H), 7.2–7.6 (m, 8H). *Anal.* calcd. for $C_{22}H_{28}N_2S_2O_2$: C 63.43, H 6.77, N 6.72, S 15.39; found: C 63.54, H 6.59, N 6.60, S 15.56.

Kinetics

Stock solutions of the thiol amides **1** were prepared by taking up the product from 22.5 mg of **2** in 5.0 mL dioxane as described above. The resulting 0.03 *M* solution when stored under N_2 proved to be stable for periods of up to one week. Kinetic runs were initiated by injecting 15 μL of this stock solution into 2.50 mL of aqueous buffer which had been temperature-equilibrated for at least 30 min in the thermostatted sample compartment of the spectrophotometer. Reacting solutions were maintained at 40.0 (±0.1)°C unless otherwise noted and the ionic strength (μ) was kept constant at 1.0 with KCl. The initial concentration of **1** was 1.8×10^{-4} *M* in the solution which also contained 0.6% dioxane. Quartz cuvettes equipped with tight-fitting Teflon stoppers were used throughout. Successive scans of the uv spectrum of a reaction mixture containing **1** clearly revealed the appearance of absorption maxima near 240 and 265 nm due to **2**. An isosbestic point is found near 231 nm. Reactions were monitored by taking absorbance readings at 265 nm over 75–90% reaction; an "infinity" value (A_∞) was taken after at least 10 half-lives. Rate-constants (k_{obs}) were calculated from the linear plots of ln ($A_\infty - A$) vs. *t* in the usual way. Runs having kinetic plots with correlation coefficients (*r*) <0.999 over at least two half-lives were rejected. The very slow runs in 1.0 *M* KCl ($\tau_{1/2} \simeq 17$ h) were followed to about 30% reaction and the A_∞ value estimated to be the same as that obtained from a reaction mixture containing an identical injection of the same stock solution which was followed to completion. Three independent runs using different stock solutions gave excellent plots, the resulting k_{obs} values agreeing to within 4%. The pH of all solutions was taken before and after the kinetic runs; agreement was within 0.02 pH units except for the very dilute HCl solutions and in 1.0 *M* KCl where the amine produced during the reaction caused appreciable pH changes. In these cases, the average a_{H^+} during the runs was calculated from the initial and final pH values. After the kinetic run, the solution was carefully examined for turbidity (a fine white precipitate of disulfide). While the presence of trace amounts of precipitate appeared to have little effect on the linearity of the kinetic plots or the derived k_{obs} values, appreciable amounts were invariably accompanied by erratic absorbance readings, A_∞ values which were too low, and curved kinetic plots. Such runs were routinely rejected. The formation of disulfide concurrent with thiolactonization hampered many of our early kinetic trials. The problem was overcome for the acidic and weakly basic solutions by using only freshly prepared stock solutions of **1**, degassing all solutions before use, carrying out the reactions under N_2 in cuvettes sealed off with Parafilm, and maintaining all kinetic solutions at 1.0×10^{-4} *M* in EDTA (17). However, even these precautions could not prevent disulfide formation during the very slow runs at pH ≥ 8.5 and these trials were abandoned. Quoted k_{obs} values are the average of at least duplicate runs; agreement between replicate runs was always within 10% and normally within 5–6%.

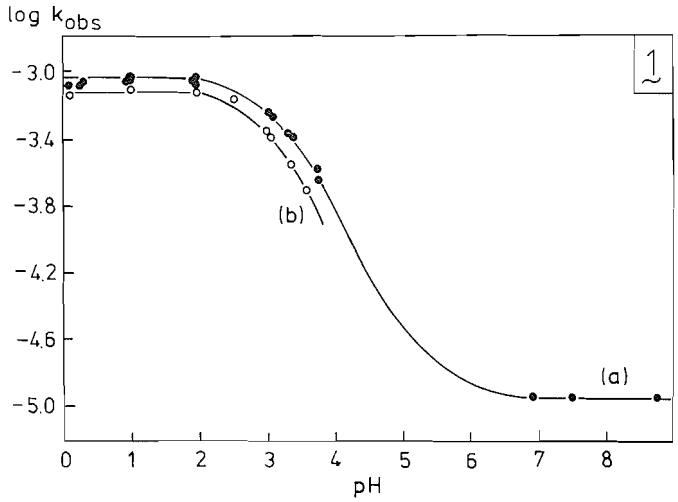

FIG. 1. The pH–log rate constant (k_{obs}) profiles for thiolactonization of (a) **1***a* and (b) **1***b* at 40.0°C, μ = 1.0.

Product

The appearance of absorption maxima near 240 and 265 nm gives clear evidence for the formation of **2** during the hydrolysis of thiol amides **1**. The final absorbances at these wavelengths typically were 80–90% of those of an equal concentration of **2** under identical conditions. The product is invariably contaminated by a small amount of disulfide which remains in solution and has no appreciable effect on the kinetics under investigation.

Product isolation was carried out as follows. Thiol n-propylamide **1***a* prepared from 75 mg of **2** was taken up in 5.0 mL dioxane and added slowly to 1.75 L of degassed 0.10 *M* HCl at 25°C. The solution was stirred vigorously under N_2 in the dark for 18 h. A fine suspension of disulfide (10 mg, 13%) was removed by filtration and the resulting solution extracted with three 250-mL portions of ether. The combined ether extracts were dried ($MgSO_4$) and concentrated to dryness to yield 53 mg (71%) of **2** (identified by nmr), contaminated by a trace (<5%) of disulfide.

Results

The hydrolysis of thiol amides **1** provides clear evidence for nucleophilic participation by the thiol group during amide hydrolysis. The characteristic uv absorptions of **2** appear during the reaction and this product can be isolated in good yield from

[6]Chemical shift incorrect in ref. 15.

[7]After shaking with D_2O, the variable broad NH signal near δ 6.5–8 was removed and the δ 3.39 resonance became a triplet (—CH_2CH_2ND—).

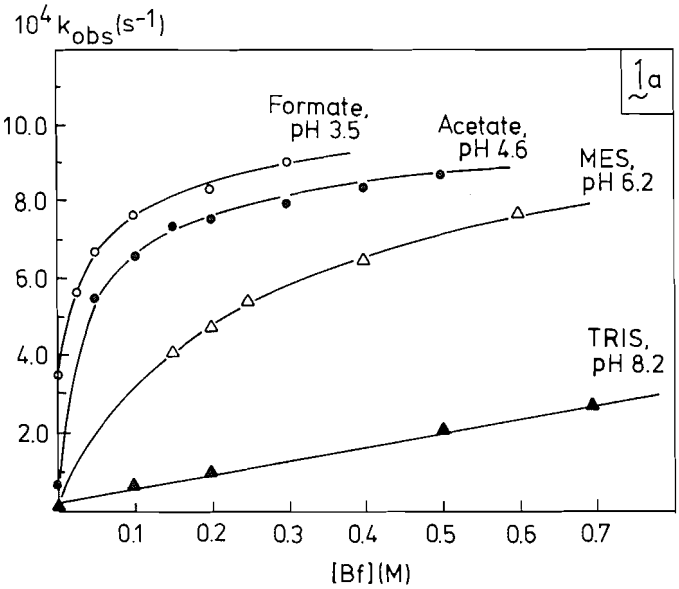

FIG. 2. Buffer catalysis plots for the thiolactonization of **1***a* at 40.0°C, μ = 1.0 (the fraction of the buffer in its basic form is 0.5 in each case).

the reaction mixture. No base-catalyzed hydrolysis pathway (with or without sulfur participation) could be detected for **1***a* up to pH 8.7, and the subsequent basic hydrolysis of **2** did not interfere with our measurements.[8]

The pH–log rate constant (k_{obs}) profiles for appearance of **2** from **1***a* and **1***b* at 40.0°C are illustrated in Fig. 1. Both amides exhibit a rate plateau from pH 0–2 which then falls off with decreasing acidity to a slow spontaneous (water-catalyzed) process above pH 6. The average value of k_{obs} on the low pH plateau is 8.5 (±0.5) × 10^{-4} s^{-1} for **1***a* and 7.3 (±0.4) × 10^{-4} s^{-1} for **1***b*. The inflection points in both curves in Fig. 1 occur at a pH of 3.3 and, since there is no group in either **1** which has a pK near this value,[9] this behavior must be indicative of a change in rate-determining step from one which is uncatalyzed at low pH to one which is acid-catalyzed at pH >3.5.

Although buffer catalysis was examined only for **1***a*, it is clear that the thiolactonization is strongly catalyzed by the carboxylate, amine, and phosphate buffers used to maintain constant pH over the pH range 3.5–8.3. Some typical buffer catalysis plots are illustrated in Fig. 2. The saturation behavior observed for buffer catalysis is again consistent with a change in rate-determining step. The maximum value of k_{obs} at high concentration of buffer or HCl varied randomly with pH over the pH range 0–7 within the limits 8.0–9.8 × 10^{-4} s^{-1}. Catalytic effectiveness of the buffers decreases as the pK_a of the conjugate acid of the buffer increases (Fig. 2) and, for a given buffer, as the pH increases.

The minimum mechanistic pathway required to account for the results above is the two-step, one-intermediate (I_0), scheme below.

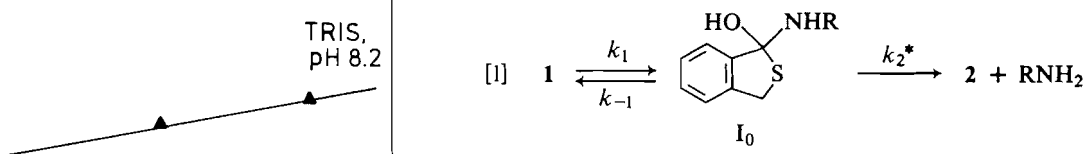

Under our reaction conditions (low [RNH_2], pH < 9), the reverse of the second reaction can be neglected.[10] In analogy with mechanisms proposed for the reverse reaction, thiolester aminolysis (17, 23–26), and thioimidate ester hydrolysis (27), we propose that formation of I_0 from **1** is uncatalyzed and that its breakdown is subject to acid and buffer catalysis. Making the steady-state assumption for I_0 (repetitive scans of the uv spectrum of reacting **1** gave no evidence for the accumulation of an intermediate), solution of the rate equation gives:

$$[2] \quad k_{obs} = k_1 \cdot k_2^*/(k_{-1} + k_2^*)$$

where, in general, k_2^* is given by

$$[3] \quad k_2^* = k_{H_2O} + k_H \cdot a_{H^+} + k_{Bf} \cdot [Bf]$$

Rearranging eq. [2] gives, after substitution of eq. [3],

$$[4] \quad k_{obs}/(1 - k_{obs}/k_1) = k'_{H_2O} + k'_H \cdot a_{H^+} + k'_{Bf} \cdot [Bf]$$

where

$$k'_{H_2O} = k_1 \cdot k_{H_2O}/k_{-1}, \; k'_H = k_1 \cdot k_H/k_{-1}$$

and

$$k'_{Bf} = k_1 \cdot k_{Bf}/k_{-1}$$

Kinetic data were analyzed as follows. At low pH or high [Bf], $k_2^* \gg k_{-1}$ and eq. [2] becomes: $k_{obs} = k_1$, independent of pH and [Bf]. The low pH rate plateau and the limiting rate constant extrapolated from buffer catalysis data (*vide infra*) give values for k_1 in the range 9.8 (±1.8) × 10^{-4} s^{-1} (pH 0–7.5).

Three runs in 1.0 *M* KCl at pH 6.9–8.7 gave an average value of k_{obs} = 1.11 (±0.02) × 10^{-5} s^{-1}. Clearly the last two terms in eq. [3] can be neglected in this range and eq. [4] becomes

$$k'_{H_2O} = k_1 - k'_{obs}(k_1 - k_{obs})$$

[8]We have measured the rate of basic hydrolysis of **2** in dilute NaOH solution at 40°C, μ = 1.0 (k_{OH} = 7.7 × 10^{-2} M^{-1} s^{-1}). Thus at pH 8.7, hydrolysis of **2** occurs at a rate only 6% of that of its rate of formation in 1.0 *M* KCl and none of the k_{obs} values have been corrected for this effect.

[9]The acidity constants of the amide carbonyl and the thiol group in **1***a* are estimated as follows. Yates and co-workers (18) recently determined the pK_{BH^+} values of a large number of *N*-substituted benzamides and although the n-propyl derivative was not reported, its value must be close to −1.5. Since the —CH_2OH and —CH_2SH have very similar electronic and steric effects (19), we assume that the *o*-CH_2SH group will have the same effect on this pK_{BH^+} as an *o*-CH_2OH group has on the pK_a of benzoic acid, i.e. acid strengthening by 0.3 ± 0.1 pK units (20). Similarly, we assume that the *o*-carbamido substituent will have the same effect on the pK of the thiol group in benzylmercaptan (pK_{SH} = 9.43 (21)) as it does on the pK_a of benzoic acid, acid-strengthening by 0.4 ± 0.2 pK units (22). Thus, our estimates for pK_{BH^+} and pK_{SH} of **1***a* are −1.8 ± 0.1 and 9.0 ± 0.2, respectively.

[10]Kinetics of the aminolysis of thiolactone **2** with n-propylamine and 2-methoxyethylamine have been studied in aqueous solution at 40°C, μ = 1.0 (unpublished results from this laboratory). Partially acidified amine solutions at high concentrations (0.25–1.0 *M*) served as their own buffers (pH 9.7–11.3). The kinetic data were analyzed in terms of the general rate law used previously (23). Under thiolactonization conditions (low [RNH_2], pH < 9) only the term first-order in amine contributes significantly to the thiolester aminolysis rate. This allows calculation of the maximum value of the [**2**]/[**1**] ratio under thiolactonization conditions to be in the range 1–2 × 10^3 for **1***a* or **1***b* at pH 8.5. Since this ratio increases as pH decreases, we conclude that the thiolactonization reaction **1** → **2** proceeds essentially to completion at pH ≤ 8.5 and $k_{-2} \simeq 0$.

Can. J. Chem. Downloaded from www.nrcresearchpress.com by 210.87.254.5 on 09/06/12
For personal use only.

TABLE 1. Collected kinetic data for the thiolactonization of **1***a* in aqueous solution, 40.0°C, $\mu = 1.0$

Buffer (% free base; concentrations)	pH[a]	n[b]	$10^2 k'_{Bf}$ ($M^{-1}s^{-1}$)[c]	$10^4 k_1$ (s^{-1})[c]
HCl (1.0−0.0003)	0−3.8	17	165 (±0.15)	8.9(±0.2)
Formate (50; 0.025−0.90)	3.47	9	3.79 (±0.15)	9.3(+0.2)
Acetate (25; 0.025−0.10)	4.01	3	3.85 (±0.25)	9.5(±0.5)
Formate (75; 0.05−0.20)	4.07	3	2.07 (±0.12)	9.6(±0.1)
3-Chloropropanoate (75; 0.05−0.20)	4.34	6	1.89 (±0.12)	9.3(±0.2)
Formate (90; 0.05−0.20)	4.55	3	0.76 (±0.03)	8.9(±0.3)
Acetate (50; 0.05−1.0)	4.57	18	2.75 (±0.21)	8.8(±0.2)
3−Chloropropanoate (90; 0.05−0.20)	4.85	3	0.81 (±0.03)	10.1(±0.4)
Acetate (75; 0.05−0.40)	5.07	12	1.29 (±0.09)	9.1(±0.4)
Phosphate (10; 0.04−0.16)	5.48	3	2.01 (±0.07)	9.8(±0.3)
Acetate (90; 0.10−0.40)	5.55	3	0.53 (±0.03)	10.5(±0.4)
MES (25; 0.10−0.25)	5.72	3	0.75 (±0.07)	10.2(±1.7)
Trifluoroethylamine (50; 0.10−0.40)	5.73	3	1.41 (±0.05)	10.1(±0.2)
Phosphate (25; 0.048−0.40)	5.94	4	1.69 (±0.09)	10.8(±0.4)
MES (50; 0.15−0.60)	6.21	5	0.42 (±0.03)	10.7(±0.3)
Phosphate (50; 0.05−0.40)	6.48	6	1.03 (±0.07)	10.3(±0.6)
Phosphate (75; 0.12−0.36)	7.08	6	0.64 (±0.03)	12.8(±0.6)
Tris (10; 0.10−1.0)	7.25	8	0.067 (±0.005)	11.0(±2.9)
Phosphate (90; 0.10−0.30)	7.56	8	0.37 (±0.03)	11.2(±1.3)
Tris (25; 0.40−1.0)	7.77	3	0.059 (±0.002)	15.8(±0.1)
Tris (50; 0.10−1.0)	8.25	6	0.0355(±0.0004)	[d]
2-Methoxyethylamine (10; 0.50−1.0)	8.25	3	0.0177(±0.0007)	[d]

[a]Measurements of pH were made at 25°C.
[b]n = number of runs.
[c]The errors quoted are standard deviations.
[d]The buffer catalysis plots were essentially linear up to [Bf] = 1.0 *M*.

Taking $k_1 = 9.8 \times 10^{-4}$ s^{-1} yields $k'_{H_2O} = 1.12 \times 10^{-5}$ s^{-1}.

In the dilute HCl solutions over the pH region 1−3.4, the contribution of k_{H_2O} to k_2* can be neglected and eq. [2] becomes, after substitution,

$$k_{obs} = k_1 \cdot k_H \cdot a_{H^+}/(k_{-1} + k_H \cdot a_{H^+})$$

Now, a double reciprocal plot (of k_{obs}^{-1} vs. $a_{H^+}^{-1}$) should be linear, yielding values for k'_H and k_1 from the slope and intercept, respectively. The plot for **1***a* gave $k'_H = 1.66\ (\pm 0.06)\ M^{-1}$ s^{-1} and $k_1 = 8.9\ (\pm 0.2) \times 10^{-4}$ s^{-1} ($r = 0.998$). An alternative analysis of the HCl data involves eq. [4] in the form

$$k'_H = [k_{obs}/(1 - k_{obs}/k_1) - k_{H_2O}]a_{H^+}^{-1}$$

Now, using values for k_1 and k'_{H_2O} obtained above allows calculation of an average value of k'_H of 1.65 (±0.15) M^{-1} s^{-1} for the eight runs on **1***a* over the pH range 3−3.8. A similar analysis of the kinetic data for **1***b* using values for k_1 of 7.5×10^{-4} s^{-1} and k'_{H_2O} of 9.7×10^{-6} s^{-1} (lower by 15% than the value observed for **1***a*) gave $k'_H = 1.03\ (\pm 0.12)\ M^{-1}$ s^{-1}.

The distinct curvature in most of the buffer catalysis plots (Fig. 2) over the pH range 3.5−8 indicated that, in general, solution of eq. [4] was necessary to evaluate k'_{Bf}. However, we found that the buffers studied at pH > 8 gave linear plots of k_{obs} vs. [Bf] up to 1.0 *M*. Under these conditions then, $k_2^* \ll k_{-1}$ and eq. [2] becomes, after substitution,

$$k_{obs} = k'_{H_2O} + k'_H \cdot a_{H^+} + k'_{Bf} \cdot [Bf]$$

Thus k'_{Bf} is obtained from the slope of these plots (see the Tris plot in Fig. 2 and the last two entries in Table 1).

In the pH region 5.5−8, neglecting the contribution of k_{H_2O} and $k_H \cdot a_{H^+}$ to k_2*, eq. [2] becomes, after substitution,

$$k_{obs} = k_1 \cdot k_{Bf}\,[Bf]/(k_{-1} + k_{Bf} \cdot [Bf])$$

Plots of k_{obs}^{-1} vs. $[Bf]^{-1}$ were reasonably linear, yielding values for k'_{Bf} and k_1 from the slope and intercept, respectively. The value of k_1 so determined was then used in eq. [4] to calculate another value for k'_{Bf} where now the k'_{H_2O} and k'_H contributions were considered. The values of k'_{Bf} calculated by these two methods agreed to within 5%.

Over the pH range 3.5−5.5 now the general form of eq. [4] was used to calculate k'_{Bf}, using 8.9×10^{-4} s^{-1} as an initial estimate for k_1. Only data where $k_{obs} \leq 0.75k_1$ were used in these calculations (see form of eq. [4]). We found it necessary to use an iterative procedure, making small adjustments in the value of k_1 to achieve constant values for k'_{Bf}. The values of k'_{H_2O} and k'_H were those calculated above. The values of k'_H and k'_{Bf} and the optimized values for k_1 are collected in Table 1.

Changing the pK_a[11] of the amine leaving group in **1** from 10.43 (n-propylamine) to 9.31 (2-methoxyethylamine) decreases the rate of formation of I_0 by 15% and also decreases the rate of its subsequent acid-catalyzed breakdown (*vide supra*).

Activation parameters for the thiolactonization of **1***a* were determined in 0.10 *M* HCl where formation of I_0 is solely rate-determining. The kinetic data are collected in Table 2 and the linear plot of $\ln kT^{-1}$ vs. T^{-1} gave $\Delta H^{\ddagger} = 18.5\ (\pm 0.6)$ kcal mol^{-1} (77.7 kJ mol^{-1}) and $\Delta S^{\ddagger} = -14\ (\pm 2)$ cal K^{-1} mol^{-1} (−59 J K^{-1} mol^{-1}), $r = 0.997$.

Where buffer catalysis was examined at more than one buffer ratio, plots of k'_{Bf} vs. f_B (the fraction of the buffer in its basic form) are linear with intercepts, at $f_B = 1$, of essentially zero. Intercepts of these plots at $f_B = 0$ gave k'_{HA}, the second-order rate constants for apparent general acid catalysis. The k'_{HA} values for all general acids including H_3O^+ and H_2O are collected

[11]See footnote *a* in Table 3.

Can. J. Chem. Downloaded from www.nrcresearchpress.com by 210.87.254.5 on 09/06/12
For personal use only.

TABLE 2. Temperature dependence of rate of thiolactonization of **1***a* in 0.10 *M* HCl, μ = 1.0

t (°C)[a]	$10^4 k_{obs}$ (s^{-1})[b]	n[c]
25.0	1.93(±0.09)	4
30.7	3.49(±0.10)	2
35.3	5.33(±0.39)	2
40.0	9.00(±0.27)	3
46.9	17.1(±0.2)	2

[a]±0.1°C.
[b]Errors quoted are standard deviations.
[c]n = number of runs.

in Table 3 along with values for k'_B, the corresponding rate constants for general base-catalyzed breakdown of the cationic tetrahedral intermediate ($k'_B = k'_{HA} \cdot K_{I+}/K_{HA}$). The statistically corrected Brønsted plot for such general base catalysis is illustrated in Fig. 3.

Our kinetic results in the imidazole buffers have been omitted from the analysis above since they differ in several important respects from those observed in the other buffers studied. For example, the buffer catalysis plots over the [Bf] range 0.20–1.0 *M* are essentially linear, such that there appears to be no upper limit to the value of k_{obs}. The maximum catalytic effect is observed in the buffer at f_B = 0.5 (pH 7.1). Presentation and discussion of these results will be deferred until our continuing investigation of this behaviour is completed. However, it should be pointed out that these results may be particularly relevant to the mechanism of action of papain in which an imidazole group has been assigned a general acid–base role in acylation by amide substrates (5, 6).

Discussion

The neighbouring thiol group has a very dramatic effect on the rate of hydrolysis of amides **1**. In the pH region 3–4 where the H_3O^+-catalyzed thiolactonization dominates, the rate constant k_H for **1***a* is 1.65 M^{-1} s^{-1} at 40°C, roughly 10^7 times that calculated for the H_3O^+-catalyzed hydrolysis of *N*-propylbenzamide.[12] Calculation of the effective concentration of the thiol group in **1***a* is not possible since the bimolecular thiolysis of an unactivated amide has not been reported.

The following general mechanism (an expansion of eq. [1]) is proposed to account for the observed kinetic results:

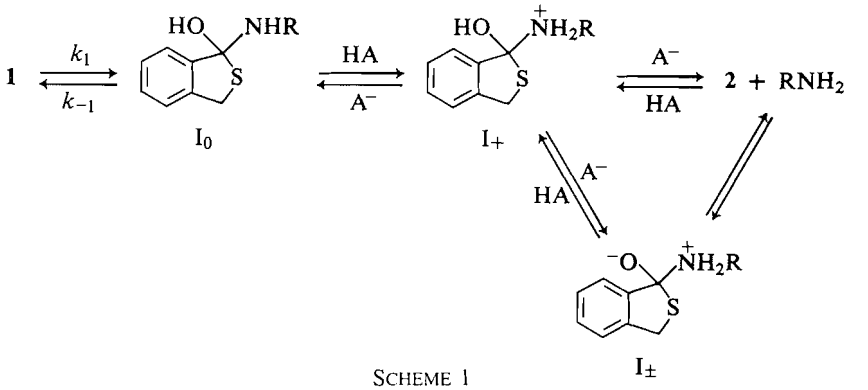

SCHEME 1

The two alternative pathways for breakdown of I_+ will be discussed later. The intermediates involved in Scheme 1 are analogous to those proposed by Jencks and Barnett (17) for the intramolecular sulfur-to-nitrogen acetyl transfer in *S*-acetyl-2-aminoethanethiol. There appears to be no need to invoke any significant reaction via an anionic tetrahedral intermediate (I_-) or the O-protonated form of the substrate.

The uncatalyzed pathway

At low pH or high buffer concentration, we propose the rate-determining step on the thiolactonization pathway to be the uncatalyzed ring-closure of **1** to form I_0. The values of k_1 extrapolated from HCl- and buffer-catalyzed data in Table 1 give an average value for k_1 of 9.7 (±1.1) × 10^{-4} s^{-1} at 40°C up to pH 7. The fact that k_{obs} in 1.0 *M* HCl is roughly 10% lower than that observed in 0.10 *M* HCl may be attributed to a lowering of water activity in the more concentrated acid (27).

However, there does appear to be a systematic (although somewhat erratic) upward trend in the extrapolated values of k_1 at higher pH. Due to the rather long extrapolations involved and the difficulty of obtaining reliable kinetic data for the very slow reactions above pH 8, we have not pursued this matter and simply ascribe this behaviour to a small medium, or pH, effect on k_1. The $\Delta S^{\ddagger}$ associated with the cyclization step (−14 cal $K^{-1}mol^{-1}$) is consistent with the loss of rotational freedom on forming the five-membered ring.

Further support for this assignment comes from studies by Schmir and co-workers (27) on the pH-dependence of products formed in thioimidate ester hydrolysis. This reaction provides an independent method of generating the same type of intermediates as those involved in thiolester aminolysis and amide thiolysis. In every case studied, Schmir found that, at low pH, the products were thiolester and amine exclusively, implying that the rate-determining step in amide thiolysis under these conditions would be formation of neutral tetrahedral intermediate, I_0.

However, conclusions drawn from the results of kinetic studies on thiolester aminolysis (26) and product studies of the hydrolysis of 2-methyl-Δ^2-thiazoline (17, 25) introduce the kinetically equivalent possibility that breakdown of $I_\pm$ to **2** and amine (Scheme 1) may be solely or partially rate-determining at low pH. In order to investigate this possibility in our case, the rate of hydrolysis of the 2-methoxyethylamide (**1***b*), which has a considerably better leaving group than the propylamide

[12]The acid-catalyzed hydrolysis rate constant (k_H) for *N*-methylbenzamide in HCl solution at 100.4°C is 6.13 × 10^{-5} M^{-1} s^{-1} (29). Using $\Delta H^{\ddagger}$ = 21.2 kcal mol^{-1} (30), we calculate k_H = 2.07 × 10^{-7} M^{-1} s^{-1} at 40°C. Making a correction of 1.35-fold for the lower reactivity of the *N*-propyl derivative (31) gives k_H = 1.54 × 10^{-7} M^{-1} s^{-1} at 40°C.

Can. J. Chem. Downloaded from www.nrcresearchpress.com by 210.87.254.5 on 09/06/12
For personal use only.

TABLE 3. Rate constants for catalysis of the thiolactonization of **1***a* at 40.0°C, $\mu = 1.0$

	Acid	pK_a[a]	k'_{HA} (M^{-1} s^{-1})[b]	k'_B (M^{-1} s^{-1})[c]
1.	H_3O^+	−1.74	1.65(±0.15)	1.20×10^{-7}
2.	HCO_2H	3.47	$7.82(\pm0.46) \times 10^{-2}$	9.2×10^{-4}
3.	$ClCH_2CH_2CO_2H$	3.88	$7.83(\pm0.27) \times 10^{-2}$	2.36×10^{-3}
4.	CH_3CO_2H	4.57	$5.27(\pm0.23) \times 10^{-2}$	7.79×10^{-3}
5.	$CHF_3CH_2NH_3^+$	5.32	$2.82(\pm0.10) \times 10^{-2}$	2.35×10^{-2}
6.	MES (H^+)	6.21	$9.2\ (\pm0.8) \times 10^{-3}$	5.94×10^{-2}
7.	$H_2PO_4^-$	6.48	$2.27(\pm0.29) \times 10^{-2}$	2.73×10^{-1}
8.	Tris (H^+)	7.85	$7.5\ (\pm0.5) \times 10^{-4}$	2.11×10^{-1}
9.	$CH_3OCH_2CH_2NH_3^+$	9.31	$1.97(\pm0.08) \times 10^{-4}$	1.60
10.	H_2O	15.27	$2.03(\pm0.04) \times 10^{-7}$[d]	1.50×10^3

[a]Except for H_3O^+ and H_2O, the pK_a values were calculated from the pH values of half-neutralized solutions at 25°C, $\mu = 1.0$, and corrected to 40°C (28).
[b]The errors quoted are standard deviations.
[c]Calculated from $k'_B = k'_{HA} \cdot K_{I+}/K_{HA}$ where $pK_{I+} = 5.4$ (see text).
[d]The value of k'_{H_2O} has been converted to a second-order rate constant by dividing by 55.1.

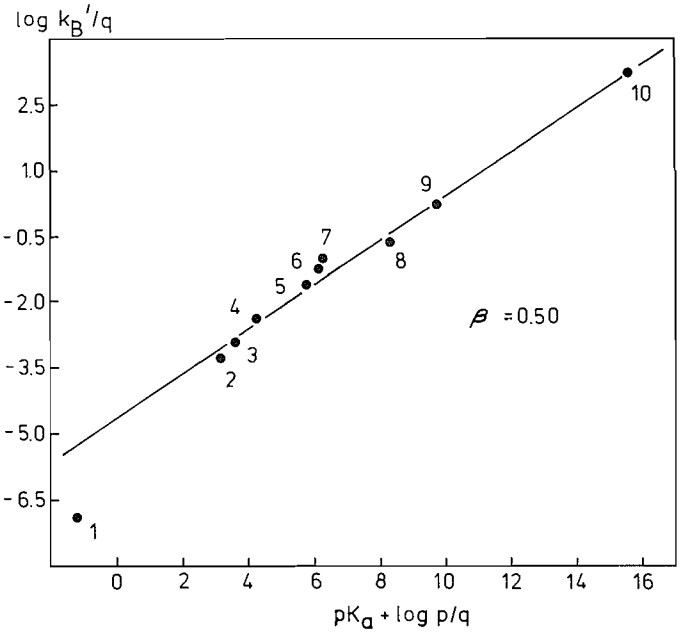

FIG. 3. The statistically-corrected Brønsted plot for the general base-catalyzed step in the thiolactonization of **1***a* at 40.0°C, $\mu = 1.0$ (the numbers refer to the conjugate base of the species in Table 3).

(**1***a*), was investigated. We anticipated that if breakdown of $I_\pm$ were rate-limiting, **1***b* should hydrolyze more rapidly than **1***a* at low pH. In fact, **1***b* reacts more slowly than **1***a* over the pH range 0−4 (Fig. 1), a result more in accord with formation of I_0 being rate-determining.

It should be pointed out that the formation of I_0 from **1** may also proceed via one or more intermediates which cannot be detected kinetically. For example, I_0 may be formed by the cyclization of zwitterion **3** formed in a highly unfavorable equilibrium from **1** (31, 32) or by way of H_3O^+-catalyzed conversion of I_- formed by the cyclization of the thiolate ion of **1** (26).

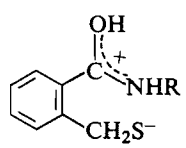

3

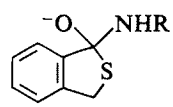

I_-

The general acid-catalyzed pathway

At pH ≥3.5 and low buffer concentration, the thiolactonization of **1***a* exhibits apparent general acid catalysis in terms of neutral substrate (or neutral tetrahedral intermediate) and we propose that breakdown of I_0 becomes rate-determining under these conditions. For general acid catalysis to be observed, this breakdown must proceed via I_+ rather than I_- (see Scheme 1). The $I_0 \rightarrow$ **2** conversion requires two proton transfers and a carbon−nitrogen bond breaking. Presumably loss of amine can occur only in a step following or concerted with *N*-protonation and will occur in the last step of the reaction.[13] This then requires the formation of I_+ or $I_\pm$ or both of these intermediates on the breakdown pathway. Now if either proton transfer in Scheme 1 were solely rate-determining, the Brønsted plot for acid catalysis should show all the characteristics of rate-determining diffusion-controlled proton transfer which have been summarized by Barnett and Jencks (17) and Kirby and co-workers (33). One characteristic of such a plot is a slope of zero or unity or curvature of the type discussed by Eigen (34) with limiting slopes of zero (at low pK_a) and unity (at high pK_a). The Brønsted plot of the k'_{HA} data in Table 3 (not shown) does exhibit some curvature for acids having a $pK_a < 4$ but the limiting slope for weaker acid catalysts is only 0.5. Thus we conclude that the proton transfer is occurring in a step concerted with loss of amine and, referring to Scheme 1, that the rate-determining step in the breakdown of I_0 is the general base-catalyzed conversion of I_+ to **2**, thus avoiding formation of $I_\pm$ as a discrete intermediate. The proposed specific acid−general base catalysis is kinetically equivalent to the general acid catalysis observed. The pK_a values of the two potentially acidic sites in I_+ have been estimated by the method of Fox and Jencks (35) to be 5.4 (ammonium group) and 8.3 (hydroxyl group).[14] Clearly then, over much of the pH range used in this study, a significant proportion of I_0 is converted to I_+ and $I_\pm$ would be the highest energy intermediate at pH ≤ 8. The above estimate of the pK_a of I_+ (to form I_0) allows calculation of the rate constants for general base-catalyzed breakdown of I_+, k'_B ($= k'_{HA} \cdot K_{I+}/K_{HA}$), which are collected in

[13]This follows from the fact that the initial step in the aminolysis of a thiolester is believed to involve attack by amine on the neutral thiolester (24).

[14]The pK_a of I_0 (to form I_-) is similarly estimated to be 11.0. The error in these pK_a values is estimated to be ±1 unit.

Can. J. Chem. Downloaded from www.nrcresearchpress.com by 210.87.254.5 on 09/06/12
For personal use only.

Table 3 and the Brønsted plot is illustrated in Fig. 3. If the point for H_2O is omitted, the correlation is good ($r = 0.993$) with a Brønsted coefficient, β, of 0.50 ± 0.02, consistent with the mechanism proposed.

The interconversion of a neutral tetrahedral intermediate and thiolester (and amine) has been previously proposed to be rate-determining at high pH in the hydrolysis of thioimidate esters (27), in the aminolysis of thiolesters (17, 26), and in the hydrolysis of 2-methyl-Δ^2-thiazoline (17, 25). Further, in each case where buffer catalysis was examined (17, 26, 27), the reaction showed general acid catalysis (or a kinetic equivalent) with a Brønsted plot indicative of rate-determining diffusion-controlled proton transfer. Specifically, these authors proposed that the slow step involves the protonic interconversion of tetrahedral intermediates analogous to I_+ and $I_\pm$. The Brønsted plot in Fig. 3 provides clear evidence that this is not the case for our reaction.

The pK_a estimates described above allow calculation of the equilibrium constant for the conversion I_0 into $I_\pm$ to be $\sim 1 \times 10^{-3}$ (17, 33). Thus $I_\pm$ is roughly 4 kcal mol^{-1} (17 kJ mol^{-1}) higher in energy than I_0 and the concerted pathway proposed must provide a lower energy pathway to product.

Acknowledgements

The financial assistance of the Natural Sciences and Engineering Research Council of Canada is gratefully acknowledged. This manuscript was prepared during a sabbatical leave spent by R. S. M. in the Chemistry Department at the University of British Columbia. We wish to thank members of this department for their hospitality, Mr. P. Borda for performing the microanalyses, and Dr. S. O. Chan and his associates for recording the Bruker WP-80 spectra.

1. Y. M. TORCHINSKI. Sulfhydryl and disulfide groups of proteins. *Translated by* H. B. F. Dixon. Plenum Publ. Corp., New York, NY. 1974. pp. 172–177; A. L. FLUHARTY. *In* Chemistry of the thiol group. Vol. 2. *Edited by* S. Patai. Interscience Publ., John Wiley and Sons, Ltd., New York, NY. 1974. pp. 608–616.
2. (*a*) W. P. JENCKS. *In* The enzymes. Vol. 9. Part B. 3rd ed. *Edited by* P. D. Boyer. Academic Press. New York, NY. 1973. Chapt. 11; (*b*) A. OHNO AND S. OAE. *In* Organic chemistry of sulfur. *Edited by* S. Oae. Plenum Press, New York, NY. 1977. pp. 174–178.
3. J. I. HARRIS and M. WATERS. *In* The enzymes. Vol. 13. Part C. 3rd. ed. *Edited by* P. D. Boyer. Academic Press, New York, NY. 1976. Chapt. 1; C. WALSH. Enzymatic reaction mechanisms. W. H. Freeman and Co., San Francisco, CA. 1979. pp. 322–330.
4. A. N. GLAZER and E. L. SMITH. *In* The enzymes. Vol. 3. 3rd ed. *Edited by* P. D. Boyer. Academic Press, New York, NY. 1971. Chapt. 14.
5. G. LOWE. Tetrahedron, **32**, 291 (1976).
6. S. BLACKBURN. Enzyme structure and function. Marcel Dekker, Inc., New York, NY. 1976. Chapt. 6; A. FERSHT. Enzyme structure and mechanism. W. H. Freeman and Co., San Francisco. CA. 1977. pp. 312–315.
7. (*a*) A. J. KIRBY and A. R. FERSHT. Prog. Bioorg. Chem. **1**, 1 (1971); (*b*) T. H. FIFE. *In* Bioorganic chemistry. Vol. 1. *Edited by* E. E. van Tamelen. Academic Press, New York, NY. 1977. Chapt. 5.
8. T. H. FIFE. Adv. Phys. Org. Chem. **11**, 1 (1975).
9. A. J. KIRBY. Adv. Phys. Org. Chem. **17**, 183 (1980).
10. W. P. JENCKS and J. CARRIUOLO. J. Biol. Chem. **234**, 1280 (1959).
11. G. A. DAFFORN and D. E. KOSHLAND, JR. J. Am. Chem. Soc. **99**, 7246 (1977).
12. R. C. WEAST (*Editor*). Handbook of chemistry and physics. 61st ed. CRC Press, Boca Raton, FL. 1980. p. C–376.
13. R. S. MCDONALD and E. V. MARTIN. Can. J. Chem. **57**, 506 (1979); R. S. MCDONALD and C. E. SIBLEY. Can. J. Chem. **59**, 1061 (1981).
14. M. PROTIVA, M. RAJSNER, E. ADLEROVA, V. SEIDLOVA, and Z. J. VEJDELEK. Collect. Czech. Chem. Commun. **29**, 2161 (1964).
15. D. R. STORM and D. E. KOSHLAND, JR. J. Am. Chem. Soc. **94**, 5815 (1972).
16. W. C. LUMMA, JR., G. A. DUTSA, and C. A. VOLKER. J. Org. Chem. **35**, 3442 (1970).
17. R. E. BARNETT and W. P. JENCKS. J. Am. Chem. Soc. **91**, 2358 (1969).
18. R. A. COX, L. M. DRUET, A. E. KLAUSNER, T. A. MODRO, P. WAN, and K. YATES. Can. J. Chem. **59**, 1568 (1981).
19. M. CHARTON. J. Org. Chem. **29**, 1222 (1964).
20. J. F. BUNNETT and C. F. HAUSER. J. Am. Chem. Soc. **87**, 2214 (1967); D. R. STORM and D. E. KOSHLAND, JR. J. Am. Chem. Soc. **94**, 5805 (1972).
21. M. M. KREEVOY, E. T. HARPER, R. E. DUVALL, H. S. WILGUS III, and L. T. DITSCH. J. Am. Chem. Soc. **82**, 4899 (1960).
22. H. MORAWETZ and J. SHAFER. J. Am. Chem. Soc. **84**, 3783 (1962); G. DALGREN and N. L. SIMMERMAN. J. Phys. Chem. **69**, 3626 (1965); M. D. HAWKINS. J. Chem. Soc. Perkins Trans. 2, 642 (1976).
23. K. A. CONNORS and M. L. BENDER. J. Org. Chem. **20**, 2498 (1961); B. BOOPSINGH and D. P. N. SATCHELL. J. Chem. Soc. Perkins Trans. 2, 1702 (1972).
24. T. C. BRUICE. J. Am. Chem. Soc. **81**, 5444 (1959); T. C. BRUICE, J. J. BRUNO, and W.-S. CHOU. J. Am. Chem. Soc. **85**, 1659 (1963); T. C. BRUICE and L. R. FEDOR. J. Am. Chem. Soc. **86**, 738, 4117 (1964); **86**, 4886 (1964); M. J. GREGORY and T. C. BRUICE. J. Am. Chem. Soc. **89**, 2121 (1967); T. C. BRUICE and S. M. FELTON. J. Am. Chem. Soc. **91**, 2799 (1969); **91**, 6721 (1969); G. J. KASPEREK and T. C. BRUICE. J. Org. Chem. **37**, 1456 (1972).
25. R. B. MARTIN, S. LOWEY, E. L. ELSON, and J. T. EDSALL. J. Am. Chem. Soc. **81**, 5089 (1959); R. B. MARTIN and R. I. HEDRICK. J. Am. Chem. Soc. **84**, 106 (1962); R. B. MARTIN, R. I. HEDRICK, and A. PARCELL. J. Org. Chem. **29**, 3197 (1964).
26. G. M. BLACKBURN. J. Chem. Soc. Chem. Commun. 249 (1970).
27. R. K. CHATURVEDI, A. E. MACMAHON, and G. L. SCHMIR. J. Am. Chem. Soc. **89**, 6984 (1967); R. K. CHATURVEDI and G. L. SCHMIR. J. Am. Chem. Soc. **91**, 737 (1969).
28. D. D. PERRIN. Dissociation constants of organic bases in aqueous solution. Butterworths, London, England. 1965; G. KORTUM, W. VOGEL, and K. ANDRUSSOW. Dissociation constants of organic acids in aqueous solution. Butterworths, London, England. 1961.
29. C. A. BUNTON, S. J. FARBER, A. J. G. MILBANK, C. J. O'CONNOR, and T. A. TURNEY. J. Chem. Soc. Perkin Trans. 2, 1869 (1972).
30. C. R. SMITH and K. YATES. J. Am. Chem. Soc. **93**, 6578 (1971).
31. A. J. KIRBY and P. W. LANCASTER. J. Chem. Soc. Perkins Trans. 2, 1206 (1972).
32. A. R. FERSHT. J. Am. Chem. Soc. **93**, 3504 (1971).
33. M. F. ALDERSLEY, A. J. KIRBY, P. W. LANCASTER, R. S. MCDONALD, and C. R. SMITH. J. Chem. Soc. Perkins Trans. 2, 1487 (1974).
34. M. EIGEN. Angew. Chem. Int. Ed. Engl. **3**, 1 (1964).
35. J. P. FOX and W. P. JENCKS. J. Am. Chem. Soc. **96**, 1436 (1974).

Can. J. Chem. Downloaded from www.nrcresearchpress.com by 210.87.254.5 on 09/06/12
For personal use only.

Kinetics of carbon monoxide oxidation over Co_3O_4 containing catalysts studied by the reversed-flow technique

GEORGE KARAISKAKIS, NICHOLAS A. KATSANOS, AND ALEXIS LYCOURGHIOTIS
Physical Chemistry Laboratory, University of Patras, Patras, Greece

Received October 19, 1982

GEORGE KARAISKAKIS, NICHOLAS A. KATSANOS, and ALEXIS LYCOURGHIOTIS. Can. J. Chem. **61**, 1853 (1983).

The reversed-flow technique, used previously to measure gas diffusion coefficients, heterogeneous catalysis of simple first-order reactions, and other processes, is now extended to the study of the kinetics of a more complicated reaction, namely, the oxidation of carbon monoxide over solid catalysts containing Co_3O_4. The reactants are allowed to diffuse slowly onto the catalyst bed and the reaction is sampled at various times by repeatedly reversing the direction of flow of a gas chromatographic carrier gas passing perpendicularly to the diffusion current.

Rate constants, calculated under steady-state conditions with a second-and first-order rate law, conform to the latter, and this is explained by assuming a reaction between adsorbed carbon monoxide and surface lattice oxygen. Activation energies, calculated from the variation of rate constants with temperature, show a minimum of 14 kJ mol^{-1} for 0.984 mmol of Ca^{2+} per g of the catalyst support. This value is lower than that found by others for pure Co_3O_4 over a similar temperature range.

GEORGE KARAISKAKIS, NICHOLAS A. KATSANOS et ALEXIS LYCOURGHIOTIS. Can. J. Chem. **61**, 1853 (1983).

On a déjà utilisé la technique de l'écoulement inversé pour mesurer les coefficients de diffusion des gaz, la catalyse hétérogène des réactions simples d'ordre un et d'autres processus. On étend maintenant cette technique à l'étude de la cinétique d'une réaction plus compliquée à savoir l'oxydation du monoxyde de carbone sur un catalyseur solide contenant du Co_3O_4. On permet aux réactifs de diffuser lentement dans le lit catalytique et on prélève des échantillons à différents intervalles en inversant de façon répétée la direction d'écoulement du gaz vecteur d'un chromatographe qui passe perpendiculairement à la direction du courant de diffusion.

Les constantes de vitesse, calculées dans les conditions d'état stationnaire avec une loi de vitesse d'ordre deux et d'ordre un, sont en accord avec cette dernière, et on l'explique en supposant qu'il se produit une réaction entre le monoxyde de carbone adsorbé et l'oxygène du réseau de la surface. Les énergies d'activation calculées à partir de la variation des constantes de vitesse avec la température passent par un minimum de 14 kJ mol^{-1} pour 0,984 mmol de Ca^{2+} par gramme de catalyseur. Cette valeur est plus faible que celle trouvée par d'autres chercheurs pour le Co_3O_4 pur dans des intervalles identiques de température.

[Traduit par le journal]

Introduction

Gas chromatography offers many possibilities for physicochemical measurements and some of them are based on perturbations imposed on the carrier gas flow. One such perturbation is to *reverse* the direction of flow of the carrier gas from time to time. Each reversal creates perturbations on the chromatographic elution curve, having the form of extra peaks recorded by the detector system. These peaks constitute a kind of "chromatographic sampling" technique, the rate process taking place within the chromatographic column being the phenomenon sampled.

In its simplest form the above technique was used to measure mutual diffusion coefficients in binary gas mixtures (1), and their temperature variation (2). The diffusion cell consists of an empty chromatographic column $l' + l$ and a diffusion column L connected perpendicularly to the first, around its midpoint (cf. Fig. 1 of ref. 1). The one gas component A (solute) is injected as a pulse at the closed end of the diffusion column, while the other component B (carrier gas) flows continuously through $l' + l$, filling also L. At known times the direction in the flow of B is reversed by means of a suitable valve (cf. Fig. 2 of ref. 1), thus creating sample peaks of A in the detector trace. When the time elapsing between any two successive reversals of the flow is greater than the total gas hold-up time $t'_M + t_M$ in column $l' + l$, a sample peak follows *every* reversal (1). But when the time passing between two successive reversals is less than both t'_M and t_M, only one (symmetrical) sample peak appears after the two successive reversals (2). The dependence of the heights of the sample peaks on the time when the last reversal was made has been derived in an analytical mathematical form and used to calculate the diffusion coefficient of A into B.

A second application of the reversed-flow method was to measure adsorption equilibrium constants of gaseous hydrocarbons on γ-aluminium oxide (3). The adsorbent in this case filled the lower part of the diffusion column L (cf. Fig. 1 of ref. 3), and the hydrocarbon was injected on the top of this column, while carrier gas helium was passing through the empty chromatographic column.

A variation of this method (4) relating to catalysis was to study the kinetics of the drying of a catalytic support impregnated with an organic solvent.

In another series of papers (5–8) the reversed-flow technique was applied to real heterogeneous catalysis. After a general theoretical analysis (6) in which the relevant mathematical equations were derived, the method was used to study the kinetics of alcohols dehydration and of some deaminations over 13X molecular sieve and γ-aluminium oxide (6–8).

In these catalytic studies only the chromatographic column $l' + l$ was employed, filled with the catalyst, and the reactant was injected as a pulse at a middle position of the column, which was also used to separate the products from the reactants (cf. Fig. 3 of ref. 6). However, the theoretical analysis (6) was made only for the case of a reactant A more strongly adsorbed on the catalyst surface than the product(s). Only the latter are eluted from the column, while the reactant, owing to its high adsorption equilibrium constant and to the repeated flow reversals, never is eluted from the column, and also it approximately retains its original space distribution along the column.

In the present paper the reversed-flow technique was applied to a quite different case of heterogeneous catalysis, with *two* gaseous reactants, namely, carbon monoxide and oxygen, neither of which could be retained in the catalytic bed for a long time. Both reactants, together with the product carbon dioxide,

Can. J. Chem. Downloaded from www.nrcresearchpress.com by 210.87.254.42 on 09/06/12
For personal use only.

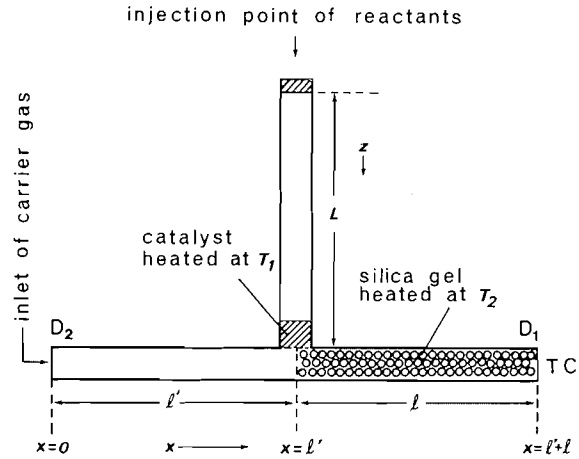

FIG. 1. Schematic representation of the cell used to study heterogeneous catalysis, feeding the catalyst bed by diffusion of the reactants from a remote point of injection.

were rapidly eluted from the catalytic column. In order to extend the reversed-flow method to this type of reactions, we combined the experimental arrangements used to study diffusion coefficients on the one hand (1) and heterogeneous catalysis on the other (6), with the result shown schematically in Fig. 1. A mixture of the reactants is introduced as a pulse at the top of the column L and is allowed to diffuse slowly onto the catalyst retained within a short section at the lower part of the column, and heated to a temperature T_1. The concentration of the reactants at the junction $x = l'$ depends on: (*a*) the time, (*b*) their diffusion coefficient, modified to an effective value because of possible adsorption inside the catalyst bed (3), (*c*) the rate of the chemical reaction on the catalyst, (*d*) the mass of the catalyst, and (*e*) the volume flow-rate of the carrier gas. The concentration of the product at the same point $x = l'$ is determined by: (*a*) the reaction rate which in turn depends on the concentration(s) of reactants, (*b*) the catalyst mass, and (*c*) the carrier gas flow-rate.

A sampling of all concentrations issuing from L can be made by reversing the direction of the carrier gas flow for a short time, and then restoring it in its original direction from D_2 to D_1. Following this flow perturbation, fairly symmetrical sample peaks are recorded by the thermal conductivity detector (TC). These peaks appear separate for the reactants and products, since the chromatographic material (silica gel), filling the column section l and heated at a different temperature (T_2) from that of the catalyst (T_1), causes separation of the various substances.

The above are an obvious extension of the technique reported earlier (6). They continuously sample the catalytic reactor by repeatedly reversing the gas flow direction and measuring the sample signals produced in a chromatographic detector. If the reactants have considerably bigger adsorption equilibrium constants on the catalyst surface than the products, only column $l' + l$, filled with catalyst, is necessary. This acts both as a catalytic reactor and a chromatographic column, and the reactants are injected directly onto it, at some intermediate position along the column (6). Then only the products are eluted and recorded, whereas the reactants approximately retain their original space distribution in the column. If, on the other hand, the adsorption equilibrium constants of the reactants are comparable to those of the products, so that no separation can be effected by the catalytic bed itself, the arrangement of Fig. 1 is employed, i.e. a separate chromatographic material is placed within the system to cause separation of the various substances. Moreover, the catalyst is restricted to a small column length and is fed with reactants by their diffusion from a remote point of injection. This arrangement ensures the presence of reactants over the catalyst for a long time period, and also that the space within which reaction takes place is confined near the junction of the two columns and is not spread with time along the column $l' + l$.

The reversed-flow method is a differential technique for studying heterogeneous catalysis, not suffering from a possible disadvantage of the stopped-flow method (9), consisting in continuously switching the system under study from a flow dynamic one to a static system and vice versa. This permits diffusion and other related phenomena to come into play when the flow is stopped. Compared to the sample vacancy chromatography (10), it is simpler experimentally, since it is not necessary to pass the reactants, mixed with the carrier gas, continuously through the catalyst. Moreover, a whole range of reactants composition is possible within one single experiment, by feeding the catalyst through the diffusion column L.

The oxidation of carbon monoxide was chosen because of the well known interest in this reaction in connection with control of automotive emissions (11) and in order to study the activity for the above reaction of some catalysts newly synthesized in this laboratory (12).

Experimental

Materials

The carrier gas helium and the oxygen were of gas chromatographic grade (Linde, ≥ 99.99% purity). Carbon monoxide and carbon dioxide were obtained from Matheson Gas Products.

The catalysts, designated as Ca-X-Co-420, contained X mmol Ca^{2+} per g of γ-Al_2O_3, and 2.8 g of Co_3O_4 per 100 g of the modified support. They were calcined at 420°C and prepared as already reported (12).

Silica gel 100–120 mesh from Matheson Coleman and Bell was used for gas chromatography.

Apparatus

The apparatus is shown diagrammatically in Fig. 2 and was a variation of that used to measure diffusion coefficients (1). It consisted of a simple gas chromatograph (Pye series 104) with a thermal conductivity detector (TC), incorporating the cell of Fig. 1 and a suitable valve S (four-port or six-port with two alternate ports connected through a small piece of 1/16 in. tube).

The three arms of the cell had lengths L = 70.5 cm (stainless steel), $l = l'$ = 40 cm (glass), and a common i.d. 4 mm. The catalytic bed was 2.8 cm long and contained 0.35 g of catalyst each time.

The flow reversals were made by switching the gas valve S from one position (solid lines) to the other position (dotted lines) and vice versa.

The column length l' was an open tube, while the column length l was filled with silica gel effecting the separation of the reactants CO + O_2 from the product CO_2. Both column sections l' and l were kept at 323 K by means of the chromatograph oven. The catalyst bed always was heated to a higher temperature by means of a heated injector block, incorporating a thermocouple and regulated through the electrical control unit of the chromatograph. Temperature variations along the bed were smaller than 3 K.

Procedure

Before measurements, the whole system was conditioned by heating *in situ* the catalyst at 673 K and the silica gel column at 473 K, both for 20 h, under helium flow. The reactants were premixed at room temperature and atmospheric pressure in a proportion by volume 3:1 $CO:O_2$. Some preliminary injections of this mixture were made

Can. J. Chem. Downloaded from www.nrcresearchpress.com by 210.87.254.42 on 09/06/12
For personal use only.

Can. J. Chem. Downloaded from www.nrcresearchpress.com by 210.87.254.42 on 09/06/12
For personal use only.

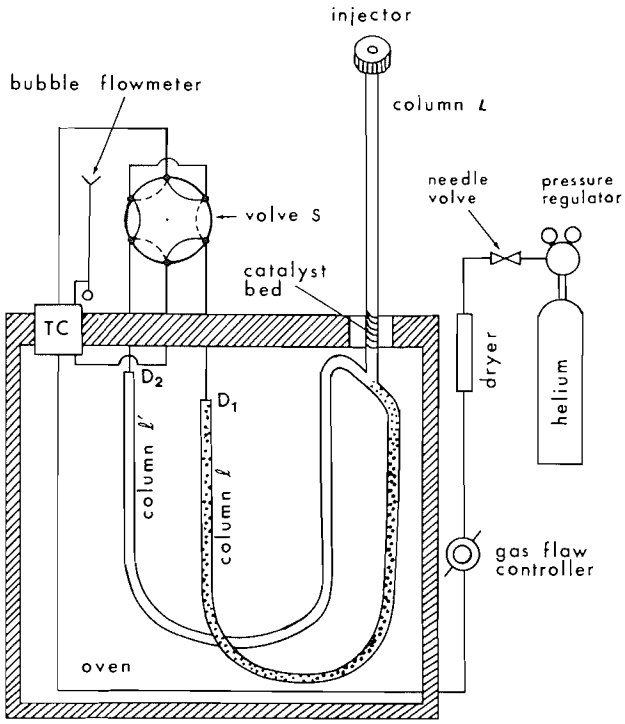

FIG. 2. Experimental set-up to study heterogeneous catalysis by the reversed-flow method.

to stabilise the catalyst, and then, with the carrier gas flowing in direction from D_2 towards D_1 (cf. Figs. 1 and 2) with a flow rate 0.281 $cm^3 s^{-1}$, 2 cm^3 of the reacting mixture were rapidly introduced with a gas-tight syringe at the top of the diffusion column L.

After some time (usually about 15 min or more), a detectable continuous signal appeared in the chromatographic trace, being obviously due to both reactants and products. Then, the direction of the carrier gas flow was reversed by switching valve S to its dotted position, the exact time of the reversal being noted. This reversed flowing was maintained for a period of 12 s, which was less than the gas hold-up time in the empty column section l'. Then the flow was restored to its original direction by valve S. After a dead time of about 12 s, the continuous chromatographic signal is reestablished and on it appear two fairly symmetrical and relatively narrow *sample* peaks, as Fig. 3 shows. The first of these peaks is due to a mixture of CO and O_2, while the second to CO_2. Both constitute what was called in the Introduction "chromatographic sampling" of the chemical reaction at the time of the flow reversal. This sampling is repeated several times with always the same duration (12 s) of reverse flow, giving a series of pair peaks, corresponding to various times from the injection of the reactants. The pressure at the injection point was 1.2 atm. The pressure change in tube L at each flow reversal was small because of the small pressure drop along the filled column l (about 0.2 atm), and also because of the short reversal duration (12 s). In cases of large pressure drops along l, the column section l' should also be filled with the same material as l to minimize pressure changes at the exit of L.

It was not found possible to separate all the three substances CO, O_2, and CO_2 after each flow reversal, since this would require a rather long time compared to the time of the reaction. Thus, we confined ouselves to the separation of the product CO_2 from the reaction mixture CO + O_2. The relative sensitivity of the thermal conductivity detector for CO and O_2 was determined by injecting a mixture of known composition in these two gases at the top of a column L which did not contain any catalyst, while the separation column l contained molecular sieve 5A 80–100 mesh. By applying the same reversed-flow technique, a series of pair peaks was obtained. Plotting the height of CO peaks and the height of O_2 peaks separately as described elsewhere (2), the effective diffusion coefficients of the two gases in

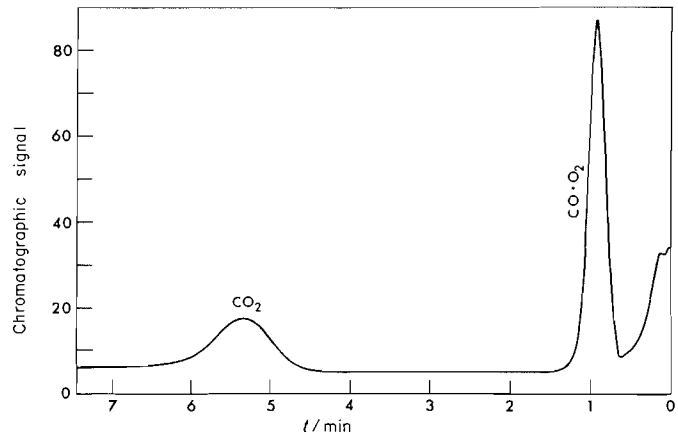

FIG. 3. Chromatographic sampling of the reaction CO + $\frac{1}{2}O_2 \rightarrow CO_2$ at 552.2 K, 44 min after injection of the reactants.

helium were determined. They were found 0.578 and 0.604 $cm^2 s^{-1}$ for CO and O_2, respectively, reduced to 1.2 atm. These differ by about 5% from the theoretically calculated values at the same pressure and temperature. The relative sensitivity for the detector used, found from the ratio of the intercepts of ln $(ht_0^{1/2})$ against $1/t_0$ plots, gave a response of O_2 to that of CO 1.05, when the response was measured as the height of the peak maximum above the continuous signal. The relative sensitivity of CO and CO_2 was found in a similar way without catalyst, but with silica gel in column l. Measured in peak heights to the maximum it was CO_2:CO = 1:5.37, while in peak areas CO_2:CO = 1:1.62.

Results and discussion

The chromatographic sampling equation has been derived in special forms (1, 6), as well as in a general form (2):

$$\begin{aligned} c_x = {} & c_{x,1}(l', t_0 + t' + \tau)\cdot u(\tau) + c_{x,2}(l', t_0 + t' - \tau) \\ & \cdot[1 - u(\tau - t')]\cdot[u(\tau) - u(\tau - t'_M)] \\ & + c_{x,3}(l', t_0 - t' + \tau)\cdot u(t_0 + \tau - t') \\ & \cdot\{u(t - t')[1 - u(\tau - t'_M)] \\ & - u(\tau - t')[u(\tau) - u(\tau - t'_M)]\} \end{aligned} \quad [1]$$

where c_x is the concentration of the various substances at the detector, $c_{x,1}(l',\ldots)$, $c_{x,2}(l',\ldots)$, $c_{x,3}(l',\ldots)$ are concentrations at the point $x = l'$ (cf. Fig. 1) for the times shown, the various u's are unit step functions for the arguments shown in parentheses, and τ was taken to mean $t - t_M$, i.e. the time from the last restoration of the carrier gas flow diminished by the gas hold-up time in section l of the column. Now that this section is filled with a solid adsorbent, the retention time t_R of the various substances for linear ideal chromatography on column l must be substituted for t_M. This can easily be proved by starting from eq. [5] of ref. 2 which now must be written as:

$$(1 + k_A)\frac{\partial c_x}{\partial t} = -v\frac{\partial c_x}{\partial x} + v(c_x)_{x=l'}\delta(x - l')$$

k_A being the partition ratio of each substance A on column l. This amounts to a substitution of v by $v/(1 + k_A)$, or $l/v = t_M$ by $(1 + k_A)l/v = (1 + k_A)t_M = t_R$. Thus, for the present situation

$$\tau = t - t_R \quad [2]$$

and since t_R is different for the reactants CO + O_2 and the product CO_2, eq. [1] predicts a separation for two out of the three terms $c_{x,1}^{(r)}$, $c_{x,2}^{(r)}$, $c_{x,3}^{(r)}$ of the reactants, from two out of the three $c_{x,1}^{(p)}$, $c_{x,2}^{(p)}$, $c_{x,3}^{(p)}$ terms of the product, as depicted in

Can. J. Chem. Downloaded from www.nrcresearchpress.com by 210.87.254.42 on 09/06/12
For personal use only.

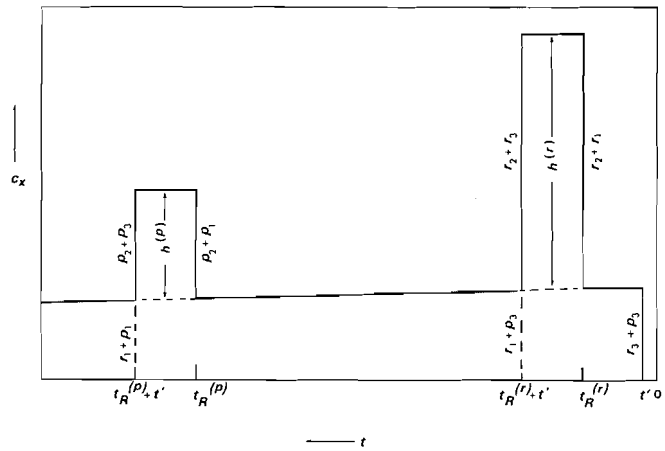

FIG. 4. Values of the time variable t, at which the various terms of eq. [1] for the reactants and the product appear and cut down, for linear ideal chromatography in column l. r_1, r_2, r_3, p_1, p_2, p_3 stand for $c_{x,1}^{(r)}$, $c_{x,2}^{(r)}$, $c_{x,3}^{(r)}$, $c_{x,1}^{(p)}$, $c_{x,2}^{(p)}$, $c_{x,3}^{(p)}$, respectively.

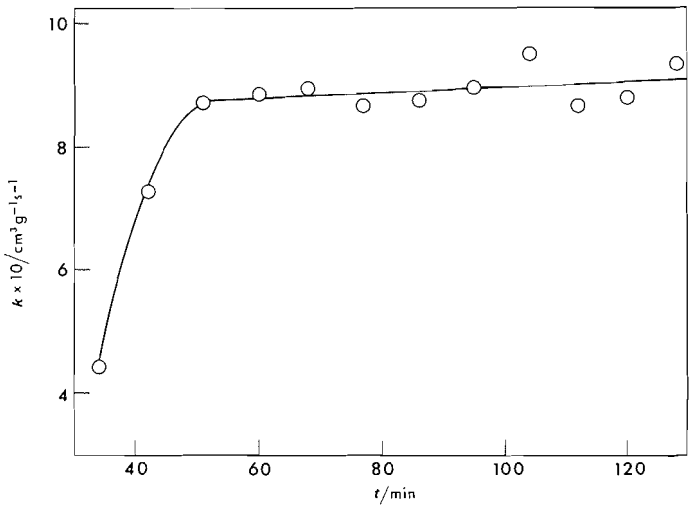

FIG. 5. An example of attainment of a steady-state condition in the reaction rate for the catalyst containing 0.392 mmol Ca^{2+} per g γ-Al_2O_3 at 526.2 K.

Fig. 4. Comparison of this figure with the experimental Fig. 3 shows that eq. [1] correctly predicts the elution curve after each flow reversal, apart from a different normal spreading of the two peaks. This is due to non-ideality (axial diffusion in column l, mass transfer resistance in the stationary phase, non-equivalent flow paths in the packed bed), and also to the fact that there is a small volume between the tube l' and the bottom of the catalyst bed in L which, on restoring the original gas flow direction, is "drained" by an exponential dilution phenomenon.

The height h of the maximum of the peaks, measured from the steady continuous signal, is equal to the sum $c_{x,2} + c_{x,3}$ and corresponds to time $t_R + t'/2$ or $\tau = t'/2$ (cf. Fig. 4). From eq. [1], by putting $\tau = t'/2$ in these two terms, we obtain

$$[3] \quad h = c_{x,2}(l', t_0 + t'/2) + c_{x,3}(l', t_0 - t'/2)$$

for both reactants and product. Since the times in the two terms on the r.h.s. differ only by t' (= 12 s), both terms can be taken at a mean time t_0. Then eq. [3] reduces to

$$[4] \quad h^{(r)} \simeq 2c_x^{(r)}(l', t_0) \qquad \text{and} \qquad h^{(p)} \simeq 2c_x^{(p)}(l', t_0)$$

for reactans and product, respectively.

There remains to be seen what the two concentrations $c_x^{(r)}$ and $c_x^{(p)}$, measured by the respective heights $h^{(r)}$ and $h^{(p)}$, represent. If $r(t_0)$ is a mean reaction rate at time t_0 for the whole catalyst bed in mol CO_2 s^{-1} g^{-1} catalyst, the concentration of CO_2, at $z = L$, $x = l'$ is given by

$$[5] \quad c_x^{(p)}(l', t_0) = \frac{r(t_0)M}{\dot{V}}$$

and thus $h^{(p)}$ is a measure of the mean reaction rate at the time of each flow reversal. The height $h^{(r)}$ of the other peak clearly measures the sum of the concentrations of the non reacted CO + O_2 diffusing out of the catalyst bed at $x = l'$ and time t_0.

In steady-state conditions, assumed to be established after a certain time, the relative concentrations of the three substances will depend on the concentrations of reactants reaching the catalyst bed by diffusion and the stoichiometry of the reaction, $CO + \frac{1}{2}O_2 \rightarrow CO_2$, since no accumulation of reactants or product occurs in the catalyst bed. Then, if $3a$ is the concentration of CO diffusing into the bed at any time, the respective O_2 concentration will be a, since the two reactants were introduced at the top of the diffusion column in a volume ratio 3:1 and their effective diffusion coefficients in the inert helium were found approximately equal. Thus, at any time after steady state the three concentrations detected will be $[CO_2] = y$, $[CO] = 3a - y$, $[O_2] = a - y/2$. Since $h^{(r)} = 2[CO] + 2[O_2] = 8a - 3y$ and $h^{(p)} = 2[CO_2] = 2y$, the two concentrations [CO] and $[O_2]$ can be expressed in terms of $h^{(r)}$ and $h^{(p)}$, the measured $h^{(p)}$ being multiplied by 5.37 to correct it for relative sensitivities of the detector (cf. Experimental section):

$$[6] \quad [CO] = \frac{3}{8}h^{(r)} + \frac{1}{16}h^{(p)} \qquad \text{and} \qquad [O_2] = \frac{1}{8}h^{(r)} - \frac{1}{16}h^{(p)}$$

Because of the small concentrations of both reactants over the catalyst surface, linear Henry-type adsorption isotherms can be assumed. Therefore, if the reaction follows a simple Langmuir–Hinshelwood or Rideal mechanism, a second-order rate law is expected, $r = k[CO][O_2]$, where k is an apparent rate constant. Combining this rate law with eqs. [4], [5], and [6], one obtains

$$[7] \quad k = \frac{32\dot{V}}{M} \cdot \frac{h^{(p)}}{(3h^{(r)} + h^{(p)}/2)(h^{(r)} - h^{(p)}/2)}$$

However, the experimental data do not conform to this equation, since the k values calculated using eq. [7] increase with time continuously without limit. Thus, a mechanism involving a reaction between adsorbed carbon monoxide and adsorbed or gaseous oxygen or vice versa does not seem to be supported by the present experimental evidence.

Another mechanism, pointed out by Mehandjien and Nikolova-Zhecheva (13), namely, a reaction between adsorbed carbon monoxide and surface lattice oxygen, would follow a phenomenological rate law $r = k[CO]$, if the mass of the catalyst is big enough. Then, instead of eq. [7], we would have

$$[8] \quad k = \frac{4\dot{V}}{M} \cdot \frac{h^{(p)}}{3h^{(r)} + h^{(p)}/2}$$

Rate constants calculated from the experimental $h^{(r)}$ and $h^{(p)}$ values, using eq. [8] for all catalysts studied and at all temperatures, initially increase but then reach a limiting value and remain constant, within the limits of experimental error, after a certain time. An example is shown in Fig. 5, while Table 1 lists the mean limiting values of this rate constant. It is seen

Can. J. Chem. Downloaded from www.nrcresearchpress.com by 210.87.254.42 on 09/06/12
For personal use only.

TABLE 1. Limting rate constants k for the oxidation of carbon monoxide over Co_3O_4 supported on γ-Al_2O_3 doped with Ca^{2+}, for various support compositions and at various temperatures*

Ca^{2+} content (mmol per g γ-Al_2O_3)	T (K)	t_0† (min)	$k \times 10$ ($cm^3\ g^{-1}\ s^{-1}$)
0.392	466.2	63–123	2.80(5) ±0.05
	487.2	30–93	3.8 (7) ±0.1
	526.2	51–128	8.93(10)±0.09
	552.2	90–125	9.4 (3) ±0.2
0.621	441.2	90–110	1.86(3) ±0.04
	466.2	95–135	3.2 (4) ±0.1
	500.2	95–125	4.02(4) ±0.08
0.984	466.2	64–107	3.80(6) ±0.05
	487.2	50–110	4.42(6) ±0.05
	509.2	86–107	5.41(3) ±0.09
	552.2	36–108	6.5 (8) ±0.3
1.560	441.2	77–107	0.80(4) ±0.02
	466.2	104–144	1.36(5) ±0.03
	500.2	75–125	1.89(6) ±0.05
	535.2	93–124	2.92(4) ±0.08
	544.2	100–144	3.22(5) ±0.09
2.470	466.2	49–96	1.39(6) ±0.05
	487.2	86–102	1.40(3) ±0.03
	509.2	77–120	3.20(5) ±0.02
	526.0	62–91	4.18(4) ±0.03
	552.2	76–100	7.0 (4) ±0.1

*Each k value is a mean of a number of k's shown in parentheses, measured in the time interval under t_0. The ± values are standard errors of the mean.

†Each final entry in the intervals given corresponds to the time of the last flow reversal, but does not include the final elution time of the product CO_2 (ca. 8 min).

TABLE 2. Activation energies for the oxidation of carbon monoxide over Co_3O_4 supported on γ-Al_2O_3 doped with Ca^{2+}, for various support compositions; the ± values are standard errors from the regression analysis

Ca^{2+} content (mmol per g γ-Al_2O_3)	E_a (kJ mol^{-1})
0.392	33±5
0.621	24±7
0.984	14±1
1.560	26±1
2.470	44±6

from this table that there exists a variation in the time required for attainment of the steady state (initial entries under t_0). This is probably due to the pure repeatability of introducing the gaseous reacting mixture of CO and O_2, since the time required for the model to apply (and the rate coefficients to become constant) depends mainly on the time required for a steady-state situation to be attained in the diffusion tube and catalyst bed. Anyhow, the constancy of k after some time is consistent with the mechanism implied by eq. [8] in agreement with the findings of Mehandjiev and Nikolova-Zhecheva (13), who established that at temperatures between 250 and 350°C the catalyst (Co_3O_4) stoichiometry changes under the effect of the reactants.

The relevant activation energies, calculated from conventional Arrhenius plots, are collected in Table 2. A remarkable fact is immediately apparent from this table, namely that the activation energy decreases almost linearly with increasing Ca^{2+} content of the catalyst support, until a minimum value at 0.984 mmol Ca^{2+} per g γ-Al_2O_3, and then increases again linearly with Ca^{2+} content. The minimum value (3.2 ± 0.3 kcal mol^{-1}) is rather smaller than that found by others (13) for pure Co_3O_4 (4.6 ± 0.5 kcal mol^{-1}) at a comparable temperature range, but discussion of this behaviour is beyond the scope of this article.

Acknowledgement

The authors wish to thank Mrs. Anna Sinou-Karahaliou for assistance.

1. N. A. KATSANOS and G. KARAISKAKIS. J. Chromatogr. **237**, 1 (1982).
2. N. A. KATSANOS and G. KARAISKAKIS. J. Chromatogr. **254**, 15 (1983).
3. G. KARAISKAKIS, N. A. KATSANOS, and A. NIOTIS. J. Chromatogr. **245**, 21 (1982).
4. G. KARAISKAKIS, A. LYCOURGHIOTIS, and N. A. KATSANOS. Chromatographia, **15**, 351 (1982).
5. N. A. KATSANOS and I. GEORGIADOU. J. Chem. Soc. Chem. Commun. 242 (1980); 640 (1980).
6. N. A. KATSANOS. J. Chem. Soc. Faraday Trans. I, **78**, 1051 (1982).
7. G. KARAISKAKIS, N. A. KATSANOS, I. GEORGIADOU, and A. LYCOURGHIOTIS. J. Chem. Soc. Faraday Trans. I, **78**, 2017 (1982).
8. M. KOTINOPOULOS, G. KARAISKAKIS, and N. A. KATSANOS. J. Chem. Soc. Faraday Trans. I, **78**, 3379 (1982).
9. C. S. G. PHILLIPS, A. J. HART-DAVIS, R. G. L. SAUL, and J. WORMALD. J. Gas Chromatogr. **5**, 424 (1967).
10. C. S. G. PHILLIPS and C. R. MCLLWRICK. Anal. Chem. **45**, 782 (1973).
11. F. G. DWYER. Catalysis reviews. Vol. 6. *Edited by* H. Heinemann. Dekker, New York. 1972. p. 261.
12. A. LYCOURGHIOTIS, A. TSIATSIOS, and N. KATSANOS. Z. phys. Chem. **126**, 95 (1981).
13. D. MEHANDJIEV and E. NIKOLOVA-ZHECHEVA. J. Catal. **65**, 475 (1980).

Appendix

c_x = concentration of the reactants and products at the detector (mol cm^{-3})
h = height of the maximum of extra peaks above the continuous signal (mol cm^{-3})
l, l' = lengths of the two sections of the chromatographic column (cm)
L = length of diffusion column (cm)
k = apparent rate constant for the reaction
M = catalyst mass (g)
$r(t_0)$ = mean reaction rate at time t_0 (mol $g^{-1}\ s^{-1}$)
t_0 = time measured from the injection of reactants to the last backward reversal of gas flow (min)
t' = time interval of backward flow of carrier gas (s)
t = time measured from the last restoration to forward direction of the gas flow (s)
t_M, t'_M = gas hold-up time of column section l or l', respectively (s)
t_R = ideal retention time on column section l (s)
$\dot{V}$ = volume flow-rate of carrier gas ($cm^3\ s^{-1}$)
x, z = distance coordinates along the chromatographic and the diffusion column, respectively (cm)
τ = time defined by eq. [2]

Modified Curtius rearrangements in the selective cleavage of β-D-glucosiduronic acid and β-D-glucosiduronamide linkages[1]

GERALD OLIVER ASPINALL,[2] HANY KAMAL FANOUS, NIMAL SAVITRI KUMAR,[3] AND VELUPILLAI PUVANESARAJAH
Department of Chemistry, York University, Downsview, Toronto, Ont., Canada M3J 1P3

Received January 27, 1983

GERALD OLIVER ASPINALL, HANY KAMAL FANOUS, NIMAL SAVITRI KUMAR, and VELUPILLAI PUVANESARAJAH. Can. J. Chem. **61**, 1858 (1983).

The selective cleavage of β-D-glucosiduronic acid linkages in permethylated carbohydrates is achieved by modified Curtius rearrangements involving (a) reaction of glycosiduronic acids with diphenylphosphoroazidate or (b) treatment of glycosiduronamides with lead tetraacetate, each in the presence of *tert*-butanol or benzyl alcohol to give 5-*tert*-butyloxycarbonylamino- or 5-benzyloxycarbonylaminopentopyranosides, followed by mild acid hydrolysis (for *tert*-butyl) or hydrogenolysis (for benzyl) of the carbamates to give pentodialdoses (from uronic acids) with retention of substituents, and with exposure of aglyconic hydroxyl groups. The liberated functional groups are available for derivative formation. These reaction sequences have been performed on permethylated derivatives of D-glucuronic acid, gentiobiouronic acid, 2-*O*-β-D-glucopyranosyl-D-galacturonic acid, and gum arabic.

GERALD OLIVER ASPINALL, HANY KAMAL FANOUS, NIMAL SAVITRI KUMAR et VELUPILLAI PUVANESARAJAH. Can. J. Chem. **61**, 1858 (1983).

On a clivé sélectivement la liaison reliant l'acide β-D-glucosiduronique aux carbohydrates perméthylés en utilisant une transposition de Curtius modifiée qui implique les étapes suivantes: (a) la réaction de l'acide glycosiduronique avec la phosphoroazidate de diphényle ou (b) la réaction des glycosiduronamides avec le tétraacétate de plomb. La réaction dans les deux cas a lieu en présence de l'alcool *tert*-butylique ou de l'alcool benzylique et conduit aux *tert*-butyloxycarbonylamino-5 ou aux benzyloxycarbonylamino-5 pentopyranosides. L'hydrolyse acide douce (du *tert*-butyle) ou l'hydrogénolyse (du benzyle) des carbamates donne les pentoaldioses (à partir de l'acide uronique) avec rétention des substituants et avec exposition des groupes hydroxyles de l'aglyconique. On peut utiliser les groupes fonctionnelles ainsi libérés pour préparer des dérivés. On a réalisé cette suite de réactions sur les dérivés perméthylés de l'acide D-glucuronique, de l'acide gentiobiouronique, de l'acide *O*-2-β-D-glucopyranosyl-D-galacturonique et de la gomme arabique.

[Traduit par le journal]

The selective cleavage of glucosiduronamide linkages in polysaccharides by the Hofmann degradation was first performed by Kochetkov *et al.* (1) with the net liberation, after mild acid treatment of the reaction mixture, of a pentodialdose and an aglycone. We have previously shown (2) that this degradation (see Scheme 1) may be carried out on permethylated polysaccharides containing nonterminal glucuronic acid residues so that (*i*) pentodialdoses (B″) derived from the uronic acid residues (B) are reduced to pentitols (B‴) with glycosyl substituents (A) still attached, and (*ii*) the sites of former attachment of glycosyluronic acid residues may be ascertained by further reactions of the exposed hydroxyl groups (in C′). The reaction sequence, however, suffers from disadvantages in that (a) it is carried out under strongly basic conditions, and (b) that the isolation and characterization of products only at the end of a lengthy series of operations does not permit the detection of incomplete reaction in the early steps of the sequence. We now describe two modified Curtius rearrangements, carried out under neutral conditions in nonaqueous solvents, in which the intermediate isocyanates (B*), common to Hofmann and Curtius rearrangements, are converted into isolable *tert*-butyl or benzyl carbamates (B′) without rupture of glycosidic linkages. Cleavage of glycosidic linkages in the structurally modified methylated oligo- or polysaccharides may then be effected by decomposition of the carbamates with the same net formation of pentodialdoses from hexuronic acid units and liberation of aglycones as in the Hofmann degradation. Fragmentations leading to the same products have been achieved by oxidative decarboxylation with lead tetraacetate (3) via 5-acetoxypentopyranosides (B^+).

Methyl 2,3,4-tri-*O*-methyl-β-D-glucopyranosiduronic acid (**1**) and the permethylated derivative (**5**) of methyl β-gentiobiosiduronic acid (3) were used as substrates for the modified Curtius rearrangement described by Yamada and coworkers (4, 5). Treatment of the glycosiduronic acids with diphenylphosphorazidate in *tert*-butanol in the presence of 1 molar equivalent of triethylamine furnished *tert*-butyl carbamates **3** and **8** as crystalline rearrangement products in high yield. The available nmr data did not define the stereochemistry at C-5 of the modified sugar residues but retention of configuration is assumed as with other Curtius rearrangements (5). Alternatively, *tert*-butyl carbamates **3** and **8** were prepared in similar yield by reaction of the corresponding glycosiduronamides **2** and **7** with lead tetraacetate in *tert*-butanol (6, 7). For polysaccharide substrates we have found this latter procedure to be superior in degree of structural modification and in ease of product isolation. The same two procedures have been used for the preparation of the analogous benzyl carbamates **4** and **9**, reactions being performed in benzene solution with only a small excess of benzyl alchol.

Controlled cleavage of the *tert*-butyl carbamates was achieved with formic acid at room temperature, intermediate pentodialdoses were reduced with sodium borohydride, and the products were acetylated to give the corresponding pentitol diacetates. Thus carbamate **3** afforded 2,3,4-tri-*O*-methylxylitol diacetate which was characterized by glc – mass spectrometry. With 1,6-anhydro-2,3,4-tri-*O*-methyl-β-D-galactopyranose as internal standard, analysis of the products similarly

[1]Presented in part at the Canadian Institute of Chemistry Conference, Vancouver, B.C., June 3–6, 1979, and at the 10th International Symposium on Carbohydrate Chemistry, Sydney, New South Wales, Australia, July 7–11, 1980.

[2]Author to whom correspondence should be addressed.

[3]On leave from the University of Peradeniya, Sri Lanka (1977–1978).

Can. J. Chem. Downloaded from www.nrcresearchpress.com by 210.87.254.5 on 09/06/12
For personal use only.

Can. J. Chem. Downloaded from www.nrcresearchpress.com by 210.87.254.5 on 09/06/12
For personal use only.

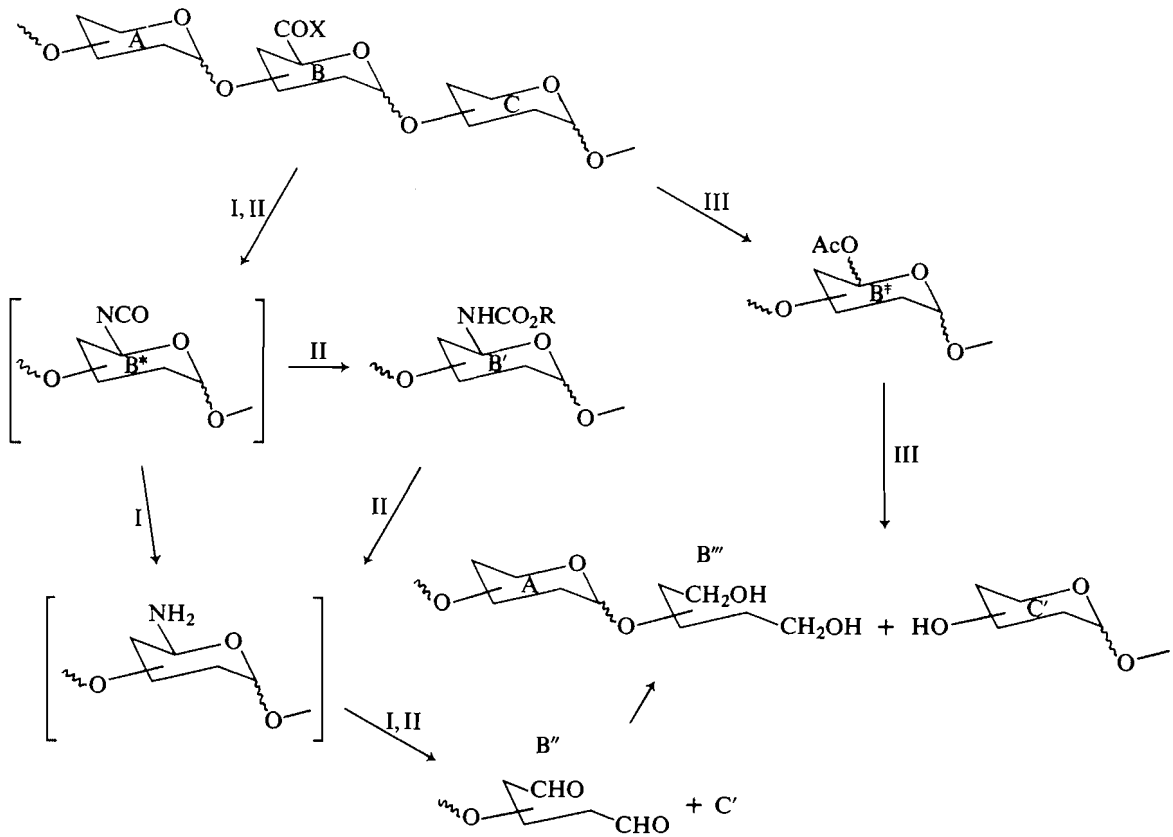

SCHEME 1. Selective cleavage of internal glycosiduronic acid (X = OH) or glycosiduronamide (X = NH_2) linkages (B) and formation of stable derivatives (—A—B‴ and C′—) initiated by (I) Hofmann rearrangement, (II) Curtius rearrangement, or (III) lead tetraacetate decarboxylation–acetoxylation.

1 R = CO_2H
2 R = $CONH_2$
3 R = $NH{\cdot}CO_2$ *t* Bu (Bu = butyl)
4 R = $NH{\cdot}CO_2$ Bn (Bn = benzyl)

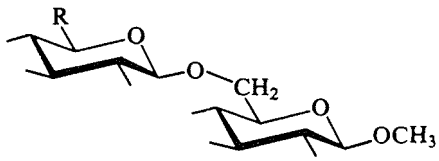

5 R = CO_2H
6 R = CO_2CH_3
7 R = $CONH_2$
8 R = $NH{\cdot}CO_2$ *t* Bu
9 R = $NHCO_2$ Bn

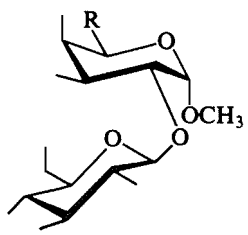

10 R = $CONH_2$
11 R = $NH{\cdot}CO_2$ *t* Bu
12 R = —CO_2H

Unless otherwise specified, substituents are OCH_3

generated from the disaccharide carbamate **8** showed liberation of aglycone as methyl 6-*O*-acetyl-2,3,4-tri-*O*-methyl-β-D-glucopyranoside, in 95% yield, but only 35% of the above pentitol derivative was detected, probably due to inadvertent loss of this substance or its precursors during the various concentration steps. Degradations of benzyl carbamates **4** and **9** were carried out by hydrogenolysis over palladium–charcoal, followed by mild treatment with aqueous acid to ensure complete hydrolysis of intermediate 5-aminopentopyranosides to pentodialdose, and then reduction with sodium borohydride and acetylation as for the products from the *tert*-butyl carbamates. Again, product analysis by glc – mass spectrometry indicated liberation of aglycone in greater than 90% yield but overall formation of uronic acid-derived pentitol derivative in only 35–40% yield.

In order to furnish substrates yielding relatively nonvolatile products, and also to provide a basis for comparison of the new procedure with the lead tetraacetate degradation (3) and related reactions, samples of the permethylated pseudoaldobiouronic ester, methyl [methyl 2-*O*-(2,3,4,6-tetra-*O*-methyl-β-D-glucopyranosyl)-3,4-di-*O*-methyl-α-D-galactopyranosid]uronate (8), were converted into the amide (**10**) and thence to the *tert*-butyl carbamate (**11**) and, by saponification, to the acid (**12**). Hydrolysis of the carbamate **11**, followed by reduction and acetylation, gave products which were examined by glc – mass spectrometry. Using 1,6-anhydro-hexa-*O*-methyl-β-maltose as internal standard, the results indicated the formation of the disaccharide alditol, 1,5-di-*O*-acetyl-2-*O*-(2,3,4,6-tetra-*O*-methyl-β-D-glucopyranosyl)-3,4-di-*O*-methyl-L-arabinitol (**13**), as the major product in 67% yield. Side-reactions resulted in the liberation of some 2,3,4,6-tetra-*O*-methyl-D-glucose

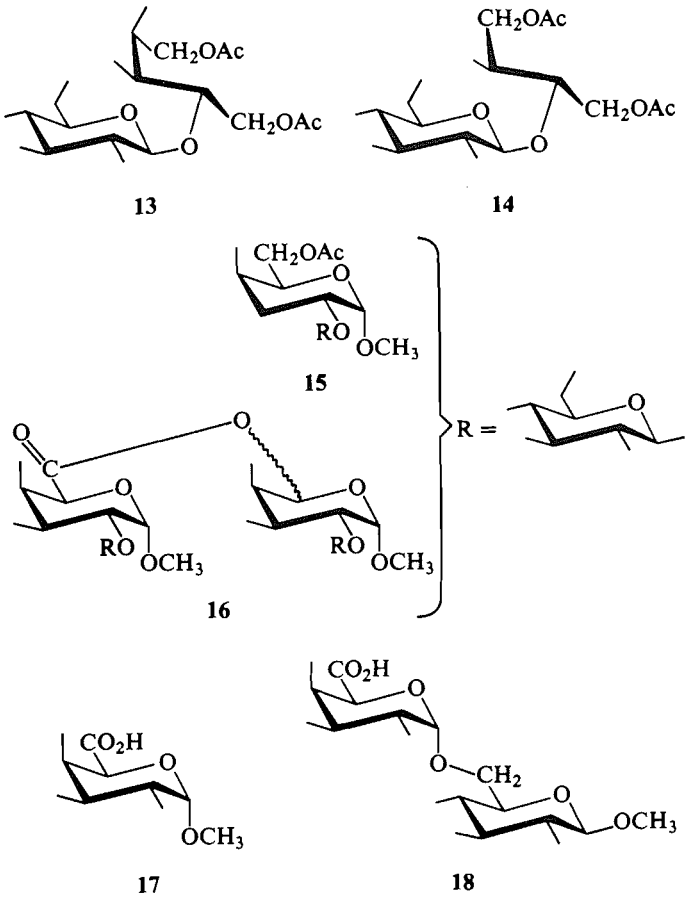

from nonreducing units, as shown by the detection of the derived partially methylated alditol acetate, and a third component, whose mass spectrum showed the presence of an intact nonreducing end group but did not define the nature of the modified unit as aglycone.

In a separate series of reactions the permethylated pseudoaldobiouronic acid **12** was treated with lead tetraacetate in boiling benzene, as described previously (3), and reaction of the products with sodium borohydride followed by acetylation afforded the same disaccharide alditol derivative **13** in 45% yield. Side-reactions resulted in the formation of two other disaccharide derivatives. The mass spectrum of the product of lower retention time pointed to the formation of a tetritol-terminated derivative **14** from more extensive oxidative degradation of the uronic acid **12**. The mass spectrum of the second by-product indicated the formation of a mono-*O*-acetyl-hexa-*O*-methyl disaccharide methyl glycoside, probably **15**. Such a compound could arise from the reduction of the uronic acid residue of a dimeric ester (**16**) formed during the lead tetraacetate reaction, cf. Kitagawa *et al.* (9). These investigators also observed that methyl 2,3,4-tri-*O*-methyl-α-D-galactopyranosiduronic acid (**17**) reacted with lead tetraacetate much more slowly than the corresponding β-D-glucopyranosiduronic acids. In our hands, examination of the products of reaction of this compound (**17**) with lead tetraacetate, followed by reduction and acetylation, showed the formation of 2,3,4-tri-*O*-methylarabinitol diacetate (85%), a di-*O*-methyltetritol diacetate (8%), and methyl 6-*O*-acetyl-2,3,4-tri-*O*-methyl-α-D-galactopyranoside (5%) from reduction of dimeric ester. In the degradation of methyl hexa-*O*-methyl-β-melibiosiduronic acid (**18**) previously reported (3), complete liberation of aglycone was observed but the pentitol derivative was formed in slightly lower yield (~80%). Re-examination of these products has shown that ~12% of the corresponding tetritol was formed from further degradation of the uronic acid residue, but no reduced disaccharide was detected. In the case of the permethylated pseudoaldobiouronic acid **12**, larger amounts of reagent and extended reaction time were required to effect complete disappearance of starting material. In the lead tetraacetate reaction sequence, the products from these side-reactions are apparently formed in significant proportions only when the main reaction takes place slowly. The corresponding by-products have not been detected in reactions of β-D-glucopyranosiduronic acid derivatives, either in model compounds or in more complex polysaccharides.

Kitagawa *et al.* (10) have shown that uronic acid glycosides may be decarboxylated by anodic oxidation in acetic acid solution to give the same 5-acetoxypentopyranosides that are formed in the lead tetraacetate reaction (9). The permethylated pseudoaldobiouronic acid **12** was submitted to anodic oxidation, the reaction mixture was treated directly with sodium borohydride and then acetylated, and the products were examined by glc – mass spectrometry. The disaccharide alditol derivative **13** was formed in ~75% yield, and the tetritol-terminated derivative **14** was detected as a by-product together with traces of the reduced disaccharide methyl glycoside **15**. Although this degradation effected a more satisfactory conversion of this uronic acid glycoside into disaccharide alditol, other experiments showed that no detectable reaction occurred at the electrode surface with methylated polysaccharide substrates.

As for the lead tetraacetate degradation (3), permethylated gum arabic was used as a substrate for the modified Curtius rearrangement and subsequent carbamate degradation. The methylated polysaccharide was converted into the corresponding amide, completeness of reaction being checked by ir spectroscopy. *tert*-Butyl and benzyl carbamates were formed separately by reaction of polysaccharide amide with lead tetraacetate in the presence of the appropriate alcohol. Completeness of the desired structural modification was checked (a) by disappearance of amide carbonyl absorption at 1700 cm^{-1}, and (b) by glc examination of methyl glycosides formed on methanolysis which showed, within the limits of detection, that reaction had resulted in complete modification of methylated glucuronic acid residues. Quantitative analysis of the constituent sugars in the methylated polysaccharide carbamates by glc of the partially methylated alditol acetates formed on hydrolysis, reduction, and acetylation showed that structural modification had been effected without change in neutral sugar composition (Table 1). The modified methylated polysaccharides containing *tert*-butyl and benzyl carbamate residues were degraded by controlled formic acid hydrolysis, and by hydrogenolysis followed by mild acid treatment, respectively, and the reaction mixtures were treated with sodium borohydride and then acetylated. In each case products of low molecular weight were separated by fractional precipitation and/or chromatography on Sephadex LH-20. Further separation of the fractions of low molecular weight gave two main components, which were shown by glc – mass spectrometry to be indistinguishable from the previously characterized (3) 1,5-di-*O*-acetyl-2,3,4-tri-*O*-methylxylitol and 1,5-di-*O*-acetyl-2,3-di-*O*-methyl-4-*O*-(2,3,4-tri-*O*-methyl-α-L-rhamnopyranosyl)-D-xylitol (**19**). For the sample of disaccharide alditol (**19**) formed from the *tert*-butyl carbamate, the ^{13}C nmr spectrum

Can. J. Chem. Downloaded from www.nrcresearchpress.com by 210.87.254.5 on 09/06/12
For personal use only.

TABLE 1. Preparation of carbamates from glycosiduronic acids and glycosiduronamides

Starting material	Product	Method	Yield %	Melting point °C	$[\alpha]_D^\circ$	Analysis % Calculated C	Calculated H	Calculated N	Found C	Found H	Found N
1	**3**	A	87	123.5–125	−12.4	52.32	8.47	4.38	52.41	8.39	4.36
2	**3**	B	84								
1	**4**	A	87	137	−14.2	57.45	7.09	3.94	57.07	7.11	3.85
2	**4**	B	85								
5	**8**	A	86	128–130	−3	52.56	8.25	2.66	52.44	8.21	2.70
7	**8**	B	92								
5	**9**	A	92	177–179	−3	55.80	7.88	2.50	56.02	7.45	2.63
7	**9**	B	84								
10	**11**	B	86	107	+77	52.56	8.25	2.66	52.72	8.59	2.79

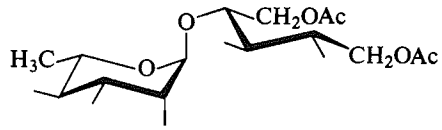

19

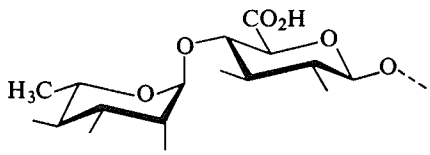

20

showed a value of $^1J_{^{13}C_1,^1H_1}$ = 167.5 Hz and thus confirmed (11) the previously assigned α-L-rhamnopyranosyl configuration (2) for this compound, and hence for terminal units in methylated gum arabic (**20**). Methylated sugar analysis for the degraded methylated polysaccharides showed that the reaction sequences had resulted in the removal of at least 90% of the terminal rhamnose residues external to the modified uronic acid residues without alteration in the proportions of arabinose and galactose methyl ethers (Table 1).

The Curtius rearrangement of permethylated glycosiduronamides followed by controlled cleavage of carbamates and the associated modified glycosidic linkages provides a satisfactory alternative procedure to the lead tetraacetate decarboxylation–acetoxylation reaction sequence for the selective cleavage of β-D-glucopyranosiduronic acid derivatives with formation of the same final products. The formation of *tert*-butyl carbamates is experimentally more satisfactory than that of benzyl carbamates, and no inadvertent hydrolysis of other glycosidic linkages has yet been detected in the cleavage of the *tert*-butyl carbamates with formic acid. The undefined side-reactions in the degradations of these carbamates do not detract from the value of the degradations for glucuronic acid-containing polysaccharide substrates which are described in this and the following paper (12). In the following paper we show that both reaction procedures may be used to generate oligosaccharide fragments of structural significance from the cleavage of interior glucosiduronic acid linkages. In the lead tetraacetate degradation, side-reactions of the types shown in the fragmentation of α-D-galactopyranosiduronic acid linkages in mono- and disaccharide derivatives have not been detected in the cleavage of β-D-glucopyranosiduronic acid linkages in methylated polysaccharide substrates. Neither procedure, however, has yet proved suitable for the corresponding depolymerization of polysaccharides containing α-D-galactopyranosyluronic acid residues, and an entirely different approach to this problem is now being explored.

Experimental

Evaporations were carried out under diminished pressure at temperatures of 40°C or less. Optical rotations were measured in chloroform solution with a Perkin–Elmer model 141 polarimeter at 20 ± 2°C. The ir spectra were measured on a Unicam SP 200 spectrophotometer. The ^{1}H nmr spectra were recorded on a Varian EM 360 spectrophotometer in deuteriochloroform with tetramethylsilane as internal standard. The ^{13}C nmr spectrum was measured on a Bruker WH 400 spectrophotometer. Gas–liquid chromatography was performed on a Perkin–Elmer Sigma 3B chromatograph using a S.C.O.T. column coated with silicone gum OV-225. For glc – mass spectrometry, the column in a Pye 204 chromatograph was attached by a jet separator to a VG Micromass 16F mass spectrometer operated with an inlet temperature of 250°C, an ionization potential of 70 eV, and an ion-source temperature of ~250°C.

Preparation of tert-*butyl and benzyl carbamates*

Method A

An equimolar (0.5–1.0 mmol each) mixture of glycosiduronic acid, diphenyl phosphorazidate, and triethylamine was heated under reflux overnight in (*i*) anhydrous *tert*-butanol (15 mL) or (*ii*) benzyl alcohol (1.2 molar proportions) in benzene (15 mL). The reaction mixture was concentrated, the residue in benzene was washed successively with aqueous 5% citric acid, water, aqueous sodium hydrogen carbonate, and water, and the dried solution was concentrated. The product was chromatographed on silica gel with ether–hexane (4:1) and the resulting carbamate was recrystallized from ether – light petroleum.

Starting materials were methyl 2,3,4-tri-*O*-methyl-β-D-glucopyranosiduronic acid (**1**) (13) and methyl hexa-*O*-methyl-β-gentiobiosiduronic acid (**5**) (3).

Method B

Methyl permethylated glycosiduronates were converted into the corresponding glycosiduronamides by treatment with methanolic ammonia. A mixture of permethylated glycosiduronamide (1 mmol), pyridine (1 mmol), and lead tetraacetate (4.5 mmol) in (*i*) *tert*-butanol (15 mL) or (*ii*) benzene (15 mL) containing benzyl alcohol (1.2 mmol) was heated under reflux for 4 h. A further quantity (4. 5 mmol) of lead tetraacetate was added and the mixture was heated under reflux overnight. The reaction mixture was concentrated, the residue was extracted with ether or ethyl acetate, and the extract was washed with water, dried, and concentrated. The product was chromatographed as above and the carbamate was recrystallized.

Starting materials were methyl 2,3,4-tri-*O*-methyl-β-D-glucopyranosiduronamide (**2**) (14), methyl hexa-*O*-methyl-β-gentiobiosiduronamide (**7**), and methyl 3,4-di-*O*-methyl-2-*O*-(2,3,4,6-tetra-

Can. J. Chem. Downloaded from www.nrcresearchpress.com by 210.87.254.5 on 09/06/12
For personal use only.

Can. J. Chem. Downloaded from www.nrcresearchpress.com by 210.87.254.5 on 09/06/12
For personal use only.

O-methyl-β-D-glucopyranosyl)-α-D-galactopyranosiduronamide (**10**). Amide **7** had mp 199–200°C, $[\alpha]_D$ −62°. *Anal.* calcd. for $C_{19}H_{35}NO_{11}$: C 50.32, H 7.78, N 3.09; found: C 50.19, H 8.07 N 3.40. Amide **10** had mp 189–190°C, $[\alpha]_D$ +52.7°. *Anal.* calcd. for $C_{19}H_{35}NO_{11}$: C 50.32, H 7.78, N 3.09; found: C 50.34, H 7.83, N 3.00.

The following carbamates were prepared: methyl (5*S*)-5-*tert*-butyloxycarbonylamino-2,3,4-tri-*O*-methyl-β-D-xylopyranoside (**3**), methyl (5*S*)-5-benzyloxycarbonylamino-2,3,4-tri-*O*-methyl-β-D-xylopyranoside (**4**), methyl 2,3,4-tri-*O*-methyl-6-*O*-[(5*S*)-5-*tert*-butyloxycarbonylamino-2,3,4-tri-*O*-methyl-β-D-xylopyranosyl]-β-D-glucopyranoside (**8**), methyl 6-*O*-[(5*S*)-5-benzyloxycarbonylamino-2,3,4-tri-*O*-methyl-β-D-xylopyranosyl]-2,3,4-tri-*O*-methyl-β-D-glucopyranoside (**9**), and methyl 3,4-di-*O*-methyl-2-*O*-(2,3,4,6-tetra-*O*-methyl-β-D-glucopyranosyl)-5-(5*S*)-*tert*-butyloxycarbonylamino-β-L-arabinopyranoside (**11**). Methods of preparation, yields, physical constants, and elemental analyses for these compounds are given in Table 1. The ir spectra of all carbamates showed absorption at 3330–3350 (NH), 1710–1730 (CO), and 1550 cm^{-1} (NH), and the ^{1}Hmr spectra gave signals for the correct ratios of OCH_3 (δ 3.4–3.6) and *Ph*—CH_2 (δ 7.3) or *tert*-Bu (δ 1.45) groups.

Degradations of tert-*butyl carbamates*

Weighed quantities (10–20 mg) of *tert*-butyl carbamate and internal standard (1,6-anhydro-2,3,4-tri-*O*-methyl-β-D-galactopyranose (15) for carbamates **3** and **8** and 1,6-anhydro-2,2′,3,3′,4′,6′-hexa-*O*-methyl-β-maltose (16) for carbamate **11**) in approximately equimolar proportions were treated with 98% formic acid (2 mL) at room temperature for 2 h. Formic acid was removed by codistillation with toluene under diminished pressure without increase in temperature, the residue in water (1 mL) was treated with sodium borohydride (50 mg) for 5 h, excess hydride was destroyed and sodium ions were removed with Amberlite resin IR-120(H), and the filtered solution was concentrated by codistillation with toluene and then methanol. The residue was acetylated in acetic anhydride – pyridine (1:1) (1 mL), the products were examined by glc (at 150°C for monosaccharide derivatives or 210°C for disaccharide derivatives) for quantitative analysis, and their identities were confirmed by glc – mass spectrometry using authentic samples, when available, for comparison.

Carbamate **3** afforded 2,3,4-tri-*O*-methylxylitol diacetate (*m/e* 117, 161). Carbamate **8** furnished 2,3,4-tri-*O*-methylxylitol diacetate (40%) and methyl 6-*O*-acetyl-2,3,4-tri-*O*-methyl-β-D-glucopyranoside (95%) (*m/e* 187, 247). Carbamate **11** afforded a major product (67%), $T_{1,6\text{-anhydro-hexamethylmaltose}}$ 1.57, which showed prominent fragment ions at *m/e* 307, 247, 219, 187, 161 and was assigned the structure **13**. Other products in the mixture were 2,3,4,6-tetra-*O*-methylglucitol diacetate (*m/e* 205, 161, 145, 129, 117, 101) (~10%), and two incompletely identified disaccharide derivatives at $T_{1,6\text{-anhydro-hexamethylmaltose}}$ 0.85 and 2.10, both of whose mass spectra showed ions at *m/e* 219 and 187 arising from tetra-*O*-methylglucopyranosyl residues.

Degradations of benzyl carbamates

Weighed quantities (10–20 mg each) of benzyl carbamate and 1,6-anhydro-2,3,4-tri-*O*-methyl-β-D-galactopyranose in approximately equimolar proportions in ethanol (10 mL) were hydrogenolysed at atmospheric pressure over 10% palladium–charcoal overnight, the filtered solutions were concentrated, and the products in water (5 mL), brought to pH 5 by the addition of acetic acid, were kept overnight. The resulting solutions were treated with sodium borohydride (50 mg) for 4 h, and the reduction products were worked up and acetylated as described above for analysis by glc – mass spectrometry.

Carbamate **4** afforded 2,3,4-tri-*O*-methylxylitol diacetate (40%). Carbamate **9** furnished 2,3,4-tri-*O*-methylxylitol diacetate (35%) and methyl 6-*O*-acetyl-2,3,4-tri-*O*-methyl-β-D-glucopyranoside (95%).

Degradations of permethylated galactopyranosiduronic acids with lead tetraacetate

Degradations were performed as described earlier (3) with the addition of one or other of the above-mentioned internal standards, but for longer reaction times (up to 48 h) than for the corresponding glucopyranosiduronic acids, to ensure complete disappearance of starting material. The products were treated with sodium borohydride and then acetylated for examination by glc – mass spectrometry.

Methyl 2,3,4-tri-*O*-methyl-α-D-galactopyranosiduronic acid (**17**) from the corresponding methyl ester (17) afforded 2,3,4-tri-*O*-methylarabinitol diacetate (85%), $T_{1,6\text{-anhydro-tri-}O\text{-methylgalactose}}$ 3.38, an incompletely identified product (8%), $T_{1,6\text{-anhydro-tri-}O\text{-methylgalactose}}$ 1.19, whose mass spectrum with fragment ions at *m/e* 161, 143, 129, 117, and 101 was consistent with that of a di-*O*-methyltetritol diacetate, and a compound (5%), $T_{1,6\text{-anhydro-tri-}O\text{-methylgalactose}}$ 3.69, which was indistinguishable from methyl 6-*O*-acetyl-2,3,4-tri-*O*-methyl-α-D-galactopyranoside and showed fragment ions at *m/e* 247, 215, 187. Re-examination of the products from methyl hexa-*O*-methyl-β-melibiosiduronic acid (**18**) (3) showed, in addition to the major products, a minor product (12%) which was indistinguishable from the above-mentioned di-*O*-methyltetritol diacetate. Methyl 3,4-di-*O*-methyl-2-*O*-(2,3,4,6-tetra-*O*-methyl-β-D-glucopyranosyl)-α-D-galactopyranosiduronic acid (**12**) furnished as the major product the disaccharide alditol (**13**) (45%), which was identical (glc – ms) to the previously characterized compound, together with two minor disaccharide derivatives (each 15%) and 2,3,4,6-tetra-*O*-methylglucitol diacetate (12%). The first disaccharide derivative, $T_{1,6\text{-anhydrohexamethylmaltose}}$ 0.90, showed fragment ions at *m/e* 263, 219, 203, 161, 155, 143, and 117 and was assigned structure **14**. The second disaccharide derivative, $T_{1,6\text{-anhydro-hexa-}O\text{-methylmaltose}}$ 2.10, showed fragment ions at *m/e* 307, 247, 219, 215, 187, 161, and 155, and was indistinguishable (glc – ms) from methyl 6-*O*-acetyl-3,4-di-*O*-methyl-2-*O*-(2,3,4,6-tetra-*O*-methyl-β-D-glucopyranosyl)-α-D-galactopyranoside (**15**) prepared from the methyl ester (8) by reduction with lithium aluminum hydride followed by acetylation.

Anodic oxidation of permethylated pseudoaldobiouronic acid **12**

Permethylated pseudoaldobiouronic acid (**12**) (14.6 mg) and 1,6-anhydro-hexa-*O*-methyl-β-maltose (9.9 mg) in acetic acid (20 mL) containing triethylamine (0.5 mL) were electrolyzed at 20°C for 24 h (50 V, 120 mA). After work-up, the reaction products were treated with sodium borohydride and acetylated as in the lead tetraacetate degradations, and the resulting compounds were examined by glc – mass spectrometry. The major product was the disaccharide alditol **13** (75%); the tetritol-terminated derivative **14** (10%) was a minor product, but only traces (~1%) of the reduced disaccharide methyl glycoside **15** could be detected.

Preparation and degradation of tert-*butyl carbamate from methylated gum arabic*

Methylated gum arabic was converted into the methylated polysaccharide amide as described previously (2) and completeness of reaction was checked by disappearance of ester carbonyl absorption in the ir spectrum at 1740 cm^{-1}. Methylated gum arabic amide (150 mg) in benzene (5 mL) and *tert*-butanol (5 mL) containing pyridine (0.2 mL) and lead tetraacetate (500 mg) were heated under reflux for 4 h, a further quantity (500 mg) of lead tetraacetate was added, and heating under reflux was continued overnight. The cooled reaction mixture was diluted with benzene, filtered, and the filtrate was washed with water, dried, and concentrated. The residue was purified by chromatography on Sephadex LH-20 with dichloromethane–acetone (1:1) to give the polysaccharide *tert*-butyl carbamate (135 mg). Completeness of reaction was shown (a) by ir absorption at 1740 cm^{-1} (carbamate C=O) but none at 1700 cm^{-1} (amide C=O), and (b) by the absence of peaks with the retention times of methyl ester methyl glycosides of 2,3,4-tri- and 2,3-di-*O*-methylglucuronic acid on glc examination of the methanolysis products.

Methylated gum arabic *tert*-butyl carbamate (150 mg) was kept in 98% formic acid for 4 h at room temperature. The formic acid was removed by codistillation with toluene under reduced pressure. The residue in water–methanol (3:2) (5 mL) was treated with sodium borohydride (50 mg) for 4 h. The solution was treated with Amberlite resin IR-120(H) to destroy excess of hydride and remove sodium ions,

TABLE 2. Methylation analyses of neutral sugar components of methylated gum arabic and derived methylated polysaccharides

		Derived alditol acetates[b] (mol% of neutral sugar components)			
	T^a	A	B	C	D
2,3,4-Me_3 Rha[c]	0.44	8	8	1	1
2,3,5-Me_3 Ara[c]	0.44	17	17	18	17
2,3,4-Me_3 Ara	0.55	2	2	3	3
2,5-Me_2 Ara	0.87	17	17	16	15
2,3,4,6-Me_3 Gal	1.10	13	13	12	11
2,4,6-Me_3 Gal	1.95	3	3	5	5
2,3,4-Me_3 Gal	3.04	4	4	6	6
2,4-Me_2 Gal	4.83	23	23	26	24
2-Me Gal	6.02	13	13	14	13

[a]Retention times of partially methylated alditol acetates relative to those of 1,5-di-*O*-acetyl-2,3,4,6-tetra-*O*-methyl-D-glucitol at 170°C.

[b]A, Neutral sugar constituents only from methylated gum arabic; B, neutral sugar constituents from methylated gum arabic *tert*-butyl and benzyl carbamates; C, neutral sugar constituents from degraded methylated polysaccharides formed from both *tert*-butyl and benzyl carbamates; D, calculated from C allowing for loss of ~7% of rhamnose residues.

[c]The relative proportions of these two sugars were estimated separately by glc of the methyl glycosides formed on methanolysis of the methylated polysaccharides.

and the filtrate was concentrated by codistillation with toluene and then methanol. The product showed a weak ir absorption at 1740 cm^{-1}, and the whole procedure was repeated (treatment with formic acid for 2 h) to give material with no residual ir absorption at 1740 cm^{-1}. The residue was acetylated with acetic anhydride – pyridine (1:1) (1 mL) and, after normal work-up, addition of light petroleum to the products in ether afforded degraded methylated gum arabic (110 mg), which was washed thoroughly to remove products of low molecular weight (detected on tlc) and then chromatographed on Sephadex LH-20 using dichloromethane as eluant.

The supernatant liquid from the above precipitation was chromatographed on silica gel using dichloromethane–acetone (4:1) as eluant to give three fractions. Fraction (*i*) (5 mg) was identified as 2,3,4-tri-*O*-methylxylitol diacetate by glc – mass spectrometry. Fraction (*ii*) (15 mg) was indistinguishable by glc – mass spectrometry from 1,5-di-*O*-acetyl-2,3-di-*O*-methyl-4-*O*-(2,3,4-tri-*O*-methyl-α-L-rhamnopyranosyl)-D-xylitol (**19**) (*1*); ^{1}H nmr ($CDCl_3$) δ: 1.28 (d, 3H, $J_{5,6}$ = 6 Hz, H-6 of Me_3 rhamnopyranose residue), 2.09, 2.10 (2s, 2 × 3H, 2 × OAc), 3.44, 3.50, 3.51, 3.52, 3.55 (5s, 5 × 3H, 5 × OCH_3); ^{13}C nmr ($CDCl_3$) δ: 97.10 (C1′, $^1J_{^{13}C_1,^1H_1}$ = 167.5 Hz). Fraction (*iii*) (3 mg) was shown by glc–ms to contain a main component, $T_{\text{fraction}(ii)}$ 0.56, whose mass spectrum included fragment ions at *m/e* 189 and 157 indicating the presence of a tri-*O*-methylrhamnopyranosyl residue.

Preparation and degradation of benzyl carbamate from methylated gum arabic

Methylated gum arabic amide (150 mg) in benzene (10 mL) containing pyridine (0.2 mL), benzyl alcohol (27 mg), and lead tetraacetate (500 mg) was heated under reflux for 4 h, further lead tetraacetate (500 mg) was added, and refluxing was continued overnight. The cooled solution was diluted with benzene, filtered, and concentrated. The residue in water was dialysed against distilled water, the solution was concentrated, and the product was extracted with dichloromethane and then purified by chromatography on Sephadex LH-20 with dichloromethane–acetone (1:1) as eluant to give the polysaccharide benzyl carbamate (120 mg). Completeness of reaction was checked as for the methylated polysaccharide *tert*-butyl carbamate.

Methylated gum arabic benzyl carbamate (150 mg) in ethanol (10 mL) was hydrogenolysed at atmospheric pressure over 10% palladium–charcoal overnight. The filtered solution was concentrated, the residue in water (5 mL) was acidified to pH 5 with acetic acid and kept overnight, and the products were treated with sodium borohydride (50 mg) for 4 h. The reaction mixture was worked up as described for that from the *tert*-butyl carbamate, the products were acetylated, and fractional precipitation of the polysaccharide component and chromatographic separations furnished (*i*) degraded methylated gum arabic (110 mg), (*ii*) 1,5-di-*O*-acetyl-2,3,4-tri-*O*-methylxylitol (5 mg), and (*iii*) 1,5-di-*O*-acetyl-2,3-di-*O*-methyl-4-*O*-(2,3,4-tri-*O*-methyl-α-L-rhamnopyranosyl)-D-xylitol (13 mg). Fractions (*ii*) and (*iii*) were characterized by glc – mass spectrometry.

Compositional analysis of methylated polysaccharides

The sugar components of methylated gum arabic, methylated polysaccharide *tert*-butyl and benzyl carbamates, and the degraded methylated polysaccharides after carbamate cleavage were analyzed as partially methylated alditol acetates formed on hydrolysis, followed by reduction with sodium borohydride and acetylation, by glc (170°C). Average values for two determinations are shown in Table 2. For separations of derivatives of 2,3,4-tri-*O*-methylrhamnose and 2,3,5-tri-*O*-methylarabinose, methylated polysaccharides were heated under reflux with methanolic 5% hydrogen chloride and the resulting methyl glycosides were examined by glc (130°C, 5°/min to 180°C). The results are shown in Table 2.

Acknowledgements

The authors are grateful for financial support from the Natural Sciences and Engineering Research Council of Canada, for the award of a Royal Society Commonwealth Bursary (to N.S.K.), for the recording of mass spectra by Dr. B. H. Khouw, and for the recording of the ^{13}C nmr spectrum by the Southwestern Ontario NMR Centre at the University of Guelph.

1. N. K. KOCHETKOV, O. S. CHIZHOV, and A. F. SVIRIDOV. Carbohydr. Res. **14**, 277 (1970).
2. G. O. ASPINALL and K.-G. ROSELL. Can. J. Chem. **56**, 685 (1978).
3. G. O. ASPINALL, H. K. FANOUS, N. S. KUMAR, and V. PUVANESARAJAH. Can. J. Chem. **59**, 935 (1981).
4. K. NINOMIYA, T. SHIOIRI, and S. YAMADA. Tetrahedron, **30**, 2151 (1974).
5. K. NINOMIYA, T. SHIOIRI, and S. YAMADA. Chem. Pharm. Bull. **22**, 1398 (1974).
6. B. ACOTT, A. J. L. BECKWITH, and A. HASSANALI. Aust. J. Chem. **21**, 197 (1968).
7. H. E. BAUMGARTEN, H. L. SMITH, and A. STAKLIS. J. Org. Chem. **40**, 3554 (1975).
8. J. HIRSCH, P. KOVÁČ, V. KOVÁČIK, and V. MIHÁLOV. Chem. Zvesti, **30**, 674 (1976).
9. I. KITAGAWA, M. YOSHOKAWA, and A. KADOTA. Chem. Pharm. Bull. **26**, 484 (1978).
10. I. KITAGAWA, T. KAMIGAUCHI, H. OHMORI, and M. YOSHIKAWA. Chem. Pharm. Bull. **28**, 3078 (1980).
11. K. BOCK and C. PEDERSEN. J. Chem. Soc. Perkin Trans. 2, 293 (1974); Acta Chem. Scand. Ser. B, **29**, 258 (1975).
12. G. O. ASPINALL and V. PUVANESARAJAH. Can. J. Chem. **61**, 1864 (1983).
13. S. W. CHALLINOR, W. N. HAWORTH, and E. L. HIRST. J. Chem. Soc. 258 (1931).
14. F. SMITH. J. Chem. Soc. 571 (1939).
15. D. MCCREATH and F. SMITH. J. Chem. Soc. 387 (1939).
16. G. O. ASPINALL, O. IGARASHI, W. MITURA, and M. FUNABASHI. Can. J. Chem. **54**, 1708 (1976).
17. P. A. LEVENE and L. C. KREIDER. J. Biol. Chem. **120**, 597 (1937).

Can. J. Chem. Downloaded from www.nrcresearchpress.com by 210.87.254.5 on 09/06/12
For personal use only.

The selective fragmentation of methylated leiocarpan A by β-D-glucosiduronic acid and β-D-glucosiduronamide cleavage[1]

GERALD OLIVER ASPINALL[2] AND VELUPILLAI PUVANESARAJAH
Department of Chemistry, York University, Downsview, Toronto, Ont., Canada M3J 1P3

Received January 27, 1983

GERALD OLIVER ASPINALL and VELUPILLAI PUVANESARAJAH. Can. J. Chem. **61**, 1864 (1983).

Selective cleavage of internal β-D-glucopyranosiduronic acid linkages in permethylated leiocarpan A has been achieved by two procedures for structural modification involving (a) decarboxylation–acetoxylation using lead tetraacetate or (b) *tert*-butyl carbamate formation by a modified Curtius rearrangement, followed by controlled fragmentation of the modified polysaccharides to yield the same two main partially methylated pentitol-terminated oligosaccharides. Chemical and spectroscopic characterization of these oligosaccharides and their substitution products has shown them to be derivatives of *O*-β-D-xylopyranosyl-(1 → 6)-*O*-α-D-mannopyranosyl-(1 → 4)-D-xylitol and *O*-β-L-arabinofuranosyl-(1 → 3)-[*O*-β-D-xylopyranosyl-(1 → 6)]-*O*-α-D-mannopyranosyl-(1 → 4)-D-xylitol. These observations provide new information on the anomeric configuration and mode of attachment of side-chains in the polysaccharide.

GERALD OLIVER ASPINALL et VELUPILLAI PUVANESARAJAH. Can. J. Chem. **61**, 1864 (1983).

On a clivé sélectivement des liaisons internes de l'acide β-D-glucopyranosiduronique des leiocarpanes perméthylés, selon deux méthodes dans le but d'apporter des modifications structurales impliquant: (a) une décarboxylation–acétoxylation par le tétraacétate de plomb ou (b) la formation du *tert*-butylcarbamate selon une transposition modifiée de Curtius suivie de la fragmentation contrôlée des polysaccharides modifiés pour aboutir à deux oligosaccharides principaux terminés par un pentitol partiellement méthylé. La caractérisation chimique et spectroscopique de ces oligosaccharides et de leurs produits de substitutions révèlent qu'ils sont des dérivés du *O*-β-D-xylopyranosyl-(1 → 6) *O*-α-D-mannopyranosyl-(1 → 4)-D-xylitol et du *O*-β-L-arabinofuranosyl-(1 → 3) [*O*-β-D-xylopyranosyl-(1 → 6)] *O*-α-D-mannopyranosyl-(1 → 4)-D-xylitol. Ces observations fournissent de nouvelles informations sur la configuration de l'anomère et sur le mode de liaison des chaines latérales du polysaccharide.

[Traduit par le journal]

We have recently described two procedures for the selective cleavage of glycosiduronic acid or glycosiduronamide linkages in permethylated polysaccharides (1, 2). Each procedure involves modification of uronic acid residues prior to depolymerization, followed by selective glycoside cleavage at the altered sugar residues. In the first method (1), reaction of permethylated uronic acid residues with lead tetraacetate results in decarboxylation and acetoxylation giving epimeric 5-acetoxypentopyranose units. Reductive cleavage of these units with sodium borohydride affords pentitol-terminated fragments with exposure of aglyconic hydroxyl groups at the former sites of attachment of uronic acid residues. In the second method (2), the same net transformation is achieved by Curtius rearrangement of glycosiduronic acid or glycosiduronamide residues to 5-*tert*-butyloxycarbonyl (or benzyloxycarbonyl) aminopentopyranose residues, followed by carbamate cleavage and reduction of liberated pentodialdoses. These methods, developed for monosaccharide and disaccharide model compounds, have been used also for the cleavage of glucosiduronic acid linkages in the outer chains of methylated gum arabic. Polysaccharides containing a high proportion of uronic acid residues in interior chains present a more stringent test of the general applicability of these methods since fragmentation to the desired neutral oligosaccharide alditols will only occur if (*i*) a high degree of structural modification of uronic acid residues is achieved, and (*ii*) selective cleavage of the modified polysaccharide proceeds to completion with minimum formation of by-products. We describe here the application of both methods to methylated leiocarpan A (3). Leiocarpan A, the major polysaccharide component of *Anogeissus leiocarpus* gum (4), contains a backbone with alternating 4-*O*-substituted β-D-glucuronic acid and 2-*O*-substituted α-D-mannopyranose residues (5) with terminal D-xylopyranose and L-arabinofuranose residues attached variously to mannose residues (**1**). A base-catalyzed degradation of the methylated polysaccharide has provided direct evidence for the site of attachment and anomeric configuration of the terminal

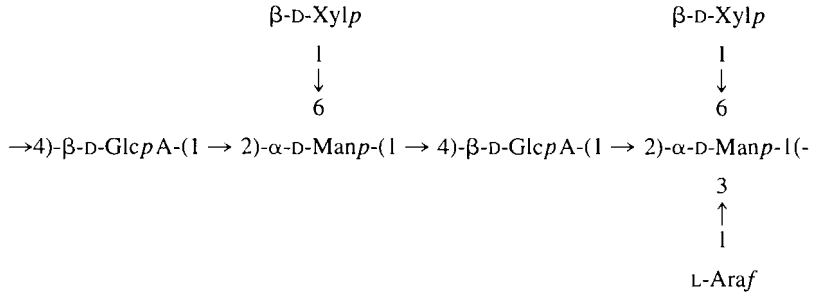

1

[1]Presented in part at the 11th International Symposium on Carbohydrate Chemistry, Vancouver, B.C., August 23–27, 1982.
[2]Author to whom correspondence should be addressed.

Can. J. Chem. Downloaded from www.nrcresearchpress.com by 210.87.254.105 on 09/06/12
For personal use only.

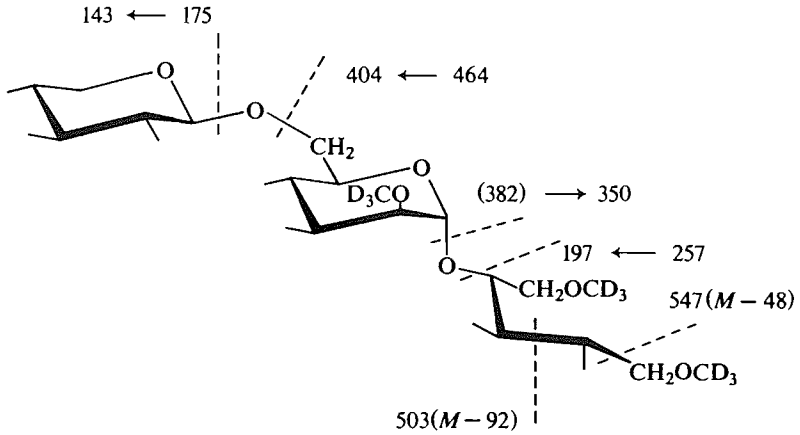

2

FIG. 1. Mass spectral fragmentation of peralkylated oligosaccharide alditol **2**; unless otherwise specified substituents are OCH_3.

β-D-xylopuranose residues (6). The provisionally assigned site of attachment of L-arabinofuranose residues at O-3 mannose units was inferred from methylation studies on the parent gum and on the arabinose-free degraded gum (4, 5), but no information was available on the anomeric configuration of these residues.

Methylated leiocarpan A was treated with aqueous alkali at pH 12 and 0°C to ensure complete ester hydrolysis with no detectable accompanying β-elimination. As shown previously (1), the methylated polysaccharide underwent decarboxylation and accompanying acetoxylation on heating with lead tetraacetate in benzene. Completeness of reaction was ascertained by withdrawal of aliquot samples for ir spectroscopic examination which showed disappearance of ionizable carboxyl groups. Samples of modified methylated polysaccharide were also methanolyzed and examination of the products by glc showed, within the limits of detection, the absence of methyl ester methyl glycosides of uronic acids. Treatment of the modified methylated polysaccharide with sodium borohydride, followed by methanolysis and acetylation, and glc examination showed the formation of units of 2,3-di-*O*-methylxylitol (from the corresponding residues of 2,3-di-*O*-methylglucuronic acid) together with those of the unaltered neutral sugars, 2,3,5-tri-*O*-methylarabinose, 2,3,4-tri-*O*-methylxylose, and 3,4-di- and 4-*O*-methylmannose. The suitably modified methylated polysaccharide containing epimeric 5-acetoxypentopyranose residues was then treated with sodium borohydride to effect deacetylation and reduction of exposed pentodialdose to pentitol residues.

The partially methylated oligosaccharides thus generated were separated most satisfactorily by preparative hplc of their *O*-benzoyl derivatives. Although a small degree of mutual contamination was observed, the results of the following experiments left no doubt as to the identities of the major component in each fraction. The oligosaccharide fractions were de-*O*-benzoylated and samples were withdrawn for hydrolysis, followed by reaction with hydroxylamine and acetylation to form partially methylated alditol acetates and partially methylated aldononitriles which were examined by glc – mass spectrometry. The partially methylated oligosaccharides were further alkylated with trideuteriomethyl iodide, and the fully alkylated oligosaccharides were characterized by ^1H and ^{13}C nmr spectroscopy, mass spectrometry, and methylated sugar analysis.

Hydrolysis of oligosaccharide fraction I gave, as major components, 2,3,4-tri-*O*-methylxylose, 3,4-di-*O*-methylmannose, and 2,3-di-*O*-methylxylitol. After trideuteriomethylation, hydrolysis of the fully alkylated oligosaccharide furnished 2,3,4-tri-*O*-methylxylose, 2-*O*-[$^2H_3$]methyl-3,4-di-*O*-methylmannose, and 1,5-di-*O*-[$^2H_3$]methyl-2,3-di-*O*-methylxylitol whose derivatives were identified by glc – mass spectrometry. The mass spectrum of the peralkylated oligosaccharide fraction gave fragment ions at *m/e* values shown in Fig. 1 and was consistent with proposed structure **2**. The ^1H nmr spectrum showed signals for two anomeric protons at δ 5.15 (broad singlet) and 4.26 (doublet, $J_{1,2}$ = 7.3 Hz), in accord with previous evidence for β-D-xylopyranose and α-D-mannopyranose residues in the polysaccharide. Signals in the Cmr spectrum for anomeric carbon atoms at δ_C 102.3 and 96.2 in the corresponding residues further supported the conclusions.

Hydrolysis of oligosaccharide fraction II gave, as major components, 2,3,5-tri-*O*-methylarabinose, 2,3,4-tri-*O*-methylxylose, 4-*O*-methylmannose, and 2,3-di-*O*-methylxylitol. After trideuteriomethylation, hydrolysis of the fully alkylated oligosaccharide afforded 2,3,5-tri-*O*-methylarabinose, 2,3,4-tri-*O*-methylxylose, 2-*O*-[$^2H_3$]methyl-4-*O*-methylmannose, and 1,5-di-*O*-[$^2H_3$]methyl-2,3-di-*O*-methylxylitol. The mass spectrum of the peralkylated oligosaccharide gave fragment ions at the *m/e* values shown in Fig. 2 for the proposed structue **3**. The ^1Hmr spectrum showed the same two signals for anomeric protons at δ 5.12 (broad singlet) and 4.27 (doublet, $J_{1,2}$ = 7.3 Hz), together with a third signal at δ 5.19 (doublet, $J_{1,2}$ = 4.3 Hz). Similarly, the Cmr spectrum showed a signal for a third anomeric carbon atom at δ_C 104.1, in addition to those assigned to anomeric centres in β-D-xylopyranose and α-D-mannopyranose residues at δ_C 102.7 and 97.9. The additional anomeric signals are in agreement with other assignments for β-L-arabinofuranose residues (7, 8). These observations provide direct confirmation that O-3 of D-mannose residues is the site of attachment of L-arabinofuranose residues in leiocarpan A and show that these units have the β-L-configuration.

The methylated oligosaccharide fraction II contained a small proportion (~10%) of contaminating trisaccharide alditol from fraction I, as shown by the formation of 3,4-di-*O*-methylmannose on hydrolysis. However, after trideuteriomethylation, hydrolysis of the peralkylated oligosaccharide fraction gave a rather higher proportion (~20%) of the corresponding 2,3,4-tri-*O*-methylmannose and the mass spectrum of the derived partially methylated alditol acetate showed the presence of

Can. J. Chem. Downloaded from www.nrcresearchpress.com by 210.87.254.105 on 09/06/12
For personal use only.

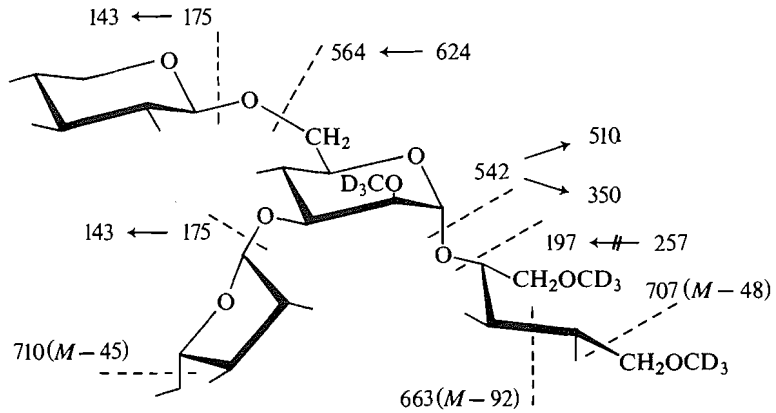

3

FIG. 2. Mass spectral fragmentation of peralkylated oligosaccharide alditol **3**.

some trideuteriomethyl substituent at O-3 in addition to that expected at O-2. Such a substituent probably arose from a trisaccharide fragment originating from a less than fully methylated region of the polysaccharide. However, in view of the detection of only one site of incomplete methylation, we consider it more likely that the exposed hydroxyl group arose from the inadvertent loss of an arabinofuranosyl residue during the preparation of the original sample of methylated leiocarpan A rather than from incomplete alkylation.

The importance of achieving complete structural modification of uronic acid residues prior to depolymerization was shown in an earlier series of experiments. Saponification of methylated leiocarpan A for a period sufficient for complete reaction of mono- and disaccharide derivatives resulted in less than complete (but still >80%) de-esterification. Since uronic esters are stable to reaction with lead tetraacetate (1), subsequent treatment of the modified polysaccharide with sodium borohydride resulted in less than complete depolymerization, but was accompanied by reduction of esterified 2,3-di-*O*-methylglucuronic acid to the corresponding 2,3-di-*O*-methylglucose units. Separation of the reaction products led to the isolation and characterization in terms of sugar composition of a higher oligosaccharide (or possibly a mixture of closely related species). The proposed structure **4** for this oligosaccharide fraction indicates the presence of a tetrasaccharide al-

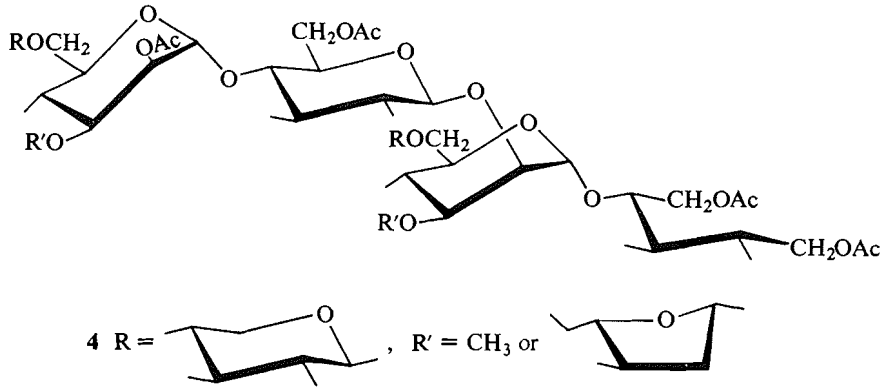

ditol segment derived from the glucuronomannan main chain with three or four attached pentose residues in side-chains.

A further sample of methylated leiocarpan A was treated with methanolic ammonia, care being taken to ensure completeness of amidation. Reaction of the polysaccharide amide with lead tetraacetate in *tert*-butanol furnished (5*S*)-5-*tert*-butyloxycarbonylamino-2,3-di-*O*-methyl-β-D-xylopyranose in place of 2,3-di-*O*-methyl-β-D-glucuronic acid residues. Completeness of reaction was ascertained by (a) disappearance of amide carbonyl absorption at 1700 cm^{-1}, and (b) by glc analysis of methyl glycoside acetates formed on methanolysis followed by acetylation, which showed that all 2,3-di-*O*-methylglucuronic acid units had been modified. The modified polysaccharide was selectively hydrolyzed with formic acid at room temperature and the hydrolyzate was treated with sodium borohydride. The resulting mixture of partially methylated oligosaccharides was fractionated, as for the products of the lead tetraacetate degradation, by preparative hplc of the *O*-benzoyl derivatives. The two main oligosaccharide fractions were shown to be identical to those formed in the lead tetraacetate degradation. On trideuteriomethylation they gave the same fully alkylated oligosaccharides as shown by their mass spectra and by glc – mass spectrometry of the sugar derivatives formed on hydrolysis.

These experiments have shown that both the lead tetraacetate decarboxylation–acetoxylation procedure (1) and the Curtius rearrangement to furnish *tert*-butyl carbamate-containing derivatives (2) may be used to effect structural modification of internal glucuronic acid residues in methylated polysaccharides, and that selective glycoside cleavage at the altered sugar residues, followed by reduction, results in the formation of pentitol-terminated oligosaccharides. The oligosaccharides thus generated retain all the structural information of the corre-

Can. J. Chem. Downloaded from www.nrcresearchpress.com by 210.87.254.105 on 09/06/12
For personal use only.

Can. J. Chem. Downloaded from www.nrcresearchpress.com by 210.87.254.105 on 09/06/12
For personal use only.

sponding segments of the parent polysaccharide other than that on configuration at C-5 and the anomeric centre of the uronic acid residues. Completeness of reaction at each modification step is essential if the desired depolymerization is to be achieved.

Experimental

Unless otherwise stated, general experimental methods were as described in the preceding paper (2). Most ^{1}H and all ^{13}C nmr spectra were measured on a Bruker WH 400 spectrophotometer. High-pressure liquid chromatography (hplc) was performed on a Waters Associates μ-Porasil column (3.9 × 300 mm, 10 μ silica), the solvent gradient was delivered by two model 6000A pumps controlled by a Waters Associates model 660 programmer, and a model 440 uv absorbance detector set at 254 nm was used. Elution at a flow rate of 2 mL/min was performed with chloroform for 5 min, followed by a linear gradient over 20 min to a final solvent composition of chloroform–acetonitrile (70:30), and isocratic elution at that solvent composition for a further 10 min.

Lead tetraacetate degradation of methylated leiocarpan A

Methylated leiocarpan A (200 mg) was saponified at 0°C and at pH 12 as described previously (1) but for a period of 6 h to ensure complete de-esterification. The resulting methylated polysaccharide acid (180 mg) in benzene (10 mL) containing pyridine (0.2 mL) and lead tetraacetate (1 g) was heated under reflux for 15 h.[3] A sample from the reaction mixture was methanolyzed, the products were acetylated, and glc analysis (120°C, 5°/min to 180°C and hold) showed the presence of acetylated (if possible) methyl glycosides of 2,3,4-tri-*O*-methylxylose, 2,3,5-tri-*O*-methylarabinose, 3,4-di- and 4-*O*-methylmannose, but the absence of derivatives of 2,3-di-*O*-methylglucuronic acid. The remainder of the reaction solution was filtered, the precipitate was washed with benzene, and the combined filtrate and washings were washed several times with water, dried, and concentrated to give modified methylated leiocarpan A (150 mg), ν_{max} 1750 cm^{-1} but no absorption at 1600 cm^{-1} on treatment with triethylamine. The modified methylated polysaccharide (150 mg) in tetrahydrofuran–water (1:1, 3 mL) was treated with sodium borohydride (100 mg) for 15 h. Excess of hydride was destroyed, the pH of the solution was brought to 5 by the addition of Dowex-50 (H) resin, and the filtered solution was repeatedly concentrated with methanol to a mixture of partially methylated oligosaccharide alditols (140 mg). A portion of the mixture was methanolyzed, the products were acetylated, and glc (as above) showed the formation of derivatives of 2,3,4-tri-*O*-methylxylose and 2,3,5-tri-*O*-methylarabinose (incompletely separated), and 3,4-di- and 4-*O*-methylmannose, together with 2,3-di-*O*-methylxylitol triacetate.

The mixture of partially methylated oligosaccharide alditols (140 mg) in pyridine (2 mL) was treated with benzoyl chloride (0.25 mL) at 0°C and then kept at room temperature for 24 h. Ice was added to destroy excess benzoyl chloride, and the mixture was poured into water and then extracted with dichloromethane. The extract was washed with aqueous sodium hydrogen carbonate and then with water, dried, and concentrated to a syrup (250 mg). Thin-layer chromatography (dichloromethane–acetone, 8:1) of the syrup showed the presence of two major components. A portion of the mixture was separated in batches by hplc (flow rate, 2 mL/min) with initial elution with chloroform for 5 min, followed by gradient elution over 20 min to a final solvent composition of chloroform–acetonitrile (70:30), and isocratic elution for a further 10 min. The *O*-benzoyl derivatives of partially methylated oligosaccharide alditols I and II (~30 mg each) were eluted at 22.5 and 26 min, and the collected fractions contained less than 10% of cross-contamination. The benzoylated oligosaccharide fractions were each de-*O*-benzoylated with catalytic quantities of sodium methoxide in methanol, the solutions were treated with Amberlite resin IR-120(H) to remove sodium ions, and the filtrates were concentrated to give the respective partially methylated oligosaccharide alditols.

Partially methylated oligosaccharide alditol I

A sample of the oligosaccharide was hydrolyzed and the resulting mixture of sugars was heated with hydroxylamine hydrochloride in pyridine, and again after addition of acetic anhydride (9). Analysis of the products by glc – mass spectrometry (column temperature 180°C, 1°/min to 220°C) showed the presence of 2,3-di-*O*-methylxylitol triacetate and of partially methylated aldononitrile acetates from 2,3,4-tri-*O*-methylxylose and 3,4-di-*O*-methylmannose in approximately equimolar proportions, and from 2,3,5-tri-*O*-methylarabinose and 4-*O*-methylmannose in much smaller proportions. The oligosaccharide was further alkylated with trideuteriomethyl iodide by the Hakomori procedure (10). The fully alkylated oligosaccharide alditol gave significant fragment ions in the mass spectrum at *m/e* values shown with formula **2**; ^{1}H nmr ($CDCl_3$) δ: 5.15 (broad s, 1H, H-1 of α-D-mannopyranose residue), 4.26 (d, 1H, $J_{1,2}$ = 7.3 Hz, H-1 of β-D-xylopyranose residue); ^{13}C nmr ($CDCl_3$) δ_C: 102.3 (C-1 of β-D-xylopyranose residue), 96.2 (C-1 of α-D-mannopyranose residue). Hydrolysis of the fully alkylated oligosaccharide alditol, followed by treatment with sodium borohydride and acetylation, gave the following partially alkylated alditols, the identities of whose acetates were established by glc – mass spectrometry: 1,5-di-*O*-[$^2H_3$]methyl-2,3-di-*O*-methylxylitol, 2,3,4-tri-*O*-methylxylitol, 2-*O*-[$^2H_3$]methyl-3,4-di-*O*-methylmannitol, and, in trace amount, 2,3,5-tri-*O*-methylarabinitol.

Partially methylated oligosaccharide alditol II

Hydrolysis of the oligosaccharide, followed by analysis of the liberated sugars as for oligosaccharide I, showed the formation of derivatives of 2,3-di-*O*-methylxylitol, 2,3,5-tri-*O*-methylarabinose, 2,3,4-tri-*O*-methylxylose, and 4-*O*-methylmannose in approximately equimolar proportions, with a much smaller proportion of 3,4-di-*O*-methylmannose. Further alkylation with trideuteriomethyl iodide gave fully alkylated oligosaccharide alditol II, whose mass spectrum gave significant fragment ions at *m/e* values shown with formula **3**; ^{1}H nmr ($CDCl_3$) δ: 5.19 (d, 1H, $J_{1,2}$ = 4.3 Hz, H-1 of β-L-arabinofuranose residue), 5.12 (broad s, 1H, H-1 of α-D-mannopyranose residue), 4.27 (d, 1H, $J_{1,2}$ = 7.3 Hz, H-1 of β-D-xylopyranose residue); ^{13}C nmr ($CDCl_3$) δ_C: 104.1 (C-1) of β-L-arabinofuranose residue), 102.7 (C-1 of β-D-xylopyranose residue), 97.9 (C-1 of α-D-mannopyranose residue). Hydrolysis of the fully alkylated oligosaccharide alditol II, followed by reduction and acetylation, gave derivatives of the following partially alkylated alditols, whose identities were established by glc – mass spectrometry as 1,5-di-*O*-[$^2H_3$]methyl-2,3-di-*O*-methylxylitol, 2,3,5-tri-*O*-methylarabinitol, 2,3,4-tri-*O*-methylxylitol, and 2-*O*-[$^2H_3$]methyl-4-*O*-methylmannitol. A further compound formed in much smaller amount was 2-*O*-[$^2H_3$]methyl-3,4-di-*O*-methylmannitol, in which ~50% of OCH_3 groups at C-3 carried deuterium labelling.

*Lead tetraacetate degradation of methylated leiocarpan A and partial characterization of a higher oligosaccharide (**4**)*

Methylated leiocarpan A (200 mg) was saponified at 0°C and at pH 12 for 2 h as described previously (1), and the ir spectrum of the methylated polysaccharide acid showed that more than 80% of uronic esters groups had been saponified. Methylated polysaccharide acid (175 mg) in benzene (8 mL) containing pyridine (0.5 mL) and lead tetraacetate (1 g) was heated under reflux for 15 h, the reaction mixture was worked up as described above, and the products were treated with sodium borohydride and then acetylated to give partially methylated oligosaccharide alditol acetates (100 mg). The mixture was chromatographed on a column of Sephadex LH-20 with dichloro-

[3]This reaction may also be carried out in *N*,*N*-dimethylformamide at *room temperature* for 20 h. The advantage of lower reaction temperature with less decomposition of lead tetraacetate is more than offset by the much less clean work-up procedure. The reaction at lower temperature achieves no more satisfactory modification of polysaccharides containing α-D-galactopyranosyluronic acid residues (cf. refs. 1 and 2).

methane as eluant to give fractions A (28 mg), B (40 mg), and C (22 mg). Thin-layer chromatographic examination with dichloromethane–acetone mixtures as eluant and analysis of sugar composition of fractions B and C showed that they were partially separated mixtures of acetylated derivatives of partially methylated oligosaccharide alditols I and II. Fraction A had much lower tlc mobility and the ^{1}H nmr spectrum showed O—CH_3 and O—$COCH_3$ protons in a ratio to be expected for a hepta- or octasaccharide derivative (**4**). The sugar composition of the fraction was determined by (*i*) methanolysis and acetylation of the resulting mixture of alditol and methyl glycosides, and (*ii*) hydrolysis, reduction, and acetylation of the resulting mixture of partially methylated alditols, followed by glc analysis. The results showed the presence of the following constituents: 2,3,4-trimethylxylose, 2,3,5-tri-*O*-methylarabinose, 3,4-di- and 4-*O*-methylmannose, 2,3-di-*O*-methylglucose, and 2,3-di-*O*-methylxylitol, the last two in approximately equimolar proportions.

Preparation and degradation of tert*-butyl carbamate from methylated leiocarpan A*

Methylated leiocarpan A (3) (150 mg) in methanol (10 mL) and liquid ammonia (20 mL) was kept under pressure at room temperature for 24 h, and removal of solvent furnished methylated leiocarpan A amide (130 mg), ν_{max} 1700 cm^{-1}. Methylated leiocarpan A amide (130 mg) in *tert*-butanol (8 mL) containing pyridine (0.2 mL) and lead tetraacetate (700 mg) was heated under reflux for 15 h. The reaction mixture was diluted with *tert*-butanol and filtered, the insoluble residue was washed several times with *tert*-butanol, and the combined filtrate and washings were concentrated. The product was chromatographed on Sephadex LH-20 with dichloromethane as eluant to give methylated leiocarpan A *tert*-butyl carbamate (110 mg), ν_{max} 1740 cm^{-1} with no absorption at 1700 cm^{-1}. A portion of the methylated polysaccharide carbamate was methanolyzed and the products were acetylated, and glc showed the formation of derivatives of 2,3,4-tri-*O*-methylxylose, 2,3,5-tri-*O*-methylarabinose, and 3,4-di- and 4-*O*-methylmannose, but not of 2,3-di-*O*-methylglucuronic acid. The methylated leiocarpan A carbamate (110 mg) was kept in 98% formic acid (2 mL) for 4 h at room temperature. The solution was poured into water, the diluted solution was extracted with dichloromethane, and the extract was dried and concentrated to a syrup. Since the ir spectrum showed residual absorption at 1740 cm^{-1}, the formic acid treatment was repeated to yield a syrup (90 mg) with no absorption at 1740 cm^{-1}. The syrup was reacted with sodium borohydride (75 mg) in water (2 mL) for 15 h, and normal work-up afforded a mixture of partially methylated alditol acetates. Methanolysis of a sample of this mixture, followed by acetylation and glc analysis, showed the formation of derivatives of the same sugars as derived from the corresponding oligosaccharide fraction generated by the lead tetraacetate procedure. As above, the partially methylated oligosaccharide alditols were fractionated by hplc of the *O*-benzoyl derivatives to give two main fractions which were de-*O*-benzoylated to furnish partially methylated oligosaccharide alditols I and II. The oligosaccharide alditols were shown to be identical to those formed by the lead tetraacetate method by (a) characterization of hydrolysis products, (b) the mass spectrum of the fully alkylated derivatives formed on further trideuteriomethylation, and (c) characterization of the hydrolysis products from the fully alkylated derivatives.

Acknowledgements

The authors thank the Natural Sciences and Engineering Research Council of Canada for financial support, Dr. B. H. Khouw for recording mass spectra, and the Southwestern Ontario NMR Centre at the University of Guelph for recording nmr spectra.

1. G. O. Aspinall, H. K. Fanous, N. S. Kumar, and V. Puvanesarajah. Can. J. Chem. **59**, 935 (1981).
2. G. O. Aspinall, H. K. Fanous, N. S. Kumar, and V. Puvanesarajah. Can. J. Chem. **61**, 1858 (1983).
3. G. O. Aspinall and J. J. Carlyle. J. Chem. Soc. C, 851 (1969).
4. G. O. Aspinall, J. J. Carlyle, J. M. McNab, and A. Rudowski. J. Chem. Soc. C, 840 (1969).
5. G. O. Aspinall and J. M. McNab. J. Chem. Soc. C, 845 (1969).
6. G. O. Aspinall and A. S. Chaudhari. Can. J. Chem. **53**, 2189 (1975).
7. J.-P. Joseleau, G. Chambat, M. Vignon, and F. Barnoud. Carbohydr. Res. **58**, 165 (1977).
8. T. Usui, T. Tsushima, N. Yamaoka, and K. Matsuda. Agric. Biol. Chem. **38**, 1409 (1974).
9. F. R. Seymour, R. D. Plattner, and M. E. Slodki. Carbohydr. Res. **44**, 181 (1975).
10. S. Hakomori. J. Biochem. Tokyo, **55**, 205 (1964).

Can. J. Chem. Downloaded from www.nrcresearchpress.com by 210.87.254.105 on 09/06/12
For personal use only.

Methyl substituted thioxanthones and thioxanthone-10,10-dioxides

IAN D. BRINDLE[1] AND PAUL P. DOYLE
Department of Chemistry, Brock University, St. Catharines, Ont., Canada L2S 3A1

Received December 10, 1982

IAN D. BRINDLE and PAUL P. DOYLE. Can. J. Chem. **61**, 1869 (1983).

The preparation of all four monomethylthioxanthones and their corresponding dioxides is described. A previously published synthesis of the 2- and 3-methylthioxanthones by Gilman and Diehl has been shown to produce the 2- and 4-methyl isomers.

IAN D. BRINDLE et PAUL P. DOYLE. Can. J. Chem. **61**, 1869 (1983).

On décrit la préparation des quatre monométhylthioxanthones et de leurs dioxydes correspondants. On montre qu'une synthèse des méthyl-2 et méthyl-3 thioxanthones, publiée antérieurement par Gilman et Diehl donne les isomères méthyl-2 et méthyl-4.

[Traduit par le journal]

Can. J. Chem. Downloaded from www.nrcresearchpress.com by 210.87.254.5 on 09/06/12
For personal use only.

The methyl substituted thioxanthones and corresponding dioxides have not been well studied. Although the 2-methylthioxanthone and the 2- and 4-methylthioxanthone-10,10-dioxides were known before 1910 (1, 2), of the remaining five compounds only the 3-methylthioxanthone-10,10-dioxide has been reported (3). We required methyl substituted thioxanthones and their dioxides for long range nmr coupling experiments, the results of which will be published elsewhere, thus we undertook the synthesis of the title compounds.

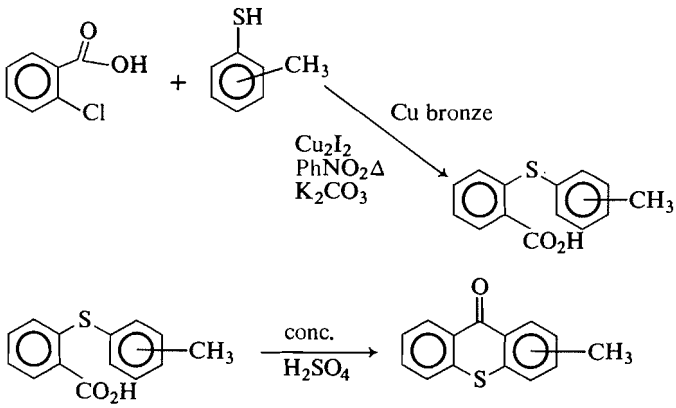

The Ullman reaction has been used to prepare 2-carboxyl diphenyl sulfides (4). These sulfides were readily cyclized by concentrated sulfuric acid to thioxanthones in about 60% yield by the procedure of Mayer (2). 2-Carboxy-3′-methyldiphenyl sulfide cyclized to the 1- and 3-methylthioxanthones in almost equal yields and the two isomers were readily separated by column chromatography. The identity of the two isomers was readily established by comparison of the nmr spectra of the two isomers with the known xanthones.[2] The thioxanthones were readily oxidized to the dioxides, using 30% hydrogen peroxide in glacial acetic acid, in 90% yield.

The large discrepancy between the reported melting point of 3-methylthioxanthone-10,10-dioxide and our compound led us to investigate the work of Gilman and Diehl (3). In their work, 2-mercaptobenzoic acid was condensed with toluene in the presence of sulfuric acid to give a mixture of isomers which could not be separated. Subsequent treatment of the mixture with 30% hydrogen peroxide gave a mixture which was separable by fractional crystallization into 2-methylthioxanthone-10,10-dioxide and a lower-melting material tentatively identified as the 3-methyl isomer on the basis of infrared evidence.

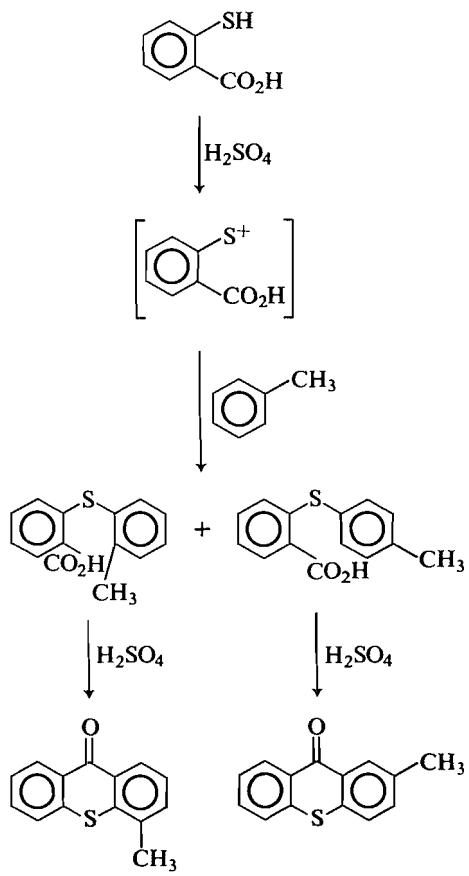

SCHEME 1

We have repeated this experiment under the same conditions used by Gilman and Diehl. After the disulfide by-product was removed, the remaining yellow product was subjected to hplc analysis which showed two components which were identified, on the basis of retention time and addition of the known isomers, as the 2- and 4-methylthioxanthones in the ratio 3:1.[3]

The products and the product ratio suggest an attack by an electrophilic sulfur on toluene on the *o*- and (preferred) *p*-positions, followed by sulfuric acid mediated ring closure to the observed products (Scheme 1). The sulfenium ion equivalent

[1]Author to whom correspondence may be addressed.

[2]I. D. Brindle, J. M. Miller, and T. R. B. Jones, unpublished observations.

[3]NOTE ADDED IN PROOF: The structure of 4-methylthioxanthone has now been established by single-crystal X-ray diffraction studies by M. F. Richardson (personal communication).

TABLE 1. 2-Carboxy-x'-methyldiphenyl sulfides

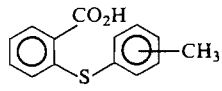

Isomer	Yield %	Melting point °C	Lit. melting point (ref.)	Microanalyses
2'-Methyl	75	175–176	—	C 68.88, H 4.81, S 12.92
3'-Methyl	80	180–182	—	C 68.70, H 4.92, S 12.87
4'-Methyl	85	214–216	215–216(4)	
				$C_{14}H_{12}SO_2$ requires: C 68.83, H 4.95, S 13.12%

TABLE 2. x-Methylthioxanthones

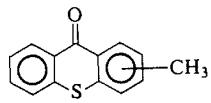

Isomer	Yield %	Melting point°C	Lit. melting point (ref.)	Microanalyses
1-Methyl	28	93–95	—	C 74.49, H 4.44, S 13.81
2-Methyl	60	122–124	123(2)	
3-Methyl	29	115–116	—	C 74.17, H 4.44, S 13.93
4-Methyl	66	146–148	—	C 74.33, H 4.34, S 14.04
				$C_{14}H_{10}SO$ requires: C 74.31, H 4.45, S 14.7

TABLE 3. x-Methylthioxanthone-10,10-dioxides

Isomer	Yield %	Melting point °C	Lit. melting point (ref.)	Microanalysis
1-Methyl	90	201–203	—	C 65.02, H 3.93, S 12.31
2-Methyl	91	204–206	199(2)	
3-Methyl	91	206–207	158.5–160(3)	C 64.97, H 3.89, S 12.43
4-Methyl	91	181–182	172(1)	
				$C_{14}H_{10}SO_3$ requires: C 65.10, H 3.90, S 12.41

could be derived from sulfenic acid, as suggested by Gilman and Diehl. The product distribution is, in fact, what would be predicted by the mechanism suggested by Gilman and Diehl. The low melting point obtained by Gilman and Diehl for the compound isolated probably resulted from the cocrystallization of both the 2- and 4-methylthioxanthone-10,10-dioxides.

Experimental

The series of reactions to make the thioxanthone-10,10-dioxides was similar in each case, so the preparation from *m*-thiocresol will be illustrative of the method.

Analyses were performed by Dr. Franz Pascher Microanalytisches Laboratorium, Buchstr., 45, 5300 Bonn, West Germany. Melting points are uncorrected.

2-Carboxy-3'-methyldiphenyl sulfide

o-Chlorobenzoic acid (5.0 g; 0.032 mol), *m*-thiocresol (4.0 g; 0.032 mol), dry potassium carbonate (13.2 g; 0.096 mol), copper I iodide (0.2 g), and copper bronze (93.3% Cu, 4.98% Sn, 1.55% Zn, and 0.08% Pb; 0.2 g) were stirred together in dry nitrobenzene (40 mL). The reaction mixture was heated to reflux and maintained, with stirring, for 10 min.

The nitrobenzene was removed by steam distillation and the tars were removed by filtering with charcoal. The filtrate was treated with hydrochloric acid to pH 1 and the solid was filtered off and dried to give the crude product (3.1 g, 80%) as a tan powder melting at 170–174°C. Crystallization from methanol gave *2-carboxy-3'-methyldiphenyl sulfide* as white needles, mp 180–182°C (microanalysis given in Table 1).

1- and 3-Methylthioxanthone

2-Carboxy-3'-methyldiphenyl sulfide (14.6 g; 0.060 mol) was stirred in sulfuric acid (146 mL) under nitrogen for 1.5 h at 100°C. The cooled mixture was poured onto ice and the crude product was filtered off and taken up in chloroform. Unreacted starting material was removed by shaking with 10% sodium carbonate. The chloroform was washed with water, dried ($MgSO_4$), and evaporated to dryness. The resultant yellow oil solidified on standing (9.00 g, 66%), mp 55–90°C; ^{1}Hmr ($CDCl_3$) showed two methyl singlets at δ 2.46 (54%) and δ 2.91 (46%).

The yellow oil was dissolved in a minimum volume of toluene and chromatographed on 60–100 mesh Florisil. Elution with hexane, and hexane–ether, 9:1, 8:2, 7:3 gave two bands which were examined by tlc (silica gel, CCl_4). The first fraction (R_f 0.81) gave 1-methylthioxanthone (3.75 g; 28%) as pale yellow blades after crystallization from hexane, mp 93–95°C. The second fraction (R_f 0.58) yielded *3-methylthioxanthone* (3.87; 29%) as pale yellow needles from hexane, mp 115–116°C (microanalysis given in Table 2).

1-Methylthioxanthone-10,10-dioxide

1-Methylthioxanthone (3.0 g; 0.13mol) was dissolved in 50 mL of hot glacial acetic acid. The solution was heated to reflux and 30%

Can. J. Chem. Downloaded from www.nrcresearchpress.com by 210.87.254.5 on 09/06/12
For personal use only.

hydrogen peroxide (18 mL) was added in 6-mL portions at half hour intervals. The reaction mixture was maintained at reflux, with stirring, for 3 hours. A pale yellow crystalline solid separated upon cooling and was filtered off (3.0 g; 88%). An additional 0.07 g precipitated when the filtrate was poured over ice. The product was dissolved in chloroform and passed through a short column of acid-washed alumina with 200 mL of chloroform. A small amount of unidentified material remained at the top of the column. *1-Methylthioxanthone-10,10-dioxide* (2.6 g) was obtained as pale yellow rods from glacial acetic acid, mp 201–203°C (microanalysis given in Table 3).

Reaction of o-*mercaptobenzoic acid and toluene*

The reaction was carried out under the same conditions used by Gilman and Diehl (3). The yellow solid recovered after the removal of the disulfide was subjected to hple analysis on a Partisil PSX 10–25 column and eluted with 50% hexane in chloroform at 2 mL/min. Retention times for the two components were 3.3 min and 3.8 min corresponding to the 2- and 4-methylthioxanthones; these were in the ratio 3:1.

Acknowledgement

The authors wish to thank the Natural Sciences and Engineering Research Council of Canada for a grant (for PPD).

1. F. ULLMANN and A. LEHNER. Ber., **38**, 740 (1905).
2. F. MAYER. Ber. **43**, 584 (1910).
3. H. GILMAN and J. W. DIEHL. J. Org. Chem. **24**, 1914 (1959).
4. J. GOLDBERG. Ber. **37**, 4526 (1904).

Can. J. Chem. Downloaded from www.nrcresearchpress.com by 210.87.254.5 on 09/06/12
For personal use only.

2-Mercaptoaldehyde dimers and 2,5-dihydrothiophenes from 1,3-oxathiolan-5-ones[1,2]

JOHN M. MCINTOSH AND MAQBOOL A. SIDDIQUI
Department of Chemistry, University of Windsor, Windsor, Ont., Canada N9B 3P4

Received December 16, 1982

JOHN M. MCINTOSH and MAQBOOL A. SIDDIQUI. Can. J. Chem. **61**, 1872 (1983).

Representative 1,3-oxathiolan-5-ones (**6**), prepared from 2-mercaptoacids, have been reduced to 2-mercaptoaldehydes **1** with diisobutylaluminum hydride. The aldehydes **1**, which appear to exist in several dimeric forms, react with vinyltriphenylphosphonium bromide to give 2,5-dihydrothiophenes.

JOHN M. MCINTOSH et MAQBOOL A. SIDDIQUI. Can. J. Chem. **61**, 1872 (1983).

On a réduit les oxa-1,3 thiolanones-5 (**6**) typiques obtenues à partir des mercapto-2 acides, en mercapto-2 aldéhydes **1** avec l'hydrure de diisobutylaluminium. Les aldéhydes **1** qui semblent exister sous plusieurs formes dimères réagissent avec le bromure de vinyltriphénylphosphonium en donnant les dihydro-2,5 thiophènes.

[Traduit par le journal]

Can. J. Chem. Downloaded from www.nrcresearchpress.com by 210.87.254.40 on 09/06/12
For personal use only.

For a number of years we have been interested in the formation and synthetic applications of substituted and functionalized 2,5-dihydrothiophenes (**2**) (Scheme 1). We have shown that these molecules can be prepared simply and in high yield by the reaction of 2-mercaptocarbonyl compounds (**1**) with vinylphosphonium salts (1) or vinylphosphonates (2) and that they are efficient precursors of conjugated dienes (1, 2) and substituted thiophenes (3). In order to use this methodology in the synthesis of more complex systems, it became imperative to develop ways of introducing the 2-mercaptoaldehyde or ketone into a molecule which also contained other functional groups or, conversely, carrying this combination of reactive functionalities in some protected or latent form from which they could be generated under mild and specific conditions.

2-Mercaptoaldehydes and ketones have usually been prepared from the parent carbonyl compounds by bromination (which must be regiospecific in the case of ketones), followed by reaction with a salt of hydrogen sulfide. The conditions for the latter reaction are necessarily strongly basic, conditions which are normally avoided with molecules containing an aldehyde group. Compounds **1** exist largely in dimeric forms. Several different structural types have been identified (Scheme 1), two of which are represented by **3** and **4** (4). Form **3***a* is

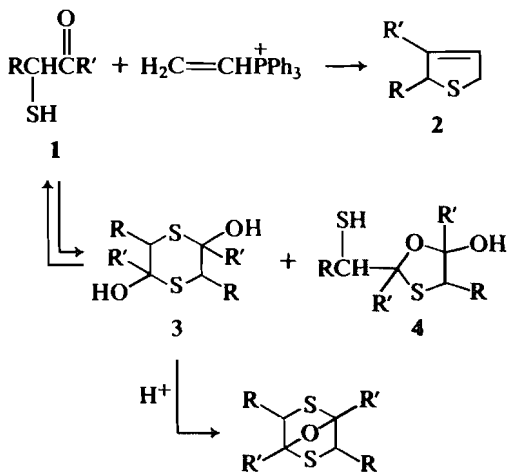

SCHEME 1

[1]Dihydrothiophenes 9. For part 8, see ref. 2*b*.

[2]Taken in part from the M.Sc. thesis of M.A.S. University of Windsor, December 1982.

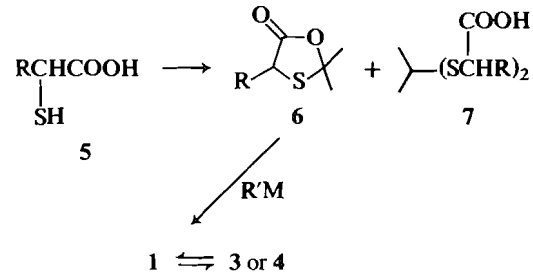

SCHEME 2

sensitive to acid-catalyzed dehydration (4*a*) but these revert to **1** under basic conditions. The liberated groups are sensitive to acid, base, and oxidizing conditions. A suitable solution to the problem would involve the use of a heterocyclic species which would be easily formed from readily available precursors, stable to a variety of reaction conditions, and which would generate the desired 2-mercaptocarbonyl compound in a chemospecific and regiospecific way.

We chose the 1,3-oxathiolane-5-one system (**6**) (5) as an ideal point to begin our investigation. It possesses the following advantages: (1) it is easily prepared from 2-mercaptoacids; (2) it offers the possibility of being alkylated at the 4-position, thus allowing the direct introduction of the desired functionalities into a larger molecule in the protected form; (3) the reaction of the ester carbonyl with either hydride or organometallic reagents should lead to the mercaptoaldehydes or ketones (Scheme 2). Our results on the hydride reduction reaction are the subject of this report.

Preparation of 1,3-oxathiolan-5-ones

Acetone was chosen as the blocking group for the mercaptoacids in order to give the simplest possible nmr spectra in a compound which had no potentially troublesome protons at C2. Also, the presence of the *gem*-dimethyl substituents should materially reduce difficulties arising from reactions at the nucleophilic sulfur atom. Compounds **6***a*–*e* (Table 1) were prepared from the corresponding mercaptoacids **5** by condensation either with acetone (6) or 2-methoxypropene (7). In some cases one of these methods was superior and in other cases the reverse situation occurred. The spectroscopic data for compounds **6** are contained in Table 2.

Reduction of 1,3-oxathiolan-5-ones

Unless the initial adduct formed by hydride attack on **6** is

TABLE 1. Preparation of oxathiolanones from the corresponding acids

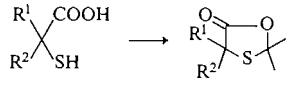

		Acid				Oxathiolanone				
R^1	R^2	No.	Yield (%)[a]	[bp °C(Torr)]	Ref.	No.	Method	Yield (%)	bp °C (Torr)	Ref.
H	H	**5***a*	[b]	—		**6***a*	A	42	90–93(20)	6
Me	H	**5***b*	[b]	—		**6***b*	A	63	98–103(20)	7
Et	H	**5***c*	75	[105–110(9.3)]	12	**6***c*	B	85	79–82(9)	
Me	Me	**5***d*	49	[105–110(16)]	13	**6***d*	B	53	86–90(24) (mp 52–54)	
Ph	H	**5***e*	67	mp 57–60	10	**6***e*	B	85	mp 85–88 (hexane)	

[a]From 2-bromo acid via the xanthate.
[b]Commercially available.

TABLE 2. Spectroscopic data for 1,3-oxathiolan-5-ones

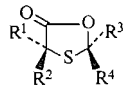

			Cmr						
Compound	Infrared[a] (cm^{-1})	^{1}Hmr[b] (δ)	C2	C4	C5	R^1	R^2	$R^3(CH_3)$	$R^4(CH_3)$
6*a*	1775, 1230 1095, 982	3.84(s, 2H), 1.78(s, 6H)	88.9	33.3	172.0	—	—	30.7	30.7
6*b*	1770, 1228 1175, 1050	4.16(q, 1H, J = 7 Hz), 1.75(s, 6H) 1.60(d, 3H, J = 7 Hz)	86.0	42.4	174.6	17.9	—	30.9	31.3
6*c*	1760, 1230 1178, 980	4.14(dd, 1H, J = 5,8 Hz), 2.38–1.60 (m, 2H), 1.64(s, 6H), 1.0(t, 3H, J = 7 Hz)	86.3	50.2	174.0	26.3 11.9	—	31.2	31.8
6*d*	1765, 1745 1175, 1078	1.78(s, 6H), 1.68(s, 6H)	84.5	52.8	177.8	30.2	30.2	32.6	32.6
6*e*	1768, 1250 1108, 990	7.51(s, 5H), 5.31(s, 1H), 1.85(s, 6H)	86.0	52.7	172.7	128.8 128.6	—	31.0	31.7

[a]Four most intense peaks.
[b]Coding follows the following scheme: chemical shift (multiplicity, integrated intensity, coupling constant).

stable, further reduction to the alcohol is to be expected. Therefore the reduction conditions must allow the lactol intermediate to survive until all the hydride has been consumed. Initial investigations using LAH at −78°C were not encouraging. Significant overreduction to mercaptoalcohols was observed, even when the consumption of **6** was incomplete. The known (8) ability of diisobutylaluminum hydride (DIBAL) to reduce lactones and nitriles to the aldehyde stage led us to consider this reagent. It should be noted that potentially troublesome Lewis acid–base interactions can occur in this combination of reagents. However, when the reduction was carried out in toluene at −78°C, the 2-mercaptoaldehydes were obtained in their dimeric forms **3** and **4**. In several cases more than one dimeric form was isolated. Some were crystalline, others were not. In at least one case (**3***d*), significant portions of the product showed a carbonyl absorption in the infrared spectrum suggesting the presence of monomeric species. In all cases, either the separated forms or the mixture reacted equally well in the formation of 2,5-dihydrothiophenes mentioned below. Thus the overall yields of **3** are calculated on the basis of the combined yields of all forms. In most cases, the major dimeric form appeared to be **3**, but most of these can exist in diastereomeric forms and the nmr spectra of such materials indicate such mixtures. In addition, **3** are only very sparingly soluble in organic solvents and resort had to be made to either DMSO or pyridine. In these solvents, the dimer(s) and monomer are in equilibrium and, for this reason, the nmr spectra of **3** are difficult to interpret and thus are omitted from this paper.

The yields (Table 3) of **3** range from 14 to 70%. In general, our experience in preparing these compounds via the reaction of 2-haloaldehydes with sodium hydrosulfide (9, 1*d*) suggests that the described method is superior in all respects. The 2-haloaldehydes, prepared by the chlorination (sulfuryl chloride) or bromination of aldehydes, are extemely fragile molecules which polymerize readily and cannot be purified. The reaction of these with sodium hydrosulfide gives the dimers **3** in a maximum yield of 50% and many are formed in much lower amounts (cf. 6% yield of **3***b*) (1*d*)). In contrast, the present method starts with either the much more stable haloacids or with commercially available mercaptoacids (**5***a*, *b*).

Each of the dimers **3** and **4** was used to prepare the dihydrothiophenes **2** by reaction with vinyltriphenylphosphonium bromide (1). The yields and spectroscopic data for **2** are given in Table 4.

Further work is in progress on the reaction of **6** with alkylating and organometallic reagents as potential routes to homologated and functionalized mercaptoaldehydes and ketones and the results will be reported in due course.

Can. J. Chem. Downloaded from www.nrcresearchpress.com by 210.87.254.40 on 09/06/12
For personal use only.

TABLE 3. Preparation of aldehydes **3** from lactones **6**

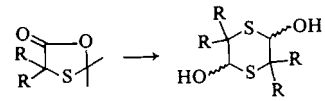

Lactone	Aldehyde	(yield(%))[a]	Melting point[b]	Ref.	Comments
6*a*	**3***a*	(14)	122–125	14	ca. Equal amounts of liquid and solid forms
6*b*	**3***b*	(39)	139–143	1*d*	ca. 4:1 solid – liquid form
6*c*	**3***c*	(70)	143–149	9	ca. 7:1 solid – liquid form
6*d*	**3***d*	(47)	Very broad		ca. 5:4 solid – liquid; liquid contains some monomeric species (ir)
6*e*	**3***e*	(66)	175–178		ca. 4:3 solid – liquid forms

[a]Combined yield products as dimeric forms, both of which afforded **2** in comparable yields.
[b]Of solid portion.

TABLE 4. Yields and spectral data for 2,5-dihydrothiophenes (**2**)

Compound No.	R^1	R^2	Time (h)	Yield (%)	^{1}Hmr[a]	Cmr C2	C3	C4	C5	R^1	R^2
2*a*[b]	H	H	5	44	5.88(s, 2H), 3.76(s, 4H)	38.9	128.6	128.6	38.9	—	—
2*b*	Me	H	6	42	5.78(s, 2H), 4.3(m, 1H), 3.77(m, 2), 1.39(d, 3H, J = 6 Hz)	49.7	135.1	127.0	39.1	24.2	—
2*c*[c]	Et	H	14	75	5.75(s, 2H), 4.20(m, 1H), 3.68(m, 2H), 1.95–1.41(m, 2H), 0.93(t, 3H, J = 7 Hz)	57.4	133.2	128.5	38.5	{31.1, 11.6}	—
2*d*	Me	Me	24	59	5.60(s, 2H), 3.75(s, 2H), 1.45(s, 6H)	59.8	140.5	124.9	39.1	32.4	32.4
2*e*	Ph	H	12	48	7.34(s, 5H), 5.87(m, 2H), 5.36(m, 1H), 3.89(m, 2H)	58.8	133.2	128.8	39.6	{129.5, 128.5, 127.6, 127.2}	—

[a]Coding as in Table 2.
[b]Reference 15.
[c]Reference 1*c*.

TABLE 5. Analytical data for previously unreported compounds

Compound	Formula	Analyses Calcd. (%) C	H	S	Found (%) C	H	S
6*c*	($C_7H_{12}O_3S$)	52.47	7.55	20.01	52.43	7.57	19.67
6*d*	($C_7H_{12}O_2S$)	52.47	7.55	20.01	52.55	7.42	19.86
6*e*	($C_{11}H_{12}O_2S$)	63.43	5.81	15.39	63.53	5.67	15.39
3*d*[a,b]	($C_8H_{16}O_2S_2$)	46.12	7.74	30.78	(m/z = 208, 104)		
3*e*[a]	($C_{16}H_{16}O_2S_2$)	63.13	5.30	21.06	63.21	5.19	20.84

[a]Of solid form dimer.
[b]Insufficient sample available.

Experimental

Melting points are corrected; boiling points are uncorrected. Infrared spectra were run on a Beckman IR-12 instrument in chloroform solution. The ^{1}Hmr spectra were run at 60 MHz in deuterochloroform and are reported in the following format: chemical shift (δ) (multiplicity, number of protons, coupling constant). The Cmr spectra were run in deuterochloroform at 22.64 MHz in the FT mode using a flip angle of 45° on a Bruker CXP-100 instrument and are reported in ppm relative to internal TMS as standard. The aquisition time was 0.7 s and 8K data points were collected. Gas chromatographic analyses were performed using either 10% or 20% SE30 on Chromosorb W columns as previously described (1), solvents were removed at reduced pressure, and the drying agent used was anhydrous magnesium sulfate. Satisfactory C, H, and S analyses were obtained on all new compounds (Table 5) except **3***d* which gave a mass spectrum (molecular weight and fragmentation pattern) consistent with the assigned structure.

Mercaptoacids **5***a* and **5***b* are commercially available. Acids **5***c*, *d*, and *e* were prepared from the corresponding 2-bromoacids by treatment with potassium *O*-ethyl xanthate, followed by alkaline hydrolysis according to literature precedents (10).

Can. J. Chem. Downloaded from www.nrcresearchpress.com by 210.87.254.40 on 09/06/12
For personal use only.

Can. J. Chem. Downloaded from www.nrcresearchpress.com by 210.87.254.40 on 09/06/12
For personal use only.

Preparation of 1,3-oxathiolan-5-ones

Two methods (A and B) were used.

Method A (7)

To the appropriate mercaptoacid (0.2 mol) was added 2-methoxypropene (0.8 mol), dropwise with stirring at 0°C. After the addition was complete, the mixture was refluxed for 24 h, cooled, diluted with ether, and the mixture successively washed with 1 *N* sodium carbonate solution (3 × 50 mL), water (3 × 50 mL), and dried. Removal of the solvent gave **6**, which was purified by distillation or crystallization. Physical constants and spectroscopic data are given in Tables 1 and 2. In the case of **6***a*, a solid product sometimes formed which was shown to be **7** (11) by its melting point and spectral features.

Method B (6)

To a solution of mercaptoacid (0.4 mol) in 100 mL of benzene in a 250-mL flask fitted with a Dean–Stark water separator was added 3 equiv. of acetone and a catalytic amount of toluene sulfonic acid. The mixture was refluxed for 24 h, at which point no more water was separating. The cooled solution was diluted with ether (200 mL) and washed and dried as described under Method A. The products obtained are described in Tables 1 and 2.

Preparation of 2-mercaptoaldehyde dimers **3** *and* **4**

To a solution of the lactone **6** (0.02 mol) in 5 mL of dry toluene which had been cooled to −78°C was added 4 equiv. of DIBAL-H (25% in toluene), dropwise with stirring under a nitrogen atmosphere. Stirring was continued at −78°C for 2 h after the final addition and then the mixture was poured slowly into 200 mL of 50% aqueous acetic acid and 100 g of ice. The mixture was stirred vigorously for 15 min and extracted with chloroform (3 × 100 mL). The extracts were washed successively with saturated sodium bicarbonate solution (until the extracts were basic) and water and dried. Evaporation gave a semi-solid product which was treated with ether and then filtered. The filtrate was evaporated, treated again with ether, and refiltered. In this manner, the solid form (**3**) of **1** was obtained, which appeared from ir and ^{1}Hmr data to be a diastereomeric mixture of dimers **3**. The ^{1}Hmr spectra of the liquid material obtained from the ether filtrate showed many absorptions which, taken in conjunction with the infrared spectra, suggested mixtures of **3**, **4**, and in the case of **6***d*, **1**. These spectra were strongly solvent dependent. On the basis of their subsequent reaction with vinyltriphenylphosphonium bromide, the liquid portions are considered to be equivalent to the solids and the yields reported in Table 3 are calculated on this basis.

Dihydrothiophene formation

Each of the DIBAL-H products **3** and **4** were converted to the 2,5-dihydrothiophenes **2** in the following manner (1). To a solution of vinyltriphenylphosphonium bromide (4 g, 0.01 mol) in 50 mL of dry pyridine containing 0.015 mol of triethylamine was added a pyridine solution of 5 mmol of **3** or **4**, dropwise with stirring under a nitrogen atmosphere. After addition was complete, the solution was refluxed for the time indicated in Table 4, cooled, poured into water (500 mL), and extracted with ether (2 × 100 mL) and pentane (2 × 100 mL). The combined extracts were washed with 10% hydrochloric acid, water, and dried. Evaporation to ca. 10 mL, followed by filtration through a short column of acidic alumina using pentane as eluant, afforded **2**, free of colored or phosphorus-containing impurities. Gas–liquid chromatographic analysis showed them to be >95% pure. The yields and spectral data are given in Table 4.

Acknowledgements

The financial assistance of the Natural Sciences and Engineering Research Council of Canada made this work possible and is gratefully acknowledged.

1. (*a*) J. M. McINTOSH and H. B. GOODBRAND. Tetrahedron Lett. 3157 (1973); (*b*) J. B. McINTOSH, H. B. GOODBRAND, and G. M. MASSE. J. Org. Chem. **39**, 202 (1974); (*c*) J. M. McINTOSH and R. S. STEEVENSZ. Can. J. Chem. **52**, 1934 (1974); (*d*) J. M. McINTOSH and G. M. MASSE. J. Org. Chem. **40**, 1294 (1975); (*e*) J. M. McINTOSH and R. S. STEEVENSZ. Can. J. Chem. **55**, 2442 (1977).
2. (*a*) J. M. McINTOSH and R. A. SIELER. Can. J. Chem, **56**, 226 (1978); (*b*) J. Org. Chem. **43**, 4431 (1978).
3. J. M. McINTOSH and H. KHALIL. Can. J. Chem. **53**, 209 (1975).
4. (*a*) G. GEISELER and F. STACHE. Chem. Ber. **94**, 337 (1961); (*b*) F. ASINGER, M. THIEL, and H. KALTWASSER. Ann. Chem. **606**, 67 (1957); (*c*) A. KIRRMANN, J. CANTACUZÈNE, L. VIO, and M. MARTIN. Bull. Soc. Chim. Fr. 1067 (1963).
5. T. B. CAMERON and H. W. PINNICK. J. Am. Chem. Soc. **102**, 744 (1980), and references therein.
6. K. PIHLAJA, A. NIKKILÄ, K. NEUVONEN, and R. KESKINEN. Acta Chem. Scand. Ser. A, **30**, 457 (1976).
7. Y. K. YEE. Ph.D. Dissertation, Cornell University, 1978; Diss. Abstr. Int. B., **39**, 3847 (1979).
8. E. WINTERFELDT. Synthesis, 617 (1975).
9. A. KIRRMANN, J. CANTACUZÈNE, and L. VIO. Rev. Chim. Acad. Repub. Pop. Roum. **7**, 1011 (1962); Chem. Abstr. **61**, 8180a (1962).
10. W. A. BONNER. J. Org. Chem. **33**, 1831 (1968).
11. S. WAKAKI, T. ASAHIMA and Y. TOHMON. J. Agric. Chem. Soc. Jpn. **28**, 174 (1954).
12. E. BILLMAN. Ann. Chem. **348**, 128 (1906).
13. E. BILLMAN. Ann. Chem. **339**, 351 (1905).
14. G. HESSE and F. JÖRDER. Chem. Ber. **85**, 930 (1952).
15. R. H. EVERHARDUS, R. GRÄFING, and L. BRANDSMA. Recl. Trav. Chim. Pays-Bas, **95**, 153 (1976).

Excess enthalpies, heat capacities, and volumes of trialkylamine and cyclohexane systems: NR_3 + NR'_3 and c-C_6 + NR_3. Effect of correlations of molecular orientations and steric hindrance

BERNARD RIEDL AND GENEVIÈVE DELMAS[1]

Département de chimie, Université du Québec à Montréal, C.P. 8888, Succ. A, Montréal (Qué.), Canada H3C 3P8

Received July 6, 1982

BERNARD RIEDL and GENEVIÈVE DELMAS. Can. J. Chem. **61**, 1876 (1983).

A Picker flow calorimeter has been used to obtain molar excess heat capacities, c_p^E, through the concentration range at 25°C for the NR_3 + NR'_3 systems where R = C_nH_{2n+1} and n = 2, 3, 4, 5, 6, 8, 12. Excess heats, h^E and c_p^E are also given for the mixtures of four trialkylamines with cyclohexane. Excess volumes V^E have been also measured on the same systems. Two contributions to the three thermodynamic functions were investigated, namely, that of disordering the long chains and that called steric hindrance. The steric hindrance has been found to occur with molecules having a highly substituted central atom. The corresponding contribution has an unexpected sign for non-polar systems, i.e., negative for h^E and positive for c_p^E, indicative of a loss of molecular mobility on passing from the pure liquid to the solution. The mixtures of the globular NR_3 give small negative c_p^E (≥ -0.7 J K^{-1} mol^{-1}) except for one. For the systems involving globular + linear molecules, the c_p^E are also negative but larger (down to -3.7 J K^{-1} mol^{-1}) due principally to the disordering contribution. The c_p^E confirm the small steric hindrance contribution seen on the h^E. The cyclohexane + NR_3 systems have positive h^E (varying between 275 and 660 J mol^{-1}) and negative c_p^E (varying between -1.6 and -5.2 J K^{-1} mol^{-1}) typical of a disordering effect and/or of a small force field difference. The parameter characteristic of the disappearance of order with temperature, obtained from the slope of h^E versus c_p^E, is found to be 90 K, understandably in between the value for the linear alkanes (50 K) and the SnR_4 (140 K). The V^E are well predicted by the Prigogine–Patterson–Flory equation of state theory, in particular, the contrast between the all positive values for the cyclohexane systems and the negative ones for the NR_3 mixtures due to the much higher cohesive energy of cyclohexane compared to that of the trialkylamines.

BERNARD RIEDL et GENEVIÈVE DELMAS. Can. J. Chem. **61**, 1876 (1983).

Nous avons utilisé le calorimètre à flux Picker pour mesurer à 25°C les capacités calorifiques d'excès, c_p^E, en fonction de la concentration pour les systèmes NR_3 + NR'_3 avec R = C_nH_{2n+1} et n = 2, 3, 4, 5, 6, 8, 12. Les enthalpies d'excès h^E et c_p^E sont données aussi pour les mélanges de quatre trialkylamines avec le cyclohexane. Pour les mêmes systèmes, nous avons mesuré aussi les volumes de mélange V^E. Deux contributions à ces trois fonctions thermodynamiques étaient l'objet de ce travail, la contribution de désordre des longues chaines et la contribution d'empêchement stérique. Cette dernière se retrouve avec des molécules qui ont un atome central très substitué. Le signe de la contribution correspondante est plutôt inattendu pour les systèmes non-polaires puisqu'il est négatif pour h^E et positif pour c_p^E révélant une diminution de mobilité moléculaire en solution. Les mélanges de NR_3 globulaires (sauf un) ont des c_p^E négatives (≥ -0.7 J K^{-1} mol^{-1}). Pour les mélanges de molécules globulaires et linéaires, les c_p^E sont aussi négatives mais la plus grande valeur absolue (qui atteint -3.7 J K^{-1} mol^{-1}) est due à la contribution de désordre. Les valeurs de c_p^E confirment la modeste contribution d'empêchement stérique vue sur les h^E. Les systèmes cyclohexane + NR_3 ont des valeurs positives de h^E (variant entre 275 et 660 J mol^{-1}) et négatives de c_p^E (variant entre -1.6 et -5.2 J K^{-1} mol^{-1}) typiques d'une contribution de désordre et d'une petite différence d'énergie de cohésion. Le paramètre caractéristique de la disparition de l'ordre avec la température τ obtenu par la pente de h^E en fonction de c_p^E a une valeur de 90 K intermédiaire entre celle pour les alcanes linéaires (50 K) et les SnR_4 (140 K). Les V^E sont bien prédits par la théorie de Prigogine, Patterson et Flory et en particulier le contraste entre les valeurs positives pour les systèmes SnR_4 et négatives pour les NR_3, différence due à la valeur élevée de l'énergie de cohésion du cyclohexane comparée à celle des trialkylamines.

Introduction

This work is part of an investigation of the effect of molecular shape on the thermodynamic properties of mixtures. The NR_3 series (R = C_nH_{2n+1}) is convenient for this purpose since in the passage from n = 2 for the first member of the series to n = 12 for the longest studied here, the molecular shape changes from globular to linear without too much modification of the component chemical nature. The aim of the present paper is to confirm by c_p^E and V^E measurements, the information previously (1) obtained from the h^E of the NR_3 + NR'_3 systems and of the NR_3 + linear and branched alkane (2) systems on two contributions to the thermodynamic functions, namely, the disordering contribution and the steric hindrance contribution.

The disordering contribution h^E(dis) occurs when an ordered liquid (A) is mixed with a non-ordered one (B). Most of the ordered, non-polar liquids studied have been made of long-chain anisotropic molecules and the non-ordered ones are made of globular isotropic molecules. Rayleigh scattering data on pure components and solutions (3) confirm and complete the information on orientational order obtained by thermodynamic methods. The effect of molecular size, free volume, and temperature on h^E(dis) have been discussed in previous work on small molecule systems (1–4) and on polymeric solutions (5). An enthalpy–entropy compensation reduces the effect of disordering on the free energy of mixing (6, 7) when the solution is made of small molecules but, in polymeric systems, correlations of molecular orientations stabilize the solution (8, 9). In binary systems, the label of steric hindrance effect has been given to systems having an unexpected value of the heat which could be either exothermic or less endothermic than forecast and containing a molecule with a highly substituted atom. The presence of two neighbouring substituted atoms or of a substituted atom situated in the center of the molecule appears to be a favorable factor for the steric hindrance effect (10, 11) since 2,3-dimethylpentane gives the steric hindrance effect, but 2,4-dimethylpentane does not. Surprisingly 3-methylhexane gives a more exothermic contribution than 2-methylhexane (8). The

[1]To whom all correspondence should be addressed.

Can. J. Chem. Downloaded from www.nrcresearchpress.com by 210.87.254.42 on 09/06/12
For personal use only.

Can. J. Chem. Downloaded from www.nrcresearchpress.com by 210.87.254.42 on 09/06/12
For personal use only.

SnR_4 (21, 22) (with R = ethyl and propyl) and 3,3-diethylpentane (4) (which can be written C(ethyl)$_4$ or 3,3-DEP), which show an important effect, have been studied extensively (2, 11). The sign of the heat indicates that there is less mobility in the solution than in the pure components. This contribution, also called "condensation contribution" by Patterson (11) and "coupling of torsionnal oscillations" by de Ligny (12), may be correlated with the mean number of *gauche* configurations Z_g (13) in the case of the branched alkanes.

The h^E data on mixtures of NR_3 with normal and branched alkanes (2) and with other trisubstituted amines have shown a small steric hindrance effect in the triethylamine and tripropylamine systems (1). The present measurements aim at confirming the characteristic features of the NR_3 + NR'_3 mixtures seen for the h^E data. The c_p^E data have been obtained on the following systems: five type-A systems made of all the binary combinations of the globular NR_3 (triethyl-, tripropyl-, tributyl-, and tri-(methyl-2-butyl)-) except one and nine type-B binary systems containing a long chain trialkylamine (hexyl, octyl, and dodecyl) with the three lower amines compounds (triethyl, tripropyl, and tributyl amines).

V^E values have been also measured for these systems to follow the effect of the cohesive energy difference on V^E and to compare it with the predicted values. The investigation of steric hindrance using *c*-C_6 as second component is reported in Part 2 of this work (19). In the course of this study, h^E, c_p^E, and V^E have been measured for *c*-C_6 for four long chain compounds: the trihexyl-, trioctyl-, tridodecyl-, and dimethyl dodecyl amines. However, as the data are interpreted mainly in terms of correlations of orientations destructions, the presentation and discussion of the results, more fitted to the present paper, will be given here.

In the following text, the names of the NR_3 compounds will be shortened to NEt_3, NPr_3, etc, as listed in the tables. *N*-(methyl-2-butyl)$_3$ has been written $NIsopent_3$.

Experimental

Materials

The amines come from the same source as in previous work (1, 2, 14), namely, Eastman (Rochester), Aldrich (Milwaukee), and the Chemical Procurement Laboratories (College Point, NY) and cyclohexane from the Chemical Samples Co. (Colombus, OH). Their physicochemical properties, density (d), expansion coefficient (α), thermal pressure coefficient (γ), and molecular (V^*, P^*) and shape (s) parameters are given in Table 1. (See Appendix for their interrelationships and the definitions of the surface-to-volume ratios (s).)

The lower amines which adsorb readily water are kept on molecular sieves. For each new batch of compound, the known heat of mixing with *c*-C_6 is re-measured as well as the refractive index and the density in order to test the quality of the compound.

Apparatus

The excess heat capacities c_p^E have been obtained at 25°C throughout the concentration range using the Picker flow calorimeter (Technorep, Montreal and Setaram, Lyon) which has been used (15, 21) and described (16) previously. The precision and accuracy of the present measurements for the reference system, *c*-C_6 + *n*-C_{16} are within 0.02 J K^{-1} mol^{-1} of the published data (−6.67 J K^{-1} mol^{-1} compared to −6.69 (16) at the maximum). For a given system, the reproducibility of the measurements of solution density and heat capacity data are about the same. For the $NDodec_3$ systems, the reproducibility is poorer (0.05 to 0.1 J K^{-1} mol^{-1}) due to the viscosity of this compound (17). The enthalpies of mixing are obtained with a tilting Tian Calvet calorimeter with the usual two compartment cells. The h^E of a reference system, CCl_4 + benzene, are obtained within 1−2% of the published results. The excess volumes are calculated from densities determined with an Anton Paar precision densitometer (Fisher Co.).

Results and discussion

The c_p^E, V^E, and h^E have been fitted through the concentration range to the Redlich−Kister equations:

$$c_p^E = x_1x_2 \sum_{i=0}^{i=2} B_i(x_1 - x_2)^i$$

[1] $$V^E = x_1x_2 \sum_{i=0}^{i=2} C_i(x_1 - x_2)^i$$

$$h^E = x_1x_2 \sum_{i=0}^{i=2} A_i(x_1 - x_2)^i$$

The concentration and values at the maximum have been listed in Tables 2, 3, and 5 as well as the A_i, B_i, and C_i parameters.

For analysing the data more easily, the heats of mixing have been written in previous work as the sum of different contributions:

[2] $$h^E_{exp} = h^E(\text{chem}) + h^E(\text{free volume}) + h^E(\text{disorder}) + h^E(\text{steric hindrance})$$

even if their independence and additivity have not been proven. h^E(chem) and h^E(free volume) correspond, respectively, to the terms having their origin in the force field and the free volume difference. h^E(chem) should be small in mixtures of alkane-like systems as the present ones (except possibly for NEt_3) and h^E(f.v.) can be calculated from an equation of state term. By analogy, c_p^E may be written under the same format:

[3] $$c_p^E = c_p^E(\text{chem}) + c_p^E(\text{f.v.}) + c_p^E(\text{dis}) + c_p^E(\text{steric hindrance})$$

The expected temperature dependence of the h^E contributions will permit the prediction of the sign of c_p^E for the corresponding contribution. As reported in Table 4, the steric hindrance and disordering contributions diminish when the temperature is raised, so the corresponding c_p^E is positive for the first (h^E being negative) and negative for the second (h^E being positive). The free volume contribution increases with T so that c_p^E is negative (h^E being negative). The different signs of c_p^E for the contributions investigated in this work are an advantage for the separation of the different terms in h^E and c_p^E. Since h^E(chem) does not vary much with temperature the corresponding contribution to c_p^E is negligible. In systems containing only globular or short chain amines, or A-type mixtures, the disordering contribution prevalent in the long-chain B-type mixtures is negligible so that eq. [3] becomes:

[4] $$c_p^E(\text{exp}) - c_p^E(\text{f.v.}) = c_p^E(\text{steric hindrance}) \text{ for the A-type mixtures}$$

and

[5] $$c_p^E(\text{exp}) - c_p^E(\text{f.v.}) = c_p^E(\text{dis}) + c_p^E(\text{steric hindrance}) \text{ for the B-type mixtures}$$

The free volume contributions (see Appendix) to c_p^E have been listed in the last but one column of the tables. $(c_p^E)_v$ is the experimental c_p^E divided by $x_1V_1^* + x_2V_2^*$ where V_1^* and V_2^* are the core volumes of the two components.

Mixtures of globular NR_3: type-A systems

The small values of h^E found on these systems (<32 J mol^{-1})

Can. J. Chem. Downloaded from www.nrcresearchpress.com by 210.87.254.42 on 09/06/12
For personal use only.

TABLE 1. Physicochemical data (d, α, γ), equation of state parameters (P^*, V^*) and shape factor, s, for the pure compounds: NR_3, SnR_4, and c-C_6

Compounds	$d_{25°C}$[a] (g cm^{-3})	$10^3\,\alpha_{25°C}$[a] (K^{-1})	γ[a] (J cm^{-3} K^{-1})	P^* (J cm^{-3})	V^* (cm^3 mol^{-1})	$s = S/V^{**}$ [c] (Å^{-1})
NEt_3	0.7238	1.290[b]	0.906	459.1	107.3	0.85[d]
NPr_3	0.7531	1.064[b]	0.865	409.6	151.1	0.90
$NBut_3$	0.7740	0.97[b]	0.963	442.3	192.7	0.88
$NIsopent_3$	0.7790	0.92	0.917	419.2	235.7	0.86
$NHex_3$	0.7967	0.879	0.993	442.1	276.9	0.85
$NOct_3$	0.8098	0.832	1.029	450.5	359.9	0.84
$NDodec_3$	0.8206	0.787	1.104	475.5	528.7	0.83
$(CH_3)_2NDodec$	0.7846	0.91	1.016	457.1	221.3	0.92
c-C_6	0.7739	1.217		530	84.3	0.93[d]
$SnMe_4$[e]	1.2805	1.28	0.809	409	106.7	0.96[d]
$SnEt_4$[e]	1.1955	1.00	0.977	454	158.6	0.86
$SnPr_4$[e]	1.0992	0.89	1.071	479	215.8	0.84
$SnBut_4$[e]	1.0456	0.818	1.006	439	271.6	0.83

[a]Reference 14.
[b]Reference 15.
[c]Where s and V^{**} are the molecular surface and core volume in a cylindrical model (see Appendix).
[d]Using a spherical model.
[e]Used in Part 2 (19).

indicate that these solutions are almost ideal. The small negative c_p^E are due in part only to the free volume difference since $c_p^E(\text{exp}) - c_p^E(\text{f.v.})$ is still negative. The sign of the difference would correspond to a larger decrease of h^E at higher temperature than expected from the free volume term. The molecular origin of this exothermic heat or better cohesion in solution is not easy to guess. It could be of the dipole–dipole type which would be more stable in solution than in the pure components.

$NIsopent_3$ + $NBut_3$ system is interesting since h^E and c_p^E are both positive. Contrary to the four other systems, h^E is predicted to increase with increasing temperature. An indication of the existence of subtle effects in these systems is given by the two different signs of c_p^E for the apparently quite similar systems $NIsopent_3$ + $NBut_3$(0.125) and $NIsopent_3$ + NPr_3-(−0.50) systems which are likely to have similar shape and equation of state parameters. Perhaps the investigation of other systems where the effects would be larger may help to see the origin of these differences.

Mixtures of globular + linear NR_3 (type-B systems)

In order to compare the experimental values for the different systems, $c_p^E(\text{exp})$ per cm^3 at the maximum of the concentration have been plotted in the bottom part of Fig. 1 versus the molar volume of the second component. Lines are drawn through the systems containing $NDodec_3$, $NOct_3$, and $NHex_3$. The same plot is made in the top part of Fig. 1 with the h_v^E the heats per cm^3 for the same systems. The characteristic features of these NR_3 mixtures given by this figure are the following: (*1*) the c_p^E are large and negative and their absolute values increase between $NHex_3$ and $NDodec_3$; (*2*) the irregularities observed in h_v^E with NEt_3 and NPr_3 are seen on the c_p^E; (*3*) the c_p^E are mirror images of the h^E indicating probably the dominance of one contribution or of two contributions which are not independent.

Quantitative evaluation of the disordering contribution on c_p^E

Temperature variation of the order in long-chain liquids

The temperature variation of the heats of mixing (15) or of other thermodynamic property such as the excess viscosity of mixtures (18), of a globular molecule with an ordered liquid, is indicative of the fast decrease of orientational order when the

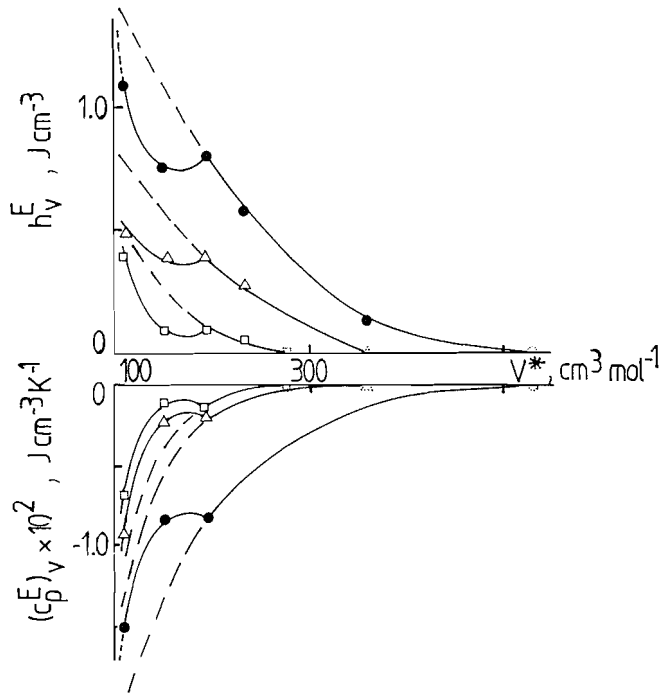

FIG. 1. Excess heats h_v^E in J cm^{-3} (upper part) and excess heat capacities, $(c_p^E)_v$ in J cm^{-3} K^{-1} (lower part) for $NHex_3$ (□), $NOct_3$ (△), and $NDodec_3$ (●) mixed with NEt_3, NPr_3, $NBut_3$ plotted against the core volume V^* of the smaller NR_3. The main contribution comes from the disordering of the long chains, bringing about h^E positive and c_p^E negative. The difference between the curves and the dotted lines corresponds to the extra steric hindrance contribution with NEt_3 and NPr_3 ($h^E < 0$ and $c_p^E > 0$).

temperature is raised. If the order is assumed to diminish exponentially with temperature with a characteristic temperature, τ, the disordering contribution to h^E and c_p^E can be written (15) as

$$h^E(\text{dis}) = h_0 e^{-T/\tau}$$

$$[6]\quad c_p^E(\text{dis}) = -(h_0/\tau)e^{-T/\tau}$$

$$h^E(\text{dis})/c_p^E(\text{dis}) = -\tau$$

Can. J. Chem. Downloaded from www.nrcresearchpress.com by 210.87.254.42 on 09/06/12
For personal use only.

TABLE 2. Excess heat capacities, c_p^E for the $NR_3 + NR'_3$ systems at the concentration x_1 of the maximum, the B_i parameters are the coefficients of the Redlich–Kister equation, c_p^E(f.v.) have been calculated at the same concentration

Class	Component 1	Component 2	c_p^E (J K^{-1} mol^{-1})	x_1	B_0 (J K^{-1} mol^{-1})	B_1 (J K^{-1} mol^{-1})	B_2 (J K^{-1} mol^{-1})	$10^2\,(c_p^E)_v$ (J cm^{-3} K^{-1})	c_p^E(f.v.) (J K^{-1} mol^{-1})	$c_p^E - c_p^E$(f.v.) (J K^{-1} mol^{-1})	h^E (J mol^{-1})
A	NEt_3	+ NPr_3	−0.06	0.72	−0.210	−9.179	−0.143	−0.05	−0.101	0.04	10.6
	NEt_3	+ $NBut_3$	−0.69	0.64	−2.649	−1.484	−1.155	−0.50	−0.242	0.45	16.3
	NPr_3	+ $NBut_3$	−0.23	0.67	−0.879	−0.228	—	—	−0.026	0.20	17.5
	NPr_3	+ $NIsopent_3$	−0.50	0.65	—	—	—	—	−0.07	−0.43	31.6
	$NBut_3$	+ $NIsopent_3$	0.125	0.50	—	—	—	0.060	—	+0.12	7.1
B	NEt_3	+ $NHex_3$	−1.15	0.66	−3.965	−4.768	3.565	−0.697	−0.457	−0.69	40
	NEt_3	+ $NOct_3$	−1.83	0.65	−6.317	−1.831	—	−0.936	−0.600	−1.23	86
	NEt_3	+ $NDodec_3$	−3.66	0.68	−13.396	−7.108	−6.791	−1.51	−0.732	−2.93	296
	NPr_3	+ $NHex_3$	−0.27	0.43	−1.080	0.196	0.529	−0.12	−0.14	−0.13	18
	NPr_3	+ $NOct_3$	−0.58	0.58	−1.184	−0.452	−0.227	−0.24	−0.26	−0.32	92
	NPr_3	+ $NDodec_3$	−2.30	0.68	−8.525	−3.599	−5.583	−0.845	−0.390	−1.91	225
	$NBut_3$	+ $NHex_3$	−0.36	0.41	−1.374	0.773	0.202	−0.15	−0.04	−0.32	20
	$NBut_3$	+ $NOct_3$	−0.55	0.60	−2.165	−0.650	−0.242	−0.21	−0.09	−0.46	104
	$NBut_3$	+ $NDodec_3$	−2.74	0.60	−10.708	−3.445	−0.477	−0.830	−0.177	−2.56	260

TABLE 3. Excess volume V^E for the $NR_3 + NR'_3$ systems at the concentration x_1 of the maximum. The C_i parameters are the coefficients of the Redlich–Kister equation. The three contributions to V^E calculated and the interchange energy parameter $X_{12}s_1^{-1}$ have been added.

Class	Component 1	Component 2	V^E (cm^3 mol^{-1})	x_1	C_0 (cm^3 mol^{-1})	C_1 (cm^3 mol^{-1})	C_2 (cm^3 mol^{-1})	V^E_{calcd} (cm^3 mol^{-1})	$V^E_{exp} - V^E_{calcd}$ (cm^3 mol^{-1})	$V^E(h^E)$ (cm^3 mol^{-1})	$V^E(P^*)$ (cm^3 mol^{-1})	V^E(f.v.) (cm^3 mol^{-1})	$X_{12}s_1^{-1}$ (J cm^3 Å^{-1})
A	NEt_3	+ NPr_3	0.125	0.41	0.47	−0.16	−0.15	0.089	0.036	0.021	0.157	−0.089	0.72
	NEt_3	+ $NBut_3$	−0.125	0.50	−0.47	−0.20	−0.08	−0.089	−0.036	0.033	0.083	−0.205	1.28
	NPr_3	+ $NBut_3$	−0.052	0.50	—	—	—	−0.067	0.015	0.017	−0.062	−0.023	0.51
	NPr_3	+ $NIsopent_3$	−0.082	0.35	0.32	−0.05	0.34	−0.024	−0.058	0.032	−0.023	−0.033	0.80
	$NBut_3$	+ $NIsopent_3$	<0.04	—	—	—	—	—	—	—	—	—	0.15
B	NEt_3	+ $NHex_3$	−0.293	0.64	−1.11	−0.61	−0.15	−0.148	−0.145	0.071	0.098	−0.317	2.41
	NEt_3	+ $NOct_3$	−0.487	0.68	−1.82	0.87	−0.53	−0.351	0.136	0.122	0.078	−0.552	3.81
	NEt_3	+ $NDodec_3$	−0.643	0.65	−2.02	0.87	−1.92	−0.647	0.003	0.270	−0.177	−0.743	8.32
	NPr_3	+ $NHex_3$	−0.116	0.55	−0.435	0.017	−0.016	−0.229	0.107[a]	0.025	−0.145[a]	−0.109	0.69
	NPr_3	+ $NOct_3$	−0.295	0.64	−1.18	−0.25	−0.49	−0.358	0.063[a]	0.088	−0.254[a]	−0.193	2.30
	NPr_3	+ $NDodec_3$	−0.377	0.70	−1.28	−1.06	−0.76	−0.662	0.285[a]	0.180	−0.535[a]	−0.307	4.61
	$NBut_3$	+ $NHex_3$	−0.077	0.55	−1.288	0.108	−0.178	−0.013	−0.064	0.018	−0.001	−0.032	0.46
	$NBut_3$	+ $NOct_3$	−0.099	0.62	−0.399	−0.155	−0.134	−0.036	−0.063	0.081	−0.034	−0.082	1.33
	$NBut_3$	+ $NDodec_3$	−0.106	0.75	−0.316	−0.96	−0.24	−0.195	+0.089	0.184	−0.210	−0.169	3.18

[a]The possible overestimation of the term coming from the difference in P^* may be the cause of this large positive value of $V^E_{exp} - V^E_{calcd}$.

Can. J. Chem. Downloaded from www.nrcresearchpress.com by 210.87.254.42 on 09/06/12
For personal use only.

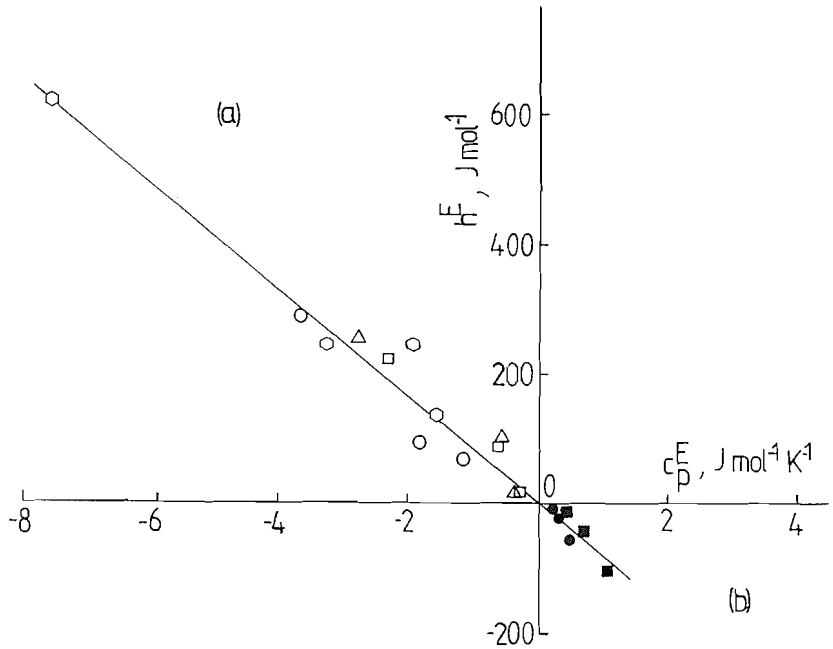

FIG. 2. Correlation between the h^E and c_p^E for the disordering contribution (curve *a*) of the long chain NR_3 mixed with NEt_3 (○), NPr_3 (□), NBut (△), and *c*-C_6 (⬡) and for the steric hindrance contribution (curve *b*). From eq. [6], the characteristic temperature is found to be 90 K for the disordering and about 100 K for the steric hindrance effect.

TABLE 4. Expected signs of h^E, V^E, and c_p^E for the different contributions

	Sign			
Parameter	Force field difference	Free volume difference	Disordering	Steric hindrance
h^E	+[a]	−[b,d]	+	−
Change of h^E when T increases	Little change	More −	Less +	Less −
c_p^E	About 0	−[b,d]	−	+
V^E	+	−[b,c,d]	+	−

[a]In non-polar systems.
[b]Depends mostly on the difference in expansion coefficients.
[c]Depends also on the relative cohesive energy of the two components.
[d]Values have been calculated in ref. 1 and Table 5 for h^E in Tables 2, 3, and 5 for c_p^E and V^E.

Equation [6] predicts a linear relationship between h^E(dis) and c_p^E(dis).

In the upper part of Fig. 2, one can see such a relationship for the nine B-type systems. The experimental h^E and c_p^E have been used instead of eq. [5] for the sake of simplicity. A similar line would be obtained by subtracting the free volume terms. The systems involving NEt_3 and NPr_3 for which steric hindrance has been found from the heats are also in the graph because of the relatively small part of the total heat due to steric hindrance. The characteristic temperature τ is found to be about 90 K, which is higher than the value (50 K) found for the linear alkanes. A greater stability with temperature of the correlations of molecular orientations between the NR_3 molecules could be expected since the branched character of the NR_3 more than two molecules can be involved in the correlations and also because of the lower free volume of these compounds compared to the linear alkanes of the same carbon atom number in the chain.

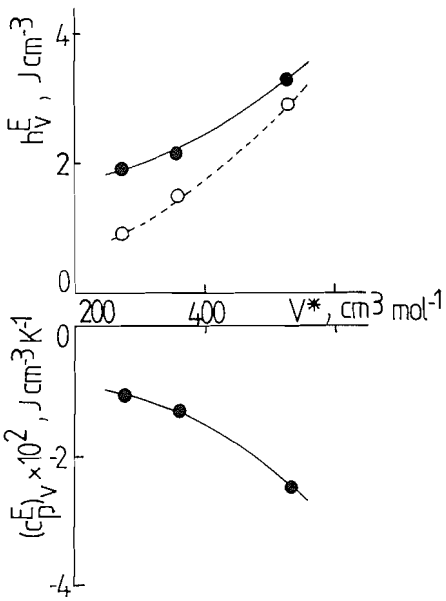

FIG. 3. h_v^E and $(c_p^E)_v$ for the mixtures of three long chain trialkyl amines with *c*-C_6 plotted against the volume V^* of the NR_3. The dotted line represents the disordering contribution (values used for the *c*-C_6 points in Fig. 2 (⬡)). The force field contribution or "rotation" contribution needed to make the separation is described in Part 2.

The results of theories developed for order in the linear alkanes or for liquid crystals which do not predict a linear temperature-independent relation between h^E(dis) and c_p^E(dis) are discussed in ref. 14.

Evaluation of the steric hindrance contribution to c_p^E

In the SnR_4 + SnR'_4 systems, the irregularities (21) of the h^E and of the c_p^E indicated a steric hindrance contribution more important for the $SnEt_4$ and $SnPr_4$ than for the $SnMe_4$ and $SnBut_4$ systems. By analogy, one can extend this property to the NR_3 compounds. The steric hindrance contribution will be

Can. J. Chem. Downloaded from www.nrcresearchpress.com by 210.87.254.42 on 09/06/12
For personal use only.

TABLE 5. Excess enthalpies, heat capacities, and volumes of the long chain trialkylamines + cyclohexane mixtures, the free volume contributions and other calculated terms are similar to those of Tables 3 and 4

Component 1	Component 2	h^E (J mol^{-1})	x_1	A_0 (J mol^{-1})	A_1 (J mol^{-1})	A_2 (J mol^{-1})	h_v^E (J cm^{-3})	h^E(f.v.) (J mol^{-1})	$X_{12}s_1^{-1}$ (J cm^{-3} Å^{-1})
c-C_6 +	$NHex_3$	272	0.65	958.008	684.48	454.119	1.89	−24.0	8.65
c-C_6 +	$NOct_3$	380	0.66	1381.898	1083.138	839.471	2.13	−44.8	11.9
c-C_6 +	$NDodec_3$	660	0.73	1998.249	1535.995	2899.663	3.25	−69.7	18.2
c-C_6 +	$N(CH_3)_2Dodec$	375	0.70	1274.643	910.756	1494.178	3.15	−23.1	13.2

Component 1	Component 2	c_p^E (J mol^{-1} K^{-1})	x_1	B_0 (J mol^{-1} K^{-1})	B_1 (J mol^{-1} K^{-1})	B_2 (J mol^{-1} K^{-1})	$10^2(c_p^E)_v$ (J cm^{-3} K^{-1})	c_p^E(f.v.) (J mol^{-1} K^{-1})	$c_p^E - c_p^E$(f.v.) (J mol^{-1} K^{-1})
c-C_6 +	$NHex_3$	−1.62	0.65	−5.200	−4.533	−3.722	−1.07	−0.28	−1.34
c-C_6 +	$NOct_3$	−1.92	0.73	−5.968	−9.326	1.211	−1.30	−0.44	−1.48
c-C_6 +	$NDodec_3$	−7.50	0.72	−28.311	−20.223	—	−2.50	−0.62	−6.88
c-C_6 +	$N(CH_3)_2Dodec$	−3.25	0.56	−12.823	3.204	1.647	−2.25	−0.14	−3.11

Component 1	Component 2	V_{exp}^E (cm^3 mol^{-1})	x_1	C_0 (cm^3 mol^{-1})	C_1 (cm^3 mol^{-1})	C_2 (cm^3 mol^{-1})	V_{calcd}^E (cm^3 mol^{-1})	$V_{exp}^E - V_{calcd}^E$ (cm^3 mol^{-1})	$V^E(h^E)$ (cm^3 mol^{-1})	$V^E(P^*)$ (cm^3 mol^{-1})	V^E(f.v.) (cm^3 mol^{-1})
c-C_6 +	$NHex_3$	0.419	0.63	1.441	1.040	0.861	0.415	0.004	0.226	0.412	−0.222
c-C_6 +	$NOct_3$	0.460	0.67	1.459	1.160	2.130	0.448	0.012	0.301	0.482	−0.335
c-C_6 +	$NDodec_3$	0.647	0.70	2.107	1.724	1.784	0.409	0.238[a]	0.474	0.407	−0.472
c-C_6 +	$N(CH_3)_2Dodec$	0.566	0.66	2.031	0.760	2.257	0.414	0.152[a]	0.303	0.271	−0.160

[a]If calculated per cm^3 of the mixture, the values of $V_{exp}^E - V_{calcd}^E$ are the same for these two systems.

Can. J. Chem. Downloaded from www.nrcresearchpress.com by 210.87.254.42 on 09/06/12
For personal use only.

obtained from the difference between the expected value of the h^E and c_p^E (dotted line in Fig. 1) at the abscissa of $V^*(NEt_3)$ and $V^*(NPr_3)$, and the experimental value. The lack of data for h^E and c_p^E data for the volatile NMe_3 system diminishes greatly the reliability of the c_p^E(steric hindrance) values since the position of the dotted line is ambiguous. The more positive values of c_p^E(exp) in Fig. 1 for the six points corresponding to the NEt_3 and NPr_3 systems are in agreement with a positive contribution coming from c_p^E(steric hindrance). On the lower part of Fig. 2, the estimated c_p^E(steric hindrance) have been plotted against the h^E(steric hindrance) found previously. The value of the characteristic temperature is found to be 100 K compared to 70–80 K for the steric hindrance contribution for the $SnPr_4$ and $SnEt_4$ derivatives, but it should be considered as an approximate value because of the method of separation of the contribution used.

Excess volumes

Table 3 gives the experimental V^E at the concentration of the maximum, the parameters of eq. [1], and the different contributions to V^E for the two series. The seventh column lists V^E(exp) − V^E(calcd) and the last, the interchange energy parameter $X_{12}s_1^{-1}$ (see Appendix). The Prigogine–Patterson–Flory theory, using the Van der Waals model for energy, can predict V^E usually quite successfully. In this calculation, the steric hindrance and disorder contributions are included in $V^E(h^E)$ or $V^E(X_{12})$, the contribution calculated from the experimental heats of mixing. The free volume term V^E(f.v.) depends on $\tilde{v}_1 - \tilde{v}_2$ and is always negative (third term in the table). The second term $V^E(P^*)$, proportional to $(\tilde{v}_1 - \tilde{v}_2)(P_1^* - P_2^*)$, can change sign depending on the relative cohesive energy of the expanded and less expanded component. It gives a quantitative expression to the fact that an expanded but cohesive (high P^*) component will contract less in solution with a non-expanded second component than a less cohesive liquid would do and vice versa. For the A-type systems, $V^E_{exp} - V^E_{calcd}$ is less than 0.04 $cm^3\ mol^{-1}$ except for one system (0.058). For the B-type systems, the three contributions are large since the h^E can reach 300 J mol^{-1}, the difference in free volume is important between NEt_3 and $NDodec_3$ and the difference in P^* varies from 20 to 65 J cm^{-3} between the members of the series. A perfect prediction of the V^E in these systems would be somewhat surprising with such a simple model, the van der Waals model (see Appendix), for the energy. For six systems out of nine, $V^E_{exp} - V^E_{calcd}$ is less than 0.10 $cm^3\ mol^{-1}$. With the NPr_3 systems, the large difference in P^* with the long-chain component (32 to 64 J cm^{-3}) produces a large $V^E(P^*)$ contribution which is probably overestimated in the case of the NPr_3 + $NDodec_3$ for which $V^E_{exp} - V^E_{calcd}$ reaches 0.28. In the NEt_3 systems, the $(\tilde{v}_1 - \tilde{v}_2)(P_1^* - P_2^*)$ is now positive which, in these cases, does not improve the agreement between V^E_{calcd} and V^E_{exp} although one can find other cases where the $V^E(P^*)$ term is quite instrumental in giving a good theoretical prediction of V^E_{exp}.

Long-chain trialkylamines + c-C_6 systems: h^E, c_p^E, *and* V^E

One can expect that the dominant contribution for these systems will be the disordering of the long chains of the NR_3 molecules by the globular *c*-C_6. h^E will be positive and since orientational order in the pure components diminishes at higher temperature, c_p^E is expected to be negative and to increase with the size of the ordered component. In Fig. 3, one can see the familiar occurrence, that h_v^E and $(c_p^E)_v$ are mirror images of each other with respect to the *x* axis. In Figs. 1 and 3, the lines have different slopes because in one case (Fig. 1) the points with the same long chain compounds and in the other (Fig. 3) the points with the same globular molecule are joined. Comparing Table 5 with Table 2 (last column), one cannot miss the fact that the h^E values are systematically larger when *c*-C_6 replaces NR_3 as the order-breaker. One of the sources of this difference is the force field contribution to h^E in the case of the *c*-C_6 mixtures. The method developed in Part 2 (19) has been used here to obtain h^E(chem) for these systems and calculate h^E(dis) (--- in Fig. 3) by subtraction from h^E_{exp}. The corresponding heat capacity contribution was not subtracted in the lower part of Fig. 3 because the available data on several systems did not permit to ascertain a special contribution to c_p^E coming from the difference in the force field. After the subtraction of the force field contribution, h^E(dis) is still consistently much larger with *c*-C_6 than with the NR_3 molecules. For instance, h^E(dis) of $NDodec_3$ is found to be 2.90 J cm^{-3} with *c*-C_6 and 1.1 J cm^{-3} with NEt_3, both having about the same expansion coefficient. The reason for this effect may come from the method of separation of the contribution, or of a lack of additivity of the contributions due to a cross term, depending on a large force field difference as it is the case here. The molecular shape and cohesive energy of the order breaker may have an effect on the magnitude of the disorder in solution (1, 2). However, the characteristic temperature of the orientational order in the NR_3 molecules which is a property of the pure component is found the same if the order breaker is a globular NR_3 or *c*-C_6 as can be seen in Fig. 2 in which the points representing the *c*-C_6 + NR_3 mixtures, except one, fall on the same h^E, c_p^E, correlation line as the NR_3 + NR'_3 systems.

The experimental values of V^E are given in the bottom part of Table 5. The different columns give the same parameters as Table 3 for the NR_3 + NR'_3 systems. Although the three contributions to V^E have comparable magnitude and different signs, the value of $V^E_{exp} - V^E_{calcd}$ is smaller than 0.02 $cm^3\ mol^{-1}$ for two systems out of four. On the other hand, for the two systems containing the dodecyl chain the excess volume is much more positive than calculated. This may correspond to a real physical effect, i.e., the uneasy packing of molecules of quite different shape like *c*-C_6 and the long NR_3 molecules. Such a large value for $V^E_{exp} - V^E_{calcd}$ (0.28 $cm^3\ mol^{-1}$) is found for only one system (NPr_3 + $NDodec_3$) in the NR_3 + NR'_3 series. It is difficult to decide between the packing effect and the overestimation of $V^E(P^*)$ as given above. In a qualitative analysis, it is interesting to compare the two series of systems NR_3 + NR'_3 and *c*-C_6 + NR'_3 viewed from their excess volumes (here R′ stands for a long chain). A rapid guess would make one predict similar V^E since a long chain amine (NR'_3) is mixed in each case with a globular, volatile component, NR_3 or *c*-C_6 but the experiments show that the V^E are all negative in the amine mixtures and all positive in the *c*-C_6 ones. Two of the present systems, NEt_3 + $NDodec_3$ and *c*-C_6 + $NDodec_3$, illustrate the difficulty of guessing V^E, since one is −0.64 $cm^3\ mol^{-1}$ and the other is +0.65 $cm^3\ mol^{-1}$. This constitutes a striking case of the resistance to the contraction in solution of a volatile but highly cohesive molecule like cyclohexane, when mixed with a low free volume second component. This effect is well predicted by the Prigogine–Patterson–Flory theory with a Van der Waals model for the energy.

Acknowledgements

The support of the NSERC and of the University of Quebec

(CAFIR) is acknowledged. We thank P. C. Nkinamubanzi for some of the calculations.

1. (*a*) R. PHILIPPE, G. DELMAS, and H. PHUONG-NGUYEN. Can. J. Chem. **56**, 2856 (1978); (*b*) R. PHILIPPE and G. DELMAS. Int. Data Ser. A, **1**, 6 (1980).
2. R. PHILIPPE, G. DELMAS, and H. PHUONG-NGUYEN. Can. J. Chem. **57**, 517 (1979).
3. P. TANCRÈDE, P. BOTHOREL, and D. PATTERSON. J. Chem. Soc. Faraday II, **73**, 29 (1977).
4. P. TANCRÈDE, P. BOTHOREL, P. DE SAINT-ROMAIN, and D. PATTERSON. J. Chem. Soc. Faraday II, **73**, 15 (1977).
5. H. PHUONG NGUYEN and G. DELMAS. Macromolecules, **12**, 740 (1979).
6. M. BARBE and D. PATTERSON. J. Phys. Chem. **82**, 40 (1978).
7. G. DELMAS and P. PURVES. J. Chem. Soc. Faraday Trans. II, **73**, 1838 (1977).
8. M. COUCHON, H. PHUONG-NGUYEN, and G. DELMAS. Can. J. Chem. **56**, 2472 (1978).
9. (*a*) D. FILIATRAULT, H. PHUONG-NGUYEN, and G. DELMAS. J. Polym. Sc. **19**, 763 (1981); (*b*) D. FILIATRAULT and G. DELMAS. Macromolecules, **12**, 65 (1979).
10. H. PHUONG-NGUYEN and G. DELMAS. Macromolecules, **12**, 746 (1979).
11. P. DE ST-ROMAIN, H. TRA VAN, and D. PATTERSON. J. Chem. Soc. Faraday **1**, 75 (1979); **1**, 1700 (1979).
12. C. L. DE LIGNY and W. E. HAMMERS. J. Solution Chem. **7**, 155 (1978).
13. G. MANN. Tetrahedron, **23**, 3375 (1967).
14. R. PHILIPPE, G. DELMAS, and M. COUCHON. Can. J. Chem. **56**, 370 (1978).
15. S. N. BATTACHARYYA and D. PATTERSON. J. Solution Chem. **9**, 247 (1980).
16. P. TANCRÈDE, L. V. LAM, P. PICKER, and D. PATTERSON. J. Chem. Soc. Faraday II, **70**, 1465 (1974).
17. B. RIEDL. M.Sc. thesis, Université du Québec à Montréal. 1980.
18. G. DELMAS, P. PURVES, and P. DE SAINT-ROMAIN. J. Phys. Chem. **79**, 1970 (1975).
19. H. PHUONG-NGUYEN, B. RIEDL, and G. DELMAS. Can. J. Chem. **61**, 1885 (1983).
20. D. PATTERSON and G. DELMAS. Discuss. Faraday Soc. **49**, 98 (1970).
21. B. RIEDL and G. DELMAS. J. Sol. Chem. To be published.
22. H. PHUONG-NGUYEN, B. RIEDL, and G. DELMAS. J. Phys. Chem. To be published.

Can. J. Chem. Downloaded from www.nrcresearchpress.com by 210.87.254.42 on 09/06/12
For personal use only.

Appendix

List of symbols

The density (d), expansion coefficient (α), and thermal pressure coefficient (γ) are measurable parameters from which the volume at 0 K or "core volume", V^*, can be calculated as well as P^*, the cohesive energy per cm^3. The surface-to-volume ratio (s) can be calculated from a model (sphere, cylinder etc...). c_p^E is an experimental quantity defined as the difference between the experimental c_p of the solution and the c_p obtained by a molar fraction average of the c_p for the two pure components. The values of v, U, c_p, and T with a tilde are dimensionless reduced values used in the theory. They can be obtained from an equation and experimental data (d, α, and γ). The interchange energy parameter X_{12} is obtained essentially from the heat of mixing of 1 and 2 after subtracting the free volume term. ψ and θ are respectively energy and surface fraction averages defined as below.

Calculation of the free volume terms

$h^E(f.v.)$ *and* $X_{12}s_1^{-1}$

The free volume term depends only on the difference between the reduced volume of the pure components. We apply an approximate (19) form of the Prigogine–Flory theory which separates the interactional and free volume contributions. The free volume contribution h^E(f.v.) is defined as:

$$[1]\quad h^E(\text{f.v.})/(x_1U_1^* + x_2U_2^*) = \tilde{c}_p(\tilde{T}_u)(\psi_1\tilde{T}_1 + \psi_2\tilde{T}_2 - \tilde{T}_u)$$

Here $\tilde{T}_u$ is the average reduced temperature for the solution appropriate to the energy $\tilde{U}$ and is defined by:

$$\tilde{U}(\tilde{T}_u) = \psi_1\tilde{U}(\tilde{T}_1) + \psi_2\tilde{U}(\tilde{T}_2)$$

With the Van der Waals model, $\tilde{U}(\tilde{T}_u) = -1/\tilde{v}$, so that the volume corresponding to $\tilde{T}_u$ is $1/\tilde{v}_u = \psi_1/\tilde{v}_1 + \psi_1/v_1$, where $\psi_1 = x_1U_1^*/(x_1U_1^* + x_2U_2^*)$. In this model, the reduced volume of a pure component is obtained from its expansion coefficient, α, and $\tilde{v}^{1/3} = ((\frac{4}{3}\alpha T) + 1)/(\alpha T + 1)$. The reduced temperature is calculated from the reduced volume and $\tilde{T} = \tilde{v}^{-1}(1 - \tilde{v}^{-1/3})$. Also, $\tilde{c}_p(\tilde{T}_u) = (\frac{4}{3}\tilde{v}_u^{-1/3} - 1)^{-1}$, $U^* = P^*V^*$ and $P^* = \gamma\tilde{v}^2T$ where γ is the thermal pressure coefficient. Equation [1] does not depend on the surface-to-volume ratio. In the Flory terminology, the interactional contribution, which is the difference between the experimental value of the heat and the free volume contribution, is expressed through the X_{12} parameter. In the present form, X_{12} is obtained by eq. [2]:

$$[2]\quad h^E(\text{exp}) - h^E(\text{f.v.})/(x_1U_1^* + x_2U_2^*) = (X_{12}/P_1^*)\theta_2\psi_1 f(\tilde{v})$$

$f(\tilde{v})$ is defined as $(\tilde{v}^{-1} + \tilde{T}\tilde{c}_p)$ and is not very different from 1. ψ_1 and θ_2 ($\theta_2 = x_2V_2^*s_2/(x_1V_1^*s_1 + x_2V_2^*s_2)$) are used rather than the mole fractions. The units of X_{12} are energy per cm^3. The parameter $X_{12}s_1^{-1}$ is independent of the choice of 1 or 2 as a second component, i.e. $X_{12}s_1^{-1} = X_{21}s_2^{-1}$. The left side of eq. [2] does not depend on the surface-to-volume ratios s_1 and s_2 while X_{12} and θ_2 do to some extent. $X_{12}s_1^{-1}$ also relies very little on the s's. The core volume, V^*, is obtained from the molar volume V and $\tilde{v} = V/V^*$.

$c_p^E(f.v.)$

It is given by the equation:

$$[3]\quad c_p^E = \tilde{c}_{p,s}[x_1U_1^*/T_1^*) + x_2(U_2^*/T_2^*)] - x_1\tilde{c}_{p_1}(U_1^*/T_1^*) - x_2\tilde{c}_{p_2}(U_2^*/T_2^*)$$

The reduced volume of the solution $\tilde{v}_s$ used to calculate $\tilde{c}_{p,s}$ is obtained from the solution reduced temperature $\tilde{T}_s$ defined as an energy average.

$$\tilde{T}_s = (\psi_1\tilde{T}_1 + \psi_2\tilde{T}_2)(1 - X_{12}\psi\theta_2/P_1^*)$$

The X_{12} term does not have a large effect on $\tilde{T}_s$ in the present systems.

V^E

According to ref. 20, the excess volume can be written using the Van der Waals model:

$$[4]\quad \frac{V^E}{x_1V_1^* + x_2V_2^*} = \tilde{T}_v\frac{\partial\tilde{v}}{\partial\tilde{T}_v}\psi_1\theta_2(X_{12}/P_1^*) + (\tilde{v}_1 - \tilde{v}_2) \times (\psi_1 - \phi_1) - \frac{1}{2}\left(\frac{\tilde{v}_1 - \tilde{v}_2}{\partial\tilde{v}/\partial\tilde{T}_v}\right)^2\frac{\partial^2\tilde{v}}{\partial\tilde{T}_v^2}\{\psi_1\psi_2 + (\psi_1 - \phi_1)^2\}$$

here $\tilde{v}_v = \phi_1\tilde{v}_1 + \phi_2\tilde{v}_2$ and $\tilde{T}_v$ corresponds to $\tilde{v}_v$ so defined. By developing the second term of eq. [4], we can show that $\psi_1 - \phi_1$ varies as $P_1^* - P_2^*$. The first term of eq. [4] is $V^E(h^E)$, the second $V^E(P^*)$, and the last V^E(f.v.) as listed in Tables 3 to 5.

Surface-to-volume ratios

In order to compare the cohesive energies of molecules of different shapes, models have been detailed in ref. 14. For the globular molecules, assimilated to a sphere of a radius R, $s = (4/3)\pi R^3(\pi R^2)^{-1} = 4.083(V^*)^{-1/3}$. For linear- and branched-alkanes, the model used is that of a right cylinder with a 4.98 Å and 6.98 Å diameter. The NR_3 and SnR_4 molecules are assimilated to a group of three and four cylinders if the chain is longer than two carbons. Probably, for the ethyl derivatives, neither model is very realistic.

Can. J. Chem. Downloaded from www.nrcresearchpress.com by 210.87.254.42 on 09/06/12
For personal use only.

Excess heats, heat capacities, and volumes of globular non-polar molecules: mixtures of trialkylamine and tetraalkyltin compounds with cyclohexane

H. PHUONG-NGUYEN, BERNARD RIEDL, AND GENEVIÈVE DELMAS[1]

Département de chimie, Université du Québec à Montréal, C.P. 8888, Succ. A, Montréal, (Qué.), Canada H3C 3P8

Received July 6, 1982

H. PHUONG-NGUYEN, BERNARD RIEDL, and GENEVIÈVE DELMAS. Can. J. Chem. **61**, 1885 (1983).

h^E, c_p^E, and V^E have been measured at 25°C over the whole composition range for eight mixtures of cyclohexane (c-C_6) with $N(C_nH_{2n+1})_3$ (n = 2, 3, 4, 5) and with $Sn(C_nH_{2n+1})_4$ (n = 1, 2, 3, 4). The effect of sterically hindered molecules on the thermodynamic functions of mixtures containing a globular second component like c-C_6 was investigated. For the $Sn(C_nH_{2n+1})_4$ + c-C_6 systems, the c_p^E values are positive; this is quite unusual for non-polar systems. It is found that the sterically hindered molecules do not lower h^E as is the case with long chain alkanes or the NR_3 or SnR_4 molecules. On the other hand, h^E for these systems and for others of the type c-C_6 + A (A being a globular molecule) when plotted versus α_A, the expansion coefficient of A, fall on a smooth curve which increases with α_A. This is interpreted as an increase of the mobility or/and rotation of c-C_6 in high free volume solvents. A maximum of 1.8 J K^{-1} mol^{-1} in c_p^E for the c-C_6 + Sn(propyl)$_4$ system is in agreement with the rapid change of h^E around $\alpha_A = 0.9 \times 10^{-3}$ K^{-1}. The negative values of c_p^E for the NR_3 systems probably indicate a weak association between the NR_3 molecules. The V^E values follow quite well the predictions made using h^E and the Prigogine–Patterson–Flory equation of state theory.

H. PHUONG-NGUYEN, BERNARD RIEDL et GENEVIÈVE DELMAS. Can. J. Chem. **61**, 1885 (1983).

h^E, c_p^E et V^E ont été mesurés à 25°C en fonction de la concentration pour huit mélanges de c-C_6 avec $N(C_nH_{2n+1})_3$ (n = 2, 3, 4, 5) et avec $Sn(C_nH_{2n+1})_4$ (n = 1, 2, 3, 4). On étudie l'effet d'empêchement stérique dans le cas de mélanges dont le deuxième composant est une molécule globulaire comme c-C_6. Pour les mélanges c-C_6 + $Sn(C_nH_{2n+1})_4$, les c_p^E sont positifs ce qui est inhabituel dans les systèmes non-polaires. On trouve que les composés empêchés stériquement ne diminuent pas les h^E comme c'était le cas avec des deuxièmes constituants en chaine. De plus, h^E pour ces systèmes et pour d'autres du type c-C_6 + A (A étant une molécule globulaire) quand portés en fonction de α_A, le coefficient d'expansion de A, se retrouvent sur une courbe régulière qui augmente avec α. Cet effet est interprété comme indiquant une augmentation de mobilité ou/et de rotation du c-C_6 dans les solvants de volume libre élevé. Un maximum de 1.8 J K^{-1} mol^{-1} pour le c_p^E du système c-C_6 + Sn(propyl)$_4$ est consistant avec la variation rapide de h^E autour de $\alpha = 0.9 \times 10^{-3}$ K^{-1}. Les valeurs négatives de c_p^E pour les systèmes contenant les trialkylamines sont probablement dues à une faible association entre les molécules NR_3. Les V^E suivent bien les prédictions faites par la théorie développée par Prigogine, Patterson et Flory.

Introduction

In the preceding paper (1) the information given by h^E, c_p^E, and V^E for mixtures of trialkyl amines (NR_3 + NR_3') and long chain amines mixed with c-C_6 have been interpreted in terms of two contributions, associated with disorder and steric hindrance. The disordering contribution occurs when a globular molecule is mixed with a long-chain ordered liquid. The decrease of the cohesive energy in solution due to the loss of the correlation of molecular orientations present in the pure liquid corresponds to a positive contribution to h^E. The steric contribution is associated with the presence of a crowded central atom in a molecule. The resulting effect in solution, since the excess heat is exothermic, is to diminish the overall mobility or to improve the packing. More details about non-thermodynamic methods used to study orientational order or about the effect of temperature, free volume, or molecular shape can be found in references 1 and 2 for the disordering contribution and in references 1 to 3 for steric hindrance. In several instances, both contributions are met in the same system and understandably so, because in mixtures of long-chain molecules the heats are larger and irregularities in the thermodynamic functions can be seen and interpreted with less ambiguity than in mixtures of globular non-polar molecules in which the effects are usually small. This is illustrated by the h^E values of the SnR_4 + SnR_4' (3*a*, *e*) (R = C_nH_{2n+1}, and $n \leq 4$) system which do not exceed 65 J mol^{-1}.

In systems where a steric hindrance effect is expected, an indication of the importance of the molecular shape of the second component is given by the results of h^E of n-C_{16}, on one hand, and c-C_6 on the other hand, with two branched nonanes. At the equimolar concentration, the h^E of n-C_{16} with the highly sterically hindered 3,3-diethylpentane (3,3-DEP) is 18 J mol^{-1}, i.e. 300 J lower than the value with the non-sterically hindered 2,2,5-trimethylhexane (317 J mol^{-1}) (4). On the other hand, the corresponding h^E of the same branched nonanes with c-C_6 are, respectively, 179 and 192 J mol^{-1} (3*d*), showing that the steric hindrance contribution, familiar with the 3,3-DEP systems, is almost zero when c-C_6 is the second component. Similar results are found for other cycoalkanes such as methylcyclohexane, cycloheptane, and cyclooctane for which the sterically hindered component gives even higher h^E (3*d*).

The aim of the present paper is to investigate the steric hindrance effect of the NR_3 and SnR_4 molecules in solution with c-C_6. The relatively large h^E found systematically in systems containing c-C_6 (5–7) even when no force field difference contribution or no disordering contribution occurs, should facilitate the analysis of the results. The c_p^E and V^E data will be obtained on the same systems to see if these functions may detect, better than h^E, the steric hindrance effect in c-C_6 mixtures. Furthermore, the c-C_6 + NR_3 and c-C_6 + SnR_4 systems promise to be a good series to test the effect on V^E of the difference in cohesive energy as predicted by the equation of state theories (8, 9), since the pressure reduction parameter P^* which reflects the cohesive energy is high (530 J cm^{-3}) for c-C_6 compared to those of the NR_3 and SnR_4 compounds (ref. 1, Table 1). The present paper reports the h^E, c_p^E, and V^E data of four globular amines N(ethyl)$_3$, N(propyl)$_3$, N(butyl)$_3$, N(2-methylbutyl)$_3$ with c-C_6 and four tetraalkyltin compounds Sn(methyl)$_4$, Sn(ethyl)$_4$, Sn(propyl)$_4$, Sn(butyl)$_4$ with c-C_6 at

[1]To whom all correspondence should be addressed.

Can. J. Chem. Downloaded from www.nrcresearchpress.com by 210.87.254.105 on 09/06/12
For personal use only.

TABLE 1. Excess heats h^E for the cyclohexane + NR_3 and cyclohexane + SnR_4 systems at the concentration x_1 of the maximum; the A_i parameters are the coefficients of the Redlich–Kister equation; h^E(f.v.) and $X_{12}s_1^{-1}$ have been calculated at the same concentration

Component 1	Component 2	h^E (J mol^{-1})	x_1	A_0 (J mol^{-1})	A_1 (J mol^{-1})	A_2 (J mol^{-1})	h_v^E (J cm^{-3})	h^E(f.v.) (J mol^{-1})	$X_{12}s_1^{-1}$ (U cm^{-3} Å^{-1})
c-C_6	NEt_3	230	0.55	900.25	176.86	432.95	2.43	−0.92	10.38
c-C_6	NPr_3	226	0.55	885.10	195.15	445.46	1.99	−5.50	8.08
c-C_6	$NBut_3$	158	0.65	602.12	437.08	—	1.33	−15.5	5.63
c-C_6	$Nisopent_3$	140	0.55	539.68	180.19	−289.96	0.92	−18.39	5.19
c-C_6	$SnMe_4$	186	0.60	720.60	323.07	48.39	1.99	−0.62	8.42
c-C_6	$SnEt_4$	244	0.65	892.76	455.55	481.37	2.22	−10.72	9.89
c-C_6	$SnPr_4$	136	0.65	478.44	364.58	115.05	1.04	−30.5	5.65
c-C_6	$SnBut_4$	88	0.725	251.54	293.01	316.73	0.64	−48.1	4.39

25°C over the whole concentration range. The names of the compounds are abbreviated as shown in the tables, NEt_3 for N(ethyl)$_3$, $SnMe_4$ for Sn(methyl)$_4$, and so on.

Experimental

Materials

Cyclohexane was purchased from the Chemical Samples Co. (Columbus, OH). The amines came from the same sources as in Part 1 (Eastman, Aldrich, and Chemical Procurement), the SnR_4 from the Organisch Chemisch Instituut (Utrecht) or the K and K company. Their physicochemical characteristics are given in Table 1 of the preceding paper (Part 1).

Apparatus

The c_p^E and V^E values are obtained as in Part 1 with a Picker Flow calorimeter (Sodev, Sherbrooke, Canada) and an Anton-Paar precision densitometer (Fisher Co.). The heats of mixing were obtained with an adiabatic Calvet calorimeter (10).

Equation of state contributions

The contributions to h^E, h^E (f.v.), c_p^E, c_p^E (f.v.), and V^E, V^E (f.v.) coming from the difference in state of expansion of the two components have been calculated from the equations given in the Appendix of Part 1 and are listed in Tables 1–3. The contribution to V^E coming from h^E and the difference of P^* are added in Table 3. $X_{12}s_1^{-1}$ corresponds to the part of h^E not associated with the free volume difference.

Results and discussion

The h^E, c_p^E, and V^E have been fitted through the concentration range to the Redlich–Kister equations:

$$h^E = x_1x_2 \sum_{i=0}^{i=2} A_i(x_1 - x_2)^i$$

$$[1] \quad c_p^E = x_1x_2 \sum_{i=0}^{i=2} B_i(x_1 - x_2)^i$$

$$V^E = x_1x_2 \sum_{i=0}^{i=2} C_i(x_1 - x_2)^i$$

Heats of mixing

Table 1 gives h^E at the maximum, the concentration of the maximum, the parameters of eq. [1], the heat per cm^3 h_v^E, and two calculated parameters h^E (f.v.), and $X_{12}s_1^{-1} \cdot h_v^E$ is obtained through

$$h_v^E = h^E/(x_1V_1^* + x_2V_2^*)$$

V_1^* and V_2^* are the core volumes (or volumes at 0 K) of the two components (see Appendix of Part 1).

In previous work (2*a*) with long-chain alkanes as the second component, the steric hindrance contribution was seen in the following way: h^E or h_v^E was plotted against $V^*(SnR_4)$ and the points joined by a line. It was found that the points for $SnEt_4$ (1.71) and $SnPr_4$ (1.16) were situated well below the expected value between the $SnMe_4$ (3.08) and $SnBut_4$ (1.38) values. The figures in parentheses correspond to h_v^E with n-C_{16}. The difference between the expected value and the experimental ones was assumed to correspond to the negative steric hindrance contribution which could amount to −200 J mol^{-1}. A similar plot of the present data will not show a special lower h^E for the $SnEt_4$ and $SnPr_4$ derivatives so that it is concluded that the steric hindrance contribution does not occur, in its usual form, with a globular second component like c-C_6, a feature already seen with 3,3-DEP as the sterically hindered molecule. On the other hand, the jump towards more positive h^E between $SnPr_4$ and $SnEt_4$ is similar to that obtained (13) with *trans*-decalin or three highly branched alkanes as a second component.

In order to see some trend in the h^E with c-C_6, the h_v^E have been plotted in Fig. 1*a* versus α, the expansion coefficient of the NR_3 (□) or SnR_4 (○) compounds. On the same curve, h_v^E of other globular molecules such as the very branched alkanes 2,2,4-trimethylpentane, 2,2,4,6,6-pentamethylheptane, and 2,2,4,4,6,8,8,-heptamethylnonane have been added (△). The h_v^E values of two branched nonanes, (▲) 3,3-DEP and 2,2,5-dimethylpentane (11), of n-C_6 (●) and CCl_4 (■) have been joined to complete the present data. The free volume term would be represented by a curve going from 0 for $\alpha = 1.22 \times 10^{-3}$ (that of c-C_6) to −0.4 J cm^{-3} for $\alpha = 0.8 \times 10^{-3}$. If $h_v^E - h_v^E$ (f.v.) were plotted instead of h_v^E, the points would be displaced towards more positive values by the corresponding amount. However, it is preferable to plot just the experimental data for the sake of simplicity and also because the theory overestimates the free volume contribution to h^E when the difference of expansion coefficients of the two components increases.

The large h_v^E values found in non-polar systems when one of the components is c-C_6 have always been puzzling, particularly in mixtures with branched alkanes whose chemical groups CH_2 and CH_3 are rather similar to those of c-C_6. The explanation is given in terms of the larger cohesive energy of c-C_6 compared to the branched alkanes. The curve shown in Fig. 1*a* may help to obtain a more molecular picture of the origin of these relatively large heats. The variation of h^E with the expansion coefficient of the second component indicates that the perturbation or loss of cohesion or disorder introduced in c-C_6 is very dependent on the free volume of the second component. The mixing may have changed a particularly good and cohesive packing between the c-C_6 molecules. This hypothesis is not too satisfactory because one would then expect that if there were

Can. J. Chem. Downloaded from www.nrcresearchpress.com by 210.87.254.105 on 09/06/12
For personal use only.

Can. J. Chem. Downloaded from www.nrcresearchpress.com by 210.87.254.105 on 09/06/12
For personal use only.

TABLE 2. Excess heat capacities, c_p^E for the cyclohexane + NR_3 and cyclohexane + SnR_4 systems at the concentration x_1 of the maximum; the B_i parameters are the coefficients of the Redlich–Kister equation; c_p^E(f.v.) has been calculated at the same concentration

Component 1	Component 2	c_p^E (J mol^{-1} K^{-1})	x_1	B_0 (J mol^{-1} K^{-1})	B_1 (J mol^{-1} K^{-1})	B_2 (J mol^{-1} K^{-1})	10^2 $(c_p^E)_v$ (J cm^{-3} K^{-1})	c_p^E(f.v.) (J mol^{-1} K^{-1})	$c_p^E - c_p^E$(f.v.) (J mol^{-1} K^{-1})
c-C_6	+ NEt_3	−0.77	0.65	−2.910	−1.568	—	−0.83	−0.11	−0.53
c-C_6	+ NPr_3	−1.23	0.60	−6.058	1.839	14.334	−1.12	−0.07	−1.06
c-C_6	+ $NBut_3$	−1.0	0.65	−3.495	−3.658	−0.009	−0.82	−0.12	−0.88
c-C_6	+ $NIsopent_3$	−0.94	0.50	−3.610	0.432	−0.879	−0.59	−0.16	−0.70
c-C_6	+ $SnMe_4$	0.84	0.60	2.945	2.073	1.100	0.90	−0.11	0.95
c-C_6	+ $SnEt_4$	1.61	0.47	6.443	0.308	1.830	1.30	−0.11	1.72
c-C_6	+ $SnPr_4$	2.78	0.37	10.163	−4.497	8.847	1.67	−0.26	3.04
c-C_6	+ $SnBut_4$	0.85	0.60	2.406	3.462	1.764	0.50	−0.40	1.2

TABLE 3. Excess volume V^E for the cyclohexane + NR_3 and cyclohexane + SnR_4 systems at the concentration x_1 of the maximum; the C_i parameters are the coefficients of the Redlich–Kister equation; the three contributions to V^E calculated have been added

Component 1	Component 2	x_1	V^E (cm^3 mol^{-1})	C_0 (cm^3 mol^{-1})	C_1 (cm^3 mol^{-1})	C_2 (cm^3 mol^{-1})	V^E_{calcd} (cm^3 mol^{-1})	$V^E - V^E_{calcd}$ (cm^3 mol^{-1})	$V^E(h^E)$ (cm^3 mol^{-1})	$V^E(P^*)$ (cm^3 mol^{-1})	V^E(f.v.) (cm^3 mol^{-1})
c-C_6	+ NEt_3	0.50	0.293	1.209	0.266	—	0.113	0.180	0.178	−0.055	−0.010
c-C_6	+ NPr_3	0.60	0.401	1.487	1.022	—	0.364	0.037	0.203	0.192	−0.031
c-C_6	+ $NBut_3$	0.55	0.386	1.557	0.039	1.286	0.307	0.093	0.144	0.215	−0.113
c-C_6	+ $Nisopent_3$	0.60	0.177	0.695	0.400	0.275	0.399	−0.190	0.129	0.410	−0.140
c-C_6	+ $SnMe_4$	0.50	0.150	0.535	0.165	0.099	0.123	0.027	0.183	−0.056	−0.039
c-C_6	+ $SnEt_4$	0.37	0.535	1.952	−1.021	1.020	0.291	0.244	0.204	0.147	−0.06
c-C_6	+ $SnPr_4$	0.40	−0.220	−0.822	0.487	−0.052	0.121	−0.341	0.115	0.170	−0.164
c-C_6	+ $SnBut_4$	0.65	0.205	0.76	—	—	0.204	−0.004	0.079	0.359	−0.234

Can. J. Chem. Downloaded from www.nrcresearchpress.com by 210.87.254.105 on 09/06/12
For personal use only.

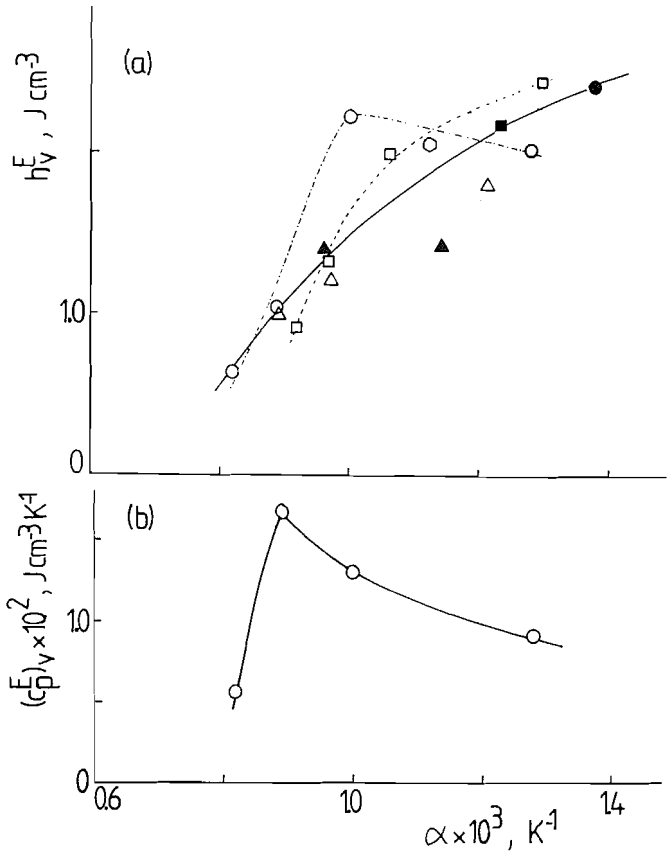

FIG. 1. (*a*) h_v^E, the excess heat per cm^3 at the maximum at 25°C, for the (□) NR_3 + *c*-C_6 and (○) SnR_4 + *c*-C_6 systems plotted against the expansion coefficient of the NR_3 or SnR_4 compounds. Seven other systems have been added: (△) the three highly branched alkanes 2,2,4-trimethylpentane, 2,2,4,6,6-pentamethylheptane, and 2,2,4,4,6,8,8-heptamethylnonane, (●) *n*-hexane, (■) CCl_4, (▲) two branched nonanes, and (⬡) *cis*-1,3-dimethylcyclohexane. Full curve through all the points. Dotted lines with inflexion points for the NR_3 and SnR_4 sytems. (*b*) $(c_p^E)_v$ for the SnR_4 + *c*-C_6 systems in J K^{-1} cm^{-3} plotted against α, the expansion coefficient of the SnR_4 compound.

really a random mixing, this packing is destroyed whatever the free volume of the second component. A change which could be related more to the free volume than the molecular shape of the neighbours would be the rotations of the symmetrical *c*-C_6. A more extensive rotation in a large free volume solution could explain the large variation of the heats with the free volume. If this is so, one would expect a smaller variation of h^E if a less symmetrical molecule like methylcyclohexane were mixed with the same series of globular compounds.

Other systems containing c-C_6

h^E data have been obtained recently (12) for *c*-C_6 with methylcyclohexane and six dimethylcyclohexane, the methyl conformation being either equatorial–axial or equatorial–equatorial. For all systems except one, h^E is very small so that the representative points for h_v^E situated between 0.20 and 0.95 J cm^{-3} for $\alpha = 1.13 \times 10^{-3}$ K^{-1} are quite outside the main curve. h_v^E is almost zero (<0.1 J cm^{-3}) (11) for *c*-C_6 mixed with *c*-C_7 and *c*-C_8. This means that the other cycloalkanes keep the cohesive energy of *c*-C_6 unchanged. Surprisingly, the *cis*-1,3-dimethylcyclohexane with its two equatorial methyl groups has a large h^E value and produces apparently the same effect as the branched alkanes, or the NR_3 or SnR_4 compounds of loosening the *c*-C_6 "structure". ((⬡) in Fig. 1).

Excess heat capacities

SnR_4 systems

In Table 4 of Part 1 the expected temperature dependence of the known contributions to h^E is given and consequently the expected c_p^E for each contribution. The total c_p^E may either be the balance of the different c_p^E or it may reflect the dominance of one contribution as is often the case for h^E (disorder) or h^E (free volume). The occurrence of $h^E > 0$ and $c_p^E > 0$, which means that the heat of mixing becomes more endothermic at higher temperature, is not listed because it does not correspond to any of the usual contributions described for non-polar systems in the present work. However, the experimental curve of Fig. 1*b* would provide an obvious reason for having in *c*-C_6 mixtures a positive c_p^E. When *T* increases, the h^E for systems with a free volume lower than that of *c*-C_6 should be moving towards higher values corresponding to systems with larger α. Furthermore, one would expect that the fastest changes in h^E would occur for systems situated in the lower part of the $h^E(\alpha)$ curve. The *c*-C_6 + SnR_4 systems fall in this category of $h^E > 0$ and $c_p^E > 0$ systems with c_p^E ranging from 0.8 to 2.8 J K^{-1} mol^{-1}. A confirmation of the hypothesis that, in the SnR_4 + *c*-C_6 systems, the main contribution to h^E comes from the change of cohesion or order in *c*-C_6 induced by a change in the free volume of the solution, can be seen in Fig. 1*b*, where $(c_p^E)_v$ has been plotted against α. $(c_p^E)_v$ is seen to go through a maximum for $SnPr_4$. This maximum of $(c_p^E)_v$ with $SnPr_4$ is due to this system approaching the domain of free volume (or of α) corresponding to the fastest change in the state of rotation of *c*-C_6. With $SnEt_4$ and $SnBut_4$, the $(c_p^E)_v$ are smaller because the change of rotation has reached its peak at 25°C in $SnEt_4$ mixtures and is on the contrary too far away in temperature for the $SnBut_4$ solutions.

Other systems

c_p^E have been obtained for several branched nonanes (such as 2,2,4,4-tetramethylpentane, 3,3-diethylpentane) mixed with *c*-C_6 (Huu Tra Van and D. Patterson, to be published). The fact that the $c_p^E(x)$ have an *S*-shaped curve with maxima around +0.3 and −0.3 J K^{-1} mol^{-1} makes it difficult to predict the change of h^E with *T*. The c_p^E obtained for three highly branched alkanes (2,2,4-trimethylpentane, 2,2,4,6,6-pentamethylheptane, and 2,2,4,4,6,8,8,-heptamethylnonane are negative and small (−0.12, −0.22, −0.55 J K^{-1} mol^{-1}) (7). It is possible that the temperature dependence of the effect of the branched alkanes on *c*-C_6 is different from that of the SnR_4 compounds due to their quite different shape. An indication of this fact can be seen in Fig. 1*a* where a line going only through the branched alkanes (△) would increase more gently with α than the main curve.

NR_3 systems

Table 2 lists the c_p^E of the NR_3 + *c*-C_6 systems which are all negative, in contrast to those for the SnR_4 + *c*-C_6 mixtures. The free volume contribution (varying between −0.07 and −0.15 J mol^{-1} K^{-1}) represents only a small part of the experimental value. The decrease of h^E with *T* predicted for the NR_3 + *c*-C_6 systems is encountered in ordered pure components whose order diminishes through thermal agitation with temperature. It is possible that a small contribution in the total h^E comes from a disordering type contribution to h^E. The structure or order in the pure NR_3 compounds may be due to the non-symmetrical character of these molecules whose arrangement in the liquid at 25°C may involve some kind of order among the molecules, in order to avoid the electron pair of the nitrogen atom of two NR_3

molecules being next neighbours. In the more isotropic SnR_4 molecules such structure would not be necessary. The sign of c_p^E for the above system does not put in question the interpretation of the data given in Fig. 1*b*. Due to the moderate magnitude of the positive and negative c_p^E, a $h^E(\alpha)$ curve with the same overall trend is likely to be found even at temperatures higher than 25°C.

Excess volumes

Table 3 gives the V^E values at the maximum and the concentration of the maximum, the Redlich–Kister parameters, and the calculated V^E obtained from the sum of the usual three contributions $V^E(h^E)$, $V^E(P^*)$, and V^E(f.v.). As said more explicitly in Part 1, $V^E(h^E)$ has the sign of h^E, V^E(f.v.) is always negative, and $V^E(P^*)$ is proportional to $(\tilde{v}_1 - \tilde{v}_2)(P_1^* - P_2^*)$. This last term goes from negative to positive in the two series because $\tilde{v}_1 - \tilde{v}_2$ changes sign in the series, but not $P_1^* - P_2^*$ which is always > 0 due to the higher P^* value of c-C_6. The sixth column gives $V^E - V^E$(calcd). The agreement between the experimental and calculated values is very good. Possibly, the more positive values obtained with volatile second components may have a physical significance, that reveals that an increase of volume is needed to accommodate the increase of motion in c-C_6.

Acknowledgements

The support of the ministry of Education (Province of Quebec) and of Imperial Oil of Canada is gratefully acknowledged.

1. B. RIEDL and G. DELMAS. Can. J. Chem. **61**, 000 (1983).
2. *a*, G. DELMAS and S. TURRELL. J. Chem. Soc. Faraday 2, **70**, 572 (1974); *b*, G. DELMAS and NG. T. THANH. J. Chim. Phys. **72**, 1285 (1975); *c*, G. DELMAS and P. PURVES. J. Chem. Soc. Faraday 2, **73**, 1828 (1977); **73**, 1838 (1977); *d*, G. DELMAS and NG. T. THANH. J. Chem. Soc. Faraday 2, **71**, 1172 (1975).
3. *a*, G. DELMAS and NG. T. THANH. J. Phys. Chem. **81**, 1730 (1977); *b*, R. PHILIPPE, G. DELMAS, and H. PHUONG-NGUYEN. Can. J. Chem. **56**, 2856 (1978); *c*, C. L. DE LIGNY and W. E. HAMMERS. J. Solution Chem. I, 155 (1978); *d*, P. DE ST-ROMAIN, H. TRA VAN, and D. PATTERSON. J. Chem. Soc. Faraday 1, **75**, 1700 (1979); *e*, B. RIEDL and G. DELMAS. J. Phys. Chem. To be published.
4. P. TANCREDE, P. BOTHOREL, P. DE SAINT-ROMAIN, and D. PATTERSON. J. Chem. Soc. Faraday 2, **73**, 15 (1977).
5. P. TANCREDE, D. PATTERSON, and V. T. LAM. J. Chem. Soc. Faraday 2, **71**, 985 (1975).
6. V. T. LAM, P. PICKER, D. PATTERSON, and P. TANCREDE. J. Chem. Soc. Faraday 2, **70**, 1465 (1974).
7. S. N. BATTACHARYYA and D. PATTERSON. J. Solution Chem. (*a*) **9**, 267 (1980); (*b*) J. Phys. Chem. **83**, 2979 (1979).
8. G. DELMAS, P. DE SAINT ROMAIN, and P. PURVES. J. Chem. Soc. Faraday, **71**, 481 (1975).
9. D. PATTERSON and G. DELMAS. Discuss. Faraday Soc. **49**, 98 (1970).
10. G. DELMAS and P. TANCRÈDE. Eur. Polymer J. **9**, 199 (1973).
11. P. DE ST-ROMAIN, HUU TRA VAN, and D. PATTERSON. J. Chem. Soc. Faraday 1, **75**, 1700 (1979); **75**, 1708 (1979).
12. H. B. EWING and K. N. MARSH. J. Chem. Thermodyn. **9**, 863 (1977).
13. B. REIDL, H. PHUONG-NGUYEN, and G. DELMAS. J. Phys. Chem. To be published.

Can. J. Chem. Downloaded from www.nrcresearchpress.com by 210.87.254.105 on 09/06/12
For personal use only.

The electrochemical behavior and structure of silver salts of imides and carboxamides[1,2]

JEAN-YVES HUOT,[3] DENIS SERVE,[4] AND JEAN LESSARD[5]

Département de chimie, Université de Sherbrooke, Sherbrooke (Qué.), Canada J1K 2R1

Received September 30, 1982

JEAN-YVES HUOT, DENIS SERVE, and JEAN LESSARD. Can. J. Chem. **61**, 1890 (1983).

Silver salts of amides (imides and carboxamides), containing silver cations and amide anions in a one-to-one ratio, have been studied by electrochemical, potentiometric, and spectroscopic means. They have the structure [Amide–Ag–Amide]Ag with a linear nitrogen–silver–nitrogen bond and a silver cation loosely bound to the oxygens of the amide moieties. For instance, (*i*) the electrochemical data show that half of the silver ions are tightly bound (more difficult to reduce); (*ii*) only the loosely bound half can be titrated with chloride ions; (*iii*) according to ^{1}H and ^{13}C nmr spectroscopy, the silver salt of succinimide (**1**) is symmetric. The selective reduction of the loosely bound silver ions in acetonitrile containing tetraethylammonium tetrafluoroborate consumes 0.5 F/mol and leads to the mixed salt [Amide–Ag–Amide]Et_4N; further reduction at a more negative potential leads to the formation of the tetraethylammonium salt, Et_4NAmide. The latter two salts derived from succinimide have been prepared by a chemical route. The silver, mixed silver–tetracthylammonium, and tetraethylammonium salts are electroactive in oxidation.

JEAN-YVES HUOT, DENIS SERVE et JEAN LESSARD. Can. J. Chem. **61**, 1890 (1983).

Nous avons étudié, par des méthodes électrochimiques, potentiométriques et spectroscopiques, quelques sels d'argent d'amides (imides et carboxamides) formés par une mélange équimolaire de cations argent et d'anions d'amides. Les résultats permettent de déduire la structure [Amide–Ag–Amide]Ag comportant une liaison azote–argent–azote linéaire et un cation argent faiblement lié aux oxygènes des groupements amides. Par exemple, (*i*) les études électrochimiques montrent que la moitié des ions argent sont fortement liés (plus difficle à réduire); (*ii*) uniquement les cations argent faiblement liés peuvent être titrés par les ions chlorures; (*iii*) selon les spectres rmn de proton et du carbone-13, le sel d'argent du succinimide (**1**) est symétrique. La réduction sélective des ions argent faiblement liés, dans l'acétonitrile contenant du tétrafluoroborate de tétraéthylammonium, donne le sel mixte [Amide–Ag–Amide]Et_4N; une réduction plus poussée à un potentiel plus négatif conduit au sel de tétraéthylammonium, Et_4NAmide. Ces deux derniers sels ont été préparés par voie chimique dans le cas du succinimide. Les sels d'argent, les sels mixtes d'argent et de tétraéthylammonium et les sels de tétracthylammonium sont électroactifs en oxydation.

Introduction

Our interest in the oxidation of imide and amide anions in a nonaqueous medium led us to prepare their silver salts which are more soluble in acetonitrile than the alkali metal salts. Furthermore, the silver salts should be readily converted to tetraalkylammonium salts by deposition of silver on a cathode in a medium containing a tetraalkylammonium salt as supporting electrolyte.

The silver salt of formanilide was prepared by Comstock and Kleeberg (1) in 1890 and those of benzamide, proprionamide, and acetamide by Titherley (2) in 1897. Conductometric (3) and electrochemical (4) studies of the silver salt of acetamide in melted acetamide led to the identification of a soluble 2:1 (amide anion – silver ion) complex, $[(CH_3CONH)_2Ag]Na$, and an insoluble 1:1 complex, $CH_3CONHAg$. From studies on the site of alkylation of ambident anions, Stein and Tan (5) concluded that, in the silver salts of carboxamides, the silver ion (a soft acid) is bound to the nitrogen (the softer site of the amide anion).

Thermodynamic analysis of the silver salt of succinimide in water revealed the existence of a 1:1 and a 2:1 complex (6); the small contribution from entropy would be characteristic of a soft–soft (nitrogen–silver ion) interaction. According to potentiometric and thermodynamic data on silver complexes of uracil, the monoanion forms a 2:1 complex and the dianion, a 1:1 complex (7). In the dianion salt, one silver ion would be attached to the more basic nitrogen and the other to the neighboring carbonyl group (7). Recently, Guay and Beauchamp (8) have reported the X-Ray crystallographic structure of the silver salt of 1-methyl thymine: two imide anions are bound to one silver ion through the nitrogens and in a linear fashion.[6]

This paper deals with the structure of some silver salts of imides and carboxamides determined from electrochemical, potentiometric, and spectroscopic data.

Results and discussion

The stoichiometry of the silver salts of imides and carboxamides corresponds to a one-to-one ratio of amide anion and silver cation according to the method of preparation and to the analytical data (see the Experimental). The electrochemical behavior of the silver salt of succinimide, AgSucc (**1**), on a platinum electrode and in acetonitrile containing tetraethylammonium tetrafluoroborate (TEAFB) as supporting electrolyte, is summarized in Table 1 and is representative of the behavior of the other silver salts.

The linear voltammogram of **1** (Fig. 1, A) shows three diffusion controlled waves having the same amplitude (I_l/C): one

[1]Abbreviated from the M.Sc. Dissertation of J. Y. Huot, Université de Sherbrooke, Sherbrooke, Québec. 1980.

[2]Presented in part at the 64th Canadian Chemical Conference, Halifax, Nova Scotia. June, 1981.

[3]NSERC of Canada (1978–1980) and "Ministère de l'Education du Québec" (1978–1980) predoctorate fellow.

[4]France–Quebec visiting Scientist (Sept.–Dec. 1977). Present address: Laboratoire de photochimie, Université scientifique et médicale de Grenoble, 38041 Grenoble Cedex, France.

[5]Author to whom correspondence should be addressed.

[6]The X-ray structure of gold(I) salt of *N*-methyl hydantoin also shows a nitrogen–gold(I)–nitrogen linear bond with two amide anions (9). A 2:1 structure has been accepted since 1940 for the mercuric complexes of succinimide and acetamide (10). Like the Ag^+ ion, the Au^+ and Hg^{2+} ions have a d^{10} configuration.

Can. J. Chem. Downloaded from www.nrcresearchpress.com by 210.87.254.6 on 09/06/12
For personal use only.

TABLE 1. Electrochemical[a] and ultraviolet spectroscopic data for AgSucc (**1**) in acetonitrile–TEAFB (0.1 *M*)

Solution	Linear voltammetry[b] $E_{1/2}$[d] (V)	I_l/C[e] (μA/m*M*)	αn	Cyclic voltammetry[c] E_p[d] (V)	I_p/C (μA/m*M*)	$\lambda_{max}(\epsilon)$[f] (nm)	Electrodeposition of Ag^0 E_{appl}[d] (V)	n_{app} (F/mol)	Yield[g] (%)
Initial	−0.18	7	1.2	−0.25	9	233(4500)	−0.50	0.49	54
	−1.30	6	0.5	−1.50	4				
	(+1.48)	7	0.3	(0.00)[h]	Very large				
After reduction at −0.50 V (0.49 F/mol)	−1.35	6	0.3	−1.55	5	233(4500)	−1.50	0.52	51
	(+1.48)	7	0.3	(−0.29)[h]	3				
				(0.00)[h]	Very large				
After further reduction at −1.50 V (1.01 F/mol)	(+1.90)[i]	13	0.7			227(11 000)			
	(+1.69)[j]	13	1.0						

[a]The electrochemical analyses were carried out on a Pt electrode using a 3.35 m*M* solution.
[b]On a rotating disc electrode (ω = 600 rpm). The anodic waves are given between parentheses.
[c]Range: 0.00 to −2.00 V. The anodic peaks are indicated between parentheses.
[d]*E* vs. Ag^0/Ag^+ 0.01 *M*.
[e]The limiting current is diffusion controlled.
[f]For the uv spectra, 0.5 mL of the electrochemical solution was diluted to 5 mL with dry acetonitrile. The extinction coefficients (L mol^{-1} cm^{-1}) are based on the concentration of the succinimide moieties (anions).
[g]Calculated from the weight of Ag^0 deposited on the cathode and based on the total amount of silver ions initially present in **1**.
[h]Oxidation of electrodeposited Ag^0.
[i]Forward scan.
[j]Backward scan.

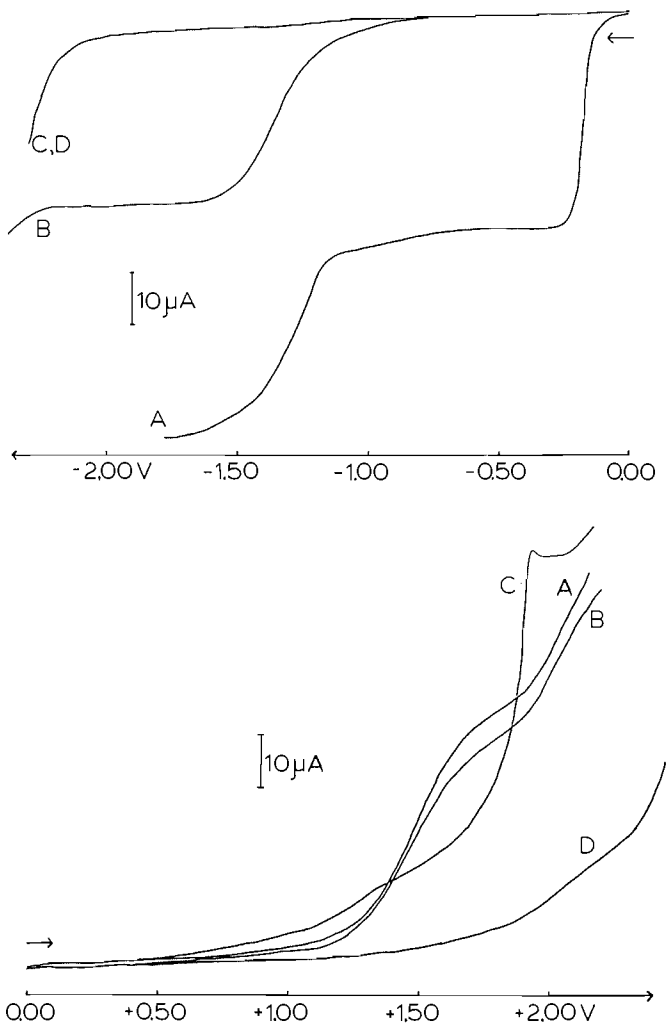

FIG. 1. Linear voltammetry of [Succ–Ag–Succ]Ag (**1**) in acetonitrile–TEAFB (0.1 *M*) on a Pt electrode (ω = 600 rpm, sweep rate = 16 mV/s): A, before reduction; B, after reduction at −0.50 V; C, after reduction at −1.50 V; D, residual current.

anodic wave and *two cathodic waves*.[7] The corresponding cathodic peaks of the cyclic voltammogram are shown in Fig. 2, A; the large anodic peak at 0 V is due to the oxidation of Ag^0 deposited on the electrode during the cathodic sweep. Upon reduction at −0.50 V, 50% of the silver present in **1** is deposited. The first cathodic wave disappears while the second cathodic wave and the anodic wave remain unchanged (Fig. 1, B). The cyclic voltammogram (Fig. 2, B) shows the second cathodic peak only and a new anodic peak at −0.29 V. There is no change in the uv spectrum (Table 1). Further reduction at −1.50 V leads to the deposition of the remaining 50% of the silver initially present in **1**. In the uv spectrum, there is a small bathochromic shift and an hyperchromic effect. The linear voltammogram (Fig. 1, C) shows the anodic wave only, which now appears at a more anodic potential; its amplitude has increased by a factor of two (Table 1).

The above results can only be accounted for if salt **1** has the structure [Succ–Ag–Succ]Ag in which there are two different types of silver ions in a one-to-one ratio. The silver ion tightly bound to two succinimide anions should be more difficult to reduce than the other. Therefore, the first cathodic wave ($E_{1/2}$ = −0.2 V) corresponds to process [1] and the second cathodic wave ($E_{1/2} \simeq -1.35$ V), to process [2].

[1] [Succ–Ag–Succ]Ag + Et_4NBF_4 + $e^- \xrightarrow{-0.2\ V}$ **1** [Succ–Ag–Succ]Et_4N + Ag^0 + BF_4^- **1***a*

[2] [Succ–Ag–Succ]Et_4N + Et_4NBF_4 + $e^- \xrightarrow{-1.35\ V}$ **1***a* 2 Et_4NSucc + Ag^0 + BF_4^- **1***b*

[7]The fact that the αn value for the first cathodic wave is larger than 1.0 can probably be ascribed to the modification of the nature and surface of the electrode with the deposition of Ag^0. The same phenomenon was observed when reducing silver nitrate on platinum in acetonitrile–TEAFB (0.1 *M*) (see Table 3, last entry). The αn values have been obtained by plotting log $[(i_l - i)/i]$ versus potential according to the relationship given in ref. 11 for irreversible processes.

Can. J. Chem. Downloaded from www.nrcresearchpress.com by 210.87.254.6 on 09/06/12
For personal use only.

Can. J. Chem. Downloaded from www.nrcresearchpress.com by 210.87.254.6 on 09/06/12
For personal use only.

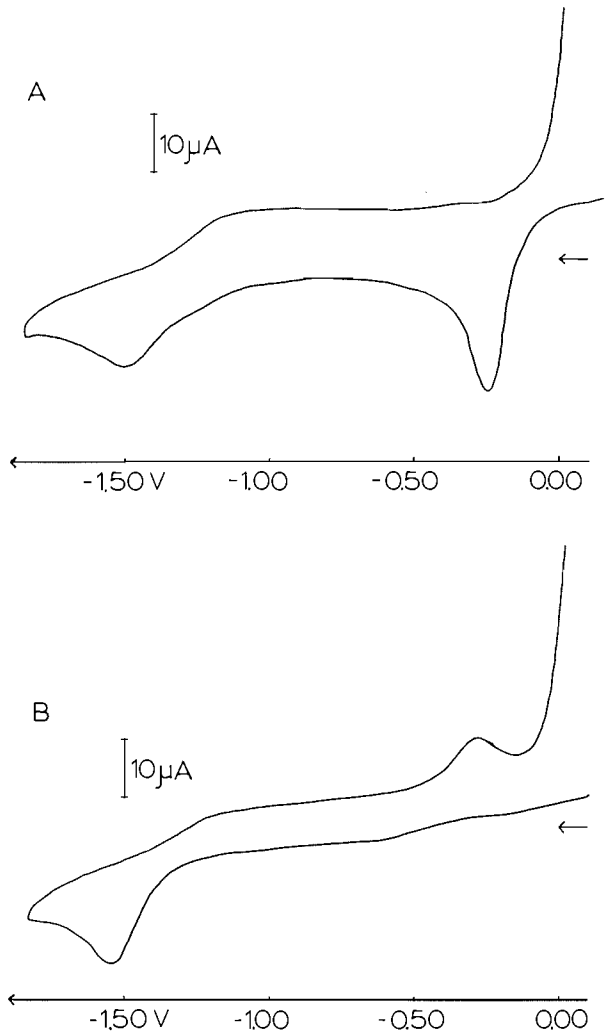

FIG. 2. Cyclic voltammetry of [Succ–Ag–Succ]Ag (**1**) in acetonitrile–TEABF (0.1 *M*) on a Pt electrode (sweep rate = 200 mV/s): A, before reduction; B, after reduction at −0.50 V.

The mixed silver tetraethylammonium salt **1***a* and the tetraethylammonium salt **1***b* have been prepared chemically (see the Experimental) and their electrochemical and uv spectroscopic behavior were identical to those of the species obtained from the electrochemical reduction of AgSucc (**1**) after passing 0.49 F/mol at −0.50 V, then 0.52 F/mol at −1.50 V, respectively. The mixed salt **1***a* is oxidized at the same potential and gives a uv spectrum practically identical to that of the silver salt **1** in agreement with the conclusion that the same species, the Succ–Ag–Succ anion, is involved in both salt **1** and salt **1***a*. Reduction of **1***a* at −1.50 V liberates two succinimide anions (eq. [2]), which accounts for the two-fold increase of the amplitude of the anodic wave.[8] The succinimide anion (see **1***b*) is more difficult to oxidize ($E_{1/2}$ = +1.90 V) and absorbs at a longer wavelength (λ_{max} = 227 nm) than the Succ–Ag–Succ anion (see **1** or **1***a*, $E_{1/2}$ = +1.48 V, λ_{max} = 223 nm). The extinction coefficient of 4500 L mol^{-1} cm^{-1} reported for **1** and **1***a* (Table 1) is based on the concentration of succinimide anions; it becomes 9000 (as compared to 11 000 for **1***b*) when based on the concentration of Succ–Ag–Succ anions.

Further confirmation of structure [Succ–Ag–Succ]Ag for **1** is provided by the following potentiometric and amperometric titrations. First, as shown in Table 3, only half of the silver ions present in **1**, the loosely bound ones, can be titrated with tetraethylammonium chloride (eq. [3]). The protonolysis of **1** with nitric acid (eq. [4]) liberates the tightly bound silver ions

[3] $\underset{\mathbf{1}}{[Succ-Ag-Succ]Ag} + Et_4NCl \rightarrow \underset{\mathbf{1}a}{[Succ-Ag-Succ]Et_4N} + AgCl$

[4] $\underset{\mathbf{1}}{[Succ-Ag-Succ]Ag} + 2HNO_3 \rightarrow 2HSucc + 2AgNO_3$

which can then be titrated with chloride ions (Table 3). Secondly, the potentiometric titration of silver nitrate with the sodium salt of succinimide in 50% ethanol gives one end point at 2.0 equivalents (Fig. 3) and is thus described by reaction [5]. Thirdly, the amperometric titration of the tetraethylammonium

[5] $AgNO_3 + 2NaSucc \rightarrow [Succ-Ag-Succ]Na + NaNO_3$

salt of succinimide (**1***b*) with silver nitrate (Fig. 4) shows clearly that the mixed silver–tetraethylammonium salt **1***a*, where only the tightly bound silver ions are present, is formed first (eq. [6]). Indeed when about 0.4 equivalent of silver nitrate has been added, the cyclic voltammogram shows a

[6] $\underset{\mathbf{1}b}{2Et_4NSucc} + AgNO_3 \rightarrow \underset{\mathbf{1}a}{[Succ-Ag-Succ]Et_4N} + Et_4NNO_3$

[7] $\underset{\mathbf{1}a}{[Succ-Ag-Succ]Et_4N} + AgNO_3 \rightarrow \underset{\mathbf{1}}{[Succ-Ag-Succ]Ag} + Et_4NNO_3$

cathodic peak at −1.45 V, an anodic peak at −0.20 V, and the large anodic peak at 0 V; thus, this voltammogram corresponds to the cyclic voltammogram of **1***a* (see Fig. 2, B). As more silver nitrate is added, the cathodic peak at −0.20 V due to the reduction of the loosely bound silver ions in **1** first appears, then increases in intensity,[9] while the intensity of the cathodic peak at −1.45 V remains more or less constant (Fig. 4). The anodic peak at −0.30 V decreases in intensity and disappears when **1***a* has been completely converted to **1** (eq. [7]). Finally, the amperometric titration of the silver salt **1** with the tetraethylammonium salt **1***b* followed by cyclic voltammetry (Fig. 5) shows clearly the formation of the mixed silver–tetraethylammonium salt **1***a*, according to eq. [8]. As salt **1** is converted to salt **1***a*, the amount of loosely bound silver ions

[8] $\underset{\mathbf{1}}{[Succ-Ag-Succ]Ag} + \underset{\mathbf{1}b}{2Et_4NSucc} \rightarrow 2\underset{\mathbf{1}a}{[Succ-Ag-Succ]Et_4N}$

(limiting current of the cathodic peak at −0.20 V) decreases while that of the tightly bound silver ions (limiting current of the cathodic peak at −1.45 V) increases. Surprisingly, when the loosely bound silver ions (salt **1**) have completely disappeared, further addition of succinimide anions leads to a steeper increase of the limiting current at −1.45 V; a plateau is reached when about 2 equivalents of **1***b* have been added, as if the effective concentration of tightly bound silver ions (of **1***a*) was

[8]The *n* value for the oxidation of the Succ–Ag–Succ anion is ≤1.2 and that for the oxidation of the succinimide anion is 0.97 (see footnote 11).

[9]Since the peak potentials for the reduction of $AgNO_3$ and the reduction of the loosely bound silver ion of **1** are quite close, a single peak at ca. −0.2 V is observed when the two species are present, that is, when there is an excess of $AgNO_3$.

TABLE 2. ^1H and ^{13}C nuclear magnetic resonance and infrared data for succinimide and salts **1**, **1***a*, and **1***b*

Compound	^1H nmr[a] CH_2 (ppm)	^{13}C nmr[b] CH_2 (ppm)	^{13}C nmr[b] C=O (ppm)	Infrared[c] ν C=O (cm^{-1})
HSucc	2.58	30.5	181.6	1770, 1725
Et_4NSucc(**1***b*)[d]	2.42	32.9	198.3	1650, 1600
[Succ–Ag–Succ]Et_4N (**1***a*)[d]	2.59[e]	32.4	194.5	1640
[Succ–Ag–Succ]Ag (**1**)	2.55	32.4	194.7	1650

[a]In CD_3CN–D_2O (9:1) with TMS as reference.
[b]In CH_3CN–D_2O (8:2) using CH_3CN as reference.
[c]In dry CH_3CN.
[d]In the ^{13}C nmr spectrum, the carbons of the tetraethylammonium cation absorb at 7.7 (CH_3) and 53.1 pm (CH_2).
[e]In CD_3CN–D_2O (8:2).

TABLE 3. Electrochemical[a] and potentiometric[b] data for the silver salts of imides and carboxamides

Silver salts of	Concentration[c] (m*M*)	Linear voltammetry[c] $E_{1/2}$[f,g] (V)	Linear voltammetry[c] I_l/C (μA/m*M*)	Linear voltammetry[c] αn	Cyclic voltametry[d] E_p[f] (V)	Cyclic voltametry[d] I_p/C (μA/m*M*)	Potentiometric titration of Ag^+ ion (%)	Potentiometric titration of Ag^+ ion $+HNO_3$[h] (%)
Succinimide (**1**)	5.7	−0.18	7	1.2	−0.25	9	50	99
		−1.30	6	0.5	−1.50	4		
		(+1.48)	7	0.3	(0.0)	Very large		
Glutarimide (**2**)	4.5	−0.18	6	1.5	−0.48	5	48	
		−1.38	5	0.8	−1.66	4		
		(+1.45)	8	0.3	(0.0)	Very large		
Tetramethyl-succinimide (**3**)	2.3	−0.16	10	2.1	−0.26	8	51	
		−1.52	8	0.8	−1.70	8		
		(+1.50)	11	0.2	(0.0)	Very large		
Phthalimide (**4**)	1.3	−0.17	8	1.0	−0.22	10	50	
		−1.30	7	0.7	−1.46	8		
		(+1.52)	8	0.3	(−0.35)	2		
					(0.0)	Very large		
Benzoylimide (**5**)	2.2	−0.20	5	1.3	−0.30	8	54	108
		−0.5[i]	3	0.4	−0.54	5		
		(+1.04)	6	0.4	(0.0)	Very large		
Formanilide (**6**)	<1.2[j]	−0.27	5	0.8	−0.30	—	50	105
		−1.38	6	0.5	−1.74	—		
		(+0.41)	6	1.0	(+0.10)	Very large		
Benzamide (**7**)	<1.9[j]	−0.26	2	1.0				
		−1.41	2	—				
$AgOCOCH_3$	2.9	−0.23	2	0.7	−0.40	4	100	
					(−0.10)	2		
$AgNO_3$	3.6	−0.10	13	3.1			100	
		−0.17[k]	13	1.1				

[a]The electrochemical analyses were carried out on a Pt electrode in acetonitrile–TEABF (0.1 *M*).
[b]The potentiometric titrations were carried out in acetonitrile with tetraethylammonium chloride using a silver wire vs. Ag/Ag^+ 0.01 *M*.
[c]On a rotating disc electrode (ω = 600 rpm except in the case of salt **7** where ω = 4000 rpm). The anodic waves are given between parentheses.
[d]Range: 0.00 to −2.00 V. The anodic peaks are indicated between parentheses.
[e]The concentration is based on the formula (Ag Amide)·xH_2O determined from the analytical data (see Experimental).
[f]*E* vs. Ag/Ag^+ 0.01 *M*.
[g]After electrodeposition of all the silver ions, the amplitude of the *anodic wave* increases by a factor two and its half-wave potential changes with the direction of the scan; for **1**, see Table 1; for **2**, reduction at −1.60 V, $E_{1/2}$ = +1.71 V (forward) and +1.64 V (backward); for **3**, reduction at −1.60 V, $E_{1/2}$ = +1.16 V (forward) and +1.46 V (backward); for **4**, reduction at −1.50 V, $E_{1/2}$ = +2.02 V (forward) and +1.50 V (backward); for **5**, reduction at −0.90 V, $E_{1/2}$ = +0.93 V (no change with the direction of scanning); for **6**, reduction at −1.50 V, $E_{1/2}$ = +0.16 V (no change with the direction of scanning).
[h]One equivalent of concentrated nitric acid with respect to AgSucc (**1**) was added.
[i]Ill-defined wave (see Fig. 6).
[j]The amount of salt added could not be solubilized completely.
[k]In the presence of 1 equiv. of succinimide (HSucc).

Can. J. Chem. Downloaded from www.nrcresearchpress.com by 210.87.254.6 on 09/06/12
For personal use only.

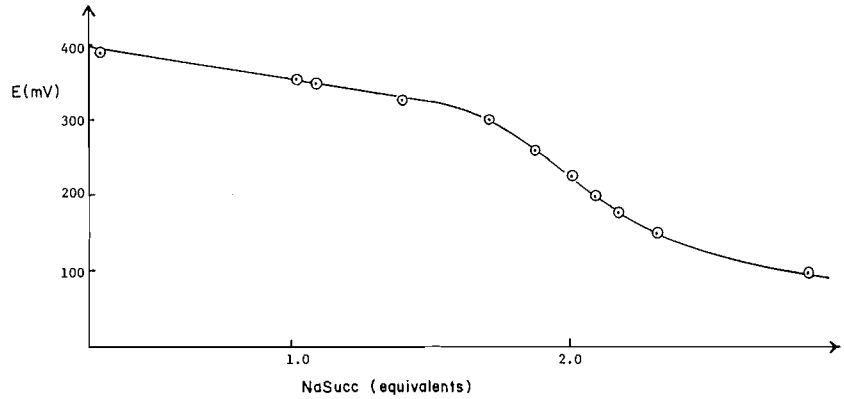

FIG. 3. Potentiometric titration of silver nitrate by the sodium salt of succinimide in 50% ethanol.

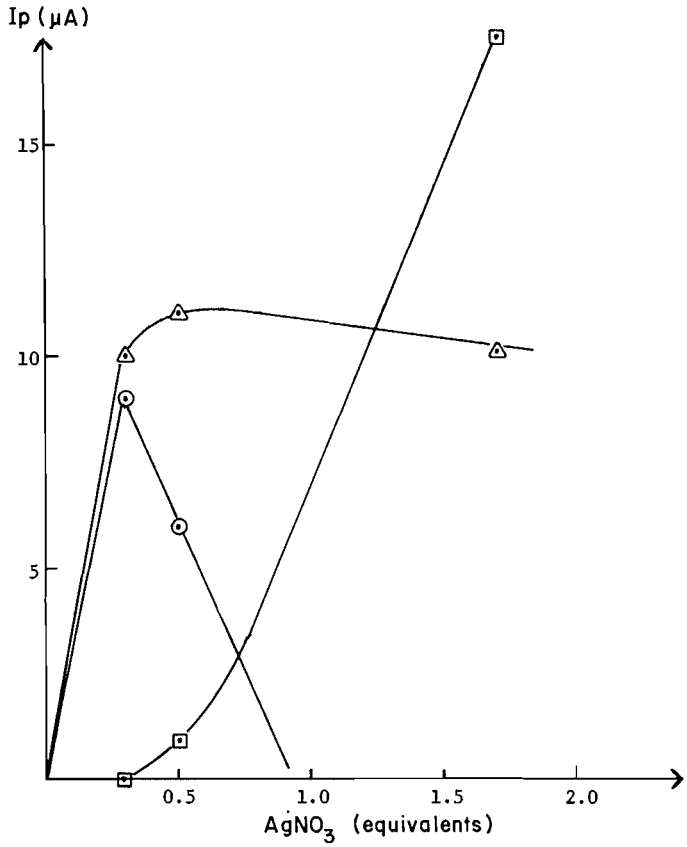

FIG. 4. Amperometric titration (cyclic voltammetry) of Et_4NSucc (**1***b*) (prepared by reduction of AgSucc (**1**) (3.40 m*M*) at −1.70 V in acetonitrile–TEAFB (0.1 *M*)) by silver nitrate: △, current of the cathodic peak at −1.48 V; ⊡, current of the cathodic peak at −0.20 V; ⊙, current of the anodic peak at −0.30 V.

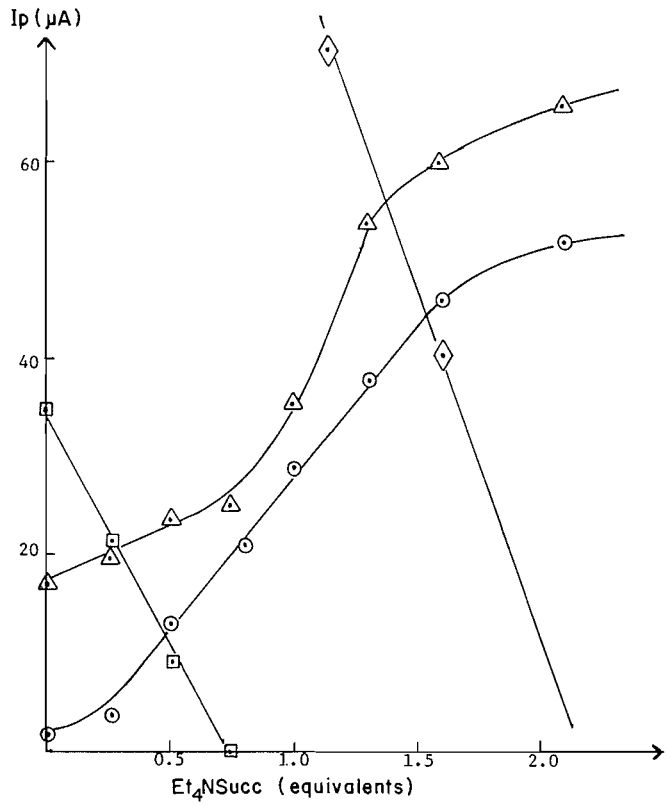

FIG. 5. Amperometric titration (cyclic voltammetry) of [Succ–Ag–Succ]Ag (**1**) (4.39 m*M*) by Et_4NSucc (**1***b*) (the equivalents of **1***b* are calculated using the formula AgSucc for **1**) in acetonitrile–TEAFB (0.1 *M*): △, current of the cathodic peak at −1.45 V; ⊡, current of the cathodic peak at −0.20 V; ⊙, current of the anodic peak at −0.30 V; ◇, current of the anodic peak at 0 V.

twice as large in the presence of a 100% excess of succinimide anions. We have no satisfactory explanation for that phenomenon.

The origin of the anodic peak at −0.30 V in the cyclic voltammogram of the mixed salt **1***a* (Fig. 2, B) can be ascribed to the oxidation of electrodeposited silver to a tightly bound silver ion in the presence of succinimide anions at the surface of the electrode (eq. [9]). Succinimide anions are liberated by

$$[9]\quad Ag^0 + 2Succ^- \xrightarrow{-0.30\ V} [Succ{-}Ag{-}Succ]^- + e^-$$

$$[10]\quad Ag^0 + BF_4^- \xrightarrow{0\ V} Ag^+BF_4^- + e^-$$

the reduction of tightly bound silver ions (reduction of **1***a*, eq. [2]) during the cathodic sweep. However, because reaction [8] is rapid, succinimide anions cannot be present at the electrode, during the anodic sweep, as long as there is still some salt **1** left. Indeed, as shown in Figs. 4 and 5, the anodic peak at −0.30 V appears only when there are no more loosely bound silver ions left. Furthermore, its limiting current increases with the concentration of succinimide anions. In Fig. 4, the maximum value of the limiting current at −0.30 V corresponds to the highest concentration of mixed salt **1***a*, as expected. In Fig. 5, however, the limiting current reaches a plateau when there is a 100% excess of succinimide anions with respect to salt **1**, a phenomenon which is also observed for the cathodic wave at

Can. J. Chem. Downloaded from www.nrcresearchpress.com by 210.87.254.6 on 09/06/12
For personal use only.

Can. J. Chem. Downloaded from www.nrcresearchpress.com by 210.87.254.6 on 09/06/12
For personal use only.

−1.45 V and for which we cannot provide a satisfactory explanation as stated above. In the absence of succinimide anions, all the electrodeposited silver is oxidized according to eq. [10]. Since there is a large excess of tetrafluoroborate anions, the rate of this process is limited by the diffusion of silver ions into the solution and the current of the anodic peak at 0 V is large; this current decreases as the peak at −0.30 V (the amount of succinimide anions) increases, as expected (see Fig. 4).

The fact that there are two types of silver ions in silver salt **1** derived from succinimide eliminates structure A in which the two silver ions would be equivalent. The ^1H and ^{13}C nmr data recorded in Table 2 show clearly that the [Succ–Ag–Succ]Ag complex (**1**) must be symmetric and have structure B in which the tightly bound silver ion is linked linearly to each nitrogen of the two succinimide anions. Indeed, the eight protons of the two succinimide moieties give rise to a singlet; the four carbons

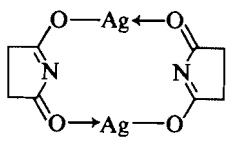

A

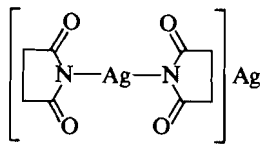

B

of the carbonyl groups give a single signal, as do the four carbons of the methylene groups. The loosely bound silver ions, which are more difficult to reduce ($E_{1/2}$ = −0.20 V) than silver nitrate ($E_{1/2}$ = −0.10 V), probably interact with the carbonyl groups of the two succinimide anions. In solution, this interaction is not strong enough to make the rotation around the N—Ag—N bond a slow process on the nmr time scale. Structure B is in agreement with the classical theory according to which an Ag—N bond should be stronger than an Ag—O bond (12). It also agrees perfectly with the X-ray crystallographic structure of the silver salt of 1-methyl thymine determined by Guay and Beauchamp (8): half of the silver ions are bound linearly to the nitrogens of two imide anions and the other half interact with four carbonyl groups. The nmr and ir data for the mixed silver–tetraethylammonium salt **1***a* (Table 2) are very similar to those for the silver salt **1** since the same species, the Succ–Ag–Succ anion, is responsible for the absorptions. We have already pointed out the similarity of the uv spectra (Table 1).

As shown in Table 3, the electrochemical and potentiometric behavior of all the silver salts studied is perfectly analogous to that of salt **1**. Reduction at a potential ($-E_{appl} \simeq -E_{1/2}$ + 200 mV) corresponding to the first cathodic wave leads to the deposition of only 50% of the silver ions and the remaining 50% are deposited upon reduction at a potential corresponding to the second cathodic wave. Thus, all the silver salts must have the same [Amide–Ag–Amide]Ag structure. The silver salts and the corresponding mixed tetraethylammonium salts are oxidized at nearly the same potentials as in the case of salts **1** and **1***b* derived from succinimide (see Fig. 6 for salts **5** and **5***a* derived from benzoylimide). The tetraethylammonium salts of glutarimide (**2***b*) and phthalamide (**4***b*) are more difficult to oxidize than the corresponding silver (**2** and **4**) and mixed silver–tetraethylammonium (**2***a* and **4***a*) salts as in the succinimide case (see Table 1 and Fig. 1, C), whereas the reverse situation is found for the tetraethylammonium salts of tetramethylsuccinimide (**3***b*), benzoylimide (**5***b*) (see Fig. 6), and formanilide (**6***b*). The oxidation of the silver salt of formanilide (**6**), a carboxamide, is much easier than that of silver salts of imides because the energy of the HOMO of the Amide–

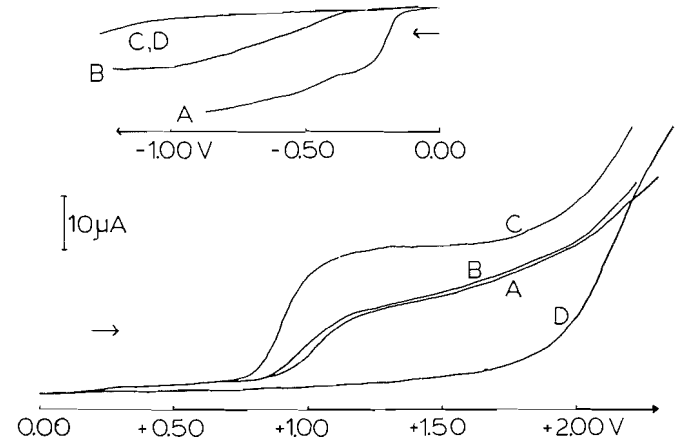

FIG. 6. Linear voltammetry of the silver salt of benzoylimide (**5**) (2.15 m*M*) in acetonitrile–TEAFB (0.1 *M*) on a Pt electrode (ω = 600 rpm, sweep rate = 16 mV/s): A, before reduction; B, after reduction at −0.25 V; C, after reduction at −0.90 V; D, residual current.

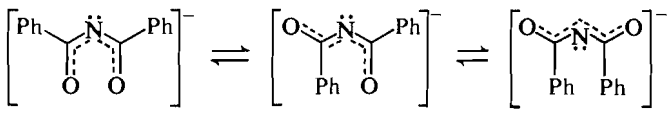

trans–trans *cis–trans* *cis–cis*

SCHEME 1

Ag–Amide anion must be lower when the anionic ligands are derived from an imide (two carbonyl groups) than when they are derived from a carboxamide (one carbonyl group) (13). We could not obtain a satisfactory oxidation wave for the silver salt of benzamide (**7**).[10]

The silver salt of benzoylimide (**5**) is the sole salt derived from an acyclic imide and is less stable than the other salts. We also tried to prepare $[(CH_3\overset{O}{\overset{\|}{C}})_2N—Ag—N(\overset{O}{\overset{\|}{C}}CH_3)_2]Ag$ but this salt was still less stable and was too sensitive to hydrolysis to be isolated and studied under the standard conditions. The electrochemical behavior of salt **5** is somewhat different from that of the other silver salts since the two cathodic waves are separated by about 0.3 V as compared to 1.1–1.3 V for the other salts. Furthermore, as shown in Fig. 6, the second cathodic wave is not very well defined, being spread over a 0.5 V range. In salt **5**, the ligands (the benzoylimide anions) could *a priori* exist under the three planar conformations shown (Scheme 1). For the free anion, the *cis–cis* conformation should be much less stable than the two others because of steric interactions between the two phenyl rings which would tend to orient themselves into the OCNCO plane to allow some delocalization of the electrons of the imide anion onto the aromatic rings. However, if the *cis–cis* benzoylimide ((*cis–cis*)Bzmide) anion is a better ligand to Ag^+ than the two other conformers, the [(*cis–cis*)Bzmide–Ag–(*cis–cis*)Bzmide]$^-$ anion could be present in significant amount together with the other complex anions: [(*cis–trans*)Bzmide–Ag–(*cis–trans*)Bzmide]$^-$, [(*trans–trans*)Bzmide–Ag–(*trans–*

[10]Further work on the oxidation of the silver salts of imides and carboxamides is in progress and will be reported in a forthcoming paper.

TABLE 4. Ultraviolet spectral data of the salts of imides and carboxamides in acetonitrile–TEABF (0.01 *M*)[a]

Silver salt of	Concentration[b] (10^{-4} *M*)	$\lambda_{max}(\epsilon)$(nm) Before reduction	After reduction 0.5 F/mol	After reduction 1 F/mol	Parent amide[c]
Succinimide (**1**)	3.35	223(4500)[d]	223(4500)[d]	227(11 000)[d]	224(100), 230 (93), 245(73)
Glutarimide (**2**)	1.02	231(9000)	213(9300)	237(9900)	233(215), shoulder
Tetramethyl-succinimide (**3**)	2.34	227(4000)	227(4150)	230(5750)	233(150), 251(130)
Phthalimide (**4**)	1.58	230(15 600) 236(15 500) 226(9100)	230(15 700) 236(15 600) 226(9100)	230(17 850) 238(17 200) 246(10 400)	230(9600), 238(9200), 234(8400)
Benzoylimide (**5**)	0.28	241(28 000)	—	237(21 000)	243(22 400)
Formanilide (**6**)	0.95	242(10 500) 209(8900)	242(11 000) 209(9500)	242(11 000)	243(12 900)

[a]0.5 mL of the electrochemical solution was diluted to 5 mL with dry acetonitrile.
[b]Based on the concentration of amide anions.
[c]In dry CH_3CN without any supporting electrolyte.
[d]Taken from Table 1.

trans)Bzmide]$^-$, [(*cis*–*cis*)Bzmide–Ag–(*cis*–*trans*)Bzmide]$^-$, etc. The fact (*i*) that salt **5** is less stable than the other silver salts, and (*ii*) that the reduction of the tightly bound silver ion in **5** and **5***a* occurs at potentials lower than those observed with the other silver and mixed silver–tetraethylammonium salts, shows that the benzoylimide anion binds Ag^+ less tightly than a carboxamide anion or a cyclic imide anion. The presence of a mixture of benzoylimide–Ag–benzoylimide complexes, which differ from one another by the conformation of the benzoylimide anions and which have different reduction potentials, could explain the spreading of the cathodic wave due to the reduction of [Bzmide–Ag–Bzmide]$^-$ in **5** and **5***a*.

We have included silver acetate in Table 3 for comparison purposes. The low cathodic half-wave potential as well as the precipitation of 100% of the silver ions by tetraethylammonium chloride shows that Ag—O bonds are weaker than Ag—N bonds and thus confirms the conclusions of the classical theory (12). The structure of silver carboxylates has been determined by potentiometry (14), linear voltammetry (15), and X-ray diffraction (16–18) and corresponds to:

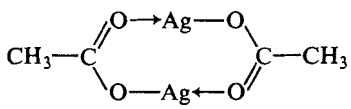

The one cathodic wave and the one cathodic peak observed in the voltammograms for silver acetate show that the silver ions are all equivalent, in agreement with the structure shown above.

Table 4 summarizes the uv spectral data, in acetonitrile, of the various salts studied. The parent amides (imides and carboxamides) are included for comparison. As in the case of succinimide, the uv spectra before any reduction and after reduction of the loosely bound silver ions (0.5 F/mol) are identical because the same species, the amide–Ag–amide anion, is responsible for the absorption. The salts derived from imides bearing no aromatic ring(s) show a large hyperchromic effect when compared to the parent imide. However, since succinimide shows a strong band at 190 nm (ϵ = 15 000) in acetonitrile (19), the formation of the imide anion must be accompanied by a ca. 35 nm bathochromic shift of the 190 nm band.[11] As for salt **1***a* (0.5 F/mol), further reduction of salts **2***a* and **3***a* to give the corresponding tetraethylammonium salts **2***b* and **3***b* (1 F/mol) is accompanied by a small bathochromic shift. However, the hyperchromic effect was observed only in the case of salt **1***a*.

Experimental

General

Melting points were determined on a Buchi apparatus and are uncorrected. Infrared (ir) spectra were obtained using a Perkin–Elmer 257 spectrophotometer. Ultraviolet (uv) spectra were recorded with a Varian–Techtron 635 spectrophotometer. Proton magnetic resonance (^{1}H nmr) spectra were measured using Bruker WP-60 and Varian A-60 instruments. Carbon magnetic resonance (^{13}C nmr) spectra were recorded on a Bruker HX-90 spectrometer. Mass spectra were taken on Hitachi RMU-6E instrument. Microanalysis were carried out by Mr. H. Seguin, National Research Council of Canada, Ottawa.

Solvent and electrolyte

Technical grade acetonitrile was purified as reported in ref. 21. Tetraethylammonium tetrafluoroborate (TEAFB), prepared from tetrafluoroboric acid and tetraethylammonium bromide (22), was recrystallized from 95% ethanol until the silver ion test was negative. It was then dried in a vacuum oven for 2 days at 80°C.

Electrochemical instrumentation and methods

Solutions were deoxygenated with dry and oxygen-free nitrogen saturated with acetonitrile. A nitrogen atmosphere was maintained over the solutions throughout the experiments. A three-electrode system and a PAR cell (type K0060) were used for the voltammetric analyses and the electrodepositions of silver. The auxiliary electrode was a platinum wire. Potentials were measured with respect to an Ag^0/Ag^+ (0.01 *M*) electrode (23).

The voltammetric analyses were carried out with a homemade potentiostat. A Tacussel rotating electrode type ED1 (with Controvit speed controller) having a platinum 20 mm^2 disc was used at rotation rates of 500 to 5000 rpm for the linear voltammograms; the sweep rate was 16 mv/s. The same electrode served as a stationary electrode for the cyclic voltammograms; the sweep rate was 200 mV/s. The plat-

[11]The ionization of phenol to phenolate causes a 25 nm bathochromic shift of the 210 nm band (20).

Can. J. Chem. Downloaded from www.nrcresearchpress.com by 210.87.254.6 on 09/06/12
For personal use only.

Can. J. Chem. Downloaded from www.nrcresearchpress.com by 210.87.254.6 on 09/06/12
For personal use only.

inum disc was washed with nitric acid, rinsed with water, dried, then polished on a Carbimet-600A paper (Buehler) before each use.

The electrodepositions of silver were performed with a Tacussel type ASA-100 potentiostat having both a Tacussel type IG-5 integrator and an ammeter connected in series within the auxiliary circuit. The working electrode was a 18 cm^2 platinum plate. After the deposition of silver, the electrode was washed with acetonitrile, dried, and the amount of silver deposited was determined by weight.

Amides and imides

Succinimide, glutarimide, phthalamide, and benzanilide were obtained from commercial sources.

Tetramethylsuccinimide

It was prepared according to the method described by Bickel and Waters (24) in a 22% yield, mp 186°C (lit. (23) mp 187–188°C); ν_{max} ($CHCl_3$): 3510, 3220, 1790 and 1740 cm^{-1}; δ ($CDCl_3$): 1.18 and 1.21 (not resolved, 12 H) and 8.56 ppm (m, NH).

Benzoylimide

It was obtained as described by Titherley (25) in a 10% yield; mp 144–145°C (lit. (24) mp 144°C); ν_{max} ($CHCl_3$): 3440, 3380, 1750, 1690, 1600, and 1580 cm^{-1}; δ ($CDCl_3$): 7.40 (m, 6H) and 7.75 ppm (m, 4H), the NH absorption could not be seen.

Formanilide

It was prepared in a 72% yield by refluxing equimolar quantities of aniline and formic acid for 5 h while removing water with a Dean–Stark separator, mp 47°C (lit. (26) mp 50°C); ν_{max} ($CHCl_3$): 3420, 3380, 1690, and 1600 cm^{-1}; δ ($CDCl_3$): 7.15–7.48 (5H), 8.32 (d, J = 1.7 Hz, 0.7H), and 8.66 ppm (d, J = 11.4 Hz, 0.3H). Thus the conformer with C—H and N—H in a *cis* relationship predominates.

Silver salts

Silver acetate is commercially available. The silver salts of imides and amides were prepared according to the following general procedure (27). Equimolar amounts of silver nitrate and imide or carboxamide were dissolved in 50% ethanol (between 1 and 2 mL per mol of amide except in the case of benzoylimide where 6 mL per mol of imide was used). The solution was heated to reflux and an equimolar quantity of sodium hydroxide (a 1.00 *M* or a 5.00 *M* aqueous solution) was then added dropwise and slowly. The precipitate formed was filtered, washed with 95% ethanol, then with ether. It was dried at room temperature and in the dark in a vacuum desiccator containing phosphorus pentoxide.

The ir spectra of all the silver salts in KBr show a broad band in the 1600 cm^{-1} region for the C=O stretching vibration and a broad absorption around 3400–3500 cm^{-1} due to the presence of water in the crystals. Except for the silver salt of succinimide (**1**), the silver salts of imides and carboxamides were generally not soluble enough in acetonitrile to yield satisfactory ir (dry CH_3CN) and nmr (CD_3CN–D_2O) spectra.

Salt 1 (succinimide)

It was isolated as a greyish solid, dec. at 250°C (72% yield); ν_{max} (CH_3CN): 3640 and 3540 (water), 1650 (C=O) cm^{-1}; δ (CH_3CN, 20% D_2O): 2.56 ppm (s). *Anal.* calcd. for $C_4H_4NO_2Ag \cdot \frac{1}{2}H_2O$: C 22.34, H 2.37, N 6.51, Ag 50.18; found: C 22.72, H 2.27, N 6.68, Ag 49.30.

Salt 2 (glutarimide)

It was isolated as a brown solid, dec. at 220°C (81% yield). *Anal.* calcd. for $C_6H_6NO_2Ag$: C 27.29, H 2.75, N 6.37, Ag 49.04; found: C 27.04, H 2.79, N 6.52, Ag 48.88.

Salt 3 (tetramethylsuccinimide)

It was isolated as a brown solid which melted above 280°C (69% yield). *Anal.* calcd. for $C_8H_{12}NO_2Ag$: C 36.64, H 4.58, N 5.34, Ag 41.20; found: C 36.17, H 4.43, N 5.17, Ag 40.70.

Salt 4 (phthalimide)

It was isolated as a beige solid melting above 345°C (92% yield). *Anal.* calcd. for $C_8H_4NO_2Ag \cdot \frac{1}{2}H_2O$: C 36.53, H 1.92, N 5.33, Ag 41.02; found: C 37.01, H 1.89, N 5.40, Ag 40.39.

Salt 5 (benzoylimide)

It was isolated as a brownish solid, mp 265°C (91% yield). *Anal.* calcd. for $C_{14}H_{10}NO_2Ag \cdot \frac{1}{2}H_2O$: C 49.46, H 3.27, N 4.12, Ag 31.73; found: C 49.67, H 3.22, N 4.04, Ag 31.48.

Salt 6 (formanilide)

It was isolated as a greyish solid, mp 182–185°C (90% yield). *Anal.* calcd. for $C_7H_6NOAg \cdot \frac{1}{2}H_2O$: C 35.47, H 2.98, N 5.91, Ag 45.51; found: C 35.97, H 2.75, N 6.02, Ag 47.01.

Salt 7 (benzamide)

The orange-brown solid obtained was not pure according to the elemental analysis and was most probably contaminated with silver oxide. *Anal.* calcd. for $C_7H_6NOAg \cdot \frac{1}{2}H_2O + \frac{1}{6}Ag_2O$: C 30.50, H 2.20, N 5.08, Ag 52.18; found: C 30.06, H 2.18, N 5.36, Ag 53.73.

Mixed silver–tetraethylammonium salt of succinimide (1a)

To a stirred mixture of succinimide (2.00 g, 20.2 mmol), tetraethylammonium hydroxide (14.4 mL of 1.40 *M* aqueous solution, 20.2 mmol), and water (15 mL) was added dropwise to a solution of silver nitrate (1.72 g, 10.1 mmol) in water (30 mL). No precipitation occurred. The reaction mixture took a greyish-blue color. The solvent was removed in a rotatory evaporator and the resulting greyish-blue solid was washed with methylene chloride, mp 190–192°C (3.26 g, 69%); ν_{max} (CH_3CN): 3620, 3540, and 3420 (water), 1640 (C=O) cm^{-1}; δ (CD_3CN, 20% D_2O): 1.20 (t of t, J = 8 and 2 Hz, 12H), 2.59 (s, 8H), and 3.16 ppm (q, J = 8 Hz, 8H). *Anal.* calcd. for $C_{16}H_{28}N_3O_4Ag \cdot 2H_2O$: C 40.85, H 6.87, N 8.94; found: 40.35, H 6.82, N 8.85.

Tetraethylammonium salt of succinimide (1b)

Tetraethylammonium bromide (42.0 g, 0.20 mol) was dissolved in the minimum amount of hot 95% ethanol. Silver sulfate (31.2 g, 0.10 mol) was added. Silver bromide was removed by filtration and the solvent was removed with a rotatory evaporator. The residue was recrystallized from ethanol–acetone to afford tetraethylammonium sulfate, mp 164–165°C (5.5 g, 15%). The sodium salt of succinimide was then prepared from succinimide (0.458 g, 4.6 mmol) and sodium ethoxide (30 mL of 0.15 *M* solution in absolute ethanol, 4.5 mmol). Tetraethylammonium sulfate (0.800 g, 2.25 mmol) in absolute ethanol (4 mL) was added to the previous solution which became clouded. Part of the solvent was removed in a rotatory evaporator. The addition of acetonitrile caused the quantitative precipitation of sodium sulfate which was removed by filtration. The solvent was stripped off in a rotatory evaporator, then the residue was dried in a vacuum desiccator over phosphorous pentoxide to afford salt **1***b* as a white solid, mp 72–73°C (sealed tube) (0.806 g, 76%); ν_{max} (CH_3CN): 3600 (b, water), 1650 and 1600 (C=O) cm^{-1}; δ (CD_3CN): 1.22 (t of t, J = 7 and 2 Hz, 12 H), 2.33 (s, 4H), and 3.20 ppm (q, J = Hz, 8H).

Sodium salt of succinimide

The salt was prepared from succinimide and sodium ethoxide (see above). It was also obtained *in situ* for the amperometric titration of silver nitrate by adding sodium hydroxide (1.30 mL of a 1.0 *N* solution, 1.30 mmol) to a solution of succinimide (0.127 g, 1.28 mmol) in 50% ethanol (250 mL).

Acknowledgements

We are grateful to the "Ministère de l'Education du Québec" and to the Natural Sciences and Engineering Research Council of Canada for financial assistance. We thank Professor F. M. Kimmerle for helpful discussions and Mr. H. Seguin of the National Research Council of Canada for microanalyses.

1. W. J. COMSTOCK and F. KLEEBERG. Am. Chem. J. **12**, 493 (1890).
2. A. W. TITHERLEY. J. Chem. Soc. **71**, 490 (1897).
3. G. JANDER and G. WINKLER. J. Inorg. Nucl. Chem. **9**, 24 (1959).
4. S. GUIOT and B. TREMILLON. J. Electroanal. Chem. **22**, 147 (1969).
5. A. R. STEIN and S. H. TAN. Can. J. Chem. **52**, 4050 (1974).

6. M. J. BLAIS, O. ENEA, and G. BERTHON. Thermochim. Acta, **30**, 37 (1979).
7. J. R. DEMEMBER and F. A. WALLACE. J. Am. Chem. Soc. **97**, 6240 (1975).
8. F. GUAY and A. L. BEAUCHAMP. J. Am. Chem. Soc. **101**, 6260 (1979).
9. N. A. MALIK, P. J. SADLER, S. NEIDLE, and G. L. TAYLOR. J. Chem. Soc. Chem. Commun. 711 (1978).
10. N. V. SUBBARAO and T. R. SESHADRI. Proc. Indian Acad. Sci. Sect. A, 1 (1940).
11. Z. GALUS. Fundamentals of electrochemical analysis. Ellis Horwood Ltd., Westergate, G. B. 1976. p. 249.
12. M. ISRAELI and L. D. PETTIT. J. Inorg. Nucl. Chem. **37**, 999 (1975).
13. I. FLEMING. Frontier orbitals and organic chemical reactions. John Wiley and Sons Ltd., New York, NY. 1976.
14. R. ALEXANDER, E. C. F. KO, Y. C. MAC, and A. J. PARKER. J. Am. Chem. Soc. **89**,. 3703 (1967).
15. S. H. COHEN, R. T. IWAMOTO, and J. KLEINBERG. J. Am. Chem. Soc. **82**, 1844 (1960).
16. R. L. GRIFFITH. J. Chem. Phys. **11**, 499 (1943).
17. A. E. BLAKESLEE and J. L. HOARD. J. Am. Chem. Soc. **78**, 3029 (1956).
18., P. COGGON and A. T. MCPHAIL. J. Chem. Soc. Chem. Commun. 91 (1972).
19. D. W. TURNER. J. Chem. Soc. 4555 (1957).
20. A. I. SCOTT. Ultraviolet spectra of natural products. Pergamon Press, Ltd., New York. 1964. p. 93.
21. D. BERUBE and J. LESSARD. Can. J. Chem. **60**, 1127 (1982).
22. H. O. HOUSE, E. FENB, and N. P. PEET. J. Org. Chem. **36**, 2371 (1971).
23. J. P. BILLON. J. Electroanal. Chem. **1**, 486 (1959/60).
24. A. F. BICKEL and W. A. WATERS. Recl. Trav. Chim. Pays-Bas, **69**, 1490 (1950).
25. A. W. TITHERLEY. J. Chem. Soc. **85**, 1673 (1904).
26. R. C. WEAST (*Editor*). Handbook of Chemistry and Physics. 53th ed. CRC Press, Cleveland. 1972. p. C-303.
27. R. P. BELL and J. P. BROWN. J. Org. Chem. **1**, 1520 (1936); L. I. SMITH and J. NICHOLS. J. Org. Chem. **6**, 489 (1941).

Can. J. Chem. Downloaded from www.nrcresearchpress.com by 210.87.254.6 on 09/06/12
For personal use only.

Nuclear analogs of β-lactam antibiotics. XVII.[1] Stereospecific synthesis of penem and carbapenem precursors

ALAIN MARTEL,[2] JEAN-PAUL DARIS, CAROL BACHAND, MARCEL MÉNARD, TONY DURST,[3] AND BERNARD BELLEAU[4]
Bristol Laboratories of Canada, 100 Industrial Boulevard, Candiac, P.Q., Canada J5R 1J1

Received February 9, 1983

ALAIN MARTEL, JEAN-PAUL DARIS, CAROL BACHAND, MARCEL MÉNARD, TONY DURST, and BERNARD BELLEAU. Can. J. Chem. **61**, 1899 (1983).

The transformation of methyl 6-α-bromopenicillanate (**6**) to *N*-methoxalyl-(3*S*)-bromo-(4*R*)-chloro-2-azetidinone (**8**) is described. Azetidinone **8** was converted, in a stereoselective manner, to (3*S*)-bromo-(4*R*)-tritylthio-2-azetidinone (**9**). Subsequent reduction of the 4-bromo substituent with zinc afforded the chiral (4*R*)-tritylthio-2-azetidinone (**10**), a useful intermediate for the synthesis of penems. Azetidinone **8** was also converted to the reactive (3*S*)-bromo-(4*R*)-chloro-2-azetidinone (**11**). Treatment of the (4*R*)-chloroderivative **11** with *n*-butyl or allylcuprate afforded the (4*R*)-butyl and (4*R*)-allylazetidinones **12** and **13** as the predominant diastereomers. Finally, an improved synthesis of **11** to **13** using tetraallyltin is also described.

ALAIN MARTEL, JEAN-PAUL DARIS, CAROL BACHAND, MARCEL MÉNARD, TONY DURST et BERNARD BELLEAU. Can. J. Chem. **61**, 1899 (1983).

On décrit la transformation de l'α-bromo-6 pénicillanate de méthyle (**6**) en *N*-méthoxalyl-bromo (3*S*) chloro (4*R*) azétidinone-2 (**8**). On transforme l'azétidinone (**8**) d'une façon stéréosélective en bromo (3*S*) tritylthio (4*R*) azétidinone-2 (**9**). La réduction subséquente du brome en position 4, par le zinc, permet d'obtenir le composé chiral: la tritylthio (4*R*) azétidinone-2 (**10**), un intermédiaire utile pour la synthèse des pénems. On a également transformé l'azétidinone (**8**) en bromo (3*S*) chloro (4*R*) azétidinone-2 (**11**). La réaction du dérivé chloré (4*R*) (**11**) avec le *n*-butyle ou l'allylcuprate donne les butyles (4*R*) et les allyl (4*R*) azétidinones **12** et **13** comme diastéréoisomères majoritaires. On décrit également une synthèse améliorée des composés **11** à **13** qui fait appel au tétraallylétain.

[Traduit par le journal]

Can. J. Chem. Downloaded from www.nrcresearchpress.com by 210.87.254.40 on 09/06/12
For personal use only.

The discovery of thienamycin (**1**) (2) and the subsequent disclosure of the penem system (**2**) by Woodward (3) opened new synthetic challenges to organic chemists. The accessibility to both nuclei via a common chiral intermediate became highly desirable in terms of synthetic strategy. An enormous amount of work has already been documented for the manipulation and transformation of penicillins to various azetidinone nuclei (for a recent review, see ref. 4). The pioneering work of Kukolja (5) on the chlorinolysis of penicillins and the subsequent work by Wolfe *et al.* (6) and Sheehan *et al.* (7) first demonstrated the potential of a 3-substituted 4-chloro-2-azetidinone. The penicillin nucleus, because of its low cost and chirality, remains the substrate of choice for degradation to a precursor giving access to both chiral penems (8) and carbapenems.

Our approach was based on the conversion of a penicillin to a chiral azetidinone derivative, such as **3**, having (a) a leaving group (X) at position 4 and (b) a 3-α substituent (Y) that would be bulky enough to induce a stereoselective β-face entry of the incoming nucleophile (Scheme 1).

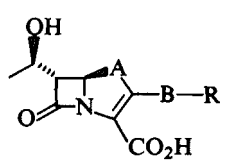

1, A = CH_2, B = S
2, A = S, B = CH_2

We found that the α-bromine substituent in the readily available methyl 6-α-bromopenicillanate (**6**) (9) was indeed capable of inducing complete chiralty when SNi displacement reactions (10) were performed at the adjacent position. Consequently we now report (1) the transformation of **6** to *N*-methoxalyl-(3*S*)-bromo-(4*R*)-chloro-2-azetidinone (**8**) and (3*S*)-bromo-(4*R*)-chloro-2-azetidinone (**11**), (2) the conversion of **8** or **11** to (4*R*)-tritylthio-2-azetidinone (**10**), and (3) the synthesis of (3*S*)-bromo-(4*R*)-allyl-2-azetidinone (**13**) from **11**.

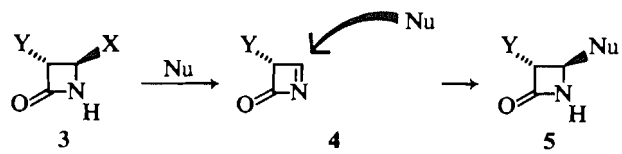

SCHEME I

Treatment of methyl 6-α-bromopenicillanate (**6**) (obtained in 93% yield from the corresponding acid (MeI, DMF)) with chlorine (2.6 equiv., CH_2Cl_2) at low temperature gave the *trans* 4-chloroazetidinone **7**[5] in excellent yield (86%). The ^{1}Hmr spectrum of derivative **7** (see Table 1) showed, for H-3 and H-4 respectively, two doublets centered at 4.90 and 5.84 with a small coupling constant (ref. 11) ($J_{3,4}$ = 1.0 Hz). Interestingly, the corresponding *cis* isomer was not observed in the reaction mixture. Ozonolysis of methyl α-[(3*S*)-bromo-(4*R*)-chloro-2-azetidinon-1-yl]-β-methylcrotonate (**7**) (12) in CH_2Cl_2 (−78°C) with subsequent reduction of the ozonide with $(CH_3)_2S$ (13) gave, after careful work-up, the labile *N*-methoxalyl derivative **8** (yield 94%). Azetidinone **8** revealed a carbonyl absorption at remarkably high frequency in the infrared (ν_{max} (CH_2Cl_2): 1840 (s), 1805 (sh), 1760 (s), and 1730 (s) cm^{-1}).

When treated with 2,4-dinitrophenylhydrazine (THF, room temperature, 18 h) compound **8** gave the labile (3*S*)-bromo-(4*R*)-chloro-2-azetidinone **11** (yield 71%) that could be isolated from the reaction residue by extraction and crystallization from hexane. Although unstable at room temperature in the presence of moisture, the crystalline[6] **11** could be kept in an

[1]For part XVI see ref. 1.
[2]Author to whom correspondence may be addressed.
[3]University of Ottawa.
[4]McGill University.

[5]Satisfactory analytical data were obtained for all new compounds.
[6]Since decomposition of **11** occurred upon heating, no melting point was observed.

Can. J. Chem. Downloaded from www.nrcresearchpress.com by 210.87.254.40 on 09/06/12
For personal use only.

TABLE 1. ^{1}H magnetic resonance spectral data*

Compound	H-3	H-4	Others
7	4.90 (d) J = 1.0	5.84 (d) J = 1.0	3.79 (s, 3H, OCH_3), 2.31 (s, 3H, CH_3) 2.02 (s, 3H, CH_3)
8	4.99 (d) J = 1.7	5.94 (d) J = 1.7	3.98 (s, 3H, OCH_3)
9	4.64 (t) J = 2.0	4.50 (d) J = 2.0	7.49–7.25 (m, 15H, aromatic-H) 4.9 (bs, 1H, NH)
10	3.28, 2.83 (dd) J = 15 J = 15 J = 5.2 J = 2.9 J = 2.0 J = 1.5	4.43 (dd) J = 5.2 J = 2.9	7.55–7.15 (m, 15H, aromatic-H) 6.9 (bs, 1H, NH)
11	4.90 (dd) J = 1.0 J = 2.5	5.62 (d) J = 1.0	6.44 (bs, 1H, NH)
12	4.37 (dd) J = 1.9 J = 2.2	3.75 (dt) J = 1.9 J = 6.6	6.12 (bs, 1H, NH), 1.83–1.26 (m, 6H, CH_2) 0.93 (t, 3H, CH_3)
13	4.42 (t) J = 2.1	3.89 (dt) J = 1.8 J = 6.6	6.05 (bs, 1H, NH), 6.06–5.55 (m, 1H, CH_2—CH=), 5.29–5.23 (m, 1H, 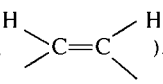), 5.16–5.04 (m, 1H, 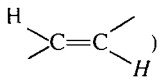) 2.54–2.36 (m, 2H, CH_2)

*Recorded at 80 MHz in $CDCl_3$ using tetramethylsilane as internal standard. The chemical shifts are recorded in δ (ppm) and the J's in Hz.

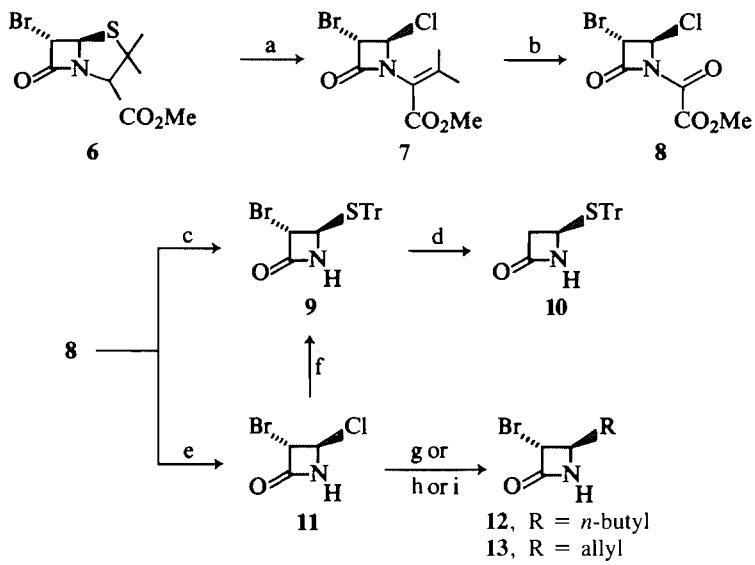

(a) Cl_2, CH_2Cl_2, −78° to 0°C, 1h; (b) O_3, CH_2Cl_2, −78°C, $(CH_3)_2S$; (c) TrSNa, MeOH, −15°C, 30 min; (d) Zn, MeOH, CH_3CO_2H, −15°C, 20 min; (e) 2,4-dinitrophenylhydrazine, THF, 18 h, 20°C; (f) TrSNa, i-PrOH/H_2O, 3:1, 0°C, 30 min; (g) Li Cu(n-butyl)$_2$, ether, THF, −78° to −40°C, 1.25 h; (h) Li Cu(CH_2CH=CH_2)$_2$, THF, ether, −78°C, 20 min; (i) Sn(CH_2CH=CH_2)$_4$, CH_2Cl_2 or THF, −78° to 20°C, 3.5 h.

SCHEME 2

air-tight container at low temperature (Dry Ice) for months without serious degradation.

Addition of azetidinone **11** to a solution of sodium triphenylmethyl mercaptide (1.5 equiv.) in isopropanol–water gave the chiral *trans* azetidinone **9** ($J_{3,4}$ = 2 Hz, mp 130–131°C, $[\alpha]_D^{25}$ +48.2° (c 0.305, MeOH)) in 25% yield. As observed for 4-acetoxazetidinone (10) and other *N*-unsubstituted azetidinones (14*a*), conversion of **11** to **9** presumably proceeds

Can. J. Chem. Downloaded from www.nrcresearchpress.com by 210.87.254.40 on 09/06/12
For personal use only.

through intermediate **4** (Y = Br). None of the possible *cis*-diastereomers of **9** could be detected in the reaction mixture, which indicated the high stereocontrol (10, 14) exerted by the 3-α-bromine atom on the nucleophilic attack at position 4. Removal of bromine with zinc in methanol afforded the pure (4*R*)-tritylthio-2-azetidinone (**10**) (mp 119−119.5°C, $[\alpha]_D^{25}$ +70.5° (*c* 0.112, MeOH)) in 76% yield. Racemic **10** has already been described as a key intermediate in the synthesis of 6-unsubstituted and substituted penems (8, 15).

Alternatively, the azetidinone **9** could be obtained in one step from **8** by using an excess (2 equiv., MeOH) of triphenylmethyl mercaptide. Presumably the nucleophile first cleaved the *N*-methoxalyl group to liberate **11** *in situ*, which then reacted with a second molecule of the nucleophile as described above. Thus addition of **8** to sodium triphenylmethyl mercaptide gave, after filtration on silica gel, the desired azetidinone **9** (yield 49%) which was identical with the sample described above.

Onoue *et al.* (16) have reported the coupling of allylcopper with *N*-substituted 4-chloroazetidinone to give mixtures of the corresponding 4-α and 4-β-allylazetidinones. Due to the facile formation of reactive intermediates such as **4**, *N*-unsubstituted azetidinones usually undergo nucleophilic substitution at position 4 more readily than their *N*-substituted counterparts. Accordingly, the coupling of cuprates with azetidinone **11** was attempted. Treatment of **11** with lithium di-*n*-butylcuprate (17) gave a 57% yield of the corresponding (4*R*)-*n*-butyl-(3*S*)-bromo-2-azetidinone (**12**, $J_{3,4}$ = 1.9 Hz).

Since 4-allylazetidinones have been reported as useful intermediates for carbapenems (16, 18), the coupling of lithium diallylcuprate (generated from tetraallyltin or triphenylallyltin) (19) with azetidinone **11** was carried out. In this way a good yield (75%) of the allylazetidinone **13** was obtained, with the desired *trans* diastereomer as the major component (95:5, *trans*/*cis*, estimated by ^{1}Hmr). The pure *trans* isomer **13** ($J_{3,4}$ = 1.8 Hz $[\alpha]_D^{25}$ +38.6° (*c* 0.78, MeOH)) could be isolated by column chromatography (silica gel, 2−8% ether/CH_2Cl_2). Since tin derivatives are reported to react with acid chlorides (20), it was speculated that azetidinone **11**, via **4** (Y = Br), might react with tetraallyltin directly. Indeed, treatment of **11** with tetraallyltin in CH_2Cl_2 also gave a high yield (86%) of **13** as a mixture of *trans* (82%) and *cis* (18%) diastereomers.[7] This reaction was also found to be solvent dependent, with the ratio being greatly improved in favor of the *trans* isomer **13** (*trans*/*cis*, 92.5:7.5)[7] when THF was used as solvent. To our knowledge, this is the first report of a C4—C azetidinone coupling reaction of this type.

In summary, (3*S*)-bromo-(4*R*)-chloro-2-azetidinone (**11**) was prepared in high overall yield (53%) from 6-α-bromopenicillanic acid. Azetidinones **11** and **8** are key intermediates for the preparation of chiral penem and carbapenem precursors (**10**, **13**). The preparation of allylazetidinone **13** was greatly improved by using tetraallyltin instead of allylcuprate.

Acknowledgements

We would like to thank Drs. Y. Ueda and E. Ruediger for helpful discussion during the preparation of the manuscript. The technical assistance of R. Droghini, J. Lajeunesse, and M. Endo is gratefully acknowledged. We would also like to thank Bristol-Myers, Syracuse, for the supply of 6-α-bromopenicillanic acid.

[7]Determined by hplc on a Waters Associates PrePak-500 silica column.

1. A. MARTEL, J. COLLERETTE, J. BANVILLE, J. P. DARIS, P. LAPOINTE, B. BELLEAU, and M. MÉNARD. Can. J. Chem. **61**, 613 (1983).
2. (*a*) H. KROPP, J. S. KAHAN, J. SUNDELOF, G. DARLAND, and J. BIRNBAUM. Abstract 228, 16th Intersci. Conf. Antimicr. Agents and Chemotherapy, Chicago (1976); (*b*) G. ALBERS-SCHONBERG, B. H. ARISON, O. D. HENSENS, J. HIRSHFIELD, K. HOOGSTEEN, E. A. KACZKA, R. E. RHODES, J. S. KAHAN, F. M. KAHAN, R. W. RATCLIFFE, E. WALTON, L. J. RUSWINKLE, R. B. MORIN, and B. G. CHRISTENSEN. J. Am. Chem. Soc. **100**, 6491 (1978).
3. R. B. WOODWARD. *In* Recent advances in the chemistry of β-lactam antibiotics. *Edited by* J. Elks. Chem. Soc. Spec. Publ. No. 28. 1977. Chapt. 18.
4. R. D. G. COOPER. *In* Topics in antibiotic chemistry. Vol. 3. Part B. *Edited by* P. G. Sammes. Ellis Horwood Publishers, Chichester. 1980; F. A. JUNG, R. PILGREM, J. P. POYSER, and P. J. SIRET. *In* Topics in antibiotic chemistry. Vol. 4.
5. (*a*) S. KUKOLJA. J. Am. Chem. Soc. **93**, 6267 (1971); (*b*) **93**, 6269 (1971).
6. S. WOLFE, W. S. LEE, G. KANNENGIESSER, and J.-B. DUCEP. Can. J. Chem. **50**, 2894 (1972).
7. J. C. SHEEHAN, D. BEN-ISHAI, and J. U. PIER. J. Am. Chem. Soc. **95**, 3064 (1973).
8. (*a*) M. MÉNARD and G. CARON (Bristol-Myers Co.). U.S. Patent No. 4,155,912 (1979); (*b*) Y. UEDA (Bristol-Myers Co.). U.S. Patent No. 4,182,711 (1980); (*c*) M. MÉNARD and A. MARTEL (Bristol-Myers Co.). U.S. Patent No. 4,262,437 (1981); (*d*) M. MÉNARD and A. MARTEL (Bristol-Myers Co.). U.S. Patent No. 4,282,150 (1981).
9. (*a*) G. CIGNARELLA, G. PIFFERI, and E. TESTA. J. Org. Chem. **27**, 2668 (1962); (*b*) J. P. CLAYTON. J. Chem. Soc. (C) 2123 (1969).
10. K. CLAUSS, D. GRIMM, and G. PROSSEL. Justus Liebigs Ann. Chem. 539 (1974).
11. P. V. DEMARCO and R. NAGARAJAN. *In* Cephalosporins and penicillins: chemistry and biology. *Edited by* E. H. Flynn. Academic Press, New York. 1972. pp. 330−340.
12. R. D. G. COOPER and F. L. JOSÉ. J. Am. Chem. Soc. **94**, 1021 (1972).
13. J. J. PAPAS and W. P. KEAVENEY. Tetrahedron Lett. 4273 (1966).
14. (*a*) J. C. SHEEHAN. Ger. Pat. No. 1,943,161 (1971); Chem. Abstr. **75**, 49103 (1973); (*b*) M. D. BACHI and A. GROSS. J. Chem. Soc. Chem. Commun. 959 (1981).
15. J. BANVILLE, B. BELLEAU, P. DEXTRAZE, J. L. DOUGLAS, F. LEITNER, A. MARTEL, M. MÉNARD, R. SAINTONGE, and Y. UEDA. ACS Annual Meeting, New York City. Aug. 23−28, 1981.
16. H. ONOUE, M. NARISADA, S. UYAO, H. MATSUMURA, K. OAKADA, T. YANO, and W. NAGATA. Tetrahedron Lett. 3867 (1979).
17. G. H. POSNER. *In* Organic reactions. *Edited by* W. G. Dauben *et al.* John Wiley & Sons Inc., New York. 1975. pp. 253−400.
18. A. J. G. BAXTER, K. H. DICKINSON, P. M. ROBERTS, T. C. SMALE, and R. SOUTHGATE. J. Chem. Soc. Chem. Commun. 236 (1979).
19. D. SEYFERTH and M. A. WEINER. J. Org. Chem. **26**, 4797 (1961).
20. G. HIMBERT and L. HENN. Tetrahedron Lett. 2637 (1981).

Thermodynamics of H^+/Na^+ exchange on amorphous zirconium phosphate in mixed solvents

N. Z. MISAK AND E. M. MIKHAIL

Nuclear Chemistry Department, Atomic Energy Establishment, Cairo, Egypt

Received June 9, 1982[1]

N. Z. MISAK and E. M. MIKHAIL. Can. J. Chem. **61**, 1902 (1983).

ΔG^0 of the H^+/Na^+ exchange on zirconium phosphate is positive and changes a little on addition of up to 90% methanol. On addition of isopropanol and acetone, ΔG^0 becomes less positive. Both ΔH^0 and ΔS^0 become progressively less negative on adding increasing amounts of the organic solvents. The decrease of ΔG^0 on addition of isopropanol and acetone is at least partly due to effects on the ion–solvent interactions in the liquid phase. In the case of methanol, these effects lead to a decrease of ΔG^0 but the decrease is mostly balanced by an increase due to effects on the interactions in solid phase. The latter effects involve an increase of enthalpy and a decrease of entropy, these changes are larger the higher the methanol content. Possible reasons for these enthalpy and entropy changes are discussed.

N. Z. MISAK et E. M. MIKHAIL. Can. J. Chem. **61**, 1902 (1983).

Le ΔG^0 d'échange de H^+/Na^+ sur le phosphate de zirconium est positif et varie légèrement lorsqu'on ajoute du méthanol à une concentration allant jusqu'à 90%. L'addition d'isopropanol et d'acétone rend le ΔG^0 moins positif. Les ΔH^0 et le ΔS^0 deviennent progressivement moins négatifs lorsqu'on ajoute des quantités croissantes de solvants organiques. La diminution de ΔG^0 lors de l'addition d'isopropanol et d'acétone est due partiellement aux effets des interactions ion–solvant dans la phase liquide. Dans le cas du méthanol, ces effets provoquent une diminution de ΔG^0, mais la diminution est contre-balancée par une augmentation due aux effets des interactions dans la phase solide. Les derniers effets impliquent une augmentation d'enthalpie et une diminution d'entropie qui sont plus fortes lorsque la teneur en méthanol est très élevée. On discute des causes possibles de ces variations d'enthalpie et d'entropie.

[Traduit par le journal]

Introduction

In a previous paper (1), we reported on tracer equilibria, capacity and kinetics of exchange on amorphous zirconium phosphate (ZrP) in mixed solvents. It was established that in mixed solvents of up to 90% methanol and acetone and 60% isopropanol, Na^+ is sorbed by ZrP by an ion exchange mechanism. With the exception of 90% methanol, the Na-capacity increases with the increase of the concentration of added organic solvent. The diffusion of Na^+ in ZrP is slackened in the presence of methanol and acetone. These results were tentatively discussed in terms of the possible effects of organic solvents on the hydration and solvation of Na^+, the basicity of the organic solvents, and the decrease of the dielectric constant inside the exchanger.

The present paper reports on the thermodynamics of H^+/Na^+ exchange on amorphous ZrP in solutions containing up to 90% methanol and 60% isopropanol and acetone. The study of the thermodynamics of ion exchange in mixed solvents is important in revealing, through the examination of the role of solvent, the various phenomena underlying the selectivity behaviour of the exchanger. Amorphous ZrP was used because ion exchange on the crystalline material has been shown to be thermodynamically irreversible (2–4). On the crystalline material, the isotherms for the forward and reverse processes do not coincide and considerable hysteresis is observed.

Experimental

Zirconium phosphate

ZrP was prepared by addition at about 60°C of equal volumes of 0.8 *M* zirconyl chloride and 2 *M* H_3PO_4 to the same volume of distilled water. After washing with water till a pH of about 4 of the washings, the solid was air-dried at 50°C, soaked in 1 *M* HCl, washed with distilled water, and redried at 50°C. It was then sieved to different sizes and stored over saturated NH_4Cl in a nitrogen atmosphere. The prepared exchanger is a partially hydrolysed $Zr(HPO_4)_2$ having a PO_4/Zr ratio of 1.33 and a weight loss at 1000°C of 24.8%, which corresponds to the empirical formula $ZrO_2.0.67\ P_2O_5.4H_2O$. The Na-capacity of the exchanger in water, 30% methanol, 60% methanol, 90% methanol, 30% isopropanol, 60% isopropanol, 30% acetone, and 60% acetone (weight percents of the organic solvents), determined by equilibration with 0.1 *m* NaCl solutions tagged with ^{22}Na, is 1.35, 1.51, 1.58, 1.21, 1.46, 1.72, 1.61, and 1.72 mequiv./g, respectively (1). These values are practically independent of temperature in the 25–65°C range studied.

Ion exchange isotherms

Precalculated amounts of standard NaCl and HCl, and of water, organic solvent, and tracer ^{22}Na were added to weighed amounts of the H-form of ZrP. The concentration of NaCl + HCl was kept constant at a total molality of 0.1 and the initial concentration of Na^+ in solution was varied from 0.01 to 0.1 *m*. All samples were shaken for 48 h (sufficient to attain equilibrium) in a shaker thermostat adjusted at 25, 45, and 65 ± 0.5°C. The solution was separated from the solid and analysed for Na^+ and Cl^- ions. The solid was washed with a small amount of alcohol and analysed for Na^+. In all the media, Cl^- was found to retain its initial concentration, indicating the absence of electrolyte invasion and that only ion exchange took place. The reversibility of the isotherms was tested and proved in all media at 25°C by making isotherms in the same conditions but starting with the Na-form of the exchanger and excluding ^{22}Na. The Na^+ ion concentration was also determined in both solution and solid. Isopropanol and acetone concentrations higher than 60% were not used due to the precipitation of NaCl.

Analyses

In the forward isotherms (starting with the H-form of ZrP), Na^+ was determined by γ-counting of the solution and the solid, using a NaI scintillation head connected to a scaler of the type Nuclear Chicago, Model 186A, USA. The γ-activity of the solid was measured either directly or after elution with 1 *N* HCl. In the reverse isotherms (starting with the Na-form of ZrP), the Na^+ content of the solution and of the solid, after elution with HCl, was determined by atomic absorption, using a Pye Unicam SP 90A atomic absorption spectrophotometer.

[1]Revision received January 4, 1983.

Can. J. Chem. Downloaded from www.nrcresearchpress.com by 210.87.254.105 on 09/06/12
For personal use only.

Can. J. Chem. Downloaded from www.nrcresearchpress.com by 210.87.254.105 on 09/06/12
For personal use only.

Results and discussion

The selectivity coefficient K is given by the equation:

$$[1] \quad K = \frac{q/q_0(1 - m/m_0)}{m/m_0(1 - q/q_0)}$$

q_0 is the Na-capacity in the respective medium in mequiv./g, m_0 is the total molality of solution and is constant and equal to 0.1. q is the concentration at equilibrium of Na^+ in ZrP in mequiv./g and m is its respective molality in solution. q and m are obtained from the analysis of the solid and weighed aliquots of the solution. Higher values of q/q_0 are obtained by increasing the relative concentration of Na^+ in solution, and the values of K at the different values of q/q_0 are calculated by the use of eq. [1] and the respective values of m/m_0. The ion exchange isotherms (not given here to save space) which are drawn as q/q_0 versus m/m_0 have shown that the forward and reverse exchanges coincide.

The corrected selectivity coefficient K' is given by:

$$[2] \quad K' = K\frac{\gamma_{\pm}^2(\mathrm{HCl})}{\gamma_{\pm}^2(\mathrm{NaCl})}$$

where $\gamma_{\pm}$ is the mean activity coefficient in the respective medium. Once K' is known, the thermodynamic equilibrium constant K_a can be obtained from the well-known Gaines–Thomas equation (5). This equation applies at total molalities ≤ 0.1 for both aqueous and mixed media (6, 7) provided that the solvent composition remains the same (7), which is the case with ZrP displaying no swelling (1). The equation has the following form:

$$[3] \quad \log K_a = \int_0^1 \log K' \mathrm{d}(q/q_0)$$

With regard to the values of $\gamma_{\pm}^2(\mathrm{HCl})/\gamma_{\pm}^2(\mathrm{NaCl})$, this ratio can be considered equal to unity in the aqueous medium (8). In the mixed solvents, many authors assume this ratio to be equal to unity (7, 9–11). This is based on Harned's rule (12) stating that the ratio of the mean molal activity coefficients of two electrolytes at a given concentration and temperature is independent of solvent composition. However, the examination of many data in the literature (13–15) shows that Harned's rule is not always applicable. The above mentioned ratio can be far from unity and is actually dependent on solvent composition.

Data on the activity coefficients of HCl and NaCl in mixed solvents are available only in methanolic solutions (13–18). We have plotted $\gamma_{\pm}(\mathrm{HCl})$ and $\gamma_{\pm}(\mathrm{NaCl})$ against the weight percent of methanol and from these plots we obtained the required values at 30, 60, and 90% methanol. As to the other mixed solvent solutions, we used the following approximate equation (8) to obtain the values of $\gamma_{\pm}(\mathrm{HCl})$ (or $\gamma_{\pm}(\mathrm{NaCl})$) in 30 or 60% isopropanol and acetone from the values of $\gamma_{\pm}(\mathrm{HCl})$ (or $\gamma_{\pm}(\mathrm{NaCl})$) in 30% or 60% methanol:

$$[4] \quad \frac{\log \gamma_{\pm}}{\log \gamma'_{\pm}} = \left(\frac{D'}{D}\right)^{3/2}$$

$\gamma_{\pm}$ and $\gamma'_{\pm}$ are the mean activity coefficients in solvents of dielectric constants D and D', respectively. The application of eq. [4] to obtain activity coefficient values for HCl in the various mixed media from values in aqueous methanol gave figures which are in reasonable agreement with the experimental figures given in the literature for these systems (13, 19). Agreement to better than 10% for 60% organic solvent contents and 5% for 30% organic solvent contents was obtained. Unfortunately, there are no experimental values for NaCl in solvents other than methanol, but it may be anticipated that the agreement will be as good.

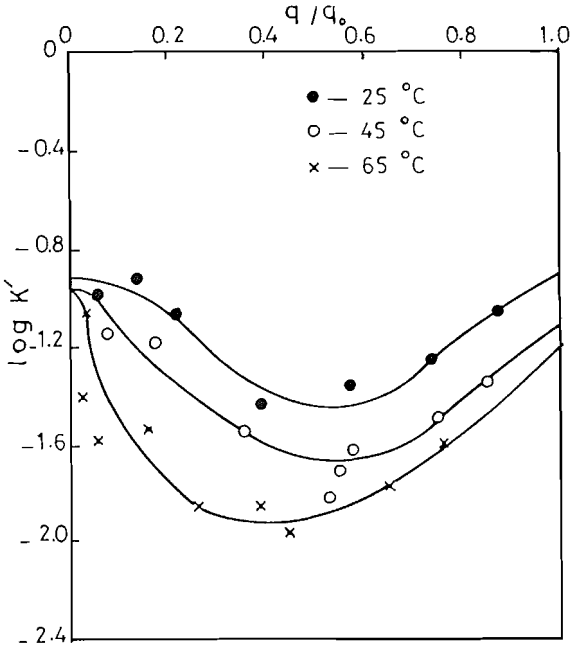

FIG. 1. Variation of log K' with q/q_0 for exchange from the aqueous medium at different temperatures.

The mean activity coefficients of HCl and NaCl in presence of each other are obtained from the values for the single electrolytes by the use of the Glueckauf equation (20). The calculated values of $\gamma_{\pm}(\mathrm{HCl})/\gamma_{\pm}(\mathrm{NaCl})$ were found to be constant regardless of the relative amounts of the two electrolytes in solution. The values of $\gamma_{\pm}^2(\mathrm{HCl})/\gamma_{\pm}^2(\mathrm{NaCl})$, necessary for the calculation of K' (eq. [2]), are 1.06, 1.12, and 1.49 in 30%, 60%, and 90% methanol, respectively, 1.08 and 1.19 in 30% and 60% isopropanol, respectively, and 1.06 and 1.14 in 30% and 60% acetone, respectively. It is seen, therefore, that this ratio cannot be put equal to unity at the relatively high organic solvent concentrations.

The variation of log K' with q/q_0 is exemplified by Fig. 1 for the aqueous medium, Fig. 2 for 60% methanol, and Fig. 3 for 60% isopropanol. The figures not given here are similar in shape to those for the aqueous medium. Considering this variation, it can be said that except in 60% isopropanol, log K' first decreases with increase of loading and then increases with a minimum at values of q/q_0 around 0.5. In 60% isopropanol, log K' first decreases with loading and then tends to be more or less constant. Such a complex nature of the log K' – loading plots may be related to the proportions and properties of energetically different exchange sites in the exchanger (21).

Having obtained the values of K_a by integration under the curves in the log K' – q/q_0 plots, standard thermodynamic equations are used for the calculation of ΔG^0, ΔH^0, and ΔS^0. ΔH^0 is calculated from the slopes of the straight lines given in Fig. 4.

The various thermodynamic data are given in Table I for the different conditions. ΔS^0 is split in the case of the aqueous medium into two terms (22), one belonging to the solution phase, ΔS^h, and the other belonging to the exchanger phase, ΔS^e. ΔS^h is equal to the difference in the hydration entropies of the two ions (H^+ and Na^+) and is obtained from the data of Rosseinsky (23). ΔS^e is obtained by subtraction of ΔS^h from

Can. J. Chem. Downloaded from www.nrcresearchpress.com by 210.87.254.105 on 09/06/12
For personal use only.

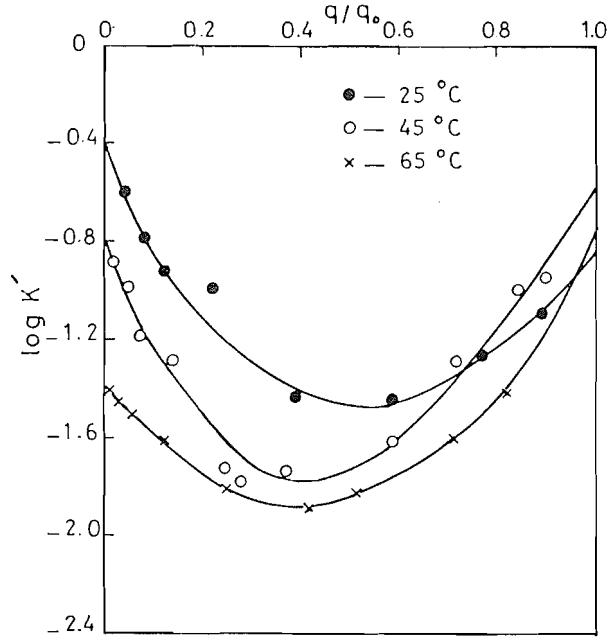

FIG. 2. Variation of log K' with q/q_0 for exchange from 60% methanol at different temperatures.

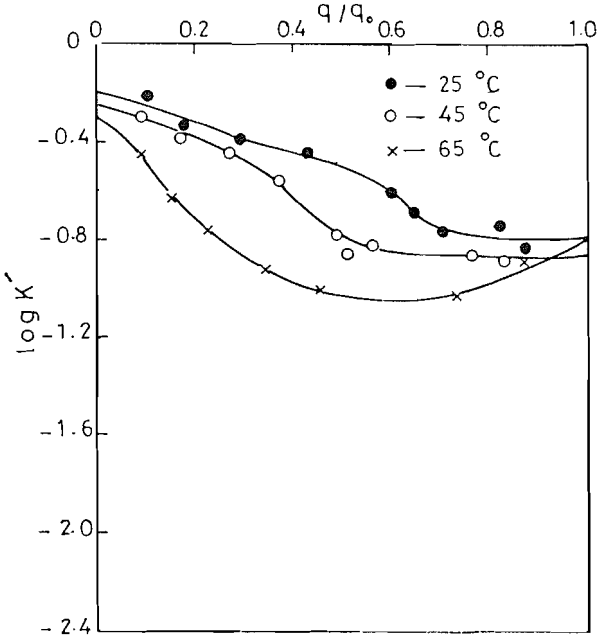

FIG. 3. Variation of log K' with q/q_0 for exchange from 60% isopropanol at different temperatures.

ΔS^0. The estimated accuracy for the ΔG^0 values is generally ± 0.1 kJ/mol, for the ΔH^0 values, ± 1.0 kJ/mol, and for the ΔS^0 values, ± 4 J/mol deg.

Table 1 shows that in all media, H^+/Na^+ exchange is an entropy-directed reaction. In the aqueous medium, this is in qualitative agreement with previous studies (24, 25). In this medium, $\overline{\Delta S}^e$ is negative, showing a decrease of entropy when H^+ in ZrP is replaced by Na^+. Since the alkali ions are retained in a hydrated state inside ZrP (26), such an entropy decrease is presumably due to a water transfer from the aqueous solution to the solid phase. Such a transfer results in the decrease of the entropy of the whole system because the water molecules have less degrees of freedom in the solid phase than in the liquid phase (22). In the methanolic solutions, Table 1 shows that ΔG^0 is only little changed, while in the other media ΔG^0 decreases (becomes less positive) in the presence of the organic solvents. The decrease is progressive in the case of isopropanol while a small decrease is observed when going from 30 to 60% acetone. ΔH^0 and ΔS^0 increase (become less negative) with increasing additions of the organic solvents. However, in the methanolic solutions, this increase is appreciable only in 90% methanol. In acetone, little change is observed, as in the case of ΔG^0, on going from 30 to 60% of the organic solvent.

Changes in the values of ΔG^0, ΔH^0, and ΔS^0, obtained in the aqueous medium, due to addition of organic solvents should be sought in the effect of this addition on the ion–solvent interactions in solution and on the various interactions in the solid exchanger. Effects on ion–solvent interactions are related to the thermodynamics of transfer of the exchanging ions from water to the respective mixed-solvent solution, while the effects on the interactions in the solid phase are related to the thermodynamics of similar transfer of the Na- and H-forms of ZrP. The latter transfer depends on the solvent composition of liquid and solid phases and on the extent of solvent imbibition by the solid (6, 7, 27). Changes in ΔG^0, ΔH^0, and ΔS^0 due to effects on the interactions in the solid phase may be obtained by subtraction of changes due to effects on ion–solvent interactions (which may be estimated in many cases) from the values of ΔG^0, ΔH^0, and ΔS^0, obtained experimentally.

With regard to ΔG^0, it is seen from the data given in the literature and involving the free energies of transfer ΔG_t^0 or the medium effect ${}_m\gamma$ ($\Delta G_t^0 = RT \ln {}_m\gamma$) for H^+ and the alkali ions (28–37) that for transfer from water to mixtures of water and methanol, ethanol, or acetone, ΔG_t^0 for H^+ is more negative than for any of the alkali ions. Besides, this trend is generally more profound the higher the crystallographic radius of the alkali ion and the higher the organic solvent content. Changes on addition of organic solvents in the value of ΔG^0, obtained in the aqueous medium, due to effects on ion–solvent interactions in the liquid phase may be put equal to $\Delta G_t^0(H^+) - \Delta G_t^0(Na^+)$ (7, 27). Hence, it can be deduced that the addition of methanol, acetone, and presumably also isopropanol should lead to a lower ΔG^0, i.e., to the increase of the selectivity constant.

The decrease (Table 1) of ΔG^0 on addition of isopropanol and acetone should be therefore, at least partly, attributed to effects on ion–solvent interactions in the liquid phase. The very little changes in the presence of methanol mean that the effects on interactions in the solid exchanger mostly balance the effects in the liquid phase. Quantitative evaluation is possible only with methanol, since the transfer free energy data in acetone (37) do not include the Na^+ ion and there are no data at all in isopropanol. Even in the case of methanol, a strictly quantitative evaluation is possible only for the interrelation of the results in 30% and 60% methanol. This is due to the fact that at these methanol concentrations, the Na-capacity is almost the same (see Experimental). Hence the standard states of the solid phase, involving the pure cationic form in equilibrium with an infinitely dilute solution of the respective electrolyte in the respective solvent (5), can be considered as consistent.

One can write the following equality in the case of ion–solvent interaction effects in the liquid-phase being the only factor responsible for change of ΔG^0 on increase of the methanol content from 30 to 60%:

[5] $\Delta G^0(60\%) = \Delta G^0(30\%) + \Delta G_t^0(H^+) - \Delta G_t^0(Na^+)$

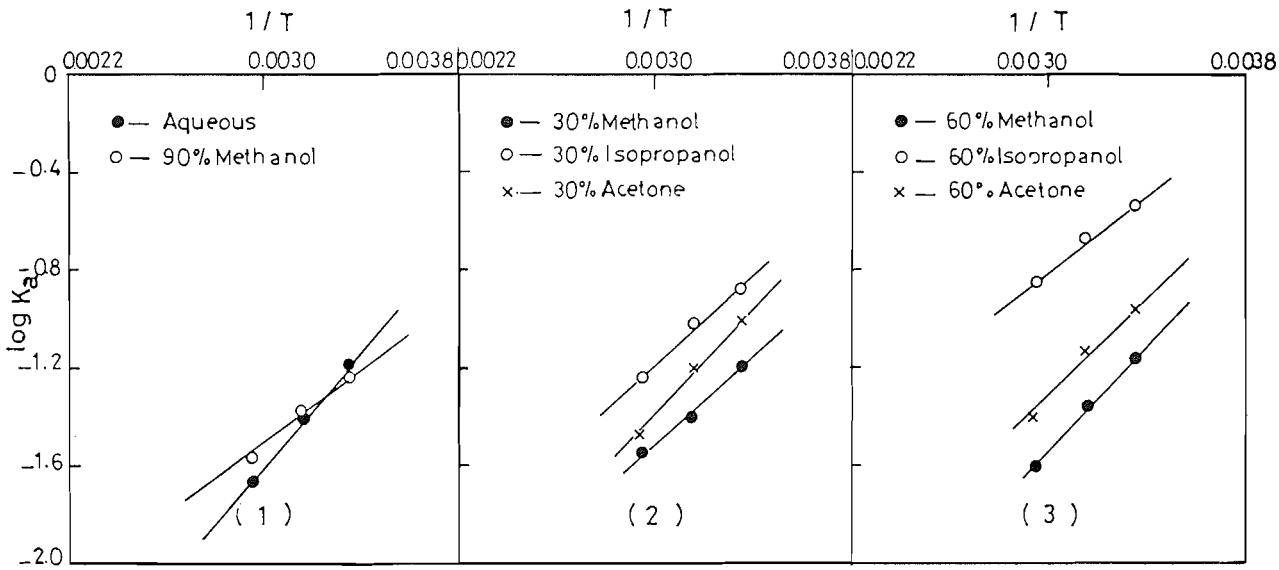

FIG. 4. Variation of log K_a with $1/T$ for exchange from: (*1*) aqueous and 90% methanol solutions; (*2*) 30% methanol, isopropanol, and acetone; and (*3*) 60% methanol, isopropanol, and acetone.

TABLE 1. Thermodynamic data for H^+/Na^+ exchange at 25°C on ZrP in aqueous and mixed-solvent solutions

Medium	ΔG^0 (kJ/mol)	ΔH^0 (kJ/mol)	ΔS^0 (J/mol deg)	ΔS^h	$\overline{\Delta S^e}$
Aqueous	6.91	−8.30	−51.1	−21.4	−29.7
30%Methanol	6.96	−8.17	−50.8	—	—
60%Methanol	6.70	−7.75	−48.5	—	—
90%Methanol	7.12	−5.24	−41.5	—	—
30% Isopropanol	5.07	−5.87	−36.7	—	—
60% Isopropanol	3.10	−5.03	−27.3	—	—
30% Acetone	5.87	−7.21	−43.9	—	—
60%Acetone	5.53	−6.83	−41.5	—	—

$\Delta G^0(30\%)$ and $\Delta G^0(60\%)$ are the free energies of exchange obtained experimentally in 30 and 60% methanol, respectively. $\Delta G_t^0(H^+)$ and $\Delta G_t^0(Na^+)$ are the free energies of transfer of H^+ and Na^+ ions from 30 to 60% methanol. Using for the calculation of $\Delta G_t^0(H^+) - \Delta G_t^0(Na^+)$ the most recent and accurate data of Bax *et al.* (35), the value −3.52 kJ/mol is obtained. Thus, $\Delta G^0(60\%)$ should be less than $\Delta G^0(30\%)$ by 3.52 kJ/mol if ion–solvent interactions are the only factor. The fact that $\Delta G^0(60\%)$ is almost equal to $\Delta G^0(30\%)$ (Table 1) shows that major changes in ZrP occur on the increase of methanol concentration from 30 to 60%. These changes involve an increase of ΔG^0 by about 3.52 kJ/mol on going from 30 to 60% methanol, probably due to more sorption of methanol by ZrP.

The evaluation of the changes in ΔH^0 and ΔS^0, occurring on addition of organic solvents, due to solid phase interactions is of interest. It may allow to make a semiquantitative judgement about the changes occurring in the solid phase and leading to changes in ΔG^0, and consequently to a modification of the selectivity of the exchanger in presence of organic solvents. However, such an evaluation is possible only in the case of methanol where values for ΔH_t^0 and ΔG_t^0 of both HCl and NaCl are available (29, 32). From these values ΔS_t^0 is obtained and the changes in ΔH^0 and ΔS^0 on addition of the organic solvent due to effects on ion–solvent interactions in solution can be taken equal to $\Delta H_t^0(HCl) - \Delta H_t^0(NaCl)$ and $\Delta S_t^0(HCl) - \Delta S_t^0(NaCl)$. From the values obtained either directly or by interpolation, it can be readily deduced that ΔH^0 may decrease due to these effects by values of 84 and 335 J/mol on addition of 30 and 60% methanol, respectively. At 90% methanol, an increase of 84 J/mol is expected. With regard to ΔS^0, increases of 11.3, 26, and 36.9 J/mol deg at 30, 60, and 90% methanol, respectively, are expected due to these effects. From these values and the differences between the values of ΔH^0 and ΔS^0 in the aqueous and mixed-solvent solutions (representing overall changes due to ion–solvent and solid phase interactions), the effects of methanol addition on solid phase interactions are evaluated. These effects give rise to an increase in ΔH^0 of 214, 885, and 2976 J/mol at 30, 60, and 90% methanol, respectively, and a decrease in ΔS^0 of 11, 23.4, and 27.3 J/mol deg, respectively, at these same methanol concentrations. Thus, the rather significant increase of ΔH^0 on addition of 90% methanol (Table 1) comes almost exclusively from the effects of this addition on the solid phase. The increase of ΔS^0 is the outcome of effects on the liquid phase outweighing those on the solid phase.

The expected major effects of addition of methanol on the solid phase are connected with sorption–desorption processes of the two components of solvent (H_2O and CH_3OH) and dehydration of ingoing Na^+ with its subsequent stronger, relative to the aqueous medium, interaction with the exchange sites.

Can. J. Chem. Downloaded from www.nrcresearchpress.com by 210.87.254.105 on 09/06/12
For personal use only.

Methanol has been reported to be chemisorbed by ZrP and an indication has been found for an esterification reaction between the alcohol and the P—OH groups of ZrP (38). Water in ZrP is either interstitially sorbed water or water weakly sorbed by hydrogen bonds to the P—OH of ZrP (39, 40). The dehydration of Na^+ ions with their subsequent stronger interaction with the exchange sites is expected to give rise to positive enthalpy and entropy changes (41, 42). It seems therefore possible that the decrease of entropy on addition of methanol due to effects on the solid is mainly connected with the chemisorption of methanol. The increase of enthalpy is probably connected with the sorption of Na^+ in a less hydrated state from the mixed solvent than from the aqueous medium. This seems to be particularly true at relatively high methanol concentrations where the increase of enthalpy is rather significant.

1. N. Z. MISAK and E. M. MIKHAIL. Radiochim. Acta, **30**, 111 (1982).
2. G. ALBERTI, S. ALLULLI, V. COSTANTINO, M. A. MASSUCCI, and E. TORRACA. Society of Chemical Industry. London, 1970. p. 318.
3. A. CLEARFIELD, A. OSKARSSON, and O. OSKARSSON. Ion Exch. Membr. **1**, 91 (1972).
4. G. ALBERTI, V. COSTANTINO, and J. S. GILL. J. Inorg. Nucl. Chem. **38**, 1733 (1976).
5. G. L. GAINES and H. C. THOMAS. J. Chem. Phys. **21**, 714 (1953).
6. A. R. GUPTA. J. Phys. Chem. **75**, 1152 (1971).
7. A. M. EL-PRINCE and K. L. BABCOCK. J. Phys. Chem. **79**, 1550 (1975).
8. H. S. HARNED and B. B. OWEN. The physical chemistry of electrolyte solutions. Reinhold Pub. Co., New York. 1958.
9. A. SCHWARZ. J. Phys. Chem. **72**, 789 (1968).
10. Z. DIZDAR. J. Inorg. Nucl. Chem. **34**, 1069 (1972).
11. K. A. BONI and H. A. STROBLE. Z. Phys. Chem. Neue Folge, **87**, 169 (1973).
12. H. S. HARNED. J. Phys. Chem. **66**, 589 (1962).
13. N. A. IZMAILOV. Elektrokhimiya Rastvorov (Electrochemistry of solutions). Izd. Khim. Moscow. 1976.
14. G. AKERLOV. J. Am. Chem. Soc. **59**, 1916 (1937).
15. S. MINE and J. JASTRZEBSKA. Rocz. Chem. **42**, 719 (1968).
16. Y. MARCUS and A. S. KERTES. Ion exchange and solvent extraction of metal complexes. Wiley-Interscience, New York. 1969.
17. K. JACKOWSKA. Rocz. Chem. **45**, 87 (1971).
18. S. MINE and J. JASTRZEBSKA. Rocz. Chem. **47**, 1775 (1973).
19. R. E. JERVIS and K. NEELOKANTAN. J. Inorg. Nucl. Chem. **37**, 531 (1975).
20. E. GLUECKAUF. Nature, **163**, 414 (1949).
21. R. M. BARRER and J. KLINOWSKI. Trans. Faraday Soc. **1**, 73 (1972).
22. H. S. SHERRY. Ion exchange. *Edited by* J. A. Marinsky. Vol. 2. Dekker, New York. 1969. Chapt. 3.
23. D. R. ROSSEINSKY. Chem. Rev. **65**, 467 (1965).
24. E. M. LARSEN and D. R. VISSERS. J. Phys. Chem. **64**, 1732 (1960).
25. V. PEKAREK and V. VESELY. Talanta, **19**, 219 (1972).
26. G. H. NANCOLLAS and B. V. TILAK. J. Inorg. Nucl. Chem. **31**, 3642 (1969).
27. D. NANDAN and A. R. GUPTA. J. Phys. Chem. **79**, 180 (1975).
28. D. FEAKINS and P. WATSON. J. Chem. Soc. 4734 (1963).
29. D. FEAKINS. Physico-chemical processes in mixed aqueous solvents. *Edited by* F. Franks. Heinemann Educational Books Ltd., London. 1967. p. 71.
30. B. CASE and R. PARSOUS. Trans. Faraday Soc. **63**, 1224 (1967).
31. A. J. DILL, L. M. ITZKOWITZ, and O. POPOVYCH. J. Phys. Chem. **72**, 4580 (1968).
32. A. L. ANDREWS, H. P. BENNETTO, D. FEAKINS, K. G. LAWRENCE, and R. P. T. TOMKINS. J. Chem. Soc. A, 1486 (1968).
33. O. POPOVYCH. Crit. Rev. Anal. Chem. **1**, 73 (1970).
34. O. POPOVYCH, A. GIBOFSKY, and D. H. BERNE. Anal. Chem. **44**, 811 (1972).
35. D. BAX, C. L. DELIGNY, and M. ALFENAAR. Rec. Trav. Chim. **91**, 452 (1972).
36. D. BAX, C. L. DELIGNY, and A. G. REMIJNSE. Rec. Trav. Chim. **91**, 966 (1972).
37. D. BAX, C. L. DELIGNY, and A. G. REMIJNSE. Rec. Trav. Chim. **91**, 1225 (1972).
38. T. A. KARASEVA, Z. D. SKRIPNIK, and V. V. STRELKO. Ukr. Khim. Zhur. No. 5, 479 (1976).
39. A. CLEARFIELD and J. STYNES. J. Inorg. Nucl. Chem. **26**, 117 (1964).
40. A. CLEARFIELD and G. D. SMITH. Inorg. Chem. **8**, 431 (1969).
41. W. J. HAMER. Structure of electrolyte solutions. John Wiley and Sons Inc., New York. 1959.
42. G. H. NANCOLLAS. Interactions in electrolyte solutions. Elsevier, Amsterdam. 1966.

Can. J. Chem. Downloaded from www.nrcresearchpress.com by 210.87.254.105 on 09/06/12
For personal use only.

The existence of binuclear species in the nickel(II)/azide system

M. E. V. SUÁREZ, E. A. NEVES, AND R. TOKORO

Instituto de Química da Universidade de São Paulo, Cx. Postal 20780, São Paulo, Brazil

Received July 5, 1982[1]

M. E. V. SUÁREZ, E. A. NEVES, and R. TOKORO. Can. J. Chem. **61**, 1907 (1983).

The binuclear species $Ni_2N_3^{3+}$ has been found by potentiometric and spectrophotometric measurements to coexist with the monoazide species NiN_3^+ at $C_{Ni(II)} \gg C_{N_3^-}$ conditions. The formation constants β_{11} and β_{21} are 7.5 M^{-1} and 4.3 M^{-2} respectively, as determined potentiometrically at 25.0°C, with a glass electrode at an ionic strength of 2.00 M held with $NaClO_4$. The molar absorptivities ϵ_{11} and ϵ_{21} have been determined in the 302−290 nm wavelength range.

M. E. V. SUÁREZ, E. A. NEVES et R. TOKORO. Can. J. Chem. **61**, 1907 (1983).

Les mesures potentiométriques et spectrophotométriques ont permis de découvrir l'existence d'espèce binucléaires du type $Ni_2N_3^{3+}$ à côté du monoazothydrure NiN_3^+ dans des conditions où $C_{Ni(II)} \gg C_{N_3^-}$. Par potentiométrie à 25°C en utilisant une électrode de verre avec une force ionique de 2,0 M dans du $NaClO_4$, on trouve des constantes de formation β_{11} et β_{21} de 7,5 M^{-1} et de 4,3 M^{-2} respectivement. On a déterminé les absortivités ϵ_{11} et ϵ_{21} dans l'intervalle de longueur d'onde de 302−290 nm.

[Traduit par le journal

Can. J. Chem. Downloaded from www.nrcresearchpress.com by 210.87.254.6 on 09/06/12
For personal use only.

Knowledge of the overall stepwise formation constants of the nickel(II)/azide complexes is desirable in order to better interpret the electrochemical behaviour of nickel(II) in an azide supporting electrolyte without hydrazoic acid (1, 2) or in the N_3^-/HN_3 buffer, where two catalytic waves occur (3). An earlier equilibrium study of the cobalt(II)/azide/hydrazoic acid system (4) was very helpful in the interpretation of these catalytic waves (5), which present many different characteristics when compared with the analogous nickel(II) system. There have been reports of spectrophotometric studies of the monoazide specie (1, 6, 7), NiN_3^+, and of potentiometric studies of the monoazide and successive complexes of up to three ligands (8, 9), $Ni(N_3)_3^-$.

There is disagreement as to the magnitude of the β_1 formation constant. In one of these studies, a dispersion of the $\bar{n}$ data (average ligand number) with the free ligand concentration can be observed at several metal cation concentrations, which could be the evidence for the existence of polynuclear species (8). However, the presence of polynuclear species was not considered.

A potentiometric study of the nickel(II)/azide system was undertaken and it was found that polynuclear species were present whereas in the corresponding cobalt(II) system none was detectable. The former system is so complicated that it will be described separately.

The present paper deals with spectrophotometric and potentiometric studies in which the ratio $C_{Ni(II)}/C_{N_3^-} \gg 1$, the main purpose being to check the possibility of the existence of species like $Ni_mN_3^{(2m-1)}$ where m could be 1 and 2.

Experimental

Reagents and solutions

All reagents were of chemically pure or analytical grade.

Sodium perchlorate (Merck) was used to prepare 6.5 M solutions. Standardization was performed gravimetrically by drying 3−4 mL of the solution in an oven at 110°C to constant weight.

Nickel perchlorate was prepared by treating cobalt-free nickel carbonate (Baker Analyzed) with 4.0 M perchloric acid at room temperature, stirring for three days, and filtering. Standard perchloric acid was added to give a solution with an excess of 0.01000 M hydrogen ion concentration, $C_{H^+,M}$. Standardization was performed electrogravimetrically in the presence of hydrazine sulfate to avoid anodic oxidation of the ammonia buffer.

Sodium azide (Fischer) was washed with pure alcohol, vacuum dried, and oven dried at 110°C; after this it was used as a primary standard.

Instruments and methods

An Orion Research model 801 A digital potentiometer, adapted to a Metrohm EA 121 glass electrode, combined with an Ag/AgCl reference electrode filled with 3.0 M sodium chloride, was used in the pH measurements. The glass electrode was maintained in thermostated 2.0 M sodium perchlorate for at least 30 min prior to all measurements. A 1.99 M $NaClO_4$ solution with a free hydrogen concentration of 0.01000 M was used to standardize the glass electrode to a conditional pH = 2.000, refering to the hydrogen ion concentration instead of activity. The calibrated electrode was then employed for the pH measurements on the azide buffer solutions at the same ionic strength. All solutions were gently stirred during measurements and a small constant flux of reference electrode solution (1 drop per hour) was maintained to provide a reproducible electrolyte junction.

The standard nickel(II) solution was added to 5.000 mL of the N_3^-/HN_3 buffer, where a change from pH_1 to pH_2 was observed. The data treatment was carried out using a HP-97 calculator as described previously (4). The original program was slightly modified in order to provide only ΔN_3^- data instead of $\bar{n}$ (see Results and discussion).

The spectrophotometric measurements were taken with 1.000 cm quartz cells in a Carl Zeiss PM-QII instrument. The same azide concentration in the blank solution, without nickel(II), was used.

All measurements were done at 2.00 M ionic strength, maintained with $NaClO_4$, at (25.0 ± 0.2)°C.

Results and discussion

Spectrophotometric measurements

Evidence of species other than NiN_3^+ was obtained from the application of the McConnell and Davidson spectrophotometric method (10), modified for the conditions in which the ligand forms a weak acid (11, 12). This method is applied at different $C_{Ni(II)}$ levels and it is expected to provide constant values for β_1 in each set of results, independent of the nickel(II) concentration.

The basis of the method in its final form (12) results in the application of the following equation, when only NiN_3^+ exists,

$$[1]\qquad \underbrace{\underbrace{\frac{C_{Ni(II)}C_{N_3^-}}{A\left(1+\frac{|H^+|}{K_{HN_3}}\right)}}_{y}+\frac{A}{\epsilon_1^2\left(1+\frac{|H^+|}{K_{HN_3}}\right)}}_{y'}=\underbrace{\frac{1}{\epsilon_1\beta_1}+\frac{1}{\epsilon_1}\times\underbrace{\frac{C_{Ni(II)}+C_{N_3^-}}{\left(1+\frac{|H^+|}{K_{HN_3}}\right)}}_{x}}_{y'}$$

[1]Revision received February 11, 1983.

Can. J. Chem. Downloaded from www.nrcresearchpress.com by 210.87.254.6 on 09/06/12
For personal use only.

TABLE 1. Values of absorbance, at different wave lengths, and pH, corresponding to $C_{Ni(II)} = 5.014 \times 10^{-2}$ *M* and several $C_{N_3^-}$; final β_1' and ϵ_1' values

	λ (nm)						
$C_{N_3^-} \times 10^3$	302	299	296	293	290	287	pH
6.542	0.470	0.506	0.541	0.561	0.553	0.544	5.011
5.997	0.424	0.456	0.488	0.506	0.499	0.492	4.969
5.535	0.385	0.414	0.443	0.459	0.454	0.447	4.928
5.140	0.351	0.378	0.405	0.419	0.415	0.409	4.893
4.797	0.323	0.348	0.372	0.385	0.381	0.376	4.861
β_1'	14.6	15.2	15.4	14.1	16.9	18.4	
ϵ_1'	215	226	240	263	231	216	

TABLE 2. β_1' values obtained at different wave lengths and $\overline{\beta}_1'$ corresponding to the various $C_{Ni(II)}$ values

	λ (nm)						
$C_{Ni^{2+}} \times 10^2$	203	299	296	293	290	287	$\overline{\beta}_1'$
2.149	—	8.86	9.79	9.78	10.5	12.9*	9.73±0.67
3.223	—	11.1	11.5	10.7	12.3	14.7*	11.4±0.68
5.014	14.6	15.2	15.4	14.1	16.9	18.4*	15.2±1.06
6.089	18.0	17.5	17.9	14.4*	17.0	21.3*	17.6±0.46

*Due to discrepancies these values were ignored in the calculation of β_1'.

TABLE 3. Formation constant of NiN_3^+ from the literature

β_1 values	Remarks	Ionic strength	References
11±1	Potentiometric	3 *M*	9
6.9±0.1	Spectrophotometric	1 *M*	6
42.6	Spectrophotometric	?	7
6±1	Spectrophotometric	2 *M*	1
7.4±0.4	Potentiometric	1 *M*	8
7.5±0.1	Final potentiometric value value from present paper	2 *M*	—

where A, ϵ_1, K_{HN_3}, $C_{Ni(II)}$ and $C_{N_3^-}$ are the absorbance, molar absorptivity of the first complex, the stoichiometric ionization constant of the HN_3 acid, and the analytical concentration of the metal cation and ligand, respectively.

This is not an exact equation when considering only "y" and "x". The term containing ϵ_1^2 is normally neglected, but it can be introduced iteratively to convert "y" into "y'", after previous estimation of β_1 and ϵ_1 until these parameters converge to constant values.

If there is more than one species, instead of NiN_3^+, as $Ni_2N_3^{3+}$ or $Ni_2(N_3)_2^{2+}$, an apparent β_1' "constant" will be obtained as well as an average ϵ_1', which changes in magnitude with the metal cation concentration.

Table 1 presents a typical set of experimental data of absorbance measured at six different wave lengths to give the apparent formation constant in a particular $C_{Ni(II)}$, β_1'. There are three other series like this one. The final β_1' and ϵ_1' after the iterative procedure are also presented. The K_{HN_3} value was potentiometrically determined at 2.00 *M* ionic strength and at 25°C to be 2.46×10^{-5} *M* by a similar procedure which has been used previously (12).

We observed that β_1' determined as above changes with nickel(II) concentration over the range $(2.0-6.1) \times 10^{-2}$ *M*. This is a clear evidence that β_1' does not remain constant with nickel(II) concentration as would happen if only the monoazide species were formed. All results for different concentrations of nickel(II) at six wave lengths and also the average $\overline{\beta}_1'$ are presented in Table 2.

If the β_1' data are extrapolated to zero concentration of nickel(II) an almost linear plot results from which the true β_{11}, related to NiN_3^+, may be obtained. However, a much better extrapolation was obtained through a least-squares fit of the data to a parabolic equation with the following interception:

$$\beta_{11} = 6.90\ M^{-1}$$

This extrapolated value is coincident with the one found by Senise and Godinho (6) (Table 3). They worked at varying nickel(II) concentration. This procedure probably results in compensation for the formation of the binuclear species during extrapolation of the "y" term in eq. [1] to the zero value of "x". They were unable to detect the $Ni_2N_3^{3+}$ complex formation by their procedure.

More reliable results are expected from potentiometric measurements at comparable conditions of $C_{Ni(II)}/C_{N_3^-}$ than in the spectrophotometric study. The basis of this method has been described earlier (4). It depends on the change of a conditional pH in N_3^-/HN_3 buffers by the introduction of an analytical concentration of the metal cation.

It is expected that at least species like NiN_3^+, $Ni_2N_3^{3+}$, $Ni_2(N_3)_2^{2+}$ can coexist under the working conditions. Thus, the original program, slightly changed, can provide $\Delta|N_3^-|$ data, which are related with the bonded nickel(II) concentration by:

$$[2\text{-A}] \quad \Delta|N_3^-| = |NiN_3^+| + |Ni_2N_3^{3+}| + 2|Ni_2(N_3)_2^{2+}| + \ldots\ldots$$

The combination of this with the formation constants β_{ml} refering to $Ni_m(N_3)_l^{2m-l}$ complexes gives

$$[2\text{-B}] \quad \Delta|N_3^-| = \beta_{11}|Ni^{2+}||N_3^-| + \beta_{21}|Ni^{2+}|^2|N_3^-| + 2\beta_{22}|Ni^{2+}|^2|N_3^-|^2 + \ldots\ldots\ldots\ldots$$

A subsidiary F_1 function can be derived:

$$[3\text{-A}] \quad F_1 = \frac{\Delta|N_3^-|}{|Ni^{2+}||N_3^-|} = \beta_{11} + \beta_{21}|Ni^{2+}| + 2\beta_{22}|Ni^{2+}||N_3^+| + \ldots\ldots\ldots\ldots$$

These F_1 data can be easily calculated because the calculator program also provides $|N_3^-|$ data. As $C_{Ni(II)} \gg C_{N_3^-}$, the $|Ni^{2+}|$ data can be obtained as a first approximation by:

$$|Ni^{2+}| \cong C_{Ni(II)} - \Delta|N_3^-|$$

If only NiN_3^+ exists several terms in eq. [3-A] will disappear and is reduced to

$$[3\text{-B}] \quad F_1 = \text{constant} = \beta_{11}$$

This was not actually found when different values of $C_{Ni(II)}$ were added to solutions with the $|N_3^-|/|HN_3|$ ratio equal to 10:10, 14:14, and 20:20 (m*M*). Table 4 shows that F_1 changes linearly with $|Ni^{2+}|$ which suggests that:

$$[3\text{-C}] \quad F_1 \cong \beta_{11} + \beta_{21}|Ni^{2+}|$$

The linear regression with the three series of data leads to values of β_{11} and β_{21} which are approximately equal. The $|Ni^{2+}|$ data were then corrected again by solving the second degree equation obtained by

Can. J. Chem. Downloaded from www.nrcresearchpress.com by 210.87.254.6 on 09/06/12
For personal use only.

$$[4\text{-A}] \quad C_{Ni(II)} = |Ni^{2+}| + \beta_{11}|Ni^{2+}||N_3^-| + 2\beta_{21}|Ni^{2+}|^2|N_3^-|$$

$$[4\text{-B}] \quad 2\beta_{21}|Ni^{2+}|^2|N_3^-| + (1 + \beta_{11}|N_3^-|)|Ni^{2+}| - C_{Ni(II)} = 0$$

The final values of the formation constants are:

$$\beta_{11} = \frac{|NiN_3^+|}{|Ni^{2+}||N_3^-|} = 7.5 \pm 0.1\ M^{-1}$$

$$\beta_{21} = \frac{|Ni_2N_3^{3+}|}{|Ni^{2+}|^2|N_3^-|} = 4.3 \pm 0.1\ M^{-2}$$

This β_{11} value is doubtless more reliable than the value 6.9 M^{-1} obtained from spectrophotometric data.

However, another explanation for this higher stoichiometric β_{11} constant can be proposed on the basis of the reasonable assumption that two monoazide species exist in equilibrium: a true complex and an ion pair. Thus, the spectrophotometric measurements at the ultraviolet region would provide a lower constant value because it brings up spectral differences between the outer-sphere complex and the inner one. Such a situation has been described by Posey and Taube (13) and Bell and Panckhurst (14).

Other attempts to solve a 3 × 3 matrix from simultaneous equations with the data of Table 4 by including in [2-B] the terms corresponding to $Ni_2(N_3)_2^{2+}$ or $Ni(N_3)_2$ were unsuccessful. This result is expected because the $C_{N_3^-}$ is maintained at a very low level and the formation of those two species requires the addition of a quadratic term, $|N_3^-|^2$, which is very low (see eq. [2-B]). However, solution of the 2 × 2 matrix confirmed the values for β_{11} and β_{21}.

These constants are expected to describe in a better way the system at high $C_{Ni^{2+}}/C_{N_3^-}$ ratio. They can also be used in the calculation of the individual values of ϵ_{11} and ϵ_{21} from the spectrophotometric measurements, where the following equation can be derived:

$$[5\text{-A}] \quad A = A_{NiN_3^+} + A_{Ni_2N_3^{3+}}$$

$$[5\text{-B}] \quad A = \epsilon_{11}|NiN_3^+| + \epsilon_{21}|Ni_2N_3^{3+}|$$

$$[5\text{-C}] \quad A = \epsilon_{11}\beta_{11}|Ni^{2+}||N_3^+| + \epsilon_{21}\beta_{21}|Ni^{2+}|^2|N_3^-|$$

Table 5 presents the absorbance values and the ϵ_{11} and ϵ_{21} data from the matrix solution of simultaneous equations such as [5-C], from the absorbance measured at known $|Ni^{2+}|$ and $|N_3^-|$ calculated by iteration from eq. [4-B] and:

$$[6\text{-A}] \quad C_{N_3^-} = |N_3^-| + |HN_3| + \beta_{11}|Ni^{2+}||N_3^-| + \beta_{21}|Ni^{2+}|^2|N_3^-|$$

$$[6\text{-B}] \quad |N_3^-| = (C_{N_3^-} - |HN_3|)/(1 + \beta_{11}|Ni^{2+}| + \beta_{21}|Ni^{2+}|^2)$$

$$[7] \quad |HN_3| = C_{HClO_4} + C_{H^+,Ni^{2+}}$$

We can observe that ϵ_{11} reaches a maximum value at 293 nm while ϵ_{21} shows a regular increase toward lower wave lengths. These different tendencies may explain why the apparent constant, β_1', increases at lower wave lengths where the species $Ni_2N_3^{3+}$ absorbs preferentially.

These spectrophotometric and potentiometric measurements confirm that azide ion can behave as a bridge ligand to nickel(II) cations, which is not the case with a similar cobalt(II) system. Thus it is expected that at higher azide concentrations many other polynuclear species can be formed with more than one ligand, due to a more favorable exponential factor. These results will be reported later.

Finally, it should be pointed out that the effect of hydrolysis on the present measurements should be negligible because the pH of the majority of the working solutions was lower than 5.

TABLE 4. Data obtained from potentiometric measurements

	$C_{N_3^-}$ = 19.99 mM				$C_{N_3^-}$ = 27.99 mM				$C_{N_3^-}$ = 39.98 mM			
$C_{Ni^{2+}}$	$\|N_3^-\|\times10^3$	$\Delta\|N_3^-\|\times10^3$	$\|Ni^{2+}\|_f$*	$F_{1(i)}$*	$\|N_3^-\|$	$\Delta\|N_3^-\|\times10^3$	$\|Ni^{2+}\|_f$*	$F_{1(i)}$*	$\|N_3^-\|$	$\Delta\|N_3^-\|\times10^3$	$\|Ni^{2+}\|_f$*	$F_{1(i)}$*
5.957×10^{-2}	6.116	2.740	5.679×10^{-2}	7.889	8.671×10^{-3}	3.750	5.570×10^{-2}	7.764	1.256×10^{-2}	5.214	5.413×10^{-2}	7.669
7.816×10^{-2}	5.332	3.174	7.490×10^{-2}	7.948	7.570×10^{-3}	4.372	7.361×10^{-2}	7.846	1.100×10^{-2}	6.092	7.173×10^{-2}	7.721
9.591×10^{-2}	4.694	3.479	9.230×10^{-2}	8.030	6.674×10^{-3}	4.813	9.087×10^{-2}	7.936	9.717×10^{-3}	6.739	8.876×10^{-2}	7.814
1.124×10^{-1}	4.186	3.678	1.086×10^{-1}	8.091	5.959×10^{-3}	5.103	1.070×10^{-1}	8.003	8.690×10^{-3}	7.170	1.047×10^{-1}	7.880
1.323×10^{-1}	3.653	3.839	1.283×10^{-1}	8.191	5.218×10^{-3}	5.335	1.266×10^{-1}	8.076	7.619×10^{-3}	7.524	1.242×10^{-1}	7.951

*Final values calculated iteratively.

TABLE 5. Experimental data and composition of working solutions (*1*), (*2*), and (*3*) used to calculate ϵ_{11} and ϵ_{21}

Parameter	Value (*1*)	(*2*)	(*3*)	ϵ_{11}	ϵ_{21}
C_{NaN_3}	1.999×10^{-2}	1.999×10^{-2}	1.999×10^{-2}		
C_{HClO_4}	1.004×10^{-2}	1.004×10^{-2}	1.004×10^{-2}		
$C_{Ni(II)}$	2.686×10^{-2}	3.134×10^{-2}	3.582×10^{-2}		
C_{NaClO_4}	1.90	1.89	1.87		
$\lvert Ni^{2+}\rvert$	2.524×10^{-2}	2.949×10^{-2}	3.375×10^{-2}		
$\lvert N_3^-\rvert$	8.313×10^{-3}	8.082×10^{-3}	7.861×10^{-3}		
$\lvert HN_3\rvert$	1.008×10^{-2}	1.009×10^{-2}	1.010×10^{-2}		
A (302 nm)	0.491	0.558	0.623	309	221
A (299 nm)	0.527	0.599	0.669	331	271
A (296 nm)	0.562	0.638	0.714	352	347
A (293 nm)	0.580	0.660	0.738	362	475
A (290 nm)	0.570	0.650	0.726	354	542

In this regard, the data compiled by Sillén and Martell (15) imply that significant hydrolysis of nickel(II) cations occurs only above pH 5.5.

Acknowledgements

The authors are greatly indebted to CNPq and FINEP (Brazilian Foundations) for financial support.

1. W. KUTNER and Z. GALUS. J. Electroanal. Chem. **51**, 363 (1974).
2. P. SENISE and E. A. NEVES. Ann. Acad. Brasil. Ciênc. **41**, 333 (1969).
3. E. A. NEVES, M. E. V. SUÁREZ, and R. TOKORO. Unpublished results.
4. E. A. NEVES, R. TOKORO, and M. E. V. SUÁREZ. J. Chem. Res. (M), 4401 (1979); J. Chem. Res. (S), 376 (1979).
5. R. TOKORO and E. A. NEVES. J. Electroanal. Chem. **125**-1, 115 (1981).
6. P. SENISE and O. E. S. GODINHO. J. Inorg. Nucl. Chem. **32**, 3641 (1970).
7. R. ABU-EITTAH and S. ELMAKABATY. J. Inorg. Nucl. Chem. **35**, 291 (1973).
8. S. AHRLAND and E. AVSAR. Acta Chem. Scand. A**29**, 881 (1975).
9. F. MAGGIO, V. ROMANO, and L. PELLERITO. J. Electroanal. Chem. **15**, 227 (1967).
10. H. MCCONNELL and N. DAVIDSON. J. Am. Chem. Soc. **72**, 3164 (1950).
11. G. SAINI and G. OSTACOLI. J. Inorg. Nucl. Chem. **8**, 346 (1958).
12. E. A. NEVES and P. SENISE. J. Inorg. Nucl. Chem. **34**, 1915 (1972).
13. F. A. POSEY and H. TAUBE. J. Am. Chem. Soc. **78**, 15 (1956).
14. R. P. BELL and M. H. PANCKHURST. Rec. Trav. Chim. **75**, 725 (1956).
15. L. G. SILLÉN and A. E. MARTELL. Stability constants supplement No. 1. Special Publication 25. The Chemical Society, London. 1964.

Can. J. Chem. Downloaded from www.nrcresearchpress.com by 210.87.254.6 on 09/06/12
For personal use only.

Nucleic acid related compounds. 41. Restricted furanose conformations of 3′,5′-*O*-(1,1,3,3-tetraisopropyldisilox-1,3-diyl)nucleosides provide a convenient evaluation of anomeric configuration[1,2]

MORRIS J. ROBINS[3] AND JOHN S. WILSON
Department of Chemistry, The University of Alberta, Edmonton, Alta., Canada T6G 2G2

AND

LINDSAY SAWYER[4] AND MICHAEL N. G. JAMES[3]
Department of Biochemistry, The University of Alberta, Edmonton, Alta, Canada T6G 2H7

Received November 16, 1982

MORRIS J. ROBINS, JOHN S. WILSON, LINDSAY SAWYER, and MICHAEL N. G. JAMES. Can. J. Chem. **61**, 1911 (1983).

Treatment of ribonucleosides (and related furanosyl compounds) with 1,3-dichloro-1,1,3,3-tetraisopropyldisiloxane in pyridine gave high yields of 3′,5′-*O*-(1,1,3,3-tetraisopropyldisilox-1,3-diyl)nucleosides (3′,5′-*O*-TPDS-nucleosides). The ^{1}H nmr coupling parameters of the sugar backbone of the β-D-ribofuranosyl anomers of these *trans*(1,2)-fused 8 to 5 membered ring TPDS compounds indicated a remarkably consistent range of furanose conformations. The data are compatible with a predominant population of conformers in the general ^3E (C3′-*endo*) range found for a large series of rigidly *trans*-fused 6 to 5 membered ring nucleoside cyclic 3′,5′-monophosphates. X-ray crystallographic analysis of 3′,5′-*O*-TPDS-cytidine revealed an almost perfect ^3E sugar envelope conformation (P = 19.7°, τ_m = 41.9°) in agreement with the ^{1}H nmr solution data. Attachment of two bulky isopropyl groups to each silicon atom and expansion of the Si—O—Si bond angle to 155° gives an essentially planar six atom segment of the 8-membered ring. Apparently this demands a distinctly preferred conformation for the fused ring system. The readily prepared 3′,5′-*O*-TPDS-β-D-ribofuranosyl derivatives have $J_{1'-2'} \leq 1.5$ Hz in most cases. This provides a rapid and convenient evaluation of the H1′—H2′ *trans* configuration in these structures.

MORRIS J. ROBINS, JOHN S. WILSON, LINDSAY SAWYER et MICHAEL N. G. JAMES. Can. J. Chem. **61**, 1911 (1983).

Les ribonucléosides (et les composés furannosyles apparentés) réagissent avec le dichloro-1,3 tétraisopropyl-1,1,3,3 disiloxane dans la pyridine en donnant les *O*-(tétraisopropyl-1,1,3,3 disiloxydiyl-1,3)-3′,5′ nucléosides (*O*-TPDS-3′,5′ nucléosides) avec de forts rendements. Les paramètres de couplage en rmn du ^{1}H, de l'unité sucre des anomères du β-D-ribofurannosyle de ces composés TPDS à noyaux condensés de 5 à 8 chainons en position *trans*(1,2) indiquent un nombre très important de conformations du furannose. Les données sont en accord avec une population prédominante de conformères dans le domaine général ^3E (C′3-*endo*) trouvés pour un très grand nombre de nucléosides monophosphates-3′,5′ cycliques à noyaux condensés de 6 à 5 chainons en position *trans*. L'analyse par cristallographie de rayons X de la *O*-TPDS-3′,5′ cytidine révèle une conformation enveloppe presque parfaite de sucre du type ^3E (P = 19,7°, τ_m = 41,9°) en accord avec les données de la rmn du ^{1}H en solution. La fixation de deux groupes isopropyles encombrants sur chaque atome de silicium et l'expansion de l'angle de liaison Si—O—Si à 155°C donne essentiellement un segment plan de 6 atomes dans le cycle à 8 chainons. Apparemment ceci requiert une conformation préférée distincte du système cyclique condensé. Les dérivés du *O*-TPDS-3′,5′ β-D-ribofurannosyle ont un $J_{1'-2} \leq 1,5$ Hz dans la plupart des cas. Cette donnée fournit une évaluation rapide et convenable de la configuration *trans* H1′—H2′ de ces structures.

[Traduit par le journal]

A variety of chemical, chiroptical, and nmr methods have been used to determine the anomeric configuration of ribonucleosides (for a critical survey of the major methods see ref. 1). However, many of these criteria are based on unique and/or empirical properties of specific nucleoside structures and the majority require both anomers for comparison. We have described a general and unequivocal method for the independent assignment of β or α anomers based on ^{1}H nmr analysis of the rigid geometric orientation of the anomeric proton (H1′) and H2′ on the *trans*(1,2)-fused 6 to 5 membered ring system of nucleoside cyclic 3′,5′-monophosphates (1). However, this procedure suffers from the experimental involvement required to synthesize and purify these cyclic nucleotides. We now wish to report application of the easily prepared 3′,5′-*O*-(1,1,3,3-tetraisopropyldisilox-1,3-diyl)nucleoside (3′,5′-*O*-TPDS-nucleoside) derivatives for the convenient anomeric configuration assignment of applicable β-ribofuranosyl structures.

Markiewicz and Wiewiorowski described the synthesis of 1,3-dichloro-1,1,3,3-tetraisopropyldisiloxane (TPDS dichloride) and its reaction with ribonucleosides to give their 3′,5′-*O*-TPDS derivatives (2). Others (3) and ourselves (4) have used this novel protecting group with related furanosyl compounds. Most ribo- and arabinofuranosyl compounds were converted smoothly into their 3′,5′-*O*-TPDS derivatives upon treatment with TPDS dichloride in pyridine (4, 5). Guanosine required a cosolvent and by-product formation (3) occurred when *N*,*N*-dimethylformamide (DMF) was used (4*b*). Extended heating of 3′,5′-*O*-TPDS derivatives in protic solvents and acid treatment (3) should be avoided. The 3′,5′-*O*-TPDS-guanosine derivative was obtained in ~70% yield, but no difficulties were encountered with the other products in our studies and high yields were easily obtained (4*b*).

It is noteworthy that the arabinofuranosyl nucleosides of adenine (4*b*) and cytosine (4*b*, 5) gave the 3′,5′-*O*-TPDS derivatives exclusively. Cyclization of ribonucleoside 5′-monophosphates was known to proceed at O3′ to give the cyclic 3′,5′-monophosphates (6), whereas analogous treatment of the 2′-epimeric arabinonucleoside 5′-monophosphates gave

[1]This paper is dedicated to Professor Raymond U. Lemieux on the occasion of his sixty-third birthday.

[2]For the previous paper in this series see ref. 26.

[3]Author to whom correspondence should be addressed.

[4]On sabbatical leave from the Chemistry Department, Napier College of Commerce and Technology, Edinburgh, Scotland, 1980–1981.

Can. J. Chem. Downloaded from www.nrcresearchpress.com by 210.87.254.5 on 09/06/12
For personal use only.

Can. J. Chem. Downloaded from www.nrcresearchpress.com by 210.87.254.5 on 09/06/12
For personal use only.

the cyclic 2′,5′-monophosphates (7) uniquely. Verification of the O3′ linkage of the present 3′,5′-*O*-TPDS structures was provided by acylation of the 2′-hydroxyl group and observation of the marked downfield shift of the nmr signal for H2′ ($\Delta\delta$ = 1.1 to 1.5 ppm for 2′-OH → 2′-OAc; and $\Delta\delta \sim 2$ ppm for 2′-OH → 2′-OCSOPh).

It has been concluded that vicinal proton–proton coupling values of $J \lesssim 1$ Hz on a 5-membered ring provide definitive verification of their *trans* orientation (8) since *cis* coupling values of $\lesssim 2$ Hz are precluded geometrically. The anomeric proton nmr signal in over 200 examples of various types of β-D-ribonucleoside cyclic 3′,5′-monophosphates appeared as a sharp singlet without a reported exception (1). Coupling values of $J_{1'-2'} < 0.7$ Hz were found in all cases examined by double resonance (1, 9).

Experimental

The ^1H nmr spectra were recorded in the Fourier transform mode using Bruker WH-200 and WH-400 spectrometers by the High-Field NMR Laboratory of the Department of Chemistry. Spectra were determined in Me_2SO-d_6 solutions with Me_4Si as internal standard. Poorly resolved spectra were improved by dilution of the sample with Me_2SO-d_6 or other solvents as indicated. Additional spectra were determined in the other solvents indicated, with Me_4Si as internal standard. First order spectral analysis was performed with the aid of double resonance decoupling. No coupling values are given when resolution or spectral complexity was prohibitive at 400 MHz. Ambient spectrometer temperatures were employed. Insignificant effects on coupling parameters were observed over a 10°C range and major effects were not apparent over a 30°C range with compound **1**.

X-ray crystallographic analysis was performed on a crystal of 3′,5′-*O*-TPDS-cytidine (**8**) that measured 0.7 × 0.55 × 0.25 mm. A final *R*-factor of 0.059 (R_w = 0.070) was obtained.[5] The description of an independent structure determination of **8** was published subsequent to the completion of our analysis (10). A comparison of temperature effects on this molecular structure at 116 K (10) and 289 K[5] was thereby afforded.

Synthesis of the 3′,5′-O-(1,1,3,3-tetraisopropyldisilox-1,3-diyl) compounds was effected by a general procedure illustrated by the following preparation.

3′,5′-O-TPDS-adenosine (1)

To 267 mg (1 mmol) of dried adenosine suspended in 10 mL of dry pyridine was added 320 μL (316 mg, 1 mmol) of 1,3-dichloro-1,1,3,3-tetraisopropyldisiloxane and the mixture was stirred at room temperature for 3 h. Pyridine was evaporated and the residue was partitioned between EtOAc and H_2O. The organic phase was washed with 2 × 20 mL of cold 1 *N* HCl/H_2O, H_2O, saturated $NaHCO_3$/H_2O, saturated NaCl/H_2O, dried (Na_2SO_4), filtered, and evaporated. The resulting amorphous product contained only minor impurities (tlc).

For characterization, this material was chromatographed on a column of silica gel (2 × 10 cm, 10 g) using $CHCl_3$ followed by 2% MeOH/$CHCl_3$ for elution. Appropriately pooled fractions were evaporated and the residue was crystallized from CH_3CN to give 433 mg (85%) of **1** with mp 98–99.5°C; uv (0.1 *N* HCl) max 257 nm (ε 14 900), (0.1 *N* NaOH) max 259 nm (ε 15 100). *Anal.* calcd. for $C_{22}H_{39}N_5O_5Si_2$: C 51.84, H 7.71, N 13.74; found: C 51.65, H 7.92, N 13.73.

Isolation methods and characterization data for compounds **1***a*, **4**, **4***a*, **5**, **5***a*, **6**, **6***a*, **7**, **7***a*, **8***b*, **8***c*, **11** will be published separately (11) with details of our 2′-deoxygenation procedures (4*a*). Isolation, yields, and data for compounds **3**, **8**, **8***a*, **13** may be found in ref. 4*b*. Compounds **2**, **4***b*, **4***c*, **9**, **10**, **12**, **12***a*, **14**, **15**, **16**, **17**, **19**, **20**, **21**, **22**, **23** were prepared by treatment of a 0.1 mmol sample of the precursor nucleoside with 2.5 mL of dry pyridine and 32 μL (0.1 mmol) of 1,3-dichloro-1,1,3,3-tetraisopropyldisiloxane according to the general procedure. The standard processing was followed by chromatography of the residue on preparative silica gel plates (5 × 20 cm) using 5% MeOH/$CHCl_3$. The product zone was scraped from the plate and the compound was eluted with 7% MeOH/$CHCl_3$. The filtered eluate was evaporated and the tlc homogeneous oils had the spectral properties listed in Tables 2–6.

Compound **18** was prepared by the procedure used for **11** (4*b*).

Compounds **19***a* and **23***a* were prepared by the general procedure using 0.1 mmol samples of the precursor nucleosides and 32 μL of the bifunctional silylating reagent in 5 mL of dry pyridine. After stirring for 3 h, 20 μL (2 mmol) of acetic anhydride was added and stirring was continued for 4 h. Volatile materials were evaporated and the residues were chromatographed on columns (1.5 × 7 cm, 6 g) of silica gel using $CHCl_3$. Evaporation of appropriate fractions gave **19***a* (76%) and **23***a* (77%) as tlc homogeneous oils with the spectral properties listed in Tables 4–6.

Results and discussion

Table 1 presents the 36 structures of the 3′,5′-*O*-TPDS-furanosyl derivatives examined in this study. Table 2 contains the chemical shift data and Table 3 the first order spin–spin coupling parameters for 25 β-D-ribofuranosyl compounds. Table 4 contains the chemical shift data and Table 5 the coupling parameters for α-D-ribo-, β-D-arabino-, and α-D-arabino-furanosyl derivatives. Table 6 contains the high resolution mass spectral data and uv absorbance maxima for characterization of the 3′,5′-*O*-TPDS derivatives prepared for this study. The X-ray crystallographic positional and equivalent isotropic thermal parameters for the non-hydrogen atoms of 3′,5′-*O*-TPDS-cytidine (**8**) are given in Table 7.

A. Determination of anomeric configuration

As seen in Table 3, the coupling of H1′ with H2′ was less than the limit of resolution ($J_{1'-2'} < 0.5$ Hz) resulting in the appearance of a sharp singlet for the anomeric proton signal for 13 β-D-ribofuranosyl derivatives (**5**, **6**, **7**–**12***a*). The anomeric proton signal for 9 additional compounds (**1**–**4**, **4***b*, **4***c*, **5***a*, **6***a*) appeared as a narrowly split doublet with $J_{1'-2'} \leq 1.5$ Hz. Exceptions to this $J_{1'-2'} \leq 1.5$ Hz limit were observed with the 3′,5′-*O*-TPDS derivatives of the C-nucleoside antibiotics formycin (**13**, $J_{1'-2'}$ = 2.0 Hz) and pyrazofurin (**14**, $J_{1'-2'}$ = 2.7 Hz) as well as with the 2′-*O*-phenoxythiocarbonyl derivative (**4***a*, $J_{1'-2'}$ = 2.6 Hz) of 3′,5′-*O*-TPDS-guanosine.

Examination of the types of compounds reveals that all ten pyrimidine-type derivatives gave anomeric proton singlets. This includes three pyrimidine *N*-nucleosides with free 2′-hydroxyl functions (**7**, **8**, **8***b*), three with 2′-*O*-phenoxythiocarbonyl groups (**7***a*, **8***a*, *c*), two 3-deazapyrimidine *N*-nucleosides (**9**, **10**), and two pyrimidine C-nucleosides (pseudouridine, **12**, and the antibiotic oxazinomycin, **12***a*) each with free 2′-hydroxyl functions. Additional examples of related pyrimidine C-nucleoside derivatives have been reported very recently.[6] Anomeric proton singlets were also observed for the 3′,5′-*O*-TPDS derivatives of methyl β-D-ribofuranoside (**11**), and the two pyrrolo[2,3-*d*]pyrimidine antibiotics tuber-

[5]A discussion of the crystal data and detailed structure features as well as tables of anisotropic thermal factors, hydrogen parameters, and calculated and observed structure factor amplitudes (19 pages) have been placed in the Depository of Unpublished Data, CISTI, National Research Council of Canada, Ottawa, Ont., Canada K1A 0S2, and may be obtained from that depository at a nominal cost.

[6]Four pyrimidine C-nucleosides with a free 2′-hydroxyl and two with 2′-*O*-imidazolylthiocarbonyl groups were reported by Pankiewicz *et al.* (12) to have anomeric proton singlets.

TABLE 1. 3′,5′-*O*-TPDS derivative structures[a]

A. β-D-Ribofuranosyl

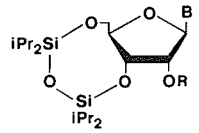

B =

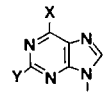

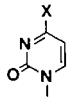

1	X=NH_2, Y=R=H	7	X=OH, R=H
1a	X=NH_2, Y=H, R=CSOPh	7a	X=OH, R=CSOPh
2	X=Y=NH_2, R=H	8	X=NH_2, R=H
3	X=OH, Y=R=H	8a	X=NH_2, R=CSOPh
4	X=OH, Y=NH_2, R=H	8b	X=NHAc, R=H
4a	X=OH, Y=NH_2, R=CSOPh	8c	X=NHAc, R=CSOPh
4b	X=SH, Y=NH_2, R=H		
4c	X=Cℓ, Y=NH_2, R=H		

B =

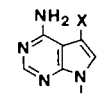

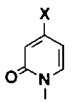

5	X=R=H	9	X=OH, R=H
5a	X=H, R=CSOPh	10	X=NH_2, R=H
6	X=CN, R=H		
6a	X=CN, R=CSOPh		

11	B=OCH_3, R=H

B =

12	X=NH, R=H
12a	X=O, R=H

13 B =

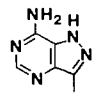

, R=H

14 B =

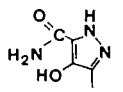

, R=H

B. α-D-Ribofuranosyl

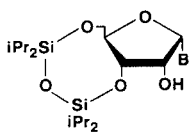

B =

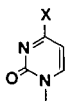

15	X=OH
16	X=NH_2

17 B =

18 B = OCH_3

C. β-D-Arabinofuranosyl

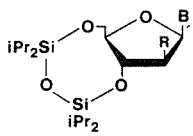

B =

19	X=NH_2, R=OH
19a	X=NHAc, R=OAc
20	X=NH_2, R=Cℓ
21	X=NH_2, R=N_3

22 B =

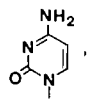

, R=OH

D. α-D-Arabinofuranosyl

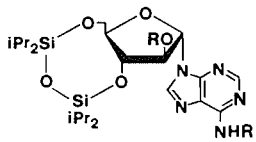

23	R=H
23a	R=Ac

[a]The indicated hydroxy-purine and pyrimidine compounds occur as their keto tautomers in solution.

cidin (**5**) and toyocamycin (**6**), each with a free 2′-hydroxyl group. The purine nucleoside derivatives with free 2′-hydroxyl functions (**1**, **2**, **3**, **4**, **4***b*, **4***c*) had narrow anomeric proton doublets with $J_{1'-2'}$ = 0.9–1.5 Hz. The 2′-*O*-phenoxythiocarbonyl derivatives of the purine and pyrrolo[2,3-*d*]-pyrimidine compounds (**1***a*, **4***c*, **5***a*, **6***a*) exhibited anomeric proton doublets with $J_{1'-2'}$ = 1.2–1.5 Hz with the exception of the above noted $J_{1'-2'}$ = 2.6 Hz for **4***a*.

A minor increase in the anomeric proton coupling constant of **1** was observed with an ~80°C increase in temperature in dimethylsulfoxide (DMSO) solution. However, solvent effects were more substantial. The spectrum of **1** in DMSO had $J_{1'-2'}$

Can. J. Chem. Downloaded from www.nrcresearchpress.com by 210.87.254.5 on 09/06/12
For personal use only.

TABLE 2. ^{1}H nuclear magnetic resonance chemical shifts of 3′,5′-*O*-TPDS-β-D-ribofuranosyl compounds[a,b]

Compound	Base H's[c]	H-1′[c,d]	H-2′[c]	H-3′[c]	H-4′[f]	H-5′[c]	H-5″[c]	2′-OH[d]	NH_2[c]	Solvent[g]
1	8.19, 8.10	5.86	4.51[h]	4.78	4.00[i]	4.05	3.92	5.60	7.30	A
1*a*	8.32, 8.08	6.36	6.53	5.53	4.00	4.05	3.98	—	7.43	A
2	7.82	5.86	4.55	4.80	4.13	4.15[f]	4.08[f]	4.60[f]	6.32 5.38	C
3	8.18, 8.00	5.88	4.45	4.60	4.04[f]	4.10	3.95	5.70[f]	—	A
4	7.76	5.68	4.26	4.35	4.00[f]	4.08	3.92	5.61	6.50	A
4*a*	7.96	6.11	6.26	4.89	4.04	4.07[f]	3.98[f]	—	6.43	A
4*b*	7.94	5.70	4.25	4.32	4.00	4.09	3.91	5.68	6.86	A
4*c*	8.16	5.80	4.40[f]	4.40[f]	4.04[f]	4.12	3.95	5.68	7.00	A
5	8.04, 7.26,[d] 6.59[d]	5.96[c]	4.28	4.60	3.96	4.05	3.92	5.52	7.06	A
5*a*	8.28, 7.17,[d] 6.40[d]	6.30	6.32	5.22	4.08	4.15	4.06	—	5.35	B
6	8.21, 8.18	5.99[c]	4.35[h]	4.50	4.06[i]	4.16	3.96	5.75	6.90	A
6*a*	8.36, 8.17	6.32	6.44	5.30	4.01	4.01[f]	4.01[f]	—	7.02	A
7	7.69,[d] 5.53[d]	5.54[c]	4.14[f]	4.16	3.97[f]	4.12	3.92	5.58	—	A
7*a*	7.80,[d] 5.85[d]	6.00[c]	6.08[d]	4.60	4.16	4.20[f]	4.10[f]	—	—	B
8	7.72,[d] 5.68[d]	5.57[c]	3.92[h]	4.09	4.01[f]	4.17	3.92	5.61	7.16[d]	A
8*a*	7.71,[d] 5.78[d]	5.80[c]	6.08	4.84	3.94	4.14	4.03	—	7.34	A
8*b*	8.16,[d] 7.23[d]	5.62[c]	4.08[f]	4.08[f]	4.08	4.24	3.94	5.83	—	A
8*c*	8.10,[d] 7.24[d]	5.88[c]	6.12	4.75	4.00	4.20[f]	4.00[f]	—	—	A
9	7.65,[d] 5.82,[c] 5.55[d]	5.75[c]	4.10[f]	4.16[f]	4.05	4.00[f]	4.00[f]	5.80[f]	—	A
10	7.52,[d] 5.60,[d] 5.50	5.85[c]	4.16[f]	4.25	4.16	4.18[f]	3.95	4.20[f]	7.20	B
11	3.22[j]	4.64[c]	3.84[f]	4.29	3.84	3.89	3.80[f]	5.10	—	A
12	7.32	4.52[c]	3.96[d]	4.13	3.84	4.04[f]	3.87[f]	5.20	—	A
12*a*	7.64	4.56[c]	4.00[f]	4.17	3.85	4.05[f]	3.87[f]	5.25	—	A
13	8.46	5.30	4.70	4.89	4.16	4.09	4.04	4.09[f]	6.90	C
14	—	5.04	4.52	4.33	4.00	4.16[f]	4.10[f]	5.16	—	C

[a]Shifts δ (ppm) measured from internal Me_4Si.
[b]The four isopropyl groups on silicon produced complex multiplets at δ ~1.05–1.10. The phenyl ring protons on the phenoxythiocarbonyl-substituted compounds produced multiplets at δ ~7.17(*o*), 7.52(*m*), and 7.37(*p*).
[c]Singlet (unless noted).
[d]Doublet (unless noted).
[e]Doublet of doublets (unless noted).
[f]Unresolved multiplet (unless noted).
[g]A = Me_2So-d_6, B = $CDCl_3$, C = Me_2CO-d_6.
[h]Apparent triplet.
[i]Doublet of triplets.
[j]Singlet —OCH_3.

= 0.9 Hz, but in chloroform it increased to $J_{1'-2'}$ = 1.4 Hz. Compound **5** in DMSO had an anomeric proton singlet, but in chloroform $J_{1'-2'}$ = 1.5 Hz was observed. The anomeric proton coupling of **13** was reduced to $J_{1'-2'}$ = 2.0 Hz in acetone, but increased to $J_{1'-2'}$ = 3.2 Hz in chloroform.

It is apparent that the conformations of these *trans*(1,2)-fused 8 to 5 membered ring 3′,5′-*O*-TPDS-β-compounds reside in a *preferred range* rather than the rigidly fixed geometry of the *trans*(1,2)-fused 6 to 5 membered cyclic 3′,5′-monophosphates (1). The purine-type 3′,5′-*O*-TPDS derivatives exhibit larger anomeric proton couplings and are subject to temperature and solvent effects. Significant increases in the H1′ coupling constant occur with several of the present derivatives upon acylation of O2′ to give phenyl thionocarbonate esters in contrast with negligible effects observed upon substitution of O2′ with the cyclic 3′,5′-monophosphates (1).

Four α-D-ribofuranosyl 3′,5′-*O*-TPDS derivatives (**15–18**) were examined. As seen in Table 5, their anomeric proton coupling values ($J_{1'-2'}$ = 3.5–4.0 Hz) are closely similar to those observed with the cyclic α-D-3′,5′-monophosphates (1, 13). Likewise, five β-D-arabinofuranosyl 3′,5′-*O*-TPDS derivatives (**19–22**) had *cis* $J_{1'-2'}$ = 6.0–6.7 Hz couplings in harmony with the cyclic 3′,5′-monophosphate analogues (1).

With the evidence at hand we consider that an anomeric proton coupling of $J_{1'-2'} \leq 1.5$ Hz provides a safe criterion for assignment of the β configuration to a ribofuranosyl 3′,5′-*O*-TPDS derivative. It would appear that the corresponding α anomers have $J_{1'-2'} \geq 3.5$ Hz. However, owing to the exceptions noted, couplings of $J_{1'-2'} \gtrsim 2$ Hz could be ambiguous and corroborative methods (1) should be employed.

B. X-ray crystal structure of 3′,5′-O-TPDS-cytidine (8)

Final positional and isotropic thermal parameters for the atoms of compound **8** are listed in Table 7.[5] Figure 1 shows a stereo ORTEP (14) diagram of the molecule with identification of the atomic numbering scheme used for the crystallographic analysis. Bond lengths (no corrections were made for riding motion) and bond angles are given in Fig. 2. A stereoscopic diagram of the crystal packing of **8** is presented in Fig. 3.

1. *General structure features*

The endocyclic bond lengths and angles in the sugar moiety of **8** are compatible with those found in nucleoside cyclic 3′,5′-monophosphates (15). However, they deviate from certain trends noted in "free" nucleoside furanosyl structures (16). The expanded Si—O—Si bond angle of 155.1° allows formation of a "flattened" disiloxane ring with Si1, Si2, O12, O3′, O5′, and C4′ coplanar within a mean deviation of 0.037 Å. The C3′ and C5′ atoms lie 0.81 Å and 0.78 Å, respectively, on opposite sides of the plane, resulting in an overall "twist" conformation for the 8-membered ring. Large variations in

Can. J. Chem. Downloaded from www.nrcresearchpress.com by 210.87.254.5 on 09/06/12
For personal use only.

TABLE 3. Proton spin–spin coupling values of 3′,5′-*O*-TPDS-β-D-ribofuranosyl compounds[a]

Compound	$J_{1'-2'}$	$J_{2'-3'}$	$J_{3'-4'}$	$J_{4'-5'}$	$J_{4'-5''}$	$J_{5'-5''}$	$J_{2'-2'OH}$
1	0.9	5.0	8.0	3.2	2.6	−12.6	4.7
1*a*	1.2	5.5	8.7	4.1	[b]	−13.0	—
2	1.5	5.0	7.5	3.5	2.0	−11.5	[b]
3	1.5	5.2	8.4	2.8	3.2	−12.8	[b]
4	1.6[c]	5.0	8.0	3.2	2.6	−13.0	5.2
4*a*	2.6	5.8	7.0	[b]	[b]	[b]	—
4*b*	1.5	5.0	8.3	3.0	2.5	−13.0	~3.5
4*c*	1.5	~4.5	8.3	3.3	2.5	−12.5	4.8
5	[d]	5.5	7.7	2.0	2.3	−12.5	4.7
5*a*	1.5	5.2	8.6	3.2	2.7	−13.0	—
6	[d]	5.0	8.5	2.6	2.4	−13.0	5.0
6*a*	1.5	5.2	8.4	2.8	3.2	−12.8	—
7	[d]	4.4	8.4	2.6	2.6	−13.2	4.5
7*a*	[d]	5.3	9.5	[b]	[b]	[b]	—
8	[d]	4.4	8.8	2.2	2.7	−13.0	4.4
8*a*	[d]	5.5	8.5	3.5	2.5	−12.8	—
8*b*	[d]	[b]	[b]	2.0	2.5	−14.0	4.0
8*c*	[d]	5.0	8.7	[b]	[b]	[b]	—
9	[d]	[b]	[b]	[b]	[b]	[b]	[b]
10	[d]	5.0	9.0	[b]	2.5	−13.0	[b]
11	[d]	4.5	7.5	3.0	[b]	−11.5	4.0
12	[d]	4.5	8.5	[b]	[b]	−12.5	4.0
12*a*	[d]	4.5	8.4	[b]	[b]	[b]	4.0
13	2.0	5.2	7.5	5.0	2.7	−11.5	[b]
14	2.7	5.6	8.0	4.8	3.0	−12.5	[b]

[a]Coupling values in Hz.
[b]Unresolved.
[c]Coupling reduced to 1.2 Hz by addition of MeOD and D_2O.
[d]Sharp singlet ($J_{1'-2'} < 0.5$ Hz).

TABLE 4. ^{1}H nuclear magnetic resonance chemical shifts of α-D-ribo, β-D-arabino, and α-D-arabino 3′,5′-*O*-TPDS-furanosyl compounds[a]

Compound	Base H's[e]	H-1′[d]	H-2′[e]	H-3′[e]	H-4′[f]	H-5′[e]	H-5″[e]	2′-OH[d]	NH_2[e]	Solvent[g]
15	7.47,[d] 5.67[d]	6.01	4.13	4.33	4.07[i]	4.00	3.86	5.62	—	A
16	7.54,[d] 5.57[d]	6.02	4.18[f]	4.36	4.13[i]	4.03	3.87	5.40	7.07	A
17	8.26, 8.18	6.38	4.34[f]	4.50	4.20	4.02	3.91	5.79	7.30	A
18	3.34[i]	4.79	3.97	4.08[h]	3.84	3.89[f]	3.76[f]	4.07[f]	—	A
19	8.11, 8.04	6.21	4.55[f]	4.55[f]	3.80	4.12	3.92	5.80	7.30	A
19*a*	8.58, 8.40	6.56	5.64	5.08[f]	4.05	4.05[f]	4.05[f]	—	—	A
20	8.35, 8.14	6.50	4.66	4.79[h]	3.94	4.23	4.10	—	5.95	B
21	8.11, 8.10	6.40	4.90[f]	4.90[f]	3.94	4.24	3.94[f]	—	7.36	A
22	7.44,[d] 5.66[d]	6.07	4.22	4.07	3.68	3.98	3.92	5.63	7.11	A
23	8.26, 7.98	5.81	4.78	4.54	4.16[i]	4.10	4.04	[f]	5.91	B
23*a*	8.69, 8.64	6.20	6.26	4.61[f]	4.61	4.02[f]	3.92[f]	—	—	A

[a]See footnotes *a–j* of Table 2 which apply also to this table.

Si—O—Si bond angles have been reported (17). The glycosyl torsion angle χ_{CN} (O4′-C1′—N1-C6) is 16.9°, in the normal *anti* range. The C4′—C5′ rotamer is *gauche*$^+$ (gg) with a torsion angle of 45.9°. The nearly perfect ^3E (C3′-*endo* envelope) conformation of the furanose ring has a pseudorotation angle of $P = 19.7°$ with a maximum puckering amplitude of $\tau_m = 41.9°$, in harmony with the normal *N*-hemisphere ranges (18) and our ^{1}H nmr solution results (see section C.2.).

2. *Temperature effects*

Crystals of 3′,5′-*O*-TPDS-cytidine (**8**) decrease in their unit cell volume by 3.7% on cooling from 289 K[5] to 116 K (10). This decrease is due completely to a 1.07 Å shrinkage in the *c* unit cell dimension (the *a* and *b* cell axes lengths increase slightly). In spite of the large change in unit cell dimension, the molecular dimensions of 3′,5′-*O*-TPDS-cytidine are very similar. Bond lengths C2—N3, C2′—C3′, and C4′—O4′ differ by 3σ to 4σ between the two determinations. However, the largest discrepancies of up to 0.07 Å are in the disordered region of the four isopropyl groups. In our room temperature structure determination the equivalent isotropic B factors are in the range 9–18 Å^2 (Table 7)[5] whereas the liquid nitrogen temperature has reduced these values by a factor of approximately three to 3.1–8.7 Å^2 (10).

The two structures have been compared by a rigid body rotation and translation least-squares minimization program. The rms difference in positional coordinates after the refinement is 0.081 Å for the 32 non-hydrogen atoms. The largest atomic position differences are in the isopropyl groups (0.10–0.16 Å) and for the amino-nitrogen atom of the cytosine

Can. J. Chem. Downloaded from www.nrcresearchpress.com by 210.87.254.5 on 09/06/12
For personal use only.

TABLE 5. Proton spin–spin coupling values of α-D-ribo, β-D-arabino, and α-D-arabino 3′,5′-*O*-TPDS-furanosyl compounds[a]

Compound	$J_{1'-2'}$	$J_{2'-3'}$	$J_{3'-4'}$	$J_{4'-5'}$	$J_{4'-5''}$	$J_{5'-5''}$	$J_{2'-2'OH}$
15	3.5	4.0	9.1	3.0	2.5	−12.8	4.4
16	3.6	4.0	9.0	2.8	2.4	−13.0	4.4
17	4.0	5.0	8.0	4.0	3.0	−12.5	[b]
18	4.0	5.0	8.0	3.0	4.0	−10.5	[b]
19	6.3	8.0	8.0	4.0	2.5	−12.5	5.8
19*a*	6.7	8.0	8.5	[b]	[b]	[b]	—
20	6.0	8.0	8.0	4.0	3.0	−13.0	—
21	6.6	[b]	[b]	5.5	[b]	−13.0	—
22	6.2	7.0	7.8	3.8	3.0	−13.0	5.8
23	5.7	8.1	8.7	3.0	3.0	−13.2	[b]
23*a*	5.8	7.5	[b]	[b]	[b]	−13.0	—

[a]Coupling values in Hz.
[b]Unresolved.

TABLE 6. Ultraviolet absorbance maxima and high resolution mass spectral data for the 3′-5′-*O*-TPDS compounds

3′,5′-*O*-TPDS-(derivative of)	Ultraviolet(MeOH) max(nm)	Characteristic mass spectral ions		
		Calculated (M^+)	m/z (%)	m/z (M − *i*Pr) (%)
Adenosine (**1**)	260	509.2490 ($C_{22}H_{39}N_5O_5Si_2$)	509.2485 (9)	466.1924 (100)
2-Aminoadenosine (**2**)[a]	280, 258, 217	524.2599 ($C_{22}H_{40}N_6O_5Si_2$)	524.2598 (18)	481.2053 (16)
Inosine (**3**)[b]	249	510.2328 ($C_{22}H_{38}N_4O_6Si_2$)	510.2331 (4)	467.1774 (100)
Guanosine (**4**)	256	525.2435 ($C_{22}H_{39}N_5O_6Si_2$)	525.2443 (24)	482.1876 (91)
6-Thioguanosine (**4***b*)[c]	344, 260	541.2210 ($C_{22}H_{39}N_5O_5SSi_2$)	541.2219 (24)	498.1653 (86)
2-Amino-6-chloro-9-(β-D-ribofuranosyl)purine (**4***c*)	308, 245	543.2099 ($C_{22}H_{38}{}^{35}ClN_5O_5Si_2$)	543.2095 (8)	500.1545 (100)
Tubercidin (**5**)	270, 227	508.2528 ($C_{23}H_{40}N_4O_5Si_2$)	508.2547 (8)	465.1980 (60)
Toyocamycin (**6**)	280, 232	533.2492 ($C_{24}H_{39}N_5O_5Si_2$)	533.2478 (4)	490.1938 (100)
Uridine (**7**)	262	486.2268 ($C_{21}H_{38}N_2O_7Si_2$)	486.2262 (12)	443.6678 (100)
Cytidine (**8**)[d]	273	485.2378 ($C_{21}H_{39}N_3O_6Si_2$)	485.2384 (12)	442.1833 (96)
N^4-Acetylcytidine (**8***b*)	297, 247	527.2533 ($C_{23}H_{41}N_3O_7Si_2$)	527.2524 (0.3)	484.2006 (7)
3-Deazauridine (**9**)	280	485.2265 ($C_{22}H_{39}NO_7Si_2$)	485.2262 (12)	442.1718 (100)
3-Deazacytidine (**10**)	262	484.2424 ($C_{22}H_{40}N_2O_6Si_2$)	484.2429 (2)	441.1870 (10)
Methyl β-D-ribofuranoside (**11**)	[e]	363.1661 ($C_{15}H_{31}O_6Si_2$)[f]		363.1686 (4)
Pseudouridine (**12**)	260	443.1670 ($C_{18}H_{31}N_2O_7Si_2$)[f]		443.1667 (10)
Oxazinomycin (**12***a*)	[e]	444.1506 ($C_{18}H_{30}NO_8Si_2$)[f]		444.1516 (31)
Formycin (**13**)	304,[g] 294, 287[g]	509.2480 ($C_{22}H_{39}N_5O_5Si_2$)	509.2479 (14)	446.1936 (100)
Pyrazofurin (**14**)	266	458.1779 ($C_{18}H_{32}N_3O_7Si_2$)[f]		458.1775 (13)
1-α-D-Ribofuranosyluracil (**15**)	262	443.1670 ($C_{18}H_{31}N_2O_7Si_2$)[f]		443.1677 (67)
1-α-D-Ribofuranosylcytosine (**16**)	270	485.2378 ($C_{21}H_{39}N_3O_6Si_2$)	485.2380 (9)	442.1832 (100)
1-α-D-Ribofuranosyladenine (**17**)	260	509.2490 ($C_{22}H_{39}N_5O_5Si_2$)	509.2489 (6)	466.1942 (100)
Methyl α-D-ribofuranoside (**18**)	[e]	363.1661 ($C_{15}H_{31}O_6Si_2$)[f]		363.1686 (33)
9-β-D-Arabinofuranosyladenine (**19**)	260	509.2490 ($C_{22}H_{39}N_5O_5Si_2$)	509.2483 (5)	466.1927 (100)
N^6,$O^{2'}$-Diacetyl-9-β-D-arabinofuranosyladenine (**19***a*)	271	593.2701 ($C_{26}H_{43}N_5O_7Si_2$)	593.2690 (1)	550.2151 (100)
9-(2-Chloro-2-deoxy-β-D-arabinofuranosyl)adenine (**20**)	259	527.2167 ($C_{22}H_{38}{}^{35}ClN_5O_4Si_2$)	527.2170 (8)	484.1612 (100)
9-(2-Azido-2-deoxy-β-D-arabinofuranosyl)adenine (**21**)	261	534.2557 ($C_{22}H_{38}N_8O_4Si_2$)	534.2521 (3)	491.2008 (30)
1-β-D-Arabinofuranosylcytosine (**22**)	270	485.2378 ($C_{21}H_{39}N_3O_6Si_2$)	485.2386 (1)	492.1832 (10)
9-α-D-Arabinofuranosyladenine (**23**)	260	509.2490 ($C_{22}H_{39}N_5O_5Si_2$)	509.2484 (2)	466.1945 (100)
N^6,$O^{2'}$-Diacetyl-9-α-D-arabinofuranosyladenine (**23***a*)	271	593.2701 ($C_{26}H_{43}N_5O_7Si_2$)	593.2690 (1)	550.2151 (100)

[a]White needles from EtOH with mp 190–192°C.
[b]Crystals from 50% CH_3CN/EtOH with mp 219–220.5°C.
[c]Yellow needles from EtOH with mp > 255°C (dec).
[d]Crystals from $CHCl_3$ with mp 267–269°C.
[e]Ultraviolet transparent.
[f]No molecular ion was observed. Calculated value and formula are for the (M − *i*Pr) ion.
[g]Shoulder.

base, N4 (Δ = 0.14 Å). Slight differences in some of the molecular torsional angles can be attributed to the rearranged packing interactions that result in crystal cooling. χ_{CN}, the glycosidic torsion angles, differ by 4.5°; other torsional angles

Can. J. Chem. Downloaded from www.nrcresearchpress.com by 210.87.254.5 on 09/06/12
For personal use only.

Can. J. Chem. Downloaded from www.nrcresearchpress.com by 210.87.254.5 on 09/06/12
For personal use only.

TABLE 7. Fractional coordinates and equivalent isotropic temperature factors (B_{eq}, Å^2) for the non-hydrogen atoms of 3′,5′-*O*-TPDS-cytidine. The atomic positional parameters have been multiplied by 10^4; the estimated standard deviations in the parameters are given in parentheses

Atom	x/a	y/b	z/c	B_{eq}
O12	−809 (4)	5540 (3)	3951 (1)	6.63 (15)
N1	4254 (4)	2898 (3)	3416 (1)	5.34 (14)
C2	4817 (5)	2355 (4)	3011 (1)	5.93 (19)
N3	4583 (5)	1081 (3)	2923 (1)	6.30 (17)
C4	3811 (6)	390 (4)	3223 (2)	5.95 (20)
C5	3198 (6)	919 (4)	3648 (2)	6.42 (21)
C6	3455 (5)	2196 (4)	3727 (1)	5.89 (19)
O2	5523 (5)	3057 (3)	2741 (1)	8.60 (20)
N4	3591 (5)	−870 (3)	3125 (2)	7.03 (20)
O4′	4356 (4)	4583 (3)	3966 (1)	5.86 (12)
C1′	4594 (5)	4291 (4)	3489 (1)	5.43 (17)
C2′	3577 (5)	5168 (4)	3200 (1)	5.44 (17)
C3′	2351 (4)	5458 (3)	3563 (1)	4.85 (15)
C4′	3288 (5)	5610 (3)	4004 (1)	5.23 (16)
C5′	2431 (6)	5529 (4)	4454 (1)	5.88 (19)
O2′	4338 (4)	6308 (3)	3087 (1)	7.00 (15)
O3′	1452 (3)	6551 (2)	3471 (1)	5.72 (12)
O5′	1408 (4)	4473 (3)	4459 (1)	6.23 (14)
Si1	−413 (2)	6435 (1)	3506 (1)	6.31 (5)
C12	−1211 (8)	5688 (6)	2976 (2)	9.58 (38)
C122	−731 (12)	4270 (8)	2910 (4)	13.39 (59)
C121	−775 (13)	6474 (11)	2544 (3)	15.71 (70)
C11	−1060 (7)	8125 (6)	3591 (3)	9.70 (36)
C111	−2765 (8)	8262 (9)	3577 (5)	18.54 (83)
C112	−370 (11)	8739 (7)	4013 (3)	13.35 (56)
Si2	−416 (2)	4606 (1)	4397 (0)	6.25 (5)
C21	−956 (8)	2904 (6)	4288 (2)	9.23 (34)
C211	−513 (12)	2008 (6)	4685 (3)	12.43 (51)
C212	−2519 (9)	2623 (8)	4127 (4)	13.53 (57)
C22	−1301 (8)	5254 (10)	4916 (3)	12.17 (52)
C221	−376 (10)	5944 (11)	5268 (3)	13.75 (57)
C222	−2915 (7)	5777 (8)	4848 (3)	11.22 (43)

agree more closely.

It can be seen in Fig. 3 that there are 4 molecules stacked parallel to the *c* axis. Thus, the large shrinkage of 1.07 Å in the *c* dimension can occur by relatively small movements of ~0.25 Å between the layers relative to one another. This movement is probably a result of the reduced amplitude of thermal motion of the isopropyl groups in the hydrophobic layer. Also contributing is an apparent change in the intermolecular hydrogen bonding involving O2′ and N3 on 2_1 related molecules. The low temperature structure has a bifurcated hydrogen bond for the hydrogen atom on atom O2′ (to N3 and O2 respectively) whereas in our room temperature structure the O2′—H···O2 interaction is not consistent with hydrogen bonding even though the O2′···O2 distance is short (O---O: 2.99 Å, O---H: 2.41 Å). Theoretical analysis of these two structures should contribute to an understanding of the molecular dynamics involved in the structural changes.

C. ^{1}H nuclear magnetic resonance solution studies

1. *General considerations*

Conversion of the 2′-hydroxyl groups of 3′,5′-*O*-TPDS-ribonucleosides to their phenyl thionocarbonate esters resulted in downfield shifts of $\Delta\delta$ = 1.94–2.16 ppm for the H2′, 0.44–0.80 ppm for the H3′, and 0.22–0.50 ppm for the H1′ signals (see Table 2). The $J_{1'-2'}$ values increased upon thioacylation of O2′ for the purine-type compounds (**1**, **4**, **5**, **6** → **1***a*, **4***a*, **5***a*, **6***a*), but remained at $J_{1'-2'} < 0.5$ Hz for the pyrimidine derivatives (**7**, **8**, **8***b* → **7***a*, **8***a*, **8***c*). The $J_{2'-3'}$ values increased significantly upon thioacylation of O2′ for both purine and pyrimidine compounds (**1**, **4**, **7**, **8** → **1***a*, **4***a*, **7***a*, **8***a*), but remained essentially constant for tubercidin and toyocamycin (**5**, **6** → **5***a*, **6***a*) (see Table 3).

A remarkably consistent environment in the C4′—C5′ region of these 3′,5′-*O*-TPDS derivatives is indicated by the chemical shift and coupling data for H4′, H5′, and H5″ in Tables 2–5. Only minor perturbations in these parameters occur upon changing the base substituent at C1′ or upon thioacylation of O2′. A nearly symmetrical *gauche*$^+$ equilibrium for the C4′—C5′ orientation in harmony with the crystal data (see section B.1.) is suggested from the $J_{4'-5'}$ and $J_{4'-5''}$ values. The absence of trends relating minor changes in $J_{3'-4'}$ with changes in $J_{1'-2'}$, base substituent type at C1′, or thioacylation of O2′ argues for restricted conformational mobility and/or a consistent equilibrium population in the C3′—C4′—C5′ molecular fragment.

Reliable conformational analysis of these 3′,5′-*O*-TPDS derivatives in solution by ^{1}H nmr is complicated by several factors. (1) Karplus equation constants are sensitive to the electronegativity of substituents as well as to bond length and angle distortions. The disiloxane bridge represents a new substituent and furanose ring distortions similar to those seen in cyclic 3′,5′-monophosphates (15) are present. (2) Nucleosides, nucleotides, and nucleoside cyclic 2′,3′-monophosphates have been treated as pseudorotating equilibrium mixtures (19–21) whereas nucleoside cyclic 3′,5′-monophosphates have been regarded as rigid single conformers in solution (1, 9, 13, 22). Crystallographic thermal parameters of **8** are high for the isopropyl groups. Temperature and solvent effects on the coupling parameters of certain 3′,5′-*O*-TPDS compounds also would suggest conformational flexibility for the fused ring system. However, the X-ray structure of **8** as well as consistency in coupling values in the C3′—C4′—C5′ region are more compatible with the restricted cyclic 3′,5′-monophosphate features. (3) The two-state *N* ⇄ *S* (C3′-*endo* C2′-*exo* ⇄ C3′-*exo* C2′-*endo*) pseudorotational model of Altona and Sundaralingam (18*a*, 19) assumes a small rotation barrier about C2′—C3′ on a "symmetrical" furanose ring and is in harmony with a large data base of crystal structures for nucleosides and "open" nucleotides. However, in the present 3′,5′-*O*-TPDS-ribonucleosides, there are no clear reciprocal trends relating $J_{1'-2'}$ and $J_{3'-4'}$ or ($J_{1'-2'}$ + $J_{3'-4'}$) and $J_{2'-3'}$. Therefore, flattening of the molecule and fluctuations of the pucker in the O4′—C1′—C2′ region might add further complexity.

First-order analysis of the 400 MHz ^{1}H nmr spectrum of **8** gave coupling parameters that were not altered significantly by computer simulation. No attempt was made to further refine the data for the other compounds since first-order values were similar for a sizeable number of resolved spectral peaks. The pseudorotational model involves major assumptions (19, 23) and the resulting analyses, while providing very useful results, must be recognized as somewhat uncertain approximations.

2. *3′,5′-O-TPDS-β-D-ribofuranosyl compounds*

Mean average coupling parameters for nine 3′,5′-*O*-TPDS ribonucleoside derivatives (**1**, **1***a*, **2**–**4**, **4***b*, **4***c*, **5***a*, **6***a*) from Table 3 are $J_{1'-2'}$ = 1.4 ± 0.2 Hz, $J_{2'-3'}$ = 5.1 ± 0.2 Hz, $J_{3'-4'}$ = 8.2 ± 0.3 Hz, and ($J_{1'-2'}$ + $J_{3'-4'}$) = 9.6 ± 0.4 Hz. The Altona–Sundaralingam numerical treatment (19) gives a "best fit" for an 85% *N* (15% *S*) equilibrium composition (K_{eq} = 0.18) with pseudorotational parameters of P_N = 4.3°, $^N\tau_m$ =

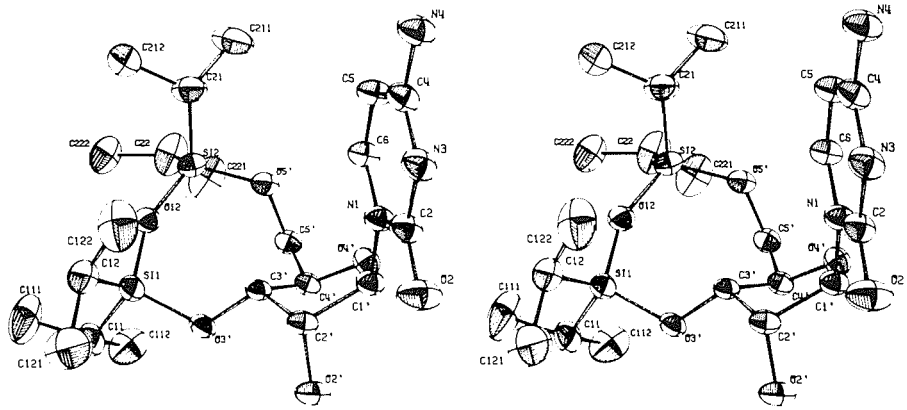

FIG. 1. ORTEP stereodrawing of 3′,5′-*O*-TPDS-cytidine showing the atom numbering used in this analysis. The thermal ellipsiods enclose 20% probability. The glycosyl torsion angle χ_{CN} (O4′-C1′—N1-C6) is 16.9°. The β-D-ribose ring has the ^3E conformation. The fused 8-membered trioxadisilacyclooctane is flattened with six atoms approximately coplanar (mean Δ = 0.037 Å). Atoms C3′ and C5′ deviate by −0.81 Å and 0.78 Å on opposite sides of this plane.

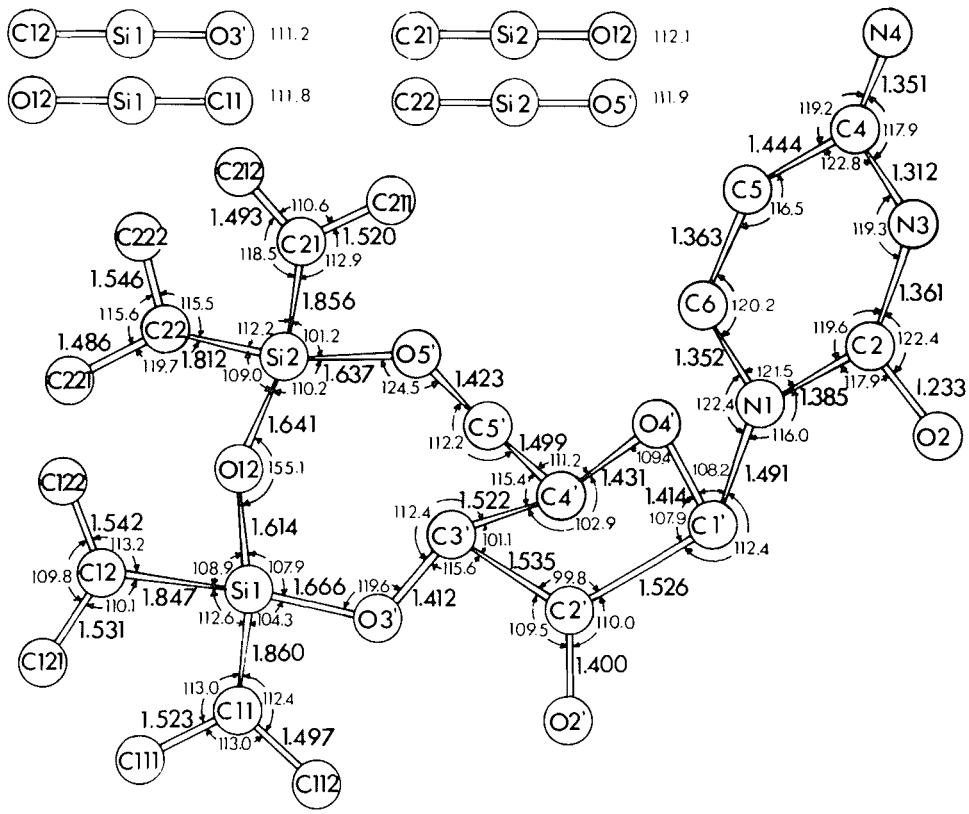

FIG. 2. Bond distances and interbond angles for 3′,5′-*O*-TPDS-cytidine at $R = 0.059$. The average esd's in bond lengths are 0.006 Å, in bond angles 0.4°.

35.6°; $P_S = 170.4°$, $^S\tau_m = 36°$; $^NJ_{1'-2'} = 0$ Hz, $^NJ_{3'-4'} = 9.6$ Hz; $^SJ_{1'-2'} = 9.5$ Hz, $^SJ_{3'-4'} = 0.1$ Hz. A modified Karplus vicinal proton coupling equation ($J_{H-H} = A\cos^2\phi_{H-H} - B\cos\phi_{H-H}$) with $A = 10.5$ and $B = 1.2$ was used (19). The related graphical analysis of Davies and Danyluk with Karplus constants of $A = 9.8$ and $B = 0.9$ calculated for ribonucleotides (20*a*) gave an 87% *N* (13% *S*, $K_{eq} = 0.15$) composition with $P_N = 21°$, $^N\tau_m = 37°$; $P_S = 163°$, $^S\tau_m = 39.5°$.

These parallel pseudorotational treatments indicate an $N \rightleftarrows S$ equilibrium with ~85% population in the ^3E–$^3T_2$ sector of *N*-pseudorotamers and ~15% in the ^2E–$^2T_3$ *S*-range (19). The calculated parameters fall within the most highly populated ranges found for β-D-ribofuranosyl compounds in the solid state (18*a*) and those indicated for the *N*-conformer average are compatible with the crystallographic structure of **8** (see section B.1.). It is noteworthy that the averaged coupling values are in harmony with the Case D pseudorotational composition of Altona and Sundaralingam,[7] but not with any single "ideal" conformation derived directly.

The derivatives (**5**, **6**, **7**–**8***a*, **8***c*, **10**–**12***a*) with vanishingly small anomeric proton coupling constants ($J_{1'-2'} < 0.5$ Hz) have a slightly smaller $J_{2'-3'} = 4.9 \pm 0.4$ Hz mean coupling

[7]See Table IV of ref. 19.

Can. J. Chem. Downloaded from www.nrcresearchpress.com by 210.87.254.5 on 09/06/12
For personal use only.

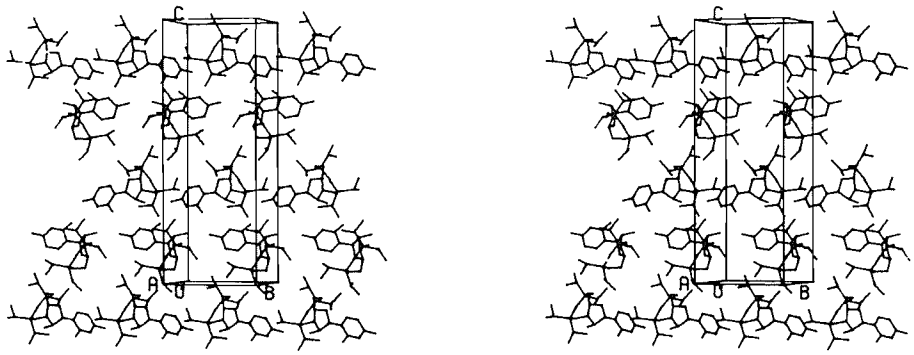

FIG. 3. The packing of the molecules of 3′,5′-*O*-TPDS-cytidine in the unit cell. The hydrogen-bonded chains of molecules run parallel to the 2_1 screw axes that are parallel to the crystallographic *b* axes.

Can. J. Chem. Downloaded from www.nrcresearchpress.com by 210.87.254.5 on 09/06/12
For personal use only.

and a slightly larger $J_{3'-4'} = 8.5 \pm 0.4$ Hz mean than the above group of nine compounds. However, the variation in these couplings is greater and the mean limits overlap the former series. The sum ($J_{1'-2'} + J_{3'-4'}$) is smaller in the latter group owing to the decrease in $J_{1'-2'}$. This would suggest a more flattened ring, but no significant increase in $J_{2'-3'}$ is observed as would be expected from an "ideal" pseudorotating furanose system (19). By comparison, mean coupling values for four nucleoside cyclic 3′,5′-monophosphates (*c*AMP, *c*GMP, *c*UMP, *c*CMP) were reported to be $J_{1'-2'} < 0.7$ Hz, $J_{2'-3'} = 5.4 \pm 0.2$ Hz, and $J_{3'-4'} = 9.9 \pm 0.2$ Hz (1, 22*c*). *Both* $J_{2'-3'}$ and $J_{3'-4'}$ are significantly larger than in the present series of 3′,5′-*O*-TPDS derivatives. The cyclic 3′,5′-monophosphates have been assumed to exist in an essentially rigid $^3T_4$ to ^3E conformation range. Distortions resulting from the strained fused ring system have been assumed to cause deviations in coupling values from those expected for an ideal ^3E conformer.

A "relaxed" C3′—C4′ region with a more flattened furanose ring in the *N* (^3E–$^3T_2$) range distorted by fusion with the hindered disiloxane fragment (in pseudorotational equilibrium with a minor population of *S*-forms) probably represents the best estimation of the solution conformation of these 3′,5′-*O*-TPDS-β-D-ribofuranosyl compounds. The series with $J_{1'-2'} < 0.5$ Hz appears to shift toward a more nearly pure *N*-type population with additional furanose distortions. However, a more nearly rigid conformation with significant angle distortions cannot be exluded completely.

3. *3′,5′-O-TPDS-α-D-ribofuranosyl compounds*

Mean coupling values for the four α-D-ribofuranosyl anomers (**15**–**18**) in Table 5 are $J_{1'-2'} = 3.8 \pm 0.2$ Hz, $J_{2'-3'} = 4.5 \pm 0.5$ Hz, and $J_{3'-4'} = 8.5 \pm 0.5$ Hz. These parameters compare favorably with those found for four α-D-ribofuranosyl cyclic 3′,5′-monophosphates ($J_{1'-2'} = 3.9 \pm 0.6$ Hz, $J_{2'-3'} = 4.2 \pm 0.4$ Hz, and $J_{3'-4'} = 10.0 \pm 0.2$ Hz) (13) except, again, for the more "relaxed" H3′—H4′ coupling. The slightly increased $J_{2'-3'}$ mean and sizeably reduced $J_{3'-4'}$ couplings in the 3′,5′-*O*-TPDS compounds are compatible with flattening of the furanose ring in the *N*-range (19) relative to the "maximally puckered" cyclic 3′,5′-monophosphates (13).

4. *3′,5′-O-TPDS-arabinofuranosyl compounds*

Mean coupling values for the five β-D-arabinofuranosyl derivatives (**19**,. **19***a*, **20**–**22**) in Table 5 are $J_{1'-2'} = 6.4 \pm 0.2$ Hz, $J_{2'-3'} = 7.8 \pm 0.4$ Hz, and $J_{3'-4'} = 8.1 \pm 0.2$ Hz. Directly derived mean angles from $J_{H-H} = 10.5 \cos^2 \phi_{H-H} - 1.2 \cos \phi_{H-H}$ are $\phi_{1'-2'} = 33°$, $\phi_{2'-3'} = 144°$, and $\phi_{3'-4'} = 145°$. This clearly, indicates a conformer population in the *N* ($_2T^3$–$_2E$) range in harmony with partial coupling data for β-D-arabinofuranosyl cyclic 3′,5′-monophosphates (1) and in constrast with the "pure" *S* (^2E) conformers observed for arabinofuranosyl cyclic 2′,5′-monophosphates (9, 24, 25). This also provides corroboration of the 3′,5′-*O*-TPDS (vs. the possible 2′,5′-*O*-linkage) structure for these arabino derivatives.

Two 3′,5′-*O*-TPDS-α-D-arabinofuranosyl anomers (**23** and **23***a*) were prepared. The $J_{1'-2'} = 5.7$ Hz, $J_{2'-3'} = 8.1$ Hz, and $J_{3'-4'} = 8.7$ Hz values for **23** and $J_{1'-2'} = 5.8$ Hz and $J_{2'-3'} = 7.5$ Hz for **23***a* are again compatible with an *N*-type conformation population.

Conclusions

A strong preponderance of *N*-type conformers with a remarkably consistent range of $J_{3'-4'}$ values is seen throughout the 3′,5′-*O*-TPDS nucleosides in the present study irrespective of the type of base substituent at C1′, the anomeric configuration at C1′, and the epimeric configuration or substituent at C2′. This indicates a rather demanding conformational preference for the tetraisopropyl-substituted *trans*(1,2) 1,3,5-trioxa-2,4-disilacyclooctane to furanose ring fusion. The powerful bias for the *N*-range of conformers is responsible for the small anomeric proton (H1′) to H2′ coupling values observed in the 3′,5′-*O*-TPDS-β-D-ribofuranosyl derivatives. An apparent low limit of $J_{1'-2'} \geq 3.5$ Hz exists for α-D-ribofuranosyl 3′,5′-*O*-TPDS compounds in agreement with their cyclic 3′,5′-monophosphate analogues (1). Larger anomeric proton coupling values occur with both α-D- and β-D-arabinofuranosyl 3′,5′-*O*-TPDS derivatives.

The β configuration of a ribofuranosyl 3′,5′-*O*-TPDS derivative can be assigned with confidence when $J_{1'-2'} \lesssim 1.5$ Hz. It should be recognized that *this is not an empirical criterion*, but is dependent on the geometrical constraints of the fused ring system. It is *definitive for the β anomeric assignment* whenever $J_{1'-2'} \lesssim 1.5$ Hz is observed directly, or is realized by alteration of solvent or temperature. Alternative methods (1) should be employed to corroborate β assignments in cases of $J_{1'-2'} \gtrsim 1.6$ Hz and to verify α assignments ($J_{1'-2'} \geq 3.5$ Hz). The latter ranges of couplings might be found to overlap with certain anomeric pairs owing to the potential flexibility of the 8 to 5 fused ring system.

The commercial availability of 1,3-dichloro-1,1,3,3-tetraisopropyldisiloxane[8] makes this determination readily applicable.

Acknowledgments

We thank the Natural Sciences and Engineering Research

[8]Available from Aldrich Chemical Co.

Council of Canada (A5890), the National Cancer Institute of Canada, the Medical Research Council of Canada (grant to the MRC Group in Protein Structure and Function), and The University of Alberta for generous support. M.J.R. thanks Professor A. D. Broom for facilities and hospitality provided during a visiting professorship at the University of Utah 1981–1982.

1. M. J. ROBINS and M. MACCOSS. J. Am. Chem. Soc., **99**, 4654 (1977).
2. (*a*) W. T. MARKIEWICZ and M. WIEWIOROWSKI. Nucleic Acids Res., Spec. Publ. No. 4. s185 (1978); (*b*) W. T. MARKIEWICZ. J. Chem. Res. Synop. 24 (1979).
3. C. H. M. VERDEGAAL, P. L. JANSSE, J. F. M. DE ROOIJ, and J. H. VAN BOOM. Tetrahedron Lett. **21**, 1571 (1980).
4. (*a*) M. J. ROBINS and J. S. WILSON. J. Am. Chem. Soc. **103**, 932 (1981); (*b*) J. S. WILSON. Ph.D. Dissertation, The University of Alberta, 1981.
5. W. T. MARKIEWICZ, N. SH. PADYUKOVA, Z. SAMEK, and J. SMRT. Collect. Czech. Chem. Commun. **45**, 1860 (1980).
6. M. SMITH, G. I. DRUMMOND, and H. G. KHORANA. J. Am. Chem. Soc. **83**, 698 (1961).
7. (*a*) W. J. WECHTER. J. Org. Chem. **34**, 244 (1969); (*b*) M. Hubert-Habart and L. GOODMAN. Chem. Commun. 740 (1969).
8. (*a*) R. U. LEMIEUX and D. R. LINEBACK. Annu. Rev. Biochem. **32**, 155 (1963); (*b*) K. L. RINEHARDT, JR., W. S. CHILTON, M. HICKENS, and W. VON PHILLIPSBORN. J. Am. Chem. Soc. **84**, 3216 (1962); (*c*) J. A. MAY, JR. and L. B. TOWNSEND. J. Org. Chem. **41**, 1449 (1976).
9. M. KAINOSHO and K. AJISAKA. J. Am. Chem. Soc. **97**, 6839 (1975).
10. C. H. M. VERDEGAAL, A. J. DE KOK, H. P. WESTERINK, J. H. VAN BOOM, and C. ROMERS. Acta Crystallogr. Sect. B, **37**, 1924 (1981).
11. M. J. ROBINS, J. S. WILSON, and F. HANSSKE. J. Am. Chem. Soc. In press.
12. K. PANKIEWICZ, A. MATSUDA, and K. A. WATANABE. J. Org. Chem. **47**, 485 (1982).
13. M. MACCOSS, F. S. EZRA, M. J. ROBINS, and S. S. DANYLUK. J. Am. Chem. Soc. **99**, 7495 (1977).
14. C. K. JOHNSON. ORTEP Report ORNL-3794. Oak Ridge National Laboratory, Tennessee, 1965.
15. (*a*) C. L. COULTER. Acta Crystallogr. Sect. B, **25**, 2055 (1969); (*b*) M. SUNDARALINGAM and J. ABOLA. J. Am. Chem. Soc. **94**, 5070 (1972); (*c*) A. K. CHWANG and M. SUNDARALINGAM. Acta Crystallogr. Sect. B, **30**, 1233 (1974).
16. (*a*) M. SUNDARALINGAM. Ann. N.Y. Acad. Sci. **255**, 3 (1975); (*b*) P. PRUSINER and M. SUNDARALINGAM. Acta Crystallogr. Sect. B, **34**, 517 (1978).
17. N. G. BOKII and YU. T. STRUCHKOV. Zh. Strukt. Khim. **9**, 722 (1968).
18. (*a*) C. ALTONA and M. SUNDARALINGAM. J. Am. Chem. Soc. **94**, 8205 (1972); (*b*) S. T. RAO, E. WESTHOF, and M. SUNDARALINGAM. Acta Crystallogr. Sect. A, **37**, 421 (1981).
19. C. ALTONA and M. SUNDARALINGAM. J. Am. Chem. Soc. **95**, 2333 (1973).
20. (*a*) D. B. DAVIES and S. S. DANYLUK. Biochemistry, **13**, 4417 (1974); (*b*) **14**, 543 (1975).
21. R. D. LAPPER and I. C. P. SMITH. J. Am. Chem. Soc. **95**, 2880 (1973).
22. (*a*) M. SMITH and C. D. JARDETZKY. J. Mol. Spectrosc. **28**, 70 (1968); (*b*) B. J. BLACKBURN, R. D. LAPPER, and I. C. P. SMITH. J. Am. Chem. Soc. **95**, 2873 (1973); (*c*) C-H. LEE and R. H. SARMA. J. Am. Chem. Soc. **98**, 3541 (1976); (*d*) M. J. ROBINS, M. MACCOSS, and J. S. WILSON. J. Am. Chem. Soc. **99**, 4660 (1977).
23. (*a*) W. K. OLSON and J. L. SUSSMAN. J. Am. Chem. Soc. **104**, 270 (1982); (*b*) W. K. OLSON. J. Am. Chem. Soc. **104**, 278 (1982).
24. M. MACCOSS, F. S. EZRA, M. J. ROBINS, and S. S. DANYLUK. Carbohydr. Res. **62**, 203 (1978).
25. M. MACCOSS, C. F. AINSWORTH, G. LEO, F. S. EZRA, and S. S. DANYLUK. J. Am. Chem. Soc. **102**, 7353 (1980).
26. E. DE CLERCQ, J. DESCAMPS, J. BALZARINI, J. GIZIEWICZ, P. J. BARR, and M. J. ROBINS. J. Med. Chem. In press.

Can. J. Chem. Downloaded from www.nrcresearchpress.com by 210.87.254.5 on 09/06/12
For personal use only.

Cholesteric type II Micellar mesophases prepared from two different single centre chiral amphiphiles

D. D. LASIČ
Institut 'Josef Stefan', University of Ljubljana, Ljubljana, Yugoslavia

AND

M. E. MARCONDES HELENE AND L. W. REEVES[1]
Chemistry Department, University of Waterloo, Waterloo, Ont., Canada N2L 3G1

Received February 10, 1983

D. D. LASIČ, M. E. MARCONDES HELENE, and L. W. REEVES. Can. J. Chem. **61**, 1921 (1983).

A mixed micellar cholesteric mesophase has been prepared using sodium L-lauroylalaninate (L-LAK) and sodium D-lauroylserinate (D-LSK). The cholesteric mesophase can be synthesized with all mixtures of these amphiphiles from 100% L-LAK to 100% D-LSK in the micelle. The measurement of the pitch length at constant temperature has been accomplished for the whole range of relative composition of the two different single chiral centre amphiphiles at constant water content and with all other components unchanged in composition. The inverse pitch length is not a simple function of composition as has been found in thermotropic cholesterics. The sign of the helix is the same for L-LAK and D-LSK. Temperature dependence of the pitch in both the single chiral amphiphile and mixed chiral amphiphile mesophases gives longer pitches as the temperature is raised in all cases.

D. D. LASIČ, M. E. MARCONDES HELENE et L. W. REEVES. Can. J. Chem. **61**, 1921 (1983).

On a préparé une mésophase cholestérique micellaire mixte en utilisant le L-lauroylalaninate de sodium (L-LAK) et le D-lauroylsérinate de sodium (D-LSK). On peut synthétiser la mésophase cholestérique avec tous les mélanges possibles de ces amphiphiles en partant de 100% de L-LAK jusqu'à 100% de D-LSK dans la micelle. On a mesuré la longueur du pas à température constante pour tout le domaine de composition relative des deux différents amphiphiles de centre chiral simple pour une teneur constante en eau sans changer la composition des autres composants. La longueur du pas inverse n'est pas une fonction simple de la composition comme on l'a trouvé dans les cholestériques thermotropiques. L'hélice a le même signe dans le L-LAK et dans le D-LSK. L'effet de la température sur le pas de l'hélice dans le cas de l'amphiphile simple et dans le cas des mésophases amphiphiles chiraux mixtes, se traduit dans tous les cas par une augmentation du pas lorsque la température s'élève.

[Traduit par le journal]

Introduction

A type II cholesteric liquid crystal based on finite micelles, containing a single centre resolved optically active amphiphile, was recently prepared for the first time (1). The negative diamagnetic anisotropy, perpendicular to the helix axis, requires that the latter axis aligns parallel to a magnetic field (2). The procedure of locating a type II DM nematic phase, and then at the same composition unbalancing the mixture of *d* and *l* forms of the amphiphile, was successful in creating three more type II cholesterics based on potassium lauroyl alaninate, serinate, and valinate (3). The pitch length of the aligned mesophases was determined as a function of the mole fraction of D and L forms, the water content, the concentration of some highly dissymmetric solutes, and the presence of such solutes at a fixed concentration in the bilayers (3). In the simplest case of mixtures of D and L forms the inverse pitch obeyed the equation

$$[1] \quad \frac{1}{2p} = \beta(2x_L - 1)$$

where p = the helical pitch length, β is the twisting power of the single centre amphiphile, and x_L = mole fraction of the L form of this amphiphile in the bilayer of the mesophase. The mole fractions of all components in the mesophases made from potassium lauroylalaninate (LAK) and potassium lauroyl serinate (LSK) were the same and, consequently, mixed phases using the L form of one and the D form of the other are accessible. The cholesteric behaviour in these micellar liquid crystals is a secondary consequence of the dissymmetric amphiphile, which resides in a micelle bilayer (3). The agreement with eq. [1] gives no information that the twist is a secondary consequence of interactions between molecules. The present article is devoted to a study of the cholesteric pitch resulting from the use of two different amphiphiles where the cross term in the interaction model is not zero (4). In addition, the opportunity has been afforded to study the pitch length as a function of temperature.

Experimental

Sodium D-*N*-lauroylserinate(D-LSK) and sodium L-*N*-lauroylalaninate (L-LAK) were synthesized according to published procedures for acylation of amino acids (5). Mesophases which were type II cholesteric were prepared using mixtures of D-LSK and L-LAK, in which the mole fractions of all components, amphiphiles, electrolyte, and water, were maintained constant. The mesophase compositions in terms of moles were: 1.175 mol of L-LAK + D-LSK, 0.337 mol of Na_2SO_4, 0.446 mol of decanol, and 38.9 mol of $H_2O(D_2O)$. The ratio of moles of the L-LAK and D-LSK used in the mixture of chiral amphiphiles were 1:0, 0.8:0.2, 0.6:0.4, 0.4:0.6, 0.2:0.8, and 0:1. The pitch lengths were measured by laser diffraction in aligned or unaligned samples with the wavelength 632.8 nm at room temperature.

Results

The inverse pitch versus mole fraction of D-LSK in the mixture of optically active amphiphiles is plotted in Fig. 1. Unlike mesophases prepared from single optically active amphiphiles, the dependence is not linear (3). The mixture produces a nematic mesophase at 0.72 mole fraction D-LSK in the mixture at 30°C.

The inverse pitch versus temperature for the mesophases

[1]Author to whom correspondence may be addressed.

Can. J. Chem. Downloaded from www.nrcresearchpress.com by 210.87.254.105 on 09/06/12
For personal use only.

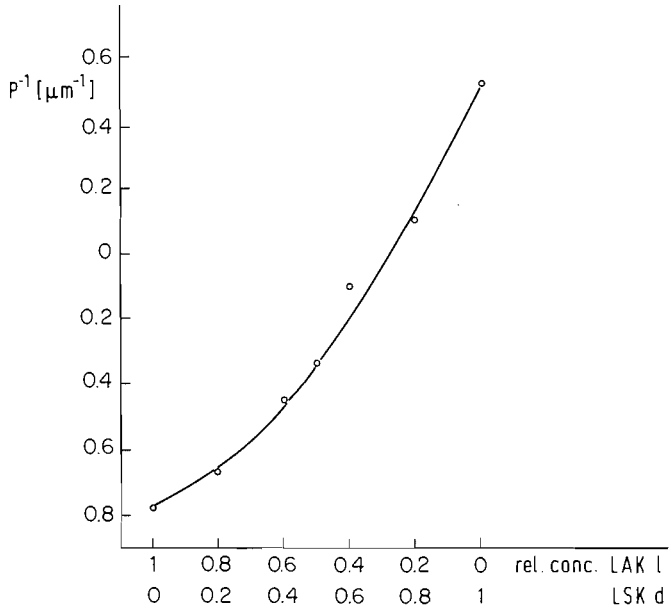

FIG. 1. Variation of the inverse pitch versus composition.

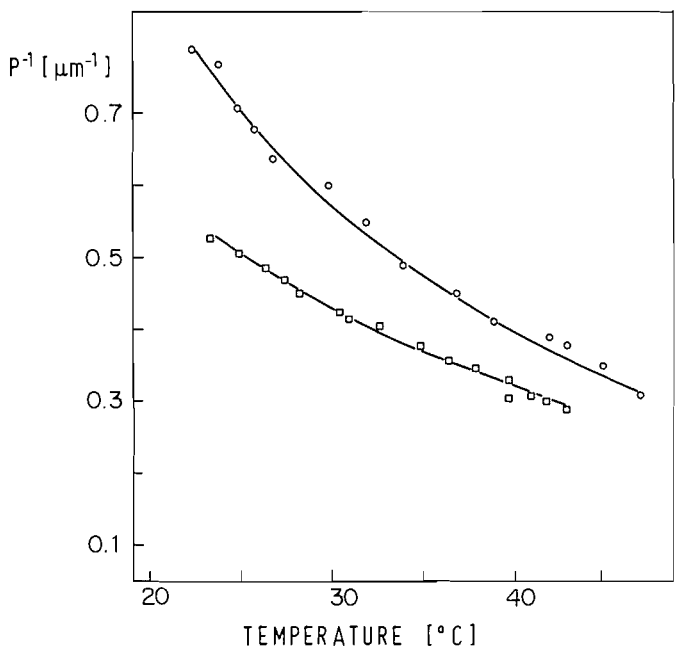

FIG. 2. Temperature dependence of the inverse pitch of pure L-LAK (circles) and pure D-LSK (squares).

containing pure D-LSK and pure L-LAK is plotted in Fig. 2. In both cases the pitch length increases with temperature and the inverse pitch is not a linear function. In Fig. 3 the inverse pitch of two mixtures of the two amphiphiles is represented as a function of temperature. A similar nonlinear dependence is found with the pitch lengthening with temperature rise.

Discussion

Cholesteric liquid crystals derived from orientationally ordered finite micelles (6) are fundamentally different from thermotropic liquid crystals from a molecular viewpoint. The system is compartmentalized into nonmixing regions, the finite micelles, and the aqueous compartment. In this and prior cases (1, 3) the optically active components are contained within the

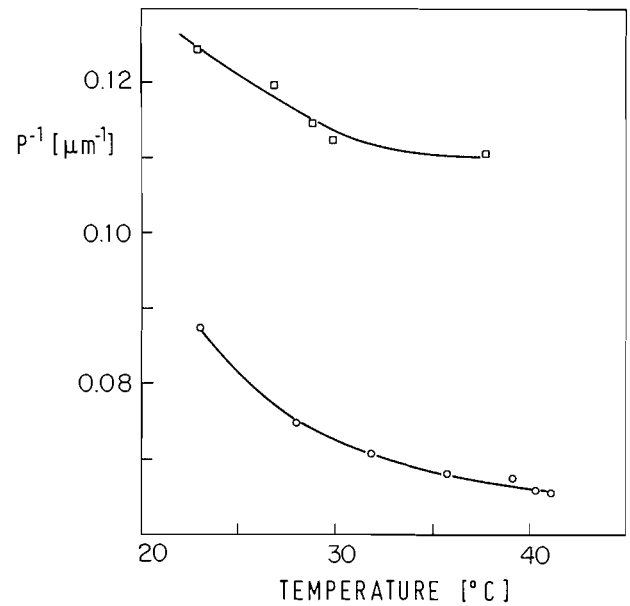

FIG. 3. Temperature dependence of the inverse pitch of sample with 0.4 L-LAK and 0.6 D-LSK (squares) and of sample with 0.2 L-LAK and 0.8 D-LSK (circles).

micelles, being amphiphilic compounds. The nematic phase is obtained from equimolar concentrations of D and L forms of the same amphiphile, in which case the micelles are known to be bilayer disks which are planar. The micellar liquid crystals have, in the present case, no chiral components in the aqueous compartment. The twisting action at short range between dissymmetric components can only proceed within the micelle to the extent of its major dimension distance. The micelle is then isolated from the next neighbour by components such as water and simple spherical ions which have no chiral aspect. It was suggested in two prior publications (1, 3) that the long range helical orientational order of the cholesteric phase derives from a partial twisting of individual micelles which then pack more efficiently with helical rather than nematic order. However, there are other explanations of the reduction of asymmetric micelles.[2] The same chiral amphiphiles in lower concentrations of water form *lamellar* phases, which can have no helical axis formed from a transmission of chiral information across the intervening water barrier between infinite micelles.

It is known (6) that the finite micelle nematics have different mean micelle sizes over the range of water content of the nematic system. At the highest water content the planar disk micelles are smaller. Correspondingly, because the cholesteric phase is derived from the nematic phase merely by preparing it with an unbalanced mixture of D and L forms, the micelle size in the cholesteric phase decreases as water content increases. Since the pairwise interaction over long range between amphiphiles may proceed only as far as the major dimension of the micelle, then this factor must enter into the equations affecting the pitch length. For this reason it was shown (3) that the pitch length depends in a complex manner on water content.

[2]D. D. Lasič, unpublished results. The chiral molecules dissolved in the micelle may induce tilted bilayers in the disklike micelles. In the rodlike micelles the lipid micelles may also not be perpendicular to the water surface. The same effect may also have chiral amphiphiles. Such asymmetric micelles can be packed into a helical order rather than in nematic order.

Can. J. Chem. Downloaded from www.nrcresearchpress.com by 210.87.254.105 on 09/06/12
For personal use only.

The equation of Bak and Labes (4) for thermotropic cholesteric mixtures, applies to D and L mixtures of the same amphiphile in the finite micelle case for fixed water content. The mole fraction taken for the D or L form is that in the micelle, and the number of moles of water and other nonchiral components are kept constant. The twist coefficients β are much smaller for the lyotropic case. The equation for a mixture of two optically active compounds (4) is

$$[2] \quad \frac{1}{2p} = \frac{1}{n_A + n_B} \{\beta_A n_A^2 + 2\beta_{AB} n_A n_B + \beta_B n_B^2\}$$

where β_A and β_B are twist coefficients for compound A and compound B and β_{AB} is a mutual twisting coefficient for the pairwise interaction of A with B. n_A and n_B are the number of moles of A and B. p is the helical pitch length. This equation is based on a model for the thermotropic case, where intermolecular pairwise interactions are continuous throughout the mesophase with no interruptions. In the lyotropic case, the water compartment interrupts the transmission of chiral information. In the form where β_A and β_B are obtained from the pitch in pure L-LAK and pure D-LSK mesophases, the equation is *not* obeyed in the present experiments. A much more complex theory is first required, which can account for such events as the change in micelle size with water content for the related nematic phases.

Figure 1 reveals that the sign of the helix in mesophases prepared from L-LAK is opposite to those prepared from D-LSK, because the pitch passes to infinity at an intermediate composition, to give a nematic phase.

The pitch length increases as the temperature is raised in all cases and this is unusual for thermotropic cholesterics; nevertheless an increase was previously observed in some thermotropic mixtures and induced cholesteric phases (7).

Acknowledgements

LWR wishes to thank the Natural Sciences and Engineering Research Council of Canada for operating grants and DDL, the Institut 'Josef Stefan' Ljubljana, for leave of absence permission.

1. M. ACIMIS and L. W. REEVES. Can. J. Chem. **58**, 1533 (1980).
2. E. SACKMANN, S. MEIBOOM, L. C. SNYDER, A. E. MEIXNER, and R. E. DIETZ. J. Am. Chem. Soc. **90**, 3567 (1968).
3. P. S. COVELLO, B. J. FORREST, M. E. MARCONDES HELENE, L. W. REEVES, and M. VIST. J. Phys. Chem. **87**, 176 (1983).
4. C. S. BAK and M. M. LABES. J. Chem. Phys. **62**, 3066 (1975); **63**, 805 (1975).
5. E. JUNGERMANN, J. F. GERECHT, and I. J. KREMS. J. Am. Chem. Soc. **78**, 172 (1956).
6. B. J. FORREST and L. W. REEVES. Chem. Rev. **81**, 1(1981).
7. P. G. DE GENNES. The physics of liquid crystals. Clarendon Press, Oxford. 1974.

Can. J. Chem. Downloaded from www.nrcresearchpress.com by 210.87.254.105 on 09/06/12
For personal use only.

Cyclohexanones: evidence of chair inversion and estimate for barriers to planarity from the far-infrared spectra

TRACY L. SMITHSON, NAN IBRAHIM, AND HAL WIESER[1]

Department of Chemistry, University of Calgary, Calgary, Alta., Canada T2N 1N4

Received February 23, 1983

TRACY L. SMITHSON, NAN IBRAHIM, and HAL WIESER. Can. J. Chem. **61**, 1924 (1983).

The far-infrared spectra in the region of 50–450 cm^{-1} are reported for the vapours of cyclohexanone and the structurally related compounds tetrahydro-4*H*-pyran-4-one, tetrahydro-4*H*-thiopyran-4-one, tetrahydro-4*H*-pyran-3-one, 1,3-dioxan-5-one, and 4*H*-pyran-4-one. Except for the last mentioned, the spectra are characterized by two or in some cases three sequences of Q branches which are assigned to the out-of-plane deformations of the cyclohexanone ring. The lowest wavenumber sequence in each compound is believed to arise from a vibration which, if completely executed, would take the chair conformation to its equivalent via an inversion through the planar form. Each sequence is amenable to solution by a one-dimensional Hamiltonian incorporating a quadratic–quartic potential function, providing estimates for the magnitudes of the barriers to planarity.

TRACY L. SMITHSON, NAN IBRAHIM et HAL WIESER. Can. J. Chem. **61**, 1924 (1983).

On rapporte les spectres dans l'infrarouge lointain (région de 50 à 450 cm^{-1}) des vapeurs de cyclohexanone et des composés structurellement apparentés: la tétrahydro-4*H*-pyranone-4, la tétrahydro 4*H*-thiopyranone-4, la tétrahydro 4*H*-pyranone-3, la dioxane-1,3 one-5 et la 4*H*-pyranone-4. A l'exception du dernier composé, les spectres sont caractérisés par deux ou, dans certain cas, trois séquences de Q raies que l'on attribue aux déformations hors plan du cycle de la cyclohexanone. On pense que la séquence ayant la plus faible longueur d'onde dans chaque composé, provient d'une vibration qui si elle est complète transformerait la conformation chaise en son équivalent via une inversion en passant par la forme plane. Chaque séquence peut être résolue par un Hamiltonien unidimensionnel impliquant une fonction de potentiel quadratique–quartique et fournit ainsi des évaluations de l'ordre de grandeur des barrières à la planéarité.

[Traduit par le journal]

Can. J. Chem. Downloaded from www.nrcresearchpress.com by 210.87.254.6 on 09/06/12
For personal use only.

Introduction

In its ground state, cyclohexanone is believed to exist in a chair conformation that is somewhat flattened at the carbonyl end (1). In a fashion similar to cyclohexane, the ketone will pass from one chair conformation to its equivalent via several higher energy flexible forms. The inversion process is thought to reach a position of maximum energy with a transition state that is partially on its way to a symmetric boat form, and an intermediate metastable state with a symmetric twist form. Enthalpy differences between these two and the chair are estimated to be of the order of 26 and 13 kJ/mol (2140 and 1120 cm^{-1}), respectively (1). A corresponding experimental number quoted in terms of the free energy of activation of the transition state is 21 kJ/mol at −170°C (2). To our knowledge, no estimates of the barrier to planarity are available at this time.

The cyclohexanone ring gives rise to three out-of-plane deformation vibrations, at least one of which should exhibit a fair degree of anharmonicity. Carreira and Lord (3) some years ago have searched for evidence of these anharmonic motions in the far-infrared spectrum of the vapour without success. They reported a relatively strong B band at 182.0 cm^{-1}, and a much weaker and unresolved C band at 92.1 cm^{-1}, concluding harmonic behaviour from these observations. A hint that the situation may be more complicated comes from the microwave spectrum (4) which apparently was difficult to assign because of its richness, as indeed one would expect if a number of vibrational states were accessible at ambient temperature.

We have recorded recently the far-infrared spectra in the region of 50–450 cm^{-1} of cyclohexanone (**I**) and the structurally related compounds tetrahydro-4*H*-pyran-4-one (**II**), tetrahydro-4*H*-thiopyran-4-one (**III**), tetrahydro-4*H*-pyran-3-one (**IV**), 1,3-dioxan-5-one (**V**), and 4*H*-pyran-4-one (**VI**):

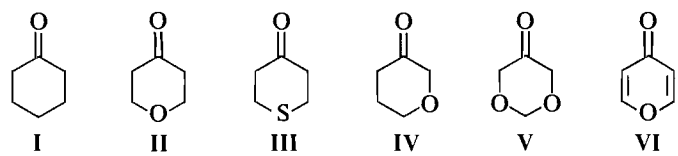

I **II** **III** **IV** **V** **VI**

All of these compounds but one (**VI**) show absorptions with the fine structure that is characteristic of anharmonic skeletal deformations. In the following the spectra and their interpretations are reported, together with estimates for the barriers to planarity where appropriate.

Experimental

The compounds **II**, **III**, and **VI** were purchased from Aldrich Chemicals and **I** from Matheson, with quoted purities of at least 99%. After verifying by nmr we used these materials without further purification. Drying was necessary only for **I** and was achieved by storing it over KOH. The compounds **IV** and **V** were synthesized as follows.

Tetrahydro-4*H*-pyran-3-one (**IV**): The 3-hydroxy precursor was first prepared by hydroboration of dihydropyran with sodium borohydride and borontrifluoride-etherate (5) in 21% yield, followed by oxidation (in 19% yield) with Jones' reagent (6, 7) to give the desired compound, bp 76–80°C/23 mm (lit. bp 57–58°C/9 mm (8)). NMR (60 MHz, $CDCl_3$): δ 3.91 (singlet, 2H, CH_2—O); 3.75 (triplet, 2H, CH_2—O); 2.60–2.30 (multiplet, 2H, CH_2); 2.26–1.81 (multiplet, 2H, CH_2). After fractional distillation the compound was about 91% pure, the impurity being the alcohol precursor. No attempt was made at further purification since the alcohol has a much lower vapour pressure and therefore did not cause any interference in the vapour phase far-infrared spectra.

1,3-Dioxan-5-one (**V**): In the first step, glycerol was acetalated with paraformaldehyde in an acidic medium following the method of Hibbert and Trister (9). The mixed acetals were equilibrated with a trace of acid to give the 5-hydroxy precursor in 36% yield. Subsequent oxidation with CrO_3–pyridine–CH_2Cl_2 complex (10) gave the target compound in 12% yield, bp 51–52°C/20 mm (semi-solid at room temperature). NMR (60 MHz, $CDCl_3$): δ 4.88 (singlet, 2H,

[1]To whom all correspondence should be addressed.

Can. J. Chem. Downloaded from www.nrcresearchpress.com by 210.87.254.6 on 09/06/12
For personal use only.

O—CH_2—O); 4.23 (singlet, 4H, CH_2). Purification was achieved by fractional distillation. The final product was 90% pure, pyridine being the impurity. Interference in the far-infrared spectra from the latter material was removed by computer subtraction.

All the spectra were obtained with a Nicolet 8000 Fourier Transform Interferometer. The samples were contained in either a matched 60 m variable path gas cell manufactured by the same company, or a commercial Wilks 20 m variable path cell. The spectra were taken with 45 or 18.75 m, respectively, with sample pressures adjusted to give reasonable absorbancies for the features of interest. In most instances this meant near saturated vapour pressures. The resolution was set at 0.12 or 0.24 cm^{-1} with boxcar apodization. We used a liquid nitrogen cooled MCT-B detector above 400 cm^{-1}, and below that a liquid helium cooled bolometer operating at 4.2 K, equipped with the appropriate cut-on filters. The mirror velocity was adjusted for optimum signal-to-noise in the specific regions under study. Either a KBr beamsplitter, or a 3, 6, or 12 μm Mylar beamsplitter was used as appropriate. Between 200–500 scans were accumulated as required to achieve good signal-to-noise. The spectrometer was calibrated against standard water absorptions, and the reported positions of the sharp lines are believed to be accurate to at least 0.02 cm^{-1}.

The spectra and their interpretation

The three out-of-plane deformation modes of the cyclohexanone ring span $2A' + A''$ in the C_s symmetry point group. For the present purposes we will label them at $\nu_1(A')$, $\nu_2(A'')$, and $\nu_3(A')$ in increasing energy. In the liquid phase they have been assigned to the lowest three absorptions at 106, 188, and 312 cm^{-1}, respectively (11). The moments of inertia are such that the A' modes should display C-type contours and the A'' mode a B-type (4). Based on an extensive valence force field analysis (11), ν_1 is described as a ring distortion in which all the CCC angles change and the CC torsions and the C=O out-of-plane wag also participate, ν_2 is described essentially as a ring twisting deformation involving the β-CC bonds (a "partial flipping toward a chair–boat conformation inversion" (11)), and ν_3 as mostly a twisting of the γ-CC bonds. In addition, we may expect some involvement from the "in-plane" and "out-of-plane" wagging of the carbonyl group the latter of which we designate here by ν_{op}, not meaning to imply, however, that these vibrations are so localized.

The survey spectra of the six compounds in the region of 75–435 cm^{-1} are displayed in Fig. 1. Clearly, the most prominent common feature is ν_1 with its distinct C-type contour. The position is remarkably uniform, excepting **III** for which it is shifted to lower wavenumber due possibly to the increased reduced mass, and **VI** for which in any case one would expect a shift to higher wavenumbers. These findings agree with the description of ν_1 as involving the ring as a whole, with perhaps a greater contribution from the C=O end. The second mode is characterized by B contours at nearly the same position for **I**, **II**, and **III**. With the introduction of the oxygen atoms, the band contour changes for **IV** and **V**. In **VI** this vibration is infrared forbidden. These observations are in keeping with the notion that ν_2 represents primarily a twisting of the middle part of the chair. Finally, the C band of ν_3 shows little intensity in **I** and **III**, is prominent in **II** and **IV**, and weaker again in **V** and **VI**. The relative intensity of this mode in **I** as compared to **II**, **IV**, and **V** would suggest that the vibration involves a significant amount of that end of the ring which is diagonally opposite to the C=O group, also agreeing with the earlier assignment (11). The positions are summarized in Table 1.

The ν_1 mode of all compounds except for **VI** clearly exhibits the characteristic sequences of Q branches. This structure is not so apparent for the parent, although there too it can be seen distinctly upon expansion. The bands for **I** and **II** are shown on an enlarged scale in Fig. 2. The assignment for **I** is not immediately obvious, but can be made with confidence by comparing with **II**. For the latter, ν_3 also shows combination structure (Fig. 3), as well as a much weaker difference series near 240 cm^{-1} (Fig. 4). These sequences together provide an unambiguous assignment of all the transitions involved, yielding the unique energy level diagram depicted in Fig. 5. Accordingly, the structure of the ν_1 band in **I** and **II** must arise from the sequence of transitions in the ground state of all other modes and in the first excited state of ν_3. The ground state separations of ν_1 in **II** are confirmed by combination series based on ν_{op}, namely ν_{op} in several excited state of ν_1 starting at 504.57 cm^{-1}, and the corresponding sum bands $\nu_1 + \nu_{op}$, starting at 599.89 cm^{-1}, both progressing to lower wavenumbers (see Fig. 6). The ν_1 sequences of **IV** and **V** are expanded in Fig. 7. While for **III** the Q branches are so closely spaced as to be poorly resolved even with 0.06 cm^{-1} resolution (spectrum not shown), those of **IV** and **V** are widely separated as evident already in the survey spectra (cf. Fig. 1). There is some indication of ν_1 in the excited state of another mode for both **IV** and **V**, but in the absence of any sum or difference bands no clear assignment can be made. The modes ν_2 and ν_3 of the same molecules also show the distinctive multiplet structure (see Fig. 1), but again no unambiguous correlations are possible. For **V** the sequence of ν_2 appears to be that of a purely quartic oscillator for which reason it is reproduced on an expanded scale in Fig. 8.

The positions of ν_1 in the ground state of all other modes for compounds **I** to **V** are summarized in Table 2. In Table 3 are given the ν_1 separations in several excited states of ν_3 for **I** and **II**, as well as the separations of ν_2 for **V**. The positions of the other sequences in **II** are tabulated in Table 4.

Inversion of the cyclohexanone ring

For cyclohexane Pickett and Strauss pictured the three out-of-plane coordinates as deforming the planar ring to a boat-like, to a twist-like, and to a chair-like form (13). The corresponding vibrations, designated ω_1, ω_2, and ω_3, respectively, are assigned to absorptions at 243 cm^{-1} for the degenerate pair of ω_1 and ω_2, and 384 cm^{-1} for ω_3 (14). Hendrickson classified the same modes of inversion as symmetrical and pseudorotation (15). There are two of the former, namely the transition from chair to boat to chair maintaining a plane of symmetry, and from chair to "twist-boat" and back to chair maintaining an axis of symmetry. The pseudorotation mode is said to describe the passage from the boat to the twist forms.

Following the discussion in the preceding section, we visualize the coordinates of cyclohexanone as follows. While the twist, ν_2, is essentially equivalent to its cyclohexane counterpart ω_2, the other two modes may be viewed as "weighted" out-of-phase (ν_1) and in-phase (ν_3) combinations of a simultaneous folding about the C2—C6 and C3—C5 diagonals. The word "weighted" is meant to imply that the folding about the two diagonals may not be taking place to the same extent, but rather would be quite different for the two modes. In terms of these three coordinates the potential energy forms a four dimensional surface with the origin at the central maximum corresponding to the planar conformation. Any one of the coordinates in zero displacement of the other two may follow a double minimum potential function. The extent of coupling between them would depend on the energies of the three conformers relative to one another, to the barriers to interconversion, and

Can. J. Chem. Downloaded from www.nrcresearchpress.com by 210.87.254.6 on 09/06/12
For personal use only.

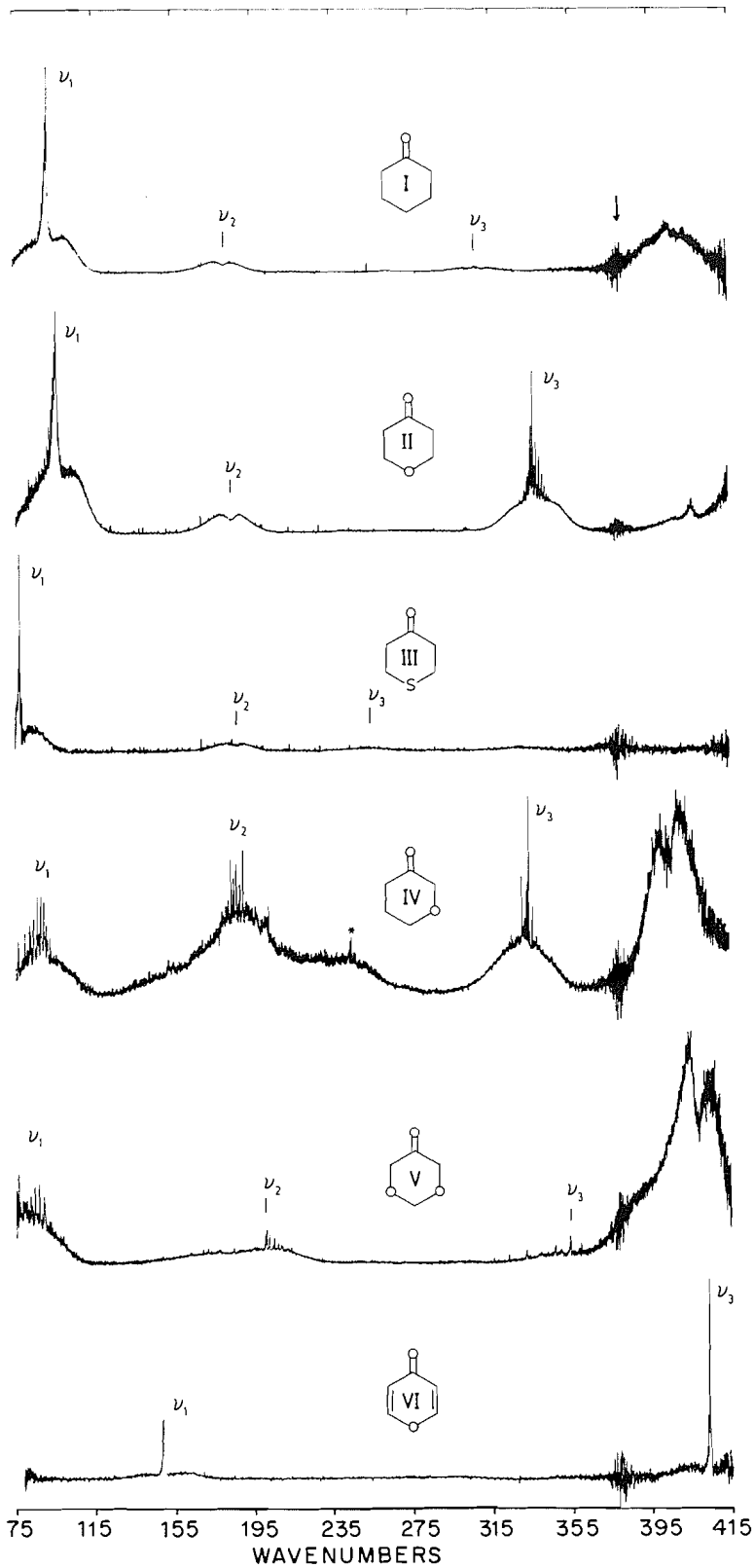

FIG. 1. Survey spectra of cyclohexanone and related compounds. Near saturated vapour pressures, 45 m path, 0.12 cm^{-1} resolution, 3 μm Mylar beamsplitter, 300 scans. Band marked with an asterisk in **IV** is residual pyridine impurity. The noise in the region of 380 cm^{-1} in all the spectra, marked with an arrow in **I**, is due to the strong absorption of the Mylar cut-on filter.

to the central barrier to planarity. The actual interconversion between the conformers, of course, would follow the path of minimum energy.

Since the ground state conformation of the ring is the chair form, we expect ν_1 to be the dominant vibration. If, therefore, that mode gives rise to a diminishing sequence of absorptions we might attempt in the first instance to model these transitions by a one-dimensional Hamiltonian incorporating a quadratic–

TABLE 1. Comparison of the out-of-plane ring deformations in cyclohexanone and a series of related compounds

Compound	$\nu_1(A')/cm^{-1}$	$\nu_2(A'')/cm^{-1}$	$\nu_3(A')/cm^{-1}$
I, Cyclohexanone	92.39	181.51	307.62
II, Tetrahydro-4*H*-pyran-4-one	97.16	184.44	336.87
III, Tetrahydro-4*H*-thiopyran-4-one	77.48	186.2	253.6
IV, Tetrahydro-4*H*-pyran-3-one	90.48	186.43	336.64
V, 1,3-Dioxan-5-one	89.04	201.24	353.96
VI, 4*H*-Pyran-4-one	148.76	—[a]	423.92

[a]Infrared forbidden.

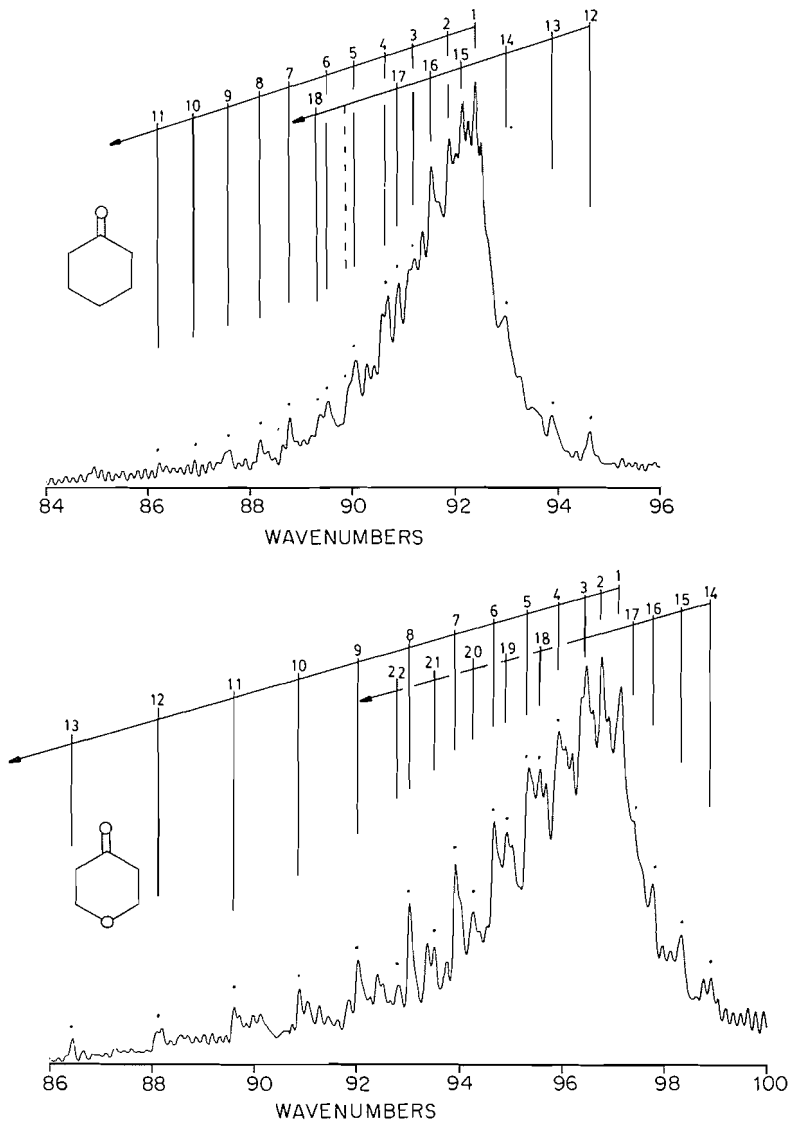

FIG. 2. Sequences of ν_1. Near saturated vapour pressure, 45 m path, 0.12 cm^{-1} resolution, 12 μm Mylar beamsplitter, 400 scans. Numbered peak positions are tabulated in Tables 2 and 3.

quartic potential function. This is tantamount to saying that the coupling between the ν_1 mode and the other two is not too severe so as not to affect seriously its vibrational spacings. Such an assumption is not unreasonable in view of the considerable energy difference between the chair and the other two conformers. In that case, ν_2 and ν_3 would resemble near-harmonic vibrations in the deep potential well of the chair. The situation is similar to the bend/twist coupling in cyclohexene-type molecules, although there the twist, which is the higher energy mode, is the dominant one and the lower energy bend is a near-harmonic vibration constrained in the well of the twisted ground state conformation (16). It is important to note that in these molecules both the twist and the bend vibration exhibit diminishing absorption sequences, reflecting some coupling between the two.

For the one-dimensional calculations we used the standard Hamiltonian in a computer program described elsewhere (12). As mentioned earlier, the assignments of all the ν_1 sequences

Can. J. Chem. Downloaded from www.nrcresearchpress.com by 210.87.254.6 on 09/06/12
For personal use only.

Can. J. Chem. Downloaded from www.nrcresearchpress.com by 210.87.254.6 on 09/06/12
For personal use only.

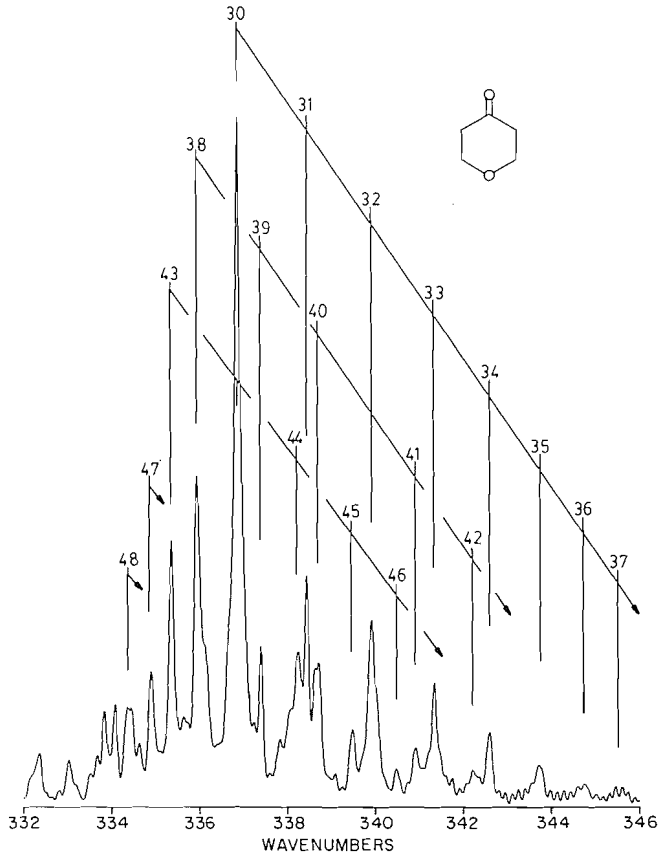

FIG. 3. Sequences of ν_3. Reduced vapour pressure, 45 m path, 0.12 cm^{-1} resolution, 6 μm Mylar beamsplitter, 400 scans. Numbered peak positions are tabulated in Table 4.

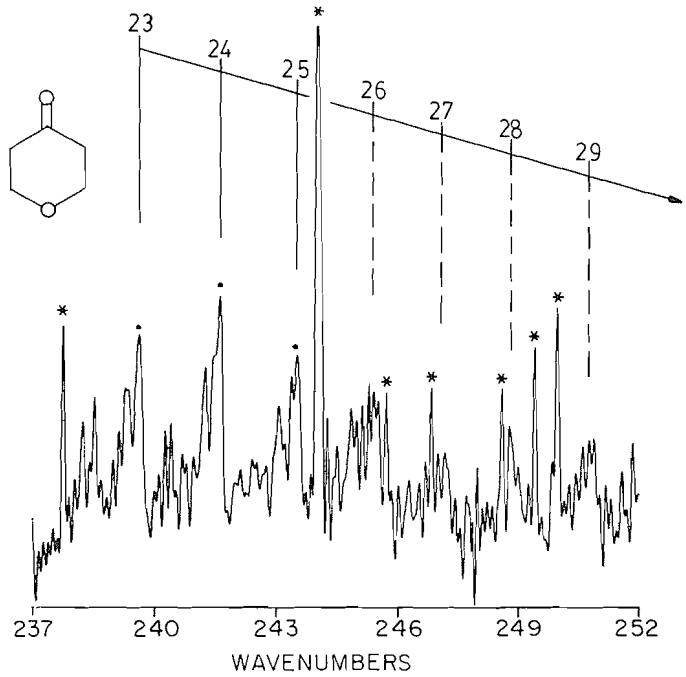

FIG. 4. Difference sequence, $\nu_3 - \nu_1$. Saturated vapour pressure, 45 m path, 0.12 cm^{-1} resolution, 6 μm Mylar beamsplitter, 600 scans. Lines marked with an asterisk are D_2O and HOD absorptions. Numbered peak positions are tabulated in Table 4.

are based on those of **II**. For compound **V** we used only the first three absorptions (labelled 1 to 3 in Fig. 7) in the initial calculation which then predicted the next three positions (peaks 4 to 6 in Fig. 7). The results of all the calculations are listed in Table 2 in terms of the observed − calculated values for the transitions. The best fitting dimensionless quadratic and quartic potential constants and the corresponding barriers (equal to $V_2^2/4V_4$) are also given.

Since compound **II** yielded the most complete information not only for ν_1 but also for ν_3 (see Fig. 5), we used its data for several tests. We first confirmed that the double minimum barrier for ν_1 is well determined by the observed transitions and is not affected by extrapolation errors. In order to establish the role of ν_3 we then attempted to fit its sequence, which also progresses to lower wavenumbers, with the one-dimensional quadratic–quartic potential. While the fit was very good, it suggested an unrealistic barrier height of about 16 000 cm^{-1}. We therefore concluded that the diminishing sequence for ν_3 could result from coupling with one or both of the two other modes. It is of interest to note that the ν_1 separations in the excited state of ν_3 in **I** and **II**, as they are either observed in the spectra or determined from the combination principle, are also amenable to modelling with the quadratic–quartic Hamiltonian (see Table 3). The effective excited state barriers are clearly different from those in the ground state, confirming that some degree of coupling must exist between at least these two modes. If the coupling were taking place preferentially between ν_1 and ν_3, a coupled oscillator approach might be successful. We therefore tried to determine a best fitting two-dimensional potential surface described by a function of the form

$$V(x_1, x_3) = V_{21}x_1^2 + V_{23}x_3^2 + V_{41}x_1^4 + V_{43}x_3^4 + V_{\text{mix}}x_1^2x_3^2$$

in the appropriate Hamiltonian, x_1 and x_3 being the dimensioned coordinates corresponding to ν_1 and ν_3, using a computer program outlined elsewhere (17). Taking ν_3 as a harmonic oscillator with the appropriate scaling coefficient, constraining V_{21} and V_{41} to the one-dimensional values, and using all the data for ν_1 and ν_3, we first allowed V_{mix} to seek its own value. The least-squares refinement forced V_{mix} to zero. Including a small quartic anharmonicity in ν_3 did not assist in determining the coupling constant. Allowing V_{23} to vary simultaneously with V_{mix} also did not improve the results. When all constants were allowed to float the calculation became ill-conditioned as the estimated standard deviation on V_{mix} was consistently larger than the computed value. While the spectra indicate that some coupling must exist, this two-dimensional analysis clearly is not possible. One reason could be that the extent of coupling is too small for a meaningful determination of V_{mix}. Another reason could be that the current method, containing only the fourth power mixing term which is quadratic in both coordinates, is insensitive to coupling in this case when the conformers are so different in energy and the barrier between them is that large, and that perhaps other coupling terms would be more effective. Indeed, ν_3 in the ground state of the ν_1 mode (i.e. ν_3 in the chair conformer) may resemble more a vibration with cubic anharmonicity than follow a quadratic dependence. Still another possibility is that the projection of the four-dimensional potential surface into three dimensions simply is inappropriate in this case.

At this stage we are left with the conclusion that the one-dimensional double minimum potential function which suc-

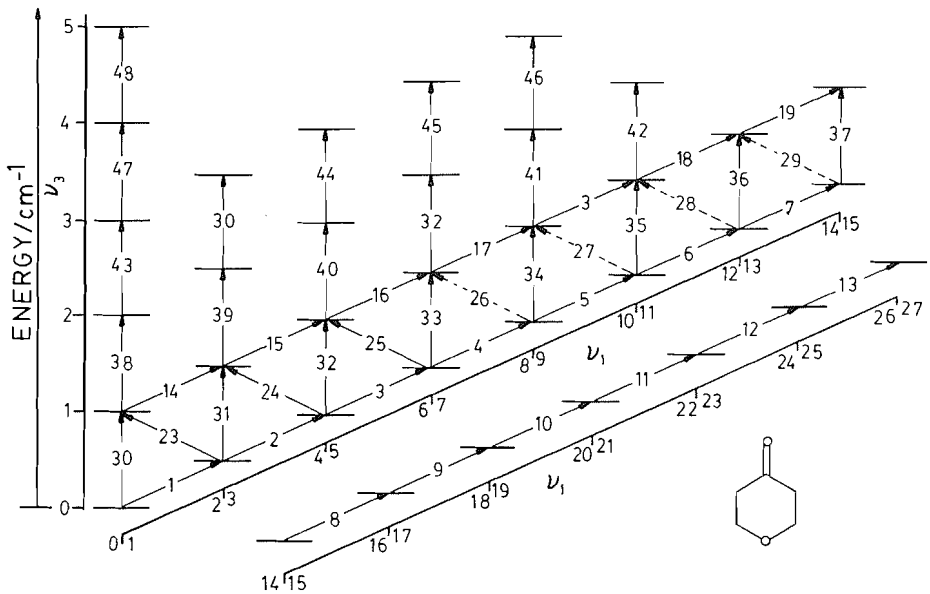

FIG. 5. Energy level diagram for ν_1 and ν_3. Numbered transitions correspond to peak positions labelled in Figs. 2 and 3, and tabulated in Tables 2, 3, and 4.

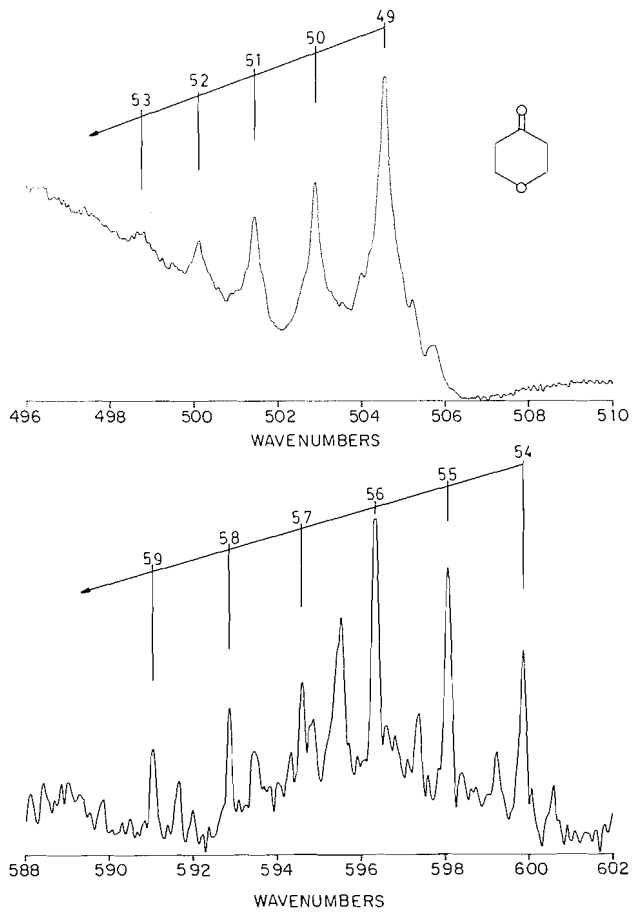

FIG. 6. Combination sequences of ν_{op} with ν_1. Reduced and saturated vapour pressure, respectively, 18.75 m path, 0.12 cm^{-1} resolution, Ge/KBr beamsplitter, 500 scans. Numbered peak positions are tabulated in Table 4.

cessfully reproduces the energy level spacings of ν_1 and represents a section through the potential energy surface at zero displacement of the other two coordinates, provides a reasonable estimate for the barrier to planarity of the cyclohexanone

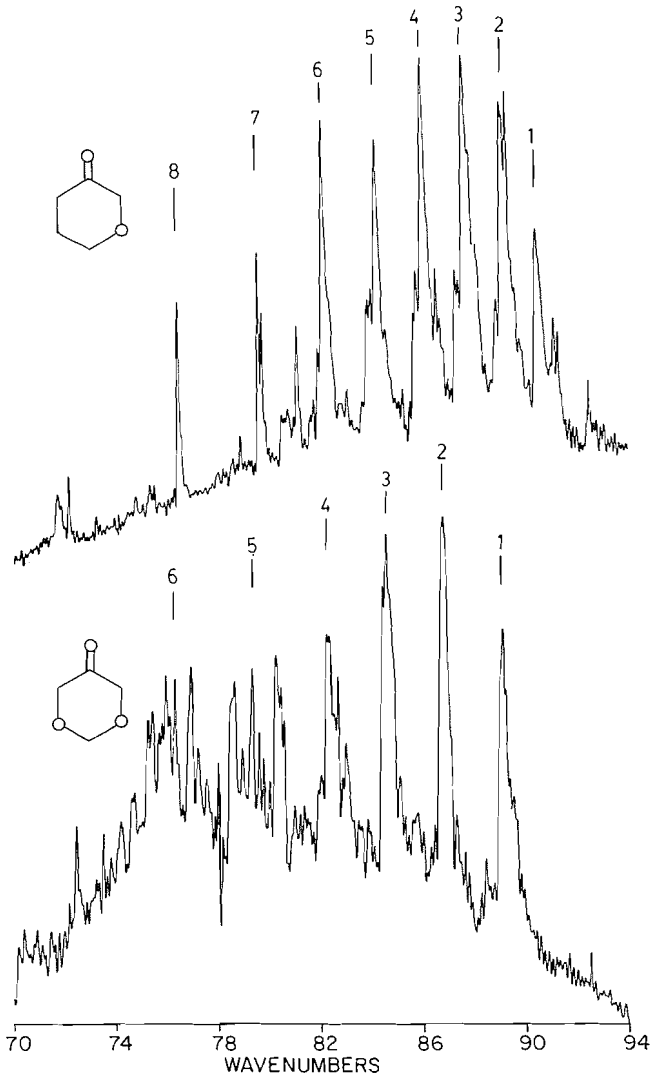

FIG. 7. Sequences of ν_1. Near saturated vapour pressures, 45 m path, 0.12 cm^{-1} resolution, 12 μm Mylar beamsplitter, 300 (upper trace) and 500 (lower trace) scans. Numbered peak positions are tabulated in Table 2.

Can. J. Chem. Downloaded from www.nrcresearchpress.com by 210.87.254.6 on 09/06/12
For personal use only.

TABLE 2. Positions of ν_1 (cm^{-1}) in the ground state of all other modes

Transition[a]			Peak	I		II		IV		V	
ν_u	←	ν_l	No.[b]	Obs.	Δ[c]	Obs.	Δ[c]	Obs.	Δ[c]	Obs.	Δ[c]
3, 2		1, 0	1	92.39	−0.02	97.16	−0.62	90.48	−0.43	89.04	0.06
5, 4		3, 2	2	91.89	0.05	96.77	−0.33	89.10	−0.19	86.71	−0.14
7, 6		5, 4	3	91.22	−0.05	96.38	−0.03	87.64	0.05	84.52	−0.04
9, 8		7, 6	4	90.70	0.02	95.95	0.24	86.03	0.25	82.21	0.14
11,10		9, 8	5	90.08	0.00	95.34	0.35	84.22	0.37	79.32	−0.01
13,12		11,10	6	89.54	0.06	94.68	0.42	82.15	0.38	76.30	0.06
15,14		13,12	7	88.78	−0.07	93.94	0.43	79.63	0.12		
17,16		15,14	8	88.20	−0.02	93.06	0.32	76.47	−0.55		
19,18		17,16	9	87.60	0.03	92.06	0.11				
21,20		19,18	10	86.92	0.01	90.92	−0.22				
23,22		21,20	11	86.22	−0.01	89.64	−0.67				
25,24		23,22	12			(88.16)	(−1.29)[d]				
27,26		25,24	13			(86.46)	(−2.11)[d]				
Derived parameters[e]											
Std. dev./cm^{-1}				0.04		0.43		0.39		0.10	
$(V_4/(m\gamma)^2)/cm^{-1}$				−27.008(15)		−30.282(158)		−21.368(118)		−20.691(33)	
$(V_2/m\gamma)/cm^{-1}$				0.06200(40)		0.08267(43)		0.1069(29)		0.1327(8)	
Barrier/cm^{-1}[f]				2940±21		2772±165		1068±40		806±8	

[a]Quantum numbers of the upper (u) and lower (l) energy levels. Each level is doubly degenerate as reflected by the labelling.
[b]The peak numbers correspond to the observed peak positions marked in Figs. 2 and 7.
[c]Observed − calculated.
[d]Observed but not included in the fitting process.
[e]Evaluated with a potential function $V(q) = (V_2/m\gamma)q^2 + (V_4/m^2\gamma^2)q^4$, q the dimensionless coordinate (12). Fixed parameters: $m = 100.0u$; $\gamma = 4\pi^2 c\nu/h$; $\nu = 80.00\ cm^{-1}$ for **I** and **II**, $100.0\ cm^{-1}$ for **IV** and **V**; 350 basis functions were used for **I** and **II**, and 150 for **IV** and **V**.
[f]Uncertainties reflect the estimated standard deviations for the potential constants.

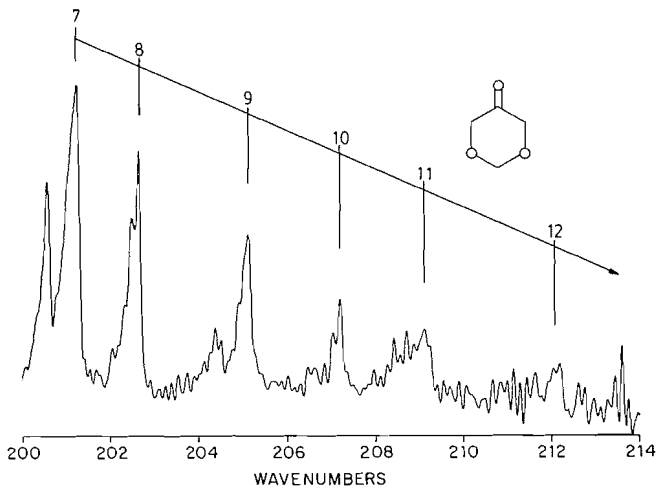

FIG. 8. Sequence of ν_2. Near saturated vapour pressure, 45 m path, 0.12 cm^{-1} resolution, 6 μm Mylar beamsplitter, 500 scans. Numbered peak positions are tabulated in Table 3.

ring. The trend in the barrier heights displayed by the various compounds (see Table 2) is consistent with what one would expect for the successive replacement of methylene groups by oxygen atoms. For the sulfur compound the unresolved ν_1 transitions indicate a higher barrier than for any of the other molecules. Comparing **II** and **IV** it appears that an oxygen atom in the 3 position of the cyclohexanone ring more effectively reduces the barrier than when it occupies the 4 position.

The barrier is lowest for **V** where the methylene groups have been isolated so that the driving force towards an aplanar form is mainly the steric requirement of the bond angles. As a consequence, the twist in the zero displacements of the other two modes would be a single minimum vibration. Indeed, the ν_2 sequence of **V** (Fig. 8) is reproduced remarkably well by a one-dimensional quartic oscillator (see last columns in Table 3). If the twist in this case were a relatively independent single minimum vibration, we would not expect to find a twisted conformation either as a metastable or as a transition state. The most stable conformer most likely still is a chair. It is not certain, however, whether the inversion takes place via a boat-like form or the planar conformation.

Summary[2]

The far-infrared spectra in the region of 50–450 cm^{-1} of gaseous cyclohexanone (**I**) and the related compounds tetrahydro-4*H*-pyran-4-one (**II**), tetrahydro-4*H*-thiopyran-4-one (**III**), tetrahydro-4*H*-pyran-3-one (**IV**), and 1,3-dioxan-5-one (**V**), reveal distinctive absorptions several of which exhibit characteristic sequences of Q branches. Based on the relative band positions, intensities, and contours these absorptions are assigned to the three out-of-plane deformations of the cyclohexanone ring skeleton. In all five compounds the lowest energy vibration, designated ν_1, gives rise to a prominent di-

[2]NOTE ADDED IN PROOF

A recent microwave study of tetrahydro-4*H*-pyran-4-one (**II**) (18) confirmed the chair conformation as the most stable form. The microwave spectrum also showed evidence of the four excited states of ν_1 and the first excited state of ν_2 (referred to by the author as ring bending and twisting modes, respectively). The far-infrared positions of the fundamentals were reported as very broad lines at about 100 and 185 cm^{-1}. The rotational constants when plotted against the "bending" quantum number deviated slightly from linearity, indicating an anharmonic potential function. For tetrahydro-4*H*-thiopyran-4-one (**III**) the ground state chair conformation was confirmed by electron diffraction (19).

Can. J. Chem. Downloaded from www.nrcresearchpress.com by 210.87.254.6 on 09/06/12
For personal use only.

Can. J. Chem. Downloaded from www.nrcresearchpress.com by 210.87.254.6 on 09/06/12
For personal use only.

TABLE 3. Positions of ν_1 (cm^{-1}) in several excited states of ν_3 in **I** and **II**, and of ν_2 in **V**

Compound **I** (ν_1)					Compound **II** (ν_1)							Compound **V** (ν_2)				
Transition[a]		$\nu_3 = 1$			$\nu_3 = 1$			$\nu_3 = 2$		$\nu_3 = 3$		Trans.[a]				
ν_u ← ν_l		No.[b]	Obs.	Δ[d]	No.[b]	Obs.	Δ[d]	Ded.[c]	Δ[d]	Ded.[c]	Δ[d]	ν_u ← ν_l		No.[b]	Obs.	Δ[d]
3, 2	1, 0	12	94.62	0.09	14	98.88	−0.13	100.02	0.02	101.70	−0.04	1	0	7	201.22	0.48
5, 4	3, 2	13	93.88	0.06	15	98.33	0.05	99.56	−0.02	100.93	−0.01	2	1	8	202.64	−0.38
7, 6	5, 4	14	92.98	−0.10	16	97.78	0.04	99.02	0.06	100.27	0.14	3	2	9	205.12	−0.11
9, 8	7, 6	15	92.14	−0.19	17	97.34	0.24	98.21	−0.12	99.20	−0.09	4	3	10	207.20	−0.17
11,10	9, 8	16	91.55	−0.01	3	96.51	0.08	97.76	0.07			5	4	11	209.13	−0.33
13,12	11,10	17	90.91	0.14	18	95.70	−0.05					6	5	12	212.01	0.52
15,14	13,12				19	94.94	−0.12									
17,16	15,14	18	(89.38)	(0.20)[e]	20	(94.26)	(−0.08)[e]									
19,18	17,16				21	(93.53)	(−0.11)[e]									
21,20	19,18				22	(92.84)	(−0.06)[e]									
Derived parameters:[f]																
Std. Dev./cm^{-1}			0.14			0.14			0.09		0.12				0.70	
$(V_2/m\gamma)/cm^{-1}$			−28.346(74)			−31.016(73)			−31.740(57)		−32.847(94)				196.817(876)	
$(V_4/(m\gamma)^2)/cm^{-1}$			0.08220(380)			0.07881(55)			0.07813(35)		0.1057(70)				3.1398(1600)	
Barrier/cm^{-1}[g]			2443±115			3052±133			3233±150		2551±127				0	

[a]Quantum numbers of the upper (u) and lower (l) energy levels, designated with double labels if degenerate.
[b]The numbers correspond to the observed peak positions marked in Fig. 2 for **I** and **II**, and in Fig. 8 for **V**.
[c]Deduced from the energy level diagram in Fig. 5.
[d]Observed − calculated, or deduced − calculated.
[e]Observed but not included in the fitting process.
[f]Evaluated with a potential function $V(q) = (V_2/m\gamma)q^2 + (V_4/m^2\gamma^2)q^4$, q the dimensionless coordinate (12). Fixed parameters: $m = 100.0u$; $\gamma = 4\pi^2 c\nu/h$; $\nu = 80.00\ cm^{-1}$ for **I** and **II**, $100.0\ cm^{-1}$ for **V**; 350 basis functions were used for **I** and **II**, and 150 for **V**.
[g]Uncertainties reflect the estimated standard deviations for the potential constants.

TABLE 4. Other ν_1 combination sequences (in cm^{-1}) in **II**

Transition[a]						Transition[a]						Transition[a]					
$(\nu_3,\nu_1)_u \leftarrow (\nu_3,\nu_1)_l$				No.[b]	Obs.	$(\nu_3,\nu_1)_u \leftarrow (\nu_3,\nu_1)_l$				No.[b]	Obs.	$(\nu_{op},\nu_1)_u \leftarrow (\nu_{op},\nu_1)_l$				No.[b]	Obs.
1	1, 0	0	3, 2	23	234.65	1	15,14	0	15,14	37	345.60	1	1, 0	0	1, 0	49	504.57
	3, 2		5, 4	24	241.58	2	1, 0	1	1, 0	38	335.94		3, 2		3, 2	50	502.93
	5, 4		7, 6	25	243.51		3, 2		3, 2	39	337.41		5, 4		5, 4	51	501.43
	7, 6		9, 8	26	245.40		5, 4		5, 4	40	338.70		7, 6		7, 6	52	500.14
	9, 8		11,10	27	247.26		7, 6		7, 6	32	339.93		9, 8		9, 8	53	498.73
	11,10		13,12	28	249.05		9, 8		9, 8	41	340.93	1	3, 2	0	1, 0	54	599.89
	13,12		15,14	29	250.82		11,10		11,10	42	342.22		5, 4		3, 2	55	598.10
1	1, 0	0	1, 0	30	336.87	3	1, 0	2	1, 0	43	335.36		7, 6		5, 4	56	596.37
	3, 2		3, 2	31	338.43		3, 2		3, 2	30	336.87		9, 8		7, 6	57	594.61
	5, 4		5, 4	32	339.93		5, 4		5, 4	44	338.24		11,10		9, 8	58	592.88
	7, 6		7, 6	33	341.35		7, 6		7, 6	45	339.49		13,12		11,10	59	591.05
	9, 8		9, 8	34	342.60		9, 8		9, 8	46	340.48						
	11,10		11,10	35	343.73	4	1, 0	3	1, 0	47	334.90						
	13,12		13,12	36	344.76	5	1, 0	4	1, 0	48	334.40						

[a]Quantum numbers of the upper (u) and lower (l) levels, designated with double labels if degenerate.
[b]The numbers correspond to observed peak positions marked in Figs. 3, 4, and 6, and the numbered transitions in the energy level diagram in Fig. 5.
[c]Determined by combination principle from Fig. 5.

minishing series of Q branches below 100 cm^{-1}. The other two modes, ν_2 and ν_3 near 180 and 300 cm^{-1}, respectively, vary in intensity and band contour for the different molecules. Supported by earlier force field calculations on the parent the ν_1 and ν_3 modes are described, respectively, as an out-of-phase and in-phase combination of an unequal though simultaneous folding about the C2—C6 and C3—C5 diagonals, whereas ν_2 is described as a twisting of the central part of the skeleton.

The spectrum of **II** provides the most comprehensive information about the ν_1 and ν_3 modes, leading to an extensive energy level diagram. The ν_1 sequences in the ground state of all other modes and in several excited states of ν_3 are amenable to solution with a one-dimensional Hamiltonian containing a quadratic–quartic potential function. Combined solution with a corresponding two-dimensional Hamiltonian was not possible. It is concluded, therefore, that the double minimum potential function for ν_1 represents a section along that coordinate in the potential energy surface at zero displacement of the other two modes. The inversion barrier resulting from that function is thought to give a reasonable estimate of the barrier to planarity for the six-membered ring skeleton.

In **I**, **IV**, and **V** only the ν_1 mode can be dealt with in a similar fashion. For **III** the fine structure though clearly present could not be resolved. The barriers to planarity so derived are 2940, 2772, 1068, and 806 cm^{-1}, respectively, for **I**, **II**, **IV**, and **V**. For the sulfur compound the barrier is expected to be higher than that for the parent. The present analysis yields no information about the relative stabilities of the various possible conformers nor about the barriers to interconversion between them. For **V** there are reasons to suggest that the symmetric twist conformation does not exist as either a metastable or a transition state, and that the energetically favoured chair–chair inversion may pass through the planar form.

Acknowledgements

This research is supported by a special project fund from the Alberta Environment Research Trust and by an Operating Grant from the Natural Sciences and Engineering Research Council of Canada (NSERC), both of which are hereby gratefully acknowledged. T.L.S. also wishes to thank NSERC for the award of a Postgraduate Scholarship during the tenure of which the work described here was carried out.

1. R. BUCOURT. *In* Topics in stereochemistry. Vol. 8. *Edited by* E. L. Eliel and N. L. Allinger. John Wiley and Sons, New York. 1974. pp. 183–187.
2. F. R. JENSEN and B. H. BECK. J. Am. Chem. Soc. **90**, 1066 (1968).
3. L. A. CARREIRA and R. C. LORD. J. Chem. Phys. **51**, 3225 (1969).
4. Y. OHNISHI and K. KOZIMA. Bull. Chem. Soc. Jpn. **41**, 1323 (1968).
5. G. ZWEIFEL and H. C. BROWN. Org. Reactions, **13**, 1 (1963).
6. K. B. WIBERG. Oxidation in organic chemistry. Part A. Academic Press, New York. 1965. p. 145.
7. A. BOWERS, T. G. HALSALL, E. R. H. JONES, and A. J. LEMIN. J. Chem. Soc. 2555 (1953).
8. J. A. HIRSCH and A. A. JARMAS. J. Org. Chem. **43**, 4106 (1978).
9. H. HIBBERT and S. TRISTER. Can. J. Res. **14B**, 415 (1936).
10. R. RATCLIFFE and R. RODEHORST. J. Org. Chem. **35**, 4000 (1970).
11. H. FUHRER, V. B. KARTHA, P. J. KRUEGER, H. H. MANTSCH, and R. N. JONES. Chem. Rev. **5**, 439 (1973).
12. J. A. DUCKETT, T. L. SMITHSON, and H. WIESER. J. Molec. Spectrosc. **78**, 407 (1979).
13. H. M. PICKETT and H. L. STRAUSS. J. Am. Chem. Soc. **92**, 7281 (1970).
14. H. M. PICKETT and H. L. STRAUSS. J. Chem. Phys. **53**, 376 (1970).
15. J. B. HENDRICKSON. J. Am. Chem. Soc. **89**, 7047 (1967).
16. E. A, DIXON, G. S. S. KING, T. L. SMITHSON, and H. WIESER. J. Molec. Struct. **71**, 97 (1981).
17. T. L. SMITHSON, J. A. DUCKETT, and H. WIESER. To be published.
18. J. L. ALONSO. J. Mol. Spectrosc. **84**, 520 (1980).
19. R. SEIP, H. M. SEIP, and Z. SMITH. J. Mol. Struct. **32**, 279 (1976).

Can. J. Chem. Downloaded from www.nrcresearchpress.com by 210.87.254.6 on 09/06/12
For personal use only.

Vapor-phase charge-transfer complexes. 11. Ethyl methyl sulfide – iodine

SUNNY J. LO AND MILTON TAMRES

Department of Chemistry, University of Michigan, Ann Arbor, MI 48109, U.S.A.

Received July 6, 1982[1]

SUNNY J. LO and MILTON TAMRES. Can. J. Chem. **61**, 1933 (1983).

The spectral and thermodynamic properties of the ethyl methyl sulfide – iodine complex were determined in the vapor phase by both a modified Benesi–Hildebrand method and the constant activity method. The former method also was used to study this complex in *n*-heptane solution. The results in both phases are compared with those for diethyl sulfide – iodine and dimethyl sulfide – iodine. Since solution data were lacking for the latter complex, it was studied in *n*-heptane in the present work. Trends in the homologous series and solvent effects are noted.

SUNNY J. LO et MILTON TAMRES. Can. J. Chem. **61**, 1933 (1983).

Faisant appel à la méthode modifiée de Bénési–Hildebrand et à la méthode d'activité constante, on a déterminé les propriétés spectrales et thermodynamiques du complexe de: iode–sulfure d'éthyle méthyle en phase gazeuse. On également utilisé la première méthode pour étudier ce complexe en solution dans le *n*-heptane. On a comparé les résultats relatifs aux deux phases avec ceux des complexes de: iode–sulfure de diéthyle et iode–sulfure de diméthyle. En l'absence de données relatives au deuxième complexe en solution, on a choisi de l'étudier en solution dans le *n*-heptane. On a relevé les tendances des séries homologues et les effets de solvant.

[Traduit par le journal]

Can. J. Chem. Downloaded from www.nrcresearchpress.com by 210.87.254.40 on 09/06/12
For personal use only.

Introduction

Thermodynamic and spectral properties of iodine complexes with homologous series of donors have been studied extensively in solution (1–4), but relatively few comparable studies have been made in the vapor phase (5). In the special case of sulfide–iodine complexes, only the following donors have been studied in the vapor phase: diethyl sulfide (6–10), dimethyl sulfide (8–10), and tetramethylene sulfide (8). For the last donor, except for establishing the position of the charge-transfer (CT) band maximum, the remaining data are suspect due to a slow reaction (9). Also, of these three sulfide complexes, the dimethyl sulfide – iodine has been studied primarily in the visible region in solution (in CCl_4) (11). Very little has been reported for the CT band in solution (8).

To further enhance the comparison between vapor and solution studies, the ethyl methyl sulfide – I_2 complex was investigated in the vapor phase using both the conventional (modified Benesi–Hildebrand) method (2, 12, 13) and the constant activity method (14–16). It was studied as well in *n*-heptane solution by the conventional method, as was also the dimethyl sulfide – I_2 complex.

Experimental section

Material

Ethyl methyl sulfide and dimethyl sulfide (Eastman Kodak Co.) were distilled through a 27-cm insulated Vigreux column packed with glass helices, and a middle cut was taken. Vapor phase chromatography showed the absence of impurities.

The purification of iodine and the synthesis of tetramethylammonium pentaiodide followed procedures described elsewhere (17–19).

Apparatus and procedures

A Cary 14 spectrophotometer was used for all spectral measurements. Details regarding the apparatus and the procedures used for studies in the vapor phase and in solution have been described in earlier papers (8–10, 20, 21, and in the thesis of Lo (22)).

Calculations

The spectrophotometric equation which applies to the conventional method of studying the interaction of donor (D) with an acceptor (A) to form complex (C) is given by eq. [1]. D_0 and A_0 are the initial concentrations of donor and acceptor, respectively, K_c is the equilibrium constant, l is the cell path, ϵ_c is the molar absorptivity, and

$$[1]\quad \frac{D_0 l A_0}{\mathrm{ABS}'} = \frac{D_0 + A_0}{\epsilon_c'} + \frac{1}{K_c \epsilon_c'} - \frac{\mathrm{ABS}'}{l(\epsilon_c')^2}$$

ABS is the absorbance. The primes on ABS and ϵ_c signify values corrected for the contributions of free donor and free acceptor. Equation [1] is quadratic in ϵ_c. For rather weak complexes, the last term may be dropped with very little effect on K_c and ϵ_c (23, 24). The resulting equation, of Scott type (13), is linear in ϵ_c.

In the constant activity method, the iodine content was controlled by the equilibrium between tetramethylammonium polyiodides, e.g.,

$$[2]\quad \mathrm{TMAI_5(solid)} \rightleftarrows \mathrm{TMAI_3(solid)} + \mathrm{I_2(vapor)}$$

In this method the spectrophotometric equation which applies, for the condition $D_0 \gg C$, is

$$[3]\quad \mathrm{ABS} = K_c \epsilon_c l D_0 [\mathrm{I_2}]_{0,T}$$

where $[\mathrm{I_2}]_{0,T}$ is the fixed iodine concentration for the polyiodide mixture at a specified temperature T.

The change in internal energy of complexation (ΔE_c^0) in the vapor phase, or in the heat of complexation (ΔH_c^0) in solution, was determined and checked by several methods: (*1*) from the temperature dependence of log K_c; (*2*) from the temperature dependence of log $K_c\epsilon_c$ (for those cases where the complex is too weak to get good separation of K_c and ϵ_c from the $K_c\epsilon_c$ product); and (*3*) from the temperature dependence of log ABS for a single donor–acceptor mixture. The last applies to the constant activity study (10, 25) provided data are available for the temperature dependence of the equilibrium in eq. [2]. It is readily shown for the vapor phase that eq. [3] becomes

$$[4]\quad \frac{-\Delta E_c^0}{2.303R} = \frac{\mathrm{d}\log K_c\epsilon_c}{\mathrm{d}(1/T)} = \frac{\mathrm{d}\log \mathrm{ABS}}{\mathrm{d}(1/T)} - \frac{\mathrm{d}\log [\mathrm{I_2}]_{0,T}}{\mathrm{d}(1/T)}$$

This technique holds approximately in the conventional study if the change in concentration of the lesser component is small over the temperature range (e.g., for weak complexes) (5).

Results

Ethyl methyl sulfide – I_2

For the vapor phase conventional study, four experiments were performed with varying donor and acceptor concen-

[1]Revision received February 9, 1983.

TABLE 1. Regression analysis[a] of K_c and ϵ_{max}^{CT} for the ethyl methyl sulfide – iodine complex in the vapor phase

T (°C)	$K_c\epsilon_{max}^{CT} \times 10^{-5}$ (M^{-2} cm^{-1})	K_c (M^{-1})	$\epsilon_{max}^{CT} \times 10^{-4}$ (M^{-1} cm^{-1})	Correlation constant
104.4	1.284±0.037	8.95±1.80	1.435±0.254	0.997
108.8	1.143±0.029	8.05±1.55	1.420±0.287	0.997
113.4	1.030±0.025	7.97±1.49	1.291±0.215	0.997
119.0	0.914±0.030	7.57±2.02	1.207±0.289	0.994
124.4	0.792±0.040	7.46±3.06	1.062±0.392	0.987

[a]Error limits for 95% confidence level.

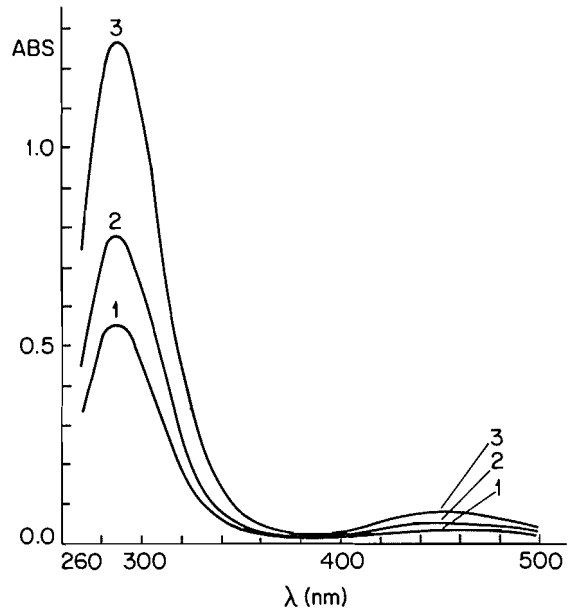

FIG. 1. The charge-transfer band and complexed visible iodine band for the ethyl methyl sulfide – iodine complex in the vapor phase: cell path = 75 cm; $[(CH_3)(C_2H_5)S] = 7.587 \times 10^{-3}$ M; (*1*) 70.0°C, $[I_2] = 2.790 \times 10^{-6}$ M; (*2*) 80.0°C, $[I_2] = 5.470 \times 10^{-6}$ M; (*3*) 95.8°C, $[I_2] = 1.466 \times 10^{-5}$ M. These are difference spectra with $TMAI_5/TMAI_3$ in the sample and reference cells.

trations and cell paths.[2] A charge-transfer band with a maximum at 289 nm was observed. The peak decreased in intensity with increasing temperature.[2] A regression analysis of log ABS vs. $1/T$ was made for each of the four mixtures. The average internal energy change (ΔE_c^0) was -7.1 ± 0.4 kcal mol^{-1} (correlation constant 0.998).

K_c and the molar absorptivity of the charge-transfer band, ϵ_{max}^{CT}, were determined by the usual regression analysis of eq. [1]. For this particular system, absorbance corrections due to contributions from the donor and acceptor species were small because of their low molar absorptivities in the region of the charge-transfer band maximum. The results of the analysis are listed in Table 1.

The rather large decrease in ϵ_{max}^{CT} with increase in temperature indicates that the separation of K_c and ϵ_{max}^{CT} from the $K_c\epsilon_{max}^{CT}$ product is poor. This may be due to a slow reaction. It was found for experiments where the sulfide concentration was high (>0.008 M) that it was not possible to return to the same absorbance at a fixed temperature at the end of a run. Therefore, a calculation of ΔE_c^0 was made based on a plot of log $K_c\epsilon_{max}^{CT}$ vs. $1/T$. This gave a value of -7.4 ± 0.8 kcal mol^{-1} which is in good agreement with that cited from the plot of the log ABS vs. $1/T$. (It is estimated (9) that the difference in ΔE_c^0 in the two methods for sulfide–I_2 complexes at elevated temperatures is ~0.3 kcal mol^{-1}.)

For the vapor phase constant activity method, $TMAI_5/TMAI_3$ was used as the iodine source. The spectrum of the charge-transfer band and the complexed visible iodine band is shown in Fig. 1 at 70.0°C, 80.0°C, and 95.8°C. (The spectrum also was recorded, although not shown in the figure, at 74.9°C, 85.2°C, and 89.2°C.) The charge-transfer band is well defined with a maximum at 289 nm. The complexed visible iodine band is less well defined due to the low absorbance in this region. The maximum does seem to occur at approximately 450 nm. The iodine spectrum cannot be studied in the vapor phase above 498 nm due to the onset of iodine's vibrational structure.

The experimental absorbance values and the $K_c\epsilon_{max}^{CT}$ values, calculated using eq. [3], are shown in Table 2, along with the $\epsilon_{max}^{CT}/\epsilon_{max}^{BS}$ ratio. The small variation in the ratio is probably due to small baseline shifts. A change of only 0.005 absorbance can change the ratio significantly. The average value of the ratio from this run and from a duplicate experiment is 17.1.

As derived in eq. [4], from the known temperature dependence of log ABS, and also, the saturation pressure curve for the $TMAI_5/TMAI_3$ equilibrium, the internal energy of complex formation can be calculated. The internal energy of vaporization, ΔE_{sat}, for this polyiodide system is 16.14 ± 0.76 kcal mol^{-1} (10). A regression analysis of the data at 289 nm in Table 2 gave a ΔE_c^0 of -8.19 ± 0.32 kcal mol^{-1}. This is slightly more negative than the value of -7.4 ± 0.8 kcal mol^{-1} obtained by the conventional method.

For the *n*-heptane solution study by the conventional method, the same solutions were used in both the uv and visible regions.[2] Matched far-uv glass-stoppered silica cells 0.100 cm in length were used in the ultraviolet spectral region. In the visible region, 1.000 cm cells were used. The charge-transfer band maximum[2] is at 301 nm. The visible absorbance data at 24.5°C are shown in Fig. 2. There is a well-defined isosbestic point at 492 nm. A slight temperature dependence of the isosbestic point was observed. At 4.7°C the crossing occurred at 490.5 nm. No shift in the maximum of the complexed visible iodine band or of the charge-transfer band was observed over the concentration range studied. The complexed visible iodine band[2] was obtained by subtracting the absorbance due to free

[2]Tables of concentration and spectral data in the vapor phase and in solution, and figures of spectra of the charge-transfer and blue-shifted visible iodine bands in the vapor phase and in solution, are available as supplementary material, at a nominal charge, from the Depository of Unpublished Data, CISTI, National Research Council of Canada, Ottawa, Ont., Canada K1A 0S2.

Can. J. Chem. Downloaded from www.nrcresearchpress.com by 210.87.254.40 on 09/06/12
For personal use only.

TABLE 2. Temperature dependence study[a] of ethyl methyl sulfide[b] – iodine in the vapor phase by the constant acitivity method ($TMAI_5/TMAI_3 = I_2$ source)

T (°C)	$[I_2]$ ($M \times 10^6$)	Corrected absorbance[c] CT band	Corrected absorbance[d] complexed visible iodine band	$K_c\epsilon_{max}^{CT} \times 10^{-5}$[e] ($M^{-2}$ cm^{-1})	$\frac{\epsilon_{max}^{CT}}{\epsilon_{max}^{BS}}$
70.0	2.790	0.552	0.033	3.477	16.7
74.9	3.905	0.664	0.043	3.007	15.4
80.0	5.470	0.772	0.049	2.480	15.8
85.2	7.639	0.908	0.056	2.089	16.2
89.2	9.182	1.022	0.061	1.831	16.8
95.8	14.66	1.265	0.073	1.521	17.3

[a]In a 75.0-cm cell.
[b]$[(CH_3)(C_2H_5)S] = 0.007587\ M$.
[c]Using a 0–2.0 absorbance scale, readings taken at 289 nm.
[d]Using a 0–0.2 absorbance scale, readings taken at 450 nm.
[e]Calculated using eq. [3].

TABLE 3. Regression analysis[a] of K_c, ϵ_{max}, and ϵ_{max}^{BS} for the ethyl methyl sulfide – iodine complex in *n*-heptane

T (°C)	$K_c\epsilon_{max} \times 10^{-6}$ (M^{-2} cm^{-1})	K_c (M^{-1})	ϵ_{max} (M^{-1} cm^{-1})	Correlation constant
	Ultraviolet region $\lambda_{max}^{CT} = 301$ nm			
24.5	3.504±0.046	124.2±3.4	28220±420	0.99997
19.4	4.553±0.134	159.1±8.6	28610±760	0.99992
14.3	5.445±0.057	187.8±3.4	28990±240	0.99999
9.7	7.066±0.089	244.2±4.8	28940±220	0.99999
4.7	9.008±0.197	315.8±9.4	28520±280	0.99999
	Visible region $\lambda_{max}^{BS} = 438$ nm			
24.5	0.2320±0.0075	121.7±8.2	1906±71	0.99986
19.4	0.3019±0.0071	156.3±6.8	1932±42	0.99995
14.3	0.3630±0.0179	188.1±16	1930±75	0.99985
9.7	0.4683±0.0114	244.2±8.2	1918±28	0.99997
4.7	0.5905±0.271	307.3±20	1922±41	0.99995

[a]Error limits for the 95% confidence level.

TABLE 4. Regression analysis[a] of K_c, ϵ_{max}, and ϵ_{max}^{BS} for the dimethyl sulfide – iodine complex in *n*-heptane

T (°C)	$K_c\epsilon_{max} \times 10^{-6}$ (M^{-2} cm^{-1})	K_c (M^{-1})	ϵ_{max} (M^{-1} cm^{-1})	Correlation constant
	Ultraviolet region $\lambda_{max}^{CT} = 300$ nm			
19.4	2.853±0.078	102.1± 6.3	27950±1020	0.99987
14.3	3.794±0.118	136.6± 8.4	27760± 910	0.99989
9.7	4.758±0.108	171.4± 7.0	27760± 540	0.99996
4.8	6.050±0.544	215.6±31.0	28060±1640	0.99966
	Visible region $\lambda_{max}^{BS} = 441$ nm			
19.4	0.1858±0.0084	102.2± 1.1	1818± 11	0.99999
14.3	0.2516±0.0161	142.1±17.1	1771±115	0.99959
9.7	0.3089±0.0090	170.1± 8.9	1816± 45	0.99993
4.8	0.3738±0.0176	202.6±15.6	1845± 60	0.99989

[a]Error limits for the 95% confidence level.

iodine from the total visible absorbance at each wavelength. This requires a knowledge of the equilibrium constant, which was determined from the data in the ultraviolet region. The complexed visible iodine band maximum is at 438 nm.

K_c, ϵ_{max}^{CT}, and ϵ_{max}^{BS} were determined by the usual regression analysis of eq. [1]. While corrections in the ultraviolet region are small because the free donor and free acceptor contribute very little to the absorbance near the charge-transfer band maximum, in the region of the complexed visible iodine band maximum they are significant because of the free iodine absorption.

The results of the analysis are shown in Table 3. The ultraviolet and visible molar absorptivities, ϵ_{max}^{CT} and ϵ_{max}^{BS}, respectively, show small variations over the limited temperature range. The average of the five ϵ_{max}^{CT} and ϵ_{max}^{BS} values is 28 660 M^{-1} cm^{-1} and 1 922 M^{-1} cm^{-1}, respectively. The $\epsilon_{max}^{CT}/\epsilon_{max}^{BS}$

Can. J. Chem. Downloaded from www.nrcresearchpress.com by 210.87.254.40 on 09/06/12
For personal use only.

Can. J. Chem. Downloaded from www.nrcresearchpress.com by 210.87.254.40 on 09/06/12
For personal use only.

TABLE 5. Spectral and thermodynamic properties of sulfide–iodine complexes in the vapor phase and in solution[a,b]

Parameter	Dimethyl sulfide – iodine		Ethyl methyl sulfide – iodine		Diethyl sulfide – iodine	
	Vapor[c]	*n*-Heptane[d]	Vapor[d]	*n*-Heptane[d]	Vapor[c]	*n*-Heptane
Spectral, CT band						
λ_{max} (nm)	285	300 (299)[e]	289	301	290	303[f]
ϵ_{max} (M^{-1} cm^{-1})	13 430±2 550[g]	27 880±1 030[h]	14 350±2 540[i]	28 660±385[j]	16 800±2 230[k]	26 400±1 050[f,l] (29 800)[m]
$\Delta\bar{\nu}_{1/2}{}^{n}$ (cm^{-1})	5 400±150	5 380 (5 300±150)[e]	5 900	5 370	5 800±150	5 400±150[e]
f^0	0.33	0.65	0.37	0.66	0.42	0.615[e] (0.695)[m]
$\mu_{mn}{}^{P}$ (D)	4.5	6.4	4.7	6.5	5.1	6.30[e] (6.69)[m]
$K_c\epsilon_{max}{}^{q}$ (M^{-2} cm^{-1}) (t, °C)	102 000±3 000 (100°C)		143 000±3 500[r] (100°C) (136 000)[s] (100°C)		193 200±3 000 (100°C)	
		2 220 000±210 000 (25.0°C)		3 430 000±105 000 (25.0°C)		4 750 000 ±390 000 (25.0°C) (5 370 000)[m] (25.0°C)
Spectral, visible I_2 band						
λ_{max} (nm)	457	441	(~450)[t]	438	452 (453)	437[f]
ϵ_{max}(M^{-1} cm^{-1})	703[u]	1 810±60[h]	839[v]	1 920±50[j]	1 050	1 930±55[f,l] (1 960)[m]
$\Delta\bar{\nu}_{1/2}{}^{n}$ (cm^{-1})	4 350	3 940	3 820	4 050	4 800	4 200[m]
f^0	0.013	0.031	0.014	0.034	0.022	0.0350[f] (0.0355)[m]
$\mu_{mn}{}^{p}$ (Debye)	1.13	1.70	1.15	1.77	1.45	1.80[f] (1.82)[m]
$K_c\epsilon_{max}$ (M^{-2} cm^{-1}) (t, °C)	5 340[w] (100°C)		8 360[w] (100°C)		12 100[w] (100°C)	
		148 300±12 800[q] (25.0°C)		229 000±63 000[q] (25.0°C)		347 000 (25.0°C)
f^{CT}/f^{BS}	24	21	26	20	19	18[f] (20)[m]
$\epsilon_{max}^{CT}/\epsilon_{max}^{BS}$	19.1	15.4	17.1	14.9	16.0	13.7 (15.2)[m]

Can. J. Chem. Downloaded from www.nrcresearchpress.com by 210.87.254.40 on 09/06/12
For personal use only.

TABLE 5 *(Concluded)*

Parameter	Dimethyl sulfide – iodine		Ethyl methyl sulfide – iodine		Diethyl sulfide – iodine	
	Vapor[c]	*n*-Heptane[d]	Vapor[d]	*n*-Heptane[d]	Vapor[c]	*n*-Heptane
Thermodynamic						
K_c (M^{-1})	7.5±1.3		9.97±2		11.5±1.1	
(t, °C)	(100°C)		(100°C)		(100°C)	
		78.1±4.8		119±5		180±7[f,s]
		(25.0°C)		(25.0°C)		(25.0°C)
$-\Delta E_c^0$ (kcal mol^{-1})	7.1±0.4		8.2±0.3[s]		8.3±0.2	
$-\Delta H_c^0$ (kcal mol^{-1})	7.8±0.4	8.3±1.2	8.9±0.3	7.8±0.8	9.0±0.2	8.9±0.6[f,x,y]
						8.3±0.2[f,x,y]
$-\Delta S_c^0$ (cal mol^{-1} deg^{-1})	15.1±1.0	19.2	17.4	16.7	17.3±0.5	19.4±2.0[f,x,y]
						17.5±0.5[f,x,y]

[a]Standard state of 1 M.
[b]Error limits at 95% confidence level.
[c]From this laboratory; refs. 9 and 10.
[d]Present study.
[e]Reference 8.
[f]Reference 39.
[g]Average over temperature range 90–120°C, ref. 9.
[h]Average over temperature range 4.8–19.4°C.
[i]At the lowest temperature 104.4°C; no average taken because of systematic decrease in ϵ_{max} with increase in temperature due possibly to a slow reaction.
[j]Average over temperature range 4.7–24.5°C.
[k]Average over temperature range 105.2–127.1°C, ref. 9.
[l]Average over temperature range 5.6–40.2°C.
[m]Reference 40.
[n]Half-width; difference in $\bar{\nu}$ at half the maximum intensity on the high- and low-energy side of the band, except for the EtMeS–I_2 CT band in the vapor phase where it is twice the difference between the band peak and half of the maximum intensity on the low-energy side.
[o]Oscillator strength (27*a*).
[p]Electronic transition dipole (27*a*).
[q]From a plot of log $K_c\epsilon_{max}$ vs. $1/T$.
[r]From data obtained by the conventional method.
[s]From data obtained by the constant activity method.
[t]Not well defined because of low absorbance (see Fig. 1).
[u]Calculated from the experimentally determined average value for ϵ_{max}^{CT} and theobserved ratio of $\epsilon_{max}^{CT}/\epsilon_{max}^{BS}$.
[v]Calculated from the value of ϵ_{max}^{CT} obtained at the lowest temperature (104.4°C) and the observed ratio of $\epsilon_{max}^{CT}/\epsilon_{max}^{BS}$.
[w]Calculated by multiplying ϵ_{max}^{BS} and K_c.
[x]For other literature values see ref. 9.
[y]Standard error.

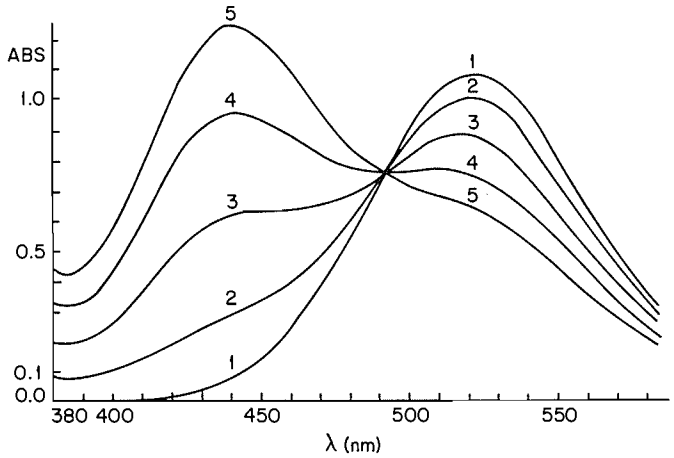

FIG. 2. The visible spectra of the ethyl methyl sulfide – iodine complex at 24.5°C in *n*-heptane; isosbestic point at 492 nm; cell path = 1.000 cm; (*1*) $[I_2] = 1.190 \times 10^{-3}$ *M*; (*2*) $[I_2] = 1.189 \times 10^{-3}$ *M*, $[(CH_3)(C_2H_5)S] = 1.001 \times 10^{-3}$ *M*; (*3*) $[I_2] = 1.188 \times 10^{-3}$ *M*, $[(CH_3)(C_2H_5)S] = 2.996 \times 10^{-3}$ *M*; (*4*) $[I_2] = 1.184 \times 10^{-3}$ *M*, $[(CH_3)(C_2H_5)S] = 5.990 \times 10^{-3}$ *M*; (*5*) $[I_2] = 1.185 \times 10^{-3}$ *M*, $[(CH_3)(C_2H_5)S] = 1.004 \times 10^{-2}$ *M*.

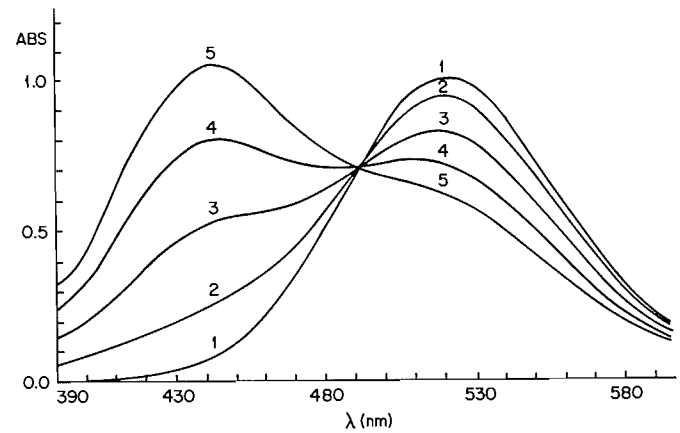

FIG. 3. The visible spectra of the dimethyl sulfide – iodine complex at 19.4°C in *n*-heptane; isosbestic point at 492.3 nm; cell path = 1.000 cm; (*1*) $[I_2] = 1.087 \times 10^{-3}$ *M*; (*2*) $[I_2] = 1.091 \times 10^{-3}$ *M*, $[(CH_3)_2S] = 1.051 \times 10^{-3}$ *M*; (*3*) $[I_2] = 1.090 \times 10^{-3}$ *M*, $[(CH_3)_2S] = 3.190 \times 10^{-3}$ *M*; (*4*) $[I_2] = 1.086 \times 10^{-3}$ *M*, $[(CH_3)_2S] = 6.365 \times 10^{-3}$ *M*; (*5*) $[I_2] = 1.091 \times 10^{-3}$ *M*, $[(CH_3)_2S] = 1.055 \times 10^{-2}$ *M*.

ratio is 14.8. At 24.5°C the equilibrium constant is 124.2 ± 3.4 M^{-1}. This agrees well with a previously reported equilibrium constant of 136.2 ± 15.8 M^{-1} at 25°C via an nmr study in CCl_4 (26).

A plot of D_0lA_0/ABS versus $(D_0 + A_0)$ at different temperatures for both the ultraviolet and visible data gave parallel slopes which is indicative of the small variation in the molar absorptivity with temperature.

The enthalpy of complexation, ΔH_c^0, was determined via a regression analysis of $\log K_c\epsilon_{max}^{CT}$ versus $1/T$ and also of $\log K_c$ versus $1/T$. ΔH_c^0 values of −7.8 ± 0.8 kcal mol^{-1} (correlation constant 0.998) and −7.6 ± 1.0 kcal mol^{-1} (correlation constant 0.998), respectively, were obtained. The two ΔH_c^0 values are the same within experimental error, indicating good $K_c\epsilon_{max}^{CT}$ separation. The thermodynamic data for K_c obtained in the visible spectral region are within experimental error of the data obtained in the ultraviolet region as Table 3 shows.

Dimethyl sulfide – I_2

The ultraviolet and visible spectral characteristics of the dimethyl sulfide – iodine complex were investigated via the conventional method in *n*-heptane. The temperature dependence of the complex was studied in the range 4.8–19.4°C at approximately 5° intervals. The volatility of the donor made it difficult to study this complex at higher temperatures. Again, 0.100-cm cells were used in the ultraviolet spectral region, and 1.000-cm cells were used in the visible spectral region. The charge-transfer band maximum[2] is at 300 nm. The visible absorbance data at 19.4°C are shown in Fig. 3. The isosbestic point occurs at 492.3 nm and shows a slight temperature dependence (490.5 nm at 4.8°C, 491.3 nm at 9.7°C, and 491.6 nm at 14.3°C). The complexed visible iodine band[2] has a maximum at 441 nm. From the absorbance data[2] of the charge-transfer and complexed visible iodine bands, K_c, ϵ_{max}^{CT}, and ϵ_{max}^{BS} were determined by the usual regression analysis of eq. [1], and the results are given in Table 4. The average molar absorptivity for the charge-transfer and complexed visible iodine bands, 27 850 and 1 813 M^{-1} cm^{-1}, respectively, shows no significant variation over this limited temperature range. The $\epsilon_{max}^{CT}/\epsilon_{max}^{BS}$ was calculated at each of the four temperatures studied. The average of the four ratios was 15.4.

A regression analysis of $\log K_c\epsilon_{max}^{CT}$ versus $1/T$ and, also, of $\log K_c$ versus $1/T$ gave ΔH_c^0 values of −8.29 ± 1.22 kcal mol^{-1} (correlation constant 0.999), and −8.24 ± 1.58 kcal mol^{-1} (correlation constant 0.998), respectively, based on the absorbance data at the charge-transfer band maximum. The agreement in the ΔH_c^0 values again is indicative of good separation of the $K_c\epsilon_{max}^{CT}$ product. The determination of ΔH_c^0 from only four temperatures probably accounts for the higher error limits compared to the ethyl methyl sulfide – iodine case.

The ΔH_c^0 results from the ultraviolet absorbance data are expected to be more accurate than those based on the visible data. Analysis of the visible data gave $\Delta H_c^0 = -7.68 \pm 2.74$ kcal mol^{-1} (correlation constant 0.992) from the $\log K_c\epsilon_{max}^{CT}$ versus $1/T$ plot, and −7.45 ± 3.81 kcal mol^{-1} (correlation constant 0.986) from the $\log K_c$ versus $1/T$ plot.

Discussion

The complete spectral and thermodynamic properties of the three sulfide–I_2 complexes in the vapor phase and in *n*-heptane solution are summarized in Table 5. It would be expected that these properties would show a systematic trend within each phase for a homologous series of donors with a common acceptor. However, the error limits in the determination of ϵ_{max}^{CT}, of ϵ_{max}^{BS}, of K_c, and of ΔE_c^0 (or ΔH_c^0) generally mask any correlation of these properties with strength of complexation. Only in two instances is it clear that the sequence of donor strength is Et_2S > EtMeS > Me_2S: (*1*) the solution values of K_c (at 25°C), where the error limits are relatively small, and (*2*) the $K_c\epsilon_c$ product in both phases. In the latter case, the precision in determining the $K_c\epsilon_c$ product is better than that obtained when this product is separated into its components, especially for weak complexes. Further, if K_c and ϵ_c follow a similar trend, then the $K_c\epsilon_c$ product should magnify that trend.

Band intensities are measured by the transition dipole (27*a*) μ ($\simeq 0.0958(\epsilon_{max}\Delta\bar{\nu}_{1/2}/\bar{\nu})^{1/2}$), and the oscillator strength (27*a*), f ($= 4.704 \times 10^{-7}\bar{\nu}_{max}\mu^2$). Here, $\Delta\bar{\nu}_{1/2}$ is the half-width of the band in cm^{-1}, and $\bar{\nu}$ is the average wave number in cm^{-1} (usually approximated as the wave number at the absorption maximum, $\bar{\nu}_{max}$). The values of $\Delta\bar{\nu}_{1/2}$ for the CT bands are

Can. J. Chem. Downloaded from www.nrcresearchpress.com by 210.87.254.40 on 09/06/12
For personal use only.

TABLE 6. Charge-transfer and ionization energy data for sulfide complexes with iodine and with tetracyanoethylene

Sulfide	I_D^v (eV)	Iodine in vapor phase $h\nu_{max}^{CT}$ (eV)	Iodine in *n*-heptane $h\nu_{max}^{CT}$ (eV)	TCNE in methylene chloride[a] $h\nu_{max}^{CT}$ (eV)
1. $(CH_3)_2S$	8.67[a](8.685)[b]	4.35_0	4.13_3	2.53_0
2. $(C_2H_5)(CH_3)S$	(8.55)[b]	4.29_0	4.11_9	
3. $(C_2H_5)_2S$	8.44[a](8.43)[b]	4.27_5	4.09_2	2.45_5
4. $(CH_2)_4S$	8.40[a]	4.23_1[c]	4.05_2[d]	2.40_3
5. $(CH_2)_3S$	8.65[a]		4.05_2[d]	2.54_7
6. $(CH_2)_5S$	8.45[a]		4.10_5[d]	2.50_5

[a]Reference 38.
[b]Reference 41.
[c]Reference 8.
[d]Reference 39.

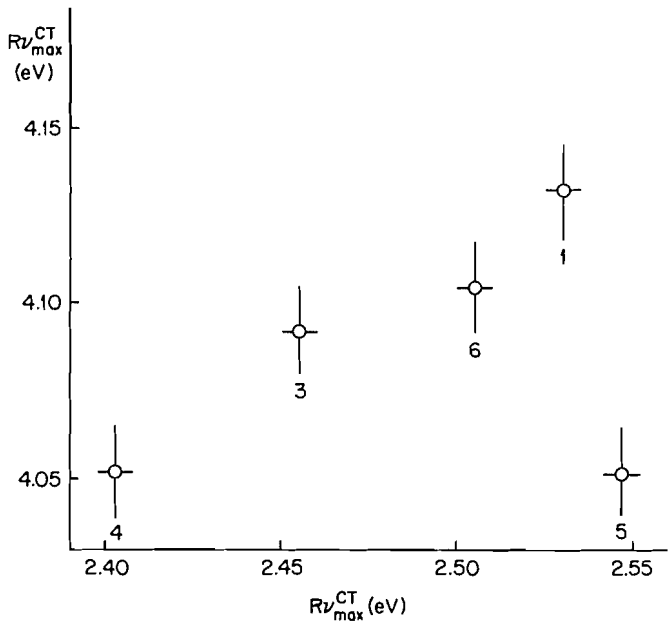

FIG. 4. Correlation between the charge-transfer band position of sulfide–iodine complexes in *n*-heptane (*Y*-axis) vs. that of sulfide–TCNE complexes in methylene chloride (*X*-axis); numbering corresponds to that in Table 6.

rather comparable for all the complexes, as is also the case for the blue-shifted iodine bands. Further, the variation in $\bar{\nu}_{max}$ for the three complexes, both for the charge-transfer and blue-shifted iodine bands, is very small. Consequently, the trends in the magnitude of μ and of f follow essentially those for ϵ.

The solvent effect on the thermodynamic properties of the sulfide–I_2 complexes is relatively small. Taken as a whole, the values for ΔH_c^0 in the vapor phase and in solution are comparable. Further, extrapolation of the solution data to 100°C, or the vapor phase data to 25°C, shows that K_c is about the same in the two phases (9, 22).

It is of interest to compare the spectral properties of the complexes between the two phases. ϵ_{max} is an order of magnitude greater for the charge-transfer band than for the blue-shifted iodine band, as seen in the $\epsilon_{max}^{CT}/\epsilon_{max}^{BS}$ (or f^{CT}/f^{BS}) ratio. This ratio is larger in the vapor phase than in solution. Analysis of the data shows that both the charge-transfer band and the blue-shifted iodine band are increased in intensity in going from the vapor phase to solution. However, the solvent effect on the band intensity is *relatively greater* for the blue-shifted iodine band than for the charge-transfer band, thereby decreasing the $\epsilon_{max}^{CT}/\epsilon_{max}^{BS}$ ratio.

Several of the theories which have been proposed to account for the solvent influence on the properties of complexes have been discussed earlier (5, 22, 25). However, one model bears special mention in the light of some recent experimental results, namely, the solvent cage effect (28). Creation of a solvent cavity requires energy and, therefore, the cavity will tend to be of minimum size, causing the complex within the cavity to be compressed. This compression in going from the vapor phase to solution has been proposed to account for (*a*) the red shift in the CT band of weak complexes (28), (*b*) the blue shift in the iodine visible band (5, 29), and (*c*) an increase in band intensity due to greater orbital overlap (27*d*).

The solvent cage effect has been compared to pressure effects on these complexes (28, 30). A study by Suzuki *et al.* of the effect of pressure on the CT band (31, 32) and on the visible I_2 band (33) of the diethyl sulfide–I_2 complex in *n*-heptane solution supports the solvent cage model. These authors noted the following changes as the pressure increased from 1 to 3300 bar: (*1*) initial increase in pressure caused red shifts in the CT band (but increasing the pressure still further reversed the trend and caused blue shifts); (*2*) ϵ_{max}^{CT} was enhanced; (*3*) there was a blue shift in the visible iodine band; (*4*) ϵ_{max}^{BS} was enhanced; (*5*) the enhancement was greater for ϵ_{max}^{BS} than for ϵ_{max}^{CT}, so that the $\epsilon_{max}^{CT}/\epsilon_{max}^{BS}$ ratio decreased from 11.9 at 1 bar to 10.7 at 3300 bar.

Further support for a solvent cage model stems from a recent study (34) of iodine complexes formed with donors in supersonic molecular beams. A typical system is dimethyl sulfide – iodine in He as a diluent gas. The fluorescence excitation spectra of the "cold clusters" are attributed to a blue-shifted absorption of the complexed I_2, followed by emission from free I_2 when the complex dissociates. Comparison of these spectra with the absorption spectra of donor–iodine complexes in the vapor phase and in *n*-heptane solution shows they resemble more closely the spectra in solution.

It has been found for iodine complexes that a relation exists, although with much scatter, between the blue shift of the visible iodine band and the strength of complexation (as, say, measured by ΔH_c^0) (27*c*). Paetzold (35–37) has found, for a homologous series of donor–iodine complexes, that quite a good linear correlation exists between the blue-shifted visible iodine band and several parameters which are a measure of bond strength (e.g., ΔH_c^0, ΔG_c^0, force constants). Comparison

Can. J. Chem. Downloaded from www.nrcresearchpress.com by 210.87.254.40 on 09/06/12
For personal use only.

of the solution data in Table 5 shows a consistent decrease in λ_{max}^{BS} with increased donor strength. However, in the vapor phase, λ_{max}^{BS} for EtMeS–I_2 was not sufficiently resolved for quantitative comparison.

For a homologous series of donors with a common acceptor, theory (27*b*) predicts a correlation between the charge-transfer band position, $h\nu_{max}^{CT}$, and the vertical ionization energy of the donor, I_D^v. Table 6 lists data for the sulfide–I_2 complexes in the vapor phase and in *n*-heptane solution. Corresponding data are given for these sulfides complexed with TCNE in methylene chloride (38). The range in values of I_D^v and of $h\nu_{max}^{CT}$ is rather small, and makes their correlation seem more scattered. When $h\nu_{max}^{CT}$ data for sulfides complexed with iodine in *n*-heptane are plotted versus comparable data for the same sulfides complexed with TCNE in methylene chloride the correlation is improved (Fig. 4), except the point for $(CH_2)_3S$ which is significantly out of line. The value for $h\nu_{max}^{CT}$ for the iodine complex in *n*-heptane was rechecked by the constant activity method, using $TMAI_5$, and the result was the same.

Acknowledgment

The authors thank Professor Hans Bock for sending us a copy of the thesis of W. Schulz.

1. G. BRIEGLEB. Elektronen-donator–acceptor komplexe. Springer-Verlag, Berlin. 1961.
2. R. FOSTER. Organic charge-transfer complexes. Academic Press, New York. 1969.
3. C. N. R. RAO, S. N. BHAT, and P. C. DWIVEDI. Appl. Spect. Rev. **5**, 1 (1971).
4. E. N. GUR'YANOVA, I. P. GOL'DSHTEIN, and I. P. ROMM. Donor–acceptor bond. Moscow. 1973; English Transl. John Wiley and Sons, New York. 1975.
5. M. TAMRES. Molecular complexes. Vol. 1. *Edited by* R. Foster. Paul Elek Ltd., London. 1973. Chapt. 2.
6. J. M. GOODENOW and M. TAMRES. J. Chem. Phys. **43**, 3393 (1965).
7. M. TAMRES and J. M. GOODENOW. J. Phys. Chem. **71**, 1982 (1967).
8. M. KROLL. J. Am. Chem. Soc. **90**, 1097 (1968).
9. M. TAMRES and S. N. BHAT. J. Am. Chem. Soc. **94**, 2577 (1972).
10. M. TAMRES and S. N. BHAT. J. Am. Chem. Soc. **95**, 2516 (1973).
11. N. W. TIDESWELL and J. D. MCCULLOUGH. J. Am. Chem. Soc. **79**, 1031 (1957).
12. H. A. BENESI and J. H. HILDEBRAND. J. Am. Chem. Soc. **71**, 2703 (1949).
13. R. L. SCOTT. Rec. Trav. Chim. Pays-Bas. **75**, 787 (1956).
14. J. D. CHILDS. Ph.D. Thesis, University of Oklahoma, Norman, OK. 1971.
15. J. D. CHILDS, S. D. CHRISTIAN, J. GRUNDNES, and S. R. ROACH. Acta. Chem. Scand. **25**, 1679 (1971).
16. J. D. CHILDS, S. D. CHRISTIAN, and J. GRUNDNES. J. Am. Chem. Soc. **94**, 5657 (1972).
17. M. BRANDON, M. TAMRES, and S. SEARLES, JR. J. Am. Chem. Soc. **82**, 2129 (1960).
18. F. D. CHATTAWAY and G. HOYLE. J. Chem. Soc. **123**, 654 (1923).
19. A. I. POPOV and R. E. BUCKLES. Inorg. Synth. **5**, 172 (1957).
20. M. TAMRES and J. GRUNDNES. J. Am. Chem. Soc. **93**, 801 (1971).
21. H. C. TSE and M. TAMRES. J. Phys. Chem. **81**, 1367 (1977).
22. S. J. LO. Ph.D. Thesis. The University of Michigan, Ann Arbor, MI. 1981.
23. M. TAMRES. J. Phys. Chem. **65**, 654 (1961).
24. R. A. LABUDDE and M. TAMRES. J. Phys. Chem. **74**, 4009 (1970).
25. M. TAMRES and J. YARWOOD. Spectroscopy and structure of molecular complexes. *Edited by* J. Yarwood. Plenum Press, New York. 1973. Chapt. 3.
26. E. T. STROM, W. L. ORR, B. S. SNOWDEN, JR., and D. E. WOESSNER. J. Phys. Chem. **71**, 4017 (1967).
27. R. S. MULLIKEN and W. B. PERSON. Molecular complexes: a lecture and reprint volume. John Wiley and Sons, New York. 1969. (*a*) p. 26; (*b*) p. 118; (*c*) p. 159; (*d*) Chapt. 3.
28. J. PROCHOROW and A. TRAMER. J. Chem. Phys. **44**, 4545 (1966).
29. M. TAMRES and S. N. BHAT. J. Phys. Chem. **75**, 1057 (1971).
30. P. J. TROTTER. J. Am. Chem. Soc. **88**, 5721 (1966).
31. S. SAWAMURA, Y. TANIGUCHI, and K. SUZUKI. Bull. Chem. Soc. Jpn. **52**, 284 (1979).
32. S. SAWAMURA, Y. TANIGUCHI, and K. SUZUKI. Bull. Chem. Soc. Jpn. **52**, 3511 (1979).
33. S. SAWAMURA, Y. TANIGUCHI, and K. SUZUKI. Bull. Chem. Soc. Jpn. **52**, 281 (1979).
34. K. L. SAENGER, G. M. MCCLELLAND, and D. R. HERSCHBACH. J. Phys. Chem. **85**, 3333 (1981).
35. R. PAETZOLD. Chem. Script. **8A**, 64 (1975).
36. R. PAETZOLD. Z. Chem. **15**, 377 (1975).
37. R. PAETZOLD and K. NIENDORF. Z. Phys. Chem. Leipzig, **256**, 361 (1975).
38. W. SCHULZ. Ph.D. Thesis, Johann Wolfgang Goethe University. Frankfurt/Main, Germany. 1979.
39. M. TAMRES and S. SEARLES. J. Phys. Chem. **66**, 1099 (1962).
40. H. TSUBOMURA and R. LANG. J. Am. Chem. Soc. **83**, 2085 (1961).
41. K. WATANABE, T. NAKAYAMA, and J. MOTTL. J. Quant. Spectrom. Radiative Transfer, **2**, 369 (1962).

Can. J. Chem. Downloaded from www.nrcresearchpress.com by 210.87.254.40 on 09/06/12
For personal use only.

Ternary complexes of Pb(II) with itaconic acid and nicotinic acid: a polarographic study

VILAS KASHINATH CHITALE AND KRISHNA SADASHIV PITRE
Department of Chemistry, University of Saugar, Sagar (M.P.), India 470 003

Received February 24, 1983

VILAS KASHINATH CHITALE and KRISHNA SADASHIV PITRE. Can. J. Chem. **61**, 1941 (1983).

Polarographic measurements have been used to evaluate the overall formation constants of simple and mixed complexes of Pb(II) with itaconic acid and nicotinic acid at (25 ± 0.1) °C (abbreviated as ICA and NA). It is observed that Pb(II) forms 1:1, 1:2, and 1:3 binary complexes with ICA, whereas 1:1 and 1:2 binary complex species are formed with NA. The reduction of binary as well as ternary complexes is found to be reversible and diffusion controlled, involving two electrons at constant ionic strength $I = 1.0$ adjusted with the necessary addition of potassium nitrate.

For ternary system the reduction of Pb(II) has been carried out at two fixed concentrations of nicotinic acid, whereas itaconic acid concentration is varied. Schaap and McMaster's treatment reveals the formation of $[Pb(ICA)(NA)]^-$, $[Pb(ICA)(NA)_2]^{2-}$, and $[Pb(ICA)_2(NA)]^{3-}$ with $\log \beta_{11} = 3.00 \pm 0.03$, $\log \beta_{12} = 5.35 \pm 0.028$, and $\log \beta_{21} = 5.52 \pm 0.032$, respectively. The numbers after the ± signs stand for the standard deviation.

Addition and substitution of the ligand species in the ternary complexes have also been discussed.

VILAS KASHINATH CHITALE et KRISHNA SADASHIV PITRE. Can. J. Chem. **61**, 1941 (1983).

On a utilisé des mesures polarographiques pour évaluer la constante de formation globale des complexes simples et mixtes du Pb(II) avec l'acide itaconique et avec l'acide nicotinique à (25 ± 0,1)°C (AIC et AN). On a observé que le Pb(II) forme des complexes binaires du type 1:1, 1:2 et 1:3 avec le AIC tandis qu'il forme des complexes binaires du type 1:1 et 1:2 avec le AN. On a trouvé que la réduction des complexes binaires aussi bien que celle des complexes ternaires est réversible et contrôlée par la diffusion. Elle implique deux électrons à une force ionique constante de $I = 1,0$ que l'on ajuste en ajoutant nécessairement du nitrate de potassium.

Dans le cas des systèmes ternaires on effectue la réduction du Pb(II) pour deux concentrations fixes d'acide nicotinique tandis qu'on fait varier la concentration de l'acide itaconique. Le traitement de Schaap et McMaster révèle la formation du $[Pb(AIC)(AN)]^-$, du $[Pb(AIC)(AN)_2]^{2-}$ et du $[Pb(AIC)_2(AN)]^{3-}$ avec $\log \beta_{11} = 3,00 \pm 0,03$, $\log \beta_{12} = 5,35 \pm 0,028$ et $\log \beta_{21} = 5,52 \pm 0,032$ respectivement. Les nombres entre parenthèses indiquent la déviation normale.

On discute également de l'addition et de la substitution des ligands dans les complexes ternaires.

[Traduit par le journal]

Introduction

In continuation of our previous work on the polarographic study of mixed complexes of Pb(II) with some organic ligands (1, 2), the present paper deals with the ternary complexes of Pb(II) with itaconic acid and nicotinic acid. This system has not been reported so far polarographically.

Experimental

All the chemicals used were of analytical reagent grade and their solutions were prepared in doubly distilled water. The ionic strength was adjusted at $I = 1.0$ by necessary addition of KNO_3, used as supporting electrolyte (0.01%). Gelatin was used as maxima suppressor, sodium itaconate and sodium nicotinate were used as ligands. The concentration of Pb(II) was maintained at 1×10^{-3} *M*.

Polarograms were recorded on a CIC (Baroda, India) automatic pen recording polarograph. The characteristics of the DME used were $m = 2.37$ mg, $s = 3.0$ s at 35 cm, the effective height of the mercury column, open circuit, when measured in air-free 1.0 *M* KNO_3 ($m^{2/3} t^{1/6} = 2.136\ mg^{2/3} s^{-1/2}$). The pH of the test solution was adjusted at pH 6.5 ± 0.1 by necessary addition of nitric acid/sodium hydroxide solutions. For pH measurements, an Elico digital pH meter (model LI-120) was used. Pure nitrogen gas was passed through test solutions before recording the polarograms. All the measurement were made at room temperature 25 ± 0.1°C.

Results and discussion

Pb(II) gives a single, well-defined reversible reduction wave in potassium nitrate. The reduction of Pb(II) as well as its binary and ternary complexes with itaconic acid and nicotinic acid are diffusion controlled, as revealed from the straight line plots of i_d vs. $\sqrt{h}$ passing through the origin. The plot of $\log i/i_d - i$ vs. E_{dc} for each polarogram was found to be linear with a slope of 30 ± 2 mV indicating the reversibility of the electrode process involving two electrons.

(A) Binary systems

The stability constants of simple binary complexes of Pb(II) with itaconic acid and nicotinic acid were evaluated separately prior to the study of ternary system. Identical conditions were maintained in both the simple as well as mixed systems.

(i) Pb(II)–itaconate system

A plot of $-E_{1/2}$ vs. $\log C_x$ (logarithm of the concentration of itaconate) was a smooth curve (Fig. 1*a*), thereby suggesting the formation of successive complexes. The Deford and Hume method (3) was applied to determine the formation constants of the successive complexes. Three complexes were formed (4):

$[Pb(ICA)]$	$\log \beta_{10} = 2.17;$	$\beta_{10} = 150$
$[Pb(ICA)_2]^{2-}$	$\log \beta_{20} = 3.30;$	$\beta_{20} = 2000$
$[Pb(ICA)_3]^{4-}$	$\log \beta_{30} = 5.30;$	$\beta_{30} = 200000$

$F_j(X)$ functions of simple complexes of Pb(II) with itaconate are presented in Table 1.

(ii) Pb(II)–nicotinate system

In this case the plot of $-E_{1/2}$ vs. $\log [NA]$ was again a smooth curve, thereby showing the formation of successive complexes (Fig. 1*b*). The stability constants of the successive complexes were evaluated by the Deford and Hume method (3). Two successive complexes were formed:

$[Pb(NA)]^+$	$\log \beta_{01} = 1.24;$	$\beta_{01} = 17.5$
$[Pb(NA)_2]$	$\log \beta_{02} = 2.32;$	$\beta_{02} = 210$

Can. J. Chem. Downloaded from www.nrcresearchpress.com by 210.87.254.6 on 09/06/12
For personal use only.

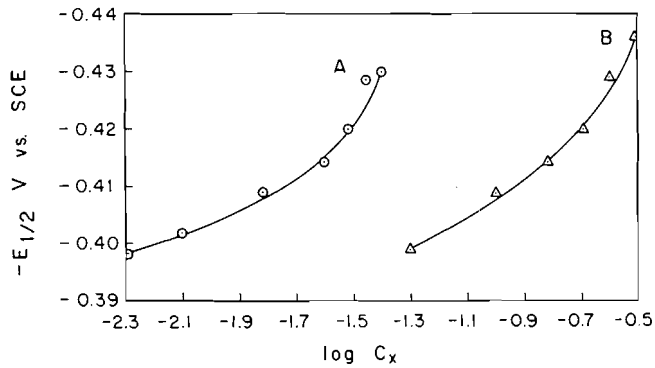

FIG. 1. Plots of $-E_{1/2}$ vs. $-\log C_x$ for (*A*) Pb(II)–itaconate system; (*B*) Pb(II)–nicotinate system.

TABLE 1. Polarographic characteristics and $F_j(X)$ values for the Pb(II)–itaconate system

C_x (mol)	$-E_{1/2}$ (V) vs. sce	i_d (div)	$F_0(X)$	$F_1(X)$	$F_2(X)$	$F_3(X)$
0.00	0.390	80	—	—	—	—
0.005	0.398	78	1.914	182.8	—	—
0.010	0.402	76	2.68	168	1800	—
0.015	0.408	74	4.40	222.6	5166	231066
0.025	0.414	74	7.04	241	3640	—
0.030	0.42	72	11.55	351.6	6700	166666
0.035	0.428	70	22.196	605.6	13000	322857
0.040	0.430	68	26.7	642.4	12300	265000

$\beta_{00} = 1$, $\beta_{10} = 150$, $\beta_{20} = 2000$, $\beta_{30} = 200\,000$

TABLE 2. Polarographic characteristics and $F_j(X)$ values of Pb(II)–nicotinate system

C_x (mol)	$-E_{1/2}$ (V) vs. sce	i_d (div)	$F_0(X)$	$F_1(X)$	$F_2(X)$
0.00	0.390	80	—	—	—
0.05	0.398	78	1.914	18.28	156.0
0.10	0.408	86	4.29	32.9	154.0
0.15	0.414	74	7.03	40.2	151.3
0.20	0.420	72	11.55	52.75	176.35
0.25	0.428	70	22.19	84.76	269.04
0.35	0.436	68	26.71	73.45	159.79

$\beta_{00} = 1.0$, $\beta_{01} = 17.5$, and $\beta_{02} = 210$

$F_j(X)$ functions of simple complexes of Pb(II) with NA are tabulated in Table 2. The shift in $E_{1/2}$ and the reduction of i_d values is exactly according to the scheme of complexation satisfying polarographic requirements. This also rules out any adsorption of the charged and neutral species formed. Polarographic studies of Pb(II)–nicotinate system as carried out by Gaur *et al.* (5) also supports the above observation.

(B) Ternary system

In this case the concentration of sodium itaconate was varied and that of sodium nicotinate was kept constant at 0.1 *M* and 0.25 *M*, respectively. It was noted that $E_{1/2}$ values were greater as compared to those observed in binary systems, thereby showing the formation of mixed complexes.

The method of Schaap and McMasters (6) was used to evaluate the overall formation constants of the ternary system. The polarographic measurements and $F_{ij}(X)$ functions of mixed complexes of Pb(II) with itaconic and nicotinic acids at fixed concentrations of the latter at 0.1 *M* and 0.25 *M* have been listed in Tables 3 and 4 respectively.

The overall formation constants calculated from the functions *A*, *B*, *C*, and *D* were:

$[Pb(ICA)(NA)]^-$	$\log \beta_{11} = 3.00$;	± 0.030
$[Pb(ICA)(NA)_2]^{2-}$	$\log \beta_{12} = 5.35$;	± 0.028
$[Pb(ICA)_2(NA)]^{3-}$	$\log \beta_{21} = 5.52$;	± 0.032

The numbers after the ± signs stand for the standard deviation.

The mixing constant K_M (equilibrium constant) for reaction

$$\tfrac{1}{2}[Pb(ICA)_2]^{2-} + \tfrac{1}{2}[Pb(NA)_2] \rightleftharpoons [Pb(ICA)(NA)]^-$$

is a measure of relative stability of mixed complexes in solution as compared to simple binary complexes. This is expressed (7, 8) as

$$K_M = \frac{\beta_{11}}{\sqrt{\beta_{02}\,\beta_{20}}}$$

In the present case the value of log K_M comes to be 0.1883 and that of stabilization constant K_S expressed as

$$\log K_S = \log K_M - \log 2$$

and it comes to be −0.1127.

The positive value of log K_M and the negative value of log K_S thus show that mixed complexation is preferred over simple bis-complexation.

Pb(II) is hexa-coordinated. Three mixed complexes existing

TABLE 3. Polarographic characteristics and $F_{ij}(X)$ functions of Pb(II)–itaconate–nicotinate system, fixed concentration of nicotinc acid = 0.1 *M*

C_x (mol)	$-E_{1/2}$ (V) vs. sce	i_d (div)	$F_{00}(X)$	$F_{10}(X)$	$F_{20}(X)$	$F_{30}(X) \times 10^5$
0.00	0.39	80	—	—	—	—
0.010	0.40	76	2.29	—	—	—
0.015	0.410	72	5.29	152.6	—	—
0.020	0.414	70	7.44	272.0	5600	—
0.030	0.428	66	23.54	684.6	17486	4.10
0.040	0.434	62	40.03	948.25	19705	3.60
0.050	0.440	58	68.36	1327	23340	3.60

$A = 3$, $B = 160$, $C = 5000$, and $D = 3.5 \times 10^5$

Can. J. Chem. Downloaded from www.nrcresearchpress.com by 210.87.254.6 on 09/06/12
For personal use only.

TABLE 4. Polarographic characteristics and $F_{ij}(X)$ functions of Pb(II)–itaconate–nicotinate system, fixed concentration of nicotinic acid = 0.25 *M*

C_x (mol)	$-E_{1/2}$ (V) vs. sce	i_d (div)	$F_{00}(X)$	$F_{10}(X)$	$F_{20}(X)$	$F_{30}(X)$ $\times 10^5$
0.00	0.39	80	—	—	—	—
0.010	0.410	74	5.49	—	—	—
0.015	0.418	70	10.16	344.0	2933	—
0.020	0.424	66	17.23	661.5	18075	7.5
0.030	0.432	62	34.24	1008.0	23600	6.8
0.040	0.438	58	58.48	1363.0	27550	6.1
0.050	0.446	54	117.29	2265.8	39300	7.2

$A = 5$, $B = 300$, $C = 3000$, and $D = 6.0 \times 10^5$

TABLE 5. Equilibria involved in three mixed complexes and equilibrium constants (K) values

No.	Equilibria	log K at 25°C
[1]	$Pb^{2+} + ICA^{2-} + NA^- \rightleftarrows [Pb(ICA)(NA)]^-$	3.0
[2]	$Pb^{2+} + ICA^{2-} + 2NA^- \rightleftarrows [Pb(ICA)(NA)_2]^{2-}$	5.35
[3]	$Pb^{2+} + 2ICA^{2-} + NA^- \rightleftarrows [Pb(ICA)_2(NA)]^{3-}$	5.52
[4]	$[Pb(ICA)(NA)]^- + NA^- \rightleftarrows [Pb(ICA)(NA)_2]^{2-}$	2.35
[5]	$[Pb(ICA)(NA)]^- + ICA^{2-} \rightleftarrows [Pb(ICA)_2(NA)]^{3-}$	2.52
[6]	$[Pb(NA)_2] + ICA^{2-} \rightleftarrows [Pb(ICA)(NA)_2]^{2-}$	3.03
[7]	$[Pb(ICA)]^{2-} + NA^- \rightleftarrows [Pb(ICA)(NA)]^-$	0.83
[8]	$[Pb(ICA)_2]^{2-} + NA^- \rightleftarrows [Pb(ICA)_2(NA)]^{3-}$	2.22
[9]	$[Pb(ICA)_3]^{4-} + NA^- \rightleftarrows [Pb(ICA)_2(NA)]^{3-} + ICA^{2-}$	0.22
[10]	$[Pb(ICA)(NA)_2]^{2-} + ICA^{2-} \rightleftarrows [Pb(ICA)_2(NA)]^{3-} + NA^-$	0.17

in solution have the equilibria as listed in Table 5. The equilibrium constants (log values) have been calculated and written in front of each equilibrium as also reported earlier by Shivhare and Singh (9).

From the equilibrium constants the tendency of a ligand to add to a complex and to substitute another ligand may be compared. It is seen that ICA^{2-} adds readily to $[Pb(ICA)(NA)]^-$ as compared to NA^- (equilibria [4], [5]). It is also observed that the complexing tendency of ICA^{2-} is much more than NA^- (equilibria [6], [7]). The stability of three complexes as seen from their overall formation constants follow the order:

$$Pb(ICA)(NA)]^- < [Pb(ICA)(NA)_2]^{2-} < [Pb(ICA)_2(NA)]^{3-}$$

Acknowledgements

The authors are thankful to Professor A. V. Mahajani, Head, Department of Chemistry, University of Saugar, Sagar M.P. for laboratory facilities. One of the authors V.K.C. is thankful to the U.G.C., New Delhi and Government of M.P. for the award of a teacher fellowship.

1. V. K. CHITALE and K. S. PITRE. J. Electrochem. Soc. India. In press.
2. V. K. CHITALE and K. S. PITRE. Polyhedron. To be published.
3. D. D. DEFORD and D. N. HUME. J. Am. Chem. Soc. **73**, 5321 (1951).
4. V. K. CHITALE AND K. S. PITRE. J. Electrochem. Soc. India. **31**, 133 (1982).
5. OM PRAKASH, S. K. BHASIN, D. S. JAIN, and J. N. GAUR. J. Indian Chem. Soc. **55**, 1307 (1978).
6. W. B. SCHAAP and D. L. MCMASTERS. J. Am. Chem. Soc. **83**, 4699 (1961).
7. R. SUNDERSAN and A. K. SUNDARAM. Proc. Ind. Acad. Sci. **79**A, 161 (1974).
8. S. L. JAIN, J. KISHAN, and R. C. KAPOOR. Indian J. Chem. **18**A, 133 (1979).
9. M. SHIVHARE and M. SINGH. J. Indian Chem. Soc. **58**, 647 (1981).

Can. J. Chem. Downloaded from www.nrcresearchpress.com by 210.87.254.6 on 09/06/12
For personal use only.

Comment: Temperature profiles for reactions with self-heating: thermal explosion in the sphere

TERRY BODDINGTON, PETER GRAY, AND STEPHEN SCOTT
School of Chemistry, University of Leeds, Leeds LS2 9JT, U.K.

Received January 4, 1983
(Ref.: Can. J. Chem. **60**, 2012 (1982))

TERRY BODDINGTON, PETER GRAY, and STEPHEN SCOTT. Can. J. Chem. **61**, 1944 (1983).

Attention is drawn to two unifying treatments of self-heating and self-cooling in chemical systems. They lead to simple but accurate expressions not only for temperature–position "profiles" but also for all the other important aspects of non-isothermal behaviour, up to and including the point of critical ignition.

TERRY BODDINGTON, PETER GRAY et STEPHEN SCOTT. Can. J. Chem. **61**, 1944 (1983).

On met l'accent sur deux études unifiées de l'autochauffage et de l'autorefroidissement dans les systèmes chimiques. Ces études conduisent à des expressions simples et précises non seulement pour les profils de température vs la position mais aussi pour tous les autres aspects importants du comportement non isotherme, jusqu'à inclure le point d'inflammation critique.

[Traduit par le journal]

Can. J. Chem. Downloaded from www.nrcresearchpress.com by 210.87.254.40 on 09/06/12
For personal use only.

In a recent article, Moise and Pritchard (1) offer an approximate alternative to the tabulated solutions of Chandrasekhar and Wares (2) for temperature–position profiles in an exothermic reactant of spherical geometry, and for the connection between the dimensionless centre temperature θ_0 and the value of Frank–Kamenetskii's parameter δ. Their approach is said to require no more than a hand-held, programmable calculator to yield profiles that are nowhere in error by more than 1% for $\delta \leqq 3$ nor by more than 5% for $\delta = 3.3$. The purpose of the present note is to point out that precision of this level and better is attainable with more illumination and less effort. It can also be got with greater generality, since the treatment copes easily both with general boundary conditions (arbitrary Biot number) from the Frank–Kamenetskii to the Semenov extremes, and also with endothermic reactions. It also requires a minimum of manipulation to lead to other important properties of the system, such as the corrections that are to be made to Arrhenius parameters when kinetic measurements are made without regard for self-heating.

Although our earliest accounts (3) of this work go back to 1970 and routes to temperature–position profiles are given (4) in full in 1971, the most complete studies (5, 6) overlap in time with Moise and Pritchard, appearing in 1981 whilst their work was being printed. Only the main points need to be made here. We focus these comments on spherical geometry.

(*1*) Two independent, analytical routes (6) are now available. One proceeds via a quintic approximation (7) to the Arrhenius temperature-dependence; the other uses a second-order reversion (3, 4) of a series solution, invoking the exponential approximation to the Arrhenius term. (Moise and Pritchard use the exponential approximation also.)

(*2*) Although these analytical treatments are not exact, they yield algebraic solutions of kinds that are rarely in error by more than 1 or 2%, and that apply without difficulty right up to criticality.

(*3*) Explicit (and fairly simple) algebraic equations can be set out for:

(*a*) temperature–position profiles, central excess temperatures, and temperature gradients at the surface for stable stationary states;

(*b*) the same quantities for unstable states and for criticality;

(*c*) rate-constant correction factors f;

(*d*) errors in kinetic parameters (e.g. E_{act}) from criticality to limiting forms for very small self-heating;

(*e*) generalized heat-transfer conditions at the boundary where the algebra is heavier, but quite manageable;

(*f*) endothermic systems, which can be treated easily and yield parallel expressions. These often differ by no more than the sign of a single coefficient.

All this is not to deny the possible value in other contexts of approaches like Moise and Pritchard's, but so far as the topic of thermal explosion in the sphere is concerned, it seems an arduous, lonely, and obscure path to results that can be reached more easily and by routes that offer clearer views.

Acknowledgement

We thank British Gas for a post-doctoral fellowship.

1. A. MOISE and H. O. PRITCHARD. Can. J. Chem. **60**, 2012 (1982).
2. S. CHANDRASEKHAR and G. W. WARES. Astrophys. J. **109**, 551 (1949).
3. T. BODDINGTON and P. GRAY. Proc. R. Soc. London, A**320**, 71 (1970).
4. T. BODDINGTON, P. GRAY, and D. I. HARVEY. Phil. Trans. R. Soc. London, A**270** 467 (1971).
5. T. BODDINGTON, P. GRAY, and S. K. SCOTT. Proc. R. Soc. London, A**378**, 27 (1981).
6. T. BODDINGTON, P. GRAY, and S. K. SCOTT. J. Chem. Soc. Faraday Trans. II, **78**, 1721 (1982); **78**, 1731 (1982).
7. B. F. GRAY. Combust. Flame, **11**, 86 (1969); P. GRAY, P. R. LEE, and J. A. MACDONALD. Combust. Flame, **11**, 461 (1969).

COMMUNICATION

Homoenolization of 3,3,6,6-tetramethylbicyclo[2.2.1]heptan-2-one and 1,3,3-trimethylbicyclo[2.2.1]heptan-2-one. Preferential *syn* exchange at C-7

NICK HENRY WERSTIUK, SHAHIN YEROUSHALMI, AND GEORGE TIMMINS
Department of Chemistry, McMaster University, Hamilton, Ont., Canada L8S 4M1

Received March 29, 1983

NICK HENRY WERSTIUK, SHAHIN YEROUSHALMI, and GEORGE TIMMINS. Can. J. Chem. **61**, 1945 (1983).

Preliminary studies of the KO*t*Bu-catalyzed H−D exchange of 3,3,6,6-tetramethylbicyclo[2.2.1]heptan-2-one (**1***b*) and 1,3,3-trimethylbicyclo[2.2.1]heptan-2-one(fenchone, **1***c*) in *t*-BuOD at elevated temperatures have been carried out. We find that **1***b* undergoes H−D exchange at the bridgehead α to the carbonyl group and at C-7 with a *syn*/*anti* preference of 5:1, establishing that C-7 of a bicyclo[2.2.1]heptan-2-one is an homoenolizable site. A similar preference was observed for exchange at C-7 of fenchone. These exchange studies also indicate that significant dilution of the deuterium pool occurs when a solution of KO*t*Bu/*t*-BuOD is heated at elevated temperatures for extended periods.

NICK HENRY WERSTIUK, SHAHIN YEROUSHALMI et GEORGE TIMMINS. Can. J. Chem. **61**, 1945 (1983).

On a effectué des études préliminaires sur l'échange H−D de la tétraméthyl-3,3,6,6 bicyclo[2.2.1] heptanone-2 (**1***b*) et la tétraméthyl-1,3,3 bicyclo[2.2.1] heptanone-2 (fenchone, **1***c*) catalysée par le KO*t*-Bu dans le *t*-BuOD à des températures élevées. Nous avons trouvé que le composé **1***b* subit un échange H−D au niveau de la tête de pont en α du carbonyle et au niveau du C-7 avec une préférence *syn*/*anti* de 5:1 qui permet d'établir que le carbone en position 7 du bicyclo[2.2.1] heptanone-2 est un site homoénolisable. On a noté une préférence analogue pour l'échange au niveau C-7 de la fenchone. Ces études d'échange indiquent également qu'il se produit une dilution significative du deutérium lorsqu'on chauffe une solution KO*t*-Bu/*t*-BuOD à des températures élevées pendant des périodes assez longues.

[Traduit par le journal]

Following the report of Nickon and Lambert (1) on the base-catalyzed homoenolization of 3,3-dimethylbicyclo-[2.2.1]heptan-2-one (camphenilone, **1***a*), a number of ketones have been studied and information has been obtained regarding the factors which determine the rates and stereochemistry of H−D exchange and the propensity for skeletal rearrangement. Reviews (2−5) of the subject have been published. While Nickon and Lambert established that **1***a* incorporated three deuterium atoms at C-1 and C-6 quite readily in KO*t*Bu/*t*BuOD at 185°C and racemized at essentially the same rate, they were unable to quantify the rate of bridgehead H−D exchange because C-1 and C-6 become equivalent in the homoenolate anion. Subsequently, Nickon *et al.* (6) studied the

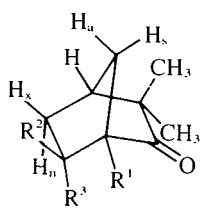

1

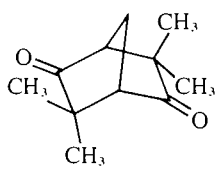

2

a, $R^1 = R^2 = R^3 = H$
b, $R^1 = H$; $R^2 = R^3 = CH_3$
c, $R^1 = CH_3$; $R^2 = R^3 = H$

exchange of 7-D-**1***a* in KO*t*Bu/*t*-BuOH, detected no loss of deuterium when the deuterated ketone was heated for 98 h at 185°C, then recycled at 185°C for 200 h, and stated that C-7 was not an homoenolizable site. The lack of reactivity at C-7 was noteworthy because the hydrogens, like those at C-6, are β to the carbonyl group. Ring strain and poor orbital alignment were invoked to account for the lack of reactivity at C-7 (6). Stothers and co-workers, in an apparently complete study of the homoenolization of 1,3,3-trimethylbicyclo[2.2.1]heptan-2-one (fenchone, **1***c*), established that the *exo*/*endo* rate ratio for exchange at C-6 was ~3.5, but did not observe exchange at C-7 (7). In contrast, studies in this laboratory showed that 3,3,6,6-tetramethylbicyclo[2.2.1]heptane-2,5-dione (**2**) undergoes relatively rapid exchange at the bridgeheads ($k \sim 1.5 \times 10^{-5}$ s^{-1}) and at C-7 ($k \sim 9 \times 10^{-6}$ s^{-1}) (8).

In this communication we provide evidence that monoketone **1***b* undergoes exchange *at C-1 and C-7* as well as the methyls. In contrast to the *exo* preference observed for exchange at C-6 of **1***c*, exchange at C-7 of **1***b* occurs preferentially *syn* to the carbonyl group. We have reexamined the homoenolization of fenchone (**1***c*) that was studied by Stothers and find that slow exchange also occurs at C-7, again with a *syn* preference. Table 1 lists the data on the homoenolizations of **1***b* and **1***c*. The crucial assignments of the $^1H(^2H)$ resonances used in determining the deuterium distributions were accomplished using double irradiation experiments.[1]

From entries 1, 2, and 4 it is clear that exchange at C-7 of **1***b* and **1***c* is slower than exchange at C-1 of **1***b* and the *exo*-3-methyls of **1***b* and **1***c*. Significant deuterium incorporation at C-7 occurs above 200°C. The approximate pseudo-first-order rate constants for exchange of *syn*-7-H, *anti*-7-H, and H-1 of **1***b* at 185°C are estimated to be $\sim 1.5 \times 10^{-8}$, $\sim 3 \times 10^{-9}$, and

[1]Irradiation of H-4 (δ 2.13) of **1***b* resulted in loss of a 4.4 Hz coupling in a high-field component (centered at δ 1.4) of an AB quartet and thereby identified H-5x, and also H-5n. Irradiation of H-5n resulted in a loss of coupling (2.6 Hz, W-type) in a low-field component (centered at δ 1.95) of an AB quartet and thereby identified H-7s, and H-7a (δ 1.85) as well. Even at 400 MHz, all the resonances of **1***c* are not resolved. From double irradiation experiments and by analogy to **1***b*, a complex multiplet centered at δ 1.7 was assigned to H-7s, H-5x, and H-5n. Our assignment of H-6x, which according to our analysis overlaps with H-7a, and the other resonances, H-6n and the methyls, agreed with Stothers' assignments (7).

Can. J. Chem. Downloaded from www.nrcresearchpress.com by 210.87.254.42 on 09/06/12
For personal use only.

Can. J. Chem. Downloaded from www.nrcresearchpress.com by 210.87.254.42 on 09/06/12
For personal use only.

TABLE 1. H−D Exchange of bicyclic ketones

Entry	Substrate	[K] (wt. in g)	[KO*t*Bu][a] (vol. in mL)	Temp (°C), h	Excess D per molecule[b]	Distribution[c]						
						C-1	C-6x	C-6n	C-7s	C-7a	Bridgehead methyl	Other methyls[n]
1	**1***b*	0.23(0.131)	1.2(3.5)	175±2,[c] 403	0.56	0.280[d]			0.020[d]	—		0.260[f]
2	**1***b*	0.073(0.060)	1.2(4.0)	185±2, 504	0.60	0.250			0.030	—		0.320
3	**1***b*	0.33(0.150)	1.3(2.8),	220±5, 300;	—[e]	—[e]			—	—		—
		0.30(0.102)[f]	1.3(2.0)	220±5, 300	1.67	0.500[g]			0.120	0.024		1.020
4	**1***c*	0.22(0.150)	0.9(4.5)	175±2, 650	1.70		0.690	0.710	0.030	—[i]	0.040	0.240
5	**1***c*	1.06(0.484)	1.1(3.0)	175±2, 180;								
				205±5, 400	1.44		0.360	0.400	0.070	—	0.060	0.550
6	**1***c*	0.33(0.256)	1.2(5.0)	220±5, 300;	1.62		—[e]	—	—	—	—	—
		0.32(0.137)[f]	1.3(2.8)	220±5, 300	2.51		0.390	0.390	0.120	—	0.24	1.370

[a]The base solutions were prepared in a dry-box or glove bag.
[b]Determined mass spectrometrically at low voltage. Recoveries of the ketone usually were ~70%.
[c]Determined by ^{2}Hmr at 38.4 MHz. Incorporations were determined by computerized curve-fitting of the spectra to Lorentzian line shapes and are averages of at least three fittings. The average error is in the order of ±10%.
[d]Determined by ^{2}Hmr at 61.4 MHz using Eu(fod)$_3$.
[e]Not determined.
[f]The deuterated ketone was isolated from the first exchange and recycled.
[g]A very weak signal (<0.020) which overlapped partially with D-1 was assigned to D-4, indicating that very slow exchange was occurring at C-4 as well.
[h]From ^{1}Hmr it was deduced that one of the methyls, most likely the *exo*-C-3-methyl, had exchanged preferentially.
[i]The signal due to H-7a overlaps H-6x.

~3×10^{-7} s^{-1}, respectively, by a one-point kinetic analysis of the data in entries 1, 2, and 3. Thus, α exchange is ~20 times faster than *syn* exchange at C-7 and ~100 times faster than *anti* exchange. While the *syn*/*anti* preference is ~5:1 for **1***b*, it is difficult to establish the ratio exactly for **1***c* because the *anti*-7-D resonance overlaps with the *exo*-6-D resonance (*vide supra*). Since the deuterium incorporation in the *syn*-7-position of **1***c* is essentially the same as the incorporation in **1***b* and the *exo* and *endo* incorporations at C-6 of **1***c* are identical within experimental error, a comparable *syn* preference is indicated for **1***c*. From entry 6 it is seen that the rate of exchange of *syn*-7-H of **1***c* is approximately equal to the rate of exchange of the bridgehead methyl on a per hydrogen basis. Since the *syn*- and *anti*-hydrogens of **1***b* are in nearly identical steric environments and *syn* exchange is preferred, the interpretation of the *exo* preference observed for exchange at C-6 of **1***c* on the basis of a homoconjugative effect must be reconsidered because *exo* approach to **1***c* is less hindered than the *endo* approach. Perhaps electrostatic stabilization (5, 9) of the inside anions at C-7 of **1***b* and **1***c* is greater than stabilization of the outside anions. Additional studies are planned to probe this possibility.

Since the rate of *exo* ($k \sim 7 \times 10^{-6}$ s^{-1}) H−D exchange at C-6 of fenchone (**1***c*) (7) should be a good measure of *exo* exchange of camphenilone (**1***a*) at C-6, our studies establish, using the bridgehead exchange of **1***b*, that *exo* exchange at C-6 of camphenilone should be ~25 times as fast as bridgehead exchange. This analysis is in keeping with the observation that the rates of H−D exchange and racemization of camphenilone are equal within experimental errors (6).

As is indicated in entries 3 and 6, an attempt was made to increase the deuterium incorporation by heating **1***b* and **1***c* at 220°C for 300 h and then recycling the deuterated ketones. While more deuterium was incorporated into the ketones, the reactive positions − C-1 and the *exo*-3-methyl of **1***b* and C-6 and the *exo*-3-methyl of **1***c* − did not contain the expected amounts of deuterium. In fact, more deuterium is incorporated at C-6 of **1***c* in shorter reaction periods (entry 4). The data in entry 6 also indicate that the *exo*- and *endo*- positions at C-6, and most likely the *exo*-2-methyl as well, were equilibrated with the deuterium pool. The low deuterium incorporations at C-6 and the *exo*-methyl which equilibrate rapidly with the deuterium pool clearly indicate that the pool is being diluted by a process other than exchange of the ketone, that we calculate to be not greater than 10% after two cycles. While the mode of the dilution is not known, *tert*-butyl alcohol must be the source of the protons. It is conceivable that *tert*-butoxide promotes $\overline{O}D$ elimination at elevated temperatures, forming *t*-BuOH and isobutene that can undergo H−D exchange as well. A substantial dilution of the deuterium pool would result and a decrease in the basicity of the medium would occur, which appears to be the case when homoenolizations are run at elevated temperatures or for long periods. This interesting possibility will be probed by carrying out the homoenolization of **1***c* in perdeuterated *tert*-butyl alcohol. Deuterium incorporation should increase and the activity of the base should be maintained for a longer period. The study of exchange at fairly unreactive positions, a necessity if the exact role of the carbonyl group in stabilizing remote anions is to be detailed, will be facilitated.

Acknowledgement

We thank the Natural Sciences and Engineering Research Council of Canada for financial support.

1. A. NICKON and J. L. LAMBERT. J. Am. Chem. Soc. **84**, 4609 (1962).
2. E. BUNCEL. Reaction mechanisms in organic chemistry. Monograph 9. Elsevier, Amsterdam. 1975. pp. 116–122 and 161–167.
3. D. H. HUNTER. *In* Isotopes in organic chemistry. Vol. 1. *Edited by* E. Buncel and C. C. Lee. Elsevier, Amsterdam. 1975. pp. 197–203.
4. D. H. HUNTER, J. B. STOTHERS, and E. W. WARNHOFF. *In* Rearrangements in ground and excited states. Vol. 1. *Edited by* P. de Mayo. Academic Press, New York. 1980. pp. 393–461.
5. N. H. WERSTIUK. Tetrahedron, **39**, 205 (1983).
6. A. NICKON, J. L. LAMBERT, and J. E. OLIVER. J. Am. Chem. Soc. **88**, 2787 (1966).
7. A. L. JOHNSON, J. B. STOTHERS, and C. T. TAN. Can. J. Chem. **53**, 212 (1975).
8. N. H. WERSTIUK. Can. J. Chem. **53**, 2211 (1975).
9. A. J. NOEST and N. M. M. NIBBERING. J. Am. Chem. Soc. **102**, 6427 (1980).

Can. J. Chem. Downloaded from www.nrcresearchpress.com by 210.87.254.42 on 09/06/12
For personal use only.

The determination of technetium-99 in urine[1]

GARY H. KRAMER

Biomedical Research Branch, Health Sciences Division, Atomic Energy of Canada Limited, Research Company, Chalk River Nuclear Laboratories, Chalk River, Ont., Canada K0J 1J0

Received December 21, 1982

GARY H. KRAMER. Can. J. Chem. **61**, 1949 (1983).

A method has been developed for the routine radiochemical analysis of technetium-99 in human urine. The excreted technetium is coprecipitated from a 200 mL urine sample with CuS. Valence state adjustments are performed with $K_2S_2O_8$. The precipitate is dissolved in ammoniacal peroxide and, after the Cu(II) is removed by ion exchange, the Tc-99 is extracted with 2-butanone (MEK). Subsequent evaporation of the organic solvent gives an essentially weightless source that if counted with a gas proportional counter will give a better limit of detection than liquid scintillation methods. The recovery of Tc-99 using this procedure is 80% (σ = 4%) and the limit of detection is 20 mBq (0.6 pCi) at the 95% confidence level for a routine sample – counting time 20 minutes, counting efficiency 24%, ambient background 1.3 counts per minute (cpm).

GARY H. KRAMER. Can. J. Chem. **61**, 1949 (1983).

On a mis au point une méthode d'analyse radiochimique courante du technétium-99 dans l'urine humaine. A partir d'un échantillon de 200 mL d'urine, on fait coprécipiter le technétium excrété avec du CuS. On réalise des ajustements de la valence avec du $K_2S_2O_8$. On dissout le précipité dans du peroxyde ammoniacal et on extrait le Tc-99 avec la butanone-2 (MEK) après avoir enlevé le Cu(II) par échange d'ions. L'évaporation subséquente du solvant organique donne essentiellement une source impondérable qui si elle est comptée avec un compteur proportionnelle de gaz donnera une meilleure limite de détection que les méthodes de scintillation liquide. Par cette méthode on récupère le Tc-99 à 80% (σ = 4%) et la limite de détection est de 20 mBq (0,6 pCi) avec une certitude de 95% pour un echantillon courant. Le temps de comptage est de 20 minutes, l'efficacité de comptage est de 24%, le bruit de fond est de 1,3 compte par minute (cpm).

[Traduit par le journal]

Introduction

Technetium-99 is produced either as a fission product in nuclear reactors or by the thermal neutron bombardment of Mo-98. In both cases, the initial product is Tc-99m that decays by internal transfer with the emission of 140 keV γ-rays to Tc-99. The half-life of Tc-99m is 6.0 hours. This metastable state of Tc-99 is one of the most widely used clinical radionuclides; however, Tc-99 finds virtually no commercial use except for investigations into the physical and chemical properties of technetium. Technetium-99 is the longest lived of all the technetium isotopes (half-life = 2.1×10^5 a) and decays by beta particle emission (E_{max} = 0.292 MeV). There are no accompanying gamma emissions.

To design an effective analysis method for Tc-99 it is necessary to estimate the level of activity in urine for the most conservative case. Assuming the ALI (annual limit on intake) to be 2×10^{-9} Sv/Bq and that personnel are sampled monthly, then the activity in a 24 hour urine sample is estimated to be 1.3 kBq. Typically, 200 mL of urine is collected and analysed so that the estimate of activity becomes 186 Bq. These figures are estimated for a Class W inhalation incident as described elsewhere (1). Similar calculations performed for a Class D inhalation case give a level of activity in a urine sample of 235 Bq and for an ingestion incident the level of activity in urine would be 224 Bq. Hence, the DIL (derived investigation limit) should be 186 Bq and the analytical method should be capable of estimating a value less than the DIL.

There are many methods in the literature for radiochemical analysis of technetium, but most of them are not designed to deal with low levels of activity that are usually found in bioassay and environmental samples. Typical of these are the methods of Anders (2) and Embleton and Foreman (3). Technetium urinalysis has received very little attention except by Fairman and Sedlet (4) and Walker *et al.* (5). The former procedure does not provide adequate separation from some interfering activities and does not have adequate sensitivity (6). The latter procedure can only deal with a small sample size and also suffers from inadequate sensitivity. Pacer (7) has recently described the counting efficiency and quenching characteristics of liquid scintillation counting of Tc-99, and Zodda *et al.* (8) have described an analysis method for pertechnetate using hplc; however, neither method is suitable for bioassay. Foti *et al.* (9) have described a method for measuring Tc-99 in environmental samples using neutron activation that gives good recovery of Tc-99 and a low detection limit.

It has often been stated that any analytical scheme for technetium must avoid heating because of the high vapour pressure of Tc_2O_7 and $HTcO_4$. Indeed, Boyd and co-workers (10) have shown the vapour pressures to be considerable at 100°C; Tc_2O_7, 13.3 Pa; $HTcO_4$ (saturated aqueous solution), 9.3 Pa. The results given in this work indicate that loss of technetium by evaporation is not a problem because the results obtained under reflux conditions are identical to those obtained under "open-beaker" conditions.

This paper describes a method (that is designed for routine personnel monitoring) for the determination of small amounts of inorganic or weakly bound Tc-99 in urine. Analysis time is approximately 6 hours prior to radioactive counting.

Experimental

Reagents

2-Butanone (MEK): a "Baker analysed" reagent was obtained from the J. T. Baker Chemical Company and used without further purification.

Tracers

Technetium-99 was obtained from New England Nuclear Canada Limited as an aqueous solution of ammonium pertechnetate. The activity was determined to 98% precision by 4π beta counting. Appropriate dilutions of the initial solution in 1 *M* NH_4OH were prepared for routine use.

[1]AECL-8026.

Can. J. Chem. Downloaded from www.nrcresearchpress.com by 210.87.254.105 on 09/06/12
For personal use only.

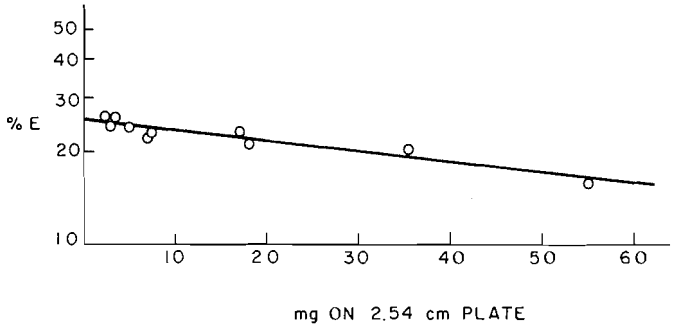

FIG. 1. Calibration curve for technetium-99.

Equipment

Beta counting was performed with a gas proportional (GP) counter. The average background for the 5.6 cm (diameter) detector was 1.3 counts per minute (cpm). The instrument calibration curve is shown in Fig. 1.

Procedure

The urine sample (200 mL) is acidified with 6 mL concentrated H_2SO_4. Ten grams of $K_2S_2O_8$ are added and the solution is heated with stirring. The heating is continued until the pale yellow solution begins to turn orange again. Two milliliters of the Cu(II) carrier solution (5 mg Cu(II)/mL) are added to the cooled solution. A thioacetamide solution is also added (200 mg/10 mL). The solution is heated with stirring to 70°C ± 5°C for 30 min and then allowed to cool to room temperature. The CuS precipitate is removed by vacuum filtration through a sintered glass frit (fine) and washed with 30 mL of 0.1 *M* H_2SO_4. The CuS precipitate is also washed with 30 mL of methanol to remove the coprecipitated organics which appear as a dark brown impurity in the methanol wash. The precipitate is dissolved by adding NH_4OH – 30% H_2O_2 (5–10 mL) (5:1, v:v) in small amounts (1–2 mL). After the dissolution is complete the solution is drawn through the frit into the collection vessel and the procedure repeated until all the precipitate is dissolved. If all the organics have not been washed out with methanol the solution will appear green, otherwise it will be predominately blue. The solution is transferred to a covered beaker and heated on a hot plate to destroy any residual H_2O_2 and to convert all the sulfo salts of technetium to TcO_4^-. After the completion of this step the solution will be blue. The solution is cooled and the pH adjusted to 10, or greater. The Cu(II) ions are removed by adding sufficient cation exchange resin (Bio-Rad AG 50W) in the NH_4^+ form until the solution is either colourless or *very* pale yellow. The resin is removed by passing the solution through a glass wool filter. The resin is washed with a dilute NH_4OH wash solution (5 mL). The filtrate is transferred to a round bottom flask and treated with 3–5 drops of 30% H_2O_2. Sufficient Na_2CO_3 is added to make the solution 0.25 *M* and an equal volume of MEK is added. The flask is shaken for 10 min. The organic layer is removed and retained. Another extraction is performed and the two organic layers are combined in a beaker and evaporated to a small volume (5–10 mL) under a heat lamp in a fume cupboard. Finally, the remaining MEK is transferred to a weighed aluminum counting dish (2.5 cm diameter) and evaporated to dryness. The beaker is rinsed with a few mL of MEK and this is also added to the counting dish and evaporated.The dish is counted for Tc-99.

Results and Discussion

Gerlit (11) has shown that Tc(VII) is quantitatively carried by CuS coprecipitation but that other valence states are not. It was, therefore, necessary to preadjust the technetium valence state in urine by oxidation. Although an intake of technetium would probably be originally a pertechnetate intake, the chemical environment in the body and, certainly, in the urine could reduce a significant portion to the lower valence states. To simulate this, all spiked urine samples were allowed 24 h to equilibrate prior to analysis.

TABLE 1. Some typical experimental data for Tc-99 recovery

Sample[a]	Recovered (cpm)	Counting efficiency (%)	% Recovered
1	188	24	84
2	158	22	77
3	189	24	83
4	172	23	81

[a]Sample volume 200 mL; added activity 15.4 Bq; counting time 20 min; ambient background ~1.3 cpm.

A sulphate medium was selected for the following reasons. Copper sulphide will dissolve in hot 2 *M* nitric acid and also at lower acidities if large quantities of ammonium nitrate are present. The sulphide ion is oxidized to elemental sulphur under these conditions. Hydrochloric acid was rejected because it will rapidly reduce Tc(VII) to lower valence states (12). Some attempts have been made to utilize this fact to design a radiochemical separation procedure (12–14). Therefore, sulphuric acid was chosen as the acidic medium and $K_2S_2O_8$ was chosen as the oxidizing agent because its decomposition product, SO_4^{2-}, does not interfere with the subsequent CuS coprecipitation. Other oxidizing agents were tried, but only H_2O_2 was potentially suitable in leaving no interfering products. Unfortunately, H_2O_2 is not completely decomposed during the oxidation step and the residual peroxide reacts with the thioacetamide to form elemental sulphur. Interferences from sulphate precipitates were not found to be a problem.

The dissolution of CuS by ammoniacal hydrogen peroxide is a well known method (4, 15, 16) and, provided that it is carried out carefully, is quite satisfactory. It is important to add small amounts of the dissolving solution, otherwise the reaction will become very violent and a significant portion of the sample may be lost. Other workers have used acidic peroxide dissolution solutions (6) but this method cannot be conveniently interfaced with the MEK extraction.

The MEK extraction from a basic 0.25 *M* Na_2CO_3 solution has a distribution coefficient of about 16 (17). The two extractions should recover 99.5% of the technetium that is maintained as Tc(VII) by the addition of peroxide. A further advantage is the ease of evaporation of MEK to give essentially weightless sources for beta counting. In practice, between 3 and 6 mg residues were found on the counting dishes and the counting efficiency was approximately 24%; however, the limit of detection is still improved over liquid scintillation methods. To obtain the same detection limit given below, a liquid scintillation sample would have to be counted for approximately 50 min. The evaporation of MEK on the counting dish was tested for volatilization of technetium. No noticeable decrease in activity was observed between samples that were counted, exposed to the heat lamp for six hours, and then recounted.

The method has been tested on 14 spiked (15 Bq) urine samples that were analysed under reflux conditions. The amount of added activity was chosen to be an order of magnitude less than the DIL (see Table 1). The mean recovery was 81% (σ = 6%). A further five samples were analysed under "open-beaker" conditions and the mean recovery was 79% (σ = 4%). Obviously volatilization is not a problem. To check the efficiency of the oxidation step, three urine samples were spiked with Tc(IV), prepared by reducing Tc(VII) with hydrazine (2), and the mean recovery was 85% (σ = 5%). The amount of oxidant was also optimized by studying the mean

Can. J. Chem. Downloaded from www.nrcresearchpress.com by 210.87.254.105 on 09/06/12
For personal use only.

recovery as a function of weight of added $K_2S_2O_8$/200 mL urine. At 10 g and above, the recovery of Tc-99 remained constant at 82% (σ = 5%) whereas at lower weights there was a significant drop in recovery, i.e., at 5 g, recovery was 59%.

Further investigations were carried out using Tc-95m (78 kBq) to find where the major source of loss of technetium was occurring. No activity was found in the trap above the reflux condenser. The major source of loss was found to be at the CuS precipitation step. The results of six experiments showed that 16 ± 5% Tc-95m remained in solution after CuS had precipitated. The balance of the activity (84%) was found in the redissolved CuS fraction. The source of this loss was thought to be incomplete oxidation but the earlier results, where the recovery of Tc-99 was investigated as a function of the amount of oxidant, refutes this hypothesis; nevertheless, if the oxidation step is removed, and Tc-95m is prereduced, then the recovery and loss are both 50%, indicating that oxygen is converting much of the Tc(IV) to Tc(VII). Similarly, experiments have shown that prereduced Tc-95m can be recovered to the extent of 85% when the oxidation step is included in the analysis. Clearly some component of urine is acting as a holdback carrier because a second CuS precipitation does not recover any further activity.

This method compares favourably with the results found by Foti *et al.* (9). Their quoted recoveries were 80% and the detection limit for vegetation varied from 9×10^{-12} to 3×10^{-11} g Tc-99 (i.e., 6 to 19 mBq/25 g sample). The mean recovery of the method described in this paper was 81% but the detection limits are poorer than those of Foti *et al.*. It is estimated that the detection limit (18) for this procedure at the 95% confidence level is 20 mBq (0.6 pCi) for a routine sample that would have a counting efficiency of approximately 24%, a counting time of 20 min, and a chemical recovery of 80%; however, if the counting time is extended to 200 min, then the detection limit falls to 6.5 mBq.

1. J. R. JOHNSON and M. B. CARVER. Health Phys. **41**, 341 (1981).
2. E. ANDERS. The radiochemistry of technetium. AEC Report NAS-NS-3021, November 1960.
3. J. R. EMBLETON and J. K. FOREMAN. Technetium-99: isolation of milligram quantities from irradiated uranium and fission product waste solutions and a note on its analytical chemistry. UKAEA Report, PGR 93(w), March 1960.
4. W. FAIRMAN and J. SEDLET. The determination of technetium-99 in urine. AEC Report TID-7696, October 1963.
5. C. R. WALKER, B. C. SHORT, and H. S. SPRING. The determination of technetium-99 by liquid scintillation counting. Goodyear Atomic Corporation Report, GAT-T-2953, October 1979.
6. N. W. GOLCHERT and J. SEDLET. Anal. Chem. **41**, 669 (1969).
7. R. A. PACER. Int. J. Appl. Radiat. Isot. **31**, 731 (1980).
8. J. P. ZODDA, W. R. HEINEMAN, T. W. GILBERT, and E. DEUTSCH. J. Chromatogr. **227**, 249 (1982).
9. S. FOTI, E. DELUCCHI, and V. AKAMIAN. Anal. Chim. Acta, **60**, 269 (1972).
10. W. T. SMITH, J. W. COBBLE, and G. E. BOYD. J. Am. Chem. Soc. **75**, 5773 (1953).
11. J. B. GERLIT. Proc. Int. Conf. Peaceful Uses of Atomic Energy. Vol. 7. Geneva. 1955. p. 145.
12. L.OSSICINI, F. SARACINO, and M. LEDERER. J. Chromatogr.**16**, 524 (1964).
13. F. JASIM, R. J. MAGEE, and C. L. WILSON. Talanta, **4**, 17 (1960).
14. S. J. RIMSHAW. U. S. Patent No. 3,005,683 (October, 1961).
15. G. E. BOYD and Q. U. LARSON. J. Phys. Chem. **60**, 707 (1956).
16. B. T. KENNA and P. K. KURODA. J. Inorg. Nucl. Chem. **27**, 142 (1961).
17. S. J. RIMSHAW and G. F. MALLING. Anal. Chem. **33**, 751 (1961).
18. L. CURRIE. Anal. Chem. **40**, 586 (1968).

Can. J. Chem. Downloaded from www.nrcresearchpress.com by 210.87.254.105 on 09/06/12
For personal use only.

Quenching of the fluorescence of substituted benzenes by halomethanes

H. A. KHWAJA, G. P. SEMELUK, AND I. UNGER

Department of Chemistry, University of New Brunswick, Fredericton, NB., Canada E3B 6E2

Received November 25, 1982

H. A. KHWAJA, G. P. SEMELUK, and I. UNGER. Can. J. Chem. **61**, 1952 (1983).

Rate constants, k_q, for the quenching of the singlet state of benzene, toluene, *p*-xylene, fluorobenzene, trifluoromethyl benzene, *p*-bis(trifluoromethyl)benzene, and aniline by CCl_4, CH_3CCl_3, $CHCl_3$, and $CFCl_3$ in the gas phase have been determined. In each instance the quenching is via a charge-transfer complex with the aromatic acting as donor. There is a linear dependence between ln k_q and IP (ionization potential) of the aromatics which supports Klein's model for exciplex formation. The most effective quencher is CCl_4 while the least effective is $CFCl_3$. The most effective donor was aniline while the least effective one was *p*-bis(trifluoromethyl)benzene. In general, fluorinated aromatics are less effective donors than the corresponding protonated molecules.

H. A. KHWAJA, G. P. SEMELUK et I. UNGER. Can. J. Chem. **61**, 1952 (1983).

On a déterminé la constante de vitesse, k_q, de rupture de l'état triplet du benzène, du toluène, du *p*-xylène, du fluorobenzène, du trifluorométhylbenzène, du *p*-bis(trifluorométhyl) benzène et de l'aniline par le CCl_4, le CH_3CCl_3, le $CHCl_3$ et le $CFCl_3$ en phase gazeuse. Dans chaque cas la rupture se fait par l'intermédiaire d'un complexe de transfert de charge où le noyau aromatique joue le rôle de donneur. Il y a une relation linéaire entre ln k_q et le PI (potentiel d'ionisation) des composés aromatiques qui vient à l'appui du modèle de Klein relatif à la formation d'un exciplexe. Le CCl_4 est le meilleur agent de rupture tandis que le $CFCl_3$ est le moins efficace. L'aniline est le meilleur donneur tandis que le *p*-bis(trifluorométhyl) benzène est le moins efficace. En général les composés aromatiques fluorés sont des donneurs moins efficaces que les molécules protonées correspondantes.

[Traduit par le journal]

Can. J. Chem. Downloaded from www.nrcresearchpress.com by 210.87.254.42 on 09/06/12
For personal use only.

Introduction

Exciplex and excimer formation has been shown to be responsible for the quenching of the excited states of a large variety of molecules in solid, liquid, and vapor phases (see, for example, ref. 1). Exciplex formation may be due to charge transfer or to hydrogen bonding, or to a combination of both (2). In the case of charge-transfer (CT) complex formation, a model proposed by Klein (3) based on the absolute rate theory of Eyring has been tested by various authors (4, 5) and found to hold. Klein's model requires that there be a linear dependence of the overall second-order quenching rate constant, k_q, on the exponential of some measure of the free energy change associated with the formation of the complex. The two most important factors in CT exciplex formation are the ionization potential (IP) of the donor and the electron affinity (EA) of the acceptor. Thus the common method of investigating for the formation of CT exciplexes, when no spectral change in the emission of the excited state of the monomer is observed, is to vary either the EA of a number of acceptors while holding the IP of the donor constant, or the IP of a number of donors while holding the EA of the acceptor constant. The excited molecule may act either as donor or acceptor. If the resulting plot of ln k_q vs. EA or IP is linear it is considered likely that a CT exciplex is responsible for quenching. Recently we reported (6) on the quenching of benzene fluorescence by a number of halocarbons in the gas phase. In that study a good Klein correlation between k_q and EA of the halocarbons was established, thus suggesting a CT exciplex and charge transfer from benzene to halocarbon. In order to complete the study we have examined the fluorescence quenching of a number of aromatics by several halocarbons, thus allowing for an examination of the variation of k_q with IP as well as the influence of benzene ring charge density on charge transfer. The study was carried out in gas phase in order to eliminate solvent effects.

Experimental

Materials

Toluene was obtained from J. T. Baker Chemical Company as GC spectrophotometric quality and was used without any further purifications. Benzotrifluoride was obtained from PCR Research Chemicals Inc. with a stated minimum purity of 99.5%. Fluorobenzene and *p*-xylene were from Aldrich Chemical Company and 1,4-bistrifluoromethylbenzene was from Pfaltz and Bauer Inc. The research grade aniline (Anachemia Chemical Company) was purified by a conventional fractional distillation procedure, in which only the middle fraction was collected. None of the aromatics exhibited detectable impurity emission under the conditions of excitation and detection utilized here.

CCl_4 (GC spectrophotometric quality) was obtained from J. T. Baker Chemical Co., 1,1,1-trichloroethane (analytical reagent grade, 99.5%) was from BDH Chemicals Ltd., and $CHCl_3$ (spectrograde) was from Caledon Laboratories. These halogenated methanes were further purified by gas–liquid chromatography using an HP Model 7620 A chromatograph attached to a 5797A collecting unit, with He as the carrier gas; detection was by flame ionization. The chromatographic procedure gave a purity of >99.9% for each of the materials. $CClF_3$ was obtained from Matheson Company with a stated purity of >99% and was used as received.

Apparatus and procedures

Absorption spectra were obtained with a Perkin-Elmer 330 spectrophotometer. Fluorescence spectra were recorded with a modified Aminco-Bowman spectrophotofluorométer (SPF) using a quartz cuvette with inside dimensions 1 cm × 1 cm × 4.5 cm.

Samples were admitted to the working manifold from sample reservoirs attached to the vacuum line and were degassed by the freeze–pump–thaw method with a minimum of three cycles at better than 5×10^{-6} Torr. The pressures of aromatics in the quenching experiments were: benzene, 20 Torr; toluene, 3.5 Torr; *p*-xylene, 3 Torr; fluorobenzene, 1.0 Torr; trifluoromethyl benzene, 2.0 Torr; *p*-bis(trifluoromethyl)benzene, 2.0 Torr; aniline, 0.3 Torr. The pressures of halocarbon quencher ranged from 20 to 80 Torr.

For each point to be determined, a freshly prepared mixture of quencher and aromatic was admitted to the cell. Fluorescence spectra of aromatic were measured as a function of quencher concentration (up to 80 Torr). Details of pressure measurements, quantum yield determination, etc. have been given in ref. 6.

A full description of the apparatus, data collection, and processing used in this study has been given elsewhere (6, 7).

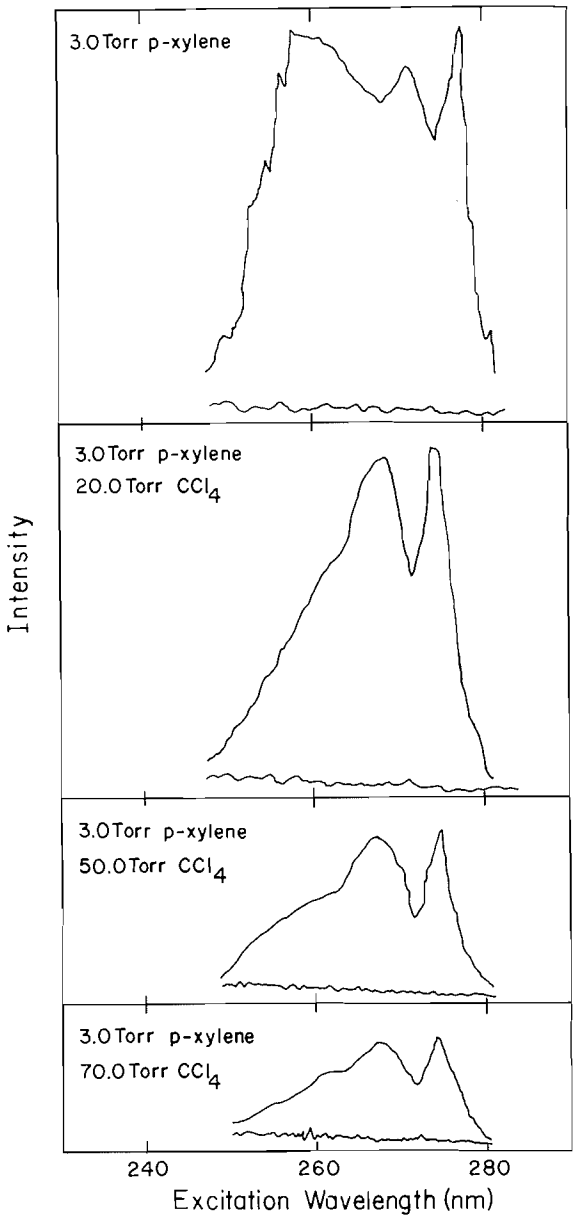

FIG. 1. Fluorescence excitation spectra of *p*-xylene in the presence of CCl_4, λ_{em} = 296 nm.

Results and discussion

Absorption, fluorescence emission, and excitation spectra of each of the aromatics in the absence and presence of each of the quenchers at the highest pressures used were recorded. The absorption and emission spectra were identical to that reported previously (8) and have therefore not been reproduced here. The absorption spectra of the aromatics with and without quencher were identical, thus ruling out the possibility of ground state complexation. Moreover, mixtures of aromatic and halocarbon that had been left in the cell in the dark for periods of up to 24 h showed no change in absorptivity.

With the exception of 1,4-$C_6H_4(CH_3)_2$ the excitation spectra of the aromatics exhibit the same maxima as do the absorption spectra and they are unaltered by the addition of halocarbons. The fluorescence excitation spectrum of 1,4-$C_6H_4(CH_3)_2$ is changed by the addition of CCl_4. Figure 1 demonstrates this effect for CCl_4, showing that the addition of CCl_4 strongly quenches the fluorescence of 1,4-$C_6H_4(CH_3)_2$ by preferential

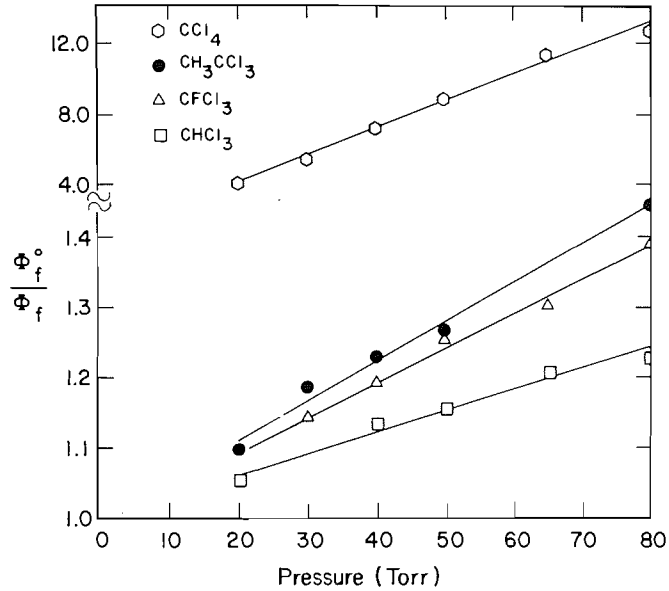

FIG. 2. Stern–Volmer plots for the quenching of *p*-xylene fluorescence by CCl_4, CH_3CCl_3, $CHCl_3$, and $CFCl_3$ (P(1,4-$C_6H_4(CH_3)_2$) = 3.0 Torr, λ_{ex} = 272 nm, T = 297.9 ± 0.2 K).

quenching of the shortest wavelength excitation sub-band; at 70 Torr of CCl_4 the yield from excitation into this sub-band is almost zero and there is simultaneously a shift of the longer wavelength excitation sub-bands to higher energies (CH_3CCl_3 and $CFCl_3$ also alter the excitation spectrum of 1,4-$C_6H_4(CH_3)_2$ but not as dramatically with the middle sub-band least affected). However, the shape of the fluorescence emission spectrum is unaffected by the addition of CCl_4. These observations indicate that the fluorescence observed in 1,4-$C_6H_4(CH_3)_2$ originates solely from the vibrationally relaxed excited singlet state and that there is a vibronic interaction between the excited state of the aromatic and some vibrational motion in CCl_4.

Fluorescence yields, Φ_f, of each of the aromatics were determined as a function of halocarbon pressure and are based on Φ of benzene being 0.183 (9). For every aromatic halocarbon pair, Φ_f was found to decrease with increasing quencher pressure. Plots of Φ_f^0/Φ_f vs. the quencher pressure obeyed the Stern–Volmer expression

$$[1] \quad \Phi_f^0/\Phi_f = 1 + k_q\tau[Q]$$

where Φ_f^0 and Φ_f refer to fluorescence yields of aromatics in absence and presence of halogenated methane, k_q is the bimolecular quenching rate constant, and τ is the lifetime of the excited singlet aromatic. A typical plot is given in Fig. 2. k_q was evaluated from the slopes of the plots and literature values of τ taken under similar conditions of excitation wavelength, aromatic pressure, etc. as those used in this study. The results are summarized in Table 1. It is evident from Table 1 that quenching by CCl_4, CH_3CCl_3, $CHCl_3$, and $CFCl_3$ of the excited singlet states of most of the aromatic molecules studied is a highly efficient process. k_q ranges from 5.2×10^8 L mol^{-1} s^{-1} for the $C_6H_5CH_3$–$CFCl_3$ pair to 9.4×10^{11} L mol^{-1} s^{-1} in the $C_6H_5NH_2$–CCl_4 system. Comparison of the quenching rate constants for aromatics by CCl_4 and $CHCl_3$ reveals a dramatic difference in quenching efficiency, see Table 1. The greater quenching efficiency of CCl_4 as compared with $CHCl_3$ is related to their difference in electron affinity. Similarly, for any single quencher, the magnitude of k_q increases with the

Can. J. Chem. Downloaded from www.nrcresearchpress.com by 210.87.254.42 on 09/06/12
For personal use only.

TABLE 1. Vapor phase quenching rate constants, cross sections, and ΔG^* for substituted benzenes with halogenated methanes (T = 297.9 ± 0.2 K)

Aromatic	Quencher	λ_{ex} (nm)	τ (ns)	k_q (L mol^{-1} s^{-1})	IP[i] (eV)	EA[h] (eV)	E_{0-0}[j] (eV)	ΔG^*[k] (eV)
Aniline	CCl_4	282	5.1[a]	9.41×10^{11}	7.69	2.12[f]	4.22[d]	1.35
	CH_3CCl_3	282	5.1[a]	7.03×10^{10}		1.88[f]		1.59
	$CHCl_3$	282	5.1[a]	5.57×10^{10}		1.75[f]		1.72
	$CFCl_3$	282	5.1[a]	1.06×10^{11}		1.1[g]		2.37
p-Xylene	CCl_4	272	44[b]	6.31×10^{10}	8.45	2.12[f]	4.51	1.80
	CH_3CCl_3	272	44[b]	2.35×10^{9}		1.88[f]		2.04
	$CHCl_3$	272	44[b]	1.26×10^{9}		1.75[f]		2.17
	$CFCl_3$	272	44[b]	2.05×10^{9}		1.1[g]		2.82
Toluene	CCl_4	264	56[b]	1.58×10^{10}	8.82	2.12[f]	4.62	2.05
	CH_3CCl_3	264	56[b]	1.13×10^{9}		1.88[f]		2.29
	$CHCl_3$	264	56[b]	7.16×10^{8}		1.75[f]		2.42
	$CFCl_3$	264	56[b]	5.16×10^{8}		1.1[g]		3.07
Fluorobenzene	CCl_4	265	9.5[c]	3.27×10^{9}	9.20	2.12[f]	4.69	2.39
	CH_3CCl_3	265	9.5[c]	3.05×10^{9}		1.88[f]		2.63
	$CFCl_3$	265	9.5[c]	8.19×10^{8}		1.1[g]		3.41
Benzotrifluoride	CCl_4	265	19.0[d]	3.82×10^{9}	9.68	2.12[f]	4.69	2.87
	CH_3CCl_3	265	19.0[d]	2.86×10^{9}		1.88[f]		3.11
	$CHCl_3$	265	19.0[d]	2.40×10^{9}		1.75[f]		3.24
	$CFCl_3$	265	19.0[d]	2.59×10^{9}		1.1[g]		3.89
1,4-Bistrifluoro-methylbenzene	CCl_4	267	10.7[d]	1.42×10^{9}	10.1[b]	2.12[f]	4.64	3.34
	CH_3CCl_3	267	10.7[d]	1.15×10^{9}		1.88[f]		3.58
	$CHCl_3$	267	10.7[d]	1.35×10^{9}		1.75[f]		3.71
	$CFCl_3$	267	10.7[d]	8.99×10^{8}		1.1[g]		4.36
Benzene	CCl_4	254	75[e]	31.9×10^{8}	9.25	2.12[f]	4.72	2.41
	CH_3CCl_3	254	75[e]	8.65×10^{8}		1.88[f]		2.65
	$CHCl_3$	254	75[e]	5.56×10^{8}		1.75[f]		2.78
	$CFCl_3$	254	75[e]	2.46×10^{8}		1.10[g]		3.43

[a]Reference 16.
[b]Reference 17.
[c]Reference 18.
[d]Reference 19.
[e]Reference 20.
[f]Reference 5.
[g]Reference 13.
[h]EA value was interpolated from the relationship of electron affinity with thermal electron attachment rate for gaseous chloromethanes.
[i]Reference 21.
[j]Reference 22.
[k]$\Delta G^* = \Delta G + C + P$; however, C and P are constant throughout.

electron-donating power of the substituents in the aromatics.

In the benzene – halogenated methane systems π-bonding is possible between the electron cloud of the benzene ring and the empty 3*d* levels of the Cl atoms in the chloralkane. One would expect therefore that formation of the complex would be enhanced by substituents on the benzene ring that increase the electron density of the ring, and would be hindered by groups that withdraw electrons from the ring. If, on the other hand, the interaction is between the electron-deficient carbon atom on the halocarbon and the π ring electrons, changing electron density of the latter will have the same effect as above. Methyl substitution leads to increasing effectiveness. For example, the magnitude of k_q is increased by a factor of 5 in going from the benzene–CCl_4 pair (31.8×10^8 L mol^{-1} s^{-1}) to the toluene–CCl_4 pair. Similarly the higher quenching constants observed for 1,4-$C_6H_4(CH_3)_2$ compared to those for $C_6H_5CH_3$ must be due to the inductive effect of two such substituents. This concurs with the trends seen in fluorescence quenching of pyrazoline derivatives by halomethanes (10), where the formation of a donor–acceptor complex has been postulated. The same behavior has been observed in the quenching of aliphatic ketones (4), where successive substitution of methyl groups around the carbonyl chromophore promotes quenching by CCl_4. When an amino donor group is introduced into the benzene chromophore, k_q increases by nearly two orders of magnitude (see Table 1). In contrast, electrophilic fluorine atoms would be expected to effectively deactivate the aromatic ring and reduce the donor ability. Comparison of the quenching rate constants of the C_6H_5F–CCl_4 pair and C_6H_6–CCl_4 pair confirms this point. k_q for the $C_6H_5CF_3$–CCl_4 pair is found to be smaller than k_q for the C_6H_5F–CCl_4 pair, as expected for such an electron-withdrawing substituent. Further, the second trifluoromethyl group increases the electron affinity over that of the monosubstituted molecule by ~1 eV (11), which should make donor–acceptor complex formation less favourable and k_q smaller; this is indeed observed here.

The fluorescence quenching observed here cannot be due to ground state complexation or to chemical reaction since samples exposed for prolonged periods showed no evidence of product formation. In the case of $C_6H_5NH_2$, quenching with $CHCl_3$ and CH_3CCl_3 could be due to hydrogen bonding, but the literature suggests that this is unlikely (12).

The charge transfer exciplex model of quenching is based on eq. [2]

Can. J. Chem. Downloaded from www.nrcresearchpress.com by 210.87.254.42 on 09/06/12
For personal use only.

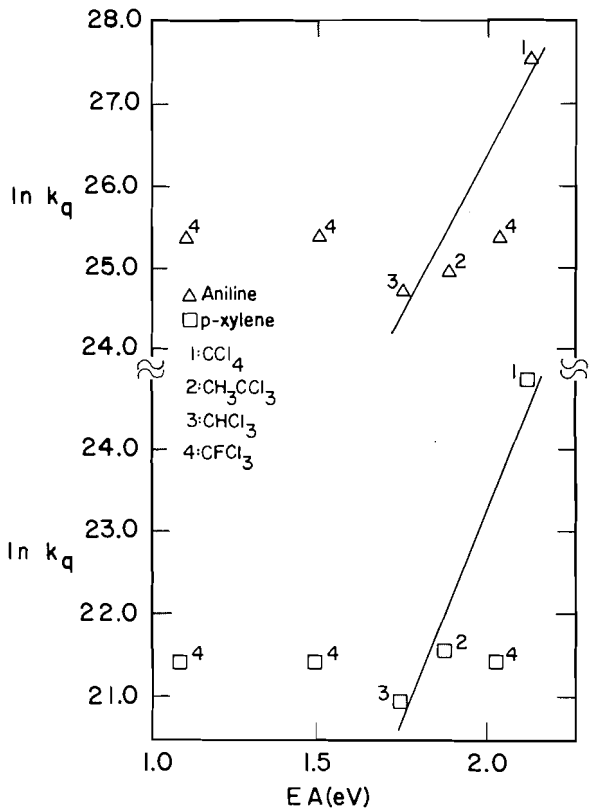

FIG. 3. Plot of ln k_q vs. EA for aniline and *p*-xylene singlet quenching by CCl_4, CH_3CCl_3, $CHCl_3$, and $CFCl_3$ in the vapor phase. Three different values for EA ($CFCl_3$) are given in the literature (5, 14, 15).

$$[2]\quad {}^1D^* + Q \underset{k_{-1}}{\overset{k_1}{\rightleftharpoons}} {}^1(\delta+\ \ \delta-)^* \xrightarrow{k_2} D + Q \text{ or products}$$

where D* represents the fluorescent donor aromatic; Q, the ground state halogenated methanes; and $(D^{\delta+}.....Q^{\delta-})^*$, an exciplex. Applying the steady-state approximation gives

$$[3]\quad k_q = \frac{k_1 k_2}{k_{-1} + k_2}$$

and if $k_{-1} \gg k_2$,

$$[4]\quad k_q = Kk_2$$

$$[5]\quad \ln k_q = -\frac{\Delta G}{RT} + \ln k_2$$

$$[6]\quad \ln k_q \propto |-(IP_D - EA_A - E_{S^1} - C - P)|/RT$$

where k_q is the overall quenching rate constant, IP_D is the ionization potential of the donor, EA_A is the electron affinity of the acceptor, C is the Coulomb energy, P is the polarization energy of the separated charges, and E_{S^1} represents the energy of the first excited state.

In the case of benzene and a large number of halocarbons it has been shown that ln k_q does indeed vary linearly with EA_A, all the other terms of eq. [6] being constant. In the present case the dependency of ln k_q vs. EA_A was examined for each aromatic and a reasonably linear relationship holds. Typical plots are given in Fig. 3. That the point for $CFCl_3$ falls far off the line is not surprising since widely divergent values for E_A of this molecule are given in the literature (5, 13, 14). It is also possible to test eq. [6] by plotting ln k_q vs. IP_D; the results of this plot are shown in Fig. 4. A combination of all the free energy parameters allows one to plot ln k_q vs. ΔG^* ($\Delta G^* = \Delta G + C + P$ where $C + P$ are constant throughout), the results are given in Fig. 5. The deviation from linearity is undoubtedly due to the assumption $k_{-1} \gg k_2$ not being equally valid for all fluorophore quencher pairs.

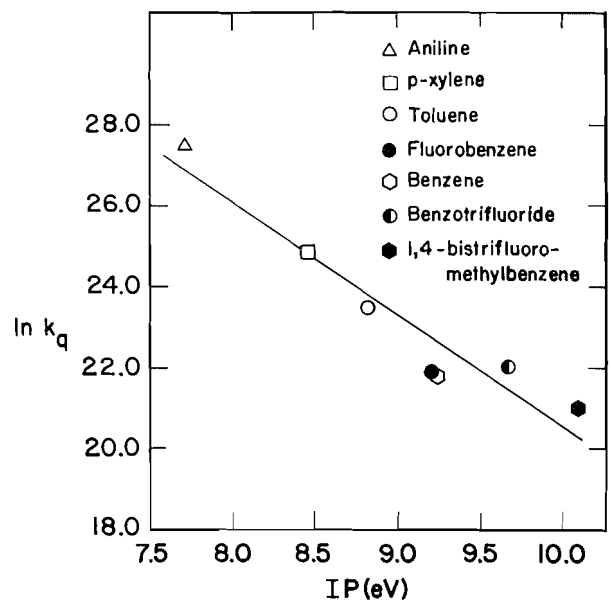

FIG. 4. Variation of ln k_q with IP(aromatic) for quenching by CCl_4.

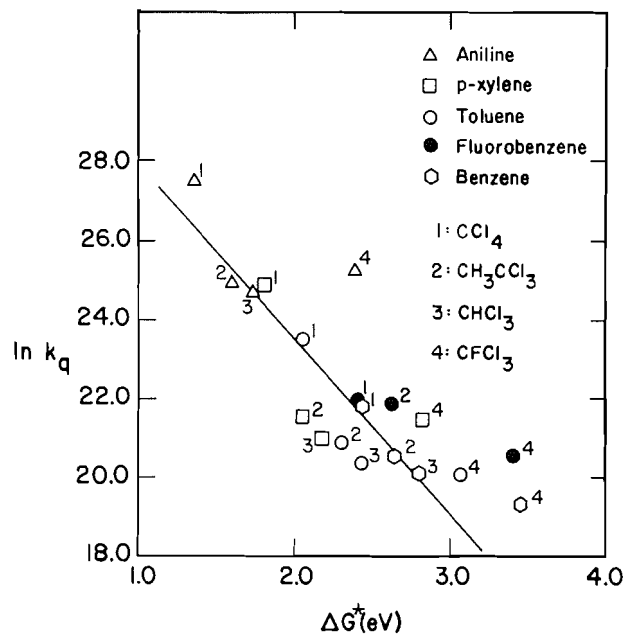

FIG. 5. Variation of ln k_q with free energy change for various quenchers.

Finally, if full electron-transfer from excited aromatic to quencher occurs, the maximum slope should be $1/RT \simeq 39$ eV^{-1}. From Fig. 4, a gradient of 2.72 eV^{-1} is obtained. The degree of charge transfer is therefore relatively small (~7%) and is comparable with the value of ~4 eV^{-1} quoted by Loutfy *et al.* (15) for the quenching of triplet acetone by olefins and ~6 eV^{-1} given by Saperstein and Levin (5) for the quenching of singlet aromatics by chloroform.

Can. J. Chem. Downloaded from www.nrcresearchpress.com by 210.87.254.42 on 09/06/12
For personal use only.

Acknowledgement

The authors are grateful to the Natural Sciences and Engineering Research Council of Canada for financial support of this work.

1. P. G. SENNIKOV, V. A. KUZNETSOV, and A. N. EGOROCHKIN. Adv. Mol. Relaxation Interaction Processes, **20**, 89 (1981) and references therein.
2. T. KUROI, Y. GONDO, M. KUWABARA, R. SHIMADA, and Y. KANDA. Bull. Chem. Soc. Jpn.. **54**, 2243 (1981).
3. J. KLEIN, V. PLAZANET, and G. LAUSTRIAT. J. Chim. Phys. Physicochim. Biol. **67**, 302 (1970).
4. R. O. LOUTFY and A. C. SOMERSALL. Can. J. Chem. **54**, 760 (1976).
5. D. SAPERSTEIN and E. LEVIN. J. Chem. Phys. **62**, 3560 (1975).
6. H. A. KHWAJA, G. P. SEMELUK, and I. UNGER. Can. J. Chem. **60**, 1767 (1982).
7. J. B. ADDISON, G. P. SEMELUK, and I. UNGER. J. Lumin. **15**, 323 (1977).
8. I. B. BERLMAN. Handbook of fluorescence spectra of aromatic molecules. 2nd ed. Academic Press, New York. 1971.
9. W. A. NOYES, JR., W. A. MULAC, and D. A. HARTER. J. Chem. Phys. **44**, 2100 (1966).
10. O. V. BUTRIMOVICH, L. A. ISACHENKOVA, and A. M. SARZHEVSKII. Zh. Prik. Spek. **32**, 876 (1980).
11. R. G. BROWN and D. PHILLIPS. J. Am. Chem. Soc. **96**, 4784 (1972).
12. T. KUROI, Y. GONDO, M. KUWABARA, R. SHIMADA, and Y. KANDA. Bull. Chem. Soc. Jpn. **54**, 2248 (1981).
13. H. DISPERT and K. LACMANN. Int. J. Mass Spectrom. Ion Phys. **28**, 49 (1978).
14. H. J. T. PRESTON and J. J. KAUFMAN. Chem. Phys. Lett. **50**, 157 (1977).
15. R. O. LOUTFY, S. K. DOGRA, and R. W. YIP. Can. J. Chem. **57**, 342 (1979).
16. H. VON WEYSSENHOFF and F. KRAUS. J. Chem. Phys. **54**, 2387 (1971).
17. G. M. BREUER and E. K. C. LEE. Chem. Phys. Lett. **14**, 404 (1972).
18. G. L. LOPER and E. K. C. LEE. Chem. Phys. Lett. **13**, 140 (1972).
19. G. M. BREUER, P. A. HACKETT, D. PHILLIPS, and M. G. ROCKLEY. Trans. Faraday Soc. **68**, 1995 (1972).
20. G. M. BREUER AND E. K. C. LEE. J. Chem. Phys. **51**, 3130 (1969).
21. V. I. VEDENEYEV, L. V. GURVICH, V. N. KONDRAT'YEV, V. A. MEDVEDEV, and YE L. FRANKEVICH. Bond energies, ionization potentials, and electron affinities. Edward Arnold Publishers Ltd. 1966.
22. D. PHILLIPS. J. Photochem. **1**, 97 (1972/73).

Can. J. Chem. Downloaded from www.nrcresearchpress.com by 210.87.254.42 on 09/06/12
For personal use only.

Reactions of the trisulfur trinitride anion, $S_3N_3^-$, with halogens and other electrophilic substrates

TRISTRAM CHIVERS AND M. N. SUDHEENDRA RAO
Department of Chemistry, University of Calgary, Calgary, Alta., Canada T2N 1N4

Received December 16, 1982

TRISTRAM CHIVERS and M. N. SUDHEENDRA RAO. Can. J. Chem. **61**, 1957 (1983).

The reactions of the trisulfur trinitride anion, $S_3N_3^-$, with halogens (Cl_2, Br_2, I_2), AsF_5, $SOCl_2$, SO_2Cl_2, S_2Cl_2, $COCl_2$, CS_2, Me_3SiCl, and Ph_2PCl have been investigated. In all cases these reactions gave mixtures of known sulfur–nitrogen compounds. Thus the halogens react with $S_3N_3^-$ to give mainly S_4N_4, $S_4N_3^+X^-$ (X = Br, Cl), $(SN)_x$, and $S_3N_3X_3$ (X = Cl), while AsF_5 oxidizes $S_3N_3^-$ to $S_4N_4 \cdot AsF_5$. The major products of the reaction of $S_3N_3^-$ with $SOCl_2$ or SO_2Cl_2 were S_4N_4, $S_4N_3^+Cl^-$, and (for $SOCl_2$ only) $S_3N_2O_2$. S_3N_2Cl was the main product of the reaction of $S_3N_3^-$ with S_2Cl_2, whereas $COCl_2$ yielded $(SN)_x$ in addition to S_3N_2Cl and S_4N_4. Carbon disulfide reacts with $S_3N_3^-$ to give S_4N_2, S_4N_4, and CNS^-. The cyclophosphathiazenes, $(Ph_2PN)(SN)_2$, 1,3- and 1,5-$(Ph_2PN)_2(SN)_2$, in addition to $(Ph_2PN)_x$ (x = 3, 4), $(Ph_2PN)_3 \cdot HCl$ and $(Ph_2PN)_2NSCl$ were isolated from the reactions of Ph_2PCl with $S_3N_3^-$ in various molar ratios. The latter reaction represents a useful alternative synthesis of the 1,5-isomer of the eight-membered ring $(Ph_2PN)_2(SN)_2$.

TRISTRAM CHIVERS et M. N. SUDHEENDRA RAO. Can. J. Chem. **61**, 1957 (1983).

On étudie les réactions de l'anion trinitrure de soufre $S_3N_3^-$ avec les halogènes (Cl_2, Br_2, I_2), le AsF_5, le $SOCl_2$, le S_2Cl_2, le $COCl_2$, le CS_2, le Me_3SiCl et le Ph_2PCl. Dans tous les cas ces réactions donnent des mélanges de composés connus de l'azote avec le soufre. Ainsi les halogènes réagissent avec le $S_3N_3^-$ en donnant principalement le S_4N_4, le $S_4N_3^+X^-$ (X = Br, Cl), le $(SN)_x$ et le $S_3N_3X_3$ (X = Cl), tandis que le AsF_5 oxyde le $S_3N_3^-$ en $S_4N_4 \cdot AsF_5$. Le $S_3N_3^-$ réagit avec le $SOCl_2$ ou le SO_2Cl_2 en donnant comme produits majoritaires le S_4N_4, le $S_4N_3^+Cl^-$ et (dans le cas du SO_2Cl_2 seulement) le $S_3N_2O_2$. La réaction avec le S_2Cl_2 donne le S_3N_2Cl comme produit principal tandis qu'avec le $COCl_2$ on obtient surtout du $(SN)_x$ en plus du S_3N_2Cl et du S_4N_4. Le bisulfure de carbone réagit avec le $S_3N_3^-$ en donnant du S_4N_2, du S_4N_4 et du CNS^-. En faisant réagir le Ph_2PCl avec le $S_3N_3^-$ et en faisant varier les rapports molaires on obtient les cyclophosphathiazènes $(Ph_2PN)(SN)_2$, les $(Ph_2PN)_2(SN)_2$-1,3 et -1,5 en plus du $(Ph_2PN)_x$ (x = 3, 4), du $(Ph_2PN)_3 \cdot HCl$ et du $(Ph_2PN)_2NSCl$. La dernière réaction représente une autre synthèse utile de l'isomère-1,5 du cycle à 8 chainons: $(Ph_2PN)_2(SN)_2$.

[Traduit par le journal]

Introduction

The trisulfur trinitride anion, $S_3N_3^-$, has been thoroughly characterized both structurally (1) and spectroscopically (ir and Raman (1), uv–visible (1, 2), MCD (2), and ^{15}N nmr (3)). This thermally unstable and oxygen-sensitive anion is a planar six-membered ring (1). *Ab initio* Hartree–Fock–Slater SCF calculations show that it is a six orbital 10π-electron system in which the degenerate π* levels are fully occupied (1, 4) and this view of the electronic structure has been confirmed by experiment (2).

Some aspects of the chemical behaviour of $S_3N_3^-$ have been investigated and a variety of transformations including oxidation ($S_3N_3O^-$, ref. 5), ring contraction ($CCl_3CON{-}S_3N_2$, ref. 6), cage formation ($S_4N_5^-$, ref. 6), and ring opening (S_4N^-, ref. 7) have been observed (see Fig. 1). Of particular interest to us is the preparation of monosubstituted derivatives, S_3N_3X,[1] and the cation $S_3N_3^+$.[2] We have, therefore, conducted a study of the reactions of $S_3N_3^-$ with halogens, AsF_5, and other electrophilic substrates and we report the details of our findings here.

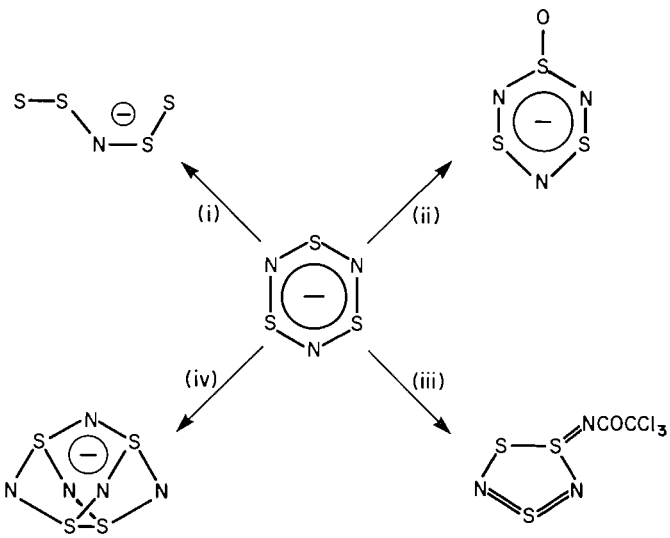

FIG. 1. Some reactions of the trisulfur trinitride anion, $S_3N_3^-$. (*i*) In CH_3CN at reflux (7), (*ii*) O_2 in CH_3CN (5), (*iii*) CCl_3COCl in CH_2Cl_2 (6), (*iv*) S_4N_4 in C_2H_5OH (6).

Experimental

Reagents and general procedures

$Cs^+S_3N_3^-$ (6) and $PPN^+S_3N_3^-$ (7) (PPN = Ph_3PNPPh_3) were prepared by the literature procedures. The following chemicals were obtained commercially and used as received: chlorine (Matheson), bromine (Fisher Scientific Co.), iodine (J.T. Baker Chemical Co.), arsenic pentafluoride (Ozark-Mahoning), chlorotrimethylsilane (Pen-

[1]Reference 8*a*. There are conflicting literature reports on the preparation of S_3N_3Cl from the reaction of $S_3N_3Cl_3$ and S_4N_4 and, recently, this reaction has been shown to produce $S_5N_5^+Cl^-$ (8*b*). A report of the formation of S_3N_3Br by bromination of S_4N_4 in CS_2 (8*c*) must be viewed with caution in view of more recent work which identified $S_4N_3^+Br^-$, $S_4N_3^+Br_3^-$, and $CS_3N_2Br_2$ as the products of this reaction (8*d*).

It has been claimed that the dark red amorphous solid which precipitates when S_4N_4 reacts with I_2 in boiling inert solvents is S_3N_3I (8*c*). However, the characterization is based entirely on analytical data. We were unable to repeat this synthesis.

[2]Planar $S_3N_3^+$ is expected to be a diradical (see ref. 1). However, if the symmetry of the ring is lower than D_{3h}, the degeneracy of the antibonding levels would be removed and a stable 8 π-electron system might result (cf. $Ph_2PS_2N_3$, ref. 9).

Can. J. Chem. Downloaded from www.nrcresearchpress.com by 210.87.254.6 on 09/06/12
For personal use only.

TABLE 1. Reactions of $S_3N_3^-$ with halogens and electrophilic substrates

Reactants[a]		Reaction conditions[b]	Products isolated[c,d]	Comments
$PPN^+S_3N_3^-$ (0.42 g; 0.62 mmol)	+ Cl_2	No solvent, 23°C, 1 h	$S_3N_3Cl_3$ (7%) PPN^+Cl^-	NH_4Cl was detected in the precipitate. An unidentified dark volatile product which hydrolyzed to NH_4Cl was also obtained
$PPN^+S_3N_3^-$ (2.43 g; 3.60 mmol)	+ Cl_2	CH_2Cl_2 (40 mL), −78°C, 16 h	S_4N_4 (40%) S_4N_3Cl S_8 (trace) PPN^+Cl	Small amounts of NH_4Cl in precipitate and filtrate
$PPN^+S_3N_3^-$ (2.55 g; 3.77 mmol)	+ Br_2 (3.8 mmol)	CH_2Cl_2 (50 mL), −60°C, 20 h	S_4N_4 (40%) $(SN)_x$ (trace) PPN^+Br^-	Small amount of NH_4Br in the precipitate
$PPN^+S_3N_3^-$ (1.17 g; 1.71 mmol)	+ Br_2 (1.7 mmol)	No solvent, 23°C, 24 h	S_4N_4 S_4N_3Br PPN^+Br (1.1 g; 1.8 mmol)	Small amount of NH_4Br in the precipitate
$PPN^+S_3N_3^-$ (1.33 g; 1.97 mmol)	+ I_2 (2.0 mmol)	CH_2Cl_2 (40 mL), −60°C, 6 h	S_4N_4 (47%) PPN^+I^- (0.63 g; 0.95 mmol)	An unidentified blue–black solid (0.03 g) was obtained in the precipitate
$PPN^+S_3N_3^-$ (2.38 g; 3.52 mmol)	+ Me_3SiCl (3.5 mmol)	CH_2Cl_2 (50 mL), −78°C, 20 h	S_4N_4 (56%) PPN^+Cl^- (1.85 g; 3.23 mmol)	
$Cs^+S_3N_3^-$ (1.68 g; 6.20 mmol)	+ SO_2Cl_2 (3.1 mmol)	CH_2Cl_2 (50 mL), −78°C, 16 h	S_4N_4 (53%) CsCl (1.05 g; 6.23 mmol)	Gas evolution observed. At low temperature, reaction mixture changed colour from dark green → dark purple → reddish brown → reddish yellow
$Cs^+S_3N_3^-$ (0.9 g; 3.32 mmol)	+ $SOCl_2$ (3.8 mmol)	CH_3CN (30 mL), 23°C, 7 h	S_4N_4 (39%) S_4N_3Cl $S_3N_2O_2$ (50%) CsCl (0.56 g; 3.32 mmol)	Reaction mixture changed colour from reddish brown → cherry red → yellowish green → orange
$Cs^+S_3N_3^-$ (1.0 g; 3.69 mmol)	+ S_2Cl_2 (1.9 mmol)	CH_3CN (25 mL), 23°C, 20 h	S_4N_4 S_3N_2Cl S_4N_3Cl (trace) CsCl	
$Cs^+S_3N_3^-$ (1.36 g; 5.01 mmol)	+ $COCl_2$	CH_3CN (50 mL), −78°C, 18 h	S_4N_4 (56%) $(SN)_x$ (22%)[e] CsCl (0.80 g; 4.75 mmol)	An unidentified carbonyl-containing product was obtained in the precipitate
$Cs^+S_3N_3^-$ (2.11 g; 7.78 mmol)	+ AsF_5	CH_2Cl_2 (60 mL), −78°C, 24 h	S_4N_4 (10%) $S_4N_4 \cdot AsF_5$ (2%) $(SN)_x$ (13%) $Cs^+AsF_6^-$	A small amount of unreacted $Cs^+S_3N_3^-$ was present in the precipitate
$PPN^+S_3N_3^-$ (1.73 g; 2.56 mmol)	+ CS_2	CS_2 (25 mL), 0°C, 16 h	S_4N_2 (13%) S_4N_4 (8%) PPN^+CNS^- (100%)	Blood red reaction mixture. Ir spectrum indicated another product in the filtrate, which could not be isolated
$Cs^+S_3N_3^-$ (0.48 g; 1.77 mmol)	+ Ph_2PCl (1.8 mmol)	CH_2Cl_2 (25 mL), 0°C, 16 h	$(Ph_2PN)(SN)_2$ 1,5-$(Ph_2PN)_2(SN)_2$ S_8 S_4N_4 $Ph_2P(S)Cl$ CsCl (0.27 g; 1.60 mmol)	Reaction mixture was a reddish purple colour. Products were isolated by chromatography on Bio-Beads S-X8

Can. J. Chem. Downloaded from www.nrcresearchpress.com by 210.87.254.6 on 09/06/12
For personal use only.

TABLE 1 *(Concluded)*

Reactants[a]		Reaction conditions[b]	Products isolated[c,d]	Comments
$Cs^+S_3N_3^-$ (2.00 g; 7.38 mmol)	+ Ph_2PCl (14.8 mmol)	CH_2Cl_2 (70 mL), 0°C, 20 h	$(Ph_2PN)_3$ $(Ph_2PN)(SN)_2$ (trace) 1,5-$(Ph_2PN)_2(SN)_2$ S_8 S_4N_4 $Ph_2P(S)Cl$ CsCl	As above
$Cs^+S_3N_3^-$ (0.93 g; 3.93 mmol)	+ Ph_2PCl (13.7 mmol)	CH_3CN (25 mL), 23°C, 38 h	1,3-$(Ph_2PN)_2(SN)_2$ 1,5-$(Ph_2PN)_2(SN)_2$ $(Ph_2PN)_4$ (trace) S_8 $Ph_2P(S)Cl$ $(Ph_2PN)_3 \cdot HCl$ CsCl	Products were isolated by fractional crystallization. A small amount of the hydrolysis product $[H_2NPPh_2NPPh_2NH_2]^+Cl^-$ was also isolated
$Cs^+S_3N_3^-$ (5.42 g; 20.0 mmol)	+ Ph_2PCl (49.9 mmol)	CH_3CN (100 mL), 0°C, 15 h	$(Ph_2PN)_3$ 1,5-$(Ph_2PN)_2(SN)_2$ $(Ph_2PN)_2NSCl$ S_8 S_4N_4 $Ph_2P(S)Cl$ $(Ph_2PN)_3 \cdot HCl$ CsCl	Products were separated by chromatography. $[H_2NPPh_2NPPh_2NH_2]^+Cl^-$ was also isolated

[a]The stoichiometry is indicated except for gaseous reagents (see Experimental section).
[b]The identity and volume of the solvent, the temperature, and the time of reaction are indicated in that order.
[c]Products were isolated from both the precipitate and filtrate portions of the reaction mixture. Only the S—N products are shown with yields of pure products based on sulfur in parentheses. The products in the precipitate were usually mixed with PPN^+ or Cs^+ halides and were not always obtained pure, in which case no yield is indicated.
[d]The structures of $(Ph_2PN)(SN)_2$ (**1**), 1,3-$(Ph_2PN)_2(SN)_2$ (**2**), and 1,5-$(Ph_2PN)_2(SN)_2$ (**3**) are illustrated in Fig. 2.
[e]Identifed by comparison of infrared and mass spectra and the X-ray powder diffraction pattern with the literature values (13).

insular Chem Research), chlorodiphenylphosphine (Alfa Products), and phosgene (Matheson). Sulfur monochloride (Fisher Scientific Co.), thionyl chloride (Fisher Scientific Co.), and sulfuryl chloride (Aldrich Chemical Co.) were distilled prior to use.

Methylene chloride and carbon disulfide were dried over P_2O_5 and distilled from P_2O_5 before use. Acetonitrile (reagent grade) was dried by distillation from P_2O_5 followed by distillation from CaH_2. All reactions and distillations were carried out under an atmosphere of nitrogen (99.99% purity) passed through Ridox and silica gel. Air-sensitive materials were manipulated under an atmosphere of dry nitrogen in a Vacuum Atmospheres Dri-Lab fitted with a Dri-Train.

Instrumentation

Routine infrared spectra (CsI windows) were recorded as Nujol mulls on a Perkin-Elmer 467 grating spectrometer. Ultraviolet–visible spectra were obtained by using a Cary 219 spectrophotometer. ^{31}P nmr spectra were recorded on a Varian XL-200 NMR spectrometer. Routine EI (70 eV) mass spectra were run on a Varian CH5 mass spectrometer. Chemical analyses were performed at the Department of Chemistry, University of Calgary (C, H, N) and at M.H.W. Laboratories, Phoenix, AZ (C, H, N, S, P, and halogens).

Reactions of $PPN^+S_3N_3^-$ with halogens and other electrophilic reagents

The experimental details for the reactions of $S_3N_3^-$ salts with various reagents are summarized in Table 1. The reactions were carried out by adding the stoichiometric amount of the reagent to a stirred solution of the $S_3N_3^-$ salt at the temperature indicated. For gaseous reagents (Cl_2, $COCl_2$, AsF_5), a moderate flow of gas was passed into the solution for 2–4 min. In the case of the low temperature reactions, the reaction mixture was allowed to reach ambient temperature slowly. At the conclusion of each reaction solid products were filtered off and solvent was removed from the filtrate *in vacuo*. The products from the precipitate and filtrate portions of the reaction mixture were treated separately and pure components were isolated by solvent extraction and fractional crystallization. This was particularly difficult in the case of the precipitates due to the presence of large amounts of PPN^+ or Cs^+ halides. All the products isolated were known compounds which were identified by ir and mass spectra and, in some cases, by uv–visible and ^{31}P nmr spectra. Good agreement with spectroscopic data quoted in the literature was found for the following products: $S_3N_3Cl_3$ (10), S_4N_4 (11), S_4N_3Cl and S_4N_3Br (12), S_3N_2Cl (12), $(SN)_x$ (13), $S_4N_4 \cdot AsF_5$ (14), S_4N_2 (15), $S_3N_2O_2$ (16), $(Ph_2PN)_3$ and $(Ph_2PN)_4$ (17), $(Ph_2PN)(SN)_2$ (18), 1,3- and 1-5,$(Ph_2PN)_2(SN)_2$ (19), and $(Ph_2PN)_2NSCl$ (20).

Characterization of $(Ph_2PN)_3 \cdot HCl$

In the reaction of Ph_2PCl with $Cs^+S_3N_3^-$ (2.5:1 and 4:1 molar ratios) an air-stable, white crystalline solid (ca. 200 mg) was isolated and identified as $(Ph_2PN)_3 \cdot HCl$. *Anal.* calcd. for $C_{36}H_{31}ClN_3P_3$: C 68.19, H 4.94, Cl 5.59, N 4.94, P 14.65; found: C 68.25, H 5.03, Cl 5.86, N 5.03, P 14.27. The major bands in the infrared spectrum (Nujol mull) were at 3080 (sh)w, 3057 w, 1440 s, 1242 vs, 1235 (sh), vs, 1205 s, 1200 (sh)s, 1186 s, 1130 m, 955 s, 734 s, 728 (sh)m, 702 m, 550 vs, 523 m, 516 (sh)m, 509 m cm^{-1}.

The mass spectrum showed major peaks at m/e 597 ($Ph_6P_3N_3^+$, 19%), 520 ($Ph_5P_3N_3^+$, 15%), 38 ($H^{37}Cl$, 33%), and 36 ($H^{35}Cl$, 100%). The ^{31}P nmr spectrum (in $CDCl_3$) showed a broad singlet at $\delta = +21.9$ (ref. external 85% H_3PO_4). The reaction of the adduct $(Ph_2PN)_3 \cdot HCl$ with triethylamine in boiling benzene gave $(Ph_2PN)_3$, identified by comparing its infrared spectrum with that of an authentic sample, and $Et_3N \cdot HCl$.

Results and discussion

Reactions of $S_3N_3^-$ with halogens and AsF_5

The products of the reactions of S_4N_4 with halogens are dependent on the reaction conditions. Thus the final product of the chlorination of S_4N_4 at ambient temperature is $S_3N_3Cl_3$ (10), but at −60°C the thermally unstable $S_4N_4Cl_2$ is formed (21).

Can. J. Chem. Downloaded from www.nrcresearchpress.com by 210.87.254.6 on 09/06/12
For personal use only.

Can. J. Chem. Downloaded from www.nrcresearchpress.com by 210.87.254.6 on 09/06/12
For personal use only.

With an excess of *liquid* bromine S_4N_4 forms the salt $S_4N_3^+Br_3^-$ quantitatively (22), whereas the reaction of bromine *vapour* with *solid* S_4N_4 gives the conducting polymer $(SNBr_{0.4})_x$ (23). We have, therefore, carried out the reactions of $S_3N_3^-$ with halogens (Cl_2, Br_2, and I_2) under a variety of conditions.

With all three halogens the major reaction product was S_4N_4 and there was no evidence for the formation of monosubstituted products S_3N_3X. Differences were observed, however, in the identities of the minor products obtained when the reactions were carried out under different conditions. Thus Cl_2 reacted with $PPN^+S_3N_3^-$ *in solution* to give $S_4N_3^+Cl^-$ (in addition to S_4N_4) whereas with *solid* $PPN^+S_3N_3^-$ the only S—N product was $S_3N_3Cl_3$. The latter is probably formed by the reaction of excess chlorine with S_4N_4 (10). The minor products of the reactions of $PPN^+S_3N_3^-$ with bromine were $(SN)_x$ (CH_2Cl_2 solvent) and $S_4N_3^+Br^-$ (solid state reaction). The reaction of I_2 with $PPN^+S_3N_3^-$ in CH_2Cl_2 gave S_4N_4 as the only identifiable S—N product.

The formation of $S_4N_3^+X^-$ (X = Cl, Br) probably occurs by the known reaction of S_4N_4 with S_2X_2 (24), the latter being formed by the reaction of halogen with sulfur produced in the reaction.

$$3S_4N_4 + 2S_2X_2 \rightarrow 4S_4N_3^+X^-$$

The absence of $S_4N_3^+I^-$, a thermally unstable salt (25), is accounted for by the instability of S_2I_2 (26).

The oxidation of $Cs^+S_3N_3^-$ by AsF_5 in CH_2Cl_2 gave three S—N products: S_4N_4, $S_4N_4 \cdot AsF_5$, and $(SN)_x$. It should be noted that the oxidation of S_4N_4 with excess AsF_5 in SO_2 produces the cation $S_4N_4^{2+}$ directly (27), but the adduct $S_4N_4 \cdot AsF_5$ is obtained when the reaction is conducted in CCl_4 (14*a*).

Reactions of $S_3N_3^-$ with $SOCl_2$, SO_2Cl_2, S_2Cl_2, $COCl_2$, and Me_3SiCl

The reactions of $SOCl_2$ and SO_2Cl_2 with $Cs^+S_3N_3^-$ produced an interesting sequence of colour changes (see Table 1) suggesting the formation of unstable intermediates. S_4N_4 was a major product in both reactions and, in the case of $SOCl_2$, $S_3N_2O_2$ was also isolated in ca. 50% yield. It should be mentioned that the related anion $S_4N_5^-$ also produces $S_3N_2O_2$ on reaction with $SOCl_2$ (28), as does S_4N_4 (29). The latter reaction also yields $S_4N_3^+Cl^-$ (29), but this cannot be the only source of $S_3N_2O_2$ in the $S_3N_3^-/SOCl_2$ reaction since only a small amount of $S_4N_3^+Cl^-$ was obtained. The main product of the reaction of S_2Cl_2 with $S_3N_3^-$ was S_3N_2Cl.

When $COCl_2$ gas was passed into a solution of $Cs^+S_3N_3^-$ in acetonitrile at −78°C a substantial amount of good quality $(SN)_x$ was obtained in addition to S_4N_4. The reaction of $PPN^+S_3N_3^-$ with Me_3SiCl in CH_2Cl_2 produced S_4N_4 in 56% yield.

Comments on the mechanism of the reactions of $S_3N_3^-$ with halogens and other electrophilic substrates

The ready oxidation of $S_3N_3^-$ is expected in view of its electronic structure (*vide supra*) and the initial oxidation product is expected to be the $S_3N_3^{\bullet}$ radical, which has been identified as one of the products of the pyrolysis of S_4N_4 over quartz or silver wool (30). However, there is disagreement over its structure. An open chain structure has been suggested on the basis of LCAO-SCF (minimal basis set) calculations (31), while more recent studies by photoelectron spectroscopy have led to the conclusion that $S_3N_3^{\bullet}$ is cyclic (32). It seems reasonable to rationalize the formation of S_4N_4 and, in some cases, smaller amounts of $(SN)_x$ from the oxidation of $S_3N_3^-$ with halogens or other electrophilic substrates by the initial formation of $S_3N_3^{\bullet}$ which rearranges quickly to give the observed products before further oxidation can take place. It is worth noting that the reaction of $S_3N_3Cl_3$, $S_3N_2Cl_2$, or S_3N_2Cl with Me_3SiN_3 also produces $(SN)_x$ and S_4N_4. The $S_3N_3^{\bullet}$ radical has been proposed as an intermediate in the formation of $(SN)_x$ in these reductions (13), and it is conceivable that the reduction of $S_3N_3Cl_3$ and the oxidation of $S_3N_3^-$ to $(SN)_x$ and S_4N_4 proceed via the same intermediate.

Reaction of $S_3N_3^-$ with CS_2

During the attempted removal of elemental sulfur from $PPN^+S_3N_3^-$ by washing with CS_2, a blood-red solution was observed. Tetrasulfur dinitride, S_4N_2, was isolated from the reaction mixture in addition to S_4N_4 and PPN^+CNS^-. Since the yield of S_4N_2 is only ca. 15%, this reaction does not represent an improvement over existing syntheses (15*b*, 33). It is clear, however, that CS_2 should be avoided as a solvent for reactions of $S_3N_3^-$.

Reaction of $S_3N_3^-$ with Ph_2PCl

The reaction of $Cs^+S_3N_3^-$ with Ph_2PCl in CH_2Cl_2 or acetonitrile yielded a complex mixture of products whose composition was dependent on the molar ratio of the reactants. The known cyclophosphathiazenes (**1**, ref. 18), (**2** and **3**, ref. 19) (see Fig. 2) and $(Ph_2PN)_2NSCl$ (20), in addition to small amounts of the cyclophosphazenes $(Ph_2PN)_x$ (x = 3, 4) and the adduct $(Ph_2PN)_3 \cdot HCl$ were isolated and identified (see Table 1 and Experimental section). A stoichiometry of 1:1 favours the formation of the six-membered ring (**1**), but an increase in the molar ratio $Ph_2PCl:S_3N_3^-$ leads to preferential formation of the eight-membered rings (**2** and **3**, see Table 1). The cyclophosphathiazenes can be separated by gel permeation chromatography but the pure products are obtained in fairly low yields. Consequently, this synthesis is not superior to the reaction of Ph_2PH (or Ph_2PPPh_2) with S_4N_4 for the preparation of these inorganic heterocycles with the exception of **3** which is only obtained in very low yields (ca. 1%) by the latter route (19).

In attempting to rationalize the formation of the cyclophosphathiazenes (**1**–**3**), we propose that the reaction of Ph_2PCl with $S_3N_3^-$ proceeds via the formation of an open-chain intermediate $Ph_2P—N=S=N—S—N=S$, **4**, which cyclizes with loss of S, to give **1** (cf. the formation of $Ph_3P=N—S_3N_3$ via an open-chain intermediate in the reaction of Ph_3P with S_4N_4 (34)). The formation of the isomers **2** and **3** can then be explained by a head-to-tail dimerization of **4** with loss of $(SN)_xS$ units (x = 0 and 2, **2**; x = 1, **3**). In support of this proposal S_8 and S_4N_4 (in the case of the 1:1 reaction) were isolated as reaction products. In the presence of excess Ph_2PCl, S_4N_4 would undergo the following sequence of known reactions (20), thus accounting for the formation of $(Ph_2PN)_2NSCl$ and its hydrolysis product $[H_2NPPh_2NPh_2PNH_2]^+Cl^-$ in reactions in which the molar ratio $Ph_2PCl:S_4N_4$ exceeded 2:1.

$$S_4N_4 \xrightarrow{Ph_2PCl} (Ph_2PN)_2NSCl \xrightarrow{2H_2O} [H_2NPPh_2NPh_2PNH_2]^+Cl^- + SO_2$$

The isolation of the adduct $(Ph_2PN)_3 \cdot HCl$ was unexpected since HCl adducts of cyclophosphazenes are formed readily only when the substituents on phosphorus are alkyl or dialkylamino groups (17). However, it has been suggested that the adduct $(Ph_2PN)_3 \cdot HICl_2$, formed by the reaction of $(Ph_2PN)_3$

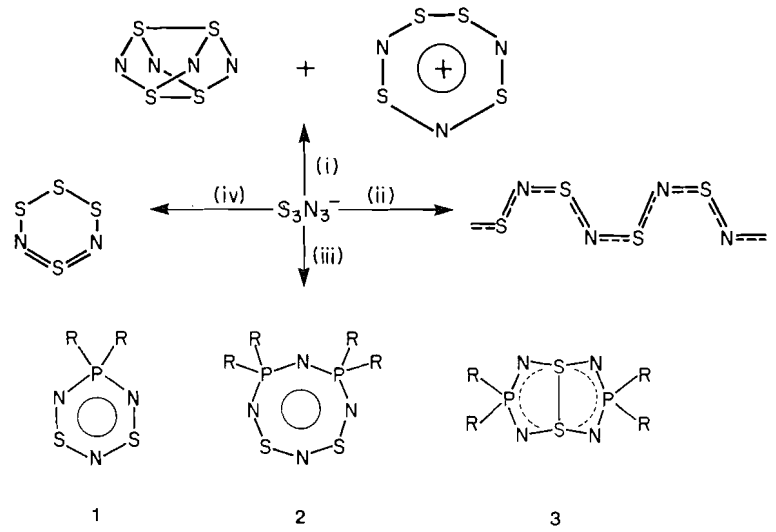

FIG. 2. Major products from the reactions of $S_3N_3^-$ with (*i*) halogens, (*ii*) $COCl_2$, (*iii*) Ph_2PCl, and (*iv*) CS_2.

with ICl in the presence of moisture, contains the cation $Ph_6P_3N_3H^+$ but no spectroscopic data were given (35). In the infrared spectrum of $(Ph_2PN)_3 \cdot HCl$ the degenerate ring stretching vibration, $\nu(P{=}N)$, is shifted to higher wavenumbers by ca. 50 cm^{-1} compared to the free base, $(Ph_2PN)_3$, as expected for protonation at a ring nitrogen atom (17).

Summary and conclusions

The reactions of $S_3N_3^-$ with halogens and other electrophilic substrates gave a complex mixture of products in which S_4N_4 is the major component. In some cases, smaller amounts of $(SN)_x$ were also isolated. These results are best rationalized in terms of initial oxidation of the electron-rich $S_3N_3^-$ ion to the $S_3N_3^{\cdot}$ radical, which rearranges quickly to S_4N_4 or $(SN)_x$ before further oxidation can take place. It is conceivable that the electrochemical oxidation of $S_3N_3^-$ will produce the corresponding cation, $S_3N_3^+$, and this possibility is under investigation. The reaction of $S_3N_3^-$ with Ph_2PCl yields the cyclophosphathiazenes **1**–**3**, but it is only synthetically useful for the preparation of the 1,5-isomer, **3**.

Acknowledgements

We thank Mr. N. Burford for providing spectral data (ir and ^{31}P nmr) for compounds **1**–**3** and the Natural Sciences and Engineering Research Council of Canada for financial support.

1. J. BOJES, T. CHIVERS, W. G. LAIDLAW, and M. TRSIC. J. Am. Chem. Soc. **101**, 4517 (1979).
2. J. W. WALUK and J. MICHL. Inorg. Chem. **20**, 963 (1981).
3. T. CHIVERS, R. T. OAKLEY, O. J. SCHERER, and G. WOLMERSHÄUSER. Inorg. Chem. **20**, 914 (1981).
4. T. CHIVERS, W. G. LAIDLAW, R. T. OAKLEY, and M. TRSIC. Inorg. Chim. Acta, **53**, L189 (1981).
5. T. CHIVERS, R. T. OAKLEY, A. W. CORDES, and W. T. PENNINGTON. J. Chem. Soc. Chem. Commun. 1214 (1981); T. CHIVERS, A. W. CORDES, R. T. OAKLEY, and W. T. PENNINGTON. Inorg. Chem. In press.
6. J. BOJES and T. CHIVERS. Inorg. Chem. **17**, 318 (1978).
7. T. CHIVERS, W. G. LAIDLAW, R. T. OAKLEY, and M. TRSIC. J. Am. Chem. Soc. **102**, 5773 (1980).
8. (*a*) H. G. HEAL. The inorganic heterocyclic chemistry of sulfur, nitrogen and phosphorus. Academic Press, London. 1980. Chapt. 7, p. 136; (*b*) L. ZBORILOVA and P. GEBAUER. Z. Anorg. Allg. Chem. **483**, 44 (1981); (*c*) Y. MONTEIL and H. VINCENT. Z. Naturforsch. B. **31b**, 673 (1978); (*d*) G. WOLMERSHÄUSER, G. B. STREET, and R. D. SMITH. Inorg. Chem. **18**, 383 (1979).
9. N. BURFORD, T. CHIVERS, A. W. CORDES, W. G. LAIDLAW, M. C. NOBLE, R. T. OAKLEY, and P. N. SWEPSTON. J. Am. Chem. Soc. **104**, 1282 (1982).
10. G. G. ALANGE, A. J. BANISTER, and B. BELL. J. Chem. Soc. Dalton Trans. 2399 (1972).
11. M. VILLENA-BLANCO and W. L. JOLLY. Inorg. Synth. **9**, 98 (1967).
12. W. L. JOLLY and K. D. MAGUIRE. Inorg. Synth. **9**, 102 (1967).
13. F. A. KENNETT, G. K. MACLEAN, J. PASSMORE, and M. N. S. RAO. J. Chem. Soc. Dalton Trans. 851 (1982), and references cited therein.
14. (*a*) R. MEWS, D.-L. WAGNER, and O. GLEMSER. Z. Anorg. Allg. Chem. **412**, 148 (1975); (*b*) R. J. GILLESPIE, J. P. KENT, and J. F. SAWYER. Acta Crystallogr. B**36**, 655 (1980).
15. (*a*) J. NELSON and H. G. HEAL. J. Chem. Soc. A. 136 (1971); (*b*) T. CHIVERS, P. W. CODDING, W. G. LAIDLAW, S. W. LIBLONG, R. T. OAKLEY, and M. TRSIC. J. Am. Chem. Soc. **105**, 1186 (1983).
16. D. A. ARMITAGE and A. W. SINDEN. Inorg. Chem. **11**, 1151 (1972).
17. S. S. KRISHNAMURTHY, A. C. SAU, and M. WOODS. Adv. Inorg. Chem. Radiochem. **21**, 41 (1978).
18. N. BURFORD, T. CHIVERS, A. W. CORDES, W. G. LAIDLAW, M. C. NOBLE, R. T. OAKLEY, and P. N. SWEPSTON. J. Am. Chem. Soc. **104**, 1282 (1982).
19. N. BURFORD, T. CHIVERS, and J. F. RICHARDSON. Inorg. Chem. In press.
20. T. CHIVERS, M. N. S. RAO, and J. F. RICHARDSON. J. Chem. Soc. Chem. Commun. 982 (1982).
21. L. ZBORILOVA and P. GEBAUER. Z. Chem. **19**, 32 (1979); L. ZBORILOVA and P. GEBAUER. Z. Anorg. Allg. Chem. **448**, 5 (1979).
22. G. B. WOLMERSHÄUSER and G. B. STREET. Inorg. Chem. **17**, 2685 (1978).
23. (*a*) G. B. STREET, R. L. BINGHAM, J. I. CROWLEY, and J. KUYPER. J. Chem. Soc. Chem. Commun. 464 (1977); (*b*) M. AKHTAR, C. K. CHIANG, A. J. HEEGER, and A. G. MACDIARMID. J. Chem. Soc. Chem. Commun. 846 (1977).
24. H. G. HEAL. Adv. Inorg. Chem. Radiochem. **15**, 375 (1972).
25. (*a*) S. C. PEAKE and A. J. DOWNS. J. Chem. Soc. Dalton Trans. 859 (1974); (*b*) H. VINCENT, Y. MONTEIL, and M. P. BERTHET. J. Inorg. Nucl. Chem. **42**, 5 (1980).
26. H.-J. MÄUSLE and R. STEUDEL. Z. Anorg. Allg. Chem. **463**, 27 (1980).

Can. J. Chem. Downloaded from www.nrcresearchpress.com by 210.87.254.6 on 09/06/12
For personal use only.

27. R. J. GILLESPIE, J. P. KENT, J. F. SAWYER, D. R. SLIM, and J. D. TYRER. Inorg. Chem. **20**, 3799 (1981).
28. T. CHIVERS and J. PROCTOR. Can. J. Chem. **57**, 1286 (1979).
29. A. J. BANISTER and J. S. PADLEY. J. Chem. Soc. A. 1437 (1967).
30. R. D. SMITH. J. Chem. Soc. Dalton Trans. 478 (1979).
31. P. W. DEUTSCH and L. A. CURTISS. Chem. Phys. Lett. **51**, 125 (1977).
32. W. M. LAU. Ph.D. Thesis, University of British Columbia. 1982.
33. R. W. H. SMALL, A. J. BANISTER, and Z. V. HAUPTMAN. J. Chem. Soc. Dalton Trans. 2188 (1981), and references cited therein.
34. J. BOJES, T. CHIVERS, A. W. CORDES, G. MACLEAN, and R. T. OAKLEY. Inorg. Chem. **20**, 16 (1981).
35. R. D. WHITAKER, J. C. CARLETON, and H. H. SISLER. Inorg. Chem. **2**, 420 (1963).

Can. J. Chem. Downloaded from www.nrcresearchpress.com by 210.87.254.6 on 09/06/12
For personal use only.

An improved procedure for the conversion of certain coumarins to 2,2-dimethylchromenes: efficient transformation of umbelliferone to precocene 1

GEORGE M. STRUNZ, DENIS BRILLON,[1] AND PIERRE GIGUÈRE

Maritimes Forest Research Centre, Canadian Forestry Service, Department of the Environment, P.O. Box 4000, Fredericton, N.B., Canada E3B 5P7

Received March 1, 1983

GEORGE M. STRUNZ, DENIS BRILLON, and PIERRE GIGUÈRE. Can. J. Chem. **61**, 1963 (1983).

An improved method for transforming certain coumarins to 2,2-dimethylchromenes has been developed. Umbelliferone (**1***b*) was efficiently converted to precocene I (**2***b*) (73%) by etherification to herniarin (**1***c*) with tetramethylorthocarbonate, followed by reaction with methyllithium and cyclization of the resulting phenolic alcohol on silica gel.

GEORGE M. STRUNZ, DENIS BRILLON et PIERRE GIGUÈRE. Can. J. Chem. **61**, 1963 (1983).

On a amélioré la methode de la conversion de quelques coumarines au diméthyles-2,2-chromènes. L'umbelliférone (**1***b*) était transformé efficacement en précocène I (**2***b*) (73%) par préparation de l'éther méthylique herniarin (**1***c*), utilisant le tetraméthylorthocarbonate, suivi de la réaction avec le méthyllithium et cyclisation de l'alcool phénolique résultant avec le gel de silice.

The methoxy-2,2-dimethylchromenes **2***b* and **2***c* (1) were observed by Bowers to exhibit antiallatotropic activity in several hemimetabolous insect species (2), i.e. they disrupt juvenile hormone production, and cause precocious metamorphosis and sterility when administered to these insects. The compounds, designated precocenes 1 and 2 respectively (2), appear to be metabolized to the cytotoxic 3,4-epoxides in the corpus allatum, accounting for their selective effects against this endocrine organ (3).

The precocenes have been synthesized via 4-chromanones produced by condensation of appropriately substituted phenols or phenol derivatives with dimethylacrylic acid or its chloride (2, 4).

An alternative approach, which has been employed with variable success in the synthesis of substituted 2,2-dimethylchromenes, involves reaction of appropriate coumarins with methyl magnesium halides and cyclization of the product by acid treatment and/or distillation (5).

We have confirmed the previous observation (5*d*) that application of the Grignard procedure to 7-methoxycoumarin (herniarin) (**1***c*) (prepared, *vide infra*, by methylation of umbelliferone (**1***b*)) gives, at best, modest yields of the corresponding

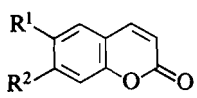

1

	R^1	R^2
a	H	H
b	H	OH
c	H	OCH_3

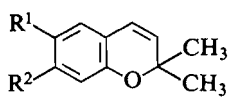

2

	R^1	R^2
a	H	H
b	H	OCH_3
c	OCH_3	OCH_3

2,2-dimethylchromene, precocene 1 (**2***b*). (Livingstone and coworkers (5*d*,*e*) reported yields of 44%, 42%, and 52% respectively for the conversion of 7-, 5-, and 8-methoxycoumarins to the corresponding 2,2-dimethylchromenes by the action of methyl magnesium iodide.) This paper reports our observation that the desired transformation to precocene 1 can be accomplished with substantially improved yield (~73%) by treatment of herniarin with methyllithium and, after careful work-up, cyclization of the phenolic alcohol product under mild conditions on silica gel.

The initial step, methylation of the phenolic hydroxyl group of umbelliferone, was executed virtually quantitatively by refluxing the latter with tetramethylorthocarbonate (6) in the presence of a catalytic amount of *p*-toluenesulfonic acid.

The methyllithium – silica gel procedure applied to coumarin itself afforded 2,2-dimethylchromene in 83% yield (cf. 59% by the Grignard method (5*b*)).

Experimental

Commercial umbelliferone (95+%) was purified prior to use by elution with acetone successively through columns of silica gel and of neutral alumina. The crystalline material obtained on removal of solvent melted at 234–237°C (hot-stage apparatus, uncorrected) (lit. (7) mp 230–231°C).

*7-Methoxycoumarin (herniarin) (***1***c)*

A solution of umbelliferone (**1***b*) (925 mg, 5.70 mmol; purified as above) in anhydrous tetrahydrofuran (12.0 mL) and tetramethylorthocarbonate (11.0 mL) containing *p*-toluenesulfonic acid (3 mg), was heated under reflux for 18 h. Distillation at atmospheric pressure until the temperature began to rise above ca. 90°C removed tetrahydrofuran and volatile products (dimethylcarbonate and methanol (6)). Additional tetramethylorthocarbonate (2–6 mL) was then added until solid material redissolved, and the resulting solution was refluxed for a further 65 h, when tlc analysis revealed that the reaction was complete. After the mixture had returned to ambient temperature, volatile material was removed by vacuum distillation (water pump). Subsequent application of high vacuum for several hours ensured that no volatile material remained. Nuclear magnetic resonance and tlc analysis demonstrated that the conversion to herniarin was virtually quantitative, and the product was sufficiently pure to be used directly in the subsequent step.[2]

*7-Methoxy-2,2-dimethylchromene (precocene I) (*2b)

Herniarin (~5.70 mmol), from the previous step, was dissolved by gentle warming in a mixture of anhydrous ether (27.0 mL) and toluene (18.0 mL). In a nitrogen atmosphere, and with a bath temperature of 38–40°C, a solution of methyllithium in ether (14.8 mmol of ca. 1.3 *M* solution) was added steadily by syringe during 1 min (it was found that if the addition of methyllithium was too slow, production of by-products increased). Vigorous agitation was necessary throughout this and the following step. After a further minute, the reaction

[1] Undergraduate cooperative program participant from University of Sherbrooke.

[2] Herniarin was also prepared in excellent yield from umbelliferone using excess methyl iodide and potassium carbonate in acetone (5*a*).

Can. J. Chem. Downloaded from www.nrcresearchpress.com by 210.87.254.6 on 09/06/12
For personal use only.

flask was cooled in a Dry Ice – ethanol bath, and a mixture of water (1.0 mL) and tetrahydrofuran (10.0 mL) was added by syringe during 3 min. The temperature was allowed to rise to ca. 0°C and 10% aqueous KH_2PO_4 solution (~11 mL) was added to bring the pH below 7.0. The mixture was poured into water (total volume ca. 100 mL), and NaCl was added to saturation. The mixture was extracted five times with ethyl acetate (total volume ~300 mL), and the extracts were dried over $MgSO_4$ and filtered. The resulting solution of phenolic alcohol was refrigerated if not used immediately.

For cyclization to the chromene, the solvent was removed *in vacuo*, and the residue in hexane (75 mL) was refluxed with stirring under nitrogen in the presence of silica gel[3] (30 g) for 6 h. The silica gel was then removed by filtration and washed with hexane. Evaporation of the filtrates under reduced pressure afforded crude precocene I. The hope that the silica gel would retain by-products produced during the sequence was only partially realized, and it was necessary to effect a final purification by flash chromatography (8) using hexane–EtOAC (96:4) as eluent.

Precocene I (pure by nmr, tlc, and glc) was obtained in an overall yield of 73% from umbelliferone, and was characterized by comparison of its spectroscopic and chromatographic characteristics with those of a commercial sample (Aldrich Chemical Co.).

2,2-Dimethylchromene (2a)

The title compound was prepared from coumarin (**1***a*) in a manner analogous to that used for the preparation of precocene I. The procedure was identical as far as the phenolic alcohol which, in the absence of the electron-donating methoxyl group on the aromatic ring, required somewhat more vigorous conditions for cyclization (toluene in lieu of hexane, 98°C, 8.5 h). The yield of pure 2,2-dimethylchromene obtained after flash chromatography (85% hexane, 15% chloroform) was 83%.

[3] Kieselgel, 100–200 mesh (Gebr. Herrmann, Köln): not specially dried before use.

1. A. R. ALERTSEN. Acta Chem. Scand. **9**, 1725 (1955); T. R. KASTURI and R. MANITHOMAS. Tetrahedron Lett. **27**, 2573 (1967).
2. W. S. BOWERS, T. OHTA, J. S. CLEERE, and P. A. MARSELLA. Science, **193**, 542 (1976).
3. G. E. PRATT, R. C. JENNINGS, A. F. HAMNETT, and G. T. BROOKS. Nature, **284**, 320 (1980).
4. R. HULS. Bull. Soc. Chim. Belg. **67**, 22 (1958).
5. (*a*) W. BRIDGE, A. J. CROCKER, T. CUBIN, and A. ROBERTSON. J. Chem. Soc. 1530 (1937); (*b*) R. L. SHRINER and A. G. SHARP. J. Org. Chem. **4**, 575 (1939); (*c*) L. I. SMITH and P. M. RUOFF. J. Am. Chem. Soc. **62**, 145 (1940); (*d*) R. LIVINGSTONE and R. B. WATSON. J. Chem. Soc. 1509 (1957); (*e*) J. D. HEPWORTH and R. LIVINGSTONE. J. Chem. Soc. C, 2013 (1966); (*f*) J. D. HEPWORTH, T. K. JONES, and R. LIVINGSTONE. Tetrahedron, **37**, 2613 (1981); (*g*) L. MERLINI. Advances in the chemistry of chrom-3-enes. *In* Advances in heterocyclic chemistry. Vol. 18. *Edited by* A. R. Katritzky and A. J. Boulton. Academic Press, New York. 1975. pp. 159–198.
6. B. SMITH. Acta Chem. Scand. **10**, 1006 (1956).
7. R. C. WEAST (*Editor*). Handbook of Chemistry and Physics. 57th ed. C.R.C. Press, Cleveland, OH. 1976.
8. W. C. STILL, M. KAHN, and A. MITRA. J. Org. Chem. **43**, 2923 (1978).

Can. J. Chem. Downloaded from www.nrcresearchpress.com by 210.87.254.6 on 09/06/12
For personal use only.

The photochemistry of 9,10-anthracenedione in sulfuric acid solution. The dependence of product yields on reaction conditions

A. Douglas Broadbent and John M. Stewart

Department of Chemistry, Mount Allison University, Sackville, N.B., Canada E0A 3C0

Received October 7, 1982

A. Douglas Broadbent and John M. Stewart. Can. J. Chem. **61**, 1965 (1983).

Irradiation of a sulfuric acid solution of 9,10-anthracenedione with near-uv light generated 2-hydroxy-9,10-anthracenedione as the major product. In addition, the 1-hydroxy and polyhydroxy derivatives and the reduction products anthrone and bianthronyl were also formed. The yields of these minor products were markedly influenced by the concentrations of water and oxygen in the sulfuric acid. At low light intensities, oxygen quenched the efficient formation of the hydroxyanthracenediones and also oxidised the initial quinone reduction products. Photoreduction of the anthracenedione and photooxidation of anthrone occurred simultaneously in the solution. The reaction mechanism is more complex than previous studies indicated.

A. Douglas Broadbent et John M. Stewart. Can. J. Chem. **61**, 1965 (1983).

L'irradiation de l'anthracènedione-9,10, en solution dans l'acide sulfurique avec une lumière du proche uv conduit à la formation de l'hydroxy-2 anthracènedione-9,10 comme produit majoritaire. De plus, il se forme également l'hydroxy-1, les dérivés polyhydroxy et les produits de la réduction de l'anthrone et du bianthronyle. Les rendements de ces produits secondaires sont fortement influencés par la concentration en eau et en oxygène dans l'acide sulfurique. Lorsqu'on utilise une lumière de faible intensité, l'oxygène bloque la formation efficace des hydroxyanthracènediones et oxyde également les produits initiaux de la réduction de la quinone. La photoréduction de l'anthracènedione et la photoxydation de l'anthrone se produisent simultanément en solution. Le mécanisme de la réaction est plus complexe que ne l'indiquent les études antérieures.

[Traduit par le journal]

Can. J. Chem. Downloaded from www.nrcresearchpress.com by 210.87.254.5 on 09/06/12
For personal use only.

Introduction

Although sulfuric acid is a widely used and excellent solvent for 9,10-anthracenedione and its derivatives (1), little is known about photochemical reactions of these compounds in this solvent. Irradiation of a 100% sulfuric acid solution of 9,10-anthracenedione-2-sulfonate, with near-uv light, has been reported to produce only 2-hydroxy-9,10-anthracenedione sulfonates, with no 1-hydroxy derivatives (2). Total regioselectivity was also found in the similar photochemical reaction of the unsubstituted 9,10-anthracenedione (OAO), which was claimed to yield 2-hydroxy-9,10-anthracenedione (2-HO—OAO) as the sole product (3). Observation of well-defined isosbestic points in a series of uv spectra of a progressively irradiated solution indicated a clean, efficient reaction. No differences in reaction rate were noted between preparative experiments using nitrogen or air bubbling. The lack of oxygen influence on the photochemical reaction of OAO in sulfuric acid was apparently confirmed by subsequent studies (4), in which 1-hydroxy- (1-HO—OAO) and 1,4-dihydroxy-9,10-anthracenedione (quinizarin) were also isolated in addition to the major 2-HO—OAO. Changes in the product distribution during the reaction suggested that the initially formed 1-HO—OAO underwent a subsequent photochemical hydroxylation reaction yielding quinizarin.

We have recently established (5) that the photochemical reaction of OAO in sulfuric acid is more complex than the earlier studies indicated. The rate of formation of 2- and 1-HO—OAO, and the yields of the minor products, are markedly affected by the concentrations of oxygen and water in the sulfuric acid solution. This paper reports our results on product isolation and identification and the dependence of product yields on the reaction conditions. In addition, since oxygen has been found to effectively quench the reaction at low light intensities, some preliminary photochemical kinetic data are included.

Results

Product yields

Irradiation of OAO in 96% sulfuric acid solution, stirred by nitrogen bubbling, gave 2-HO—OAO as the major isolated product, along with low yields of 1-HO—OAO, and the quinone reduction products 9(10*H*)-anthracenone (anthrone) and 9,9′(9*H*,9′*H*)-bianthracene-10,10′-dione (bianthronyl). Traces of polyhydroxyanthracenediones were also observed on TLC analysis, but the quantities were insufficient for identification. An identical reaction performed with oxygen bubbling yielded more 2- and 1-HO—OAO, but only a trace of bianthronyl and no detectable anthrone. Although the yields of polyhydroxyanthracenediones were always low (<1%), their formation was sufficiently enhanced by the presence of oxygen that isolation and identification of quinizarin (minor) and 1,2-dihydroxy-9,10-anthracenedione (alizarin, major) were possible. Product yields for photochemical reactions in nitrogen- and oxygen-stirred sulfuric acid solutions are given in Table 1.

In preparative experiments, the initial rate of conversion of OAO was less in solutions containing oxygen, but rapidly increased, so that the overall yields of 2- and 1-HO—OAO were larger than in the nitrogen-stirred reactions. In 100% sulfuric acid, the rate was much less than in solutions containing water.

Dark reactions

Sulfuric acid solutions of OAO and its monohydroxy derivatives were stored in the dark for one week and the quinones recovered unchanged. Since the photochemical reaction of OAO in sulfuric acid resembled that with peroxydisulfate (6), dark reactions, comparable to the photolyses, were performed with added ammonium peroxydisulfate and similarly analysed. The yields of products are given in Table 1 in parentheses. No reduction products of the OAO were detected in these dark reactions. The only polyhydroxy product found was quinizarin, which was only detected in 100% sulfuric acid reactions with a yield of 3% for either oxygen or nitrogen bubbling.

Time-lapse spectrophotometry

Because of the obvious change in product distribution in the reaction on switching from nitrogen to oxygen bubbling, and

TABLE 1. Yields of products from irradiation (3 h) of 9,10-anthracenedione (2.5 m*M*) in sulfuric acid solutions with yields of analogous dark reactions (48 h) in the presence of ammonium peroxydisulfate (25 m*M*) in parentheses

	% Yields based on OAO consumed*					
	90% H_2SO_4		96% H_2SO_4		100% H_2SO_4	
Compound	N_2	O_2	N_2	O_2	N_2	O_2
2-HO—OAO	71(62)	81(55)	74(56)	88(58)	66(64)	65(61)
1-HO—OAO	14(38)	16(45)	7(44)	11(42)	32(35)	30(37)
Anthrone	10 —	— —	6 —	— —	— —	— —
Bianthronyl	5 —	2 —	13 —	tr —	tr —	— —

*For both photochemical and dark reactions the % conversion of OAO was 75–85% except in 100% sulfuric acid where conversions of 40–60% were determined.

TABLE 2. Ultraviolet spectroscopic data for 9,10-anthracenedione and its photochemical reaction products in 96% sulfuric acid solution*

Compound	λ_{max} (nm), $\epsilon \times 10^{-4}$ ($dm^3\ mol^{-1}\ cm^{-1}$)†				
OAO	411(0.98)	311(1.21)	272(4.57)		
2-HO—OAO	484(0.77)	415(0.61)	321(1.03)	289(2.58)	248(1.48)
1-HO—OAO	458(0.94)	305(1.00)	261(2.70)	216(1.40)	
Anthrone	352(2.38)	284(1.05)	248(0.64)	212(2.42)	
Bianthronyl	348(2.80)	298(1.40)	288(1.42)	215(4.32)	
1,2-DiHO—OAO	498(1.21)	323(0.69)	286(2.73)	274(3.06)	
1,4-DiHO—OAO	548(2.55) 253(2.27)	511(1.68)	478(0.73)	330(0.68)	278(3.19)
2,3-DiHO—OAO	425(0.73)	301(3.23)	246(1.03)	206(1.52)	

*Molar absorptivities ϵ dependent on the acid concentration.
†Wavelength of maximum absorbance λ with molar absorptivity ϵ in parentheses.

the report that irradiation of a dilute sulfuric acid solution of OAO gave a series of uv spectra with well-defined isosbestic points, unaffected by the stirring gas (3), this experiment was re-examined. The series of recorded spectra resembled those already published (3), but they did depend upon the nature of the gas used for stirring. In the photochemical reaction of OAO in 96% sulfuric acid saturated with air, enhanced absorption at 547 nm was observed during the later stages of the irradiation. In a subsequent reaction performed with oxygen bubbling, this absorption was noticed much earlier and became more intense. No such absorption was seen in a nitrogen-saturated solution, even on prolonged irradiation. The spectrophotometric data in Table 2 indicate that the 547 nm absorption is characteristic of quinizarin, which is the only hydroxyanthracenedione with such long-wave absorption in sulfuric acid solution.

On irradiation of an OAO solution in 96% sulfuric acid saturated with nitrogen, an additional maximum absorption was observed at 354 nm. Furthermore, such solutions displayed a more intense absorption in the 320–370 nm range, which was not observed in aerated reaction solutions. These additional absorptions, observed only in the absence of oxygen, are typical of the OAO reduction products anthrone and bianthronyl.

The repetition of the time-lapse spectrophotometry was thus useful in confirming the conditions under which the newly established minor products were formed. In addition, a pronounced influence of the nature of the stirring gas on the rate of reaction was noted. The rate of conversion of OAO and of appearance of 2-HO—OAO was much lower in the presence of oxygen. In fact, if the sulfuric acid solution was effectively oxygen saturated prior to and during the irradiation, it was possible to almost totally inhibit all product formation in the dilute solution.

Product photostability

Both 2- and 1-HO—OAO were shown to be stable to irradiation in 96 and 100% sulfuric acid saturated with nitrogen or oxygen. No polyhydroxyanthracenedione formation was detected by TLC or uv analysis. In control experiments using NaOH solutions of hydroxy compounds, the spectrophotometric detection limit for quinizarin was found to be about 0.1% of the amount of monohydroxy compound present. The possibility of a photosensitized reaction involving OAO was eliminated when no increase in the rate of formation of polyhydroxyanthracenediones was found on irradiation of 1- and 2-HO—OAO in the presence of OAO, where the latter absorbed a considerable fraction of the incident light.

Formation of anthrone and bianthronyl

TLC analysis of samples removed during irradiation of a 96% sulfuric acid solution of OAO under nitrogen established an initial rapid increase in the amount of anthrone produced, followed by its gradual disappearance and the simultaneous formation of bianthronyl. The occurrence of such reduction products of OAO under these conditions, and their absence in solutions containing oxygen or in the more strongly oxidising 100% acid, suggested that OAO underwent solvent-induced photoreduction to 9,10-anthracenediol (HOAOH). The reaction of this oxygen-sensitive compound in sulfuric acid was therefore examined. Within 1 min, reaction in the dark gave a stable solution containing OAO, anthrone, and a trace of bianthronyl. Because of the extreme ease of oxidation of HOAOH, similar reactions of the more stable tautomeric

Can. J. Chem. Downloaded from www.nrcresearchpress.com by 210.87.254.5 on 09/06/12
For personal use only.

TABLE 3. Yields of products from dark reactions (3–5 min) of 9,10-anthracenediol and its derivatives (0.05 m*M*) in nitrogen-saturated 96% sulfuric acid

Compound	% Yields *	
	OAO	Anthrone
HOAOH	72	28
Oxanthrone	61	39
AcOAOAc	63	37

*Determined by uv spectrophotometry in 96% sulfuric acid by comparison with the known spectra of OAO and anthrone.

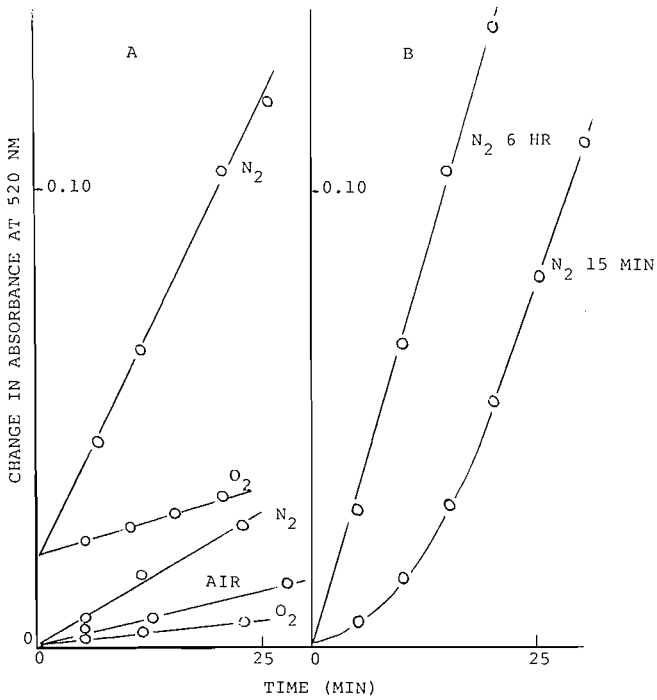

FIG. 1. Rates of product formation (change of absorbance at 520 nm) on irradiation of OAO in 96% sulfuric acid solution in a 5 cm cell. *A*: At 366 nm with gas stirring; 5.6 m*M* (upper plots offset 0.02) and 0.52 m*M*. *B*: With unfiltered radiation $\lambda > 300$ nm and manual agitation after pre-bubbling with nitrogen for stated times; 1.25 m*M*.

10-hydroxy-9(10*H*)-anthracenone (oxanthrone) and of 9,10-diacetoxyanthracene (AcOAOAc) were studied with similar results. The yields in Table 3 were determined by uv spectrophotometric analysis of the OAO/anthrone mixtures. The presence of OAO and anthrone was confirmed by TLC analysis, which also detected traces of bianthronyl.

On irradiation of OAO in 96% sulfuric acid under nitrogen, anthrone might arise by disproportionation of initially generated HOAOH. The formation of bianthronyl could then occur by the previously established photo-oxidation of anthrone (7). This photo-oxidation reaction is little affected by the presence of OAO and its hydroxy derivatives in the irradiated acid solution, because anthrone absorbs in the 350 nm region, where the other compounds are relatively transparent. On photolysis in 100% sulfuric acid, no anthrone and only a trace of bianthronyl were found. In 100% sulfuric acid, HOAOH is rapidly oxidised to OAO with little formation of anthrone, which itself is oxidised in the dark yielding OAO and bianthronyl (8).

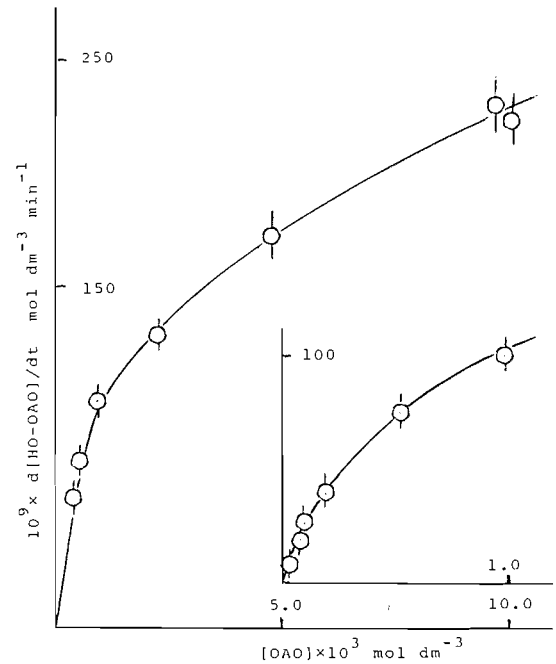

FIG. 2. The dependence of the rate of formation of HO—OAO, determined from linear plots of absorbance at 490 or 520 nm versus time, on the initial OAO concentration for irradiation at 366 nm. Solutions with initial OAO concentrations above 1×10^{-4} *M* absorbed >99% of the incident radiation. The low end of the concentration range is expanded in the box.

Photochemical kinetics

In addition to product identification, the rate of consumption of OAO and of formation of hydroxy products was examined using incident radiation at 366 nm on an optical bench. Product formation was monitored at 490 nm, or at 520 nm, if the initial concentration of OAO was sufficiently high to result in initial absorption at the shorter wavelength. The irradiated solutions were constantly stirred by gas bubbling. In reactions on the optical bench, the absorbance of the products (mainly 2-HO—OAO) was directly proportional to the irradiation time, i.e., plots of absorbance versus time were linear. Figure 1*A* illustrates the influence of the stirring gas on the initial rate of formation of the HO—OAO. The initial rate continued to increase as the starting concentration of OAO increased beyond that where more than 99% of the incident radiation was absorbed. This is shown in Fig. 2. In reactions performed with short irradiation times and intermediate manual agitation of the solution, the quantum yield was found to be 0.5. This was the maximum value recorded but solution homogeneity was not certain.

The rate measurements using different gases demonstrated that oxygen was an effective quencher of the overall reaction. Irradiation of thoroughly oxygen-saturated solutions resulted in a low rate of consumption of OAO and formation of meagre amounts of products, particularly at the low light intensities used on the optical bench. As the light intensity was increased, the low rate of reaction in the oxygen-saturated solution also increased, until it approached the rate in a nitrogen-stirred reaction at the same high light intensity. Initial inhibition in the presence of oxygen was a useful criterion of inadequate nitrogen bubbling (Figure 1*B*), but the effect of residual oxygen was less pronounced at high light intensities and OAO concentrations.

Can. J. Chem. Downloaded from www.nrcresearchpress.com by 210.87.254.5 on 09/06/12
For personal use only.

Can. J. Chem. Downloaded from www.nrcresearchpress.com by 210.87.254.5 on 09/06/12
For personal use only.

Removal of dissolved oxygen from sulfuric acid solutions, as indicated by no initial rate inhibition, required bubbling with nitrogen over several hours, and preferably overnight. Although nitrogen and oxygen are slightly soluble in this solvent, 6.8×10^{-4} and 1.3×10^{-3} M, respectively (9), the rate of exchange on bubbling was slow. The influence of oxygen on the initial rate of consumption of OAO, or of formation of HO—OAO, suggested that oxygen has a dual role in the overall reaction. Oxygen not only inhibits the photochemical reaction by quenching the excited state, but is also consumed by oxidation of OAO reduction products such as HOAOH. In relation to the quenching of the excited state by oxygen, a dull red emission was observed (by dark adapted eye) just inside the front window of an irradiated oxygen-saturated solution of OAO in 96% sulfuric acid. This emission was absent in the presence of nitrogen, was not the weak fluorescence emission of OAO or 2-HO—OAO (3), but was like the red emission of excited singlet oxygen. At low incident light intensities, quenching is most evident because the rate of formation of HOAOH, and of oxygen consumption, is low. At high intensities, the high rate of formation of HOAOH and its subsequent oxidation depletes the oxygen in the acid solution so that quenching is minimized, even though the solution is continuously bubbled with oxygen. No consumption of oxygen was detected in an experiment using a gas burette to measure the volume of oxygen absorbed by the irradiated solution. This result, and the low yields of OAO reduction products, indicated that the solvent can function as oxidising agent in place of the oxygen when the latter is absent or its concentration is low.

Discussion

The parent OAO, having $pK = -8.27$ (10), is essentially fully monoprotonated in 100% sulfuric acid. This is not the case in the 96% acid. The H_0 acidity functions for these solutions are -11.94 and -9.88, respectively (10). The various products will be present as their protonated, conjugate acids or as sulfate esters, if they have hydroxy groups. These compounds dissociate or hydrolyse on addition of water.

The results do not support the proposal of a reaction mechanism involving nucleophilic addition of bisulfate ion to the photo-excited conjugate acid of OAO (3). Although such a mechanism can be modified to account for the occurrence of reduction products, it is not consistent with the influence of the initial OAO concentration on the initial rate of formation of HO—OAO, in solutions which absorb >99% of the incident light (Fig. 2). Our observations indicate that polyhydroxyanthracenediones arise from the intervention of oxygen in the reaction, rather than from the proposed secondary photochemical process of the monohydroxy products (4). This result suggested that the reaction might proceed by an electron transfer mechanism analogous to that proposed for photochemical hydroxylation of anthracenediones in aqueous solution (11). Electron transfer from bisulfate ion to the excited state of OAO or its conjugate acid would give HOAOH, by disproportionation of the semiquinone so produced, and a sulfate radical. The hydroxy products would arise by oxidation of the sulfate radical – OAO adduct, and polyhydroxy derivatives by interception of the sulfate radical adduct by oxygen. Unfortunately, the attempt to confirm the sulfate radical mechanism by dark reactions with peroxydisulfate was not totally successful, despite the similarity of these reactions to the photochemical hydroxylations.

We have established that HOAOH in sulfuric acid undergoes rapid oxidation by oxygen, or the solvent, or disproportionates to OAO and anthrone. Such disproportionation is known in other solvents (12). Disproportionation of HOAOH or its derivatives in sulfuric acid did not give the expected equal yields of OAO and anthrone but an excess of OAO, because of oxidation by the solvent. Photochemical reduction and oxidation, involving the solvent, occur simultaneously in the same solution. The photoreduction of OAO to anthrone is favoured by the presence of water, bisulfate ion being a likely electron donor for the initial reduction of the OAO. The photo-oxidation of anthrone, or more probably the tautomeric 9-anthracenol, is diminished in the presence of water, and oxidation even occurs in the dark in 100% sulfuric acid solution (8). Sulfur trioxide, or sulfuric acid itself, could function as the oxidising agent in these reactions.

Our studies have established that the photochemical reaction of OAO in sulfuric acid solution produces 2-HO—OAO, 1-HO—OAO, and several minor products, whose yields were markedly dependent upon the concentrations of water and oxygen in the acid solution. No definitive conclusions regarding the mechanism of the overall reaction were reached, and alternatives to the proposed electron transfer process are possible. The influence of concentration on the rate of reaction could also be rationalized by a bimolecular primary photochemical step involving ground and excited state OAO molecules. Such a mechanism has been proposed for photochemical reactions of OAO derivatives in aqueous solutions but was not confirmed by triplet state lifetime measurements (13).

Experimental

Materials

The various anthracenediones were commercial samples purified by column chromatography and/or recrystallization. Column chromatography of both 1- and 2-HO—OAO was necessary (SiO_2/$CHCl_3$) to remove polyhydroxy derivatives. Anthrone (14), bianthronyl (15), oxanthrone (16), HOAOH (17), AcOAOAc (18), and hystazarin (19) were prepared by published procedures. The sulfuric acid was reagent grade 95.5–96.5%. The 100% sulfuric acid was prepared by addition of redistilled sulfur trioxide to 96% sulfuric acid to give an initial freezing temperature of 10.3°C (20) and the strength checked by volumetric analysis.

Reaction conditions

For photochemical reactions, the solutions were prepared by addition of the anthracenedione to the sulfuric acid, bubbled with the appropriate gas for at least 4 h and then irradiated with a water-cooled Hanovia 450 W mercury lamp at 15–18°C. In most cases, the solutions were saturated with the gas by bubbling overnight. The oxygen and nitrogen were passed through 96% sulfuric acid prior to passage through the reaction solution. For reactions of HOAOH and its derivatives, the solutions were prepared by addition of the appropriate solid to nitrogen-saturated sulfuric acid. These were immediately mixed under nitrogen and the uv spectra recorded.

Products were isolated by pouring the solution onto ice and extracting with $CHCl_3$. For TLC analysis, Eastman Chromagram SiO_2 plates 13181 were used with *p*-xylene as the developing solvent. The following R_f values were found: OAO, 0.60; 1-HO—OAO, 0.70; 2-HO—OAO, 0.03; anthrone, 0.52; bianthronyl, 0.09; quinizarin, 0.75; alizarin, 0.01; hystazarin, 0.01. For column chromatography $SiO_2/CHCl_3$ and Al_2O_3/ethanol were used. The % yields were determined by TLC, followed by extraction of the various zones with $CHCl_3$ and uv analysis in sulfuric acid solution with the Cary 219 UV Spectrophotometer. The uv spectrum of the isolated alizarin indicated possible contamination by hystazarin (19).

Optical bench studies

For time-lapse spectrophotometric studies, light from the Hanovia

450 W mercury lamp was passed through a glass lens ($\lambda > 300$ nm) and into the solution cell. For kinetic and quantum yield studies, an Ealing 366 nm interference filter was placed in the optical train. Light intensities were measured by ferrioxalate actinometry (21) and were in the range $1.10 \pm 0.06 \times 10^{15}$ photon cm^{-3} min^{-1}. For quantum yield measurements, the following molar absorptivities were used: $\epsilon_{490} = 8.0 \times 10^3$, $\epsilon_{520} = 5.2 \times 10^3$ dm^3 mol^{-1} cm^{-1}. These values were calculated from the absorption spectra of 1- and 2-HO—OAO in 96% sulfuric acid solution and the determined ratio of these products. For reactions involving 15 s irradiation periods with 2 min intermediate manual agitation of the solution, the maximum quantum yield was 0.5 for an OAO concentration of 1×10^{-2} *M* in sulfuric acid under nitrogen. It may be higher with optimum mixing, a situation not easily achieved with sulfuric acid solutions.

Acknowledgements

The authors gratefully acknowledge financial assistance from the Natural Sciences and Engineering Research Council, supplies from CIBA AG, Basel, and the award of Marjorie Young Bell Junior Research Fellowships (Mount Allison University) to Christopher and Joyce Milley, who assisted in part of this work.

1. K. VENKATARAMAN. The chemistry of synthetic dyes. Vol. 2. Academic Press, NY. 1952.
2. K. P. CLARK and H. I. STONEHILL. J. Chem. Soc. Faraday Trans. 1, **68**, 1676 (1972).
3. G. G. MIHAI, P. G. TARASSOFF, and N. FILIPESCU. J. Chem. Soc. Perkin Trans. **1**, 1374 (1975).
4. A. V. EL'TSOV, Y. K. LEVENTAL, and O. P. STUDZINSKII. Zh. Org. Khim. **12**, 2483 (1976).
5. A. D. BROADBENT and J. M. STEWART. J. Chem. Soc. Chem. Commun. 676 (1980).
6. L. WACKER. J. Prakt. Chem. **54**, 88 (1896).
7. N. FILIPESCU, E. AVRAM, and K. D. WELK. J. Org. Chem. **42**, 507 (1977).
8. V. V. KOZLOV and K. I. KUDELINA. J. Gen. Chem. USSR, **17**, 302 (1947).
9. International critical tables. Vol. III. McGraw-Hill Book Co. Inc., New York. 1928. p. 262.
10. C. H. ROCHESTER. Acidity functions. Academic Press, London. 1970.
11. A. D. BROADBENT and R. P. NEWTON. Can. J. Chem. **50**, 381, (1972).
12. K. H. MEYER. Justus Liebig's Ann. Chem. **379**, 37 (1911); S. COFFEY. Chem. Ind. (London), 1068 (1953); A. M. DAWSON and A. JOHNSON. J. Soc. Dyers Colorists, **82**, 49 (1966).
13. G. O. PHILLIPS, N. W. WORTHINGTON, J. F. MCKELLAR, and R. R. SHARP. J. Chem. Soc. A, 767 (1969); J. L. CHARLTON, R. G. SMERCHANSKI, and C. E. BURCHILL. Can. J. Chem. **54**, 512 (1976); V. A. KUZ'MIN, A. K. CHIBISOV, and A. V. KARYAKIN. Int. J. Chem. Kinet. **4**, 639 (1972).
14. K. H. MEYER. Org. Synth. **8**, 8 (1928).
15. O. DIMROTH. Chem. Ber. **34**, 219 (1901).
16. D. M. HERCULES and S. CARLSON. Anal. Chem. **45**, 1794 (1973).
17. M. A. MATTHEWS. J. Chem. Soc. **129**, 236 (1926).
18. E. DEB. BARNETT, N. F. GOODWAY, A. G. HIGGINS, and C. A. LAWRENCE. J. Chem. Soc. **145**, 1224 (1934).
19. T. M. FLORENCE, Y. J. FARRER, and H. E. ZITTEL. Aust. J. Chem. **22**, 2321 (1969).
20. M. LILER. Reaction mechanisms in sulphuric acid. Academic Press, London. 1971.
21. J. G. CALVERT and J. N. PITTS, JR. Photochemistry. Wiley, NY. 1966.

Can. J. Chem. Downloaded from www.nrcresearchpress.com by 210.87.254.5 on 09/06/12
For personal use only.

La photolyse du cyclohexène gazeux à 184,9 nm

GUY J. COLLIN ET HÉLÈNE DESLAURIERS
Département des Sciences Fondamentales, Université du Québec à Chicoutimi, Chicoutimi (Qué.), Canada G7H 2B1

Reçu le 10 janvier 1983

GUY J. COLLIN et HÉLÈNE DESLAURIERS. Can. J. Chem. **61**, 1970 (1983).

La photolyse du cyclohexène gazeux a été systématiquement étudiée à 184,9 nm en l'absence ou en présence d'intercepteur radicalaire tel que O_2, NO, H_2S ou HI entre 1 et 70 Torr. En outre, le propane ou le soufre hexafluoré a été utilisé comme agent stabilisant. L'éthylène et le butadiène-1,3 ont été les seuls produits majeurs observés avec des rendements quantiques supérieurs à 0,5 quelles que soient les conditions expérimentales. Les analyses isotopiques de l'éthylène formé dans la photolyse du cyclohexène-3,3,6,6-d_4 montrent la présence prépondérante de la variété perhydrogénée. Ces résultats, avec d'autres observations tirées de la littérature, favorisent un mécanisme de fragmentation de la molécule excitée en une étape ou en deux étapes, mais dans ce cas via un intermédiaire dont le temps de vie est plus court que celui de la molécule photoexcitée.

GUY J. COLLIN and HÉLÈNE DESLAURIERS. Can. J. Chem. **61**, 1970 (1983).

We have studied the 184.9 nm photolysis of gaseous cyclohexene either in the absence or in the presence of radical scavengers such as O_2, NO, H_2S, or HI at pressures between 1 and 70 Torr. Propane or sulfur hexafluoride has also been used as stabilizing agent. In all cases, ethylene and 1,3-butadiene have rather high quantum yields ($\Phi \geq 0.5$). The isotopic analysis of the ethylene formed in the photolysis of cyclohexene-3,3,6,6-d_4 shows the high importance of the perhydrogenated species. These results, together with others taken from the literature, favor a one-step fragmentation mechanism or a double-step mechanism involving an intermediate which has a lifetime shorter than that of the photoexcited molecule.

Can. J. Chem. Downloaded from www.nrcresearchpress.com by 210.87.254.40 on 09/06/12
For personal use only.

Introduction

La photochimie du cyclohexène est relativement bien connue. Déjà en 1965, DeMaré *et al.* ont étudié la mercurisensibilisation de cet hydrocarbure à 254 nm (1). L'éthylène et le butadiène-1,3, en rendements similaires, sont les produits majeurs avec toutefois des quantités fort appréciables de vinylcyclobutane et de cyclohexane. L'augmentation de la pression a un effet négatif sur les rendements des deux hydrocarbures insaturés tandis que celui du vinylcyclobutane atteint un maximum à une pression de 5–10 Torr (665–1 330 N m^{-2}). Plus tard, Lesclaux *et al.* ont étudié la photolyse directe de cet hydrocarbure cyclique à 147, 123,6 et vers 105 nm en présence ou en l'absence de divers intercepteurs radicalaires (2). A 147 nm (8,4 eV) le système est relativement simple: hormis la formation de petites quantités d'hydrogène et de pentadiènes ($\Phi \leq 0{,}04$), les produits majeurs sont l'éthylène ($\Phi = 0{,}83$) et le butadiène-1,3 ($\Phi = 0{,}71$). Il ne semble pas que des radicaux stables soient formés en quantités appréciables sauf l'atome d'hydrogène qui a un rendement de l'ordre de 0,2 (2). Finalement, il apparaît que la photolyse du tétradeutérocyclohexène-3,3,6,6-d_4 forme principalement l'éthylène-d_0 et le butadiène-1,1,4,4-d_4.

[1] $\text{cyclo-}C_6H_{10} + h\nu \longrightarrow \text{cyclo-}C_6H_{10}^{**}$

[2] 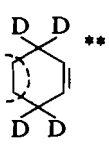 $\longrightarrow C_2H_4 + CD_2{=}CHCH{=}CD_2$

A plus courtes longueurs d'onde, 123,6 nm (10,0 eV) et 106,7–104,8 nm (11,6–11,8 eV) les mêmes processus semblent actifs, de façon prépondérante. Cependant l'augmentation de l'énergie du photon, et donc de celle de la molécule photoexcitée, favorise la fragmentation secondaire de l'éthylène et du butadiène, de telle sorte que le rapport $\Phi(C_2H_4)/\Phi(C_4H_6)$, qui est voisin de 1,2 à 147 nm, passe à 2,1 et à presque 4 à 123,6 et à 106,7–104,8 nm, respectivement (2). Il faut ajouter que l'apparition de paires d'ions – le potentiel d'ionisation du cyclohexène est de 8,94 eV (3) – vient compliquer l'interprétation quantitative relative à la fragmentation de la molécule photoexcitée.

A plus longue longueur d'onde, soit à 184,9 nm (6,4 eV), Inoue *et al.* ont également montré que les produits majeurs sont toujours l'éthylène et le butadiène-1,3 avec un rapport $\Phi'(C_2H_4)/\Phi'(C_4H_6)$ voisin de 1,05–1,10 (4). Bien que les rendements quantiques n'aient pas été mesurés, ils sont fortement affectés par l'augmentation de la pression: ils décroissent de moitié entre 5 et 30 Torr (650 et 4 000 N m^{-2}). Ces auteurs ont aussi observé la formation de mini-quantités de méthylènecyclopentane et de bicyclohexane[3.1.0] dont les rendements ne semblent pas affectés par l'augmentation de la pression (4). En phase liquide, ces deux isomères sont formés chacun avec des rendements quantiques de l'ordre de 0,06 (5).

Nous avons repris ce dernier travail avec bien entendu l'intention de le compléter en orientant nos efforts vers l'identification d'indices permettant d'apprécier à leur juste valeur, et s'ils existent, les processus d'isomérisation et de façon plus générale les comportements de la molécule photoexcitée.

Méthode expérimentale

Le cyclohexène est un produit "A.P.I." dont le contenu affiché en impuretés est de 0,023 ± 0,020 mol%. Aucune impureté couramment analysée par chromatographie en phase gazeuse à l'aide d'un double détecteur à ionisation de flamme, n'y est décelée. L'oxygène (99,99%) et l'oxyde nitrique (99,0%) sont des produits achetés chez Matheson du Canada. Le cyclohexène-3,3,6,6-d_4 a déjà été décrit (2). Les techniques photolytiques utilisées à 184,9 (6) et vers 163 nm (7), les actinométries (6, 8), les analyses chromatographiques (6, 8) de même que celles réalisées par spectrométrie de masse (2) ont toutes été décrites. Des analyses ont aussi été effectuées à l'aide d'une colonne de SE-30 afin de confirmer l'absence d'une éventuelle formation de vinylcyclobutane (1).

Résultats

a. *La formation des produits*

La photolyse à 184,9 nm du monomère pur, ou en présence

Can. J. Chem. Downloaded from www.nrcresearchpress.com by 210.87.254.40 on 09/06/12
For personal use only.

d'oxygène, d'oxyde nitrique, d'hydrogène sulfuré, d'isoprène ou d'iodure d'hydrogène, montre la présence d'éthylène et de butadiène-1,3 avec des rendements supérieurs à 0,5 quelle que soit la pression du cyclohexène entre 1 et 60 Torr (133–8 000 N m^{-2}). On observe en outre quelques produits supplémentaires avec des rendements mineurs. Il faut mentionner en présence d'iodure d'hydrogène: le méthane (Φ = 0,02), le propène (Φ = 0,01). En présence d'hydrogène sulfuré on observe, en outre, du cyclohexane: Φ = 0,12 et 0,07 à 2,5 et 30 Torr. Il faut enfin ajouter que tous les efforts réalisés en vue de mettre en évidence la formation éventuelle de composés isomères acycliques ou du vinylcyclobutane ont été vains, que ce soit en présence du cyclohexène pur ou en présence du propane ou de soufre hexafluoré à des pression de 400–500 Torr.

b. *L'effet de la pression à 184,9 nm*

La figure 1 montre la variation du rendement quantique de l'éthylène entre 10 et 70 Torr (1 330 et 9 300 N m^{-2}). Il faut tout de suite remarquer l'importance du rendement quantique un peu inférieur à l'unité à faible pression. Hormis une erreur systématique toujours possible, il est clair que la fragmentation de la molécule photoexcitée à cette longueur d'onde produit essentiellement de l'éthylène avec en contre partie du butadiène-1,3 (Fig. 2). Là encore existe un léger déficit en butadiène. L'addition de l'atome d'hydrogène sur la double liaison du monomère a déjà été signalée comme pouvant ajouter de l'éthylène (9). L'effet de la pression sur le rapport $\Phi(C_2H_4)/\Phi(C_4H_6)$ pourrait être alors expliqué sur la base de la stabilisation d'un intermédiaire:

$$[3]\quad H\cdot + \text{cyclo-}C_6H_{10} \xrightarrow{\text{cyclo-}C_6H_{11}^{\#}} C_2H_4 + C_4H_7' \qquad \Delta H = -15 \text{ kcal mol}^{-1}$$

$$[4]\quad C_4H_7' \rightarrow H\cdot + C_4H_6 \qquad \Delta H \cong 41 \text{ kcal mol}^{-1}$$

$$[5]\quad C_4H_7' \xrightarrow{(M)} C_4H_7\cdot$$

La réaction [4] étant endothermique, il est assuré que la réaction de stabilisation par collision, processus [5], lui fait une concurrence d'autant plus vive que la pression s'accroît. Il faut aussi ajouter que le butadiène-1,3 est plus sensible, réactif que l'éthylène vis-à-vis les radicaux usuels, de telle sorte qu'il peut aussi être consommé dans des réactions secondaires. Il faut finalement ajouter que la présence de quantités minimes de radicaux est révélée par la formation de méthane, de propène et de cyclohexane lorsque le monomère est photolysé en présence d'iodure d'hydrogène ou de sulfure d'hydrogène: (R = H·, CH_3·, ou C_3H_5')

$$[6]\quad R\cdot + HX \rightarrow RH + X \qquad (\text{où X = I ou HS})$$

c. *La photolyse du cyclohexène-3,3,6,6-d_4*

Le tableau 1 montre les analyses isotopiques de l'éthylène obtenu à diverses longueurs d'onde. Au fur et à mesure que celle-ci croît, l'éthylène perhydrogéné croît en importance en même temps que diminue celle de l'éthylène-d_2. Par contre, entre 147 et 184,9 nm, il semble y avoir un peu plus de C_2D_4 et de C_2D_3H. Il faut ajouter que l'addition signalée plus haut d'un atome d'hydrogène sur ce cyclohexène partiellement deutérié libère normalement une molécule d'éthylène-1,1-d_2 (9). Dans ce cas, la tendance observée dans ce tableau montre sans ambiguité possible la diminution de l'importance de ce produit avec l'allongement de la longueur d'onde.

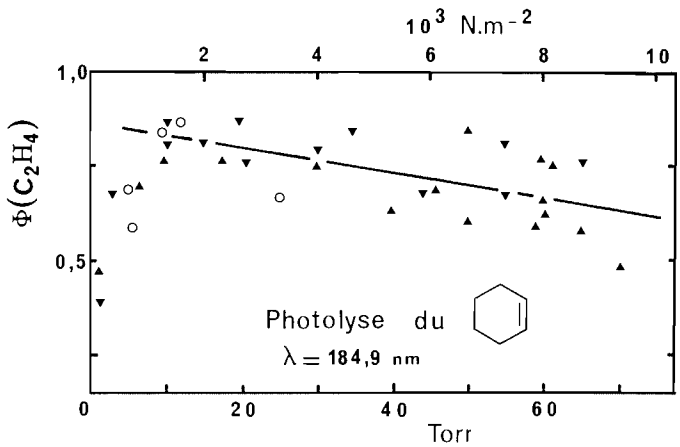

FIG. 1. Rendement quantique de l'éthylène en fonction de la pression du cyclohexène. ○: aucun additif; ▲: 10% O_2; ▼: 10% NO. Note: la décroissance du rendement quantique à des pressions inférieures à 10 Torr est liée à l'absorption partielle du faisceau photonique.

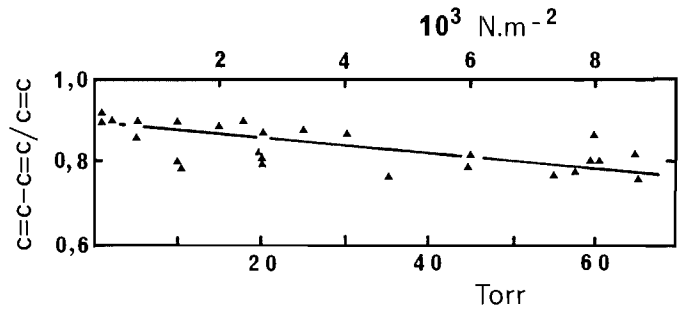

FIG. 2. Variation du rapport $\Phi(C_4H_6)/\Phi(C_2H_4)$ en fonction de la pression du cyclohexène.

Puisque le monomère contient 40% d'atomes d'hydrogène lourds, et sur la base où tous les atomes d'hydrogène seraient équivalents, l'éthylène formé devrait être constitué principalement des variétés -d_2 (43%) et -d_1 (38%). Il est évident que ce n'est pas le cas.

Discussion

La molécule, en absorbant un photon, est portée dans un état électronique, S_n. Le spectre d'absorption de la molécule n'est pas trop bavard et la nature de l'état électronique excité n'est pas évidente. La vibration d'élongation de la liaison C—C est cependant visible et le spectre présente certaines similarités avec celui du tétraméthyléthylène (10). La photochimie des alcènes acycliques en phase gazeuse a été, en général, expliquée sur la base de la rupture primaire de la liaison β(C—C) (11) et ce probablement à partir de l'état fondamental électronique vibrationnellement excité. Le mécanisme déjà proposé par ailleurs pour le cyclohexène met plus directement en cause les états électroniques S_1 et Rydberg (4, 5).

Mécanisme réactionnel

L'effet de pression est évidemment intéressant. S'il permet une estimation grossière du temps de vie d'un intermédiaire impliqué dans la formation de l'éthylène, il n'en indique pas la nature. Tous les efforts faits en vue de stabiliser un hydrocarbure acyclique en C_6 ou le vinylcyclobutane ont été vains. Cet échec est peut-être le résultat d'une pression de stabilisation insuffisante de la chambre expérimentale bien que d'autres études ont montré par ailleurs que, vers 60 Torr, la moitié des

TABLEAU 1. Photolyse du cyclohexène-3,3,6,6-d_4. Analyses isotopiques de l'éthylène

λ (nm)	Pression (Torr)	C_2D_4	C_2D_3H	$C_2D_2H_2$	C_2DH_3	C_2H_4
106,7–104,8[a]	1	4,1	5,4	29,3	0,5	54,0
	28	2,0	3,0	28,3	5,3	61,5
123,6[a]	1	1,9	2,4	17,3	1,5	76,8
	5	<0,8	1,0	13,4	1,1	83,7
147[a]	1			12,7	1,5	85,8
	5			12,9	1,1	86,0
	25			12,0	0,4	87,6
163,3	25	<0,35	≤0,35	8,1	0,5	90,7
184,9	10	3,6	<1,8	6,5	2,0	85,0
	25	n.d.[b]	3,0	5,5	2,0	89,5

[a]Tiré de la réf. 2.
[b]Non déterminé.

molécules hexène-1 (C_6H_{12}), dans l'état fondamental vibrationnellement excité à 184,9 nm, devraient être stabilisées par collision.[1] Cette pression est de l'ordre de 1 500 Torr dans le cas du pentène-1 (C_5H_{10}). Cet échec peut être aussi le résultat des propriétés physiques associées du ou des états électroniques de la molécule photoexcitées.

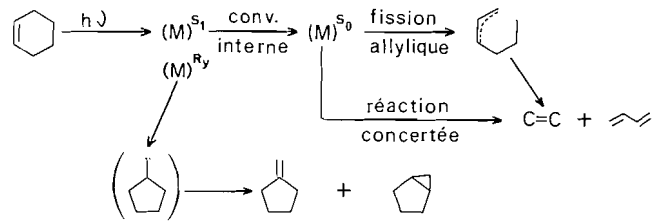

Mécanisme Réactionnel

La décomposition thermique du cyclohexène a été, elle aussi, étudiée par plusieurs laboratoires. La constante de vitesse du processus 2 – en système thermique – est telle que log $k_2 = 15{,}3 - 66900/RT$ (9) ou $14{,}93 - 65200/RT$ (12). L'énergie d'activation et le facteur de fréquence sont plus faibles que ceux observés dans le cas des ruptures de liaisons β(C—C) (13). Cette remarque a déjà été faite ailleurs (14) de telle sorte que l'éthylène et le butadiène-1,3 sont le résultat d'une fragmentation concertée du cyclohexène telle que cela a été calculé théoriquement (15) plutôt qu'en deux étapes. C'est donc une fragmentation de type rétro-Diels–Alder (16) permise selon les règles de conservation de symétrie des orbitales de Woodward et Hoffmann (17). Il est pertinent de rappeler ici que la mercurisensibilisation semble générer plutôt un mécanisme en deux étapes puisque vinylcyclobutane, qui y est observé, est le résultat de la cyclisation de l'intermédiaire radicalaire n-propylallyle.

[1] J. Gawłowski et G. J. Collin. J. Photochem. Accepté pour publication.

Remerciements

Nous voudrions remercier le ministère des Affaires Intergouvernementales du Québec (Coopération belgo-québécoise) qui a permis des échanges fructueux avec monsieur G. DeMaré (Université Libre de Bruxelles) dont le concours a été vivement apprécié. La généreuse hospitalité de monsieur P. Ausloos (NBS, Washington) a aussi contribué à enrichir cette étude.

1. G. R. DeMaré, O. P. Strausz et H. E. Gunning. Can. J. Chem. **43**, 1329 (1965).
2. R. Lesclaux, S. Searles, L. W. Sieck et P. Ausloos. J. Chem. Phys. **53**, 336 (1970).
3. D. A. Demeo et M. A. El-Sayed. J. Chem. Phys. **52**, 2622 (1970).
4. Y. Inoue, S. Takamuku et H. Sakurai. J. Chem. Soc. Perkin Trans. 2, 1635 (1977).
5. R. Srinivasan et K. H. Brown. J. Am. Chem. Soc. **100**, 4602 (1978).
6. G. J. Collin, H. Deslauriers et A. Więckowski. J. Phys. Chem. **85**, 944 (1981).
7. A. Więckowski et G. J. Collin. Can. J. Chem. **56**, 1435 (1978).
8. G. J. Collin, H. Deslauriers et B. Simard. J. Photochem. **21**, 19 (1983).
9. W. Tsang. Int. J. Chem. Kinet. **2**, 311 (1970).
10. D. F. Evans. Proc. Chem. Soc. 378 (1963).
11. G. J. Collin, H. Deslauriers et S. Auclair. Can. J. Chem. **57**, 863 (1979).
12. D. C. Tardy, R. Ireton et A. S. Gordon. J. Am. Chem. Soc. **101**, 1508 (1979).
13. A. B. Trenwith. Int. J. Chem. Kinet. **5**, 67 (1973).
14. S. W. Benson. *Dans* Thermochemical kinetics. 2e ed. J. Wiley & Sons, New York. 1976. pp. 108–114 et 140.
15. R. E. Townshend, G. Ramunni, G. Segal, W. J. Hehre et L. Salem. J. Am. Chem. Soc. **98**, 2190 (1976).
16. J. A. Barltrop et J. D. Coyle. *Dans* Principles of photochemistry. J. Wiley & Sons, New York. 1978. pp. 164–169.
17. R. B. Woodward et R. Hoffmann. *Dans* The conservation of orbital symmetry. Verlag Chemie, Weinheim. 1970.

Can. J. Chem. Downloaded from www.nrcresearchpress.com by 210.87.254.40 on 09/06/12
For personal use only.

Lanostane-to-cucurbitane transformation[1,2]

O. E. EDWARDS AND Z. PARYZEK[3]

Division of Chemistry, National Research Council of Canada, Ottawa, Ont., Canada K1A 0R6

Received February 22, 1983

O. E. EDWARDS and Z. PARYZEK. Can. J. Chem. **61**, 1973 (1983).

Westphalen-type rearrangement of a 9α-hydroxy-11-ketone derived from lanosterol resulted in formation of two 19(10 → 9β)*abeo*-lanostenes representing the first lanostane-to-cucurbitane transformation. A novel ring A aromatic 9,10-seco derivative was formed as an acid catalysed cleavage product of 11-keto cucurbitenes. A cine 9 → 12 substitution led to the first 12-substituted lanostane derivatives and the first C-nor-D-homolanostane derivatives.

O. E. EDWARDS et Z. PARYZEK. Can. J. Chem. **61**, 1973 (1983).

Une transposition du type Westphalen de l'hydroxy-9α cétone-11 provenant du lanostérol conduit à la formation de deux *abeo*-lanostènes 19(10 → 9β) qui représentent la première transformation du lanostane en cucurbitane. Le clivage, catalysé par un acide, des céto-11 curcurbitènes permet d'obtenir un nouveau cycle aromatique A le dérivé séco-9,10. Une substitution du type cine 9 → 12 conduit au premier dérivé du lanostane substitué en position 12 et au premier dérivé du C-nor-D homolanostane.

[Traduit par le journal]

Can. J. Chem. Downloaded from www.nrcresearchpress.com by 210.87.254.6 on 09/06/12
For personal use only.

Our long-standing interest in the behaviour of α-keto carbenium ions (1–3) led us to study the deamination of steroidal α-aminoketones (4). However, attempts to prepare 9α-amino-11-keto lanostane derivatives failed (5). An alternative method of generating tertiary α-keto carbenium ions appeared to be the Westphalen-type (6) dehydration (sulfuric acid in acetic acid – acetic anhydride) of the tertiary α-ketols. (Numerous studies have been made of the steric and electronic factors influencing the molecular rearrangements that usually accompany the dehydrations resulting from the use of these reagents (*7a–d*).)

Because of our hope of efficiently preparing cucurbitanes (19(10 → 9 β)*abeo*-lanostanes) and/or cycloartanes (9,19-cyclo-lanostanes) we chose to examine the behaviour under Westphalen conditions of 3β-acetoxy-9α-hydroxylanostanes with either a carbonyl or acetoxy group on C-11. A preliminary account of this work has been published (8).

The desired substrates were prepared from dihydrolanosterol by way of 3β-acetoxy-5α-lanost-9(11)-ene (**1**) (9). Hydroxylation of the double bond of **1** using osmium tetroxide in pyridine afforded the 3β-acetoxy-9α,11α-diol **2**. Acetylation of **2** gave 3β,11β-diacetoxy-5α-lanostan-9α-ol (**3**). Dehydration of **3** using thionyl chloride – collidine in chloroform gave the known 3β-acetoxy-5α-lanostan-7,9(11)-diene (10).

Oxidation of **2** using Jones' reagent gave only 32% of the desired ketol **4**. However, oxidation of **2** under Pfitzner–Moffatt conditions (11) as modified by Turnbull *et al.* (12) gave **4** (3β-acetoxy-9α-hydroxy-5α-lanostan-11-one) in 69% yield. Its structure was confirmed by dehydration using thionyl chloride – pyridine to the known 3β-acetoxy-5α-lanost-8-en-11-one (13). Since our preliminary report (8), Lawrie *et al.* have described compounds **2** and **4** with spectra corresponding to those of our specimens (14).

In contrast to the above oxidations of **2**, chromium trioxide in acetic acid converted it into an acid in 89% yield. This gave a methyl ester with ν_{max}: 1728 and 1708 cm^{-1}. The ^{13}C nmr spectrum of the acid confirmed the presence of a ketone carbonyl (215.5 ppm) as well as the carboxyl group (178.6 ppm)

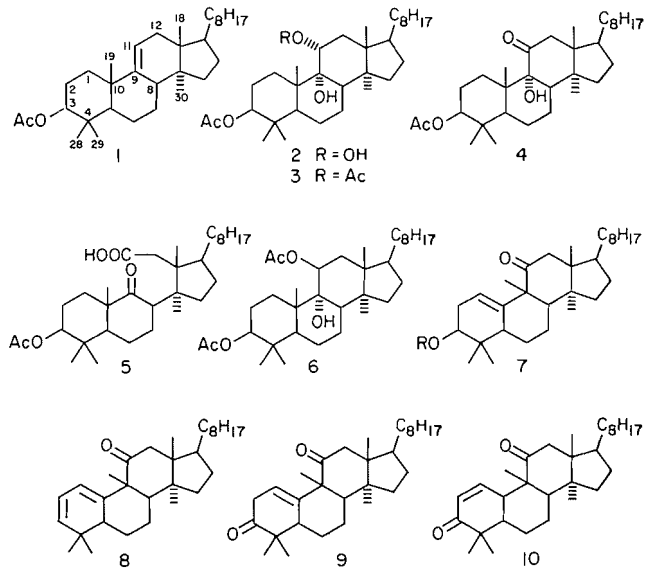

and 3-acetoxy group (171.8 ppm). This evidence, and its analysis and mass spectrum, confirmed that it was 3β-acetoxy-9-oxo-9,11-seco-5α-lanostan-11-oic acid (**5**).

Reduction of the ketone carbonyl of **4** with sodium borohydride, followed by acetylation using acetyl chloride-*N*,*N*-dimethylaniline in dichloromethane (15) gave 3β,11β-diacetoxy-5α-lanostan-9α-ol (**6**).

Westphalen dehydration of ketol **4** gave a complex mixture containing some sulfur. Three products, designated for discussion as A, B, and C, were isolated in a pure state by repeated chromatography in yields of 21, 14 and 39%, respectively.

Compound A analysed for $C_{32}H_{53}O_3$ and had ν_{max}: 1225 and 1685 cm^{-1}. Its ^{1}H nmr spectrum had signals due to an olefinic proton at δ 5.14 and the 3-hydrogen at δ 4.54. Hydrolysis of A gave the 3-hydroxy compound, which was converted to the tosylate. Elimination of *p*-toluene sulfonic acid was effected using potassium *tert*-butoxide in dimethyl sulfoxide at 75°C under argon. The resultant diene still contained the isolated carbonyl group (λ_{max}: 1695 cm^{-1}) and had ultraviolet absorption (ν_{max}: 270 nm, ε 6450) showing it to be a homoannular diene. Its ^{1}H nmr spectrum had a 3-hydrogen multiplet at δ 5.5. Thus structure **7** (R = Ac) (3β-acetoxy-19(10 → 9β)*abeo*-

[1]Issued as NRCC No. 21160.

[2]Presented in part at the Annual Conference, The Chemical Institute of Canada, Ottawa, June 1980.

[3]NRCC postdoctoral fellow. Present address, Institute of Chemistry, A. Mickiewicz University of Poznan, Poland.

Can. J. Chem. Downloaded from www.nrcresearchpress.com by 210.87.254.6 on 09/06/12
For personal use only.

11-oxo-lanost-1,(10)-ene) seemed certain for A and 19(10 → 9β)*abeo*-11-oxo-lanosta-1(10),2-diene (**8**) for the diene. Confirmation of the structure came from the action of potassium hydroxide in ethanol on the 3-ketone (**9**) derived from A. A mixture rich in the conjugated ketone **10** with λ_{max}: 229 nm (ε 7000) was formed. However, pure **10** could not be obtained by chromatography. Oxidation of ketone **9** with selenium dioxide in dioxane gave a crystalline yellow selenium-containing compound with ν_{max}: 1690 and 1646 cm^{-1}

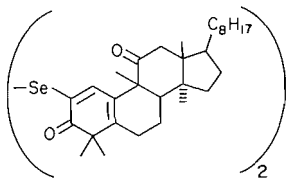

11

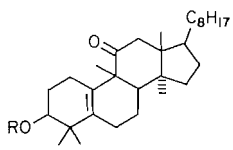

12 R = Ac
13 R = H

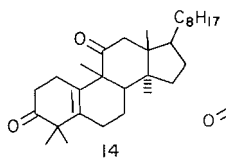

14

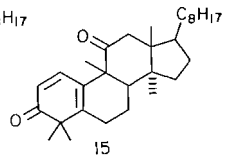

15

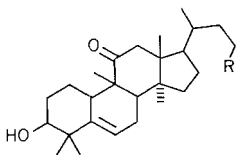

16 R = -CHOH-COH(CH3)2
17 R = -CO-CH(CH3)2
18 R = -C(=N-NHTs)-CH(CH3)2

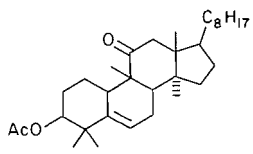

19

and λ_{max}: 270 nm (ε 12 000). It gave a one-hydrogen signal at δ 7.15. Its analysis and molecular weight were consistent with structure **11**. However, its mass spectrum gave only ions resulting from loss of selenium. Comparable diselenides have been reported previously (16). Finally, a double irradiation experiment showed that the vinyl hydrogen of **9** was coupled with a methylene group resonating at δ 2.82.

Compound B was also an unsaturated ketone isomeric with A. Alkaline hydrolysis of B gave a hydroxy ketone which was still unconjugated. Jones' oxidation of this gave a non-conjugated diketone (ν_{max}: 1713 and 1693 cm^{-1}). Its rather intense $n-\pi^*$ absorption (λ_{max}: 293 nm, ε 150) was consistent with it being the β,γ unsaturated ketone **14** (17). Thus B appeared to be 3β-acetoxy-19(10 → 9β)*abeo*-11-oxolanostan-5(10)ene (**12**) and the corresponding alcohol was **13**. Interrelation of A and B was achieved by selenium dioxide oxidation of the derived diketone **14**. A minor product was the diselenide **11** previously obtained from A. The major product was an amorphous dienone. This had ν_{max}: 1690, 1660, and 1625 cm^{-1}, and λ_{max}: 325 nm (ε 4800). The ultraviolet absorption was consistent with structure **15**, 3,11-dioxo-19(10 → 9β)-*abeo*-5α-lanosta-1,5(10)-diene (18), as was the presence of two low field ^1H nmr signals at δ 7.00 and 5.96 (doublets, J = 11 Hz). The intense cd maxima at 300 nm (ε 4.65 and 7.5, respectively) shown by A and B were also characteristic of 11-keto cucurbitanes (19), reinforcing the above structural conclusions.

Final proof of structure of A and B came from interrelation with the cucurbitacins bryodulcosigenin **16** (20) and bryogenin **17** (19) from *Bryonia alba* (20).[4] The 24-carbonyl of bryogenin was removed in two ways, by cyanoborohydride reduction (21) of its 24-tosylhydrazone (**18**) or by Wolff–Kishner reduction of the 24-semicarbazone. The resulting 24-deoxybryogenin was purified as its beautifully crystalline acetate **19** but the alcohol could not be obtained crystalline. The acetate **19** was heated with a solution of anhydrous *p*-toluenesulfonic acid in benzene. A minor product was a conjugated diene (see Discussion). The main product (60% yield) had intense end absorption in the ultraviolet, λ_{max}: 263 (ε 110) and 271 nm (ε 70) and ν_{max}: 1692 cm^{-1}. It thus appeared to be an aromatic compound with the 11-ketone intact. Its ^1H nmr spectrum contained a three hydrogen signal at δ 7.05, a two hydrogen triplet at δ 2.71 (benzylic hydrogens), and two methyl singlets at δ 2.30 and 2.24. Successive additions of $Eu(dpm)_3$ caused a methyl doublet and a broad 1H singlet to move rapidly downfield. In addition, a two hydrogen singlet attributable to the 12-hydrogens moved rapidly downfield and became a quartet with J = 16 Hz. Its ^{13}C nmr spectrum showed the presence of three substituted and three unsubstituted aromatic carbons. Thus the aromatic compound unequivocally had structure **20**.

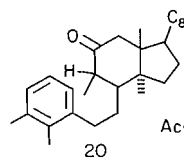

20

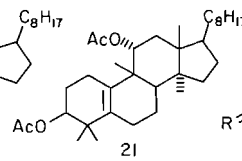

21

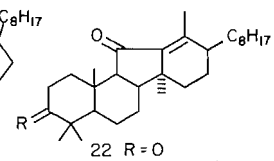

22 R = O
23 R = H, 3β-OH

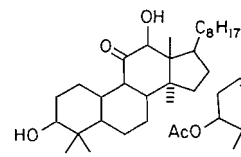

24

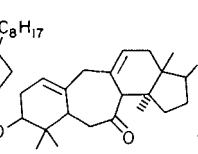

25

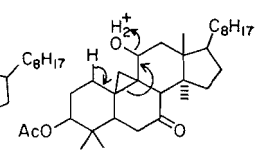

26

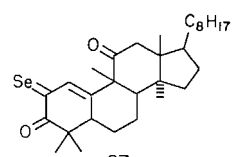

27

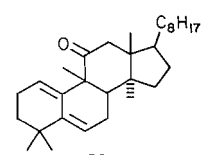

28

The same treatment of compound B gave a 19% yield of the identical aromatic compound, confirming the structures **12** and **7** assigned to it and to A.

Product C proved to be the known 3β,-11-diacetoxy-5α-lanosta-7,9(11)-diene (13*b*) which could be hydrolysed with alkali to 3β-hydroxy-5α-lanost-8-ene-11-one.

The action of sulfuric acid in acetic anhydride on ketol **4** gave similar results to those using the acetic acid–anhydride mixture. Compounds A, B, and C were isolated in 19, 13, and 27% yields, respectively.

Treatment of the 11α-acetoxy-9α-hydroxy compound **3** under Westphalen conditions gave a crude product containing 6% sulfur. From the mixture, 11% of starting material, 25% of 3β-acetoxy-5α-lanosta-7,9(11)-diene, and 14% of an unknown product were obtained. The spectral characteristics of the unknown suggested that it had structure **21**, 3β,11α-

[4]Roots supplied as *Bryonia Alba* by the S. B. Penick Co. contained glyosides yielding these two aglycones. Unpublished work with J. P. Devlin and J. W. Elder.

Can. J. Chem. Downloaded from www.nrcresearchpress.com by 210.87.254.6 on 09/06/12
For personal use only.

diacetoxy-19(10 → 9β)*abeo*-lanost-5(10)-ene. This was confirmed by hydrolysis to the diol, then Jones' oxidation to a dione which had ir and nmr spectra identical to those of dione **14** prepared earlier from compound B (**12**).

The attempted Westphalen dehydration of the 3β,11β-diacetoxy-9α-hydroxy compound **6** gave a complex mixture which was not further investigated.

In the course of studying other conditions for dehydrating ketol **4**, it was heated in benzene with *p*-toluenesulfonic acid hydrate. Neither simple elimination of water nor dehydration with migration of C-19 ensued. Instead, a mixture was produced which, after hydrolysis, could be separated into two main products. The major product (43%) had infrared absorption at 1695 and 1620 cm^{-1} and an ultraviolet maximum at 255 nm (ε 14 000). Its ^1H nmr spectrum had a 3H singlet at δ 2.08 consistent with the presence of a β-methyl group on an α,β-unsaturated ketone. Jones' reagent oxidized the compound to a diketone with ν_{max}: 1695 cm^{-1} (increased intensity) and 1620 cm^{-1}. This evidence indicates the structure of the diketone to be 3,11-dioxo-C-nor-D-homolanostan-12-ene (**22**) and hence that of the original hydrolysis product to be **23**. The minor product was a keto alcohol (ν_{max}: 3615, 3435, and 1705 cm^{-1}). A 12-hydroxy-11-ketone system was indicated by a ^1H nmr doublet at δ 4.27 (J = 8 Hz) and ^{13}C nmr signals at 214 and 72.4 ppm, in addition to the signals at δ 3.25 and 78.5 ppm due to C-3. The equatorial nature of the 12-hydroxyl group of the ketol was probable since its ultraviolet maximum was at 277 nm with ε 87 (22). The compound could be oxidized to a trione which enolized in alkali (λ_{max}: 283 nm, ε 290, shifted to λ_{max}: 330 nm, ε 3600 at high pH). Thus the structure of the ketol was 3β,12β-dihydroxy-5α-lanostane-11-one (**24**).

Discussion

Although prior to the present work, methyl migration to give 19(10 → 9β)*abeo* steroids had been observed during deamination of 9α-amino compounds (4, 23) and Lewis acid catalysed opening of 9α,11α-epoxides (24, 25), attempts to obtain the same migration in lanosterol analogues had failed (24*b*, 26). Thus the formation of **7** and **12** was the first successful production of cucurbitanes from lanostanes. Since then, superior yields of cucurbitanes were obtained by methyl migration following boron trifluoride catalysed opening of 3β-acetoxy-9β,11β-epoxylanostan-7-one by Paryzek and co-workers (27) and by Baddeley and Simes and their co-workers (28). This led to the first preparation of a true cucurbitacin (24-deoxybryogenin) (27).

Evidence for the nature of the carbocations involved in these rearrangements exists. At one extreme, the deamination of α-amino ketones and diazo ketones (2), and probably Westphalen dehydration of β-fluoro alcohols (29), the cation formation is slow and there is high retention of steric identity. This is consistent with σ-bond involvement during, or very rapidly after, cation formation. The Westphalen dehydration of tertiary alcohols with less electronegative β groups (e.g. acetoxy) has been shown to lead to tight ion pairs (30). The counter-ion location determines the stereochemistry of resulting steps. However, the epoxide opening in acetic anhydride catalysed by boron trifluoride seems to lead to a nearly planar cation, since migration of methyl groups *cis* to the epoxide can be a major event (27, 28).

Of the reactions open to a cationic center at C-9 with an 11-carbonyl, the migration of the 10-methyl group and loss or migration of the 8β-hydrogen are the most probable events. In the case of the 11α-acetoxy compound **3**, the additional possibility of loss of the 11β-hydrogen exists. The methyl migration is competitive with these hydrogen involvements, partly because of repulsive interaction between the 4β-methyl group and the 10-methyl group which is relieved as migration starts, and partly because proton loss from carbon carrying an acetoxy group appears to be disfavored (29–31).

Although the 10-methyl migration must pass through a transition state or intermediate resembling a corner-protonated cyclopropane, no evidence has been found for the formation of 9,19-cyclo compounds (cycloartanes) in the deamination or Westphalen dehydration studies. However, in the prolonged reaction at 10°C in the epoxide opening work of Baddeley *et al.* (28), the ring B expanded compound **25** was formed. This probably arose from a cycloartane (see **26**) formed by acid catalysed cyclization of the 19(10 → 9 β)*abeo* olefins.

Although they were probably formed, no products of backbone migration of the 9-hydrogen and 13- and 14-methyl groups were identified in this work.

In interesting contrast to the Westphalen-type dehydration of ketol **4**, the action of *p*-toluenesulfonic acid hydrate in hot benzene resulted in formal migration of the cationic center from C-9 to C-12. The products arising from this were the C-nor-D-homo compound **23** and the 12β-hydroxy-11-ketone **24**. A likely mechanism for the ciné substitution (32) is shown in eq. [1]. The C-nor-D-homo rearrangement is characteristic of a 12β leaving group (4, 33), suggesting that the 12β-hydroxy compound is an intermediate in the formation of **23**. This appears to be the first report of formation of a C-nor-D-homo compound in the lanostane series.

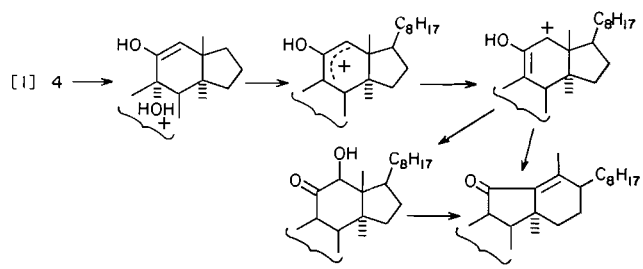

The selenium dioxide oxidation of **9** and **14** has its parallel in steroid chemistry (16). It seems likely that a seleno-ketone **27** is an intermediate. Air oxidation of its enol could give the dimer (eq. [2]).

One of the most interesting reactions encountered in this work was the aromatization of ring A resulting when olefin **12** or 24-deoxybryogenin acetate were treated with anhydrous *p*-toluenesulfonic acid in refluxing benzene. The main product **20** probably arose by the sequence shown in eq. [3]. The forma-

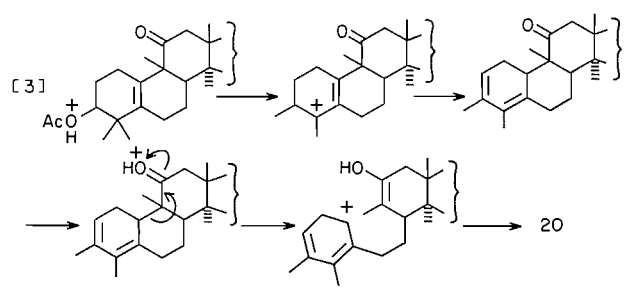

Can. J. Chem. Downloaded from www.nrcresearchpress.com by 210.87.254.6 on 09/06/12
For personal use only.

tion of an alkylic cation from an isolated carbocation, and the aromatization, provide obvious driving force for the sequence of events. A second product from 24-deoxybryogenin was a conjugated diene with λ_{max}: 242 nm. This, the absence of the 3-acetoxy group, and the presence of the 11-carbonyl and two vinyl hydrogens, make it probable that its structure was **28**, formed by elimination of acetic acid followed by double bond migration. This diene position seems specially favored for the cucurbitane skeleton (34).

The failure of the 11β-acetoxy-9α-ol **6** to give appreciable quantities of the C-19 migrated products can be attributed to the bulk of the 11-acetoxy group which opposes the movement of the methyl group toward C-9. If this is correct, the complexed 11β oxygen in the probably more planar cation arising by opening of the 9β,11β-oxide (27, 28) must have much less repulsive interaction with C-19. The methyl migration in the α-ketols is probably closer to a synchronous process because of the higher energy required to ionize the C—O bond (2, 7*c*).

Experimental

Unless otherwise stated, infrared spectra and rotations were for chloroform solutions, ultraviolet spectra for 95% ethanol solutions, and nmr spectra for deuteriochloroform solutions. Preparative tlc was done on 1000 μ SiO_2 plates with fluorescent indicator. Proton nmr spectra were obtained on a Varian EM-360 spectrometer (60 MHz) and ^{13}C spectra on Varian CFT-20 and Brüker WP-80 spectrometers. Mass spectra were produced by electron impact unless otherwise stated.

3β-Acetoxy-9α,11α-dihydroxy-5α-lanostane 2

A solution of 3.5 g of the 9,11 olefin **1** (9) and 1.5 g of osmium tetroxide in 50 mL of pyridine was stirred under nitrogen at room temperature for 15 h. An additional 0.5 g of osmium tetroxide was added, then the mixture left for 50 h. Saturated sodium hydrosulfite solution was added, then the products extracted into benzene. The benzene layers were washed with dilute hydrochloric acid, water, dilute sodium carbonate solution, water, then dried over magnesium sulfate. The 3.98 g of product recovered from the benzene crystallized from n-heptane, giving 3.45 g (92%) of the 9α,11α-diol **2**. This was recrystallized from methanol giving needles, mp 162−164°C. Since our communication (8), this has also been described by Lawrie *et al.* (14) as having mp 164.5−165.5°C. Our ir and ^1H nmr spectra accord with those reported.

3β,11α-Diacetoxy-9α-hydroxy-5α-lanostane 3

A solution of 601 mg of 9α,11α-diol **2** in 5 mL of pyridine and 2 mL of acetic anhydride was left at room temperature for two days. The reagents were removed under reduced pressure, the product dissolved in benzene, then this solution was washed with dilute acid and sodium carbonate solution. The 702 mg of crude product crystallized from methanol giving 642 mg of 3,11-diacetate **3** with mp 76−78°C. It had ν_{max}: 3580, 1725, 1260, and 1025 cm^{-1}. Its ^1H nmr spectrum gave signals at δ: 5.40 (1H, dd, J = 10 and 6.5 Hz), 4.47 (1H br t), and 2.04 (6H, singlet). *Anal.* calcd. for $C_{34}H_{58}O_5$: C 74.68, H 10.69; found: C 74.84, H 10.72.

Reaction of 3 with thionyl chloride − collidine

An ice-cold solution of 78 mg of 3β,11α-diacetoxy-9α-hydroxylanostane **3** and 0.3 mL of s-collidine in 0.3 mL of dry, ethanol-free chloroform was prepared. After addition of 0.1 mL of thionyl chloride the mixture was left at 0°C for 25 min. Ice water was then added, the products extracted into benzene, the benzene layers washed with water, dilute hydrochloric acid, then dilute sodium carbonate solution. The benzene contained 63 mg of crystalline product, which was purified on a 1000 μ silica gel plate using 5:1 benzene − ethyl acetate for development. The main zone gave 44 mg of 3β-acetoxy-5α-lanosta-7,9(11)-diene. After crystallization from acetone−dichloromethane, it had mp 163−166°C (lit. (10) mp 167−169°C). Its ir, uv, and ^1H nmr spectra were in accord with those reported.

3β-Acetoxy-9α-hydroxy-5α-lanostan-11-one 4

(a) *With DCC−DMSO − dichloroacetic acid (12)*

A solution containing 2.32 g of the diol **2**, 2.85 g of dicyclohexylcarbodiimide, 0.313 mL of dichloroacetic acid, and 10 mL of dimethylsulfoxide (added last) was left at room temperature for 5.5 h. A solution of 2.5 g of oxalic acid dihydrate in 2 mL of methanol was added. After a further 6 h, 20 mL of water was added, then the product extracted into benzene. The organic layers were washed with 5% potassium carbonate solution, then water, and dried over magnesium sulfate. The benzene solutions gave an oil which crystallized from aqueous acetone giving 1.61 g of ketol **4** which had mp 183−185°C. This has since been described by Lawrie *et al.* (14). Its ir and ^1H nmr spectra accord with those reported. Its ^{13}C nmr spectrum had signals at δ: 210.4, 171.0, 80.5, and 80.2, and its mass spectrum gave ions with m/e: 502 (M^+), 484, 442, 424, 319, 306, 293, and 137.

(b) *With Jones' reagent*

One mL of Jones' reagent (35) was added dropwise to a stirred solution of 504 mg of acetoxy diol **2** in 30 mL of acetone. Excess reagent was destroyed using 2-propanol. The acetone solution was decanted, then evaporated. The products were distributed between benzene−ether mixture and water. The organic layers gave 422 mg of light green oil. A hexane solution of this was filtered through 5.5 g of alumina (Act. III). The eluate was chromatographed on 20 g of neutral alumina (Act. III). Benzene eluted 151 mg of ketol **4** whose physical properties were the same as those described above.

The structure of the ketol **4** was firmly established by dehydration using thionyl chloride in pyridine at room temperature to give 3β-acetoxy-5α-lanost-8-en-11-one, mp 127−130°C (lit. (13) mp 130−132°C). Its ir and uv spectra agreed with the literature. Its ^1H nmr spectrum had signals at δ: 4.62 (1H, t), 2.09 (1H, s), 1.17, 1.15, 0.93, and 0.84 (methyl signals).

3β,11β-Diacetoxy-5α-lanostan-9α-ol (6)

Sodium borohydride (392 mg) was added gradually over 45 min to a refluxing solution of 512 mg of acetoxy ketol **4** in 20 mL of methanol under nitrogen. The products were distributed between benzene and water, giving 521 mg of crystalline reduction products. This was dissolved in 5 mL of dichloromethane and 2.15 mL of dimethylaniline. The solution was cooled to 0°C, then 1 mL of acetyl chloride in 5 mL of dichloromethane was added dropwise. After 21 h the mixture was added to an ethyl ether − water mixture. The organic layer was washed successively with sodium carbonate solution, dilute hydrochloric acid, then sodium bicarbonate solution. The crude product crystallized from ethanol giving the diacetate **6** with mp 178.5 − 180.5°C. It had ν_{max}: 3640, 3500, 1730, 1260, and 1030 cm^{-1} and gave ^1H nmr signals at δ: 4.96 (1H, br s), 4.56 (1H, m), 2.07 (6H, s), 1.26, 0.97, 0.93, and 0.83 (methyl signals). *Anal.* calcd. for $C_{34}H_{58}O_5$: C 74.68, H 10.69; found: C 74.62, H 10.95.

3β-Acetoxy-9-oxo-9,11-seco-5α-lanostan-12-oic acid (5)

The diol **2** (204 mg) was added to a solution of 210 mg of chromium trioxide in 10 mL of 95% acetic acid. After 25 min at room temperature, the mixture was diluted with water and the product extracted into benzene. Although the benzene layers were washed with sodium carbonate solution, the 187 mg of crude product was rich in acid, crystallizing from aqueous ethanol to give 141 mg of keto acid **5**, mp 159−162°C. It had ν_{max}: 3510, 3400−2400, 1725, 1705, and 1253 cm^{-1}. It gave ^1H nmr signals (100 MHz) at δ: 4.46 (1H, m), 2.84 and 2.48 (two 1H doublets, J = 14 Hz), 2.02 (3H, s), 1.21, 1.0, 0.95, 0.88, and 0.81 (methyl signals) and ^{13}C nmr signals at δ: 215.5, 178.6, 171.8, and 81.0 ppm. Its mass spectrum had peaks at m/e: 518 (M^+), 472, 440, 387, 363, 319, 252, and 207. *Anal.* calcd. for $C_{32}H_{54}O_5$: C 74.09, H 10.49; found: C 74.19, H 10.49.

A comparable yield of the keto acid was obtained by oxidation of the diol **2** using chromium trioxide − pyridine in dichloromethane at room temperature.

Can. J. Chem. Downloaded from www.nrcresearchpress.com by 210.87.254.6 on 09/06/12
For personal use only.

Methyl 3β-acetoxy-9-oxo-9,11-seco-5α-lanostan-12-oic acid

An ether solution of 100 mg of the keto acid **5** was treated with excess diazomethane in ether. After 10 min, the excess reagent was destroyed with acetic acid. The crude ester crystallized from aqueous ethanol, giving 73 mg with mp 89–91°C. It had ν_{max}: (CH_2Cl_2): 1728, 1708, and 1243 cm^{-1} and gave ^1H nmr signals at δ: 4.56 (1H, m), 3.70 (3H, s), 2.92 and 2.54 (pair of 1H doublets, J = 14 Hz superimposed on a broad 1H singlet), 1.29, 1.13, 0.99, 0.93, 0.88, and 0.83 (methyl signals) and ^{13}C nmr signals at δ: 214.6, 174.3, 170.5, 79.9, and 54.8. It gave *m/e*: 532 (M^+), 517, 500, 472, 387, 377, and 279. *Anal.* calcd. for $C_{33}H_{56}O_5$: C 74.39, H 10.59; found: C 74.18, H 10.32.

Westphalen dehydration of ketol (4) in acetic acid – acetic anhydride

A solution of 41 mg of concentrated sulfuric acid in 9 mL of acetic anhydride and 18 mL of acetic acid was added at room temperature to 911 mg of ketol (**4**). The mixture was agitated until the solid had dissolved (1 min), then left at room temperature for 2 h. The solution was then poured onto crushed ice. After one hour the products were extracted into pentane. The pentane layer and washings were extracted with water, then with dilute aqueous sodium hydroxide, giving 822 mg of gum. This still contained 1.58% of sulfur.

The product was absorbed from dichloromethane onto 60 g of tlc silica gel, and eluted with the same solvent. Following 20 mg of unidentified material, fractions yielding 192 mg of pure compound A or mixtures rich in this compound were eluted. The next 107 mg of eluate also contained considerable A. This was followed by mixtures of B with compound C, then C alone. Methanol in dichloromethane eluted more C. The early fractions crystallized from methanol. The mother liquors were repeatedly separated on silica gel plates using dichloromethane or 10% ethyl acetate in benzene for development. In this way 183 mg (21%) of compound A with structure (**7**) was obtained.

Compound B was separated from C by repeated purification on silica gel plates using 10% ethyl acetate in benzene as developing solvent. Finally 124 mg (14%) of compound B, to which structure (**12**) was assigned, was obtained pure. Compound C was the major product (39%). Its ir and uv spectra were in accord with the data reported for 3β,11-diacetoxy-5α-lanosta-7,9(11)-diene (13*b*) and its ^1H nmr spectrum showed signals at δ: 5.60 (1H, br t, J = 5 Hz), 4.51 (1H, br t, J = 7 Hz), 2.12, and 2.03 (2–3H, s). Alkaline hydrolysis of this compound in methanolic potassium hydroxide gave 3β-hydroxy-5α-lanost-8-en-11-one with mp 163–164°C, whose spectral properties were in accord with those reported (13).

Action of acetic anhydride – sulfuric acid on ketol 4

To a stirred solution of 222 mg of ketol **4** in 12 mL of acetic anhydride at 80°C was added dropwise a solution of 0.1 g of sulfuric acid in 0.45 mL of acetic anhydride. The reaction mixture was allowed to cool. After 15 min, water was added, then the products extracted into a 1:1 benzene–ether mixture. The organic layers were washed with sodium carbonate solution, then with water, dried with magnesium sulfate, and evaporated to give 236 mg of oil. Separation similar to that described for the preceding experiment gave compound A (19% yield), compound B (13%), and 3β,11-diacetoxy-lanosta-7,9(11)-diene (27%).

3β-Acetoxy-19(10 → 9β)abeo-5α-lanost-1(10)-en-11-one (7, R = Ac)

This crystallized as plates from methanol, mp 85°C. It had ν_{max}: 1725 and 1685 cm^{-1}. Its ^1H nmr spectrum had signals at δ: 5.14 (1H, br s), 4.54 (1H, dd, J_1 = 10.5, J_2 = 7 Hz), 2.80 and 2.40 (two-1H, d, J = 15 Hz), 2.06 (3H, s), 1.25, 1.08, 0.92, 0.82, and 0.76 (methyl signals). *Anal.* calcd. for $C_{32}H_{52}O_3$: C 79.28, H 10.81; found: C 79.45, H 10.85.

3β-Hydroxy-19(10 → 9β)abeo-5α-lanost-1(10)-en-11-one (7, R = H)

The 3-acetoxy unsaturated ketone **7**, (R = Ac) (41 mg), was hydrolysed by refluxing a solution in 3 mL of methanol containing 90 mg of potassium hydroxide under argon for 1 h. The solvent was removed under reduced pressure, then the products distributed between water and dichloromethane. The dichloromethane layer and washings gave 39 mg of amorphous keto alcohol **7** (R = H). It had λ_{max}: 296 (ε 88), cd peaks at 300 nm (ε 4.65) and 207 nm (ε 4.4); ν_{max}: 3600, 3480, and 1690 cm^{-1}; and gave ^1H nmr signals at δ: 5.2 (1H, m, $W_{1/2}$ = 8 Hz), 3.52 (1H, dd, J_1 = 9 and J_2 = 6 Hz), 2.82 and 2.41 (two 1H doublets, J = 15 Hz), 1.28, 1.11, 1.06, 0.92, 0.82, 0.73, and 0.67 (methyl signals). Its ^{13}C nmr spectrum had signals at δ: 213.9, 139.0, and 119.5 ppm. It gave *m/e*: 442 (M^+), 427, 424, 409, 250, 192, 173, and 149.

3β-Acetoxy-19(10 → 9β)abeo-lanost-5(10)-en-11-one (12)

This formed plates from methanol, mp 149°C. It had ν_{max}: 1719 and 1690 cm^{-1} and Δε +7.5 (at 300 nm). It gave ^1H nmr signals at δ 4.72 (1H, m), 2.57 (2H, br s), 2.05 (3H, s), 1.18, 1.13, 1.00, 0.98, 0.93, 0.83, and 0.72 (methyl signals). It gave ^{13}C nmr signals at δ: 216.4, 171.0, 134.4, 128.2, and 77.9 ppm and *m/e*: 482 (M^+), 469, 424, 409, 174, 145, 131, 101, and 95. *Anal.* calcd. for $C_{32}H_{52}O_3$: C 79.28, H 10.81; found: C 79.10, H 10.81.

Ring A diene 8

Fifty mg of *p*-toluenesulfonyl chloride was added to a solution of 55 mg of hydroxyketone, **7** (R = H), in 0.5 mL of dry pyridine. After three days at room temperature, benzene was added, then the solution washed with dilute hydrochloric acid, water, and sodium bicarbonate solution. The dried benzene layers yielded a thick oil which was chromatographed on 18 g of tlc silica gel using dichloromethane for elution. The main eluate gave 38 mg of tosylate which would not crystallize. Its ^1H nmr spectrum had two 1H doublets at δ 7.83 and 7.35 (J = 8 Hz), a broad singlet at δ 5.10, a 1H triplet at 4.49, a 3H singlet at δ 2.37, and methyl signals at 1.24, 1.06, 0.92, 0.81, and 0.71.

The tosylate was dissolved in 0.5 mL of dry dimethyl sulfoxide under argon at 75°C, then 37 mg of potassium *tert*-butoxide in 0.6 mL of dimethyl sulfoxide added dropwise. The mixture was stirred under argon at 75°C for 1.75 h, cooled, then diluted with benzene. The benzene solution was washed with water, dried, and distilled, giving 27 mg of oil. A benzene solution of this was filtered through a column of 1 g of neutral alumina, Act I. The eluted product (20 mg) crystallized readily. After recrystallization from methanol, 19(10 → 9β)-*abeo*-lanosta-1(10),2-diene had mp 116–117°C; ν_{max} ($CHCl_3$): 1695 cm^{-1}; and λ_{max}: 270 nm (ε 6450). Its ^1H nmr spectrum gave signals at δ: 5.5 (br 3H, m), 2.67 and 2.54 (two apparent 1H singlets) 1.42, 1.27, 1.13, 1.09, 0.98 and 0.87, and 0.82 (methyl signals). It gave *m/e*: 424 (M^+), 409, 406, 392, and 294. *Anal.* calcd. for $C_{30}H_{48}O$: C 84.84, H 11.39; found: C 83.31, H 10.92.

19(10 → 9β)abeo-5α-Lanost-1(10)-en-3,11-dione (9)

One drop of Jones' reagent (35) was added to a solution of 50 mg of hydroxy-ketone **7** (R = H) in 5 mL of acetone. After 5 min the excess reagent was reduced with methanol, then the solution evaporated to dryness. The product was distributed between water and dichloromethane, then the organic layer and washings extracted with dilute sodium carbonate solution. The gum recovered from the dichloromethane was purified on a 1000 μ silica gel plate using 0.75% ethanol in chloroform for development. A dark front zone was followed by the desired diketone **9** (R_f approx 0.6). Yield 29 mg (58%). The amorphous diketone had ν_{max}: 1710 and 1690 cm^{-1} and gave ^1H nmr (100 MHz) signals at δ: 5.26 (1H, dd, J_1 = 8 Hz, J_2 = 3 Hz), 2.61 and 2.47 (two 1H doublets, J = 14 Hz), 2.82 (2 H, m), 1.36, 1.09, 1.00, 0.92, 0.88, 0.82, and 0.77 (methyl signals). The multiplet at δ: 5.26 was coupled with one centered at δ 2.82, collapsing to a broad singlet when the latter was irradiated. Its mass spectrum had peaks at *m/e*: 440 (M^+), 425, 356, 250, 217, 190, 165, 147, and 142.

The diketone **9**, when dissolved in 15% ethanol containing potassium hydroxide under argon, rapidly gave a maximum at 229 nm, rising in intensity to an ϵ_{max} over 7000. The crude product isolated from this reaction had ν_{max}: 1695 and 1647 cm^{-1}. However, attempted purification on silica gel plates gave no pure enone **10**.

Can. J. Chem. Downloaded from www.nrcresearchpress.com by 210.87.254.6 on 09/06/12
For personal use only.

*Bis(3,11-dioxo-19(10 → 9β)abeo-lanosta-1,5(10)-dien-2-yl) diselenide (**11**)*

Thirty-three mg of diketone **9** in 3 mL of dry dioxane containing 0.15 mL of water and 10 mg of sublimed selenium dioxide was heated under reflux in an argon atmosphere for 2 h. The mixture was left overnight at room temperature, filtered, then evaporated to dryness. The residue was dissolved in dichloromethane and the solution filtered through a short bed of Act. I neutral alumina. Dichloromethane eluted 17 mg of yellow product, while 0.75% ethanol in chloroform eluted 13 mg of more polar products.

The dichloromethane eluates crystallized from 95% ethanol giving 7 mg of **11** as yellow needles, mp 205°C. This had ν_{max}: 1690, 1646, and 1623 cm^{-1} and λ_{max}: 370 nm, ϵ 12 000. It gave ^1H nmr signals at δ: 7.15 (1H, s), 2.52 (2H, s), 1.33, 1.27, 1.20, 1.06, 0.91 and 0.80, and 0.72 (methyl signals). Its mass spectrum (chemical ionization) had peaks at 518, 516, 439, 438, 437, 436, 409, and 408. *Anal.* calcd. for $C_{60}H_{90}O_4Se_2$ (1033): C 69.74, H 8.78; found: C 69.19, H 8.86; *Mol. Wt* (thermistor drop method) 1012.

*3β-Hydroxy-19(10 → 9β)abeo-lanosta-5(10)-ene-11-one (**13**)*

The acetate of the Westphalen product B (**12**) (32 mg) was dissolved in 3 mL of methanol containing 223 mg of potassium hydroxide. The solution was refluxed under argon for 2 h, then the solvent evaporated. The product was distributed between water and dichloromethane, giving 26 mg of colorless oil in the organic phase. This had ν_{max}: 3600, 3350 (broad), and 1692 cm^{-1}, λ_{max}: 296, ϵ 88; and gave ^1H nmr signals at δ: 3.4 (1H, t, J = 5 Hz), 2.51 (2H, s) 1.18, 1.14, 1.04, 0.97, 0.90, 0.80, and 0.70 (methyl signals). Its cd spectrum had $\Delta\epsilon$ +8.0 (300 nm).

*19[10 → 9β]abeo-Lanosta-5(10)-ene-3,11-dione (**14**)*

A solution of 20 mg of **13** in 3 mL of acetone was titrated with a dilute solution of Jones' reagent in acetone. The acetone solution was decanted from the precipitate, then evaporated under reduced pressure. The product was taken up in dichloromethane, the solution washed with aqueous sodium carbonate, dried, and distilled. The 19 mg of product was purified on a 10 × 20 cm 500 μ SiO_2 plate using 0.75% ethanol in chloroform for elution. Zone 1 (R_f 0.55) gave 11 mg of diketone **14** as an oil. This had ν_{max}: 1713 and 1693 cm^{-1} and λ_{max}: 293 nm, ϵ 150. It gave ^1H nmr signals at δ: 2.50 (2H, s) 1.22, 1.17, 1.12, 0.90, 0.80, and 0.72 (methyl signals).

*Action of selenium dioxide on diketone **14***

A solution of 25 mg of diketone **14** and 11 mg of selenium dioxide in 4 mL of pure dioxane and 200 μL of water was heated at 100°C under argon for 6 h. The mixture was taken to dryness on a rotating evaporator, then the product taken up in hexane. This solution was washed with dilute sodium hydroxide solution, dried, and distilled, giving 25 mg of yellow gum. This was separated on a 500 μ fluorescent silica gel plate using 2% methanol in chloroform. The fastest moving compound (R_f 0.9) gave a yellow band with strong fluorescence quenching. It yielded 4 mg of crystalline solid (needles mp 205°C from ethanol) with λ_{max}: 370 nm. Its spectral properties were identical with those of compound **11** obtained from **9**. The next zone did not strongly quench fluorescence. It gave 6 mg with a weak uv maximum at 324 nm. This was followed by a strongly quenching zone containing 9 mg of an amorphous dienone (**15**) which had ν_{max}: 1690, 1660 and 1625 cm^{-1}; λ_{max}: 325 nm (ϵ 4800). It gave ^1H nmr signals at δ: 7.00 (1H, d, J = 11 Hz), 5.96 (1H, d, J = 11 Hz), 2.58 (2H, s), 1.30, 1.23, 1.08, 0.92, 0.80, and 0.78 (methyl signals). Its mass spectrum had peaks at m/e: 438 (M^+), 423, 410 and 395. M^+ calcd. for $C_{30}H_{46}O_2$: 438.

*Action of p-toluenesulfonic acid on B (**13**)*

A solution of 47 mg of the acetoxy keto olefin B (**13**) and 184 mg of anhydrous *p*-toluenesulfonic acid in 4 mL of dry benzene was refluxed under argon for 4.5 h. A pink color developed rapidly. The red solution was cooled, washed with dilute sodium carbonate solution, dried, and evaporated. The 44 mg of residue was separated on a 1000 μ silica gel plate, developing with 0.75% ethanol in chloroform. The weakly fluorescent band with R_f approx 0.5 gave 9 mg (19%) of essentially pure aromatic ketone **20** with spectra identical to that derived from 24-deoxybryogenin acetate (see below).

*Bryogenin (**17**)*

This was prepared by the action of acid on bryodulcosigenin (**16**) from *Bryonia alba* (20). After crystallization from acetone–hexane it had mp 157–158°C. This proved homogeneous by hplc. Its ^1H nmr spectrum had signals at δ: 5.7 (1H, br d), 3.49 (1H, br s), 1.13, and 1.15 (methyl signals). Half the expected doublet of doublets for the 12-hydrogens was visible at δ 2.96 (J = 14 Hz).

*Bryogenin 24-tosylhydrazone (**18**)*

Bryogenin (350 mg) and 400 mg of *p*-toluenesulfonylhydrazine in 6 mL of ethanol containing 50 mg of acetic acid was refluxed for 5 h. The solvent was removed on a rotating evaporator. A solution of the residue in dichloromethane was washed with dilute sulfuric acid, then sodium carbonate solution, dried, and distilled, leaving 526 mg of neutral product. This was adsorbed on 11 g of neutral alumina, activity III. Elution with 1:1 ether–hexane gave 41 mg of byrogenin, followed by 392 mg of the tosylhydrazone. This was never obtained crystalline. It had ν_{max}: 3500, 3280, 3210, 1694, 1600, and 1168 cm^{-1} and gave ^1H nmr signals at δ: 7.9 and 7.32 (two 2H doublets, J = 8 Hz), 7.7 (br s, 1H, NH), 5.7 (br d, 1H, J = 6 Hz), 3.50 (1H, s), 2.50 (3H, s), 1.15, 1.03, 0.95, and 0.70 (methyl signals).

Reduction of bryogenin 24-p-toluenesulfonylhydrazone

A solution of 410 mg of the tosylhydrazone in 4 mL of methanol was prepared. To this was added 106 mg of sodium cyanoborohydride, followed by slow addition of 79 mg of *p*-toluenesulfonic acid (during 2.75 h). Finally, another 80 mg of the acid was added, leading to rapid gas evolution. The methanol was evaporated. A dichloromethane solution of the products was washed with sodium carbonate solution, then dried. The 293 mg of product was purified on four 1000 μ silica plates using 5% methanol in chloroform for development. A front zone R_f 0.7 (86 mg of unknown) was followed by 151 mg rich in the desired 24-deoxybryogenin. This was acetylated by heating for 2 h at 60°C with a 1:1 mixture of acetic anhydride – pyridine. A methanol solution of the product gave 86 mg of crystals, mp 89–94°C, which, on recrystallization, had mp 133–135°C. The mother liquors were purified on preparative tlc plates, then crystallization from methanol, giving 80 mg, mp 108–109°C. Recrystallization of this gave 40 mg, mp 116–125°C, with similar spectra to the product with mp 135°C.

Bryogenin 24-semicarbazone

Bryogenin (411 mg, mp 153–155°C), semicarbazide hydrochloride (440 mg), and sodium acetate (504 mg) in 10 mL of methanol was heated to the boiling point for 10 min, then left for 22 h at room temperature. The solvent was removed under reduced pressure. A dichloromethane solution of the product was washed with dilute sulfuric acid, then dilute sodium carbonate solution. The neutral product was absorbed from chloroform onto 50 g of tlc silica gel, then eluted with 5% methanol in chloroform, giving 500 mg of quite pure semicarbazone.

A sample was purified for analysis by recrystallization from methanol, giving mp 156–164°C. It had ν_{max}: 3520, 3460, 3380, 1686, and 1560 cm^{-1} and gave ^1H nmr signals at δ: 8.35 (1H, s), 5.75 (3H, br), 1.16, 1.05, and 0.76. *Anal.* calcd. for $C_{31}H_{51}N_3O_3$: C 72.47, H 10.01; found: C 72.60, H 10.12.

Action of alkali on bryogenin semicarbazone

Bryogenin 24-semicarbazone (1.04 g) was mixed with 20 mL of diethylene glycol and 4 g of potassium hydroxide. This was heated to 190°C in an oil bath under a gentle stream of argon. As the vigorous boiling subsided, the temperature of the bath was raised to 205°C (total heating time 2 h). The mixture was cooled, then diluted with water, and extracted with dichloromethane. The dichloromethane extracts were washed with water, dried, then freed of solvent. The 832 mg of product was acetylated in 1:1 acetic anhydride – pyridine overnight. The acetate crystallized from methanol, giving 480 mg, mp 131°C and

277 mg, mp below 90°C. The first crop was nearly pure 24-deoxybryogenin acetate **19**. The second crop was a mixture of **19** with another product, giving very similar ir and ^{1}H nmr spectra. This was not further investigated.

24-Deoxybryogenin

This was not obtained crystalline. Product from reduction of the tosylhydrazone was purified by chromatography on silica gel plates using 5% methanol in chloroform for elution. Material giving a single spot on tlc (same solvent) gave ν_{max}: 3610, 3520 and 1690 cm^{-1} and ^{1}H nmr signals at δ: 5.60 (1H, br), 3.50 (1H, s), 2.97, 2.42 (two 1H doublets, J = 14 Hz), 1.15, 1.10, 1.02, 0.92, 0.85, and 0.73. It gave ^{13}C nmr signals at δ: 214.9 (s), 139.6 (s), 120.6 (d), and 76.15 (d).

24-Deoxybryogenin acetate **19**

Product with mp 135°C from reduction of tosylhydrazone **18** and Wolff–Kishner reduction of the semicarbazone **17** was further purified using silica gel plates under argon, with development using 2% methanol in chloroform. Recrystallization from methanol gave a product with mp 137–138°C. A final purification by flash chromatography on 40 times its weight of silica gel, eluting with benzene – ethyl acetate (95:5), followed by recrystallization from methanol, gave 24-deoxybrogenin acetate as laths, mp 143.5–145°C. It had ν_{max}: 1726 and 1690 cm^{-1} and gave ^{1}H nmr signals at δ: 5.67 (1H, br), 4.73 (1H, br s), 3.0, 2.46 (two 1H doublets, J = 14 Hz), 2.05 (3H, s), 1.10, 1.06, 0.92, 0.82, and 0.73. Its ^{13}C nmr spectrum had signals at δ: 214.6 (s), 170.6 (s), 139.7 (s), 119.1 (d), 78.2 (d), 49.6 (t), 48.9 (s) 43.9 (d), 40.0 (s), 39.5 (t), 36.4, 35.9, 35.6, 34.5, 28.0, 26.2, 25.0, 24.0, 22.9, 22.7, 21.3, 19.9, 18.6, 18.3, and 16.8. *Anal.* calcd. for $C_{32}H_{52}O_3$: C 79.28, H 10.81; found: C 79.36, H 10.26.

Action of p-*toluenesulfonic acid on* ***19***

A solution of 101 mg of dry 24-deoxybryogenin acetate (**19**) and 239 mg of anhydrous *p*-toluenesulfonic acid in 7 mL of dry benzene under argon was refluxed gently for 4.5 h. It was then cooled, extracted with sodium carbonate solution, dried, and distilled. The 90 mg of neutral product was put on a 1000 μ SiO_2 plate and developed with 0.75% ethanol in chloroform. A dark zone (uv light with R_f 0.8) contained 19 mg of a mixture of diene **28** with ca. 3 mg of aromatic compound **20**. A weaker fluorescent band with R_f 0.7 gave 51 mg of fairly pure amorphous aromatic compound **20**. (Estimated total yield 56%).

19(10 → 9β)abeo-Lanostan-1(10),5-diene-11-one (28)

The less polar product from the action of *p*-toluenesulfonic acid on deoxybyrogenin was further purified on a silica gel plate using 1:1 dichloromethane–benzene for development. The oil so obtained (ca. 17%) had λ_{max}: 242 nm (ε 10 500) and ν_{max}: 1690 cm^{-1}. Its ^{1}H nmr spectrum gave signals at δ: 5.43 (1H, m), 5.0 (1H, m) and methyl signals at 0.90, 0.82, and 0.74. Its mass spectrum gave ions at *m/e*: 424.3712 (M^+), 409, 278, 151, and 95. *Mol. Wt.* calcd. for $C_{30}H_{48}O$: 424.3705.

9,10-Seco-28(4 → 3)abeo-cucurbita-1,3,5(10)-triene-11-one (20)

After a second purification on silica gel plates, using 20:1 benzene – ethyl acetate for development, this crystallized and had mp 41–45°C. It had intense absorption below 225 nm and λ_{max}: 263 nm (ε 110) and 271 nm (ε 70). It had ν_{max}: 1692 cm^{-1}. Its ^{1}H nmr spectrum had signals at δ: 7.06 (3H, s), 2.71 (2H, t, J = 8 Hz), 2.54 (2H, s), 2.30 (3H, s), 2.24(3H, s), 1.28, 1.18, 1.03, 0.92, 0.83, and 0.77 (methyl signals). The signals for the aromatic protons, the low-field methyl protons (2.30, 2.24), and the benzylic hydrogens (2.71) hardly moved as Eu(dpm)$_3$ was added to the solution, although the aromatic proton signal changed from a singlet to a multiplet. The singlet at 2.54 attributable to the 12-hydrogens moved rapidly downfield as the shift reagent was added, becoming a doublet of doublets with J = 16 Hz. A broad one-hydrogen signal attributable to the 9-hydrogen and a methyl doublet (1.23, J = 6 Hz) also moved rapidly, indicating proximity of these groups to the carbonyl. Its ^{13}C nmr spectrum had signals at δ: 214.3, 140.8 (s), 136.9 (s), 134.1 (s), 127.8 (d), 127.0 (d), and 125.5 (d) and its mass spectrum gave peaks at *m/e*: 424.3700 (M^+), 304, 291, 254, 151, and 119. *Mol. Wt.* calcd. for $C_{30}H_{48}O$: 424.3705.

Westphalen dehydration of 3β,11α-diacetoxy-5α-lanostan-9α-ol

A solution of 125 mg of sulfuric acid in 2.5 mL of acetic acid was added dropwise at room temperature to a solution of 506 mg of **2** in 12.5 mL of acetic acid and 10 mL of acetic anhydride. After 3 h, a precipitate which had formed was removed by filtration. After crystallization from acetone–dichloromethane, this had mp 162–164°C and spectral properties characteristic of 3β-acetoxy-5α-lanosta-7,9(11)-diene. The filtrate was poured into water, then the products extracted into benzene. The benzene layers were washed free of acid using sodium carbonate solution, dried, and evaporated, giving 325 mg of yellow oil (at least 4 components). This was chromatographed on Act. III alumina, eluting with hexane and hexane–benzene mixtures. A further 28 mg of 3β-acetoxy-5α-lanosta-7,9(11)-diene and 57 mg of starting material were obtained. Fractions with medium polarity contained 68 mg of olefin **21** which gave ^{1}H nmr signals at δ: 5.20 (1H, m), 4.74 (1H, m) 2.08 (3H, s), and 2.05 (3H, s). This was hydrolysed using refluxing potassium hydroxide in 95% ethanol. The tlc separation of the products gave 30 mg of dihydroxy olefin with ^{1}H nmr signals at δ: 3.73 (1H, dd, J_1 = 9 Hz, J_2 = 7 Hz), 3.40 (1H, t, J = 4 Hz), 1.20, 1.02, 0.93, 0.80, and 0.70 (methyl signals). Finally, oxidation of this compound with Jones' reagent in acetone gave 28 mg of diketone. Its ir and nmr spectra were identical with those of diketone **14**.

Action of p-*toluenesulfonic acid hydrate on* ***4***

The ketol (**4**) (327 mg), mp 181°C, and 291 mg of powdered *p*-toluenesulfonic acid monohydrate was suspended in 8 mL of dry benzene. This was refluxed under argon for 2.5 h, giving a dark red solution. This was cooled, then washed with sodium carbonate solution. The dried benzene layers (Na_2SO_4) were distilled, leaving a crystalline residue. This was dissolved in 10 mL of absolute ethanol containing 230 mg of potassium hydroxide, then the solution refluxed under argon for 1 h. The ethanol was removed on a rotating evaporator, then the residue distributed between water and dichloromethane. The 317 mg of product recovered from the dichloromethane was put on two 1000 μ 20 cm × 20 cm SiO_2 plates, then developed with 20% ethyl acetate in benzene. Band 4 (R_f 0.5) gave 135 mg, which crystallized from methanol to yield 92 mg of enone **23**. Band 5 (R_f 0.4) gave 63 mg, which crystallized from methanol to yield 38 mg of ketol **24**.

3β-Hydroxy-11-oxo-C-nor-D-homo-5α-lanost-12-ene (23)

This had mp 159°C; ν_{max}: (CH_2Cl_2): 3500, 3489, 1695, and 1620 cm^{-1}; and λ_{max}: 255 nm (ε 14 000) and 356 nm (ε 100). It gave ^{1}H nmr signals at δ: 3.31 (1H, m), 2.08, 3H, s), 1.01, 0.93, 0.90, 0.85, and 0.80 (methyl signals). *Anal.* calcd. for $C_{30}H_{50}O_2$: C 81.39, H 11.38; found: C 81.28, H 11.12.

3β,12β-Dihydroxy-5α-lanostan-11-one (24)

This had mp 146°C, ν_{max} (CH_2Cl_2): 3615, 3435, and 1705 cm^{-1}; and λ_{max}: 277 nm, (ε 87). It gave ^{1}H nmr signals at δ: 4.27 (1H, br d, J = 8 Hz) and 3.25 (1H, m) and ^{13}C nmr signals at δ: 214.2, 78.5, and 72.4 ppm. *Anal.* calcd. for $C_{30}H_{52}O_3$: C 78.20, H 11.38; found: C 77.94, H 11.57.

C-nor-D-homolanost-12-en-3,11-dione (22)

Compound **23** (24 mg) in 2 mL of acetone was titrated with a dilute solution of Jones' reagent (35) in acetone. The product was purified using a 500 μ silica gel plate with 0.75% ethanol in chloroform for development. The main zone gave 12 mg of pure diketone (**22**) with mp 133°C; ν_{max}: 1695 and 1620 cm^{-1}; and λ_{max}: 255 nm (ε 15 300). It gave ^{1}H nmr signals at δ: 2.13 (3H, s), 1.30, 1.14, 1.07, 0.96, and 0.86 (methyl signals). Its mass spectrum had peaks at *m/e*: 440 (M^+), 425, 355. 327, 312, 295, 189, 175, 149, and 141.

5-α-Lanostan-3,11,12-trione

Ketol **24** (17 mg) in 2 mL of acetone was titrated with dilute solution of Jones' reagent (35) in acetone. The product crystallized from

Can. J. Chem. Downloaded from www.nrcresearchpress.com by 210.87.254.6 on 09/06/12
For personal use only.

methanol giving 13 mg of triketone **11** with mp 154–156°C. It had ν_{max}: 1722, 1705, and 1695 cm^{-1} and λ_{max}: 283 nm (ϵ 290) shifting to λ_{max}: 330 nm (ϵ 3600) in ethanol containing potassium hydroxide. Its ^1H nmr spectrum had signals at δ: 2.9 to 2.1 (3H, multiplet), 1.29, 1.09, 1.03, 0.94, and 0.83 (methyl signals).

Acknowledgements

We thank H. Seguin for analyses, Dr. I.C.P. Smith and co-workers and R. J. Kolt for ^{13}C nmr spectra, the Ottawa–Carleton Mass Spectrometry Center for the mass spectra, and R. J. Kolt for technical assistance.

1. O. E. EDWARDS and M. LESAGE. Can. J. Chem. **41**, 1592 (1963).
2. O. E. EDWARDS, J. DIXON, J. W. ELDER, R. J. KOLT, and M. LESAGE. Can. J. Chem. **59**, 2096 (1981).
3. O. E. EDWARDS. Can. J. Chem. **59**, 3039 (1981).
4. O. E. EDWARDS and T. SANO. Can. J. Chem. **47**, 3489 (1969).
5. O. E. EDWARDS and Z. PARYZEK. Can. J. Chem. **51**, 3866 (1973). Unpublished work with J. P. Devlin and J. W. Elder.
6. T. WESTPHALEN. Ber. **48**, 1064 (1915).
7. (*a*) J. M. COXON and J. R. GIBSON. Aust. J. Chem. **34**, 2577 (1981); (*b*) D. N. KIRK. Tetrahedron, **31**, 1299 (1975); (*c*) J. G. L. JONES and B. A. MARPLES. J. Chem. Soc. (C) 572 (1971); (*d*) P. KOCOVSKY, V. CERNY, and F. TURECEK. Collect. Czech. Chem. Commun. **44**, 234 (1979).
8. O. E. EDWARDS and Z. PARYZEK. Can. J. Chem. **53**, 3498 (1975).
9. J. FRIED, J. W. BROWN, and M. APPLEBAUM. Tetrahedron Lett. 849 (1965).
10. L. RUZICKA, R. DENSS, and O. JEGER. Helv. Chim. Acta, **29**, 204 (1946).
11. K. E. PFITZNER and J. G. MOFFATT. J. Am. Chem. Soc. **87**, 5661 (1965); **87**, 5670 (1965).
12. P. TURNBULL, K. SYHORA and J. H. FRIED. J. Am. Chem. Soc. **88**, 4764 (1966).
13. (*a*) J. F. MCGHIE, M. K. PRADHAN, and J. F. CAVALLA. J. Chem. Soc. 3176 (1952); (*b*) M. V. MIJOVIC, W. VOSER, H. HEUSSER, and O. JEGER. Helv. Chim. Acta, **35**, 964 (1952).
14. W. LAWRIE, W. HAMILTON, J. MCLEAN, and J. MENEY. J. Chem. Soc. Perkin Trans. 1, 471 (1978).
15. PL. A. PLATTNER. T. PETRZILKA, and W. LANG. Helv. Chim. Acta, **27**, 513 (1944).
16. K. FLOREY and A. R. RESTIVO. J. Org. Chem. **22**, 406 (1957).
17. A. I. SCOTT. Interpretation of the ultraviolet spectra of natural products. Pergamon Press, Oxford. 1964. p. 75.
18. J. W. APSIMON, R. R. KING, and J. J. ROSENFELD. Can. J. Chem. **47**, 1989 (1969).
19. G. BIGLINO, J. M. LEHN, and G. OURISSON. Tetrahedron. Lett. 1651 (1963).
20. (*a*) P. TUNMAN, W. GERNER, and G. STAPEL. Ann. **694**, 162 (1966); (*b*) G. BIGLINO and G. M. NANO. Farmaco, Ed. Sci. **22**, 140 (1967).
21. R. O. HUTCHINS, C. A. MILEWSKI, and B. E. MARYANOFF. J. Am. Chem. Soc. **95**, 3662 (1973).
22. G. BAUMGARTNER and CH. TAMM. Helv. Chim. Acta, **38**, 441 (1955).
23. L. P. MAKHUBU, Z. G. HAJOS and G. R. DUNCAN. Can. J. Chem. **52**, 1744 (1974).
24. (*a*) J. W. APSIMON, R. R. KING, and J. M. ROSENFELD. Can. J. Chem. **47**, 1989 (1969); (*b*) J. W. APSIMON and J. W. ROSENFELD. J. Chem. Soc. Chem. Commun. 1271 (1970).
25. A. C. CAMPBELL, C. L. HEWETT, M. S. MAIDMENT, and G. T. WOODS. J. Chem. Soc. Perkin Trans. 1, 1799 (1974).
26. E. C. LEVY and D. LAVIE. Israel J. Chem. **8**, 677 (1970); I. G. GUEST and B. A. MARPLES. J. Chem. Soc. (C), 1468 (1971).
27. Z. PARYZEK. Tetrahedron Lett. 4761 (1976); J. Chem. Soc. Perkin Trans. 1, 1222 (1979); Bull. Pol. Acad. Sci. **26**, 583 (1978); Z. PARYZEK and R. WYDRA. Steroids, **38**, 141 (1981).
28. G. V. BADDELEY, H. J. SAMAAN, J. J. H. SIMES, and TU HOA AI. J. Chem. Soc. Perkin Trans. 1, 7 (1979).
29. J. W. BLUNT, A. FISCHER, M. P. HARTSHORN, F. W. JONES, D. N. KIRK, and S. W. YOONG. Tetrahedron, **21**, 1567 (1965).
30. J. M. COXON and J. R. GIBSON. Aust. J. Chem. **32**, 2223 (1979); J. G. JONES and B. A. MARPLES. J. Chem. Soc (C), 572 (1971).
31. G. SNATZKE and A. VIETHEN. Ann. **703**, 159 (1967).
32. N. L. WENDLER. *In* Molecular rearrangements. Vol 2. *Edited by* P. de Mayo. Interscience Publishers, New York. 1963. p. 1127; P. A. DIASSI and R. M. PALMER. J. Org. Chem. **26**, 5240 (1961); W. F. JOHNS. J. Org. Chem. **28**. 1616 (1963).
33. R. F. HIRSCHMANN, C. S. SNODDY, JR., C. F. HISKEY, and N. L. WENDLER. J. Am. Chem. Soc. **76**, 4013 (1954); J. ELKS, G. H. PHILLIPS, D. A. H. TAYLOR, and L. J. WYMAN. J. Chem. Soc. 1739 (1954).
34. W. T. DEKOCK, P. R. ENSLIN, K. B. NORTON, D. H. R. BARTON, and A. BOTHNER-BY. J. Chem. Soc. 3828 (1963).
35. K. BOWDEN, J. M. HEILBRON, E. R. H. JONES, and B. C. L. WEEDON. J. Chem. Soc. 39 (1946).

Can. J. Chem. Downloaded from www.nrcresearchpress.com by 210.87.254.6 on 09/06/12
For personal use only.

Lewis acid complexes of 1,2-diketones and their derivatives. The synthesis of seven-membered rings

CHRISTOPHER BLACKBURN, RONALD F. CHILDS,[1] AND ROGER A. KENNEDY
Department of Chemistry, McMaster University, Hamilton, Ont., Canada L8S 4M1

Received February 24, 1983

CHRISTOPHER BLACKBURN, RONALD F. CHILDS, and ROGER A. KENNEDY. Can. J. Chem. **61**, 1981 (1983).

The structures and charge distributions of Lewis acid complexes of butane-2,3-dione, **1**, cyclohexane-1,2-dione, **2**, and 2-methoxycyclohex-2-en-1-one, **5**, have been investigated by ^{1}H nmr spectroscopy. A 1:1 complex was formed between **1** and $SnCl_4$ which appeared to have a bridged structure. In the case of **2** and **5** both oxygens were again involved in complex formation with $TiCl_4$ or $SnCl_4$. In each case the large downfield shift of the vinyl proton resonance, H3, indicated extensive charge delocalization within the complexes and that these systems can be regarded as complexed α,β-unsaturated enones. The reactions of Lewis acid complexes of **2**, **5**, and the silyl ethers 2-(trimethylsiloxy)cyclohex-2-en-1-one, and 3-(trimethylsiloxy)-but-3-en-2-one, **11**, with butadiene have been investigated. The acyclic enol ether **11** reacted with butadiene in the presence of either $TiCl_4$ or $SnCl_4$ to give products corresponding to both 4C + 3C and 4C + 2C cycloaddition reactions; in all other cases 4C + 2C products only could be isolated.

CHRISTOPHER BLACKBURN, RONALD F. CHILDS et ROGER A. KENNEDY. Can. J. Chem. **61**, 1981 (1983).

Faisant appel à la spectroscopie de rmn du ^{1}H, on a étudié les structures et les distributions de charges des complexes d'acide de Lewis de la butanedione-2,3 (**1**), de la cyclohexanedione-1,2 (**2**) et de la méthoxy-2 cyclohexène-2 one-1 (**5**). Il se forme un complexe 1:1 entre le composé **1** et le $SnCl_4$ qui semble posséder une structure pontée. Dans le cas des composés **2** et **5** les deux oxygènes sont encore impliqués dans la formation d'un complexe avec le $TiCl_4$ ou le $SnCl_4$. Dans chaque cas, le grand déplacement de la résonance du proton vinylique, H3, vers les champs faibles indique une forte délocalisation de charge à l'intérieur de ces complexes et on peut considérer ces systèmes comme des énones-α,β insaturées complexées. On a étudié les réactions des complexes d'acide de Lewis des composés **2** et **5**, et des éthers silylés: (triméthylsiloxy)-2 cyclohexène-2 one-1 et (triméthylsiloxy)-3 butène-3 one-2, **11**, avec le butadiène. L'éther énol acyclique **11** réagit avec le butadiène en présence du $TiCl_4$ ou du $SnCl_4$ en donnant des produits correspondants aux deux réactions de cycloaddition 4C + 3C et 4C + 2C. Dans tous les autres cas on obtient uniquement des produits 4C + 2C.

[Traduit par le journal]

The synthesis of carbocyclic seven-membered rings by 3C + 4C cycloaddition reactions has received much attention (1). These reactions normally involve a thermal $4\pi + 2\pi$ cycloaddition with an allyl cation adding to a 1,3-diene (2). The allyl cations are generated as transient species and the addition to the diene is but one of several competing reactions. For example, proton loss or nucleophilic capture of the allyl cation can readily occur and this leads to low yields of the desired seven-membered rings with less reactive dienes.

An attractive alternative approach would be to generate the allyl cations as long-lived species. One potential way of doing this is to react a suitably substituted α,β-unsaturated carbonyl compound with a Lewis acid. Lewis acid complexes of enones are well characterized compounds that are involved in a large variety of reactions (3) including the catalysed Diels–Alder reaction to form cyclohexenones (4). If the enone were to contain a good electron-donating group at the α-carbon, it might be possible to divert this reaction to form a cycloheptenone, eq. [1]. Indeed, as this work was underway, Sasaki *et al.* reported that such a reaction occurs with the $SnCl_4$-catalysed reaction of 1,3-butadiene with trimethylsilyl ether of pyruvaldehyde (5).

[1]

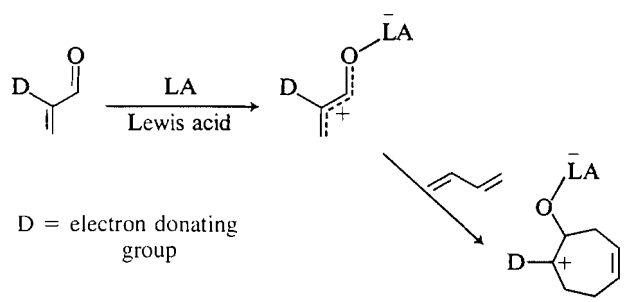

Potentially, complexation of a 1,2-diketone with a Lewis acid and subsequent removal of a proton from an adjacent carbon could give an allyl cation with an oxygen substituent at C2. We have explored this type of reaction of diketones and their derivatives and have found that, in certain cases, the resulting complexes undergo cycloadditions with dienes to form seven-membered rings (6).

Results and discussion

Complexations of 1,2-diketones

The 1,2-diketones used in this study were butane-2,3-dione, **1**, and cyclohexane-1,2-dione, **2**. The former material exists mainly in the diketo form, whereas **2***a* is present mainly as its enol tautomer **2***b*.

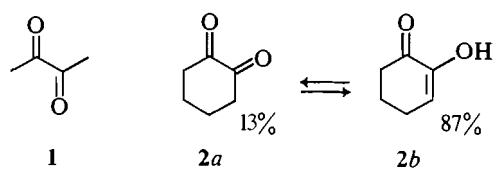

1 **2***a* **2***b*

Treatment of CH_2Cl_2 solutions of **1** with $SnCl_4$ or $TiCl_4$ at room temperature led to fairly rapid decomposition ($t_{1/2}$ ca. 1 h at 34°C). To minimize these decompositions, the reactions were studied at lower temperatures. Solubility problems made work with $TiCl_4$ difficult but a detailed examination of the $SnCl_4$ system was undertaken.

The ^{1}H nmr spectra of **1** and $SnCl_4$ mixtures in CD_2Cl_2 displayed both a concentration and temperature dependence, Table 1. At −18°C a single methyl resonance was seen irre-

[1]Author to whom correspondence may be addressed.

Can. J. Chem. Downloaded from www.nrcresearchpress.com by 210.87.254.40 on 09/06/12
For personal use only.

TABLE 1. ^{1}H nuclear magnetic resonance spectrum of **1**/$SnCl_4$ mixtures[a]

	^{1}H chemical shift methyl resonance (ppm)						
1/$SnCl_4$ ratio	−18°C	−48°C	−68°C	−78°C	−88°C	−98°C	−103°C
1/—	2.30						
1/0.33	2.59	2.85	2.90	2.91	3.2/2.4	3.31/2.39	3.31/2.39
1/1	2.84		3.28		3.29		
1/2	2.98		3.28				
1/3	3.05		3.28				
1/4	3.08		3.28				

[a]CD_2Cl_2 solutions, $CHDCl_2$ used as internal reference taken as 5.33 ppm.

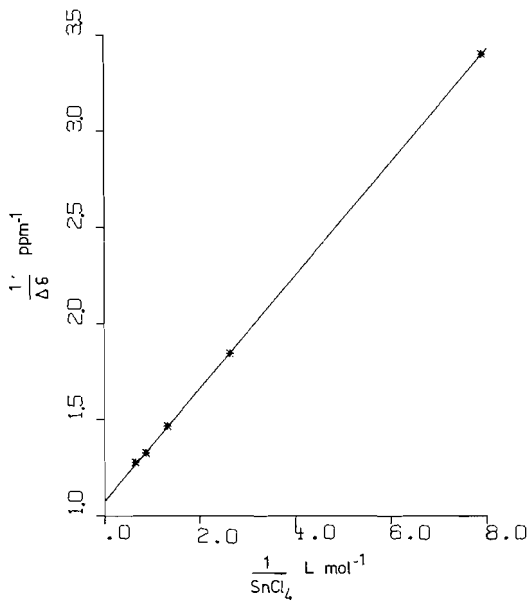

FIG. 1. Plot of $1/\Delta\delta$ of the ^{1}H chemical shift of 2,3-butanedione versus $1/[SnCl_4]$.

spective of the ratio of **1**/$SnCl_4$ used. However, the position of this resonance was shifted progressively further downfield as the ratio of Lewis acid was increased. This behavior indicates that at least one complex is being formed between **1** and $SnCl_4$ in this solvent and that at −18°C there is rapid equilibrium between free and complexed **1** which leads to an averaging of the ^{1}H nmr spectrum.

The equilibrium constant for the reaction of $SnCl_4$ with **1** was estimated from a modified Benisi–Hildebrand plot, Fig. 1, as 31.5 (7). The linearity of this plot indicates that only one equilibrium is important at −18°C.

The ^{1}H nmr spectra of **1**/$SnCl_4$ mixtures exhibited a reversible temperature dependence, Table 1. As the temperature was lowered, two different types of behavior were noted, depending on whether the ratio of $SnCl_4$ to **1** was greater or less than 1. In cases where a molar excess of $SnCl_4$ was present, a downfield shift of the methyl resonance was observed as the temperature was lowered. In each case a limiting chemical shift was reached at δ 3.28, indicating essentially complete formation of the complex at the lower temperatures. With less than one molar equivalent of Lewis acid, two methyl group resonances were observed in the nmr spectra at low temperatures. For example, with a **1** to $SnCl_4$ ratio of 1:0.33 at −100°C, resonances at δ 3.31 and 2.39 were observed with a relative area of 1:2.5, respectively. The former resonance is very close to that observed above with more than a one molar equivalent of $SnCl_4$, whereas the latter resonance is attributable to free **1**. The area ratio of these two resonances corresponded to the formation of a 1:1 complex between biacetyl and $SnCl_4$. Clearly, at −100°C, exchange between free and complexed biacetyl is slow on the nmr time scale.

Taken together, these results strongly indicate that a 1:1 complex is formed between **1** and $SnCl_4$. The question arises as to the structure of this complex. Only one methyl group resonance is observed for the complex in its nmr spectrum at low temperatures. This could be taken to mean that a symmetrical bridged structure is formed or that there is a rapid equilibration between two mono-coordinated structures, eq. [2]. This exchange could be intramolecular, eq. [2], or proceed by an intermolecular process involving a nondissociative mechanism. The limiting downfield shift of the methyl resonances seen in the ^{1}H nmr spectrum of **1** on complexation with $SnCl_4$ in 0.98 ppm. This is a considerably greater shift than normally encountered on complexation of a methyl-substituted ketone with $SnCl_4$ and would possibly indicate that the bridged structure **3** is preferred.

[2] 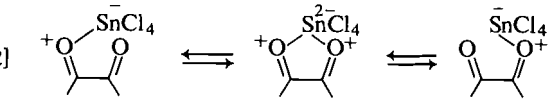

3

Attempts were made to remove a proton from the $SnCl_4$ complex of **1** by adding 2,6-di-*tert*-butylpyridine to the solutions. This base does not react with a Lewis acid such as $SnCl_4$ (8), but can form a salt with protic acids. From the ^{1}H nmr spectra of solutions of **1**/$SnCl_4$ containing 2,6-di-*tert*-butylpyridine, it was clear that some complex reaction(s) had taken place. It was not possible to identify any of the products of these reactions.

Cyclohexane-1,2-dione

It was again found necessary to use low temperatures in order to retard decomposition of the complexes of **2** and either $SnCl_4$ or $TiCl_4$. The ^{1}H nmr spectra of solutions of **2** and $TiCl_4$ were both concentration and temperature independent when the ratio of $TiCl_4$/**2** was equal to or greater than 1, Table 2. This suggests the formation of a 1:1 complex between **2** and $TiCl_4$, with a large equilibrium constant in favour of formation of the complex.

As cyclohexane-1,2-dione exists predominantly in its enol form **2***b*, there are two nonequivalent Lewis base sites available for complexation. From the changes in the ^{1}H nmr spectrum, it would appear that complexation has taken place at both the keto and enol oxygen atoms. Evidence for reaction at the former site comes from the large downfield shift of the vinyl proton reso-

Can. J. Chem. Downloaded from www.nrcresearchpress.com by 210.87.254.40 on 09/06/12
For personal use only.

TABLE 2. ^{1}H nuclear magnetic resonance spectral data for complexation of **2** and **5**

Lewis base	Lewis acid	Base/acid ratio	Temperature °C	Chemical shift (ppm)[a] H3	OH	OCH_3	H4—H3	HCl
2	—		34	6.21	6.10	—	2.65–1.8	—
2	$TiCl_4$	1:1	−18	7.30	—	—	3.09–2.25	1.35
2	$TiCl_4$	1:2	−18	7.30	—	—	3.09–2.21	1.35
2	$SnCl_4$	1:2	−18	7.19	8.00	—	3.00–2.10	1.23
2	$SnCl_4$	1:3	−18	7.20	8.45	—	3.00–2.10	1.23
2	$SnCl_4$	1:3	−88	7.33	—	—	3.06–2.10	1.23
5	—		34	5.89	—	3.64	2.59–1.88	—
5	$TiCl_4$	1:1	−18	6.93	—	4.27	3.06–2.12	—
5	$SnCl_4$	1:1	−18	6.94	—	4.27	3.04–2.00	—

[a]Solvent CD_2Cl_2 for all complexes; $CDCl_3$ for **2** and **5** in absence of any Lewis acid. Reference for complexes $CHDCl_2$ taken as 5.30 ppm.

nance of **2***b* on complexation. The magnitude of this shift is that which would be expected for complexation of a normal enone with $TiCl_4$ (9).

The hydroxy proton signal that is present in the ^{1}H nmr spectrum of **2** disappeared when the dione was complexed with $TiCl_4$. A new peak was observed at much higher field (δ 1.2). The chemical shift of this signal was shifted downfield as the temperature was lowered. The disappearance of the OH resonance of the hydroxy group and the appearance of this new signal suggested that HCl had been evolved as the complex was formed. Further evidence for the presence of HCl was obtained by the addition of the hindered base 2,6-di-*tert*-butylpyridine to the nmr tube and the formation of the 2,6-di-*tert*-butylpyridinium cation. Addition of gaseous HCl to the nmr tube enhanced the intensity of the peak at δ 1.2, confirming that it was indeed attributable to HCl. Thus the reaction of 2*b* with $TiCl_4$ may occur as shown in eq. [3], although comparable intermolecular complexes involving bonding of the titanium to oxygens of two diketones cannot be ruled out. It is likely that the small amount of **2***a* in equilibrium with **2***b* is also converted to **4**.

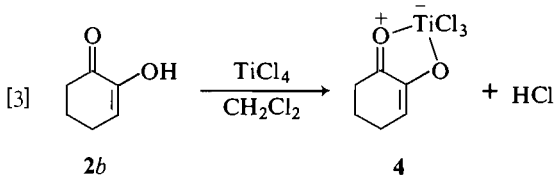

2*b* **4**

The reaction of **2** with $SnCl_4$ appears to be similar to that with $TiCl_4$ except that the loss of HCl is not complete. The complexation of the tin to the keto oxygen is indicated by the large downfield shift of the vinyl proton resonance. In addition, a broad concentration and temperature dependent signal at ca. δ 8.0 was observed, which was attributed to an OH resonance. This signal was absent at very low temperatures or in the presence of 2,6-di-*tert*-butylpyridine.

2-Methoxycyclohex-2-en-1-one, 5

The reaction of **5** with $SnCl_4$ and $TiCl_4$ was examined at −18°C. A considerable downfield shift of the vinyl proton resonance was observed with each Lewis acid, indicating that complexation had taken place at the keto oxygen, Table 2. In addition, the resonance associated with the methoxy group was also shifted downfield. This is suggestive that further complexation of the Lewis acid to the ether oxygen is occurring to some extent. No signals which could be attributed to the formation of HCl could be detected.

Addition reactions of complexes

Reactions of solutions of the above complexes with 1,3-butadiene were examined. Treatment of the $TiCl_4$ complex of **2** with butadiene and subsequent work-up gave a single product which appeared to have the structure **6** on the basis of its spectroscopic properties. This structural assignment was confirmed by catalytic hydrogenation of **6** to give **7**, a compound which has been previously described in the literature (10).

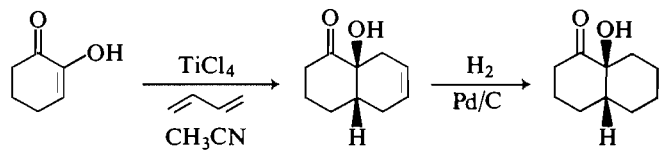

2 **6** **7**

The enol ether **5** reacted in a similar manner to **2** to give **8**. In addition to **8**, small amounts of **6** and a compound containing two butadiene residues were also isolated. Structural proof for **8** rests in its reduction to **9** and comparison of its properties to those of authentic material prepared by chlorination and methoxide displacement of 1-decalone and separation of the corresponding *cis* and *trans* isomers (10). The third component isolated from this reaction had a M^+ peak in its mass spectrum at *m/e* 202 and an elemental analysis corresponding to $C_{14}H_{18}O$. The ^{1}H nmr and ir spectra were consistent with the structure **10**, in which methanol has been lost from the original adduct **8** and a further butadiene added.

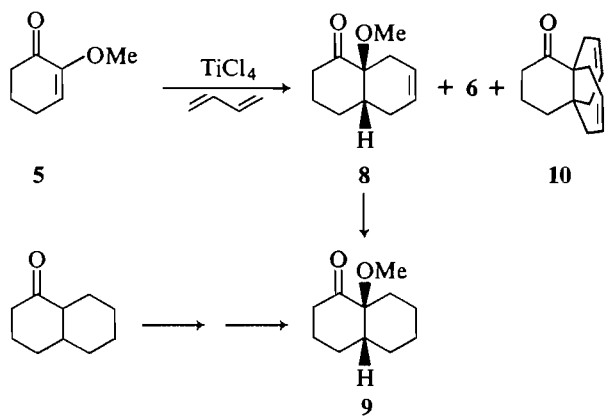

5 **8** **10**

9

Can. J. Chem. Downloaded from www.nrcresearchpress.com by 210.87.254.40 on 09/06/12
For personal use only.

Can. J. Chem. Downloaded from www.nrcresearchpress.com by 210.87.254.40 on 09/06/12
For personal use only.

The trimethylsilyl ether of **2** also reacted with $TiCl_4$ and butadiene to give **6** in 40% yield. Sasaki *et al.* have reported a similar result (5).

It would seem that all the products isolated in these reactions of **2** and its enol ethers with butadiene result from 4C + 2C cycloadditions. It should be noted that these 4 + 2 adducts would be expected to be more thermodynamically stable than the corresponding 4C + 3C adducts and that the two types of adduct can be formally interconverted by an acyloin rearrangement (11). In the absence of any materials corresponding to 4 + 3 adducts, it was not possible to test whether they would have survived the somewhat acidic reaction and work-up conditions.

As 2,3-butanedione did not form complexes which had an enol type structure, the reactions of the trimethylsilyl ether **11** with butadiene were investigated. With $TiCl_4$ as the Lewis acid, **11** reacted with butadiene to give the two isomeric products **12** and **13**, plus some uncharacterized high boiling material.

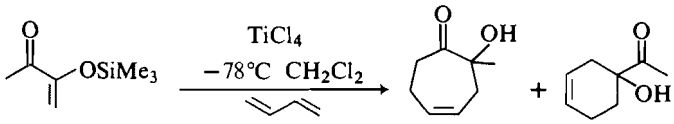

11 **12** **13**

Some difficulty was experienced in separating **12** and **13**, as **12** was relatively unstable and was converted to **13** when adsorbed on silica gel or at high temperatures on a glc column. Initial structural assignments for these materials were based on their spectroscopic properties. Infrared spectra indicated that both **12** and **13** were hydroxyketones; the ^1H nmr spectra showed that each compound had two vinyl protons, methylene protons and a methyl group. The signals of the latter protons were a singlet in each case and in characteristic positions for a methyl group on a saturated carbon, compound **12**, and adjacent to a carbonyl group, compound **13**. The structural assignment of **12** was confirmed by its reduction to **14** and subsequent independent synthesis of **14** from cycloheptan-1,2-dione, eq. [4].

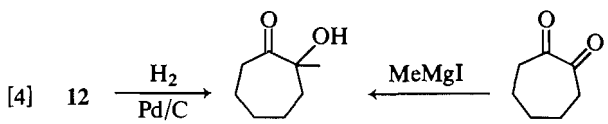

In an attempt to improve the yield of **12** and **13**, a smaller excess of butadiene was used and moisture carefully excluded from the system. Under these conditions two additional products were detected. From both the ^1H nmr and ms of these products, it was clear that they were silyl ethers. Reaction of a mixture of **12** and **13** with trimethylsilylchloride and triethylamine gave two silyl ethers which were identical to the extra materials produced in the cycloaddition reaction. On this basis these additional products were identified as **15** and **16**.

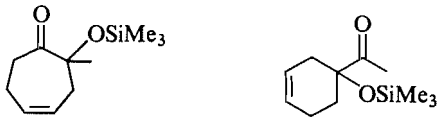

15 **16**

With limited amounts of butadiene and using $SnCl_4$ as a catalyst, **11** reacted to give **15** and **16** together with dimers of **11**. Acid hydrolysis of the mixture afforded **12** and **13** in a 1 : 1.5 ratio. This latter result contrasts with the report of Sasaki *et al.* who reported **13** as the sole product. It is possible that, during the chromatography used by these workers, **12** rearranged to **13**.

It is interesting to note that Sasaki *et al.* observed the formation of a 7-membered ring compound in the reaction of the trimethylsilyl ether of the enol of pyruvaldehyde. It might well be that the acyloin rearrangement of these seven-membered ring hydroxyketones occurs less readily with the secondary alcohol resulting from this latter reaction than the tertiary alcohols produced in the reaction of biacetyl.

In conclusion, it should be emphasized that the Lewis acid catalysed cycloaddition reactions of α,β-unsaturated carbonyl compounds, observed here to form seven-membered rings, proceed by a 4C + 3C route. The seven-membered ring products have been shown to be thermodynamically less stable than the related six-membered ring products. This means that these seven-membered ring products can only be produced directly in the reaction and not by an initial formation of the six-membered ring and subsequent ring expansion. It is not known whether the formation of the seven-membered ring is a concerted reaction; however, it is clear that the presence of a strong electron-donating group at the α-carbon of an enone can divert the normal pattern of Lewis acid catalysed cycloadditions to a 4C + 3C cycloaddition.

Experimental

General

The ^1H nmr spectra were obtained on Varian EM 390 and Bruker WP 80 instruments. CD_2Cl_2 and $CDCl_3$ were dried over freshly activated 4 Å molecular sieves before use. CH_2Cl_2 and CH_3CN were distilled from P_2O_5 and stored over molecular sieves. The Lewis acids, $SnCl_4$ and $TiCl_4$, were distilled and stored in sealed glass ampules.

The following compounds were prepared by literature procedures: 3-(trimethylsiloxy)-but-3-en-2-one, **11**, (12); cycloheptan-1,2-dione (13); 2-methoxycyclohex-2-en-1-one, **5** (14). 2-(Trimethylsiloxy)-cyclohex-2-en-1-one was prepared by silylation of **2** in acetonitrile using a similar procedure to that given above for **11**. The ^1H nmr spectrum was identical to that given in the literature (15).

Preparation of nuclear magnetic resonance samples

These were prepared under dry nitrogen. The appropriate Lewis base was weighed into a dry nmr tube, solvent added, and the tube capped with a rubber septum cap. A measured volume of a Lewis acid was added to the cooled tube (−78°C) using a 10 μL syringe. The contents of the tube were mixed by tilting the tube. Samples were kept at −78°C until their nmr spectra were obtained.

Reaction of 2 with butadiene

Compound **2** (1.6 g) in CH_3CN (1 mL) was placed in a thick-walled glass tube. The tube was blanketed with argon, cooled to −78°C, and $TiCl_4$ (1.8 mL, 1.65×10^{-2} mol) added. The solution was warmed to 0°C, further CH_3CN (6 mL) added, and the tube cooled to −78°C before 1,3-butadiene (4 mL) was condensed into the tube. The tube was sealed and allowed to warm to 25°C for 14 h. The contents of the tube were added to a 1 : 1 mixture of ether and water (20 mL) and the acid neutralized with solid $NaHCO_3$. After removal of the solids by filtration through Celite, the organic material was extracted into ether (2 × 15 mL), the ether layer dried ($MgSO_4$), and ether removed *in vacuo* to give an oil. Vacuum transfer of the oil gave **6** (0.78 g, 35%); ir (film): 3490, 3030, 1715, 1070 cm^{-1}; ^1H nmr (CCl_4), δ: 1.5–2.7 (m, 11H), 3.8 (s, 1H), 5.7 (m, 2H); ms M^+: 166. *Anal.* calcd. for $C_{10}H_{14}O_2$: C 72.26, H 8.49; found: C 72.24, H 8.55%.

Can. J. Chem. Downloaded from www.nrcresearchpress.com by 210.87.254.40 on 09/06/12
For personal use only.

*Reaction of **5** with butadiene*

An exactly comparable procedure to that given above for **2** was used. The resulting oil (0.7 g) was separated by preparative glc (15% Carbowax on Chromosorb A) at 200°C to give three compounds, **8**, 58%; **6**, 12%; **10**, (12%), plus other unidentifed minor components. Properties of **8** (10): ir (film): 3020, 1720, 1080 cm^{-1}; ^1H nmr (CCl_4), δ: 1.6–2.6 (m, 11H), 3.4 (s, 3H), 5.8 (m, 2H); ms M^+ 180. Properties of **10**: ir: 3025, 1710 cm^{-1}; ^1H nmr (CCl_4), δ: 1.15–2.8 (m, 14H), 5.3–6.0 (m, 4H); ms M^+: 202. *Anal.* calcd. for $C_{14}H_{10}O$: C 83.12, H 8.97; found: C 83.26, H 9.03%.

*Reaction of 2-(trimethylsiloxy)-but-1-en-3-one **11** with butadiene*

(a) *Excess butadiene*

A solution of **11** (2 g) in dry CH_2Cl_2 (15 mL) was cooled to −78°C under a nitrogen atmosphere and 1,3-butadiene (ca 10 mL) condensed into the reaction flask. $TiCl_4$ (1.4 mL) was added and the reaction mixture stirred for 1 h at −78°C. The reaction mixture was poured into a 1:1 mixture of ether/ice water (150 mL) and neutralized by the addition of $NaHCO_3$. The crude product was isolated as described above and the resulting oil distilled (70–75°C, 4 Torr) to give a mixture of **12** and **13** (0.42 g, 24%) in a 1.1:1 ratio. The products were separated by preparative glc (5% OV-17 on Chromosorb W) at 75°C, to give **12**; ir (film): 3490, 3040, 1710, 1095 cm^{-1}; ^1H nmr (CCl_4), δ: 1.25 (s, 3H), 2.10–2.47 (m, 4H), 2.5–2.93 (m, 2H), 3.8 (s, 1H), 5.85 (m, 2H); ms M^+: 140. *Anal.* calcd. for $C_8H_{12}O_2$: C 68.55, H 8.63; found: C 68.56, H 8.60%.

The properties of **13** were: ir (film): 3480, 3035, 1710, 1090 cm^{-1}; ^1H nmr (CCl_4), δ: 1.5–2.7 (m, 6H), 2.2 (s, 3H), 3.2 (s, 1H), 5.65 (m, 2H); ms *m/e*: 122 ($M^+ - H_2O$). *Anal.* calcd. for $C_8H_{12}O_2$: C 68.55, H 8.63; found: C 68.83, H 8.66%.

(b) *Limited butadiene*

1,3-Butadiene (0.27 g) was transferred into a 100-mL round bottom flask, the flask cooled to −78°C under N_2, and dry CH_2Cl_2 (10 mL), **11** (0.52 g), and $TiCl_4$ (0.36 mL) added successively using dry syringes. The reaction was stirred at −78°C for 6 h and worked up as above. Analysis of the resulting mixture by glc–ms indicated four major components, **12**, **13**, and the silyl derivatives **15** (ms *m/e*: 197, 169, 143, 73) and **16** (ms *m/e*: 212, 197, 169, 143, 73) (16). The ^1H nmr of the mixture indicated the presence of trimethylsilyl groups (δ 0.09 and 0.07).

The above mixture (0.2 g) was treated with chlorotrimethylsilane (1.3 mL) and triethylamine (1.4 mL) in dry CH_2Cl_2 (5 mL) for 20 h. The resulting suspension was treated with pentane (5 mL) and the precipitate removed by filtration in a nitrogen atmosphere. The residue obtained after removing the solvent was distilled (100°C, 5 Torr) to give a mixture of **15** and **16** (0.236 g; 34% based on **11**). The products were separated by preparative glc (5% OV-17 on Chromosorb W) at 105°C, to give **15** (retention time 11.5 min); ^1H nmr (CCl_4), δ: 0.09 (s, 9H), 1.6–2.3 (m, 6H), 2.15 (s, 3H), 5.60 (m, 2H). Compound **16** (retention time 13.5 min), ^1H nmr (CCl_4), δ: 0.07 (s, 9H), 1.30 (s, 3H), 2.25–2.9 (m, 6H), 5.72 (m, 2H).

(c) *$SnCl_4$ catalyst*

The procedure (b) above was employed using $SnCl_4$ (0.38 mL) as the Lewis acid. The crude product was distilled (120°C, 3 Torr) to give an oil (0.19 g). The major components were identified as **15** and **16** by ^1H nmr and glc comparison with authentic materials, and (two) dimers of **11** by glc–ms analysis; each showed *m/e*: 316, 273, 231, 143, 73; M^+ calcd. for $C_{14}H_{28}O_4Si_2$: 316 (12).

The mixture obtained above was treated with 1 *N* HCl (1 mL) in methanol (5 mL) for 30 min at 25°C and poured onto ice-water containing $NaHCO_3$. The organic material was extracted into ether and the extracts were dried ($MgSO_4$). The ^1H nmr analysis of the oil obtained on removing the solvent indicated a mixture containing **12** and **13** in a 1:1.5 ratio according to the peak heights of the methyl resonances.

Reaction of 2-(trimethylsiloxy)-cyclohex-2-en-1-one with butadiene

A solution of butadiene (0.27 g) and 2-(trimethylsiloxy)-cyclohex-2-en-1-one (0.60 g, 3.3 mmol) in dry CH_2Cl_2 (10 mL) was treated with $TiCl_4$ (0.36 mL) as described in (b) above. The reaction mixture was allowed to warm up to room temperature, stirred for a further 20 h, and worked up as described above. The oil obtained after removing the solvent was distilled (3 Torr; Kugelrohr temperature 130°C) to give **6** (220 mg, 40%); ir and ^1H nmr spectra identical to those of authentic **6** described earlier.

*Hydrogenation of **6***

A solution of **6** (44 mg) in ethanol (1 mL) was hydrogenated (1 atm) over Pd/C at room temperature. After 18 h the catalyst was removed by filtration and the solvent was evaporated under reduced pressure. The crude product was vacuum transferred to give **6** (37 mg, 83%), mp 56–60°C (lit. (10) mp 61–64°C); ir: 3490 (br), 1710 cm^{-1}; ^1H nmr (CCl_4), δ: 0.9–2.0 (m, 13H), 2.4 (m, 2H), 3.6 (s, 1H).

*Hydrogenation of **12***

Compound **12** (114 mg, 0.8 mmol) was hydrogenated as described above for compound **6**. The crude product was distilled (120°C, 4 Torr) to give **14** (60 mg, 53%). Preparative glc (5% OV-17 on Chromosorb W) at 130°C afforded the analytical sample (retention time 2.5 min); ir (CCl_4): 3520, 3220, 2980, 2940, 2870, 1715, 1460, 1370, 1340, 1185, 1050, 950 cm^{-1}; ^1H nmr (CCl_4), δ: 1.25 (s, 3H), 1.25–2.22 (m, 8H), 2.37–2.70 (m, 2H), 3.50 (s, 1H) exchanges with D_2O; ms M^+ calcd. for $C_8H_{14}O_2$: 142.0094; found: 142.0964.

Reaction of cycloheptan-1,2-dione with methylmagnesium iodide

A solution of methylmagnesium iodide (2.32 mmol) in ether (7 mL) was added dropwise to a solution of crude cycloheptan-1,2-dione (0.59 g, ca 50% dione) in dry ether (5 mL) at 0°C. The reaction mixture was stirred at the same temperature under dry nitrogen for 1.5 h and poured into ice-cold ammonium chloride solution. The organic material was extracted into ether and the extracts were washed with brine and dried ($MgSO_4$). The residue obtained after removing the solvent under reduced pressure was distilled (4 Torr; Kugelrohr temperature 140°C) and the resultant oil was subjected to preparative glc (5% OV-17 on Chromosorb W) at 125°C. Collection of the fraction with retention time 3.7 min afforded **14**; properties (retention time, ir spectrum, ^1H nmr spectrum) identical to those of the hydrogenation product of compound **12**.

Acknowledgement

This work was supported by the Natural Sciences and Engineering Research Council of Canada.

1. H. M. R. HOFFMANN. Angew. Chem. Int. Ed. Engl. **12**, 819 (1973); R. NOYORI. Acc. Chem. Res. **12**, 61 (1979).
2. H. M. R. HOFFMANN, G. F. P. KERNAGHAN, and G. GREENWOOD. J. Chem. Soc. B, 2257 (1971); H. M. R. HOFFMANN, K. E. CLEMENS, and R. H. SMITHERS. J. Am. Chem. Soc. **94**, 3940 (1972); A. E. HILL, G. GREENWOOD, and H. M. R. HOFFMANN. J. Am. Chem. Soc. **95**, 1338 (1973); H. M. R. HOFFMANN and J. MATTHEI. Chem. Ber. **113**, 3837 (1980); R. NOYORI, S. MAKINO, and H. TAKAYA. J. Am. Chem. Soc. **93**, 1272 (1971); R. NOYORI, Y. HAYAKAWA, M. FUNAKURA, H. TAKAYA, S. MURAI, R. KOBAYASHI, and S. T. SUTSUMI. J. Am. Chem. Soc. **94**, 7202 (1972); R. NOYORI, S. MAKINO, T. OKITA, and Y. HAYAKAWA. J. Org. Chem. **40**, 806 (1975); R. NOYORI, Y. HAYAKAWA, M. FUNAKURA, H. TAKAYA, S. MURAI, R. KOBAYASHI, and N. SONODA. J. Am. Chem. Soc. **100**, 1759 (1978); H. TAKAYA, S. MAKINO, Y. HAYAKAWA, and R. NOYORI. J. Am. Chem. Soc. **100**, 1765 (1978); N. SHIMIZU, M. TANAKA, and Y. TSUNO. J. Am. Chem. Soc. **104**, 1330 (1982).
3. B. B. SNIDER. J. Org. Chem. **39**, 225 (1974); **41**, 3061 (1976); S. M. MAKIN. Pure Appl. Chem. **49**, 173 (1976); T. SATO, S. YOSHIE, T. IMAMURA, K. HASEGAWA, M. MIYAHARA, S. YAMAMURA, and O. ITO. Bull. Chem. Soc. Jpn. **50**, 2714 (1977).
4. P. YATES and P. EATON. J. Am. Chem. Soc. **82**, 4436 (1960); G. I. FRAY and R. ROBINSON. J. Am. Chem. Soc. **83**, 249 (1961); H. W. THOMPSON and D. G. MELILLO. J. Am. Chem. Soc. **92**, 3218 (1970); M. KAKUSHIMA, J. ESPINOSA, and Z. VALENTA.

Can. J. Chem. **54**, 3304 (1976); M. KAKUSHIMA and D. G. SCOTT. Can. J. Chem. **57**, 1399 (1979); M. KAKUSHIMA. Can. J. Chem. **57**, 2564 (1979); M. KAKUSHIMA, L. ALLAIN, R. A. DICKINSON, P. S. WHITE, and Z. VALENTA. Can. J. Chem. **57**, 3354 (1979); M. KAKUSHIMA, J. DAS, G. R. REID, P. S. WHITE, and Z. VALENTA. Can. J. Chem. **57**, 3356 (1979).

5. T. SASAKI, Y. ISHIBASHI, and M. OHNO. Tetrahedron Lett. 1693 (1982).
6. R. A. KENNEDY. M.Sc. Thesis, McMaster University, 1982.
7. H. A. BENESI and J. H. HILDEBRAND. J. Am. Chem. Soc. **71**, 2703 (1944).
8. H. C. BROWN and B. KANNER. J. Am. Chem. Soc. **88**, 986, 1966.
9. R. F. CHILDS, D. L. MULHOLLAND, and A. NIXON. Can. J. Chem. **60**, 801 (1982).
10. H. O. HOUSE and H. W. THOMPSON. J. Org. Chem. **28**, 164 (1963).
11. C. J. COLLINS and J. F. EASTHAM. *In* The chemistry of the carbonyl group. *Edited by* S. Patai. Interscience, New York. 1966. pp. 771–783.
12. S. MURAI, I. RYCE, Y. KADONO, H. KATAYAMA, K. KONDO, and N. SONODA. Chem. Lett. 1219 (1977).
13. R. W. VANDER HAAR, R. C. VOTER, and C. V. BANKS. J. Org. Chem. **14**, 836 (1949).
14. M. S. GIBSON. J. Chem. Soc. 681 (1962).
15. C. COURET, J. SATGE, J. ESCUDIE, and F. COURET. J. Organometal. Chem. **57**, 287 (1973).
16. H. O. HOUSE, L. Z. CZUBA, M. GALL, and H. D. OLMSTEAD. J. Org. Chem. **34**, 2324 (1969).

Can. J. Chem. Downloaded from www.nrcresearchpress.com by 210.87.254.40 on 09/06/12
For personal use only.

Hydroxyacetals, phthalans, and isobenzofurans therefrom

BRIAN A. KEAY, HEINZ P. PLAUMANN, DAYANANDA RAJAPAKSA, AND RUSSELL RODRIGO
Guelph–Waterloo Centre for Graduate Work in Chemistry, Department of Chemistry, University of Waterloo, Waterloo, Ont., Canada N2L 3G1

Received January 31, 1983

BRIAN A. KEAY, HEINZ P. PLAUMANN, DAYANANDA RAJAPAKSA, and RUSSELL RODRIGO. Can. J. Chem. **61**, 1987 (1983).

A general method for the generation of isobenzofuran intermediates is described. Lithiated aromatic acetals are converted to hydroxyacetals (A) which may be cyclized to isobenzofurans by mild acid treatment through the 1-hydroxyphthalans (B). The isobenzofurans generated *in situ* are trapped by a variety of dienophiles to provide the expected oxo-bicyclo adducts (C). The mass and ^{1}Hmr spectra of B and C are discussed.

BRIAN A. KEAY, HEINZ P. PLAUMANN, DAYANANDA RAJAPAKSA et RUSSELL RODRIGO. Can. J. Chem. **61**, 1987 (1983).

On décrit une méthode générale de production des intermédiaires de l'isobenzofuranne. On transforme les acétals aromatiques lithiés en hydroxyacétals (A) que l'on peut cycliser en isobenzofurannes via les hydroxy-1 phtalanes (B) en présence d'un acide dans des conditions douces. On piège les isobenzofurannes générés *in situ* avec divers diénophiles pour obtenir les adduits oxo-bicyclo attendus (C). On discute des spectres de masse et de rmn du ^{1}H des composés B et C.
[Traduit par le journal]

Can. J. Chem. Downloaded from www.nrcresearchpress.com by 210.87.254.42 on 09/06/12
For personal use only.

The benzo[*c*]furan system, trivially called isobenzofuran (ISB), has been known (1) since 1964. In the following years, many methods were developed for the production of isobenzofurans, most of them involving retro Diels–Alder reactions of various precursors (2) and culminating in the isolation (3) of the parent benzo[*c*]furan as an unstable solid very prone to polymerization. Several theoretical calculations (2) suggest that the molecule is nonaromatic but the appearance of furanoid protons at δ 8.40 in the ^{1}Hmr spectrum of ISB implies (3) the presence of a significant ring current. The reactivity of isobenzofurans as dienes in the Diels–Alder reaction, however, is extremely well documented (2) and their widespread application[1] to the construction of aromatic and hydroaromatic natural products has hitherto been limited only by the lack of versatile methods of ISB synthesis. Syntheses not entailing Diels–Alder reversions have been reported (5) in recent years and the consequent enhancement in synthetic versatility has led to many applications of inter (6) and intramolecular (7) Diels–Alder reactions of ISB's in natural product synthesis. In this report we discuss some of our recent work on the generation of a variety of ISB's and their reactions with many common dienophiles.

The aromatic acetal route we have employed is generalized in Scheme 1. It is a "one-pot" process, although phthalans (B) and even isobenzofurans[2] may be isolated in some instances.

Preparation of hydroxyacetals (A)

Many acetals (and ketals), incorporating a variety of substituents differing in number, type, and position, were prepared. The most convenient route, also the simplest, begins with a bromoaldehyde which is converted to its dimethyl acetal (with trimethylorthoformate and Dowex 50 W-X2 resin in refluxing methanol), lithiated by halogen–lithium exchange, and reacted with formaldehyde or an aromatic aldehyde (A**1**–A**5**).

Alternatively, direct *ortho*-deprotonation (8) of aromatic acetals, followed by treatment of the ensuing *ortho*-lithio species with nonenolizable aldehydes, provides a series of contiguously substituted hydroxyacetals (A**6**–A**8**). A major shortcoming of these preparations is that the aryl lithium species is readily protonated by enolizable aldehydes or ketones, thus precluding the use of most aliphatic aldehydes and limiting the R^1 substituent to H or aryl.

One solution to this problem is to start with a bromoketal instead, and to carry out the same sequence of reactions. Thus, hydroxyketals A**9**–A**11** are obtained by halogen–lithium exchange from the corresponding bromoketal and reaction with formaldehyde (A**9**, A**10**) or piperonal (A**11**). Compounds A**9** and A**10** are precursors of 1-methyl isobenzofurans and in general this route will provide 1,3-dialkyl (or 1,3-alkyl aryl)

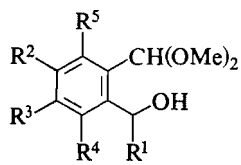

A**1** $R^2 = R^3 = OMe$, R^1 = 3,4-methylenedioxyphenyl, $R^4 = R^5 = H$
A**2** $R^2 + R^3 = OCH_2O$, R^1 = 3,4-methylenedioxyphenyl, $R^4 = R^5 = H$
A**3** $R^2 + R^3 = OCH_2O$, R^1 = 3,4-dimethoxyphenyl, $R^4 = R^5 = H$
A**4** $R^2 + R^3 = OCH_2O$, R^1 = 3,4,5-trimethoxyphenyl, $R^4 = R^5 = H$
A**5** $R^2 = R^3 = OMe$, $R^1 = R^4 = R^5 = H$
A**6** $R^3 = R^4 = OMe$, R^1 = 3,4-methylenedioxyphenyl, $R^2 = R^5 = H$
A**7** $R^2 = R^3 = R^4 = OMe$, R^1 = 3,4,5-trimethoxyphenyl, $R^5 = H$
A**8** $R^3 = R^4 = OMe$, $R^1 = R^2 = R^5 = H$
A**12** $R^2 + R^3 = OCH_2O$, $R^4 = R^5 = H$, R^1 = cyclohexyl

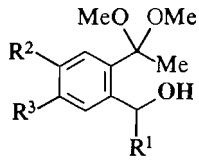

A**9** $R^2 = R^3 = OMe$, $R^1 = H$
A**10** $R^2 + R^3 = OCH_2O$, $R^1 = H$
A**11** $R^2 = R^3 = OMe$, R^1 = 3,4-methylenedioxyphenyl

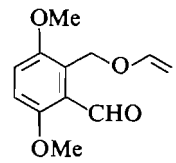

A**13**

[1]One exception has been the use of an isobenzofuran intermediate in the synthesis of an anthracyclinone (see ref. 4).
[2]D. Rajapaksa and R. Rodrigo. Unpublished results.

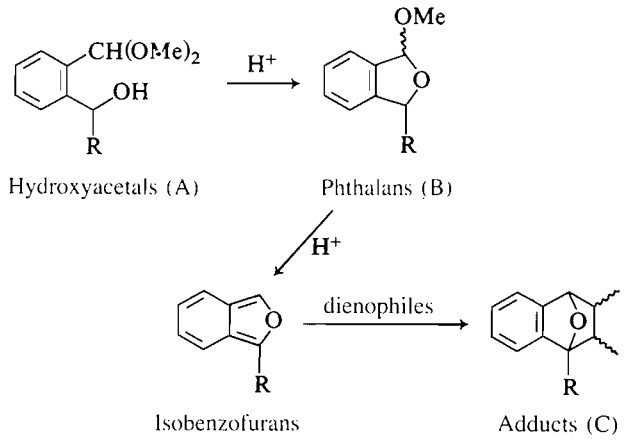

SCHEME 1

isobenzofurans.

In the course of our work we have made the fortuitous discovery that carbinolamines arising from the capture of lithiated acetals by dimethyl formamide can be selectively hydrolysed without affecting the acetal moiety to provide *ortho* formyl acetals. Thus hydroxyacetal A**12** was prepared from the 6-bromo dimethyl acetal of piperonal as illustrated in Scheme 2.

The success of this Grignard route provides another avenue of access to such hydroxyacetals (R^1 = alkyl) previously prepared by the ketal method. Furthermore, the potential of the Grignard and bromoketal technologies for assembling complex fragments, in preparation for intramolecular Diels–Alder reactions, is obvious. Investigations concerned with the synthesis of condensed hydroaromatic systems by these methods are in progress.

All but two (A**4** and A**8**) of these hydroxyacetals are oils that

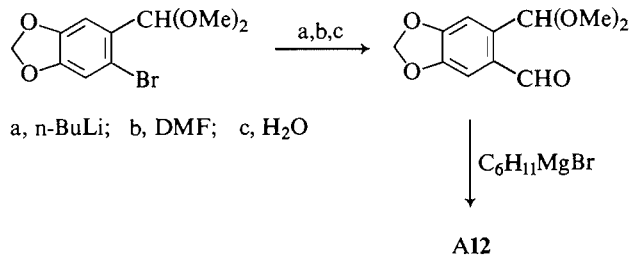

SCHEME 2

provided spectroscopic data consistent with their structures but resisted crystallization. They were used without further purification for the generation of isobenzofurans according to Scheme 1.

The mass spectra of these compounds are characterized by the presence of prominent ions resulting from sequential elimination of two molecules of methanol from the parent ion ($M - 32$, $M - 64$); an ion corresponding to loss of methanol and a methoxy radical ($M - 63$) is also found in the spectra.

Phthalans (B)

The 1-methoxy (or hydroxy) phthalans formed by mild acid treatment of the hydroxyacetals are easily detectable by ^{1}Hmr spectroscopy. Some were isolated and characterized (B**2**, B**5**, B**6**, B**7**, B**8**, B**13**, and B**14**). The known 1-hydroxyphthalan B**14** was prepared by reduction of the corresponding phthalide as previously reported (9). This is not a general route to hydroxyphthalans, however; its success depends on the presence of "peri" substituents (R4, R5 ≠ H) in the benzene ring. They prevent the ring opening and thereby forestall the further reduction of the masked aldehyde initially formed. A similar explanation has been advanced (10) for reactions where one mole of a Grignard reagent adds to certain peri-substituted phthalides to form hydroxyphthalans. The related 1-methoxyphthalan

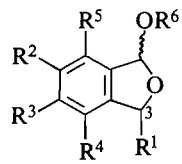

B**2** $R^2 + R^3 = OCH_2O$, R^1 = 3,4-methylenedioxyphenyl, $R^4 = R^5 = R^6 = H$
B**5** $R^2 = R^3 = OCH_3$, $R^1 = R^4 = R^5 = H$, R^6 = Me
B**6** $R^3 + R^4 = OCH_2O$, R^1 = 3,4-methylenedioxyphenyl, $R^2 = R^5 = H$, R^6 = Me
B**7** $R^2 = R^3 = R^4$ = OMe, R^1 = 3,4,5-trimethoxyphenyl, $R^5 = H$, R^6 = Me
B**8** $R^3 = R^4$ = OMe, $R^1 = R^2 = R^5 = H$, R^6 = Me
B**13** $R^4 = R^5$ = OMe, $R^1 = R^2 = R^3 = H$, R^6 = Me
B**14** $R^4 = R^5$ = OMe, $R^1 = R^2 = R^3 = R^6 = H$

B**13** was also prepared by a more direct route from 2,5-dimethoxybenzyl alcohol. Lithiation (11) of its vinyl ether and treatment and dimethylformamide provided a hydroxyacetal equivalent A**13** which, upon successive treatment with methanolic mercuric acetate and methanolic *p*-toluene sulfonic acid, gave B**13**.

Phthalans show substantial long-range coupling between protons at C-1 and C-3. It has been suggested that this is a "dual pathway" interaction ($^4J + {}^3J$) and its magnitude in several variants of 2,5-dihydrofurans has been related (12) to conformational factors. Our phthalans all possess a C-1 oxygen substituent and in every instance we have observed that $J_{1,3}$ (*trans*) is ≈2.4 Hz while $J_{1,3}$ (*cis*) ≈ 0 Hz. Although such a distinct stereochemical dependence of 1,3 coupling has not been previously reported for oxygen-substituted phthalans, similar drastic decreases in the 1,3 *cis* coupling constants of 2,5-dihydrofurans have been noted and correlated (12) with the electronic effects of a 2-oxygen substituent in the latter compounds. It thus appears that in 1- or 3-oxygenated phthalans the magnitude of the long-range ($J_{1,3}$) coupling is stereochemically diagnostic. In all our phthalans where *cis* and *trans* stereoisomers can exist we find that ring closure of the acyclic precursors takes place approximately equally in either direction to produce a 1:1 mixture of *cis* and *trans* isomers. Signals of H-1 and H-3 of both isomers are visible in the ^{1}Hmr spectrum in approximately equal intensities. The isomers must be of about

Can. J. Chem. Downloaded from www.nrcresearchpress.com by 210.87.254.42 on 09/06/12
For personal use only.

TABLE 1. Reactions of hydroxy acetals* with dimethylacetylene dicarboxylate

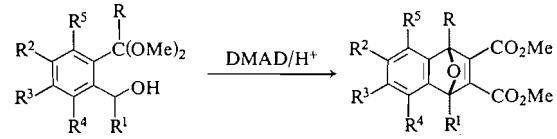

Hydroxy acetal	Adduct (yield, %)
A**1**	C**1**(65)
A**2**	C**2**(65)
A**3**	D**3**(62)†
A**4**	C**4**(65)
A**5**	C**5**(99)
A**6**	D**6**(62)†
A**7**	D**7**(73)†
A**8**	C**8**(34)
A**9**	C**9**(96)
A**10**	C**10**(96)
A**11**	C**11**(96)
A**12**	C**12**(70)

*R = H except in A**9**, C**9**–A**11**, C**11** (R = Me).
†Isolated as the naphthol.

equal stability because the 1 : 1 proportion is unaffected by the duration of acid exposure in the cyclization.

The Diels–Alder reaction and formation of adducts (C)

The Diels–Alder reactions of ISB precursors A and B were studied in two ways. In the first instance almost all precursors were reacted with dimethyl acetylenedicarboxylate in the presence of a catalytic quantity of glacial acetic acid at steam bath temperatures. With this combination of reactants both regiochemical and stereochemical problems were avoided for the time being. The bridged adducts were isolated in good yields after crystallization from ether. In a few cases care had to be taken to prevent aromatization to the naphthol. Thus adducts **C1**, **C2**, and **C4** (Table 1) were very prone to aromatization and careful control of time (25–30 min) and temperature (95–100°C) was necessary. Under these conditions the Diels–Alder reaction remains incomplete and acceptable yields of these compounds were only obtained after recycling mother liquors remaining from crystallization of the adducts. Adducts **C3** and **C10** resisted crystallization but could be converted to the crystalline naphthols D**3** and D**10** by further acid treatment. Adduct **C7** could not be obtained under any conditions. It appears that the peri-methoxy group (R_4 = OMe) hinders ISB formation below 130°C. At this temperature **C7** is rapidly isomerized to D**7**, the isolated product.

In a second study, a symmetrical ISB precursor A**5** (or B**5**) was subjected to Diels–Alder additions with a variety of dienophiles (Table 2). Regiochemical complications were thus circumvented but in every case mixtures of *endo–exo* products were isolated in good to excellent yields. *endo* Isomers generally predominated except in the case of the 2-butenolide adduct (entry 4). *endo* Isomers were crystallized from the mixture in some cases (entries 2, 5, and 8) while in others the adducts were separated by a combination of chromatography and fractional crystallization. *endo–exo* Ratios were easily estimated by ^{1}Hmr spectroscopy, aided by spectra of pure isomers where available. To illustrate the use of ^{1}Hmr spectroscopy for this purpose, a tabulation and brief discussion of the spectra of pure *exo* and *endo* C**5***i* (entry 9, Table 2) is presented below (Table 3).

Differences between the spectra of *exo* and *endo* isomers observed here are typical of all the adducts and are easily detected and explained. In the *exo* isomers bridgehead protons (H-1) are singlets; H-4 is coupled only to the β-proton at C-3 and thus appears as a doublet in both isomers. These protons are rigidly held in a plane approximating that of the adjacent benzene ring and are consequently subject to its deshielding influence. Thus H-1 and H-4 signals are both around δ 5.5 but with differing coupling patterns in the two isomers. No "phthalan-type" long range coupling was found between these two protons, however, even though the rigidity of the molecule ensures a favourable "W" pathway. Further differences between the two spectra can also be associated with the disposition of the C-2 substituent. A significant variation is found in H-9 (aldehyde proton) and H-2 resonances, an obvious consequence of differential shielding by the benzene ring. Such shielding also affects the 3α protons in both isomers making $\Delta\nu(3\alpha,3\beta)$ relatively large and thus simplifying the spectra. Slight, but consistent, differences in the absorptions of aromatic protons and substituents between *exo* and *endo* isomers are seen in all adducts. Again, it is the C-2 substituent in the *endo* configuration only that is responsible for the nonequivalence of the observed chemical shifts. All assignments and coupling constants were secured by decoupling experiments and 400 MHz spectra where necessary.

The mass spectra of all adducts were characterized by the presence of a very intense ion corresponding to a retro Diels–Alder fission of the molecular ion. This ion, the base peak in all spectra, corresponds to 5,6-dimethoxy isobenzofuran. Charge localization on the "dienophile" is also observed in many cases. The ISB ion (common at *m/z* 178 in all examples of **C5**) shows subsequent extrusions of CO, CH_3, CO, and CH_2O represented by ions at 150, 135, 107, and 77 mass units respectively. A minor decomposition pathway in all **C5** cases (except **C5***f*) involves dehydration to a naphthalene represented by an ion at $M - 18$ ($M - 19$ in 2-deutero examples).

Adducts substituted at a bridgehead position by an aryl group (e.g. **C1**–**C4**, **C6**, **C7**) were easily aromatized to the corresponding naphthols (6, 7).

Experimental

General methods

Melting point determinations were made using a Buchi SMP-20 apparatus and are uncorrected. Infrared spectra were obtained on Beckman Model IR-10 or on Acculab 10 spectrophotometers. Nuclear magnetic resonance spectra were obtained on either a Varian T-60, Perkin–Elmer R12-B, Bruker WP-80, or Bruker WH-400 spectrophotometer. Samples were run in $CDCl_3$ solutions containing tetramethylsilane as an internal standard. Low and high resolution mass spectra were measured on a Varian VG Organic 7070F mass spectrometer. Flash column chromatography was performed using Merck 0.063–0.200 mm (70–230 mesh) silica gel 60 which was packed dry into glass columns and eluted with benzene–acetone (4:1) unless otherwise noted. Combustion analyses were performed by Guelph Chemical Laboratories, Guelph, Ontario and/or Canadian Microanalytical Service Ltd, Vancouver, British Columbia.

General method for preparing benzaldehydedimethyl acetals

A stirred mixture of the benzaldehyde (0.1 mol), trimethylorthoformate (0.3 mol), absolute methanol (150 mL), and Dowex 50W-X8 acid exchange resin was refluxed for 20 h. The solution was cooled, filtered, and evporated *in vacuo*. The residual oil was distilled *in vacuo* providing the acetal in pure form.

Can. J. Chem. Downloaded from www.nrcresearchpress.com by 210.87.254.42 on 09/06/12
For personal use only.

Can. J. Chem. Downloaded from www.nrcresearchpress.com by 210.87.254.42 on 09/06/12
For personal use only.

TABLE 2. Reaction of A5 (and B5) with dienophiles

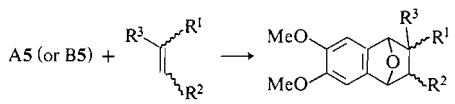

Dienophile	Yield (*endo: exo*)	Adduct (C)	
1. Benzoquinone	60(7:3)	$R^1 + R^2 =$ 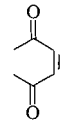 , $R^3 = H$	C5a
2. Naphthoquinone	86(3:1)*	$R^1 + R^2 =$ 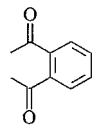 , $R^3 = H$	C5b
3. Methyl vinylketone	80(3:2)†	R^1 = COMe, $R^2 = R^3 = H$	C5c
4. 2-Butenolide	72(1:2)†	$R^1 + R^2 =$, $R^3 = H$	C5d
5. Acrylonitrile	64(9:1)*	R^1 = CN, $R^2 = R^3 = H$	C5e
6. α-Chloroacrylonitrile	70	R^1 = CN, R^3 = Cl, $R^2 = H$	C5f
7. Maleic anhydride	60(7:3)	$R^1 + R^2 =$ 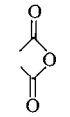 , $R^3 = H$	C5g
8. Methyl acrylate	50(3:2)	$R^1 = CO_2Me$, $R^2 = R^3 = H$	C5h
9. Acrolein	63(3:2)†	R^1 = CHO, $R^2 = R^3 = H$	C5i

**endo* Adduct crystallized.
†Adducts separated and crystallized.

TABLE 3.

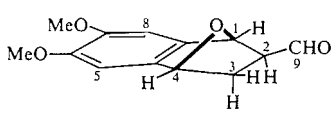

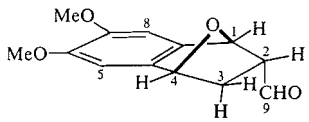

	exo			*endo*		
Proton	δ(ppm)	Multiplicity	*J* (Hz)	δ(ppm)	Multiplicity	*J* (Hz)
1	5.57	s		5.51	d	1,2 = 5.08
2	2.49	ddd	2,9 = 3.06 2,3α = 8.55 2,3β = 3.66	3.23	dddd	1,2 = 5.08 2,9 = 3.32 2,3α = 3.71 2,3β = 9.50
3α	1.67	dd	*gem* = 11.6 2,3α = 8.55	1.67	dd	*gem* = 11.8 2,3α = 3.71
3β	2.36	ddd	2,3β = 3.66 *gem* = 11.6 3β,4 = 4.88	2.35	ddd	2,3β = 9.5 *gem* = 11.8 3β,4 = 5.08
4	5.49	d	3β,4 = 4.88	5.45	d	3β,4 = 5.08
9	9.74	d	2,9 = 3.05	8.91	d	2,9 = 3.32
5,8	6.90	s		6.84,6.91	s, s	
2 × OMe	3.88	s		3.85, 3.88	s, s	

General lithium–halogen exchange procedure (A1–A5, A9–A11)

A stirred solution of the bromoacetal and dry diethyl ether (15 mL) was cooled to −78°C under N_2. n-BuLi (1.1 equiv./ mol of acetal) was added dropwise and the resulting precipitate stirred for 0.5 h before being treated with the appropriate electrophilic reagent. Increasing the scale of the reaction to 30 mmol did not noticeably affect the yields.

6-Formyl piperonal dimethyl acetal

6-Bromopiperonal dimethyl acetal (6.08 g, 22.1 mmol) was lithiated as previously described and treated with excess of dry dimethylformamide (10 g, 137 mmol) at −78°C. The reaction mixture was allowed to warm up to room temperature during 2 h and quenched with H_2O. The ether layer was separated, the aqueous layer extracted with ether (2 × 50 mL), and the combined ether extracts washed with

Can. J. Chem. Downloaded from www.nrcresearchpress.com by 210.87.254.42 on 09/06/12
For personal use only.

a saturated solution of NaCl and dried (Na_2SO_4). Evaporation of solvent gave crystalline 6-formyl piperonal dimethylacetal (4.05 g, 82%) which was recrystallized from ether–hexane, mp 80°C; ir ($CHCl_3$): 1670 (C=O) cm^{-1}; ^{1}Hmr ($CDCl_3$, 80 MHz), δ 3.40 (s, 6H, 2 OMe), 5.85 (s, 1H, C*H*$(OMe)_2$), 6.08 (s, 2H, OCH_2O), 7.18, 7.40 (s, 1H each, Ar), 10.30 (s, 1H, CHO); mass spectrum, *m/z* (assignment): 224 (M^+), 209 ($M^+ - CH_3$) 194 ($M^+ - 2\ CH_3$), 193 ($M^+ - OCH_3$). *Anal.* calcd. for $C_{11}H_{12}O_5$: C 58.92, H 5.35; found: C 58.96, H 5.26.

*Compound A***1**

6-Bromo-3,4-dimethoxybenzaldehyde dimethyl acetal (5.0 g, 17.2 mmol) was lithiated as previously described. To the stirred suspension was added a solution of piperonal (2.8 g, 18.7 mmol) and dry diethyl ether (50 mL) via a pressure-equalizing dropping funnel. The mixture was stirred for 0.5 h, poured into H_2O (50 mL), and extracted with ether (2 × 50 mL). The extract was dried (Na_2SO_4) and evaporated *in vacuo*. This afforded a light oil (16.6 g, 95%) which was not purified further; ir (neat): 3450 (OH) cm^{-1}; ^{1}Hmr ($CDCl_3$, 60 MHz), δ: 3.23 (s, 6H, —CH$(OCH_3)_2$), 3.37 (d, 1H, —OH, J = 4 Hz, exchangeable with D_2O), 3.85, 4.18 (s, 3H each, 2 × OCH_3), 5.40 (s, 1H, C*H*$(OCH_3)_2$), 5.87 (s, 2H, —OCH_2O—), 5.97 (d, 1H, —C*H*OH, J = 4 Hz, collapses to a singlet after D_2O), 6.63–6.90 (m, 4H, Ar), 7.05 (s, 1H, Ar); mass spectrum, *m/z* (assignment): 362 (M^+), 330 ($M^+ - CH_3OH$), 299 ($M^+ - CH_3OH - CH_3O$), 298 ($M^+ - 2CH_3OH$).

*Compound A***2**

6-Bromo-3,4-methylenedioxybenzaldehydedimethyl acetal (5.0 g, 18.2 mmol) was lithiated and treated with piperonal (2.87 g, 19.1 mmol) as previously described. Work-up was similar to that of A**1** and afforded an oil (6.0 g, 95%) which was not purified further; ir (neat): 3420 (OH) cm^{-1}; ^{1}Hmr ($CDCl_3$, 60 MHz) δ: 3.21 (s, 6H, 2 × OCH_3), 3.45 (br, 1H, OH, exchangeable with D_2O), 5.37 (s, 1H, C*H*$(OCH_3)_2$), 5.87 (s, 4H, 2 × —OCH_2O—), 5.96 (br, 1H, —C*H*OH, sharpens with D_2O,) 6.66–6.95 (m, 3H, Ar), 6.75, 7.02 (s, 1H, each, Ar); mass spectrum, *m/z* (assignment): 346 (M^+), 314 ($M^+ - CH_3OH$), 283 ($M^+ - CH_3OH - CH_3O$), 282 ($M^+ - 2CH_3OH$).

*Compound A***3**

6-Bromo-3,4-methylenedioxybenzaldehydedimethyl acetal (5.0 g, 18.2 mmol) was lithiated and treated with veratraldehyde (3.15 g, 1.90 mmol). Work-up as described gave A**3** as an oil (6.0 g, 91%) which was not purified further; ir (neat): 3520 (OH) cm^{-1}; ^{1}Hmr ($CDCl_3$, 60 MHz), δ: 3.25 (s, 6H, CH$(OCH_3)_2$), 3.50 (d, 1H, OH, J = 4.2 Hz, disappears with D_2O), 3.91 (s, 6H, 2 × OCH_3), 5.42 (s, 1H, C*H*$(OCH_3)_2$, 5.95 (s, 2H, —OCH_2O—), 6.1 (d, 1H, J = 4.2 Hz, collapses to a singlet with D_2O), 6.7–7.2 (m, 5H, Ar); mass spectrum, *m/z* (assignment): 362 (M^+), 330 ($M^+ - CH_3OH$), 299 ($M^+ - CH_3OH - CH_3O$), 298 ($M^+ - 2CH_3OH$).

*Compound A***4**

Treatment of lithiated 6-bromo-3,4-methylenedioxybenzaldehydedimethyl acetal (3.0 g, 10.9 mmol) with 3,4,5-trimethoxybenzaldehyde (2.3 g, 11.7 mmol) gave A**4** as an oil (4.0 g, 93%) which later crystallized from diethyl ether; mp 111–112.5°C; ^{1}Hmr ($CDCl_3$, 60 MHz), δ: 3.22, 3.30 (s, 3H each, CH$(OCH_3)_2$), 3.77 (s, 9H, —OCH_3), 3.6 (d, 1H, OH, disappears with D_2O), 5.41 (s, 1H, —C*H*$(OCH_3)_2$), 5.80 (s, 2H, —OCH_2O—), 6.01 (d, 1H, —C*H*OH, collapses to a singlet with D_2O), 6.55 (s, 2H, Ar), 6.63, 6.95 (s, 1H each, Ar); mass spectrum, *m/z* (assignment): 392 (M^+), 360 ($M^+ - CH_3OH$), 329 ($M^+ - CH_3OH - CH_3O$), 328 ($M^+ - 2CH_3OH$); hrms calcd. for $C_{20}H_{24}O_8$: 392.1471; found: 392.1414. *Anal.* calcd. for $C_{20}H_{24}O_8$: C 61.21, H 6.17; found: C 61.01, H 6.41.

*Compound A***5**

6-Bromo-3,4-dimethoxybenzaldehydedimethyl acetal (5.4 g) was lithiated and treated with anhydrous formaldehyde gas. The latter was generated by pyrolyzing paraformaldehyde (6 g) with a hot air gun and the resulting gas passed, in a stream of drynitrogen, over a boat of anhydrous $CaCl_2$ and into the lithiated solution. The mixture was stirred for 1 h at room temperature and poured into H_2O (50 mL). The ether layer was separated, dried (Na_2SO_4), and the ether removed *in vacuo* to leave an oil (95%) which resisted crystallization; ^{1}Hmr ($CDCl_3$, 80 MHz) δ: 3.01 (t, 1, OH, disappears with D_2O), 3.35 (s, 6H, —CH$(OCH_3)_2$, 3.85 (s, 6H, 2 × OCH_3), 4.59 (d, 2H, O—C*H*$_2$OH, collapses to a singlet in D_2O), 5.41 (s, 1H, —C*H*$(OCH_3)_2$), 6.82, 7.00 (s, 1H each, Ar); mass spectrum, *m/z* (assignment): 242 (M^+), 210 ($M^+ - CH_3OH$).

*Compound A***7**

2-Bromo-3,4,5-trimethoxybenzaldehydedimethyl acetal (1.46 g, 4.5 mmol) was lithiated and previously described. To the stirred suspension was added a solution of 3,4,5-trimethoxybenzaldehyde (0.891 g, 4.56 mmol) in dry ether (50 mL). Work-up as previously described gave A**7** as an oil (1.9 g, 95.6%), ir (neat): 3450 (OH) cm^{-1}; ^{1}Hmr ($CDCl_3$, 80 MHz), δ: 3.27, 3.29, 3.50, 3.74, 3.79, 3.80, 3.81, 3.83 (all s, 3H each, 8 OMe groups), 3.98 (d, 1H, OH, exchangeable with D_2O), 5.30 (s, 1H, C*H*$(OMe)_2$), 6.1 (d, 1H, C*H*OH, J = 10.7 Hz), 6.55, 6.56, 6.96 (all s, 1H each, Ar), mass spectrum, *m/z* (assignment): 438 (M^+), 406 ($M^+ - CH_3OH$), 375 ($M^+ - CH_3OH - CH_3O$), 374 ($M^+ - 2CH_3OH$).

General lithiation procedure for piperonal and veratraldehyde dimethyl acetals

A stirred solution of the acetal and dry diethyl ether (15 mL), under N_2, was cooled to 0°C and treated with n-BuLi (1.1 equiv./mole of acetal). After 1 h the mixture was treated with the appropriate electrophilic reagent.

*Compound A***6**

Veratraldehyde dimethyl acetal (2.07 g; 9.76 mmol) was lithiated and treated dropwise with an ethereal solution of piperonal (1.46 g, 9.8 mmol in 50 mL) at −78°C. It was allowed to warm up to room temperature. Work-up similar to that of A**1** afforded an oil (3.35 g, 95%) which was used in the Diels–Alder reaction without further purification; ir (neat): 3450 (OH) cm^{-1}; Hmr ($CDCl_3$, 80 MHz), δ: 3.23 (s, 6H, 2 acetal OCH_3), 3.52 (s, 3H, OCH_3), 3.80 (s, 3H, OCH_3), 4.2 (d, 1H, OH, J = 10 Hz, exchangeable with D_2O), 5.2 (s, 1H, C*H*$(OMe)_2$), 5.85 (s, 2H, —OCH_2O), 6.13 (d, 1H, C*H*OH, J = 10 Hz), 6.65–7.35 (m, 5H, Ar); mass spectrum, *m/z* (assignment): 362 (M^+), 331 ($M^+ - CH_3O$), 330 ($M^+ - CH_3OH$), 299 ($M^+ - CH_3OH - CH_3O$), 298 ($M^+ - 2CH_3OH$).

*Compound A***8**

Veratraldehyde dimethyl acetal (2.5 g) was lithiated and treated with gaseous formaldehyde as per A**5**. Similar work-up gave a white amorphous solid which later crystallized from ether (2.7 g, 95%); mp 54–56°C; ir ($CHCl_3$): 3420 (OH) cm^{-1}; ^{1}Hmr ($CDCl_3$, 60 MHz), δ: 3.0 (t, 1H, OH, disappears with D_2O), 3.35 (s, 6H, —CH$(OCH_3)_2$), 3.81 (s, 6H, 2 × OCH_3), 4.70 (d, 2H, C*H*$_2$OH), collapses to a singlet with D_2O), 5.32 (s, 1H, —CH$(OCH_3)_2$), 6.65 and 7.07 (ABq, 1H each, J_{ortho} = 8.1 Hz, Ar); mass spectrum, *m/z* (assignment): 242 (M^+), 210 ($M^+ - CH_3OH$). *Anal.* calcd. for $C_{12}H_{18}O_5$: C 59.49, H 7.49; found: C 59.22, H 7.78.

*Compound A***9**

6-Bromo-3,4-dimethoxyacetophenonedimethyl ketal (2.0 g) was lithiated and treated with formaldehyde gas (6 g of paraformaldehyde) as previously described. Similar work-up afforded an oil (86%) which resisted crystallization; ir (neat): 3450 (OH) cm^{-1}; ^{1}Hmr ($CDCl_3$, 80 MHz), δ: 1.60 (s, 3H,—CH_3), 3.2 (s, 1 1H, OH, disappears with D_2O), 3.29 (s, 6H, —C$(OCH_3)_2$)CH_3), 3.90 (s, 6H, 2 × OCH_3), 4.61 (s, 2H, —C*H*$_2$O), 6.93, 7.07 (s, 1H each, Ar); mass spectrum, *m/z* (assignment): 256 (M^+), 225 ($M^+ - CH_3O$).

*Compound A***10**

6-Bromo-3,4-methylenedioxyacetophenonedimethyl ketal (1 g) was lithiated and treated with formaldehyde gas (3 g of paraformaldehyde) as previously described. Similar work-up gave an oil (72%) which resisted crystallization; ir (neat): 3460 (OH) cm^{-1}; ^{1}Hmr ($CDCl_3$, 80 MHz), δ: 1.58 (s, 3H,—CH_3), 3.0 (t, 1H, —OH, disappears with D_2O), 3.29 (s, 6H, —C$(OCH_3)CH_3$), 4.56 (d, 2H, —CH_2OH, collapses to a singlet with D_2O), 5.96 (s, 2H, —OCH_2O—), 6.88, 7.01 (s, 1H each, Ar); mass spectrum, *m/z* (assignment): 240 (M^+), 209 ($M^+ - CH_3O$).

Can. J. Chem. Downloaded from www.nrcresearchpress.com by 210.87.254.42 on 09/06/12
For personal use only.

Compound A**11**

6-Bromo-3,4-dimethoxyacetophenonedimethyl ketal (0.434 g, 1.42 mmol) was lithiated and treated with a solution of piperonal (0.213 g, 1.42 mmol) in dry ether at −78°C. The reaction mixture was allowed to warm up to room temperature, and worked up as in A**7** to give A**11** as an oil (0.485 g, 91%); ir (neat): 3450 (OH) cm^{-1}; ^{1}Hmr ($CDCl_3$, 80 MHz), δ: 1.52 (s, 3H, Me), 3.15 3.28, 3.76 (s, 3H each, 3MeO), 3,9 (s and overlapping m, 4H, MeO and OH), 5.94 (s, 2H, OCH_2O), 6.27 (d, 1H, C*H*OH, J = 4.49 Hz, collapses to a singlet with D_20), 6.79−6.89 (m, 4H, Ar), 7.06 (s, 1H, Ar); mass spectrum, m/z (assignment): 312 ($M^+ - 2CH_3OH$).

*Compound A***12**

Bromocyclohexane (2.04 g, 10 mmol) was added dropwise under N_2 from a syringe, while stirring, to Mg turnings (0.31 g, 12.5 mmol) in dry ether (50 mL) so that the ether refluxes gently. Stirring continued for 1 h at room temperature. A solution of 6-formylpiperonal dimethyl acetal (2.24 g, 10 mmol) in ether (50 mL) was added from a dropping funnel to the ice-cold solution. The ice bath was removed and stirring at room temperature continued for 2 hours. The resulting solution was decanted from Mg and a saturated NH_4Cl solution added. It was extracted with ether (3 × 50 mL) and the combined ether extracts washed with water (50 mL) and dried (Na_2SO_4). Removal of solvent afforded A**12** as an oil (2.98 g, 97%) which was used without further purification, ir: 3450 (OH) cm^{-1}; ^{1}Hmr ($CDCl_3$, 80 MHz) δ: 0.9−2.5 (m, 11H, C_6H_{11}) 3.3 (s, 6H, 2 MeO) 4.58 (d, 1, C*H*—OH, collapses to a singlet with D_2O), 5.5 (s, 1H, C*H*$(OMe)_2$), 5.95 (s, 2H, OCH_2O) 6.95, 7.06 (s, 1H each, Ar); mass spectrum, m/z (assignment): 277 ($M^+ - CH_3OH$), 276 ($M^+ - CH_3OH$), 245 ($M^+ - CH_3OH - CH_3O$), 244 ($M^+ - 2CH_3OH$), 193 ($M^+ - CH_3OH - C_6H_{11}$).

*Compound A***13**

2,5-Dimethoxybenzyl vinyl ether (5.0 g, 25.7 mmol) was lithiated with n-BuLi (2 equiv.) at 0°C in anhydrous pentane (150 mL, distilled over CaH_2) for 6 h, under nitrogen. The flask was placed in the freezer for 6 h to allow the solid lithio derivative to sediment. The pentane was then syringed out and dry diethyl ether (100 mL) added at 0°C. Once the anion dissolved, dry DMF (5 mL, distilled *in vacuo* from CaH_2 into NaH) was added slowly, not allowing the temperature to rise above 0°C. After 12 h at room temperature, the solution was poured in H_2O (50 mL) and washed with saturated brine solution (3 × 50 mL). The ether was dried (Na_2SO_4) and removed *in vacuo* to leave an oil. Repeated crystallizations from ether afforded 0.8 g of A**13**. Final distillation of the mother liquor (120−140°C/0.01 Torr) afforded another 0.8 g (total yield: 30%), mp 82−83°C; bp 120−124°C/0.01 Torr; ir (KBr): 1695(CHO), 1625 (C=C) cm^{-1}; ^{1}Hmr ($CDCl_3$, 80 MHz), δ: 3.83, 3.87 (s, 3H each, 2 × OCH_3), 4.04 (dd, 1H, J_{gem} = 2.0, J_{cis} = 6.8 Hz, vinyl H), 4.30 (dd, 1H, J_{gem} = 2.0, J_{trans} = 14.1 Hz, vinyl H), 5.12 (s, 2H, —CH_2O—), 6.55 (dd, 1H, J_{cis} 6.8, J_{trans} = 14.1 Hz,—OC*H*CH_2), 7.12 and 6.95 (ABq, 1H each, J_{ortho} = 8.2 Hz, Ar), 10.55 (s, 1H, —CHO); mass spectrum, m/z: 222 (M^+), 179 ($M^+ - OCHCH_2$): *Anal.* calcd. for $C_{12}H_{14}O_4$: C 64.86, H 6.35; found: C 64.64, H 6.09.

*Compound B***2**

The hydroxyacetal A**2** (7.0 g) was dissolved in degassed 1,2-dimethoxyethane (70 mL) and H_2O (50 mL) was added. The mixture was stirred for 24 h under N_2. The resulting white precipitate (a mixture of *cis* and *trans*, a mixture of steroisomers) was filtered and washed with diethyl ether (72%); mp 151−152°C (scaled tube); ^{1}Hmr ($CDCl_3$, 60 MHZ), δ: 5.8−6.11 (m, 5H, 2 × OCH_2O—, C(3)H), 6.35, 6.50 (s, 1H each, *cis* and *trans* C(1)H), 6.8−7.1 (m, 5H, Ar); hrms calcd. for $C_{16}H_{12}O_6$: 300.0634; found: 300.0598. *Anal.* calcd. for $C_{16}H_{12}O_6$: C 64.00, H 4.03; found: C 64.17, H 3.99.

*Compound B***5**

The hydroxyacetal A**5** (1.0 g) was placed in methanol (5 mL) and 2 *N* HCl (3 mL) added. After stirring for 8 h at room temperature, the methanol was removed *in vacuo* and the resulting oil extracted with $CHCl_3$ (3 × 10 mL). Drying (Na_2SO_4) and removal of $CHCl_3$ afforded an oil (92%) which resisted crystallization; ^{1}Hmr ($CDCl_3$, 80 MHz), δ: 3.38 (s, 3H, C(1)—OCH_3), 3.86, 3.87 (s, 3H each, 2 × OCH_3), 4.93 (d, 1H, J_{gem} = 12.0 Hz, C(3)H), 5.16 (dd, 1H, J_{gem} = 12.0, $J_{1,3\,trans}$ = 2.2 Hz, C(3)H), 6.13 (d, 1H, $J_{1,3\,trans}$ = 2.2 Hz, C(1)H), 6.75, 6.88 (s, 1H each, Ar); mass spectrum, m/z (assignment): 210 (M^+), 179 ($M^+ - CH_3O$); hrms calcd. for $C_{11}H_{14}O_4$: 210.0892; found: 210.0889.

*Compound B***8**

Several recrystallizations of A**8** from boiling methanol gave B**8** (88%), mp 60−61.5°C; ^{1}Hmr ($CDCl_3$, 60 MHz), δ: 3.31 (s, 3H, C(1)—OCH_3), 3.80 (s, 6H, 2 × OCH_3), 4.98 (br s, 2H, C(3)H's), 5.86 (br s, 1H, C(1)H), 6.66 and 6.82 (ABq, 1H each, J_{ortho} = 8.2 Hz, Ar): *Anal.* calcd. for $C_{11}H_{14}O_4$: C 62.84, H 6.71; found: C 62.74, H 6.80.

*Compound B***13**

Aldehyde A**13** (1.5 g) was dissolved in methanol (20 mL) and treated with $Hg(OAc)_2$ (83 mg). After 1 h, *p*-toluenesulfonic acid (21 mg) was added and 0.5 h later solid sodium bicarbonate (0.2 g) was added. The mixture was filtered and the methanol removed *in vacuo* to leave an oil. This oil was extracted into ether (2 × 10 mL), washed with H_2O (10 mL), dried (Na_2SO_4), and the ether removed to leave an oil which later crystallized from ether (90%); mp 75−76°C; ^{1}Hmr ($CDCl_3$, 80 MHz), δ: 3.44 (s, 3H, C(1)—OCH_3), 3.78, 3.82 (s, 3H each, 2 × OCH_3), 4.95 (d, 1H, J_{gem} = 13.1 Hz, C(3)H), 5.15 (dd, 1H, $J_{1,3\,trans}$ = 2.0, J_{gem} = 13.1 Hz, C(3)H), 6.23 (d, 1H, $J_{1,3\,trans}$ = 2.0 Hz, C(1)H), 6.75 (s, 2H, Ar); mass spectrum, m/z (assignment): 210 (M^+), 179 ($M^+ - OCH_3$). *Anal.* calcd. for $C_{11}H_{14}O_4$: C 62.85, H 6.71; found: C 62.62, H 6.43.

*Compound B***14**

Method A. Aldehyde A**13** (1.5 g) was dissolved in dioxane−water (20 mL, 7:3) and treated with $Hg(OAc)_2$ (03 g). After 3 h at room temperature, the dioxane was removed *in vacuo* and the resulting oil extracted into the $CHCl_3$ (3 × 10 mL). Drying (Na_2SO_4) and removal of $CHCl_3$ afforded a solid which was filtered and recrystallized from CH_2Cl_2 (91%), mp 155−157°C (lit (9) mp 156−158°C); ir (KBr): 3450 (OH) cm^{-1}; ^{1}Hmr ($CDCl_3$, 80 MHz), δ: 2.97 (d, 1H, —OH, $J_{1,OH}$ = 7.0 Hz, disappears with D_2O), 3.80, 3.85 (s, 3H each, 2 × OCH_3), 4.97 (d, 1H, J_{gem} = 13.3 Hz, C(3)H), 5.27 (dd, 1H, $J_{1,3\,trans}$ = 2.15, J_{gem} = 13.3 Hz, C(3)H), 6.57 (dd, 1H, $J_{1,3\,trans}$ = 2.15, $J_{1,OH}$ = 7.0 Hz, collapses to a doublet in D_2O, C(1)H), 6.77 (s, 2H, Ar); mass spectrum, m/z (assignment): 196 (M^+), 179 (M^+—OH).

Method B. 4,7-Dimethoxyphthalide (1.94 g, 9.97 mmol) was dissolved in dry CH_2Cl_2 (from CaH_2, 163 mL) and cooled to −60 ± 5°C. Dibal-H (15 mL of 1.52 *M* in toluene, 22.8 mmol) was added over 0.25 h and the solution stirred a further 70 min. Methanol (5 mL) was added slowly and the mixture warmed to room temperature. The mixture was poured into $CHCl_3$ (200 mL), shaken with saturated NaCl (200 mL), and filtered through Celite. The $CHCl_3$ was dried (Na_2SO_4) and removed *in vacuo*, leaving a white solid. This was slurried in hexane and filtered, leaving 1.8 g (93%) of B**14**.

General procedure for dimethyl acetylenedicarboxylate (DMAD) adduct formation

The hydroxyacetal or phthalan (1 g) was dissolved in excess DMAD (5 mL). Glacial acetic acid (0.3 mL) was added and the mixture heated on a steam bath with swirling for 20−30 min. The excess DMAD was distilled *in vacuo* leaving a thick oil. Crystals formed upon the addition of ether were filtered, and examination of the mother liquor revealed unreacted phthalan. This could be recycled to optimize the yield.

*Compound C***1**

Adduct C**1** was prepared from A**1** by the above method in 65% yield. Crystals were obtained from ether; mp 178−180°C; ir ($CHCl_3$): 1725 (C=O) cm^{-1}; ^{1}Hmr ($CDCl_3$, 80 MHz) δ: 3.75, 3.78 (s, 3H each, 2 × CO_2CH_3), 3.83, 3.84 (s, 3H each, 2 × OCH_3), 6.00 (s, 3H, —OCH_2O— and bridge H), 6.8−7.2 (m, 5H, Ar); mass spectrum, m/z (assignment): 440 (M^+), 408 ($M^+ - CH_3OH$), 298 (5,6-dimethoxyisobenzofuran). *Anal.* calcd. for $C_{23}H_{20}O_9$. C 62.71,

Can. J. Chem. Downloaded from www.nrcresearchpress.com by 210.87.254.42 on 09/06/12
For personal use only.

H 4.59; found: C 62.99, H 4.59.

Compound C2

Adduct **C2** was prepared from **A2** by the above method in 65% yield. Crystals were obtained from ether; mp 129–130°C; ir ($CHCl_3$): 1725 (C=O) cm^{-1}; ^{1}Hmr ($CDCl_3$, 60 MHz), δ: 3.68, 3.72 (s, 3H each, 2 × OCH_3), 5.93 (m, 5H, 2 × —OCH_2—O, bridge H), 6.8–7.2 (m, 5H, Ar); mass spectrum, *m/z* (assignment): 424 (M^+), 282 (5,6-methylenedioxyisobenzofuran). *Anal.* calcd. for $C_{22}H_{16}O_9$: C 62.23, H 3.81; found: C 62.31, H 3.85.

Compound C4

Adduct **C4** was prepared from **A4** by the above procedure in 65% yield, mp 159°C; ir ($CHCl_3$); 1720 (C=O) cm^{-1}; ^{1}Hmr ($CDCl_3$, 80 MHz), δ: 3.73, 3.77 (s, 3H each, 2 × CO_2CH_3), 3.87 (s, 9H, 3 × OCH_3), 5.90 (close ABq, 2H, —OCH_2O—), 5.95 (s, 1H, bridge), 6.77 (s, 2H, Ar), 6.90 (s, 2H); hrms calcd. for $C_{24}H_{22}O_{10}$: 470.1213; found: 470.1241. *Anal.* calcd. for $C_{24}H_{22}O_{10}$: C 61.28, H 4.71; found: C 61.03, H 4.68.

Compound C5

Compound **A5** was treated as above and provided yellow crystals upon the addition of ether (95%); mp 139–139.5°C; ir ($CHCl_3$): 1710, 1730 (C=O) cm^{-1}; ^{1}Hmr ($CDCl_3$, 60 MHz), δ: 3.80 (s, 6H, 2 × CO_2CH_3), 3.80 (s, 6H, 2 × OCH_3), 5.93 (s, 2H, 2 bridge H), 7.10 (s, 2H, Ar); mass spectrum, *m/z* (assignment): 320 (M^+).

Compound C8

Adduct **A8** was treated as above and provided **C8** in 34% yield, mp 104–105°C; ir ($CHCl_3$): 1736, 1714 (C=O) cm^{-1}; ^{1}Hmr ($CDCl_3$, 60 MHz), δ: 3.71 (s, 9H, 2 × CO_2CH_3, 1 × OCH_3), 3.98 (s, 3H, —OCH_3), 5.78 and 6.21 (ABq, 1H each, J = 1.7 Hz, 2 bridge H), 6.4 and 6.91 (ABq, 1H each, J_{ortho} = 8.7 Hz, Ar); mass spectrum, *m/z* (assignment): 320 (M^+). *Anal.* calcd. for $C_{16}H_{16}O_7$: C 60.00, H 5.04; found: C 59.97, H 5.13.

Compound C9

Adduct **C9** was prepared from **A9** in 96% yield and failed to crystalize; ^{1}Hmr ($CDCl_3$, 80 MHz), δ: 1.96 (s, 3H, CH_3), 3.76, 3.82, 3.88, 3.89 (s, 3H each, 2 × CO_2CH_3, 2 × OCH_3), 5.85 (s, 1H, bridge H), 7.0, 7.07 (s, 1H each, Ar); mass spectrum, *m/z* (assignment): 334 (M^+), 192 (5,6-dimethoxy-1-methylisobenzofuran).

Compound C10

Adduct **C10** was prepared from **A10** in 96% yield. Addition of ether afforded yellow crystals, mp 87.5–89.5°C; ^{1}Hmr ($CDCl_3$, 80 MHz), δ: 1.92 (s, 3H, CH_3), 3.76, 3.82 (s, 3H each, 2 × CO_2CH_3), 5.80 (s, 1H, bridge H), 5.95 (close ABq, 2H, J = 1.1 Hz, —OCH_2O—), 6.87, 6.93 (s, 1H each, Ar); mass spectrum, *m/z* (assignment): 3.18 (M^+), 176 (1-methyl-5,6-methylenedioxyisobenzofuran). *Anal.* calcd. for $C_{16}H_{14}O_7$: C 60.38, H 4.43; found: C 61.07, H 4.52.

Compound D6

Diels–Alder reaction of the acetal alcohol **A6** (448 mg) was done with dimethyl acetylenedicarboxylate as described in the general procedure by heating at 130°C for 20 min. Usual work-up gave the naphthol **D6** (309 mg, 62%) as a crystalline solid, mp 167°C; ir (KBr): 1735 and 1640 (C=O) cm^{-1}; ^{1}Hmr ($CDCl_3$, 80 MHz), δ: 3.15 (s, 3H, OMe), 3.45 (s, 3H, OMe), 3.82, 3.87 (s, 3H each, $COOCH_3$), 5.85 (s, 2H, OCH_2O), 6.68 (m, 3H, Ar), 7.2, 8.2 (ABq, 2H, Ar), 12.4 (s, 1H, OH exchangeable with D_2O); mass spectrum, *m/z* (assignment): 440 (M^+), 408 ($M^+ - CH_3OH$), 393 ($M^+ - CH_3OH - CH_3$). *Anal.* calcd. for $C_{23}H_{20}O_9$: C 62.72, H 4.54; found: C 62.71, H 4.56.

Compound D7

The acetal alcohol **A7** heated wth dimethyl acetylenedicarboxylate at 130°C for 20 min with acetic acid, gave naphthol **D7** in 73% yield, mp 162°C; ip (KBr): 1720, 1645 (C=O) cm^{-1}; ^{1}Hmr ($CDCl_3$, 80 MHz), δ: 3.33, 3.52 (s, 3H each, 2 OMe), 3.8, 3.9 (s, 6H each, 4 OMe), 3.92, 4.05 (s, 3H each, 2 – OMe), 6.55 (s, 2H, Ar), 7.68 (s, 1H, Ar), 12.35 (s, 1H, OH exchanges with D_2O); mass spectrum, *m/z* (assignment): 516 (M^+), 485 ($M^+ - CH_3OH$), 484 ($M^+ - CH_3OH$), 453 ($M^+ - CH_3OH - CH_3O$). *Anal.* calcd. for $C_{26}H_{28}O_6$: C 60.46, H 5.42; found: C 60.40, H 5.34.

Compound C11

Adduct **C11** was prepared from the ketal alcohol **A11** in 72% yield by the general procedure described above. Crystallization from ether gave yellow prisms, mp 169°C; ir (KBr): 1705, 1720 (C=O) cm^{-1}; ^{1}Hmr ($CDCl_3$, 80 MHz), δ: 2.95 (s, 3H, Me), 3.69, 3.76 3.85, 3.90 (s, 3H each, 4 MeO), 6.0 (s, 2H, OCH_2O), 6.8–7.2 (m, 5H, Ar); mass spectrum, *m/z* (assignment): 454 (M^+), 408 ($M^+ - CH_3O - CH_3$). *Anal.* calcd. for $C_{24}H_{22}O_9$: C 63.43, H 4.84; found: C 63.43, H 4.84.

Compound C12

Adduct **C12** was prepared from the ketal alcohol **A12** in 70% yield. Crystallization from methanol gave light yellow prisms, mp 170°C; ir (KBr): 1700, 1725 (C=O) cm^{-1}; ^{1}Hmr ($CDCl_3$, 80 MHz) δ: 1.0–2.0 and 2.2–2.7 (m, 11H, C_6H_{11}), 3.75, 3.85 (s, 3H each, 2 MeO), 5.85 (s, 1H, bridge H), 5.92 (ABq, 2H, OCH_2O), 6.82, 6.87 (d, 2H, Ar); mass spectrum, *m/z* (assignment): 386 (M^+), 354 ($M^+ - CH_3OH$), 322 ($M^+ - 2CH_3OH$). *Anal.* calcd. for $C_{21}H_{22}O_7$: C 65.28, H 5.69; found C 65.26, H 5.70.

Compound D3

Diels–Alder reaction of **A3** with dimethylacetylenedicarboxylate in the presence of acetic acid of 100°C for 1 h gave naphthol **D3** in 62% yield, mp 167°C; ir (KBr): 1700, 1725 (C=O) cm^{-1}; ^{1}Hmr ($CDCl_3$, 80 MHz,) δ: 3.55, 3.85, 3.90, 3.92 (s, 3H each, 4 MeO), 6.05 (s, 2H, OCH_2O), 6.7–6.9 (m, 4H, Ar), 7.75 (s, 1H, Ar), 12.22 (s, 1H, OH); mass spectrum, *m/z* (assignment): 440 (M^+), 408 ($M^+ - CH_3OH$), 393 ($M^+ - CH_3OH - CH_3$). *Anal.* calcd. for $C_{23}H_{20}O_9$: C 62.72, H 4.54; found: C 62.66 H 4.60.

General procedure for the reaction of a variety of dienophiles with A5

The hydroxyacetal **A5**, glacial acetic acid, appropriate dienophile, and a suitable solvent were placed in a flask and refluxed to completion of the reaction. The flask was cooled and saturated bicarbonate added until the acetic acid was neutralized. The solvent was separated, dried (Na_2SO_4), and removed *in vacuo* to leave an oil.

Compound C5a

Acetal **A5** (0.55 g, 2.3 mmol), glacial acetic acid (0.2 mL) benzoquinone (2 equiv.), and CH_2Cl_2 (20 mL) were treated for 18 h as above. The addition of ether afforded a mixture (60%) of *endo/exo* (7:3) crystals which could not be separated. Analyses were done on the mixture; mp 10°C; ir ($CHCl_3$): 1675 (C=O), 1610 (C=C) cm^{-1}; mass spectrum, *m/z* (assignment): 286 (M^+), 278 (5,6-dimethoxyisobenzofuran). *Anal.* calcd. for $C_{16}H_{14}O_5$: C 67.12, H 4.93; found: C 67.01, H 5.09. The Hmr ($CDCl_3$, 80 MHz), endo adduct; δ: 3.65 (m, 2H, C(2), C(3)—H), 3.83 (s, 6H (2 × OCH_3) 5.68 (m, 2H, C(1), C(4)—H), 6.01 (s, 2H, —CH=CH—), 6.70 (s, 2H, Ar); exo adduct, δ: 2.80 (s, 2H, C(2), C(3)—H), 3.87 (s, 6H, 2 × OCH_3), 5.59 (s, 2H, C(1), C(4)—H) 6.80 (s, 2H, —CH=CH—), 6.90 (s, 2H, Ar).

Compound C5b

Acetal **A5** (0.5 g, 2 mmol), glacial acetic acid (0.2 mL), naphthaquinone (2.5 equiv.), and $CHCl_3$ (10 mL) were treated for 1 h as above. The excess naphthaquinone was removed on a column of silica gel using EtOAc/petrolum ether (1:1) as a solvent. The addition of ether to the resulting oil afforded the *endo* adduct but the *exo* adduct could not be isolated ^{1}Hmr showed the *endo/exo* ratio to be 3:1 and the yield was 86%. *Endo* Isomer: mp 215–217°C; ^{1}Hmr ($CDCl_3$, 80 MHz), δ: 3.63 (s, 6H, 2 × OCH_3), 3.8 (m, 2H, C(2), C(3)—H), 5.81 (m, 2H, C(1), C(4)—H), 6.63 (s, 2H, Ar), 7.47–7.85 (AA'BB' pattern, 4H, Ar); mass spectrum, *m/z* (assignment): 336 (M^+), 178 (5,6-dimethoxyisobenzofuran). *Anal.* calcd. for $C_{20}H_{16}O_5$: C 71,42, H 4.79; found: C 71.67, H 4.84.

Compound C5c

Acetal **A5** (4.3 g, 17.7 mmol), glacial acetic acid (1.9 mL), methyl vinyl ketone (3 equiv. freshly distilled, and 1% hydroquinone added as an inhibitor), and CCl_4 (100 mL) were heated t 60°C for 6 h. The addition of ether afforded *endo* crystals. The oil from the mother liquor was run through a gravity of column of silica gel using benzene/acetone (4:1). The faster spot (R_f = 0.52) afforded *endo*

Can. J. Chem. Downloaded from www.nrcresearchpress.com by 210.87.254.42 on 09/06/12
For personal use only.

crystals and the slower spot (R_f = 0.50) *exo* crystals upon the addition of ether. The yield was 78% and the *endo/exo* ratio was 3:2. *Endo* Adduct: mp 129–131°C; ir ($CHCl_3$): 1710 (C=O) cm^{-1}; ^{1}Hmr ($CDCl_3$, 80 MHz), δ: 1.83 (dd, 1H, $J_{\alpha,3\beta}$ = 11.7, $J_{2,3\alpha}$ = 4.1 Hz, C(3α)—H), 1.99 (s, 3H, $COCH_3$), 2.22 (ddd, 1H, $J_{3\alpha,3\beta}$ = 11.7, $J_{2,3\beta}$ = 9.5, $J_{3\beta,4}$ = 4.6 Hz, C(3β)—H), 3.40 (ddd, 1H, $J_{1,2}$ = 5.1, $J_{2,3\alpha}$ = 4.1, $J_{2,3\beta}$ = 9.5 Hz, C(2)—H), 3.83, 3.86 (s, 3H each, 2 × OCH_3), 5.38 (d, 1H, $J_{3\beta,4}$ = 4.6 Hz, C(4)—H), 5.53 (d, 1H, $J_{1,2}$ = 5.1 Hz, C(1)—H), 6.79, 6.87 (s, 1H each, Ar); mass spectrum, *m/z* (assignment): 248 (M^+), 178 (5,6-dimethoxyisobenzofuran). *Anal.* calcd. for $C_{14}H_{16}O_4$: C 67.73, H 6.50; found: C 67.54, H 6.87. *Exo* Adduct: mp 88–90°C; ir ($CHCl_3$): 1710 (C=O) cm^{-1}; ^{1}Hmr ($CDCl_3$ 80 MHz), δ: 1.66 (dd, 1H, $J_{3\alpha,3\beta}$ = 11.5, $J_{2,3\alpha}$ = 8.8 Hz, C(3α)—H), 2.88 (s, 3H, $COCH_3$), 2.29 (ddd, 1H, $J_{3\alpha,3\beta}$ = 11.5, $J_{3\beta,4}$ = 4.6, $J_{2,3\beta}$ = 4.4 Hz, C(3β)—H), 2.59 (dd, 1H, $J_{2,3\alpha}$ = 8.8, $J_{2,3\beta}$ = 4.4 Hz, (C(2)—H), 3.87 (s, 6H, 2 × OCH_3), 5.43 (d, 1H, $J_{3\beta,4}$ = 4.6 Hz, C(4)—H), 5.50 (s, 1H, C(1)—H), 6.89 (s, 2H, Ar); mass spectrum, *m/z* (assignment): 248 (M^+), 178(5,6-dimethoxyisobenzofuran): *Anal.* calcd. for $C_{14}H_{16}O_6$: C 67.73, H 6.50; found C 67.76, H 6.62.

*Compound C*5e

Acetal A5 (0.5 g, 2 mmol), glacial acetic acid (0.5 mL), acrylonitrile (6 equiv., freshly distilled, and 1% hydroquinone added as an inhibitor), and $CHCl_3$ (5 mL) were treated as above for 4 h. The addition of ether to the oil afforded *endo* crystals (64%). The ^{1}Hmr showed an *endo/exo* ratio 9:1 and the *exo* adduct could not be isolated. *Endo* Adduct: mp 184–187°C; ir ($CHCl_3$): 2200 (CN) cm^{-1}; ^{1}Hmr ($CDCl_3$, 80 MHz), δ: 1.61 (dd, 1H, $J_{3\alpha,3\beta}$ = 11.6, $J_{2,3\alpha}$ = 4.03 Hz, C(3α)—H), 2.52 (ddd, 1H, $J_{3\alpha,3\beta}$ = 11.6, $J_{2,3\beta}$ = 10.6, $J_{3\beta,4}$ = 4.15 Hz, C(3β)—H), 3.19 (ddd, 1H, $J_{1,2}$ = 4.15, $J_{2,3\alpha}$ = 4.03, $J_{2,3\beta}$ = 10.6 Hz, C(2)—H), 3.88 (s, 6H, 2 × OCH_3), 4.57 (t, 2H, $J_{1,2}$ = $J_{3\beta,4}$ = 4.15, C(1) and C(4)—H), 6.91, 7.05 (s, 1H each, Ar); mass spectrum, *m/z* (assignment): 231 (M^+), 178 (5,6-dimethoxyisobenzofuran). *Anal.* calcd. for $C_{13}H_{13}NO_3$: C 67.52, H 5.67, N 6.06; found: C 67.35, H 5.72, N 6.12.

*Compound C*5f

Acetal A5 (0.5 g, 2.0 mmol), glacial acetic acid (0.2 mL), α-chloroacrylonitrile (0.5 mL), and CH_2Cl_2 (10 mL) were treated as above for 18 h. The oil was run through a silica gel column, but failed to crystallize upon the addition of ether (70%). There was a major and minor isomer (7:3) but the stereochemistry could not be determined; ir ($CHCl_3$): 1205 (C—O) cm^{-1}; mass spectrum, *m/z* (assignment): 265 (M^+), 178 (5,6-dimethoxyisobenzofuran). The ^{1}Hmr ($CDCl_3$, 80 MHz), minor isomer, δ: 2.39 (d, 1H, $J_{3\alpha,3\beta}$ = 12.9 Hz, C(3β)—H), 2.75 (dd, 1H, $J_{3\alpha,3\beta}$ = 12.9, $J_{3\alpha,4}$ = 4.4 Hz, C(3α)—H), 3.91, 3.94, (s, 3H each 2 × OCH_3), 5.4–5.6 (m, 2H, C(1), C(4)—H), 7.13, 7.40 (s, 1H each, Ar); major isomer, δ: 1.84 (d, 1H, $J_{3\alpha,3\beta}$ = 12.7 Hz, C(3β)—H), 3.10 (dd, 1H, $J_{3\alpha,3\beta}$ = 12.7, $J_{3\alpha,4}$ = 4.9 Hz, C(3α)—H), 3.87 (s, 6H, 2 × OCH_3), 5.4–5.6 (m, 2H, C(1) and C(4)—H), 6.90, 7.05 (s, 1H each Ar).

Compound C5h

Acetal A5 (0.5 g, 2.0 mmol), glacial acetic acid (0.5 mL), methyl acrylate (3 equiv., freshly distilled, and 1% hydroquinone added as an inhibitor), and $CHCl_3$ (10 mL) were treated as above for 10 h. Addition of ether afforded the *endo* isomer. Attempts to isolate the *exo* isomer were unsuccessful. The *endo/exo* ratio was 3:2 and the yield was 50%. *Endo* Adduct: mp 105–107°C; ir ($CHCl_3$): 1740 (C=O) cm^{-1}; ^{1}Hmr ($CDCl_3$, 80 MHz), δ: 1.74 (dd, 1H, $J_{3\alpha,3\beta}$ = 11.6, $J_{2,3\alpha}$ = 3.8 Hz, C(3α)—H), 2.31 (ddd, 1H, $J_{3\alpha,3\beta}$ = 11.6, $J_{3\beta,4}$ = 5.16, $J_{2,3\beta}$ = 10.3 Hz, C(3β)—H), 3.4 (ddd, 1H, $J_{1,2}$ = 5.16, $J_{2,3\alpha}$ = 3.8, $J_{2,3\beta}$ = 10.3 Hz, C(2)—H), 3.52 (s, 3H, —CO_2CH_3), 3.82, 3.85 (s, 3H each, 2 × OCH_3), 5.39 (d, 1H, $J_{3\beta,4}$ = 5.16 Hz, C(4)—H), 5.50 (d, 1H, $J_{1,2}$ = 5.16 Hz, C(1)—H), 6.8, 6.85 (s, 1H each, Ar); mass spectrum, *m/z* (assignment): 264 (M^+), 178 (5,6-dimethoxyisobenzofuran). *Anal.* calcd. for $C_{14}H_{16}O_5$: 63.63, H 6.10; found: C 63.24, H 6.32.

*Compound C*5i

Acetal A5 (1.02 g), glacial acetic acid (0.41 mL), acrolein (1.14 mL), and $CHCl_3$ (10 mL) were treated as above for 30 h. The addition of ether afforded *endo* crystals. The oil from the mother liquor was placed on a silica gel column. The faster spot (R_f = 0.55) gave *endo* crystals and the slower spot (R_f = 0.52) *exo* crystas upon the addition of ether (63%; *endo/exo* ratio 3:2). *endo* Adduct:: mp 103–104°C; ir (KBr): 1720 C=O), 2720 (CHO) cm^{-1}; ^{1}Hmr ($CDCl_3$, 80 MHz), see Table 3. High resolution ms calcd. for $C_{13}H_{14}O_4$: 234.0892; found: 234.0884. *exo* Adduct: mp 73–74°C; ir (KBr):1715 (C=O), 2710 (CHO) cm^{-1}; ^{1}Hmr ($CDCl_3$, 400 MHz), see Table 3. High resolution ms calcd. for $C_{13}H_{14}O_4$: 234.0892; found: 234.0903.

*Compound C*5d

Into a refluxing solution of 2-butenolide (0.4 g, 4.75 mmol) and $CHCl_3$ (10 mL) was added a mixture of acetal A5 (0.46 g, 1.9 mmol), glacial acetic acid (0.2 mL), and $CHCl_3$ (10 mL). After 48 h at reflux, the resolution was cooled and saturated bicarbonate added until the acetic acid was neutralized. The $CHCl_3$ was separated, dried (Na_2SO_4), and removed *in vacuo* to leave an oil. The excess butenolide was removed *via* a high vacuum distillation. The remaining oil was passed through a silica gel column. The faster spot (R_f = 0.6) gave *exo* crystals and the slower (R_f = 0.53) *endo* crystals upon the addition of ether/CH_2Cl_2. The yield was 72% and the *endo/exo* ratio was 1:2 *exo* Aduct. mp 177–178°C; ir ($CHCl_3$): 1765 (C=O) cm^{-1}; ^{1}Hmr ($CDCl_3$, 80 MHz), δ: 2.6–3.0 (m, 2H, C(2) and C(3)—H), 3.85 (s, 6H, 2 × OCH_3), 4.2–4.8 (m, 2H, —CH_2O—), 5.29 (s, 1H, C(4)—H), 5.65 (s, 1H, C(1)—H), 6.87, 6.92 (s, 1H each, Ar); mass spectrum, *m/z* (assignment): 262 (M^+), 178 (5,6-dimethoxyisobenzofuran). *Anal.* calcd. for $C_{14}H_{14}O_5$: C 64.12, H 5.38; found C 63.91, H 5.33. *endo* Adduct: mp 184–185°C; ir ($CHCl_3$): 1765 (C=O) cm^{-1}; ^{1}Hmr ($CDCl_3$, 80 MHz), δ: 3.4–4.3 (m, 4H, C(2,3) and —CH_2O—), 3.85, 3.87 (s, 3H each, 2 × OCH_3), 5.4 (d, 1H, $J_{3,4}$ = 5.1 Hz, C(4)—H), 5.59 (d, 1H, $J_{1,2}$ = 5.02 Hz, C(1)—H), 6.93 (s, 2H, Ar); mass spectrum, *m/z* (assignment): 262 (M^+), 178 (5,6-dimethoxyisobenzofuran). *Anal.* calcd. for $C_{14}H_{14}O_5$: C 64.12, H 5.38; found: C 63.80, H 5.28.

*Compound C*5g

To a mixture of acetal A5 (0.5 g, 2.0 mmol) and glacial acetic acid (0.2 mL) was added acetic anhydride (0.1 mL) and maleic anhydride (0.6 g, 6.1 mmol) in CH_2Cl_2 (5 mL). The mixture was refluxed 24 h, cooled, and saturated bicarbonate added until neutral. The CH_2Cl_2 was dried (Na_2SO_4) and removed *in vacuo* to leave an oil. The addition of ether resulted in a mixture of *endo/exo* (7:3) crystals (60%) which could not be separated. Analyses were done on the mixture: mp 214–217°C; ir (KBr): 1760–1850 (C=O) cm^{-1}; mass spectrum, *m/z* (assignment): 276 (M^+), 178 (5,6-dimethoxyisobenzofuran). *Anal.* calcd. for $C_{14}H_{12}O_6$: C 60.87, H 4.38; found: C 60.53, H 4.52. The ^{1}Hmr ($CDCl_3$, 80 MHz), *endo* isomer; δ: 3.87 (s, 6H, 2 × OCH_3), 4.00 (m, 2H, C(2) and C(3)—H), 5.70 (m, 2H, C(1) and C(4)—H), 6.90 (s, 2H, Ar); *exo* isomer; δ: 3.20 (s, 2H, C(2) and C(3)—H), 3.87 (s, 6H, 2 × OCH_3), 5.85 (s, 2H, C(1) and C(4)—H), 6.96 (s, 2H, Ar).

Acknowledgements

We thank the Natural Sciences and Engineering Research Council for support of this work. The assistance of K. Hallman in the preparation of adducts B9 and B10 is also acknowledged. The 400 MHz spectra were obtained at the South-Western Ontario NMR Centre, funded by a major installation grant from NSERC Canada.

1. L. F. FIESER and M. J. HADDADIN. J. Am. Chem. Soc. **86**, 2081 (1964); Can. J. Chem. **43** 1599 (1965).
2. W. FRIEDRICHSEN. Adv. Heteocycl. Chem. **26**, 135 (1980); U. E. WIERSUM. Aldrichimica Acta, **14**, 53 (1981).
3. R. N. WARRENER. J. Am. Chem. Soc. **93**, 2346 (1971); D. WEGE. Tetrahedron Lett. 2337 (1971); U. E. WIERSUM and W. J. MIJS. J. Chem. Soc. Chem. Commun. 347 (1972).

4. A. S. KENDE, D. P. CURRAN, Y. TSAY, and J. E. MILLS. Tetrahedron Lett. 3537 (1977).
5. J. G. SMITH, S. S. WELANKIWAR, B. S. SCHANTZ, E. H. LAI, and N. G. CHU. J. Org. Chem. **45** 1817 (1980); M. A. MAKHLOUF and B. RICKBORN. J. Org. Chem. **46**, 2734 (1981). L. CONTRERAS and D. B. MACLEAN. Can. J. Chem. **58**, 2573 (1980); **58**, 2580 (1980); B. A. KEAY, D. K. W. LEE, and R. RODRIGO. Tetrahedron Lett. 3663 (1980).
6. H. P. PLAUMANN, J. G. SMITH, and R. RODRIGO. J. Chem. Soc. Chem. Commun. 354; (1980); S. O. DESILVA, C. ST. DENIS, and R. RODRIGO. J. Chem. Soc. Chem. Commun. 995 (1980); R. RODRIGO. J. Org. Chem. **45**, 4538 (1980); D. RAJAPAKSA and R. RODRIGO. J. Am. Chem. Soc. **103**, 6208 (1981); B. A. KEAY and R. RODRIGO. Can. J. Chem. **61**, 637 (1983).
7. B. A. KEAY and R. RODRIGO. J. Am. Chem. Soc. **104**, 4725 (1982).
8. H. P. PLAUMANN, B. A. KEAY, and R. RODRIGO. Tetrahedron Lett. 4921 (1979).
9. C. D. PERCHONOCK and B. LOEV. Prostaglandins, **15**, 623 (1978).
10. J. G. SMITH and R. T. WIKMAN. Tetrahedron, **30**, 2603 (1974).
11. R. C. RONALD, J. M. LANSINGER, T. S. LILLIE, and C. J. WHEELER. J. Org. Chem. **47**, 2541 (1982).
12. M. BARFIELD, R. J. SPEAR, and S. STERNHELL. J. Am. Chem. Soc. **97** 5160 (1975).

Can. J. Chem. Downloaded from www.nrcresearchpress.com by 210.87.254.42 on 09/06/12
For personal use only.

Nuclear analogs of β-lactam antibiotics. XVIII.[1] A short synthesis of 2-alkylthiocarbapen-2-em-3-carboxylate

YASUTSUGU UEDA,[2] CHRISTOPHER E. DAMAS, AND BERNARD BELLEAU
Bristol Laboratories of Canada, 100 Industrial Boulevard, Candiac, P.Q., Canada J5R 1J1

Received February 21, 1983

YASUTSUGU UEDA, CHRISTOPHER E. DAMAS, and BERNARD BELLEAU. Can. J. Chem. **61**, 1996 (1983).

A short synthesis of (±)-2-alkylthiocarbapen-2-em-3-carboxylic acid (**2**) from sorbic acid via a key intermediate **4** is described.

YASUTSUGU UEDA, CHRISTOPHER E. DAMAS et BERNARD BELLEAU. Can. J. Chem. **61**, 1996 (1983).

On décrit une synthèse courte de l'acide (±)-alkyl-2-thiocarbapenem-2-carboxylique-3 (**2**) à partir de l'acide sorbique via l'intermédiaire-clé **4**.

[Traduit par le journal]

Can. J. Chem. Downloaded from www.nrcresearchpress.com by 210.87.254.6 on 09/06/12
For personal use only.

The discovery of thienamycin **1** (1), a potent and broad spectrum β-lactam antibiotic, has initiated considerable effort in the synthesis of the carbapenem ring system (2). Several methods have recently been developed for the synthesis of thienamycin (3) and its 6-unsubstituted analogs (4). Some of these methods (4) require long synthetic sequences or the starting materials are not readily available. We wish to report a short synthesis of 6-unsubstituted 2-alkylthiocarbapen-2-em-3-carboxylic acid (**2**) from an inexpensive starting material, sorbic acid (**3***a*), through a key intermediate **4**.[3] The carbon skeleton necessary for the synthesis of a carbapenem nucleus such as **5** is built-in to this intermediate.

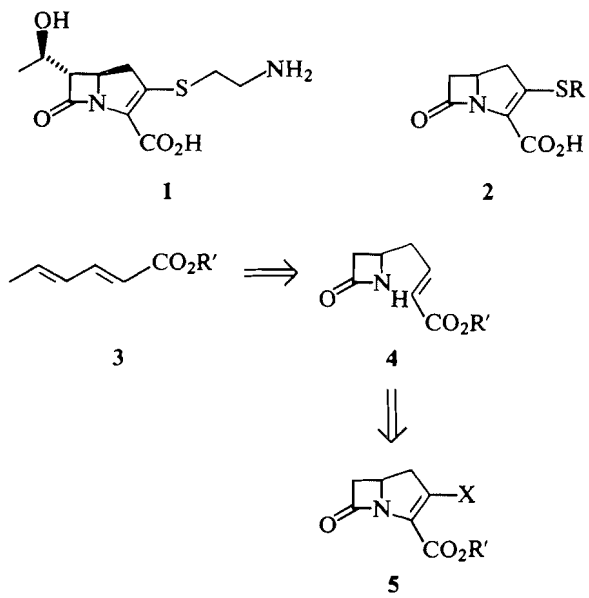

1 **2** **3** **4** **5**

Thus, methyl sorbate (**3***b*) was converted to methyl 3,5-hexadienoate (**6***a*) in 77% yield by kinetic protonation of the enolate generated with lithium diisopropylamide at −78°C in THF–HMPA (6). *p*-Nitrobenzyl 3,5-hexadienoate (**6***b*) was prepared from sorbic acid (**3***a*) as follows: since *p*-nitrobenzyl esters generally suffer from treatment with a strong base such as LDA, sorbic acid (**3***a*) was converted to 3,5-hexadienoic acid (**6***c*) by kinetic protonation of the enolate generated at −10°C with 2 equiv. of LDA in THF (7). This acid was immediately esterified at 0–5°C with *p*-nitrobenzyl bromide and triethylamine to obtain *p*-nitrobenzyl 3,5-hexadienoate (**6***b*) in 65.7% overall yield from sorbic acid (**3***a*).

Addition of chlorosulfonyl isocyanate (8) to these conjugated dienes **6***a* and **6***b* at room temperature in CH_2Cl_2 cleanly provided azetidinone sulfonyl chlorides **7***a* and **7***b* which were, without isolation, reduced by a modification (Na_2SO_3–$NaHCO_3$) of the Durst method (9) to yield azetidinones **8***a* and **8***b* in 63% and 49% yield, respectively. Use of NaOH instead of $NaHCO_3$ caused destruction of the molecule. Isomerization of the double bond in **8***a* to the conjugated system **4***a* was studied in various base–solvent systems. Triethylamine in CH_2Cl_2 did not effect the isomerization at an appreciable rate at room temperature. Triethylamine in polar aprotic solvents, such as DMSO, DMF, or CH_3CN, gave, after weeks, the desired isomerization product **4***a* together with a white solid which consisted of β-lactam opened products.[4]

These fragmentation materials were the major products when **8***a* was treated with strong bases such as 1,5-diazabicyclo[4.3.0]non-5-ene (DBN) in CH_2Cl_2, sodium methoxide in MeOH, or potassium *tert*-butoxide in *t*-BuOH. The best result was obtained by using 1,4-diazabicyclo[2.2.2.]octane (DABCO) in CH_3CN at room temperature. Thus, **8***a* and **8***b* were treated with DABCO in CH_3CN at room temperature for 3–4 days to produce the conjugated esters **4***a* and **4***b* in 87% and 73% yield, respectively.

Although intermediates **4** could be used, after protection of

[1]For Part XVII of this series see ref. 14.

[2]Author to whom correspondence should be addressed.

[3]After a major part of this work was completed, the Smith Kline & French group described a similar approach in their recent publication (5).

[4]These by-products were tentatively characterized as a mixture of **i** and **ii** based on the ^{1}Hmr spectrum, which exhibited two different methyl signals at around 3.7 ppm, and the uv spectrum, which showed a λ_{max} at 256 nm. These were presumably formed by proton abstraction, followed by the ring opening as shown in **iii** and/or **iv**, and then isomerization to each other.

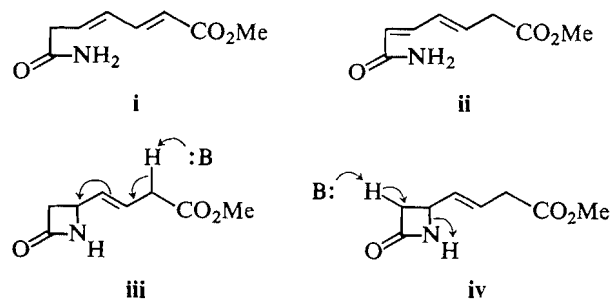

i **ii** **iii** **iv**

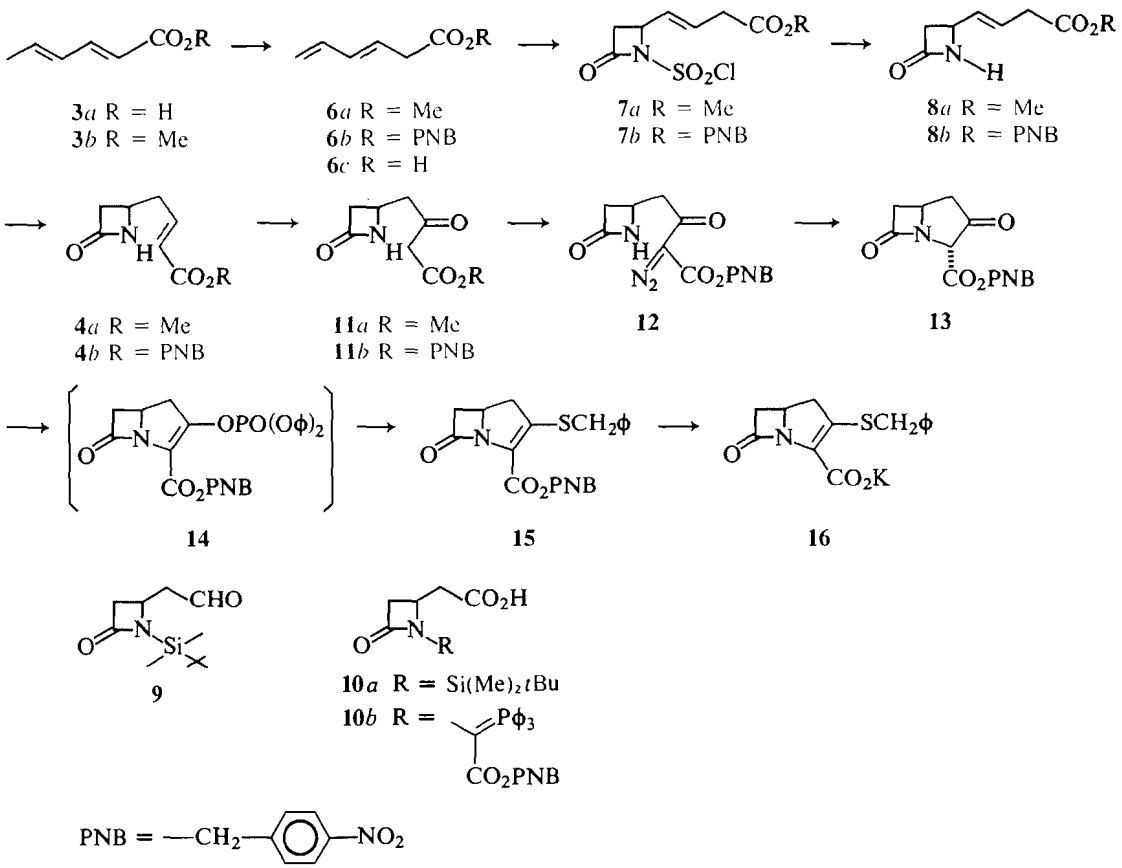

SCHEME 1

the amide, for the synthesis of carbapenems[5] by oxidation of the double bond to the aldehyde **9** (*4a*, *g*) or the carboxylic acids **10** (*3d*, *4d–f*), since they contain the carbon framework needed for the synthesis of carbapenem carboxylates, we decided to use this advantage without breaking down the molecule.

Conversion of α, β-unsaturated esters **4***a*, and **4***b* to β-keto esters **11***a* and **11***b* was readily achieved in 30% and 36% yield, respectively, by the oxypalladation method (*t*-BuOOH/$NaPdCl_4$) which was recently developed by Tsuji *et al.* (10) and employed in the synthesis of a carbapenem intermediate (*4g*). Teatment of β-keto ester **11***b* with *p*-carboxybenzenesulfonyl azide (11) gave diazo compound **12** in 88% yield, which was cyclized by $Rh_2(OAc)_4$, the Merck method (*4a*), to produce cleanly the bicyclic β-keto ester **13**. Transformation of this type of keto ester to 2-alkylthiocarbapenem was reported by the Merck group (*4a*). One example is demonstrated here. Thus **13**, treated with diphenyl chlorophosphate (diisopropylethylamine/CH_3CN, 0°C), gave enol phosphate **14** which was, without isolation, converted to 2-benzylthiocarbapenem **15** in 34% yield by reaction with benzyl mercaptan in the presence of diisopropylethylamine. Catalylic hydrogenolysis of **15** (H_2/Pd–C, $KHCO_3$) afforded carbapenem potassium salt **16**, the presence of which was confirmed by an ir absorption band at 1765 cm^{-1} and its uv spectrum (λ_{max} 299 nm). Due to the instability of this type of molecule (*4c–e*), we were unable to isolate it in a pure form.

This approach offers the following advantages over the methods previously reported. (a) The starting material is commercially available and inexpensive. (b) A variety of carboxylic acid protecting groups, particularly the *p*-nitrobenzyl group, can be easily introduced: *p*-nitrobenzyl ester is most commonly used in the penem or carbapenem synthesis since it can be cleaved to the corresponding carboxylic acid by catalytic hydrogenolysis without destruction of the labile ring system. (c) Since all the necessary carbon skeleton is constructed in one step, this is the most direct route known so far to the carbapenem ring system.

Experimental

Melting points were determined on a Gallenkamp melting point apparatus and are not corrected. The infrared spectra were recorded on a Perkin–Elmer 267 grating infrared spectrometer. The ^1H nuclear magnetic resonance spectra were taken with either the Varian EM-360 (60 MHz) or a Varian CFT-20 (80 MHz) nmr spectrometer. Tetramethylsilane (for solutions other than D_2O) and sodium 4,4-dimethyl-4-silapentane-1-sulfonate (for solutions of D_2O) were used as internal standards and chemical shifts are reported in parts per million (δ) relative to the internal standards. The ultraviolet spectra were recorded on an Unicam SP8-100 uv spectrophotometer. Tetrahydrofuran was freshly distilled from lithium aluminum hydride. Anhydrous diethyl ether (Mallinkrodt or Fisher) was used without further treatment. All other solvents were reagent grade and had been stored over molecular sieves before use. n-Butyllithium (n-BuLi) in hexane (Aldrich) was titrated periodically by the diphenylacetic acid method. Triethylamine, diisopropylamine, and diisopropylethylamine were distilled from CaH_2 and stored over NaOH. Analytical thin layer chromatography (tlc) was conducted on precoated plates (Silica Gel 60F-254, E. Merck). Visualization was effected by uv light and iodine. Preparative layer chromatography (plc) was performed on silica gel plates prepared from Silica Gel 60 GF-254 (E. Merck). For column chromatography, 70–230 mesh Silica Gel 60 (E. Merck) was

[5]The versatility of this type of intermediate **4** in the synthesis of carbapenems will be reported in a forthcoming paper.

Can. J. Chem. Downloaded from www.nrcresearchpress.com by 210.87.254.6 on 09/06/12
For personal use only.

Can. J. Chem. Downloaded from www.nrcresearchpress.com by 210.87.254.6 on 09/06/12
For personal use only.

used. The analyses were performed by Micro-Tech Laboratories, Skokie, Illinois, U.S.A. The abbreviations for ^{1}Hmr multiplicities are used as follows: s, singlet; d, doublet; dd, doublet of doublets; ddd, doublet of doublet of doublets; t, triplet, dt, doublet of triplets; td, triplet of doublets; m, multiplet; br, broad.

*Methyl 2,4-hexadienoate (methyl sorbate) (**3**b)*

Through a stirred suspension of 2,4-hexadienoic acid (**3***a*) (sorbic acid; 112 g, 1.00 mol) in methanol (0.5 L) was bubbled dry hydrogen chloride gas for 5 min, and then the mixture was heated at reflex for 4 h. After cooling, the methanol was evaporated *in vacuo* and the residual oil was diluted with CH_2Cl_2 (0.4 L), removing water which separated out. The CH_2Cl_2 solution was washed carefully with saturated $NaHCO_3$ and then brine, dried (Na_2SO_4), and evaporated. The residue was distilled under reduced pressure to obtain 98.5 g (0.782 mol, yield 78.2%) of the title compound **3***b* as a colourless liquid; bp 69°–71°C/12 Torr (lit. (12) bp 60°C/12 Torr); ir (neat) ν_{max}: 1720 (C=O), 1650 (C=C), and 1620 (C=C) cm^{-1}; R_f 0.72 (Et_2O); ^{1}Hmr ($CDCl_3$) δ: 1.87 (3H, d, J = 5 Hz, 5-Me), 3.74 (3H, s, —CO_2Me), 5.6–6.5 (3H, m, olefinic protons), and 7.05–7.5 (1H, m, 5-H) ppm.

*Methyl 3,5-hexadienoate (**6**a)*

To a stirred solution of diisopropylamine (85 mL, 0.61 mol) in THF (1.4 L) was added, at 0°–5°C under a nitrogen atmosphere, n-BuLi (396 mL, 0.61 mol; 1.54 *M* in hexane) over a period of 45 min. The resulting pale yellow solution was stirred at 0°–5°C for 15 min and then cooled to −75° to −78°C. A solution of hexamethylphosphoramide (115 mL, 0.66 mol) in THF (30 mL) was added in 30 min, and stirring continued for 30 min. To this mixture was added a solution of methyl 2,4-hexadienoate (**3***b*) (64.0 g, 0.508 mol; methyl sorbate) in THF (30 mL) during a period of 1 h at −78°C and stirred for 30 min. The dark red mixture was poured into 2 *N* HCl (900 mL) with stirring. The mixture was extracted with pentane (200 mL × 3) and these extracts combined, washed successively with H_2O (600 mL × 3), saturated $NaHCO_3$ (600 mL) and brine (600 mL), dried (Na_2SO_4), and evaporated to a yellow oil. This was distilled under reduced pressure to give 49.0 g (0.389 mol, yield 76.6%) of the title compound **6***a* as a clear liquid: bp 58°–60°C/12 Torr (lit. (6*b*) bp 73°–75°C/12 Torr); ir (neat) ν_{max}: 1735 (C=O) and 1640 (C=C) cm^{-1}; R_f 0.67 (benzene–Et_2O 4:1); ^{1}Hmr ($CDCl_3$) δ: 3.12 (2H, d, J = 6 Hz, —CH_2—), 3.69 (3H, s, —CO_2Me), 5.14 (2H, t, J = 8 Hz, olefinic protons), and 5.5–6.7 (3H, m, olefinic protons) ppm.

p-*Nitrobenzyl 3,5-hexadienoate (**6**b)*

To a stirred solution of diisopropylamine (76.5 mL, 0.55 mol) in THF (0.5 L) was added at 0°–5°C n-BuLi (344 mL, 0.55 mol; 1.6 *M* in hexane), over a period of 0.5 h under a nitrogen atmosphere, and stirred at 0°–5°C for 0.5 h. To this was added at −15° to −10°C a solution of 2,4-hexadienoic acid (**3***a*) (28.0 g, 0.25 mol) in THF (125 mL) over a period of 0.5 h. The cooling bath was removed and the mixture stirred at room temperature for 1 h. This was poured into a cold solution of concentrated HCl (125 mL) in water (500 mL). The aqueous layer was saturated with sodium chloride and extracted with EtOAc (150 mL × 3). All organic layers were combined, washed with brine (200 mL × 2), dried ($MgSO_4$), and evaporated, yielding 29.0 g of 3,5-hexadienoic acid as a crude oil: bp 61°–63°C/0.2 Torr (lit. (13) bp 102°–103°C/6 Torr); ir (neat) ν_{max}: 2500–3500 (br, CO_2H) and 1710 (CO_2H) cm^{-1}; R_f 0.57 (Et_2O); ^{1}Hmr ($CDCl_3$) δ: 3.15 (2H, d, J = 6 Hz, 2-H) and 5–6.7 (5H, m, olefinic protons) ppm. The distilled material polimerized on standing.

To a solution of this crude material (29.0 g) in DMF (250 mL) was added at 0°–5°C *p*-nitrobenzyl bromide (54.0 g, 0.25 mol) followed by triethylamine (34.75 mL, 0.25 mol). The mixture was stirred at 0°–5°C overnight (ca. 18 h). This was poured into cold water (1 L) and extracted with EtOAc (250 mL × 2), then brine (250 mL), dried ($MgSO_4$), and evaporated to yield 52.7 g of a brown oil. A major portion (30.88 g) of this crude oil was purified[6] by column chromatography (600 g, Et_2O–hexanes 1:4) to obtain 25.28 g of a yellowish oil which was crystallized from Et_2O–pentane (1:2, 15 mL) to give 23.78 g (96.3 mmol, yielded 65.7% based on 2,4-hexadienoic acid) of the title compound **6***b* as pale yellow crystals: mp 40°–41°C; ir (film) ν_{max}: 1740 (C=O), 1525 and 1350 (NO_2) cm^{-1}; R_f 0.46 (Et_2O–hex 1:1); ^{1}Hmr ($CDCl_3$) δ: 3.22 (2H, J = 6 Hz, 2-H), 5.23 (2H, s, —CO_2CH_2Ar), 5.0–6.7 (5H, m, olefinic protons), 7.48 (2H, d, J = 9 Hz, aromatic protons), and 8.16 (2H, d, J = 9 Hz, aromatic protons) ppm. *Anal.* calcd. for $C_{13}H_{13}NO_4$: C 63.15, H 5.30, N 5.67; found: C 63.02, H 5.32, N 5.56.

*Methyl 4-(2-azetidinon-4-yl)-3-butenoate (**8**a)*

To a stirred solution of methyl 3,5-hexadienoate (**6***a*) (48.85 g, 0.388 mol) in CH_2Cl_2 (1.2 L) was added, at 0°–5°C under a nitrogen atmosphere, chlorosulfonyl isocyanate (38.0 mL, 0.430 mol) in 15 min. The mixture was stirred at room temperature for 21 h. A small portion (1 mL) of the reaction mixture was added to a mixture of cold water (3 mL) and CH_2Cl_2 (3 mL), and the CH_2Cl_2 layer was dried (Na_2SO_4) and evaporated to yield methyl 4-(*N*-chlorosulfonyl-2-azetidinon-4-yl)-3-butenoate (**7***a*) as a yellowish oil: ir (neat) ν_{max}: 1815 (β-lactam) and 1730 (ester) cm^{-1}; ^{1}Hmr ($CDCl_3$) δ: 3.07 (1H, dd, J_{gem} = 16 Hz, $J_{3-4\,trans}$ = 4 Hz, 3-H_b), 3.20 (2H, d, J = 6 Hz), 3.55 (1H, dd, J_{gem} = 16 Hz, $J_{3-4\,cis}$ = 6 Hz, 3-H_a), 3.70 (3H, s, —CO_2Me), 4.80 (1H, m, 4-H), 5.5–6.4 (2H, m, olefinic protons) ppm. The rest of the reaction mixture was added slowly to a mechanically stirred slurry of sodium sulfite (242 g, 1.93 mol) in water (0.5 L), ice (0.6 L), and CH_2Cl_2 (0.5 L) at 0°–5°C. During the addition, the mixture was maintained at a pH of 7–8 by addition of saturated $NaHCO_3$ (total 1.8 L). The foaming, milky reaction mixture thus obtained was warmed to room temperature during 1.5 h. The organic layer was collected and the aqueous layer saturated with NaCl and then extracted with CH_2Cl_2 (×2). The combined organic layers were washed with brine, dried ($MgSO_4$), and evaporated to yield 66.0 g of milky yellow oil, which was purified[6] by column chromatography (1.2 kg, EtOAc) to obtain 41.3 g (0.244 mol, yield 63.0%) of the title compound **8***a* as a colourless oil: bp 126°–130°/0.01 Torr; ir (neat) ν_{max}: 3280 (NH), 1760–1730 (br, β-lactam and ester), 1670 (C=C), and 970 (*trans*-disubstituted olefin) cm^{-1}; R_f 0.32 (EtOAc); ^{1}Hmr ($CDCl_3$, 80 MHz) δ: 2.70 (1H, ddd, J_{gem} = 14.9 Hz, $J_{3'-4'\,trans}$ = 2.6 Hz, $J_{3'-1'}$ = 1.3 Hz, 3'-H_b), 3.11 (2H, d, J = 5.7 Hz, —CH_2CO_2—), 3.23 (1H, ddd, J_{gem} = 14.9 Hz, $J_{3'-4'\,cis}$ = 5.1 Hz, $J_{3'-1'}$ = 2.2 Hz, 3'-Ha), 3.69 (3H, s, —CO_2Me), 4.15 (1H, m, 4'-H), 5.5–6.1 (2H, m, olefinic protons), and 5.8 (br, 1'-H) ppm. *Anal.* calcd. for $C_8H_{11}NO_3$: C 56.79, H 6.55, N 8.28; found: C 56.77, H 6.59, N 8.39.

p-*Nitrobenzyl 4-(2-azetidinon-4-yl)-3-butenoate (**8**b)*

To a stirred solution of *p*-nitrobenzyl 3,5-hexadienoate (**6***b*) (2.47 g, 10 mmol) in CH_2Cl_2 (30 mL) was added, at 0°–5°C under a nitrogen atmosphere, chlorosulfonyl isocyanate (0.98 mL, 11 mmol), and the mixture was stirred at room temperature for 3 days. A small portion (1 mL) of the reaction mixture was shaken with a mixture of water (5 mL) and CH_2Cl_2 (5 mL). The CH_2Cl_2 layer was dried (Na_2SO_4) and evaporated to yield *p*-nitronbenzyl 4-(*N*-chlorosulfonyl-2-azetidinon-4-yl)-3-butenoate as a yellowish oil: ir (neat) ν_{max}: 1825 (β-lactam), 1745 (ester), 1520, and 1350 (NO_2) cm^{-1}; ^{1}Hmr ($CDCl_3$, 80 MHz) δ: 3.08 (1H, dd, J_{gem} = 16.7 Hz, $J_{3'-4'\,trans}$ = 4.1 Hz, 3'-H_b), 3.28 (2H, d, J = 6.1 Hz, —CH_2CO_2—), 3.54 (1H, dd, J_{gem} = 16.7 Hz, 3'-H_a), 4.79 (1H, ddd, $J_{4'-4}$ = 7.5 Hz, $J_{4'-3'\,cis}$ = 6.5 Hz, $J_{4'-3'\,trans}$ = 4 Hz, 4-H), 5.23 (2H, s, —CO_2CH_2Ar), 5.6–6.4 (2H, m, olefinic protons), 7.50 (2H, d, J = 8.7 Hz, aromatic protons), and 8.21 (2H, d, J = 8.7 Hz, aromatic protons) ppm. The rest of the reaction mixture was added slowly at room temperature to a stirred mixture of sodium sulfite (12 g, 95 mmol), water (60 mL), and CH_2Cl_2 (60 mL). During the addition, the reaction mixture was maintained at a pH of 7–9 by simultaneous addition of saturated $NaHCO_3$ (70 mL). This was stirred for another 3 h, and the CH_2Cl_2 layer washed with brine, dried (Na_2SO_4), and evaporated *in vacuo*, yielding 1.99 g of a crude oil. This was purified by column chromatography (80 g, EtOAc) to yield 1.41 g (4.86 mmol, yield 48.6%)

[6]Distillation under reduced pressure caused serious decomposition.

Can. J. Chem. Downloaded from www.nrcresearchpress.com by 210.87.254.6 on 09/06/12
For personal use only.

of the title compound **8***b* as an oil which crystallized on standing: mp 85°–87°C (recrystallized from CH_2Cl_2–Et_2O); ir (film) ν_{max}: 1745 (β-lactam and ester), 1525, and 1350 (NO_2) cm^{-1}; R_f 0.32 (EtOAc); ^{1}Hmr ($CDCl_3$, 80 MHz) δ: 2.70 (1H, ddd, J_{gem} = 15 Hz, $J_{3'-4'trans}$ = 2.6 Hz, $J_{3'-1'}$ = 1.3 Hz, 3′-H_b), 3.19 (2H, d, J = 5.4 Hz, —CH_2CO_2—), 3.23 (1H, ddd, J_{gem} = 15 Hz, $J_{3'-4'cis}$ = 5 Hz, $J_{3'-1'}$ = 2.2 Hz, 3′-H_a), 4.16 (1H, m, 3′-H), 5.22 (2H, s, —CO_2CH_2Ar), 5.5–6.1 (2H, m, olefinic protons), 7.51 (2H, d, J = 8.7 Hz, aromatic protons), and 8.23 (2H, d, J = 8.7 Hz, aromatic protons) ppm. *Anal.* calcd. for $C_{14}H_{14}N_2O_5$: C 57.93, H 4.86, N 9.65; found: C 57.61, H 4.79, N 9.57.

*Methyl 4-(2-azetidinon-4-yl)-2-butenoate (**4**a)*

A solution of methyl 4-(2-azetidinon-4-yl)-3-butenoate (**8***a*) (16.9 g, 0.100 mol) and 1,4-diazabicyclo[2.2.2]octane (22.4 g, 0.200 mol; DABCO) in CH_3CN (100 mL) was stirred at room temperature under a nitrogen atmosphere for 4 days. The solvent was evaporated at room temperature *in vacuo*, and the residue mixed with EtOAc (20 mL). The precipitates, formed were filtered and washed with cold EtOAc (20 mL). The filtrate and the washings were combined, evaporated, and the residual oil purified by column chromatography (300 g, EtOAc) to obtain 14.68 g, (86.9 mmol, yield 86.9%) of the title compound **4***a* as an amber coloured oil. This was crystallized from Et_2O at 0°C; mp 51°–52°C; ir ($CHCl_3$) ν_{max}: 3420 (NH), 1765 (β-lactam), 1720 (ester), and 1660 (C=C) cm^{-1}; R_f 0.32 (EtOAc); ^{1}Hmr ($CDCl_3$) δ: 2.55 (2H, dt, J = 6.8 Hz, J_{4-2} = 1.4 Hz, 4-H), 2.63 (1H, ddd, J_{gem} = 14.8 Hz, $J_{3'-4'trans}$ = 2.4 Hz, $J_{3'-1'}$ = 1.2 Hz, 3′-H_b), 3.14 (1H, ddd, J_{gem} = 14.8 Hz, $J_{3'-4'cis}$ = 4.8 Hz, $J_{3'-1'}$ = 2.2 Hz, 3′-H_a), 3.74 (3H, s, —CO_2Me), 3.5–3.8 (1H, m, 4′-H), 5.90 (1H, td, J_{2-3} = 16 Hz, J_{2-4} = 1.4 Hz, 2-H), 6.87 (1H, br, 1′-H), and 6.94 (1H, td, J_{3-2} = 16 Hz, J_{3-4} = 6.8 Hz, 3-H) ppm; *Anal.* calcd. for $C_8H_{11}NO_3$: C 56.79, H 6.55, N 8.28; found: C 57.00, H 6.49, N 8.13.

*Isomerization of **8**a with Et_3N in DMSO*

A mixture of methyl 4-(2-azetidinon-4-yl)-3-butenoate (**8***a*) (4.05 g, 24.0 mmol) and triethylamine (1.50 g, 15.0 mmol) in DMSO (24 mL) was stirred at room temperature for 18 days. The rection mixture was poured into a cold mixture of 1 *N* HCl (15 mL), water (85 mL), and CH_2Cl_2 (100 mL). The aqueous layer was saturated with sodium chloride and extracted with CH_2Cl_2 (35 mL × 3). All CH_2CH_2 layers were combined, washed with brine, dried (Na_2SO_4), and evaporated, yielding 3.83 g of crude oily solid. This was purified by column chromatography (60 g, MeOH–benzene 2:98) to obtain 2.12 g (12.5 mmol, yield 52.4%) of **4***a* as a colourless oil: R_f 0.33 (MeOH–benzene 1:4), and 1.32 g (7.81 mmol, yield 32.5%) of β-lactam opened materials **i** and **ii** as a white solid: mp 127°–133°C; ir (Nujol) ν_{max}: 3390, 3190 (—$CONH_2$), 1720 (ester) and 1645 (amide) cm^{-1}; uv (EtOH) λ_{max}: 256 nm (ε 26 000); R_f 0.22 (MeOH–benzene 1:4); ^{1}Hmr ($CHCl_3$, 80 MHz) δ: 3.14 (d, J = 5.7 Hz, —CH_2—), 3.21 (d, J = 5.2 Hz, —CH_2—), 3.70 (s, —CO_2Me), 3.74 (2, —CO_2Me), 5.5 (br, —$CONH_2$), 5.87 (d, J = 15.3 Hz, olefinic proton), 6.1–7.4 (m, olefinic protons) ppm.

*p-Nitrobenzyl 4-(2-azetidinon-4-yl)-2-butenoate (**4**b)*

A solution of *p*-nitrobenzyl 4-(2-azetidinon-4-yl)-3-butenoate (**8***b*) (1.16 g, 4.00 mmol) and 1,4-diazabicyclo[2.2.2]octane (900 mg, 8.00 mmol; DABCO) in CH_3CN (8 mL) was stirred at room temperature for 3 days. After evaporation of the solvent *in vacuo*, the residue, dissolved in EtOAc (40 mL), was washed with 1 *N* HCl (10 mL), then brine, dried (Na_2SO_4), and evaporated to yield 1.05 g of yellow solid. This was purified by column chromatography (50 g, EtOAc) to obtain 850 mg (2.93 mmol, yield 73.2%) of the title compound **4***b* as white crystals: mp 126°–128°C (recrystallized from EtOAc); ir (film) ν_{max}: 3200 (NH), 1755 (β-lactam), 1720 (ester), 1655 (C=C), 1510, and 1350 (NO_2) cm^{-1}; R_f 0.31 (EtOAc); ^{1}Hmr ($CDCl_3$, 80 MHz) δ: 2.57 (2H, dt, J = 7.1 Hz, J_{4-2} = 1.3 Hz, 4-H), 2.65 (1H, ddd, J_{gem} = 15 Hz, $J_{3'-4'trans}$ = 2.4 Hz, $J_{3'-1'}$ = 1 Hz, 3′-H_b), 3.15 (1H, ddd, J_{gem} = 15 Hz, $J_{3'-4'cis}$ = 5 Hz, $J_{3'-1'}$ = 2.3 Hz, 3′-H_a), 3.74 (1H, m, 4′-H), 5.27 (2H, s, —CO_2CH_2Ar), 5.97 (1H, td, J_{2-3} = 15.7 Hz, J_{2-4} = 1.3 Hz, 2-H), 6.97 (1H, dt, J_{3-2} = 15.6 Hz, J_{3-4} = 7.1 Hz, 3-H), 7.53 (2H, d, J = 8.7 Hz, aromatic protons), and 8.23 (2H, d, J = 8.7 Hz, aromatic protons) ppm. *Anal.* calcd. for $C_{14}H_{14}N_2O_5$: C 57.93, H 4.86, N 9.65; found: C 58.01, H 4.81, N 9.59.

*Methyl 4-(2-azetidinon-4-yl)-3-oxobutanoate (**11**a)*

To a mixture of sodium tetrachloropalladate (58 mg, 0.2 mmol) and *tert*-butyl hydroperoxide (193 mg, 1.5 mmol; 70% aqueous solution) in 50% aqueous HOAc (1 mL) was added a solution of methyl 4-(2-azetidinon-4-yl)-2-butenoate (**4***a*) (169 mg, 1.0 mmol) in 50% aqueous HOAc (1 mL), and the mixture was heated at 50°C for 10 h. The solvents were evaporated by a vacuum pump at 50°C and the residue was purified by plc (EtOAc) to yield 55 mg (0.30 mmol, yield 30%) of the title compound **11***a* as a yellowish oil: ir (neat) ν_{max}: 3320 (NH), 1745 (β-lactam and ester), and 1715 (C=O) cm^{-1}; R_f 0.20 (EtOAc); ^{1}Hmr ($CDCl_3$, 80 MHz) δ: 2.59 (1H, ddd, J_{gem} = 15 Hz, $J_{3'-4'trans}$ = 2.5 Hz, $J_{3'-1'}$ = 1 Hz, 3′-H_b), 2.77 (1H, dd, J_{gem} = 18 Hz, $J_{4-4'}$ = 8 Hz, 4-H_a), 3.08 (1H, dd, J_{gem} = 18 Hz, $J_{4-4'}$ = 4.6 Hz, 4-H_b), 3.16 (1H, ddd, J_{gem} = 15 Hz, $J_{3'-4'cis}$ = 5.0 Hz, $J_{3'-1'}$ = 2.4 Hz, 3′-H_a), 3.47 (2H, s, 2-H), 3.74 (3H, s, —CO_2Me), 3.9 (1H, m, 4′-H), and 6.15 (br, NH) ppm.

*p-Nitrobenzyl 4-(2-azetidinon-4-yl)-3-oxobutanoate (**11**b)*

To a mixture of sodium tetrachloropalladate (58 mg, 0.2 mmol) and *tert*-butyl hydroperoxide (193 mg, 1.5 mmol; 70% aqueous solution) in 50% aqueous HOAc (3 mL) was added a solution of *p*-nitrobenzyl 4-(2-azetidinon-4-yl)-2-butenoate (290 mg, 1.0 mmol) in 50% aqueous HOAc (3 mL) and the mixture was heated at 60°–65°C for 6 h. The resulting reddish mixture, diluted with EtOAc (30 mL), was neutralized by careful addition of saturated $NaHCO_3$ (ca. 50 mL). The organic layer was washed with brine, dried (Na_2SO_4), and evaporated to yield 187 mg of a crude oil. This was purified by column chromatography (10 g, EtOAc) to obtain 109 mg (0.356 mmol, yield 36%) of the title compound as a clear oil. This was crystallized by trituration with i-PrOH: mp 46°–48°C; ir (film) ν_{max}: 3300 (br, NH), 1745 (β-lactam and ester), 1715 (C=O), 1520, and 1350 (NO_2) cm^{-1}; R_f 0.19 (EtOAc); ^{1}Hmr ($CDCl_3$, 80 MHz) δ: 2.59 (1H, ddd, J_{gem} = 15 Hz, $J_{3'-4'trans}$ = 2.5 Hz, $J_{3'-1'}$ = 1 Hz, 3′-H_b), 2.77 (1H, ddd, J_{gem} = 18 Hz, $J_{4-4'}$ = 8 Hz, 4-H_a), 3.08 (1H, dd, J_{gem} = 18 Hz, $J_{4-4'}$ = 5 Hz, 4-H_b), 3.18 (1H, ddd, J_{gem} = 15 Hz, $J_{3'-4'cis}$ = 5 Hz, $J_{3'-1'}$ = 2.5 Hz, 3′-H_a), 3.55 (2H, s, 2-H), 3.93 (1H, m, 4′-H), 5.27 (2H, s, —CO_2CH_2Ar), 6.0 (br, NH), 7.52 (2H, d, J = 8.7 Hz, aromatic protons), and 8.24 (2H, J = 8.7 Hz, aromatic protons) ppm. *Anal.* calcd. for $C_{14}H_{14}N_2O_6$: C 54.90, H 4.61, N 9.15; found: C 54.70, H 4.80, N 9.06.

*p-Nitrobenzyl 4-(2-azetidinon-4-yl)-3-oxo-2-diazobutanoate (**12**)*

To a mixture of *p*-nitrobenzyl 4-(2-azetidinon-4-yl)-3-oxobutanoate (**11***b*) (1.38 g, 4.51 mmol) and *p*-carboxybenzenesulfonyl azide (1.27 g, 5.59 mmol) in CH_3CN (30 mL) was added, at 0°–5°C under a nitrogen atmosphere, Et_3N (2.70 mL, 19.4 mmol), causing dissolution followed by precipitation. The mixture was diluted with CH_3CN (15 mL) and stirred at room temperature for 30 min. The precipitate was filtered and washed with EtOAc. The filtrate and washings were combined and evaporated to yield 2.0 g of a greenish oil. This was purified by column chromatography (160 g, EtOAc) to give 1.32 g (3.97 mmol, yield 88.1%) of the title compound **12** as yellowish crystals: mp 109°–110°C (recrystallized from EtOAc); ir (film) ν_{max}: 3370 (NH), 2140 (C=N_2), 1760 (β-lactam), 1720 (ester), 1650 (C=O), 1520, and 1350 (NO_2) cm^{-1}; R_f 0.41 (EtOAc); ^{1}Hmr ($CDCl_3$, 80 MHz) δ: 2.65 (1H, ddd, J_{gem} = 15 Hz, $J_{3'-4'trans}$ = 2.5 Hz, $J_{3'-1'}$ = 1 Hz, 3′-H_b), 2.99 (1H, dd, J_{gem} = 18 Hz, $J_{4-4'}$ = 8.5 Hz, 4-H_a), 3.17 (1H, ddd, J_{gem} = 15 Hz, $J_{3'-4'cis}$ = 5 Hz, $J_{3'-1'}$ = 2.4 Hz, 3′-H_a), 3.38 (1H, dd, J_{gem} = 18 Hz, $J_{4-4'}$ = 4.4 Hz, 4-H_b), 3.95 (1H, m, 4′-H), 5.35 (2H, s, —CO_2CH_2Ar), 6.07 (br, NH), 7.53 (2H, d, J = 8.8 Hz, aromatic protons), and 8.25 (2H, d, J = 8.8 Hz, aromatic protons) ppm; *Anal.* calcd. for $C_{14}H_{12}N_4O_6$: C 50.61, H 3.64, N 16.86; found: C 50.72, H 3.81, N 16.80.

*p-Nitrobenzyl 2-oxocarbapenam-3-carboxylate (**13**)*

Through a suspension of *p*-nitrobenzyl 4-(2-azetidinon-4-yl)-3-oxo-

2-diazobutanoate (49 mg, 0.15 mmol) and $Rh_2(OAc)_4$ (0.1 mg) in benzene (2 mL) was bubbled dry nitrogen for 10 min, and this mixture was heated at gentle reflux under a nitrogen atmosphere for 30 min. The catalyst was filtered and washed with EtOAc. The filtrate and washings were cobmined and evaporated to yield a crude oil which was purified by column chromatography (short column, EtOAc) to obtain 37 mg (0.12 mmol, yield 81%) of the title compound **13** as an oil: ir (film) ν_{max}: 1765 (β-lactam), 1745 (ester and ketone), 1520, and 1350 (NO_2) cm^{-1}; R_f 0.60 (EtOAc); ^{1}Hmr ($CDCl_3$, 80 MHz) δ: 2.40 (1H, dd, J_{gem} = 19 Hz, J_{1-5} = 8 Hz, 1-H_a), 2.94 (1H, dd, J_{gem} = 19 Hz, J_{1-5} = 6.2 Hz, 1-H_b), 2.96 (1H, dd, J_{gem} = 16 Hz, $J_{6-5\,trans}$ = 2 Hz, 6-H_b), 3.67 (1H, dd, J_{gem} = 16 Hz, $J_{6-5\,cis}$ = 5 Hz, 6-H_a), 4.15 (1H, m, 5-H), 4.77 (1H, s, 3-H), 5.30 (2H, s, —CO_2CH_2Ar), 7.53 (2H, d, J = 8.8 Hz, aromatic protons), and 8.24 (2H, d, J = 8.8 Hz, aromatic protons) ppm.

p-*Nitrobenzyl 2-benzylthiocarbapen-2-em-3-carboxylate (15)*

To a stirred solution of freshly prepared *p*-nitrobenzyl-2-oxo-carbapenam-3-carboxylate (**13**) (151 mg, 0.496 mmol) in CH_3CN (10 mL) was added, at 0°–5°C under a nitrogen atmosphere, diisopropylethylamine (0.095 mL, 0.55 mmol), followed by diphenyl chlorophosphate (0.11 mL, 0.55 mmol). The mixture was stirred at 0°–5°C for 30 min, by which time the tlc (EtOAc–hex 1:1) indicated that the reaction was over. The enol phosphate **14** could be isolated as an off-white solid: mp 105°–111°C (dec.); ir (film) ν_{max}: 1790 (β-lactam), 1730 (ester), and 1640 (C=C) cm^{-1}; R_f 0.20 (EtOAc–hex 1:1); ^{1}Hmr ($CDCl_3$, 80 MHz) δ: 2.96 (1H, dd, J_{gem} = 17 Hz, $J_{6-5\,trans}$ = 3 Hz, 6-H_b), 3.0–3.3 (2H, m, 1-H), 3.55 (1H, dd, J_{gem} = 17 Hz, $J_{6-5\,cis}$ = 5.5 Hz, 6-H_a), 4.15 (1H, m, 5-H), 5.20 (1H, d, J = 13.8 Hz, —CO_2CH_2Ar), 5.43 (1H, d, J = 13.8 Hz, —CO_2CH_2Ar), 7.26 (10H, s, aromatic protons), 7.54 (2H, d, = 8.8 Hz, aromatic protons), and 8.15 (2H, d, J = 8.8 Hz, aromatic protons) ppm. Without isolation of the enol phosphate **14**, to this reaction mixture was added, at 0°–5°C, diisopropylamine (0.086 mL, 0.50 mmol), and then benzyl mercaptan (0.058 mL, 0.50 mmol). The mixture was stirred at room temperature (N_2) for 1 h. The solvent was evaporated *in vacuo* at room temperature and the residue (yellowish solid), dissolved in CH_2Cl_2, was washed with diluted brine, dried (Na_2SO_4), and evaporated to yield crystalline solid. This was rinsed with a small amount of cold EtOAc to obtain 70 mg (0.17 mmol, yield 34%) of the title compound **15** as yellowish crystals: mp 124°–128°C (dec.); ir (film) ν_{max}: 1765 (β-lactam), 1690 (ester), 1515, and 1340 (NO_2) cm^{-1}; uv (EtOH) λ_{max}: 319 (ε 13 300) and 266 nm (ε 11 000); R_f 0.27 (EtOAc–hex 1:1); ^{1}Hmr ($CDCl_3$, 80 MHz) δ: 2.90 (1H, dd, J_{gem} = 16.5 Hz, $J_{6-5\,trans}$ = 3.0 Hz, 6-H_b), 2.95 (1H, dd, J_{gem} = 18 Hz, J_{1-5} = 8.5 Hz, 1-H_a), 3.29 (1H, J_{gem} = 18 Hz, J_{1-5} = 8.5 Hz, 1-H_b), 3.49 (1H, dd, J_{gem} = 16.5 Hz, $J_{6-5\,cis}$ = 5.3 Hz, 6-H_a), 4.08 (2H, s, —$SCH_2\phi$), 4.15 (1H, m, 5-H), 5.23 (1H, d, J = 13.6 Hz, —CO_2CH_2Ar), 5.50 (1H, d, J = 13.6 Hz, —CO_2CH_2Ar), 7.33 (5H, s, aromatic protons), 7.63 (2H, d, J = 8.8 Hz, aromatic protons), and 8.19 (2H, d, J = 8.8 Hz, aromatic protons) ppm. This material decomposed during preparative layer chromatography on silica gel.

Potassium 2-benzylthiocarbapen-2-em-3-carboxylate (16)

A solution of *p*-nitrobenzyl 2-benzylthiocarbapen-2-em-3-carboxylate (35 mg, 0.085 mmol) in THF (6 mL) was mixed with Et_2O (6 mL), a solution of K_2HPO_4 (15 mg, 0.085 mmol) and $KHCO_3$ (8.5 mg, 0.085 mmol) in water (6 mL), and 10% Pd–C (35 mg). This mixture was shaken in a Parr apparatus under hydrogen pressure of 30 psi at room temperature for 30 min. The aqueous layer, separated, was filtered over Celite and the filtrate washed with Et_2O. Lyophilization of the aqueous phase gave 10 mg of the title compound as greyish powder: ir (KBr disc) ν_{max}: 1765 (β-lactam) and 1630 (br, —CO_2^-) cm^{-1}; uv (H_2O) λ_{max}: 299 nm (ε 1800); ^{1}Hmr (D_2O, 80 MHz) δ: 2.7–3.5 (m, 1-H and 6-H), 3.37 (dd, J_{gem} = 16 Hz, $J_{6-5\,cis}$ = 4 Hz, 6-H_a), 4.05 (s, —$CH_2\phi$), 4.1 (m, 5-H), and 7.35 (s, aromatic protons) ppm.

Acknowledgements

We would like to thank Dr. M. Ménard for his interest, Dr. A. Martel for helpful discussions, and Mr. G. Lacasse for 80 MHz ^{1}Hmr spectra during the course of this work.

1. (*a*) G. Albers-Schönberg, B. H. Arison, O. D. Hensens, J. Hirshfield, K. Hoogsteen, E. A. Kaczka, R. E. Rhodes, J. S. Kahan, F. M. Kahan, R. W. Ratcliffe, E. Walton, L. J. Ruswinkle, R. B. Morin, and B. G. Christensen. J. Am. Chem. Soc. **100**, 6491 (1978); (*b*) J. S. Kahan, F. M. Kahan, R. Geogelman, S. A. Currie, M. Jackson, E. O. Stapley, T. W. Miller, A. K. Miller, D. Hendlin, S. Mochaks, S. Hernandez, H. B. Woodruff, and J. Birnbaum. J. Antibiot. **32**, 1 (1979).
2. (*a*) T. Kametani and M. Ihara. J. Synth. Org. Chem. Jpn. **38**, 1025 (1980); (*b*) R. D. G. Cooper. *In* Topics in antibiotic chemistry. Vol. 3. *Edited by* P. G. Sammes. Ellis Horwood Ltd., Chichester. 1980. pp. 101–138; (*c*) T. Kametani, K. Fukumoto, and M. Ihara. Heterocycles, **17**, 463 (1982); (*d*) R. W. Ratcliffe and G. Albers-Schönberg. *In* Chemistry and biology of β-lactam antibiotics. Vol. 2. *Edited by* R. B. Morin and M. Gorman. Academic Press, New York. 1982. pp. 227–313.
3. (*a*) D. B. R. Johnston, S. M. Schmitt, F. A. Bouffard, and B. G. Christensen. J. Am. Chem. Soc. **100**, 313 (1978); (*b*) S. M. Schmitt, D. B. R. Johnston, and B. G. Christensen. J. Org. Chem. **45**, 1142 (1980); (*c*) D. G. Melillo, I. Shinkai, T. Liu, K. Ryan, and M. Sletzinger. Tetrahedron Lett. **21**, 2783 (1980); (*d*) T. N. Salzmann, R. W. Ratcliffe, B. G. Christensen, and F. A. Bouffard. J. Am. Chem. Soc. **102**, 6161 (1980); (*e*) S. Karady, J. S. Amato, R. A. Reamer, and L. M. Weinstock. J. Am. Chem. Soc. **103**, 6765 (1981).
4. (*a*) R. W. Ratcliffe, T. N. Salzmann, and B. G. Christensen. Tetrahedron Lett. **21**, 31 (1980); (*b*) S. M. Schmitt, D. B. R. Johnston, and B. G. Christensen. J. Org. Chem. **45**, 1135 (1980); (*c*) S. Oida, A. Yashida, and E. Ohki. Chem. Pharm. Bull. **28**, 3494 (1980); (*d*) R. J. Ponsford, P. M. Roberts, and R. Southgate. Chem. Commun. 847 (1979); (*e*) L. Cama and B. G. Christensen. Tetrahedron Lett. **21**, 2013 (1980); (*f*) M. J. Basker, J. H. Bateson, A. J. G. Baxter, R. J. Ponsford, P. M. Roberts, R. Southgate, T. C. Smale, and J. Smith. J. Antibiot. **34**, 1224 (1981), and references therein; (*g*) S. Takano, C. Kasahara, and K. Ogasawara. Chem. Lett. 631 (1982); (*h*) M. Shibasaki, A. Nishida, and S. Ikegami. Tetrahedron Lett. **23**, 2875 (1982).
5. D. A. Berges, E. R. Snipes, G. W. Chan, W. D. Kingsburry, and C. M. Kinig. Tetrahedron Lett. **22**, 3557 (1981).
6. (*a*) K. Torssell. Tetrahedron Lett. 623 (1974); (*b*) R. V. Stevens, R. E. Cherpeck, B. L. Harrison, J. Lai, and R. Lapalme. J. Am. Chem. Soc. **98**, 6317 (1976).
7. S. F. Martin, C. Tu, and T. Chou. J. Am. Chem. Soc. **102**, 5274 (1980).
8. (*a*) J. K. Rasmussen and A. Hassner. Chem. Rev. **76**, 389 (1976); (*b*) W. A. Szabo. Aldrichimica Acta, **10**, 23 (1977).
9. T. Durst and M. J. O'Sullivan. J. Org. Chem. **35**, 2043 (1970).
10. J. Tsuji, H. Nagashima, and K. Hori. Chemistry Lett. 257 (1980).
11. J. B. Hendrickson and W. A. Wolf. J. Org. Chem. **33**, 3610 (1968).
12. D. H. Wheeler. J. Am. Chem. Soc. **70**, 3467 (1948).
13. R. Paul and S. Tchelitcheff. Bull. Soc. Chim. Fr. 108 (1948).
14. A. Martel, J.-P. Daris, C. Bachand, M. Ménard, T. Durst, and B. Belleau. Can. J. Chem. **61**, 1899 (1983).

Can. J. Chem. Downloaded from www.nrcresearchpress.com by 210.87.254.6 on 09/06/12
For personal use only.

Molecular conformation of di-*o*-anisylcarbinol: an X-ray diffraction study

C. FAERMAN, H. NEGRI, AND G. PUNTE[1]

Departamento de Física, Facultad de Ciencias Exactas, Universidad Nacional de La Plata, C.C. 67, 1900 – La Plata, Argentina

AND

A. A. VITALE AND N. S. NUDELMAN[1]

Departamento de Química Orgánica, Facultad de Ciencias Exactas y Naturales, Universidad de Buenos Aires, Ciudad Universitaria, Pab. 2, Piso 3, 1428 – Buenos Aires, Argentina

Received July 15, 1982[2]

C. FAERMAN, H. NEGRI, G. PUNTE, A. A. VITALE, and N. S. NUDELMAN. Can. J. Chem. **61**, 2001 (1983).

Di-*o*-anisylcarbinol crystallizes in the triclinic system, space group $P\bar{1}$ with a = 7.50 (4), b = 10.89 (4), c = 7.98 (3) Å, α = 101.9 (1), β = 94.1 (1), γ = 94.6 (1)°, Z = 2, V = 633.11 Å^3, D_c = 1.28 mg m^{-3}, D_m = 1.26 (1) mg m^{-3}, CuK$_\alpha$ radiation, λ = 1.54178 Å, μ(CuK$_\alpha$) = 0.633 mm^{-1}, F(000) = 260. The structure has been determined by direct methods using single crystal X-ray data and refined by least-squares to the final R factors R = 5.89% and R_w = 5.35%. The molecule has a twist-skewed conformation with the phenyl rings on nearly orthogonal planes. The crystal structure shows a hydrogen-bonded dimer and a peculiar arrangement of the methoxy and phenyl groups.

C. FAERMAN, H. NEGRI, G. PUNTE, A. A. VITALE et N. S. NUDELMAN. Can. J. Chem. **61**, 2001 (1983).

Le di-*o*-anisylcarbinol cristallise dans le système triclinique et appartient au groupe d'espace $P\bar{1}$, avec a = 7,50 (4), b = 10,89 (4), c = 7,98 (3) Å, α = 101,9 (1), β = 94,1 (1), γ = 94,6 (1)°, Z = 2, V = 633,11 Å^3, D_c = 1,28 mg m^{-3}, D_m = 1,26 (1) mg m^{-3}, radiation CuK$_\alpha$, λ = 1,54178 Å, μ(CuK$_\alpha$) = 0,633 mm^{-1}, F(000) = 260. On a déterminé la structure par des méthodes directes en utilisant les données de rayons-X sur un monocristal et on l'a affinée par la méthode des moindres carrés jusqu'à des valeurs de R = 5,89% et de R_w = 5,35%. La molécule a une conformation *gauche* croisée avec les noyaux phényles dans des plans quasi orthogonaux. La structure du cristal montre un dimère lié par une liaison hydrogène et un arrangement particulier des groupes méthoxy et phényle.

[Traduit par le journal]

Introduction

As part of a study on the reaction of aryl-lithiums with carbon monoxide, initiated several years ago (1) and reviewed very recently (2), we have investigated the carbonylation reaction of *o*-anisyllithium. In this reaction di-*o*-anisylcarbinol (**1**), Fig. 1, and di-*o*-anisylketone are the only isolable reaction products (ca. 40% each) (2, 3).

Our interest in compound **1** arose by the observation of two different nmr signals for the hydrogen atoms of the methoxy groups of **1** in CCl_4 solution, suggesting a partially restricted rotation of the aryl rings.

A considerable number of molecular structure determinations, theoretical calculations, and nmr spectra on bridged diphenyl compounds have been performed by several authors (4–12). A common purpose of these works was to study the effects of different bridging atoms and phenyl substituents on the bridged diphenyl conformation. The special efforts devoted to these compounds were to some extent due to the biological importance of disclosing the relationship between conformation and activity in thyroid hormone. Some of these reported works provide theoretical as well as experimental evidence for intermolecular and intramolecular hydrogen bonding (5–9, 11, 12).

In this paper we present an X-ray single crystal molecular structure determination of **1** which supplies experimental data that may contribute to the understanding of conformation in bridged diphenyl compounds.

Experimental

Preparation of compound

Compound **1** was prepared in excellent yield (88%) by adding *o*-methoxybenzaldehyde to *o*-anisyllithium (prepared by the method described for phenyllithium (13)), in THF at room temperature. Hydrolysis and standard work-up (14) of the reaction mixture, rendered **1** (mp 82–83°C, lit. (15) mp 83°C). Compound **1** may also be obtained from the reaction of *o*-anisyllithium with carbon monoxide (2, 3). Infrared (KBr, cm^{-1}): 3300 (st O—H), 2800 (st C—H), 1580 (st C=C), 1450 (def C—H), 1220 (st C—O), 750 (def C—H ar); nmr (CCl_4) δ:3.55 (s, 3H, —OC*H*$_3$, 3.80 (s, 3H, —OC*H*$_3$), 6.35 (d, 1H, —C*H*), 7.2 (m, 9H, ar *H* and —O*H*; this signal integrates to 8H in D_2O); nmr (acetone-d_6) δ: 3.80 (s, 6H, —OC*H*$_3$), 4.26 (d, 1H, —O*H*), 6.44 (d, 1H, —C*H*), 7.1 (m, 8H, ar *H*). Colourless single crystals were grown by controlled slow evaporation from methanol solution at room temperature.

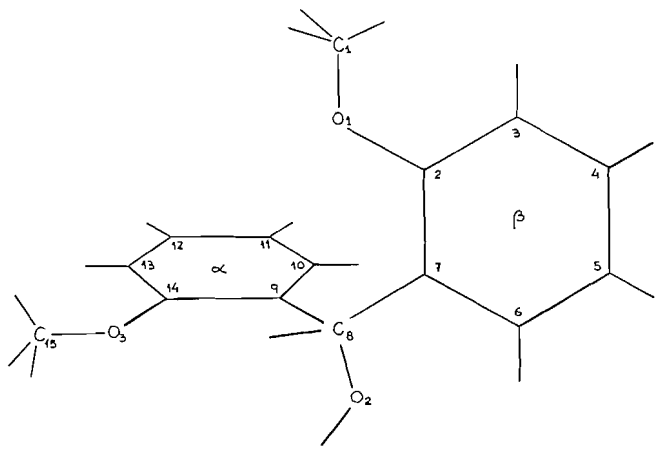

FIG. 1. Atom labelling of di-*o*-anisylcarbinol (**1**).

Structure determination and refinement

Crystal data are as stated in the abstract. An irregular specimen, mounted along ***a***, with approximate dimensions 0.55 × 0.73 × 0.91 mm was used to collect the data. Precession and Weissenberg photographs showed the crystallographic system is triclinic and were

[1]Member of Scientific Research Career, CONICET. To whom reprint requests should be addressed.

[2]Revision received January 13, 1983.

Can. J. Chem. Downloaded from www.nrcresearchpress.com by 210.87.254.6 on 09/06/12
For personal use only.

Can. J. Chem. Downloaded from www.nrcresearchpress.com by 210.87.254.6 on 09/06/12
For personal use only.

TABLE 1. Final fractional atomic coordinates ($\times 10^4$) and anisotropic temperature factors for non-hydrogen atoms ($\times 10^4$)[a]

Atom	x	y	z	U_{11}	U_{22}	U_{33}	U_{23}	U_{13}	U_{12}
C(8)	1661(5)	−3354(4)	−423(6)	463(28)	374(26)	334(27)	45(18)	−17(13)	−54(14)
O(2)	1826(3)	−4667(3)	−584(5)	719(22)	371(21)	519(24)	158(17)	−76(12)	−55(12)
C(1)	1326(10)	385(6)	2000(11)	935(58)	505(43)	954(63)	−96(37)	−21(35)	270(28)
C(2)	3171(6)	−1309(5)	1408(6)	490(33)	527(34)	366(29)	118(22)	−36(16)	36(17)
C(3)	4654(7)	−600(6)	2349(7)	732(43)	465(37)	513(37)	111(28)	−84(22)	−127(22)
C(4)	6241(8)	−1102(6)	2462(8)	545(44)	852(54)	667(43)	33(36)	−136(25)	−164(30)
C(5)	6379(7)	−2328(7)	1695(8)	354(37)	997(55)	760(43)	297(39)	−117(22)	−1(26)
C(6)	4894(6)	−3053(5)	780(7)	449(35)	609(40)	522(34)	113(26)	38(19)	105(21)
C(7)	3284(5)	−2572(4)	626(5)	438(30)	405(29)	279(24)	64(19)	−3(13)	14(15)
O(1)	1523(4)	−893(3)	1215(5)	659(23)	544(25)	606(24)	−25(18)	−69(14)	160(15)
C(9)	1389(5)	−3110(4)	−2204(6)	453(27)	317(26)	435(30)	52(20)	−5(15)	51(14)
C(10)	2706(6)	−2522(5)	−2951(6)	388(31)	614(35)	458(32)	115(24)	4(17)	−29(17)
C(11)	2463(6)	−2321(5)	−4589(7)	610(34)	655(37)	503(37)	189(28)	68(19)	−67(20)
C(12)	840(6)	−2724(5)	−5551(7)	661(35)	683(39)	398(35)	169(28)	−3(19)	−26(21)
C(13)	−495(6)	−3320(5)	−4849(6)	548(35)	705(40)	344(31)	56(26)	−85(16)	−2(21)
C(14)	−237(5)	−3508(4)	−3189(6)	443(27)	468(32)	386(30)	37(22)	−24(16)	18(17)
C(15)	−3243(7)	−4482(7)	−3356(8)	439(36)	916(50)	608(42)	226(36)	−89(21)	−66(24)
O(3)	−1548(3)	−4102(3)	−2424(4)	432(19)	651(24)	474(22)	149(17)	−43(11)	−55(12)

[a]Temperature factor expression is: $\exp(-2\pi(U_{11}h^2a^{*2} + U_{22}k^2b^{*2} + U_{33}l^2c^{*2} + 2U_{12}hka^*b^* + 2U_{13}hla^*c^* + 2U_{23}klb^*c^*))$.

TABLE 2. Final fractional atomic coordinates ($\times 10^3$) and isotropic temperature factors for hydrogen atoms ($\times 10^4$)

Atom	x	y	z	U
H(8)	56(6)	−313(5)	21(7)	65(15)
H(02)	179(7)	−494(7)	40(9)	110(26)
H(101)	4(9)	39(6)	177(9)	94(22)
H(102)	235(9)	107(8)	172(11)	127(26)
H(103)	163(11)	50(9)	329(14)	153(35)
H(3)	485(7)	31(6)	295(8)	88(19)
H(4)	731(7)	−69(6)	293(8)	77(19)
H(5)	−263(8)	−263(5)	169(7)	69(20)
H(6)	498(5)	−396(5)	23(6)	49(12)
H(10)	386(5)	−228(4)	−241(6)	35(12)
H(11)	345(5)	−192(4)	−514(6)	39(11)
H(12)	75(5)	−274(5)	−699(8)	70(14)
H(13)	−156(6)	−356(4)	−546(7)	55(14)
H(151)	−411(8)	−492(6)	−273(9)	100(21)
H(152)	−324(7)	−508(6)	−457(10)	104(22)
H(153)	−382(9)	−373(7)	−357(9)	102(23)

used to determine the preliminary cell dimensions. Single crystal diffraction data were obtained using the equi-inclination multiple film Weissenberg technique; 1431 reflections, with intensities above background, were measured on the layers (0–5, k, l) by the S.R.C. Daresbury Laboratory microdensitometer service, England.

All measurable intensities were treated as observed. The intensities from different layers were scaled according to the number of oscillations, and corrected for Lorentz and polarization factors. No extinction and absorption corrections were performed. Acurate cell dimensions were obtained from least-squares fitting of Weissenberg film coordinates.

From 798 unique measured reflections the structure was solved with the aid of the MULTAN 78 program (16), assuming the space group to be $P1$.

The solution obtained with this program not only showed all the non-hydrogen atoms but also the center of symmetry corresponding to the space group $P1$. The positions of these atoms were then refined in the latter group using the SHELX program (17), by isotropic full-matrix least-squares methods up to an R value of 13%.

A difference Fourier map phased on the refined positions of all the previously located atoms showed all the hydrogen atoms. An anisotropic refinement performed on the non-hydrogen atoms lowered the R value to 10.36%. At this stage it was necessary to refine the inter-layer scale factors. After doing this, the agreement clearly improved, the final R value being 7.52%. The methyl hydrogen atoms that had been constrained to a primary sp^3 group conformation during the initial cycles of refinement were gradually freed. Non-hydrogen and hydrogen atoms were refined respectively by anisotropic and isotropic blocked diagonal matrix least-squares methods to convergence, yielding final R values of $R = 5.89\%$ and $R_w = 5.35\%$. The weighting scheme used was $w = 1.0/0.028855F^2$.

The final refined positional and thermal parameters are given in Tables 1 and 2. Bond lengths and angles are given in the schematic drawing of the title compound shown in Fig. 2.[3]

Results and discussion

Description of the structure

The molecular conformation of the title compound is illustrated in Fig. 1. In the crystalline state the two phenyl rings adopt a twist-skewed conformation (C(7)—C(8)—C(9)—C(10) = 16.64° and C(2)—C(7)—C(8)—C(9) = 79.73°). This conformation is similar to those observed in other C-bridged diphenyl compounds (9*b*, 18–21).[4] The dihedral angle between least-squares planes for rings α and β is 88.36°, as can be seen in Table 3. A lack of planarity of ring β is observed. Each methoxy group is coplanar with its ring (Table 3) and distal to the other one. The C(7)—C(8)—C(9) angle is 112.9(4)°, which compares fairly well with the bridge angle observed in 4-(α-hydroxy-4-methoxybenzyl)-3,5-diiodobenzyl alcohol (bridge angle = 113.5(4)°) (9*b*).

The molecules related by the symmetry operation $\bar{x}, \bar{y}-1, \bar{z}$ are linked by two hydrogen bonds, bond lengths and angle being 2.99(1) Å and 169(2)°, respectively. Although the donor–acceptor distance could suggest a weak interaction, the observed directionality of the bridge, and the H-acceptor distance, 2.11 Å, allows the assumption that the molecules build

[3]Tables of the structure factors may be obtained, at a nominal charge, from the Depository of Unpublished Data, CISTI, National Reasearch Council of Canada, Ottawa, Ont., Canada K1A 0S2.

[4]The active twist-skewed conformation adopted by the molecules of thyronine and its derivatives has been associated with the presence of iodine or other bulky substituents in the two *ortho* positions of the inner ring (9*b*, 9*d*, 11).

Can. J. Chem. Downloaded from www.nrcresearchpress.com by 210.87.254.6 on 09/06/12
For personal use only.

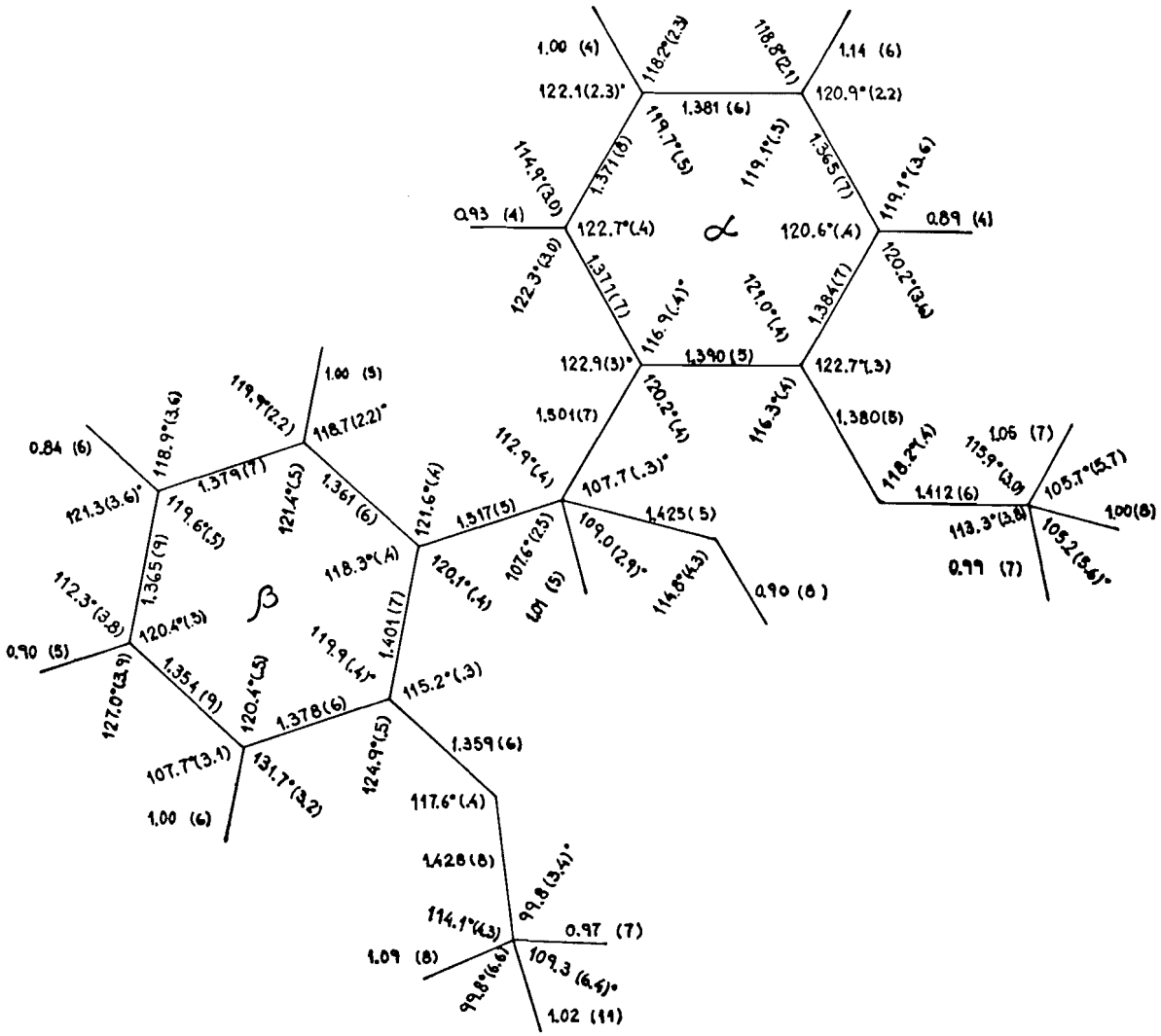

FIG. 2. Bond lengths and angles of di-*o*-anisylcarbinol.

TABLE 3. Least-squares planes

Equations of planes

Plane 1: $0.4150X - 0.8220Y - 0.3900Z - 3.7814 = 0$
Plane 2: $0.2814X + 0.4743Y - 0.8342Z + 1.0219 = 0$
Plane 3: $0.6628X - 0.6703Y - 0.3336Z - 3.5380 = 0$
Plane 4: $0.4374X - 0.8261Y - 0.3553Z - 3.7186 = 0$
Plane 5: $0.2928X + 0.4768Y - 0.8288Z + 1.0044 = 0$

Plane 1	Plane 2	Plane 3
O(3)	O(1)	C(8)
C(15)	C(1)	C(7)
C(14)	C(2)	C(9)

Deviations of atoms from the planes (Å)

Plane (4): C(9) −0.0003(44), C(10) 0.0024(52), C(11) −0.0013(54), C(12) −0.0020(54), C(13) 0.0041(52), C(14) −0.0030(44), $\chi^2 = 1.49$

Plane(5): C(2) 0.0117(49), C(3) −0.0122(57), C(4) 0.0054(63), C(5) 0.0017(65), C(6) −0.0020(54), C(7) −0.0046(40), $\chi^2 = 12.57$

Dihedral angles (°), (esd's are 0.5)

1,4	2.4	4,3	15.8	2,5	0.7	5,3	81.3	4,5	88.4

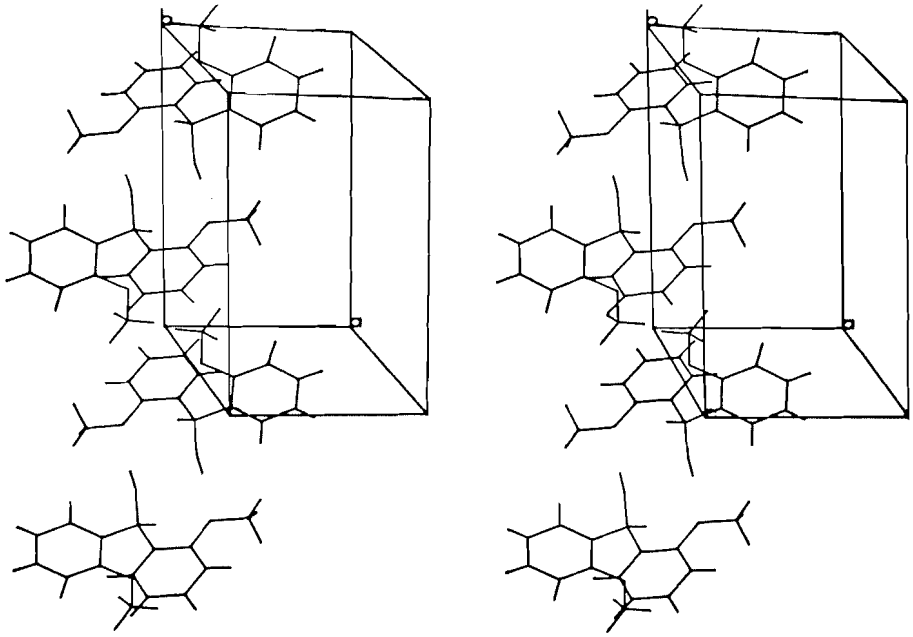

FIG. 3. Stereoscopic view of the molecular packing of di-*o*-anisylcarbinol.

centrosymmetric dimers through O(2)—H(02)··· O′(3) (the prime indicates symmetry operation: $(\bar{x}, \bar{y}-1, \bar{z})$). The distance of 2.11 Å is shorter than the 2.4 Å that can be taken as a criterion for hydrogen bonding (22) and shorter, as well, than the Rahim and Barman van der Waals criterion (23). Furthermore, the observed bond length is in good agreement with theoretical calculations (24) and statistical mechanical treatment (25) of water dimers, which give a value of $R = 3.0$ Å and 5 kcal stabilization energy.

Dimers are additionally stabilized through the dipole–dipole interaction between OH groups (the distance between dipole centers is 2.73(5) Å).

A stereoscopic view of the structure (Fig. 3) shows an unusually oriented packing of the dimers along *b*. In that direction, dimers related by the symmetry operation $(x, y, n-z)$ present the α ring of one dimer opposite to the methyl hydrogens of the α ring of the other one, and vice versa. The distance between gravity centers of facing groups is 4.47 Å. The particular reason for this special packing is not yet clear. No other signifiant short intermolecular distance was detected. Interaction between dimers in other directions seems to be through van der Waals contacts.

Comparison of experimental results

The different chemical shifts observed for the hydrogen atoms of the methoxy groups in the CCl_4 solution can be interpreted as a result of the partially restricted rotation of the aryl rings that could be, in part, due to the existence of an intramolecular hydrogen bond between the hydrogen of the OH group and one of the oxygen atoms of the methoxy groups located at the *o*-position of the phenyl rings.

Although the formation of an intermolecular hydrogen bond in solution cannot be excluded only on the basis of the nmr data, it can be assumed that at the low concentration used to run the spectra an intramolecular hydrogen bond should be preferred to an intermolecular one. When the solvent has hydrogen bond acceptor capabilities (case of acetone), the formation of stronger hydrogen bonds between the molecules of **1** and the solvent prevents the intramolecular H-bond. The rotation is no longer restricted and both methoxy groups are equivalent in the nmr spectra.

On the other hand, the crystallographic determination provides structural evidence which shows general agreement with the existence of an intermolecular hydrogen bond, since each molecule contributes with a hydrogen bond to the building of a centrosymmetric dimeric unit which is stabilized by the energy decrease produced by two hydrogen bonds and the additional dipole–dipole interaction.

Crystallographic studies of di-*o*-anisylketone, where a hydrogen bond is not expected, are in progress, since out of the present results it is not possible to establish fully whether the above-mentioned interactions may contribute to the twist-skewed conformation adopted by **1** in the crystal.

Acknowledgements

The authors are indebted to the National Research Council (CONICET) and the Science and Technology Secretariat (SUBCYT) of Argentina for financial support. Fellowships from the CICPBA (C. F. and H. N.) and from the CONICET (A. A. V.) are gratefully acknowledged.

1. L. S. TRZUPEK, T. L. NEWIRTH, E. G. KELLY, N. S. NUDELMAN, and G. M. WHITESIDES. J. Am. Chem. Soc. **95**, 8118 (1973).
2. A. A. VITALE, D. PEREZ, P. OUTUMURO, and N. S. NUDELMAN. An. Asoc. Quím. Argent. **70**, 155 (1982).
3. N. S. NUDELMAN and A. A. VITALE. Proceedings of the XIV Arg. Chem. Symposium, Santa Fe. 1978.
4. R. GOPAL, W. D. CHANDLER, and B. E. ROBERTSON. Can. J. Chem. **58**, 658 (1980), and references therein.
5. D. G. HAY and M. F. MACKAY. Acta Crystallogr. Sect. B, **35**, 2952 (1979).
6. L. DUPONT, O. DIDEBERG, J. TOUSSAINT, and J. DELARGE. Acta Crystallogr. Sect. B, **36**, 2170 (1980).
7. S. RANTSORDAS, M. PERRIN, A. THOZET, and S. LECOCQ. Acta Crystallogr. Sect. B, **37**, 1253 (1981).
8. P. VAN ROEY and K. A. KERR. Acta Crystallogr. Sect. B., **37**, 1244 (1981).
9. (*a*) V. CODY. Acta Crystallogr. Sect. B, **37**, 1685 (1981); (*b*) **37**, 763 (1981); (*c*) **36**, 1723 (1980); (*d*) Science, **201**, 1131 (1978).

Can. J. Chem. Downloaded from www.nrcresearchpress.com by 210.87.254.6 on 09/06/12
For personal use only.

10. N. CAMERMAN and A. CAMERMAN. Science, **175**, 764 (1972).
11. S. W. DIETRICH, E. C. JORGENSEN, P. A. KOLLMAN, and S. ROTHENBERG. J. Am. Chem. Soc. **98**, 8310 (1976), and references therein.
12. E. O. SCHEMPLER. Acta Crystallogr. Sect. B, **38**, 554 (1982), and references therein.
13. N. S. NUDELMAN and A. A. VITALE. Org. Prep. Proced. **13**, 144 (1981).
14. N. S. NUDELMAN and A. A. VITALE. J. Org. Chem. **46**, 4625 (1981).
15. K. ZIEGLER and C. OCHS. Ber. **55**, 2273 (1922).
16. P. MAIN, M. M. WOOLFSON, L. LESSINGER, G. GERMAIN, and J. P. DECLERCQ. MULTAN 78. A system of computer programs for the automatic solution of crystal structures from X-ray diffraction data. Univ. of York, England, and Louvain-la-Neuve, Belgium. 1978.
17. G. M. SHELDRICK. SHELX 76. Program for crystal structure determination. University of Cambridge, England. 1976.
18. V. CODY, E. C. JORGENSEN, and E. CHEUNG. Am. Crystallogr. Assoc. Meeting Abstracts, **7**(1), 23 (1979).
19. D. TRANQUI, P. RICHARD, J. VICAT, and H. FILLION. Acta Crystallogr. Sect. B, **30**, 673 (1974).
20. S. P. VAN DER HEIJDEN, W. D. CHANDLER, and B. E. ROBERTSON. Can. J. Chem. **53**, 2121 (1975).
21. G. SMITH, C. H. L. KENNARD, and J. WHITNALL. Cryst. Struct. Commun. **6**, 131 (1977).
22. I. OLOVSSON and P. J. JONSSON. The hydrogen bond. Recent developments in theory and experiments. Vol. II. *Edited by* P. Schuster, G. Zundel, and G. Sandorfy. North Holland, Amsterdam. 1976. p. 402.
23. Z. RAHIM and B. N. BARMAN. Acta Crystallogr. Sect. A, **34**, 761 (1978).
24. G. H. F. DIERCKSER. Chem. Phys. Lett. **4**, 373 (1969); D. HANKINS, J. W. MOSCOWITZ, and F. H. STILLINGER. Chem. Phys. Lett. **4**, 527 (1970); J. Chem. Phys. **53**, 4544 (1970).
25. R. W. BOLANDER, J. L. KASSMER, JR., and J. T. ZUNG. J. Chem. Phys. **50**, 4402 (1969).

Can. J. Chem. Downloaded from www.nrcresearchpress.com by 210.87.254.6 on 09/06/12
For personal use only.

2,2-Bis(ethylthio)ethanenitrile: preparation and use as a one or two carbon nucleophile

GORDON S. BATES[1] AND S. RAMASWAMY
Department of Chemistry, University of British Columbia, Vancouver, B.C., Canada V6T 1Y6

Received January 31, 1983

GORDON S. BATES and S. RAMASWAMY. Can. J. Chem. **61**, 2006 (1983).

2,2-Bis(ethylthio)ethanenitrile **1** was prepared in high yield from 2,2-bis(ethylthio)ethanal **2**. Alkylation of the potassium salt of **1** with various alkylating agents and conjugate addition to cyclic α,β-unsaturated ketones provided high yields of the alkylation products of **1**. The potential one and two carbon chain extension capability of this new reagent has been demonstrated.

GORDON S. BATES et S. RAMASWAMY. Can. J. Chem. **61**, 2006 (1983).

On a préparé, avec un bon rendement, le bis(éthylthio)-2,2 éthanenitrile **1** à partir du bis(éthylthio)-2,2 éthanal **2**. L'alkylation du sel de potassium du composé **1** avec divers agents alkylants et l'addition conjuguée sur des cétones cycliques α,β insaturées donnent les produits d'alkylation du composé **1** avec d'excellents rendements. On démontre la possibilité d'ajouter à ce nouveau réactif une à deux chaines carbonées.

[Traduit par le journal]

A reagent that can serve as a one or two carbon nucleophile would be of great applicability in organic synthesis. An investigation of the literature revealed that with the exception of diazoacetic esters there did not appear to be any reagents of *demonstrated* one and two carbon nucleophilic capability. However, there are a few reagents that are *potential* one or two carbon chain extending agents but which have been used only as single carbon reagents. These reagents fall into two categories: those in which a carbon is lost as carbon dioxide (1) and those in which a carbon is lost as a nitrile group during hydrolysis (or alcoholysis) of a transient acyl nitrile intermediate (2) or in the process of regeneration of a ketone from a cyanohydrin (3).

2,2-Bis(ethylthio)ethanenitrile **1**, which can be prepared readily from aldehyde **2** (4), appeared to be a potential one or

$(EtS)_2CHCN$ **1** $(EtS)_2CHCHO$ **2**

$(EtS)_2C{=}CHNHR$ **3** $(EtS)_2CHCO_2H$ **4**

two carbon nucleophile.[2] Alkylation of **1** should yield the two carbon chain extension product **5**.[3] Both newly added carbons can be maintained in the product during several subsequent transformations. For example, a Raney nickel desulphurization would lead to product **6**. Elimination of the elements of ethanethiol from **5** would produce the alkene **7** which has recently been shown to be an excellent dienophile in Diels–Alder reactions (8). In addition, **7** could act as an acceptor molecule in a conjugate addition reaction. The nitrile group in **5** could also be reduced to yield **8**, a precursor to an α-amino ketone.[4] All of these processes lead to products in which both carbons of the nucleophile derived from **1** have been conserved. Conversely, oxidative cleavage of the thioketal group in **5** would generate an acyl nitrile intermediate which could be

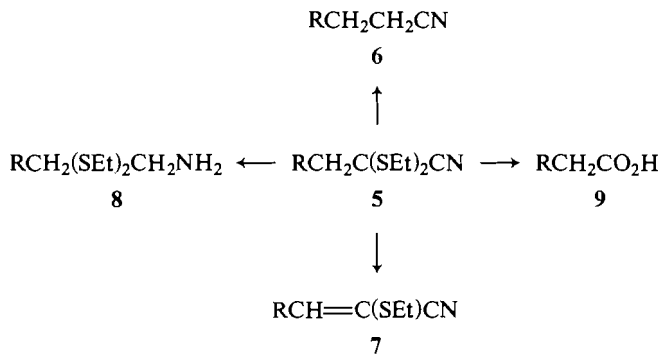

intercepted by a nucleophile such as water to provide the one carbon chain extended product **9**.

These numerous potential synthetic possibilities associated with nitrile **1** prompted an investigation of the chemistry of this compound.

The conversion of **2** into **1** was accomplished readily by stirring a dichloromethane solution of aldehyde **2** with hydroxylamine hydrochloride in the presence of three equivalents of triethylamine followed by the slow addition of two equivalents of methanesulphonyl chloride. This procedure provided an overall yield of 75–80% of **1** starting from aldehyde **2**.

Our previous experience with the enamine **3** (4) and acid **4** (10) suggested that alkylation of **1** would be best accomplished using the potassium salt of the nitrile in tetrahydrofuran. A preliminary experiment confirmed that the expected difference in reactivity of various salts of **1** was again present. For example, complete alkylation of the lithium salt of **1** with bromoethane required almost seven hours, whereas alkylation of the potassium salt was complete within 45 minutes.

The potassium salt of nitrile **1** was generated by the addition of the nitrile to one equivalent of mineral oil-free potassium hydride in tetrahydrofuran at 0°C. Deprotonation of **1** occurred essentially instantaneously to yield a yellow solution of the potassium salt which could be alkylated cleanly by a variety of halides and sulphonate esters[5] (Table 1). However, the anion apparently fails to react with carboxylate esters and aldehydes,

[1]Author to whom correspondence should be addressed.

[2]The *S*-methyl (5) and 1,3-dithiane (6) analogues of **1** have been reported.

[3]Compounds of this type have been prepared in poor yield by the reaction of various nitriles with sulphur in the presence of alkyl halides (7).

[4]Thioacetal derivatives of 2-aminoethanal have been reported (9).

[5]Benzene sulphonate esters are superior to *p*-methyl benzenesulphonates when alkylation is sluggish and elevated temperatures or prolonged reaction times are required to bring the reaction to completion.

Can. J. Chem. Downloaded from www.nrcresearchpress.com by 210.87.254.6 on 09/06/12
For personal use only.

TABLE 1. Nitrile anion alkylation

$$(EtS)_2CHCN \xrightarrow[(2)\ RX,\ 25°C]{(1)\ KH,\ THF} (EtS)_2CCN \quad (R)$$

RX	Time (h)	Yield (%) (isolated)
MeI	0.5	75
MeOBs	0.5	95
EtBr	2	90
EtOTs	2	88
2-PrI	2	80
2-PrOBs	2	77
n-BuBr	2	85
n-$C_8H_{17}Br$	2	75
c-$C_6H_{11}OBs$*	4	74
CH_2=$CHCH_2Br$	0.25	90
Me_2C=$CHCH_2Br$†	0.25	90
$PhCH_2Br$	0.5	95
$BrCH_2CO_2Me$‡	0.5	82
2-Cyclopentenone‡	0.5	98
2-Cyclohexenone‡	0.5	97
$C_6H_5CO_2Me$	2	Recovered starting material
C_6H_5CHO	2	Recovered starting material

*Alkylation at 50°C.
†S_N^2 product.
‡Alkylation at −78°C.

presumably due to a ready reversal of the initial addition step (cf. conjugate additions below).

Conjugate addition reactions of the anion of **1** were also investigated. Metallated dithioacetals, in general, show a high preference for direct addition to α, β-unsaturated ketones (11). However, substitution of carbanion stabilizing groups on the nucleophilic reagent enhances the ability of conjugate addition to occur (12). It was found that **10** and **11** were formed in virtually quantitative yield when the anion of **1** was allowed to react with 2-cyclopentenone and 2-cyclohexenone, respectively, at −78°C. No detectable amount of the direct addition product **12** was observed in these reactions.

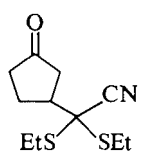

10

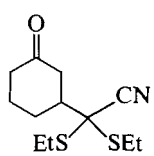

11

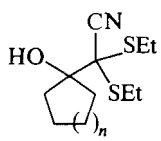

12

The conjugate addition reaction showed an interesting temperature dependence. When the reaction between 2-cyclopentenone and the anion of **1** was quenched at higher temperatures an increasing amount of nitrile **1** was reisolated (Table 2). On the basis of the temperature dependence study on the conjugate addition reaction of the anion of **1** with 2-cyclopentenone, it appears that an equilibrium exists between the starting materials and the product. Indeed, when the conjugate addition product **10** was deprotonated at 0°C with potassium bis(trimethyl)silylamide and the reaction mixture was allowed to warm to room temperature and was quenched with aqueous ammonium chloride, nitrile **1** could be isolated in high yield from the reaction mixture.

As the ability to alkylate **1** had been established, several functional group transformations on the alkylation products of

TABLE 2. Effect of temperature on the conjugate addition of **1** with 2-cyclopentenone

	Yield (%)	
Temperature (°C)	**10**	**1**
−78	100	0
−64	87	13
−23	50	50
0	40	60
20	5	95

1 were subsequently examined in order to demonstrate the one or two carbon extension capabilities of the reagent. 2,2-Bis(ethylthio)decanenitrile **5** (R = *n*-C_7H_{15}), prepared by reaction of the nitrile anion with 1-bromooctane, was chosen as a suitable substrate. Partial hydrolysis of this compound using pyridinium hydrobromide perbromide (13) in a two phase solvent system yielded the desired unsaturated nitrile **7** (R = *n*-C_7H_{15}) in 86% yield. Reduction of the decanenitrile derivative with lithium aluminum hydride produced the masked α-amino ketone **8** (R = *n*-C_7H_{15}) in 81% yield and a P-2 Raney nickel (14) desulphurization proceeded smoothly to yield decanenitrile in 76% yield. In each of the above procedures both carbons of the nucleophile derived from **1** have been retained in the product. In contrast, oxidative hydrolysis of the dithioketal group of **5** (R = *n*-C_7H_{15}) using *N*-chlorosuccinimide − silver nitrate (15) afforded the one carbon chain extension product, nonanoic acid, in 75% yield.

Thus, the readily available and inexpensive reagent **1** represents a nucleophilic reagent which may be used as a one *or* two carbon chain extension synthon. The further synthetic utility of this reagent in natural products synthesis is currently under investigation.

Experimental

General

All reactions were carried out under a nitrogen atmosphere. Stirring was accomplished using Teflon-coated magnetic stirring bars. Tetrahydrofuran was freshly distilled from sodium benzophenone ketyl under a nitrogen atmosphere. Potassium hydride was obtained as a 25% dispersion in mineral oil from Alpha Division, Ventron Corporation. All other reagents were obtained from the Aldrich Chemical Company, Inc. and were used without further purification. Methyl, ethyl, 2-propyl, and cyclohexyl arylsulphonate esters were prepared by reaction of an excess of the appropriate alcohol for 12 hours at 0°C with the appropriate sulphonyl chloride in pyridine, followed by a standard work-up. All extraction and chromatography solvents were distilled before use.

All temperatures are stated in degrees Celsius. Molecular distillations were performed by means of a Buchi Kugelrohr apparatus. Proton magnetic resonance (^{1}H nmr) spectra were obtained on the following instruments: Varian Associates T-60, EM-360L, and HA-100. Spectra were run in deuterochloroform or carbon tetrachloride solution with tetramethylsilane as an internal reference. Chemical shifts are reported on the δ scale. The multiplicity, integrated peak area, and coupling constants in Hertz (Hz) (if observable) are indicated in parentheses after each signal. Infrared spectra were recorded as liquid films using a Perkin−Elmer 700 spectrometer, and were calibrated with the 1601 cm^{-1} band of polystyrene. High resolution mass spectra were obtained using an AEI MS-50 mass spectrometer. Elemental analyses were performed at the Microanalytical Laboratory, University of British Columbia.

Merck pre-coated tlc sheets Silica Gel 60F-254 were used for analytical thin-layer chromatography. Florisil 100−200 mesh supplied by the J. T. Baker Chemical Company and Merck Silica Gel 60

Can. J. Chem. Downloaded from www.nrcresearchpress.com by 210.87.254.6 on 09/06/12
For personal use only.

Can. J. Chem. Downloaded from www.nrcresearchpress.com by 210.87.254.6 on 09/06/12
For personal use only.

(230–400 mesh) were used for column chromatography. Analytical gas chromatography was carried out on a Hewlett–Packard Model 5830-A chromatograph equipped with 1.8 m × 0.3 cm columns packed with 3% OV-101 or 5% Carbowax.

The following abbreviations are used in the description of the multiplicity of each signal in the ^{1}H nmr spectrum: s = singlet, d = doublet, t = triplet, q = quartet, sept = septet, m = multiplet, dd = doublet of doublets, dt = doublet of triplets, dm = doublet of multiplets, b = broad.

2,2-Bis(ethylthio)ethanenitrile ***1***

To a stirred solution of 12.32 g (75 mmol) of 2,2-bis(ethylthio)-ethanal (4) in 300 mL of dichloromethane was added 5.45 g (78.25 mmol) of hydroxylamine hydrochloride, followed by 45 mL (330 mmol) of triethylamine. The reaction mixture was stirred overnight at room temperature, and then was cooled to 0°C and 12.5 mL (162 mmol) of methanesulphonyl chloride in 25 mL of dichloromethane was added over 0.5 h. Stirring was continued for a further 3 h, during which time the reaction mixture was allowed to warm to room temperature. The solvent was evaporated under reduced pressure and the residue was dissolved in 300 mL of ethyl ether, washed successively with 50 mL of H_2O, 2 × 50 mL of aqueous 2 *N* HCl, 4 × 25 mL of aqueous saturated Na_2CO_3, 25 mL of H_2O, and dried ($MgSO_4$). The solvent was evaporated under reduced pressure and the crude product was distilled to afford 9.2 g (76%) of **1** as a pale yellow liquid; bp 68°C/0.2 Torr; infrared: 2230 cm^{-1}; ^{1}H nmr (CCl_4) δ: 1.31 (t, 6, *J* = 7), 2.79 (q, 4, *J* = 7), 4.55 (s, 1). *Anal.* calcd. for $C_6H_{11}NS_2$ (161.29): C 44.68, H 6.87, N 8.68; found: C 44.76, H 6.97, N 8.58. *Mol. Wt.* calcd. for $C_6H_{11}NS_2$: 161.0333; found: 161.0335.

Standard procedure for the alkylation of 2,2-bis(ethylthio)ethanenitrile

A suspension of 0.160 g (1 mmol) of 25% KH in mineral oil was washed free of oil by stirring with 3 × 5 mL portions of pentane under a N_2 atmosphere. The oil-free KH was suspended in 5 mL of tetrahydrofuran and 0.161 g (1 mmol) of **1** in 0.5 mL of tetrahydrofuran was added. An immediate evolution of H_2 gas was observed and a yellow solution of the potassium salt of the nitrile resulted. To this solution was added 1.05 mmol of the alkylating agent and the reaction mixture was stirred for 0.25–4 h at room temperature (at 50°C for cyclohexyl benzenesulphonate and at −78°C for methyl bromoacetate). The reaction mixture was diluted with 40 mL of ethyl ether, washed with 5 mL of H_2O, and dried ($MgSO_4$). The solvent was evaporated under reduced pressure to afford the alkylated nitrile. The trace of pale yellow colour in the product could be conveniently removed by filtration of the product through a small column of Florisil using 1–2% ethyl acetate in 30–60 petroleum ether (v/v) as the eluting solvent.

For the conjugate addition reactions with 2-cyclohexenone and 2-cyclopentenone, the solution of the nitrile salt was cooled to −78°C. The ketone (1 equivalent) was added in one portion and the reaction mixture was stirred at −78°C for 30 min. The reaction was quenched at −78°C with aqueous saturated NH_4Cl and worked up as above.

2,2-Bis(ethylthio)propanenitrile

Boiling point (molecular distillation) 60°C/0.1 Torr; infrared: 2240 cm^{-1}; ^{1}H nmr (CCl_4) δ: 1.28 (t, 6, *J* = 7), 1.85 (s, 3), 2.83 (q, 4, *J* = 7). *Anal.* calcd. for $C_7H_{13}NS_2$ (175.32): C 47.96, H 7.47, N 7.99; found: C 48.05, H 7.49, N 8.09. *Mol. Wt.* calcd. for $C_7H_{13}NS_2$: 175.0489; found: 175.0491.

2,2-Bis(ethylthio)butanenitrile

Boiling point (molecular distillation) 70°C/0.1 Torr; infrared: 2240 cm^{-1}; ^{1}H nmr (CCl_4) δ: 1.18 (t, 3, *J* = 7), 1.28 (t, 6, *J* = 7), 2.04 (q, 2, *J* = 7), 2.8 (q, 4, *J* = 7). *Anal.* calcd. for $C_8H_{15}NS_2$ (189.34): C 50.75, H 7.99, N 7.40; found: C 50.85, H 8.08, N 7.51. *Mol. Wt.* calcd. for $C_8H_{15}NS_2$: 189.0646; found: 189.0649.

2,2-Bis(ethylthio)-3-methylbutanenitrile

Boiling point (molecular distillation) 75°C/0.1 Torr; infrared: 2230 cm^{-1}; ^{1}H nmr (CCl_4) δ: 1.18 (d, 6, *J* = 7), 1.26 (t, 6, *J* = 7), 2.22 (sept, 1, *J* = 7), 2.8 (q, 4, *J* = 7). *Anal.* calcd. for $C_9H_{17}NS_2$ (203.37): C 53.15, H 8.43, N 6.89; found: C 52.99, H 8.54, N 6.70. *Mol. Wt.* calcd. for $C_9H_{17}NS_2$: 203.0803; found: 203.0809.

2,2-Bis(ethylthio)hexanenitrile

Boiling point (molecular distillation) 80°C/0.1 Torr; infrared: 2230 cm^{-1}; ^{1}H nmr (CCl_4) δ: 0.91 (t, 3, *J* = 6.5), 1.25 (t, 6, *J* = 7), 1.15–1.8 (m, 4), 2.02 (m, 2), 2.8 (q, 4, *J* = 7). *Anal.* calcd. for $C_{10}H_{19}NS_2$ (217.40): C 55.25, H 8.81, N 6.44; found: C 55.49, H 8.96, N 6.49. *Mol. Wt.* calcd. for $C_{10}H_{19}NS_2$: 217.0959; found: 217.0962.

2,2-Bis(ethylthio)decanenitrile

Boiling point (molecular distillation) 100°C/0.2 Torr; infrared: 2230 cm^{-1}; ^{1}H nmr ($CDCl_3$) δ: 0.90 (t, 3, *J* = 6.5), 1.33 (t, 6, *J* = 7), 1.1–2.05 (m,12), 2.88 (q, 4, *J* = 7). *Anal.* calcd. for $C_{14}H_{27}NS_2$ (273.51): C 61.48, H 9.95, N 5.23; found: C 61.65, H 9.85, N 5.12. *Mol. Wt.* calcd. for $C_{14}H_{27}NS_2$: 273.1584; found: 273.1585.

2,2-Bis(ethylthio)-2-cyclohexylethanenitrile

Boiling point (molecular distillation) 90°C/0.1 Torr; infrared: 2207 cm^{-1}; ^{1}H nmr (CCl_4) δ: 1.25 (t, 6, *J* = 7), 1.1–2.3 (m, 11), 2.78 (q, 4, *J* = 7). *Anal.* calcd. for $C_{12}H_{21}NS_2$ (243.44): C 59.21, H 8.70, N 5.75; found: C 59.02, H 8.79, N 5.86. *Mol. Wt.* calcd. for $C_{12}H_{21}NS_2$: 243.1116; found: 243.1119.

2,2-Bis(ethylthio)pent-4-enenitrile

Boiling point (molecular distillation) 70°C/0.1 Torr; infrared: 2240, 1640 cm^{-1}; ^{1}H nmr ($CDCl_3$) δ: 1.28 (t, 6, *J* = 7), 2.71 (dm, 2), 2.81 (q, 4, *J* = 7), 5.08–5.32 (m, 2), 5.9 (m, 1). *Anal.* calcd. for $C_9H_{15}NS_2$ (201.36): C 53.69, H 7.51, N 6.96; found: C 54.00, H 7.55, N 7.23. *Mol. Wt.* calcd. for $C_9H_{15}NS_2$: 201.0647; found: 201.0647.

2,2-Bis(ethylthio)-5-methylhex-4-enenitrile

Boiling point (molecular distillation) 80°C/0.1 Torr; infrared: 2220, 1667 cm^{-1}; ^{1}H nmr (CCl_4) δ: 1.26 (t, 6, *J* = 7), 1.66 (bs, 3), 1.76 (bs, 3), 2.74 (dm, 2), 2.82 (q, 4, *J* = 7), 5.3 (tm, 1). *Anal.* calcd. for $C_{11}H_{19}NS_2$ (229.41): C 57.59, H 8.35, N 6.11; found: C 57.66, H 8.39, N 6.21. *Mol. Wt.* calcd. for $C_{11}H_{19}NS_2$: 229.0959; found: 229.0959.

2,2-Bis(ethylthio)-3-phenylpropanenitrile

Boiling point (molecular distillation) 100°C/0.1 Torr; infrared: 2225 cm^{-1}; ^{1}H nmr (CCl_4) δ: 1.16 (t, 6, *J* = 7), 2.65 (m, 4), 3.16 (s, 2), 7.14–7.36 (m, 5). *Anal.* calcd. for $C_{13}H_{17}NS_2$ (251.42): C 62.11, H 6.82, N 5.57; found: C 62.00, H 6.75, N 5.44. *Mol. Wt.* calcd. for $C_{13}H_{17}NS_2$: 251.0803; found: 251.0804.

Methyl 3,3-bis(ethylthio)-3-cyanopropanoate

Boiling point (molecular distillation) 70°C/0.05 Torr; infrared: 2235, 1745 cm^{-1}; ^{1}H nmr ($CDCl_3$) δ: 1.34 (t, 6, *J* = 7), 2.93 (q, 4, *J* = 7), 3.09 (s, 2), 3.8 (s, 3). *Anal.* calcd. for $C_9H_{15}NO_2S_2$ (233.36): C 46.32, H 6.48, N 6.00, S 27.48; found: C 46.46, H 6.52, N 6.17, S 27.28. *Mol. Wt.* calcd. for $C_9H_{15}NO_2S_2$: 233.0544; found: 233.0543.

2,2-Bis(ethylthio)-2-(3'-oxocyclopentyl)ethanenitrile

Boiling point (molecular distillation) 100°C/0.1 Torr; infrared: 2200, 1740 cm^{-1}; ^{1}H nmr ($CDCl_3$) δ: 1.34 (t, 6, *J* = 7), 1.95–3.0 (m, 7), 2.9 (q, 4, *J* = 7). *Anal.* calcd. for $C_{11}H_{17}NOS_2$ (243.39): C 54.28, H 7.04, N 5.75, S 26.35; found: C 53.96, H 7.13, N 5.71, S 26.11. *Mol. Wt.* calcd. for $C_{11}H_{17}NOS_2$: 243.0752; found: 243.0762.

2,2-Bis(ethylthio)-2-(3'-oxocyclohexyl)ethanenitrile

Boiling point (molecular distillation) 110°C/0.05 Torr; infrared: 2230, 1710 cm^{-1}; ^{1}H nmr ($CDCl_3$) δ: 1.34 (t, 6, *J* = 7), 1.4–2.6 (m, 9), 2.88 (q, 4, *J* = 7). *Anal.* calcd. for $C_{12}H_{19}NOS_2$ (257.42): C 55.99, H 7.44, N 5.44, S 24.91; found: C 56.09, H 7.46, N 5.40, S 24.77. *Mol. Wt.* calcd. for $C_{12}H_{19}NOS_2$: 257.0908; found: 257.0912.

Temperature dependence on the addition of the anion of ***1*** *to 2-cyclopentenone*

Generation of the anion of nitrile **1** and the addition of 2-cyclopentenone at −78°C was carried out as described above. The

Can. J. Chem. Downloaded from www.nrcresearchpress.com by 210.87.254.6 on 09/06/12
For personal use only.

reaction mixture was allowed to warm to the indicated temperatures (−64°C, −23°C, 0°C, 20°C) and allowed to stir for 30 min to reach equilibrium. The reaction mixture was quenched with aqueous saturated NH_4Cl and worked up as described earlier. The relative amounts of the nitrile **1** and the conjugate addition product **10** were established by the relative integration of the methine singlet of **1** at δ 4.55 with respect to the ethyl triplet at δ 1.34 (corrected for **1**) in the ^1H nmr spectrum of the product mixture.

Reverse conjugate addition of ***1***

A suspension of 0.160 g (1 mmol) of 25% KH in mineral oil was washed free of oil by stirring with 3 × 5 mL portions of pentane under a N_2 atmosphere. The oil-free KH was suspended in 5 mL of tetrahydrofuran and 0.210 mL (1 mmol) of *N,N*-bis(trimethyl)-silylamine was added. The mixture was stirred until evolution of H_2 gas ceased. The resulting solution was cooled to 0°C and 0.100 g (0.41 mmol) of the conjugate adduct **10** in 0.5 mL of tetrahydrofuran was added in one portion. The reaction mixture was allowed to warm to room temperature and was stirred at room temperature for a further 30 min. The reaction mixture was quenched with aqueous saturated NH_4Cl and diluted with ethyl ether, washed with 5 mL of H_2O, and dried ($MgSO_4$). The solvent was evaporated under reduced pressure to afford a yellow oil which upon molecular distillation gave 0.055 g (83%) of nitrile **1**.

Preparation of decanenitrile

To 2.4 g (10 mmol) of $NiCl_2 \cdot 6H_2O$ dissolved in 8 mL of ethanol was added 0.75 g (20 mmol) of $NaBH_4$ in small portions over 5 min with vigorous stirring. After 0.5 h, 0.273 g (1 mmol) of 2,2-bis-(ethylthio)decanenitrile was added and the reaction mixture refluxed for 12 h. The reaction mixture was cooled to room temperature and the solvent was evaporated under reduced pressure. The residue was triturated with 5 × 10 mL of ethyl ether and the combined washings dried ($MgSO_4$) and then filtered through 20 g of Florisil using 5% ethyl acetate in 30−60 petroleum ether (v/v) as the eluting solvent. The eluent was evaporated under reduced pressure and the oily residue was subjected to molecular distillation (70°C/0.1 Torr) to afford 0.116 g (76%) of a product whose spectral data were in agreement with those of authentic decanenitrile.

2-Ethylthio-2-decenenitrile

A mixture of 0.273 g (1 mmol) of 2,2-bis(ethylthio)decanenitrile, 0.400 g (1.25 mmol) of pyridinium hydrobromide perbromide, and 0.01 g of tetra-*n*-butylammonium bromide in 4 mL of dichloromethane and 4 mL of H_2O was stirred vigorously for 6 h. The reaction mixture was diluted with ethyl ether, washed with 2 × 5 mL of H_2O, and dried ($MgSO_4$). The solvent was evaporated under reduced pressure and the residue subjected to molecular distillation to afford 0.181 g (86%) of the desired product as a mixture of *E* and *Z* isomers; bp (molecular distillation) 90°C/0.1 Torr; infrared: 2240, 1705 cm^{-1}; ^1H nmr ($CDCl_3$) δ: 0.88 (t, 3, J = 7), 1.25, 1.28 (t, 3, J = 7), 1.1−2.5 (m, 10), 2.38 (m, 2), 2.8 (m, 2), 6.59, 6.63 (t, 1, J = 7.75). *Anal.* calcd. for $C_{12}H_{21}NS$ (211.37): C 68.19, H 10.01, N 6.63; found: C 68.04, H 10.00, N 6.60. *Mol. Wt.* calcd. for $C_{12}H_{21}NS$: 211.1395; found: 211.1398.

2,2-Bis(ethylthio)decanamine

A mixture of 0.273 g (1 mmol) of 2,2-bis(ethylthio)decanenitrile and 0.114 g (3 mmol) of $LiAlH_4$ in 10 mL of tetrahydrofuran was stirred vigorously for 12 h. The excess $LiAlH_4$ was decomposed by the cautious addition of $Na_2SO_4 \cdot 10H_2O$. The mixture was filtered and the solvent evaporated under reduced pressure. The residue was chromatographed on silica using 5% ethanol in 30−60 petroleum ether (v/v) as the eluting solvent to afford 0.214 g (77%) of the desired product. Infrared: 3600−3200 cm^{-1}; ^1H nmr ($CDCl_3$) δ: 0.85 (t, 3, J = 7), 1.0−1.4 (m, 20), 1.4−1.8 (m, 4), 2.6 (q, 4, J = 7). *Anal.* calcd. for $C_{14}H_{31}NS_2$ (277.54): C 60.59, H 11.26, N 5.05; found: C 60.42, H 11.11, N 5.13. *Mol. Wt.* calcd. for $C_{14}H_{31}NS_2$: 277.1898; found: 277.1901.

Nonanoic acid

To a stirred solution of 0.400 g (3 mmol) of *N*-chlorosuccinimide and 0.519 g (3 mmol) of $AgNO_3$ in 4 mL of acetonitrile and 1 mL of H_2O was added 0.273 g (1 mmol) of 2,2-bis(ethylthio)decanenitrile in 1 mL of acetonitrile. The reaction mixture was stirred for 0.5 h and then 0.5 g of Na_2SO_3 was added and stirring continued for a further 10 min. The reaction mixture was diluted with 20 mL of ethyl ether and the organic phase decanted. The residue was washed with a further 2 × 10 mL portion of ethyl ether. The combined organic phase was washed with 5 × 5 mL of H_2O and then extracted with 1 mL of aqueous 2 *N* NaOH. The basic aqueous phase was washed with 10 mL of ethyl ether, acidified with aqueous 2 *N* HCl, and extracted with 2 × 20 mL of ethyl ether. The organic extract was dried ($MgSO_4$) and then evaporated under reduced pressure to afford 0.118 g (75%) of a product whose spectral data were identical to those of authentic nonanoic acid.

Acknowledgements

This work was supported by the Natural Sciences and Engineering Research Council of Canada and in part by a Cottrell Research Grant provided by the Research Corporation.

1. M. S. NEWMAN and B. J. MAGERLEIN. Org. React. **5**, 413 (1949); M. BALLESTER. Chem. Rev. **55**, 283 (1955); J. ADAMS, L. HOFFMAN, JR., and B. M. TROST. J. Org. Chem. **35**, 1600 (1970).
2. D. H. R. BARTON, R. D. BRACHO, and D. A. WIDDOWSON. J. Chem. Soc. Chem. Commun. 781 (1973); D. R. WHITE and D. K. WU. J. Chem. Soc. Chem. Commun. 989 (1974); S. E. DENIZO, R. W. FREEKSEN, W. E. PABST, and D. S. WATT. J. Am. Chem. Soc. **99**, 182 (1977).
3. G. STORK and L. MALDONADO. J. Am. Chem. Soc. **93**, 5286 (1971).
4. G. S. BATES and S. RAMASWAMY. J. Chem. Soc. Chem. Commun. 904 (1980).
5. K. HARTKE and J. QUANTE. Arch. Pharm. Weinheim, **313**, 1029 (1980).
6. S. HAYASHI, M. FURUKAWA, Y. FUJINO, N. NAKAO, and S. INOUE. Chem. Pharm. Bull. Jpn. **19**, 1557 (1971); H. N. KHATRI and H. M. WALBROSKY. J. Org. Chem. **43**, 734 (1978); P. PHILIPPE, B. W. METCALF, and J. S. WISEMAN. Chem. Abstr. **95**, 98321q (Patent) (1981).
7. E. MARCHAND, G. MOREL, and A. FOUCAUD. C. R. Acad. Sci. Ser. C, **289**, 57 (1979).
8. L. STELLA and J. L. BOUCHER. Tetrahedron Lett. **23**, 953 (1982).
9. H. HAMBERGER, P. STUTZ, and G. SCHULZ. Tetrahedron Lett. 3623 (1977).
10. G. S. BATES and S. RAMASWAMY. Can. J. Chem. **58**, 716 (1980).
11. D. SEEBACH. Synthesis, 17 (1969).
12. A. RAHMAN, B. MANAS, and R. A. J. SMITH. J. Chem. Soc. Chem. Commun. 216 (1975); R. J. CREGGE, J. L. HERRMANN, J. E. RICHMANN, R. F. ROMANET, and R. H. SCHLESSINGER. Tetrahedron Lett. 2595 (1973).
13. G. S. BATES and J. O'DOHERTY. J. Org. Chem. **46**, 1745 (1981).
14. C. A. BROWN and V. K. AHUJA. J. Org. Chem. **38**, 2226 (1973).
15. E. J. COREY and B. W. ERICKSON. J. Org. Chem. **36**, 3553 (1971).

Chemical studies on oils derived from aspen poplar wood, cellulose, and an isolated aspen poplar lignin[1]

RICHARD L. EAGER, JAMES M. PEPPER,[2] AND JIBEN C. ROY
Department of Chemistry, University of Saskatchewan, Saskatoon, Sask., Canada S7N 0W0

AND

JOSEPH F. MATHEWS
Department of Chemical Engineering, University of Saskatchewan, Saskatoon, Sask., Canada S7N 0W0

Received August 25, 1982[3]

RICHARD L. EAGER, JAMES M. PEPPER, JIBEN C. ROY, and JOSEPH F. MATHEWS. Can. J. Chem. **61**, 2010 (1983).

An initial study has been made of the chemical nature of the oil phase resulting from the the conversion of aspen poplar wood, cellulose, and an isolated lignin from the aspen poplar as a result of their interactions with water and carbon monoxide in the presence of sodium carbonate at 360°C. Gas chromatographic analysis of the sodium hydroxide soluble fractions from each substrate revealed similar spectra of alkyl-substituted phenols. The relative abundance of identified low molecular weight phenolic compounds decreased from lignin to wood to cellulose. This was in agreement with the known phenolic nature of lignin. As well, it confirmed the synthesis during reaction of such compounds from a carbohydrate substrate. Gas chromatographic analysis of the whole oils also revealed the presence in each case of several alkyl-substituted cyclopentanones whose relative abundance decreased from cellulose to wood to lignin. Silica gel column separation of the oils, after a charcoal treatment, followed by capillary gas chromatographic – mass spectrometric analyses of the resulting fractions indicated the presence of other higher molecular weight phenols, napthols, cycloalkanols, cycloalkanones, and polycyclic and long chain alkanes and alkenes.

RICHARD L. EAGER, JAMES M. PEPPER, JIBEN C. ROY et JOSEPH F. MATHEWS. Can. J. Chem. **61**, 2010 (1983).

On a fait une étude préliminaire sur la nature chimique de la phase huileuse résultant de la transformation du bois de peuplier, de la cellulose et de la lignine isolée du peuplier par suite de leurs interactions avec l'eau, et le monoxyde de carbone en présence du carbonate de sodium à 360°C. L'analyse chromatographique en phase gazeuse des fractions de ces substrats, solubles dans l'hydroxyde de sodium, révèle des spectres identiques de phénols portant des substituants alkyles. L'abondance relative des composés phénoliques de faible masse molaire que l'on a identifiés, diminue lorsqu'on passe de la lignine, au bois et à la cellulose. Ce fait s'accorde très bien avec la nature phénolique connue de la lignine. Ce fait est également confirmé lors de la synthèse de tels composés à partir d'un carbohydrate. L'analyse chromatographique de toutes les huiles révèle également dans chaque cas la présence de plusieurs cyclopentanones portant un substituant alkyle dont l'abondance relative diminue lorsqu'on passe de la cellulose, au bois et à la lignine. La séparation des huiles sur gel de silice, après traitement au charbon, suivie d'une analyse par cpg sur colonne capillaire couplée à un spectromètre de masse indique la présence d'autres composés de poids moléculaires plus élevés: des phénols, des naphtols, des cycloalcanols, des cycloalcanones et des alcanes et des alcènes polycycliques et à longues chaines.

[Traduit par le journal]

Introduction

Considerable attention has been given lately to studies on the conversion of biomass to a fuel oil to function as an alternative energy source. Some of these reported studies (1–5) have been based on the early work of Appell *et al.* (6) who reported that a variety of lignocellulosic materials (wood products, agricultural and civic wastes) could be converted, in part, into a fuel oil by reaction with carbon monoxide and water at elevated temperatures in the presence of sodium carbonate as a catalyst. Other studies (7, 8) involved the use of metallic catalysts in the presence of either hydrogen or mixtures of hydrogen and carbon monoxide. In each case complete conversion of the lignocellulosic material occurred to produce an oil fraction, a water-soluble fraction, and a residual gaseous fraction. In this laboratory attention has been directed (9) towards the use of local aspen poplar as the lignocellulosic raw material. Factorial design experiments were made to determine the optimum reaction conditions in the batch process (temperature, reaction time, water-to-wood ratio, nature of and amount of catalyst, and initial gas (carbon monoxide and/or nitrogen) pressure). The black, moderately viscous oil, obtainable in yields of 35–45 percent of the wood, was, to a first approximation, qualitatively similar to that reported by other workers using varied raw materials. The residual oxygen content was 15–20 percent and, of the 70–75 percent carbon content, 36 percent was unsaturated and/or aromatic in nature as revealed by ^{13}C nmr. As an initial step to learn more about the chemical composition of the conversion products which, in turn, would lead to a better understanding of the mechanisms of the reactions involved, a study was made of the apparently less complex water-soluble products. Several highly oxygenated products were identified (10), including a mixture of low-molecular weight (C_1–C_7) aliphatic alcohols, ketones, and acids. This paper reports on the initial study of the chemical nature of the components comprising the oil fraction. A similar study was made using separately the cellulose and lignin components of the aspen wood as reaction substrates in order that some conclusions may be drawn with respect to the origin of the identified compounds.

The oil samples were prepared, according to the procedure reported previously (10), from aspen poplar wood (*Populus tremuloides* Michx), cellulose, and an isolated aspen poplar lignin (11, 12). All such samples subsequently referred to as total oil were air-dried in a fumehood at room temperature for

[1]Presented, in part, at the 28th Congress, International Union of Pure and Applied Chemistry, Vancouver, B.C., Canada, August 1981.

[2]Author to whom correspondence should be addressed.

[3]Revision received March 25, 1983.

Can. J. Chem. Downloaded from www.nrcresearchpress.com by 210.87.254.105 on 09/06/12
For personal use only.

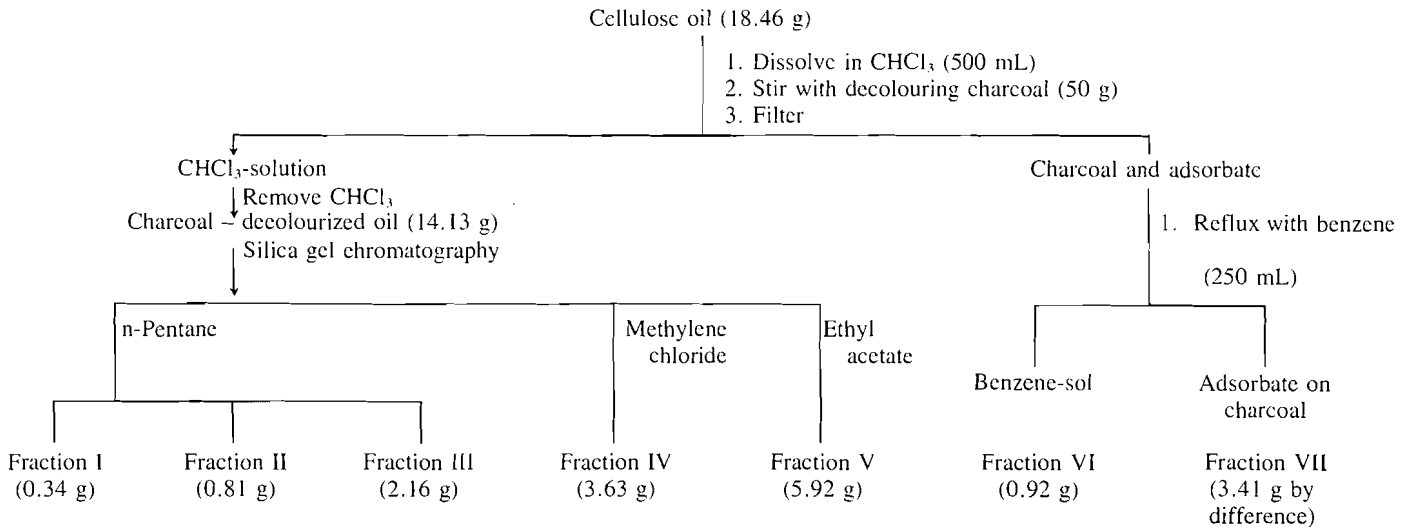

FIG. 1. Fractionation of oil from cellulose.

2–3 days, until the moisture content as determined by Karl Fischer titration was less than one percent. A preliminary examination of these oils indicated a similar carbon, hydrogen, and oxygen analysis (C 74%, H 7.5%, and O (by difference) 18.5%) for wood and cellulose and a slightly different analysis (C 66%, H 6.5%, and O (by difference) 27.5%) for the isolated lignin. There were strong infrared absorption bands for hydroxyl and carbonyl functional groups, and evidence by ^1H and ^{13}C nmr for the presence of unsaturated and/or aromatic ring structures. The ^{13}C analysis indicated that 36, 32, and 49 percent of the total carbon present in the oils obtained from the wood, cellulose, and lignin, respectively, was of an aromatic and/or unsaturated nature.

A preliminary study of the oil obtained from the wood by column chromatographic separation, using silica gel and elution with n-hexane – acetone (1:1), toluene – dioxane (6:1), toluene – ethyl formate – formic acid (4:5:1), showed that separation, as monitored by thin-layer chromatography, was not effected. Similarly, solvent extraction in a Soxhlet extractor, using solvents of increasing polarity (n-hexane, benzene, diethyl ether, acetone) gave rise to black viscous fractions representing approximately 7, 67, 8, and 12 percent respectively of the oil and char-like residue of 9 percent. Neither procedure was suitable to produce fractions that were amenable for further identification studies.

A useful chemical separation was achieved by extraction of acidic (later shown to be essentially phenolic) components using five percent sodium hydroxide solution. Acidification of these alkaline extracts from the oils obtained from wood, cellulose, and lignin and the subsequent examination of the ether-soluble fractions by gas chromatography indicated a similarity of composition. Mass spectrometry, along with a comparison with authentic compounds, permitted the identification of several mononuclear alkyl-substituted phenols. In earlier work, extractions of these oils had been made with five percent sodium bicarbonate in an attempt to isolate any strong acidic compounds. Such extracts were found to be similar to those later made using sodium hydroxide. This similarity was presumably the result of the water solubility of the phenolic products.

A similar gas chromatographic analysis of the whole oils from wood, cellulose, and lignin permitted the identification of several alkyl-substituted cyclopentanones.

With recognition that phenolic compounds were being derived not only from the initially phenolic lignin but from all the carbohydrate sources examined, attention was directed to a detailed study of the oil obtained from the cellulose component only. Such a product would be free of whatever different compounds may arise from the hemicellulose and lignin components. Treatment of a chloroform solution of the originally black oil with decolourizing charcoal and subsequent silica gel column separation (Fig. 1) was useful in obtaining fractions amenable for further study. No compounds were detected in a chloroform extract of the charcoal alone. Each Fraction (I to VI) was examined by gas chromatography and/or gas chromatography – mass spectrometry. Invidual compounds were identified by analysis of their mass spectra and, in some cases, also by comparison with authentic reference samples.

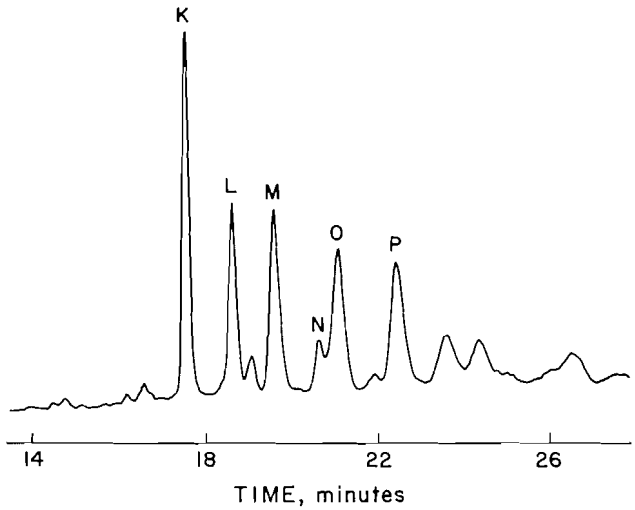

FIG. 2. Typical gas chromatogram of sodium hydroxide extract of oil from aspen wood (see Table 1 for compound identification).

Experimental results

Extraction with five percent sodium hydroxide of the product oils from wood, cellulose, and the isolated lignin led to fractions which were examined by gas chromatography using a SP-1200/1% H_3PO_4 on Chromosorb column. A typical chromatogram (from wood) serves to represent each of these fractions and is shown as Fig. 2. Identifications of the compounds

Can. J. Chem. Downloaded from www.nrcresearchpress.com by 210.87.254.105 on 09/06/12
For personal use only.

Can. J. Chem. Downloaded from www.nrcresearchpress.com by 210.87.254.105 on 09/06/12
For personal use only.

TABLE 1. Phenolic components of oil from wood, cellulose, and lignin

Peak[a]	Compound	Oil from wood %[b]	Oil from cellulose %[b]	Oil from lignin %[b]
K	Phenol	0.22	0.07	0.67
L	*o*-Cresol and 2,6-dimethylphenol	0.12	0.10	0.17
M	*m* and/or *p*-Cresol	0.13	0.13	0.32
N	2-Ethylphenol	0.05	0.06	0.11
O	2,4-Dimethylphenol and/or 2,5-dimethylphenol	0.08	0.14	0.14
P	3-Ethylphenol and/or 4-ethylphenol and/or 2,3-dimethylphenol	0.12	0.16	0.32
	Total	0.72	0.66	1.73

[a]See Fig. 2.
[b]Calculated as percent of total oil. Data in each case are the averages of duplicate experiments (±0.02).

TABLE 2. Additional compounds identified from NaOH extracts of the oils from wood, cellulose, and an isolated lignin

Compound[a]	Oil from wood	Oil from cellulose	Oil from lignin
Guaiacol	−[b]	−	+[b]
4-Ethyl-1,3-benzenediol	−	−	+
4-Methylguaiacol	−	−	+
Ethylmethylphenol	+	+	+
p-Isopropylphenol	+	+	+
p-Propylphenol and/or *o*-propylphenol	+	+	+
4-Ethylguaiacol	−	−	+
Diethylphenol	+	+	−
4-Propylguaiacol	−	−	+
1-Indanol	+	+	+
3,4-Dimethylbenzaldehyde	+	+	+
2,6-Dimethoxyphenol	−	−	+
4-Propenylguaiacol	−	−	+
1- and/or 2-Naphthol	−	−	+
2-Methyl-1-naphthol	+	+	+
3-Methyl-1-naphthol	−	−	+
Dimethylnaphthol	+	+	+
2,5,8-Trimethyl-1-naphthol	+	−	+
2-(Phenylmethyl)phenol	−	−	+

[a]Compounds are listed in order of increasing retention times.
[b]+ and − indicate present and absent, respectively.

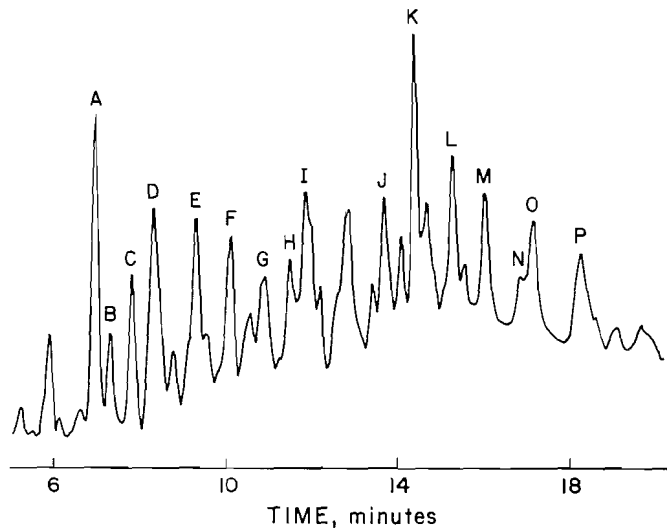

FIG. 3. Gas chromatogram of original oil from aspen poplar wood (see Tables 1 and 3 for compound identification).

represented by the various peaks were made on samples collected using a column splitter and were analysed by ultraviolet absorption spectroscopy and mass spectrometry and by comparison with authentic samples. The nature of these compounds and their relative abundance are given in Table 1.

Subsequently a more detailed qualitative analysis of the alkali-soluble fractions with boiling points and retention times higher than those reported in Table 1 was obtained using capillary gas chromatography – mass spectrometry. The presence of several other mono- and dinuclear phenols was confirmed. These are given in Table 2.

The product oils produced earlier (10) as a result of treating each of cellobiose, glucose, fructose, xylose, and glycerol under the same conditions as used for the cellulose were available in the laboratory. Extraction of these oils with sodium bicarbonate and gas chromatographic examination of the recovered acidic products showed that very similar profiles were obtained in each case and were similar to that derived from the oil from cellulose. Three other model substances, formaldehyde, acetaldehyde, and glycolaldehyde, were also treated under the same reaction conditions. In each case an oil was obtained which contained an alkali-soluble fraction which gave a gas-chromatographic profile indicating the presence of phenolic compounds.

Furthermore, samples of the whole oils from wood, cellulose, and lignin were gas-chromatographed using the same column as that used for the phenolic fractions. A typical chromatogram (from wood) serves to represent each of these fractions and is shown as Fig. 3. Identifications of the compounds represented by the labelled peaks were made on samples collected using a column splitter and analyses by infrared spectrophotometry, mass spectrometry, and comparison with authentic reference samples. The nature of these compounds and their relative abundance is given in Table 3. Data from several runs agreed closely. Table 3 shows a typical analysis.

Since it was now apparent that cellulose could be a precur-

TABLE 3. Cyclopentanone components of oil from wood, cellulose, and lignin

Peak[a]	Compound	Oil from wood %[b]	Oil from cellulose %[b]	Oil from lignin %[b]
A	2-Methylcyclopentanone	0.49	0.54	0.12
B	3-Methylcyclopentanone	0.18	0.28	0.08
C	2,5-Dimethylcyclopentanone	0.08	0.10	—
D	2,3-Dimethylcyclopentanone and/or 2,4-dimethylcyclopentanone	0.61	0.80	0.59
E	2-Ethylcyclopentanone	0.34	0.41	0.12
F	2-Ethyl-5-methylcyclopentanone	0.21	0.44	0.12
G	3-Ethyl-2-methylcyclopentanone and/or 4-ethyl-2-methylcyclopentanone	0.27	0.38	0.11
H	2-Propylcyclopentanone	0.34	0.39	0.12
I	2-Methyl-5-propylcyclopentanone	0.37	0.44	0.19
J	2-Butylcyclopentanone	0.40	0.32	0.12
	Total	3.29	4.01	1.59

[a]See Fig. 3.
[b]Calculated as percent of total oil.

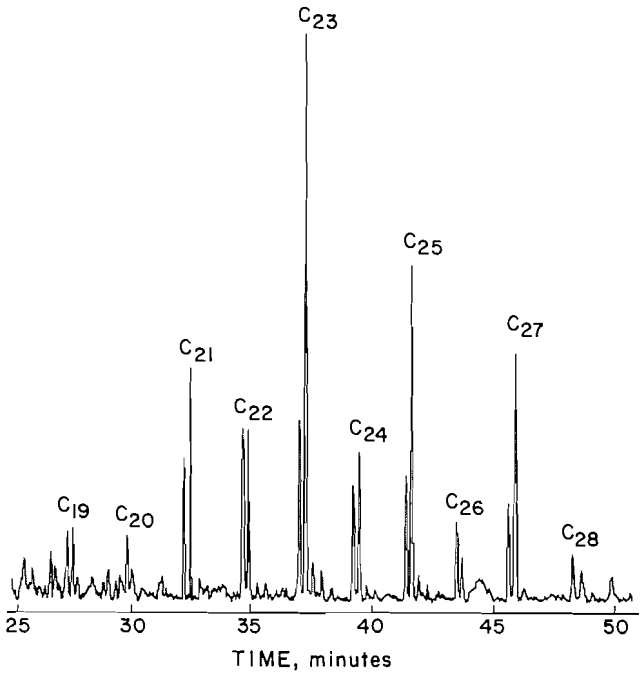

FIG. 4. Capillary gas chromatogram of alkane/alkene components of Fraction I of oil from cellulose.

sor, although not the only precursor, of the majority of the various types of products comprising the oil produced from wood, it alone was used as the raw material for further studies. The black, moderately viscous oil produced in 28% yield was examined as illustrated in Fig. 1, with the disposition of the original amount of oil among the separated fractions as shown. An examination of Fractions I through VI by capillary gas chromatography – mass spectrometry revealed the following.

Fraction I

The presence of the following compounds was confirmed:[4] methylindan, ethylindan, dimethylindan, trimethylindan, ethyltetralin, diphenyl ether, and a series of both long chain alkanes and alkenes (C_nH_{2n+2} and C_nH_{2n} where n = 19 to 28). The chromatograms (Fig. 4) representing the alkane/alkenes exhibited a characteristic series of doublet peaks with the peak of shorter retention time corresponding to the alkane. The mass spectra of the alkanes displayed the characteristic fragmentation pattern with groups of peaks spaced 14 mass units apart and each group having, as the most abundant species, the C_nH_{2n+1} ion which occurred with gradually decreasing abundance with increasing mass. On the other hand, mass spectra of the alkenes were dominated by ions of the general formula C_nH_{2n-1}, which also gradually declined in abundance with increasing mass.

Fraction II

Some of the indans found in Fraction I were also found here but the poor resolution of peaks prevented further identification.

Fraction III

This fraction contained the ketonic derivatives. Those listed in Table 3 were identified, along with 2-pentylcyclopentanone, 2-cyclopentylcyclopentanone, 2-ethylcyclohexanone, β-hydrindanone, methyl-β-hydrindanone, methylindanone, dimethylindanone, and methyltetralone.

Fractions IV and V

The chromatograms of these fractions were very similar and represented primarily the phenolic compounds listed in Tables 1 and 2. Also identified was a series of alcohols including cyclopentanol, 2-methylcyclopentanol, 2,5-dimethylcyclopentanol, 5-methylcyclohexanol, and 3-cyclohexen-1-ol. Mass fragmentation patterns of two sizable peaks at higher retention times gave a strong indication for the presence of hexadecanoic acid and a C_{18} or C_{19} alcohol.

Fraction VI

The chromatogram of this fraction was very similar to that shown in Fig. 3 indicating that some of the phenols and cyclopentanones originally present in the oil had been adsorbed and removed by the charcoal.

Discussion

It is now abundantly evident from this research and from

[4]All possible sources of contaminants (grease, pump oil) were checked as potential precursors of these compounds. No evidence was found.

Can. J. Chem. Downloaded from www.nrcresearchpress.com by 210.87.254.105 on 09/06/12
For personal use only.

Can. J. Chem. Downloaded from www.nrcresearchpress.com by 210.87.254.105 on 09/06/12
For personal use only.

earlier reports (3–5) that the alkaline degradation of whole biomass or of its separate constitutent components leads to a very complex mixture of chemical products. In turn, these compounds, due to their greater variance in structure, must involve extensive and complex mechanistic pathways for their production. Clarification of these mechanisms should lead to a better understanding of the conversion process and ultimately to the recognition of those reaction conditions whereby potentially valuable chemical products may be obtained in economically acceptable yields. This complexity has been supported herein by the identification of several distinctly different classes of compounds including mono- and dinuclear phenols, cycloalkanones and cycloalkanols, and polycyclic and long-chain alkanes and alkenes. Sufficient specific examples of each such group have been identified to characterize the group.

The identification of the alkyl-substituted phenols obtained by the sodium hydroxide extraction of the oil from wood, cellulose, and isolated lignin (Table 1) strongly suggests, as expected, that the aromatic nature of lignin results in significantly more phenolic degradation products (although of the same type) than are observed from wood or cellulose. Under these reaction conditions carbohydrates function as precursors for phenolic substances and, in the case of wood, the net result of converting both the carbohydrate and the lignin is the larger percentage yield of phenolic compounds over that from cellulose alone. On the other hand, the origin of the cyclopentanones (Table 2) would appear to be primarily the hexose-based cellulose, with lesser yields from wood with only 50% cellulose and much less from the lignin preparation which is primarily aromatic but most likely contains carbohydrate impurities.

Little can yet be said about the mechanism of formation of any of these varied products. The alkaline conversion of carbohydrates to aromatic materials, including phenols, has been recognized for a long time and recently has been studied extensively by Theander and Westerlund (13). The current study emphasizes the apparent role of smaller (1-, 2-, or 3-carbon) fragments being involved in the synthetic pathways. In particular, the multiple methyl-substituted phenols and cyclopentanones suggest the involvement of a one-carbon reactant. As well, in the homologous series of higher molecular weight alkanes and alkenes (Fig. 4), there are indications of either one- or two-carbon fragments being involved. The predominance of the odd numbered carbon units may be synthetically significant but is as yet not understood. It must be recognized that the relatively long times of reaction at an elevated temperature, due to the extended heating-up and cooling-off periods, contribute to the complexity of the rections involved. Currently studies are underway to examine the nature of the oil produced in short periods of time using a small-scale semicontinuous reactor (14). These studies, together with concurrent ones using model substances, may provide more useful information about the overall mechanism of the reactions involved and will be reported at a later date.

Experimental

The apparatus and the standard experimental conditions used to prepare oil fractions by the high temperature (360°C), alkaline (Na_2CO_3) catalyzed degradation of aspen wood (*Populus tremuloides* Michx) (100 g), cellulose (MN-Cellulose Powder for Column Chromatography) (100 g), and an isolated aspen poplar lignin (11, 12) (25 g) were described earlier (10). The time of extraction of the lignin was 1.5 h.

The lignin sample analyzed for C 57.7%, H 5.76%, suggesting the presence of some carbohydrate impurity since similarly isolated samples (15) analyzed for C 59.3%, H 6.0% (average).

Sodium hydroxide extraction

A solution of oil (1 g) dissolved in $CHCl_3$ (75 mL) was extracted with 5% NaOH (10 × 40 mL). The combined extracts, after acidifying with HCl, were extracted with diethyl ether, the extract dried over anhydrous Na_2SO_4, and excess solvent removed. The residue weights from wood, cellulose, and lignin were 28, 22, and 32.5% of original oil respectively.

Gas chromatographic analysis for relative abundance studies

The sodium hydroxide soluble fractions (Fig. 2) and the whole oil fractions (Fig. 3) were chromatographed on a HP Model 5750 instrument using a 6 ft × 1/8 in. od stainless steel column packed with 10% SP-1200/1% H_3PO_4 on Chromosorb W (80–100 mesh, AW). The detector temperature was maintained at 310 ± 10°C and the injector temperature at 250 ± 10°C. Hydrogen was passed at 40 mL/min and the air flow rate at 500 mL/min. To produce Fig. 2, the temperature was held constant at 50°C for one minute, then programmed from 50°C to 180°C at 10°/min and held at 180°C, using nitrogen as the carrier gas, at 15 mL/min until no further peaks appeared. To produce Fig. 3, similar conditions were used except that the initial temperature was 55°C and the carrier gas flow rate was 25 mL/min. Calibration curves for each of the standards were prepared by injecting varying amounts to cover the expected range in the sample for analysis.

Capillary gas chromatographic analyses

Gas chromatographic – mass spectrometric analyses of Fractions I through V and the alkaline extracts were made using a Finnigan Model 4000 system interfaced to an INCOS Model 2300 data acquisition system. The column was fused silica (25 m × 0.25 mm id) coated with OV-17. The initial temperature of 30°C was raised rapidly to 60°C and programmed from 60°C to 200°C (hold) at 4°/min. Electron impact mass spectra were obtained respectively every 1.5 s by scanning from m/z 41 to m/z 650 at 70 eV.

Sources of reference compounds

All the alkyl-substituted cyclopentanones were synthesized, using the general procedure reported by Stork *et al.* (16) starting from cyclopentanone or previously prepared 2-methylcyclopentanone or 3-ethylcyclopentanone, synthesized from β-ethyladipic acid using the method of Thorpe and Kon (17). All structures were confirmed by an examination of their mass spectral fragmentation patterns.

Acknowledgements

The authors gratefully acknowledge financial assistance from the Canadian Forestry Service, Department of Environment (ENFOR Programme), and the award (to J.C.R.) of three University of Saskatchewan Graduate Fellowships. The capillary column gc–ms analyses were performed by Mr. L. Hogge, Prairie Regional Laboratory, NRC, Saskatoon, Saskatchewan.

1. H. R. APPELL. The production of oil from wood waste. Fuels from waste. Academic Press. Inc., New York. 1977. Chapt. VIII.
2. J. C. CAVALIER and E. CHORNET. Fuel, **56**, 57 (1977).
3. P. M. MOLTON, R. K. MILLER, J. M. DONOVAN, and T. F. DEMMITT. Carbohydr. Res. **75**, 199 (1979).
4. D. C. ELLIOTT. Can. J. Chem. Eng. **58**, 730 (1980).
5. P. M. MOLTON, R. K. MILLER, J. A. RUSSELL, and J. M. DONOVAN. Biomass as a non-fossil fuel source. ACS Symposium Series 144, 137 (1981).
6. H. R. APPELL, Y. C. FU, S. FRIEDMAN, P. M. YAVORSKY, and I. WENDER. Converting organic wastes to oil. U.S. Bureau of Mines Report of Investigation No. 7560. 1971.
7. D. G. B. BOOCOCK, D. MACKAY, M. MCPHERSON, S. NADEAU, and R. THURIER. Can. J. Chem. Eng. **57**, 98 (1979).

8. D. G. B. BOOCOCK, D. MACKAY, H. FRANCO, and P. LEE. Can. J. Chem. Eng. **58**, 466 (1980).
9. R. L. EAGER, J. F. MATHEWS, and J. M. PEPPER. Can. J. Chem. Eng. **60**, 289 (1982).
10. R. L. EAGER, J. F. MATHEWS, J. M. PEPPER, and H. ZOHDI. Can. J. Chem. **59**, 2191 (1981).
11. J. M. PEPPER, P. E. I. BAYLIS, and E. ADLER. Can. J. Chem. **37**, 1241 (1959).
12. J. M. PEPPER and M. SIDDIQUEULLAH. Can. J. Chem. **39**, 390 (1961).
13. O. THEANDER and E. WESTERLUND. Acta Chem. Scand. Ser. B, **34**, 701 (1980), and references therein.
14. R. L. EAGER, J. M. PEPPER, and J. F. MATHEWS. Can. J. Chem. Eng. **61**, 189 (1983).
15. J. M. PEPPER and M. SIDDIQUEULLAH. Can. J. Chem. **39**, 1454 (1961).
16. G. STORK, A. BRIZZOLARA, H. LANDESMAN, J. SZMUSZKOVICZ, and R. TERRELL. J. Am. Chem. Soc. **85**, 207 (1963).
17. J. F. THORPE and G. A. R. KON. Org. Synth. Coll. Vol. 1, 192 (1947).

Can. J. Chem. Downloaded from www.nrcresearchpress.com by 210.87.254.105 on 09/06/12
For personal use only.

Enamines and iminium salts from amido-acids[1]

JOHN M. MCINTOSH, LILIANNA Z. PILLON, SAMUEL O. ACQUAAH, JAMES R. GREEN,[2] AND GRAHAM S. WHITE[2]
Department of Chemistry, University of Windsor, Windsor, Ont., Canada N9B 3P4

Received January 10, 1983

JOHN M. MCINTOSH, LILIANNA Z. PILLON, SAMUEL O. ACQUAAH, JAMES R. GREEN and GRAHAM S. WHITE. Can. J. Chem. **61**, 2016 (1983).

Distillation of ω-carboxyalkyl lactams from soda-lime leads to the formation of bicyclic enamines or imines with concomitant loss of carbon dioxide and water. Monoamides of dicarboxylic acids afford cyclic ketones. A mechanistic rationale is presented and it is concluded that the reaction is a variant of the classical Ruzicka cyclization of dicarboxylic acids. The method allows the regiospecific formation of iminium salts of bicyclic nitrogen heterocycles.

JOHN M. MCINTOSH, LILIANNA Z. PILLON, SAMUEL O. ACQUAAH, JAMES R. GREEN et GRAHAM S. WHITE. Can. J. Chem. **61**, 2016 (1983).

La distillation des lactames ω-carboxyalkyles sur de la chaux sodée conduit à la formation d'énamines bicycliques ou d'imines avec une perte concomittante de bioxyde de carbone et d'eau. Les monamides d'acides dicarboxyliques conduisent à des cétones cycliques. On propose un mécanisme réactionnel et on conclut que la réaction est une variante de la cyclisation des acides dicarboxyliques selon la méthode classique de Ruzicka. La méthode permet la formation régiospécifique des sels d'iminium des hétérocycles azotés bicycliques.

[Traduit par le journal]

Can. J. Chem. Downloaded from www.nrcresearchpress.com by 210.87.254.40 on 09/06/12
For personal use only.

The enamine functionality is one of the most versatile in the array of processes available to the synthetic chemist (1). The interconversion between the iminium and enamine forms, a process which can frequently be controlled and which is of central importance in the synthetic and biosynthetic elaboration of many alkaloids (1), allows the manipulation of electrophilic and nucleophilic sites with remarkable ease. Reactions can then be effected with nucleophilic (e.g. Grignard reagents) or electrophilic reagents (e.g. acyl or alkyl halides) (Scheme 1).

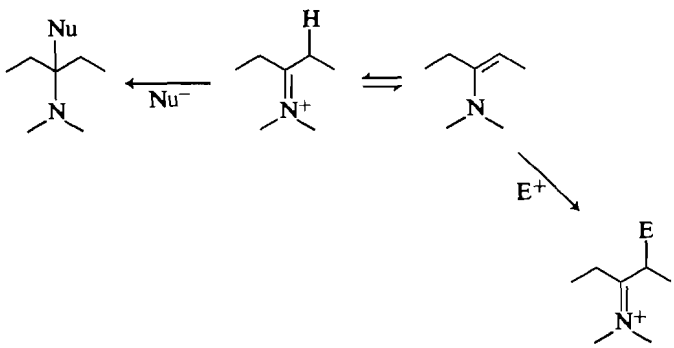

SCHEME 1

. Enamines are most frequently prepared (1) by interaction of secondary amines with aldehydes or ketones (i.e. a C—N bond-forming process). Another process used, particularly in bicyclic materials, is the mercuric acetate oxidation of tertiary amines, a method pioneered by Leonard *et al.* (2) and used to great advantage in alkaloid synthesis. Another very useful process, which has been described recently by Rapoport and coworkers (3), involves decarboxylation of α-amino acids. The iminium salts so obtained can be isomerized to the enamine form under the usual conditions.

An ongoing project in our laboratories is directed toward the synthesis of substituted tricyclic ammonium salts of type **1**. Antithetical analysis suggested that appropriate precursors would be the bicyclic salts **2** (Scheme 2). Results already

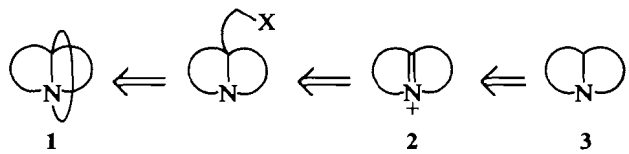

SCHEME 2

reported (4) have verified the proposed route for **2** → **1**. However, the project demanded the synthesis of **1** with varying ring sizes and substituents present in the rings. For Leonard's oxidative procedure to be useful, the synthesis of the saturated bicyclic amines **3** with these points satisfied was required. Such syntheses appeared to be long and the regiospecific oxidation of several of these was problematical.

Our attention was attracted by a report by Miyano *et al.* (5) of the preparation of dehydropyrrolizidine (**5**) by the simple expedient of distilling the carboxy-lactam **4** from soda-lime (eq. [1]). Such an operation, if generally applicable, would be

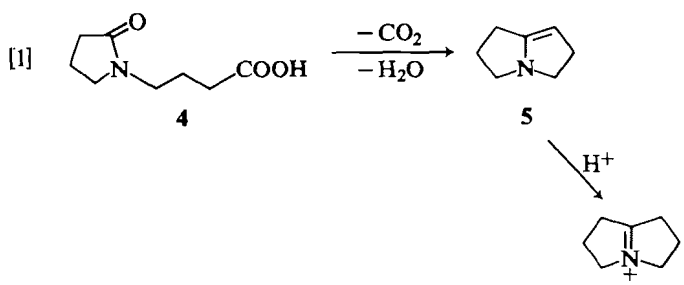

highly attractive in that the lactams are relatively easily prepared and the overall sequence from commercially available materials would be quite short. In addition, it represents a method of enamine formation by a C—C bond-forming process.

A literature review showed that this reaction had been investigated by Murakoshi *et al.* in the late 1960's (6, 7). This work, which appeared largely in Japanese, does not seem to have been widely recognized. From these reports it can be seen that 5-, 6-, and 7-membered rings can be formed, the stereochemistry at the C—N center is retained, and that the presence of N—H bonds does not interfere with the cyclization. Further-

[1]Presented in part at the 65th Annual Meeting of the Chemical Institute of Canada, Toronto, Ontario, June 1982.

[2]Holder, NSERC summer undergraduate scholarship.

Can. J. Chem. Downloaded from www.nrcresearchpress.com by 210.87.254.40 on 09/06/12
For personal use only.

more, both Murakoshi and Alder[3] have shown that esters can be used in place of the acids. In view of the importance of this method to our research, we undertook to explore its limits more fully and our results are the subject of this report.

One can envisage several different types of amido-acids which might undergo this reaction. Both *C*- and *N*-(ω-carboxyalkyl)lactams, as well as ω-acylaminocarboxylic acids, are potential substrates for the reaction. In each of these, the effect of ring size (both of the existing and cyclizing rings) and substituents on nitrogen and/or the chains are possible variables.

Results

Our first investigations centered on the use of *N*-(ω-carboxyalkyl)lactams. We have already reported, in the context of the synthesis of **1** (4), the preparation of **6***a* and **6***b* and their conversion to **7***a* and **7***b* respectively. An improved procedure for the preparations of **6***a*,*b* is included in the experimental section of this paper. The procedure is simple and easily carried out. In addition, Miyano *et al.* have recently reported the formation of **7***c* (8) as well as **5** (5). To investigate the application

[2] 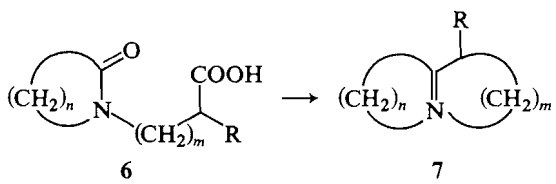

6 **7**

a $n = 4$, $m = 3$, R = H
b $n = 4$, $m = 2$, R = H
c $n = 3$, $m = 2$, R = CH_3
d $n = 4$, $m = 4$, R = H
e $n = 5$, $m = 2$, R = H

to the annulation of larger rings, the homologous lactam **6***d* was prepared. Pyrolysis afforded a complex mixture of products, as was evidenced by glc analysis. A crystalline perchlorate salt (**7***d*) could be isolated, but the yield was only 14%. An unidentified side-product was also obtained which was clearly ketonic in nature (ir, ms). The difficulty in forming seven-membered rings is well-known and has recently been encountered by Rapoport (3). It appears that this situation applied also to the pyrolysis reaction, although the formation of the seven-membered imine from 6-acetamidohexanoic acid is successful (7).

Annulated seven-membered rings can be approached from the other direction as is evidenced by the formation of **7***e*. In this case, the previously described (9) strategy for assembling the *N*-alkylated piperidones was not applicable. However, *N*-alkylation of caprolactam with 5-chloro-1-pentene (10) under phase-transfer (PT) conditions (11) followed by permanganate oxidation, also using PT methodology (12), gave **6***e* in acceptable amounts.

Simple alkyl substituents do not interfere with the reaction whether they are at the reacting center or elsewhere. This is shown by the formation of **7***c* (8) as well as the two new transformations leading to **10** and **14**. Two points of interest regarding **10** and **14** can be noted.

The cyanide addition products **11** and **15** appear to be stereochemically homogeneous, based primarily on ^{13}C evidence. However, in both cases, we were unable to effect replacement

[3] 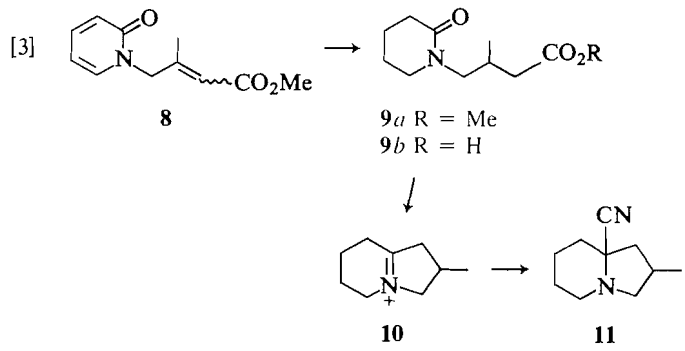

8 **9***a* R = Me; **9***b* R = H **10** **11**

[4] 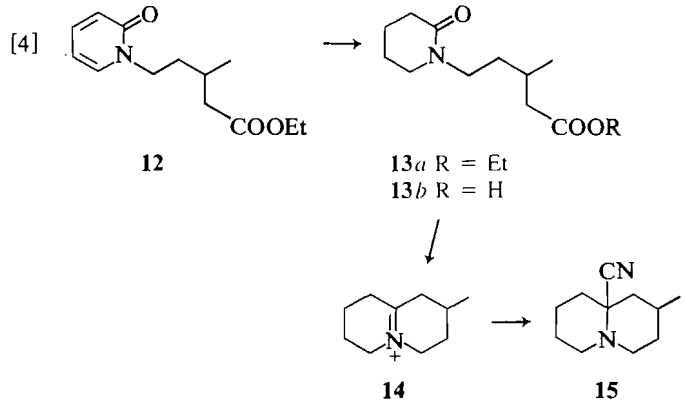

12 **13***a* R = Et; **13***b* R = H **14** **15**

of the cyano group with Grignard reagents. Prolonged reaction times with large excess of 4-phenoxybutylmagnesium bromide led to only 10% conversion of starting material.

We next turned our attention to *C*-(ω-carboxyalkyl)lactams. It was of interest to determine if cyclization would occur to give fused bicyclic systems in which nitrogen was not at the bridgehead position. To this end, lactams **16***ab* and **19** were prepared and subjected to the pyrolysis reaction. Lactam **16***a* afforded **17***a* in 61% crude yield. The perchlorate **18***a* was not crystalline but a low yield of a hygroscopic hexachloroplatinate could be isolated. Lactam **16***b* gave 78% of enamine **17***b* which was pure according to glc analysis. The hexachloroplatinate was extremely hygroscopic and could not be isolated in a crystalline form. The nmr of **17***a* showed that it existed primarily

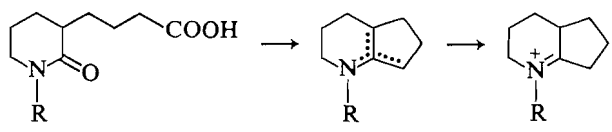

16*a* R = H **17** **18**

[5] **16***b* R = Me

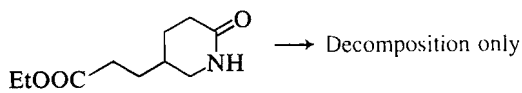

19

in the imine form, while that of **17***b* showed the two possible enamine forms in approximately equal amounts. As expected, **19** gave a complex mixture of products which remain unidentified.

Cyclization of monoamides of α,ω-dicarboxylic acids would be expected to lead to enamines of cycloalkanones. In the event, reaction of **20***a* or **20***b* led to the formation of the cycloalkanone directly. That these products were not formed

[3]R. W. Alder, private communication.

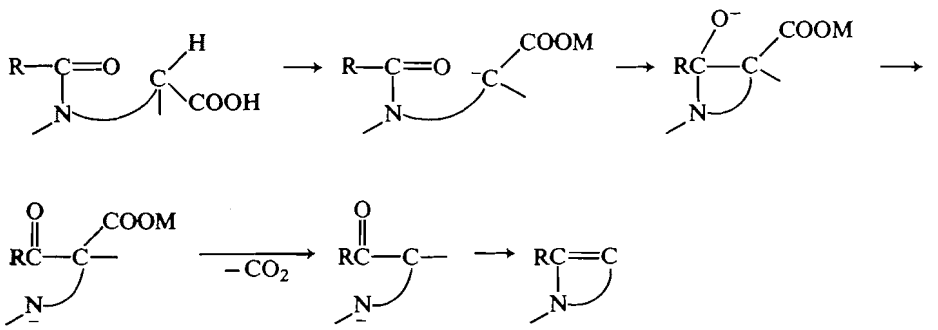

SCHEME 3

[6] $HOOC(CH_2)_nCONR_2 \longrightarrow (CH_2)_n + R_2NH + CO_2$

20 **21**

a $n = 6$, R = C_2H_5
b $n = 4$, R = $(CH_2)_4$

by hydrolysis of the enamine was shown by including authentic samples of these in a pyrolysis reaction and isolating them unchanged.

Murakoshi's work (6) has delineated the cyclization of ω-acylaminocarboxylic acids to cyclic imines and iminium salts (6, 7). We repeated his work using the commercially available **22**. In this case the cyclization occurred in two ways to afford **23** and **24**, the latter being obtained in 74% yield.

[7] $AcNH(CH_2)_5COOH \longrightarrow$ 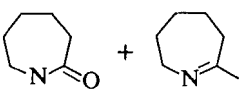

22 **23** **24**

Finally the possibility of intermolecular reactions was investigated briefly. Attempts to condense hexanoic acid with hexanamide or phenylacetic acid with *N,N*-dimethyl hexanamide were unsuccessful. The use of the primary amide led to the precedented (13) formation of hexanonitrile plus 6-undecanone, while the reaction involving the tertiary amide led to a mixture of 1,3-diphenylacetone and 1-phenyl-2-heptanone in low yield.

Discussion

Speculation on the mechanism of reactions occurring under the heterogeneous and high-temperature conditions employed is unproductive. However, a rationale has been developed based on the observations of the ketone-forming reactions. Such products are reminiscent of the classical Ruzicka reaction (14) which involves the pyrolysis of dicarboxylic acid salts over barium, calcium, or thorium oxide. Both radicals and anionic routes have been postulated (15), although it is difficult to explain the reported (16) formation of 2,2,5,5-tetramethylcyclopentanone from 2,2,5,5-tetramethylsuccinnic acid using an anionic mechanism. Nevertheless, our results allow the use of the pathway shown in Scheme 3 to be used as a predictive tool. The formation of ketonic products from the monoamides **20** would be expected if the nitrogen atom is not "tied" to the rest of the molecule. Similarly, the cyclization of **19** would involve a very strained intermediate and failure to cyclize is predictable. Finally, the observation of ketonic material from **6***d* can be viewed as support for this rationale, as such molecules might be expected to be more resistant to intramolecular enamine formation than would the related ten- and nine-membered ring analogs. The intervention of an aminoketone intermediate would, of course, obviate the attractive possibility of a regiospecific enamine synthesis.

The formation of bicyclic enamines by a C—C bond-forming process is a very useful adjunct to the usual methodology. Particularly important for our purposes is that it allows the regiospecific preparation of substituted bicyclic iminium salts. It is worthy of note that hydrolysis of the iminium salts (e.g. **18**, **24**) provides molecules which are related to the amino acids by apparent N → C acyl transfer and results in the effective transformation of an acid to a ketone. While we feel that hetero substituents are unlikely to survive the conditions, the point remains to be tested. In any case, the method allows the synthesis of enamines without the necessity of prior preparation of amino ketones and thus provides a rapid formation of these materials from precursors which are easily prepared and stable to many common reaction conditions.

Experimental

Melting points are corrected; boiling points are uncorrected. Infrared spectra were run on a Beckman IR-12 instrument. The ^{1}Hmr spectra were run at 60 MHz and are reported in the following format: chemical shift (δ) (multiplicity, number of protons, coupling constant). The Cmr spectra were run at 22.64 MHz in the FT mode using a flip angle of 45° on a Bruker CXP-100 instrument. Mass spectra were obtained on a Varian MATCH5-DF instrument in one of two modes coded FDMS (field desorption mode) or FIMS (field ionization mode). Gas chromatographic analyses were performed using either 10% or 20% SE30 on Chromosorb W columns, solvents were removed at reduced pressure, and the drying agent used was anhydrous magnesium sulfate.

Syntheses of amidoacids

Improved preparation of N-*(3-carboxypropyl)-2-piperidinone (**6**a) and* N-*(4-carboxybutyl)-2-piperidinone (**6**b)*

The reaction between 2-methoxypyridine and either ethyl 4-bromobutyrate or ethyl 5-bromovalerate was carried out as previously described (9). The mixture was distilled to a head temperature of ca. 120°C (0.15 Torr) to remove *N*-methylpyridone and other low-boiling impurities. The brown residue was then hydrogenated at 60 psi initial pressure over a 10%Pd/C catalyst and the hydrogenated material was hydrolyzed as previously described (9). The method avoids the difficult distillation of the pyridone esters, a procedure which causes significant decomposition and consequent loss of material.

N-*(5-carboxypentyl)-2-piperidinone (**6**d)*

Ethyl 6-bromohexanoate was prepared from ϵ-caprolactone by saturating an ice-cold ethanolic solution of the lactone with hydrogen bromide, allowing the mixture to stir at ambient temperature overnight, pouring onto ice, and extracting with dichloromethane. Dis-

Can. J. Chem. Downloaded from www.nrcresearchpress.com by 210.87.254.40 on 09/06/12
For personal use only.

Can. J. Chem. Downloaded from www.nrcresearchpress.com by 210.87.254.40 on 09/06/12
For personal use only.

tillation afforded a 44% yield of the bromoester, bp 69–72°C (0.13 Torr) (20). Alternatively, the bromoester could be purified using silica gel chromatography and 3:1 petroleum ether/ether as eluant. Using this procedure, the yield of pure product was 56%; ir ($CHCl_3$): 2950, 2880, 1730, 1465, 1380 cm^{-1}; ^{1}Hmr ($CDCl_3$): 4.2 (q, 2H, J = 8 Hz), 3.5 (t, 2H, J = 7 Hz), 2.6–1.1 (m, 8H), 1.25 (t, 3H, J = 8 Hz); Cmr ($CDCl_3$): 173.1, 60.1, 34.0, 33.2, 32.6, 27.7, 24.2, 14.3. The bromoester (6.5 g, 0.06 mol) was heated to 195°C under a nitrogen atmosphere and 10 g (0.045 mol) of 2-methoxypyridine was added dropwise by a syringe over 4 h. Methyl bromide was evolved. The mixture was heated at 195°C for 3 h and then stirred at ambient temperature overnight.

Distillation gave a large forerun consisting largely of *N*-methylpyridone (bp 66–67°C (0.15 Torr)). The desired product, *N*-(5-carbethoxypentyl)-2-pyridone, remained as the residue after removal of this fraction. The crude yield was 6.9 g (64%) and the material was used directly in the succeeding step; ^{1}Hmr ($CDCl_3$): 7.6 (m, 2H), 6.8 (dd, 1H, J = 1, 8 Hz), 6.45 (dt, 1H, J = 1, 6 Hz), 4.15 (m, 4H), 2.5–1.2 (m, 8H), 1.25 (t, 3H, J = 7 Hz).

The crude ester (6.0 g, 0.025 mol) was dissolved in 30 mL of ethanol and hydrogenated over platinum oxide. Hydrogen absorption was complete in 6 h. Filtration and evaporation afforded 6.0 g (100%) of *N*-(5-carbethoxypentyl)-2-piperidinone as a clear liquid which was pure according to glc analysis; ^{1}Hmr ($CDCl_3$): 4.2 (q, 2H, J = 7 Hz), 3.7–3.2 (m, 4H), 2.6–2.1 (m, 4H), 2.1–1.1 (m, 10H), 1.25 (t, 3H, J = 7 Hz).

The amidoester (5.5 g, 0.023 mol) was dissolved in 25 mL of ethanol and a solution of 1.85 g (0.033 mol) of KOH in 10 mL of water was added. The mixture was stirred at ambient temperature overnight, evaporated, diluted with water, and extracted with ether. The aqueous phase was acidified and extracted with chloroform (4 × 75 mL). The extracts were dried and evaporated, the last traces of solvent being removed at 0.05 Torr. The white solid remaining (**6***d*) (3.5 g, 71%) had mp 72–74°C; ir ($CHCl_3$): 3500–2400, 1715, 1630, 1510, 670 cm^{-1}; ^{1}Hmr ($CDCl_3$): 10.7 (s, 1H), 3.6–3.2 (m, 4H), 2.5–2.0 (m, 4H), 2.0–1.2 (m, 10H); Cmr ($CDCl_3$): 177.2, 170.5, 48.0, 47.3, 34.1, 32.0, 26.7, 26.4, 24.7, 23.6, 21.2. *Anal.* calcd. ($C_{11}H_{19}NO_3$): C 61.95, H 8.98, N 6.57; found: C 62.16, H 9.37, N 6.36.

N-*(3-carboxy-2-methylpropyl)-2-piperidinone (**9**b)*

A stereoisomeric mixture of methyl 4-bromo-3-methylbut-2-enoate (17) (10 g, 0.052 mol) was heated to 160°C under nitrogen. 2-Methoxypyridine (10 g, 0.092 mol) was added in the usual manner. After heating at 165°C for 3 h, the mixture was distilled. The product **8** (4.2 g, 31%) was obtained, bp 130–140°C (0.15 Torr). The ^{1}Hmr and glc analyses showed this material to be a 60:40 mixture of the *E* and *Z* isomers. *Anal.* calcd. ($C_{11}H_{17}NO_3$): C 63.56, H 6.37, N 6.76; found: C 63.41, H 6.42, N 6.79.

Ester **8** (3.5 g, 0.017 mol) was hydrogenated in methanol solution over a 5% Rh/Al_2O_3 catalyst at one atmosphere pressure. Three equivalents of hydrogen were absorbed in 3 h. Filtration and evaporation gave **9***a* as a yellow liquid which required no further purification; ^{1}Hmr ($CDCl_3$): 3.70 (s, 3H), 3.34 (m, 4H), 2.30 (m, 5H), 1.80 (m, 4H), 0.95 (d, 3H, J = 6 Hz).

Ester **9***a* (3.3 g, 0.015 mol) was added to a solution of 1.0 g KOH in 80 mL of ethanol and 10 mL of water. The mixture was stirred at ambient temperature overnight and then evaporated to remove the alcohol. Water (30 mL) was added and the solution was washed with ether. The aqueous phase was acidified to pH 3 and extracted thoroughly with chloroform (5 × 50 mL). The dried extracts were evaporated to give a clear oil which solidified when final traces of solvents were removed at 0.1 Torr pressure. There was obtained 2.4 g (78%) of **9***b*, mp 94–96°C; ir ($CHCl_3$): 3600–2400, 1715, 1630, 1510 cm^{-1}; ^{1}Hmr ($CDCl_3$): 12.2 (s, 1H), 3.35 (m, 4H), 2.38 (m, 5H), 1.82 (m, 4H), 1.00 (d, 3H, J = 8 Hz); Cmr ($CDCl_3$): 175.5, 171.4, 52.4, 48.3, 39.2, 31.9, 28.6, 23.1, 21.0, 17.8. *Anal.* calcd. ($C_{10}H_{17}NO_3$): C 60.28, H 8.70, N 7.03; found: C 60.70, H 9.02, N 7.00.

N-*(4-carboxy-3-methylbutyl)-2-piperidinone (**13**b)*

3-Methyl-δ-valerolactone (Aldrich) (7 g, 0.06 mol) was converted to ethyl-5-bromo-3-methylvalerate (9.7 g, 88%) according to a published procedure (18). The ester (9 g, 0.04 mol) was heated to 180°C under nitrogen. 2-Methoxypyridine (10 g, 0.09 mol) was added dropwise with stirring via syringe in the usual manner and then the liquid was distilled. Ester **12** (3.68 g, 38.5%) was obtained (bp 139–150°C (0.2 Torr)) as a clear liquid; ir (film): 2980, 1730, 1660, 1590, 1540 cm^{-1}; ^{1}Hmr ($CDCl_3$): 7.63 (d, 1H, J = 6 Hz), 7.42 (dd, 1H, J = 2, 4 Hz), 6.73 (d, 1H, J = 9 Hz), 6.38 (td, 1H, J = 6, 1 Hz), 4.07 (m, 4H), 2.4–1.45 (m, 5H), 1.23 (t, 3H, J = 7 Hz), 1.02 (d, 3H, J = 6 Hz); Cmr ($CDCl_3$): 172.3, 162.5, 140.3, 138.2, 120.2, 107.6, 60.2, 48.3, 41.4, 36.0, 28.1, 19.7, 14.3.

Hydrogenation over platinum oxide, followed by hydrolysis as described for **9***b*, afforded **13***b* (83%) as a white solid after trituration with petroleum ether, mp 91–93°C; ^{1}Hmr ($CDCl_3$): 11.6 (s, 1H), 3.33 (m, 4H), 2.65–1.20 (m, 11H), 1.00 (d, 3H, J = 8 Hz); Cmr ($CDCl_3$): 176.4, 170.6, 47.8, 45.3, 41.5, 33.5, 32.0, 28.1, 21.2, 19.8. *Anal.* calcd. ($C_{11}H_{19}NO_3$): C 61.95, H 8.98, N 6.57; found: C 61.93, H 9.15, N 6.82.

N-*(3-carboxypropyl)caprolactam (**6**e)*

A solution of 2.8 g (0.025 mol) of caprolactam and 2.6 g (0.025 mol) of 5-chloro-1-pentene (10) in 20 mL of dry THF was added to a suspension of 1.3 g (0.023 mol) of finely ground KOH and 5 mmol of tetrabutylammonium bromide in 50 mL of dry THF. The addition required 1 h and vigorous stirring was used. The mixture was then refluxed for 8 h, the precipitate removed by filtration, and the filtrate evaporated. The residue was diluted with methylene chloride and the solution was washed with water, saturated brine, and dried. Evaporation gave an oil which upon distillation gave 2.8 g (62%) of *N*-(4-pentenyl)carpolactam, bp 95–98°C (0.7 Torr); ir (film): 3080, 2950, 2855, 1660, 1635, 1470, 1350, 975, 900 cm^{-1}; ^{1}Hmr ($CDCl_3$): 6.00–5.33 (m, 1H), 5.05–4.55 (m, 2H), 3.30–3.08 (m, 4H), 2.48–2.13 (m, 2H), 2.10–1.80 (bt, 2H, J = 6 Hz), 1.78–1.20 (m, 8H); Cmr ($CDCl_3$): 175.6, 138.0, 114.9, 49.7, 48.0, 37.4, 31.2, 30.1, 28.9, 27.5, 23.6.

To a vigorously stirred cold solution of 9.8 g (0.062 mol) of potassium permanganate in 100 mL of water was added a solution of 3.6 g (0.02 mol) of the olefinic lactam in 15 mL of acetic acid over 30 min. Stirring was continued for 12 h at ambient temperature. Sodium bisulfite (3 g) was added slowly to the cooled solution, followed by enough 6 *N* hydrochloric acid to bring the pH to 1. The solution was extracted with methylene chloride (4 × 25 mL), and the organic extracts washed with cold water and dried. Evaporation and trituration with ether gave **6***e* (48%) as a white solid, mp 73–75°C; ir ($CHCl_3$): 3600–2400, 1730, 1600, 1500, 1450, 1400, 1210, 1010, 890, 750, 620 cm^{-1}; ^{1}Hmr ($CDCl_3$): 9.3 (s, 1H), 3.5 (m, 2H), 2.5 (m, 4H), 2.0 (m, 8H); Cmr ($CDCl_3$): 176.8, 176.4, 49.9, 47.8, 36.9, 31.5, 28.5, 23.3. *Anal.* calcd. ($C_{10}H_{17}NO_3$): C 60.28, H 8.60, N 7.03; found: C 60.17, H 8.60, N 7.16.

*3-(3-Carboxypropyl)-2-piperidinone (**16**a)*

To a mixture of 6.9 g of potassium *tert*-butoxide (0.061 mol) in 50 mL of *tert*-butyl alcohol was added 10.5 g (0.061 mol) of 3-carbethoxy-2-piperidinone. The solution was stirred at ambient temperature for 40 min and then ethyl 4-bromobutyrate (11.9 g, 0.061 mol) was added dropwise. After stirring overnight the solution was refluxed for 30 min, evaporated, diluted with chloroform, washed once with water, dried, and evaporated. The residue was treated with petroleum ether and filtered to remove residual starting material. Evaporation of the filtrate gave 9.4 g (54%) of a colorless oil (3-carbethoxy-3-(3-carbethoxypropyl)-2-piperidinone) which was purified using silica gel chromatography (ether); ir ($CHCl_3$): 3420, 3015, 1730, 1670, 1470, 1380, 1360, 1250, 1200 cm^{-1}; ^{1}Hmr ($CDCl_3$): 7.7 (s, 1H), 4.2 (qq, 4H, J = 7, 7 Hz), 3.6–3.2 (m, 2H), 2.5–1.7 (m, 10H), 1.25 (t, 3H, J = 7 Hz); Cmr ($CDCl_3$): 172.2, 171.9, 170.1, 60.2, 59.2, 52.6, 41.1, 33.9, 33.5, 28.7, 19.1, 18.8, 13.1; FDMS m/z = 285. *Anal.* calcd. ($C_{14}H_{23}NO_5$): C 58.96, H 8.06, N 4.91; found: C 58.61, H 8.00, N 4.90.

The diester (7.35 g, 0.025 mol) was heated at reflux with 30 mL of 50% sodium hydroxide for 2 h. The cooled solution was diluted with

Can. J. Chem. Downloaded from www.nrcresearchpress.com by 210.87.254.40 on 09/06/12
For personal use only.

water, washed with chloroform, acidified, and evaporated to dryness. The residue was slurried with absolute ethanol and filtered. The filtrate was evaporated to give 3-carboxy-3-(3-carboxypropyl)-2-piperidinone (5.4 g, 95%) as white crystals, mp 181–183°C; ir (KBr): 3400–2600, 1720, 1650, 1620, 1470, 1440, 1300, 810 cm^{-1}; ^{1}Hmr (DMSO): 8.2 (bs, 1H), 2.7 (m, 2H), 2.3–1.2 (m, 10H).

The diacid (5.0 g, 0.021 mol) was heated at 180–190°C for 5 h. Carbon dioxide was evolved. The yellow oil was purified by silica gel chromatography (ethanol/methylene chloride) to give 3.6 g (97%) of acid **16***a*; ir (film): 3500–2500, 1740, 1630, 1510, 1455, 1400, 1280, 1200, 1060, 880 cm^{-1}; ^{1}Hmr (D_2O): 3.4 (m, 2H), 2.9 (m, 3H), 2.6–1.9 (m, 8H).

*3-(3-Carboxypropyl)-1-methyl-2-piperidionone (**16**b)*

Sodium hydride (0.021 mol) which had been washed three times with hexane was added to a solution of 2.37 g (0.021 mol) of *N*-methyl-2-piperidinone in toluene (40 mL) and the mixture was refluxed overnight. To the cooled mixture was added dropwise 4.3 g (0.022 mol) of ethyl 4-bromobutyrate and the mixture was refluxed overnight. The cooled solution was filtered and the residue washed with chloroform. The filtrates were evaporated to give 3.8 g (80%) of the ethyl ester of **16***b* as a colorless oil which was pure according to glc analysis; ^{1}Hmr ($CDCl_3$): 4.15 (q, 2H, J = 7 Hz), 3.7 (t, 1H, J = 6 Hz), 3.3 (m, 2H), 2.95 (s, 3H), 2.7–1.5 (m, 10H), 1.25 (t, 3H, J = 7 Hz).

The ester (3.4 g, 0.017 mol) was hydrolyzed using 25 mL of 50% sodium hydroxide at ambient temperature for 3 days. The basic solution was washed once with chloroform, acidified, evaporated to dryness and worked up as described for **16***a* to give 3.1 g (92%) of **16***b* as a colorless oil which crystallized on standing to give oily crystals, mp 40–43°C; ir (KBr): 3300–2500, 1735, 1470, 1435, 1230, 1200, 1100, 950 cm^{-1}; ^{1}Hmr (D_2O): 3.6 (m, 3H), 3.3 (s, 3H), 3.2–2.0 (m, 10H).

*Ethyl 2-piperidinone-5-propionate (**19**)*

Compound **19** was prepared from diethyl 4-cyanopimelate (19) by hydrogenation over platinum oxide and heating the resulting aminodiester to achieve cyclization. The crude product (90% by glc analysis) was used directly in the pyrolysis experiment; ir ($CHCl_3$): 3425, 3000–2880, 1720, 1655 cm^{-1}; ^{1}Hmr ($CDCl_3$): 4.10 (q, 2H, J = 7 Hz), 3.20 (m, 2H), 2.30 (m, 3H), 1.70 (m, 4H), 1.23 (t, 3H, J = 7 Hz).

General procedure for soda-lime pyrolyses

The procedure was the same in all cases. The acid was thoroughly mixed with twice its weight of finely ground soda-lime. The soda-lime used contained an indicator which turned blue in the presence of carbon dioxide. Frequently the mixture became sticky and turned blue as soon as mixing began. The pasty mass was transferred to a flask which was fitted with a short-path distillation apparatus, purged with nitrogen, and the flask was heated with a free flame. The contents of the flask turned blue, evolved carbon dioxide, and then turned white again. Water distilled, followed by organic material (head temperature 140–200°C). After all the material had distilled, the two-phase distillate was diluted with ether, the phases were separated, and the aqueous phase extracted with ether. The combined ethereal extracts were dried and evaporated to give the crude enamine which was treated with either 70% perchloric acid in ethanol (1:1) or 10% hexachloroplatinic acid hydrate in absolute ethanol as outlined below for each individual case. It is noteworthy that many of the enamines appear to react with chloroform over a period of several hours, leading to discolored solutions. Fresh samples were used for all spectral investigations.

From **6***a* and **6***b*, salts **7***a* and **7***b* were obtained in 71% and 78% yields respectively. The physical and spectroscopic data for these compounds have been reported previously (1, 9).

From **6***d*, the enamine was obtained in 49% crude yield. Gas-liquid chromatographic analysis showed the enamine to constitute approx. 70% of the mixture; ir ($CHCl_3$): 2960, 1640 cm^{-1}; ^{1}Hmr ($CDCl_3$): 4.55 (bs, 1H), 3.3 (m, 4H), 2.5–2.1 (m, 12H); Cmr ($CDCl_3$): 115.7, 65.7, 49.6, 48.0, 37.1, 33.6, 29.8, 26.0, 23.1. The perchlorate **7***d* was obtained in 30% yield from this mixture, mp 150–152°C (from ethanol after precipitation from ether with ethanolic perchloric acid); ir ($CHCl_3$): 2950, 1680, 1470, 1450, 1100 cm^{-1}; ^{1}Hmr ($CDCl_3$): 3.6 (m, 4H), 2.55 (m, 4H), 1.55 (m, 10H); Cmr ($CDCl_3$): 193.7, 59.7, 55.6, 37.2, 34.8, 29.1, 23.9, 21.3, 20.8, 16.7; FDMS m/z = 152. *Anal.* calcd. ($C_{10}H_{18}NClO_4$): C 47.72, H 7.16, N 5.56; found: C 48.28, H 6.44, N 4.72. (The hygroscopic nature of the crystals made better analyses impossible.)

From the distillation of **6***e* there was obtained a 95% yield of a clear oil which rapidly turned brown on contact with air. Gas-liquid chromatographic analysis showed this material to be 95% pure; ir ($CHCl_3$): 2920, 2850, 1650, 1425 cm^{-1}; ^{1}Hmr ($CDCl_3$): 3.15 (t, 1H, J = 6 Hz), 2.88 (m, 4H), 2.68–1.1 (m, 10H). Acidification of an ethanolic solution of this enamine with perchloric acid, followed immediately by treatment with saturated sodium cyanide solution in the usual manner (9), gave a clear oil whose ^{1}Hmr was featureless but whose Cmr was entirely consistent with the expected cyano adduct of **7***e*; Cmr ($CDCl_3$): 120.1, 65.5, 55.0, 51.1, 40.4, 38.1, 27.0, 25.9, 23.8, 21.3; FIMS m/z = 164.

From **9***b*, the perchlorate **10** was obtained in 75% overall yield, mp 210–212°C (from acetone/ethanol) (hygroscopic white crystals); ^{1}Hmr: 4.4–3.5 (m, 4H), 3.4–2.4 (m, 5H), 2.3–1.7 (m, 4H), 1.28 (d, 3H, J = 6 Hz); Cmr ($CDCl_3$): 190.4, 66.8, 48.0, 45.9, 27.5, 20.1, 18.4, 16.4. *Anal.* calcd. ($C_9H_{16}NClO_4$): C 45.48, H 6.79, N 5.89; found: C 45.47, H 6.69, N 6.23. Treatment of this salt with saturated aqueous sodium cyanide (1) gave the cyano derivative **11** (90%) as a colorless liquid; Cmr ($CDCl_3$): 118.9, 60.4, 59.0, 48.0, 46.0, 45.2, 34.4, 28.4, 24.6, 21.6.

From **13***b* salt **14** (as the perchlorate) was obtained in 61% yield, mp 208–209°C (from ethanol); ^{1}Hmr ($CDCl_3$): 3.80 (m, 4H), 2.78 (m, 5H), 2.02 (m, 6H), 1.10 (d, 3H, J = 5 Hz); Cmr ($CDCl_3$): 186.7, 54.6, 53.9, 40.5, 32.6, 28.5, 23.4, 20.5, 16.6. *Anal.* calcd. ($C_{10}H_{18}NClO_4$): C 47.71, H 7.21, N 5.59; found: C 48.17, 7.13, 5.32.

Treatment of this salt with sodium cyanide as described above gave the cyano derivative **15** in 92% yield as a clear oil which solidified in the freezer; Cmr ($CDCl_3$): 118.0, 60.9, 52.4, 52.1, 45.1, 37.0, 33.7, 28.1, 25.1, 21.4.

From **16***a*, the crude organic material was obtained in 61% yield. From this mixture, the hexachloroplatinate **18***a* was obtained in 15% yield as a yellow solid, mp 162–163°C; ir (KBr): 3190, 2990, 1630, 1500, 1100 cm^{-1}; ^{1}Hmr (DMSO): 7.4 (s, 2H), 3.6 (m, 4H), 2.9 (m, 4H), 2.3–1.3 (m, 18H); FDMS m/z = 124. Correct analytical data could not be obtained because of the highly hygroscopic nature of this salt.

From **16***b*, the enamine(s) **17***b* were obtained in 78% yield. Gas-liquid chromatographic analysis showed this material to be ca. 90% pure, but attempts to isolate salts **18***b* were unsuccessful because of their extremely hygroscopic nature; ir ($CHCl_3$): 2990, 2900, 1640, 1520, 1475, 1370, 1110 cm^{-1}; ^{1}Hmr ($CDCl_3$): 3.4 (m, 2H), 3.05 (s, 3H), 2.7–1.5 (m, 11H); ms m/z = 137 (M^+).

From **20***a*, a distillate was obtained which was shown by glc to consist mainly of cycloheptanone (**21***a*). The melting point of the 2,4-DNP derivative (147°C) was undepressed by admixture of an authentic sample. The yield was 47%.

From **20***b*, a distillate was obtained which was shown by glc to consist mainly of piperidine and cyclopentanone (**21***b*). Distillation of an authentic sample of the piperidine enamine of **21***b* from soda-lime led to its recovery in 70% yield.

From **22** was obtained a mixture of a solid and liquid product. The solid was removed by filtration of an ether solution and shown to be **23** by mixture melting point and spectral comparison with an authentic sample. The remaining material was imine **24** (74%). The hexachloroplatinate had mp 160–162°C (absolute ethanol); ir (KBr): 3480, 3230, 2960, 1720, 1485, 1390 cm^{-1}; ^{1}Hmr (DMSO): 7.5 (bs, 2H), 3.0–2.2 (m, 4H), 2.1 (s, 6H), 1.8–0.9 (m, 12H); Cmr (DMSO): 43.3, 39.5, 39.3, 30.5, 27.5, 26.1, 23.5. *Anal.* calcd. ($C_{14}H_{28}N_2PtCl_6$): C 26.68, H 4.16, N 4.44; found: C 26.11, H 4.87, N 4.56.

NOTE ADDED IN PROOF:

It has recently come to our attention that a similar type of reaction has been reported by Mundy (21). Alkali ring-opening of the acyl lactams described would lead to the same intermediates invoked to rationalize our results.

Acknowledgements

The financial assistance of the Natural Sciences and Engineering Research Council of Canada made this work possible and is gratefully acknowledged. The financial assistance provided to J.G. and G.W. by NSERC in the form of undergraduate summer research scholarships is also acknowledged.

1. A. G. COOK. Enamines. Marcel Decker, New York. 1969; H. P. HUSSON. *In* Indole and biogenetically related alkaloids. *Edited by* J. O. Phillipson and M. H. Zenk. Academic Press, New York. 1980. Chapt. 10; H. BOHME and H. G. VIEHE. *In* Advances in organic chemistry, methods and results. Vol. 9. *Edited by* E. C. Taylor. Academic Press, New York. 1976.
2. N. J. LEONARD, A. S. HAY, R. W. FULMER, and V. W. GASH. J. Am. Chem. Soc. **77**, 439 (1956).
3. I. G. CSENDES, Y. Y. LEE, H. C. PADGETT, and H. RAPOPORT. J. Org. Chem. **44**, 4173 (1979).
4. J. M. McINTOSH. Can. J. Chem. **58**, 2604 (1980).
5. S. MIYANO, T. SOMEHARA, M. NAKAO, and K. SUMOTO. Synthesis, 701 (1978).
6. I. MURAKOSHI, K. TAKADA, and J. HAGINAWA. Chem. Abstr. **72**, 55217 (1970); I. MURAKOSHI, S. YOSHIDA, and J. HAGINAWA. Chem. Abstr. **61**, 9465a (1964); **61**, 9465c (1964); I. MURAKOSHI, A. KUBO, J. SAITO and J. HAGINAWA. Chem. Abstr. **70**, 47269 (1969).
7. I. MURAKOSHI, A. KUBO, J. SAITO, and J. HAGINAWA. Chem. Pharm. Bull. **12**, 1747 (1964).
8. S. MIYANO, S. FUJII, O. YAMOSHITA, N. TORAISHI, and K. SUMOTO. J. Org. Chem. **46**, 1737 (1981).
9. J. M. McINTOSH. Tetrahedron, **38**, 261 (1982).
10. M. F. ANSELL and S. S. BROWN. J. Chem. Soc. 1788 (1957).
11. H. TAKAHATA, T. HASHIZUMA, and Y. YAMAZAKI. Heterocycles, **12**, 1449 (1979).
12. A. P. KRAPCHO, J. R. LARSON, and J. M. ELDRIDGE. J. Org. Chem. **42**, 3749 (1977).
13. D. T. MOWRY. Chem. Rev. **42**, 262 (1948).
14. L. RUZICKA. Helv. Chim. Acta, **9**, 230 (1926).
15. R. H. HITES and K. BIEMANN. J. Am. Chem. Soc. **94**, 5772 (1972).
16. L. RAND. J. Org. Chem. **27**, 1034 (1962).
17. I. AHMAD, R. N. GEDYE, and A. NECHVATAL. J. Chem. Soc. (C), 185 (1968).
18. J. GOOTJES and W. T. NANTA. Recl. Trav. Chim. Pays-Bas, **84**, 1427 (1965).
19. S.-O. LAWESSON, E. H. LARSEN, and H. J. JAKOBSEN. Ark. Kemi, **23**, 453 (1964).
20. H. KAMEOKA and K. KINOSHITA. Kogyo Kagaka Zasshi, **72**, 1204 (1969).
21. B. P. MUNDY and Y. KIM. J. Heterocycl. Chem. **19**, 1221 (1982).

Can. J. Chem. Downloaded from www.nrcresearchpress.com by 210.87.254.40 on 09/06/12
For personal use only.

La dissolution de l'anode de cuivre dans les solutions faiblement chlorurées

ROBERT-LOUIS BROSSARD

Institut de recherche d'Hydro-Québec, C.P. 1000, 1800 Montée Ste-Julie, Varennes (Qué.), Canada J0L 2P0

Reçu le 21 décembre 1982

ROBERT-LOUIS BROSSARD. Can. J. Chem. **61**, 2022 (1983).

La dissolution de l'anode de cuivre a été étudiée en solution aqueuse de pH égal à 4 et dont la concentration en LiCl dissous a été variée de 0,005 *M* à 0,1 *M*. Dans la zone de dissolution active, la valence de dissolution est égale à 1 entre 0,03 *M* et 0,1 *M* pour être comprise entre 1 et 2 en-dessous de 0,03 *M*. Entre 0,03 *M* et 0,1 *M*, l'étape qui contrôle la vitesse de dissolution est presque entièrement attribuable à la diffusion des ions $CuCl_2^-$ dans la solution pour les tensions les plus faibles. La mesure de l'ordre de la réaction par rapport aux ions Cl^- qui est proche de un pour des tensions voisines de la tension réversible ($E_{Cu/CuCl}$) de la réaction $Cu + Cl^- = CuCl + 1e$, suggère que la diffusion des ions Cl^- dans la solution tend aussi à devenir une étape contrôlante lorsque la tension devient voisine de $E_{Cu/CuCl}$.

Pour sa part, le CuCl fait son apparition dès que la tension atteint $E_{Cu/CuCl}$ alors que les courbes en balayage linéaire de tension présentent deux sommets. Ces deux pics ont comme étape limitante la diffusion des ions dans la solution. La hauteur des deux pics est entièrement explicable à partir de la diffusion des ions Cl^- dans la solution comme étape la plus lente. Par ailleurs, le rapport entre le sommet de la deuxième vague et le sommet de la première vague est de 2,14. Ce comportement est en harmonie avec le fait que la valence de dissolution du cuivre augmente depuis le premier pic jusqu'au deuxième.

ROBERT-LOUIS BROSSARD. Can. J. Chem. **61**, 2022 (1983).

The dissolution of a copper anode has been studied in aqueous solution at pH 4 and in which the dissolved LiCl was varied between 0.005 *M* and 0.1 *M*. In the dissolution zone, the dissolution valence is unity between 0.03 *M* and 0.1 *M* and the step controlling the speed of dissolution is almost entirely attributable to the diffusion of $CuCl_2^-$ ion in solution for the weakest voltage. The order of reaction with respect to the chloride ion (Cl^-) is close to unity for voltage close to the reversible voltage ($E_{Cu/CuCl}$) of the reaction $Cu + Cl^- = CuCl + 1e$, suggesting that diffusion of Cl^- ions in solution tends also to become a controlling step when the voltage is close to $E_{Cu/CuCl}$.

CuCl appears when the voltage reaches $E_{Cu/CuCl}$, that is when the linear sweep voltage curves show two peaks. These two peaks have the diffusion of ions in the solution as their limiting step. The height of these two peaks is explicable by the diffusion of Cl^- ions in solution as the slowest step. On the other hand, the ratio between the peak of the second wave and that of the first is 2.14. This behaviour is in agreement with the fact that the valence of dissolution of copper increases from the first peak to the second.

[Journal translation]

Can. J. Chem. Downloaded from www.nrcresearchpress.com by 210.87.254.40 on 09/06/12
For personal use only.

1. Introduction

L'usage de solutions qui contiennent des ions Cl^- tend à se répandre dans les procédés d'usinage et de polissage du cuivre par voie électrochimique. Il est aussi reconnu que les ions Cl^- jouent un rôle prédominant dans le processus de corrosion de ce métal (1 à 8). Ainsi, de nombreuses recherches se sont penchées sur l'étude des mécanismes de dissolution du cuivre en présence des ions chlorures (1 à 20).

Dans les solutions acides ou voisines de la neutralité, l'étape déterminante de la dissolution active du cuivre est imputée à la diffusion d'une espèce ionique dans la solution. Les espèces envisagées sont le Cl^- (1), le Cu^+ (13, 14) ou, plus généralement, un chlorocomplexe de cuivre (2–8, 18–20). L'anode a cependant tendance à se recouvrir de CuCl (16) lorsque la tension devient suffisamment anodique. Dans ces conditions, les auteurs (5, 13, 14, 18) pensent que l'étape limitante est la diffusion des ions Cl^- dans la solution. Ces études ont été conduites pour des concentrations en Cl^- supérieures à 0,1 *M* soit en milieu de pH 3 (1, 5, 13, 14, 16), soit dans une gamme de pH comprise entre 4 et 7 (8, 19, 21, 22), alors que Braun et Nobe (1) prévoient un changement de mécanisme en-dessous de 0,1 *M* en Cl^-.

Le présent travail se propose d'approfondir l'étude de la dissolution anodique du cuivre en solution aqueuse de pH = 4 dont la concentration en Cl^- est comprise entre 0,005 *M* et 0,1 *M*.

2. Partie expérimentale

2.1 *La cellule et ses accessoires*

Les détails relatifs à la cellule et ses accessoires ainsi qu'aux électrodes de travail sont donnés dans un article précédent (20).

2.2 *La préparation des essais*

Un barbotage d'azote de 6 h précédait l'immersion de l'électrode de cuivre dans la solution. Les solutions contenaient entre 0,05 et 0,1 *M* de LiCl dissous. Un tampon à base de phtalate de potassium a été utilisé pour stabiliser le pH à 4.

La méthode employée par Shoesmith *et al.* (23, 24) a été retenue pour le polissage du cuivre: l'échantillon était poli mécaniquement par abrasion avec du papier au carbure de silicium pour se terminer par un polissage avec l'alumine de 1 μ. L'échantillon était alors rincé à l'alcool, à l'acétone puis à l'eau distillée avant son immersion.

2.3 *Les techniques expérimentales utilisées*

Les courbes en balayage linéaire de la tension ont été obtenues par les méthodes courantes. Un bain thermostatique a servi au contrôle de la température. La valence de dissolution a été déterminée dans la zone de dissolution active avec 0,1 *M* en LiCl dissous. Elle a été mesurée par perte de poids (11, 21) après que l'électrode de cuivre, soumise à une tension constante, ait été traversée par une charge de 50 C.

3. Résultats expérimentaux

3.1 *Apparition du produit de corrosion*

L'enregistrement obtenu en balayage linéaire de la tension, reproduit à la fig. 1, et qui correspond à une vitesse de balayage en tension de 1 mV/s, est représentatif du comportement de l'anode de cuivre. La courbe montre deux vagues d'oxydation. La vague "1" est bien définie et son maximum a comme coordonnées 0 mV_{ecs} et 5,3 mA/cm^2. La vague "2", plus diffuse, a un maximum en courant voisin de 12 mA/cm^2. D'après les travaux réalisés dans les solutions chlorurées acides (14), la valence de dissolution est proche de un dans la région de la première vague pour être voisine de deux dans la région de la deuxième vague.

Par ailleurs, la relation E vs. $\log_{10} i$ est linéaire dans la partie

Can. J. Chem. Downloaded from www.nrcresearchpress.com by 210.87.254.40 on 09/06/12
For personal use only.

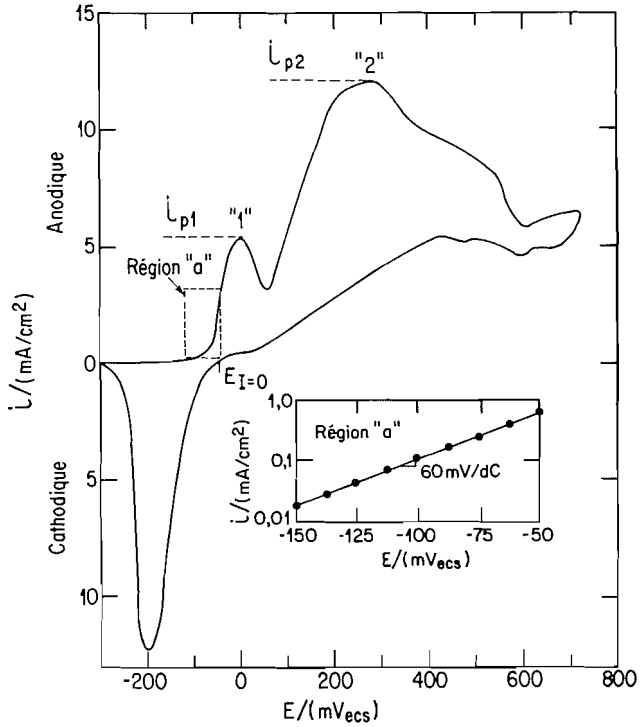

FIG. 1. Courbe de polarisation en balayage linéaire de la tension sur un fil de cuivre. Balayage à 1 mV/s. LiCl: 0,1 *M*. La solution est non agitée et l'électrode est en position stationnaire. $E_{I=0}$: tension à courant nul. La région "a" en médaillon correspond à la première portion de la partie ascendante de la première vague d'oxydation.

ascendante de la vague "1" alors que l'examen de la surface de l'anode par le microscope a permis d'observer que le cuivre reste à nu jusqu'au voisinage de la tension réversible ($E_{Cu/CuCl}$) de la réaction:

[1] $\quad Cu + Cl^- = CuCl + e$

qui est donné par (25):

[2] $\quad E_{Cu/CuCl} = 0{,}109 - 0{,}0591 \log_{10} (Cl^-)$

où $E_{Cu/CuCl}$ est en volt par rapport à l'électrode au calomel saturé.

Le produit de corrosion s'accumule sur l'électrode dès que la tension imposée dépasse de quelques mV la tension réversible $E_{Cu/CuCl}$ (Fig. 2). Dans le cas reproduit à la fig. 2, $E_{Cu/CuCl}$ est de -50 mV$_{ecs}$ (25) alors que l'échantillon a été polarisé jusqu'à -25 mV$_{ecs}$. On remarque que la surface est non uniformément recouverte par le produit de corrosion.

Pour sa part, la relation E vs. $\log_{10} i$ cesse d'être linéaire lorsque le produit de corrosion fait son apparition et le sommet de la première vague de passivation est atteint lorsque E dépasse $E_{Cu/CuCl}$ de 50 mV environ. Ce comportement laisse entrevoir un changement au niveau du mécanisme de dissolution avec l'apparition du produit de corrosion.

3.2 *Comportement du cuivre dans la zone de dissolution active* ($E \leq E_{Cu/CuCl}$)

Les valeurs expérimentales de la valence de dissolution sont rassemblées au tableau 1 pour des concentrations en ions Cl^- comprises entre 0,005 et 0,1 *M*. On remarque que la valence de dissolution dépend de la concentration en ions Cl^-. Elle est de 1,0 entre 0,1 et 0,03 *M* pour augmenter avec une concentration

FIG. 2. Aspect de la surface de l'anode en présence du produit de corrosion. Retrait de l'électrode: -25 mV$_{ecs}$. Conditions expérimentales données à la fig. 1.

TABLEAU 1. Valeurs expérimentales de la valence de dissolution à différentes concentrations en ions Cl^-

Cl^- (*M*)	n^a
0,005	1,65
0,01	1,65
0,02	1,35
0,03	1,0
0,05	1,0
0,07	1,0
0,1	1,0[b]

[a] Valeurs calculées à partir de la pente $(\partial E/\partial \log_{10} i)$ à 22°C.

[b] Valeur confirmée expérimentalement par perte de poids.

décroissante en Cl^- et atteindre 1,65 à 0,005 *M*. Ce comportement tend à confirmer les prévisions faites à partir des calculs théoriques de Braun et Nobe (1) qui suggèrent, notamment, qu'une portion non négligeable du cuivre se dissous sous forme de Cu^{2+} lorsque la concentration en ions Cl^- est en dessous d'une valeur voisine de 0,05 *M*.

Les particularités de l'anode de cuivre, polarisée à des tensions inférieures à $E_{Cu/CuCl}$, et dans la gamme de concentration comprise entre 0,03 et 0,1 *M*, sont:

(a) la relation E vs. $\log_{10} i$ est linéaire avec une pente voisine de 60 mV/décade (Fig. 3). $(\partial E/\partial \log_{10} i)_{Cl^-} = 60$ mV/décade;

(b) la relation i vs. $\omega^{1/2}$ est linéaire pour $\omega \leq 375$ rad/s et l'ordonnée à l'origine passe près de zéro (Fig. 4), i.e. $(\partial i/\partial \omega^{1/2})_{E,Cl^-}$ est constante;

(c) la relation E vs. $\log_{10} i\omega^{-1/2}$ donne une droite avec une

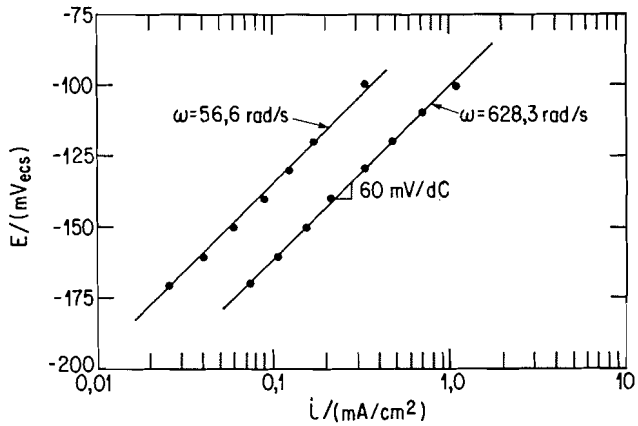

FIG. 3. Relations E vs. $\log_{10} i$ à différentes valeurs de ω. Balayage à 0,5 mV/s; LiCl: 0,1 M. $E \leq E_{Cu/CuCl}$.

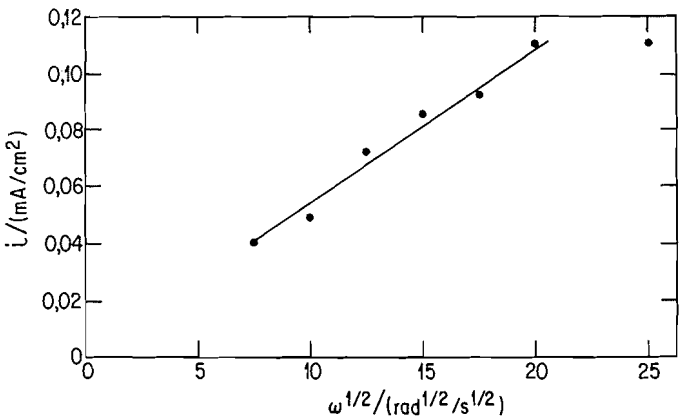

FIG. 4. Courant de dissolution anodique en fonction de $\omega^{1/2}$ avec E et Cl^- fixes. $E = -160$ mV_{ecs} ($E \leq E_{Cu/CuCl}$); LiCl: 0,1 M.

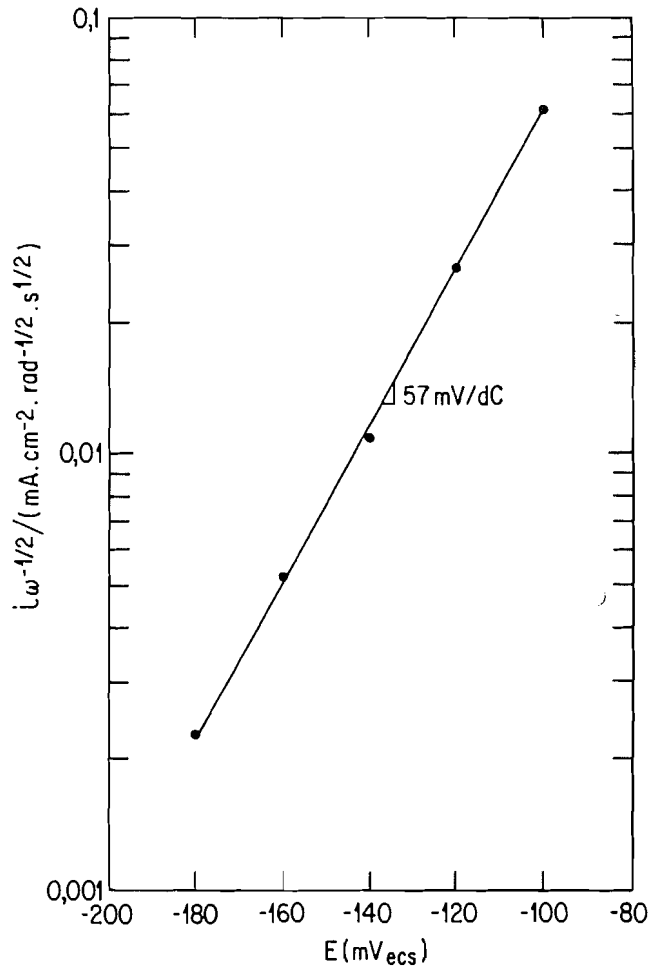

FIG. 5. $i\omega^{-1/2}$ en fonction de la tension imposée. LiCl = 0,1 M; $E \leq E_{Cu/CuCl}$.

pente de 60 mV/décade approximativement (Fig. 5), i.e. $(\partial E/\partial \log_{10} i\omega^{-1/2})_{Cl^-,T} = 60$ mV/décade. Le produit $i \cdot \omega^{-1/2}$ représente la pente de la relation i vs. $\omega^{1/2}$ dans la zone où cette relation est linéaire et où l'ordonnée à l'origine passe par 0 (Fig. 4). Une valeur de $i \cdot \omega^{-1/2}$ correspond à une tension et une concentration en Cl^- fixées;

(d) l'ordre de la réaction par rapport aux ions Cl^- dépend de la tension (Fig. 6). Il est proche de 1 lorsque la tension est élevée i.e. −20 mV pour tendre vers 2 lorsque la tension va décroissant. Ainsi, il atteint 1,83 pour une tension de −140 mV;

(e) la valence de dissolution est égale à 1 (Tableau 1).

De plus, lorsque l'échantillon est soumis à un balayage de retour rapide, une vague de réduction est observée (Fig. 7). Le courant qui correspond au sommet de la vague de réduction (i_p) est proportionnel au courant d'oxydation (i_{ox}). Dans l'exemple choisi ici, le balayage est dix fois plus rapide lors du retour. Enfin, la quantité d'électricité mise en jeu lors du balayage de retour (Q_{cat}) est inférieure à celle mise en jeu lors de l'aller (Q_{an}).

3.3 *Comportement du cuivre en présence du produit de corrosion*

3.3.1 *Nature et caractéristiques du film formé*

L'utilisation du microscope à balayage a permis d'observer la surface de l'électrode durant l'oxydation anodique (Figs. 2, 8). Rappelons que la présence du produit de corrosion est perceptible dès que E dépasse $E_{Cu/CuCl}$ (Fig. 2) alors que le sommet de la première vague d'oxydation coïncide avec le recouvrement complet de l'électrode (Fig. 8). Pour sa part, le courant de dissolution demeure élevé malgré la présence du produit de corrosion sur toute la surface. Après un balayage anodique de 1 mV/s, l'examen de l'électrode révèle un dépôt de plusieurs microns d'épaisseur (à l'oeil nu) dans la partie descendante de la deuxième vague.

Par ailleurs, la diffraction aux rayons-X a permis l'identification d'un seul composé, le chlorure cuivreux, jusqu'à une tension de +800 mV_{ecs}. La présence du CuCl sur l'électrode est associée: (a) à la vague cathodique qui est la signature de la réduction du CuCl (20) formé par voie électrochimique; (b) au fait que la tension à courant nul ($E_{I=0}$), lors du balayage de retour, est de quelques mV inférieure à la tension réversible $E_{Cu/CuCl}$ (Fig. 9).

L'ensemble de ces observations autorise à penser que le CuCl formé est peu protecteur et que le cuivre en présence de CuCl se conduit comme une électrode de second genre où le métal est en équilibre avec un de ses sels insolubles.

3.3.2 *Etape déterminante de la dissolution*

La présence d'une légère agitation dans la solution se traduit par une augmentation considérable du courant de dissolution. La diffusion d'une espèce ionique dans la solution est donc susceptible de contrôler la dissolution du cuivre.

Les courbes $i(E)$, obtenues en balayage linéaire de la tension (Figs. 1, 10), montrent qu'une augmentation de la vitesse de balayage se traduit par une augmentation de courant. Le phé-

Can. J. Chem. Downloaded from www.nrcresearchpress.com by 210.87.254.40 on 09/06/12
For personal use only.

Can. J. Chem. Downloaded from www.nrcresearchpress.com by 210.87.254.40 on 09/06/12
For personal use only.

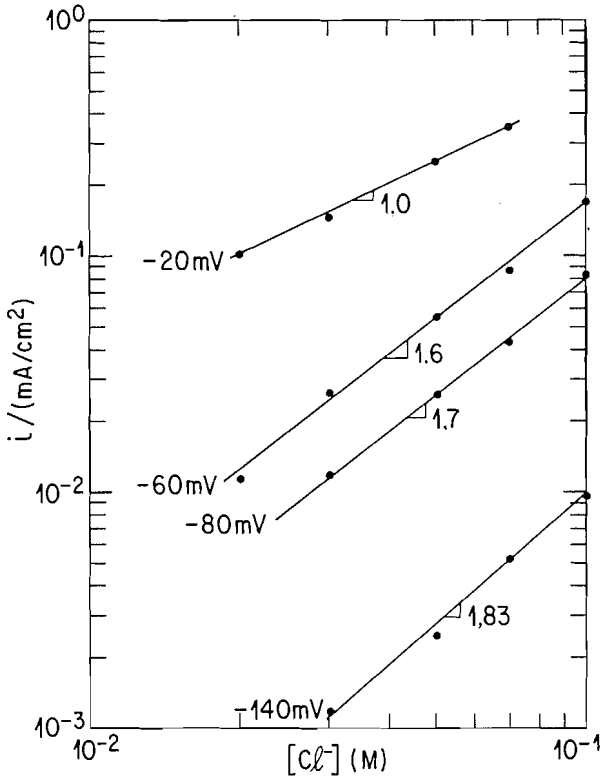

FIG. 6. Influence de la concentration en Cl^- sur le courant de dissolution anodique à différentes valeurs de la tension d'électrode. Balayage à 0,2 mV/s ($E \leq E_{Cu/CuCl}$). La solution est non agitée et l'électrode, un fil de cuivre, est en position stationnaire.

FIG. 8. Apparence de la surface de l'électrode au sommet de la première vague de dissolution. Conditions d'oxydation données à la fig. 1.

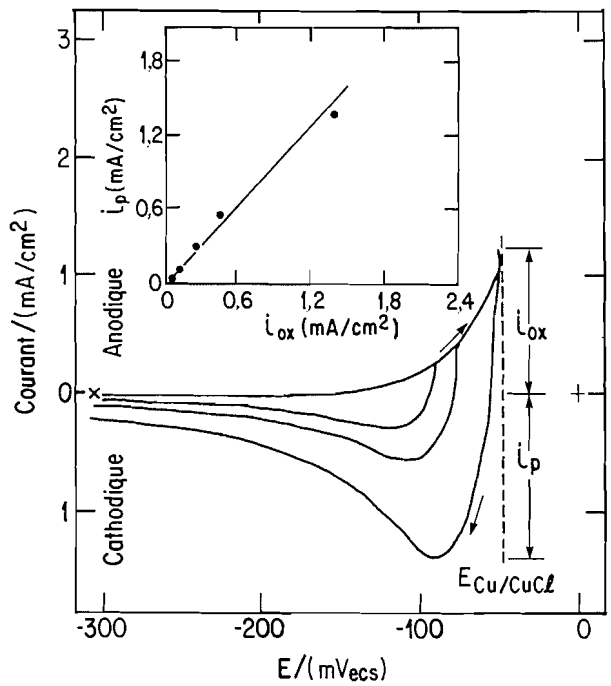

FIG. 7. Vagues de réduction du cuivre immédiatement après un balayage anodique. Balayage à 4 mV/s à l'aller, à 40 mV/s au retour. $E \leq E_{Cu/CuCl}$; LiCl = 0,1 M; × point de départ. L'électrode est en position stationnaire et la solution est non agitée.

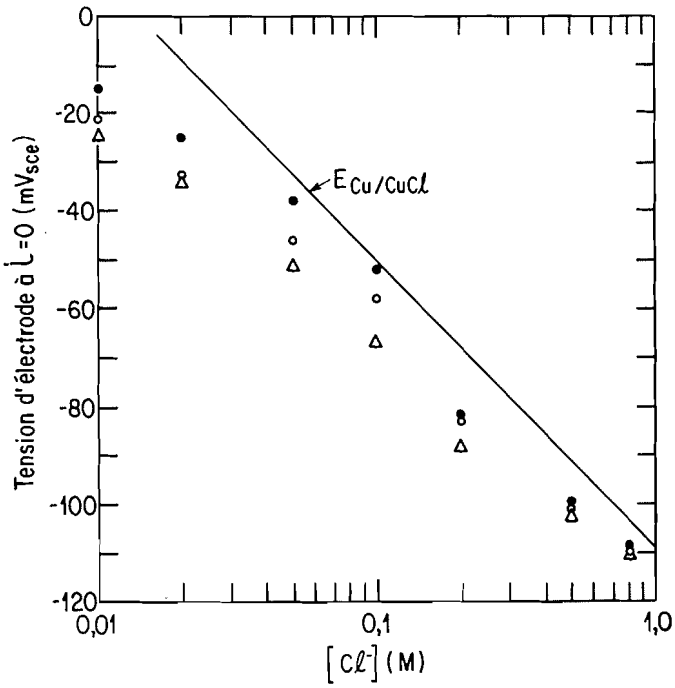

FIG. 9. $E_{Cu/CuCl}$ et $E_{I=0}$ en fonction de la concentration en Cl^-. Tension où la direction du balayage est inversée: (●) +800 mV_{ecs}; (○) +500 mV_{ecs}; (△) +100 mV_{ecs}. Vitesse de balayage de 1 mV s^{-1} à l'aller et au retour. Autres conditions expérimentales données à la fig. 1.

nomène de diffusion a été mis en évidence à partir des relations entre le sommet de la vague d'oxydation (i_{p1} et i_{p2}) et la vitesse de balayage dE/dt sur un fil de cuivre (Fig. 11). La relation qui lie i_{p1} et i_{p2} à la racine carrée de la vitesse de balayage est bien représentée par une droite dont l'ordonnée à l'origine passe par

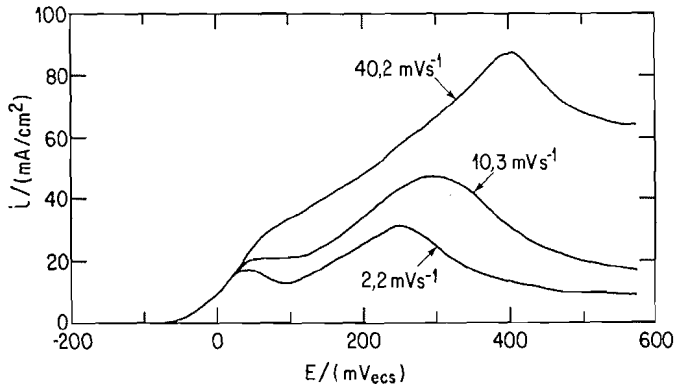

FIG. 10, Influence de la vitesse de balayage sur les courbes $i(E)$ obtenues en balayage linéaire de la tension sur un fil de cuivre. LiCl: 0,1 *M*. La solution est non agitée et l'électrode est en position stationnaire.

zéro. Ce comportement est la signature d'un processus contrôlé par la diffusion en phase liquide (26). Pour les solutions 0,1 *M* LiCl, les relations trouvées sont:

$$[3] \quad i_{p1} = 0{,}21 \left(\frac{dE}{dt}\right)^{1/2}$$

$$[4] \quad i_{p2} = 0{,}45 \left(\frac{dE}{dt}\right)^{1/2}$$

où i_{p1} et i_{p2} sont exprimées en A cm^{-2} et dE/dt en V s^{-1}.

4. Discussion

Dans un premier temps, la dissolution active du cuivre est discutée. La tension imposée est alors inférieure à la tension réversible $E_{Cu/CuCl}$ et le cuivre reste à nu durant la dissolution. Dans un second temps, on discute de la dissolution du cuivre lorsqu'il y a présence de CuCl sur la surface; la tension imposée est alors supérieure à la tension réversible $E_{Cu/CuCl}$.

4.1 *Dissolution active du cuivre*

Les relations i vs. $\omega^{1/2}$ (Fig. 4) suggèrent que la diffusion d'une espèce ionique en solution est l'étape lente de la dissolution du cuivre. Par ailleurs, l'espèce la plus stable pour le cuivre dissous est le $CuCl_2^-$ (1, 25, 27) dans la gamme de concentration en Cl^- comprise entre 0,05 et 0,1 *M* (1). Lorsque la dissolution du cuivre sous forme de $CuCl_2^-$ est envisagée, les étapes les plus probables sont (2, 28):

$$[5] \quad Cu + 2Cl^- = (CuCl_2^-)_i + 1e \text{ (étape rapide)}$$

qui est suivie de:

$$[6] \quad (CuCl_2^-)_i \rightarrow (CuCl_2^-)_s \text{ (étape lente)}$$

les indices i et s indiquent la concentration à la surface de l'électrode et au sein de la solution, respectivement. La deuxième étape, qui est l'étape lente, correspond à la diffusion du $CuCl_2^-$ depuis la surface de l'anode jusqu'au coeur de la solution. La première étape, qui est l'oxydation du cuivre en $CuCl_2^-$, est susceptible d'être dans un état très voisin de l'équilibre, ce qui autorise à utiliser l'équation de Nernst:

$$[7] \quad E = E^0_{Cu/CuCl_2^-} + \frac{RT}{F} \ln \frac{(CuCl_2^-)_i}{(Cl^-)^2}$$

Le réarrangement des termes donne:

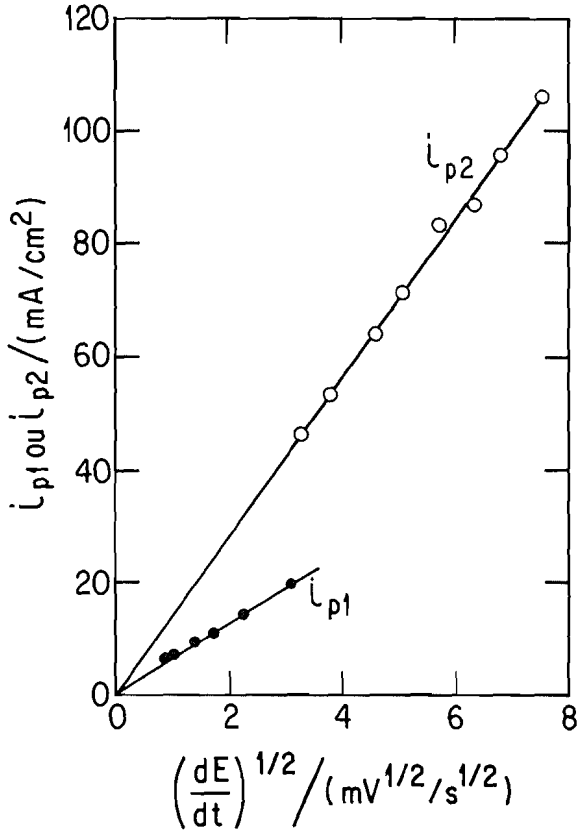

FIG. 11. Influence de la vitesse de balayage sur le sommet des vagues d'oxydation. LiCl: 0,1 *M*.

$$[8] \quad (CuCl_2^-)_i = (Cl^-)^2 \exp \frac{F}{RT} (E - E^0_{Cu/CuCl_2^-})$$

On suppose que la concentration en ions (Cl^-) demeure la même à l'interface, (Cl_i^-), que dans la solution (Cl_s^-). Par ailleurs, l'étape lente en est une de diffusion et la vitesse de la réaction est donnée par la première loi de Fick, dont la forme simplifiée est:

$$[9] \quad i = ZFD \frac{(CuCl_2^-)_i - (CuCl_2^-)_s}{\delta}$$

La relation [9] devient:

$$[10] \quad i = ZFD \frac{(CuCl_2)_i}{\delta}$$

lorsque $(CuCl_2)_i \gg (CuCl_2^-)_s$.

La combinaison des relations [7], [8] et [10] donne:

$$[11] \quad i = \frac{ZFD}{\delta} (Cl^-)^2 \exp \frac{F}{RT} (E - E^0_{Cu/CuCl_2^-})$$

L'utilisation de l'électrode à disque tournant permet d'écrire (29):

$$[12] \quad \delta = 1{,}63\, D^{1/3}_{(CuCl_2^-)}\, \nu^{1/6}\, \omega^{-1/2}$$

La substitution de δ dans la relation [11] donne:

$$[13] \quad i = 0{,}62\, ZF\, \nu^{-1/6}\, D^{2/3}_{(CuCl_2^-)}\, \omega^{1/2}\, (Cl^-)^2 \times \exp \frac{F}{RT} (E - E^0_{CuCl_2^-})$$

où Z, la charge de l'espèce qui diffuse, est égale à 1; ν, la viscosité cinématique, est voisine de $0{,}96 \times 10^{-2}$ cm^2/s (30);

Can. J. Chem. Downloaded from www.nrcresearchpress.com by 210.87.254.40 on 09/06/12
For personal use only.

Can. J. Chem. Downloaded from www.nrcresearchpress.com by 210.87.254.40 on 09/06/12
For personal use only.

$D_{(CuCl_2^-)}$ est le coefficient de diffusion de l'espèce $CuCl_2^-$; ω est la vitesse de rotation de l'électrode en radians par seconde; E est la tension d'électrode alors que $E^0_{Cu/CuCl_2^-}$ est la tension d'équilibre standard pour la réaction [4].

Les dérivées partielles de la relation [13] sont:

[14] $\left(\frac{\partial E}{\partial \log_{10} i}\right)_{298\,K,Cl^-} = 59$ mV/décade (Fig. 3)

[15] $\left(\frac{\partial i}{\partial \omega^{1/2}}\right)_{E,Cl^-} =$ constante (Fig. 4)

[16] $\left(\frac{\partial E}{\partial \log_{10} (i\omega^{-1/2})}\right)_{298\,K,Cl^-} = 59$ mV/décade (Fig. 5)

Les équations [14], [15] et [16] sont semblables aux particularités (a), (b) et (c) trouvées pour la dissolution active du cuivre (Figs. 3–5) entre 0,03 et 0,1 *M* en LiCl dissous. La valeur expérimentale de l'ordre de la réaction par rapport aux ions Cl^-, qui tend vers 2 lorsque la tension va décroissant (Fig. 6), est conforme avec la relation [13]. On est alors conduit à penser que l'espèce ionique qui diffuse dans la solution est le $CuCl_2^-$ plutôt qu'une autre espèce comme le Cl^-, dans la gamme de tension et de concentration considérées. L'existence du $CuCl_2^-$ est d'ailleurs en harmonie avec le fait que le cuivre dissous a une forte tendance à être associé aux ions Cl^- pour former des complexes (25, 27) lorsque la concentration en ions Cl^- dépasse 0,05 *M* (1).

Le coefficient de diffusion du $CuCl_2^-$ est calculable à partir de l'équation [13].

Les termes Z, F, V et F/RT ont été remplacés par leur valeur respective. Pour sa part, $E^0_{Cu/CuCl_2^-}$ est égal à $+208$ mV_{enh} ou -38 mV_{ecs} (25). Il suffit de connaître $i\omega^{-1/2}$ pour des valeurs de Cl^- et de E données (Fig. 5). C'est ainsi que les coefficients de diffusion donnés au tableau 2 ont été calculés. Ils sont voisins de 1×10^{-5} cm^2/s et dépendent peu de la tension imposée. Ils sont tout à fait conformes aux valeurs de $D_{CuCl_2^-}$ données dans la littérature (18, 26).

Enfin, dans le cas où l'étape déterminante est entièrement imputée à la diffusion des ions Cl^- dans la solution, le courant doit être indépendant de la tension imposée et l'ordre de la réaction par rapport aux ions Cl^- doit être égale à 1 (5). Ces particularités sont incompatibles avec les caractéristiques (a), (c) et (d) trouvées pour l'anode de cuivre aux tensions les plus faibles. Néanmoins, l'ordre de la réaction est compris entre 1 et 2 lorsque la tension s'élève pour atteindre 1 à -20 mV (Fig. 6). La tension de -20 mV est proche de la tension réversible $E_{Cu/CuCl}$ donnée par la relation [2]. Ce comportement laisse croire que la diffusion des ions Cl^- tend aussi à devenir une étape contrôlante à mesure que la tension devient voisine de $E_{Cu/CuCl}$.

Les caractéristiques de la vague de réduction, observée durant le balayage de retour (Fig. 7), sont aussi tout à fait compatibles avec le mécanisme de dissolution formé par les étapes [5] et [6].

En effet, l'équation [10] est équivalente à:

[17] $(CuCl_2^-)_i = (ZFD)^{-1}\,\delta\, i$

Pour un fil de cuivre en l'absence d'agitation imposée, l'écriture de la relation [17] se simplifie:

[18] $(CuCl_2^-)_i = k_1\, i$

où k_1 est une constante de proportionnalité.

TABLEAU 2. Valeurs expérimentales du coefficient de diffusion déterminé à partir de la relation [13]

E (mV_{ecs})	$Cl^- = 0{,}1$ *M*	$Cl^- = 0{,}04$ *M*
-180	$0{,}91 \times 10^{-5}$ cm^2/s	$1{,}3 \times 10^{-5}$ cm^2/s
-160	$1{,}0 \times 10^{-5}$ cm^2/s	$1{,}3 \times 10^{-5}$ cm^2/s
-140	$1{,}0 \times 10^{-5}$ cm^2/s	$1{,}2 \times 10^{-5}$ cm^2/s
-120	$1{,}1 \times 10^{-5}$ cm^2/s	$1{,}2 \times 10^{-5}$ cm^2/s

Pour sa part, le sommet de la vague de réduction (i_p), lors du balayage de retour, est susceptible d'être d'autant plus élevé que la concentration en $CuCl_2^-$ au voisinage de la surface de l'électrode est grande. Ce qui autorise à écrire:

[19] $i_p \propto (CuCl_2^-)_i$

Les relations [18] et [19] donnent:

[20] $i_p \propto i$

C'est à dire que i_p doit augmenter avec l'intensité du courant d'oxydation. Cette prévision est conforme aux résultats expérimentaux (Fig. 7).

Enfin, les courbes voltamétriques de la fig. 7 présentent une particularité supplémentaire. La tension à courant nul, durant le balayage de retour ($E_{i=0}$), est très voisine de la tension où le sens du balayage est inversé (E_{inv}). D'après le modèle envisagé, il est prévisible que la concentration en $CuCl_2^-$ à la surface de l'électrode, $(CuCl_2^-)_i$, change peu entre les instants où $E = E_{inv}$ et où $E = E_{i=0}$ si la vitesse de balayage en retour est suffisamment élevée. Puisque $(CuCl_2^-)_i$ change peu et que E est fixé par $(CuCl_2^-)_i$, à une concentration en Cl^- donnée (relation [7]), il est envisageable que E change peu, i.e. que E_{inv} soit très voisin de $E_{i=0}$.

4.2 *Dissolution du cuivre dans la zone des vagues d'oxydation*

4.2.1 *Pic de la première vague d'oxydation*

On a vu que la première vague d'oxydation est contrôlée par la diffusion d'une espèce dans la solution (Fig. 11). Pour un procédé d'électrode contrôlé par la diffusion, le sommet de la vague est relié à la vitesse de balayage selon (26):

[21] $i_{pi} = (3{,}76 \times 10^5)\, n^{3/2}\, D_i^{1/2} \left(\frac{dE}{dt}\right)^{1/2} C_i$

où i_{pi} est le sommet de la vague en A cm^{-2}, D_i le coefficient de diffusion en $cm^2\ s^{-1}$, dE/dt la vitesse de balayage en V s^{-1}, C_i la concentration de l'espèce qui diffuse en mol cm^{-3} et n le nombre d'électrons.

Dans les solutions acides de LiCl, la valeur élevée du courant de dissolution fait penser selon Kozin *et al.* (13, 14) que la première vague d'oxydation est limitée par la diffusion des ions Cl^-, depuis le coeur de la solution jusqu'à la surface de l'électrode. Le courant qui correspond au maximum de la première vague d'oxydation est aussi de plusieurs mA cm^{-2} pour le cuivre immergé en solution 0,1 *M* LiCl (Fig. 1). Par ailleurs, on a vu que la diffusion des ions Cl^- tend à devenir une étape contrôlante de la dissolution active du cuivre lorsque la tension devient voisine de $E_{Cu/CuCl}$. Il semble donc raisonnable d'envisager la diffusion des ions Cl^- comme étape contrôlante. Pour une solution 0,1 *M* en Cl^- i.e. pour C_i de $0{,}1 \times 10^{-3}$ mol cm^{-3}, $D_{Cl^-} \simeq 1{,}94 \times 10^{-5}$ $cm^2\ s^{-1}$ (31), alors que $n \simeq 1{,}2$ (21). La substitution de ces valeurs dans la relation [21] conduit à:

[22] $i_{pl} = 0{,}21 \left(\frac{dE}{dt}\right)^{1/2}$

où i_{p1} est exprimé en A cm^{-2} et correspond au sommet de la vague lorsque la diffusion des ions Cl^- est considérée; (dE/dt) est en V s^{-1}. i_{p1} donné par la relation [22] est donc en bon accord avec i_{p1} trouvé expérimentalement, i.e. la relation [3].

4.2.2 *Deuxième vague d'oxydation*

Dans le cas où l'étape déterminante est attribuée à la diffusion des ions Cl^- dans la solution, les valeurs de D_{Cl^-} et de (Cl^-) sont identiques à celles utilisées dans la relation [22]. Pour sa part, $n \simeq 2$ (25). On obtient alors:

$$[23] \quad i_{p2} = 0{,}45 \left(\frac{dE}{dt}\right)^{1/2}$$

Ainsi, i_{p2} donné par la relation [23] est en harmonie avec i_{p2} trouvé expérimentalement i.e. la relation [4]. On envisage donc la formation d'intermédiaire comme le $CuCl^+$ ou le Cu^{2+} (25) dans la région de la 2e vague alors que l'étape déterminante de la dissolution est entièrement imputable à la diffusion des ions Cl^- dans la solution.

Conclusion

La surface de cuivre reste complètement à nu durant la dissolution anodique de ce métal à des tensions inférieures à $E_{Cu/CuCl}$. La valence de dissolution est égale à 1 entre 0,03 *M* et 0,1 *M* en LiCl dissous pour être comprise entre 1 et 2 en dessous de 0,03 *M*. Entre 0,03 *M* et 0,1 *M*, la vitesse de dissolution est presque entièrement expliquable à partir de la diffusion du $CuCl_2^-$ dans la solution pour les tensions les plus faibles. La diffusion des ions Cl^- tend aussi à devenir une étape contrôlante à mesure que la tension devient voisine de $E_{Cu/CuCl}$.

Il y a apparition de chlorure cuivreux à la surface de l'anode de cuivre en position stationnaire et en contact avec une solution non agitée lorsque la tension imposée est voisine de la tension réversible $E_{Cu/CuCl}$.

Les courbes en balayage linéaire de tension présentent deux vagues de dissolution. La hauteur de la 2e vague est environ 2,2 fois la hauteur de la première.

Dans le cas de la première vague, son sommet (i_{p1}) augmente de façon linéaire avec la racine carrée de la vitesse de balayage. Les valeurs expérimentales de i_{p1} sont en harmonie avec les valeurs théoriques du sommet de la vague qui sont calculées en considérant la diffusion des ions Cl^- comme étape déterminante.

Dans le cas de la deuxième vague, son sommet (i_{p2}) augmente de façon linéaire avec la racine carrée de la vitesse de balayage. Les valeurs expérimentales de i_{p2} sont en accord avec les valeurs théoriques du sommet de la vague qui sont calculées en considérant la diffusion des ions Cl^- comme étape déterminante.

Remerciements

L'auteur tient à remercier monsieur M. Pelletier, en stage à l'I.R.E.Q., ainsi que monsieur G. Larochelle pour leur contribution au travail expérimental.

1. M. Braun et K. Nobe. J. Electrochem. Soc. **126**, 1666 (1979).
2. A. L. Bacarella et J. C. Griess. J. Electrochem. Soc. **120**, 459 (1973).
3. R. S. Cooper et J. H. Bartlett. J. Electrochem. Soc. **105**, 109 (1958).
4. R. K. Astakhova et B. S. Krasikov. Zh. Prikl. Khim. **44**, 363 (1972).
5. A. Moreau. Electrochim. Acta, **26**, 1609 (1981).
6. L. Kiss, J. Farkas et A. Korosi. Acta Chim. Acad. Sci. Hung. **67**, 179 (1971).
7. L. Kiss, J. Farkas et A. Korosi. Magy. Kem. Foly. **77**, 35 (1971).
8. T. Hurlen. Acta Chem. Scand. **15**, 1231 (1961).
9. V. K. Altukhov, A. V. Vvedenskii, I. K. Marshadov et T. N. Kledinina. Sov. Electrochem. **15**, 242 (1979).
10. D. J. G. Ives et A. E. Rawson. J. Electrochem. Soc. **109**, 462 (1962).
11. A. I. Golubev, M. Kh. Kadyrov et R. I. Nazarova. Prot. Met. USSR, **5**, 230 (1969).
12. C. H. Bonfiglio, H. C. Albaya et O. A. Cobo. Corros. Sci. **13**, 717 (1973).
13. L. F. Kozin, K. K. Ledesov et S. N. Nagibin. Izv. Akad. Nauk Kaz. SSR Ser. Khim. **4**, 11 (1980).
14. L. F. Kozin, K. K. Lepesov et S. N. Nagibin. Izv. Akad. Nauk Kaz. SSR Ser. Khim. **6**, 28 (1980).
15. F. M. Al-Kharafi et Y. A. El-Tantawy. J. Electrochem. Soc. **128**, 2073 (1981).
16. M. Turner et P. A. Brook. Corros. Sci. **13**, 973 (1973).
17. S. Nageswar et T. H. V. Setty. Proc. Indian Acad. Sci. Sect. A, **71**, 282 (1972).
18. A. Moreau. Electrochim. Acta, **26**, 497 (1981).
19. G. Faita, G. Fiori et D. Salvadore. Corros. Sci. **15**, 383 (1975).
20. R. L. Brossard. Can. J. Chem. **60**, 616 (1982).
21. K. Kinoshita, D. Landolt, R. H. Muller et C. W. Tobias. J. Electrochem. Soc. **117**, 1246 (1970).
22. H. Sugarawa. Sci. Rep. Res. Inst. Tohoku Univ. Ser. A., **18**, 86 (1966).
23. D. W. Shoesmith, T. E. Rummery, D. Owen et W. Lee. J. Electrochem. Soc. **123**, 790 (1976).
24. D. W. Shoesmith et W. Lee. Electrochim. Acta, **22**, 1411 (1977).
25. J. Van Muylder, N. de Zoubov et M. Pourbaix. Cebelcor. Rapp. Tech. No. 101. Bruxelles, juillet 1962.
26. P. Delahey. New instrumental methods in electrochemistry. Interscience, New York. 1954. p. 124.
27. I. A. Semenov, V. F. Lazare et A. I. Levin. Sov. Electrochem. **11**, 1013 (1975).
28. L. Brossard. J. Electrochem. Soc. **130**, 403 (1983).
29. V. G. Lévich. Physicochemical hydrodynamics. Prentice Hall, Englewood Cliffs, NJ. 1962. p. 69.
30. R. Parsons. Handbook of electrochemical constants. Butterworths, London. 1959. p. 77.
31. A. J. Bard et L. R. Faulkner. Electrochemical methods. J. Wiley & Sons, New York. 1980. p. 80.

Can. J. Chem. Downloaded from www.nrcresearchpress.com by 210.87.254.40 on 09/06/12
For personal use only.

Kinetics and isotope effects on the proton transfer reaction of 4-nitrophenylphenylcyanomethane with tetramethylguanidine in acetonitrile and benzonitrile solvents

ARNOLD JARCZEWSKI AND PRZEMYSLAW PRUSZYNSKI
Institute of Chemistry, Adam Mickiewicz University, Poznan, Poland

AND

KENNETH T. LEFFEK
Department of Chemistry, Dalhousie University, Halifax, N.S., Canada B3H 4H6

Received February 2, 1983

ARNOLD JARCZEWSKI, PRZEMYSLAW PRUSZYNSKI, and KENNETH T. LEFFEK. Can. J. Chem. **61**, 2029 (1983).

The kinetic deuterium isotope effect for the proton transfer reaction between 4-nitrophenylphenylcyanomethane and tetramethylguanidine, k_H/k_D, at 25°C, is 10.7 in acetonitrile solvent and 12.5 in benzonitrile. The enthalpy of activation difference, $(\Delta H^{\ddagger}_D - \Delta H^{\ddagger}_H)$, in both solvents is large, 2.2 kcal mol^{-1}, and 2.4 kcal mol^{-1}; respectively, indicating a significant contribution from proton tunnelling to the reaction. The equilibrium constants, K, measured spectrophotometrically are large, 6000 dm^3 mol^{-1} in acetonitrile and 2000 dm^3 mol^{-1} in benzonitrile and in good agreement with the values calculated from the kinetic measurements.

ARNOLD JARCZEWSKI, PRZEMYSLAW PRUSZYNSKI et KENNETH T. LEFFEK. Can. J. Chem. **61**, 2029 (1983).

L'effet isotopique cinétique du deutérium dans la réaction de transfert de proton entre le nitrophényl-4 phénylcyanométhane et la tétraméthylguanidine k_H/k_D à 25°C est de 10,7 dans l'acétonitrile et de 12,5 dans le benzonitrile. Il y a une grande différence d'enthalpie d'activation $(\Delta H^{\ddagger}_D - \Delta H^{\ddagger}_H)$ dans les deux solvants. Elle est respectivement de 2,2 kcal mol^{-1} et de 2,4 kcal mol^{-1} ce qui indique une contribution importante de l'effet tunnel du proton à la réaction. Les constantes d'équilibre mesurées par spectrophotométrie sont élevées, 6000 dm^3 mol^{-1} dans l'acétonitrile et 2000 dm^3 mol^{-1} dans le benzonitrile et s'accordent bien avec les valeurs calculées à partir des mesures cinétiques.

[Traduit par le journal]

Introduction

Primary deuterium isotope effects can vary over a wide range, from $k_H/k_D \sim 2$ up to more than 20 at 25°C, depending on a number of factors. It has been known for a long time (1–3) that reactions involving extensive steric hindrance may have high narrow potential energy barriers which give rise to large isotope effects, $k_H/k_D > 7$, as a result of proton tunnelling. A significant contribution to the isotope effect from proton tunnelling has been noted in reactions with symmetrical transition states (4–6) and also in reactions in solvents of low polarity (7). In such solvents the proton transfer takes place independently of solvent reorganization which allows the tunnel effect to exert a maximum influence on the rate.

Caldin and Mateo (7) found very high isotope effects up to $k_H/k_D \sim 50$ at 25°C, for proton transfer reactions to tetramethylguanidine base. However, Rogne and co-workers (8, 9) have suggested that these extremely large values in nonpolar solvents are artefacts of deuterium scrambling during the reaction. Melander and Saunders (10) have given a kinetic treatment of this case and demonstrated that the standard equation [1] for a reversible deuteron transfer reaction, where k_{obs} is the

$$[1] \quad k_{obs} = k_f b + k_b$$

observed pseudo-first order rate constant when the base concentration b is in large excess and k_f and k_b are the rate constants for the forward and backward reactions respectively, is changed to [2] when the equilibrium constant k_f/k_b is small and deuterium exchange is rapid. Thus, fitting the deuteron transfer

$$[2] \quad k_{obs} = k_f b$$

reaction to eq. [1] instead of eq. [2] would yield a k_{fD} value lower than its true value and hence an abnormally large k_H/k_D isotopic ratio.

One manifestation of deuterium scrambling is that the equilibrium constant, determined from optical density measurements on reaction solutions which have reached equilibrium, does not agree with that calculated from k_f/k_b (9). This may be used as a test that deuterium scrambling is not significant when it can be shown that the two determinations of the equilibrium constant are the same within experimental error. However, the rate constant k_f is always determined correctly whether or not deuterium scrambling takes place, i.e. whether eq. [1] or eq. [2] is appropriate.

The present work extends the range of the experimental observations for systems where a large isotope effect due to proton tunnelling may be expected. A carbon acid with increased steric hindrance relative to *p*-nitrophenylnitromethane studied by Caldin and Mateo (7), and which could show no secondary isotope effect, was selected, *p*-nitrophenylphenylcyanomethane. This reacts with tetramethylguanidine (TMG) but the reaction could be followed only in fairly polar solvents where the equilibrium constants for proton transfer were large.

Results and discussion

The reaction of 4-nitrophenylphenylcyanomethane with TMG base gives a violet-blue product, $\lambda_{max} = 590$ nm in both acetonitrile and benzonitrile solvents. The absorbance measurements of the product gave good linear plots of a/A versus $1/b$ as required by eq. [3], where a and b are the initial concentrations of the acid and base respectively, A is the absorbance

$$[3] \quad a/A = \frac{1}{Kb\epsilon} + \frac{1}{\epsilon}$$

at equilibrium, ϵ the molar extinction coefficient of the product, and K is the equilibrium constant. Equation [3] is derived on the assumption that the product is an ion-pair, so the reaction is represented by eq. [4].

Can. J. Chem. Downloaded from www.nrcresearchpress.com by 210.87.254.42 on 09/06/12
For personal use only.

TABLE 1. Rate constants for the reaction of 4-nitrophenylphenylcyanomethane with tetramethylguanidine

Temp (°C)	10^4[Base] (M)	k_{obs} (s^{-1})	10^{-3} k_f (dm^3 mol^{-1} s^{-1})	k_b (s^{-1})	k_{HH}/k_{HD}
(a) Acetonitrile solvent					
(i) $NO_2C_6H_4(C_6H_5)CH(CN)$ initial conc. 8×10^{-6} M					
15.0	4.9–19.7	3.8–12.5	5.85 ± 0.2	1.0 ± 0.2	
20.0	4.9–19.7	4.4–14.1	6.64 ± 0.1	1.2 ± 0.1	
25.0	4.9–19.7	5.4–16.9	7.86 ± 0.2	1.5 ± 0.2	
30.0	4.9–19.7	6.5–18.6	8.36 ± 0.5	2.5 ± 0.2	
35.0	4.9–19.7	7.6–21.4	9.46 ± 0.5	3.2 ± 0.6	
40.0	4.9–19.7	8.7–24.8	10.88 ± 0.5	3.7 ± 0.6	
(ii) $NO_2C_6H_4(C_6H_5)CD(CN)$ initial conc. 8×10^{-6} M					
15.0	11.0–44.0	0.74–2.4	0.51 ± 0.2	0.15 ± 0.07	11.5
20.0	11.0–44.0	0.98–3.1	0.63 ± 0.03	0.23 ± 0.09	10.5
25.0	11.0–44.0	1.3–3.7	0.73 ± 0.03	0.44 ± 0.08	10.7
30.0	11.0–44.0	1.7–4.6	0.88 ± 0.03	0.70 ± 0.08	9.5
35.0	11.0–44.0	2.1–5.6	1.08 ± 0.04	0.84 ± 0.12	8.8
(a) Benzonitrile solvent					
Temp (°C)	10^4[Base] (M)	k_{obs} (s^{-1})	10^{-3} k_f (dm^3 mol^{-1} s^{-1})	k_b (s^{-1})	k_{HH}/k_{HD}
(i) $NO_2C_6H_4(C_6H_5)CH(CN)$ initial conc. 4×10^{-5} M					
10.0	6.4–17.1	13.5–22.0	11.8 ± 0.6	5.6 ± 0.7	
15.0	6.4–17.1	17.3–27.9	14.8 ± 0.5	7.6 ± 0.6	
20.0	6.4–17.1	21.7–42.1	19.0 ± 0.5	9.3 ± 0.6	
25.0	6.4–17.1	27.2–53.0	23.9 ± 0.6	11.6 ± 0.8	
30.0	6.4–17.1	34.1–66.0	29.8 ± 1.1	14.5 ± 1.4	
35.5	6.4–17.1	45.5–83.0	35.0 ± 2.7	21.6 ± 3.5	
40.0	6.4–17.1	55.5–105.5	46.4 ± 1.8	24.9 ± 2.2	
(ii) $NO_2C_6H_4(C_6H_5)CD(CN)$ initial conc. 4×10^{-5} M					
10.0	6.9–17.1	0.90–1.1	0.76 ± 0.04	0.40 ± 0.05	15.6
15.0	6.9–17.1	1.3–2.3	1.03 ± 0.05	0.59 ± 0.06	14.3
20.0	6.9–17.1	1.6–3.0	1.31 ± 0.01	0.74 ± 0.02	14.5
25.0	6.9–17.1	2.1–4.1	1.92 ± 0.06	0.79 ± 0.08	12.5
30.0	6.9–17.1	3.2–5.8	2.47 ± 0.03	1.54 ± 0.04	12.0
35.0	6.9–17.1	4.1–7.6	3.36 ± 0.01	1.83 ± 0.02	10.4
40.0	6.9–17.1	5.3–9.7	4.26 ± 0.05	2.10 ± 0.07	10.9

[4] $NO_2C_6H_4\underset{\underset{C_6H_5}{|}}{C}HCN + HN{=}C(N(CH_3)_2)_2 \underset{k_b}{\overset{k_f}{\rightleftharpoons}}$

$$NO_2C_6H_4\underset{\underset{C_6H_5}{|}}{\bar{C}}CN\cdots H_2\overset{+}{N}{=}C(N(CH_3)_2)_2$$

The data did not fit the analogous equation derived on the assumption that the product consists of separate ions (11).

The equilibrium constant for both reactions is high, K = 6000 dm^3 mol^{-1} and 2000 dm^3 mol^{-1} for acetonitrile and benzonitrile respectively, at 20°C. The molar extinction coefficient in both solvents is equal to 4000 dm^3 mol^{-1} cm^{-1}.

The value of the equilibrium constant depends on the polarity of the solvent and, in the case of a reaction with more polar products than reactants, should be higher for the more polar solvent, as is the case for this reaction.

Pseudo-first order rate constants were determined using an acid concentration of 8×10^{-6} M in acetonitrile solvent and 4×10^{-5} M in benzonitrile solvent, with varying base concentrations always in large excess. The rate constants for the forward and backward reactions of eq. [4] were calculated using eq. [1] and are collated in Table 1. The errors quoted for k_f and k_b are the standard deviations.

It may be noted that the rate constants for the backward reaction are small. Thus, this cyano-carbon acid does not show the very rapid reaction of its carbanion with acids which was observed by Hibbert *et al.* (12, 13) for malononitriles. Rather, it reacts very much like the acid studied by Caldin *et al.* (14, 15), 4-nitrobenzyl cyanide. This suggests that, as expected (16), the negative charge in the carbanion is delocalized into the nitrophenyl ring.

The values of the equilibrium constants for the normal acid, calculated from k_f/k_b, are 5700 dm^3 mol^{-1} and 2000 dm^3 mol^{-1} in acetonitrile and benzonitrile respectively, at 20°C, in good agreement with the results obtained from equilibrium measurements, showing that the proton transfer is free from side reactions, such as decomposition of the ion-pair to products other than the original substrate and base. This confirms that eq. [4] is the correct description of the reaction, the kinetic equation for which gives eq. [1] as the expression for the observed first-order rate constant.

The equilibrium constants, calculated from k_f/k_b, for the deuterated substrate at 20°C are 2700 dm^3 mol^{-1} and 1800 dm^3 mol^{-1} in acetonitrile and benzonitrile respectively. The isotope effect on the equilibrium constant should be approximately unity, as is the case in benzonitrile. The apparent equilibrium isotope effect of about 3 in acetonitrile shows that some deuterium exchange is taking place and that the results do not fit

Can. J. Chem. Downloaded from www.nrcresearchpress.com by 210.87.254.42 on 09/06/12
For personal use only.

Can. J. Chem. Downloaded from www.nrcresearchpress.com by 210.87.254.42 on 09/06/12
For personal use only.

eq. [1] exactly. If exchange were complete and eq. [2] were followed, the apparent isotope effect on the equilibrium constant would be infinity. Thus, the reaction in acetonitrile falls between eq. [1] and eq. [2], leading to k_b values which are in error. The k_f values, however, are valid. Thus, the k_b values in acetonitrile cannot be used to interpret the reaction.

It has been suggested (17) that traces of water, which always remain in TMG after drying and purification, could give rise to $\bar{O}H$ ion which might be the proton abstracting base rather than the TMG. To test this possibility, experiments were carried out in which the solvent benzonitrile was saturated with D_2O before purification by the Coetzee and McGuire method (18). Previously dried and purified TMG was also equilibrated with about 1% D_2O and then redried and distilled. Observed pseudo-first order rate constants for the deuterated substrate at 20°C for the same TMG concentrations in line 3 of Table 1 (b) (ii) were 1.7 to 3.0 s^{-1} yielding $k_f = 1.32$ dm^3 mol^{-1} s^{-1} and $k_b = 0.76$ s^{-1}, in excellent agreement with the values in the table. If $\bar{O}H$ had been replaced by $\bar{O}D$ as the reagent base, an isotope effect from about 50% up to 80% (19) should have been observed. The influence of $\bar{O}H$ or the ion-pair $TMGH^+\bar{O}H$ on the reaction rates and isotope effects, therefore, appears to be negligible.

The k_f rate constants for the reaction in Table 1 are about 3 times smaller in acetonitrile than in benzonitrile. This is not expected from the dielectric constants for these solvents. However, Caldin and Mateo (7) found a similar rate reversal for 4-nitrophenylnitromethane, although it was not as large. From Caldin's study of ten solvents, the rate constants in acetonitrile seem to be abnormally small. For such a rate reversal to occur in a reaction in which the transition state is more polar than the initial state, the transition state must come early along the reaction coordinate, before much charge development has taken place.

The activation parameters, together with their standard deviations, for the proton and deuteron transfer reactions are shown in Table 2. The forward reaction shows rather small enthalpy of activation values and negative entropy of activation values, typical of proton transfer reactions. It may be seen that the enthalpy of activation is smaller in acetonitrile than in benzonitrile, as would be expected from the dielectric constants of the solvents, and that the rate reversal is brought about by the much larger negative entropy of activation in acetonitrile.

The activation parameters for the reverse reaction are determined with considerably less precision, but this reaction also shows a large negative entropy of activation.

The values of the primary deuterium isotope effect (Table 1) are large, and larger in the less polar benzonitrile ($k_H/k_D = 12.5$ at 25°C) than in the more polar acetonitrile (10.7 at 25°C). These values are larger than can be explained by the loss of the zero-point energy of the C—H stretching vibration, although not beyond the limits of a zero-point energy effect involving the loss of the C—H stretch and changes in the two C—H bending modes. However, the large isotopic difference in the enthalpies of activation for the forward reaction ($\Delta H_D^{\ddagger} - \Delta H_H^{\ddagger}$) = 2.2 to 2.4 kcal mol^{-1} indicates a significant contribution from the tunnelling effect to the proton transfer reaction.

TABLE 2. Activation parameters for the reaction of 4-nitrophenylphenylcyanomethane with tetramethylguanidine

Parameter	Proton transfer	Deuteron transfer
(a) Acetonitrile solvent		
$\Delta H_f^{\ddagger}$ (kcal mol^{-1})	3.7±0.2	5.9±0.2
$\Delta S_f^{\ddagger}$ (cal mol^{-1} deg^{-1})	−28.3±0.7	−25.6±0.8
$\Delta H_b^{\ddagger}$ (kcal mol^{-1})	9.9±0.9	—
$\Delta S_b^{\ddagger}$ (cal mol^{-1} deg^{-1})	−24±3	—
(b) Benzonitrile solvent		
$\Delta H_f^{\ddagger}$ (kcal mol^{-1})	7.3±0.2	9.7±0.2
$\Delta S_f^{\ddagger}$ (cal mol^{-1} deg^{-1})	−14.0±0.6	−11.1±0.7
$\Delta H_b^{\ddagger}$ (kcal mol^{-1})	8.2±0.4	9.9±0.9
$\Delta S_b^{\ddagger}$ (cal mol^{-1} deg^{-1})	−26±1.3	−25±3

Experimental

Materials

p-Nitrophenylphenylacetonitrile was prepared by the procedure of Neresheimer and Rupple (20) for the condensation of phenylacetonitrile with *p*-nitrochlorobenzene. A mixture of *p*-nitrochlorobenzene (10 g), pyridine (100 g), and a paste obtained by grinding pyridine (21 g) and potassium hydroxide (21 g) in a ball mill under a nitrogen atmosphere, was cooled to −5°C. Phenylacetonitrile (7.5 g) was added, with stirring, during a period of 10 minutes. This mixture was maintained at 0°C and stirred for 10 hours, then benzene (100 mL) was added with stirring and the blue-violet mixture was suction-filtered. The solid material was washed with benzene, then with diethyl ether, and then with cold water. The solid was then placed in water (1 L) and acetic acid (50 g) was added slowly. The precipitated product was filtered, washed with water, and vacuum dried. After recrystallization from 95% ethanol, the product had a mp of 70–72°C; nmr, aliphatic proton, δ 5.6 ppm; ratio of aromatic to aliphatic hydrogen, 9.2:1.

The deuterated carbon acid was obtained by exchanging 0.2 g of the above product with dioxan/D_2O (5:1) in which a small amount of sodium had been dissolved. After 1 or 2 minutes the mixture was neutralized with DCl in D_2O and the solvent evaporated. The carbon acid was extracted with dioxan and the exchange procedure was repeated four times. After the fourth exchange the deuterated substrate was recovered by extracting the sediment with dry chloroform and pouring this solution into an excess of dry petroleum ether. The nmr spectrum showed that the signal from the aliphatic proton was reduced to the background. Therefore, the carbon acid was at least 98% deuterated in the aliphatic position.

Reagent grade acetonitrile was purified by the method of O'Donnell *et al.* (21), with a final fractional distillation from P_2O_5.

Reagent grade benzonitrile was purified by the method of Coetzee and McGuire (18) by drying with CaH_2, followed by fractional distillation at reduced pressure over a small amount of P_2O_5.

Tetramethylguanidine was dried with KOH and then fractionally distilled under reduced pressure. The middle fraction, about 25% of the total, was used.

Equilibrium and kinetic measurements

The optical density measurements were made on Specord UV-VIS and VSU-2P spectrophotometers fitted with a constant temperature bath to control the temperature of the cell block within 0.1°C.

The kinetic runs were performed under pseudo-first order conditions with the base always in at least 50-fold excess. The solvents were always freshly distilled and the deuterated carbon acid stock solutions were always freshly prepared to avoid the possibility of a slow exchange of the deuterium atom with the solvent. The kinetic measurements for the normal and deuterated carbon acids were made in a stopped-flow spectrophotometer and the pseudo-first order rate constants were calculated using the Guggenheim method. The second-order rate constants were calculated from eq. [1] and the activation parameters were evaluated from these by means of a least-squares fit to the transition state theory equation.

1. E. S. LEWIS and L. H. FUNDERBURK. J. Am. Chem. Soc. **89**, 2322 (1967).

2. R. P. BELL and D. M. GOODALL. Proc. R. Soc. Ser. A, **294**, 273 (1966).
3. R. P. BELL, W. H. SACHS, and R. L. TRANTER. Trans. Faraday Soc. **67**, 1995 (1971).
4. J. E. DIXON and T. C. BRUICE. J. Am. Chem. Soc. **92**, 905 (1970).
5. R. A. MARCUS. J. Phys. Chem. **72**, 891 (1968).
6. E. F. CALDIN. Chem. Rev. **69**, 135 (1969).
7. E. F. CALDIN and S. MATEO. J. Chem. Soc. Faraday Trans. 1, **71**, 1876 (1974).
8. J. H. BLANCH and O. ROGNE. J. Chem. Soc. Faraday Trans. 1, **74**, 1254 (1978).
9. O. ROGNE. Acta Chem. Scand. Ser. A, **32**, 559 (1978).
10. L. MELANDER and W. H. SAUNDERS. Reaction rates of isotopic molecules. Wiley, New York. 1980. Chapt. 10.
11. E. F. CALDIN, A. JARCZEWSKI, and K. T. LEFFEK. Trans. Faraday Soc. **67**, 110 (1971).
12. F. HIBBERT, F. A. LONG, and E. A. WALTERS. J. Am. Chem. Soc. **93**, 2829 (1971).
13. F. HIBBERT and F. A. LONG. J. Am. Chem. Soc. **93**, 2836 (1971).
14. E. F. CALDIN, M. KASPARIAN, and G. TOMALIN. Trans. Faraday Soc. **64**, 2802 (1968).
15. E. F. CALDIN and G. TOMALIN. Trans. Faraday Soc. **64**, 2814 (1968).
16. R. P. BELL. The proton in chemistry. 2nd ed. Cornell Univ. Press., Ithaca, NY. 1973. p. 212.
17. I. HEGGEN, J. LINDSTROM, and O. ROGNE. J. Chem. Soc. Faraday Trans. 1, **74**, 1263 (1978).
18. J. F. COETZEE and D. K. MCGUIRE. J. Phys. Chem. **67**, 1810 (1963).
19. C. G. SWAIN and R. F. W. BADER. Tetrahedron, **10**, 182 (1960).
20. H. NERESHEIMER and W. RUPPLE. U.S. Pat. 2,080,057 (1937).
21. J. F. O'DONNELL, J. T. AYERS, and C. K. MANN. Anal. Chem. **37**, 1161 (1965).

Can. J. Chem. Downloaded from www.nrcresearchpress.com by 210.87.254.42 on 09/06/12
For personal use only.

Induction periods in the formation of ethane from the pyrolysis of ethylene

ALLAN L. MACKENZIE, PHILIP D. PACEY,[1] AND JAYANTHA H. WIMALASENA[2]
Department of Chemistry, Dalhousie University, Halifax, N.S., Canada B3H 4J3

Received February 2, 1983

ALLAN L. MACKENZIE, PHILIP D. PACEY, and JAYANTHA H. WIMALASENA. Can. J. Chem. **61**, 2033 (1983).

Induction periods have been observed in the formation of C_2H_6 from C_2H_4 pyrolysis at 895 K and 23 to 78 Torr. The induction periods were interpreted as evidence of the approach to the steady-state concentration of radicals. The observed inverse pressure dependence of the induction periods was an indication that both chain initiation and termination were bimolecular. Taking the termination rate constant as 1.3×10^{10} L mol^{-1} s^{-1} and neglecting autocatalysis, for the most likely initiation reaction,

$$2C_2H_4 \rightarrow C_2H_3 + C_2H_5$$

the rate constant was found to be 2.3×10^{-4} L mol^{-1} s^{-1}. Assuming further that termination is dominated by recombination and disproportionation of C_2H_5, the rate constant for

$$C_2H_5 + C_2H_4 \rightarrow C_2H_6 + C_2H_3$$

was found to be 8×10^4 L mol^{-1} s^{-1}.

ALLAN L. MACKENZIE, PHILIP D. PACEY et JAYANTHA H. WIMALASENA. Can. J. Chem. **61**, 2033 (1983).

On a observé des périodes d'induction lors de la formation du C_2H_6 à partir de la pyrolyse du C_2H_4 à 895 K et à des pression entre 23 et 78 Torr. On considère que ces périodes d'induction soient une preuve de l'évolution des radicaux vers la concentration de l'état stationnaire. L'influence inverse de la pression sur la période d'induction indique que l'amorçage et la rupture des chaînes sont bimoléculaires. En utilisant la constante de vitesse de $1{,}3 \times 10^{10}$ L mol^{-1} s^{-1} pour la rupture des chaînes et en négligeant l'autocatalyse on trouve une constante de vitesse de $2{,}3 \times 10^{-4}$ L mol^{-1} s^{-1} pour la réaction d'amorçage la plus courante:

$$2C_2H_4 \rightarrow C_2H_3 + C_2H_5$$

De plus, en supposant que la combinaison et la dismutation du C_2H_5 sont responsables de la rupture des chaînes, on trouve une constante de vitesse de 8×10^4 L mol^{-1} s^{-1} pour la réaction:

$$C_2H_5 + C_2H_4 \rightarrow C_2H_6 + C_2H_3$$

[Traduit par le journal]

Introduction

The pyrolysis of ethylene at 750–900 K has proved to be difficult to study (1–7) for the following reasons: (*i*) rates have been found to increase with increasing reaction times, a phenomenon attributed to autocatalysis; (*ii*) some products may be formed by several pathways, making it impossible to determine the rate of any one of these paths; and (*iii*) several radicals are believed to participate in the reaction and it has not been possible to demonstrate conclusively which radical is dominant.

In the present work, these difficulties have been addressed in the following ways: (*i*) a flow system has been used to study the system at short reaction times, before autocatalysis becomes dominant; (*ii*) the product, ethane, has been studied, as this product is formed mainly by one path; and (*iii*) temperatures and pressures have been chosen so that reactor residence times would be similar to the times necessary to establish the steady state concentrations of the radicals. Experiments satisfying the latter criterion are capable of providing information about chain initiation and termination processes (8, 9).

The mechanism for the formation of ethane in ethylene pyrolysis has been proposed to be as follows (6):

[1] $2C_2H_4 \rightarrow C_2H_3 + C_2H_5$

[2] $C_2H_5 + C_2H_4 \rightarrow C_2H_6 + C_2H_3$

. . . . . .

[3*a*] $2C_2H_5 \rightarrow n\text{-}C_4H_{10}$

[3*b*] $2C_2H_5 \rightarrow C_2H_4 + C_2H_6$

Here the dots stand for various omitted addition, abstraction, isomerization, and decomposition reactions of the radicals.

The chain lengths are believed to be long (6), so the propagation reaction, [2], occurs many times more often than the termination, [3*b*], and the rate of formation of C_2H_6 can be identified with the rate of reaction [2].

The rate constant, k_1, has previously been estimated by comparing rates of formation of products in the presence and absence of additional initiation processes (5–7). These studies agree that initiation in pure C_2H_4 is second order, but do not agree on the absolute initiation rate.

During the establishment of the steady-state concentration of C_2H_5, it may be shown (8, 10) that the chordal rate of formation of C_2H_6 should be given by the following expression:

$$[4] \quad [C_2H_6]/t = (b/t) \ln [1 + \exp(at)]/2 - ab/2$$

Here it has been assumed that the above mechanism is correct, that autocatalysis has not begun, that chains are long, and that the pseudo-stationary state approximation (11) is valid for all radical species except C_2H_5. The parameters a and b in eq. [4] may be shown by the methods of ref. 8 to be given by:

$$[5] \quad a = 4[C_2H_4](k_1k_3)^{1/2}$$

and

$$[6] \quad ab = 2k_2(k_1/k_3)^{1/2}[C_2H_4]^2$$

[1]To whom all correspondence should be addressed.

[2]Present address: Department of Chemistry, University of Sri Jayewardenepura, Nugegoda, Sri Lanka.

Can. J. Chem. Downloaded from www.nrcresearchpress.com by 210.87.254.105 on 09/06/12
For personal use only.

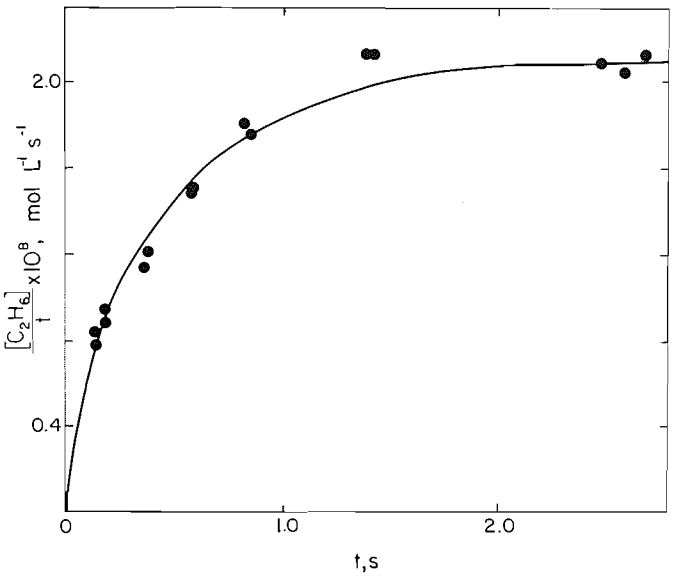

FIG. 1. Dependence of the chordal rate of formation of C_2H_6 on the reactor residence time at 73 Torr and 896 K: (●) experimental; (—) least-squares fit to eq. [4].

where $k_3 = k_{3a} + k_{3b}$. The parameter a has the units, s^{-1}, and is related to the inverse of the induction period, the time during which radical concentrations build up toward their steady-state values. This induction period should occur much earlier in the course of the reaction than the induction period for establishment of a steady-state concentration of 1-C_4H_8, investigated in ref. 1. The product, ab, is twice the steady rate of formation of C_2H_6.

The experimental temperature, 895 K, has been chosen so that C_2H_6 yields are great enough to be measured and induction periods long enough to be accessible with the equipment available (10).

Experimental section

The apparatus and experimental technique were similar to those used in refs. 8 and 10. Three cylindrical quartz reactors were used, with internal diameters and surface-to-volume ratios (S/V) of, respectively, (*i*) 1.7 cm, 3.1 cm^{-1}, (*ii*) 0.8 cm, 9.9 cm^{-1}, and (*iii*) 0.4 cm, 8.8 cm^{-1}. Along the axes of reactors i and ii were placed 0.4 cm o.d. quartz thermocouple wells. Reactor iii was placed along the axis of a 1.1 cm i.d. quartz tube, which held a moveable platinum – platinum – 13% rhodium thermocouple. The temperature profile was used in a computer program (12) to calculate the length of the reaction zone.

Reactant and product concentrations were analyzed in a gas chromatograph with a 1-m, 10% NaOH on alumina column at 23°C. The chromatograph was calibrated each day with mixtures containing small concentrations of ethane diluted with nitrogen. Ethylene (Matheson, research purity, 99.98%) was degassed at the melting temperature of isopentane. The principal impurities remaining were CH_4 (1–1.5 ppm), C_2H_6 (1–2 ppm), 1,3-C_4H_6 (<0.4 ppm), and C_4H_{10} (<0.3 ppm).

Results

Experiments[3] have been performed at reactor temperatures of 892–900 K, reactant pressures from 23 to 78 Torr, and residence times from 0.136 to 5.7 s.

[3]Tables of experimental results are available from the Depository of Unpublished Data, CISTI, National Research Council of Canada, Ottawa, Ont., Canada K1A 0S2.

TABLE 1. Parameters at 895 K determined by least-squares fits to eq. [4] as in Fig. 1

P, Torr	Reactor diameter, cm	$10^{-6}a^2/(4[C_2H_4])^2$ (L^2 mol^{-2} s^{-2})	$10^2ab/(2[C_2H_4]^2)$ (L mol^{-1} s^{-1})
23	1.7	2.9	1.01
35	0.8	3.3	0.97
35	0.8	3.5	0.80
42	0.8	3.1	0.94
47	0.8	2.8	1.08
52	0.4	3.5	1.15
58	0.4	2.5	1.03
61	0.8	2.0	0.97
73	0.4	2.9	1.25
78	0.4	3.7	1.03
Ave.		3.0±0.5	1.02±0.12

Results of a series of experiments at 896 K and 73 Torr are shown in Fig. 1. The points are experimental; the solid curve is a non-linear least-squares fit to eq. [4], representing the establishment of the steady state.

The results of this and other least-squares fits at other pressures are summarized in Table 1. Parameters determined at experimental temperatures other than 895 K have been adjusted slightly to 895 K by multiplying by exp $[-E_a((R895\ \mathrm{K})^{-1} - (RT)^{-1}))$. For the third column in Table 1, equal to $10^{-6}k_1k_3$ by eq. [5], E_a was taken as 269 kJ mol^{-1} from ref. 7. For the final column, equal to $10^2k_2(k_1/k_3)^{1/2}$ by eq. [6], E_a was taken as 176 kJ mol^{-1}, from ref. 2. The quoted uncertainties in the averages are standard deviations of the tabulated values.

It can be seen from the table that parameters obtained in different reactors and at different pressures are in satisfactory agreement. When the logarithms of the parameters were plotted against the logarithm of the pressure, it was possible to find the orders for these parameters. The orders were found to be 1.93 ± 0.17 for a^2 and 2.16 ± 0.10 for ab, in agreement with eqs. [5] and [6], within experimental uncertainty.

Taking $k_3 = 1.3 \times 10^{10}$ L mol^{-1} s^{-1} from ref. 8 and assuming eqs. [5] and [6] are correct, one obtains from the average values in Table 1, $k_1 = 2.3 \times 10^{-4}$ L mol^{-1} s^{-1} and $k_2 = 8 \times 10^4$ L mol^{-1} s^{-1}.

Discussion

Possible competing processes

For an alternative initiation reaction,

[7] $C_2H_4 + M \rightarrow C_2H_3 + H + M$

k_7, when M = Ar, is calculated (13) to be five orders of magnitude slower than k_1 at this temperature. Although C_2H_4 is likely to be more efficient at energy exchange than Ar, reaction [1] should still be much faster than [7].

Similarly, the rate of decomposition (8) of the major impurity, C_2H_6, is calculated to be three orders of magnitude slower than reaction [1] and the concentration of C_4H_{10} impurity was much less than that which was found to have an effect on the rate in ref. 6. Other possible initiation reactions have been shown not to be significant in ref. 5.

Using the rate constants from the previous section, one can calculate that the chain length is about 50. Following the argument in the Introduction, 99% or more of the C_2H_6 should be formed by reaction [2].

We now consider whether reactions [3*a*] and [3*b*] are the

Can. J. Chem. Downloaded from www.nrcresearchpress.com by 210.87.254.105 on 09/06/12
For personal use only.

Can. J. Chem. Downloaded from www.nrcresearchpress.com by 210.87.254.105 on 09/06/12
For personal use only.

principal termination reactions. The yield of CH_4, probably formed by

[8] $CH_3 + C_2H_4 \rightarrow CH_4 + C_2H_3$

was found in this work to be 10% of the yield of C_2H_6 from reaction [2]. Similarly, the yield of C_4H_{10}, formed partly by reaction [3*a*] and partly, perhaps, by the reaction

[9] $C_4H_9 + C_2H_4 \rightarrow C_4H_{10} + C_2H_3$

has been shown (2) to be 7% of the rate of formation of C_2H_6. Since the rate constants of reactions [8] and [9] are probably similar to that for reaction [2], it may be concluded that the concentration of C_2H_5 is greater than that of CH_3 or C_4H_9 and that C_2H_5 is the dominant alkyl radical.

If a first-order termination, with rate constant k_w, were dominant, then the induction period would be k_w^{-1}, independent of pressure (14, 15). If this termination were a kinetically controlled surface process, the induction period would be inversely proportional to S/V. Instead, the induction period, related to a^{-1}, was found to be inversely proportional to pressure and independent of S/V in accord with eq. [5] and with the hypothesis that second-order homogeneous terminations are dominant.

The observed pressure dependence of a could also be explained by an alternative bimolecular termination, for example,

[10] $2C_2H_3 \rightarrow C_4H_6$

Delliste *et al.* (6) have shown that the ratio $[C_2H_3]/[C_2H_5]$ is approximately equal to k_2/k_{11}, where reaction [11] is

[11] $C_2H_3 + C_2H_4 \rightarrow C_4H_7$

Based on Arrhenius parameters (16) for other radical additions to C_2H_4 and on the value of k_2 from the Results section, it may be estimated that $[C_2H_3]$ is 1 or 2% of $[C_2H_5]$ and hence that reaction [10] may be neglected.

A possible alternative cause of induction periods in pyrolysis reactions is the delay in warming the reactant after it enters the reactor. The steady-state rates in the cylindrical reactor, iii, would be reduced (17) by a fraction approximately equal to $r^2/\kappa t$, where r is the reactor radius, t the residence time, and κ the thermal diffusivity, which equals $\lambda/([C_2H_4]C_p)$. Here λ, the thermal conductivity, has been calculated by the method of ref. 18 and C_p, the heat capacity, has been obtained from ref. 19. The maximum reduction in apparent rate from this source in the present work would be 4% and would occur for the shortest times in Fig. 1. Any errors from this source will be neglected in this work.

In deriving eqs. [4] to [6] it was assumed that autocatalysis does not affect the results under the present experimental conditions. Boyd, Wu, and Back (2) found that there was a period of steady formation of C_2H_6 before the onset of catalysis. Other workers (1, 6) did not observe this steady period, and Delliste *et al.* (6) fitted their results to the following expression:

$$[12] \quad \frac{[C_2H_6]}{t} = k_2\left(\frac{k_1}{k_3}\right)^{1/2}[C_2H_4]^2(1 + ct)$$

Here the parameter c is a combination of rate constants important in the formation and decomposition of 1-C_4H_8. The possibility of autocatalysis during the establishment of the steady state may be approximately taken into account by multiplying eq. [4] by the factor $(1 + ct)$ from eq. [12]:

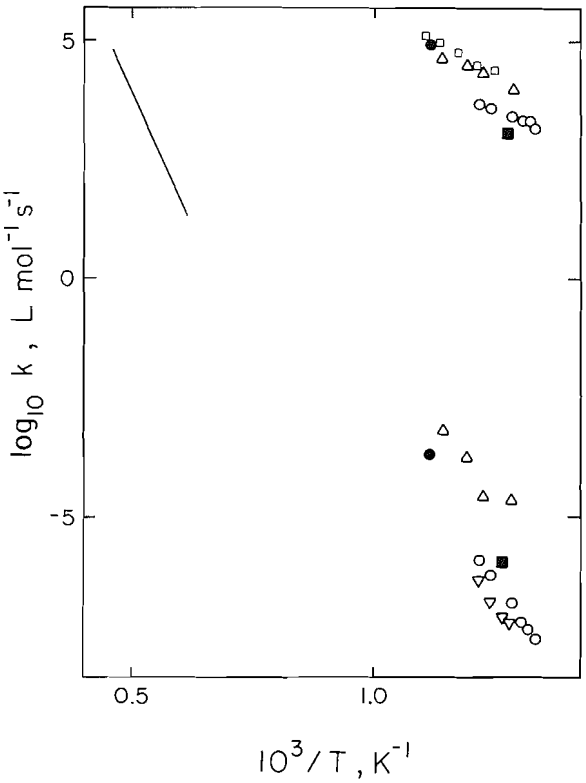

FIG. 2. Arrhenius plots for reactions [1] (lower right), [2] (upper right), and [7] (upper left); □, ref. 1; △, ref. 2; ■, ref. 6; ○, ref. 7, $C(CH_3)_4$ addition; ▽, ref. 7, C_2H_6 addition; —, ref. 13; ●, this work.

$$[13] \quad \frac{[C_2H_6]}{t} = \left[\frac{b}{t}\ln\{[1 + \exp(at)]/2\} - \frac{ab}{2}\right](1 + ct)$$

This equation may be justified in the same way as the use of the factor $(1 - ct)$ to account for self-inhibition in ref. 10.

Equations [12] and [13] have been fitted to the data in Fig. 1 by least squares. Equation [12], the equation of a straight line, has a sum of squares of residuals five times as large as for eq. [4] and does not fit the data well. For eq. [13], a is increased by 18%, b is decreased by 23%, and the sum of squares of residuals is decreased by 6% compared to the fit to eq. [4]. By the method of analysis of variance (20), it is found that the third parameter, c, is significant only at the 50% confidence level. Henceforth, we will adopt the values of a and b from fits to eq. [4], but recognize that the possibility of autocatalysis introduces an uncertainty in these parameters.

Comparison with other work

Values of k_1 are shown in the form of an Arrhenius plot in the lower part of Fig. 2. Values based on acceleration by 1-butene, whether added initially (5) or formed as a product (6), have been omitted, because of a ten-fold uncertainty in the rate constant of the reference reaction

[14] 1-$C_4H_8 \rightarrow CH_3 + C_3H_5$

Instead, k_1 has been estimated, using the following equation (6, 21), from initial rates of formation of n-C_4H_{10} reported in refs. 2 and 6:

$$[15] \quad 1.14R^0_{C_4H_{10}} = k_1[C_2H_4]^2$$

Use of this equation is supported by the observation that C_4H_{10} formation is second order and has an activation energy of 290

kJ mol^{-1} (2), similar to values for reaction [1] obtained by other techniques.

The values of k_1 obtained by the different techniques do not agree well. Each technique has its own weaknesses. The present technique assumes that autocatalysis does not affect the induction period and assumes a value for the termination rate constant. The acceleration technique assumes a mechanism for acceleration and a value for the reference rate constant. Equation [15] is based on the assumption that reactions [3*a*] and [3*b*] are the only termination steps and that there are no other sources of C_4H_{10}. Preparations are being made to use the latter technique in this laboratory for comparison with the present results. Values of the rate constant for the high temperature initiation reaction, [7], are shown at the left in Fig. 2.

In the upper right hand corner of Fig. 2 are shown values for the abstraction rate constant, k_2. In most cases, values of $k_2 k_1^{1/2} k_3^{-1/2}$ have been taken from the steady-state rate of formation of C_2H_6, k_3 has been taken from ref. 8, and k_1 has been taken as the corresponding value from the lower part of Fig. 2. Values of k_2 calculated from observed C_2H_6 and C_4H_{10} yields in ref. 1 have been adjusted to take into account the more recent value of k_3 (8). Again there are differences between the results of different techniques.

In conclusion, we note that there are still aspects of C_2H_4 pyrolysis that are not completely understood. Studies of induction periods do introduce a new perspective on the problem. The observed pressure dependence of the induction periods can be simply explained only if the initiation and termination reactions are both bimolecular. The observed pressure dependence of the product *ab* is in agreement with the hypothesis that reactions [3*a*] and [3*b*] are the main termination reactions. Values of the parameters, *a* and *b*, would be somewhat affected if autocatalysis occurs, but there is no evidence that autocatalysis is significant at these early reaction times. Subject to the above assumptions and limitations, it has been possible to estimate values of k_1 and k_2.

Acknowledgments

The authors wish to thank the Natural Sciences and Engineering Research Council of Canada for a grant in support of this research. J.H.W. thanks the Dorothy J. Killam Trust for the award of a scholarship.

1. M. P. HALSTEAD and C. P. QUINN. Trans. Faraday Soc. **64**, 103 (1968).
2. M. L. BOYD, T. M. WU, and M. H. BACK. Can. J. Chem. **46**, 2415 (1968).
3. M. SIMON and M. H. BACK. Can. J. Chem. **47**, 251 (1969).
4. M. H. BACK and R. MARTIN. Int. J. Chem. Kinet. **9**, 757 (1979).
5. G. AYRANCI and M. H. BACK. Int. J. Chem. Kinet. **13**, 897 (1981).
6. D. DELLISTE, C. RICHARD, and R. MARTIN. J. Chim. Phys. **78**, 655 (1981).
7. G. AYRANCI and M. H. BACK. Int. J. Chem. Kinet. In press.
8. P. D. PACEY and J. H. WIMALASENA. Chem. Phys. Lett. **76**, 433 (1980).
9. S. CORBEL, P.-M. MARQUAIRE, and G.-M. CÔME. Chem. Phys. Lett. **80**, 34 (1981).
10. P. D. PACEY and J. H. WIMALASENA. J. Phys. Chem. **84**, 2221 (1980).
11. G.-M. CÔME. J. Phys. Chem. **81**, 2560 (1977).
12. P. D. PACEY and J. H. PURNELL. Int. J. Chem. Kinet. **4**, 657 (1972).
13. T. JUST, P. ROTH, and R. DAMM. Sixteenth Symp. Int. Comb. 961 (1976).
14. R. M. MARSHALL and G. SHAHKAR. J. Chem. Soc. Faraday Trans. I **72**, 2271 (1981).
15. P. D. PACEY and J. H. WIMALASENA. Can. J. Chem. **61**, 1086 (1983).
16. J. A. KERR and M. J. PARSONAGE. Evaluated kinetic data on gas phase addition reactions: reactions of atoms and radicals with alkenes, alkynes and aromatic compounds. Butterworths, London. 1972.
17. H. FURUE and P. D. PACEY. J. Phys. Chem. **84**, 3139 (1980).
18. J. O. HIRSCHFELDER, C. F. CURTISS, and R. B. BIRD. Molecular theory of gases and liquids. Wiley, New York. 1954.
19. AMERICAN PETROLEUM INSTITUTE. Selected values of properties of hydrocarbons and related compounds. Vol. 6. Texas A & M University, College Station. 1975.
20. C. A. BENNETT and N. L. FRANKLIN. Statistical analysis in chemistry and the chemical industry. Wiley, New York. 1954.
21. H. ADACHI, N. BASCO, and D. G. L. JAMES. Int. J. Chem. Kinet. **11**, 995 (1979).

Can. J. Chem. Downloaded from www.nrcresearchpress.com by 210.87.254.105 on 09/06/12
For personal use only.

Absolute rate constants for hydrocarbon autoxidation. 33. A product study of the self-reaction of α-tetralylperoxyls in solution[1]

A. BAIGNÉE,[2] J. H. B. CHENIER, AND J. A. HOWARD[3]

Division of Chemistry, National Research Council of Canada, Ottawa, Ont., Canada K1A 0R9

Received January 28, 1983

A. BAIGNÉE, J. H. B. CHENIER, and J. A. HOWARD. Can. J. Chem. **61**, 2037 (1983).

The major initial products of the self-reaction of α-tetralylperoxyls ($C_{10}H_{11}O_2^{\cdot}$) in chlorobenzene at 303–353 K are equal concentrations of α-tetralol and α-tetralone in ~90% yield based on the number of initiating radicals. These yields are consistent with the non-radical (Russell) mechanism for self-reaction. Low concentrations of bis(α-tetralyl) peroxide are produced, indicating that there is a small but detectable free-radical contribution towards termination. $C_{10}H_{11}O_2^{\cdot}$ undergoes β-scission in this temperature range but steady-state concentrations of $C_{10}H_{11}^{\cdot}$ are too low to influence the termination rate constant $2k_t$, or react with $C_{10}H_{11}O_2^{\cdot}$ to give $(C_{10}H_{11})_2O_2$. α-Tetralol to α-tetralone ratios and total yields of these products are significantly less than 1 and 100%, respectively, in methanol and acetonitrile. Formaldehyde is produced in methanol indicating the involvement of α-hydroxymethylperoxyls, derived from the solvent, in termination. There is no evidence for a chain reaction or a zwitterion intermediate for self-reaction of $C_{10}H_{11}O_2^{\cdot}$ in solution.

A. BAIGNÉE, J. H. B. CHENIER et J. A. HOWARD. Can. J. Chem. **61**, 2037 (1983).

Les produits initiaux majoritaires de l'autoréaction des α-tétralylpéroxyles ($C_{10}H_{11}O_2^{\cdot}$) dans le chlorobenzène à 303–353 K correspondent à des concentrations égales d'α-tétralol et d'α-tétralone avec un rendement approximatif de 90% basé sur le nombre de radicaux initiateurs. Ces rendements sont en accord avec le mécanisme d'autoréaction non radicalaire (Russell). Les faibles concentrations de bis(α-tétralyl) peroxyde obtenues indiquent que la contribution du radical libre à la rupture est faible mais décelable. Le composé $C_{10}H_{11}O_2^{\cdot}$ subit une scission β dans cet intervalle de température mais les concentrations de l'état stationnaire du $C_{10}H_{11}^{\cdot}$ sont trop faibles pour influencer la constante de vitesse de rupture $2k_t$, ou pour réagir avec le radical $C_{10}H_{11}O_2^{\cdot}$ pour donner le $(C_{10}H_{11})_2O_2$. Les rapports α-tétralol/α-tétralone et les rendements totaux de ces produits sont de façon significative inférieures à 1 et à 100% respectivement dans le méthanol et l'acétonitrile. Dans le méthanol, il se forme de la formaldéhyde, ce qui indique que des α-hydroxyméthylpéroxyles provenant du solvant sont impliqués dans la rupture. Il n'y a pas de preuve d'une réaction en chaine ou de la présence d'une paire d'ions intermédiaires dans l'autoréaction du $C_{10}H_{11}O_2^{\cdot}$ en solution.

[Traduit par le journal]

Introduction

Kinetic studies of the self-reaction of alkylperoxyls ($RO_2^{\cdot}$) in solution below 403 K have revealed that absolute rate constants for self-reaction ($2k_t$) of primary ($R^1CH_2O_2^{\cdot}$) and secondary alkylperoxyls ($R^1R^2CHO_2^{\cdot}$) are several orders of magnitude larger than rate constants for tertiary alkylperoxyls ($R^1R^2R^3CO_2^{\cdot}$) (1). Self-reactions of peroxyls with and without a hydrogen atom on the α-carbon atom would, therefore, appear to involve different mechanisms. Product studies have, in general, supported this conclusion, since primary and secondary alkylperoxyls give products indicative of a non-radical mechanism (Russell mechanism) while tertiary alkylperoxyls give products consistent with the intermediacy of tertiary alkoxyls.

The mechanism for self-reaction of tertiary alkylperoxyls has been well estabished (2–4). These radicals exist in dynamic equilibrium with a tetroxide which decomposes to give two caged alkoxyls and oxygen. A fraction (~10%) of these alkoxyls combine to give di-*tert*-alkyl peroxide while the remainder escape the solvent cage and undergo H-atom abstraction, β-scission, or rearrangement (3, 4).

Secondary alkylperoxyls (and probably $R^1CH_2O_2^{\cdot}$) also exist in equilibrium with tetroxide at low temperatures and values of the thermodynamic parameters ΔH^0 and ΔS^0 appear identical, within experimental error, to values for $R^1R^2R^3CO_2^{\cdot}$ (5). This suggests that $2k_t$ (primary and secondary) are $>2k_t$ (tertiary) because primary and secondary alkyl tetroxides decompose faster than tertiary alkyl tetroxides, either because of a change in mechanism or because primary and secondary alkyl tetroxides homolyze much faster than tertiary alkyl tetroxides.

Russell (6) over 20 years ago suggested that $R^1R^2CHO_2^{\cdot}$ and $R^1CH_2O_2^{\cdot}$ undergo self-reaction via a cyclic intermediate which decomposes by a non-radical mechanism to give alcohol, ketone (or aldehyde), and oxygen in equal yields.

[1] $2R^1R^2CHO_2^{\cdot} \rightleftharpoons$ 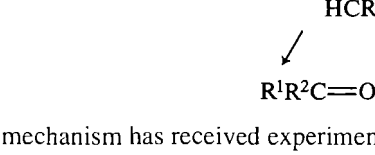

$R^1R^2C{=}O + O_2 + R^1R^2CHOH$

This mechanism has received experimental support from the observation of a primary kinetic isotope effect on $2k_t$ when the H attached to the α carbon is replaced by deuterium (7), the evolution of $^1\Sigma_g^+$ and $^1\Delta_g$ oxygen (8, 9), and the production of equal yields of alcohol and ketone (10–14). Product yields are, however, not always compatible with this mechanism. For instance, Bennett and Summers (15) reported high ketone-to-alcohol ratios from self-reaction of several secondary alkylperoxyls at low temperatures. Furthermore, at ambient temperatures, a considerable fraction of 1-ethoxyethylperoxyls and 1,2-diphenylethylperoxyls give free alkoxyls (16).

It has been argued (17), with the aid of thermochemical calculations, that the activation energy for non-radical tetroxide decomposition would have to be very small or even negative to compensate for the entropy loss in the formation of the cyclic transition state. In actual fact, overall pre-exponential factors

[1]Issued as NRCC No. 21229.
[2]NRCC Summer Student 1982.
[3]Author to whom correspondence should be addressed.

Can. J. Chem. Downloaded from www.nrcresearchpress.com by 210.87.254.6 on 09/06/12
For personal use only.

of $10^8-10^9\ M^{-1}\ s^{-1}$ and overall activation averages of 1–2 kcal mol^{-1} have been determined by kinetic electron spin resonance studies of the decay of secondary alkylperoxyls (18).

In an attempt to account for the kinetics and products of self-reaction of $R^1CH_2O_2^{\cdot}$ and $R^1R^2CHO_2^{\cdot}$, Nangia and Benson (19) have proposed the following chain mechanism which involves the intermediacy of a diradical, $R\dot{C}HO\dot{O}$, or zwitterion, $R\overset{+}{C}HO\bar{O}$.

[2] $2RCH_2O_2^{\cdot} \longrightarrow RCH_2OOH + R\dot{C}HO\dot{O}$

[3] $R\dot{C}HO\dot{O} + RCH_2O_2^{\cdot} \longrightarrow RCHO + RCH_2O_3^{\cdot}$

[4] $RCH_2O_3^{\cdot} \longrightarrow RCH_2O^{\cdot} + O_2$

[5] $RCH_2O^{\cdot} + RCH_2O_2^{\cdot} \longrightarrow RCH_2OH + R\dot{C}HO\dot{O}$

[6] $RCH_2O^{\cdot} + RCH_2O_2^{\cdot} \longrightarrow RCHO + RCH_2OOH$

[7] $RCH_2O^{\cdot} + RCH_2O_2^{\cdot} \rightleftharpoons RCH_2OOOCH_2R$

[8] $RCH_2O^{\cdot} + RCH_2OOH \longrightarrow RCH_2OH + RCH_2O_2^{\cdot}$

[9] $R\dot{C}HO\dot{O} + RCHO \longrightarrow$ 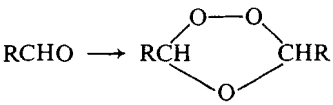 $\longrightarrow RCHO + R\dot{C}H\text{–}O^{\cdot} \longrightarrow RCOOH$

Reaction [2] is a disproportionation reaction which would be expected to have a small activation energy and an A-factor of $\sim 10^9\ M^{-1}\ s^{-1}$. Reactions [3] to [5] constitute a chain cycle with aldehyde (or ketone) and alcohol as the reaction products, and chain lengths of 2–10. In solution, in the presence of a good H-atom donor such as an aralkane or aralkyl hydroperoxide, the diradical should react to give an α-hydroperoxyalkyl which would undergo β-scission to give ketone or aldehyde and hydroxyl

[10] $R\dot{C}HO\dot{O} + RH \longrightarrow R\dot{C}HOOH + R^{\cdot}$

[11] $R\dot{C}HOOH \longrightarrow RCHO + HO^{\cdot}$

There have been several careful kinetic and product studies of the self-reactions of alkylperoxyls ($CH_3O_2^{\cdot}$, $C_2H_5O_2^{\cdot}$, $(CH_3)_2CHO_2^{\cdot}$, and $(CH_3)_3CO_2^{\cdot}$) in the gas phase (20–26) and absolute termination rate constants are very similar in the gas and liquid phases. It has been concluded that $CH_3O_2^{\cdot}$, for example, interact by terminating and non-terminating mechanisms with the ratio of rate constants k_{12b}/k_{12a}, falling in the range 1.3 to 2 at ambient temperatures.

[12] $2CH_3O_2^{\cdot} \xrightarrow{a} CH_3OH + CH_2O + O_2$

$2CH_3O_2^{\cdot} \xrightarrow{b} 2CH_3O^{\cdot} + O_2$

$2CH_3O_2^{\cdot} \xrightarrow{c} CH_3OOCH_3 + O_2$

In several of these studies, in marked contrast to solution studies (27), dialkyl peroxide has been tentatively identified and a value of the rate constant ratio $k_{12c}/k_{12} \leq 0.14$ has been calculated.

Apart from H-atom abstraction and β-scission, the alkoxyls formed in reaction [12b] are believed to undergo self-reaction to give carbonyl and alcohol (reaction [13]), react with oxygen to give carbonyl and hydroperoxyl (reaction [14]), and react with alkylperoxyl to give carbonyl and hydroperoxide (reaction [15]).

[13] $2CH_3O^{\cdot} \longrightarrow CH_3OH + CH_2O$

[14] $CH_3O^{\cdot} + O_2 \longrightarrow CH_2O + HO_2^{\cdot}$

[15] $CH_3O^{\cdot} + CH_3O_2^{\cdot} \longrightarrow CH_2O + CH_3OOH$

Clearly there are some quite marked differences in the behaviour of primary and secondary alkylperoxyls in the gas phase and in solution. In an attempt to study the self-reaction of secondary alkylperoxyls more thoroughly in solution, we have determined the products of the autoxidation of tetralin, the induced decomposition of α-tetralin hydroperoxide, the thermolysis of azotetralin in the presence of oxygen, and the metal-catalyzed decomposition of α-$C_{10}H_{11}OOH$ by high performance liquid chromatography under a wide variety of reaction conditions. The results of this study are reported here.

Experimental

Materials

α-Tetralol and α-tetralone were obtained from Aldrich and were used as received. Tetralin was purified by washing with concentrated sulfuric acid, sodium bicarbonate solution, and water, then dried, distilled, and chromatographed on alumina under argon. α-Tetralin hydroperoxide was prepared by the cobalt naphthanate-initiated autoxidation of tetralin at 50°C. The crude hydroperoxide, obtained by removal of the excess hydrocarbon, was recrystallized from toluene.

2,2,3,3-Tetraphenylbutane and di-*tert*-butyl hyponitrite had been prepared previously in our laboratory. Azo-bis-isobutyronitrile was recrystallized from methanol below 40°C. Methanol, chlorobenzene, and acetonitrile were carefully dried and distilled. Lead oxide (Anachemia) and cobalt acetylacetonate (Ventron) were used as received. Cobalt stearate and naphthanate were prepared by standard procedures.

Bis(α-tetralyl) peroxide was prepared from α-tetralin hydroperoxide by the method of Triebs and Pellman (28). The product, after having been recrystallized from hexane, had a mp 90–91°C.

Azo-bis-α-tetralin was prepared from α-tetralone and hydrazine by the method of Cohen and Wang (29, 30). The final product gave one peak in the hplc chromatogram. The ultraviolet spectrum (Hewlett–Packard 8450A) gave $\lambda_{max} = 364$ mμ (the azo linkage) and $\epsilon = 90\ M^{-1}\ cm^{-1}$. Complete decomposition in chlorobenzene at 323 K gave 1 mole of N_2 per mole of azotetralin. A 9.6 mM solution in C_6H_5Cl at 323 K evolved N_2 with a rate of $2.3 \times 10^{-8}\ M\ s^{-1}$; giving $k_d = 2.4 \times 10^{-6}\ s^{-1}$ where k_d is the first-order rate constant for decomposition of $(C_{10}H_{11})_2N_2$.

Product studies

Oxidation and decomposition products were identified and quantified by high performance liquid phase chromatography using a Varian 5000 liquid chromatograph in conjunction with a Vista 401 chromatography data system. The chromatograph was equipped with a reverse phase column and the eluting solvent was a mixture of acetonitrile and water. Formaldehyde was converted to the formylhydrazone by reaction with a slight excess of 2,4-dinitrophenylhydrazine after trap-to-trap distillation (31). Autoxidations were performed at O_2 pressures of 1 to 100 atm as described previously (3). Yields, unless stated otherwise, were based on the total number of radicals produced in the initiation reaction and were accurate to ~5%.

Results

Products of autoxidation of tetralin

The initial rate of autoxidation of tetralin (1 M) in chlorobenzene, intitiated by di-*tert*-butyl hyponitrite (10.8 mM), under oxygen (1 atm) at 303 K was $5.4 \times 10^{-7}\ M\ s^{-1}$ and the kinetic chain length was 9–10. The major reaction products

Can. J. Chem. Downloaded from www.nrcresearchpress.com by 210.87.254.6 on 09/06/12
For personal use only.

TABLE 1. Products yields as a function of time for thermally initiated autoxidation of tetralin (1 *M*) in chlorobenzene at 303 K[a]

Reaction time (h)	3	9	23	45	120	216
Product	Yield (m*M*)					
$\Delta[BON_2OB]$	0.33	1.0	2.3	4.1	7.7$_4$	9.7
$[O_2]_{abs}$	5.5	16.2	47.5	78	—	—
$C_{10}H_{10}O$	0.29	0.9	3.0	6.25	12	18
$C_{10}H_{11}OH$	0.27	0.8$_2$	1.85	3.5	4.7	4.6
$C_{10}H_{11}OOH$	6.2	12	32	80	90	130
$(C_{10}H_{11})_2O_2$	—	—	0.03	0.06	0.1	0.25
[A]/[K]	0.91	0.91	0.62	0.55	0.4	0.25
$[A]+[K]/[BO^{\cdot}]_f$	0.92	0.95	1.17	1.25	1.2	1.3

[a] P_{O_2} = 1 atm; $[BON_2OB]_0$ = 10.8 m*M*.

TABLE 2. Product yields as a function of time for thermally initiated autoxidation of tetralin (1 *M*) in chlorobenzene at 303 K and 100 atm of O_2

Reaction time (h)	3	7	19	43	73	135
Product	Yield (m*M*)					
$\Delta[BON_2OB]$[a]	0.29	0.67	1.2	3	4.4	6.2
$C_{10}H_{10}O$	0.31	0.54	2.2	5.6	8.7	15.5
$C_{10}H_{11}OH$	0.2	0.34	0.65	1.6	2.4	3.9
$C_{10}H_{11}OOH$	6	7.5	30	55	60	130
$(C_{10}H_{11})_2O_2$	—	—	0.024	0.05	0.055	0.06
[A]/[K]	0.64	0.63	0.3	0.28	0.28	0.25
$[A]+[K]/[BO^{\cdot}]_f$	0.98	0.73	1.3	1.3	1.4	1.7

[a] $[BON_2OB]_0$ = 8.2 m*M*.

TABLE 3. Product yields as a function of time for the thermally initiated autoxidation of tetralin (1 *M*) in chlorobenzene at 353 K[a]

Reaction time (h)	1	4	23
Product	Yield (m*M*)		
$C_{10}H_{10}O$	0.2	0.5	2.1
$C_{10}H_{11}OH$	0.29	0.625	1.4
$C_{10}H_{11}OOH$	11	25	48
$(C_{10}H_{11})_2O_2$	—	0.013	0.027
[A]/[K]	1.4	1.25	0.7

[a] $[AIBN]_0$ = 0.5 m*M*.

were α-tetralin hydroperoxide, α-tetralone, and α-tetralol in the yields given in Table 1. The initial ratio of α-tetralol to α-tetralone, [A]/[K], was 0.9 and decreased gradually as the reaction proceeded. The total yield of alcohol plus ketone was initially ~90% per chain initiated. Clearly α-tetralol and α-tetralone were the major termination products and they were formed in almost equal yields. As the reaction proceeded, the yield of ketone became greater than the yield of alcohol, the latter being close to the yield expected from the toal number of termination reactions. At high conversions (1–2%) there was a minor peak in the hplc with a retention time identical to that for bis(α-tetralyl) peroxide. The maximum yield of this termination product was ~0.7% per initiation radical.

Autoxidation of tetralin under 100 atm of O_2 at 303 K gave the same products as were formed at 1 atm; there was, however, some perturbation of the product yields (Table 2). The yield of alcohol was reduced slightly while the yield of ketone was increased slightly, although the total initial yield was close to 100%. The high pressure of O_2 had no noticeable effect on the rate of decomposition of BON_2OB, very little influence on the rate of autoxidation, and no effect on the yield of $(C_{10}H_{11})_2O_2$.

The AIBN initiated autoxidation of tetralin in chlorobenzene at 353 K gave [A]/[K] = 1.4 after 1 h and 0.7 after 23 h. $(C_{10}H_{11})_2O_2$ was produced with a maximum yield of 2% based on the alcohol yield after 23 h (Table 3).

Autoxidation of tetralin in methanol at 303 K gave the products listed in Table 4. Values of [A]/[K] were much lower than in chlorobenzene and were of the order of 0.1 or less. In addition, the total yield of [A] + [K] was initially only 35–40% and $(C_{10}H_{11})_2O_2$ was not produced. The low yield of tetralol was not due to autoxidation of this product, because the concentration of initially added tetralol (2.7 m*M*) did not decrease in autoxidizing tetralin under standard conditions for 48 h. Separate experiments showed that formaldehyde was formed in this solvent in yields ~ [K] − [A].

Inclusion of benzaldehyde into this system did not influence the yields of alcohol, ketone, and peroxide or [A]/[K] to any appreciable extent. Very little benzoic acid was produced and there was no additional peak in the peroxide region of the chromatogram which could be attributed to ozonide formation.

Induced decomposition of α-tetralin hydroperoxide

The major products of the induced decomposition of $C_{10}H_{11}OOH$ in chlorobenzene, methanol, methanol containing LiCl, and acetonitrile under argon at 303 K were α-tetralol and α-tetralone in the yields summarized in Table 5.

The initial [A]/[K] in chlorobenzene was ~0.9 and decreased to ~0.6 when all the initiator had decomposed. The stoichiometry of the reaction, *n*, ($\Delta[ROOH]/\Delta[BO^{\cdot}]$) was 1 and most of the hydroperoxide decomposed could be accounted for as alcohol and ketone. Bis(α-tetralyl) peroxide was formed with a maximum yield of 0.023 m*M* or 0.3%. [A]/[K] was not influenced to any appreciable extent by an increase in tem-

Can. J. Chem. Downloaded from www.nrcresearchpress.com by 210.87.254.6 on 09/06/12
For personal use only.

TABLE 4. Product yields as a function of time for thermally initiated autoxidation of tetralin (1 *M*) in CH_3OH at 303 K[a]

Reaction time (h)	3	24	45	75	168
Product	Yield (m*M*)				
$\Delta[BON_2OB]$	0.25	1.8	3.0	5.8	6.6
$C_{10}H_{10}O$	0.17	0.9	2.6	6.25	12.5
$C_{10}H_{11}OH$	~0.015	0.25	0.46	0.86	1.2
$C_{10}H_{11}OOH$	1.8	13	16	19	26
$(C_{10}H_{11})_2O_2$	—	—	—	—	~0.007
[A]/[K]	0.09	0.14	0.06	0.08	0.09
$[A]+[K]/[BO^{\cdot}]_t$	0.4	0.35	0.57	0.68	1.1

[a]P_{O_2} = 5 atm; $[BON_2OB]_0$ = 8.0 m*M*.

TABLE 5. Product yields from the induced decomposition of α-tetralin hydroperoxide at 303 K

Time (h)	$[C_{10}H_{11}OOH]$ (m*M*)	$[BON_2OB]$ (m*M*)	Solvent	$[C_{10}H_{11}OH]$ (m*M*)	$[C_{10}H_{10}O]$ (m*M*)	$\frac{[A]}{[K]}$	$\frac{[A]+[K]}{[BO^{\cdot}]_t}$	$\frac{[ROOH]_d}{[BO^{\cdot}]_t}$
0	18.6	5.1	C_6H_5Cl	—	—	—	—	
24.0	16.5	4.0		0.95	1.1	0.9	1.0	1.0
53.2	15.0	2.9		1.65	2.0	0.8	0.9	0.9
119.5	13.5	1.4		2.25	3.0	0.75	0.8	0.8
173	13.0	0.8		2.3	3.4	0.7	0.7	0.7
215.5	12.5	0.53		2.4	3.9	0.6	0.8	1.0
0	17.4	5.7	CH_3OH	—	—	—	—	
19.5	13.0	4.6		0.16	3.0	0.04	1.6	2.2
45.3	12.0	3.5		0.23	4.4	0.05	1.2	1.4
155	10.5	1.1		0.46	8.0	0.06	1.0	0.8
0	21.6	5.5	CH_3OH/LiCl	—	—	—	—	—
5.25	18.0	5.2		0.13	1.6	0.1	3.2	7.0
65.95	7.5	2.7		1.5	15	0.1	3.3	2.8
71.1	0	2.6		1.64	17.4	0.1	1.9	—
434	0	0.06		1.6	17.4	0.1	1.9	—
0	10.0	7.4	CH_3CN	—	—	—	—	—
4	9.5	7.1		0.04	0.25	0.2	0.4	0.9
18.75	7.7	6.1		0.32	0.8	0.4	0.5	1.0
53.1	6.0	4.2		1.0	2.35	0.4	0.6	0.7
95.6	5.4	2.7		1.55	3.6	0.4	0.6	0.5
162	0.7	1.3		1.85	7.0	0.3	0.8	0.85
318	0.1	0.3		1.65	7.8	0.2	0.7	0.8

perature to 353 K, whereas there was a small increase in the yield of $(C_{10}H_{11})_2O_2$. Again, almost all of the hydroperoxide decomposed could be accounted for as $C_{10}H_{10}O$ and $C_{10}H_{11}OH$.

In methanol, [A]/[K] was about 1/20 of the ratio in chlorobenzene and most of the hydroperoxide decomposed gave $C_{10}H_{10}O$ and $C_{10}H_{11}OH$. Formaldehyde was produced in yields ~ [K] − [A]. Initial stoichiometric factors fell between 1 and 2, suggesting some induced decomposition. At higher conversions, where yields could be measured more accurately, *n* values were 1. $(C_{10}H_{11})_2O_2$ was not produced in this solvent and there was no evidence for the formation of methyl α-hydroperoxytetralyl ether. Replacing the argon with 5 atm of O_2 and increasing the temperature to 353 K had no effect on [A]/[K], and $(C_{10}H_{11})_2O_2$ was not produced in either of these experiments. In methanol containing LiCl, [A]/[K] was low, $(C_{10}H_{11})_2O_2$ was not detected, and there was no significant peak in the chromatogram which could be assigned to α-chloro-α-hydroperoxytetralin. The hydroperoxide was, however, decomposed much more rapidly in this system.

[A]/[K] in acetonitrile was less than the value in chlorobenzene but greater than the value in methanol. In this solvent there was no evidence for induced hydroperoxide decomposition since *n* was ~1 throughout the reaction. The yields of alcohol and ketone were, however, consistently just less than 1. The yield of $(C_{10}H_{11})_2O_2$ in CH_3CN was ~0.1%.

It is conceivable that β-scission of $C_{10}H_{11}O_2^{\cdot}$ to give $C_{10}H_{11}^{\cdot}$ and O_2 could play an important role in the chemistry of this peroxyl at ambient temperatures. Decompositions of $C_{10}H_{11}OOH$ were, therefore, conducted under an atmosphere of $^{36}O_2$ at 303, 343, and 353 K. $C_{10}H_{11}{}^{18}OH$ and $C_{10}H_{10}{}^{18}O$ were definitely formed under these conditions but their yields were extremely low (Table 6).

Decomposition of azotetralin in the presence of oxygen

Azotetralin decomposed slowly in solution at 303 K to give α-tetralyls which, in the presence of O_2, were rapidly converted to α-tetralylperoxyls. The major products in chlorobenzene, acetonitrile, and methanol were $C_{10}H_{10}O$, $C_{10}H_{11}OH$, and $C_{10}H_{11}OOH$ in the yields given in Table 7. $C_{10}H_{11}OH$ only appeared after prolonged oxidation and [A]/[K] < 1. $C_{10}H_{11}OOH$ was almost certainly produced by reaction of $C_{10}H_{11}O_2^{\cdot}$ with $(C_{10}H_{11})_2N_2$ and/or the solvent.

Decomposition of azotetralin was faster at 323 K and a 9.6 m*M* solution in C_6H_5Cl absorbed O_2 (1 atm) with a rate of 2.9

Can. J. Chem. Downloaded from www.nrcresearchpress.com by 210.87.254.6 on 09/06/12
For personal use only.

TABLE 6. Product yields from induced decomposition of $C_{10}H_{11}OOH$ in chlorobenzene under an atmosphere of $^{36}O_2$

Temperature	$C_{10}H_{11}OH$ (mM)	$C_{10}H_{11}{}^{18}OH$ (mM)	$C_{10}H_{10}O$ (mM)	$C_{10}H_{10}{}^{18}O$ (mM)
303	6.1	0.5	21.3	1.7
323	0.087	0.009	0.086	0.009
353	1.67	0.33	3.65	0.65

TABLE 7. Product yields in the thermolysis of azotetralin under oxygen (1 atm)

Time (h)	Solvent	Temperature (K)	$[C_{10}H_{11}OH]$ (mM)	$[C_{10}H_{10}O]$ (mM)	$[C_{10}H_{11}OOH]$ (mM)	$\frac{[A]}{[K]}$
16	C_6H_5Cl	303	—	0.04	0.085	—
91			—	0.06	0.24	—
185			2.1	5.5	12.8	0.4
90.83	CH_3CN	303	—	0.26	0.4	—
203.7			0.62	1.3	1.37	0.48
94.3	CH_3OH	303	—	0.2	0.1	—
15	C_6H_5Cl	323	1.65	1.5	6.0	1.1

TABLE 8. Product yields from metal catalyzed decomposition of $C_{10}H_{11}OOH$ at 303 K

Metal	Solvent	$[C_{10}H_{11}OH]$ (mM)	$[C_{10}H_{10}O]$ (mM)	$[C_{10}H_{11}OOH]_0$ (mM)	$[C_{10}H_{11}OOH]_t$ (mM)	$[(C_{10}H_{11})_2O_2]$ (mM)
$Co(acac)_2$	CH_3OH	1.1	0.7	7.4	4.5	0.013
$Co(acac)_2$	C_6H_5Cl	1.5	4	7	~0.1	0.022
$CoSt_2$	C_6H_5Cl	0.3	1.0	8	6.5	—
PbO_2	CH_3OH	2.1	2.3	6.1	2	0.015
PbO_2	C_6H_5Cl	1.65	1.6	6	2.8	0.023

$\times 10^{-8}$ M s^{-1}, suggesting very little induced decomposition of the azo compound. $C_{10}H_{10}O$ and $C_{10}H_{11}OH$ were formed in equal yields and $[C_{10}H_{11}OOH]/([A] + [K])$ was ~1.9.

Induced decomposition of α-$C_{10}H_{11}OOH$ by metal catalysts

The behaviour of $C_{10}H_{11}O_2^{\cdot}$ in solution, at higher steady-state radical concentrations than are encountered in autoxidation and in systems where alkoxyls as well as alkylperoxyls are produced, has been investigated by product studies of the induced decomposition of $C_{10}H_{11}OOH$ by metal catalysts. The results of these studies are summarized in Table 8.

Lead dioxide, which oxidizes a hydroperoxide to its peroxyl, gave $([A] + [K])/\Delta[C_{10}H_{11}OOH] \sim 1$, $[A]/[K] \sim 1$, and $[(C_{10}H_{11})_2O_2]/\Delta[C_{10}H_{11}OOH] = 0.004-0.007$ in chlorobenzene and methanol.

Decomposition of $C_{10}H_{11}OOH$ by $Co(acac)_2$, which gives alkoxyls as well as peroxyls, in chlorobenzene was fast, and ~80% of the hydroperoxide gave $[A]/[K] \sim 0.4$ and $[(C_{10}H_{11})_2O_2]/\Delta[C_{10}H_{11}OOH] \sim 0.003$. Decomposition by $Co(acac)_2$ was much slower in methanol and $([A] + [K])/\Delta[C_{10}H_{11}OOH] \sim 0.62$, $[A]/[K] \sim 1.6$, and $[(C_{10}H_{11})_2O_2]/\Delta[C_{10}H_{11}OOH] \sim 0.004$. Cobalt stearate is less reactive than $Co(acac)_2$ and in chlorobenzene $([A] + [K])/\Delta[C_{10}H_{11}OOH] \sim 0.87$, $[A]/[K] = 0.3$, and no $(C_{10}H_{11})_2O_2$ could be detected. Clearly, in systems which give alkoxyls as well as peroxyls, $[A]/[K]$ is <1 in chlorobenzene and >1 in methanol.

Discussion

Self-reaction of $C_{10}H_{11}O_2^{\cdot}$, prepared by autoxidation of tetralin, induced decomposition of $C_{10}H_{11}OOH$, and autoxidation of azotetralin in chlorobenzene in the temperature range 303–353 K, initially gives equal yields of α-tetralone and α-tetralol with a total yield of ~90%. Low yields of $(C_{10}H_{11})_2O_2$ are, however, definitely produced. These results are contrary to those of Fukuzumi and Ono (32) who found $(C_{10}H_{11}OH]/[C_{10}H_{10}O] = 1.72$ at 291 K for the PbO_2–$C_{10}H_{11}OOH$ initiated autoxidation of tetralin. As the autoxidation of tetralin proceeds, $[A]/[K]$ decreases because of the formation of excess α-tetralone which is almost certainly produced by autoxidation of accumulated α-tetralin hydroperoxide. Thus, at 5–10% conversion, $C_{10}H_{11}O_2^{\cdot}$ has about the same probability of abstracting the α-tertiary hydrogen atom from $C_{10}H_{11}OOH$ as it does reacting with $C_{10}H_{12}$. The resulting α-hydroperoxytetralyl undergoes very rapid β-scission, even in the presence of O_2, to give α-tetralone (reaction [16]).

[16] 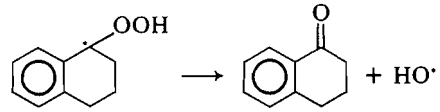

In chlorobenzene, there is no evidence for the involvement of a chain process in the self-reaction of $C_{10}H_{11}O_2^{\cdot}$ and the free-radical induced decomposition of $C_{10}H_{11}OOH$. Furthermore, experiments performed in methanol and in the presence of lithium chloride and benzaldehyde give no evidence for the intermediacy of a zwitterion, which would be expected to give methyl α-hydroperoxytetralyl ether in methanol, α-chloro-α-hydroperoxytetralin in the presence of LiCl, and the ozonide **1** in the presence of benzaldehyde.

[17] 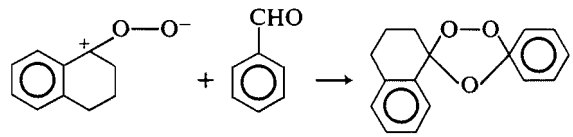

1

Can. J. Chem. Downloaded from www.nrcresearchpress.com by 210.87.254.6 on 09/06/12
For personal use only.

The low yields of bis(α-tetralyl) peroxide and the fact that [A]/[K] in C_6H_5Cl is initially >1 at 323 K do suggest a minor contribution from the free-radical mechanism,

[18] $2C_{10}H_{11}O_2^{\bullet} \rightleftarrows C_{10}H_{11}OOOOC_{10}H_{11} \rightarrow 2C_{10}H_{11}O^{\bullet} + O_2$

$C_{10}H_{11}OOOOC_{10}H_{11} \rightarrow (C_{10}H_{11})_2O_2 + O_2$

This mechanism can, however, only account for ~5–10% of the products at 303 K and is significantly less important in solution than it is in the gas phase.

It could, perhaps, be argued that $(C_{10}H_{11})_2O_2$ is formed by combination of $C_{10}H_{11}^{\bullet}$ and $C_{10}H_{11}O_2^{\bullet}$, since $C_{10}H_{11}O_2^{\bullet}$ undergoes β-scission in the temperature range 303–323 K. The value of the rate constant for β-scission estimated from yields of $C_{10}H_{10}{}^{18}O$ and $C_{10}H_{11}{}^{18}OH$ is, however, less than the value of 2 s^{-1} for α-cumylperoxyl (3) which is in line with the relative stabilization energies of α-tetralyl and cumyl. The steady-state concentration of α-tetralyl would, therefore, be far too low to influence the magnitude of the overall termination rate constant for $C_{10}H_{11}O_2^{\bullet}$ and to be responsible for the low concentrations of $(C_{10}H_{11})_2O_2$ produced by autoxidation of tetralin and induced decomposition of tetralin hydroperoxide. In addition, the yield of $(C_{10}H_{11})_2O_2$ produced by autoxidation of tetralin does not depend on the oxygen pressure, as would be expected if combination of $C_{10}H_{11}^{\bullet}$ and $C_{10}H_{11}O_2^{\bullet}$ is the principal reaction pathway to peroxide formation.

The gas phase reaction of alkoxyl with oxygen to give ketone and hydroperoxyl (reaction [14]) is not an important source of ketone in solution. This is because an alkoxyl, e.g., isopropoxyl, reacts 166 times faster with hydroperoxide than with O_2 at 302 K (23). Consequently, their reactivity towards hydrocarbon and O_2 must be very similar (33). In solution $C_{10}H_{11}O^{\bullet}$ would, therefore, react with $C_{10}H_{12}$ or $C_{10}H_{11}OOH$ rather than O_2.

The low values of [A]/[K] and the low yields of termination products derived from $C_{10}H_{11}O_2^{\bullet}$, given by autoxidation of tetralin and induced decomposition of tetralin hydroperoxide in methanol and acetonitrile, suggest the involvement of solvent derived peroxyls in termination.[4] Thus, in methanol, reaction of α-hydroxylmethylperoxyl with α-tetralylperoxyl to give α-tetralone, formaldehyde, and water should be faster than reaction to give α-tetralol and formic acid because the transfer of a tertiary hydrogen from $C_{10}H_{11}O_2^{\bullet}$ will be faster than the transfer of a secondary hydrogen from $HOCH_2O_2^{\bullet}$ in the cyclic transition state (34).

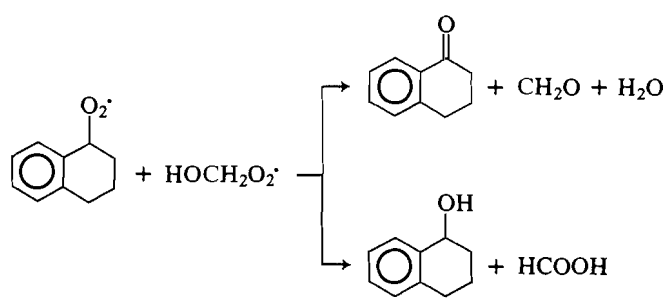

The termination rate constant for $C_{10}H_{11}O_2^{\bullet}$ does not appear to be influenced by a change of solvent from tetralin to methanol (35). This is probably because the radicals in methanol were generated by reaction of $C_{10}H_{11}OOH$ with Ce^{4+}, which oxidizes the hydroperoxide very rapidly, and the present study shows that solvent-derived radicals are not involved under these conditions.

In conclusion, it is apparent from the results presented here that product yields from self-reaction of peroxyls in solution depend on the method of radical generation, the extent of reaction, and the solvent. Mechanistic conclusions from such studies should, therefore, be treated with some caution.

[4]We thank Dr. K. U. Ingold for this suggestion.

1. J. A. HOWARD. Adv. Free Radical Chem. **4**, 49 (1972).
2. J. A. HOWARD. ACS Symp. Ser. **69**, 413 (1978).
3. J. A. HOWARD, J. E. BENNETT, and G. BRUNTON. Can. J. Chem. **59**, 2253 (1981).
4. J. A. HOWARD, J. H. B. CHENIER, and T. YAMADA. Can. J. Chem. **60**, 2566 (1982).
5. E. FURIMSKY, J. A. HOWARD, and J. SELWYN. Can. J. Chem. **58**, 677 (1980).
6. G. A. RUSSELL. J. Am. Chem. Soc. **78**, 1047 (1957).
7. J. A. HOWARD and K. U. INGOLD. J. Am. Chem. Soc. **90**, 1058 (1968).
8. J. A. HOWARD and K. U. INGOLD. J. Am. Chem. Soc. **90**, 1056 (1968).
9. M. NAKANO, K. TAKAYAMA, Y. SHIMIZU, Y. TSUJI, H. INABA, and T. MIGITA. J. Am. Chem. Soc. **98**, 1974 (1976).
10. T. MILL and R. S. STRINGHAM. J. Am. Chem. Soc. **90**, 1062 (1968).
11. R. L. MCCARTHEY and A. MACLACHLAN. J. Chem. Phys. **35**, 1625 (1961).
12. W. A. CRAMER. J. Phys. Chem. **71**, 1171 (1967).
13. A. MACLACHLAN. J. Am. Chem. Soc. **87**, 960 (1965).
14. B. J. BOGAN, J. J. HAVEL, R. A. COVELESKIE, F. CELLII, B. J. STAMMERJOHN, W. A. SANDERS, F. W. WILLIAMS, and H. W. CARHART. Proc. 18th Symp. on Combustion, The Combustion Institute, 1981. p. 843.
15. J. E. BENNETT and R. SUMMERS. Can. J. Chem. **52**, 1377 (1974).
16. D. LINDSAY, J. A. HOWARD, E. C. HORSWILL, L. ITON, and K. U. INGOLD. Can. J. Chem. **51**, 870 (1973).
17. K. ADAMIC, D. F. BOWMAN, T. GILLAN, and K. U. INGOLD. J. Am. Chem. Soc. **93**, 902 (1971).
18. J. A. HOWARD and J. E. BENNETT. Can. J. Chem. **50**, 2374 (1972).
19. P. S. NANGIA and S. W. BENSON. Int. J. Chem. Kinet. **12**, 43 (1980).
20. D. A. PARKES. Int. J. Chem. Kinet. **9**, 451 (1977).
21. K. SELBY and D. J. WADDINGTON. J. Chem. Soc. Perkin Trans. 2, 1259 (1979).
22. C. S. KAN, J. G. CALVERT, and J. H. SHAW. J. Phys. Chem. **84**, 3411 (1980).
23. L. T. COWLEY, D. J. WADDINGTON, and A. WOOLLEY. J. Chem. Soc. Faraday Trans. 1, **78**, 2535 (1982).
24. H. NIKI, P. D. MAKER, C. M. SAVAGE, and L. P. BREITENBACK. J. Phys. Chem. **85**, 877 (1981).
25. H. NIKI, P. D. MAKER, C. M. SAVAGE, and L. P. BREITENBACK. J. Phys. Chem. **86**, 3825 (1982).
26. C. ANASTASI, D. J. WADDINGTON, and A. WOOLLEY. J. Chem. Soc. Faraday Trans. 1, **79**, 505 (1983).
27. R. HIATT and L. ZIGMUND. Can. J. Chem. **48**, 3967 (1970); R. HIATT, T. MILL, K. C. IRWIN, and J. K. CASTLEMAN. J. Org. Chem. **33**, 1428 (1968).
28. W. TRIEBS and G. PELLMAN. Ber. **87**, 1201 (1954).
29. S. G. COHEN and C. H. WANG. J. Am. Chem. Soc. **77**, 2457 (1955).
30. S. SELTZER. J. Am. Chem. Soc. **83**, 2626 (1961).
31. H. TUSS, V. NEITZERT, W. SEILER, and R. NEEB. Fresenius Z. Anal. Chem. **312**, 613 (1982).
32. S. FUKUZUMI and Y. ONO. J. Phys. Chem. **80**, 2973 (1976).

Can. J. Chem. Downloaded from www.nrcresearchpress.com by 210.87.254.6 on 09/06/12
For personal use only.

33. H. PAUL, R. D. SMALL, and J. C. SCAIANO. J. Am. Chem. Soc. **100**, 4520 (1978).
34. J. A. HOWARD and K. U. INGOLD. J. Am. Chem. Soc. **90**, 1058 (1968).
35. J. R. THOMAS and K. U. INGOLD. Adv. Chem. Ser. **75**, 258 (1968).

Can. J. Chem. Downloaded from www.nrcresearchpress.com by 210.87.254.6 on 09/06/12
For personal use only.

Hydrogen bonding and other polar interactions of 1-, 2-, and 4-octyne with organic solvents

JOHN H. HALLMAN, W. KIRK STEPHENSON, AND RICHARD FUCHS
Department of Chemistry, University of Houston, Houston, TX 77004, U.S.A.

Received January 3, 1983

JOHN H. HALLMAN, W. KIRK STEPHENSON, and RICHARD FUCHS. Can. J. Chem. **61**, 2044 (1983).

The heats of vaporization of 1-octyne (10.11 ± 0.02 kcal/mol), 2-octyne (10.63 ± 0.03 kcal/mol), and 4-octyne (10.21 ± 0.02 kcal/mol) have been determined. Heats of solution of the liquid octynes and *n*-octane have been measured in heptane, cyclohexane, 1,2-dichloroethane, *n*-butyl ether, ethanol, triethylamine, dimethyl sulfoxide, butyrolactone, dimethylformamide, and hexamethylphosphoric triamide. Enthalpies of transfer from vapor to each solvent have been calculated. Enthalpies of hydrogen bond formation, calculated by the pure base method, become more exothermic in the above solvent order. Correlations with the Taft–Kamlet solvent parameters π^* and β indicate that other polar interactions (presumably dipole – induced dipole) are appreciably larger for 1-octyne than for 2- and 4-octyne.

JOHN H. HALLMAN, W. KIRK STEPHENSON et RICHARD FUCHS. Can. J. Chem. **61**, 2044 (1983).

On a déterminé les chaleurs de vaporisation de l'octyne-1 (10,11 ± 0,02 kcal/mol), de l'octyne-2 (10,63 ± 0,03 kcal/mol) et de l'octyne-4 (10,21 ± 0,02 kcal/mol). On a mesuré les chaleurs de solution des octynes et du *n*-octane à l'état liquide dans l'heptane, le cyclohexane, le dichloro-1,2 éthane, l'éther *n*-butylique, l'éthanol, la triéthylamine, le diméthylsulfoxyde, la butyrolactone, le diméthylformamide et le triamide de l'acide hexaméthylphosphorique. On a calculé les enthalpies de transfert de la vapeur vers chaque solvant. Les enthalpies de formation de la liaison hydrogène, calculées selon la méthode de base pure, deviennent plus exothermiques quand on passe d'un solvant à un autre dans l'ordre mentionné ci-dessus. Les corrélations avec les paramètres de solvant de Taft–Kamlet π^* et β indiquent que d'autres interactions polaires (possiblement dipole – dipole induit) sont notamment plus grandes pour l'octyne-1 que pour l'octyne-2 et l'octyne-4.

[Traduit par le journal]

Can. J. Chem. Downloaded from www.nrcresearchpress.com by 210.87.254.6 on 09/06/12
For personal use only.

Hydrogen bonding by the acetylenic hydrogen (—C≡C—H) to electron-pair donating solvents has been examined (1) by infrared spectroscopy (1, 2), ^{1}H and ^{13}C nmr (1, 3), thermodynamically (1, 4), and by other methods (1). Enthalpies of hydrogen bond formation (ΔH_f) have been evaluated from (*i*) the temperature variation in equilibrium constants (3) (*K* measured by ir or nmr), (*ii*) enthalpies of transfer of alkynes from an "inert" solvent to basic solvents, determined from differences in the enthalpies of transfer from vapor to solvents ($\Delta H(v \rightarrow S)$) (derived from the temperature variation of partition coefficients measured by gas chromatography) (4), and (*iii*) the combination of equilibrium constants from spectrophotometric measurements and calorimetric enthalpies of mixing (2).

Each of these methods has some inherent problems. Equilibrium constants measured by ir or nmr are believed to reflect only hydrogen bonding interactions, but the sometimes poor agreement between the two methods, and the variation in *K* with the "inert" solvent medium are distressing. After measurement of the temperature variation of *K*, the resulting uncertainties in ΔH_f (0.3–0.6 kcal/mol) are typically 20–30% of the experimental values (1–3 kcal/mol). Direct enthalpy measurements, whether by gc or calorimetrically, are intrinsically less uncertain, but provide no information about the nature of the solute–solvent interactions, the completeness of the interactions, and other factors, which determine that enthalpy. Kurkchi and Iogansen's enthalpies of transfer of acetylene, propyne, and 1-butyne from "isooctane" to basic solvents (4) have been correlated (5) with the solvent parameters π^* and β, representing the dipolarity–polarizability and H-bond acceptor abilities, respectively:

$$\Delta H_{tr}(H—C\equiv C—H) = -0.10 - 1.56\pi^* - 3.56\beta \text{ kcal/mol}$$

$n = 8$ solvents; correlation coefficient, $r = 0.997$;

standard deviation, sd = 0.14 kcal/mol

$$\Delta H_{tr}(CH_3C\equiv CH) = -0.06 - 1.24\pi^* - 1.17\beta \text{ kcal/mol}$$

$r = 0.980$, sd = 0.15 kcal/mol

$$\Delta H_{tr}(CH_3CH_2C\equiv CH) = -0.04 - 1.12\pi^* - 0.88\beta \text{ kcal/mol}$$

$r = 0.976$, sd = 0.15 kcal/mol

The correlations indicate that each of the two H-bonds of acetylene, and the H-bonds of propyne and 1-butyne are comparable to the other solvent – alkyne polar interactions (mainly dipole – induced dipole). Kamlet and Taft (5) note that the solvents are all H-bond acceptors at an oxygen atom, and the enthalpy correlations with π^* and β would likely be poorer for solvents with other acceptor sites. This follows from the observation (6) that ΔH and ΔG of H-bonding of *p*-fluorophenol with a wide variety of solvents are poorly correlated except within closely related families, and the suggestion (7) that the solvatochromic parameters are generally correlated with ΔG.

There are other reservations about the above correlation (5) of the ΔH_{tr} data (4). One is the substantial correlation of π^* and β for this particular group of solvents ($\pi^* = 0.156 + 0.921\beta$, $r = 0.881$, sd = 0.123), which makes the quantitative separation of H-bonding and other polar interactions somewhat tenuous. The other problem is more serious. ΔH_{tr} (isooctane → solvent) results not only from exothermic H-bonding and other polar interactions with the solvent, but also from an endothermic contribution from the enthalpy of cavity formation within the solvent structure. The latter quantity tends to increase with increasing solvent polarity, and with increasing solute size. The apparent decreasing response to changes in solvent π^* and β in the series acetylene > propyne > 1-butyne, attributed (5) to the electronic properties of the H, CH_3, and CH_3CH_2 substituents, may result, in part, from failure to take into account variations in the cavity formation term.

With these reservations in mind, we have undertaken a cal-

TABLE 1. Heats of solution of 1-, 2-, and 4-octyne and *n*-octane (kcal/mol)[a]

Solvent	ΔH_s			
	n-C_8	1-Octyne	2-Octyne	4-Octyne
n-Heptane	−0.01±0.01	0.54±0.02	0.44±0.02	0.35±0.01
Cyclohexane	0.43±0.02	0.89±0.01	0.69±0.02	0.53±0.02
1,2-Dichloroethane	2.41±0.06	0.83±0.02	0.77±0.02	0.87±0.03
n-Butyl ether	0.08±0.01	−0.21±0.02	−0.08±0.01	−0.07±0.01
γ-Butyrolactone	3.03±0.05	0.77±0.02	1.26±0.02	1.32±0.05
Triethylamine	0.08±0.02	−0.43±0.04	−0.10±0.01	−0.08±0.01
Ethanol	0.93±0.03	0.33±0.01	0.67±0.02	0.63±0.01
N,*N*-Dimethylformamide	2.52±0.07	0.04±0.01	0.91±0.01	1.08±0.02
Hexamethylphosphoric triamide	1.36±0.04	−1.76±0.03	0.02±0.05	0.06±0.02
Dimethyl sulfoxide	4.03±0.28	1.23±0.05	1.70±0.02	1.72±0.09

[a]The indicated uncertainties are twice the standard deviations.

TABLE 2. Enthalpies of transfer of 1-, 2-, and 4-octyne and *n*-octane from vapor to solvents (kcal/mol)

Solvent	$-\Delta H(v \rightarrow S)$			
	n-Octane	1-Octyne	2-Octyne	4-Octyne
n-Heptane	9.93±0.01	9.57±0.03	10.19±0.04	9.86±0.02
Cyclohexane	9.49±0.03	9.22±0.03	9.94±0.04	9.68±0.03
1,2-Dichloroethane	7.51±0.07	9.28±0.03	9.86±0.04	9.34±0.03
n-Butyl ether	9.84±0.01	10.32±0.03	10.71±0.03	10.28±0.02
Butyrolactone	6.89±0.08	9.34±0.03	9.37±0.04	8.89±0.05
Triethylamine	9.84±0.03	10.54±0.05	10.73±0.03	10.29±0.02
Ethanol	8.99±0.03	9.78±0.03	9.96±0.04	9.58±0.02
DMF	7.40±0.07	10.07±0.03	9.72±0.03	9.13±0.03
HMPT	8.56±0.04	11.87±0.07	10.61±0.06	10.15±0.03
DMSO	5.89±0.28	8.88±0.06	8.93±0.04	8.49±0.09

orimetric study of the interactions of 1-, 2-, and 4-octyne and *n*-octane with 10 solvents, *n*-heptane, cyclohexane, 1,2-dichloroethane, *n*-butyl ether, butyrolactone, triethylamine, ethanol, dimethylformamide, hexamethylphosphoric triamide, and dimethyl sulfoxide. This solvent group has a much reduced correlation of π^* with β, and includes triethylamine, with a non-oxygen H-bond acceptor atom. The use of *n*-octane as a nonpolar model compound for the octynes is intended to eliminate cavity formation considerations. 2-Octyne and 4-octyne cannot donate a hydrogen for H-bonding, but are capable of other polar (dipole − induced dipole) interactions; in this way they may be useful models for evaluating H-bonding by 1-octyne.

Experimental

The solvents were commercial samples in excess of 99% purity, dried over 3A molecular sieve (ethanol), 10X (HMPT), or 4A molecular sieve. Triethylamine was distilled from ninhydrin to remove primary and secondary amine impurities. The octynes (Farchan Labs) were freshly fractionally distilled, and refrigerated. Heat of vaporization samples were 1-octyne (99.96%), 2-octyne (99.80%), 4-octyne (99.95%), and *n*-octane (99.9%). Purities were established by gas chromatography using a Shimadzu Mini 2 gc with a glass lined system, a 30 m × 0.25 mm id SE-30 silica capillary column, and a Hewlett-Packard 3390A integrator.

The calorimetric procedure and apparatus have previously been described (8). The calorimeter was immersed in a 25.0°C water bath regulated to ±0.002°C. Liquid solutes were introduced from 20- or 50-μL syringes, and corrections in ΔH_s were made for the heat capacity of the samples which were at 21−23°C. The uncertainties reported for ΔH_s in Table 1 are twice the standard deviation of three or more determinations. In measuring ΔH_s of *n*-octane in DMSO the glass top of the vacuum jacketed solution calorimeter was replaced by a Teflon top which nearly eliminates vapor space above the liquid.

Heats of vaporization were determined by evaporation of 100 μL samples into a slow stream of nitrogen (0.5−3 mL/min) under reduced pressure (12−49 torr) at 25.0°C. The vaporization calorimeter consists of a coiled 4.76 mm od nickel tube imbedded in a copper heat sink in which are mounted a thermistor and heater. The assembly is contained in a vacuum jacketed solution calorimeter. The evaporative cooling was compensated by heating powered by a timed constant current source (9). The values of ΔH_v are averages of 4−6 determinations, and the uncertainties are twice the standard deviation.

Results and discussion

The measured values of ΔH_v are: *n*-octane, 9.91 ± 0.02 kcal/mol (reported (10) 9.92 ± 0.01); 1-octyne, 10.11 ± 0.02; 2-octyne, 10.63 ± 0.03; and 4-octyne, 10.21 ± 0.02. These values have been combined with heats of solution (Table 1) to obtain the enthalpies of transfer from vapor to solvents in Table 2: $\Delta H(v \rightarrow S) = \Delta H_s - \Delta H_v$.

Two methods may be used to evaluate the enthalpies of H-bonding (ΔH_f) of 1-octyne. In one (the $\Delta\Delta H(v \rightarrow S)$ method) (11) the assumption is made that the more exothermic value of $\Delta H(v \rightarrow S)$ for 1-octyne, relative to the values of comparable non-donor model compounds (2-octyne, 4-octyne), can be attributed entirely to the enthalpy of hydrogen bond formation. It has been pointed out (11), however, that the H-bond donor and model compound must be very carefully matched with respect to molar volume and the ability to undergo other interactions. The solute molar volumes are: *n*-octane, 162.6 mL; 1-octyne, 147.7 mL; 2-octyne, 145.1 mL; and

Can. J. Chem. Downloaded from www.nrcresearchpress.com by 210.87.254.6 on 09/06/12
For personal use only.

TABLE 3. Enthalpies of hydrogen bond formation (kcal/mol)

	(1-Octyne) − (2-octyne)		(1-Octyne) − (4-octyne)	
Solvent	$\Delta\Delta H$(v → S)	ΔH_f pure base	$\Delta\Delta H$(v → S)	ΔH_f pure base
n-Heptane	0.62	0.00	0.29	0.00
Cyclohexane	0.72	0.10	0.45	0.17
1,2-Dichloroethane	0.58	−0.04	0.06	−0.23
n-Butyl ether	0.39	−0.23	−0.04	−0.33
Butyrolactone	0.03	−0.59	−0.45	−0.74
Triethylamine	0.19	−0.43	−0.25	−0.54
Ethanol	0.18	−0.44	−0.20	−0.49
DMF	−0.35	−0.97	−0.94	−1.23
HMPT	−1.26	−1.88	−1.72	−2.01
DMSO	0.05	−0.57	−0.39	−0.68

4-octyne, 146.8 mL. The MV increment for the CH_2 group is ~ 16 mL. The octynes are well matched in this respect, but at this point we cannot confidently equate the polar interactions (other than H-bonding) of each.

An alternative approach is the pure base method (12), by which ΔH_f is evaluated in a basic solvent with reference to a nonpolar solvent incapable of H-bonding (heptane):

$$\Delta H_f = (\Delta H_s^A - \Delta H_s^M)_B - (\Delta H_s^A - \Delta H_s^M)_{ref}$$

where A is the H-bond donor solute (1-octyne), M is the model compound (2- or 4-octyne), B is a basic (H-bond acceptor) solvent, and ref is the nonpolar reference solvent.

ΔH_f values for 1-octyne have been calculated by both methods using both model compounds (Table 3). It has been demonstrated (11) that the two methods are equivalent only when

$$\Delta H^A(v \rightarrow ref) = \Delta H^M(v \rightarrow ref)$$

and that is not the case for this system (Table 2). The values of ΔH_f for 1-octyne in heptane calculated by the $\Delta\Delta H_f$ (v → S) method (0.62 vs. 2-octyne, 0.29 vs. 4-octyne) are indications of the degree to which the model compounds are inappropriate. One could normalize the values of ΔH_f by assigning the value ΔH_f(heptane = 0, and adjusting ΔH_f in other solvents accordingly, but this is exactly what is accomplished by the pure base method without the need of measuring ΔH_v values and calculating ΔH (v → S). However, the pure base method is also dependent on appropriate model compounds. If we fail to obtain values of ΔH^A (v → ref) and ΔH^M (v → ref), there will be no independent way to assess the quality of the model compound. It should be noted that the difference of 0.62 kcal/mol between ΔH (v → heptane) for 1-octyne and 2-octyne leads to an error at least this large in ΔH_f values in each solvent by the $\Delta\Delta H$ (v → S) method, but this error is partially cancelled by the pure base method. But if 1-octyne and the model compound have different values of ΔH (v → S) in nonpolar, non-hydrogen bonding heptane due to differences in molar volume, dipole moment, steric hindrance to solvation, etc., then the difference in the other more polar and associated solvents may very well be larger. In the pure base method we must assume that the 0.62 kcal/mol correction (for 1-octyne vs. 2-octyne) remains substantially unchanged in other solvents, but this cannot be experimentally verified. Values of ΔH_f by the pure base method (Table 3) for 1-octyne vs. 2-octyne indicate that (within little more than the combined uncertainties) no H-bonding occurs in *n*-heptane, cyclohexane, and 1,2-dichloroethane. ΔH_f in butyl ether is surprisingly weak, although this may reflect, in part, incomplete complexation. It was also unexpected that ΔH_f is more exothermic in butyrolactone and DMF than in DMSO. Values in butyl ether and HMPT are somewhat less exothermic than previous values for phenylacetylene (2, 3) (−1.4 ± 0.3 kcal/mol in ethyl ether, −3.7 ± 0.3 kcal/mol in HMPT).

In order to examine correlations of polar interactions of the octynes with the Taft−Kamlet solvent parameters π^* and β (13) in the absence of substantial solvent cavity formation enthalpy complications, the enthalpies of polar interaction (ΔH_p) (including ΔH_f for 1-octyne) have been calculated. This is entirely analogous to the pure base method except that the model compound for all the octynes is *n*-octane. These results are presented in Table 4.

The resulting regression equations are:

$$\Delta H_{f,p}\text{ (1-octyne)} = -0.03 - 2.62\pi^* - 1.05\beta$$

$$n = 9,\ r = 0.993,\ \text{sd} = 0.114$$

$$\Delta H_p\text{ (2-octyne)} = -0.18 - 2.28\pi^*$$

$$r = 0.982,\ \text{sd} = 0.134$$

$$\Delta H_p\text{ (4-octyne)} = -0.11 - 2.16\pi^*$$

$$r = 0.977,\ \text{sd} = 0.151$$

Ethanol has been omitted from the correlations because of the present uncertainty in the solvent parameter values for amphiprotic solvents. The non-zero intercept results, in part, from our use of *n*-heptane as the reference solvent, whereas the π^* scale uses cyclohexane as the reference (π^*(heptane) = −0.08, π^* (cyclohexane) = 0.00). Multiple correlations with π^* and β for 2-octyne and 4-octyne lead to inappreciable improvement in the correlation coefficients and standard deviations. This would be expected for species which are not H-bond donors. Because of the substantial uncertainty in π^* and β values for hexamethylphosphoric triamide (13) the regression equation for 1-octyne has been recalculated omitting HMPT (and ethanol):

$$\Delta H_{p,f}\text{ (1-octyne)} = -0.08 - 2.63\pi^* - 0.82\beta$$

$$n = 8,\ r = 0.996,\ \text{sd} = 0.080$$

We suspect that this is a more accurate representation of the weak H-bonding behavior of 1-octyne. Values for HMPT of $\pi^* = 0.71$, $\beta = 2.10$ would fit the present data rather well, but there is no reason to believe that these are appropriate to

Can. J. Chem. Downloaded from www.nrcresearchpress.com by 210.87.254.6 on 09/06/12
For personal use only.

TABLE 4. Enthalpies of total polar interactions of 1-, 2-, and 4-octyne (vs. *n*-octane) by the pure base method (kcal/mol)

Solvent	π^{*a}	β^b	$-\Delta H_{t,p}$ (1-octyne)	$-\Delta H_p$ (2-octyne)	$-\Delta H_p$ (4-octyne)
n-Heptane	−0.08	0.00	0.00	0.00	0.00
Cyclohexane	0.00	0.00	0.09	0.19	0.10
1,2-Dichloroethane	0.81	0.00	2.13	2.09	1.90
n-Butyl ether	0.24	0.46	0.84	0.61	0.51
Butyrolactone	0.87	0.49	2.81	2.22	2.07
Triethylamine	0.14	0.71	1.06	0.63	0.63
Ethanol	0.54	0.77	1.15	0.71	0.66
DMF	0.88	0.69	3.03	2.06	2.06
HMPT	0.87	1.05	3.67	1.79	1.79
DMSO	1.00	0.76	3.35	2.78	2.78

[a]Solvent dipolarity−polarizability parameters from ref. 13.
[b]Solvent H-bond acceptor parameters from ref. 13.

other systems. It is noteworthy that correlations for the solvent triethylamine are excellent; this contrasts with the expectations of Kamlet and Taft (5).

Acknowledgements

The authors wish to thank Dr. Mortimer J. Kamlet for helpful discussion, and both Dr. Kamlet and Professor Stanley N. Deming for the least-squares correlation equations. This study was supported by the Robert A. Welch Foundation (Grant E-136).

1. R. D. GREEN. Hydrogen bonding by C-H groups. Wiley, New York. 1974.
2. J. C. BRAND, G. EGLINTON, and J. F. MORMAN. J. Chem. Soc. 2526 (1960).
3. V. D. ZIESSOW and E. LIPPERT. Ber. Bunsenges. Physik. Chem. **74**, 13 (1970).
4. G. A. KURKCHI and A. V. IOGANSEN. Russ. J. Phys. Chem. **41**, 283 (1967).
5. M. J. KAMLET and R. W. TAFT. Pol. J. Chem. 1341 (1981).
6. E. M. ARNETT, E. J. MITCHELL, and T. S. S. R. MURTY. J. Am. Chem. Soc. **96**, 3875 (1974).
7. R. W. TAFT, N. J. PIENTA, M. J. KAMLET, and E. M. ARNETT. J. Org. Chem. **46**, 661 (1981).
8. R. FUCHS and P. P. S. SALUJA. Can. J. Chem. **54**, 3857 (1976).
9. R. FUCHS. J. Chem. Educ. **58**, 594 (1981).
10. J. D. Cox and G. PILCHER. Thermochemistry of organic and organometallic compounds. Academic Press, New York. 1970.
11. R. FUCHS, L. A. PEACOCK, and W. K. STEPHENSON. Can. J. Chem. **60**, 1953 (1982).
12. E. M. ARNETT, L. JORIS, E. J. MITCHELL, T. S. S. R. MURTY, T. M. GORRIE, and P. V. R. SCHLEYER. J. Am. Chem. Soc. **92**, 2365 (1970).
13. M. J. KAMLET, J. L. M. ABBOUD, and R. W. TAFT. Progr. Phys. Org. Chem. **13**, 485 (1981).

Can. J. Chem. Downloaded from www.nrcresearchpress.com by 210.87.254.6 on 09/06/12
For personal use only.

Raman spectra of sodium sulphamate single crystal

P. MUTHUSUBRAMANIAN AND A. SUNDARA RAJ
School of Physics, Madurai Kamaraj University, Madurai - 625 021, India

Received March 16, 1982

P. MUTHUSUBRAMANIAN and A. SUNDARA RAJ. Can. J. Chem. **61**, 2048 (1983).

Vibrational assignments are proposed for solid $NaNH_2SO_3$ on the basis of room temperature polarized Raman spectra of single crystals. Infrared data for the region 4000–50 cm^{-1} of the polycrystalline sample are also presented. The results indicate that (*1*) there is no water of crystallization, (*2*) the hydrogen bonding is extremely weak, and (*3*) the strength of N—S bond is stronger than in sulphamic acid.

P. MUTHUSUBRAMANIAN et A. SUNDARA RAJ. Can. J. Chem. **61**, 2048 (1983).

On propose des attributions vibrationnelles pour le $NaNH_2SO_3$ à l'état solide sur la base du spectre Raman polaire à température ambiante de cristaux uniques. On présente également les données IR s'étendant de 4000 à 50 cm^{-1} se rapportant à un échantillon polycristallin. Les résultats indiquent que (*1*) il n'y a pas d'eau de cristallisation, (*2*) les liaisons hydrogènes sont entièrement faibles et (*3*) la force de la liaison N—S est supérieure à celle de l'acide sulphamique.
[Traduit par le journal]

Can. J. Chem. Downloaded from www.nrcresearchpress.com by 210.87.254.42 on 09/06/12
For personal use only.

Introduction

The wide industrial applications of the salts of sulphamic acid necessitate a thorough study of their various physical and chemical properties in the crystalline state. The review article by Benson and Spillane (1) describes the present status of these salts in the literature. We have already reported the polarized Raman spectra of potassium (2) and ammonium (3) sulphamates. We report here the results obtained for the laser Raman spectra of a single crystal of sodium sulphamate ($NaNH_2SO_3$) together with the ir spectra of the polycrystalline sample.

Some pre-laser Raman (4) and ir studies (4, 5) have been reported. Katiyar and Krishnan (4) observed only eight lattice modes and this is the latest Raman data on this crystal. Also, there is a discrepancy regarding the presence of water molecules in the crystal. The present study was undertaken in order to investigate this discrepancy and the nature of hydrogen bonding as well as to make a complete analysis of the vibrational spectra of the crystalline solid.

Experimental

Single crystals of sodium sulphamate were grown by slow evaporation at room temperature (30–35°C) from a solution of sulphamic acid neutralized with sodium carbonate. From the small needle-type crystals a rectangular parallelopiped of size 3 × 1.5 × 1 mm with its faces parallel to the crystallographic axes was cut using crossed polaroids. The axes were identified by X-ray photographs. The Raman spectra were excited using a 40 mW He–Cd laser (4416 Å) and recorded on a double monochromator of resolution about 2.5 cm^{-1}. A constant scanning speed of 40 cm^{-1}/min was employed throughout the experiment with a time constant of 10 s. The other experimental details about the recording of polarized Raman spectra have been described in an earlier paper (2).

The ir spectrum of polycrystalline $NaNH_2SO_3$ (KBr pellet) in the 4000–200 cm^{-1} region was recorded on a Perkin-Elmer Model 577 spectrophotometer. The far-ir spectrum (500–50 cm^{-1}) was recorded using a Polytec FIR 30 spectrometer.

Crystal structure

No complete crystal structure data are yet available for $NaNH_2SO_3$. However, the preliminary X-ray diffraction study (6) shows that the compound crystallizes in the orthorhombic system with 12 molecules per unit cell and belongs to the space group D_2^4 ($P2_12_12_1$). There is no water of crystallization in this crystal. The site symmetry of the sulphamate ion is C_1. Finally, sodium sulphamate is not isomorphous to the potassium salt (7).

TABLE 1. Mode distribution of the $NaNH_2SO_3$ crystal

	A	B_1	B_2	B_3	Total
Internal	45	45	45	45	180
Libratory	9	9	9	9	36
Translatory	18	17	17	17	69
Acoustic		1	1	1	3

Factor group analysis

The symmetry of the sulphamate ion is C_s, which is lowered to C_1 in the crystal. Correlating the free state symmetry with the factor group D_2 of the crystal through the site symmetry leads to the distribution of modes shown in Table 1. Since the crystal is noncentrosymmetric, all modes are Raman-active and all modes except those belonging to A species are ir-active. Out of the total 288 modes, 180 are internal modes of the $(NH_2SO_3)^-$ ion and they are equally distributed in the four different representations. The free state distribution is $\Gamma_{int.}^{free} = 9A' + 6A''$. Thus, we expect a triplet for each internal vibration in each species of the polarized Raman spectra. The remaining 108 modes are due to the external vibrations consisting of (*i*) libratory modes of $(NH_2SO_3)^-$, (*ii*) translatory modes of $NaNH_2SO_3$, and (*iii*) acoustic modes. The polarizability tensors (8) for this crystal are the same as those of the space group D_{2h}.

Results and discussion

The observed Raman and ir frequencies are given in Tables 2 and 3. The Raman and ir measurements are accurate to ±2 cm^{-1} and ±1 cm^{-1} respectively. Due to practical difficulties, the α_{zz} component of the Raman spectra was not recorded. The assignments of external and internal modes are discussed separately in the following sections.

External modes

From the factor group analysis, there are nine libratory modes in each representation. Also, a total of 69 translatory modes is expected. This large number of modes is due to the presence of 12 molecules in the unit cell. However, we observed only 13 libratory and 15 translatory modes. Even though fewer modes than expected are detected, the observed frequencies contain the three libratory and six translatory modes. The large number of missing bands may be due to very small correlation field splitting.

The observed Raman and far-ir frequencies along with their assignments are given in Table 2. Typical Raman spectra in different orientations are shown in Fig. 1 and the far-ir spec-

TABLE 2. Frequencies (in cm^{-1}) observed in Raman and far-ir spectra of crystalline $NaNH_2SO_3$ in the external mode region*

A		B_1	B_2	B_3		
xx	*yy*	*xy*	*zx*	*zy*	Far ir	Assignment
		34(m)				*T'*
		44(w)	41(w)			*T'*
		70(vw)	72(w)	67(w)	68	*T'*
79(w)	77(vw)		76(w)			*T'*
	89(w)	84(vw)	92(vw)	85(vw)	87	*T'*
101(w)		95(w)			94	*T'*
114(w)	118(vw)				117	*R'*
128(m)		123(vw)	123(vw)			
134(vw)				133(w)		*R'*
143(w)			149(vw)		148	
		172(vw)	176(w)		170	*R'*
196(vw)			190(w)		212	

*The letters m, w, and vw given in parentheses represent medium, weak, and very weak intensities respectively. $T' \rightarrow$ translatory; $R' \rightarrow$ libratory.

TABLE 3. Frequencies (in cm^{-1}) observed in Raman and ir spectra of crystalline $NaNH_2SO_3$ in the region 250–3600 cm^{-1}

A		B_1	B_2	B_3		
xx	*yy*	*xy*	*zx*	*zy*	Infrared	Assignment
		285(vw)	286(vw)	285(vw)	301(vw)	$\nu_{15}(A'')$ N—S torsion
	326(vw)		329(w)	330(vw)	323(w)	?
350(w)	351(vw)	340(w)	353(w)	349,355(w)	364(vw)	$\nu_9(A')$ SO_3 sym. rocking
398(m)	400(w)	400(m)	400(s)	398(w)	385(w)	$\nu_{14}(A'')$ SO_3 asym. rocking
		416(m)	418(m)			
			473(w)	473(vw)		$\nu_8(A')$ SO_3 sym. deformation
500(w)				498(vw)		
559(m)	559(vw)	558(s)	559(m)	563(m)	567(s)	$\nu_7(A')$ SO_3 sym. deformation
572(s)	575(w)		573(w)	575(s)	575(s)	
		589(vw)	587(w)	590(s)	595(m)	$\nu_{13}(A'')$ SO_3 asym. deformation
592(m)	595(m)	599(w)	595(w)		604(m)	
680(w)					712(vw)	$2\nu_9$
789(s)	791(w)	790(vw)	791(vw)	789(w)	792(s)	$\nu_6(A')$ N—S stretching
867(vs)	869(m)	871(vw)	871(w)	869(w)	886(m)	$\nu_5(A')$ NH_2 sym. wagging
898(s)	904(m)	911(w)	906(w)	904(w)	910(w)	
1046(s)	1050(m)	1053(vw)	1049(w)	1049(w)	1057(s)	
1067(vs)	1071(vs)	1069(vw)	1065(w)	1071(w)	1070(w)	$\nu_4(A')$ SO_3 sym. stretching
			1077(w)		1081(s)	
		1121,1131(w)	1134(w)	1122(w)	1139(m)	$\nu_{12}(A'')$ NH_2 asym. rocking
1183(s)	1184(m)	1195(w)	1187(m)	1191(m)	1194(s)	$\nu_3(A')$ SO_3 sym. stretching
1232(vw)	1233(w)	1235(m)		1232(w)		
1248(vw)		1242(m)	1243(w)		1244(m)	$\nu_{11}(A'')$ SO_3 asym. stretching
1269(w)	1269(vw)			1266(w)	1256(vw)	
		1286(vw)	1277(w)		1293(m)	$\nu_5+\nu_{14}$?
1536(vw)		1542(vw)	1548(w)	1554(vw)	1563(w)	$\nu_2(A')$ HNH bending
			1604(vw)			$2\nu_6$
		2975(vw)		2693(vw)		
					3076(vw)	$2\nu_2$
3208(m)	3213(vw)				3190(w)	$\nu_1(A')$ NH_2 sym. stretching
	3251(vw)		3250(w)		3266(m)	
3286(w)	3285(w)					
3309(w)	3304(w)	3308(w)	3312(w)	3310(w)	3312(m)	$\nu_{10}(A'')$ NH_2 asym. stretching
	3363(w)	3374(vw)		3374(w)	3352(m)	

*The letters s, vs, m, w, and vw given in parentheses represent strong, very strong, medium, weak, and very weak intensities respectively.

trum in Fig. 2. The assignment of the frequencies has been made on the basis of a comparison of the lattice modes in other sulphamates (2, 3). Also, it has been assumed that the moment of inertia of sulphamate ion is smaller than the mass of sodium sulphamate molecule. The assignments reveal that the frequencies of libratory modes of $(NH_2SO_3)^-$ ion in this crystal are slightly higher than those in potassium and ammonium sulphamates. In the *A* species of the spectrum, the *xx* polarization

Can. J. Chem. Downloaded from www.nrcresearchpress.com by 210.87.254.42 on 09/06/12
For personal use only.

Can. J. Chem. Downloaded from www.nrcresearchpress.com by 210.87.254.42 on 09/06/12
For personal use only.

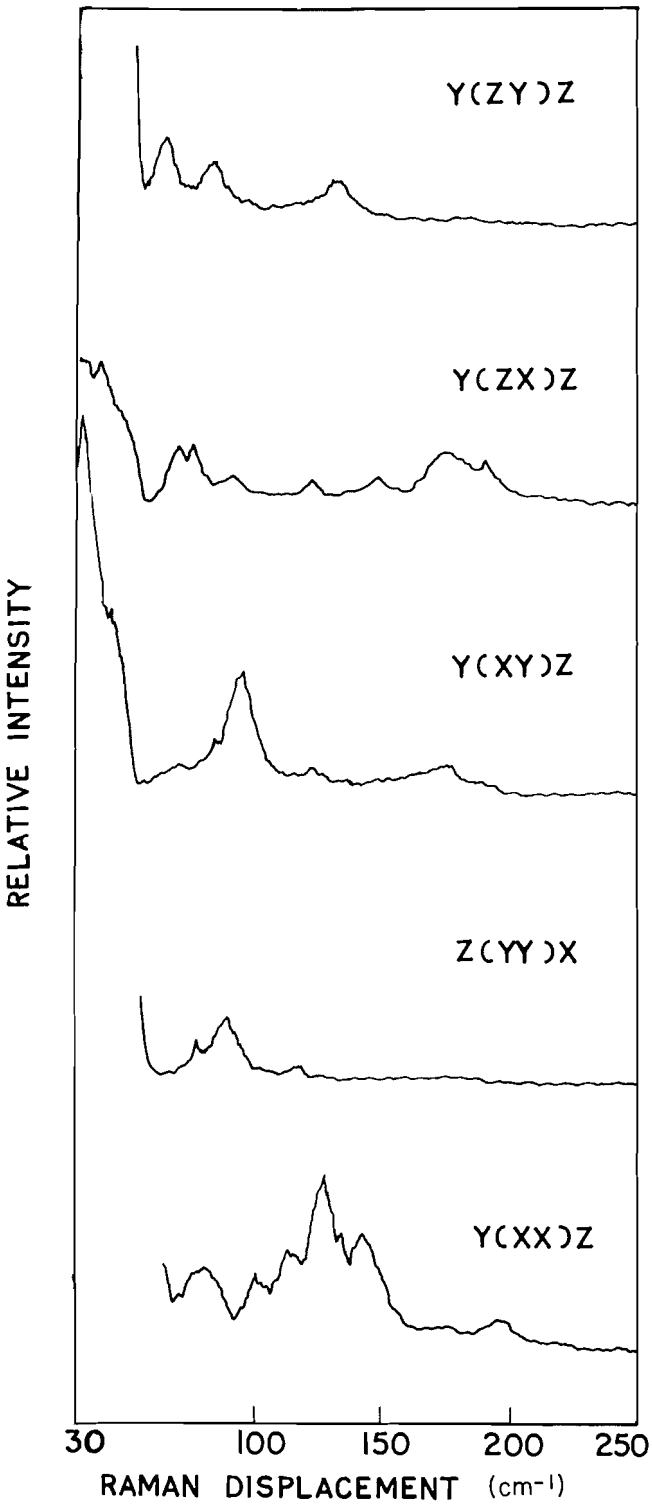

FIG. 1. Raman spectra of $NaNH_2SO_3$ (single crystal) in the 250–30 cm^{-1} region.

component is much stronger than the *yy* polarization component. The intensities given in parentheses are relative intensities of bands throughout the whole region (3600–30 cm^{-1}) including the internal modes. In the far-ir spectra, seven bands are observed and they have been assigned in conjunction with the Raman frequencies.

Internal modes

The observed Raman displacements of crystalline

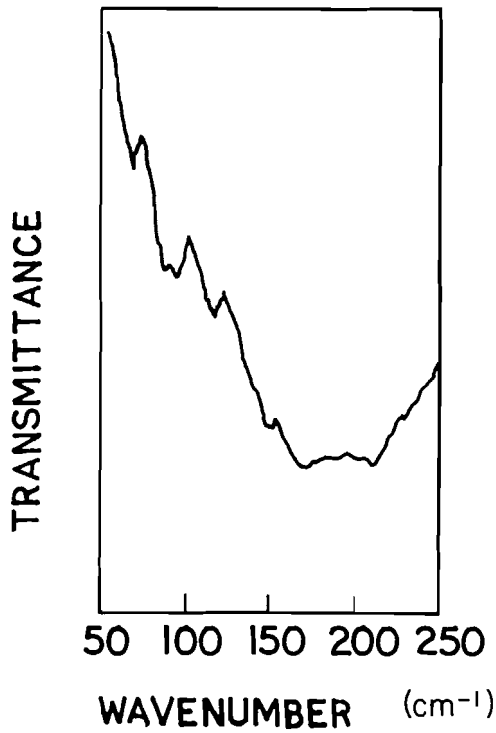

FIG. 2. Far-ir spectra (250–50 cm^{-1}) of polycrystalline $NaNH_2SO_3$.

$NaNH_2SO_3$ together with their assignments (based on the free molecular symmetry, C_s) are given in Table 3. Infrared frequencies of the polycrystalline samples are entered in column six of this table. The internal mode frequencies of $(NH_2SO_3)^-$ ion appear almost at the same region as those of potassium or ammonium sulphamates with a small shift or broadening. Theoretically, triplets are expected for each vibration; but, except in one or two cases, doublets or singlets are observed.

Katiyar and Krishnan (4) reported H—O—H bending modes at 1590 cm^{-1} in both the Raman and the ir. However, we observed no such band in the ir spectrum. A very weak band at 1604 cm^{-1} was detected in the B_2 component of the Raman spectra which may be due to the overtone of $\nu_6(A')$, the N—S stretching vibration. Katiyar and Krishnan assigned the bands observed at 3370 cm^{-1} in the Raman and 3392 cm^{-1} in the ir to the O—H stretching mode. Normally, in crystals, the OH stretching frequencies of water never appear below 3400 cm^{-1} unless strong hydrogen bonding is present. We observed bands around 3370 cm^{-1} (Raman) and 3352 cm^{-1} (ir). The region 3530–3000 cm^{-1} for different orientations of the Raman spectra are shown in Fig. 3. The ir spectrum in the 4000–250 cm^{-1} region is shown in Fig. 4. As seen in the figures, the bands at 3370 and 3352 cm^{-1} are not so broad as expected for OH stretching frequencies. In calcium sulphamate, we observed the OH stretching frequencies around 3510 cm^{-1} in the Raman and 3526 cm^{-1} in the ir with broad peaks (to be published). The X-ray diffraction study at room temperature (6) and the thermogravimetric analysis also do not show any evidence for the presence of water molecule. Moreover, if there is a H_2O in sodium sulphamate, it amounts to $12H_2O$ in the unit cell which should split the fundamental frequencies. These splittings are also absent. Also, the broad bands due to rocking and wagging modes of lattice water are found missing in the librational region (<1000 cm^{-1}) (9). Based on these considerations, it is clear that the frequency at 3370 cm^{-1} is due to the NH_2 asym-

Can. J. Chem. Downloaded from www.nrcresearchpress.com by 210.87.254.42 on 09/06/12
For personal use only.

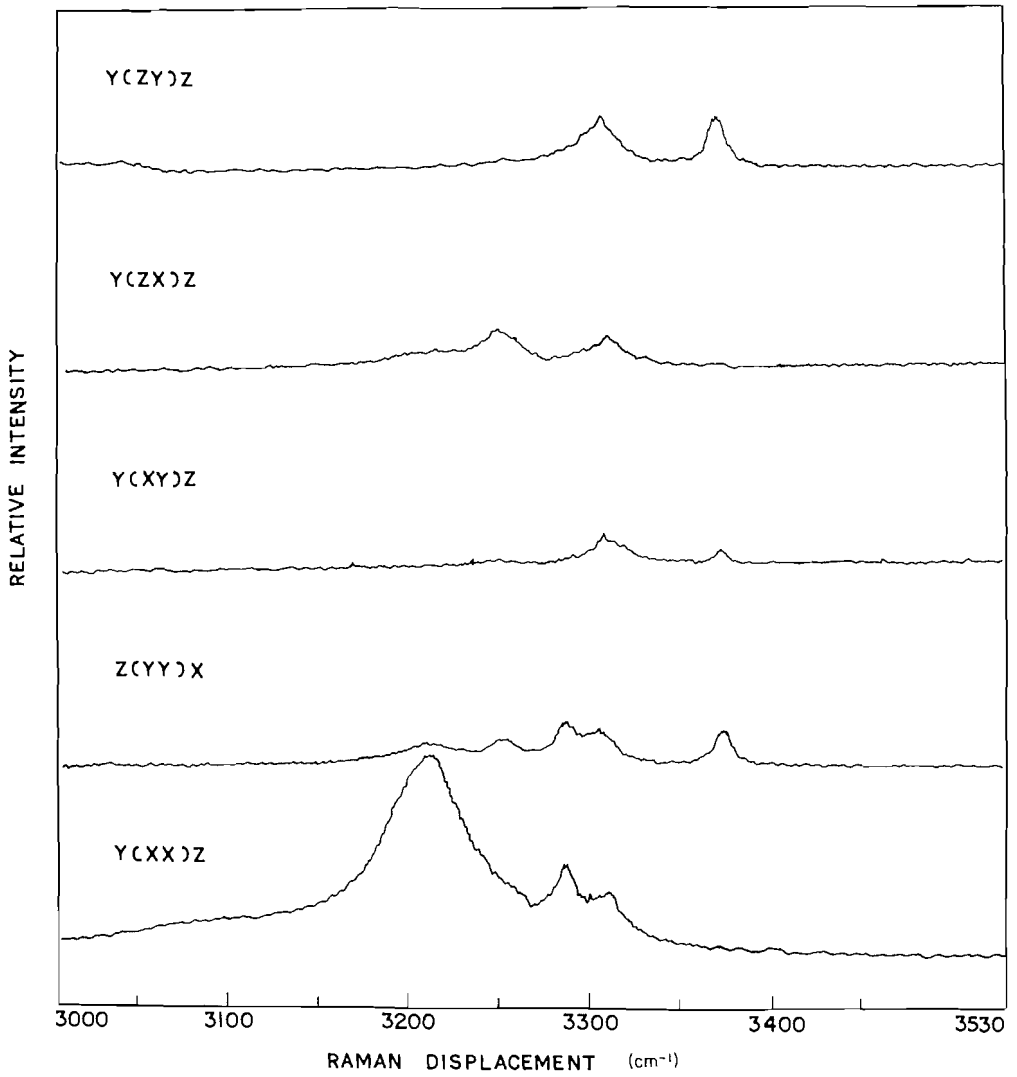

FIG. 3. Raman spectra of $NaNH_2SO_3$ (single crystal) in the region 3530–3000 cm^{-1}.

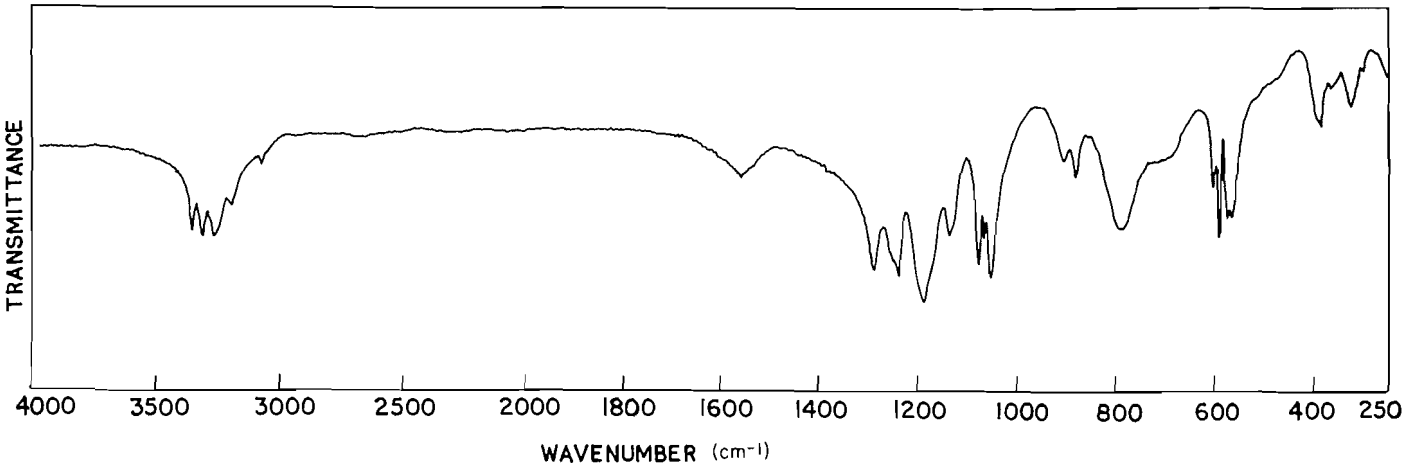

FIG. 4. Infrared spectra (4000–250 cm^{-1}) of polycrystalline $NaNH_2SO_3$.

metric stretching mode (ν_{10}).

The band at 285 cm^{-1} was assigned to N—S torsion, which was not observed in potassium and ammonium sulphamates. Lucazeau *et al.* (10) observed this around 244 cm^{-1} in sulphamic acid, having medium strength hydrogen bonding. We found the same at 300 cm^{-1} in calcium sulphamate and at 288 cm^{-1} in barium sulphamate (to be published).

The N—S stretching frequency appears around 790 cm^{-1} in sodium sulphamate. According to Banister *et al.* (11), this higher value of N—S stretching frequency in sulphamate as compared to sulphamic acid is due to the increase in double bond character of the N—S bond. In sulphates, the S—O

stretching modes have been reported below 1200 cm^{-1} by different workers (12, 13). But, in $NaNH_2SO_3$, we observed the SO_3 asymmetric stretching above 1200 cm^{-1} and this shows that the NSO_3 structure is not tetrahedral and the strength of S—O bond is larger. The correlation field splitting (about 35 cm^{-1}) is at a maximum for this mode.

When we analyse and compare the frequencies in different sulphamates, we find that the hydrogen bonding in $NaNH_2SO_3$ is extremely weak. In KNH_2SO_3, the NH_2 asymmetric stretching (ν_{10}) appears at 3320 cm^{-1} and in ammonium sulphamate at 3307 cm^{-1}. However in $NaNH_2SO_3$, it is at 3370 cm^{-1}. Thus ν_{10} is approaching the free NH_2 stretching frequency (14) of 3410 cm^{-1}. The lowering of NH_2 symmetric wagging frequency (ν_5) also indicates that the magnitude of hydrogen bonding is very small in this crystal.

Acknowledgements

The authors thank Drs. N. S. Satya Murthy, A. P. Roy, and M. L. Bansal (Nuclear Physics Division, BARC, Bombay) for providing facilities to record the Raman spectra, and Dr. N. Krishnamurthy for his helpful discussions. One of us (A.S.R.) is grateful to the Department of Atomic Energy, Government of India, Bombay for the award of a Junior Research Fellowship (B).

1. G. A. BENSON and W. J. SPILLANE. Chem. Rev. **80**, 151 (1980).
2. A. SUNDARA RAJ, P. MUTHUSUBRAMANIAN, and N. KRISHNAMURTHY. J. Raman Spectrosc. **11**, 127 (1981).
3. A. SUNDARA RAJ and P. MUTHUSUBRAMANIAN. J. Raman Spectrosc. **12**, 24 (1982).
4. R. S. KATIYAR and R. S. KRISHNAN. Indian J. Pure Appl. Phys. **6**, 686 (1968).
5. A. M. VUAGNAT and E. L. WAGNER. J. Chem. Phys. **26**, 77 (1957).
6. R. MANICKKAVASAGAM, R. K. RAJARAM, and K. S. CHANDRASEKARAN. Z. Kristallogr. In press.
7. G. W. COX, T. M. SABINE, V. M. PADMANABHAN, N. T. BAN, M. K. CHUNG, and A. J. SURJADI. Acta Crystallogr. **23**, 578 (1967).
8. R. LOUDON. Adv. Phys. **13**, 423 (1964).
9. V. M. MALHOTRA, H. A. BUCKMASTER, and H. D. BIST. Can. J. Phys. **58**, 1667 (1980).
10. G. LUCAZEAU, A. LAUTIE, and A. NOVAK. J. Raman Spectrosc. **3**, 161 (1975).
11. A. J. BANISTER, L. F. MOORE, and J. S. PADLEY. Spectrochim. Acta, **23**A, 2705 (1967).
12. A. TORRES, F. RULL, and J. A. DE SAJA. Spectrochim. Acta, **36**A, 425 (1980).
13. S. MONTERO, R. SCHMÖLZ, and S. HAUSSÜHL. J. Raman Spectrosc. **2**, 101 (1974).
14. J. BUKOWSKA. Spectrochim. Acta, **35**A, 985 (1979).

Can. J. Chem. Downloaded from www.nrcresearchpress.com by 210.87.254.42 on 09/06/12
For personal use only.

Dielectric evidence for the formation of a clathrate hydrate by sulfuryl chloride[1]

S. R. GOUGH, J. A. RIPMEESTER, and D. W. DAVIDSON
Division of Chemistry, National Research Council of Canada, Ottawa, Ont., Canada K1A 0R9

Received March 24, 1983

S. R. GOUGH, J. A. RIPMEESTER, and D. W. DAVIDSON. Can. J. Chem. **61**, 2053 (1983).

A hydrate formed by SO_2Cl_2 at −20°C is shown by its low temperature dielectric absorption to be a structure II clathrate hydrate. The activation energy for reorientation of encaged SO_2Cl_2 molecules is 1.1 kcal mol^{-1} between 19 and 41 K.

S. R. GOUGH, J. A. RIPMEESTER et D. W. DAVIDSON. Can. J. Chem. **61**, 2053 (1983).

On rapporte qu'un hydrate, formé par SO_2Cl_2 à −20°C, possède la structure II d'un hydrate clathrate tel que démontré par son absorption diélectrique à basse température. L'énergie d'activation pour la réorientation des molécules de SO_2Cl_2 encageés est de 1.1 kcal mol^{-1} entre 19 et 41 K.

Can. J. Chem. Downloaded from www.nrcresearchpress.com by 210.87.254.5 on 09/06/12
For personal use only.

In 1901 Baeyer and Villiger reported (1) the formation of a crystalline hydrate when sulfuryl chloride was poured into ice-cold water. The hydrate was found to have a composition of $SO_2Cl_2 \cdot 15.9\ H_2O$, and, since it readily reformed after heating and recooling, was considered not to contain chemically-bound water. There appear to have been no other experimental studies of this hydrate. In a review (2) written after gas hydrates had been found to be clathrates, it was suggested that SO_2Cl_2 is too large to form a normal clathrate hydrate and that impurities such as SO_2 and Cl_2 (which individually form clathrate hydrates) could have been responsible for Baeyer and Villiger's "sulfuryl chloride hydrate".

Since dipolar molecules encaged in clathrate hydrates undergo rapid reorientation which characteristically gives radio-frequency absorption at very low temperatures (2, 3), dielectric measurements may be used to show the existence (or not) of a clathrate hydrate of SO_2Cl_2 even in the presence of such impurities as acidic hydrolysis products, ice, and solid SO_2Cl_2. The values of the permittivity and loss so obtained, however, do not quantitatively characterize the pure homogeneous hydrate.

Addition of commercial sulfuryl chloride (Matheson, Coleman and Bell) to cold water failed to produce hydrate. However, hydrate formed immediately as a white solid when water was sprayed as a fine mist into liquid SO_2Cl_2 at −20°C. The solid was filtered at −20°C and stored in liquid nitrogen. Sample conditioning was avoided because of the tendency of SO_2Cl_2 to hydrolyse. Sample disks were prepared by pressing the powder in a cold mould before insertion into the dielectric cell which was mounted in a cryostat (4). Dielectric measurements (5) were made at frequencies between 1 Hz and 10 MHz and at temperatures between 4 and 200 K.

The dielectric absorption and dispersion measured below 100 K are illustrated in Fig. 1. The reproducible loss peak observed at low temperatures (e.g., at 28 K and 10 kHz) is ascribed to reorientation of encaged SO_2Cl_2 molecules. The rise in absorption and permittivity at higher temperatures continues monotonically to above 200 K where the values reached are much higher than can be ascribed to simple reorientation of water molecules in the hydrate lattice. Such irreproducible polarization effects must be attributed to acidic impurities and the attendant large proton conductance of the host lattice. Hydrolysis of SO_2Cl_2 to HCl, HSO_3Cl, and H_2SO_4 is well known (6).

There is no evidence of dielectric absorption from encaged species other than SO_2Cl_2. In particular, exploratory studies of

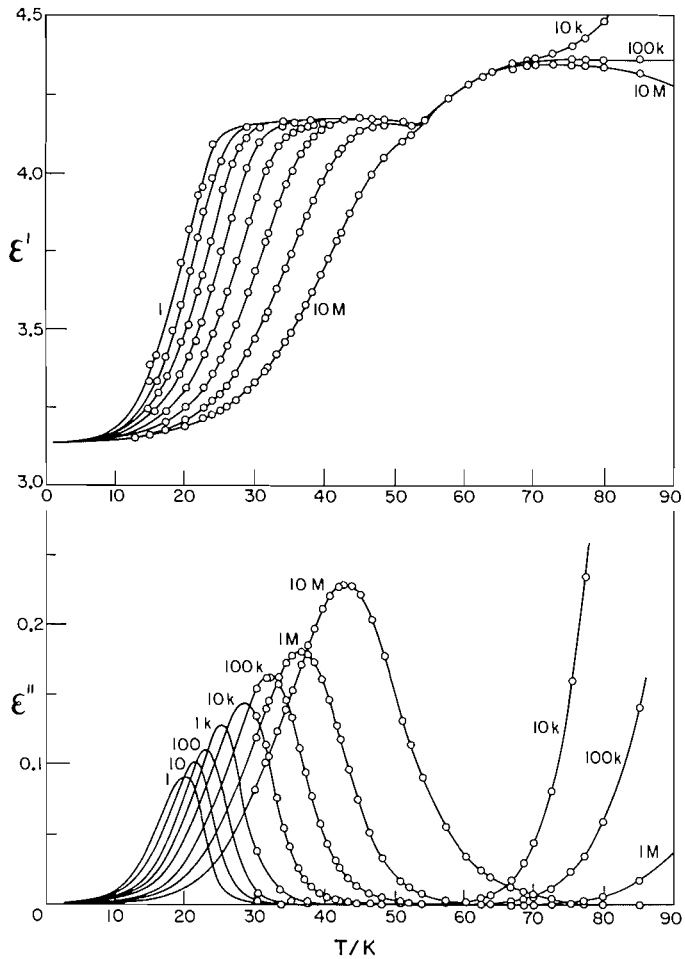

FIG. 1. Dielectric permittivity (ε′) and loss (ε″) curves of sulfuryl chloride hydrate at the frequencies indicated (in Hz). Many experimental points have been omitted for reasons of clarity.

SO_2 hydrate show the absorption of SO_2 to occur at much lower temperatures (e.g., 14 K for the loss maximum at 10 kHz) than the absorption found here.

The dielectric behaviour of enclathrated SO_2Cl_2 shows the features common to guest molecule reorientation in 22 other clathrate hydrates for which low-temperature dielectric measurements have been made (7): broad absorption–dispersion curves which are skewed in the direction of increased absorption at high frequencies, and permittivities on the low-frequency (high-temperature) side of the guest-molecule dispersion region which hardly change with decreasing

[1] NRCC No. 21271.

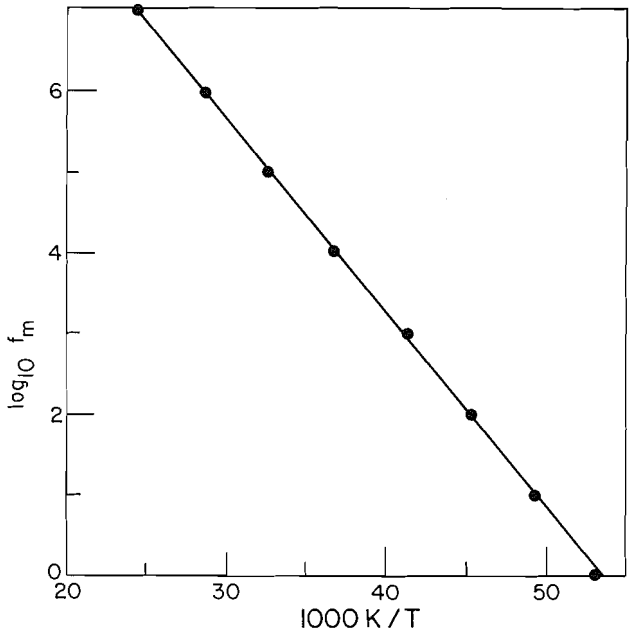

FIG. 2. Temperature dependence of the frequency of maximum dielectric absorption by SO_2Cl_2 in the hydrate.

temperature. Such features are attributable to the presence of orientations of different energy in individual cages and to a distribution of such energies in different cages arising from the disordered orientations of the lattice water molecules.

The linear Arrhenius plot between 19 and 41 K of the frequency of maximum absorption (Fig. 2) gives an "activation energy" of 1.1$_1$ kcal mol^{-1}, a fairly average value for guest-molecule reorientation in structure II clathrate hydrates (7).

From the geometry of SO_2Cl_2 (8) and van der Waals radii r_v of 1.40 Å for O and 1.80 Å for Cl, the sphere of minimum size which can enclose SO_2Cl_2 is 6.79 Å in diameter. The average free diameter of the largest clathrate cage, the 16-hedron of structure II, is only 6.56 Å for a unit cell dimension of 17.3 Å (2). However, in addition to 12 pentagonal faces, this cage consists of four almost planar hexagonal rings of hydrogen-bonded water molecules which are tetrahedrally disposed with respect to the cage centre. Since SO_2Cl_2 has a distorted tetrahedral shape, it is possible for this molecule to be accommodated within the cage by protrusion of the O and Cl atoms into the free space within the hexagonal rings. A similar situation occurs for CCl_4 which has a van der Waals diameter of 7.13 Å and yet forms a structure II hydrate stable up to 0.67°C (9).

We conclude that SO_2Cl_2 forms a structure II clathrate hydrate with composition close to $SO_2Cl_2 \cdot 17H_2O$. Remeasurement of the low temperature dielectric properties after heating the sample to a variety of temperatures and recooling showed eutectic melting of excess SO_2Cl_2 to occur near −75°C and the hydrate to decompose near −14°C. The hydrate formed by Baeyer and Villiger at 0°C probably was SO_2Cl_2 hydrate stabilized by the incorporation of SO_2 and/or Cl_2 "help gas" impurities in the small, otherwise empty cages of the structure II lattice (2).

1. A. BAEYER and V. VILLIGER. Ber. Dtsch. Chem. Ges. **34**, 736 (1901).
2. D. W. DAVIDSON. *In* Water: a comprehensive treatise. Vol. 2. *Edited by* F. Franks. Plenum Press, New York. 1973. p. 115.
3. D. W. DAVIDSON, S. R. GOUGH, F. LEE, and J. A. RIPMEESTER. Rev. Chim. Miner. **14**, 447 (1977).
4. S. R. GOUGH. J. Phys. E, **15**, 530 (1982).
5. S. R. GOUGH, R. E. HAWKINS, B. MORRIS, and D. W. DAVIDSON. J. Phys. Chem. **77**, 2969 (1973).
6. J. W. MELLOR. Comprehensive treatise on inorganic and theoretical chemistry. Vol. 10. Longmans, London. 1930. p. 672.
7. D. W. DAVIDSON and J. A. RIPMEESTER. *In* Inclusion compounds. Vol. 2. Academic Press, New York. 1983. In press.
8. M. HARGITTAI and I. HARGITTAI. J. Mol. Struct. **73**, 253 (1981).
9. G. H. LAMERIS. Thesis, Technische Hogeschool, Delft. 1976.

Can. J. Chem. Downloaded from www.nrcresearchpress.com by 210.87.254.5 on 09/06/12
For personal use only.

Structure of rhodocladonic acid. X-ray crystal structure analysis of its triacetate

STEWART MCLEAN, PAUL MAHLER, STANLEY C. NYBURG, JEFFERY F. SAWYER, COLIN J. WEBSTER, AND WINNIE WONG-NG

Department of Chemistry, University of Toronto, Toronto, Ont., Canada M5S 1A1

Received January 28, 1983

STEWART MCLEAN, PAUL MAHLER, STANLEY C. NYBURG, JEFFERY F. SAWYER, COLIN J. WEBSTER, and WINNIE WONG-NG. Can. J. Chem. **61**, 2055 (1983).

The structure of the lichen pigment rhodocladonic acid, 2-acetyl-3,4,6-trihydroxy-7-methoxynaphtho[2,3-*b*]furan-5,8-dione (**1***a*), has been assigned on the basis of an X-ray crystal structure analysis of its triacetate (**1***c*). Crystals of the triacetate are triclinic, space group $P\bar{1}$ with cell dimensions a = 13.609(3) Å, b = 15.009(3) Å, c = 5.456(2) Å, α = 106.66(4)°, β = 103.45(3)°, γ = 72.30(4)°, U = 1004(1) Å^3, and D_{calc} = 1.47 g cm^{-3} for Z = 2; R_1 = 0.0505 for 1644 observed ($F > 6\sigma(F)$) reflections.

STEWART MCLEAN, PAUL MAHLER, STANLEY C. NYBURG, JEFFERY F. SAWYER, COLIN J. WEBSTER et WINNIE WONG-NG. Can. J. Chem. **61**, 2055 (1983).

On a déterminé la structure du pigment du lichen: l'acide rhodocladonique, acétyle-2 trihydroxy-3,4,6 méthoxy-7 naphto[2,3-*b*] furannedione-5,8 (**1***a*) en analysant la structure du cristal de son triacétate (**1***c*) par cristallographie de rayons-X. Les cristaux du triacétate sont tricliniques et appartiennent au groupe d'espace $P\bar{1}$ avec a = 13,069(3) Å, b = 15,009(3) Å, c = 5,456(2) Å, α = 106,66(4)°, β = 103,45(3)°, γ = 72,30(4)°, U = 1004(1) Å^3 et D_{calc} = 1,47 g cm^{-}3, Z = 2; R_1 = 0,0505 pour 1644 réflexions ($F > 6\sigma$ (F)) observées.

[Traduit par le journal]

The structure of rhodocladonic acid, a red pigment of many lichens in the genus *Cladonia*, has been a subject of interest for many years. In 1941 Shibata (1) assigned it a substituted anthraquinone structure on the basis of an erroneous molecular formula. Baker and Bullock (2) determined the correct molecular formula, established that rhodocladonic acid is a naphthoquinone (unprecedented in lichens), and, on the basis of degradative studies, assigned it a furonaphthoquinone structure having an acetyl side chain, three hydroxyl substituents, and one methoxyl substituent; structures **1***a* and **1***b* were considered

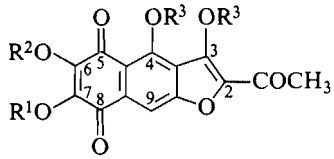

1*a* R^1 = Me; R^2 = R^3 = H
b R^2 = Me; R^1 = R^3 = H
c R^1 = Me; R^2 = R^3 = Ac

the most reasonable on biogenetic grounds, but the location of the methoxyl group in the native pigment could not be assigned since the key degradation was carried out on the trimethyl ether.

Our own independent investigation had led us to the same conclusion concerning the naphthoquinone part of the skeleton and the hydroxyl and methoxyl substituents, but we felt that the identity of the third ring, undoubtedly corresponding to a condensed polyketonic unit, could not be assigned unequivocally on the basis of an alkali-induced degradation (3). For this reason we undertook to determine the complete structure unambiguously by X-ray crystal structure analysis. Because of its extreme insolubility in common solvents, crystals of rhodocladonic acid itself suitable for this purpose were not available; of the simple derivatives that could reasonably be expected to be prepared without risk of skeletal rearrangement, the triacetate proved the most suitable.

Experimental

Rhodocladonic acid was isolated from the apothecia of *Cladonia cristatella* collected in southern Ontario. Treatment of the pigment with acetic anhydride and triethylamine overnight at room temperature afforded the triacetate which was carefully recrystallized from acetone and obtained as a yellow aggregate, mp 211–213°C (lit. (2) mp 210–212°C). Individual crystals appear as almost colorless plates,

TABLE 1. Fractional atomic coordinates ($\times 10^4$) of non-hydrogen atoms

Atom	x	y	z
C(1)	−6281(3)	3248(3)	895(7)
C(2)	−7064(3)	3883(3)	−236(8)
O(3)	−6665(2)	4261(2)	−1693(5)
C(4)	−5620(3)	3848(3)	−1448(8)
C(5)	−5331(3)	3203(3)	157(7)
C(6)	−4288(3)	2712(3)	629(6)
C(7)	−3556(3)	2852(3)	−532(7)
C(8)	−3892(3)	3524(3)	−2072(7)
C(9)	−4925(3)	4029(3)	−2557(9)
C(10)	−3129(3)	3714(3)	−3295(8)
C(11)	−2013(3)	3177(3)	−2903(8)
C(12)	−1711(3)	2538(3)	−1434(8)
C(13)	−2435(3)	2326(3)	−178(8)
O(14)	−2083(2)	1748(2)	1167(6)
O(15)	−3408(2)	4300(2)	−4613(6)
O(16)	−1445(2)	3440(2)	−4108(6)
C(17)	−382(5)	2927(7)	−4328(15)
O(18)	−664(2)	2086(2)	−780(6)
C(19)	−368(4)	1104(4)	−1822(12)
O(20)	−954(3)	687(3)	−3328(8)
C(21)	744(5)	705(7)	−829(18)
O(22)	−3996(2)	2124(2)	2328(5)
C(23)	−3988(4)	1173(3)	1366(9)
O(24)	−4272(4)	876(3)	−825(7)
C(25)	−3581(8)	637(5)	3438(14)
O(26)	−6346(2)	2751(2)	2581(5)
C(27)	−6885(4)	2053(3)	1665(10)
O(28)	−7290(3)	1869(3)	−507(7)
C(29)	−6847(8)	1598(7)	3749(15)
C(30)	−8192(4)	4216(3)	−240(10)
O(31)	−8576(3)	3954(3)	1135(7)
C(32)	−8816(5)	4849(5)	−2007(14)

Can. J. Chem. Downloaded from www.nrcresearchpress.com by 210.87.254.40 on 09/06/12
For personal use only.

Can. J. Chem. Downloaded from www.nrcresearchpress.com by 210.87.254.40 on 09/06/12
For personal use only.

TABLE 2(a). Bond lengths (Å)

Bond	Length	Bond	Length
C(1)—C(2)	1.356(5)	C(11)—C(12)	1.334(7)
C(1)—C(5)	1.417(7)	C(11)—O(16)	1.323(7)
C(1)—O(26)	1.373(6)	C(12)—C(13)	1.472(8)
C(2)—O(3)	1.376(7)	C(12)—O(18)	1.390(5)
C(2)—C(30)	1.463(6)	C(13)—O(14)	1.214(6)
O(3)—C(4)	1.359(5)	O(16)—C(17)	1.432(7)
C(4)—C(5)	1.398(6)	O(18)—C(19)	1.387(7)
C(4)—C(9)	1.361(7)	C(19)—O(20)	1.186(7)
C(5)—C(6)	1.388(5)	C(19)—C(21)	1.481(8)
C(6)—O(22)	1.372(5)	O(22)—C(23)	1.369(5)
C(6)—C(7)	1.390(7)	C(23)—O(24)	1.168(6)
C(7)—C(8)	1.401(6)	C(23)—C(25)	1.481(10)
C(7)—C(13)	1.485(5)	O(26)—C(27)	1.372(7)
C(8)—C(9)	1.382(5)	C(27)—O(28)	1.176(6)
C(8)—C(10)	1.488(7)	C(27)—C(29)	1.467(13)
C(10)—O(15)	1.213(6)	C(30)—O(31)	1.211(8)
C(10)—C(11)	1.486(6)	C(30)—C(32)	1.486(9)
Range C—H 0.78(10) to 1.05(9)			

TABLE 2(b). Bond angles (deg)

Bonds	Angle	Bonds	Angle
C(5)—C(1)—C(2)	108.6(4)	C(11)—C(10)—O(15)	119.4(5)
C(5)—C(1)—O(26)	123.7(3)	C(11)—C(10)—C(12)	119.0(5)
C(2)—C(1)—O(26)	127.6(4)	C(10)—C(11)—O(16)	111.7(4)
C(1)—C(2)—O(3)	109.6(4)	C(12)—C(11)—O(16)	129.3(4)
C(1)—C(2)—C(30)	133.8(5)	C(11)—C(12)—C(13)	123.3(4)
O(3)—C(2)—C(30)	116.6(4)	C(11)—C(12)—O(18)	121.7(5)
C(2)—O(3)—C(4)	106.8(3)	C(13)—C(12)—O(18)	114.8(4)
O(3)—C(4)—C(5)	110.8(4)	C(12)—C(13)—C(7)	119.0(4)
O(3)—C(4)—C(9)	126.1(4)	C(12)—C(13)—O(14)	118.4(4)
C(5)—C(4)—C(9)	123.1(4)	C(7)—C(13)—O(14)	122.5(5)
C(4)—C(5)—C(6)	118.8(4)	C(11)—O(16)—C(17)	121.7(5)
C(4)—C(5)—C(1)	104.2(3)	C(12)—O(18)—C(19)	116.0(4)
C(1)—C(5)—C(6)	136.9(4)	O(18)—C(19)—O(20)	121.9(4)
C(5)—C(6)—C(7)	120.0(4)	O(18)—C(19)—C(21)	110.5(5)
C(5)—C(6)—O(22)	118.7(4)	O(20)—C(19)—C(21)	127.6(6)
C(7)—C(6)—O(22)	121.3(3)	C(6)—O(22)—C(23)	118.5(3)
C(6)—C(7)—C(8)	118.3(3)	O(22)—C(23)—O(24)	121.1(5)
C(6)—C(7)—C(13)	122.9(4)	O(22)—C(23)—C(25)	110.9(4)
C(8)—C(7)—C(13)	118.9(4)	O(24)—C(23)—C(25)	128.0(5)
C(7)—C(8)—C(9)	123.0(5)	C(1)—O(26)—C(27)	118.5(3)
C(7)—C(8)—C(10)	120.0(3)	O(26)—C(27)—O(28)	122.2(6)
C(9)—C(8)—C(10)	117.0(4)	O(26)—C(27)—C(29)	110.1(5)
C(4)—C(9)—C(8)	116.7(4)	O(28)—C(27)—C(29)	127.8(7)
C(4)—C(9)—H(91)	120.(3)	C(2)—C(30)—O(31)	119.4(4)
C(8)—C(9)—H(91)	123.(3)	C(2)—C(30)—C(32)	117.4(6)
C(8)—C(10)—C(11)	119.9(4)	O(31)—C(30)—C(32)	123.2(5)
C(8)—C(10)—O(15)	120.8(4)		
Ranges C—C—H 100(3) – 120(4)			
H—C—H 91(8) – 125(7)			

most of which are too small for practical use. A specimen of dimensions 0.10 × 0.03 × 0.20 mm was chosen and used throughout.

Crystal data $M = 444.34$

$C_{21}H_{16}O_{11}$ Triclinic, $P\bar{1}$ or $P1$

($P\bar{1}$ by successful analysis), $a = 13.609(3)$, $b = 15.009(3)$, $c = 5.456(2)$ Å, $\alpha = 106.66(4)°$, $\beta = 103.45(3)°$, $\gamma = 72.30(4)°$, $U = 1004(1)$ Å^3, $F(000) = 460$, and $D_{calc} = 1.47$ g cm^{-3} for $Z = 2$; CuK$\bar{\alpha}$ radiation (Ni-filtered, $\lambda = 1.5418$ Å), μ(CuK$\bar{\alpha}$) = 9.4 cm^{-1}.

X-Ray crystal structure determination

Preliminary Weissenberg photographs indicated no symmetry higher than triclinic, and cell parameters were obtained from the diffraction angles of 14 well-centred reflections on an automated Picker four-circle diffractometer by the use of Ni-filtered Cu K$\bar{\alpha}$ radiation. Reflections were collected in the $\theta-2\theta$ mode on the same instrument using an orientation matrix based on this cell. For each reflection the scan range was 1° to either side of the $\alpha_1\alpha_2$ peaks using a scan rate of 2° min^{-1}; stationary counter background levels were obtained at each side of the reflection. A standard reflection measured after every 50 reflections collected showed no systematic variations with time. Of a total of 3138 independent reflections collected within the limits $0.1 < \sin\theta < 0.88$, 1494 were considered significant on

TABLE 3. Deviations (Å) of atoms from best least-squares planes

Plane 1	$-0.241X - 0.5522Y - 0.8057Z = -1.3212$				
C(1)*	−0.018(4)	C(9)*	−0.000(5)	O(16)	0.006(3)
C(2)*	0.009(4)	C(10)*	−0.007(4)	C(17)	0.222(8)
O(3)*	0.025(3)	C(11)*	0.019(4)	O(18)	−0.086(3)
C(4)*	0.008(4)	C(12)*	0.027(4)	O(22)	−0.144(3)
C(5)*	−0.018(4)	C(13)*	0.023(4)	O(26)	−0.098(3)
C(6)*	−0.038(4)	O(14)*	0.004(3)	C(30)	0.044(5)
C(7)*	−0.003(4)	O(15)*	−0.024(3)	O(31)	−0.052(4)
C(8)*	−0.008(4)	H(91)	0.01(4)	C(32)	0.230(7)
Plane 2	$0.5416X + 0.3630Y - 0.7582Z = 1.5017$				
O(18)*	0.001(3)	O(20)*	0.001(4)	C(12)	−0.094(4)
C(19)*	−0.007(6)	C(21)*	0.005(9)		
Plane 3	$0.9691X - 0.1574Y - 0.1899Z = -5.2784$				
O(22)*	0.000(3)	O(24)*	0.001(6)	C(6)	0.086(4)
C(23)*	−0.001(6)	C(25)*	0.001(12)		
Plane 4	$0.7316X - 0.6307Y - 0.2430Z = -8.2663$				
O(26)*	0.001(3)	O(28)*	0.001(4)	C(1)	0.014(4)
C(27)*	−0.005(5)	C(29)*	0.005(11)		
Plane 5	$-0.2151X - 0.6468Y - 0.7317Z = -1.8429$				
C(2)*	0.002(4)	O(31)*	0.002(4)	C(30)*	−0.008(5)
C(32)*	0.005(7)				
Angles (deg) made with plane 1					
Plane 2: 72.9	Plane 3: 88.1		Plane 4: 67.0		Plane 5: 6.9

*Asterisked atoms used to determine planes.

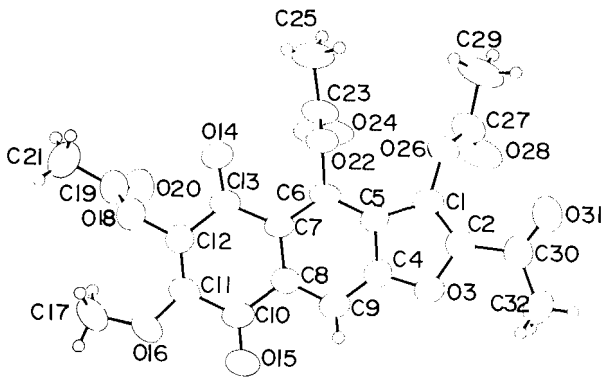

FIG. 1. ORTEP view of the molecule showing the numbering scheme used in the structure determination. Thermal ellipsoids are drawn at the 50% probability level. All hydrogen atoms are drawn with uniform isotropic thermal parameters.

the criterion $F > 6\sigma(F)$[1] and were used in subsequent refinements.

Structure solution

Initial attempts at structure solution in the centric space group $P\bar{1}$ (indicated by statistical tests on the E values) by the use of direct method routines in the programs MULTAN (4) and SHELX (5) only led to confusing "chicken-wire" patterns of hexagonal rings. Inspection of a sharpened $E \times F$ Patterson map indicated that the plane of the molecule was virtually parallel to (131), and a single hexagonal ring in this plane was developed using damped least-squares and Fourier refinements into a crude distorted fragment of a postulated condensed tricyclic structure with a residual $R \sim 0.50$. Subsequent direct-method phasing with the original origin and starting reflections as well as several phases calculated on the basis of the current model gave several further E-maps in which the model was shifted with respect to the (131) plane, but invariably it was too close to one of the centres of symmetry in the unit cell. An expanded fragment of the molecule in one E-map did, however, serve as a good phasing model in the acentric space group $P1$ and enabled a second molecule related by a noncrystallographic centre of symmetry to be located. This arrangement was then shifted to conform to the space group $P\bar{1}$, and subsequent least-squares and Fourier refinements proceeded routinely. All hydrogen atoms were successfully located in a Fourier map calculated using a Sims weighting scheme. Least-squares refinement minimizing $\Sigma w(|F_o| - |F_c|)^2$ converged (max. shift/error = 0.17) to the final agreement indices $R_1 = 0.0505$ and $R_2 = 0.0560$. In the final cycles of refinement the weights used were $1/\sigma(F)^2$ such that $\langle w\Delta F^2 \rangle$ was independent of F_{obs} and sin θ everywhere. A final ΔF-map was featureless.

All calculations were performed on an SEL 75 computer, using the programs MULTAN (4), SHELX (5), and ORTEP (6), as well as local programs. Neutral-atom scattering factors were taken from International Tables (7). The final atomic positional parameters are given in Table 1; anisotropic thermal parameters and parameters for hydrogen atoms have been deposited.[2] Interatomic distances and bond angles and some least-squares mean planes in the molecule are given in Tables 2 and 3.[3] Of the three acetoxy substituents, those at C(1) and C(6) exhibit large librational motion about their O—CO bonds, giving rise to quite large temperature factors for O(28), C(29), and O(24), C(25). There seems to be no similar large libration of the acetate at C(12).

Results and discussion

The X-ray analysis establishes unequivocally that the tri-

[1] $\sigma(F) = \{[\sigma(I)\cdot Lp]^2 + 0.02F_o^4\}^{1/2}/2F_o$ and $\sigma(I) = [a\ (\text{peak} + \text{background})]^{1/2}$ where a = attenuation factor and Lp is the Lorentz-polarization correction for each reflection.

[2] These tables, along with tables of observed and calculated structure factors and of temperature factors, are available, at a nominal charge, from the Depository of Unpublished Data, CISTI, National Research Council of Canada, Ottawa, Ont., Canada K1A 0S2.

[3] The atomic numbering system used in all tables corresponds to that defined by the connectivity map shown in Fig. 1. This system is used for clarity when molecular geometry is discussed. The locants required for purposes of systematic nomenclature are shown in structure **1**.

Can. J. Chem. Downloaded from www.nrcresearchpress.com by 210.87.254.40 on 09/06/12
For personal use only.

acetate of rhodocladonic acid has structure **1***c* (2-acetyl-3,4,6-triacetoxy-7-methoxynaphtho[2,3-*b*]furan-5,8-dione). Since it can safely be assumed that the acetate was formed without rearrangement of the molecule, it follows that rhodocladonic acid is the corresponding trihydric phenol, **1***a*. The novel structural features proposed by Baker and Bullock (2) are confirmed, and the ambiguity concerning the position of the methoxyl group is removed.

In the crystal, the naphtho[2,3-*b*]furan-5,8-dione framework is planar to within ±0.027 Å and is virtually parallel to the (131) plane. Bond distances and bond angles within this unit are normal, being comparable to those in analogous compounds. The C-acetyl substituent has normal dimensions and is approximately coplanar with the molecular framework. The three acetoxy groups at C(1), C(6), and C(12)[3] have the same dimensions, within the measured standard deviations, and appear normal; their planes (Table 3) are rotated from the plane of the tricyclic framework by angles of 67.0(2)°, 88.1(2)°, and 72.9(2)°, respectively. The methoxyl group at C(11) has a C(12)—C(11)—O(16)—C(17) torsion angle of 6.9(1)°.

The closest intermolecular contact is H(91)···O(15) ($\bar{x}$ $\bar{y}$ $\bar{z}$) of length 2.57(2) Å.

Acknowledgement

This work was supported by grants from the Natural Sciences and Engineering Research Council of Canada.

1. S. J. SHIBATA. Pharm. Soc. Jpn. **61**, 320 (1941).
2. P. M. BAKER and E. BULLOCK. Can. J. Chem. **47**, 2733 (1969).
3. R. H. THOMSON. Naturally occurring quinones. Academic Press, London. 1971. p. 317.
4. G. GERMAIN, P. MAIN, and M. M. WOOLFSON. Acta Crystallogr. Sect. A, **27**, 368 (1971).
5. G. M. SHELDRICK. Computing in crystallography. *Edited by* H. Schenk *et al.* Delft University Press, 1978.
6. C. K. JOHNSON. ORTEP Report ORNL-3794. Oak Ridge National Laboratory, Tennessee, U.S.A. 1965.
7. INTERNATIONAL TABLES FOR X-RAY CRYSTALLOGRAPHY. Vol. IV. Kynoch Press, Birmingham. 1974. p. 72, *seq.*

Can. J. Chem. Downloaded from www.nrcresearchpress.com by 210.87.254.40 on 09/06/12
For personal use only.

Hydrolysis rates of some acetylimidazole derivatives

B. J. GOUR-SALIN[1]

Department of Chemistry, University of Alberta, Edmonton, Alta., Canada T6G 2E1

Received September 1, 1982[2]

B. J. GOUR-SALIN. Can. J. Chem. **61**, 2059 (1983).

N-Acetylbenzimidazole (**4**), *N*-acetyl-*N'*-methylbenzimidazolium acetate (**5**), and *N*-acetyl-*N'*-methyltetrahydrobenzimidazolium acetate (**6**) were synthesized and their hydrolysis rates were studied.

B. J. GOUR-SALIN. Can. J. Chem. **61**, 2059 (1983).

On rapporte la synthèse de la *N*-acetylbenzimidazole (**4**), de l'acétate de *N*-acétyl-*N'*-méthylbenzimidazolium (**5**) et de l'acetate de *N*-acétyl-*N'*-méthyltétrahydrobenzimidazolium (**6**), de même que l'étude de leurs viteses d'hydrolyse.

[Traduit par le journal]

Can. J. Chem. Downloaded from www.nrcresearchpress.com by 210.87.254.105 on 09/06/12
For personal use only.

The imidazole group of a histidine residue has been implicated as a necessary part of the catalytically active centre of a large number of enzymes. Its exact role has not as yet been established and the studies reported here were carried out to define more fully the properties and mechanisms of reaction of acylimidazole compounds in nonenzymatic reactions in order to provide a more complete background for consideration of their possible role in enzymatic catalysis.

Jencks and Carriuolo (1*a*) have shown that *N*-acetylimidazole (**1**) hydrolyzes by acid, neutral, and base pathways according to eq. [1] (Scheme 1).

$$[1] \quad v = 2.8\,[H^+] + 0.005\,[\mathbf{1}] + 19000\,[\mathbf{1}]\,[OH^-]$$

At low pH, the rate is controlled by the reaction of [**1**H$^+$] (pK_a = 3.6) (1*a*) and the pH rate profile is level at pH's where the imidazole is completely protonated (k_{obs} = 2.8 min^{-1}, ref. 1*a*). In a later study Marlburg and Jencks (1*c*) showed that [**1**H$^+$] and its *N*-methyl analogue (**2**) decomposed rapidly in

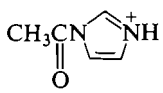

1H$^+$

k_{H_2O} = 2.8 min^{-1}
k_{H_2O/D_2O} = 2.5

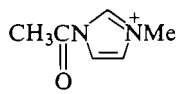

2

k_{H_2O} = 2.8 min^{-1}
k_{H_2O/D_2O} = 2.6

H_2O and exhibited solvent isotope effects. Proton inventory studies (2) indicate that the pH-dependent, water-catalyzed hydrolysis of 1-acetylimidazolium ion probably involves a transition state such as that shown in **3**.

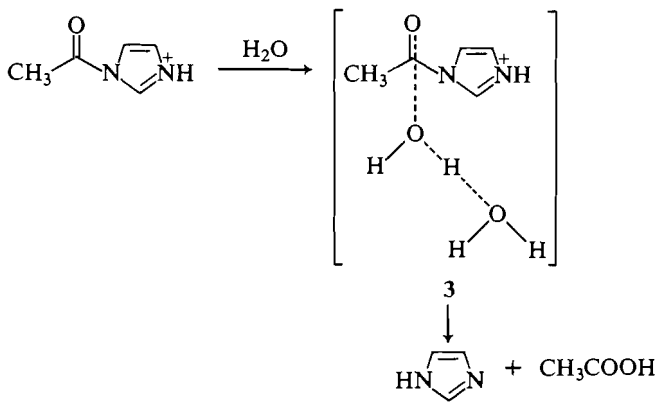

3

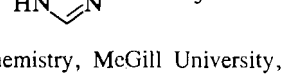

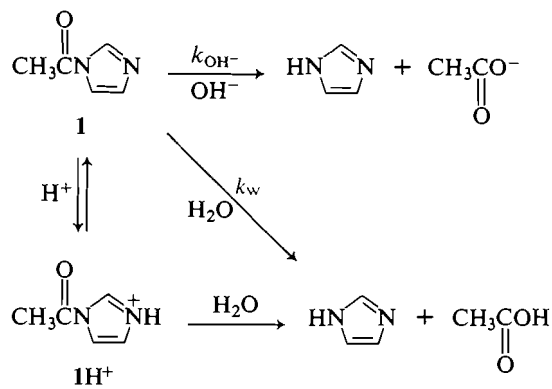

SCHEME 1

To further this examination of the hydrolysis rates of *N*-acetylimidazole compounds, *N*-acetylbenzimidazole (**4**), *N*-acetyl-*N'*-methylbenzimidazolium acetate (**5**), and *N*-acetyl-*N'*-methyltetrahydrobenzimidazolium acetate (**6**) were synthesized and their hydrolysis rates studied.

Results and discussion

N-Acetylbenzimidazole (**4**) was synthesized from the reaction of acetyl chloride with benzimidazole, while both

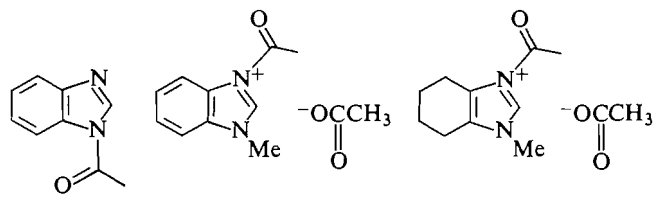

4 **5** **6**

N-acetyl-*N'*-methylbenzimidazolium acetate (**5**) and *N*-acetyl-*N'*-methyltetrahydrobenzimidazolium acetate (**6**) were synthesized by reacting the corresponding *N*-methylimidazole compounds with acetic anhydride. The hydrolysis of *N*-acetylbenzimidazole (**4**) and *N*-acetyl-*N'*-methylbenzimidazolium acetate (**5**) was followed spectrophotometrically at 290 nm while the decomposition of *N*-acetyl-*N'*-methyltetrahydrobenzimidazolium acetate was monitored at 265 nm. In Fig. 1 are shown the hydrolysis rates for compounds **4**, **5**, and **6** in 29.4% EtOH/H_2O at 25°C as a function of pH, obtained by determining the rate at each pH at several different buffer concentrations and then extrapolating to zero buffer concentration. For *N*-acetylbenzimidazole (**4**) the rate of hydrolysis increases sharply above and below neutrality. The rate law can be formulated as in eq. [2].

[1]Present address: Department of Chemistry, McGill University, Montreal, P.Q., H3A 2K6.

[2]Revision received March 7, 1983.

Can. J. Chem. Downloaded from www.nrcresearchpress.com by 210.87.254.105 on 09/06/12
For personal use only.

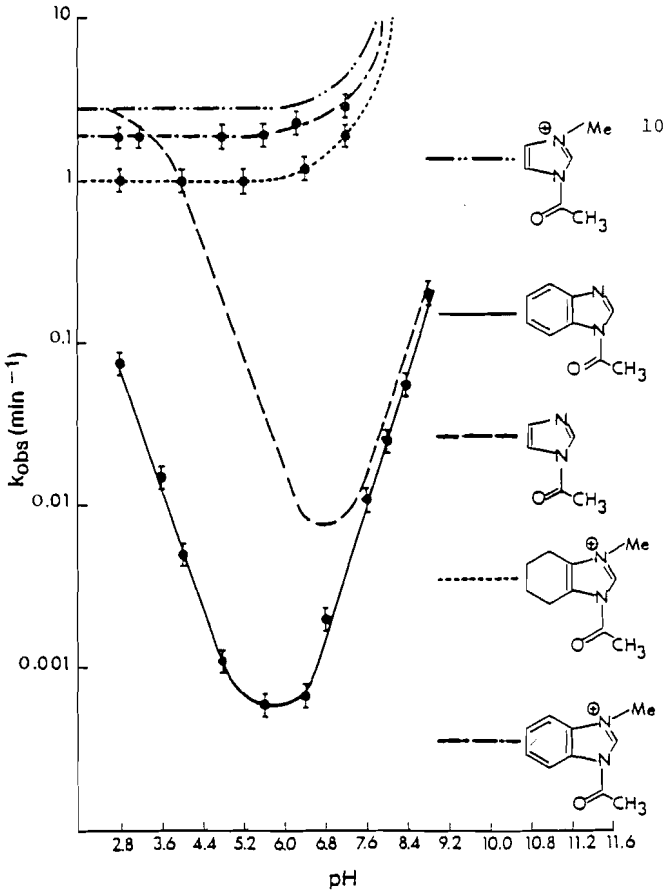

FIG. 1. The pH–rate profiles for the hydrolysis of *N*-acetylbenzimidazole (**4**), *N*-acetyl-*N'*-benzimidazolium acetate (**5**), and *N*-acetyl-*N'*-tetrahydrobenzimidazolium acetate (**6**) in 29.4% (v/v) ethanol–H_2O at 25°C. The pH–rate profiles for the hydrolysis of *N*-acetylimidazole and *N*-acetyl-*N'*-methylimidazole in H_2O at 25°C as reported by Jencks and co-workers (1).

$$[2] \quad \nu = 5.3 \pm 0.7 \times 10^{1} [H^+][\mathbf{4}] + 3.7 \pm 1.4 \times 10^{-4} [\mathbf{4}] + 2.8 \pm 0.4 \times 10^{4} [\mathbf{4}][OH^-]$$

The pH–rate profile found for *N*-acetylbenzimidazole (**4**) and that found for *N*-acetylimidazole (**1**) (*1a*) appear to be quite similar, with the exception that for *N*-acetylbenzimidazole (**4**) a plateau region in the pH–rate profile, in the pH range studied, is not visible, indicating a lower pK_a for this compound. Again, as in Jencks' results (1) for *N*-acetyl-*N'*-methylimidazolium chloride (**2**), whose rate law is formulated in eq. [3], the pH–rate profiles for *N*-acetyl-*N'*-methylbenzimidazolium acetate (**5**) and *N*-acetyl-*N'*-methyltetrahydrobenzimidazolium acetate (**6**) remain constant from pH 1 to pH 6 and

$$[3] \quad \nu = 2.8 [\mathbf{2}] + 9.0 \times 10^{6} [\mathbf{2}][OH^-]$$

increase as neutrality is approached (Fig. 1). The rate laws obtained for compounds **5** and **6** are formulated in eqs. [4] and [5] respectively.

$$[4] \quad \nu = 1.9 \pm 0.1 [\mathbf{5}] + 1.2 \pm 0.1 \times 10^{7} [\mathbf{5}][OH^-]$$

$$[5] \quad \nu = 1.0 \pm 0.05 [\mathbf{6}] + 6 \pm 0.1 \times 10^{6} [\mathbf{5}][OH^-]$$

It appears that all three classes of imidazole compounds act in a similar manner in spite of the uncertain differences in resonance stabilization and steric effects amongst them. It is interesting to note that the parent imidazole compounds have widely varying pK_a values (Table 1). These differences in basicities do not appear to affect the hydrolysis rates of the *N*-acyl derivatives extensively. For the *N*-acetylimidazole compounds studied, it appears that the hydrolysis rates remain reasonably constant as long as the imidazole ring is maintained in its protonated form, the driving force for the hydrolysis presumably being the gain in resonance stabilization obtained.

TABLE 1. Dissociation constants of imidazole derivatives

Compound	pK_a
Imidazole	6.9[a]
Benzimidazole	5.54[b]
1-Methylbenzimidazole	5.44[b]
1-Methyltetrahydrobenzimidazole	8.20[b]

[a]Determined in 23.3% ethanol/H_2O (v/v) solvent (ref. 6).

[b]Typically 0.025 mmol of the substance to be titrated was dissolved in 2 mL ethanol, 3.0 mL 0.5 *N* KCl, and 1 mL 0.1051 *N* HNO_3 and titrated with 0.1000 *N* NaOH.

Experimental

N-*Acetylbenzimidazole (4)*

Benzimidazole (1 g, 0.0085 mol) and 1.1 equivalents of acetyl chloride were added to dry THF (100 mL) and stirred for 1 h. The hydrochloride salt of benzimidazole precipitated out of solution and was filtered off. The THF was then removed *in vacuo* and the residue washed with ether. Any precipitate which formed was filtered off and the ether removed under reduced pressure. The product could be recrystallized from benzene/pentane: mp 112–114°C (lit. (3) mp 113°C). The hydrochloride salt of 1-acetylbenzimidazole could be made directly by bubbling dry HCl gas through the ethereal solution to precipitate 0.3 g (0.0015 mol, 18% yield) of product: mp 195–196°C; ir (KBr disc): 1760, 1545, 1490, 1315, 1245, 1170, 760 cm^{-1}; nmr $C_9H_8N_2O \cdot HCl$ (DMSO-d_6, 100 MHz), δ: 2.78 (s, 3H, CH_3), 7.38–8.26 (m, 4H), and 9.00 (s, 1H). Mass spectrum *m/e* (rel. intensity): 160 (M^+, 77), 118 (100). *Exact Mass* calcd. for $C_9H_8N_2O$: 160.0632; found: 160.0635.

N-*Acetyl*-N'-*methylbenzimidazolium acetate (5)*

The hydrochloride salt of 1-methylbenzimidazole (1 g, 0.0059 mol) was added to acetic anhydride (10 mL) and stirred at room temperature until all of the solid had dissolved. Dry ether was then added until the solution became cloudy and 0.7 g of a mixture of the chloride and acetate salts of 1-acetyl-3-methylbenzimidazole and 1-methylbenzimidazole precipitated out of solution.

Due to the extremely labile nature of this salt, separation from the unreacted starting material could not be effected. The mixture was used for pseudo-first order decomposition kinetics. Spectral analyses of the kinetic mixtures after reaction were identical with those made up from *N*-methylbenzimidazole in the same buffer.

Infrared (KBr, disc): 1765, 1752, 1570, 1460, 1375, 1330, 1230, 1130, 770 cm^{-1}; nmr (DMSO-d_6, 100 MHz), δ: 1.92 (s, 3H, OAc), 2.92 (s, 3H, NAc), 4.22 (s, 3H, NMe), 7.70–8.44 (m, 4H), and 9.68 (s, 1H). D_2O exchange yielded 1-methylbenzimidazole. Mass spectrum *m/e* (rel. intensity): 160 (M^+ – Me, 1.85), 133 (23), 131 (100). *Exact Mass* calcd. for $C_{10}H_{11}N_2O$ – Me: 160.0637; found: 160.0639.

N-*Methyltetrahydrobenzimidazole*

1-Methylbenzimidazole (1 g, 0.0076 mol), 5% rhodium on carbon (1 g), glacial acetic acid (20 mL), and 1.1 equivalents of concentrated HCl were placed in a hydrogenation bomb and heated at 120°C under 1000 lb H_2 pressure overnight (4). After cooling, the rhodium was filtered off and the acetic acid removed under reduced pressure (rotoevaporator at 60°C). The residue was dissolved in H_2O (20 mL) and taken to a pH of 9–10 with saturated aqueous potassium carbonate, and the aqueous layer extracted several times with chloroform. The

Can. J. Chem. Downloaded from www.nrcresearchpress.com by 210.87.254.105 on 09/06/12
For personal use only.

combined chloroform extracts were dried with $MgSO_4$ and the solvent removed under reduced pressure. The gummy residue was then dissolved in dry Et_2O (200 mL) and dry HCl gas was bubbled through the solution. A white powder precipitated which was recrystallized from 98% EtOH/ether to give 0.5 g (0.0029 mol, 38% yield) of 1-methyltetrahydrobenzimidazole: mp 194–195°C.

Infrared ($CHCl_3$, cast): 1670, 1500, 1450, 800 cm^{-1}; nmr $C_8H_{11}N_2$ ($CDCl_3$, 90 MHz), δ: 1–1.9 (m, 4H), 2.35–2.7 (m, 4H), 2.48–2.64 (m, 4H), 3.70 (s, 3H, NCH_3), and 8.90 (s, 1H). Mass spectrum *m/e* (rel. intensity): 136 (M^+, 96), 135 (80), 108 (100). *Exact Mass* calcd. for $C_8H_{11}N_2$: 136.1000; found: 136.0998. *Anal.* calcd. for $C_8H_{11}N_2 \cdot HCl$: C 55.65, H 7.59, N 16.22; found: C 55.38, H 7.49, N 16.28.

N-*Acetyl*-N′-*methyltetrahydrobenzimidazolium acetate* (**6**)

The hydrochloride salt of 1-methyltetrahydrobenzimidazole (1 g, 0.0058 mol) was added to acetic anhydride (10 mL) and stirred at room temperature until all of the solid had dissolved. Dry ether was then added until the solution became cloudy and 0.65 g of a mixture of the chloride and acetate salts of 1-acetyl-3-methyltetrahydrobenzimidazole and 1-methyltetrahydrobenzimidazole precipitated out of solution. Due to the extremely labile nature of this salt, separation from the unreacted starting material could not be effected. The mixture was used for pseudo-first order decomposition kinetics. Spectral analyses of the kinetic mixtures after reaction were identical with those made up from *N*-methyltetrahydrobenzimidazole in the same buffer.

Infrared (KBr, disc): 1641, 1543, 1445, 740, 628 cm^{-1}; nmr (DMSO-d_6, 100 MHz), δ: 1.6–1.9 (m, 4H), 1.92 (s, OAc^-), 1.4–2.0 (m, 4H), 2.74 (s, NAc), 3.86 (s, NMe), and 8.94 (s, 1H). Addition of D_2O results in spectrum of 1-methyltetrahydrobenzimidazole. Mass spectrum *m/e* (rel. intensity): 164 (M^+ − Me, 0.1), 108 (100). *Exact Mass* calcd. for $C_{10}H_{15}N_2O - CH_3$: 164.0095; found: 164.0022.

Determination of dissociation constants

The pK_a's were determined potentiometrically using a modified version of Albert and Sergeant's method (5). The pK_a determinations were performed in a jacketed cell kept at 25 + 0.1°C with a Colora Ultra Thermostat constant temperature bath. Air was excluded from the cell by passing a gentle stream of nitrogen through the cell. The pH was recorded as a function of added 0.1000 *N* NaOH (delivered by a Radiometer ABU12) using a titration assembly consisting of a Radiometer TTT2 titrator and PHA943B titration module in conjunction with a Radiometer 6K2402B combined electrode and recorded on a Radiometer SBR3 titrigraph. The electrode was standardized by using dilute acid solutions in the ethanol/H_2O medium in the low pH region and dilute base solutions in the high pH region. A typical run was performed by adding 3.0 mL of 0.5 *N* KCl, 1 mL of 0.1051 *N* HNO_3, 1 mL 95% ethanol, and 0.025 mmol of the substance to be titrated in 1 mL ethanol to the thermostatted cell (25°C) and titrating with 0.1000 *N* NaOH. Each pK_a was the average of at least three reproducible runs.

Rates of hydrolysis

The decomposition of *N*-acetyl-*N*′-methylbenzimidazolium acetate and *N*-acetylbenzimidazole was monitored at 290 nm in 29.4% ethanol/H_2O (v/v) with an ionic strength equal to 0.345 *M* by addition of a calculated amount of KCl (after correction for the amount of ionized buffer). The reaction was checked for buffer catalysis by using 0.21 *M*, 0.13 *M*, and 0.02 *M* buffers and the final rate constant obtained by extrapolation of k_{obs} to zero [buffer]. Sodium formate/formic acid buffer was used from pH 2.8 to 4.0, sodium acetate/acetic acid from 4.4 to 5.2, MES (2(*N*-morpholino)ethane sulfonic acid) from 5.6 to 6.4, HEPES (*N*-2-hydroxyethylpiperazine-*N*′-2-ethanesulfonic acid) from 6.8 to 7.2, TRICINE (*N*-tris(hydroxymethyl)methylglycine) from 7.6 to 8.8, CHES (2(*N*-cyclohexylamino)ethanesulfonic acid) from 9.2 to 10.0. Buffer reagents were used as supplied from Sigma. Data were fit to a nonlinear least-squares program and each rate constant was the result of at least three reproducible results. Product analysis was done by comparison of the final spectrum of the kinetic run with the uv–vis spectrum of the corresponding "NH" compound. In all three cases the expected products were obtained.

Acknowledgements

The author thanks the Natural Sciences and Engineering Research Council of Canada and the University of Alberta for support. The experimental work was done from 1976–1980 in the laboratories of Professor R. S. Brown (University of Alberta) as part of an ongoing program modelling cysteine protease mediated hydrolyses.

1. (*a*) W. P. JENCKS and J. CARRIUOLO. J. Biol. Chem. **234**, 1272 (1959); (*b*) R. WOLFENDEN and W. P. JENCKS. J. Am. Chem. Soc. **83**, 4390 (1961); (*c*) S. M. MARLBURG and W. P. JENCKS. J. Am. Chem. Soc. **84**, 232 (1962).
2. (*a*) J. L. HOGG, M. K. PHILLIPS, and D. E. JERGENS. J. Org. Chem. **42**, 2459 (1977); (*b*) J. L. HOGG and M. K. PHILLIPS. Tetrahedron Lett. 3011 (1977); (*c*) J. L. HOGG and W. P. HUSKEY. J. Org. Chem. **46**, 53 (1981).
3. M. A. STAAB. Ber. **90**, 1320 (1957).
4. I. BUTULA. Croat. Chem. Acta, **45**, 297 (1973).
5. A. ALBERT and E. P. SERJEANT. *In* Ionization constants of acids and bases. J. Wiley and Sons, New York. 1962.
6. T. C. BRUICE and G. L. SCHMIR. J. Am. Chem. Soc. **79**, 1663 (1957).

The cycloaddition of norbornadiene to (triphenylphosphoranediyl)aminocyclotrithiatriazene; the crystal and molecular structure of $Ph_3PN—S_3N_3 \cdot C_7H_8$

STEPHEN W. LIBLONG AND RICHARD T. OAKLEY[1]
Department of Chemistry, University of Calgary, Calgary, Alta., Canada T2N 1N4

AND

A. WALLACE CORDES AND MARK C. NOBLE
Department of Chemistry, University of Arkansas, Fayetteville, AR 72701, U.S.A.

Received February 7, 1983

STEPHEN W. LIBLONG, RICHARD T. OAKLEY, A. WALLACE CORDES, and MARK C. NOBLE. Can. J. Chem. **61**, 2062 (1983).

The reaction of norbornadiene with (triphenylphosphoranediyl)aminocyclotrithiatriazene produces the cycloadduct $Ph_3PN—S_3N_3 \cdot C_7H_8$. The crystal and molecular structure of this compound has been determined by X-ray crystallography. Crystals of $Ph_3PN—S_3N_3 \cdot C_7H_8$ are monoclinic, space group $P2_1/c$, a = 9.757(1), b = 15.114(1), c = 16.535(2) Å, β = 100.73(1)°, V = 2395.7(9) Å^3, and Z = 4. The structure was solved by direct methods and refined by Fourier and full-matrix least-squares procedures to give a final R of 0.040 and R_w of 0.058 for 2620 observed reflections. The structure reveals that the S_3N_3 ring adds to norbornadiene in an *exo* fashion via two sulphur atoms. The S_3N_3 ring adopts a chair conformation with the three ligands occupying axial positions on the same side of the ring. The relative rates of this and other cycloadditions involving SN substrates and olefins are discussed in terms of the energies of the interacting frontier orbitals. The results suggest that HOMO(olefin)–LUMO(SN substrate) interactions control the kinetics of these reactions.

STEPHEN W. LIBLONG, RICHARD T. OAKLEY, A. WALLACE CORDES et MARK C. NOBLE. Can. J. Chem. **61**, 2062 (1983).

La réaction du norbornadiène avec le (triphénylphosphoranediyl)aminocyclotrithiatriazène conduit au produit de cycloaddition: $Ph_3PN—S_3N_3 \cdot C_7H_8$. On a déterminé la structure du cristal et la structure moléculaire de ce composé par cristallographie de rayons-X. Les cristaux de $Ph_3PN—S_3N_3 \cdot C_7H_8$ sont monocliniques et appartiennent au groupe d'espace $P2_1/c$ avec a = 9,757(1), b = 15,114(1), c = 16,535(2) Å, β = 100,73(1)°, V = 2395,7(9) Å^3 et Z = 4. On a résolu la structure par les méthodes directes et on l'a affinée par la méthode de Fourier et la méthode des moindres carrés (matrice entière) jusqu'à des valeurs de R = 0,040 et de R_w = 0,058 pour 2620 réflexions observées. La structure révèle que le cycle S_3N_3 s'additionne sur le norbornadiène d'une façon *exo* par l'intermédiaire de deux atomes de soufres. Le cycle S_3N_3 adopte une conformation chaise avec trois ligands en position axiale du même côté du cycle. On discute des vitesses relatives de cette réaction ainsi que celles d'autres réactions de cycloaddition impliquant des substrats du type SN et des oléfines en fonction des énergies d'interaction des orbitales frontières. Les résultats suggèrent que les interactions HOMO(oléfine)–LUMO(SN) contrôlent la cinétique de ces reactions.

[Traduit par le journal]

Introduction

The rates of organic electrocyclic reactions have been successfully interpreted using frontier molecular orbital (FMO) theory (1, 2). Although the same concepts are equally applicable to the study of the analogous reactions of conjugated inorganic systems, insufficient experimental and theoretical information has been available to allow the extrapolation of ideas. However, recent work on the cycloaddition of 2e-olefins to binary sulphur–nitrogen (SN) derivatives suggests that such studies would be useful. For example, the regiochemistry of the addition of norbornadiene (NBD) to tetrasulphur tetranitride S_4N_4 (3) and phosphadithiatriazenes $R_2PS_2N_3$, **1** (4) (equation [1]) can be rationalized in terms of the symmetries of the interacting frontier orbitals. As a development of this work we are currently examining the reactions of closely related SN ring systems with different olefins. Through studies of this kind the relationships between the energies and distributions of the interacting frontier orbitals and overall reaction rates can be assessed. In the present paper we report the preparation and molecular structure of the cycloadduct **4** formed between (triphenylphosphoranediyl)aminocyclotrithiatriazene, **3**, and norbornadiene (equation [2]). The relative reactivities of **1** and **3** with olefins are discussed in the light of their π-electronic structures.

[1] 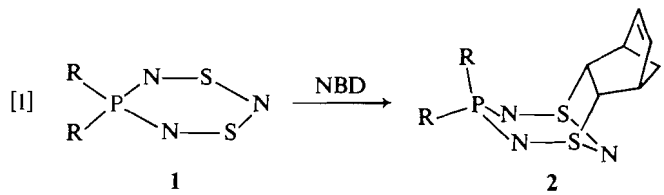

1 2

[2] 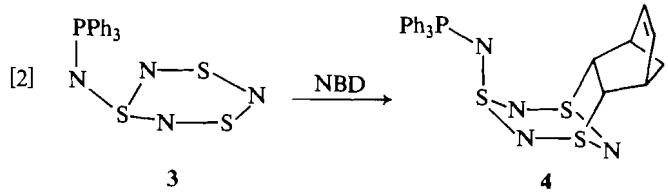

3 4

Experimental

Starting materials

(Triphenylphosphoranediyl)aminocyclotrithiatriazene, **3**, was prepared by the reaction (5) of S_4N_4 (6) with *N*-trimethylsilyltriphenylphosphinimine (7). Norbornadiene was a commercial product (Aldrich). Methylene chloride (reagent grade) was purified by distillation from phosphorus pentoxide. Nuclear magnetic resonance spectra were obtained using a Varian XL-200 nmr spectrometer. Chemical analyses were performed by Mr. Lada Malek of the Department of Chemistry, University of Calgary.

Preparation of $Ph_3PN—S_3N_3 \cdot C_7H_8$

A large excess of norbornadiene (1.40 g, 15 mmol) was added to

[1]To whom all correspondence should be addressed.

Can. J. Chem. Downloaded from www.nrcresearchpress.com by 210.87.254.42 on 09/06/12
For personal use only.

Can. J. Chem. Downloaded from www.nrcresearchpress.com by 210.87.254.42 on 09/06/12
For personal use only.

a solution of $Ph_3PN—S_3N_3$ (0.349 g, 0.84 mmol) in 15 mL methylene chloride, and the mixture heated to reflux under an atmosphere of nitrogen. After 36 h the light brown solution was cooled to room temperature and concentrated *in vacuo* to a volume of ca. 5 mL. Diethyl ether (50 mL) was then added, inducing the precipitation of an off-white solid. This material was filtered off and recrystallized from methylene chloride/acetonitrile to give colourless crystalline blocks of $Ph_3PN—S_3N_3 \cdot C_7H_8$, **4** (0.26 g, 0.51 mmol, 61%), decomp. >140°C. *Anal.* calcd. For $C_{25}H_{23}N_4PS_3$: C 59.3, H 4.6, N 11.1; found: C 59.0, H 4.5, N 11.3. ^1H nmr ($CDCl_3$) δ: 7.0–8.0 (15H, m, phenyl rings), 6.43 (2H, s, $H_{5,6}$), 5.39 (2H, s, $H_{1,4}$), 3.19 (2H, s, $H_{2,3}$), 1.90 and 1.19 (2H, AB, $H_{7,7'}$ = 8.5). ^{31}P nmr ($CDCl_3$, ref. ext. H_3PO_4) δ, 18.7.

X-ray analysis of $Ph_3PN—S_3N_3 \cdot C_7H_8$

Crystals of **4** suitable for X-ray work were obtained by slow evaporation of a methylene chloride/acetonitrile solution. The 0.31 × 0.30 × 0.51 mm crystal used for data collection was mounted with epoxy on a glass fiber. All data were collected using an Enraf-Nonius CAD-4 diffractometer and graphite-monochromated MoK_α (λ = 0.71073 Å) radiation. A least-squares calculation using the diffractometer settings for 25 carefully centred reflections gave the following cell dimensions (at 21°C): a = 9.757(1), b = 15.114(1), c = 16.535(2) Å, β = 100.73(1)°, V = 2395.7(9) Å^3. For $PS_3N_4C_{25}H_{23}$ with mw = 506.65 and Z = 4, D_c = 1.41 g cm^{-3}, F_{000} = 1056 and $\mu(MoK_\alpha)$ = 3.84 cm^{-1}.

Systematic absences of $h0l$ for l odd and $0k0$ for k odd uniquely indicated the space group $P2_1/c$. A total of 4550 unique reflections were measured using θ–θ scans for 2θ from 4 to 50 (h = −11 to 11, k = 0 to 18, l = 0 to 19). The scan range was (1.2 + 0.35 tan θ) and the scan speeds varied from 5 to 20 deg min^{-1}. 1930 reflections had $I < 3\sigma(I)$ and were considered unobserved. The intensities of three reflections (0 1 4, 3 3 0, 6 1 0) which were measured periodically during the data collection varied by less than 2.5% and thus indicated crystal and electronic stability. An absorption correction based on ψ scans gave correction factors which varied from 97.9 to 99.9.

The structure was solved by direct methods (MULTAN 78) (8) and refined by Fourier and least-squares techniques. The final full-matrix least-squares refinement based on F^2 included 298 parameters (positional and anisotropic thermal parameters for all non-hydrogen atoms) and had a parameter:reflection ratio of 1:8.8. Hydrogen atoms were not refined but were included in the structure factor calculations at calculated positions with isotropic thermal parameters of 5.0 Å^2. The weighting scheme, based on counting statistics with an instability factor of 5%, gave no systematic variation of $\Delta F/\sigma(F)$ as a function of either F or sin θ. No secondary extinction correction was made. In the final cycle of refinement the maximum shift/error was 0.06, R = 0.040, R_w = 0.058, and GOF = 1.21. The final difference map had a maximum value of 0.24 e Å^{-3}. Neutral atom scattering factors corrected for real and imaginary anomalous dispersion corrections were used (9). The computer programmes used were those provided by the Enraf-Nonius SDP programme package.

Molecular orbital calculations

The modified neglect of diatomic overlap (MNDO) method (10) is recognized as providing reliable estimates of occupied orbital energies (i.e. ionization potentials) for sulphur–nitrogen derivatives (11). Calculations using this procedure were carried out on several model compounds related to **1** and **3**. Numerical results relating to $R_2PS_2N_3$ molecules refer to a calculation on a $H_2PS_2N_3$ model, for which the geometry was fully optimized within the bounds of C_{2v} symmetry. In the case of **3**, calculations were performed on a $H_3PN—S_3N_3$ model. Full geometry optimization (within C_s symmetry) was again invoked, except for the following restrictions: the ligand geometry was held fixed (d(P—N) = 1.65 Å, d(P—H) = 1.4 Å, ∠SNP = 120°) as was the angle (40°) between the S_2N_3 plane and the plane formed by the substituted sulphur and its two endocyclic neighbours. Variations in either of the models produced small changes in orbital energies (<0.2 eV), but the orbital ordering remained essentially unchanged.

*Electrochemistry of **1** (R = Ph) and **3***

Electrochemical oxidation of **1** (R = Ph) and **3** was carried out in acetonitrile at a rotating platinum electrode with 0.1 *M* $Bu_4N^+ClO_4^-$ as supporting electrolyte. Reductions were performed at a dropping mercury electrode using the same solvent and electrolyte. Half-wave potentials are quoted with reference to a saturated calomel electrode (sce).

Results and discussion

Molecular structure of $Ph_3PN—S_3N_3 \cdot C_7H_8$

The crystal structure of the title compound is composed of discrete molecules of **4**; there are no unusually short intermolecular contacts. Figure 1 shows an ORTEP drawing of the molecule and indicates the atom numbering scheme. Table 1 provides a limited compilation of nonhydrogen atom coordinates (all those designated in Fig. 1) and Table 2 gives a listing of the bond lengths and angles relevant to the present discussion.[2]

Molecules of **4** consist of a six-membered S_3N_3 ring possessing three S-ligands. The orientation of the norbornenyl residue indicates that, as in all other SN–olefin electrocyclic reactions reported to date, the $Ph_3PN—S_3N_3$ molecule **3** adds to NBD in an *exo* fashion.[3] The S_3N_3 ring adopts a chair conformation, with the ligands occupying axial positions. While this orientation is dictated for the S—C bonds by the chelating nature of the norbornenyl group, the —NPPh$_3$ ligand is, in principle, free to occupy either an equatorial or axial position. In $Ph_3PN—S_3N_3$ itself, the choice is equatorial (13). The substitution pattern of the S_3N_3 ring is reminiscent of that observed in $S_3N_3Cl_3$ (14) and $S_3N_3F_3$ (15), where the ligands also occupy axial positions. However, although these structures tend towards chair conformations, the rings are, as a whole, much flatter. The dihedral angles between the planes of three-atom segments and the planes of the four atoms flanking the segment in these molecules are given in Table 6. The more acute puckering in the present case can be attributed to the small "bite" size of the norbornenyl group, which draws the S4 and S6 atoms together. This effect is most easily demonstrated through a comparison of the N5 angle (106.2°) with the angles at N7 (118.2°) and N3 (118.9°). In $S_3N_3Cl_3$ and $S_3N_3F_3$ the mean angles at nitrogen are still larger (at 123.3° and 123.2° respectively). Thus, in order to achieve the small angles at nitrogen without affecting the corresponding angles at sulphur (all of which are similar to those observed in $S_3N_3Cl_3$ and $S_3N_3F_3$), the ring is forced to fold into a more pronounced chair shape.

*Reactivity of **1** and **3** olefins*

In our recent discussion of the electronic structures of $R_2PS_2N_3$ molecules **1** we noted that the symmetries of the highest occupied and lowest unoccupied molecular orbitals (HOMO and LUMO) were such that the concerted addition of a 2e-olefin, e.g. equation [1], was a symmetry-allowed process (4). MNDO molecular orbital calculations on a model

[2]A structure factor table and tables containing the coordinates of the phenyl hydrogen atoms (Table 3), the structural parameters for the phenyl groups (Table 4), and anisotropic thermal parameters for all non-hydrogen atoms (Table 5) are available at a nominal charge from the Depository of Unpublished Data, CISTI, National Research Council of Canada, Ottawa, Ont., Canada K1A 0S2.

[3]This stereochemistry is consistent with recent calculations on the geometry of norbornadiene (12), which reveal a slight pyramidalization of the olefinic CH bonds in the *endo* direction, and hence a slight preference for *exo* addition.

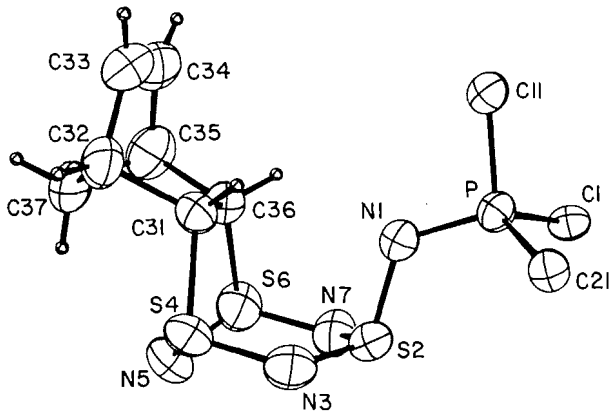

FIG. 1. ORTEP drawing (50% probability ellipsoids) of $Ph_3PN—S_3N_3 \cdot C_7H_8$.

TABLE 1. Positional parameters (and their standard deviations) for the non-hydrogen atoms of $Ph_3PN—S_3N_3 \cdot C_7H_8$*

Atom	x	y	z	B (Å^2)
P	0.40812(9)	0.48686(6)	0.21419(5)	2.84(2)
S2	0.2783(1)	0.31851(7)	0.19425(6)	3.95(2)
S4	0.0294(1)	0.28891(7)	0.08127(6)	4.79(2)
S6	0.2573(1)	0.21518(6)	0.05077(7)	4.66(2)
N1	0.3259(3)	0.0881(2)	0.6582(2)	3.53(7)
N3	0.1067(3)	0.3191(2)	0.1722(2)	4.79(8)
N5	0.0936(4)	0.1956(2)	0.0539(2)	5.40(9)
N7	0.3455(3)	0.2567(2)	0.6408(2)	4.37(7)
C1	0.5884(3)	0.4593(2)	0.2545(2)	2.96(7)
C2	0.6708(3)	0.5138(2)	0.3112(2)	3.48(8)
C3	0.8112(4)	0.4950(3)	0.3353(2)	4.49(9)
C4	0.8679(4)	0.4239(3)	0.3028(3)	4.8(1)
C5	0.7866(4)	0.3693(3)	0.2467(3)	4.70(9)
C6	0.6459(4)	0.3867(2)	0.2226(2)	3.74(8)
C11	0.4070(3)	0.5803(2)	0.1463(2)	2.89(7)
C12	0.4352(4)	0.6653(3)	0.1747(2)	4.29(9)
C13	0.4292(5)	0.7345(3)	0.1201(3)	5.4(1)
C14	0.3978(4)	0.7197(3)	0.0368(2)	5.0(1)
C15	0.3724(4)	0.6355(3)	0.0082(2)	5.1(1)
C16	0.3761(4)	0.5661(3)	0.0620(2)	4.07(9)
C21	0.3319(3)	0.5215(2)	0.3004(2)	2.81(7)
C22	0.3733(4)	0.4852(3)	0.3775(2)	4.47(9)
C23	0.3030(5)	0.5074(3)	0.4405(2)	5.3(1)
C24	0.1925(4)	0.5649(3)	0.4262(2)	4.86(9)
C25	0.1501(4)	0.5996(3)	0.3494(3)	5.3(1)
C26	0.2193(4)	0.5780(3)	0.2868(2)	4.35(9)
C31	0.0992(4)	0.3616(2)	0.0087(2)	3.30(8)
C32	0.0026(4)	0.3689(3)	−0.0778(2)	4.6(1)
C33	0.0759(4)	0.4347(3)	−0.1227(2)	5.1(1)
C34	0.1879(4)	0.3967(3)	−0.1377(2)	5.6(1)
C35	0.1938(4)	0.3042(3)	−0.1047(2)	5.1(1)
C36	0.2304(3)	0.3178(2)	−0.0099(2)	3.33(8)
C37	0.0382(5)	0.2841(3)	−0.1186(2)	5.7(1)

*Anisotropically refined atoms are given in the form of the isotropic equivalent thermal parameter B defined as $(4/3)[a^2\beta_{11} + b^2\beta_{22} + c^2\beta_{33} + ab\beta_{12} \times \cos\gamma + ac\beta_{13}\cos\beta + bc\beta_{23}\cos\alpha]$.

$H_3PN—S_3N_3$ derivative indicate that the analogous cycloaddition for **3** (equation [2]) is equally allowed. The π-like frontier orbitals for the $H_3PN—S_3N_3$ model are illustrated in Fig. 2. However, in spite of the correct symmetry conditions for both reactions (equations [1] and [2]), one is considerably faster than the other. Although we have not measured the actual rate constants for the addition of NBD to **1** and **3**, it is clear

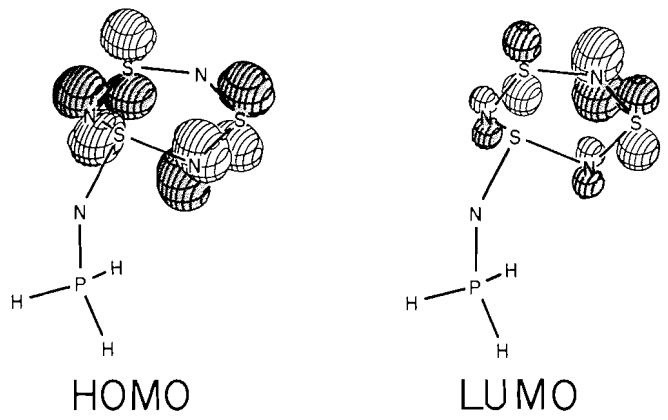

FIG. 2. Frontier orbitals of $H_3PN—S_3N_3$.

from the preparative procedures for **2** and **4** that they must differ by several orders of magnitude. Thus, while the reaction of **1** (R = Ph, Me) with a 10% excess of NBD is complete within 2–3 min, that involving **3** requires a large excess of NBD, prolonged reaction times (~36 h), and elevated temperatures (40°C). In addition to this dichotomy, we also point out that if norbornadiene is replaced by cyclohexene, no addition occurs to either **1** or **3**. It is therefore apparent that simple symmetry rules are, by themselves, inadequate guides to the reactivity of SN systems with olefins. A better understanding can be developed through an analysis of the relative energies of the interacting frontier orbitals.

Frontier molecular orbital analysis

As a standard application of frontier orbital theory (1, 2), the stabilization term ΔE_{FMO} for the concerted addition of an olefin to either **1** or **3** may be written as:

$$[3]\quad \Delta E_{FMO} = 2\beta_{sc}^2 \frac{2C_s(\text{HOMO})C_c(\text{LUMO})}{|E_s(\text{HOMO}) - E_c(\text{LUMO})|} + \frac{2C_s(\text{LUMO})C_c(\text{HOMO})}{|E_s(\text{LUMO}) - E_c(\text{HOMO})|} = 2\beta_{sc}^2(\Delta E_1 + \Delta E_2)$$

where β_{sc} is the resonance integral for the interaction of a sulphur $3p$ with a carbon $2p$ orbital, and C and E refer respectively to the eigenvector coefficients and eigenvalues associated with a given orbital (HOMO or LUMO) of the SN ring (subscript s) or olefin (subscript c). As in many organic cycloadditions, for which similar expressions can be written, one of the terms $\Delta E_{1,2}$ can be expected to dominate the value of ΔE_{FMO} (by virtue of a small denominator for that term). Using these principles Fukui and co-workers have recently pointed out that the addition of 2e-olefins to S_4N_4 is governed by the interaction of the LUMO of S_4N_4 with the HOMO of the olefin (3). In accord with this interpretation, less nucleophilic olefins, i.e., those with a lower lying HOMO, do not react with S_4N_4 (16).

The reactivities of **1** and **3** with olefins can be rationalized similarly. Evidence regarding the relative frontier orbital energies E_s(HOMO) and E_s(LUMO) for the two types of molecule has been obtained from a variety of physical measurements (e.g. $\pi^* \rightarrow \pi^*$ transition energies, redox potentials) as well as from theoretical (MNDO) calculations. However, before discussing the numerical details it is instructive to examine qualitatively the differences in the electronic structures of the two

Can. J. Chem. Downloaded from www.nrcresearchpress.com by 210.87.254.42 on 09/06/12
For personal use only.

TABLE 2. Selected bond lengths (Å) and angles (deg) for $Ph_3PN—S_3N_3 \cdot C_7H_8$

Atom 1	Atom 2	Distance	Atom 1	Atom 2	Distance
P	N1	1.583(3)	S6	N5	1.634(3)
P	C1	1.810(3)	S6	N7	1.631(3)
P	C11	1.803(3)	S6	C36	1.840(3)
P	C21	1.805(3)	C31	C32	1.563(5)
S2	N1	1.634(4)	C31	C36	1.523(4)
S2	N3	1.646(3)	C32	C33	1.500(5)
S2	N7	1.649(3)	C32	C37	1.519(5)
S4	N3	1.617(3)	C33	C34	1.299(5)
S4	N5	1.640(3)	C34	C35	1.498(6)
S4	C31	1.848(3)	C35	C36	1.555(5)
			C35	C37	1.523(6)

Atom 1	Atom 2	Atom 3	Angle	Atom 1	Atom 2	Atom 3	Angle
N1	P	C1	113.8(2)	S4	C31	C32	113.8(2)
N1	P	C11	104.6(2)	S4	C31	C36	107.3(2)
N1	P	C21	115.5(2)	C32	C31	C36	103.5(3)
C1	P	C11	107.6(1)	C31	C32	C33	103.7(3)
C1	P	C21	106.9(1)	C31	C32	C37	101.4(3)
C11	P	C21	108.0(1)	C33	C32	C37	99.7(3)
N1	S2	N3	105.1(2)	C32	C33	C34	107.3(4)
N1	S2	N7	103.4(2)	C33	C34	C35	108.7(4)
N3	S2	N7	112.0(2)	C34	C35	C36	103.3(3)
N3	S4	N5	111.3(2)	C34	C35	C37	99.3(3)
N3	S4	C31	105.8(2)	C36	C35	C37	102.4(3)
N5	S4	C31	97.3(2)	S6	C36	C31	107.2(2)
N5	S6	N7	111.8(2)	S6	C36	C35	114.9(3)
N5	S6	C36	97.4(2)	C31	C36	C35	102.5(3)
N7	S6	C36	106.0(2)	C32	C37	C35	94.0(3)
P	N1	S2	123.5(2)				
S2	N3	S4	118.9(2)				
S4	N5	S6	106.2(2)				
S2	N7	S6	118.2(2)				

TABLE 6. Dihedral angles in $Ph_3PN—S_3N_3 \cdot C_7H_8$, $S_3N_3Cl_3$, and $S_3N_3F_3$

Molecule	Plane 1	Plane 2	Angle (deg)
$Ph_3PN—S_3N_3 \cdot C_7H_8$	N3—S2—N7	N3—S4—N7—S6	155.3
	N3—S4—N5	N3—S2—N5—S6	130.0
	N5—S6—N7	N5—N4—N7—S2	140.4
	S4—N5—S6	N3—S4—N7—S6	124.4
	S2—N3—S4	N7—S2—N5—S4	144.6
	S2—N7—S6	N3—S2—N5—S6	145.5
$S_3N_3Cl_3$	N—S—N (ave)	N—S—N—S	160.6
	S—N—S (ave)	N—S—N—S	158.5
$S_3N_3F_3$	N—S—N (ave)	N—S—N—S	156.6
	S—N—S (ave)	N—S—N—S	154.0

compounds. This can achieved by means of a simple perturbation treatment in which the π-system of each molecule (**1** or **3**) is generated by the incorporation of either (*i*) a $[>PR_2]^+$ group or (*ii*) a $[>S—NPPh_3]^+$ group into an open chain 5-atom NSNSN fragment with 8 π-electrons. The fusion of a $[>PR_2]^+$ group into this fragment to produce **1** will extend the π-system of the latter to include the 3*d*-orbitals of phosphorus. As our earlier *ab initio* Hartree–Fock–Slater MO analysis of $H_2PS_2N_3$ has shown (4), the magnitude of the 3*d*-orbital mixing is small, but it will lead to a slight stabilization of the HOMO and the LUMO levels of the pentadienyl-like $S_2N_3^-$ unit (see Fig. 3). By contrast, the introduction of a $[>S—NPPh_3]^+$ moiety will, to a first approximation, leave the HOMO unaffected, since the orbital is nodal at the substituted sulphur atom (*d*-orbital effects will be smaller than in **1**). However, the interaction of the lone pair orbital on sulphur with the LUMO of $S_2N_3^-$ will cause a substantial destabilization of this orbital and a consequent increase in the HOMO–LUMO gap (relative to **1**).

The redox potentials and the $\pi^* \rightarrow \pi^*$ (HOMO–LUMO) transition energies (4, 17, 18) for **1** (R = Ph) and **3** (Table 7) substantiate the conclusions of this simple description. $Ph_3PN—S_3N_3$ is more readily oxidized than $Ph_2PS_2N_3$, and is less easily reduced, in agreement with the frontier orbital ordering illustrated in Fig. 3. Likewise the larger $\pi^* \rightarrow \pi^*$ transition energy for $Ph_3PN—S_3N_3$ is consistent with a larger HOMO–LUMO gap. MNDO molecular orbital calculations on two model compounds $H_2PS_2N_3$ and $H_3PN—S_3N_3$ also support

Can. J. Chem. Downloaded from www.nrcresearchpress.com by 210.87.254.42 on 09/06/12
For personal use only.

TABLE 7. $\pi^* \rightarrow \pi^*$ (HOMO $\rightarrow$ LUMO) transition energies (eV) and redox potentials (V, vs. sce) for $Ph_2PS_2N_3$, **1**, and $Ph_3PN—S_3N_3$, **3**

Compound	$E(\pi^* \rightarrow \pi^*)$	$E^{1/2}_{redn}$	$E^{1/2}_{oxidn}$
1 (R = Ph)	2.25	−1.10	+0.91
3	2.59	−1.25	+0.83

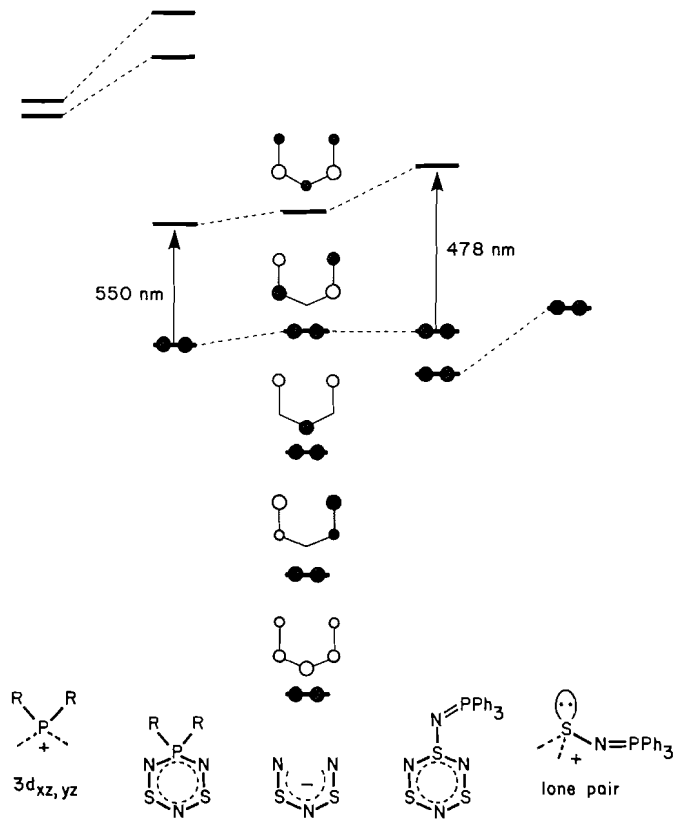

FIG. 3. Qualitative correlation diagram illustrating the interaction of (*i*) a PR_2^+ group and (*ii*) a $S—NPR_3^+$ group with the π-system of a hypothetical $S_2N_3^-$ ion.

the above description, but provide a HOMO–LUMO gap which is unrealistically large. However, the energies of the HOMO's are probably quite reliable (in terms of their correspondence to ionization potentials) (11); for $H_2PS_2N_3$ and $H_3PN—S_3N_3$ the calculated values are −8.7 and −8.5 eV, respectively. Using these numbers (which are not critical) to approximate E_s (HOMO) in **1** and **3** and the $\pi^* \rightarrow \pi^*$ transition energies of $Ph_2PS_2N_3$ and $Ph_3PN—S_3N_3$ to represent the HOMO–LUMO gap, the frontier orbital energy diagram shown in Fig. 4 can be constructed. Inspection of the energy separations of the interacting HOMO–LUMO pairs for the reaction of **1** and **3** with an arbitrary olefin[4] reveals at once that the ΔE_2 term will dominate the ΔE_{FMO} expression. Furthermore it is readily apparent that the higher lying LUMO of **3** will give rise to a larger denominator for the ΔE_2 term of eq. [3], and hence a smaller ΔE_{FMO}. The lower reactivity of **3** can thus be attributed, at least in part, to this effect. The fact that neither **1** nor **3** react with less electron-rich olefins can also be understood. If E_{HOMO}(olefin) is lowered, the ΔE_2 term and hence ΔE_{FMO} will be reduced.

[4]HOMO and LUMO energies indicated for the olefin in Fig. 4 represent an average value obtained from several electron rich olefins (see ref. 19).

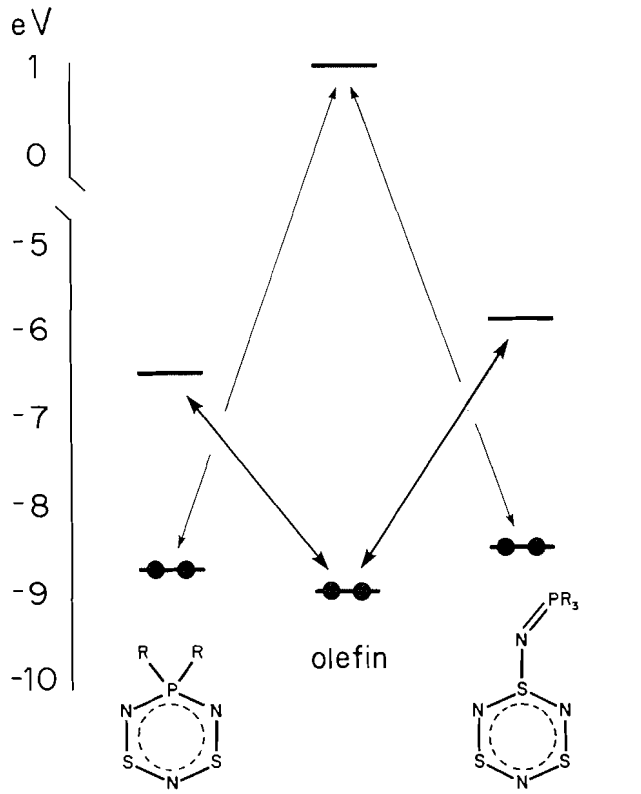

FIG. 4. Frontier orbital energies (estimated) for $Ph_2PS_2N_3$, $Ph_3PN—S_3N_3$, and an arbitrary electron-rich 2e-olefin.

Conclusion

The results reported here suggest that the concerted addition of 2e-olefins to conjugated binary sulphur nitrogen systems is under strong kinetic control; reactivity is dependent on the interaction of the HOMO(olefin) with the LUMO(SN substrate). Further studies of the electrocyclic reactions of SN molecules with olefins should take into consideration the need for (*a*) electron-rich olefins and (*b*) SN substrates with a sufficiently low lying acceptor orbital (of the correct symmetry). However, reactions involving reverse electron demand may also be possible.

Acknowledgements

We thank the Natural Sciences and Engineering Research Council of Canada, the Research Corporation, and the National Science Foundation (EPSCOR grant ISP 8011447) and the State of Arkansas for financial support. We also acknowledge NSERC for a University Research Fellowship (to R.T.O.). We thank Dr. M. Hojo for carrying out the electrochemical measurements.

1. I. FLEMING. Frontier orbitals and organic chemical reactions. John Wiley and Sons.1976.
2. J. SAUER and R. SUSTMANN. Angew. Chem. Int. Ed. **19**, 779 (1980).
3. T. YAMABE, K. TANAKA, A. TACHIBANA, K. FUKUI, and H. KATO. J. Phys. Chem. **83**, 767 (1979).
4. N. BURFORD, T. CHIVERS, A. W. CORDES, W. G. LAIDLAW, M. C. NOBLE, R. T. OAKLEY, and P. N. SWEPSTON. J. Am. Chem. Soc. **104**, 1282 (1982).
5. I. RUPPERT, V. BASTIAN, and R. APPEL. Chem. Ber. **107**, 3426 (1974).
6. (*a*) L. BIRKHOFER, A. RITTER, and P. RICHTER. Chem. Ber. **96**,

Can. J. Chem. Downloaded from www.nrcresearchpress.com by 210.87.254.42 on 09/06/12
For personal use only.

2760 (1963); (*b*) L. BIRKHOFER and A. RITTER. Angew. Chem. Int. Ed. **4**, 417 (1965).
7. M. VILLENA-BLANCO and W. L. JOLLY. Inorg. Synth. **9**, 98 (1977).
8. P. MAIN, S. E. HULL, L. LESSINGER, G. GERMAIN, J-P. DECLERCQ, and M. M. WOOLFSON. MULTAN 78 - a system of computer programmes for the automatic solution of crystal structures from X-ray diffraction data. Universities of York, England and Louvain, Belgium. 1978.
9. International tables for X-ray crystallography. Vol. IV. Kynoch Press, Birmingham. 1974.
10. M. J. S. DEWAR and W. THIEL. J. Am. Chem. Soc. **99**, 4399 (1977).
11. R. GLEITER and R. BARTETZKO. Z. Naturforsch. **36**b, 492 (1981).
12. N. A. RONDAN, M. N. PADDON-ROW, P. CARAMELLA, and K. N. HOUK. J. Am. Chem. Soc. **103**, 2436 (1981).
13. E. M. HOLT, S. L. HOLT, and K. J. WATSON. J. Chem. Soc. Dalton Trans. 1357 (1974).
14. G. A. WIEGERS and A. VOS. Acta Crystallogr. **20**, 192 (1966).
15. B. KREBS, S. POHL, and O. GLEMSER. J. Chem. Soc., Chem. Commun. 548 (1972).
16. M. R. BRINKMAN and C. W. ALLEN. J. Am. Chem. Soc. **94**, 1550 (1972).
17. J. BOJES, T. CHIVERS, A. W. CORDES, G. MACLEAN, and R. T. OAKLEY. Inorg. Chem. **20**, 16 (1981).
18. J. W. WALUK, T. CHIVERS, R. T. OAKLEY, and J. MICHL. Inorg. Chem. **21**, 832 (1982).
19. K. N. HOUK. J. Am. Chem. Soc. **95**, 4092 (1973).

Can. J. Chem. Downloaded from www.nrcresearchpress.com by 210.87.254.42 on 09/06/12
For personal use only.

Concerning the orientation in free radical additions to olefins

JOSEP M. POBLET AND ENRIC CANADELL[1]
Departamento de Química Física, Facultad de Química, Tarragona, Spain
AND
TOMÁS SORDO
Departamento de Química Física, Facultad de Ciencias, Oviedo, Spain

Received December 22, 1982

JOSEP M. POBLET, ENRIC CANADELL, and TOMÁS SORDO. Can. J. Chem. **61**, 2068 (1983).

On the basis of MNDO, MINDO/3, and STO-3G calculations, the regioselectivity of radical additions to substituted olefins is rationalized in terms of an electronic effect.

JOSEP M. POBLET, ENRIC CANADELL et TOMÁS SORDO. Can. J. Chem. **61**, 2068 (1983).

A partir de calculs MNDO, MINDO/3 et STO-3G, on montre que la regioselectivité des additions radicalaires à des olefines substituées peut être rationalisée par un éffet orbitalaire.

Can. J. Chem. Downloaded from www.nrcresearchpress.com by 210.87.254.6 on 09/06/12
For personal use only.

The interplay of polar, steric, and bond strength effects has been invoked to explain the orientation of free radical additions to olefins (1). Usually, the attack is at the less substituted end of the olefin. It is well known that both the SOMO–LUMO and SOMO–HOMO interactions can be important to explain the reactivity of radicals. In a study of the addition of $\dot{C}H_3$ to ethylene, Fukui and co-workers (2) proposed that the SOMO–LUMO interaction was more important than the SOMO–HOMO one. This is rather surprising if we take into account the ionization potential and the electronic affinity of ethylene (−10.5 and 1.8 eV, respectively) and the ionization potential of $\dot{C}H_3$ (−9.8 eV). Recent results of Ponec and Malek (3), as well as Arnaud *et al.* (4) do not support the suggestion of Fukui and co-workers (2). In the course of a general theoretical study of these reactions (5, 6) we have found evidence in favour of the dominance of the SOMO–HOMO interaction in the first steps of the reaction even for the addition of a radical traditionally considered to be a nucleophile as the $\dot{C}H_3$.

The relative importance of the two interactions can be inferred by inspection of the shape of the SOMO of the system methyl + olefin. This orbital initially localized on the methyl radical correlates with the SOMO of the product, mostly localized on the α carbon (1).[2] The transfer of the radical character from the incoming radical to the C_α center is made by mixing of the SOMO ($\dot{C}H_3$) with π (out-of-phase) and π* (in phase) as represented in **2**. As long as the SOMO–HOMO interaction predominates the *p* orbitals on the ethylene stay in phase in the SOMO of the supersystem.

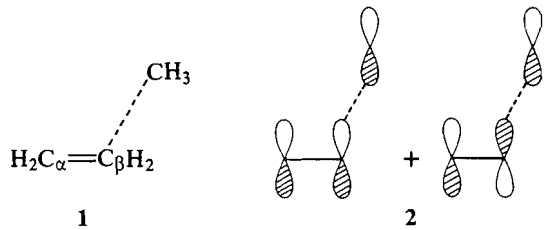

1 **2**

We have examined the shape of this orbital along a reaction coordinate defined by the distance of approach C_{methyl}—C_β. For different values of the approach distance the structure was optimized with respect to all other geometrical parameters at the MNDO and MINDO/3 levels. Using these geometries, the orbitals were recalculated at the STO-3G level. The additions studied were those of $\dot{C}H_3$ to CH_2=CHX (X = H, CH_3, F, Cl) and CH_2=CF_2. All these reactions involve a reactant-like transition state with a σ type geometry. The olefinic bond remains practically unaltered and the C...C_β approach distance lies between 2.40 and 2.25 Å, depending on the olefin (5, 6).

In all cases, the contribution at C_β along the reaction coordinate and even at the transition state remains noticeable and in phase with the contribution at C_α.[3] We can therefore be confident that the SOMO–HOMO interaction is dominating in the first steps of the reaction.[4] Model calculations show this three-electron interaction is stabilizing[5] and, consequently, the addition should preferentially occur at the carbon having the larger coefficient in the π orbital.

As pointed out by Libit and Hoffman (9), the alkyl substituents increase the coefficient at the non-substituted end of the ethylene HOMO. So, as long as alkyl substituents are considered, the addition will always be at the less substituted end of the olefin. Experimental proof comes, among others, from the systematic work by Boldt and co-workers (10).

The rule can be made more general if we recall that fluorines (and halogens in general) polarize the ethylene HOMO in the same way as CH_3 (11). Extending the conjugation or substitution with acceptor groups like CO or CN places the greater coefficient at the less substituted end of the olefin in both the HOMO and LUMO. Consequently, **the addition at the less substituted end of the olfein has an electronic origin**. Let us point out that even if steric and electronic effects go in the same direction, it is difficult to believe that steric effects are behind the regioselectivity in the additions of hydrogen atoms (12)

[1]To whom all correspondence should be addressed.

[2]SOMO: singly occupied orbital in open shell Nesbet type calculations or highest occupied α spin-orbital in UHF calculations.

[3]See Fig. 3 of ref. 4 and ref. 7.

[4]Consequently, the $\dot{C}H_3$ radical should be considered electrophilic. The charge density for the $\dot{C}H_3$ fragment in the transition states substantiate this conclusion. The same result was found for other alkyl radicals as the cyclopropyl radical (5).

[5]The calculations were done for the attack of $\dot{C}H_3$ to CH_2=CHX (X = H, CH_3, F) and CF_2=CHX (X = H, F) with the usual perturbation expressions with overlap (8). The approach distance was taken to be 3.0 Å. The interfragment overlaps were calculated with standard Slater orbitals and the fragment orbitals were both MINDO/3 and INDO. The results are completely coincident in both cases (6).

which, in turn, can be easily explained by the electronic effect.[6]

It is clear that the model developed in this paper is oversimplified.[7] Nevertheless, the experimental results for the most part (1) substantiate it. Only few exceptions have been noticed. For instance, the additions of $\dot{C}H_3$ and $\dot{C}H_2F$ to $CF_2{=}CHF$ are at the more substituted end of the olefin. Strikingly, both the polarization of the HOMO and full MNDO determination of the transition state predict the wrong product in this case. This reversal in the orientation can not be attributed to an increase in the SOMO–LUMO interaction overriding the effect of the SOMO–HOMO one. Experimental ionization potentials and STO-3G calculations (15) both place the SOMO of $\dot{C}Cl_3$ higher than that of $\dot{C}H_3$ and indeed, the addition of $\dot{C}Cl_3$ (like the more electrophilic $\dot{C}F_3$) is at the less substituted end of the olefin. Extended basis set *ab initio* calculations for these systems are now under way in order to clarify the origin of these few exceptions to the rule.

Acknowledgment

We are grateful to Dr. Odile Eisenstein for her comments on the manuscript.

1. J. M. TEDDER. Angew. Chem. Int. Ed. Engl. **21**, 401 (1982); J. M. TEDDER and J. C. WALTON. Tetrahedron, **36**, 701 (1980); J. M. TEDDER and J. C. WALTON. Adv. Phys. Org. Chem. **16**, 51 (1978).
2. H. FUJIMOTO, S. YAMABE, T. MINATO, and K. FUKUI. J. Am. Chem. Soc. **94**, 9205 (1972).
3. R. PONEC and J. MALEK. J. Mol. Struct. Theochem. **88**, 295 (1982).
4. R. ARNAUD, R. SUBRA, and V. BARONE. Nouv. J. Chim. **6**, 91 (1982).
5. E. CANADELL, J. M. POBLET, and S. OLIVELLA. J. Phys. Chem. **87**, 424 (1983); S. OLIVELLA, E. CANADELL, and J. M. POBLET. To be published.
6. J. M. POBLET. M. Sci. Thesis, Tarragona. 1980.
7. R. ARNAUD, J. DOUADY, and R. SUBRA. Nouv. J. Chim. **5**, 181 (1981).
8. A. IMAMURA. Mol. Phys. **15**, 225 (1968).
9. L. LIBIT and R. HOFFMANN. J. Am. Chem. Soc. **96**, 1370 (1974).
10. K. RIEMENSCHNIDER, E. DRECHSEL-GRAU, and P. BOLDT. Tetrahedron Lett. 185 (1979); K. RIEMENSCHNIDER, H. BARTELS, W. EICHEL, and P. BOLDT. Tetrahedron Lett. 189 (1979) and references therein.
11. M.-H. WHANGBO, D. MITCHELL, and S. WOLFE. J. Am. Chem. Soc. **100**, 3698 (1978).
12. K. R. JENNINGS and R. J. CVETANOCIC. J. Chem. Phys. **35**, 1233 (1961).
13. H. FISCHER and H. KOLLMAR. Theoret. Chim. Acta, **16**, 163 (1970); M. J. S. DEWAR and D. H. LO. J. Am. Chem. Soc. **93**, 7201 (1971); L. M. MOLINO and E. CANADELL. Theoret. Chim. Acta, **60**, 299 (1981).
14. V. BONACIC-KOUTECKY, J. KOUTECKY, and L. SALEM. J. Am. Chem. Soc. **99**, 842 (1977).
15. R. J. ELLIOT and W. G. RICHARDS. J. Chem. Soc. Perkin Trans. 2, 943 (1982).

[6]For bulkier radicals or substituents the relative weight of both effects can be different. The relative importance of both effects could be determined by an energy partitioning analysis in local contributions (13).

[7]For a different and more refined model, see ref. 14.

Can. J. Chem. Downloaded from www.nrcresearchpress.com by 210.87.254.6 on 09/06/12
For personal use only.

Condensed-phase reactions of O_3 with NH_3 and NH_2OH[1,2]

THERESA HUSTON, I. C. HISATSUNE, AND JULIAN HEICKLEN

Department of Chemistry and Center for Air Environment Studies, The Pennsylvania State University, University Park, PA 16802, U.S.A.

Received November 17, 1982

THERESA HUSTON, I. C. HISATSUNE, and JULIAN HEICKLEN. Can. J. Chem. **61**, 2070 (1983).

The reactions of O_3 with NH_3 and NH_2OH were studied in the condensed phase. A yellow ozonide was formed immediately upon the addition of O_3 to the NH_2OH solid maintained at $-190°C$, but the yellow–orange ozonide seen in the NH_3 case was not formed until the system was warmed to $-170°C$. These ozonides could be reconverted to reactants by photolysis with near ultraviolet light or by heating to $-90°C$ ($NH_3^+O_3^-$) or $-115°C$ ($NH_2OH^+O_3^-$).

Upon warming the NH_3-O_3 system to $-130°C$, $NH_4NO_3 \cdot 3NH_3$ appeared. It started to deamminate at about $-105°C$ to give NH_4NO_3. In the NH_3-O_3 system a second species, tentatively identified as $NH_2O^+HO_2^-$, was also formed at $-170°C$. It began to decompose with the evolution of O_2 at about $-10°C$.

In the NH_2OH-O_3 system, HNO_3 was also seen immediately upon addition of O_3 to NH_2OH. It appeared as $NH_2OH \cdot HNO_3$, a hydrogen-bonded complex with NH_2OH. At about $-100°C$, NH_2OH started to anneal and the $NH_2OH \cdot HNO_3$ bands grew rapidly and converted to $NH_3OH^+NO_3^-$.

There was no evidence of NH_2OH as an intermediate in the NH_3-O_3 system, but since NH_2OH reacted so readily with O_3, this possibility could not be ruled out. These ozonolysis reactions may be represented as

$$NH_3^+O_3^- + O_3 \xrightarrow{NH_3} NH_4NO_3 + H_2O + O_2$$

and

$$NH_2OH^+O_3^- \xrightarrow{NH_2OH} NH_3OH^+NO_3^- + H_2O$$

THERESA HUSTON, I. C. HISATSUNE et JULIAN HEICKLEN. Can. J. Chem. **61**, 2070 (1983).

On a étudié les réactions du O_3 avec le NH_3 en phase condensée. Il se forme immédiatement un ozonide jaune lorsqu'on ajoute du O_3 au NH_2OH solide maintenu à $-190°C$, mais l'ozonide jaune orange observé dans le cas du NH_3 ne se forme pas tant que l'on ne chauffe pas le système à $-170°C$. On peut retransformer ces ozonides en réactifs par photolyse dans le proche ultraviolet ou par chauffage à $-90°C$ ($NH_3^+O_3^-$) ou à $-115°C$ ($NH_2OH^+O_3^-$). Il se forme du $NH_4NO_3 \cdot 3NH_3$ lorsqu'on chauffe le système NH_3-O_3 à $-130°C$. Le $NH_4NO_3 \cdot 3NH_3$ commence à se désaminer à environ $-105°C$ en donnant du NH_4NO_3. Dans le système NH_3-O_3 il se forme également une deuxième espèce à $-170°C$ que l'on pense être le $NH_2O^+HO_2^-$. Il commence à se décomposer à environ $-10°C$ en dégageant de l'oxygène.

Dans le système NH_2OH-O_3 il se forme également du HNO_3 dès qu'on ajoute du O_3 au NH_2OH. Il se manifeste sous la forme d'un complexe de $NH_2OH \cdot HNO_3$ lié au NH_2OH par des liaisons hydrogènes. Le NH_2OH commence à se décomposer à environ $-100°C$, les raies du $NH_2OH \cdot HNO_3$ croissent rapidement, et se transforme en $NH_3OH^+NO_3^-$.

Il n'y a pas de preuve de l'existence d'un intermédiaire du type NH_2OH dans le système NH_3-O_3, mais puisque le NH_2OH réagit facilement avec O_3 on ne peut pas écarter cette éventualité.

On peut représenter ces réactions d'ozonolyse de la façon suivante:

$$NH_3^+O_3^- + O_3 \xrightarrow{NH_3} NH_4NO_3 + H_2O + O_2$$

et

$$NH_2OH^+O_3^- \xrightarrow{NH_2OH} NH_3OH^+NO_3^- + H_2O$$

[Traduit par le journal]

Introduction

The NH_3-O_3 reaction has been studied for over 70 years. Early studies (1) showed that an intense reddish-orange color was produced when O_3 was bubbled into liquid ammonia cooled to $-78°C$. As the sample was warmed the color became fainter and disappeared by $-60°C$. If the ammonia was evaporated or if it was reacted with O_3 in the gas phase at room temperature, major products were NH_4NO_3, O_2, and H_2O, with the overall reaction being

[1] $2NH_3 + 4O_3 \rightarrow NH_4NO_3 + 4O_2 + H_2O$

Spectroscopic studies of the reddish-orange compound have been performed in several investigations. Solomon *et al.* (2) took an esr spectrum of the solid which showed a *g*-value of 2.0119 indicating an unpaired electron. They identified the compound as ammonium ozonide $NH_4^+O_3^-$. The ir spectrum was obtained by Herman and Giguère (3) who found two strong bands at 800 and 1140 cm^{-1} and two weak bands at 1260 and 2053 cm^{-1} which they assigned to ν_2, ν_3, ν_1, and $\nu_1 + \nu_2$ modes of O_3^-, respectively. The ir spectrum also showed the characteristic bands of NH_4^+ and NO_3^- ions.

Jacox and Milligan (4) examined the spectra of alkali metal ozonides at 14 K. In all cases a band at about 800 cm^{-1} was present. By isotopic studies, they showed that this band belonged to O_3^- and should be assigned as the ν_3 fundamental of

[1]CAES Report No. 643-82.

[2]Taken from the Ph.D. Thesis of Theresa Huston.

Can. J. Chem. Downloaded from www.nrcresearchpress.com by 210.87.254.6 on 09/06/12
For personal use only.

Can. J. Chem. Downloaded from www.nrcresearchpress.com by 210.87.254.6 on 09/06/12
For personal use only.

the ion. The other absorptions reported by Herman and Giguère (3) were not observed, thus showing that at least the 1140 cm^{-1} band was not due to the ozonide ion.

Spiker and Andrews (5) and Thomas and Andrews (6) also obtained the ir spectra of the alkali metal ozonides at 15 K. They found the intense band near 800 cm^{-1} assigned to ν_3 and also weak bands in the 500–600 cm^{-1} region which were assigned to ν_2. Raman studies performed by Andrews and Spiker (7) showed a band at about 1010 cm^{-1} which was assigned to ν_1, the symmetric stretch mode.

Several studies have been done on the uv–visible spectrum of the ozonide. The reddish-orange solid from the NH_3–O_3 reaction showed an absorption peak at 460 nm (2). Jacox and Milligan (4) showed that $Na^+O_3^-$ had an absorption between 510 and 370 nm with an average vibrational spacing of 819 cm^{-1} corresponding to the O_3^- ν_3 band. Giguère and Herman (8) found $K^+O_3^-$ to absorb between 300 and 600 nm with a peak at 457 nm. This absorption was confirmed by Andrews (9) and by Ault and Andrews (10).

The kinetics of the NH_3–O_3 reaction to produce NH_4NO_3 were studied in aqueous solution by Papko (11) and by Hoigné and Bader (12), and in the gas phase by Olszyna and Heicklen (13). In solution the reaction was found to be first order in each reactant at pH < 9, but for pH > 9 or in the gas phase the rate law was complex and indicated a free-radical chain oxidation. Because of the complexity of the reaction kinetics, it was decided to re-examine the low-temperature condensed-phase reaction between NH_3 and O_3 to see if reaction intermediates could be identified.

Experimental

Ammonia and ozone gases were introduced separately into a reaction cell at liquid nitrogen temperature and then warmed slowly. Infrared and uv–visible spectra were taken after the warmed samples were recooled.

The cells were evacuated for at least 12 h before cooling with liquid nitrogen in preparation for the condensation of reactants onto the cold window. Low-temperature cells, similar to those described by Miller (14), were used. The bodies of the cells were made of Pyrex glass and fitted with external CsBr or fused quartz windows. An inner window of AgCl, CsBr, CsI, KBr, or fused quartz was attached to the cold finger in different experiments.

The gases were handled in conventional vacuum lines with Teflon stopcocks fitted with Viton "O" rings and ground-glass stopcocks lubricated with Dow Corning Silicon High Vacuum Grease. After deposition of each gas, the cell was opened to vacuum. After evacuation the cell was removed from the vacuum line to examine its spectrum.

Both Perkin-Elmer Model 225 and 521 grating infrared spectrophotometers were used in this study. Spectra were scanned from 4000 to 250 cm^{-1}. A Cary Model 14 uv–visible spectrophotometer whose sample compartment was modified to accommodate the low-temperature cell was used to scan from 650 to 190 nm.

Ammonia (Matheson Co.) was liquefied in a vacuum line and then distilled at 50 Torr vapor pressure, with the central fraction being collected in one-liter storage bulbs. Deuterated ammonia (Merck, Sharp, and Dohme of Canada, Ltd.) was used directly.

Ozone was prepared immediately before each use by means of a Tesla coil discharge through purified oxygen at a reduced pressure and immersed in a liquid nitrogen bath. Any excess oxygen was removed by pumping with an oil diffusion pump on the liquid ozone maintained at −196°C. The oxygen (Philip Wolf and Sons) was purified by collecting it as a liquid in a trap cooled with liquid nitrogen. About half of this liquid was allowed to boil off slowly, after which samples were collected in one-liter gas storage bulbs. The last fraction was discarded.

Nitric acid was prepared by the distillation of an H_2SO_4–HNO_3 solution as described by Nightingale *et al.* (15). Also, nitric acid and deuterated nitric acid were prepared by the addition of H_2O or D_2O to N_2O_5. The pentoxide was made by the ozonolysis of NO_2, which was prepared by the reaction of oxygen with nitric oxide. Nitric oxide (Matheson Co.) was purified by fractional distillation.

Tertiary hydroxylammonium phosphate was prepared from hydroxylamine hydrochloride and tertiary sodium phosphate after the method described by Uhlenhuth (16). All condensable material produced during the thermal decomposition of the phosphate salt was collected in a tube cooled by liquid nitrogen. The pressure in the vacuum line was kept at about 200 mTorr or less during this time because Back and Betts (17) found the NH_2OH thermal decomposition to be enhanced by increasing NH_2OH pressure. After any noncondensable gas had been pumped away, the material in the tube was warmed slowly by replacing a Dewar flask around it. About half of this material was removed, by which time the pressure during pumping was steady. The sample was then recooled while any noncondensable gas was removed by evacuation. The NH_2OH again was warmed slowly and the amount needed for that day's experiment was deposited on the cold window while pumping through the low-temperature cell. Any remaining material was discarded. No impurities were ever detected in these samples by ir spectroscopy.

When a larger amount of NH_2OH (estimated to be enough for ten experiments) was produced at one time, purification problems were encountered. All the decomposition products except H_2O were removed by passing the sample through a trap maintained at −95°C. When kept in an ice–water bath the NH_2OH formed a white solid ring above the level of liquid H_2O in the bottom of the tube. Before each use this sample was evacuated for 1 to 10 min until a steady pressure of about 200 mTorr was obtained. The ice–water bath was then removed from the storage tube and NH_2OH was deposited on the cold window for 1 to 3 min. The first three samples obtained in this manner had no observable ir bands due to H_2O. The next six samples showed increasing amounts of H_2O as the amount of NH_2OH solid in the sample tube decreased.

NH_3–O_3 reaction

Various amounts of NH_3, ranging from 1.2×10^{-6} to 1.0×10^{-4} mol, and O_3, ranging from 9.3×10^{-6} to 5.7×10^{-5} mol, were condensed separately onto the cold window at −196°C and then warmed slowly to initiate the reaction. The first sign of reaction occurred at −170°C at the same time that the solid NH_3 was annealing on the cold window and ozone was already in the vapor phase. Even though the liquid O_3 had wetted the window earlier, no reaction was evident until this temperature. By comparison, proton transfer reaction from gaseous HCl to solid NH_3 was seen to occur only from −145°C when the hydrogen bonds of solid NH_3 evidently became weaker (18).

By observing and plotting the growth and decay of the bands first appearing at −170°C, it became evident that two species were always forming at the same time. One of these substances, which we identified as the charge-transfer complex $NH_3^+O_3^-$ was yellow to orange in color depending on the amount produced. The other compound was tentatively identified as $NH_2O^+HO_2^-$. The ir bands for both products along with their deuterated analogs can be found in Table 1. In order to enhance the spectral features, a sample was warmed to −130°C and then recooled to −190°C to give the spectrum shown in Fig. 1. Because of this warming a small amount of the product $NH_4NO_3 \cdot 3NH_3$ also was formed and gave rise to a weak peak due to NO_3^- at 830 cm^{-1} on the high frequency shoulder of the 800 cm^{-1} peak of the ozonide species. Other bands (18) of $NH_4NO_3 \cdot 3NH_3$ overlapped those listed in Table 1 and also those of solid NH_3 whose spectrum is the upper curve in Fig. 1.

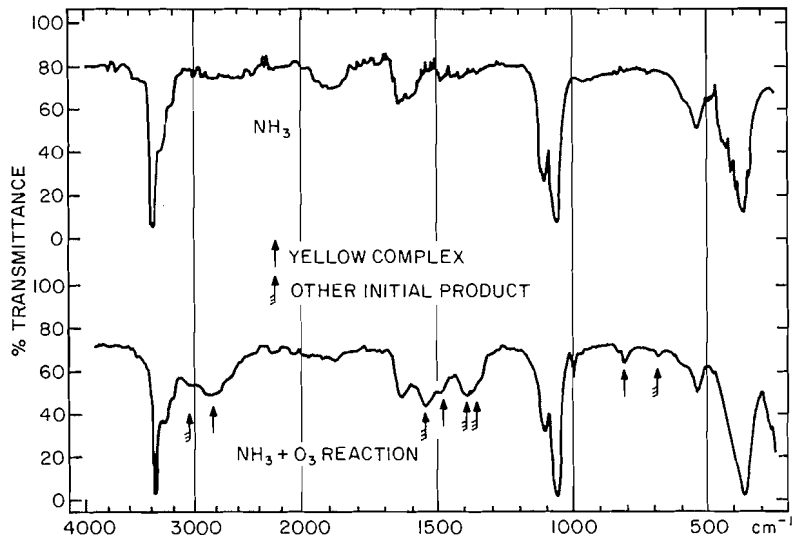

FIG. 1. Infrared spectra of NH_3 before reaction and of the two initial products in the NH_3-O_3 reaction. Spectra recorded at −190°C. The absorption at 1000 cm^{-1} is an artifact caused by changing gratings.

TABLE 1. Infrared frequencies (cm^{-1}) of the initial products of the NH_3-O_3 reaction

Infrared frequency			
$NH_3 + O_3$	$ND_3 + O_3$	ν_H/ν_D	Assignment
	$NH_3^+O_3^-$		
~2800 s	~2120 s	1.32	N—H stretch
~1490 w	~1125 w	1.32	N—H bend
800 s	795 s	1.01	ν_3 of O_3^-
	$NH_2O^+HO_2^-$		
3440 w			O—H stretch
~3020 s	~2350 s	1.29	N—H stretch
1550 s	1530 m	1.01	N—O stretch
	~1430 w		
~1400 m	~1080 w	1.30	N—H bend
~1370			O—H bend
~1120 w			OOH bend
~800 vw	~800 vw	~1.0	O—O stretch
675 w	605 w	1.12	N—O bend

We identified the colored complex to be $NH_3^+O_3^-$ rather than $NH_4^+O_3^-$ as reported by Solomon *et al.* (2) and by Herman and Giguère (3) for the following reasons. First, all bands in Table 1 assigned to this ozonide, including those associated with N—H vibrational modes, disappeared when the ozonide was photolyzed with a mercury lamp. Ammonium ion bands, when they were present in the spectrum, did not disappear during photolysis. Second, during the initial formation of the ozonide, no bands due to such ions as the nitrate or the nitrite were generated. The infrared bands of NO_3^- and NO_2^- are much more intense than those from NH_4^+, and they would have been detected were they formed in our system. Hence, there were no ready sources of proton to form the ammonium ion at −170°C.

The most distinguishing feature in the spectrum of $NH_3^+O_3^-$ is the band at 800 cm^{-1}. Upon deuteration this band shifted only slightly from 800 to 795 cm^{-1} indicating that a hydrogen atom was not directly involved with this vibrational mode. Bands at similar frequencies were observed by Spiker and Andrews (5) and by Thomas and Andrews (6) in alkali and alkaline earth metal ozonides, respectively. These authors had assigned this band to ν_3, the antisymmetric stretch fundamental, of the ozonide ion. Small shifts were seen by them due to the different metal cations used. A similar interpretation can be made for our 800 cm^{-1} band from the NH_3-O_3 reaction: the small shift observed upon deuteration was attributed to the cation effect. The small frequency shift upon deuteration is further evidence that the cation is NH_3^+ where bonding with the O_3 can occur through the nitrogen atom. If the cation had been the ammonium ion, the O_3^- anion would have had to bond to it through a hydrogen atom and a much larger isotopic shift should have been observed. For example, a shift of 15 cm^{-1} was observed in the ν_3 stretching fundamental of the nitrate ion when the cation is changed from NH_4^+ to ND_4^+. Our yellow–orange color is also consistent with the yellow to red colors reported previously for metal ozonides.

The deuterated studies showed that the 2800 and 1490 cm^{-1} bands were shifted by the amount expected for N—H stretching and bending vibrations, respectively. The low value of 2800 cm^{-1} suggests hydrogen bonding. For example, the ν_1 fundamental of the ammonium ion in $NH_4NO_3 \cdot 3NH_3$ is at 2800 cm^{-1} (18). Furthermore, the bending mode ν_4 of the NH_4^+ ion in this ammoniated species is also at 1490 cm^{-1}. The NH_3 molecule was still very likely hydrogen bonded to other NH_3 molecules in the solid matrix since it was seen in separate experiments (18) to be unreactive to HCl at these temperatures. Because the present reaction took place between gaseous ozone and solid ammonia, it is unlikely that the ammonium ion could have formed at these low temperatures.

Additional experiments were done following the uv–visible spectra of the reaction system. For these runs the O_3/NH_3 ratio was varied between 0.5 and 3.0. The sample sizes ranged from 4.4×10^{-6} to 4.3×10^{-5} mol for NH_3 and from 9.9×10^{-6} to 2.4×10^{-5} mol for O_3. For this study the low-temperature cell had outer SiO_2 windows and either a thin CsBr or SiO_2 inner window. The temperature of the SiO_2 window was more difficult to control, so the CsBr window was used for about half of the experiments. This CsBr window had good transmission from 650 to 250 nm but began absorbing strongly below this. The instrument cut-off was 190 nm and the SiO_2 windows still transmitted most of the radiation down to that wavelength.

Initially, NH_3 absorbed from the cut-off limit to about 250

Can. J. Chem. Downloaded from www.nrcresearchpress.com by 210.87.254.6 on 09/06/12
For personal use only.

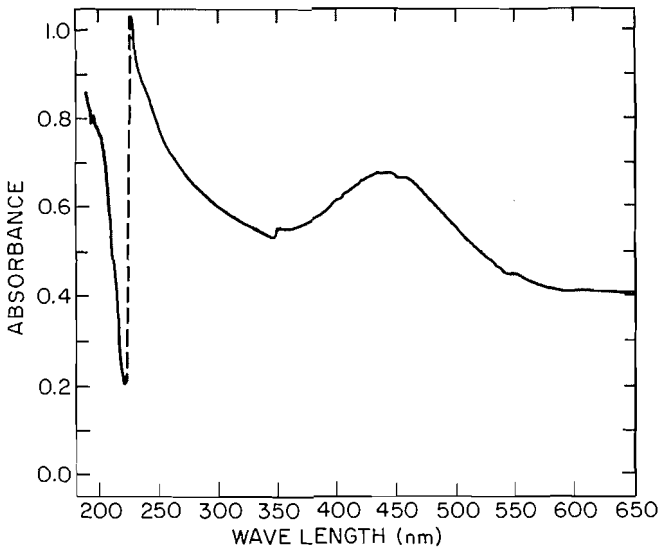

FIG. 2. Ultraviolet–visible spectrum of ammonia ozonide at −190°C.

nm for a typical sample used in these experiments. If more material was deposited on the window, it absorbed to a longer wavelength. No sign of absorption near 250 nm could be found when O_3 was introduced into the low-temperature cell. If the cell was allowed to warm slowly and the 250 nm wavelength was followed with time, O_3 was detected as it formed a liquid film on the window before vaporizing. Many attempts to keep the O_3 on the cold window either alone or on top of NH_3 failed. When both the NH_3 and O_3 were in the cell, and O_3 was allowed to form a liquid film on the window before recooling the cell, no change at all in the spectrum could be found from the initial spectrum. It was discovered that ozone had to be in the gas phase before any reaction occurred at about −170°C with the still solid NH_3.

The initial change in the spectrum came with the formation of the yellow complex. The visible absorption consisted of a broad band from 550 to 350 nm with the peak occurring at 438 nm as shown in Fig. 2. In the deuterated analog the band seemed to be shifted slightly with the peak at 435 nm. The 438 nm band had the same temperature dependence as that shown by $NH_3{}^+O_3{}^-$ in the ir scans. It started to form at −170°C, reached its maximum value at about −105°C, and decreased upon further warming. If the sample was warmed until −90°C when the sample had become clear and the 438 nm peak had disappeared, recooled to −196°C and then rewarmed to only −125°C, both the yellow color and the absorption peak returned, although not as strong as before warming to −90°C. The absorption seen here agrees with visible spectra recorded for ozonide species by many workers listed in the Introduction. The assignment of the yellow species as an ozonide is thus strengthened by this spectrum.

The initial reaction

[1] $NH_3 + O_3 \rightarrow NH_3{}^+O_3{}^-$

was never seen to be complete. The purple color of O_3 could be seen upon recooling the sample, sometimes surviving to room temperature, even when unreacted NH_3 was still present in the cell. This had also been seen in the gas cell when NH_3 and O_3 both remained for several hours. The O_3 was found to decrease slowly with no further consumption of NH_3. Thus the ammonia molecule in reaction [1] appears to require activation in addition to having its nitrogen atom exposed for attack by the ozone molecule.

Ammonia ozonide can be photolyzed. A medium-pressure mercury lamp which transmitted light in the 300–760 nm region (Pyrex envelope) was used for this purpose. Photolysis was done through either the Pyrex glass walls of the cell or through a quartz window. The complete photolysis of the material seemed to take less time when a quartz window was used but no other differences were noted. The yellow complex was bleached white by the exposure to the Hg lamp, regenerating O_3. Infrared and uv–visible scans after photolysis showed that all the bands of $NH_3{}^+O_3{}^-$ had disappeared and a weak band at 1230 cm^{-1} (1240 cm^{-1} in the deuterated case) had appeared. There was also some increase in absorptions where NH_4NO_3 had strong bands. The ratio of the decrease in the absorbance of the 800 cm^{-1} band to the increase of the 1230 cm^{-1} band ranged from 1.6 to 3.2. This would indicate that more than one reaction was involved in the photolysis. This 1230 cm^{-1} band remained until about −110°C, but there was no indication of its altering the rest of the reaction in any way. In most cases both the O_2 and any excess O_3 were evacuated from the cell before photolysis. This was to insure that any spectroscopic changes were not due to the photolysis of O_3 with subsequent reaction of its products. Since the lamp produced a large amount of heat, and the outer body of the cell became warm even when air was constantly circulated around the lamp, the noncondensable gas had to be removed in larger samples to insure a vacuum within the cell so as to keep the sample at −190°C. Several samples were photolyzed while keeping both the O_2 and O_3 in the cell. No spectroscopic differences were observed from those samples in which these two compounds had been removed. If excess O_3 and O_2 had been removed from the cell before photolysis, only a small amount of O_2 was found to have formed during irradiation but enough O_3 was generated to show its purple color when condensed on the cold finger. The yellow ozonide reformed upon warming, but not as much as before photolysis. If the O_3 released during photolysis was removed by evacuation before the sample was rewarmed, no ozonide reformed.

Apparently, the main photolytic reaction is

[2] $NH_3{}^+O_3{}^- + h\nu \rightarrow NH_3 + O_3$

but some of the time the product with the weak 1230 cm^{-1} band and very likely the final reaction product NH_4NO_3 must also be produced. The 1230 cm^{-1} band is in the N—O stretch region of the spectrum, and the small shift to 1240 cm^{-1} upon deuteration would indicate that H-atoms were not directly involved in this band. The small amount of O_2 produced during photolysis could come from the same reaction producing this ir band. One attractive assignment of this band is to the species NH_3O formed by reaction [3].

[3] $NH_3{}^+O_3{}^+ + h\nu \rightarrow NH_3O + O_2$

Theoretical studies on ammonia oxide (NH_3O) have been carried out by Hart (19) who deduced that it has a bound ground state with an unusually long N—O bond. This oxide was found to be less stable by 30 kcal/mol than its tautomeric form of hydroxylamine (NH_2OH) and correlated with the dissociation products $NH_3(^1A_1) + O(^1D)$ in a well of depth 35 kcal/mol. This makes NH_3O unstable to dissociation to the spin forbidden products $NH_3(^1A_1) + O(^3P)$. Presumably the latter spin-forbiddenness and hydrogen-bonding in the NH_3 matrix at low temperatures may contribute to the stability of NH_3O if it is

Can. J. Chem. Downloaded from www.nrcresearchpress.com by 210.87.254.6 on 09/06/12
For personal use only.

produced by reaction [3]. Since the presence of the 1230 cm^{-1} band did not affect the course of the overall reaction, NH_3O can generate the observed products by reaction [4].

$$[4]\quad NH_3O + O_3 \xrightarrow{NH_3} NH_4NO_3 + H_2O$$

The assignment of the infrared bands of the second product listed in Table 1 to NH_3O can be ruled out. According to Hart's calculation (19), the reaction

$$[5]\quad NH_3 + O_3 \rightarrow NH_3O + O_2$$

in the gas phase is endothermic by 35 kcal/mol. It is, therefore, unlikely that reaction [5] can be initiated thermally by warming the reactants from liquid nitrogen temperature to −170°C, which was the experimental condition when the second product was generated. Furthermore, the N—O bond in NH_3O is reported to be a weak single bond (19), whereas the value of 1550 cm^{-1} for the stretching frequency of the second product suggests a double bond.

In order to establish the identity of the second product, a closer examination of the experimental results is required. It formed at −170°C with essentially no evolution of oxygen and continued to grow at the same rate as the ozonide until about −110°C, after which it remained constant. The spectroscopic data show that this colorless solid possesses an N—H bond, an N—O double bond, and possibly an O—O bond. It remained stable until about −10°C when it decomposed with the evolution of oxygen. These results suggest that the atomic compositions of the ozonide and this second product may be similar, and that both may be ion pairs.

In spite of these similarities in behavior, the electronic structures of the ozonide and this second product are very different. The ozonide is photolyzed readily but the second product is not when they are exposed to the 300–760 nm radiation from a mercury lamp at liquid nitrogen temperature. Thus, the second product may be a tautomer of the ozonide, and we tentatively suggest it to be $NH_2O^+HO_2^-$. Fox and co-workers (20) have shown that the very toxic and reactive gas NF_3O, which is distinct from NF_2OF, combines readily with acceptors of fluoride ion, such as BF_3, SbF_5, and AsF_5, to form relatively stable 1:1 adducts. For example, $NF_2O^+SbF_6^-$ is reported to be stable even at 100°C but reacts violently with water at room temperature. The association of the hydroperoxide anion HO_2^- with the ozonide ion is based on the studies of Landi and Heidt (21). These authors observed the formation of O_3^- during flash photolysis of basic aqueous hydrogen peroxide and showed that the kinetics of the system involved both O_3^- and HO_2^- ions. An ir spectrum of solid $NH_4^+HO_2^-$ was obtained by Knop and Giguère (22). This sample was prepared by depositing a layer of NH_3 on top of a layer of H_2O_2 on an ir window at −190°C. Upon warming to −80°C $NH_4^+HO_2^-$ formed. Other than the NH_4^+ ion absorptions a broad band at 1100 cm^{-1} and a weaker but sharper band at 836 cm^{-1} were seen. These were assigned as the bending and O—O stretching vibrations, respectively, of the HO_2^- ion. The bands seen at 1120 and 800 cm^{-1} in the second product are assigned in like manner. No NH_4^+ bands were present in the spectrum of our product. $NH_4^+HO_2^-$ had been found by Maass and Hatcher (23) to have a melting point of 24.5°C and to be stable in the absence of H_2O. Although our second product was normally stable until −10°C, when H_2O was added to the NH_3–O_3 system it decomposed at −85°C as the H_2O left the cold window.

The $NH_4NO_3 \cdot 3NH_3$ was seen to start forming at −130°C as the NH_3 matrix bands began to decrease. Copious amounts of O_2 were released simultaneously. The spectrum of $NH_4NO_3 \cdot 3NH_3$ was identical to that produced when HNO_3 was reacted with excess NH_3, a reaction which also started at about −130°C (18). The $NH_4NO_3 \cdot 3NH_3$ started to deammonate at about −105°C to form NH_4NO_3 simultaneously with the disappearance of the remaining $NH_3^+NO_3^-$. When the final reaction mixtures were recondensed back onto the low-temperature window, their spectra showed the presence of water.

A possible reaction sequence for this system may be as follows:

$$[1]\quad NH_3 + O_3 \rightarrow NH_3^+O_3^-$$

$$[6]\quad NH_3^+O_3^- + O_3 \xrightarrow{NH_3} NH_4NO_3 + H_2O + O_2$$

$$[7]\quad NH_3 + O_3 \rightarrow NH_2O^+HO_2^-$$

$$[8]\quad 2NH_2O^+HO_2^- \rightarrow 3O_2 + 2NH_3$$

Reactions [1] and [6] show an O_3-to-NH_3 consumption ratio of 1.0. Reactions [7] and [8] are essentially a catalytic decomposition of O_3. In a number of experiments we measured, although with great difficulty and experimental uncertainty, the O_3-to-NH_3 consumption ratio and found it to vary between 1.1 and 2.3, consistent with the ratio of 2.0 found by Strecker and Thieneman (1*c*). From the reaction sequence, it can be seen that this ratio would vary depending on the amount of $NH_2O^+HO_2^-$ that formed in each separate experiment.

NH_2OH–O_3 reaction

A possible mechanism for the ozonolysis of NH_3 could include NH_2OH as an intermediate. Therefore we thought it would be useful to examine the ozonolysis of NH_2OH. The reaction of NH_2OH with O_3 in the low-temperature cell can be divided into two groups. The reaction pattern of each sample depended upon whether the NH_2OH had been annealed before the O_3 was added to the cell. Annealed and unannealed solid NH_2OH had readily distinguishable spectra (18). The results of the annealed samples will be discussed first.

The reaction of annealed NH_2OH solid with gaseous O_3 was not seen until about −65°C when NH_2OH started to sublime off the low-temperature window. At about −50°C, a hydrogen-bonded complex $NH_2OH \cdot HNO_3$ was seen with the subsequent appearance of crystalline $NH_3OH^+NO_3^-$ at −10°C. The latter solid remained unchanged while kept under vacuum at room temperature overnight but subsequently it slowly changed to NH_4NO_3 with evolution of non-condensable gas presumably according to reaction [9].

$$[9]\quad 2NH_3OH^+NO_3^- \rightarrow 2NH_4NO_3 + O_2$$

In many runs it was evident that much of the reaction took place after NH_2OH had sublimed off the window. In these cases $CsNO_3$ was observed on the inner and outer windows of the cell. Similar results were obtained when HNO_3 was reacted with NH_2OH in the low-temperature cell (18).

Quite a different reaction pattern was observed when O_3 was introduced into the low-temperature cell containing unannealed NH_2OH. The samples were seen to turn from white to yellow as soon as the O_3 being introduced into the cell struck the surface of the NH_2OH on the cold window. The ir spectrum also showed changes after the introduction of O_3: a band at 1035 cm^{-1} and $NH_2OH \cdot HNO_3$ were both observed.

The yellow color was present from −190°C to about −115°C. It sometimes grew deeper in color during the warm-

Can. J. Chem. Downloaded from www.nrcresearchpress.com by 210.87.254.6 on 09/06/12
For personal use only.

Can. J. Chem. Downloaded from www.nrcresearchpress.com by 210.87.254.6 on 09/06/12
For personal use only.

ing cycles, but it did not approach the intensity of the yellow color seen in the NH_3-O_3 reaction from $-170°C$ to its decrease at $-105°C$. Photolysis of the sample while kept at $-190°C$ with a medium-pressure mercury lamp caused the material to turn white, but no change in the ir spectrum could be detected. The mercury lamp used here transmitted from 300 to 760 nm. The sample again turned yellow when it was warmed to about $-120°C$, but no change in the ir spectrum could be attributed to this yellow color. In the NH_3-O_3 system the ir bands at 800 and 2800 cm^{-1} belonging to the yellow species were detectable before the yellow color was visible. Thus in the NH_2OH-O_3 system not only was less charge-transfer complex formed but its ir bands appear to be much weaker. During all this time the major portion of the O_3 could be seen on the colder Cu frame and cold finger. This was especially noticeable when the samples were first recooled and the purple color of the ozone could be seen very distinctly on the cold finger.

The 1035 cm^{-1} band which was present at $-190°C$ disappeared, or at least significantly decreased, upon the first warming. The only other change at this temperature was a small increase in $NH_2OH \cdot HNO_3$. The 1035 cm^{-1} band was unchanged by photolysis. Once this band disappeared it was never seen to reform upon recooling and rewarming. There was always a large portion of the O_3 still present in the cell at this time because its purple color could be seen upon recooling. It could also be seen to wet the window upon warming. The NH_2OH did not anneal at these low temperatures. In the samples with the largest absorption of the 1035 cm^{-1} band, this band was completely gone by $-105°C$. The intensity of the 1035 cm^{-1} band increased with the amount of material used, but there was no definite dependence upon the amount of either reactant.

$NH_2OH \cdot HNO_3$, which was also seen in the ir spectra immediately after O_3 introduction into the cell, exhibited slow growth during warming until NH_2OH started to anneal around $-100°C$. At this temperature $NH_2OH \cdot HNO_3$ grew rapidly and converted to amorphous $NH_3OH^+NO_3^-$ as all the unreacted NH_2OH annealed. The intensity of the ir bands of amorphous $NH_3OH^+NO_3^-$ continued to increase up to room temperature. After the sublimation of NH_2OH and H_2O (another reaction product), this was the only change seen in the spectrum for some runs. In other cases NH_4NO_3 formed at room temperature as the NH_3OH^+ ion converted to NH_4^+ ion.

Only in two runs did crystalline $NH_3OH^+NO_3^-$ form at $-15°C$. No amorphous $NH_3OH^+NO_3^-$ was seen in these runs,. and the crystalline $NH_3OH^+NO_3^-$ formed as the $NH_2OH \cdot HNO_3$ disappeared.

Experiments were also performed following the $NH_2OH + O_3$ reaction by uv–visible spectroscopy. Solid NH_2OH itself absorbed from 220 nm to the instrumental cut-off at 190 nm. An increase in absorption due to sample scattering occurred at $-90°C$ as the hydroxylamine annealed and turned milky white. Sublimation from both CsBr and SiO_2 windows was noted at $-40°C$. Only NH_3 gas was observed in the low-temperature cell when a uv–visible spectrum was recorded at room temperature.

In only one experiment was a weak absorption observed at 255 nm when liquid O_3 was alone in the low-temperature cell. The CsBr window had been cooled with liquid nitrogen for a long time before O_3 was introduced into the cell and was evidently cold enough for some liquid O_3 to remain on it. Most of the ozone could be seen to have condensed on the Cu frame and cold finger.

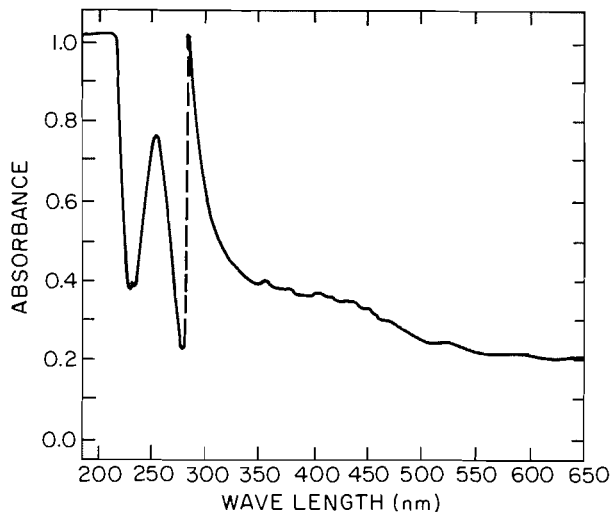

FIG. 3. Initial uv–visible spectrum of $NH_2OH + O_3$ at $-190°C$.

As soon as O_3 was introduced into the low-temperature cell already containing condensed NH_2OH, two new peaks appeared in the spectrum. They can be seen in Fig. 3. One was in the visible region exhibiting a broad peak at 440 nm and corresponded to the yellow color of the sample. The 440 nm peak was present in 3 out of 5 runs using the distilled NH_2OH and in 2 out of 4 runs using the partially decomposed samples. Since none of these samples had been annealed before O_3 was added, the yellow color was expected to be present in every sample as was seen in the ir studies. It was then noted that the yellow color and the 440 nm peak were never observed in those samples in which a uv–visible spectrum of the NH_2OH alone was recorded before the O_3 was added. When the O_3 was added to the NH_2OH in the low-temperature cell before a uv–visible spectrum was taken, the yellow color appeared as expected. These phenomena were observed when both the SiO_2 and CsBr window were used. The cell was always placed in the instrument so that the sample was on the side of the cold window towards the light source. However, the yellow color was seen when O_3 was added to NH_2OH after its ir spectrum had been recorded. Thus, only the shorter wavelength ultraviolet radiation appears to destroy the trapping sites for the yellow complex.

The intensity of the 440 nm absorption remained unchanged until about $-130°C$ when it started to decrease. This band disappeared upon photolysis with a medium-pressure mercury lamp and reappeared upon rewarming, as did the yellow color. No ir band had exhibited this same behavior, so the species corresponding to this 440 nm band must have absorbed only very weakly and below our detection limit in the ir region. This visible band behaved essentially the same as the 438 nm band seen in the NH_3-O_3 reaction. In that reaction the absorption was much stronger and was present from -170 to $-105°C$ where it started to decrease in intensity. Due to the great similarity in absorption and behavior, we believe that an ozonide also formed with NH_2OH and absorbed at 440 nm.

The other initial peak had its maximum absorption at about 255 nm. In the only case already mentioned when O_3 itself produced an absorption at 255 nm, the intensity of the absorption increased by a factor of 15 when NH_2OH was condensed on the CsBr window on top of this O_3. The absorption again increased slightly when more O_3 was introduced into the cell. In all of these experiments the major portion of the O_3 was seen

Can. J. Chem. Downloaded from www.nrcresearchpress.com by 210.87.254.6 on 09/06/12
For personal use only.

to condense on the Cu frame. When O_3 was introduced into the low-temperature cell in several portions instead of all at one time, the 255 nm band was seen to increase a small amount with each addition. The major part of the absorption was produced by the first addition of O_3. At the same time no change was seen in the 440 nm band. The absorbance of the 255 nm band increased with the amount of O_3 used for each experiment, but a graph of these results produced a random scattering of data points. This peak started to decrease as soon as the sample was warmed. In the run containing the strongest 255 nm absorbance the peak was completely gone by −130°C. When the samples were photolyzed with the Hg lamp, the intensity of the 255 nm band either remained unchanged or decreased. The decrease could have been caused by the heating effect of the lamp. One sample displayed different results: the 255 nm peak had already disappeared before photolysis but reappeared even stronger than initially as the 440 nm peak disappeared upon photolysis.

This 255 nm band agreed with the temperature dependence and photolysis results of the 1035 cm^{-1} band seen in the ir work. As with the 1035 cm^{-1} band, once it disappeared upon warming it could not be made to reappear by recooling and rewarming to a temperature at which it had previously been present. The similarity of the 255 nm uv band to that of ozone and the close approximation of the 1035 cm^{-1} ir band seen here with the strong ν_3 band of O_3 indicate that these absorptions are due to ozone adsorbed on active surface sites of solid NH_2OH.

Other than the change in absorption from the annealing of NH_2OH, no other change was seen in the spectra until the NH_2OH started to sublime off the window. Only then was it possible to observe a white solid on the window with a continuously increasing absorption from 450 nm to the instrument cut-off at 190 nm. In thicker samples the absorption due to this solid extended even farther into the visible region. This solid remained on the window even at room temperature. In all samples using the SiO_2 window, a small peak at 200 nm was also seen at room temperature and remained upon recooling of the sample. It was already seen at −60°C in one case but only after warming to room temperature in the other three cases. Since the CsBr window itself completely absorbed the radiation at this wavelength, it was impossible to tell if the 200 nm peak was ever present in about half of the experiments performed. Since the 200 nm absorption was seen using both distilled and partially decomposed NH_2OH, its presence was not determined by the initial state of this reactant. The presence or absence of the 440 nm band did not affect its formation. This peak was never seen in the NH_4NO_3 formed from the reaction of NH_3 with O_3. Since the only other solid ever seen in the ir spectra at room temperature was $NH_3OH^+NO_3^-$, this would be the most likely compound absorbing at 200 nm.

We were unable to observe in the NH_2OH-O_3 system any reaction intermediates common to those observed in the NH_3-O_3 system. The NH_2OH-O_3 system was more reactive since $NH_2OH \cdot HNO_3$ was seen even at −190°C. Thus, the possibility that NH_2OH may be an intermediate in the NH_3-O_3 system cannot be ruled out. In the NH_2OH-O_3 system, reaction sequences similar to those with NH_3 occur, i.e.

$$[9] \quad NH_2OH + O_3 \rightarrow NH_2OH^+O_3^-$$

$$[10] \quad NH_2OH^+O_3^- \xrightarrow{NH_2OH} NH_3OH^+NO_3^- + H_2O$$

The charge-transfer complex $NH_2OH^+O_3^-$ is decomposed into reactants either by photolysis or thermally. Active surface sites, where the charge-transfer complexes are formed, are destroyed by ultraviolet radiation. In order to account for O_2 and N_2O evolution, both of which were seen, we propose the additional reaction

$$2NH_2OH^+O_3^- \rightarrow N_2O + 3H_2O + 2O_2$$

1. (*a*) W. MANCHOT and W. KAMPSCHULTE. Ber. Dtsch. Chem. Ges. **40**, 4984 (1907); (*b*) W. MANCHOT. Ber. Dtsch. Chem. Ges. **46**, 1089 (1913); (*c*) W. STRECKER and H. THIENEMAN. Ber. Dtsch. Chem. Ges. **53**, 2096 (1920).
2. I. J. SOLOMON, K. HATTORI, A. J. KACMAREK, G. M. PLATZ, and M. J. KLEIN. J. Am. Chem. Soc. **84**, 34 (1962).
3. K. HERMAN and P. A. GIGUÈRE. Can. J. Chem. **43**, 1746 (1965).
4. M. E. JACOX and D. E. MILLIGAN. J. Mol. Spectrosc. **43**, 148 (1972).
5. R. C. SPIKER, JR., and L. ANDREWS. J. Chem. Phys. **59**, 1851 (1973).
6. D. M. THOMAS and L. ANDREWS. J. Mol. Spectrosc. **50**, 220 (1974).
7. L. ANDREWS and R. C. SPIKER, JR. J. Chem. Phys. **59**, 1863 (1973).
8. P. A. GIGUÈRE and K. HERMAN. Can. J. Chem. **52**, 3941 (1974).
9. L. ANDREWS. J. Chem. Phys. **63**, 4465 (1975).
10. B. S. AULT and L. ANDREWS. J. Mol. Spectrosc. **65**, 437 (1977).
11. S. I. PAPKO. Zhur. Priklad. Khim. **22**, 667 (1949); **23**, 8 (1950).
12. J. HOIGNÉ and H. BADER. Environ. Sci. Technol. **12**, 79 (1978).
13. K. OLSZYNA and J. HEICKLEN. Adv. Chem. Ser. No. 113, 191 (1972) and Center for Air Environment Studies Report No. 322-73, The Pennsylvania State University. 1975.
14. P. MILLER. M.Sc. Thesis, The Pennsylvania State University. 1962.
15. R. NIGHTINGALE, A. DOWNIE, D. ROTENBERG, B. CRAWFORD, JR., and R. OGG, JR. J. Phys. Chem. **58**, 1047 (1954).
16. R. UHLENHUTH. Liebig Ann. Chem. **311**, 117 (1900).
17. R. A. BACK and J. BETTS. Can. J. Chem. **43**, 2157 (1965).
18. T. HUSTON, I. C. HISATSUNE, and J. HEICKLEN. Can. J. Chem. **61**, 2077 (1983).
19. B. T. HART. Aust. J. Chem. **29**, 231 (1976); **29**, 241 (1976).
20. (*a*) W. B. FOX, J. S. MACKENZIE, E. R. MCCARTHY, J. R. HOLMES, R. F. STAHL, and R. JUURIK. Inorg. Chem. **7**, 2064 (1968); (*b*) W. B. FOX, C. A. WAMSER, R. EIBECK, D. K. HUGGINS, J. S. MACKENZIE, and R. JUURIK. Inorg. Chem. **8**, 1247 (1969); (*c*) C. A. WAMSER, W. B. FOX, B. SUKORNICK, J. R. HOLMES, B. B. STEWART, R. JUURIK, N. VANDERKOOI, and D. GOULD. Inorg. Chem. **8**, 1249 (1969).
21. V. R. LANDI and L. J. HEIDT. J. Phys. Chem. **73**, 2361 (1969).
22. O. KNOP and P. A. GIGUÈRE. Can. J. Chem. **37**, 1794 (1959).
23. O. MAASS and W. H. HATCHER. J. Am. Chem. Soc. **44**, 2472 (1922).

Low-temperature infrared studies of some acid–base reactions[1,2]

THERESA HUSTON, I. C. HISATSUNE, AND JULIAN HEICKLEN
Department of Chemistry and Center for Air Environment Studies, The Pennsylvania State University, University Park, PA 16802, U.S.A.

Received November 17, 1982

THERESA HUSTON, I. C. HISATSUNE, and JULIAN HEICKLEN. Can. J. Chem. **61**, 2077 (1983).

Low-temperature infrared spectroscopy has been used to examine the systems $NH_3 + H_2O$, $NH_3 + HCl$, $H_2O + HCl$, $NH_3 + HNO_3$, and $NH_2OH + HNO_3$. Hydrogen-bonding in the solid states greatly reduces the reactivities in these systems. Temperatures where reactions initiated in the systems $NH_3(s) + HCl(g)$, $HNO_3(s) + NH_3(g)$, $H_2O(s) + HCl(g)$, and $NH_2OH(s) + HNO_3(s)$ were, respectively, −145, −130, −127, and −125°C. Infrared spectra of $2NH_3 \cdot H_2O$, $NH_3 \cdot H_2O$, $NH_4Cl \cdot 3NH_3$, $NH_4NO_3 \cdot 3NH_3$, $NH_4NO_3 \cdot 2HNO_3$, $NH_2OH_2^+NO_3^-$, $NH_3OH^+NO_3^-$, $H_3O^+Cl^-$, $H_5O_2^+Cl^-$, and $H_5O_2^+Cl^- \cdot H_2O$ have been identified in these reaction systems.

THERESA HUSTON, I. C. HISATSUNE et JULIAN HEICKLEN. Can. J. Chem. **61**, 2077 (1983).

On a fait appel à la spectroscopie infrarouge à basse température pour étudier les systèmes suivants: $NH_3 + H_2O$, $NH_3 + HCl$, $H_2O + HCl$, $NH_3 + HNO_3$ et $NH_2OH + HNO_3$. La présence de liaisons hydrogènes dans l'état solide réduit de beaucoup la réactivité de ces systèmes. On a initié les systèmes: $NH_3(s) + HCl(g)$, $HNO_3(s) + NH_3(g)$, $H_2O(s) + HCl(g)$ et $NH_2OH(s) + HNO_3(s)$ à des températures respectives de: −145, −130, −127 et −125°C. Dans ces systèmes on a identifié les spectres infrarouges des composés suivants: $2NH_3 \cdot H_2O$, $NH_3 \cdot H_2O$, $NH_4Cl \cdot 3NH_3$, $NH_4NO_3 \cdot 3NH_3$, $NH_4NO_3 \cdot 2HNO_3$, $NH_2OH_2^+NO_3^-$, $NH_3OH^+NO_3^-$, $H_3O^+Cl^-$, $H_5O_2^+Cl^-$ et $H_5O_2^+Cl^- \cdot H_2O$.

[Traduit par le journal]

Introduction

In the infrared spectroscopic studies (1) of low-temperature ozonolysis of NH_3 and NH_2OH, numerous absorption bands other than those from the expected products NH_4NO_3 and H_2O were observed. These bands showed complex temperature dependences, suggesting formation and breaking of hydrogen-bonds and changes in molecular structures at different temperatures. In order to identify the origins of these absorption bands, we have found it necessary to examine the infrared spectra of various mixtures of NH_3, NH_2OH, H_2O, HCl, and HNO_3 at liquid nitrogen temperature and to follow their changes with temperature. The experimental results from these studies are presented here.

Experimental

Spectroscopic equipment used in this work has been described already in the companion report (1). Various combinations of NH_3, NH_2OH, H_2O, HCl, and HNO_3 were deposited on a liquid-nitrogen cooled window (AgCl, CsBr, or CsI) of a low-temperature cell either as mixtures or as separate layers. These samples were warmed to various temperatures and then recooled to examine their spectra. Window temperatures were determined by a copper–constantan thermocouple attached to the metal window bracket (2).

Preparations of most of the chemicals used here have been described before (1). The reagents H_2O (triply distilled) and D_2O (Volk Radiochemical Co., 99.8%) were degassed and distilled in the vacuum line before use. Hydrogen chloride (Matheson Co.) was also subjected to a low-temperature fractional distillation. Gas pressures were measured on either a mercury manometer or a manometer containing Ke1-F3 polymer oil (3M Co.) with a density of 1.93 g/cm^3 at 23°C.

Results and discussion

NH_3–H_2O system

The infrared spectrum of NH_3 at liquid nitrogen temperature has been reported by Reding and Hornig (3). Our results at −190°C were in agreement with this earlier study. Prominent bands of NH_3 and of ND_3 in parentheses were at ν_3 = 3380 s (2508 s), ν_1 = 3290 m (2390 vw), ν_4 = 1650 m (1198 m), and ν_2 = 1060 vs (816 vs) in cm^{-1} units. Solid NH_3 also has a moderately intense lattice mode band at 360 cm^{-1}. Typical samples of NH_3 were already crystalline when they were deposited on the cooled window, but in thicker samples some amorphous forms were trapped. Annealing of the latter to −165°C caused the relative intensities of ν_3, ν_2, and the lattice band to increase while the other bands in the spectrum became weaker. Sublimation of the samples started at about −160°C.

Our spectrum of water at −190°C also agreed with the earlier results of Hornig *et al.* (4). Although the bands were all broad, annealing effects were evident when samples were warmed to about −90°C and recooled. The initial spectrum with bands at ν_1 = 3400 w (2530 w), ν_3 = 3220 vs (2430 s), ν_2 = 1620 w (1210 vw), and ν_L = 780 s (580 w) shifted on annealing to ν_1 = 3350 w (2550 w), ν_3 = 3200 s (2400 s), ν_2 = 1570 w (1210 vw), and ν_L = 810 s (610 w) where the frequencies are in cm^{-1} units and those of the deuterated species are given in parentheses. At about −85°C water began to sublime off the cooled window.

Two ammoniates of water, $NH_3 \cdot H_2O$ and $2NH_3 \cdot H_2O$, are known, and their thermodynamic properties have been measured by Hildenbrand and Giauque (5). The crystal structures of $NH_3 \cdot H_2O$ and $2NH_3 \cdot H_2O$ have been determined, respectively, by Olovsson and Templeton (6) and by Siemons and Templeton (7). When our experiments were done (late 1970s), the only infrared study of these complexes appeared to be one of a preliminary nature reported by Waldron and Hornig (8*a*). Because of severe overlapping of the spectra of these ammoniates, Waldron and Hornig were able to assign clearly only a single band at 1120 cm^{-1} for $NH_3 \cdot H_2O$ and three bands at 3140, 1091, and 1020 cm^{-1} for $2NH_3 \cdot H_2O$. Peaks at 3365, 3220, 2950, and 1625 cm^{-1} were assigned commonly to both complexes. Since our work has been completed there have been numerous studies of the infrared spectra of the ammonia hydrates (8*b*–*f*).

In the present investigation, the identity of the complex $2NH_3 \cdot H_2O$ was readily established. When gaseous mixtures of NH_3 and H_2O with mole ratio NH_3/H_2O ranging from 2.0 to 36.5 were condensed on the low-temperature window, the

[1]CAES Report No. 657-82.
[2]Taken in part from the Ph.D. Thesis of Theresa Huston.

Can. J. Chem. Downloaded from www.nrcresearchpress.com by 210.87.254.105 on 09/06/12
For personal use only.

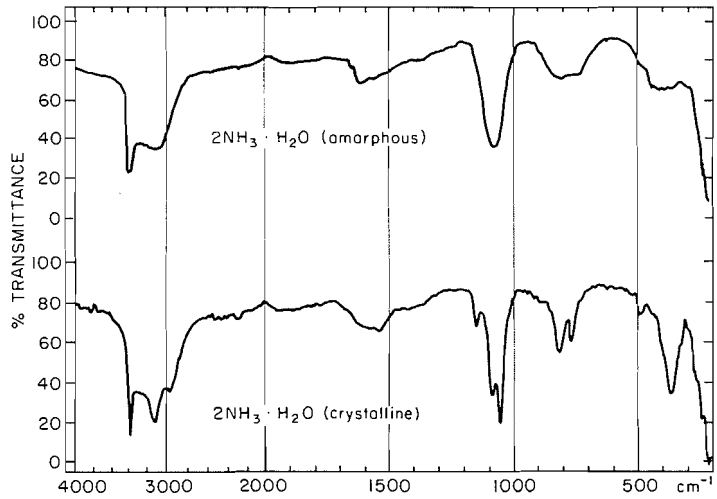

FIG. 1. Infrared spectra of amorphous and crystalline $2NH_3 \cdot H_2O$ at $-190°C$.

TABLE 1. Infrared spectra of $2NH_3 \cdot H_2O$ at $-190°C$ (cm^{-1} units)

Amorphous		Crystalline		
$2NH_3 \cdot H_2O$	$2ND_3 \cdot D_2O$	$2NH_3 \cdot H_2O$	$2ND_3 \cdot D_2O$	Assignment
3360 vs	2490 s	3370 vs	2490 s	$\nu(NH_3)$
~3120 s	~2340 m	3135 s	~2320 m	$\nu(NH)$, $\nu(OH)$
		~2975 w	~2220 w	
~2310 w		~2280 w		
~1870 vw	1460 w	~1880 w	1465 m	
	1250 w		~1250 w	
1615 m	1175 m	1615 m	~1170 m	$\delta(NH)$
~1530 w		~1550 w		$\delta(OH)$
		~1150 w	~875 vw	
		~1085 m		$\delta(NH)$
1090 vs	830 vs	1055 vs	845 vs	$\delta(NH)$
800 m	600 m	810 s	605 s	$L(H_2O)$
~750 m	~550 w	760 m	~560 w	$L(H_2O)$
	~400 w	525 vw	~410 w	
		480 w		
~400 s		353 s	~275 s	$L(NH_3)$
		245 w		

same product whose spectrum is shown in Fig. 1 (upper curve) was obtained. In these experiments each gaseous mixture was allowed to stand at least for 12 h at room temperature to insure complete mixing of the components, and the total pressure of H_2O in the mixture was kept below about one-half the equilibrium vapor pressure of H_2O. Higher H_2O pressures caused condensation in the gas storage bulb. At lower ratios of NH_3/H_2O, some ice formation was also observed, but the initial product of these excess NH_3 samples was amorphous $2NH_3 \cdot H_2O$ which appeared as a glassy solid. Warming of these samples to about $-150°C$ caused the samples to become crystalline white which upon recooling to $-190°C$ produced the spectrum shown in Fig. 1 (lower curve). During recooling excess NH_3 had sublimed off the cooled window. Peak frequencies in the spectra of amorphous and crystalline $2NH_3 \cdot H_2O$ are listed in Table 1.

When a white crystalline sample of $2NH_3 \cdot H_2O$ from excess NH_3 matrices was warmed to $-130°C$ and then recooled to $-190°C$, it changed into a clear crystalline solid having the spectrum shown in Fig. 2 (lower curve). This clear crystal melted at about $-100°C$ and upon recooling to $-190°C$ changed into a glassy solid whose spectrum is the upper curve in Fig. 2. At about $-85°C$, the samples sublimed off the cooled window. When the cell contents in these experiments were recondensed on the low-temperature window, the entire sequence of spectroscopic changes could be reproduced by warming to various temperatures and then recooling to liquid nitrogen temperature.

The spectra shown in Fig. 2 and peak frequencies given in Table 2 are attributed to the complex $NH_3 \cdot H_2O$. When a gaseous mixture with a composition of $NH_3/H_2O = 1.0$ was deposited on the liquid nitrogen cooled window, the initial spectrum was identical to the upper curve of Fig. 2. Warming of this sample to $-125°C$ and then recooling caused the spectrum to change to the lower curve in this figure.

Experiments were also performed in which NH_3 was deposited on top of a previously deposited layer of H_2O, or *vice versa*. The initial spectra were indistinguishable from those of NH_3 or H_2O alone at $-190°C$. First changes in the spectra of these layered samples occurred at about $-125°C$ when the ammonia bands began to get weaker. By $-115°C$, the strongest bands of crystalline $NH_3 \cdot H_2O$ and $2NH_3 \cdot H_2O$ became visible. Further warming to higher temperatures caused the formation of ice without a significant increase in the yield of either com-

Can. J. Chem. Downloaded from www.nrcresearchpress.com by 210.87.254.105 on 09/06/12
For personal use only.

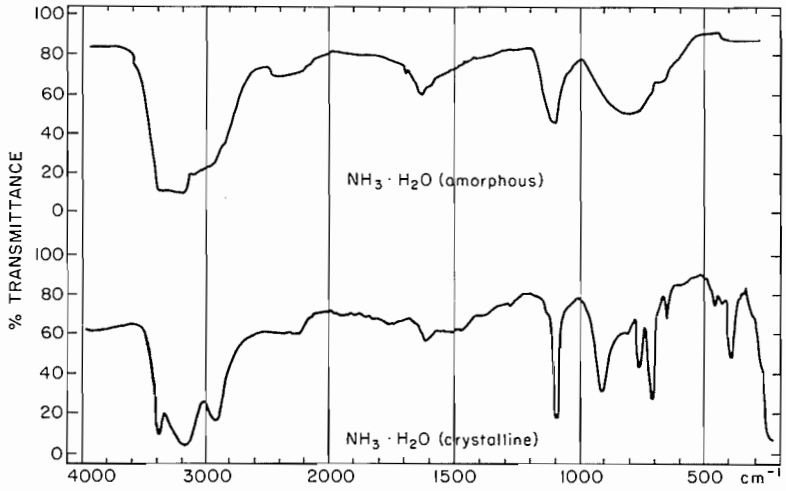

FIG. 2. Infrared spectra of amorphous and crystalline $NH_3 \cdot H_2O$ at −190°C.

TABLE 2. Infrared spectrum of $NH_3 \cdot H_2O$ at −190°C (cm^{-1} units)

Amorphous		Crystalline		
$NH_3 \cdot H_2O$	$ND_3 \cdot D_2O$	$NH_3 \cdot H_2O$	$ND_3 \cdot D_2O$	Assignment
3380 vs		3384 m	2515 m	ν(NH)
			2495 w	
3220 vs	2400 s	~3200 vs	~2350 s	ν(NH), ν(OH)
3100 w		~3130 w		
2980 vw	~2150 w	~2900 m	~2170 w	
2400 w		2410 w		
		~1810 w		
		~1740 w		
		1645 w		
1630 m	1180 vw	1620 m	~1170 w	δ(NH), δ(OH)
		~1130 w		
1100 s	850 w	1090 s	840 s	δ(NH)
	~800 vw	1035 w	~800 w	
800 vs	600 m	~890 vs	~650 s	L(H_2O)
		755 m		L(H_2O)
~680 vw		703 s	505 m	L(H_2O)
		~400 w		
400 w		382 s	275 vw	L(NH_3)

plex. Thus, the data summarized in Tables 1 and 2 were obtained from gaseous reactant mixtures. The deuterium work was done with a mixture having the composition ND_3/D_2O = 22.0.

Bertie and Morrison (8*b*, *d*) obtained the ir spectra of these two ammonia hydrates as mulls in various substances at −178°C. Using an FTIR spectrometer they were able to obtain better resolution of the broad peaks than we were with our instrumentation. This is most evident in the N—H stretching region of the spectra. Their reported absorption frequencies and assignments for the major peaks agree with our results within the error limits for these broad absorption bands. With the $2NH_3 \cdot H_2O$ species, their reported values of 1092 and 1083 cm^{-1} for δ(NH) are much closer to the value of 1090 cm^{-1} that we found for the amorphous solid than to the 1085 and 1055 cm^{-1} values found after crystallization (Table 1). The spectrum of $NH_3 \cdot H_2O$ reported by Sill *et al.* (8*c*) is very similar to that of Bertie and Morrison (8*b*) with the exception of a stronger absorption at 1542 cm^{-1}. We found only a very weak absorption at 1540 cm^{-1}.

Solid NH_3 by itself did not react with the AgCl window, but as $2NH_3 \cdot H_2O$ or $NH_3 \cdot H_2O$ it combined with AgCl to form $Ag(NH_3)_2Cl$. Infrared bands of the $Ag(NH_3)_2^+$ ion appeared as the NH_3 hydrates upon warming to about −70°C and then disappeared at about −45°C, leaving behind a coarse white layer of crystalline AgCl. The spectrum of $Ag(NH_3)_2Cl$ is shown in Fig. 3 and band assignments based on a previous work on $Ag(NH_3)_2NO_3$ by Geddes and Bottger (9) are summarized in Table 3.

NH_3–HCl system

Pure HCl could be kept on the cooled window of our cell only by pumping on the liquid nitrogen refrigerant. At −198°C the spectrum of solid HCl showed two peaks at 2700 and 2745 cm^{-1} in agreement with the report by Hornig and Osberg (10). When HCl was introduced into the low-temperature cell with a previously deposited film of solid NH_3 at −190°C, it immediately sublimed to the coldest metal parts of the refrigerant compartment. No reaction was observed until the cell was warmed to −145°C when absorption bands of NH_4Cl started to appear. In contrast to this behavior, NH_3 and HCl isolated in a N_2 matrix at 15 K first forms the hydrogen-bonded complex

Can. J. Chem. Downloaded from www.nrcresearchpress.com by 210.87.254.105 on 09/06/12
For personal use only.

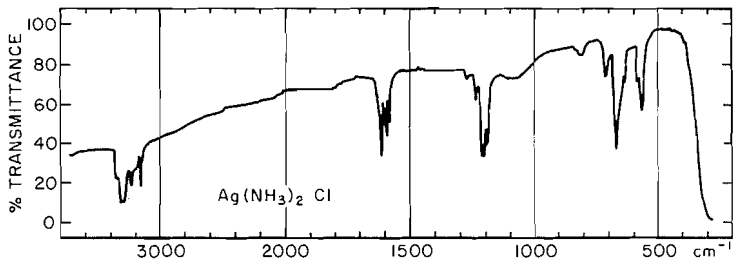

FIG. 3. Infrared spectrum of $Ag(NH_3)_2Cl$ on AgCl window at −190°C.

TABLE 3. Fundamental frequencies of silver diammine complexes (cm^{-1} units)

Species[a]	Assignment[a]	Frequency			
		$Ag(NH_3)_2NO_3$[a] (25°C)	$Ag(ND_3)_2NO_3$[a] (25°C)	$Ag(NH_3)_2Cl$[b] (−190°C)	$Ag(ND_3)_2Cl$[b] (−190°C)
A_1	ν(NH)			~3210 w	2307 vw
A_1	δ(NH_3)	1214	932	1178 m	~905 vw
A_1	ν(AgN)	386	363	440 vw	
$\bar{A}_1$	τ(NH_3)				
$\bar{A}_2$	ν(NH)	3180	2320	3154 m	2302 m
$\bar{A}_2$	δ(NH_3)	1246	953	1196 vs	919 s
A_2	ν(AgN)	470		510 vw	
E	ν(NH)	3270	2375	~3290 s	2456 s
		3320	2465	3307 w	2366 w
E	δ(NH_3)	1602	1167	1579 s	
		1624	1177	1597 s	1166 vw
E	ρ(NH_3)	610	479	555 s	408 m
		660	495	565 w	~422 vw
E	δ(AgN_2)	176	166		
		208	200		
$\bar{E}$	ν(NH)			3238 m	2392 w
				3246 vw	~2410 vw
$\bar{E}$	δ(NH_3)	1642	1240	1609 s	1179 m
				1624 vw	1250 w
$\bar{E}$	ρ(NH_3)	590?		660 vs	490 s
				698 m	~510 w

[a]From Geddes and Bottger (9).
[b]This study.

$NH_3 \cdot HCl$ which on warming to 40 K produces NH_4Cl (11). Thus, the hydrogen-bonded NH_3 matrix is substantially less reactive toward HCl. In fact, the reaction in the latter case was relatively slow until at about −115°C when NH_3 itself started to sublime off the window. By about −90°C, however, the reaction was complete and no further increase in the product spectrum was observed. The infrared spectrum of the product NH_4Cl at −190°C and at 25°C agreed with that reported by Schumaker and Garland (12).

Just as NH_3 started to leave the cooled window at −115°C, new bands appeared in the spectrum of the reaction system near 1450 and 1140 cm^{-1}. These bands are assigned to $NH_4Cl \cdot 3NH_3$ whose crystal structure and phase properties have been reported, respectively, by Olovsson (13) and by Billy and Jarrige (14). The yield of this ammoniate was generally low and its spectrum is compared to that of NH_4Cl in Fig. 4. Peak frequencies in this spectrum are summarized in Table 4. They compare reasonably well with those reported by Corset *et al.* (15) who dissolved NH_4Cl in liquid NH_3 and then cooled the solution to −130°C. The complex $NH_4Cl \cdot 3NH_3$ deamminated at about −95°C. Interestingly, when NH_3 was deposited on top of a film of solid NH_4Cl and then warmed to −100°C, no bands due to this ammoniate were observed. The presence of water also complicated the spectra of the reaction mixtures through formation of hydrates of NH_3 and HCl. Temperatures where NH_4Cl first formed and where reaction was complete were also increased somewhat when water was in the system. For example, when NH_3 was reacted with a mixture having a mole ratio HCl/H_2O = 1.0, NH_4Cl appeared at −117°C and the reaction was complete at −75°C. With dry HCl the respective temperatures were −145°C and −90°C.

H_2O–HCl system

Infrared spectra of hydrates of HCl were studied by examining the temperature dependencies of matrices formed from reactant mixtures with the mole ratio HCl/H_2O ranging from 0.13 to 7.3. Partial pressures of H_2O were kept below the equilibrium vapor pressure in order to prevent condensation of the reactant mixtures before use. Only an AgCl cooled window was used in this series of experiments.

When HCl/H_2O mole ratios were 1.0 or greater, identical initial spectra were displayed by the samples. A spectrum is illustrated in Fig. 5 (upper curve) and peak frequencies are listed in Table 5. This spectrum is assigned to the monohydrate of HCl and its agreement with earlier results of Ferriso and Hornig (16) and of Gilbert and Sheppard (17) is reasonable in

Can. J. Chem. Downloaded from www.nrcresearchpress.com by 210.87.254.105 on 09/06/12
For personal use only.

TABLE 4. Infrared spectra of triammine complexes of NH_4Cl and NH_4NO_3 (cm^{-1} units)

Frequency				
$NH_4Cl \cdot 3NH_3$[a] (−190°C)	$NH_4Cl \cdot 3NH_3$[b] liq. NH_3 (−130°C)	$NH_4NO_3 \cdot 3NH_3$[a] (−130°C)	$NH_4NO_3 \cdot 3NH_3$[c] liq. NH_3 (−40°C)	Assignment
~3380 w	~3386 w			
3350 s	3352 s	3390 s	3382 m	$\nu(NH_3)$
			3294 s	$\nu(NH_3)$
	3230 w	3250 w	3218 s	
	3186 w			
3090 m	~3090 m	~3100 m	3034 w	$\nu(NH_4^+)$
~2740 m	~2750 s	~2800 s	2777 m	$\nu(NH_4^+)$
	~2250 w			
	~2020 m	2080 w		
		1730 vw	1700 vw	$\delta(NH_4^+)$
			1657 w	$2\delta(NO_3^-)$
~1620 w	1626 w	1630 w	1637 m	$\delta(NH_3)$
1500 m	~1460 m			
1468 m	1454 s	~1490 m	1436 vw	$\delta(NH_4^+)$
1450 s	1401 m			
		1370 s	1375 m	$\nu(NO)$
		1345 vs	1336 m	
1140 s	1142 s	~1140 vw		
1118 m	1119 m			
1080 s	1079 vs	1090 s	1090 m	$\delta(NH_3)$
			1042 s	$\nu(NO)$
		830 vw		$\delta(NO_3^-)$
			707 m	$\delta(NO_3^-)$
570 w				
430 m		410 s		$L(NH_3)$

[a]This study.
[b]From Corset *et al.* (15).
[c]From Lundeen and Tobias (29) Raman study.

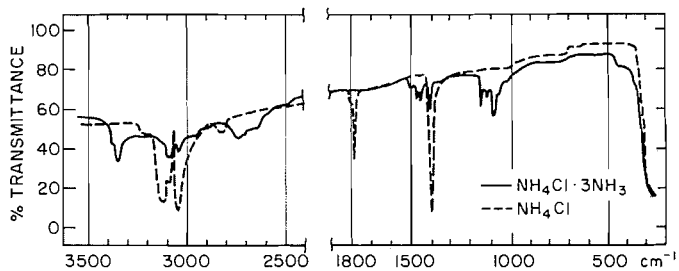

FIG. 4. Infrared spectra of NH_4Cl and $NH_4Cl \cdot 3NH_3$ at −190°C.

view of the very broad bands. Warming of the samples to −125°C caused an abrupt change in the spectra characterized by sharpening and increases in absorbances as illustrated by the lower curve in Fig. 5. Since this type of change often occurs when amorphous solids transform into crystalline phases, we make a similar interpretation and assign the upper and lower curves of Fig. 5 to amorphous and crystalline monohydrate of HCl, respectively. Peak frequencies of our crystalline sample agreed with those reported by Desbat and Huong (18) and also by Gilbert and Sheppard (17) who, however, attributed this spectrum to the dihydrate of HCl. The latter investigators found their complex to be formed at −103°C and to remain on the cooled window until −83°C. The best yield of the crystalline monohydrate of HCl in the present study was when the reactant mixture mole ratio HCl/H_2O was 5.0 or greater. The crystal structure of the monohydrate has been reported by Yoon and Carpenter (19) to be $H_3O^+Cl^-$ with H_3O^+ having a C_{3v} symmetry with an H—O—H angle of 117°.

Additional changes in the spectrum occurred when a sample of crystalline $H_3O^+Cl^-$ was warmed to −95°C. The bands became very broad once again as illustrated in Fig. 6 (upper curve). Peak frequencies are summarized in the first column of Table 6. A better yield of this spectrum was obtained when the mole ratio HCl/H_2O was 1.0. Continued warming of the sample caused the matrix to sublime off the cooled window at −80°C. The entire change described above could be repeated many times by recondensing the recovered reactant mixture and subjecting these matrices to warming and recooling cycles.

When the HCl/H_2O mole ratios were less than 1.0, these samples had clear glassy appearances and showed initial spectra resembling the upper curve of Fig. 6 more than they did of amorphous $H_3O^+Cl^-$ (Fig. 5). In fact, essentially the same spectrum as that of Fig. 6 was obtained when samples with mole ratio HCl/H_2O near 0.5 were warmed to −130°C. Thus, the origin of this spectrum is attributed to the dihydrate of HCl. When HCl/H_2O was less than 0.5, less dihydrate was formed and the spectra were overlapped with that of amorphous ice which has a characteristic strong band at 780 cm^{-1}. Continued warming of samples with $HCl/H_2O < 1$ to −120°C caused the matrices to become crystalline white and their spectra to change to that illustrated by the lower curve in Fig. 6. We assigned this spectrum to that of crystalline dihydrate of HCl whose ir and Raman spectra have been reported by Rozière and Potier (20). Peak frequencies in the spectrum of this dihydrate are given in Table 6. Also listed here are two sets of data from the work of Gilbert and Sheppard (17). These authors assigned one set to the trihydrate because it was formed from the "dihydrate" in the

Can. J. Chem. Downloaded from www.nrcresearchpress.com by 210.87.254.105 on 09/06/12
For personal use only.

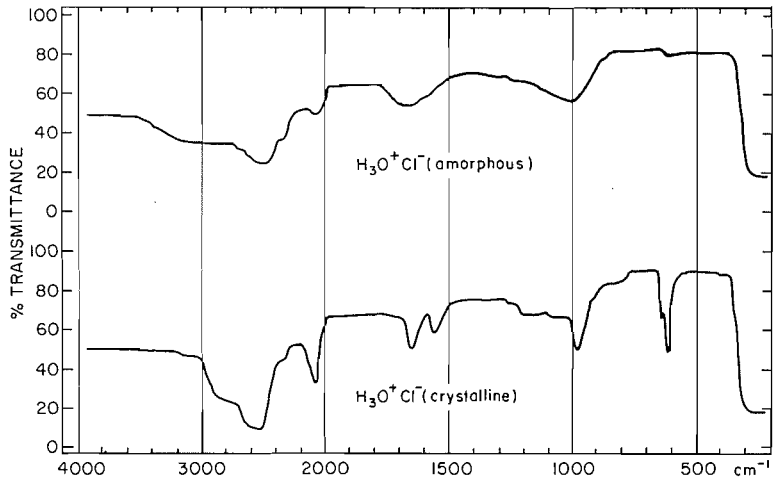

FIG. 5. Infrared spectra of amorphous and crystalline $H_3O^+Cl^-$ at −190°C.

TABLE 5. Infrared spectrum of $H_3O^+Cl^-$ at −190°C (cm^{-1} units)

Frequency						
Amorphous			Crystalline			
This study	G and S[a]	F and H[b]	This study	G and S[c]	D and H[d]	C_{3v} assignment
~3100 s	3150 s	3235 s	~3100 w	3142 m	3140 w	ν_3
~2700 w			~2840 m	2850 m	2840 vs	
2500 s	2555 s	2590 s	~2520 vs	2540 s	2610 s	ν_1
~2320 w			~2340 w			
				2238 vw		
2070 m	2100 m	2109 m	2080 s	2080 s	2060 m	
1660 m	1685 s	1700 m	1650 m	1653 s	1650 s	ν_4
1590 w	1600 w		1550 m	1553 m	1550 w	
			1200 w	1197 w	1230 m	
		~1150 w	1150 w	1149 w		
			~1080 m	1082 m		
~1020 m	1045 s	1060 s	975 s	997 s	(970 w)	ν_2
	775 w	770 w				
			~640 w	642 m	(625 w)	Lattice
			605 vs	612 s	(615 s)	Lattice
570 vw						
470 vw	490 w			484 w		
	210 s			242 s	(245 s)	Lattice

[a]From Gilbert and Sheppard (17).
[b]From Ferriso and Hornig (16).
[c]From Gilbert and Sheppard (17) but assigned to the dihydrate.
[d]From Desbat and Huong (18). Frequencies in parentheses are from Raman spectrum; infrared frequencies read from text figure.

temperature range of −83 to −53°C and the second set to the tetrahydrate since it was produced from the "trihydrate" by warming from −53 to −38°C. Our crystalline dihydrate sublimed off the cooled window at −70°C.

In one experiment H_2O was condensed first to give amorphous ice and then HCl was introduced into the low-temperature cell. No reaction was observed until −127°C when a large amount of amorphous dihydrate formed. It began to decay at −80°C but only a small amount of crystalline dihydrate was detected in the temperature range of −88 to −65°C.

Lundgren and Olovsson (21) have determined the crystal structure of the HCl dihydrate and showed it to be $H_5O_2^+Cl^-$. The cation $[H_2O—H—OH_2]^+$ has a relatively short central oxygen–oxygen distance of 2.41 Å. Rozière and Potier (20) have made a tentative assignment of their spectra based on this cation structure. Our assignments given in Table 6 essentially follow those of the latter authors with only minor modifications. Uncertainties in these assignments suggest more spectroscopic investigation of carefully prepared samples.

Very little crystalline dihydrate was formed when the HCl/H_2O ratio was 0.25 or less. Warming of these matrices to −120°C produced instead a new set of absorption bands characterized by relatively sharp peaks at 615 and 1625 cm^{-1} which were visible even when amorphous ice was present in the sample. The spectrum of this species and that of amorphous ice are shown in Fig. 7. Distinction of this hydrate from the monohydrate and dihydrate is particularly evident in the 400–800

Can. J. Chem. Downloaded from www.nrcresearchpress.com by 210.87.254.105 on 09/06/12
For personal use only.

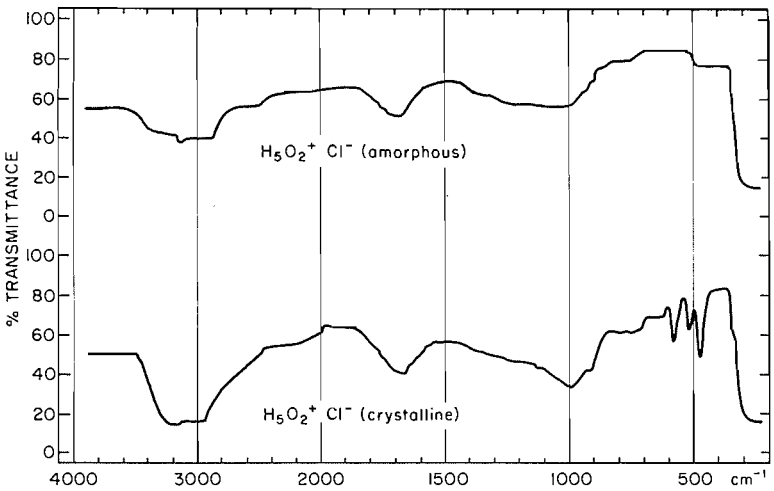

FIG. 6. Infrared spectra of amorphous and crystalline $H_5O_2^+Cl^-$ at −190°C.

TABLE 6. Infrared spectrum of $H_5O_2^+Cl^-$ at −190°C (cm^{-1} units)

Frequency					
Amorphous		Crystalline			$[H_2O—H—OH_2]^+$
This study	G and S[a]	This study	G and S[b]	R and P[c]	assignment
	~3400 s		3300 s		
~3100 s	3180 s	3200 s	3229 s	3250 s	ν(OH)
			3065 s	~3150 s	
	2961 s	~2960 m	2962 s	~3000 s	ν(OH)
	2884 s			~2800 s	
				2350 m	
	2170 w	2200 w	2235 w	2240 m	
1680 s	1700 s	1675 s	1696 s	1700 m	δ(OH_2), ν(OHO)
			~1600 w		
~1350 m			1328 m		
~1250 m	1210 m	~1200 m		1270 m	δ(OHO)
~1100 s	~1130 s	~1100 s	1079 s	~1100 m	δ(H_2O)
		1000 s	1007 s	1000 m	
~920 w		915 m	923 m	930 m	ρ(H_2O)
~860 w		800 vw	820 m	820 vw	
770 m	780 m	755 vw	767 w		ρ(H_2O)
			731 w		
		720 w	716 w	710 m	ν(OHO)
	679 w	640 m	663 w	660 m	ω(H_2O)
			~654 w		
	560 m	575 s	580 m	570 s	ω(H_2O)
	485 m	515 m	519 m	520 m	τ(H_2O)
			~488 w		
		470 s	476 m	465 vs	τ(H_2O)
~400 m	420 s		420 w		
			226 w	224 s	
	190 s			194 m	

[a]From Gilbert and Sheppard (17) but assigned to the trihydrate.
[b]From Gilbert and Sheppard (17) but assigned to the tetrahydrate.
[c]From Rozière and Potier (20).

cm^{-1} region in the spectra of Figs. 5, 6, and 7. Although the vibrational spectrum of the trihydrate apparently has not been reported, its crystal structure has been determined by Lundgren and Olovsson (22) to be represented by $H_5O_2^+Cl^- \cdot H_2O$. Also, the spectrum of $HBr \cdot 4H_2O$ has been reported by Rudolph and Zimmerman (23), and it differs considerably from that shown in Fig. 7. Therefore, we assign the lower spectrum of Fig. 7 to that of crystalline $H_5O_2^+Cl^- \cdot H_2O$ with peaks at 3410 m, 3330 vs, 3200 s, 1625 m, 1140 w, 1050 m, 790 m, and 615 s in cm^{-1} units. The trihydrate sublimed off the cooled window at −70°C. Absorption bands attributable to another known hydrate $HCl \cdot 6H_2O$ (24) or to complexes such as $HCl \cdot H_2O$ (25, 26) or $2HCl \cdot H_2O$ (26) observed in Ar and N_2 matrices at 15 K were not detected in the present work.

Complex mixtures of products were obtained when NH_3 was present in the H_2O–HCl system. A matrix with $NH_3/H_2O = 20$ reacted with HCl to produce NH_4Cl at −140°C with the reaction being over at −75°C. During this reaction in the tem-

Can. J. Chem. Downloaded from www.nrcresearchpress.com by 210.87.254.105 on 09/06/12
For personal use only.

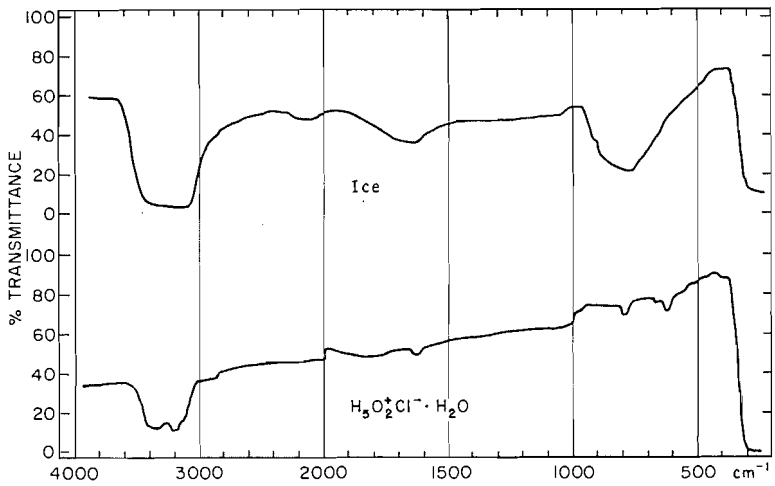

FIG. 7. Infrared spectra of amorphous H_2O and crystalline $H_5O_2^+Cl^- \cdot H_2O$ at −190°C.

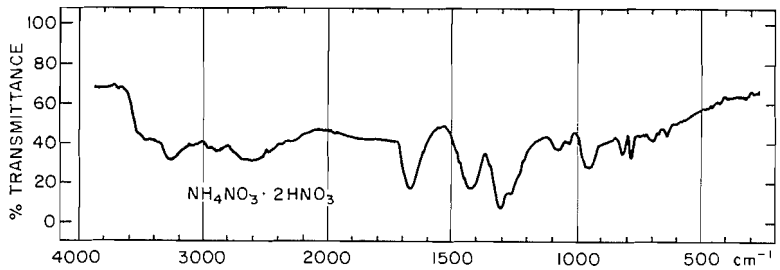

FIG. 8. Infrared spectrum of $NH_4NO_3 \cdot 2HNO_3$ at −190°C.

perature range of −160°C to −83°C, $2NH_3 \cdot H_2O$, $NH_3 \cdot H_2O$, $H_3O^+Cl^-$, $H_5O_2^+Cl^-$, and $NH_4Cl \cdot 3NH_3$ were detected. When NH_3 was decreased to $NH_3/H_2O = 1.0$, NH_4Cl continued to be formed until −60°C and $NH_3 \cdot H_2O$, $H_5O_2^+Cl^-$, and $H_5O_2^+Cl^- \cdot H_2O$ were observed.

NH_3–HNO_3 system

A large difference in sublimation temperatures of these reactants required HNO_3 to be deposited on the cooled window first. Mole ratios of NH_3/HNO_3 ranged from 0.5 to 60, and both CsBr and AgCl windows were used. By the time the initial amorphous HNO_3 transformed into a crystalline solid (27) at −140°C, NH_3 had sublimed off the cooled window. The first sign of reaction occurred at −130°C when a set of new absorption bands appeared in the spectrum. These new bands were assigned to $NH_4NO_3 \cdot 3NH_3$ which has a melting point of about −40°C according to phase studies of Kuriloff (28). Peak frequencies of this triammoniate spectrum obtained at −190°C are listed in Table 4. This spectrum was similar to that of $NH_4Cl \cdot 3NH_3$ (Fig. 4) except for the presence of bands due to the NO_3^- ion. Frequencies from the most recent Raman studies of liquid NH_3 solutions of NH_4NO_3 by Lundeen and Tobias (29) are also listed in Table 4 for comparison. The band assignments given here are essentially those of the latter authors. Deammination of $NH_4NO_3 \cdot 3NH_3$ began at about −100°C under our experimental conditions.

Matrices with $NH_3/HNO_3 < 1$ also showed signs of reaction at −130°C. At this temperature NH_3 was already off the cooled window, and HNO_3 had annealed and was decreasing. The product bands at 1420 and 1305 cm^{-1} were the first to become evident, and they continued to grow until about −70°C when the reaction was complete. The spectrum of the resulting sample recooled to −190°C is illustrated in Fig. 8, and it is due to the complex $NH_4NO_3 \cdot 2HNO_3$. The composition of this complex had been determined by Potier and Potier (30) from phase studies, and subsequent refinement of X-ray data by Einstein and Tuck (31) has shown that the structure of this complex may be represented by $NH_4^+[NO_3 \cdot 2HNO_3]^-$ where the nitrate is hydrogen-bonded to two HNO_3 molecules. Peak frequencies in the spectrum of Fig. 8 are 3460 m, 3240 s, 2950 w, 2600 s, 1660 s, 1420 s, 1345 w, 1305 vs, 1260 m, 1070 m, 1045 w, 950 m, 815 m, 775 m, 705 w, and 695 w in cm^{-1} units. Prominent peaks in this set are in reasonable agreement with those reported earlier by Diop and Potier (32) who also presented a tentative assignment of the spectrum. The trinitrate complex on the cooled window started to decompose at −50°C and only NH_4NO_3 remained upon warming to 25°C. If HNO_3 was deposited on top of NH_4NO_3 and then warmed to −90°C, the same complex was formed.

In experiments with excess HNO_3, only the CsBr cooled window was used. It was noted that during the final warming of these samples to room temperature, $CsNO_3$ was being formed causing the band intensity ratio of NH_4^+/NO_3^- to vary from that in NH_4NO_3. In a pair of comparison experiments where HNO_3 or NH_3 was in excess but the amount of the second limiting reagent was the same, the intensity of the NH_4^+ ion band was only about one-half of that expected when HNO_3 was in excess. In the excess HNO_3 case, the NO_3^- ion band was three times stronger than expected. Thus, in addition to the reaction with the CsBr window, HNO_3 appeared to be destroying the NH_4^+ ion although the cell contents after completion of the experiments contained no detectable noncondensable gas. Also, when HNO_3 was deposited on top of NH_4NO_3 on the cooled window and the sample was warmed to

Can. J. Chem. Downloaded from www.nrcresearchpress.com by 210.87.254.105 on 09/06/12
For personal use only.

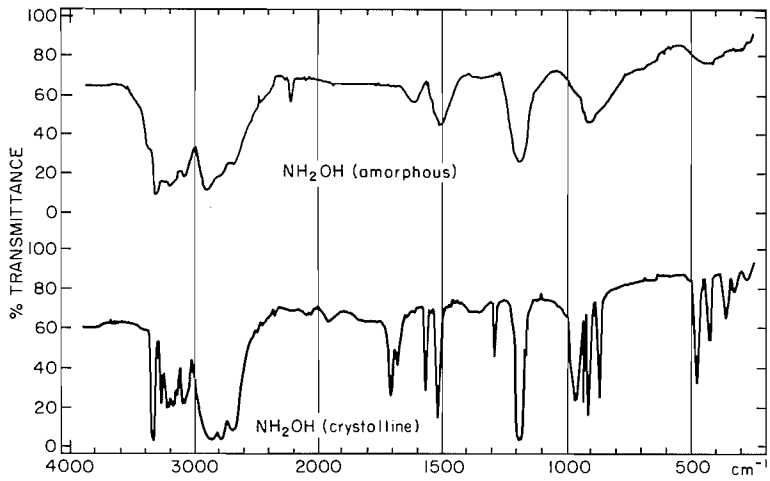

FIG. 9. Infrared spectra of amorphous and crystalline NH_2OH at −190°C.

TABLE 7. Infrared spectra of gaseous, amorphous, and crystalline NH_2OH (cm^{-1} units)

Frequency						
Gas, 25°C	Amorphous, −190°C		Crystalline, −190°C			
G and L[a]	This study	N and W[b]	G and L[a]	This study	N and W[b]	Assignment[b]
3350 w	3315 s	3293 s	3331 s	3335 vs	3302 s	ν(NH)
3297 m	3250 w		3268 s	3270 s	3245 w	
			3207 s	3205 s		
	3200 s	3195 s		3170 s	3173 s	ν(NH)
	3080 m	3080 m		3080 s	3065 m	
3656 s	~2900 s	2908 vs		2860 vs	2867 vs	ν(OH)
2740 vw	~2800 w			2780 m	2787 m	
	~2700 m	2700 s		2700 m	2675 s	
				2670 m		
				1710 s	1697 m	
1605 m	1610 m	1605 w	1657 m	1685 m	1675 w	
	1565 vw			1570 s	1564 w	
1357 s	1515 s	1505 m	1502 m	1520 vs	1515 s	δ(NH_2)
1297 w	1285 vw			1290 m	1287 w	
1120 vs	1190 vs	1185 s	1187 vs	1190 vs	1191 vs	δ(NOH)
				1170 vs		
	~960 w			963 s	950 m	ρ(NH_2)
				953 s		
				935 s	932 w	
895 m	~900 s	900 m	926 s	917 vs	912 s	ν(NO)
765 w			845 m	870 vs	867 m	ω(NH_2)
430 vw	~430 m		490 vw	475 vs	~535 w	τ(OH)
				428 s		
				360 m		
	~310 w			325 w		

[a]From Giguère and Liu (35). One-meter gas cell and cooled solid mull used.
[b]From Nightingale and Wagner (34).

room temperature, there was about a 30% decrease in the absorbance of the NH_4^+ ion band and an increase of about 50% in the strength of the NO_3^- ion band. Since the outer CsBr windows of the cell were also attacked by HNO_3 the acid was removed from the cell at about −50°C as the trinitrate complex decomposed. The spectra of NH_4NO_3 and ND_4NO_3 at 25 and −190°C were in agreement with the results of Thèorêt and Sandorfy (33).

NH_2OH–HNO_3 system

The investigation of this reaction system was complicated by severe changes with temperature in the spectrum of solid NH_2OH itself as Nightingale and Wagner (34) had observed previously. When solid NH_2OH at room temperature was sublimed onto a cooled window at −190°C, it formed a clear amorphous film with a spectrum as shown in Fig. 9. The sharp peak near 2200 cm^{-1} in this spectrum is due to N_2O, a known decomposition product of NH_2OH. Warming of the amorphous solid to −90°C caused the sample to become white, and the spectrum changed irreversibly to that of crystalline NH_2OH. At −45°C, NH_2OH samples sublimed off the cooled window. Peak frequencies in the spectra of amorphous and crystalline NH_2OH are summarized in Table 7. Earlier data from Nightingale and Wagner (34) and from Giguère and Liu (35)

Can. J. Chem. Downloaded from www.nrcresearchpress.com by 210.87.254.105 on 09/06/12
For personal use only.

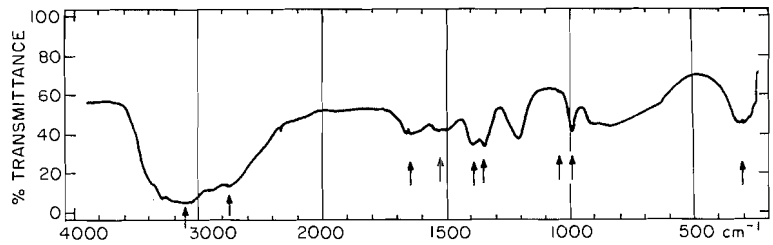

FIG. 10. Infrared spectrum of $NH_2OH_2^+NO_3^-$ in NH_2OH matrix at −190°C. Arrows identify peak positions of this complex.

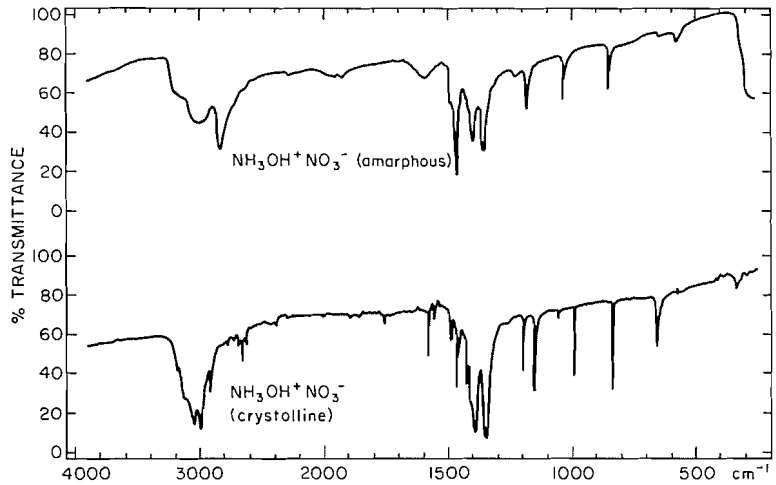

FIG. 11. Infrared spectra of amorphous and crystalline $NH_3OH^+NO_3^-$ at −190°C.

TABLE 8. Infrared spectrum of $NH_2OH_2^+NO_3^-$ at −190°C (cm^{-1} units)

Frequency, cm^{-1}	Assignment
~3100 s	ν(NH), ν(OH)
2760 s	ν(OH)
~1650 m	$\delta(OH_2^+)$
~1540 m	$\delta(NH_2)$
1390 vs	$\nu(NO_3^-)$
1350 vs	$\nu(NO_3^-)$
1040 w	$\nu(NO_3^-)$
995 s	$\delta(OH_2^+)$
835 vw	$\delta(NO_3^-)$
~300 s	Lattice

are also presented here for comparison. Assignments of the fundamentals are those of Nightingale and Wagner.

When HNO_3 was deposited on top of a film of amorphous NH_2OH at −190°C or *vice versa*, there was no reaction. Warming of these layered samples to −135°C caused HNO_3 to become crystalline. Only at about −125°C was there evidence of any chemical change, and new infrared bands first appeared at 1335 and 1390 cm^{-1}. These bands as well as others shifted slightly on warming and are listed in Table 8. They continued to grow as the temperature of the matrix approached the annealing temperature of −90°C. An example of a spectrum of amorphous NH_2OH with HNO_3 reaction intermediate but without excess HNO_3 is shown in Fig. 10. Arrows identify peaks whose frequencies are identical to those formed from the $NH_2OH-HNO_3$ reaction and are listed in Table 8. This spectrum was obtained from the reaction of amorphous NH_2OH and O_3 at low temperatures (1). When amorphous NH_2OH at −190°C was exposed to O_3, the same HNO_3 reaction intermediate was formed immediately. Growth of infrared bands of this intermediate was slow as the matrix was warmed but it became rapid as NH_2OH started to anneal at −90°C. At the same time new absorption bands due to amorphous $NH_3OH^+NO_3^-$ or occasionally crystalline $NH_3OH^+NO_3^-$ began to appear. As NH_2OH started to sublime off the cooled window at about −45°C, the absorption bands of the hydroxylammonium nitrate became stronger and remained to room temperature. In contrast to the above behavior, crystalline NH_2OH reacted with O_3 only on warming to −50°C, but it too formed the same HNO_3 reaction intermediate. The intermediate from the latter reaction as well as that from the $NH_2OH-HNO_3$ reaction converted into amorphous or crystalline hydroxylammonium nitrate at about −45°C as the remaining NH_2OH sublimed off the cooled window. Spectra of amorphous and crystalline $NH_3OH^+NO_3^-$ at −190°C are illustrated in Fig. 11 and their frequencies are summarized in Table 9. In this table, data for the room temperature sample are from Rocchiccioli (36) and those for the chloride salt are from Frasco and Wagner (37).

Our experimental evidence from the $NH_2OH-HNO_3$ and NH_2OH-O_3 reaction systems suggests that the HNO_3 reaction intermediate is a precursor of the final product $NH_3OH^+NO_3^-$ and that it is a complex of NH_2OH and HNO_3. A reasonable structure of this complex is one in which the proton transfer from the acid occurs at the oxygen atom to give $NH_2OH_2^+NO_3^-$. The absence of the characteristic strong $-NH_3^+$ group deformation fundamental at 1465 cm^{-1} (Table 9) and the presence of hydronium ion-like bands at 2760, 1650, and 995 cm^{-1} in Table 8 provide additional support for the proposed structure of this intermediate. For example, in the spectrum of $H_3O^+NO_3^-$, Savoie and Giguère (38) have reported bands at 2780 s, 1680 m, 1386 s, 1340 m, 1253 w, 1135

Can. J. Chem. Downloaded from www.nrcresearchpress.com by 210.87.254.105 on 09/06/12
For personal use only.

TABLE 9. Infrared spectra of amorphous and crystalline NH_3OH^+ salts (cm^{-1} units)

$NH_3OH^+NO_3^-$			$NH_3OH^+Cl^-$	
Amorphous[a] (−190°C)	Crystalline[a] (−190°C)	Crystalline[b] (25°C)	Crystalline[c] (−190°C)	Assignment[c]
~3200 m	~3120 m		3160 w	ν(OH)
~3020 s	3045 s	3045 w	3072 vs	ν(NH)
2830 s	2990 vs	2995 s	3006 vs	ν(NH)
	2920 m	2900 s	2925 vw	
	2780 vw		2790 vw	
			2756 w	
	2730 vw		2731 vw	
	2680 vw		2677 m	
	2660 m	2655 m		
	2620 w			
	2385 vw	2380 vw		
~1920 w	1890 vw	1895 w	1902 m	
	1860 vw		1819 w	
	1755 m			
1590 m	1580 m	1580 s	1575 m	δ(NH_3)
	1560 w	1559 w	1560 w	
1490 w	1490 m	1505 vw	1505 w	
1465 vs	1465 vs	1470 m	1475 s	δ(NH_3)
	1425 m			
1390 vs	1385 vs			
1358 vs	1350 vs	1365 s		ν(NO_3^-)
1346 vs	1340 vs			
1230 w	1260 vw			
1185 m	1198 s	1193 s	1197 s	δ(OH)
	1150 s	1165 s	1172 s	ρ(NH_3)
1027 m	995 s	998 s	997 s	ν(NO)
845 m	837 s	830 m		δ(NO_3^-)
	655 s		585 s	τ(OH)
565 w	555 w	529 m		
~260 s	330 m			

[a]This study.
[b]From Rocchiccioli (36), mull sample.
[c]From Savoie and Giguère (37), sublimed film.

s, 930 w, and 815 s in cm^{-1} units. Thus, the data in Table 8 have been assigned on the basis of the structure $NH_2OH_2^+NO_3^-$.

Summary

Acid–base reactions among various pairs of reactants NH_3, NH_2OH, H_2O, HCl, and HNO_3 have been examined by low-temperature infrared spectroscopy. Hydrogen-bonding in the solid state greatly reduces the reactivities of these reagents. In the systems $NH_3(s) + HCl(g)$, $HNO_3(s) + NH_3(g)$, $H_2O(s) + HCl(g)$, and $NH_2OH(s) + HNO_3(s)$ reactions become observable at −145, −130, −127, and −125°C, respectively. In the $NH_3–H_2O$ system, no proton transfer took place and the products were $2NH_3 \cdot H_2O$ and $NH_3 \cdot H_2O$. In the $NH_2OH–HNO_3$ system, both $NH_2OH_2^+NO_3^-$ and $NH_3OH^+NO_3^-$ were observed. Other species whose spectra were observed were $NH_4Cl \cdot 3NH_3$, $NH_4NO_3 \cdot 3NH_3$, $NH_4^+[NO_3 \cdot 2HNO_3]^-$, $H_3O^+Cl^-$, $H_5O_2^+Cl^-$, and $H_5O_2^+Cl^- \cdot H_2O$.

1. T. HUSTON, I. C. HISATSUNE, and J. HEICKLEN. **61**, 2070 (1983).
2. L. A. HULL, I. C. HISATSUNE, and J. HEICKLEN. J. Am. Chem. Soc. **94**, 4856 (1972).
3. F. P. REDING and D. F. HORNIG. J. Chem. Phys. **19**, 594 (1951); **23**, 1053 (1955).
4. D. F. HORNIG, H. F. WHITE, and F. P. REDING. Spectrochim. Acta, **12**, 338 (1958).
5. D. L. HILDENBRAND and W. F. GIAUQUE. J. Am. Chem. Soc. **75**, 2811 (1953).
6. I. OLOVSSON and D. H. TEMPLETON. Acta Crystallogr. **12**, 827 (1959).
7. W. J. SIEMONS and D. H. TEMPLETON. Acta Crystallogr. **7**, 194 (1954).
8. (*a*) R. D. WALDRON and D. F. HORNIG. J. Am. Chem. Soc. **75**, 6079 (1953); (*b*) J. E. BERTIE and M. M. MORRISON. J. Chem. Phys. **73**, 4832 (1980); (*c*) G. SILL, U. FINK, and J. R. FERRARO. J. Chem. Phys. **74**, 997 (1981); (*d*) J. E. BERTIE and M. M. MORRISON. J. Chem. Phys. **74**, 4361 (1981); (*e*) C. THORNTON, M. S. KHATKALE, and J. P. DEVLIN. J. Chem. Phys. **75**, 5609 (1981); (*f*) B. NELANDER and L. NORD. J. Phys. Chem. **86**, 4375 (1982).
9. A. L. GEDDES and G. L. BOTTGER. Inorg. Chem. **8**, 802 (1969).
10. D. F. HORNIG and W. E. OSBERG. J. Chem. Phys. **23**, 662 (1955).
11. B. S. AULT and G. C. PIMENTEL. J. Phys. Chem. **77**, 1649 (1973).
12. N. E. SCHUMAKER and C. W. GARLAND. J. Chem. Phys. **53**, 392 (1970).
13. I. OLOVSSON. Acta Chem. Scand. **14**, 1453 (1960).
14. M. BILLY and J. JARRIGE. Bull. Soc. Chim. Fr. 2924 (1970).
15. J. CORSET, P. V. HUONG, and J. LASCOMBE. Spectrochim. Acta, **24**A, 2045 (1968).
16. C. C. FERRISO and D. F. HORNIG. J. Chem. Phys. **23**, 1464 (1955).

Can. J. Chem. Downloaded from www.nrcresearchpress.com by 210.87.254.105 on 09/06/12
For personal use only.

17. A. S. GILBERT and N. SHEPPARD. J. Chem. Soc. Faraday Trans. II, **69**, 1628 (1973).
18. B. DESBAT and P. V. HUONG. Spectrochim. Acta, **31**A, 1109 (1975).
19. Y. K. YOON and G. B. CARPENTER. Acta Crystallogr. **12**, 17 (1959).
20. J. ROZIÈRE and J. POTIER. J. Mol. Struct. **13**, 91 (1972).
21. J.-O. LUNDGREN and I. OLOVSSON. Acta Crystallogr. **23**, 966 (1967).
22. J.-O. LUNDGREN and I. OLOVSSON. Acta Crystallogr. **23**, 971 (1967).
23. J. RUDOLPH and H. ZIMMERMAN. Z. Phys. Chem. **43**, 311 (1964).
24. G. VUILLARD. Ann. Chim. Paris, **2**, 233 (1957).
25. B. S. AULT and G. C. PIMENTEL. J. Phys. Chem. **77**, 57 (1973).
26. A. SCHRIVER, B. SILVA, D. MAILLARD, and J. P. PERCHARD. J. Phys. Chem. **81**, 2095 (1977).
27. G. E. MCGRAW, D. L. BERNITT, and I. C. HISATSUNE. J. Chem. Phys. **42**, 237 (1965).
28. B. KURILOFF. Z. Physik. Chem. **25**, 107 (1898).
29. J. W. LUNDEEN and R. S. TOBIAS. J. Chem. Phys. **63**, 924 (1975).
30. A. POTIER and J. POTIER. Bull. Soc. Chim. Fr. **311** (1959).
31. F. W. B. EINSTEIN and D. G. TUCK. Acta Crystallogr. B**26**, 1117 (1970).
32. L. DIOP and J. POTIER. J. Mol. Struct. **36**, 191 (1977).
33. A. THÈORÈT and C. SANDORFY. Can. J. Chem. **42**, 57 (1964).
34. R. E. NIGHTINGALE and E. L. WAGNER. J. Chem. Phys. **22**, 203 (1954).
35. P. A. GIGUÈRE and I. D. LIU. Can. J. Chem. **30**, 948 (1952).
36. C. ROCCHICCIOLI. Compt. Rend. **253**, 838 (1961).
37. D. L. FRASCO and E. L. WAGNER. J. Chem. Phys. **30**, 1124 (1959).
38. R. SAVOIE and P. A. GIGUÈRE. J. Chem. Phys. **41**, 2698 (1964).

Can. J. Chem. Downloaded from www.nrcresearchpress.com by 210.87.254.105 on 09/06/12
For personal use only.

Spectrométrie de masse du chloro-1 diméthoxy-2,6 naphtalène; comparaison de données théoriques et expérimentales

JEAN-CLAUDE RICHER
Département de Chimie, Université de Montréal, B.P. 6210, Montréal (Qué.), Canada H3C 3V1

ET

SIMONE ODIOT
Département de Recherches Physiques, Université Pierre et Marie Curie, 4 Place Jussieu, 75230 Paris, France

Reçu le 30 juin 1981[1]

JEAN-CLAUDE RICHER et SIMONE ODIOT. Can. J. Chem. **61**, 2089 (1983).

Nous avons synthétisé, d'une façon non ambigue, le chloro-1 diméthoxy-2,6 naphtalène-d_3 (**5**) et nous avons examiné son spectre de masse sous impact électronique. Nous rapportons aussi des calculs théoriques sur les stabilités relatives des chloro-1 et chloro-5 méthoxy-6 naphtols-2 (**4***a* et **4***b*) et sur les stabilités relatives des liaisons O—CH_3 en positions 2 et 6 du composé **5**.

JEAN-CLAUDE RICHER and SIMONE ODIOT. Can. J. Chem. **61**, 2089 (1983).

In an unambiguous manner we have synthesized 1-chloro-2,6-dimethoxy-d_3-naphthalene (**5**) and examined its electron impact mass spectrum. We report here calculations on the relative stabilities of 1-chloro and 5-chloro-6-methoxy-2-naphthols (**4***a* and **4***b*) and on the relative stabilities of the O—CH_3 bond in the 2 and 6 positions of compound **5**.

[Journal translation]

Introduction

Au cours d'une étude antérieure (1) sur la spectrométrie de masse du diméthoxy-2,6 naphtalène et de ses dérivés, nous avons suggéré que ces composés subissent la perte d'un radical méthyle (voir Schéma 1) et nous avons indiqué (1) que le choix du méthyle éliminé est arbitraire. Nous avions d'ailleurs noté, dans le cas de **1***a* (X^1 = Cl et X^2 = H), que l'ion à (M − 15) est plus intense que l'ion correspondant pour la molécule non substituée, **1***b* (X^1 = X^2 = H); nous avons supposé qu'un tel comportement peut être dû à la tendance marquée du chlore à partager l'un de ses doublets non liant et à stabiliser ainsi l'ion de type quinonique qui peut être formé (Schéma 2).

C'est dans le but de confirmer expérimentalement cette hypothèse que nous avons synthétisé des dérivés marqués d'une façon spécifique; nous avons ensuite comparé les résultats expérimentaux obtenus par spectrométrie de masse avec les résultats des calculs théoriques relatifs aux forces des diverses liaisons O—CH_3.

Résultats et discussion

Les produits dérivés ont été obtenus en effectuant les réactions représentées dans le schéma 3.

La structure **4***a* plutôt que **4***b* est attribuée sur la base du spectre rmn du ^{13}C. La première observation a trait au fait que le spectre du produit **4***a* ne comporte qu'un signal pour un O$\underline{C}H_3$. Cette observation suggère que la chloration de **3** ne conduit qu'à un seul dérivé chloré et cette sélectivité doit probablement être attribuée à une interaction entre le réactif SO_2Cl_2 et le OH libre du naphtol. Ces considérations suggèrent donc la structure **4***a* pour le produit chloré. Cette conclusion est

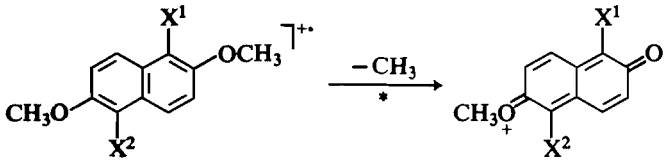

SCHÉMA 1

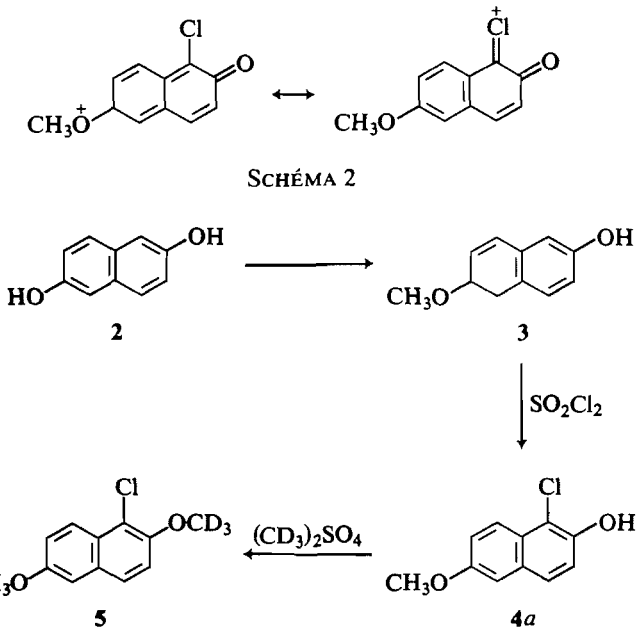

SCHÉMA 3

confirmée par l'examen du tableau 1 où sont rassemblés les déplacements chimiques des OCH_3 de naphtalènes apparentés. Ces données mettent en évidence le fait que les déplacements chimiques des OCH_3 qui ne sont pas soumis à l'influence d'un chlore en *ortho* sont de l'ordre de 55,5 ± 0,2 ppm alors que les valeurs équivalentes pour des OCH_3 en *ortho* d'un chlore sont de l'ordre de 57,5 ppm. La structure des composés **4***a* et **5** est donc établie sans ambiguité.

Sous impact électronique, la molécule **5** perd beaucoup plus facilement le CD_3 que le CH_3; le rapport est de 95:5 (voir Fig. 1) correspondant à une différence d'énergie de rupture d'environ 1,7 kcal/mol. Des calculs théoriques portant sur une évaluation des énergies relatives de dissociation des deux types de liaisons O—CH_3 vont dans le sens de cette observation, même s'ils sont loins d'être concluants; la différence liée à la présence du chlore est évaluée à 0,13 kcal/mol.

[1] Révision reçue le 17 mars 1983.

Can. J. Chem. Downloaded from www.nrcresearchpress.com by 210.87.254.105 on 09/06/12
For personal use only.

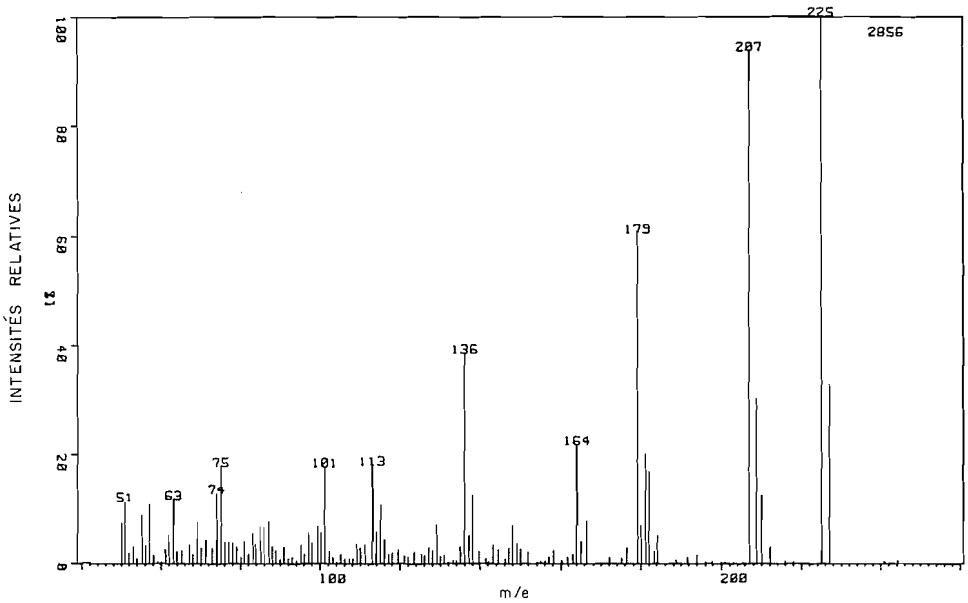

FIG. 1. Spectre de masse du chloro-1 diméthoxy-2,6 naphtalène-d_3 (**5**).

TABLEAU 1. Déplacements chimiques, en rmn du ^{13}C, des OCH_3

Composés	Déplacements chimiques (ppm/TMS)
3	55,44
4*	55,44
5 (léger)*	55,70 et 57,39
5-d_3*	55,76
5-d_3†	55,71 et 57,53

* Les spectres ont été enregistrés pour des solutions saturées dans l'acétone-d_6 sur un appareil Bruker WH-90 opérant à 22,63 MHz dans le mode de découplage en large bande. Les paramètres d'acquisition des spectres réalisés par transformation de Fourier sont: largeur spectrale 6024 Hz; temps d'acquisition −0,655 s; délai entre deux impulsions: 7 μs.

† Le spectre a été enregistré sur un appareil Bruker WP-80 opérant à 20,15 MHz et avec lequel un délai de 25 s était accordé entre deux impulsions.

Partie expérimentale

Les techniques expérimentales générales ont été décrites antérieurement (voir par exemple les réfs. 2, 3).

Synthèse des produits

Méthoxy-6 naphtol-2 (3)

La méthylation du dihydroxy-2,6 naphtalène est conduite d'après les indications de Downing et Woodcock (4).

Chloro-1 méthoxy-6 naphtol-2 (4a)

On ajoute 0,5 g de **3** en solution dans 10 mL de chloroforme dans 0,37 g de SO_2Cl_2 en solution dans 10 mL de chloroforme et l'on maintient le mélange dans un bain de glace pendant 15 h. On ajoute alors 21 mL d'éther puis 10 mL d'eau pour décomposer l'excès de SO_2Cl_2. La solution ainsi obtenue est décantée, lavée à l'eau, séchée sur du Na_2SO_4 et évaporée. On obtient ainsi 0,2 g (34% de rendement) de **4***a*; pf: 110–112°C (après sublimation).

Chloro-1 diméthoxy-2,6 naphtalène-d_3 *(5)*

On traite une solution de 1,6 g (8 mmol) de chloro-1 méthoxy-6 naphtol dissous dans 8 mL de méthanol par 1,1 mL de diméthylsulfate deutéré en présence de soude en suivant le procédé suggéré par Vyas et Shah (5). On obtient ainsi 625 mg (35% de rendement théorique) de **5**, pf 118–120°C (litt. (4) pf 117–118°C) dont le spectre de masse (Figs. 1 et 2) a été déterminé sur un appareil Micromass 12-12F de la compagnie VG opérant à 70 eV.

Calculs théoriques

Les calculs ont été effectués dans le cadre classique de la méthode

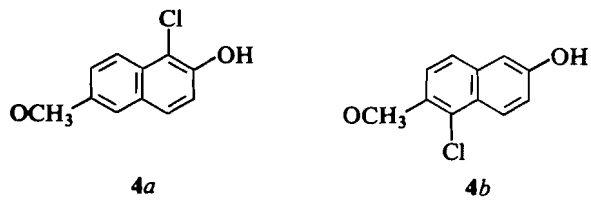

4a **4b**

FIG. 2

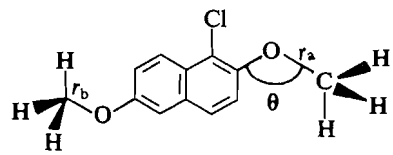

FIG. 3

C—C du cycle = 1,40 Å; C—O = 1,36 Å; O—CH_3 fixe = 1,35 Å soit pour r_b ou r_a; r = O—CH_3 variable soit pour r_a ou r_b; C—H = 1,09 Å; θ = C—O—C = 121°; H—CH—(H) = 109° 28′. Tous les autres angles du cycle sont pris égaux à 120°.

CNDO/2 (6, 7) après optimisation de la géométrie et minimisation de l'énergie E sur le paramètre géométrique θ = C—O—H (conformation s-*cis* de la figure 3). On obtient les valeurs suivantes:

4*a*	E = −138,094563 ua	θ = 108° 16′
4*b*	E = −138,090350 ua	θ = 108° 31′

On note que l'angle θ est insensible au voisinage soit de Cl ou de H et que le composé **4***a* est plus stable que **4***b* par 4213×10^{-6} ua soit 2,6 kcal/mol. L'évaluation des énergies relatives de dissociation des liaisons O—CH_3 (qui sont identifiées aux valeurs correspondantes pour O—CD_3) du composé **5** donnée par la différence d'énergie ΔE entre la valeur calculée pour la distance r_e à l'équilibre (O—CH_3) et celle pour r (limite de convergence du calcul) est en rapport avec la fragilité relative de ces liaisons (Tableau 2).

Cette différence d'énergie $\Delta_{\Delta E} = \Delta E_{OCH_3(2)} - \Delta E_{OCH_3(6)} = 0{,}355586 - 0{,}355794 = 208 \times 10^{-6}$ ua = 130 cal/mol. La géométrie adoptée est donnée dans la figure 3 où la forme s-*trans*, θ = 121° est la plus stable.

Conclusion

Les résultats expérimentaux obtenus au cours de ce travail

Can. J. Chem. Downloaded from www.nrcresearchpress.com by 210.87.254.105 on 09/06/12
For personal use only.

TABLEAU 2. Variation de l'énergie en fonction de la distance r (O—CH_3)

r_a	E (ua)	r_b	E (ua)
1,15	−146,586947	1,35	−146,76748
1,25	−146,721776	1,36	−146,768487
1,35	−146,767488	1,37	−146,768950
r_e = 1,38063	−146,768925	r_e = 1,37238	−146,768989
1,45	−146,756508	1,38	−146,768914
1,80	−146,54445	1,39	−146,768392
		1,40	−146,767413
2,00	−146,413339	2,00	−146,413195
Limite de convergence		Limite de convergence	
	ΔE_{ua} = 0,355586		ΔE_{ua} = 0,355794

nous permettent donc de confirmer l'hypothèse formulée dans le travail antérieur (1) selon laquelle la liaison du O—CH_3 en position 2 du Cl se rompt plus aisément que la liaison du O—CH_3 en position 6 par rapport au chlore (voir Schéma 1).

On a aussi démontré, par des calculs théoriques semi-empiriques relativements simples que l'énergie de dissociation de la liaison O—CH_3 du groupement en α du chlore est plus faible que l'énergie de dissociation du O—CH_3 en position 6; ces calculs confirment l'expérience ainsi que l'hypothèse préconisée antérieurement et représentée dans les schémas 1 et 2.

Remerciements

Les auteurs remercient vivement le CRSNG et les autorités chargées d'administrer les accords scientifiques franco-québécois pour l'aide apportée sous forme d'octrois et de frais de mission. Les auteurs remercient aussi Madame Monique Blain, Mlle Carole Lépine et M. Robert Mayer et le Dr. H. Martineau pour l'aide technique.

1. J. CASTONGUAY, A. ROSSI, J. C. RICHER et Y. ROUSSEAU. Org. Mass Spectrom. **6**, 1225 (1972).
2. J. C. RICHER, M. A. POIRIER, YVETTE MARONI et G. MANUEL. Can. J. Chem. **58**, 39 (1980).
3. J. C. RICHER et A. ROSSI. Can. J. Chem. **47**, 3935 (1969).
4. D. F. DOWNING et D. WOODCOCK. J. Chem. Soc. 531 (1958).
5. G. N. VYAS et N. M. SHAH. Org. Synth. Coll. Vol. **4**, 837, note 5 (1963).
6. J. A. POPLE, D. P. SANTRY et G. A. SEGAL. J. Chem. Phys. **43**, 5129 (1965).
7. J. A. POPLE et G. A. SEGAL. J. Chem. Phys. **43**, 5136 (1965).

Can. J. Chem. Downloaded from www.nrcresearchpress.com by 210.87.254.105 on 09/06/12
For personal use only.

Solvolytic studies with 2-methyl[1-^{13}C]-1-propyl tosylate

CHOI CHUCK LEE AND HUSSEIN F. ZOHDI

Department of Chemistry, University of Saskatchewan, Saskatoon, Sask., Canada S7N 0W0

Received March 11, 1983

CHOI CHUCK LEE and HUSSEIN F. ZOHDI. Can. J. Chem. **61**, 2092 (1983).

Solvolysis of 2-methyl[1-^{13}C]-1-propyl tosylate was carried out in HOAc or CF_3COOH without or with the presence of 2.0 equivalents of NaOAc or CF_3COONa, respectively. Isobutyl, *sec*-butyl and *tert*-butyl products were obtained. With the use of ^{13}C as label, isotopic scramblings were analyzed by ^{13}C nmr, avoiding the necessity of chemical degradations associated with the use of ^{14}C. There was no isotopic scrambling in the isobutyl product and scrambling of the ^{13}C-label was observed only between C-2 and C-3 in the *sec*-butyl product, indicating 1,2-hydride shifts in the *sec*-butyl cation. In contrast to the involvement of equilibrating protonated methylcyclopropane intermediates observed in the trifluoroacetolysis of [1-^{14}C]-1-butyl tosylate, the present results indicated that protonated methylcyclopropane intermediates did not play a significant role in the acetolysis or trifluoroacetolysis of isobutyl tosylate.

CHOI CHUCK LEE et HUSSEIN F. ZOHDI. Can. J. Chem. **61**, 2092 (1983).

On a effectué la solvolyse du tosylate de méthyle-2 [^{13}C-1] propyle-1 dans du AcOH ou du CF_3COOH en présence ou non de 2 équivalents de AcONa ou de CF_3COONa respectivement. On a obtenu des produits du type isobutyle, *sec*-butyle et *tert*-butyle. Faisant appel au marquage par le ^{13}C on a analysé le mélange isotopique par la rmn du ^{13}C évitant ainsi la nécessité de recourir à des dégradations chimiques associées à l'utilisation du ^{14}C. Il n'y a pas de mélange isotopique dans le cas de l'isobutyle et on a observé un mélange du marqueur au ^{13}C uniquement entre le C-2 et le C-3 du *sec*-butyle, ce qui indique un glissement 1,2 d'hydrure dans le cation *sec*-butyle. Contrairement à l'implication des intermédiaires méthylcyclopropane protonés à l'équilibre observés dans la trifluoroacétolyse du tosylate de [^{14}C-1] butyle-1 les résultats actuels indiquent que les intermédiaires méthylcyclopropanes protonés ne jouent pas un rôle significatif dans l'acétolyse ou la trifluoroacétolyse du tosylate d'isobutyle.

[Traduit par le journal]

In the trifluoroacetolysis of [1-^{14}C]-1-butyl tosylate, extensive isotopic scramblings were observed in the chief product, *sec*-butyl trifluoroacetate, the mean ^{14}C distribution at C-1, C-2, C-3, and C-4, respectively, being 48.1, 2.3, 3.3, and 46.3% (1). These results were explained by invoking the occurrence of two processes, the main pathway being the degenerate rearrangement interconverting *sec*-butyl cations through 1,2-hydride shifts, with a minor process involving equilibrating protonated methylcyclopropanes as reaction intermediates (eq. [1]) to account for the small amounts of scrambling of the label into the C-2 and C-3 positions (1). Similar scrambling

[1] 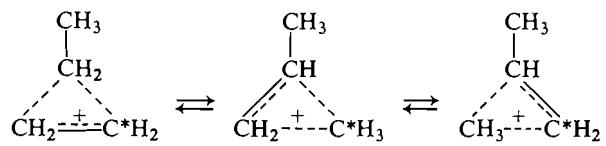

results indicating a minor contribution by protonated methylcyclopropane intermediates have also been observed in the trifluoroacetolysis of [1-^{14}C]-1-butylmercuric perchlorate (2) and in the HNO_2 deamination of [1-^{14}C]-1-butylamine (3). It is of interest to find out whether protonated methylcyclopropane intermediates would play a part in solvolytic reactions with the isobutyl system. In the present work, 2-methyl[1-^{13}C]-1-propyl tosylate (**1**-OTs-1-^{13}C) was solvolyzed in HOAc or CF_3COOH in order to ascertain if the isotopic scrambling data would indicate a role for protonated methylcyclopropanes in these reactions. ^{13}C instead of ^{14}C was used as label and the scrambling was analyzed by ^{13}C nmr so as to avoid the chemical degradations required in the use of ^{14}C.

The solvolysis of **1**-OTs-1-^{13}C was carried out in HOAc or CF_3COOH, without or with the presence of 2.0 equivalents of NaOAc or CF_3COONa, respectively. The ester products obtained in each experiment were hydrolyzed to give a mixture of isobutyl, *sec*-butyl, and *tert*-butyl alcohols (**1**-OH-*x*-^{13}C, **2**-OH-*x*-^{13}C, and **3**-OH-*x*-^{13}C, respectively) which were separated by preparative vpc. The yields of these alcohols are summarized in Table 1.

To determine the ^{13}C distributions in the **1**-OH-*x*-^{13}C and **2**-OH-*x*-^{13}C, these alcohols were converted to the corresponding phenylurethanes and the ^{13}C nmr spectra of these solid derivatives were obtained in the presence of 0.1 *M* $Cr(AcAc)_3$ (chromium acetylacetonate) as a relaxation agent. The presence of the $Cr(AcAc)_3$ strongly quenched the nuclear Overhauser enhancements, thus allowing for a quantitative correlation between peak intensity and ^{13}C content (4). Shown in Fig. 1A is the ^{13}C spectrum, obtained in $CDCl_3$ in the presence of 0.1 *M* $Cr(AcAc)_3$, for a typical sample of isobutyl phenylurethane prepared from **1**-OH-*x*-^{13}C derived from a solvolysis reaction. This spectrum indicated that only the C-1 CH_2 carbon was enriched with ^{13}C, the integrated intensity of the two CH_3 groups being very similar to those of the two *o*- or *m*-carbons of the phenyl group, and the integrated intensity of the C-2 CH carbon being very similar to that of the one carbon absorption of the *p*-carbon of the phenyl group. Thus there was essentially no scrambling of the ^{13}C-label from C-1 and the **1**-OH-*x*-^{13}C obtained from all of the solvolysis reactions studied was actually the unrearranged **1**-OH-1-^{13}C.

Figures 1B and 1C, respectively, are the ^{13}C spectra, obtained in the presence of 0.1 *M* $Cr(AcAc)_3$, for the *sec*-butyl phenylurethane prepared from **2**-OH-*x*-^{13}C derived from Run 1 of Experiment 1 (acetolysis, no added NaOAc) and from Run 1 of Experiment 4 (trifluoroacetolysis, 2.0 equiv. CF_3COONa). The assignments for C-1, C-2, C-3, and C-4 of the *sec*-butyl group and the *o*-, *m*-, and *p*-carbons of the phenyl group are shown in the spectra, the remaining two downfield peaks being due to the quarternary carbon of the phenyl group and the carbonyl carbon of the urethane function. From the integrated intensities as shown in Tables 2 and 3, the ^{13}C enrichments in the *sec*-butyl carbons were calculated using the integrated in-

Can. J. Chem. Downloaded from www.nrcresearchpress.com by 210.87.254.40 on 09/06/12
For personal use only.

TABLE 1. Yields of butyl alcohols derived from the products of solvolysis of 2-methyl[1-^{13}C]-1-propyl tosylate and ^{13}C scrambling between C-2 and C-3 in the *sec*-butyl product[a]

Expt.	Medium	Total yield (%)		Relative yields (%)[b]						^{13}C-Distribution in *sec*-BuOH (%)[c]			
				iso-BuOH		*sec*-BuOH		*t*-BuOH		C-2		C-3	
		Run 1	Run 2	Run 1	Run 2	Run 1	Run 2	Run 1	Run 2	Run 1	Run 2	Run 1	Run 2
1	HOAc	31	38	76	77	14	13	10	11	29±11	29±17	71±11	71±17
2[d]	HOAc−NaOAc	55	54	98	98	1.5	1.5	0.5	0.5	12±10	15±3	88±10	85±3
3	CF_3COOH	18	18	24	28	57	53	19	19	50±4	50±1	50±4	50±1
4[d]	$CF_3COOH-CF_3COONa$	51	56	28	34	15	13	57	53	38±0.5	40±0.3	62±0.5	60±0.3

[a]The isomeric butyl alcohols were derived from hydrolysis of the butyl esters obtained in each experiment.
[b]Based on vpc.
[c]Calculated as shown in Tables 2 and 3.
[d]Two molar equivalents of NaOAc or CF_3COONa were present in the reaction mixture.

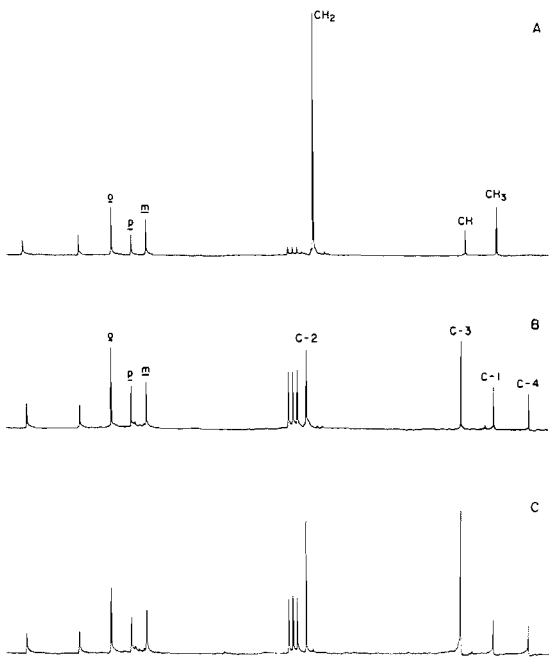

FIG. 1. ^{13}C nuclear magnetic resonance spectra in $CDCl_3$ containing 0.1 *M* $Cr(AcAc)_3$. A. [*x*-^{13}C]Isobutyl phenylurethane; B. [*x*-^{13}C]-*sec*-butyl phenylurethane derived from Run 1, Expt. 1; C. [*x*-^{13}C]-*sec*-butyl phenylurethane derived from Run 1, Expt. 4.

tensity of the *o*-, *m*-, or *p*-carbon of the phenyl group as a reference standard.

It is seen from Tables 2 and 3 that, for both of these experiments, there was no ^{13}C enrichment in C-1 and C-4, but there was scrambling of the ^{13}C between C-2 and C-3. Although the precision obtained for the extent of scrambling in the acetolysis experiment was relatively poor, the present results did show that, with the use of $Cr(AcAc)_3$, the ^{13}C spectra were capable of being used to measure the extents of scrambling of the ^{13}C-label. Similar treatment of the data from the ^{13}C spectra of samples of *sec*-butyl phenylurethane derived from the other experiments also showed scramblings between C-2 and C-3, but no scrambling to C-1 and C-4. The extents of such scramblings between C-2 and C-3 for all of the solvolysis reactions studied in the present work are included in Table 1.

The kinetics of solvolysis of **1**-OTs, including acetolysis and trifluoroacetolysis, have been studied by Winstein and coworkers (5, 6). At 75°C, the titrimetric rate constants for the acetolysis and trifluoroacetolysis of **1**-OTs were found to be 0.234×10^{-6} s^{-1} and 55.4×10^{-6} s^{-1}, respectively. These results were interpreted as indicating anchimeric assistance in CF_3COOH due to participation of the neighboring H or CH_3 to give the *tert*-butyl or *sec*-butyl product (6). The present results are in agreement with Winstein's conclusions and the use of the isotopic label further showed that, in the *sec*-butyl cation, 1,2-hydride shifts took place, leading to the scrambling of the label between C-3 and C-2.

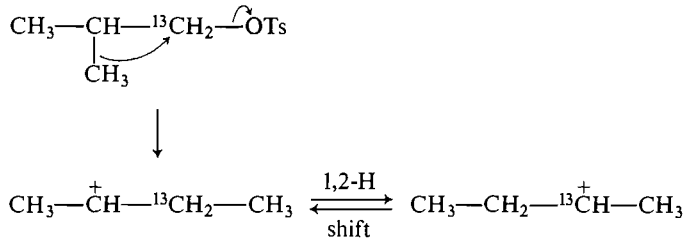

For the reaction under the least nucleophilic conditions, i.e. trifluoroacetolysis with no added CF_3COONa (Experiment 3), complete equilibration of the label between C-3 and C-2 in the *sec*-butyl product was observed. On the other hand, as would be expected, the least extent of scrambling was found for the acetolysis carried out in the presence of added NaOAc (Experiment 2).

In the trifluoroacetolysis of [1-^{14}C]-1-butyl tosylate (1), small amounts of scrambling to the C-2 and C-3 positions of the *sec*-butyl product were observed. Consideration of the possible mechanisms that might be responsible for the appearance of the label at C-2 and C-3 led to the conclusion favoring the involvement of equilibrating protonated methylcyclopropane intermediates rather than the occurrence of 1,2-ethyl shifts in the 1-butyl cation (1). A similar involvement of protonated methylcyclopropanes in the solvolysis of **1**-OTs-1-^{13}C would lead to the scrambling of the label into C-1 and C-4 of the *sec*-butyl product. In the present work, the complete absence of any ^{13}C enrichment in C-1 and C-4 of the *sec*-butyl product, as well as the absence of any scrambling in the isobutyl product, indicated that, in contrast to the trifluoroacetolysis of 1-butyl tosylate, protonated methylcyclopropane intermediates did not play any significant part in the formation of products during the acetolysis or trifluoroacetolysis of **1**-OTs-1-^{13}C. This conclusion is also in agreement with the findings of Karabatsos *et al.* (7) that the aqueous acid deamination of 2-methyl(1,1-$^2H_2$)-1-propylamine (**1**-NH_2-1,1-d_2) did not give any isotopic scrambling results in support of protonated methylcyclopropanes.

Can. J. Chem. Downloaded from www.nrcresearchpress.com by 210.87.254.40 on 09/06/12
For personal use only.

TABLE 2. ^{13}C-enrichments and ^{13}C-distribution in the *sec*-butyl groups of the *sec*-butyl phenylurethane derived from Run 1, Expt. 1

	Integrated intensity	^{13}C-Enrichment calcd. from				
		o-C[a]	*m*-C[b]	*p*-C[c]	Mean[d]	^{13}C-Distribution (%)
C-1	0.97	−0.03	0.13	−0.21	−0.04±0.17	—
C-2	1.47	0.47	0.63	0.29	0.46±0.17	29±11
C-3	2.13	1.13	1.29	0.95	1.12±0.17	71±11
C-4	0.77	−0.23	−0.07	−0.41	−0.24±0.17	—

[a]The integrated intensity of the *o*-carbons was 2.00 or 1.00 per C, the enrichments being the difference between the observed intensity of C-1, C-2, C-3, or C-4 and 1.00.
[b]The integrated intensity of the *m*-carbons was 1.67 or 0.84 per C, the enrichments being the difference between the observed intensity of C-1, C-2, C-3, or C-4 and 0.84.
[c]The integrated intensity of the *p*-carbon was 1.18, the enrichments being the difference between the observed intensity of C-1, C-2, C-3, or C-4 and 1.18.
[d]Mean value ± maximum deviation from the mean.

TABLE 3. ^{13}C-enrichments and ^{13}C-distribution in the *sec*-butyl group of the *sec*-butyl phenylurethane derived from Run 1, Expt. 4

	Integrated intensity	^{13}C-Enrichment calcd. from				
		o-C[a]	*m*-C[b]	*p*-C[c]	Mean[d]	^{13}C-Distribution (%)
C-1	0.96	−0.04	−0.01	−0.11	−0.05±0.06	—
C-2	4.90	3.90	3.93	3.83	3.89±0.06	38±0.5
C-3	7.43	6.43	6.46	6.36	6.42±0.06	62±0.5
C-4	0.83	−0.17	−0.14	−0.24	−0.18±0.06	—

[a]The integrated intensity of the *o*-carbons was 2.00 or 1.00 per C, the enrichment being the difference between the observed intensity of C-1, C-2, C-3, or C-4 and 1.00.
[b]The integrated intensity of the *m*-carbons was 1.94 or 0.97 per C, the enrichments being the difference between the observed intensity of C-1, C-2, C-3, or C-4 and 0.97.
[c]The integrated intensity of the *p*-carbon was 1.07, the enrichment being the difference between the observed intensity of C-1, C-2, C-3, or C-4 and 1.07.
[d]Mean value ± maximum deviation from the mean.

Experimental

*2-Methyl[1-^{13}C]-1-propyl tosylate (**1**-OTs-1-^{13}C)*

The substrate, **1**-OTs-1-^{13}C, was prepared using conventional methods. Treatment of isopropylmagnesium bromide with [^{13}C]CO_2 (from 90% enriched [^{13}C]$BaCO_3$ supplied by MSD Isotopes of Montreal) gave the labeled isobutyric acid which was reduced with $LiAlH_4$ to isobutyl alcohol and then treated with *p*-toluenesulfonyl chloride in pyridine to give **1**-OTs-1-^{13}C, mp 11−12°C (lit. (5) mp 12.0−12.5°C).

Solvolysis reactions

In the acetolysis, 5.0 g (22 mmol) of **1**-OTs-1-^{13}C in 50 mL of HOAc was heated under reflux at 100 ± 2°C for 13 days. The reaction time was chosen after nmr monitoring of preliminary trial reactions, with the disappearance after 13 days of the doublet due to the C-1 CH_2 of the substrate as an indication of complete reaction. From the kinetic data of Winstein and Marshall (5), for the acetolysis, a reaction time of 13 days at 100°C would correspond to about 6 half-lives. For the acetolysis in the presence of NaOAc, the same conditions were used except that the reaction mixture also contained 3.6 g (44 mmol) of NaOAc.

In the trifluoroacetolysis, a solution of 5.0 g (22 mmol) of **1**-OTs-1-^{13}C in 50 mL of CF_3COOH, without or with the presence of 6.0 g (44 mmol) of CF_3COONa, was heated under reflux at 60 ± 1°C for 60 h, the reaction time again being chosen after preliminary monitoring by nmr. According to the data of Winstein and co-workers (6), the half-life for the trifluoroacetolysis at 75°C was about 3.5 h.

Each reaction mixture was worked up using a procedure similar to that employed in the trifluoroacetolysis of [1-^{14}C]-1-butyl tosylate (1). This involved the addition of a sufficient amount of aqueous KOH to neutralize the reaction mixture and leave a final solution containing 20% KOH, the refluxing of the basic solution overnight to effect the hydrolysis of the ester products, and the recovery of the isomeric butyl alcohols by continuous ether extraction. A small amount of the recovered products was used for vpc analysis through a capillary column packed with Carbowax 20M to give the relative yields of the isobutyl, *sec*-butyl, and *tert*-butyl alcohols (**1**-OH-*x*-^{13}C, **2**-OH-*x*-^{13}C, and **3**-OH-*x*-^{13}C, respectively). The remainder of the product mixture, with some added carriers if necessary, was separated by preparative vpc to give samples of **1**-OH-*x*-^{13}C, **2**-OH-*x*-^{13}C, and **3**-OH-*x*-^{13}C, the first two of these alcohols being converted to the corresponding phenylurethanes for nmr analysis in $CDCl_3$ in the presence of 0.1 *M* $Cr(AcAc)_3$.

Acknowledgment

The financial support given by the Natural Sciences and Engineering Research Council of Canada is sincerely acknowledged.

1. C. C. LEE, A. J. CESSNA, E. C. F. KO, and S. VASSIE. J. Am. Chem. Soc. **95**, 5688 (1973).
2. C. C. LEE and R. REICHLE. J. Org. Chem. **42**, 2058 (1977).
3. C. C. LEE, R. REICHLE, and U. WEBER. Can. J. Chem. **56**, 658 (1978).
4. J. N. SHOOLERY. Prog. Nucl. Magn. Reson. Spectrosc. **11**, 79 (1977).
5. S. WINSTEIN and H. MARSHALL. J. Am. Chem. Soc. **74**, 1120 (1952).
6. I. L. REICH, A. DIAZ, and S. WINSTEIN. J. Am. Chem. Soc. **91**, 5635 (1969).
7. G. J. KARABATSOS, N. HSI, and S. MEYERSON. J. Am. Chem. Soc. **92**, 621 (1970).

Can. J. Chem. Downloaded from www.nrcresearchpress.com by 210.87.254.40 on 09/06/12
For personal use only.

Sulfoxydes et sulfones hétérobicycliques dérivés de l'α-thioglycérol. 2,8-Dioxa-6-oxo-6-thiabicyclo[3.2.1]octanes et 2,8-dioxa-6,6′-dioxo-6-thiabicyclo[3.2.1]octanes[1]

PIERRE CALINAUD ET JACQUES GELAS

Université de Clermont-Ferrand, École Nationale Supérieure de Chimie, Ensemble Scientifique des Cézeaux, BP 45, 63170 Aubière, France

Reçu le 21 decembre 1982

PIERRE CALINAUD et JACQUES GELAS. Can. J. Chem. **61**, 2095 (1983).

Les réactions d'oxydation de sulfures hétérobicycliques dérivés de l'α-thioglycérol (alkyl-2,8-dioxa-6-thiabicyclo-[3.2.1]octanes), menant respectivement aux sulfoxydes et aux sulfones correspondants, ont été étudiées. La stéréochimie de l'oxydation en fonction de l'agent utilisé (eau oxygénée, acide *méta*-chloroperbenzoïque, hypochlorite de *tert*-butyle) a été examinée. L'attribution de la structure des sulfoxydes repose sur la discussion d'un ensemble de critères spectrographiques et chimiques propre à ce type de composé.

PIERRE CALINAUD and JACQUES GELAS. Can. J. Chem. **61**, 2095 (1983).

The oxidation reactions of heterobicyclic sulfides derived from α-thioglycerol (alkyl-2,8-dioxa-6-thiabicyclo[3.2.1]-octanes), leading to sulfoxides and the corresponding sulfones, have been studied. The stereochemistry of the oxidation as a function of the reagent used (H_2O_2, *meta*-chloroperbenzoic acid, and *tert*-butyl hypochlorite) has been examined. Structural assignments of the sulfoxides arise from the spectroscopic and chemical properties of these compounds.

[Journal translation]

Can. J. Chem. Downloaded from www.nrcresearchpress.com by 210.87.254.6 on 09/06/12
For personal use only.

Depuis une dizaine d'années un intérêt considérable est apparu concernant la détermination des préférences conformationnelles des substituants portés par un hétéroatome d'un cycle (Fig. 1) et ceci particulièrement pour les hétérocycles à six maillons (3). En effet, outre l'intérêt fondamental évident que présentent ces études, les conséquences d'une telle détermination pourraient être particulièrement utiles dans l'avenir pour les substances douées d'activité biologique.

Disposant avec les 2,8-dioxa-6-thiabicyclo[3.2.1]octanes préparés au laboratoire (1) d'un modèle particulièrement approprié (équilibre conformationnel pratiquement bloqué) pour envisager les problèmes posés par l'oxydation au niveau de l'atome de soufre, nous avons entrepris l'étude des sulfoxydes et sulfones de cette série. Nous y avons été d'autant plus incités que les seuls travaux dans cette dernière ont été publiés sous forme d'une note préliminaire (4) décrivant la formation des deux sulfoxydes stéréoisomères correspondant au dioxathiabicyclooctane non substitué et préparé à partir du 1,6-anhydro-β-D-glucopyranose. Une tentative d'attribution de la stéréochimie respective de ces deux sulfoxydes était proposée sur la base de la vitesse de réduction par le diborane plus grande pour le sulfoxyde à liaison S—O *axiale* que pour l'isomère à liaison S—O *équatoriale*. En revanche l'étude des sulfoxydes dérivés des 2-hydroxy ou 2-méthoxy-1,4-oxathiannes a été plus approfondie et constitue d'ailleurs une des toutes premières définition de critères d'attribution de la stéréochimie *axiale* ou *équatoriale* de la liaison S—O dans les hétérocycles à six maillons (5).

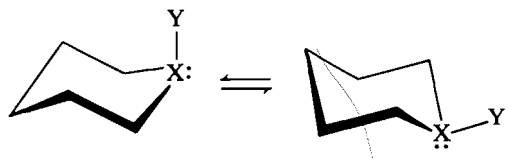

FIG. 1.

TABLEAU 1. Sulfoxydes dérivés des 2,8-dioxa-6-thiabicyclo[3.2.1]octanes

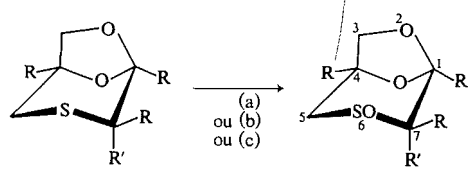

(a) H_2O, Me_2CO
(b) *m*-$ClC_6H_4CO_3H$, CH_2Cl_2
(c) *tert*-BuOCl, MeOH

Composés	R-1	R-4	R-7	R′-7
1	H	H	H	H
2	Me	H	H	H
3	Me	H	Me	H
4	Me	H	Me	Me
5	Me	Me	H	H
6	Ph	H	H	H

2,8-Dioxa-6-oxo-6-thiabicyclo[3.2.1]octanes

Les dioxathiabicyclooctanes de départ ont été décrits précédemment (1). Les sulfoxydes correspondants (Tableau 1) ont été obtenus par trois méthodes.

(a): L'oxydation par l'eau oxygénée selon Rigau *et al.* (6); l'agent oxydant est utilisé en quantité stoechiométrique, seul le sulfoxyde est obtenu à côté d'une très faible quantité de sulfone et du sulfure de départ inattaqué.

(b): L'oxydation par l'acide *méta*-chloroperbenzoïque en solution dans le dichlorométhane (7) semble être plus rapide et surtout moins dangereuse que la précédente pour laquelle nous avons observé un cas d'explosion violente.

(c): L'oxydation par l'hypochlorite de *tert*-butyle selon la méthode décrite par Johnson et McCants (8) a été utilisée pour obtenir préférentiellement des sulfoxydes à liaison S—O *axiale* (proportion S—O *axiale* environ 70%), alors que les deux méthodes précédemment citées conduisent essentiellement dans notre cas à des sulfoxydes où la liaison S—O est *équatoriale* (plus de 90%). La préparation du couple de stéréoisomères dans un certain nombre de cas (sulfoxydes **1**, **2** et **4**) a permis de lever toute ambigüité quant à l'attribution de la

[1]Recherches dans la série des acétals cycliques: Partie XXVI; Partie XXV: voir réf. 1. Pour une Note Préliminaire voir réf. 2.

TABLEAU 2. Déplacements chimiques (ppm) des protons en α du groupement sulfinyle dans le sulfoxyde **5**

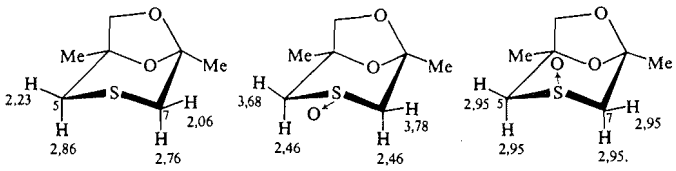

	H-5 *ax*	H-7 *ax*	H-5 *éq*	H-7 *éq*
Δδ (S → SO *éq*)	−0,40	−0,30	+1,45	+1,72
Δδ (S → SO *ax*)	+0,09	+0,19	+0,72	+0,89

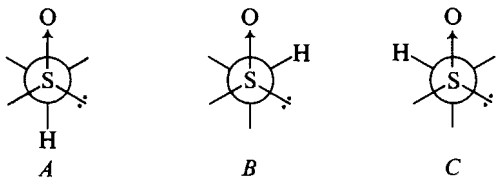

FIG. 2.

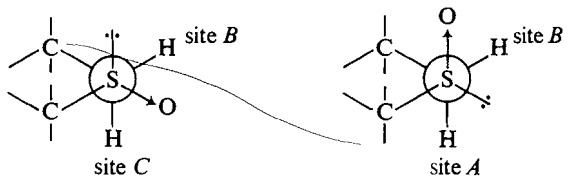

FIG. 3.

stéréochimie des sulfoxydes pratiquement purs obtenus par les deux autres méthodes.

Critères d'attribution de la structure et de la configuration des sulfoxydes

Bien que d'autres critères d'identification (voir notamment points de fusion et R_f dans la partie expérimentale) puissent être utiles, ce sont certaines données de spectrographie de rmn qui apparaissent en fait des moins discutables pour attribuer la configuration d'un sulfoxyde. (Pour une revue critique de ces critères se reporter à la publication de Lett et Marquet (9) et références citées.)

1. *Déplacements chimiques*

Si l'on compare les sulfoxydes aux dioxathiabicyclooctanes de départ (1) l'effet le plus remarquable est l'inversion des déplacements chimiques des protons portés par les atomes de carbone en α du groupement sulfinyle, particulièrement dans le cas d'un sulfoxyde *équatorial*: les protons *équatoriaux* (qui résonnent à champ plus fort que les protons *axiaux* dans les sulfures) résonnent à champ faible dans les sulfoxydes alors que les protons *axiaux* résonnent à champ fort. L'attribution *équatoriale–axiale* des protons en 5 a pu être faite grâce à la constante de couplage à longue distance en W $^4J_{3,5}$ qui n'existe qu'entre le proton H-3 *exo* et le proton H-5 *axial*. Nous détaillons dans le tableau 2 un exemple particulièrement net fourni par les spectres des sulfoxydes **5** *axial* et *équatorial* pour lesquels on a rappelé les déplacements chimiques pour le sulfure de départ. Ces déplacements s'expliquent très bien en reprenant l'interprétation du blindage ou du déblindage de protons par un groupe sulfinyle (9). Si on considère les différents sites spatiaux possibles (Fig. 2), un proton dans le site *B* sera le plus

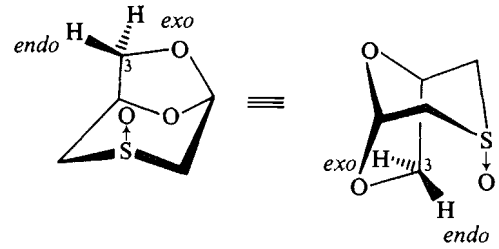

FIG. 4.

TABLEAU 3. Effets de déblindage exercé sur le proton H-3 *endo* par un groupe sulfinyle *axial* (solvant Me_2CO-d_6)

Proton	Composés	δ SO *éq*	δ SO *ax*	Δδ
H-3 *endo*	**1**	4,60	4,90	+0,30
	2	3,90	4,77	+0,87
	5	3,91	4,82	+0,91
H-3 *exo*	**1**	3,93	3,92	+0,01
	2	3,90	3,92	+0,02
	5	3,41	3,53	+0,12

TABLEAU 4. Différences entre les déplacements chimiques des protons géminés en α du groupe sulfinyle

Composés	Δν H-5	Δν H-7
2 *éq*	1,07	0,99
2 *ax*	0,69	0,69
5 *éq*	1,22	1,32
5 *ax*	0,10	0,10

déblindé de tous alors que les protons dans les sites *A* ou *C* seront soit légèrement déblindés, soit blindés. Si nous reprenons ce modèle pour nos propres sulfoxydes on constate (Fig. 3) que pour le sulfoxyde *équatorial* le proton *axial* en α est dans un site *C* (*anti* par rapport à la paire libre et *gauche* par rapport à SO) et le proton *équatorial* en α dans un site *B* (*gauche* par rapport à la paire libre et à la liaison SO). Inversement, pour le sulfoxyde *axial* le proton *axial* en α est dans un site *A* (*anti* par rapport à la liaison SO et *gauche* par rapport à la paire libre) et le proton *équatorial* en α dans un site *B*. Les effets observés (Tableau 2) sont conformes aux prévisions tirées du modèle de la figure 2. Cependant en général l'effet de déblindage est de l'ordre de 0,4 ppm (9). L'écart entre nos propres valeurs peut être dû à au moins deux facteurs: (*i*) nos composés sont pratiquement dans une conformation bloquée et de ce fait les effets peuvent être plus marqués; (*ii*) si on admet (ainsi qu'on a déjà eu l'occasion de le discuter pour les homologues oxygénés (1)) que le cycle 1,4-oxathianne des bicycles est aplati dans la région C-5—S-6—C-7, on doit obtenir un effet de déblindage d'autant plus prononcé pour un site *B* et pour un sulfoxyde *équatorial* (tendance à éclipser le proton avec la paire libre); inversement le léger blindage observé pour les protons *axiaux* d'un sulfoxyde *équatorial* serait dû à la tendance à éclipser le proton dans le site *C* avec la liaison SO.

Une observation intéressante est l'effet de déblindage exercé sur H-3 *endo* par l'atome d'oxygène du groupe sulfinyle lorsque celui-ci est *axial* (Fig. 4). A titre d'exemple nous indiquons dans le tableau 3 les valeurs relevées pour les couples des sulfoxydes **1**, **2** et **5**.

Un autre critère d'attribution de la configuration de la liaison SO est l'examen de la différence des déplacements chimiques

Can. J. Chem. Downloaded from www.nrcresearchpress.com by 210.87.254.6 on 09/06/12
For personal use only.

TABLEAU 5. Effets de solvant sur les déplacements chimiques des sulfoxydes *équatoriaux* et *axiaux*

$\Delta\delta = \delta_{Me_2CO\text{-}d_6} - \delta_{C_6D_6}$

Composés	H-4	H-3 *endo*	H-3 *exo*	H-5 *ax*	H-5 *éq*	H-7 *ax*	H-7 *éq*
1 *éq*	1,26	0,23	0,40				
2 *éq*	0,73	0,43	0,40	−0,09	0,52	−0,04	0,42
2 *ax*	0,72	0,11	0,17	—	—	—	—
4 *éq*	0,55	0,16	0,16	—	0,31	—	—
5 *ax*	—	0,34	0,31	0,07	0,65	0,04	0,65

TABLEAU 6. Constantes de couplages entre protons géminés en α de la liaison S → O (solvant C_6D_6)

	SO *équatorial*		SO *axial*	
Composés	$^2J_{H\text{-}5ax,\ H\text{-}5éq}$	$^2J_{H\text{-}7ax,\ H\text{-}7éq}$	$^2J_{H\text{-}5ax,\ H\text{-}5éq}$	$^2J_{H\text{-}7ax,\ H\text{-}7éq}$
1	13,0	13,0	16,0	16,0
2	12,6	12,4	14,8	14,2
5	12,6	12,4	15,6	14,0

entre le proton *axial* et le proton *équatorial* en α du groupe sulfinyle (règle du ΔνHα (9)). La littérature indique qu'en général ΔνHα est plus grand pour un sulfoxyde *équatorial* (par exemple pour les sulfoxydes du thiacyclohexane on trouve (10): Δν 0,87 et 0,48 ppm). Pour nos sulfoxydes les valeurs relevées (Tableau 4) sont en accord avec ce principe, ainsi qu'avec le fait que ΔνHα est sensible à la substitution où qu'elle soit dans la molécule.

2. *Effets de solvant*

Il est possible (9) d'appliquer aux sulfoxydes le modèle du complexe de collision proposé par Ledaal (11) (solvatation du site polaire par l'extrémité positive du dipôle) qui implique que les protons situés sur la face opposée à la liaison SO soient les plus blindés lorsqu'on compare les spectres réalisés dans la tétrachlorure de carbone à ceux obtenus dans le benzène (axe du benzène colinéaire avec l'axe du dipôle). Nos résultats (Tableau 5) sont en accord avec ces propositions. Les effets les plus marquants sont ceux observés pour les protons *équatoriaux* dans les cas de sulfoxydes *équatoriaux*. En ce qui concerne les sulfoxydes *axiaux* la complexité des signaux ne permet pas une attribution sûre des déplacements en cause.

3. *Constantes de couplage*

Les constantes de couplage entre protons géminés sont nettement différentes de celles observées (1) pour les dioxathiabicyclooctanes. En accord avec la littérature (voir la réf. 9 et réfs. citées), les constantes de couplage entre les protons géminés situés en α du groupe sulfinyle (Tableau 6) sont plus fortes lorsque la liaison SO est *axiale* ($|^2J|$14–15 Hz) que lorsque celle-ci est *équatoriale* ($|^2J|$ 11–13 Hz). Ce critère d'attribution de stéréochimie parait être le plus précieux de tous ceux utilisés jusqu'ici.

Les constantes entre protons géminés en C-3 (cyclo dioxolanne) sont du même ordre de grandeur (~7,2 Hz) que celles correspondant aux protons en même position dans les trioxabicyclooctanes (~7,0 Hz) (12), mais légèrement plus fortes que celles mettant en cause les mêmes protons dans les dioxathiabicyclooctanes (~6,5 Hz) (1). En revanche, aux erreurs de mesure près, on n'observe pas de différence lorsqu'on compare la constante de couplage des protons géminés en C-3 pour un sulfoxyde *axial* ou pour un sulfoxyde *équatorial*.

Ainsi que nous l'avons déjà signalé, un couplage ^4J (en W) met en cause le proton *exo* sur C-3 et le proton *axial* porté par C-5. Son intensité (mesurée directement sur le spectre analysable au premier ordre) atteint parfois une valeur anormalement importante (par exemple 2,8 Hz pour le composé **5**).

Stéréochimie de l'oxydation

Il est intéressant de revenir brièvement sur l'origine de l'importante *stéréo*sélectivité observée dans les réactions d'oxydation des dioxathiabicyclooctanes. En effet, l'utilisation comme agent oxydant de l'eau oxygénée ou de l'acide *méta*-chloroperbenzoïque conduit presqu'exclusivement aux sulfoxydes *équatoriaux;* même la mise en jeu de l'hypochlorite de *tert*-butyle, connu (8) pour donner très préférentiellement des sulfoxydes *axiaux*, ne mène dans notre cas qu'à 70% environ de composés présentant cette stéréochimie. Des facteurs stériques sont très vraisemblablement responsables en majeure partie de cette *stéréo*sélectivité. On peut en effet rapprocher nos résultats de ceux obtenus (Schéma 1) pour le thiacyclohexane (13) et pour les 6-méthoxy-2-hydroxyméthyl-1,4-oxathiannes (5) qui montrent l'influence déterminante de la présence d'un groupement *axial* en β de l'atome de soufre. On peut considérer que les dioxathiabicyclooctanes possèdent effectivement en β de l'atome de soufre un pont méthylènoxy stériquement proche de deux groupements en interaction *syn–axiale* avec une éventuelle liaison SO *axiale* (cf. Fig. 4).

Deutériation en α du groupe sulfinyle

Toutes nos attributions de la stéréochimie de nos sulfoxydes reposant jusqu'ici sur des critères de rmn, il était logique de tenter de les confirmer par une méthode chimique. Nous avons envisagé l'échange qui peut être réalisé entre un proton en α du groupement sulfinyle et un atome de deutérium. Katritsky et coll. (14) ont montré que le proton en conformation *trans* s'échange préférentiellement aux autres (l'échange pouvant être compétitif et mener aux deux composés en concurrence). Pour un sulfoxyde où la liaison S—O est *équatoriale*, c'est donc le proton *équatorial* en α qui doit s'échanger avec le deutérium. Nous avons étudié cette réaction en mettant en jeu le sulfoxyde **4** (Schéma 2), qui ne pose pas de problème de *régio*sélectivité. Après avoir été porté à 90°C pendant 72 h au sein de soude et dans l'oxyde de deutérium, le sulfoxyde **4** présente un spectre de rmn où le proton *équatorial* en 5 a disparu à plus de 95%; seul le signal du proton *axial* est observé

Can. J. Chem. Downloaded from www.nrcresearchpress.com by 210.87.254.6 on 09/06/12
For personal use only.

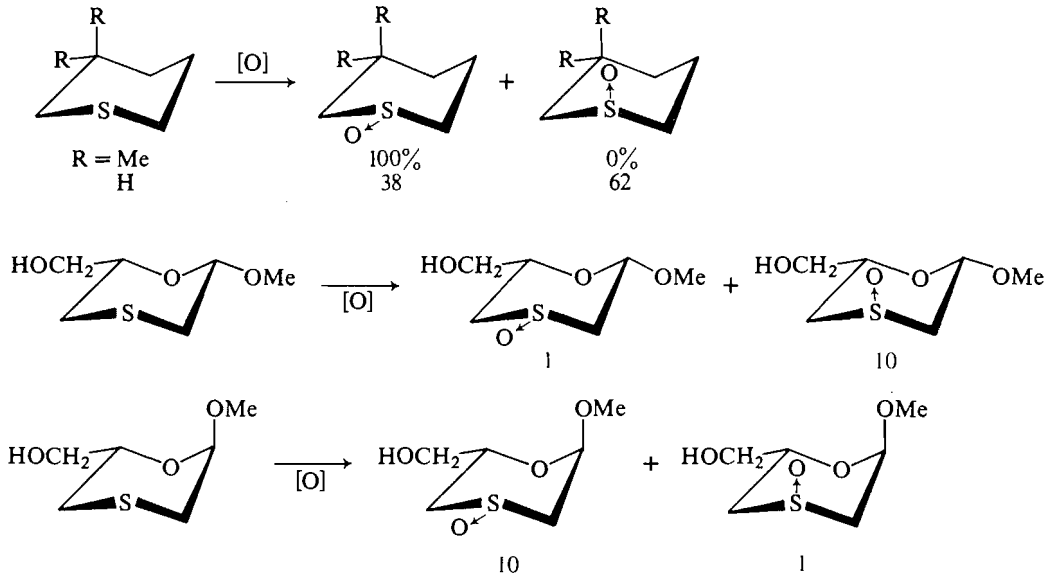

SCHÉMA 1

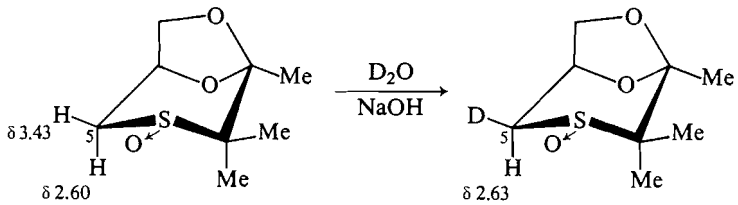

SCHÉMA 2

TABLEAU 7. Sulfones dérivés des 2,8-dioxa-6-thiabicyclo[3.2.1.]octanes

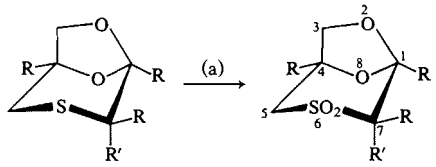

(a): *m*-$ClC_6H_4CO_3H$, CH_2Cl_2

Composés	R-1	R-4	R-7	R′-7
7	H	H	H	H
8	Me	H	H	H
9	Me	H	Me	H
10	Me	H	Me	Me
11	Me	Me	H	H
12	Ph	H	H	H

(à la précision près des mesures par spectrographie de rmn).

La position *axiale* du proton résiduel est déduite sans ambigüité de (*i*) la valeur du déplacement chimique du signal correspondant et (*ii*) de la présence d'un couplage ($^4J_{3,5}$ 1,5 Hz) en W avec le proton H-3 *exo*. Il semble que dans les conditions réactionnelles il n'y ait pratiquement pas de compétition entre les deux échanges stéréochimiques possibles. Ceci pourrait être dû à l'absence quasi-totale d'équilibre conformationnel dans la molécule de départ.

2,8-Dioxa-6,6′-dioxo-6-thiabicyclo[3.2.1]octanes

Les sulfones rassemblées dans le tableau 7 peuvent être préparées par oxydation des sulfoxydes correspondants par l'eau oxygénée en quantité stoechiométrique dans un solvant (généralement l'acétone); la réaction présente un rendement médiocre et n'est pas sans danger. Nous avons préféré opérer par oxydation directe du sulfure par un excès d'acide *méta*-chloroperbenzoïque.

L'intérêt de ces sulfones réside en premier lieu dans la comparaison de leurs caractéristiques spectrales (notamment en spectrographie de masse (15)) avec celles des sulfoxydes. Par ailleurs ces sulfones bicycliques sont intéressantes sur le plan synthétique notamment en raisons des possibilités de modifications structurales offertes par la réaction de Ramberg-Bäcklund.

On trouvera dans la partie expérimentale les critères d'identification des sulfones préparées. Indiquons simplement ici les points les plus importants concernant leurs spectres de rmn.

Si on compare les déplacements chimiques des sulfones à ceux des sulfoxydes correspondants, l'effet le plus remarquable est la disparition du déblindage que l'on pouvait observer sur les protons *axiaux* en α du groupe sulfinyle (particulièrement lorsque la liaison SO est *équatoriale*). Sauf pour le composé **12** les valeurs de $\Delta\delta$ ($\delta_{SO_2} - \delta_{SO}$) sont comprises entre 0,5 et 1,0 ppm. Cet effet peut être expliqué par la présence sur l'atome de soufre à la fois d'une liaison SO *équatoriale* et d'une liaison SO *axiale*.

En ce qui concerne les constantes de couplage entre les protons géminés en α du groupement sulfonyle, par exemple en position 5, leurs valeurs sont intermédiaires entre celles observées pour les protons portés par C-5 en α du groupe sulfinyle selon que la liaison SO est *axiale* ou *équatoriale*. (Exemple: $|^2J_{5,5}|$ 13,4 et 13,2 Hz pour les sulfones **8** et **11**; comparer avec les valeurs identiques dans le tableau 6 pour les sulfoxydes **2** et **4**.) Pour les autres protons de la molécule les valeurs des

Can. J. Chem. Downloaded from www.nrcresearchpress.com by 210.87.254.6 on 09/06/12
For personal use only.

TABLEAU 8. Déplacements chimiques en rmn ^{13}C des atomes de carbone des 2,8-dioxa-6-thiabicyclo[3.2.1]octanes et de leurs sulfoxydes et sulfones dérivés (solvant $CDCl_3$)

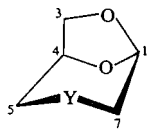

Atome de carbone	Y = S[a]				Y = SO						Y = SO_2			
					SO *équatorial*				SO *axial*					
	13	**14***éq*	**14***ax*	**15**	**2**	**3**	**4**	**5**	**2**	**5**	**8**	**9**	**10**	**11**
C-1	105,5	108,4	108,4	111,2	106,2	108,9	111,5	106,3	104,2	105,5	106,5	108,9	111,5	106,5
C-3	69,2	69,5	68,7	69,4	69,1	69,4	69,2	79,3	68,5	73,5	68,3	68,3	68,6	73,5
C-4	74,5	73,6	73,6	74,7	73,3	73,2	78,0	79,9	71,8	78,2	72,3	72,1	72,0	79,2
C-5	34,9	41,9	42,1	30,7	53,7	54,9	51,0	58,1	47,7	52,2	56,7	57,3	54,5	61,3
C-7	28,9	32,0	32,0	47,9	60,5	67,5	63,3	59,5	53,3	52,2	62,7	66,1	68,3	61,3
Me-1	24,8	23,5	23,5	26,9	24,6	22,0	20,9	25,0	25,5	25,8	24,9	22,4	21,1	25,2
Me-4	—	—	—	—	—	—	—	22,4	—	24,0	—	—	—	23,3
Me-7*éq*	—	16,5	—	19,8	—	11,8	14,5	—	—	—	—	6,7	15,9	—
Me-6*ax*	—	—	22,4	25,6	—	—	20,5	—	—	—	—	—	20,3	—

[a]Les déplacements chimiques des atomes de carbone des sulfures **13**, **14** (deux stéréoisomères Me-7*éq* et Me-7*ax*) et **15**, correspondant respectivement aux sulfoxydes **2**, **3** et **4** sont donnés ici à titre de comparaison.

constantes de couplage sont du même ordre de grandeur (cf. partie expérimentale) que celles relevées dans le cas des sulfoxydes.

Spectres de rmn ^{13}C des dioxathiabicyclooctanes, de leurs sulfoxydes et de leurs sulfones

Les données de la littérature sur la rmn ^{13}C des molécules hétérobicycliques étant restreintes[2] nous pensons utile de commenter brièvement les résultats marquants, volontairement limités à l'étude des seuls déplacements chimiques (Tableau 8).

Si on compare les spectres des dioxathiabicyclooctanes à ceux des trioxabicyclooctanes homologues[3] on constate un déplacement important à champ fort des atomes de carbone en α de l'atome de soufre, tandis que cet effet est beaucoup moins marqué pour les autres atomes du bicycle.

Pour les sulfures, l'atome présentant le plus fort déplacement est le carbone acétalique C-1 tri ou tétrasubstitué et voisin de deux atomes d'oxygène. Son déplacement chimique augmente quand le nombre des substituants porté par l'atome de carbone voisin C-7 augmente. A 30 ppm environ à champ plus fort on trouve l'atome C-4 trisubstitué et voisin d'un atome d'oxygène. L'atome C-3 résonne environ à 4 ppm plus bas. Enfin les deux atomes C-5 et C-7 porteurs de l'atome de soufre résonnent à champ beaucoup plus fort et l'écart qui est observé entre leurs signaux respectifs (6 à 9 ppm) est attribuable à la différence d'environnement due à l'atome C-3 et à l'atome O-2 du pont méthylènoxy.

Quand on passe des sulfures aux sulfoxydes on observe un déblindage important (de 14 à 25 ppm) sur les atomes C-5 et C-7 dû à l'effet de l'atome d'oxygène de la liaison SO qui diminue la densité électronique sur ces atomes de carbone, ainsi qu'au changement d'hybridation de l'atome de soufre. Il est particulièrement intéressant de déceler les éventuels effets de la configuration *axiale* ou *équatoriale* de la liaison SO. Les rares travaux réalisés dans ce domaine (par exemple pour des sulfites cycliques (19), pour le sulfoxyde 1,4-oxathianne (20) ou pour les *cis* et *trans* 4-*tert*-butyle-5-thiane oxyde (21)) indiquent un blindage des atomes de carbone en β de la liaison SO *axiale*. Pour notre part lorsqu'on passe d'un sulfoxyde *équatorial* à un sulfoxyde *axial* on constate pour les atomes de carbone en β (atomes de carbone en tête de pont) un effet de blindage faible, bien que net, d'environ 1 à 2 ppm. Un effet de même sens est observé en ce qui concerne les atomes de carbone en α du groupe sulfinyle (Δδ 6 à 7 ppm).

Enfin il est intéressant de noter que l'atome de carbone C-3 du pont méthylèneoxy subit un blindage de 1 à 6 ppm lorsque le sulfoxyde est *axial*.

Un autre déblindage se manifeste quand on compare les déplacements de C-5 et C-7 dans les sulfoxydes à ceux observés dans les sulfones (de 2 à 5 ppm quand on passe du sulfoxyde *équatorial* à la sulfone, et de l'ordre de 9 ppm quand on passe du sulfoxyde *axial* à la sulfone). Il parait concevable que la présence de deux atomes d'oxygène sur l'atome de soufre modifie plus encore l'environnement des carbones voisins C-5 et C-7 et peut être tenu pour responsable du déblindage observé. Il est alors logique de penser que l'introduction d'un atome d'oxygène *axial* sur un sulfoxyde *équatorial* (où l'effet de blindage est le plus important) provoque un déplacement plus faible que dans le cas contraire où un atome d'oxygène vient en position *équatoriale* sur un sulfoxyde *axial*.

Partie expérimentale

Les points de fusion ont été déterminés sur un appareil Büchi SMP 20 K et ne sont pas corrigés. Les chromatographies en couches minces (ccm) ont été réalisées sur des plaques 5 × 2 cm prêtes à l'emploi Merck (couche de 0,25 mm de gel de silice 60); la détection est obtenue par projection d'une solution aqueuse d'acide sulfurique (30%), et chauffage à 150°C. Les R_f ont été mesurés sur des plaques de 20 cm de longueur, et leurs valeurs sont suivies de l'indication,

[2]Pour des séries hétérocycliques apparentées on peut citer les travaux réalisés sur les 1,4-oxathiannes (16), les sulfites cycliques (17) ou sur les sulfoxydes de pénicillines (18).

[3]P. Calinaud et J. Gelas, résultats inédits.

Can. J. Chem. Downloaded from www.nrcresearchpress.com by 210.87.254.6 on 09/06/12
For personal use only.

TABLEAU 9. Constantes physiques et analyses des sulfoxydes dérivés des dioxathiabicyclooctanes

Composés	pf °C	R_f[a]	Analyses				
1 *éq*	102–103	0,48	Calc. pour $C_5H_8O_3S$:	C 40,54;	H 5,41;	O 32,43;	S 21,62
1 *ax*	121–122	0,38	tr.:[b]	40,12	5,60	32,87	21,30
2 *éq*	96–97	0,55	Calc. pour $C_6H_{10}O_3S$:	C 44,44;	H 6,17;	O 29,63;	S 19,75
2 *ax*	111–112	0,38	tr.:[b]	43,98	5,95	30,01	19,25
3	97–98	0,56	Calc. pour $C_7H_{12}O_3S$:	C 47,74;	H 6,82;	O 27,27;	S 18,18
			tr.:	47,08	6,80	27,52	17,92
4	148–149	0,56	Calc. pour $C_8H_{14}O_3S$:	C 50,53;	H 7,37;	O 25,26;	S 16,84
			tr.:	49,97;	7,14	25,72	16,74
5 *éq*	88–88,5	0,58	Calc. pour $C_7H_{12}O_3S$:	C 47,73;	H 6,82;	O 27,27;	S 18,18
5 *ax*	127–128	0,42	tr.:[b]	47,39	6,72	27,51	18,23
6	102–103	0,73	Calc. pour $C_{11}H_{12}O_3S$:	C 58,93;	H 5,36;	O 21,43;	S 14,29
			tr.:	58,98	5,40	21,35	14,18

[a]Eluant: acétate d'éthyle – méthanol 4:1.
[b]Analyse effectuée sur le mélange des stéréoisomères.

entre parenthèses, de l'éluant utilisé. Les séparations sur colonne ont été obtenues avec le gel de silice 60 (granulométrie 70–230 ASTM, Merck). Les solvants utilisés ont été séchés selon les méthodes classiques et distillés sur une colonne statique de 130 cm de longueur. Les analyses par chromatographie en phase vapeur (cpv) ont été réalisées sur un appareil Hewlett–Packard modèle 5750 équipé d'une colonne Carbowax 20 M (3 mm × 3 m) et d'un détecteur à catharomètre (gaz vecteur: 30 mL d'hydrogène par minute). Les séparations d'échantillons par cpv ont été effectuées sur un appareil Varian–Aerograph 705 N muni d'une colonne Carbowax 20 M (9 mm × 6 m), détecteur à ionisation de flamme (gaz vecteur: 120 mL d'azote par minute). Les analyses ont été réalisées au Service Central de Microanalyse du CNRS. Les spectres de rmn du proton ont été réalisés sur les appareils Varian A 60 et Varian T 60 (découplage de spin); les abréviations classiques sont utilisées dans la description de ces spectres: s: singulet; d: doublet; dd: doublet de doublet; t: triplet; q: quadruplet; m: multiplet. Les déplacements chimiques sont indiqués en ppm par rapport au tétraméthylsilane; l'intensité relative de chaque signal est indiquée entre parenthèses; les constantes de couplage mesurées sur les agrandissements sont exprimées en Hz. Les spectres de rmn ^{13}C ont été enregistrés sur un appareil Brucker HFX 90 ou sur un appareil JEOL FX 60 avec découplage des protons par bruit. Les spectres ir ont été enregistrés sur un appareil Beckman IR 8.

L'étude de la fragmentation de ces composés sous l'impact électronique et (pour certains d'entre eux) par ionisation chimique a été publiée par ailleurs (15).

*2,8-Dioxa-6-oxo-6-thiabicyclo[3.2.1]octanes (**1–6**)*

Synthèse

(*i*) *Oxydation des sulfures par l'eau oxygénée*

A une solution de 20 mmol de dioxathiabicyclooctane (préparée selon la réf. 1) dans 40 mL d'acétone refroidie par un bain d'eau glacée, on ajoute en deux ou trois portions 20 à 25 mmol d'eau oxygénée à 110 volumes (solution commerciale). On agite et laisse le mélange revenir à température ambiante. On suit par ccm (éluant: acétate d'éthyle – méthanol 4:1) l'avancement de l'oxydation. Quand celle-ci est pratiquement terminée, on vérifie l'absence de peroxyde dans la solution et chasse l'acétone. Le résidu qui cristallise contient plus de 90% de sulfoxyde pour moins de 10% de produit de départ et des traces de sulfone. Le sulfoxyde est purifié par chromatographie sur colonne de gel de silice (éluant: acétate d'éthyle – méthanol 4:1). Rdt environ 50%.

(*ii*) *Oxydation par l'acide* méta-*chloroperbenzoïque*

On ajoute goutte à goutte un équivalent d'acide *méta*-chloroperbenzoïque en solution dans le chlorure de méthylène (20 mmol dans 20 mL de solvant) à une solution de 20 mmol de sulfure dans 40 mL de chlorure de méthylène refroidie à 0°C et agitée. On abandonne pendant une nuit au réfrigérateur. On filtre le précipité d'acide benzoïque, lave le filtrat avec une solution saturée de $NaHCO_3$, sèche (Na_2SO_4) et évapore le chlorure de méthylène après avoir vérifié l'absence de peroxyde. Rdt environ 90%.

(*iii*) *Oxydation par l'hypochlorite de* tert-*butyle*

A une solution de 10 mmol de sulfure dans 50 mL de méthanol, refroidie à −70°C et agitée magnétiquement, on ajoute, assez rapidement, 10 mmol d'hypochlorite de *tert*-butyle fraîchement préparé (22). On laisse la température remonter à −40°C et ajoute Na_2CO_3 anhydre. Quand le mélange est revenu à température ambiante, on filtre et chasse le méthanol. La ccm du résidu cristallisé indique alors la présence des deux sulfoxydes qui sont séparés par chromatographie sur colonne de gel de silice (éluant acétate d'éthyle – méthanol 8:1).

Identification

Les constantes physiques sont rassemblées dans le tableau 9. Dans tous les cas où la paire de sulfoxydes *axial* et *équatorial* a été obtenue, le point de fusion du stéréoisomère *axial* est supérieur (de 20 à 40°) à celui du sulfoxyde *équatorial*. Ceci est en accord avec ce qui est généralement observé dans la littérature (9). Nous mesurons des R_f plus faibles pour les sulfoxydes *axiaux* que pour les sulfoxydes *équatoriaux*.

Tous les composés décrits montrent en spectrographie ir une bande entre 1026 et 1046 cm^{-1} (solutions à 0,2% dans le méthanol) caractéristique (23) du groupement sulfinyle.

Les déplacements chimiques des protons sont donnés dans le tableau 10.

Deutériation en α du groupement sulfinyle

Elle est réalisée selon la méthode décrite par Katritzky et coll. (14). A une solution de 0,8 g du sulfoxyde **4** dans 10 mL de D_2O est additionné 0,2 g de NaOH pure. On porte alors au bain-marie pendant 72 h. Après retour à la température ambiante on extrait trois fois la solution par 30 mL de chloroforme, sèche (Na_2SO_4) et distille le solvant. Le produit brut isolé (0,7 g, rdt·87%) et purifié par chromatographie sur colonne de gel de silice (éluant: acétate d'éthyle – méthanol 4:1) est identifié au deutéro-5 triméthyl-1,7,7 dioxa-2,8 oxo-6 thia-6 bicyclooctane **4***d* (pf 146–147°C).

*2,8-Dioxa-6,6'-dioxo-6-thiabicyclo[3.2.1]octanes (**7–12**)*

Ces sulfones ont été préparées selon le mode opératoire décrit pour les sulfoxydes et utilisant l'acide *méta*-chloroperbenzoïque (soit une

Can. J. Chem. Downloaded from www.nrcresearchpress.com by 210.87.254.6 on 09/06/12
For personal use only.

TABLEAU 10. Spectres de rmn ^1H des sulfoxydes dérivés des dioxathiabicyclooctanes (solvant[a] Me_2SO-d_6)

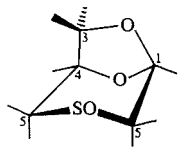

Composés	R-1	H-3 *endo*	H-3 *exo*	R-4	H-5 *éq*	H-5 *ax*	R-7 *éq*	R-7 *ax*
1 *éq*	m 6,05	dd 4,60	m 3,93	m 5,06	← m 3,73–3,33 →			
1 *ax*	m 5,92	dd 4,90	m 3,92	m 5,36	← m 3,63–2,67 →			
2 *éq*	s 1,46	dd 3,90	m 3,90	m 4,96	dd 3,70	m 2,63	d 3,65	d 2,66
2 *ax*	s 1,49	dd 4,77	m 3,92	m 4,97	← m 3,36–2,67 →			
3 *éq*	s 1,40	dd 3,88	m 3,86	m 4,93	dd 3,70	m 2,83	d 1,46	q 2,60
4 *éq*	s 1,43	← m 4,00–3,73 →		m 4,80	d 3,43	dd 2,60	s 1,20	s 1,36
5 *éq*	s 1,46	dd 3,91	m 3,41	s 1,46	m 3,68	m 2,46	m 3,78	m 2,46
5 *ax*	s 1,50	dd 4,82	m 3,53	s 1,47	← m 2,95 →			
6 *éq*	m 7,60	dd 4,75	m 4,13	m 5,36	← m 3,70 →			

Couplages géminés			Couplages vicinaux				Couplage à longue distance
$^2J_{3,3}$	$^2J_{5,5}$	$^2J_{7,7}$	$^3J_{3endo,4}$	$^3J_{3exo,4}$	$^3J_{5ax,4}$	$^3J_{5éq,4}$	$^4J_{3exo,5ax}$
7,0–7,4	cf. Tableau 6		1,0–1,4	6,2–6,4	3,6–3,8	2,8–3,0	1,5–2,8

[a]Les déplacements chimiques indiqués dans ce tableau correspondent tous à des spectres pris dans Me_2CO-d_6; en revanche un certain nombre de constantes de couplage (notamment celles indiquées dans le tableau 6) ont été mesurées sur des spectres pris dans C_6D_6, en raison d'une meilleure résolution des signaux correspondants permettant une analyse proche du premier ordre.

TABLEAU 11. Constantes physiques et analyses des sulfones dérivées des dioxathiabicyclooctanes

Composés	pf °C	R_f[a]	Analyses				
7	185	0,90	Calc. pour $C_5H_8O_4S$:	C 36,59;	H 4,88;	O 39,02;	S 19,51
			tr.:	36,28	4,81	38,78	19,23
8	119–120	0,82	Calc. pour $C_6H_{10}O_4S$:	C 40,45;	H 5,62;	O 35,96;	S 17,98
			tr.:	40,15	5,58	35,72	17,56
9	130–131	0,88	Calc. pour $C_7H_{12}O_4S$:	C 43,75;	H 6,25;	O 33,33;	S 16,67
			tr.:	43,50	6,21	33,22	16,59
10	183	0,71	Calc. pour $C_8H_{14}O_4S$:	C 46,60;	H 6,80;	O 31,06;	S 15,53
			tr.:	47,02	6,45	30,99	S 15,42
11	155–156	0,78	Calc. pour $C_7H_{12}O_4S$:	C 43,75;	H 6,25;	O 33,33;	S 16,67
			tr.:	43,83	6,33	32,65	16,85
12	149–150	0,86	Calc. pour $C_{11}H_{12}O_4S$:	C 55,00;	H 5,00;	O 26,67;	S 13,33
			tr.:	54,78	5,02	26,61	13,16

[a]Éluant: acétate d'éthyle – méthanol 4:1.

TABLEAU 12. Spectres de rmn ^1H des sulfones dérivées des dioxathiabicyclooctanes (solvant Me_2Co-d_6)

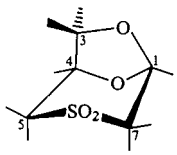

Composés	R-1	H-3 *endo*	H-3 *exo*	R-4	H-5*éq*	H-5*ax*	R-7	R-7
7	m 5,91	2d 4,60	m 3,92	m 4,97	← m 3,67–3,08 →			
8	s 1,55	d 4,43	m 3,93	m 5,06	m 3,38	m 3,38	m 3,38	m 3,38
9	s 1,46	d 4,36	m 3,92	m 5,00	m 3,45	m 3,45	d 1,32	m 3,30
10	s 1,46	d 4,36	m 3,91	m 4,93	m 3,53	m 3,23	s 1,33	s 1,43
11	s 1,53	m 4,46	m 3,53	s 1,50	m 3,45	m 3,25	← m 2,80–3,00 →	
12	m 7,67	2d 4,77	m 4,15	m 5,37	m 3,67	m 3,67	m 3,67	m 3,67

Couplages géminés			Couplages vicinaux				Couplage à longue distance
$^2J_{3,3}$	$^2J_{5,5}$	$^2J_{7,7}$	$^3J_{3endo,4}$	$^3J_{3exo,4}$	$^3J_{5ax,4}$	$^3J_{5éq,4}$	$^4J_{3exo,5ax}$
7,0–7,4	13,2–14,2	15,0	0,8–1,2	5,6–6,0	3,5–3,6	2,4	0,8–1,4

Can. J. Chem. Downloaded from www.nrcresearchpress.com by 210.87.254.6 on 09/06/12
For personal use only.

quantité stoechiométrique au départ des sulfoxydes, soit une quantité double au départ des sulfures). Rendements de 80 à 97% en produit purifié.

Les points de fusion des sulfones (Tableau 11) sont beaucoup plus élevés que ceux des sulfoxydes correspondants ce qui est sans doute l'indice d'une asymétrie moins prononcée pour la molécule. Les R_f des sulfones sont plus élevés que ceux des sulfoxydes correspondants et plus faibles que ceux des sulfures du départ. Ceci pourrait traduire une diminution de la polarisation (ou de la polarisabilité) de la liaison SO.

Toutes les sulfones décrites présentent en spectrographie ir une bande vers 1300–1301 cm^{-1} caractéristique (24) du groupement sulfonyle.

Les déplacements chimiques des protons sont donnés dans le tableau 12.

1. J. GELAS et M. TEPPAZ-MISSON. Can. J. Chem. **61**, 000 (1983).
2. P. CALINAUD et J. GELAS. Abstr. Papers 5th Int. Congr. Heterocycl. Chem. 314 (1975).
3. J. B. LAMBERT et S. I. FEATHERMAN. Chem. Rev. **75**, 611 (1975).
4. K. W. BUCK, A. B. FOSTER, A. R. PERRY et J. M. WEBBER. Chem. Commun. 433 (1965).
5. (*a*) K. W. BUCK, A. B. FOSTER, W. D. PARDOE, M. H. QUADIR et J. M. WEBBER. Chem. Commun. 759 (1966); (*b*) A. B. FOSTER, Q. H. QUASAN, D. R. HAWKINS et J. M. WEBBER. Chem. Commun. 1084 (1968).
6. J. J. RIGAU, C. C. BACON et C. R. JOHNSON. J. Org. Chem. **35**, 3655 (1970).
7. U. E. EISNER, M. Z. HAQ, J. FLIPPER et I. KARTE. J. Chem. Soc. Perkin Trans. **1**, 357 (1972).
8. C. R. JOHNSON et D. MCCANTS. J. Am. Chem. Soc. **87**, 5404 (1965).
9. R. LETT et A. MARQUET. Tetrahedron, **30**, 3379 (1974).
10. J. B. LAMBERT et R. G. KESKE. J. Org. Chem. **31**, 3429 (1966).
11. T. LEDAAL. Tetrahedron, **14**, 1683 (1968).
12. P. CALINAUD et J. GELAS. Can. J. Chem. **56**, 2292 (1978).
13. J. B. LAMBERT, D. S. BAILEY et C. E. MIXAN. J. Org. Chem. **37**, 377 (1972).
14. B. J. HUTCHINSON, K. K. ANDERSEN et A. R. KATRITZKY. J. Am. Chem. Soc. **91**, 3839 (1969).
15. P. CALINAUD, J. GELAS, D. HORTON et J. D. WANDER. Org. Mass Spectrom. **13**, 438 (1978).
16. W. A. SZAREK, D. M. YVAS, A. M. SEPULCHRE, S. D. GERO et G. LUKAS. Can. J. Chem. **52**, 2041 (1974).
17. G. W. BUCHANAN, J. B. STOTHERS et G. WOOD. Can. J. Chem. **51**, 3746 (1973).
18. R. A. ARCHER, R. D. G. COOPER, P. V. DEMARCO et L. F. JOHNSON. Chem. Commun. 1291 (1970).
19. N. K. WILSON et J. B. STOTHERS. Top. Stereochem. **8**, 1 (1974), et références citées.
20. D. M. FRIEZE et S. A. EVANS. J. Org. Chem. **40**, 2690 (1975).
21. G. W. BUCHANAN et T. DURST. Tetrahedron Lett. 1683 (1975).
22. M. J. MINTZ et C. WALLING. Org. Synth. **49**, 9 (1969).
23. (*a*) P. D. DE LAMARE, D. J. MILLEN, J. G. TILLET et D. WATSON. J. Chem. Soc. 1619 (1963); (*b*) T. CAIRNS, G. ELLINGTON et D. T. GIBSON. Spectrochim. Acta, **20**, 159 (1964).
24. K. C. SHREIBER. Anal. Chem. **21**, 1168 (1949).

Can. J. Chem. Downloaded from www.nrcresearchpress.com by 210.87.254.6 on 09/06/12
For personal use only.

Réaction de Pummerer en série hétérobicyclique. 5-Acétoxy- et 7-acétoxy-2,8-dioxa-6-thiabicyclo[3.2.1]octanes[1]

PIERRE CALINAUD ET JACQUES GELAS

Université de Clermont-Ferrand, École Nationale Supérieure de Chimie, Ensemble Scientifique des Cézeaux, BP 45, 63170 Aubière, France

Reçu le 21 décembre 1982

PIERRE CALINAUD et JACQUES GELAS. Can. J. Chem. **61**, 2103 (1983).

La réaction de transformation de sulfoxydes hétérobicycliques (alkyl-2,8-dioxa-6-oxo-6-thiabicyclo[3.2.1]octanes) en α-acétoxysulfures (5-acétoxy- ou 7-acétoxy-2,8-dioxa-6-thiabicyclo[3.2.1]octanes) sous l'action de l'anhydride acétique (réaction de Pummerer) est décrite. La *régio-* et la *stéréo*-sélectivités de la réaction sont discutées.

PIERRE CALINAUD and JACQUES GELAS. Can. J. Chem. **61**, 2103 (1983).

The transformation of heterobicyclic sulfoxides (alkyl-2,8-dioxa-6-oxo-6-thiabicyclo[3.2.1]octanes) to α-acetoxysulfides (5-acetoxy- or 7-acetoxy-2,8-dioxa-6-thiabicyclo[3.2.1]octanes) by acetic anhydride (Plummerer reaction) is described. The regio- and stereoselectivities of the reaction are discussed.

[Journal translation]

Can. J. Chem. Downloaded from www.nrcresearchpress.com by 210.87.254.42 on 09/06/12
For personal use only.

Il a été montré par Pummerer (2) que l'anhydride acétique réagit sur les sulfoxydes au sein d'un solvant pour donner un α-acétoxysulfure. Bien qu'étendu à de nombreux sulfoxydes (3) le champ d'application de cette transposition n'a été que peu élargi à des molécules d'intérêt biologique. On peut cependant citer les travaux (*i*) de McCormick et McElhinney (4) qui préparent des analogues de sucres à atome de soufre dans le cycle à partir de composés thiophanniques; (*ii*) de Szarek et coll. (5) accédant à des modèles de nucléosides dérivés de 1,4-oxathiannes; (*iii*) de Kuszmann et Sohar (6) étudiant le réarrangement des sulfoxydes de thioanhydrohexitols; (*iv*) enfin de Matsumoto *et al.* (7) dans la série des illudines.

Les sulfoxydes des 2,8-dioxa-6-thiabicyclo[3.2.1]octanes (Fig. 1) constituent une base d'étude particulièrement intéressante puisque les α-acétoxysulfures *B* qu'ils peuvent permettre d'atteindre sont des hémiacétals cycliques sulfurés homologues structuraux de 1,6-anhydropyranoses et que les données physiques (concernant notamment l'effet anomère) ou chimiques de tels modèles ne sont pas nombreuses.

L'action de l'anhydride acétique à reflux sur les 2,8-dioxa-6-oxo-6-thiabicyclo[3.2.1]octanes (préparés par ailleurs (1)) permet d'accéder aux acétoxy-2,8-dioxa-6-thiabicyclo[3.2.1]-octanes. Un double problème est posé par une telle réaction: il s'agit d'une part de celui de la *régio*sélectivité de la réaction (le groupement acétoxyle pouvant être introduit en position 5 ou 7) et d'autre part de celui de la stéréochimie du groupement acétoxyle soit *axial*, soit *équatorial*. La détermination des déplacements chimiques et des constantes de couplages protoniques en rmn permet de résoudre ces deux problèmes, grâce à la connaissance de ces paramètres dans les dioxathiabicyclo-octanes (8).

Lorsqu'on met en jeu successivement les trois sulfoxydes **1**, **2** et **3** (Schéma 1), on obtient dans chaque cas avec un bon rendement (environ 75% après purification) le produit majoritaire de la réaction. Les spectres de rmn de ces composés (Tableau 1) sont très proches les uns des autres et correspondent aux structures des α-acétoxysulfures **6**, **7** et **8** pour les raisons suivantes. D'une part, tous ces spectres montrent vers 2,0 ppm un unique singulet dû au groupe acétoxyle. D'autre part, un doublet également unique apparait vers 6,0 ppm et correspond à un proton au pied du groupe acétoxyle. La cohérence de ces caractéristiques dans cette série fait attribuer la position 5 au groupe acétoxyle; en effet: (*i*) dans le cas du sulfoxyde **3** aucune *régio*isomérie n'est possible et le doublet à champ faible ne peut être dû qu'à un proton sur C-5; (*ii*) le spectre du composé **7** montre la persistance du quadruplet vers 3,30 ppm dû au proton *axial* sur C-7; (*iii*) le spectre du composé **6** montre par rapport à celui du sulfure homologue **1** (8) le maintien du signal dû aux protons en C-7. Enfin, dans les trois cas la valeur de la constante de couplage pour ce doublet (3,2 Hz) est compatible avec une stéréochimie *axiale* (H-5) et *équatoriale* (H-4) des protons en cause. Ce point est confirmé par la présence d'une structure fine sur les signaux de H-5 *axial* et H-3 *exo* et qui est due au couplage ^4J 0,8 Hz.

Que le produit nettement majoritaire dans ces réactions soit le dérivé *équatorial* 5-acétoxy est confirmé par le spectre de rmn effectué sur le produit brut de la réaction. Par exemple dans le cas de la réaction menant au dérivé **8**, on observe (outre un doublet à 6,18 ppm, J 3,2 Hz) un doublet (proportion environ 20%) dont les caractéristiques (δ 5,48 ppm, J 2,2 Hz) sont celles du proton H-5 *équatorial*.

Une confirmation est également fournie par l'observation du

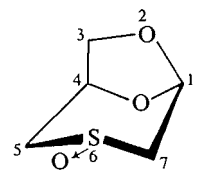

FIG. 1.

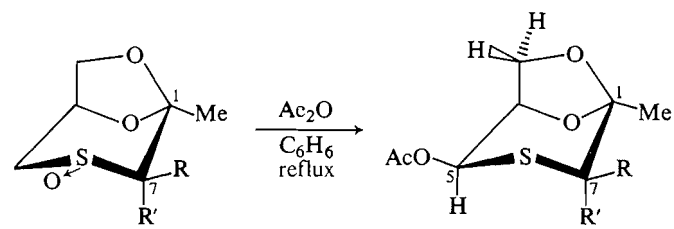

R = R′ = H	**1**	**6**
R = Me, R′ = H	**2**	**7**
R = R′ = Me	**3**	**8**[a]

SCHÉMA 1

[a]Un dérivé deutérié homologue (CD_3COO-5) a été préparé en utilisant l'anhydride acétique deutérié en vue de l'étude de sa fragmentation sous impact électronique (9).

[1]Recherches dans la série des acétals cycliques: Partie XXVII; Partie XVI: voir réf. 1.

TABLEAU 1. Spectres de rmn ^1H des α-acétoxysulfures[a]

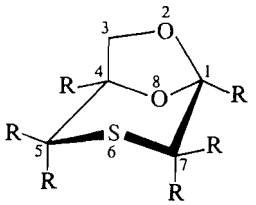

Composés	R-4	R-5 *éq*	R-5 *ax*	R-7 *éq*	R-7 *ax*	R-1	H-3 *exo*	H-3 *endo*
	m 4,53(1)	s 2,07 (3)	d 6,01 (1)	m 2,50 (1)	m 3,12 (1)	s 1,46 (3)	m 3,90 (1)	m 4,46 (1)
		d 5,27 (1)	s 2,13 (3)	m 3,56–2,76 (2)		s 1,36 (3)		
6	m 4,70 (1)	m 3,56–2,76 (2)		s 5,16 (1)	s 2,20 (3)	s 1,36 (3)	⟵ m 3,80–3,43 (2) ⟶	
		m 3,56–2,76 (2)		s 2,10 (3)	s 5,77 (1)	s 1,50 (3)		
7	m 4,58 (1)	s 2,05 (3)	d 6,03 (1)	d 1,10 (3)	q 3,28 (1)	s 1,40 (3)	m 3,90 (1)	m 4,41 (1)
8	m 4,52 (1)	s 2,05 (3)	d 6,05 (1)	s 1,18 (3)	s 1,55 (3)	s 1,35 (3)	d 3,86 (1)	dd 4,35 (1)
		s 5,17 (1)	s 2,10 (3)					
9	m 4,83 (1)	s 2,06 (3)	s 6,00 (1)	⟵ m 4,83–2,35 (5) ⟶				
		s 5,32 (1)	s 2,12 (3)					
		s 2,08 (3)	s 5,60 (1)					
10	s 1,30 (3)	s 2,10 (3)	s 5,23 (1)	d 2,27 (1)	d 3,00 (1)	s 1,35 (3)	d 3,53 (1)	d 4,33 (1)

Couplages géminés		Couplages vicinaux			Couplages à longue distance	
$^2J_{3,3}$	$^2J_{7,7}$	$^3J_{5ax,4éq}$	$^3J_{5éq,4e8q}$	$^3J_{7ax,Me\text{-}7éq}$	$^4J_{5ax,3exo}$	$^4J_{5éq,7éq}$
8,0	12,4	3,2	2,4	6,8	0,8–1,0	<0,5

[a]Solvant: tétrachlorure de carbone. Les déplacements chimiques sont indiqués en ppm par rapport au tétraméthylsilane. Multiplicité: s, singulet; d, doublet; q, quadruplet; m, multiplet. Les constantes de couplage indiquées en valeur absolue sont les espacements de signaux mesurés sur les agrandissements et sont exprimées en Hz.

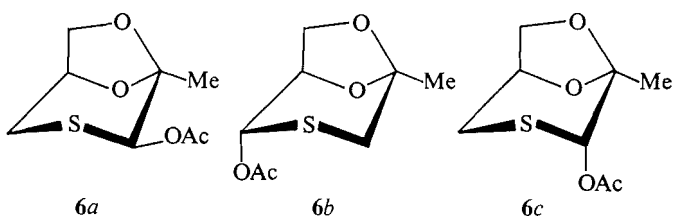

6a **6b** **6c**

FIG. 2.

déplacement chimique du quadruplet dû à H-7 *axial* pour le composé **7**: ce proton résonne à la même fréquence que celle observée dans le sulfure homologue non acétoxylé préparé par ailleurs (8) et on est contraint de rejeter la stéréochimie *axiale* de OAc-5 qui n'aurait pas manqué de déblinder le proton *syn–axial* H-7.

Lorsqu'on examine les spectres de rmn des fractions de purification contenant éventuellement des substances très minoritaires, il est parfois possible de faire des hypothèses sur la nature des sous-produits. Ainsi dans le cas de la mise en jeu du sulfoxyde **1** il nous a été possible d'isoler, avec un rendement n'atteignant pas 5%, un mélange dont le spectre de rmn montre, notamment, à champ faible, trois signaux d'inégale intensité, successivement: un singulet à 5,77 ppm attribuable à H-7 *axial* dans le dérivé **6***a* (Fig. 2); un doublet (δ 5,27 ppm, *J* 2,4 Hz) attribuable au proton H-5 *équatorial* dans le sulfure **6***b*; un singulet large (δ 5,16 ppm) attribuable au proton H-7 *équatorial* du composé **6***c*, l'élargissement observé étant très vraisemblablement dû à un couplage en W à travers l'atome de soufre avec le proton H-5 *équatorial* ($^4J < 0,5$ Hz).

Afin de confirmer la très forte *régio*sélectivité ainsi observée, nous avons examiné le cas du réarrangement des sulfoxydes **4** et **5** (Schéma 2). Pour ces deux cas l'analyse des produits de la réaction est plus délicate. Le sulfoxyde **4** conduit

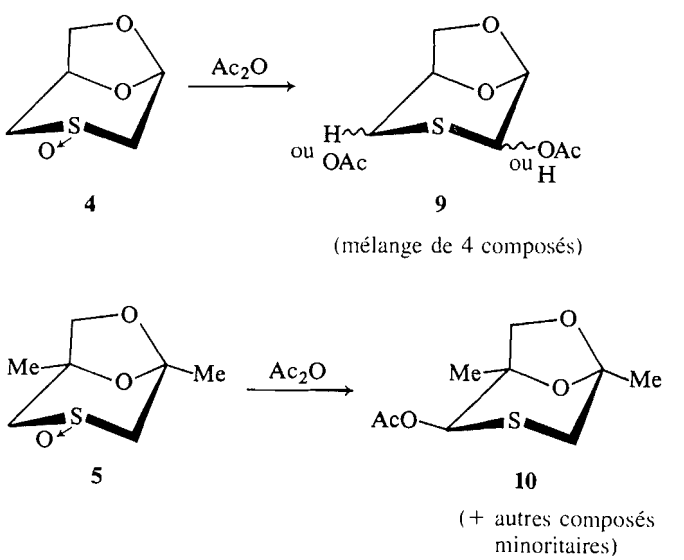

4 **9**

(mélange de 4 composés)

5 **10**

(+ autres composés minoritaires)

SCHÉMA 2

à un mélange complexe qui ne peut être résolu par chromatographie sur colonne (pratiquement une seule tache en ccm, mais quatre pics très mal résolus en cpv). Son spectre de rmn révèle à champ faible quatre signaux dont les déplacements et les multiplicités sont en faveur de l'existence des quatre *régio* et *stéréo*isomères possibles du sulfure **9**. En revanche, il est possible d'isoler le composé majoritaire du mélange obtenu à partir du sulfoxyde **5**.

Son spectre de rmn est compatible avec la structure **10** (couplage ^4J en W) observé pour les protons H-5 *axial* et H-3 *exo* d'une part et d'autre part spectre de masse (9) cohérent avec les fragmentations observées pour les composés **6**, **7** et **8** et

Can. J. Chem. Downloaded from www.nrcresearchpress.com by 210.87.254.42 on 09/06/12
For personal use only.

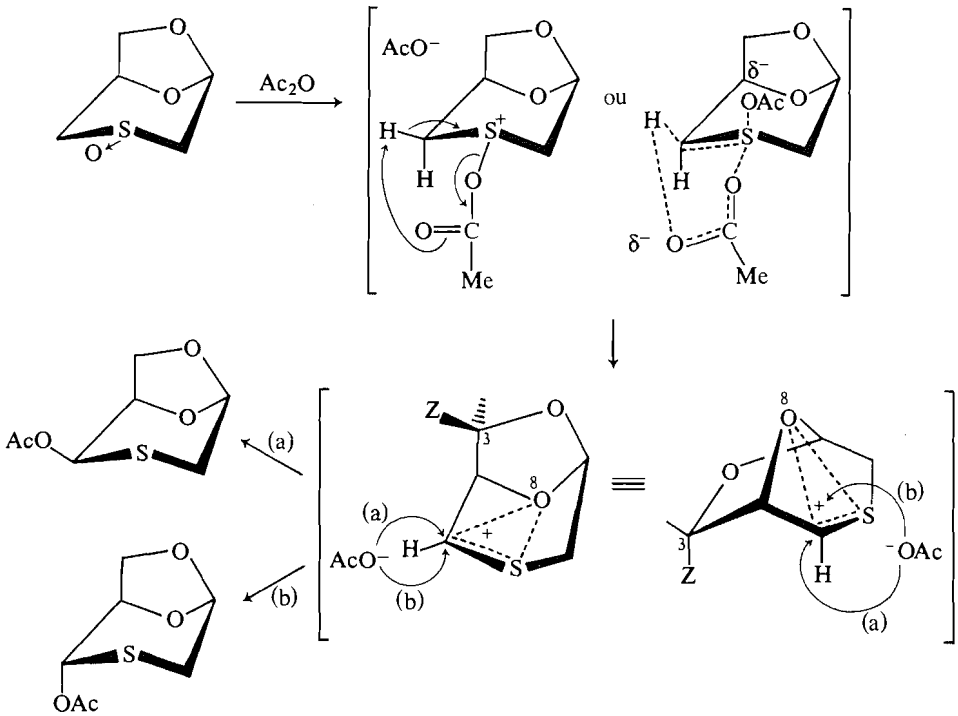

SCHÉMA 3

TABLEAU 2. Constantes physiques et analyses des α-acétoxysulfures

Composés	pf °C	R_f[a]	Analyses				
6	83–84	0,88	Calc. pour $C_8H_{12}O_4S$:	C 47,06;	H 5,88;	O 31,37;	S 15,69
			tr.:	46,96	5,87	31,56	15,51
7	71–72	0,90	Calc. pour $C_9H_{14}O_4S$:	49,54	6,42	29,36	14,68
			tr.:	49,38	6,42	28,81	14,43
8	74–75	0,91	Calc. pour $C_{10}H_{16}O_4S$:	51,72	6,90	27,59	13,79
			tr.:	51,58	6,88	27,05	14,10
9	Huile	0,84	Calc. pour $C_7H_{10}O_4S$:	44,21	5,26	33,69	16,84
			tr.:	43,97	5,15	33,58	16,70
10	102–103	0,88	Calc. pour $C_9H_{14}O_4S$:	49,54	6,42	29,36	14,68
			tr.:	49,77	6,40	29,34	14,90

[a]Éluant: acétate d'éthyle – méthanol 4:1.

démontrant[2] que le groupe OAc est fixé sur C-5.

En conclusion, nos observations peuvent se résumer de la manière suivante: une forte *régiosélectivité* est observée dans le réarrangement, le groupement acétoxyle se fixant de préférence sur C-5; une forte *stéréosélectivité* est constatée puisque le composé majoritaire (sinon unique) est celui où le groupe acétoxyle est en conformation *équatoriale*.

La connaissance du mécanisme du réarrangement de Pummerer a progressé considérablement, particulièrement ces dernières années (voir notamment la réf. 10, et références citées). Les auteurs s'accordent en général (11) pour proposer l'intervention d'un ion sulfocarbénium mésomère. Dans notre cas, il parait possible de proposer un mécanisme tel que celui indiqué sur le schéma 3. Selon ce mécanisme l'atome d'hydrogène en α de l'atome de soufre qui serait éliminé dans la première étape serait celui (*équatorial*) que nous avons par ailleurs reconnu comme étant spécifiquement échangeable par du deutérium (1). Un composé *équatorial* serait obtenu finalement par l'attaque selon (a), l'isomère *axial* étant obtenu par l'attaque (b) concurrente. On peut imaginer une participation de l'atome d'oxygène O-8 qui stabiliserait l'ion sulfocarbénium et modifierait la conformation du bicycle pour favoriser l'attaque selon (a) tant que le substituant Z (ici Z = H) en position 3 n'est pas suffisament encombrant pour l'empêcher.

Il est à remarquer enfin que l'effet anomère (qui est présent dans les trioxabicyclooctanes (12) et stabilise un groupement tel que OR en α de l'atome d'oxygène en conformation *axiale*) entre vraisemblablement en jeu dans nos modèles. Le caractère "cinétique" des produits obtenus semble donc acquis, mais il demande cependant à être confirmé par l'équilibration de ceux-ci. Malheureusement, nous n'avons pu jusqu'ici dans les conditions utilisées (acide paratoluènesulfonique ou éthérate de trifluorure de bore ou chlorure de zinc anhydre) réaliser cette anomérisation sans décomposition importante.

[2]Dans ce cas, il ne serait pas prudent de tirer des conclusions basées sur des spectres de rmn de mélange; en effet, en raison de la présence de deux groupements méthyle en tête de pont les protons au pied des groupes OAc se présentent tous sous forme de singulet plus ou moins large, et seule la spectrométrie de masse (9) permet une attribution définitive de structure.

Can. J. Chem. Downloaded from www.nrcresearchpress.com by 210.87.254.42 on 09/06/12
For personal use only.

Partie expérimentale

Pour les méthodes et indications générales, ainsi que pour la synthèse des sulfoxydes (**1–5**) voir la réf. 1.

*Synthèse des α-acétoxysulfures (**6–10**)*

Une solution du sulfoxyde (1 g) dans l'anhydride acétique (1 g) et 30 mL de benzène sec sont chauffés à reflux avec une trace d'acide paratoluènesulfonique pendant 3 à 12 h (on suit la disparition du sulfoxyde par ccm). On laisse refroidir la solution, neutralise ($NaHCO_3$) et distille le benzène. Les α-acétoxysulfures sont ensuite purifiés par chromatographie sur gel de silice (éluant: acétate d'éthyle – méthanol 5:1).

Identification

Les constantes physiques des acétoxydioxathiabicyclooctanes sont indiquées dans le Tableau 2. Tous les composés décrits montrent en spectrographie ir, par rapport aux sulfures de départ, l'apparition d'une bande située vers 1735–1745 cm^{-1} (solutions dans CCl_4) caractéristique du groupement OAc. Les spectres de rmn ont été décrits dans la partie théorique. Les spectres de masse ont été discutés par ailleurs (9).

1. P. CALINAUD et J. GELAS. Can. J. Chem. **61**, 2095 (1983).
2. R. PUMMERER. Chem. Ber. **42**, 1401 (1910).
3. (*a*) G. A. RUSSEL et G. J. MIKOL. *Dans* Mechanisms of molecular migrations. Vol. 1. *Edité par* B. S. Thyagarajan. Interscience, New York. 1968. p. 157; (*b*) W. E. PARHAM et L. D. EDWARDS. J. Org. Chem. **33**, 4150 (1968); (*c*) T. DURST. Adv. Org. Chem. **6**, 285 (1969).
4. J. E. MCCORMICK et R. S. MCELHINNEY. Chem. Commun. 171 (1969); J. E. MCCORMICK et R. S. MCELHINNEY. J. Chem. Soc. Perkin Trans. **1**, 1335 (1972); 2795 (1972).
5. (*a*) D. M. VYAS et W. A. SZAREK. Carbohydr. Res. **30**, 225 (1973); (*b*) W. A. SZAREK, D. M. VYAS, S. D. GERO et G. LUKACS. Can. J. Chem. **52**, 2041 (1974); (*c*) W. A. SZAREK et D. M. VYAS. J. Heterocycl. Chem. **12**, 123 (1975).
6. J. KUSZMANN et P. SOHAR. Acta Chim. Acad. Sci. Hung. **88**, 167 (1976).
7. T. MATSUMOTO, H. SHIRAHAMA, F. SAKAN et K. TAGIKAWA. Bull. Chem. Soc. Jpn. **50**, 325 (1977).
8. J. GELAS et M. TEPPAZ-MISSON. Can. J. Chem. **61**, 000 (1983).
9. P. CALINAUD, J. GELAS, D. HORTON et J. D. WANDER. Org. Mass Spectrom. **12**, 438 (1978).
10. (*a*) S. WOLFE et P. M. KAZMAIER. Can. J. Chem. **57**, 2388 (1979); (*b*) S. WOLFE et P. M. KAZMAIER. Can. J. Chem. **57**, 2397 (1979); (*c*) S. WOLFE, P. M. KAZMAIER et H. AUKSI. Can. J. Chem. **57**, 2404 (1979).
11. (*a*) C. R. JOHNSON et W. G. PHILIPS. J. Am. Chem. Soc. **91**, 682 (1969); (*b*) G. E. WILSON et C. J. STRONG. J. Org. Chem. **37**, 2376 (1972); (*c*) K. OMURA, A. K. SHARMA et D. SCWERN. J. Org. Chem. **41**, 957 (1976).
12. J. GELAS. Bull. Soc. Chim. Fr. 4045 (1970).

Can. J. Chem. Downloaded from www.nrcresearchpress.com by 210.87.254.42 on 09/06/12
For personal use only.

Dielectric relaxation processes of some dialkyl disulfides

H. A. KHWAJA AND S. WALKER

Department of Chemistry, Lakehead University, Thunder Bay, Ont., Canada P7B 5E1

Received January 4, 1983

H. A. KHWAJA and S. WALKER. Can. J. Chem. **61**, 2107 (1983).

Dielectric relaxation studies have been performed for dimethyl, diethyl, di-isopropyl, di-n-butyl, di-*tert*-butyl, and di-n-octyl disulfides in a polystyrene matrix. For the last five compounds the absorption appears in two temperature regions. The relaxation data for the higher temperature regions are consistent with intramolecular rotation around the S—S bond with accompanying flexibility in the alkyl chains. The enthalpy barrier to this relaxation process is ~29 kJ mol^{-1} and is the *trans* (lower) barrier. This value is typical for all six dialkyl disulfides. The most likely interpretation of the low temperature process is that there is segmental relaxation of the alkyl chains which also involves movement of the main dipoles (S—S and S—C).

H. A. KHWAJA et S. WALKER. Can. J. Chem. **61**, 2107 (1983).

On a effectué des études de relaxation diélectrique sur les disulfures de méthyle, d'éthyle, d'isopropyle, de n-butyle, de *tert*-butyle et de n-octyle dans un support de polystyrène. Pour les 5 derniers composés l'absorption se manifeste dans deux zones de température. Les données de relaxation pour la région de haute température sont en accord avec une rotation intramoléculaire autour de la liaison S—S avec une flexibilité dans la chaine alkylée. La barrière d'enthalpie de ce processus de relaxation est de 29 kJ mol^{-1} environ et c'est la barrière *trans* (la plus basse). Cette valeur est typique pour tous les six disulfures d'alkyle. L'interprétation la plus courante de processus à basse température préconise une relaxation segmentaire des chaines d'alkyles qui implique également le mouvement des dipoles principaux (S—S et S—C).

[Traduit par le journal]

Can. J. Chem. Downloaded from www.nrcresearchpress.com by 210.87.254.6 on 09/06/12
For personal use only.

Introduction

The existence of a barrier to rotation around the S—S link of a disulfide was established at least two decades ago, but experimentally determined barrier heights span quite a range. The rotation was frequently treated on a two-fold energy barrier model although in many measured values the *cis* and *trans* barriers were not separately identified. Two of the earlier studies on infrared spectra of dialkyl disulfides were those of Thompson and Trotter (1) and of Sheppard (2). At about the same time Scott and co-workers (3) reported the vibrational assignments of dimethyl disulfide (3*a*), diethyl disulfide (3*b*), and dimethyl di-n-propyl disulfide (3*c*), together with the collection of early data of infrared and Raman frequencies for thermodynamic studies. Detailed infrared and Raman spectra of di-*tert*-butyl disulfide were measured later by Scott and co-workers (3*d*). These investigations showed the presence of some rotational freedom about the S—S link. Through the use of calculated and observed entropy and heat capacity, an effective barrier height of 28.4 kJ mol^{-1} (3*c*) for the internal rotation around the S—S bond of dimethyl disulfide was deduced. El-Sabban and Scott (3*e*), using infrared data, reported a similar barrier height of 30.5 kJ mol^{-1}. From the Raman torsional frequencies for the S—S bond, barrier heights for dimethyl disulfide of 39.7 kJ mol^{-1} and 55.2 kJ mol^{-1} (3*b*) were obtained. Nuclear magnetic resonance data (4) yielded a somewhat larger barrier, 51.4 kJ mol^{-1} (*cis* barrier). By means of the millimeter-wave rotational spectrum of H_2S_2, Gordy and coworkers (5) concluded that the barrier to internal rotation is considerably higher than for the analogous H_2O_2 molecule (*cis* barrier, 29.3 kJ mol^{-1}; *trans* barrier, 4.6 kJ mol^{-1}) (6).

Molecular orbital studies on the H_2S_2 molecule have yielded barrier heights in the range 11.3–45.6 kJ mol^{-1} (*cis*) and 3.3–25.1 kJ mol^{-1} (*trans*). Boyd (7), using the EH method, has calculated a somewhat lower barrier for H_2S_2 of 6.3 kJ mol^{-1} (*cis*) and a *trans* barrier of 3.8 kJ mol^{-1}. For dimethyl disulfide, the PC1LO method (8) provided an equilibrium CS—SC dihedral angle of 100°, a *cis* barrier of 12.1 kJ mol^{-1}, and a *trans* barrier of 5.4 kJ mol^{-1}. Unlike the PC1LO method (8), the EH calculations produced a dihedral angle of about 90°, staggered methyl groups, and a barrier for rotation about the S—S bond of 29.3 kJ mol^{-1} (*cis*) and 9.2 kJ mol^{-1} (*trans*). More recently, Allinger *et al.* (9) have examined a two-fold barrier for dimethyl disulfide with a *cis* barrier height of 44.4 kJ mol^{-1} and a *trans* barrier height of 29.3 kJ mol^{-1}. Using the ZDO-SCF method, Perahia and Pullman (10), however, have estimated a surprisingly high *cis* barrier (~192 kJ mol^{-1}) and a *trans* barrier (60.7 kJ mol^{-1}).

Barrier heights to rotation about the C—S link in some dialkyl disulfides are reported in the literature. From an entropy approach (3*a*), a barrier height of 4.8 kJ mol^{-1} was determined for methyl group rotation in dimethyl disulfide. The EH calculation (7) indicated that, when the CSSC dihedral angle is large enough to avoid steric hindrance between the methyl groups, the barrier to rotation around C—S bonds in $(CH_3)_2S_2$ is 5.0 kJ mol^{-1}, which is in agreement with the experimental (11) barrier of 6.7 kJ mol^{-1}.

No dielectric study of the intramolecular energy barriers in dialkyl sulfides exists, and this approach offers a means of determining this and of studying the flexibility within these systems.

Experimental

The dialkyl disulfides treated here have the general formula R—SS—R (where R is methyl, ethyl, isopropyl, n-butyl, *tert*-butyl, and n-octyl). All of them were commercial samples (K & K and Aldrich Chemical Company) and their physical properties were in accord with the literature values. Each solute molecule was examined in a polystyrene matrix. The concentrations of solute in the polymer disks were sufficiently low (~5% by weight) to eliminate concentration effects (12). Atactic polystyrene was used which had a molecular weight ($\bar{M}_w$) value of 230 000. The preparation of the polystyrene matrices was the same as described by Davies and Swain (13).

Dielectric constants and the loss factor of solutes in the polymer matrix were obtained in the frequency range 50 to 10^5 Hz using a General Radio 1615A capacitance bridge incorporated with a suitable measuring cell from liquid nitrogen temperature to approximately 350 K. A detailed description of the apparatus, measurement techniques, and accuracy of the measurements is reported elsewhere (14, 15). In one case additional measurements were made on a Hewlett–Packard Q-meter type HP 4342A in the range 2.2×10^4 to 2.7×10^7 Hz.

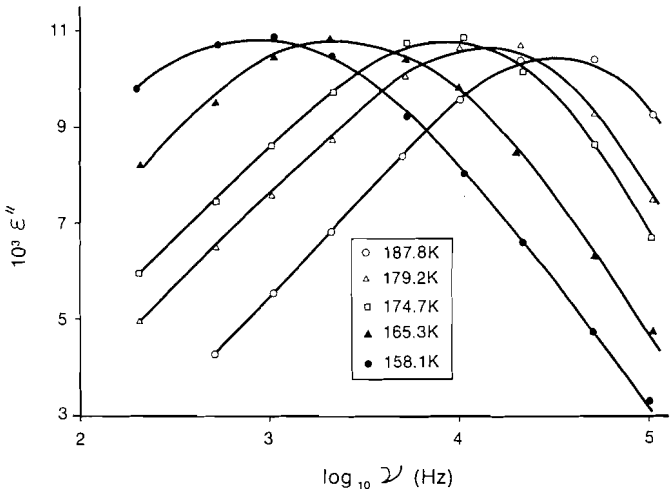

FIG. 1. Plot of loss factor against $\log_{10}$(frequency) at five temperatures for dimethyl disulfide in a polystyrene matrix.

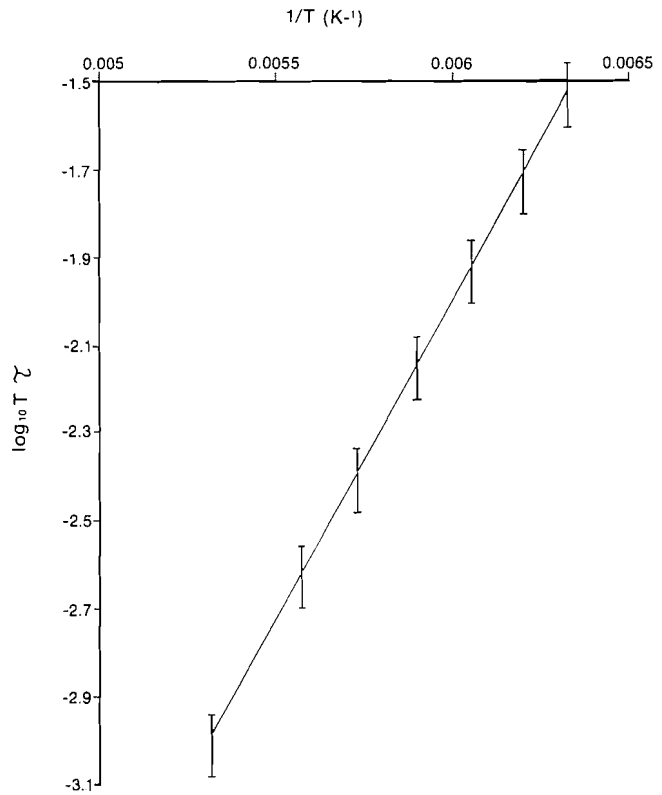

FIG. 2. Eyring plot for dimethyl disulfide in a polystyrene matrix.

Results

The loss due to the solute itself (ϵ''_{solute}) is calculated by subtracting the loss value of the pure polystyrene itself at that frequency and the same temperature. Thus, the loss due to the solute itself is given by

$$[1] \quad \epsilon''_{solute} = \epsilon''_{measured} - \epsilon''_{polystyrene} = \epsilon''$$

In Fig. 1 the ϵ'' values are plotted against $\log_{10}$(frequency) for dimethyl disulfide at five temperatures. Analyses of such curves through the use of the Fuoss–Kirkwood equation (16) (eq. [2]) yielded the maximum loss factor, ϵ''_{max}, mean relaxation time, $\tau\left(\frac{1}{2\pi\nu_{max}}\right)$, and the distribution parameter, β.

$$[2] \quad \cosh^{-1}(\epsilon''_{max}/\epsilon'') = 2.303\ \beta \log (\nu_{max}/\nu)$$

The resultant data for the molecules examined at a variety of temperatures are summarized in Table 1.

The energy barriers opposing the dipole reorientation were evaluated by using the Eyring rate expression:

$$[3] \quad \ln (T\tau) = \frac{\Delta H_E}{RT} - \frac{\Delta S_E}{R} + \ln (h/k)$$

where the terms have their usual significance. The enthalpies of activation and the entropies of activation were obtained from the slope and intercept, respectively, of the plot of $\ln (T\tau)$ against $1/T$, and with the help of a computer program. The program also calculated the relaxation time and the free energies of activation at different temperatures where:

$$[4] \quad \Delta G_E = \Delta H_E - T\Delta S_E$$

The Eyring analysis results are recorded in Table 2.

Standard statistical techniques were employed in the fitting and analyses of the data with the various computer programs, and the results such as the activation enthalpies and entropies were obtained with different confidence interval widths (17). For the present purpose, however, the 95% confidence interval was chosen as a good representation of experimental error: the error in ΔH_E was at worst $\pm 10\%$ or ± 3 kJ mol^{-1}, whichever is the greater, and the error of ΔS_E may be as high as $\pm 50\%$ of the nominal value in some cases, since the latter is often a small part of the intercept of the Eyring plot (1, 15). The errors could be reduced by extending the temperature and/or the frequency range.

Discussion

In symmetrical dialkyl disulfides, the components of the dipole moment of the two substituent groups along the long axis of the molecule (S—S bond) cancel, thus leaving zero permanent molecular dipole moment component along that axis. However, if there is no freedom of rotation about the S—S bond, the perpendicular components of the moment lead to a permanent dipole moment (μ). This is a similar situation to that of 1,4-diacetyl benzene (18) and terephthaldehyde (19). The possible relaxation processes relating to the perpendicular components of the μ are (*i*) molecular rotation, (*ii*) motion involving rotation about the S—S bond, or (*iii*) segmental motion involving rotation about flexible bonds which results in the movement of the S—S group.

All the dialkyl disulfides examined here except dimethyl disulfide exhibited two distinct families of absorption peaks, one in the 80–150 K region and the other in the 160–220 K region.

For dimethyl disulfide, a high temperature absorption in the range 158–188 K was observed with $\Delta H_E = 28$ kJ mol^{-1} and $\Delta S_E = 10$ J K^{-1} mol^{-1}. With rising temperature, the magnitude of ϵ''_{max} decreases for these dialkyl disulfides, which is in line with the observation of Davies and Swain (13) who recorded similar behaviour for an intramolecular process in cyclohexyl chloride and cyclohexyl bromide in polystyrene matrices. Also, the appreciably large Fuoss–Kirkwood distribution parameter, $\beta \sim 0.4$, is greater than that normally found for a molecular process in this temperature region. Such a large β suggests an intramolecular process.

The next member of the dialkyl disulfide series, diethyl disulfide, yields an activation enthalpy of 26 kJ mol^{-1} and absorbs around 180 K, which is in similar ranges of tem-

Can. J. Chem. Downloaded from www.nrcresearchpress.com by 210.87.254.6 on 09/06/12
For personal use only.

Can. J. Chem. Downloaded from www.nrcresearchpress.com by 210.87.254.6 on 09/06/12
For personal use only.

TABLE 1. Relaxation times, distribution parameters, and maximum loss factors for some dialkyl disulfides in polystyrene matrices at various temperatures (solute concentrations are in parentheses)

T(K)	$10^6\tau$(s)	β	$10^3\epsilon''_{max}$
Dimethyl disulfide (0.95 *M*)			
158.1	188	0.37	11.02
161.3	118	0.37	11.09
165.3	71.7	0.36	10.99
169.4	41.4	0.37	10.97
174.7	22.8	0.36	10.95
179.2	13.6	0.36	10.86
187.8	5.2	0.37	10.57
Diethyl disulfide (0.72 *M*)			
(Higher temperature absorption)			
161.3	246	0.40	10.48
165.8	140	0.40	10.40
170.3	83.5	0.40	10.35
175.6	46.5	0.40	10.17
186.2	16.3	0.41	9.89
193.6	7.9	0.41	9.59
199.9	4.7	0.45	9.47
(Lower temperature absorption)			
80.9	26.5	0.24	8.18
83.6	14.9	0.24	8.49
84.2	14.0	0.23	8.62
86.8	7.8	0.25	8.98
89.6	4.4	0.25	9.33
90.8	3.8	0.26	9.45
92.1	3.3	0.27	9.69
Di-isopropyl disulfide (0.56 *M*)			
(Higher temperature absorption)			
176.0	227	0.32	10.69
180.5	127	0.35	10.57
185.1	69.3	0.34	10.36
190.5	42.0	0.37	10.08
195.0	23.4	0.36	9.84
199.6	16.2	0.39	9.67
204.7	10.0	0.39	9.42
209.5	6.6	0.40	9.17
(Lower temperature absorption)			
100.6	211	0.24	9.83
104.3	107	0.24	10.41
106.4	72.9	0.24	10.76
110.9	38.8	0.24	11.46
113.6	18.4	0.25	11.90
115.9	12.1	0.25	12.33
121.1	4.9	0.26	13.28
125.1	3.0	0.27	14.04

TABLE 1 *(Concluded)*

T(K)	$10^6\tau$(s)	β	$10^3\epsilon''_{max}$
Di-n-butyl disulfide (0.48 *M*)			
(Higher temperature absorption)			
173.8	218	0.30	11.72
178.0	123	0.30	11.89
182.7	63	0.29	12.07
187.0	39	0.31	12.14
191.5	23	0.33	12.30
197.0	14	0.35	12.39
201.6	8.5	0.37	12.45
206.6	5.7	0.38	12.36
(Lower temperature absorption)			
101.8	328	0.29	7.50
105.3	176	0.29	7.96
109.3	84	0.29	8.42
113.3	41	0.28	8.92
115.3	27	0.28	9.18
120.6	11	0.29	9.89
125.4	5.2	0.29	10.51
128.5	3.5	0.30	10.99
Di-*tert*-butyl disulfide (0.48 *M*)			
(Higher temperature absorption)			
170.6	281	0.34	8.16
175.0	161	0.35	8.14
180.4	82.7	0.36	8.07
184.9	50.3	0.37	8.00
190.3	28.5	0.39	7.89
195.7	16.5	0.40	7.82
199.8	11.3	0.41	7.76
205.9	6.5	0.43	7.60
(Lower temperature absorption)			
85.8	46.3	0.19	4.59
90.6	19.0	0.19	4.91
94.3	9.5	0.19	5.19
99.2	4.3	0.20	5.53
101.3	3.2	0.20	5.59
Di-n-octyl disulfide (0.30 *M*)			
(Higher temperature absorption)			
181.3	230	0.24	6.28
185.4	150	0.26	6.44
190.8	83	0.26	6.66
194.4	62	0.24	6.69
199.8	36	0.23	6.88
205.9	22	0.23	7.12
210.5	15	0.22	7.24
216.0	9.3	0.21	7.43
(Lower temperature absorption)			
130.4	204	0.34	7.17
135.6	86	0.33	7.53
140.3	39	0.34	8.03
144.8	19	0.34	8.41
149.8	9.2	0.36	8.92
155.0	4.4	0.36	9.35
157.9	3.4	0.39	9.69

perature and frequency to dimethyl disulfide. As the data in Table 1 clearly show, the distribution parameter, β, values are significantly large (0.4–0.45) while the maximum loss factor, ϵ''_{max}, decreases with increasing temperature. The free energy of activation (ΔG_E = 28 kJ mol^{-1}) and relaxation time ($\tau = 4.6 \times 10^{-6}$ s) at 200 K also compare reasonably well with the corresponding data for dimethyl disulfide (ΔG_{E200} = 26 kJ mol^{-1} and $\tau_{200} = 1.7 \times 10^{-6}$ s). Such close similarity in relaxation data for the two systems of different molecular size suggests a common intramolecular process. For dimethyl disulfide, rotation about the S—S bond is the only feasible detectable dielectric absorption process for an intramolecular motion. This absorption cannot be attributed to an impurity in the polystyrene itself as this is taken into account in eq. [1] in the $\epsilon''_{polystyrene}$ term which includes the loss due to any impurity. Further, the difference in loss factor between the intramolecular process and $\epsilon''_{polystyrene}$ is appreciable, since the ϵ''_{max} of the intramolecular process is $\sim 11 \times 10^{-3}$ whereas the highest loss exhibited by the $\epsilon''_{polystyrene}$ at any of the temperatures and frequencies is 0.7×10^{-3}. Thus, even if $\epsilon''_{polystyrene}$ were neglected in eq. [1], it would not alter appreciably the Eyring parameters derived from the loss data.

For the high temperature absorption, when the size of the alkyl group is increased, di-isopropyl, di-n-butyl, di-*tert*-butyl,

TABLE 2. Relaxation data and the Eyring activation parameters for some dialkyl disulfides in a polystyrene matrix

Solute	ΔH_E (kJ mol^{-1})	ΔS_E (J K^{-1} mol^{-1})	τ(s) 100 K	τ(s) 200 K	ΔG_E (kJ mol^{-1}) 100 K	ΔG_E (kJ mol^{-1}) 200 K	T(K)
Dimethyl disulfide	28	10		1.7×10^{-6}		26	158–188
Diethyl	26	−9		4.6×10^{-6}	27	28	161–200
disulfide	11	−8	2.9×10^{-7}	5.3×10^{-10}	12	13	81–92
Di-isopropyl	31	4		1.5×10^{-5}	30	30	176–210
disulfide	18	10	2.6×10^{-4}	3.1×10^{-9}	17	16	101–125
Di-n-butyl	32	13		1.0×10^{-5}	31	29	174–207
disulfide	18	5	5.3×10^{-4}	6.0×10^{-9}	17	17	102–129
Di-*tert*-butyl	30	1		1.1×10^{-5}	30	29	171–206
disulfide	12	−15	3.8×10^{-6}	1.6×10^{-9}	13	15	85–101
Di-n-octyl	28	−15		3.6×10^{-5}	30	31	181–216
disulfide	25	23	2.8×10^{-1}	4.7×10^{-8}	23	20	130–158

and di-n-octyl disulfides, activation enthalpies of 31, 32, 30, and 28 kJ mol^{-1}, respectively, are obtained. For the temperature range of absorption in a given frequency range, significantly high "β" values (~0.4) and the decreasing behaviour of ϵ''_{max} with the rise of temperature (exception being the di-n-octyl disulfide) for these systems in each instance show similarity with the high temperature process of dimethyl and diethyl disulfides. In addition, the activation enthalpy does not reveal any sign of appreciable increase with increasing size of the molecule (20) on passing from dimethyl to di-n-octyl disulfide. On the contrary, it shows little variation, within the limits of experimental accuracy, and immediately discounts the relaxation of the molecule as a whole in favour of intramolecular relaxation in each of these dialkyl disulfides. Thus, altogether, the compounds have a similar ΔH_E value for the higher temperature process; in fact, the variation is only between 28 to 32 kJ mol^{-1} and shows no dependence on size or shape. This is in harmony with an intramolecular process and is strongly supported by the relatively high β values.

It is perhaps surprising that in the series dimethyl disulfide, diethyl disulfide, di-n-butyl disulfide, and di-n-octyl disulfide the ΔH_E values are 28, 26, 32, and 28 kJ mol^{-1}, and there is no increasing trend in the energy barrier as the size of the alkyl group increases since the activation energy for the intramolecular process may be expected to increase as the substituent size increases. In fact, the experimental error being ±3 kJ mol^{-1}, all the barriers are about 29 kJ mol^{-1}. An analogous study was made by Mazid *et al.* (21) on phenyl-alkyl ketones (C_6H_5COR, where R was varied between CH_3 to $C_{10}H_{21}$) in a polystyrene matrix. For eight such compounds the ΔH_E values ranged between 30 to 25 kHJ mol^{-1} with no apparent trend with increasing size of R. The main conclusion to be drawn from these Eyring activation parameters is that the length of the alkyl chain does not appreciably influence the energy barrier of the intramolecular process, which is essentially the same as that for acetyl group relaxation in acetophenone. It would seem likely that there is facile rotation about the $C_{aliphatic}$—$C_{aliphatic}$ bonds and that the effective volume swept out in the intramolecular motion is similar in each case.

Probably the results for the disulfide could be interpreted in precisely the same way where: (a) for dimethyl disulfide the rotation is about the S—S bond (and C—S bonds, but this would not be detected dielectrically for dimethyl disulfide); (b) for the other disulfides, relaxation about the S—S, C—S, and C—C bonds may occur. There is excellent agreement between our energy barrier value (ΔH_E = 28 kJ mol^{-1}) for intramolecular rotation in dimethyl disulfide and the 29.3 kJ mol^{-1} obtained for the *trans* barrier by Allinger *et al.* (9), one of the most recent studies on dimethyl disulfide. As Tay *et al.* (15) observed, for a two-fold energy barrier system the dielectric absorption technique yields a ΔH_E corresponding to the switch from the isomer with the higher energy to that of the lower. In the case of dimethyl disulfide, in terms of literature terminology this is described as the *trans* barrier. Allinger *et al.* (9) reviewed both the experimental and theoretical studies and concluded "that the *trans* barrier height of 29.3 kJ mol^{-1} is in good agreement" with those found from calorimetric data (3*d*) and from infrared data (3).

Dimethyl disulfide did not show a low temperature absorption although it was carefully measured from the lowest available temperature (77 to 300 K); this was also the case when the frequency range was extended to 2×10^7 Hz by measurement on a Hewlett–Packard Q-meter. The low temperature absorption of diethyl disulfide, di-isopropyl disulfide, di-n-butyl disulfide, and di-*tert*-butyl disulfide yielded enthalpies of activation of 11, 18, 18, and 12 kJ mol^{-1}, respectively. Examination of the data in Table 2 indicates similarity in behaviour amongst diethyl disulfide, di-isopropyl disulfide, di-n-butyl disulfide, and di-*tert*-butyl disulfide in the temperature range of absorption, the activation enthalpy and entropy, the relaxation of time, and free energy of activation at 100 K.

For the low temperature process there is probably an increase in ΔH_E with increasing size for the straight chain compounds. Thus, the ΔH_E values for diethyl, di-n-butyl, and di-n-octyl disulfides are 11, 18, and 25 kJ mol^{-1}. The relaxation times at 100 K follow the sequence 5.3×10^{-7}, 5.3×10^{-4}, and 2.8×10^{-1} s and also suggest that the size of the relaxing unit increases with increasing chain length. This is not the case, however, for the two non-straight chain compounds diisopropyl disulfide (ΔH_E = 18 kJ mol^{-1}, $\tau_{100\ K} = 2.6 \times 10^{-4}$ s), the values of which are correspondingly greater than for the slightly larger molecule di-*tert*-butyl disulfide (ΔH_E = 12 kJ mol^{-1}, $\tau_{100\ K} = 2.8 \times 10^{-6}$ s). The most likely interpretation of the low temperature process is that there occurs segmental relaxation of the alkyl chains which also involves movement of the main dipoles (S—S and S—C). For the straight chain compounds the longer chains involve contributions from larger reorienting units and in the limit could involve contributions from a molecular process. These concepts are in line with the findings of Khwaja and Walker (22) in a detailed study of

Can. J. Chem. Downloaded from www.nrcresearchpress.com by 210.87.254.6 on 09/06/12
For personal use only.

relaxation processes in alkyl-CHO compounds.

For all the five R—S—S—R compounds from dimethyl disulfide to di-*tert*-butyl disulfide, the temperature regions for relaxation of types (*ii*) and (*iii*) are well separated. However, in the case of di-n-octyl disulfide the two regions almost merge and the relaxation parameters will thus be subject to greater error.

The absence of the low temperature process for dimethyl disulfide is quite striking. This molecule is capable only of dielectric absorption involving molecular rotation and relaxation about the S—S bonds. A small molecule such as pyridine absorbs in the region of liquid nitrogen temperature (23). However, dimethyl disulfide is a significantly smaller molecule than this and would absorb at lower temperatures than liquid nitrogen (the lowest we have available) in our frequency range since the molecular relaxation time of the polar solute in a polystyrene matrix is highly dependent on size (20).

Conclusion

All the higher temperature dielectric relaxation data are consistent with the notion that in all dialkyl disulfides an intramolecular relaxation process occurs around the S—S bond with the enthalpy of activation barrier around 29 kJ mol^{-1}. The enthalpies of activation do not alter significantly when the size of the molecule is varied, and they all fall in the range 29 ± 3 kJ mol^{-1}. There is probably considerable flexibility about the C—C bonds in the alkyl groups.

Tay *et al.* (15) showed that the nmr, ultrasonic, and dielectric methods, which all employ transition state theory, yield similar energy barriers for intramolecular processes. However, the calorimetric, Raman, microwave, and infrared approaches yield barriers based upon the representation of the barrier (V) in terms of a Fourier series expansion and do not invoke the concept of entropy of activation. Only when the ΔS_E value is small, would agreement between ΔH_E and V values be sought. It is striking that for the intramolecular processes of dimethyl disulfide, where ΔS_E is quite small, there is excellent agreement between our ΔH_E, and the ones from theoretical calculations, and infrared and calorimetric methods (9). The main objectives of our work were to study flexibility in the dialkyl disulfides and to establish an intramolecular energy barrier from transition state theory for rotation about the S—S bond.

Acknowledgements

The authors wish to acknowledge the financial assistance of the National Research Council of Canada and to express their appreciation to Mr. B. K. Morgan for technical help.

1. W. H. THOMPSON and I. F. TROTTER. J. Chem. Soc. 481 (1946).
2. N. SHEPPARD. Trans. Faraday Soc. **46**, 429 (1950).
3. (*a*) D. W. SCOTT, H. L. FINKE, M. E. CROSSE, G. B. GUTHRIE, and H. M. HUFFMAN. J. Am. Chem. Soc. **72**, 2424 (1950); (*b*) D. W. SCOTT, H. L. FINKE, J. P. MCCULLOUGH, M. E. GROSS, R. E. PENNINGTON, and G. WADDINGTON. J. Am. Chem. Soc. **74**, 2478 (1952); (*c*) W. N. HUBBARD, D. R. DOUSLIN, J. P. MCCULLOUGH, D. W. SCOTT, S. S. TODD, I. A. HOSSENLOPP, A. GEORGE, and G. WADDINGTON. J. Am. Chem. Soc. **80**, 3547 (1958); (*d*) J. H. S. GREEN, D. J. HARRISON, W. KYNASTON, and D. W. SCOTT. Spectrochim. Acta, Part A, **25**, 1313 (1969); (*e*) M. Z. EL SABBAN and D. W. SCOTT. U. S. Bur. Mines, Bull. No. 654, 1970.
4. G. CLAESON, G. ANDROES, and M. CALVIN. J. Am. Chem. Soc. **83**, 4357 (1961).
5. G. WINNEWISSER, M. WINNEWISSER, and W. GORDY. J. Chem. Phys. **49**, 3465 (1968).
6. R. H. HUNT, R. A. LEACOCK, C. W. PETERS, and K. T. HECHT. J. Chem. Phys. **42**, 1931 (1965).
7. D. B. BOYD. J. Am. Chem. Soc. **94**, 8799 (1972).
8. S. D. THOMPSON, D. G. CARROLL, F. WATSON, M. O'DONNELL, and S. P. MCGLYNN. J. Chem. Phys. **45**, 1367 (1966).
9. N. L. ALLINGER, M. J. HICKEY, and J. KAO. J. Am. Chem. Soc. **98**, 2741 (1976).
10. D. PERAHIA and B. PULLMAN. Biochem. Biophys. Res. Commun. **43**, 65 (1971).
11. D. SUTTER, H. DREIZLER, and H. D. RUDOLPH. Z. Naturforsch. 1676 (1965).
12. T. I. BORISOVA and V. N. CHRIKOV. Russ. J. Phys. Chem. **47**, 949 (1973).
13. M. DAVIES and J. SWAIN. Trans. Faraday Soc. **67**, 1637 (1971).
14. S. P. TAY and S. WALKER. J. Chem. Phys. **63**, 1634 (1975).
15. S. P. TAY, S. WALKER, and E. WYN-JONES. Adv. Mol. Relaxation Interact. Processes, **13**, 47 (1978).
16. R. M. FUOSS and J. G. KIRKWOOD. J. Am. Chem. Soc. **63**, 385 (1941).
17. B. OSTLE. Statistics in research. 2nd ed. Iowa State University Press, Ames, IA. 1963.
18. C. K. MCLELLAN and S. WALKER. Can. J. Chem. **55**, 583 (1977).
19. A. LAKSHMI, S. WALKER, N. A. WEIR, and J. H. CALDERWOOD. Trans. Faraday Soc. **74**, 727 (1978).
20. H. A. KHWAJA and S. WALKER. Adv. Mol. Relaxation Interact. Processes, **19**, 1 (1981).
21. M. A. MAZID, S. WALKER, and N. A. WEIR. Adv. Mol. Relaxation Interact. Processes, **19**, 249 (1981).
22. H. A. KHWAJA and S. WALKER. Adv. Mol. Relaxation Interact. Processes, **22**, 27 (1982).
23. J. P. SHUKLA, S. WALKER, and J. WARREN. J. Chem. Soc. Faraday Trans. 2, **74**, 2045 (1978).

Can. J. Chem. Downloaded from www.nrcresearchpress.com by 210.87.254.6 on 09/06/12
For personal use only.

Structural analysis of 3-*C*-phosphonates, -phosphinates, and -phosphine oxides of branched-chain sugars[1,2]

JEAN-RICHARD NEESER,[3] JEAN M. J. TRONCHET,[4] AND ETIENNE J. CHAROLLAIS
Institut de Chimie Pharmaceutique et Pavillon des Isotopes de l'Université, 30 quai Ernest Ansermet, CH 1211, Genève 4, Switzerland

Received February 8, 1983

JEAN-RICHARD NEESER, JEAN M. J. TRONCHET, and ETIENNE J. CHAROLLAIS. Can. J. Chem. **61**, 2112 (1983).

A complete nmr study (^{1}H, ^{13}C, ^{31}P) of twelve 3-*C*-phosphonates, -phosphinates, and -phosphine oxide derivatives of 3-*C*-branched-chain pento- and hexo-furanoses is reported. For all compounds the configuration at C_3 is determined and, for oxaphospholanes **9** to **12**, the configuration at the asymmetric phosphorus atom. The $^3\boldsymbol{T}_2$ conformation of the furanose ring of acyclic derivatives **1** to **8** and the conformationally rigid *cis*-fused oxaphospholane-furanose bicyclic systems of **9** to **12** have been used to study the $^3J_{PCCH}$ vs. $\theta_{P,H}$ and $^3J_{PCCC}$ vs. $\theta_{P,C}$ relationships which are specific to this series of compounds. The use of the ν P=O ir stretching frequency, δ ^{31}P chemical shift, and $^1J_{P,C}$ coupling constant values in structural analysis of *C*-phosphorus-bearing sugars is also reported and discussed.

JEAN-RICHARD NEESER, JEAN M. J. TRONCHET et ETIENNE J. CHAROLLAIS. Can. J. Chem. **61**, 2112 (1983).

Nous décrivons l'étude par rmn (^{1}H, ^{13}C, ^{31}P) de douze dérivés ramifiés et phosphorés en C_3 (*C*-phosphonates, -phosphinates et -oxydes de phosphine) de pento- et d'hexo-furannoses. Pour tous les composés, la configuration en C_3 a été attribuée, de même que la configuration au niveau de l'atome de phosphore asymétrique pour les oxaphospholannes **9** à **12**. L'adoption de la conformation $^3\boldsymbol{T}_2$ par le cycle furannique des dérivés **1** à **8** d'une part, et la rigidité conformationnelle des systèmes bicycliques oxaphospholanno-furannosiques présentés par les produits **9** à **12** d'autre part, ont servi de base à l'établissement des relations $^3J_{PCCH}$ vs. $\theta_{P,H}$ et $^3J_{PCCC}$ vs. $\theta_{P,C}$, spécifiques à cette série de composés. Nous décrivons également comment les valeurs de la fréquence de vibration ir ν P=O, du déplacement chimique δ ^{31}P et de la constante de couplage $^1J_{P,C}$ peuvent contribuer à l'analyse structurale des dérivés phosphorés de sucres.

Can. J. Chem. Downloaded from www.nrcresearchpress.com by 210.87.254.42 on 09/06/12
For personal use only.

Considering the increasing importance of branched-chain sugars, together with the biological interest of *C*-phosphorus-bonded derivatives of carbohydrates (as analogues of naturally occurring sugar phosphates), we were prompted to study the synthesis and the spectroscopic properties of a series of 3-*C*-phosphorus-bearing 3-*C*-branched chain sugars.

Syntheses, analytical data, and experimental details for compounds **1** to **12** (Fig. 1) have been reported elsewhere (2, 3). The present study concerns the spectroscopic properties and the structural analysis of the new derivatives, including configurational assignments at the new asymmetric centers (C_3 for **1** to **12** and the phosphorus atom for **9** to **12**) and conformational determinations. The ir P=O stretching frequency values for all compounds are given in Table 1 and the nmr data in Tables 2 to 6. The present work completes our previous spectroscopic studies of phosphate esters of pentofuranoses (1).

1. Structural analysis of phosphine-oxide derivatives 1 and 2

Examination of Table 2 immediately shows that configurational assignments at the C_3 atom for **1** and **2** can be simply deduced from a comparison between the δ H—C_1 chemical shift values of both of these compounds. Indeed, this proton is shielded by 0.72 ppm for **2**, compared with compound **1**. Such a strong shielding effect is best explained by postulating a preferred conformation for one of the phenyl groups attached to the phosphorus of **2**. Examination of Dreiding models clearly shows that only the *xylo* configuration (S_{C3}) allows a spatial arrangement for a phenyl group such that its anisotropic effect could influence the shift of the H—C_1 resonance of **2**.

Looking now at the coupling constant values (Table 2), it appears that the vicinal couplings $^3J_{PCCH}$ for **1** and **2** are very different: $J_{2,P}$ = 0 (**1**) or 8.3 Hz (**2**) and $J_{4,P}$ = 5.3 (**1**) or 22.6 Hz (**2**). The dependence of $^3J_{PCCH}$ values on dihedral angles has already been reported and related "Karplus-like" correlation relationships have already been proposed (4–8). As will be discussed later in the text, the literature survey shows that almost all previous studies are limited to the phosphonate derivatives (5–8). On the other hand, it is well known that such ^3J vs. θ relationships are always susceptible to factors other than dihedral angles, such as the electronegativity of the coupled atom substituents, the electronegativity of the substituents on the coupling route (as well as the orientation of these substituents), ring strain, and bond angle distortions. This observation rules out any hope of using a correlation established with phosphonate model-compounds for conformational assignment of the furanose ring of phosphine oxides **1** and **2**. However, a wide range of 1,2-*O*-isopropylidene-furanose derivatives has been extensively studied in many previous works (1, 9–11), including studies of 3-*O*-phosphate derivatives (1) and 3-*C*-phosphonate derivatives (10, 11). In almost all the cases, the $^3\boldsymbol{T}_2$ conformation (or the $_2\boldsymbol{T}^3$, which is very similar) was assigned as being preferred for the furanose ring; furthermore, this same conformation for the sugar ring enabled Evelyn and Hall (10, 11) to rationalize the very different $J_{2,P}$ and $J_{4,P}$ values of 1,2-*O*-isopropylidene-3-*C*-phosphonate derivatives of pento- and hexo-furanoses, which are epimeric at C_3. In like fashion, assignment of the $^3\boldsymbol{T}_2$ conformation (see Fig. 2) for the furanose ring of **1** and **2**, leads to a unique assignment of the *ribo* configuration for **1** (R_{C3}) and the *xylo* for **2** (S_{C3}). Thus, the $^3\boldsymbol{T}_2$ conformation for the furanose ring of **1** (*ribo* configuration) is consistent with the zero value of $J_{2,P}$ and the same twist form for **2** (*xylo* configuration) explains the large $J_{4,P}$ value (22.6 Hz) observed for this derivative. It is interesting to note that this latter coupling constant is much smaller than the same one measured by Evelyn and Hall (10, 11) on the spectra of similar

[1] Phosphorated sugars VII; V (ref. 1); VI (ref. 2).
[2] This work constitutes a part of the Ph.D. Thesis of J.-R.N. (3).
[3] Present address: Research Department, Nestlé Products Technical Assistance Co. Ltd., 1000 Lausanne, Switzerland.
[4] Author to whom correspondence should be addressed.

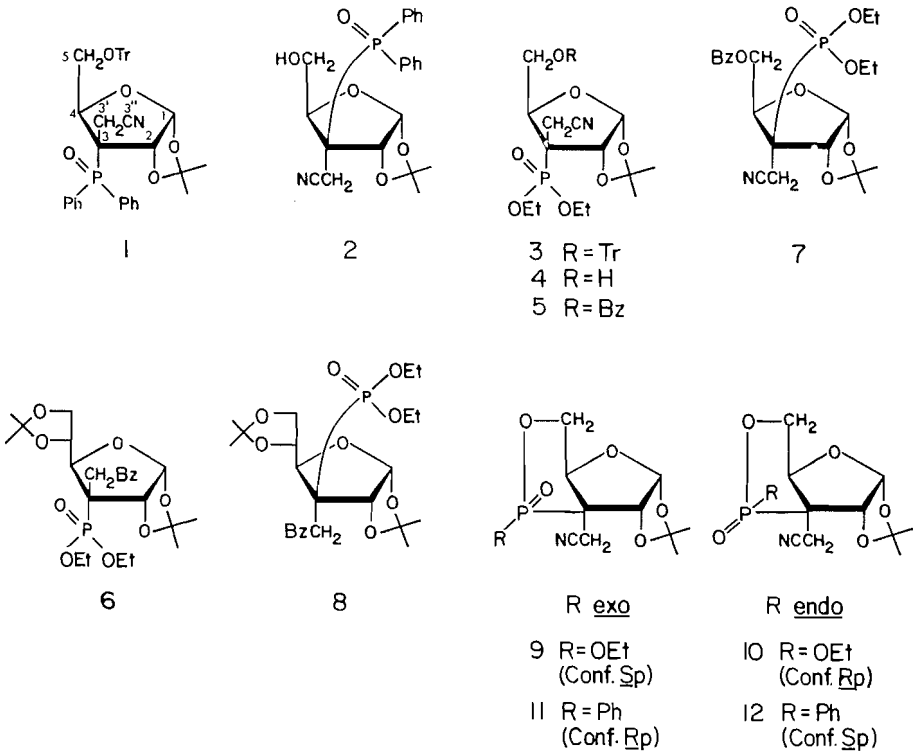

FIG. 1.

TABLE 1. Infrared spectroscopy; stretching ν P=O of 3-*C*-phosphorus-bearing derivatives **1** to **12**

Compound	ν P=O (cm^{-1})	Compound	ν P=O (cm^{-1})
Phosphine oxides		Acyclic phosphonates	
1	1185	**3**	1255
2	1180	**4**	1255
	1165		1245
Cyclic phosphonates			
9	1260	**5**	1260
10	1260	**6**	1255
Cyclic phosphinates			
11	1240	**7**	1255
12	1230	**8**	1250
	1220		

TABLE 2. ^1H nuclear magnetic resonance chemical shifts[a] and coupling constants of phosphine oxides **1** and **2**

	Compounds			Compounds	
Chemical shifts (δ)	**1** *ribo*: R_{C3}	**2** *xylo*: S_{C3}	*J* (Hz)	**1** *ribo*: R_{C3}	**2** *xylo*: S_{C3}
H—C_1	6.00	5.28	$J_{1,2}$	3.5	4.0
H—C_2	4.83	5.13	$J_{2,P}$	0	8.3
H—C_4	4.50	4.64	$J_{4,P}$	5.3	22.6
H_A—C_5	3.79	4.28	$J_{4,5A}$	1.6	6.0
H_B—C_5	3.39	4.11	$J_{4,5B}$	7.1	6.0
H_A—$C_{3'}$	2.89	3.03	$J_{P,3'A}$	9.0	11.0
H_B—$C_{3'}$	2.58	2.82	$J_{P,3'B}$	15.3	8.7

[a] δ, ^1H, 90 Mz, $CDCl_3$.

phosphonate derivatives. This difference can be attributed to the difference of electronegativity of the phosphorus substituents between diphenylphosphine oxide derivatives (**2**) and dimethoxyphosphonate derivatives (10, 11).

Can. J. Chem. Downloaded from www.nrcresearchpress.com by 210.87.254.42 on 09/06/12
For personal use only.

Can. J. Chem. Downloaded from www.nrcresearchpress.com by 210.87.254.42 on 09/06/12
For personal use only.

TABLE 3. Chemical shifts (δ) ^1H, ^{13}C, ^{31}P of acyclic phosphonates **3** to **8**

	Compounds					
	Configuration: R_{C3}				Configuration: S_{C3}	
	ribo			*allo*	*xylo*	*gluco*
Chemical shifts (δ)	**3**	**4**	**5**	**6**	**7**	**8**
H—C_1	6.02[a]	5.98[a]	5.93[b]	5.84[a]	5.83[b]	5.88[a]
H—C_2	4.77	4.79	4.77	5.44	4.82	5.43
H—C_4	4.71	4.55	4.77	4.67	4.39	4.29 to 3.80
H_A—C_5	3.42	3.90	4.62	H—C_5 { 4.29 to 3.88	4.74	3.80 H—C_5: 4.78
H_B—C_5	3.20	3.79	4.31		4.54	
H_A—$C_{3'}$	2.72	2.93	2.83	3.72	2.91	4.29 to 3.80
H_B—$C_{3'}$	2.45	2.67	2.56	2.90	2.80	3.08
$C_{3'}$[c]	116.55	116.94	116.15	197.78	116.17	195.74
C_1	103.97	104.02	103.87	104.32	104.88	104.82
C_4	85.52	85.81	85.29	85.07	82.27	84.86
C_2	78.73	79.76	77.19	82.44	80.51	82.68
C_5	61.80	59.97	61.70	73.48	63.67	74.23
C_3	51.33	51.26	51.07	53.03	49.93	52.92
$C_{3'}$	17.82	17.63	17.20	35.45	17.37	37.30
^{31}P[d]	−18.80	−21.11	−20.00*	−21.21	−22.80*	−23.32

[a] δ, ^1H, 90 MHz, $CDCl_3$.
[b] δ, ^1H, 360 MHz, $CDCl_3$.
[c] δ, ^{13}C, 25.2 MHz, $CDCl_3$.
[d] δ, ^{31}P, 40.5 MHz, $CDCl_3$ (reference 10% H_3PO_4 in acetone-d_6) (*reference 85% H_3PO_4 in D_2O).

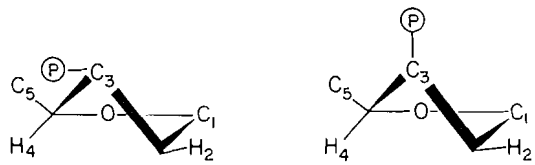

Configuration: R_{C3} Configuration: S_{C3}

Conformation: $^3T_2$

θ (H—C_2; P) ≃ 90°	θ (H—C_2; P) ≃ 40°
θ (H—C_4; P) ≃ 45° to 50°	θ (H—C_4; P) ≃ 160°
θ (C_1; P) ≃ 150°	θ (C_1; P) ≃ 80°
θ (C_5; P) ≃ 70° to 75°	θ (C_5; P) ≃ 40°

FIG. 2. Configuration at C_3 and conformation of the furanose ring of acyclic derivatives **1** to **8**.

2. Structural analysis of acyclic phosphonate derivatives 3 to 8[5]

(A) *^1H nuclear magnetic resonance*

Examination of the data in Table 3 shows the influence of the diethoxyphosphono group on the chemical shift of the protons in its close neighbourhood. For pentofuranose derivatives epimeric at C_3 (e.g. **5** and **7**), H—C_4 of **5** is deshielded by 0.38 ppm with respect to its chemical shift value for compound **7**. A similar difference is observed for the chemical shifts of hexofuranose derivatives epimeric at C_3; thus for **6**, H—C_4 is deshielded with respect to **8** and an analogous deshielding for H—C_5 of **8** is observed with respect to the shift for **6**. Assuming that the three oxygenated substituents of the diethoxyphosphono group are responsible for such through-space deshielding effects, these observations immediately suggest assignment of the R_{C3} configuration for **5** and **6** (*ribo* for **5** and *allo* for **6**) and the S_{C3} configuration for **7** and **8** (*xylo* for **7** and *gluco* for **8**).

Looking now at the values of the $^3J_{PCCH}$ coupling constants for compounds **3** to **8**, Table 4 clearly shows the occurrence of differences which are of the same order of magnitude as those mentioned above for **1** and **2**. The comparison between **5** (**3**, **4**, **6**) and **7** (**8**) includes the zero value of $J_{2,P}$ for **5** (**3**, **4**, **6**) and the very large value of $J_{4,P}$ = 31.3 Hz for **7**. There are many previous reports relating the "Karplus-like" dependency of the $^3J_{PCCH}$ vicinal coupling constants on dihedral angles, for phosphonate derivatives. The first studies on this topic were made by Benezra and Ourisson (5, 6). Evelyn *et al.* (8), as well as Benezra (7), have extended this approach to various phosphonate derivatives, including phosphonates attached to 3-, 5-, or 6-membered rings, linear phosphonates, and α-hydroxy-phosphonates; Benezra has proposed the following $^3J_{PCCH}$ vs. θ_{PH} relationship (7):

$$^3J_{PCCH} = 18 \cos^2 \theta; \quad 0° < \theta < 90° \qquad [1]$$

$$^3J_{PCCH} = 41 \cos^2 \theta; \quad 90° < \theta < 180°$$

Application of the above equation seems, however, limited to the linear phosphonates and those attached to 5- and 6-membered rings; the α-hydroxy-phosphonates and the 3-membered ring containing derivatives involve much smaller vicinal coupling constant values. In the case of compounds **3** to

[5] In this text, the term "acyclic" refers to the phosphorus atom, where it is not involved in a heterocycle, distinguishing compounds **1** to **8** from "cyclic" derivatives having an oxaphospholane ring (**9** to **12**). Compounds **1** to **12** all contain a furanose ring.

TABLE 4. Coupling constants of acyclic phosphonates **3** to **8**

	Compounds					
	Configuration: R_{C3}				Configuration: S_{C3}	
	ribo			*allo*	*xylo*	*gluco*
J (Hz)	**3**	**4**	**5**	**6**	**7**	**8**
$J_{1,2}$	3.6	3.7	3.8	3.2	3.6	3.4
$J_{2,P}$	0	0	0	0	7.2	6.8
$J_{4,P}$	5.1	6.0	5.2	5.2	31.3	?
$J_{4,5A}$	3.2	4.0	3.7	$J_{4,5} = 5.2$	4.1	$J_{4,5} = 8.5$
$J_{4,5B}$	5.1	5.1	6.8		7.5	
$J_{P,3'A}$	10.4	10.0	8.0	7.3	11.7	?
$J_{P,3'B}$	17.7	17.4	19.3	24.9	17.6	27.0
$^1J_{P,C3}$	151.0	151.6	151.2	150.2	143.8	140.9
$^2J_{P,C2}$	7.4	7.6	5.3	7.5	2.5	7.3
$^2J_{P,C3'}$	0	0	0	2.4	0	0
$^2J_{P,C4}$	4.4	4.9	3.9	4.5	3.8	2.9
$^3J_{P,C5}$	0	0	0	0	3.9	3.8
$^3J_{P,C1}$	10.1	10.1	10.2	10.9	0	0
$^3J_{P,C3''}$	8.7	10.0	8.9	5.9	7.5	<4

8, smaller ^3J values than the ones predicted by eq. [1] can be anticipated, because of the presence of the electronegative $-O_2$ substituent on the $J_{2,P}$ coupling route and the electronegative $-O_4$ substituent on the $J_{4,P}$ coupling route. But, on the other hand, the $J_{2,P}$ and $J_{4,P}$ values typical for compounds **3** to **8** are very close to the ones measured by Evelyn and Hall for similar derivatives (10, 11) and, again, examination of Dreiding models leads to the unambiguous assignment of the same $^3T_2$ conformation for the furanose ring of all these derivatives (**3** to **8**), together with the R_{C3} configuration for **3**–**6** and the S_{C3} one for **7** and **8** (see Fig. 2).

(B) *^{13}C nuclear magnetic resonance*

Table 4 shows that another series of differences between **5** (**3**, **4**, **6**) and **7** (**8**) can be emphasized, based on the $^3J_{PCCC}$ coupling constant values measured from the ^{13}C nmr spectra of compounds **3** to **8**. Thus $J_{P,C1} = 10.1$–10.9 Hz (**3**–**6**) or zero (**7**, **8**), and $J_{P,C5} = 0$ (**3**–**6**) or 3.8–3.9 Hz (**7**, **8**). Previous workers have already reported a "Karplus-like" $^3J_{PCCC}$ vs. $\theta_{P,C}$ correlation for phosphonate derivatives (12, 13), and have discussed (14, 15) the susceptibility of this relationship to the electronegativity of substituents on the coupling route, their orientation, as well as its susceptibility to ring strain and bond angle distortions. From the $^3J_{PCCC}$ coupling constants measured on the ^{13}C nmr spectrum of a conformationally rigid phosphonate derivative of camphane, Thiem and Meyer have established the following correlation (16):

$$[2] \cdot \ ^3J_{PCCC} = 7.35 - 1.76 \cos\theta + 7.86 \cos 2\theta$$

These authors noted that α-hydroxy- or α-alkoxy-phosphonates involved coupling constant values 2–5 Hz smaller than those predicted by the above equation (16). More recently, consideration of various conformationally rigid 2-phosphorus-bearing norbornyl derivatives led Quin *et al.* to propose the following general equation (17):

$$[3] \quad ^3J_{PCCC} = A \cos^2\theta + B \cos\theta + C$$

with the following A, B, C values for the phosphonates:

$$A = 17.3; \qquad B = -4.7; \qquad C = -0.9$$

In the case of compounds **3** to **8**, we can expect smaller ^3J values than those predicted by eq. [2] or [3], because of the presence of the electronegative $-O_2$ and $-O_4$ substituents on the $J_{P,C1}$ and $J_{P,C5}$ coupling routes, respectively. However, examination of Dreiding models clearly shows that, in complete agreement with our previous conformational and configurational assignments, the large $J_{P,C1}$ values for **3**–**6** correspond to a large dihedral angle ($\theta \approx 150°$), the $J_{P,C5}$ values for **7** and **8** (3.8–3.9 Hz) for a θ angle close to 40°, and the zero values for $J_{P,C1}$ (**7**, **8**) and $J_{P,C5}$ (**3**–**6**) are typical for angles close to 70–80° (see Fig. 2 and Table 4). It is of interest to note that, if the $^3J_{PCCC}$ vs. $\theta_{P,C}$ relationship specific to our compounds has the same general form as that predicted by eq. [3], the typical minimum value has to correspond to a dihedral angle close to 80°. Thus, from the above correlations, we can infer that the $^3J_{PCCC}$ vicinal couplings typical for phosphonates **3** to **8** describe a "Karplus-like" dependency.

Examination of the $^1J_{P,C3}$ coupling constants for compounds **3** to **8** (Table 4) leads to the following observation: $^1J_{P,C3}$ for derivatives of R_{C3} configuration (**3**–**6**) is larger than the same value for derivatives of S_{C3} configuration (**7**, **8**). In previous works (15, 18–20) it has been reported that the values of one-bond ^{13}C—^{31}P couplings depend on the orientation of the phosphorus atom, when the dialkoxy-phosphoryl group substitutes a ring: $^1J_{C,Peq} > {}^1J_{C,Pax}$ (ref. 18). Thus from a comparison between this value for either **5** (151.2 Hz) and **7** (143.8 Hz) or **6** (150.2 Hz) and **8** (140.9 Hz), we observe differences of the order of 7.4 and 9.3 Hz, which are in complete agreement with previously reported values (18) between an equatorial orientation of the phosphorus atom and an axial one. In our case, this observation is an additional proof for our conformational and configurational assignments (see Fig. 2).

(C) *^{31}P nuclear magnetic resonance*

Examination of the δ ^{31}P chemical shift values (Table 3) for C_3 epimeric phosphonate derivatives leads to the following observation: this value is larger for **5** (R_{C3}) than for **7** (S_{C3}) and for **6** (R_{C3}) than for **8** (S_{C3}). Paulsen and Greve have already reported (21) a dependence of δ ^{31}P on the orientation of the phosphorus atom, similar to that of $^1J_{P,C}$: δ ^{31}Peq > δ ^{31}Pax (ref. 21). Again we consider this difference between the δ ^{31}P

Can. J. Chem. Downloaded from www.nrcresearchpress.com by 210.87.254.42 on 09/06/12
For personal use only.

TABLE 5. Chemical shifts (δ) ^1H, ^{13}C, ^{31}P of cyclic oxaphospholanes **9** to **12**

Chemical shifts (δ)	Compounds			
	9	**10**	**11**	**12**
H—C_1	5.91[a]	6.07[a]	6.18[b]	5.22[a]
H—C_2	4.82	5.00	5.06	4.26
H—C_4	4.73	4.60	4.78	4.79
H_R—C_5	4.41	4.19	4.56	4.74
H_S—C_5	4.34	4.40	4.84	4.64
H_A—$C_{3'}$	3.01	2.84	2.64	3.12
H_B—$C_{3'}$	2.98	2.80	2.33	3.09
$C_{3'}$	116.44[d]	116.40[c]	115.62[c]	117.01[d]
C_1	106.47	106.56	106.99	105.72
C_4	84.52	84.58	83.99	85.17
C_2	82.24	82.32	82.05	82.44
C_5	68.73	68.08	73.06	71.39
C_3	46.93	47.27	52.13	52.46
$C_{3'}$	16.34	16.55	16.68	16.31
^{31}P[e]	−38.87	−37.73	−50.76	−52.61

[a] δ, ^1H, 360 MHz, $CDCl_3$.
[b] δ, ^1H, 90 MHz, $CDCl_3$.
[c] δ, ^{13}C, 25.2 MHz, $CDCl_3$.
[d] δ, ^{13}C, 90 MHz, $CDCl_3$.
[e] δ, ^{31}P, 40.5 MHz, $CDCl_3$ (reference 10% H_3PO_4 in acetone-d_6).

chemical shift of epimeric phosphonate derivatives **5** and **7** (or **6** and **8**) as an additional proof of structure (see Fig. 2).

3. Structural analysis of oxaphospholane-ring-containing derivatives 9 to 12

(A) *Configurational assignment at the phosphorus atom of phosphinates 11 and 12*

Examination of Table 5 shows that the chemical shift values of the sugar ring protons for derivatives **9** to **12** provide excellent information for configurational assignment at the phosphorus atom of **11** and **12**; however, for phosphonates **9** and **10** the proton chemical shifts are much too close to allow any interpretation. For **11** and **12** the most important source of chemical shift differences between H—C_1 and H—C_2 (0.96 and 0.80 ppm respectively) must be the close proximity of the phenyl group to H—C_1 and H—C_2. Examination of Dreiding models immediately shows that the phosphorus configuration arising from an *endo* substitution of the phosphorus by the phenyl group (with respect to the oxaphospholane-furanose bicyclic fusion) is the only one which allows the appropriate orientation of the phenyl ring. This leads directly to the assignment of the *endo* configuration at the phosphorus atom of **12** (S_P) and to the assignment of the *exo* one for **11** (R_P).

(B) *Configurational assignment at the phosphorus atom of phosphonates 9 and 10*

Assignment of the configuration at the phosphorus atom for **9** and **10** poses a more difficult problem than for **11** and **12**. Dealing first with the $J_{P,H}$ coupling constant values, it appears that three groups of ^3J vicinal couplings emphasize the difference between **9** (**11**) and **10** (**12**): $J_{4,5proR}$ and $J_{4,5proS}$, $J_{P,5proR}$ and $J_{P,5proS}$, and finally $J_{P,3'A}$ and $J_{P,3'B}$; the first two groups of two coupling constants concern the conformation of the oxaphospholane ring for **9** to **12**, although the last two ^3J values relate to the conformational equilibria around the C_3—$C_{3'}$ bond. Compounds **9** to **12** present conformationally very restricted oxaphospholane-furanose bicyclic systems and the preferred conformation of the phosphorated heterocycle comes very probably as a result of the varying degrees of steric hindrance that both the *endo* or *exo* configurations at phosphorus can imply. The very similar $J_{4,5proR}$, $J_{4,5proS}$, $J_{P,5proR}$, and $J_{P,5proS}$ couplings for **9** and **11**, as well as the similarity between these same values for **10** and **12**, lead then to assignment of the same *endo* configuration at the phosphorus atom for **10** and **12** and the same *exo* one at this atom for **9** and **11**. Furthermore, examination of Dreiding models shows that the position of the phosphorus substituents can widely influence the conformational equilibria around the C_3—$C_{3'}$ bond, as a result of the close juxtaposition between the phosphorus substituents and the —CH_2CN chain. Thus the similar $J_{P,3'A}$ and $J_{P,3'B}$ coupling constants for **9** and **11** and the same relationship between these values for **10** and **12** confirms the above configurational assignment for **9** and **10**.

TABLE 6. Coupling constants of cyclic oxaphospholanes **9** to **12**

J (Hz)	Compounds			
	9	**10**	**11**	**12**
$J_{1,2}$	3.5	3.3	3.7	4.0
$J_{2,P}$	6.0	6.0	5.7	7.4
$J_{4,P}$	24.5	24.3	19.9	20.7
$J_{4,5proR}$	2.4	2.0	3.0	2.0
$J_{4,5proS}$	0	0	0	0
$J_{P,5proR}$	4.0	2.2	6.3	0
$J_{P,5proS}$	12.0	21.0	11.0	22.0
$J_{P,3'A}$	16.5	20.0	17.5	15.0
$J_{P,3'B}$	18.0	14.0	17.5	10.0
$^1J_{P,C3}$	122.2	122.5	79.5	79.3
$^2J_{P,C2}$	6.1	8.7	7.3	12.2
$^2J_{P,C3'}$	0	3.4	1.5	0
$^2J_{P,C4} + {}^3J_{P,C4}$	9.2	7.6	6.5	0
$^2J_{P,C5} + {}^3J_{P,C5}$	6.1	6.3	0	0
$^3J_{P,C1}$	0	0	0	0
$^3J_{P,C3''}$	6.1	3.8	4.3	<2
$^1J_{P,C(Ph)}$	—	—	138.5	144.0

Considering now the $J_{P,C}$ coupling constants, examination of Table 6 suggests the following comment: for compounds **9** to **12**, the $J_{P,C4}$ and $J_{P,C5}$ values represent the sum of a ^2J geminal coupling ($^2J_{POC}$ or $^2J_{PCC}$) plus a ^3J vicinal coupling ($^3J_{POCC}$ or $^3J_{PCCC}$). For P=O phosphoryl bond-containing organophosphorus compounds, the $^2J_{POC}$ (probably negative (14)) and the $^2J_{PCC}$ (which can change sign (14)) couplings are dependent on the ring strain (22), and on the stereochemistry of the phosphorus atom (23, 24); thus, it appears that the analysis of the $J_{P,C4}$ and $J_{P,C5}$ values cannot be completed for oxaphospholanes **9** to **12** because too many factors are responsible for both the $^2J_{P,C}$ and $^3J_{P,C}$ couplings.

Finally, observation of the $^3J_{P,C3''}$ couplings for compounds **9** to **12** suggests the following comment (see Table 6): a desire to estimate the precise contribution of this $^3J_{P,C}$ vicinal coupling in the conformational analysis of the rotameric composition around the C_3—$C_{3'}$ bond for **9** to **12** prompts comparison of this last constant with the $^3J_{P,3'A}$ and $^3J_{P,3'B}$ proton–phosphorus couplings, assuming that these three values represent the average between populations of three low-energy rotamers. In this regard, because $J_{P,3'A} + J_{P,3'B} = 35$ Hz for **11** and 25 Hz for **12**, we can anticipate a larger $J_{P,C3''}$ value for **12** than for **11**. Surprisingly, it is not so and $J_{P,C3''}$ is larger for **11** (4.3 Hz) than for **12** (<2 Hz); this observation emphasizes a probable susceptibility of the $^3J_{PCCC}$ couplings on the stereochemistry of the asymmetric phosphorus atom for phosphinates **11** and **12**: an

Can. J. Chem. Downloaded from www.nrcresearchpress.com by 210.87.254.42 on 09/06/12
For personal use only.

Can. J. Chem. Downloaded from www.nrcresearchpress.com by 210.87.254.42 on 09/06/12
For personal use only.

anticlinal or *antiperiplanar* orientation between P=O and the C_3—$C_{3'}$ bond (*exo* configuration: **11**) implies a larger $^3J_{P,C3''}$ value than a *synperiplanar* one (*endo* configuration: **12**), against the anticipation deduced from the rotameric composition around the C_3—$C_{3'}$ bond. It is now of interest to note that similarly, $^3J_{P,C3''}$ is larger for phosphonate **9** than for **10**, together with the same value of $(J_{P,3'A} + J_{P,3'B})$ for both compounds. Thus, if the susceptibility of the $^3J_{P,C3''}$ coupling on the stereochemistry of the phosphorus atom for phosphonates **9** and **10** is similar to the one for phosphinates **11** and **12**, this observation would confirm the above configurational assignment for **9** and **10**.

(C) *Conformational assignment of the oxaphospholane-furanose bicyclic system for derivatives 9 to 12*

Use of ^3J coupling constants for conformational analysis requires careful selection of the constants and of the ^3J vs. θ correlation equations. Many authors have previously proposed correlation equations related to such proton–proton and proton–phosphorus couplings for various 1,2-*O*-isopropylidene-furanose derivatives (9), sugar-phosphates (1, 25), or phosphonate derivatives (see eq. [1]) (7). Given that the ^{1}H nmr spectra of compounds **9** to **12** exhibit three sets of vicinal coupling constants, $^3J_{HCCH}$ ($J_{1,2}$, $J_{4,5proR}$, and $J_{4,5proS}$), $^3J_{POCH}$ ($J_{P,5proR}$ and $J_{P,5proS}$), and $^3J_{PCCH}$ ($J_{2,P}$ and $J_{4,P}$), these compounds provide a stringent test. Furthermore, because these bicyclic systems are rigid and because the $J_{4,5proR}$ and $J_{4,5proS}$ values (as well as $J_{P,5proR}$ and $J_{P,5proS}$) are complementary, these couplings can be interpreted *qualitatively* by comparison of the observed values with those established for other derivatives. Thus the couplings between both the H—C_5 protons and the proton H—C_4 or the phosphorus atom can be compared with the values predicted by both the Lee and Sarma relationships (25) (which are well established for conformational assignment of 6-membered phosphate rings fused *cis* or *trans* to a five-membered sugar ring):

[4] $^3J_{HCCH} = 10.5 \cos^2 \theta - 1.2 \cos \theta$ (25)

[5] $^3J_{POCH} = 18.1 \cos^2 \theta - 4.8 \cos \theta$ (25)

In the same way, the $J_{2,P}$ and $J_{4,P}$ values can be compared with those predicted by the Benezra relationship (7) (see section 2, eq. [1]).

Dealing first with the $J_{4,P}$ values for derivatives **9** to **12** (Table 6), the large value of this coupling constant (19.9 to 24.5 Hz) implies an *anti-periplanar* orientation between H—C_4 and the phosphorus atom. Secondly, the small $J_{4,5proR}$ value (2–3 Hz), together with the zero $J_{4,5proS}$ value, indicates a very restricted conformational mobility around the C_4—C_5 bond. Examination of Dreiding models clearly shows that the couplings for compounds **9** to **12** are only compatible with five possible forms ($^3T_2$, ^3E, $^3T_4$, E_4, and $^0T_4$) for the furanose ring and three (^4E, $^4T_5$, and E_5) for the oxaphospholane ring.

The $J_{P,5proR}$ and $J_{P,5proS}$ values emphasize the difference between the preferred conformation of the oxaphospholane ring of **9** and **11**, and that preferred for the same ring of **10** and **12**. Thus, from examination of Dreiding models, together with the order of magnitude of these coupling constants, we derive:

for **9** and **11**:

$J_{P,5proR} = 4.0–6.3$ Hz; $90° < \theta \leq 120°$

$J_{P,5proS} = 11–12$ Hz; $120° < \theta < 150°$

for **10** and **12**:

$J_{P,5proR} = 0–2.2$ Hz; $\theta < 90°$

$J_{P,5proS} = 21–22$ Hz; $\theta > 150°$

Even from these approximate dihedral angles, we can assign unambiguously the ^4E conformation for the oxaphospholane ring of **9** and **11**, and a conformation intermediate between $^4T_5$ and E_5 for **10** and **12**. The adoption of this last conformation for **10** and **12** implies that the furanose ring is held in a conformation intermediate between the E_4 and the $^0T_4$ forms, which completes the conformational assignment for both the heterocycles of **10** and **12**.

The $J_{1,2}$, $J_{2,P}$, and $J_{4,P}$ values (Table 6) are very similar for compounds **9** to **12**. They clearly indicate that the furanose rings of **9** and **10** adopt the same form, which was assigned above for **10**, as $E_4/^0T_4$. The smaller value of $J_{2,P}$ for **11** than for **12** implies an increase of the related dihedral angle ($\theta < 90°$) for **11** and, in the context of the ^4E from previously assigned for the oxaphospholane ring, this requirement is only compatible with the $^3T_2$ conformation for the furanose ring of **11**. The above conformational assignments for derivatives **9** to **12** are depicted in Fig. 3.

Finally, it is of interest to note that, for dioxaphosphorinane derivatives of phosphonates, the ν P=O stretching frequency, the δ^{31}P chemical shift, and the $^1J_{P,C}$ coupling constant between an aliphatic substituent on phosphorus and this last atom, all these three values can be used in structural analysis, because of their dependence on the orientation of the P=O bond with respect to the ring conformation (26). For derivatives **9** to **12**, it has not been possible to study if such a dependence existed in the case of oxaphospholane rings, because the ^4E form (**9**, **11**) as well as the $^4T_5/E_5$ one (**10**, **12**) allow an isoclinal orientation of both the substituents on phosphorus. Thus **9** and **10** (and **11** and **12**) cannot be compared with respect to the orientation of the P=O bond, this orientation being the same for the four compounds.

4. Spectroscopic properties of 3-*C*-phosphorus-bearing derivatives of pento- and hexo-furanoses

(A) *"Karplus like" relationships for* $^3J_{P,H}$ *vs.* $\theta_{P,H}$

As discussed in sections 1 and 2, the available nmr data suffice for assignment of the $^3T_2$ conformation for the furanose ring of acyclic derivatives **1** to **8**; furthermore, the conformational rigidity of the bicyclic systems for **9** to **12** allows for the assignments given in section 3. Thus, we can now measure the relevant dihedral angles from Dreiding models of the assigned conformations (for **1** to **8**, see Fig. 2; for **9** to **12**, see Fig. 3), and finally report the $^3J_{PCCH}$ coupling constants as a function of the dihedral angles; this is summarized graphically in Fig. 4. Some comments are appropriate.

Assuming that the $^3J_{PCCH}$ dependence on dihedral angle can be represented by a function having the form $[A \cos^2 \theta + B \cos \theta + C]$, the values for the phosphonate derivatives **3** to **8** correspond to eq. [6]:

[6] $^3J_{PCCH} = 24.8 \cos^2 \theta - 10.0 \cos \theta$

A comparison between the above equation and the Benezra relationship (7) (eq. [1]) leads to the conclusion that the typical vicinal coupling constants for phosphonates **3** to **8** are slightly smaller than those predicted by the Benezra equation. As anticipated, very probably this is because of the presence of electronegative substituents along the coupling routes ($-O_2$ for $J_{2,P}$ and $-O_4$ for $J_{4,P}$) in the carbohydrate derivatives.

From a comparison of the $^3J_{PCCH}$ values of the phosphine oxide derivatives **1** and **2** with those of the phosphonates **3** to **8**, it is clear that those of the phosphine oxides (**1**, **2**) are

Can. J. Chem. Downloaded from www.nrcresearchpress.com by 210.87.254.42 on 09/06/12
For personal use only.

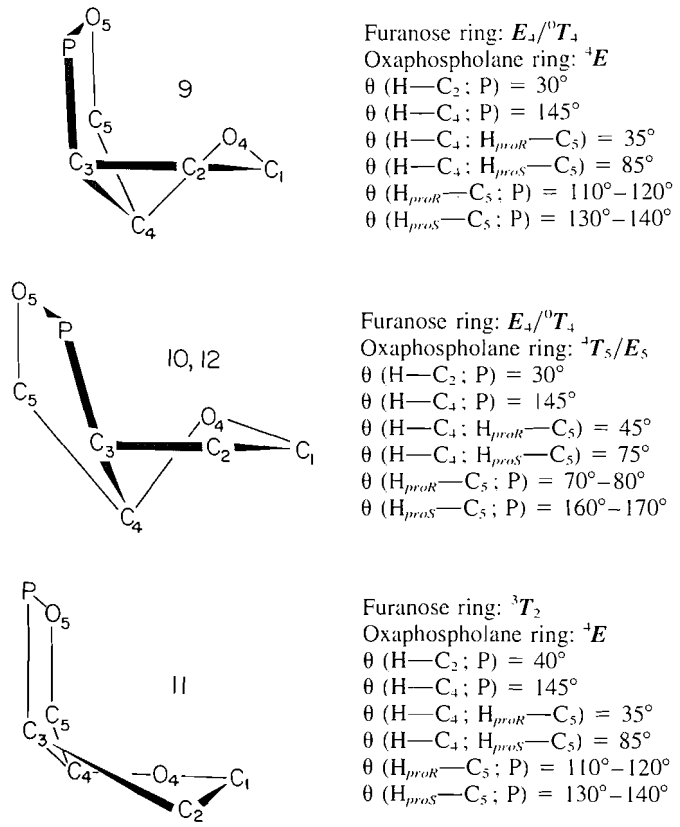

FIG. 3. Conformations of furanose and oxaphospholane rings of cyclic derivatives **9** to **12**.

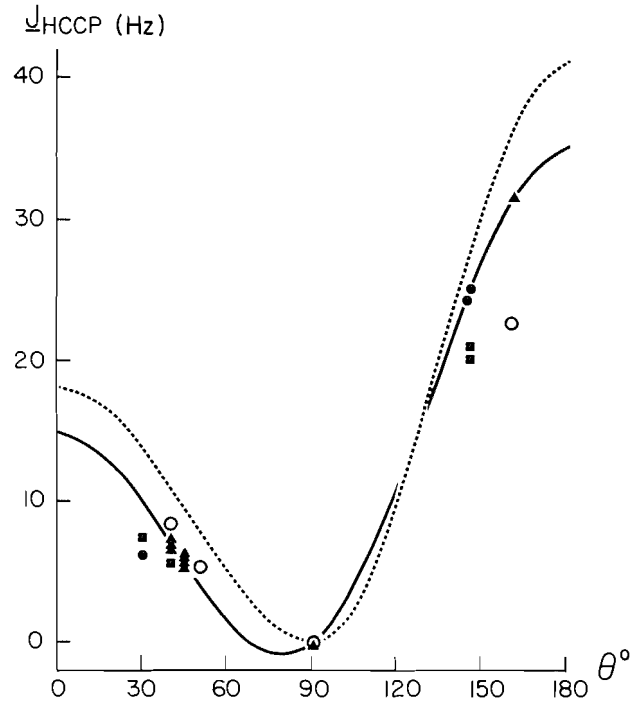

FIG. 4. $^3J_{HCCP}$ vs. $\theta_{P,H}$ relationships; (——) ▲, acyclic phosphonates **3** to **8**; ○, phosphine oxides **1** and **2**; ●, cyclic phosphonates **9** and **10**; □, cyclic phosphinates **11** and **12**; (- - -) phosphonates studied in ref. 7.

slightly larger in the first part of the curve ($0 \leq \theta < 90°$), but smaller for $90° < \theta \leq 180°$ (see Fig. 4). This observation suggests that in the general "Karplus-like" correlation equation, the importance of the *B* factor (operating on the cos θ term) decreases with the electronegativity of the phosphorus substituents; similar observations can be deduced from a comparison of the $^3J_{POCH}$ values of phosphonates and phosphates (27), as well as from a comparison of the $^3J_{PCCC}$ values of phosphonates and phosphine oxides (17).

To estimate the effect of the *cis*-fused oxaphospholane ring closure on the $^3J_{PCCH}$ coupling constants, we can now compare the typical values reported for the phosphonates **9** and **10** with the specific ones for acyclic derivatives **3** to **8** (see Fig. 4). Thus, although closure of the oxaphospholane ring seems to affect drastically the $^3J_{PCCH}$ value related to $\theta = 30°$, its effect on the coupling corresponding to $\theta = 145°$ is very small. In this regard, it is of interest to note that the $^3J_{HCCH}$ coupling constants specific for phosphonates **9** and **10** ($J_{4,5proR}$ and $J_{4,5proS}$), which correspond to small dihedral angles, are drastically smaller than those predicted by the Lee and Sarma relationship (25) (eq. [4]); on the other hand, the $^3J_{POCH}$ coupling constants specific for the same phosphonates **9** and **10** ($J_{P,5proR}$ and $J_{P,5proS}$), but which correspond to large dihedral angles, are in complete agreement with the Lee and Sarma relationship (25) (eq. [5]). Thus, it seems that the $^3J_{HCCH}$, $^3J_{PCCH}$, and $^3J_{POCH}$ vicinal coupling constant values are susceptible to the closure of a *cis*-fused oxaphospholane ring only when they are related to small dihedral angles ($0° < \theta < 90°$).

(B) *"Karplus-like" relationships for* $^3J_{P,C}$ *vs.* $\theta_{P,C}$

Here too, examination of Dreiding models permitted measurement of the typical carbon–phosphorus dihedral angles which could be correlated with the $^3J_{PCCC}$ coupling constants of the acyclic phosphonate derivatives **3** to **8**. Again, assuming that the dependence of these coupling constants on the dihedral angles has the general form predicted by eq. [3], the corresponding $^3J_{PCCC}$ vs. $\theta_{P,C}$ relationship (Fig. 5) is summarized in eq. [7]:

$$[7] \quad {}^3J_{PCCC} = 10.3 \cos^2 \theta - 3.0 \cos \theta$$

A comparison between the above equation and that proposed by Quin *et al.* (17) (eq. [3]) shows that the specific vicinal coupling values for compounds **3** to **8** are much smaller than those predicted by eq. [3]. If this decrease in ^3J values is attributed solely to the presence of electronegative substituents along the coupling routes for **3** to **8**, it is interesting to note that these substituent effects are much larger on the $^3J_{PCCC}$ values than on the $^3J_{PCCH}$ couplings.

(C) *Use of* ν P=O, δ ^{31}P, *and* $^1J_{P,C}$ *values in structural analysis of* C-*phosphorus-bearing carbohydrates*

Many empirical "rules" have already been reported whereby the value of the ν P=O stretching frequency, the δ ^{31}P chemical shift value, or the $^1J_{P,C}$ coupling constant can be used for the structural analysis of organophosphorus compounds (1, 15, 18–21, 26, 28–32). It appears that these three parameters are frequently dependent on the same structural factors. Fig. 6 illustrates this dependence for compounds **3** to **12**, and three points merit comment.

(*i*) Examination of Table 1 clearly shows that the ν P=O ir stretching frequency value, as expected, decreases with the electronegativity of the phosphorus substituents. A comparison of the δ ^{31}P and $^1J_{P,C}$ values of **9** (**10**) and **11** (**12**) leads to the same observation (see Fig. 6).

(*ii*) As already stated (see sections 2(B) and 2(C)) two C_3-epimeric 3-*C*-phosphonate derivatives (**5** and **7**, or **6** and **8**)

Can. J. Chem. Downloaded from www.nrcresearchpress.com by 210.87.254.42 on 09/06/12
For personal use only.

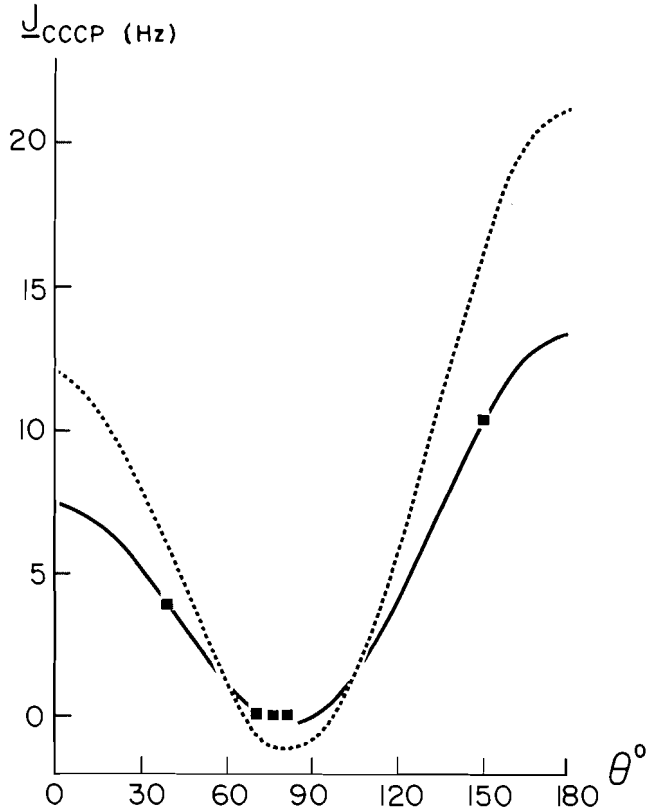

FIG. 5. $^3J_{CCCP}$ vs. $\theta_{P,C}$ relationships; (——) ■, acyclic phosphonates **3** to **8**; (- - -) phosphonates studied in ref. 17.

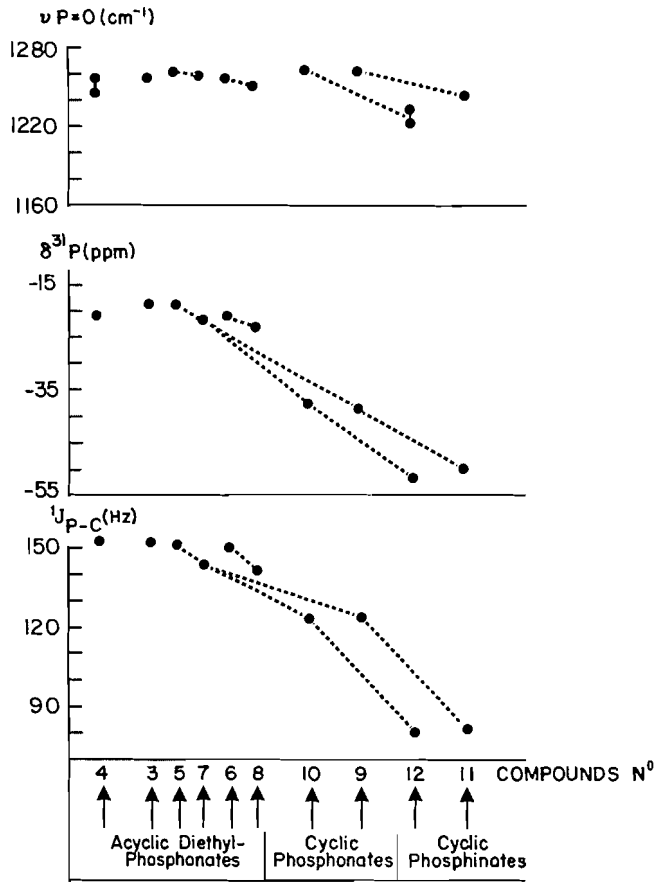

FIG. 6. Correlations of ir/nmr data and structure of *C*-phosphorus-bearing sugars.

can be compared using these values because of their dependence on the orientation of the phosphorus atom with respect to the furanose ring conformation.

(*iii*) The oxaphospholane ring closure does not affect the ν P=O stretching frequency value, although it does affect both the δ ^{31}P and the $^1J_{P,C}$ values (compare **7** and **9** (**10**)).

Acknowledgements

This work was supported by the Fonds National Suisse de la Recherche Scientifique (no. 2.781.77 and 2.070.081). The authors would like to thank Dr. U. Bürger and Mr. J. P. Saulnier for the 25.2 MHz ^{13}C nmr spectra, Professor B. Gross, Miss F. Chrétien, and Mr. P. Simon (Université de Nancy, France) for the ^{31}P nmr spectra, Dr. B. Willhalm and Mr. W. Thommen (Firmenich & Co., S. A., Genève) for the 360 MHz ^{1}H and 90 MHz ^{13}C nmr spectra. It is a pleasure for one of us (J.R.N.) to thank Professor L. D. Hall for helpful discussions.

1. J. R. NEESER, J. M. J. TRONCHET, and E. J. CHAROLLAIS. Can. J. Chem. **61**, 1387 (1983).
2. J. M. J. TRONCHET, J. R. NEESER, E. J. CHAROLLAIS, and (in part) L. GONZALEZ. J. Carbohydr. Chem. (1983). In press.
3. J. R. NEESER. Nouveaux types de sucres phosphorés: synthèse, propriétés spectroscopiques, en particulier RMN-^{1}H, -^{13}C, -^{31}P. Thèse de doctorat es Sciences No. 1999. Université de Genève (1981).
4. A. A. BOTHNER-BY and R. H. COX. J. Phys. Chem. **73**, 1830 (1969).
5. C. BENEZRA and G. OURISSON. Bull. Soc. Chim. Fr. 1825 (1966).
6. C. BENEZRA. Tetrahedron Lett. 4471 (1969).
7. C. BENEZRA. J. Am. Chem. Soc. **95**, 6890 (1973).
8. L. EVELYN, L. D. HALL, P. R. STEINER, and D. H. STOCKES. Org. Magn. Reson. **5**, 141 (1973).
9. R. J. ABRAHAM, L. D. HALL, L. HOUGH, and K. A. MCLAUCHLAN. J. Chem. Soc. 3699 (1962).
10. L. EVELYN and L. D. HALL. J. Chem. Soc. Chem. Commun. 576 (1969).
11. L. EVELYN and L. D. HALL. Carbohydr. Res. **27**, 21 (1973).
12. R. B. WETZEL and G. L. KENYON. J. Am. Chem. Soc. **96**, 5189 (1974).
13. C. A. KINGSBURY and D. THOENNES. Tetrahedron Lett. 3037 (1976).
14. G. W. BUCHANAN and C. BENEZRA. Can. J. Chem. **54**, 231 (1976).
15. G. W. BUCHANAN and F. G. MORIN. Can. J. Chem. **55**, 2885 (1977).
16. J. THIEM and B. MEYER. Org. Magn. Reson. **11**, 50 (1978).
17. L. D. QUIN, M. J. GALLAGHER, G. T. CUNKLE, and D. B. CHESNUT. J. Am. Chem. Soc. **102**, 3136 (1980).
18. J. THIEM and B. MEYER. Tetrahedron Lett. 3573 (1977).
19. J. THIEM, B. MEYER, and H. PAULSEN. Chem. Ber. **111**, 3325 (1978).
20. G. ADIWIDJAJA, B. MEYER, H. PAULSEN, and J. THIEM. Tetrahedron, **35**, 373 (1979).
21. H. PAULSEN and W. GREVE. Chem. Ber. **106**, 2114 (1973).
22. Y. KASHMAN, I. WAGENSTEIN, and A. RUDI. Tetrahedron, **32**, 2427 (1976).
23. G. A. GRAY and S. E. CREMER. J. Org. Chem. **37**, 3470 (1972).
24. Y. KASHMAN and A. RUDI. Tetrahedron Lett. 2819 (1976).
25. C. H. LEE and R. H. SARMA. J. Am. Chem. Soc. **98**, 3541 (1976).
26. W. J. STEC, K. LESIAK, D. MIELCZAREK, and B. STEC. Z. Naturforsch. Teil B, **30**, 710 (1975).
27. L. D. HALL and R. B. MALCOLM. Can. J. Chem. **50**, 2092 (1972).
28. D. B. COOPER, T. D. INCH, and G. J. LEWIS. J. Chem. Soc.

Perkin Trans. **1**, 1043 (1974).
29. W. J. STEC and A. LOPUSINSKI. Tetrahedron, **29**, 547 (1973).
30. J. P. MAJORAL and J. NAVECH. Bull. Soc. Chim. Fr. 1331 (1971).
31. J. P. MAJORAL and J. NAVECH. Bull. Soc. Chim. Fr. 2609 (1971).
32. L. D. HALL and R. B. MALCOLM. Can. J. Chem. **50**, 2102 (1972).

Can. J. Chem. Downloaded from www.nrcresearchpress.com by 210.87.254.42 on 09/06/12
For personal use only.

Réduction électrochimique de cétones aromatiques encombrées en milieu aprotique et en présence de chlorure de manganèse

FRANÇOISE FOURNIER, JACQUES BERTHELOT ET YVES-LOUIS PASCAL
Laboratoire de Chimie Organique Structurale, CNRS ERA 557, Université Pierre et Marie Curie, Bâtiment F, 4 Place Jussieu, 75230 Paris Cedex 05, France

Reçu le 27 janvier 1983

FRANÇOISE FOURNIER, JACQUES BERTHELOT et YVES-LOUIS PASCAL. Can. J. Chem. **61**, 2121 (1983).

La réduction électrochimique de cétones aromatiques encombrées et peu réductibles est réalisable en milieu aprotique (DMF), sur cathode de mercure, en présence de chlorure de manganèse, à un potentiel correspondant au système Mn(II)/Mn(0), mais beaucoup moins négatif que celui de réduction de la cétone elle-même. Il y a hydrodimérisation sélective en glycol-α et absence totale de polymérisation. Dans le cas de cétones dissymétriques, les diastéréoisomères *dl* sont formés préférentiellement. L'action du manganèse est dûe soit à la réduction d'un complexe de manganèse (à bas degré d'oxydation) – cétone, soit à la réduction de la cétone par un film de manganèse colloïdal sur la surface de l'électrode.

FRANÇOISE FOURNIER, JACQUES BERTHELOT, and YVES-LOUIS PASCAL. Can. J. Chem. **61**, 2121 (1983).

The electrochemical reduction of hindered aromatic ketones which are difficult to reduce can be achieved in an aprotic medium (DMF) on a mercury pool cathode, in presence of Mn(II) chloride, at the reduction potential of the Mn(II)/Mn(0) system, but less negative than that of the ketone itself. There is selective hydrodimerization into an α-glycol, with total lack of polymerization. With dissymmetric ketones, the *dl* diastereoisomers of the diols are produced preferentially. The effect of manganese is due either to the reduction of a Mn(I) or Mn(0) – ketone complex or to the reduction of the ketone by a film of colloidal manganese on the electrode surface.

Introduction

La réduction électrochimique d'aldéhydes et cétones aromatiques en milieu aprotique, en particulier dans le diméthylformamide (DMF), a suscité quelques travaux (1). L'avantage d'un tel milieu est surtout une grande étendue de la zone d'électroactivité d'où une bonne séparation des potentiels de réduction correspondant aux différents transferts électroniques. Selon les cas, l'électrolyse conduit à des glycols-α et à des alcools, mais les rendements sont souvent très diminués par des réactions de polymérisation.

La réduction de cétones aromatiques dans le DMF en présence de Cr(II), électrogénéré à partir de sels de Cr(III) favorise souvent l'hydrodimérisation en diol et inhibe totalement les polymérisations. En règle générale, que la cétone seule soit plus facile ou plus difficile à réduire que Cr(II), la réduction en présence du métal se fait toujours à un potentiel moins négatif que le $E_{1/2}$ de la cétone (2–5). Malgré tout, la sélectivité de cette réaction d'électroréduction assistée est difficile à relier aux valeurs respectives des potentiels de réduction des composés organiques et du sel métallique. De plus, pour les cétones dont le $E_{1/2}$ est plus positif que celui de Cr(II), on pourrait penser qu'il s'agit là de réduction chimique par les espèces Cr(II) électrogénérées; en effet les résultats sont les mêmes que ceux obtenus par action du chlorure ou de l'acétate chromeux (5).

Nous présentons ici les résultats de la réduction électrochimique de cétones aromatiques, en milieu organique aprotique, en présence de sel de manganèse Mn(II). Par rapport aux sels de chrome précédemment étudiés (4, 5), ce système ne présente pas la complexité engendrée par l'existence du système Cr(III)/Cr(II) et évite la compétition entre le phénomène électrochimique et la réduction chimique par le chrome(II). Les cétones étudiées dans ce travail sont représentées dans Fig. 1.

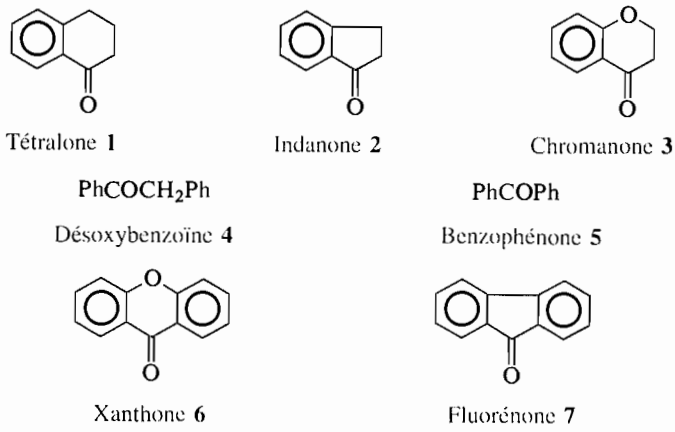

FIG. 1

Résultats et discussion

Analyse polarographique et voltammétrique

Les mesures ont été effectuées par rapport à l'électrode au calomel saturé (ECS) à double jonction, l'électrolyte support étant une solution de bromure de tétrabutyl ammonium (TBABr) 0,1 *M* dans le diméthylformamide (DMF).

Dans ces conditions, le polarogramme d'une solution de $MnCl_2 \cdot 4H_2O$ (10^{-3} *M*) présente une seule vague de réduction biélectronique, irréversible à $E_{1/2} = -1{,}55$ V (système Mn(II)/Mn(0)); dans le DMSO, pour le même système, $E_{1/2} = -1{,}68$ V (6). En voltammétrie cyclique, en utilisant une goutte de mercure chaque fois renouvelée (électrode de Kémula) et pour des balayages effectués après agitation sous argon, de la solution de chlorure de manganèse, on observe une variation linéaire du potentiel du pic de réduction du système Mn(II)/Mn(0) avec le logarithme de la vitesse de balayage v (dans l'intervalle 5 mV s^{-1} à 500 mV s^{-1}), avec une pente très faible d'environ 20 mV par décade de v. Avec une goutte non renouvelée, les voltamogrammes se modifient à chaque cycle.

Les cétones étudiées (Tableau 1) présentent toutes une première vague polarographique de nature réversible. Cette vague correspond à l'échange d'un électron comme le montre la comparaison avec le polarogramme du benzaldéhyde (à 10% près) dont la première vague est monoélectronique (7) et le coefficient de diffusion peu différent de ceux des cétones étudiées. Leur deuxième vague de réduction (monoélectronique et irréversible) n'est pas toujour visible car masquée par la décharge du sel de fond.

Can. J. Chem. Downloaded from www.nrcresearchpress.com by 210.87.254.6 on 09/06/12
For personal use only.

TABLEAU 1. Résultats des électrolyses en présence de Mn^{2+} et de Cr^{3+}

Cétone	$-E_{1/2}{}^{a}$ (V) Cétone 10^{-3} *M*	$-E_{1/2}{}^{b}$ (V) Cétone 10^{-3} *M* + Mn^{2+} 10^{-3} *M*	Electrolyse en présence de Mn^{2+}	$-E_{1/2}{}^{c}$ (V) Cétone 10^{-3} *M* + Cr^{3+} 10^{-3} *M*	Electrolyse en présence de Cr^{3+}
1	1,97	1,55	Diol 84% *d, l* 65% *méso* 19%	1,53	Diol 85% *d, l* 68% *méso* 17%
2	2,01	1,57	Diol 66% *d, l* 51% *méso* 15%	1,53	Diol 63% *d, l* 48% *méso* 15%
3	1,90	1,565	Diol 74% *d, l* 63% *méso* 11%	1,53	Diol 78% *d, l* 62% *méso* 16%
4	1,89	1,56	Diol 64% → *d, l* 37%; Alcool 6% → *méso* 27%	1,48	Diol 64% → *d, l* 47%; Alcool 11% → *méso* 17%
5	1,72 et 2,01	1,57	Alcool 87%	1,45	Diol 74% Alcool 18%
6	1,63	1,505	Xanthone	1,44	Alcool 90%
7	1,24 et 1,91	1,15	Fluorénone	1,08	Diol 38% Alcool 48%

$^{a}E_{1/2}$ (V) = potentiel de demi-vague polarographique, par rapport à l'électrode à calomel au KCl saturé. Solvant DMF; sel de fond TBABr 0,1 *M*.
$^{b}E_{1/2}$ (V) = vague du complexe cétone – Mn(II).
$^{c}E_{1/2}$ (V) = vague du complexe cétone – Cr(II).

Si à une solution 10^{-3} *M* en cétone, on ajoute des quantités croissantes de Mn(II), on observe d'abord une diminution régulière des vagues de la cétone tandis qu'apparaît une nouvelle vague aux alentours de −1,50 V. La hauteur de cette vague devient maximale pour un mélange équimoléculaire de cétone et de sel de manganèse. Pour ce rapport 1:1 les vagues de la cétone ont complètement disparu.

De la même façon, lorsqu'on ajoute la cétone à une solution 10^{-3} *M* de chlorure de manganèse(II), la vague de réduction Mn(II)/Mn(0) se déplace très peu jusqu'à la valeur précédemment obtenue (−1,50 V) (mélange cétone – sel de manganèse). Après l'équimolarité, les vagues propres à la cétone se superposent à la courbe $i-E$ précédente.

Les mêmes observations avaient été faites dans le cas d'un mélange cétone – sel de chrome. Dans ce dernier cas, à l'équimolarité, la vague polarographique unique (système Cr(II)/Cr(0)) est controlée par la diffusion et avait été attribuée à l'existence d'un complexe chrome(II)–cétone (2–5).

L'analyse par voltammétrie cyclique de ce mélange Mn(II)–cétone a été réalisée en prenant la tétralone comme exemple.

Sur le voltammogramme du mélange équimolaire (Fig. 2) le pic de réduction Mn(II) en Mn(0) n'est pas modifié par la présence de la cétone; de même le pic de réduction de la cétone n'est pas modifié par la présence de l'espèce Mn(II). Enfin au balayage retour, apparaît le pic de réoxydation de la cétone (système réversible). Cette indépendance des deux systèmes en présence est vérifiée pour toute vitesse de balayage supérieure à 5 mV s^{-1}. Pour 5 mV s^{-1} (vitesse d'enregistrement usuelle du polarogramme), il apparaît un seul pic de réduction à un potentiel voisin du potentiel de réduction Mn(II)/Mn(0) et en balayage retour n'apparaît aucun pic de réoxydation de la cétone. A cette vitesse, la seule espèce réduite forme avec son produit de réduction un système irréversible.

Pour un mélange équimolaire de sel de manganèse et de cétone, la variation avec la vitesse de balayage (v) du potentiel E_{Pc} du premier pic de réduction (réaction Mn(II) → Mn(0)) est la même qu'en absence de cétone ($\partial E_{Pc}/\partial \log v \simeq -20$ mV) dans l'intervalle 10 à 500 mV s^{-1} et dans le même temps, il apparaît le pic de réduction de la tétralone libre vers −1,975 V pour $v > 10$ mV s^{-1}. Celui-ci d'intensité d'abord très faible et

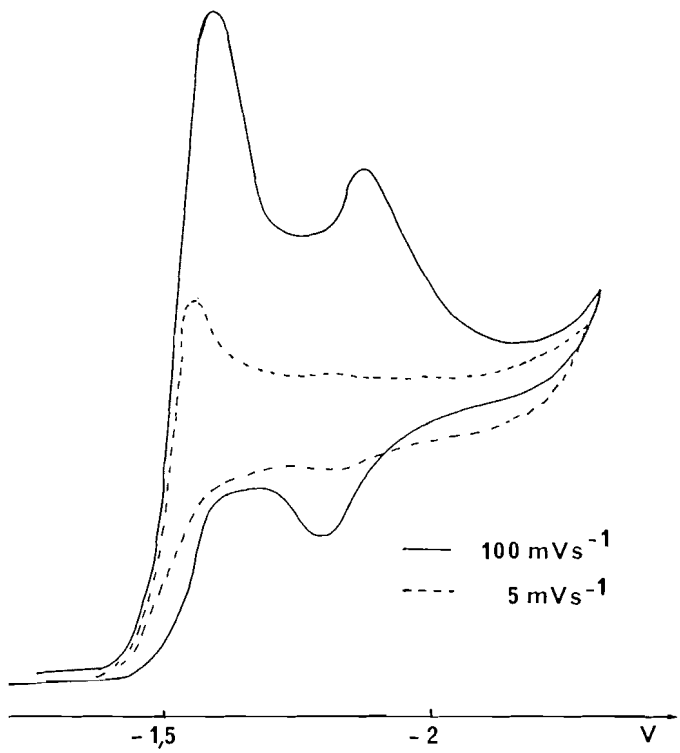

FIG. 2. Voltammogrammes du mélange tétralone (10^{-3} *M*) et Mn(II) (10^{-3} *M*) dans DMF, TBABr 0,1 *M*.

se déplaçant légèrement vers des potentiels moins négatifs se fixe à −1,96 V à partir de 100 mV s^{-1} tandis que sa hauteur relative croît et que le système devient de plus en plus réversible.

Il apparaît donc que le complexe cétone–manganèse, mis en évidence par la polarographie, ne se forme que très lentement et n'affecte les voltammogrammes que pour des balayages à très faible vitesse. Une confirmation est apportée par l'étude de l'influence de la concentration en cétone en présence de Mn(II) (10^{-3} *M*) pour une vitesse de balayage fixée à 50 mV s^{-1}. Le premier pic de réduction reste fixe, celui de la cétone n'apparaissant que pour une concentration de 0,75 × 10^{-3} *M*

Can. J. Chem. Downloaded from www.nrcresearchpress.com by 210.87.254.6 on 09/06/12
For personal use only.

Can. J. Chem. Downloaded from www.nrcresearchpress.com by 210.87.254.6 on 09/06/12
For personal use only.

(−1,955 V) et se déplaçant légèrement vers des potentiels plus négatifs, pour atteindre −2,015 V pour une concentration en cétone de 10^{-2} *M*. Tout au long de cette étude, il a été vérifié qu'une goutte de mercure non renouvelée reste passivée, et entraîne en conséquence la non-reproductibilité des voltammogrammes. Tout cela semble indiquer en fait, la formation d'un film, les modifications irréversibles de la surface de l'électrode étant imputables aux espèces Mn(0) formées (amalgame ou film de métal colloïdal); le film superficiel formé sur l'électrode étant plus ou moins inhibiteur pour la réduction des ions complexes métalliques mais non pour les molécules de cétone. On peut penser qu'il en est de même dans les conditions d'une électrolyse préparative à un potentiel contrôlé plus négatif que celui de la réduction de Mn(II) en Mn(0).

Electrolyse à potentiel contrôlé

Une autre méthode d'étude de la réaction qui se produit au niveau du pic correspondant au complexe manganèse–cétone est l'identification des produits préparés par électrolyse au potentiel de ce pic. Ces réductions ont été conduites sur des mélanges, en proportions équimolaires de cétone et chlorure de manganèse. Le résultat des électrolyses préparatives pour chaque cétone étudiée est consigné dans le tableau 1 et peut être comparé aux résultats obtenus pour ces mêmes cétones en présence de chlorure de chrome (4, 5).

Le potentiel de demi-vague correspondant au complexe manganèse–cétone permet de classer les cétones **1** à **7** en 3 catégories.

(*i*) Les cétones beaucoup moins réductibles que Mn(II) et dont le $E_{1/2}$ du complexe est voisin de celui de Mn(II)/Mn(0) seul: **1** à **4**. Pour ces composés, la réduction électrochimique en présence de Mn(II) conduit à des résultats semblables à ceux de la réduction effectuée en présence de Cr(II) en imposant le potentiel de la vague du complexe Cr(II)–cétone.

(*ii*) Une cétone de potentiel de réduction légèrement inférieur à celui de Mn(II) et dont le $E_{1/2}$ du complexe est voisin de celui de Mn(II): la benzophénone **5** qui conduit quantitativement au benzhydrol alors qu'avec Cr(III) on isolait à côté du benzhydrol (18%), un pourcentage assez élevé de diol (74%).

(*iii*) Les cétones de potentiel de réduction voisin ou supérieur à celui de Mn(II) et dont le $E_{1/2}$ du complexe est déplacé vers les potentiels moins négatifs: la xanthone **6** et la fluorénone **7** où il y a récupération quantitative du produit de départ alors qu'avec Cr(III) la xanthone **6** donnait le xanthol et la fluorénone **7** un mélange du diol (38%) et du fluorénol (48%). Pour ces trois dernières cétones (**5**, **6**, **7**), nous ne pouvons actuellement apporter une explication satisfaisante de ces différences expérimentales. Une électrolyse à un potentiel correspondant au palier de la vague de réduction du complexe manganèse–cétone, permet d'obtenir avec un bon rendement les glycols-α d'hydrodimérisation lorsque le potentiel de demi-vague de la cétone est beaucoup plus négatif que celui de Mn(II). Les glycols-α obtenus avec les cétones dissymétriques sont en majorité comme avec le chrome (4, 5) les diastéréoisomères *dl*, ce qui s'explique bien par des effets stériques, si on admet qu'au moment de la soudure des radicaux ions cétyles, ceux-ci sont fixés au manganèse par leurs atomes d'oxygène, conduisant alors au pinacolate fixé sous sa forme cisoïde, dont la configuration, *dl* est beaucoup moins encombrée (un raisonnement analogue est développé dans la ref. 8 pour la réduction chimique de l'indanone). Seules les configurations des diols correspondants à **1** et **2** ont été jusque là déterminées de façon rigoureuse (8, 9), mais nous avons pu mettre au point une méthode spectrale d'attribution de toutes les configurations (10). Il est à remarquer que la réduction directe des cétones dans le DMF au potentiel de leur première vague polarographique donne surtout des polymères (plus de 80%).

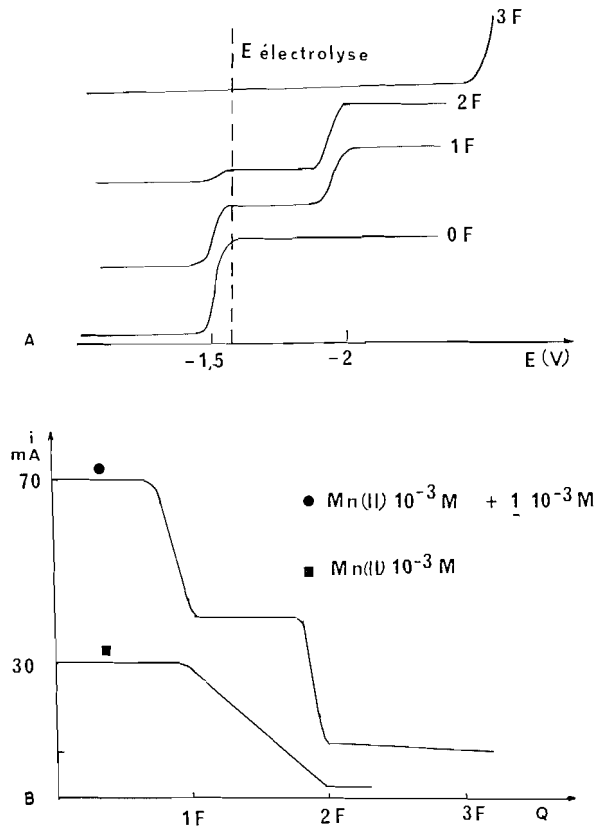

FIG. 3. Electrolyse de **1** dans le DMF–TBABr en présence de Mn(II) en quantité équimolaire. A. Polarogrammes enregistrés à 0, 1, 2 et 3 Faradays. B. Courbe $i = f(Q)$ pour la même électrolyse.

Pour tenter d'analyser le mécanisme de la réduction indirecte, en présence de sel de manganèse, particulièrement dans le cas des cétones les moins réductibles, nous avons enregistré les polarogrammes sur des échantillons prélevés en cours d'électrolyse et ramenés à des concentrations de 10^{-3} *M* (Fig. 3). Pour l'équimolarité entre le manganèse et la tétralone **1** par exemple, au début de l'électrolyse, le polarogramme présente la seule vague de réduction du complexe manganèse – cétone. Pendant le passage du premier Faraday, outre la décroissance de cette vague proportionnellement au nombre de coulombs consommés on note l'apparition de la vague de la cétone libre. Pour 1 Faraday, les deux vagues ont même hauteur. Entre 1 et 2 Faradays, la vague du complexe cétone – manganèse continue à décroître pour disparaître à 2 Faradays et alors seule la vague de réduction de la cétone libre apparaît. Après 2 Faradays la vague de la cétone diminue et disparaît peu après 3 Faradays. L'intensité du courant d'électrolyse (Fig. 3) est faible et constante (70 mA) jusque vers 0,6 F, décroît linéairement jusque 1 F à 40 mA, reste de nouveau constante jusque 1,6 F, décroît de nouveau linéairement pour rester sensiblement constante et très faible (de l'ordre de 10 mA) entre 2 et 3 F. Pour une électrolyse de Mn(II) seul, le courant initial est très faible vers 30 mV, constant jusque 0,6 F puis décroît linéairement pour s'annuler à 2 F. Il y a donc libération d'une partie de la cétone en cours d'électrolyse, cela pourrait s'expliquer par la disparition progressive de Mn(II) sous forme de

Can. J. Chem. Downloaded from www.nrcresearchpress.com by 210.87.254.6 on 09/06/12
For personal use only.

métal déposé et en suspension, ce qui libérerait les molécules de cétone complexées, quant aux courbes $i = f(Q)$ elles seraient en faveur d'un complexe Mn(I)–cétone montré par l'existence d'un palier de courant de 1 à 1,6 F lors de l'électrolyse du mélange équimolaire cétone – Mn(II). L'électrolyse a nécessité le passage total de 3 F pour obtenir les produits de réduction et disparition totale de la cétone initiale (1 F est nécessaire à la réduction de la cétone, 2 F pour réduire Mn(II) au stade Mn(0)).

Une autre façon d'évaluer le nombre d'électrons consommés par la réaction est d'arrêter l'électrolyse avant qu'elle soit terminée. Après passage de 2,2 F et traitement immédiat, on récupère 19% de cétone (tétralone **1**) et il s'est formé 63% de diol (*d, l:* 45%; *méso:* 18%); 80% du produit initial a donc réagi dès le passage d'environ 2 F. D'autre part, en amenant Mn(II) sous forme Mn(0) par électrolyse puis en ajoutant ensuite la tétralone **1** dans le milieu, la cétone de départ est récupérée intégralement que l'on maintienne ou non le potentiel de réduction imposé lors des électrolyses normales.

Il semble donc, que l'hydrodimérisation se fait pendant l'électrolyse par réaction entre la cétone et une espèce électrogénérée instable contenant du manganèse à bas état d'oxydation. Une condition impérative étant la présence de la cétone dès le début de l'électrolyse pour obtenir les meilleurs rendements (Tableau 1) (85% de diol pour la tétralone **1**), en effet, l'addition de la cétone à 1,5 F puis poursuite normale de l'électrolyse jusqu'à 3 F fournit 65% de diol (*d, l:* 50%; *méso:* 15%) et polymérisation.

Conclusion

Comme dans le cas du chrome (2–5), le système actif est le système Mn(II)/Mn(0). L'avantage certain du manganèse par rapport à Cr(II) est la stabilité de l'espèce Mn(II), ce qui entraine une plus grande simplicité du système et notamment supprime toute sorte de réactions parasites. Il faut aussi bien sûr pour le temps d'électrolyse décompter l'étape Cr(III)/Cr(II) inutile à la réduction électrochimique. Ceci permet de distinguer la réaction électrocatalysée (uniquement présentée avec Mn(II)) de la réduction chimique (cas de Cr(II)). Cette réduction parasite, qui complique les phénomènes, explique peut-être la non-réactivité de la xanthone et de la fluorénone avec Mn(II) (Tableau 1), bien que les 2 systèmes soient actifs avec Cr(III).

L'existence d'un complexe entre le métal et le composé carbonylé n'a pas pu être établie avec certitude mais est hautement probable. Pour les cétones **1** à **4** (plus difficiles à réduire que Mn(II) ou Cr(II)) où ΔV ($E_{1/2}$ métal $-$ $E_{1/2}$ cétone) est de l'ordre de 400 mV, les résultats sont à toute fin pratique identiques en présence de Mn(II) et en présence de Cr(II): rendements, proportions de glycol et d'alcool, proportions de diastéréoisomères *dl* et *méso*. Il semble que le mécanisme puisse être le même avec les deux espèces métalliques: réduction d'un complexe entre le métal à bas degré d'oxydation (I ou 0) et la cétone ou le radical cétyle, soit encore formation d'un film de métal colloïdal à la surface de l'électrode (5) sans toutefois éliminer complètement la réduction d'un complexe avec Cr(II) ou Mn(II) (2–5). Par contre, avec les cétones **5** et **6**, où ΔV est voisin de 150 mV, le mécanisme serait différent selon l'espèce métallique formée à l'électrode. Avec la cétone **7**, plus réductible que Cr(II) ou Mn(II) (ΔV de l'ordre de -300 mV), la réduction pourrait être, au moins en partie, réalisée directement par le métal(II) électrogénéré pendant la durée de l'électrolyse, comme le montre la similitude des résultats des réactions chimiques et électrochimiques (5). Pour rendre compte de l'inhibition de la polymérisation, il semble nécessaire que le radical électrogénéré directement ou indirectement, soit fixé par coordination ou chimisorption grâce à son atome d'oxygène sur un site agissant comme acide de Lewis. Cela explique en même temps la formation préférentielle des isomères *dl* des diols quand la cétone est dissymétrique, ainsi que le gain d'énergie d'activation observé pour la réduction de la cétone.

Nous ne pouvons, faute de données suffisantes, proposer pour l'instant un mécanisme précis quant à cette réduction. Nous avons entrepris l'étude du film par des méthodes spectroscopiques et électrochimiques. Cependant, un premier mécanisme peut être envisagé pour l'ensemble des différentes étapes réactionnelles:

L = DMF

$L_6\,Mn^{II} + \bar{e} \rightleftarrows L_6\,Mn^{I}$ rapide

$L_6\,Mn^{I} + R^1\,R^2\,C{=}O \rightleftarrows$ "complexe cétone – Mn^{I}" lent

"Complexe" $+ \bar{e} \rightleftarrows$ cétone $+ Mn^0$ (colloïdal) rapide

$Mn^0 + R^1\,R^2\,C{=}O \rightarrow$ produits de réduction (diols ou alcool) $+ Mn^{I}$ lent

(ou M^0 + cétone $\rightarrow M^0\cdots$ cétone adsorbée $\xrightarrow{\bar{e}}$ produits de réduction)

Ce mécanisme rend compte de l'apparition de la cétone libre en cours d'électrolyse et du caractère catalytique de la réduction (5). Nous poursuivons l'étude de cette réaction électrochimique avec d'autres sels de métaux de transition.

Partie expérimentale

Les points de fusion ont été déterminés au banc de Köfler et au microscope à platine chauffante Leitz. Les spectres ir ont été obtenus avec un spectromètre Pye–Unicam SP 3 200; ceux de rmn ^{1}H avec les appareils Bruker WP 80 et Bruker SY 250. Les chromatographies sur couche mince ont été réalisées sur gel de silice fluorescente "Merck PF-254", (plaque 20 × 20, e = 0,1 cm).

En électrochimie, tous les potentiels ont été mesurés par rapport à une électrode de référence au calomel et KCl saturé, à double jonction Tacussel RDJ/C 10. Les polarogrammes ont été enregistrés sur une table traçante XY Iffelec IF 3802 couplée à un polarographe PAR 174 A. Les voltammogrammes ont été réalisés grâce à un potentiostat PAR 173 gouverné par un générateur de signaux PAR 175, sur goutte de mercure fournie par une électrode de Kémula à piston micrométrique.

Les électrolyses ont été réalisées en atmosphère d'argon, à 20°C, avec un potentiostat PAR 173 muni d'un coulomètre PAR 179, sur une cathode de mercure de 26 cm^2 environ de surface et agitée avec un barreau aimanté. Les compartiments anodique et cathodique sont séparés par une pastille de verre fritté de porosité 4 et de 2,5 cm de diamètre. L'anode est un disque de platine de 2 cm de diamètre.

Le DMF utilisé contient du bromure de tétrabutylammonium 0,1 M et un peu d'eau 2×10^{-2} M environ (dosage de Karl–Fischer). Ainsi pour les analyses voltammétriques avec des concentrations en $MnCl_2 \cdot 4H_2O$ de 10^{-3} M, la concentration d'eau est de l'ordre de 2 à 3×10^{-2} M, pour les électrolyses où la concentration de sel de manganèse est en général de 7×10^{-2} M (5×10^{-3} mol dans 70 cm^3 de solvant), la concentration d'eau est de 0,45 M environ.

En fin de réaction (déterminée par analyse polarographique) le mélange obtenu est versé dans un grand volume d'eau (700 cm^3 au moins), extrait à l'éther et séché sur sulfate de sodium. Le solvant est chassé sous vide, le résidu séparé par chromatographie en couche mince de silice.

Beaucoup de produits obtenus sont connus (11–14) et nous les avons identifiés par leurs caractéristiques physiques et spectroscopiques, par comparaison avec celles d'échantillons authentiques. Les particularités observées et les spectres de rmn des glycols obtenus sont donnés dans les réfs. 5 et 10.

1. J. P. SEGUIN, J. P. DOUCET et R. UZAN. C. R. Acad. Sci. Ser. C, **278**, 129 (1974); M. A. MICHEL, G. MOUSSET et J. SIMONET. J. Electroanal. Chem. **98**, 319 (1979); C. P. ANDRIEUX et J. M. SAVEANT. Bull. Soc. Chim. Fr. 2090 (1973); E. LAMY, L. NADJO et J. M. SAVEANT. Electroanal. Chem. **50**, 141 (1974); W. R. FAWCETT et A. LASIA. Can. J. Chem. **59**, 3256 (1981); P. H. GIVEN, M. E. PEOVER et J. SCHOEN. J. Chem. Soc. 2674 (1958); A. BEWICK et H. CLEGHORN. J. Chem. Soc. Perkin Trans. **2**, 140 (1973).
2. M. PERRIN, P. POUILLEN, G. MOUSSET et P. MARTINET. Tetrahedron, **36**, 221 (1980); C. R. Acad. Sci. Ser. C, **284**, 955 (1977).
3. D. W. SOPHER et J. H. P. UTLEY. J. Chem. Soc. Chem. Commun. 1087 (1979).
4. F. FOURNIER, J. BERTHELOT et Y. L. PASCAL. C. R. Acad. Sci. **294**, série II, 849 (1982).
5. F. FOURNIER, J. BERTHELOT et Y. L. PASCAL. Tetrahedron. À paraître.
6. F. C. FREDERICK et K. E. JOHNSON. J. Electrochem. Soc. 2070 (1981).
7. G. ANTHOINE, J. NASIELSKI et B. WILMET-DEVOS. Bull. Soc. Chim. Belg. **78**, 465 (1969).
8. G. MAJERUS, E. YAX et G. OURISSON. Bull. Soc. Chim. Fr. 4143 (1967).
9. D. SEEBACH, H. A. OEI et H. DAUM. Chem. Ber. **110**, 2316 (1977).
10. Y. L. PASCAL, O. CONVERT, J. BERTHELOT et F. FOURNIER. Tetrahedron. Soumis à publication.
11. G. MAJERUS, E. YAX et G. OURISSON. Bull. Soc. Chim. Fr. 4143 (1967).
12. D. SEEBACH, H. A. OEI et H. DAUM. Chem. Ber. **110**, 2316 (1977).
13. H. GOTH, P. CERUTTI et H. SCHMIDT. Helv. Chim. Acta, **48**, 1395 (1965).
14. Y. ALTMAN et D. GINSBURG. J. Chem. Soc. 1498 (1961).

Can. J. Chem. Downloaded from www.nrcresearchpress.com by 210.87.254.6 on 09/06/12
For personal use only.

Synthèse et thermolyse de vinyl-2 aziridines N-non substituées

MOHAMED EL MEKKI ATTIA, YVONNE GELAS-MIALHE ET ROGER VESSIERE
Ecole Nationale Supérieure de Chimie, Université de Clermont 2, B.P. 45, 63170 Aubiere, France

Reçu le 16 décembre 1982

MOHAMED EL MEKKI ATTIA, YVONNE GELAS-MIALHE et ROGER VESSIERE. Can. J. Chem. **61**, 2126 (1983).

Les vinyl-2 aziridines N-non substituées sont préparées par action de phosphoranes sur des acyl-2 aziridines N-non substituées. L'étude de leurs spectres de rmn permet de préciser leur stéréochimie. Leur thermolyse conduit à des imines formées par ouverture vraisemblablement hétérolytique de la liaison carbone–carbone du cycle et migration du proton initialement lié à l'atome d'azote.

MOHAMED EL MEKKI ATTIA, YVONNE GELAS-MIALHE, and ROGER VESSIERE. Can. J. Chem. **61**, 2126 (1983).

N-unsubstituted 2-vinylaziridines are prepared from N-unsubstituted 2-acylaziridines and phosphoranes. Their stereochemistry is established from a study of their nmr spectra. Thermal isomerization of these compounds gives imines by a reaction involving heterolytic cleavage of the carbon–carbon bond of the ring and migration of hydrogen initially bound to nitrogen.

Can. J. Chem. Downloaded from www.nrcresearchpress.com by 210.87.254.42 on 09/06/12
For personal use only.

Plusieurs études consacrées à l'isomérisation thermique de vinyl-2 aziridines tertiaires ont mis en évidence le rôle important des substituants portés par l'hétérocycle sur l'évolution de la réaction. Celle-ci fait généralement intervenir, soit une rupture hétérolytique de la liaison carbone–carbone du cycle, soit une transposition sigmatropique (1).

Il nous a semblé intéressant de poursuivre les travaux que nous avions engagés dans ce domaine par l'étude du comportement thermique des vinyl-2 aziridines secondaires (N-non substituées) pour lesquelles aucun résultat n'était connu.

Seules, quelques méthodes particulières avaient été publiées concernant la synthèse des vinyl-2 aziridines secondaires (2), aussi avons-nous cherché, préalablement à notre étude, à mettre au point un procédé de préparation de ces produits aussi général que possible.

I. Préparation des vinyl-2 aziridines secondaires

Les vinyl-2 aziridines secondaires ont été préparées par un procédé identique à celui que nous avons mis en oeuvre pour accéder aux vinyl-2 aziridines tertiaires (1*a*) (Schéma 1).

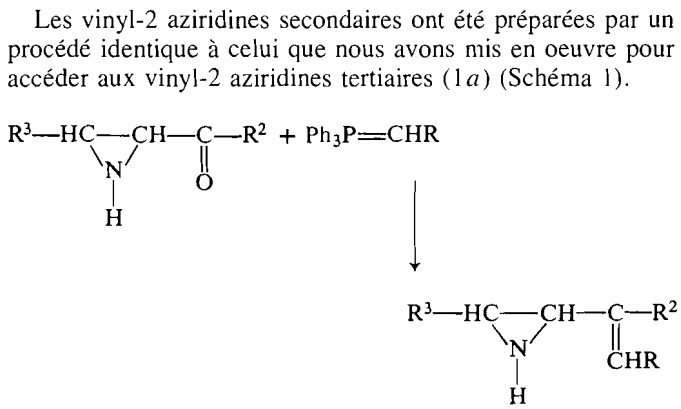

SCHÉMA 1

Les acyl-2 aziridines **1**, **2** et **3** (Tableau 1) utilisées dans cette réaction sont obtenues par action de l'ammoniac sur des cétones α,β-dibromées (réaction de Cromwell (3)). L'action sur ces dérivés de divers phosphoranes permet d'obtenir les vinyl-2 aziridines **4** à **11** (Tableau 1) avec des rendements en produits purs compris le plus souvent entre 40 et 60%.

Deux vinyl-2 aziridines isomères sont obtenues dans les expériences 4, 5 et 6 (Tableau 1). Seuls ont pu être séparés par chromatographie sur colonne les composés **9***a* et **9***b*.

La préparation du composé **11** (réaction 8, Tableau 1) n'est past toujours reproductible en raison de la grande sensibilité de ce produit à la chaleur (*vide infra*); il peut également être obtenu par une réaction de Horner entre la cétone **1** et le

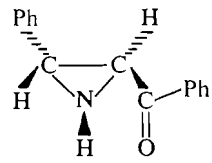

1 *S*R* trans*

SCHÉMA 2

diéthylphosphonoacétate d'éthyle; cette dernière réaction présente l'avantage d'être réalisée à température ambiante, toutefois son rendement est inférieur à celui de la réaction précédente.

L'identification et la détermination de la stéréochimie des acyl-2 et vinyl-2 aziridines ont été réalisées par étude de leurs spectres de résonance magnétique nucléaire. La configuration relative *S*R** ou *R*R** des atomes de carbone C-2 et C-3 du cycle[1] est déduite de la valeur de la constante de couplage $J_{H\text{-}2—H\text{-}3}$. Dans le cas des composés **4**, **7**, **8** et **9***b* cette constante ne peut être mesurée. Cependant, les résultats des expériences 2, 3, 6, 7 et 8 montrent que, comme pour les aziridines tertiaires (1*a*) la configuration relative des atomes de carbone C-2 et C-3 de la vinyl-2 aziridine est la même que celle de l'acyl-2 aziridine qui lui a donné naissance. Par analogie, nous avons donc attribué une configuration *R*R** aux dérivés **4**, **7**, **8** et **9***b*.

La position de l'atome d'hydrogène lié à l'atome d'azote par rapport aux substituants du cycle peut également être précisée; elle est déduite de la valeur des couplages $^3J_{H—N—C—H\text{-}2}$ et $^3J_{H—N—C—H\text{-}3}$ (4). Dans le cas des composés **1** et **9***a*, la mise en évidence de ces couplages (voir partie expérimentale) à 25°C et à 60°C montre que dans cet intervalle de température les deux molécules possèdent la configuration pour laquelle l'atome d'hydrogène lié à l'atome d'azote et le substituant fixé sur le carbone C-2 sont en position *cis* (Schéma 2). Une constatation identique a été faite par Lopez (5).

Le spectre de l'aziridine **4** est mal résolu à température ambiante. Par contre, il peut être analysé à −40°C, il indique

[1]Dans le cas d'une acyl-2 aziridine de configuration *S*R** les atomes d'hydrogène liés aux atomes de carbone C-2 et C-3 du cycle sont en *trans* par rapport au plan du cycle (schéma 2). Ces mêmes atomes sont, par contre, en *cis* chez la vinyl-2 aziridine de configuration de même désignation *S*R**. L'aziridine est dite *trans* (*cis*) lorsque l'atome d'hydrogène lié à l'atome d'azote est en position *trans* (*cis*) par rapport à l'atome d'hydrogène porté par le carbone C-2.

TABLEAU 1. Vinylaziridines préparées par réaction de Wittig sur les acyl-2 aziridines

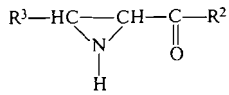

Exp No	Composé	R^3	R^2	Stéréochimie[a]	Phosphorane	Composé	Stéréochimie[a]	Rdt (%)
1	**1**	Ph	Ph	*S*R* trans*	$Ph_3P{=}CH_2$	**4**	**4** *cis*/**4** *trans* = 47:53	59
2	**2**	CH_3	Ph	*S*R**	$Ph_3P{=}CH_2$	**5**	*R*R**	48
3	**3**	CH_3	Ph	*R*R**	$Ph_3P{=}CH_2$	**6**	*S*R**	46
4	**1**	Ph	Ph	*S*R**	$Ph_3P{=}CH{-}CH_3$	**7***a*/**7***b* = 45:55	*Z*/*E*	62
5	**2**	CH_3	Ph	*S*R**	$Ph_3P{=}CH{-}CH_3$	**8***a*/**8***b* = 50:50	*Z*/*E*	44
6	**1**	Ph	Ph	*S*R**	$Ph_3P{=}CHPh$	**9***a*/**9***b* = 70:30	*R*R*Z*/*R*R*E*[b]	58
7	**2**	CH_3	Ph	*S*R**	$Ph_3P{=}CHPh$	**10**	*R*R**	12,5
8	**1**	Ph	Ph	*S*R**	$Ph_3P{=}CH{-}COOEt$	**11**	*R*R**	20

[a]Déterminée par rmn de ^1H; les symboles *R** et *S** définissent la configuration relative des atomes de carbone C-2 et C-3 du cycle; les symboles *E* et *Z* concernent la configuration de la double liaison. L'aziridine est dite *trans* (*cis*) lorsque l'atome d'hydrogène lié à l'atome d'azote est en position *trans* (*cis*) par rapport à l'atome d'hydrogène porté par le carbone C-2.
[b]L'aziridine **9***a* possède la configuration *trans*.

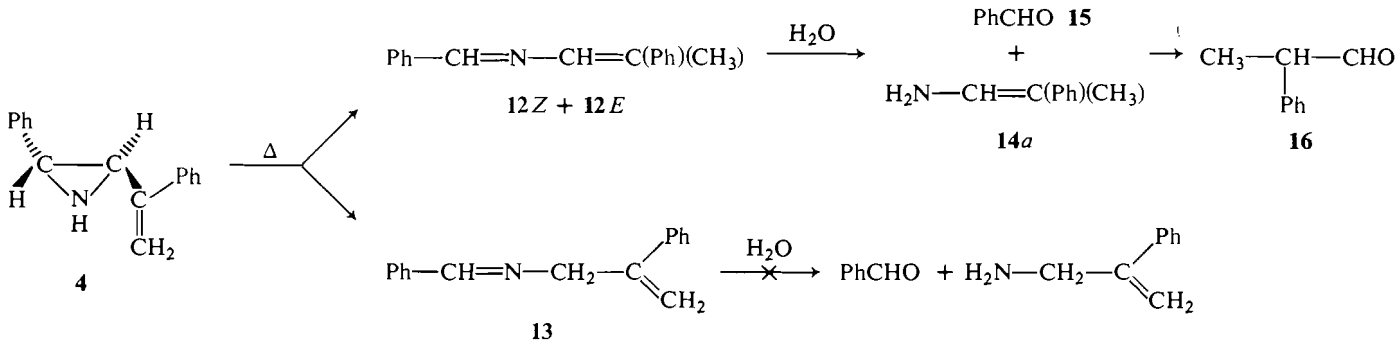

SCHÉMA 3

que l'on est alors en présence des deux invertomères *cis* et *trans* de l'aziridine **4** dans les proportions *cis*/*trans* = 47:53, ce qui correspond pour le phénomène d'inversion à une énergie libre $\Delta G_0 = -0{,}05$ kcal/mol. Le spectre obtenu à +60°C montre qu'à cette température la vitesse d'inversion est importante; la température de coalescence correspond à la température ambiante (les spectres sont donnés dans la partie expérimentale).

L'étude des spectres de rmn ^1H des vinyl-2 aziridines permet également de déterminer la configuration de la double liaison. La configuration *E* des composés **7***b* et **8***b* est déduite de la présence d'un couplage homoallylique entre le proton H-2 et le groupement méthyle fixé sur la double liaison; ce couplage correspond à une disposition transoïde des protons considérés. La configuration *Z* de l'isomère **9***a* se déduit du déplacement vers les champs faibles du proton H-2 par rapport à celui de **9***b*; en effet, dans cette configuration, le groupement phényle situé dans le plan du proton H-2 provoque son déblindage.

II. Isomérisation thermique des vinyl-2 aziridines

Les conditions optimales dans lesquelles les réactions d'isomérisation ont été réalisées, ainsi que la nature des produits identifiés, sont précisées dans le tableau 2.

L'examen par rmn du produit brut de thermolyse de l'aziridine **4** (expérience 9) permet d'identifier les composés **12** et **13** que nous avons séparés par chromatographie liquide à haute pression. Le composé **12** est, d'après son spectre, un mélange des deux isomères éthyléniques *E* et *Z*, l'isomère le plus abondant étant le dérivé *E* pour lequel le signal du groupement méthyle résonne au champ le plus faible en raison de sa situation en *cis* par rapport à l'atome d'azote. Le produit brut de thermolyse se décompose au cours de la séparation de ses constituants par chromatographie sur colonne de gel de silice. En sortie de colonne on obtient un mélange des produits **14***a*, **15** et **16** identifiés par comparaison avec des échantillons authentiques. L'hydrolyse du produit brut de thermolyse conduit à la formation de ces trois mêmes composés que l'on obtient également en abandonnant le produit brut quelques jours à température ambiante. Ces résultats montrent clairement que le produit primaire de l'isomérisation thermique de l'aziridine **4** est constitué des imines **12** et **13**, lesquelles sont facilement hydrolysées en benzaldéhyde et énamine **14***a*; cette dernière donne naissance à l'aldéhyde **16** (Schéma 3).

La (phényl-2 éthyl)amine, produit d'hydrolyse de l'imine **13**, n'est pas isolée. On peut penser qu'elle s'isomérise dans le milieu réactionnel en amine conjuguée **14***a*. On peut également envisager que l'isomérisation de l'imine **13** en imine conjuguée **12** est plus rapide que son hydrolyse.

Les expériences 10, 11 et 16 (Tableau 2) montrent que les réactions d'isomérisation thermique des aziridines **9***a*, **9***b* et **11** se déroulent de façon analogue à la réaction précédemment décrite; les produits primaires sont constitués par des imines dont l'hydrolyse (expérience 10) conduit à un mélange d'aldéhyde et d'amine. On peut rapprocher de l'expérience 16 la réaction décrite par Heine *et al.* (6) concernant l'action de l'éthoxycarbonylméthylènetriphénylphosphorane sur la *p*-nitrophényl-3 benzoyl-2 aziridine, réaction dans laquelle seule une imine est isolée (Schéma 4).

Dans les expériences 12, 13, 14 et 15, nous avons uniquement identifié les dérivés d'hydrolyse des produits de thermolyse. Les produits isolés dans l'expérience 13 sont les mêmes

Can. J. Chem. Downloaded from www.nrcresearchpress.com by 210.87.254.42 on 09/06/12
For personal use only.

TABLEAU 2. Thermolyse des vinyl-2 aziridines

Exp No	Aziridines	Conditions opératoires optimales[a] Temps	θ°C	Produits identifiés Après hplc	Après lc sur colonne de silice
9	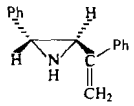 **4**	2h30	100	75% Ph—CH=N—CH=C(Ph)(CH$_3$) **12** E/**12** Z = 90:10 25% Ph—CH=N—CH$_2$—C(Ph)=CH$_2$ **13**	(Ph)(CH$_3$)C=CH—NH$_2$ **14**a PhCHO **15** PhCH(CH$_3$)—CHO **16**
10	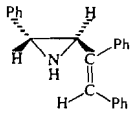 **9**b	2h30	100	35% Ph—CH$_2$—N=CH—C(Ph)=CHPh **17**a 50% Ph—CH=N—CH=C(Ph)CH$_2$Ph **18** 15% Ph—CH=N—CH$_2$—C(Ph)=CHPh **19**	PhCHO **15** Ph—CH$_2$—C(Ph)=CH—NH$_2$ **20** Ph—CH=C(Ph)—CHO **21** Ph—CH$_2$—CHPh—CHO **22**
11	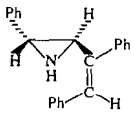 **9**a	2h30	100	25% Ph—CH=N—CH=C(Ph)—CH$_2$Ph **18** 75% Ph—CH$_2$—N=CH—C(Ph)=CHPh **17**a/**17**b = 55:45	
12	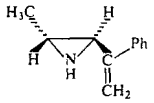 **5**	2h	200		(Ph)(CH$_3$)C=CH—NH$_2$ **14**b
13	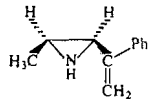 **6**	2h	200		(Ph)(CH$_3$)C=CHNH$_2$ **14**a CH$_3$—CH(Ph)—CHO **16**
14	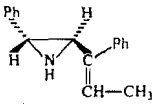 **7**a/**7**b = 45:55	3h	100		**7**b CH$_3$—CH=C(Ph)—CHO **23** 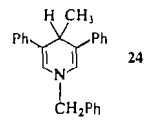 **24**
15	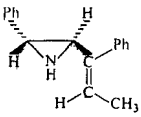 **7**b	2 h	150		**24**
16	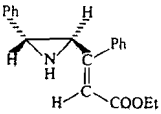 **11**	4 Jours, CHCl$_3$ à reflux			Ph—CH=N—CH$_2$—C(Ph)=CH—COOC$_2$H$_5$ **25**

[a]Conditions optimales établies après avoir fait varier température et temps de thermolyse, le produit brut étant analysé par rmn ^{1}H. Dans ces conditions, à l'exception de l'expérience 14, le rendement de la thermolyse est quantitatif.

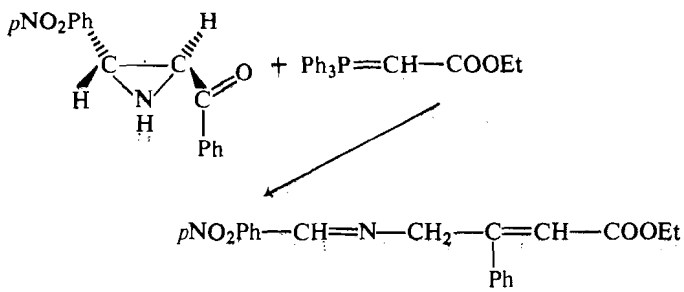

SCHÉMA 4

que ceux obtenus dans l'expérience 9, indiquant un comportement analogue des composés **4** et **6**. L'énamine **14**b isolée dans l'expérience 12 est le stéréoisomère du dérivé **14**a isolé dans les expériences 9 et 13. Le groupement méthyle du produit **14**b (δ = 2,60 ppm) résonne à champ plus faible que celui de **14**a (δ = 2,53 ppm), ce qui nous incite à lui attribuer la configuration E.

L'α-phénylcrotonaldéhyde **23** isolé dans l'expérience 14 provient très vraisemblablement de l'hydrolyse de l'imine formée dans l'ouverture thermique de l'aziridine **7** (schéma 5).

Le deuxième produit d'hydrolyse de cette imine, la benzylamine, n'est pas isolé; cependant, sa formation est prouvée par l'obtention de la dihydropyridine **24**. En effet, nous avons vérifié que ce produit se formait par action de la benzylamine sur l'α-phénylcrotonaldéhyde; il résulte très vraisemblablement de la dimérisation de l'imine née de la condensation de l'amine sur l'aldéhyde (7).

Au cours de l'expérience 14 seule est isomérisée l'aziridine **7**a; la purification du produit brut de thermolyse permet alors d'obtenir l'isomère **7**b pur. A température plus élevée (150°C)

Can. J. Chem. Downloaded from www.nrcresearchpress.com by 210.87.254.42 on 09/06/12
For personal use only.

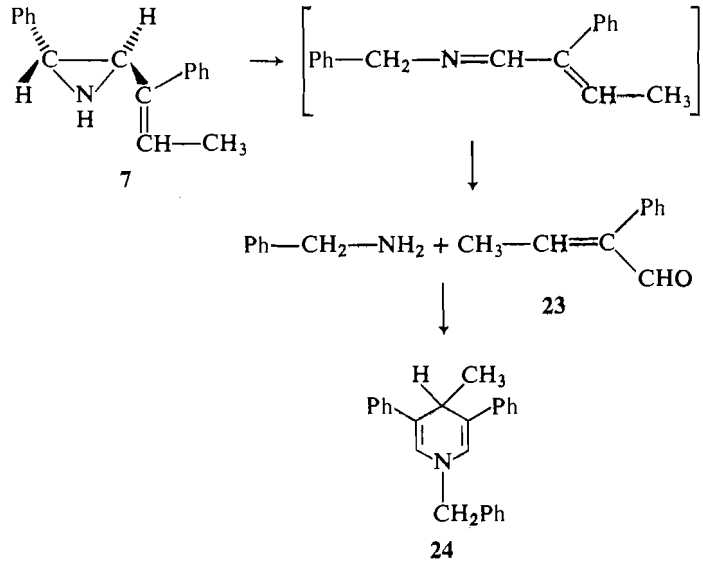

SCHÉMA 5

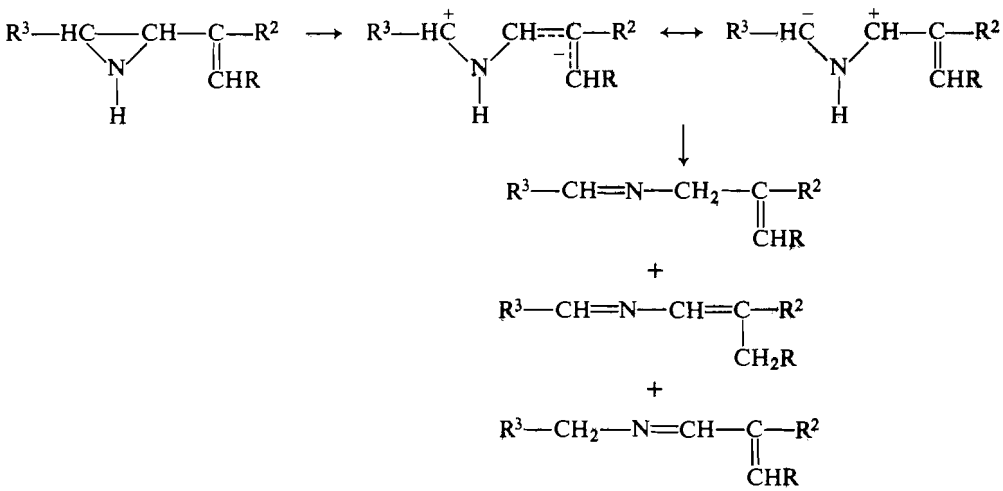

SCHÉMA 6

ce dernier se réarrange, conduisant à la dihydropyridine **24** (exp. 15).

Discussion des résultats

La structure des produits de thermolyse implique une rupture de la liaison carbone–carbone du cycle aziridine, rupture favorisée par la présence d'un groupement phényle sur le carbone C-3 comme le montre la comparaison des expériences 9 et 12. Une ouverture radicalaire semble peu probable. En effet, on ne connaît pas d'exemple d'ouverture thermique d'aziridines par homolyse de la liaison carbone–carbone du cycle. Cette isomérisation met plus vraisemblablement en jeu une ouverture conrotatoire de l'aziridine en ylure d'azométhine suivie d'une migration intramoléculaire de proton vers le centre le plus nucléophile du dipôle (schéma 6).

III. Conclusion

Au cours de ce travail, nous avons montré que les vinyl-2 aziridines secondaires étaient aisément accessibles à partir des acyl-2 aziridines secondaires par réaction de Wittig. Leur thermolyse conduit à des imines formées par ouverture vraisemblablement hétérolytique de la liaison carbone–carbone du cycle et migration du proton initialement lié à l'atome d'azote.

Ce comportement, différent de celui des vinyl-2 aziridines tertiaires pour lesquelles on observe généralement un agrandissement de cycle (1), met parfaitement en évidence le rôle capital du substituant lié à l'atome d'azote pour l'évolution des thermolyses des vinylaziridines.

Partie expérimentale

Les spectres de résonance magnétique nucléaire ont été enregistrés à l'aide des appareils Varian A 60, Varian T 60 ou Jeol 60 pour ^1H et Jeol FX 60 pour ^{13}C en utilisant le tétraméthylsilane comme référence interne. Les déplacements chimiques sont exprimés en ppm et les constantes de couplage en Hertz. Les solutions utilisées pour étudier le phénomène d'inversion de l'atome d'azote ont été soigneusement séchées, soit sur alumine, soit sur pastilles de soude. Les spectres infrarouge ont été effectués sur un spectrophotomètre Perkin–Elmer 157. Les spectres uv ont été enregistrés sur un appareil Cary 14. Les chromatographies sur colonne ont été réalisées, soit sur gel de silice (Merck 7734), soit à moyenne pression sur Lichoprep Si 60 (colonnes Merck Lobar). Les chromatographies liquides à haute pression ont été effectuées sur un appareil Waters 440 avec pompe M 6000 A et réfractomètre différentiel R 401 (colonnes Microporasil).

Préparation des acyl-2 aziridines 1, 2 et 3

Préparées selon le mode opératoire décrit par Weber et Bandlow (8).

Can. J. Chem. Downloaded from www.nrcresearchpress.com by 210.87.254.42 on 09/06/12
For personal use only.

Can. J. Chem. Downloaded from www.nrcresearchpress.com by 210.87.254.42 on 09/06/12
For personal use only.

Phényl-3 benzoyl-2 aziridine ***1***

Rdt = 82%; F = 97−98°C (litt. (9) F = 100−102°C); ir (cm^{-1}): 1670, 3235; rmn ^1H ($CDCl_3$): 2,72 (t large, N—H), 3,17 (dd, H-2, J = 2,4 (*trans*), J = 8,8 (*cis*)), 3,50 (dd, H-3, J = 2,4 (*trans*), J = 6,8 (*trans*)), 7,20 à 7,80 (m, C_6H_5); rmn ^{13}C ($CDCl_3$): 43,5 (C-2), 44,1 (C-3), 126,4, 128,1, 128,5, 128,7, 129,0, 134,0, 136,1, 138,5, (C_6H_5), 196,0 (C=O).

Méthyl-3 benzoyl-2 aziridines ***2*** *et* ***3***

Le produit brut (Rdt = 88%) est constitué d'un mélange des isomères **2** (50%) et **3** (50%). Ils sont séparés par chromatographie sur colonne (chloroforme/acétate d'éthyle 1:1).

Isomère ***2*** S*R*: ir (cm^{-1}): 3325, 1680; rmn ^1H ($CDCl_3$): 2,72 (pic large, N—H), 2.18 (dq, H-3, J = 2,5 (*trans*), J = 5,3), 3,24 (d, H-2, J = 2,5), 1,33 (d, CH_3, J = 5,3), 7,20 à 8,20 (m, C_6H_5); rmn ^{13}C ($CDCl_3$): 18,6 (CH_3), 38,1 (C-3), 40,5 (C-2), 128,1, 128,6, 133,4, 136,2 (C_6H_5), 196,8 (C=O).

Isomère ***3*** R*R*: ir (cm^{-1}): 3320, 1680; rmn ^1H ($CDCl_3$): 2,26 (pic large, N—H), 2,55 (dq, H-3, J = 6,2 (*cis*), J = 5,8), 3,53 (d, H-2, J = 6,2 (*cis*)), 1,11 (d, CH_3, J = 5,8), 7,25 à 8,20 (m, C_6H_5); rmn ^{13}C ($CDCl_3$): 12,7 (CH_3), 36,6 (C-2), 39,8 (C-3), 128,1, 128,7, 133,5, 136,6 (C_6H_5), 195,9 (C=O).

Préparation des vinyl-2 aziridines

Dans un réacteur muni d'un agitateur et traversé par un courant d'argon, on place 0,045 mol d'hydrure de sodium préalablement lavé au pentane et ajoute 35 mL de diméthylsulfoxyde sec. On chauffe à 75−80°C pendant 45 min puis, le mélange étant refroidi par un bain glace−sel, on ajoute 0,045 mol de sel de phosphonium en solution dans 40 mL de diméthylsulfoxyde et poursuit l'agitation pendant 45 min à température ambiante. On introduit alors 0,03 mol d'acyl-2 aziridine en solution dans 20 mL de diméthylsulfoxyde. L'agitation est maintenue pendant 14 h à température ambiante, puis pendant 2 h à 60°C. Le mélange réactionnel est alors refroidi et versé dans l'eau glacée. On extrait à l'éther, lave les extraits à l'eau, sèche et concentre. Les produits sont alors purifiés.

Phényl-3 (phényl-1 vinyl)-2 aziridine ***4***

Le produit brut est purifié par chromatographie sur colonne (benzène/acétone 9:1): Rdt = 59%; F = 73−75°C; ir (cm^{-1}): 3270, 1640, 1600; rmn ^1H (CCl_4 + NaOH) −40°C: 0,98 (t, 0,47 H, J = 9, J = 8), 1,38 (t, 0,53 H, J = 9, J = 8), 2,40 à 3 (m, 2H), 4,98 et 5,30 à 5,50 (m, 2H, $=CH_2$), 7 à 7,50 (m, C_6H_5); +25°C: 1,05 (m, 1H, signal très large, largeur à mi-hauteur = 37 Hz), 2,65 (m de quatre pics mal résolus, 2H, largeur à mi-hauteur = 27 Hz), 5,0 et 5,32 (2 pics larges, 2H, $=CH_2$), 7,0 à 7,50 (m, C_6H_5); +60°C: 1,15 (m, 1H, N—H), 2,75 (2 pics larges séparés par 8,2 Hz, largeur à mi-hauteur = 15 Hz, 2H), 5,10 et 5,38 (s, 2H, $=CH_2$), 7 à 7,50 (m, C_6H_5); rmn ^1H ($CDCl_3$): 1,45 (s large, 1H, N—H), 2,83 (s, 2H, H-2 et H-3), 5,23 et 5,43 (s, 2H, $=CH_2$), 7,10 à 7,60 (m, C_6H_5); rmn ^{13}C ($CDCl_3$): 42,1, 43,8, 125,7, 126,2, 127,3, 128,0, 128,5, 128,6, 139,0, 139,6, 110,4, 146,6. *Anal.* calc. pour $C_{16}H_{15}N$: C 86,88, H 6,79, N 6,33; trouvé: C 86,69, H 6,85, N 6,38.

Méthyl-3 (phényl-1 vinyl)-2 aziridine ***5***

Le produit brut est purifié par chromatographie sur colonne (chloroforme/acétate d'éthyle 1:1): Rdt = 48%; ir (cm^{-1}): 3220, 1630, 1600; rmn ^1H ($CDCl_3$): 0,95 (s large, 1H, N—H), 1,27 (d, 3H, J = 5, CH_3), 1,81 (dq, 1H, H-3, J = 5, J = 2,8 (*trans*)), 2,35 (d, pics larges, 1H, H-2, J = 2,8 (*trans*)), 5,10 dd et 5,29 d (2H, $=CH_2$, J = 0,8 (*gem*) et ^4J = 1); rmn ^{13}C ($CDCl_3$): 19,2 (CH_3), 35,3 (C-3), 40,5 (C-2), 126,0, 128,3, 127,7, 139,4 (C_6H_5), 110,2 et 146,9 (C=C). *Anal.* calc. pour $C_{11}H_{13}N$: C 83,02, H 8,18, N 8,81; trouvé: C 82,83, H 8,34, N 8,89.

Méthyl-3 (phényl-1 vinyl)-2 aziridine ***6***

Purifiée par chromatographie sur colonne (chloroforme/acétate d'éthyle 1:1): Rdt = 46%; ir (cm^{-1}): 3220, 1630, 1600; rmn ^1H ($CDCl_3$): 0,95 (d, 3H, CH_3, J = 5,2), 1,20 (s large, N—H), 2,25 (dq, 1H, H-3, J = 6,2 (*cis*), J = 5,2), 2,75 (d, 1H, H-2, J = 6,2 (*cis*)), 5,31 d et 5,59 d (2H, $=CH_2$, J = 0,7 (*gem*)), 7,15 à 7,60 (m, C_6H_5). *Anal.* calc. pour $C_{11}H_{13}N$: C 83,02, H 8,18, N 8,81; trouvé: C 83,12, H 8,14, N 8,83.

Phényl-3 (phényl-1 propène-1 yl)-2 aziridine ***7***

Purifiée par chromatographie sur colonne (chloroforme/acétone 98:2). On obtient un mélange des isomères **7***a* et **7***b* dans le rapport **7***a*/**7***b* = 55:45: Rdt = 62%; ir (cm^{-1}): 3200, 1600; rmn ^1H ($CDCl_3$) de **7***a*: 1,1 (s large, 1H, N—H), 1,52 (d, 3H, J = 6,9, CH_3), 2,73 (s, 2H, H-2 et H-3), 5,79 (dq, 1H, =CH, ^4J = 1,6, J = 6,9), 7,10 à 7,50 (m, C_6H_5); rmn ^1H ($CDCl_3$) de **7***b*: 1,84 (dd, 3H, CH_3, ^5J = 0,8, ^3J = 6,9), 2,80 (m, 2H, H-2 et H-3), 5,92 (dq, 1H, =CH, ^3J = 6,9, ^4J = 1,4), 7,10 à 7,50 (m, C_6H_5); rmn ^{13}C ($CDCl_3$) de **7***a*: 14,6, 39,2, 46,7, 123,4, 126,2, 127,4, 129,1, 136,7, 139,9; rmn ^{13}C ($CDCl_3$) de **7***b*: 14,3, 39,8, 41,3, 125,7, 127,0, 127,2, 127,6, 128,2, 128,4, 138,8, 139,8. *Anal.* calc. pour $C_{17}H_{17}N$: C 86,81, H 7,23, N 5,96: trouvé: C 86,61, H 7,13, N 5,91.

Méthyl-3 (phényl-1 propène-1 yl)-2 aziridine ***8***

Le produit brut est, d'après son spectre de rmn ^1H, constitué d'un mélange des isomères **8***a* et **8***b* dans le rapport **8***a*/**8***b* = 50:50; on relève en effet sur le spectre deux doublets à 1,85 (J = 7) et 1,50 (J = 7) et deux quadruplets à 5,73 et 5,85. Il est purifié par chromatographie sur colonne (chloroforme/acétate d'éthyle 1:1). On obtient l'isomère **8***b* pur: Rdt = 44%; ir (cm^{-1}): 3220, 1670, 1610; rmn ^1H ($CDCl_3$): 1,22 (d, 3H, J = 5,5), 1,85 (dd, 3H, J = 7, J = 0,8), 2 à 2,70 (m, 3H), 5,80 (dq, 1H, J = 7, ^4J = 1,2), 7 à 8,10 (m, C_6H_5). *Anal.* calc. pour $C_{12}H_{15}N$: C 83,24, H 8,67, N 8,09; trouvé: C 83,51, H 8,63, N 8,28.

Phényl-3 (phényl-1 styryl)-2 aziridine ***9***

Le produit brut est purifié par chromatographie sur colonne (benzène/acétate d'ethyle 80:20). On obtient un mélange des isomères **9***a* et **9***b* dans le rapport **9***a*/**9***b* = 70:30: Rdt = 58%. Ils sont séparés par chromatographie sur colonne (éther de pétrole/acétate d'éthyle 85:15).

Isomère ***9***a: F = 106−107°C; ir (cm^{-1}): 3200, 1600, 1590; rmn ^1H ($CDCl_3$): 1,20 (s large, 1H, N—H), 2,81 (d, 1H, H-3, J = 2,8 (*trans*)), 3,08 (dd, 1H, H-2, J = 2,8 (*trans*), ^4J = 1), 6,89 (s large, 1H, =CH), 7,10 à 7,70 (m, C_6H_5); rmn ^1H (C_6H_6 + NaOH), +25°C: 0,97 (t, pics larges, 1H, N—H, J = 9,2 (*cis*), J = 8,4 (*trans*)), 2,62 (dd, 1H, H-3, J = 9,2 (*cis*), J = 3 (*trans*)), 2,98 (d, pics larges, largeur à mi-hauteur = 6,4 Hz, 1H, H-2, J = 8,4 (*trans*)); rmn ^1H (C_6H_6 + NaOH), +60°C: 1,0 (t, 1H, N—H, J = 8,4 (*trans*), J = 9,2 (*cis*)), 2,75 (dd, H-3, J = 3 (*trans*), J = 9,2 (*cis*)), 3,08 (ddd, H-2, ^4J = 1,5, J = 3 (*trans*), J = 8,4 (*trans*)); rmn ^{13}C ($CDCl_3$): 41,3, 42,6, 125,9, 127,1, 127,3, 127,9, 128,3, 128,9, 129,0, 129,4, 131,2, 136,4, 139,4, 139,6, 139,9. *Anal.* calc. pour $C_{22}H_{19}N$: C 88,89, H 6,40, N 4,71; trouvé: C 88,71, H 6,47, N 4,76.

Isomère ***9***b: F = 101−102°C; ir (cm^{-1}): 3200, 1600, 1590; rmn ^1H ($CDCl_3$): 1,62 (s large, 1H, N—H), 2,83 (s large, 2H, H-2 et H-3), 6,71 (s, 1H, =CH), 6,90 à 7,60 (m, C_6H_5); rmn ^{13}C ($CDCl_3$): 39,6, 47,6, 125,9, 126,8, 127,1, 127,5, 127,9, 128,4, 128,9, 129,0, 129,2, 136,3, 136,8, 139,6, 139,7. *Anal.* calc. pour $C_{22}H_{19}N$: 88,89, H 6,40, N 4,71; trouvé: C 88,93, H 6,52, N 4,64.

Méthyl-3 (phényl-1 styryl)-2 aziridine ***10***

Le produit brut est purifié par chromatographie sur colonne (chloroforme/acétate d'éthyle 1:1): Rdt = 12,5%; ir (cm^{-1}): 3250, 1600, 1580; rmn ^1H ($CDCl_3$): 1,21 (d, 3H, CH_3, J = 5,2), 1,80 (dq, 1H, H-3, J = 5,2, J = 2,5 (*trans*)), 2,72 (dd, 1H, H-2, J = 2,5 (*trans*), ^4J = 1), 6,80 (d, 1H, =CH, ^4J = 1), 7,15 à 7,70 (m, C_6H_5). *Anal.* calc. pour $C_{17}H_{17}N$: C 86,81, H 7,23, N 5,96; trouvé: C 86,41, H 7,10, N 5,76.

Phényl-3 (éthoxycarbonyl-2 phényl-1 vinyl)-2 aziridine ***11***

(a) On chauffe à reflux pendant 24 h une solution de 0,005 mol d'aziridine **1** et de 0,005 mol d'éthoxycarbonylméthylènetriphénylphosphorane dans 150 mL de chloroforme anhydre. On évapore ensuite le solvant, reprend à l'alcool, filtre et concentre. Le produit brut est purifié par chromatographie sur colonne (éther de pétrole/acétate d'éthyle 85:15): Rdt = 20%; ir (cm^{-1}): 3200, 1720, 1640, 1600; rmn ^1H ($CDCl_3$): 1,50 (s large, 1H, N—H), 2.78 (spectre AB, 2H, H-2 et H-3, J = 2,5), 6,15 (s, 1H, =CH), 1,03 (t, 3H, J = 7), 3,98 (q, 2H, J = 7), 7,10 à 7,60 (m, C_6H_5). *Anal.* calc. pour $C_{19}H_{19}NO_2$: C 77,82, H 6,48, N 4,78; trouvé: C 77,42, H 6,42, N 4,83.

Can. J. Chem. Downloaded from www.nrcresearchpress.com by 210.87.254.42 on 09/06/12
For personal use only.

(b) A 0,005 mol de NaH mis en suspension dans 10 mL de THF, on ajoute 0,005 mol de phosphonate en solution dans 10 mL de THF. On laisse 45 min sous agitation et sous argon puis on ajoute 0,005 mol d'aziridine **1** dissoute dans 15 mL de THF. Après 5 heures de réaction à température ambiante on verse le mélange réactionnel dans de l'eau glacée, extrait à l'éther, sèche puis concentre. Le produit brut est ensuite purifié comme précédemment: Rdt = 10%.

Isomérisation thermique des vinyl-2 aziridines

Un échantillon de 5 mmol de vinyl-2 aziridine pure, en ampoule scellée sous argon, est chauffé au bain d'huile. Les conditions expérimentales particulières à chaque composé sont données dans le tableau 2. En fin de réaction le produit brut est analysé en rmn puis purifié.

Isomérisation de la phényl-3 (phényl-1 vinyl)-2 aziridine ***4***

La purification du produit de thermolyse par hplc (isooctane/acétate d'éthyle 98:2) permet de séparer les imines **12** et **13**.

N-*benzylidène méthyl-2 styrylamine* ***12***: F = 64−66°C; ir (cm^{-1}): 1680, 1627, 1602; rmn ^1H ($CDCl_3$): 2,22 (s large, 0,3H), 2,51 (s large, 2,7H), 7 à 8 (m, C_6H_5 et CH=C), 8,28 (s large, 1H, CH=N); rmn ^{13}C ($CDCl_3$): 15,5, 125,8, 127,5, 128,4, 128,6, 130,7, 136,8, 139,2, 141,1, 159,2.

N-*benzylidène phényl-2 allylamine* ***13***: ir (cm^{-1}): 1680, 1642, 1600; rmn ^1H ($CDCl_3$): 4,62 (m, 1H), 4,80 (m, 1H), 5,25 (m, 1H), 5,50 (m, 1H), 7 à 8 (m, C_6H_5), 8,28 (s large, 1H); rmn ^{13}C ($CDCl_3$): 64,1, 96,0, 113,5, 125,3, 126,0, 126,5, 127,0, 127,2, 128,3, 130,7, 162,2.

L'hydrolyse en milieu chlorhydrique du produit de thermolyse conduit à un mélange des aldéhydes **15** et **16** identifiés par comparaison avec des échantillons authentiques et de l'énamine **14***a* identifiée par comparaison avec un échantillon préparé selon une méthode décrite (10).

Enamine ***14***a: rmn ^1H ($CDCl_3$): 2,53 (s large, 3H), 7 à 8 (m, 8H).

Isomérisation thermique de la phényl-3 (phényl-1 styryl)-2 aziridine ***9***

Le produit de thermolyse de **9***b* est purifié par chromatographie liquide haute pression (isooctane/acétate d'éthyle 98:2). On obtient l'imine **17***a* pure et un mélange des dérivés **18** et **19** (**18**/**19** = 75:25).

Imine ***17***a: ir (cm^{-1}): 1600, 1615, 1660, 1685, 1715; rmn ^1H ($CDCl_3$): 4,7 (pic large, 2H), 8,30 (s large, 1H), 6,90 à 7,90 (m, C_6H_5 et C=CH); rmn ^{13}C ($CDCl_3$): 65,0, 127,0, 127,8, 128,0, 128,3, 128,6, 129,0, 129,2, 129,4, 129,7, 129,9, 130,8, 162,0.

Imine ***18***: ir (cm^{-1}): 1600, 1685; rmn ^1H ($CDCl_3$): 4,5 (pic large, 2H), 8,15 (s large, 1H), 6,90 à 7,90 (m, C_6H_5 et C=CH); rmn ^{13}C ($CDCl_3$): 35,3, 125,7, 126,6, 126,9, 127,4, 128,3, 128,6, 129,4, 129,9, 130,1, 130,9, 139,9, 140,5, 160,0.

Imine ***19***: rmn ^1H ($CDCl_3$): 4,20 (pic large, 2H), 8,40 à 8,60 (s large, 1H), 6,90 à 7,90 (m, C_6H_5 et C=CH).

Le produit de thermolyse de l'aziridine **9***a* est, d'après ses spectres de rmn, composé des imines **17***a* (40%), **17***b* (35%) et **18** (25%); rmn ^1H ($CDCl_3$): 4,5 (pic large, 0,5H), 4,7 (pic large, 0,8H), 4,8 (pic large, 0,7H), 6,90 à 7,90 (m, C_6H_5 et C=CH), 8,15 (s large, 0,25H), 8,30 (s large, 0,75H); rmn ^{13}C ($CDCl_3$): 35,3, 59,3, 65,0, 125,7, 125,9, 126,6, 126,8, 127,0, 127,2, 127,5, 128,4, 129,0, 129,4, 129,8, 130,1, 130,7, 131,4, 131,6, 136,4, 136,8, 137,3, 138,4, 139,4, 139,5, 140,0, 140,5, 140,7, 160,0, 161,6, 161,9.

Le produit d'hydrolyse du produit de thermolyse de **9***a* est purifié par chromatographie sur colonne (chloroforme/acétone 99:1). On identifie le benzaldéhyde, l'énamine **20**: ir (cm^{-1}): 1590, 1600, 1680, 3400; rmn ^1H ($CDCl_3$): 4,30 (s, 2H), 7,20 à 8,20 (m, C_6H_5, C=CH et NH_2); et l'aldéhyde α-phénylcinnamique **21**: ir (cm^{-1}): 1605, 1615, 1685; rmn ^1H ($CDCl_3$): 9,87 (s, 1H), 7,10 à 7,90 (m, C_6H_5 et C=CH). Spectre de masse: 208 (96, $M^{+\cdot}$), 207 (45, $M^{+\cdot} - H^{\cdot}$), 179 (53, $M^{+\cdot} - {}^{\cdot}CHO$), 105 (76), 102 (25, 179 − $^{\cdot}C_6H_5$), 77 (32, $C_6H_5^+$), 71 (32), 44 (42), 40 (100).

Le produit de thermolyse de l'aziridine **9** est purifié par chromatographie sur colonne (chloroforme/acétone 99:1). On identifie les aldéhydes **15** et **21** et l'énamine **20** par comparaison avec des échantillons précédemment décrits. On isole également l'aldéhyde **22**: ir (cm^{-1}): 1610 1730; rmn ^1H ($CDCl_3$): 2,88 (dd, 1H, J = 8 et J = 14), 3,45 (dd, 1H, J = 7,5 et J = 14), 3,78 (4 doublets, 1H, J = 7,5, J = 8 et J = 1,5), 7 à 8 (m, C_6H_5), 9,67 (d, 1H, J = 1,5). Spectre de masse: 210 (10, $M^{+\cdot}$), 181 (6, $M^{+\cdot} - {}^{\cdot}CHO$), 107 (37), 106 (95), 105 (98), 104 (4, 181 − $^{\cdot}C_6H_5$), 94 (35), 92 (13), 91 (50, $PhCH_2^+$), 79 (61), 78 (85), 77 (76, $C_6H_5^+$), 63 (65), 52 (25), 51 (97), 50 (51), 44 (82), 40 (100).

Isomérisation de la méthyl-3 (phényl-1 vinyl)-2 aziridine ***5***

Le produit brut est purifié par chromatographie sur colonne ($CHCl_3$). On isole la phényl-2 propèn-1 yl amine **14***b*: ir (cm^{-1}): 1615, 1690, 3250, 3400; rmn ^1H ($CDCl_3$): 2,60 (s, 3H), 7,25 (s, 1H), 7,30 à 7,80 (m, C_6H_5 et NH_2).

Isomérisation de la méthyl-3 (phényl-1 vinyl)-2 aziridine ***6***

Le produit brut est purifié par chromatographie sur colonne ($CHCl_3$). Les dérivés **14***a* et **16** sont identifiés par comparaison avec des échantillons précédemment décrits.

Isomérisation de la phényl-3 (phényl-1 propèn-1 yl)-2 aziridine ***7***

(a) Le produit de thermolyse d'un mélange **7***a*/**7***b* = 45:55 est purifié par chromatographie sur colonne (chloroforme/acétone 98:2). On sépare ainsi l'isomère **7***b* des produits de thermolyse qui sont ensuite séparés par chromatographie sur colonne (chlorure de méthylène/éther de pétrole 3:2).

α-*Phénylcrotonaldéhyde* ***23***

Identifié par comparaison avec un échantillon authentique préparé selon un mode opératoire décrit (11): Eb_8 = 103−103,5°C (litt. (11) Eb_{750} = 233−235°C); ir (cm^{-1}): 1610, 1645, 1700; rmn ^1H ($CDCl_3$): 2,0 (d, 3H, J = 7), 6,85 (q, 1H, J = 7), 7,20 à 7,50 (m, C_6H_5), 9,6 (s, 1H).

N-*benzyl diphényl-3,5 méthyl-4 dihydropyridine* ***24***

Spectre ir (cm^{-1}): 1600, 1665. Spectre uv (EtOH): 375 nm (ε 3360), 290 nm (ε 4440), 240 nm (ε 11 645); rmn ^1H ($CDCl_3$): 1,23 (d, 3H, J = 6,5), 4,14 (q, 1H, J = 6,5), 4,50 (s, 2H), 6,53 (s, 2H), 7 à 7,60 (m, 15H); rmn ^{13}C ($CDCl_3$): 21,8, 31,3, 57,8, 114,0, 124,1, 125,3, 126,9, 127,6, 128,5, 128,8, 129,2, 138,5, 139,3. Spectre de masse: 337 (10, $M^{+\cdot}$), 323 (22), 322 (81, $M^{+\cdot} - {}^{\cdot}CH_3$), 260 ($M^{+\cdot} - {}^{\cdot}C_6H_5$), 246 ($M^{+\cdot} - {}^{\cdot}C_6H_5 - {}^{\cdot}CH_2$), 245 (3, 322 − $^{\cdot}C_6H_5$), 232 ($M^{+\cdot}$ − Ph—CH=NH), 231 (3, 232 − $^{\cdot}H$), 106 (9), 105 (13, $Ph—CH=\overset{+}{N}H^{\cdot}$), 92 (9), 91 (100, $Ph—\overset{+}{C}H_2$), 88 (4), 86 (26), 85 (15), 84 (40), 83 (22), 77 (12, Ph^+), 65 (7), 47 (13). Préparation de la pyridine **24**: une solution composée de 0,009 mol de phényl-2 crotonaldéhyde, 0,015 mol de benzylamine et 0,5 mL d'acide acétique dans 50mL de méthanol anhydre est chauffée à reflux pendant 2 h. On évapore le solvant et purifie le résidu par chromatographie sur colonne (chlorure de méthylène/éther de pétrole 3:2). On obtient 1,35 g de produit pur identifié à la pyridine **24**: F = 130−131°C.

(b) Le produit de thermolyse de l'isomère **7***b* est purifié par chromatographie sur colonne (chlorure de méthylène/éther de pétrole 3:2). On obtient un produit dont le spectre de rmn est identique à celui décrit pour la dihydropyridine **24**.

Isomérisation thermique de la phényl-3 (phényl-1 éthoxycarbonyl-2 vinyl)-2 aziridine ***11***

Une solution de 0,2 g d'aziridine **11** dans 5 mL de chloroforme est chauffée à reflux pendant 4 jours. Après concentration, le produit brut constitué de l'imine **25** est purifié par chromatographie sur colonne (éther de pétrole/acétate d'éthyle 85:15): ir (cm^{-1}): 1730, 1710, 1660, 1645, 1605; rmn ^1H ($CDCl_3$): 1,18 (t, 3H, J = 7), 4,10 (q, 2H, J = 7), 4,08 (s, 2H), 7 à 8 (m, 11H), 8,30 (s, 1H); rmn ^{13}C ($CDCl_3$): 14,1, 35,4, 60,5, 126,0, 127,7, 128,6, 131,0, 133,6, 136,5, 139,4, 141,3, 160,5, 171,8.

1. (*a*) D. BOREL, Y. GELAS-MIALHE et R. VESSIERE. Can. J. Chem. **54**, 1590 (1976), et références citées; (*b*) J. SAULEAU, A. SAULEAU et J. HUET. Bull. Soc. Chim. (II), 97 (1978); (*c*) H. P. FIGEYS et R. JAMMAR. Tetrahedron Lett. **21**, 2995 (1980); **22**, 637 (1981).
2. (*a*) E. L. STOGRYN et S. J. BROIS. J. Am. Chem. Soc. **89**, 605 (1967); (*b*) A. MISHRA, S. N. RICE et N. LWOWSKI. J. Org.

Chem. **33**, 481 (1968); (*c*) G. RICART, D. COUTURIER et C. GLACET. C. R. Acad. Sci. C, **277**, 519 (1973); (*d*) G. RICART. Bull. Soc. Chim. 2607 (1974); (*e*) L. FERRERO, S. GERIBALDI, M. ROUILLARD et M. AZZARO. Can. J. Chem. **53**, 3227 (1975); (*f*) R. CHAABOUNI et A. LAURENT. Synthesis, 464 (1975); (*g*) A. G. HORTMANN et J. Y. KOO. J. Org. Chem. **39**, 3781 (1974); (*h*) A. HASSNER, R. D'COSTA, A. T. MC PHAI et N. BUTLER. Tetrahedron Lett. **22**, 3691 (1981).

3. (*a*) N. H. CROMWELL et H. HOEKSEMA. J. Am. Chem. Soc. **71**, 708 (1949); (*b*) N. H. CROMWELL et G. D. MERCER. J. Am. Chem. Soc. **79**, 3819 (1957).
4. T. J. BARDOS, C. SZANTAY et C. K. NAVADA. J. Am. Chem. Soc. **87**, 5796 (1965); R. G. KOSTYANOVSKII et A. A. FOMICHEV. Bull. Acad. Sci. USSR, 815 (1971); R. MARTINO, J. ABEBA et A. LATTES. Tetrahedron Lett. 433 (1973); H. NAKANISHI et O. YAMAMOTO. Tetrahedron, **30**, 2115 (1974).
5. A. LOPEZ. Thèse de Docteur-Ingénieur, Toulouse. 1974.
6. H. W. HEINE, G. B. LOWRIE et K. C. IRVING. J. Org. Chem. **35**, 444 (1970).
7. J. GELAS. Bull. Soc. Chim. 3093 (1967).
8. F. WEBER et C. BANDLOW. Z. Chem. **13**, 467 (1973).
9. P. L. SOUTHWICK et C. R. CHRISTMAN. J. Am. Chem. Soc. **74**, 1886 (1952).
10. N. KRABE, A. SEHER et E. POLZIN. Chem. Ber. **74**, 1892 (1941).
11. R. KUHN et J. MICHEL. Chem. Ber. **71**, 119 (1938).

Can. J. Chem. Downloaded from www.nrcresearchpress.com by 210.87.254.42 on 09/06/12
For personal use only.

Spectre de vibration de quelques *N*-méthyl-halogénotriazoles-1,2,4

M. Saidi Idrissi et M. Senechal
Laboratoire de spectroscopie infrarouge, Faculté des Sciences, Rabat, Maroc
H. Sauvaitre
Laboratoire de chimie structurale, Faculté des Sciences, Pau, France
ET
C. Garrigou-Lagrange
CRPP, Domaine Universitaire, 33405 Talence, France

Reçu le 13 janvier 1983

M. Saidi Idrissi, M. Senechal, H. Sauvaitre et C. Garrigou-Lagrange. Can. J. Chem. **61**, 2133 (1983).

Les spectres vibrationnels d'une série de *N*-méthyl-chloro et *N*-méthyl-bromotriazoles-1,2,4 ont été étudiés, et une interprétation en a été proposée dans le but d'essayer de résoudre le problème de la tautomérie des triazoles-1,2,4 *C*-substitués.

M. Saidi Idrissi, M. Senechal, H. Sauvaitre, and C. Garrigou-Lagrange. Can. J. Chem. **61**, 2133 (1983).

Vibrational spectra of some *N*-methyl chloro and *N*-methyl bromotriazoles-1,2,4 are reported. An assignment of the normal modes is proposed. This study was done in order to find new elements to solve the problem of tautomerism in *C*-substituted triazoles-1,2,4.

Can. J. Chem. Downloaded from www.nrcresearchpress.com by 210.87.254.5 on 09/06/12
For personal use only.

I. Introduction

Dans le cadre de nos travaux sur la tautomérie des halogénotriazoles-1,2,4 (1–3), nous nous sommes intéressés à l'étude par spectroscopie de vibration de leurs dérivés *N*-méthylés dans lesquels l'hydrogène mobile a été substitué par un groupement CH_3 ou CD_3 noté ci-dessous Y, empêchant ainsi toute possibilité de tautomérie.

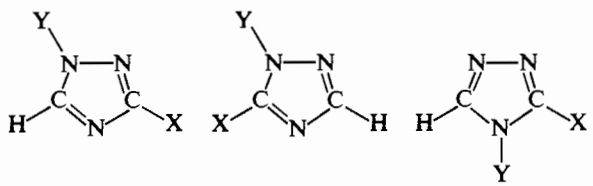

On peut penser a priori que ce groupement influence peu le spectre du noyau triazolique et que les résultats que nous obtiendrons avec ces molécules "bloquées" comme modèle pourront se transposer aux halogénotriazoles *C*-substitués.

Les spectres vibrationnels de ces composés n'ont fait l'objet d'aucune analyse détaillée. Seuls à notre connaissance Mel'nikov *et al.* (4, 5) ont publié les spectres infrarouges et Raman de quelques méthyl-1-nitro-3 triazoles-1,2,4 et ont proposé une attribution basée sur un calcul de modes normaux.

Dans ce travail, nous avons étudié les *N*-méthyl-chlorotriazoles et *N*-méthyl-bromotriazoles dont nous avons analysé les spectres infrarouges dans différents états physiques (état condensé, solution dans CCl_4 ou CS_2, vapeur) et les spectres Raman (liquide, solide ou solution aqueuse). L'examen des spectres vibrationnels de quelques molécules marquées au deutérium nous a permis de justifier nos attributions.

Nous discuterons, séparément, les modes de vibration cycliques et extracycliques (6–9) ce qui n'exclut pas la possibilité d'interaction entre ces deux catégories.

Les nombres d'onde attribués aux vibrations fondamentales du noyau triazolique et du groupement méthyle (CH_3 ou CD_3) sont consignés dans les tableaux 1 et 2 respectivement. A titre d'illustration, nous présentons dans les figures 1 et 2 les spectres infrarouges des trois Me-1Cl-3 TA étudiés dans les régions 3300–2000 cm^{-1} et 1600–200 cm^{-1}.

L'analyse des spectres se fera par région.

II. Discussion des attributions

II-1. *Région 3200–2000 cm^{-1}*

Dans ce domaine spectral, on attend toutes les vibrations de valence ν CH (ou ν CD) du cycle triazolique et du groupement méthyle.

II-1-1. *Vibrations de valence ν CH (ou ν CD) triazolique*

Entre 3150 et 3100 cm^{-1}, le spectre infrarouge du Me-1 TA présente une seule bande large attribuable aux vibrations de valence des deux vibrateurs CH aromatiques (Tableau 1). Dans le cas des *N*-méthyl-halogenotriazoles, la seule absorption relevée dans cette région est due à la vibration de valence de l'unique vibrateur CH de ces molécules. Cette bande se déplace vers 2300 cm^{-1} sur les spectres de leurs homologues *C*-deutériés (Fig. 1). La fréquence de ce mode n'est pas sensible à la nature du substituant.

II-1-2. *Vibrations du groupement méthyle*

Les spectres infrarouges de tous les composés étudiés présentent entre 3030 et 2800 cm^{-1} des bandes d'absorption dont les positions et les intensités sont caractéristiques des vibrations du groupement CH_3. Elles sont déplacées vers 2200 cm^{-1} sur le spectre du CD_3-1-Cl-5 TA (Fig. 1). La bande observée vers 2950 cm^{-1} sur les spectres Raman des méthyl-1 halogénotriazoles est due à la superposition des vibrations ν_s et ν'_s CH_3. Dans le cas du Me-4Br-3TA, une bande infrarouge assez intense à 2918 cm^{-1} pourrait correspondre à la vibration ν_s CH_3. L'absorption relevée vers 3000 cm^{-1} sur les spectres infrarouges de l'ensemble des dérivés examinés est attribuée au mode ν_a CH_3.

II-2. *Région 1600–900 cm^{-1}*

Les calculs de modes normaux effectués sur des hétérocycles, et en particulier sur le triazole-1,2,4 (10) et le chloro triazole-1,2,4 (11) montrent qu'il est impossible d'individualiser les vibrations des différentes liaisons du cycle, et qu'elles sont toutes couplées. C'est pourquoi, dans la suite de ce mémoire, nous notons les vibrations du squelette triazolique R_1 à R_9.

Seules certaines vibrations planes du squelette (R_1 à R_7, δ CH) et cinq vibrations de déformation du groupement méthyle sont attendues dans cette zone spectrale. L'approximation des vibrations de groupe dans ce domaine est moins rigoureuse que

TABLEAU 1. Fréquences des vibrations fondamentales du squelette triazolique des *N*-méthyltriazoles-1,2,4

Me-1TA	Me-1Cl-3TA	CD_3-1Cl-3TA	Me-1Cl-5TA	Me-1Br-3TA	Me-1Br-3D-5TA	Me-1Br-5TA	Me-4Br-3TA	Attributions
3 130	3 120	3 120	3 120	3 130	2 310	3 120	3 110	ν CH(CD)
1 515	1 510	1 502	1 495	1 510	1 480	1 485	1 517	R_1
1 420	1 428	1 412	1 425	1 425	1 419	1 415	1 419	R_2
1 348	1 360	1 362	1 360	1 350	1 322	1 345	1 349	R_3
1 278	1 285	1 289	1 270	1 272	1 265	1 270	1 275	R_4
1 215	1 195	1 197	1 180	1 186	876	1 175	1 200	δ CH (CD)
1 145	—	—	—	—	—	—	—	δ CH
1 070	1 065	1 096	1 140	1 070	1 070	1 115	1 145	R_5
1 008	1 020	1 018	1 010	1 020	1 017	1 005	994	R_6
960	998	996	960	986	998	965	946	R_7
882	—	—	880	—	—	880	—	γ C_3H
850	860	856	—	860	562	—	848	γ C_5H
680	708	708	696	710	702	690	680	R_8
640	635	626	660	635	634	656	644	R_9
680	708	666	705	702	690	700	680	ν N—CH_3
465	425	404	430	413	402	435	424	δ C—CH_3
—	480	472	512	356	351	360	349	ν CX
—	306	295	—	286	278	270	247	δ CX

TABLEAU 2. Attribution des vibrations fondamentales des groupements CH_3 et CD_3

Composé	Vibration							
	ν_a	ν'_s	ν_s	δ_a	δ'_s	δ_s	$r_\perp$	$r_\parallel$
Me-1TA	3 000	2 950	2 950	1 446	1 490	1 368	1 055	968
Me-1Cl-3TA	3 005	2 958	2 958	1 440	1 470	1 360	1 065	960
Me-1Cl-3D-5TA	3 000	2 956	2 949	1 457	1 464	1 362	1 073	960
Me-1Br-3TA	3 000	2 958	2 958	1 440	1 470	1 360	1 070	—
Me-1Br-3D-5TA	3 000	2 950	2 950	1 447	1 480	1 350	1 071	—
Me-1Cl-5TA	3 002	2 956	2 956	1 445	1 510	1 390	1 080	970
Me-1Br-5TA	3 000	2 960	2 950	1 450	1 510	1 385	1 070	968
Me-4Br-3TA	3 012	2 956	2 918	1 448	1 468	1 371	1 067	946
CD_3-1Cl-3TA	—	2 260	2 130	1 046	1 046	1 096	856	—

dans le domaine des hautes fréquences. Néanmoins, nous l'utiliserons pour proposer une interprétation des spectres et nous discuterons successivement les vibrations δ CH, les vibrations du noyau triazolique et les vibrations du groupement méthyle.

II-2-1. *Vibrations de déformation δ CH (ou δ CD)*

Les deux vibrations de déformation dans le plan δ CH du Me-1TA sont attribuées aux bandes observées vers 1215 et 1145 cm^{-1} (Tableau 1). Les spectres infrarouges des *N*-méthyl-halogénotriazoles présentent une absorption moyenne à forte vers 1200 cm^{-1} que nous attribuons au mode δ CH de ces composés car cette bande n'apparait pas sur les spectres de leurs homologues *C*-deutériés. La vibration δ CD est relevée vers 880 cm^{-1} (Fig. 2).

II-2-2. *Vibrations du cycle triazole-1,2,4*

Aux vibrations R_1 à R_7, nous avons fait correspondre des bandes infrarouges et des raies Raman de fréquences voisines de celles observées dans le cas du triazole-1,2,4 (1, 10) (Tableau 1). La position de la vibration R_1 est fonction de la position de l'halogène sur le cycle. Dans le cas des Me-1TA et Me-1X-3TA, le mode R_5 est observée à fréquence plus basse, les modes R_6 et R_7 à fréquences plus élevées que sur les spectres des autres composés (Tableau 1). Rappelons que dans les halogénotriazoles, les vibrations R_5 et δ CH sont en forte interaction (2).

Remarque: lors de son étude des spectres des monohalogénotriazoles et de leurs sels de potassium et d'argent, Grinshtein *et al.* (12) avaient observé un multiplet vers 1270 cm^{-1} qu'ils avaient expliqué par l'existence de plusieurs formes isomères.

Sur les spectres des *N*-méthyl-halogénotriazoles que nous avons examinés, alors que l'absorption attribuée au mode R_4 vers 1275 cm^{-1} est simple dans le cas des Me-1TA et Me-1X-5TA, elle apparait sous forme de multiplet sur les spectres des Me-1X-3TA (Fig. 2). Le spectre du Me-4Br-3TA présente dans cette région deux bandes de faible intensité. L'apparition du multiplet sur les spectres de ces "formes bloquées" nous amène à exclure l'hypothèse de Grinshtein.

Il ne peut s'agir d'une autoassociation mettant en jeu le vibrateur CH en position 5, le plus acide (cf. partie expérimentale), puisque ce multiplet existe sur les spectres des Me-1diX-3,5TA.[1] Il ne peut pas s'agir non plus d'une harmonique car la région de 600–700 cm^{-1} est assez semblable pour tous les composés. Seule reste donc, pour expliquer l'existence de ces bandes multiples, l'hypothèse d'une ou plusieurs combinaisons.

II-2-3. *Vibrations de déformation et de balancement du groupement méthyle*

Par analogie avec les interprétations déjà proposées pour les spectres de molécules aromatiques méthylées (13), nous attribuons l'absorption faible observée vers 1480 cm^{-1} sur les spectres infrarouges des Me-1TA, Me-1X-3TA, Me-4Br-3TA et l'épaulement relevé à 1510 cm^{-1} sur les spectres des

[1] M. Saidi Idrissi, travaux non publiés.

Can. J. Chem. Downloaded from www.nrcresearchpress.com by 210.87.254.5 on 09/06/12
For personal use only.

Can. J. Chem. Downloaded from www.nrcresearchpress.com by 210.87.254.5 on 09/06/12
For personal use only.

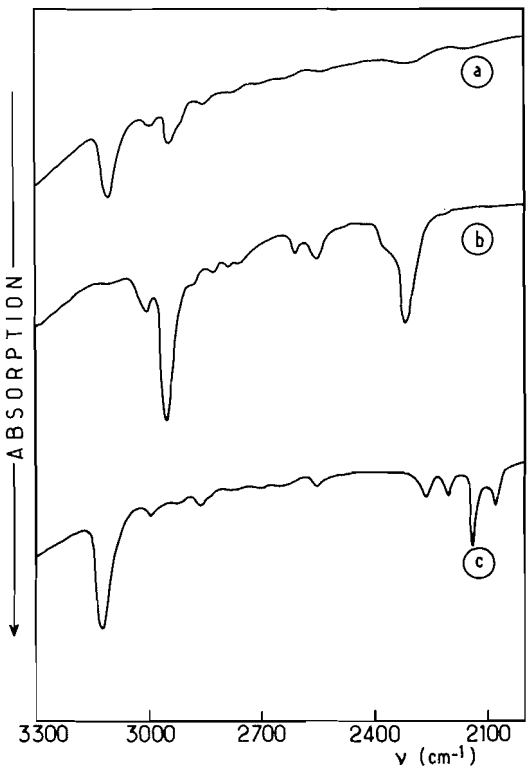

FIG. 1. Spectres infrarouges des Me-1Cl-3TA (a), Me-1Cl-3D-5TA (b) et CD_3-1Cl-3TA (c) à l'état liquide entre 3300 et 200 cm^{-1}.

Me-1X-5TA à la vibration de déformation δ_s' CH_3 (Tableau 2). Les modes δ_a et δ_s sont situés vers 1450 et 1370 cm^{-1} respectivement. Notons que, dans le cas du Me-1Cl-3TA, la bande à 1360 cm^{-1} correspond à une superposition des modes δ_s CH_3 et R_3.

Les vibrations de balancement du groupement méthyle $r_\perp$ et $r_\parallel$ sont observées vers 1070 et 960 cm^{-1} respectivement (Tableau 2). Le spectre du CD_3-1-Cl-3TA confirme ces attributions (Fig. 2).

II-3. *Région 900–200 cm^{-1}*

On attend cinq vibrations de type A" (γ CH, R_8, R_9, γ C—X, γ N—CH_3) et quatre vibrations A' (ν N—CH_3, δ N—CH_3, ν C—X, δ C—X) dans la région 900–200 cm^{-1}, la vibration de torsion du groupement méthyle ayant très vraisemblablement une fréquence inférieure à 200 cm^{-1}.

II-3-1. *Vibrations de symétrie A"*

La vibration γ CH des Me-1X-5TA est relevée vers 880 cm^{-1} (Tableau 1), celle des Me-1X-3TA vers 860 cm^{-1}. Sur le spectre infrarouge du Me-1TA à l'état dissous, on observe deux absorptions à 882 et 850 cm^{-1}; nous les attribuons, par comparaison avec les molécules précédentes, aux deux modes γ CH faisant intervenir respectivement les vibrateurs CH en positions 3 et 5 du cycle. La vibration γ CH du Me-4Br-3TA est relevée à 848 cm^{-1}, fréquence voisine de celle observée dans le cas des Me-1X-3TA (Tableau 1). Notons que dans ces deux cas, l'hydrogène occupe une position analogue par rapport au groupement méthyle. Cette interprétation est confirmée par le déplacement de ces bandes vers 560 cm^{-1} après deutériation sur le carbone (Fig. 2).

Les mouvements de déformation du cycle triazole R_8 et R_9 donnent lieu aux absorptions situées respectivement vers 700 et 630 cm^{-1} sur les spectres infrarouges de tous les composés (Tableau 1, Fig. 2).

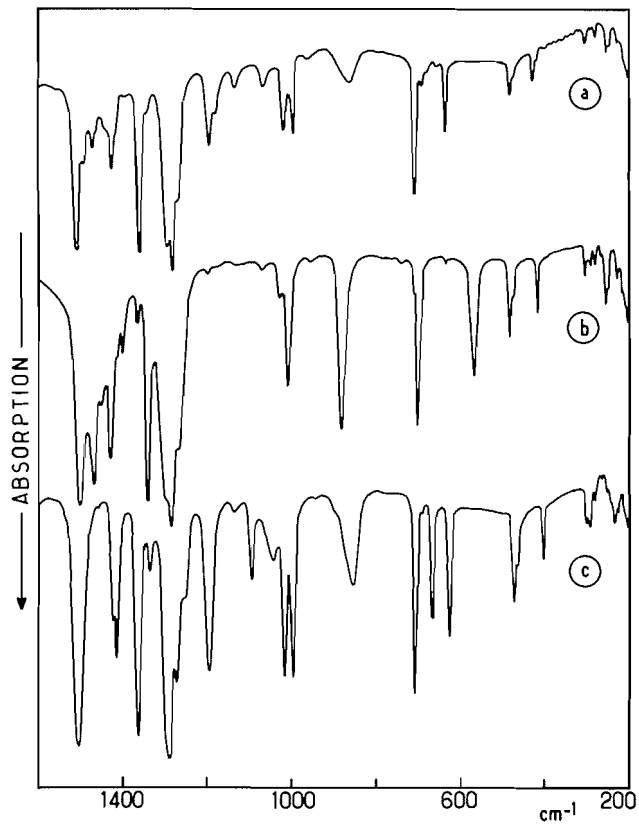

FIG. 2. Spectres infrarouges des Me-1Cl-3TA (a), Me-1Cl-3D-5TA (b) et CD_3-1Cl-3TA (c) à l'état liquide; région 1600–200 cm^{-1}.

Toutes ces bandes présentent bien un contour de type C sur les spectres de l'état gazeux (14).

Notons, comme prévu, qu'aucune de ces vibrations n'a été observée sur les spectres Raman des solutions aqueuses.

Les vibrations γ N—CH_3 et γ C—X n'ont pas pu être localisées, soit parce qu'elles sont en dehors de notre domaine d'étude en infrarouge, soit parce qu'elles sont d'intensité trop faible.

II-3-2. *Vibrations de symétrie A'*

La bande moyenne à forte relevée vers 700 cm^{-1} sur les spectres infrarouges de l'ensemble des molécules et à laquelle correspond une raie Raman intense et polarisée est due à la vibration ν N—CH_3. Cette attribution est en accord avec celle donnée pour le *N*-méthyl pyrrole (15).

A la vibration de déformation dans le plan δ N—CH_3, nous rattachons les fréquences observées vers 420 cm^{-1}.

Une absorption infrarouge et une raie Raman très forte et polarisée sont observées vers 480 cm^{-1} sur les spectres des Me-1Cl-3TA (Tableau 1, Fig. 2); nous les attribuons à la vibration ν C—Cl. Dans le cas des Me-1Cl-5TA, on retrouve cette vibration vers 512 cm^{-1} (Fig. 2). La vibration de déformation δ C—Cl est située vers 300 cm^{-1}.

La vibration ν C—Br apparait sur les spectres des *N*-méthyl bromotriazoles sous la forme d'une raie Raman intense et polarisée et d'une absorption moyenne vers 360 cm^{-1}; le mode δ C—Br est observée vers 280 cm^{-1} (Tableau 1).

Ces attributions sont proches de celles données dans le cas des ClTA (2) et BrTA (14, 16).

III. Conclusion

Les spectres de vibration des *N*-méthyl monohalogénotriazoles-1,2,4 ont été analysés. Une attribution pour l'ensemble

des mouvements a été proposée. Toutefois, contrairement à d'autres techniques physicochimiques, notamment la détermination de moments dipolaires en solution (17), l'étude par la spectroscopie de vibration de ces "formes bloquées" n'a pas permis d'apporter des éléments nouveaux à l'élucidation du problème de la tautomérie des *C*-halogénotriazoles-1,2,4. En effet, les spectres des composés examinés présentent une grande similitude et il nous a été impossible de relever une région spectrale présentant une variation notable entre les spectres des différents *N*-méthyl halogénotriazoles-1,2,4.

IV. Conditions expérimentales

IV-1. *Synthèse des composés étudiés*

Les *N*-méthyl halogénotriazoles-1,2,4 ont été obtenus selon le mode opératoire décrit dans les réfs. 1 et 17, les composés *C*-deutériés ont été préparés par échange avec D_2O à 120°C pendant une journée pour les Me-1X-3TA et une semaine pour les Me-1X-5TA.

Le CD_3-1Cl-3TA a été synthétisé en milieu neutre en utilisant ICD_3 comme agent méthylant.

IV-2. *Étude spectroscopique*

Les spectres infrarouges dans la région 4000–200 cm^{-1} ont été enregistrés avec des spectromètres P.E. 225 et 577.

Les échantillons ont été étudiés dans différents états physiques (solide dispersé dans le Nujol ou le Fluorolube ou en pastille de KBr, liquide pur et vapeur). Des cellules à fenêtres en CsI et une cellule chauffante P.E. ont été utilisées.

Les spectres Raman des composés liquides ou des solutions aqueuses ont été obtenus en utilisant deux spectromètres Coderg, l'un équipé d'un laser à Argon ionisé émettant à 4880 Å, l'autre d'un laser Hélium Néon (λ = 6328 Å).

Remerciements

Nous sommes reconnaissants à Monsieur A. Bernardini de l'école des Sciences et Techniques de Montpellier, à Mme E. Dupart du Centre de Recherche Paul Pascal de nous avoir aidés à obtenir certains composés et à Mme C. Dacié d'avoir enregistré pour nous quelques spectres de composés à l'état gazeux.

1. M. Saidi Idrissi. D.E.S., Rabat (1977).
2. M. Saidi Idrissi, M. Senechal, H. Sauvaitre, M. Cotrait et C. Garrigou-Lagrange. J. Chim. Phys. **77**, 195 (1980).
3. M. Saidi Idrissi, P. Lalanne et C. Garrigou-Lagrange. J. Chim. Phys. **78**, 511 (1981).
4. V. V. Mel'nikov, V. V. Stolpakova, M. S. Pevzner et B. V. Gidaspov. Khim. Geterotsikl. Soedin. 707 (1973); trad. angl. p. 651.
5. V. V. Mel'nikov, V. V. Stolpakova, M. S. Pevzner et B. V. Gidaspov. Khim. Geterotsikl. Soedin. 1194 (1973); trad. angl. p. 1085.
6. C. Garrigou-Lagrange, J. M. Lebas et M. L. Josien. Spectrochim. Acta, **16**, 106 (1960).
7. N. Claverie et C. Garrigou-Lagrange. J. Chim. Phys. **61**, 889 (1964).
8. G. Davidovics, C. Garrigou-Lagrange, P. Roepstorff et J. Chouteau. Spectrochim. Acta, Part A, **23**, 2669 (1967).
9. A. M. Bellocq et C. Garrigou-Lagrange. J. Chim. Phys. **66**, 1511 (1969).
10. D. Bougeard, N. le Calve, B. Saint-Roch et A. Novak. J. Chem. Phys. **64**, 5152 (1976).
11. M. Saidi Idrissi, C. Garrigou-Lagrange et E. Pouchan. Can. J. Chem. **59**, 3341 (1981).
12. V. Ya. Grinshtein, A. A. Strazdin et A. K. Grinvalde. Khim. Geterotsikl. Soedin. **6**, 248 (1970).
13. M. T. Forel. Thèse, Bordeaux (1962).
14. M. Saidi Idrissi. Thèse, Rabat (1981).
15. W. Scott. J. Mol. Spectrosc. **37**, 77 (1971).
16. M. Saidi Idrissi, H. Sauvaitre et C. Garrigou-Lagrange. J. Iraqi Chem. Soc. **5**, 109 (1980).
17. A. Bernardini. Thèse, Montpellier (1975).

Can. J. Chem. Downloaded from www.nrcresearchpress.com by 210.87.254.5 on 09/06/12
For personal use only.

The crystal structure of *N*-[[6-methoxy-5-(trifluoromethyl)thio-1-naphthalenyl]thioxomethyl]-*N*-methylglycine, $C_{16}H_{14}F_3NO_3S_2$ [1]

KOTTAYIL I. VARUGHESE AND MARIA PRZYBYLSKA
Division of Biological Sciences, National Research Council of Canada, Ottawa, Ont., Canada K1A 0R6

AND

KAZIMIR SESTANJ, FRANCESCO BELLINI, AND LESLIE G. HUMBER
Chemistry Department, Ayerst Research Laboratories, Montreal, P.Q., Canada H4R 1J6

Received Feburary 9, 1983

KOTTAYIL I. VARUGHESE, MARIA PRZYBYLSKA, KAZIMIR SESTANJ, FRANCESCO BELLINI, and LESLIE G. HUMBER. Can. J. Chem. **61**, 2137 (1983).

The crystals of $C_{16}H_{14}F_3NO_3S_2$ belong to the monoclinic space group $P2_1/c$ with a = 11.577(1), b = 12.404(1), c = 12.366(1) Å, β = 90.01(1)°, and Z = 4. The structure was solved by MULTAN 78. The parameters were refined by block-diagonal least-squares to a final R of 0.047 for 2679 observed reflections. Of particular interest is an intramolecular attractive interaction between the sulfur and oxygen atoms with an S···O distance of 2.879(2) Å, in which oxygen appears to act as an electrophile. Intermolecular hydrogen bonds between the hydroxyl and keto groups join the molecules related through a centre of symmetry into dimers.

KOTTAYIL I. VARUGHESE, MARIA PRZYBYLSKA, KAZIMIR SESTANJ, FRANCESCO BELLINI et LESLIE G. HUMBER. Can. J. Chem. **61**, 2137 (1983).

Les cristaux de $C_{16}H_{14}F_3NO_3S_2$ appartiennent au groupe d'espace monoclinique $P2_1/c$ avec a = 11,577(1), b = 12,404(1), c = 12,366(1) Å, β = 90,01(1)° et Z = 4. On a résolu la structure par la méthode MULTAN 78 et on l'a affinée par la méthode des moindres carrés jusqu'à une valeur de R = 0,047 pour 2679 réflexions observés. L'attraction intramoléculaire entre l'atome de soufre et les atomes d'oxygènes avec une distanee S···O de 2,879(2) Å dans laquelle l'oxygène semble agir comme un électrolyte est d'un intérêt particulier. Les liaisons hydrogènes intermoléculaires entre les groupes hydroxyle et cétone réunissent en dimères les molécules apparentées via un centre de symétrie.

[Traduit par le journal]

Introduction

N-[[6-Methoxy-5-(trifluoromethyl)thio-1-naphthalenyl]thioxomethyl]-*N*-methylglycine, **1**, is a compound which inhibits aldose reductase (1), an enzyme which reduces glucose to sorbitol in certain tissues, and which is involved in the manifestation of some of the disabling complications of chronic diabetes (2).

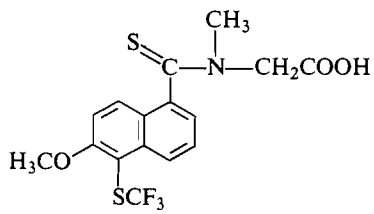

1

Compound **1** contains a thioamide grouping in the side chain, wherein the zwitterionic iminothiol resonance structures can exist in *cis* or *trans* forms. In addition, free rotation of the side chain about the bond joining it to the naphthalene ring is likely restricted due to the bulk of the sulfur atom as well as the peri effect of the hydrogen atom at position 8.

For these reasons a crystallographic study was undertaken to determine the structure of **1** and the conformation of the side chain.

Experimental

Crystal data:

$C_{16}H_{14}F_3NO_3S_2$ fw = 389.4

Monoclinic, $P2_1/c$, a = 11.577(1), b = 12.404(1), c = 12.366(1) Å, β = 90.01(1)°, Z = 4, ρ_c = 1.46 g cm^{-3}, λ(CuKα) = 1.54178 Å, μ(CuKα) = 31.0 cm^{-1}.

[1]NRCC No. 21306.

The crystals of the title compound, mp 168–169°C, were obtained from a mixture of ethyl acetate and ether (~1:2). The data were measured at room temperature on a Nonius CAD-4 diffractometer using a crystal of dimensions 0.5 × 0.3 × 0.25 mm and Ni-filtered Cu radiation. The cell parameters were derived from the least-squares fit to the angular settings of 25 well-centered reflections with 2θ values from 38.2 to 50°. The scan mode ω–2θ was used to a limit of 2θ = 140°. The peaks were scanned at a 4° take-off angle with $\Delta\omega = (0.7 + 0.25 \tan\theta)°$ extended 25% on each side for background, and at a maximum speed of 5°/min for strong reflections. Three reflections were used to monitor the changes in intensities and no systematic decrease was observed.

A total of 3370 unique reflections was measured of which 2679 (79%) were above threshold of 1.43$\sigma(I_{net})$. The net intensities were corrected for Lorentz and polarization effects but not for absorption.

The structure was solved by MULTAN 78 (3) and refined by block-diagonal least-squares to an R = 0.047 and R_w = 0.055 for observed reflections.

The weighting scheme was $\sqrt{w} = 1/\{1 + [(|F_o| - 10)/15]^2\}^{1/2}$ if $\sin^2\theta \geq 0.27$ and $\sqrt{w} = [1/\{1 + [(|F_o| - 10)/15]^2\}^{1/2}]$ $(\sin^2\theta/0.27)$ if $\sin^2\theta < 0.27$. The constants were chosen to make $\Sigma w(|F_o| - |F_c|)^2$ independent of $|F_o|$. During the final stages of refinement three reflections ($20\bar{2}$, 012, $12\bar{4}$) which showed extinction effects were excluded.

Mean and maximum shifts/esd for all atoms were 0.07 and 0.98, respectively. The scattering factors were those of Hanson, Herman, Lea, and Skillman (4) for non-hydrogen atoms and of Stewart, Davidson, and Simpson (5) for H. All calculations were carried out with the NRCC crystallographic computer programs by Ahmed, Hall, Pippy, and Huber (6).

The refined atomic coordinates are given in Table 1.[2]

[2]Tables of observed and calculated structure factors and of temperature factors are available, at a nominal charge, from the Depository of Unpublished Data, CISTI, National Research Council of Canada, Ottawa, Ont., Canada K1A 0S2.

Can. J. Chem. Downloaded from www.nrcresearchpress.com by 210.87.254.105 on 09/06/12
For personal use only.

TABLE 1. Fractional coordinates (for S × 10^5; for C, N, O, F × 10^4; for H × 10^3) and isotropic temperature factors with esd's in parentheses; H(1) is attached to O(3); $B_{eq} = \frac{8}{3}\pi^2 \sum_i \sum_j U_{ij} a_i^* a_j^* a_i a_j$

Atom	x	y	z	B_{eq} or B (Å^2)
S(1)	84600(5)	39344(5)	4212(6)	5.0
S(2)	144085(6)	24350(5)	23175(7)	5.2
F(1)	8650(2)	1830(2)	460(2)	8.6
F(2)	6936(2)	2485(2)	449(3)	9.2
F(3)	7936(3)	2499(2)	1885(2)	9.1
O(1)	8679(1)	4996(2)	2481(2)	5.5
O(2)	14307(1)	4916(2)	3823(1)	4.7
O(3)	16182(1)	4649(2)	4133(1)	5.3
N	14554(1)	4450(1)	1665(1)	3.4
C(1)	12916(2)	3437(2)	968(2)	3.4
C(2)	12962(2)	2934(2)	−10(2)	4.5
C(3)	11961(3)	2815(2)	−632(2)	5.1
C(4)	10916(2)	3165(2)	−258(2)	4.6
C(5)	9751(2)	4063(2)	1176(2)	3.9
C(6)	9716(2)	4611(2)	2144(2)	4.2
C(7)	10738(2)	4759(2)	2746(2)	4.3
C(8)	11760(2)	4374(2)	2371(2)	3.7
C(9)	11846(2)	3832(2)	1375(2)	3.2
C(10)	10821(2)	3674(2)	751(2)	3.6
C(11)	7990(3)	2630(2)	826(3)	5.9
C(12)	8655(3)	5722(3)	3371(4)	7.1
C(13)	13987(2)	3512(2)	1641(2)	3.4
C(14)	14143(2)	5434(2)	1142(2)	4.4
C(15)	15575(2)	4551(2)	2341(2)	4.0
C(16)	15280(2)	4717(2)	3509(2)	3.9
H(1)	1597(3)	476(3)	480(3)	7.2(8)
H(2)	1368(3)	268(3)	−29(2)	5.1(6)
H(3)	1205(4)	244(3)	−132(3)	7.1(8)
H(4)	1025(3)	307(3)	−70(3)	5.3(6)
H(7)	1067(3)	511(3)	340(3)	5.5(7)
H(8)	1243(2)	448(2)	277(2)	4.4(5)
H(12,1)	791(4)	590(3)	342(3)	7.5(9)
H(12,2)	920(3)	626(3)	321(3)	7.1(8)
H(12,3)	886(5)	529(5)	407(5)	10.0(12)
H(14,1)	1473(3)	575(3)	81(2)	5.3(6)
H(14,2)	1383(3)	584(3)	164(3)	5.5(7)
H(14,3)	1363(3)	525(3)	63(3)	5.3(6)
H(15,1)	1602(3)	519(3)	204(3)	5.2(6)
H(15,2)	1608(3)	391(3)	230(2)	4.9(6)

Discussion

The stereochemistry of the molecule is shown in Fig. 1 and the bond lengths and angles are presented in Fig. 2. The C—H bonds are in the range 0.87 to 1.04 Å (mean = 0.94 Å and esd ≤ 0.04 except for C(12)—H(12,3) for which it is 0.06 Å). The bond lengths of the naphthalene moiety agree well with those in naphthalene (7) and perdeuteronaphthalene (8) (cf. values in Table 2), with the exception of C(4)—C(10) and symmetrically related C(8)—C(9), which are significantly shorter (1.402(3) and 1.406(3) Å). It is interesting that these bond lengths match the corresponding values in 1,5-dimethylnaphthalene obtained from a neutron diffraction study (9), but not those from the less accurate X-ray analysis of 1,5-dimethylnaphthalene (10). The endocyclic angles fall into two categories: the smaller angles at C(9) and C(10) vary from 118.3 to 119.0°; the remaining angles range from 119.8 to 122.0°. Similar differences, although smaller, were observed in naphthalene, perdeuteronaphthalene, and in 1,5-dimethylnaphthalene (9).

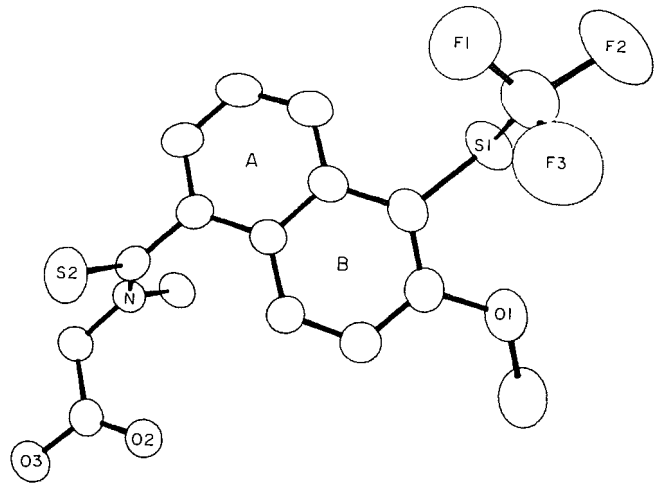

FIG. 1. An ORTEP drawing showing thermal ellipsoids at the 50% probability level.

The lengthening of C—F bonds (1.319−1.331(4) Å) and the shortening of S(1)—C(11) to 1.779(3) Å seem to be due to the attraction of electrons by the CF_3 group. In (R)-*N*-trifluoroacetyl-1-(1-naphthyl)ethylamine (11) the C—F bonds vary from 1.303−1.314(7) Å. The S(1)—C(sp^2) bond is 1.770(2) Å.

The C(13)—N bond length is 1.336(3) Å, suggesting considerable double bond character. A stereoscopic pair (Fig. 3) shows that the naphthalene moiety and the acetic acid chain are *trans* to each other with respect to that C—N bond, and that S(2) is far removed from the hydrogens at positions 2 and 8 of the naphthalene ring (3.35(3) and 3.46(3) Å, respectively). The shortest S(2) intramolecular contact is 2.66(3) Å, with H(15,2).

The naphthalene moiety deviates significantly from planarity. The distances of its atoms from the calculated plane, given by $0.1582X + 0.8768Y - 0.4542Z = 5.5754$, where X, Y, Z are orthogonal coordinates in Å, are shown in Table 3. Both S(1) and O(1) atoms are situated above that plane and the S···O intramolecular distance is 2.879(2) Å, which is considerably shorter than the sum of the van der Waals radii of 3.32 Å (r(O) = 1.52 Å, r(S) = 1.80 Å (12)). The angles S(1)—C(5)—C(6) and O(1)—C(6)—C(5) are appreciably smaller (118.5 and 117.9°, respectively) than the adjoining C(10)—C(5)—S(1) and C(7)—C(6)—O(1) (120.5 and 122.3°). All these observations indicate the presence of an attractive S···O interaction.

Rosenfield, Parthasarathy, and Dunitz (13) examined nonbonded atomic contacts with divalent sulfur in 69 structures and found directional preferences for the approach of electrophiles and nucleophiles to the sulfur atom. Electrophiles tend to approach S roughly 20° from the perpendicular to the plane through atoms Y—S—Z, with values ranging from 0° to 40°. In terms of the "frontier orbital" model (14, 15), this direction corresponds to the highest occupied molecular orbital (HOMO), which is a sulfur lone-pair orbital. Nucleophiles, on the other hand, were shown to approach the sulfur atom approximately along the extension of one of the two covalent bonds to S, which was identified as the lowest unoccupied molecular orbital (LUMO), the antibonding orbital, σ*.

In a later study Row and Parthasarathy (16) surveyed structures with S···S intermolecular interactions and found that the majority of these contacts correspond to electrophile−nucleo-

Can. J. Chem. Downloaded from www.nrcresearchpress.com by 210.87.254.105 on 09/06/12
For personal use only.

Can. J. Chem. Downloaded from www.nrcresearchpress.com by 210.87.254.105 on 09/06/12
For personal use only.

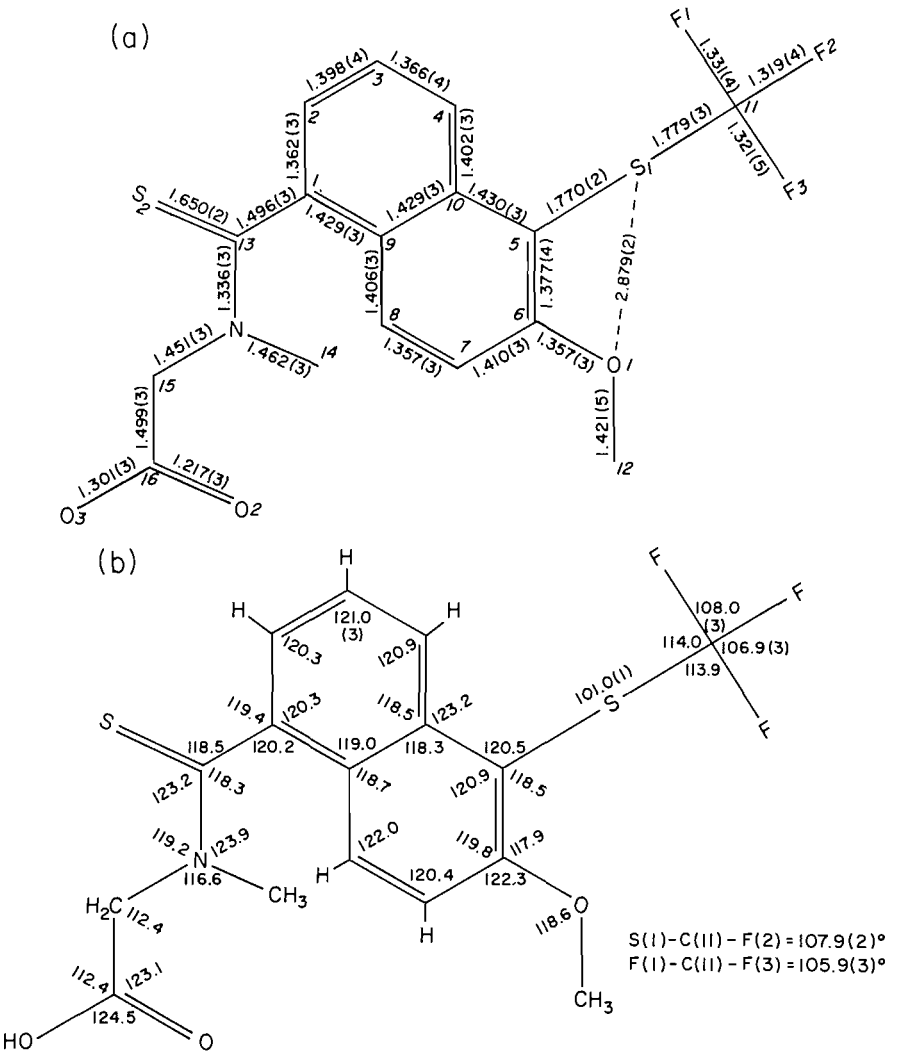

FIG. 2. (*a*) Bond lengths (Å) with their esd's; (*b*) valency angles (deg); the esd is 0.2° with the exception of those given in brackets.

TABLE 2. Comparison of bond lengths (Å) in naphthalene, with estimated standard deviations in parentheses

Bond	Title compound	$C_{10}H_8$[a]	$C_{10}D_8$[b]	$C_{12}H_{12}$[c]	$C_{12}H_{12}$[d]
C(1)—C(2)	1.362(3)	1.376(2)	1.372(5)	1.413(14)	1.375(19)
C(5)—C(6)	1.377(4)	1.376(2)	1.372(5)	1.403(14)	1.355(19)
C(3)—C(4)	1.366(4)	1.378(2)	1.372(5)	1.392(14)	1.380(16)
C(7)—C(8)	1.357(3)	1.378(2)	1.372(5)	1.380(12)	1.389(15)
C(1)—C(9)	1.424(3)	1.423(2)	1.423(5)	1.408(11)	1.446(14)
C(5)—C(10)	1.430(3)	1.423(2)	1.423(5)	1.418(10)	1.436(14)
C(4)—C(10)	1.402(3)	1.424(2)	1.423(5)	1.406(13)	1.444(19)
C(8)—C(9)	1.406(3)	1.424(2)	1.423(5)	1.402(14)	1.432(19)
C(2)—C(3)	1.398(4)	1.411(2)	1.401(7)	1.416(13)	1.428(32)
C(6)—C(7)	1.410(3)	1.411(2)	1.401(7)	1.422(12)	1.422(28)
C(9)—C(10)	1.429(3)	1.421(2)	1.412(7)	1.444(10)	1.380(24)

[a]Naphthalene, study at −150°C (7).
[b]Perdeuteronaphthalene, a neutron diffraction study (8).
[c]1,5-Dimethylnaphthalene, a neutron diffraction study (9).
[d]1,5-Dimethylnaphthalene, an X-ray analysis (10).

phile pairing involving a HOMO orbital of one sulfur atom and LUMO of the other.

In most cases the S···O interactions (17, 18) are along one of the covalent bonds to S, the oxygen atom acting as a nucleophile. However, the examination of the stereochemistry of the title compound revealed that O(1) acts as an electrophile, as it is approaching the sulfur atom at 36.0° to the perpendicular to the plane defined by C(5), S(1), and C(11), i.e. along the HOMO orbital of S.

The S···O interaction is also nearly along the extension of

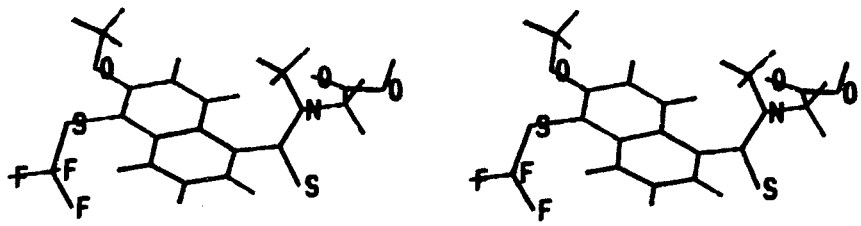

FIG. 3. Stereoscopic view of the molecule.

TABLE 3. Distances of atoms from the mean plane of the naphthalene moiety ($\times 10^3$) and their esd's[a]

Atom	Distance (Å)	Atom	Distance (Å)
C(1)	−16(2)	C(8)	2(2)
C(2)	−4(3)	C(9)	−11(2)
C(3)	31(3)	C(10)	−20(2)
C(4)	10(3)	S(1)*	16(1)
C(5)	−31(2)	O(1)*	53(2)
C(6)	14(2)	C(12)*	339(4)
C(7)	24(3)	C(13)*	−116(2)

[a]Atoms marked by an asterisk were not included in the calculation of the plane.

the O(1)—C(12) bond (<S(1)···O(1)—C(12) = 166.5(2)°), and is therefore directed towards the σ* orbital of O(1). It brings the C(12) atom close to the plane of the naphthalene moiety (Δ = 0.339 Å; see Table 3) and leads to the small value of 10.8(4)° for the torsion angle C(7)—C(6)—O(1)—C(12).

The hydrogen atoms of C(12) straddle H(7) giving smallest possible H···H contacts of 2.23(5) and 2.26(6) Å (see Fig. 3). The repulsion between these hydrogens is responsible for the widening of C(7)—C(6)—O(1) to 122.3° as compared to the corresponding angle C(10)—C(5)—S(1) of 120.5°, and to the increase of the C(6)—O(1)—C(12) angle to 118.6°. All these observations indicate that the sterically strained orientation of the methoxy group must be caused by a rather strong S···O interaction. This preferred orientation may be of importance in the biological activity of this compound.

Intermolecular hydrogen bonds between O(3) and O(2′) as well as between O(2) and O(3′) join the molecules related through a centre of symmetry into dimers. The pertinent data are: O(3)—H···O(2′) = 172.9(3.9)°, O(3)···O(2′) = 2.646(3) Å, O(3)—H = 0.87(4) Å, and H···O(2′) = 1.78(4) Å. There are no other short intermolecular contacts.

1. European Patent Application No. 82300940.2, published September 8, 1982.
2. D. DVORNIK. *In* Annual reports in medicinal chemistry. Vol. 13. *Edited by* F. H. Clarke. Academic Press, New York. 1978. p. 159.
3. P. MAIN, S. E. HULL, L. LESSINGER, G. GERMAIN, J. P. DECLERCQ, and M. M. WOOLFSON. MULTAN 78. A system of computer programs for the automatic solution of crystal structures from X-ray diffraction data. Universities of York, England, and Louvain-La-Neuve, Belgium. 1978.
4. H. P. HANSON, F. HERMAN, J. D. LEA, and S. SKILLMAN. Acta Crystallogr. **17**, 1040 (1964).
5. R. F. STEWART, E. R. DAVIDSON, and W. T. SIMPSON. J. Chem. Phys. **42**, 3175 (1965).
6. F. R. AHMED, S. R. HALL, M. E. PIPPY, and C. P. HUBER. NRC crystallographic programs for the IBM 360 system, accession Nos. 133–147. J. Appl. Crystallogr. **6**, 309 (1973).
7. V. I. PONOMAREV, O. S. FILIPENKO, and L. O. ATOVMYAN. Kristallografiya, **21**, 392 (1976).
8. G. S. PAWLEY and E. A. YEATS. Acta Crystallogr. B**25**, 2009 (1969).
9. J. BEINTEMA. Acta Crystallogr. **18**, 647 (1965).
10. G. FERRARIS, D. W. JONES, J. YERKESS, and K. D. BARTLE. J. Chem. Soc. Perkin II, 1628 (1972).
11. S. WEINSTEIN and L. LEISEROWITZ. Acta Crystallogr. B**36**, 1406 (1980).
12. A. BONDI. J. Phys. Chem. **68**, 441 (1964).
13. R. E. ROSENFIELD, JR., R. PARTHASARATHY, and J. D. DUNITZ. J. Am. Chem. Soc. **99**, 4860 (1977).
14. K. FUKUI, T. YONEZAWA, C. NAGATA, and H. SHINGU. J. Chem. Phys. **22**, 1433 (1954).
15. G. KLOPMAN. J. Am. Chem. Soc. **90**, 223 (1968).
16. T. N. GURU ROW and R. PARTHASARATHY. J. Am. Chem. Soc. **103**, 477 (1981).
17. D. G. GARRATT, M. PRZYBYLSKA, and M. CYGLER. Can. J. Chem. **61**, 1176 (1983).
18. A. KÁLMÁN and L. PÁRKÁNYI. Acta Crystallogr. B**36**, 2372 (1980).

Can. J. Chem. Downloaded from www.nrcresearchpress.com by 210.87.254.105 on 09/06/12
For personal use only.

The electrochemical synthesis of β-diketonato complexes of cadmium(II), and their adducts; the crystal and molecular structure of $Cd(acac)_2phen$

LUIS BUSTOS, JAMES H. GREEN, J. LAWRENCE HENCHER, MASOOD A. KHAN, AND DENNIS G. TUCK[1]

Department of Chemistry, University of Windsor, Windsor, Ont., Canada N9B 3P4

Received October 21, 1982

LUIS BUSTOS, JAMES H. GREEN, J. LAWRENCE HENCHER, MASOOD A. KHAN, and DENNIS G. TUCK. Can. J. Chem. **61**, 2141 (1983).

The cadmium β-diketonate complexes $Cd(RCOCHCOR')_2$ (R = CH_3, R' = CH_3; R = CF_3, R' = CH_3, *i*-C_3H_7, *i*-C_4H_9, *t*-C_4H_9, C_6H_5, 2-naphthyl) can be prepared in good yield by the direct room temperature electrochemical oxidation of the metal into a solution of the parent diketone in acetonitrile. Adducts of the type $Cd(RCOCHCOR')_2L$ (L = 2,2'-bipyridine, 1,10-phenanthroline, *N,N,N',N'*-tetramethylethylenediamine) can be prepared *in situ*, or by subsequent addition of the ligand to the electrolytic solution. X-ray studies show that the molecular structure of both $Cd(acac)_2phen$ and $Cd(CF_3COCHCOC_6H_5)_2phen$ is based on a CdO_4N_2 kernel, distorted from octahedral stereochemistry by the bite of the ligands.

LUIS BUSTOS, JAMES H. GREEN, J. LAWRENCE HENCHER, MASOOD A. KHAN et DENNIS G. TUCK. Can. J. Chem. **61**, 2141 (1983).

On peut préparer les complexes de β-dicétonates de cadmium $Cd(RCOCHCOR')_2$ (R = CH_3, R' = CH_3; R = CF_3, R' = CH_3, *i*-C_3H_7, *i*-C_4H_9, *t*-C_4H_9, C_6H_5, naphtyl-2) avec un bon rendement en réalisant une oxydation électrochimique directe, du métal en présence de la dicétone en solution dans l'acétonitrile à la température de la pièce. On peut préparer *in situ* les adduits du type $Cd(RCOCHCOR')_2L$ (L = bipyridine-2,2'; phénanthroline-1,10, *N,N,N',N'*-tétraméthyléthylène diamine) ou par addition subséquente du ligand à la solution électrolytique. Les études de rayons-X révèlent que la structure moléculaire des deux $Cd(acac)_2phen$ et $Cd(CF_3COCHCOC_6H_5)_2phen$ comprend un noyau de CdO_4N_2, et a une stéréochimie octaédrique déformée par le pincement du ligand.

[Traduit par le journal]

Introduction

Complexes of cadmium(II) with neutral or anionic oxygen-donor ligands have received some attention in the study of the coordination chemistry of this element. A number of adducts of cadmium halides with urea and similar ligands are known (1), and X-ray structural results have been reported for some of these (2). The most common coordination number is six, but four- and five-coordinate species have also been identified, and in keeping with other features of the coordination chemistry of cadmium and other d^{10} metal ions, relatively slight alteration in ligand properties, reaction conditions etc., may bring about changes in the coordination number. One especially interesting example of such effects is the compound $CdZn_2(PO_4)_2$, in which cadmium is found in CdO_4, CdO_5, and CdO_7 coordination (3). More relevant to the present work are the compounds $Cd(acac)_2$ (4) and $K[Cd(acac)_3]\cdot H_2O$ (5) (acac = 2,4-pentanedionate), both of which involve a CdO_6 kernel, with an infinite chain structure in $Cd(acac)_2$ giving rise to the increase in coordination number beyond the expected value of four.

We have now investigated the acceptor properties of $Cd(acac)_2$ and some analogous complexes in a preparative study involving the direct electrochemical synthesis of these compounds and their adducts. This aspect of the work follows previous electrochemical syntheses of other β-diketonate complexes in this laboratory (6–8). X-ray crystallographic studies show that the molecular structure of both of the adducts $Cd(acac)_2phen$ and $Cd(CF_3COCHCOC_6H_5)_2phen$ (phen = 1,10-phenanthroline) is based on a pseudo-octahedral CdO_4N_2 kernel.

Experimental

General

Cadmium metal was used as supplied, in the form of flattened sheets (ca. 1 × 1 cm, 1–2 g). All other materials were as in previous work (9). Cadmium analysis was by atomic absorption spectrophotometry.

Infrared spectra were recorded on a Beckman IR-12 spectrometer; ^1H and ^{19}F nmr spectra were run on a Bruker CXP-100 instrument. Mass spectra were recorded with a Varian MAT CH-5DF instrument operating in the field desorption mode, and interfaced with an Incos Model 2000 computer.

Electrochemical procedures

The electrochemical methods were essentially those used in previous experiments (6–8). A 100 mL beaker containing approximately 50 mL of solution phase served as the reaction vessel; the cathode was a thin platinum plate, and the cadmium anode (1–2 g) was a flattened sheet suspended on a platinum wire. One important experimental point which quickly emerged is that too high a current caused disintegration of the anode, with consequent contamination of the product. The conditions quoted in Table 1 gave a reasonable rate of reaction without such complications. Details of some specific preparations are given below.

The products were characterised by cadmium analysis, infrared spectroscopy, and in some cases mass spectrometric determination of molecular weight. Analytical results are given in Table 2. The ^1H nmr spectra, detailed in Table 3, are very similar to these reported for complexes of indium with the same β-diketonates (10).

Preparative

(a) Bis(2,4-pentanedionate)cadmium(II). As the electrochemical oxidation proceeded, hydrogen gas was evolved at the cathode, and a colourless precipitate formed at the anode. This air-stable material was collected by filtration and dried *in vacuo*.

(b) Adducts of $Cd(acac)_2$. The oxidation was carried out using the conditions given in Table 1. The products deposited in the cell were collected, washed with acetonitrile and petroleum ether, and dried *in vacuo*.

(c) $Cd(CF_3COCHCOR)_2$. The products of the electrochemical oxidation of cadmium in the presence of CF_3COCH_2COR (see Table 1) are soluble in the reaction mixture. The solution was filtered after electrolysis to remove any particles of cadmium metal etc., and solvent removed from the filtrate *in vacuo*. The resultant oil was dissolved in the minimum amount of acetone, and petroleum ether added to precipitate the product, which was collected and dried *in vacuo*.

[1]To whom all correspondence should be addressed.

Can. J. Chem. Downloaded from www.nrcresearchpress.com by 210.87.254.42 on 09/06/12
For personal use only.

Can. J. Chem. Downloaded from www.nrcresearchpress.com by 210.87.254.42 on 09/06/12
For personal use only.

TABLE 1. Reaction conditions for the direct electrochemical synthesis of cadmium(II)-β-diketonates, and adducts

Compound	Vol. of acetonitrile (mL)	Vol. (or wt.) of diketone[a]	Voltage (V)	Initial current (mA)	Time (h)	Cd dissolved (g)	Product obtained (g)	Yield (%)
$Cd(acac)_2$	40	10 mL	16	20	4.0	0.15	0.26	63
$Cd(acac)_2bipy$	40	10 mL[b]	8	20	2.4	0.11	0.28	61
$Cd(acac)_2phen$	40	5 mL[c]	11	20	12.0	0.37	0.57	65
$Cd(acac)_2tmed$	40	5 mL[d]	16	20	6.4	0.18	0.38	56
$Cd(CF_3COCHCOCH_3)_2$	20	2 mL	18	10	12.0	0.12	0.29	69
$Cd(CF_3COCHCOC_3H_7^i)_2$	20	3 mL	26	30	16.0	0.16	0.46	68
$Cd(CF_3COCHCOC_4H_9^t)_2$	20	2 mL	45	30	16.0	0.16	0.45	63
$Cd(CF_3COCHCOC_4H_9^t)_2$	20	1 mL	44	20	5.0	0.11	0.36	74
$Cd(CF_3COCHCOC_6H_5)_2$	45	1.8 g	11	20	15.0	0.31	0.89	60
$Cd[CF_3COCHCO(2\text{-naphthyl})]_2$	40	1.4 g	10	20	14.0	0.41	1.65	70

[a]Plus 25 mg Et_4ClO_4 in each case.
[b]Plus 0.79 g 2,2′-bipyridine (bipy).
[c]Plus 1.0 g 1,10-phenanthroline (phen).
[d]Plus 5 mL *N,N,N′,N′*-tetramethylethylenediamine.

TABLE 2. Analytical results for cadmium β-diketonates and adducts

Compound	Melting point (°C)	Cd analysis (%) Found	Cd analysis (%) Calcd.	Mol. wt.[a] Found	Mol. wt.[a] Calcd.
$Cd(acac)_2$	235	36.4	36.2	—	—
$Cd(acac)_2bipy$[b]	252	24.3	24.1	—	—
$Cd(acac)_2phen$[b]	259	22.9	22.8	—	—
$Cd(acac)_2tmed$[b]	243	26.5	26.3	—	—
$Cd(CF_3COCHCOCH_3)_2$	78	26.7	26.8	420	420
$Cd(CF_3COCHCOC_3H_7^i)_2$	71	23.9	23.7	476	476
$Cd(CF_3COCHCOC_4H_9^t)_2$	76	22.5	22.4	504	504
$Cd(CF_3COCHCOC_4H_9^t)_2$	77	22.5	22.4	504	504
CdL_2[c]	110	20.8	20.7	544	544
CdL_2'[c]	115	17.4	17.5	644	644
CdL_2bipy[b,c]	178	15.2	16.1	—	—
CdL_2phen[b,c]	189	15.5	15.5	—	—
$CdL_2'bipy$[b,c]	187	13.0	14.1	—	—

[a]Nearest integral *m/e* for most abundant molecular ion peak.
[b]bipy = 2,2′-bipyridine; phen = 1,10-phenanthroline; tmed = *N,N,N′,N′*-tetramethylethylenediamine.
[c]L = $CF_3COCHCOC_6H_5$; L′ = $CF_3COCHCO$(2-naphthyl).

TABLE 3. ^1H nmr spectra of cadmium β-diketonates, and adducts (ppm, from Me_4Si)

Compound	Solvent	CH_3, R	γ-CH	Donor ligand
$Cd(acac)_2$	d_6-dmso	2.19 s (5.5H)	5.15 s (1H)	—
$Cd(acac)_2bipy$[a]	$CDCl_3$	1.90 s (5.5H)	5.20 s (1H)	7.8–9.1 m (3.9H)
$Cd(acac)_2phen$[a]	CD_2Cl_2	1.83 s (6H)	5.17 s (1H)	7.6–8.8 m (4.7H)
$Cd(acac)_2tmed$[a]	$CDCl_3$	1.92 (6.2 H)	5.42 s (1H)	2.25 s (12.4H) $N(CH_3)$[b] 2.40 s (3H) NC_2H_4N
CdL_2[c]	d_6-acetone	7.6–8.1 m (5H)	6.40 s (1H)	—
CdL_2bipy[a,c]	d_6-acetone	7.6–8.0 m[c]	6.30 s	8.0–9.1 m[d]
CdL_2phen[a,c]	d_6-acetone	7.6–8.0[c]	6.35 s	8.0–9.0 m[d]
CdL_2'[d]	CD_3CN	7.3–8.7 m (7H)	6.55 s (1H)	—
$CdL_2'bipy$[a,d]	d_6-acetone	7.3–9.4 m[c,e]	6.52	

[a]bipy = 2,2′-bipyridine; phen = 1,10-phenanthroline; tmed = *N,N,N′,N′*-tetramethylethylenediamine.
[b]Integration of low accuracy.
[c]L = $CF_3COCHCOC_6H_5$; L′ = $CF_3COCHCO$(2-naphthyl).
[d]Integration not attempted.
[e]Naphthyl and donor ligand resonances not resolved.

(d) Adducts of $Cd(CF_3COCHCOR)_2$ (R = C_6H_5, 2-naphthyl). A solution of the cadmium β-diketonate and an equimolar quantity of 2,2′-bipyridine or 1,10-phenanthroline was stirred at room temperature for ca. 3 h. The solvent was removed by evaporation, and diethyl ether, and then petroleum ether, added to precipitate the adduct, which was collected and dried *in vacuo*. Yields were in the range of 70–80%. The product of the reaction of 1,10-phenanthroline and $Cd[CF_3COCHCO(2\text{-naphthyl})]_2$ did not analyse satisfactorily.

TABLE 4. Summary of crystal data, intensity collections, and structural refinement for $Cd(acac)_2phen$, $C_{22}H_{22}CdN_2O_4$ (**1**) and $Cd(CF_3COCHCOC_6H_5)_2phen$, $C_{32}H_{20}CdF_6N_2O_4$ (**2**)

Parameters	Value	
	1	**2**
Cell constants	a = 16.159(1) Å b = 10.292(2) Å c = 12.694(3) Å	a = 9.069(2) Å, α = 94.45(2)° b = 10.952(2) Å, β = 94.89(2)° c = 15.849(4) Å, γ = 104.94(2)°
Cell volume (Å^3)	2111(1)	1507(1)
Space group	*Pbcn* (No. 60)	*PT* (No. 2)
Z	4	2
M_r	490.83	722.91
ρ(calcd)(g cm^{-3})	1.544	1.593
Abs coeff (cm^{-1})	9.61	7.14
Radiation (λ = 0.71069 Å)	MoK_α	MoK_α
Min/max abs correct	2.32/2.82	—
2θ angle	4–50°	4–50°
Scan width	K_α − 1° to $K_{\alpha 2}$ + 1°	$K_{\alpha 1}$ − 1° to $K_{\alpha 2}$ + 1°
Scan speed	2.02–4.88° min^{-1}	2.02–4.88° min
Bkgd time/scan time	0.5	0.5
Total reflections measd	2169 (h, k, l)	5337 (h, ±k, ±l)
Unique average data	$1324[F_o^2 > 3\sigma(F_o)^2]$	$4288[F_o^2 > 2\sigma(F_o)^2]$
$R = (\Sigma\Delta/\Sigma\lvert F_o\rvert)$	0.0233	0.0691
$R_w = [\Sigma w\Delta^2/\Sigma wF_o^2]^{1/2}$	0.0280	0.0715

TABLE 5. Atomic coordinates for non-hydrogen atoms in $Cd(acac)_2phen$

	x	y	z
Cd	0.0	0.03320(3)	0.25
O(1)	0.0647(1)	0.1702(2)	0.3575(2)
O(2)	0.1268(1)	0.0292(2)	0.1723(2)
N	−0.0341(2)	−0.1540(2)	0.1506(2)
C(1)	0.1417(2)	0.1746(3)	0.3751(3)
C(2)	0.2032(2)	0.1185(4)	0.3140(3)
C(3)	0.1933(2)	0.0505(4)	0.2198(3)
C(4)	0.1661(3)	0.2492(4)	0.4728(4)
C(5)	0.2703(3)	−0.0045(6)	0.1678(3)
C(11)	−0.0680(2)	−0.1548(3)	0.0560(2)
C(12)	−0.0885(2)	−0.2679(3)	0.0023(2)
C(13)	−0.0733(2)	−0.3843(3)	0.0484(2)
C(14)	−0.0371(2)	−0.3899(3)	0.1489(2)
C(15)	−0.0187(2)	−0.2702(3)	0.1978(2)
C(16)	−0.0177(2)	−0.5089(4)	0.2017(3)

Crystal structure determination

The crystal data for $Cd(acac)_2phen$ are given in Table 4. A suitable crystal with dimensions of 0.2 × 0.2 × 0.3 mm was chosen, and the data were collected on a Syntex $P2_1$ diffractometer. The procedure for data collection and processing is described elsewhere (11). During the data collection, the intensities of three monitor reflections decreased by 4% and this was accounted for by applying appropriate scaling factors. The space group *Pbcn* (No. 60) was determined from the systematic absences ($0kl$, $k = 2n$; $h0l$, $l = 2n$; $hk0$, $h + k = 2n$). The data were corrected for Lorentz and polarization effects, and an analytical absorption correction was also applied.

The position of the cadmium atom on a two-fold axis was obtained from a sharpened Patterson synthesis, and the subsequent difference Fourier map revealed the positions of all other non-hydrogen atoms. The structure was refined anisotropically by full-matrix least-squares methods to $R = 0.0369$. A difference map at this stage showed peaks for some plausible hydrogen atom positions, and all the hydrogen atoms were included in the subsequent refinement in the "idealized" position (C—H = 0.95 Å, $U = 0.06$ Å^2 for phenyl hydrogens and $U = 0.11$ Å^2 for methyl hydrogens). Full-matrix least-squares refinement yielded the final values $R = 0.0233$, $R_w = 0.0280$, for 1324 "observed" reflections. In the last cycle the largest shift/error ratio was 0.01 and the final difference map had no features of chemical significance, the maximum peak being ~0.2 e Å^{-3}. Least-squares refinement minimized the function $\Sigma w(\lvert F_o\rvert - \lvert F_c\rvert)^2$. Unit weights were used in the initial stages of refinement, while in the final cycles of calculation a weighting scheme of the form $w = (1/(\sigma^2(F) + 0.02F^2))$ was employed.

Scattering factors for all non-hydrogen atoms, including the anomalous disperson correction terms $\Delta f'$ and $\Delta f''$ of cadmium were obtained from ref. 12, and for the hydrogen atoms from ref. 13. All calculations were carried out on the University of Windsor IBM 3031 computer with the programmes CHECK and PROC (14), ABSORB (15), SHELX 77 (16), XANADU (17), and ORTEP (18). The final atomic coordinates[2] are given in Table 5, and bond lengths and angles are presented in Table 6. Figure 1 illustrates the molecular structure, with the atomic numbering scheme, and the unit cell packing is shown in Fig. 2.

A single crystal of $Cd(CF_3COCHCOC_6H_5)_2phen$ was subjected to an exactly analogous treatment and refined to $R = 0.0691$ (see Table 4). At this stage it was clear that the molecular geometry of this molecule is essentially identical to that of $Cd(acac)_2phen$ insofar as the CdO_4N_2 kernel is concerned.

Results and discussion

Preparative

The experiments described above demonstrate another application of the method of direct electrochemical synthesis in the preparation of cadmium β-diketonates and their adducts. This latter group of new complexes can be synthesised in a one-step procedure, or by using solutions of the cadmium diketonates prepared previously. The $Cd(CF_3COCHCOR)_2$ compounds have not been previously reported.

The mechanism of the electrochemical synthesis of β-diketonate complexes has been described earlier in terms of

[2]The observed and final calculated structure amplitudes, calculated hydrogen atom coordinates, and the anisotropic thermal parameters are available, at a nominal charge, from the Depository of Unpublished Data, CISTI, National Research Council of Canada, Ottawa, Ont., Canada K1A 0S2.

Can. J. Chem. Downloaded from www.nrcresearchpress.com by 210.87.254.42 on 09/06/12
For personal use only.

Can. J. Chem. Downloaded from www.nrcresearchpress.com by 210.87.254.42 on 09/06/12
For personal use only.

TABLE 6. Bond distances (Å) and angles (deg) in $Cd(acac)_2phen$[a]

Bond	Distance (Å)	Bond	Distance (Å)
Cd—O(1)	2.224(2)	Cd—O(2)	2.274(2)
Cd—N	2.368(2)		
O(1)—C(1)	1.264(4)	O(2)—C(3)	1.252(4)
C(1)—C(2)	1.387(5)	C(2)—C(3)	1.394(6)
C(1)—C(4)	1.511(5)	C(3)—C(5)	1.519(6)
N—C(11)	1.319(3)	N—C(15)	1.361(4)
C(11)—C(12)	1.389(4)	C(12)—C(13)	1.356(4)
C(13)—C(14)	1.405(4)	C(14)—C(15)	1.411(4)
C(14)—C(16)	1.431(5)	C(15)—C(15)′	1.457(6)
C(16)—C(16)′	1.354(8)		

Bonds	Angle (deg)	Bonds	Angle (deg)
O(1)—Cd—O(1)′	101.3(1)	O(1)—Cd—O(2)	81.6(1)
O(1)—Cd—O(2)′	99.7(1)	O(1)—Cd—N	162.3(1)
O(1)—Cd—N′	94.6(1)	O(2)—Cd—O(2)′	177.9(1)
O(2)—Cd—N	87.9(1)	O(2)—Cd—N′	90.4(1)
N—Cd—N′	71.1(1)	Cd—O(1)—C(1)	126.4(2)
Cd—O(2)—C(3)	124.2(2)	Cd—N—C(11)	125.9(2)
Cd—N—C(15)	116.0(2)	C(11)—N—C(15)	118.1(3)
O(1)—C(1)—C(2)	126.3(3)	O(1)—C(1)—C(4)	114.8(3)
C(2)—C(1)—C(4)	118.9(3)	C(1)—C(2)—C(3)	127.3(3)
O(2)—C(3)—C(2)	126.8(3)	O(2)—C(3)—C(5)	115.4(3)
C(2)—C(3)—C(5)	117.8(4)	N—C(11)—C(12)	123.4(3)
C(11)—C(12)—C(13)	119.0(3)	C(12)—C(13)—C(14)	120.2(3)
C(13)—C(14)—C(15)	116.8(3)	C(13)—C(14)—C(16)	123.4(3)
C(15)—C(14)—C(16)	119.7(3)	N—C(15)—C(14)	122.4(3)
N—C(15)—C(15)′	118.5(3)	C(14)—C(15)—C(15)′	119.2(3)
C(14)—C(16)—C(16)′	121.1(3)		

[a]Symmetry equivalent position: prime denotes $(-x, y, 1/2 - z)$.

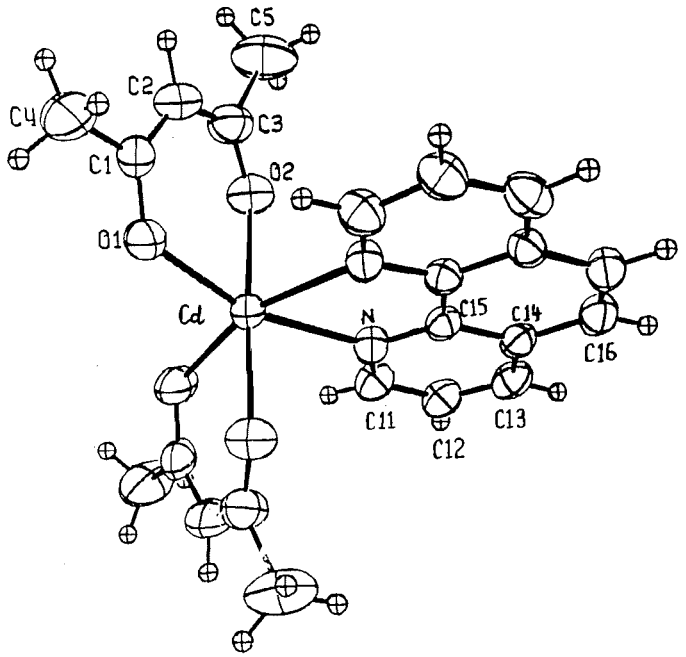

FIG. 1. Stereochemistry of $Cd(acac)_2phen$, $CdC_{22}H_{22}N_2O_4$.

the following processes:

cathode: $n\text{Hacac} + ne \rightarrow n\text{acac}^- + (n/2)H_2$

anode: $n\text{acac}^- + M \rightarrow M(acac)_n$

In keeping with this mechanism, we observed formation of gas at the cathode; equally the electrochemical efficiency, defined as moles of metal dissolved per Faraday, was close to the calculated value of 0.5 mol F^{-1} (experimental, for Cd/Hacac 0.54 mol F^{-1}; for Cd/Hacac/bipy 0.52 mol F^{-1}). The chemical yields, measured in terms of moles of product per mole metal dissolved, are in the range 55–75% (Table 1), so that the method is a simple and efficient route to these chelate complexes.

Electrochemical synthesis is also a convenient route to adducts of cadmium β-diketonates with bidentate ligands. The compound $Cd(acac)_2bipy$ has been previously prepared from $Na[Cd(acac)_3]$, but the product of this method with 1,10-phenanthroline is the hydrate $Cd(acac)_2phen \cdot H_2O$ (19). The formation of such adducts is a reflection of the Lewis acid character of $Cd(acac)_2$, as is the solid state homopolymeric structure of this compound, and the preparative results show that this property is retained even when bulky β-diketonate ligands such as $[CF_3COCHCO(2\text{-naphthyl})]^-$ are used. This electron pair acceptor character is one of the many examples of the tendency of d^{10} metal ions to exceed the four-coordination predicted by the inert gas configuration rule. We were unable to obtain adducts of $Cd(acac)_2$ with monodentate ligands such as pyridine, dimethylsulphoxide, or acetonitrile by the electrochemical method, although adducts of $Cd(acac)_2$ with R_3PO (R = *n*-octyl, phenyl) have been reported (20).

Finally, we note that the presence of bulky substituents in the β-diketonate ligand does not inhibit the acceptor character of the resultant CdL_2 species toward bidentate ligands, and pre-

Can. J. Chem. Downloaded from www.nrcresearchpress.com by 210.87.254.42 on 09/06/12
For personal use only.

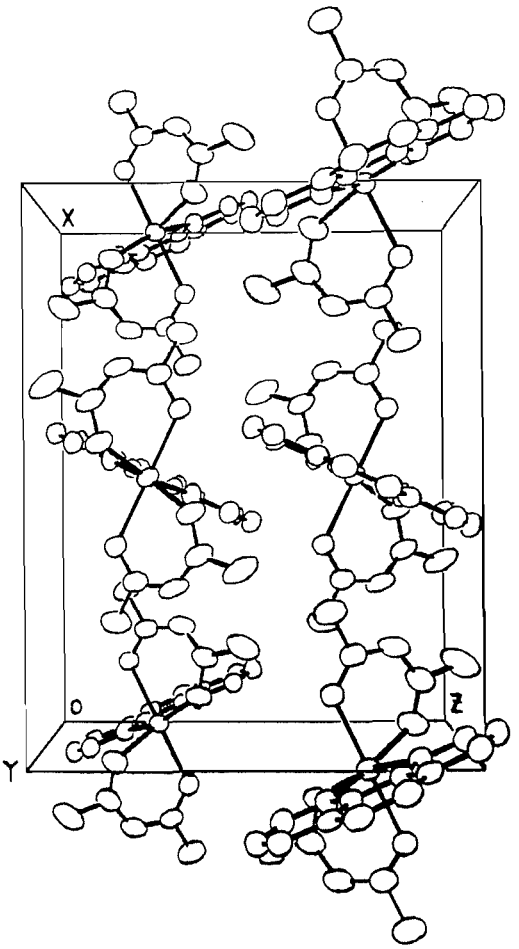

FIG. 2. Packing diagram for $Cd(acac)_2phen$, $CdC_{22}H_{22}N_2O_4$.

liminary X-ray investigation confirmed that $Cd(CF_3COCHCOC_6H_5)_2phen$ has essentially the same CdO_4N_2 structure as $Cd(acac)_2phen$. It is unfortunate that we were not able to obtain samples of any of the $Cd(CF_3COCHCOR)_2$ compounds in sufficiently good quality for X-ray structural determination, so that the question of the molecularity of these compounds in the solid state presently remains unanswered.

Structure of $Cd(acac)_2phen$

The molecular structure of $Cd(acac)_2phen$ (Fig. 1) is based on CdO_4N_2 octahedral coordination, necessarily distorted as the result of the bidentate character of the ligands. The Cd—O bond distances are in the middle of the range of 2.25–2.50 Å derived earlier (2) for six-coordinate species, but the detailed values show a clear *trans*-effect, in that Cd—O bonds opposite oxygen are significantly longer (2.272(3) Å) than Cd—O *trans* to nitrogen (2.223(3) Å). This is readily understood in terms of the formal negative charge distributed between the two oxygen atoms of $acac^-$, as opposed to the neutral nitrogen atoms of 1,10-phenanthroline. Comparison of the Cd—O bond distances with those in $Cd(acac)_2$, or $Cd(acac)_3^-$, are rendered difficult by the range of values in these compounds. For $Cd(acac)_2$, Cd—O_{br} spans the range 2.288(4)–2.353(4) Å, while for the non-bridging oxygen atoms Cd—O is 2.221(5) and 2.250(4) Å. In $Cd(acac)_3^-$, the values range from 2.247(9) to 2.325(9) Å, with an average of 2.28 Å, close to the present result for Cd—O *trans* to oxygen. The O—Cd—O angles within the chelate ring are in good agreement in all three compounds, namely, 80.4° in $Cd(acac)_2$, 79.5° in $Cd(acac)_3^-$, and 81.5(1)°, in $Cd(acac)_2phen$; the values for the first two compounds are the mean angles for the various independent ligands (4, 5). The CdO_2C_3 ring formed by the β-diketonate ligand is almost planar, with the maximum deviation of 0.017 Å at C(1). The C—C and C—O bond lengths are again close to those published for this ligand in complexes with cadmium (4, 5), and with the isoelectronic In^{3+} ion (21).

The literature contains two previous reports of structures involving cadmium complexed by 1,10-phenanthroline, namely, $(phen)Cd[Mn(CO)_5]_2$ (22) and $(phen)Cd(S_2COEt)_2$ (23). The Cd—N distances and the N—Cd—N angle found in the present work agree with the earlier values within experimental error. Results for other neutral donors (2) yield Cd—N distances in the range 2.10–2.80 Å, with a mean value of ca. 2.40 Å, in agreement with the experimental result given in Table 6. The structure of the coordinated 1,10-phenanthroline calls for little comment; the aromatic rings are planar, and the C—C and C—N bond lengths are in keeping with published values.

As noted earlier, the structure of $Cd(CF_3COCHCOC_6H_5)_2phen$ has been refined to $R = 0.069$. The average bond distances are Cd—O = 2.25(3) Å, and Cd—N = 2.32(3) Å, the mean O—Cd—O angle is 80(1)°, and N—Cd—N is 72(1)°. In all respects then the structure is the same as that reported for $Cd(acac)_2phen$ within the experimental error. The structure of the ammonium salt of the anion $Cd[CF_3COCHCO(2\text{-furyl})]_3^-$ shows very similar values (24), and given these similarities the refinement was not carried further.

Mass spectrometric results

We have commented elsewhere (25) on the advantages of field desorption mass spectrometry in inorganic and organometallic chemistry. The case of $Cd(CF_3COCHCOR)_2$ complexes is further evidence of this, with the spectra all being effectively identical. That of $Cd(CF_3COCHCOC_6H_5)_2$ consists of two main features, to wit, a group of peaks corresponding to the molecular ions $CdL_2^{+\cdot}$ of various isotopes and ions of the neutral ligand $HL^{+\cdot}$. The intensities of the $CdL_2^{+\cdot}$ region are in agreement, within experimental error, with those calculated on the basis of the known isotopic masses and abundances. Certain significant low mass species are tentatively identified on the basis of m/e values as $CF_2^{+\cdot}$ (50.0), $F_2^{+\cdot}$ (38.00) and $FO^{+\cdot}$ (35.00). These low mass ions represent less than 20% of the total ion intensity, of which 65% is in the $CdL_2^{+\cdot}$ manifold.

Acknowledgement

This work was supported in part by Operating Grants (to D.G.T.) from the Natural Sciences and Engineering Research Council of Canada.

1. B. J. AYLETT. Comprehensive inorganic chemistry. Vol. 3. *Edited by* A. F. Trotman-Dickenson. Pergamon Press, Oxford. 1973. p. 273.
2. D. G. TUCK. Rev. Inorg. Chem. **1**, 209 (1979).
3. C. CALVO and J. S. STEPHENS. Can. J. Chem. **46**, 903 (1968).
4. E. N. MASLEN, T. M. GREANEY, C. L. RASTON, and A. H. WHITE. J. Chem. Soc. Dalton Trans. 400 (1975).
5. T. M. GREANEY, C. L. RASTON, A. J. WHITE, and E. N. MASLEN. J. Chem. Soc. Dalton Trans. 876 (1975).
6. J. J. HABEEB, D. G. TUCK, and F. H. WALTERS. J. Coord. Chem. **8**, 27 (1978).
7. J. J. HABEEB and D. G. TUCK. Inorg. Synth. **19**, 257 (1979).
8. N. KUMAR and D. G. TUCK. Can. J. Chem. **60**, 2579 (1982).
9. J. J. HABEEB and D. G. TUCK. J. Organomet. Chem. **146**, 213 (1978).

10. H. L. CHUNG and D. G. TUCK. Can. J. Chem. **52**, 3944 (1974).
11. M. A. KHAN, R. C. STEEVENSZ, D. G. TUCK, J. G. NOLTES, and P. W. R. CORFIELD. Inorg. Chem. **19**, 3407 (1980).
12. International tables for X-ray crystallography. Vol. IV. Kynoch Press, Birmingham. 1974. pp. 99, 149.
13. R. F. STEWART, E. R. DAVIDSON, and W. T. SIMPSON. J. Chem. Phys. **42**, 3175 (1965).
14. P. W. CORFIELD and W. SCHMONSEES. CHECK and PROC: Data reduction. 1972.
15. D. TEMPLETON and L. TEMPLETON. ABSORB: A programme for applying analytical absorption correction to data. 1973.
16. G. M. SHELDRICK. SHELX 77: A programme for crystallographic calculations, University Chemical Laboratory, Cambridge, England. 1977.
17. P. ROBERTS and G. SHELDRICK. XANADU: A programme for mean plane and torsion angle calculations. 1975.
18. C. K. JOHNSON. ORTEP: Thermal ellipsoid plotting programme. 1965.
19. R. B. BIRDY and M. GOODGAME. Inorg. Chim. Acta, **36**, 281 (1979).
20. G. N. RAO and N. C. LI. J. Inorg. Nucl. Chem. **28**, 2931 (1966).
21. J. G. CONTRERAS, F. W. B. EINSTEIN, and D. G. TUCK. Can. J. Chem. **52**, 3793 (1974).
22. W. CLEGG and P. J. WHEATLEY. J. Chem. Soc. Dalton Trans. 511 (1974).
23. C. L. RASTON and A. H. WHITE. Aust. J. Chem. **29**, 739 (1976).
24. W. O. MCSHARRY, M. CEFOLA, and J. G. WHITE. Inorg. Chim. Acta, **38**, 161 (1980).
25. D. G. TUCK, G. W. WOOD, and S. ZHANDIRE. Can. J. Chem. **58**, 833 (1980).

Can. J. Chem. Downloaded from www.nrcresearchpress.com by 210.87.254.42 on 09/06/12
For personal use only.

Excess volumes of binary mixtures of cyclohexanone with some monosubstituted benzenes at 298.15 K

B. CHAWLA,[1] S. K. MEHTA, R. V. JASRA, AND S. K. SURI[2]

Department of Chemistry, Indian Institute of Technology, New Delhi - 110016, India

Received May 13, 1982[3]

B. CHAWLA, S. K. MEHTA, R. V. JASRA, and S. K. SURI. Can. J. Chem. **61**, 2147 (1983).

Molar excess volumes for the binary mixtures of cyclohexanone with benzene and some monosubstituted benzenes, namely, toluene, ethylbenzene, isopropylbenzene, tertiary butylbenzene, chlorobenzene, bromobenzene, iodobenzene, *N*,*N*-dimethylaniline, nitrobenzene, benzaldehyde, and benzonitrile have been calculated from the precise and accurate experimental density data at 298.15 K over the entire composition range. The results have been discussed in terms of the strength of molecular interactions in the binary mixtures.

B. CHAWLA, S. K. MEHTA, R. V. JASRA et S. K. SURI. Can. J. Chem. **61**, 2147 (1983).

Faisant appel aux données précises de densité expérimentale à 298,1 K sur toute l'étendue de de composition, on a calculé les volumes molaires en excès des mélanges binaires de quelques benzènes monosubstitués tels le toluène, l'éthylbenzène, l'isopropylbenzène, le *tert*-butylbenzène, le chlorobenzène, le bromobenzène, l'iodobenzène, la *N*,*N*-diméthylaniline, le nitrobenzène, la benzaldéhyde et le benzonitrile. On discute des résultats en fonction de la force des interactions moléculaires dans les mélanges binaires.

[Traduit par le journal]

Can. J. Chem. Downloaded from www.nrcresearchpress.com by 210.87.254.6 on 09/06/12
For personal use only.

Introduction

In continuation of our earlier studies on thermodynamic properties of binary liquid mixtures (1–4), we report in this paper the results of molar excess volumes for mixtures of cyclohexanone with benzene and some monosubstituted benzenes at 298.15 K. The monosubstituted benzenes studied are toluene, ethylbenzene, isopropylbenzene, tertiary butylbenzene, chlorobenzene, bromobenzene, iodobenzene, *N*,*N*-dimethylaniline, benzaldehyde, nitrobenzene, and benzonitrile. These studies were aimed to determine the effect of changing polarity of monosubstituted benzenes on the volumetric behaviour of their cyclohexanone solutions with a view to understand the factors determining the unlike interactions between molecules in such mixtures.

Experimental

Analar reagent grade samples of benzene, toluene, and benzaldehyde and commercial laboratory reagent grade samples of ethylbenzene, chlorobenzene, bromobenzene, nitrobenzene, benzonitrile, *N*,*N*-dimethylaniline, and cyclohexanone supplied by BDH, and samples of isopropylbenzene and iodobenzene supplied by Aldrich were purified according to established procedures (5). The sample of tertiary butylbenzene was prepared by reacting tertiary butylchloride (obtained by reacting tertiary butylalcohol with concentrated hydrochloric acid) with benzene in presence of anhydrous aluminium chloride (6). The resultant material was first dried over anhydrous magnesium sulphate and then fractionally distilled. All of the reagents were stored in brown bottles and fractionally distilled immediately before use. The densities and refractive indices of the solvents have been compared with the accepted literature values (5, 7–9) in Table 1.

The molar excess volumes of mixing have been calculated from the experimental density data. The solutions for the measurement of densities were prepared by weight and corrections for buoyancy were applied. The details of the experimental technique for the preparation of solutions have been described earlier (10).

The densities were measured with a vibrating tube digital density meter Model DMA 602/DMA 60 (Anton Paar, Austria). Water from a constant temperature bath was circulated through the metal block of the density meter at a flow rate of ~ 3 dm^3 min^{-1}. The temperature of the water bath was controlled to $\pm 1 \times 10^{-3}$ K using a Tronac PTC 40 proportional temperature controller. The density meter was calibrated with dried air and degassed ion-exchanged water. The density of water was taken to be 0.9970429 g cm^{-3} at 298.15 K (11). Duplicate densities of liquids and liquid mixtures studied agreed within 3×10^{-5} g cm^{-3}. This propagates a maximum uncertainty of about ± 0.008 cm^3 mol^{-1} in molar excess volumes.

Results and discussion

The molar excess volumes, V_m^E, for the binary mixtures at 298.15 K are recorded in Table 2 and plotted as a function of solution composition in Fig. 1. Each set of results was fitted with a polynomial form:

$$[1] \quad V_m^E/(\text{cm}^3\ \text{mol}^{-1}) = x(1-x)\sum_{i=0}^{n-1} A_i(2x-1)^i$$

where x is the mole fraction of a cyclohexanone. Values of the coefficients A_i were determined by the method of (unweighed) least squares. It was found that the best fit was obtained using three to four parameters in the equation. The values of A_i along with the standard derivation for the molar excess volume $\sigma(V^E)$ are listed in Table 3.

It is observed from Fig. 1 that V_m^E varies almost symmetrically with the mole fraction of cyclohexanone and shows a maximum (or minimum) somewhere around $x = 0.50 \pm 0.15$ for all the binary systems reported in this paper. For binary mixtures of cyclohexanone with benzaldehyde, iodobenzene, nitrobenzene, and *N*,*N*-dimethylaniline, V_m^E at 298.15 K is positive over the entire composition range whereas for all other solutions, it is negative. Solutions containing bromobenzene and benzonitrile were found to exhibit only small negative values of V_m^E. To the best of our knowledge, no V_m^E data have been reported in the literature to compare with our results.

The large negative V_m^E values for the binary mixtures of cyclohexanone with benzene are indicative of specific interactions between the lone pair of electrons on the oxygen of

[1]To whom all correspondence should be addressed at: Department of Chemistry, Duke University, Durham, NC 27707, U.S.A.

[2]Present address: Hindustan Lever Research Centre, Andheri (East), Bombay 400 099, India.

[3]Revision received March 24, 1983.

Can. J. Chem. Downloaded from www.nrcresearchpress.com by 210.87.254.6 on 09/06/12
For personal use only.

TABLE 1. Densities (g cm^{-3}) and refractive indices of liquids used at 298.15 K

Liquid	Density		Refractive index (n_D)	
	Our value	Lit. value (ref. 7)	Our value	Lit. value (ref. 7)
Benzene	0.87372	0.87366	1.4980	1.49793
Toluene	0.86207	0.86232	1.4945	1.4939
Ethylbenzene	0.86274	0.86264	1.4930	1.4932
Isopropylbenzene	0.85806	0.85751	1.4890	1.4889
tert-Butylbenzene	0.86228	0.86240	1.4895	1.49024
Chlorobenzene	1.10107	1.10118	1.5215	1.5219
Bromobenzene	1.48891	1.48824	1.5580	1.55709
Iodobenzene	1.82361	1.82377[a]	1.5865	1.56915[a,d]
Nitrobenzene	1.19847	1.19833	1.5505	1.5499
Benzaldehyde	1.04323	1.0434[b]	1.5440	1.5428[b]
Benzonitrile	1.00064	1.00071[c]	1.5285	1.5265[b,d]
N,*N*-Dimethylaniline	0.95168	0.95177[a]	1.5550	—
Cyclohexanone	0.94194	0.94207[b,d]	1.4015	1.41061[b,d]

[a]Calculated from data in ref. 8.
[b]From ref. 5.
[c]From ref. 9.
[d]Extrapolated value.

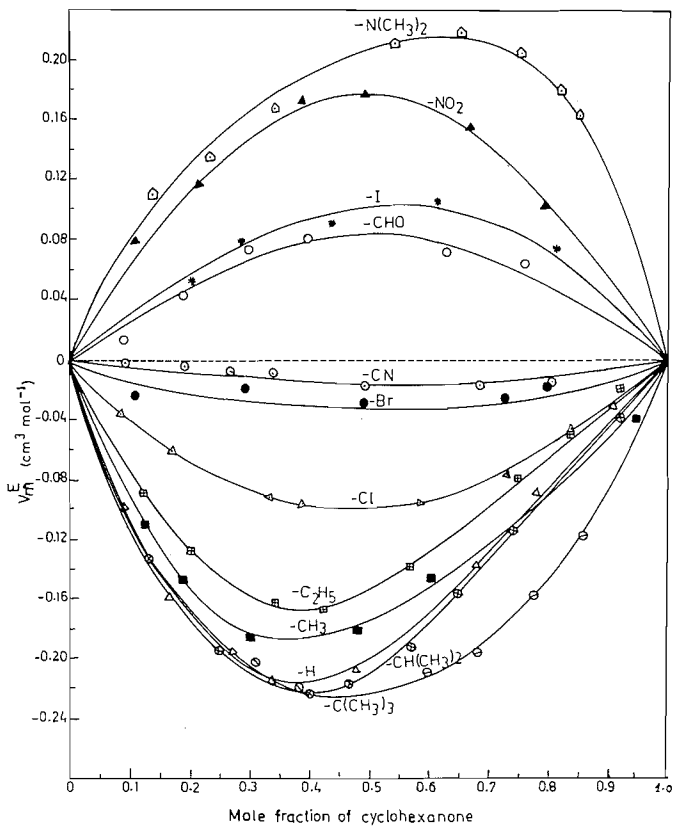

FIG. 1. Molar excess volumes, V_m^E, as a function of composition at 298.15 K for the binary mixtures of cyclohexanone with various monosubstituted benzenes: △, benzene; ■, toluene; ⊞, ethylbenzene; ⊗, isopropylbenzene; ∅, tertiary-butylbenzene; △, chlorobenzene; ●, bromobenzene; ✻, iodobenzene; ⬠, *N*,*N*-dimethylaniline; ▲, nitrobenzene; ○, benzaldehyde; ⊙, benzonitrile.

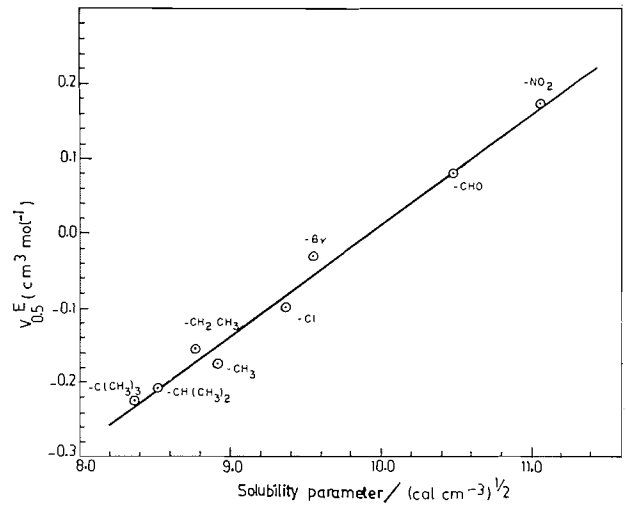

FIG. 2. Molar excess volumes for the binary mixtures at equimolar concentration, $V_{0.5}^E$ plotted against the solubility parameter of the monosubstituted benzenes at 298.15 K.

cyclohexanone and the easily polarizable π-electron system of the benzene ring (12). The V_m^E for *n*-alkyl substituted benzenes follow the order: ethylbenzene > toluene > benzene. This can be attributed to the increased positive contribution to V_m^E arising from an increase in π-electron density on the benzene ring (due to the *n*-alkyl substitution) (12). It is observed that the branched chain alkyl substitution, in spite of the significant contribution to the increase in π-electron density of the aromatic ring (and hence increased positive contribution to the polarity component of V_m^E) tend to decrease V_m^E, the magnitude of which has been found to be dependent on the extent of branching. It is apparent that the steric factors in isopropylbenzene and tertiary butylbenzene play predominant role in determining the volumetric behaviour of their cyclohexanone solutions. A similar observation has been made for the binary mixtures of cyclohexanone with alkanes (4).

The excess volumes for the binary mixtures at equimolar concentration, $V_{0.5}^E$, have been tabulated in Table 4 along with

TABLE 2. Excess volume of mixing, V_m^E, for binary mixtures of cyclohexanone and substituted benzenes at 298.15 K

Mole fraction of $C_6H_{10}O$	V_m^E ($cm^3\ mol^{-1}$)	Mole fraction of $C_6H_{10}O$	V_m^E ($cm^3\ mol^{-1}$)
$C_6H_{10}O + C_6H_6$		$C_6H_{10}O + C_6H_5Br$	
0.0906	−0.0997	0.1079	−0.0244
0.1609	−0.1591	0.2947	−0.0204
0.2655	−0.1948	0.4913	−0.0306
0.3376	−0.2132	0.7314	−0.0245
0.4791	−0.2074	0.7998	−0.0163
0.6777	−0.1367	$C_6H_{10}O + C_6H_5I$	
0.7767	−0.0897	0.2041	0.0495
0.9019	−0.0305	0.2886	0.0794
$C_6H_{10}O + C_6H_5CH_3$		0.4371	0.0854
0.1254	−0.1093	0.6114	0.1040
0.1848	−0.1473	0.8116	0.0732
0.2982	−0.1842	$C_6H_{10}O + C_6H_5N(CH_3)_2$	
0.4795	−0.1805	0.1400	0.1103
0.6044	−0.1454	0.2334	0.1350
0.9448	−0.0397	0.3445	0.1664
$C_6H_{10}O + C_6H_5CH_2CH_3$		0.5410	0.2105
0.1223	−0.0881	0.6530	0.2184
0.1998	−0.1279	0.7517	0.2056
0.3412	−0.1613	0.8224	0.1814
0.4230	−0.1665	0.8544	0.1631
0.5687	−0.1385	$C_6H_{10}O + C_6H_5NO_2$	
0.7451	−0.0780	0.1108	0.0793
0.8336	−0.0493	0.2138	0.1163
0.9218	−0.0166	0.3887	0.1735
$C_6H_{10}O + C_5H_5CH(CH_3)_2$		0.4922	0.1767
0.1310	−0.1340	0.6675	0.1545
0.2454	−0.1933	0.7927	0.1225
0.3839	−0.2170	$C_6H_{10}O + C_6H_5CHO$	
0.4612	−0.2167	0.0897	0.0132
0.5644	−0.1920	0.1914	0.0424
0.6498	−0.1572	0.3013	0.0751
0.7366	−0.1139	0.3991	0.0823
0.9149	−0.0412	0.6252	0.0727
$C_6H_{10}O + C_6H_5C(CH_3)_3$		0.7655	0.0641
0.3075	−0.2009	$C_6H_{10}O + C_6H_5CN$	
0.3944	−0.2206	0.0951	−0.0010
0.5986	−0.2080	0.1960	−0.0044
0.6761	−0.1961	0.2736	−0.0078
0.7706	−0.1571	0.3371	−0.0099
0.8556	−0.1166	0.4938	−0.0182
$C_6H_{10}O + C_6H_5Cl$		0.6854	−0.0184
0.0856	−0.0347	0.8026	−0.0141
0.1731	−0.0601		
0.3295	−0.0908		
0.3868	−0.0941		
0.5859	−0.0940		
0.7280	−0.0783		
0.8374	−0.0492		

some of the physical properties of benzene and the mono-substituted benzenes. For *n*-alkyl substituted and halo substituted benzenes, $V_{0.5}^E$ show an increase with decreasing ionization potential. Other binary mixtures studied do not show any systematic relationship with the electron-donor, -acceptor ability or with the polarity parameters (Hammett or Taft inductive effect parameters) of the component molecules (13). This is an indication of the presence of the combined contribution of steric and polarity factors to the volumetric behaviour of these solutions. In order to determine the extent of specific like and unlike interactions present in these mixtures, it is necessary to evaluate the contribution to V_m^E by size and polarity components. The attempts in this direction are being made and will be discussed subsequently.

It is interesting to observe a linear relationship between $V_{0.5}^E$ of these mixtures and solubility parameter values of the substituted benzenes at 298.15 K (Fig. 2). A tentative explanation for this seems to be the presence of dipoles in the mixtures.

Can. J. Chem. Downloaded from www.nrcresearchpress.com by 210.87.254.6 on 09/06/12
For personal use only.

TABLE 3. Parameters of eq. [1] and the standard deviations $\sigma(V_m^E)$ ($cm^3\ mol^{-1}$) at 298.15 K for binary mixtures of cyclohexanone with benzene and monosubstituted benzenes

Systems	A_0	A_1	A_2	A_3	$\sigma(V_m^E)$
$C_6H_{10}O$ + C_6H_6	−0.8029	0.4640	0.0330	0.1213	±0.004
+ $C_6H_5CH_3$	−0.6943	0.4541	−0.2368	−0.4021	±0.003
+ $C_6H_5CH_2CH_3$	−0.6224	0.3550	0.1163	—	±0.003
+ $C_6H_5CH(CH_3)_2$	−0.8159	0.4308	−0.0776	—	±0.004
+ $C_6H_5C(CH_3)_3$	−0.8942	0.0854	−0.2240	—	±0.005
+ C_6H_5Cl	−0.3954	0.0195	0.0030	0.0579	±0.005
+ C_6H_5Br	−0.0932	0.0508	−0.1671	—	±0.006
+ C_6H_5I	0.3961	0.1276	0.0120	—	±0.008
+ $C_6H_5N(CH_3)_2$	0.7910	0.4145	0.6082	−0.2544	±0.005
+ $C_6H_5NO_2$	0.6947	−0.0001	0.1411	—	±0.008
+ C_6H_5CHO	0.3285	−0.1052	0.0298	0.5022	±0.005
+ C_6H_5CN	−0.0660	−0.1302	−0.0044	0.2895	±0.004

TABLE 4. Molar volume (V), heats of vaporization (ΔH_{vap}), solubility parameter (δ), and ionization potentials (I) of various monosubstituted benzenes and $V_{0.5}^E$ of their cyclohexanone solutions at 298.15 K

Substituent	V ($cm^3\ mol^{-1}$)	ΔH_{vap} (kcal mol^{-1}) (ref. 14)	δ* $(cal\ cm^{-3})^{1/2}$	I (eV) (ref. 15)	$V_{0.5}^E$ ($cm^3\ mol^{-1}$)
—H	89.41	8.1	9.16	9.24	−0.201
—CH_3	106.78	9.1	8.93	8.82	−0.174
—CH_2CH_3	123.07	10.1	8.79	8.76	−0.156
—$CH(CH_3)_2$	140.17	10.8	8.53	8.69	−0.205
—$C(CH_3)_3$	155.64	11.5	8.37	8.68	−0.223
—Cl	102.63	9.6	9.37	9.07	−0.100
—Br	108.42	10.5	9.56	8.98	−0.029
—I	111.84	†	—	8.73	0.099
—$N(CH_3)_2$	126.80	†	—	7.12	0.198
—NO_2	123.11	13.19	11.07	9.92	0.175
—CHO	101.71	11.8	10.50	9.52	0.082
—CN	103.06	†	—	9.70	−0.018

*Calculated from $\delta = \left[\frac{\Delta H_{vap} - RT}{V}\right]^{1/2}$

†Reliable ΔH_{vap} data are not available.

Acknowledgment

The authors thank Professor J. C. Ahluwalia, Indian Institute of Technology, New Delhi, India for the use of digital density meter.

1. S. K. SURI. Can. J. Chem. **25**, 2839 (1981).
2. S. K. SURI. J. Chem. Eng. Data, **25**, 390 (1981).
3. S. K. SURI. Thermochim. Acta, **39**, 325 (1980).
4. B. CHAWLA, R. PRAKASH, and S. K. SURI. Can. J. Chem. **61**, 1647 (1983).
5. J. A. RIDDICK and W. B. BUNGER. Techniques of organic chemistry. Vol. II. Organic solvents. Wiley-Interscience, New York. 1970.
6. A. I. VOGEL. A textbook of practical organic chemistry. 3rd ed. Longmans. 1959.
7. J. TIMMERMANS. Physico-chemical constants. Vol. II, Elsevier, Amsterdam. 1965.
8. G. KÖRÖSI and E. SZ. KOVÁTS. J. Chem. Eng. Data, **26**, 323 (1981).
9. L. P. MILLER, H. N. WACHTER, and V. FRIED. J. Chem. Eng. Data, **20**, 417 (1975).
10. R. C. MAHESHWARI, S. K. SURI, and U. S. TEWARI. J. Chem. Eng. Data, **24**, 239 (1979).
11. H. WAGENBRETH and H. BLANKE. PTB-Mitt. **6**, 412 (1971).
12. T. KAGIYA, Y. SUMIDA, and T. INOUE. Bull. Chem. Soc. Jpn. **41**, 767 (1968).
13. S. EHRENSON, R. T. C. BROWNLEE, and R. W. TAFT. Progress in physical organic chemistry. *Edited by* A. Streitwieser and R. W. Taft. Vol. 10. John Wiley and Sons, New York. 1973.
14. R. R. DREISBACH. Physical properties of chemical compounds. Vol. II. ACS Publication. 1959.
15. R. C. WEAST (*Editor*). Handbook of chemistry and physics. CRC Press Inc., Florida, 1980–81. pp. E76–80.

Can. J. Chem. Downloaded from www.nrcresearchpress.com by 210.87.254.6 on 09/06/12
For personal use only.

Stereoselective effect on ternary complexation of copper ions with *N,N'*-dimethyltartramide and mandelic acid

MICHELLE M. PETIT-RAMEL

Laboratory of Analytical Chemistry II, 43 Boulevard du 11 novembre 1918, 69622 Villeurbanne Cedex, France

AND

GAËL DE RYCKE, ANDRÉ RIO, AND PIERRE E. BLOND

Laboratory of Organic Chemistry and Kinetics, I.C.P.I., 31, place Bellecour F. 69288 Lyon Cedex 1, France

Received July 14, 1982[1]

MICHELLE M. PETIT-RAMEL, GAËL DE RYCKE, ANDRÉ RIO, and PIERRE E. BLOND. Can. J. Chem. **61**, 2151 (1983).

The binary and ternary complexation in aqueous solution between copper(II) ion, *N,N'*-dimethyltartramide (H_2A) and mandelic acid (HB), were studied by potentiometric measurements in the 5–10 pH range at 25°C and μ = 1 *M* in $NaClO_4$. The titrations were analyzed using a pit-mapping method and the concentration distribution of the various simple and mixed complexes were plotted versus a pH gradient. A significant stereoselective effect is displayed in the ternary complexes only.

MICHELLE M. PETIT-RAMEL, GAËL DE RYCKE, ANDRÉ RIO et PIERRE E. BLOND. Can. J. Chem. **61**, 2151 (1983).

Les complexations binaires et ternaires des ions Cu^{2+} par le *N,N'*-dimethyltartramide (H_2A) et l'acide mandélique (HB) ont été étudiées, en solution aqueuse, entre les pH 5 et 10, à 25°C et à une force ionique μ = 1 *M* en $NaClO_4$. Les données expérimentales ont été analysées à l'aide d'une méthode de pit-mapping et les courbes de distribution de chacune des espèces simple et mixte ont été tracées en fonction du pH. Un effet stéréoselectif significatif n'est observé que dans le cas des complexes ternaires formés avec les énantiomères de l'acide malique.

Introduction

The dependance of the thermodynamic stability of copper complexes with optically active ligands on the resolution of racemates was first reported about ten years ago during ligand exchange chromatography of racemates by Davankov and Rogozhin (1, 2), mainly for α-amino acids (3–5). On the other hand, little work has appeared on the separation of α-hydroxy-acids or diols enantiomers, probably because these compounds show a less uniform behaviour than the amino acids. However, the complexing properties of dihydroxy compounds such as mandelic acid (6, 7) or catechol derivatives (8) with some metals, especially Cu, Zn, and Cd, have already been described and used in several analytical techniques (9, 10).

Preliminary to a chromatographic study, it is necessary to follow the formation of the copper complexes with amides derived from tartaric acid, such as *N,N'*-dimethyltartramide (H_2A), and hydroxyacid such as mandelic acid (HB):

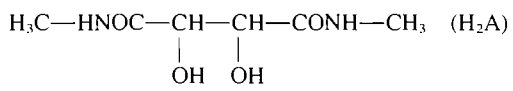

In order to examine the complexing properties of the hydroxyl groups of the asymmetric carbons, the ends of the amide structure were deliberately blocked with non-ionizable protecting groups for the range of pH corresponding to the ionization of the alcoholic functions.

In this paper, we wish to report the possibility of obtaining: firstly a ternary complex between copper ions, *N,N'*-dimethyltartramide and mandelic acid; and secondly, a significant stereoselective interaction when the ternary complexation occurs with enantiomeric forms of mandelic acid.

Results

(1) Binary complexation of copper ions with N,N'*-dimethyltartramide (H_2A)*

Quantitative information about the interactions, firstly between protons and the hydroxyl groups of a ligand A, and secondly between copper ions, M, and the same ligand in a protic solvent, may be conventionally given (11) by the apparent equilibrium constant β_{pqr} of the species H_qA (β_{0q1}) and $M_pH_qA_r$ (β_{pqr}). Considering

$$[1] \quad A + qH \rightleftarrows H_qA$$

and

$$[2] \quad pM + qH + rA \rightleftarrows M_pH_qA_r$$

with

$$[3] \quad \beta_{0q1} = \frac{[H_qA]}{[H]^q[A]}$$

and

$$[4] \quad \beta_{pqr} = \frac{[M_pH_qA_r]}{[M]^p[H]^q[A]^r}$$

For every pH corresponding to the experimental curve, we can define an average number of undissociated protons per mol of ligand:

$$[5] \quad \bar{q} = \frac{C_H - [H] + [OH]}{C_A}$$

where C_A is the total concentration of ligand, [H] and [OH] the concentrations at equilibrium of H^+ and OH^-, respectively, and C_H the concentration of protons.

$$[6] \quad C_H = qC_A - B'$$

where B' is the concentration of hydroxide added.

We can obtain the transformed analogue of the titration curve, $\bar{q} = f(pH)$. The function becomes linear by a development in Fourier series. The normal equation drawn from this new expression is derived by the Gauss technique, and the derivation corresponds to minimization of the sum $\Sigma(\bar{q}_{exp} - \bar{q}_{calcd})^2$. Standard deviations are calculated by a pit-mapping method from the residual variance and the matrix of the covariances.

[1] Revision received April 5, 1983.

Can. J. Chem. Downloaded from www.nrcresearchpress.com by 210.87.254.105 on 09/06/12
For personal use only.

TABLE 1. Stability constants β_{pqrs} of copper complexes with *N,N'*-dimethyltartramide and mandelic acid; $NaClO_4$, 1 *M*; *T*, 25°C

N,N'-Dimethyltartramide (A)	*pqrs*	*log* $\beta_{pqrs} \pm 2\sigma$*	
HA	0110	13.00	
H_2A	0210	25.00	
CuA	1010	14.56	(0.02)
CuA_2	1020	22.98	(0.02)
Mandelic acid (B)			
HB	0101	3.10	(0.05)
CuB	1001	2.70	(0.05)
N,N'-Dimethyltartramide (A), mandelic acid (B)			
		CuA(−)B	CuA(+)B
CuAB	1011	17.78 (0.10)	17.06 (0.10)

*The numbers in parentheses are the confidence limits.

For *N,N'*-dimethyltartramide, as is usually justifiable in the case of substituted amides, the acidities of the amide groups are neglected, the ligand being considered bidentate with a general formula H_2A. The presence of two amide groups enhances the polarization of the OH bonds and provides them with a certain mobility in very alkaline medium. Unfortunately, the only potentiometric data are inadequate in this pH range, and it is useful to complete them by one other parameter, the rotatory power, whose value is in direct connection with the releasing of the two alcoholic protons (12). Discontinuous polarimetric measurements are performed on various solutions of *N,N'*-dimethyltartramide using known additions of super-concentrated sodium hydroxide solution (16 *N*). The successive deprotonation constants β_{021} and β_{011} can then be refined with a convenient precision between the two polarimetric levels corresponding with the H_2A and A^- forms respectively (Fig. 1).

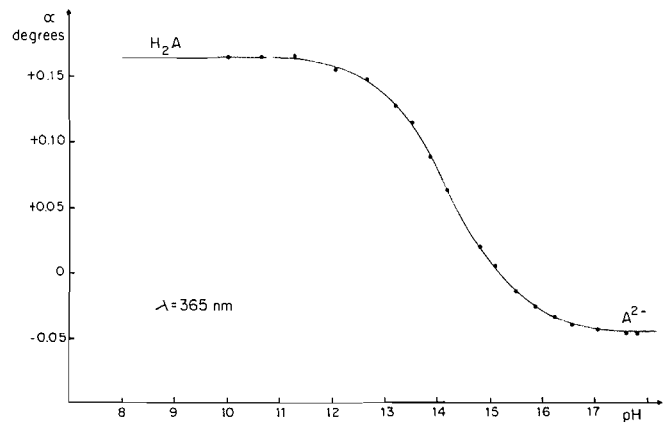

FIG. 1. Cu–*N,N'*-dimethyltartramide system: rotatory power versus pH in high-alkalinity region [A] = 2×10^{-3} *M*.

To establish the stability of the copper complexes, pH measurements were performed on solutions containing the same ligand concentration, C_A, and the various concentrations of metallic ion, C_M. For the different ratios C_A/C_M, one can superpose the formation curves, which implies the formation of two successive complexes MA and MA_2 without the formation of protonated species. The β_{0q1} constants (ligand) and β_{10r} constants (complexes) given in Table 1 allow us to determine the proportions of each species for each concentration of metallic ion and chelating agent.

(2) Binary complexation of copper ions with mandelic acid (HB)

Although metallic mandelate complexes have previously been reported (6, 7, 13), a quantitative study of the equilibria involved does not seem to have been undertaken under our experimental conditions. We have found very little information about the soluble MB complex; Meites (14) and Sengupta *et al.* (15) have described a way of obtaining information about the dissociation constant of the slightly soluble MB_2 complex, as well as the solubility product of the salt. The neutralization curves show no evidence of the ionization of two protons, but only that from the carboxyl group since the hydroxyl group does not dissociate below pH 13. Potentiometric determinations are limited by the precipitation of the MB_2 copper mandelate near pH 4, though the appearance of this complex, already mentioned, was verified by rapid experimentation. Only the formation of the MB complex can be interpreted in terms of equilibrium constants.

The titration curves for racemic and optically active mandelic acid are exactly superposable. In the presence of copper ions, they are again superposable, leading to identical $\bar{q}$, pH plots and hence to identical stability constants.

(3) Ternary complexation of copper ions with N,N'*-dimethyltartramide (H_2A) and mandelic acid (HB)*

According the general equilibrium:

[7] $pM + qH + sB \rightleftarrows M_pH_qB_s$

or, in absence of polynuclear and protonated species,

[8] $M + rA + sB \rightleftarrows MA_rB_s$

the stability constant of the MA_rB_s ternary complex is expressed by:

$$[9] \quad \beta_{10rs} = \frac{[MA_rB_s]}{[M][A]^r[B]^s}$$

Numerous potentiometric investigations (16, 17) dealing with the formation of ternary chelates with different ligands have appeared. Significant differences in the neutralization curves in this system indicate the formation of only one MAB mixed species, as long as there are no interactions between the ligands themselves. Its stoichiometry may be directly determined by a detailed numerical analysis of the data, and calculations lead to a precise value of the stability constant (Table 1) and show there is a significant stereoselectivity in the ternary complexes with tartramide and mandelic acid enantiomers.

In conclusion, the present work is preliminary to a chromatographic separation of mandelic enantiomers on an active

Can. J. Chem. Downloaded from www.nrcresearchpress.com by 210.87.254.105 on 09/06/12
For personal use only.

Can. J. Chem. Downloaded from www.nrcresearchpress.com by 210.87.254.105 on 09/06/12
For personal use only.

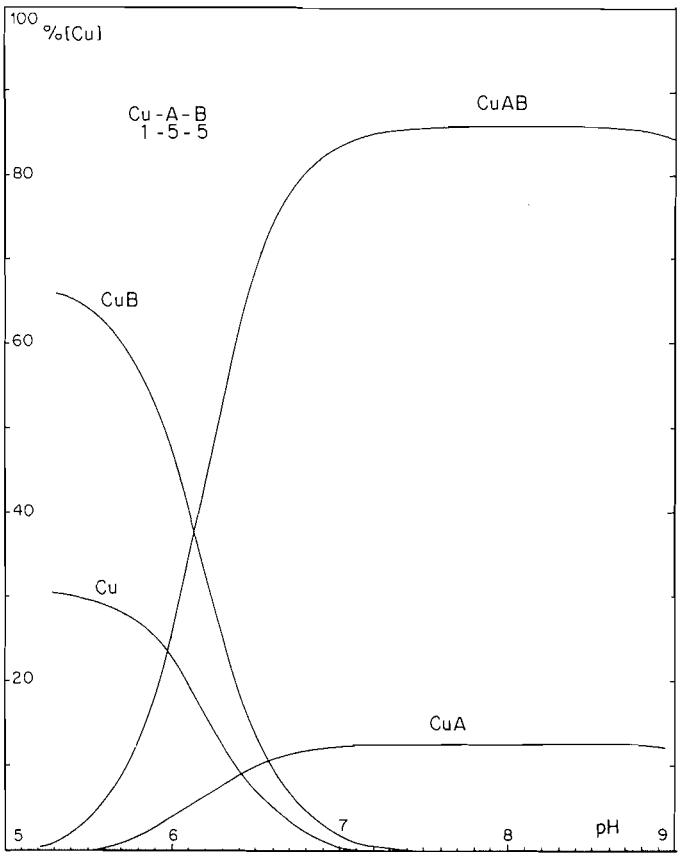

FIG. 2. Cu – *N,N'*-dimethyltartramide (A) – mandelic acid (B) system: distribution curves [Cu] = 10^{-3} *M*; [A] = 5×10^{-3} *M*; [B] = 5×10^{-3} *M*.

TABLE 2. pH = $f(N_{NaOH})$; [*N,N'*-dimethyltartramide] = 2×10^{-3} *M*

NaOH (*N*)	pH	NaOH (*N*)	pH
0.16	13.20	6.53	15.50
0.49	13.60	8.16	15.85
0.81	13.85	9.79	16.20
1.63	14.20	11.42	16.60
3.26	14.80	13.06	17.10
4.89	15.15	14.69	17.55

support based on tartramide groups. The ligands of the stationary and mobile phases must permit the formation of the previous mixed species and the difference in retention of the antipode must reflect a significant stereoselective effect. Obviously the efficacy of this mechanism depends on the difference between the stability constants of the CuA(+)B and CuA(−)B complexes which are proportional to the stereoselectivity of the mixed species. Distribution curves (Fig. 2) show that the optimal pH of the separation is near 8.

Experimental

Potentiometric titrations were conducted under a nitrogen atmosphere in a water-jacketed glass titration cell whose temperature was maintained at 25 ± 0.1°C by a circulating bath. Measurements were performed using a Philips PW 9409 pH meter with a combined Philips CA 11 electrode. In the 2–11 pH range, an average linear correction to the measured pH was made (ΔpH = 0.21) based on the usual calibration with Bates standard buffers, under the same conditions of ionic strength. The OH^- concentration was evaluated from the ionic product of water at 25°C in $NaClO_4$ 1 *M*, in this work pK_w = 13.770. Beyond pH 11, the alkaline medium concerning the two successive deprotonations of the *N,N'*-dimethyltartramide is obtained with the Scharzenbach and Sulberger's abacus (18) which permits the reaching of the theoretical pH values between 11 and 17 by using a serie of super-concentrated sodium hydroxide solutions. The correlation between the pH and the sodium hydroxide solution normalities is given in Table 2.

Rotatory powers were taken on a Perkin-Elmer M141 spectropolarimeter at 365 nm at room temperature with a 1 dm cell.

Mandelic acid was a Fluka puriss product. The *N,N'*-dimethyltartramide was synthesized in our laboratory from anhydrous and gaseous Roth methylamine and a chilled Merck ethyl tartrate alcoholic solution. After recrystallisation, the optical activity of the product was tested and found in good agreement with the values of Frankland and Slator (19).

1. V. A. DAVANKOV and S. V. ROGOZHIN. Dokl. Akad. Nauk. USSR, **193**, 94 (1970).
2. V. A. DAVANKOV and S. V. ROGOZHIN. J. Chromat. **60**, 28 (1971).
3. B. L. LEFEBVRE, R. AUDEBERT, and C. QUIVORON. Isr. J. Chem. **15**, 69 (1977).
4. O. YA MAUCHI, T. SAKURAI, and A. NAKA HARA. Bull. Chem. Soc. Jpn. **50**, 1776 (1977).
5. V. A. DAVANKOV and P. R. MITCHELL. J. Chem. Soc. Dalton, 1012 (1972).
6. S. K. VERMA and R. P. AGARWAL. J. Less Common Metals, **12**, 221 (1967).
7. J. E. POWELL and W. F. S. NEILLIE. J. Inorg. Nucl. Chem. **29**, 2371 (1967).
8. R. F. JAMESON and W. F. S. NEILLIE. J. Chem. Soc. 2391 (1965).
9. F. BOIS, A. BEROD, H. CHERMETTE, J. F. PUJOL, and P. BLOND. Mikrochim. Acta, 213 (1978).
10. L. JOHANSSON. Acta Chem. Scand. **34**, 495 (1980).
11. M. M. PETIT-RAMEL and I. KHALIL. Bull. Soc. Chim. Fr. **11–12**, 1127 (1977).
12. M. M. PETIT-RAMEL and C. M. BLANC. J. Inorg. Nucl. Chem. **34**, 1233 (1972).
13. P. V. KHADIKAR and R. L. AMERIA. J. Indian Chem. Soc. **47**, 1201 (1970).
14. L. MEITES. J. Am. Chem. Soc. **75**, 2859 (1953).
15. K. K. SENGUPTA, A. K. CHATTERJEE, and S. P. MOULIK. Indian J. Chem. **14A**, 331 (1976).
16. A. E. MARTELL. *In* Proceed. 3rd Symp. Coord. Chem. Vol. 2, DEBRECEN (1970).
17. R. P. MARTIN, M. M. PETIT-RAMEL, and J. P. SCHARFF. *In* Metal ions in biological systems. Vol. 2, *Edited by* Sigel. Dekker, New York. 1973.
18. G. SCHWARZENBACH and R. SULBERGER. Helv. Chim. Acta, **37**, 348 (1944).
19. F. FRANKLAND and A. SLATOR. J. Chem. Soc. **83**, 1349 (1903).

The isotropic hyperfine interaction in ternary complexes of copper(II) with 8-hydroxyquinoline and various salicylic acids

Y. ANJANEYULU,[1] N. V. S. RAO, R. Y. SWAMY, AND R. P. RAO
Department of Chemistry, Nagarjuna University, Nagarjunanagar 522 510, India

AND

V. G. K. M. PISIPATI
Department of Physics, Nagarjuna University, Nagarjunanagar 522 510, India

Received January 7, 1983

Y. ANJANEYULU, N. V. S. RAO, R. Y. SWAMY, R. P. RAO, and V. G. K. M. PISIPATI. Can. J. Chem. **61**, 2154 (1983).

Electron spin resonance and optical absorption studies are carried out on bis(8-hydroxyquinolinato)copper(II) and seven ternary copper(II) complexes with 8-hydroxyquinoline and salicylic acid or substituted salicylic acids. Electron spin resonance spectra of all these complexes give well-resolved lines. An unusual splitting of the parallel lines in frozen solution spectra and four line fluid (DMF) solution spectra at room temperature are observed. It is explained on the basis of either partial dissociation of 8-hydroxyquinoline ligand or the solvation effect of DMF which solvates some copper chelate molecules even at room temperature. This is more prominent on the parallel lines in frozen solution spectra of all the ternary complexes. The molecular orbital coefficients are estimated assuming an axial symmetry and these indicate that the in-plane π bonding is weak compared to σ-bond in the ternary complexes. The value of χ, which is proportional to hyperfine constants, indicates that it is quite independent of either ligand substitutions or substitutions in the ligand, but purely depends upon the immediate environment which constitutes the coordination around the paramagnetic ion.

Y. ANJANEYULU, N. V. S. RAO, R. Y. SWAMY, R. P. RAO et V. G. K. M. PISIPATI. Can. J. Chem. **61**, 2154 (1983).

On a étudié l'absorption en rpe at l'absorption optique du bis(hydroxy-8 quinolinato) de cuivre(II) et de sept complexes ternaires du cuivre(II) avec l'hydroxy-8 quinoléine, l'acide salicylique ou avec des acides salicyliques substiutés. Les spectres rpe de tous ces complexes donnent des raies bien résolues. On observe un dédoublement inhabituel des raies parallèles dans les spectres en solution gelée et quatre raies dans les spectres en solution fluide (DMF) à la température de la pièce. On explique ces faits en fonction d'une dissociation partielle du ligand hydroxy-8 quinoléine ou en fonction de l'effet de solvatation du DMF qui solvate quelques molécules de chélate de cuivre même à la température de la pièce. Cet effet est plus marqué dans les raies parallèles des spectres de tous les complexes ternaires en solution gelée. On évalue les coefficients d'orbitale moléculaire en supposant une symétrie axiale et ces coefficients indiquent que la liaison π dans le plan est faible comparativement à la liaison σ des complexes ternaires. La valeur de χ qui est proportionnelle aux constantes hyperfines, indique qu'elle est tout à fait indépendante des substitutions des ligands ou des substitutions dans le ligand, mias qu'elle dépend de l'environnement immédiat qui constitue la coordination autour de l'ion paramagnétique.

[Traduit par le journal]

Introduction

Electron spin resonance measurements of ternary copper(II) complexes are meagre compared to those of simple complexes (1–3). Particular importance is attached to the esr study on ternary complexes due to their prominence in biological systems. In these complexes, copper(II) is bound to two chelating ligands and the way in which each ligand influences the formation of a typical structure is important. No systematic study of esr of biologically active ternary copper(II) complexes regarding the hyperfine contact term in the hyperfine interactions of the paramagnetic ion was made.

The parameter χ proposed by Abragam *et al.* (4) and related to the hyperfine contact term K, is

$$[1] \quad \chi = \frac{4\pi}{S_T} \left\langle \psi \left| \sum_i \delta(r_i)\, S_{zi} \right| \psi \right\rangle$$

where χ = the effective field per unpaired electron, S_T = the total spin of the ion, $\delta(r_i)$ = the delta function term (the Fermi contact term), and S_{zi} = the spin of the ith electron. The parameter χ is negative and nearly constant in magnitude for the ions in the first row of transition element series (5). McGarvey extensively carried out the calculations on χ for the first row transition elements with different ligands and concluded that the value can vary 30% in magnitude depending upon the ligand, the host lattice, and the geometry of the chelate. Allen *et al.* (6) studied the nature of χ for a number of tetradentate Schiff base complexes of copper(II), where the immediate environment is two nitrogen atoms and two oxygen atoms, with the nitrogen atoms *cis* to each other. They concluded that the χ value is constant and quite independent of ligand substitution, with an average value = −3.918. It has been reported that the nature of χ in aliphatic polyamine complexes of copper(II) (7, 8), where the immediate environment is four nitrogen atoms, is nearly constant with a value = −3.700, confirming that the χ is nearly independent of ligand substitution but only depends upon the immediate environment. This paper presents esr and optical absorption data on bis(8-hydroxyquinolinato)copper(II) and ternary copper(II) complexes formed with 8-hydroxyquinoline and salicylic acid or substituted salicylic acids in an attempt to understand the nature of the metal–ligand bond and the parameter χ. The details of the complexes studied are shown in Fig. 1*a* and *b*.

Experimental

Equimolar solutions (0.2 *M*) of copper(II) acetate monohydrate, 8-hydroxyquinoline, and salicylic acid (or substituted salicylic acid) are prepared in 80% aqueous methanol from AnalaR Chemicals.

For preparing the ternary complexes (2–8), 50 mL each of copper(II) acetate monohydrate and the corresponding salicylate solution are mixed and stirred for half an hour. To this mixture, 50 mL of 8-hydroxyquinoline is added slowly whereby the solid mixed complex

[1] To whom all correspondence should be addressed.

Can. J. Chem. Downloaded from www.nrcresearchpress.com by 210.87.254.40 on 09/06/12
For personal use only.

Can. J. Chem. Downloaded from www.nrcresearchpress.com by 210.87.254.40 on 09/06/12
For personal use only.

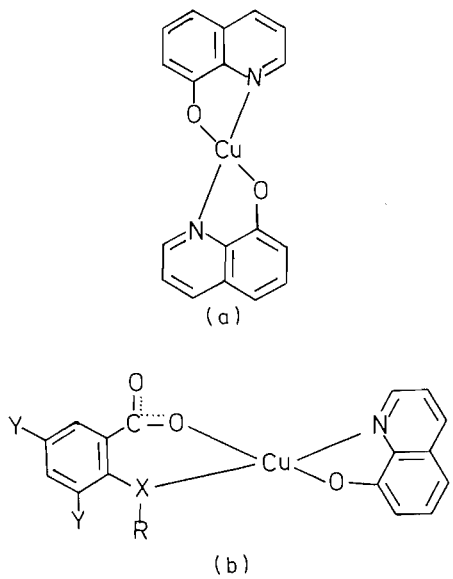

FIG. 1. (*a*) **1** $Cu(OX)_2$ bis(8-hydroxyquinolinato)copper(II); (*b*) ternary complexes of copper(II) with 8-hydroxyquinoline and salicylic acid or substituted salicylic acid, where R = H or $COCH_3$; X = O or S; Y = Cl, Br, I, NO_2, H. **2**, Cu(OX)(SA); **3**, Cu(OX)(Ace-SA); **4**, Cu(OX)(Cl-SA); **5**, Cu(OX)(2Br-SA); **6**, Cu(OX)(2I-SA); **7**, Cu(OX)(2NO_2-SA); **8**, Cu(OX)(Thio-SA) where OX = 8-hydroxyquinoline, SA = salicylic acid, Ace-SA = acetylsalicylic acid, Cl-SA = 5-chlorosalicylic acid, 2Br-SA = 3,5-dibromosalicylic acid, 2I-SA = 3,5-diiodosalicylic acid, 2NO_2-SA = 3,5-dinitrosalicylic acid, Thio-SA = thiosalicylic acid.

separates. After stirring for another half an hour the solid product is removed by filtration and washed with several volumes of distilled water. The solid is then boiled in acetone to remove any trace of excess ligand. In the case of binary complex **1**, 1 mol of copper(II) acetate monohydrate (25 mL) and 2 mol of 8-hydroxyquinoline (50 mL) are mixed. All the complexes are dried at 110°C for 12 h.

The first derivative tracings of the esr signals in dimethyl formamide (DMF) solutions of the complexes are recorded at room and liquid nitrogen temperatures using Varian E4 X-band ESR spectrometer. The optical absorption spectra are recorded in solution using Beckman DK-2 ratio recording spectrophotometer.

Theoretical background

In all these complexes, the crystal field symmetry of the copper ion may be taken as tetragonal (distorted), arising out of two oxygen atoms and two nitrogen atoms with a *trans* configuration in complex **1** and two oxygen atoms of salicylic acids and nitrogen and oxygen atoms of 8-hydroxyquinoline in complexes **2** to **7**, while in complex **8** sulphur replaces one oxygen atom in the salicylic acid, forming a distorted square planar coordination (distorted D_{4h} symmetry). Electronic and esr spectra of copper(II) complexes with square planar or square pyramidal stoichiometry can be easily understood using Fig. 2. Such a distortion will be smallest for strongly coordinating axial ligands and will increase when the coordinating power of the axial ligands decreases, resulting in the observation of only one overlapping band (9). Gersmann and Swalen (10) reported three d–d optical transitions for $Cu(OX)_2$ in a frozen solution for which the solvent was a mixture of chloroform and toluene while Kokoszka *et al.* (11) observed three d–d optical transitions for the $Cu(OX)_2 \cdot 2\,H_2O$ polycrystalline sample. In the present work all these complexes exhibited only a broad maximum in solution around ~15 000 cm^{-1} to 16 000 cm^{-1} at room temperature. Hence we believe that the three d–d optical

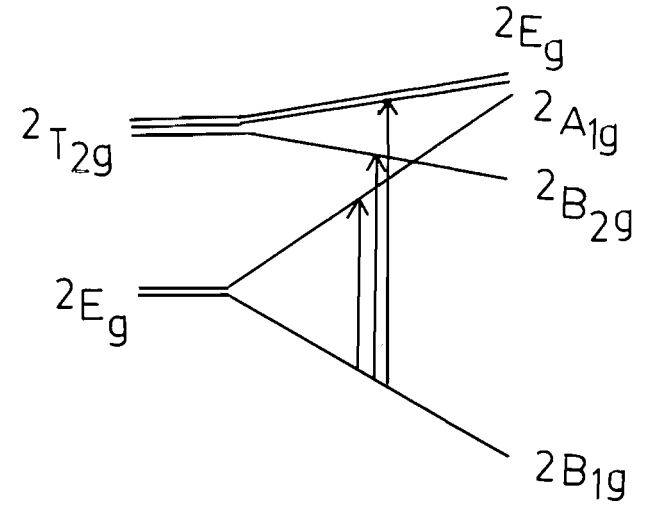

FIG. 2. Ligand-field splittings for tetragonal copper(II) complexes.

transitions observed by the other authors are due to the different experimental conditions.

The metal–ligand antibonding molecular orbitals are constructed taking $2s$, $2p_x$, $2p_y$, and $2p_z$ orbitals of the four ligand atoms into coordination with copper $3d$ orbitals and they are (10)

$$B_{1g} = \alpha d_{x^2-y^2} - \frac{1}{2}\alpha' [-\sigma_x^{(1)} + \sigma_y^{(2)} + \sigma_x^{(3)} - \sigma_y^{(4)}]$$

$$B_{2g} = \beta d_{xy} - \frac{1}{2}(1-\beta^2)^{1/2} [p_y^{(1)} + p_x^{(2)} - p_y^{(3)} - p_x^{(4)}]$$

[2] $$A_{1g} = \gamma d_{3z^2-r^2} - \frac{1}{2}(1-\gamma^2)^{1/2} [\sigma_x^{(1)} + \sigma_y^{(2)} - \sigma_x^{(3)} - \sigma_y^{(4)}]$$

$$E_g = \delta d_{xz} - \sqrt{\frac{(1-\delta^2)}{2}} [p_z^{(1)} - p_z^{(3)}]$$

$$= \delta d_{yz} - \sqrt{\frac{(1-\delta^2)}{2}} [p_z^{(2)} - p_z^{(4)}]$$

The wave functions are written in order of increasing energy. The locations of A_{1g} are uncertain but this state does not effect the magnetic parameters and, hence, is unobservable (γ^2). The B_{1g} and A_{1g} states account for the in-plane σ bonding (α^2) to the copper. The B_{2g} state represents the in-plane π bonding (β^2). Of the molecular orbital coefficients, δ^2 could not be calculated, since no higher d–d transitions are observed. It is further noted (6, 7) that the value of δ^2 varies from 0.9 to 1.0 and that the change in χ value is only about 2%. In view of this, δ^2 is taken as equal to 1 while calculating the other parameters.

sp-Hybridized ligand σ orbitals are represented by

[3] $$\sigma = np \mp (1-n^2)^{1/2} s$$

Overlap is included only for the B_{1g} state, where α and α' are related by

[4] $$\alpha^2 + \alpha'^2 - 2\alpha\alpha' S = 1$$

where S is the overlap integral between the $d_{x^2-y^2}$ and the normalised ligand σ orbitals.

When the wave functions for the ground state B_{1g} are applied to the Hamiltonian,

[5] $$\mathcal{H} = g_\parallel \beta_e H_z S_z + g_\perp \beta_e (H_x S_x + H_y S_y) + A_\parallel S_z I_z + A_\perp (S_x I_x + S_y I_y)$$

Can. J. Chem. Downloaded from www.nrcresearchpress.com by 210.87.254.40 on 09/06/12
For personal use only.

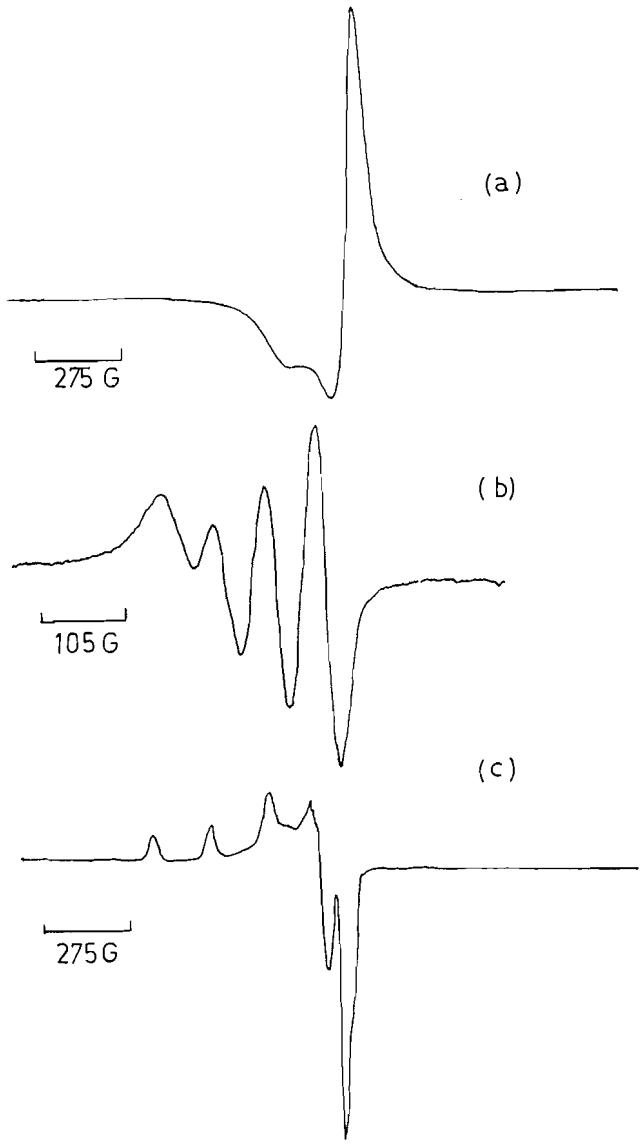

FIG. 3. Electron spin resonance spectra of $Cu(OX)_2$: (*a*) powder at room temperature; (*b*) in DMF at room temperature; (*c*) in DMF at liquid nitrogen temperature.

the principal values of the g and A tensors in the above equation are related to the free ion spin–orbital coupling constant (λ), the electronic energy levels (ΔE), and the molecular orbital coefficients through the following simplified (assuming $\delta^2 = 1$) equations (5, 12).

$$[6] \quad (g_\parallel - 2.0023) = \frac{-8\lambda\beta}{\Delta E}\left[\alpha^2\beta - \alpha\alpha'\beta S + \frac{\alpha\alpha'}{2}(1-\beta^2)^{1/2}T(n)\right]$$

and

$$[7] \quad A_\parallel = -K - \frac{4}{7}\alpha^2 P + (g_\parallel - 2.0023)PZ_\parallel + \frac{3}{7}(g_\perp - 2.0023)PZ_\perp$$

$$[8] \quad A_\perp = -K + \frac{2}{7}\alpha^2 P + \frac{11}{14}(g_\perp - 2.0023)PZ_\perp$$

where

$$[9] \quad Z_\parallel = \frac{\alpha\beta}{\alpha\beta - \alpha'\beta S - \frac{1}{2}\alpha'(1-\beta^2)^{1/2}T(n)}$$

$$[10] \quad Z_\perp = \left[\frac{\alpha}{\alpha - \alpha' S}\right]$$

The values of α^2 and K can be easily calculated from eqs. [7] and [8] and in the approximation $Z_\parallel = Z_\perp = 1$ the equation for the isotropic contact term K is

$$[11] \quad A_{ave} = -K + (g_{ave} - 2.0023)P$$

the isotropic contact term K is related to χ through the relationship (5)

$$[12] \quad \chi = -\frac{3}{2}\left[\frac{hca_0^3}{2.0023 g_N \beta_e \beta_N}\right] K$$

in atomic units. The values of the parameters (13) used in this work are $P = 0.0036\ cm^{-1}$, $T(n)_N = 0.333$, $T(N)_O = 0.220$, $T(N)_S = 0.440$, $\lambda = -828\ cm^{-1}$, $S_N = 0.093$, $S_O = 0.076$, and $S_S = 0.005$.

Results and the treatment of the data

The esr spectra of complexes **1**, **3**, and **7** as powder at room temperature and in solution (DMF) at room and liquid nitrogen temperatures are shown in Figs. 3 to 5. The room temperature spectra in solution of complexes **1**, **2**, **3**, and **8** (DMF) show four spin-dependent hyperfine lines as expected (Fig. 3) whereas the other complexes exhibit an unusual line shape, showing (Fig. 5) an extra line; each line with slightly different line widths. Similar observations were recorded at room temperature in the case of complex bis(*n*-methylbenzothiohydroxamato)copper(II) at Q band (14) in DMF and acetonitrile solvents. It was explained that either dimethylformamide or acetonitrile solvates some of the copper chelate molecules such that the tumbling molecules can be differentiated even at room temperature. This solvation effect is clearly observed in case of frozen solution spectra of ternary complexes by the splitting of axial lines (Figs. 4 and 5), giving rise to a spectrum due to isolated ions of two species. We believe that the species **I** belongs to all the ternary copper complexes reported (**2**–**8**) in the present work, while species **II** can be identified as $Cu(OX)_2$ (1). This identification is made from the reasonable agreement of the computed values of $g_\parallel$ and $A_\parallel$ for the species **II** in all the complexes (**2**–**8**) with the value of $Cu(OX)_2$ (Table 2). This may be arising out from the partial dissociation of the ternary complex into $Cu(OX)_2$.

The average g_0 and A_0 values obtained from the solution spectra at room temperature together with ΔE values are given in Table 1. The $g_\parallel$ and $A_\parallel$ values are obtained from frozen solution spectra by the method developed by Neiman *et al.* (15). The values of $g_\perp$ and $A_\perp$ obtained from the following equations

$$g_0 = (g_\parallel + 2g_\perp)/3 \text{ and } A_0 = (A_\parallel + 2A_\perp)/3$$

are given in Table 2 together with the g values obtained from polycrystalline spectra.

The molecular orbital parameters are calculated assuming an axial symmetry and assuming $\delta^2 = 1$. Initial values of α^2 are obtained from eqs. 7 and 8 assuming $Z_\parallel = Z_\perp = 1$. α' is then calculated using eq. [4], while β^2, the in-plane π-bonding coefficient, is calculated using eq. [6]. These values, together with the value of $\delta^2 = 1$, allow one to obtain the values of $Z_\parallel$

Can. J. Chem. Downloaded from www.nrcresearchpress.com by 210.87.254.40 on 09/06/12
For personal use only.

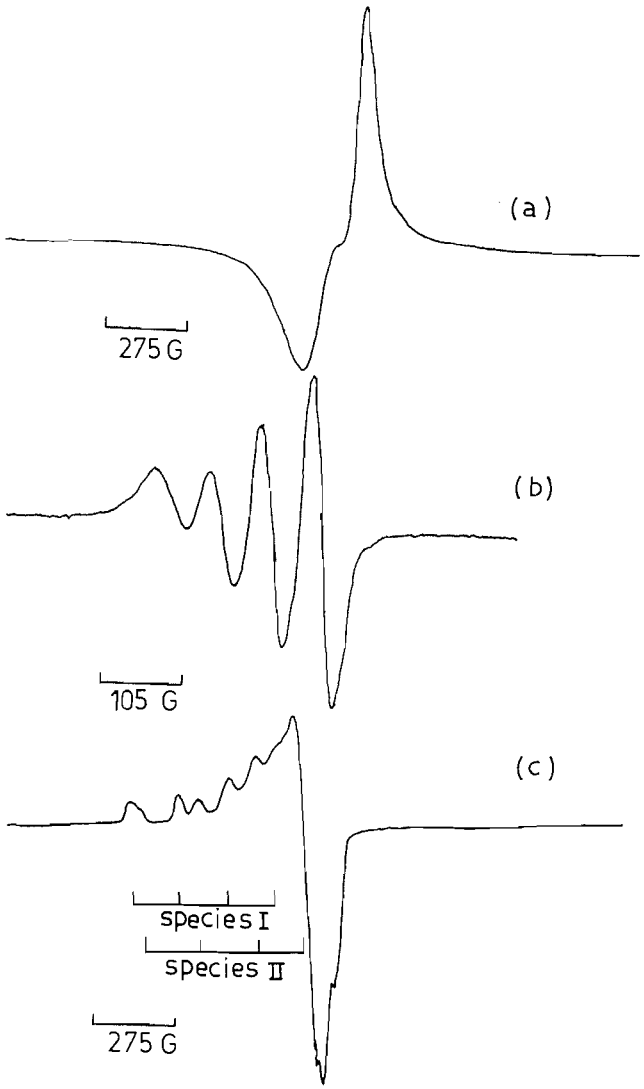

FIG. 4. Electron spin resonance spectra of Cu(OX)(Ace-SA): (*a*) powder at room temperature; (*b*) in DMF at room temperature; (*c*) in DMF at liquid nitrogen temperature.

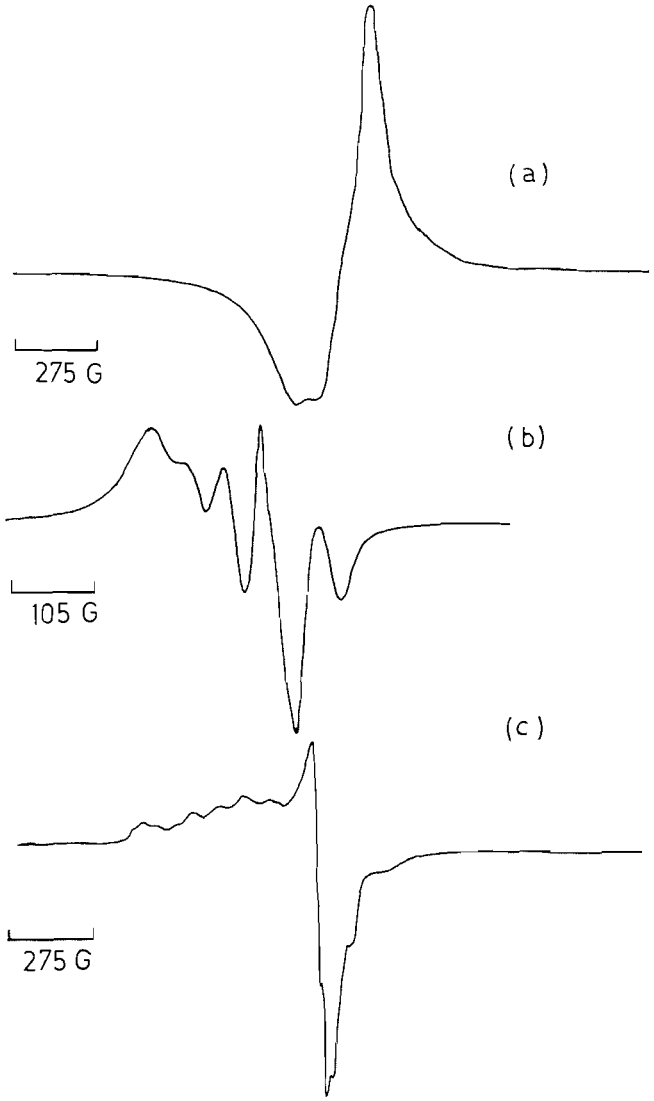

FIG. 5. Electron spin resonance spectra of Cu(OX)(2NO_2-SA): (*a*) powder at room temperature; (*b*) in DMF at room temperature; (*c*) in DMF at liquid nitrogen temperature.

TABLE 1. Values of g_0, A_0, and ΔE in DMF solution

Complex No.	g_0	$A_0 \times 10^4$ (cm^{-1})	ΔE (cm^{-1})
1	2.130	71	16 000
2	2.127	66	16 340
3	2.129	70	16 340
4	2.136	64	14 815
5	2.140	67	16 000
6	2.137	70	15 385
7	2.141	70	16 000
8	2.135	72	15 385

and $Z_\perp$ which are used to recalculate a better approximation of α^2.

This iteration is continued until there is no change in the molecular orbital coefficients. Three to four iterations are usually sufficient. The spin Hamiltonian parameters (Table 2) and the molecular orbital coefficients (Table 3) are somewhat different from those reported earlier for compound **1** (10, 11). This difference probably arises due to the following reasons: (*a*) the studied compounds are different, $Cu(OX)_2$ in DMF and the polycrystalline sample is anhydrous $Cu(OX)_2$, whereas Gersmann and Swalen (10) used $Cu(OX)_2$ in solvent (60% $CHCl_3$ + 40% toluene) and Kokoszka *et al.* (11) used hydrated polycrystalline sample $Cu(OX)_2 \cdot 2H_2O$; (*b*) the difference may be due to the different ligands on the *Z*-axis. Similar difference in magnetic properties is reported for copper diethyl dithiocarbamates in different solvents and the difference is identified due to the solvent effect (10). The value of K is calculated using eqs. [7] and [8] and using it, the value of χ is obtained using eq. [12]. The results are presented in Table 3.

Discussion

From a study of the molecular orbital coefficients (Table 3) it is inferred that in all the ternary complexes **2** to **8** the in-plane π bonding is weak compared to the σ bond. The β^2 value tends to unity in other complexes except in the case of complex **4**. Comparing the β^2 values of these ternary complexes with the binary $Cu(OX)_2$, it is clear that by replacing a molecule of 8-hydroxyquinoline either by salicylic acid or substituted salicylic acids, the strength of in-plane π bonding is decreased irrespective of the type of substitution in salicylic acid. This is

TABLE 2. Principal g and A values

Complex No.	g-Values from powder spectra g_1 $g_\parallel$	g_2	g_3 $g_\perp$	Principal g and A values[a] $g_\parallel$	$g_\perp$	$A_\parallel \times 10^4$ cm^{-1}	$A_\perp \times 10^4$ cm^{-1}
1	2.196		2.047	2.244	2.075	167	23
2	2.167		2.050	2.299	2.041	149	25
				(2.236)[b]		(172)[b]	
3	2.161		2.047	2.291	2.048	158	26
				(2.236)		(172)	
4	2.273		2.022	2.297	2.055	153	20
				(2.247)		(172)	
5	2.186		2.045	2.299	2.060	149	26
				(2.255)		(172)	
6	2.168		2.063	2.309	2.053	151	30
				(2.249)		(172)	
7	2.204	2.088	2.055	2.302	2.060	149	31
				(2.236)		(172)	
8	2.168		2.065	2.298	2.053	158	29
				(2.247)		(167)	

[a] The accuracies in the evaluated values of $g_\parallel$, $g_\perp$, $A_\parallel$, and $A_\perp$ are ± 0.004, ± 0.006, $\pm 5 \times 10^{-4}$, and $\pm 10 \times 10^{-4}$, respectively.
[b] Values in parentheses indicate corresponding values of species **II**.

TABLE 3. Values of $Z_\parallel$, $Z_\perp$, molecular orbital coefficients, and χ

Complex No.	$Z_\parallel$	$Z_\perp$	α^2	α'^2	β^2	$-\chi$
1	1.119	1.060	0.748	0.337	0.824	3.923
2	1.087	1.087	0.735	0.345	~1.000	3.820
3	1.073	1.053	0.771	0.307	0.968	3.803
4	1.088	1.050	0.798	0.278	0.865	3.754
5	1.081	1.061	0.721	0.367	0.967	3.831
6	1.065	1.057	0.746	0.334	0.992	3.886
7	1.069	1.062	0.708	0.375	0.995	3.868
8	1.069	1.040	0.765	0.295	0.930	3.908

quite reasonable as 8-hydroxyquinoline is a much better π acceptor than salicylic acids due to the difference in bonding parameters of heterocyclic nitrogen and carboxylato group. Similar type of consistency is observed in $Z_\parallel$ and $Z_\perp$ values for all these complexes.

The χ value of -3.923 for complex **1** with a copper(II) environment of two oxygen atoms and two nitrogen atoms in *trans* position is consistent with the average value of -3.918 reported for other copper complexes with similar type of environment (6, 16) formed with different types of ligands. In the case of ternary complexes **2** to **7**, where the immediate environment of copper(II) is different from complex **1**, with three oxygen atoms and a nitrogen atom, the χ value varies from -3.754 (complex **4**) to -3.886 (complex **6**) giving rise to an average value of -3.827, which lies in between the value reported for other systems, -3.918 for complex **1** and -3.700 for complexes of copper(II) with four nitrogen atoms in the immediate environment (7, 8). In the case of complex **8**, in which the environment of Cu(II) is different from other ternary complexes by the replacement of oxygen atom by sulphur from thiosalicylic acid, the value is -3.908.

Conclusions

From a study of the molecular orbital coefficients and the parameter in these ternary complexes the salient features are: *1*, the in-plane π bonding is weak compared to that in $Cu(OX)_2$ and *2*, the characteristic χ value is found to be independent of ligand substitution but depends on the immediate coordination environment.

Acknowledgements

The authors are grateful to Professor Jan Reedijk and Mr. F. B. Hulsbergen, Department of Chemistry, State University Leiden, Gorlaeus Laboratories, The Netherlands, for their kind help in getting the esr and electronic spectra, and specially to Professor Reedijk for his constant encouragement and valuable suggestions.

The financial support given by U.G.C. and C.S.I.R., India for carrying this work is gratefully acknowledged.

1. A. M. MAKI and B. R. MCGARVEY. J. Chem. Phys. **29**, 31 (1958).
2. B. A. SASTRY, S. MD. ASADULLAH, and K. V. G. REDDY. J. Mol. Struct. **55**, 143 (1979).
3. W. J. NEWTON and B. J. TABNER. J. Chem. Soc. Dalton, 466 (1981).
4. A. ABRAGAM, J. HOROWITZ, and M. H. L. PRYCE. Proc. R. Soc. London Ser. **230**, 169 (1955).
5. B. R. MCGARVEY. J. Phys. Chem. **71**, 51 (1967).
6. H. C. ALLEN, JR. and M. I. SCULLANE. J. Coord. Chem. **8**, 93 (1978).
7. V. G. K. M. PISIPATI, G. SATYANANDAM, and N. V. S. RAO. Org. Magn. Res. **17**, 235 (1981).
8. R. L. LANCIONE, H. C. ALLEN, JR., and J. R. BUNTAINE. J. Coord. Chem. **8**, 201 (1979).
9. J. REEDIJK. Transition Met. Chem. **6**, 195 (1981).
10. H. R. GERSMANN and J. D. SWALLEN. J. Chem. Phys. **36**, 3221 (1962).
11. G. H. KOKOSZKA, H. C. ALLEN, JR., and G. GORDON. J. Chem. Phys. **42**, 3730 (1965).
12. D. E. BILLINGS and B. J. HATHAWAY. J. Chem. Phys. **50**, 2258 (1969).
13. D. KIVELSON and R. NEIMAN. J. Chem. Phys. **35**, 149 (1961).
14. J. BECHER, D. J. BROCKWAY, K. S. MURRAY, R. E. NEWMANN, and H. TOFTLUND. Inorg. Chem. **21**, 1791 (1982).
15. R. NEIMAN and D. KIVELSON. J. Chem. Phys. **35**, 156 (1961).
16. M. I. SCULLANE and H. C. ALLEN, JR. J. Coord. Chem. **7**, 181 (1978).

Can. J. Chem. Downloaded from www.nrcresearchpress.com by 210.87.254.40 on 09/06/12
For personal use only.

Mass spectrometric analysis of the products from the isotopomeric cationic intermediates in the solvolysis of 1,2-dianisyl-2-*p*-($^2H_3$)methoxyphenyl[2-^{13}C]vinyl bromide in 70% HOAc – 30% H_2O

CHOI CHUCK LEE, XIAN-DA YU, AND CHARLES Y. FIAKPUI

Department of Chemistry, University of Saskatchewan, Saskatoon, Sask., Canada S7N 0W0

Received January 24, 1983

CHOI CHUCK LEE, XIAN-DA YU, and CHARLES Y. FIAKPUI. Can. J. Chem. **61**, 2159 (1983).

Solvolyses were carried out with 6.0 m*M* doubly labeled 1,2-dianisyl-2-*p*-($^2H_3$)methoxyphenyl[2-^{13}C]vinyl bromide in 70% HOAc – 30% H_2O in the presence of 0, 1, 5, 10, or 400 molar equivalents of added NaOAc. The distributions of products derived from the 4 possible isotopomeric trianisylvinyl cationic intermediates were determined from the mass spectra of the isotopomeric dianisyl ketones obtained from degradation of the reaction products, the spectra being obtained by the chemical ionization teehnique in order to minimize possible complications by multiple fragmentations. The mass speetrometrie results obtained showed agreement with previously obtained ^{14}C serambling data and with the ^{13}C scramblings obtained in the present study using ^{13}C nmr. Increasing amounts of added NaOAc had the effect of decreasing the extents of scrambling from 1,2-anisyl shifts as previously observed. However, the formation of products from all 4 possible doubly labeled isotopomeric trianisylvinyl cations definitely demonstrated the occurrence of successive 1,2-anisyl shifts in the trianisylvinyl cation, and the detection of sueh successive shifts was not possible in previous work using a singly labeled substrate. The observed distribution of products derived from the 4 isotopomeric cations could be calculated assuming various contributions from equilibrations among these isotopomeric cations, and the mechanistic implications of the results are discussed.

CHOI CHUCK LEE, XIAN-DA YU et CHARLES Y. FIAKPUI. Can. J. Chem. **61**, 2159 (1983).

On a solvolysé des solutions 6,0 m*M* de bromure de dianisyl-1,2-*p*-($^2H_3$) méthoxyphényl[^{13}C-2] vinyle-2 doublement marqué dans un mélange à 70% de AcOH et 30% de H_2O en présence de 0, 1, 5, 10 ou 400 équivalents molaires de AcONa ajouté. On a déterminé les distributions des produits provenant des 4 intermédiaires cationiques trianisylvinyles isotopomères obtenus à partir de la dégradation des produits de la réaction. On a obtenu les spectres par la technique d'ionisation chimique afin de minimiser les complications possibles dues aux fragmentations multiples. Les résultats obtenus en spectrométrie de masse sont en accord avec les données de mélange du ^{14}C obtenues précédemment et avec les données de mélange du ^{13}C obtenues dans ce travail à l'aide de la rmn du ^{13}C. Des quantités croissantes de AcONa ajouté ont pour effet de diminuer le taux de mélange provenant des glissements 1,2 d'anisyle tels qu'observés antérieurement. Cependant la formation des produits à partir des 4 cations trianisylvinyles isotopomères possibles doublement marqués démontrent de façon définitive la présence successive de glissement anisyle-1,2 dans le cation trianisylvinyle que l'on ne pouvait déceler dans un travail antérieur en utilisant des substrats contenant un seul marqueur. On peut calculer la distribution des produits provenant des 4 cations isotopomères en supposant des contributions diverses des phénomènes d'équilibration parmi ces cations isotopomères et on discute de l'importance de ces résultats dans le mécanisme réactionnel.

[Traduit par le journal]

The first study on the trianisylvinyl cation was reported in 1969 by Rappoport and Gal (1). These workers investigated the kinetics of solvolysis of trianisylvinyl bromide and chloride (**1**-Br and **1**-Cl) in 80% ethanol and concluded that these reactions proceeded via the intermediate trianisylvinyl cation. Subsequently, additional solvolytic studies with trianisylvinyl substrates by Rappoport and co-workers (2–5) all provided further kinetic results in support of the intermediacy of the trianisylvinyl cation. The first observation of a degenerate rearrangement arising from 1,2-anisyl shifts in the trianisylvinyl cation was reported from this laboratory in 1975 (6). The reaction of trianisyl[2-^{13}C]vinyl bromide (**1**-Br-2-^{13}C) with HOAc–AgOAc or with CF_3COOH–CF_3COOAg was found to give 20% or 50% scrambling, respectively, of the label from C-2 to C-1 in the reaction product (6). Similarly, 1,2-anisyl shifts in the trianisylvinyl cation were also observed in the solvolysis of 1,2-dianisyl-2-*p*-($^2H_3$)methoxyphenylvinyl bromide (**1**-Br-2-methoxy-d_3) in a number of solvent systems (7). Subsequently, the extents of isotopic scrambling resulting from the solvolysis of **1**-Br-2-^{14}C under a variety of experimental conditions have been investigated using a 9:1 mixture of HOAc–Ac_2O (8) or 70% HOAc – 30% H_2O (9) as solvent.

In giving rise to degenerate rearrangements in triarylvinyl cations, it is probable that repeated cycles of 1,2-aryl shifts may take place. In the acetolysis of **1**-Br-2-^{14}C, for example, scrambling of the label from C-2 to C-1 was found in both the reaction product and the recovered, unconsumed reactant (8). In the latter stages of reaction, the scrambling in the recovered reactant was higher than in the corresponding product and it was suggested (8) that this finding indicated the occurrence of many cycles of ionization, 1,2-shift, and return to covalent bonding, leading to the accumulation of large amounts of scrambled reactant. A more definitive measure of successive 1,2-shifts in a triarylvinyl cation could be obtained from studies using a doubly labeled substrate. With a single isotopic label, such as **1**-Br-2-^{14}C or **1**-Br-2-methoxy-d_3, only two isotopomers could arise from the 1,2-shift process as shown in eqs. [1] and [2].

$$[1]\quad An_2C^*{=}\overset{+}{C}An \underset{2k_r}{\overset{2k_r}{\rightleftharpoons}} An\overset{+}{C}^*{=}CAn_2$$

$$[2]\quad An(An^*)C{=}\overset{+}{C}An \underset{2k_r}{\overset{k_r}{\rightleftharpoons}} An^*\overset{+}{C}{=}CAn_2$$

With a doubly labeled substrate, as illustrated in Scheme 1 for the trianisylvinyl system, four isotopomeric cations, **2**, **3**, **4**, and **5**, would be possible and their detection would demonstrate unequivocally the occurrence of successive 1,2-shifts.

Can. J. Chem. Downloaded from www.nrcresearchpress.com by 210.87.254.5 on 09/06/12
For personal use only.

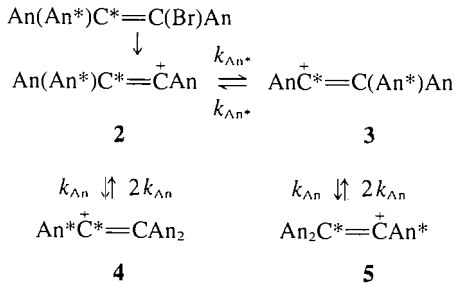

SCHEME 1

An earlier study on the acetolysis of **1**-Br labeled with ^{13}C and ^{14}C, namely, 1,2-dianisyl-2-*p*-[^{14}C]methoxyphenyl[2-^{13}C]-vinyl bromide (**1**-Br-2-^{13}C-2-methoxy-^{14}C), however, failed to demonstrate the formation of isotopomeric ions **2**, **3**, **4**, and **5** (10). The scrambling results obtained from the acetolysis of **1**-Br-2-^{13}C-2-methoxy-^{14}C were the same as those derived from analogous reactions with a 1:1 mixture of singly labeled **1**-Br-2-^{13}C and **1**-Br-2-methoxy-^{14}C because the ^{13}C and ^{14}C contents were determined by two independent methods (10). Since labeling with a radioisotope would involve a tracer amount of the label, double labeling with two radioisotopes would only give an intermolecular mixture of singly labeled substrates. To obtain a truly doubly labeled substrate, two highly enriched stable isotopes could be employed. Recently, we have prepared such a doubly labeled system, namely, 1,2-diphenyl-2-($^2H_5$)phenyl[2-^{13}C]vinyl bromide (**6**-Br-2-^{13}C-2-Ph-d_5), and studied its solvolysis in 70% HOAc – 30% H_2O (to be designated 70% HOAc; the solvolysis of **6**-Br in HOAc alone would be too slow) (11). In this study, the formation of the isotopomeric products derived from cations analogous to **2**, **3**, **4**, and **5** was analyzed by mass spectrometry (11). In the present work, such studies were extended to include an investigation on the solvolysis in 70% HOAc of a doubly labeled **1**-Br, namely, 1,2-dianisyl-2-*p*-($^2H_3$)methoxyphenyl[2-^{13}C]-vinyl bromide (**1**-Br-2-^{13}C-2-methoxy-d_3).

The doubly labeled **1**-Br-2-^{13}C-2-methoxy-d_3 was prepared in the same way as described in the preparation of **1**-Br-2-^{13}C-2-methoxy-^{14}C (10) except that the Grignard reagent from *p*-($^2H_3$)methoxybromobenzene instead of that from *p*-[^{14}C]methoxybromobenzene was employed in the reaction with 1,2-dianisyl[1-^{13}C]ethanone, the reactions utilized being given below:

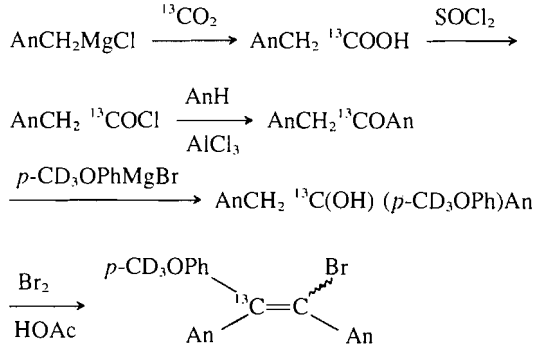

1-Br-2-^{13}C-2-methoxy-d_3

No attempt was made in separating the possible *Z*- and *E*-isomers of the **1**-Br-2-^{13}C-2-methoxy-d_3. The isotopic enrichments, as indicated by the supplier, were 90 and 99%, respectively, for ^{13}C and D (as $Ba^{13}CO_3$ and CD_3I). However, for most of the experiments, the doubly labeled substrate was prepared from [^{13}C]$BaCO_3$ slightly diluted to 80% enrichment. The **1**-Br-2-^{13}C-2-methoxy-d_3 that was obtained was analyzed by mass spectrometry (described in the experimental section) and the 80% ^{13}C enrichment and essentially complete deuteration were confirmed.

Solvolytic experiments were carried out with 6.0 m*M* **1**-Br-2-^{13}C-2-methoxy-d_3 in 70% HOAc in the presence of 0, 1, 5, 10, or 400 molar equivalents of added NaOAc. These conditions were similar to some of those employed in the studies with **1**-Br-2-^{14}C (9). Again, as in the previous study with **1**-Br-2-^{14}C (9), the product mixtures of isotopomeric trianisylvinyl acetates and 1,2,2-trianisylethanones were reduced with $LiAlH_4$ to give the labeled 1,2,2-trianisylethanols **7**, **8**, **9**, and **10** derived, respectively, from the isotopomeric cations **2**, **3**, **4**, and **5**. Since the ^{13}C enrichment was 80%, 20% of the isotopomeric 1,2,2-trianisylethanols would contain no ^{13}C. Thus along with **7**, **8**, **9**, and **10**, **7′**, **8′**, **9′**, and **10′**, respectively, would also be derived from cations **2**, **3**, **4**, and **5**, the ratio of **7**:**7′**, **8**:**8′**, **9**:**9′**, and **10**:**10′** being 80:20.

p-$CH_3OC_6H_4$(*p*-$CD_3OC_6H_4$)^{13}CHCH(OH)$C_6H_4OCH_3$-*p*

7

p-$CD_3OC_6H_4{}^{13}$CH(OH)CH($C_6H_4OCH_3$-*p*)$_2$

9

p-$CH_3OC_6H_4$(*p*-$CD_3OC_6H_4$)CHCH(OH)$C_6H_4OCH_3$-*p*

7′

p-$CD_3OC_6H_4$CH(OH)CH($C_6H_4OCH_3$-*p*)$_2$

9′

p-$CH_3OC_6H_4{}^{13}$CH(OH)CH(*p*-$CD_3OC_6H_4$)$C_6H_4OCH_3$-*p*

8

(*p*-$CH_3OC_6H_4$)$_2{}^{13}$CHCH(OH)$C_6H_4OCD_3$-*p*

10

p-$CH_3OC_6H_4$CH(OH)CH(*p*-$CD_3OC_6H_4$)$C_6H_4OCH_3$-*p*

8′

(*p*-$CH_3OC_6H_4$)$_2$CHCH(OH)$C_6H_4OCD_3$-*p*

10′

In the work with the doubly labeled triphenylvinyl system, **6**-Br-2-^{13}C-2-Ph-d_5, it was found that electron impact (EI) mass spectrometry on the mixture of isotopomeric 1,2,2-triphenylethanones or 1,2,2-triphenylethanols failed to give consistent or reproducible results on the relative amounts of products derived from the various possible isotopomeric triphenylvinyl cations (11). To minimize complications arising from possible multiple fragmentations in the EI spectrum, chemical ionization (CI) mass spectrometry (12, 13) was utilized in evaluating the distribution of products from various precursor triphenylvinyl cations (11). Thus in the present work, each sample of isotopomeric 1,2,2-trianisylethanols derived from a given

Can. J. Chem. Downloaded from www.nrcresearchpress.com by 210.87.254.5 on 09/06/12
For personal use only.

TABLE 1. CI spectra in the $[M + H]^+$ region for the isotopomeric dianisyl ketones derived from the products of solvolysis of **1**-Br-2-^{13}C-2-methoxy-d_3 in 70% HOAc

	Relative abundance[a]									
	Expt. 1[b]		Expt. 2		Expt. 3		Expt. 4		Expt. 5	
m/z	Run 1	Run 2	Run 1	Run 2	Run 1	Run 2	Run 1	Run 2	Run 1	Run 2
242	1.77	1.23	1.91	2.08	2.27	2.17	2.04	2.10	1.09	0.78
243	23.21	22.47	23.33	29.67	24.36	24.00	20.26	23.60	17.48	15.74
244	10.55	7.66	10.30	12.31	11.65	11.00	9.53	10.30	6.94	6.17
245	—	0.35	5.08	5.34	5.14	4.80	5.05	5.60	—	2.87
246	33.69	34.92	49.89	46.74	46.14	43.83	43.57	42.10	38.63	37.48
247	100.00	100.00	100.00	100.00	100.00	100.00	100.00	100.00	100.00	100.00
248	15.00	15.66	17.37	17.80	15.33	15.77	15.25	16.50	14.33	15.15
249	2.39	1.92	2.35	2.97	2.12	2.07	2.04	1.70	1.60	2.19

[a] Experiments 1, 2, 3, 4, and 5, respectively, were carried out with 6.0 m*M* **1**-Br-2-^{13}C-2-methoxy-d_3 in 70% HOAc – 30% H_2O in the presence of 0, 1, 5, 10, and 400 molar equivalents of NaOAc at 120 ± 1°C for 2 h. Titration of the liberated Br^- ion showed that the reaction was essentially complete in all of these experiments.
[b] The ^{13}C enrichment in the doubly labeled substrate for Expt. 1 was 90%; for the other experiments, the ^{13}C enrichment was 80%.

TABLE 2. Distribution of products from isotopomeric cations **2**, **3**, **4**, and **5** calculated from the data in Table 1 and scrambling of the ^{13}C label from C-2 to C-1 from ^{13}C nmr

	Distribution of products from precursor ions (%)										Scramble of ^{13}C from C-2 to C-1 (%)		Scrambling of ^{14}C from C-2 to C1 (%)[a]
	2		**3**		**4**		**5**		**3** + **4**				
Expt.	Run 1	Run 2	Run 1	Run 2	Run 1	Run 2	Run 1	Run 2	Run 1	Run 2	Run 1	Run 2	
1	66.6	67.5	14.5	15.6	14.0	14.0	4.9	2.9	28.5	29.6	28.2	28.0	27.9[b]
2	67.4	66.1	15.3	13.0	12.7	15.9	4.6	5.0	28.0	28.9	27.0	27.6	27.7[c]
3	68.3	69.7	12.9	11.8	13.0	13.1	5.8	5.4	25.9	24.9	25.4	24.8	25.9[d]
4	71.9	71.0	11.9	10.9	11.3	13.2	4.9	4.9	23.2	24.1	23.0	23.8	25.3[e]
5	76.3	78.3	9.6	8.9	10.5	9.7	3.6	3.1	20.1	18.6	18.4	17.6	18.2[f]

[a] Data from similar solvolysis of **1**-Br-2-^{14}C in 70% HOAc (9).
[b] Solvolysis of 5.9 m*M* **1**-Br-2-^{14}C with no added salt, Expt. 2, Table 2, ref. 9.
[c] Solvolysis of 6.0 m*M* **1**-Br-2-^{14}C in the presence of 6.0 m*M* NaOAc, Expt. 9, Table 2, ref. 9.
[d] Solvolysis of 6.0 m*M* **1**-Br-2-^{14}C in the presence of 30 m*M* NaOAc, Expt. 10, Table 2, ref. 9.
[e] Solvolysis of 5.9 m*M* **1**-Br-2-^{14}C in the presence of 60 m*M* NaOAc, Expt. 11, Table 2, ref. 9.
[f] Solvolysis of 6.0 m*M* **1**-Br-2-^{14}C in the presence of 2500 m*M* NaOAc, Expt. 25, Table 2, ref. 9.

experiment was oxidized to the corresponding dianisyl ketones, the CI spectrum of which was used to determine the distribution of products derived from isotopomeric cations **2**, **3**, **4**, and **5**.

The CI spectrum, with NH_3 as the reagent gas, for ordinary dianisyl ketone, $(p\text{-}CH_3OC_6H_5)_2CO$, gave the molecular ion, $[M + H]^+$, at m/z 243 as the base peak. The relative abundance of the peaks in the molecular ion region were 4.11, 100.00, 17.97, and 2.11%, respectively, for m/z 242, 243, 244, and 245. The only other peak, with a relative abundance of 5.24%, appeared at m/z 135 for $[p\text{-}CH_3OC_6H_4CO]^+$.

From each solvolysis experiment, oxidation of the isotopomeric 1,2,2-trianisylethanols gave a mixture of isotopomeric dianisyl ketones, $(p\text{-}CH_3OC_6H_4)_2CO$, $(p\text{-}CH_3OC_6H_4)_2{}^{13}CO$, $p\text{-}CH_3OC_6H_4(p\text{-}CD_3OC_6H_4)CO$, and $p\text{-}CH_3OC_6H_4(p\text{-}CD_3OC_6H_4)^{13}CO$, with $[M + H]^+$ ions appearing, respectively, at m/z 243, 244, 246, and 247. The relative abundances of these molecular ions, after appropriate corrections, were then utilized to calculate the distrbution of products derived from precursor trianisylvinyl cations **2**, **3**, **4**, and **5**. Given in Table 1 are the observed relative abundances of the peaks in the $[M + H]^+$ region of the CI spectra for the isotopomeric dianisyl ketones derived from the various solvolysis reactions with **1**-Br-2-^{13}C-2-methoxy-d_3. After correcting for the $[M + H + 1]^+$ and $[M + H + 2]^+$ peaks and for the presence of only 90 or 80% enrichment of the ^{13}C label, the distributions of products formed from cations **2**, **3**, **4**, and **5** were calculated, a detailed illustration of the calculations being given in the experimental section. The results are summarized in Table 2.

In our previous work on the solvolysis of **1**-Br-2-^{14}C in 70% HOAc (9), the extents of scrambling of the ^{14}C label from C-2 to C-1 were determined. Included in Table 2 are the ^{14}C scrambling results obtained for the solvolysis of **1**-Br-2-^{14}C under conditions that were similar, though not identical, to those used in the present studies. It may be noted from Scheme 1 that if the substrate were labeled only with ^{13}C, the sum of the products from cations **3** and **4** would be equal to the scrambling of the ^{13}C label from C-2 to C-1. Such ^{13}C scramblings from C-2 to C-1 were measured in the present work from the ^{13}C nmr spectra of the 1,2,2-trianisylethanols derived from the various solvolysis reactions using the method previously described by Oka and Lee (6). The results are also included in Table 2. It is seen from Table 2 that the products derived from cations **3** and **4** are in fairly good agreement with the corresponding extents of scrambling of the ^{13}C or ^{14}C label from C-2 to C-1.

In the solvolysis of **1**-Br-2-^{14}C in 70% HOAc (9), it was found that the extent of scrambling was decreased with in-

Can. J. Chem. Downloaded from www.nrcresearchpress.com by 210.87.254.5 on 09/06/12
For personal use only.

Can. J. Chem. Downloaded from www.nrcresearchpress.com by 210.87.254.5 on 09/06/12
For personal use only.

creasing amounts of added NaOAc. The present results, as indicated by the amounts of product derived from ions **3**, **4**, and **5**, also showed this trend. As previously suggested (9), these results were interpreted as support for the formation of the dissociated trianisylvinyl cation as reaction intermediate. Since such dissociated ions could competitively give rise to 1,2-anisyl shifts and be captured by nucleophiles to give product, the presence of the more nucleophilic acetate ion in the reaction mixture would favor the formation of more unscrambled product at the expense of 1,2-shifts, resulting in the observed decrease in the extents of scrambling with increasing amounts of added NaOAc. On the other hand, with the triphenylvinyl cationic system, solvolysis in 70% HOAc for both the singly labeled **6**-Br-2-^{14}C (9) or the doubly labeled **6**-Br-2-^{13}C-2-Ph-d_5 (11) resulted in isotopic scramblings the extent of which was not significantly affected by the presence of added NaOAc. It has been shown recently that both common ion rate depression and ^{82}Br exchange took place in the solvolysis in 70% HOAc of **1**-Br or **6**-Br, indicating the involvement of the dissociated trianisylvinyl or triphenylvinyl cation, and it was suggested that the insensitivity of the extent of scrambling in the solvolysis of labeled **6**-Br might be due to a low selectivity of the less stable triphenylvinyl cation (14).

As pointed out earlier in this paper, with the use of a singly labeled substrate, successive 1,2-shifts would not be directly detectable. With the use of double labeling, the formation of products derived from all isotopomeric cations **2**, **3**, **4**, and **5** from **1**-Br-2-^{13}C-2-methoxy-d_3 as observed in the present work (Table 2), and the formation of such products from the 4 analogous cations from **6**-Br-2-^{13}C-2-Ph-d_5 (11), definitely demonstrated the occurrence of successive 1,2-aryl shifts in the trianisylvinyl and triphenylvinyl cations. Aside from this conclusion, it may also be of interest to compare in more detail the results in Table 2 with the analogous data derived from **6**-Br-2-^{13}C-2-Ph-d_5 (11).

Similar to Scheme 1, the 4 isotopomeric cations derived from **6**-Br-2-^{13}C-2-Ph-d_5 may be designated as **2′**, **3′**, **4′**, and **5′** as shown in Scheme 2. From 9 solvolysis experiments with

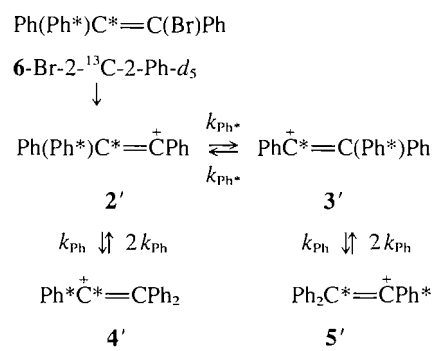

SCHEME 2

6-Br-2-^{13}C-2-Ph-d_5 carried out in 70% HOAc containing 0, 5, or 10 molar equivalents of NaOAc, the mean values for the products derived from **2′**, **3′**, **4′**, and **5′** were found to be 84.7 ± 2.2, 7.3 ± 1.2, 6.6 ± 1.2, and 1.5 ± 0.5%, respectively (11). Since the initially formed ion **2′** would rearrange to ions **3′** and **4′** in the first stage of the 1,2-shift process while ion **5′** was formed subsequently from ion **3′**, it was suggested that one-half of **2′** could be equilibrated between ions **2′** and **4′** and the other half equilibrated between **2′**, **3′**, and **5′** (11). Such a mechanism would qualitatively explain the observation that roughly the same amounts of products were derived from ions **3′** and **4′** while the least amount of product was derived from ion **5′**.

Taking into account the statistical factors involved in the equilibration processes, complete equilibration of 50% of **2′** between **2′** and **4′** would give 33.3% of **2′** and 16.7% of **4′**. Similarly, complete equilibration of 50% of **2′** between **2′**, **3′**, and **5′** would give 25% of **2′**, 16.7% of **3′**, and 8.3% of **5′**. The net result in the distribution of products derived from **2′**, **3′**, **4′**, and **5′** would be 58.3 (33.3 + 25.0), 16.7, 16.7, and 8.3%, respectively. The observed result of about 85% product from **2′**, 6–7% from **3′** or **4′**, and about 2% from **5′** clearly showed that not all of ion **2′** has undergone equilibration (11).

The above interpretations, which were discussed in the previous study (11), may be modified by assuming that only part of ion **2′** would equilibrate through 1,2-shifts while the rest could be captured directly by nucleophiles to give unscrambled product. If only 36% of **2′** were to equilibrate and 64% were captured directly to give unscrambled product, equilibration of one-half of the 36% of **2′** between **2′** and **4′** would give 12% **2′** and 6% **4′**. Similarly, equilibration of the other 18% between **2′**, **3′**, and **5′** would give 9% **2′**, 6% **3′**, and 3% **5′**. The net distribution of products from **2′**, **3′**, **4′**, and **5′** would be 85 (64 + 12 +9), 6, 6, and 3%, respectively. One could make a further assumption that complete equilibration between **3′** and **5′** was not quite achieved since it took place in a later stage subsequent to the formation of **3′** from **2′**. Instead of the statistical 2:1 distribution of 6% **3′** and 3% **5′**, the products from **3′** and **5′** could be modified to 7% and 2%, respectively. With such a modification, the overall distribution of products from **2′**, **3′**, **4′**, and **5′** would be 85, 7, 6, and 2%, respectively, in excellent agreement with the results observed in the solvolysis of **6**-Br-2-^{13}C-2-Ph-d_5 in 70% HOAc (11).

Similar treatments can be applied to the data in Table 2 obtained in the present studies with **1**-Br-2-^{13}C-2-methoxy-d_3. For example, in Expt. 1 (solvolysis in 70% HOAc with no added NaOAc), the observed average distributions of products from ions **2**, **3**, **4**, and **5**, respectively, were 67, 15, 14, and 4%. Assuming that 16% of **2** was captured directly to give unscrambled product, 42% of **2** was equilibrated between **2** and **4** to give 28% **2** and 14% **4**, and the other 42% of **2** was equilibrated between **2**, **3**, and **5** to give 21% **2**, 14% **3**, and 7% **5**, the net distribution of products from **2**, **3**, **4**, and **5** would be 65 (16 + 28 + 21), 14, 14, and 7%, respectively. Again, if complete equilibration between **3** and **5** was not achieved, the 14% product from **3** and 7% product from **5** could be modified to 15% and 6%, respectively, giving an overall distribution of products from **2**, **3**, **4**, and **5** of 65, 15, 14, and 6%, respectively, in reasonably good agreement with the observed data.

In the same way as described above for Expt. 1, the distributions of products derived from **2**, **3**, **4**, and **5** were calculated for the other experiments and the results are summarized in Table 3. For Expt. 2, the same calculated distribution of products as for Expt. 1 could be utilized, suggesting that the presence of 1 equiv. of added NaOAc did not materially affect the scrambling processes. In Expts. 3–5, as expected, the proportion of ion **2** that was captured directly to give unscrambled product was found to increase with increasing amounts of added NaOAc. It is also of interest to note from Table 3 that the statistical distribution of 2:1 for the products from **3** and **5** was not achieved in Expts. 1 and 2, suggesting that equilibration was more complete when the solvolysis was carried out in the presence of more added NaOAc as in Expts. 3–5. A similar

Can. J. Chem. Downloaded from www.nrcresearchpress.com by 210.87.254.5 on 09/06/12
For personal use only.

TABLE 3. Calculated distribution of products from isotopomeric cations **2**, **3**, **4**, and **5**

		Distribution of products from precursor ions (%)											
		2					**3**		**4**		**5**		
Expt.	Added NaOAc (equiv.)	Direct capture	**2** ⇄ **4**	**2** ⇄ **3** ⇄ **5**	Sum	Observed[a]	**2** ⇄ **3** ⇄ **5**	Observed[a]	**2** ⇄ **4**	Observed[a]	**2** ⇄ **3** ⇄ **5**	Observed[a]
1	0	16	28	21	65	67	14(15)[b]	15	14	14	7(6)[b]	4
2	1	16	28	21	65	67	14(15)[b]	14	14	14	7(6)[b]	5
3	5	22	26	20	68	69	13	12	13	13	6	6
4	10	28	24	18	70	71	12	11	12	12	6	5
5	400	48	17	13	78	77	9	9	9	10	4	3

[a] Averaged values from the duplicate runs recorded in Table 2.
[b] Assuming that the statistical 2:1 distribution from the equilibration of **3** and **5** was not achieved and the calculated distribution of 14% **3** and 7% **5** was modified to 15% **3** and 6% **5**.

conclusion was reached in the previous study on the acetolysis of **1**-Br-2-^{13}C-2-methoxy-^{14}C (10). In this earlier work, comparisons of the extents of rearrangements of the ^{13}C chain label and the ^{14}C ring label led to the conclusion that more complete equilibration of the labels was achieved when the reaction was carried out in the presence of high concentrations of added salts.

To account for the effect of added salts, it was suggested (10) that in the absence or presence of low concentrations of added salts, some of the 1,2-shifts might have occurred in the ion-pair stage and the presence of the leaving group as the counterion would give a frontside hindrance to the 1,2-migration, preventing a complete equilibration. On the other hand, in the more polar medium with the presence of higher concentrations of added salts, dissociation would proceed further, the 1,2-shifts would be unhindered by any counterion and more complete equilibration would be attained. A similar mechanism may be used to account for the present results. In the solvolysis of **1**-Br-2-^{13}C-2-methoxy-d_3 in 70% HOAc, under conditions of Expts. 1 and 2, a small portion of the 1,2-shifts may have taken place in the ion-pair stage, while under conditions of Expts. 3–5, the 1,2-shifts occurred essentially with dissociated ions. Support for a minor role for ion-pairs in the process of 1,2-anisyl shifts has also been obtained recently by Ikeda *et al.* (15). These workers studied the solvolysis of 2,2-dianisyl-1-phenylvinyl bromide specifically labeled by *p*-(^{2}H$_3$)CH$_3$O (methoxy-d_3) in the *cis*- or *trans*-anisyl group. A slight preference, 53:47 or 51:49, respectively, was found for the migration of the anisyl group *trans* to bromine for the solvolysis in 2,2,2-trifluoroethanol/2,6-lutidine or in HOAc/AgOAc. It was proposed that this preference was due to the intervention of ion-pairs in the rearrangement process, with the leaving group as the counterion hindering the migration of the anisyl group *cis* to bromine.

Experimental

*1,2-Dianisyl-2-*p*-($^2H_3$)methoxyphenyl[2-^{13}C]vinyl bromide (**1**-Br-2-^{13}C-2-methoxy-*d*$_3$)*

The doubly labeled substrate, **1**-Br-2-^{13}C-2-methoxy-d_3, was prepared in the same way as previously described for the preparation of 1,2-dianisyl-2-*p*-[^{14}C]methoxyphenyl[2-^{13}C]vinyl bromide (10), except that CD_3I instead of [^{14}C]methyl iodide was used to methylate *p*-bromophenol to give the labeled *p*-methoxybromobenzene, which in turn was converted to the Grignard reagent for reaction with 1,2-dianisyl[1-^{13}C]ethanone, eventually leading to **1**-Br-2-^{13}C-2-methoxy-d_3.

The isotopically labeled starting materials, [^{13}C]$BaCO_3$ and CD_3I, were supplied by MSD Isotopes of Montreal and the enrichments for the ^{13}C and D were specified as 90 and 99%, respectively. For most of the solvolysis reactions, the substrate was prepared from [^{13}C]$BaCO_3$ diluted to 80% enrichment. A sample of **1**-Br-2-^{13}C-2-methoxy-d_3 obtained from 80% enriched [^{13}C]$BaCO_3$ and 99% enriched CD_3I gave a CI spectrum with relative intensities at m/z 428, 429, 430, 431, and 432, respectively, of 2.71, 10.34, 5.42, 10.84, and 2.96% of the base peak, the base peak being m/z 349 for the $[M + H - Br]^+$ ion. For **1**-Br containing ^{79}Br, the $[M + H]^+$ peaks with only the methoxy-d_3 label and with both methoxy-d_3 and ^{13}C labels would appear at m/z 428 and 429, respectively. Since the relative intensities for m/z 428 and 429 were 2.71 and 10.34, the presence of **1**-Br-2-methoxy-d_3 and **1**-Br-2-^{13}C-2-methoxy-d_3 would correspond to 2.71/(2.71 + 10.34) and 10.34/(2.71 + 10.34) or 21 and 79%, respectively. Similarly, for **1**-Br containing ^{81}Br, the $[M + H]^+$ peaks with only the methoxy-d_3 label and with both methoxy-d_3 and ^{13}C labels appeared at m/z 430 and 431, respectively, with relative intensities of 5.42 and 10.84. Since there was an m/z 432 peak with

Can. J. Chem. Downloaded from www.nrcresearchpress.com by 210.87.254.5 on 09/06/12
For personal use only.

relative intensity of 2.96 or 27.3% of the intensity of the 431 peak, a correction for $[M + H + 1]^+$ was made on m/z 430, the correction being 27.3% of the intensity of m/z 429. The corrected intensity for m/z 430 would thus be $5.42 - (0.273 \times 10.34) = 2.50$. With relative intensities of 2.50 and 10.84 for m/z 430 and 431, the presence of **1**-Br-2-methoxy-d_3 and **1**-Br-2-^{13}C-2-methoxy-d_3 would correspond to 19 and 81%, respectively. The mean values from the ^{79}Br and ^{81}Br peaks of 20% **1**-Br labeled only with methoxy-d_3 and 80% **1**-Br labeled with both methoxy-d_3 and ^{13}C thus may be regarded as a confirmation of the 80% ^{13}C enrichment and essentially complete deuteration for the doubly labeled substrate.

Solvolysis reactions

The solvolysis of **1**-Br-2-^{13}C-2-methoxy-d_3 in 70% HOAc in the presence of various amounts of NaOAc was carried out in a similar manner as previously described for the solvolysis of **1**-Br-2-^{14}C in 70% HOAc (9). Typically, a solution of 258 mg (0.60 mmol) of **1**-Br-2-^{13}C-2-methoxy-d_3 and 49 mg (0.60 mmol) of NaOAc in 100 mL of 70% HOAc in a sealed tube was heated at 120 ± 1°C for 2 h. Similar reactions were carried out in the absence of any NaOAc or in the presence of 5, 10, or 400 molar equivalents of NaOAc. After cooling in an ice bath, the sealed tube was opened and each reaction mixture was extracted with $CHCl_3$ (3 × 50 mL). The extract was washed with a dilute $NaHCO_3$ solution and then with H_2O. Titration of the liberated Br^- ion in the combined aqueous phase showed that in all of these experiments, the reaction was essentially complete. The $CHCl_3$ extract was dried over $MgSO_4$ and the solvent was removed by distillation. The residual organic product was reduced twice with $LiAlH_4$ (6) to give the isotopomeric 1,2,2-trianisylethanols. Samples of the 1,2,2-trianisylethanols were analyzed for the extents of scrambling of the ^{13}C label from C-2 to C-1 using ^{13}C nmr as described by Oka and Lee (6). $KMnO_4$ oxidation (8, 16) of the isotopomeric 1,2,2-trianisylethanols obtained from each solvolysis reaction gave the isotopomeric dianisyl ketones for mass spectral analysis.

Mass spectral analysis

The CI spectra of the various samples of dianisyl ketones were obtained with 0.3 torr of NH_3 as reagent gas. A gc–ms instrument was employed, each sample being passed through the gc before the CI spectrum was obtained using a VG-16F mass spectrometer supplied by Micromass Ltd. Given in Table 1 are the CI spectra in the $[M + H]^+$ region for the isotopomeric dianisyl ketones derived from the various solvolysis experiments with **1**-Br-2-^{13}C-2-methoxy-d_3, the $[M + H]^+$ ions for $(p\text{-}CH_3OC_6H_4)_2CO$, $(p\text{-}CH_3OC_6H_4)_2\ ^{13}CO$, $p\text{-}CH_3OC_6H_4(p\text{-}CD_3OC_6H_4)CO$, and $p\text{-}CH_3OC_6H_4(p\text{-}CD_3OC_6H_4)^{13}CO$ appearing at m/z 243, 244, 246, and 247, respectively.

As an illustration of the calculations, consider the data for run 1 of Expt. 2 in Table 1. Since the abundance of $[M + H + 1]^+$ and $[M + H + 2]^+$ at m/z 248 and 249, respectively, were 17.37% and 2.35% of the abundance of m/z 247, corrections were made as follows:

$$\begin{array}{lcl} \text{Corrected abundance of } m/z \text{ 247} & = & \text{Observed abundance of 247} - \text{17.37\% of the abundance of 246} - \text{2.35\% of the abundance of 245} \\ & = & 100.00 - (0.1737 \times 49.85) - (0.0235 \times 5.08) = 91.22 \end{array}$$

Similarly, the corrected abundance of m/z 246 would equal (the observed abundance of 246) − (17.37% of the abundance of 245) − (2.35% of the abundance of 244). In this way, the corrected relative abundances for m/z 247, 246, 244, and 243, respectively, were calculated to be 91.22, 48.73, 6.21, and 23.00.

Since the ^{13}C enrichment was 80%, cation **2**, for example, would give rise to an 80:20 mixture of **7** and **7′**, and oxidation of **7** and **7′** would give, respectively, $p\text{-}CH_3OC_6H_4(p\text{-}CD_3OC_6H_4)^{13}CO$ ($[M + H]^+$ at m/z 247) and $p\text{-}CH_3OC_6H_4(p\text{-}CD_3OC_6H_4)CO$ ($[M + H]^+$ at m/z 246). Similarly, **3** would give rise to an 80:20 mixture of **8** and **8′**, both of which would oxidize to $p\text{-}CH_3OC_6H_4(p\text{-}CD_3OC_6H_4)CO$ ($[M + H]^+$ at m/z 246). In the same way, the isotopomeric dianisyl ketones derived from the products of ions **4** and **5** could also be deduced, the overall results being summarized in eqs. [3] to [6].

[3] **2** → 80% **7** + 20% **7′** → 80% m/z 247 + 20% m/z 246

[4] **3** → 80% **8** + 20% **8′** → 100% m/z 246

[5] **4** → 80% **9** + 20% **9′** → 100% m/z 243

[6] **5** → 80% **10** + 20% **10′** → 80% m/z 244 + 20% m/z 243

From eqs. [3] to [6], the sources of the m/z 247, 246, 244, and 243 peaks could be obtained as summarized in eqs. [7] to [10].

[7] Abundance of m/z 247 = 0.80 (product from **2**)

[8] Abundance of m/z 246 = product from **3** + 0.20 (product from **2**)

[9] Abundance of m/z 244 = 0.80 (product from **5**)

[10] Abundance of m/z 243 = product from **4** + 0.20 (product from **5**)

Using the corrected relative abundances of 91.22, 48.73, 6.21, and 23.00, respectively, for m/z 247, 246, 244, and 243 and applying eqs. [7] to [10], the relative amounts of products from ions **2**, **3**, **4**, and **5** were calculated to be 114.03, 25.93, 21.45, and 7.76, respectively. Expressing these amounts of products on a percentage basis, the distribution of products from **2**, **3**, **4**, and **5**, respectively, would become 67.4, 15.3, 12.7, and 4.6%, as given in Table 2.

Acknowledgments

We wish to express our sincere thanks to Professor K. K. Midha of the College of Pharmacy of this University for permission to use the VG-F16 mass spectrometer, to Mr. K. Hall for obtaining the CI spectra, and to the Natural Sciences and Engineering Research Council of Canada for financial support.

1. Z. Rappoport and A. Gal. J. Am. Chem. Soc. **91**, 5246 (1969).
2. Z. Rappoport and Y. Apeloig. Tetrahedron Lett. 1817 (1970).
3. Z. Rappoport and A. Gal. Tetrahedron Lett. 3233 (1970).
4. Z. Rappoport and J. Kaspi. J. Am. Chem. Soc. **92**, 3220 (1970).
5. Z. Rappoport and J. Kaspi. J. Chem. Soc. Perkin Trans. **2**, 1102 (1972).
6. M. Oka and C. C. Lee. Can. J. Chem. **53**, 320 (1975).
7. Y. Houminer, E. Noy, and Z. Rappoport. J. Am. Chem. Soc. **98**, 5632 (1976).
8. C. C. Lee, U. Weber, and C. A. Obafemi. Can. J. Chem. **57**, 1384 (1979).
9. C. C. Lee, E. C. F. Ko, and Z. Rappoport. Can. J. Chem. **58**, 2369 (1980).
10. C. C. Lee, C. A. Obafemi, J. W. Quail, and Z. Rappoport. Can. J. Chem. **59**, 2342 (1981).
11. C. C. Lee, C. Y. Fiakpui, and K. K. Midha. J. Org. Chem. **48**, 1025 (1983).
12. I. Howe, D. H. Williams, and R. D. Bowen. Mass spectrometry, principles and applications. 2nd ed. McGraw–Hill, New York. 1981. pp. 43–48; 178–186.
13. W. J. Richter and H. Schwarz. Angew. Chem. Int. Ed. Engl. **17**, 424 (1978).
14. C. C. Lee, C. A. Obafemi, and Z. Rappoport. Can. J. Chem. **60**, 3019 (1982).
15. T. Ikeda, S. Kobayashi, H. Taniguchi, and Z. Rappoport. J. Org. Chem. **47**, 1916 (1982).
16. C. C. Lee, A. J. Cessna, B. A. Davis, and M. Oka. Can. J. Chem. **52**, 2679 (1974).

Reactions of steroidal 4,5- and 5,6-epoxides with strong bases

HERBERT L. HOLLAND AND JAHANGIR

Department of Chemistry, Brock University, St. Catharines, Ont., Canada L2S 3A1

Received February 17, 1983

HERBERT L. HOLLAND and JAHANGIR. Can. J. Chem. **61**, 2165 (1983).

A series of C-3 oxygenated and unsubstituted (4,5)α, (4,5)β, (5,6)α, and (5,6)β epoxy steroids has been prepared, and the reactions of these compounds with strong bases (potassium *tert*-butoxide, LDA, and LDEA) were investigated. Only LDEA gave rise to product formation; β elimination of the epoxide to give a β-hydroxy olefin was observed in this case. The regioselectivity of product formation is consistent with a mechanism of rearrangement involving removal of a hydrogen located *syn* to the epoxide oxygen. In some cases, a directing influence from a polar substituent (OH) of the starting material was also apparent. The ^{13}C nmr spectra of the steroidal epoxides used in this study were assigned; these data are diagnostic of the conformation of ring A of (4,5)α and (4,5)β epoxy steroids.

HERBERT L. HOLLAND et JAHANGIR. Can. J. Chem. **61**, 2165 (1983).

On a préparé une série d'époxy stéroides du type (4,5)α, (4,5)β, (5,6)α et (5,6)β oxygénés en position C-3 et non substitués et on a étudié leurs réactions avec des bases fortes (*tert*-butylate de potassium, LDA et LDEA). Seule la LDEA conduit à la formation de produits; on a observé dans ce cas une élimination β de l'époxyde qui conduit à la β-hydroxy oléfine. La régiosélectivité de la formation du produit est en accord avec un mécanisme de transposition qui implique une élimination d'hydrogène situé en position *syn* de l'oxygène de l'époxyde. On note également dans quelques cas, une influence directrice du substituant polaire (OH) du produit de départ. On a identifié les spectres de rmn du ^{13}C des époxy stéroides utilisées; ces données permettent de prédire la conformation du cycles A des (4,5)α et (4,5)β époxy stéroides.

[Traduit par le journal]

Can. J. Chem. Downloaded from www.nrcresearchpress.com by 210.87.254.40 on 09/06/12
For personal use only.

The base catalysed rearrangement of epoxides to allylic alcohols, involving β-hydrogen abstraction (eq. [1]), can be performed by strong bases such as alkyl lithiums (1), alkoxide

[1] 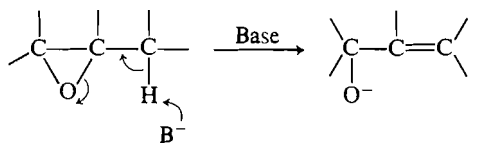

[2] 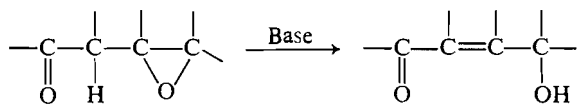

salts (2, 3), or lithium dialkylamides (4, 5). In the steroid field, a variant of this reaction has been widely used in the preparation of γ-hydroxy-α,β-unsaturated ketones by base catalysed rearrangement of β,γ epoxy ketones such as **3***b* and **6***b* (eq. [2]), in which case weaker bases such as triethylamine are successful in promoting rearrangement (6, 7).

In cases where the stereochemical details of eq. [1] have been investigated, a requirement for a *syn* coplanar arrangement of β hydrogen and epoxide oxygen has been proposed (lithium diethylamide, LDEA, as base) (8). The regioselectivity of the LDEA promoted reaction has also been studied (9); attack occurs at the least hindered site with large factors separating primary, secondary, and tertiary proton abstraction.

In an attempt to delineate the steric requirements and regioselectivity of eq. [1] when applied to the preparation of steroidal γ-hydroxy olefins, we have studied the reactions of a series of 5,6 epoxy (**1**−**6**) and 4,5 epoxy (**7**−**12**) steroids of defined configuration and conformation with several strong bases.

Epoxides **1**−**12** were prepared by published procedures. Hitherto unreported ^{13}C chemical shifts are presented in Tables 1−4. The values for the 5,6-epoxides **1**, **3***c*, **4**, and **6***c* (Tables 1 and 2) were assigned by comparison with those reported for similar androstane derivatives (10). Those for the C-3α derivatives **2** and **5**, and for the unsubstituted epoxides **3***a* and **6***a*, were thence derived by a consideration of the shifts

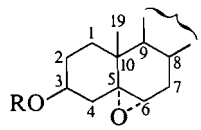

1 *a* R = H
b R = Ac

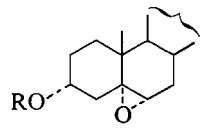

2 *a* R = H
b R = Ac

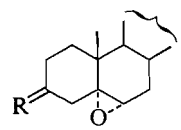

3 *a* R = H_2
b R = O
c R = OCH_2CH_2O

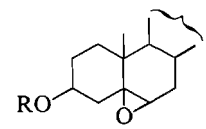

4 *a* R = H
b R = Ac

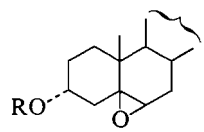

5 *a* R = H
b R = Ac

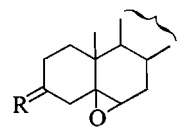

6 *a* R = H_2
b R = O
c R = OCH_2CH_2O

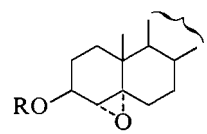

7 *a* R = H
b R = Ac

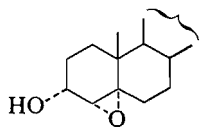

8

caused by substitution at C-3 (11).

The spectra of the (4,5)α epoxides (Table 3) were assigned by reference to the published data for 5α-cholestan-5-ol (and derivatives) (11) and support the conformation for ring A shown in Fig. 1; the γ upfield shift of C-1 caused by the C-5α pseudo axial epoxide oxygen, and the lack of a similar shift dependent upon the stereochemistry of oxygen substitution at C-3, are particularly diagnostic of the diaxial relationships involved. The spectra of the (4,5)β epoxides **10**−**12** were

Can. J. Chem. Downloaded from www.nrcresearchpress.com by 210.87.254.40 on 09/06/12
For personal use only.

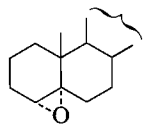

9

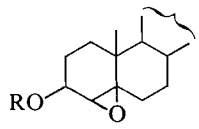

10 *a* R = H
b R = Ac
c R = Bz

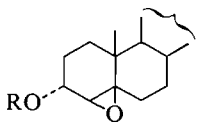

11 *a* R = H
b R = Ac

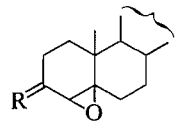

12 *a* R = H_2
b R = O

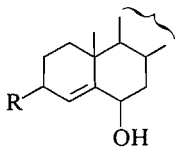

13 *a* R = OH
b R = H

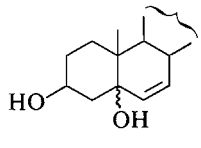

14 *a* 5αOH
b 5βOH

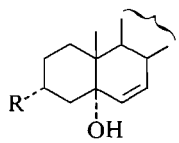

15 *a* R = OH
b R = H

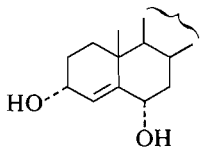

16

assigned by reference to the spectra of 5β-cholestane and derivatives (11), and by the use of heteronuclear ($^1H/^{13}C$) decoupling and/or SFORD data. Carbons 3−5, 8−10, and 19 were thus readily assignable. The remaining rings A and B carbons were assigned by a consideration of the effects of substitution at C-3. Thus the resonance position of C-7 does not vary greatly over the series, while carbons 2, 4, and 6 show the anticipated effects caused by substitution at C-3. The values reported for **12***b* represent a correction of our previously published assignments for C-1 and C-7 (12); these latter were made without benefit of the variation in substitution pattern at C-3 available in the series now under study.

When compared with the spectrum of the alcohol **10***a*, the esters **10***b* and **10***c* show shifts (in addition to the anticipated effects at C-2 and C-4) at C-1 and C-9, which are characteristic of a change in conformation in ring A (Fig. 2). The chemical shift assignments for **10***a*, **11***a*, **11***b*, **12***a*, and **12***b* are consistent with conformation A; thus C-1 of **12***a* shows a γ upfield shift relative to the corresponding carbon of 5β-cholestane (11) characteristic of 1,3-diaxial interaction with the C-5β epoxide oxygen. A further γ upfield shift of C-1 in **10***a* and **11***a* occurs as a consequence of substitution at C-3, the interactions being 1,3 axial hydroxyl (−3.8 ppm) in the case of **10***a*, and 1,3 equatorial hydroxyl (−3.6 ppm) for **11***a* (11). In **10***b* and **10***c*, however, the greater bulk of the 3β substituent now necessitates that it occupy an equatorial position (conformation B, Fig. 2) in which the C-5 β − C-1β diaxial interaction is lost. A comparison of the chemical shifts at C-1 in **10***b* and **10***c* with that of **12***a* confirms that this is so. If the effect of oxygen substitution at C-1 is removed from the observed shifts in **10***b* and **10***c* (see above), then C-1 of these compounds would resonate at significantly lower field (ca. 3−4 ppm) than that observed for C-1 of **12***a*. In addition, the chemical shifts of C-9 in **10***b* and **10***c* are characteristic of the absence in these compounds of the interaction between the C-2α and C-9α hydrogens present in normal C-5β steroids (13), and the presence of an eclipsing γ interaction from the C-1α hydrogen possible in conformation B. The chemical shift of C-9 is particularly diagnostic of the stereochemistry of the A/B ring function in saturated steroids (11, 13), and the variations observed here are consistent with the interpretation of the effects of stereochemistry and conformation on the resonance position of C-9 (13).

TABLE 1. ^{13}C Chemical shifts of (5,6)α epoxy steroids **1**−**3**

	δ ppm					
Carbon*	**1***a*	**1***b*	**2***a*	**2***b*	**3***a*	**3***c*
1	32.5	32.2	28.7	28.0	34.5	31.4
2	31.0	27.3	29.0	26.0	21.8	31.0
3	68.5	71.4	68.0	69.6	23.4	109.0
4	39.9	36.2	36.5	33.8	31.0	39.2
5	66.0	66.1	65.5	63.5	66.1	64.1
6	59.5	59.2	57.8	56.7	60.3	57.5
7	28.1	28.0	28.1	28.4	28.1	28.0
8	29.9	29.9	29.8	29.7	29.9	29.9
9	42.6	42.5	42.8	42.4	43.0	42.2
10	34.9	35.1	35.7	35.4	36.3	35.1
19	15.9	15.9	15.4	15.6	15.9	15.6

*In this and subsequent tables, carbons 11−18 and 20−27 had chemical shifts close to those of other ring A and/or B substituted cholestanes (11).

TABLE 2. ^{13}C Chemical shifts of (5,6)β epoxy steroids **4**−**6**

	δ ppm					
Carbon	**4***a*	**4***b*	**5***a*	**5***b*	**6***a*	**6***c*
1	37.2	36.7	33.2	33.8	35.8	36.2
2	31.0	27.3	28.5	25.5	21.7	30.9
3	69.4	71.4	67.2	70.5	28.1	109.6
4	42.2	38.0	40.0	36.7	32.9	41.6
5	63.0	62.6	62.2	61.7	65.8	63.0
6	63.7	63.6	63.7	63.3	63.7	63.3
7	32.7	32.6	32.5	32.5	32.9	32.4
8	29.8	29.8	29.9	29.8	30.1	29.8
9	51.4	51.0	50.5	50.3	51.7	49.9
10	34.9	35.1	35.6	35.5	36.0	35.1
19	17.0	17.0	17.0	17.2	17.2	17.1

TABLE 3. ^{13}C Chemical shifts of (4,5)α epoxy steroids **7**−**9**

	δ ppm			
Carbon	**7***a*	**7***b*	**8**	**9**
1	28.7*	29.8*	27.8	31.3
2	27.1	23.2	27.0	22.5
3	66.0	68.0	63.3*	28.5
4	64.9	62.0	63.2*	60.8
5	67.5	66.8	69.9	66.1
6	29.8	30.4	29.9	30.4
7	28.5*	29.6*	28.5	28.5
8	35.7	35.5**	35.5	35.7
9	50.1	50.0	50.6	50.4
10	35.7	35.3**	35.5	35.9
19	17.8	17.5	17.3	16.0

*Chemical shifts marked with asterisks may be interchanged.

TABLE 4. ^{13}C Chemical shifts of (4,5)β epoxy steroids **10**–**12**

Carbon	δ ppm						
	10*a*	**10***b*	**10***c*	**11***a*	**11***b*	**12***a*	**12***b*
1	26.0*	29.7	30.0	26.2**	25.8	29.8	26.2
2	26.4*	22.6	22.7	25.9**	22.1	17.4	32.6
3	63.8	66.8	66.7	66.0*	69.0	23.9	206.9
4	64.3	61.3	61.5	66.9*	63.1	61.5	62.8
5	69.0	69.1	69.8	66.9*	66.3	65.7	70.4
6	31.2	31.3	31.3	31.0	30.7	31.6	29.9
7	30.4	30.4	30.4	30.4	30.3	30.7	30.5
8	35.2	35.3	35.8	35.2	35.1	35.2	35.1
9	47.3	49.1	49.4	46.1	46.2	46.6	46.6
10	35.8	35.8	35.2	36.2	36.0	35.2	37.2
19	19.0	18.4	18.4	18.7	18.6	19.3	19.0

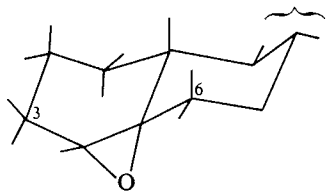

FIG. 1. Conformation of (4,5)α epoxy steroids **7**–**9**.

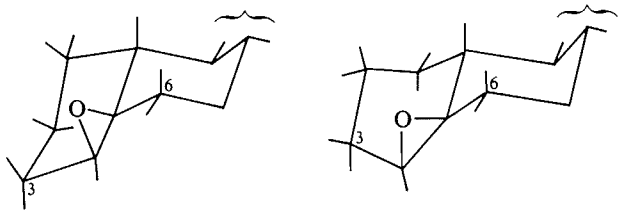

FIG. 2. Conformations of (4,5)β epoxy steroids **10**.

None of the epoxides treated with potassium *tert*-butoxide or lithium diisopropyl amide (LDA) (see Experimental) resulted in the formation of products. In all cases, only starting material was recovered. Presumably, the steric bulk of these reagents prevents hydrogen abstraction in the cases studied. The failure to observe any rearrangements resulting from α hydrogen abstraction (14–16) by LDA may also be attributable to steric factors. Since reactions with LDA could be carried out only at low temperatures (17), further experiments used the more versatile diethyl amide LDEA. This latter reagent has proven useful in carrying out the reaction of eq. [1] in cases where LDA gave only poor yields (18, 19).

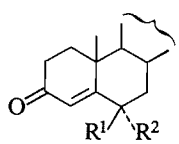

17 *a* R^1 = H, R^2 = OH
b R^1 = OH, R^2 = H

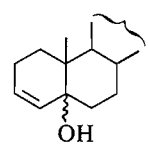

18 *a* 5αOH
b 5βOH

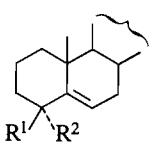

19 *a* R^1 = H, R^2 = OH
b R^1 = OH, R^2 = H

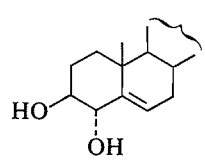

20

TABLE 5. Reactions of epoxides **1**–**12** with LDEA

Starting material	Products (isolated %)
1*a*	**14***a* (56)
2*a*	**15***a* (18), **16** (18)
3*a*	**15***b* (72)
3*c*	**17***a* (60)
4*a*	**13***a* (17), **14***b* (33)
5*a*	No reaction
6*a*	**13***b* (5)
6*c*	**17***b* (29)
7*a*	**20** (10)
8	No reaction
9	**18***a* (40), **19***a* (15)
10*a*	No reaction
11*a*	No reaction
12*a*	**18***b* (60), **19***b* (30)

The reactions of epoxides **1**–**12** with LDEA are summarized in Table 5. Products were characterized as described in the Experimental section, and hitherto unreported ^{13}C chemical shifts are listed in Table 6. The assignments were routine and relied heavily on published values for steroid substituent shift parameters (11).

The product distributions summarized in Table 5 are consistent with the proposals made earlier concerning the steric requirements for opening of epoxides (8) and also suggest the presence of a directing influence from the oxygen substituents of C-3 (see Figs. 2 and 3). Thus whereas the unsubstituted (5,6)α epoxide **3***a* gave only a Δ^6 product (**15***b*), presumably via a facile *syn* elimination involving the axial C-7α hydrogen, and the equatorial C-3β alcohol **1***a* also opened only from C-7, giving **14***a*, the corresponding C-3α alcohol **2***a*, in which coordination of base to the axial alcohol group might be expected to direct subsequent proton removal from C-4α, gave rise to both Δ^4 (**16**) and Δ^6 (**15***a*) products. The 3-ethylene ketal **3***c* gave only the 6β hydroxy-Δ^4-3-ketone **17***a* (following hydrolytic work-up) (Fig. 3).

The (5,6)β epoxides gave only low yields of allylic alcohols on treatment with LDEA. Here, none of the C-4 or C-7 hydrogens is located ideally *syn* to the epoxide oxygen; the closest to a *syn* relationship exists with that at C-4β, but the latter is also located 1,3 diaxial to the C-19 methyl group, and therefore hindered to attack by base (Fig. 3).

The unsubstituted (5,6)β epoxide **6***a* therefore gave only a low yield of Δ^4-6β-ol **13***b* and the axial C-3α alcohol **5***a* was not affected by treatment with LDEA. In the latter case, additional coordination of base to the alcohol group would not only render the reagent sterically ineffective in promoting epoxide opening, but also increase electrostatic charge on the α face of the molecule, thus making the alternative (8) *anti* removal of the C-7α hydrogen unfavourable.

It is interesting that transannular reaction leading to 3,5 oxetane formation (20), even in sterically ideal cases such as **5***a*, is not an observed pathway of reaction. The C-3β hydroxy-(5,6)β-epoxide **4***a* gave a low yield of products arising from removal of either the C-4 (**13***a*) or the C-7 (**14***b*) hydrogen. The latter product is presumably formed by *anti* removal of the axial C-7α hydrogen, a possible pathway for epoxide opening in the absence of a *syn* hydrogen (8). This route can become operative in the absence of the electrostatic charge on the α face of the molecule, which would prevent such a process occurring with epoxide **5***a* (see above). The 3-ketal **6***c* gave only a low yield

Can. J. Chem. Downloaded from www.nrcresearchpress.com by 210.87.254.40 on 09/06/12
For personal use only.

TABLE 6. ^{13}C Chemical shifts of alcohols **14**–**18**

	δ ppm						
Carbon	**14***a*	**14***b*	**15***b*	**16**	**17***a*	**18***a*	**18***b*
1	28.6	23.8	29.3	32.1	35.8	31.9	28.9
2	30.6	27.9	20.6*	27.5	33.8	22.6	22.6
3	67.2	67.4	20.2*	63.9	198.1	130.7	130.7
4	45.0	43.5	35.9	116.9	117.2	133.6	133.6
5	73.9	75.8	72.0	150.0	174.7	72.0	71.9
6	133.3	129.0	133.9*	68.8	77.1	35.1	35.1
7	133.3	133.9	132.8*	42.2	37.7	26.7	27.7
8	38.5	37.3	38.5	34.2	34.2	34.8	34.8
9	40.1	40.0	40.1	53.6	53.2	43.2	43.2
10	38.3	38.9	40.4	38.0	38.5	37.3	39.0
19	14.7	17.7	14.5	19.0	18.5	14.1	16.4

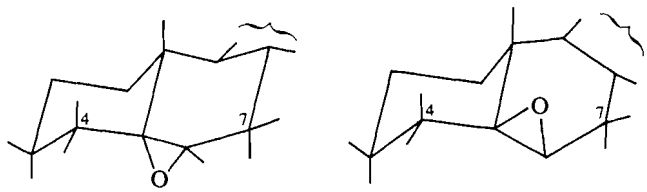

1–3 **4–6**

FIG. 3. Conformations of (5,6)α and (5,6)β epoxy steroids.

of the product of opening from C-4, **17***b*, on treatment with LDEA.

The epoxide oxygen of (4,5)α epoxy steroids (Fig. 1) does not have an ideal *syn* relationship with either the C-3α or C-6α hydrogens; the dihedral angles concerned (ca. 30° in each case) are small, however, and epoxide opening occurs from both C-3 and C-6 in the case of the unsubstituted epoxide **9**. The favoured route of opening involves loss of hydrogen from C-3, giving **18***a*; in the presence of a C-3α hydroxyl group (as in **8**), the absence of a hydrogen at C-3 *syn* to the epoxide oxygen prevents reaction from occurring. The corresponding β alcohol epoxide **7***a* opens only from C-6, a result consistent with prior coordination of base to the C-3β alcohol group: in this event, removal of the C-3α hydrogen would become electrostatically unfavourable, involving as it would the development of negative charge density at a carbon (C-3) carrying a partially ionized hydroxyl function.

Of the (4,5)β epoxides, only the unsubstituted example **12***a* was opened by LDEA. In this case, both the C-3β and C-6β hydrogens are located on the same side of the molecule as the epoxide oxygen: the predominance of the Δ^3 product **18***b* may reflect the greater accessibility of the C-3β hydrogen than that at C-6β, the latter being located 1,3 diaxially to the C-19 methyl.

The results discussed above are entirely compatible with a *syn* mechanism of β epoxide opening by LDEA, and therefore complement those of Thummel and Rickborn (8). However, the application of this reaction to the preparation of hydroxy substituted steroidal olefins would seem to be limited to those examples (e.g. **15***b*) in which a simple *syn* β elimination occurs without the complication of directing influences from existing polar substituents.

Experimental

Apparatus, materials, and methods

Melting points were determined on a Kofler heating stage and are uncorrected. Infrared spectra were recorded with a Perkin–Elmer 237B spectrometer. Proton nmr spectra were obtained at 60 MHz with a Varian A-60 or Bruker WP 60, or at 80 MHz with a Bruker WP 80 CW, and ^{13}C nmr spectra with a Bruker WP 60 or WH 400 (at the Southwestern Ontario nmr Centre, Guelph) using $CDCl_3$ as solvent and TMS as internal standard. Mass spectra were obtained with an AEI MS 30 spectrometer fitted with a Kratos DS-55 data system. Thin layer chromatography was performed on Merck silica gel 60 F-254, and column chromatography on silica gel (60–200 mesh) or alumina. Elemental analyses were performed by Guelph Chemical Laboratories, Guelph, Ontario or by Galbraith Laboratories Inc., Knoxville, Tennessee.

Preparation of epoxides

The following epoxides were prepared by published procedures and exhibited satisfactory spectral, analytical and chromatographic properties. The ^{13}C nmr data are listed in the tables. (5,6)α-Epoxy-5α-cholestan-3β-ol (**1***a*) (21); (5,6)α-epoxy-5α-cholestan-3α-ol (**2***a*) (22, 23); (5,6α)-epoxy-5α-cholestane (**3***a*) (22); (5,6α)-epoxy-5α-cholestan-3-one, 3-cyclic ethylene ketal (**3***c*) (24); (5,6β)-epoxy-5β-cholestan-3β-ol (**4***a*) (24); (5,6β)-epoxy-5β-cholestan-3α-ol (**5***a*) (23, 26); (5,6β)-epoxy-5β-cholestan-3-one, 3-cyclic ethylene ketal (**6***c*) (24); (4,5α)-epoxy-5α-cholestan-3β-ol (**7***a*) (27, 28); (4,5α)-epoxy-5α-cholestane (**9**) (22); (4,5β)-epoxy-5β-cholestan-3β-ol (**10***a*) (12, 27, 28); (4,5β)-epoxy-5β-cholestan-3α-ol (**11***a*) (12, 28, 29); (4,5β)-epoxy-5β-cholestane (**12***a*) (22); and (4,5β)-epoxy-5β-cholestan-3-one (**12***b*) (12).

*(5,6β)-Epoxy-5β-cholestane (**6**b)*

This was prepared by the procedure of Watabe *et al.* (30); in our hands, the results outlined below were obtained.

A solution of *N*-bromosuccinimide (2.35 g) in perchloric acid (20 mL, 5%), was added over 30 min to a stirred solution of cholest-5-ene (2.22 g) (31) in THF (90 mL) at room temperature. The mixture was stirred for an additional 30 min, then diluted with chloroform (150 mL), neutralized (5% potassium carbonate), and saturated with sodium chloride. The organic layer was separated, washed, dried, and evaporated. The residue was then dissolved in methanol (60 mL) containing sodium hydroxide (3 g), and the solution refluxed for 30 min. Evaporation then gave a residue which was dissolved in chloroform to give a solution which was then washed, dried, and evaporated to a residue which was chromatographed (silica) using hexane–benzene gradient elution and afforded 5,6β-epoxy-5β-cholestane (**6***a*), (1.08 g), mp 53–55°C (lit. (27) mp 55–57°C). Further elution gave 5α-cholestan-5-ol-6-one (0.3 g), mp 150–152°C (lit. (32) mp 152–153°C), followed by 5α-cholestane-5, 6β-diol (0.09 g), mp 121–124°C (lit. (33) mp 125.5°C).

*(4,5α)-Epoxy-5α-cholestan-3α-ol (**8**)*

A solution of *m*-chloroperoxybenzoic acid (0.8 g) in methylene chloride (20 mL) was added to a solution of cholest-4-en-3α-ol (34) in methylene chloride (20 mL), and the resulting mixture kept at 0°C

Can. J. Chem. Downloaded from www.nrcresearchpress.com by 210.87.254.40 on 09/06/12
For personal use only.

Can. J. Chem. Downloaded from www.nrcresearchpress.com by 210.87.254.40 on 09/06/12
For personal use only.

for 20 h. The solution was then washed (sodium bicarbonate), dried, and evaporated to give noncrystalline **8**. Crystallization from methanol gave a sample of mp 92–94°C (lit. (35) mp 91–92°C).

Preparation of epoxyesters

The epoxyesters listed below were prepared by standard procedures from the corresponding alcohols, and gave satisfactory spectral and analytical data:

1*b*, **2***b* (23), **4***b* (25), **5***b* (36), **7***b* (28), **10***b* (37), **10***c* (37), and **11***b* (38).

Treatment of epoxides with potassium tert*-butoxide*

A solution of potassium *tert*-butoxide in *tert*-butyl alcohol (100 mL, 0.06 *M*) was added to a solution of the steroidal epoxide (0.1 g) in ether or THF (10 mL), and the resulting mixture refluxed under an atmosphere of dry nitrogen. After three days, the steroid was re-isolated following the addition of water and a conventional work-up. The following were obtained unchanged from this procedure: **1***a*, **2***a*, **3***a*, **3***c*, **4***a*, **5***a*, **6***a*, **6***c*, **7***a*, **8**, **9**, **10***a*, **11***a*, and **12***a*.

Treatment of epoxides with LDA

Diisopropylamine (0.8 mL) was added over 15 min to a solution of methyl lithium (3.3 mL, 1.56 *M* in ether) in dry THF (100 mL) at −20°C. The resulting mixture was stirred at −20°C for an additional 15 min and then cooled to −78°C. A solution of epoxide (0.1 g) in THF (5 mL) was then added. The reaction mixture was stirred at −78°C for 12 h, after which time the temperature was allowed to come to −10°C, and then stirring was continued for an additional 3 days. Butanol (2 mL) was then added, and the mixture neutralized (1 *M* HCl), diluted with water, and extracted with chloroform. After isolation in the conventional way, the following epoxides were obtained unreacted by the above procedure: **1***a*, **2***a*, **3***a*, **3***c*, **4***a*, **5***a*, **6***a*, **6***c*.

Treatment of epoxides with LDEA

The following general procedure was used. LDEA was generated as described above from diethyl amine (2.0 mL) and *n*-butyl lithium (5.16 mL, 2.4 *M* in hexane) in ether solution (100 mL). A solution of the epoxide (0.3 g) in THF (5 mL) was then added at −15°C, and the resulting mixture heated under reflux. Water (10 mL) was then added dropwise, and the resulting mixture washed with saturated ammonium chloride solution. Chloroform was then added, and the solution washed further (water), dried (sodium sulphate), and evaporated. Previously unpublished ^{13}C nmr data for the products described below are listed in the tables. All the compounds listed below also gave satisfactory ^{1}H nmr and mass spectral data. Yields refer to isolated, purified material. No significant amounts of other products were detected by tlc.

*(5,6α)-Epoxy-5α-cholestan-3β-ol (1*a*)*

Treatment of **1***a* as described above with LDEA for 24 h gave a residue which was chromatographed (neutral alumina) to give cholest-6-ene-3β,5α-diol (**14***a*) (56%) as the only product, mp 146–150°C (from methanol) (lit. (39) mp 147–150°C).

*(5,6α)-Epoxy-5α-cholestan-3α-ol (2*a*)*

The residue from treatment of **2***a* with LDEA for 3 days was crystallized from ethyl acetate – hexane to give cholest-4-ene-3α,6α-diol (**16**) (19%), mp 191–193°C (lit. (40) mp 189–191°C). Chromatography of the mother liquor (silica gel, gradient elution from chloroform to ethyl acetate) gave **2***a* (25%) followed by cholest-6-ene-3α,5α-diol (**15***a*) (18%), mp 146–149°C (from hexane). M^+ calcd. for $C_{27}H_{46}O_2$: 402.349; found: 402.346. R_f's: ethyl acetate, 0.55; 5% methanol/chloroform, 0.37; ether, 0.75.

*(5,6α)-Epoxy-5α-cholestane (3*a*)*

Crystallization from ethyl acetate – hexane of the residue from a 1 h reaction of **3***a* with LDEA gave 5α-cholest-6-en-5α-ol (**15***b*) (72%), mp 86°C. M^+ calcd. for $C_{27}H_{46}O$: 386.348; found: 386.354. R_f's: ether, 0.9; ethyl acetate, 0.65; 5% methanol/chloroform, 0.65.

*(5,6α)-Epoxy-5α-cholestan-3-one, 3-cyclic ethylene ketal (3*c*)*

Chromatography of the residue from a 3 day reaction of **3***c* with LDEA (silica gel, benzene–ether gradient elution), afforded cholest-4-en-6α-ol-3-one (**17***a*) (60%), identical in all respects with an authentic sample.

*(5,6β)-Epoxy-5β-cholestan-3α-ol (4*a*)*

The residue from treatment of **4***a* with LDEA for 3 days was dissolved in hexane and allowed to stand at 0°C, whereupon cholest-4-ene-3β,6β-diol (**13***a*) (17%) was obtained, identical in all respects with an authentic sample. The mother liquor was chromatographed (neutral alumina, hexane to ether gradient elution) and gave 5β-cholest-6-ene-3β,5β-diol (**14***b*) (33%), mp 137–140°C (lit. (41) mp 139–140°C).

*(5,6β)-Epoxy-5β-cholestan-3α-ol (5*a*)*

Treatment of **5***a* with LDEA for 3 days resulted in the recovery of starting material (75%) as the only identifiable steroid.

*(5,6β)-Epoxy-5β-cholestane (6*a*)*

Treatment of **6***a* with LDEA for 3 days gave a residue from which only **6***a* (85%) and cholest-4-en-6β-ol (**13***b*) (5%) (identical with an authentic sample (42)) were obtained.

*(5,6β)-Epoxy-5β-cholestan-3-one, 3-cyclic ethylene ketal (6*c*)*

The residue from treatment of **6***c* with LDEA for 3 days was chromatographed (silica, chloroform to ethyl acetate gradient elution) to give cholest-4-en-6β-ol-3-one (**17***b*) (29%) as the only identifiable steroid, identical in all respects with an authentic sample.

*(4,5α)-Epoxy-5α-cholestan-3β-ol (7*a*)*

Chromatography of the residue from a three day reaction of **7***a* with LDEA (neutral alumina, hexane to ether gradient elution) gave **7***a* (50%), followed by cholest-5-ene-3β,4α-diol (**20**) (10%), mp 216–219°C (from aqueous methanol) (lit. (43) mp 223°C from acetone).

(4,5α)-Epoxy-5α-cholestan-3α-ol (8)

Treatment of **8** with LDEA for three days gave no detectable reaction products (tlc).

(4,5α)-Epoxy-5α-cholestane (9)

The residue from a three day reaction of **9** with LDEA was chromatographed (neutral alumina, hexane to ether gradient elution) to give 5α-cholest-3-en-5α-ol (**18***a*) (40%), mp 79–80°C (from aqueous acetone) (lit. (44) mp 75–76°C), followed by cholest-5-en-4α-ol (**19***a*) (15%), mp 140–142°C (from acetone–pentane) (lit. (45) mp 144–145°C).

*(4,5β)-Epoxy-5β-cholestan-3β-ol (10*a*) and (4,5)β-epoxy-5β-cholestan-3-α-ol (11*a*)*

Treatment of **10***a* or **11***a* with LDEA for three days resulted in the recovery of unreacted starting materials only.

*(4,5β)-Epoxy-5β-cholestane (12*a*)*

The residue from a three day reaction of **12***a* with LDEA was dissolved in ether, passed through a short column of neutral alumina, and then subjected to preparative tlc (silica gel, hexane–ether, 1:1). The band of higher R_f was identified as cholest-5-en-4β-ol (**19***b*) (30%), mp 128–130°C (from aqueous methanol) (lit. (43) mp 131–132°C) and the other as 5β-cholest-3-en-5β-ol (**18***b*) (60%), mp 90–92°C (from aqueous methanol) (lit. (45) mp 89–91°C).

Acknowledgements

Financial support was supplied by the Natural Sciences and Engineering Research Council of Canada. We are grateful to Mr. T. Jones for his assistance in obtaining spectral data, and to the staff of the Southwestern Ontario nmr centre, University of Guelph, for their help in obtaining ^{1}H and ^{13}C nmr spectra.

1. H. Nozaki, T. Mori, and R. Noyori. Tetrahedron, **22**, 1207 (1966).
2. E. H. Eschinasi. Israel J. Chem. **6**, 713 (1968).

3. C. C. PRICE and D. D. CARMELITE. J. Am. Chem. Soc. **88**, 4039 (1966).
4. A. C. COPE and J. K. HEEREN. J. Am. Chem. Soc. **87**, 3125 (1965).
5. J. K. WHITESELL and P. D. WHITE. Synthesis, 602 (1975).
6. D. H. R. BARTON and Y. HOUMINER. J. Chem. Soc. Perkin Trans. 1, 919 (1972).
7. P. B. D. DE LA MARE and R. D. WILSON. J. Chem. Soc. Perkin Trans. 2, 975 (1977).
8. R. P. THUMMEL and B. RICKBORN. J. Org. Chem. **36**, 1365 (1971).
9. B. RICKBORN and R. P. THUMMEL. J. Org. Chem. **34**, 3582 (1969).
10. H. L. HOLLAND, P. R. P. DIAKOW, and G. J. TAYLOR. Can. J. Chem. **56**, 3121 (1978).
11. J. W. BLUNT and J.B. STOTHERS. Org. Magn. Reson. **9**, 439 (1977).
12. H. L. HOLLAND, E. RIEMLAND, and U. DAUM. Can. J. Chem. **60**, 1919 (1982).
13. D. LIEBFRITZ and J. D. ROBERTS. J. Am. Chem. Soc. **95**, 4996 (1973).
14. J. K. CRANDALL and L.-H. LIN. J. Org. Chem. **32**, 435 (1967); **32**, 532 (1967).
15. J. K. CRANDALL and L.-H. LIN. J. Org. Chem. **33**, 2375 (1968).
16. A. C. COPE, H.-H. LEE, and H. E. PETREE. J. Am. Chem. Soc. **80**, 2849 (1958).
17. E.-I. NEGISH. *In* Organometallics in organic synthesis. Vol. 1. John Wiley, New York. 1980. p. 100.
18. D. DE KEUKELEIRE, H. DE WILDE, F. VERZELE, W. WYFFELS, and M. VANDEWALLE. Bull. Soc. Chim. Belg. **88**, 79 (1979).
19. C. K. KISSEL and B. RICKBORN. J. Org. Chem. **37**, 2060 (1972).
20. T. MASAMUNE, S. SATO, A. ABIKO, M. ONO, and A. MURAI. Bull. Chem. Soc. Jpn. **53**, 2895 (1980).
21. L. F. FIESER and M. FIESER. Reagents for organic synthesis. Vol. 1. Wiley, New York. 1967. p. 136.
22. Y. HOUMINER. J. Chem. Soc. Perkin Trans 1, 1663 (1973).
23. M. MOUSSERON-CANET and J.-C. GUILLEUX. Bull. Soc. Chim. Fr. 3853 (1966).
24. D. J. COLLINS, C. M. HORN, and V. J. WECKER. Aust. J. Chem. **29**, 2077 (1976).
25. S. G. LEVINE and M. E. WALL. J. Am. Chem. Soc. **81**, 2826 (1959).
26. P. TSUI and G. JUST. Can. J. Chem. **51**, 3502 (1973).
27. D. J. COLLINS. Aust. J. Chem. **16**, 658 (1963).
28. H. B. HENBEST and R. A. WILSON. J. Chem. Soc. 1958 (1957).
29. D. J. COLLINS. J. Chem. Soc. 3919 (1959).
30. T. WATABE, M. KANAI, M. ISOBE, and N. OZAWA. J. Biol. Chem. **256**, 2900 (1981).
31. R. B. TURNER, W. R. MEADER, and R. E. WINKLER. J. Am. Chem. Soc. **79**, 4122 (1957).
32. H. REICH, F. E. WALKER, and R. W. COLLINS. J. Org. Chem. **16**, 1753 (1951).
33. L. RUZICKA and G. THOMANN. Helv. Chim. Acta, **16**, 216 (1933).
34. R. SCHOENHEIMER and E. A. EVANS. J. Biol. Chem. **114**, 567 (1936).
35. E. GLOTTER, P. KRINSKY, M. REJTO, and M. WEISSENBERG. J. Chem. Soc. Perkin Trans 1, 1442 (1976).
36. H. L. HOLLAND and JAHANGIR. J. Org. Chem. In press.
37. R. LORNE and S. JULIA. Bull. Soc. Chim. Fr. 1357 (1973).
38. P. A. PLATTNER, H. HEUSER, and A. B. KULKARNI. Helv. Chim. Acta, **31**, 1822 (1948); **31**, 1885 (1948).
39. A. NICKON and J. F. BAGLI. J. Am. Chem. Soc. **83**, 1498 (1961).
40. P. KOCOVSKY and V. CERNY. Collect. Czech. Chem. Commun. **42**, 2415 (1977).
41. V. PRELOG, L. RUZICKA, and P. STEIN. Helv. Chim. Acta, **26**, 2222 (1943).
42. A. NICKON and W. L. MENDELSON. Can. J. Chem. **43**, 1419 (1965).
43. L. F. FIESER and R. STEVENSON. J. Am. Chem. Soc. **76**, 1728 (1954).
44. P. S. WHARTON and D. H. BOHLEN. J. Org. Chem. **26**, 3615 (1961).
45. D. N. JONES, J. R. LEWIS, C. W. SHOPPEE, and G. H. R. SUMMERS. J. Chem. Soc. 2876 (1955).

Can. J. Chem. Downloaded from www.nrcresearchpress.com by 210.87.254.40 on 09/06/12
For personal use only.

On the reaction of furan with bromine in aqueous solution. Observation of the slow hydration of malealdehyde

OSWALD S. TEE[1] AND B. E. SWEDLUND[2]

Department of Chemistry, Concordia University, 1455 de Maisonneuve Ouest, Montreal, P.Q., Canada H3G 1M8

Received February 2, 1983

OSWALD S. TEE and B. E. SWEDLUND. Can. J. Chem. **61**, 2171 (1983).

The rate of reaction of furan with bromine in aqueous solution has been measured and the rate constant obtained by Williamson and Coller is confirmed. However, it is now found that the reaction of bromine with furan in water has two distinct stages: attack of bromine leading to the formation of malealdehyde **3** and hydration of **3** to a 2:1 mixture of the geometrical isomers of its cyclic hydrate **4**. This second, slower process is observable by stopped-flow uv spectrophotometry occurring after the consumption of bromine. The observed kinetics are very similar to those recently found for the analogous hydration of phthalaldehyde by McDonald and Martin.

OSWALD S. TEE et B. E. SWEDLUND. Can. J. Chem. **61**, 2171 (1983).

On a mesuré la vitesse de la réaction du furanne avec le brome en solution aqueuse et on a confirmé la constante de vitesse obtenue par Williamson et Coller. Cependant on trouve maintenant que la réaction du brome avec le furanne dans l'eau a deux étapes distinctes: l'attaque du brome qui conduit à la formation du maléaldéhyde **3** et l'hydratation du composé **3** qui conduit à un mélange 2:1 des isomères géométriques de son hydrate cyclique **4**. Ce second processus, le plus lent, peut être observé par la spectrophotométrie uv à flux stoppé que l'on utilise après la disparition du brome. Les cinétiques observées sont semblables à celles trouvées récemment pour l'hydratation analogue du phthalaldéhyde par McDonald et Martin.

[Traduit par le journal]

Can. J. Chem. Downloaded from www.nrcresearchpress.com by 210.87.254.40 on 09/06/12
For personal use only.

The halogenation of furans is complex with the nature of products varying widely with the substrate, reagent, solvent, and reaction conditions (1–4). However, two broad classes of reaction may be recognized, viz. addition and substitution, with the former often leading to ring-opening (1–4).

Bromination of furan in CCl_4 gives a mixture of 2-bromo- and 2,5-dibromofuran (5). Using ^{1}Hmr spectroscopy, Baciocchi *et al.* (6) observed the formation of 1,4- and 1,2-dibromo adducts from furan and bromine in the non-nucleophilic solvent carbon disulphide, at low temperature. With time, and on warming, the adducts underwent elimination to 2-bromofuran (6).

In hydroxylic solvents the reaction of furan (**1**) follows a different course. With bromine (or chlorine) in an alcohol solvent at low temperatures, reaction leads to the formation of a

[1] 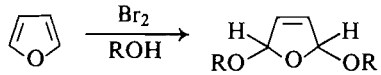

1 **2**

2,5-dialkoxy-2,5-dihydro derivative, **2** (7, 8). Similarly, in acetic acid containing potassium acetate, the corresponding diacetoxy compound **2** (R = Ac) is obtained (9). Recently, Williamson and Coller studied the reaction of furan with bromine, generated electrochemically, in aqueous solution (10).

[2] 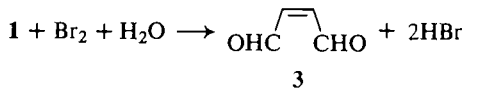

3

They diagnosed the product as being butenedial **3** (malealdehyde), eq. [2], on the basis of being able to form its bis-phenylhydrazone from the product mixture. They also measured the rate of reaction of bromine with furan using a coulochronopotentiometric method (10).

In contrast to these results, Linda and Marino (11) reported

[3] 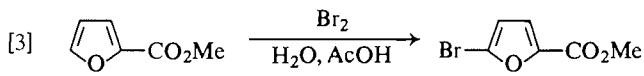

that bromination of methyl furoate in 50% aqueous acetic acid gives the substitution product, eq. [3], the same product as can be obtained under other reaction conditions (12).

We have begun to study the bromination of furans systematically to try to ascertain why some derivatives undergo addition, whereas others show substitution. Our initial approach to this problem was to study the effect of substituents and solvents upon the rate of bromination.[3,4] To anchor a correlation of results for aqueous solution a reliable value for furan was required.[5] During measurement of this value we found that another, slower process is observable, which is the subject of the present paper.

Results

Kinetic studies

We first measured the second-order rate constant (k_2) for the reaction of bromine with furan in aqueous solution. We found $k_2 = 1.4 \times 10^6\ M^{-1}\ s^{-1}$ (25°C, $I = 0.1\ M$ (KBr)), as measured by the stopped-flow uv method (13–15). This value is in reasonable agreement with $k_2 = 1.8 \times 10^6\ M^{-1}\ s^{-1}$ (25°C, extrapolated[6] to $I = 0$), obtained electrochemically by Williamson and Coller (10).

While we were carrying out the above measurement we observed that the final absorbance value slowly drifted downwards, suggesting a second, slower process occurring after the

[1]Author to whom correspondence may be addressed.

[2]Permanent address: Department of Chemistry, University of Auckland, Private Bag, Auckland, New Zealand.

[3]E. Ostrowski-Janik (Honours Thesis, Concordia University, 1981) studied 2-furoic acid, its anion, and methyl 2-furoate in aqueous solution.

[4]L. Bloomfield (Honours Thesis, Concordia University, 1981) studied furan, 2-furoic acid, methyl 2-furoate, and thiophene in 50% aqueous acetic acid.

[5]The second-order rate constant obtained by Williamson and Coller seemed high on the basis of the correlation line defined by Janik's results for substituted furans.[3]

[6]Measurements were made in 2–5 *M* aqueous KBr and then linearly extrapolated to zero concentration (10).

Can. J. Chem. Downloaded from www.nrcresearchpress.com by 210.87.254.40 on 09/06/12
For personal use only.

TABLE 1. Effect of concentration changes on k_{obs} for intermediate disappearance, at 25°C

pH	$[\mathbf{1}]\times10^4$ (M)	$[Br_2]\times10^4$ (M)	Medium[a]	k_{obs} (s^{-1})
3.12	5.0	5.0		0.643
	5.0	10.0		0.643
5.20	5.5	0.48		0.153
	2.2	1.9		0.149
5.19	5.0	5.0	0.1 M $NaClO_4$	0.148
5.16	5.0	5.0	1.0 M KBr	0.0992
5.28	5.0	5.0	1.0 M $NaClO_4$	0.0847
4.49	5.0	5.0	[Buffer] = 0.005 M	0.156
			= 0.010 M	0.161
			= 0.015 M	0.165
			= 0.020 M	0.171
4.46	5.0	5.0	50% Dioxane	0.0297

[a]Supporting medium is 0.1 M KBr, [buffer] = 0.01 M, except where noted otherwise.

TABLE 2. pH Dependence of k_{obs} for the disappearance of the intermediate[a]

pH	$k_{obs}(s^{-1})$	$k_{cal}(s^{-1})$[b]	log k_{obs}
1.27[c]	39.2	35.4	1.593
2.14[c]	4.46	4.90	0.649
3.12	0.643	0.638	−0.192
3.98[d]	0.199	0.209	−0.701
4.49	0.161	0.162	−0.793
5.09	0.157	0.147	−0.804
5.30	0.147	0.146	−0.833
5.86	0.151	0.149	−0.821
6.54	0.175	0.179	−0.757
7.12	0.247	0.286	−0.607
7.30[e]	0.401	0.362	−0.397
7.57[e]	0.568	0.552	−0.246

[a]At 25°C. I = 0.1 M (KBr). Total buffer concentration = 0.01 M. Normally $[\mathbf{1}]_0 = [Br_2]_0 = 5 \times 10^{-4}$ M, but values not critical (see text).

[b]Calculated from eq. [4] using the parameters given in the text.

[c]Using $HClO_4$ + NaBr, due to low solubility of $KClO_4$.

[d]$[\mathbf{1}]_0 = 5.5 \times 10^{-4}$ M, $[Br_2]_0 = 4.8 \times 10^{-5}$ M.

[e][Buffer] = 0.02 M.

consumption of bromine. This behaviour is most evident at 230−240 nm. At these wavelengths there is a sizeable absorption which appears on the side of the large absorption at 200−220 nm due to the various other species in solution. Monitoring the disappearance of the transient absorption gave excellent first-order kinetics, and appropriate rate constants (k_{obs}) were obtained in the normal way (14).

Table 1 shows values of k_{obs} found under various conditions; Table 2 and Fig. 1 show how k_{obs} varies with pH. The rate is essentially invariant in the pH region 4.5−6, and so most of the data in Table 1 pertain to this region.

The value of k_{obs} is unaffected by the initial concentration of furan or bromine (Table 1). Moreover, the same value is obtained in 0.1 M $NaClO_4$ as in 0.1 M KBr. In addition, the intensity of the initial absorbance at 240 nm varies in proportion to the concentration of the limiting reagent, be it furan or bromine. These observations are all consistent with the transient absorption being due to an intermediate which is formed rapidly and essentially irreversibly from furan and bromine.

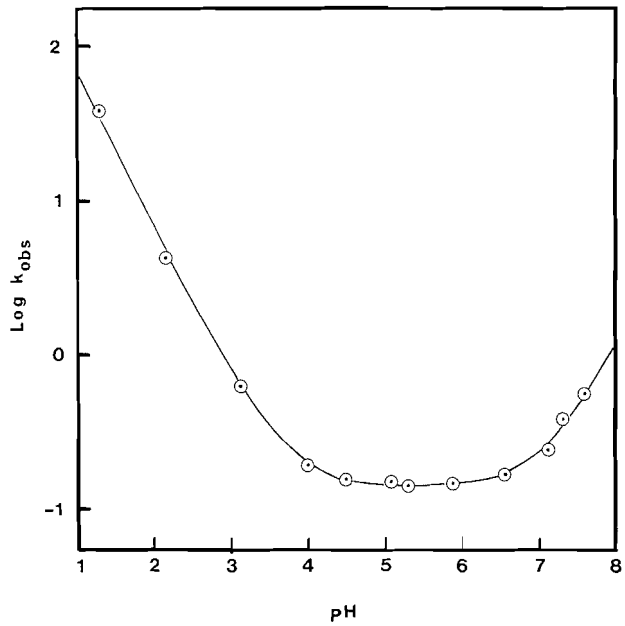

FIG. 1. The pH−rate profile for disappearance of the intermediate. Data in Table 2.

Increasing the ionic strength with KBr or $NaClO_4$ causes similar reductions in rate (Table 1). These experiments are evidence against the intermediate being a bromo species undergoing solvolysis (*vide infra*). The observation that k_{obs} is reduced (0.15 to 0.03 s^{-1}) in 50% aqueous dioxane is not inconsistent with water being involved in the process being followed.

The pH−rate profile (Fig. 1)[7] can be described by eq. [4] with $k_0 = 0.140$ s^{-1}, $k_H = 657$ M^{-1} s^{-1}, and $k_{OH} = 1.11 \times 10^6$ M^{-1} s^{-1}.

$$[4] \quad k_{obs} = k_H[H^+] + k_0 + k_{OH}[OH^-]$$

Furthermore, the reaction is subjected to buffer catalysis. Data obtained at pH 4.49 (Table 1) show that increasing the buffer (acetic acid/acetate) concentration causes a linear increase in k_{obs} (intercept = 0.151 s^{-1}, slope = 0.980 M^{-1} s^{-1}, r = 0.997). Likewise, on the basic side of the profile, values of k_{obs} (not shown) obtained at [buffer] = 0.08 M fall above those shown in Fig. 1.[8] Given then that buffer catalysis occurs, the values of k_0, k_H, and k_{OH} quoted above may be somewhat elevated. However, since the data on which they are based were obtained at low buffer concentration, the elevation is probably no more than 10−20%.

Product studies

Using normal titrimetric methods, we confirmed that the 1:1 reaction of furan with bromine in water does indeed produce two mole equivalents of hydrobromic acid, as required by eq. [3] (10). There is a reaction with a second equivalent of bromine, but it occurs much more slowly.

Proton nmr analysis of reaction mixtures was most re-

[7]Below pH 1 the rate of disappearance of the intermediate approaches that of bromine attack on furan. Above pH 5 the rate of bromination decreases due to the formation of HOBr (15). Around pH 8 this reduction begins to interfere with the process of interest. These factors limit the pH range accessible for the rate profile.

[8]For example, at pH = 7.42, [buffer] = 0.08 M, we found k_{obs} = 0.84, whereas interpolating between the last two points in Table 2 gives k_{obs} = 0.47.

vealing. We observed only two major signals not arising from the medium: a broadened singlet at δ 6.20 and a fairly sharp singlet at δ 5.90, with integrated areas in the ratio of about 2:1. These peaks are not attributable to malealdehyde **3**, which should give two doublets of equal intensity at about δ 10.3 and 6.5 (16). They can, however, be explained by a mixture of the *cis* and *trans* isomers (**4***c*, **4***t*) of the cyclic hydrate of **3**. The sharp singlet at δ 5.90 is assigned to the methine protons of the *cis* isomer **4***c*. The broadened larger peak at δ 6.20 is attributed

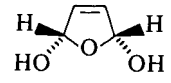

4*c*

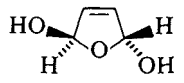

4*t*

to the vinylic protons of **4***c* and to the methine *and* vinylic protons of the *trans* isomer **4***t*. A 2:1 mixture of **4***c* and **4***t* then gives rise to the observed peak ratios.

These assignments are supported by experiments we have carried out, as well as by the nmr spectra of many derivatives of the general type **2** observed by earlier workers (6, 17–21). In general, the methine protons of *cis* adducts appear upfield of those of the *trans* (6, 17–21). The position of both these types relative to the vinylic protons varies depending upon the particular structure and the solvent (17, 18). Often, however, the vinylic protons of the geometrical isomers are essentially coincident (17, 18, 20). For comparative purposes, Table 3 shows data we have obtained, together with that for three closely related cases from the literature.

For the dimethoxy compound **2** (R = Me), which exists as a 7:3 mixture of the *cis* and *trans* isomers (17), we find that in D_2O the vinyl protons of both isomers are at δ 6.20, the *cis* methine protons at δ 5.71, and the *trans* methine protons at δ 6.02. In CCl_4 the same relative peak positions are maintained, but signals are shifted upfield by ~0.2 ppm (17). Table 3 also contains data for the diacetoxy isomers **2** (R = Ac) and the cyclic hydrates **5**. The last (**5**) were prepared by anodic oxidation[9] of 3,4-diethylfuran in acetonitrile containing saturated aqueous sodium bicarbonate (19). The methine protons of the two isomers of **5** appear as broadened singlets at δ 5.71 and 6.05 (19).

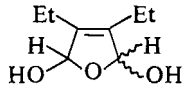

5

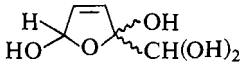

6

We also observed the hydrolysis of the dimethoxy compounds **2** (R = Me) in D_2O containing a few drops of DCl. The peaks due to **2** (R = Me) gradually diminish and eventually a stage is reached in which the hydrates **4** predominate. However, there are other signals in the same area attributable to partial hydrolysis (**2** with one hydroxyl and one methoxyl). Presumably, at the concentration of **2** used, there is insufficient driving force for total conversion to the hydrates **4**.

As a final point supporting the assignment of **4**, we note that the isomeric hydrates **6** have been observed (by nmr) among the products obtained from the reaction of furfural (furan-2-carboxaldehyde) with aqueous bromine (22).

Discussion

From the evidence just presented it seems clear that the stoichiometry of the 1:1 reaction of furan with bromine in water is as shown in eq. [5]. The organic product is the cyclic hydrate **4**, which is formed as a 2:1 mixture of the *cis* and *trans*

[5] $\mathbf{1} + Br_2 + 2H_2O \longrightarrow \mathbf{4} + 2HBr$

isomers (**4***c*, **4***t*). Thus the overall reaction in water is completely analogous to the reaction in methanol, eq. [1], which produces a similar 7:3 mixture of diastereomers (17), and to the reaction in acetic acid (9).

The conclusion of Williamson and Coller that the product is malealdehyde was based upon the isolation of an appropriate derivative (10). This result in no way conflicts with our conclusion that the product is **4**, since it is well-known that the hydration of aldehydes is sufficiently reversible that free aldehyde can be trapped by suitable reagents (23).

Initially we made another observation which appears at variance with **4** being the reaction product. As noted above, there is reaction with a second equivalent of bromine, but it is very slow. At first glance one expected the CC double bond of **4** to be fairly reactive towards bromine, whereas, of course, that of malealdehyde should be quite unreactive.[10] However, we find that the dimethoxy compound **2** (R = Me) also reacts only slowly with bromine. Clearly then, the oxygens of **2** and **4** substantially reduce the reactivity of their double bonds, compared to what is normal for an alkene (24, 25). Presumably this is due to the combined inductive effects of all three oxygens.

We now consider the nature of the process that can be observed by uv spectrophotometry and for which we have obtained kinetic data. We believe this to be the relatively slow hydration of malealdehyde to produce the hydrates **4** (eq. [6]).

[6] 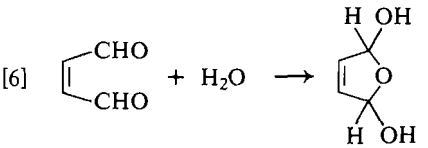

3 **4**

The strong transient absorption observed below 245 nm is consistent with the intermediacy of malealdehyde (20, 26). Moreover, other potential intermediates are insufficiently conjugated to absorb significantly above 220 nm. However, the strongest evidence for the process in eq. [6] is the similarity of

TABLE 3. Proton chemical shifts for cyclic hydrates and cyclic acetals

Compound	Isomer	Solvent	δ (ppm) Methine	δ (ppm) Vinylic	Ref.
4	*cis*	D_2O	5.90	6.20	[a]
	trans		6.20	6.20	
2(R = Me)	*cis*	D_2O	5.71	6.20	[a]
	trans		6.02	6.20	
	cis	CCl_4	5.54	5.99	17
	trans		5.74	5.99	
2(R = Ac)	*cis*	CCl_4	6.58	6.12	18
	trans		6.80	6.12	
5	*cis*	$CDCl_3$	5.71	—	19
	trans		6.05	—	

[a]This work.

[9]Anodic oxidation of furans in hydroxylic media is the other principal route to compounds of type **2** (4, 19, 20, and refs. therein).

[10]Diethyl fumarate reacts very slowly with aqueous bromine (24). Malealdehyde should be less reactive still.

Can. J. Chem. Downloaded from www.nrcresearchpress.com by 210.87.254.40 on 09/06/12
For personal use only.

TABLE 4. Catalytic constants for the hydration of malealdehyde **3** and phthalaldehyde **7**

Constant	**3**[a]	**7**[b]	Ratio
k_0 (s^{-1})[c]	0.140	5.6×10^{-3}	25
k_H (M^{-1} s^{-1})	657	70	9.4
k_{OH} (M^{-1} s^{-1})	1.11×10^6	7.9×10^4	14
k_{AcOH} (M^{-1} s^{-1})	0.98[d]	0.044	22

[a]At 25°C, I = 0.1 M.
[b]At 28°C, I = 1.0 M, from ref. 27.
[c]Following McDonald and Martin, we take this to be due to water acting as a general base (27).
[d]Approximate value based on one series of measurements at pH 4.49 (Table 1).

our kinetic results to those of McDonald and Martin (27). They recently reported a thorough study of the analogous hydration of phthalaldehyde **7** to its cyclic hydrate **8**, eq. [7]. Our rate

[7] 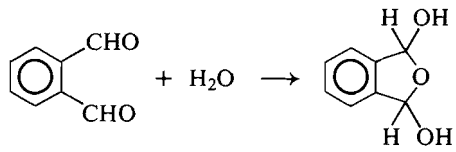

7 **8**

profile (Fig. 1) is very similar to theirs (Fig. 5, ref. 27), but it is displaced vertically since the process we have followed is about 15 times faster. Correspondingly, the catalytic constants for the two studies are quite similar (Table 4), with those from the present work being 9–25 times larger.

It seems reasonable that the rate constants for the hydration of **3** should be somewhat greater than those for the hydration of **7**. In malealdehyde the transmission of the conjugative effect from one formyl group to the other occurs through a simple CC double bond. In phthalaldehyde the corresponding transmission is through a benzene ring that is stabilized by aromaticity. Accordingly, the transmission of the conjugative effects in **7** may be attenuated relative to that in **3**, and the rate constants for **7** thus be somewhat smaller. A further point which supports these arguments concerns the position of the hydration equilibrium. McDonald and Martin observed 10% free phthalaldehyde in equilibrium with its hydrate **8**. In contrast, we observe no appreciable free malealdehyde in equilibrium with its hydrate **4**. This is also consistent with the view that the formyl groups of malealdehyde exert a stronger influence on one another than those in phthalaldehyde.

Mechanisms

The observations and the kinetic results obtained in the present study clearly point to the reaction of bromine with furan in water having two distinct stages (eq. [8]): attack of bromine leading to the formation of malealdehyde **3** and hydration of **3** to the cyclic hydrate **4**.

[8] **1** $\xrightarrow[-2HBr]{Br_2,H_2O}$ **3** $\xrightarrow{H_2O}$ **4**

The sequence of steps involved in the formation of **3** are probably those shown in Scheme 1. Attack of bromine upon furan gives a transient cation **9** which is captured by water to produce the 2-bromo-5-hydroxy adduct **10**.[11] Ionization of this

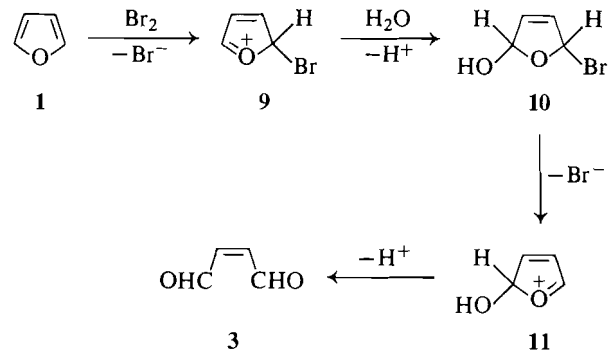

1 **9** **10** **3** **11**

SCHEME 1

intermediate should be facile since it is an allylic bromide and an α-bromo ether, and the process leads to the delocalized cation **11**. Proton loss and CO bond cleavage, probably concerted, then converts **11** into malealdehyde **3**.

In an alcohol solvent a similar sequence of steps presumably takes place, except that the alkoxy cation analogous to **11** is captured by solvent to give the product **2**. At the outset we favored such a mechanism for the reaction in water, expecting that the cation **11** would be captured by solvent to give the hydrate **4**, which subsequently equilibrated with malealdehyde **3**. However, our results are much more consistent with **3** being formed first and equilibration with **4** occurring second.[12]

The steps involved in the hydration of malealdehyde are presumably analogous to those for phthalaldehyde hydration (27). On the basis of buffer catalysis studies, McDonald and Martin argued convincingly that the slow step involves hydration of one formyl group and that the subsequent cyclization is relatively fast (27). Since the catalytic constants we have obtained are all elevated to a similar extent relative to those for phthalaldehyde hydration (Table 4), the Bronsted α and β for malealdehyde hydration must be similar.[13] It seems reasonable, therefore, to postulate that malealdehyde hydration likewise involves rate-limiting hydration of one formyl group, followed by fast cyclization (Scheme 2). The slow step may be either general acid- or general base-catalyzed (Scheme 2), as indicated by the kinetic results, and as is normal for aldehyde hydration (23, 28).

Experimental

Furan (Aldrich) was distilled before use. 2,5-Dihydro-2,5-dimethoxyfuran (**2**, R = Me) (Aldrich) was used as received. Solutions (buffers, bromine, etc.) used in kinetics experiments were as in other recent work (13–15, 29).

Ultraviolet spectral measurements were made with Unicam SP 800 and Aminco DW-2 spectrophotometers. The proton nmr spectra re-

[11]Several authors have written the reaction in alcoholic solvents as involving a 2,5-dibromo adduct, analogous to **10** (e.g. ref. 22). It seems more likely to us that the cation **9** is largely captured by solvent in nucleophilic solvents, such as water and methanol (7).

[12]As a referee has pointed out, we cannot exclude the partitioning of the intermediate cation **11** since the actual concentration of malealdehyde **3** is unknown. If the capture of **11** by water (to give hydrates **4**) is similar in rate to the ring-opening (**11** → **3**), then a significant proportion of **4** may be formed directly. In this case the observed kinetics pertain to that fraction of the reaction which is temporarily diverted to malealdehyde **3** and which subsequently equilibrates with the hydrates **4**.

[13]From the catalytic constants for hydronium ion and acetic acid one can estimate α = 0.43. Likewise, from the values for water (see Table 4, footnote *c*) and hydroxide ion we estimate β = 0.40. For comparison, the values for phthalaldehyde hydration are α = 0.52, β = 0.51 (27) and for acetaldehyde hydration α = 0.54, β = 0.45 (28).

Can. J. Chem. Downloaded from www.nrcresearchpress.com by 210.87.254.40 on 09/06/12
For personal use only.

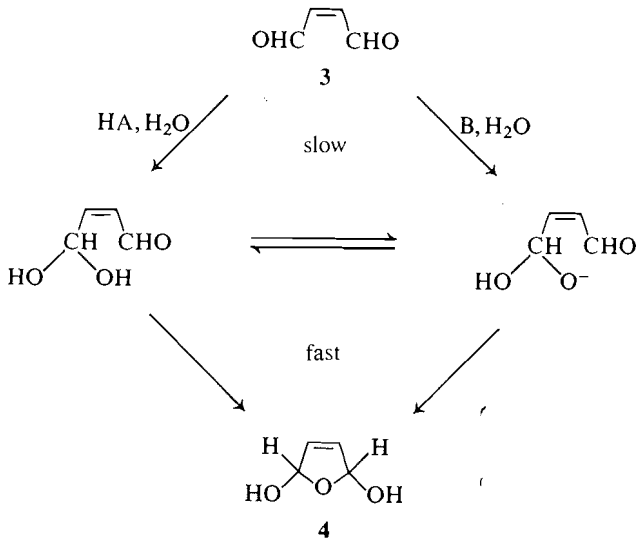

SCHEME 2

ported above were recorded on a Varian T-60 machine, using D_2O as solvent and DSS as internal standard.

Kinetics

Measurements of rates were made using an Aminco DW-2 spectrophotometer with stopped-flow accessory. Data acquisition employed the equipment recently described (14) and data analysis followed standard practice (13–15, 29).

The rate of reaction of furan with bromine was measured by monitoring the disappearance of bromine (λ = 267 nm, tribromide ion band) under pseudo first-order conditions (furan = 10^{-4} *M*, bromine = 10^{-5} *M*) in acetate buffer (pH = 3.98) and in 0.1 *M* KBr, at 25°C (15). The second-order rate constant given in the text was obtained from the observed first-order rate constant (45.2 s^{-1}) by correcting for the substrate concentration and for the actual concentration of free bromine in the normal way (15).

Since the solubility of furan in water is quite low, a concentrated stock solution was made up in methanol. Furan solutions for kinetics experiments were made up by diluting a few microlitres of this stock into an appropriately large volume of the desired medium.

Monitoring the disappearance of the tail-end absorption at 230–240 nm, ascribed to malealdehyde **3**, gave excellent first-order kinetics in the pH range 1–8. Final absorbance values (more than 10 half-lives) were stable and rate constants calculated by the normal, Kezdy–Swinbourne, and Guggenheim methods (30) agreed very well. Outside of the pH range 1–8, rate constants were not obtained for the reasons given above.[7]

Product studies

Because of the low solubility of furan in water and its propensity for resinification in the presence of acid, the analysis of product mixtures by nmr was not easy. Two basic approaches were employed, as detailed below.

In the first, a small amount of bromine was weighed into a small test-tube and covered with sufficient sodium bicarbonate to neutralize the acid to be produced.

An appropriate volume of deuterium oxide was added to these reagents and then a known amount of furan was added as a layer on top of the heavy water. The total mixture was cooled in ice and then was very *gently* stirred to bring about gradual reaction of the furan and bromine in the D_2O. After reaction was complete any residual solid was filtered off and the filtrate was submitted to nmr analysis.

The second approach was essentially the same, except that the furan was added gradually as a solution in dioxane. The two approaches gave the same results. The only nmr peaks of any significance, other than HDO (or dioxane), were those ascribed to the cyclic hydrates **4**.

Various unsuccessful attempts were made to isolate malealdehyde **3**. Unfortunately, as earlier workers have found (31), it is quite labile. It undergoes rapid polymerization in concentrated solutions and isomerization to the *E*-isomer (fumaric dialdehyde) in dilute solution (31). Formation of the latter causes solutions to turn yellow due to an absorption band at 354 nm (31). This yellowing was evident in product solutions left to stand for prolonged periods of time.

Acknowledgements

The authors are grateful to the Natural Sciences and Engineering Research Council of Canada for an operating grant (to O.S.T.) and to the University of Auckland for leave of absence (for B.E.S.).

1. A. P. DUNLOP and F. N. PETERS. The furans. Reinhold, New York. 1953. Chapt. 3.
2. F. M. DEAN. Naturally occurring oxygen ring compounds. Butterworths, London. 1963. Chapt. 1.
3. G. MARINO. Adv. Heterocycl. Chem. **13**, 235 (1971).
4. F. M. DEAN. Adv. Heterocycl. Chem. **30**, 167 (1982).
5. H. GILMAN and G. F. WRIGHT. Chem. Rev. **11**, 323 (1932).
6. E. BACIOCCHI, S. CLEMENTI, and G. V. SEBASTIANI. J. Chem. Soc. Chem. Commun. 875 (1975).
7. J. A. JOULE and G. F. SMITH. Heterocyclic chemistry. Van Nostrand Reinhold, London. 1972. p. 242.
8. D. M. BURNESS. Org. Synth. Coll. Vol. V, 403 (1973); J. LEVISALLES. Bull. Soc. Chim. Fr. 997 (1957); N. CLAUSON-KAAS, F. LIMBORG, and J. FAKSTORP. Acta Chem. Scand. **2**, 109 (1950); J. FAKSTORP, D. RALEIGH, and L. E. SCHIEPP. J. Am. Chem. Soc. **72**, 869 (1950).
9. N. CLAUSON-KAAS. Acta Chem. Scand. **1**, 379 (1947).
10. J. WILLIAMSON and B. A. W. COLLER. Aust. J. Chem. **32**, 2423 (1979).
11. P. LINDA and G. MARINO. J. Chem. Soc. (B). 392 (1968).
12. D. G. MANLY and E. D. AMSTUTZ. J. Org. Chem. **21**, 516 (1956).
13. O. S. TEE and M. PAVENTI. J. Am. Chem. Soc. **104**, 4142 (1982).
14. O. S. TEE, M. TRANI, R. A. MCCLELLAND, and N. E. SEAMAN. J. Am. Chem. Soc. **104**, 7219 (1982).
15. O. S. TEE and C. G. BERKS. J. Org. Chem. **45**, 830 (1980).
16. W. ADAM and I. ERDEN. Angew. Chem. Int. Ed. Engl. **17**, 211 (1978).
17. Y. AITO, T. MATSUO, and C. ASO. Bull. Chem. Soc. Jpn. **40**, 130 (1967).
18. C. BARBIER, D. GAGNAIRE, and P. VOTTERO. Bull. Soc. Chim. Fr. 2330 (1968).
19. J. FROBORG, G. MAGNUSSON, and S. THOREN. J. Org. Chem. **40**, 122 (1975).
20. J. A. HIRSCH and A. J. SZUR. J. Heterocycl. Chem. **9**, 523 (1972).
21. K. C. RICE and J. R. DYER. J. Heterocycl. Chem. **12**, 1325 (1975).
22. H. GREUTER and T. WINKLER. Helv. Chim. Acta, **61**, 3103 (1978).
23. R. P. BELL and P. G. EVANS. Proc. R. Soc. London Ser. A, **291**, 297 (1966); L. H. FUNDERBURK. L. ALDWIN, and W. P. JENCKS. J. Am. Chem. Soc. **100**, 5444 (1978).
24. J. R. ATKINSON and R. P. BELL. J. Chem. Soc. 3260 (1963).
25. M. F. RUASSE and J. E. DUBOIS. J. Am. Chem. Soc. **97**, 1977 (1975).
26. A. I. SCOTT. Interpretation of the ultraviolet spectra of natural products. MacMillan, New York. 1964. pp. 61–69.
27. R. S. MCDONALD and E. V. MARTIN. Can. J. Chem. **57**, 506 (1979).
28. T. H. LOWRY and K. S. RICHARDSON. Mechanism and theory in organic chemistry. 2nd ed. Harper and Row, New York. 1981. p. 598.
29. O. S. TEE and M. PAVENTI. J. Org. Chem. **46**, 4172 (1981).

Can. J. Chem. Downloaded from www.nrcresearchpress.com by 210.87.254.40 on 09/06/12
For personal use only.

30. E. S. SWINBOURNE. Analysis of kinetic data. Nelson, London. 1971. pp. 78–84.

31. D. L. HUFFORD, D. S. TARBELL, and T. R. KOSZALKA. J. Am. Chem. Soc. **74**, 3014 (1952).

Can. J. Chem. Downloaded from www.nrcresearchpress.com by 210.87.254.40 on 09/06/12
For personal use only.

Preparation and stereochemistry of 8- and 9-hydroxy-2,5-ethano-3-benzazocines

PATRICE C. BÉLANGER, JOHN SCHEIGETZ, AND ROBERT N. YOUNG

Medicinal Chemistry Department, Merck Frosst Canada Inc., P.O. Box 1005, Pointe-Claire/Dorval, P.Q., Canada H9R 4P8

Received October 21, 1982[1]

PATRICE C. BÉLANGER, JOHN SCHEIGETZ, and ROBERT N. YOUNG. Can. J. Chem. **61**, 2177 (1983).

Two isomers of a novel ring system, 1,2,3,4,5,6-hexahydro-2,5-ethano-3-benzazocine, were prepared by a Beckmann rearrangement of *syn*- and *anti*-2-hydroxy-11-oximino-6,9-methano-5,6,7,8,9,10-hexahydrobenzocyclooctene, **4***a* and **4***b* respectively. Because of the similarity in their ir, nmr, and ms, it was impossible to distinguish between the different isomers. To resolve this problem, selective benzylic oxidation and nmr shift reagent studies gave results that determined the structures.

PATRICE C. BÉLANGER, JOHN SCHEIGETZ et ROBERT N. YOUNG. Can. J. Chem. **61**, 2177 (1983).

Deux isomères d'un nouveau système polycyclique, l'hexahydro-1,2,3,4,5,6-ethano-2,5-benz-3-azocine ont été préparés en effectuant le réarrangement de Beckmann sur les isomères *syn* et *anti* de l'hydroxy-2-oximino-11-méthano-6,9-hexahydro-5,6,7,8,9,10-benzocyclooctene **4***a* et **4***b* respectivement. La similarité de leur spectre infrarouge, de résonance magnétique nucléaire et de masse a rendu impossible la distinction des isomères. Il a fallu effectuer une oxydation sélective du carbone benzylique *para* au groupe méthoxy. Des études de résonance magnétique nucléaire avec des réactifs de contact ont résolu ce problème et ont permis d'assigner de façon non ambiguë les structures.

Introduction

The benzomorphan ring system has been a popular model for structural modifications in the preparation of analgesics (1). The system is a 3-benzazocine and is further characterized by a 2,6-methano bridge. While preparation and analgesic properties of other methano bridged benzazocines have been reported (2), the corresponding 2,5-ethano bridged 3-benzazocine is a novel system. During our investigation of the chemistry of the 5,6,7,8,9,10-hexahydro-6,9-methanobenzocyclooctene (3) system, we found that such a ring system **1** may be used to generate isomeric 3-benzazocines **2** and **3**. The analgesic properties of derivatives of these and related novel systems will be the subject of a future publication. In this paper we wish to report on the preparation and the proof of structure of two isomers of the 3-benzazocine system.

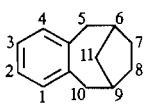

1

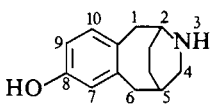

2

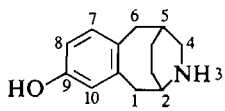

3

Discussion

A mixture of *syn*- and *anti*-2-hydroxy-11-oximino-6,9-methano-5,6,7,8,9,10-hexahydrobenzocyclooctene **4***a*, **4***b* was prepared as previously reported (3). The separation of the *syn* and *anti* isomers was easily accomplished by preparative high pressure liquid chromatography (hplc) on silica gel. The definitive assignment of their structures was not possible either by ^{1}H or ^{13}C nmr. Each of the oxime isomers was converted to its corresponding isomeric 3-benzazocine as is outlined in Scheme 1.

The key step in generating this novel 2,5-ethano-3-benzazocine ring system from the 6,9-methanobenzocyclooctene ring system is based on the Beckmann rearrangement (4). Several conditions were tried and the best results for ring expansion to the cyclic amides were obtained by using *p*-toluenesulfonyl chloride in pyridine (5). The product from the Beckmann rearrangement is known to be highly dependent on the stereochemistry of the starting oxime (6). Thus it was expected that the *syn* isomer would lead to only the 8-hydroxy-2,5-ethano-3-benzazocine **6** after hydrolysis of the *p*-toluenesulfonate **5***a* and lithium aluminium hydride reduction of the resulting amide **5***b*. Similarly, the *anti* isomer **4***b*

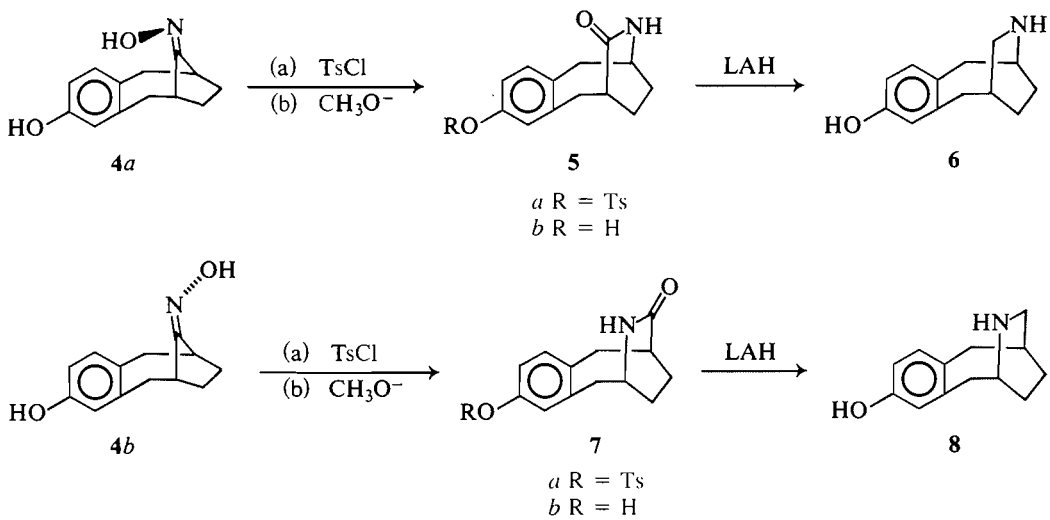

SCHEME 1

[1]Revision received April 29, 1983.

Can. J. Chem. Downloaded from www.nrcresearchpress.com by 210.87.254.105 on 09/06/12
For personal use only.

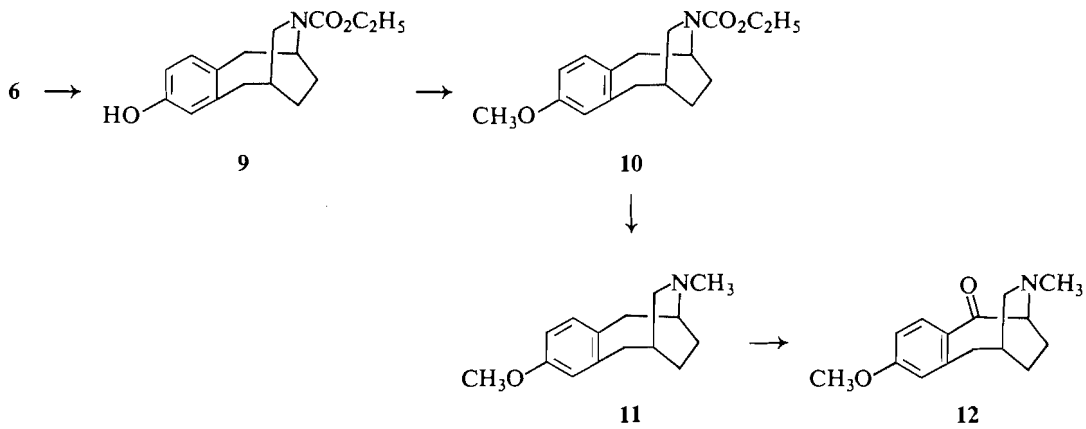

SCHEME 2

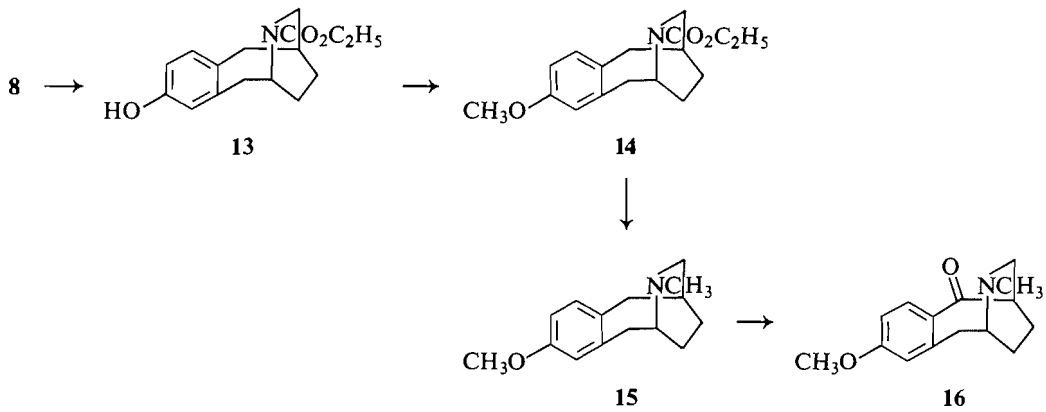

SCHEME 3

would be converted to 9-hydroxy-2,5-ethano-3-benzazocine **8**.

The structure assignment of the isomeric Beckmann rearrangement products could not be deduced by conventional methods. Thus, it was decided that the selective oxidation of the benzylic methylene group *para* to the phenolic hydroxyl would produce a β-aminoketone **16** versus an α-aminoketone **12**, therefore permitting better nmr differentiation of the bridgehead protons in **6** and **8**.

Direct oxidation on the free phenolamine **6** or **8** gave only decomposition products. To avoid these complications it was necessary to protect the phenol function as its methyl ether. The synthetic sequence utilized in the preparation of the isomeric ketones **12** and **16** is outlined in Schemes 2 and 3.

Reaction of **7***b* with ethyl chloroformate gave a product in which both the phenol and the amine were protected. On treatment with base, the carbonate was hydrolyzed rapidly. The carbamate **9** was now methylated with dimethylsulfate and potassium carbonate in acetone and the resulting methoxy derivative **10** was reduced with LAH/THF to give the methoxy-*N*-methylamine **11** in an overall yield of 87% from amine **6**. Oxidation with CrO_3/10% H_2SO_4 as reported in the preparation of ethylketocyclazocine (7) gave the desired ketone **12**. The isomer **16** was prepared in a similar manner.

Although the oxidation yields were not optimized, the isomer **15** gave better yields of the corresponding ketone **16** which seemed to be more stable in the oxidation mixture. The ketone **12** obtained from the oxidation of the isomer **11** is an α-aminoketone and as such appears to be much more susceptible to overoxidation. We speculate that the reason for the low yield is due to possible β-elimination, giving a product subject to further degradation.

Nuclear magnetic resonance shift reagent studies

A nmr shift reagent study, using $Eu(fod)_3$, was undertaken on ketones **12** and **16** to prove unambiguously their structure.

In the 90 MHz spectrum of ketone **16**, the bridgehead proton H-5 signal is buried in complex absorptions around 3.1 ppm. The gradual downfield displacement of the absorption due to H-5, using various amounts of shift reagent, can be followed as shown in Table 1. After the addition of 1.0 mmol of $Eu(fod)_3$ to 1.5 mmol of ketone, proton H-5 is shifted to 6.13 ppm and, as can be seen in Fig. 1, it has the characteristics of a poorly resolved multiplet, which is expected from the bridgehead proton of isomer **16** on coupling with three adjacent protons. Somewhat surprisingly (8), the europium appears to complex most strongly with the carbonyl oxygen. This is apparent from the doublet observed for H-7 which is most affected by the shift reagent.

The 90 MHz spectrum of the ketone **12** was in excellent agreement with that expected of isomer **12**. As seen in Fig. 2, the absorption due to the bridgehead proton H-2 is clearly visible at 3.5 ppm without the use of shift reagent and its position corresponds to the expected value from shielding constants (9).

Nevertheless, the addition of $Eu(fod)_3$ was carried out and the results are listed in Table 2. As is the case for isomer **16**, the complexation of europium is with the carbonyl oxygen. Proton H-2 appears as a doublet of doublets with coupling

Can. J. Chem. Downloaded from www.nrcresearchpress.com by 210.87.254.105 on 09/06/12
For personal use only.

Can. J. Chem. Downloaded from www.nrcresearchpress.com by 210.87.254.105 on 09/06/12
For personal use only.

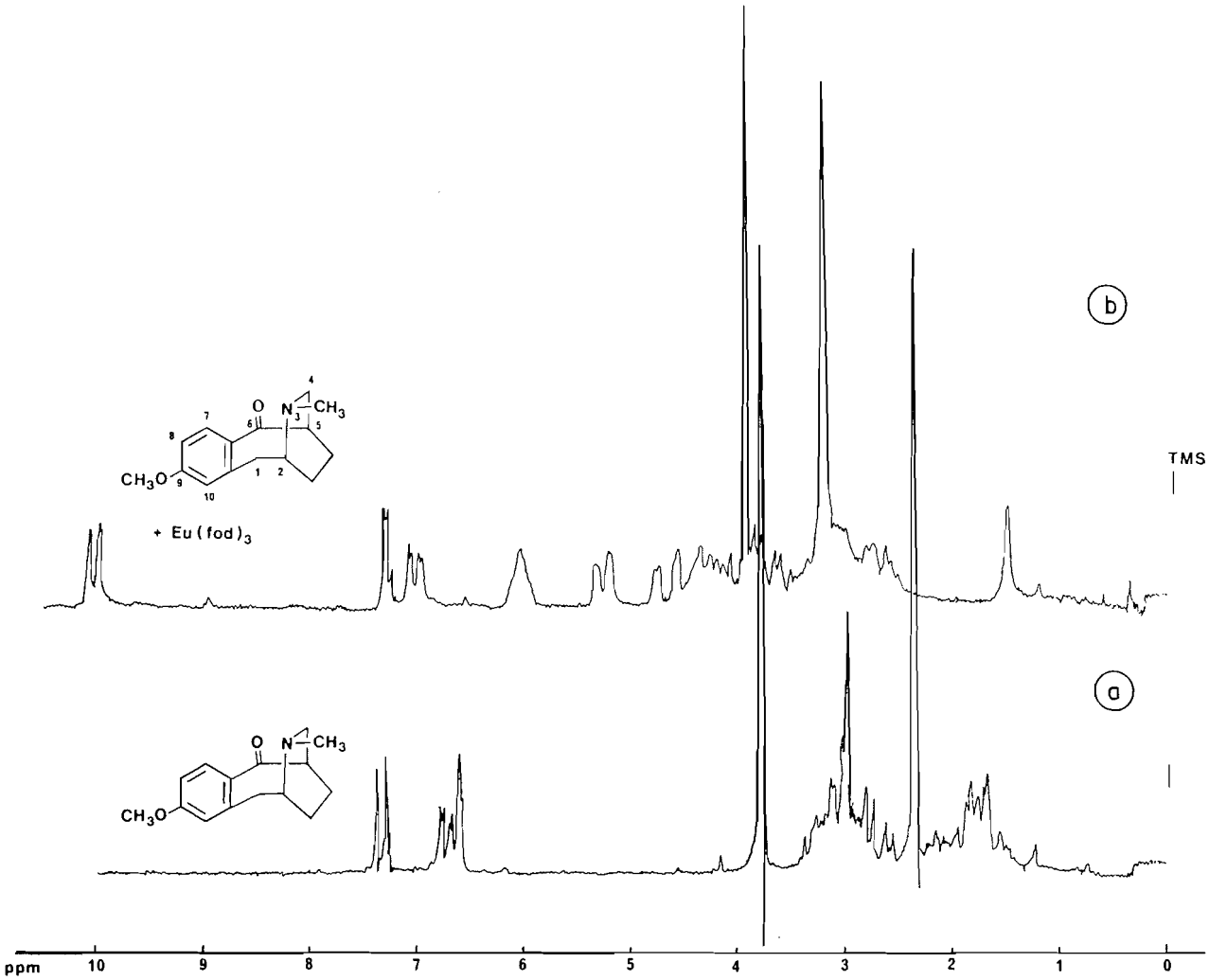

FIG. 1. The ^1H nmr spectra of **16** without shift reagent (spectrum a) and with 0.45 equivalents $Eu(fod)_3$ (spectrum b).

TABLE 1. $Eu(fod)_3$ induced chemical shifts of selected protons of **16**

$Eu(fod)_3$ equivalents	H_5	H_{10}	H_8	H_7	H_{11} H_{12}	CH_3O	CH_3N
0	3.1*	6.63	6.77	7.37	1.80	3.83	2.40
0.07	3.3	6.70	6.80	7.60	1.90	3.83	2.50
0.16	3.6	6.80	6.87	8.17	2.10	3.87	2.65
0.23	4.33	6.97	6.93	8.60	2.40	3.93	2.83
0.33	5.10	7.17	7.00	9.23	2.70	4.00	3.03
0.45	6.13	7.37	7.10	10.07	3.00	4.03	3.30
0.61	7.47	7.67	7.23	11.17	3.40	4.10	3.67
0.86	9.33	8.10	7.40	12.73	4.00	4.20	4.20

*Chemical shift expression in ppm downfield from TMS.

constants of 2 Hz and 7 Hz. Examination of molecular models indicates that the piperidine ring in **12** can exist in two possible conformations. In one conformer (A) the methylene protons at C-11 are bisected by the bridgehead proton H-2 when viewing along the (C_2—C_{11}) bond and one would expect to observe a triplet for H-2 with a coupling constant of about 4 Hz.

In the other conformer (B) the dihedral angles between H-2 and the adjacent methylene protons are about 90° and about 30° giving expected couplings of 1–2 Hz and 7–8 Hz respectively according to Karplus (10). Therefore, the doublet of doublets at 3.5 ppm, having coupling constants of 7 Hz and 2 Hz, appears to correspond to this particular conformer.

This nmr study clearly established the structure of both isomers **12** and **16** and, therefore, their relationship to *syn* and *anti* oximes **4***a* and **4***b*. Compound **16** was obtained from the more polar *syn* isomer **4***a*, whereas **12** originated from the less polar *anti* isomer **4***b*.

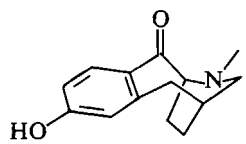

A

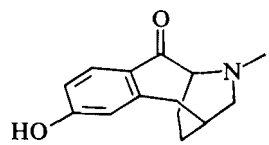

B

Can. J. Chem. Downloaded from www.nrcresearchpress.com by 210.87.254.105 on 09/06/12
For personal use only.

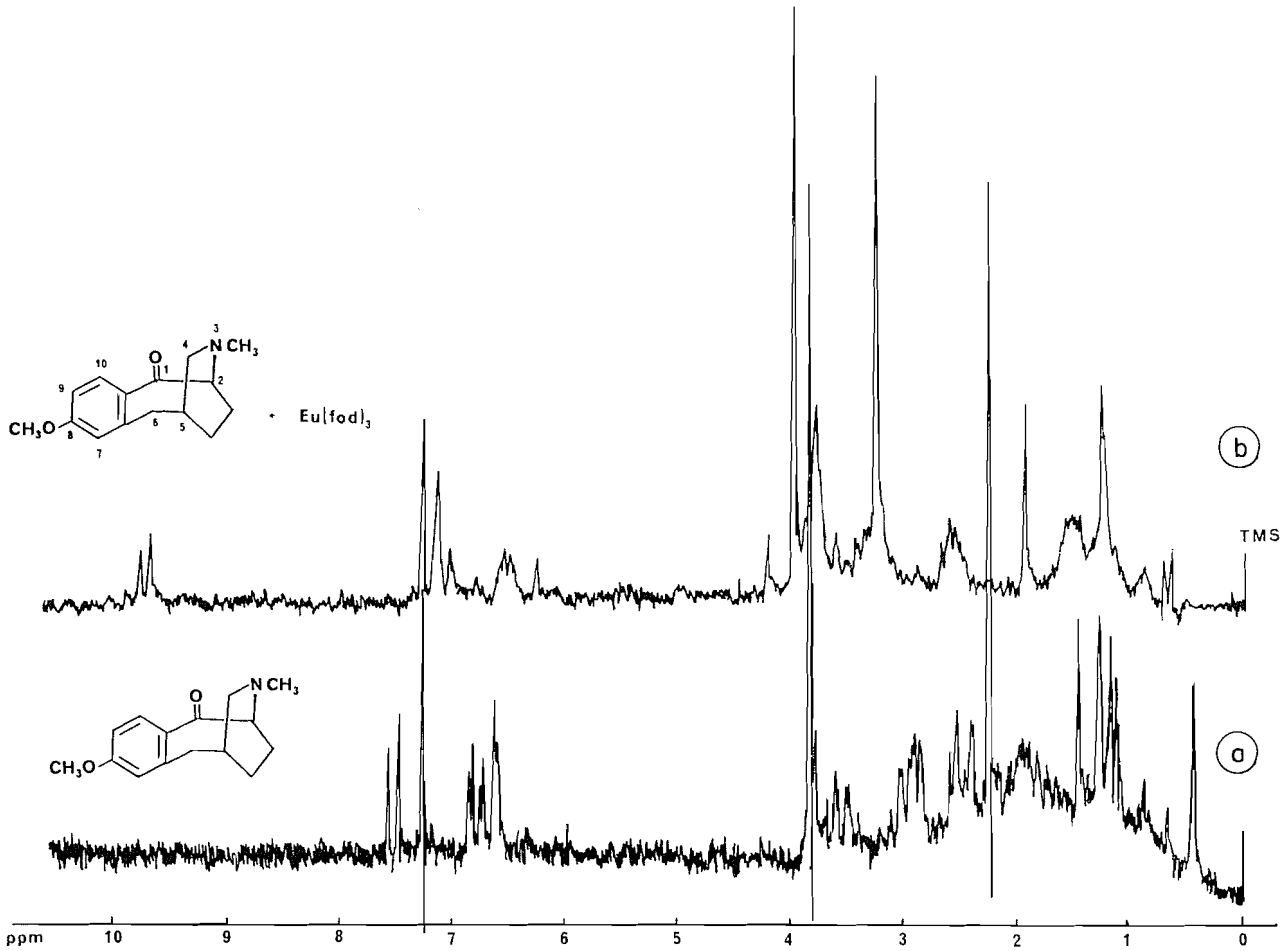

FIG. 2. The ^1H nmr spectra of **12** without shift reagent (spectrum a) and with 0.34 equivalents $Eu(fod)_3$ (spectrum b).

TABLE 2. $Eu(fod)_3$ induced chemical shifts of selected protons of **12**

$Eu(fod)_3$ equivalents	H_2	H_7	H_9	H_{10}	H_{11} H_{12}	CH_3O	CH_3N
0	3.53*	6.67	6.78	7.50	1.83	3.80	2.33
0.04	3.63	6.67	6.80	7.60	1.90	3.83	2.33
0.09	4.13	6.77	6.87	8.03	2.03	3.87	2.50
0.20	5.30	7.00	7.00	8.83	2.20	3.93	2.87
0.34	6.53	7.07	7.13	9.73	2.60	3.97	3.27
0.52	7.63	7.33	7.23	10.50	2.90	4.03	3.63
0.73	9.40	7.70	7.33	11.80	3.43	4.17	4.30

*Chemical shift expression in ppm downfield from TMS.

Mass spectral analyses

The mass spectral analyses of all the 8-hydroxy-2,5-ethano-3-benzazocine analogues, as well as all the 9-hydroxy-2,5-ethano-3-benzazocine analogues, were found to produce similar fragmentation patterns. They all produced as major fragments a dihydropyridinium ion and a *p*-hydroxy or *p*-methoxy-2-methyl tropylium ion. In this series of derivatives there was only one notable exception. The keto derivative **12**, besides giving the above fragmentation, also fragmented the bridge containing the amine as seen by the $M - 57$ peak. The significance of the relative abundance of the $M - 57$ peak (58%) can be interpreted as due to the α-amino ketone nature of this derivative **12**.

Experimental

Melting points were taken on a Thomas–Hoover apparatus in open capillary tubes and are uncorrected. Infrared spectra were recorded on a Perkin-Elmer 267 grating spectrophotometer. A Varian EM-390 spectrometer was used to record nmr spectra. Proton chemical shifts are relative to tetramethylsilane (TMS) as internal standard. A Waters Prep LC/500 System was used to perform the hplc preparative separations, using one silica gel cartridge with a flow rate of 250 mL/min. Elemental analyses were performed by Galbraith and Associates, Knoxville, TN. The low resolution mass spectral analyses were performed by the Morgan-Schaffer Corporation, Montreal.

All reactions as well as column chromatography were monitored routinely with the aid of thin layer chromatography (tlc) using precoated 0.25 mm silica gel plates (Eastman Kodak) or silica gel GF plates (Analtech).

syn- *and* anti-*2-Hydroxy-11-oximino-6,9-methano-5,6,7,8,9,10-hexahydrobenzocyclooctene (4*a *and 4*b*)*

The oxime mixture **4** was prepared as described in ref. 3. Fifteen grams of the mixture were chromatographed on a Waters Prep

Can. J. Chem. Downloaded from www.nrcresearchpress.com by 210.87.254.105 on 09/06/12
For personal use only.

LC/500, eluting with hexane/ethyl acetate, 1:1 v/v, to provide 7.3 g of the more polar *syn*-isomer **4***a* and 7.6 g of the less polar *anti*-isomer **4***b*.

Isomer **4**a: mp 190–192°C; (EtOAc/hexane 1:10 v/v); ir (KBr): 3300 (OH^-), 1680 (C=N) cm^{-1}; nmr ($CDCl_3$): 6.4–7.1 (m, 3H), 3.2–3.8 (m, 2H), 2.6–3.0 (m, 4H), 1.1–1.9 (m, 4H). *Anal.* calcd. for $C_{13}H_{15}NO_2$: C 71.86, H 6.95, N 6.44; found: C 71.82, H 6.76, N 6.41.

Isomer **4**b: mp 178–180°C; (EtOAc/hexane 1:1 v/v); ir (KBr): 3320 (OH^-), 1690 (C=N) cm^{-1}; nmr ($CDCl_3$): 6.4–7.1 (m, 3H), 3.2–3.8 (m, 2H), 2.6–3.0 (m, 4H), 1.1–1.9 (m, 4H). *Anal.* calcd. for $C_{13}H_{15}NO_2$: C 71.86, H 6.95, N 6.44; found: C 71.79; H 6.73, N 6.64.

*2,5-Ethano-8-*p*-toluenesulfonyloxy-4-oxo-1,2,3,4,5,6-hexahydro-3-benzazocine (**5**a)*

syn-2-Hydroxy-11-oximino-6,9-methano-5,6,7,8,9,10-hexahydrobenzocyclooctene (**4***a*) (3.0 g, 13.8 mmol) and *p*-toluenesulfonyl chloride (5.8 g, 30.4 mmol) in pyridine (50 mL) was stirred at room temperature overnight. The reaction mixture was concentrated *in vacuo* to a residue that was purified by chromatography ($CH_3OH/CHCl_3$, 1:100 v/v) to yield 3.18 g (70%) of the title compound; mp 128–131°C; ir (KBr): 3400 (NH), 1660 (C=O) cm^{-1}; nmr ($CDCl_3$): 6.4–7.8 (m, 7H), 3.5–4.0 (m, 2H), 2.6–3.2 (m, 4H), 2.4 (s, 3H), 1.4–2.1 (m, 4H). *Anal.* calcd. for $C_{20}H_{21}NSO_4$: C 64.66, H 5.69, N 3.77, S 8.63; found: C 64.51, H 5.88, N 3.72, S 8.89.

*2,5-Ethano-9-*p*-toluenesulfonyloxy-4-oxo-1,2,3,4,5,6-hexahydro-3-benzazocine (**7**a)*

By the same procedure used for the preparation of **5***a*, *anti*-2-hydroxy-11-oximino-6,9-methano-5,6,7,8,9,10-hexahydrobenzocyclooctene (**4***b*) (3.0 g, 13.8 mmol) was converted to 3.13 g (69%) of the title compound, mp 182–186°C; ir (KBr): 3300 (NH), 1670 (C=O) cm^{-1}; nmr ($CDCl_3$): 6.4–7.8 (m, 7H), 3.5–4.0 (m, 2H), 2.6–3.2 (m, 4H), 2.4 (s, 3H), 1.4–2.1 (m, 4H). *Anal.* calcd. for $C_{20}H_{21}NSO_4$: C 64.66, H 5.69, N 3.77, S 8.63; found: C 64.50, H 5.57, N 3.75, S 8.81.

*2,5-Ethano-8-hydroxy-4-oxo-1,2,3,4,5,6-hexahydro-3-benzazocine (**5**b)*

A solution of 2,5-ethano-8-*p*-toluenesulfonyloxy-4-oxo-1,2,3,4,-5,6-hexahydro-3-benzazocine (**5***a*) (3.55 g, 9.56 mmol) and sodium methoxide (1.9 g, 36.0 mmol) in methanol (17 mL) was stirred at room temperature overnight. Hydrochloric acid (3 *N*; 35 mL) was added and the reaction mixture extracted twice with chloroform. The combined organic layers were washed with water, dried (Na_2SO_4), and concentrated *in vacuo* to yield an oil. After triturating in water, the solid was filtered and dried to yield 1.58 g (76%) of the title compound, mp 241–245°C; ir (KBr): 3400 (OH^-), 3320 (NH), 1650 (C=O) cm^{-1}; nmr (CD_3OD): 6.4–7.0 (m, 3H), 3.6–4.1 (m, 2H), 2.6–3.2 (m, 4H), 1.5–2.1 (s-broad, 4H).

*2,5-Ethano-9-hydroxy-4-oxo-1,2,3,4,5,6-hexahydro-3-benzazocine (**7**b)*

By the same procedure used for the preparation of **5***b*, 2,5-ethano-9-*p*-toluenesulfonyloxy-4-oxo-1,2,3,4,5,6-hexahydro-3-benzazocine (**7***b*) (3.25 g, 8.76 mmol) was converted to 1.66 g (87%) of the title compound, mp 305–309°C; ir (KBr): 3400 (OH^-) 3300 (NH), 1650 (C=O) cm^{-1}; nmr (DMSO-d_6): 6.3–7.0 (m, 3H), 3.3–3.9 (m, 2H), 2.7–3.0 (m, 4H), 1.4–1.9 (bs, 4H). *Anal.* calcd. for $C_{13}H_{15}NO_2$: C 71.86, H 6.95, N 6.44; found: C 71.46, H 6.90, N 6.18.

*2,5-Ethano-8-hydroxy-1,2,3,4,5,6-hexahydro-3-benzazocine hydrochloride (**6**)*

To a solution of 2,5-ethano-8-hydroxy-4-oxo-1,2,3,4,5,6-hexahydro-3-benzazocine (**5***b*) (1.54 g, 7.07 mmol) in tetrahydrofuran (70 mL) was added, in small portions, lithium aluminium hydride (1.34 g, 35 mmol). The mixture was refluxed overnight. The reaction mixture was treated with a saturated ammonium chloride solution (3 mL) and then with 1 *N* sodium bicarbonate (8 mL). The mixture was stirred for 15 min and then filtered. The filtrate was concentrated *in vacuo*. The oil was taken up in methanol, treated with hydrogen chloride, and evaporated to dryness. The residue was triturated in ether to yield 1.04 g (62%) of a solid which, after recrystallization from methanol/chloroform, had mp 234–240°C; ir (KBr): 3400 (OH^-), 3360 (NH) cm^{-1}; nmr (CD_3OD): 6.4–7.1 (m, 3H), 3.7–4.2 (m, 1H), 2.5–3.5 (m, 7H), 1.4–2.2 (m, 4H). *Anal.* calcd. for $C_{13}H_{17}NO \cdot HCl$: C 65.12, H 7.56, N 5.84, Cl 14.78; found: C 64.56, H 7.65, N 5.65, Cl 14.69.

*2,5-Ethano-9-hydroxy-1,2,3,4,5,6-hexahydro-3-benzazocine hydrochloride (**8**)*

Similarly, 2,5-ethano-9-hydroxy-4-oxo-1,2,3,4,5,6-hexahydro-3-benzazocine (**7***b*) (1.40 g, 6.45 mmol) in tetrahydrofuran (65 mL) was reduced by lithium aluminium hyride (1.2 g, 32 mmol) to yield 1.33 g (87%) of the title compound, mp 275°C; ir (KBr): 3440 (OH^-), 3320 (NH) cm^{-1}; nmr (CD_3OD): 6.4–7.1 (m, 3H), 3.7–4.2 (m, 1H), 2.5–3.5 (m, 7H), 1.4–2.2 (m, 4H). *Anal.* calcd. for $C_{13}H_{17}NO \cdot HCl$: C 65.12, H 7.56, N 5.84, Cl 14.78; found: C 65.09, H 7.60 N 5.77, Cl 15.37.

*N-Ethoxycarbonyl-2,5-ethano-8-hydroxy-1,2,3,4,5,6-hexahydro-3-benzazocine (**9**)*

To a solution of 2,5-ethano-8-hydroxy-1,2,3,4,5,6-hexahydro-3-benzazocine (**6**) (200 mg, 0.98 mmol), 1.0 mL of triethylamine, and 40 mL of THF was added a solution of ethyl chloroformate (122 mg, 1.14 mmol) in 1 mL of THF. The reaction mixture became slightly warm and after stirring for 30 min was concentrated. The residue was partitioned between chloroform and 1 *N* HCl. The chloroform layer was washed with water, dried (Na_2SO_4), and concentrated to yield an oil. An infrared spectrum showed a carbonate band at 1755 cm^{-1} and a carbamate band at 1680 cm^{-1}.

The unpurified *N*-ethoxycarbonyl-2,5-ethano-8-ethoxycarbonyloxy-1,2,3,4,5,6-hexahydro-3-benzazocine was dissolved in 25 mL of methanol and 4 mL of 3 *N* NaOH solution was added. After 5 minutes, the mixture was concentrated and the residue partitioned between 15 mL of 1 *N* HCl and chloroform. The chloroform layer was dried (Na_2SO_4) and concentrated to yield 233 mg (85%) of the title compound, mp 127–131°C; ir (KBr): 3340 (OH^-), 1665 (C=O) cm^{-1}; nmr ($CDCl_3$): 6.3–7.0 (m, 3H), 4.2–4.5 (m, 1H), 3.8–4.2 (q, 2H), 3.4–3.8 (t, 1H), 2.2–3.2 (m, 7H), 0.9–1.9 (m, 7H); *m/e*: 275 (M^+, 67%), 154 (90%), 153 (41%), 122 (100%), 121 (48%). *Anal.* calcd. for $C_{16}H_{21}NO_3$: C 69.79, H 7.68, N 5.08; found: C 69.10, H 7.80, N 4.94.

*N-Ethoxycarbonyl-2,5-ethano-9-hydroxy-1,2,3,4,5,6-hexahydro-3-benzozocine (**13**)*

By the same procedure used for the preparation of **9**, 2,5-ethano-9-hydroxy-1,2,3,4,5,6-hexahydro-3-benzazocine (**13**) (910 mg, 4.48 mol) was converted to 1.1 g (90%) of the title compound. The product was triturated with hexane; mp 103–106°C; ir (KBr): 3340 (OH^-), 1665 (C=O) cm^{-1}; nmr ($CDCl_3$): 6.1–7.0 (m, 3H), 4.2–4.6 (m, 1H), 3.75–4.2 (q, 2H), 3.3–3.75 (t, 1H), 2.2–2.3 (m, 7H), 0.9–2.0 (m, 7H); *m/e*: 275 (M^+, 81%), 154 (83%), 121 (100%). *Anal.* calcd. for $C_{16}H_{21}NO_3$: C 69.79, H 7.68, N 5.08; found: C 69.68, H 7.68, N 5.12.

*N-Ethoxycarbonyl-2,5-ethano-8-methoxy-1,2,3,4,5,6-hexahydro-3-benzazocine (**10**)*

A mixture of *N*-ethoxycarbonyl-2,5-ethano-8-hydroxy-1,2,3,4,5,6-hexahydro-3-benzazocine (**9**) (233 mg, 0.84 mmol), dimethyl sulfate (0.23 g; 8.0 mmol), and anhydrous potassium carbonate (0.47 g, 1.7 mmol) in acetone (20 mL) was stirred at room temperature for 3 days. The mixture was filtered and the filtrate concentrated *in vacuo*. The residue was taken up in chloroform and washed with water, dried (Na_2SO_4), filtered, and concentrated *in vacuo* to yield 227 mg (93%) of the title compound as an oil; ir (thin film): 1690 (C=O) cm^{-1}; nmr ($CDCl_3$): 6.5–7.0 (m, 3H), 4.2–4.6 (m, 1H), 3.8–4.2 (q, 2H), 3.75 (s, 3H), 3.4–3.8 (m, 1H), 2.2–3.2 (m, 7H), 1.0–1.9 (m, 7H); *m/e*: 289 (M^+, 37%), 154 (25%), 153 (12%), 136 (100%), 135 (24%).

Anal. calcd. for $C_{17}H_{23}NO_3 \cdot \frac{1}{2}H_2O$: C 68.43, H 8.10, N 4.69; found: C 68.08, H 8.02, N 4.57.

N-*Ethoxycarbonyl-2,5-ethano-9-methoxy-1,2,3,4,5,6-hexahydro-3-benzazocine (**14**)*

By the same procedure used for the preparation of **10**, *N*-ethoxycarbonyl-2,5-ethano-9-hydroxy-1,2,3,4,5,6-hexahydro-3-benzazocine (**13**) (1.0 g, 3.6 mmol) was converted to 1.04 g (96%) of the title compound as an oil; ir (thin film): 1690 (C=O) cm^{-1}; nmr ($CDCl_3$): 6.5−7.0 (m, 3H), 4.2−4.6 (m, 1H), 3.8−4.2 (q, 2H), 3.75 (s, 3H), 3.4−3.8 (m, 1H), 2.2−3.2 (m, 1H), 2.2−3.2 (m, 7H), 1.0−1.9 (m, 7H); *m/e*: 289 (M^+, 9%), 154 (26%), 135 (100%). *Anal.* calcd. for $C_{17}H_{23}NO_3$: C 70.56, H 8.01, N 4.84; found: C 69.97, H 8.13, N 4.68.

N-*Methyl-2,5-ethano-8-methoxy-1,2,3,4,5,6-hexahydro-3-benzazocine (**11**)*

To a solution of *N*-ethoxycarbonyl-2,5-ethano-8-methoxy-1,2,3,4,-5,6-hexahydro-3-benzazocine (**10**) (277 mg, 0.768 mmol) in 10 mL of THF was added lithium aluminum hydride (175 mg, 4.6 mmol) under a nitrogen atmosphere. The mixture was refluxed for 1 hour. After cooling to room temperature, the mixture was treated with a saturated NH_4Cl solution (2.1 mL) followed by 1 *N* $NaHCO_3$ (5.7 mL). The mixture was filtered and the salts washed with THF. The filtrate was concentrated *in vacuo*. The residue was dissolved in chloroform, dried (Na_2SO_4), filtered, and concentrated *in vacuo* to yield 200 mg (85%) of the title compound as an oil. The hydrochloride melted at 160°C; ir (KBr): 1605, 1580, 1260, 1040 cm^{-1}; nmr ($CDCl_3$): 6.5−7.1 (m, 3H), 3.8 (s, 3H), 2.5−3.4 (m, 8H), 2.4 (s, 3H), 1.1−2.0 (m, 4H); *m/e*: 231 (M^+, 14%), 96 (100%), 94 (25%).

N-*Methyl-2,5-ethano-9-methoxy-1,2,3,4,5,6-hexahydro-3-benzazocine (**15**)*

By the same procedure used for the preparation of **11**, *N*-ethoxycarbonyl-2,5-ethano-9-methoxy-1,2,3,4,5,6-hexahydro-3-benzazocine (**14**) (703 mg, 18.5 mmol) was reduced to 831 mg (90%) of the title compound as an oil. The hydrochloride melted at 255−258°C; ir (thin film): 1610, 1585, 1270, 1050 cm^{-1}; nmr ($CDCl_3$): 6.5−7.1 (m, 3H), 3.8 (s, 3H), 2.5−3.4 (m, 8H), 2.4 (s, 3H), 1.1−2.0 (m, 4H); *m/e*: 231 (M^+, 21%), 135 (11%), 96 (100%). *Anal.* calcd. for $C_{15}H_{21}NO \cdot H_2O$: C 72.25, H 9.29, N 5.61; found: C 72.19, H 8.67, N 5.78.

N-*Methyl-2,5-ethano-8-methoxy-1-oxo-1,2,3,4,5,6-hexahydro-3-benzazocine (**12**)*

To a mixture of *N*-methyl-2,5-ethano-8-methoxy-1,2,3,4,5,6-hexahydro-3-benzazocine (**11**) (200 mg, 0.86 mmol) in 5 mL of 10% H_2SO_4 was added, in one portion, a solution of chromium trioxide (135 mg, 1.35 mmol) in 5 mL of 10% H_2SO_4. The resultant mixture was heated in an oil bath at 65°C for 1 hour. The mixture was brought to room temperature and basified with NH_4OH. After diluting with THF and stirring for 5−10 minutes, the salts were filtered off and washed with THF. The THF layer was separated and concentrated *in vacuo*. The residue was dissolved in chloroform, dried (Na_2SO_4), filtered, and concentrated *in vacuo* to an oil, which was purified on a silica gel preparative plate, developing with 2% $CH_3OH/CHCl_3$ plus NH_3 vapour to yield 10 mg (5%) of the ketone (**12**): ir (thin film): 1665 (C=O), 1600, 1260 cm^{-1}; nmr ($CDCl_3$): 7.4−8.6 (d, 1H), 6.5−6.8 (m, 2H), 3.8 (s, 3H), 3.4−3.6 (d, 1H), 2.2−3.1 (m, 5H), 2.2 (s, 3H), 1.0−2.2 (m, 4H); *m/e*: 245 (M^+, 50%), 188 (58%), 96 (100%), 94 (68%).

N-*Methyl-2,5-ethano-9-methoxy-6-oxo-1,2,3,4,5,6-hexahydro-3-benzazocine (**16**)*

By the same procedure used for the preparation of **12**, *N*-methyl-2,5-ethano-9-methoxy-1,2,3,4,5,6-hexahydro-3-benzazocine (**15**) (231 mg, 1.0 mmol) was oxidized to 204 mg (83%) of the title compound as an oil. The hydrochloride melted at 233−235°C; ir (thin film): 1670 (C=O), 1260, 1050 cm^{-1}; nmr ($CDCl_3$): 7.2−7.4 (d, 1H), 6.5−6.8 (m, 2H), 3.8 (s, 3H), 2.5−3.4 (m, 6H), 2.4 (s, 3H), 1.4−2.4 (m, 4H); *m/e*: 245 (M^+, 14%), 149 (23%), 96 (100%). *Anal.* calcd. for $C_{15}H_{19}NO_2 \cdot H_2O$: C 68.41, H 8.03, N 5.31; found: C 69.22, H 7.56, N 5.65.

Acknowledgement

The authors wish to thank Dr. J. Rokach for valuable discussions.

1. G. Proctor and F. J. Smith. J. Chem. Soc. Perkin Trans 1, 1754 (1981).
2. P. H. Mazzocchi and A. M. Harrison. J. Med. Chem. **21**, 238 (1978); P. M. Mazzocchi and B. C. Stahly. J. Med. Chem. **24**, 457 (1981).
3. P. C. Bélanger, R. N. Young, J. Scheigetz, C. Dufresne, and J. P. Springer. J. Org. Chem. **47**, 4329 (1982).
4. L. G. Donaruma and W. Z. Heldt. Organic reactions. Vol. II. John Wiley and Sons, Inc., New York, NY. 1960. pp. 1−156.
5. W. G. Dauben, R. C. Tweit, and R. L. MacLean. J. Am. Chem. Soc. **77**, 48 (1955).
6. J. Kenyon and D. P. Young. J. Chem. Soc. 263 (1941); A. Campbell and J. Kenyon. J. Chem. Soc. 25 (1946).
7. W. F. Michne and N. F. Albertson. J. Med. Chem. **15**, 1278 (1972).
8. J. K. M. Sanders and D. H. Williams. J. Am. Chem. Soc. **93**, 641 (1971).
9. R. M. Silverstein, G. C. Bassler, and T. C. Morrill. Spectrometric identification of organic compounds. 3rd ed. John Wiley and Sons, Inc., New York, NY. 1974. p. 159.
10. M. Karplus. J. Chem. Phys. **30**, 11 (1959).

Can. J. Chem. Downloaded from www.nrcresearchpress.com by 210.87.254.105 on 09/06/12
For personal use only.

Equilibrium decomposition pressures of the compounds Cs_2ZrCl_6 and Cs_2HfCl_6 and X-ray identification of Na_2HfCl_6, K_2HfCl_6, and Cs_2HfCl_6

G. J. KIPOUROS[1] AND S. N. FLENGAS

Department of Metallurgy and Materials Science, University of Toronto, Toronto, Ont., Canada M5S 1A4

Received November 9, 1982

G. J. KIPOUROS and S. N. FLENGAS. Can. J. Chem. **61**, 2183 (1983).

The chemical equilibria representing the reactions

$$Cs_2ZrCl_{6(s\text{ or }l)} = 2CsCl_{(s\text{ or }l)} + ZrCl_{4(vap,P,T)}$$

and

$$Cs_2HfCl_{6(s\text{ or }l)} = 2CsCl_{(s\text{ or }l)} + HfCl_{4(vap,P,T)}$$

were investigated by direct vapour pressure measurements and thermodynamic data such as free energies and enthalpies of reaction have been calculated. The X-ray powder patterns of the compounds Na_2HfCl_6, K_2HfCl_6, and Cs_2HfCl_6 are also reported.

With reference to the separation of Hf from Zr by a recently developed process based on the selective reactivity of $ZrCl_4$ and $HfCl_4$ vapours with alkali chlorides, it is shown that the efficiency of alkali chlorides as separating agents increases in the order CsCl → LiCl → NaCl → KCl.

G. J. KIPOUROS et S. N. FLENGAS. Can. J. Chem. **61**, 2183 (1983).

On a étudié les équilibres chimiques suivants:

$$Cs_2ZrCl_{6(s\text{ ou }l)} = 2CsCl_{(s\text{ ou }l)} + ZrCl_{4(vap,P,T)}$$

et

$$Cs_2HfCl_{6(s\text{ ou }l)} = 2CsCl_{(s\text{ ou }l)} + HfCl_{4(vap,P,T)}$$

en faisant appel aux mesures directes de pression de vapeur et aux données thermodynamiques telles que les énergies libres et les enthalpies de réaction que l'on a calculées. On rapporte également les diagrammes de poudre de rayons-X des composés suivants: Na_2HfCl_6, K_2HfCl_6 et $CsHfCl_6$.

En ce qui concerne la séparation du Hf à partir du Zr selon un procédé mis au point récemment et qui fait appel à la réactivité sélective des vapeurs de $ZrCl_4$ et de $HfCl_4$ avec les chlorures de métaux alcalins, on montre que l'efficacité des chlorures de métaux alcalins, en tant qu'agents de séparation, augmente dans l'ordre suivant: CsCl → LiCl → NaCl → KCl.

[Traduit par le journal]

Can. J. Chem. Downloaded from www.nrcresearchpress.com by 210.87.254.40 on 09/06/12
For personal use only.

Introduction

In previous publications from this laboratory the vapour pressures of $ZrCl_4$ in equilibrium with its solutions containing alkali chlorides such as LiCl (1), NaCl (2, 3), KCl (4, 5), and CsCl (6), and of $HfCl_4$ in equilibrium with its solutions containing alkali chlorides such as LiCl (1), NaCl (3), KCl (5), and CsCl (6), have been determined by direct experimental techniques involving the use of a spoon type Bourdon gauge (2, 4), a molten tin isoteniscope (1, 6), or a quartz spiral type Bourdon gauge (3, 5).

In the present investigation, a fused silica spiral type Bourdon gauge has been applied to the determination of the vapour pressures of $ZrCl_4$ and $HfCl_4$ in equilibrium with the two pure compounds Cs_2ZrCl_6 and Cs_2HfCl_6, respectively, over a temperature range extending below and above their melting points. The compounds Na_2HfCl_6, K_2HfCl_6, and Cs_2HfCl_6 were synthesized and were identified by means of their X-ray powder diffraction patterns.

From the results of this study, the equilibrium dissociation constants, free energies, and enthalpies for the reactions

$$[1]\quad Cs_2MCl_{6(s)} \leftrightarrows 2CsCl_{(s)} + MCl_{4(vap)}$$

where M represents Zr or Hf, have been calculated.

The equilibrium constant for the exchange reaction

$$[2]\quad \underset{\text{(in solid or liquid solution)}}{Cs_2ZrCl_6} + \underset{\text{(vapour)}}{HfCl_4} \leftrightarrows \underset{\text{(in solid or liquid solution)}}{Cs_2HfCl_6} + \underset{\text{(vapour)}}{ZrCl_4}$$

was also calculated and the theoretical efficiency for the separation of hafnium from zirconium by a previously developed process based on the selective reactivity of $ZrCl_4$ and $HfCl_4$ vapours with alkali chlorides (7–9) has been calculated.

Experimental

At specific partial pressure and temperature pure $ZrCl_4$ and $HfCl_4$ vapours react with solid alkali chlorides to form the stoichiometric solid complex compounds A_2ZrCl_6 and A_2HfCl_6, respectively, where A is an alkali metal like Na, K, or Cs.

The general method applied for the preparation of the pure stoichiometric compounds was developed in this laboratory earlier (1, 2) and involves the reaction of finely ground alkali chloride, having a particle size of less than 325 mesh, with $ZrCl_4$ or $HfCl_4$ vapours at 1 atm pressure.

The $ZrCl_4$ and $HfCl_4$ salts were purchased from the Wah Chang Corporation of America, Albany, NY. As they were always received in a partially hydrolyzed condition, they were purified by repeated sublimations in vacuum through a molten tin plug, as reported earlier (1).

The alkali chlorides used in the present investigation were reagent grade containing less than 0.01% total impurities, were supplied by Cerac Inc., and were dried under vacuum, at 500°C.

[1]Present address: Department of Materials Science and Engineering, Massachusetts Institute of Technology, Cambridge, MA 02139, U.S.A.

TABLE 1. Indexed powder X-ray diffraction patterns for the compounds Na_2HfCl_6, K_2HfCl_6, and Cs_2HfCl_6

Na_2HfCl_6				K_2HfCl_6				Cs_2HfCl_6			
Intensity	d_{obs} (Å)	d_{calcd} (Å)	(hkl)	Intensity (I/I_0)	d_{obs} (Å)	d_{calcd} (Å)	(hkl)	Intensity	d_{obs} (Å)	d_{calcd} (Å)	(hkl)
S	6.57	6.50	002	100	5.78	5.79	111	50	5.93	5.99	111
VVW	4.25	4.29	222	40	4.99	5.01	002	100	3.66	3.67	022
M	3.78	3.77	330	70	3.53	3.54	022	20	3.12	3.13	113
S	3.57	3.57	420	100	3.02	3.02	113	60	2.99	3.00	222
W	3.42	3.42	402	10	2.890	2.897	222	40	2.589	2.599	004
S	2.816	2.826	440	75	2.506	2.509	004	10	2.383	2.385	133
W	2.736	2.742	350	40	2.299	2.302	133	40	2.118	2.122	224
W	2.529	2.528	260	20	2.242	2.244	024	10	2.000	2.000	115/333
VVW	2.156	2.161	116	20	2.047	2.048	224	40	1.836	1.838	044
VVW	2.117	2.123	026	30	1.929	1.931	115/333	10	1.755	1.757	135
S	1.991	1.998	080	50	1.774	1.774	044	15	1.642	1.644	026
VVW	1.912	1.913	082	30	1.697	1.696	135	8	1.566	1.567	226
W	1.803	1.802	156	10	1.528	1.530	335	7	1.499	1.500	444
M	1.624	1.625	347	12	1.448	1.448	444	10	1.457	1.456	177/155
M	1.415	1.415	358	15	1.405	1.405	117/155	10	1.390	1.389	246
M	1.259	1.258	288	10	1.307	1.307	137/355	—	1.354	1.353	137/355
M	1.148	1.150	389					—	1.302	1.299	008
								—	1.226	1.225	228/066
								—	1.200	1.200	157/555
								—	1.163	1.162	048
Crystal structure: tetragonal a = 15.99 Å, c = 13.21 Å				Crystal structure: cubic a = 10.036 ± 0.003 Å				Crystal structure: cubic a = 10.3945 ± 0.004 Å			

Handling of materials, preparation of samples, and transfer to the reaction cells were conducted in a dry box filled with helium gas.

The apparatus for measuring the equilibrium vapour pressures of $ZrCl_4$ and $HfCl_4$ over the pure complex compounds Cs_2ZrCl_6 and Cs_2HfCl_6, respectively, consisted of a hollow fused silica Bourdon spiral pressure gauge connected to a fused silica reaction cell as has been described elsewhere (5).

For these measurements the temperature of the sample container was varied between 360 and 930°C while the upper part of the apparatus containing the Bourdon spiral was maintained at temperatures about 30°C higher than the corresponding normal sublimation points of pure $ZrCl_4$ and $HfCl_4$.

The Cs_2ZrCl_6 or Cs_2HfCl_6 compounds were introduced into the sample container of the apparatus in the form of powders. It was found that large quantities of absorbed gas were released from the salt upon heating. This introduced a systematic error into the measurements. Accordingly, an elaborate degassing procedure was employed in which the cell was repeatedly heated, cooled, reopened, and evacuated. When the residual gas was no longer present upon cooling, equilibrium vapour pressures were measured.

Experimental results

(a) X-ray diffraction powder patterns

The X-ray powder patterns of the compounds Na_2HfCl_6, K_2HfCl_6, and Cs_2HfCl_6 were obtained with a Debye-Scherrer 114.8 mm camera, exposed for various periods of time (1 to 12 h) to CuK_α radiation (λ = 1.5418 Å) filtered through nickel. The diffractometer powder method was also used.

The specimens which were the stoichiometric compounds were ground and screened to −200 mesh in a dry box filled with argon. Then they were hermetically sealed in 0.3 mm silica glass capillaries.

Radiated Cs_2HfCl_6 produced the diffraction pattern shown in Table 1. The results of this work are in agreement with earlier work by Barskaya and Toptygina (10) who prepared their sample by precipitation using hafnium oxychloride as starting material. The extra lines reported by these authors are due to the use of unfiltered radiation.

The X-ray diffraction patterns for the compounds Na_2HfCl_6 and K_2HfCl_6 obtained in this laboratory are also given in Table 1. This study was the first to identify these compounds and no comparison can be made with existing data.

Tentative crystal structures of the hexachlorohafnate compounds were also determined. Although the data in Table 1 are those of polycrystalline samples, it was possible to test whether the structures were cubic, tetragonal, or hexagonal by means of nomographs (11).

Indexed powder X-ray diffraction patterns for the compounds Na_2HfCl_6, K_2HfCl_6, and Cs_2HfCl_6 are given in Table 1, and include the calculated values.

Good agreement with the measured pattern of Na_2HfCl_6 was obtained by assuming this compound to have a tetragonal structure, having a = 15.99 Å and c = 13.21 Å. Table 1 compares the data with the spectrum of the proposed structure.

As seen in Table 1, the measured powder pattern of K_2HfCl_6 and that generated on the assumption that the crystal structure is cubic with a cell dimension having a = 10.036 Å are in good agreement.

The measured powder pattern of Cs_2HfCl_6 is compared with that generated on the assumption that its crystal structure is cubic with a cell dimension a = 10.395 Å. The agreement between observed and calculated d-spacings is excellent. A cubic structure has also been assumed in an earlier investigation (10).

(b) Determination of equilibrium vapour pressures

The vapour pressures of $ZrCl_4$ and $HfCl_4$, in equilibrium with the pure compounds Cs_2ZrCl_6 and Cs_2HfCl_6 respectively, were determined and are given in Table 2. In Fig. 1 these data are plotted as $\ln P_{MCl_4}$ vs. $1/T$. The lines shown on the graphs are calculated by the least-squares method, while the points are experimental.

Some experimental points for the equilibrium decomposition

Can. J. Chem. Downloaded from www.nrcresearchpress.com by 210.87.254.40 on 09/06/12
For personal use only.

Can. J. Chem. Downloaded from www.nrcresearchpress.com by 210.87.254.40 on 09/06/12
For personal use only.

TABLE 2. Measured vapour pressures* of $ZrCl_4$ and $HfCl_4$ over the pure compounds Cs_2ZrCl_6 and Cs_2HfCl_6, respectively

$ZrCl_4$		$HfCl_4$	
T (°C)	P (mm Hg)	T (°C)	P (mm Hg)
352.0	5.2	372.1	4.3
421.4	6.6	400.4	4.8
449.0	6.9	460.6	5.8
576.6	9.3	517.5	6.8
666.8	11.1	565.2	7.4
727.0	12.3	670.3	9.3
752.6	15.5	707.4	9.9
774.1	21.7	763.2	12.6
796.5	41.8	803.4	17.3
810.4	101.8	813.9	31.6
815.1	109.8	825.9	41.8
841.8	145.5	838.1	94.0
859.5	173.7	844.3	102.8
869.8	200.2	863.3	132.0
883.0	230.5	903.4	238.2
895.2	261.8	876.4	178.2
921.7	336.4	856.9	140.2
927.5	357.9	829.5	93.0
909.0	293.3	822.2	45.9
850.6	161.3	809.2	28.8
825.9	125.6	799.9	19.7
817.5	111.4	779.6	15.3
806.9	86.9	730.0	10.7
802.2	63.3	657.7	9.6
791.9	32.4	608.0	8.3
785.2	24.9	544.6	7.2
771.9	21.5	488.0	6.3
741.2	13.0	431.2	5.4
694.1	11.3		
565.9	9.7		
538.0	8.5		
474.9	7.4		
385.7	6.0		

*Pressures were measured in mm Hg, and corrections were made for mercury expansion and for gravity effects (12, 13) to convert to standard conditions, i.e. at 273.15 K and an acceleration of free fall of 9.80665 m/s^2. Pressures given in mm Hg may be converted to bars by multiplying by the factor 1.333×10^{-3}. Temperatures reported in this table are based on the IPTS-68 (14).

pressures of Cs_2ZrCl_6 and Cs_2HfCl_6 obtained previously in the laboratory (6) using a molten tin isoteniscope are also shown in Fig. 1 and are in good agreement with the present work for the Cs_2ZrCl_6 compound. These previous data were obtained only at higher temperatures near the melting temperature of Cs_2ZrCl_6 as at lower temperatures the measurements became unreliable due to gases absorbed by the sample. The previous vapour pressure data over Cs_2HfCl_6 are substantially higher than those obtained in the present study and they become even higher as the temperature increases, due to the evolution of the residual gas which probably had remained in the system.

As was pointed out above, the spiral type gauge used in the present work can withstand large pressure gradients and sudden decompression and is well suited for extensive degassing procedures, thus making possible accurate measurements at low pressures.

Also shown in Fig. 1 are equilibrium pressures reported by Morozov and Sun-In-Chzu (15), which are in disagreement with the values measured in the present study. Transportation techniques have been employed by these authors and no mention was made of the problem of depleting $ZrCl_4$ or $HfCl_4$ from the condensed Cs_2ZrCl_6 and Cs_2HfCl_6 phases during the course of an experiment. The quantitative determination of transported $ZrCl_4$ and $HfCl_4$ was done colorimetrically and by flame photometry.

The corresponding equations for the temperature dependence of the equilibrium pressures within the characteristic temperature ranges were calculated and are given in Table 3.

Reaction [1] in Table 3 defines the equilibrium pressure of $ZrCl_4$ over pure solid Cs_2ZrCl_6 and solid CsCl at temperatures lower than the eutectic temperature shown in Fig. 1.

Reaction [2] in Table 3 represents the equilibrium pressure of $ZrCl_4$ over pure solid Cs_2ZrCl_6 at temperatures higher than the eutectic temperature and in the presence of a solution of CsCl and Cs_2ZrCl_6 of liquidus composition, as given by the phase diagram (6). Due to the temperature dependence of the activity of CsCl in this region, the $\ln P_{ZrCl_4}$ vs. $1/T$ plot exhibits the curvature shown.

Reaction [3] in Table 3 represents the equilibrium pressure of $ZrCl_4$ over pure molten Cs_2ZrCl_6 at temperatures higher than its melting point.

Similar considerations apply to reactions [4], [5], and [6] for Cs_2HfCl_6 given in Table 3. It should be noted that the non-linear and upper linear portions of the pressure curves for Cs_2ZrCl_6 and Cs_2HfCl_6 in Fig. 1 intercept at temperatures which are in agreement with the corresponding melting points of the compounds.

Discussion

The alkali metal hexachlorozirconates and hexachlorohafnates represent stable compounds in which the activities of the corresponding tetrachlorides are particularly low. This is manifested by the dramatic reduction in the pressures of MCl_4 over the pure A_2MCl_6 compounds, shown in Fig. 2 which represents the temperature dependence of the partial pressure of $ZrCl_4$ and $HfCl_4$ in equilibrium with alkali hexachlorozirconates and hexachlorohafnates. As shown in Fig. 2 the vapour pressure of pure $ZrCl_4$, at 450°C, is about 25 atm (16) as compared to the partial pressure of $ZrCl_4$ of 0.01 atm over the pure Cs_2ZrCl_6 at 450°C.

The thermodynamic stability of the A_2MCl_6 compounds, where A represents an alkali metal and M represents Zr or Hf, may be related to the size of the alkali cation A^+. In Fig. 2 the decomposition temperature of the alkali metal hexachlorozirconate and hexachlorohafnate compounds, which is defined as the temperature at which the partial vapour pressure of MCl_4 over the pure A_2MCl_6 compound becomes 1 atm, increases as in the sequence $Li_2MCl_6 \rightarrow Na_2MCl_6 \rightarrow K_2MCl_6 \rightarrow Cs_2MCl_6$, i.e. as the size of the alkali metal cation increases.

Thermodynamic data for the decomposition of the compounds Cs_2ZrCl_6 and Cs_2HfCl_6 may be obtained from the following considerations.

Below the corresponding eutectic temperatures of the pseudobinary systems $CsCl-Cs_2ZrCl_6$ and $CsCl-Cs_2HfCl_6$ respectively, the thermal decomposition of the chlorozirconate and chlorohafnate complex compounds are described by the reactions:

[3] $Cs_2ZrCl_{6(s)} = 2CsCl_{(s)} + ZrCl_{4(vap)}$

[4] $Cs_2HfCl_{6(s)} = 2CsCl_{(s)} + HfCl_{4(vap)}$

By choosing the standard states for the condensed phases as

Can. J. Chem. Downloaded from www.nrcresearchpress.com by 210.87.254.40 on 09/06/12
For personal use only.

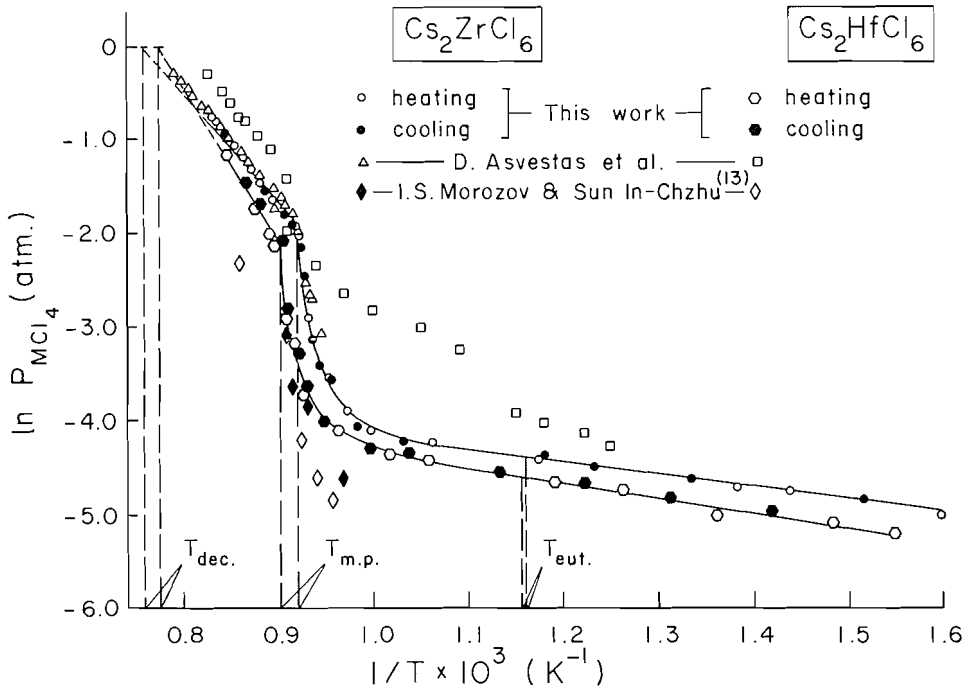

FIG. 1. ln P_{MCl_4} versus $1/T$ diagram for the pure complex compounds Cs_2ZrCl_6 and Cs_2HfCl_6.

TABLE 3. Equilibrium vapour pressures of $ZrCl_4$ and $HfCl_4$ over the pure compounds Cs_2ZrCl_6 and Cs_2HfCl_6, respectively

Equilibrium reactions	Temperature range (K)	ln P_{MCl_4} (atm) = $A + B/T$			
		A	B	Corr. coeff. $\hat{r}$	Std. error $\hat{s}$
[1] $Cs_2ZrCl_{6(s)} = 2CsCl_{(s)} + ZrCl_{4(v)}$	625–862	−2.752	−1 392	0.9927	0.0217
[2] $Cs_2ZrCl_{6(s)} = \underline{2CsCl}_{(l)} + ZrCl_{4(v)}$	862–1083		Non-linear		
[3] $\underline{Cs_2ZrCl_6}_{(l)} = \underline{2CsCl}_{(l)} + ZrCl_{4(v)}$	1083–1200	10.726	−13 788	0.9996	0.0126
[4] $Cs_2HfCl_{6(s)} = 2CsCl_{(s)} + HfCl_{4(v)}$	645–864	−2.781	−1 536	0.9984	0.0604
[5] $Cs_2HfCl_{6(s)} = \underline{2CsCl}_{(l)} + HfCl_{4(v)}$	864–1100		Non-linear		
[6] $\underline{Cs_2HfCl_6}_{(l)} = \underline{2CsCl}_{(l)} + HfCl_{4(v)}$	1100–1177	13.974	−17 790	0.9840	0.0626

the pure solids at all temperatures and for the vapour phase, the pure vapour at 1 atm, the thermodynamic equilibrium constants for the decomposition reactions [3] and [4] can be written as:

$$[5] \quad K = P_{ZrCl_{4(vap)}}$$

$$[6] \quad K = P_{HfCl_{4(vap)}}$$

Actual pressures have been used in these equations, instead of fugacities, as the zirconium tetrachloride vapour is known to be unimolecular and ideal (17, 18), and hafnium tetrachloride vapour would be expected to be quite similar.

The standard heat ΔH_R^0 for the decomposition reactions may be obtained from the van't Hoff equation, written as:

$$[7] \quad \mathrm{d} \ln K/\mathrm{d}T = -\Delta H_R^0/RT^2$$

while the standard free energy and the average standard entropy can be determined from the well known equations

$$[8] \quad \Delta G_R^0 = -RT \ln K$$

$$[9] \quad \Delta G_R^0 = \Delta H_R^0 - T\Delta S_R^0$$

The results of these calculations for pure Cs_2ZrCl_6 and Cs_2HfCl_6 are given in Table 4, including the thermodynamic values for the decomposition of the other pure alkali hexachlorozirconate and hexachlorohafnate compounds (19). From these data the equilibrium constant of the exchange reaction:

$$[10] \quad \underset{(vap)}{HfCl_4} + \underset{\text{(as a solid solution of } Cs_2ZrCl_6 \text{ in } Cs_2HfCl_6)}{Cs_2ZrCl_6} = \underset{(vap)}{ZrCl_4} + \underset{\text{(as a solid solution of } Cs_2HfCl_6 \text{ in } Cs_2ZrCl_6)}{Cs_2HfCl_6}$$

is calculated as

$$[11] \quad K_{ex} = \left(\frac{P_{ZrCl_4}}{P_{HfCl_4}}\right)_{vap} \left(\frac{X_{Cs_2HfCl_6}}{X_{Cs_2ZrCl_6}}\right)_{\text{in solid solution}}$$

In this equation, mole fractions (X's) have been substituted for activities, because of the suggested ideal behaviour of the solid solutions (19).

Since [10] was derived by subtracting [3] from [4] given in Table 3, the temperature dependence of the equilibrium constant given by [11] may be calculated by combining [5] and [6] as:

$$[12] \quad \ln K_{ex} = 0.029 + 144/T$$

A plot of K_{ex} vs. T (in °C) is shown in Fig. 3. Data for the previously investigated systems employing LiCl (1), NaCl (3),

Can. J. Chem. Downloaded from www.nrcresearchpress.com by 210.87.254.40 on 09/06/12
For personal use only.

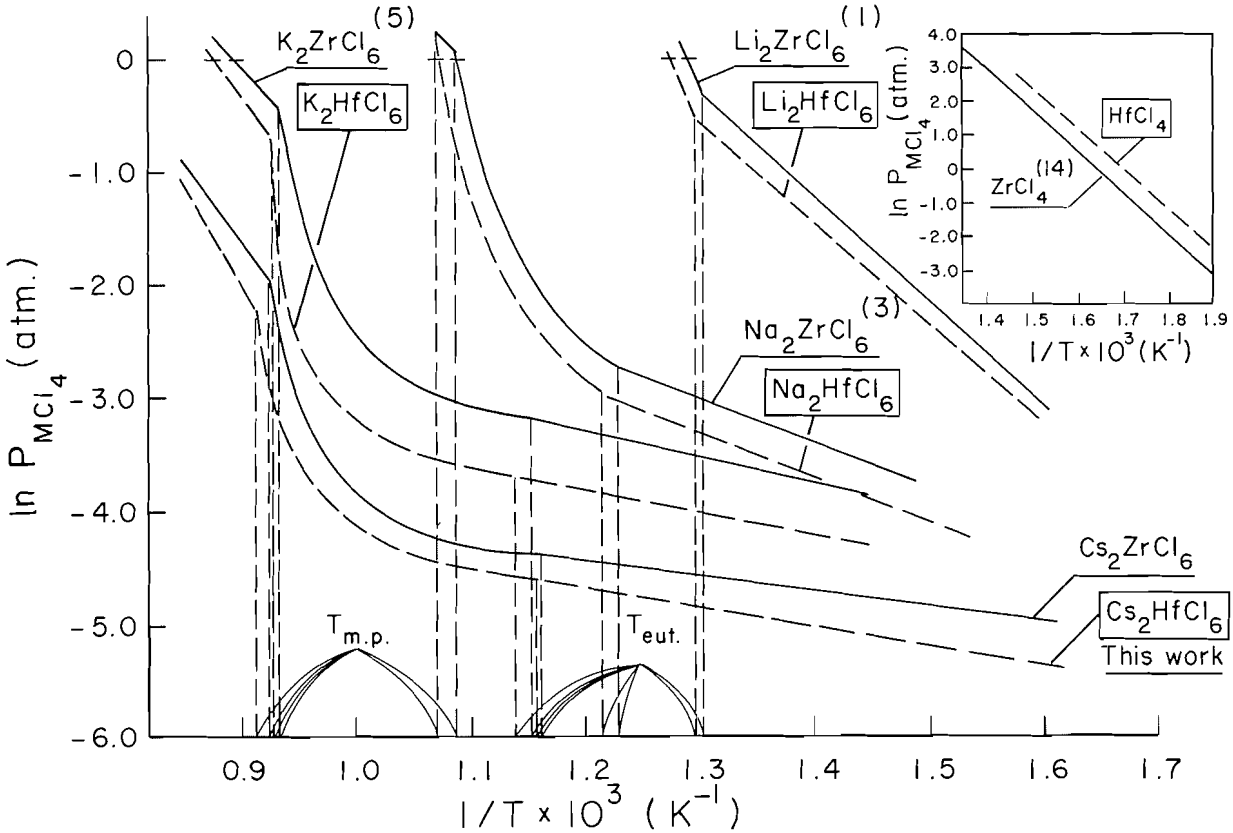

FIG. 2. Temperature dependence of the partial pressure of $ZrCl_4$ and $HfCl_4$ in equilibrium with the various alkali hexachlorozirconate and hexachlorohafnate compounds.

TABLE 4. Thermodynamic* values for the decomposition of pure alkali hexachlorozirconates and hexachlorohafnates

Compound	Temperature range (K)	ΔH^0_R(dec.) (cal/mol)	ΔS^0_R(dec.) (eu)	Reference
Li_2ZrCl_6	633–769	7 888	9.97	1
Na_2ZrCl_6	672–821	7 807	4.16	3
K_2ZrCl_6	694–867	4 570	−1.08	5
Cs_2ZrCl_6	625–862	2 766	−5.47	This work
Li_2HfCl_6	623–773	7 570	9.32	1
Na_2HfCl_6	653–813	7 485	3.09	3
K_2HfCl_6	700–877	2 678	−4.66	5
Cs_2HfCl_6	645–864	3 052	−5.53	This work

*Enthalpies and entropies given in cal/mol and eu may be converted to the corresponding SI units of J/mol and J/deg-mol by multiplying by the factor 4.184.

and KCl (5) are also included in this figure for comparison purposes.

It has been shown in a previous publication (8) that impure $ZrCl_4$ containing $HfCl_4$ may be purified in a closed two-compartment reaction cell in which the impure $Zr(Hf)Cl_4$ mixture is placed in the first compartment, which is kept at a temperature T_1, while the alkali chloride ACl is placed in the second compartment which is kept at a temperature T_2.

The separation proceeds through the formation of the complex compounds A_2ZrCl_6 and A_2HfCl_6 which appear in the second compartment as a solid solution. The efficiency of the separation process depends upon the magnitude of the equilibrium constant for the exchange reaction [10].

The efficiency of separation η defined as:

$$[13]\quad \eta = \frac{(\text{wt\% } HfCl_4)_{initial} - (\text{wt\% } HfCl_4)_{final}}{(\text{wt\% } HfCl_4)_{initial}} \times 100$$

may be calculated from the previously derived relationship (8)

$$[14]\quad K_{ex} = \frac{2(X'_{ZrCl_4})a - b + 2Z}{2(X'_{HfCl_4})a - 2Z}\left(\frac{P^0_{ZrCl_4}}{P^0_{HfCl_4}}\right)_{T_1}\frac{2Z}{b - 2Z}$$

where X'_{ZrCl_4} and X'_{HfCl_4} are the mole fractions of $ZrCl_4$ and $HfCl_4$ respectively in the $Zr(Hf)Cl_4$ mixture initially present in the first compartment of the separation cell prior to reaction; a represents the total number of moles of $Zr(Hf)Cl_4$ present in the first compartment of the reactor, prior to separation; b represents the number of moles of ACl present in the second compartment of the reactor; Z is the number of moles of $HfCl_4$

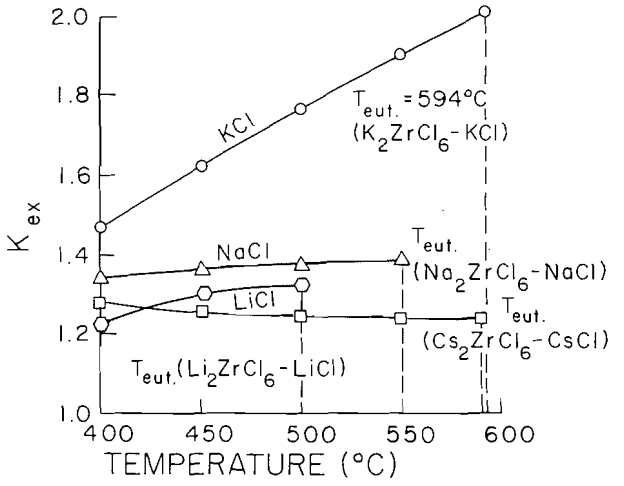

FIG. 3. Temperature dependence of the equilibrium constants K_{ex} for the exchange reactions:

$$HfCl_{4(v)} + A_2ZrCl_{6(sol.solution)} \leftrightarrows A_2HfCl_{6(sol.solution)} + ZrCl_{4(v)}$$

where A = Li^+, Na^+, K^+, or Cs^+.

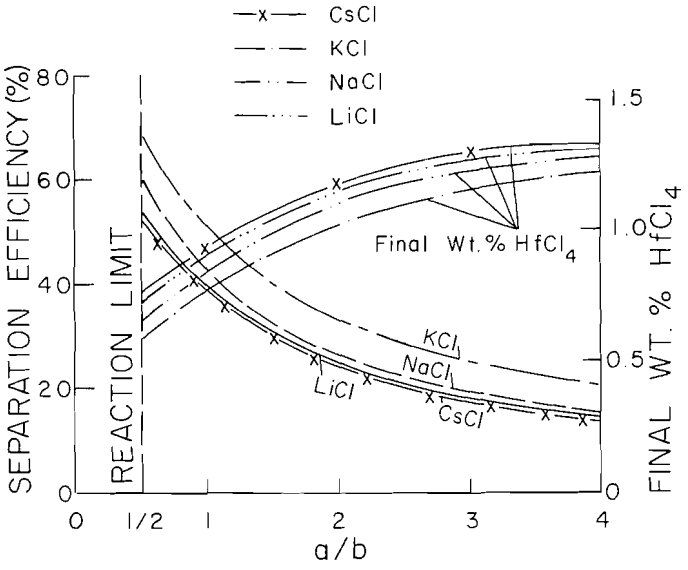

FIG. 4. Variation of the separation efficiency and of the final wt% $HfCl_4$ with the molar ratio a/b of Zr(Hf)Cl_4 to ACl, for a Zr(Hf)Cl_4 mixture initially containing 1.54 wt% $HFCl_4$. T_1 and T_2 are respectively 330 and 450°C.

which have reacted with ACl and are retained in the second compartment of the reactor after equilibrium has been reached; $P^0_{ZrCl_4}$ and $P^0_{HfCl_4}$ are the sublimation pressures (16) of pure $ZrCl_4$ and $HfCl_4$ respectively, at temperature T_1.

Considering a reactor containing CsCl and T_1 and T_2 temperatures of 330 and 450°C respectively, the separation efficiency factor η may be calculated from the determined values of K_{ex} and for various ratios of a/b.

Figure 4 illustrates the variation of η with the a/b ratio for LiCl, NaCl, KCl, or CsCl. As is seen, η increases as the a/b ratio decreases. Hence the separation becomes more efficient when the amount of Zr(Hf)Cl_4 mixture placed in compartment I is close to that required by the stoichiometry for the formation of Cs_2ZrCl_6 and Cs_2HfCl_6. The reaction limit is reached at a/b = 0.5, at which point all the added tetrachloride vapours react with the CsCl. On the other hand, as the a/b ratio approaches the value of 0.5, most of the Zr(Hf)Cl_4 is present as a Cs_2ZrCl_6–Cs_2HfCl_6 solid solution in compartment II. Hence for practical purposes, the a/b ratio must be larger than 0.5, and a value of about 0.8 to 1.0 appears optimum. At a/b = 0.8 the calculated separation efficiency is about 40%.

By comparing LiCl, NaCl, KCl, and CsCl as separating agents for Hf, it is evident that at 450°C the separation efficiency increases in the order CsCl → LiCl → NaCl → KCl.

In a recent publication from this laboratory (9) the separation of Hf from Zr has been described using a liquid alkali chloride or mixtures of alkali chlorides as separating agents. When liquid CsCl is used the exchange reaction may be written as:

[15] $HfCl_4$ (vap) + Cs_2ZrCl_6 (as a liquid solution of Cs_2ZrCl_6 in Cs_2HfCl_6) = $ZrCl_4$ (vap) + Cs_2HfCl_6 (as a liquid solution of Cs_2HfCl_6 in Cs_2ZrCl_6)

the equilibrium constant of which may also be approximated to that given by [12].

Acknowledgement

The authors are grateful to the Natural Sciences and Engineering Research Council of Canada for a grant in support of this work.

1. J. E. DUTRIZAC and S. N. FLENGAS. Advances in Extractive Metallurgy Symposium, paper 24, April 17–20. The Institution of Mining and Metallurgy, London, England. 1967.
2. R. L. LISTER and S. N. FLENGAS. Can. J. Chem. **43**, 2947 (1965).
3. G. J. KIPOUROS and S. N. FLENGAS. Can. J. Chem. **59**, 990 (1981).
4. R. L. LISTER and S. N. FLENGAS. J. Electrochem. Soc. **111**, 343 (1964).
5. G. J. KIPOUROS and S. N. FLENGAS. Can. J. Chem. **56**, 1549 (1978).
6. D. A. ASVESTAS, P. PINT, and S. N. FLENGAS. Can. J. Chem. **55**, 1154 (1977).
7. J. E. DUTRIZAC and S. N. FLENGAS. Canadian Patent No. 863,258 (February 9, 1971).
8. S. N. FLENGAS and J. E. DUTRIZAC. Metall. Trans. B, **8B**, 377 (1977).
9. C. A. PICKLES and S. N. FLENGAS. *In* Extractive metallurgy of refractory metals. *Edited by* H. Y. Sohn, O. Norman Carlson, and J. T. Smith. 1981, AIME. p. 107.
10. I. B. BARSKAYA and G. M. TOPTYCINA. Russ. J. Inorg. Chem. **12**, 14 (1967).
11. E. W. NUFFIELD. X-ray diffraction methods. John Wiley and Sons, Inc., New York, 1966. p. 120.
12. D. AMBROSE. Vapour pressures. *In* Chemical thermodynamics, Vol. I. *Edited by* M. L. McGlashan. The Chemical Society, 1973. Chapt. 7.
13. W. G. BROMBACHER, D. R. JOHNSON, and J. L. CROSS. Mercury barometers and manometers. National Bureau of Standards, Washington, D.C. Monograph 8. 1960.
14. R. L. POWELL *et al.* Thermocouple reference tables based on the IPTS-68. National Bureau of Standards, Washington, D.C. Monograph 125. 1974.
15. I. S. MOROZOV and SUN-IN-CHZHU. Zh. Neorg. Khim. **4**, 678 (1959); Russ. J. Inorg. Chem. **4**, 307 (1959).
16. A. A. PALKO, A. D. RYON, and D. W. KUHN. J. Phys. Chem. **62**, 319 (1958).
17. O. RAHLES and W. SISCHER. Z. Anorg. Allg. Chem. **21**, 349 (1933).
18. J. A. FRIEND, A. T. W. COLLEY, and R. S. HAYES. J. Chem. Soc. 494 (1930).
19. S. N. FLENGAS and P. PINT. Can. Metall. Q. **8**, 151 (1969).

Can. J. Chem. Downloaded from www.nrcresearchpress.com by 210.87.254.40 on 09/06/12
For personal use only.

Quantitative determination of hafnium in mixtures of zirconium–hafnium hexachloro alkali compounds by neutron activation analysis and X-ray fluorescence

C. A. PICKLES, G. J. KIPOUROS,[1] AND S. N. FLENGAS

Department of Metallurgy and Materials Science, University of Toronto, Toronto, Ont., Canada M5S 1A4

AND

R. G. V. HANCOCK

SLOWPOKE Nuclear Reactor Facility, University of Toronto, Toronto, Ont., Canada M5S 1A4

Received November 9, 1982

C. A. PICKLES, G. J. KIPOUROS, S. N. FLENGAS, and R. G. V. HANCOCK. Can. J. Chem. **61**, 2189 (1983).

A procedure for the determination of Hf in both mixtures of $HfCl_4-ZrCl_4$ and $A_2HfCl_6-A_2ZrCl_6$, where A = Li, Na, K, Rb, or Cs, is described. The method involves conversion of the chlorocompounds into HfO_2-ZrO_2 mixtures and subsequent analysis by either X-ray fluorescence or neutron activation analysis. The two analytical techniques are compared with regard to accuracy and simplicity.

C. A. PICKLES, G. J. KIPOUROS, S. N. FLENGAS et R. G. V. HANCOCK. Can. J. Chem. **61**, 2189 (1983).

On décrit une méthode de détermination du HF dans les mélanges de $HfCl_4-ZrCl_4$ et de $A_2HfCl_6-A_2ZrCl_6$, ou A = Li, Na, K, Rb ou Cs. La méthode fait intervenir la transformation des composés chlorés en des mélanges de HfO_2-ZrO_2 suivie d'une analyse par fluorescence de rayons-X ou d'une analyse par activation neutronique. On a comparé ces deux techniques d'analyse dans le but de déterminer la technique la plus précise et la plus simple.

[Traduit par le journal]

Introduction

Hafnium and zirconium have almost identical chemical properties and therefore separation of the two elements is both difficult and expensive. At the present time hafnium is separated from zirconium by solvent extraction (1, 2). This process has certain disadvantages and therefore a number of alternative processes have been proposed, which include fractional crystallization (3), ion exchange (4), and fractional distillation (5). It is also possible to separate hafnium from zirconium by the selective reaction of $HfCl_4-ZrCl_4$ vapour mixtures with either solid or molten alkali chlorides (ACl where A = Li, Na, K, Rb, or Cs) (6, 7). In order to determine the separation efficiency of the process, a method was devised for determining the concentration of hafnium in both mixtures of $HfCl_4-ZrCl_4$ and in mixtures of A_2HfCl_6 and A_2ZrCl_6, where the hafnium concentration ranged from 0.1 to 3.9 wt.% $HfCl_4$ in the $HfCl_4-ZrCl_4$ mixtures. Quantitative chemical analysis of hafnium–zirconium systems is impossible by standard chemical methods. X-ray fluorescence has been employed successfully under carefully controlled conditions for analysis of mixtures of zirconium and hafnium oxides in the concentration range from 0.5 to 99.5 wt.% hafnium (8). This technique suffers from both matrix effects and a strong dependence on the sample preparation method. To avoid these potential problems neutron activation analysis was employed and compared with the X-ray fluorescence technique.

Sample preparation

Because the chlorocompounds of zirconium and hafnium hydrolyse readily it is necessary to convert them to a stable form which in this case is the respective oxide. The synthetic standards were prepared by weighing the appropriate amounts of spectrographic grade $ZrCl_4$ and $HfCl_4$ containing less than 100 ppm $HfCl_4$ and $HgCl_4$ in a dry box. Then the sample was dissolved in distilled water and the HfO_2-ZrO_2 mixture was precipitated by the addition of ammonium hydroxide. The oxide was filtered, dried, and fired at 1000°C in a platinum crucible for 12 h. This method results in mixtures which are more homogeneous than those obtained by the mechanical mixing of the oxides.

X-ray powder diffraction patterns were employed to verify that the hydrolysis of the chlorides to the oxides was complete, and the results confirmed that $HfCl_4$ and $ZrCl_4$ were completely converted to the respective oxides. Furthermore, to confirm that the hydrolysis of A_2MCl_6 proceeded according to the reaction:

$$[1] \quad 2A_2MCl_6 + H_2O \rightarrow 2MO_2 + 8HCl + 4ACl$$

the filtrate, which contained dissolved ACl, was evaporated to dryness. The X-ray powder pattern of the dried filtrate corresponded to that of ACl in each case.

Results

Neutron activation analysis

Powdered samples, weighing approximately 300 mg, were placed in polyethylene vials. They were irradiated in the SLOWPOKE nuclear reactor in a neutron flux of 1.0×10^{11} n/cm^2 s for 10 s. The hafnium isotope measured was ^{179m}Hf with a γ-ray energy of 214.3 keV and a half-life of 19.0 s. After a decay time of about 180 s, the irradiated samples were counted for 20 s. Thus, the total cycle time for a single analysis was less than 1 min. Measurements of γ-ray activities were made with a Canberra Ge–(Li) detector coupled to a Canberra 8180 series 4096 channel analyzer. The detector had a nominal relative counting efficiency of 6.7% and FWHM resolution of 1.9 keV for the 1332 keV γ-ray of ^{60}Co. It is mounted horizontally in a model 7600 cryostat. γ-Ray peak intensities were evaluated by automatic analyzer integration of suitable manually selected spectral regions of interest at each peak. The teletype output integrals were then processed using a Texas Instrument TI-55 calculator to determine elemental concentrations.

Whenever a set of samples was analyzed, a standard was also irradiated. The hafnium measurements of the standards were best represented by a least-square line. Thus, the elemental hafnium content of a sample was determined by comparison with the standard line.

[1]Present address: Department of Materials Science and Engineering, Massachusetts Institute of Technology, Cambridge, MA 02139, U.S.A.

Can. J. Chem. Downloaded from www.nrcresearchpress.com by 210.87.254.42 on 09/06/12
For personal use only.

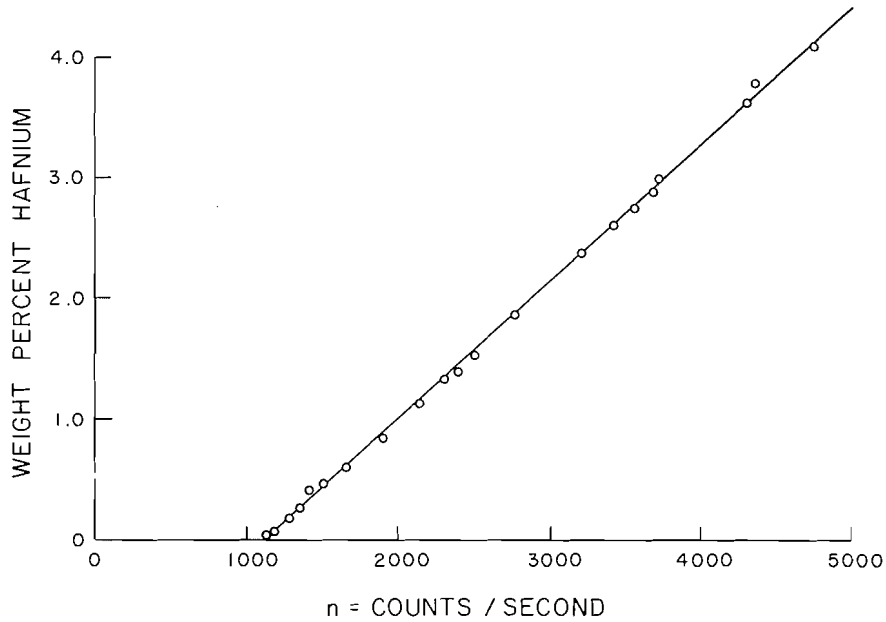

FIG. 1. Calibration curve for hafnium contents in the range 0 to 4 wt.% by neutron activation analysis.

Typical results are as follows:
In the range $0 < \text{wt.\% Hf} < 4$

$$[2] \quad \text{wt.\% Hf} = 2.63 \times 10^{-5}\, n - 1.62 \times 10^{-1}$$

where n is the number of counts per s. The correlation coefficient was $r = 0.9986 \pm 0.0018$ to within 95% certainty and the standard error of estimate was $S_{y.x} = 1.22$. The results of the analyses and the least-square line are shown in Fig. 1.

The corresponding amount of HfO_2 present in the sample was then calculated, and the difference between this and the total mass of the sample was presumed to be the mass of ZrO_2. From this value the mass of elemental zirconium was calculated. The zirconium concentration was reported as wt.% zirconium in the ZrO_2-HfO_2 mixture. The hafnium concentration had an absolute error estimate of less than 0.1 wt.% for hafnium contents of less than 4%. The lower limit of detection by this method using samples such as those described herein was determined to be about 100 ppm of hafnium in ZrO_2 (10).

This method is accurate provided that the sample consists of only HfO_2-ZrO_2. In order to check the analysis, the entire γ spectrum of each sample was examined to detect the presence of any other metals. In samples prepared from the tetrachloride mixtures only zirconium and hafnium were found. However, samples prepared from $A_2ZrCl_6-A_2HfCl_6$ mixtures contained small but measurable amounts of alkali metals. The concentration of these metals was less than 5% of the total mass of the sample. Since the chlorine content was below the lower limit of detection (about 50 μg) it was concluded that the alkali metal was not present as a chloride. Therefore it was assumed that the alkali metal was present as oxide, A_2O, and the appropriate small correction was made to the zirconium concentration. Table 1 gives the isotope which was measured for each element.

X-ray fluorescence analysis

A weighed amount (1 g) of the prepared standard was ground to minus 325 mesh, mixed with 1/2 g of methylcellulose and pressed to form tablets.

The hafnium line L_{β_2} at $2\theta = 38.47°$, was resolved from the zirconium second order K_{β_1} line at $2\theta = 40.14°$ and the counts over 40 s were measured in a SIEMENS SRI spectrometer with a tungsten target and a lithium fluoride (200) diffracting crystal. The counts over 40 s were also measured at an angle at which there was no peak present and the intensity was found to be independent of the hafnium content. This angle was found at 35°.

TABLE 1. Nuclear data for sample analysis (9)

Element	Isotope measured	Half-life	γ-Ray (keV)
Hf	^{179m}Hf	19.0 s	214.3
Na	^{24}Na	15 h	1368.4
K	^{42}K	12.52 h	1524.7
Rb	^{80m}Rb	1.02 min	2118.6
Cs	^{134m}Cs	3.15 h	127.4
Cl	^{38}Cl	37.29 min	1642.0

The hafnium measurement on the standards was best represented by a least-square line and the elemental hafnium content of the sample was determined by comparison with the standard line.
In the range $0 < \text{wt.\% Hf} < 4$

$$[3] \quad \text{wt.\% Hf} = 1.14 \times 10^{-3}\, n - 1.28$$

where n is the number of counts per s. The correlation coefficient was $r = 0.9955 \pm 0.0006$ to within 95% certainty and the standard error of estimate was $S_{y.x} = 1.32$. The results of the analyses and the least-square line are shown in Fig. 2. Again the absolute error estimate was less than 0.1 wt.% and the detection limit was about 100 ppm.

From a comparison of the correlation coefficients and the standard errors of estimate for both neutron activation and X-ray fluorescence, it is clear that the accuracy of the methods is similar for hafnium contents in the composition range up to 4 wt.%. However, the neutron activation technique requires less sample preparation and the cycle time is reduced, and for the same accuracy it should be considered as superior to the X-ray fluorescence technique.

Can. J. Chem. Downloaded from www.nrcresearchpress.com by 210.87.254.42 on 09/06/12
For personal use only.

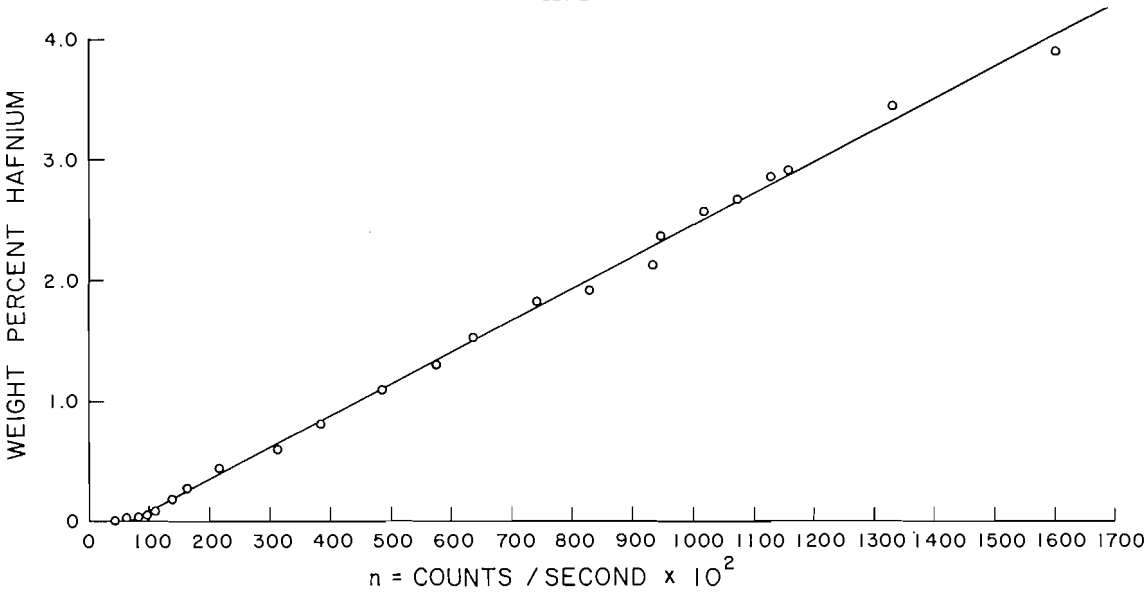

FIG. 2. Calibration curve for hafnium contents in the range 0 to 4 wt.% by X-ray fluorescence.

1. H. F. REICHARD and R. H. NEILSEN. J. Metals, **28**, 28 (1976).
2. W. A. STICKNEY. U.S. Bureau of Mines, RI-S499 (1959).
3. N. P. SAJIN and E. A. PEPELYAEVA. Proc. Int. Conf. Peaceful Uses Atomic Energy, Geneva, 1955, United Nations, NY (8), 559 (1956).
4. M. QUERESHI and K. HUSAIN. Anal. Chem. **43**, 447 (1971).
5. L. A. NISEL'SON, T. D. SOKOLOVA, and V. I. STOLYAROV. Dokl. Akad Nauk. SSSR, **168**, 1107 (1966).
6. S. N. FLENGAS and J. E. DUTRIZAC. Met. Trans. B, **8B**, 377 (1977).
7. C. A. PICKLES and S. N. FLENGAS. *In* Extractive metallurgy of refractory metals. *Edited by* R. O. Carlsson, AIME, New York. 1981. pp. 315–339.
8. A. K. MUKHERJI. *In* Analytical chemistry of zirconium and hafnium. Pergamon Press. 1970. pp. 226–246.
9. F. ADAMS and R. DAMS. J. Radioanal. Chem. **3**, 99 (1969).
10. R. JENKINS and J. L. DEVRIES. Practical X-ray spectrometry, New York. 1967.

Can. J. Chem. Downloaded from www.nrcresearchpress.com by 210.87.254.42 on 09/06/12
For personal use only.

Bis(diethylammonium) hexachlorostannate(IV), $(Et_2NH_2)_2SnCl_6$, and tris-(di-*n*-propylammonium) hexachlorostannate(IV) chloride, $(n\text{-}Pr_2NH_2)_3(SnCl_6)Cl$: crystal structure and hydrogen bonding[1]

T. STANLEY CAMERON, MARGARET ANN JAMES, AND OSVALD KNOP

Department of Chemistry, Dalhousie University, Halifax, N.S., Canada B3H 4J3

AND

MICHAEL FALK

Atlantic Research Laboratory, National Research Council of Canada, Halifax, N.S., Canada B3H 3Z1

Received March 1, 1983

T. STANLEY CAMERON, MARGARET ANN JAMES, OSVALD KNOP, and MICHAEL FALK. Can. J. Chem. **61**, 2192 (1983).

The crystal structure of $(Et_2NH_2)_2SnCl_6$ ($P2_1/n$, $Z = 2$, $a = 9.078(1)$ Å, $b = 10.644(2)$ Å, $c = 9.801(2)$ Å, $\beta = 93.02(1)°$) consists of a monoclinically distorted antifluorite arrangement of $Et_2NH_2^+$ and $SnCl_6^{2-}$ ions. The $SnCl_6$ octahedra are linked by hydrogen bonds to form infinite chains separated from one another by the Et groups. The temperature variation of the spectral features in the NH and ND stretching regions points to the existence of a transition in the vicinity of 320 K. The structure of $(n\text{-}Pr_2NH_2)_3(SnCl_6)Cl$ ($P2_1/c$, $Z = 4$, $a = 10.265(4)$ Å, $b = 30.428(4)$ Å, $c = 10.380(2)$ Å, $\beta = 92.75(3)°$) consists of $n\text{-}Pr_2NH_2^+$ cations of three types, $SnCl_6^{2-}$, and Cl^-. All the ions are interconnected by hydrogen bonds, those to Cl^- being of a strength comparable to the strength of the short, linear N—H···Cl^- bond in Et_3NHCl. Spectroscopic evidence indicates the probable existence of a transition at ~170 K.

T. STANLEY CAMERON, MARGARET ANN JAMES, OSVALD KNOP et MICHAEL FALK. Can. J. Chem. **61**, 2192 (1983).

Le composé $(Et_2NH_2)_2SnCl_6$ cristallin représente une variété monocline ($P2_1/n$, $Z = 2$, $a = 9{,}078(1)$ Å, $b = 10{,}644(2)$ Å, $c = 9{,}801(2)$ Å, $\beta = 93{,}02(1)°$) de la structure antifluorine déformée comportant les ions $Et_2NH_2^+$ et $SnCl_6^{2-}$. Les octaèdres $SnCl_6$ sont reliés par des liaisons hydrogène; les chaînes infinies qui en résultent sont séparées l'une de l'autre par des groupes éthyle. Les variations thermiques des caractéristiques spectrales, dans les régions d'élongation du NH et du ND, indiquent une transition à environ 320 K. La structure cristalline du $(n\text{-}Pr_2NH_2)_3(SnCl_6)Cl$ ($P2_1/c$, $Z = 4$, $a = 10{,}265(4)$ Å, $b = 30{,}428(4)$ Å, $c = 10{,}380(2)$ Å, $\beta = 92{,}75(3)°$) comprend des cations $n\text{-}Pr_2NH_2^+$ de trois types et des anions $SnCl_6^{2-}$ ainsi que Cl^-. Tous les ions sont reliés par des liaisons hydrogène. La force de la liaison hydrogène dans le cas de l'ion Cl^- s'approche de celle de la courte liaison rectiligne N—H···Cl^- du Et_3NHCl. Les preuves spectroscopiques indiquent l'existence probable d'une transition à 170 K environ.

In previous papers (1, 2) we dealt at some length with the structural and hydrogen-bonding aspects of a number of alkylammonium hexachlorostannates(IV), $(R_nNH_{4-n})_2SnCl_6$. Among the ir spectra described in ref. 2 were those of $(Et_2NH_2)_2SnCl_6$ (2EHS) and $(n\text{-}Pr_2NH_2)_3(SnCl_6)Cl$ (2PHS.PCl) (the last-named compound having been initially taken for $(n\text{-}Pr_2NH_2)_2SnCl_6$ = 2PHS), but in the absence of crystal-structure determinations of the two compounds the interpretation of the spectra was largely tentative.

The crystal structures of these two salts have now been determined and are described below, together with additional information on the NH and ND stretching regions of the ir spectra. Details of the preparation and crystal-structure determination are given in ref. 2 and will not be repeated here. The crystal data of both compounds are presented in Table 1.

$(Et_2NH_2)_2SnCl_6$

From optical measurements Ries (3) concluded that the point-group symmetry of 2EHS was C_{2h} (the same as that of the corresponding hexachloroplatinate, ref. 4). This agrees with our observation. With the N—H and C—H bond lengths constrained to 1.02 and 1.08 Å, respectively, the structure was refined anisotropically (except for the isotropic temperature factors on the hydrogens) to $R = 0.030$. The positional parameters are listed in Table 2, the thermal parameters in Table 3,[2]

TABLE 1. Crystallographic data of $(Et_2NH_2)_2SnCl_6$ and $(n\text{-}Pr_2NH_2)_3SnCl_7$*

Parameter	Value	
	$C_8Cl_6H_{24}N_2Sn$	$C_{18}Cl_7H_{48}N_3Sn$
Formula weight	479.70	673.46
a, Å	9.078(1)	10.265(4)
b, Å	10.644(2)	30.428(4)
c, Å	9.801(2)	10.380(2)
β, deg	93.02(1)	92.75(3)
V, Å^3	945.7(2)	3238.4(4)
Z	2	4
d_{obs}, g/cm^3	1.680†	1.372
d_{calcd}, g/cm^3	1.685(3)	1.381(4)
Space group	$P2_1/n$ (No. 14)‡	$P2_1/c$ (No. 14)§
$F(000)$	476	1384
μ_{Mo}, cm^{-1}	20.3	12.7
θ range, deg	2–23	2–23
Reflections:		
Total counted	1844	4729
Unique, total	1643	4391
Unique, used‖	1468	3094
$100R$; $100R_w$	3.0; 2.9	4.4; 4.5

*Radiation, Mo $K\alpha_1$; $\lambda = 0.70926$ Å.

†Reference 3.

‡Systematic absences: $h0l$, $h + l = 2n + 1$; $0k0$, $k = 2n + 1$. All atoms except Sn in general positions.

§Systematic absences: $h0l$, $l = 2n + 1$; $0k0$, $k = 2n + 1$. All atoms in general positions.

‖$I > 1\sigma(I)$.

[1]NRCC No. 21280.

[2]This Table has been deposited. Copies are available, at a nominal charge, from the Depository of Unpublished Data, CISTI, National Research Council of Canada, Ottawa, Ont., Canada K1A 0S2.

Can. J. Chem. Downloaded from www.nrcresearchpress.com by 210.87.254.5 on 09/06/12
For personal use only.

TABLE 2. $(Et_2NH_2)_2SnCl_6$: positional parameters*

Atom	Positional parameter			Atom	Positional parameter		
	x	*y*	*z*		*x*	*y*	*z*
Sn	½	½	½	H(11)	6851(18)	1856(53)	8445(60)
Cl(1)	3422(1)	3979(1)	6602(1)	H(12)	5701(53)	2711(36)	7630(31)
Cl(2)	7075(1)	3755(1)	5872(1)	H(111)	5559(49)	2108(34)	10519(36)
Cl(3)	4387(1)	3397(1)	3308(1)	H(112)	4380(34)	3149(45)	9559(51)
N	5770(1)	2116(2)	8447(2)	H(121)	6336(56)	4553(39)	9165(40)
C(11)	5446(4)	2782(4)	9739(4)	H(122)	6452(67)	4292(53)	10944(36)
C(12)	6481(5)	3884(4)	9962(5)	H(123)	7579(35)	3581(53)	9931(62)
C(21)	4781(5)	1031(4)	8114(4)	H(211)	4942(53)	0380(39)	8905(40)
C(22)	5146(5)	0441(5)	6774(5)	H(212)	3691(37)	1375(55)	7962(60)
				H(221)	4980(59)	1077(43)	5935(41)
				H(222)	6253(40)	0131(64)	6791(88)
				H(223)	4523(77)	−0348(49)	6488(82)

*All nonspecial parameter values have been multiplied by 10^4.

TABLE 5. $(Et_2NH_2)_2SnCl_6$: interatomic distances (Å) and bond angles (deg)*

Atom	Distance	Atoms	Angle
Sn—Cl(1)	2.436(1)	Cl(1)—Sn—Cl(2)	90.1(0)
Sn—Cl(2)	2.422(1)	Cl(1)—Sn—Cl(3)	90.3(0)
Sn—Cl(3)	2.424(1)	Cl(2)—Sn—Cl(3)	90.1(0)
N—H(11)	[1.02]†	N—H(11)—Cl(3A)	170(5)
N—H(12)		N—H(11)—Cl(2)	86(4)
N···Cl(2)	3.336(3)	N—H(12)—Cl(1)	129(4)
N···Cl(3A)	3.338(2)	N—H(12)—Cl(2)	145(4)
N···Cl(1)	3.367(3)	Cl(1)—H(12)—Cl(2)	85(3)
N···Cl(1A)	3.991(3)		
N···Cl(2′A)	4.115(3)		
H(11)···Cl(3A)	2.33(3)		
H(11)···Cl(2)	3.25(8)		
H(11)···Cl(1A)	3.45(7)		
H(11)···Cl(2′A)	3.50(7)		
H(12)···Cl(2)	2.45(6)		
H(12)···Cl(1)	2.63(7)		
H(12)···Cl(3′)	4.24(4)		

*Symmetry code (Fig. 2): Cl(3′): $1-x, 1-y, 1-z$; Cl(1A), Cl(3A): $\frac{1}{2}+x, \frac{1}{2}-y, \frac{1}{2}+z$; Cl(2′A): $\frac{3}{2}-x, y-\frac{1}{2}, \frac{3}{2}-z$.
†Constrained in refinement.

the structure factors in Table 4,[2] and interatomic distances and bond angles in Table 5.

The cation/anion packing in 2EHS is yet another example of the antifluorite arrangement, monoclinically distorted (cf. refs. 2 and 5) (Fig. 1). The centrosymmetric $SnCl_6$ octahedra are practically regular, the mean of d(Sn—Cl) being 2.427(8) Å. This is statistically indistinguishable from the mean for $(R_nNH_{4-n})_2SnCl_6$, 2.425(12) Å (2). There is only one type of NH_2 group in the structure. One of the N-hydrogens, H(12), participates in a slightly asymmetrically bifurcated N—H···2Cl bond, with H···Cl distances of ~2.45 and ~2.63 Å and NHCl angles of 145° and 129°, respectively.[3] The other hydrogen, H(11), forms a slightly bent N—H···Cl bond, H···Cl ~ 2.33 Å, NHCl ~ 170° (Fig. 2).

As would be expected for an $(R_2NH_2)_2SnCl_6$ structure containing small alkyls (cf. ref. 2), the hydrogen bonds join the $SnCl_6$ octahedra so as to form infinite chains separated from one another by the Et groups (Fig. 1). 2EHS is thus similar to the corresponding Me salt, 2MHS. However, both salts undergo thermally induced transitions, 2MHS at ~100 K (2) and 2EHS to all appearances at ~320 K (*vide infra*), i.e. at room temperature 2MHS is above but 2EHS below T_{tr}. This difference is reflected in the two room-temperature structures. High-temperature polymorphs generally have higher symmetries than the corresponding low-temperature forms. Indeed, the $Me_2NH_2^+$ ion in 2MHS has C_s symmetry at room temperature, with the two N—H bonds equivalent, but this equivalence is destroyed by cooling through T_{tr} (2). This would suggest that the N—H(11) and N—H(12) bonds, which are dissimilar in the room-temperature structure of 2EHS, become equivalent on heating through T_{tr}, so that the 2EHS structure would then resemble even more closely the room-temperature structure of 2MHS.

Features of the ir spectra in the NH and ND stretching regions and their temperature dependence have already been described (2). Their interpretation is now supported by the knowledge of the crystal structure. The nonequivalent N—H(11) and N—H(12) bonds would be expected to give rise to 1:1 NH and ND stretching doublets, and this is what is observed at all temperatures below 293 K (Fig. 21 of ref. 2).

[3]The N—H(12)···Cl(1),Cl(2) grouping is close to planar.

Can. J. Chem. Downloaded from www.nrcresearchpress.com by 210.87.254.5 on 09/06/12
For personal use only.

TABLE 6. $(n\text{-}Pr_2NH_2)_3(SnCl_6)Cl$: positional parameters (except for alkyl hydrogens)*

Atom	Positional parameter			Atom	Positional parameter		
	x	y	z		x	y	z
Sn	−0446(0)	6513(0)	2321(0)	C(111)	0747(9)	6923(4)	7018(12)
Cl(1)	0983(2)	6059(1)	1097(1)	C(112)	1319(13)	6517(4)	7544(15)
Cl(2)	−2305(2)	6206(1)	1156(2)	C(113)	2709(11)	6467(3)	7045(11)
Cl(3)	1443(2)	6859(1)	3414(2)	C(121)	−1520(10)	6699(4)	7265(13)
Cl(4)	−0539(4)	5976(1)	3977(3)	C(122)	−2882(13)	6928(7)	7350(16)
Cl(5)	−1841(2)	6993(1)	3507(3)	C(123)	−3895(14)	6583(5)	7494(17)
Cl(6)	−0306(3)	7085(1)	0676(2)	C(211)	4525(9)	6854(2)	1614(8)
Cl	4622(2)	5702(1)	0027(2)	C(212)	3763(10)	6966(3)	0395(10)
N(1)	−0558(7)	7044(1)	7510(1)	C(213)	4262(10)	7418(4)	−0118(10)
H(11)	−085(2)	733(1)	706(3)	C(221)	4741(8)	6313(3)	3298(7)
H(12)	−043(2)	711(1)	847(1)	C(222)	4362(9)	5865(3)	3746(9)
N(2)	4047(1)	6420(1)	2057(4)	C(223)	5188(11)	5739(3)	4974(11)
H(21)	422(3)	619(1)	138(2)	C(311)	1974(8)	−0009(3)	3425(7)
H(22)	307(1)	644(1)	217(3)	C(312)	2835(11)	−0049(4)	2292(9)
N(3)	2807(2)	0109(1)	4610(5)	C(313)	1908(10)	−0200(3)	1119(10)
H(31)	344(2)	−014(1)	483(2)	C(321)	1870(7)	0170(2)	5643(7)
H(32)	330(3)	039(1)	445(2)	C(322)	2595(9)	0295(3)	6896(9)
				C(323)	1608(12)	0356(4)	7972(9)

*All values for nonhydrogen atoms have been multiplied by 10^4 and those for hydrogens by 10^3.

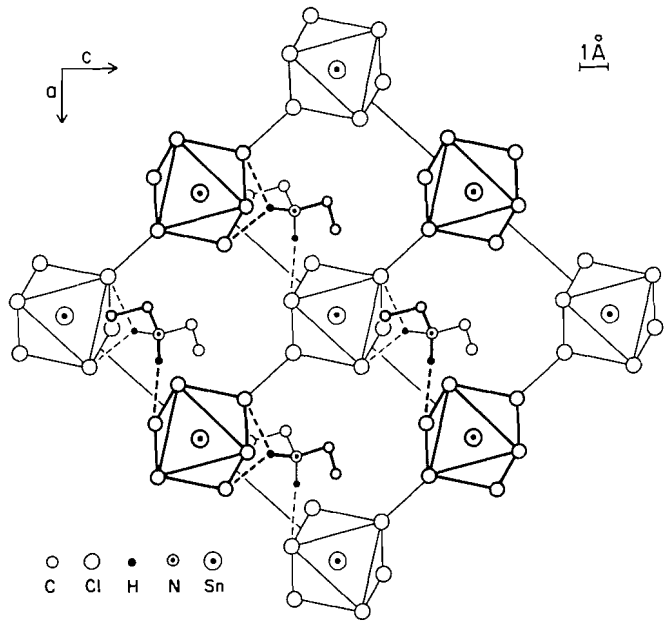

FIG. 1. Projection of the 2EHS structure on (010) displaying the antifluorite-type cation/anion packing. Only one half of the unit cell is shown; the other half is obtained by inversion in a centre of symmetry in one of the Sn atoms. The ethyl hydrogens have been omitted.

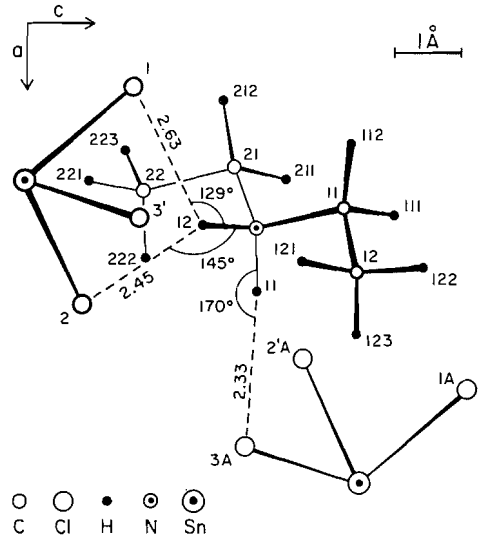

FIG. 2. Hydrogen bonding in 2EHS. Projection on (010). The distances are in Å. For additional interatomic distances, bond angles, and symmetry code, see Table 5.

Attention is drawn to the temperature dependence of the ν(NH) and ν(ND) doublets (Fig. 20 of ref. 2) which indicates the existence of a thermal collapse of the two components of each doublet somewhere in the vicinity of 320 K, pointing to a structural transition. From the similarity with 2MHS and a number of complex NH_4 halides (6, 7) the high-frequency branch of the ν vs. T plot can be expected to have its continuation in a single ν vs. T line above T_{tr}, while the lower-frequency branch increasingly approaches the high-frequency branch and disappears at T_{tr}. Furthermore, the temperature coefficient of the upper branch is negative and that of the lower branch positive. This behaviour indicates that the high-frequency component, which corresponds to a weaker hydrogen bond, originates in a highly bent N—H···Cl bond (8) and the lower-frequency component in a stronger, more normal hydrogen bond. The hydrogen-bonding geometry (Fig. 2) is in agreement with the spectroscopic evidence. The bifurcated bond, although involving longer H···Cl distances and small NHCl angles, 145° and 129°, is not appreciably weaker than the normal bond, as indicated by the doublet splitting of only 29 cm^{-1} for ν(NH) and 12 cm^{-1} for ν(ND) at 10 K.

Since the quality of the probe-ion spectra deteriorated rapidly as the sample temperature approached 293 K, attempts to obtain usable spectra in the vicinity of the expected T_{tr} seemed unpromising and no effort was made to extend the investigation of 2EHS above room temperature. A direct demonstration of the transition will have to rely on another method.

(n-Pr_2NH_2)$_3$($SnCl_6$)Cl

As reported in ref. 2, preparations intended to yield 2PHS

Can. J. Chem. Downloaded from www.nrcresearchpress.com by 210.87.254.5 on 09/06/12
For personal use only.

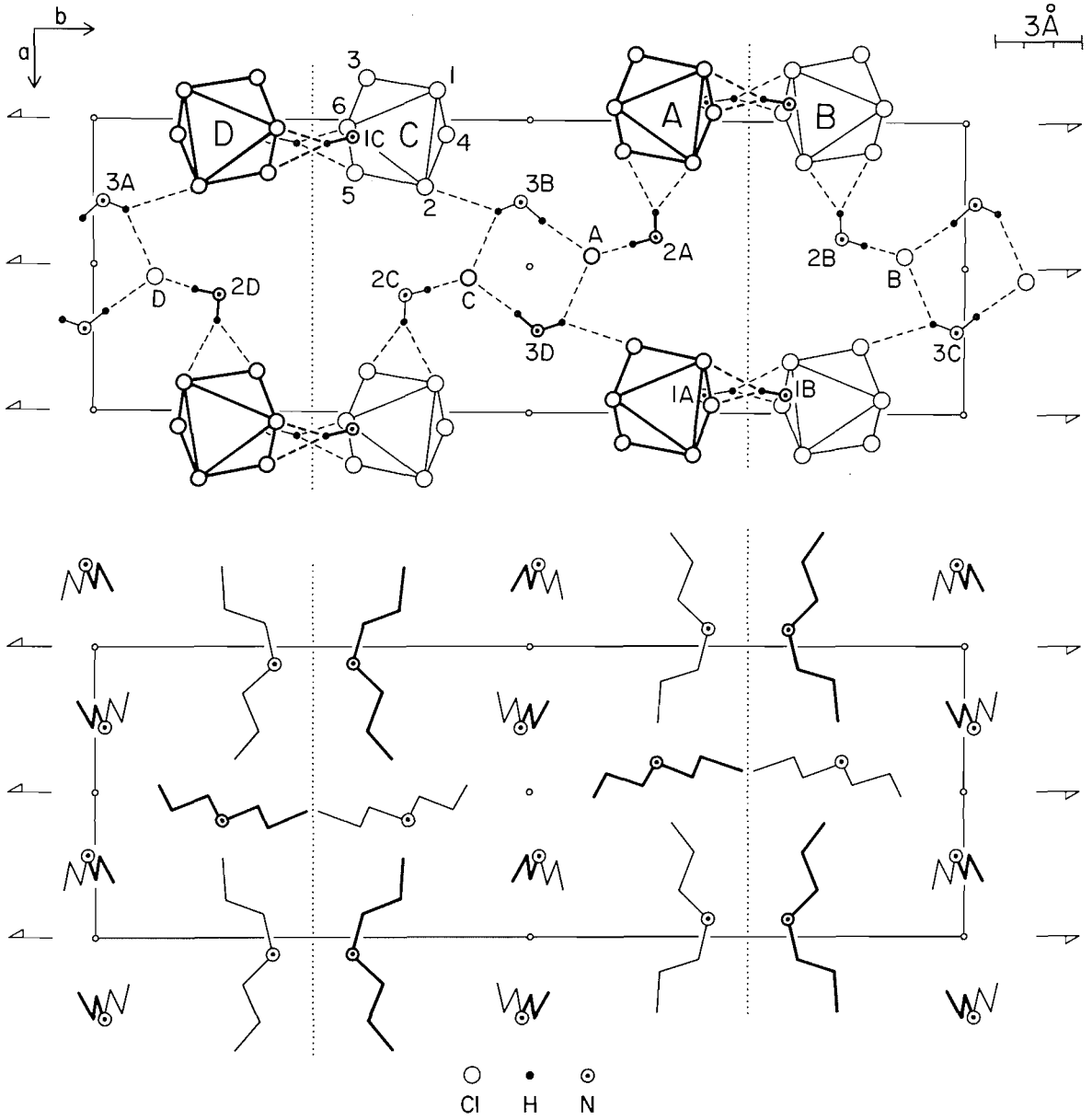

FIG. 3. Projection of the $(n\text{-}Pr_2NH_2)_3(SnCl_6)Cl$ structure on (001). (*A*) (top) Exclusive of the alkyl groups. The H(12) are in each case masked by the Cl(6) atoms to which they are hydrogen-bonded. (*B*) (bottom) The cations exclusive of the H atoms. For symmetry code, see Table 10.

TABLE 10. Hydrogen bonding in $(n\text{-}Pr_2NH_2)_3(SnCl_6)Cl$: N···Cl and H···Cl distances (Å) and bond angles (deg)*

Atom			Distance		
N	H	Cl	N···Cl	H···Cl	Angle
1	11	6B	3.281(5)	2.37(5)	148(2)
		5B	3.394(7)	2.77(5)	120(2)
1	12	6A″	3.286(3)	2.29(1)	165(2)
		5B	3.394(7)	3.09(4)	98(2)
2	21	A	3.111(6)	2.09(4)	173(3)
2	22	3A	3.357(5)	2.51(4)	141(2)
		1A	3.434(4)	2.64(3)	135(2)
3	31	B	3.110(6)	2.10(4)	170(2)
3	32	D	3.206(5)	2.37(4)	139(2)
		2D	3.467(6)	2.74(4)	129(2)

*Symmetry code: A, x, y, z; B, x, $\frac{1}{2} - y$, $\frac{1}{2} + z$; C, $\bar{x}$, $\bar{y}$, $\bar{z}$; D, $\bar{x}$, $\frac{1}{2} + y$, $\frac{1}{2} - z$; X′ = X + (100); X″ = X + (001).

have resulted in 2PHS.PCl instead. This mixed-anion salt does not properly belong to the hexachlorostannate(IV) series investigated in refs. 1 and 2, but its crystal structure was determined regardless of this, partly to account for the unexpected features of the ir spectrum in the region of NH and ND stretching absorptions (cf. ref. 2) and partly because it was considered opportune to augment the meager inventory of known structures of this type $((NH_4)_3(SiF_6)F$ (9), $K_3(SiF_6)F$ (10), and the thermochromic $[(NH_3CH_2CH_2)_2NH_2](CuCl_4)Cl$ (11)).

With the N—H and C—H bond lengths constrained to 1.02 and 1.08 Å, respectively, the structure was refined isotropically (except for the anisotropic Sn and Cl) to $R = 0.044$. The positional parameters are listed in Table 6, those of the alkyl hydrogens in Table 7,[2] the thermal parameters in Table 8,[2] and the structure factors in Table 9.[2]

The structure consists of $SnCl_6^{2-}$ and Cl^- anions and of $n\text{-}Pr_2NH_2^+$ cations of three types (Fig. 3). All the H_N atoms

Can. J. Chem. Downloaded from www.nrcresearchpress.com by 210.87.254.5 on 09/06/12
For personal use only.

Can. J. Chem. Downloaded from www.nrcresearchpress.com by 210.87.254.5 on 09/06/12
For personal use only.

TABLE 11. $(n\text{-}Pr_2NH_2)_3(SnCl_6)Cl$: geometry of the $SnCl_6$ octahedron

Atom	d(Sn—Cl), Å	H-bonded to*	d(Cl···H), Å	SnClH, deg
Cl(4)	2.377(3)	—	—	—
Cl(2)	2.399(2)	H(32)	2.74(4)	139(1)
Cl(1)	2.419(2)	H(22)	2.64(3)	92(1)
Cl(5)	2.423(2)	H(11)	2.77(5)	86(1)
		H(12)	3.09(4)	104(1)
Cl(3)	2.438(2)	H(22)	2.51(4)	94(1)
Cl(6)	2.447(2)	H(12)	2.29(1)	136(1)
		H(11)	2.37(5)	95(1)

*Each of these hydrogens participates in a bifurcated N—H···2Cl bond (see Table 10 for symmetry equivalence of the H atoms).

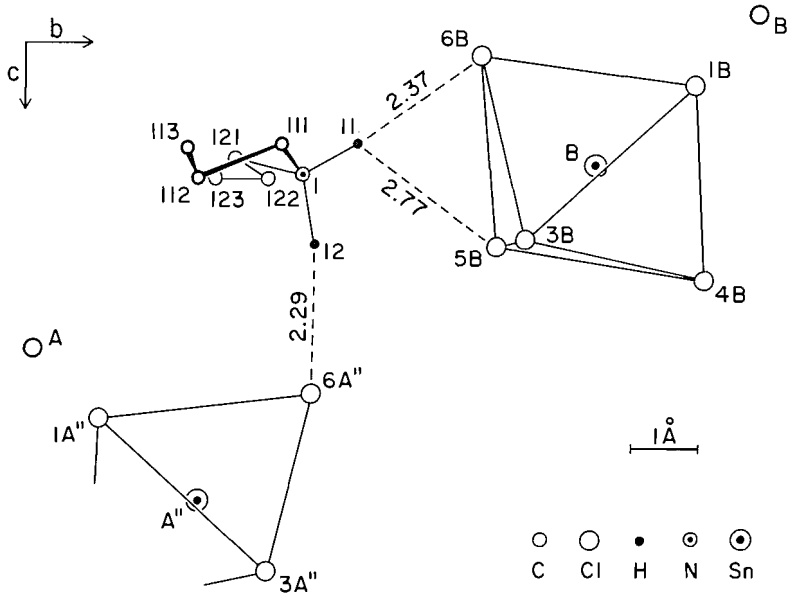

FIG. 4. Environment of N(1) in $(n\text{-}Pr_2NH_2)_3(SnCl_6)Cl$ (projection on (100)).

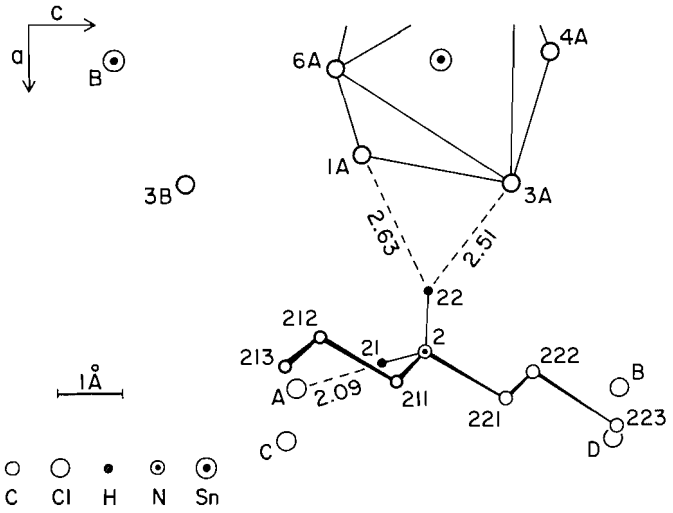

FIG. 5. Environment of N(2) in $(n\text{-}Pr_2NH_2)_3(SnCl_6)Cl$ (projection on (010)).

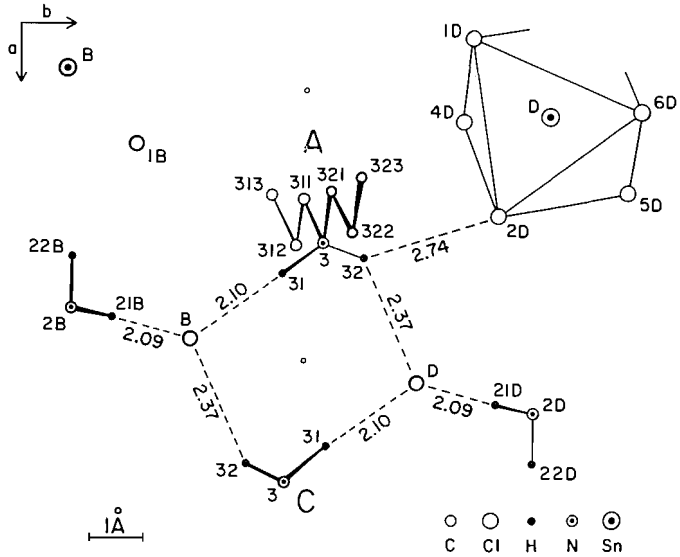

FIG. 6. Environment of N(3) and Cl^- in $(n\text{-}Pr_2NH_2)_3(SnCl_6)Cl$ (projection on (001)).

engage in hydrogen bonding: H(21) and H(31) exclusively to Cl^-; H(11), H(12), and H(22) exclusively to Cl_{Sn}; and H(32) to one Cl^- and one Cl_{Sn} (Table 10, Figs. 4–6). The H(21)···Cl^- and H(31)···Cl^- distances are quite short and correspond to almost straight N—H···Cl bonds. All the other hydrogen bonds are bifurcated, although N(1)—H(12)···Cl(6A") is only marginally so, the H(12)···Cl(5B) distance being 3.09 Å and

Can. J. Chem. Downloaded from www.nrcresearchpress.com by 210.87.254.5 on 09/06/12
For personal use only.

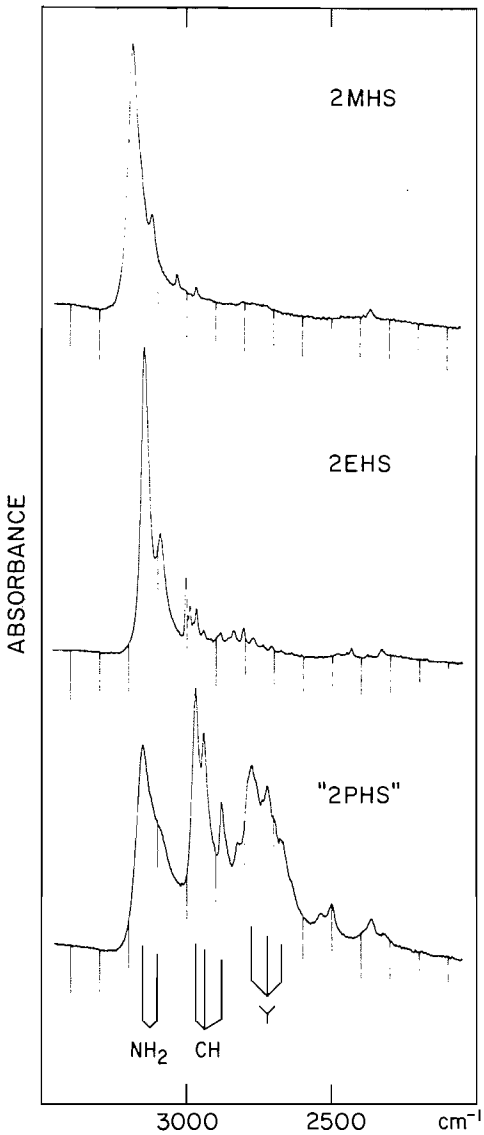

FIG. 7. Room-temperature spectra of undeuterated $(Me_2NH_2)_2SnCl_6$ (2MHS), $(Et_2NH_2)_2SnCl_6$ (2EHS), and $(n\text{-}Pr_2NH_2)_3(SnCl_6)Cl$ ("2PHS") in the NH stretching region (mulls in fluorocarbon oil). The bands marked *Y* correspond to the strongly hydrogen-bonded N—H···Cl^- groupings.

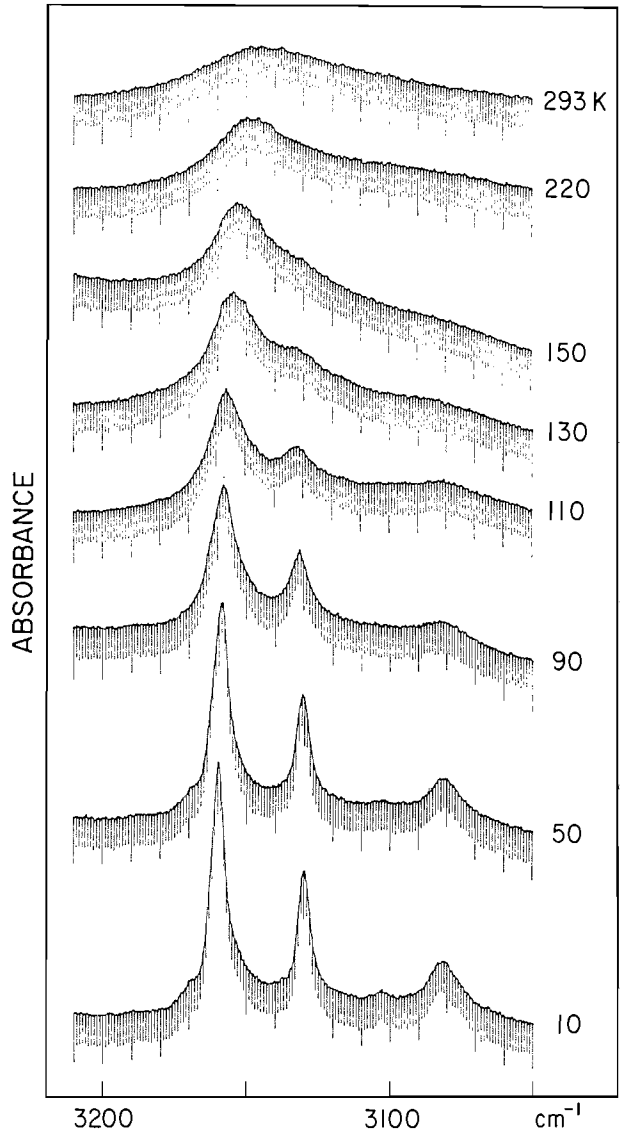

FIG. 8. The high-wavenumber portion of the NH stretching fundamental of $(n\text{-}Pr_2NH_2)_3(SnCl_6)Cl$ (94% D) at different temperatures (mulls in fluorocarbon oil).

the N(1)—H(12)—Cl(5B) angle only 98°.

Each Cl^- is the recipient of three hydrogen bonds, from H(21), H(31), and H(32), the last-named hydrogen being involved through one component of a bifurcated bond (Fig. 6). The first two of these H···Cl^- distances are considerably shorter than the other H···Cl distances and about the same as the H···Cl^- distance in Et_3NHCl, ~2.08 Å (N···Cl, 3.11 Å), where the N—H···Cl^- bond is linear by symmetry (12).

The Sn—Cl distances (Table 11) range from ~2.38 to ~2.45 Å (mean, 2.417(30) Å). This fairly large spread, ca. 0.07 Å ~ 3% of *d*(Sn—Cl), is explained by the asymmetry of the hydrogen-bonding scheme in which the $SnCl_6^{2-}$ ion is involved. With the exception of Sn—Cl(5), *d*(Sn—Cl) increases steadily with the decrease in the Cl_{Sn}···H distance, i.e., with the strength of the Cl_{Sn}···H bond. Some of the SnClH angles are quite small.

The structure as a whole may be viewed as an arrangement of flat, almost planar bands of alternating $SnCl_6$ octahedra and N(1)H_2 groups. The axes of the bands are parallel to the *c*-axis and their planes to (100) (Figs. 3*A* and 4). Each band consists of two parallel rows of $SnCl_6$ octahedra related by a glide mirror plane and cross-linked into zig-zag chains by the H(11) and H(12) hydrogens. The bands in turn are cross-linked by a system of hydrogen bonds involving the N(2)H_2 and N(3)H_2 groups and the Cl^- ions (Fig. 3*A*). The alkyl groups extend their carbon chains in directions more or less parallel to the crystallographic axes, those on N(1) to *a*, those on N(2) to *b*, and those on N(3) to *c* (Fig. 3*B*). This, together with the mutually more or less perpendicular systems of *inter*- and *intra*-band hydrogen bonds, makes the structure a truly three-dimensional edifice. At the same time, the presence of the alkyl groups renders the structural arrangement quite dissimilar to that found for $(NH_4)_3(SiF_6)F$ (9).

Figure 7 contrasts the spectrum of undeuterated 2PHS.PCl in the NH stretching region with the corresponding spectra of 2MHS and 2EHS. The 2PHS.PCl spectrum exhibits absorption in the 3100−3150 cm^{-1} region which matches that in the spectra of 2MHS and 2EHS and clearly corresponds to the stretch-

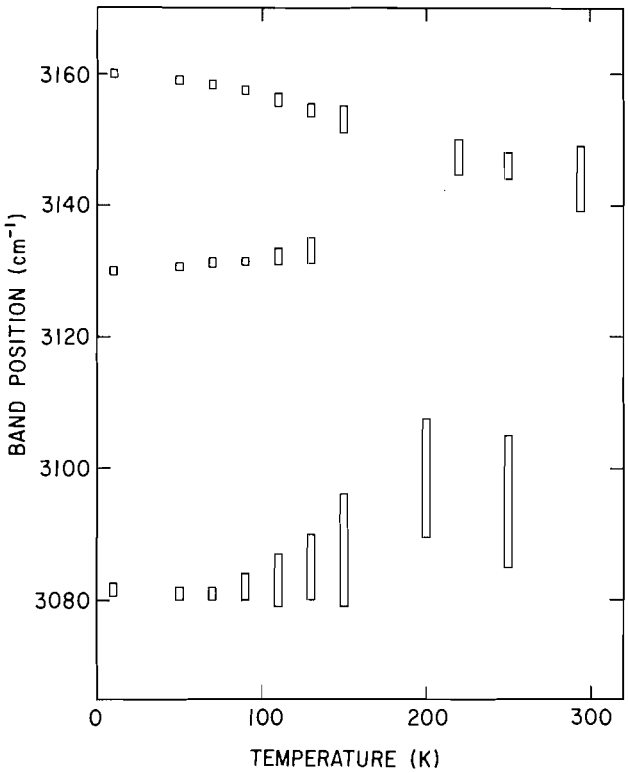

FIG. 9. Positions of the high-wavenumber NH stretching maxima vs. temperature for $(n\text{-}Pr_2NH_2)_3(SnCl_6)Cl$ (from Fig. 8).

ing of $—NH_2^+$ groups hydrogen-bonded to the $SnCl_6^{2-}$ anions (cf. also $MeNH_3^+$ in $(MeNH_3)_2PtCl_6$ (13) and $(MeNH_3)_2CdCl_4$ (14)). In addition, the spectrum contains a complex absorption (*Y* in Fig. 7) between 2500 and 2900 cm^{-1}. NH stretching absorptions at wavenumbers as low as this have been reported to occur in the spectrum of solid Et_3NHCl (refs. 15, 16; unpublished work) as well as in the solution spectra of Et_3NH^+ salts (17); corresponding absorptions in crystalline methylammonium halides, $Me_nNH_{4-n}X$ (X = F, Cl, Br, I) are well documented (18–20). It is thus reasonable to attribute *Y* to NH stretching modes arising from the $—NH_2^+$ groups strongly hydrogen-bonded to the Cl^- ions. Such absorptions are notorious for undergoing complicated Fermi resonance (17). They are unlikely to be understood in detail without extensive ancillary experiments. No attempt has therefore been made to assign the individual features of these spectra to the structurally distinct NH protons.

The temperature shifts of the NH stretching fundamentals in a highly deuterated sample (Figs. 8 and 9) show a gradual collapse of the high-wavenumber doublet, pointing to a probable transition at about 170 K.

Acknowledgments

This investigation was supported by research grants from the Natural Sciences and Engineering Research Council of Canada to two of the authors (T.S.C. and O.K.), and by a grant from the Walter J. Sumner foundation to M.A.J.

1. O. KNOP, T. S. CAMERON, M. A. JAMES, and M. FALK. Can. J. Chem. **59**, 2550 (1981).
2. O. KNOP, T. S. CAMERON, M. A. JAMES, and M. FALK. Can. J. Chem. (in press).
3. A. RIES. Z. Kristallogr. **39**, 49 (1904).
4. A. RIES. Z. Kristallogr. **36**, 321 (1902).
5. O. KNOP. J. Solid State Chem. **45**, 223 (1982).
6. O. KNOP, I. A. OXTON, W. J. WESTERHAUS, and M. FALK. J. Chem. Soc. Faraday 2, **77**, 309 (1981).
7. O. KNOP, I. A. OXTON, W. J. WESTERHAUS, and M. FALK. J. Chem. Soc. Faraday 2, **77**, 811 (1981).
8. O. KNOP, W. J. WESTERHAUS, and M. FALK. Can. J. Chem. **58**, 867 (1980).
9. J. L. HOARD and M. B. WILLIAMS. J. Am. Chem. Soc. **64**, 633 (1942).
10. D. L. DEADMORE and W. F. BRADLEY. Acta Crystallogr. **15**, 186 (1962).
11. B. ZASLOW and G. L. FERGUSON. Chem. Commun. 822 (1967).
12. F. GENET. Bull. Soc. Fr. Min. Crist. **88**, 463 (1965).
13. I. A. OXTON, O. KNOP, and J. L. DUNCAN. J. Mol. Struct. **38**, 25 (1977).
14. I. A. OXTON and O. KNOP. J. Mol. Struct. **37**, 59 (1977).
15. R. C. LORD. Unpublished work quoted in G. C. Pimentel and A. L. McClellan. The hydrogen bond. W. H. Freeman and Co., San Francisco. 1960. Fig. 3-21, p. 107.
16. R. S. MCDOWELL. Doctoral thesis. Massachusetts Institute of Technology, Cambridge, MA. 1960.
17. V. P. GLAZUNOV, A. A. MASHKOVSKY, and S. E. ODINOKOV. J. Chem. Soc. Faraday 2, **75**, 629 (1979).
18. E. A. V. EBSWORTH and N. SHEPPARD. Spectrochim. Acta, **13**, 261 (1959).
19. A. CABANA and C. SANDORFY. Spectrochim. Acta, **18**, 843 (1962).
20. A. THÉORÊT and C. SANDORFY. Spectrochim. Acta A, **23**, 519 (1967).

Can. J. Chem. Downloaded from www.nrcresearchpress.com by 210.87.254.5 on 09/06/12
For personal use only.

Chalcogenide esters as reactive intermediates in selenium and tellurium purifications

SANTOKH S. BADESHA,[1] PAUL MONCZKA,[2] AND STEVEN D. SMITH[2]
Xerox Corporation, Webster Research Center, Webster, NY 14580, U.S.A.

Received March 7, 1983

SANTOKH S. BADESHA, PAUL MONCZKA, and STEVEN D. SMITH. Can. J. Chem. **61**, 2199 (1983).

This paper describes a novel application of chalcogenide esters to purify selenium and tellurium to the 99.999% purity level. The chalcogenide esters were prepared from a variety of source materials which include: crude selenium and tellurium and commercial grade selenium dioxide, tellurium dioxide, and selenous acid. Crude selenium and tellurium were first converted to their respective oxides by treatment with concentrated nitric acid. The oxides were condensed with alcohols or diols to obtain the corresponding esters which, on reduction with hydrazine in organic media, provided high purity elemental selenium and tellurium.

SANTOKH S. BADESHA, PAUL MONCZKA et STEVEN D. SMITH. Can. J. Chem. **61**, 2199 (1983).

On décrit une nouvelle utilisation des chalcogénures dans la purification du sélénium et du tellure avec une pureté de 99,999%. On a préparé les chalcogénures à partir de divers produits de départ tels le sélénium et le tellure à l'état brut, le bioxyde de sélénium, le bioxyde de tellure et l'acide séléneux de qualité commerciale. On a d'abord transformé le sélénium et le tellure à l'état brut en oxydes en les faisant réagir avec l'acide nitrique concentré. On a ensuite condensé les oxydes sur des alcools ou des diols afin d'obtenir les esters correspondants qui par réduction avec l'hydrazine en milieu organique donnet le sélénium et le tellure avec une grande pureté.

[Traduit par le journal]

Can. J. Chem. Downloaded from www.nrcresearchpress.com by 210.87.254.40 on 09/06/12
For personal use only.

Introduction

The purity of selenium, tellurium, and their alloys for use in electrophotographic and semiconductor devices is very important. Materials less than 99.999% purity level are considered unsuitable for such devices. The contaminants which are generally found in chalcogenide materials are Mo, Mn, Ni, Pb, Sb, Sn, Si, Ti, Tl, Zn, W, Ag, Al, As, B, Ba, Bi, Ca, Cd, Co, Cr, Cu, Fe, Hg, Na, Mg, S, Cl, and O, depending on the source and method of recovery.

Selenium purification has been reviewed briefly by Scholten (3), Lumbroso (4), Pleteneva (5), and more extensively by Chizhikov and Schastlivyi (6), and Jennings and Yannopoulos (7). There are relatively few reports in the literature on the purification of tellurium (8, 9). Procedures for purification of these chalcogenides are very diversified; however, they can be divided into two major categories, namely chemical and physical. These two methods are usually employed in a sequential fashion, in that high temperature distillations generally are used in the final step. Chemical methods of purification have a common objective; the preparation of an intermediate compound amenable to purification and from which chalcogens can be easily recovered. The intermediate compounds which have been reported to date in the literature are selenides and tellurides, oxides, chlorides, and cyanates. To arrive at the 99.999% purity level, the manufacturers of selenium and tellurium must go through several derivatization and purification stages. The most difficult and expensive of these are repeated ion-exchange and high temperature distillations. It is worth noting that while most manufacturers use similar purification steps, samples of high purity selenium obtained from different sources have significantly different electrical properties. Electrolytic reduction of selenium(IV) on a mercury cathode has also been used for purification. Similarly, electrochemical methods have been exploited to effect separations of tellurium as its salts from impurities, especially selenium (10). These salts are then removed from the anode compartment, dissolved in strong alkali, and chemically reduced to elemental tellurium. Zone refining has also been used extensively for small scale purification of tellurium (11), whereas its application to selenium has been reported ineffective (12).

Despite the fact that selluranes and telluranes have been known since the early 1960's, very little has been done in exploring their chemistry and their possible use as reaction intermediates. In this paper we describe a novel chemical process in which these chalcogenide esters have been reduced to high purity (99.999%) selenium and tellurium.

Results and discussion

Tetraalkoxytelluranes have been prepared by the condensation of tellurium tetrachloride with sodium alkoxides in the presence of excess alcohols (13). Aromatic (14) and aliphatic (15) diols have also been reported to condense with tellurium dioxide or telluric acid to give the corresponding tetraalkoxytelluranes. The tellurane (**1**) used in this report was prepared from two source materials which include: crude tellurium and commercial grade tellurium dioxide. The procedure used by Simon and Heintz (15) for the condensation of tellurium dioxide with ethylene glycol was modified by using *p*-toluenesulfonic acid as reaction catalyst. It was observed that use of the catalyst reduces the reaction time and improves the yield of the product (**1**) over that period earlier (15).

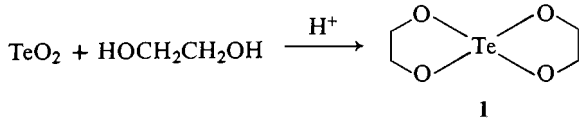

1

In the case of crude tellurium as source material, it was first converted to a mixture of tellurium dioxides by treatment with hot nitric acid. The completion of the reaction was generally indicated by the disappearance of black metallic tellurium. The white precipitate of tellurium oxides was collected in quantitative yield by filtration, washed free of acid with water, and dried. Sulfuric acid or its mixtures with nitric acid, hydrogen peroxide, or molecular oxygen at elevated temperatures can also be used for this oxidation reaction (8). The resulting tellu-

[1]To whom correspondence should be addressed.
[2]Co-op students from Rochester Institute of Technology, New York.

Can. J. Chem. Downloaded from www.nrcresearchpress.com by 210.87.254.40 on 09/06/12
For personal use only.

TABLE 1. Emission spectral analysis of selenium and tellurium samples[a]

Element	Detection limits	Commercial grade selenium	Sample #1	Sample #2	Sample #3	Samples #4 and 5
Ag	(<05)	1	—	—	—	—
Al	(<1)	5+	—	—	1	—
As	(<5)	m	—	—	—	—
B	—	—	—	—	—	—
Ba	—	—	—	—	—	—
Bi	—	m	—	—	—	—
Ca	(<1)	10+	—	—	2	1[b]
Cd	(<1)	20+	—	—	—	2
Co	(<5)	—	—	—	—	—
Cr	(<1)	10+	—	—	—	—
Cu	(<0.01)	2	—	—	0.1	—
Fe	(<0.5)	m	1[b]	1	2[b]	—
Hg	(<5)	10	—	—	—	—
Na	(<10)	20	—	—	—	—
Mg	(<1)	20	1[b]	—	4[b]	2[b]
Mn	(<1)	10	—	—	—	—
Mo	(<5)	15	—	—	—	—
Ni	(<1)	10	—	—	—	—
Pb	(<3)	m	—	—	—	—
Sb	(<5)	20+	—	—	—	—
Sn	(<1)	20+	—	—	—	—
Si	(<1)	20+	3[b]	—	1[b]	5[b]
Te	(<5)	10+	—	—	—	Balance
Ti	(<10)	20+	—	—	—	—
Tl	—	—	—	—	—	—
Zn	(<1)	5+	—	—	—	—
Se	(<1)	Balance	Balance	Balance	Balance	—

[a]The values are in ppm. At values above 1 ppm, a variability of ±1 ppm may be expected; "m" means that amount is >500 ppm; "—" means that the element is not expected.
[b]These impurities come from glass apparatus and spatula used in the process.

rium dioxide was then heated at 120°C for 1 h in excess ethylene glycol using *p*-toulenesulfonic acid as a catalyst. The temperature of the reaction mixture was raised to 150°C for 5 min during which time the solution became clear. On cooling to room temperature, a white crystalline solid separated out, which was filtered out and recrystallized from 2-ethoxyethanol, yielding tetraalkoxytellurane (**1**) in 80–85% yields. The yield can be further improved by reducing the volume of the filtrates.

The literature reports that strongly acidic solutions of tellurium dioxide (16, 17) and telluric acid (16) have been reduced with ammonia or hydrazinium hydroxide. We have found that tetraalkoxytellurane (**1**) can be easily reduced to high purity tellurium with hydrazine in organic media.

$$\mathbf{1} + H_2NNH_2 \rightarrow Te^0 + N_2\uparrow + HOCH_2CH_2OH + H_2O$$

The reaction is exothermic and the completion is generally indicated by the cessation of nitrogen gas. The black precipitate of elemental tellurium is collected in quantitative yield by filtration. We have also found that ascorbic acid and sulfur dioxide can be used to reduce **1** to elemental tellurium. The optical emission spectral analysis indicated that the resulting tellurium is of the 99.999% purity level (see Table 1, samples #4 and 5).

The chemistry of tetracoordinated selenium is somewhat less developed than tellurium; it has been reviewed by Paetzold and Reichenbacher (18) and Irgolic and Kudchadker (19). Dialkyl selenites have been prepared by the action of (*a*) alkyl halides on silver selenite (20), (*b*) sodium alkoxide on selenyl chloride (21), and (*c*) selenium dioxide on alcohols (22, 23), and dialkyl sulfites (24). Simon and Paetzold (25) have prepared dimethyl and diethyl selenites employing methylene insertion reaction on selenium dioxide dissolved in methanol or ethanol while Mehrotra and co-workers (26) have prepared alkyl selenites by the action of selenous acid on alcohols. We prepared dimethyl and diethyl selenites from a variety of source materials which include: crude selenium, commerical grade selenium dioxide, and commerical grade selenous acid. In the case of crude selenium as source material, it was first converted to a mixture of selenium oxides by treatment with concentrated nitric acid. Sulfuric acid or its mixture with nitric acid or molecular oxygen at elevated temperatures can also be used for this reaction (27). The oxides were then dissolved in ethanol and filtered, any residue being discarded. The filtrate was then converted to diethyl selenite by azeotropic removal of water. The diethyl selenite is purified by vacuum distillation. A variety of aliphatic and aromatic hydrocarbons can be used to make binary and ternary azeotropes with water (28). Those which we have used include pentane, cyclohexane, benzene, and toluene, with pentane being preferred. Diethyl selenite distills as a colorless liquid at 78°C/11 mm Hg in yields in excess of 90%. The residue left in the flask after the distillation can be again dissolved in ethanol and another crop of diethyl selenite can be obtained. This reaction is depicted in the following scheme:

$$\begin{matrix} SeO_2 \\ \text{or} \\ H_2SeO_3 \end{matrix} + ROH \xrightarrow[R = \text{alkyl}]{} (RO)_2SeO + H_2O$$

2

Can. J. Chem. Downloaded from www.nrcresearchpress.com by 210.87.254.40 on 09/06/12
For personal use only.

Pure diethyl selenite was also prepared by the literature method (26) by the condensation of commercial grade selenous acid or selenium dioxide with ethanol. Pentane was used for azeotropic removal of water.

Alicino and Kowald (29) have reviewed the use of different reducing agents for reduction of selenous acid to elemental selenium. Detailed kinetic studies have also been made on the reduction of selenous acid in acidic media with hydrazine (30) and sulfur dioxide (31).

We have found that diethyl selenite can be reduced to high purity selenium by chemical methods. Chemical reagents used to reduce the selenium ester (**2**) in this study include hydrazine and sulfur dioxide. In both cases, the precipitated selenium is of the 99.999% purity level. In a typical procedure, a solution of diethyl selenite in 2-ethoxyethanol was reduced to selenium by the dropwise addition of hydrazine. The reaction is exothermic and nitrogen gas is evolved. The cessation of nitrogen gas normally indicates the completion of the reaction. The resulting black powder was collected by filtration, washed with cellosolve, and dried, affording high purity selenium in quantitative yield (see Table 1, sample #2). The reaction is shown in the following scheme:

$$(RO)_2SeO + H_2NNH_2 \rightarrow ROH + Se^0 + N_2\uparrow + H_2O$$

In the case of the sulfur dioxide reduction, sulfur dioxide gas was bubbled through an aqueous solution of the ester (**2**) at 75°C and selenium was precipitated in quantitative yield. The resulting black precipitate was washed several times with hot water to ensure the complete removal of sulfate ions and was then dried. The emission spectral analysis performed on the powders obtained above indicates that the selenium is of high purity (see Table 1, samples #1 and 3).

$$(RO)_2SeO \xrightarrow{SO_2/H_2O} H_2SO_4 + Se^0 + ROH$$

Other reducing agents which can be used include: hydroxylamine salts, thioureas, hydroquinones, ascorbic acid, glyoxal, phosphines, and active methylene compounds, etc.

Experimental section

General comments

The following instruments were used for spectral measurements: Bruker WP-80 (nmr), Nuclide model-12-90G (mass spectrum), Perkin-Elmer 267 (ir), Baird-Atomic (optical emission spectrograph). The pyrex glass apparatus was bought from Ace Glass, Inc. All the chemicals were commercial grade and obtained from either VWR Scientific or Aldrich Chemical Co. Commercial grade selenium and tellurium were obtained from CCR[R] and Fisher Scientific Co., respectively, and the purity levels were determined by optical emission spectral analysis. The standards used in optical emission spectral analysis were obtained from National Bureau of Standards (SRM #726). The amounts of the reagents and the reaction conditions are not optimized; the same high purity level is maintained on scaling down to a 5 g scale.

Preparation of diethyl selenite from crude selenium

Crude selenium powder (453 g) was dissolved in 1 L of concentrated nitric acid by stirring and warming over a period of 3 h. When a clear solution was obtained, nitric acid was distilled off at 110–112°C. The traces of nitric acid were then removed under high vacuum. The resulting white residue was dissolved in 700 mL of absolute ethanol and water was removed azeotropically with 600 mL of benzene. The solvents were removed by distillation at atmospheric pressure and the residue was then fractionally distilled under high vacuum. Diethyl selenite which distills at 78°C/11 Torr (lit. (26) 76°C/10 Torr) was collected. The grey residue left in the flask was again dissolved in absolute ethanol (800 mL) and benzene (600 mL). The water was removed azeotropically as before and an additional crop of diethyl selenite was collected by fractional distillation. Overall yield of diethyl selenite was 956 g (90%). One can improve the yield of the ester further by recycling the grey residue left in the flask.

Preparation of diethyl selenite from commercial grade selenous acid (94%)

Diethyl selenite was preopared from commercial grade selenous acid in 91% yield (lit (26), 84%) using *n*-pentane to remove water azeotropically.

Preparation of diethyl selenite from commercial grade selenium dioxide

Diethyl selenite was also prepared in 73% yield by the condensation of commercial grade selenium dioxide with absolute ethanol (26).

Reduction of diethyl selenite obtained from crude selenium with hydrazine

Diethyl selenite (956 g) was dissolved in 1 L of cellosolve in a 2 L 3-necked RB flask equipped with reflux condenser, graduated addition funnel, and a Teflon[R] paddle stirrer. A solution of 175 g of hydrazine in 200 mL of cellosolve was added dropwise over a 2 h period through the addition funnel to the stirred solution of the ester. The reaction was exothermic and N_2 gas was evolved. The resulting black precipitate was collected by filtration on a sintered glass filter, washed with 200 mL (4 × 50 mL) of cellosolve, dried, and weighed. The overall yield of the high purity selenium is 403 g (99%). Emission spectral analysis indicated that the material was 99.999% pure and the details are shown in Table 1 (sample #1).

Reduction of diethyl selenite from commercial grade selenous acid with hydrazine

A solution of diethyl selenite obtained from commercial grade selenous acid in cellosolve was reduced with hydrazine, yielding high purity selenium in 99% yield. The purity was determined by emission spectral analysis and the results are summarized in Table 1 (sample #2).

Reduction of diethyl selenite from commercial grade selenous acid with sulfur dioxide

Sulfur dioxide gas was slowly bubbled at room temperature through a solution of 400 g of diethyl selenite in 1 L of deionized water in a 2 L Erlenmeyer flask. Red precipitates of amorphous selenium separate out. Sulfur dioxide was bubbled through the above slurry for 2 h at 85°C. The precipitate was then collected by filtration, washed several times with water until the washings were neutral, vacuum dried, and weighed. A total yield of 163 g (96%) of red amorphous selenium was obtained. The yield can be improved by increasing the reaction temperature and by bubbling sulfur dioxide until no more red color develops in the filtrate. Emission spectral analysis indicated that material is 99.999% pure. The details are given in Table 1 (sample #3).

Preparation of high purity tellurium from commercial grade tellurium dioxide

A mixture of commercial grade tellurium dioxide (160 g), *p*-toluenesulfonic acid (5 g), and ethylene glycol (1600 mL) was heated and stirred under argon atmosphere at 120°C for 3 h and then at 160°C until a clear solution resulted. The above solution was cooled to room temperature and then allowed to stand on the bench for 5 h. Tetraalkoxytellurane, which separated as white needles, was collected by filtration, washed with 100 mL (2 × 50 mL) of cellosolve, and recrystallized from cellosolve. The overall yield of the ester was 86%; mp 203–204°C (lit. (15) 207–218°C). The filtrates were discarded. One can obtain an additional crop of tetraalkoxytellurane by concentrating the above filtrates.

The above tellurium ester was dissolved in 1 L of warm cellosolve. A solution of 35 g of hydrazine in 100 mL of cellosolve was added dropwise through an addition funnel over a period of 30 min. The

reaction was exothermic and N_2 gas was evolved. The black slurry was further stirred for 1 h and filtered. The black precipitate was collected, washed with 100 mL (2 × 50 mL) cellosolve, dried, and weighed. A total yield of 84% high purity tellurium was obtained. The purity was determined by emission spectroscopy and the details are given in Table 1 (sample #5).

Purification of commercial grade tellurium

Concentrated nitric acid (300 mL) was charged into a 1 L RB flask equipped with a reflux condenser. Commercial grade tellurium (50 g) was added to the above flask. The suspension was stirred and refluxed until all the tellurium dissolved and a white slurry resulted. This conversion takes approximately 6 h. Nitric acid was then distilled off at 110–112°C. The traces of nitric acid were removed under high vacuum. The white residue, which is tellurium dioxide, was converted to tetraalkoxytellurane by treatment with 500 mL of ethylene glycol and 5 g of *p*-toluenesulfonic acid as above.

Pure tetraalkoxytellurane was then dissolved in 500 mL of cellosolve by stirring and warming. A solution of 15 g of hydrazine in 50 mL of cellosolve was then added dropwise over a period of 20 min. The reaction is exothermic and N_2 is evolved. The black precipitate was collected by filtration, washed with 50 mL (2 × 25 mL) of cellosolve, dried, and weighed. A total of 42 g (84%) of high purity tellurium was obtained. The purity was determined by emission spectroscopy and the details are given in Table 1 (sample #4).

Acknowledgments

We wish to thank D. Shuba for emission spectral analysis, CCR[R] for a sample of crude selenium, and A. S. Dellario for typing the manuscript.

1. C. S. FULLER. Ultrapurification of semiconductor materials. *Edited by* M. S. Brooks and J. F. Kennedy. MacMillan Company, New York. 1964. pp. 3–24.
2. N. P. SAZHIN. Zh. Vses. Khim. Obshchest. **13**, 499 (1968); Chem. Abstr. **70**, 13037 (1968).
3. J. J. SCHOLTEN. Chem. Weekblad. **51**, 583 (1955); Chem. Abstr. **49**, 13852 (1955).
4. H. LUMBROSO. Nouveau Traité de Chimie Minerale. *Edited by* P. Pascal and Masson. Paris. pp. 1651–1912, 1961.
5. N. B. PLETENEVA. Tsvet. Metal, **34** (1961).
6. D. M. CHIZHIKOV, V. P. SCHASTLIVYI. Selenium and selenide (Selen i selenidy), Moscow. 1964.
7. P. H. JENNINGS and J. C. YANNOPOULOS. Selenium. *Edited by* R. A. Zingar and W. C. Cooper. Van Nostrand Reinhold. 1974; and references therein.
8. W. C. COOPER. Tellurium. Van Nostrand Reinhold. 1971; U.S. Patent 3,922,511.
9. K. J. IRGOLIC. The organic chemistry of tellurium. Gordon and Breach, New York. 1974.
10. J. W. MELLOR. A comprehensive treatise on inorganic and theoretical chemistry. Vol. XI. Longmans, Green and Co., London 1931. pp. 1–121; R. BRANNU. J. Chem. Soc. **55**, 382 (1889); A. VANHIPPEL and M. C. BLOOM. J. Chem. Phys. **18**, 1243 (1950).
11. L. V. KOZHITOU, A. V. VANYUKOV and P. B. SHAPKIN. Tsevetnye Metally, **40**, 89 (1967).
12. R. TSUZUKI. Nippon Kinzoku Gakkaishi. **25**, 721 (1961); Chem. Abstr. **60**, 14149 (1961).
13. H. MEERWEIN and T. BERSIN. Justus Liebigs Ann. Chem. **476**, 113 (1929); R. C. MEHROTRA and S. N. MATHUR. J. Indian Chem. Soc. **42**, 749 (1965).
14. V. P. J. ANTIKAINEN and P. J. MALKONEN. Z. Anorg. Allg. Chem. **299**, 292 (1959).
15. A. SIMON and G. HEINTZ. Naturwissenschaften. **47**, 468 (1960); D. B. DENNEY, D. Z. DENNEY, P. J. HAMMOND, and Y. F. HUS. J. Am. Chem. Soc. **103**, 2340 (1981); R. C. MEHROTRA and S. N. MATHUR. J. Indian Chem. Soc. **42**, 748 (1965).
16. M. I. GOLOVEI, J. M. PEKAR, I. I. TUROK, and G. N. SHPYRKO. U.S.S.R., SU 935, 475; Chem. Abstr. **97**, 111919*d* (1982).
17. F. FEHEH. Handbook of preparative inorganic chemistry. Vol. 1. *Edited by* G. Brauer. Academic Press, New York. 1963. Chapt. 7.
18. R. PAETZOLD and M. REICHENBACHER. Organic selenium compounds, their chemistry and biology. *Edited by* D. L. Klayman and W. H. H. Gunther. Wiley, New York. 1973. Chapt. IX.
19. K. J. IRGOLIC and M. V. KUDCHADKER. Selenium. *Edited by* R. A. Zingaro and W. C. Cooper. Van Nostrand Reinhold, New York. 1974. Chapt. 8.
20. A. MICHAELIS and B. LANDMANN. Liebigs Ann. **241**, 150 (1887), Ber dt. Chem. Ges. **20**, 625 (1887).
21. W. STRECKER and W. DAINEL. Liebigs Ann. **462**, 186 (1928).
22. H. P. KAUFMANN and D. B. SPANNUTH. Chem. Ber. **91**, 2127 (1958).
23. C. A. BUNTON and B. N. HENDY. J. Chem. Soc. 3137 (1963).
24. R. C. PAUL, K. K. BHASIN, and R. C. SHARMA. Indian J. Chem. **13**, 292 (1975).
25. A. SIMON and R. PAETZOLD. Z. Anorg. Allg. Chem. **303**, 53 (1960).
26. R. C. MEHROTRA and S. N. MATHUR. J. Indian Chem. Soc. **41**, 111 (1964); N. N. MEL'NIKOV; M. S. ROKITSKAYA. J. Gen. Chem. (U.S.S.R.), **7**, 1543 (1937); C. A. **31**, 8502 (1937).
27. S. ATO and J. ICHIOKA. Repts. Sci. Research Int. Jpn, **1**, 27 (1956); Chem. Abstr. **50**, 10352 (1956).
28. R. C. WEAST (*Editor*). CRC handbook of chemistry and physics. Edition CRC Press, Inc., 1978. p. D-36.
29. J. F. ALICINO and J. A. KOWALD. Organic selenium compounds, their chemistry and biology. *Edited by* D. L. Klayman and W. H. H. Gunther. Wiley, New York. 1973. Chapt. XVII.
30. S. B. SANT. React. Kinet. Catal. Lett. **5**, 107 (1976).
31. K. HAMADA. J. Sci. Hirosima, Univ. Ser. A-11, **25**, 281; L. M. VINOGRADOV and G. F. PINAEV. (U.S.S.R.), Obshch. Prikl. Khim. **4**, 49 (1972); G. G. BABAYAN, G. S. CHTYAN, G. S. PANOSYAN, O. A. ADZHEMYA and D. R. ANDREASYAN. Arm Khim, Zh. **26**, 202 (1973); T. A. CHIU, J. S. HORNG, and Y. C. HOH. Hydrometallurgy, **7**, 135 (1981).

Can. J. Chem. Downloaded from www.nrcresearchpress.com by 210.87.254.40 on 09/06/12
For personal use only.

Dissolution enthalpies of NaI in binary mixtures of water with aliphatic alcohols and methylcellosolve at 298.15 K. Enthalpic pair interaction coefficients of NaI–nonelectrolyte in water solution

HENRYK PIEKARSKI

Department of Physical Chemistry, Institute of Chemistry, University of Łódź, ul. Nowotki 18, 91-416 Łódź, Poland

Received December 15, 1982

HENRYK PIEKARSKI. Can. J. Chem. **61**, 2203 (1983).

The enthalpy of solution, ΔH_{sol}, of NaI in methanol + water, ethanol + water, *n*-propanol + water, isopropanol + water, and methoxyethanol + water at all compositions and ΔH_{sol} of NaI in *s*-butanol + water and *tert*-butanol + water from 0 to 5 mol% alcohol was measured.

The NaI–nonelectrolyte pair interaction enthalpies were determined and correlated with the functions describing some properties of the nonelectrolyte. A functional group additivity concept, introduced by Savage and Wood for non-ionic solutes, was applied to the interactions between NaI and nonelectrolytes.

HENRYK PIEKARSKI. Can. J. Chem. **61**, 2203 (1983).

On a mesuré l'enthalpie de solution ΔH_{sol} du NaI en solution dans les solvants suivants: méthanol + eau, éthanol + eau, *n*-propanol + eau, isopropanol + eau et méthoxyéthanol + eau en toutes proportions et on a mesuré le ΔH_{sol} du NaI en solution dans les mélanges de *s*-butanol eau et de *tert*-butanol eau dont la teneur en alcool varie de 0 à 5 mol%.

On a déterminé les enthalpies d'interaction de la paire: NaI–nonélectrolyte et on les a reliées aux fonctions qui décrivent certaines propriétés d'un non électrolyte. On a appliqué un concept d'addivité de groupe fonctionnel, introduit par Savage et Wood pour les solutés non ioniques, aux interactions entre le NaI et les non électrolytes.

[Traduit par le journal]

Can. J. Chem. Downloaded from www.nrcresearchpress.com by 210.87.254.5 on 09/06/12
For personal use only.

Introduction

A simple way of representing solute–solute interactions in dilute solutions is through virial expansion in solute concentration, as shown by McMillan and Mayer (1). The virial coefficients of such an expansion represent, respectively, pair, triplet, and higher order interactions between the molecules of the same dissolved substance in two-component systems, as well as among different molecules in three-component systems. Any changes in the solute–solvent interactions are considered to be contained in the coefficients of interactions between the molecules of the solutes. Enthalpic pair interaction coefficients in both two- and three-component systems have been dealt with in a number of studies, but few of them concerned interactions between electrolyte and nonelectrolyte (2–6). The aim of this study was to fill this gap, if only to some extent. The systems studied were aqueous mixtures of NaI and alcohols at 298.15 K. Sodium iodide was used as the electrolyte due to its relatively good solubility in the investigated mixtures.

As is well known, enthalpic interaction coefficients may be determined on the basis of dissolution enthalpies in a two- or three-component system (2–5, 7). Accordingly, the enthalpies of NaI dissolution in methanol, ethanol, propanol, isopropanol, and methoxyethanol + water mixtures were determined over the entire range of concentrations of the mixed solvent as well as in *s*-butanol and *tert*-butanol + water in the range of several mol% of alcohol at 298.15 K. Some of the above mentioned systems had previously been studied by calorimetric method (8–12). However, in view of the small number of experimental points in the water-rich mixtures, those data could not be used for the present purpose.

Experimental

Materials

Sodium iodide, "Baker Analyzed", manufactured by J. T. Baker Chemicals B.V. (Holland), crystallized from a water–acetone mixture, was dried under vacuum for several days at ca. 335 K. Methanol, ethanol, propanol, and isopropanol — all analytically pure — manufactured by POCh Gliwice (Poland): *s*-butanol and *tert*-butanol — A. R. manufactured by Reanal (Hungary) were purified and dried by standard methods (13). Methoxyethanol p.a. manufactures by Merck (Germany) was subjected to fractional distillation. All solvents were kept over molecular sieves 3A. The water content in alcohols was determined by the Fischer method and it did not exceed 0.02% by weight. The water was deionized and twice distilled. The water–alcohol mixtures were prepared by weight.

Apparatus and method of measurement

Enthalpies of NaI dissolution in water–methoxyethanol mixtures were determined using an LKB 8700-1 calorimeter provided with a 100 cm^3 glass measuring vessel.[1]

All other measurements were made using a home-made non-isothermic, non-adiabatic calorimeter with the surrounding medium at constant temperature as described in an earlier paper (14).

Results and discussion

Enthalpy of NaI dissolution

Enthalpies of NaI dissolution in water + alcohol mixtures were determined in the range of small electrolyte concentrations (0.002–0.02 mol dm^{-3}). The measured enthalpies were extrapolated to infinitely dilute solution using the method of Criss and Cobble (15). The dielectric permittivity and density of the water + alcohol mixtures required for the calculations were taken from the literature (16–19). The calculated standard enthalpies of NaI dissolution in methanol, ethanol, propanol, isopropanol, *s*-butanol, *tert*-butanol, and methoxyethanol mixtures with water at 298.15 K are presented in Table 1 and Fig. 1. The literature data concerning the systems under study are also included in Table 1 and Fig. 1.

As can be seen in Fig. 1, the $\Delta H^0 = f(x)$ plot for the water + alcohol mixtures under study shows a maximum in the range of small alcohol concentrations, similar to the case of other electrolyte + water + alcohol systems studied earlier (8–12, 14, 20–27). The maximum in question is generally taken to be connected with the ordering or stabilization of water structure

[1]The research was done by the author while on a post-doctoral fellowship at the Physical Chemistry Department of Free University, Amsterdam.

TABLE 1. Standard enthalpies of solution of NaI in water + alcohol mixtures at 298.15 K

X_{Alc} (mol%)	ΔH^0 (J mol^{-1})						
	Methanol	Ethanol	Propanol	Isopropanol	*s*-Butanol	*tert*-Butanol	Methoxyethanol
0[a]	−7 575	−7 575	−7 575	−7 575	−7 575	−7 575	−7 575
1	−7 220	−6 920	−6 700	−6 460	−6 235	−6 000	—
2	−6 900	−6 280	−5 835	−5 360	−4 850	−4 480	−7 345
4	−6 280	−4 960	−4 130	−3 180	−2 340	−1 570	—
5	−5 980	−4 310	−3 290	−2 050		−420	−7 845
6	—	−3 675	−2 450	−1 000			—
8	−5 190	−2 430	−2 510	−630			—
10	−4 690	−1 760	−3 975	−1 210			−10 775
12	—	−1 670	—	−1 970			—
15	−4 020	−2 340	−6 610	−3 470			−14 350
20	—	—	—	−6 190			—
30	−6 300	−7 780	−13 300	−10 880			−25 900
50	−10 020	−14 020	−18 115	−18 280(11)			—
60	—	−15 440	—	—			−42 050
70	−15 690	−16 400	−21 130	−23 640(11)			—
80	−19 920	−17 910	−22 490	—			—
90	−25 310	−20 605	−23 760	−26 700(11)			−55 230
100	−32 010	−24 770	−24 980	−27 950			−59 330
	−32 050(9)	−24 518(28)	−24 700(30)				
	−29 290(8)	−24 142(29)	−23 525(31)				

[a]Other values of ΔH^0 NaI in water: −7 533 (29); −7 615 (32).

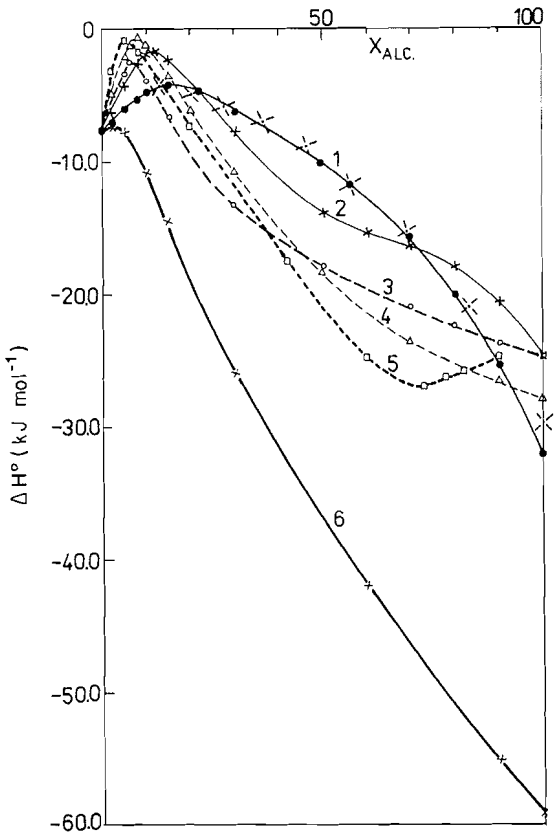

FIG. 1. Standard solution enthalpy of NaI in the mixtures of water with alcohols as a function of solvent composition at 298.15 K: (*1*, methanol; *2*, ethanol; *3*, propanol; *4*, isopropanol; *5*, *tert*-butanol; *6*, methoxyethanol)× literature data (8).

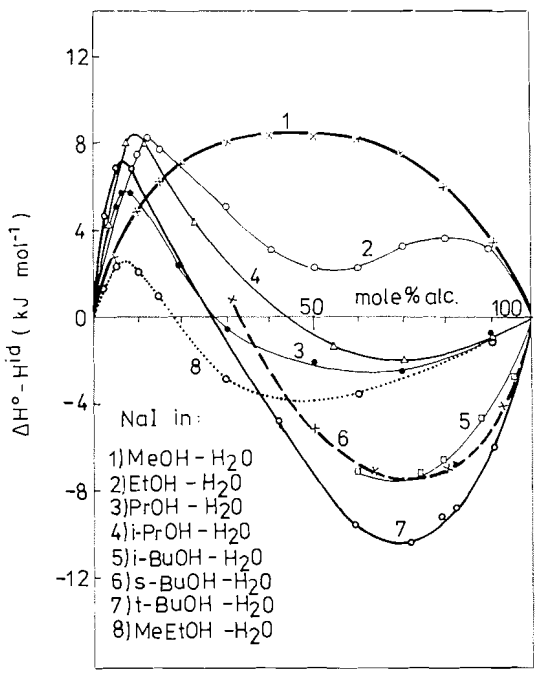

FIG. 2. Deviations from the additivity of the standard solution enthalpy of NaI in water−alcohol mixtures at 298.15 K.

by alcohol molecules (32−36). It follows from the literature data as well as from the results of this study, that the shape and position of the ΔH^0 peak depends on the size of the alcohol molecules. As the molecule size increases, the peak shifts towards smaller alcohol content in the mixture.

It is interesting to compare the course of the $\Delta H^0 = f(x)$ NaI plots for mixtures of the different alcohols with water, from methanol to *tert*-butanol (Fig. 1). The plots change their courses as the size of the alcohol molecule increases, similar to the heats of mixing curves for the same alcohols with water (37). This correspondence becomes even more obvious if NaI dissolution enthalpy is replaced by a function which represents deviations from additivity of NaI dissolution enthalpies in the above mixtures (Fig. 2).

Can. J. Chem. Downloaded from www.nrcresearchpress.com by 210.87.254.5 on 09/06/12
For personal use only.

$$\delta\Delta H^0 = \Delta H^0 - \Delta H^{id}$$

This similarity may well reflect the effect of changes in the structure of water–alcohol mixture on ion solvation in these mixtures.

Thermochemically, the NaI–water–methoxyethanol system behaves similarly to known NaI–water–alcohol systems. This is in agreement with the finding of Petrucci (38) who observed a similar behaviour of water–methylcellosolve and water–methanol mixtures as solvents of electrolytes. The standard enthalpy of NaI dissolution determined in the present study passes through a maximum in the range of small cellosolve contents (ca. 2 mol%). However, this maximum is considerably lower than the ones in other water–alcohol solvents (Fig. 1).

Also noteworthy is the large thermal effect of NaI dissolution in pure methoxyethanol (59.3 kJ mol^{-1}) which is comparable to the enthalpy of NaI dissolution in DMF (57.1 kJ mol^{-1}) (39), but quite different from the enthalpy of NaI dissolution in simple aliphatic alcohols (Table 1). This is probably due to the presence of an internal H-bond in methylcellosolve molecule (40, 41) which makes the formation of a more complex structure in pure solvent difficult, as in the case of the structure of lower aliphatic alcohols. Consequently, less energy is required to break a methoxyethanol molecule from its surrounding medium in order to form an ion solvation shell and, as a result the enthalpy of solution becomes more exothermic.

Enthalpic pair interaction coefficients

In order to calculate the enthalpic interaction coefficient h_{EN} for pairs NaI + alcohol in water solution, the method proposed by Friedman and Krishnan (4) and Desnoyers *et al.* (7) as modified by Heuvelsland *et al.* (3) was used. The standard enthalpy of NaI dissolution in mixtures of water with a small amount of alcohol was presented as a function.

$$[1] \quad \Delta H^0(\text{E in N + W}) = \Delta H^0(\text{E in W}) + bX_N + cX_N^2$$

where E is the electrolyte, N the cosolvent, W, water, X_N is molar fraction of the cosolvent, and b and c are coefficients which can be determined by the least-squares method.

Parameter b in eq. [1], which represents limiting slope of function ΔH^0(E in N + W), is connected with the McMillan–Mayer interaction coefficient h_{EN}:

$$[2] \quad b = 2\nu h_{EN}(\partial m_N/\partial X_N)_{X_N \to 0}$$

Denoting the molecular weight of water by M_w, we have, for dilute solutions

$$[3] \quad \left(\frac{\partial m_N}{\partial X_N}\right)_{X_N \to 0} = \frac{1}{M_w}$$

where m_N is in mol kg^{-1}, M_w in kg mol^{-1}. Hence

$$[4] \quad h_{EN} = b\frac{M_w}{2\nu}$$

where ν is the number of ions. The pair interaction coefficient defined as above constitute, for the systems containing an electrolyte of the 1–1 type, a half of the sum of the enthalpic effect of the interaction between a molecule of a given nonelectrolyte and cation (K^+) and anion (A^-)

$$[5] \quad h_{NE} = (1/2)\, h(K^+A^- - \text{nonelectrolyte}) = (1/2)[h(K^+ - \text{nonelectrolyte}) + h\,(A^- - \text{nonelectrolyte})]$$

TABLE 2. Enthalpic pair interaction coefficients for electrolyte–nonelectrolyte pairs in water solution at 298.15 K

	h_{EN} (J kg mol^{-2})	
Nonelectrolyte	NaI	NaCl
Methanol	+157	+150(2)
Ethanol	+298	+290(2)
Propanol	+395	+370(2)
Isopropanol	+509	
Isobutanol	+600[b]	
s-Butanol	+643	
tert-Butanol	+720	+483(2)
	+711(2)	
Methoxyethanol	+97	
THF	+172[b]	−200[b]
DMF	−212[b]	
DMSO	−314[b]	
Formamide	−348[b]	
Sulpholane[a]	−542[b]	
Acetone	−46[b]	

[a] T = 303.15 K.

[b] The values calculated from literature data: isobutanol (14), DMF and formamide (39), DMSO (42), THF (43), sulpholane (44), acetone (45).

The values of h_{EN} calculated this way are collected in Table 2. For the sake of comparison, the table also contains pair interaction coefficients for the NaI–nonelectrolyte system calculated on the basis of literature data (39, 42–44) as well as h_{EN} values obtained by other authors for the same or similar systems (2).

It follows from the data above that the pair interaction coefficients obtained exhibit considerable variation depending on the kind of nonelectrolyte; there are both negative and positive values of h_{EN}. The pair parameters for systems containing one of the first three aliphatic alcohols have values similar — within the limit of error — to the corresponding parameters for NaCl + alcohol + water system. This coincides with the finding of Perron *et al.* (2) about the weak dependence of parameters h_{EN} on ion size. However, in the case when the nonelectrolyte is TBA or THF, the values of h_{EN} coefficients for NaI and NaCl exhibit considerable differences. Considering the results of Perron (2), it seems that the differences observed in the present study may have been due to specific behaviour of I^- ion in the systems under investigation.

When analyzing the pair interaction coefficients obtained in this study, an attempt was made to find out whether simple relations could be established between h_{EN} and the functions characterizing the different properties of the nonelectrolytes under study. The interaction parameters h_{EN} relative to the polarizability (α) of the nonelectrolyte molecule are presented in Fig. 3. As can be seen, the pairwise interaction coefficients for NaI with MeOH, EtOH, PrOH, *i*-PrOH, *i*-BuOH, *s*-BuOH produce a linear function when plotted against polarizability of the alcohol. It may well be that in the systems mentioned above electrostatic interactions make the leading contribution to h_{EN} coefficients.

Electrolyte–nonelectrolyte interactions are to some extent connected with the donor–acceptor properties of the nonelectrolyte molecule. Therefore, an analysis was made of the dependence of h_{EN} for NaI–nonelectrolyte on the various parameters which define the acidic and basic properties of the

Can. J. Chem. Downloaded from www.nrcresearchpress.com by 210.87.254.5 on 09/06/12
For personal use only.

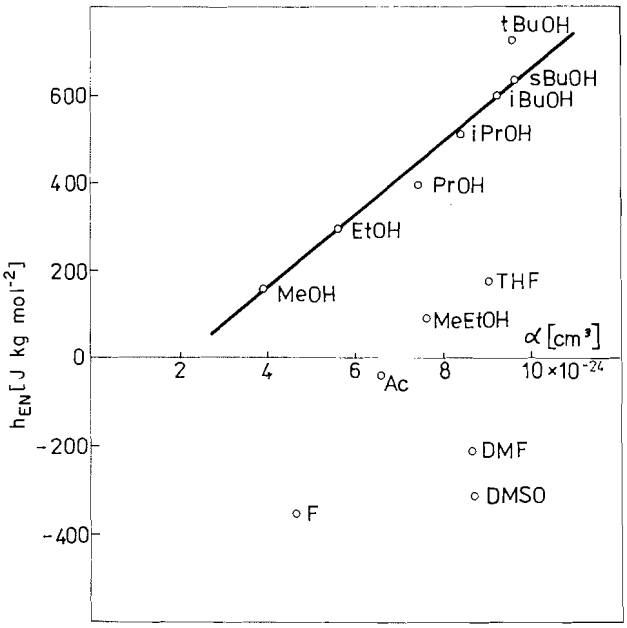

FIG. 3. Plot of enthalpic pair interaction coefficients of NaI–nonelectrolyte in water solutions versus the polarizability of the nonelectrolyte molecule.

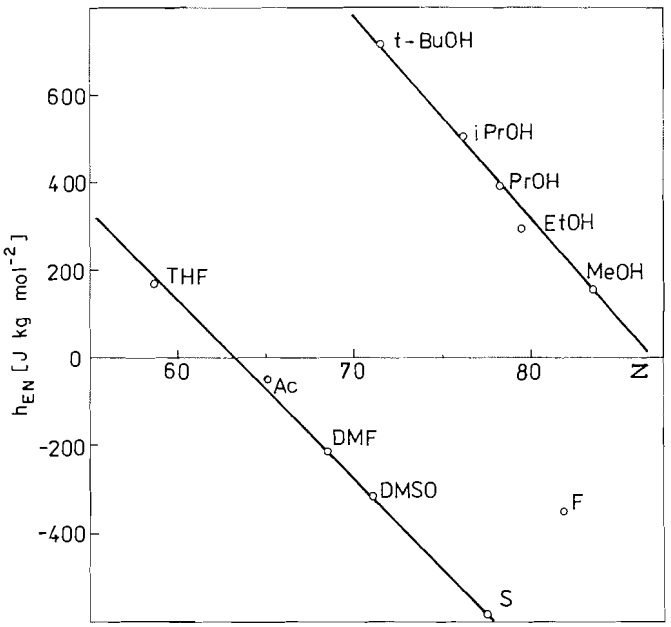

FIG. 4. Plot of h_{EN}(NaI–nonelectrolyte) vs. the Kosower acidity parameter (Z).

cosolvent. It turned out that there is no direct correlation between the enthalpic interaction coefficients obtained by us and the functions defining the basic properties of the nonelectrolyte, such as Gutmann donor number DN (46) or the Kamlett–Taft β_{KT} (47) or Koppel–Paiu β (48) basicity parameter. By contrast, there exists a correlation in the case of acidity functions, as can be seen in Fig. 4, which shows the plot of h_{EN} vs. the Kosower acidity parameter Z (49).

Here there are two, almost parallel straight-line segments one of which refers to aliphatic alcohols and the other represents nonelectrolytes whose molecules are aprotic in character (DMF, sulpholane, THF, acetone, DMSO). The h_{EN} value corresponding to the NaI + formamide interaction is not located on either of the two straight lines. The plots of the interaction coefficients under discussion against the other acidity functions, such as the Dimrot–Reichardt parameter E_T (50), present a similar picture.

The observed dependence of h_{EN} vs. Z makes it possible to divide the nonelectrolytes under study into two groups. The first group contains aliphatic alcohols which are known to bring about stabilization or ordering of the water structure (32–39). Their molecules exhibit both electron-donor and electron-acceptor properties. The second group comprises (as follows from Fig. 4) DMF, THF, DMSO, acetone, and sulpholane which, although they do affect water structure in different ways, all exhibit electron-donor properties.

The above findings seem to permit the conclusion that enthalpic pair interaction coefficients for an NaI–nonelectrolyte–water system depend primarily on two effects: a structural-hydration one and an electrostatic one. The former divides nonelectrolytes because of differences in the mechanism of their hydration, while within a given group of nonelectrolytes it is the electrostatic interactions that seem to play the most important role (Fig. 3).

On the other hand, the coefficients h_{EN} of NaI interaction with nonelectrolyte calculated in the present work constitute, according to formula [5], half of the sum of the enthalpic effect of the interaction between a molecule of a given nonelectrolyte

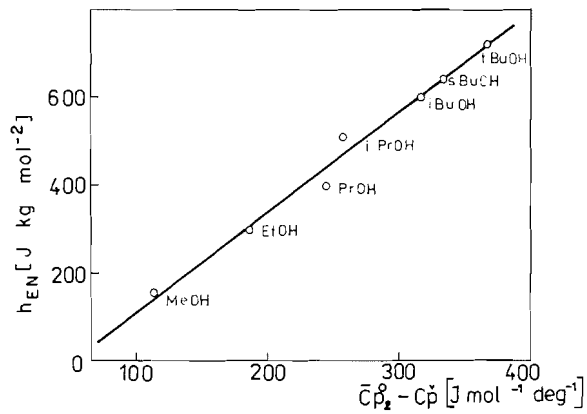

FIG. 5. Correlation of h_{EN}(NaI–alcohol) and heat capacity ($\bar{C}^0_{p_2} - C^v_p$) of transfer of the alcohols from the vapor phase to high dilution in water.

and cation (Na^+) and anion (I^-). The absence of an electron acceptor group in a DMF, DMSO, THF, acetone, and sulpholane may be responsible for the weak interaction between the molecules of the above mentioned substances with the anion under study. The parallel shift of the straight line segments $h_{EN} = f(Z)$ for the two nonelectrolyte groups discussed above (Fig. 4) may thus be due to differences in the effect of iodide ion interactions with a molecule of group one or group two nonelectrolyte.

In order to find out which of the above interpretations of the course of functions $h_{EN} = f(Z)$ is correct, one would have to divide coefficient h_{EN} into ionic contributions. This, however, is not possible at the moment in view of insufficient data.

Since heat capacity data are known to be very sensitive to structural changes in solution (51), it seemed interesting to find out whether the h_{EN} coefficients obtained in this study correlate with the C_p data for water solutions of the nonelectrolytes under investigation.

As can be seen in Fig. 5, there is a linear dependence between h_{EN} and ($\bar{C}^0_{p_2} - C^v_p$) for the alcohols where $\bar{C}^0_{p_2}$ denotes partial molal heat capacity of alcohol in high dilution in water,

Can. J. Chem. Downloaded from www.nrcresearchpress.com by 210.87.254.5 on 09/06/12
For personal use only.

Can. J. Chem. Downloaded from www.nrcresearchpress.com by 210.87.254.5 on 09/06/12
For personal use only.

and C_p^v is heat capacity of pure vapour of alcohol. The observed dependences seems particularly interesting in view of the fact that, as established by Arnett, Kover, and Carter ($\bar{C}_{p_2}^0 - C_p^v$), the heat capacity of solution for alcohols from the vapour phase to water does give some correlation with the entropies ΔS^0 for the same process (52). It follows that the interaction coefficients h_{EN}(NaI−alcohol) also correlate with transfer entropy ΔS^0. Unfortunately, since appropriate data were not available, it was not possible to find out whether the h_{EN} vs. ($\bar{C}_{p_2}^0 - C_p^v$) plots obtained also hold for the other nonelectrolytes of Table 2.

It follows from the data collected in Table 2 that the h_{EN} coefficients for all NaI + alcohol pairs in water are positive and they increase steadily with increasing alkyl group size. A similar effect of the alkyl group size on h_{EN} values was observed in the case of other systems described in the literature (3, 5, 53, 54). This regularity suggested that the interaction coefficients might have an additive nature. As is well known, Savage and Wood (53) have found that coefficients h_{EN} for nonelectrolytes are made up additively from contributions of the different functional groups. Basic to their approach is the assumption that each functional group in molecule "E" interacts with each functional group in molecule "N" and that each of these interactions has its own contribution to the enthalpy, regardless of the nature of the molecule. Steric effects are neglected and, consequently, it is assumed that interactions between the given groups are independent of their position in the molecule. In their study, Savage and Wood (53) selected the methyl (CH_2), hydroxymethylene (CHOH), and amide (HNCO) groups as the functional groups and, as a result, they considered six possible interactions corresponding to the following pairs: CH_2−CH_2, CH_2−CHOH, CH_2−HNCO, CHOH−CHOH, CHOH−HNCO, and HNCO−HNCO.

In the present study we are dealing with an electrolyte−alcohol system. Since without additional extra thermodynamic assumptions it is impossible to divide h_{EN} into ionic contributions, the values calculated by us represent mean ionic coefficient of the ion − alcohol molecule interaction or, more accurately, (1/2) (Na^+I^-)−alcohol molecule. The model assumed takes account of three types of interaction in the systems under study: (1/2) (Na^+I^-)−CH_2, (1/2) (Na^+I^-)−OH, and (1/2) (Na^+I^-)−O ether oxygen atom. In such a case, h_{EN} may be represented in the form of a summation

$$[6] \quad h_{EN} = \sum_i n_{Ei} h_{Ei}$$

where h_{Ei} is the characteristic contribution to coefficient h_{EN} from mean ionic interactions with the selected group of type "i" in molecule "N". Following other authors (3, 5, 53, 54), we assumed the CH_3 group to be equivalent to 1.5 of the CH_2 group. In order to solve eq. [6] for the seven h_{EN} values available, multiple linear regression was employed and the following group contributions to h_{Ei}: (1/2)(NaI−CH_2) = +(140.6 ± 5.7) J kg mol^{-2}, (1/2)(NaI−OH) = −(61.8 ± 22.4) J kg mol^{-2}, (1/2)(NaI−O) = −(333.3 ± 171.8) J kg mol^{-2}, were obtained.

In Fig. 6 are collected the values of h_{EN} determined from experimental data as well as those calculated on the basis of the above mentioned contributions of the interactions from the different selected groups.

As can be seen, in spite of the simplicity of the model of interactions the two sets of data are in satisfactory agreement. Further work of electrolyte−nonelectrolyte interaction coefficients is envisaged for other electrolytes in order to gain a better understanding of the electrochemistry of three-component systems, when one of the components is an electrolyte.

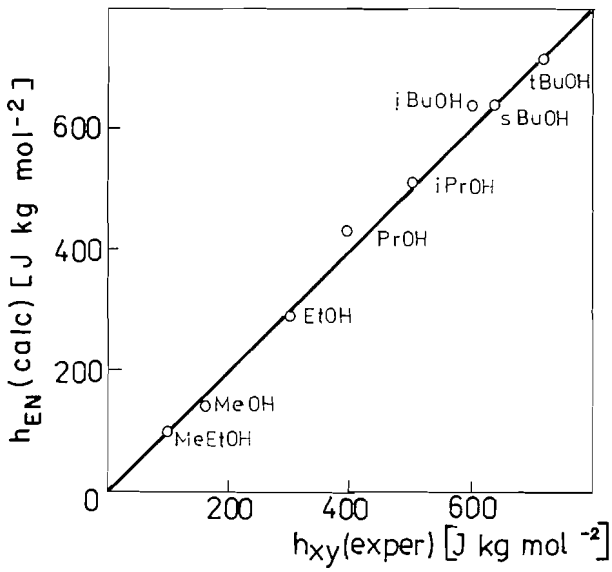

FIG. 6. Plot of calculated versus experimental values of h_{EN}(NaI−alcohol) in water at 298.15 K.

Acknowledgements

I would like to thank the authorities of the Free University of Amsterdam for the generous grant of a post-doctoral fellowship at their Thermochemical Laboratory. I have a special debt of gratitute to Professor G. Somsen (Free University of Amsterdam) and Professor S. Taniewska-Osińska (University of Łódź) for discussing with me earlier drafts of the paper and offering valuable comments and useful suggestions.

1. W. G. MCMILLAN, JR. and J. E. MAYER. J. Chem. Phys. **13**, 276 (1945).
2. G. PERRON, D. JOLY, J. E. DESNOYERS, L. AVEDIKIAN, and J.-P. MOREL. Can. J. Chem. **56**, 552 (1978).
3. W. J. M. HEUVELSLAND, C. DE VISSER, and G. SOMSEN. J. Chem. Soc. Faraday Trans. I, **77**, 1191 (1981).
4. H. L. FRIEDMAN and C. V. KRISHNAN. J. Solution Chem. **2**, 119 (1973).
5. W. J. M. HEUVELSLAND. Thesis. Free University of Amsterdam, Amsterdam. 1980.
6. C. DE VISSER, W. J. M. HEUVELSLAND, and G. SOMSEN. J. Solution Chem. **7**, 193 (1978).
7. J. E. DESNOYERS, G. PERRON, L. AVEDIKIAN, and J.-P. MOREL. J. Solution Chem. **5**, 631 (1976).
8. C. M. SLANSKY. J. Am. Chem. Soc. **62**, 2430 (1940).
9. G. V. KARPENKO, K. P. MISHCHENKO, and G. M. POLTORATSKII. Zhur. Strukt. Khim. **8**, 416 (1967).
10. B. G. PERELYGIN, YU. A. BYVALCEV, and A. F. VOROB'EV. Zhur. Fiz. Khim. **52**, 1558 (1978).
11. S. TANIEWSKA-OSIŃSKA and H. PIEKARSKI. Zhur. Fiz. Khim. **44**, 1665 (1974).
12. S. TANIEWSKA-OSIŃSKA and H. PIEKARSKI. Thermodynamika i Stroeniye Rastvorov, Ivanovo. **6**, 15 (1979).
13. A. WEISSBERGER, E. S. PROSKAUER, J. A. RIDDICK, and E. E. TOOPS, JR. Organic solvents. Interscience Publishers Inc., New York. 1955.
14. S. TANIEWSKA-OSIŃSKA and H. PIEKARSKI. J. Solution Chem. **7**, 891 (1978).
15. C. M. CRISS and J. W. COBBLE. J. Am. Chem. Soc. **83**, 3223 (1961).
16. J. TIMMERMANS. The physico-chemical constants of binary sys-

tems in concentrated solutions. Interscience Publisher Inc., New York. 1959.
17. G. AKERLÖF. J. Am. Chem. Soc. **54**, 4125 (1932).
18. G. ROUX, G. PERRON, and J. DESNOYERS. J. Solution Chem. **7**, 639 (1978).
19. S. TANIEWSKA-OSIŃSKA and S. WITKOWSKI. Acta Univ. Lodz. Folia Chim. Ser. II, **24**, 3 (1978).
20. R. L. MOSS and J. H. WOLFENDEN. J. Chem. Soc. London, 118 (1939).
21. G. A. KRESTOV. Termodynamika ionnykh procesov v rastvorakh. *Edited by* Khimiya, Leningrad. 1973.
22. B. G. PERELYGIN, YU. A. BYVALCEV, and A. F. VOROB'EV. Zhur. Fiz. Khim. **52**, 484 (1978); **52**, 1836 (1978).
23. R. K. MOHANTY, T. S. SARMA, S. SUBRAMANIAN, and J. C. AHLUWALIA. Trans. Faraday Soc. **67**, 305 (1971).
24. R. K. MOHANTY, S. SUNDER, and J. C. AHLUVALIA. J. Phys. Chem. **76**, 2577 (1973).
25. L. AVEDIKIAN, J. JUILLARD, J-P. MOREL, and M. DUCROS. Thermochim. Acta, **6**, 283 (1973).
26. Y. POINTUD, J. JUILLARD, L. AVEDIKIAN, and J-P. MOREL. Thermochim. Acta, **8**, 423 (1974).
27. N. DOLLET and J. JUILLARD. J. Solution Chem. **5**, 77 (1976).
28. K. P. MISHCHENKO, V. V. SUBBOTINA, and B. S. KRUMGALZ. Teoret. i Eksper. Khim. **5**, 268 (1969).
29. M. H. ABRAHAM., E. AH-SING, A. F. DANIL DE NAMOR, T. HILL, A. NASEHZADEH, and R. A. SCHULZ. J. Chem. Soc. Faraday Trans. I, **74**, 359 (1978).
30. I. I. LONKEVICH, K. P. MISHCHENKO, and S. V. SHADSKII. Zhur. Obshch. Khim. **40**, 723 (1970).
31. M. H. ABRAHAM, A. F. DANIL DE NAMOR, and R. A. SCHULZ. J. Solution Chem. **6**, 491 (1977).
32. K. P. MISHCHENKO and G. M. POLTORATSKII. Problems of thermodynamics and structure of aqueous and nonaqueous electrolyte solutions. Plenum Publishing Corp., New York. 1972.
33. G. NEMETHY. Ann. Ist. Super. Sanita, **6**, 487 (1970).
34. O. YA. SAMOILOV. Zhur. Strukt. Khim. **7**, 15 (1964); **7**, 175 (1964).
35. G. NEMETHY and H. A. SCHERAGA. J. Phys. Chem. **66**, 1773 (1962).
36. M. N. BUSLAEVA and O. YA. SAMILOIV. Zhur. Strukt. Khim. **4**, 502 (1963).
37. F. FRANKS and D. S. REID. Water, a comprehensive treatise. Vol. 2. *Edited by* F. Franks. Plenum Press. 1973.
38. S. PETRUCCI. Acta Chem. Scand. **16**, 760 (1962).
39. S. TANIEWSKA-OSIŃSKA and A. PIEKARSKA. Bull. Acad. Pol. Sci., Ser. Sci. Chim. **26**, 612 (1978).
40. G. V. MERKEN, H. P. THUN, and F. VERBEEK. Electrochim. Acta, **21**, 11 (1976).
41. C. V. MERKEN, H. P. THUN, and F. VERBEEK. Bull. Soc. Chim. Belg. **86**, 649 (1977).
42. R. FUCHS and C. P. HAGAN. J. Phys. Chem. **77**, 1797 (1973).
43. S. TANIEWSKA-OSIŃSKA, B. PIESTRZYŃSKA, and R. ŁOGWINIENKO. Can. J. Chem. **58**, 1584 (1980).
44. M. CASTAGNOLO, G. PETRELLA M. DELLA MONICA, and A. SACCO. J. Solution Chem. **8**, 501 (1979).
45. J. MOKRZAN. To be published.
46. V. GUTMANN and R. SCHMID. Coord. Chem. Rev. **12**, 263 (1974).
47. M. J. KAMLET and R. W. TAFT. J. Am. Chem. Soc. **98**, 377 (1977).
48. J. A. KOPPEL and A. I. PAJU. Reakts. Sposobn. Organ. Soedin. **11**, 121 (1974).
49. E. M. KOSOWER. J. Am. Chem. Soc. **80**, 3253 (1958); **80**, 3261 (1958); **80**, 3267 (1958).
50. C. REICHARDT. Lösungsmittel effekte in der organische chemie. Verlag Chemie, Weinheim/Bergstr. Germany. 1973.
51. H. S. FRANK and W. Y. WEN. Discuss. Faraday Soc. **24**, 133 (1957).
52. E. M. ARNETT, W. B. KOVER, and J. V. CARTER. J. Am. Chem. Soc. **91**, 4028 (1969).
53. J. J. SAVAGE and R. H. WOOD. J. Solution Chem. **5**, 733 (1976).
54. C. DE VISSER, W. J. M. HEUVELSLAND, and G. SOMSEN. J. Solution Chem. **6**, 525 (1977).

Can. J. Chem. Downloaded from www.nrcresearchpress.com by 210.87.254.5 on 09/06/12
For personal use only.

On the analysis of calorimetric data in the study of dimerization of carboxylic acids in nonpolar solvents

PAWEŁ GÓRALSKI AND STEFANIA TANIEWSKA-OSIŃSKA
Department of Physical Chemistry, University of Łódź, ul. Nowotki 18, 91-416 Łódź, Poland

Received September 17, 1982[1]

PAWEŁ GÓRALSKI and STEFANIA TANIEWSKA-OSIŃSKA. Can. J. Chem. **61**, 2209 (1983).

The calorimetric dilution method was analyzed for the accuracy with which the equilibrium constant (K_d) and dimerization enthalpy (ΔH_d) can be determined. The calculations were carried out using the ideal monomer–dimer model. It was found that the error in determining the functions describing dimerization increases strongly with rising K_d values but is independent of ΔH_d values. Doubt is expressed whether dimerization and trimerization can be studied simultaneously by the calorimetric method. A suggestion is made to use spectroscopy and calorimetry jointly rather than separately to determine K_d and ΔH_d values rapidly and conveniently, producing, in many cases, more accurate results.

PAWEŁ GÓRALSKI et STEFANIA TANIEWSKA-OSIŃSKA. Can. J. Chem. **61**, 2209 (1983).

On a évalué la précision de la méthode de dilution calorimétrique dans la détermination de la constante d'équilibre (K_d) et de l'enthalpie de dimérisation (ΔH_d). On a effectué les calculs en utilisant un modèle monomère–dimère idéal. En déterminant les fonctions qui décrivent la dimérisation on trouvé que l'erreur augmente de façon márquée lorsque la valeur de K_d augmente mais elle ne dépend pas de ΔH_d. On doute que l'on puisse étudier simultanément la dimérisation et la trimérisation par la méthode calorimétrique. On propose d'utiliser la spectroscopie conjointement avec la calorimétrie et non séparément pour déterminer rapidement de façon convenable les valeurs de K_d et de ΔH_d. On obtient dans plusieurs cas des résultats plus précis.
[Traduit par le journal]

Introduction

The vast majority of studies devoted to self-association of carboxylic acids in nonpolar solvents have assumed the monomer–dimer equilibrium to be the only equilibrium present in the system. Such was the case, e.g., with calorimetric studies of a number of acids conducted by Calvet and Paoli (1), Mokrzan *et al.* (2), or Zaugg and co-workers (3–6). Zaugg *et al.* (6) and Krishnan *et al.* (7) were the first to employ the technique of minimizing the experimental data to determine K_d and ΔH_d values from calorimetric measurements. Such a method of treating the results was also employed (7) to determine the equilibrium constant and enthalpy of trimerization of benzoic acid (HBz) in benzene. That trimers, dimers, and monomers coexist in solutions of carboxylic acids has also been suggested in osmometric studies (8, 9).

The present study analyzes the error involved in K_d and ΔH_d values determined with the calorimetric method for the case in which the data are subjected to minimization. Also discussed will be the possibility of studying trimerization of carboxylic acids by the calorimetric method.

Methods

The use of minimization in determining K_d *and* ΔH_d *of carboxylic acids*

Application of minimization to calorimetric heat measurements makes it possible to avoid errors typical of other data processing procedures such as, e.g., the extrapolation error involved in determining the apparent relative molar enthalpy (ϕ_L). The one snag of minimization is the subjective choice of the criterion of minimization which, in principle, can be any of the measuring or searched quantities or their combination (sum, product, weighted average, etc.). Our calculations, performed on the data obtained by Krishnan *et al.* (7), show that the use of different criteria can produce K_d and ΔH_d values differing by as much as 50–70%. The discussion is based on the monomer–dimer type association model. Using the procedure described by Rollett (10), we have calculated standard deviation (SD) values for both quantities sought (δK_d and $\delta \Delta H_d$).

$$\delta K_d = \sqrt{\sum_i \left(\frac{\partial X_i}{\partial \Delta H_d}\right)^2 \Big/ \det} \cdot \delta_X$$

$$\delta \Delta H_d = \sqrt{\sum_i \left(\frac{\partial X_i}{\partial K_d}\right)^2 \Big/ \det} \cdot \delta_X$$

where:

$$\delta_X = \sqrt{\frac{\sum_i (X^i_{exp} - X^i_{calc})^2}{n - 2}}$$

$$\det = \sum_i \left(\frac{\partial X_i}{\partial \Delta H_d}\right)^2 \cdot \sum_i \left(\frac{\partial X_i}{\partial K_d}\right)^2 - \left[\sum_i \left(\frac{\partial X_i}{\partial K_d} \cdot \frac{\partial X_i}{\partial \Delta H_d}\right)\right]^2$$

X is the parameter selected as the criterion of minimization (ΔH_{dil}, Q_{exp}, etc.) and n is the number of experimental measurements.

In spite of the divergences in K_d and ΔH_d values mentioned above and related to the use of different minimization criteria, the determined SD values never exceeded ca. 10% of the values sought. This makes the SD values of K_d and ΔH_d an insufficient indicator of the accuracy of the results obtained. It seems to us that an acceptable degree of accuracy of results would be achieved if it gave some indication of the differences between results obtained for a variety of reasonably selected minimization criteria. In the case under discussion the set of relevant quantities relating to the data of ref. 7 obtained for HBz solution in a Picker calorimeter are collected in Table 1.

As can be seen from the above, the assumed resultant error may be as much as 4–5 times higher than the calculated δK_d and $\delta \Delta H_d$, when ΔH_{dil} is selected as the minimization criterion. A similar ratio of uncertainty intervals relative to the SD of dimerization enthalpy was found by Zaugg *et al.* (6) for ΔH_d of a series of acetic and propionic acid derivatives. Thus the resultant error given in Table 1 should be taken to faithfully represent the error involved in the values obtained.

[1]Revision received December 10, 1982.

Can. J. Chem. Downloaded from www.nrcresearchpress.com by 210.87.254.6 on 09/06/12
For personal use only.

TABLE 1. The effect of choice of minimization criteria of experimental calorimetric data on the obtained values of K_d and ΔH_d and the error involved

Minimization criterion	K_d	$-\Delta H_d$	δK_d	$\delta \Delta H_d$	Resultant error: err K_d	Resultant error: err ΔH_d
$\sum_i (\Delta H^i_{d(exp)} - \Delta H_{d(calc)})^2$	500*	35.1*	—	—	±100*	±2.1*
$\sum_i \omega (Q^i_{exp} - Q^i_{calc})^2$	530	36.0	±30	±0.8	±75	±1.7
$\sum_i (\Delta H^i_{dil(exp)} - \Delta H^i_{dil(calc)})^2$	575	36.8	±25	±0.4	±100	±2.1

*See ref. 7.
†$\omega = Q^{i}_{calc}{}^{-2}$, K_d (L/mol), ΔH (kJ/mol).

TABLE 2. The values of various kind of errors in K_d and ΔH_d for benzoic acid in benzene*

Errors determined	Magnitude of error: K_d (L/mol)	Magnitude of error: ΔH_d (kJ/mol)
Pre-experimentally predicted†	$\delta K_d = \pm 9$	$\delta \Delta H_d = \pm 0.21$
After experiment (Table 1)	$\delta K_d = \pm 25$	$\delta \Delta H_d = \pm 0.42$
Real (resultant) error (Table 1)	err $K_d = \pm 100$	err $\Delta H_d = \pm 2.1$

*We adopted K_d = 575 L/mol and $\Delta H_d = -36.8$ kJ/mol, resulting from minimizing ΔH_{dil}, Table 1, $N = 2.0$.
†Assumed in test $N = 2.0$ ($N = C_{initial}/C_{final}$).

Pre-experimental prediction of error in K_d *and* ΔH_d

There is no information in the relevant literature on the relation between the values of K_d and ΔH_d and the accuracy with which they are determined using the calorimetric method. An attempt to predict the error involved was made using the following assumptions.

(*i*) The minimization criterion was always the same:

$$\sum_i (\Delta H^i_{dil(exp)} - \Delta H^i_{dil(calc)})^2 \rightarrow \min \text{ [as in ref. 7]}$$

(*ii*) Only monomer–dimer equilibrium is present in the solution, i.e. the concentration dependence of the heat of dilution results only from the shifting of that equilibrium. The system is perfectly associated.

(*iii*) The set of "experimental" points consisted in each case of 25 single "measurements" evenly spaced in the function of concentration with constant accuracy of heat measurement ±0.5%.

The choice of the limits of concentrations for testing was determined by the possibility of measuring the heat with the required accuracy. For Picker's calorimeter we assumed minimal $Q_{dil} = 0.008$ J, while for batch solution calorimeter it was $Q_{dil} = 0.2$ J.

Standard deviation values (δK_d and $\delta \Delta H_d$) were calculated on the basis of the 0.5% error in the "measurement" of the dilution enthalpy whose values were determined for the assumed K_d and ΔH_d of the process. It should be stressed that, thus calculated, the δK_d and $\delta \Delta H_d$ values are not to be identified with the expected error in the experimental determination of the two quantities. The differences between the two sets of quantities are shown in Table 2 for the HBz + C_6H_6 system. The fact that in the case of experimental results the SD values are higher than those calculated before the experiment may be due to the presence, in the experiment, of accidental errors exceeding 0.5%, as well as to the possibility of a systematic error in the model for which it was impossible to make allowances during testing. The uncertainty vs. predicted SD ratio is ca. 10:1. Figures 1 and 2 show the effect of the dimerization constant (log K_d) on δK_d and $\delta \Delta H_d$ for different values of the $C_{initial}/C_{final}$ ratio (N).

The assumed error of calorimetric measurement Q_{exp} (±0.5%), which is constant regardless of the effect measured, coincides with the constant values of the relative error ΔH_{dil}. Consequently, the value of dimerization enthalpy has no effect whatever on δK_d or $\delta \Delta H_d$. Assuming that the ratio of real error to that calculated before experiment is approximately constant (10:1) and independent of K_d, it can be noticed that heat of dilution measurements yield the most accurate results when: a low N dilution calorimeter is used (error is lowest when $N = 4$ for log $K_d > 1.5$ and $N = 2$ for log $K_d < 1.5$); and the expected value of the dimerization constant is low. The minimum error for both quantities (K_d, ΔH_d) occurs when $50 > K_d > 5$ L/mol.

Regardless of the above, the accuracy increases when a wide range of acid concentrations in nonpolar medium is employed, although high concentrations should be avoided because of the possibility of specific and nonspecific interactions which are not taken into account in the model. One can expect that for systems for which $K_d < 1000$ L/mol, the accuracy of K_d and ΔH_d determination by the calorimetric method should be satisfactory (err. $K_d < 25\%$, err. $\Delta H_d < 10\%$), and it will rise as the value of K_d decreases.

Trimerization of carboxylic acids and calorimetric measurements

Minimizing experimental calorimetric data ΔH_{dil}, Krishnan *et al.* (7) described in thermodynamic terms the process of benzoic acid trimerization in benzene. According to the authors, the following considerations suggest that the solution contains trimers: (*a*) the calorimetrically determined dimerization constant of HBz in benzene is lower than those reported in the literature and obtained in other ways; (*b*) the plot of ϕ_L vs. $(-\phi_L/C)^{1/2}$ diverges from linearity (ϕ_L is the relative apparent molar enthalpy of acid in benzene); and (*c*) there is a distinct (the authors claim) concentration dependence on K_d obtained for the monomer–dimer model. The analysis and calculations we have carried out on Krishnan's results suggest that the above divergences may be accounted for in some other way. Let us thus consider the trimerization evidence (7) item by item.

(*a*) It seems to us that the difference between the K_d value obtained by Krishnan (500 L/mol) and those obtained by other

Can. J. Chem. Downloaded from www.nrcresearchpress.com by 210.87.254.6 on 09/06/12
For personal use only.

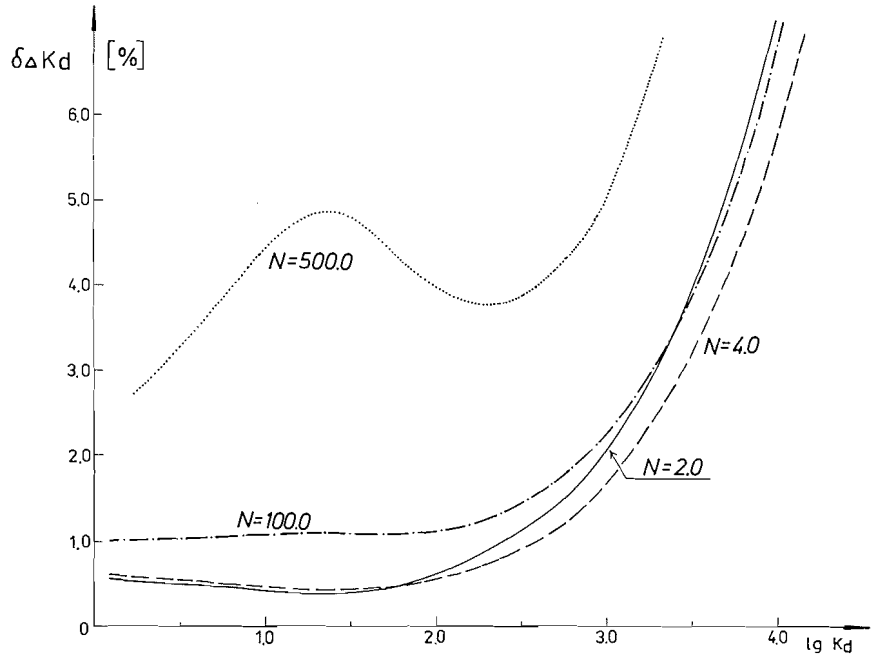

FIG. 1. The effect of the equilibrium constant of dimerization (as log K_d) on the SD of calorimetrically determined K_d values. (ΔQ_{exp} = ±0.5%).

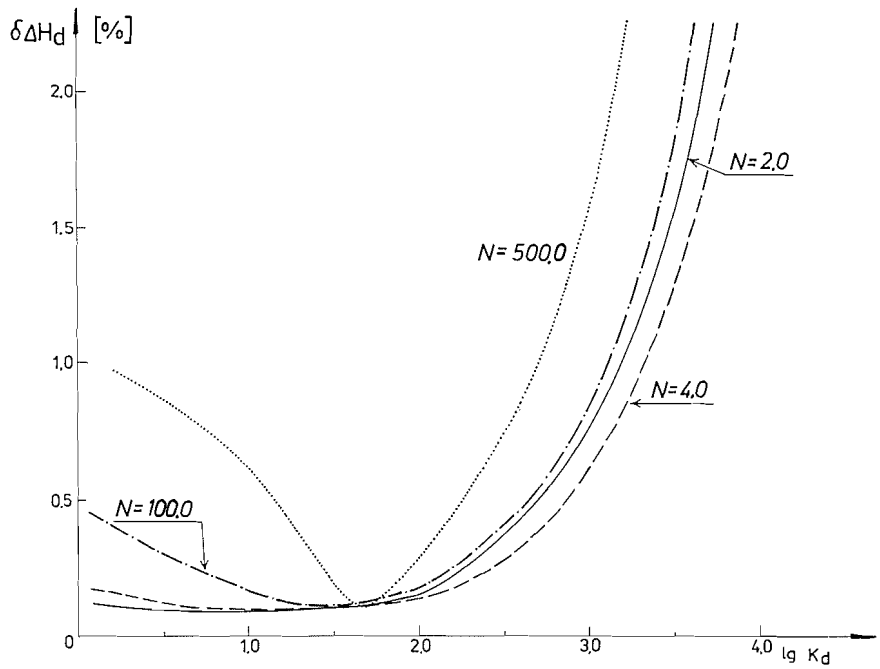

FIG. 2. The effect of the equilibrium constant of dimerization (as log K_d) on the SD of calorimetrically determined ΔH_d values.

methods (11–14), which amounts to about 100 L/mol, does not necessarily have to indicate the presence of trimers in the HBz–benzene system. As can be seen in Table 1, the use of ΔH_{dil} as the minimization criterion produces K_d values of 575 L/mol, δK_d = 25 L/mol, which practically coincide with literature data. Krishnan used the same minimization criterion for the description of the monomer–dimer–trimer model and obtained K_d = 625 L/mol. The convergence of all the data becomes especially evident when account is taken of the error in K_d determination, usually set at ca. 15–20%, which corresponds to ~100 L/mol independent of the method used.

(*b*) The curvature of the plot ϕ_L vs. $(-\phi_L/C)^{1/2}$ observed by Krishnan becomes considerably less pronounced when it is drawn on the basis of ϕ_L values with the lower limit of error reported in the cited work. The error in the value of ϕ_L is in this case ~1000 J/mol, which corresponds to 7–15% of the absolute value of ϕ_L. The slight divergence from linearity can be reduced still further if concentration is replaced by unknown activity; in concentrated solutions "*a*" may well be smaller than "*C*", with the difference growing with increasing concentration. The distinct nonideality of the system may be due to interactions between systems of π-electrons in the rings of both the acid and benzene molecules. Another type of interaction may be weak H-bonds of H···π type arizing with monomers whose number changes with changes in the concentration, or 1.5% hydration of monomers (7).

Can. J. Chem. Downloaded from www.nrcresearchpress.com by 210.87.254.6 on 09/06/12
For personal use only.

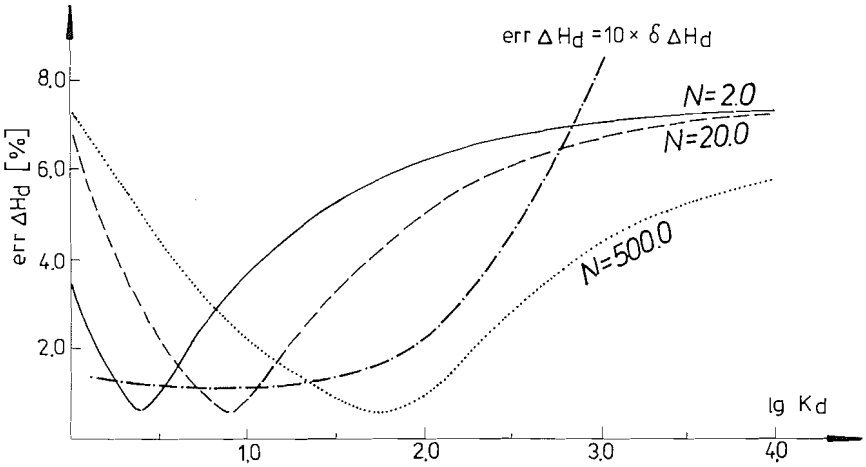

FIG. 3. Plot of the predicted error in ΔH_d vs. dimerization constant in the approach combining spectroscopy and calorimetry (dot-and-dash line, estimated; approximate error involved in calorimetry used alone, err $\Delta H_d = 10 \times \delta\Delta H_d$, see text).

(*c*) The strong, systematic dependence of the dimerization constant on the concentration may, in fact, indicate the presence of another equilibrium, not included in the model employed. Using the "best" of the values obtained by us $\Delta H_d = -36.81$ kJ/mol (Table 1), we calculated once again the K_d values for all the experimental points (7). The plot of $K_d = f[(C_i + C_f)/2]$, where C_i is the initial concentration and C_f is concentration of the acid after dilution, appears to be a collection of points which does not exhibit any distinct (rising or falling) functional dependence. The strong random scatter of K_d values (from ~450 L/mol to ~650 L/mol) is doubtless related to the considerable sensitivity of the equilibrium constant to even slight (±0.5%) error in ΔH_{dil}. It seems to us that the calorimetric method used alone should not be employed in studies of the other forms of association in acid solutions. The reason is the weak sensitivity of thermal effects to the presence (or absence) of relatively minor amounts of different stoichiometry associates.

Determination of ΔH_d by the combined use of spectroscopy and calorimetry

The analysis carried out above of the accuracy with which the functions of dimerization are determined made us look for ways of improving that accuracy. This, we think, is possible if calorimetry is used together with spectroscopy. The approach, which consists in determining the thermal effects calorimetrically and the equilibrium constant spectroscopically, has not, so far, been used in studies of carboxylic acid dimerization. Nevertheless, already in the 1960's Lamberts *et al.* (15, 16) and Arnett *et al.* (17, 18) combined the spectroscopically determined value of the equilibrium constant with calorimetric heat measurements in an attempt to establish the enthalpy of 1 : 1 donor–acceptor complex formation. The combined use of the two methods has also been found useful in studies of relatively complex associative systems (19, 20).

The value of K_d, established by spectroscopy, makes it possible to calculate the value of ΔH_d on the basis of a single calorimetric experiment, for all the variables appearing in the function $\Delta H_d = f(K_d, \Delta H_{dil}, C_{initial}, C_{final})$ are known. Practically speaking, the required number of measurements is such that the obtained value of ΔH_{dil} should not involve random error exceeding the assumed level of ±0.5%. We have considered the applicability of such a combined approach to the monomer–dimer equilibrium. The aim of the exercise was to find the range of K_d and ΔH_d values for which the combined approach produces more accurate ΔH_d data than either method employed independently of the other. The expected error in ΔH_d determination was calculated using the differential method. The constant sources of error adopted in the calculations included the value quoted, e.g., by Zhukova *et al.* (21) ($\Delta K_d = 15\%$) and $\Delta Q_{exp} = 0.5\%$ (error in calorimetric measurement). We found that the error due to possible inaccuracy of concentration measurement was negligible. The results obtained for different values of N are presented in Fig. 3 as plots of err $\Delta H_d = f(\log K_d)$.

Similarly, as before, the change of ΔH_d has no effect on the magnitude of the predicted error (err ΔH_d). Also the value of concentration C_i at which the experiment is carried out has little effect on it. As can be seen from Fig. 3, for equilibrium constants for which $\log K_d > 1.5$, the most accurate ΔH_d value can be achieved using 500 times dilution with, e.g., a batch solution calorimeter. Of greatest importance for the experimenter is the range of K_d values which closely approaches the minimum of the function err $\Delta H_d = f(\log K_d)$ as well as the fact that it shifts as N changes. The spectroscopically determined value of K_d makes it possible to select the experimental conditions (i.e. N) in such a way that the sought value of ΔH_d involves minimum error. By appropriately selecting the ratio of initial and final concentrations in heat measurements, it is possible to determine the value of ΔH_d for any K_d (when $\log K_d > 0.2$) more accurately than when calorimetry alone is used (Fig. 3). Regardless of the value of the dimerization constant, the procedure proposed here should yield more accurate results than the spectroscopic method, where the error in ΔH_d determination is estimated to be 10% or more (22).

It is thus possible to select optimal experimental conditions and the most appropriate method of determining the parameters which describe the equilibrium state in a solution even before measurements are carried out. We hope that it will also be possible to predict errors and to identify ways of reducing them in the case of more complex donor–acceptor systems, such as those we dealt with in earlier studies (19, 20).

1. E. CALVET and C. PAOLI. C. R. Acad. Sci. **257**, 3376 (1963).
2. J. MOKRZAN, S. TANIEWSKA-OSIŃSKA, and M. ŁAŹNIEWSKI. Rocz. Chem. **43**, 1523 (1969).
3. N. S. ZAUGG, S. P. STEED, and E. M. WOOLLEY. Thermochim. Acta, **3**, 349 (1972).

Can. J. Chem. Downloaded from www.nrcresearchpress.com by 210.87.254.6 on 09/06/12
For personal use only.

4. N. S. ZAUGG, L. E. TREJO, and E. M. WOOLLEY. Thermochim. Acta, **6**, 293 (1973).
5. E. M. WOOLLEY and N. S. ZAUGG. Anal. Calorim. **3**, 479 (1974).
6. N. S. ZAUGG, J. KELLEY, and E. M. WOOLLEY. J. Chem. Eng. Data, **24**, 218 (1979).
7. T. KRISHNAN, W. C. DUER, S. GOLDMAN, and J. L. FORTIER. Can. J. Chem. **57**, 530 (1979).
8. O. LEVY, G. Y. MARKOVITS, and I. PERRY. J. Phys. Chem. **79**, 239 (1975).
9. N. SUGAWARA, E. S. STEVENS, G. M. BONORA, and C. TONIOLO. J. Am. Chem. Soc. **102**, 7044 (1980).
10. J. S. ROLLETT. *In* Crystallographic computing. *Edited by* F. R. Ahmed. Munksgaard International Booksellers and Publishers Ltd., Copenhagen. 1970. pp. 167–181.
11. G. ALLEN, J. G. WATKINSON, and K. H. WEBB. Spectrochim. Acta, **22**, 807 (1966).
12. F. T. WALL and F. W. BANES. J. Am. Chem. Soc. **67**, 898 (1945).
13. G. ALLEN and E. F. CALDIN. Trans. Faraday Soc. **49**, 895 (1953).
14. B. C. BARTON and C. A. KRAUS. J. Am. Chem. Soc. **73**, 4561 (1951).
15. L. LAMBERTS and TH. ZEEGERS-HUYSKENS. J. Chim. Phys. **60**, 435 (1963).
16. L. LAMBERTS. J. Chim. Phys. **62**, 1404 (1965).
17. E. M. ARNETT, T. S. S. R. MURTY, P. VON R. SCHLEYER, and L. JORIS. J. Am. Chem. Soc. **89**, 5955 (1967).
18. E. M. ARNETT, L. JORIS, E. MITCHELL, T. S. S. R. MURTY, T. M. GORRIE, and P. VON. R. SCHLEYER. J. Am. Chem. Soc. **92**, 2365 (1970).
19. S. TANIEWSKA-OSIŃSKA and P. GÓRALSKI. J. Chem. Soc. Faraday Trans. 1, **77**, 969 (1981).
20. S. TANIEWSKA-OSIŃSKA and P. GÓRALSKI. J. Chem. Soc. Faraday Trans. 1, **78**, 1755 (1982).
21. W. A. ZHUKOVA, L. I. TARASOVA, and M. I. SZEICH-ZADE. Teor. Eksp. Khim. **14**, 396 (1978).
22. S. SINGH and C. N. R. RAO. J. Phys. Chem. **71**, 1074 (1967).

Can. J. Chem. Downloaded from www.nrcresearchpress.com by 210.87.254.6 on 09/06/12
For personal use only.

Complexes of platinum group metals with the ambidentate ligands $Ph_2P(CH_2)_nSPh$ (n = 1, 2)

ALAN R. SANGER

Alberta Research Council, 11315 - 87 Avenue, Edmonton, Alta., Canada T6G 2C2

Received November 24, 1982

ALAN R. SANGER. Can. J. Chem. **61**, 2214 (1983).

The potentially bidentate ligands $Ph_2P(CH_2)_nSPh$ (n = 1, 2) form complexes of rhodium(I), iridium(I), palladium(II), or platinum(II) in which ligands are coordinated to a metal centre either by the phosphine function alone, or by the phosphine and thioether functions, or both. Successive displacement of chloro-ligands from $[MCl_2(Ph_2PCH_2CH_2SPh)_2]$ (M = Pd, Pt) gives the cationic complexes $[MCl(Ph_2PCH_2CH_2SPh)_2]^+$ and $[M(Ph_2PCH_2CH_2SPh)_2]^{2+}$. In the latter each ligand is chelating, but in the former, one ligand is monodentate and the other bidentate. Homopolynuclear complexes may also be synthesized in which metal centres are bridged by $Ph_2P(CH_2)_nSPh$. The complex $[RhCl(Ph_2PCH_2SPh)(C_8H_{12})]$ contains cyclooctadiene as a monodentate ligand.

ALAN R. SANGER. Can. J. Chem. **61**, 2214 (1983).

Les ligands potentiellement bidentates du type $Ph_2(CH_2)_nSPh$ (n = 1, 2) forment des complexes de rhodium (I), d'iridium (I), de palladium (II) ou de platine (II) dans lesquels les ligands sont coordonnés au centre métallique soit par la fonction phosphine uniquement, soit par les fonctions phosphine et thioéther, ou par les deux. Les déplacements successifs des ligands chlorés du $[MCl_2(Ph_2PCH_2CH_2SPh)_2]$ (M = Pd, Pt) donnent les complexes cationiques de $[MCl(Ph_2PCH_2CH_2SPh)_2]^+$ et de $[M((Ph_2PCH_2CH_2SPh)_2]^{2+}$. Dans ce dernier, chaque ligand est chélatant, mais dans le premier complexe un ligand est monodentate, et l'autre est bidentate. On peut également synthétiser des complexes homopolynucléaires dans lesquels les centres métalliques sont pontés par le $Ph_2P(CH_2)_nSPh$. Le complexes $[RhCl(Ph_2PCH_2SPh)(C_8H_{12})]$ contient le cyclooctadiène comme ligand monodentate.

[Traduit par le journal]

Can. J. Chem. Downloaded from www.nrcresearchpress.com by 210.87.254.40 on 09/06/12
For personal use only.

Introduction

Potentially bidentate ligands may form a variety of complexes in which such ligands are monodentate, bidentate chelating, or bidentate bridging in behaviour (1). Within each of these classes further variation can arise depending on the site(s) of coordination of the ligand, mutual conformation of ligands about each metal centre, and, especially in the case of the bidentate bridging mode, the presence or absence of a metal–metal interaction and any other bridging ligand. Previously, we in this laboratory have shown that the diphosphines $Ph_2P(CH_2)_nPPh_2$ (n = 1–4) or the dithioethers $PhS(CH_2)_nSPh$ (n = 1–6) form platinum-group metal complexes of each type (2–5). The coordination mode of a bidentate ligand and degree of aggregation of each complex depend upon not only the nature and oxidation state of the central metal atom, but also steric effects. These effects are largely determined by the angle that a ligand would subtend at the metal centre if it chelated the metal ion, and this in turn is directly determined by the value of n (2–5). In each case the thioether ligands are more labile than the corresponding phosphine ligands.

Recently, interest has grown in complexes of ligands with dissimilar donor sites (6–10). These have included phosphine or arsine ligands which also contain nitrogen or oxygen donor sites (e.g., refs. 6, 7), or dissimilar phosphorus donor sites (e.g., ref. 8). 2-Diphenylphosphinoethanethiol, or its derived anion, has been considered as a 1-, 2-, 3-, or 5-electron donor ligand (9), demonstrating the versatility of such a system. A small number of other P and S donor ligands have been investigated, but much less intensely than either (P, P) or (S, S) bidentate ligands (10).

In addition to features in common with other potentially bidentate ligands, the ligands $Ph_2P(CH_2)_nSPh$ (herein abbreviated as "PS(n)") are of interest for the following reasons. (*1*) When the phosphine and thioether functions are both coordinated to a platinum-group metal the thioether is expected to be more labile than the phosphine, permitting facile generation of a "vacant site" at the metal centre. Consequently, oxidative addition or substitution reactions may be more readily effected. Further, the phosphine function may confer sufficient stability to an intermediate containing a vacant site to permit such a complex to behave as an effective catalyst. (*2*) Preferential coordination of phosphine and thioether functions to different metals offers the possibility of formation of heterodinuclear complexes, in a manner similar to that of 2-diphenylphosphinopyridine (6). (*3*) There exists the potential for both geometric and coordination isomerism in complexes of these ligands. Consequently, an investigation into the chemistry of systems containing the ligands PS(n) and platinum-group metals is being performed. Data concerning some complexes of rhodium(I) have been reported in a letter (5), and a series of complexes of ruthenium(II) and -(III) with PS(2) has been described (11). Herein the preparation of complexes of PS(1) and PS(2) with rhodium(I), iridium(I), palladium(II), and platinum(II) will be reported.

Experimental

All manipulations were performed in dry, oxygen-free solvents, except where so noted. Analyses were performed by Alfred Bernhardt Mikroanalytisches Laboratorium, Germany, or Canadian Microanalytical Service Ltd., Vancouver, B.C. Spectra were obtained using the following instruments: ir, Perkin Elmer 283; nmr, Bruker WP80. Conductivities were determined for solutions in acetone (2×10^{-4} to 2×10^{-3} M) or other solvents using a Radiometer CDM2e conductivity meter.

The metal complexes $[RhCl(cod)]_2$, $[RhCl(CO)_2]_2$, $[IrCl(cod)]_2$, $PdCl_2$, $[PdCl_2(PhCN)_2]$, $K_2[PtCl_4]$, and $[PtCl_2(PhCN)_2]$ (cod is 1,5-cyclooctadiene) were either commercially available (Strem, Alfa, Terochem) or synthesized using standard procedures. The ligand $Ph_2PCH_2CH_2SPh$, PS(2), was prepared by a published method (12).

Preparation of Ph_2PCH_2SPh, PS(1) (synthesis by C. G. Lobe)

CAUTION! Chloromethyl sulfides are suspected carcinogens, and should be treated as hazardous materials.

Chloromethylphenylsulfide (7.89 g, 0.05 mol) was added dropwise

TABLE 1. Preparation of complexes

Complex	Reagents	Atmosphere	Solvents
1, [RhCl(CO){PS(2)}]	$[RhCl(cod)]_2$ + 2PS(2)	CO	CH_2Cl_2
2, *trans*-[RhCl(CO){PS(1)}$_2$]	$[RhCl(cod)]_2$ + 4PS(1)	CO	CH_2Cl_2
3, *trans*-[RhCl(CO){PS(2)}$_2$]	$[RhCl(cod)]_2$ + 4PS(2)	CO	CH_2Cl_2
4, [RhCl{PS(1)}(η^1-cod)]	$[RhCl(cod)]_2$ + 4PS(1)	N_2	EtOH
5, [Rh{PS(2)}$_2$]BPh_4	$[RhCl(cod)]_2$ + 4PS(2) + $2NaBPh_4$	N_2	EtOH
6, [Rh(CO){PS(2)}$_2$]BPh_4	**5** + CO	CO	CH_2Cl_2
7, [IrCl{PS(1)}$_2$(cod)]	$[IrCl(cod)]_2$ + 4PS(1)	N_2	EtOH
8, [IrCl{PS(2)}$_2$]	$[IrCl(cod)]_2$ + 4PS(2)	N_2	EtOH
9, [Ir{PS(1)}$_2$]BPh_4	**7** + $NaBPh_4$	N_2	EtOH
10, [Ir{PS(2)}$_2$]BPh_4	**8** + $NaBPh_4$	N_2	EtOH
11, [Ir(CO){PS(2)}$_2$]BPh_4	**10** + CO	CO	CH_2Cl_2
12, *trans*-[IrCl(CO){PS(2)}$_2$]	$[IrCl(cod)]_2$ + 4PS(2)	CO	CH_2Cl_2
13, *trans*-[$PdCl_2${PS(1)}]$_4$	$[PdCl_2(PhCN)_2]$ + PS(1)	N_2	Acetone
14, *cis*-[$PdCl_2${PS(2)}]	$[PdCl_2(PhCN)_2]$ + PS(2)	N_2	Acetone
15, *trans*-[$PdCl_2${PS(1)}$_2$]	$[PdCl_2(PhCN)_2]$ + 2PS(1)	N_2	Acetone
16, *trans*-[$PdCl_2${PS(2)}$_2$]	$[PdCl_2(PhCN)_2]$ + 2PS(2)	N_2	Acetone
17, *trans*-[$PtCl_2${PS(2)}]	$K_2[PtCl_4]$ + PS(2)	N_2	H_2O/CH_2Cl_2
18, *cis*-[$PtCl_2${PS(2)}]	**17**	N_2	CH_2Cl_2
19, *cis*-[$PtCl_2${PS(1)}$_2$]	$[PtCl_2(PhCN)_2]$ + 2PS(1)	N_2	Acetone
20, *cis*-[$PtCl_2${PS(2)}$_2$]	$[PtCl_2(PhCN)_2]$ + 2PS(2)	N_2	Acetone
21, [PdCl{η^1-PS(2)}{η^2-PS(2)}]BPh_4	**16** + $NaBPh_4$	N_2	Ethanol
22, [PtCl{η^1-PS(2)}{η^2-PS(2)}]BPh_4	**19** + $NaBPh_4$	N_2	Ethanol
23, [Pd{η^2-PS(2)}$_2$]$(BPh_4)_2$	**21** + $NaBPh_4$ (excess)	N_2	Acetone
24, [Pt{η^2-PS(2)}$_2$]$(BPh_4)_2$	**22** + $NaBPh_4$ (excess)	N_2	Acetone

to a stirred solution of potassium diphenylphosphide (0.05 mol) in tetrahydrofuran (70 mL). The mixture was successively stirred overnight at room temperature, refluxed (4 h), and cooled to room temperature. Water (50 mL) was added to destroy remaining $KPPh_2$ and to dissolve KCl. The organic layer was then separated, and most of the solvent was removed under reduced pressure. The white wax so formed was dissolved in acetone, water was added, and the mixture was filtered to give $Ph_2PCH_2CH_2SPh$ as white crystals (6.9 g, 45%) which were then dried under vacuum. Evaporation of acetone from the mother liquor gave further crops of impure material. *Anal.* calcd.: C 74.00, H 5.56; P 10.04, S 10.40%; found: 73.93, H 5.63, P 9.46, S 10.32. NMR: ^{1}H: doublet (CH_2) δ 3.6 (J = 3.1 Hz), multiplet (Ph) δ 7.4 ppm (vs. $(CH_3)_4Si$); ^{31}P: δ_P −18.0 ppm (vs. 85% H_3PO_4). $Ph_2P(CH_2)_nSPh$ (n = 3, 4) and related materials may be prepared in a similar manner.

Both PS(1) and PS(2) are white, crystalline materials. The former is much more sensitive to both oxidation and thermal decomposition than the latter. PS(3) and 2-diphenylphosphinothiophene are extremely air-sensitive waxy or oily materials which are difficult to manipulate.

Preparation of metal complexes of PS(1) or PS(2)

These syntheses were each performed at room temperature or gentle reflux, and are listed in Table 1. Examples are given below. Analyses and conductivities of the products are listed in Table 2, and the ir and ^{31}P nmr spectra are listed in Table 3.

Example 1: Preparation of [Rh($Ph_2PCH_2CH_2SPh$)$_2$]BPh_4 and [Rh(CO)($Ph_2PCH_2CH_2SPh$)$_2$]BPh_4

A mixture of ethanol (50 mL), $Ph_2PCH_2CH_2SPh$ (0.591 g, 1.835 mmol) and $[RhCl(cod)]_2$ (0.224 g, 0.455 mmol) was stirred (1 h) under an atmosphere of nitrogen. A solution of Na[BPh_4] (0.4 g, excess) in ethanol (20 mL) was slowly added, and a yellow precipitate formed rapidly. The mixture was stirred (15 min), filtered, and the precipitate washed with ethanol and then dried under vacuum to give, as a yellow product, [Rh($Ph_2PCH_2CH_2SPh$)$_2$]BPh_4 (0.775 g, 80%).

A sample of the above complex (0.270 g, 0.253 mmol) was dissolved in dichloromethane (25 mL) under an atmosphere of CO. Ethanol (40 mL) was added to form a separate layer. The layers were gradually mixed, and the dichloromethane slowly evaporated to give, as a yellow, microcrystalline product, [Rh(CO)($Ph_2PCH_2CH_2SPh$)$_2$]-BPh_4 (0.223 g, 80%). Further evaporation of solvents gave additional product.

Example 2: Preparation of trans-*[IrCl(CO)($Ph_2PCH_2CH_2SPh$)$_2$]*

Under an atmosphere of carbon monoxide $[IrCl(cod)]_2$ (0.142 g, 0.212 mmol) was added to a solution of $Ph_2PCH_2CH_2SPh$ (0.279 g, 0.868 mmol) in dichloromethane (25 mL), and the mixture was stirred until a lemon−yellow solution was formed. Ethanol (10 mL) was added, and the mixture allowed to slowly evaporate under a stream of CO to leave a sticky mass. Pentane (25 mL) was added and the mixture successively stirred (1.5 h), filtered, and the bright lemon−yellow product dried under vacuum. The first crop of *trans*-[IrCl(CO)-($Ph_2PCH_2CH_2SPh$)$_2$] was 0.184 g (48%). Successive crops could be retrieved by further trituration of the sticky material in the flask under pentane.

Results and discussion

(A) Complexes of rhodium(I) and iridium(I)

In this and the following section complexes will be designated by the appropriate number from Tables 1−3.

Cleavage of the dinuclear complexes $[MCl(cod)]_2$ (M = Rh or Ir) occurs upon reaction with PS(1). The 1:1 complex [RhCl{PS(1)}(cod)], **4**, was readily isolated (eq. [2]), but the analogous iridium complex was not.

[2] $[RhCl(cod)]_2 + 2Ph_2PCH_2SPh \rightarrow 2[RhCl(cod)(Ph_2PCH_2SPh)]$

The ir spectrum of **4** exhibits a band assigned as Rh—Cl stretch, and the material is a non-electrolyte in solution in acetone. The ^{31}P nmr parameters are appropriate for a square-planar complex of rhodium(I). The ^{1}H nmr spectrum at 223 K of a solution of **4** in $CDCl_3$ revealed signals appropriate for the ligand PS(1) and 1,5-cyclooctadiene (1:1). The signals for PS(1) are at δ_H 4.1 (J(PH) = 5.4 Hz) and 7−8 ppm (($Si(CH_3)_4$ = 0), in the ratio 2:15. The cyclooctadiene signals at δ_H 5.6, 3.0, and 1.4−2.8 ppm, in the ratio 2:2:8, demonstrate that this ligand is monodentate in this complex. No coupling to rhodium was observed; signals for cyclooctadiene protons are each 10−15 Hz wide at half-heights, compared to 2−4 Hz for

Can. J. Chem. Downloaded from www.nrcresearchpress.com by 210.87.254.40 on 09/06/12
For personal use only.

TABLE 2. Analyses

Complex	Colour	Elemental analyses[a] C	H	Cl	P	S	Conductivity[b] (S cm^2 mol^{-1})	Comments[c]
1	Yellow	51.5 (51.6)	4.0 (3.9)	7.4 (7.25)	6.3 (6.3)	6.5 (6.6)		
2	Yellow	58.3 (59.8)	4.4 (4.4)	4.6 (4.5)	8.0 (7.9)	8.1 (8.2)		
3	Yellow	59.8 (60.7)	4.7 (4.7)	4.4 (4.4)	7.5 (7.6)	7.7 (7.9)		
4	Yellow	57.6 (58.4)	5.4 (5.3)	6.3 (6.4)	6.0 (5.6)	—		
5	Yellow	70.8 (72.05)	5.45 (5.5)	(0)	5.6 (5.8)	5.7 (6.0)	99	
6	Yellow	70.6 (71.3)	5.6 (5.3)	(0)	5.5 (5.7)	5.8 (5.9)	95	
7	Yellow	57.7 (58.0)	5.1 (4.9)	3.8 (3.7)	7.4 (6.5)	—	0.3	
8	Yellow	54.9 (55.1)	4.8 (4.4)	3.7 (4.1)	6.8 (7.1)	6.2 (7.4)		
9	Brown	64.5 (66.0)	5.4 (4.9)	(0)	6.1 (5.5)	4.6 (5.7)	74	
10	Cream	67.2 (66.5)	5.8 (5.1)	(0)	5.9 (5.4)	4.4 (5.5)	86	
11	Pale yellow	64.9 (65.9)	5.1 (4.9)	(0)	5.8 (5.2)	4.2 (5.4)	87	
12	Yellow	54.4 (54.7)	4.4 (4.3)	4.1 (4.0)	7.8 (6.9)	—	7.6	
13	Yellow	48.0 (47.0)	3.7 (3.5)	14.0 (14.6)	6.4 (6.4)	6.4 (6.6)		*M*, 1698 (486)
14	Yellow	48.1 (48.1)	3.8 (3.8)	14.25 (14.2)	—	6.7 (6.4)		
15	Pale yellow	55.55 (57.5)	4.0 (4.3)	—	7.6 (7.8)	7.8 (8.1)		
16	Pale yellow	58.4 (58.4)	4.7 (4.7)	8.2 (8.6)	—	8.2 (7.8)	5 (CH_2Cl_2) 113 (CH_3CN) 40 (Acetone)	
17	White	40.2 (40.8)	3.1 (3.25)	11.45 (12.05)	5.5 (5.3)	5.85 (5.45)		
18	Pale yellow	41.75 (40.8)	3.1 (3.25)	12.3 (12.05)	5.7 (5.3)	5.5 (5.45)		
19	White	51.7 (51.7)	3.9 (3.9)	—	—	7.1 (7.3)	9	
20	White	52.8 (52.75)	4.1 (4.2)	8.1 (7.8)	6.4 (6.8)	7.1 (7.0)		*M*, 844 (883)
21	Pale yellow	69.5 (69.5)	5.4 (5.3)	—	4.6 (5.6)	5.7 (5.8)	80	*M*, 912 (1106)
22	White	66.4 (64.35)	5.1 (4.9)	2.3 (3.0)	4.7 (5.2)	5.7 (5.4)	109	
23	Orange	73.3 (76.1)	5.5 (5.7)	(0)	—	4.8 (4.6)	180	
24	Yellow	70.8 (72.0)	5.4 (5.4)	(0)	—	4.1 (4.4)		

[a]Calculated values in parentheses.
[b]In acetone solutions, except where so noted.
[c]Molecular weights were determined by osmometry, using acetone solutions between 2×10^{-4} and 2×10^{-3} *M*.

signals for the PS(1) protons. The ^{1}H nmr of either $[MCl(cod)]_2$ (M = Rh or Ir) exhibits signals at δ 4.3 and 0.8–2.8 ppm in the ratio 4:8; no coupling to rhodium is observed. Therefore **4** contains PS(1) as a bidentate ligand. With an excess of PS(1), the iridium complex isolated from a reaction similar to [2], above, is the 2:1 complex $[IrCl\{PS(1)\}_2(cod)]$, **7**. In the absence of a metal–phosphorus coupling constant the ^{31}P nmr spectrum is less informative about the nature of **7** than of **4**. However, it should be noted that the phosphorus atoms are equivalent. An Ir—Cl stretching band is observed in the ir

Can. J. Chem. Downloaded from www.nrcresearchpress.com by 210.87.254.40 on 09/06/12
For personal use only.

TABLE 3. Infrared and nmr spectra

Complex	Infrared[a] ν(M—Cl)	Infrared[a] ν(CO)	^{31}P nmr[b] δ_P	^{31}P nmr[b] J(M—P)
1	291	2000	70.7	156.4
2	302	1957	24.2	123.3
3	308	1964	30.6	117.3
4	274	—	27.5	151.4
5	—	—	65.1	160.5
6	—	1974	54.4	100.7
7	310	—	−8.6	
8	—	—	29.5	
9	—	—	4.9	
10	—	—	47.3	
11	—	1962	17.3	
12	320	1954	17.0	
13	358	—	30.7	
14	317, 282	—	64.8	
15	323	—	43.5 (broad)	
16	363, 325	—	16.1 (broad)	
17	308	—	—	
18	323, 292	—	40.3	3594
19	325, 297	—	8.1	3691
20	322, 294	—	13.2	3528
21	310	—	43.5 (broad)	
22	310	—	P_A 49.8[c]	3508
			P_B 13.5[c]	3200
23	—	—	61.8	
24	—	—	45.9	3041

[a]Values in wavenumbers.
[b]Spectra were normally obtained at 223 K from solutions in dichloromethane-d_2 except where so noted in the text, and are ^{1}H-decoupled. Chemical shifts are in ppm versus external 85% H_3PO_4, and coupling constants are in Hz.
[c]$^2J(P_A—P_B)$ = 14.9 Hz.

spectrum, and the material is a non-electrolyte. If complex **7** contained a chloro-ligand, coordinated cyclooctadiene, and two bidentate PS(1) ligands it would be a 20- or 22-electron complex, and so it must instead be a five-coordinate complex of iridium containing two equivalent monodentate(P) PS(1) ligands.

Reaction of **7** with Na[BPh_4] gave the complex [Ir{PS(1)}$_2$]-BPh_4, **9**, in which the phosphorus ligands are again equivalent (^{31}P nmr) (eq. [3]).

[3] [IrCl(cod)(η^1-Ph_2PCH_2SPh)$_2$] + Na[BPh_4] → NaCl + [Ir(η^2-Ph_2PCH_2SPh)$_2$]BPh_4 + cod

Reaction of an excess of PS(2) with [IrCl(cod)]$_2$ gave the complex [IrCl{PS(2)}$_2$], **8**. The rhodium analog has not been isolated in an analytically pure state, but its existence in solution can be inferred from a subsequent reaction. Reaction of a solution of either chloro-complex with Na[BPh_4] gave [M{PS(2)}$_2$]BPh_4 (**5**, M = Rh; **10**, M = Ir). In each case the product is of limited solubility in ethanol but readily soluble in either dichloromethane or acetone, in which they are 1:1 electrolytes. Reaction of solutions of **5** or **10** with CO gave the corresponding monocarbonyl complexes, **6** or **11**. The phosphorus atoms are in each case equivalent down to 203 K (^{31}P nmr), and the phosphorus−rhodium coupling constant (100.7 Hz) is appropriate for equatorial phosphine ligands. For [Rh(CO)$_2$(η^1-diop)(η^2-diop)]$^+$ the corresponding values are J(Rh—P_{ax}) = 131 Hz and J(Rh—P_{eq}) = 106 Hz, and for [Rh(CO)(η^2-$Ph_2PCH_2CH_2CH_2PPh_2$)$_2$]$^+$ they are J(Rh—P_{ax}) = 115 Hz and J(Rh—P_{eq}) = 86 Hz (2). For the phosphorus atoms to be equivalent each PS(2) must be coordinated to Rh the same. These data are consistent with complexes **6** and **11** being trigonal bipyramidal, with axial thioether ligands (Fig. 1), or being a square-pyramidal structure. However, this latter option is less-precedented.

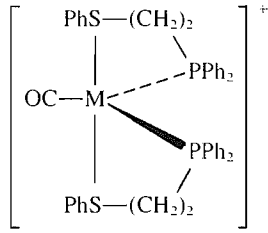

FIG. 1. Trigonal bipyramidal complexes with axial thioether ligands (M = Rh, Ir).

Although addition of CO to the complex cation, [Rh($Ph_2PCH_2CH_2CH_2PPh_2$)$_2$]$^+$, to form trigonal bipyramidal [Rh(CO)($Ph_2PCH_2CH_2CH_2PPh_2$)$_2$]$^+$ is facile, no similar reaction occurs for [Rh($Ph_2PCH_2CH_2PPh_2$)$_2$]$^+$ (2). The ready formation of **6** by addition of CO to **5** is therefore noteworthy. The ring size in chelated complexes of $Ph_2PCH_2CH_2PPh_2$ and $Ph_2PCH_2CH_2SPh$ will be very similar, and addition of CO to square-planar complexes to form trigonal bipyramidal complexes of each would be expected to affect each in a similar manner. The thioether functions in the latter, however, furnish one pendant phenyl group less than the corresponding phosphine function, thereby removing some of the potential steric constraints to formation of a five-coordinate, bis-chelated, complex. The singular inability of [Rh($Ph_2PCH_2CH_2PPh_2$)$_2$] to add CO to form such a five-coordinated complex cation must therefore be due to the unfavourability of the required conformation of the pendant phenyl groups in the anticipated product. The longer chain-length of $Ph_2PCH_2CH_2CH_2PPh_2$ requires that the conformations of the phenyl groups in the corresponding carbonyl complex are different, and do not prevent the formation of the five-coordinate complex.

Reaction of either [RhCl(CO)$_2$]$_2$ or [RhCl(cod)]$_2$ under an atmosphere of CO, with an equivalent amount of PS(2) gave the *cis*, chelated, mononuclear complex **1** (Fig. 2). The ir and ^{31}P nmr parameters of **1** are entirely comparable with the parameters of the corresponding complex of $Ph_2PCH_2CH_2PPh_2$ (2), or of [RhCl(CO)($Ph_2PC_6H_4NMe_2$)] (14).

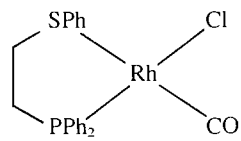

FIG. 2. Chelated, *cis*-, mononuclear complex **1**.

Reaction of either [MCl(cod)]$_2$ (M = Rh or Ir) or [RhCl-(CO)$_2$]$_2$, under an atmosphere of CO, with an excess of either PS(1) or PS(2) gave in each case the complexes [MCl(CO)(L)$_2$], **2**, **3**, and **12**. The ir spectrum of each product features single carbonyl and metal−chlorine stretching bands. The ^{31}P nmr spectra show that the phosphorus nuclei are equivalent in each complex. Complexes **2**, **3**, and **12** are therefore each of *trans* geometry, and each PS(1) or PS(2) ligand is monodentate (P) (Fig. 3).

Can. J. Chem. Downloaded from www.nrcresearchpress.com by 210.87.254.40 on 09/06/12
For personal use only.

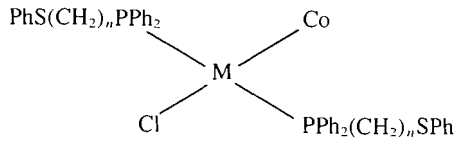

FIG. 3. Geometry (*trans*-) of **2**, **3**, and **12** (M = Rh, Ir).

Although attempts to prepare the homodinuclear complexes $[MCl(CO)\{PS(1)\}]_2$ have so far only given impure materials, complexes related to "A-frame" complexes of $Ph_2PCH_2PPh_2$ have been prepared. Attempts to prepare the above dinuclear complexes in an analytically pure state are continuing.

(B) Complexes of palladium(II) or platinum(II)

Reaction of an equivalent amount of PS(2) with $[PdCl_2(PhCN)_2]$ slowly displaced benzonitrile to give the 1:1 complex $[PdCl_2(Ph_2PCH_2CH_2SPh)]$, **14**. The observation of two metal–chlorine stretching bands in the ir spectrum is consistent with a *cis*, chelated structure (Fig. 4), analogous to $[PdCl_2(o\text{-}Ph_2PC_6H_4SPh)]$ (15). In contrast, the 1:1 product (**13**) of the reaction of $[PdCl_2(PhCN)_2]$ with an equimolar amount of PS(1) exhibits only one ir band assigned as a metal–chlorine stretch.

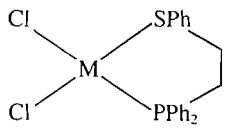

FIG. 4. Chelated (*cis*) structure (M = Pd, Pt).

Although the limited solubility of complex **13** in appropriate solvents renders a determination of the molecular weight less reliable than is desirable, the value obtained indicates that the product is tetranuclear. All phosphorus atoms are equivalent (^{31}P nmr). Because only one Pd—Cl band was observed in the ir spectrum it is unlikely that two phosphine moieties are coordinated to two palladium atoms while two thioether moieties are coordinated to the other two. Complex **13** is therefore presumed to have the structure shown in Fig. 5.

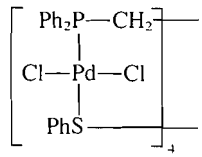

FIG. 5. Cyclic complex.

Reaction of $[MCl_2(PhCN)_2]$ (M = Pd, Pt) with an excess of PS(1) or PS(2) gives the corresponding 2:1 complexes **15** or **16** (M = Pd) and **19** or **20** (M = Pt) respectively. Reaction of an ethanolic solution of **16** or **20** with an equimolar amount of $NaBPh_4$ gave in each case the 1:1 electrolyte $[MCl\{\eta^1\text{-}PS(2)\}\{\eta^2\text{-}PS(2)\}]BPh_4$, **21** (M = Pd) or **22** (M = Pt). Reaction of an acetone solution of **21** or **22** with an excess of $NaBPh_4$ gave the 2:1 electrolytes $[M\{\eta^2\text{-}PS(2)\}_2](BPh_4)_2$, **23** and **24**, respectively.

Complex **15** is a non-electrolyte and exhibits only one Pd—Cl band in the ir spectrum, and is therefore presumed to be of *trans* geometry with monodentate(P) PS(1) ligands. The ^{31}P nmr spectrum at 309 K or 223 K exhibits only a broad signal; the reason for the breadth of this signal at all temperatures is not yet clear. Complexes **19** and **20** each exhibit two Pt—Cl bands in the ir spectra and a single environment for phosphorus in the ^{31}P nmr spectra. These complexes are therefore of *cis* geometry, also with monodentate PS(1) or PS(2) ligands respectively. Complex **16** exhibits not only an ir band at 325 cm^{-1}, close to the Pd—Cl band for **15**, but also a strong band at 363 cm^{-1}, the origin of which is not yet clear. Complex **16** is a 1:1 electrolyte in acetonitrile, but a weak electrolyte in dichloromethane, suggesting that an equilibrium (eq. [4]) may exist.

[4] 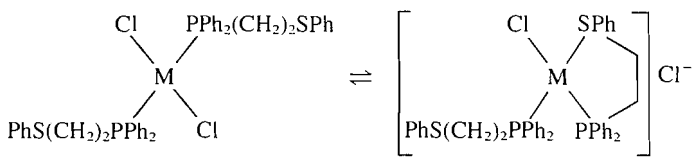

The ^{31}P nmr spectra of CD_2Cl_2 solutions of the 1:1 electrolytes **21** and **22** at room temperature each show only a single, very broad signal. However, for a solution of **22** at 233 K signals due to different phosphorus nuclei are resolved, each of which is coupled to ^{195}Pt, corresponding to mono- and bidentate PS(2) ligands. At 203 K fine structure due to coupling of each to ^{195}Pt and to each other is resolved. The values for $^1J(Pt—P_A)$ and $^1J(Pt—P_B)$ demonstrate that each phosphorus is coordinated to platinum. The value of $^2J(P_A—P_B)$ shows that the phosphine ligating moieties are mutually *cis*. Unfortunately, attempts to obtain comparable spectra for **21** again gave only broad signals to 223 K. The ^1H nmr spectrum for each complex is unexceptional, with signals appropriate for the methylene and aromatic protons in approximately correct ratios for the monocationic tetraphenylborate complexes.

The dicationic complexes **23** or **24** are 2:1 electrolytes in acetone, and the ^{31}P nmr spectra show a single environment for phosphorus in each complex. It is noteworthy that the more rigid related ligand $o\text{-}Ph_2PC_6H_4SPh$ is constrained to exhibit only bidentate, chelating behaviour in its complexes with palladium (15).

Intimate agitation of an aqueous solution of $K_2[PtCl_4]$ and a dichloromethane solution of PS(2) gave the 1:1 complex, **17**, as a white precipitate. Complex **17** exhibits only one Pt—Cl band in the ir spectrum, and is therefore presumed to be of *trans* geometry. Attempts to recrystallize this material, or to prepare solutions for nmr or molecular weight determination, gave pale yellow solutions. When evaporated to dryness these solutions yielded a pale yellow powder of which the ir spectrum was dissimilar from that of **17**. This novel material, **18**, exhibits two Pt—Cl bands, and the ^{31}P nmr parameters (δ_p 40.3 ppm, $^1J(Pt—P)$ 3.594 Hz) are very similar to those of $[PtCl_2(Ph_2PCH_2CH_2PPh_2)]$ (δ_p 45.3, $^1J(Pt—P)$ 3.618 Hz) (16). Therefore it is deduced that **18** is a *cis*, mononuclear, chelated complex (Fig. 4), while **17** is considered to be a *trans*, polynuclear, bridged complex, similar to **13** (Fig. 5).

(C) Attempts to prepare heterodinuclear complexes

To date all attempts using **2** or **3** to prepare complexes of PS(1) or PS(2) containing both a rhodium and a palladium or

Can. J. Chem. Downloaded from www.nrcresearchpress.com by 210.87.254.40 on 09/06/12
For personal use only.

platinum centre have been unsuccessful.

Reaction of *trans*-[RhCl(CO){PS(2)}$_2$] with [PdCl$_2$(PhCN)$_2$] or K$_2$[PtCl$_4$] gave a mixture of [RhCl(CO){PS(2)}], **1**, and [PdCl$_2${PS(2)}], **14**, or [PtCl$_2${PS(2)}], **18**, respectively. Similarly, reaction of *trans*-[RhCl(CO){PS(1)}$_2$], **2**, with [PdCl$_2$-(PhCN)$_2$] gave, as a bright orange precipitate, [PdCl$_2${PS(1)}]$_4$, **13**, and a solution containing a rhodium complex which has not yet been fully characterized. From none of these reactions was a complex containing P-coordinated rhodium and S-coordinated palladium or platinum isolated. A number of dithioether complexes of palladium and platinum have been prepared which are very stable and contain bridging dithioether ligands (4, 17). The failure to isolate bridged heterodinuclear complexes is therefore ascribed not to any lack of propensity to form Pd—S or Pt—S bonds in such complexes, but to the lability of the Rh—P bond which permits rapid internuclear exchange of ligands.

In contrast, reactions with mercury halides have given a series of mercury and either rhodium or palladium heterodinuclear complexes (18).

Conclusions

Complexes of rhodium(I), iridium(I), palladium(II), and platinum(II) containing the ligands Ph$_2$PCH$_2$SPh or Ph$_2$PCH$_2$-CH$_2$SPh have been synthesized. These ligands may be monodentate, coordinating via the phosphine function only, or bidentate(P, S) bridging or chelating. When the central metal atom is coordinated by two such ligands but no others, they are both bidentate and chelating. When the central metal nucleus is also coordinated to a chloro, cyclooctadiene, or carbonyl ligand, one or two Ph$_2$P(CH$_2$)$_n$SPh ligands may be monodentate(P). However, in the cationic complexes, [M(CO)(Ph$_2$PCH$_2$CH$_2$SPh)$_2$]BPh$_4$ (M = Rh, Ir), each such ligand remains bidentate and chelating.

1. A. R. SANGER. *In* Homogeneous catalysis with metal phosphine complexes. *Edited by* L. H. Pignolet. Plenum, New York. In press, Chapt. 6.
2. A. R. SANGER. J. Chem. Soc. Dalton, 120 (1977).
3. A. R. SANGER. J. Chem. Soc. Dalton, 1971 (1977).
4. A. R. SANGER and J. E. WEINER-FEDORAK. Inorg. Chim. Acta, **42**, 101 (1980); S. G. MURRAY, W. LEVASON, and H. E. TUTTLEBEE. Inorg. Chim. Acta, **51**, 185 (1981).
5. A. R. SANGER, C. G. LOBE, and J. E. WEINER-FEDORAK. Inorg. Chim. Acta, **53**, L123 (1981).
6. J. P. FARR, M. M. OLMSTEAD, and A. L. BALCH. J. Am. Chem. Soc. **102**, 6654 (1980); J. P. FARR, M. M. OLMSTEAD, C. H. LINDSAY, and A. L. BALCH. Inorg. Chem. **20**, 1182 (1981).
7. I. M. KITTANEH, H. A. HODALI, and H. A. TAYIM. Inorg. Chim. Acta, **60**, 223 (1982).
8. D. W. MEEK, R. WAID, K. D. TAN, R. M. KIRCHNER, and C. N. MORIMOTO. Inorg. Chim. Acta, **64**, L221 (1982).
9. M. SAVIGNAC, P. CADIOT, and F. MATHEY. Inorg. Chim. Acta, **45**, L43 (1980) and references therein.
10. O. STELZER. Transition metal complexes of phosphorus ligands. *In* Topics in phosphorus chemistry. Vol. 9. *Edited by* E. J. Griffith and M. Grayson. Wiley-Interscience, New York. 1977. p. 65.
11. A. R. SANGER and R. W. DAY. Inorg. Chim. Acta, **62**, 99 (1982).
12. D. L. DUBOIS, W. H. MYERS, and D. W. MEEK. J. Chem. Soc. Dalton, 1011 (1975).
13. J. T. MAGUE and A. R. SANGER. Inorg. Chem. **18**, 2060 (1979); A. R. SANGER. J. Chem. Soc. Dalton, 228 (1981); D. M. HOFFMAN and R. HOFFMAN. Inorg. Chem. **20**, 3543 (1981).
14. D. M. ROUNDHILL, R. A. BECHTOLD, and S. G. N. ROUNDHILL. Inorg. Chem. **19**, 284 (1980).
15. G. DYER, M. O. WORKMAN, and D. W. MEEK. Inorg. Chem. **6**, 1404 (1967).
16. T. G. APPLETON, M. A. BENNETT, and I. B. TOMKINS. J. Chem. Soc. Dalton, 439 (1976).
17. J. PLUSCEC and A. D. WESTLAND. J. Chem. Soc. 5371 (1965); F. R. HARTLEY, S. G. MURRAY, W. LEVASON, H. E. SOUTTER, and C. A. MCAULIFFE. Inorg. Chim. Acta, **35**, 265 (1979).
18. A. R. SANGER. Can. J. Chem. To be published.

Can. J. Chem. Downloaded from www.nrcresearchpress.com by 210.87.254.40 on 09/06/12
For personal use only.

COMMUNICATION

The synthesis of cofacial porphyrin dimers

JOHN HIOM, JOHN B. PAINE III, UDO ZAPF, AND DAVID DOLPHIN
Department of Chemistry, The University of British Columbia, Vancouver, B.C., Canada V6T 1Y6

Received May 31, 1983

JOHN HIOM, JOHN B. PAINE III, UDO ZAPF, and DAVID DOLPHIN. Can. J. Chem. **61**, 2220 (1983).

A cofacial dimeric porphyrin joined by two hydrocarbon chains has been prepared using a bis-porphyrin already linked by a single hydrocarbon chain. When each porphyrin bears an acetylenic group, copper catalyzed coupling followed by catalytic hydrogenation gives a doubly linked cofacial porphyrin. However, a far superior and more flexible route, involving the use of a dimeric biladiene-*ac*, gives in one step the same cofacial porphyrin. This latter route has been used to prepare dimeric porphyrins with hydrocarbon linkages of varying lengths.

JOHN HIOM, JOHN B. PAINE III, UDO ZAPF et DAVID DOLPHIN. Can. J. Chem. **61**, 2220 (1983).

On a préparé une porphyrine cofaciale dimère liée par deux chaînes carbonées en faisant appel à une bis-porphyrine déjà liée par une seule chaîne carbonée. Lorsque chaque porphyrine porte un groupe acétylène, un couplage catalysé par le cuivre, suivi par une hydrogénation catalytique, conduit à une porphyrine cofaciale doublement liée. Toutefois, une autre voie beaucoup plus flexible et supérieure, impliquant l'utilisation d'un biladiène *ac* dimère conduit à la même porphyrine cofaciale en une étape. On a utilisé cette dernière voie pour préparer des porphyrines dimères comportant des chaînes carbonées de diverses longueurs.

[Traduit par le journal]

Our interest in the synthesis and study of covalently-linked bis-porphyrins has continued since we first reported such compounds in 1972 (1). Although these first examples were linked via the readily-synthesized amide function, it soon became apparent, even though others have followed these early strategies, that the improved stability and solubility conferred by inert hydrocarbon (polymethylene) linkages could lead to superior substrates for subsequent study.

Our initial studies in these areas resulted in the preparation of dimeric porphyrins singly linked by polymethylene chains (2). The starting point for those compounds and the ones reported here were the bispyrroles (**1**) (the initial reaction described in Scheme I was for R′ = R = Et in **2**–**6**). It was apparent at the outset of our work that dimeric pyrromethenes of type **4** could in principle be made to couple in head-to-tail fashion, to afford doubly linked cofacial porphyrin dimers (**6**). Only the Johnson porphyrin synthesis (3) (cyclization of 1-bromo-19-methyl-biladienes-*ac*) held any reasonable hope of success and to this end a convenient, high yielding route to brominated dimeric pyrromethenes (**4**) had to be found. The traditional bromination (bromine in hot acetic or formic acid) of the dimeric pyrromethene **3** led only to intractable tars. A new procedure was devised whereby the pyrromethene **3** was allowed to stand at room temperature for several days with a modest excess of bromine in dichloromethane (or 1,2-dichloroethane) containing up to 40% (by volume) trifluoroacetic acid. These mild conditions ensure negligible loss to over-oxidation, hydrolysis, or self-condensation and provided the brominated pyrromethene (**4**) pure and in near quantitative yield.

The high dilution coupling of the brominated pyrromethene (**4**) with its precursor **3** was achieved by adding dilute dichloromethane solutions of the components to stannic chloride in dichloromethane–nitromethane. The dimeric biladienes-ac (**5**) were isolated in a crude form and cyclized to porphyrin in dimethylsulfoxide–pyridine for several days at room temperature in the dark. The product (**6**) was then isolated chromatographically. Using the route outlined in Scheme 1 the symmetric porphyrins $m = n = 10$ and 8 (R′ = R = Et) and $m = n = 5$ (R′ = R = octyl) have been prepared. In addition, by using two different chain lengths at the pyrromethene stage (**3**, **4**) cofacial porphyrins with unequal chain-lengths can be made and we have prepared the "clam-shell" porphyrins, $m = 8$, $n = 6$ (R′ = R = Et) and $m = 6$, $n = 5$ (R′ = Et, R = octyl).

While all the spectroscopic and analytical evidence[1] is consistent with the cofacial formulation for the products obtained in the reaction sequences outlined in Scheme 1, we have so far not obtained a crystal suitable for X-ray analysis for any of the dimeric porphyrins. In order to definitively establish the nature of our systems we have devised a rational stepwise synthesis of a cofacial porphyrin. Diborane reduction of 2-benzyloxycarbonyl-4-(2-methoxycarbonylethyl)-3,5-dimethylpyrrole (5) gave the corresponding 3-hydroxypropyl analog which was acetylated and then hydrogenated (Pd/C, THF) to give 4-(3-acetoxypropyl-3,5-dimethylpyrrole-2-carboxylic acid which, condensed with 3-ethyl-2-formyl-4-methylpyrrole, gave the pyrromethene **7** (Scheme 2). Bromination of **7** in the manner described above gave **8** which was condensed with the C-10 bis-dipyrromethene (**3**, R = Et, $n = 10$) to give **9** which was cyclized to the singly linked porphyrin **10**. The acetoxy groups were converted by standard means (6, 7) to the terminal acetylenes (**11**–**13**). Copper catalyzed oxidative coupling of the terminal acetylenic groups of the zinc complex of **13** gave, in moderate yield, the deca-4,6-diynl-10-ylidene decamethylbisporphyrin **14**. Careful hydrogenation (palladium oxide, formic acid) of **14** followed by aerial oxidation of the intermediary porphodimethene gave the bis-porphyrin **15** which proved identical to the porphyrin **6** ($n = m = 10$) prepared by the route outlined in Scheme 1. While the stepwise synthesis establishes the nature of the dimeric porphyrins, the synthetic route outlined in Scheme 1 is clearly the synthetic procedure of choice.

Using polymethylene chains as bridging groups we have overcome one of the major problems of stability, namely hydrolytic cleavage of the bridge if amide or ester linkages are employed. However, the dimeric porphyrins reported here ex-

[1]Satisfactory mass and nmr spectra were obtained for all new compounds.

Can. J. Chem. Downloaded from www.nrcresearchpress.com by 210.87.254.6 on 09/06/12
For personal use only.

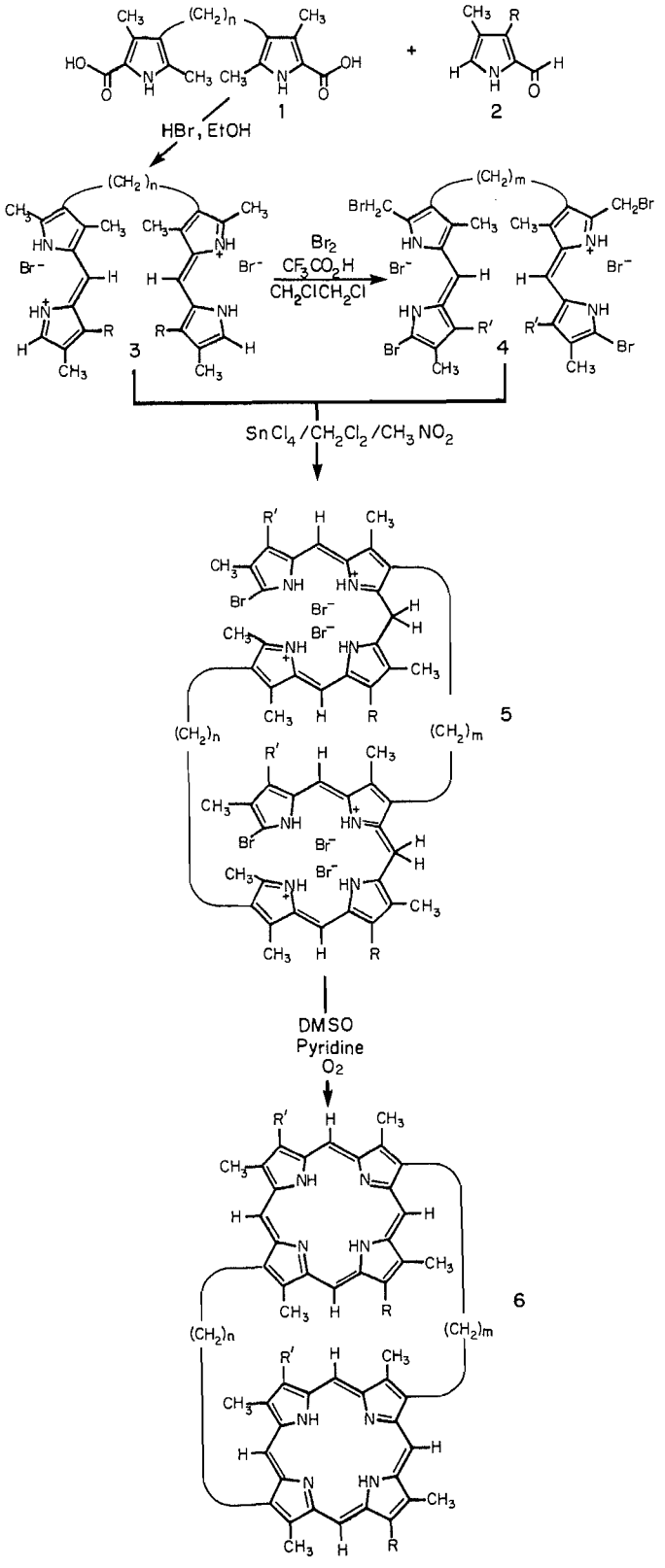

SCHEME 1

hibited low solubility, like previously reported dimeric porphyrins (8). In order to overcome these problems of solubility we have modified the reactions outlined in Scheme 1 by incorporating two octyl side chains in **3** (R = octyl, instead of ethyl as above). This dramatically increases the solubility of the final dimeric products and we now have in hand soluble stable

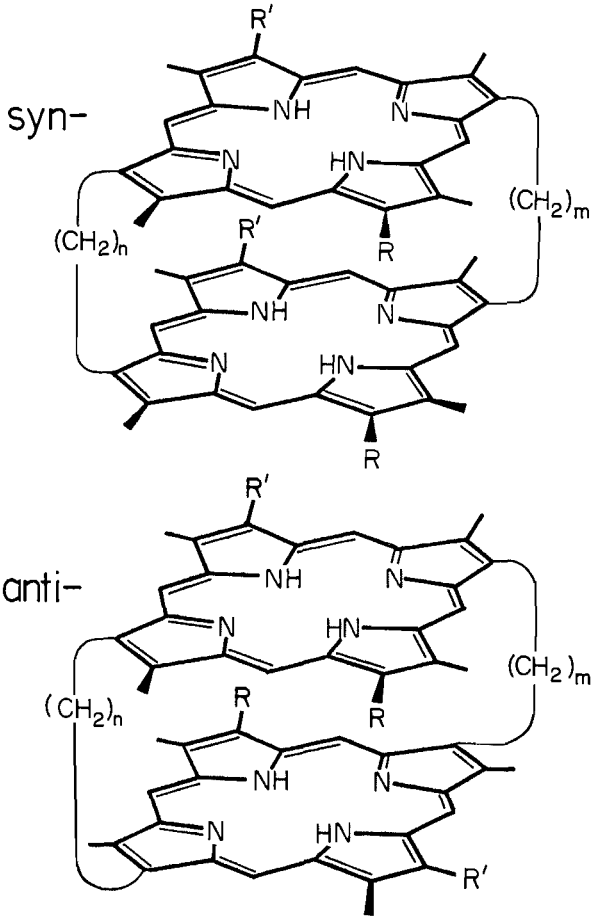

FIG. 1

dimers for future investigation.

The optical spectra of cofacial porphyrins have been reported, and varying degrees of interactions between the porphyrin rings have been observed. Both Chang (9) and Collman *et al.* (10) have observed a blue-shift of about 15 nm in the Soret bands of their cofacial systems with smaller bathochromic shifts in the visible region. Table 1 shows the same qualitative changes with the present systems. However, not only is there an hypsochromic shift in the Soret region, but these bands become progressively broader as the distance between the rings lessens. Furthermore, not only is the distance between the rings important but their relative geometries play a role in these interactions, thus the C_{6-8} dimer shows less of a change relative to etioporphyrin I[2] than the C_{8-8} dimer. Similar but smaller changes were observed (Table 1) with the zinc complexes (prepared by treating the free base in CH_2Cl_2 with zinc acetate in methanol, followed by chromatography over silica), and with the tetraprotonated salts.

During the purification of **6** (m = 6, n = 5; R′ = Et, R = octyl) and **6** (m = n = 5; R′ = R = octyl) two chromatographically separable isomers were obtained in each case. While each pair of isomers show identical mass spectra, their ^{1}H nmr spectra show the same pattern but with slightly different chemical shifts (Table 2). The possibility of forming *syn* and *anti* isomers (Fig. 1) has been alluded to previously for cofacial

[2]Etioporphyrin I (2,7,12,17-tetraethyl-3,8,13,18-tetramethyl-porphyrin) has the same structure as all of the porphyrins described here except that the groups at C_2 and C_{12} are replaced by ethyl groups.

Can. J. Chem. Downloaded from www.nrcresearchpress.com by 210.87.254.6 on 09/06/12
For personal use only.

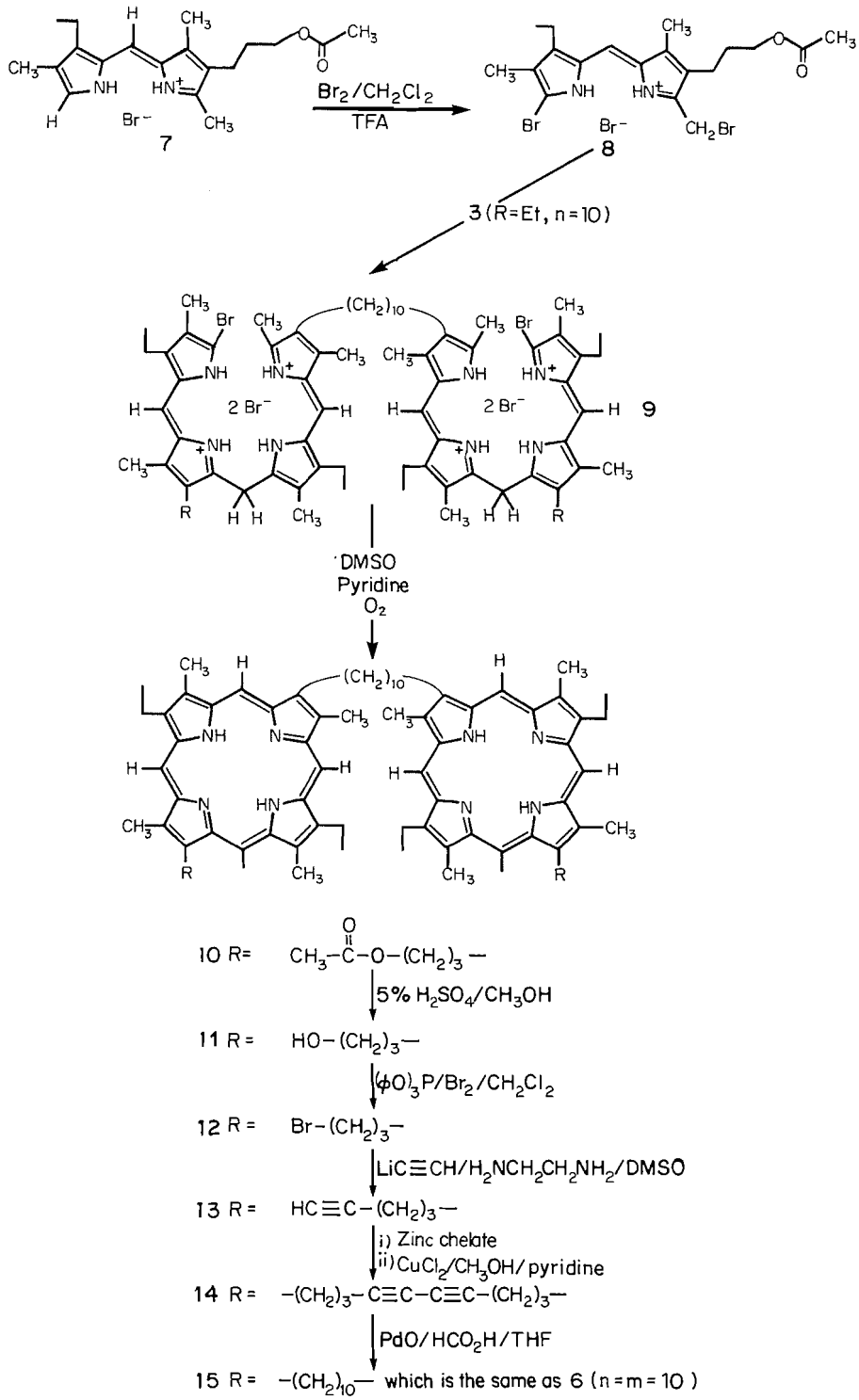

SCHEME 2

porphyrins and such isomers are known when two porphyrins are held cofacial by a common mercuric ion (11). We suspect, in the formation of cofacial porphyrins linked by amides or esters (8, 9), that a single isomer is formed due to the highly strained tetrahedral transition state generated during the formation of the last linkage. However, in the chemistry outlined in Scheme 1, the final intermediate, before oxidation to a porphyrin, is the very flexible porphodimethene. Thus intermediates leading to both *syn* and *anti* isomers will be formed. In the cases **6** ($m = 6$, $n = 5$) and **6** ($m = n = 5$), where the two rings are sufficiently close together that equilibrium between the *syn* and *anti* isomers cannot occur, then both are isolated. However, as the joining chains become longer, equilibrium may occur and, as in the case of **6** ($m = n = 10$), only one isomer is isolated.

Collman, Anson, and their colleagues (4) have shown that dramatic changes in the chemistry of cofacial dimeric porphyrins occur when the rings are forced to be very close (particularly when there are no more than four linking atoms). Our initial attempts at the preparation of **6** ($m = n = 4$) have given

Can. J. Chem. Downloaded from www.nrcresearchpress.com by 210.87.254.6 on 09/06/12
For personal use only.

TABLE 1. Optical spectra of dimeric porphyrins (CH_2Cl_2; the tetraprotonated salts are in the presence of excess CF_3CO_2H)

Free bases	Etio I	375 (sh)	396	496	531	566	619
	C_{5-5} (I)	378 (sh)	385	498	532	567	620
	C_{5-5} (II)	376 (br)		498	532	567	620
	C_{6-5} (I)	378 (sh)	387	498	532	567	620
	C_{6-5} (II)	373 (br)	—	498	533	567	620
	C_{6-8}	375 (sh)	390	497	531	567	620
	C_{8-8}	375 (sh)	388	501	534	569	623
	C_{10-10}	376 (sh)	392	502	535	570	622
Zn complexes	Etio I	408		537		574	
	C_{5-5} (I)	391		536		573	
	C_{5-5} (II)	391		536		573	
	C_{6-5} (I)	400		536		572	
	C_{6-5} (II)	398		536		572	
	C_{6-8}	403		538		574	
	C_{8-8}	400		535		572	
	C_{10-10}	390		536		571	
Tetraprotonated salts	Etio I	401		546		590	
	C_{5-5} (I)	387		546		588	
	C_{5-5} (II)	388		547		590	
	C_{6-5} (I)	398		546		590	
	C_{6-5} (II)	387		546		591	
	C_{6-8}	399		545		590	
	C_{8-8}	398		545		590	
	C_{10-10}	398		546		590	

TABLE 2. ^1H nuclear magnetic resonance chemical shifts (δ, $CDCl_3$)

Compound		*meso*-H	Ring methyl
6*a*[a] $m = n = 5$	R = R' = octyl	9.10, 9.08	3.43, 3.48
6*b*[a] $m = n = 5$	R = R' = octyl	9.25, 9.28	3.38, 3.44
6*a*[b] $m = 6$, $n = 5$	R = ethyl, R' = octyl	9.28, 9.31, 9.36, 9.40,	3.14, 3.23, 3.48, 3.48
6*b*[b] $m = 6$, $n = 5$	R = ethyl, R' = octyl	9.00, 9.16, 9.31, 9.41	3.25, 3.28, 3.35, 3.48
6[c] $m = n = 6$	R' = R = ethyl	10.12, 10.06	3.36, 3.27
6[c] $m = n = 8$	R' = R = ethyl	10.26, 10.23	3.34, 3.33
6[d] $n = m = 10$	R = R' = ethyl	10.39, 10.43	3.44, 3.50

[a]A compound with either C_{2h} or D_{4h} symmetry shows two sets of *meso* and methyl protons.
[b]A compound with either C_s or C_2 symmetry shows four sets of *meso* and methyl protons.
[c]Spectrum measured in $CDCl_3$/TFA (1%).
[d]Spectrum measured in CF_3CO_2H since material was too insoluble in $CDCl_3$.

low yields of material too insoluble to handle. We are now repeating the chemistry outlined in Scheme 1 using more soluble intermediates in order that the more soluble dimeric porphyrins will be available.

Acknowledgement

This work was supported by the Natural Sciences and Engineering Research Council of Canada and the United States National Institutes of Health (AM 17989).

1. F. P. SCHWARTZ, M. GOUTERMAN, Z. MULJIANI, and D. H. DOLPHIN. Bioinorg. Chem. **2**, 1 (1972).
2. J. B. PAINE III and D. DOLPHIN. Can. J. Chem. **56**, 1710 (1978).
3. A. W. JOHNSON. The porphyrins. Vol. 1, *Edited by* D. Dolphin. Academic Press, New York. (1978). Chapt. 5. p. 235.
4. J. P. COLLMAN, P. DENISEVICH, Y. KONAI, M. MARROCCO, C. KOVAL, and F. C. ANSON. J. Am. Chem. Soc. **102**, 6027 (1980).
5. A. W. JOHNSON, E. MARKHAM, and K. B. SHAW. J. Chem. Soc. 4254 (1958).
6. D. G. COE, S. R. LAUDAUER, and H. N. RYDON. J. Chem. Soc. 2281 (1954).
7. J. U. HUFFMANN and P. G. ARAPAKOS. J. Org. Chem. **30**, 1604 (1965).
8. J. P. COLLMAN, A. O. CHONG, G. B. JAMESON, R. T. OAKLEY, E. ROSE, E. R. SCHMITTON, and J. A. IBERS. J. Am. Chem. Soc. **103**, 516 (1981).
9. C. K. CHANG. J. Heterocycl. Chem. **14**, 1285 (1977).
10. J. P. COLLMAN, C. M. ELLIOT, T. R. HALBERT, and B. S. TOVNOG. Proc. Natl. Acad. Sci. U.S.A. **74**, 18 (1977).
11. M. F. HUDSON and K. M. SMITH. Tetrahedron, **31**, 3077 (1975).

Can. J. Chem. Downloaded from www.nrcresearchpress.com by 210.87.254.6 on 09/06/12
For personal use only.

REVIEW/SYNTHÈSE

Acidity functions: an update

ROBIN A. COX AND KEITH YATES
Department of Chemistry, University of Toronto, 80 St. George St., Toronto, Ont., Canada M5S 1A1

Received February 14, 1983

ROBIN A. COX and KEITH YATES. Can. J. Chem. **61**, 2225 (1983).

The subject of acidity functions is reviewed, with emphasis on modern developments. H_0 and other scales determined in acid media, using the Hammett cancellation assumption (zero'th order approximation) are discussed briefly. The extension to strongly basic systems is also documented. Literature references to acidity function scales in aqueous acid, aqueous acid/organic solvent, and aqueous base media are tabulated, together with those in aqueous base/organic solvent mixtures at both variable and fixed base concentration. Over 400 acidity functions are referenced, including several electrochemical scales. Various approaches to developing universal functions from the data are discussed. Proton activity scales, based on the Yates–McClelland method of pK_{BH^+} determination, and on electrochemical H_{GF} scales, are prominent among these. Carpentier's method is mentioned, and the first-order approximation, assumed linearity among log activity coefficient ratios, is used to introduce the Bunnett–Olsen and excess acidity (X-function) methods. A brief critical discussion of which method to use is provided. Future developments anticipate the second-order approximation, with a quadratic dependence of log ionization ratios upon X-functions. The review cites 337 individual references.

ROBIN A. COX et KEITH YATES. Can. J. Chem. **61**, 2225 (1983).

On étudie de nouveau les fonctions d'acidité en tenant compte des nouvelles théories. On discute brièvement des échelles H_0 et des autres échelles déterminées en milieu acide en utilisant l'hypothèse d'annulation de Hammett (approximation d'ordre zéro). On a également étudié les échelles en milieu fortement basique. On a compilé les références de la littérature portant sur les échelles de fonctions d'acidité en milieu acide, en milieu aqueux/solvant organique, et en milieu basique aqueux ainsi que celles portant sur les fonctions en milieu basique aqueux/mélanges de solvants organiques à des concentrations fixes et à des concentrations variables de bases. On a dressé une liste de plus de 400 fonctions d'acidité incluant plusieurs échelles électrochimiques. On discute des différentes approches utilisées pour développer des fonctions universelles à partir des données. Les échelles d'activité du proton basées sur la méthode de détermination du pK_{BH^+} de Yates–McClelland et sur les échelles électrochimiques H_{GF} tiennent la première place. On mentionne la méthode de Carpentier et on utilise l'approximation d'ordre un en supposant la linéarité du logarithme des rapports du coefficient d'activité pour introduire la méthode d'acidité en excès de Bunnett–Olsen (fonction X). On discute brièvement de l'utilisation de telle ou telle méthode. Les développements futurs anticipent une approximation d'ordre deux, avec une influence quadratique des fonctions X sur le logarithme des rapports d'ionisation. La nouvelle étude comporte 337 références.

[Traduit par le journal]

Introduction

The pH scale is open-ended. Just as a hydrogen ion concentration of 1×10^{-4} M translates to a pH of 4, logically it would seem that a 10 M solution should have a pH of -1. Similarly a pH of 15 should apply to a 10 M hydroxide solution. The difficulty, of course, is that these concentrated solutions are non-ideal. Below a pH of about 1.5, and above one of about 13, solutions of acids and bases become much more "acidic" and "basic" than their concentrations would suggest. Since the pH scale cannot be used, acidity scales in non-ideal media have to be measured; these are known as acidity functions, or more recently as excess acidities or basicities.

With acidity scales available, acidity constants outside the range accessible in water can be estimated (1–8), and much useful information concerning the mechanisms of acid- (1–3, 9) and base-catalyzed (1, 11–14) reactions obtained. The subject in its various aspects has been extensively reviewed (4–20); three books have been written on it (1–3), and it is covered in many physical organic textbooks (19, 21–25). An extensive tabulation of acidity functions is available (10). Here we will only be concerned with aqueous or aqueous/organic media, the developments subsequent to 1970 are emphasized. The literature coverage extends to the end of 1982.

Theory

In acid solutions, K_{BH^+} (i.e. K_a) is defined as the dissociation constant of the conjugate acid BH^+ of base B, eq. [1]; in terms of activity a its value is given by eq. [2]. Taking logs and substituting the ionization ratio $I = C_{BH^+}/C_B$ ($= a_{BH^+}/a_B$ in ideal solution) gives the familiar eq. [3]. The standard state is a hypothetical acid solution of unit activity, and the reference state (unit activity coefficients) is infinite dilution in water, for eq. [3] and most other equations in this review.

$$[1] \quad B + H^+ \overset{K_{BH^+}}{\rightleftharpoons} BH^+$$

$$[2] \quad K_{BH^+} = a_B a_{H^+}/a_{BH^+}$$

$$[3] \quad pK_{BH^+} = \log I + pH$$

$$[4] \quad K_{BH^+} = C_B C_{H^+} f_B f_{H^+}/C_{BH^+} f_{BH^+}$$

$$[5] \quad pK_{BH^+} = \log I - \log C_{H^+} - \log (f_B f_{H^+}/f_{BH^+})$$

In the non-ideal solutions under consideration here activities and concentrations cannot be equated; using molarities C and molar activity coefficients f, eqs. [2] and [3] become eqs. [4] and [5], respectively. The acidity function problem then becomes, essentially, a question of how to deal with the activity coefficient term in eq. [5].

Zero'th order approximation

$$[6] \quad pK_{AH^+} - \log I_A = -\log C_{H^+} - \log (f_A f_{H^+}/f_{AH^+}) = H_0$$

$$[7] \quad pK_{BH^+} - \log I_B = -\log C_{H^+} - \log (f_B f_{H^+}/f_{BH^+}) = H_0$$

Can. J. Chem. Downloaded from www.nrcresearchpress.com by 210.87.254.105 on 09/06/12
For personal use only.

Can. J. Chem. Downloaded from www.nrcresearchpress.com by 210.87.254.105 on 09/06/12
For personal use only.

[8] $$pK_{AH^+} - \log I_A - pK_{BH^+} + \log I_B = \log (f_B f_{AH^+}/f_A f_{BH^+}) = H_0$$

Paraphrasing Hammett (19, 26), the Hammett acidity function H_0 is defined, so as to be similar to pH, by eqs. [6] and [7] for bases A and B. On subtracting these, eq. [8] is obtained; the *Hammett cancellation assumption* is that of equating this to zero. This is the zero'th order approximation. If this is true then immediately a way of measuring pK_{BH^+} values outside the readily accessible range is available from eq. [8], if pK_{AH^+} of an *anchor* compound is known, by measuring ionization ratios as a function of some measure of acidity, usually % acid w/w or molarity. With an overlapping series of these available, H_0 values can be calculated, using eqs. [6] and [7] in a stepwise manner. Once derived, H_0 can be used directly, like pH, to obtained unkown acidity constants from ionization ratio measurements: $pK_{BH^+} = H_0 + \log I$.

Hammett acidity functions

By 1964 it was generally realized that the cancellation assumption was only adequate for weak bases which were closely related in structure (27–29). Nowadays the symbolism H_0 is restricted to acidity functions obtained using nitro-substituted primary aromatic amines only (30). H_0 scales are available for a very wide variety of aqueous acid systems, the same one often having been studied by several different groups (one receives the distinct impression that several pounds of *p*-nitroaniline must have been used for this purpose over the last 50 years). We do not propose to quote them here except for the tabulated references in Tables 1 and 2 (based on ones given by Capen (180)).

Tables 1 and 2 are confined to the most widely used aqueous and aqueous/organic solvent systems; within these bounds an attempt has been made to be comprehensive, at least as far as the readily available literature is concerned. In the authors' experience (83, 181) it is usually necessary to have all the available data on hand when deciding on a suitable acidity function to use in a given medium. Not included are (*a*) superacid systems (41, 182), (*b*) wholly non-aqueous systems (183), (*c*) systems containing added salts (184), (*d*) molten salt systems (185), (*e*) ternary systems (102, 186, 187), (*f*) solid surfaces (188), (*g*) micelles (189), or (*h*) acidity functions obtained at fixed acid concentration and variable organic solvent content (190).

Almost all existing H_0 scales have been obtained using the overlap method outlined above (for details see refs. 1 and 2), although very recently Cox and Yates have described a method for calculating H_0 scales from ionization ratio data which requires neither an "anchor" compound nor overlap between adjacent indicators (83). H_0 scales are useful for comparing different acid media for strength; in Fig. 1 plots of H_0 against mole fraction of acid are given for some representative aqueous systems. The change which several of them exhibit at the 0.5 mole fraction point shows that H_0 scales can also reflect the structure of acid media, at least to some extent.

Other acidity functions

Equation [8] does not apply when A is a primary aromatic amine and B is, say, an amide or a tertiary amine or a thioester. If a set of ionization ratios is plotted against H_0, compounds are said not to "follow" H_0 if the slope of the graph differs from unity (the plots are usually linear). However, it is quite possible to obtain acidity functions using series of amides, tertiary amines, etc., and many of these are available. They are given here in Tables 1 and 2. Perhaps the most widely used after H_0 is the H_A scale, originally derived using amides (29), which is followed by several other carbonyl compounds (191–193), by some heterocycles (54, 55), and by pyridine *N*-oxides (44, 53).

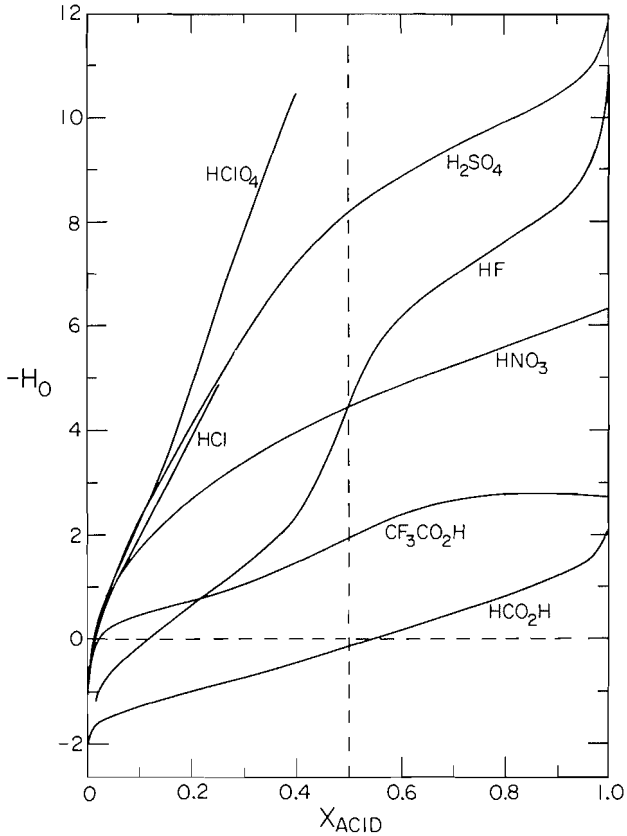

FIG. 1. H_0 vs. mole fraction of acid, for aqueous $HClO_4$ (83), H_2SO_4 (39, 41), HCl (83), HNO_3 (111), HF (112, 113), CF_3CO_2H (128), and HCO_2H (132).

[9] $$R_3COH + H^+ \overset{K_{R^+}}{\rightleftharpoons} R_3C^+ + H_2O$$

[10] $$H_R = pK_{R^+} - \log I = -\log C_{H^+} - \log (f_{R_3COH} f_{H^+}/f_{R_3C^+}) + \log a_w$$

The H_R acidity function is defined for protonation–dehydration processes, eq. [9], in eq. [10], where a_w is the activity of water (48); it is usually measured using triarylcarbinol indicators (49). From this, $H_R' = H_R - \log a_w$ can be defined. This is comparable to the other acidity functions and has been used, for instance, in alkene protonation studies (194).

Strongly basic media

[11] $$HA + HO^- \overset{K_b}{\rightleftharpoons} A^- + H_2O$$

[12] $$H_- = pK_{HA} + \log (C_{A^-}/C_{HA}) = pK_w + \log C_{HO^-} - \log a_w - \log (f_{A^-}/f_{HA} f_{HO^-})$$

For the deprotonation of eq. [11] we can write eq. [12], since K_{HA} (i.e. K_a) $= K_w/K_b$, which defines the acidity function H_-. (The usual terminology is H_- for neutral species → negative ion, H_0 for positive ion → neutral species, H_{2-} for negative ion → dinegative ion, etc. (11).) Two methods for producing strongly basic media are in common use. Firstly, the base concentration can be increased, affecting the last three terms in eq. [12], and secondly, the water activity can be progressively

TABLE 1. Acidity functions for aqueous acid media

AF[a]	T[b]	In.[c]	Acid conc.[d]	Year	Comments	Reference
	H_2SO_4					
"H_0"	?	15	0.3–100.1%	1932	Colourimetry. See refs. 1, 15, 17, 18	26
H_0	?	1	0.352–2.11 *M*	1954	Poor *p*-nitroaniline pK_a	31
H_0	20,40,60,80	7	4–100%	1956	See ref. 16	32
H_0	17	5	2.20–29.2 *N*	1958		33
H_0	25	6	0.005–38.6%	1959	See ref. 1. Best near water	34
H_0	15,25	1	85.46–99.94%	1959	2,4,6-Trinitroaniline	35
H_0	22	2	0.032–1.28 *M*	1962		36
H_0	?	4	60–99.44%	1963	See refs. 1, 7, 18	30
H_0	24	12	1–100%	1964,1966	See refs. 1, 2, 16	37
H_0	?	1	92.0–99.9%	1968	2,4,6-Trinitroaniline	38
H_0	25,40,60,80,90	12	2–99%	1969	Best general-purpose scales	39
H_0	15,25,35,45,55	10	4–98%	1970	See ref. 1	40
H_0	22	4	98.0–100.0%	1971	Best near 100% acid	41
H_0	25	2	0.25–24%	1972,1982		42
H_0	25	5	0–44%	1972	Fluorinated primary amines	43
"H_0"	25,40,60,80,90	9	14–58%	1974	Substituted pyridines	44
H_0	25	2	0.20–2.80 *M*	1976		45
H_0	25	3	0.5–20.0%	1979		46
H_0	25,60	6	20.9–58.9%	1980		47
"H_R"	25	—	5–95%	1951	By calculation from H_0	48
H_R	25	17	0.5–98%	1955	See refs. 1, 2, 15, 17, 18	49
H_R	0,15,30,45	8	0.75–98%	1964	See refs. 1, 15	50
"H_R"	20	11	28–86%	1971	Benzhydrols	51
H_R	25,40,60,80,90	13	6–90%	1975	Disagrees with ref. 50	52
H_R	25	2	0.5–20.0%	1979		46
H_A	25	10	16.1–81.8%	1964	See refs. 2, 17, 18	29
H_A	?	1	82–93%	1967	Phenazine-9,10-dioxide	53
H_A	25,40,60,80,90	9	2–80%	1974	Azine *N*-oxides	44
H_A	25	4	85.0–100.0%	1975	Pyrimidine monocations	54
H_A	25	3	2.5–90%	1977	Re-anchors H_A scale	55
H_A	15,25,40	5	1.0–45.0%	1982	2 H_0 indicators, 3 amides	56
H_C	25	10	0.5–14.0 *M*	1969	Azulenes, carbon bases. See ref. 17	57
H_C	25	7	0–80%	1968–1971	Azulenes	58
H_C	25	3	0.5–20.0%	1979	Azulenes	46
H_0'''	26	14	1–94%	1964	Tertiary amines. See refs. 2, 17, 18	27
H_0'''	25	3	0.5–20.0%	1979	Tertiary aromatic amines	46
H_0'''	25	7	2–70%	1978	Secondary aromatic amines	59
H_-	25	3	0.25–10 *M*	1961,1963	Cyanocarbons. See refs. 2, 17, 18	60
H_-	25	1	0.5–4.0 *M*	1964	Formate ion oxidation kinetics	61
H_-	?	1	$10^{-1.5}$–$10^{0.4}$ *M*	1973	Graphical only. Picrate ion	62
H_+	25	12	0.02–15.0 *M*	1968	1,2-Phenylenediamines. See ref. 2	63
H_T	25	11	10–80%	1972	Thiocompounds	64
H_T	25	16	10–90%	1977	Thiocompounds	65
H_I	25	9	0.1–12.0 *M*	1964	Indoles. See refs. 2, 17, 18	28
H_B	?	13	40–90%	1966	Benzophenones. See ref. 18	66
H_{ROH}	0	1	33–93%	1971	Ethanol	67
H_{PO}	?	12	4.9–78.0%	1973	Phosphine oxides	68
H_E	37	2	60–98%	1974	Aliphatic esters	69
H_{CA}	37	2	55–85%	1976	Aliphatic carboxylic acids	70
H'_{CA}	37	2	60–90%	1976	Halogenated carboxylic acids	70
$H_{C(OH)_2}$	25	3	0.005–10.3 *M*	1981	Hydrated aldehydes	71
H_D	25	5	3.1–49.5%	1983	1,3-Dioxan-2-ylium cations	72
$H_S^{\ddagger}$	25	9	1–12 *M*	1972	Styrene hydration kinetics	73
$H_C^{\ddagger}$	?	1	5–100%	1977,1979	H/D exchange kinetics	74
"p*H*"	?	3	2.00–8.88 *N*	1942	Thiazines	75
R_0	25	1	17.8–100%	1961	Fe^{+}/Fe^{2+}	76
R_0	20	1	0.027–0.326*x*	1972	Fe^{+}/Fe^{2+}	77
H_{GF}	25	1	0.25–11.0 *M*	1972	Fe^{+}/Fe^{2+}	78

Can. J. Chem. Downloaded from www.nrcresearchpress.com by 210.87.254.105 on 09/06/12
For personal use only.

TABLE 1 *(Continued)*

AF[a]	T[b]	In.[c]	Acid conc.[d]	Year	Comments	Reference
	$HClO_4$					
"H_0"	?	6	6.0–63.9%	1932	Colourimetry. See ref. 15	26
H_0	?	1	0.101–2.41 *M*	1954	Poor *p*-nitroaniline pK_a	31
"H_0"	?	2	49.6–71.3%	1957	See ref. 16	79
H_0	25	11	4.9–78.6%	1964	See refs. 1, 16–18	80
H_0	25	7	0.5–21.0%	1071		81
H_0	25	2	0.25–20%	1972,1982		42
H_0	15,25,35,45	6	0.5–16.5 *m*	1974		82
H_0	25	2	0.04–3.00 *M*	1976		45
H_0	25	13	0.1–78%	1981	Recalculated and updated	83
H_R	25	9	0.5–60%	1959	See refs. 1, 17	84
H_R	25	3	1.59–24%	1972,1982		42
H_A	25	8	5.5–74.4%	1973		85
H_A	15,25,35,45	3	2.0–14.0 *m*	1975		86
H_C	25	6	5–60%	1964,1969	Calculated in ref. 17, data in ref. 87	17
H_C	25	7	0.5–9.5 *M*	1969	Azulenes, carbon bases. See ref. 17	57
H_C	25	6	1–60%	1970	Azulenes	88
H_C	25	3	61.6–71.6%	1971	Alkoxybenzenes	89
H_0'''	25	13	0.2–75.4%	1973	Tertiary aromatic amines	85
H_-	25	3	0.1–10.0 *M*	1961,1963	Cyanocarbons. See ref. 17	60
H_-	25	1	0.5–6.0 *M*	1964	Formate ion oxidation kinetics	61
H_I	25	4	0.1–6.0 *M*	1964	Indoles. See ref. 17	28
H_{Azo}	?	6	0.5–7.25 *M*	1970	Azo-compounds	90
$H_C^{\ddagger}$	25	—	$H_C^{\ddagger} = 0.611\ H_C$	1979	H/D exchange. H_C from ref. 57	91
H_{GF}	25	1	0.25–7.5 *M*	1972	Fec/Fec$^+$	78
	HCl					
H_0	?	4	0.00949–6.88 *m*	1934	Colourimetry. See refs. 1, 15, 16, 18	92
H_0	?	1	0.02–3.0 *M*	1948		93
H_0	25	4	0.02–10.4%	1954	See refs. 1, 15, 18	94
H_0	?	1	0.022–3.08 *M*	1954	Poor *p*-nitroaniline pK_a	31
"H_0"	?	3	2.24–9.90 *M*	1955	See refs. 1, 15, 16, 18	95
H_0	24	3	8.9–40.5%	1956	See refs. 1, 15, 16, 18	96
H_0	20,40,60,80	3	0.14–6.44 *m*	1956	Recalculated in ref. 16. See ref. 1	97
H_0	25	—	0.1–10.0 *M*	1957	Summarizes earlier work	15
H_0	25	1	0.08–0.8 *M*	1957		98
H_0	17	2	0.113–8.61 *N*	1958		33
H_0	22	2	0.10–5.47 *M*	1962		36
H_0	26	5	0.10–38%	1964,1966	See ref. 17	99
H_0	25	1	0.05–1.00 *M*	1966		100
H_0	25	3	0.25–14%	1972,1982		42
H_0	25	3	0–25.1%	1974		101
H_0	23	4	0.02–0.22*x*	1978		102
H_0	25	9	0.1–40%	1981	Recalculated and updated	83
H_R	20	2	1.47–21.61%	1962		103
H_R	26	5	0.10–36%	1964,1966	See refs. 1, 17	99
H_R	25	3	1.15–12%	1972,1982		42
H_A	25	7	3–35%	1965		104
H_0'''	26	8	0.10–38%	1964,1966	Tertiary amines. See ref. 17	99
H_-	20	4	0.10–10.0 *M*	1961	Phosphorus-containing anions	105
	H_3PO_4[e]					
H_0	19	5	5–80%	1949	See ref. 15	107
"H_0"	4,20,40,60,80	5	3.6–83.8% P_2O_5	1956	See refs. 1, 16	97
H_0	26	2	65–86% P_2O_5	1961	See refs. 1, 16	108
H_0	25	6	5–85% P_2O_5	1964	See ref. 1, 17	109
H_0	26	5	0.54–85%	1964,1966	See ref. 18	99
H_0	23	4	0.05–0.75*x*	1978		102
H_R	26	5	0.54–80%	1964,1966	See refs. 1, 17	99
H_0'''	26	7	0.54–85%	1964,1966	Tertiary amines. See ref. 17	99
H_{GF}	25	1	2.5–60.0% P_2O_5	1975	Fec/Fec$^+$	110

Can. J. Chem. Downloaded from www.nrcresearchpress.com by 210.87.254.105 on 09/06/12
For personal use only.

TABLE 1 *(Continued)*

AF[a]	T[b]	In.[c]	Acid conc.[d]	Year	Comments	Reference
	HNO_3					
H_0	?	3	0.091–9.57 *m*	1934	Colourimetry. See refs. 1, 15	92
H_0	?	1	0.186–0.930 *M*	1954	Poor *p*-nitroaniline pK_a	31
H_0	17	3	0.772–8.67 *N*	1958		33
"H_0"	20	7	2–100%	1960	See refs. 1, 16, 17	111
H_0	25	2	0.20–3.40 *M*	1976		45
H_R	25	4	0.2–58%	1959	See refs. 1, 17	84
H_-	25	1	0.5–4.0 *M*	1964	Formate ion oxidation kinetics	61
	HF					
H_0	25	3	2.1–42.7%	1956	See ref. 1, 15–17	112
"H_0"	25	5	39.6–100%	1957	See ref. 1, 16, 17	113
H_0	?	4	37.5–100%	1970	Disagrees with refs. 113	114
R_0	?	1	2–68.4%	1973	Fec/Fec$^+$	115
R_0	?	1	75–100%	1975	Fec/Fec$^+$	116
R_+	?	1	85–100%	1975	Perylene$^+$/perylene^{2+}	116
	HBr					
H_0	24	5	0.3–56.5%	1956	Revised in ref. 16. See ref. 1, 15, 17	96
H_0	25,60	6	22.1–58.6%	1980		47
H_0	25	9	0.1–6.0%	1981	Recalculated and updated	83
	H_3PO_3					
H_0	25	3	0.44–46.1%	1959	See refs. 1, 17	34
H_{GF}	25	1	2.5–85.0%	1975	Fec/Fec$^+$	110
	H_2SeO_4					
H_0	?	6	2.8–85.7%	1966		117
H_B	25	8	54–95%	1967	Benzophenones. See ref. 1	118
	$KHSO_4$					
H_0	?	1	0.241–2.66 *M*	1954	Poor *p*-nitroaniline pK_a	31
H_0	23	3	0.25–2.25 *M*	1958	See refs. 1	119
	D_2SO_4					
D_0	22	4	10–4–1 *M*	1960	Also $H_0 = D_0$ for HCl. See ref. 1	120
D_0	25	11	8–97%	1970		121
	$DClO_4$					
D_0	22	7	0.05–9.0 *M*	1979		122
	HIO_3					
H_0	?	2	0.025–5.5 *M*	1965	See refs. 1, 17	123
	HIO_4					
H_0	?	2	0.05–2.5 *M*	1965	See refs. 1, 17	123
	BF_3					
"H_0"	25	5	32.8–100%	1957	See ref. 1	124
	$(CF_3)_2C(OH)_2$					
H_{GF}	25	1	0.580–5.402 *M*	1979	Fec/Fec$^+$	125
	CF_3CO_2H					
H_0	?	3	0.00071–0.62*x*	1955	See refs. 1, 17	126
H_0	23	2	0.99–6.73 *M*	1958	See ref. 1	119
H_0	20	1	0.528–1.00*x*	1966		127
H_0	25	4	0.1–12.97 *N*	1976	Includes data from ref. 126	128
H_R	25	12	0.1–12.97 *N*	1976	Also $H_R = D_R$	128
H_-	?	1	0.0081–0.14*x*	1955	Picrate ion	126
H_{GF}	25	1	0.002–0.998*x*	1979	Fec/Fec$^+$	125
	CCl_3CO_2H					
H_0	?	1	0.294–5.58 *M*	1954	Poor *p*-nitroaniline pK_a	31
H_0	?	2	0.025–0.42*x*	1955	See ref. 1	126
H_0	?	3	0.197–8.6 *M*	1956	See ref. 1	129
H_0	25	2	4.0–78.6%	1959	See refs. 1, 17	34
H_-	?	1	0.0052–0.20*x*	1955	Picrate ion	126
?R_0	?	1	1.5–90.0%	1971	Electrochemical functions	130
	$CHCl_2CO_2H$					
H_0	?	1	0.535–4.68 *M*	1954	Poor *p*-nitroaniline pK_a	31
H_0	23	5	0.05–12.13 *M*	1958	See ref. 1	119
H_0	25	1	3.1–85.5%	1959	See refs. 1, 17	34

Can. J. Chem. Downloaded from www.nrcresearchpress.com by 210.87.254.105 on 09/06/12
For personal use only.

TABLE 1 *(Concluded)*

AF[a]	T[b]	In.[c]	Acid conc.[d]	Year	Comments	Reference
	CH_2ClCO_2H					
H_0	25	2	3.38–81.6%	1959	See refs. 1, 17	34
$?R_0$	?	1	2.8–82.1%	1971	Electrochemical functions	130
	CH_3CO_2H					
H_0	17	1	0.722–16.06 *N*	1958	See ref. 1	33
R_0	25	1	10.4–70.6%	1969	Fec/Fec^+	131
	HCO_2H					
H_0	17	1	0.89–21.95 *N*	1958	See ref. 1	33
H_0	25	2	0.92–100%	1960	See refs. 1, 17	132
H_0	25	3	0.015–100%	1980		133
H_R	25	3	4.4–99.5%	1960	See refs. 1, 17	132
$?R_0$	?	1	0.01–0.99*x*	1971	Electrochemical functions	134
	$p\text{-}CH_3\text{–}C_6H_4\text{–}SO_3H$					
H_0	26	2	0.50–55%	1964,1966		99
H_R	26	2	0.50–55%	1964,1966	See refs. 1, 17	99
H_0'''	26	2	0.50–55%	1964,1966	Tertiary amines. See ref. 17	99
H_{GF}	25	1	1.0–62.5%	1975	Fec/Fec^+	110
	CH_3SO_3H					
H_0	25	6	3.0–100.0%	1959	See refs. 1, 16, 17	34
H_0	?	3	10–0% water	1981		135
H_{GF}	25	1	1.0–87.6%	1975	Fec/Fec^+	110
	$C_6F_5SO_3H$					
H_0	25	4	0.1–85.0%	1982		136
	1,3,5-Trifluoro-2,4-disulfonic acid					
H_0	25	4	0.1–64.0%	1982		137
	CF_3SO_3H					
"H_0"	25	4	0.50–8.50 *M*	1982		138
H_{GF}	25	1	0.564–8.322 *M*	1979	Fec/Fec^+	125
	$H_3PW_{12}O_{40}$[f]					
H_0	20	2	0.0104–0.251 *M*	1982		139

[a]Acidity function; see text and comments. Quotes indicate that other than "usual" indicators were used.
[b]Temperature, °C. A query means value unreported, presumably "room temperature", about 22°C.
[c]Number of indicators used.
[d]Concentration range studied. % = percent by weight; *M* = molarity; *N* = normality; *m* = molality; *x* = mole fraction.
[e]A qualitative study is given in ref. 106.
[f]Also given are H_0 scales for 0.010–0.240 *M* solutions in 40 vol.% dioxane and 0.00406–0.203 *M* solutions in 94.5 vol.% HOAc (139).

reduced by replacing the water by a dipolar aprotic solvent such as DMSO or sulfolane, at fixed hydroxide concentrations. This affects only the last two terms in eq. [12]. Suitable series of overlapping indicators can be used, in the same way as in acidic media, to give acidity functions; see the reviews by Bowden (11) and Rochester (1, 12). Superscripts are used to delineate the indicator type, H_-^I for indoles, H_-^P for purines and pyrimidines, etc. H_- scales themselves are obtained with substituted aniline and diphenylamine indicators (205), and H_{2-} scales with diphenylamine carboxylates or sufonates, or aminobenzoates (207).

Scales of the first type have received comparatively little attention; tabulated references to those that exist are given in Tables 3 and 4. The H_-^I scales of Yagil (198) are shown in Fig. 2 as a function of log hydroxide concentration. As can be seen, little deviation from ideality is apparent until pH 13, or even pH 14 for NaOH, and although NaOH and KOH are much more basic than their concentrations would predict at, say 5 *M*, LiOH solutions are not. Scales for hydroxide *addition*, as in eq. [13], are known as J_- (200) and are defined as in eq. [12] but without the log a_w term (compare eqs. [11] and [13]); some have been measured by Zuman *et al.* for the addition of hydroxide ion to a series of substituted benzaldehydes (201, 208).

$$[13] \quad S + HO^- \rightleftharpoons [SOH]^-$$

Scales of the second type are more common. Those available are summarized in Table 5; various acidity scales for 0.011 *M* tetramethylammonium hydroxide in aqueous dimethyl sulfoxide, as a function of mole fraction DMSO, are shown in Fig. 3. Aqueous DMSO is the most widely studied medium of this type, and one of the most useful. As Fig. 3 shows, a basicity range of at least 14 orders of magnitude is available, depending on the indicator system used. Figure 3 also shows, however, that different indicator types lead to very different acidity functions, in this medium as in most others. A J_- scale is available (108) as are W_0 scales, measured by Stewart and Van Dyke (222). These refer to the hydration of a series of substituted trifluoroacetophenones, eq. [14], rather than a reaction involving base.

$$[14] \quad ArC(OH)_2CF_3 \overset{K_d}{\rightleftharpoons} ArCOCF_3 + H_2O$$

Electrochemical scales

It is apparent that an acidity function measurable over a wide range using a single indicator would have advantages when compared to functions obtained by the overlap of several indicators. The very low indicator concentrations necessarily re-

Can. J. Chem. Downloaded from www.nrcresearchpress.com by 210.87.254.105 on 09/06/12
For personal use only.

TABLE 2. Acidity functions for organic solvent/aqueous acid media

%v/v Org.[a]	AF[b]	T[c]	In.[d]	Acid conc.[e]	Year	Comments	Reference
	H_2SO_4/EtOH						
67%	H_0	47.7	5	13.0–35.8%	1978		140
50%	H_0	30	8	0.001–6.8 *M*	1977		141
50%	H_0	47.7	5	12.5–34.7%	1978		140
50%	"H_0'"	25	8	0.2–5.0 *N*	1974	Substituted triazines	142
33%	H_0	47.7	5	12.1–29.6%	1978		140
20%	H_0	25	8	0.202–27.34 *N*	1972		143
20%	H_0	25	4	0.10–10.80 *N*	1979	No *o*-substituents	144
20%	H_A	25	7	0.50–12.00 *M*	1979		145
20%	H_0''	25	17	0.0163–11.22 *M*	1967	Diphenylamines	146
20%	H_{Azo}	25	32	0.20–19.0 *N*	1958–1959	Azo-compounds	147
20%	H_{Azo}	25	1	0.202–17.96 *N*	1972	Corrects scale of refs. 147	143
20%	H_{GF}	25	1	0.25–10.0 *M*	1972	Fec/Fec$^+$	78
20%	H_{GF}	?	1	0.04–5.9 *M*	1979	Fec/Fec$^+$	145
	H_2SO_4/dioxane						
60%	H_0	22	3	0.085–4.85 *M*	1962		36
60%	H_0	25	7	0.05–5.50 *M*	1981		148
60%	H_A	25	4	1.00–5.50 *M*	1981		148
60%	H_{GF}	25	1	0.25–5.5 *M*	1972	Fec/Fec$^+$	78
60%	H_{GF}	25	1	0.20–1.50 *M*	1981	Fec/Fec$^+$	148
40%	H_0	22	3	0.10–4.82 *M*	1962		36
40%	H_{GF}	25	1	0.25–8.5 *M*	1972	Fec/Fec$^+$	78
5%	"H_0"	23	8	2–75%	1961–1962		149
	H_2SO_4/HOAc[f]						
99%	H_0	?	3	0.12–12%	1957		151
95%	H_0	?	3	2–18%	1957		151
90%	H_0	20	1	0.20–1.00 *M*	1956		152
90%	H_0	?	3	2–22%	1957		151
90%	H_0	25	2	0.30–0.80 *M*	1976		45
85%	H_0	?	3	2–28%	1957		151
80%	H_0	22	2	0.07–2.78 *M*	1962		36
80%	H_0	25	2	0.30–1.40 *M*	1976		45
80%	H_R	24	8	4–86%	1962	% w/w benzhydrols	153
80%	H_R	?	15	10–90%	1972	% w/w benzhydrols	154
60%	H_0	25	2	0.30–2.40 *M*	1976		45
50%	H_0	?	2	0.1–0.4 *M*	1957		155
50%	H_R	?	5	14–50%	1972	% w/w benzhydrols	154
40%	H_0	25	2	0.40–2.80 *M*	1976		45
20%	H_0	25	2	0.30–3.00 *M*	1976		45
20%	H_R	?	18	24–80%	1972	% w/w benzhydrols	154
10%	H_R	?	10	24–86%	1972	% w/w benzhydrols	154
	H_2SO_4/Ethylene glycol						
50%	R_0	25	1	0.1178–6.00 *M*	1975	Fec/Fec$^+$	156
	H_2SO_4/Sulfolane						
80%	H_0	25	2	0.80–2.40 *M*	1976		45
60%	H_0	25	2	0.30–3.20 *M*	1976		45
40%	H_0	25	2	0.20–3.20 *M*	1976		45
20%	H_0	25	2	0.30–3.00 *M*	1976		45
	H_2SO_4/MeOH						
70%	H_0	?	1	1.80–3.60 *M*	1969		157
70%	H_R	?	2	1.80–3.60 *M*	1969		157
61%	H_0	20	7	2.5–85.0%	1971		158
50%	H_0	25	3	0.10–5.00 *M*	1973		159
	H_2SO_4/DMSO						
70%	H_0	25	14	1–90%	1972		160
70%	H_0'''	25	14	2–84%	1972	Tertiary amines	160
	H_2SO_4/CH_3CN						
1:1 w/w	H_{Fec}	25	9	0.005–4.00 *M*	1979	Substituted ferrocenes	161
75%	H_{GF}	25	1	0.25–4.5 *M*	1972		78

Can. J. Chem. Downloaded from www.nrcresearchpress.com by 210.87.254.105 on 09/06/12
For personal use only.

TABLE 2 *(Continued)*

%v/v Org.[a]	AF[b]	T[c]	In.[d]	Acid conc.[e]	Year	Comments	Reference
	$HClO_4$/EtOH						
90%	H_0	25	1	0.80–0.20 *M*	1977		162
50%	H_0	30	4	0.001–2.4 *M*	1977		141
50%	H_{Azo}	20	9	0.1–7.5 *M*	1969–1970	Azobenzenes	163
	$HClO_4$/dioxane						
90%	H_0	15,25,35	1	0.01–0.20 *M*	1973		164
60%	H_0	?	3	0.195–4.376 *M*	1957	See ref. 15	165
60%	H_0	20	1	0.100–0.995 *M*	1962		166
60%	H_R	?	3	0.021–3.89 *m*	1960		167
50%	H_0	25	3	0.005–1.00 *M*	1969		168
50%	H_0	10,15	1	0.01–0.10 *M*	1973		164
40%	H_0	?	3	0.217–4.423 *M*	1957	See ref. 15	165
40%	H_0	?	3	0.01–4.14 *m*	1960		167
	$HClO_4$/HOAc						
95%	H_0	?	2	0.015–0.300 *M*	1958		169
91%	H_0	?	2	0.015–0.300 *M*	1958		169
90%	H_0	?	3	0.25–14%	1957		151
90%	H_0	25	6	0.2–10%	1973		170
90%	H_0	25	2	0.02–0.60 *M*	1976		45
85%	H_0	?	2	0.015–0.300 *M*	1958		169
80%	H_0	22	1	0.10–2.49 *M*	1962		36
80%	H_0	25	2	0.04–1.20 *M*	1976		45
70%	H_0	25	7	0.3–20.3%	1973		170
70%	H_0	25	2	0.06–1.60 *M*	1976		45
60%	H_0	25	2	0.08–2.00 *M*	1976		45
51%	H_0	?	2	0.015–0.300 *M*	1958		169
50%	H_0	25	7	0.6–24.2%	1973		170
50%	H_0	25	2	0.08–2.20 *M*	1976		45
40%	H_0	?	2	1.015–0.300 *M*	1958		169
40%	H_0	25	2	0.10–2.40 *M*	1976		45
30%	H_0	25	7	0.6–23.8%	1973		170
30%	H_0	25	2	0.08–2.60 *M*	1976		45
25%	H_0	?	2	0.015–0.300 *M*	1958		169
20%	H_0	25	2	0.08–2.80 *M*	1976		45
10%	H_0	?	2	0.015–0.300 *M*	1958		169
10%	H_0	25	7	0.4–25.0%	1973		170
10%	H_0	25	2	0.06–2.80 *M*	1976		45
	$HClO_4$/Ethylene glycol						
90%	H_0	30	2	0.1–1.14 *M*	1961		171
50%	H_0	30	3	0.06–4.10 *M*	1961		171
	$HClO_4$/Sulfolane						
95%	H_0	25	7	0.2–6.3%	1971		81
95%	H_0	25	2	0.08–0.60 *M*	1976		45
90%	H_0	25	7	0.6–11.2%	1971		81
90%	H_0	25	2	0.20–1.20 *M*	1976		45
80%	H_0	25	2	0.30–1.80 *M*	1976		45
70%	H_0	25	7	0.8–19.1%	1971		81
70%	H_0	25	2	0.30–2.40 *M*	1976		45
60%	H_0	25	2	0.30–2.80 *M*	1976		45
50%	H_0	25	7	0.6–20.0%	1971		81
50%	H_0	25	2	0.20–3.00 *M*	1976		45
40%	H_0	25	2	0.20–3.20 *M*	1976		45
30%	H_0	25	7	0.4–21.5%	1971		81
30%	H_0	25	2	0.10–3.20 *M*	1976		45
20%	H_0	25	2	0.10–3.20 *M*	1976		45
10%	H_0	25	7	0.4–21.0%	1971		81
10%	H_0	25	2	0.06–3.00 *M*	1976		45
	$HClO_4$/MeOH						
91%	H_0	18	1	0.92–5.74 *N*	1953		172
90%	H_0	25	1	0.025–0.13 *M*	1977		162

Can. J. Chem. Downloaded from www.nrcresearchpress.com by 210.87.254.105 on 09/06/12
For personal use only.

TABLE 2 *(Concluded)*

%v/v Org.[a]	AF[b]	T[c]	In.[d]	Acid conc.[e]	Year	Comments	Reference
	$HClO_4$/DMSO						
50%	H_0	25	1	0.08–0.20 *M*	1977		162
	$HClO_4$/2-Butoxyethanol						
80%	H_0	25	3	0.5–3.0 *M*	1968		173
60%	H_0	25	3	0.5–3.5 *M*	1968		173
40%	H_0	25	3	0.5–4.0 *M*	1968		173
	HCl/EtOH						
95%	H_0	20	5	0.006–8.83 *M*	1968		174
71.88%	H_0	25	1	0.05–1.00 *M*	1966		100
52%	H_0	18	3	0.05–6.20 *M*	1957		175
50%	H_0	30	8	0.001–6.8 *M*	1977		141
40%	H_0	25	1	0.05–1.00 *M*	1966		100
19.99%	H_0	25	1	0.05–1.00 *M*	1966		100
10%	H_0	25	1	0.05–1.00 *M*	1966		100
	HCl/dioxane						
60%	"H_0"	22	3	0.19–5.0 *M*	1962		36
60%	H_0	25	1	0.05–1.00 *M*	1966		100
44%	H_0	25	1	0.05–1.00 *M*	1966		100
40%	H_0	22	3	0.12–5.78 *M*	1962		36
40%	H_0	25	3	0.250–4.50 *M*	1970		176
30%	H_0	25	1	0.05–1.00 *M*	1966		100
20%	H_0	25	1	0.05–1.00 *M*	1966		100
10%	H_0	25	1	0.05–1.00 *M*	1966		100
	HCl/HOAc[g]						
90%	H_0	20	1	0.20–1.00 *M*	1956		152
	HCl/ethylene glycol						
50%	H_0	30	3	0.06–4.00 *M*	1961		171
	HCl/MeOH						
91%	H_0	18	1	1.08–11.40 *N*	1953		172
73%	H_0	18	1	3.38–7.63 *N*	1953		172
	HCl/acetone						
50%	H_0	?	1	0.15–2.45 *M*	1976		177
	DCl/acetone						
50%	D_0	?	1	0.01–2.42 *M*	1976		177
	HBr/Dioxane						
40%	H_0	25	3	0.500–4.00 *M*	1970		176
	HBr/HOAc						
95.40%	H_0	25	1	0.017–0.810 *M*	1965		178
92.41%	H_0	25	1	0.022–0.810 *M*	1965		178
89.43%	H_0	25	1	0.066–0.820 *M*	1965		178
84.47%	H_0	25	2	0.014–0.880 *M*	1965		178
69.56%	H_0	25	1	0.013–0.790 *M*	1965		178
39.75%	H_0	25	1	0.019–0.810 *M*	1965		178
	HNO_3/HOAc						
10%	H_0	25	2	0.0193–1.737 *M*	1971		179
	HNO_3/Sulfolane						
40%	H_0	25	2	0.20–3.00 *M*	1976		45
20%	H_0	25	2	0.30–3.00 *M*	1976		45
	H_3PO_4/HOAc						
99%	H_0	?	3	2–28%	1957		151
95%	H_0	?	3	2–28%	1957		151
90%	H_0	?	3	2–28%	1957		151

[a]Percent organic component by volume.
[b–e]As footnotes *a–d* of Table 1.
[f]Also see ref. 150.
[g]Also see ref. 101.

sulting can best be measured electrochemically. Strehlow *et al.* (234) suggested the use of the ferrocene/ferricinium ion (Fec/Fec^+) and cobalticinium ion/cobaltocene (Coc^+/Coc) redox systems as a reference against which to measure hydrogen electrode potentials. Subsequently Strehlow and Wendt (76) measured the redox function $R_0(H)$ (abbreviated R_0 in Tables 1 and 2); $R_0(H) = F[E(x) - E(1)]/RT \ln 10$, where $E(1)$ is the emf of the cell

Can. J. Chem. Downloaded from www.nrcresearchpress.com by 210.87.254.105 on 09/06/12
For personal use only.

TABLE 3. Acidity functions for aqueous basic media

AF[a]	T[b]	In.[c]	Base conc.[d]	Year	Comments	Reference
	NaOH					
"H_-"	20	9	1–18 *M*	1944	Indigo derivatives. See refs. 1, 11, 12	195
"H_-"	25	1	0.0097–8.45 *M*	1962	Thioacetamide. See ref. 11	196
"H_-"	?	—	1.62–10.55 *M*	1980	p*H*-meter readings	197
H_-^I	25	6	0.1–16 *M*	1967	Indoles. See ref. 1	198
H_{2-}	20	23	0.001–12 *M*	1969		199
J_-	25	1	0.2–3.93 *M*	1967	Aromatic S_N2 kinetics	200
J_-	25	12	0.01–12.0 *M*	1973	Benzaldehydes, HO^- addition	201
H_{HC}	25	1	0.25–6.50 *M*	1974	Coc^+/Coc	202
	KOH					
"H_-"	20	4	1–12 *M*	1944	Indigo derivatives. See refs. 1, 11, 12	195
"H_-"	?	—	0.915–10.10 *M*	1979	p*H*-meter readings	203
H_-^I	25	12	0.1–15 *M*	1967	Indoles. See ref. 1	198
H_{2-}	20	14	0.001–12 *M*	1969		199
H_{2-}	25	5	0.1–11.0 *M*	1967	Indole carboxylates	198
H_{2-}	20	2	0.001–1 *M*	1969	Indole carboxylates	199
H_{HC}	25	1	0.25–7.50 *M*	1974	Coc^+/Coc	202
	LiOH					
"H_-"	25	1	1.2–10.7%	1965	Kinetics. Inferred from ref. 195	204
H_-	25	?	1.0–5.0 *M*	1964	See refs. 11, 12	205
"H_-"	?	—	1.09–4.30 *M*	1980	p*H*-meter readings	197
H_-^I	25	?	0.5–4.5 *M*	1967	Indoles. See ref. 1	198
H_{2-}	20	10	0.001–5 *M*	1969		199
	CsOH					
"H_-"	25	1	9.4–35.7%	1965	Kinetics. Inferred from ref. 195	204
	Tetramethylammonium hydroxide (TMAH)					
H_{GC}	25	1	0.1–2.8 *M*	1973	Coc^+/Coc	206
	Tetraethylammonium hydroxide (TEAH)					
H_{GC}	25	1	0.1–1.2 *M*	1973	Coc^+/Coc	206
	Tetra-n-butylammonium hydroxide					
H_{GC}	25	1	0.1–1.4 *M*	1973	Coc^+/Coc	206
	Benzyltrimethylammonium hydroxide (BzTMAH)					
H_-	25	5	0.01–2.38 *M*	1964	See ref. 11	205
H_{2-}	?	?	0.0114–2.48 *M*	1966		207
H_{GC}	25	1	0.5–2.6 *M*	1973	Coc^+/Coc	206

[a–d]As in Table 1.

$$Pt|H_2(g, 1\ atm)|aq.\ acid\ (a_{H^+} = 1),\ Fec/Fec^+\ (1:1)|Pt$$

R_0 scales have been measured for several acid media (76, 77, 115, 116, 130, 134, 156).

$$[15] \quad -H_{GF} = \log a_{H^+} + \log (f_{Fec}/f_{Fec^+})$$

Janata and Jansen (78) refined this approach by introducing a polarographic procedure to measure the Fec/Fec^+ half-wave potential, using this as a reference for a glass electrode. The resulting scales are called H_{GF} (glass, ferrocene), and are now available for quite a number of acid media (78, 110, 125, 145, 148). H_{GF} is defined like the other acidity functions, eq. [15], with the addition of the polarographic assumption that the diffusion coefficients for the oxidized and reduced species approximately cancel (see the discussion in ref. 78). In basic media the Coc^+/Coc redox couple is used, and several H_{GC} (glass, cobaltocene) scales are listed in Tables 3 and 5 (202, 206, 221). Janata and Taylor (202) have shown that the glass and hydrogen electrodes give the same scales in basic solution, and report some H_{HC} (hydrogen, cobaltocene) functions.

Universal functions

It is evident that Tables 1–5 summarize almost too much information to be useful, insofar as the requirement for a simple method for studying rates and equilibria in these non-ideal systems is concerned. Several approaches to the goal of determining one universal function per medium form most of the remainder of this review.

Yates–McClelland method

The Hammett H_0 has acquired, perhaps deservedly, some of the status of a "universal" acidity function for various reasons, among them its use in the Yates–McClelland and Bunnett–Olsen methods.

$$[16] \quad \log I = mH_0 + pK_{BH^+}$$

It has long been observed that log ionization ratios obtained for compounds other than primary aromatic amines give straight lines when plotted against H_0, see eq. [16], although the slopes often differ from unity. From these graphs, the log $I = 0$ intercept gives H_0 values at half-protonation $(H_0)_{1/2}$, useful in their own right for comparison purposes (235); multiplication by the slope m can then give a pK_{BH^+} estimate as the $H_0 = 0$ intercept (6, 8, 236). This allows bases treated in this way essentially to define their own acidity functions, *vide infra* (236, 237). However, the approach is empirical, and runs into trouble near the aqueous region, since in the p*H* range all slopes must be unity, see eq. [3] (8, 42).

Can. J. Chem. Downloaded from www.nrcresearchpress.com by 210.87.254.105 on 09/06/12
For personal use only.

TABLE 4. Acidity functions for organic solvent (fixed)/aqueous base (variable) media

Medium	AF[a]	T^b	In.[c]	Base conc.[d]	Year	Comments	Reference
NaOH/1% EtOH	J_-	?	19	0.01–12.0 *M*	1976	[e]	208
NaOH/10% EtOH	J_-	?	10	0.1–5.0 *M*	1976	[e]	208
NaOH/50% EtOH	J_-	?	7	0.1–3.0 *M*	1976	[e]	208
NaOH/90% EtOH	J_-	?	10	0.1–1.89 *M*	1976	[e]	208
NaOH/10% DMSO	J_-	?	10	0.01–5.0 *M*	1076	[e]	208
NaOH/50% DMSO	J_-	?	6	0.01–1.5 *M*	1076	[e]	208
NaOH/80% DMSO	J_-	?	4	0.005–0.07 *M*	1976	[e]	208
NaOH/90% DMSO	J_-	?	3	0.001–0.04 *M*	1976	[e]	208
KOH/40% dioxane	H_-	?	2	0.001–0.385 *M*	1970		209
TMAH/95% DMSO	H_-[c]	25	4	2.5×10^{-5}–0.067 *M*	1973	[f]	210
TMAH/15.9% DMF	H_-	25	1	0.0066–0.138 *M*	1970	[g,h]	211
TMAH/32.6% DMF	H_-	25	1	0.0066–0.269 *M*	1970	[g,h]	211
TMAH/55.5% DMF	H_-	25	1	0.0066–0.0725 *M*	1970	[g,h]	211
BzTMAH/50% pyridine	H_-	25	?	0.01–2.12 *M*	1964	[g,i]	205
BzTMAH/30% pyridine	H_-	25	?	0.03–2.38 *M*	1964	[g,i]	205
PTMAH/95.0% sulfolane	"H_-"	?	2	0.0032–0.0193 *M*	1960	[g,i,j]	212
PTMAH/90.5% sulfolane	"H_-"	?	1	0.0174–0.0520 *M*	1960	[g,i,j]	212
PTMAH/78.9% sulfolane	"H_-"	?	4	0.0123–0.0707 *M*	1960	[g,i,j]	212
PTMAH/65.2% sulfolane	"H_-"	?	2	0.0294–0.0541 *M*	1960	[g,i,j]	212
PTMAH/9% sulfolane	"H_-"	?	2	0.012–0.0210 *M*	1960	[g,i,j]	212

[a–d]As in Table 1.
[e]Addition of hydroxide to substituted benzaldehydes.
[f]Carbon bases.
[g]Mole% organic component.
[h]Of limited utility, since HO^- and DMF react (211).
[i]See ref. 11.
[j]PTMAH is phenyltrimethylammonium hydroxide.

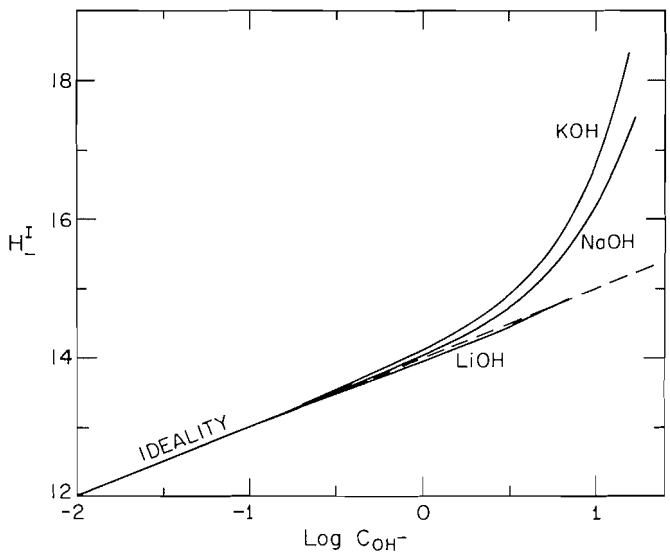

FIG. 2. H_-^I vs. log hydroxide concentration, for aqueous KOH, NaOH, and LiOH (198).

Proton activity scales

Related to the above method of pK_{BH^+} determination is the observation that, at least away from the origin, all acidity functions are linear in each other (236). Also the differences between acidity functions, $H_X - H_Y = \log(f_X f_{YH^+}/f_Y f_{XH^+})$, are reasonably linear functions of acid molarity (85, 99). Yates *et al.* showed that lines with similar slopes result if the activity coefficients of suitable compounds are used directly (85). Solubilities of neutral bases can be used to obtain f_B, and solubilities of pentacyanopropenide (PCP^-) salts give estimates of f_{BH^+}, using the Boyd approximation (17, 238) that the activity coefficient of the tetraethylammonium ion (TEA^+) does not vary greatly with acidity, see eq. [17]. With these available, it becomes possible to calculate a scale of log $a^*_{H^+}$ values using acidity functions and the activity coefficients of suitable indicators, eq. [18] (20, 85).

$$[17]\quad f^*_{BH^+} = [f_{\pm(BH^+PCP^-)}]^2/[f_{\pm(TEA^+PCP^-)}]^2 = (f_{BH^+}f_{PCP^-})/(f_{TEA^+}f_{PCP^-}) = f_{BH^+}/f_{TEA^+}$$

$$[18]\quad \log a^*_{H^+} = \log f^*_{XH^+} - \log f_X - H_X$$

Scales of log $a^*_{H^+}$, derived from a number of acidity functions, have been calculated for aqueous H_2SO_4 and $HClO_4$ (20, 85), and the former confirmed by H_{GF} measurements (239). More recent proton activity scales are available from H_{GF} for several acid media (110), those for H_2SO_4 and $HClO_4$ agreeing well with the ones given by Haldna and Koppel (240). They have found use in the investigation of reaction mechanisms in strong acids, since they enable estimation of transition state activity coefficients (TSAC), and the behaviour of these as a function of acidity is mechanistically revealing (110, 241–243). They have not so far been used for pK_{BH^+} determinations.

Carpentier's method

Carpentier noticed that the differences between certain acidity functions are approximately equal at given acidities: $(H_0 - H_0''') = (H_0''' - H_C) = (H_C - H_R) = \Delta(S)$. Acidity functions can be redefined on the basis of this "fundamental variable" $\Delta(S)$ using the "solvation coefficient" τ as a proportionality constant; $H_X = pH(H_2O) + \tau\Delta(S)$ where τ is one of seven whole numbers (46, 244). Values of log $a^*_{H^+}$ identical to those obtained from H_{GF} (110) were derived using this treatment (244). Accordingly there would be only seven fundamental acidity functions, which Carpentier distinguishes by prefixes: ${}^0H \equiv H_R$, ${}^1H \equiv H_C$, ${}^2H \equiv H_0'''$, and ${}^3H \equiv H_0$ (46), with ${}^4H$, ${}^5H$,

Can. J. Chem. Downloaded from www.nrcresearchpress.com by 210.87.254.105 on 09/06/12
For personal use only.

TABLE 5. Acidity functions for organic solvent (variable)/aqueous base (fixed) media

Range of solvent composition	Fixed base concentration	AF[a]	T^b	Year	Comments	Reference
DMSO						
5.0–70.0 mol%	0.001 *M* TMAH	H_-	25	1964	See ref. 11	205
10.32–99.59 mol%	0.011 *M* TMAH	H_-	25	1967	See refs. 1, 11	213
0.4–43.2 mol%	0.011 *M* TMAH	H_-	25	1973		214
2.1–44.1 mol%	0.011 *M* TMAH	H_-	25	1973		215
0–99.61 mol%	0.011 *M* TMAH	H_-	25	1976	Summarizes refs. 205, 213, 214	216
42.39–95.19 mol%	0.0471 *M* TMAH	H_-^F	25	1970	Substituted fluorenes	217
25.35–65.26 mol%	0.0471 *M* TMAH	H_-^F	25	1971	9-Phenylfluorenes	218
0–32.44 mol%	0.011 *M* TMAH	H_-^O	25	1973	Hindered phenols	214
0–17.43 mol%	0.011 *M* TMAH	(H_-^O)	25	1973	2,4-Diisopropylphenol	214
0.3–87.6 mol%	0.011 *M* TMAH	H_-^P	?	1977	Purines, pyrimidines	219
0–50.4 mol%	0.0471 *M* TMAH	H_0^Q	?	1973,1976	[c]	220
1.0–96.9 mol%	0.011 *M* TMAH	H_{2-}	?	1966	See ref. 1	207
2.1–44.1 mol%	0.011 *M* TMAH	H_{2-}	25	1973		215
0–88.2 mol%	0.011 *M* TMAH	H_{GC}	25	1973	Coc^+/Coc	221
0–62.8 mol%	0.047 *M* TMAH	H_{GC}	25	1973	Coc^+/Coc	221
0–70.0 mol%	0.011 *M* TEAH	H_{GC}	25	1973	Coc^+/Coc	221
50–98 vol%	0.01 *M* NaOH	J_-	?	1976	Benzaldehyde HO^- addn.	208
100–1 mol% water	None	W_0	31.4	1970,1972	[d]	222
Sulfolane						
1.79–93.4 mol%	0.011 *M* TMAH	H_-	25	1964	See ref. 11	205
1.0–95.1 mol%	0.011 *M* TMAH	H_{2-}	?	1966		207
0–75 mol%	0.011 *M* TMAH	H_{GC}	25	1974	Coc^+/Coc	202
0–75 mol%	0.011 *M* TMAH	H_{HC}	25	1974	Coc^+/Coc	202
100–1 mol% water	None	W_0	31.4	1970,1972	[d]	222
Dioxane						
0–40 mol%	0.001 *M* NaOH	H_-	?	1965		223
0–40 mol%	0.005 *M* NaOH	H_-	?	1965	See ref. 11	223
40–80 vol%	0.011 *M* TMAH	(H_-)	?	1971	Not a unique scale	224
0–54.7 mol%	0.011 *M* TMAH	H_{GC}	25	1973	Coc^+/Coc	221
Ethylene diamine						
5–85%	None	"H_-"	?	1955	See ref. 11	225
9.2–31.0 mol%	None	H_-	25	1964	Recalculated from ref. 225	205
5–100 wt.%	None	H_-	20	1965		226
10–100 mol%	None	H_{GC}	25	1973	Coc^+/Coc	206
Hydrazine						
5–60 wt.%	None	"H_-"	?	1952	See refs. 11, 230	227
5–70%	None	"H_-"	?	1959	See ref. 11	228
23.2–95.0 mol%	None	H_-	25	1964	Recalculated from ref. 228	205
10–60 wt.%	None	"H_-"[e]	20	1970	Calculated in ref. 230	229
10–50 mol%	None	H_{GC}	25	1073	Coc^+/Coc. See ref. 230	206
Pyridine						
1.0–59.7 mol%	0.011 *M* TMAH	H_-	25	1964	See ref. 11	205
1.0–63.5 mol%	0.011 *M* TMAH	H_{2-}	?	1966		207
0–50 mol%	0.011 *M* TMAH	H_{GC}	25	1973	Coc^+/Coc	221
DMF						
0–70.90 mol%	0.019 *M* TMAH	H_-	25	1970	HO^- and DMF react	211
10.47–67.09 mol%	0.019 *M* NaOH	H_-	25	1970	HO^- and DMF react	211
2-Aminoethanol						
5–100%	None	"H_-"	?	1956	See ref. 11	231
1.616–16.75 *M*	None	"H_-"	?	1979	p*H*-meter readings	203
Methanol						
0–100 mol%	0.001 *M* NaOH[f]	H_-	?	1965		223
0–100 mol%	0.005 *M* NaOH[f]	H_-	?	1965		223
Ethanol						
0–100 mol%	0.001 *M* NaOH[f]	H_-	?	1965		223
0–100 mol%	0.005 *M* NaOH[f]	H_-	?	1965	See ref. 11	223
Isopropanol						
0–100 mol%	0.001 *M* NaOH[f]	H_-	?	1965		223
0–100 mol%	0.005 *M* NaOH[f]	H_-	?	1965	See ref. 11	223

Can. J. Chem. Downloaded from www.nrcresearchpress.com by 210.87.254.105 on 09/06/12
For personal use only.

TABLE 5 *(Concluded)*

Range of solvent composition	Fixed base concentration	AF[a]	T^b	Year	Comments	Reference
t-Butanol						
0–100 mol%	0.001 *M* NaOH[f]	H_-	?	1965		223
0–100 mol%	0.005 *M* NaOH[f]	H_-	?	1965	See ref. 11	223
t-Pentanol						
0–100 mol%	0.001 *M* NaOH[f]	H_-	?	1965		223
0–100 mol%	0.005 *M* NaOH[f]	H_-	?	1965	See ref. 11	223
Ethylene glycol						
0–100 mol% water	0.01 *M* NaOH[f]	H_-	25	1971		232
10–90 mol%	0.01 *M* NaOH[f]	H_-	25	1972		233
Propylene glycol						
0–100 mol% water	0.01 *M* NaOH[f]	H_-	25	1971		232

[a,b]As in Table 1.
[c]Quaternary heterocyclic salts.
[d]Trifluoroacetophenone hydration.
[e]Electrochemical scale. Also given in ref. 229 are emf values for various hydroxide concentrations in hydrazine–water mixtures.
[f]Added as the alkoxide.

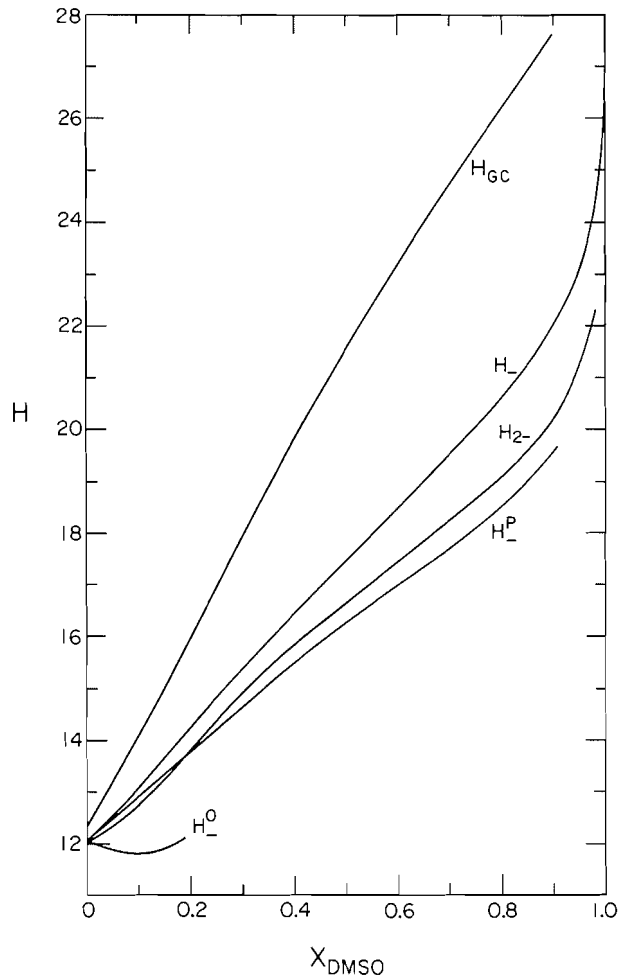

FIG. 3. Acidity functions vs. mole fraction dimethyl sulfoxide, for aqueous DMSO media containing 0.011 *M* tetramethylammonium hydroxide; H_- (216), H_{2-} (207), H_-^P (219), H_-^O (214), and H_{GC} (221).

and ^6H for pyridine *N*-oxides, amides, ketones, alcohols, etc. (245). The method has not been widely adopted; τ is essentially a whole-number variant of m^* and $(1 - \phi_e)$, see below.

First-order approximation

Most reasonable uses of acidity functions require two parameters; if one is pK_{BH^+} the other may be the slope m of eq. [16], or a specification of which acidity function is being followed, or τ. Several other two-parameter treatments are available, based on the assumption that activity coefficient ratios of the form $\log (f_B f_{H^+}/f_{BH^+})$ are linear functions of one another, rather than cancelling out. This is the first-order approximation.

Bunnett–Olsen method

This widely-used method was first proposed in 1966 (246). Taking the definition of H_0, eqs. [6] and [7], and writing the activity coefficient term as an "average" for the amines used in measuring H_0, Am, gives eq. [19]. Assuming that an equivalent term for any one base B is linear in this is eq. [20], which, on substituting into eq. [5] and suitable rearrangement gives the Bunnett–Olsen equation [21].

$$[19] \quad H_0 + \log C_{H^+} = -\log (f_{Am} f_{H^+}/f_{AmH^+})$$

$$[20] \quad \log (f_B f_{H^+}/f_{BH^+}) = (1 - \phi_e) \log (f_{Am} f_{H^+}/f_{AmH^+}) = (\phi_e - 1)(H_0 + \log C_{H^+})$$

$$[21] \quad \log I + H_0 = \phi_e (H_0 + \log C_{H^+}) + pK_{BH^+}$$

Using eq. [21], ionization ratio measurements give pK_{BH^+} values in the standard state by extrapolation, together with a slope parameter ϕ_e (ϕ_e, equilibrium, to distinguish it from the related kinetic parameter ϕ_r or $\phi_\ddagger$ (247)). The method has been widely accepted and works well in acids (see refs. 7, 65, 69, 246, 248, 249, etc.), acid/organic solvent media (145, 148), and basic solutions (216, 220).

Excess acidity method

This is referred to in the literature as the "Marziano–Cimino–Passerini" or the "Cox–Yates" method, which is unfortunate since both are the same. The term "excess acidity method" is preferred; "*X*-function method" is also used.

$$[22] \quad \log I - \log C_{H^+} = \log (f_B f_{H^+}/f_{BH^+}) + pK_{BH^+} = n \log (f_{B^*} f_{H^+}/f_{B^*H^+}) + pK_{BH^+} = nM_C + pK_{BH^+}$$

In its original form, pioneered by Marziano *et al.* in 1973 (250), an anchor compound B* and a series of overlapping

Can. J. Chem. Downloaded from www.nrcresearchpress.com by 210.87.254.105 on 09/06/12
For personal use only.

Can. J. Chem. Downloaded from www.nrcresearchpress.com by 210.87.254.105 on 09/06/12
For personal use only.

indicators were utilized, but not to derive an acidity function. The anchor pK_{BH^+}, say of *p*-nitroaniline, is used with eq. [5] to calculate values of log $(f_B f_{H^+}/f_{BH^+})$, abbreviated M_C (250), in dilute acid. The second set of ionization ratios, extending to more concentrated acid, are then plotted against these according to eq. [22], within the region of overlap, giving the second pK_{BH^+} as an intercept, and a slope n. These known values can then be used to extend M_C, working backwards, see eq. [22]. The process is repeated stepwise until the entire acidity range is covered. "Graphical" M_C scales of this type are available for aqueous H_2SO_4 and $HClO_4$ (250), DMSO/water basic mixtures (216), and aqueous KOH (251); they can easily be derived from existing sets of ionization ratios as necessary (216, 251).

Subsequently, Marziano's group introduced a refined computerized calculation method (252), enabling many sets of data to be treated simultaneously. In the course of this work, they extensively tested the concept of linearity of activity coefficient ratios assumed in this section (slopes n_{ij}), and found it valid in all cases (253); this assumption thus acquires the status of an "empirical fact" (J. F. Bunnett, personal communication). Cox and Yates confirmed and extended this work (83, 181), preferring the terminology m^* for the slope parameters and X for the activity coefficient ratio, eq. [23]. X represents the "excess acidity" (a term first used by Perrin (254)) as it is the difference between the observed acidity and that which the system would have if it were ideal (83, 181).

$$[23] \quad \log I - \log C_{H^+} = m^*X + pK_{BH^+}$$

The computer calculation method has several advantages. Any number of bases of widely differing types can be accommodated; X for aqueous sulfuric acid is derived from 165 different compounds, covering protonation at N, O, C, and S atoms, and negative, neutral, positive, and dipositive bases (181). Overlap between adjacent indicators is unnecessary (83, 181). Anchoring with a compound of known pK_a is also unnecessary, since X or M_C automatically becomes zero in the standard state (compare eqs. [22] and [23] with eq. [3]). Scales obtained in this way are available for aqueous HCl (83), and aqueous H_2SO_4 and $HClO_4$ (181, 252, 255), and the method has been used to calculate H_0 scales (essentially) for aqueous HBr (83) and $DClO_4$ (122). The latest refinement, again due to Marziano *et al.* (255), is to calculate scales for H_2SO_4 and $HClO_4$ simultaneously, ensuring that indicators have the same pK_{BH^+} regardless of medium, as they should.

There is no doubt that excess acidity scales represent the closest approach so far to "universal" acidity functions. They have been used to calculate pK_{BH^+} values (eq. [23]) by several groups (42, 83, 181, 193, 255–258). A method for evaluating pK_{BH^+} and m^* in the presence of quite severe medium effects has been developed (259) and used (260). The excess acidity method has been extended to reaction kinetics (261) and used to investigate the mechanisms of a number of different reactions (256, 257, 261–165). Temperatures other than 25°C can be easily accommodated (257), and the thermodynamics of ionization of 48 compounds in aqueous H_2SO_4 have been investigated (266).

Which method to use?

This is a valid question, considering the number of different methods of pK_{BH^+} determination already mentioned. Each method has its equivalent for kinetic studies also, and there are others not specifically discussed here, for instance the various hydration parameter treatments (1–3, 267–268).

The Bunnett–Olsen and excess acidity methods differ insofar as the former uses H_0, and hence the cancellation assumption involved in its derivation, whereas the latter only uses the linearity assumption of eq. [22]. There are other minor differences. Bunnett and Olsen in 1966 used the acid molarity as C_{H^+} in eq. [21], which may result in degrees of dissociation being included in the activity coefficient ratio, for instance of HSO_4^- in H_2SO_4 media (246). Subsequent physical studies produced better values of C_{H^+} in H_2SO_4; those given by Robertson and Dunford (169) are used with M_C (252), and recalculated literature values are used with X (83, 181). It has been found that these different C_{H^+} values cannot be interchanged among the latter two methods (270), although there is no reason in principle why either could not be used with the Bunnett–Olsen method. In sulfuric acid, differences in the pK_{BH^+} values supplied by the three methods appear at very high acidity (270), probably due to the very long extrapolations necessary. The Bunnett–Olsen method has been found to be less reliable when used with acidity functions other than H_0 (271), not that the use of other acidity functions has ever been advocated in this connection.

These differences, however, are theoretical rather than practical. The Bunnett–Olsen and excess acidity methods have been shown to be essentially equivalent, giving the same pK_{BH^+} and $(m^* = 1 - \phi_c)$ values (272). In practice the Yates–McClelland method often gives similar results too, despite its more empirical nature; many authors list pK_{BH^+} values obtained using all three methods. Probably the excess acidity method is to be preferred, if only because of the large amount of data used in calculating X, in well-studied acid media. X is not based on a single set of overlapping indicators, as is H_0. In less well-studied acid systems, where only H_0 may be available, the Bunnett–Olsen method is still unsurpassed. In basic DMSO media, the excess acidity and Bunnett–Olsen methods have been found to be practically equivalent; for the latter the choice of acidity function makes little difference to the pK_a values found (216).

Acidity functions themselves, apart from H_0 (H_- in basic media), are probably declining in importance. The newer methods have shown up several discrepancies in existing scales. For instance the Bunnett–Olsen (246), excess acidity (181), and Carpentier (273) methods all show that the original H_A scale was mis-anchored by 0.3 units, a point later confirmed directly by Edward and Wong (55). It has been suggested (216) that a variation among m^* values of less than 0.1 is necessary to define a good "acidity function" set of compounds, and several exisiting scales have been found wanting in this regard (181, 216). However, in those cases where only poor ionization ratio data for a single compound are available, good pK_a estimates can still be obtained by using the most "likely" acidity function from Tables 1–5 (219).

H_0 will probably continue to be useful in kinetic applications, at least pictorially. Plots of log rate constants against H_0 or pH/H_0 are qualitatively useful; they illustrate rate accelerations, rate maxima, etc. in an easily-understood way. For more quantitative information in the well-studied media, however, the excess acidity method is undoubtedly superior, if for no other reason than that it encompasses most of the other kinetic treatments; for details see ref. 261. It provides standard-state rate constants (256, 261, 263) and activation enthalpies and entropies (257, 262), and for reactions involving water, kinetically-involved water molecules are easily distinguished

Can. J. Chem. Downloaded from www.nrcresearchpress.com by 210.87.254.105 on 09/06/12
For personal use only.

from solvation water (262). In sulfuric acid, reaction with the other species present (274, 275) can readily be studied, e.g. with undissociated H_2SO_4 (237, 263), $H_3SO_4^+$ (274), and HSO_4^- (256, 262, 276). In cases where the activity coefficient of the substrate can be measured, the TSAC treatment is useful, enabling straightforward mechanistic distinctions (241, 242). Note that neither of these methods uses a traditional acidity function. In less well-studied media, again the Bunnett–Olsen method (247) is probably best; related kinetic treatments are available for basic solutions (277).

Second-order approximation

All of the methods discussed so far are approximations, and, one hopes, of increasing accuracy. Occasionally papers appear which remind us of the assumptions inherent in both the zero'th (278) and first-order (279) approximations; for instance Wojcik points out that either one leads to pK_{BH^+} values containing an "indeterminate constant" (279). This is thought to be small in most cases, however, as large discrepancies would cause noticeable effects in several of the above treatments.

Recently Edward, Sjöström, and Wold (280) subjected to factor analysis some data obtained in basic aqueous DMSO mixtures by Hallé *et al.* (281). These data consist of ionization ratios obtained using buffers at particular solvent compositions, and the resulting pK_a values refer to a standard state of infinite dilution in that solvent mixture. Thus acidity functions comparable to those discussed here were not derived (although it is possible to extrapolate to the aqueous standard state (282)), and the data are not strictly comparable to those used in compiling standard acidity functions. Nevertheless the factor analysis result, that *two* principal factors rather than one are required to explain the data (280), undoubtedly shows that even the first-order approximation is, in the limit, inaccurate. Indicated was a quadratic term (280); in the language of the excess acidity method this would necessitate an expansion of eq. [23] to eq. [24], which defines the second-order approximation.

$$[24] \quad \log I - \log C_{H^+} = pK_{BH^+} + m^*X + m^{**}X^2$$

Future acidity function work will probably concentrate on evaluating terms such as m^{**}. This is not going to be easy, as a great deal of accurate ionization ratio data will be necessary. Using Marziano's refinement, i.e. necessarily allowing only one value for pK_{BH^+} while using data in several different acid media (255), with the assumption that m^* is medium invariant, enough data probably exist at present to enable calculation of m^{**} and refined X values for perhaps three acid systems. Whether or not this is warranted at this time, whether or not m^* is really medium invariant, and what the physical meaning of m^{**} would be, are open questions. Preliminary work (P. G. Traverso, private communication) indicates that m^{**} may be very small in H_2SO_4 and $HClO_4$ media.

This is still a very healthy area of physical organic chemistry, as a glance at the list of references makes clear; 60% of them have appeared since the publication of Rochester's book (1) in 1970. We can certainly continue to expect new insights into equilibria and reactions in non-ideal media, resulting from the development and use of acidity functions.

Acknowledgements

We would like to thank the many people who discussed this work with us, particularly Professors J. F. Bunnett, Ülo Haldna, A. J. Kresge, Ross Stewart, and P. G. Traverso. Financial support is by the Natural Sciences and Engineering Research Council of Canada.

1. C. H. ROCHESTER. Acidity functions. Academic Press, New York. 1970.
2. M. LILER. Reaction mechanisms in sulfuric acid. Academic Press, New York. 1971.
3. F. COUSSEMANT, M. HELLIN, and B. TORCK. Les fonctions d'acidité et leurs utilizations en catalyse acido-basique. Gordon and Breach, Paris. 1969.
4. E. M. ARNETT. Prog. Phys. Org. Chem. **1**, 223 (1963).
5. N. C. DENO. Survey Prog. Chem. **2**, 155 (1964).
6. R. F. COOKSON. Chem. Revs. **74**, 5 (1974).
7. E. M. ARNETT and G. SCORRANO. Adv. Phys. Org. Chem. **13**, 83 (1976).
8. Ü. L. HALDNA. Usp. Khim. **49**, 1174 (1980); Russ. Chem. Rev. **49**, 623 (1980).
9. L. P. HAMMETT. Chem. Rev. **16**, 67 (1935); F. A. LONG and M. A. PAUL. Chem. Rev. **57**, 935 (1957).
10. V. A. PALM, (*Editor*). Tables of rate and equilibrium constants of heterolytic organic reactions. Vol. 5. Part 1. Moscow. 1978. pp. 524–656.
11. K. BOWDEN. Chem. Rev. **66**, 119 (1966).
12. C. H. ROCHESTER. Q. Rev. Chem. Soc. **20**, 511 (1966).
13. J. R. JONES. Prog. Phys. Org. Chem. **9**, 241 (1972).
14. J. R. JONES. The ionization of carbon acids. Academic Press, New York. 1973.
15. M. A. PAUL and F. A. LONG. Chem. Rev. **57**, 1 (1957).
16. M. I. VINNIK. Usp. Khim. **35**, 1922 (1966); Russ. Chem. Rev. **35**, 802 (1966).
17. R. H. BOYD. *In* Solute solvent interactions. *Edited by* J. F. Coetzee and C. D. Ritchie. Marcel Dekker, New York. 1969. pp. 97–218.
18. C. J. O'CONNOR. J. Chem. Ed. **46**, 686 (1969).
19. L. P. HAMMETT. Physical organic chemistry. 2nd. ed. McGraw-Hill, New York. 1970. pp. 263–314.
20. K. YATES and R. A. MCCLELLAND. Prog. Phys. Org. Chem. **11**, 323 (1974).
21. J. E. LEFFLER and E. GRUNWALD. Rates and equilibria of organic reactions. Wiley, New York. 1963. pp. 269–281.
22. J. HINE. Structural effects on equilibria in organic chemistry. Wiley, New York. 1975. pp. 138–150.
23. J. E. GORDON. The organic chemistry of electrolyte solutions. Wiley, New York. 1975. pp. 63–91.
24. J. MARCH. Advanced organic chemistry. 2nd ed. McGraw-Hill, New York. 1977. pp. 232–235.
25. T. H. LOWRY and K. S. RICHARDSON. Mechanism and theory in organic chemistry. 2nd. ed. Harper and Row, New York. 1981. pp. 232–250.
26. L. P. HAMMETT and A. J. DEYRUP. J. Am. Chem. Soc. **54**, 2721 (1932).
27. E. M. ARNETT and G. W. MACH. J. Am. Chem. Soc. **86**, 2671 (1964).
28. R. L. HINMAN and J. LANG. J. Am. Chem. Soc. **86**, 3796 (1964).
29. K. YATES, J. B. STEVENS, and A. R. KATRITZKY. Can. J. Chem. **42**, 1957 (1964).
30. M. J. JORGENSON and D. R. HARTTER. J. Am. Chem. Soc. **85**, 878 (1963).
31. R. P. BELL and A. H. BROWN. J. Chem. Soc. 774 (1954).
32. A. I. GEL'BSHTEIN, G. G. SHCHEGLOVA, and M. I. TEMKIN. Zh. Neorg. Khim. **1**, 506 (1956); Russ. J. Inorg. Chem. **1**(3), 167 (1956).
33. N. M. MILYAEVA. Zh. Neorg. Khim. **3**, 2011 (1958); Russ. J. Inorg. Chem. **3**(9), 27 (1958).
34. K. N. BASCOMBE and R. P. BELL. J. Chem. Soc. 1096 (1959).
35. M. I. VINNIK, R. S. RYABOVA, and N. M. CHIRKOV. Zh. Fiz. Khim. **33**, 2677 (1959); Russ. J. Phys. Chem. **33**, 575 (1959).
36. B. TORCK, M. HELLIN, and F. COUSSEMANT. Bull. Soc. Chim.

Can. J. Chem. Downloaded from www.nrcresearchpress.com by 210.87.254.105 on 09/06/12
For personal use only.

Fr. 1657 (1962).
37. M. I. VINNIK and R. S. RYABOVA. Zh. Fiz. Khim. **38**, 606 (1964); Russ. J. Phys. Chem. **38**, 320 (1964); R. S. RYABOVA, I. M. MEDVETSKAYA, and M. I. VINNIK. Zh. Fiz. Khim. **40**, 339 (1966); Russ. J. Phys. Chem. **40**, 182 (1966).
38. O. I. KACHURIN and L. P. MEL'NIKOVA. Izv. Vyssh. Ucheb. Zaved., Khim. Khim. Tekhnol. **11**, 1079 (1968); Chem. Abstr. **70**, 32128j (1969).
39. C. D. JOHNSON, A. R. KATRITZKY, and S. A. SHAPIRO. J. Am. Chem. Soc. **91**, 6654 (1969).
40. P. TICKLE, A. G. BRIGGS, and J. M. WILSON. J. Chem. Soc. B, 65 (1970).
41. R. J. GILLESPIE, T. E. PEEL, and E. A. ROBINSON. J. Am. Chem. Soc. **93**, 5083 (1971).
42. A. J. KRESGE, H. J. CHEN, and Y. CHIANG. J. Chem. Soc. Chem. Commun. 969 (1972); A. J. KRESGE, H. J. CHEN, G. L. CAPEN, and M. F. POWELL. Can. J. Chem. **61**, 249 (1983).
43. K. YATES and S. A. SHAPIRO. Can. J. Chem. **50**, 581 (1972).
44. M. J. COOK, N. L. DASSANYAKE, C. D. JOHNSON, A. R. KATRITZKY, and T. W. TOONE. J. Chem. Soc. Perkin Trans. II, 1069 (1974).
45. A. JUSSIAUME, M. GODEL, and F. COUSSEMANT. Bull. Soc. Chim. Fr. 1625 (1976).
46. P. DOMINIQUE and J.-M. CARPENTIER. J. Chem. Res. (S), 58 (1979).
47. Y. MARCUS, E. PROSS, and N. SOFFER. J. Phys. Chem. **84**, 1725 (1980).
48. V. GOLD and B. W. V. HAWES. J. Chem. Soc. 2102 (1951).
49. N. C. DENO, J. J. JARUZELSKI, and A. SCHRIESHEIM. J. Am. Chem. Soc. **77**, 3044 (1955).
50. E. M. ARNETT and R. D. BUSHICK. J. Am. Chem. Soc. **86**, 1564 (1964).
51. J. MINDL and M. VEČEŘA. Coll. Czech. Chem. Commun. **36**, 3621 (1971).
52. M. J. COOK, N. L. DASSANAYAKE, C. D. JOHNSON, A. R. KATRITZKY, and T. W. TOONE. J. Am. Chem. Soc. **97**, 760 (1975).
53. C. D. JOHNSON, A. R. KATRITZKY, and N. SHAKIR. J. Chem. Soc. B, 1235 (1967).
54. G. D. FREDERICK and C. D. POULTER. J. Am. Chem. Soc. **97**, 1797 (1975).
55. J. T. EDWARD and S. C. WONG. Can. J. Chem. **55**, 2492 (1977).
56. M. LILER and D. MARKOVIĆ. J. Chem. Soc. Perkin Trans. II, 551 (1982).
57. M. T. REAGAN. J. Am. Chem. Soc. **91**, 5506 (1969).
58. T. K. RODIMA, Ü. L. HALDNA, and E. VARJEND. Reakts. Sposobn. Org. Soedin. **5**, 466 (1968); T. K. RODIMA and Ü. L. HALDNA. Reakts. Sposobn. Org. Soedin. **6**, 227 (1969); T. K. RODIMA, Ü. L. HALDNA, and V. PALM. Reakts. Sposobn. Org. Soedin. **8**, 1165 (1971).
59. J.-M. CARPENTIER and P. LEMETAIS. Can. J. Chem. **56**, 954 (1978).
60. R. H. BOYD. J. Am. Chem. Soc. **83**, 4288 (1961); J. Phys. Chem. **67**, 737 (1963).
61. B. G. COX and P. T. MCTIGUE. J. Chem. Soc. 3893 (1964).
62. E. PATTON and R. WEST. J. Am. Chem. Soc. **95**, 8703 (1973).
63. P. VETEŠNÍK, J. BIELAVSKÝ, and M. VEČEŘA. Coll. Czech. Chem. Commun. **33**, 1687 (1968).
64. C. TISSIER and M. TISSIER. Bull. Soc. Chim. Fr. 2109 (1972).
65. J. T. EDWARD, I. LANTOS, G. D. DERDALL, and S. C. WONG. Can. J. Chem. **55**, 812 (1977).
66. T. G. BONNER and J. PHILLIPS. J. Chem. Soc. B. 650 (1966).
67. D. G. LEE and R. CAMERON. J. Am. Chem. Soc. **93**, 4724 (1971).
68. N. K. SKVORTSOV, G. F. TERESHCHENKO, B. I. IONIN, and A. A. PETROV. Zh. Obshch. Khim. **43**, 981 (1973); J. Gen. Chem. USSR, **43**, 976 (1973).
69. D. G. LEE and M. H. SADAR. J. Am. Chem. Soc. **96**, 2862 (1974).
70. D. G. LEE and M. H. SADAR. Can. J. Chem. **54**, 3464 (1976).
71. J. SEGRETARIO, J. F. RUSLING, and P. ZUMAN. J. Electroanal. Chem. **117**, 341 (1981).
72. R. A. MCCLELLAND and P. W. K. LAM. Can. J. Chem. **61**, (1983), in press.
73. F. COUSSEMANT. J. Chim. Phys. Phys.-Chim. Biol. **69**, 100 (1972).
74. C. C. GREIG, C. D. JOHNSON, S. ROSE, and P. G. TAYLOR. J. Org. Chem. **44**, 745 (1979); P. G. TAYLOR, C. D. JOHNSON, and S. ROSE. J. Chem. Soc. Chem. Commun. 101 (1977).
75. L. MICHAELIS and S. GRANICK. J. Am. Chem. Soc. **64**, 1861 (1942).
76. H. STREHLOW and H. WENDT. Z. Phys. Chem. Frankfurt, **30**, 141 (1961).
77. D. BAUER and M. BOUCHET. C. R. Acad. Sci. Paris, Ser. C, **275**, 21 (1972).
78. J. JANATA and G. JANSEN. J. Chem. Soc. Faraday Trans. 1, **68**, 1656 (1972).
79. T. G. BONNER and J. C. LOCKHART. J. Chem. Soc. 2840 (1957).
80. K. YATES and H. WAI. J. Am. Chem. Soc. **86**, 5408 (1964).
81. A. JUSSIAUME, M. GODEL, and F. COUSSEMANT. J. Chim. Phys. Phys.-Chim. Biol. **68**, 1315 (1971).
82. S. A. ATTIGA and C. H. ROCHESTER. J. Chem. Soc. Perkin Trans. II, 1624 (1974).
83. R. A. COX and K. YATES. Can. J. Chem. **59**, 2116 (1981).
84. N. C. DENO, H. E. BERKHEIMER, W. L. EVANS, and H. J. PETERSON. J. Am. Chem. Soc. **81**, 2344 (1959).
85. K. YATES, H. WAI, G. WELCH, and R. A. MCCLELLAND. J. Am. Chem. Soc. **95**, 418 (1973).
86. S. A. ATTIGA and C. H. ROCHESTER. J. Chem. Soc. Perkin Trans. II, 1411 (1975).
87. F. A. LONG and J. SCHULZE. J. Am. Chem. Soc. **86**, 327 (1964).
88. T. K. RODIMA and Ü. L. HALDNA. Reakts. Sposobn. Org. Soedin. **7**, 391 (1970).
89. A. J. KRESGE, H. J. CHEN, L. E. HAKKA, and J. E. KOUBA. J. Am. Chem. Soc. **93**, 6174 (1971).
90. S. B. SAVVIN, T. YA. BELOVA, and L. A. OKHANOVA. Zh. Anal. Khim. **25**, 1280 (1970); Russ. J. Anal. Chem. **25**, 1104 (1970).
91. C. D. JOHNSON, S. ROSE, and P. G. TAYLOR. J. Org. Chem. **44**, 753 (1979).
92. L. P. HAMMETT and M. A. PAUL. J. Am. Chem. Soc. **56**, 827 (1934).
93. E. A. BRAUDE. J. Chem. Soc. 1971 (1948).
94. M. A. PAUL. J. Am. Chem. Soc. **76**, 3236 (1954).
95. R. P. BELL, A. L. DOWDING, and J. A. NOBLE. J. Chem. Soc. 3106 (1955).
96. M. I. VINNIK, R. N. KRUGLOV, and N. M. CHIRKOV. Zh. Fiz. Khim. **30**, 827 (1956).
97. A. N. GEL'BSHTEIN, G. G. SHCHEGLOVA, and M. I. TEMKIN. Zh. Neorg. Khim. **1**, 282 (1956); Russ. J. Inorg. Chem. **1**(2), 96 (1956).
98. P. SALOMAA. Acta Chem. Scand. **11**, 125 (1957).
99. E. M. ARNETT and G. W. MACH. J. Am. Chem. Soc. **88**, 1177 (1966); G. W. MACH. Ph.D. Thesis, University of Pittsburgh. 1964.
100. H. SADEK, M. S. ABU ELAMAYEM, and I. M. SIDAHMED. Suomen. Kemi. **39B**, 225 (1966).
101. T. M. GORRIE and H. ZOLLINGER. Helv. Chim. Acta, **57**, 690 (1974).
102. A. P. BRYNZA, I. G. VINICHENKO, and V. A. ZOLOTONOSHA. Zh. Prikl. Khim. (Leningrad), **51**, 554 (1978); J. Appl. Chem. USSR, **51**, 543 (1978).
103. G. V. ÉPPLE, V. P. ODINTSOVA, and S. G. ÉNTELIS. Izv. Akad. Nauk SSSR, Otd. Khim. Nauk, 1365 (1282 in Eng. Edn.) (1962).
104. K. YATES and J. C. RIORDAN. Can. J. Chem. **43**, 2328 (1965).

Can. J. Chem. Downloaded from www.nrcresearchpress.com by 210.87.254.105 on 09/06/12
For personal use only.

105. J. N. PHILLIPS. Aust. J. Chem. **14**, 183 (1961).
106. N. C. DENO, G. SAINES, and M. SPANGLER. J. Am. Chem. Soc. **84**, 3295 (1962).
107. E. HEILBRONNER and S. WEBER. Helv. Chim. Acta, **32**, 1513 (1949).
108. R. G. DOWNING and D. E. PEARSON. J. Am. Chem. Soc. **83**, 1718 (1961).
109. A. I. GEL'BSHTEIN, R. P. AIRAPETOVA, G. G. SHCHEGLOVA, and M. I. TEMKIN. Zh. Neorg. Khim. **9**, 1502 (1964); Russ. J. Inorg. Chem. **9**, 816 (1964).
110. T. A. MODRO, K. YATES, and J. JANATA. J. Am. Chem. Soc. **97**, 1492 (1975).
111. J. G. DAWBER and P. A. H. WYATT. J. Chem. Soc. 3589 (1960).
112. R. P. BELL, K. N. BASCOMBE, and J. C. MCCOUBREY. J. Chem. Soc. 1286 (1956).
113. H. H. HYMAN, M. KILPATRICK, and J. J. KATZ. J. Am. Chem. Soc. **79**, 3668 (1957).
114. G. DALLINGA, J. GAAF, and E. L. MACKOR. Recl. Trav. Chim. Pays-Bas, **89**, 1068 (1970).
115. A. VAILLANT, J. DEVYNCK, and B. TRÉMILLON. Anal. Lett. **6**, 1095 (1973).
116. H. MÉNARD, J. P. MASSON, J. DEVYNCK, and B. TRÉMILLON. J. Electroanal. Chem. **63**, 163 (1975).
117. D. H. MCDANIEL and L. H. STEINERT. J. Am. Chem. Soc. **88**, 4826 (1966).
118. S. WASIF. J. Chem. Soc. A, 142 (1967).
119. D. P. N. SATCHELL. J. Chem. Soc. 3904 (1958).
120. E. HÖGFELDT and J. BIGELEISEN. J. Am. Chem. Soc. **82**, 15 (1960).
121. J. SIERRA, M. OJEDA, and P. A. H. WYATT. J. Chem. Soc. B, 1570 (1970).
122. R. A. COX, S.-O. LAM, R. A. MCCLELLAND, and T. T. TIDWELL. J. Chem. Soc. Perkin Trans. II, 272 (1979).
123. J. G. DAWBER. J. Chem. Soc. 4111 (1965).
124. M. I. VINNIK, G. B. MANELIS, and N. M. CHIRKOV. Zh. Neorg. Khim. **2**, 1643 (1957); Russ. J. Inorg. Chem. **2**(7), 306 (1957).
125. R. A. COX, U. J. KRULL, M. THOMPSON, and K. YATES. Anal. Chim. Acta, **106**, 51 (1979).
126. J. E. B. RANDLES and J. M. TEDDER. J. Chem. Soc. 1218 (1955).
127. C. EABORN, P. M. JACKSON, and R. TAYLOR. J. Chem. Soc. B, 613 (1966).
128. U. A. SPITZER, T. W. TOONE, and R. STEWART. Can. J. Chem. **54**, 440 (1976).
129. H. BURKETT, R. MURPHY, and D. YARIAN. Proc. Indiana Acad. Sci. **66**, 86 (1956).
130. E. M. SEMENOVA, M. A. TROFIMOV, A. A. PENDIN, and B. P. NIKOL'SKII. Elektrokhimiya, **7**, 1557 (1971); Soviet Electrochem. **7**, 1507 (1971).
131. A. A. PENDIN and YU. S. BRODSKAYA. Zh. Fiz. Khim. **43**, 1512 (1969); Russ. J. Phys. Chem. **43**, 840 (1969).
132. R. STEWART and T. MATHEWS. Can. J. Chem. **38**, 602 (1960).
133. I. M. MEDVETSKAYA, L. R. ANDREEVA, and M. I. VINNIK. Zh. Fiz. Khim. **54**, 2304 (1980); Russ. J. Phys. Chem. **54**, 1313 (1980).
134. E. M. SEMENOVA, S. N. MASLENITSKII, and A. A. PENDIN. Elektrokhimiya, **7**, 1446 (1971); Sovient Electrochem. **7**, 1393 (1971).
135. R. C. PAUL, V. P. KAPILA, R. KUMAR, and S. K. SHARMA. J. Inorg. Nucl. Chem. **43**, 171 (1981).
136. W. HABEL and P. SARTORI. J. Fluorine Chem. **19**, 311 (1982).
137. W. HABEL and P. SARTORI. J. Fluorine Chem. **21**, 351 (1982).
138. P. J. ATKINS, D. J. PALLING, N. L. POON, and C. D. HALL. J. Chem. Soc. Perkin Trans. II, 1107 (1982).
139. S. M. KULIKOV and I. V. KOZHEVNIKOV. Izv. Akad. Nauk SSSR, Ser. Khim. 492 (441 in Eng. Edn.) (1982).
140. B. FLORIS and G. ILLUMINATI. J. Organomet. Chem. **150**, 101 (1978).
141. W. N. WHITE, T. VOGELMANN, M. MORSE, and H. S. WHITE. J. Org. Chem. **42**, 162 (1977).
142. M. SAFTA and G. OSTROGOVICH. Rev. Roum. Chim. **19**, 1621 (1974).
143. A. J. KRESGE and H. J. CHEN. J. Am. Chem. Soc. **94**, 8192 (1972).
144. S. YAMAMOTO, Y. TENNO, and N. NISHIMURA. Aust. J. Chem. **32**, 41 (1979).
145. C. CAPOBIANCO, F. MAGNO, and G. SCORRANO. J. Org. Chem. **44**, 1654 (1979).
146. D. DOLMAN and R. STEWART. Can. J. Chem. **45**, 903 (1967).
147. H. H. JAFFÉ and R. W. GARDNER. J. Am. Chem. Soc. **80**, 319 (1958); S.-J. YEH and H. H. JAFFÉ. J. Am. Chem. Soc. **81**, 3274 (1959).
148. U. QUINTILY, G. SCORRANO, and F. MAGNO. Gazz. Chim. Ital. **111**, 401 (1981).
149. D. S. NOYCE and M. J. JORGENSON. J. Am. Chem. Soc. **83**, 2525 (1961); **84**, 4312 (1962).
150. R. STEWART and F. BANOO. Can. J. Chem. **47**, 3207 (1969).
151. J. ROČEK. Coll. Czech. Chem. Commun. **22**, 1 (1957).
152. Y. OGATA and M. OKANO. J. Am. Chem. Soc. **78**, 5423 (1956).
153. W. N. WHITE and C. A. STOUT. J. Org. Chem. **27**, 2915 (1962).
154. J. MINDL. Coll. Czech. Chem. Commun. **37**, 585 (1972).
155. O. WICHTERLE and P. ČEFELÍN. Coll. Czech. Chem. Commun. **22**, 1083 (1957).
156. V. S. RAO and C. KALIDAS. Bull. Chem. Soc. Jpn. **48**, 2957 (1975).
157. F. BANOO and R. STEWART. Can. J. Chem. **47**, 3199 (1969).
158. K. UNVERFERTH, D. ZSCHIESCHE, and K. SCHWETLICK. Z. Phys. Chem. (Leipzig), **247**, 302 (1971).
159. P. B. TALUKDAR and A. CHAKRABORTY. Indian J. Chem. **11**, 556 (1973).
160. K. YATES and G. WELCH. Can. J. Chem. **50**, 1513 (1972).
161. C. A. BUNTON, N. CARRASCO, and W. E. WATTS. J. Chem. Soc. Perkin Trans. II, 1267 (1979).
162. L. L. LEVESON and C. W. THOMAS. J. Chem. Soc. Perkin Trans. II, 302 (1977).
163. P. VETĚSNÍK, K. ROTHSCHEIN, J. SOCHA, and M. VEČEŘA. Coll. Czech. Chem. Commun. **34**, 1087 (1969); K. ROTHSCHEIN, J. SOCHA, P. VETĚSNÍK, and M. VEČEŘA. Coll. Czech. Chem. Commun. **35**, 3128 (1970).
164. C. W. THOMAS and L. L. LEVESON. J. Chem. Soc. Perkin Trans. II, 20 (1973).
165. C. A. BUNTON, J. B. LEY, A. J. RHIND-TUTT, and C. A. VERNON. J. Chem. Soc. 2327 (1957).
166. D. V. BANTHORPE, E. D. HUGHES, C. INGOLD, and J. ROY. J. Chem. Soc. 3294 (1962).
167. H. DAHN, L. LOEWE, and G. ROTZLER. Chem. Ber. **93**, 1572 (1960).
168. L. L. LEVESON and C. W. THOMAS. J. Chem. Soc. B, 1051 (1969).
169. K. B. WIBERG and R. J. EVANS. J. Am. Chem Soc. **80**, 3019 (1958).
170. M. GODEL, A. JUSSIAUME, and F. COUSSEMANT. Tetrahedron, **29**, 2889 (1973).
171. C. KALIDAS and R. S. PALIT. J. Chem. Soc. 3998 (1961).
172. C. EABORN. J. Chem. Soc. 3148 (1953).
173. J. G. TILLETT and R. C. YOUNG. J. Chem. Soc. B, 209 (1968).
174. B. NÁHLOVSKÝ and V. CHVALOVSKÝ. Coll. Czech. Chem. Commun. **33**, 3122 (1968).
175. D. P. N. SATCHELL. J. Chem. Soc. 2878 (1957); 3524 (1957).
176. S. AZIZ, A. F. COCKERILL, and J. G. TILLETT. J. Chem. Soc. B, 416 (1970).
177. R. KLUGER and J. L. W. CHAN. J. Am. Chem. Soc. **98**, 4913 (1976).
178. W. W. ZAJAC and R. B. NOWICKI. J. Phys. Chem. **69**, 2649 (1965).
179. A. R. BUTLER and A. P. SANDERSON. J. Chem. Soc. B, 2264 (1971).

Can. J. Chem. Downloaded from www.nrcresearchpress.com by 210.87.254.105 on 09/06/12
For personal use only.

180. G. L. CAPEN. Ph. D. Thesis. Illinois Institute of Technology. 1976.
181. R. A. COX and K. YATES. J. Am. Chem. Soc. **100**, 3861 (1978).
182. R. J. GILLESPIE and T. E. PEEL. J. Am. Chem. Soc. **95**, 5173 (1973); J. GRONDIN, R. SAGNES, and A. COMMEYRAS. Bull. Soc. Chim. Fr. 1779 (1976).
183. E. M. ARNETT and C. F. DOUTY. J. Am. Chem. Soc. **86**, 409 (1964); A. G. COOK and G. W. MASON. J. Inorg. Nucl. Chem. **28**, 2579 (1966); J.-C. FISCHER and M. WARTEL. Bull. Soc. Chim. Fr. 3302 (1972).
184. E. HÖGFELDT and P. J. STAPLES. J. Chem. Soc. A, 2074 (1971); A. P. BRYNZA, I. G. VINICHENKO, and R. N. GRISHKO. Zh. Fiz. Khim. **48**, 2477 (1974); Russ. J. Phys. Chem. **48**, 1464 (1974).
185. J. A. DUFFY and M. D. INGRAM. Inorg. Chem. **16**, 2988 (1977); **17**, 2798 (1978); R. D. DYER, R. M. FRONKO, M. D. SCHIAVELLI, and M. D. INGRAM. J. Phys. Chem. **84**, 2338 (1980).
186. N. K. PYATAKINA, YU. V. MOISEEV, and M. I. VINNIK. Zh. Fiz. Khim. **44**, 1985 (1970); Russ. J. Phys. Chem. **44**, 1122 (1970).
187. A. P. BRYNZA, I. G. VINICHENKO, and N. V. PARUSOVA. Zh. Prikl. Khim. (Leningrad), **53**, 1887 (1980).
188. T. YAMANAKA and K. TANABE. J. Phys. Chem. **79**, 2409 (1975); P. RYS and W. J. STEINEGGER. J. Am. Chem. Soc. **101**, 4801 (1979).
189. C. A. BUNTON and L. ROBINSON. J. Phys. Chem. **73**, 4237 (1969); G. MEYER, P. VIOUT, and B. TCHOUBAR. Tetrahedron Lett. 2487 (1974).
190. A. R. TOURKY, A. A. ABDEL-HAMID, and I. Z. SLIM. Z. Phys. Chem. (Leipzig), **250**, 49 (1972); **250**, 61 (1972); J. P. H. BOYER, R. J. P. CORRIOU, R. J. M. PERZ, and C. G. REYE. Tetrahedron, **31**, 2075 (1975).
191. R. I. ZALEWSKI and G. E. DUNN. Can. J. Chem. **46**, 2469 (1968).
192. J. L. JENSEN and A. I. THIBEAULT. J. Org. Chem. **42**, 2168 (1977).
193. S. GERIBALDI, A. GREC-LUCIANO, P.-C. MARIA, and M. AZZARO. J. Chim. Phys. Phys.-Chim. Biol. **79**, 103 (1982).
194. N. C. DENO, P. T. GROVES, and G. SAINES. J. Am. Chem. Soc. **81**, 5790 (1959).
195. G. SCHWARZENBACH and R. SULZBERGER. Helv. Chim. Acta, **27**, 348 (1944).
196. J. T. EDWARD and I. C. WANG. Can. J. Chem. **40**, 399 (1962).
197. J. VERDU and F. PEREDA. An. Quim. **76**, 261 (1980).
198. G. YAGIL. J. Phys. Chem. **71**, 1034 (1967).
199. J.-C. HALLÉ, F. TERRIER, and R. SCHAAL. Bull. Soc. Chim. Fr. 4569 (1969).
200. C. H. ROCHESTER. J. Chem. Soc. B, 1076 (1967).
201. W. J. BOVER and P. ZUMAN. J. Am. Chem. Soc. **95**, 2531 (1973).
202. J. JANATA and J. TAYLOR. J. Chem. Soc. Perkin Trans. II, 356 (1974).
203. J. VERDU and F. PEREDA. An. Quim. **75**, 58 (1979).
204. V. I. LAZAREV and YU. V. MOISEEV. Zh. Fiz. Khim. **39**, 445 (165); Russ. J. Phys. Chem. **39**, 231 (1965).
205. R. STEWART and J. P. O'DONNELL. J. Am. Chem. Soc. **84**, 493 (1962); Can. J. Chem. **42**, 1681 (1964).
206. J. JANATA and R. D. HOLTBY-BROWN. J. Electroanal. Chem. **44**, 137 (1973).
207. K. BOWDEN, A. BUCKLEY, and R. STEWART. J. Am. Chem. Soc. **88**, 947 (1966).
208. T. J. M. POUW and P. ZUMAN. J. Org. Chem. **41**, 1614 1976); T. J. M. POUW, W. J. BOVER, and P. ZUMAN. Adv. Chem. Ser. **155**, 343 (1976).
209. R. CURCI and G. MODENA. Tetrahedron, **26**, 4189 (1970).
210. G. GOUTINES and A. MATHIEU. Analusis, **2**, 584 (1973).
211. E. BUNCEL, E. A. SYMONS, D. DOLMAN, and R. STEWART. Can. J. Chem. **48**, 3354 (1970).
212. C. H. LANGFORD and R. L. BURWELL. J. Am. Chem. Soc. **82**, 1503 (1960); C. H. LANGFORD. Ph. D. Thesis, Northwestern University, 1960.
213. D. DOLMAN and R. STEWART. Can. J. Chem. **45**, 911 (1967).
214. A. ALBAGLI, A. BUCKLEY, A. M. LAST, and R. STEWART. J. Am. Chem. Soc. **95**, 4711 (1973).
215. O. W. KOLLING. Trans. Kans. Acad. Sci. **76**, 193 (1973).
216. R. A. COX and R. STEWART. J. Am. Chem. Soc. **98**, 488 (1976).
217. K. BOWDEN and A. F. COCKERILL. Chem. Commun. 989 (1967); J. Chem. Soc. B, 173 (1970).
218. A. F. COCKERILL and J. E. LAMPER. J. Chem. Soc. B, 503 (1971).
219. R. STEWART and M. G. HARRIS. Can. J. Chem. **55**, 3807 (1977).
220. R. A. COX, R. STEWART, M. J. COOK, A. R. KATRITZKY, and R. D. TACK. Can. J. Chem. **54**, 900 (1976); M. J. COOK, A. R. KATRITZKY, P. LINDA, and R. D. TACK. J. Chem. Soc. Perkin Trans. II, 1080 (1973).
221. J. JANATA and R. D. HOLTBY-BROWN. J. Chem. Soc. Perkin Trans. II, 991 (1973).
222. R. STEWART and J. D. VAN DYKE. Can. J. Chem. **48**, 3961 (1970); **50**, 1992 (1972).
223. K. BOWDEN. Can. J. Chem. **43**, 2624 (1965).
224. K. BOWDEN, R. S. COOK, and M. J. PRICE. J. Chem. Soc. B, 1778 (1971).
225. R. SCHAAL. C. R. Acad. Sci. Paris, **238**, 2156 (1954); J. Chim. Phys. Phys.-Chim. Biol. **52**, 784 (1955); **52**, 796 (1955).
226. C. VERMESSE-JACQUINOT. J. Chim. Phys. Phys.-Chim. Biol. **62**, 235 (1965).
227. N. C. DENO. J. Am. Chem. Soc. **74**, 2039 (1952).
228. R. SCHAAL and P. FAVIER. Bull. Soc. Chim. Fr. 2011 (1959); P. FAVIER and R. SCHAAL. C. R. Acad. Sci. Paris, **249**, 1231 (1959).
229. J.-L. BRISSET, R. GABORIAUD, and R. SCHAAL. J. Chim. Phys. Phys.-Chim. Biol. **67**, 1726 (1970).
230. D. BAUER and P. GAILLOCHET. *In* Chemistry of non-aqueous solvents. Vol. 5A. *Edited by* J. J. Lagowski. Academic Press, New York. 1978. pp. 251–275.
231. F. MASURE and R. SCHAAL. Bull. Soc. Chim. Fr. 1138 (1956).
232. N. CHATTANATHAN and C. KALIDAS. Indian J. Chem. **9**, 169 (1971).
233. K. K. KUNDU and L. AIYAR. J. Chem. Soc. Perkin Trans. II, 715 (1972).
234. H.-M. KOEPP, H. WENDT, and H. STREHLOW. Z. Elektrochem. **64**, 483 (1960).
235. P. HAAKE, R. D. COOK, and G. H. HURST. J. Am. Chem. Soc. **89**, 2650 (1967); R. A. COX and E. BUNCEL. Can. J. Chem. **51**, 3143 (1973); T. J. GILBERT and C. D. JOHNSON. J. Am. Chem. Soc. **96**, 5946 (1974); F. JOÓ and M. T. BECK. Acta Chim. Acad. Sci. Hung. **100**, 421 (1979).
236. K. YATES and R. A. MCCLELLAND. J. Am. Chem. Soc. **89**, 2686 (1967).
237. R. A. COX and E. BUNCEL. J. Am. Chem. Soc. **97**, 1871 (1975).
238. R. H. BOYD. J. Am. Chem. Soc. **85**, 1555 (1963).
239. K. YATES and R. A. MCCLELLAND. J. Am. Chem. Soc. **95**, 3055 (1973).
240. Ü. L. HALDNA and I. A. KOPPEL. Org. React. USSR, **13**, 89 (1976).
241. K. YATES and T. A. MODRO. Acc. Chem. Res. **11**, 190 (1978).
242. R. A. MCCLELLAND, T. A. MODRO, M. F. GOLDMAN, and K. YATES. J. Am. Chem. Soc. **97**, 5223 (1975); T. A. MODRO and K. YATES. J. Am. Chem. Soc. **98**, 4247 (1976); T. A. MODRO, K. YATES, and F. BEAUFAYS. Can. J. Chem. **55**, 3050 (1977); P. WAN, T. A. MODRO, and K. YATES. Can. J. Chem. **58**, 2423 (1980).
243. J. T. EDWARD and S. C. WONG. J. Am. Chem. Soc. **99**, 7224 (1977); J. T. EDWARD, G. D. DERDALL, and S. C. WONG. J. Am. Chem. Soc. **100**, 7023 (1978).

244. J.-M. CARPENTIER and M. B. FLEURY. Bull. Soc. Chim. Fr. 1075 (1976).
245. P. LEMETAIS and J.-M. CARPENTIER. J. Chem. Res. (S), 282 (M), 3369 (1981); J. Chem. Res. (S), 204, (M), 2101 (1982).
246. J. F. BUNNETT and F. P. OLSEN. Can. J. Chem. **44**, 1899 (1966).
247. J. F. BUNNETT and F. P. OLSEN. Can. J. Chem. **44**, 1917 (1966); V. LUCCHINI, G. MODENA, G. SCORRANO, and U. TONELLATO. J. Am. Chem. Soc. **99**, 3387 (1977).
248. A. LEVI, G. MODENA, and G. SCORRANO. J. Am. Chem. Soc. **96**, 6585 (1974); G. SCORRANO and V. LUCCHINI. J. Org. Chem. **44**, 1726 (1979).
249. C. J. GIFFNEY and C. J. O'CONNOR. J. Chem. Soc. Perkin Trans. II, 706 (1975); J. T. EDWARD and S. C. WONG. J. Am. Chem. Soc. **99**, 4229 (1977).
250. N. C. MARZIANO, G. M. CIMINO, and R. C. PASSERINI. J. Chem. Soc. Perkin Trans. II, 1915 (1973).
251. T. J. HANNIGAN and W. J. SPILLANE. J. Chem. Soc. Perkin Trans. II, 851 (1982).
252. N. C. MARZIANO, P. G. TRAVERSO, A. TOMASIN, and R. C. PASSERINI. J. Chem. Soc. Perkin Trans. II, 309 (1977).
253. R. PASSERINI, N. C. MARZIANO, and P. G. TRAVERSO. Gazz. Chim. Ital. **105**, 901 (1975); N. C. MARZIANO, P. G. TRAVERSO, and R. C. PASSERINI. J. Chem. Soc. Perkin Trans. II, 306 (1977).
254. C. PERRIN. J. Am. Chem. Soc. **86**, 256 (1964).
255. N. C. MARZIANO, A. TOMASIN, and P. G. TRAVERSO. J. Chem. Soc. Perkin Trans. II, 1080 (1981).
256. R. A. COX, C. R. SMITH, and K. YATES. Can. J. Chem. **57**, 2952 (1979).
257. R. A. COX, M. F. GOLDMAN, and K. YATES. Can. J. Chem. **57**, 2960 (1979).
258. J. T. EDWARD and S. C. WONG. Can. J. Chem. **57**, 1980 (1979); F. DORION and R. GABORIAUD. J. Chim. Phys. Phys.-Chim. Biol. **77**, 1057 (1980); G. ALBERGHINA, M. E. AMATO, S. FISICHELLA, and S. OCCHIPINTI. J. Chem. Soc. Perkin Trans. II, 1721 (1980); P. J. BATTYE, J. F. CASSIDY, and R. B. MOODIE. J. Chem. Soc. Chem. Commun. 68 (1981).
259. R. A. COX and K. YATES. Can. J. Chem. **59**, 1560 (1981).
260. R. A. COX, L. M. DRUET, A. E. KLAUSNER, T. A. MODRO, P. WAN, and K. YATES. Can. J. Chem. **59**, 1568 (1981).
261. R. A. COX and K. YATES. Can. J. Chem. **57**, 2944 (1979).
262. R. A. COX and K. YATES. Can. J. Chem. **59**, 2853 (1981).
263. R. A. COX and K. YATES. Can. J. Chem. **60**, 3061 (1982).
264. P. G. TRAVERSO, N. C. MARZIANO, and R. C. PASSERINI. J. Chem. Soc. Perkin Trans. II, 845 (1977); N. C. MARZIANO, P. G. TRAVERSO, and G. G. CIMINO. J. Chem. Soc. Perkin Trans. II, 574 (1980).
265. A. SALEH and J. G. TILLETT. J. Chem. Soc. Perkin Trans. II, 132 (1981); Z. SAID and J. G. TILLETT. J. Chem. Soc. Perkin Trans. II, 701 (1982).
266. R. A. COX and K. YATES. Can. J. Chem. In press.
267. J. F. BUNNETT. J. Am. Chem. Soc. **83**, 4956 (1961); **83**, 4968 (1961); **83**, 4973 (1961); **83**, 4978 (1961).
268. K. YATES. Acc. Chem. Res. **4**, 136 (1971).
269. E. B. ROBERTSON and H. B. DUNFORD. J. Am. Chem. Soc. **86**, 5080 (1964).
270. Ü. L. HALDNA and H. J. KUUS. Org. React. USSR, **16**, 5 (1979); Ü. L. HALDNA. Org. React. USSR; **16**, 129 (1979); **17**, 233 (1980).
271. Ü. L. HALDNA, I. A. KOPPEL, and H. J. KUURA. Org. React. USSR, **14**, 235 (1977); **15**, 11 (1978).
272. V. LUCCHINI, G. MODENA, G. SCORRANO, R. A. COX, and K. YATES. J. Am. Chem. Soc. **104**, 1958 (1982).
273. J.-M. CARPENTIER and P. LEMETAIS. Bull. Soc. Chim. Fr. 553 (1975).
274. R. A. COX. J. Am. Chem. Soc. **96**, 1059 (1974).
275. R. A. COX, Ü. L. HALDNA, K. L. IDLER, and K. YATES. Can. J. Chem. **59**, 2591 (1981).
276. R. A. COX, A. J. DOLENKO, and E. BUNCEL. J. Chem. Soc. Perkin Trans. II, 471 (1975).
277. D. J. KROEGER and R. STEWART. J. Chem. Soc. B, 217 (1970); R. A. MORE O'FERRALL. J. Chem. Soc. Perkin Trans. II, 976 (1972).
278. M. M. KREEVOY and E. H. BAUGHMAN. J. Am. Chem. Soc. **95**, 8178 (1973).
279. J. F. WOJCIK. J. Phys. Chem. **86**, 145 (1982).
280. J. T. EDWARD, M. SJÖSTRÖM, and S. WOLD. Can. J. Chem. **59**, 2350 (1981).
281. J.-C. HALLÉ, F. TERRIER, and R. SCHAAL. Bull. Soc. Chim. Fr. 1225 (1973); J.-C. HALLÉ. Bull. Soc. Chim. Fr. 1553 (1973); J. T. EDWARD, P. G. FARRELL, J. KIRCHNEROVA, J.-C. HALLÉ, and R. SCHAAL. Can. J. Chem. **54**, 1899 (1976).
282. R. GABORIAUD, J.-C. HALLÉ, and P. LETELLIER. Bull. Soc. Chim. Fr. 1093 (1976).

Can. J. Chem. Downloaded from www.nrcresearchpress.com by 210.87.254.105 on 09/06/12
For personal use only.

The molecular conformations of the stereoisomers of 4-methyl-5,6-benzo-2-oxo-1,3,2-dioxathiepin and of the 4,7-dimethyl derivative

A. LACHAPELLE AND M. ST-JACQUES[1]

Département de Chimie, Université de Montréal, C.P. 6210, Succ. A., Montréal (Qué.), Canada H3C 3V1

AND

A. C. GUIMARAES AND P. DE ALMEIDA

Departamento de Quimica, Universidade Federal de Minas Gerais, Cidade Universitaria – Pampulha, 30 000 Belo Horizonte, Brazil

Received February 17, 1983

A. LACHAPELLE, M. ST-JACQUES, A. C. GUIMARAES, and P. DE ALMEIDA. Can. J. Chem. **61**, 2244 (1983).

The conformational and dynamic properties of the stereoisomers of 4-methyl-5,6-benzo-2-oxo-1,3,2-dioxathiepin (**5**) and of the 4,7-dimethyl derivative (**6**) have been investigated by ^1H and ^{13}C dnmr methods, as well as by ir spectroscopy. Analysis of the nmr spectra at low temperature (−125°C), together with the conformational interpretation of the stretching vibration bands of the S=O bond in the ir spectra, indicate that the most stable conformations detected for solutions in CHF_2Cl are *C*-a (82%) and *TB*-*t*-Me_e (18%) for **5***a*, *TB*-*c*-Me_e (96%) and *TB*-*c*-Me_a (4%) for **5***b*, *C*-a for **6***a*, *TB*-*t*-Me_e, *c*-Me_e for **6***b* and *C*-e for **6***c*. The substituent effects of a methyl group at the benzylic position on both the conformational and dynamic properties of the seven-membered sulfite are discussed.

A. LACHAPELLE, M. ST-JACQUES, A. C. GUIMARAES et P. DE ALMEIDA. Can. J. Chem. **61**, 2244 (1983).

Les propriétés dynamiques et conformationnelles des stéréoisomères de la méthyl-4 benzo-5,6 oxo-2 dioxa-1,3,2 thiépine (**5**) et du dérivé diméthyl-4,7 ont été étudiées à l'aide des méthodes de rmn dynamique du ^1H et du ^{13}C ainsi que de la spectroscopie ir. L'analyse des spectres de rmn à basse température (−125°C), de concert avec l'interprétation conformationnelle des bandes de vibration d'élongation de la liaison S=O observées sur les spectres ir, indique que les conformations les plus stables en solution dans le CHF_2Cl sont *C*-a (82%) et *TB*-*t*-Me_e (18%) pour le composé **5***a*, *TB*-*c*-Me_e (96%) et *TB*-*c*-Me_a (4%) pour le composé **5***b*, *C*-a pour le composé **6***a*, *TB*-*t*-Me_e, *c*-Me_e pour le composé **6***b* et *C*-e pour le composé **6***c*. Les effets d'un ou deux groupes méthyles en position benzylique sur les propriétés dynamiques et conformationnelles des sulfites à sept chaînons sont discutés.

Introduction

Sulfites (**1**) have drawn particular attention over the years owing to the stereochemical rigidity of the pyramidal S atom. But while 5- and 6-membered sulfites have been extensively investigated by numerous techniques (ir (2–4), ^1H and ^{13}C nmr (1, 2, 5–12), dipolar moments measurements (7)), only a few studies of the larger cyclic molecules have been reported (13–16).

It is now well known that 2-oxo-1,3,2-dioxathiane (**1**) exists exclusively in the chair form (17), with the S=O bond axially oriented; furthermore, this *C*-a form has been estimated to be about 2–3 kcal/mol more stable than the equatorial form (*C*-e) in CCl_4 (18). While many reports (7, 19–21) have shown that the *C*-a form is the only one observed for *trans*-4-methyl-2-oxo-1,3,2-dioxathiane (**2**), the conformational assignment for *cis*-4-methyl-2-oxo-1,3,2-dioxathiane (**3**) has been the subject of much debate (18, 21, 22) during the last decade. Recently, Cazaux *et al.* (23), using nmr and ir techniques as well as dipolar moments calculations, proposed that **3** exists as a rapidly equilibrating mixture of *C*-a (**3***a*), *C*-e (**3***b*), and two twist forms (*TOA*-**3***c* and *TS*-**3***d*) at room temperature. On the other hand, recent reports by Pihlaja and co-workers (4) question the reliability of the ir method for identifying the existence of twist forms, and the authors interpret experimental data uniquely in terms of **3***a* and **3***b*.

Seven-membered cyclic sulfites, such as **4** and its methyl derivatives, in principle provide a better model to study the properties of twist forms because, contrary to six-membered cyclic sulfites, there can be only one *TB* ring geometry. Recent (24) ir and ^1H and ^{13}C dynamic nmr results for **4** showed the existence of a 1:1 mixture of *C*-a and *TB* in CHF_2Cl at −100°C. That result, although consistent with the fact that dipole–dipole interactions and stereoelectronic back-donation should disfavor *C*-e relative to *C*-a and *TB*, is in marked contrast with the absence of a conformational equilibrium noted for trimethylene sulfite (**1**).

Our interest in seven-membered cyclic molecules, combined with the uncertainty for *cis*-4-methyl-2-oxo-1,3,2-dioxathiane (**3**), led us to investigate the conformational dynamics

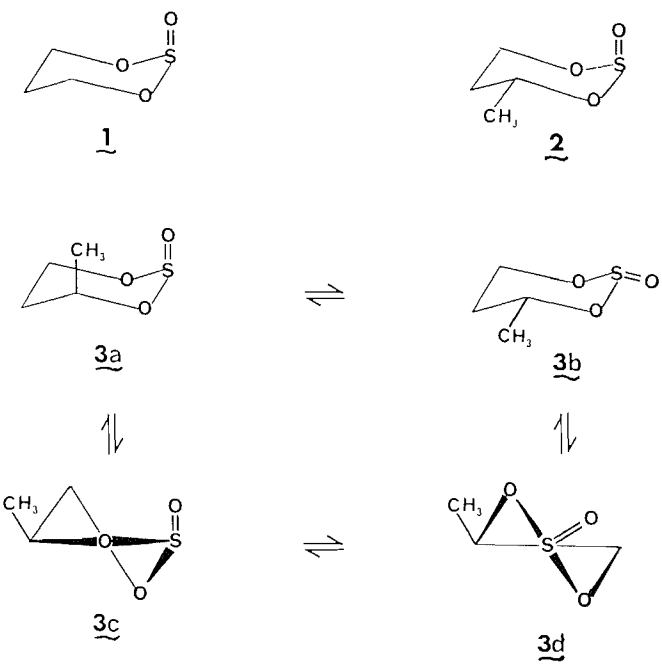

[1]Author to whom correspondence should be addressed.

Can. J. Chem. Downloaded from www.nrcresearchpress.com by 210.87.254.42 on 09/06/12
For personal use only.

TABLE 1. Infrared spectral description of the S=O stretching band in compounds **4**, **5***a*, **5***b*, **6***a*–**6***b*, and **6***c* in different solvents

Compound	Solvent	ν_s = 0 stretching band (cm^{-1})	Relative integration
4	CCl_4[a]	1220(s); 1184(s)	45:55
	CH_3CN[a]	1210(s); 1179(s)	55:45
	CS_2	1223(s); 1184(s)	46:54
5*a*	CCl_4	1225(m); 1186(s)	25:75
	CH_3CN	1218(m); 1184(s)	35:65
5*b*	CCl_4	1226(s)	100
	CH_3CN	1215(s)	100
6*a*–**6***b*	CCl_4	1223(s) and 1221(s);[b] 1187(m)	90:10
	CH_3CN	1212(s) and 1209(s);[b] 1183(m)	90:10
6*c*	CS_2	1240(s); 1225(s)	41:59
	CH_3CN	1231(s) and 1220(s)[b]	~100

[a] Taken from refs. 23 and 24.
[b] The two preceding values represent the individual components of a split band (23) whose center is considered in the text.

properties of *trans*-4-methyl-2-oxo-1,3,2-benzodioxathiepin[2] (**5***a*), *cis*-4-methyl-2-oxo-1,3,2-benzodioxathiepin (**5***b*), *trans,trans*-4,7-dimethyl-2-oxo-1,3,2-benzodioxathiepin (**6***a*), *cis,trans*-4,7-dimethyl-2-oxo-1,3,2-benzodioxathiepin (**6***b*), and *cis,cis*-4,7-dimethyl-2-oxo-1,3,2-benzodioxathiepin (**6***c*) using ir and ^1H and ^{13}C dynamic nmr. Our observations, in addition to characterizing the effects of methyl substitution on the ring conformation of the seven-membered sulfite, confirm the utility of the combined ir–dnmr approach.

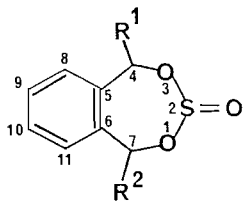

4 $R^1=R^2=H$
5a $R^1=CH_3, R^2=H$ (trans)
5b $R^1=CH_3, R^2=H$ (cis)
6a $R^1=CH_3, R^2=CH_3$ (trans,trans)
6b $R^1=CH_3, R^2=CH_3$ (cis,trans)
6c $R^1=CH_3, R^2=CH_3$ (cis,cis)

Results

Sulfites **5***a* and **5***b* were prepared from the reaction of α-methyl-*o*-xylene-α,α′-diol and thionyl chloride; after separation they were first identified by comparison with dipole moments of the six-membered sulfite analogs (21) (the *trans* isomer being less polar (μ = 3.25 D in CCl_4) than the *cis* isomer (μ = 4.66 D in CCl_4) in that series). The first compound isolated from an hplc run is therefore considered as the *trans*-isomer (**5***a*), while the second compound eluted is the *cis*-isomer (**5***b*). The interpretation of the spectroscopic data that follows confirms this assignment.

Sulfites **6***a*, **6***b*, and **6***c* were obtained in a two-step synthesis involving: (1) a Grignard reaction with methylmagnesium iodide on benzene-1,2-dicarboxaldehyde to yield α,α′-dimethyl-*o*-xylene-α,α′-diol and (2) a reaction with thionyl chloride. As was the case for isomers **5***a* and **5***b*, isomers **6***a*, **6***b*, and **6***c* were first identified by comparison with the dipolar moments of the 4,6-dimethyl-2-oxo-1,3,2-dioxathiane isomeric analogs for which the *trans,trans* and *cis-trans* isomers have very similar polarity (μ = 3.51 D and 3.93 D respectively, in CCl_4) (21), while the *cis,cis* isomer is much more polar (μ = 5.31 D in CCl_4) (21). This trend was reflected on the hplc chromatogram. The product mixture, on separation, first gave a substance consisting of a mixture of two isomers tentatively identified as the *trans,trans* (**6***a*) and *cis,trans* (**6***b*) isomers, and then a third compound, identified as the *cis,cis* isomer (**6***c*). The isomeric mixture of **6***a* and **6***b* was used without further separation for the spectroscopic investigations because several attempts to separate them were not successful. Spectroscopic data presented later confirm this assignment.

[2] The terms *trans* and *cis* define here the relationship between the methyl group(s) and the S=O bond orientation.

Infrared spectra

The ir spectra of 0.05 *M* solutions of compounds **5***a*, **5***b*, and of the isomeric mixture **6***a*–**6***b*, recorded in CCl_4 and in CH_3CN, showed stretching vibrations for the S=O bond in the 1175–1260 cm^{-1} region, as reported in Table 1. Compound **5***a* showed two bands of unequal intensity in both solvents: the most intense band at 1186 cm^{-1} (s) and the other at 1225 cm^{-1} (m) in CCl_4 integrated for 75:25 respectively. In CH_3CN the two bands shifted to 1184 cm^{-1} (s) and 1218 cm^{-1} (m), integrating for 65:35 respectively. Compound **5***b*, on the other hand, showed only one band, both in CCl_4 (1226 cm^{-1}) and in CH_3CN (1215 cm^{-1}). The mixture **6***a*–**6***b* showed a slightly split band centered at 1222 cm^{-1} (s) (i.e. 1223 cm^{-1} and 1221 cm^{-1}) and a less intense band at 1187 cm^{-1} (m) in CCl_4. In CH_3CN the spectrum revealed a slightly split band centered at 1211 cm^{-1} (s) (i.e. 1212 cm^{-1} and 1209 cm^{-1}) and a band at 1183 cm^{-1} (m).

Because of solubility problems, the ir spectra of compound **6***c* were taken as a 0.001 *M* solution in CS_2 instead of CCl_4 and as a 0.01 *M* solution in CH_3CN. The spectrum in CS_2 showed two bands of unequal intensity, one at 1240 cm^{-1} and the other at 1225 cm^{-1}, integrating for 41:59 respectively. The spectrum in CH_3CN, on the other hand, showed only one split band centered at 1225 cm^{-1} (i.e. 1231 cm^{-1} and 1220 cm^{-1}). The very small trough between these two maxima supports the description as a split band (3). The ir spectrum of **4** was taken in CS_2 for reference purposes. Table 1 contains a summary of the ir results.

Can. J. Chem. Downloaded from www.nrcresearchpress.com by 210.87.254.42 on 09/06/12
For personal use only.

Can. J. Chem. Downloaded from www.nrcresearchpress.com by 210.87.254.42 on 09/06/12
For personal use only.

Nuclear magnetic resonance spectra

^1H (400 MHz) and ^{13}C (100.62 MHz) nuclear magnetic resonance spectra of compounds **5***a*, **5***b*, and of the isomeric mixture **6***a*–**6***b* were taken at different temperatures in the range −10° to −135°C. The ^1H spectra of compound **6***c* were also studied at different temperatures, whereas the ^{13}C spectra could be taken only at room temperature in $CDCl_3$, owing to solubility problems.

Compound **5***a* showed a spectral modification in both the ^1H and ^{13}C spectra in CHF_2Cl at low temperatures, as illustrated in Fig. 1. The ^{13}C spectra at −10°C show nine well-resolved signals (chemical shifts are given in Table 2) which were identified by substituent effects and off-resonance decoupling. At −125°C, each signal has split into a doublet of unequal intensity (82:18; the taller signals are labelled "c" while the smaller ones are labelled "b"). A free energy of activation of about 8.6 kcal/mol was estimated at −80°C (T_c) using standard equations and a transmission coefficient of 1.

The ^1H spectrum of **5***a* at −10°C (a summary of ^1H nmr parameters is given in Table 3) shows an AB pattern for the C-7 methylene protons, a quartet for the C-4 methine proton, and a doublet for the methyl protons. All signals broadened on lowering the temperature and the modified spectrum at −125°C shows a major set of signals (labelled "c", in accordance with the convention established in the ^{13}C spectra), consisting of an AB pattern, a quartet, and a doublet; the observed set of minor signals is labelled "b" and also consists of an AB pattern, a quartet, and a doublet.

The ^{13}C spectrum of compound **5***b* at −10°C also shows nine well-resolved signals which were identified by the same procedure as for those of **5***a* (Table 2). All signals broadened and split at low temperature so that, at −125°C, doublets of very unequal intensity are observed, the most intense lines accounting for 96% of the total spectrum (the minor components of quaternary C-5 and C-6 could, however, not be observed). A free energy of activation of about 8.9 kcal/mol was estimated at −85°C (T_c), using standard equations and a transmission coefficient of 1. The ^1H spectrum of **5***b* at −10°C (Table 3) shows, like that of **5***a*, an AB pattern for the C-7 methylene protons, a quartet for the C-4 methine proton, and a doublet for the methyl protons. All signals broadened at lower temperature, but no ^1H spectral splitting was observed down to −135°C.

The ^{13}C nmr spectrum of the isomeric mixture **6***a*–**6***b* at −10°C (Table 2) revealed the presence of fifteen signals which, through intensity consideration, were separated into two sets and assigned with the help of off-resonance decoupling. The major set consists of 10 lines: two quaternary aromatic carbons, four protonated aromatic carbons, two tertiary aliphatic carbons, and two methyl carbons. The minor set consists of 5 lines: one quaternary aromatic carbon, two protonated aromatic carbons, one tertiary aliphatic carbon, and one methyl carbon. No spectral change was observed down to −135°C. The ^1H spectrum of the same isomeric mixture, at −10°C (Table 3), also revealed two sets of aliphatic signals, a major set consisting of two quartets (methine protons) and two doublets (methyl protons) and a minor set consisting of only one quartet and one doublet. Again, at lower temperature, no spectral change was observed down to −135°C.

The ^{13}C spectrum of compound **6***c* (Table 2), as discussed earlier, was taken only at 25°C in $CDCl_3$: it showed five signals, which were readily identified by an off-resonance experiment. The ^1H spectrum of **6***c* in CHF_2Cl (Table 3), at −15°C, revealed, besides the aromatic resonances, one quartet (methine protons) and one doublet (methyl protons) which did not split further down to −135°C.

Discussion

Ring conformations from infrared spectra

Extensive ir investigation of the six-membered cyclic sulfites has led to the proposal that specific frequency domains are characteristic of each of the three possible arrangements (axial, equatorial, or isoclinal) of the sulfite moiety when molecular association effects are negligible, as is the case for concentrations of 0.05 *M* or less (3). Recent ir work (24) on compound **4** showed that these conformational frequency domains still hold for 7-membered cyclic sulfites. Thus, the straightforward observation of the S=O stretching bands for the isomeric compounds **5***a* and **5***b*, as well as for **6***a*, **6***b*, and **6***c*, could potentially identify the sulfite bond arrangement and thereby provide information on the different ring conformations present in solution.

The ir spectra of **5***a* (*trans* isomer) reveal two bands in both CCl_4 and CH_3CN, as summarized in Table 1. The more intense band (75%) at 1186 cm^{-1} is characteristic of an axially oriented S=O moiety and compatible with the *C*-a form because the axial boat form (*B*-a) can be excluded by the results (24) on **4**. The less intense band (25%) at 1225 cm^{-1} indicates the presence of the *TB* form. The induced solvent shifts of 2 cm^{-1} for the *C*-a band and of 7 cm^{-1} for the *TB* band, on going from CCl_4 to CH_3CN, are similar to those observed for six-membered cyclic sulfites (23) and for the parent compound **4**. Furthermore, the slight increase in amount of *TB* (Table 1) in the more polar solvent is expected since *TB* is more polar than *C*-a (24).

The fact that the ir spectra of **5***b* (*cis* isomer) reveal the existence of only one band at 1226 cm^{-1} in CCl_4 and 1215 cm^{-1} in CH_3CN is compatible with the existence of a *TB* form as the predominant or sole conformation.

Band assignment in the ir spectra of the mixture of compounds **6***a*–**6***b* made use of the integration results obtained from the ^1H and ^{13}C nmr spectra for the same mixture of isomers, as discussed later in the text. Thus, the more intense slightly split band centered at 1222 cm^{-1} in CCl_4 and at 1211 cm^{-1} in CH_3CN was assigned to the *cis*–*trans* isomer (**6***b*). These values, together with the solvent-induced shift of 11 cm^{-1}, suggest that the ring of this compound adopts a *TB* geometry. The absence of symmetry for this isomer is explicit in the ^{13}C nmr spectra discussed later. The less intense band at 1187 cm^{-1} in CCl_4 and at 1183 cm^{-1} in CH_3CN could then be attributed to the *C*-a form of the *trans*–*trans* isomer (**6***a*); the small solvent-induced shift of 4 cm^{-1} confirms that deduction. The presence of symmetry for this isomeric conformation is confirmed by the ^{13}C nmr spectrum which shows only half as many lines as that of **6***b*.

Because the ir spectrum of **6***c* could not be recorded in CCl_4, CS_2 was chosen as a replacement solvent of low polarity and compound **4** was used as reference to establish the characteristic *C*-a and *TB* S=O band. Thus, the CS_2 the spectrum of **4** showed two bands at 1223 cm^{-1} and 1184 cm^{-1} which compare well with values observed in CCl_4 (1220 cm^{-1} and 1184 cm^{-1}) for the *TB* and *C*-a forms (24).

The ir spectrum of **6***c* in CS_2 showed two bands at 1240 cm^{-1} and 1225 cm^{-1} in the ratio 41:59 respectively. Thus, the band at 1225 cm^{-1} suggests a *TB* ring geometry while the band at 1240 cm^{-1} (not detected in compounds **5***a* and **5***b*) falls well within the frequency domain (1242 ± 2 cm^{-1}) attributed to the

Can. J. Chem. Downloaded from www.nrcresearchpress.com by 210.87.254.42 on 09/06/12
For personal use only.

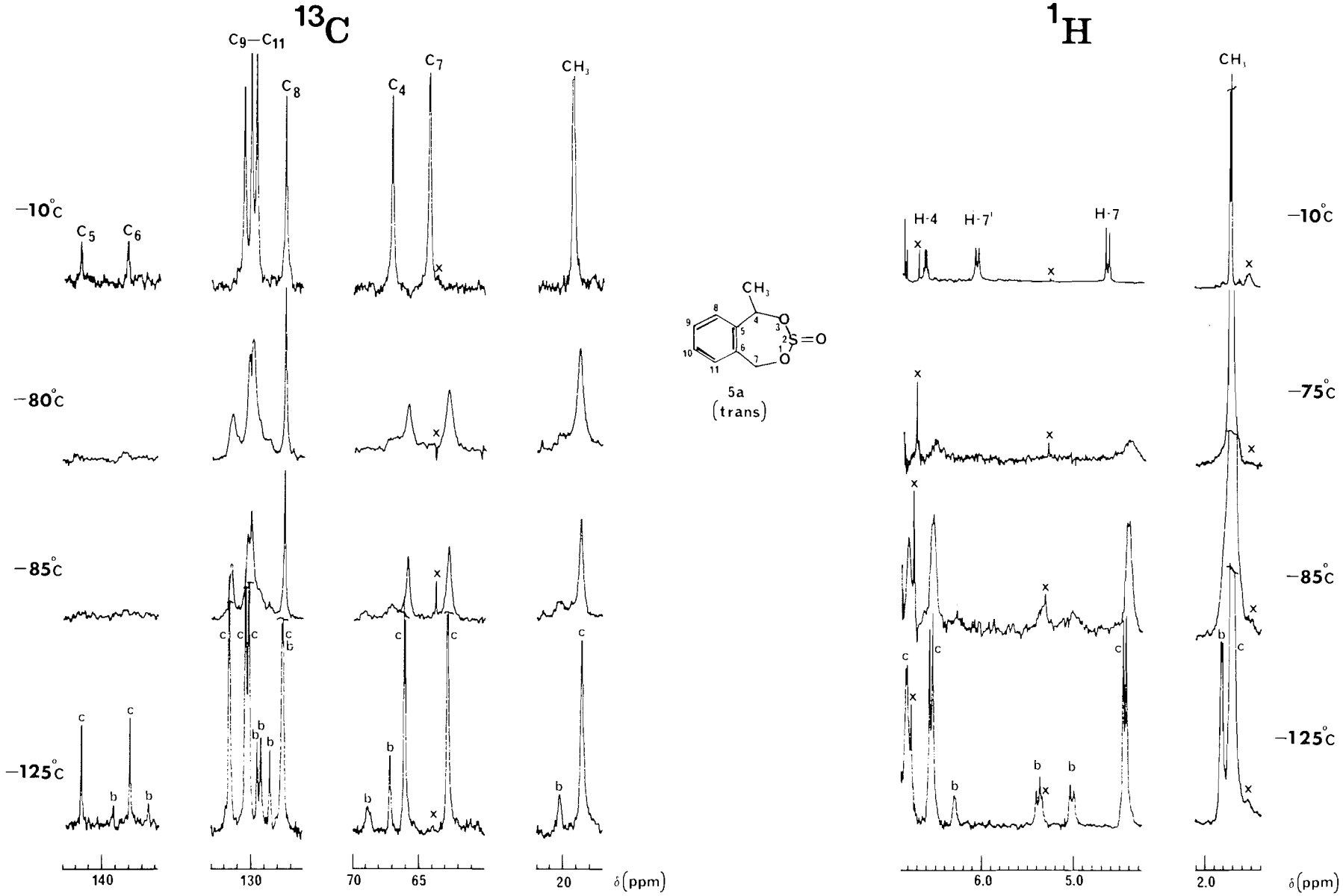

FIG. 1. Partial 100.62 MHz ^{13}C nmr (left-hand side) and 400 MHz ^{1}H nmr (right-hand side) spectra of **5***a* in CHF_2Cl at several temperatures. The meaning of the letters b and c is given in the text. Small impurity signals are denoted by x.

TABLE 2. Carbon-13 chemical shift and dynamic data for compounds **5***a*, **5***b*, **6***a*–**6***b*, and **6***c* at high and low temperatures[a]

Compound	Temperature (°C)	C-4 (ppm)	C-5 (ppm)	C-6 (ppm)	C-7 (ppm)	C-8 (ppm)	C-9–C-11 (ppm)	CH_3 (ppm)	$\Delta G^{\ddagger}$ kcal/mol
5*a*	−10	66.99	141.71	138.19	64.18	127.33	130.48, 129.56	19.84	
	(CH)	(CH)			(CH_2)		127.83		
5*a*	−125	66.07(c)[b]	141.63(c)	137.96(c)	62.79(c)	127.50(c)	131.58(c), 130.34(c)	18.59(c)	
							130.16(c)		8.6
		68.84(b)	139.44(b)	136.70(b)	67.19(b)	127.5(b)	129.45(b), 129.18(b)	20.28(b)	(−80°C)
							128.50(b)		
5*b*	−10	71.68	140.84	135.87	64.10	127.43	129.53 129.12	20.51	
		(CH)			(CH_2)		128.77		
5*b*	−125	71.70[c]	140.70	135.30	63.91	127.70	129.54 129.13	20.38	
							128.74		8.9
		71.21	—	—	66.58	127.09	131.48 131.05	18.68	(−85°C)
							130.70		
6*a*–**6***b*	−10	65.92[d]	141.66	141.66	65.92	127.28	127.28 129.72	19.20	
							129.72		
		72.29	141.39	140.38	68.74	127.38	129.24 129.20	21.10	
						127.65		20.71	
6*a*–**6***b*	−125	65.55[d]	—	—	65.55	127.40	127.40 130.03	18.69	
		72.12	141.00	139.57	68.60	127.61	129.29 129.45	20.86	
						127.87		20.51	
6*c*	25	70.92	138.15	138.15	70.92	126.13	126.13, 128.77, 128.77	20.15	

[a]The spectra were recorded at 100.62 MHz in CHF_2Cl with internal TMS.
[b]The letters (c) and (b) identify signals of different conformations as explained in the text and shown in Fig. 1. The c/b ratio at −125°C is 82:18.
[c]The first row of chemical shifts refers to the most intense set of signals.
[d]The first row of chemical shifts refers to the less intense set of signals.

TABLE 3. ^1H nuclear magnetic resonance spectral parameters of the benzylic and of the methyl protons for compounds **5***a*, **5***b*, **6***a*–**6***b*, and **6***c* at high and low temperatures[a]

Compound	Temperatures °C	δ H-4 (ppm)	δ H-7 (ppm)	δ H-7 (ppm)	$2J_{77'}$ (Hz)	δ CH_3 (ppm)
5*a*	−10	6.61	4.64	6.06	−14.2	1.71
5*a*	−125	6.81(c)[b]	4.46(c)	6.66(c)	−13.7	1.72(c)
		6.32(b)	5.01(b)	5.38(b)	—	1.83(b)
5*b*	−10	5.51	4.71	6.04	−14.4	1.80
5*b*	−125	5.51	4.77	6.10	−14.6	1.85
6*a*–**6***b*	−10		6.71[c]			1.71[c]
			5.50 6.32		—	1.80 1.84
6*a*–**6***b*	−125		6.73[c]			1.70[c]
			5.53 6.36		—	1.79 1.82
6*c*	−15		5.90		—	1.84
6*c*	−125		5.82		—	1.88

[a]The spectra were taken at 400 MHz with TMS as internal reference.
[b]The labels b and c are defined in the text; the ratio of c/b at −125°C is 82:18.
[c]The first row of chemical shifts refers to the less intense set of signals.

C-e form in the six-membered sulfites (23). Furthermore, the ir spectra of **6***c* in CH_3CN showed only a single split band centered at 1225 cm^{-1}, which suggests a shift in equilibrium towards a single *C*-e form. This tentative conclusion is corroborated by the large induced solvent shift of 15 cm^{-1} on going from CS_2 to CH_3CN, which is comparable to values commonly observed for the *C*-e form in six-membered cyclic sulfites, on going from CCl_4 to CH_3CN (23), and by the fact that the population of the more polar conformer (*C*-e form) increases on going from a less polar CS_2 solvent (41%) to a more polar CH_3CN solvent (~100%).

Although the analysis of the ir spectra provides valuable information on the ring geometry, it is of little value to locate the methyl groups which, as molecular models show, can adopt two different positions in the *TB* forms of **5***a*, **5***b*, and **6***b*, namely a pseudo-equatorial or axial position as shown in structures **7** (*TB*-*t*-Me_e) and **8** (*TB*-*t*-Me_a) for compound **5***a*, structures **9** (*TB*-*c*-Me_e) and **10** (*TB*-*c*-Me_a) for compound **5***b*, and structures **11** (*TB*-*t*-Me_e, *c*-Me_e) and **12** (*TB*-*t*-Me_a, *c*-Me_a) for compound **6***b*. (The letters *c* and *t* refer to *cis* and *trans* while a and e after Me refer to pseudoaxial and pseudoequatorial positions for the methyl groups.) Fortunately, ^1H and ^{13}C nmr parameters can give information on the methyl group orientation which is required to distinguish between the two possible

Can. J. Chem. Downloaded from www.nrcresearchpress.com by 210.87.254.42 on 09/06/12
For personal use only.

TB conformers for each of these three compounds, as discussed next. Furthermore, the nmr data provide confirmation for the ring conformations deduced tentatively above from the ir data.

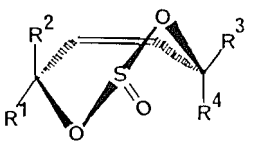

7 $R^3=CH_3, R^1=R^2=R^4=H$ (TB-t-Me_e)
8 $R^2=CH_3, R^1=R^3=R^4=H$ (TB-t-Me_a)
9 $R^1=CH_3, R^2=R^3=R^4=H$ (TB-c-Me_e)
10 $R^4=CH_3, R^1=R^2=R^3=H$ (TB-c-Me_a)
11 $R^1=R^3=CH_3, R^2=R^4=H$ (TB-t-Me_e, c-Me_e)
12 $R^2=R^4=CH_3, R^1=R^3=H$ (TB-t-Me_a, c-Me_a)

Methyl orientation from ^1H nuclear magnetic resonance spectra

The variable temperature 400 MHz ^1H nmr spectra of compound **5***a* (*trans* isomer) revealed only one spectral modification in the temperature range of −10° to −135°C, as shown in Fig. 1. Thus, the existence of two conformations of unequal populations, corresponding to the b and c signals, is indicated. Assuming that the $C \rightleftharpoons TB$ interconversion process is responsible for the spectral change (24), then distinct ^1H signals should be observed for a chair and *TB* forms at −125°C. The more intense AB pattern of the H-7 methylene protons (labelled c in Fig. 1), with a chemical shift difference of 2.2 ppm, identifies the *C*-a form because of the well-known anisotropic chemical shift effect of the axial S=O bond which strongly deshields the *syn*-1,3-axial proton relative to the equatorial one (8, 11). This effect, though, is more severe in the *C*-a form of **5***a* than in the *C*-a form of 2-oxo-1,3,2-dioxathiane (**1**) because of the greater puckering of the seven-membered cyclic sulfite. The quartet at 6.81 ppm can be ascribed to the axial H-4, in agreement with the fact that the axial S=O anisotropy effect should also deshield this proton somewhat comparably to the axial H-7 (6.66 ppm).

Interpretation of the ^1H nmr signals of the *TB* conformer of **5***a*, however, is not as straightforward. Firstly, our inability to slow down the pseudorotation process of the *TB* conformers at −135°C suggests two possibilities: (a) the existence of one predominant *TB* form (**7** or **8**) or (b) the existence of a mixture of **7** and **8** in rapid equilibrium at −135°C. Fortunately, closer examination of the ^1H chemical shifts leads to further insight into this question. The ^1H spectrum at −125°C (Fig. 1) shows a minor AB pattern labelled b (δ_A = 5.38 and δ_B = 5.01), showing a chemical shift difference of only 0.37 ppm. Results reported (24) for the *TB* form of the parent compound **4** show that the AB pattern of the CH_2 group *syn* to the S=O bond has a proton chemical shift difference of 1.2 ppm which is reduced to 0.3 ppm for the CH_2 group *anti* to the S=O bond. The result for **5***a* therefore suggests a predominant *TB* form of structure **7** (*TB*-*t*-Me_e) for which the methylene group is *anti* to the S=O bond. Molecular models of **7** reveal that the axial methine proton (H-4) should be well deshielded by the anisotropic effects of the S=O moiety and the presence of a broadened quartet at 6.32 ppm is clearly due to its axial-like position. It therefore appears that **7** is the predominant conformation for **5***a* although a minor amount of conformer **8** cannot be rigorously ruled out.

A similar analysis of the ^1H spectral data at −125°C for compound **5***b* (*cis*-isomer) shows a large chemical shift difference (Δ = 1.33 ppm) for the H-7 methylene protons, which correlated well with the chemical shift difference (Δ = 1.2 ppm) observed for the CH_2 group *syn* to the S=O bond in the *TB* form of **4**. It is significant that the methine proton (H-4) of **5***b* is less deshielded (5.51 ppm) than the methine proton of the *TB* form **7** of compound **5***a* (6.32 ppm). Thus H-4 in **5***b* cannot be axial-like and *syn* to the S=O bond. These parameters are therefore compatible with the *TB* form **9** as the predominant conformation of **5***b* in which H-4 is axial but *anti* to S=O.

The ^{13}C spectra confirm the above conclusions for **5***a* and **5***b*. In addition, the low temperature spectrum of **5***b* reveals the existence of another minor *TB* form as discussed later.

Finally, it should be noted that the orientation of the S=O bond in the *TB* forms **7** and **9** seems to have little influence on the ^1H chemical shifts of the equatorial methyl groups (1.83 ppm in conformation **7** and 1.85 in conformation **9**).

Conclusions derived from the ^1H spectra of monomethylated compounds **5***a* and **5***b* are useful to interpret the proton spectra of compounds **6***a*, **6***b*, and **6***c*. Firstly, the invariance of the ^1H spectra of the mixture of isomers **6***a*–**6***b* suggests either the presence of a single conformer for each isomer in the temperature range studied or the existence for each isomer of a very rapid equilibrium between two or more different conformers. The following analysis is compatible with single conformations for each of **6***a* and **6***b*.

Examination of the ^1H spectra at −125°C for the isomeric mixture **6***a*–**6***b* revealed two sets of signals of unequal intensities (Table 3). The minor set of signals (~10% of the intensity), consisting of a well-deshielded quartet (methine proton signal somewhat broadened by viscosity increase) at 6.73 ppm and of a doublet (methyl protons) at 1.70 ppm, exhibits chemical shifts similar to those of the *C*-a form of **5***a* for which the methine proton is at 6.81 ppm and the methyl protons is at 1.72 ppm. The ^1H nmr results therefore support the earlier ir suggestion that **6***a* existed solely under the *C*-a form. The plane of symmetry passing through the S=O bond of the *C*-a form explains the degenerated methine and methyl signals.

The major set of signals belonging to **6***b* (about 90% of the intensity), on the other hand, consists of two quartets and two doublets, indicating a non-symmetrical conformation for **6***b*. Furthermore, the relative integration of the major and the minor set of signals gives the same results as were determined from the two S=O bands in the ir spectrum in CCl_4 (Table 1). It therefore appears that the signals of **6***b* ought to correspond to a non-symmetrical *TB* conformation. The ^1H chemical shifts at −125°C support this ring conformation and provide information on the position of the methyl group. The quartet (methine proton) at 5.53 ppm is close to the methine proton of the *anti* carbon in the *TB*-*c*-Me_e form (**9**) of compound **5***b* (5.51 ppm), while the other quartet at 6.36 ppm has a chemical shift very similar to that of the methine proton of the *TB*-*t*-Me_e form (**7**) of compound **5***a* (6.32 ppm). Furthermore, the methyl groups of compound **6***b* (1.79 and 1.82 ppm) have about the same chemical shifts as the methyl groups of the monomethylated analogs, namely the *TB*-*t*-Me_e form (**7**) of compound **5***a* (1.83 ppm) and the *TB*-*c*-Me_e form (**9**) of compound **5***b* (1.85 ppm). Finally, the chemical shift difference between the methine protons in compound **6***b* (Δ = 0.83 ppm) is about the same as that between the two axial-like protons of the *TB* form of the parent compound **4** (Δ = 0.8 ppm) (24), therefore indicating that compound **6***b* exists under a *TB* conformer with structure **11**

Can. J. Chem. Downloaded from www.nrcresearchpress.com by 210.87.254.42 on 09/06/12
For personal use only.

TABLE 4. Carbon-13 chemical shift substituent effects[a] (Δ values) produced by methyl substitution on the benzylic carbons of 2-oxo-1,3,2 benzodioxathiepin (**4**)

Compound	Ring conformation[b]	Methyl substituent effect (Δ values)				
		α	β	γ[c]	δ[d]	γ'[e]
5*a*	*C*-a (Me_e)	+3.50	+3.28	−0.39	+0.22	−3.47[f]
5*a*	*TB*-*t*-Me_e (**7**)	+5.75	+4.72	+0.55	+0.78	−1.0[f,g]
5*b*	*TB*-*c*-Me_e (**9**)	+5.29	+4.55	+0.58	+0.82	−0.81[f]

[a] All methyl substituent effects are calculated using ^{13}C parameters of **5***a* and **5***b* at −125°C, in Table 2, relative to ^{13}C parameters of **4** in ref. 24. For γ', see footnote *f* below. A positive sign indicates a downfield shift.

[b] As determined previously in the text by ir, ^1H, and ^{13}C analysis.

[c] Defined as the methyl substituent effect on C-6. For the *TB* forms of **5***a* and **5***b*, the reference parameters for the *TB* form of **4** have assumed that the signal at 134.72 ppm belongs to the aromatic quaternary carbon adjacent to the benzylic carbon *syn* to S=O, whereas the signal at 136.15 ppm is assigned to the other quaternary carbon (24).

[d] Defined as the methyl substituent effect on C-7.

[e] Defined as the methyl substituent effect on C-8.

[f] The γ' values are obtained relative to the C-8 chemical shifts in the *C*-a or *TB* forms of **4**. These protonated carbons were assigned experimentally for a solution of **4** in CH_3OCH_3 at −125°C from the analysis of the effects of selective ^1H decoupling of the methylene protons on the coupled ^{13}C nmr spectrum. It was assumed that this assignment is also valid for a solution in CHF_2Cl at −150°C, so that C-8 (*TB*) is taken as 128.51 and C-8 (*C*-a) is taken as 130.97 ppm.

[g] The C-8 resonance of the *TB* form of **5***a* is partially obscured by the C-8 resonance of the *C*-a form of **5***a*.

(*TB*-*t*-Me_e, *c*-Me_e).

The absence of a ^1H nmr spectral change for compound **6***c* in CHF_2Cl down to −135°C suggests that, in this solvent, one conformation is strongly predominant. The observation of only one methine proton quartet at 5.82 ppm and only one methyl doublet at 1.88 ppm in the spectrum at −125°C indicates the existence of symmetry. These nmr data are compatible with the earlier suggestion from the ir spectral analysis that the *C*-e form is very predominant for **6***c* in a polar solvent. Because the *C*-e form has not been detected for other seven-membered sulfites, confirmation is less straightforward. However, since *C*-a can confidently be rejected from ^1H chemical shift and ir considerations, *C*-e is therefore reasonable. On the other hand, a small amount of the *TB* form cannot be excluded since the ir data show that in CS_2 the *TB* form is slightly favored. The ^{13}C spectra discussed next are also compatible with the strong predominance of the *C*-e form in CHF_2Cl.

^{13}C spectra

^{13}C nuclear magnetic resonance has proven to be a powerful technique sensitive to small stereochemical changes which often translate into large chemical shift differences. In compound **4** (24), the chemical shifts of the benzylic carbons (C-4 and C-7) were found to be characteristic of both the conformation (*C*-a vs. *TB* form) and the relative orientation of the S=O bond with respect to the C—O bonds in the *TB* form (*syn* carbon vs. *anti* carbon). Therefore, the methylene carbon (C-7 in Table 2) chemical shift should provide a valuable stereochemical probe for the monomethylated isomers, especially when the methyl group chooses to adopt a pseudoequatorial position as was suggested earlier for **5***a* and **5***b*.

The ^{13}C spectrum of the major conformation of **5***a*, at −125°C, shows a methylene carbon at 62.79 ppm, which is close to the reference value for the *C*-a form of **4** (62.49 ppm), while the minor conformation of **5***a* shows a methylene carbon at 67.19 ppm, fairly close to the *anti*-methylene carbon of the reference *TB* form of **4** (66.41 ppm). These results confirm the conclusions reached earlier from ir and ^1H spectra, that **5***a* exists as a mixture of *C*-a and *TB*-*t*-Me_e (**7**) conformers for which the former is predominant.

Similarly, the ^{13}C spectrum of the major conformation of **5***b*, at −125°C, indicates that the methylene carbon at 63.91 ppm is close to the *syn*-methylene carbon of the *TB* form of **4** (63.09 ppm), in agreement with the conclusion from ir and ^1H spectra that the major conformation of **5***b* should be *TB*-*c*-Me_e (**9**).

Methyl substituent effects (α, β, γ, δ, and γ') have been determined (Table 4) for the C4, C5, C6, C7, and C8 atoms of the *C*-a form of **5***a* and of the *TB* forms of **5***a* and **5***b*, relative to the same conformation of compound **4**, used as reference. The Δ parameters in Table 4 differ significantly for the *C*-a form and the *TB* form of **5***a*, as could be expected from the geometrical differences between the two conformations. However, the remarkable similarity between the methyl-substitution effects for the *TB* forms of compounds **5***a* and **5***b* supports the previous suggestion that the methyl groups are located in very similar environments for both *TB* forms, namely the pseudo-equatorial benzylic position as shown in **7** for **5***a*, and **9** for **5***b*.

The equatorial nature of these methyl groups provides interesting consequences. A close examination of molecular models of *C*-a and *TB* forms having an equatorial methyl group reveals that the angle between the C8—H bond and the C4—CH_3 bond is closer to 0° in the *C*-a form than in the *TB* form, suggesting that the γ' interaction between the C-8 hydrogen atom and the methyl group should be stronger for the *C*-a form. In fact, the 3.47 ppm upfield shift of the C-8 carbon (Table 4), for the *C*-a form of **5***a*, falls well in line with the 3.7 ppm upfield shift observed for the C-8 carbon of 1-methylnaphthalene (25). The weaker γ' interaction in the *TB* forms **7** (*TB*-*t*-Me_e) and **9** (*TB*-*c*-Me_e) leads to upfield shifts of only 1.0 ppm and 0.81 ppm respectively. Similar differences were also observed for 4-methyl-1,3-dioxa-5,6-benzocycloheptene,[3] where C-8 is shielded by 3.23 ppm in the *C*-a form and by only 0.91 ppm in the *TB* form.

Interpretation of the ^{13}C nmr signals of the minor confor-

[3] R. St-Amour and M. St-Jacques, unpublished work.

Can. J. Chem. Downloaded from www.nrcresearchpress.com by 210.87.254.42 on 09/06/12
For personal use only.

Can. J. Chem. Downloaded from www.nrcresearchpress.com by 210.87.254.42 on 09/06/12
For personal use only.

mation of **5***b* must be made with caution, since neither ^{1}H nor ir signals were detected for that form. A priori, those ^{13}C signals can be attributed to three possible conformations, namely a *C*-a form with an axial methyl (**13**), a *C*-e form with an equatorial methyl (**14**), and the *TB* form of **10** with a pseudoaxial methyl. The problem can, however, be reduced to a choice between the *TB*-*c*-Me_a form (**10**) and the *C*-e form (**14**), since the *C*-a form cannot account for the deshielding of the C-7 methylene carbon on introducing an axial methyl group on the C-4 carbon.

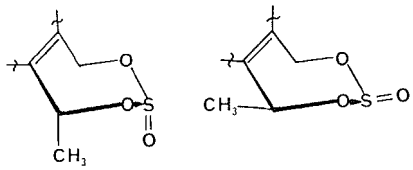

13 **14**

The chemical shift of the methylene carbon (66.58 ppm) of the minor conformation of **5***b* is in fact very similar to that of the *anti*-methylene carbon of the *TB* form of **4** (66.41 ppm), as would be expected for the *TB*-*c*-Me_a form (**10**). Data allowing the *C*-e form to be ruled out, however, require the analysis of the ^{13}C data observed for the *cis,cis* dimethyl isomer **6***c*. Consequently, the ^{13}C parameters of the three dimethylated isomeric compounds will now be considered.

As described earlier, the constancy of the ^{13}C spectra on going from −10°C to −135°C for the mixture of **6***a*–**6***b* indicates a single conformation for each stereoisomer. The presence of only five resonances for the *trans,trans* isomer **6***a*, as described earlier, indicates a symmetrical conformation for that isomer which must be the *C*-a form, to account for the well-shielded methine carbon (65.55 ppm) from the γ-*gauche* effect of the S=O bond. Furthermore, the upfield γ shift of C-8 (3.57 ppm) and the methyl chemical shift (18.89 ppm), being similar to the analogous values for the *C*-a form of **5***a* (3.47 ppm and δ_{Me} = 18.59 ppm), support the conclusion for **6***a*.

The stable conformation of the *cis,trans* isomer **6***b* is nonsymmetrical, as shown by its 10-line ^{13}C nmr spectrum. It is found to have a chemical shift difference of 3.50 ppm between C-4 and C-7 which is similar to the value observed for the benzylic carbons of the *TB* form of the parent compound (**4**), namely 3.32 ppm. Furthermore, the upfield γ-effect on C-8 (−0.77 ppm) and the methyl chemical shifts of 20.49 and 20.85 ppm closely resemble those of the *TB* form **7** for **5***a* (*TB*-*t*-Me_e) (γ_{effect} = −1.0 ppm and δ_{Me} = 20.28 ppm) and the *TB* form **9** for **5***b* (*TB*-*c*-Me_e) (γ_{effect} = −0.81 ppm and δ_{Me} = 20.38 ppm). The above analysis confirms the earlier conclusion that **6***b* adopts the *TB* form (**11**).

Conformational assignment in the case of isomer **6***c* proved more difficult than for the other compounds because the ^{13}C nmr spectrum of this rather insoluble product could be studied only in $CDCl_3$ at room temperature, rather than in CHF_2Cl at low temperatures. Direct comparison of chemical shifts between **6***c* and the other compounds must therefore be made with caution. The ir and ^{1}H parameters suggested that, in a polar solvent ($CDCl_3$ or CHF_2Cl), there is only one conformation for **6***c*, namely the symmetrical *C*-e with two equatorial methyl groups. The C4 and C7 signals have a chemical shift of 70.92 ppm, which is consistent with an *anti* relationship with respect to the S=O bond as revealed from a comparison with the *anti* carbon in *TB*-*c*-Me_e (**9**) located at 71.70 ppm. All spectroscopic data presented so far indicate that *C*-e is the predominant conformation of **6***c* in polar solvents.

The conclusion for isomer **6***c* can now be used to reexamine the earlier conformational assignment for the minor signals of compound **5***b*. Since the *C*-e form (**14**) possible for **5***b* differs from the *C*-e form of **6***c* only by the presence of an equatorial hydrogen atom at the C-7 position instead of a methyl group, it should in principle exhibit similar methyl and methine carbon chemical shifts if both exist in the same ring conformation. Close examination of the ^{13}C chemical shifts of **6***c* and of the minor conformation of **5***b* shows that a similarity exists for the methine carbons (70.92 ppm for **6***c* and 71.21 ppm for **5***b*) but not for the methyl group.

Recalling that both C4 and C7 chemical shifts constitute sensitive conformational probes, it was shown earlier that the CH_2 signal of the minor form of **5***b* pointed to the *TB* form **10**, based on a comparison with signals from the *TB* form of **4** used as model. The limited number of reference ^{13}C parameters for seven-membered rings limits our ability to distinguish clearly between *C*-e (**14**) and *TB* (**10**). Certainly, the observation of an ir S=O band for this minor conformer would have helped. If it is argued that the C7 methylene is a more reliable probe than the C4 methine signal, then the *TB*-*c*-Me_a form (**10**) would be preferred as the minor conformer of **5***b* and this might explain why the methyl chemical shifts differ for **5***b* and **6***c* (18.68 and 20.15 ppm respectively). But the solubility problem and the different spectral temperature limit the value of comparisons with **6***c*.

Conformational dynamic properties of **5**a

The interconversion scheme for cycloheptene consists of two basic molecular motions, namely a $C \rightleftharpoons B$ transformation and a $B \rightleftharpoons TB$ pseudorotation. This scheme (26) must be modified for **5***a* by taking into account the pyramidal nature of the S atom and the orientation of both the S=O bond and the methyl group. The appropriate interconversion pathways are indicated in Scheme 1, where letters a and e after *C* and *B* refer to the S=O orientation and the letters after Me describe the methyl group environment. This scheme supposes that flipping of the sulfite end of the molecules is less energetic than is wagging of the benzo part for the $C \rightleftharpoons B$ step, as was suggested in a previous study (24).

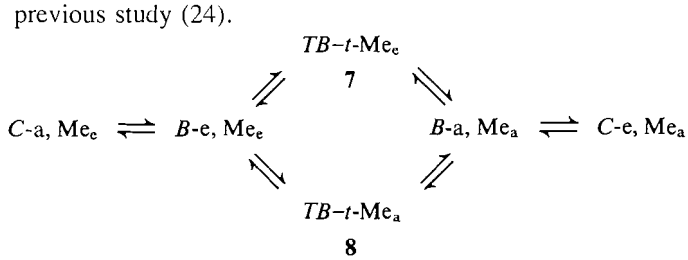

SCHEME 1

Because **7** is the only detected *TB* conformation for **5***a*, it is not possible to derive the pseudorotation barrier from the nmr spectra. On the other hand, compound **5***a* shows a *C*-a to *TB* interconversion barrier of about 8.6 kcal/mol which lies very close to that of compound **4** (9.0 kcal/mol) (24). This result could be explained by a similar molecular motion for **4** and **5***a*, as shown in Scheme 1. Since the environment of the methyl group remains essentially unchanged on going from *C*-a, Me_e to *B*-e, Me_e (the effect of the remote S=O bond being neglected), any significant methyl effect would necessarily be constant over the whole energy profile of this interconversion

step in agreement with the observed $\Delta G^{\ddagger}$ values for **4** and **5***a*. A flip of the benzo part, which would transform *C*-a, Me_c into *B*-a, Me_a, cannot explain the similar $\Delta G^{\ddagger}$ values for **4** and **5***a* since it would create 1,3-diaxial CH_3---O=S as well as 1,5-diaxial benzylic CH_3---H interactions in the transition state, which cannot exist in the preferred molecular motion of **4**.

Experimental

Melting points are uncorrected and were determined using a Büchi melting point apparatus. High-resolution spectra at 70 eV were recorded using a modified MS-9 spectrometer. The medium pressure liquid chromatography was performed on 0.040–0.063 μm silica gel (Merck no. 9385) with an ALTEX model 150 pressure regulator and a 254 nm uv detector. Solvents were distilled prior to use.

The ir spectra of the monomethylated derivatives **5***a* and **5***b* were taken as 0.05 *M* solutions in CCl_4 and in CH_3CN, in a 0.5 mm KBr cell using a Beckmann IR-20 spectrometer for the normal spectra and a Beckmann IR-9 spectrometer for the scale expansions. Integrations were made using a DuPont model 310 curve synthesizer which decomposes overlapping peaks by generation of Lorentzian functions.

The ir spectra of the dimethylated compounds **6***a*–**6***b* were taken as 0.05 *M* solutions in CCl_4 and in CH_3CN, but those of compound **6***c* were taken as 0.001 *M* and 0.01 *M* solutions in CS_2 and in CH_3CN respectively. Spectra of thin films between KBr windows (0.05 mm cell: nominal value) were recorded on a Digilab FTS-15C/D Fourier transform infrared spectrometer, equipped with a wide range photoconductive mercury cadmium telluride detector, a KBr beam splitter, and a LOBAR source. The instrument was purged with nitrogen before use. Typically, 200 interferograms of 2096 points each, recorded with a maximum optical retardation of 0.50 cm^{-1} and an optical velocity of 1.2 cm s^{-1}, were co-added, apodized with a triangular function, and Fourier transformed with 8 levels of zero filling, resulting in a spectral resolution of 2 cm^{-1}. The base line was corrected using multiple linear least-square functions. Integrations were performed using a PEAKAREA program (Digilab) which uses the trapezoidal rule, with a first point – last point approximation. This kind of operation leads to approximate values in the case of **6***a*–**6***b*, where partially overlapping peaks occur.

Routine ^1H nmr spectra were taken on a Bruker WH-90 spectrometer; solutions were typically 10% (w/v) in $CDCl_3$ containing Me_4Si as reference. Routine ^{13}C nmr spectra were taken on a Bruker WP-80 spectrometer; solutions were typically 15% (w/v) in $CDCl_3$ containing Me_4Si as reference.

The variable temperature ^1H nmr spectra at 400 MHz and ^{13}C nmr spectra at 100.62 MHz were obtained using a Bruker WH-400 spectrometer equipped with a variable temperature unit B-VT-1000. Temperatures were determined directly using the B-VT-100 unit. Calibration, using a thermocouple inside a solvent-containing nmr tube, indicates that the low temperatures reported are exact within 2°C.

The ^1H samples were studied as solutions in chlorodifluoromethane (5–6 mg in 0.55 mL of solution) containing Me_4Si and about 13% of CD_2Cl_2 (for locking purposes), in standard 5 mm tubes which had been degassed and sealed. The following parameters were used: flip angle = 60–65°; SW = 4000 Hz; pulse delay = none; data size = 4K; acquisition time = 0.512 s. The ^{13}C spectra were recorded with proton noise decoupling for solutions in CHF_2Cl (60–70 mg in 2.2 mL of solution) containing Me_4Si and about 13% of CD_2Cl_2, as locking agent, in standard 10 mm tubes which had been degassed and sealed. The following instrumental parameters were used: flip angle = 65–70°; SW = 17 000–22 000 Hz; data size: 16K; acquisition time = 0.328 s or 0.482 s; pulse delay = none.

Selective decoupling in the case of compound **4** was done using a decoupling power corresponding to 175.9 Hz. The rate constants were determined at the coalescence temperature using the equation $k = \pi\Delta\nu/\sqrt{2}$ for singlet to doublet splitting in ^1H (methyl signals of **5***a*) and ^{13}C nmr spectra (the equation provides an acceptable estimate for lines of unequal intensity (27)). The free energy barriers were calculated from standard equations (28) using a transmission coefficient of 1.

*α-Methyl-o-xylene-α,α′-diol (**15**)*

This compound was prepared from 2-acetyl benzoic acid (Aldrich) by a procedure already published (29). It was characterized by its melting point (65–67°C) and by its ^1H nmr spectrum, which were identical with those published.

4-Methyl-5,6-benzo-2-oxo-1,3,2dioxathiepin (cis *and* trans *isomers) (**5**)*

A solution of freshly distilled (30) thionyl chloride (1.19 g, 0.01 mol) in 50 mL of anhydrous ether was added dropwise during 30 min, at 0°C and under a nitrogen atmosphere, to a mixture of α-methyl-*o*-xylene-α,α′-diol (**15**) and triethylamine (2.02 g, 0.02 mol). After two hours at 0°C, the reaction is complete as shown by the ^1H spectrum of an aliquot. The mixture is then filtered and evaporated under reduced pressure, giving 1.5 g (76%) of a yellow oil containing the two isomers. Column chromatograpy on 15 μm silica gel (Merck 60H), using pentane/ether (97.5:2.5) as eluant, gave in the first fractions the *trans* isomer **5***a* (mp: 36–37°C) and in the last fractions the *cis* isomer **5***b* (mp: 56–57°C). The ^1H and ^{13}C nmr spectra (Tables 3 and 2) as well as high resolution mass spectra confirm their identity. *Mol. Wt.* calcd. for **5***a*, $C_9H_{10}O_3S$: 198.0351; found (mass spectrum at 70 eV): 198.0383. *Mol. Wt.* calcd. for **5***b*, $C_9H_{10}O_3S$: 198.0351; found (mass spectrum at 70 eV): 198.0339.

*α,α′-Dimethyl-o-xylene-α,α′-diol (**16**)*

This compound was prepared from 1,2-benzodicarboxaldehyde (Aldrich) by a procedure already published (31). The oily diastereoisomeric mixture thus obtained was used without further purification. The ^1H, ^{13}C nmr, and high-resolution mass spectra confirm its identity; ^1H nmr, δ: 1.47, 1.45 (2d, 6H, 2×Me), 5.15, 5.07 (2q, 2H, 2×CH), 7.52–7.20 (m, 4H, aromatic H's); ^{13}C nmr, δ: 24.4, 23.3 (2×Me), 67.1, 64.9 (2×CH), 127.7, 127.7, 126.1, 125.2 (4 × aromatic protonated carbons), 142.1, 141.9 (2 × aromatic quaternary carbons). *Mol. Wt.* calcd. for **16** – H_2O, $C_{10}H_{12}O$: 148.0888, found (mass spectrum at 70 eV): 148.0037 (no molecular ion peak could be detected).

4,7-Dimethyl-5,6-benzo-2-oxo-1,3,2-dixathiepin (trans,trans (**6**a), cis,trans (**6**b), *and* cis,cis (**6**c) *isomers)*

A solution of freshly distilled (30) thionyl chloride (2.77 g, 0.023 mol) in 120 mL of anhydrous ether was added dropwise (2 hours), at 0°C and under nitrogen, to a mixture of α,α′-dimethyl-*o*-xylene-α,α′-diol (3.9 g, 0.023 mol) and triethylamine (4.75 g, 0.046 mol). After two more hours at 0°C, the temperature was allowed to rise to 25°C overnight. The reaction was then complete, as shown by the ^1H nmr spectrum of an aliquot. The mixture was filtered and evaporated under reduced pressure, giving 3.28 g (66%) of a yellow oil containing the three isomers. Column chromatography on 0.040–0.063 μm silica gel (Merck no. 9385) using a hplc apparatus and hexane/ethyl acetate (98:2) as eluant gave, in the first fractions, a mixture of **6***a*–**6***b* and, in the last fractions, **6***c* (mp: 151–152°C). The ^1H and ^{13}C nmr spectra (Tables 3 and 2) as well as high-resolution mass spectra (at 70 eV) confirm their identity. *Mol. Wt.* calcd. for **6***a*–**6***b*, $C_{10}H_{12}O_3S$: 212.0507; found (mass spectra at 70 eV): 212.0547. *Mol. Wt.* calcd. for **6***c*, $C_{10}H_{12}O_3S$: 212.0507 (mass spectra at 70 eV): 212.0499.

Acknowledgements

We wish to acknowledge the technical assistance of Mr. Jean-Claude Bolduc, of the "Laboratoire de spectroscopie infrarouge par transformée de Fourier" and of Dr. Phan Viet Minh Tan, of the "Laboratoire régional de RMN à haut champ", both situated at the Université de Montréal. We are grateful to S. Désilets for assistance in preparing the dimethyl derivatives. We thank Dr. L. Cazaux, Toulouse, France, for helpful discussions duirng a stay at Toulouse by P. de Almeida.

Can. J. Chem. Downloaded from www.nrcresearchpress.com by 210.87.254.42 on 09/06/12
For personal use only.

We also wish to thank the National Research Council of Canada for its financial assistance.

1. H. F. VANWOERDEN. Chem. Rev. **63**, 557 (1963).
2. D. G. HELLIER, J. G. TILLET, H. F. VANWOERDEN, and R. F. WHITE. Chem. Ind. 1956 (1963).
3. L. CAZAUX, J. D. BASTIDE, G. CHASSAING, and P. MARONI. Spectrochim. Acta Part A, **35**, 15 (1979), and references cited.
4. (*a*) H. NIKANDER, K. PIHLAJA, and T. VIRTANEN. Acta. Chem. Scand. Ser. B, **36**, 117 (1982); (*b*) T. VIRTANEN, H. NIKANDER, and K. PIHLAJA. Tetrahedron, **38**, 2821 (1982); (*c*) B. A. ARBUSOV, E. N. KLIMOVITSKII, A. B. REMIGOV, A. V. AGANOV, I. V. ANONIMOVA, G. N. SERGEEVA, and V. V. KLOCHKOV. Dokl. Akad. Nauk SSSR, **239**, 109 (1979).
5. G. W. BUCHANAN and D. G. HELLIER. Can. J. Chem. **54**, 1428 (1976), and references cited.
6. C. H. GREEN and D. G. HELLIER. J. Chem. Soc. Perkin Trans. 2, 190 (1975), and references cited.
7. G. WOOD, J. M. MCINTOSH, and M. H. MISKOW. Can. J. Chem. **49**, 1202 (1971).
8. C. H. GREEN and D. G. HELLIER. J. Chem. Soc. Perkin Trans. 2, 458 (1972).
9. G. W. BUCHANAN, C. M. E. COUSINEAU, and T. C. MUNDELL. Can. J. Chem. **56**, 2019 (1978), and references cited.
10. C. G. OVERBERGER, T. KURTZ, and S. YAROSLAVSKY. J. Org. Chem. **30**, 4363 (1965).
11. P. ALBRIKTSEN. Acta Chem. Scand. **26**, 3678 (1972).
12. D. G. HELLIER and A. M. PHILIPS. Org. Magn. Reson. **18**, 178 (1982).
13. (*a*) R. RIEMCHNEIDER and V. WUSCHERPFENNIG. Z. Naturforsch. Teil B, **17**, 516 (1962); (*b*) **17**, 585 (1962).
14. S. E. FORMAN, A. J. BURBETAKI, M. V. COHEN, and R. A. OLOFSON. J. Org. Chem. **30**, 169 (1965).
15. A. C. GUIMARAES, J. B. ROBERT, L. CAZAUX, C. PICARD, and P. TISNES. Tetrahedron Lett. **21**, 1039 (1980).
16. T. NISHIYAMA, Y. NAKAI, H. SHISHIBORI, and F. YAMADA. Bull. Chem. Soc. Jpn. **54**, 1410 (1981).
17. C. ALTONA, H. J. GEISE, and C. ROMERS. Recl. Trav. Chim. Pays-Bas, **85**, 1197 (1966).
18. H. F. VANWOERDEN and A. T. DE VRIES-MIEDEMA. Tetrahedron Lett. 1687 (1971).
19. G. W. BUCHANAN, J. B. STOTHERS, and G. WOOD. Can. J. Chem. **51**, 3746 (1973).
20. P. MARONI, L. CAZAUX, J. P. GORRICHON, P. TISNES, and J. G. WOLF. Bull. Soc. Chim. Fr. **5**, 1253 (1975).
21. G. WOOD, G. W. BUCHANAN, and M. H. MISKOW. Can. J. Chem. **50**, 521 (1972).
22. K. PIHLAJA, H. NIKANDER, V.-M. MUKKALA, and T. NURMI. Org. Magn. Reson. **8**, 375 (1976).
23. L. CAZAUX, G. CHASSAING, and P. MARONI. J. Chem. Res. (M), 68 (1982).
24. H. FAUCHER, A. C. GUIMARAES, J. B. ROBERT, F. SAURIOL, and M. ST-JACQUES. Tetrahedron, **37**, 689 (1981).
25. T. DRAKENBERG, J. SANDSTROM, and J. SEITA. Org. Magn. Reson. **11**, 243 (1978).
26. S. KABUSS, A. LUTTRINGHAUS, H. FRIEBOLIN, H. G. SCHMID, and R. MECKER. Tetrahedron Lett. 719 (1966).
27. D. KOST, E. H. CARLSON, and M. RABAN. Chem. Commun. 565 (1971), and references cited therein.
28. F. A. L. ANET, P. J. DEGEN, and J. KRANE. J. Am. Chem. Soc. **98**, 2059 (1976).
29. M. BARFIELD, R. J. SPEAR, and S. STERNHELL. J. Am. Chem. Soc. **97**, 5165 (1975).
30. L. FIESER. Experiments in organic chemistry. 3rd ed. D. C. Heath, Boston, Mass. 1955. p. 345.
31. S. GOLDSCHMIDT and A. ZOEBELEIN. Chem. Ber. **94**, 169 (1961).

Can. J. Chem. Downloaded from www.nrcresearchpress.com by 210.87.254.42 on 09/06/12
For personal use only.

A serendipitous, high yield conversion of norbornenone to tricyclo[3.2.1.$0^{2,7}$]octan-4-one[1]

ARTHUR J. RAGAUSKAS AND J. B. STOTHERS
Department of Chemistry, University of Western Ontario, London, Ont., Canada N6A 5B7

Received February 4, 1983

ARTHUR J. RAGAUSKAS and J. B. STOTHERS. Can. J. Chem. **61**, 2254 (1983).

Simmons-Smith cyclopropanation of the trimethylsilyl enol ether of norbornenone has been found to generate the 2-trimethylsilyl ether of homoquadricyclene, homoketonization of which affords the symmetrical tricyclo[3.2.1.$0^{2,7}$]octan-4-one regiospecifically with high stereoselectivity favoring inversion of configuration.

ARTHUR J. RAGAUSKAS et J. B. STOTHERS. Can. J. Chem. **61**, 2254 (1983).

On a trouvé que la réaction de cyclopropanation de Simmons-Smith, appliquée a l'éther d'énol triméthylsilyle du norbornénone, conduit à l'éther triméthylsilyle-2 de l'homoquadricyclène. L'homocétonisation de ce dernier fournit le composé symétrique tricyclo[3.2.1.$0^{2,7}$] de façon regiospécifique et possédant un haut degré de stéréosélectivité favorisant l'inversion de configuration.

[Traduit par le journal]

Can. J. Chem. Downloaded from www.nrcresearchpress.com by 210.87.254.40 on 09/06/12
For personal use only.

As an extension of our examination of ring expansion by homoketonization of cyclopropoxide derivatives, we were interested in the conversion of norbornenone (**1**) to bicyclo[3.2.1]oct-6-en-2-one (**2**) through cyclopropoxide **3***a*, by analogy with our results for bicyclooctenone **4** (1). We wish to describe the rather unexpected finding that the reaction sequence leads to the formation of tricyclo[3.2.1.$0^{2,7}$]octan-4-one in very good yield.

In the general sequence (1), the ketone of interest is converted to the corresponding trimethylsilyl enol ether which is then cyclopropanated with a zinc–silver couple and methylene iodide. For a variety of bicyclic ketones a single cyclopropyl derivative is formed. Cleavage of the resulting cyclopropyl ether can be accomplished with dilute HCl in THF to produce the cyclopropanol which upon addition to base readily undergoes ring opening to ketonic products, i.e. homoketonization. Alternatively, treatment of the cyclopropyl ether with base directly effects cleavage and homoketonization. Since, with ketones having bridges of two carbons or less, this sequence leads preferentially to the ring expanded ketone, we anticipated a smooth conversion of **1** → **2**.

Reaction of **1** with lithium diisopropylamide followed by the addition of trimethylsilyl chloride and triethylamine gave **5** in 79% isolated yield. Cyclopropanation afforded a single product quantitatively, having no olefinic absorption in either the ^{1}H or ^{13}Cmr spectra. Its ^{1}H spectrum consisted of four multiplets (δ(C_6D_6): 1.16 (2H), 1.76 (4H), 1.97 (2H), and 2.12 (1H)) and a strong singlet at δ 0.20 (Me_3Si), while the ^{13}C spectrum exhibited two methylene signals (δ_C 25.3, 30.7), five methine peaks (20.1, 21.5, 24.4, 27.4, and 33.7), a quaternary signal (69.2), and trimethylsilyl absorption at δ_C 1.1. The molecular formula, $C_{11}H_{18}OSi$, shown by precise mass measurement, confirmed the addition of one methylene group and readily dismissed the possibility of double cyclopropanation, i.e., at the double bond of **3***b*. High regioselectivity has been found for monocyclopropanations of trimethylsilyl enol ethers of unsaturated ketones, such that addition occurs exclusively at the enolic double bond provided a large excess of the Simmons-Smith reagent is avoided (1, 2). Nevertheless the product cannot be **3***b*.

Since it is well established that halocarbenes add to norbornadienes by both 1,2- and homo-1,4-addition (3), the product could conceivably be a bishomoprismane derivative **6**. The analog of **6***a* was found as a minor product from the reaction of difluorocarbene with **5** (4). Thus, **6***a* and **6***b* were plausible structures for the addition product. Also, in the earlier studies of halocarbene additions to norbornadiene (4) and substituted derivatives (5), it was discovered that the 1,2-adducts, corre-

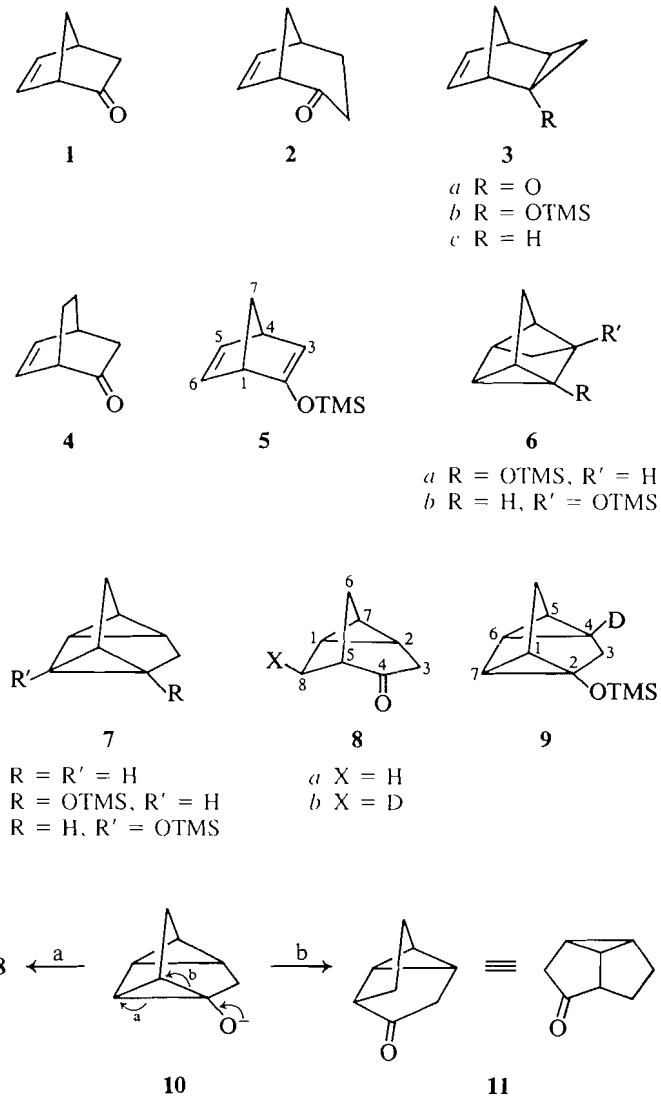

[1] Part 105 in the series ^{13}Cmr studies; for part 104 see ref. 11.

Can. J. Chem. Downloaded from www.nrcresearchpress.com by 210.87.254.40 on 09/06/12
For personal use only.

sponding to **3***c*, are thermally labile. While several are transformed to bicyclo[3.2.1]octa-3,6-dienyl derivatives, certain adducts undergo cycloaddition upon heating to form homoquadricyclene derivatives having carbon skeleton **7***a*. Analogy suggested that **7***b* could be our addition product, with **7***c* as a less likely possibility.

On treatment with base, the addition product gave a single ketone in essentially quantitative yield, having carbonyl absorption (ir 1727 cm^{-1}, δ_C 211.7) indicative of a six-membered ring ketone. The ^{13}Cmr spectrum contained five signals, in addition to the carbonyl peak: δ_C 9.2 (CH), 14.4 (2CH), 28.6 ($2CH_2$), 33.3 (CH_2), and 47.8 (CH). The two more intense signals remained as singlets in the presence of shift reagent ($Eu(fod)_3$), showing the ketone to be symmetric. Only **8***a*, of the several ketones which could form by homoketonization of **6***a*, **6***b*, **7***b*, and **7***c*, fits these data and the mp of the 2,4-dinitrophenylhydrazone agreed with literature values (6). The ^{1}H spectrum gave further confirmation. A 1-proton multiplet at δ 1.03 coupled to a sharp 2-proton doublet (J = 2.7 Hz) at 2.525 and a broad 2-proton doublet (J = 7.5 Hz) at 1.46 were readily ascribed to H-2, -3, and -1,7, respectively. A broadened triplet ($J \sim$ 5.3 Hz) at δ 2.50, due to H-5, and an "AB" pattern for the 6,8-protons were apparent. The A part (δ 2.01) was also coupled to H-5 ($J \sim$ 5.3 Hz) and H-1,7 ($J \sim$ 2 Hz), while the B part (δ 1.85) was a clean doublet (J_{AB} = 12.2 Hz) undoubtedly due to the *endo*-6,8-protons which have dihedral angles of ~ 90° with respect to H-5 and -1,7. All spin coupling interactions were confirmed by decoupling experiments. With ketone **8***a* identified, it followed that the addition product must be **7***b*.

To complete the ^{13}C assignments for **7***b*, the cyclopropanation was repeated using **5**-3-d_1 to generate **9** (0.8 D/molecule). In its ^{13}C spectrum the most shielded methine singlet was highly attenuated and accompanied by the expected triplet, J_{CD} = 26 Hz, exhibiting an isotope shift of −0.32 ppm. In addition, three other absorptions were altered, with the signals corresponding to those for **7***b* strongly attenuated and accompanied by prominent singlets 0.1 ppm toward higher field. These patterns are typically exhibited by carbons geminal to ^{2}H (7) and served to identify C-3, -5, and -6 at δ_C 30.7, 21.5, and 24.4, respectively. The remaining methylene signal, δ_C 25.3, was, therefore, due to C-8 and the signals at δ_C 27.4 and 33.6 arise from C-1 and -7.

Presumably cyclopropanation of **5** generates **3***b* initially, which undergoes facile intramolecular cycloaddition to form **7***b*. While it may be suggested that the cycloaddition may be catalyzed by silver, cyclopropanation with the more usual zinc–copper couple also gave **7***b*, although in lower yield (72%). It is known that **3***c* complexes with silver (8) but there are no reports of rearrangement of the complex. At present, it seems most reasonable to conclude that **3***b* is more prone to thermally induced cycloaddition than the corresponding dihalocarbene adducts which exhibit the same isomerization at higher temperatures.

Two aspects of the homoketonization merit comment. Although there are two modes of ring opening for the β-enolate formed from **7***b*, shown as a and b in **10**, the cyclopropoxide cleavage is apparently regiospecific. Since cleavage a and b both lead to secondary carbanions, the exclusive formation of **8***a* is an illustration of thermodynamic control of homoketonization, a feature which has been recognized for some years (9) and indicates that **8***a* is more stable than **11**. The second aspect, stereoselectivity of protonation (deuteriation) at the carbanionic site, required additional evidence for its clarification. For this purpose, the homoketonization was examined in a deuterated medium.

Treatment of **7***b* with *t*-BuO^-/*t*-BuOD gave **8**-d_x (1.12 D/molecule), which, from the ^{13}C spectrum, had incorporated ca. 0.9 atoms D at C-6,8 and ca. 0.2 atoms D at C-3. In the ^{1}H spectrum, the absorption for *exo*-6(8)-H was significantly attenuated while the clean doublet for *endo*-6(8)-H (δ 1.853) was accompanied by a triplet, J_{HD} = 1.85 Hz, at 1.837. Clearly ring opening of **10** proceeded primarily to **8***b* with inversion of configuration at the carbanionic site. Minor deuteration at C-3 undoubtedly occurred through α-exchange upon generation of the ketone in the deuterated medium. To check for small amounts of deuterium at the *endo*-6(8)-position, the ^{2}Hmr spectrum of the ketone was also examined. This spectrum contained signals at δ 1.85, 2.0, and 2.5 in the ratio 1.0:12.3:3.1, corresponding to 0.21 atoms D at C-3 and 0.91 atoms D at C-6(8) with the latter in the ratio of 12:1 favoring *exo*-D. Further confirmation of the marked preference for *exo*-deuteration at the β-methylene position was obtained by examination of the ketone generated by homoketonization of **9** in *t*-BuO^-/*t*-BuOD. The product (2.14 D/molecule) gave a ^{2}H spectrum having signals at δ 1.45, 1.85, 2.0, 2.5 with relative intensities 11.6:1.0:12.1:10.0 corresponding to 0.72, 0.062, 0.75, and 0.62 atoms D at C-2, *endo*-6(8), *exo*-6(8), and C-3, respectively. More extensive exchange occurred at C-3 because of a longer reaction time (11.5 vs. 3 h). In any event, homoketonization proceeds with high stereoselectivity (92 ± 1%) favoring inversion of configuration which is in agreement with findings for a wide variety of β-enolates (9).

Experimental

Gas–liquid chromatography (glc) was carried out on a Varian 920 instrument using columns (5.5 m × 0.64 cm) packed with 6% FFAP or 20% Carbowax 20 M on Chromosorb W. Infrared (ir) spectra were recorded with a Beckman 4250 spectrophotometer. Mass spectrometric (ms) data were obtained with a Varian MAT-311A instrument. The nmr spectra were recorded using a Varian XL-200 instrument at 30.7 (^{2}H), 50.3 (^{13}C), and 200 MHz (^{1}H).

Norbornenone (1)

After dropwise addition of α-chloroacrylonitrile (8.9 g, 0.1 mol) to freshly distilled cyclopentadiene (8.3 g, 0.125 mol) in benzene (17 mL), the solution was stirred at 45°C for 36 h, under a nitrogen atmosphere. Distillation gave 2-chloro-2-cyanobicyclo[2.2.1]hept-5-ene (15.1 g, 97%), bp 58–61°C/1.5 Torr; ir (film): 2235 (CN) cm^{-1}. The ^{13}Cmr spectrum indicated the presence of both epimers. The total product was dissolved in DMSO (88 mL) and a solution of KOH (16.5 g) in water (5.6 mL) was added with stirring. After 30 h, a saturated aqueous solution of NaCl (88 mL) was added, and the product extracted with pentane (4 × 50 mL). The combined extracts were washed with saturated salt solution until the washings were neutral, then once with water. The organic layer was dried ($MgSO_4$) and the solvent evaporated to give 8.7 g of product containing (glc) **1** (86%) and starting material (14%). Preparative glc (FFAP) furnished pure **1** as determined by glc and ^{13}Cmr (10).

[3,3-$^2H_2$]norbornenone

Freshly cut sodium metal (400 mg) was added to D_2O (32 mL, 99.7% D) in a flame-dried flask fitted with a reflux condenser and nitrogen purge. After cooling to room temperature, **1** (2 g) in pentane (1 mL) was added and the solution refluxed for 9.5 h. Pentane extraction as described above gave **1**-d_x (1.1 g); ms: 27.5% d_1, 66.7% d_2 (total 1.60 D/molecule).

Trimethylsilyl enol ether of 1 (5)

Freshly distilled THF (8 mL) containing diisopropylamine (1.4

Can. J. Chem. Downloaded from www.nrcresearchpress.com by 210.87.254.40 on 09/06/12
For personal use only.

mL, 0.01 mol), which had been dried over molecular sieves, was placed in a flask having a N_2 purge and cooled to −78°C. Upon addition of *n*-butyllithium (0.0078 mol) in *n*-hexane (3.7 mL) via syringe, the mixture was stirred for 30 min before **1** (760 mg, 0.007 mol) in THF (3 mL) was added by syringe. While stirring was continued for 30 min, a quenching solution (THF (3 mL), chlorotrimethylsilane (1.3 mL, 0.01 mol), and triethylamine (0.5 mL, 0.0037 mol)) was placed in a flame-dried, N_2-purged centrifuge tube. Traces of precipitate were removed by centrifugation and the clear quenching solution added by syringe to the cold enolate solution. The reaction mixture was maintained at −78°C for another 30 min before slowly warming to room temperature over 1 h. The mixture was then poured into a saturated aqueous solution of Na_2CO_3 (18 mL) and the product extracted with *n*-pentane (3 × 20 mL). The combined extracts were washed with saturated Na_2CO_3 and with water before drying over $MgSO_4$. After evaporation of the solvent, Kugelrohr distillation (95°C, 5 Torr) gave **5** (1.0 g, 79% yield); ir (film): 1610 cm^{-1}; ^{13}Cmr ($CDCl_3$) δ_C: 173.0 (C-2), 145.4, 141.2 (C-5, -6), 109.1 (C-3), 72.5 (C-7), 53.6 (C-1), 48.1 (C-4), 0.0 (Me_3Si).

Cyclopropanation of **5**

To a flask fitted with a reflux condenser, nitrogen purge, and magnetic stirrer was added zinc–silver couple (1.2 g, 0.018 mol) and the apparatus flame-dried. After cooling, methylene iodide (0.76 mL, 9.4 mmol) and Et_2O (3 mL) were added and the mixture warmed until refluxing occurred without external heating. Upon cessation of reflux a solution of **5** (990 mg, 5.5 mmol) in Et_2O (13 mL) was added and this mixture was refluxed for 19 h with stirring. After cooling to 0°C, pyridine (1.5 mL) was slowly added with stirring. The resulting precipitate was removed by filtration and washed with Et_2O. After removal of solvent from the filtrate, the residue was taken up in *n*-pentane; further filtration was required to remove the last traces of precipitate. Evaporation of the solvent gave **7***b* (1.06 g, 99%) which glc (FFAP) indicated to contain traces (<2%) of two impurities; ^{13}Cmr (C_6D_6) δ_C: 27.4 (C-5), 69.2 (C-4), 30.7 (C-3), 20.1 (C-2), 21.5 (C-1), 24.4 (C-7), 33.6 (C-6), 25.3 (C-8), 1.1 ($SiMe_3$). *Exact Mass* calcd. for $C_{11}H_{18}OSi$: 194.1127; found: 194.1127.

Repetition of the sequence **1** → **5** → **7***b* with [3,3-$^2H_2$]-**1** as starting material afforded **9**, ms: 20% d_0, 80% d_1 (total 0.80 D/molecule).

Homoketonization of 7b

To 28 mL of 3 *M* methanolic NaOH was added **7***b* (550 mg) and the mixture stirred for 20 min at room temperature. After the addition of H_2O (25 mL), the product was extracted with *n*-pentane (3 × 20 mL). The combined extracts were washed with saturated aqueous NaCl solution and with water. After drying and removal of the solvent, the organic phase afforded 254 mg of product while re-extraction of the aqueous phase furnished an additional 79 mg. Gas–liquid chromatography (FFAP) showed the combined product **8** (99% yield) to be reasonably pure (>98%); ir (film): 1727 cm^{-1}, ^{13}C ($CDCl_3$) δ_C: 211.8 (C=O), 47.8 (C-5), 33.3 (C-3), 28.6 (C-6,8), 14.4 (C-1,7), 9.2 (C-2). *Exact Mass* calcd. for $C_8H_{10}O$: 122.0732; found: 122.0735.

Ketone **8** gave a 2,4-dinitrophenylhydrazone, mp 191–192°C (lit. (6*a*) mp 192.5–193°C; (6*b*) mp 190–190.5°C; (6*c*) mp 194.5–195°C. *Exact Mass* calcd. for $C_{14}H_{14}O_4N_4$: 302.1016; found: 302.1017.

Preparation of **8**a-d_x

A sample of **7***b* (200 mg) was placed in 1 *M* *t*-BuO^- in *t*-BuOD (10 mL) and the solution stirred at room temperature for 3 h. After quenching with water (10 mL), the ketone was extracted with *n*-pentane as described above and purified by glc to give **8***a*-d_x; ms: 71.3% d_1, 17.3% d_2, 2.1% d_3 (total 1.12 D/molecule).

A sample of **9** (0.8 D/molecule), prepared as described above, was homoketonized in a similar fashion with an extended reaction time (11.5 h) to furnish **8***a*-d_x; ms: 19.1% d_1, 40.9% d_2, 27.3% d_3, 7.8% d_4 (total 2.14 D/molecule).

Acknowledgements

We are grateful for the financial support of the Natural Sciences and Engineering Research Council of Canada.

1. Y. HOYANO, V. PATEL, and J. B. STOTHERS. Can. J. Chem. **58**, 2730 (1980).
2. C. GIRARD and J. M. CONIA. Tetrahedron Lett. 3333 (1974).
3. C. W. JEFFORD and P. T. HUY. Tetrahedron Lett. **23**, 391 (1982).
4. C. W. JEFFORD, M. MAREDA, J.-C. E. GEHRET, T. KABENGELE, W. D. GRAHAM, and U. BURGER. J. Am. Chem. Soc. **98**, 2585 (1976); C. W. JEFFORD, V. d.l. HEROS, and U. BURGER. Tetrahedron Lett. 703 (1976).
5. C. W. JEFFORD and P. T. HUY. Tetrahedron Lett. **21**, 755 (1980).
6. (*a*) M. GEISEL, C. A. GROB, W. SANTI, and W. TSCHUDI. Helv. Chim. Acta, **56**, 1046 (1973); (*b*) R. R. SAUERS, J. A. BEISLER, and H. FEILICH. J. Org. Chem. **32**, 569 (1967); (*c*) G. T. LUMB and G. W. WHITMAN. Tetrahedron, **21**, 499 (1965).
7. R. J. ABRAHAM and P. LOFTUS. Proton and carbon 13 nmr spectroscopy. Heyden & Sons, London. 1978. pp. 145–148.
8. B. C. MENON and R. E. PINCOCK. Can. J. Chem. **47**, 3327 (1969).
9. D. H. HUNTER, J. B. STOTHERS, and E. W. WARNHOFF. Rearrangements in ground and excited states. Vol. 1. *Edited by* P. de Mayo. Academic Press, New York. 1980. Chapt. 6. pp. 430–437; N. H. WERSTIUK. Tetrahedron, **39**, 205 (1983).
10. J. B. STOTHERS, J. R. SWENSON, and C. T. TAN. Can. J. Chem. **53**, 581 (1975).
11. A. STOESSL and J. B. STOTHERS. Can. J. Chem. **61**, 1766 (1983).

Nuclear analogs of β-lactam antibiotics. XIX.[1] Syntheses of racemic and enantiomeric *p*-nitrobenzyl carbapen-2-em-3-carboxylates

YASUTSUGU UEDA,[2] CHRISTOPHER E. DAMAS, AND VIVIANNE VINET
Bristol Laboratories of Canada, 100 Industrial Boulevard, Candiac, P.Q., Canada J5R 1J1

Received March 1, 1983

YASUTSUGU UEDA, CHRISTOPHER E. DAMAS, and VIVIANNE VINET. Can. J. Chem. **61**, 2257 (1983).

Racemic and enantiomeric *p*-nitrobenzyl carbapen-2-em-3-carboxylates **3**, **3***a*, and **3***b* were prepared starting from inexpensive sorbic acid through the key intermediates, azetidinone esters **4**, thus establishing a total synthesis of the *p*-nitrobenzyl ester of a natural product SQ 27,860. Optical resolution was achieved readily on azetidinone menthyl esters, **12**. The absolute configurations were also established.

YASUTSUGU UEDA, CHRISTOPHER E. DAMAS et VIVIANNE VINET. Can. J. Chem. **61**, 2257 (1983).

On a préparé les carbapeneme-2 carboxylates-3 de *p*-nitrobenzyle racémiques et énantiomères **3**, **3***a* et **3***b* en partant d'un réactif peu coûteux, l'acide sorbique, et en passant par des intermédiaires clés, des esters de l'azétidinone **4**; on a donc réalisé ainsi une synthèse totale de l'ester *p*-nitrobenzyle du produit naturel SQ 27,860. On a facilement effectué la résolution des antipodes optiques des esters menthyliques de l'azétidinone **12** et on a également établi les configurations absolues.

[Traduit par le journal]

In our previous paper (1) we reported a simple route to (±)-2-alkylthiocarbapen-2-em-3-carboxylate **1** (R = S-alkyl), starting from inexpensive sorbic acid via an intermediate **4** (R = PNB). Now we wish to describe the versatility of intermediates **4** by preparing racemic and enantiomeric carbapenems **3**, **3***a*, and **3***b* from **4** (R = Me, *l*-menthyl). Although racemic carbapen-2-em-3-carboxylic acid esters **2** and **3** have

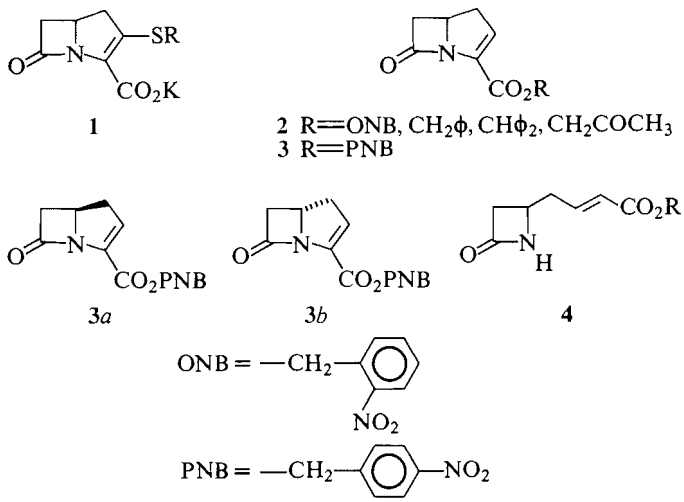

been reported (2–5), their enantiomers have not been prepared in pure form.[3] The Squibb scientists (7) recently isolated a simple carbapenem antibiotic SQ 27,860 as the *p*-nitrobenzyl ester, from bacterial sources, which was found to be (+)-*p*-nitrobenzyl carbapen-2-em-3-carboxylate. Therefore, a part of this report represents a total sysnthesis of the *p*-nitrobenzyl ester of the natural product from sorbic acid.

Racemic parent carbapen-2-em-3-carboxylate **3** was synthesized by the well-established method (3, 8), originated by Woodward and co-workers , from our key intermediate **4** (R = Me). Condensation of **3** (R = Me) (1) with *p*-nitrobenzyl glyoxylate hydrate gave carbinolamides **5** as a diastereomeric mixture which was converted to chloro-compounds **6** by thionyl chloride and pyridine. Treatment of **6** with triphenylphosphine and 2,6-lutidine provided phosphorane **7** in 64% overall yield from **4** (R = Me) as yellowish crystals. Ozonolysis of **7** in CH_2Cl_2 in the presence of trifluoroacetic acid (8*c*), followed by reduction of the ozonide with dimethyl sulfide, then regeneration of the phosphorane with $NaHCO_3$, yielded aldehyde **8** which spontaneously cyclized at 35°–40°C to give racemic carbapenem ester **3** as yellowish crystals (mp 153.5°–155°C) in 60% yield (Scheme 1). This material had spectroscopic properties (^{1}Hmr, ir) consistent with data reported by Bateson *et al.* (3*b*). Preparation of carbapenem salt **2** (R = K, Na) was attempted by hydrogenolysis (H_2/Pd–C, phosphate buffer) of **3**. Although the presence of **2** (R = K, Na) was detected in the crude, dilute solution by the uv spectrum ($\lambda_{shoulder}$ ~262 nm), it was not possible to isolate it, due to the instability of the molecule (2, 3*b*, 5, 17).

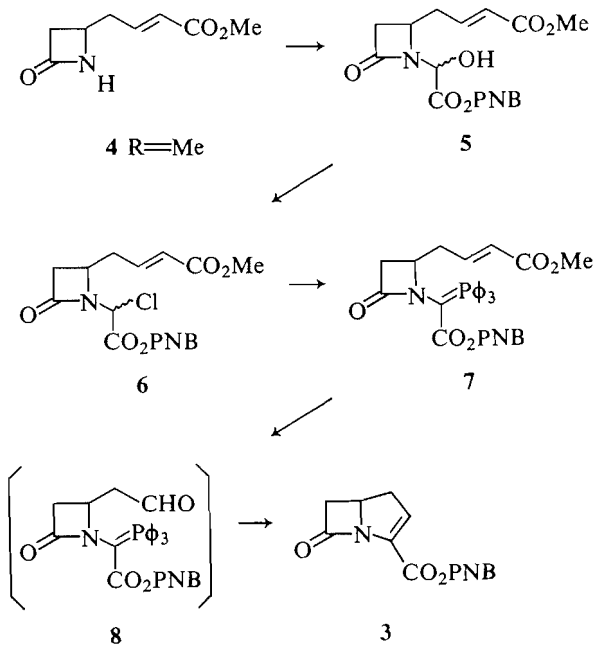

SCHEME 1

Bearing a carboxylic acid ester group in the molecule, the

[1] For Part XVIII of this series, see ref. 1.

[2] Author to whom correspondence should be addressed.

[3] The Beecham group describes the preparation of enantiomeric carbapenem esters **3***a* and **3***b* in their recent patent application (6), but their method is cumbersome and, furthermore, the enantiomeric purities are low.

Can. J. Chem. Downloaded from www.nrcresearchpress.com by 210.87.254.105 on 09/06/12
For personal use only.

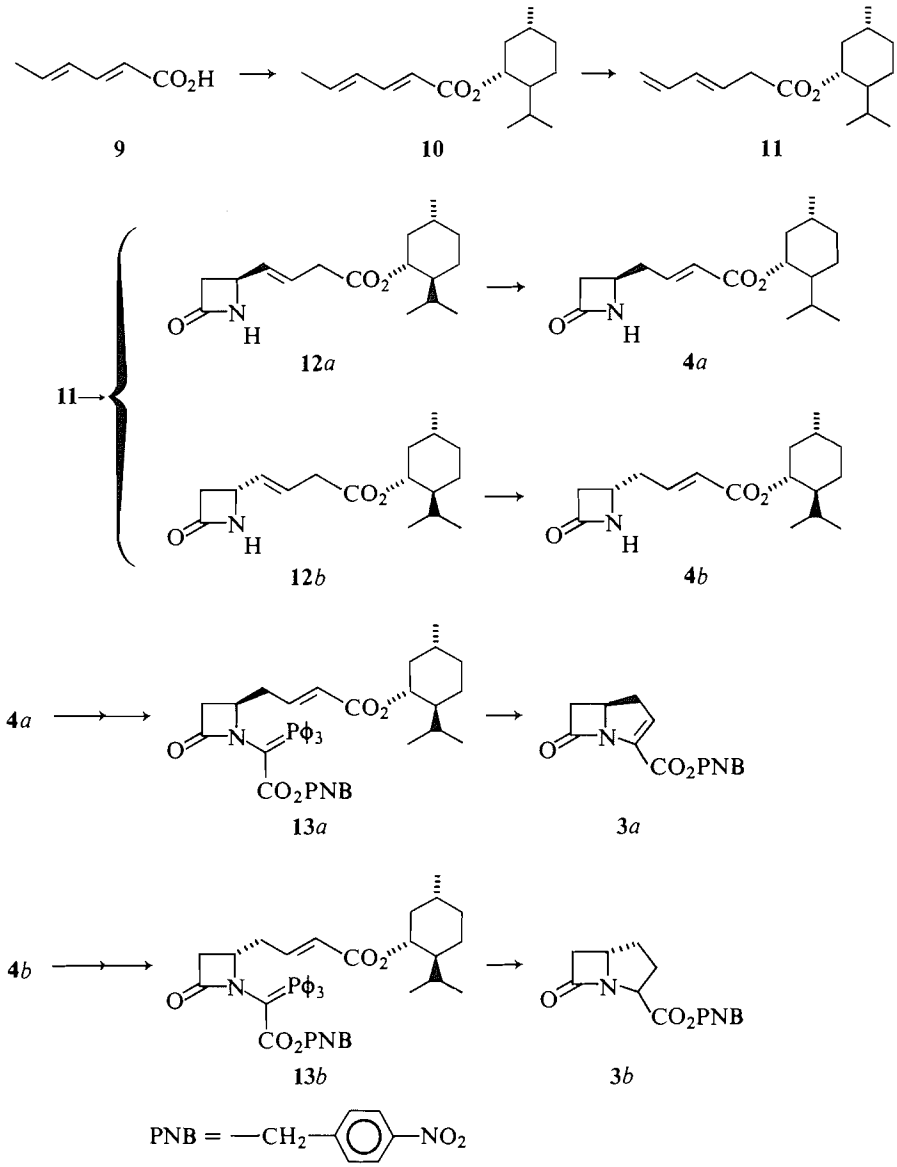

SCHEME 2

intermediate **4** provides a possibility of preparing optically active parent carbapenem carboxylates **3***a* and **3***b*. Instead of a methyl ester, an optically active ester grouping such as *l*-menthyl ester could be introduced into the intermediate **4**, producing a mixture of two diastereomers. This could make resolution of the racemate possible. After the resolution is achieved, this ester moiety is removed from the molecule to prepare optically active carbapenems.[4]

We found that although optical resolution on the intermediate **4** (R = *l*-menthyl) was possible, it was performed more conveniently on azetidinone menthyl ester **12**.

The diastereomeric mixture **12** was prepared following the method used for the preparation of methyl ester **4** (R = Me) (1), starting from sorbic acid (**9**) and optically active *l*-menthol (Scheme 2). Thus, esterification of sorbic acid (**9**) with *l*-menthol gave *l*-menthyl sorbate (**10**) which was isomerized to *l*-menthyl 3,5-hexadienoate (**11**) in 95% yield by kinetic protonation of the enolate generated from **10** with lithium diisopropylamide in THF–HMPA. Cycloaddition of chlorosulfonyl isocyanate (10) to this conjugated diene **11**, followed by a reductive work-up (11), yielded two diastereomeric azetidinones **12** in 54% yield. These two diastereomers were readily separated by crystallization to give **12***a* and **12***b* in 28% and 21% yield respectively. This facile resolution of the racemic modification depends on different solubilities of these two diastereomers in Et_2O. One crystallization from Et_2O was enough to obtain one diastereomer **12***a* (mp 120°–125°C) in a reasonably pure form. The other diastereomer **12***b* (mp 75°–78°C), which was more soluble in Et_2O, crystallized from the mother liquor by addition of pentane in the cold. In both cases, their mp and optical rotation did not change significantly by further recrystallization. Upon isomerization of the carbon–carbon double bond with 1,4-diazabicyclo[2.2.2]-octane (DABCO) in CH_3CN as described before (1), each diastereomer **12***a* and **12***b* gave **4***a* and **4***b* in good yield.

The independent transformation of the two diastereomers **4***a* and **4***b* into the optically active *p*-nitrobenzyl (5*R*)-carbapen-2-em-3-carboxylate (**3***a*): mp 123°–124°C; $[\alpha]_D$ +127.5° (*c* 1.0, CH_2Cl_2), and its 5*S*-enantiomer **3***b*: mp 122°–124°C;

[4]A similar approach has been used by Pfaendler *et al.* (9) in the preparation of enantiomeric penem-3-carboxylic acids.

Can. J. Chem. Downloaded from www.nrcresearchpress.com by 210.87.254.105 on 09/06/12
For personal use only.

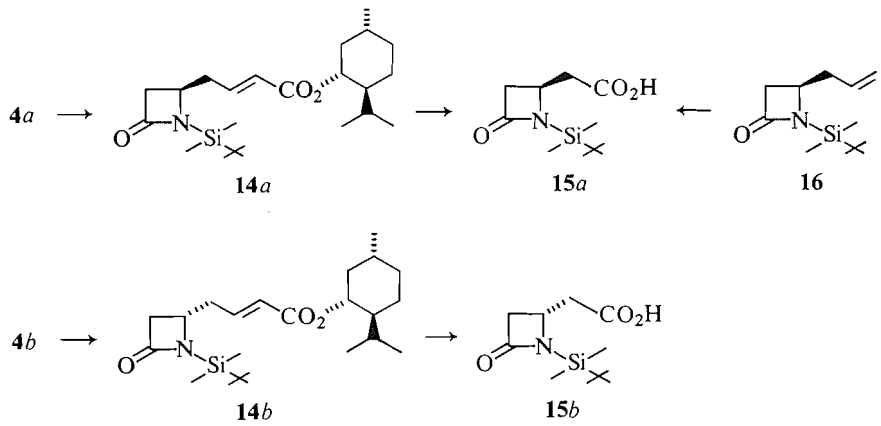

SCHEME 3

$[\alpha]_D$ −110.8° (*c* 1.0, CH_2Cl_2), was achieved through phosphoranes **13***a* and **13***b* (Scheme 2) by the same method used for the racemic series. These enantiomers had ^{1}Hmr and ir spectra identical to the racemic material. Determination of enantiomeric purities by ^{1}Hmr spectroscopic means was attempted using a chiral shift reagent (12). Examination of ^{1}Hmr spectra of racemic and each enantiomeric material obtained revealed that Eu(dcm)$_3$ (12*b*) caused separation of a doublet (a part of an AB quartet) for one of the methylene protons of the *p*-nitrobenzyl group into two sets of the doublet. The one in **3***a* appeared at slightly lower field than the one in **3***b*, $\Delta\Delta\delta$ being 0.07 ppm. Any peaks which correspond to **3***b* were not detected in the ^{1}Hmr spectrum of the enantiomer obtained with $[\alpha]_D$ of +127.5°. The isomer with $[\alpha]_D$ −110.8° showed the major peaks corresponding to the enantiomer **3***b* and a trace of peaks from the enantiomer **3***a*, indicating some contamination of **3***a* (ca. 10%). Because of the noise associated with these spectra, accurate measurements were not obtained. Nonetheless we believe that one of the isomers, **3***a*, was prepared with high enantiomeric purity.

The *l*-menthyl group, which served for racemate resolution, was removed at the last stage of the sequence (see Scheme 2). Combined with the fact that the resolution was achieved at an earlier stage, this provided the possibility of yielding a better optical purity of each final enantiomer, because further enrichment is possible at each step (e.g. **4**).

The absolute configurations were established as compounds **12***b*, **4***a*, **13***a*, and **3***a* (*R*-series) and compounds **12***a*, **4***b*, **13***b*, and **3***b* (*S*-series) by two-step conversion of **4***a* and **4***b* to **15***a*, $[\alpha]_D$ −67.5° (*c* 1.0, CH_2Cl_2), and **15***b*, $[\alpha]_D$ +36.6° (*c* 1.0, CH_2Cl_2) respectively (Scheme 3). This conversion involved protection of the β-lactam by *tert*-butyldimethylsilyl chloride and triethylamine in DMF and subsequent oxidation of the double bond by potassium permanganate under phase transfer conditions (13). The acid **15***a* was correlated to the one obtained, $[\alpha]_D$ −80.3° (*c* 1.0, CH_2Cl_2), by permanganate oxidation of allylazetidinone **16**[5] whose absolute configuration was known. Consequently, the absolute configuration of the *p*-nitrobenzyl ester of SQ 27,860, having an optical rotation $[\alpha]_D^{22}$ of +104° (7) was determined to be (5*R*)-*p*-nitrobenzyl carbapen-2-em-3-carboxylate (**3***a*).

Since racemic carbapenem ester **3** has been used as an intermediate in the preparation of 6-unsubstituted analogs of olivanic acid (6, 14), the synthesis of the (5*R*)-isomer **3***a*, described here, provides a useful and practical entry to the natural enantiomers of 6-unsubstituted carbapenem antibiotics.

In summary, we have described the syntheses of racemic and enantiomeric carbapen-2-em-3-carboxylates starting from inexpensive sorbic acid. The compounds **4** were found to be very versatile intermediates in the synthesis of carbapenems.

Experimental

Melting points were determined on a Gallenkamp melting point apparatus and are not corrected. The infrared spectra were recorded on a Perkin–Elmer 267 grating infrared spectrometer. The ^{1}H nuclear magnetic resonance spectra were taken with either a Varian EM-360 (60 MHz) or a Varian CFT-20 (80 MHz) nmr spectrometer. Tetramethylsilane was used as an internal standard and chemical shifts are reported in parts per million (δ) relative to the internal standard. The ultraviolet spectra were recorded on an Unicam SP8-100 uv spectrophotometer. Optical rotations were measured with a Perkin–Elmer Model 141 polarimeter. Tetrahydrofuran was freshly distilled from lithium aluminum hydride. Anhydrous diethyl ether (Fisher) was used without further treatment. All other solvents were reagent grade and had been stored over molecular sieves before use. n-Butyllithium (n-BuLi) in hexane and tris[*d*,*d*-dicampholylmethanato]europium (III) (Eu(dcm)$_3$) were purchased from Alfa Products and used as such. Triethylamine and diisopropylamine were distilled from CaH_2 and stored over NaOH. *p*-Nitrobenzyl glyoxylate hydrate (15) was prepared from di-*p*-nitrobenzyl fumarate by ozonolysis (CH_2Cl_2, −78°C) followed by reduction with dimethylsulfide (16). Analytical thin layer chromatography (tlc) was conducted on precoated plates (Silica Gel 60F-254, Merck). Preparative layer chromatography (plc) was performed on silica gel plates prepared from Silica Gel 60GF-254 (E. Merck). Column chromatography was carried out on Silica Gel 60 (70–230 mesh, E. Merck). The analyses were performed by Micro-Tech Laboratories, Skokie, Illinois, U.S.A.

p-Nitrobenzyl [4-(3-carbomethoxy-2-propen-1-yl)azetidin-2-on-1-yl] hydroxyacetates (5)

A mixture of 4-(3-carbomethoxy-2-propen-1-yl)-2-azetidinone (**4**, R = Me) (1) (3.19 g, 18.9 mmol) and *p*-nitrobenzyl glyoxylate hydrate (4.72 g, 20.8 mmol) in benzene (200 mL) was heated at reflux with a Dean–Stark trap for 3 h. Evaporation of the solvent gave 8.08 g of the title compound **5** as yellow foam; R_f 0.37 (Et_2O–EtOAc 1:1); ir (neat) ν_{max}: 3400 (OH), 1750 (br, β-lactam and ester), 1725 (conj. ester), 1660 (C=C), 1520, and 1350 (NO_2) cm^{-1}; ^{1}Hmr ($CDCl_3$, 60 MHz) δ: 2.3–2.9 (2H, m, 1″-H), 2.65 (1H, dd, *J* = 15 and 3 Hz, 3′-H_a), 3.12 (1H, dd, *J* = 15 and 5 Hz, 3′-H_b), 3.72 (3H, s, —CO_2Me), 3.95 (1H, m, 4′-H), 4.97 (1H, br, —OH), 5.33 (2H, s, —CO_2CH_2Ar), 5.48 (1H, br, 1-H), 5.85 (1H, d, *J* = 16 Hz, 3″-H), 6.6–7.2 (1H, m, 2′-H), 7.55 (2H, d, *J* = 9 Hz, ArH's), and 8.20 (2H,

[5] This compound was derived from a natural product, penicillin. A highly stereoselective conversion of 6α-bromopenicillanic acid to optically active allylazetidinone **16** is reported in Part XVII of this series. We thank Dr. A. Martel for the procedures of this conversion.

Can. J. Chem. Downloaded from www.nrcresearchpress.com by 210.87.254.105 on 09/06/12
For personal use only.

Can. J. Chem. Downloaded from www.nrcresearchpress.com by 210.87.254.105 on 09/06/12
For personal use only.

d, J = 9 Hz, ArH's) ppm. This crude material was used in the next step without any purification.

p-*Nitrobenzyl [4-(3-carbomethoxy-2-propen-1-yl)azetidin-2-on-1-yl] chloroacetates (6)*

To a stirred solution of crude *p*-nitrobenzyl [4-(3-carbomethoxy-2-propen-1-yl)azetidin-2-on-1-yl]hydroxyacetates (**5**) (8.08 g) and pyridine (2.14 mL) in THF (190 mL) was added, at −15°C to −20°C, thionyl chloride (1.66 mL) over a period of 5 min under an atmosphere of nitrogen. The mixture was stirred for 20 min at −15°C. After filtration of white precipitates and washing the precipitates with benzene, the filtrate and washings were combined and evaporated to dryness. The residue, extracted with benzene, was treated with Norit and evaporation of the solvent gave 6.64 g (16.7 mmol, crude yield 88.6% based on **4**, R = Me) of the title compounds **6** as a crude oil; R_f 0.72 (Et_2O–EtOAc 1:1); ir (neat) ν_{max}: 1770 (br, β-lactam and ester), 1660 (C=C), 1525, and 1355 (NO_2) cm^{-1}; ^{1}Hmr ($CDCl_3$, 60 MHz) δ: 2.2–3.4 (4H, m, 3′-H's and 1″-H's), 3.73 (3H, s, —CO_2Me), 4.2 (1H, m, 4′-H), 5.35 (2H, s, —CO_2CH_2Ar), 5.88 (1H, d, J = 16 Hz, 3″-H), 6.23 (1H, s, 1-H), 6.5–7.2 (1H, m, 2″-H), 7.55 (2H, d, J = 9 Hz, ArH's), and 8.26 (2H, d, J = 9 Hz, ArH's) ppm. This crude material was used in the next reaction without further purification.

p-*Nitrobenzyl [4-(3-carbomethoxy-2-propen-1-yl)azetidin-2-on-1-yl] triphenylphosphoranylideneacetate (7)*

To a stirred solution of crude *p*-nitrobenzyl [4-(3-carbomethoxy-2-propen-1-yl)azetidin-2-on-1-yl]chloroacetates (**6**) (6.60 g, 16.6 mmol) and triphenylphosphine (4.78 g, 18.3 mmol) in dioxane (166 mL) was added 2,6-lutidine (2.12 mL) at room temperature under a nitrogen atmosphere. The mixture was stirred (room temp., N_2) overnight (23 h). The precipitate was filtered and washed with dioxane. The filtrate and washings were combined and evaporated. The residue, redissolved in EtOAc (100 mL), was washed with 1 *N* HCl (20 mL × 2), saturated $NaHCO_3$ and then brine, dried (Na_2SO_4), and evaporated to give 11.68 g of crude phosphorane. This was purified by column chromatography (300 g, EtOAc) followed by crystallization from EtOAc–Et_2O to yield 6.64 g (10.7 mmol, yield 64.3%) of the title compound 7 as light yellow crystals; mp 172°–173°C (recrystallized from EtOAc); R_f 0.40 (EtOAc); ir (film) ν_{max}: 1745 (β-lactam), 1720 (conj. ester), 1660 (C=C), 1625 (ester), 1520, and 1350 (NO_2) cm^{-1}; ^{1}Hmr ($CDCl_3$, 60 MHz) δ: 3.70 (3H, s, —CO_2Me), 4.83, 5.17 (2H, 2s, —CO_2CH_2Ar), 7.55 (15H, s, φH's), and 8.19 (2H, d, J = 10 Hz, ArH's) ppm, the others are not well resolved. *Anal.* Calcd. for $C_{35}H_{31}N_2O_7P$: C 67.52, H 5.02, N 4.50; found: C 67.70, H 5.00, N 4.47.

*(±)-*p*-Nitrobenzyl carbapen-2-em-3-carboxylate (3)*

To a stirred solution of *p*-nitrobenzyl [4-(3-carbomethoxy-2-propen-1-yl)azetidin-2-on-1-yl]triphenylphosphoranylideneacetate (7) (1.24 g, 2.00 mmol) in CH_2Cl_2 (40 mL) was added, at 0°–5°C, trifluoroacetic acid (2 mL), and the yellowish mixture was cooled to −78°C. A stream of ozone was introduced until the blue colour was retained, and the solution was stirred at −78°C for another 5 min. Nitrogen was passed through the solution to remove excess ozone and then dimethyl sulfide (2 mL) was added. After removing the cooling bath, the solution was stirred at 0°–5°C for 1 h. This mixture was washed with saturated $NaHCO_3$ (50 mL × 2) and then brine, dried (Na_2SO_4), and evaporated *in vacuo* (bath temperature 35°–40°C). The residue was purified by column chromatography (30 g, EtOAc–hex 1:1), followed by crystallization from CH_2Cl_2–Et_2O to give 343 mg (1.19 mmol, yield 59.5%) of the title compound **3** as yellowish crystals; mp 153.5°–155°C; R_f 0.35 (EtOAc–hex 1:1); ir (film) ν_{max}: 1780 (β-lactam), 1730 (ester), 1520, and 1350 (NO_2) cm^{-1}; uv (EtOH) λ_{max}: 267 nm (ε 15 900); ^{1}Hmr ($CDCl_3$, 80 MHz) δ: 2.72 (1H, ddd, J_{gem} = 19 Hz, J_{1-5} = 9 Hz, J_{1-2} = 3 Hz, 1-H_a), 2.98 (1H, dd, J_{gem} = 17 Hz, $J_{6-5\,trans}$ = 3 Hz, 6-H_a), 3.02 (1H, ddd, J_{gem} = 19 Hz, J_{1-5} = 9.5 Hz, J_{1-2} = 3 Hz, 1-H_b), 3.54 (1H, dd, J_{gem} = 17 Hz, $J_{6-5\,cis}$ = 5.6 Hz, 6-H_b), 4.3 (1H, m, 5-H), 5.16–5.33–5.38–5.55 (2H, ABq, —CO_2CH_2Ar), 6.58 (1H, t, J = 3 Hz, 2-H), 7.60 (2H, d, J = 8.8 Hz, ArH's), and 8.23 (2H, d, J = 8.8 Hz, ArH's) ppm; ^{1}Hmr (**3**, 5 mg, and Eu(dcm)$_3$, 25 mg, in $CDCl_3$, 0.5 mL; 80 MHz) δ: 5.98–6.15–6.26–6.43 (1H, ABq, —CO_2CH_2Ar in the 5*S*-isomer), 5.98–6.15–6.32–6.50 (1H, ABq, —CO_2CH_2Ar in the 5*R*-isomer), 7.01 (t, J = 3 Hz, 2-H in the 5*R*-isomer), and 7.05 (t, J = 3 Hz, 2-H in the 5*S*-isomer) ppm. *Anal.* calcd. for $C_{14}H_{12}N_2O_5$: C 58.33, H 4.20, N 9.72; found: C 58.34, H 4.15, N 9.60.

(−)-Menthyl 2,4-hexadienoate (10)

A solution of 2,4-hexadienoic acid (112 g, 1.00 mol; sorbic acid), *l*-menthol (172 g, 1.10 mol), and concentrated sulfuric acid (10.3 mL) in benzene (1.85 L) was heated at reflux with a Dean–Stark trap for 5 days. The mixture was cooled and basified by slow addition of saturated $NaHCO_3$ (400 mL) with vigorous stirring. The organic layer was separated and further washed with saturated $NaHCO_3$ (2 × 400 mL). The aqueous layers were combined and extracted with EtOAc (400 mL). All organic layers were combined and washed with brine (2 × 500 mL), dried (Na_2SO_4), and evaporated *in vacuo* to obtain 191 g of amber oil. This was purified by a silica pad consisting of Mallinekrodt silicic acid (100 mesh, 1.4 L) on top of Merck silica gel 60 (70–230 mesh, 1.4 L), eluting with hexanes and then 2 and 5% Et_2O in hexanes to yield 116.9 g (0.467 mol, yield 46.7%) of the title compound **10** as an oil; bp 112°–114°C/0.3 Torr (lit. (17) bp 173°C/14 Torr); R_f 0.42 (Et_2O–hex 1:9); $[\alpha]_D^{23}$ −83.5° (*c* 0.60, CH_2Cl_2); ir (neat) ν_{max}: 1705 (ester), 1645, and 1620 (C=C) cm^{-1}; ^{1}Hmr ($CDCl_3$, 60 MHz) δ: 0.77 (3H, d, J = 7 Hz, —Me), 0.90 (6H, d, J = 7 Hz, *gem*-Me), 0.8–2.2 (9H, m, —CH, CH_2—), 1.85 (3H, d, J = 4.5 Hz, 5-Me), 4.73 (1H, td, J_{a-a} = 9 Hz, J_{a-e} = 2 Hz, —CO_2CH—), 5.6–6.2 (3H, m, olefinic protons), and 7.0–7.45 (1H, m, 5-H) ppm.

(−)-Menthyl 3,5-hexadienoate (11)

To a stirred solution of diisopropylamine (140 mL, 1.01 mmol) in THF (2.4 L) was added at 0°–5°C, under a nitrogen atmosphere, n-butyllithium (500 mL, 2.02 *M* in hexane, 1.01 mol) over a period of 30 min. After stirring for 30 min, the light yellow solution was cooled to −75° to −78°C. A solution of hexamethylphosphoramide (180 mL, 1.00 mol) in THF (100 mL) was added over a period of 20 min, and the mixture stirred for 1 h. To this mixture was added a solution of (−)-menthyl 2,4-hexadienoate (**10**) (200 g, 0.80 mol) in THF (100 mL) during a 15 min period, and the resulting dark red mixture was stirred (−78°C, N_2) for 2 h. This was poured into a solution of concentrated HCl (200 mL) in water (800 mL) and extracted with EtOAc (3 × 500 mL). The EtOAc extracts were washed with water (5 × 500 mL) and then brine (500 mL), dried (Na_2SO_4), and evaporated *in vacuo* to yield 189.2 g (0.756 mol, crude yield 94.5%) of the title compound **11** as an amber oil. This crude oil was used in the subsequent reaction without any purification. An analytical sample was obtained by distillation followed by plc (Et_2O–hex 1:9); bp 95°–97°C/0.2 Torr; R_f 0.52 (Et_2O–hex 1:9); $[\alpha]_D^{23}$ −70.2° (*c* 1.0, CH_2Cl_2); ir (neat) ν_{max}: 1735 (ester), 1650, and 1605 (C=C) cm^{-1}; ^{1}Hmr ($CDCl_3$, 60 MHz) δ: 0.77 (3H, d, J = 7 Hz, —Me), 0.90 (6H, d, J = 7 Hz, *gem*-Me), 0.8–2.2 (9H, m, —CH— and —CH_2—), 3.10 (2H, d, J = 6 Hz, 2-H's), 4.69 (1H, td, J_{a-a} = 9 Hz, J_{a-e} = 4 Hz, —CO_2—CH—), 5.0–5.4 (2H, m, olefinic protons), and 5.7–6.7 (3H, m, olefinic protons) ppm. *Anal.* calcd. for $C_{16}H_{26}O_2$: C 76.75, H 10.47; found: C 77.02, H 10.56.

4(S)- and 4(R)-(3-carbomenthyloxy-1-propenyl)-2-azetidinones (12a and 12b)

To a stirred solution of crude (−)-menthyl 3,5-hexadienoate (**11**) (184.2 g, 0.737 mol) in CH_2Cl_2 (2.3 L) was added at 0°–5° C, under a nitrogen atmosphere, chlorosulfonyl isocyanate (72.0 mL, 0.819 mol) over a period of 22 min. The mixture was stirred at room temperature for 24 h. This mixture was added slowly to a mechanically stirred mixture of sodium sulfite (460 g, 3.65 mol) in water (2.3 L) and CH_2Cl_2 (0.9 L) at 0°–5°C. During the addition, the mixture was adjusted to pH 7–9 by simultaneous addition of saturated $NaHCO_3$

Can. J. Chem. Downloaded from www.nrcresearchpress.com by 210.87.254.105 on 09/06/12
For personal use only.

(2.0 L). After removing the cooling bath, the milky yellow mixture was stirred for another 2 h. The cloudy organic phase was collected. The aqueous phase was saturated with sodium chloride and extracted with CH_2Cl_2 (1.0 L × 2). All organic extracts were combined, washed with brine (2L), dried (Na_2SO_4), and evaporated to yield a yellow semi-solid. This was dissolved in EtOAc and any insoluble materials were removed. Evaporation of the solvent gave 200 g of yellow oil which was crystallized from Et_2O to obtain 61.3 g (0.209 mol, yield 28.4%) of the 4*S*-isomer of the title compound **12***a*, in two crops, as yellowish powder: mp 120°–125°C; R_f 0.42 (Et_2O); $[\alpha]_D^{21}$ −69° (*c* 0.5, $CHCl_3$); ir (CH_2Cl_2) ν_{max}: 3420 (NH), 1765 (β-lactam), 1725 (ester), and 1670 (C=C) cm^{-1}; ^{1}Hmr ($CDCl_3$, 60 MHz) δ: 0.75 (3H, d, J = 7 Hz, —Me), 0.89 (6H, J = 7 Hz, *gem*-Me), 0.7–2.2 (9H, m, —CH— and —CH_2—), 2.67 (1H, ddd, J_{gem} = 15 Hz, $J_{3-4\,trans}$ = 2.5 Hz, J_{3-1} = 1.5 Hz, 3-H_β), 3.07 (2H, d, J = 6 Hz, 3′-H's), 3.22 (1H, ddd, J_{gem} = 15 Hz, $J_{3-4\,cis}$ = 5 Hz, J_{3-1} = 2 Hz, 3-H_α), 4.13 (1H, m, 4-H_α), 4.67 (1H, td, J_{a-a} = 10 Hz, J_{a-e} = 4 Hz, —CO_2CH—), 5.65–5.9 (2H, m, olefinic protons), and 6.42 (br, 1-H) ppm. An analytical sample was obtained by several recrystallizations from EtOAc–Et_2O; mp 125°–128°C; $[\alpha]_D^{21}$ − 71.4° (*c* 0.42, $CHCl_3$). *Anal.* calcd. for $C_{17}H_{27}NO_3$: C 69.59, H 9.28, N 4.77; found: C 69.06, H 9.08, N 4.58.

The mother liquor was evaporated and crystallized from Et_2O–pentane at 0°–5°C to obtain 45.93 g (0.157 mol, yield 21.3%) of the 4*R*-isomer of the title compound **12***b* as off-white powder; mp 75°–78°C; R_f 0.42 (Et_2O); $[\alpha]_D^{21}$ −56° (*c* 0.50, $CHCl_3$); ir (CH_2Cl_2) ν_{max}: 3420 (NH), 1765 (β-lactam), 1725 (ester), and 1670 (C=C) cm^{-1}; ^{1}Hmr ($CDCl_3$, 60 MHz) δ: 0.77 (3H, d, J = 7 Hz, —Me), 0.90 (6H, d, J = 7 Hz, *gem*-Me), 0.7–2.2 (9H, m, —CH—, and —CH_2—), 2.67 (1H, ddd, J_{gem} = 15 Hz, $J_{3-4\,trans}$ = 2.5 Hz, J_{3-1} = 1.5 Hz, 3-H_α), 3.08 (2H, d, J = 6 Hz, 3′-H's), 3.23 (1H, ddd, J_{gem} = 15 Hz, $J_{3-4\,cis}$ = 5 Hz, J_{3-1} = 2 Hz, 3-H_β), 4.16 (1H, m, 4-H_β), 4.70 (1H, td, J_{a-a} = 10 Hz, J_{a-e} = 4 Hz, —CO_2CH—), 5.6–5.9 (2H, m, olefinic protons), and 6.58 (br, 1-H) ppm. An analytical sample was obtained by two recrystallizations from Et_2O–pentane; mp 77.5°–78.5°C; $[\alpha]_D^{21}$ −57.0° (*c* 0.50, $CHCl_3$). *Anal.* calcd. for $C_{17}H_{27}NO_3$: C 69.59, H 9.28, N 4.77; found: C 69.70, H 9.10, N 4.57.

*4(*R*)-(3-carbomenthyloxy-2-propen-1-yl)-2-azetidinone (**4**a)*

A suspension of 4(*S*)-(3-carbomenthyloxy-1-propenyl)-2-azetidinone (**12***a*) (14.65 g, 50.0 mmol; mp 120°–125°C) and 1,4-diazabicyclo[2.2.2]octane (16.8 g, 150 mmol) in CH_3CN (150 mL) was stirred at room temperature under a nitrogen atmosphere for 7 days. The cloudy mixture was filtered over Celite and washed with EtOAc. The filtrate and washings were combined and evaporated. The residue, redissolved in EtOAc (100 mL), was cooled and shaken with cold 1 *N* HCl (300 mL). The aqueous layer was saturated with sodium chloride and extracted with EtOAc (30 mL × 2). All EtOAc layers were combined, washed successively with 1 *N* HCl (30 mL), saturated $NaHCO_3$ and then brine, dried (Na_2SO_4), and evaporated, yielding 14.89 g of a crude oil. This oil was crystallized from pentane to give 8.55 g (29.1 mmol, yield 58.3%) of the title compound **4***a* as white crystals; mp 74°–76°C; R_f 0.34 (Et_2O). An exiguous amount of the starting material **12***a* (R_f 0.42) was detected in this material. An analytical sample was obtained by plc (EtOAc–Et_2O 1:6) followed by recrystallization from pentane as pure white crystals; mp 80°–81°C; $[\alpha]_D^{20}$ −55.0° (*c* 1.0, CH_2Cl_2); ir (film) ν_{max}: 3300 (br, NH), 1765 (β-lactam), 1710 (conj. ester), and 1655 (C=C) cm^{-1}; ^{1}Hmr ($CDCl_3$, 80 MHz) δ: 0.76 (3H, d, J = 7 Hz, —Me), 0.85 (6H, d, J = 7 Hz, *gem*-Me), 0.8–2.2 (9H, m, —CH— and —CH_2—), 2.52 (2H, td, J = 7 Hz, $J_{1'-3'}$ = 1.4 Hz, 1′-H's), 2.54 (1H, ddd, J_{gem} = 14.9 Hz, $J_{3-4\,trans}$ = 2.5 Hz, J_{3-1} = 1.2 Hz, 3-H_β, partially seen), 3.14 (1H, ddd, J_{gem} = 14.9 Hz, $J_{3-4\,cis}$ = 4.9 Hz, J_{3-1} = 2.3 Hz, 3-H_α), 3.75 (1H, m, 4-H_α), 4.74 (1H, td, J_{a-a} = 10 Hz, J_{a-e} = 4 Hz, —CO_2CH—), 5.87 (1H, dt, $J_{2'-3'}$ = 15.6 Hz, $J_{3'-1'}$ = 1.4 Hz, 3′-H), 5.9 (br, 1-H), and 6.85 (1H, dt, $J_{2'-3'}$ = 15.6 Hz, $J_{2'-1'}$ = 7 Hz, 2′-H) ppm. *Anal.* calcd. for $C_{17}H_{27}NO_3$: C 69.59, H 9.28, N 4.77; found: C 69.84, H 9.41, N 4.80.

*4(*S*)-(3-carbomenthyloxy-2-propen-1-yl)-2-azetidinone (**4**b)*

The crude title compound (14.62 g) was obtained from 4(*R*)-(3-carbomenthyloxy-1-propenyl)-2-azetidinone (**12***b*) (14.65 g, 50.0 mmol) by the method used for the 4*R*-isomer. This crude material was purified by column chromatography (500 g, Et_2O) to yield 12.98 g (44.3 mmol, yield 88.6%) of the pure title compound **4***b* as an oil; R_f 0.34 (Et_2O); $[\alpha]_D^{21}$ −72.1° (*c* 1.0, CH_2Cl_2); ir (neat) ν_{max}: 3300 (br, NH), 1765 (β-lactam), 1715 (conj. ester), and 1660 (C=C) cm^{-1}; ^{1}Hmr ($CDCl_3$, 60 MHz) δ: 0.77 (3H, d, J = 7 Hz, —Me), 0.90 (6H, d, J = 7 Hz, *gem*-Me), 0.8–2.2 (9H, m, —CH— and —CH_2—), 2.54 (2H, td, J = 7 Hz, $J_{1'-3'}$ = 1 Hz, 1′-H's), 2.60 (1H, ddd, J_{gem} = 15 Hz, $J_{3-4\,trans}$ = 2 Hz, J_{3-1} = 1 Hz, 3-H_α, partially seen), 3.13 (1H, ddd, J_{gem} = 15 Hz, $J_{3-4\,cis}$ = 4.5 Hz, J_{3-1} = 2 Hz, 3-H_β), 3.75 (1H, m, 4-H), 4.73 (1H, td, J_{a-a} = 10 Hz, J_{a-e} = 4 Hz, —CO_2CH—), 5.87 (1H, dt, $J_{3'-2'}$ = 16 Hz, $J_{3'-1'}$ = 1 Hz, 3′-H), 6.57 (br, 1-H), and 6.86 (1H, dt, $J_{2'-3'}$ = 16 Hz, $J_{2'-1'}$ = 7 Hz, 2′-H) ppm. *Anal.* calcd. for $C_{17}H_{27}NO_3$: C 69.59, H 9.28, N 4.77; found: C 69.46, H 9.34, N 4.75.

p-*Nitrobenzyl [4(*R*)-(3-carbomenthyloxy-2-propen-1-yl)azetidin-2-on-1-yl]triphenylphosphoranylideneacetate (**13**a)*

A mixture of 4(*R*)-(3-carbomenthyloxy-2-propen-1-yl)-2-azetidinone (**4***a*) (2.93 g, 10.0 mmol) and *p*-nitrobenzyl glyoxylate hydrate (2.38 g, 10.5 mmol) in benzene (100 mL) was heated at reflux with a Dean–Stark trap for 3 h. Evaporation of the solvent gave 5.22 g of carbinolamides (epimeric mixture) as crude foam; R_f 0.57 (EtOAc–Et_2O 1:1); ir (neat) ν_{max}: 3440 (OH), 1760 (β-lactam and ester), 1715 (conj. ester), 1660 (C=C), 1525, and 1355 (NO_2) cm^{-1}; ^{1}Hmr ($CDCl_3$, 60 MHz) δ: 0.76 (3H, d, J = 7 Hz, —Me), 0.88 (6H, d, J = 7 Hz, *gem*-Me), 0.8–2.2 (9H, m, —CH— and —CH_2—), 2.4–3.3 (4H, m), 4.00 (1H, m, 4′-H), 4.65 (br, OH), 4.5–4.85 (1H, br, —CO_2CH—), 5.33 (2H, s, —CO_2CH_2Ar), 5.47 (1H, s, 1-H), 5.80, 5.86 (1H, 2d, J = 16 Hz, 3″-H), 6.5–7.2 (1H, m, 2″-H), 7.53 (2H, d, J = 9 Hz, ArH's), and 8.20 (2H, d, J = 9 Hz, ArH's) ppm.

The crude mixture of the two epimeric carbinolamides (4.71 g) was dissolved in THF (90 mL) and to this was added at −15° to −20°C pyridine (1.09 mL, 13.5 mmol), followed by thionyl chloride (0.92 mL), under a nitrogen atmosphere. The mixture was stirred (−15°C, N_2) for 30 min. After filtration of the white precipitate and washing with benzene, the filtrate and washings were combined and evaporated to dryness. The residue, extracted with benzene, was treated with Norit and evaporation of the solvent gave 5.26 g of *p*-nitrobenzyl [4(*R*)-(3-carbomenthyloxy-2-propen-1-yl)azetidin-2-on-1-yl]chloroacetates (epimeric mixture) as crude yellowish oil; ir (neat) ν_{max}: 1765 (β-lactam and ester), 1710 (conj. ester), 1660 (C=C), 1525, and 1350 (NO_2) cm^{-1}; ^{1}Hmr ($CDCl_3$, 60 MHz) δ: 0.76 (3H, d, J = 7 Hz, —Me), 0.89 (6H, d, J = 7 Hz, *gem*-Me), 0.8–2.1 (9H, m), 2.4–3.0 (3H, m, 3′-H_β and 1″-H's), 3.20 (1H, dd, J_{gem} = 15 Hz, $J_{3'-4'\,cis}$ = 5 Hz, 3′-H_α), 4.17 (1H, m, 4′-H), 4.72 (1H, m, —CO_2CH—), 5.33 (2H, s, —CO_2CH_2Ar), 5.85 (1H, d, J = 16 Hz, 3″-H), 6.23 (1H, s, 1-H), 6.5–7.2 (1H, m, 2″-H), 7.55 (2H, d, J = 9 Hz, ArH's), and 8.26 (2H, d, J = 9 Hz, ArH's) ppm.

To a stirred solution of the crude mixture of the two epimeric chloro compounds (5.23 g) and triphenylphosphine (2.60 g, 9.91 mmol) in dioxane (90 mL) was added 2,6-lutidine (1.16 mL, 10.0 mmol) at room temperature under a nitrogen atmosphere. The mixture was stirred overnight (20 h) and the precipitate was filtered and washed with EtOAc. The filtrate and washings were combined and evaporated. The residue, redissolved in EtOAc (50 mL), was washed with 1 *N* HCl (20 mL × 2) and then brine, dried (Na_2SO_4), and evaporated, yielding a crude oil. This was purified by column chromatography (120 g, EtOAc–Et_2O 1:1) to give 3.89 g (5.21 mmol, yield 58.1% based on **4***a*) of the title compound **13***a* as yellowish foam; R_f 0.47 (EtOAc–Et_2O 1:1); $[\alpha]_D^{21}$ − 51.5° (*c* 1.7, CH_2Cl_2); ir (film) ν_{max}: 1750 (β-lactam) 1715 (conj. ester), 1655 (C=C), 1625 (ester), 1520, and 1350 (NO_2) cm^{-1}; ^{1}Hmr ($CDCl_3$, 60 MHz) δ: 0.77 (3H, d, J = 7 Hz, —Me), 0.90 (6H, d, J = 7 Hz, *gem*-Me), 4.85, 5.2 (2H, 2s, —CO_2CH_2Ar), 7.2–8.0 (17H, m, ArH's), and 8.20 (2H, d, J = 9 Hz, ArH's) ppm, the rest are not well resolved. *Anal.* calcd. for

Can. J. Chem. Downloaded from www.nrcresearchpress.com by 210.87.254.105 on 09/06/12
For personal use only.

$C_{44}H_{47}N_2O_7P$: C 70.76, H 6.34, N 3.75; found: C 71.02, H 6.41, N 3.51.

p-*Nitrobenzyl [4(S)-(3-carbomenthyloxy-2-propen-1-yl)azetidin-2-on-1-yl]triphenylphosphoranylideneacetate (**13**b)*

The title compound, 4.12 g (5.52 mmol, yield 68.0% based on **4***b*), was prepared as yellow foam from 4(*S*)-(3-carbomenthyloxy-2-propen-1-yl)-2-azetidinone (**4***b*) (2.93 g, 10.0 mmol) by the method described above for the 4*R*-isomer, through the corresponding intermediates; R_f 0.47 (EtOAc–Et_2O 1:1); $[\alpha]_D^{21}$ −0.2° (*c* 1.3, CH_2Cl_2); ir (film) ν_{max}: 1750 (β-lactam), 1715 (conj. ester), 1655 (C=C), 1630 (ester), 1420, and 1350 (NO_2) cm^{-1}; ^{1}Hmr ($CDCl_3$, 60 MHz) δ: 0.75 (3H, d, *J* = 7 Hz, —Me), 0.88 (6H, d, *J* = 7 Hz, *gem*-Me), 7.2–8.0 (17H, m, ArH's), and 8.2 (2H, d, *J* = 9 Hz, ArH's) ppm, the rest are not well resolved. *Anal.* calcd. for $C_{44}H_{47}N_2O_7P$: C 70.76, H 6.34, N 3.75; found: C 70.47, H 6.42, N 3.69.

p-*Nitrobenzyl 5(R)-carbapen-2-em-3-carboxylate (**3**a)*

To a stirred solution of *p*-nitrobenzyl [4(*R*)-(3-carbomenthyloxy--2-propen-1-yl)azetidin-2-on-1-yl]triphenylphosphoranylideneacetate (**13***a*) (747 mg, 1.00 mmol) in CH_2Cl_2 (20 mL) was added at 0°–5°C trifluoroacetic acid (2 mL) and the resulting yellow solution was cooled to −78°C. A stream of ozone was introduced until the blue colour was retained and the mixture was stirred at −78°C for another 5 min. Nitrogen was bubbled through the solution to remove excess ozone and then dimethyl sulfide (1.5 mL) was added. After removing the cooling bath, the mixture was stirred at 0°–5°C for 1 h and washed successively with saturated $NaHCO_3$ (50 mL × 2) and brine. The organic layer was dried (Na_2SO_4) and evaporated *in vacuo* (bath temperature 35°–40°C) to yield a crude oil. This was purified by column chromatography (30 g, Et_2O) to give 197 mg (0.683 mmol, yield 68.3%) of the title compound **3***a* as a yellow solid. An analytical sample was obtained, by recrystallization from CH_2Cl_2–Et_2O, as white crystals; mp 123°–124°C; R_f 0.35 (EtOAc–hex 1:1); $[\alpha]_D^{21}$ +127.5° (*c* 1.0, CH_2Cl_2); ir (film) ν_{max}: 1780 (β-lactam), 1725 (ester), 1520, and 1350 (NO_2) cm^{-1}; uv (EtOH) λ_{max}: 267 nm (ε 14 800); ^{1}Hmr ($CDCl_3$, 80 MHz) δ: 2.72 (1H, ddd, J_{gem} = 19 Hz, J_{1-5} = 9 Hz, J_{1-2} = 3 Hz, 1-H_a), 2.98 (1H, dd, J_{gem} = 17 Hz, $J_{6-5\,trans}$ = 3.3 Hz, 6-H_β), 3.02 (1H, ddd, J_{gem} = 19 Hz, J_{1-5} = 9 Hz, J_{1-2} = 3 Hz, 1-H_b), 3.54 (1H, dd, J_{gem} = 17 Hz, $J_{6-5\,cis}$ = 5.5 Hz, 6-H_α), 4.3 (1H, m, 5-H_α), 5.16–5.33–5.38–5.55 (2H, ABq, —CO_2CH_2Ar), 6.58 (1H, t, *J* = 3 Hz, 2-H), 7.60 (2H, d, *J* = 8.8 Hz, ArH's), and 8.23 (2H, d, *J* = 8.8 Hz, ArH's) ppm; ^{1}Hmr (**3***a*, 5 mg, and Eu(dcm)$_3$, 25 mg, in $CDCl_3$, 0.5 mL; 80 MHz) δ: 5.98–6.15–6.32–6.49 (2H, ABq, —CO_2CH_2Ar), and 7.01 (1H, t, *J* = 3 Hz, 2-H) ppm. *Anal.* calcd. for $C_{14}H_{12}N_2O_5$: C 58.33, H 4.20, N 9.72; found: C 58.37, H 4.18, N 9.72.

p-*Nitrobenzyl 5-(S)-carbapen-2-em-3-carboxylate (**3**b)*

The crude title compound was obtained from *p*-nitrobenzyl [4(*S*)-(3-carbomenthyloxy-2-propen-1-yl)azetidin-2-on-1-yl]triphenylphosphoranylideneacetate (**13***b*) (747 mg, 1.00 mmol) by the method described for the 5*R*-isomer. This material was purified by column chromatography (20 g, EtOAc–hex 1:1) to yield 182 mg (0.791 mmol, yield 79.1%) of menthyl glyoxylate hydrate as white solid; mp 78°–81°C (Et_2O–pentane); R_f 0.75 (EtOAc–hex 1:1); $[\alpha]_D^{21}$ −77.0° (*c* 1.0, CH_2Cl_2); ir (film) ν_{max}: 3420 (OH) and 1740 (ester) cm^{-1}; and 197 mg (0.683 mmol, yield 68.3%) of the title compound as a white solid; mp 122°–124°C (recrystallized from CH_2Cl_2–Et_2O); R_f 0.35 (EtOAc–hex 1:1); $[\alpha]_D^{21}$ −110.8° (*c* 1.0, CH_2Cl_2); ir (film) ν_{max}: 1780 (β-lactam), 1730 (ester), 1520, and 1350 (NO_2) cm^{-1}; uv (EtOH) λ_{max}: 267 nm (ε 15 600); ^{1}Hmr ($CDCl_3$, 80 MHz) δ: 2.73 (1H, ddd, J_{gem} = 19 Hz, J_{1-5} = 9 Hz, J_{1-2} = 3 Hz, 1-H_a), 2.98 (1H, dd, J_{gem} = 17 Hz, $J_{6-5\,trans}$ = 3 Hz, 6-H_α), 3.03 (1H, ddd, J_{gem} = 19 Hz, J_{1-5} = 9.5 Hz, J_{1-2} = 3 Hz, 1-H_b), 3.55 (1H, dd, J_{gem} = 17 Hz, $J_{6-5\,cis}$ = 5.5 Hz, 6-H_β), 4.3 (1H, m, 5-H_β), 5.16–5.34–5.38–5.56 (2H, ABq, —CO_2CH_2Ar), 6.59 (1H, t, *J* = 3 Hz, 2-H), 7.60 (2H, d, *J* = 8.8 Hz, ArH's), and 8.23 (2H, d, *J* = 8.8 Hz, ArH's) ppm; ^{1}Hmr (**3***b*, 5 mg, and Eu(dcm)$_3$, 25 mg, in $CDCl_3$, 0.5 mL; 80 MHz) δ: 5.98–6.15–6.27–6.45 (2H, ABq, —CO_2CH_2Ar), 6.34 (a part of the ABq in the 5*R*-isomer), and 7.05 (1H, t, *J* = 3 Hz, 2-H) ppm. *Anal.* calcd. for $C_{14}H_{12}N_2O_5$: C 58.33, H 4.20, N 9.72; found: C 58.08, H 4.26, N 9.93.

N-tert-*butyldimethylsilyl-4(R)-(3-carbomenthyloxy-2-propen-1-yl)-2-azetidinone (**14**a)*

To a stirred solution of 4(*R*)-(3-carbomenthyloxy-2-propen-1-yl)-2-azetidinone (**4***a*) (1.91 g, 6.52 mmol) and *tert*-butyldimethylsilyl chloride (1.11 g, 7.37 mmol) in dimethylformamide (20 mL) was added at 0°C under a nitrogen atmosphere triethylamine (1.04 mL, 7.5 mmol), causing white precipitation. The mixture was stirred at room temperature overnight (18 h), and then diluted with water (100 mL) and Et_2O (65 mL). After shaking, the separated organic layer was washed with water (80 mL × 3), then brine, dried (Na_2SO_4), and evaporated to 2.56 g of an oil. This was crystallized from pentane at 0°C, yielding 2.10 g (5.15 mmol, yield 79.0%) of the title compound **14***a* as off-white crystals; mp 80.5°–81.5°C; R_f 0.54 (EtOAc–hex 1:4); $[\alpha]_D^{20}$ −116.0° (*c* 1.0, CH_2Cl_2); ir (film) ν_{max}: 1750 (β-lactam), 1715 (conj. ester), and 1655 (C=C) cm^{-1}; ^{1}Hmr ($CDCl_3$, 80 MHz) δ: 0.23 (3H, s, Si-Me), 0.25 (3H, s, Si-Me), 0.76 (3H, d, *J* = 7 Hz, —Me), 0.89 (6H, d, *J* = 7 Hz, *gem*-Me), 0.96 (9H, s, Si-*t*Bu), 2.64 (1H, dd, J_{gem} = 15 Hz, $J_{3-4\,trans}$ = 3 Hz, 3-H_β), 3.19 (1H, dd, J_{gem} = 15 Hz, $J_{3-4\,cis}$ = 5 Hz, 3-H_α), 3.65 (1H, m, 4-H_α), 4.75 (1H, td, J_{a-a} = 10 Hz, J_{a-e} = 4 Hz, —CO_2CH—), 5.85 (1H, dt, $J_{3'-2'}$ = 15.7 Hz, $J_{3'-1'}$ = 1.4 Hz, 3'-H), and 6.83 (1H, dt, $J_{2'-3'}$ = 15.7 Hz, $J_{2'-1'}$ = 7 Hz, 2'-H) ppm. *Anal.* calcd. for $C_{23}H_{41}NO_3Si$: C 67.76, H 10.14, N 3.44; found: C 67.85, H 10.07, N 3.76.

N-tert-*butyldimethylsilyl-4(S)-(3-carbomenthyloxy-3-propen-1-yl)-2-azetidinone (**14**b)*

The crude title compound (9.0 g) was prepared as an oil from 4(*S*)-(3-carbomenthyloxy-2-propen-1-yl)-2-azetidinone (**4***b*) (6.70 g, 22.87 mmol) by the method described for the 4(*R*)-isomer. This was purified by column chromatography (270 g, EtOAc–hex 1:4) to obtain 8.10 g (19.9 mmol, yield 87.0%) of the title compound **14***b* as a colourless oil; R_f 0.54 (EtOAc–hex 1:4); $[\alpha]_D^{21}$ +9.0° (*c* 1.0, CH_2Cl_2); ir (neat) ν_{max}: 1750 (β-lactam), 1715 (conj. ester), and 1655 (C=C) cm^{-1}; ^{1}Hmr ($CDCl_3$, 80 MHz) δ: 0.22 (3H, s, Si-Me), 0.24 (3H, s, Si-Me), 0.75 (3H, d, *J* = 7 Hz, —Me), 0.88 (6H, d, *J* = 7 Hz, *gem*-Me), 0.95 (9H, s, Si-*t*Bu), 2.63 (1H, dd, J_{gem} = 15 Hz, $J_{3-4\,trans}$ = 3 Hz, 3-H_α), 3.18 (1H, dd, J_{gem} = 15 Hz, $J_{3-4\,cis}$ = 5 Hz, 3-H_β), 3.6 (1H, m, 4-H_β), 4.74 (1H, td, J_{a-a} = 10 Hz, J_{a-e} = 4 Hz, —CO_2CH—), 5.85 (1H, dt, $J_{3'-2'}$ = 15.7 Hz, $J_{3'-1'}$ = 1.4 Hz, 3'-H), and 6.82 (1H, td, $J_{2'-3'}$ = 15.7 Hz, $J_{2'-1'}$ = 7 Hz, 2'-H.

N-tert-*butyldimethylsilyl-3(S)-carboxymethyl-2-azetidinone (**15**a)*

(a) *From compound **14**a*

A suspension of potassium permanganate (474 mg, 3.00 mmol) in water (5 mL) was vigorously stirred for 10 min and cooled to 5°–10°C while toluene (2 mL), tetrabutylammonium bromide (50 mg), and a solution of *N-tert*-butyldimethylsilyl-4(*R*)-(3-carbomenthyloxy-2-propen-1-yl)-2-azetidinone (**14***a*) (408 mg, 1.00 mmol) in EtOAc (3 mL) were added successively. The mixture was stirred at room temperature for 1 h and then the reaction was quenched by successive addition of a solution of sodium bisulfite (937 mg) in water (9 mL), EtOAc (10 mL), and then 3 *N* HCl (3 mL). The organic layer was collected and the aqueous layer extracted with EtOAc. All organic layers were combined, washed with brine, dried (Na_2SO_4), and evaporated to obtain 507 mg of a crude gum. This was purified by column chromatography (30 g, acetone–toluene 1:1) to yield 123 mg (0.505 mmol, yield 50.5%) of the title compound **15***a* as an amorphous solid; mp 100°–105°C; R_f 0.4 (acetone–toluene 1:1, elongated spot); $[\alpha]_D^{21}$ −67.5° (*c* 1.0, CH_2Cl_2); ir (film) ν_{max}: 2500–3500 (br, —CO_2H), 1730 (β-lactam), and 1680 (—CO_2H) cm^{-1}; ^{1}Hmr ($CDCl_3$, 80 MHz) δ: 0.22 (3H, s, Si-Me), 0.25 (3H, s, Si-Me), 0.95 (9H, s, Si-*t*Bu), 2.50 (1H, dd, J_{gem} = 16 Hz, $J_{1'-4}$ = 9.8 Hz, —*CH*—CO_2H), 2.79 (1H, dd, J_{gem} = 15.7 Hz, $J_{3-4\,trans}$ = 2.8 Hz), 2.93 (1H, dd, J_{gem} = 16 Hz, $J_{1'-4}$ = 4.1 Hz, —CH—CO_2H), 3.33 (1H, dd, J_{gem} = 15.7 Hz, $J_{3-4\,cis}$ = 5.3 Hz, 3-H_α), 3.9 (1H, m, 4-H_α), and 6.25 (br, —CO_2H) ppm.

(b) *From compound* **16**

The title compound **15***a* (97 mg, 0.40 mmol, yield 40%) was prepared as white foam from *N-tert*-butyldimethylsilyl-4(*R*)-allyl-2-azetidinone (**16**) (224 mg, 1.00 mmol) by the method described above; R_f 0.4 (acetone–toluene 1:1, elongated spot); $[\alpha]_D^{21}$ −80.3° (*c* 1.0, CH_2Cl_2). The ^{1}Hmr ($CDCl_3$, 80 MHz) and ir (film) spectra were identical with those obtained from **14***a*.

N-tert-*butyldimethylsilyl-3(*R*)-carboxymethyl-2-azetidinone (**15**b)*

The title compound **15***b* (5.07 mg, 2.08 mmol, yield 69.3%) was obtained as off-white foam from *N-tert*-butyldimethylsilyl-4(*S*)-(3-carbomenthyloxy-2-propen-1-yl)-2-azetidinone (**14***b*) (1.223 g, 3.00 mmol) by the method described above for the 4*S*-isomer; R_f 0.4 (acetone–toluene 1:1, elongated spot); $[\alpha]_D^{21}$ +36.6° (*c* 1.0, CH_2Cl_2). The ^{1}Hmr ($CDCl_3$, 80 MHz) and ir (film) spectra were identical with those of the 4*S*-isomer.

Acknowledgements

We would like to thank Professor B. Belleau of McGill University and Dr. M. Ménard for their interest in this work. We also thank Mr. G. Lacasse for 80 MHz ^{1}Hmr spectra.

1. Y. Ueda, C. E. Damas, and B. Belleau. Can. J. Chem. **61**, 1996 (1983).
2. L. D. Cama and B. G. Christensen. J. Am. Chem. Soc. **100**, 8006 (1978).
3. (*a*) A. J. G. Baxter, K. H. Dickinson, P. M. Roberts, T. C. Small, and R. Southgate. J. Chem. Soc. Chem. Commun. 236 (1979); (*b*) J. H. Bateson, A. J. G. Baxter, P. M. Roberts, T. C. Small, and R. Southgate. J. Chem. Soc. Perkin Trans. 1, 3242 (1981).
4. H. Onoue, M. Narisada, S. Uyeo, H. Matsumura, K. Okada, T. Yano, and W. Nagata. Tetrahedron Lett. 3867 (1979).
5. H. R. Pfaendler, J. Gosteli, R. B. Woodward, and G. Rihs. J. Am. Chem. Soc. **103**, 4526 (1981).
6. J. H. Bateson and P. M. Roberts. (Beecham Pharmaceuticals). European Patent Application 0 008 888 (1980); Chem. Abstr. **94**, P3917f (1981).
7. W. L. Parker, M. L. Rathnum, J. S. Wells, Jr., W. H. Trejo, P. A. Principe, and R. B. Sykes. J. Antibiot. **35**, 653 (1982).
8. (*a*) R. Scartazzini, H. Peter, H. Bickel, K. Heusler, and R. B. Woodward. Helv. Chim. Acta, **55**, 408 (1972); (*b*) R. B. Woodward, K. Heusler, I. Ernest, K. Burri, R. J. Friary, F. Haviv, W. Oppolozer, R. Paioni, K. Syhora, R. Wenger, and J. K. Whitesell. Nouv. J. Chim. **1**, 85 (1977); (*c*) I. Ernest, J. Gosteli, C. W. Greengrass, W. Holick, D. E. Jackman, H. R. Pfaendler, and R. B. Woodward. J. Am. Chem. Soc. **100**, 8214 (1978).
9. H. R. Pfaendler, J. Gosteli, and R. B. Woodward. J. Am. Chem. Soc. **101**, 6306 (1979).
10. (*a*) J. K. Rasmussen and A. Hassner. Chem. Rev. **76**, 389 (1976); (*b*) W. A. Szabo. Aldrichimica Acta, **10**, 23 (1977).
11. T. Durst and M. J. O'Sullivan. J. Org. Chem. **35**, 2043 (1970).
12. (*a*) G. R. Sullivan. *In* Topics in stereochemistry. Vol. 10. *Edited by* E. L. Eliel and N. L. Allinger. Interscience – John Wiley and Sons, New York. 1978. pp. 288–329; (*b*) M. D. McCreary, D. W. Lewis, D. L. Wernick, and G. M. Whitesides. J. Am. Chem. Soc. **96**, 1038 (1974).
13. A. W. Herriott and D. Picker. Tetrahedron Lett. 1511 (1974).
14. M. J. Basker, J. H. Bateson, A. J. G. Baxter, R. J. Ponsford, P. M. Roberts, R. Southgate, T. C. Smale, and J. Smith. J. Antibiot. **34**, 1224 (1981).
15. E. G. Brain, A. J. Eglington, J. H. C. Nayler, N. F. Osborne, R. Southgate, and P. M. Tolliday. J. Chem. Soc. Perkin Trans. 1, 2479 (1977).
16. M. Ménard and A. Martel. (Bristol-Myers Co.). U.S. Patent 4,282,150 (1981).
17. H. Rupe. Justus Liebigs Ann. Chem. **327**, 157 (1903).

Can. J. Chem. Downloaded from www.nrcresearchpress.com by 210.87.254.105 on 09/06/12
For personal use only.

Hydrolysis of phosphoranes containing a perfluoropinacolyl ring[1]

ALEXANDER F. JANZEN, ALBERTA E. LEMIRE, RONALD KIRK MARAT, AND ALAN QUEEN
Department of Chemistry, University of Manitoba, Winnipeg, Man., Canada R3T 2N2

Received January 26, 1983

ALEXANDER F. JANZEN, ALBERTA E. LEMIRE, RONALD KIRK MARAT, and ALAN QUEEN. Can. J. Chem. **61**, 2264 (1983).

The hydrolysis of phosphoranes $Ph_2P(pfp)Cl$, $Ph_2P(pfp)OR$, $PhP(pfp)(OR)_2$, and $(RO)_3P(pfp)$, containing a perfluoropinacolyl (pfp) ring, occurs under neutral, basic, or acidic conditions and leads to the formation of acyclic perfluoropinacolyl products, i.e. $R_2P(O)OC(CF_3)_2C(CF_3)_2OH$, as determined by ^1H, ^{19}F, ^{31}P, ^{13}C nmr and ir studies. In the presence of a base, all trifluoromethyl groups in $Ph_2P(O)OC(CF_3)_2C(CF_3)_2OH$ are equilibrated, as verified by ^{19}F and ^{13}C nmr; and from the variable temperature ^{19}F nmr line-shape analysis the activation parameters for this exchange process were found to be: E_a = 36.0 ± 3 kJ mol^{-1}, $\Delta H^{\ddagger}$ = 33.5 ± 3 kJ mol^{-1}, $\Delta S^{\ddagger}$ = −86 ± 8 J K^{-1} mol^{-1}, $\Delta G^{\ddagger}_{298}$ = 59.0 ± 0.6 kJ mol^{-1}. The reactions of phosphoranes with HF were briefly investigated.

ALEXANDER F. JANZEN, ALBERTA E. LEMIRE, RONALD KIRK MARAT et ALAN QUEEN. Can. J. Chem. **61**, 2264 (1983).

L'hydrolyse des phosphoranes: $Ph_2P(pfp)Cl$, $Ph_2P(pfp)OR$, $PhP(pfp)(OR)_2$ et $(RO)_3P(pfp)$ contenant le cycle perfluoropinacolyle (pfp) se produit en milieu neutre, acide ou basique et conduit à la formation de perfluoropinacolyles acycliques i.e. $R_2P(O)OC(CF_3)_2C(CF_3)_2OH$ comme l'indiquent la rmn du ^1H, du ^{19}F, du ^{31}P, du ^{13}C et les études en ir. La rmn du ^{19}F et du ^{13}C révèle qu'en milieu basique tous les groupes trifluorométhyle du $Ph_2P(O)OC(CF_3)_2C(CF_3)_2OH$ sont équilibrés. L'analyse de la forme des raies de la rmn du ^{19}F à température variable donne les paramètres d'activation suivants: E_a = 36,0 ± 0,3 kJ mol^{-1}, $\Delta H^{\ddagger}$ = 33,5 ± 3 kJ mol^{-1}, $\Delta S^{\ddagger}$ = −86,8 J K^{-1} mol^{-1}, $\Delta G^{\ddagger}$ = 59,0 ± 0,6 kJ mol^{-1}. On discute brièvement des réactions des phosphoranes avec le HF.

[Traduit par le journal]

Can. J. Chem. Downloaded from www.nrcresearchpress.com by 210.87.254.42 on 09/06/12
For personal use only.

The hydrolysis of phosphoranes containing a five-membered ring may produce either an acyclic phosphoryl compound **A** or a cyclic hydroxyphosphorane **B**. In some instances, an equilibrium between isomers **A** and **B** has been observed and the equilibrium may be shifted by varying the temperature or the

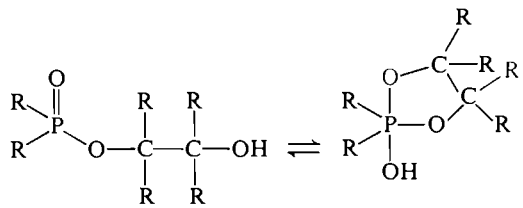

A **B**

base concentration (1−5). Such equilibria, of interest because of their role in the hydrolysis of phosphorus esters in organic and biological systems, may be studied by ^{19}F nmr since the trifluoromethyl groups are often equivalent in cyclic perfluoropinacolyl phosphoranes, but non-equivalent in acyclic analogues. Recent studies with $Me_2P(O)OC(CF_3)_2C(CF_3)_2OH$ have demonstrated that ^{19}F nmr can be used to monitor an equilibrium between cyclic and acyclic phosphorus compounds (6).

In some early work, we prepared the perfluoropinacolyl derivative **1** from chlorodiphenylphosphine and hexafluoroacetone and observed its rapid hydrolysis to $Ph_2P(pfp)OH$ (7).

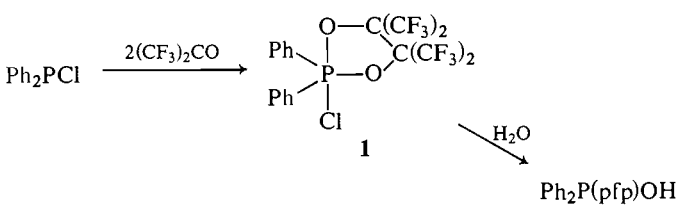

1

Although **1** gave a single fluorine nmr peak in the pfp region (pfp = —$OC(CF_3)_2C(CF_3)_2O$—) and ir bands characteristic of a cyclic pfp derivative, our evidence did not distinguish between an acyclic **A** or cyclic **B** structure for the hydrolysis product. More recently, as part of a kinetic study of the hydrolysis of $PhP(pfp)[OCH(CF_3)_2]_2$ (8), we required structural information about the hydrolysis product; consequently, we have re-examined the synthesis and hydrolysis of **1**, and also studied the hydrolysis of a variety of other perfluoropinacolyl phosphoranes using ^{19}F, ^{31}P, and ^{13}C nmr to distinguish between acyclic and cyclic products and using dynamic nmr techniques to investigate the equilibrium between acyclic **A** and cyclic **B** products.

Phosphoranes **1**−**8** were prepared from hexafluoroacetone and the corresponding phosphines and identified by a combination of nmr, ir, ms, and elemental analysis. The chlorophosphorane **1**, although stable in a sealed tube, hydrolyzed rapidly and was conveniently identified by its reaction with $(CF_3)_2CHOH$ to give **2**.

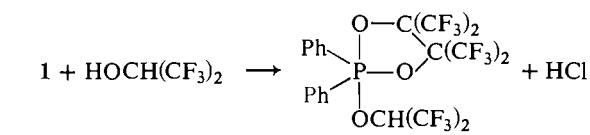

2

Those ir bands previously found to be characteristic of cyclic pfp derivatives (9) are present in phosphoranes **1**−**8** (Table 1).

The fluorine nmr spectra of **1**−**8** gave single peaks in the pfp region, thus showing that the trifluoromethyl groups are equivalent in the cyclic phosphoranes. This equivalence is also evident in the carbon nmr spectra of **2** and **6** (Table 2) which show only one CF_3 and one O—C peak assigned to the pfp ring. Other perfluoropinacolyl phosphoranes also show this equivalence in their carbon nmr spectra (10).

The hydrolysis of cyclic phosphoranes **1**, **3**−**8** was carried out under neutral, basic, or acidic conditions to give products **9**−**11**. In some instances, further reaction occurred and free

[1]Presented at the 63rd C.I.C. Conference, Ottawa, Ont., Canada, June 8−11, 1980.

Can. J. Chem. Downloaded from www.nrcresearchpress.com by 210.87.254.42 on 09/06/12
For personal use only.

TABLE 1. Infrared bands (cm^{-1}) characteristic of cyclic pfp derivatives

Compound	Infrared band
1	1095 998 954 878 743
2	1109 1001 963 888 745
3	1108 1001 966 888 736
6	1120 1005 968 888 743
7	1120 1020 958 882 750
8	1124 998 965 880 745

perfluoropinacol was liberated but, as described in the Experimental section, products **9**–**11** could be isolated in 10–75% yield. Hydrolysis of **1** occurred on exposure to air or in solvents containing trace amounts of water or in aqueous acetonitrile. Hydrolysis of **3**–**5** was carried out in 99% ethanol or in dilute NaOH solution. Hydrolysis of **6**–**9** was accomplished with concentrated H_2SO_4 at 25°C; at higher temperatures, perfluoropinacol is liberated (11).

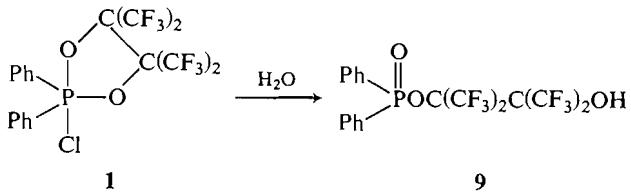

1 **9**

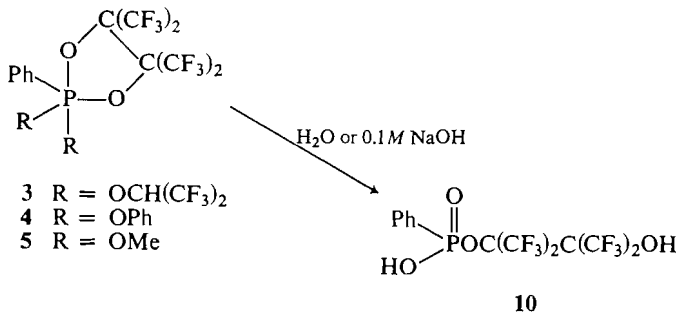

3 R = $OCH(CF_3)_2$
4 R = OPh
5 R = OMe

10

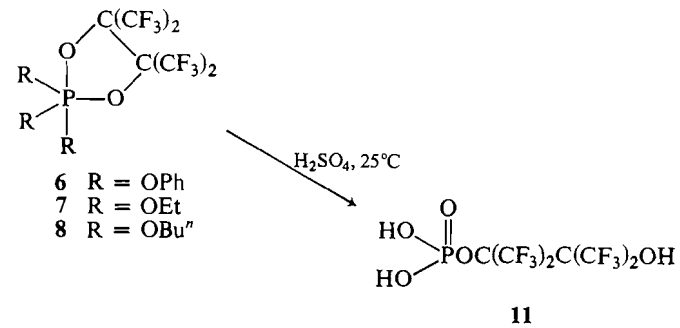

6 R = OPh
7 R = OEt
8 R = OBu″

11

An acyclic **A** or cyclic **B** structure was considered for the hydrolysis products **9**–**11**. Although a cyclic structure $(HO)_3P(pfp)$ has been proposed for the hydrolysis product of $(EtO)_3P(pfp)$, **7** (12), the following spectral evidence is entirely consistent with an acyclic phosphoryl structure **A** for **9**–**11**: (*a*) The ^{19}F nmr spectra of **9**–**11** show, in each case, two septets with $^5J_{FF}$ = 10 Hz (Table 2). A typical spectrum is shown in Fig. 1. A cyclic structure would be expected to give only a single perfluoropinacolyl peak, as found for the cyclic phosphoranes **1**–**8**. (*b*) The ^{13}C nmr spectra of **9**–**11** show non-equivalent CF_3 groups as well as non-equivalent ring carbons, whereas the ^{13}C nmr spectra of cyclic phosphoranes **2** and **6** show equivalent CF_3 groups and equivalent ring carbons in the pfp region (Table 2). (*c*) A comparison of the phosphorus chemical shifts of the cyclic phosphoranes **1**–**8** with the hydrolysis products **9**–**11** shows a significant downfield shift for **9**–**11** (Table 2). For example, on hydrolysis of **1** to **9** there is a shift from −5.4 to 41.3 ppm; from **3** to **10** there is a shift from −38.6 to 12.2 ppm; and from **7** to **11** there is a shift from −53.2 (13) to −8.6 ppm. The phosphorus chemical shift of $Ph_2P(O)OCH(CF_3)_2$ (**12**) 39.2 ppm (14), however, is very similar to that of $Ph_2P(O)OC(CF_3)_2C(CF_3)_2OH$ (**9**) 41.3 ppm, as expected if **9** has an acyclic structure.

Compound **9** was used to study the equilibrium between acyclic **A** and cyclic **B** isomers. The doublet of septets in the ^{19}F nmr spectrum of **9** collapsed to a single peak as the rate of exchange of trifluoromethyl groups increased. In solvents such as acetone, dioxane, dichloromethane, or toluene, exchange is evident above 60°C. At 25°C exchange is promoted by bases such as pyridine, imidazole, quinoline, and excess dimethylsulfoxide. Typical pyridine-promoted temperature-dependent ^{19}F nmr spectra are shown in Fig. 1. A line-shape analysis of the variable temperature spectra gave the following activation parameters: E_a = 36.0 ± 3 kJ mol^{-1}, $\Delta H^{\ddagger}$ = 33.5 ± 3 kJ mol^{-1}, $\Delta S^{\ddagger}$ = −86 ± 8 J K^{-1} mol^{-1}, $\Delta G^{\ddagger}_{298}$ = 59.0 ± 0.6 kJ mol^{-1}.

Deprotonation, following by ring-closure, adequately accounts for the nmr results. An exchange mechanism involving

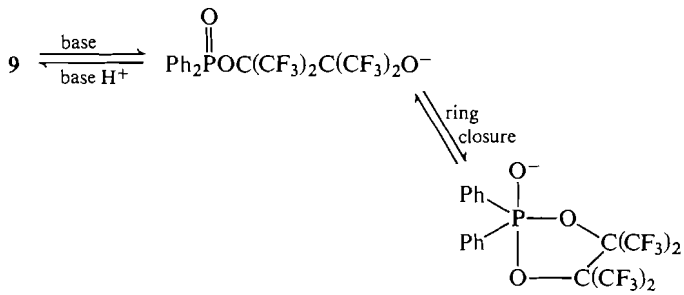

complete loss of the perfluoropinacolyl ligand was eliminated by adding perfluoropinacol to a rapidly exchanging system and observing separate ^{19}F nmr peaks for bound and free perfluoropinacol. That exchange in **9** can occur by a ring-closing and ring-opening process, with rates that are rapid on the nmr time scale, is of interest in view of alternative mechanisms of exchange in cyclic phosphoranes such as Berry pseudorotation or turnstile rotation (15).

Attempts to observe exchange of the $OCH(CF_3)_2$ group in $PhP(pfp)[OCH(CF_3)_2]_2$ (**3**) with free $HOCH(CF_3)_2$ in solvent dimethoxyethane, or with $HOCH(CF_3)_2$ in the presence of pyridine, or with $NaOCH(CF_3)_2$ in dimethylformamide, all at 25°C, were unsuccessful; in each case separate fluorine nmr signals were observed for free and bound $OCH(CF_3)_2$ groups.

Finally, as part of our interest in reactions of HF, we briefly investigated the reactions of phosphoranes with anhydrous HF. With 1 mol HF, $PhP(pfp)[OCH(CF_3)_2]_2$ (**3**) gave a mixture of $PhPF(pfp)OCH(CF_3)_2$ and $PhPF_2(pfp)$ while adding 2–4 mol HF gave mainly $PhPF_2(pfp)$, but on standing at 25°C, perfluoropinacol was liberated. After 6 days, $PhP(pfp)(OPh)_2$ and 2 mol HF showed mainly $PhPF_2(pfp)$ and perfluoropinacol. Reaction of $(PhO)_5P$ with 1 or 2 mol HF gave $(PhO)_4PF$ and $(PhO)_3PF_2$ but on standing at 25°C or on increasing the ratio of HF, the formation of $(PhO)_4P^+PF_6^-$ (16) was favoured. $PhP(OMe)_2(pfp)$ (**5**) with 1 mol HF liberated perfluoropinacol.

TABLE 2. Nmr spectral parameters of some perfluoropinacolyl phosphorus compounds[a]

Compound	δ_P	δ_F	δ_C (CF_3)	δ_C (—OC)
1	−5.4	−67.4		
2	−18.7	−67	121.9	82.4
		−72	121.2 (J_{CP}4.9)	72.7 ($^1J_{CH}$149.5, $^2J_{CP}$11.1, $^2J_{CF}$33.2)
3	−38.6	−67		
		−72		
5	−31.2	−68		
6		−68	120.9 ($^3J_{CP}$8.9)	81.7
8		−68.9		
9	41.3	−67.3 ($^5J_{FF}$10)	121.7	88.0 (J_{CP}14.4)
		−69.4	120.7 (J_{CP}4.8)	81.9
10	12.2	−67.3 ($^5J_{FF}$10)	121.3	86.6 (J_{CP}15.3)
		−69.4	120.5 (J_{CP}5.5)	81.7
11	−8.6	−67 ($^5J_{FF}$10)	122.2	85.5 (J_{CP}8.8)
		−68	121.3	83.1
12			122	69.2 ($^2J_{CP}$5.0, $^2J_{CF}$34.6)

[a]Chemical shifts in ppm are positive to low field of TMS, $CFCl_3$, and 85% H_3PO_4. Coupling constants in Hz.

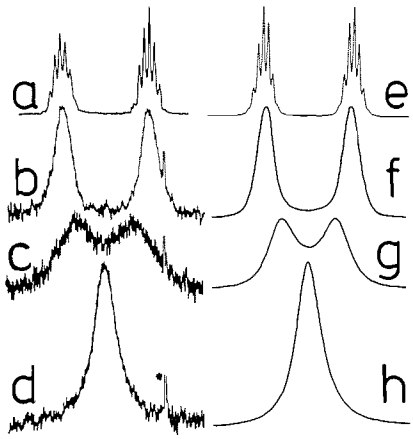

FIG. 1. Typical pyridine-promoted, temperature-dependent experimental (left) and calculated (right) ^{19}F nmr spectra of $Ph_2P(O)OC(CF_3)_2C(CF_3)_2OH$, **9** (0.19 *M*), in 1:1 CD_2Cl_2−toluene. (*a*) 300 K, [py] = 0 *M*; (*b*) 270 K, [py] = 0.20 *M*; (*c*) 300 K, [py] = 0.20 *M*; (*d*) 320 K, [py] = 0.21 *M*; (*e*) τ = 0.2 s; (*f*) τ = 0.02 s; (*g*) τ = 0.0044 s; (*h*) τ = 0.00125 s. *Impurity peak is perfluoropinacol.

$PhP(OPh)_2$ with 2 mol HF gave a mixture of PhPF(OPh), $PhPF_2$, and $PhPF_3H$, while $PhP[OCH(CF_3)_2]_2$ with 2 mol HF gave a mixture of $PhPFOCH(CF_3)_2$, $PhPF_2$, and $PhPF_3H$.

Experimental

Infrared spectra were measured on a Perkin-Elmer 337 spectrophotometer in Nujol and hexachlorobutadiene on NaCl plates. Mass spectra were obtained on a Finnigan 1015 quadrupole instrument operating at 70 eV. ^1H, ^{13}C, ^{19}F, and ^{31}P nmr spectra were recorded on a Bruker WH-90 spectrometer at 90, 22.63, 84.66, and 36.44 MHz, respectively. Fluorine decoupling of ^{13}C nmr spectra was accomplished with a modified Bruker BSV3 decoupler operating at 84.7 MHz with a power level of 10 W and a 3 dB noise bandwidth of 500 Hz. The nmr lineshapes were calculated with a matrix-expanded and modified version of the program DNMR3 (17) on an Amdahl 470-V7 computer with the IBM Fortran H (extended) compiler. Elemental analyses were carried out by Micro-Tech Laboratories, Skokie, Illinois.

The following compounds were prepared by the literature methods: $PhP(pfp)[OCH(CF_3)_2]_2$ (**3**), ref. 8; $PhP(pfp)(OPh)_2$ (**4**), ref. 18; PhP(pfp)$(OMe)_2$ (**5**), ref. 18; $(PhO)_3P(pfp)$ (**6**), ref. 19; $(EtO)_3P(pfp)$, ref. 13; $Ph_2P(O)OCH(CF_3)_2$ (**12**), ref. 22; $PhP[OCH(CF_3)_2]_2$, ref. 20; $(PhO)_5P$, ref. 21; and perfluoropinacol, ref. 11. Other compounds were commercial samples. HF solutions were made by condensing anhydrous HF into acetonitrile to give approximately 0.7 *M* solutions. Solvents were dried and redistilled prior to use. The following compounds were not isolated but identified by their published spectra: $(PhO)_4P^+PF_6^-$ (16), $(PhO)_3PF_2$ (23), and $PhPF_2(pfp)$ (24).

$Ph_2P(pfp)Cl$ (1)

Ph_2PCl (2.54 g, 11.5 mmol) and $(CF_3)_2CO$ (4.5 g, 27 mmol) were sealed in a tube and kept at 25°C for 1 week. Excess $(CF_3)_2CO$ was removed and an oil remained which decomposed in air. It was identified as $Ph_2P(pfp)Cl$ (**1**) by ir (Table 1), ^{19}F and ^{31}P nmr (Table 2), and by its reaction with an equimolar amount of $HOCH(CF_3)_2$ in toluene−C_6D_6 to give $Ph_2P(pfp)OCH(CF_3)_2$ (**2**).

Under the same conditions, $PhPCl_2$ and $(CF_3)_2CO$ did not react to give a phosphorane product.

$Ph_2P(pfp)OCH(CF_3)_2$ (2)

$Ph_2POCH(CF_3)_2$ (5.6 g, 16 mmol) and excess $(CF_3)_2CO$ were sealed in a reaction tube and kept at 25°C for 3 days. Volatile products were removed and an oily liquid solidified on standing. Recrystallization from petroleum ether gave white crystals identified as $Ph_2P(pfp)OCH(CF_3)_2$ (**2**), 10%, mp 61−62°C, stable in air and soluble in benzene, dichloromethane, dimethoxyethane, and dioxane. *Anal.* calcd. for $C_{21}H_{11}F_{18}O_3P$: C 36.86, H 1.62, F 49.98; found: C 35.63, H 1.52, F 50.55. A variable temperature fluorine nmr spectrum of **2** showed only slight changes over temperature range +25 to −65°C.

(n-$C_4H_9O)_3P(pfp)$ (8)

Excess $(CF_3)_2CO$ (4.0 g, 24 mmol) was added to $(n\text{-}C_4H_9O)_3P$ (2.79 g, 11.1 mmol) and the reaction tube sealed and kept at 25°C for 4 days. Vacuum fractionation of the mixture yielded $(n\text{-}C_4H_9O)_3P(pfp)$ (**8**) (95%), identified by ir (Table 1) and ^{19}F nmr (Table 2). *Anal.* calcd. for $C_{18}H_{27}F_{12}O_5P$: C 37.12, H 4.67; found: C 36.92, H 4.63.

$Ph_2P(O)OC(CF_3)_2C(CF_3)_2OH$ (9)

Water was added to $Ph_2P(pfp)Cl$ (**1**), prepared as described above, in acetonitrile until a solid precipitated. The solid was filtered, washed with water, and recrystallized by dissolving in a minimum of hot CH_2Cl_2, adding hexane, and then evaporating on a rotary evaporator until the solid just begins to precipitate. The solid, identified as $Ph_2P(O)OC(CF_3)_2C(CF_3)_2OH$ (**9**) (44%, mp 125−126°C) by ^{19}F, ^{31}P, and ^{13}C nmr (Table 2), is air stable and soluble in CH_2Cl_2, dioxane, acetone, and acetonitrile. *Anal.* calcd. for $C_{18}H_{11}F_{12}O_3P$: C 40.47, H 2.07, F 42.68; found: C 40.49, H 1.96, F 41.28. Infrared (hexachlorobutadiene): 3100 (b, OH); on deuteration, 2310 (b, OD) cm^{-1}.

Can. J. Chem. Downloaded from www.nrcresearchpress.com by 210.87.254.42 on 09/06/12
For personal use only.

Can. J. Chem. Downloaded from www.nrcresearchpress.com by 210.87.254.42 on 09/06/12
For personal use only.

$PhP(O)(OH)OC(CF_3)_2C(CF_3)_2OH$ (10)

Ethanol (containing 1% water) was added, with stirring, to $PhP(pfp)[OCH(CF_3)_2]_2$ (**3**) (0.5 g, 0.6 mmol). Ethanol was removed under vacuum and benzene added, repeatedly, until no free $HOCH(CF_3)_2$ remained in the oil, as monitored by ^{19}F nmr. A solid precipitated on adding CH_2Cl_2 which was washed with cold CH_2Cl_2, dried under vacuum, and sublimed to give $PhP(O)(OH)OC(CF_3)_2C(CF_3)_2OH$ (**10**) (45%, mp 98–99°C), identified by nmr (Table 2) and ir: 3200 (b, OH) cm^{-1}. *Anal.* calcd. for $C_{12}H_7F_{12}O_4P$: C 30.39, H 1.49, F 48.09; found: C 30.26, H 1.51, F 50.43.

The neutral and basic (0.1 *M* NaOH) hydrolysis of $PhP(pfp)(OPh)_2$ (**4**) and $PhP(pfp)(OMe)_2$ (**5**) also gave **10** as a major product, as determined by nmr.

$(HO)_2P(O)OC(CF_3)_2C(CF_3)_2OH$ (11)

Concentrated H_2SO_4 (6 mL) was added with stirring to $(EtO)_3P(pfp)$ (**7**) (2.5 g, 10 mmol) at 25°C. A precipitate formed immediately, which was filtered, washed with hexane, and dried under vacuum to give a white solid identified as $(HO)_2P(O)OC(CF_3)_2C(CF_3)_2OH$ (**11**), 75%, ir: 3400 (b, OH) cm^{-1}; nmr (Table 2). It is soluble in H_2O and CH_3CN. A portion of this solid was sublimed to yield a product with mp 99–100°C. Another portion was recrystallized from hexane to give fine needle crystals with mp 104–105°C. Sublimed and recrystallized products had identical ^{19}F nmr spectra. *Anal.* calcd. for $C_6H_3F_{12}O_5P$: C 17.40, H 0.73, F 55.07; found: C 16.80, 15.26, H 0.92, 1.48, F 51.22. The elemental analyses are low in C and F but high in H, suggesting the presence of water in the sample.

A similar procedure was used to prepare **11** from $(PhO)_3P(pfp)$ (**6**).

Mass spectra

The characteristic peaks in the mass spectra are given below:

Compound	Peaks
1	M−19, M−35, M−69, M−77, M−167
2	M−19, M−69, M−77
3	M−19, M−69, M−77, M−167
4	M, M−19, M−69, M−93
5	M, M−19, M−31, M−69
6	M−77, M−93
8	M, M−18, M−69, M−87
9	M, M−18, M−69, M−77
10	M, M−1, M−19

Acknowledgement

The continued financial support of the Natural Sciences and Engineering Research Council of Canada is greatly appreciated.

1. F. RAMIREZ, B. HANSEN, and N. B. DESAI. J. Am. Chem. Soc. **84**, 4588 (1962); F. H. WESTHEIMER. Acc. Chem. Res. **1**, 70 (1968); P. GILLESPIE, F. RAMIREZ, I. UGI, and D. MARQUARDING. Angew. Chem. Internat. Edit. **12**, 91 (1973).
2. G. KEMP and S. TRIPPETT. Tetrahedron Lett. 4381 (1976).
3. A. MUNOZ, M. GALLAGHER, A. KLAEBE, and R. WOLF. Tetrahedron Lett. 673 (1976); F. RAMIREZ, M. NOWAKOWSKI, and J. F. MARACEK. J. Am. Chem. Soc. **99**, 4515 (1977).
4. I. GRANOTH and J. C. MARTIN. J. Am. Chem. Soc. **100**, 5229 (1978); Y. SEGALL and I. GRANOTH. J. Am. Chem. Soc. **101**, 3687 (1979).
5. M. VOLKHOLZ, O. STELZER, and R. SCHMUTZLER. Chem. Ber. **111**, 890 (1978); G.-V. RÖSCHENTHALER, K. SAUERBREY, and R. SCHMUTZLER. Israel J. Chem. **17**, 141 (1978).
6. D. SCHOMBURG, O. STELZER, N. WEFERLING, R. SCHMUTZLER, and W. S. SHELDRICK. Chem. Ber. **113**, 1566 (1980).
7. R. POLLITT. M.Sc. Thesis, University of Manitoba. 1969.
8. A. QUEEN, A. E. LEMIRE, and A. F. JANZEN. Internat. J. Chem. Kinet. **13**, 411 (1981).
9. M. ALLAN, A. F. JANZEN, and C. J. WILLIS. Can. J. Chem. **46**, 3671 (1968).
10. J. A. GIBSON and G.-V. RÖSCHENTHALER. J. Chem. Soc. Dalton, 1440 (1976).
11. N. P. GAMBARYAN, YU. A. CHEBURKOV, and I. L. KNUNYANTS. Izv. Akad. Nauk SSSR, Ser. Khim. 1526 (1964); Chem. Abstr. **64**, 14082*a* (1966).
12. V. P. EVDAKOV, L. I. MIZRAKH and L. YU. SANDALOVA. Zh. Obshch. Khim. **37**, 1818 (1967); Chem. Abstr. **68**, 59507*c* (1968).
13. F. RAMIREZ, C. P. SMITH, J. F. PILOT, and A. S. GULATI. J. Org. Chem. **33**, 3787 (1968).
14. F. RAMIREZ, C. P. SMITH, and J. F. PILOT. J. Am. Chem. Soc. **90**, 6726 (1968).
15. R. LUCKENBACH. Dynamic stereochemistry of pentaco-ordinated phosphorus and related elements. Georg Thieme Publishers, Stuttgart. 1973.
16. L. KOLDITZ, K. LEHMANN, W. WIEKER, and A.-R. GRIMMER. Z. anorg. allg. Chem. **360**, 259 (1968).
17. D. A. KLEIER and G. BINSCH. Program 165, Quantum Chemistry Program Exchange, Indiana University. 1970.
18. R. A. BRAUN. Chem. Abstr. **68**, P114058*j* (1968).
19. F. RAMIREZ, C. P. SMITH, A. S. GULATI, and A. V. PATWARDHAN. Tetrahedron Lett. 2151 (1966).
20. D. DAKTERNIEKS, G.-V. RÖSCHENTHALER, and R. SCHMUTZLER. Z. Naturforsch. **33b**, 507 (1978).
21. F. RAMIREZ, A. J. BIGLER, and C. P. SMITH. J. Am. Chem. Soc. **90**, 3507 (1968).
22. P. HAAKE and C. E. DIEBERT. J. Am. Chem. Soc. **93**, 6931 (1971).
23. S. C. PEAKE, M. FILD, M. J. C. HEWSON, and R. SCHMUTZLER. Inorg. Chem. **10**, 2723 (1971).
24. H.-B. EIKMEIER, K. C. HODGES, O. STELZER, and R. SCHMUTZLER. Chem. Ber. **111**, 2077 (1978).

Thiirene formation in the reactions of sulfur atoms with alkynes

BELA VERKOCZY
Saskatchewan Oil and Gas Corporation, 1500 Chateau Tower, 1920 Broad Street, Regina, Sask., Canada S4P 3V2
ALDEN G. SHERWOOD
Department of Chemistry, Simon Fraser University, Burnaby, B.C., Canada V5A 1S6
AND
IMRE SAFARIK AND OTTO P. STRAUSZ
Department of Chemistry, University of Alberta, Edmonton, Alta., Canada T6G 2G2

Received February 10, 1983

This article is dedicated to Professor Harry E. Gunning on the occasion of his 65th birthday

BELA VERKOCZY, ALDEN G. SHERWOOD, IMRE SAFARIK, and OTTO P. STRAUSZ. Can. J. Chem. **61**, 2268 (1983).

The gas phase reactions of $S(^1D_2)$ and $S(^3P_J)$ atoms with alkynes have been studied by photolyzing COS in the presence of CH≡CH, $CF_3C{\equiv}CH$, and $CF_3C{\equiv}CCF_3$. In the reactions with CH≡CH, CS_2, benzene, and thiophene were formed; with $CF_3C{\equiv}CH$, eight products were found with disubstituted thiophenes and trisubstituted benzenes as the major products. In the case of $CF_3C{\equiv}CCF_3$, only perfluorotetramethylthiophene was detected at low conversion but at long photolysis several new products were observed. Many of the reaction products characterized here have not been reported before.

The formation and distribution of the reaction products could be rationalized by an overall mechanism in which the formation of the highly reactive primary adducts, thiirene and thioformylmethylene, is followed by bimolecular reactions yielding the principal end products. The formation of minor products could be explained by secondary photoisomerizations, secondary photolysis, and by secondary decompositions and the secondary reactions of sulfur atoms with primary products.

BELA VERKOCZY, ALDEN G. SHERWOOD, IMRE SAFARIK et OTTO P. STRAUSZ. Can. J. Chem. **61**, 2268 (1983).

On a étudié les réactions en phase gazeuse des atomes de $S(^1D_2)$ et de $S(^3P_J)$ avec les alcynes en photolysant le COS en présence du CH≡CH, du $CF_3C{\equiv}CH$ et du $CF_3C{\equiv}CCF_3$. Les réactions impliquant le CH≡CH conduisent à la formation du CS_2, du benzène et du thiophène. Celles impliquant le $CF_3C{\equiv}CH$ donnent 8 produits comprenant des thiophènes disubstitués et des benzènes trisubstitués comme produits principaux. Dans le cas du $CF_3C{\equiv}CCF_3$ on a décelé uniquement du fluorotétraméthylthiophène au début de la photolyse, mais sur une longue période on observe plusieurs produits nouveaux. Plusieurs des produits caractérisés dans ce travail ne sont pas répertoriés dans la littérature.

On peut rationaliser la formation et la distribution des produits de la réaction en faisant appel à un mécanisme global dans lequel la formation des adduits primaires très réactifs, thiirène et thioformylméthylènes, est suivie de réactions bimoléculaires qui conduisent aux produits finaux principaux. On peut expliquer la formation des produits secondaires par des photo-isomérisations secondaires, par une photolyse secondaire, par des décompositions secondaires et par des réactions secondaires des atomes de soufre avec les produits primaires.

[Traduit par le journal]

Introduction

Systematic studies in the last two decades (1–4) have provided a comprehensive knowledge of the reactions of sulfur atoms with olefins. Both ground ^3P_J and excited $^1D_2$ state atoms react readily with olefins but the type of reaction depends on the spectroscopic state. The reaction with ^3P_J atoms yields the corresponding lowest excited triplet state thiirane as the sole product in a single step, stereospecific cycloaddition followed by collisional deactivation to the ground state. $S(^1D_2)$ atoms, on the other hand, react via simultaneous, competing cycloaddition to give vibrationally excited singlet ground state thiiranes and C—H insertion to yield the corresponding thiols.

Both $S(^3P_J)$ and $S(^1D_2)$ atoms have also been found to react with acetylenes, but the elucidation of the mechanism of these reactions proved to be difficult because of the inherent instability of the primary products (5, 6). These reactions are generally characterized by low product recovery and extensive polymerization. When COS was photolyzed with acetylene, propyne, 2-butyne, or hexafluoro-2-butyne, the products were small amounts of CS_2, benzenes, and thiophenes. The primary sulfur adducts were detected in flash photolysis – kinetic mass spectrometric studies and their mean lifetimes determined to be between 0.1 and 7 seconds. These were postulated to be thiirenes formed in the symmetry allowed addition of $S(^1D_2)$ atoms to the acetylenes. Absolute rate constants and Arrhenius parameters have been determined for the addition of $S(^3P_J)$ atoms to a number of alkynes (7, 8) by flash photolysis with vacuum uv kinetic absorption spectroscopy. The room temperature rate constants are somewhat lower and the activation energies and preexponential factors somewhat higher for the alkynes than those for the corresponding olefins. The variation in activation energies, however, shows the same decreasing trend with increasing alkyl substitution on the acetylenic carbon atoms in accordance with the electrophilic character of the $S(^3P_J)$ atoms.

In our continuing effort aimed at the elucidation of the reactivity of sulfur atoms and at gaining an insight into the chemistry of thiirenes we have carried out further, more comprehensive studies on their reactions with alkynes. The results of these studies are being reported here.

Experimental

The high vacuum apparatus and procedures employed were similar to those described in previous reports from this laboratory (4).

The light source was a Hanovia medium pressure mercury arc equipped with a 6 mm Vycor 7910 filter ($\lambda \geq 240$ nm). Photolyses were carried out in cylindrical quartz cells 10.0 cm long and 5.0 cm in diameter, connected through stainless steel high temperature Hoke valves to a conventional grease-free vacuum system. One of the quartz cells was placed in an aluminum block furnace (2.5 cm thick) equipped with four 500 watt pencil heaters, powered and regulated by

Can. J. Chem. Downloaded from www.nrcresearchpress.com by 210.87.254.5 on 09/06/12
For personal use only.

Can. J. Chem. Downloaded from www.nrcresearchpress.com by 210.87.254.5 on 09/06/12
For personal use only.

an API 2 Mode proportional electronic controller, for temperature studies. Temperatures, accurate to ±0.5°C, were measured with an iron–constantan thermocouple.

After photolysis, the noncondensable gas, CO, was quantitatively collected and measured in a gas buret with the aid of a Toepler pump. Substrates and products were then separated by trap-to-trap distillations at 1–3 Torr pressure. Product separation was achieved by passing the photolyzed mixture through three traps at −196°C and a solid N_2 (−210°C), then through three traps at −98°C. The product fraction was distilled into an evacuated gas chromatograph sample loop and passed through a 2 mm id × 122 cm glass column containing 60/80 mesh Chromosorb W.A. coated with 10% tricresyl phosphate, and maintained at 23°C. A microthermistor cell fitted with Gow-Mac 13-502 thermistors was employed as a detector and was operated at 30°C with a bridge current of 8.0 mA. Helium was used as the carrier at a flow rate of 25 cm^3/min. Retention times are listed in Tables 3, 4, and 9. Product samples were collected downstream from the detector for identification.

Mass spectra were obtained on an AEI MS 12 instrument with the ion source operating at 70 eV and the ionization chamber kept at about 50°C. The resulting data were interpreted using a computer, Data General Nova 3, employing a DS 50 program.

Ultraviolet spectra were recorded on a Unicam 1800 spectrometer using a 10.0 × 1.6 cm quartz cell equipped with a cold finger.

Infrared spectra of Ar matrix-isolated species were recorded by a Nicolet 7199 FT infrared spectrophotometer at 1 cm^{-1} resolution. The samples were prepared by an Air-Products and Chemicals Inc., Model CS-202 Displex closed-cycle helium refrigeration system coupled to a high vacuum line.

Three nmr spectrometers were used for structural determination: Bruker WP-60, Bruker 200 and 400 MHz instruments, equipped with proton (^1H) or fluorine (^{19}F) probes. Gas samples were condensed into medium walled nmr sample tubes containing degassed, solidified $CDCl_3$ as solvent and as an internal standard. In the case of ^{19}F nmr, trifluoroacetic acid was employed as an external standard. The nmr samples were run either at room temperature (24°C) or −30°C, depending on the stability of the material.

Materials

Carbonyl sulfide (Matheson) was purified as described previously (2). Carbon dioxide (Airco, 99.9%) was used as such. Acetylene (Matheson, 99%) was degassed at −186°C.

3,3,3-Trifluoropropyne (Columbia Organic Chemicals, 99.0%) was distilled repeatedly at −115°C and the purity checked on a 6 ft gc Porapak N column, and by gc–ms.

Perfluoro-2-butyne (Columbia Organic Chemicals, 99.0%) was distilled at −98°C several times. The remaining impurities, as analyzed by gc were less than 0.2%.

Perfluorotetramethylthiophene (PFTMT) was prepared according to Krespan (9) for calibration purposes.

Results

1. *$COS + C_2H_2$*

We have photolyzed 80 Torr COS with 240 Torr C_2H_2 at 160°C, hoping for improved product recovery at higher temperature. Recovery was found to be very low, only about 5%, in the room temperature study. The product yields are given in Table 1. As can be seen, CS_2, benzene, and thiopene are formed in the photolysis with relative yields of 10:3:1. In the room temperature photolysis, the same products were found with relative yields of 4:3:1 at the same $[C_2H_2]/[COS]$ ratio of 3 (5). The product recovery showed a substantial increase at the higher temperature, the combined yield of CS_2 and thiophene being about 86% in terms of sulfur atoms consumed.

In a subsequent experiment, 80 Torr COS and 240 Torr C_2H_2 were photolyzed with 1400 Torr added CO_2 at 144°C. CO_2 deactivates the excited $S(^1D_2)$ atoms to the ground state; this way the yields and distribution of the products in the reaction of the $S(^3P_J)$ atoms with C_2H_2 can be determined. The results are shown in Table 2. The same products, CS_2, benzene, and thiophene are formed with relative yields of 3.5:1.5:1, as in the absence of CO_2 at room temperature. Product yields were low, on the order of 4% in terms of sulfur atoms consumed.

TABLE 1. Product yields from the S + C_2H_2 reaction at 160°C[a]

Product	Yield (μmol)
Carbon disulfide	0.426
Benzene	0.124
Thiophene	0.041

[a]λ > 240 nm; photolysis time = 4.0 min; $P(C_2H_2)$ = 240 Torr; $P(COS)$ = 80 Torr; R^0_{CO} = 0.726 μmol min^{-1}; R_{CO} = 0.465 μmol min^{-1}.

TABLE 2. Product yield from the $S(^3P_J)$ + C_2H_2 reaction at 144°C[a]

Product	Yield (μmol)
Carbon disulfide	0.040
Benzene	0.0182
Thiophene	0.0118

[a]λ > 240 nm; photolysis time = 20.0 min; $P(COS)$ = 40 Torr; $P(C_2H_2)$ = 120 Torr; P_{CO_2} = 1400 Torr; R^0_{CO} = 0.325 μmol min^{-1}; R_{CO} = 0.208 μmol min^{-1}.

2. *COS + 3,3,3-trifluoropropyne*

Photolysis of a mixture of 80 Torr COS and 480 Torr C_3HF_3 at 150°C led to the formation of eight products, the structure, relative yield, and modes of identification of which are presented in Table 3. With the exception of CS_2, none of these compounds have been previously reported in the literature. A short description of the assignment of the structure together with mass and ^{19}F nmr spectra are given in paragraph 9 of this section.

The yields of all the major products were lower at 25°C but their relative distribution was unchanged, indicating that all the observed products are thermally stable.

3. *$COS + C_3HF_3 + C_2H_2$*

The photolysis for 60 min of a mixture of 80 Torr COS, 510 Torr C_3HF_3, and 170 Torr C_2H_2 at 150°C yielded no additional products, but it was observed that the product yields were considerably lower than those obtained in the absence of C_2H_2.

4. *$COS + C_3HF_3$ + perfluoro-2-butyne (PFB-2)*

Eighty Torr COS was photolyzed with a mixture of 300 Torr C_3HF_3 and 300 Torr PFB-2 at 150°C for 60 min. The observed products, together with their relative distribution, are given in Table 4.

One of the major products, compound **9**, is also a novel structure previously unreported in the literature (*vide infra*). The other major product of this sytem is perfluorotetramethylthiophene (PFTMT), **10**. The preparation and spectral and thermal properties of this compound have been described by Krespan (9).

Products **11** and **12** were only formed in trace amounts and hence could not be characterized. The tentative structure given in Table 4 are based partly on their ms and partly on kinetic considerations (*vide infra*).

The yields of products **6** and **8** were very small. The tri-

TABLE 3. Product yields from the reactions of sulfur atoms with 3,3,3-trifluoropropyne at 150°C[a]

Compound number	Relative glc peak area	Products	Molecular weight	Elution time (min)	Identified by
1	Trace	$S{=}C{=}CH{-}CF_3$	126	1.0	ms
2	0.01	CS_2	76	4.0	ms, elution time
3	0.14	?	288	9.0	ms
4	1.00	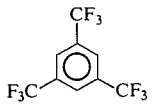	282	9.5	ms, nmr
5	0.17	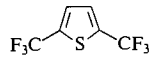	220	31.0	ms, uv, nmr
6	0.90	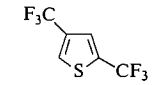	220	30.0	ms, nmr, uv
7	0.18	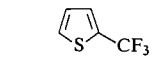	152	36.0	ms, uv, nmr
8	0.50	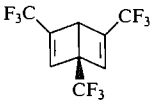	282	63.0	ms, nmr, uv

[a] $\lambda > 240$ nm; photolysis time = 130 min; $P(C_3HF_3) = 480$ Torr; $P(COS) = 80$ Torr.

TABLE 4. Product yields from the reaction of sulfur atoms with a 1:1 mixture of $CF_3{-}C{\equiv}CH$ and $CF_3{-}C{\equiv}C{-}CF_3$ at 150°C[a]

Compound number	Relative glc peak area	Products	Molecular weight	Elution time (min)	Identified by
1	Unresolved	$S{=}C{=}CH{-}CF_3$	126	1.0	ms
2	0.01	CS_2	76	4.0	ms, elution time
9	1.00	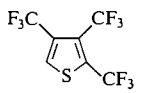	288	9.0	ms, nmr, uv
10	1.00	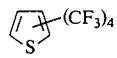	356	19.0	ms, nmr, uv, elution time
6	0.06	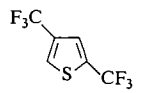	220	30.0	ms, nmr, uv
11	0.03	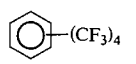	350	41.0	ms
8	0.05	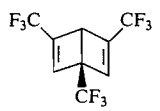	282	63.0	ms, nmr, uv
12	<0.01	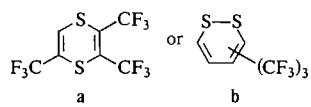 a or b	320	83.0	ms

[a] $\lambda > 240$ nm; photolysis time 60 min; $P(C_3HF_3) = 300$ Torr; $P(C_4F_6) = 300$ Torr; $P(COS) = 80$ Torr.

substituted benzene, **4**, the monosubstituted thiophene, **7**, and the unknown compound, **3**, were demonstrably absent.

5. *COS + PFB-2*

In order to assess the absorption characteristics of the substrate at room temperature, the gas phase uv spectrum of 422 Torr PFB-2 was obtained. Absorption begins at about $\lambda \sim 250$ nm, becoming quite strong below 234 nm. $\epsilon \simeq 5 \times 10^{-6}$ Torr^{-1} cm^{-1} at 240 nm and 1.7×10^{-4} Torr^{-1} cm^{-1} at 228 nm. Gas-chromatographic analysis of a sample of 500 Torr C_4F_6, photolyzed for 60 min, showed no sign of products, as expected, owing to the very small extinction coefficient at the effective photolyzing wave length ($\lambda \geq 240$ nm).

In the photolysis of COS with C_4F_6 under conditions of low conversion the only detectable product, besides CO, is PFTMT. The yields of both products depend on the substrate pressure, as shown in Fig. 1. With increasing C_4F_6 pressure, the PFTMT yield increases; the CO yield decreases, ap-

Can. J. Chem. Downloaded from www.nrcresearchpress.com by 210.87.254.5 on 09/06/12
For personal use only.

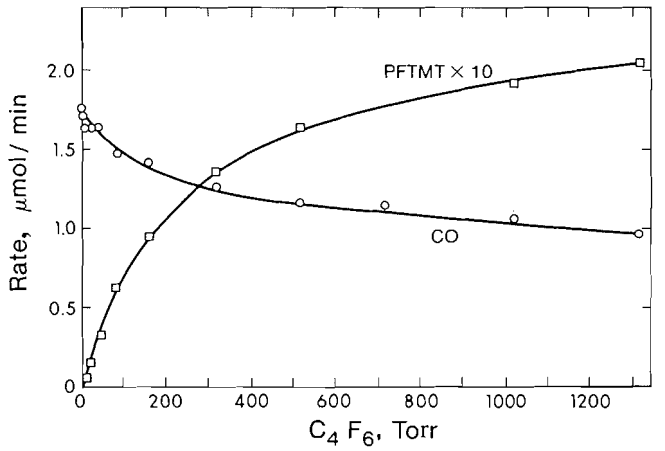

FIG. 1. The effect of PFB-2 pressure on the yields of PFTMT and CO. $P(COS)$ = 300 Torr.

proaching half of its initial value at high pressures.

Increasing the total pressure from 200 to 1200 Torr at a constant $[C_4F_6]/[COS]$ ratio of 1.0 effected a small but definite enhancement in the PFTMT yield.

In order to study the reactions of $S(^3P_J)$ atoms separately, 40 Torr COS and 120 Torr C_4F_6 were photolyzed in the presence of increasing amounts of CO_2 to deactivate the $S(^1D_2)$ atoms. The PFTMT yield gradually decreased with increasing CO_2 concentrations to a limiting value of about 14% of the primary generated sulfur atoms at 1500 Torr CO_2. No new products were detected and further increase of the C_4F_6 content resulted only in a slightly higher PFTMT yield.

Next we have investigated the effect of temperature on the product yields of the photolysis. Blank experiments showed that both PFB-2 and PFTMT are stable at 160°C and, moreover, allowing the photolyzate to remain standing for 3 hours at room temperature, do not affect the product yields.

The variation of product yields with the temperature is shown in Table 5. It is seen that the PFTMT yield increases with increasing temperature and at 160°C reaches 60−100% of the primarily formed sulfur atom. The CO yield from abstraction shows similar increase with the temperature, which is probably due mainly to the increased competition from the reaction of $S(^3P_J)$ with COS at higher temperatures. The results of a temperature study carried out in the presence of a large excess of added CO_2 also gave similar results for $S(^3P_J)$ atoms, as seen from the data in Table 6.

6. *COS + PFB-2 + C_2H_2*

Photolysis of COS with mixtures of PFB-2 and C_2H_2 yielded PFTMT and 2,3-bis(trifluoromethyl)thiophene (b-TFMT) as major products, together with traces of a symmetrical bis(trifluoromethyl)thiophene (2,5 or 3,4) and CS_2. Benzene and thiophene were demonstrably absent.

The effect of C_2H_2 pressure on the PFTMT and b-TFMT yields at two different temperatures, 25 and 132°, are given in Tables 7 and 8, respectively. As is seen, a sharp initial drop is followed by a gradual decrease in the PFTMT yield with an increase of the added C_2H_2; the b-TFMT yield shows a gradual increase in the whole pressure range. Temperature has a significant effect on the yield of both products; at 130°C the yield of PFTMT increased about three-fold and that of b-TFMT over ten-fold compared to the yields at room temperature.

7. *COS + PFB-2 (high conversion experiments)*

The photolysis of a mixture of 280 Torr COS and 480 Torr C_4F_6 for 192 min at 25°C led to the formation of ten products, the elution times and tentative structure assignments of which are listed in Table 9. The spectral and thermal characteristics of the products, together with the pertinent ms and ^{19}F nmr spectra, are given in paragraph 9 of this section.

The products of **15**, **16**, **19**, and **20** were detected only in very small amounts, and because of their thermal and surface instabilities it was not possible to characterize them further.

The dependence of the yields of the major products on exposure time is given in Table 10, and illustrated in Fig. 2. It is seen that the rate of increase of **10** is increasing slightly less than linear with time whereas the yields of **13** and **17** increase dramatically after ca. 10 min exposure time. The yields for **16** and **18** are rather scattered but they indicate a trend towards stationary concentrations. The other products **14**, **15**, **19**, **20**, and **21** were not detected in the first 15 minutes and formed only in traces at 30 minutes photolysis time.

At very long exposure time (192 min) the following general trends were observed.

(a) A near correspondence between the rate of increase of **13** and the rate of decrease of **10**, suggesting that the former arises from photoconversion of the major product PFTMT, **10**.

(b) The yield of **14** increased slightly.

(c) Several large and unresolved peaks appeared at elution times corresponding to those of the trimer **17** and dimer **18**.

(d) The trimers **19**, **20**, and compound **21** were detected.

The effect of exposure time on the yields of products **14**, **15**, **16**, **18**, **19**, and **20**, was found to be small and appeared to indicate that the concentration of these products had reached a photostationary state.

When a mixture of 280 Torr COS and 480 Torr C_4F_6 was photolyzed for 46 min the yield of the trimer, **17**, increased approximately two-fold as compared to that from a mixture of 280 Torr COS and 240 Torr C_4F_6 at 46 min photolysis time. Thus the yield of **17** is not only a function of exposure time but also of the PFB-2 concentration and probably the photostationary state concentration of **16** which may be one of the immediate precursors of **17**. Assuming equal detector responses, the other products, **13**, **16**, and **18** were formed in the ratio 1:1:1.

Photolysis of 80 Torr COS and 240 Torr C_4F_6 for 36 min led to the formation of the compounds **10**, **13**, **16**, **17**, and **18**. Compounds **17** and **18** were formed in a 1:1 ratio but **13** only in small amounts. In order to establish the effect of COS pressure on the product yields, 200 Torr COS was added to this mixture and photolyzed. At 16 minutes photolysis time the yield of the dimer, **16**, doubled but remained unchanged at longer exposure time. Only a small amount of trimer **17** was detected for the 16 minutes photolysis but longer exposure time, 46 min, greatly enhanced its yield (approximately six-fold increase). This confirms the above conclusion that **16** is one of the principal precursors of **17**. The effect of added PFTMT on the product yields has also been studied. Photolysis of a mixture of 280 Torr COS and 480 Torr C_4F_6 with 2.5 Torr added PFTMT led to: (a) a 25-fold increase in the yield of PFTMDT, **13**, a clear indication that this product arises from secondary photolysis of PFTMT; (b) a substantial increase in the yield of compound **14**; (c) a 35−40% decrease in the yield of trimer **17** and a slight decrease in the yield of dimer **18**.

In order to examine the thermal stabilities of the products, 80 Torr COS with 240 Torr C_4F_6 was photolyzed for 30 min at 160°C. Only the yields of products **10** and **13** increased as compared to room temperature experiments.

Can. J. Chem. Downloaded from www.nrcresearchpress.com by 210.87.254.5 on 09/06/12
For personal use only.

Can. J. Chem. Downloaded from www.nrcresearchpress.com by 210.87.254.5 on 09/06/12
For personal use only.

TABLE 5. Effect of temperature on the PFTMT yield from the $S(^1D_2, {}^3P_J)$ + PFB-2 reaction[a]

Temperature °C	Rate, μmol min^{-1}			$R_{CO} - R^0_{CO}/2$	PFTMT yield (%)[b]
	CO^0	CO	PFTMT		
24	0.336	0.205	0.032	0.039	24.5
61	0.393	0.257	0.053	0.061	39.2
82	0.440	0.305	0.079	0.085	58.6
108	0.518	0.370	0.121	0.111	81.8
125	0.585	0.432	0.157	0.140	102.8
160	0.726	0.510	0.221	0.147	102.3

[a]λ > 240 nm; photolysis time = 4.0 min; $P(COS)$ = 80 Torr; $P(C_4F_6)$ = 240 Torr.
[b]Based on $R^0_{CO} - R_{CO}$.

TABLE 6. Effect of temperature on the yield of PFTMT from the $S(^3P_J)$ + PFB-2 reaction[a]

Temperature °C	Rate, μmol min^{-1}			$R_{CO} - R^0_{CO}/2$	PFTMT yield (%)[b]
	CO^0	CO	PFTMT		
23	0.164	0.095	0.009	0.013	13.6
58	0.217	0.131	0.022	0.023	25.6
83	0.244	0.151	0.033	0.029	35.7
111	0.265	0.174	0.063	0.041	69.1
144	0.325	0.225	0.097	0.062	96.5

[a]λ > 240 nm; $P(COS)$ = 40 Torr; $P(C_4F_6)$ = 120 Torr; $P(CO_2)$ = 1400 Torr; photolysis time = 15 min.
[b]Based on $R^0_{CO} - R_{CO}$.

TABLE 7. Effect of acetylene pressure on the rates of PFTMT and b-TFMT formation at 25°C[a]

$P_{C_2H_2}$ (Torr)	Rate, μmol min^{-1} × 10^3		% Product recovery[b] (Σ(PFTMT + b-TFMT))
	PFTMT	b-TMFT	
0	86.7	—	27.1
25	54.0	Trace	16.9
50	46.0	2.3	15.1
100	34.4	5.1	12.4
200	23.0	6.3	9.2
500	6.3	16.7	7.2
500	5.7	16.2	6.9

[a]λ > 240 nm; P_{COS} = 80 Torr; $P_{C_4F_6}$ = 500 Torr; R^0_{CO} = 0.639 μmol min^{-1}; photolysis time: 4.0 min.
[b]Based on $R^0_{CO} - R_{CO}$.

TABLE 8. Effect of acetylene pressure on the rates of PFTMT and b-TFMT formation at 132°C[a]

$P_{C_2H_2}$ (Torr)	Rate, μmol min^{-1} × 10^3		% Product recovery[b] (Σ(PFTMT + b-TFMT))
	PFTMT	b-TMFT	
0	250	—	78.1
25	162	9.3	53.5
50	141	15.0	48.8
100	106	23.0	40.3
200	70	30.0	31.3

[a]λ > 240 nm; $P(COS)$ = 80 Torr; $P(C_4F_6)$ = 500 Torr; R^0_{CO} = 0.640 μmol min^{-1}; photolysis time: 4.0 min.
[b]Based on $R^0_{CO} - R_{CO}$.

8. *Secondary reactions of PFTMT,* ***10***

A mixture of 300 Torr COS and 3.3 Torr PFTMT was photolyzed for 40 min to establish the possible secondary reaction with S atoms. The major reaction product identified was compound **21** (Table 9). Small amounts of compound **13** and traces of an unidentified compound (possibly an isomer of

TABLE 9. Products detected from reactions of sulfur atoms with PFB-2[a]

Compound number	Compound name	Structure[b]	Molecular weight	Elution time (min)	Identified by
13	Perfluorotetramethyl-Dewar-thiophene (PFTMDT)	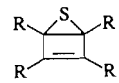	356	2.7	ms, uv
14		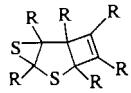	550	5.6	ms, nmr
10	Perfluorotetramethyl thiophene (PFTMT)	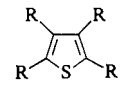	356	19.0	ms, uv, nmr
15	Dimer	$(C_4F_6S)_2$	388	33.0	ms
16		$(C_4F_6)_3S_2$	550	45.0	ms
17	Trimer	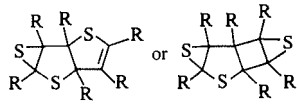 (a) or (b)	582	56.0	ms, nmr
18	Perfluoro 3,4,5,6-tetramethyl 1,2-dithiin	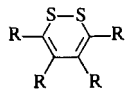	388	77.0	ms, nmr
19	Trimer	$(C_4F_6S)_3$	582	98.0	ms
20	Trimer	$(C_4F_6S)_3$	582	124.0	ms
21		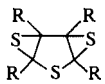	420	156.0	ms, nmr

[a] $\lambda > 240$ nm; $P(C_4F_6) = 480$ Torr; $P(COS) = 280$ Torr; photolysis time = 192 min, $T = 25°C$.
[b] R = CF_3.

TABLE 10. Exposure time dependence of the product yields in the S + C_4F_6 reaction[a]

Time (min)	Yield, μmol			Peak area in planimeter units				
	CO	$CO^0 - CO$	**10**	**10**	**13**	**16**	**17**	**18**
5	7.69	2.76	0.71	21100	5	365	700	240
10	13.71	7.19	1.05	31500	54	387	1802	346
20	26.04	15.76	1.77	53300	385	750	6005	430
30	41.51	21.19	2.37	71100	893	775	11110	690

[a] $\lambda > 240$ nm; $T = 23°C$; $P(C_4F_6) = P(COS) = 300$ Torr; $R^0_{CO} = 2.09$ μmol min^{-1}.

$(C_4F_6S)_2$) were also detected.

The photolysis of a mixture of 300 Torr C_4F_6 and 3.3 Torr PFTMT for 40 min led to the exclusive formation of **13**. The original concentration of **10** was depleted by half.

9. *Identification of the photolysis products*[1]

Product 1

Product **1** was only obtained in trace amounts, but its ms fragmentation pattern is consistent with the 3,3,3-trifluoromethylthioketene structure. The molecular ion ($M^+ = 126$) signal has a relative intensity of 74.4. The $(M - 32)^+$ signal, of relative intensity 37.2, likely corresponds to the loss of a sulfur atom. The most intense peak $(M - 51)^+$ may be associated with the loss of S and F atoms. This type of fragmentation pattern strongly militates against the $CF_3C{\equiv}C{-}SH$ isomeric structure.

Product 4

The mass spectrum featured the parent ion ($M^+ = 282$) at a relative intensity of 87.6. The ^{19}F nmr spectrum (Appendix I) consists of a single peak at 99.35 ppm, which resolves into a complex quartet under high resolution.

The uv spectrum of **4** consists of an absorption maximum at 201 nm and a less intense one at 272 nm. These features are similar to those of the uv spectrum reported by Barlow *et al.* (10) for hexakis(trifluoromethyl)benzene in n-pentane, which has an absorption maximum at 212 nm.

The proposed structure (Table 3) of **4** is consistent with the above spectral properties; moreover, by analogy with the S + C_3H_6 reaction (5), 1,3,5-tris(trifluoromethyl)benzene was expected to be a product in the S + C_3F_3H system.

[1]The detailed mass spectra are available as supplementary material and may be obtained, at nominal charge, from the Depository of Unpublished Data, CISTI, National Research Council of Canada, Ottawa, Ont., Canada K1A 0S2.

Can. J. Chem. Downloaded from www.nrcresearchpress.com by 210.87.254.5 on 09/06/12
For personal use only.

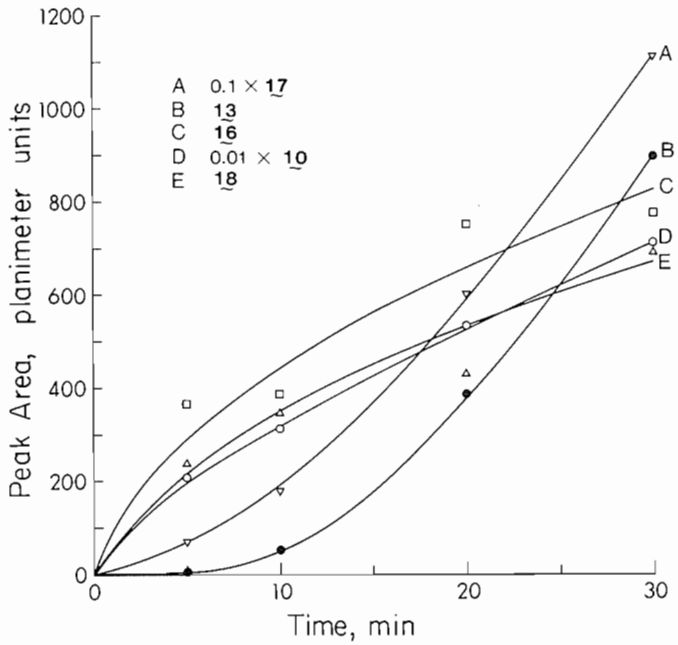

FIG. 2. Exposure time dependence of the product yields in the photolysis of 300 Torr COS and 300 Torr PFB-2. Product **10**: ○; product **13**: ●; product **16**: □; product **17**: ▽; product **18**: △.

Product 5

The mass spectrum yielded the parent ion ($M^+ = 220$) as the most intense peak. The uv spectrum shows one maximum at $\lambda = 226$ nm, suggesting a substituted thiophene. Since the 2,3- and 2,4-isomers can be discounted on the basis of the ^{1}H nmr spectra (Appendix II), this product is therefore either 2,5- or 3,4-bis(trifluoromethyl)thiophene.

Product 6

The mass spectrum features the parent ion ($M^+ = 220$) as the second most intense peak, with relative intensity of 98.0. The uv spectrum of this product features an absorption maximum at $\lambda = 226$ nm. This absorption is common to all CF_3 substituted thiophenes (5, 9) examined to date and may vary by ±2 nm depending on the degree and type of substitution.

The ^{19}F nmr spectrum yields two single peaks of equal intensity at 99.66 and 103.65 ppm.Under high resolution both peaks give rise to complex doublets. 2,3-Bis(trifluoromethyl)-thiophene has been synthesized, and the recorded ^{1}H and ^{19}F nmr spectra (Appendices I and II) and its uv spectrum differ from the ones described above; therefore the only remaining reasonable structure for **6** is 2,4-bis(trifluoromethyl)thiophene.

Product 7

The parent ion ($M^+ = 152$) is the most intense peak in the mass spectrum. In the uv spectrum a strong absorption occurs at $\lambda = 224$ nm and a weak one at $\lambda = 272$ nm, in good agreement with the uv spectrum obtained for 2,3,4-tris(trifluoromethyl)thiophene (*vide infra*). The ^{19}F nmr spectrum of **7** yields a single peak at 100.29 ppm. This chemical shift is consistent with that observed for **6** (99.66 ppm). A careful study of all the available ^{19}F nmr spectra of various CF_3-substituted thiophenes strongly suggests that the high field shifted positions (i.e., 99.66 ppm as compared to 103.65 ppm in **6**) correspond to a CF_3 group adjacent to the sulfur atom. On this basis **7** is tentatively identified as 2-trifluoromethylthiophene.

Product 8

The relative intensity of the parent ion ($M^+ = 282$) is 98.1. The ^{19}F nmr spectrum featured two peaks integrating into 2:1 at 99.81 and 96.06 ppm, respectively, indicating that two equivalent and one nonequivalent CF_3 groups are present in the molecule. High resolution of the first peak at 99.81 ppm led to a very complex pattern but the other one remained a broad single peak.

The uv spectrum features three absorption maxima, a strong one at 203 nm and two weak ones of equal intensity at 263 and 269 nm. The first absorption is in agreement with the value $\lambda_1 = 202.5$ nm reported by Barlow *et al.* (10) for hexakis(trifluoromethyl)dewar benzene. Moreover, exposure time studies have shown that **8** is a photolysis product of **4** and thus the assigned Dewar benzene structure is the most reasonable one.

Product 9

Its mass spectrum yields the parent ion ($M^+ = 288$) as the most intense peak. The uv spectrum features a strong absorption maximum at 226 nm and a weak one at 272 nm, in close resemblance to the uv spectrum of 2-trifluoromethylthiophene. Its ^{19}F nmr spectrum consists of three peaks of equal intensity, indicating that three chemically distinct CF_3 groups are present in the molecule. Under high resolution the peak at 105.02 ppm yields a complex quartet, the peak at 103.26 ppm a quartet, and the third peak at 101.57 ppm also resolves into a set of quartets. On the basis of these spectral data and those of similar systems (5, 9), it is reasonable to assign the 2,3,4-tris(trifluoromethyl)-thiophene structure to **9**.

Product 13: perfluorotetramethylDewar-thiophene (PFTMDT)

The ms gives the parent ion ($M^+ = 356$) as the second most intense peak at 99.0 on the relative scale. The gas phase uv spectrum of PFTMDT features two maxima at 247.5 and 336.5 nm, with corresponding extinction coefficients of 1.3×10^{-2} and 2.7×10^{-3} $Torr^{-1}$ cm^{-1}, respectively. The uv and ms spectra of this compound have been described by Heicklen and co-workers (11) in detail and are identical to those of product **13**.

At room temperature **13** is stable; its conversion to PFTMT at higher temperature was described by Kobayashi *et al.* (12) who found the uncatalyzed reaction to be very slow even at 160°C ($\tau_{1/2} \approx 5$ h in benzene).

Product 14

The structural assignment for this compound was made partly on the basis of kinetic considerations and partly on the basis of its ms and ^{19}F nmr spectra, listed in Appendix I. The ms gives only a low intensity peak (7.5) for the parent ion ($M^+ = 550$). The ^{19}F nmr spectrum consists of four single peaks which integrate in the ratio 2:2:1:1. The high resolution spectrum leaves the low field peak at 109.70 ppm unresolved (integration 2), resolves the second peak at 103.19 into two similar complex structures (integration 2), the third peak at 99.74 ppm leads to a very complex structure (integration 1), and the high field peak at 87.00 ppm is again resolved into a very complex structure. This product appears to be unstable in the gas phase at room temperature, and disappears after several hours without forming any recoverable products.

Product 17

The mass spectrum features only a low intensity signal, 9.3 for the parent ion ($M^+ = 582$). The ^{19}F nmr spectrum consists of six lines of equal intensities at 106.38, 106.04, 101.93, 98.61, 97.88, and 89.21 ppm. The high resolution spectrum is described in Appendix I.

The uv spectrum of **17** shows continuous absorption from

Can. J. Chem. Downloaded from www.nrcresearchpress.com by 210.87.254.5 on 09/06/12
For personal use only.

190 to about 320 nm, with several maxima of comparable intensities at λ = 208, 225, 244, 256, 288 nm.

The FT−ir spectrum was obtained in an argon matrix at 10 K; however, the weak absorptions observed in the region 1600−1650 cm^{-1} could not be clearly assigned to the $\diagdown C{=}C \diagup$ stretching frequency.

On the basis of the molecular weight and the ^{19}F nmr spectrum, which shows the presence of six unequivalent CF_3 groups, the most reasonable structures for this product are **17***a* and **17***b* (Table 9), although a more definitive structural assignment cannot be made.

Gas-chromatographic analysis of a gaseous sample of **17**, stored in a quartz cell for about 16 h at room temperature, showed the presence of PFTMT and traces of undecomposed trimer. No products could be detected after storage in a quartz tube at −196°C for 48 h; however, the original peak size decreased by about 30%.

Product 18: perfluoro 3,4,5,6-tetramethyl 1,2-dithiin

This compound is thermally unstable and sensitive to surfaces. When a gaseous sample of the dimer **18** was stored in a quartz cell at room temperature for about 16 h it decomposed completely. Gas-chromatographic analysis of the decomposition products showed the presence of PFTMT, PFB-2, and a very broad trailing peak having variable elution times (7 to 15 min). Storage at −196°C in a quartz tube for about 14 h effected 50% decomposition. Only very small amounts of PFTMT and PFB-2 were detected, and the broad peak was absent.

The relative intensity of the parent ion (M^+ = 388) is only 39.5. The uv spectrum of **18** is ill defined; the weak absorption range is between ~280 to 190 nm, but features at least one maximum at 250 nm. The ^{19}F nmr spectrum (Appendix I) shows the presence of two equivalent pairs of CF_3 groups at 108.47 and 99.45 ppm. Under high resolution both peaks yield complex spectra. The FT-ir spectrum (in argon matrix at 10 K) features weak absorptions in the region 1600−1650 cm^{-1}, suggesting the presence of double bonds in this molecule.

Only 1,4-dithiins have been reported in the literature but, in their photolysis studies on substituted thiadiazoles, Zeller *et al.* (13) postulated the transient existence of 1,2-dithiins in order to explain the mode of formation of some of the products. The 1,2-dithiin structure for product **18** is consistent with the above spectral data and also with kinetic mechanistic considerations (*vide infra*).

Product 21

The parent ion (M^+ = 420) is a medium intensity signal 37.9 in the mass spectrum of **21**.

The ^{19}F nmr spectrum features two signals of 1:1 integration, hence two sets of equivalent pairs of CF_3 groups are present in the molecule. High resolution yields two sets of very complex spectra at 103.50 and 101.00 ppm, respectively.

Additional support for the structure assigned to **21**, given in Table 9 on the basis of molecular weight and the ^{19}F nmr spectrum, comes from the kinetic mechanistic considerations (*vide infra*).

Storage of product **21** for several days at 25°C in a quartz tube effected no appreciable loss; therefore, it appears to be thermally stable. Its thermal stability at higher temperatures was not investigated.

The remaining products of the high conversion experiments, **15**, **16**, **19**, and **20**, were detected only in very small amounts and because of their thermal and surface instabilities, it was not possible to characterize them further.

Discussion

The primary adducts formed in the reactions of $S(^1D_2)$ and $S(^3P_J)$ atoms with the acetylenes studied to date (5), HC≡CH, $CH_3C{\equiv}CH$, $CH_3C{\equiv}CCH_3$, $CF_3C{\equiv}CH$, and $CF_3C{\equiv}CCF_3$, are all highly reactive and can readily undergo further bimolecular reactions to yield the observed principal end products, dimer, trimer benzene, thiophene, polymeric solid, etc. According to *ab initio* SCF MO CI calculations (14), sulfur atoms may interact with the parent acetylene in the following exothermic, spin and orbital symmetry-allowed, elementary reactions:

[1] $S(^1D_2) + HC{\equiv}CH \rightarrow$ (S_0) $\Delta H \sim -60$ kcal/mol

[2] $S(^1D_2) + HC{\equiv}CH \rightarrow H\dot{C}{=}CH{-}\dot{S}\ (S_1)$ $\Delta H \sim -46$ kcal/mol

[3] $S(^1D_2) + HC{\equiv}CH \rightarrow HC{\equiv}CSH$ $\Delta H \sim -87$ kcal/mol

[4] $S(^3P_J) + HC{\equiv}CH \rightarrow H\dot{C}{=}CH{-}\dot{S}\ (T_0)$ $\Delta H \sim -6$ kcal/mol

The cycloadduct, thiirene, formed in [1] is 27 kcal/mol less stable than the insertion product, ethynylthiol, formed in [3] and about 14 kcal/mol more stable than its ring opened isomer, the S_1 state thioformylmethylene from reaction [2]. The $4n-\pi$ electron antiaromatic character of thiirene is manifested by the low C—S bond energy, 14 kcal/mol (14), as compared to that in the saturated counterpart, thiirane, which has a value of >40 kcal/mol (14−16) and explains the ability of thiirene to undergo a facile ring expansion reaction with acetylene to give thiophene

[5] 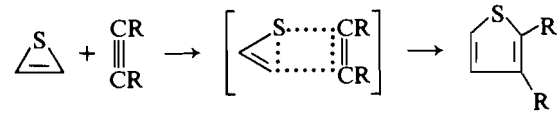

Since the late seventies, thiirene and a series of its derivatives, thioketene and ethynylthiol, have been isolated and identified by ir spectroscopy in low temperature inert matrices from the photolysis of 1,2,3,-thiadiazoles (17−20), where the intervention of thiirene as a novel intermediate had been postulated a decade earlier (3, 5, 6). Recently, the photolysis of trithiocarbonates has been shown to be a superior source of thiirene (19) and the isolation and esr identification of a thioketocarbene, namely, the T_0 state thiobenzoylphenylmethylene, has also been accomplished (21). The T_0 state of the thioketocarbene, formed in [4], is nearly isoenergetic with the S_1 state; both are double open shell species and are better represented by the 1,3-diradical structure as indicated above. The closed shell thioketocarbene $H\ddot{C}{-}C(=S){-}H$ is the S_2 state of the diradical lying 17 kcal/mol above the T_0 ground state. The isomerization of the S_1 state diradical to the thioketene or thiirene features a very small energy barrier and therefore it could not be isolated to date. The stabilization of the T_0 state diradical could not be accomplished to date either, probably because intersystem crossing on account of the small T_0-S_1 energy splitting, ~1 kcal/mol (computed), is quite efficient and isomerization to the thioketene, ethynylthiol, and thiirene on the lowest singlet energy surface cannot be arrested. In the case of thiobenzoylphenylmethylene, the experimental T_0-S_1 energy splitting is about 5 kcal/mol and that is the reason why it could

Can. J. Chem. Downloaded from www.nrcresearchpress.com by 210.87.254.5 on 09/06/12
For personal use only.

Can. J. Chem. Downloaded from www.nrcresearchpress.com by 210.87.254.5 on 09/06/12
For personal use only.

be readily stabilized below ca. 150 K in the solid matrix of its precursor 4,5-diphenyl-1,2,3-thiadiazol polycrystal (21). The near degeneracy of the T_0-S_1 states in HĊ=CH—Ṡ and probably in its mono- and dimethyl derivatives, as well, explains why the electronic state does not have a major impact on the nature of their chemistry, although the distribution of the products from them is somewhat affected. The direct insertion of $S(^1D_2)$ atoms into the C—H bond has been well documented (3) and in the gas phase it is nearly statistical with alkanes. In its reaction with ethylene, $S(^1D_2)$ atom gives vibrationally excited thiirane via cycloaddition and vinylthiol via direct insertion into the C—H bonds in a ratio of 0.9 (4). Since the rate of cycloaddition with $S(^1D_2)$ atoms should be about the same to the triple bond in acetylene as to the double bond in ethylene, but the number of C—H bonds in the former are less and their strength is higher (by 10 kcal/mol), insertion would be expected to be inefficient and negligible. Nonetheless, ethynyl thiol may form in the secondary photolysis of thiirene or the diradical, as in the low temperature matrix photolysis of thiirene and trifluoromethyl thiirene, or via the spontaneous, pressure dependent unimolecular isomerization of the initially hot cycloadducts, as in the gas phase addition of $S(^1D_2)$ atoms to ethylene, propylene, allene, and methylallene. The unimolecular isomerization reactions again would be less important than in the case of hot thiirane because the excess energy available is considerably lower, 60 kcal/mol compared to 87 kcal/mol in the case of thiirane. Therefore we conclude that ethynylthiol plays a minor role, if any, in the gas phase reaction of $S(^1D_2)$ atoms with acetylenes.

The gas phase photolysis of COS at $\lambda = 230-250$ nm yields about 70% $S(^1D_2)$ and 30% $S(^3P_J)$ atoms while, in the presence of >14-fold excess of CO_2, nearly all $S(^1D_2)$ atoms are deactivated to the ^3P_J ground state prior to reaction with the substrate

$$[6a]\quad COS + h\nu \xrightarrow{\lambda > 230\ nm} CO + S(^1D_2) \qquad 70\%$$

$$[6b]\quad \xrightarrow{\lambda > 230\ nm} CO + S(^3P_J) \qquad 30\%$$

$$[7]\quad COS + h\nu \xrightarrow[CO_2]{\lambda > 230\ nm} CO + S(^3P_J) \qquad 100\%$$

followed by

$$[8]\quad COS + S(^1D_2) \rightarrow CO + S_2$$

$$[9]\quad COS + S(^3P_J) \rightarrow CO + S_2$$

The S + C_2H_2 system

The yield of retrievable products, CS_2, benzene, and thiophene, is low at 25°C from both the $S(^1D_2)$ and $S(^3P_J)$ atom reactions. Raising the temperature to 160°C causes a large increase in product yields from 5% to 86% in the $S(^1D_2)$ atom reaction but has no observable effect on the $S(^3P_J)$ atom reactions, Tables 1 and 2.

The products can be rationalized in terms of the reaction sequence [6] or [7], [1], [2], [4], followed by [5], and

$$[10]\quad \dot{S}—CH=\dot{C}H(T_0) + HC\equiv CH \rightarrow \dot{S}(CH)_3\dot{C}H(T_0) \xrightarrow{C_2H_5} \text{(benzene)} + S(^3P_J)$$

$$\dot{S}(CH)_3\dot{C}H(T_0) \xrightarrow{M} \text{(thiophene)}$$

$$[11]\quad \dot{S}(CH)_3\dot{C}H \xrightarrow{nC_2H_2} \text{polymer}$$

$$[12]\quad \text{(thiirene)} + \text{(vinylthiol)} \rightarrow CS_2 + C_3H_4$$

$$[13]\quad H\dot{C}=CH—\dot{S}(S_1) \rightleftarrows H\dot{C}=CH—\dot{S}(T_0)$$

$$[14a]\quad H\dot{C}=CH—\dot{S}(S_1) \rightarrow H_2C=C=S$$

$$[14b]\quad \rightarrow \text{(thiirene)}$$

The low yield of recoverable products from the reactions of $S(^3P_J)$ atoms (~4%) suggests that, as with other free radicals, polymerization of the acetylene is efficient and it is the main sink of sulfur.

The higher yields of CS_2, benzene, and thiophene from the reactions of $S(^1D_2)$ atoms at elevated temperature show that the corresponding steps, [5], [10], and [12] are more efficient here.

The S + $CF_3C\equiv CH$ system

The major products, Table 3, are 2,4-bis(trifluoromethyl)-thiophene, **6**, and 1,3,5-tris(trifluoromethyl)benzene, **4**, in analogy to the reactions of S atoms with $CH_3C\equiv CH$ where trimethylbenzene and dimethylthiophene have been observed as major products (6).

The disubstituted thiophenes are formed in the addition reactions between S and the substrate followed by

$$[15]\quad \text{(CF}_3\text{-substituted thiirene)} + \text{(CF}_3\text{-substituted acetylene)} \rightarrow \text{(thiophene)}$$

The preponderance of **6** over **5** may be explained with the preferential opening of the substituted side of the C—S bond in thiirene, which is a trend opposite to that found before for methylthiirene (22) probably owing to the inverse polarities of the CH_3 and CF_3 groups and with the preferential addition of the substituted acetylenic carbon to the sulfur of the thiirene ring (*vide infra*). The Dewar benzene, **8**, and thiophene, **5**, may then result from the secondary photoisomerization of **4** and **6**, respectively, and **7** from the secondary photolysis of **5** and **6**. Alternatively, **5** may form from reactions of $S(^3P_J)$ atoms. CS_2 and the trifluoromethyl thioketene are formed in trace quantities.

The S + $CF_3C\equiv CH$ + $CF_3C\equiv CCF_3$ system

When sulfur atoms are reacted with an equimolar mixture of the above two substrates, the yields of disubstituted thiophenes and trisubstituted benzenes are drastically suppressed and tri- and tetra-substituted thiophenes become the dominant products, Table 4. A plausible way to rationalize product distribution is to assume that $S(^1D_2)$ atoms react with approximately equal rates with the two substrates,

$$[16]\quad S(^1D_2) + CF_3C\equiv CH \xrightarrow{k_{16}} \text{(thiophene)}$$

$$[17]\quad S(^1D_2) + CF_3C\equiv CCF_3 \xrightarrow{k_{17}} \text{(thiophene)}$$

where $k_{16} \approx k_{17}$, but scavenging of thiirenes occurs preferentially with C_4F_6.

[18] 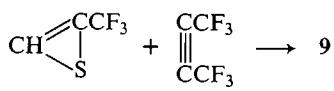 → **9**

[19] 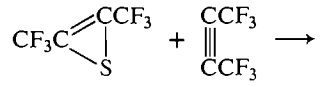 → **10**

[20] $S + 2CF_3C{\equiv}CH + C_4F_6 \longrightarrow \mathbf{11} + S$

The dimeric product(s) **12***a* and/or **12***b* appears to form from the dimerization of two primary adducts. The quantities of these products were too small for structural identification.

The S + C_4F_6 system

In low conversion experiments the only measurable sulfur product is **10**, PFTMT. The effect of the concentration of C_4F_6 on product yields at 23°C is shown in Fig. 1. As seen, the CO yield drops first more steeply up to ca. 80 Torr C_4F_6, owing to preferential scavenging of $S(^3P_J)$ atoms by C_4F_6 which becomes complete at ca. 80 Torr, and then more gradually on account of the competition between C_4F_6 and COS for $S(^1D_2)$ atoms,

[21] $S(^3P_J) + C_4F_6 \longrightarrow \cdot S{-}C(CF_3){=}\dot{C}{-}CF_3$ (T_0)

and

[22] $S(^1D_2) + C_4F_6 \longrightarrow$

[8] $S(^1D_2) + COS \longrightarrow CO + S_2$

where $k_{22} \approx k_8$. The yield of **10** is 25% in terms of sulfur atoms consumed in the addition reaction at the highest pressure of C_4F_6 employed, 1320 Torr. The rest of the sulfur appears to end up in the solid polymer.

The effect of temperature on the yield of **10** was examined in a series of experiments reported in Table 5. As seen from the data, the yield of **10** increases with rising temperature. Here, the possibility of a minor contribution to the CO yield from the attack on COS of any of the free radicals involved in the reaction

[23] $COS + R^{\cdot} \rightarrow RS^{\cdot} + CO$

cannot be excluded with certainty. Therefore the percentage yields for **10**, listed in Table 5, represent a lower limit if reaction [23] does contribute to CO formation and the correct values if [23] is not operative. At the highest temperature this lies between 60 and 97% theoretical. This temperature effect is due to the scavenging reaction of the thiirene with the acetylene

[19] 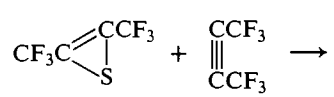 → **10**

A similar study on the reactions of $S(^3P_J)$ atoms from the photolysis of 40 Torr COS in the presence of 120 Torr C_4F_6 and 1400 Torr CO_2, which yields over 90% $S(^3P_J)$ atoms, gave entirely analogous results, Table 6. Even though at room temperature the yield of **10** is lower here, 14% versus 25% from $S(^1D_2)$ atoms, at 144°C the yields become identical, 60−100%.

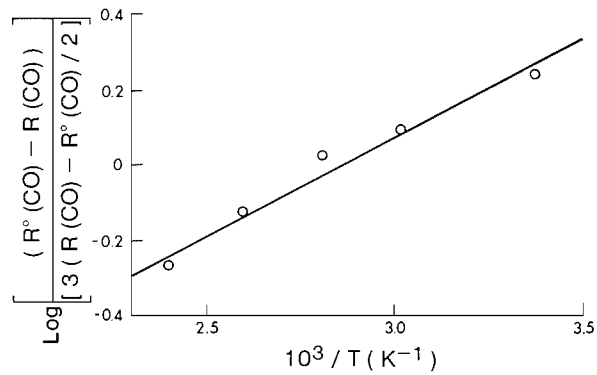

FIG. 3. Arrhenius plot for the $S(^3P_J)$ + PFB-2 system.

In this system it is possible to assess the importance of reaction [23] because the rate constants for the reaction

[9] $COS + S(^3P_J) \rightarrow CO + S_2$

and

[21] $C_4F_6 + S(^3P_J) \rightarrow \cdot S{-}C(CF_3){=}\dot{C}{-}CF_3$ (T_0)

are known. From simple kinetic treatment

$$\frac{R_{21}}{R_9} = \frac{k_{21}[S(^3P_J)]\,[C_4F_6]}{k_9[S(^3P_J)]\,[COS]} = \frac{R^0_{CO} - R_{CO}}{R_{CO} - R^0_{CO}/2}$$

if [23] is inoperative. Values for the expression $\{[R^0_{CO} - R_{CO}] \cdot [COS]\}/\{[R_{CO} - R^0_{CO}/2][C_4F_6]\}$, which is equal to k_{21}/k_9, have been calculated at different temperatures using the data in Table 6 and have been plotted in the Arrhenius form, Fig. 3. The plot gives a good straight line; from the slope, $E_9 - E_{21} = 2.4 \pm 0.2$ and from the intercept, $A_{21}/A_9 = 0.032 \pm 0.005$. Since $k_9 = (9.2 \pm 1.2) \times 10^{11} \exp[-(3630 \pm 120)/RT]$ cm^3 mol^{-1} s^{-1} (23), the Arrhenius parameters for the addition of $S(^3P_J)$ atoms to C_4F_6 would be

$$k_{21} = (2.95 \pm 0.59) \times 10^{10} \exp[-(1240 \pm 200)/RT] \text{ cm}^3 \text{ mol}^{-1} \text{ s}^{-1}$$

At room temperature, $k_{21} = 3.8 \times 10^9$ cm^3 mol^{-1} s^{-1}, a value far too low compared to the value, $k_{21} = 2.1 \times 10^{11}$ cm^3 mol^{-1} s^{-1} obtained from direct flash photolysis/kinetic absorption spectroscopic measurements (8).

Therefore we are forced to conclude that reaction [23] does indeed contribute to the rate of CO formation in the triplet and, by inference, in the singlet system as well, and the true yield of **10** in both systems at 144−160°C may be estimated to be slightly above 60%. The loss is due to polymerization and the ratio of the product-forming steps to the polymer-forming steps can be estimated by

[22] $$\frac{R_{PFTMT}}{R_{(loss)}} = \frac{\%\ \text{PFTMT yield}}{100 - \%\ \text{PFTMT yield}}$$

The RHS of eq. [22] calculated from the data in Tables 5 and 6 when plotted in the Arrhenius form gives a straight line in the region of lower temperatures. The slope of the obtained straight line gives an activation energy of $\Delta E = 4.4$ kcal/mol. It is reasonable to assume that the polymerization reactions feature activation energies which are small but not zero, hence $E_a(\mathbf{10}) > 4.4$ kcal/mol.

Thus, for the overall reaction, the following scheme may be considered:

Can. J. Chem. Downloaded from www.nrcresearchpress.com by 210.87.254.5 on 09/06/12
For personal use only.

Can. J. Chem. Downloaded from www.nrcresearchpress.com by 210.87.254.5 on 09/06/12
For personal use only.

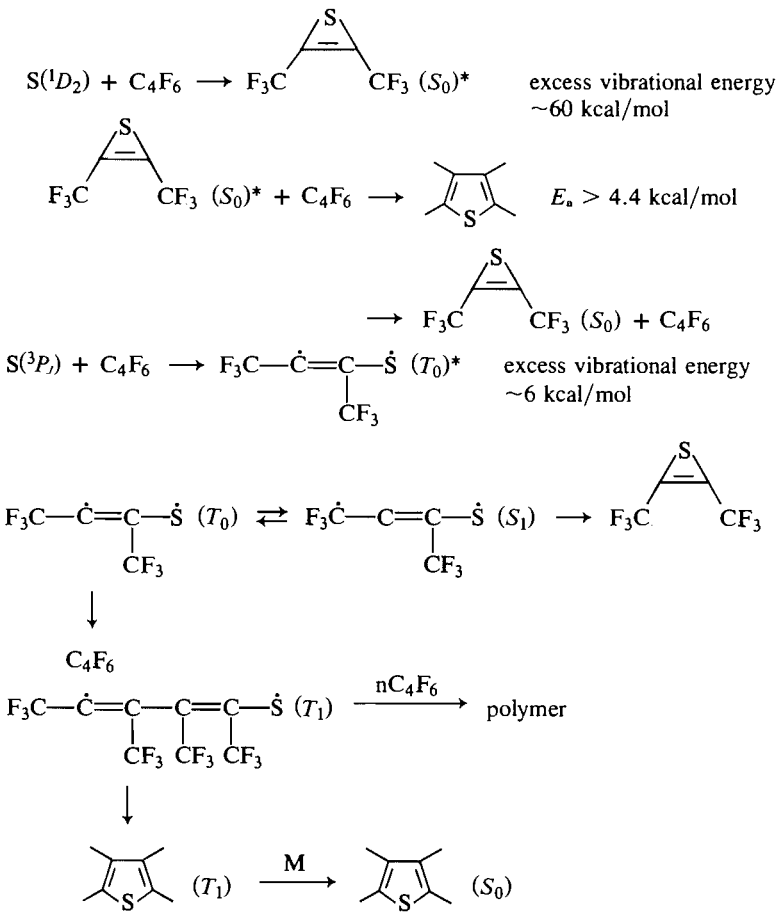

In higher conversion experiments several additional products could be detected in small quantities and in some cases identified. At least three of them appear to be primary products, Table 9 and Fig. 3, and others are clearly secondary products. Thus, compound **18**, identified as the novel perfluoro-3,4,5,6-tetramethyl-1,2-dithiin is a primary product formed in small yields, probably from the symmetrical dimerization of vibrationally relaxed thiirenes along with another isomeric dimer,

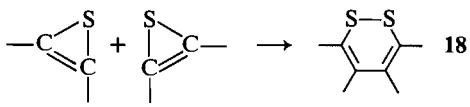

15, whose structure could not be established. The stability of **18** is attributable to the strong electron withdrawing effect of the four CF_3 groups. Also, three isomeric trimers **17**, **19**, and **20** were detected, of which the structure of only **17** could be established as

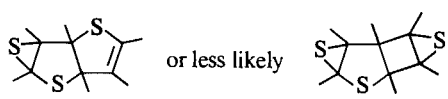

17*a* **17***b*

They could be formed either via the addition of S to **16** or via the addition of another thiirene molecule to the dimers

$$(C_4F_6S)_2 + C_4F_6S \rightarrow (C_4F_6S)_3$$

Product **16** is apparently also a primary product and could be formed via the addition of a secondary triplet adduct to a primary adduct

$$\dot{C}=C-C=C-\dot{S} + \dot{C}_4F_6\dot{S} \rightarrow (C_4F_6)_3S_2 \qquad \mathbf{16}$$

The Dewar thiophene **13** is a known photolysis product of the thiophene **10** (11) and, accordingly, its yield rapidly increases with photolysis time at the expense of **10**, Fig. 2. Its formation from **10** was confirmed in separate experiments by photolyzing 280 Torr COS and 480 Torr C_4F_6 with 2.5 Torr added **10** which resulted in a 25-fold increase in the yield of **13**. Since in the above experiment the yield of **14** has also shown a substantial increase, it would appear that it is formed via the steps

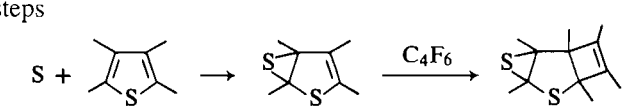

And finally the novel compound, product **21**, forms by the stepwise addition of two sulfur atoms to **10**, as shown by the photolysis of 300 Torr COS in the presence of 3.3 Torr of **10** which resulted in the formation of **21** as the major product.

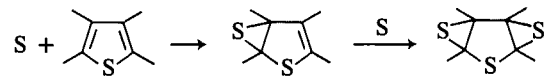

The superior scavenging ability of the strongly nucleophile C_4F_6 among acetylenes for thiirenes was recognized at the earliest stage in the study of thiirene chemistry (6). In order to get a better insight into these reactions the effect of varying amounts of added C_2H_2 was examined on the photolysis of 80

Torr COS in the presence of 500 Torr C_4F_6, cf. paragraph 6 in Results and Tables 7 and 8. $S(^3P_J)$ atoms have equal rate constants for addition to C_2H_2 and C_4F_6 (k = 2.3 and 2.1 $\times 10^{11}$ cm^3 mol^{-1} s^{-1}) (8) and the rate constants for reaction with the $S(^1D_2)$ atoms should also be nearly equal. Yet, from the data presented in Tables 7 and 8, it is clear that addition of even small quantities of C_2H_2, ~5%, has a much larger suppressing effect on the yield of **10** with the simultaneous appearance of the cross product, bis(2,3-trifluoromethyl)thiophene. This occurs at both temperatures, 25 and 132°C, studied and, while increasing amounts of added C_2H_2 increase the yield of b-TFMT, the sum of PTMT and b-TFMT decreases as the concentration of added C_2H_2 increases. This strongly suggests that C_2H_2 is capable of intercepting bis(trifluoromethyl)thiirene even more efficiently than C_4F_6, but that the adduct is largely a diradical which undergoes polymerization with the excess acetylenes resulting in a decrease of recoverable product yields,

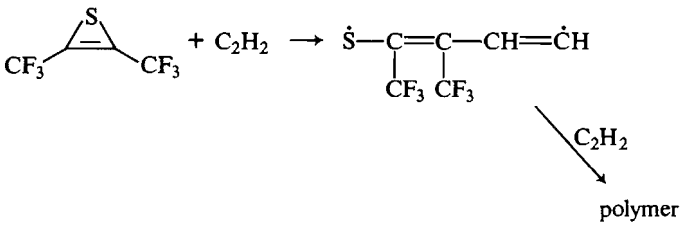

This observation is in line with the results of earlier studies on S + C_2H_2, CH_3—C≡CH, and CH_3—C≡C—CH_3 (5, 6) and also of studies on the photolysis of 1,2,3-thiadiazoles in the presence of acetylenes (22).

Bis(trifluoromethyl)thiirene is probably more stable than any of the other thiirenes discussed in this article and it is possible that, at sufficiently low temperature in the presence of low concentrations of C_4F_6, it would be sufficiently stable to study its spectroscopic properties in the gas phase.

The study of the reaction of sulfur atoms with acetylenes, apart from its inherent interest, has shed new light on the gas phase chemistry of thiirenes and their isomeric thioketocarbenes and resulted in the synthesis of a series of novel and interesting molecules.

Acknowledgements

We thank the Natural Sciences and Engineering Research Council of Canada for continuing financial support, Dr. T. Nakashima and Mr. G. Bigam for the nmr, and Drs. E. M. Lown and M. Torres for helpful assistance.

1. O. P. STRAUSZ and H. E. GUNNING. J. Am. Chem. Soc. **84**, 4080 (1962).
2. A. R. KNIGHT, O. P. STRAUSZ, S. M. MALM, and H. E. GUNNING. J. Am. Chem. Soc. **86**, 4243 (1964).
3. O. P. STRAUSZ. Pure Appl. Chem. Suppl. **4**, 165 (1972).
4. A. G. SHERWOOD, I. SAFARIK, B. VERKOCZY, G. ALMADI, H. A. WIEBE, and O. P. STRAUSZ. J. Am. Chem. Soc. **101**, 3000 (1979).
5. E. L. DEDIO. Ph.D. Thesis, University of Alberta, 1967.
6. O. P. STRAUSZ, J. FONT, E. L. DEDIO, P.KEBARLE, and H. E. GUNNING. J. Am. Chem. Soc. **89**, 4805 (1967).
7. D. J. LITTLE and R. J. DONOVAN. J. Photochem. **1**, 371 (1972/73).
8. A. VAN ROODSELAAR, I. SAFARIK, O. P. STRAUSZ, and H. E. GUNNING. J. Am. Chem. Soc. **100**, 4068 (1978).
9. C. G. KRESPAN. J. Am. Chem. Soc. **83**, 3434 (1961).
10. M. G. BARLOW, R. HASZELDINE, and R. HUBBARD. J. Chem. Soc. (C), 1232 (1970).
11. H. A. WIEBE, S. BRASLAVSKY, and J. HEICKLEN. Can. J. Chem. **50**, 2721 (1972).
12. Y. KOBAYASHI, I. KUMADAKI, A. OSHAWA, and Y. SEKINE. Tetrahedron Lett. 1639 (1975).
13. K. P. ZELLER, H. MEIER, and E. MULLER. Tetrahedron Lett. 537 (1971); Justus Liebigs Ann. Chem. **32**, 766 (1972).
14. R. K. GOSAVI and O. P. STRAUSZ. To be published.
15. P. VITINS. Ph.D. Thesis, University of Alberta, 1973.
16. O. P. STRAUSZ, H. E. GUNNING, A. S. DENES, and I. G. CSIZMADIA. J. Am. Chem. Soc. **94**, 8317 (1972).
17. J. LAURENI, A. KRANTZ, and R. H. HAJDU. J. Am. Chem. Soc. **96**, 6768 (1974); A. KRANTZ and J. LAURENI. J. Am. Chem. Soc. **103**, 486 (1981).
18. M. TORRES, A. CLEMENT, J. E. BERTIE, H. E. GUNNING, and O. P. STRAUSZ. J. Org. Chem. **43**, 2490 (1978).
19. M. TORRES, A. CLEMENT, H. E. GUNNING, and O. P. STRAUSZ. Nouv. J. Chim. **3**, 149 (1979).
20. M. TORRES, I. SAFARIK, A. CLEMENT, J. E. BERTIE, and O. P. STRAUSZ. Nouv. J. Chim. **3**, 365 (1979).
21. H. MURAI, M. TORRES, and O. P. STRAUSZ. J. Am. Chem. Soc. **101**, 3976 (1979).
22. J. FONT, M. TORRES, H. E. GUNNING, and O. P. STRAUSZ. J. Org. Chem. **43**, 2487 (1978).
23. R. B. KLEMM and D. D. DAVIS. J. Phys. Chem. **78**, 1137 (1974).

Can. J. Chem. Downloaded from www.nrcresearchpress.com by 210.87.254.5 on 09/06/12
For personal use only.

Can. J. Chem. Downloaded from www.nrcresearchpress.com by 210.87.254.5 on 09/06/12
For personal use only.

Appendix I

TABLE A-I. ^{19}F nuclear magnetic resonance spectral data[a]

Compound number	Structure	Peak description	Chemical shift (ppm)[b]	Integration
4[c]	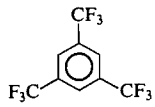	Complex quartet	99.35	1
6[d]	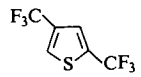	Complex doublets Complex doublets	103.65 99.66	1 1
[e]	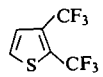	Quartet (complex doublets) Quartet (complex unresolved)	105.51 101.80	1 1
7[c]	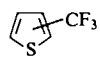	Complex	100.29	1
8[c]	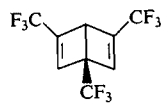	Very broad Broad	99.81 96.06	2 1
9[d]	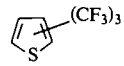	Complex quartet Quartet Quartet	105.02 103.26 101.57	1 1 1
10[f]	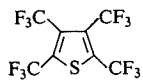	Complex Complex	105.76 103.93	1 1
14[g]	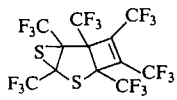	Single Complex (2 similar) Very complex Very complex	109.70 103.19 99.74 87.00	2 2 1 1
17*a*[g] or **17***b*[g]	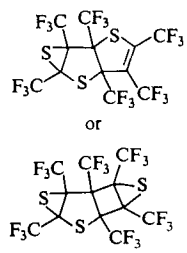	Quartet Quartet Broad Broad Quartet Very broad	106.38 106.04 101.93 98.61 97.88 98.21	1 1 1 1 1 1
18[g]	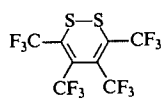	Complex Complex	108.74 99.45	1 1
21[g]	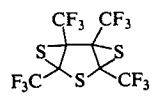	Very complex Very complex	103.50 101.00	1 1

[a] ^{19}F frequency = 376.31 MHz; solvent $CDCl_3$; T = 25°C.
[b] All chemical shifts are referenced to hexafluorobenzene as external standard.
[c] Compound reference numbers are from Table 3.
[d] Compound reference numbers are from Table 4.
[e] From ref. 5.
[f] From ref. 9.
[g] Compound reference numbers are from Table 9.

Appendix II

TABLE A-II. ^{1}H nuclear magnetic resonance spectral data[a]

Compound number	Structure	Peak description	Chemical shift (ppm)[b]	Integration
5[c]	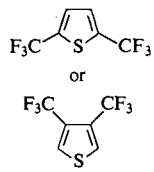	Complex	7.67	1
6[c]	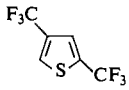	Complex Complex	7.96 7.67	1 1
[d]		Complex Complex	7.58 7.38	1 1
9[e]	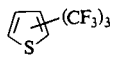	Broad	7.66	1

[a] ^{1}H frequency = 400 MHz; solvent, $CDCl_3$; T = 25°C.
[b] Referenced to TMS, as internal standard.
[c] Reference number from Table 3.
[d] From ref. 5.
[e] Reference number from Table 4.

Can. J. Chem. Downloaded from www.nrcresearchpress.com by 210.87.254.5 on 09/06/12
For personal use only.

Low frequency vibrational spectra of lithium formate monohydrate and its aqueous solutions

A. AGARWAL, D. P. KHANDELWAL, AND H. D. BIST
Department of Physics, Indian Institute of Technology, Kanpur-208016, India

Received February 14, 1983

A. AGARWAL, D. P. KHANDELWAL, and H. D. BIST. Can. J. Chem. **61**, 2282 (1983).

The far infrared and Raman spectra of polycrystalline lithium formate monohydrate and the Rayleigh wing scattering of its aqueous solutions are reported. Three new bands in solid and bands due to librations of $HCOO^-$ and the quasi-tetrahedral structure of water in solutions have been identified.

A. AGARWAL, D. P. KHANDELWAL et H. D. BIST. Can. J. Chem. **61**, 2282 (1983).

On rapporte les spectres dans l'infrarouge lointain et les spectres Raman du monohydrate de formiate de lithium polycristallin et la dispersion de Rayleigh Wing de sa solution aqueuse. On a identifié: trois nouvelles raies dans le solide, les raies dues aux librations du $HCOO^-$ ainsi que la structure quasi-tétraédrique de l'eau dans les solutions.

[Traduit par le journal]

Can. J. Chem. Downloaded from www.nrcresearchpress.com by 210.87.254.6 on 09/06/12
For personal use only.

Introduction

The spectrum of lithium formate monohydrate in the low frequency region, which covers the librations of the non-spherical $HCOO^-$ ion, has been studied by the Raman technique in the solid state (1, 2); however, the corresponding infrared (ir) spectrum has not been reported. The spectra of aqueous solutions have not been examined by either method. In the present work the ir spectrum of a microcrystalline sample in the low frequency region (300−20 cm^{-1}) and the Raman spectra of aqueous solutions of various concentrations in the same region are being presented for the first time, along with a re-examination of the Raman spectrum of the solid. The Raman spectra of the solutions are examined in the $R_2(\nu)$ format (3−5), which is useful for an analysis of the Rayleigh wing scattering. Since the bands of the $HCOO^-$ librations in the aqueous solutions are masked by two characteristic translational bands of water falling in the same region (4−9), we have used the technique of suitable subtractions of the $R_2(\nu)$ contribution due to pure water from those of the solutions so as to get better information about the $HCOO^-$ librations in the solution phase.

Experimental

For Raman spectra the samples were excited with the 514.5 nm line from a Spectra Physics 165 Ar^+ laser, using ~150 mW power at the sample. The spectra were recorded using the Spex 1403 double monochromator with a digital detection and recording system (DPC-2 and Linear chart recorder). The far ir spectrum was recorded in a polystyrene pellet on the Polytex FTIR instrument at the Regional Sophisticated Instruments Centre, IIT, Madras. The accuracy of measurements for the sharper bands is ±1 cm^{-1} and for the broader resolved components from the $R_2'(\nu)$ curves (see below) is about ±4 cm^{-1}.

Results

Figure 1(*a*) shows the Raman spectrum of polycrystalline $HCOOLi.H_2O$ along with the corresponding ir spectrum. Figure 1(*b*), (*c*), and (*d*) show the Raman spectra of 4 *M*, 2 *M*, and 0.5 *M* aqueous solutions, respectively, taken under identical excitation and other conditions. The curves are given in the $R_2'(\nu)$ format (see below) and the contour in each case is resolved into the minimum number of Lorentzian bands warranted by the peaks or humps. These components are shown by dotted curves, and the pertinent data are presented in Table 1.

The $R_2'(\nu)$ format was obtained as follows. The observed $I(\nu)$ versus ν curves were first recast into the $R_2(\nu)$ format (3), showing $\nu^2\bar{I}(\nu)$ versus ν, where $\bar{I}(\nu)$ is the mean of the Stokes and anti-Stokes intensities at ν. The $R_2(\nu)$ format of the curves makes it possible to compare the Raman spectra with the ir spectra, the Rayleigh scattering being appropriately suppressed (3). From this $R_2(\nu)$ curve for the solution a suitable fraction of the $R_2(\nu)$ curve for pure water was subtracted to optimize the information about contributions of the $HCOO^-$ ion in the solution phase. We call this the $R_2'(\nu)$ format of the curve. The fraction, f, of the $R_2(\nu)$ of water to be subtracted was decided as follows. For the solution with the highest concentration the value of f was set so as to keep the lowest $R_2'(\nu) = 0$. The same fraction f was then used to deduce the $R_2'(\nu)$ for the other solutions.

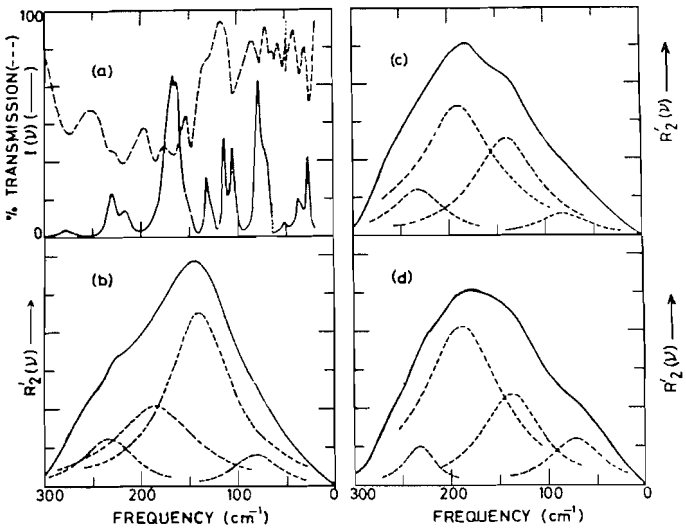

FIG. 1. (*a*) The infrared and Raman spectra of microcrystalline solid lithium formate monohydrate; the broken-line curve is for infrared, and the continuous curve for Raman. (*b*), (*c*), and (*d*) are the Raman $R_2'(\nu)$ spectra respectively of 4 *M*, 2 *M*, and 0.5 *M* solutions of the salt; the dotted curves under each spectrum are the resolved bands with Lorentzian shape.

Discussion

Polycrystalline solid

Our Raman spectrum of the solid sample essentially agrees with that reported by Hase (1), except for the bands at 70, 37, and 27 cm^{-1} which were not reported earlier. The assignments

TABLE 1. Peak positions of the bands for lithium formate monohydrate at 300 K[a]

Solid					Aqueous solutions, Raman $R_2'(\nu)$ format[b]			
Infrared		Raman		Assignment	4 *M*	2 *M*	0.5 *M*	Assignment
274	s	277	w	T(F), T(W)				
					232	232	232	
231	m	230	m	T(F)	(2.5, 64; 38)	(2.4, 64; 22)	(2.0, 40; 10)	ν(W)
219	s	216	w	T(F), T(W)				
					186	190	188	T_1(W)
183	s			129+70	(4.2, 100; 100)	6.8, 100; 100)	(8.2, 100; 100)	
165	s	166	s	ω(F)				
		163	s	ω(F)				
148	s			2×78[c]				
					140	140	136	ω(F), τ(F)
					(9.0, 80; 170)	(5.1, 80; 60)	(4.7, 76; 44)	
138	sh	132	m	τ(F)				
131	sh	129	sh	τ(F)				
104	s	113	s	T(F)				
		105	s	T(F), T(W)				
					82	82	72	
					(1.6, 56; 20)	(1.1, 60; 10)	(2.4, 64; 18)	ρ(F), T_2(W)
78	m	78	s	ρ(F)				
68	sh	70	sh	ρ(F)				
62	w			?				
53	m	51	m	T(F)				
36	m	37	m	105−70				
25	s	27	s	78−51				

[a]The positions are in cm^{-1}. The quantities in parentheses after the band positions are the peak intensities, half widths (cm^{-1}), and relative integrated intensities, respectively. The symbols have the following meanings: (F) = formate; (W) = water; T = translation, τ = twist, ω = wag, ρ = rock; s = strong, m = medium, w = weak, sh = shoulder; T_1, T_2 = hindered translations.

[b]See text.

[c]Overtone of 78 cm^{-1} band.

in column 3 of Table 1 follow Hase, who used isotopic shifts with $^6Li/^7Li$, H/D in the formate group, and H/D in water for the purpose. We have assigned the second rocking mode of formate ion, $\rho(F)$ to the 70 cm^{-1} band, now observed, instead of the 51 cm^{-1} band. This shows the two $\rho(F)$ modes occurring as a close doublet (78 and 70 cm^{-1}), like the two twisting, $\tau(F)$, and the two wagging, $\omega(F)$ modes of formate ion. The 51 cm^{-1} band is now assigned to a translational mode, T(*F*), so that the second set of three T(*F*) modes is now placed at 113, 105, and 51 cm^{-1}, like the first set placed at 277, 230, and 216 cm^{-1}. The information obtained by Hase (1) from the isotopic shift studies is not violated in these changed assignments.

The far ir bands agree with the Raman bands, including those at 70, 37, and 27 cm^{-1}. Three additional bands show up in ir at 183, 148, and 62 cm^{-1}. These are apparently second order bands. The $\omega(F)$ and one T(*F*) (at 113−105 cm^{-1}) doublets in the Raman spectrum are unresolved in the ir spectrum.

Aqueous solutions

(i) The band around 140 cm^{-1}

The band around 140 cm^{-1} is the strongest resolved band in the $R_2'(\nu)$ spectrum for 4 *M* solution (Fig. 1(*b*)). This band exhibits considerable diminution in intensity as the concentration is decreased, suggesting that the band is associated with the $HCOO^-$ group.

From the Raman spectra of microcrystalline (1) and single crystal samples (2), the twisting and wagging modes of the $HCOO^-$ ion in this salt are known to fall around 129−133 cm^{-1} and 164−174 cm^{-1}, respectively. Our ir spectrum (Table 1) of the solid supports these assignments. In the aqueous solutions the environment around the $HCOO^-$ ion will be quite different, since the probability of coordination with Li^+ will be replaced by that with the oxygen of free water with increasing dilution. The wagging and twisting modes of $HCOO^-$ could therefore have frequencies quite different from those in the solid. In any case the corresponding bands would be much broader due to diffusional motion. The 140 cm^{-1} band in aqueous solutions, with its large half-width (~80 cm^{-1}), thus represents the unresolved twisting and wagging motions of the formate ion. That its frequency (140 cm^{-1}) is lower than the weighted mean of the twist and wag frequencies in the solid (~150 cm^{-1}) means the coordination around $HCOO^-$ is weaker in solution than in solid, as is to be expected.

(ii) The band around 188 cm^{-1}

The next prominent band in the $R_2'(\nu)$ curves of aqueous solutions is around 188 cm^{-1}. This band shows continuous decrease in intensity as we go from pure water to the solution having the highest concentration (4 *M*). Therefore, it may pertain to free water in the solutions also. In free water the corresponding band has position 191 cm^{-1} and it is assigned to hindered translation of the centre of mass parallel to the molecular plane (4, 6). With increasing amount of the solute, this band could weaken on two counts. Firstly, increasing fractions of water molecules will go into coordination with the solute, leaving smaller fractions as free water. Secondly, the hydrogen bonding between the free water molecules will also decrease, if the structure around the formate ion does not fit that of free water (4), as in the present case (see section (*iv*)). The effect is not a pH effect because in these solutions the pH changes very marginally with concentration: 7.36 for 0.5 *M* to 7.60 for 4 *M* solution.

Can. J. Chem. Downloaded from www.nrcresearchpress.com by 210.87.254.6 on 09/06/12
For personal use only.

(iii) The lowest frequency band

The lowest frequency band in the $R_2'(\nu)$ spectra of the aqueous solutions appears at 82 cm^{-1} for the 4 *M* and 2 *M* solutions (with almost equal intensities) and at 72 cm^{-1} for the 0.5 *M* solution with increased intensity. In the Raman spectrum of the microcrystalline solid the rocking doublet falls at 78 and 70 cm^{-1} (Fig. 1(*a*)). In the single crystal Raman spectra the four components appear in the range 70−80 cm^{-1} for different symmetry species (2). Thus the above-mentioned band in the $R_2'(\nu)$ spectra can be assigned to the rocking mode of $HCOO^-$ ion.

The changes in intensity and peak frequency of the band on reducing the concentration from 2 *M* to 0.5 *M* are not clearly understood. One suggestion could be that it has some contribution from the reported hindered translation perpendicular to the molecular plane (hydrogen bond bending mode) of water at 60 cm^{-1} (5−9). Though Brooker *et al.* (4) raise doubt on the presence of this band, the model calculations for liquid water (6, 7) support the earlier experimental evidence. Its contribution will distinctly increase at low concentration, as is observed.

(iv) The band around 232 cm^{-1}

The fourth band in the $R_2'(\nu)$ spectra of aqueous solutions is around 232 cm^{-1}. The diminution in the integrated intensity of this band with decreasing concentrations of the solute may suggest that this band originates from the free formate ions. However, this view is ruled out because the $R_2'(\nu)$ curve for acetone solution (not shown here) did not give any trace of such a band.

Liquid water has a quasi-tetrahedral structure in which each water molecule is striving to bond itself tetrahedrally to four neighbouring molecules (10, 11). Though the bonds are continuously breaking and reforming, the tetrahedral features may be revealed in Raman scattering which involves short-time interactions (5). Eriksson and Lindgren (12) calculated a vibrational frequency for water in the tetrahedral environment at 239 cm^{-1}. In the lithium solution the Li^+ ions coordinate tetrahedrally with the surrounding water molecules forming a tetrahedral $Li(OH_2)_4^+$ complex (13). As in the tetrahedral complex the lithium atom does not move in a totally symmetric Li—O vibration and only the reduced mass of water enters into the corresponding **G** matrix (13), it is only slightly different from the water vibration considered by Eriksson and Lindgren (12) for pure water in tetrahedral environment. Thus we suggest that the 232 cm^{-1} band is the totally symmetric vibration of the tetrahedrally surrounded water molecules against the central lithium ion. The enhancement in the intensity of this band with increasing solute concentration is accounted for by the fact that the more available the lithium ions in the solution, the more stable the tetrahedral structure of water becomes.

1. Y. HASE. Spectrochim. Acta, **37**A(4), 275 (1981).
2. J. C. GALZERANI, R. SRIVASTAVA, R. S. KATIYAR, and S. P. S. PORTO. J. Raman Spectrosc. **6**(4), 174 (1977).
3. M. PERROT, M. H. BROOKER, and J. LASCOMBE. J. Chem. Phys. **74**(5), 2787 (1981).
4. M. H. BROOKER and M. PERROT. J. Chem. Phys. **74**(5), 2795 (1981).
5. O. F. NIELSEN. Chem. Phys. Lett. **60**, 515 (1979).
6. R. W. IMPEY and P. A. MADDEN. Mol. Phys. **46**(3), 513 (1982).
7. O. WERES and S. A. RICE. J. Am. Chem. Soc. **94**, 8983 (1972).
8. M. MOSKOVITS and K. H. MICHAELIAN. J. Chem. Phys. **69**, 2306 (1978).
9. D. EISENBERG and W. KAUZMANN. The structure and properties of water. Oxford University Press, London. 1969. p. 228.
10. J. MORGAN and B. E. WARRAN. J. Chem. Phys. **6**, 666 (1938).
11. G. W. ERADY and W. J. ROMANOW. J. Chem. Phys. **32**, 306 (1960).
12. A. ERIKSSON and J. LINDGREN. J. Mol. Struct. **48**, 417 (1978).
13. K. H. MICHAELIAN and M. MOSKOVITS. Nature, **273**, 135 (1978).

Can. J. Chem. Downloaded from www.nrcresearchpress.com by 210.87.254.6 on 09/06/12
For personal use only.

Pentaketide metabolites from *Potebniamyces gallicola* n. sp.

CAMILLE A. BOULET AND GERALD A. POULTON[1]
Department of Chemistry, University of Victoria, Victoria, B.C., Canada, V8W 2Y2

Received March 7, 1983

CAMILLE A. BOULET and GERALD A. POULTON. Can. J. Chem. **61**, 2285 (1983).

The fungus *Potebniamyces gallicola* n. sp. has been isolated from cankered swellings of western hemlock (*Tsuga heterophylla* (Raf.) Sarg.) produced by the dwarf mistletoe (*Arceuthobium tsugense* (Rosendahl) G. N. Jones), and has been implicated in the induction of disease in the infected trees. *P. gallicola* was cultured on malt extract, and four isoprenylated pentaketide metabolites were isolated by extraction; these were identified as the known compounds fuscin **1** and dihydrofuscin **2**, and two related compounds secofuscin **3** and dihydrosecofuscin **4**, not previously reported in nature.

CAMILLE A. BOULET et GERALD A. POULTON. Can. J. Chem. **61**, 2285 (1983).

On a isolé le champignon *Potebniamyces gallicola* n. sp. du gonflement nécrosé de la cigue de l'ouest (*Tsuga hétérophylla* (Raf.) Sarg.) produit par le gui nain (*Arceuthobium tsugense* (Rosendahl) G.N. Jones). Ce champignon est impliqué dans l'induction de la maladie des arbres infestés. On a cultivé le *P. gallicola* dans un extrait de malt et on en a extrait quatre métabolites pentacétides isoprénylés. On a identifié ces derniers comme étant les composés connus: la fuschine **1** et la dihydrofuschine **2** et deux composés apparentés la sécofuschine **3** et la dihydrosécofuschine **4** non encore répertorié dans la nature.

[Traduit par le journal]

Can. J. Chem. Downloaded from www.nrcresearchpress.com by 210.87.254.105 on 09/06/12
For personal use only.

The fungus *Potebniamyces gallicola* n. sp. has been isolated (1) from cankered swellings of western hemlock (*Tsuga heterophylla* (Raf.) Sarg.) produced by the dwarf mistletoe (*Arceuthobium tsugense* (Rosendahl) G.N. Jones). Slant agar cultures of this fungus showed visible amounts of a metabolite as surface rosettes. Since the metabolite of a related pathogenic fungus, *Potebniamyces balsamicola* Smerlis var. *boycei* Funk, had been shown (2) to possess interesting anti-fungal and anti-bacterial activity, we undertook the isolation and structure elucidation of the metabolites of *P. gallicola*.

P. gallicola was cultured on 3% malt extract, unshaken, at 15°C, and the metabolites were isolated by extraction of the homogenized culture medium. Examination of the crude extract by hplc showed the presence of two pairs of compounds; the main metabolite was isolated by trituration with pentane. Recrystallization from benzene/pentane gave yellow crystals, mp 225–227°C, which were identified as the known compound fuscin **1** (Experimental), and confirmed by comparison with an authentic sample of fuscin obtained from Prof. D. H. R. Barton. Fuscin (9,10-dihydro-5-hydroxy-4,8,8-trimethyl-2*H*,4*H*-benzo[1,2-*b*;4,3-*c*']dipyran-2,6(8*H*)dione) has previously only been isolated from two closely related species of *Oidiodendron* (3–9).

The presence of a second metabolite was obvious from the crude nmr spectrum and hplc of the extract. An interpretation of the spectrum suggested that it was closely related to that of fuscin, and it was assumed that the metabolite could be the known dihydrofuscin **2**; this identity was confirmed by chemical conversion of fuscin into dihydrofuscin, and by co-injection on the hplc.

Extraction of a second culture series containing greater amounts of the second pair of metabolites was carried out in a manner similar to that described above. Trituration of the crude extract with pentane yielded a quantity of the pure third metabolite **3**, mp 159–163°C, which proved to be isomeric with fuscin. The proton nmr of **3** showed two exchangeable protons at δ 6.72, an olefinic proton at δ 6.50, a methyl (δ 1.57) coupled to a methine (δ 5.73), and signals at δ 3.32 (2H doublet), 5.04 (1H triplet), 1.75 and 1.67 (each 3H singlets)

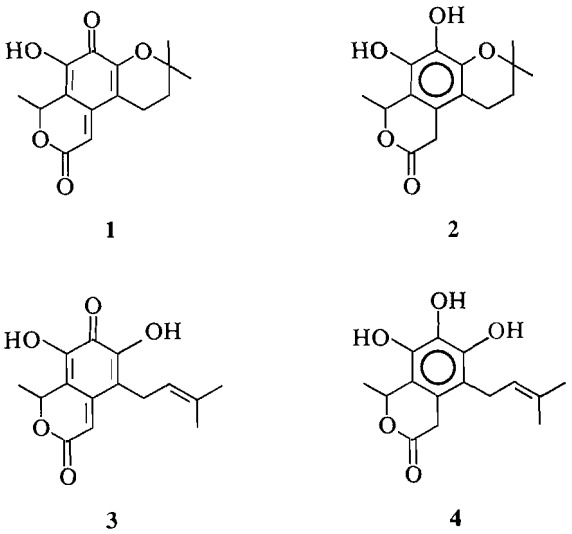

which correspond to an aromatic prenyl side chain (10). This evidence suggested that the quinonoid system is essentially the same as in fuscin with the only major change being that the pyranoid ring has not been formed. The structure of this metabolite was therefore assigned as 5,7-dihydroxy-4-methyl-8-(3'-methyl-2'-butenyl)-4*H*-benzo[*c*]pyran-2(1*H*),6-dione **3** (secofuscin). Support for this tentative identification was forthcoming from the ready cyclization of secofuscin to fuscin by dilute acid.

The hplc evidence suggested that the third and fourth metabolites were also related as an oxidation/reduction pair, and thus the fourth metabolite was assigned the structure **4**, dihydrosecofuscin, in accord with its nmr spectrum.

Secofuscin and dihydrosecofuscin have not been previously reported as natural products, although they have been described as intermediates in the total synthesis of fuscin. It is interesting to speculate that they should also co-occur with fuscin and dihydrofuscin in *Oidiodendron* species, and might have been missed during the extraction due to the work-up which was used. Secofuscin and dihydrosecofuscin complete the isolation, as compounds in nature, of all the intermediates in the biosynthetic scheme leading to fuscin (9, 11). A simple pen-

[1]Author to whom correspondence may be addressed.

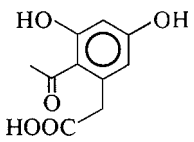

5

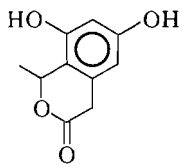

6

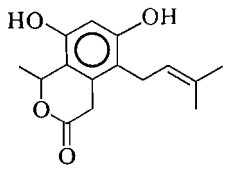

7

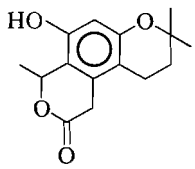

8

taketide **5** is cyclized, **6**, and prenylated, **7**, oxygen is introduced to produce dihydrosecofuscin, which is readily converted to fuscin.

Experimental

General

Melting points were determined on a Kofler hot stage and are uncorrected. Proton nmr spectra were determined on a Perkin–Elmer R32 spectrometer at 90 MHz in $CDCl_3$ solution and are with reference to TMS. Infrared spectra were obtained on a Perkin–Elmer 283 spectrometer, and ultraviolet spectra on the Beckman DU-8 spectrophotometer. The hplc analyses were made on a Varian 5000 liquid chromatograph equipped with a Varichrom detector (detection at 254 nm) and a 30 cm MCH-10 reverse phase column (4 mm id, 10 μ particle size) using the binary solvent system water–methanol. Accurate mass measurements were kindly provided by the University of British Columbia mass spectrometry centre using the Kratos MS-50 instrument.

Cultures

P. gallicola (1) was cultured on 200 mL of 3% malt extract (DIFCO) in 500 mL Erlenmeyer flasks. Three culture series of twenty flasks each were started from inocula selected from agar culture plates showing greatest production of crystals.

Extractions

Mycelial mats were removed from the culture medium after 75 days, and the medium macerated in a blender and extracted with benzene (4 × 1000 mL). The crude extract was concentrated, and the product crystallized out by the addition of a small amount of pentane. The crude crystals were dried and recrystallized from benzene–pentane. Culture series B yielded predominantly fuscin **1**, and culture series C yielded predominantly secofuscin **3**. The presence of the dihydro compounds in the extracts and the presence of all four metabolites in the culture series A was established by hplc analysis as indicated above.

Metabolites

Fuscin, **1**, mp 225–227°C (lit. (3) mp 230°C); ν_{max} (KBr disc): 3345 (OH), 1695 (C=C—COOR), 1650, 1620, 1590 (quinone) cm^{-1}; λ_{max} (log ε): 352 nm (4.92); ^{1}Hmr δ: 6.89 (1H, br s, OH), 6.35 (1H, s, H-1), 5.73 (1H, q, J = 6.6 Hz, H-4), 2.61 (2H, dt, J = 6.7, 1.5 Hz, H-10), 1.87 (2H, t, J = 6.6 Hz, H-9), 1.60 (3H, d, J = 6.6 Hz, 4-Me), 1.42, 1.39 (3H, s, 8-Me's). *Exact Mass* calcd. for $C_{15}H_{16}O_5$: 276.09978; found: 276.1000.

Dihydrofuscin, **2**, ^{1}Hmr δ: 5.84 (1H, q, J = 7.0 Hz, H-4), 3.68 and 3.38 (each 1H, d, J = 20 Hz, H-1), 2.55 and 1.83 (each 2H, t, J = 6.0 Hz, H-9 and H-10), 1.57 (3H, d, J = 7.0 Hz, 4-Me), and 1.31, 1.35 (each 3H, s, 8-Me's).

Secofuscin, **3**, mp 159–163°C; ν_{max} (KBr disc): 3440, 3250 (OH), 1690 (C=C—COOR), 1655, 1615, 1560 (quinone) cm^{-1}; λ_{max} (log ε): 349 nm (4.92); ^{1}Hmr δ: 6.72 (2H, s, D_2O exchangeable, OH), 6.50 (1H, s, H-1), 5.73 (1H, q, J = 6.6 Hz, H-4), 5.04 (1H, t, J = 7.2 Hz, H-9), 3.32 (2H, d, J = 7.0 Hz, H-10), 1.75 and 1.67 (each 3H, s, 8-Me's), and 1.57 (3H, d, J = 6.6 Hz, 4-Me). *Exact Mass* calcd. for $C_{15}H_{16}O_5$: 276.09978; found: 276.0998.

Dihydrosecofuscin, **4**, ^{1}Hmr δ: 5.79 (1H, q, J = 7.0 Hz, H-4), 5.04 (1H, t, J = 8.0 Hz, H-9), 3.74 and 3.41 (each 1H, d, J = 20 Hz, H-1), 3.24 (2H, d, J = 8.0 Hz, H-10), 1.78 and 1.70 (each 3H, s, 8-Me's), and 1.52 (3H, d, J = 7.0 Hz, 4-Me).

1. A. FUNK and R. B. SMITH. Can. J. Bot. **59**, 1610 (1981).
2. A. S. SEKHON and A. FUNK. J. Antimicrob. Chemother. **3**, 95 (1977).
3. S. E. MICHAEL. Biochem. J. **43**, 528 (1948).
4. J. H. BIRKINSHAW, A. BRACKEN, S. E. MICHAEL, and H. RAISTRICK. Biochem. J. **48**, 67 (1951).
5. D. H. R. BARTON and J. B. HENDRICKSON. Chem. Ind. 682 (1955).
6. A. J. BIRCH. Chem. Ind. 682 (1955).
7. D. H. R. BARTON and J. B. HENDRICKSON. J. Chem. Soc. 1028 (1956).
8. A. J. BIRCH. Chem. Weekbl. **56**, 597 (1960).
9. G. C. CRAWLEY. J. Chem. Soc. Perkin Trans. **1**, 222 (1981).
10. W. STECK and M. MAZUREK. Lloydia, **35**, 418 (1972).
11. A. J. BIRCH, A. J. RYAN, J. SCHOFIELD, and H. SMITH. J. Chem. Soc. 1231 (1965).

Can. J. Chem. Downloaded from www.nrcresearchpress.com by 210.87.254.105 on 09/06/12
For personal use only.

Application en série benzofurannique d'un nouveau procédé de nitration par l'acide nitrique en présence de chlorure stannique[1]

JACQUES EINHORN, PIERRE DEMERSEMAN ET RENÉ ROYER[2]

Service de Chimie de l'Institut Curie, E.R. no. 213 du CNRS 26 rue d'Ulm, 75231 Paris Cédex 05, France

Reçu le 18 janvier 1983

JACQUES EINHORN, PIERRE DEMERSEMAN et RENÉ ROYER. Can. J. Chem. **61**, 2287 (1983).

On détermine la possibilité d'étendre en série benzofurannique une nouvelle technique de nitration par l'acide nitrique, en présence de chlorure stannique, dans le chlorure de méthylène. Cette technique mérite d'être retenue pour la commodité de sa mise en oeuvre et la diversité des produits qu'elle est susceptible de fournir, selon les conditions expérimentales.

JACQUES EINHORN, PIERRE DEMERSEMAN, and RENÉ ROYER. Can. J. Chem. **61**, 2287 (1983).

A new nitration technique, using nitric acid in the presence of stannic chloride in dichloromethane, has been extended to a series of benzofurans. The ease of performing the reaction as well as the diversity of products that can be obtained under various experimental conditions make it a worthwhile technique.

[Journal translation]

Can. J. Chem. Downloaded from www.nrcresearchpress.com by 210.87.254.42 on 09/06/12
For personal use only.

Le benzofuranne et la plupart de ses dérivés dont l'hétérocycle n'est pas substitué sont trop fragiles pour que leur nitration puisse être effectuée avec des rendements satisfaisants dans les conditions usuelles, au moyen, par exemple, d'acide nitrique dans l'acide ou l'anhydride acétique (1–16). Or, nous avons récemment montré que la nitration des composés aromatiques peut être assurée de façon commode et rentable au moyen d'un complexe – $Cl_4Sn(NO_2)_2$ – que forment l'acide nitrique et le chlorure stannique dans le chlorure de méthylène (17). Il nous a semblé intéressant de préciser dans quelle mesure cette méthode pouvait être étendue en série benzofurannique, étant donné notamment la diversité et l'importance des propriétés biologiques des nitro-2 benzofurannes (10, 13, 18–24).

Nous l'avons donc appliquée au benzofuranne **1** lui-même, ainsi qu'au méthyl-2 benzofuranne **2** et, pour comparaison, au méthyl-3 benzofuranne **3**.

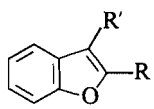

1 R = R′ = H
3 R = H; R′ = CH_3

Des résultats exposés sur le tableau ci-joint, il ressort que la méthode en question présente les mêmes avantages en série benzofurannique qu'en série benzénique. Bien qu'elle ne convienne pas mieux que d'autres pour assurer la nitration des benzofurannes **1** et **3** non substitués en position 2, elle est parfaitement utilisable dans le cas du méthyl-2 benzofuranne **2**. Si, en effet, le benzofuranne **1** ne donne ainsi que des traces de nitro-2 benzofuranne **4** (2), tandis que le méthyl-3 benzofuranne **3** est complètement décomposé, le méthyl-2 benzofuranne **2** fournit une petite quantité du dérivé nitré en 3 **9** qui avait déjà été décrit (25), à côté d'une majorité de son isomère **10** inconnu jusqu'à présent.

Par ailleurs, comme un bon nombre de nitro-2 benzofurannes ont été obtenus jusqu'ici par déplacement "ipso" d'un groupement acétyle plutôt que par substitution directe en position 2, nous avons utilisé la même méthode pour traiter l'acétyl-2 benzofuranne **5** et l'acétyl-2 triméthyl-3,5,6 benzofuranne **6**

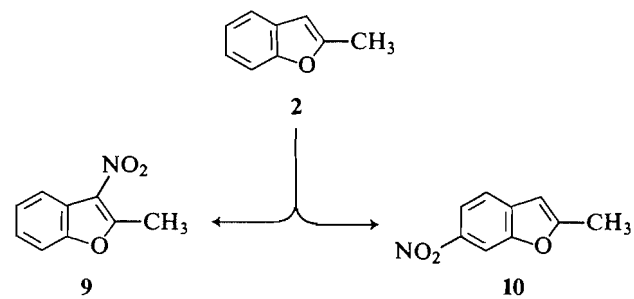

2

9 **10**

(12). Nous y avons enfin soumis, à titre complémentaire, l'acide coumarilique **7** et l'acide méthyl-3 coumarilique **8**, afin de préciser dans quelle mesure des dérivés fonctionnels relativement labiles du benzofuranne étaient susceptibles de supporter cette sorte de nitration.

La nature et le rendement des divers produits obtenus à partir de ces benzofurannes substitués en 2 par un groupement électro-attractif dépendent plus ou moins, selon les cas, de la proportion des réactifs.

C'est ainsi que l'acétyl-2 benzofuranne **5** donne pratiquement les mêmes quantités des mêmes produits **11** (14), **12** (14) et **13** (14), aussi bien avec un qu'avec cinq équivalents d'agent nitrant. Il fournit en outre, dans le premier cas, un peu de nitro-2 benzofuranne **4**.

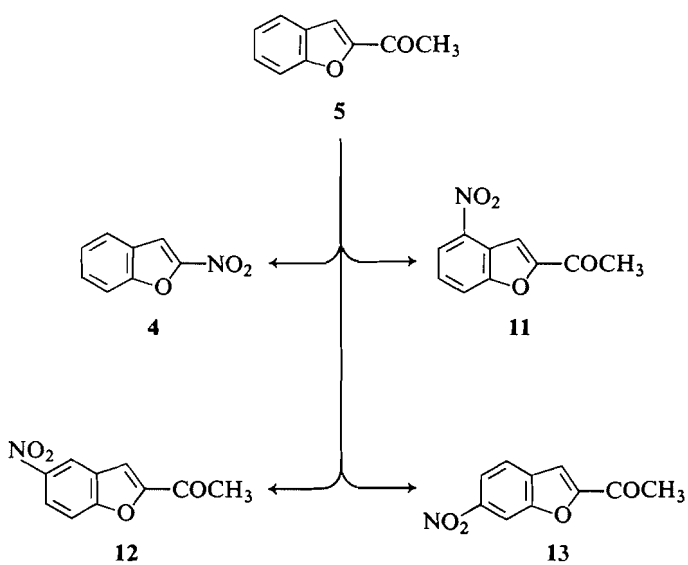

5

4 **11**

12 **13**

[1]Article LXVIII de la série: "Recherches sur le benzofuranne". LVII: voir réf. 16.

[2]A qui toute correspondance doit être adressée.

Can. J. Chem. Downloaded from www.nrcresearchpress.com by 210.87.254.42 on 09/06/12
For personal use only.

TABLEAU 1. Nitration des benzofurannes

Benzofurannes de départ	Mole d'agent nitrant	Temps de réaction (min)	Dérivé nitré formé		
			Composé	Rdt(%)	*F* (°C)(réf.)
1	1,1	10	**4**	Traces	134(2)
2	1,1	15	**9**	10	125–126(25)
			10	45	99
3	1,1	10		[a]	
5	1,1	240	**4**	2	134(2)
			11	3	196(14)
			12	48	173(14)
			13	45	147(14)
5	5	120	**11**	3	196(14)
			12	47,5	173(14)
			13	46	147(14)
6	1,1	240	**14**	21	135
			15	49	168(8)
6	5	120	**16**	66	124
7	1,1	120	**4**	5	134(2)
			17	33	295(26)
			18	33	240(27)
7	5	120	**17**	39	295(26)
			19	16	174(14)
			20	16	150(13)
8	1,1	120	**21**	13,5	98
			22	48	295
			23	32	215
8	5	120	**24**	48,5	192
			25	32,5	140

[a]Résinification.

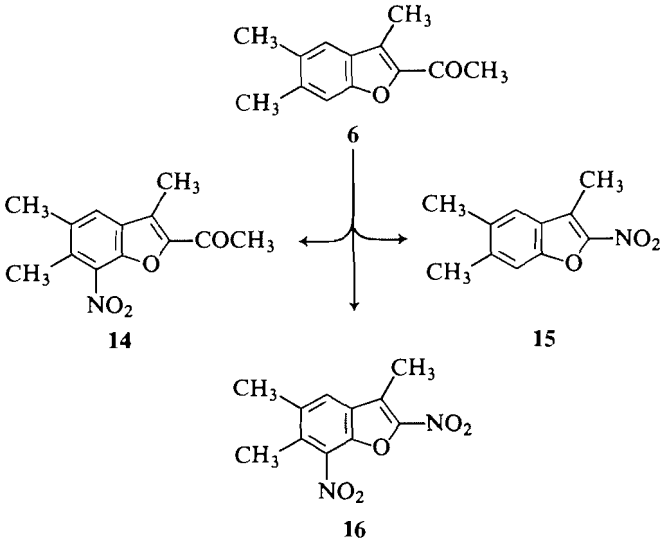

6

14 **15**

16

Dans les mêmes conditions, l'acétyl-2 triméthyl-3,5-6 benzofuranne **6** conduit respectivement aux deux dérivés mononitrés **14** et **15** (8) ou au seul dérivé dinitré **16**, dont les structures sont déduites, sans ambiguité, de leurs spectres de rmn ^1H.

L'acide coumarilique **7** quant à lui, peut donner exclusivement des dérivés mononitrés sur l'hétérocycle **4** ou sur l'homocycle **17** (26) et **18** (27) mais aussi des quantités non négligeables des dérivés dinitrés **19** (14) et **20** (13), dont la formation implique l'élimination préalable du carboxyle en 2. Il en est de même de l'acide méthyl-3 coumarilique **8** à partir duquel on peut obtenir soit des dérivés mononitrés sur l'hétérocycle **21** ou sur l'homocycle **22** et **23**, soit des dérivés dinitrés tout à la fois sur l'homocycle et sur l'hétérocycle **24** et **25**.

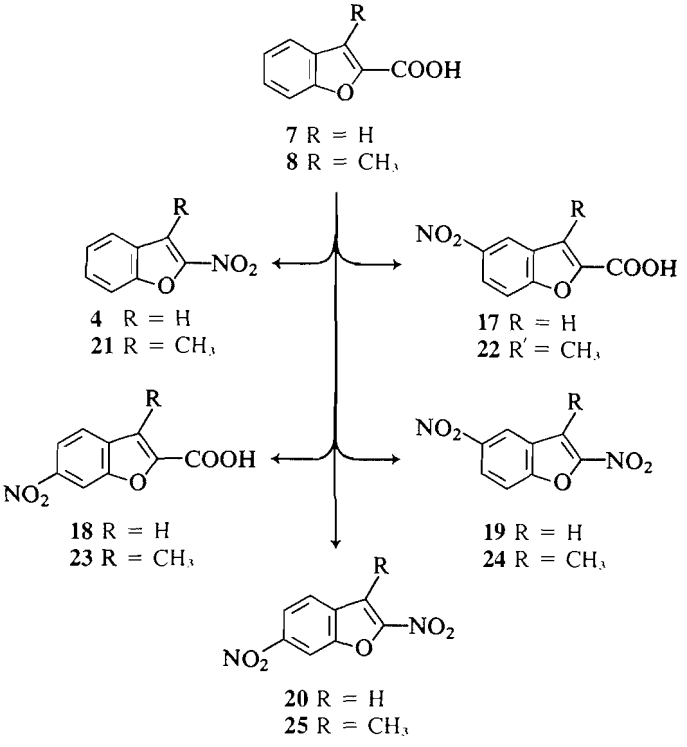

7 R = H
8 R = CH_3

4 R = H
21 R = CH_3

17 R = H
22 R′ = CH_3

18 R = H
23 R = CH_3

19 R = H
24 R = CH_3

20 R = H
25 R = CH_3

Can. J. Chem. Downloaded from www.nrcresearchpress.com by 210.87.254.42 on 09/06/12
For personal use only.

C'est dans le souci pratique d'ouvrir une nouvelle voie d'accès aux nitro-2 naphtofurannes qui se singularisent en particulier par leurs exceptionnelles propriétés mutagènes (28–31), que nous avons appliqué la même méthode de nitration à l'acide naphto[2,1-*b*]furanne carboxylique-2 **26** (32). En fait, celui-ci donne principalement (64%) de l'acide nitro-6 naphto-[2,1-*b*]furanne carboxylique-2 **27**, à côté d'une petite quantité (8%) de dinitro-2,6 naphto[2,1-*b*]furanne **28** lorsqu'on le traite pendant 2 h avec une quantité équimoléculaire de mélange nitrant. Lorsqu'on emploie un excès de ce dernier, il y a résinification importante et on obtient seulement 30% environ d'acide dinitro-5,6 naphto[2,1-*b*]furanne carboxylique-2 **29**, au bout du même temps de réaction.

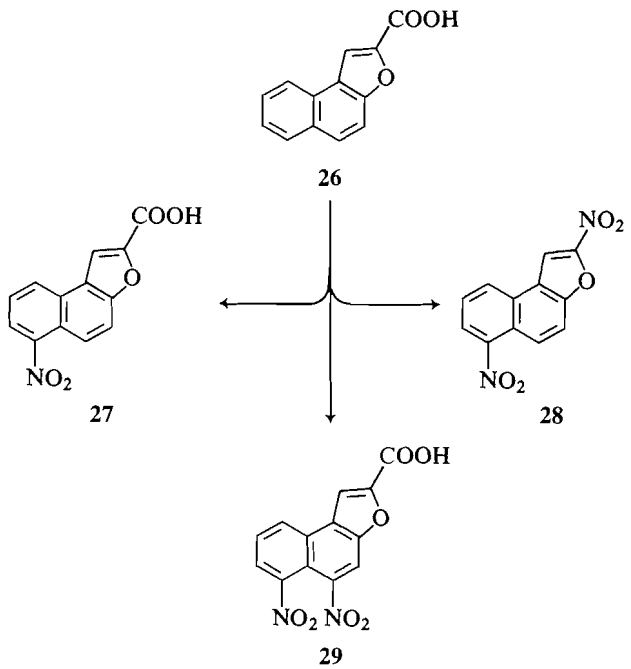

En conclusion, la méthode de nitration développée ici mérite d'être retenue tout autant pour la commodité de sa mise en oeuvre que pour la diversité des produits qu'elle est susceptible de fournir, selon les conditions expérimentales. C'est ainsi qu'elle est beaucoup moins susceptible que d'autres méthodes de nitration de provoquer l'élimination des groupements électroattractifs situés en 2 sur le benzofuranne. Elle permet ainsi de préparer avec des rendements satisfaisants des benzofurannes nitrés peu accessibles ou inaccessibles d'autre manière. C'est le cas notamment des dérivés nitrés sur l'homocycle de l'acide méthyl-3 coumarilique **22** et **23** et de l'acide nitro-6 naphto[2,1-*b*]furanne carboxylique **27**.

Partie expérimentale

Les structures des composés originaux décrits ici ont été confirmées par rmn, la position en 5 ou en 6 d'un groupe nitro sur l'homocycle benzofurannique pouvant être facilement déduite grâce aux profils particuliers des signaux présentés par l'une ou l'autre des deux substitutions (14). Les spectres rmn ^{1}H ont été enregistrés à 60 MHz ou à 90 MHz (cas des composés **26** à **29**), en utilisant le TMS comme référence interne.

Procédé général de nitration

A une solution refroidie à 0°C (ou à −50°C dans le cas des benzofurannes **1**, **2** et **3**) du composé à nitrer (0,012 mol) dans 10 mL de dichlorométhane anhydre, on ajoute en cinq minutes, sous agitation, une solution fraîchement préparée du mélange nitrant constitué avec des quantités équimolaires de chlorure stannique puis d'acide nitrique d = 1,52 dans le dichlorométhane (20 mL par gramme de NO_3H). Si la solution de mélange nitrant est conservée trop longtemps avant l'utilisation, un fin précipité incolore peut apparaître, qui ne gêne en rien la réaction. Après abandon sous agitation pendant le temps et à la température indiqués sur le tableau, on verse sur 250 mL d'eau glacée, sépare la phase organique, extrait la phase aqueuse deux fois avec du chloroforme, réunit les extraits organiques et les lave jusqu'à neutralité. Après élimination des solvants sous pression réduite à 30°C, le produit brut de la réaction est traité selon les cas, de différentes façons qui sont indiquées ci-après.

Nitration du benzofuranne 1

La chromatographie sur colonne de silice avec élution au toluène permet d'isoler de très petites quantités de nitro-2 benzofuranne **4** (2).

Nitration du méthyl-2 benzofuranne 2

Le produit brut de la réaction est d'abord débarrassé de ses résines par filtration de sa solution chloroformique sur une très courte colonne de silice. Après élimination du solvant, une chromatographie sur silice avec élution au toluène fournit d'abord le méthyl-2 nitro-3 benzofuranne **9** (25) puis le méthyl-2 nitro-6 benzofuranne **10** sous forme de microcristaux beiges, F = 99°C (de l'éthanol); rmn ^{1}H (DMSO): 2,55 (sl, 3H, CH_3), 6,85 (sl, 1H, H_3), 7,75 (d, 1H, H_4, J_{4-5} = 9 Hz), 8,10 (d de d, 1H, H_5, J_{5-4} = 9 Hz, J_{5-7} = 2,5 Hz), 8,35 (m, 1H, H_7, le profil multiplet est dû aux couplages 7–5 et 7–3). *Anal.* calc. pour $C_9H_7NO_3$: C 61,02, H 3,98, N 7,90; trouvé: C 61,12, H 3,95, N 8,01.

Nitration de l'acétyl-2 benzofuranne 5

L'identification et le dosage des composés formés sont effectués par cpv suivant les conditions que nous avons déjà décrites (14) en utilisant les composés originaux comme témoins. Chacun des benzofurannes nitrés **4**, **11**, **12** et **13** est séparé par cristallisation comme nous l'avions déjà décrit (14).

Nitration de l'acétyl-2 triméthyl-3,5,6 benzofuranne 6

Après élimination des résines par filtration sur très courte colonne de silice d'une solution chloroformique du produit brut de la réaction, on procède à une chromatographie sur soixante fois son poids de silice, avec élution par le chloroforme. On isole ainsi successivement:

(*i*) le triméthyl-3,5,6 nitro-2 benzofuranne **15**, microcristaux beiges, F = 168°C (du toluène); rmn ^{1}H ($CDCl_3$): 2,40 (sl, 6H, CH_{3_5} et CH_{3_6}), 2,60 (s, 3H, CH_{3_3}), 7,30 et 7,40 (2 × s, 2H, H_4 et H_7);

(*ii*) le triméthyl-3,5,6 dinitro-2,7 benzofuranne **16**, microcristaux paille, F = 124°C (de l'éthanol); rmn ^{1}H ($CDCl_3$): 2,30 (s, 3H, CH_{3_5}), 2,55 (s, 6H, CH_{3_3} et CH_{3_6}), 7,55 (s, 1H, H_4). L'attribution de la structure est déduite de la résonance à 2,60 ppm du méthyle le plus déblindé. Comme le méthyle en 3 du triméthyl-3,5,6 nitro-2 benzofuranne (**15**) présente également sa résonance à 2,60 ppm, il est exclu que le deuxième nitro du dérivé dinitré **16** soit en 4, c'est à dire en *péri* par rapport au méthyle en 3, ce qui entraînerait alors une résonance de ce dernier à un champ différent, nettement plus faible (33). *Anal.* calc. pour $C_{11}H_{10}N_2O_5$: C 52,85, H 4,03, N 11,21; trouvé: C 52,98, H 3,91, N 11,12.

(*iii*) L'acétyl-2 triméthyl-3,5,6 nitro-7 benzofuranne **14**, souillé du dérivé dinitré **16**, que l'on purifie par une nouvelle chromatographie sur silice ($CHCl_3$), ce qui fournit des microcristaux jaune, F = 135°C (du méthanol); rmn ^{1}H ($CDCl_3$): 2,30 (s, 3H, CH_{3_5}), 2,45 (sl, 6H, CH_{3_3} et $COCH_3$), 2,60 (s, 3H, CH_{3_6}), 7,50 (s, 1H, H_4). La situation en 7 du groupe nitro est déduite de façon analogue à celle utilisée dans le cas précédent pour le composé **16**. En effet, le méthyle le plus déblindé présente un signal à 2,60 ppm, incompatible avec une éventuelle situation du groupe nitro en *péri* du méthyle en 3. *Anal.* calc. pour $C_{13}H_{13}NO_4$: C 63,15, H 5,30, N 5,66; trouvé: C 63,00, H 5,41, N 5,70.

Nitration de l'acide coumarilique 7

(a) *Avec 1,1 mol d'agent nitrant*

La solution chloroformique du produit brut de réaction est extraite avec une solution aqueuse de CO_3Na_2 1 *N*. L'évaporation de la solution organique fournit le nitro-2 benzofuranne **4** (2) et la précipitation par l'acide chlorhydrique de la phase aqueuse basique libère un mélange en parties égales des acides **17** (26) et **18** (27) que l'on dose par rmn ^{1}H et sépare par recristallisations fractionnées de l'éthanol.

Can. J. Chem. Downloaded from www.nrcresearchpress.com by 210.87.254.42 on 09/06/12
For personal use only.

(b) *Avec 5 mol d'agent nitrant*

On procède comme ci-dessus, mais il est nécessaire de chromatographier sur silice (avec élution au toluène) le résidu obtenu par évaporation de la phase organique, pour séparer les dinitrobenzofuranes **19** (14) et **20** (13). La précipitation acide de la phase organique fournit directement l'acide **17** (26) à l'état pur.

Nitration de l'acide méthyl-3 coumarilique 8

(a) *Avec 1,1 mol d'agent nitrant*

Par extraction de la solution chloroformique du produit brut de réaction à l'aide d'une solution 1 *N* de CO_3Na_2 suivie de précipitation acide, on obtient le mélange des deux acides nitrés **22** et **23** que l'on sépare par recristallisation fractionnée de l'éthanol (35 mL par gramme de mélange). On obtient ainsi l'acide méthyl-3 nitro-5 coumarilique **22** sous forme de microcristaux jaune pâle, F = 295°C, après une nouvelle cristallisation de l'acide acétique; rmn ^{1}H (DMSO): 2,75 (s, 3H, CH_3), 8,05 (d, 1H, H_7, J_{7-6} = 9 Hz), 8,50 (d de d, 1H, H_6, J_{6-7} = 9 Hz, J_{6-4} = 2,5 Hz), 8,95 (d, 1H, H_4, J_{4-6} = 2,5 Hz), OH indiscernable. La structure de dérivé nitré en 5 est déduite de la résonance à champ faible (8,95 ppm) du proton couplé en *méta*, par rapport à celle (8,55 ppm) que l'on observe pour le proton analogue du dérivé nitré en 6, conformes à ce que l'on observe chez les acides nitro-5 coumarilique (δ = 8,90 ppm) et nitro-6 coumarilique (δ = 8,60 ppm) dont les structures étaient précédemment établies (26 et 27). *Anal.* calc. pour $C_{10}H_7NO_5$: C 54,35, H 3,19, N 6,34; trouvé: C 54,42, H 3,05, N 6,28.

La concentration de moitié des eaux-mères de recristallisation fournit l'acide méthyl-3 nitro-6 coumarilique **23** qui est purifié par une nouvelle recristallisation du toluène: microcristaux jaune pâle, F = 215°C; rmn ^{1}H (DMSO): 2,60 (s, 3H, CH_3), 7,95 (d, 1H, H_4, J_{4-5} = 9 Hz), 8,20 (d de d, 1H, H_5, J_{5-4} = 9 Hz, J_{5-7} = 2,5 Hz), 8,55 (d, 1H, H_7, J_{7-5} = 2,5 Hz), OH indiscernable. *Anal.* calc. pour $C_{10}H_7NO_5$: C 54,35, H 3,19, N 6,34; trouvé: C 54,33, H 3,25, N 6,18.

L'évaporation sous pression réduite de la phase organique fournit le méthyl-3 nitro-2 benzofuranne **21**: microcristaux beige, F = 98°C (de l'éthanol); rmn ^{1}H ($CDCl_3$): 2,40 (s, 3H, CH_3), 7,40 à 7,80 (m, 4H arom.). *Anal.* calc. pour $C_9H_7NO_3$: C 61,02, H 3,98, N 7,90; trouvé: C 59,85, H 4,00, N 7,99.

(b) *avec 5 mol d'agent nitrant*

Le produit brut de réaction est recristallisé dans un mélange toluène–cyclohexane (8:2), ce qui fournit le méthyl-3 dinitro-2,5 benzofuranne **24** sous forme de microcristaux jaune, F = 192°C; rmn ^{1}H (DMSO): 2,75 (s, 3H, CH_3), 8,05 (d, 1H, H_7, J_{7-6} = 9 Hz), 8,50 (d de d, 1H, H_6, J_{6-7} = 9 Hz, J_{6-4} = 2,5 Hz), 8,95 (d, 1H, H_4, J_{4-6} = 2,5 Hz). La structure de dérivé nitré en 5 est déduite comme ci-avant pour le cas de l'acide **22**. *Anal.* calc. pour $C_9H_6N_2O_5$: C 48,69, H 2,75, N 12,62; trouvé: C 48,75, H 2,70, N 12,57.

Les eaux-mères de cristallisation sont évaporées sous pression réduite et le résidu obtenu, recristallisé deux fois de l'éthanol, conduit au méthyl-3 dinitro-2,6 benzofuranne **25**, microcristaux jaune, F = 140°C; rmn ^{1}H (DMSO): 2,70 (s, 3H, CH_3), 8,25 (sl, 2H, H_4 et H_5), 8,70 (d, H_7, J_{7-6} = 2,5 Hz). *Anal.* calc. pour $C_9H_6N_2O_5$: C 48,69, H 2,75, N 12,62; trouvé: C 48,81, H 2,72, N 12,50.

Nitration de l'acide naphto[2,1-b]furanne carboxylique-2 26

(a) *Avec 1,1 mol d'agent nitrant*

Le produit brut de réaction est mis en solution dans le chloroforme. L'épuisement par une solution 1 *N* de CO_3Na_2 permet de libérer, par acidification, l'acide nitro-6 naphto[2,1-*b*]furanne carboxylique-2 **27**, microcristaux beige, F = 190°C (de l'acide acétique dilué); rmn ^{1}H(DMSO): 7,50 à 7,75 (m, 2H, H_8 et H_9), 7,80 (d de d, 1H, H_4, J_{4-5} = 9 Hz, J_{4-1} = 0,8 Hz), 8,05 (d, 1H, H_5, J_{5-4} = 9 Hz), 8,35 (d, 1H, H_1, J_{1-4} = 0,8 Hz), 8,55 (d de d, 1H, H_7, J_{7-8} = 9 Hz, J_{7-9} = 2,5 Hz), OH indiscernable. *Anal.* calc. pour $C_{13}H_7NO5$: C 60,76, H 2,75, N 5,45; trouvé: C 60,70, H 2,80, N 5,42.

Par évaporation de la solution chloroformique et recristallisation du résidu obtenu dans le toluène, on obtient le dinitro-2,6 naphto[2,1-*b*]-furanne **28**, microcristaux jaune, F = 170°C; rmn ^{1}H (DMSO): 7,75 (d de d, 1H, H_4, J_{4-5} = 9 Hz, J_{4-1} = 0,8 Hz), 7,95 (d, 1H, H_5, J_{5-4} = 9 Hz), 8,00 à 8,50 (m, 3H arom.), 8,60 (d, 1H, H_1, J_{1-4} = 0,8 Hz). *Anal.* calc. pour $C_{12}H_6N_2O_5$: C 55,87, H 2,34, N 10,86; trouvé: C 55,76, H 2,10, N 10,81.

(b) *Avec 5 mol d'agent nitrant*

En procédant comme ci-dessus, la solution organique ne contient que des produits résineux. La précipitation acide de la solution aqueuse fournit l'acide dinitro-5,6 naphto[2,1-*b*]furanne carboxylique-2 **29**, F > 290°C (microcristaux jaune de l'éthanol); rmn ^{1}H (DMSO): 8,00 (t, 1H, H_8, J = 9 Hz), 8,45 (d de d, 1H, H_7, J_{7-8} = 9 Hz, J_{7-9} = 2,25 Hz), 8,60 (d, 1H, H_1, J_{1-4} = 0,8 Hz), 8,90 (d de d, 1H, H_9, J_{9-8} = 9 Hz, J_{9-7} = 2,25 Hz), 8,95 (d, 1H, H_4, J_{4-1} = 0,8 Hz), OH indiscernable. *Anal.* calc. pour $C_{13}H_6N_2O_7$: C 51,70, H 2,00, N 9,28; trouvé: C 51,67, H 2,10, N 9,18.

1. R. STOERMER et O. RICHTER. Ber. **30**, 2094 (1897).
2. R. STOERMER. Ann. Chem. **312**, 237 (1900).
3. R. STOERMER et B. KAHLERT. Ber. **35**, 1640 (1902).
4. W. J. HALE. Ber. **45**, 1596 (1912).
5. E. W. SMITH. J. Sci. Iowa State Coll. **12**, 155 (1937).
6. S. TANAKA. J. Chem. Soc. Jpn. **73**, 282 (1952).
7. F. BORDIN, R. BEVILACQUA et F. DABBENI-SALA. Gazz. Chim. Ital. **99**, 1177 (1969).
8. R. ROYER et L. RENE. Bull. Soc. Chim. Fr. 1029 (1970).
9. R. ROYER et L. RENE. Bull. Soc. Chim. Fr. 3601 (1970).
10. R. ROYER, L. RENE, P. DEMERSEMAN, R. CAVIER et J. CENAC. Chim. Thér. **6**, 79 (1971).
11. R. ROYER, J.-F. ROSSIGNOL, P. DEMERSEMAN et N. PLATZER. Bull. Soc. Chim. Fr. 163 (1972).
12. R. ROYER, L. RENE et P. DEMERSEMAN. Chim. Thér. **8**, 139 (1973).
13. R. ROYER, G. LAMOTTE, P. DEMERSEMAN, R. CAVIER et J. LEMOINE. Eur. J. Med. Chem. **13**, 411 (1978).
14. G. LAMOTTE, P. DEMERSEMAN et R. ROYER. J. Heterocycl. Chem. **15**, 1343 (1978).
15. J.-P. BACHELET, J.-M. CLAVEL, P. DEMERSEMAN et R. ROYER. J. Heterocycl. Chem. **19**, 737 (1982).
16. J.-P. BACHELET, P. DEMERSEMAN et R. ROYER. J. Heterocycl. Chem. Sous presse.
17. J. EINHORN, P. DEMERSEMAN, R. ROYER et S. HALUT DESPORTES. J. Chem. Res. 98 (1983).
18. R. CAVIER, J. CENAC, R. ROYER et L. RENE. Chim. Thér. **7**, 361 (1972).
19. R. CAVIER, J. CENAC, R. ROYER, J.-P. BUISSON, L. RENE, G. LAMOTTE et P. DEMERSEMAN. Chim. Thér. **8**, 319 (1973).
20. J.-P. BUISSON, R. CAVIER, J. LEMOINE, L. RENE et R. ROYER. Eur. J. Med. Chem. **10**, 43 (1975).
21. R. ROYER, L. RENE, R. CAVIER et J. LEMOINE. Eur. J. Med. Chem. **12**, 455 (1977).
22. R. A. SCHERRER. Brevets U.S. No. 3927037 du 16. 12. 1975, no. 4.022.908 du 10. 05. 1977 et no. 4141990 du 27. 02. 1979; Brevets allemands no. 2642840 du 7. 04. 1977 et no. 2642877 du 14. 04. 1977.
23. W. J. HAMMER et M. A. RUSTAD. Brevets U.S. no. 4143152 du 6. 03. 1979 et no. 4153721 du 8. 05. 1979.
24. R. A. SCHERRER, W. J. HAMMER et R. M. STERN. Brevet U.S. no. 4143154 du 6. 03. 1979.
25. L. J. POWERS et M. P. MERTES. J. Med. Chem. **13**, 1105 (1970).
26. B. B. DEY et K. K. ROW. J. Chem. Soc. **123**, 3375 (1923).
27. P. RUMPF et C. GANSER. Helv. Chim. Acta, **37**, 435 (1954).
28. N. WEILL-THEVENET, J.-P. BUISSON, R. ROYER et M. HOFNUNG. Mutat. Res. **88**, 355 (1981).
29. S. NOCENTINI, J. COPPEY, J.-P. BUISSON et R. ROYER. Mutat. Res. **90**, 125 (1981).
30. ZAO ZHONG SU, J. J. CORNELIS et J. ROMMELAERE. Carcinogenesis, **2**, 1039 (1981).
31. N. WEILL-THEVENET, J.-P. BUISSON, R. ROYER et M. HOFNUNG. Mutat. Res. **104**, 1 (1982).
32. R. STOERMER. Ber. **30**, 1703 (1897).
33. L. M. JACKMAN et S. STERNHELL. *Dans* Application of nmr in organic chemistry. Pergamon Press, Oxford. 1969. pp. 206–207.

The structure of the benzene–maleimide photosynthetic product (mitindomide)[1]

GEORGE R. PETTIT,[2] KENNETH D. PAULL,[3] CHERRY L. HERALD, DELBERT L. HERALD, AND JOSEPH R. RIDEN[4]
Cancer Research Institute and Department of Chemistry, Arizona State University, Tempe, AZ 85287, U.S.A.

Received April 21, 1983

GEORGE R. PETTIT, KENNETH D. PAULL, CHERRY L. HERALD, DELBERT L. HERALD, and JOSEPH R. RIDEN. Can. J. Chem. **61**, 2291 (1983).

The photochemical reaction between benzene and maleic anhydride or benzene and maleimide affords respectively anhydride **6***a* and imide **6***b*. Unequivocal structures **6***a* and **6***b* were assigned on the basis of an X-ray crystal structure determination of amide **5** derived from imide **6***b*. Because of pronounced activity (e.g., PS T/C 206 at 50 mg/kg) against several of the U.S. National Cancer Institute's key experimental tumor systems, imide **6***b* has been designated mitindomide and is being prepared for eventual clinical trial.

GEORGE R. PETTIT, KENNETH D. PAULL, CHERRY L. HERALD, DELBERT L. HERALD et JOSEPH R. RIDEN. Can. J. Chem. **61**, 2291 (1983).

La réaction photochimique entre le benzène et l'anhydride maléïque ou entre le benzène et le maléimide donne respectivement l'anhydride **6***a* et l'imide **6***b*. On a établi sans équivoque les structures des composés **6***a* et **6***b* en se basant sur l'amide **5**, provenant de l'imide **6***b*, dont on a déterminé la structure par diffraction de rayons-X. La grande activité (par exemple PS T/C 206 à 50 mg/kg) de l'imide **6***b* vis à vis de plusieurs tumeurs de type expérimental de l'Institut national du cancer des Etats-Unis porte à le désigner sous le nom de mitindomide et on le prépare en vue d'un éventuel essai clinique.
[Traduit par le journal]

The photochemical addition of maleic anhydride to benzene was first recorded in 1959 (1). Shortly thereafter, the same high-melting (dec. 350°C) photoadduct was reported by other groups (2) and the mechanism was studied in detail (3). The unsensitized singlet reaction (irradiation at 50°C for 8 h) (3*d*) is believed to proceed from maleic anhydride (**1***a*) via ionic intermediate **2***a* to diene **3***a* and thence to the product formulated as anhydride **4***a* (3*a*). The sensitized addition employing benzophenone under the same conditions affords more than double the yield of anhydride **4***a* and appears to involve a triplet state where intermediate **2***a* may not be implicated (3*a*). In the latter experiments dibromomethane (as solvent) was found to promote the triplet process.

In studies of the parallel reaction involving addition of maleimide (**1***b*) to benzene, an analogous high melting (mp 345–352°C (4*a*) or dec. near 400°C (4*b*)) photoadduct was isolated (4). Irradiation at 25°C over 20 h with an acetophenone concentration of 0.16 mol per liter was found by Arkhipova *et al.* (4*b*) to give the best yield (65%) of diimide (**4***b*). Reaction of anhydride **4***a* with ammonium hydroxide or urea (at 140°C), followed by a thermally induced intramolecular cyclization, was found to yield imide **4***b* and provided evidence for the overall structure (**4***b*; ref. 4*b*). Although the structures of these classic benzene photoproducts have been deduced by chemical means (4*a*, *b*, *e*) none of them or their related derivatives (4*a*, *b*) has ever been rigorously established by X-ray crystallographic methods. We are now pleased to report (*i*) that the

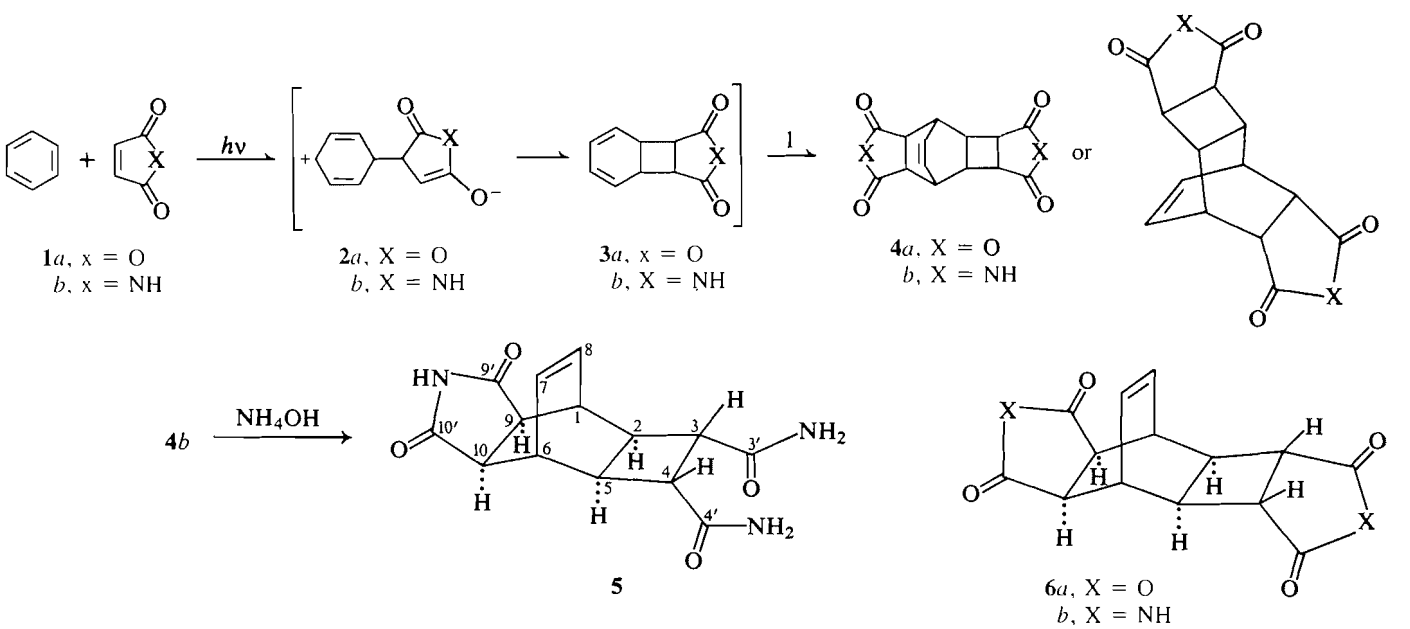

[1]Contribution 90 in the series "Antineoplastic Agents." For part 89, see ref. 9.
[2]Author to whom correspondence should be addressed.
[3]Drug Synthesis and Chemistry Br., U.S. National Cancer Institute, Bethesda, Maryland, U.S.A.
[4]Research and Development, Gulf Oil Chemical Co., Overland Park, Kansas, U.S.A.

Can. J. Chem. Downloaded from www.nrcresearchpress.com by 210.87.254.6 on 09/06/12
For personal use only.

Can. J. Chem. Downloaded from www.nrcresearchpress.com by 210.87.254.6 on 09/06/12
For personal use only.

photoaddition product **4***b*, which for the sake of simplicity[5] will be designated mitindomide (NSC 284356), strongly inhibits growth of the National Cancer Institute's 3 CD breast (T/C ~ 0, at 125 mg/kg, implanted $CD8F_1$, mammary), LE (T/C 188 at 100 mg/kg, implanted L1210 lymphocytic leukemia), and PS (T/C 206 at 50 mg/kg, implanted P388 lymphocytic leukemia) murine tumor systems, and (*ii*) the unequivocal assignment of structure **6***b* to this potentially important substance. Interpretation of the spectral data, particularly the ^{13}C nmr spectra of imide **4***b*, gave results consistent with structure **4**. But unequivocal assignment of the stereochemistry required an X-ray crystal structure determination.

A number of attempts to obtain mitindomide (**4***b*) in a crystalline form (e.g., microcrystals from DMF–water) suitable for X-ray crystallographic analysis were unsuccessful. A variety of simple derivatives such as sodium and potassium salts also proved unsatisfactory. However, when mitindomide was dissolved (over 15 min) in water using ammonium hydroxide and the solution allowed to remain at room temperature for 14 days, amide **5** crystallized as needles melting above 340°C. Recrystallization of amide **5** from ammonium hydroxide solution provided rod-like crystals. A suitable specimen (0.075 × 0.07 × 0.37 mm) was selected for diffraction studies and found to correspond with:

$C_{14}H_{15}N_3O_4$ fw 289.3

Monoclinic, a = 6.309(3), b = 9.971(3), c = 20.096(2) Å, β = 96.91°; V = 1255.05 Å^3; $F(000)$ = 304; ρ_o = 1.510 g/cc; Z = 4; ρ_c = 1.531 g/cc (25°C; CuKα, λ = 1.54184 Å).

Systematic extinctions ($0k0$ absent if $k = 2n + 1$; $h0l$ absent if $l = 2n + 1$) and achirality were consistent with space group $P2_1/c$. The observed density of ρ_o = 1.510 g/cc indicated one molecule of $C_{14}H_{15}N_3O_4$ per equivalent position (4 molecules/cell). The cell parameters were obtained by a least-squares fit of the reciprocal lattice positions of 25 diffractometer measured reflections with θ values in the range of 4–47°. Intensities of all unique reflections with $2\theta < 150°$ were measured at 25°C using a variable speed $\omega/2\theta$ scan technique on an Enraf-Nonius (Delft) CAD4 diffractometer employing graphite monochromated CuKα radiation (λ = 1.54184 Å). The scan angle was calculated for each reflection as (0.90 + 0.14 tan θ)°. The detector aperture, with a variable width of (4.0 + 0.5 tan θ) mm and a constant vertical height of 4 mm was located at a distance of 173 mm from the crystal. Maximum scan time for each reflection was 1 min. Two-thirds of that time was used to scan the peak and one-sixth in measuring each of the two backgrounds. Also the intensities of three monitor reflections were recorded every 250 min and found to have varied by a maximum of 2.66% during the entire data collection process (33.4 h). A total of 2577 unique reflections were retained for subsequent processing. All intensity data were corrected for anisotropic decay using the monitor intensities as standards. The data were corrected for Lorentz-polarization and corrections were included to the scattering factors for anomalous dispersion effects.[6] No extinction or absorption adjustments were made or were necessary (μ = 9.11 cm^{-1}).

[5]Systematically, mitindomide is 3a,3b,4,4a,7a,8,8b-octahydro-4,-8-ethenopyrrolo[3′,4′:3,4]cyclobut[1,2-*f*]isoindole-1,3,5,7[2*H*,6*H*]-tetrone.

[6]Atomic scattering factor coefficients were taken from appropriate tables (see ref. 5).

TABLE 1. Positional parameters and their estimated standard deviations

Atom	x	y	z	B(A2)
O3′	0.7140(6)	0.9108(3)	0.3185(2)	3.45(8)
O4′	0.4288(6)	0.8475(4)	0.4539(2)	3.59(8)
O9′	1.0927(6)	0.7148(3)	0.2366(2)	4.08(9)
O10′	0.3395(6)	1.2017(4)	0.3816(2)	4.18(9)
N1	0.6172(6)	1.1798(4)	0.3198(2)	2.70(9)
N2	1.0610(7)	0.9491(4)	0.3558(2)	3.1(1)
N3	0.7501(7)	0.9383(4)	0.4805(2)	3.4(1)
C1	1.1230(7)	0.9896(5)	0.1692(2)	1.84(9)
C2	1.2242(7)	1.1288(5)	0.1647(2)	1.94(9)
C3	0.9002(8)	0.7357(5)	0.3811(2)	2.1(1)
C3′	0.8875(8)	0.8728(5)	0.3491(3)	2.4(1)
C4	0.7323(8)	0.7177(5)	0.4318(3)	2.2(1)
C4′	0.6249(8)	0.8396(5)	0.4561(3)	2.9(1)
C5	1.4000(7)	1.1229(5)	0.1175(2)	1.91(9)
C6	1.4356(8)	0.9774(5)	0.0958(2)	2.1(1)
C7	1.2262(8)	0.9224(5)	0.0635(3)	2.3(1)
C8	1.0662(8)	0.9281(5)	0.1004(3)	2.2(1)
C9′	1.2417(8)	0.7590(5)	0.2109(2)	2.3(1)
C9	1.3081(8)	0.9038(5)	0.2049(2)	2.0(1)
C10′	0.4702(8)	1.2514(5)	0.3501(3)	2.5(1)
C10	1.4957(8)	0.8993(5)	0.1617(2)	2.3(1)
H1	0.997(9)	0.991(5)	0.198(3)	5.*
HN1	0.651(8)	1.093(5)	0.325(3)	5.*
HN2	1.171(8)	0.913(5)	0.376(3)	5.*
H′N2	1.059(8)	1.030(5)	0.343(2)	5.*
H2	0.751(8)	0.658(5)	0.294(3)	5.*
HN3	0.843(8)	0.906(5)	0.491(3)	5.*
H′N3	0.683(8)	1.010(5)	0.500(3)	5.*
H3	1.062(8)	0.713(5)	0.400(3)	5.*
H4	0.801(8)	0.669(5)	0.473(3)	5.*
H5	1.535(8)	1.161(5)	0.132(3)	5.*
H6	1.555(9)	0.970(5)	0.065(2)	5.*
H7	1.209(8)	0.882(5)	0.020(3)	5.*
H8	0.927(8)	0.903(5)	0.085(3)	5.*
H9	1.357(8)	0.936(5)	0.254(3)	5.*
H10	1.634(8)	0.932(5)	0.188(3)	5.*

*Starred atoms were refined isotropically. Anisotropically refined atoms are given in the form of the isotropic equivalent thermal parameter defined as: (4/3) [$a^2B(1,1) + b^2B(2,2) + c^2B(3,3) + ab(\cos\gamma)B(1,2) + ac(\cos\beta)B(1,3) + bc(\cos\alpha)B(2,3)$].

Structural determination of amide **5** was achieved by direct methods using a multisolution weighted tangent formula approach.[7] Of the 32 phase sets generated, the set with the highest figure of merit provided coordinates for all of the non-hydrogen atoms. After correct assignment of atomic species, three cycles of full matrix least-squares refinement[8] on all

[7]All crystallographic calculations were accomplished with a PDP 11/23 computer using the Enraf-Nonius (Delft) Structure Determination Package (SDP-PLUS) software system developed by B. A. Frenz and Associates, Inc., College Station, Texas, 1982. Principal programs used were; START, PAINTR, REJECT, CHORT, data reduction programs; LSB, a full-matrix least-squares refinement program; SEARCH, a connectivity peak search program; ORTEP-II, the crystallographic illustration programs; MULTAN 11/82 "A System of Computer Programs for the Automatic Solution of Crystal Structures from X-ray Diffraction Data," a direct methods program by P. Main and colleagues, University of York, York, England. For a description of MULTAN see: ref. 6.

[8]The non-Poisson contribution weighting scheme was used in least-squares refinement, where $w = 1/\sigma^2_{(F)} = 4 \times F^2/(\sigma_{F^2})^2$ and $\sigma_{(F^2)} = \sqrt{\sigma^2_{(I)} + (P \times F^2)^2}$, where P is an adjustment factor to downgrade intense reflections and w is the weight for the reflection. A value of 0.05 was used for P.

TABLE 2. Bond distances in angstroms

Atom 1	Atom 2	Distance	Atom 1	Atom 2	Distance	Atom 1	Atom 2	Distance
O3′	C3′	1.248(6)*	C1	C2	1.534(6)	C6	C7	1.504(7)
O4′	C4′	1.235(6)	C1	C8	1.515(7)	C6	C10	1.544(7)
O9′	C9′	1.208(5)	C1	C9	1.552(6)	C6	H6	1.04(5)
O10′	C10′	1.204(6)	C1	H1	1.04(6)	C7	C8	1.323(7)
N1	C10′	1.370(6)	C2	C5	1.545(7)	C7	H7	0.95(6)
N1	HN1	0.90(6)	C3	C3′	1.510(7)	C8	H8	0.93(6)
N2	C3′	1.327(6)	C3	C4	1.566(7)	C9′	C9	1.513(6)
N2	HN2	0.84(6)	C3	H3	1.07(5)	C9	C10	1.550(6)
N2	H′N2	0.85(6)	C4	C4′	1.502(7)	C9	H9	1.05(6)
N3	C4′	1.319(7)	C4	H4	1.01(5)	C10	H10	1.02(6)
N3	HN3	0.68(6)	C5	C6	1.539(7)			
N3	H′N3	0.93(6)	C5	H5	0.95(5)			

*Numbers in parentheses are estimated standard deviations in the least significant digits.

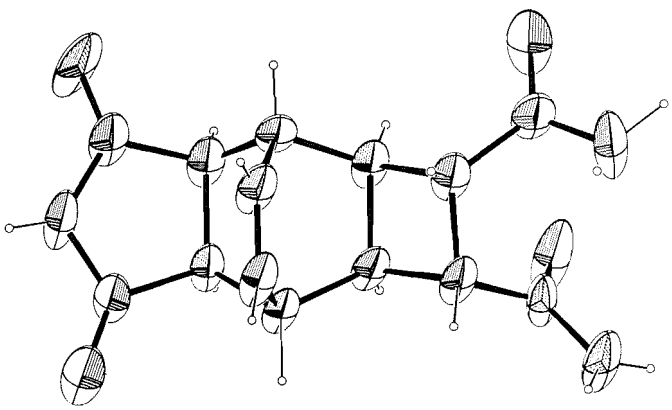

FIG. 1. Computer-generated perspective drawing of the final X-ray structure of mitindomide diamide (**5**). An ORTEP-H representation.

coordinates, scale factor, and isotropic temperature factors resulted in a rapid reduction in the conventional unweighted crystallographic discrepancy index $R(\Sigma|F_o - F_c|/\Sigma F_o|)$ to 0.080 (for observed reflections, $I > 2\sigma(I)$). A subsequent difference electron density synthesis revealed all of the hydrogen atoms in diamide **5**. Finally, several additional cycles of full-matrix least-squares refinement employing all variables (SF, x, y, z, and B's) with anisotropic nonhydrogen atoms and isotropic hydrogens (B's fixed at 5.0) caused convergence to $R = 0.045$ ($R_w = 0.049$). Refinement was discontinued when parameter shifts became insignificant (maximum shift-to-error ratio was 0.46). A final difference map showed no electron densities greater than 0.25 e Å^{-3}. All bond lengths and angles agreed well with expected values.

The relatively selective nucleophilic attack of ammonia on the cyclobutane-bearing imide that gave rise to amide **5** was confirmed by the crystal structure determination. As would be predicted, opening of this imide with concomitant release of steric compression seems a most favorable pathway. The resulting *cis*-configuration of both cyclobutane carbonyl groups indicates that no inversion of configuration took place during treatment with ammonium hydroxide. Therefore, the photoaddition product of benzene and maleic anhydride must have structure **6***a*, and mitindomide, structure **6***b*.

With the correct molecular geometry (Fig. 1) of mitindomide (**6***b*) now established, the opportunity for structure/activity and mechanism of action studies has been greatly enhanced. In respect to biological properties, particularly antineoplastic activity, the ease and direction of nucleophilic attack shown by the transformation **4***b* → **5** should prove significant. Also, the ability of mitindomide to selectively complex and remove zinc (and, under more controlled conditions, copper, see ref. 7) from aqueous solution may prove to be another important property leading to antineoplastic activity.

The very convenient one-step photosynthetic preparation of mitindomide, combined with its unique structure in terms of antineoplastic properties, suggests that a number of related systems (cf., ref. 8) derived from benzene and other aromatic and/or heterocyclic precursors should be explored. Presently mitindomide (NSC 284356) is being readied by the National Cancer Institute for eventual clinical trial.

Experimental

Melting points are uncorrected and were observed using a Koefler melting point apparatus. The ^{13}C nmr and ^{1}H nmr spectra were provided by Dr. J. Witschel, Jr. using Bruker WH-90 and Varian XL-100 nmr spectrometers. Mass spectra were determined by Mr. D. Adams with a MAT-312 mass spectrometer. Infrared spectra were obtained using a Nicolet FTIR Model MX-1 spectrometer.

Mitindomide **4**b

The benzene–maleimide photoadduct **4***b* was prepared as described previously (4) and found to exhibit: mp(dec.) > 340°C with sublimation near 300°C; ir (KBr): 3222, 3070, 2962, 2930, 1766, 1702 (very strong), 1373, 1351, 1255, 1190, 1164 cm^{-1}; ^{1}H nmr (100 MHz, DMSO-d_6 solution), δ: 2.50 (DMSO-d_6 overlap), 2.76 (s, 2H), 3.08 (br s, 2H), 3.30 (br s, 2H), 6.30 (d, J = 4 Hz, 1H), 6.34 (d, J = 4 Hz, 1H), and 11.20 (br s, 2H); ^{13}C nmr (22.63 MHz, DMSO-d_6 solution): 180.05, 179.3, 131.7 with 47.79 and 42.17 obscured by solvent, 39.09, and 34.5; mass spectrum (EI, 70 eV, m/e, 272 (M^+): 244, 201, 136, 130, 104, 78, 50, 51, 52, 44, 43, 31, 29 and 28; *Anal.* calcd. for $C_{14}H_{12}N_2O_4$: C 61.76, H 4.44, N 10.29; found: C 61.78, H 4.40, N 10.28.

*Ammonolysis of mitindomide (***4**b → **5***)*

To 64 mg of mitindomide (**4***b*) was added concentrated (28–30%) aqueous ammonium hydroxide (6 mL) and solution was complete in 15 min. After 14 days at room temperature, amide **5** crystallized as needles (4 mg) melting over 340°C; ir (KBr): 3446, 3332, 3190, 2979, 2949, 2927, 1763, 1709 (strong), 1643 (strong), 1597, 1410, 1342, and 1189 cm^{-1}. A crystal was selected for X-ray crystallographic analysis. The crystal structure (Fig. 1) was determined as summarized in the discussion and in Supplementary Material available from this journal upon request.[9]

[9]Further crystallographic details (supplementary data) including tables of observed and calculated structure factor amplitudes, fractional atomic co-ordinates, and temperature factor data are available at a nominal charge from the Depository of Unpublished Data, CISTI, National Research Council of Canada, Ottawa, Ont., Canada K1A 052.

Can. J. Chem. Downloaded from www.nrcresearchpress.com by 210.87.254.6 on 09/06/12
For personal use only.

Acknowledgments

We are very pleased to acknowledge support of this investigation by Mrs. Mary Dell Pritzlaff, the Olin Foundation (Spencer T. and Ann W.), the Fannie E. Rippel Foundation, Mr. Jack W. Whiteman, Mrs. Eleanor W. Libby, the Donald Ware Waddell Foundation, Mrs. Pearl Spear, Mr. Robert B. Dalton and grant CA-16049-07 awarded by the National Cancer Institute, DHW. We also wish to thank Drs. D. P. Gieschen, H. B. Hunnicutt, G. G. Weigend, and C. M. Woolf for very helpful assistance.

1. H. J. F. ANGUS, and D. BRYCE-SMITH. Proc. Chem. Soc. 326 (1959).
2. (*a*) G. O. SCHENCK and R. STEINMETZ. Tetrahedron Lett. 1 (1960); (*b*) E. GROVENSTEIN, JR., D. V. RAO, and J. W. TAYLOR. J. Am. Chem. Soc. **83**, 1705 (1961).
3. (*a*) D. BRYCE-SMITH, R. R. DESHPANDE, and A. GILBERT. Tetrahedron Lett. 1627 (1975); (*b*) W. HARTMANN, H. G. HEINE, and L. SCHRADER. Tetrahedron Lett. 3101 (1974); (*c*) W. M. HARDHAM and G. S. HAMMOND. J. Am. Chem. Soc. **89**, 3200 (1967); (*d*) D. BRYCE-SMITH and J. E. LODGE. J. Chem. Soc. 2675 (1962).
4. (*a*) J. S. BRADSHAW. Tetrahedron Lett. 2039 (1966); J. Org. Chem. **31**, 3974 (1966); (*b*) I. A. ARKHIPOVA, B. A. ZHUBANOV, and S. B. SAIDENOVA. Izv. Akad. Nauk Kaz. SSR, Ser. Khim. **22**, 44 (1972); Chem. Abstr. **77**, 100908k (1972); (*c*) J. M. FREY, I. RAITZYN, G. WETROFF, and A. H. PASSEDOUET. (Melle-Bezons) French Patent 1,590,119. 22 May 1970; Chem. Abstr. **74**, 141108f, (1971); (*d*) D. BRYCE-SMITH and M. A. HEMS. Tetrahedron Lett. 1895 (1966); (*e*) D. BRYCE-SMITH, B. VICKERY, and G. I. FRAY. J. Chem. Soc. (C), 390 (1967).
5. (*a*) D. T. CRAMER and J. T. WABER. International tables for X-ray crystallography. Vol. IV. The Kynoch Press, Birmingham, England. 1974. Table 2.2B; (*b*) Table 2.3.1.
6. G. GERMAIN, P. MAIN, and M. M. WOOLFSON. Acta Crystallogr. Sect. B, **26**, 274 (1970); M. M. WOOLFSON. Acta Crystallogr. Sect. B, **33**, 219 (1977).
7. (*a*) E. M. IMASHEV, I. A. ARKHIPOVA, and B. A. ZHUBANOV. Izv. Akad. Nauk Kaz. SSR, Ser. Khim. **28**, 1 (1978); Chem. Abstr. **89**, 46896n (1978); (*b*) B. A. ZHUBANOV, I. A. ARKHIPOVA, A. M. KUNAEV, M. B. LEONOVA, YU. A. KATKNOV, and E. M. IMASHEV. Otkrytiya, Izobret., Prom. Obraztsy, Tovarnye Znaki, **55**, 119 (1978); U.S.S.R. patent 594,202. 25 February, 1978; Chem. Abstr. **88**, 156390e (1978).
8. G. R. KROW, J. T. CAREY, D. E. ZACHARIAS, and E. E. KNAUS. J. Org. Chem. **47**, 1989 (1982).
9. G. R. PETTIT, C. L. HERALD, Y. KAMANO, D. GUST, and R. AOYAGI. J. Nat. Prod. **46**, 0000 (1983).

Can. J. Chem. Downloaded from www.nrcresearchpress.com by 210.87.254.6 on 09/06/12
For personal use only.

Réactions radicalaires du percarbonate de *O,O-tert*-butyle et *O*-isopropényle: acétonylations assistées par un co-amorceur

RABIH JAOUHARI, CLAUDE FILLIATRE ET JEAN-JACQUES VILLENAVE[1]

Laboratoire de Chimie Appliquée, Ecole Nationale Supérieure de Chimie et de Physique, Université de Bordeaux I, 351, cours de la Libération, 33405 Talence-cédex, France

Reçu le 4 mai 1983

RABIH JAOUHARI, CLAUDE FILLIATRE et JEAN-JACQUES VILLENAVE. Can. J. Chem. **61**, 2295 (1983).

L'acétonylation "assistée" d'alcanes, éthers, cétones, acides, esters et nitriles a été réalisée en décomposant dans ces solvants des mélanges équimoléculaires de percarbonate de *O,O-tert*-butyle et *O*-isopropényle et de peracétate de *tert*-butyle. La présence du co-amorceur permet d'accroître sensiblement l'intérêt de la méthode de synthèse radicalaire de dérivés acétonylés en supprimant la formation d'acétonylacétone, produit secondaire parfois gênant, et en améliorant nettement les rendements en dérivés acétonylés tout en conservant ou même augmentant la régiosélectivité des processus.

RABIH JAOUHARI, CLAUDE FILLIATRE, and JEAN-JACQUES VILLENAVE. Can. J. Chem. **61**, 2295 (1983).

By decomposition in alkanes, ethers, ketones, acids, esters and nitriles of equimolecular mixtures of *O,O-tert*-butyl and *O*-isopropenyl peroxycarbonate and *tert*-butyl peroxyacetate, the "assisted" acetonylation of the solvents has been accomplished. The presence of the co-initiator allows the yield of the free radical acetonylation to be markedly improved: the formation of the by-product acetonylacetone is avoided and the yield of acetonylated derivatives is strongly enhanced while the regioselectivity of the processes is preserved and even increased in some cases.

Can. J. Chem. Downloaded from www.nrcresearchpress.com by 210.87.254.40 on 09/06/12
For personal use only.

Au cours d'une étude générale (1), nous avons eu l'occasion de mettre en évidence l'aptitude du percarbonate de *O,O-tert*-butyle et *O*-isopropényle **1** à se comporter comme un agent d'acétonylation; en effet, la décomposition de cet amorceur radicalaire en solution dans divers substrats permet, par substitution d'atomes d'hydrogène plus ou moins activés, d'accéder à des dérivés acétonylés **2**. Dans de nombreux cas, cette méthode de fonctionnalisation radicalaire s'est avérée supérieure à d'autres techniques de synthèse (2, 3) mais il n'en reste pas moins qu'elle comporte un certain nombre d'inconvénients.

C'est ainsi que ses rendements ne sont pas toujours très élevés (de 30 à 50%, par rapport au percarbonate **1** mis en jeu, en fractions acétonylées purifiées par rectification). De plus, à chaque fois que le substrat comporte plusieurs sites de substitution possibles, on se rend compte que la réaction n'est sélective que si l'on opère avec des solutions de percarbonate fortement diluées mais aussi que, dans ces conditions, les rendements se trouvent abaissés de manière sensible. Ce phénomène est particulièrement marqué dans le cas des cyclanones pour lesquelles l'acétonylation ne se produit sélectivement en α du carbonyle que si les proportions initiales de percarbonate et de substraat sont dans un rapport de 1/50; dans ce cas, le rendement en dérivé acétonylé atteint à peine 30%.

Nous préoccupant de rechercher des solutions à ces divers problèmes, nous avons effectué une analyse du mécanisme, décrit dans le Schéma 1, de formation des divers produits de réaction.

Suivant ce schèma, c'est la décomposition du percarbonate **1** induite par l'addition des radicaux $S^{\cdot}$ sur sa double liaison qui constitue le processus "principal", conduisant au dérivé acétonylé **2**, l'homolyse "spontanée" étant responsable, indirectement, de la formation des produits secondaires, acétonylacétone en particulier. Dans ces conditions, il est clair que toute production de radicaux $S^{\cdot}$ indépendante de la décomposition "spontanée" du percarbonate est susceptible d'augmenter les taux de transformation en dérivés **2** et, donc, d'améliorer les rendements des réactions d'acétonylation.

Nous avons pensé que l'introduction dans le milieu réactionnel d'un amorceur susceptible de fournir, à des températures plus basses que celles provoquant l'homolyse du percarbonate, des radicaux capables d'arracher des atomes d'hydrogène au solvant pouvait constituer un bon moyen pour obtenir des radicaux $S^{\cdot}$ "supplémentaires". Nous nous sommes alors intéressés à l'acétonylation assistée par un co-amorceur définissant dans un premier temps les conditions opératoires optimales pour

Amorçage

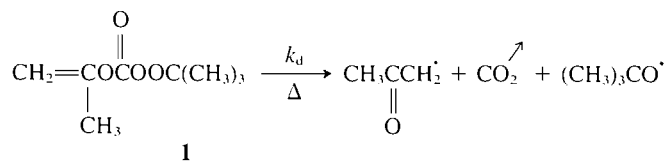

1

Propagation

$(CH_3)_3CO^{\cdot} + SH \rightarrow (CH_3)_3COH + S^{\cdot}$ et

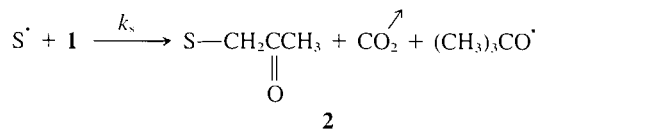

2

Terminaison

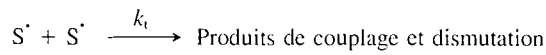

Reactions secondaires

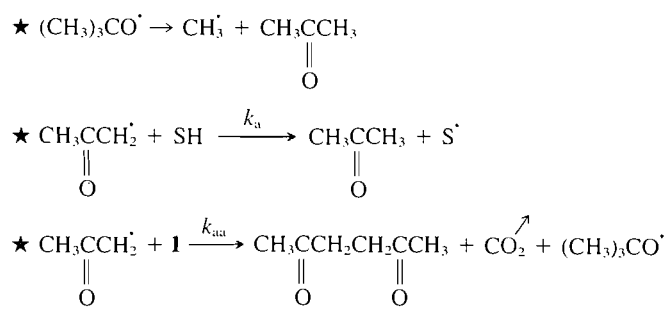

SCHÉMA I

[1]Auteur à qui toute correspondance peut être adressée.

TABLEAU 1. Décomposition du couple percarbonate **1** – peracétate **1'** dans la cyclohexanone

1/**1'**/SH (moles)	Acétonylacétone (%)[a]	Rdt en **2** (%)[b]	Substitution (%)[c] en α du C(O)	β et γ du C(O)
1/0/50	4	30	100	0
1/1/50	Traces	55	100	0
1/0/20	7	39	98	2
1/1/20	0	71	100	0
1/0/10	6	47	93	7
1/1/10	0	62	95	5
1/0/5	8	55	88	12
1/1/5	Traces	59	85	15

[a] % dans le mélange réactionnel après élimination des produits légers.
[b] Rdt, par rapport à **1**, en fraction acétonylée **2** isolée (aprés élimination de l'acétonylacétone).
[c] % dans le mélange d'isomères acétonylés.

réaliser ensuite une étude complète dans le cas de la cyclohexanone, choisie comme composé modèle, et envisager enfin l'application de la technique mise au point à diverses familles de substrats (alcanes, cétones, éthers, acides et dérivés).

Choix des conditions opératoires

Température

Pour éviter au mieux l'homolyse du percarbonate mais aussi dans le but de limiter la formation des produits de terminaison à partir des radicaux S$^{\bullet}$, on serait tenté d'opérer à une température la plus basse possible. En fait, on se heurte très rapidement à une limitation imposée par le mode de décomposition du percarbonate.

Des études cinétiques (4) nous ont permis d'établir la loi de vitesse de cette décomposition:

$$-\mathrm{d}C/\mathrm{d}t = k_d C + k_i C^2$$

la constante k_i étant proportionnelle aux constantes de vitesse k_d et k_s. Nous avons également constaté que les valeurs de k_i diminuent beaucoup plus vite, quand la température diminue, que celles de k_d. Au-dessous de 80°C, k_i est très faible ce qui signifie qu'à partir de ce seuil, l'addition des radicaux S$^{\bullet}$ sur la double liaison du percarbonate ne se produit plus que de manière négligeable. L'obtention de dérivés acétonylés n'est alors plus envisageable.

Tenant compte de cette limitation, nous avons décidé de réaliser les acétonylations assistées à 95°C, température où l'addition des radicaux S$^{\bullet}$ se produit encore de manière convenable; en corollaire, les durées de réaction ont dû être portées à 16 heures, temps nécessaire pour que la totalité du percarbonate mis en jeu ait réagi (rappelons les conditions adoptées au cours des études sur l'acétonylation non-assistée (1): 130°C; 2,5 h).

Co-amorceur

L'impossibilité d'opérer à basse température excluant l'utilisation des amorceurs "fragiles", du type dipercarbonate (décomposition rapide dès 40°C), auxquels on aurait pu penser, nous avons décidé de faire appel à des composés de stabilité thermique voisine de celle du percarbonate **1**. Entre le perbenzoate de *tert*-butyle, les percarbonates de *O,O-tert*-butyle et *O*-éthyle ou *O*-isopropyle et le peracétate de *tert*-butyle **1'** c'est le premier qui a donné les moins bons et le dernier les meilleurs résultats lors d'essais préliminaires.

Tous les essais par la suite ont été réalisés en mettant en oeuvre le peracétate de *tert*-butyle **1'** comme co-amorceur. On

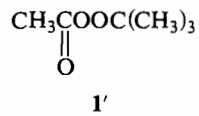

1'

peut noter à son propos que sa thermolyse donne des radicaux *tert*-butoxyle et acétoxyle capables, pour les premiers, d'arracher de l'hydrogène au solvant et, pour les derniers, de conduire par décarboxylation à des radicaux méthyle; dans la mesure où l'on ne trouve pas le produit correspondant à leur addition sur le percarbonate (méthyléthylcétone) on peut penser que l'évolution principale des radicaux méthyle est le transfert au solvant.

*Proportions relatives initiales de **1** et **1'***

Différents essais préliminaires nous ont montré qu'il était préférable d'opérer avec des quantités équimoléculaires de percarbonate et de peracétate. Avec un défaut de peracétate, la vitesse de décomposition du percarbonate est plus grande que celle du peracétate ce qui va à l'encontre du but recherché. Avec un excès de peracétate ce qui va à l'encontre du but recherché. Avec un excès de peracétate, l'augmentation du rendement en dérivé acétonylé ne compense pas les pertes liées à la séparation plus difficile de quantités sensiblement augmentées de déhydrodimère du solvant.

Décomposition "assistée" du percarbonate 1 dans la cyclohexanone

Dans le tableau 1, nous avons consigné des éléments de comparaison, pour différentes concentrations initiales en percarbonate, entre des décompositions assistées et non-assistées réalisées à 95°C.

La première constatation qui doive être faite est que les rendements sont nettement augmentés quand on opère en présence du co-amorceur mais qu'une sorte de saturation semble se produire et qu'il existe un taux de dilution optimal: proportions relatives **1**/**1'**/SH égales à 1/1/20. Ce taux de dilution est celui à partir duquel on observe une acétonylation sélective en α du carbonyle et, donc, le rendement de 71% doit être comparé non pas aux 39% ou même aux 55% obtenus pour des proportions relatives de **1** et SH égales à 1/20 ou 1/5 (le processus n'est alors pas sélectif) mais bien aux 30% de l'acétonylation, exclusivement en α, avec des proportions relatives de 1/50.

La seconde observation concerne l'absence d'acétonylacétone dans les mélanges réactionnels des acétonylations assis-

Can. J. Chem. Downloaded from www.nrcresearchpress.com by 210.87.254.40 on 09/06/12
For personal use only.

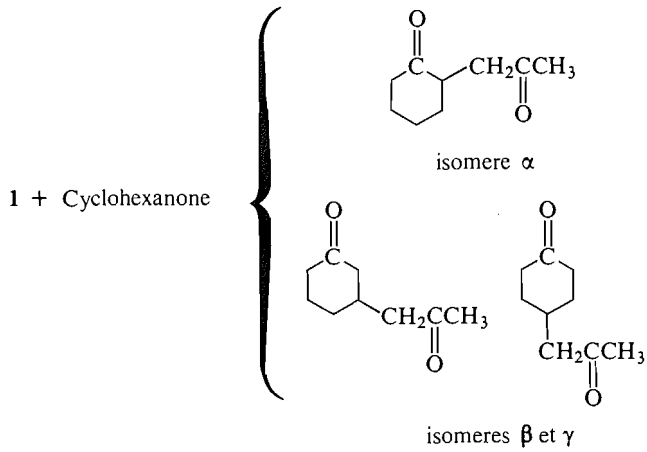

SCHÉMA 2

tées. Ceci est en bon accord avec le fait que la mise en oeuvre du co-amorceur défavorise la décomposition spontanée du percarbonate par rapport à la décomposition induite; la concentration instantanée en radicaux acétonyle $CH_3C(O)CH_2^{\bullet}$ est très abaissée et l'addition de ces radicaux sur la double liaison du percarbonate **1** ne se manifeste plus. Concernant l'acétonylacétone, on peut rappeler qu'à 130°C, les proportions de ce produit, dans le cas de la cyclohexanone, étaient de 11%. Ainsi, le fait d'opérer à plus basse température contribue à limiter la formation de l'acétonylacétone mais c'est bien l'utilisation du co-amorceur qui joue le rôle décisif dans l'élimination de ce produit secondaire des mélanges réactionnels.

En résumé, *la mise en oeuvre du co-amorceur permet d'atteindre, avec une régiosélectivité totale, des rendements très élevés en dérivé acétonylé de la cyclohexanone* (compte-tenu des pertes lors de la distillation, un rendement de 70% en produit pur correspond à un taux de transformation de **1** en **2** de l'ordre de 90%). Notons que des constatations analogues faites avec d'autres cyclanones (cycles en C_7 ou C_8) ouvrent la voie à des essais de généralisation du procédé.

Application de l'acétonylation assistée à diverses familles de substrats

Souhaitant comparer les "performances" des acétonylations assistée et non-assistée (1), nous avons repris, comme substrats, les cyclohexane, tétrahydrofuranne, cyclopentanone, acide propionique, propionate de méthyle et propionitrile représentatifs, respectivement, des alcanes, éthers, cétones, acides, esters et nitriles.

Dans le tableau 2, nous avons indiqué les rendements obtenus en opérant sans co-amorceur dans les conditions les plus favorables (130°C; 2,5 h; rapport molaire **1**/SH = 1/5) et avec le co-amorceur (95°C; 16 h; rapport molaire **1**/**1'**/SH = 1/1/20). Il convient cependant de préciser que, pour les acides, esters et nitriles, les meilleurs résultats ont été observés pour des proportions différentes de réactifs: **1**/SH = 1/50 à 130°C et **1**/**1'**/SH = 1/1/100 à 95°C.

Conclusions

L'utilisation du peracétate de *tert*-butyle comme co-amorceur lors de la décomposition du percarbonate de *O,O-tert*-butyle et *O*-isopropényle en solution permet d'augmenter sensiblement les rendements de l'acétonylation radicalaire de nombreux substrats fonctionnels ou non. En outre, lorsque des problèmes d'orientation de la réaction se posent, c'est le cas surtout avec les cétones, les rendements élevés vont de pair avec une régiosélectivité totale.

Comme la réalisation de la réaction ne pose aucun problème pratique et que les produits sont faciles à extraire des milieux réactionnels et à purifier, l'acétonylation radicalaire assistée apparaît comme une bonne méthode d'obtention de cétones, en particulier γ-fonctionnelles.

TABLEAU 2. Acétonylation assistée et non-assistée de divers substrats

Substrat	Dérivé acétonylé **2**	Rdt (%)[a] en **2** Sans **1'**	Avec **1'**
Cyclohexane	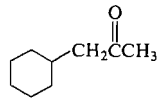	55[b]	72[c]
Tétrahydrofuranne	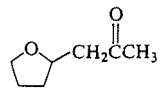	22[b]	37[c]
Cyclopentanone	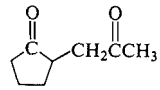	51[b]	75[c]
Acide propionique	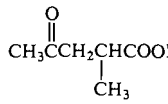	52[b']	71[c']
Propionate de méthyle	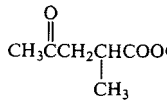	57[b']	75[c']
Propionitrile	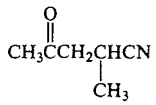	32[b']	55[c']

[a] Rdt, par rapport à **1**, en dérivé **2** isolé.
[b] Conditions opératoires: 130°C; 2,5 h; **1**/SH = 1/5.
[b'] Mêmes conditions que *b* mais **1**/SH = 1/50.
[c] Conditions opératoires: 95°C; 16 h; **1**/**1'**/SH = 1/1/20.
[c'] Mêmes conditions que [c] mais **1**/**1'**/SH = 1/1/100.

Partie expérimentale

Percarbonate 1 et peracétate 1'

La préparation du percarbonate **1**, précedemment décrite (1) consiste à condenser le chloroformiate d'isopropényle, produit commercial,[2] et l'hydroperoxyde de *tert*-butyle en présence de pyridine. Suivant cette méthode "classique" de préparation des peresters (5), le peracétate **1'** a été obtenu par réaction du chlorure d'acétyle avec l'hydroperoxyde de *tert*-butyle. Aucune purification particulière des amorceurs n'a été réalisée avant leur utilisation.

Dérivés acétonylés

Pour la plupart, ils ont été décrits lors de l'étude générale (1). Dans le cas de l'acétonylation de la cyclohexanone, l'acétonyl-2 cyclohexanone (dérivé de substitution en α du carbonyle) a été identifiée en comparant ses caractéristiques avec celles d'un échantillon préparé comme réf. 6. En ce qui concerne les isomères β et γ (acétonyl-3 et -4 cyclohexanone), leur caractérisation, en même temps que celle du dérivé α, a été réalisée après des études en spectrométrie de masse et spectroscopie de rmn ^{13}C (7).

Protocole opératoire type (dans le cas de la cyclohexanone)

Une solution de 0,01 mol de percarbonate **1** (1,74 g) et 0,01 mol de

[2] Société Nationale des Poudres et Explosifs, 12, quai Henri IV, 75181 Paris Cédex 04, France.

Can. J. Chem. Downloaded from www.nrcresearchpress.com by 210.87.254.40 on 09/06/12
For personal use only.

peracétate **1'** (1,32 g) dans 0,2 mol de solvant (~20 g) a été chauffée à 95°C pendant 16 h dans un autoclave placé dans une étuve thermorégulée. Après refroidissement, les produits secondaires (*tert*-butanol et acétone) et l'excès de solvant ont été séparés par distillation. Après rectification du résidu de distillation, le dérivé acétonylé a été obtenu pur (Eb_5 = 105–107°C; N_D^{20} = 1,4605), sa masse permettant le calcul du rendement (par rapport au percarbonate **1** mis en jeu).

Dans le cas de la cyclohexanone et pour des opérations réalisées dans des conditions où la réaction n'était pas sélective, la fraction acétonylée obtenue après distillation des produits secondaires et de l'excès de solvant a été fractionnée par chromatographie liquide–solide, sur alumine (pentane et benzène puis benzène et éther éthylique comme éluants, respectivement, de l'isomère α-acétonylé et de mélanges des isomères β- et γ-acétonylés); c'est sur les fractions obtenues que nous avons réalisé les identifications. La fraction acétonylée a été par ailleurs analysée en chromatographie en phase vapeur (chromatographe Intersmat ICG 12 à ionisation de flamme; gaz vecteur: N_2 (35 mL min^{-1}); colonnes d'acier inox (l = 1,50 m; diamètre intérieur: 2 mm) garnies de FFAP (10%) ou de SE-52 (5%) sur Chromosorb W (80–100 mesh; AW, traité DMCS)), les dosages étant réalisés suivant la méthode de l'étalon interne (benzoate d'éthyle).

Note sur la détermination des durées de réaction

L'augmentation de la vitesse de réaction que provoque l'addition du co-amorceur rendrait très imprécis tout calcul de durée de réaction à partir de données cinétiques concernant les amorceurs seuls. Dans ces conditions, nous avons réalisé un essai préalable d'acétonylation de la cyclohexanone (dans un ballon type Grignard), au cours duquel nous avons examiné par spectroscopie ir et de rmn des échantillons prélevés à différents instants. Après 15 à 16 h, nous avons constaté que les signaux caractéristiques de l'insaturation du percarbonate **1** avaient disparu.

1. R. JAOUHARI, B. MAILLARD, C. FILLIATRE et J-J. VILLENAVE. Synthesis, 760 (1982).
2. R. M. JACOBSON, R. A. RATHS et J. H. MCDONALD. J. Org. Chem. **42**, 2545 (1977).
3. A. HOSOMI, A. SHIRAHATA, Y. ARAKI et H. SAKURAI. J. Org. Chem. **46**, 4633 (1981), et références citées.
4. R. JAOUHARI, C. FILLIATRE et J-J. VILLENAVE. Thermochim. Acta, **60**, 341 (1983).
5. F. STRAIN, W. E. BISSINGER, W. R. DIAL, H. RUDOFF, A. J. DE WITT, H. C. STEVENS et H. LANGSTON. J. Am. Chem. Soc. **72**, 1254 (1950).
6. H. F. BAUMGARTEN, P. L. GREGER et C. F. VILLARS. J. Am. Chem. Soc. **80**, 6609 (1958).
7. M. BARATCHART, C. FILLIATRE, R. JAOUHARI, J-J. VILLENAVE, B. BARBE et M. PETRAUD. Analusis, **11**, 65 (1983).

Can. J. Chem. Downloaded from www.nrcresearchpress.com by 210.87.254.40 on 09/06/12
For personal use only.

FOR ERRATA SEE
v.61 1983 p. 2829

Structure and conformation of the anticodon nucleoside 5-methoxyuridine in the solid state and in solution[1]

GEORGE I. BIRNBAUM
Division of Biological Sciences, National Research Council of Canada, Ottawa, Ont., Canada K1A 0R6

AND

WAYNE J. P. BLONSKI AND FRANK E. HRUSKA
Department of Chemistry, University of Manitoba, Winnipeg, Man., Canada R3T 2N2

Received March 15, 1983

GEORGE I. BIRNBAUM, WAYNE J. P. BLONSKI, and FRANK E. HRUSKA. Can. J. Chem. **61**, 2299 (1983).

The three-dimensional structure of 5-methoxyuridine (mo^{5}U) was determined with much higher precision than in a previous study (Hillen *et al.* J. Carbohydr. Nucleosides Nucleotides, **5**, 23 (1978)). The crystals belong to the monoclinic space group $P2_1$ and the cell dimensions are a = 8.916(2), b = 14.372(2), c = 4.714(1) Å, β = 97.44(2)°. Intensity data were measured with a diffractometer and the structure was solved by direct methods. Least-squares refinement, which included all hydrogen atoms, converged at R = 0.031. The conformation about the glycosyl bond is *anti* (χ_{CN} = 23.1°), the pucker of the ribose ring is C(3′)*endo*, and the conformation of the —CH_2OH side chain is *gauche*$^+$. A comparison of the bond lengths N(3)—C(4) and C(4)—O(4) with those in uridine does not support the conclusion of Hillen *et al.* about a shift to the enol tautomer in mo^{5}U. However, there are other changes in the geometry of the pyrimidine ring due to substitution at C(5). A conformational analysis, based on ^{1}H and ^{13}C nmr data, shows that the preferred conformation in solution is that observed in the solid state.

GEORGE I. BIRNBAUM, WAYNE J. P. BLONSKI et FRANK E. HRUSKA. Can. J. Chem. **61**, 2299 (1983).

On a déterminé avec une précision supérieure à celle d'une étude antérieure (Hillen *et al.* J. Carbonhydr. Nucléosides Nucléotides, **5**, 23 (1978)) la structure tridimensionnelle de la méthoxy-5 uridine (mo^{5}U). Les cristaux appartiennent au groupe spatial monoclinique $P2_1$ avec des dimensions de maille de: a = 8,916(2), b = 14,373(2), c = 4,714(1) Å, β = 97,44(2)°. On a mesuré les intensités à l'aide d'un diffractomètre, on a résolu la structure par des méthodes directes et on l'a affinée, tous les atomes d'hydrogène inclut, par la méthode des moindres carrés jusqu'à une valeur de R = 0,031. La conformation autour de la liaison glycosyle est *anti* (χ_{CN} = 23,1°), le gauchissement du cycle ribose est C(3′) *endo* et la chaine latérale —CH_2OH a une conformation *gauche*$^+$. Une comparaison des longueurs de liaison N(3)—C(4) et C(4)—O(4) avec celles de l'uridine ne confirme pas la conclusion de Hillen *et al.* en ce qui a trait à la transformation en l'énol tautomère du mo^{5}U. Cependant il y a d'autres changements de géométrie du cycle pyrimidine provoqués par la substitution en C(5). Une analyse conformationnelle qui s'appuie sur les données de la rmn du ^{1}H et du ^{13}C montre que la conformation privilégiée en solution est celle observée à l'état solide.

[Traduit par le journal]

Introduction

5-Methoxyuridine (mo^{5}U) is one of the modified nucleosides which occur in the first anticodon ("wobble") (1) position of various tRNAs (2). It has been suggested (3) that its codon recognition is affected by a shift in the keto–enol tautomerism in the pyrimidine moiety, caused by the electron donating methoxy group.

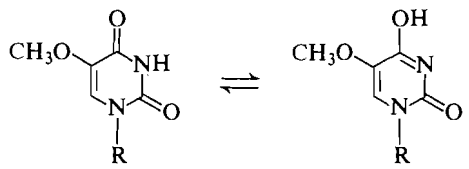

This view seemed to be supported by an X-ray analysis of 5-methoxyuridine (3) which indicated an elongation of the C(4)—O(4) carbonyl bond and a shortening of the N(3)—C(4) bond. Based on our review of 5-substituted deoxyuridines (4), we had reasons to question these results, particularly since their precision was rather low. Since a keto–enol shift has also been implicated in the mechanism of action of antiviral 5-halouridines (5), it seemed important to establish whether 5-substituents do indeed cause such shifts in uridines, giving rise to altered bond lengths. We decided, therefore, to determine the crystal structure of 5-methoxyuridine with much higher precision and, in extension of our recent studies (4, 6–9), to compare its conformation in the solid state with the solution conformation, as determined by an ^{1}H and ^{13}C nmr study.

Experimental

5-Methoxyuridine was crystallized from water to give colorless prisms. Precession photographs indicated space group $P2_1$. A crystal fragment measuring 0.15 × 0.25 × 0.40 mm was mounted on an Enraf-Nonius CAD4 diffractometer; it provided the following data: $C_{10}H_{14}N_2O_7$ fw = 274.2
Monoclinic, a = 8.916(2), b = 14.372(2), c = 4.714(1) Å, β = 97.44(2)°, V = 599.0 Å^3, ρ_o = 1.51(1), ρ_c = 1.52 g cm^{-3}, Z = 2 (21°C; CuKα$_1$, λ = 1.54056 Å); F(000) = 288, μ(CuKα) = 10.8 cm^{-1}.

Cell dimensions were determined from angular settings of 23 high-order (2θ > 90°) reflections. Intensities were measured with Ni-filtered CuKα radiation, using ω/2θ scans with variable scan ranges and speeds. There were 1296 unique reflections accessible to the diffractometer (2θ ≤ 152.0°); all of them had $I > \sigma(I)$ and were considered observed. The intensities were corrected for Lorentz and polarization factors; absorption corrections were considered unnecessary.

The structure was determined by direct methods (Hillen *et al.* (3) did not publish the atomic coordinates) with the aid of the computer program MULTAN78 (10). Of the 24 starting sets subjected to tangent refinement, the solution with the highest combined figure of merit yielded an E map on which all 19 nonhydrogen atoms were located. Atomic parameters were refined by block-diagonal least squares. All hydrogen atoms were located on difference Fourier maps and refined

[1] NRCC No. 22417.

Can. J. Chem. Downloaded from www.nrcresearchpress.com by 210.87.254.5 on 09/06/12
For personal use only.

Can. J. Chem. Downloaded from www.nrcresearchpress.com by 210.87.254.5 on 09/06/12
For personal use only.

TABLE 1. Final atomic coordinates and thermal parameters

(*A*) Nonhydrogen atoms[a]

Atom	*x*	*y*	*z*	U_{eq}
N(1)	69565(14)	55570	3738(3)	230
C(2)	58029(17)	61931(11)	3123(3)	260
O(2)	46282(14)	61599(9)	4203(3)	354
N(3)	60573(16)	68638(10)	1153(3)	279
C(4)	73213(18)	69711(12)	−189(3)	276
O(4)	73679(15)	75928(10)	−1986(3)	387
C(5)	85107(18)	63123(12)	667(3)	265
O(5)	97682(15)	64488(10)	−626(3)	383
C(6)	82975(17)	56319(11)	2541(3)	253
C(7)	109901(22)	58205(17)	144(6)	502
C(1′)	66462(17)	47783(11)	5618(3)	234
C(2′)	57492(18)	40134(11)	3908(3)	258
O(2′)	48630(14)	35506(9)	5766(3)	350
C(3′)	70329(18)	33816(11)	3176(3)	262
O(3′)	65872(15)	24695(9)	2335(2)	336
C(4′)	81444(19)	34299(11)	5913(3)	265
O(4′)	80226(12)	43850(8)	6848(2)	258
C(5′)	97560(20)	31981(13)	5631(4)	346
O(5′)	102872(15)	37493(12)	3490(3)	451

(*B*) Hydrogen atoms[b]

Atom	*x*	*y*	*z*	U_{iso}
H(3)	536(3)	722(2)	74(5)	33(5)
H(6)	902(2)	517(1)	302(4)	21(4)
H(71)	1174(4)	599(3)	−73(7)	68(9)
H(72)	1133(4)	589(3)	225(7)	76(10)
H(73)	1068(4)	523(2)	−41(7)	64(9)
H(1′)	610(2)	502(1)	700(4)	21(4)
H(2′)	509(2)	427(2)	225(4)	28(5)
H(O2′)	406(3)	328(2)	478(5)	49(6)
H(3′)	750(2)	366(2)	161(4)	27(5)
H(O3′)	627(3)	218(2)	376(6)	50(8)
H(4′)	780(3)	301(2)	725(5)	37(5)
H(5′)	978(3)	259(2)	519(6)	55(8)
H(5″)	1046(4)	340(3)	744(7)	75(9)
H(O5′)	1104(4)	346(2)	287(6)	66(8)

[a] *x* and *y* were multiplied by 10^5, *z* and U_{eq} were multiplied by 10^4.
[b] All values were multiplied by 10^3.

with isotropic temperature parameters. The scattering factors were taken from the International tables for X-ray crystallography (11) and the oxygen curve was corrected for anomalous dispersion. Throughout the refinement the function $\Sigma w(|F_o| - |F_c|)^2$ was minimized and a factor of 0.8 applied to all shifts. The following weighting scheme was used during the final stages: $w = w_1 \cdot w_2$, where $w_1 = 1$ for $|F_o| \leq 4.0$, $w_1 = 4.0/|F_o|$ for $|F_o| > 4.0$; and $w_2 = \sin^2\theta/0.2$ for $\sin^2\theta < 0.2$, $w_2 = 1$ for $\sin^2\theta \geq 0.2$. This scheme made the average values of $w(\Delta F^2)$ independent of $|F_o|$ and $\sin^2\theta$. After the final cycle the average parameter shift equalled 0.1σ and the largest one 0.8σ. The conventional residual index *R* is 0.031 and the weighted index *R′* is 0.040 for 1295 reflections (110 suffered from extinction and was given zero weight). A final difference Fourier map showed no significant features. The coordinates are listed in Table 1; lists of anisotropic temperature parameters, deviations of atoms from the mean plane of the pyrimidine ring, and of observed and calculated structure factors are available.[2]

[2] These tables may be obtained, at a nominal charge, from the Depository of Unpublished Data, CISTI, National Research Council of Canada, Ottawa, Ont., Canada K1S 0S2.

Results and discussion

A stereoscopic view of 5-methoxyuridine, showing the overall conformation in the crystal and the atomic numbering scheme, is presented in Fig. 1. Details of the conformation can be seen in the Newman projections (Fig. 2) and in Fig. 3 which also shows the bond lengths and bond angles. It should be emphasized that the precision of this structure determination is four times higher than that of Hillen *et al.* (3).

Pyrimidine moiety

Table 2 lists the bond lengths determined in this and in the previous structure analysis of mo^{5}U as well as those in the parent uridine (12). The differences between the first two columns are quite substantial, ranging up to 0.018 Å for the crucial N(3)—C(4) bond. However, owing to the high estimated standard deviations (esd's, σ's) in the previous study, this difference is equivalent to only 2σ and thus statistically not significant. A comparison of our values with those in uridine shows that, while N(3)—C(4) is somewhat shorter in mo^{5}U and C(4)—O(4) somewhat longer, these differences are also no larger than 2σ and therefore of questionable significance. Consequently, we do not believe that postulating a shift to the enol tautomer in mo^{5}U (3) can be justified.

On the other hand, the presence of a substituent at C(5) does alter the geometry of the uracil ring. We were particularly interested in the effects of substitution on endocyclic bond angles. For our comparison we used only precisely determined structures, i.e. those in which σ(C—C) ≤ 0.005 Å. The exception, for reasons given below, was 5-aminouridine (13). The results of our survey are given in Table 3. There is a definite trend in the angles at C(5) and the range of 3.0° is highly significant (with the exception noted above, the esd's of these angles are ≤0.4°). There is also a fairly good correlation between the angles at C(5) and C(4): as the former decrease, the latter increase. The angles at C(6) do not vary as much and show no clear correlation with those at C(5). The other endocyclic angles (not listed in Table 3) remain within a narrower range and vary randomly.

The angular deformations caused by substitution in aromatic systems have been extensively studied by Norrestam (14) and by Domenicano (15). In general, it has been found that π-electron-withdrawing groups cause an increase of the endocyclic bond angle at the *ipso* atom and a decrease at the *ortho* atoms. The effects on the angles at the *meta* and *para* atoms are not as large and are not significantly correlated to the electronegativities of the substituents. Of the substituents listed in Table 3, NO_2, Cl, OH, NH_2, and CH_3 also appear in a table given by Norrestam and Schepper (14). It is noteworthy that these substituents appear in the same order in both tables.

The lengthening of the ring bonds adjacent to C(5), relative to uridine, could be explained by the inductive effect of the OCH_3 group which causes a withdrawal of σ electrons from the ring. The longer C(5)—C(6) bond could also be attributed to a partial single bond character resulting from a delocalization of π electrons from the substituent to C(6).

The pyrimidine ring is significantly nonplanar, the deviations from the mean plane ranging up to −0.020(2) Å for C(2) and 0.021(2) Å for C(4). The deviations of the ring substituents range from −0.033(1) Å for O(5) to 0.128(2) Å for C(1′). We note that the ring atoms deviate from the mean plane in the same direction as the substituents attached to them. The methoxy group is almost, but not exactly, in the mean plane of the ring. Its methyl group is on the less hindered side, i.e. *syn* to

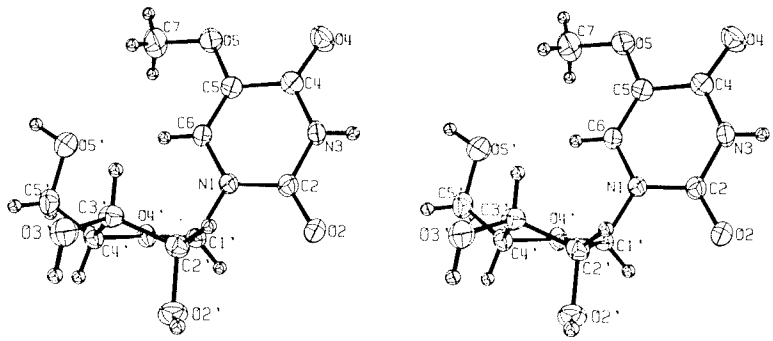

FIG. 1. Stereoscopic view of 5-methoxyuridine; the ellipsoids include 50% probability.

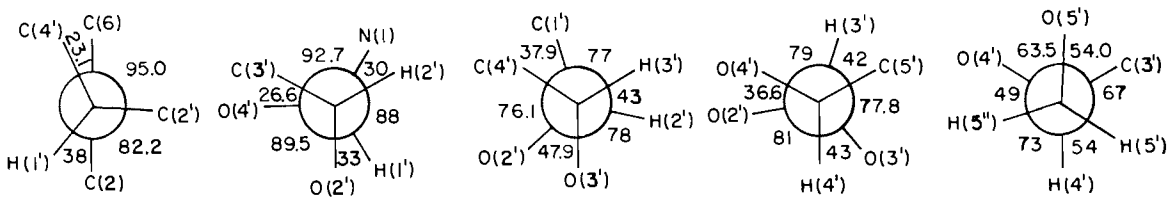

FIG. 2. Newman projections along N(1)—C(1'), C(1')—C(2'), C(2')—C(3'), C(3')—C(4'), and C(4')—C(5').

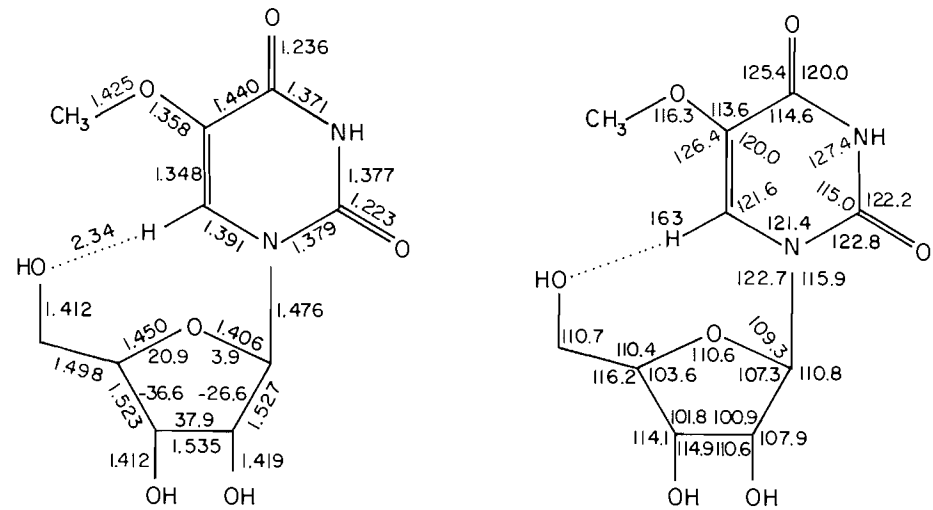

FIG. 3. Molecular geometry: (left) bond lengths and ribose ring torsion angles; esd's are 0.002 Å and 0.2°, respectively; (right) bond angles; esd's are 0.11–0.15°.

TABLE 2. Bond lengths (in Å) in mo^{5}U and in uridine

Bond	Length		
	mo^{5}U[a]	mo^{5}U[b]	Uridine[c]
N(1)—C(2)	1.367	1.379	1.371
C(2)—O(2)	1.225	1.223	1.222
C(2)—N(3)	1.390	1.377	1.370
N(3)—C(4)	1.353	1.371	1.380
C(4)—O(4)	1.244	1.236	1.231
C(4)—C(5)	1.455	1.440	1.421
C(5)—C(6)	1.355	1.348	1.334
C(6)—N(1)	1.379	1.391	1.369

[a] Reference 3; esd's are 0.009 Å.
[b] This work; esd's are 0.002 Å.
[c] Reference 12; averages of two crystallographically independent molecules in which esd's are 0.004 Å.

H(6) rather than to O(4). The conformation about the glycosyl bond is, as usual, *anti* with χ_{CN}[C(6)—N(1)—C(1')—O(4')] = 23.1°.

Ribose moiety

The ribose ring is in an envelope conformation, corresponding very closely to a C(3')*endo* (^3E) pucker. The phase angle of pseudorotation (P) is 13.0° and the maximum amplitude of puckering (τ_m) is 38.9° (16). Both P and τ_m represent average values for one of the two most common conformations of ribose rings, the other being ^2E. The bond lengths are also unexceptional and require no comments. On the other hand, some endocyclic bond angles differ from the values calculated with an equation derived by Birnbaum *et al.* (17) which correlates these angles with P and τ_m. The calculated angles at O(4'), C(1'),.....C(4') are 109.7, 107.2, 101.5, 101.9, 104.7°. The differences at O(4'), C(2'), and C(4') are statistically highly significant. Unfortunately, we are unable to explain these distortions.

The conformation of the —CH_2OH side chain is *gauche*$^+$ (Fig. 2). This rotamer is the one most commonly observed. It is stabilized not only by the *gauche* effect of the C(4')—O(4')/C(5')—O(5') interaction (18) but also by the intramolecular C(6)—H···O(5') hydrogen bond. Such hydro-

Can. J. Chem. Downloaded from www.nrcresearchpress.com by 210.87.254.5 on 09/06/12
For personal use only.

Can. J. Chem. Downloaded from www.nrcresearchpress.com by 210.87.254.5 on 09/06/12
For personal use only.

TABLE 3. Endocyclic pyrimidine bond angles (in deg) in 5-substituted uridines and deoxyuridines

Molecule	5-subst.	Angle C(4)—C(5)—C(6)	Angle N(3)—C(4)—C(5)	Angle C(5)—C(6)—N(1)
no$_2^5$dUMP[a]	NO_2	120.4	112.2	122.8
cl^{5}U[b]	Cl	120.6	113.7	122.0
cl^{5}dU[c]	Cl	120.0	114.4	121.5
mo^{5}U[d]	OCH_3	120.0	114.6	121.6
o^{5}U[e]	OH	119.8	114.1	121.9
ey^{5}dU[f]	C≡CH	119.4	114.0	122.3
n^{5}U[g]	NH_2	119.3	114.2	123.3
co$_2^5$T[h]	CH_3	118.3	115.3	122.9
		118.0	116.2	123.1
ac^{5}dU[i]	$COCH_3$	118.3	114.3	123.6
α-ac^{5}dU[j]	$COCH_3$	117.9	114.2	124.1
ip^{5}dU[k]	$C(CH_3)_2$	117.9	114.9	123.0
hm^{5}dU[l]	CH_2OH	117.4	115.4	123.3

[a] 5-Nitro-2′-deoxyuridine-5′-phosphate; ref. 32.
[b] 5-Chlorouridine; ref. 33.
[c] 5-Chloro-2′-deoxyuridine; ref. 34.
[d] 5-Methoxyuridine; this study.
[e] 5-Hydroxyuridine; ref. 35.
[f] 5-Ethynyl-2′-deoxyuridine; ref. 36.
[g] 5-Aminouridine; ref. 37.
[h] Thymidine 5′-carboxylic acid; ref. 38.
[i] 5-Acetyl-2′-deoxyuridine; ref. 39.
[j] α-5-Acetyl-2′-deoxyuridine; ref. 40.
[k] 5-Isopropyl-2′-deoxyuridine; ref. 41.
[l] 5-Hydroxymethyl-2′-deoxyuridine; ref. 4.

TABLE 4. Distances and angles for hydrogen bonds

D	*A*	*A* at	Distances, Å *D*···*A*	H···*A*	H···A_{corr}	Angles, deg *D*—H···*A*
C(6)—H···O(5′)		x, y, z	3.235	2.34	2.27	163
O(5′)—H···O(4)		$2 - x, -\frac{1}{2} + y, \frac{3}{2} - z$	2.832	1.97	1.88	168
N(3)—H···O(2′)		$1 - x, \frac{1}{2} + y, 1 - z$	2.995	2.55	2.46	116
N(3)—H···O(3′)		$1 - x, \frac{1}{2} + y, \frac{3}{2} - z$	2.832	2.14	1.96	143
O(2′)—H···O(4)		$1 - x, -\frac{1}{2} + y, \frac{3}{2} - z$	2.848	1.97	1.90	167
O(3′)—H···O(2)		$1 - x, -\frac{1}{2} + y, 1 - z$	2.800	1.97	1.88	158

gen bonds are by no means uncommon (19) and probably play a significant role in determining the overall conformation of a nucleoside.

Hydrogen bonding and packing

In addition to the intramolecular hydrogen bond mentioned above there are five intermolecular ones. All potential proton donors participate in the hydrogen bond network which can be represented schematically as follows:

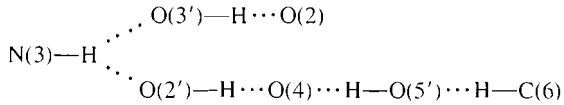

H(3) is involved in a bifurcated hydrogen bond, being donated to both O(2′) and O(3′). Such bonds have been observed in the past (20, 21); they are characterized by longer than normal H···*A* distances and larger deviations from linearity of the *D*—H···*A* angle. As expected, N(3), H(3), and the two acceptor O atoms are coplanar. The two O···H distances are unequal, indicating that this is an asymmetric bifurcated hydrogen bond. The precise geometry of all hydrogen bonds is shown in Table 4. As commonly observed in X-ray analyses, the C—H, N—H, and O—H bonds appear shorter than their real values. By extending the covalent bond lengths to their nominal values (1.00, 1.04, and 0.97 Å, respectively) one obtains corrected H···*A* distances which reflect more accurately the strengths of these hydrogen bonds. The bonds involving H(3) are relatively weak and so is the C—H···O bond. The other three hydrogen bonds are of medium strength.

The packing of the molecules in the crystal can be seen in Fig. 4. The pyrimidine rings are almost perpendicular to the *c* axis. They are hydrogen-bonded to ribose rings but not to each other. There are no base-stacking interactions, but hydrophobic and hydrophilic regions can be discerned perpendicular to the *b* axis.

Nuclear magnetic resonance solution data

For comparison with the crystal, we have obtained ^{1}H and ^{13}C nmr data for mo^{5}U in aqueous solution (Table 5). The analyses of the ^{1}H nmr spectra were carried out using standard techniques (22). The ^{13}C chemical shifts were obtained from ^{1}H-decoupled spectra; the spectral assignments were made using literature data for nucleosides (23) and confirmed with ^{13}C—^{1}H shift correlation plots (24). From $J(1',2')$ and $J(3',4')$ we calculated (22) that the C(3′)*endo* pucker (58%) is favored

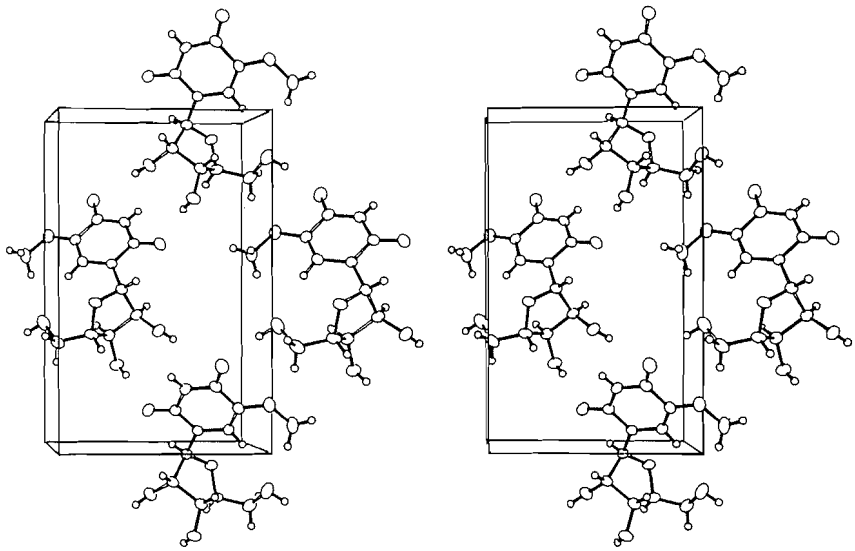

FIG. 4. Stereoscopic view along z of the molecular packing in the crystal.

over C(2′)*endo*; this distribution is similar to that in uridine (U), 53% C(3′)*endo*. From the $J(4',5')$ and $J(4',5'')$ data we estimate (25) the following populations for the side chain conformations in mo^{5}U (and U): 77% (62%) *gauche*$^+$; 18% (32%) *trans*; 4% (5%) *gauche*$^-$. Thus the sugar conformation observed in the solid state for both mo^{5}U and U (^3E, *gauche*$^+$) is also favored in aqueous solution. The enhanced *gauche*$^+$ population in mo^{5}U relative to U suggests that the C(6)—H···O(5′) hydrogen bond observed in solid state may also exist, to a small extent, in an aqueous solution.

The similarity of the ribose ^{1}H and ^{13}C nmr chemical shifts of mo^{5}U and U suggests a similar *anti-syn* distribution about their N-glycosyl bonds (22). This view is supported by the similarity in their ^3J(C6,H1′) couplings (mo^{5}U: 3.8 Hz; U: 3.7 Hz) and in their ^3J(C2,H1′) couplings (mo^{5}U: 2.2 Hz; U: 2.2 Hz) which we obtained from ^{1}H-coupled ^{13}C spectra. The fact that the ^3J(C6,H1′) couplings are greater than ^3J(C2,H1′) suggests a preference for the *anti* conformation in both instances (23). Attempts were made to estimate the *anti-syn* distribution with ^{1}H–^{1}H nOe experiments, but due to the tightly-coupled nature of the ribose protons at 90 MHz the results were inconclusive. However, the enhancement in the H(1′) intensity observed when H(6) is irradiated suggests a sizeable contribution from the *syn* conformation in some pyrimidine nucleosides (26, 27).

The OCH_3 substituent induces the following ^{13}C nmr chemical shift changes relative to uridine (a positive sign indicates a decrease in shielding): C(2) −1.7, C(4) −4.6, C(5) 34.3, C(6) −22.4 ppm. Similar trends have been observed (28) in the *free* uracil and 5-methoxyuracil bases in DMSO solution: C(2) −0.8, C(4) −3.5, C(5) 35.6, C(6) −19.5 ppm. This suggests similar electronic effects of the 5-methoxy substitution in both situations. The large deshielding of the directly substituted C(5) atom is in line with substituent electronegativities. The increased shielding of the *ortho* C(6) can be rationalized in terms of a mesomeric donation of electrons by the OCH_3 group (see above), as has been proposed for the analogous vinyl derivative (29). The much smaller changes at the *ortho* C(4) and *para* C(2) atoms indicate that the electronic interactions between the carbonyl groups and the 5-substituent are relatively unimportant. It is also interesting to report that we observed, in the ^{1}H-coupled ^{13}C spectra, ^1J(C6,H6) couplings of 181.5 and 184.0 Hz in mo^{5}U and U, respectively, whereas, for the corresponding bases in DMSO solution, couplings of 180 and 180.5 Hz were reported by Ellis *et al.* (28). Further measurements of this one-bond coupling in free bases and in their nucleosides could provide useful structural information.

Acknowledgements

Apart from the MULTAN program (10), all crystallographic computations were carried out with programs written by Ahmed *et al.* (31). Figures 1 and 4 were drawn with the ORTEP program of Johnson (32). We thank Drs. W. Niemczura and W. Gibbons for the 270 MHz spectra (Bruker WH270; Madison, Wisconsin) and Mr. K. Marat for obtaining the ^{13}C nmr spectra. F.E.H. acknowledges the Natural Sciences and Engineering Council of Canada for financial support.

1. F. H. C. CRICK. J. Mol. Biol. **19**, 548 (1966).
2. M. ALBANI, W. SCHMIDT, H. KERSTEN, K. GEIBEL, and I. LÜDERWALD. FEBS Lett. **70**, 37 (1976).
3. W. HILLEN, E. EGERT, H. J. LINDNER, H. G. GASSEN, and H. VORBRÜGGEN. J. Carbohydr. Nucleosides Nucleotides, **5**, 23 (1978).
4. G. I. BIRNBAUM, R. DESLAURIERS, T.-S. LIN, G. T. SHIAU, and W. H. PRUSOFF. J. Am. Chem. Soc. **102**, 4236 (1980).
5. E. FREESE. J. Mol. Biol. **1**, 87 (1959).
6. G. I. BIRNBAUM, T.-S. LIN, G. T. SHIAU, and W. H. PRUSOFF. J. Am. Chem. Soc. **101**, 3353 (1979).
7. I. EKIEL, E. DARZYNKIEWICZ, G. I. BIRNBAUM, and D. SHUGAR. J. Am. Chem. Soc. **101**, 4724 (1979).
8. G. I. BIRNBAUM, F. E. HRUSKA, and W. P. NIEMCZURA. J. Am. Chem. Soc. **102**, 5586 (1980).
9. G. I. BIRNBAUM, M. CYGLER, I. EKIEL, and D. SHUGAR. J. Am. Chem. Soc. **104**, 3957 (1982).
10. P. MAIN, S. E. HULL, L. LESSINGER, G. GERMAIN, J.-P. DECLERCQ, and M. M. WOOLFSON. MULTAN78, University of York, England, and University of Louvain, Belgium. 1978.
11. J. A. IBERS and W. C. HAMILTON (*Editors*). International tables for X-ray crystallography. Vol. IV. Kynoch Press, Birmingham, England. 1974.
12. E. A. GREEN, R. D. ROSENSTEIN, R. SHIONO, D. J. ABRAHAM, B. L. TRUS, and R. E. MARSH. Acta Crystallogr. Sect. B, **31**, 102 (1975).
13. E. EGERT, H. J. LINDNER, W. HILLEN, and H. G. GASSEN. Acta Crystallogr. Sect. B. **34**, 2204 (1978).

Can. J. Chem. Downloaded from www.nrcresearchpress.com by 210.87.254.5 on 09/06/12
For personal use only.

14. R. NORRESTAM and L. SCHEPPER. Acta Chem. Scand. A, **35**, 91 (1981).
15. A. DOMENICANO and P. MURRAY-RUST. Tetrahedron Lett. 2283 (1979).
16. C. ALTONA and M. SUNDARALINGAM. J. Am. Chem. Soc. **94**, 8205 (1972).
17. G. I. BIRNBAUM, M. CYGLER, L. DUDYCZ, R. STOLARSKI, and D. SHUGAR. Biochemistry, **20**, 3294 (1981).
18. S. WOLFE. Acc. Chem. Res. **5**, 102 (1972).
19. G. I. BIRNBAUM, M. CYGLER, K. A. WATANABE, and J. J. FOX. J. Am. Chem. Soc. **104**, 7626 (1982).
20. G. I. BIRNBAUM. Acta Crystallogr. Sect. B, **28**, 1248 (1972).
21. G. I. BIRNBAUM. J. Am. Chem. Soc. **96**, 6165 (1974).
22. D. B. DAVIES. Prog. Nucl. Magn. Reson. Spectrosc. **12**, 135 (1978).
23. D. B. DAVIES. Stud. Biophys. **55**, 29 (1976).
24. R. FREEMAN and G. A. MORRIS. J. Chem. Soc. Chem. Commun. 684 (1978).
25. C. A. G. HAASNOOT, F. A. A. M. DE LEEUW, and C. ALTONA. Recl. Trav. Chim. Pays-Bas, **98**, 576 (1980).
26. P. A. HART and J. P. DAVIES. J. Am. Chem. Soc. **93**, 753 (1971).
27. R. K. NANDA, R. TEWARI, G. GOVIL, and I. C. P. SMITH. Can. J. Chem. **52**, 371 (1974).
28. P. D. ELLIS, R. B. DUNLAP, A. L. POLLARD, K. SEIDMAN, and A. D. CARDIN. J. Am. Chem. Soc. **95**, 4398 (1973).
29. G. E. MACIEL. J. Phys. Chem. **69**, 1947 (1965).
30. F. R. AHMED, S. R. HALL, M. E. PIPPY, and C. P. HUBER. J. Appl. Crystallogr. **6**, 309 (1973).
31. C. K. JOHNSON. ORTEP Report ORNL-3794. 2nd revision. Oak Ridge National Laboratory, Oak Ridge, TN. 1970.
32. G. S. D. KING. Private communication.
33. S. W. HAWKINSON and C. L. COULTER. Acta Crystallogr. Sect. B, **27**, 34 (1971).
34. D. W. YOUNG and E. M. MORRIS. Acta Crystallogr. Sect. B, **29**, 1259 (1973).
35. U. THEWALT and C. E. BUGG. Acta Crystallogr. Sect. B, **29**, 1393 (1973).
36. P. J. BARR, T. A. HAMOR, and R. T. WALKER. Acta Crystallogr. Sect. B, **34**, 2799 (1978).
37. E. EGERT, H. J. LINDNER, W. HILLEN, and H. G. GASSEN. Acta Crystallogr. Sect. B, **34**, 2204 (1978).
38. D. SUCK, W. SAENGER, and W. ROHDE. Biochim. Biophys. Acta, **361**, 1 (1974).
39. P. J. BARR, P. CHANANONT, T. A. HAMOR, A. S. JONES, M. K. O'LEARY, and R. T. WALKER. Tetrahedron, **36**, 1269 (1980).
40. T. A. HAMOR, M. K. O'LEARY, and R. T. WALKER. Acta Crystallogr. Sect. B, **33**, 1218 (1977).
41. M. CZUGLER, A. KALMAN, J. T. SAGI, A. SZABOLCS, and L. ÖTVÖS. Acta Crystallogr. Sect. B, **35**, 1626 (1979).

Can. J. Chem. Downloaded from www.nrcresearchpress.com by 210.87.254.5 on 09/06/12
For personal use only.

Novel gas-phase ions. The radical cations $[CH_2XH]^{+\cdot}$ (X = F, Cl, Br, I, OH, NH_2, SH) and $[CH_2CH_2NH_3]^{+\cdot}$

JOHN L. HOLMES[1] AND F. P. LOSSING
Department of Chemistry, University of Ottawa, Ottawa, Ont., Canada K1N 9B4

AND

JOHAN K. TERLOUW[1] AND PETER C. BURGERS
Analytical Chemistry Laboratory, University of Utrecht, Croesestraat 77A, 3522 AD Utrecht, The Netherlands

Received February 28, 1983

JOHN L. HOLMES, F. P. LOSSING, JOHAN K. TERLOUW, and PETER C. BURGERS. Can. J. Chem. **61**, 2305 (1983).

The title ions have been generated by dissociative ionisation of appropriate precursor molecules and have been unequivocally identified by collisional activation and collisional ionisation mass spectrometry. Their heats of formation, $[\Delta H_f^0]$, have been measured and were found to be similar to those for their ionic isomer of conventional structure, $[CH_3X]^{+\cdot}$. The exception is $[CH_2NH_3]^{+\cdot}$ whose ΔH_f^0 is ca. 30 kcal mol^{-1} higher than that of $[CH_3NH_2]^{+\cdot}$. The shapes and appearance energies of metastable peaks in conjunction with isotopic labelling experiments, show that these novel ions do not interconvert with their conventional isomer at internal energies below the threshold for their fragmentation of lowest energy requirement, namely, loss of H$^{\cdot}$. However, unimolecular H$^{\cdot}$ loss from all $[CH_2XH]^{+\cdot}$ ions is preceded by a rate determining isomerisation to $[CH_3X]^{+\cdot}$, followed by fast dissociation. The results are generally in good agreement with recent *ab initio* calculations. Also described are the properties of the homologous ion $[CH_2CH_2NH_3]^{+\cdot}$.

JOHN L. HOLMES, F. P. LOSSING, JOHAN K. TERLOUW et PETER C. BURGERS. Can. J. Chem. **61**, 2305 (1983).

Les ions mentionnés dans le titre ont été produits par ionisation dissociante des precurseurs adéquats et identifiés sans ambiguité par spectrométrie de masse à activation et à ionisation par choc. On a mesuré leurs chaleurs de formation $[\Delta H_f^0]$ et on a trouvé qu'elles sont semblables à celles de leurs isomères ioniques à structure conventionelle $[CH_3X]^{+\cdot}$. L'ion $[CH_2NH_3]^{+\cdot}$ fait exception car son ΔH_f^0 est d'environ de 30 kcal mol^{-1} supérieure à celui de l'ion $[CH_3NH_2]^{+\cdot}$. Les formes et l'apparence des énergies des pics métastables de concert avec les expériences de marquage isotopique montrent que ces nouveaux ions ne s'interconvertissent pas en leurs isomères conventionnels à des énergies internes inférieures au seuil requis par leur plus faible énergie de fragmentation, en particulier, la perte de H$^{\cdot}$. Cependant l'étape déterminante de l'isomérisation en $[CH_3X]^{+\cdot}$ précède la perte unimoléculaire de H$^{\cdot}$ à partir de tous les ions $[CH_2XH]^{+\cdot}$ qui est suivie d'une dissociation rapide. En général les résultats s'accordent bien avec les récents calculs *ab initio*. On décrit également les propriétés de l'ion homologue $[CH_2CH_2NH_3]^{+\cdot}$.

[Traduit par le journal]

Introduction

Recently published experimental (1–7) and theoretical studies (8–12) have firmly established the existence of novel, stable, gas phase radical cations whose neutral counterparts do not represent stable molecules. For example, although the neutral species $[CH_2OH_2]$ can at best be considered as a weakly bound, transient, water–methylene complex (6), the ionised form $[CH_2OH_2]^{+\cdot}$ has been shown (4) to be thermodynamically more stable than its conventional isomer, the methanol radical cation, $[CH_3OH]^{+\cdot}$.

We have referred to these new ions as "radical–ion dipole complexes" (4); the ion $[CH_2OH_2]^{+\cdot}$, for example, can formally be represented as a tightly bound complex between ionised methylene and the dipolar water molecule, $[CH_2^{+\cdot}OH_2]$, but it may also be described as the "methylene oxonium radical cation" (3, 6). Higher homologues have been observed and could be described either as individually named onium radical cations or by placing them in two radical cation-dipole categories, one involving a carbene, e.g. $[CH_3CHClH]^{+\cdot}$ (7), and the other an olefin, e.g. $[CH_2CH_2OH_2]^{+\cdot}$ (2, 4).

The general method for the formation of the new ions involves a dissociative ionisation in which an appropriate rearrangement is followed by the elimination of a small stable molecule, such as CH_2O, CO_2, and CO, e.g.

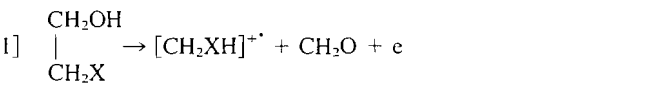

[1] $\rightarrow [CH_2XH]^{+\cdot} + CH_2O + e$

[2] $\rightarrow [CH_2XH]^{+\cdot} + CO_2 + e$

[3] $\rightarrow [CH_2XH]^{+\cdot} + CO + e$

In this paper we fully describe observations on the ions $[CH_2XH]^{+\cdot}$, X = OH, NH_2, SH, halogen, which we briefly reported earlier (4), together with those for some higher homologues.

Results and discussion

1. *Oxygen-containing ions*

$[CH_3OH]^{+\cdot}$, **1**, and $[CH_2OH_2]^{+\cdot}$, **2** (generated by all three reactions above; X = OH), have been shown to be readily distinguishable by means of their collisional activation (CA) mass spectra (3, 4) and their charge stripping (CS) mass spectra (4). The heat of formation, ΔH_f^0, of **2**, reported earlier (4) to be 195 ± 2 kcal mol^{-1}, is in good agreement with that obtained from *ab initio* calculations, 191 kcal mol^{-1} (8). These calculations also examined the barrier to interconversion of **1** and **2**, relative to the dissociation pathway of lowest energy requirement, the loss of H$^{\cdot}$. The calculated and experimental results are shown in Fig. 1*a*. That $[CH_3OH]^{+\cdot}$ dissociates by H$^{\cdot}$ loss without an excess energy requirement is known from the photoionisation appearance energy (AE) for this reaction, 11.66 eV (13); calculated for $[\dot{C}H_2OH]$ = 11.66 eV ($\Delta H_f^0[\dot{C}H_2OH]$ =

[1] To whom correspondance should be addressed.

Can. J. Chem. Downloaded from www.nrcresearchpress.com by 210.87.254.6 on 09/06/12
For personal use only.

Can. J. Chem. Downloaded from www.nrcresearchpress.com by 210.87.254.6 on 09/06/12
For personal use only.

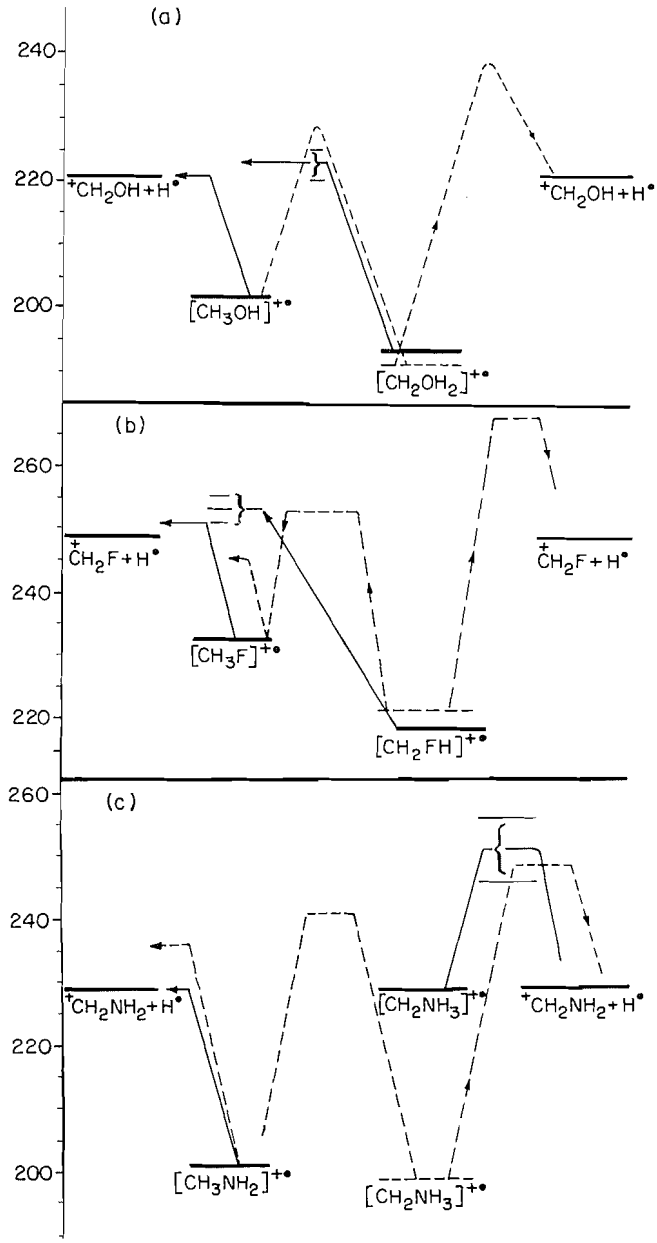

FIG. 1. (*a*) Energy diagram for the dissociation of $[CH_4O]^{+\bullet}$ ions. (*b*) Energy diagram for $[CH_3F]^{+\bullet}$ ions. (*c*) Energy diagram for $[CH_5N]^{+\bullet}$ isomers. Full lines are for experimentally determined energies (see text), broken lines are from *ab initio* calculations (8, 11, and 10) respectively.

169 kcal mol^{-1} (14), ΔH_f^0 [CH_3OH] = −48.0 kcal mol^{-1}, $\Delta H_f^0[H^{\bullet}]$ = 52.1 kcal mol^{-1} (13)). The AE for the metastable peak for loss of $H^{\bullet}$ from $[CH_2OH_2]^{+\bullet}$ was measured using $(CH_2OH)_2$ as the precursor molecule. The standard metastable peak for this comparative measurement (15) was the m/z 74 → m/z 43 fragmentation of methyl acetate. The observed AE, 12.5 ± 0.15 eV, is the same as that calculated for the overall reaction

$$(CH_2OH)_2 \rightarrow \dot{C}H_2OH + H^{\bullet} + CH_2O + e$$

($\Delta H_f^0[(CH_2OH)_2]$ = −92.6 kcal mol^{-1}, $\Delta H_f^0[CH_2O]$ = −26.0 kcal mol^{-1} (16)). The Gaussian-type metastable peaks for $H^{\bullet}$ loss from **1** and **2** have significantly different kinetic energy releases, $T_{0.5}$, measured from the peak width at half height; 9 meV for the former and 34 meV for the latter. Two explanations are formally possible: (*a*) that **2** can dissociate directly to $[\dot{C}H_2OH]$ (*without prior rearrangement* to **1**) or (*b*) that **2** dissociates via rearrangement to $[CH_3OH]^{+\bullet}$. The rearrangement must, however, be the rate determining step, in order to account for the different metastable peak shapes. With reference to Fig. 1, either of the two dissociation barriers must be lower than those from *ab initio* calculations. Explanation (*a*) requires that the ion $[CH_2OD_2]^{+\bullet}$ (produced for example from $(CH_2OD)_2$) should lose only $D^{\bullet}$ whereas (*b*) should proceed via $[CH_2DOD]^{+\bullet}$ and be capable of losing $H^{\bullet}$ or $D^{\bullet}$. The latter is indeed the case, the ion generated from $(CH_2OD)_2$, m/z 34, loses both $H^{\bullet}$ and $D^{\bullet}$, with larger $T_{0.5}$ values (55 and 68 meV respectively) indicative of an isotope effect in the rearrangement step, and in a ratio of approximately 4.6:1.

The homologous ion $[CH_2CH_2OH_2]^{+\bullet}$ has been fully described elsewhere (2, 4) and the ΔH_f^0 for its isomer $[CH_3HOCH_3]^{+\bullet}$ has been given as 176 ± 1 kcal mol^{-1} (4), making it the $[C_2H_6O]^{+\bullet}$ isomer of lowest observed ΔH_f^0. *Ab initio* calculations (9) gave a higher value for ΔH_f^0 $[CH_3HOCH_3]^{+\bullet}$, 185 kcal mol^{-1}, only 1 kcal below that for $[CH_3OCH_3]^{+\bullet}$ and the same as $\Delta H_f^0[CH_3CH_2OH]^{+\bullet}$. The optimum geometry for the ion relates it to a complex between a $CH_3^{\bullet}$ radical and the O atom in $[\dot{C}H_2OH]$ rather than one between ionised methylene and methanol (9) (i.e. the (H_3C)—O bond is longer than (H_2C)—O or H—O). Its only significant unimolecular fragmentation (other than $H^{\bullet}$ loss) is loss of $CH_3^{\bullet}$ to yield $[\dot{C}H_2OH]$, $T_{0.5}$ = 21 meV, an observation which supports its structural assignment. This fragmentation is completely absent in the MI spectra of $[CH_3OCH_3]^{+\bullet}$, $[CH_3CH_2OH]^{+\bullet}$, and $[CH_2CH_2OH_2]^{+\bullet}$. The disagreement between the *ab initio* ΔH_f^0 and the experimental value (185 vs. 176 kcal mol^{-1}) deserves comment. If one considers the ion from the point of view of the effect of methyl substitution on $[CH_2OH_2]^{+\bullet}$, it is difficult to accept the very small reduction in ΔH_f^0 resulting therefrom, 5 kcal mol^{-1}, in the *ab initio* calculations; the observed stabilisation, ca. 19 kcal mol^{-1}, is more characteristic of methyl substitution effects at formal charge bearing or sharing sites (17).

Halogen-containing ions

The ions $[CH_2XH]^{+\bullet}$, isomers of the ionised methyl halides, were made by reaction [2], with X = F, Cl, Br, and I. The ions were readily characterised by their distinctive CA mass spectra which are shown together with those for $[CH_3X]^{+\bullet}$ in Fig. 2. Major differences are apparent in all pairs of spectra except for the iodo-analogues where only small peak intensity differences serve to distinguish the species. For this pair the shapes of the $[M - 15]^{+}$ peaks are complex and different. Reasons for the complex peak shapes have been discussed elsewhere (18, 19).

The CA mass spectra of $[CH_3F]^{+\bullet}$ and $[CH_2FH]^{+\bullet}$ have already been reported (5) and the results are in fair overall agreement with those reported here. The energetics of the ion $[CH_2FH]^{+\bullet}$ have been investigated by *ab initio* calculations (11) and it was predicted to be 11 kcal mol^{-1} more stable than $[CH_3F]^{+\bullet}$. The AE of m/z 34 from FCH_2COOH was measured as 11.6 ± 0.2 eV, whence $\Delta H_f^0[CH_2FH]^{+\bullet}$ = 217 ± 4 kcal mol^{-1}. ($\Delta H_f^0[FCH_2COOH]$ = −145 kcal mol^{-1} (20), $\Delta H_f^0[CO_2]$ = −94.1 kcal mol^{-1} (13)).

The calculations also indicated that $[CH_2FH]^{+\bullet}$ rearranges to $[CH_3F]^{+\bullet}$ prior to H atom loss (the fragmentation of lowest energy requirement) rather than undergo direct dissociation. We have measured the metastable peak AE values for $H^{\bullet}$ loss

Can. J. Chem. Downloaded from www.nrcresearchpress.com by 210.87.254.6 on 09/06/12
For personal use only.

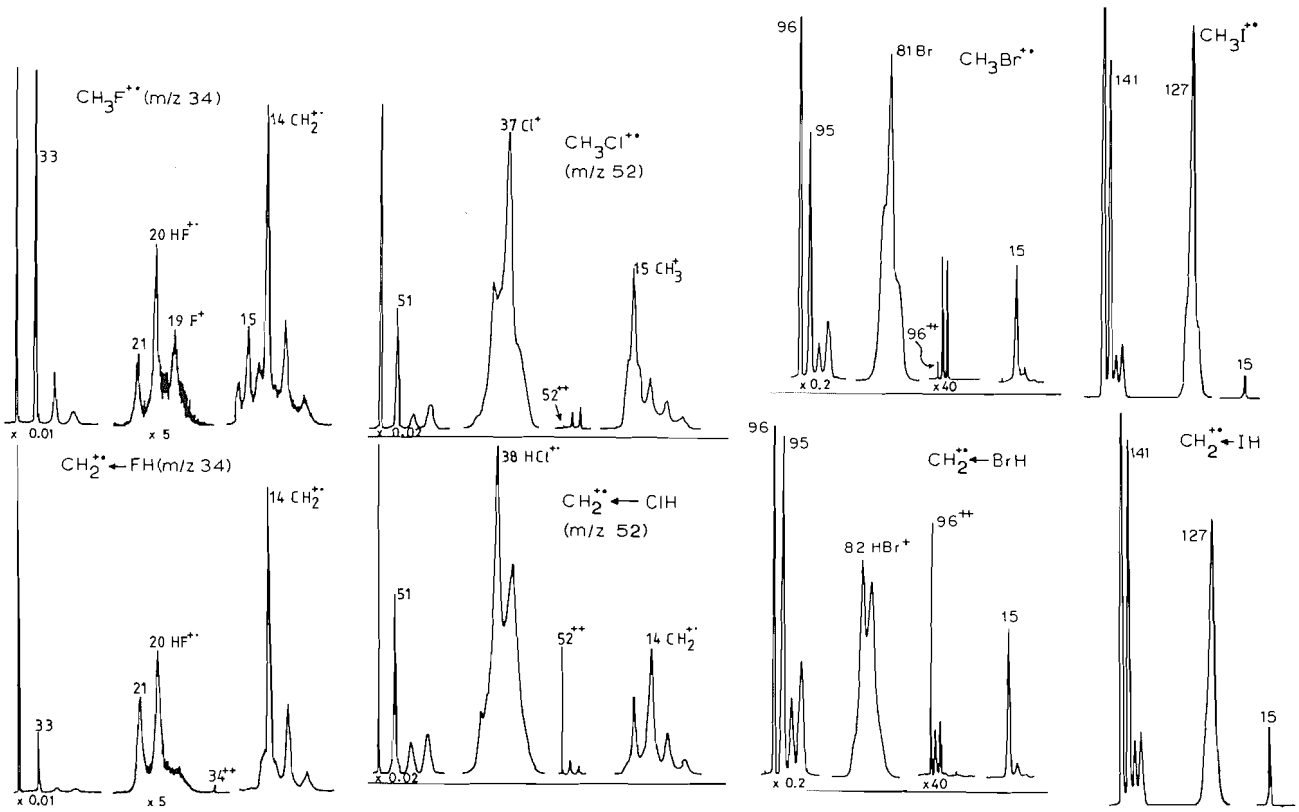

FIG. 2. Collisional activation mass spectra for $[CH_3X]^{+\cdot}$ and $[CH_2XH]^{+\cdot}$ ions, X = F, Cl, Br, I.

from the two ions and the results are shown in Fig. 1*b*. AE$[\dot{C}H_2F]$ from CH_3F was measured as 13.6 ± 0.2 eV (13.4 eV by photoionisation [13]). AE$[\dot{C}H_2F]$ from $[CH_2FH]^{+\cdot}$ generated from CH_2FCOOH was 13.4 ± 0.1 eV, calculated 13.1 eV using $\Delta H_f^0[\dot{C}H_2F]$ = 200 kcal mol^{-1} (13). This system behaves similarly to the oxy-analogue, producing Gaussian-type metastable peaks; $T_{0.5}$ for $[CH_3F]^{+\cdot} \rightarrow [\dot{C}H_2F] + H^{\cdot}$ is 12 meV; for the $[CH_2FH]^{+\cdot}$ fragmentation $T_{0.5}$ = 33 meV. The ion produced by loss of CO_2 from $[CH_2FCOOD]^{+\cdot}$ loses both $H^{\cdot}$ and $D^{\cdot}$, $T_{0.5}$ values 36 and 31 meV, respectively; relative metastable peak abundances 5.5:1 in favour of $H^{\cdot}$ loss. It is concluded that the barrier to rearrangement of $[CH_2FH]^{+\cdot}$ to $[CH_3F]^{+\cdot}$ is only slightly greater than that for the dissociation of the latter to $[\dot{C}H_2F] + H^{\cdot}$.

The heats of formation of $[CH_2ClH]^{+\cdot}$ and $[CH_2BrH]^{+\cdot}$ were measured from their AE values from chloroacetic acid and 2-bromoethanol, respectively. AE *m/z* 50 from $ClCH_2COOH$ = 11.08 ± 0.05 eV; $\Delta H_f^0[ClCH_2COOH] = -104 \pm 2$ kcal mol^{-1} (16) and AE *m/z* 94 from $BrCH_2CH_2OH$ = 11.36 ± 0.05 eV, $\Delta H_f^0[BrCH_2CH_2OH] = -51.4$ kcal mol^{-1} (20). Whence $\Delta H_f^0[CH_2ClH]^{+\cdot} = 246 \pm 3$ kcal mol^{-1} (compare $\Delta H_f^0[CH_3Cl]^{+\cdot} = 239$ kcal mol^{-1} (13)) and $\Delta H_f^0[CH_2BrH]^{+\cdot} = 237 \pm 3$ kcal mol^{-1}, allowing for ± 2 kcal mol^{-1} uncertainty in the additivity calculation (compare $\Delta H_f^0[CH_3Br]^{+\cdot} = 234$ kcal mol^{-1} (13)). Although these two methylene halonium ions clearly are stable species, unlike the oxonium ion they are not thermodynamically more stable than their isomers of conventional structure.

It is worth recording that loss of CO from ionised CH_2ClCHO and CH_2BrCHO produced a mixture of $[CH_3X]^{+\cdot}$ and $[CH_2XH]^{+\cdot}$ ions, clearly shown by the appropriate CA mass spectra. Moreover, the metastable peaks for the reactions $[CH_2XCHO]^{+\cdot} \rightarrow [CH_3X]^{+\cdot} + CO$ were both of composite shape, in keeping with the cogeneration of the above pairs of daughter ions.

Nitrogen-containing ions

The ion $[CH_2NH_3]^{+\cdot}$ is readily generated by the loss of CH_2O from ionised ethanolamine. Its CA mass spectrum, together with that of $[CH_3NH_2]^{+\cdot}$, is shown in Fig. 3. The large differences in these CA spectra and the presence of an intense *m/z* 15.5 (charge stripping) ion, $[CH_2NH_3]^{2+}$, are similar to those observed in the $[CH_3OH]^{+\cdot}$, $[CH_2OH_2]^{+\cdot}$ system and clearly show that $[CH_2NH_3]^{+\cdot}$ is a stable species. The AE of *m/z* 31 could not readily be measured because that of *m/z* 30 $[\dot{C}H_2NH_2]$ was significantly lower. However, a careful comparison of *m/z* 31 vs. *m/z* 30 at low electron energies showed that below ca. 10.9 eV *all* of *m/z* 31 consisted of the ^{13}C or ^{15}N contribution from *m/z* 30. Thus $\Delta H_f^0[CH_2NH_3]^{+\cdot} \geq 229$ kcal mol^{-1} ($\Delta H_f^0[CH_2OHCH_2NH_2] = -48.2$ kcal mol^{-1} (20)), appreciably higher than $[CH_3NH_2]^{+\cdot}$, 201 kcal mol^{-1} (13). Recent *ab initio* calculations (10) give 199 kcal mol^{-1} for $[CH_2NH_3]^{+\cdot}$; the energy diagram for $[CH_5N]^{+\cdot}$ is shown in Fig. 1*c*. Ionised methylamine fragments by $H^{\cdot}$ loss at the thermochemical threshold (21) and the accompanying Gaussian-type metastable peak is associated with only a small kinetic energy release, $T_{0.5}$ = 5 meV. The calculations (10) indicate a reverse activation energy of 6.5 kcal mol^{-1} for this fragmentation. The metastable peak for $H^{\cdot}$ loss from $[CH_2NH_3]^{+\cdot}$ is rather weak and is of composite shape with $T_{0.5}$ = 150 meV (see Fig. 4), probably consisting of a narrow Gaussian-type peak superimposed upon a broad, dished or flat-topped signal. The latter is in keeping with the large excess energy (~1 eV) required for this fragmentation. The metastable peak AE could not be accurately measured because of the low intensity of the signal; hence the

Can. J. Chem. Downloaded from www.nrcresearchpress.com by 210.87.254.6 on 09/06/12
For personal use only.

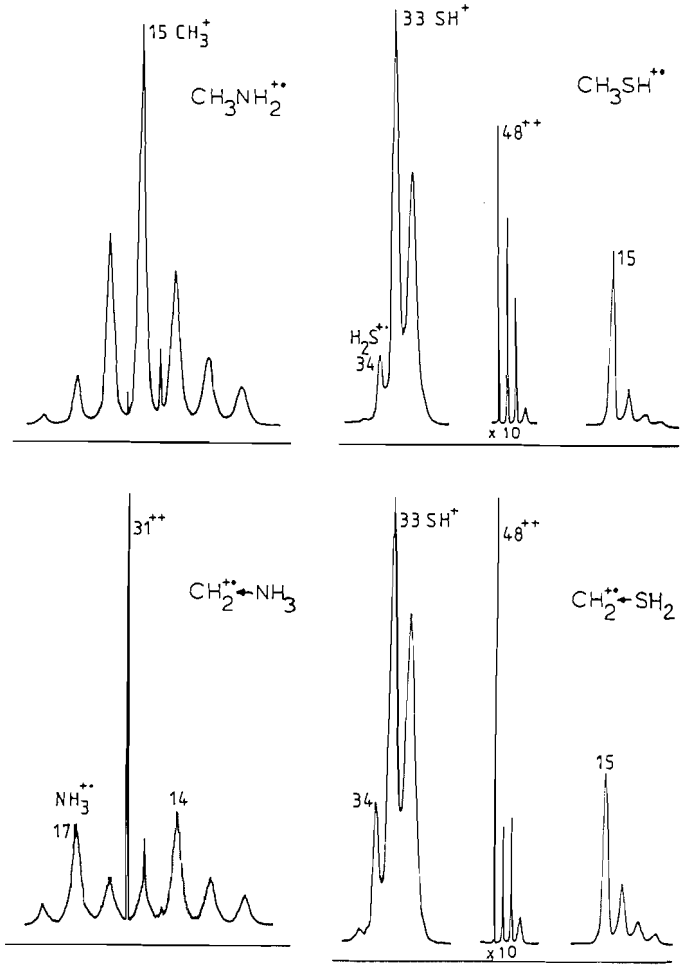

FIG. 3. Partial collisional activation mass spectra for the $[CH_5N]^{+\cdot}$ isomers (m/z 31–26 omitted) and partial collisional activation mass spectra for $[CH_3SH]^{+\cdot}$ and $[CH_2SH_2]^{+\cdot}$ ions (m/z 48 → 44 omitted).

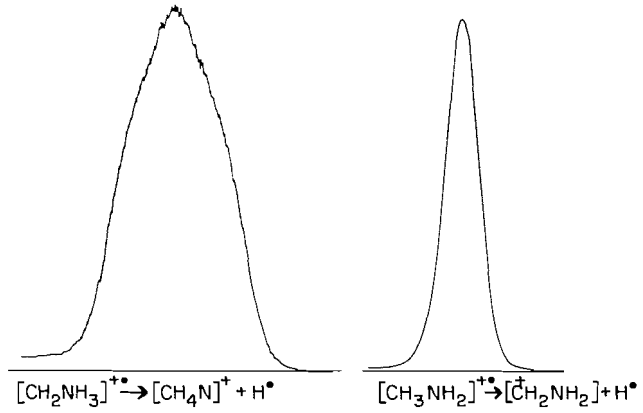

FIG. 4. Metastable peaks for loss of $H^\cdot$ from $[CH_5N]^{+\cdot}$ isomers.

wide error bars in Fig. 1*c*. The narrow component could arise from the cogeneration of an isomeric daughter ion, but ΔH_f^0 values for $CH_3\dot{N}H$ or $CH\dot{N}H_3$ are not available.

The ion derived by loss of $[CH_2NH]$ from $[H_2NCH_2CH_2CH_2NH_2]^{+\cdot}$, m/z 45, was also examined. Its CA mass spectrum was markedly different from those of $[CH_3CH_2NH_2]^{+\cdot}$ and $[(CH_3)_2NH]^{+\cdot}$, being dominated by an intense m/z 18 ion, $[NH_4]^+$, partly unimolecular in origin. The three CA mass spectra are presented in Table 1. Note that only the new ion has a charge stripping peak, m/z $[45]^{2+}$. The MI spectrum of the new ion contains only m/z 30, $[\dot{C}H_2NH_2]$ and m/z 18, abundance ratio 3:1, $T_{0.5}$ for the two Gaussian-type metastable peaks being 18 and 19 meV, respectively. The MI spectra of $[CH_3CH_2NH_2]^{+\cdot}$ and $[(CH_3)_2NH]^{+\cdot}$ are dominated by $CH_3^\cdot$ loss and $H^\cdot$ loss respectively, with minor contributions (ca. 10%) from m/z 18, $[NH_4]^+$. The new ion is best represented as $[CH_2CH_2NH_3]^{+\cdot}$, the ethylene ammonium ion (or the ethene–ammonia radical ion dipole complex), whose fragmentation behaviour is similar to that of its oxy-counterpart (2). This structure assignment is also supported by the observation that the ion $[C_2H_4D_3N]^{+\cdot}$, derived by loss of CH_2ND from $[D_2NCH_2CH_2CH_2ND_2]^{+\cdot}$, loses only $C_2H_3^\cdot$ unimolecularly and that m/z 18 and 17 in the CA mass spectrum of the unlabelled ion are cleanly shifted to m/z 21 and 20 ($[ND_3H]^+$ and $[ND_3]^{+\cdot}$). It should be noted that the facile fragmentations to $[NH_4]^+ + C_2H_3^\cdot$ and to $[\dot{C}H_2NH_2] + CH_3^\cdot$ are similarly endoergic ($\Delta H_f^0[NH_4]^+ = 155$ kcal mol^{-1} (22), $\Delta H_f^0[C_2H_3^\cdot] = 63$ kcal mol^{-1} (23); $\Delta H_f^0[\dot{C}H_2NH_2] = 178$ kcal mol^{-1} (13), $\Delta H_f^0[CH_3^\cdot] = 34$ kcal mol^{-1} (13)) and appreciably less energy demanding than dissociation to $[C_2H_4]^{+\cdot} + NH_3$ or $C_2H_4 + [NH_3]^{+\cdot}$ ($\Delta H_f^0[C_2H_4]^{+\cdot} = 255$ kcal mol^{-1} (13); $\Delta H_f^0[NH_3] = -11$ kcal mol^{-1} (13); $\Delta H_f^0[C_2H_4] = 12.5$ kcal mol^{-1} (13), $\Delta H_f^0[NH_3]^{+\cdot} = 255$ kcal mol^{-1} (13)).

The sulphur-containing ions $[CH_4S]^{+\cdot}$

The CA mass spectra of ionised thiomethanol and the ion generated by loss of CH_2O from $[CH_2OHCH_2SH]^{+\cdot}$ are shown in Fig. 3. The differences between the CA peaks are not nearly so striking as in the oxy-analogues. Nevertheless, the enhanced charge stripping peak $[CH_4S]^{2+}$ and the greater relative abundances of m/z 34 and 14, $[H_2S]^{+\cdot}$ and $[CH_2]^{+\cdot}$, are in keeping with the behaviour of the ion $[CH_2SH_2]^{+\cdot}$. The above differences are unlikely to arise from internal energy effects which are usually only important with respect to fragmentations of lowest energy requirement (25). The AE of m/z 48 from CH_2OHCH_2SH was measured as 10.42 ± 0.05 eV, leading to $\Delta H_f^0[CH_2SH_2]^{+\cdot} = 219$ kcal mol^{-1} ($\Delta H_f^0(CH_2OHCH_2SH) = -47.4$ kcal mol^{-1} (21)). $\Delta H_f^0[CH_3SH]^{+\cdot}$ is 212 kcal mol^{-1} (13). The metastable peak for $H^\cdot$ loss from the two ions were of Gaussian type and identical shape, $T_{0.5} = 28$ meV. It seems likely, therefore, that the barrier to the interconversion of these ions lies below the dissociation threshold, calculated to be 48 kcal mol^{-1} above $[CH_3SH]^{+\cdot}$; $\Delta H_f^0[\dot{C}H_2SH] = 208$ kcal mol^{-1} (24). The AE for $[\dot{C}H_2SH]$ from CH_3SH was measured in this laboratory as 11.48 ± 0.05 eV, (calculated = 11.52 eV ($\Delta H_f^0[CH_3SH] = -5.5$ kcal mol^{-1} (16)).

Experimental

Collisional activation mass spectra and metastable peak shapes were measured with the VG ZAB-2F mass spectrometer in Utrecht as described elsewhere (26). Metastable peak shapes were also obtained using an AEI MS902S mass spectrometer; all kinetic energy release values were corrected for the main beam width (27). Appearance energies (except those measured on metastable peaks) were measured with an apparatus comprising an electrostatic electron monochromator with a quadrupole mass analyser and mini computer data system (28). Metastable peak appearance energies were obtained on the AEI MS902S mass spectrometer using the metastable peaks m/z $74^{+\cdot} \rightarrow m/z$ 43^+ in methylacetate or m/z $204^{+\cdot} \rightarrow m/z$ 77^+ in iodobenzene as the standards (15).

All compounds, except those below, were commercially available and, where necessary, purified by gc. CH_2FCOOH was a gift from

TABLE 1. Collisional activation mass spectra of $[C_2H_7N]^{+\cdot}$ ions

Ion	44	43	42	41	40	39	38	30	29	28	27	26	25	22.5	18	17	16	15	14	13
$[CH_3CH_2NH_2]^{+\cdot}$	27	5.7	12	6.7	4.8	1.7	1.1	(278)	4.6	15	7.5	2.7	0.5	—	5.6	0.5	0.3	2.7	0.8	0.3
$[(CH_3)_2NH]^{+\cdot}$	(207)	20	17	6.5	5.6	2.2	1.5	1.7	2.8	24	3.9	0.6	0.1	—	5.6	—	0.2	5.8	1.3	0.4
$[CH_2CH_2NH_3]^{+\cdot}$	10	9.6	13	8.0	5.0	2.0	1.1	(20)	1.6	14	14	7.4	1.4	4	(62)	11	0.5	1.9	0.9	0.3

Prof. R.T.B. Rye (Concordia). CH_3F was synthesized as described in ref. 29. The —OD and $—ND_2$ labelled precursor molecules were obtained by exchange with D_2O in the mass spectrometer inlet system.

Acknowledgments

J.H. thanks the Natural Sciences and Engineering Research Council of Canada for continuing financial support and J.K.T. gratefully acknowledges the continuing support of the Netherlands Organisation for the Advancement of Pure Research (Z.W.O.). J.H. and J.K.T. also wish to thank the NATO Scientific Affairs Division for a collaborative research grant, No. 329.

1. F. W. CROW, M. L. GROSS, and M. M. BURSEY. Org. Mass Spectrom. **16**, 309 (1981).
2. J. K. TERLOUW, W. HEERMA, and G. DIJKSTRA. Org. Mass Spectrom. **16**, 326 (1981).
3. J. K. MCLEOD, W. BOUMA, and L. RADOM. J. Am. Chem. Soc. **104**, 2930 (1982).
4. J. L. HOLMES, F. P. LOSSING, J. K. TERLOUW, and P. C. BURGERS. J. Am. Chem. Soc. **104**, 2931 (1982).
5. H. HALIM, B. CIOMMER, and H. SCHWARZ. Angew. Chem. Int. Ed. Engl. **21**, 528 (1982).
6. Y. APELOIG, B. CIOMMER, G. FRENKING, M. KARNI, A. MANDELBAUM, H. SCHWARZ, and A. WEISZ. J. Am. Chem. Soc. **105**, 2186 (1983).
7. P. C. BURGERS, B. CIOMMER, H. HALIM, J. L. HOMES, H. SCHWARZ, and J. K. TERLOUW. Org. Mass Spectrom. **18**, 208 (1983).
8. W. J. BOUMA, R. H. NOBES, and L. RADOM. J. Am. Chem. Soc. **104**, 2929 (1982).
9 W. J. BOUMA, R. H. NOBES, and L. RADOM. Org. Mass Spectrom. **17**, 315 (1982).
10. W. J. BOUMA, R. H. NOBES, and L. RADOM. Org. Mass Spectrom. **18**, 12 (1983).
11. W. J. BOUMA, F. YATES, and L. RADOM. Chem. Phys. Lett. In press.
12. W. J. BOUMA, R. H. NOBES, and L. RADOM. J. Am. Chem. Soc. In press.
13. H. M. ROSENSTOCK, K. DRAXL, B. W. STEINER, and J. T. HERRON. J. Phys. Chem. Ref. Data Suppl. 6, No. 1 (1977).
14. F. P. LOSSING. J. Am. Chem. Soc. **99**, 7526 (1977).
15. P. C. BURGERS and J. L. HOLMES. Org. Mass Spectrom. **17**, 123 (1982).
16. J. B. PEDLEY and J. RYLANCE. Sussex – N.P.L. computer analysed thermochemical data; organic and organometallic compounds. University of Sussex. 1977.
17. J. L. HOLMES and F. P. LOSSING. Can. J. Chem. **60**, 2365 (1982).
18. R. WEBER, K. LEVSEN, P. C. BURGERS, and J. K. TERLOUW. Org. Mass Spectrom. **16**, 514 (1981).
19. E. S. MUKHTAR, I. W. GRIFFITHS, F. M. HARRIS, and J. H. BEYNON. Int. J. Mass Spectrom. Ion Phys. **42**, 77 (1982).
20. S. W. BENSON, F. R. CRUIKSHANK, D. M. GOLDEN, G. R. HAUGEN, H. E. O'NEAL, A. S. RODGERS, R. SHAW, and R. WALSH. Chem. Rev. **69**, 279 (1969).
21. F. P. LOSSING, Y. T. LAM, and A. MACCOLL. Can. J. Chem. **59**, 2228 (1981).
22. S. D. TANNER, G. I. MACKAY, A. C. HOPKINSON, and D. K. BOHME. Int. J. Mass Spectrom. Ion Phys. **29**, 153 (1979).
23. M. H. BACK and G. AYRANCI. Int. J. Chem. Kinet. **15**, 82 (1983); unpublished results, this laboratory.
24. M. ROY and T. B. MCMAHON. Org. Mass Spectrom. **17**, 392 (1982).
25. P. C. BURGERS, J. L. HOLMES, J. E. SZULEJKO, A. A. MOMMERS, and K. J. TERLOUW. Org. Mass. Spectrom. **18**, 365 (1983).
26. J. K. TERLOUW, P. C. BURGERS, and H. HOMMES. Org. Mass Spectrom. **14**, 307 (1979).
27. J. L. HOLMES and J. K. TERLOUW. Org. Mass Spectrom. **15**, 383 (1980).
28. F. P. LOSSING and J. C. TRAEGER. Int. J. Mass Spectrom. Ion Phys. **19**, 9 (1976).
29. W. F. EDGELL and L. PARTS. J. Am. Chem. Soc. **77**, 4899 (1955).

Can. J. Chem. Downloaded from www.nrcresearchpress.com by 210.87.254.6 on 09/06/12
For personal use only.

1,*n*-Radical ions: the nature of the one-electron two-centre bond in cyclopropane radical cations. An *ab initio* SCF MO approach

DANIAL D. M. WAYNER, RUSSELL J. BOYD,[1] AND DONALD R. ARNOLD[1]
Department of Chemistry, Dalhousie University, Halifax, N.S., Canada, B3H 4J3

Received February 2, 1983

DANIAL D. M. WAYNER, RUSSELL J. BOYD, and DONALD R. ARNOLD. Can. J. Chem. **61**, 2310 (1983).

The nature of the one-electron two-centre bond in the cyclopropane and 1,2-divinylcyclopropane radical cations is elucidated by use of *ab initio* self consistent field (SCF) molecular orbital (MO) calculations. The charge and spin distributions in the 90,90 and 90,0 conformations are compared at the STO-3G and 4-31G basis set levels. From energy differences between the radical cations in the 90,90 conformation and the 90,0 (transition state) conformation, the activation barriers for *cis*–*trans* isomerization in the $^2A_1$ state of $C_3H_6^+$ and of the 1,2-divinylcyclopropane radical cation are estimated. These results are compared to previous calculations and experimental data where possible.

DANIAL D. M. WAYNER, RUSSELL J. BOYD et DONALD R. ARNOLD. Can. J. Chem. **61**, 2310 (1983).

Faisant appel aux calculs *ab initio* d'orbitale moléculaire (OM) à champ autocohérent (CAC) on a élucidé la nature de la liaison à deux centres et à un électron des cations radicalaires du cyclopropane et du divinyl-1,2 cyclopropane. On a comparé la charge et les distributions de spin des conformations 90,90 et 90,0 au niveau des ensembles de base STO-3G et 4-31G. A partir des différences d'énergie entre les cations radicalaires de la conformation 90,90 et de la conformation 90,0 (état de transition), on a évalué les barrières d'activation de l'isomérisation *cis*–*trans* de l'état $^2A_1$ du $C_3H_6^+$ et du cation radicalaire du divinyl-1,2 cyclopropane. On a comparé ces résultats avec les calculs antérieurs et les données expérimentales disponibles.
[Traduit par le journal]

Can. J. Chem. Downloaded from www.nrcresearchpress.com by 210.87.254.42 on 09/06/12
For personal use only.

Introduction

The structure and reactivity of the radical cations of cyclopropane and its derivatives are of considerable interest and have been the subject of both experimental and theoretical investigation. Most of the theoretical studies (1) have been directed toward the interpretation of the photoelectron spectrum of the parent molecule. In cyclopropane, removal of the electron from either of the two degenerate Walsh MO's of *e'* symmetry (2) leads to two possible structures for the radical cation (Fig. 1). One of these species, having the trimethylene type structure, will have a $^2A_1$ ground state while the other, which resembles the π-complex between ethylene and CH_2^+, will have a $^2B_2$ ground state. Recent calculations by Collins and Gallup (1*a*), using the method of *targeted correlation*, suggest that these two species correspond to saddle points on the radical cation surface. The minimum, having C_s symmetry, is approximately halfway between these structures on the surface.

Although these theoretical studies have been useful in explaining the photoelectron spectrum of cyclopropane, they generally have not provided information that can be used to understand the reactivity of the radical cation. Evidence obtained from chemically induced dynamic nuclear polarization (CIDNP) spectra (3) indicates that most radical cations of alkyl and aryl substituted cyclopropanes tend to favour the $^2A_1$ type structure. There is evidence, however, that in some special cases, such as the radical cation of benzonorcaradiene, the radical cation may assume the $^2B_2$ structure (3*c*).

Theoretical calculations investigating some of the reactions of $C_3H_6^+$ (4) have yielded estimates of the activation energies for the loss of H, H_2, H_2^+, and CH_2^+. One important reaction, which has received little attention from a theoretical point of view, is the thermal *cis*–*trans* isomerization of the cyclopropane radical cation. This reaction is particularly interesting because of the implication of the nature of the one-electron two-centre bond.

Much that is known about the nature of bonding in cyclopropanes (5) and olefins (6) comes from experimental investigation of their thermal reactions, particularly *cis*–*trans* isomerization. Since direct observation of the parent cyclopropane radical cation is difficult, similar data for this system is not available. There is evidence, however, that the radical cation of 1,2-diphenylcyclopropane (3*a*, *b*) does *not* rapidly isomerize. In this work, however, the radical cations were generated by photosensitization (electron transfer). Under these conditions, all other reactions must compete with back electron-transfer. Since it is unlikely that there is a significant activation barrier for this process, it is impossible to determine the lower limit for the barrier to *cis*–*trans* isomerization.

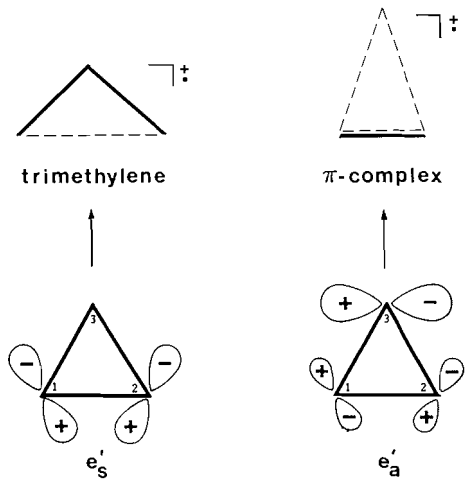

FIG. 1. Walsh MO's leading to the "trimethylene" and "π-complex" structures for the cyclopropane radical cation.

The purpose of this paper is to try to understand the nature of the one-electron two-centre bond in the cyclopropane radical cation. We have used *ab initio* calculations to obtain optimized geometries for the cyclopropane radical cation in the 90,90 conformation (7) (both $^2A_1$ and $^2B_2$ states) and in the 90,0 conformation. The difference in the energies of these species provides an estimate of the strength of the one-electron two-centre bond. This study has been extended to the 1,2-divinylcyclopropane radical cation; the results are pertinent to the

[1]Authors to whom correspondence may be addressed.

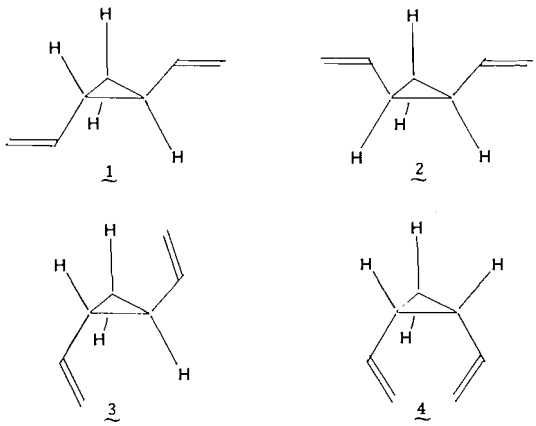

FIG. 2. Conformations of the 1,2-divinylcyclopropane radical cation used in the STO-3G calculations.

TABLE 1. 4-31G geometries of C_3H_6 and $C_3H_6^+$ [a]

Parameter	90,90($^2A_1$)	90,90($^2B_2$)	90,0[b] ($^2A''$)	C_3H_6
$r_{C_1C_2}$	1.941	1.401	(2.354)[c]	1.503
$r_{C_1C_3}$	1.483	1.713	1.448	
$r_{C_2C_3}$	1.483	1.713	1.548	
r_{C_1H}	1.072	1.072	1.077	1.072
r_{C_2H}	1.072	1.072	1.071	
r_{C_3H}	1.075	1.069	1.083	
$\angle C_1C_3C_2$ (θ)	81.7	48.3	103.6	60.0
$\angle HC_1H$	118.3	117.2	117.1	113.7
$\angle HC_2H$	118.3	117.2	120.1	
$\angle HC_3H$	113.7	120.4	110.4	
α_1[d]	179.9	126.8	183.8	150.0
α_2[d]	179.9	126.8	179.4	
E(UHF)[e]	−116.57359	−116.56373	−116.54403	

[a]All bond lengths in Å and angles in degrees.
[b]The plane of the C_3 methylene has been rotated by 90°.
[c]Internuclear distance.
[d]α_i is the angle between the C_iC_3 bond and the intersection of the plane of the C_i methylene with the plane of the carbons.
[e]Atomic units.

1,2-diphenyl derivative for which some experimental data are available.

Details of calculations

The *ab initio* MO calculations were obtained by the use of the GAUSSIAN 76 program (8*a*). The energies of the radical cations were computed using the open-shell, spin-unrestricted (UHF) procedure (8*b*). Complete geometry optimization of $C_3H_6^+$ in the $^2A_1$ and $^2B_2$ states (C_{2v} symmetry) was carried out using both STO-3G and 4-31G basis sets. The optimization of $C_3H_6^+$ in the 90,0 conformation also was carried out using both STO-3G and 4-31G basis sets; however, in this case a plane of symmetry through the centre of each methylene was maintained.

Calculations on the 1,2-divinylcyclopropane radical cation ($DVCP^+$) were carried out using only the STO-3G basis set. A complete geometry optimization was not feasible. The 4-31G optimized geometry for $C_3H_6^+$ ($^2A_1$) was used as a model for the cyclopropane group while the STO-3G optimized geometry for the allyl cation (9) was used to represent the vinyl groups. The vinyl groups were placed in the plane of the corresponding methylene to ensure maximum overlap through the π-system. In *trans*-$DVCP^+$, the C_2 axis was maintained and in *cis*-$DVCP^+$ the plane of symmetry was maintained. The conformations are best described using the nomenclature derived for conjugated polyenes (in this case 1,3,5-hexatriene), since $DVCP^+$ is structurally similar. Four conformations in the 90,90 conformation were considered (Fig. 2): 2s-*trans*-4s-*trans*-3-*trans* (**1**), 2s-*trans*-4s-*trans*-3-*cis* (**2**), 2s-*cis*-4s-*cis*-3-*trans* (**3**) and 2s-*cis*-4s-*cis*-3-*cis* (**4**). The geometry for $DVCP^+$ in the 90,0 conformation was derived using a similar approach. In this case, however, the STO-3G geometry for the allyl radical (9) was used as a model for the vinyl group on C_2, which was twisted into the plane of the cyclopropane group (*vide infra*). In all cases, the $C_1C_3C_2$ angle (θ) of the cyclopropane group was optimized.

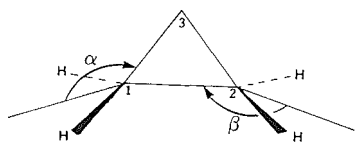

FIG. 3. Representation of the angles α and β.

TABLE 2. Mulliken overlap populations[a] for the carbons in C_3H_6 and $C_3H_6^+$

	C_3H_6	$C_3H_6^+$($^2A_1$)	$C_3H_6^+$($^2B_2$)	$C_3H_6^+$(90,0)
C_1C_2	0.1705	0.0226	0.2037	−0.0367
C_1C_3	0.1705	0.1922	0.0863	0.2505
C_2C_3	0.1705	0.1922	0.0863	0.2171

[a]4-31G.

Discussion

Structure of $C_3H_6^+$

The optimized geometries (4-31G) of the cyclopropane radical cation in the 90,90 conformations ($^2A_1$ and $^2B_2$ states) and 90,0 conformation are shown in Table 1. These structures for the $^2A_1$ and $^2B_2$ states are qualitatively similar to those using semi-empirical (1*b*,*c*,*d*, 4) and other *ab initio* methods (1*a*). The geometry in the 90,0 conformation has not been reported previously. While the structures of these species are of great interest, the changes in spin and charge distributions in relation to the structural changes are the important factors in the study of reactivity.

An interesting feature of the $^2A_1$ structure is that the value of α (defined in Table 1, Fig. 3) indicates that C_1, C_3, H_1, and H_2 lie in one plane while C_2, C_3, H_3, and H_4 lie in another plane (indicative of sp^2 hybridization at C_1 and C_2). This geometry allows effective bonding between C_1 and C_2 (Table 2) even though θ has increased relative to that of cyclopropane. The magnitude of θ (only 81.7°) is another indication that there is considerable C_1C_2 bonding interaction in this species. Another interesting aspect of this structure is the geometry at C_3. Although substantial changes have occurred at C_1 and C_2, virtually no change (relative to cyclopropane) in the C_3H bond length or the HC_3H angle occurs. This may be rationalized using the Walsh model for bonding; since the electron has been removed from a molecular orbital which is bonding between C_1 and C_2, large changes at C_3 are not expected if there is still substantial bonding between C_1 and C_2 in the radical cation.

The value of α in the $^2B_2$ structure is much smaller than that in the $^2A_1$ state. Since this structure is described as a π-complex between ethylene and CH_2^+, it is useful to consider an angle β which we define as the angle between the C_1C_2 bond and the

Can. J. Chem. Downloaded from www.nrcresearchpress.com by 210.87.254.42 on 09/06/12
For personal use only.

TABLE 3. Charge and spin distributions[a] in $C_3H_6^+$

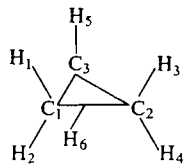

	$^2A_1$			$^2B_2$			90,0		
Atom	Atomic charge	Spin density	Fermi[b] contact	Atomic charge	Spin density	Fermi[b] contact	Atomic charge	Spin density	Fermi[b] contact
C_1	6.211	0.643	0.106	6.270	0.142	−0.002	5.935	−0.006	0.002
C_2	6.211	0.643	0.106	6.270	0.142	−0.002	6.288	1.440	0.261
C_3	6.393	−0.129	−0.057	6.315	0.896	0.150	6.504	−0.151	−0.055
H_1	0.696	−0.038	−0.017	0.688	0.004	0.004	0.676	0.000	0.000
H_2	0.696	−0.038	−0.017	0.688	0.004	0.004	0.676	0.000	0.000
H_3	0.696	−0.038	−0.017	0.688	0.004	0.004	0.724	−0.085	0.036
H_4	0.696	−0.038	−0.017	0.688	0.004	0.004	0.778	−0.091	0.036
H_5	0.701	0.031	0.016	0.696	−0.055	−0.026	0.709	0.053	0.022
H_6	0.701	0.031	0.016	0.696	−0.055	−0.026	0.709	0.053	0.022

[a]4-31G basis set.
[b]Atomic units.

intersection of the plane of the methylene with the plane of the carbons (Fig. 3). In this case, β has a value of 167.2° (for ethylene the corresponding angle would be 180.0°). The lengthening of the C_1C_3 and C_2C_3 bonds and concurrent shortening of the C_1C_2 bond are consistent with the structure predicted by the Walsh model. The antisymmetric MO extends over all three carbons; consequently, the geometries of all three methylenes in this state differ substantially from those in cyclopropane.

The cyclopropane radical cation in the 90,0 conformation shows no evidence for bonding between C_1 and C_2 (Table 2). The C_1C_3 bond has shortened while the C_2C_3 bond (the plane of the C_2 methylene has rotated 90°) has lengthened. The C_1H and C_2H bond lengths are essentially unchanged compared to cyclopropane. On the other hand, the longer C_3H bond, the large value of θ, and the smaller HC_3H angle are characteristic of a normal alkane bond. Further investigation, in fact, reveals that the C_1C_3 and C_2C_3 bond lengths are similar to those calculated for the 1-propyl cation (9). In the case of the 1-propyl cation, the C_1C_3 and C_2C_3 bond lengths (using a 3-21G basis set) were found to be 1.438 Å and 1.536 Å respectively.

The charge and spin distributions in each of these structures are shown in Table 3. In the $^2A_2$ structure only 20% of the charge is delocalized to the C_3 methylene. Similarly, most of the spin density remains between C_1 and C_2. This, of course, is consistent with the Walsh model described previously. In the $^2B_2$ structure the charge is almost equally distributed between the three methylenes, 30% on the C_3 methylene and 35% on each of the C_1 and C_2 methylenes. The spin density, however, is almost entirely localized on C_3. Thus, the description of the $^2B_2$ state as a complex between CH_2^+ and ethylene is appropriate.

The charge and spin distributions in the 90,0 conformation are also consistent with its structures. The charge is localized essentially on the C_1 methylene (71%) and to a lesser extent on C_2 and C_3 (21% and 8% respectively). The spin, on the other hand, is localized almost completely on C_2; the remainder is on C_3. These spin and charge distributions may be understood qualitatively by considering two possibilities. In the first, the spin is localized on C_2. This may be described as an "ethyl cation−methyl radical" pair. In the other case the charge is localized on C_2; this would be an "ethyl radical−methyl cation" pair. Since the ionization potential of the methyl radical is greater than the ionization potential of the ethyl radical (10) the former case would be expected to be energetically favourable. The alternate lengthening of the C_2C_3 bond and shortening of the C_1C_3 bond may be a result of the charge polarization. The C_1 carbon atom has a net positive charge (Table 3) while the C_3 carbon atom and C_2 carbon atom are both negatively charged. The Coulombic interactions between the carbons may be responsible for this alternation in bond lengths.

TABLE 4. Energies of the divinylcyclopropane radical cation[a]

Structure	Energy (kcal mol^{-1})	θ (°)[b]
1	0	77.4
2	4.25	81.7
3	13.43	77.9
4	>100	>125
90,0[c]	16.00	112.8
90,0[d]	14.23	113.0
90,0[e]	14.56	109.1

[a]STO-3G energies relative to **1** for which the STO-3G total energy is −267.34486 au.
[b]The value of θ for C_3H_6 using the STO-3G basis set is 75.8°.
[c]Angle of rotation about the C_2C_3 bond is +90°; the C_2 vinyl group has the geometry of the allyl cation.
[d]Angle of rotation about the C_2C_3 bond is +90°; the C_2 vinyl group has the geometry of the allyl radical.
[e]Angle of rotation about the C_2C_3 bond is −90°; the C_2 vinyl group has the geometry of the allyl radical.

1,2-Divinylcyclopropane radical cation

Several interesting features of the $DVCP^+$ are evident. In structures **1**, **2**, and **3** (Fig. 2) the values of θ are similar to the bond angle in the unsubstituted radical cation (Table 4). This is significant since using the geometry of the allyl cation max-

Can. J. Chem. Downloaded from www.nrcresearchpress.com by 210.87.254.42 on 09/06/12
For personal use only.

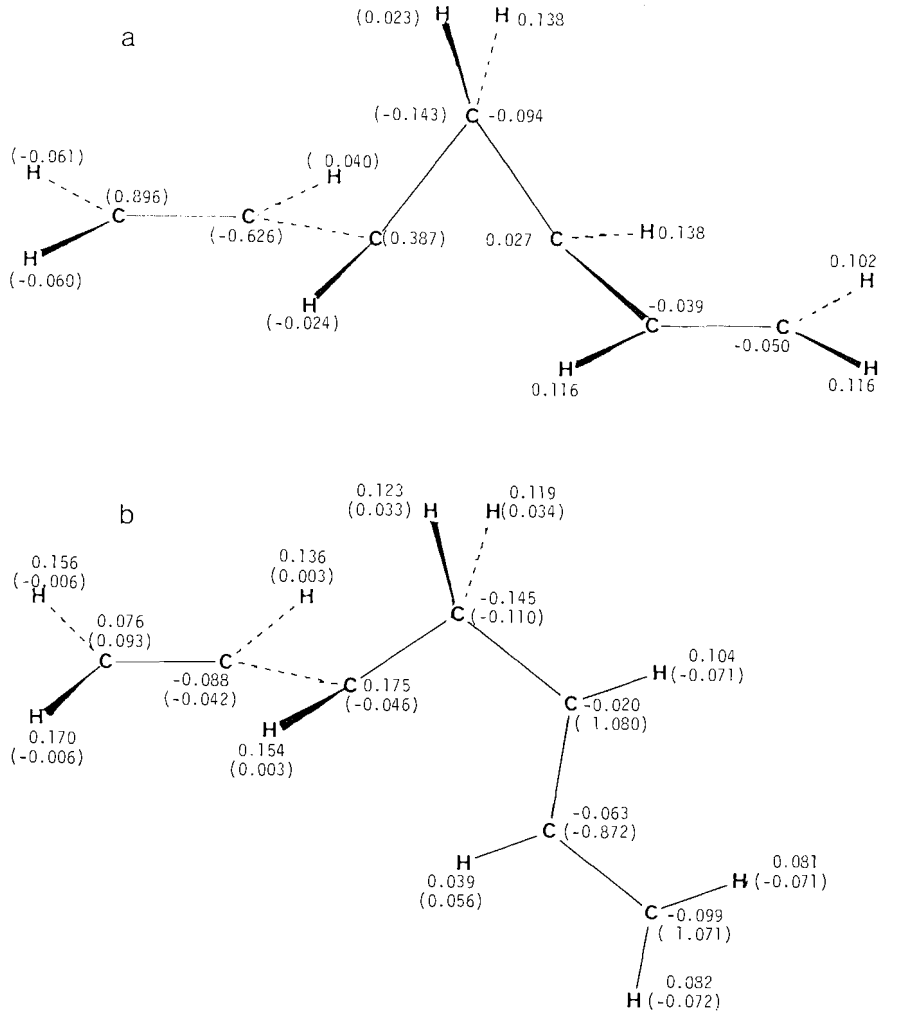

FIG. 4. Charge and spin distributions in $DVCP^+$ in the 90,90 and 90,0 conformations. The spin densities are in parentheses.

imizes the π-overlap between the vinyl groups and the respective cyclopropane carbons. This could have the result of lengthening the C_1C_2 bond since it may be expected that the more effectively the electron density is delocalized, the weaker the C_1C_2 bond should become. The value of θ in the 90,0 conformation is larger than that in the unsubstituted radical cation. This may be a consequence of the increased steric interactions with the allyl system at C_1. The steric repulsions in structure **4** are predominant. Because of CPU time restrictions it was not feasible to optimize the dihedral angles about the methylenes. However, it seems likely that the radical cation in this conformation should undergo a facile Cope rearrangement since the activation energy for the analogous rearrangement of *cis*-1,2-DVCP is only 20 kcal mol^{-1} (11).

The charge and spin distributions in the 1,2-divinylcyclopropane radical cation in the lowest energy 90,90 conformation (**1**) and in the 90,0 conformation are shown in Fig. 4. Only the $^2A_1$ structure was considered for the cyclopropane system. The experimental evidence obtained from CIDNP studies (3) is best interpreted in terms of a structure of this type. Involvement of the $^2B_2$ structure would render two substituents in spacially nonequivalent environments. The loss of the symmetry would complicate the choice of model geometries for each vinyl group. Finally, we are primarily interested in the *cis–trans* isomerization of the radical cations; it seems likely that a structure similar to the $^2A_1$ geometry would be involved.

The geometry of the vinyl groups was based on the STO-3G geometry of the allyl cation. Since almost all of the spin density appears on C_2 in the 90,0 conformation, the geometry of the allyl radical was used for the C_2 vinyl group in this case. The difference in energy using the allyl cation geometry at C_2 and that using the allyl radical geometry was only 1.8 kcal mol^{-1}.

In the 90,90 conformation, both charge and spin are delocalized into the vinyl groups. The C_3 methylene still has 18% of the charge (compared to approximately 20% in the unsubstituted case). Similarly, in the 90,0 conformation, only 10% of the charge is delocalized to the C_3 methylene and 12% to the C_2 vinyl system (compared to 8% and 21% respectively in the unsubstituted radical cation). Essentially all of the spin density remains at the C_2 vinyl system in this conformation.

Isomerization of $C_3H_6^+$

The surface for *cis–trans* isomerization of cyclopropane has been investigated (12). In this study, the activation energy was estimated as the difference in energy between cyclopropane and the trimethylene diradical in the 90,0 conformation. One interesting point which we are now able to discuss is the comparison of the calculated barrier for isomerization in cyclopropane with that in the radical cation.

A similar study investigating the rotational barrier in the ethylene radical cation has recently appeared (13). It has long been accepted that the electronic structure of cyclopropanes is

Can. J. Chem. Downloaded from www.nrcresearchpress.com by 210.87.254.42 on 09/06/12
For personal use only.

TABLE 5. Calculated activation energies for several *cis–trans* isomerization reactions

	Basis set	$E^{\ddagger}$ (kcal mol^{-1})[a]
$C_3H_6^+$ ($^2A_1$)	STO-3G	23.2
$C_3H_6^+$ ($^2A_1$)	4-31G	18.2
$C_2H_4^+$	4-31G	27.2[b]
C_3H_6	Minimal	52.6[c] (expt. 65)[d]

[a]Based on energy difference between "planar" (90,90) and "perpendicular" (90,0) geometries.
[b]Reference 13.
[c]Reference 12.
[d]Reference 5.

conceptually similar to the electronic structure of olefins (14). Another point which we are now able to discuss is whether or not this analogous behaviour is evident in the radical cations.

The calculated activation energies for isomerization of C_3H_6, $C_3H_6^+$, and $C_2H_4^+$ are shown (Table 5). There is still substantial bonding between C_1 and C_2 in $C_3H_6^+$. However, one might expect the bond strength to decrease by at least one-half of the value in cyclopropane since the electron has been removed from the symmetric Walsh orbital. The calculated activation energy for *cis–trans* isomerization of $C_3H_6^+$ is *less* than half that for C_3H_6. It is important to point out that the work of Collins and Gallup (1*a*) predicted the energy of the $^2A_1$ structure to be 6.65 kcal mol^{-1} higher than that of the $^2B_2$ structure. Our results have predicted the energy of the $^2A_1$ structure to be 6.19 kcal mol^{-1} lower than that of the $^2B_2$ structure. Interpretation of the photoelectron spectrum of cyclopropane obviously requires inclusion of correlation (1*a*). However, it is not clear how correlation would affect the relative energy of the 90,0 conformation. The geometry of the $^2A_1$ structure predicted by the calculations of Collins and Gallup still appears to have a small value of θ. It is, therefore, not unlikely that the relative energy of the 90,0 conformation would be similar to that which we predict. The qualitative conclusions in which we are interested would be essentially unchanged even if the relative energy was to change by as much as 5 kcal mol^{-1}.

It is interesting to note that the experimentally determined π-bond strength in ethylene (6) is approximately the same as the σ-bond strength in cyclopropane (5). The difference in the calculated activation energies (at the 4-31G level) of $C_3H_6^+$ and $C_2H_4^+$ should therefore be discussed. The one-electron oxidation of ethylene leads to a species which has little internal strain. We are tempted, therefore, to attribute the difference between the activation energies for *cis–trans* isomerization of $C_3H_6^+$ and $C_2H_4^+$ to the ring strain in the cyclopropane radical cation. We must use caution, however, since the difference between the calculated activation barrier for isomerization in C_3H_6 and C_2H_4 using the same basis set is, to our knowledge, not available. If the calculated activation barrier for C_2H_4 is significantly higher than that for C_3H_6, the difference in the radical cations may be meaningless. (One calculation using a double-zeta basis set with polarization and diffuse functions estimates the activation barrier for ethylene to be 62.5 kcal mol^{-1} (15)). It should be noted that the twist angle at the energy minimum in $C_2H_4^+$ is 25 degrees, apparently a compromise between π-overlap and hyperconjugation (16). The planar structure, however, is only 0.67 kcal mol^{-1} higher in energy than the twisted minimum.

Isomerization of DVCP$^+$

The *cis–trans* isomerization of the 1,2-diphenylcyclopropane radical cation has been studied by CIDNP techniques (3*a*,*b*). When 1,4-dicyanonaphthalene was used as the photosensitizer (electron transfer), *cis–trans* isomerization occurred and nuclear polarization for both isomers was observed. However, when chloranil was used as the photosensitizer (electron transfer), no isomerization was observed (3*b*) but the starting material showed nuclear polarization. The results of these CIDNP experiments led to the conclusion that, in the case of 1,4-dicyanonaphthalene, back electron-transfer in the radical ion pair generated the triplet state of 1,2-diphenylcyclopropane which then isomerized. On the other hand, back electron-transfer to the 1,2-diphenylcyclopropane radical cation from the chloranil radical anion only generated the ground state singlet of the cyclopropane since the triplet energy of the radical ion pair was insufficient to generate the triplet of the cyclopropane. The observed polarization of the starting material gave evidence for a radical cation of the $^2A_1$ type, while the lack of the other isomer indicated that the radical cation did not efficiently isomerize. Since there is probably no activation barrier for back electron-transfer in the radical ion pair, any activation barrier for isomerization will effectively inhibit this process.

An estimate of the activation barrier for isomerization of the 1,2-diphenylcyclopropane radical cation may be obtained by comparing the energies of the 90,90 and 90,0 conformations of $DVCP^+$. This is a reasonable model, considering the C—H bond dissociation energies of toluene and propene are approximately equal (17). The calculated energies of $DVCP^+$ relative to structure **1** are shown in Table 4.

The relative energies of **1**, **2**, and **3** are consistent with the results of recent calculations on vinylcyclopropane (18), s-*trans* being more stable. Structure **1** and **2** are geometric isomers having the same conformation of the vinyl groups (s-*trans*). The energy difference between **1** and **2** (4.25 kcal mol^{-1}) is similar to the energy difference observed from the thermal isomerization of 1,2-diphenylcyclopropane (about 2.3 kcal mol^{-1}) (19).

The energy difference between **1** and the radical cation in the 90,0 conformation represents the activation barrier for isomerization of the radical cation. The value of 14.23 kcal mol^{-1} indicates a bond weakening of approximately 9 kcal mol^{-1} relative to the unsubstituted radical cation (Table 5). This may be compared to the difference in σ-bond strength observed experimentally between cyclopropane and 1,2-diphenylcyclopropane, about 30 kcal mol^{-1}. The effect of the substituents on the stability of the transition state relative to the ground state in the neutral molecule is expected to be far greater than in the radical cation; there is charge and spin delocalization in both the ground and transition states in the radical cation.

In the photochemical generation of the radical ions, this activation barrier would prevent *cis–trans* isomerization of the radical cation. If a preexponential factor of 10^{14} is assumed for the isomerization (20), the rate constant for *cis–trans* isomerization of the radical cation would be only 4.3×10^3 s^{-1} at 300 K.

Conclusions

The calculated barrier to *cis–trans* isomerization (18.2 kcal mol^{-1}), the Mulliken overlap population, and the value of θ (81.7°) indicate that there is significant bonding between C_1 and C_2 in the cyclopropane radical cation ($^2A_1$). In the 90,90 conformation both spin and charge are extensively delocalized; however, in the 90,0 conformation the spin density is localized

Can. J. Chem. Downloaded from www.nrcresearchpress.com by 210.87.254.42 on 09/06/12
For personal use only.

on C_2.

The charge and spin densities in the 1,2-divinylcyclopropane radical cation are both delocalized into the vinyl groups. The small value for θ as well as the calculated barrier to *cis*–*trans* isomerization (14.2 kcal mol^{-1}) indicate that even in this species the strength of the one-electron two-centre bond is substantial. These results have been related to the 1,2-diphenyl derivative (for which experimental data are available) and indicate that *cis*–*trans* isomerization should be observed if the lifetime of the radical cation is in the order of 100 μs.

Acknowledgements

This work was supported by a grant from the Natural Sciences and Engineering Research Council of Canada (including a scholarship to D.D.M.W.). D.R.A. is grateful for a fellowship from the John Simon Guggenheim Foundation. The authors thank the Dalhousie University Computer Centre for generous amounts of computer time.

1. (*a*) J. R. COLLINS and G. A. GALLUP. J. Am. Chem. Soc. **104**; 1530 (1982); (*b*) J. A. TOSSELL, J. H. MOORE, and M. A. COPLAN. Chem. Phys. Lett. **67**, 356 (1979); (*c*) C. G. ROWLAND. Chem. Phys. Lett. **9**, 169 (1971); (*d*) E. HASELBACH. Chem. Phys. Lett. **7**, 428 (1970).
2. A. D. WALSH. Trans. Faraday Soc. **45**, 179 (1949).
3. (*a*) D. R. ARNOLD and P. C. WONG. Tetrahedron Lett. **23**, 2101 (1979); (*b*) H. D. ROTH and M. L. M. SCHILLING. J. Am. Chem. Soc. **102**, 7956 (1980); (*c*) H. D. ROTH and M. L. M. SCHILLING. Can. J. Chem. **61**, 1027 (1983).
4. S. BERÁN and R. ZAHRADNIK. Collect. Czech. Chem. Commun. **41**, 2303 (1976).
5. J. A. BERSON. Ann. Rev. Phys. Chem. **28**, 111 (1971).
6. (*a*) J. E. DOUGLAS, B. S. RABINOVITCH, and F. S. LOONEY. J. Chem. Phys. **23**, 315 (1955); (*b*) S. W. BENSON. Thermochemical kinetics. 2nd ed. Wiley, New York. 1976.
7. L. SALEM. Photochemistry-IV: plenary lectures. Butterworth and Company Ltd., Toronto, Canada. 1973.
8. (*a*) J. S. BINKLEY, R. A. WHITESIDE, P. C. HARIHARAN, R. SEEGER, J. A. POPLE, W. J. HEHRE, and M. D. NEWTON. QCPE, **11**, 368 (1978); (*b*) J. A. POPLE and R. K. NESBET. J. Chem. Phys. **22**, 571 (1954).
9. R. A. WHITESIDE, M. J. FRISCH, J. S. BINKLEY, D. J. DEFREES, H. B. SCHLEGEL, K. RAGHAVACHARI, and J. A. POPLE. Carnegie–Mellon quantum chemistry archive. 2nd ed. 1981.
10. V. I. VEDENEYEV, L. V. GURVICH, V. N. KONDRAT'YEV, V. A. MEDVEDEV, and YE. L. FRANKEVICH. Bond energies, ionization potentials and electron affinities. Edward Arnold Ltd., London. 1966.
11. J. M. BROWN, B. T. GOLDING, and J. J. STAFKO, JR. J. Chem. Soc. Chem. Commun. 319 (1973).
12. J. A. HORSLEY, Y. JEAN, C. MOSER, L. SALEM, R. M. STEVENS, and J. S. WRIGHT. J. Am. Chem. Soc. **94**, 279 (1972).
13. D. J. BELLVILLE and N.L. BAULD. J. Am. Chem. Soc. **104**, 294 (1982).
14. A. DEMEIJERE. Angew. Chem. Int. Ed. Engl. **18**, 809 (1979).
15. R. J. BUENKER and S. D. PEYERIMHOFF. Chem. Phys. **9**, 75 (1976).
16. H. KOPPEL, W. DOMCKE, L. S. CEDERBAUM, and W. J. VON NEISSEN. J. Chem. Phys. **69**, 4252 (1978).
17. D. M. GOLDEN and S. W. BENSON. Chem. Rev. **69**, 125 (1969).
18. G. R. DEMARE and M. R. PETERSON. J. Mol. Struct. **89**, 213 (1982).
19. R. J. CRAWFORD and T. R. LYNCH. Can. J. Chem. **46**, 1457 (1968).
20. D. R. ARNOLD, D. D. M. WAYNER, and M. YOSHIDA. Can. J. Chem. **60**, 2313 (1982).

Can. J. Chem. Downloaded from www.nrcresearchpress.com by 210.87.254.42 on 09/06/12
For personal use only.

Laser interferometric galvanostatic studies in the $Zn/ZnSO_4/Zn$ system with gelled electrolyte short time electrolysis

R. N. O'BRIEN AND W. MICHALIK

Department of Chemistry, University of Victoria, P.O. Box 1700, Victoria, B.C., Canada V8W 2Y2

Received January 7, 1983

R. N. O'BRIEN and W. MICHALIK. Can. J. Chem. **61**, 2316 (1983).

Electrolysis in the system $Zn/ZnSO_4/Zn$ with gelled electrolyte was followed for short times to allow use of the first term only of the solution to Fick's Second Law for transient conditions. Sufficiently good agreement was found between theory and experiment to confirm that no convection occurred in the gelled electrolyte. Similarly sufficiently good agreement with liquid electrolyte runs confirmed that no convection occurred in parallel plate, horizontal electrodes when the cathode was over the anode. The conductivity of the gelled electrolyte was about 11% lower than the liquid electrolyte.

R. N. O'BRIEN et W. MICHALIK. Can. J. Chem. **61**, 2316 (1983).

On a utilisé le système $Zn/ZnSO_4/Zn$ dans un électrolyte sous forme de gel afin d'étudier l'électrolyse pendant de courtes périodes dans le but de permettre uniquement l'emploi du premier terme de la solution de la seconde loi de Fick relative aux conditions transitoires. L'accord entre la théorie et l'expérience est sufissamment parfait pour confirmer l'absence de convection dans l'électrolyte en gel. D'une manière analogue l'accord relativement parfait avec les essais portant sur des électrolytes liquides confirme qu'il n'y a pas de convection lorsque des électrodes horizontaux sont dans un plan parallèle avec la catode placée en dessus de l'anode. La conductivité de l'électrolyte sous forme de gel est d'environ 11% plus faible que celle de l'électrolyte liquide.

[Traduit par le journal]

Can. J. Chem. Downloaded from www.nrcresearchpress.com by 210.87.254.40 on 09/06/12
For personal use only.

Introduction

In electrolysis in galvanostatic conditions, constant concentration polarization and consequently a constant concentration gradient at the working electrodes is to be expected when certain limiting conditions obtain. The simplest condition to produce a constant concentration profile at a working electrode surface is the natural convection at a vertical electrode which results from depletion (and usually a lower density) of solution at the cathode and enrichment at the anode (1). The convective flow limits the thickness of the diffusion layer and its concentration gradients.

The case of horizontal plane parallel electrodes with the anode over the cathode (A/C) results in turbulent, intense natural convection and a general average concentration polarization which is constantly changing at any individual point (1*a*). Rapid forced convection (stirring) produces a reduced and constant thickness, constant concentration gradient diffusion layer. The more sophisticated system of the rotating disc limits the diffusion layer and supplies the electroactive ion by convective diffusion (2). Thus, convective flow, the more efficient supplier of reactants to the electrode surface, replaces diffusion (and migration) as the dominant transport mechanism at all but the shortest distances from the electrode surface. A calculation of relative effects of the two mechanisms has been done (3). At short distances viscous shear forces eventually limit transport by convection.

Usually diffusion and migration are lumped together and the effect of migration in convectionless transport equations is supposed to be adequately accounted for by applying the appropriate transference number to account for the lowered concentration changes found for the unsteady state (4). However, since approximately pure migration has been observed before diffusion begins when a well characterized Teflon electret is immersed in electrolyte (5) and since constant concentration gradients, where diffusion exactly balances migration (in the absence of convection), have been observed (6), it is obvious that this method of accounting for migration is inadequate and in fact of the wrong mathematical form. The correct analytical form of the differential equation has resisted efforts to solve it to date. But it is clear that for some electrolyte concentrations, current profile, and electrode separations (in the C/A orientation), the diffusion layer will attain a constant thickness and concentration gradient while in most cases this transient condition will cause continued expansion of the diffusion layer. However, according to Wagner (7) (and observed by us qualitatively) (1*b*, 4) the concentration gradient near the electrode remains constant. Small changes do appear in the concentration gradient near the electrode with time in this work and will be discussed.

Rosebrough and Miller (8) showed that at long times of electrolysis, when the conditions could no longer be considered to conform to the semi-infinite diffusion constraints used in all recent solutions to Fick's Second Law, a straight line concentration profile should be attained. They also predicted that when this transition point is reached, new (less steep) concentration gradients near the electrode will occur.

Addressing only the case for a constant concentration gradient where migration and diffusion are equal it appears likely that if a proper solution (of mathematically correct form and fitting the best data) to the Fick's Second Law differential equation could be found, that transference numbers, diffusion coefficients, and effective electric fields would follow. The present work was undertaken to investigate, and it is hoped to settle, whether convection plays a role, other than minor in the C/A orientation where none is conventionally expected. Elimination on a truly sound experimental basis would therefore be a useful exercise, not possible by other presently forseeable means than a gelled electrolyte in an interferometric electrodeposition cell.

Theory

The complete electrochemical transport equation can be written (12)

$$[1] \quad J_i = -D_i\left(\frac{\partial C_i}{\partial x}\right) + u_i\nu_i C_i E + \nu C_i$$

where J is total flux (mol cm^{-2} s^{-1}), D is the diffusion coefficient (cm^2 s^{-1}), C_i is concentration (mol cm^{-3}), x is distance

Can. J. Chem. Downloaded from www.nrcresearchpress.com by 210.87.254.40 on 09/06/12
For personal use only.

perpendicular to the working electrode face (cm), u is mobility ($cm^2\ s^{-1}\ V^{-1}$), ν_i is the charge on the ion, E is the electric field ($V\ cm^{-1}$), and v is the fluid velocity ($cm\ s^{-1}$). The terms on the right hand side are, successively, diffusion, migration, and convection (9, 10).

Convection is eliminated by using a stagnant solution and then arranging the cathode over the anode. Because all salts are heavier than water, in water solution, this results in density layering because the concentration decreases at the top electrode (cathode) and increases at the bottom for systems of the type $Zn/ZnSO_4/Zn$. Further for any random perturbation a strong (relative to expected disturbing forces) restoring force exists and grows with time.

Considering next the remaining transport modes, no diffusion can occur unless a diffusion or concentration gradient $\partial c/\partial x$, exists since the diffusion force is a free energy gradient

$$\frac{\partial G}{\partial x} = -\mu \frac{\partial n}{\partial x}$$

where μ is the electrochemical potential. Clearly at some set of conditions of current density, concentration of electrolyte, and temperature, a balance between migration creating a concentration gradient (as adjacent ions are attracted and discharged) and diffusion eliminating it must exist and has been recently demonstrated (5). Such a condition has been attained under semi-infinite diffusion conditions (6) and under non-semi-infinite conditions (11). These data are good evidence for no convective transport because (1*b*, 4) the diffusion layer thickness is very large compared to that of convecting systems and the diffusion layer and concentration gradient grew normally for much longer times (1200 s compared to 60 s) than it does under convecting systems.

The concentration changes in the diffusion layer under galvanostatic and non-convective conditions can be obtained by solving Fick's Second Law for the appropriate conditions. If the Laplace transform solution, rather than the Fourier transform (8) is found, it is a series solution which transforms to

$$[2]\quad \Delta C_{(x,t)} = \frac{2I}{\nu F}\frac{t^{1/2}}{D^{1/2}}(1 - t_+)\left[\text{ierfc}\left(\frac{2l - x}{2\sqrt{Dt}}\right) - \text{ierfc}\left(\frac{x}{2\sqrt{Dt}}\right)\right]$$

where I is the current density ($A\ cm^{-2}$), t is time (s), ν is the number of charges per ion, F is the Faraday (coulombs per equivalent), ierfc is the integrated error function complement, t_+ the cation transference number, and the other symbols have their previously defined significance.

When the time of electrolysis is short (<180 s) only the first term is required, and if literature arguments are agreed to (12, 13) the effect of migration is taken care of by multiplying the whole expression by one minus the transport number of the electro-active ion ($1 - t_+$) in this case. Clearly this modification to the diffusion expression cannot suffice in the cases of a constant concentration gradient where t_+ must approach one and t_-, zero. This condition arises because since the anion cannot be discharged it ceases to migrate or diffuse and (at least in the bulk) merely provides electroneutrality as required.

Some optical problems require discussion. McLarnon, Muller, and Tobias have shown (14) that in thick interferometric cells, the point on which one focusses the optical recording device (a film or video camera) is important and that for any cell with a high refractive index gradient corrections are necessary to the position of the electrode and the value found for the concentration. However, errors in analysis in their paper for our thin cells used under the present conditions (low concentration, low current density, and low concentration or refractive index gradient) are less than the experimental errors encountered in hand measurements which are about $\pm 1\%$. We have, therefore, made no calculated corrections although much simpler, and for our systems, satsifactory methods have been evolved (12). In one of these systems, two selected points on an interference fringe at different distances from the electrode are evaluated for ΔC. The time is known and x is selected so using the ΔC calculated from the interference fringe, the current density, I, can be calculated from eq. [2] for each point. If the two c.d.'s are not the same, then a small increment of x is added at the anode (or subtracted at the cathode) successively until the c.d.'s approach each other which they must do in these galvanostatic experiments. Usually a minimum difference in current density is quickly found (4–6 trials) and the concentration gradient can be replotted using the new values of x.

Experimental concentrations were calculated in the usual way (4, 15, 16).

Experimental

Gels of 0.3% by weight agar containing also 0.1 *M* $ZnSO_4$ were difficult to cast in an interferometer where some wedge adjustments must be made. The liquid gel was introduced by syringe into the cell and adjustments made before and during solidification. The gel was very fragile and frequently fractures would occur and hence fringes were often unsatisfactory because they were discontinuous or blurred in some part of their length.

The cell was similar to those often described (1, 4, 16).

The zinc electrodes were recast from 99.999% pure Zn supplied by Cominco Ltd. (Trail, B.C.) to ensure a fine-grained structure. Both electrodes were mechanically polished on 600 grit emergy paper before use. All solutions were made from Analar grade materials and four times distilled water. All runs were done at a room temperature of 22 ± 0.5°C.

Only short times in some very long runs were analysed for this paper.

The electrodes were horizontal, cathode over anode, were 8 mm apart and each was 3 mm thick.

Results and discussion

It is generally considered that agar gels of less than 1% should behave as if the solution were liquid (17). This was found to be a good approximation both as regards the appearance of interferograms as shown in Fig. 1 and in a plot of the results Fig. 2, if convection is assumed absent.

Figure 1 shows interferograms at elapsed times of electrolysis of zero, 15 s, 60 s, and 180 s in the gelled electrolyte at 0.5 $mA\ cm^{-2}$. The concentration gradient can be seen to develop in a normal way for convectionless sytems with times elapsed. Figure 2 is a plot of concentration change vs. distance out from the electrode. The three times associated with the interferograms in Fig. 1 are plotted; 15 s, 60 s, and 180 s and values calculated from eq. [2] are also plotted for comparison. The experimental and calculated values obviously have the same form and the actual values agree to about within 15%, the largest absolute discrepancies being the value at the electrode surface. This discrepancy is greatest at the cathode. At both electrodes, the discrepancy at the electrode surface becomes a smaller fraction of the reading with time. Since the concentration of Zn^{2+} is 0.1 *M* and at the natural pH of 4.7 the H^+ is $\sim 2 \times 10^{-5}$ *M*, the hydrogen ion which has a molar refraction

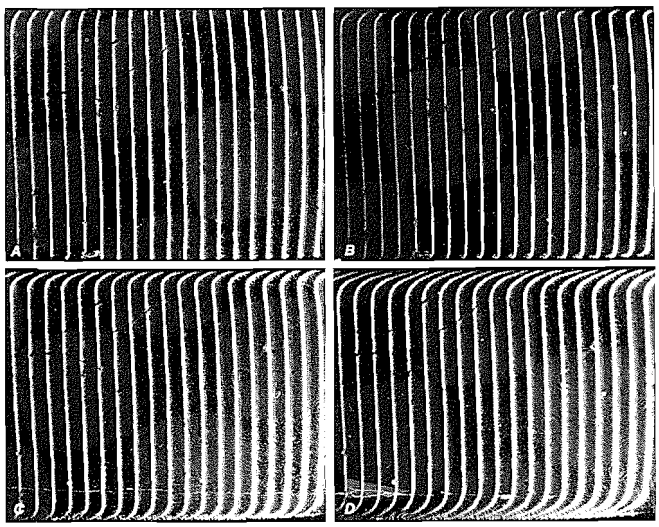

FIG. 1. Panels *a–d* show interferograms at zero, 15 s, 60 s and 120 s elapsed time of electrolysis in 0.3% agar gel, 0.1 *M* $ZnSO_4$ solution in the system $Zn/ZnSO_4/Zn$ at 22 ± 0.5°C and 0.5 mA cm^{-2} current density. The electrodes are 8 mm apart.

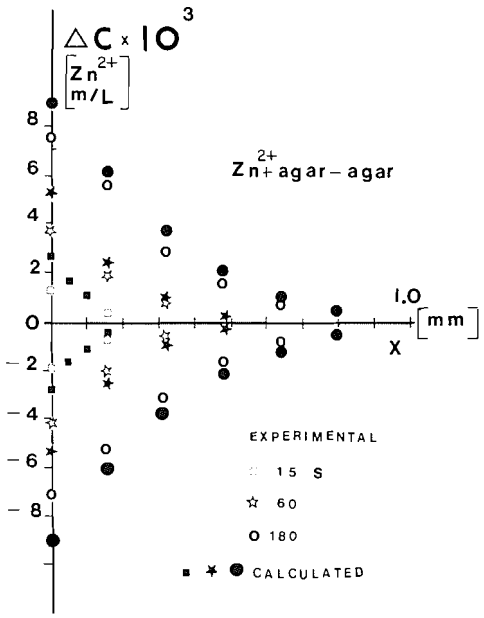

FIG. 2. Concentration change vs. distance vertically from the electrode face at three times of electrolysis, experimental and calculated values.

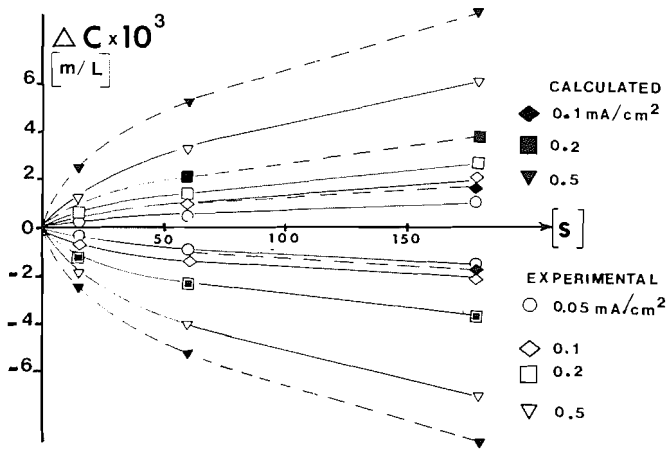

FIG. 3. Concentration change vs. time, calculated and experimental for three current densities.

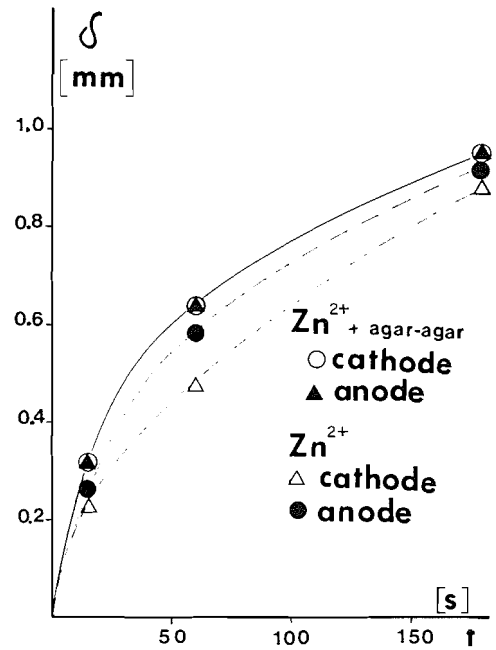

FIG. 4. Diffusion layer thickness vs. time of electrolysis in gelled and liquid electrolyte.

(14) of ~ −0.5 (compared to zinc ion at ~ +0.3) will lower the apparent concentration change at the cathode as calculated from the refractive index of the solution near the cathode (see Appendix 1). Since the mobility of the hydrogen ion is much larger than the zinc ion the effect of hydrogen ion migrating to the cathode but not being reduced and therefore forming a steep concentration gradient would be to lower the refractive index (and apparent concentration). At shorter times and shorter distances this is the effect noted, which agrees with previous work on pH changes at working electrodes (15). It is also an assumption in Wagner's electro-neutrality argument (16).

At the anode, the hydroxyl ion has greater mobility than the sulfate ion and their molal refractions are 5.15 and 7.36 respectively and again it would be expected the ΔC values would be too low especially at short times and small distances from the anode. This appears to be the case, and again this agrees with other experimental findings (13, 20, 21). At approximately 0.15 mm, these effects seem to have disappeared.

Figure 3 shows the value of ΔC at the electrode surface for 0.1, 0.2, and 0.5 mA cm^{-2} plotted against time with the calculated values also plotted. The plot shows that absolute differences increase but the relative error at the electrode decreases, the opposite tendency expected for optical anomalies (14). The D_{ZnSO_4} used was 6.87×10^{-5} cm^2 s^{-1} calculated from its infinite dilution conductivity; the anion transport number used was 0.616. Since both are limiting values, they are probably a little too high.

The thickness of the diffusion layer with time should be the same for liquid and gelled electrolytes if agar does not change the mobilities. Figures 4 and 5 show that very little change can be noted, but perhaps the attainment of a slightly thicker layer at shorter times and perhaps a slightly greater slope to diffusion

Can. J. Chem. Downloaded from www.nrcresearchpress.com by 210.87.254.40 on 09/06/12
For personal use only.

Can. J. Chem. Downloaded from www.nrcresearchpress.com by 210.87.254.40 on 09/06/12
For personal use only.

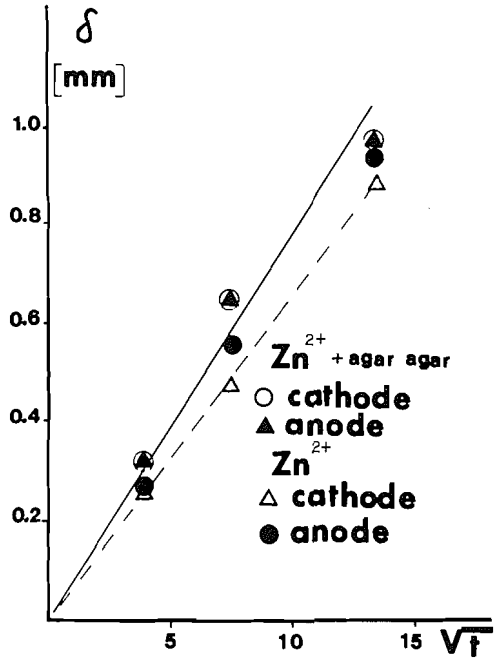

FIG. 5. Diffusion layer thickness vs. the square root of electrolysis time, experimental and calculated.

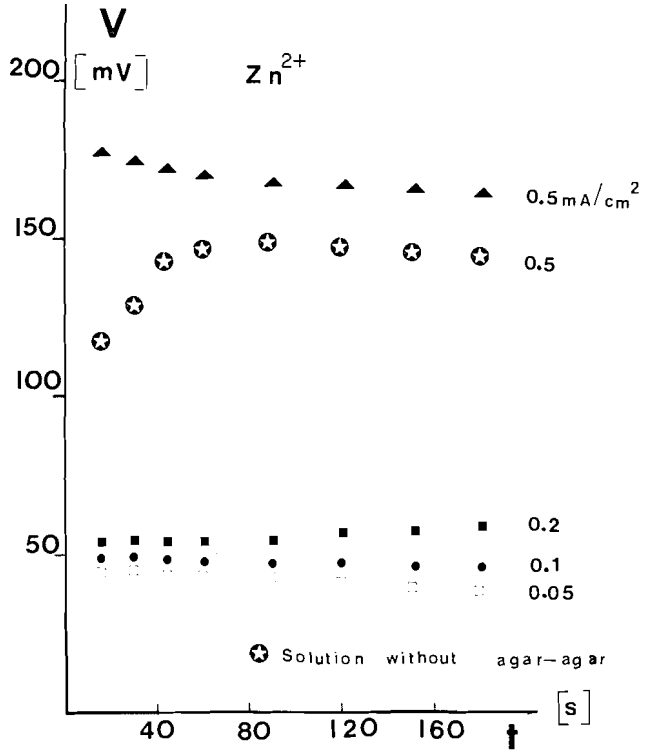

FIG. 6. Impressed potential to give various current densities vs. time.

layer thickness vs. the square root of time.[1] Figure 6 tends to confirm these results though for 0.2 mA cm^{-2}, polarisation increases with time. Concentrating on 0.5 mA cm^{-2} the liquid electrolyte conductivity (if impressed voltages are compared for identical runs in the same cell) appears to go through a maximum whereas with agar the conductivity appears to increase.[2] If hydrogen ions are associated with the polysaccharide agar then because a certain time of residence is implied and hence a slowing of the rate of migration and diffusion of hydrogen, it seems reasonable that conductivity should increase rather than go through a maximum. Note also that the conductivity and polarisation of the gelled solutions settles to about 11% less than the liquid electrolyte. Clearly Walden's rule ($\Lambda\eta = k$) is not obeyed, nor should it be expected to be obeyed in such gels. Finally Zn^{2+} is not paramagnetic and so does not give a magnetic fluid in solution and the observed magnetic field induced convection in Cu^{2+} solutions should not occur (22, 23).

Conclusions

At short times of electrolysis, gelled electrolytes at least in the $Zn/ZnSO_4/Zn$ system behave in a closely similar way to the liquid electrolyte. It can therefore be concluded that gelling with small amounts of polysaccharides, in this case agar, does not change the diffusion coefficient very much. This implies that the very open network of polysaccharide molecules which causes the gelling must allow solvated molecules and some ions almost free passage.

It is concluded that convection is absent in parallel plate horizontal electrodes in the cathode over anode configuration. The conductivity, concentration profiles and diffusion layer thickness all conform with these predicted by the transient diffusion expression as well as can be expected in its present imperfect form. It now seems possible that transport numbers will become available by calculation. Also the state of non-semi-infinite diffusion can be confidently approached.

Acknowledgement

This work was supported by an Operating Grant supplied by the Natural Science and Engineering Research Council of Canada to whom our thanks are due.

1. (*a*) R. N. O'BRIEN, W. R. YAKYMYSHYN, and J. LEJA. J. Electrochem. Soc. **110**, 820 (1963); (*b*) R. N. O'BRIEN. J. Electrochem. Soc. **119**, 589 (1972).
2. R. N. O'BRIEN. J. Electrochem. Soc. **114**, 710 (1967).
3. R. N. O'BRIEN, S. VISAISOUK, R. RAINE, and D. F. ALDERDICE. J. Fish Res. Board Can. **35**, 1316 (1976).
4. R. N. O'BRIEN. J. Electrochem. Soc. **113**, 289 (1966).
5. R. N. O'BRIEN and K. J. LUSHINGTON. Nature, London, Phys. Sci. **243**, 117 (1973).
6. R. N. O'BRIEN and H. KOLNY. Can. J. Chem. **56**, 591 (1978).
7. C. WAGNER. Trans. Electrochem Soc. **95**, 161 (1949).
8. T. R. ROSEBRUGH and W. J. MILLER. J. Phys. Chem. **14**, 816 (1910).
9. C. R. WILKE, M. EISENBERG, and C. W. TOBIAS. J. Electrochem. Soc. **100**, 513 (1953).
10. R. N. O'BRIEN and L. M. MUKHERJEE. J. Electrochem. Soc. **111**, 1358 (1964).
11. R. N. O'BRIEN, B. B. KULKARNI, W. MICHALIK, and K. S. V. SANTHANAM. Can. J. Chem. **59**, 1933 (1981).
12. C. W. TOBIAS, M. EISENBERG, and C. R. WILKE. J. Electrochem. Soc. **98**, 359C (1952).
13. J. NEWMAN. Transport processes in advances in electrochemistry and electrochemical engineering. Vol. 5. *Edited by* Paul Delahay

[1] Note that for agar-agar solution the thicknesses of diffusion layers for both anode and cathode are the same within 180 s of electrolysis.

[2] In both solutions, aqueous and agar-agar, the polarisation is a diffusion polarisation (see Fig. 5) and the gradient of concentration at the surface is very similar. Therefore the differences in the applied voltage could be referred to the differences in the conductivity of these solutions.

and C. W. Tobias. Wiley, NY. 1967. p. 96.
14. F. R. McLarnon, R. H. Muller, and C. W. Tobias. J. Electrochem. Soc. **122**, 59 (1975).
15. R. N. O'Brien and H. Kolny. Corrosion, **34**, 262 (1978).
16. R. N. O'Brien. Rev. Sci. Instrum. **35**, 803 (1964).
17. B. M. Shukla and V. N. Singh. Proc. Chem. Symp. 2nd, 1970, (Pub. 1971), **2**, 317 (Madras).
18. K. Fajans and R. Luhdeman. Z. Physik. Chem. **1329**, 150 (1935).
19. M. N. Polukarpov. J. Gen. Chem. USSR, **19**, al-a 28 (1949).
20. R. N. O'Brien, J. Leja, and E. A. Beer. J. Electrochem. Soc. **121**, 370 (1974).
21. W. F. Yakymyshyn. M.Sc. Thesis, University of Alberta, Edmonton, Alta. 1962. p. 60 at seq.
22. R. N. O'Brien and K. S. V. Santhanam. J. Electrochem. Soc. **129**, 1266 (1982).
23. R. N. O'Brien and K. S. V. Santhanam. Magnetic field effects in the C/A position. To be published.

Appendix

Polukarpov (19) found changes up to 4 pH units at the electrodes at high current densities using a universal indicator. If a pH change of 2 units at each electrode is assumed (cathode $4.7 \rightarrow 2.7$, anode $4.7 \rightarrow 6.7$), the refractive index change can be calculated. Remembering the Lorentz–Lorentz expression

$$R = \frac{M}{P}\left(\frac{n^2 - 1}{n^2 + 2}\right)$$

and for mixtures (solutions)

$$R_{sp} = \frac{p_1 R_1 + p_2 R_2 + \ldots}{p_1 + p_2}$$

where R is the molar refraction (cm^3), M the molecular weight (g), ρ the density (g cm^{-3}), n the refractive index (a ratio), R_{sp} the specific refraction, and p the proportion of the material (ion) present, and assuming electrical neutrality so that the change in hydrogen concentration ($\sim 2 \times 10^{-3}\ M$) is subtracted from the change in zinc ion concentration ($\sim 7.2 \times 10^{-3}\ M$) to give $[Zn^{2+}] \simeq 7.0 \times 10^{-3}$, then

$$\Delta C_{exp} = \frac{2 \times 10^{-3}(-0.5) + 5.2 \times 10^{-3}(0.3)}{7.2 \times 10^{-3}(0.3)} \times 9.0 \times 10^{-3}$$
$$= 2.33 \times 10^{-3}$$

which is much too low compared to 7.2×10^{-3} found and 9.0×10^{-3} calculated. For $\Delta pH = 2$ pH units

$$\Delta C_{exp} = \frac{2 \times 10^{-4}(-0.5) + 7.0 \times 10^{-3}(0.3)}{7.2 \times 10^{-3}(0.3)} \times 9.0 \times 10^{-3}$$
$$= 8.33 \times 10^{-3}\ M$$

which is too large. A pH of 3.3 would give almost the exact value or a change of 1.4 pH units which does not seem improbable.

At longer times it would be expected that the discrepancies would become smaller because the faster diffusing hydrogen ion would now replace the zinc ion. It should also be remembered the sulfate ion has a higher diffusion constant than zinc and a higher refractive index. The complications of the sulfate–bisulfate equilibrium have been dealt with by Newman (13) but, we believe, do not really alter the basic argument.

Can. J. Chem. Downloaded from www.nrcresearchpress.com by 210.87.254.40 on 09/06/12
For personal use only.

Thermodynamics of ternary mixtures of non-electrolytes: excess volumes

PREM P. SINGH[1] AND VINOD K. SHARMA

Chemistry Department, Maharshi Dayanand University, Rohtak-124001 (Haryana), India

Received September 9, 1982[2]

PREM P. SINGH and VINOD K. SHARMA. Can. J. Chem. **61**, 2321 (1983).

Molar excess volumes, V^E_{ijk}, of some $(i + j + k)$ ternary mixtures of non-electrolytes have been determined dilatometrically at 298.15 and 308.15 K and the same have been analysed in terms of (*a*) Lacombe and Sanchez theory and (*b*) an approach based on the mathematical discipline of graph theory utilizing information on the $(i + j)$, $(j + k)$, and $(k + i)$ binary mixtures alone. It has been observed that the V^E_{ijk} data predicted by the graph theoretical approach employing the graph theoretical binary interaction coefficients α_{ij}, α_{jk}, and α_{ki} compare better with the corresponding experimental values than the V^E_{ijk} values predicted by Lacombe and Sanchez theory utilizing Lacombe and Sanchez's binary interaction coefficients χ_{ij}, χ_{jk}, and χ_{ki} of the $(i + j)$, $(j + k)$, and $(k + i)$ mixtures. The V^E_{ijk} data have also been utilized to extract, via the Mayer–McMillan approach, self and cross volume interaction coefficients V_{jj}, V_{kk}, V_{jk}, V_{jjk}, and V_{jkk} and the V_{jk} values have been utilized to study molecular interactions between the *j*th and the *k*th components in the presence of the *i*th component of these $(i + j + k)$ mixtures.

PREM P. SINGH et VINOD K. SHARMA. Can. J. Chem. **61**, 2321 (1983).

On a déterminé les volumes molaires en excès V^E_{ijk} de quelques mélanges ternaires $(i + j + k)$ de non électrolytes, par dilatométrie à 298,15 et 308,15 K et on les a analysés (*a*) en fonction de la théorie de Lacombe et Sanchez et (*b*) en fonction d'une approche basée sur la théorie graphique qui utilise l'information relative à $(i + j)$, $(j + k)$ et $(k + i)$ des mélanges binaires seuls. On a observé que les données de V^E_{ijk} prédites par l'approche de la théorie graphique qui utilise la courbe théorique des coefficients d'interaction binaire α_{ij}, α_{jk} et α_{ki} s'approchent d'avantage des valeurs expérimentales correspondantes que les valeurs de V^E_{ijk} prédites par la théorie de Lacombe et Sanchez χ_{ij}, χ_{jk} et χ_{ki} des mélanges de $(i + j)$, de $(j + k)$ et de $(k + i)$. On a également utilisé les données de V^E_{ijk} pour obtenir, via l'approche de Mayer–McMillan, les coefficients d'interaction du volume et du covolume V_{jj}, V_{kk}, V_{jk}, V_{jjk} et V_{jkk}. On a utilisé la valeur de V_{jk} pour étudier l'interaction moléculaire entre les composants *j*th et *k*th en présence des *i*th composants de ces mélanges de $(i + j + k)$.

[Traduit par le journal]

Introduction

Thermodynamics of ternary mixtures of non-electrolytes has not received as much attention as the thermodynamics of binary mixtures in spite of the fact that all thermodynamic properties of ternary mixtures should, in principle, be determinable from the properties of the respective binary mixtures. Lacombe and Sanchez have recently formulated a unified molecular theory (1, 2) of fluids and fluid mixtures which defines the thermodynamic properties of ternary and higher order mixtures in terms of the pure fluid parameters and the binary interaction coefficients. This theory (2) has been shown (2–4) to be quite successful to predict molar excess volumes, V^E, and molar excess enthalpy, H^E, of a number of binary mixtures of non-electrolytes. More recently, an approach employing the graph theoretical concept of connectivity parameters has been successfully applied (5, 6) to predict V^E and H^E of quite a number of binary mixtures of non-electrolytes. This approach (5, 6) can be easily extended to ternary mixtures of non-electrolytes. It would, therefore, be interesting to see how these two approaches explain the V^E_{ijk} data of ternary $(i + j + k)$ mixtures of non-electrolytes.

Experimental

Materials and their purification

Benzene (B.D.H. A.R. grade) was purified following the method of Rastogi and Nigam (7). Toluene, *o*- and *p*-xylene (B.D.H., A.R. grade) were purified as suggested by Vogel (8). Methylene bromide (V/O Sojuzchimeyport, Moscow) was purified by treating with 5% sodium carbonate solution. If was then washed with water followed by drying over anhydrous calcium chloride and fractionally distilled.

The purity of the treated samples was checked by measuring their densities at 298.15 ± 0.01 K and they agreed to within ±0.00005 g cm^{-3} with the corresponding literature values (9–11). (The density of methylene bromide at 298.15 ± 0.01 K was obtained from the density vs. temperature plot; the necessary density data were taken from literature (11)).

Excess volumes were determined in a dilatometer similar to that used by Brown and Smith (12); the only difference being that there were now three limbs for the three components. The temperature of the bath was controlled to better than ±0.01 K by means of a toluene regulator. In order to ensure that the liquid in the capillary stem had the same composition as that of the bulk solution on mixing, the dilatometer (after mixing the components) was placed in a cold bath so that there was minimum liquid in the capillary and then again placed in the experimental water bath. This process was repeated twice or thrice. The uncertainty in our measured excess volumes is about 0.5%.

Results

V^E_{ijk} data for the various ternary mixtures as a function of composition at 298.15 and 308.15 K are recorded in Table 1 and are expressed (13) as

$$[1]\quad V^E_{ijk} = x_ix_j[A_{ij} + B_{ij}(x_i - x_j) + C_{ij}(x_i - x_j)^2] + x_jx_k[A_{jk} + B_{jk}(x_j - x_k) + C_{jk}(x_j - x_k)^2] + x_ix_k[A_{ik} + B_{ik}(x_i - x_k) + C_{ik}(x_i - x_k)^2] + x_ix_jx_k[A_{ijk} + B_{ijk}(x_j - x_k)x_i + C_{ijk}(x_j - x_k)^2x_i^2]$$

where x_i and x_j are the mole fractions of the *i*th and the *j*th components in the $(i + j + k)$ ternary mixture and A, B, and C are parameters characteristic of the $(i + j)$, $(j + k)$, and $(k + i)$ binary mixtures and are taken from literature (14). The A_{ijk}, B_{ijk}, and C_{ijk} coefficients of [1] are evaluated by fitting the V^E_{ijk} data to [2].

$$[2]\quad [V^E_{ijk} - \{x_ix_j(A_{ij}B_{ij}(x_i - x_j) + C_{ij}(x_i - x_j)^2) + x_jx_k(A_{jk} + B_{jk}(x_j - x_k) + C_{jk}(x_j - x_k)^2) + x_ix_k(A_{ik} + B_{ik}(x_i - x_k) + C_{ik}(x_i - x_k)^2)\}]/x_ix_jx_k = [A_{ijk} + B_{ijk}(x_j - x_k)x_i + C_{ijk}(x_j - x_k)^2x_i^2]$$

[1]To whom all correspondence should be addressed.

[2]Revision received March 15, 1983.

Can. J. Chem. Downloaded from www.nrcresearchpress.com by 210.87.254.40 on 09/06/12
For personal use only.

TABLE 1. Comparison of the measured V^E_{ijk} values for the various $(i + j + k)$ ternary mixtures at 298.15 and 308.15 K with their corresponding V^E_{ijk} values as evaluated from the Graph theory and the Lacombe and Sanchez theory

x_i	x_j	V^E_{ijk} cm^3 mol^{-1} Exptl.	"Graph"	Lacombe and Sanchez
Methylene bromide (i) + benzene (j) + toluene (k)				
Temperature 298.15 K				
$\alpha_{ij} = -6.7568$ cm^3 mol^{-1}, $\alpha_{jk} = -10.7167$ cm^3 mol^{-1}, $\alpha_{ki} = -2.7728$ cm^3 mol^{-1}				
0.0681	0.6597	0.100	0.065	0.068
0.1224	0.7688	0.088	0.145	0.075
0.1486	0.3086	0.147	0.140	0.121
0.1801	0.1801	0.142	0.147	0.205
0.2251	0.4615	0.192	0.156	0.052
0.3012	0.4036	0.205	0.177	0.342
0.3883	0.0971	0.197	0.252	0.197
0.4817	0.0459	0.194	0.213	0.160
0.6327	0.0680	0.185	0.275	0.256
0.6820	0.1424	0.188	0.225	0.320
0.6885	0.2156	0.184	0.183	0.242
0.7232	0.1132	0.163	0.217	0.266
0.7445	0.1940	0.163	0.155	0.195
Temperature 308.15 K				
$\alpha_{ij} = -7.2823$ cm^3 mol^{-1}, $\alpha_{jk} = -11.2151$ cm^3 mol^{-1}, $\alpha_{ki} = -2.5381$ cm^3 mol^{-1}				
0.1633	0.7313	0.168	0.091	0.114
0.1835	0.0780	0.137	0.155	0.224
0.1942	0.5993	0.212	0.122	0.130
0.2570	0.0878	0.174	0.202	0.211
0.3035	0.4125	0.289	0.183	0.398
0.3766	0.4156	0.234	0.193	0.149
0.4206	0.1786	0.225	0.254	0.230
0.4327	0.1345	0.225	0.266	0.231
0.6344	0.1807	0.235	0.236	0.256
0.7174	0.1884	0.212	0.186	0.182
Methylene bromide (i) + benzene (j) + o-xylene (k)				
Temperature 298.15 K				
$\alpha_{ij} = -6.7568$ cm^3 mol^{-1}, $\alpha_{jk} = -7.0218$ cm^3 mol^{-1}, $\alpha_{ki} = -2.2435$ cm^3 mol^{-1}				
0.0873	0.2852	0.281	0.168	0.141
0.1011	0.4942	0.316	0.186	0.135
0.1018	0.8175	0.132	0.088	0.172
0.2000	0.0550	0.242	0.231	0.210
0.2598	0.3039	0.375	0.286	0.140
0.4249	0.0829	0.341	0.391	0.287
0.6804	0.1421	0.240	0.336	0.346
0.7039	0.2402	0.237	0.188	0.175
0.7142	0.1118	0.265	0.338	0.348
0.7444	0.1260	0.229	0.290	0.244
0.7516	0.1242	0.224	0.284	0.253
0.7615	0.0929	0.216	0.312	0.348
0.9112	0.0541	0.090	0.118	0.213
Temperature 308.15 K				
$\alpha_{ij} = -7.2823$ cm^3 mol^{-1}, $\alpha_{jk} = -8.1301$ cm^3 mol^{-1}, $\alpha_{ki} = -3.4653$ cm^3 mol^{-1}				
0.0795	0.8493	0.133	0.075	0.113
0.1522	0.1043	0.246	0.197	0.146
0.1631	0.6474	0.251	0.169	0.169
0.1966	0.2247	0.295	0.251	0.275
0.2490	0.6652	0.247	0.145	0.164
0.3247	0.4188	0.325	0.273	0.224
0.3616	0.3405	0.329	0.307	0.278
0.4667	0.0788	0.403	0.410	0.465
0.4805	0.0996	0.400	0.409	0.281
0.7533	0.1349	0.254	0.201	0.373
Methylene bromide (i) + benzene (j) + p-xylene (k)				
Temperature 298.15 K				
$\alpha_{ij} = -6.7568$ cm^3 mol^{-1}, $\alpha_{jk} = -8.5182$ cm^3 mol^{-1}, $\alpha_{ki} = -2.7728$ cm^3 mol^{-1}				
0.1299	0.3636	0.275	0.178	0.231
0.1346	0.1394	0.198	0.169	0.249
0.2009	0.2320	0.278	0.223	0.249
0.2356	0.4800	0.308	0.270	0.270
0.4356	0.5052	0.256	0.166	0.185
0.4599	0.1497	0.323	0.353	0.409
0.5751	0.1658	0.313	0.340	0.313
0.6022	0.2486	0.293	0.269	0.454
0.6927	0.1265	0.250	0.310	0.414
0.7131	0.1148	0.240	0.304	0.371
0.7515	0.0785	0.222	0.305	0.260
Temperature 308.15 K				
$\alpha_{ij} = -7.2823$ cm^3 mol^{-1}, $\alpha_{jk} = -8.1301$ cm^3 mol^{-1}, $\alpha_{ki} = -3.4654$ cm^3 mol^{-1}				
0.0795	0.1452	0.181	0.125	0.112
0.1223	0.5053	0.253	0.172	0.133
0.1485	0.6733	0.226	0.141	0.189
0.1793	0.1087	0.268	0.213	0.222
0.2063	0.6985	0.216	0.181	0.147
0.2121	0.2662	0.285	0.244	0.266
0.3095	0.1488	0.314	0.311	0.291
0.4084	0.3664	0.301	0.277	0.351
0.5600	0.3224	0.269	0.245	0.288
0.8204	0.0531	0.175	0.270	0.342
0.8304	0.0530	0.163	0.256	0.214
Methylene bromide (i) + toluene (j) + o-xylene (k)				
Temperature 298.15 K				
$\alpha_{ij} = -2.5380$ cm^3 mol^{-1}, $\alpha_{jk} = -4.1818$ cm^3 mol^{-1}, $\alpha_{ki} = -2.2435$ cm^3 mol^{-1}				
0.0988	0.5872	0.112	0.080	0.075
0.1079	0.0980	0.132	0.083	0.109
0.1314	0.7371	0.104	0.142	0.119
0.2222	0.6358	0.154	0.101	0.107
0.2624	0.3394	0.235	0.141	0.127
0.3390	0.4068	0.229	0.155	0.144
0.4314	0.0755	0.306	0.219	0.209
0.4820	0.0270	0.297	0.246	0.239
0.6708	0.1215	0.248	0.213	0.268
0.6712	0.1963	0.213	0.188	0.262
0.6804	0.1302	0.237	0.210	0.256
0.7418	0.0904	0.212	0.207	0.290
0.8606	0.0801	0.117	0.122	0.247
Temperature 308.15 K				
$\alpha_{ij} = -3.5669$ cm^3 mol^{-1}, $\alpha_{jk} = -3.2727$ cm^3 mol^{-1}, $\alpha_{ki} = -2.7390$ cm^3 mol^{-1}				
0.1025	0.1393	0.118	0.076	0.154
0.1111	0.5960	0.108	0.074	0.065
0.1177	0.7588	0.087	0.063	0.080
0.1791	0.3806	0.168	0.115	0.100
0.2686	0.2514	0.243	0.170	0.169
0.3132	0.0824	0.228	0.189	0.195
0.4491	0.5085	0.193	0.148	0.141
0.6577	0.1351	0.282	0.229	0.269
0.7489	0.0866	0.246	0.213	0.301
0.7876	0.0929	0.213	0.186	0.262

Can. J. Chem. Downloaded from www.nrcresearchpress.com by 210.87.254.40 on 09/06/12
For personal use only.

TABLE 1 *(Concluded)*

x_i	x_j	V^E_{ijk} cm^3 mol^{-1} Exptl.	"Graph"	Lacombe and Sanchez	x_i	x_j	V^E_{ijk} cm^3 mol^{-1} Exptl.	"Graph"	Lacombe and Sanchez
Methylene bromide (i) + toluene (j) + p-xylene (k)									
Temperature 298.15 K, $\alpha_{ij} = -2.5380$ cm^3 mol^{-1}, $\alpha_{jk} = -4.3372$ cm^3 mol^{-1}, $\alpha_{ki} = -2.7728$ cm^3 mol^{-1}					Temperature 308.15 K, $\alpha_{ij} = -3.5669$ cm^3 mol^{-1}, $\alpha_{jk} = -4.5652$ cm^3 mol^{-1}, $\alpha_{ki} = -2.7728$ cm^3 mol^{-1}				
0.0452	0.1256	0.048	0.041	0.081	0.1018	0.0619	0.144	0.069	0.192
0.0497	0.5404	0.060	0.034	0.075	0.1040	0.5954	0.083	0.064	0.080
0.0529	0.3647	0.054	0.037	0.125	0.1090	0.2756	0.146	0.073	0.056
0.1464	0.7951	0.099	0.069	0.098	0.1357	0.1709	0.138	0.067	0.072
0.2443	0.5622	0.180	0.127	0.257	0.1429	0.7566	0.120	0.072	0.124
0.2476	0.2136	0.168	0.168	0.210	0.2319	0.3237	0.186	0.133	0.183
0.3860	0.0755	0.255	0.183	0.345	0.3787	0.2485	0.230	0.188	0.152
0.6330	0.3085	0.213	0.158	0.198	0.3827	0.5663	0.184	0.148	0.141
0.6849	0.1279	0.218	0.188	0.344	0.5352	0.1351	0.190	0.228	0.083
0.6969	0.0970	0.220	0.193	0.383	0.7188	0.1071	0.208	0.207	0.209
0.7515	0.0654	0.209	0.184	0.286	0.8024	0.1138	0.137	0.159	0.177
0.7615	0.1590	0.182	0.149	0.311					
0.8254	0.0873	0.140	0.136	0.270					

by the method of least squares and are recorded together with the standard deviation, $\sigma(V^E_{ijk})$ defined by

$$\sigma(V^E_{ijk}) = \left[\frac{\Sigma(V^E_{ijk(\text{expt})} - V^E_{ijk} \text{ from [1]})^2}{m - n}\right]^{1/2}$$

where m is the number of data points and n is the number of adjustable parameters in [1], in Table 2.

Discussion

We are unaware of any V^E data with which to compare our results for these $(i + j + k)$ mixtures.

The V^E_{ijk} data for these mixtures are analysed with Lacombe and Sanchez theory of classical fluids (1) and their mixtures (2). While the classical theory of pure fluids (1) characterizes the model fluid as an Ising or Lattice fluid (this approach has been shown (1) to be capable of describing the thermodynamic properties of a large variety of fluids), the mixture theory (2) is akin to the lattice theory of Flory and Huggins (14) but differs in the most important aspect of making an allowance for empty lattice sites thereby allowing volume change on mixing. This theory (2) expresses the molar excess volume, V^E_{ijk}, of a ternary mixture by

$$[3] \quad V^E_{ijk} = r_{\text{mix}} v^*_{\text{mix}}[\tilde{v}_{\text{mix}} - \sum_i \phi_i \tilde{v}_i]$$

where

$$[4] \quad \phi_i = m_i(\rho^*_i)^{-1}(\Sigma(m_i/\rho^*_i)^{-1})$$

$$[5] \quad m_i = x_i M_i(\Sigma x_i M_i)^{-1}$$

$$[6] \quad r_{\text{mix}} = \Sigma x_i r_i$$

$$[7] \quad r_i = r^0_i(v^*_i(v^*_{\text{mix}})^{-1})$$

$$[8] \quad v^*_{\text{mix}} = \Sigma \phi^0_i v^*_i$$

$$[9] \quad \phi^0_i = m_i(\rho^*_i v^*_i)^{-1}/\sum_i (m_i/\rho^*_i v^*_i)$$

$$[10] \quad \tilde{v}_{\text{mix}} = 1/\tilde{\rho}_{\text{mix}}$$

and all the terms have the same significance as described by Lacombe and Sanchez (2).

Evaluation of V^E_{ijk} by [3] requires a knowledge of $\tilde{\rho}_{\text{mix}}$, the reduced density of the mixture, which in principle could be calculated from the following equation of state of the mixture

$$[11] \quad (\tilde{\rho}_{\text{mix}})^2 + \tilde{P} + \frac{RT}{\epsilon^*_{\text{mix}}}[\ln(1 - \tilde{\rho}_{\text{mix}}) + (1 - \frac{1}{r_{\text{mix}}})\tilde{\rho}_{\text{mix}}] = 0$$

where

$$[12] \quad \epsilon^*_{\text{mix}} = \sum_i \phi_i \epsilon^*_{ii} - RT \Sigma\Sigma \phi_i \phi_j \chi_{ij}$$

$$[13] \quad \chi_{ij} = (\epsilon^*_{ii} + \epsilon^*_{jj} - 2\epsilon^*_{ij})/RT$$

and

$$[14] \quad \tilde{P} = P v^*_{\text{mix}}/\epsilon^*_{\text{mix}}$$

but this would require a knowledge of binary interaction energies ϵ^*_{ij}, ϵ^*_{jk}, ϵ^*_{ik} of the $(i + j)$, $(j + k)$, and $(i + k)$ binary mixtures. Such information, however, is not readily available but could be obtained from a single molar excess enthalpy datum of each of these binary mixtures by means of [11] and [15]. Since the calculations in this process are too involved, a simple approach (3) would be to evaluate ϵ^*_{ij}, ϵ^*_{jk}, and ϵ^*_{ik} for these binary mixtures from their single molar excess enthalpy, H^E, and molar excess volume, V^E, datum at $x = 0.5$ at one temperature T only by means of

$$[15] \quad H^E_{(i+j)} = 2\phi_i \phi_j r_{\text{mix}} \tilde{\rho}_{\text{mix}}[\epsilon^*_{ii} + \epsilon^*_{jj} - 2\epsilon^*_{ij}] + RTr_{\text{mix}}\left[\sum_i \left(\frac{\phi_i \tilde{\rho}_i - \tilde{\rho}_{ij}\phi_i}{T_i}\right)\right]$$

where

$$[16] \quad \tilde{T}_i = RT/\epsilon^*_{ii}$$

and

$$[17] \quad \tilde{\rho}_{\text{mix}} = [\{V^E_{(i+j)}/(\Sigma x_i r^0_i(v^*_i/\Sigma \phi_i v^*_i))(\Sigma \phi_i v^*_i)\} + \Sigma \phi_i \tilde{v}_i]^{-1}$$

Once ϵ^*_{ij}, ϵ^*_{jk}, and ϵ^*_{ik} parameters of $(i + j)$, $(j + k)$, and $(i + k)$ binary mixtures are known, $\tilde{\rho}_{\text{mix}}$ for the $(i + j + k)$ mixture

Can. J. Chem. Downloaded from www.nrcresearchpress.com by 210.87.254.40 on 09/06/12
For personal use only.

Can. J. Chem. Downloaded from www.nrcresearchpress.com by 210.87.254.40 on 09/06/12
For personal use only.

TABLE 2. Values of A, B, C parameters* of eq. [1] for the various $(i + k)$, $(j + k)$, and $(k + i)$ binary mixtures of the $(i + j + k)$ mixtures along with those of the $(i + j + k)$ mixtures together with the standard deviations $\sigma(V^E_{ijk})$ of V^E_{ijk}

System	T (K)	A	B	C	$\sigma(V^E_{ijk})$ (cm^3 mol^{-1})
Methylene bromide (i) +	298.15	−0.065	−0.8822	−23.9125	0.002
benzene (j) + toluene (k)	308.15	−1.0872	7.0868	6.0547	0.003
Methylene bromide (i) +	298.15	1.023	5.3398	23.4075	0.003
benzene (j) + o-xylene (k)	308.15	−1.4774	−4.0434	63.2566	0.003
Methylene bromide (i) +	298.15	0.6743	1.749	8.9192	0.003
benzene (j) + p-xylene (k)	308.15	−1.838	5.2633	−6.515	0.003
Methylene bromide (i) +	298.15	0.2942	−3.4533	−6.546	0.003
toluene (j) + o-xylene (k)	308.15	−1.2333	−7.3866	−107.45	0.004
Methylene bromide (i) +	298.15	2.6315	4.9187	4.7452	0.003
toluene (j) + p-xylene (k)	308.15	−1.2697	23.1512	−247.574	0.003
Methylene bromide (i) +	298.15†	0.8600	0.200	−0.3750	0.001
benzene (j)	308.15†	0.9655	0.0376	0.3222	0.001
Benzene (j) + toluene (k)	298.15†	0.3360	0.0001	−0.1313	0.0005
	308.15†	0.3600	0.0438	−0.1719	0.0006
Methylene bromide (i) +	298.15†	0.7400	0.0750	−0.0625	0.001
toluene (k)	308.15†	1.0400	0.0852	−0.1099	0.001
Benzene (j) + o-xylene (k)	298.15†	1.0600	0.05	−0.1875	0.001
	308.15†	1.0048	0.2150	−0.3819	0.001
Methylene bromide (i) +	298.15†	1.2400	0.0001	0.0002	0.001
o-xylene (k)	308.15†	1.4964	−0.01	−0.22	0.001
Benzene (j) + p-xylene (k)	298.15†	0.8400	0.1625	−0.1875	0.001
	308.15†	0.8200	0.1625	−0.1875	0.001
Methylene bromide (j) +	298.15†	1.1200	0.1600	0.0001	0.001
p-xylene (k)	308.15†	1.5600	−0.4200	0.006	0.001
Toluene (j) + o-xylene (k)	298.15†	0.1800	0.0015	−0.0594	0.0003
	308.15†	0.1444	0.0100	0.2000	0.0002
Toluene (j) + p-xylene (k)	298.15†	0.080	0.0001	−0.04	0.0001
	308.15†	0.084	0.0001	−0.03	0.0002

*The A, B, C parameters of [1] for the $(i + j)$, $(j + k)$, and $(k + i)$ mixtures denote here A_{ij}, B_{ij}, C_{ij} etc. (see text) while for the $(i + j + k)$ mixture they denote A_{ijk}, B_{ijk}, and C_{ijk} respectively.
†Reference 14.

can be evaluated from [11]−[14] and hence from a knowledge of a single V^E and H^E datum at a given temperature for an equimolar $(i + j)$, $(j + k)$, and $(i + k)$ binary mixtures it should be possible to predict V^E_{ijk} for a ternary $(i + j + k)$ mixture if it is assumed that the binary interaction coefficients χ_{ij}, χ_{jk}, and χ_{ik} for these binary mixtures are independent of composition and temperature and that these binary mixtures satisfy [11] for binary mixtures. It was, however, shown (14) that V^E and H^E values so calculated at 298.15 and 308.15 K from V^E and H^E (T = 308.15 K, x_i = 0.5) datum alone for (methylene bromide (i) + aromatic hydrocarbon (j or k) mixtures were in very poor agreement with the corresponding experimental values. This failure of the theory (2) was traced to the failure of these $(i + j$ or $k)$ mixtures to satisfy [11] for binary mixtures (perhaps due to weak donor−acceptor interactions between their j or k and i components). Consequently an alternate approach was employed to evaluate V^E or H^E values for these binary mixtures by first evaluating $\tilde{\rho}_{ij}$ and χ_{ij} through [15] and [17] utilizing the experimental V^E and H^E values for an equimolar mixture at 308.15 K and then employing them (i.e. $\tilde{\rho}_{ij}$ and χ_{ij}) to see how much the mixture deviated from [11]. (The extent to which the $(i + j)$, $(j + k)$, and $(i + k)$ binary mixtures deviated from [11] at 308.15 K (i.e. the right hand side of [11] for these mixtures) was found (14) to vary from 0.007 to 0.011). Knowing the right hand side of [11] for a binary mixture, $\tilde{\rho}_{ij}$ and hence V^E and H^E for the $(i + j)$ etc. mixture as a function of temperature and composition were shown (14) to be in reasonably good agreement with their corresponding experimental values. Since the $(i + j)$, $(j + k)$, and $(k + i)$ mixtures do not satisfy [11] but satisfy [18],

$$[18]\quad (\tilde{\rho}_{ij})^2 + \tilde{P}^2 + \frac{RT}{\epsilon^*_{mix}}[\ln(1 - \tilde{\rho}_{ij}) + (1 - r^{-1})\tilde{\rho}_{ij}] = 0.0071 \text{ to } 0.011$$

it follows that the $(i + j + k)$ mixtures would also not satisfy [11] and hence the V^E_{ijk} values predicted by [3] through [3]−[17] in the manner originally proposed by Sanchez and Lacombe would not compare well with their corresponding experimental values.

In view of the fact that the present $(i + j)$ mixtures satisfy [18], and as the addition of a k etc. component to an $(i + j)$ etc. mixture would not drastically alter the nature of i−j, j−k, and i−k interactions, the present ternary $(i + j + k)$ mixtures would also satisfy an equation of state like [18]. Now the extent to which a ternary $(i + j + k)$ mixture deviated from [11] would be nearly one third of the sum to which the $(i + j)$, $(j + k)$, and $(i + k)$ equimolar mixtures deviated at 308.15 K from [11], i.e. [11] for a ternary $(i + j + k)$ mixture (assuming it to be composed of three binary $(i + j)$, $(j + k)$, and $(i + k)$ mixtures) would reduce to

$$[19]\quad (\tilde{\rho}_{ijk})^2 + \tilde{P}^2 + \frac{RT}{\epsilon^*_{mix(i+j+k)}}[\ln(1 - \tilde{\rho}_{ijk}) + (1 - r^{-1}_{ijk})\tilde{\rho}_{ijk}] = \tfrac{1}{3}[\Sigma\text{R.H.S. of [11] for } (i + j), (j + k), \text{ and } (i + k) \text{ mixtures}]$$

Can. J. Chem. Downloaded from www.nrcresearchpress.com by 210.87.254.40 on 09/06/12
For personal use only.

where $\epsilon^{*}_{\text{mix}(i+j+k)}$ and $\tilde{\rho}_{ijk}$ are defined by [12] and [10], respectively. Once the equation of state for a ternary $(i + j + k)$ mixture, such as [19], has been established (utilizing V^{E} (x = 0.5, T = 308.15 K) and H^{E} (x = 0.5, T = 308.15 K) datum for $(x)i + (1 - x)j$, $(x)j + (1 - x)k$ and $(x)i + (1 - x)k$ mixtures), V^{E}_{ijk} for the $(i + j + k)$ mixture as a function of temperature and composition can be readily evaluated. Such V^{E}_{ijk} values at 298.15 K and 308.15 K for the various ternary mixtures are recorded in Table 1 and are also compared with their corresponding experimental values.

Examination of Table 1 reveals that the V^{E}_{ijk} values predicted by [3] compare reasonably well with the corresponding experimental values. Even in those cases where the agreement between the two values is not good, the predicted V^{E}_{ijk} values are of the right order of magnitude; in some cases, however, this is not true. Nevertheless, the present ternary $(i + j + k)$ mixtures satisfy [19] reasonably well over most of x_i and x_j. The deviations of the $V^{E}_{ijk(\text{calcd})}$ values from the corresponding experimental values at 298.15 and 308.15 K for low values of x_i, x_j, or x_k especially may be attributed to the failure of the assumption that the right hand side of [11] for the constituent $(i + j)$, $(j + k)$, and $(i + k)$ binary mixtures (evaluated from their equimolar V^{E} and H^{E} datum at 308.15 K only) was constant over the entire values of x_i, x_j, or x_k, and T.

The V^{E}_{ijk} data for these ternary mixtures are then analysed in terms of an approach (5) that employed the "graph theoretical" concept of connectivity parameters (16) to characterize its pure components. According to this approach (5) V^{E}_{ij} for a binary $(i + j)$ mixture is given by

$$[20]\quad V^{E}_{ij} = \alpha_{ij}\left[\frac{1}{\sum_i x_i({}^3\xi_i)} - \sum_i \frac{x_i}{{}^3\xi_i}\right]$$

where α_{ij} is a constant assumed to be independent of composition and characteristic of the $(i + j)$ mixture and x_i is the mole fraction of the ith component in the mixture. Further ${}^3\xi_i$ is a connectivity parameters of the third degree of the ith molecule and is defined (16) by

$$[21]\quad {}^3\xi_i = \sum_{l<m}\sum_{m<n}\sum_{n<o}(\delta_l\delta_m\delta_n\delta_o)^{-1/2}$$

where δ_l, δ_m, δ_n, and δ_o etc. denote the degrees of the l, m, n, and oth etc. vertices of the "graph" (16) of the ith molecule and were evaluated as described earlier (6). This approach (5) is based on the fact (5) that the molar volume of an ith molecule can be expressed in terms of its connectivity parameters of the first and third order by means of

$$[22]\quad V_i = (\alpha_i/{}^3\xi_i) + \beta_i{}^1\xi_i + \gamma_i$$

where α_i, β_i, and γ_i are constants and ${}^1\xi_i$ (connectivity parameters of the first degree of i) is defined by

$$[23]\quad {}^1\xi_i = \sum_{l<m}(\delta_l\delta_m)^{-1/2}$$

and that

$$[24]\quad V^{E}_{ij} = V_{\text{mix}} - V_{\text{id}} = V_{\text{mix}} - \sum x_i V_i$$

It was further assumed that V_m for the $(i + j)$ mixture should also be represented by an expression analogous to

$$[25]\quad V_m = (\alpha_m/{}^3\xi_m) + \beta_m({}^1\xi_m) + \gamma_m$$

Since the connectivity parameters of the first degree of molecule depends on the degree of the closest vertices in its molecular graph taken two at a time, it has been assumed to represent a measure of the oscillations of its C—C bond length and as mixing the ith and the jth components in the $(i + j)$ binary mixture is not going to materially alter these C—C bond lengths in this mixture, $\beta_m({}^1\xi_m)$ was assumed (5) to be given by

$$[26]\quad \beta_m({}^1\xi_m) = \sum_i x_i\beta_i({}^1\xi_i)$$

Further, $1/({}^3\xi_i)$ of an ith molecule has also been taken to represent a measure of the probability that its surface area interacts effectively with the corresponding surface areas of other molecules so that in a binary $(i + j)$ mixture containing x_i mole fraction of i, $({}^{1/3}\xi_m)$ was assumed to be given by [27].

$$[27]\quad ({}^3\xi_m)^{-1} = (\sum x_i{}^3\xi_i)^{-1}$$

Further γ_m and α_m were expressed as

$$[28]\quad \gamma_m = \sum_i x_i\gamma_i$$

$$[29]\quad \alpha_m = \alpha_i = \alpha_j = \alpha_{ij}$$

In view of this approach V^{E}_{ijk} for a ternary mixture would be given by

$$[30]\quad V^{E}_{ijk} = \alpha_{ijk}\left[\frac{1}{\sum_{i=1}^{3} x_i({}^3\xi_i)} - \sum_{i=1}^{3}\frac{x_i}{{}^3\xi_i}\right]$$

where $\alpha_m = \alpha_i = \alpha_j = \alpha_k = \alpha_{ijk}$.

Prediction of V^{E}_{ijk} for the ternary mixture by means of [30] requires a knowledge of α_{ijk} for this mixture. α_{ijk}, in principle, should be predictable from the corresponding α's of the $(i + j)$, $(j + k)$, and $(i + k)$ binary systems. A useful approximation would be to regard a ternary $(i + j + k)$ mixture to be composed of three binary $(i + j)$, $(j + k)$, and $(i + k)$ systems. Now an i and a j molecule can pack themselves in the $(i + j)$ system in two ways, i.e.

ij or *ji*

Consequently three components give six different binary arrangements in the three binary $(i + j)$, $(j + k)$, and $(i + k)$ mixtures. These six different binary packing arrangements taken two at a time will give rise to ${}^6C_2$ or 15*ijk* ternary combinations. But in actual fact, *i*, *j*, and *k* molecules can pack themselves in three ways only i.e. *ijk*, *jik*, *jki*. It is thus apparent that the number of ternary packing arrangements from the binary packing arrangements is 5 times more than the actual ternary packing arrangements. Hence it is expected that α_{ijk} should be expressible in terms of α_{ij}, α_{jk}, α_{ik}, the binary interaction coefficients, by

$$[31]\quad \alpha_{ijk} = (1/5)(\alpha_{ij} + \alpha_{jk} + \alpha_{ik})$$

so that [29] reduces to

$$[32]\quad V^{E}_{ijk} = (1/5)(\alpha_{ij} + \alpha_{jk} + \alpha_{ik})\left[\frac{1}{\sum_{i=1}^{3} x_i({}^3\xi_i)} - \sum_{i=1}^{3}\frac{x_i}{{}^3\xi_i}\right]$$

Thus if the binary interaction coefficients α_{ij}, α_{jk}, and α_{ik} are known it should be possible to predict V^{E}_{ijk} for the ternary mixture. These binary interaction coefficients were evaluated by fitting the V^{E} datum for an equimolar composition at a given temperature to [20], as described earlier (5), and then employed to predict V^{E}_{ijk} for the ternary mixture at that temperature. Such V^{E}_{ijk} values are recorded in Table 1 and are also compared with

Can. J. Chem. Downloaded from www.nrcresearchpress.com by 210.87.254.40 on 09/06/12
For personal use only.

the corresponding experimental values.

Examination of Table 1 reveals that the predicted V^{E}_{ijk} values (except in the range $x_i \leq 0.1$ for which $V^{E}_{ijk(exp)} > V^{E}_{ijk(eq.[32])}$) compare well with the corresponding experimental values. Even in those cases where the agreement between the two values is not good, the predicted V^{E}_{ijk} values are of the right order of magnitude. The failure of [32] to correctly predict V^{E}_{ijk} for most of the present $(i + j + k)$ mixtures, in the range $x_i \leq 0.1$, may be traced to the presence in them of ternary contacts (which depend on the nature of molecular interactions between the i, j, and k components of these mixtures and which have not been presently considered), other than the ijk contacts. For such solutions α_{ijk} values, as evaluated from [31], would therefore be lower than their actual values and so V^{E}_{ijk} values as calculated from [32] would be lower than their corresponding experimental values.

Thus while Lacombe and Sanchez theory (2) has the advantage of a rigorous theory of fluid and fluid mixtures which has been shown (1, 2) to describe several other aspects of binary mixtures, expressions [20] and [32] present an alternative view point (of binary and ternary mixtures of non-electrolytes) which has the advantage of simplicity and brings out the versatility of the mathematical discipline of "graph theory" (16–19). In any case these approaches cannot be expected to fare better because of: (*i*) the complicated nature of molecular interactions between the components of these ternary mixtures; and (*ii*) the still limited success with binary systems.

These approaches, however, clearly suggest that even with the present stage of knowledge about binary mixtures, it still is possible to predict, reasonably well, V^{E}_{ijk} for ternary mixtures of non-electrolytes. Preliminary studies with H^{E}_{ijk} data of ternary mixtures of non-electrolytes in terms of these two approaches support these observations and again suggest that the "graph theoretical" approach has some distinct advantages over Sanchez and Lacombe's theory (2) although it lacks the rigour of the latter theory.

We may now extract some information about the nature of molecular interactions between the components of these ternary mixtures.

Although several thermodynamic techniques (20) can be utilized for the purpose, the McMillan–Mayer formalism (21) appears to be an attractive one. According to this treatment any change in the properties of the solvent appears in the magnitudes of the solute–solute virial coefficients and the self-interaction coefficients for a binary system remain unchanged when an additional solute is added to this binary system. This is expected to be true in the present case as the solute–solute interactions would be of a short-range nature (since they have been usually expressed in terms of the Lennard–Jones potential function). According to this formalism (21) any excess function say $V^{E(3)}$ of a solution containing n solute species can be expressed as

$$[33]\quad V^{E(3)}_{(m_i \cdots m_n)} = V - V_{sol} - \sum_{i=1}^{n} V^{0}_{i} m_i$$

$$[34]\quad = \sum_{i=1}^{n}\sum_{j=1}^{n} V_{ij} m_i m_j + \sum_{i=1}^{n}\sum_{j=1}^{n}\sum_{k=1}^{n} V_{ijk} m_i m_j m_k$$

where V and $V^{E(3)}_{(m_i \ldots m_n)}$ are the volume and excess volumes respectively of a solution containing 1 kg of solvent and $m_i \ldots m_n$ moles of each solute species, V_{sol} is the standard volume of 1 kg of the solvent, and V^{0}_{i} is the partial molal volume of each solute. For a ternary $(i + j + k)$ solution, [34] reduces to

$$[35]\quad V^{E(3)}_{(m_j \cdot m_k)} = V_{jj} m_j^2 + 2V_{jk} m_j m_k + V_{kk} m_k^2 + V_{jjj} m_j^3 + 3V_{jjk} m_j^2 m_k + 3V_{jkk} m_j m_k^2 + V_{kkk} m_k^3 + \ldots.$$

and for the two binary $(i + p)(p = j \text{ or } k)$ solutions [34] yields

$$[36]\quad V^{E(3)}_{(m_j)} = V_{jj} m_j^2 + V_{jjj} m_j^3$$

$$[37]\quad V^{E(3)}_{(m_k)} = V_{kk} m_k^2 + V_{kkk} m_k^3$$

In order to evaluate the cross volume coefficients V_{jk}, V_{jkk}, and V_{jjk} from [35], we following Barone *et al.* (22), used an auxiliary function ΔV^{E*} defined as

$$[38]\quad \Delta V^{E*} = V^{E(3)}_{(m_j \cdot m_k)} - V^{E(3)}_{(m_j)} - V^{E(3)}_{(m_k)}$$

which, in view of [35]–[37], yields

$$[39]\quad \Delta V^{E*}_{(m_j \cdot m_k)^{-1}} = 2V_{jk} + 3V_{jjk} m_j + 3V_{jkk} m_k + \ldots.$$

Thus if $V^{E(3)}_{(m_j \cdot m_k)}$ data for the $(i + j + k)$ ternary mixture along with the $V^{E(3)}_{(m_p)}$ $(p = j \text{ or } k)$ for the $(i + p)$ binary mixtures are known, it should be possible to evaluate the cross volume interaction coefficients. Ideally $V^{E(3)}_{(m_j \cdot m_k)}$ or $V^{E(3)}_{(m_p)}$ $(p = j \text{ or } k)$ data for dilute solutions should be utilized to evaluate these cross volume coefficients but as the H^{E} and V^{E} data for (methylene bromide (i) + aromatic hydrocarbons (p)) mixtures at 398.15 or 298.15 K are very small ($H^{E}_{x_i=0.3} \approx 50$ J mol^{-1} or less, $V^{E}_{x_i=0.5} = 0.25$ cm^3 mol^{-1} or less), we expect [36] and [37] to be valid for a considerable larger m_p $(p = j \text{ or } k)$ values. This led to us to utilize the $V^{E(3)}_{(m_p)}$ data for methylene bromide (i) + aromatic hydrocarbons (p) mixtures in the range $0.5 \leq m_p \leq 1.8$, where $V^{E(3)}_{(m_p)^{-2}}$ are almost linear functions of m_p, to evaluate the self volume interaction coefficients V_{pp}, V_{ppp} $(p = j \text{ or } k)$ between aromatic hydrocarbon (p) molecule in the presence of i. Consequently, $V^{E(3)}_{(m_j \cdot m_k)}$ data for the methylene bromide (i) + benzene (j) + toluene or *p*-xylene or *o*-oxylene (k) ternary mixtures in the $0.5 \leq m_j, m_k \leq 1.8$ range were combined with the corresponding $V^{E(3)}_{(m_p)}$ data in the range $0.5 \leq m_p$ $(p = j \text{ or } k) \leq 1.8$ to evaluate V_{jk}, V_{jjk}, and V_{jkk} from [39] by the method of least squares. For this purpose the $V^{E}(x_j, x_k)$ data in cm^3 mol^{-1} of the methylene bromide (i) + benzene (j) + toluene or *p*-xylene or *o*-xylene (k) or methylene bromide (i) + toluene (j) + *p*-xylene or *o*-oxylene (k)) mixtures were converted to $V^{E(3)}_{(m_j \cdot m_k)}$ data in cm^3 mol^{-1} (mol kg of i)$^{-1}$ by means of

$$[40]\quad V^{E}_{(m_j \cdot m_k)}\ \text{cm}^3\ \text{mol}^{-1}\ (\text{mol kg of } i)^{-1} = [V^{E}_{x_j, x_k}\ \text{cm}^3\ \text{mol}^{-1}\ \text{of } (i + j + k)\ \text{mixture}] \times \left[\frac{1000}{x_i \cdot (\text{mol wt of } i)}\right]$$

while the m_p $(p = j \text{ or } k)$ values were obtained from

$$[41]\quad m_p = \frac{x_p \cdot 1000}{x_i \cdot (\text{mol. wt. of } i)}$$

The corresponding $V^{E}_{(m_p)}$ $(p = j \text{ or } k)$ values in cm^3 mol^{-1} (mol kg of i)$^{-1}$ in the $(p + i)$ binary mixtures were read from the $V^{E}_{(m_p)}$ vs. m_p plots; the $V^{E}_{(x_p)}$ data in cm^3 mol^{-1} of the $(p + i)$ solution were first converted to the $V^{E}_{(m_p)}$ data by means of

$$[42]\quad V^{E}_{(m_p)}\ (p = j \text{ or } k)\ \text{cm}^3\ \text{mol}^{-1}\ (\text{mol kg of } i)^{-1} = \frac{V^{E}_{(x_p)} \cdot 1000}{x_i \cdot (\text{mol. wt. of } i)}$$

TABLE 3. Self and cross volume interaction coefficients in cm^3 $(mol\ kg)^{-1}$ at 298.15 K

System	V_{jj}	V_{kk}	V_{jk}	V_{jjk}	V_{jkk}
Methylene bromide (i) + benzene (j) + toluene (k)	2.64	2.65	−0.054	−0.175	0.0032
Methylene bromide (i) + benzene (j) + *p*-xylene (k)	2.64	4.40	0.198	0.140	−0.1713
Methylene bromide (i) + benzene (j) + *o*-xylene (k)	2.64	5.60	0.655	0.082	−0.429
Methylene bromide (i) + toluene (j) + *p*-xylene (k)	2.65	4.40	−0.018	−0.013	−0.0046
Methylene bromide (i) + toluene (j) + *o*-xylene (k)	2.65	5.60	0.216	0.108	−0.1906

Such V_{jk}, V_{jjk}, and V_{jkk} values along with the V_{jj} and V_{kk} values determined earlier (14) at 298.15 K are recorded in Table 3.

Examination of Table 3 reveals that while the V_{jk} interaction coefficients of benzene (j) with toluene, *p*-xylene, and *o*-xylene (k) in the presence of methylene bromide vary in the order

toluene < *p*-xylene < *o*-xylene

those of toluene (j) with *p*-xylene and *o*-xylene (k) in the presence of methylene bromide vary as

p-xylene < *o*-xylene

and that V_{jk}^{E} (j = benzene and k = *p*-xylene or *o*-xylene) > V_{jk} (j = toluene and k = *p*-xylene or *o*-xylene). V_{jk} values thus clearly bring out the influence of the number and position of $-CH_3$ substituents in the aromatic ring of k in its interaction with j in the presence of methylene bromide (i).

It would now be instructive to compare these V_{jk} coefficients at 298.15 K with the corresponding V_{jk} coefficients at 298.15 K of *tert*-Butanol (*t*-BuOH) (j) with methanol, ethanol, *n*-propanol, and *n*-butanol (k) in the presence of water which vary in the order

n-BuOH < *n*-propanol < ethanol < methanol

If the V_{jk} data of *tert*-butanol (j) with the alkanols (k) is attributed to the mutual destructive overlapping of Gurney's cospheres (24) on alkyl chains on j and k and the subsequent repacking of j and k molecules (which would be maximum in BuOH and minimum in methanol) as the alkanols (j and k) in water come close enough to let their cospheres overlap, the V_{jk} data of benzene (j) with toluene, *p*-xylene and *o*-xylene (k) in the presence of methylene bromide (i) suggests that compared to *o*-xylene, toluene comes closer to benzene. This is understandable since the nmr data (25) on methylene bromide + benzene and methylene bromide + *p*-xylene mixtures have been interpreted to suggest contact charge transfer interactions beween the components of these mixtures; the vacant 3*d* orbitals of one bromine atom of methylene bromide accommodating the π-charge of the aromatic ring thereby shielding the methylene bromide proton and leading to the formation of a 1:1 molecular complex having the geometry

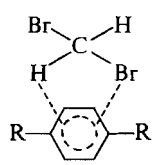

(R = H or $-CH_3$)

The addition of *o*-xylene to benzene in methylene bromide as a solvent would cause *o*-xylene to approach the now electron-deficient benzene in the above molecular complex with the electron-deficient end, i.e.

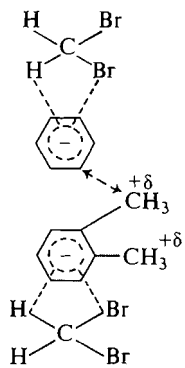

Such an interaction between benzene and toluene in the presence of methylene bromide should evidently be comparatively much stronger than that between benzene and *o*-xylene in the presence of methylene bromide. The small interaction between benzene and *p*-xylene in the presence of methylene bromide as compared to that between benzene and *o*-xylene in the presence of methylene bromide is thus understandable.

This scheme of molecular interactions would evidently envisage that if benzene is replaced by toluene in (methylene bromide (i) + benzene (j) + xylene (k)) mixtures, the jk interactions between toluene (j) and *o*-xylene (k) in the presence of methylene bromide (i) should be comparatively weaker than that between toluene and *p*-xylene in the presence of the same solvent. The V_{jk} data support this conjecture.

Acknowledgement

V.K.S. thanks the authorities of the CSIR, New Delhi, for a Senior Research Fellowship.

1. I. C. SANCHEZ and R. H. LACOMBE. J. Phys. Chem. **80**, 2352 (1976).
2. R. H. LACOMBE and I. C. SANCHEZ. J. Phys. Chem. **80**, 2568 (1976).
3. R. K. NIGAM, P. P. SINGH, K. C. SINGH, M. SINGH, and R. MISHRA. Can. J. Chem. **58**, 1902 (1980).
4. F. KIURA and S. MURAKAMI. Fluid Phase Equilibria, **3**, 93 (1979).
5. P. P. SINGH, R. K. NIGAM, K. C. SINGH, and V. K. SHARMA. Thermochim. Acta, **46**, 175 (1981).
6. P. P. SINGH, R. K. NIGAM, V. K. SHARMA, S. P. SHARMA, and

Can. J. Chem. Downloaded from www.nrcresearchpress.com by 210.87.254.40 on 09/06/12
For personal use only.

K. C. SINGH. Thermochim. Acta, **52**, 87 (1982).
7. R. P. RASTOGI and R. K. NIGAM. Trans. Faraday Soc. **55**, 2005 (1959).
8. A. I. VOGEL. A text book of practical organic chemistry. 4th ed. 1978. p. 267.
9. A. V. FEW and J. W. SMITH. J. Chem. Soc. 753 (1949).
10. A. F. FORTZIATI, A. R. GLASGOW JR., C. B. WILLINGHAM, and F. D. ROSSINI. J. Res. Natl. Bur. Stand. **36**, 129 (1946).
11. J. TIMMERMANNS. Physico-chemical constants of pure organic compounds. Elsevier Publishing Co., Inc., New York. 1950. p. 216.
12. I. BROWN and F. SMITH. Austr. J. Chem. **15**, 1 (1962).
13. J. WISNIAK and A. TAMIR. Mixing and excess thermodynamic properties. Elsevier Scientific Publishing Co., Amsterdam. 1978. p. XXV.
14. P. P. SINGH, R. K. NIGAM, and V. K. SHARMA. J. Soln. Chem. To be published.
15. P. J. FLORY. Principles of polymer chemistry. Cornell University Press, Ithaca, NY. 1953. Chapts. 12 and 13.
16. A. T. BALABAN (*Editor*). Chemical applications of graph theory. Academic Press, London. 1974.
17. R. J. WILSON and L. W. BEINEKE. Applications of graph theory. Academic Press, London. 1979.
18. D. H. ROUVARY. RIC Rev. **4**, 173 (1971).
19. C. A. COULSON. Proc. Camb. Phil. Soc. Math. Phys. Sci. **46**, 202 (1950).
20. J. E. DESNOYER, G. PERRON, L. AVEDIKIAN, and J. P. MOREL. J. Soln. Chem. **5**, 631 (1976).
21. F. FRANKS and M. D. PEDLEY. J. Chem. Soc. Faraday Trans. **177**, 1341 (1980).
22. G. BARONE, P. CACACE, G. CASTRONUOVO, and V. ELIA. J. Chem. Soc. Faraday Trans. I, **77**, 1569 (1981).
23. M. N. JONES (*Editor*). Biochemical thermodynamics. Elsevier Publishing Co., Amsterdam. 1979. p. 60.
24. R. W. GURNEY. Ionic processes in solution. Dover Publications Inc., New York. 1962.
25. P. P. SINGH, R. K. NIGAM, and V. K. SHARMA. Z. Phys. Chem. Leipzig. Acta. To be published.

Can. J. Chem. Downloaded from www.nrcresearchpress.com by 210.87.254.40 on 09/06/12
For personal use only.

Structural studies of organoboron compounds. XIV.[1] Preparation and crystal and molecular structure of 4-isopropylidene-2,5,5-triphenyl-1,3-dioxa-4-azonia-2-bora-5-boratacyclopentane

W. KLIEGEL AND D. NANNINGA

Institut für Pharmazeutische Chemie der Technischen, Universität Braunschweig, 3300 Braunschweig, Beethovenstraße 55, Bundesrepublik Deutschland

AND

STEVEN J. RETTIG AND JAMES TROTTER

Department of Chemistry, University of British Columbia, 2036 Main Mall, Vancouver, B.C., Canada V6T 1Y6

Received January 24, 1983

W. KLIEGEL, D. NANNINGA, STEVEN J. RETTIG, and JAMES TROTTER. Can. J. Chem. **61**, 2329 (1983).

Details of the synthesis, physical properties, and molecular structure of 4-isopropylidene-2,5,5-triphenyl-1,3-dioxa-4-azonia-2-bora-5-boratacyclopentane are reported. Crystals of this compound are monoclinic, a = 14.126(3), b = 16.008(1), c = 8.642(2) Å, β = 99.052(8)°, Z = 4, space group $P2_1/n$. The structure was solved by direct methods and was refined by full-matrix least-squares procedures to R = 0.032 and R_w = 0.033 for 1117 reflections with $I \geq 3\sigma(I)$. The molecule contains a nearly planar five-membered B—O—B—O—N ring which incorporates both trigonal planar boron (B—O = 1.333(4) and 1.418(4), B—C = 1.548(5) Å) and tetrahedral boron atoms (B—O = 1.495(4), B—N = 1.676(4), B—C = 2 at 1.603(5) Å). Other important libration-corrected bond distances include: C=N = 1.284(3) and N—O = 1.418(3) Å.

W. KLIEGEL, D. NANNINGA, STEVEN J. RETTIG et JAMES TROTTER. Can. J. Chem. **61**, 2329 (1983).

On rapporte les détails relatif à la synthèse, aux propriétés physiques et à la structure moléculaire de l'isopropylidène-4 triphényl-2,5,5 dioxa-1,3 azonia-4 bora-2 borata-5 cyclopentane. Les cristaux de ce composé sont monocliniques et appartiennent au groupe d'espace $P2_1/n$ avec a = 14,126(3), b = 16,008(1), c = 8,642(2) Å, β = 99,052(8)°, Z = 4. On a résolu la structure par les méthodes directes et on l'a affinée par la méthode des moindres carrés (matrice entière) jusqu'à des valeurs de R = 0,032 et de R_w = 0,033 pour 1117 réflexions avec $I \geq 3\sigma(I)$. La molécule contient un cycle à 5 chainons de B—O—B—O—N quasi planaire qui englobe à la fois l'atome de bore trigonal plant (B—O = 1,333(4) et 1,418(4), B—C = 1,548(5) Å) et l'atome de bore tétraédrique (B—O = 1,495(4), B—N = 1,676(4), B—C = 2 à 1,603(5) Å). Les autres liaisons importantes corrigées pour la libration sont: C=N = 1,284(3) et N—O = 1,418(3) Å.

[Traduit par le journal]

Introduction

An attempt to synthesize the (isopropylideniminoxy)-diphenylborane **3** (1) from acetone oxime, **1**, and oxybis-(diphenylborane) resulted in a crystalline product the elemental analysis of which indicated the formation of an adduct between the monomer **2** and "phenylboroxide" (**2** + PhBO).[2] This supposed addition compound, **4**, proved to be identical with the reaction product, obtained in nearly quantitative yield, of acetone oxime, **1**, with equivalent quantities of oxybis-(diphenylborane) and phenylboronic acid.

Compound **4** contains diphenylborinic and phenylboronic acid moieties, both of which are detectable by chemical methods such as the blue color reaction with diphenylcarbazone (2, 3) or chelate formation with 2-hydroxyethylamine (or bis(2-hydroxyéthyl)amine) which indicates the presence of diphenylborinic acid (or phenylboronic acid) (3, 4).

The ir spectrum of **4** shows a distinct absorption in the C=N stretching region at 1668 cm^{-1}. This band is shifted to a higher frequency compared with compound **3** (1639 cm^{-1}) (1) which can be explained by a more pronounced iminium salt character of **4**.

The ^{1}H-nmr spectrum of **4** features resonance signals for the 15 phenyl protons of the PhB— and Ph_2B— moieties as well as two sharp singlets, separated by 0.35 ppm, for the two magnetically non-equivalent methyl groups of the isopropylidene substituent.

According to the synthetic method, the elemental analysis, and the available spectroscopic data of **4**, both structures **4***a* and **4***b* were possible. Structure **4***a* resembles the formulation, **5**, proposed by Shitov *et al.* (5) for the decomposition product of the O-(diethylboryl) derivative of 2-aci-nitropropane which was obtained by the analogous reaction of acetone oxime and diethylborinic acid anhydride. The ^{11}B-nmr spectrum of **5** exhibits two singlets with $\delta(BF_3OEt_2)$ = −12.8 and −32 ppm indicating three- and four-coordinate boron atoms (5). Neither the ^{11}B nor the ^{1}H nmr spectra contradict an alternative structure such as **4***b* which could be understood as an addition product of **2** and "phenylboroxide" (phenylboronic acid anhydride).[2]

The mass spectrum of **4** does not show a peak corresponding to the molecular ion. This indicates the thermolability of the compound. Shitov *et al.* (5) also found only a "very weak" molecular ion peak in the mass spectrum of **5**. The base beak in the mass spectrum of **4** represents the mass (m/e) 264 which corresponds to a $(M - C_6H_5)^+$ fragment. The loss of a phenyl group is a common feature of diphenylboron chelates (6) and leads mostly to very stable fragments. A peak of m/e 264 was also observed in the mass spectrum of **3** (1) and was interpreted as a (monomer **2** + BO)$^+$ ion, like similar particles which were found as prominent peaks in the mass spectra of other (alkylideniminoxy)diorganylboranes and considered as characteristic fragments of this type of compound (7). This demonstrates the high stability of the heterocyclic particle $(4 - C_6H_5)^+$ or analogs of it. In support of these findings the mass spectrum of **5** contains the prominent fragment $(5 - C_2H_5)^+$ (5). The peak with the highest mass (m/e 312) and a relatively high abundance in the spectrum of **4** suggests the formation of $(PhBO)_3$

[1]Previous paper in this series: ref. 25.

[2]Phenylboronic acid anhydride ("phenylboroxide") exists only as the trimer $(PhBO)_3$ (triphenylboroxin) under normal conditions.

Can. J. Chem. Downloaded from www.nrcresearchpress.com by 210.87.254.42 on 09/06/12
For personal use only.

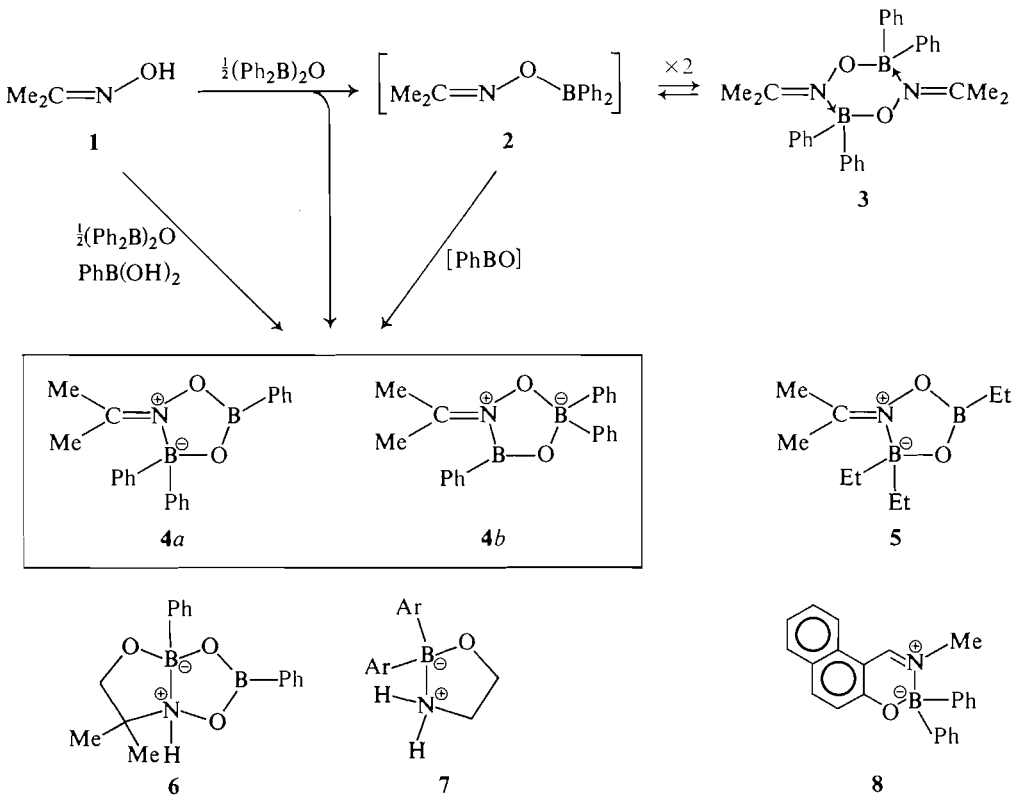

in a thermolytic reaction of **4** within the inlet system.

In view of the failure of chemical and spectroscopic methods to determine the structure of **4**, a full X-ray crystallographic analysis seemed the best way to distinguish unambiguously between the alternative formulations **4***a* and **4***b*.

Experimental

4-Isopropylidene-2,5,5-triphenyl-1,3-dioxa-4-azonia-2-bora-5-boratacyclopentane

Method a

A solution of oxybis(diphenylborane) (0.70 g, 2 mmol) and acetone oxime (0.30 g, 4 mmol) in 50 mL benzene was refluxed for 20 min using a Dean-Stark trap for the continuous removal of water. After partial evaporation of solvent and addition of petroleum ether 0.18 g (26% yield) of colorless crystals were obtained.

Method b

A solution of oxybis(diphenylborane) (0.70 g, 2 mmol), phenylboronic acid (0.49 g, 4 mmol), and acetone oxime (0.30 g, 4 mmol) in 50 mL benzene was refluxed for 45 min using a Dean-Stark trap for water removal. Partial evaporation of solvent followed by the addition of petroleum ether resulted in the precipitation of 1.25 g (92% yield) of colorless crystals which were then recrystallized from tetrahydrofuran and petroleum ether, mp 159°C. *Anal.* calcd. for $C_{21}H_{21}B_2NO_2$ (341.03): C 73.90, H 6.20, B 6.34, N 4.10; found: C 73.75, H 6.17, B 6.20, N 4.19. Ir (KBr): 1668 cm^{-1} (C=N). ^1H nmr ($CDCl_3$/TMS) δ (ppm): 1.93 (s, CH_3), 2.28 (s, CH_3), 7.2–8.0 (m, Ph_2B and PhB). Mass spectrum (70 eV, 140°C, direct inlet), *m/e* (relative abundance, assignment): 312 (80, $[PhBO]_3$), 264 (100, M − C_6H_5), 235 (12), 217 (32), 208 (22, $[PhBO]_2$), 181 (10, Ph_2BO), 165 (45, Ph_2B), 154 (22), 144 (18), 131 (38), 118 (12), 104 (58, PhBO), 87 (26), 77 (58, C_6H_5), 56 (85).

The methanolic solution of the substance gives a dark blue color reaction (2) with diphenylcarbazone and yields the well known diphenylboron chelate with 2-hydroxyethylamine (8) and monophenylboron bidentate chelate with bis(2-hydroxyethyl)amine (9) in aqueous ethanol solution.

X-ray crystallographic analysis of 4-isopropylidene-2,5,5-triphenyl-1,3-dioxa-4-azonia-2-bora-5-boratacyclopentane

A crystal bounded by the six faces (followed by their distances in mm from a common origin): ±(1 0 0), 0.100 ±(0 1 0), 0.075, ±(0 0 1), 0.190 was mounted in a general orientation. Unit-cell parameters were refined by least-squares on 2 sin θ/λ values for 25 reflections (2θ = 20–35°) measured on a diffractometer with Mo-Kα_1 radiation (λ = 0.70930 Å). Crystal data at 22°C are:

$C_{21}H_{21}B_2NO_2$ fw = 341.03

Monoclinic, a = 14.126(3), b = 16.008(1), c = 8.642(2) Å, β = 99.052(8)°, V = 1929.6(5) $Å^3$, Z = 4, ρ_c = 1.174 g cm^{-3}, $F(000)$ = 720, μ(Mo-Kα) = 0.68 cm^{-1}. Absent reflections: $h0l$, $h + l$ odd, and $0k0$, k odd, uniquely determine the space group $P2_1/n$ (nonstandard setting of $P2_1/c$, C_{2h}^5, No. 14, equivalent positions: ±(x, y, z; 1/2 − x, 1/2 + y, 1/2 − z)).

Intensities were measured with graphite-monochromatized Mo-Kα radiation (λ = 0.71073 Å) on an Enraf-Nonius CAD4-F diffractometer. An ω–2θ scan at 0.96–6.71° min^{-1} over a range of (0.70 + 0.35 tan θ) degrees in ω (extended by 25% on both sides for background measurement) was employed. Data were measured to 2θ = 52°. The intensities of three check reflections, measured every 3600 s throughout the data collection, showed a uniform decrease to final values 4.7% less than the initial values. The data were corrected for isotropic decay. Of the 3782 independent reflections measured and processed,[3] 1117 (30%) had intensities greater than 3σ(I) above background where $\sigma^2(I) = S + 2B + (0.04(S - B))^2$ with S = scan count and B = normalized background count. High-order reflections (2θ >

[3]The computer programs used include locally written programs for data processing and locally modified versions of the following: MULTAN 80, multisolution program by P. Main, S. J. Fiske, S. E. Hull, L. Lessinger, G. Germain, J. P. Declercq, and M. M. Woolfson; ORFLS, full-matrix least-squares, and ORFFE, function and errors, by W. R. Busing, K. O. Martin and H. A. Levy; FORDAP, Patterson and Fourier syntheses, by A. Zalkin; ORTEP II, illustrations, by C. K. Johnson.

Can. J. Chem. Downloaded from www.nrcresearchpress.com by 210.87.254.42 on 09/06/12
For personal use only.

Can. J. Chem. Downloaded from www.nrcresearchpress.com by 210.87.254.42 on 09/06/12
For personal use only.

TABLE 1. Final positional (fractional × 10^4, H × 10^3) and isotropic thermal parameters ($U \times 10^3$ Å^2)* with estimated standard deviations in parentheses

Atom	x	y	z	U_{eq}/U_{iso}
O(1)	5316(1)	4206(1)	3305(3)	60
O(2)	4082(1)	3253(1)	3006(2)	56
N(1)	5674(2)	3519(2)	4233(3)	52
C(1)	6525(2)	3599(2)	4982(4)	54
C(2)	7111(4)	4358(4)	4826(9)	83
C(3)	6929(4)	2902(4)	6004(7)	77
C(4)	3780(3)	4669(2)	1608(4)	55
C(5)	4172(4)	5415(3)	1220(5)	73
C(6)	3636(5)	6003(4)	309(6)	95
C(7)	2694(5)	5860(4)	−234(5)	101
C(8)	2274(4)	5126(4)	118(5)	89
C(9)	2818(3)	4535(3)	1030(5)	70
C(10)	4529(2)	2648(2)	5754(4)	55
C(11)	4837(3)	1983(3)	6740(6)	73
C(12)	4630(4)	1925(4)	8237(7)	95
C(13)	4086(4)	2521(5)	8815(8)	100
C(14)	3747(4)	3168(4)	7862(7)	94
C(15)	3962(3)	3227(3)	6370(6)	74
C(16)	5176(2)	1975(2)	3223(4)	53
C(17)	5985(3)	1925(3)	2488(4)	66
C(18)	6226(3)	1212(3)	1725(5)	77
C(19)	5651(4)	532(3)	1663(5)	78
C(20)	4841(3)	541(3)	2355(5)	76
C(21)	4614(3)	1260(3)	3107(4)	67
B(1)	4366(3)	4003(3)	2636(5)	53
B(2)	4830(3)	2784(2)	4067(5)	52
H(2a)	705(4)	471(4)	551(7)	170(30)
H(2b)	776(4)	421(3)	487(5)	161(22)
H(2c)	690(4)	472(4)	400(7)	177(30)
H(3a)	661(4)	236(4)	591(7)	191(28)
H(3b)	753(3)	282(3)	583(5)	123(19)
H(3c)	701(3)	307(3)	695(7)	153(26)
H(5)	482(3)	549(2)	159(4)	93(14)
H(6)	393(3)	649(3)	7(5)	100(17)
H(7)	230(2)	627(2)	−87(4)	89(13)
H(8)	161(3)	496(2)	−14(4)	101(15)
H(9)	255(2)	402(2)	133(4)	80(13)
H(11)	522(2)	155(2)	632(4)	81(14)
H(12)	486(3)	147(3)	891(5)	98(17)
H(13)	396(3)	249(3)	984(6)	123(22)
H(14)	339(3)	358(2)	826(5)	100(17)
H(15)	370(2)	369(2)	570(4)	80(13)
H(17)	634(2)	241(2)	248(3)	46(10)
H(18)	682(3)	122(3)	115(5)	125(16)
H(19)	582(2)	4(2)	117(4)	79(13)
H(20)	438(2)	6(2)	229(4)	96(14)
H(21)	400(2)	126(2)	358(3)	66(10)

*U_{eq} = (1/3)trace U_{diag}.

40°) were generally unobserved in spite of good crystal quality, probably due at least in part to the relatively small volume of the crystal.

The structure was solved by direct methods, all non-hydrogen atom positions being taken from an E-map. Refinement of the non-hydrogen atoms with anisotropic thermal parameters gave R = 0.078, a difference map at this point clearly revealing all 21 hydrogen atoms. Refinement with fixed contributions from the hydrogen atoms reduced R and R_w to values of 0.044 and 0.056 respectively. In spite of the small number of observed data (using a 2σ cutoff would give only 30 more reflections) the hydrogen atoms positions and isotropic thermal parameters were refined. We feel that this action is justified by the dramatic improvement in the R value. The scattering factors of ref. 10 were used for non-hydrogen atoms and those of ref. 11 for hydrogen atoms. The weighting scheme, $w = 1/\sigma^2(F)$ where $\sigma^2(F)$ is derived from the previously defined $\sigma^2(I)$, gave uniform average values of $w(|F_o| - |F_c|)^2$ over ranges of both $|F_o|$ and sin θ/λ and was employed in the final stages of refinement. Convergence was reached at R = 0.032 and R_w = 0.033 for 1117 reflections with $I \geq 3\sigma(I)$. The function minimized was $\sum w(|F_o| - |F_c|)^2$, $R = \sum||F_o| - |F_c||/\sum|F_o|$ and $R_w = (\sum w(|F_o| - |F_c|)^2/\sum w|F_o|^2)^{1/2}$.

On the final cycle of refinement the mean and maximum parameter shifts corresponded to 0.04 and 0.34σ respectively. The mean error in an observation of unit weight was 1.473. A final difference map showed maximum fluctuations of ±0.12 e Å^{-3}. The final positional and thermal parameters appear in Tables 1 and 2[4] respectively. Measured and calculated structure factors have been placed in the Depository of Unpublished Data.[4]

The ellipsoids of thermal motion for the non-hydrogen atoms are shown in Fig. 1. The thermal motion has been analysed in terms of the rigid-body modes of translation, libration, and screw motion (12). The rms standard error in the temperature factors σU_{ij} (derived from the least-squares analysis) is 0.0030 Å^2. Analysis of all 26 non-hydrogen atoms indicated significant independent motion of the phenyl groups. Four smaller groups were then separately analysed, the three PhB groups and all atoms except the unsubstituted phenyl carbon atoms (rms ΔU_{ij} = 0.0049, 0.0027, 0.0035, and 0.0059 Å^2 respectively). The appropriate bond distances have been corrected for libration (12, 13), using shape parameters q^2 of 0.08 for all atoms involved. Corrected bond lengths appear in Table 3 along with the uncorrected values; corrected bond angles do not differ by more than 1σ from the uncorrected values given in Table 4. Intra-annular torsion angles defining the conformation of five-membered heterocyclic ring are listed in Table 5. Bond lengths and angles involving hydrogen and a complete listing of torsion angles (Tables 6–8) are included as supplementary material.

Results and discussion

The X-ray crystallographic analysis of **4** unambiguously establishes **4***a* as the correct structural formulation. The two methods of preparing the adduct **4** involve different types of reactions. The low-yield method *a* proceeds via a boron–carbon bond cleavage reaction:

$$\mathbf{1} + (Ph_2B)_2O \rightarrow \mathbf{4} + C_6H_6$$

while the more efficient method *b* involves elimination of water:

$$\mathbf{1} + (1/2)(Ph_2B)_2O + PhB(OH)_2 \rightarrow \mathbf{4} + (3/2)\ H_2O$$

The crystal structure consists of discrete molecules separated by normal van der Waals distances.

The molecule contains a nearly planar B—O—B—O—N ring (χ^2 = 36.6, mean and maximum deviations from the mean plane are 0.007 and 0.010(3) Å respectively), very similar to that found in **6** (14). The trivalent atoms N(1), C(1), and B(1) exhibit planar coordination within the limits of experimental error; being displaced from the mean planes of their substituent atoms by 0.004(3), 0.008(3), and 0.010(4) Å respectively. The $Me_2C{=}N(O)B$ moiety is significantly non-planar (χ^2 = 107.6, mean and maximum deviations from the six-atom mean plane are 0.011 and 0.020(7) Å), the C(1) and N(1) coordination groups being twisted by 1.6° about the C=N double bond. The $Me_2C(1)$ moiety and the B(1) phenyl group are oriented roughly in the same plane as the five-membered heterocyclic ring (angles between normals to the mean planes being 1.7 and 5.8°

[4]The structure factor table, Table 2 (anisotropic thermal parameters) and other material mentioned in the text are available, at a nominal charge, from the Depository of Unpublished Data, CISTI, National Research Council of Canada, Ottawa, Canada K1A 0S2.

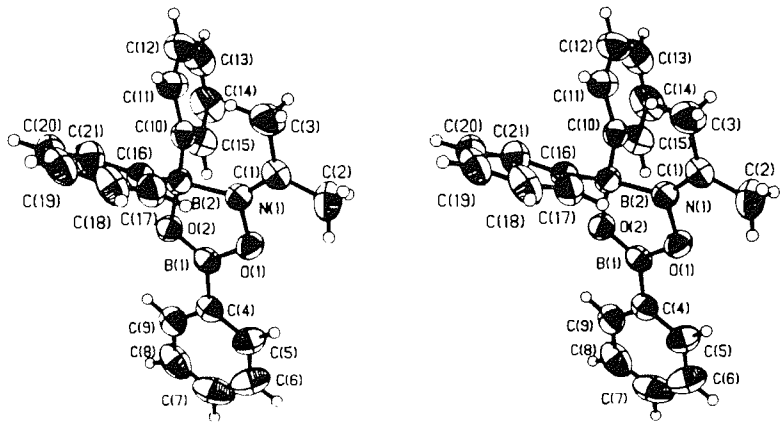

FIG. 1. Stereoscopic view of the 4-isopropylidene-2,5,5-triphenyl-1,3-dioxa-4-azonia-2-bora-5-boratacyclopentane molecule. 50% probability thermal ellipsoids are shown for the non-hydrogen atoms; hydrogen atoms have been assigned arbitrarily small thermal parameters for the sake of clarity.

TABLE 3. Bond lengths (Å) with estimated standard deviations in parentheses

	Length			Length	
Bond	Uncorr.	Corr.	Bond	Uncorr.	Corr.
O(1)—N(1)	1.408(3)	1.418	C(10)—C(11)	1.390(5)	1.403
O(1)—B(1)	1.412(4)	1.418	C(10)—C(15)	1.385(5)	1.399
O(2)—B(1)	1.322(4)	1.333	C(10)—B(2)	1.597(5)	1.603
O(2)—B(2)	1.489(4)	1.495	C(11)—C(12)	1.373(6)	1.379
N(1)—C(1)	1.279(3)	1.284	C(12)—C(13)	1.368(7)	1.382
N(1)—B(2)	1.665(4)	1.676	C(13)—C(14)	1.363(7)	1.375
C(1)—C(2)	1.488(6)	1.498	C(14)—C(15)	1.373(6)	1.379
C(1)—C(3)	1.480(5)	1.489	C(16)—C(17)	1.394(5)	1.403
C(4)—C(5)	1.380(5)	1.394	C(16)—C(21)	1.388(4)	1.396
C(4)—C(9)	1.389(5)	1.399	C(16)—B(2)	1.600(5)	1.603
C(4)—B(1)	1.542(5)	1.548	C(17)—C(18)	1.387(5)	1.390
C(5)—C(6)	1.375(6)	1.381	C(18)—C(19)	1.355(6)	1.363
C(6)—C(7)	1.359(7)	1.369	C(19)—C(20)	1.372(5)	1.382
C(7)—C(8)	1.371(6)	1.384	C(20)—C(21)	1.385(5)	1.388
C(8)—C(9)	1.385(6)	1.391			

TABLE 4. Bond angles (deg) with estimated standard deviations in parentheses

Bonds	Angle (deg)	Bonds	Angle (deg)
N(1)—O(1)—B(1)	106.6(3)	C(12)—C(13)—C(14)	118.3(6)
B(1)—O(2)—B(2)	113.2(3)	C(13)—C(14)—C(15)	120.7(6)
O(1)—N(1)—C(1)	115.8(3)	C(10)—C(15)—C(14)	122.8(5)
O(1)—N(1)—B(2)	108.4(2)	C(17)—C(16)—C(21)	114.9(4)
C(1)—N(1)—B(2)	135.8(3)	C(17)—C(16)—B(2)	125.8(3)
N(1)—C(1)—C(2)	121.8(4)	C(21)—C(16)—B(2)	119.2(3)
N(1)—C(1)—C(3)	118.1(4)	C(16)—C(17)—C(18)	123.0(4)
C(2)—C(1)—C(3)	120.1(4)	C(17)—C(18)—C(19)	119.3(5)
C(5)—C(4)—C(9)	117.0(4)	C(18)—C(19)—C(20)	120.7(5)
C(5)—C(4)—B(1)	122.5(3)	C(19)—C(20)—C(21)	118.9(4)
C(9)—C(4)—B(1)	120.5(4)	C(16)—C(21)—C(20)	123.2(4)
C(4)—C(5)—C(6)	121.7(5)	O(1)—B(1)—O(2)	114.5(3)
C(5)—C(6)—C(7)	120.2(5)	O(1)—B(1)—C(4)	117.8(3)
C(6)—C(7)—C(8)	120.1(5)	O(2)—B(1)—C(4)	127.6(3)
C(7)—C(8)—C(9)	119.4(5)	O(2)—B(2)—N(1)	97.2(2)
C(4)—C(9)—C(8)	121.5(5)	O(2)—B(2)—C(10)	111.5(3)
C(11)—C(10)—C(15)	114.9(4)	O(2)—B(2)—C(16)	111.4(3)
C(11)—C(10)—B(2)	124.1(4)	N(1)—B(2)—C(10)	107.9(3)
C(15)—C(10)—B(2)	120.9(4)	N(1)—B(2)—C(16)	110.2(3)
C(10)—C(11)—C(12)	122.5(5)	C(10)—B(2)—C(16)	116.8(3)
C(11)—C(12)—C(13)	120.8(6)		

Can. J. Chem. Downloaded from www.nrcresearchpress.com by 210.87.254.42 on 09/06/12
For personal use only.

TABLE 5. Intra-annular torsion angles (deg) standard deviations in parentheses

Atoms	Torsion angle (deg)
B(1)—O(1)—N(1)—B(2)	1.7(3)
O(1)—N(1)—B(2)—O(2)	−1.4(3)
B(1)—O(2)—B(2)—N(1)	0.6(3)
B(2)—O(2)—B(1)—O(1)	0.4(4)
N(1)—O(1)—B(1)—O(2)	−1.4(4)

respectively). The latter value is similar to those in the range 2.5−21.4° observed for other derivatives of phenylboronic acid (14−17).

The bond distances in the B—O—B—O—N ring of **4***a* are, in general, significantly different from those in **6**. These discrepancies undoubtedly arise from both steric factors (the ring in **6** being fused to another five-membered ring) and the chemical differences between corresponding nitrogen and four-coordinate boron atoms. It is noteworthy, however, that the sums of the libration-corrected bond distances in the five-membered heterocyclic rings of **4***a* and **6** are identical (7.340 Å in each case). Both **4***a* and **6** show the characteristic short anhydridic B(1)—O(2) bond (1.333(4) in **4***a*, 1.337(2) Å in **6**), believed to result from stronger π-back donation at this point in the ring. The B(1)—O(1) bonds in **4***a* and **6** (1.418(4) and 1.404(2) Å) are significantly longer than the short anhydridic bonds to B(1) but the average B(trigonal planar)—O distances in **4***a* and **6** (1.376 and 1.371 Å) compare well with a corresponding mean[5] value of 1.371(6) Å in $C_6H_5B(OH)_2$ (16). The B(2)—N(1) bond in **4***a* (1.676(4) Å) is significantly longer than the mean of 1.654(1) Å in ethanolamine esters of diarylborinic acids **7** (8, 18, 19) containing tetrahedral nitrogen, and also significantly longer than the value of 1.601(4) Å in **8** (20) which contains trigonal planar nitrogen but in a six-membered ring. This demonstrates the weaker binding and points to the lower basicity of the oxime nitrogen compared to amine or imine nitrogen. The B(2)—O(2) distance of 1.495(4) Å is significantly longer than corresponding bonds in compounds **7** (mean 1.477(2) Å) and the value of 1.467(2) Å in **6**.

The C=N and N—O distances of 1.284(3) and 1.418(3) Å are both at the long ends of the ranges previously noted for oximes (21) (1.25−1.288 and 1.32−1.426 Å respectively). A slight lengthening of the C=N bond upon coordination of nitrogen is expected relative to that of the free oxime (22). In the present case there is no significant difference between the C=N distance reported here and that found for the free oxime (23), C=N = 1.29(3) Å. For example, in salicylaldoxime (24), C=N = 1.270(5) Å, and in the complex bis-[(salicylaldoximato)phenylboron] (25), C=N = 1.278(1) Å. The B—C distances and the substituent-induced distortions of the phenyl rings are as expected (26).

[5]Here and elsewhere in this report mean values refer to weighted means with rms deviations from the mean in parentheses.

Acknowledgments

We thank the Natural Sciences and Engineering Research Council of Canada for financial support and the University of British Columbia Computing Centre for assistance. We are also indebted to the Gesellschaft für Biotechnologische Forschung mbH, Braunschweig-Stöckheim, for running the mass spectrum.

1. D. W. PALMER and K. NIEDENZU. Synth. React. Inorg. Metalorg. Chem. **9**, 13 (1979).
2. R. NEU. Z. Anal. Chem. **142**, 335 (1954); **176**, 343 (1960).
3. W. KLIEGEL and H. BECKER. Chem. Ber. **110**, 2067 (1977).
4. H. K. ZIMMERMAN. Adv. Chem. Ser. **42**, 23 (1964).
5. O. P. SHITOV, S. L. IOFFE, L. M. LEONT'EVA, and V. A. TARTAKOVSKII. J. Gen. Chem. USSR, **43**, 1257 (1973); Zh. Obshch. Khim. **43**, 1266 (1973).
6. E. HOHAUS and W. RIEPE. Z. Naturforsch. **31b**, 324 (1976); Internat. J. Mass Spectrom. Ion Phys. **31**, 113 (1979).
7. W. MARINGGELE and A. MELLER. Mh. Chem. **106**, 1369 (1975).
8. S. J. RETTIG and J. TROTTER. Can. J. Chem. **51**, 1288 (1973).
9. S. J. RETTIG and J. TROTTER. Can. J. Chem. **53**, 1393 (1975).
10. D. T. CROMER and J. B. MANN. Acta Crystallogr. Sect. A, **24**, 321 (1968).
11. R. F. STEWART, E. R. DAVIDSON, and W. T. SIMPSON. J. Chem. Phys. **42**, 3175 (1965).
12. V. SCHOMAKER and K. N. TRUEBLOOD. Acta Crystallogr. Sect. B, **24**, 63 (1968).
13. D. W. J. CRUICKSHANK. Acta Crystallogr. **9**, 747 (1956); **9**, 754 (1956); **14**, 896 (1961).
14. S. J. RETTIG, J. TROTTER, W. KLIEGEL, and H. BECKER. Can. J. Chem. **54**, 3142 (1976).
15. F. ZETTLER, H. D. HAUSEN, and H. HESS. J. Organomet. Chem. **72**, 157 (1974).
16. S. J. RETTIG and J. TROTTER. Can. J. Chem. **55**, 3071 (1977).
17. Z. V. ZVONKOVA and V. P. GLUSKOVA. Kristallografija SSSR **3**, 559 (1958).
18. S. J. RETTIG and J. TROTTER. Acta Crystallogr. Sect. B, **30**, 2139 (1974).
19. S. J. RETTIG and J. TROTTER. Can. J. Chem. **54**, 3130 (1976).
20. O. E. KOMPAN, N. G. FURMANOVA, YU. T. STRUCHKOV, L. M. SITKINA, V. A. BREN', and V. I. MINKIN. Zh. Strukt. Khim. **21**(2), 90 (1980); J. Struct. Chem. **21**, 195 (1980).
21. S. J. RETTIG and J. TROTTER. Can. J. Chem. **53**, 765 (1975), and references therein.
22. A. CHAKRAVORTY. Coord. Chem. Rev. **13**, 1 (1974).
23. T. K. BIERLEIN and E. C. LINGAFELTER. Acta Crystallogr. **4**, 450 (1951).
24. C. E. PFLUGER and R. L. HARLOW. Acta Crystallogr. Sect. B, **29**, 2608 (1973).
25. S. J. RETTIG and J. TROTTER. Can. J. Chem. **61**, 206 (1983).
26. A. DOMENICANO, A. VACIAGO, and C. A. COULSON. Acta Crystallogr. Sect. B, **31**, 221 (1975); **31**, 1630 (1975).

Can. J. Chem. Downloaded from www.nrcresearchpress.com by 210.87.254.42 on 09/06/12
For personal use only.

Structural studies of organoboron compounds. XV.[1] Crystal and molecular structures of (3-aminopropanolato)diphenylboron, (2-*N*,*N*-dimethylaminoethanolato)diphenylboron, and (2-*N*,*N*-dimethylaminoethanolato)diphenylboron − diphenylborinic acid (1:1)

STEVEN J. RETTIG AND JAMES TROTTER

Department of Chemistry, University of British Columbia, 2036 Main Mall, Vancouver, B.C., Canada V6T 1Y6

Received January 25, 1983

STEVEN J. RETTIG and JAMES TROTTER. Can. J. Chem. **61**, 2334 (1983).

Crystals of (3-aminopropanolato)diphenylboron are monoclinic, a = 9.6717(13), b = 9.8867(6), c = 14.452(2) Å, β = 99.500(7)°, Z = 4, space group $P2_1/n$; those of (2-*N*,*N*-dimethylaminoethanolato)diphenylboron are monoclinic, a = 7.0721(4), b = 16.8829(4), c = 12.0975(8) Å, β = 97.875(3)°, Z = 4, space group Cc; and those of (2-*N*,*N*-dimethylaminoethanolato)diphenylboron − diphenylborinic acid (1:1) are monoclinic, a = 11.3231(10), b = 19.3190(12), c = 12.2451(11) Å, β = 109.321(4)°, Z = 4, space group $P2_1/n$. All three structures were solved by direct methods and were refined by full-matrix least-squares procedures to final R values of 0.038, 0.031, and 0.040 for 1522, 1649, and 2420 reflections with $I \geq 3\sigma(I)$ respectively. Each structure contains a tetrahedrally coordinated boron atom. The libration-corrected B—O, B—N, and mean B—C distances are: 1.481(2), 1.643(3), and 1.623(3) Å for (3-aminopropanolato)diphenylboron; 1.476(2), 1.691 (2), and 1.625(7) Å for (2-*N*,*N*-dimethylaminoethanolato)diphenylboron. The Ph_2BOH molecule contains a trigonal-planar boron atom with B—O = 1.354(3) Å and mean B—C = 1.572(3) Å.

STEVEN J. RETTIG et JAMES TROTTER. Can. J. Chem. **61**, 2334 (1983).

Les cristaux des (aminopropanolato-3) diphénylbore sont monocliniques et appartiennent au groupe d'espace $P2_1/n$ avec a = 9,6717(13), b = 9,8867(6), c = 14,452(2) Å, β = 99,500(7)°, Z = 4. Les cristaux de (*N*,*N*-diméthylaminoéthanolato-2) diphénylbore sont monocliniques et appartiennent au groupe d'espace Cc avec a = 7,0721(4), b = 16,8829(4), c = 12,0975(8) Å, β = 97,875(3)°, Z = 4, et les cristaux de (*N*,*N*-diméthylaminoéthanolato-2) diphénylebore − acide diphénylboromique (1:1) sont monocliniques et appartiennent au groupe d'espace $P2_1/n$ avec a = 11,3231(10), b = 19,3190(12), c = 12,2451(11)Å, β = 109,321(4)°, Z = 4. On a résolu les trois structures par des méthodes directes et on les a affinées par la méthodes des moindres carrés (matrice entière) jusqu'à des valeurs respectives de R = 0,038, 0,031 et 0,040 pour 1522, 1649 et 2420 réflexions observés avec $I \geq 3\sigma(I)$. Chaque structure contient un atome de bore coordonné de façon tétraédrique. Les distances moyennes de liaison B—O, B—N et B—C corrigées pour la libration sont de 1,481(2), 1,643(3) et de 1,623(3) Å pour l'(aminopropanolato-3)diphénylbore; de 1,476(2), 1,691(2) et de 1,625(7) Å pour le (*N*,*N*-diméthylaminoéthanolato-2) diphénylbore. La molécule de Ph_2BOH contient un atome de bore plan-trigonal avec B—O = 1,354(3) Å et une distance moyenne B—C = 1,572(3) Å.

[Traduit par le journal]

Can. J. Chem. Downloaded from www.nrcresearchpress.com by 210.87.254.40 on 09/06/12
For personal use only.

Introduction

As part of a continuing structural investigation of organoboron compounds (1) we report the crystal and molecular structures of (3-aminopropanolato)diphenylboron, **1**, (2-*N*,*N*-dimethylaminoethanolato)diphenylboron, **2**, and (2-*N*,*N*-dimethylaminoethanolato)diphenylboron − diphenylborinic acid (1:1), **3**. Both **1** and **2** are closely related to the structurally characterized (2-aminoethanolato)diarylboron compounds **4** where R = H (2, 3), F (4), and CH_3 (3). Both the size of the chelate ring and, in particular, substitution at nitrogen are known to affect the rate of hydrolytic cleavage of the intramolecular N → B bond which stabilizes this type of diarylborinic ester (5). The object of this investigation is to determine if and how these factors influence the molecular geometry. The molecular complex **3** was isolated during the preparation of **2**, making possible the structure determination of the unstable parent acid Ph_2BOH.

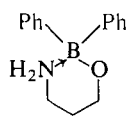

1

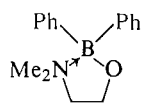

2

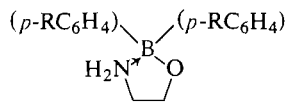

4

[1]Previous paper in this series: ref. 1.

Experimental

Compounds **1** and **2** were prepared by reacting the appropriate aminoalcohol with an equimolar quantity of diphenylborinic acid (obtained by acid hydrolysis of (2-aminoethanolato)diphenylboron) in ethanol/diethyl ether (6). A small amount of the molecular complex **3** was isolated from the reaction mixture during the preparation of **2** as colorless crystals suitable for X-ray analysis. Colorless crystals of **1** and **2** were obtained by recrystallization from ethanol.

X-ray crystallographic studies

(3-aminopropanolato)diphenylboron, 1

A crystal ca. 0.10 × 0.33 × 0.45 mm in size was mounted in a general orientation. Unit-cell parameters were refined by least-squares on 2 sin θ/λ values for 25 reflections (2θ = 30−40°) measured on a diffractometer with Mo-Kα_1 radiation (λ = 0.70930 Å). Crystal data at 22°C are:

$C_{15}H_{18}BNO$ fw = 239.13

Monoclinic, a = 9.6717(13), b = 9.8867(6), c = 14.452(2) Å, β = 99.500(7)°, V = 1363.0(3) Å^3, Z = 4, ρ_c = 1.165 g cm^{-3}, F(000) = 512, μ(Mo-Kα) = 0.66 cm^{-1}. Absent reflections: $h0l$, $h+l$ odd, and $0k0$, k odd uniquely indicate the space group $P2_1/n$ (non-standard setting of $P2_1/c$, C_{2h}^5, No. 19, equivalent positions: ± (x, y, z; 1/2 − x, 1/2 + y, 1/2 − z)).

Intensities were measured with graphite-monochromated Mo-Kα radiation (λ = 0.71073 Å) on an Enraf-Nonius CAD4-F diffractometer. An ω−2θ scan at 0.80−10.06° min^{-1} over a range of (0.60 + 0.35 tan θ) degrees in ω (extended by 25% on both sides for background measurement) was employed. Data were measured to 2θ = 55°. The intensities of three check reflections, measured every 3600 s throughout the data collection, remained constant to within 2%.

Can. J. Chem. Downloaded from www.nrcresearchpress.com by 210.87.254.40 on 09/06/12
For personal use only.

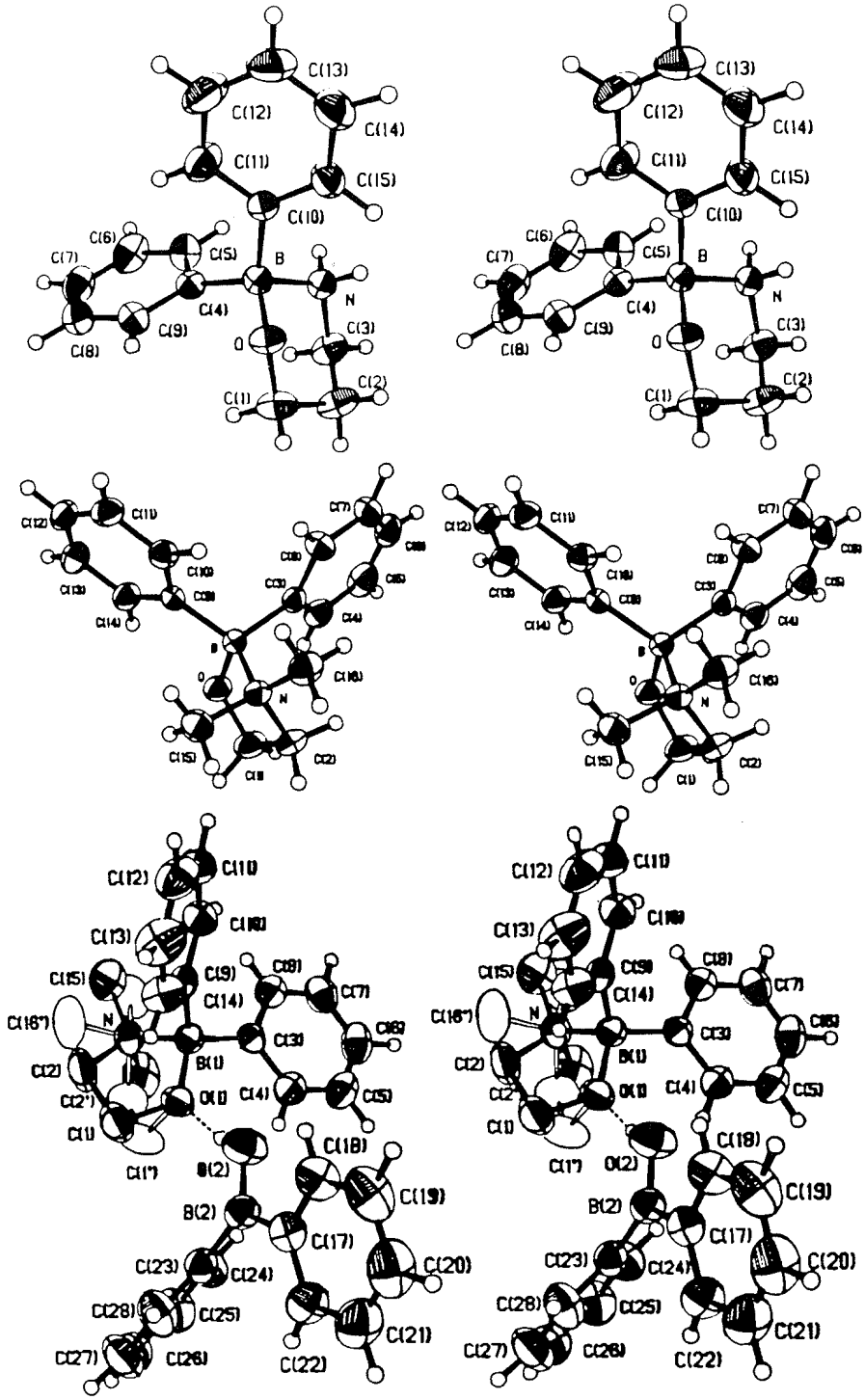

FIG. 1. Stereoscopic views of (3-aminopropanolato)diphenylboron (top), (2-*N*,*N*-dimethylaminoethanolato)diphenylboron (middle), and (2-*N*,*N*-dimethylaminoethanolato)diphenylboron − diphenylborinic acid (1:1) (bottom). 50% probability thermal ellipsoids are shown for the non-hydrogen atoms, hydrogen atoms have been assigned arbitrarily small thermal parameters for the sake of clarity.

Of the 3113 independent reflections measured and processed,[2] 1522 (48.9%) had intensities greater than $3\sigma(I)$ above background where $\sigma^2(I) = S + 2B + (0.04(S - B))^2$ with S = scan count and B = normalized background count.

The structure was solved by direct methods, the positions of all non-hydrogen atoms being determined from an *E*-map. After full-matrix least-squares refinement of the non-hydrogen atoms with anisotropic thermal parameters to $R = 0.074$, a difference map revealed the positions of all 18 hydrogen atoms which were refined with isotropic thermal parameters in subsequent least-squares cycles. The scattering factors of ref. 7 were used for non-hydrogen atoms and those of ref. 8 for hydrogen atoms. The weighting scheme, $w = 1/\sigma^2(F)$ where $\sigma^2(F)$ is derived from the previously defined $\sigma^2(I)$, gave uniform

[2]The computer programs used include locally written programs for data processing and locally modified versions of the following: MULTAN 80, multisolution program by P. Main, S. J. Fiske, S. E. Hull, L. Lessinger, G. Germain, J. P. Declerq, and M. M. Woolfson; ORFLS, full-matrix least-squares, and ORFFE, function and errors, by W. R. Busing, K. O. Martin and H. A. Levy; FORDAP, Patterson and Fourier syntheses, by A. Zalkin; ORTEP II, illustrations, by C. K. Johnson.

TABLE 1. Final positional (fractional × 10^5, disordered C and all H × 10^4) and isotropic thermal parameters ($U \times 10^3$ Å^2) with estimated standard deviations in parentheses*

Atom	x	y	z	U_{eq}/U_{iso}	Atom	x	y	z	U_{eq}/U_{iso}
		1					**2**		
O	31304(13)	41208(12)	22375(8)	37	O	98810	45492(7)	90750	39
N	22745(18)	17610(17)	21307(11)	36	N	110644(28)	44201(8)	73250(17)	33
C(1)	33261(27)	40865(24)	12758(14)	47	C(1)	116765(37)	41682(15)	92821(21)	49
C(2)	23013(31)	31228(24)	7216(15)	53	C(2)	121754(35)	38842(12)	81667(21)	42
C(3)	24764(28)	17102(23)	11275(14)	47	C(3)	77589(29)	36981(9)	76379(18)	31
C(4)	49006(18)	22480(19)	28969(12)	34	C(4)	75944(33)	31621(12)	84985(21)	42
C(5)	52301(23)	8916(23)	30925(16)	47	C(5)	64467(38)	24916(13)	83521(25)	55
C(6)	66114(26)	4382(28)	32807(17)	59	C(6)	54345(34)	23318(12)	73192(28)	56
C(7)	76981(25)	13347(33)	32758(16)	61	C(7)	55603(35)	28405(13)	64481(26)	52
C(8)	74150(25)	26703(31)	30972(16)	58	C(8)	66837(32)	35207(12)	66065(20)	42
C(9)	60388(21)	31150(24)	29099(15)	47	C(9)	78243(29)	52884(9)	75315(18)	29
C(10)	27620(19)	30396(18)	37523(12)	33	C(10)	72446(32)	55413(10)	64303(18)	36
C(11)	36732(26)	31138(28)	45992(16)	58	C(11)	60877(32)	62027(12)	61911(21)	42
C(12)	32064(30)	33383(34)	54420(17)	76	C(12)	54595(32)	66340(11)	70336(22)	44
C(13)	18141(29)	34732(28)	54764(18)	65	C(13)	60190(36)	64114(13)	81234(23)	47
C(14)	8804(26)	34226(28)	46546(18)	61	C(14)	71729(34)	57504(12)	83637(20)	39
C(15)	13545(22)	32221(25)	38104(16)	49	C(15)	120487(36)	51999(13)	73317(26)	49
B	33210(21)	28342(21)	27640(15)	31	C(16)	109899(37)	40700(13)	61936(21)	43
H(Na)	1378(24)	1999(22)	2148(15)	51(6)	B	90290(30)	44970(10)	78983(18)	28
H(Nb)	2328(22)	857(26)	2382(15)	53(6)	H(1a)	12700(48)	4568(18)	9636(28)	69(8)
H(1a)	3160(24)	4989(26)	1030(15)	62(7)	H(1b)	11708(47)	3742(19)	9752(27)	70(9)
H(1b)	4346(25)	3794(23)	1251(15)	57(6)	H(2a)	11672(33)	3329(14)	7984(19)	41(6)
H(2a)	1343(26)	3469(25)	722(16)	61(7)	H(2b)	13479(44)	3902(17)	8058(22)	57(7)
H(2b)	2480(23)	3105(25)	89(19)	68(7)	H(4)	8256(37)	3258(16)	9190(22)	56(7)
H(3a)	1797(22)	1138(23)	812(14)	48(6)	H(5)	6400(43)	2114(18)	8990(26)	65(8)
H(3b)	3450(24)	1360(24)	1145(15)	53(6)	H(6)	4763(38)	1886(17)	7267(23)	60(7)
H(5)	4444(22)	246(22)	3116(13)	48(6)	H(7)	4754(42)	2736(18)	5733(25)	66(8)
H(6)	6783(27)	−507(31)	3467(18)	83(9)	H(8)	6679(41)	3905(16)	5986(23)	55(7)
H(7)	8639(30)	965(28)	3436(18)	83(8)	H(10)	7644(37)	5234(14)	5800(22)	45(6)
H(8)	8217(31)	3319(32)	3106(20)	99(10)	H(11)	5802(45)	6366(18)	5396(27)	69(8)
H(9)	5878(25)	4119(25)	2785(17)	65(7)	H(12)	4694(38)	7076(17)	6868(23)	61(7)
H(11)	4654(26)	2982(26)	4585(16)	67(7)	H(13)	5473(42)	6704(17)	8747(24)	66(8)
H(12)	3875(28)	3423(29)	6000(20)	81(8)	H(14)	7585(35)	5593(13)	9132(20)	42(6)
H(13)	1535(24)	3592(25)	6035(18)	67(7)	H(15a)	13340(42)	5111(16)	7181(23)	55(7)
H(14)	−165(30)	3563(29)	4608(19)	84(9)	H(15b)	11343(47)	5552(17)	6828(26)	60(8)
H(15)	631(25)	3263(24)	3189(17)	67(7)	H(15c)	11931(43)	5420(16)	8037(26)	53(7)
					H(16a)	10303(35)	3567(15)	6171(20)	43(6)
					H(16b)	12199(39)	4021(14)	6027(21)	49(7)
					H(16c)	10234(42)	4408(16)	5666(25)	59(8)
							3		
O(1)	55268(13)	70349(7)	71012(12)	55	C(20)	39525(30)	58792(19)	6850(26)	85
O(2)	49069(17)	66869(9)	48205(16)	73	C(21)	47868(30)	54119(19)	13629(24)	80
N	57497(16)	76440(9)	88550(14)	53	C(22)	53361(24)	55325(14)	25344(21)	63
C(3)	35292(19)	70594(10)	76320(16)	44	C(23)	66396(20)	57845(11)	52318(18)	50
C(4)	33036(23)	63846(12)	72030(19)	54	C(24)	65434(27)	54667(14)	62126(22)	69
C(5)	22919(26)	59969(14)	72532(22)	65	C(25)	75026(31)	50843(16)	69518(28)	82
C(6)	14613(27)	62671(15)	77319(22)	70	C(26)	86062(32)	50252(16)	67531(29)	81
C(7)	16369(24)	69290(15)	81642(22)	66	C(27)	87445(28)	53202(18)	57934(31)	89
C(8)	26428(22)	73133(14)	81036(21)	58	C(28)	77689(24)	56922(16)	50347(26)	73
C(9)	43728(19)	81959(10)	67841(16)	45	B(1)	47171(22)	74841(12)	75340(19)	44
C(10)	35025(22)	86833(12)	68791(21)	57	B(2)	55341(24)	62175(13)	44093(22)	51
C(11)	32046(25)	92736(13)	61986(23)	67	C(1)′	6797(5)	7116(3)	7657(5)	80
C(12)	37529(30)	93902(16)	53785(25)	77	C(2)′	6924(4)	7673(3)	8554(4)	78
C(13)	45920(35)	89321(17)	52479(26)	85	C(15)′	5567(6)	8263(3)	9437(4)	81
C(14)	49050(28)	83454(14)	59427(22)	67	C(16)′	5842(6)	7037(4)	9638(5)	92
C(17)	50465(20)	61167(12)	30616(18)	51	C(1a)″	6503(9)	6716(5)	8066(7)	89
C(18)	42047(23)	65846(16)	23457(22)	65	C(2a)″	6352(9)	6971(5)	9156(8)	87
C(19)	36618(27)	64677(19)	11707(24)	81	C(15a)″	5260(8)	7882(5)	9802(6)	81
					C(16a)″	6706(7)	8181(5)	8815(7)	90

Can. J. Chem. Downloaded from www.nrcresearchpress.com by 210.87.254.40 on 09/06/12
For personal use only.

TABLE 1. (*Concluded*)

Atom	*x*	*y*	*z*	U_{eq}/U_{iso}	Atom	*x*	*y*	*z*	U_{eq}/U_{iso}
H(O2)	5183(27)	6739(14)	5571(27)	103(11)	H(1a)′	7169	6682	8027	93
H(4)	3891(21)	6194(11)	6840(19)	63(7)	H(1b)′	7208	7259	7103	93
H(5)	2176(24)	5534(15)	6911(23)	90(9)	H(2a)′	7015	8127	8235	90
H(6)	702(25)	5980(13)	7729(21)	86(8)	H(2b)′	7656	7582	9238	90
H(7)	1033(28)	7154(16)	8518(26)	110(11)	H(1c)″	6408	6211	8026	101
H(8)	2768(22)	7732(13)	8471(21)	71(8)	H(1d)″	7328	6840	8032	101
H(10)	3068(20)	8603(12)	7406(19)	66(7)	H(2c)″	7179	7032	9761	99
H(11)	2590(24)	9608(13)	6350(22)	81(8)	H(2d)″	5843	6663	9438	99
H(12)	3568(26)	9785(15)	4896(26)	96(10)	H(15a)′	6316	8350	10107	97
H(13)	5019(28)	8974(16)	4690(28)	117(11)	H(15b)′	5422	8655	8901	97
H(14)	5514(23)	8049(13)	5865(21)	73(8)	H(15c)′	4842	8202	9694	97
H(18)	3998(21)	6973(12)	2671(19)	63(7)	H(16a)′	5133	7043	9935	110
H(19)	3061(25)	6818(14)	708(23)	90(9)	H(16b)′	5808	6605	9200	110
H(20)	3559(24)	5782(13)	−160(26)	86(8)	H(16c)′	6627	7056	10284	110
H(21)	4958(26)	4990(15)	1040(25)	97(10)	H(15d)″	5947	7886	10541	97
H(22)	5857(24)	5165(14)	3000(22)	79(8)	H(15e)″	4912	8349	9623	97
H(24)	5723(29)	5522(14)	6354(23)	96(9)	H(15f)″	4604	7563	9848	97
H(25)	7369(26)	4865(15)	7599(27)	104(10)	H(16d)″	7358	8209	9576	109
H(26)	9257(28)	4767(15)	7236(26)	89(10)	H(16e)″	7089	8039	8235	109
H(27)	9520(31)	5294(16)	5637(26)	114(11)	H(16f)″	6299	8628	8604	109
H(28)	7837(25)	5893(14)	4347(25)	99(9)					

*Primed and double-primed atoms have occupancies of 0.60 and 0.40 respectively.

average values of $w(|F_o| - |F_c|)^2$ over ranges of both $|F_o|$ and $\sin\theta/\lambda$ and was employed in the final stages of refinement. Convergence was reached at $R = 0.038$ and $R_w = 0.047$ for 1522 reflections with $I \geq 3\sigma(I)$. For all 3113 reflections $R = 0.112$. The function minimized was $\Sigma w(|F_o| - |F_c|)^2$, $R = \Sigma||F_o| - |F_c||/\Sigma|F_o|$ and $R_w = (\Sigma w(|F_o| - |F_c|)^2/\Sigma w|F_o|^2)^{1/2}$.

On the final cycle of refinement the mean and maximum parameter shifts corresponded to 0.03 and 0.28σ respectively. The mean error in an observation of unit weight was 1.677. A final difference map showed no unusual features. The final positional and thermal parameters appear in Tables 1 and 2[3] respectively. Measured and calculated structure factors have been placed in the Depository of Unpublished Data.[3]

(2-N,N-dimethylaminoethanolato)diphenylboron, 2

Experimental details are as above except where noted. Crystal dimensions were ca. 0.10 × 0.46 × 0.50 mm. Crystal data:

$C_{16}H_{20}BNO$ fw = 253.16

Monoclinic, $a = 7.0721(4)$, $b = 16.8829(4)$, $c = 12.0975(8)$ Å, $\beta = 97.875(3)°$, $V = 1430.8(1)$ Å^3, $Z = 4$, $\rho_c = 1.175$ g cm^{-3}, $F(000) = 544$, μ(Mo Kα) = 0.67 cm^{-1}. Absent reflections: hkl, $h+k$ odd, and $h0l$, l odd, space group Cc (C_s^4, No. 9) assumed on the basis of the number of molecules in the unit-cell.

An $\omega-2\theta$ scan at 0.96−10.06° min^{-1} over a range of (0.75 + 0.35 tan θ)° in ω was employed. Of 2067 independent reflections measured (to $2\theta = 60°$), 1649(79.8%) had intensities greater than $3\sigma(I)$ above background. Data were corrected for an isotropic decay of 3.4% which occurred during the course of the data collection.

The structure was solved by direct methods. After refinement of the non-hydrogen atoms with anisotropic thermal parameters to $R = 0.067$, the coordinates of all 20 hydrogen atoms were determined from a difference map. Convergence was reached at $R = 0.031$ and $R_w = 0.040$ for 1649 reflections with $I \geq 3\sigma(I)$, for all 2067 reflections $R = 0.044$. The mean and maximum parameter shifts on the final cycle of refinement corresponded to 0.12 and 0.59σ respectively, and the mean error in an observation of unit weight was 1.392.

(2-N,N-dimethylaminoethanolato)diphenylboron − diphenylborinic acid (1:1), 3

Crystal dimensions were ca. 0.27 × 0.33 × 0.37 mm. Crystal data:

$C_{28}H_{31}B_2NO_2$ fw = 435.19

Monoclinic, $a = 11.3231(10)$, $b = 19.3190(12)$, $c = 12.2451(11)$ Å, $\beta = 109.321(4)°$, $V = 2527.7(4)$Å^3, $Z = 4$, $\rho_c = 1.144$ g cm^{-3}, $F(000) = 928$, μ(Mo Kα) = 0.65 cm^{-1}. Absent reflections: $h0l$, $h+l$ odd, and $0k0$, k odd uniquely indicate the space group $P2_1/n$.

An $\omega-2\theta$ scan at 1.34−10.06° min^{-1} over a range of (0.65 + 0.35 tan θ)° in ω was employed. Of 4422 independent reflections measured (to $2\theta = 50°$), 2420(54.7%) had $I \geq 3\sigma(I)$. Data were corrected for an isotropic decay of 3.0% during the data collection.

The structure was solved by direct methods, all non-hydrogen atoms being located from an *E*-map. After two cycles of refinement with isotropic thermal parameters to $R = 0.167$, a difference map indicated twofold conformational disorder of the five-membered chelate ring. Site occupancies of the resolved atoms C(1), C(2), C(15), and C(16) were then refined, resulting in normalized average values of 0.60 and 0.40 for the two sets of positions. These parameters were kept fixed during subsequent cycles of refinement. The non-hydrogen atoms were then refined with anisotropic thermal parameters to $R = 0.097$ at which point a difference map revealed all of the ordered hydrogen atoms, these being subsequently refined with isotropic thermal parameters. The disordered hydrogen atoms were included as fixed atoms with C—H = 0.98 Å and an isotropic thermal parameter 25% larger than that associated with the carbon atom to which it is bonded. Convergence was reached at $R = 0.040$ and $R_w = 0.049$ for 2420 observed reflections, for all 4422 reflections, $R = 0.093$. The mean and maximum parameter shifts on the final cycle of refinement were 0.16 and 0.70σ, and the mean error in an observation of unit weight was 1.760.

Analysis of thermal motion

The thermal motion in each of the three structures (Fig. 1) has been analysed in terms of the rigid-body modes of translation, libration, and screw-motion (9). The rms errors in the U_{ij} (derived from the least-squares analyses) are 0.0012, 0.0009, and 0.0015 Å^2 for **1**, **2**, and the ordered non-hydrogen atoms of **3** respectively. Analysis of entire molecules in each case indicated significant independent motion of the phenyl rings. PhB groups were separately analysed in each structure (rms ΔU_{ij} = 0.0014 − 0.0031 Å^2). The chelate rings plus atoms

[3]The structure factor table, Table 2 (anisotropic thermal parameters) and other material mentioned in the text are available, at a nominal charge, from the Depository of Unpublished Data, CISTI, National Research Council of Canada, Ottawa, Canada K1A 0S2.

Can. J. Chem. Downloaded from www.nrcresearchpress.com by 210.87.254.40 on 09/06/12
For personal use only.

Can. J. Chem. Downloaded from www.nrcresearchpress.com by 210.87.254.40 on 09/06/12
For personal use only.

TABLE 3. Bond lengths (Å) with estimated standard deviations in parentheses

Bond	Length Uncorr.	Length Corr.	Bond	Length Uncorr.	Length Corr.
			1		
O —C(1)	1.434(2)	1.437	C(6)—C(7)	1.376(4)	1.385
O —B	1.478(2)	1.481	C(7)—C(8)	1.365(4)	1.373
N —C(3)	1.495(3)	1.498	C(8)—C(9)	1.385(3)	1.389
N —B	1.638(3)	1.643	C(10)—C(11)	1.387(3)	1.403
C(1)—C(2)	1.507(3)	1.510	C(10)—C(15)	1.389(3)	1.398
C(2)—C(3)	1.513(3)	1.516	C(10)—B	1.621(3)	1.626
C(4)—C(5)	1.396(3)	1.405	C(11—C(12)	1.385(3)	1.390
C(4)—C(9)	1.393(3)	1.401	C(12)—C(13)	1.362(4)	1.374
C(4)—B	1.616(3)	1.620	C(13)—C(14)	1.369(4)	1.386
C(5)—C(6)	1.393(3)	1.397	C(14)—C(15)	1.387(3)	1.391
			2		
O —C(1)	1.415(2)	1.418	C(5)—C(6)	1.379(4)	1.385
O —B	1.470(2)	1.476	C(6)—C(7)	1.372(4)	1.380
N —C(2)	1.501(2)	1.506	C(7)—C(8)	1.395(3)	1.398
N —C(15)	1.489(2)	1.494	C(9)—C(10)	1.405(2)	1.412
N —C(16)	1.485(3)	1.490	C(9)—C(14)	1.400(2)	1.408
N —B	1.686(2)	1.691	C(9)—B	1.614(2)	1.618
C(1)—C(2)	1.518(3)	1.523	C(10)—C(11)	1.391(3)	1.394
C(3)—C(4)	1.396(3)	1.404	C(11)—C(12)	1.375(3)	1.382
C(3)—C(8)	1.402(3)	1.408	C(12)—C(13)	1.376(3)	1.382
C(3)—B	1.627(2)	1.632	C(13)—C(14)	1.389(3)	1.392
C(4)—C(5)	1.390(3)	1.394			
			3		
O(1)—B(1)	1.482(3)	1.492	C(12)—C(13)	1.346(4)	1.356
O(1)—C(1)	1.382(5)	1.388	C(13)—C(14)	1.391(4)	1.396
O(2)—B(2)	1.348(3)	1.354	C(17)—C(18)	1.393(3)	1.402
N —B(1)	1.682(3)	1.690	C(17)—C(22)	1.392(3)	1.401
N —C(2)	1.494(5)	1.505	C(17)—B(2)	1.570(3)	1.574
N —C(15)	1.442(6)	1.450	C(18)—C(19)	1.383(4)	1.388
N —C(16)	1.497(6)	1.507	C(19)—C(20)	1.373(4)	1.382
C(3)—C(4)	1.397(3)	1.406	C(20)—C(21)	1.370(4)	1.379
C(3)—C(8)	1.402(3)	1.408	C(21)—C(22)	1.382(4)	1.387
C(3)—B(1)	1.614(3)	1.617	C(23)—C(24)	1.385(3)	1.400
C(4)—C(5)	1.387(3)	1.391	C(23)—C(28)	1.389(3)	1.406
C(5)—C(6)	1.366(4)	1.372	C(23)—B(2)	1.564(3)	1.569
C(6)—C(7)	1.373(4)	1.382	C(24)—C(25)	1.376(4)	1.382
C(7)—C(8)	1.382(3)	1.386	C(25)—C(26)	1.355(4)	1.371
C(9)—C(10)	1.395(3)	1.406	C(26)—C(27)	1.361(4)	1.375
C(9)—C(14)	1.385(3)	1.399	C(27)—C(28)	1.386(4)	1.391
C(9)—B(1)	1.628(3)	1.632	C(1)—C(2)	1.510(8)	1.518
C(10)—C(11)	1.387(3)	1.391	C(1a)—C(2a)	1.485(12)	1.490
C(11)—C(12)	1.363(4)	1.377	N —C(2a)	1.458(9)	1.469
N —C(15a)	1.513(8)	1.519	N —C(16a)	1.512(8)	1.520
O(1)—C(1a)	1.460(7)	1.465			

directly bonded to these rings were also analysed (rms ΔU_{ij} = 0.0017 and 0.0015 Å^2 for **1** and **2**, 0.0060 and 0.0085 Å^2 for the alternate rings in the disordered (2-*N*,*N*-dimethylaminoethanolato)diphenylboron molecule of **3**). The appropriate bond distances have been corrected for libration (9, 10), using shape parameters q^2 of 0.08 for all atoms involved. Corrected bond lengths appear in Table 3 along with the uncorrected values; corrected bond angles do not differ by more than 1σ from the uncorrected values given in Table 4. Intra-annular torsion angles defining the conformations of heterocyclic rings are listed in Table 5. Bond lengths and angles involving hydrogen and a complete listing of torsion angles (Table 6–8) are included as supplementary material.

Results and discussion

The chelates **1** and **2** are formed by simple esterification of diphenylborinic acid (water being eliminated) followed by intramolecular N → B coordination. The molecular complex **3** (**2**·Ph_2BOH, stabilized by an O—H···O hydrogen bond) is formed as a result of the presence of excess Ph_2BOH in the reaction mixture. In reactions of this type an excess of (2-aminoethanolato)diphenylboron is employed to compensate for losses during the hydrolysis step of the synthesis.

The crystal structure of **1** consists of discrete molecules, each linked to two others by N—H···O hydrogen bonds

TABLE 4. Bond angles (deg) with estimated standard deviations in parentheses

Bonds	Angle (deg)	Bonds	Angle (deg)
	1		
C(1)—O —B	116.97(15)	C(11)—C(10)—B	121.9(2)
C(3)—N —B	113.3(2)	C(15)—C(10)—B	122.8(2)
O —C(1)—C(2)	110.5(2)	C(10)—C(11)—C(12)	122.2(2)
C(1)—C(2)—C(3)	110.8(2)	C(11)—C(12)—C(13)	121.0(2)
N —C(3)—C(2)	108.7(2)	C(12)—C(13)—C(14)	118.6(2)
C(5)—C(4)—C(9)	115.8(2)	C(13)—C(14)—C(15)	120.1(2)
C(5)—C(4)—B	123.3(2)	C(10)—C(15)—C(14)	122.8(2)
C(9)—C(4)—B	120.7(2)	O —B —N	104.88(14)
C(4)—C(5)—C(6)	121.9(2)	O —B —C(4)	113.90(15)
C(5)—C(6)—C(7)	120.0(3)	O —B —C(10)	108.32(15)
C(6)—C(7)—C(8)	119.7(2)	N —B —C(4)	108.61(15)
C(7)—C(8)—C(9)	120.0(2)	N —B —C(10)	107.96(15)
C(4)—C(9)—C(8)	122.6(2)	C(4)—B —C(10)	112.74(15)
C(11)—C(10)—C(15)	115.2(2)		
	2		
C(1)—O —B	112.52(14)	C(3)—C(8)—C(7)	121.8(2)
C(2)—N —C(15)	109.2(2)	C(10)—C(9)—C(14)	115.5(2)
C(2)—N —C(16)	109.54(15)	C(10)—C(9)—B	125.91(15)
C(2)—N —B	99.46(14)	C(14)—C(9)—B	118.47(15)
C(15)—N —C(16)	108.3(2)	C(9)—C(10)—C(11)	121.9(2)
C(15)—N —B	110.76(13)	C(10)—C(11)—C(12)	120.8(2)
C(16)—N —B	119.03(14)	C(11)—C(12)—C(13)	119.1(2)
O —C(1)—C(2)	107.36(15)	C(12)—C(13)—C(14)	120.2(2)
N —C(2)—C(1)	104.41(15)	C(9)—C(14)—C(13)	122.6(2)
C(4)—C(3)—C(8)	115.8(2)	O —B —N	98.23(12)
C(4)—C(3)—B	119.5(2)	O —B —C(3)	112.28(14)
C(8)—C(3)—B	124.55(15)	O —B —C(9)	110.33(13)
C(3)—C(4)—C(5)	122.7(2)	N —B —C(3)	109.65(12)
C(4)—C(5)—C(6)	119.8(2)	N —B —C(9)	113.51(13)
C(5)—C(6)—C(7)	119.6(2)	C(3)—B —C(9)	112.11(12)
C(6)—C(7)—C(8)	120.4(2)		
	3		
B(1)—O(1)—C(1)	115.1(3)	C(22)—C(17)—B(2)	122.2(2)
B(1)—N —C(2)	99.3(2)	C(17)—C(18)—C(19)	121.6(3)
B(1)—N —C(15)	117.4(3)	C(18)—C(19)—C(20)	119.9(3)
B(1)—N —C(16)	110.6(3)	C(19)—C(20)—C(21)	120.0(3)
C(2)—N —C(15)	112.1(4)	C(20)—C(21)—C(22)	120.1(3)
C(2)—N —C(16)	107.9(4)	C(17)—C(22)—C(21)	121.6(3)
C(15)—N —C(16)	108.9(4)	C(24)—C(23)—C(28)	115.8(2)
C(4)—C(3)—C(8)	114.5(2)	C(24)—C(23)—B(2)	121.3(2)
C(4)—C(3)—B(1)	120.0(2)	C(28)—C(23)—B(2)	122.9(2)
C(8)—C(3)—B(1)	125.5(2)	C(23)—C(24)—C(25)	122.5(3)
C(3)—C(4)—C(5)	122.6(3)	C(24)—C(25)—C(26)	120.1(3)
C(4)—C(5)—C(6)	120.6(3)	C(25)—C(26)—C(27)	119.8(3)
C(5)—C(6)—C(7)	119.3(3)	C(26)—C(27)—C(28)	120.1(3)
C(6)—C(7)—C(8)	119.8(3)	C(23)—C(28)—C(27)	121.7(3)
C(3)—C(8)—C(7)	123.3(3)	O(1)—B(1)—N	97.82(15)
C(10)—C(9)—C(14)	114.5(2)	O(1)—B(1)—C(3)	111.0(2)
C(10)—C(9)—B(1)	124.5(2)	O(1)—B(1)—C(9)	110.7(2)
C(14)—C(9)—B(1)	120.9(2)	N —B(1)—C(3)	110.7(2)
C(9)—C(10)—C(11)	122.9(2)	N —B(1)—C(9)	110.4(2)
C(10)—C(11)—C(12)	120.0(3)	C(3)—B(1)—C(9)	114.9(2)
C(11)—C(12)—C(13)	119.4(3)	O(2)—B(2)—C(17)	115.5(2)
C(12)—C(13)—C(14)	120.7(3)	O(2)—B(2)—C(23)	121.8(2)
C(9)—C(14)—C(13)	122.6(3)	C(17)—B(2)—C(23)	122.6(2)
C(18)—C(17)—C(22)	116.8(2)	O(1)—C(1)—C(2)	105.8(4)
C(18)—C(17)—B(2)	120.7(2)	N —C(2)—C(1)	106.0(4)
C(2a)—N —B(1)	101.4(4)	C(15a)—N —B(1)	111.9(3)
C(2a)—N —C(15a)	109.7(6)	C(15a)—N —C(16a)	105.4(5)
C(2a)—N —C(16a)	109.8(6)	C(16a)—N —B(1)	118.6(3)
O(1)—C(1a)—C(2a)	107.8(6)	N —C(2a)—C(1a)	104.6(7)
B(1)—O(1)—C(1a)	110.8(4)		

Can. J. Chem. Downloaded from www.nrcresearchpress.com by 210.87.254.40 on 09/06/12
For personal use only.

TABLE 5. Intra-annular torsion angles (deg) standard deviations in parentheses

Atoms	Value (deg)
1	
B —O —C(1)—C(2)	60.3(2)
O —C(1)—C(2)—C(3)	−58.8(3)
C(1)—C(2)—C(3)—N	57.9(3)
B —N —C(3)—C(2)	−55.8(2)
C(3)—N —B —O	52.0(2)
C(1)—O —B —N	−54.1(2)
2	
B —O —C(1)—C(2)	4.3(2)
O —C(1)—C(2)—N	24.4(2)
B —N —C(2)—C(1)	−38.6(2)
C(2)—N —B —O	39.70(14)
C(1)—O —B —N	−27.2(2)
3	
B(1)—O(1)—C(1)—C(2)	0.7(6)
O(1)—C(1)—C(2)—N	27.0(6)
B(1)—N —C(2)—C(1)	−38.3(4)
C(2)—N —B(1)—O(1)	35.6(3)
C(1)—O(1)—B(1)—N	−22.1(4)
B(1)—O(1)—C(1a)—C(2a)	−1.2(9)
O(1)—C(1a)—C(2a)—N	−26.7(10)
B(1)—N —C(2a)—C(1a)	40.1(8)
C(2a)—N —B(1)—O(1)	−39.3(5)
C(1a)—O(1)—B(1)—N	24.0(5)

(N—H(Nb)···O(1/2 − x, 1/2 + y, 1/2 − z), H···O = 1.88(3), N···O = 2.814(2) Å, N—H···O = 163(2)°) to form continuous spirals about the twofold screw axes. The structure of **2** consists of individual molecules separated by normal van der Waals distances, and that of **3** contains hydrogen-bonded $Ph_2BOCH_2CH_2NMe_2$—Ph_2BOH units (O(2)—H(O2)···O(1), H···O = 1.87(3), O···O = 2.729(2) Å, O—H···O = 166(3)°), separated from other such units by normal van der Waals distances.

The six-membered heterocyclic ring in **1** has a slightly distorted chair conformation (see Table 5). The intraannular bond angles in this ring are, as expected, nearer the tetrahedral value than are those in the five-membered rings of **2** and **4**. The O—B, N—B, mean[4] C—B, O—C, and N—C bond lengths in **1** (1.481(2), 1.643(3), 1.623(3), 1.437(2), and 1.498(3) Å respectively) may be compared with the corresponding mean values for compounds **4** (1.477(2), 1.654(1), 1.618(1), 1.412(2), and 1.488(2) Å). The only statistically significant differences between corresponding parameters are a lengthening of the O—C bond by 0.025(3) Å and a shortening of the N—B bond by 0.011(3) Å in **1** relative to those in compounds **4**.

The five-membered heterocyclic ring in **2** has an envelope conformation, the nitrogen atom being displaced from the approximate plane of the other four ring atoms. The two conformations of the disordered ring in the (2-*N*,*N*-dimethylaminoethanolato)diphenylboron molecule in **3**, mirror images of one another, are essentially the same as that found in the ordered structure **2** (see Table 5). Bond lengths and angles for the (2-*N*,*N*-dimethylaminoethanolato)diphenylboron molecules in **2** and **3** are generally the same; all bonds to boron are equal within experimental error except the B—O distance (1.476(2) Å in **2**, 1.492(3) Å in **3**). In spite of the fact that the ring oxygen atom in **3** is involved in a hydrogen bond,unlike that in **2**, most of this discrepancy probably arises from imperfect modelling of the conformational disorder in **3**.

The major structural differences between the (2-*N*,*N*-dimethylaminoethanolato)diphenylboron molecule and compounds **4** are the expected (on steric grounds) increases of the N—B and N—C(ring) distances (by 0.037(2) and 0.018(3) Å) to 1.691(2) and 1.506(2) Å respectively. The N—B distances in compounds **1**, **2**, and **4** are thus found to be directly proportional to the rates of hydrolytic cleavage of the N—B bonds (5, 11).

The trigonal planar boron atom in the Ph_2BOH molecule of **3** is displaced 0.017(3) Å from the plane of its substituents. The C(17) and C(23) phenyl groups are twisted out the B(2) coordination plane by 16.1 and 47.8° respectively. The C—B—C angle is 122.6(2)° while the C—B—O angles are significantly different, 115.5(2)° for C(17) and 121.8(2)° for C(23). The mean C—B(2) distance of 1.572(3) Å lies between the mean values of 1.566(3) Å in $PhB(OH)_2$ (12) and 1.580(9) Å in Ph_3B (13), and the B(2)—O(2) distance of 1.354(3) Å is significantly shorter than the corresponding mean of 1.371(6) Å in $PhB(OH)_2$.

The phenyl rings in all three structures are slightly, but significantly, non-planar (χ^2 = 12.7−70.5), the maximum deviation of any phenyl carbon atom from its respective mean plane being 0.015 Å. The geometry of the B-substituted phenyl rings is as expected (14).

[4]Here and elsewhere in this report mean values refer to weighted means with rms deviations from the mean in parentheses.

Acknowledgments

We thank the Natural Sciences and Engineering Research Council of Canada for financial support and the University of British Columbia Computing Centre for assistance.

1. W. KLIEGEL, D. NANNINGA, S. J. RETTIG, and J. TROTTER. Can. J. Chem. **61**, 2329 (1983).
2. S. J. RETTIG and J. TROTTER. Can. J.Chem. **51**, 1288 (1973).
3. S. J. RETTIG and J. TROTTER. Can. J. Chem. **54**, 3130 (1976).
4. S. J. RETTIG and J. TROTTER. Acta Crystallogr. Sect. B, **30**, 2139 (1974).
5. H. K. ZIMMERMAN. Adv. Chem. Ser. **42**, 23 (1964).
6. G. N. CHEREMOS, H. WEIDMANN, and H. K. ZIMMERMAN. J. Org. Chem. **26**, 1683 (1961).
7. D. T. CROMER and J. B. MANN. Acta Crystallogr. Sect. A, **24**, 321 (1968).
8. R. F. STEWART, E. R. DAVIDSON, and W. T. SIMPSON. J. Chem. Phys. **42**, 3175 (1965).
9. V. SCHOMAKER and K. N. TRUEBLOOD. Acta Crystallogr. Sect. B, **24**, 63 (1968).
10. D. W. J. CRUICKSHANK. Acta Crystallogr. **9**, 747 (1956); **9**, 754 (1956); **14**, 896 (1961).
11. H. K. ZIMMERMAN, D. W. MUELLER, and W. F. SEMMELROGGE, JR. Ann. Chem. **655**, 54 (1962).
12. S. J. RETTIG and J. TROTTER. Can. J. Chem. **55**, 3071 (1977).
13. F. ZETTLER, H. D. HAUSEN, and H. HESS. J. Organomet. Chem. **72**, 157 (1974).
14. A. DOMENICANO, A. VACIAGO, and C. A. COULSON. Acta Crystallogr. Sect. B, **31**, 221 (1975); **31**, 1630 (1975).

Can. J. Chem. Downloaded from www.nrcresearchpress.com by 210.87.254.40 on 09/06/12
For personal use only.

Uranium recovery from phosphate ores through sintering

L. A. GUIRGUIS
Nuclear Materials Corporation, Cairo, Egypt

Received May 7, 1982[1]

L. A. GUIRGUIS. Can. J. Chem. **61**, 2341 (1983).

The use of an alkaline reactant for phosphate processing is an alternative to the current methods of using acid reagents.

In this work the possibilities of attacking low-grade phosphate ores by sintering with sodium carbonate at moderate temperature are considered. The carbonate liquor obtained by a water leach contains uranium in the form of uranyl tricarbonate complex, as well as the equivalent dissolved phosphate. Uranium from such liquor was recovered as sodium uranate on addition of sodium hydroxide, while pure sodium phosphate, useful as a chemical, was recovered by fractional crystallization.

Finally, a flowsheet was designed for the proposed process.

L. A. GUIRGUIS. Can. J. Chem. **61**, 2341 (1983).

L'utilisation d'un réactif alcalin pour le traitement des phosphates offre la possibilité de rompre avec les méthodes usuelles basées sur les réactifs acides.

Dans ce travail, on considère la possibilité de traiter les minerais à faible teneur en phosphate en les agglomérant avec le carbonate de sodium à température modérée. La solution carbonatée obtenue par lavage à l'eau contient de l'uranium sous forme de carbonate d'uranyle, en plus de l'équivalent en phosphate dissout. On récupère l'uranium sous forme d'uranate de sodium en ajoutant de l'hydroxyde de sodium à la solution tandis qu'on récupère, par cristallisation fractionné, le phosphate à l'état pur.

Finalement on propose un cheminement pour cette technique.

[Traduit par le journal]

Introduction

To convert the phosphorus in apatite to a soluble form for use as a plant nutrient, the phosphate, along with impurities such as uranium, are commonly dissolved in sulphuric acid to produce superphosphate or phosphoric acid for further processing. Such acid processes are not so readily applied to low-grade ores; in particular, they are unsuitable for treatment of ores in which calcareous gangue would lead to acid wastage and the production of unwanted calcium salts. Thus the use of new chemical process routes is necessary.

High-temperature, or sinter-reaction, treatment of phosphate rock has been studied widely (1–3). However, most of the processes described aim at the defluorination of apatite. Separation of products of high phosphate content is not normally contemplated. The Rhenania process, thus far the most successful example of a sintering process, produces a fertilizer containing at best 30% P_2O_5. In this sinter reaction, apatite reacts with silica and sodium carbonate at a temperature in the range 1100–1200°C, yielding a complex product that may be either a sodium calcium silicophosphate or a mixture of sodium calcium orthophosphate and calcium orthosilicate. In fact, the sintering temperature used in the Rhenania process is fairly high.

In the present study, the examined phosphate sample was found to be amenable to attack by sintering with sodium carbonate in the presence of sodium fluoride at 700°C, a temperature much lower than that used in a typical Rhenania process. Moreover, the formation of the soluble uranyl tricarbonate anion, $UO_2(CO_3)_3^{4-}$ permits the use of this method for the nearly selective dissolution of uranium from the sintered material.

Experimental procedure

The present study was carried out on a low-grade phosphate sample from the Abu Shegella area, phosphate horizon (c), Red Sea region, Egypt. The analysed chemical composition (in wt%) was as follows: SiO_2 28.0, CaO 33.19, MgO 0.40, Al_2O_3 0.53, Fe_2O_3 0.38, FeO 2.28, TiO_2 0.32, Cr_2O_3 0.66, P_2O_5 13.90, Na_2O 0.54, K_2O 0.05, SO_4 1.80, Cl 0.32, F 3.71, CO_2 9.28, H_2O 0.83, organic matter 2.80, U 0.014.

TABLE 1. Effect of particle size on extraction process

Mesh size	P_2O_5 leached, %
30	7.35
100	18.58
200	40.92
325	80.00
400	79.93

Sodium carbonate and sodium fluoride were milled to the same mesh size as that of the ore, and thoroughly mixed with the ore in an agate mortar. The prepared sample fraction was placed in a fused magnesite crucible and inserted inside a tube furnace heated to the required temperature.

Atmospheric carbonate leaching experiments were done using the carbonate sintered milled ore in 1 L round bottom glass vessels with three openings. The large opening in the middle through which the stirrer rod passes was water sealed in order to minimize the evaporation of solution and subsequent increase in the pH during the leaching process. One of the smaller openings was connected to a reflux water condenser to prevent the eventual escape of condensable gases; the other opening supported a thermometer. The leaching vessels were clamped in a temperature-regulated oil bath.

Sodium bicarbonate and air or $KMnO_4$ were added in the appropriate amounts and then water was added in equal volume to the ore. After the end of a leaching experiment, an aliquot of the slurry was cooled to measure the pH, followed by filtration through Buchner funnels with suction. The spent ore cake was washed by an equal weight of hot 5 g/L Na_2CO_3 solution in two successive steps to displace the soluble values. The original filtrate and washings were collected in a measuring flask, the volume was adjusted using a 5 g/L Na_2CO_3 solution and a sample was analysed for uranium, phosphorus, and other constituents. The wet residue was weighed, dried in a drying oven at 110°C, reweighed, ground to 300 mesh size, quartered, and then analysed for its unleached uranium content.

A number of pressure-leaching tests were conducted on the sintered

[1] Revision received March 31, 1983.

Can. J. Chem. Downloaded from www.nrcresearchpress.com by 210.87.254.6 on 09/06/12
For personal use only.

TABLE 2. Effect of amount of sodium carbonate on the extraction process

Amount of Na_2CO_3 (g/kg ore)	Amount of NaF (g/kg ore)	P_2O_5 leached, %
50	2.5	34.12
100	5	46.56
200	10	62.42
300	15	80.10
400	20	79.28
500	25	80.03

ore in a stirred thermoregulated autoclave of 5-L capacity. Air was supplied from a standard cylinder by means of a 2-stage pressure regulator.

The sintered milled ore (200 g), the desired amount of sodium bicarbonate, oxidant, and water was introduced in the stainless steel reaction vessel. The autoclave was then heated to 90°C. Air was then introduced to a pressure of 5 atm and from this instant the leaching time was calculated.

Results and discussion

A large number of sintering and leaching experiments were performed on the ore, each time changing one of the different sintering factors that affect the overall extraction (sintering + leaching) process, namely, the amount of sodium carbonate, the amount of sodium fluoride, the ore grain size, the temperature, the time of sintering. Efficiency of leaching P_2O_5 did not exceed 80% at 700°C sintering temperature. The conditions of the leaching experiments were not varied.

(a) Effect of sintering time

With other parameters fixed at 300 g Na_2CO_3/kg ore, 15 g NaF/kg ore and a temperature of 700°C, the amount of P_2O_5 leached was constant at 80% ± 1% for each 5- to 30-min sintering time.

(b) Effect of grain size

Table 1 shows the effect of grain size on the sintering–extraction process. The extent of the sintering improved with the fineness of the ore. This may be due to the large surface area exposed. The optimum grain size was found to be 325 mesh.

(c) Effect of the amount of sodium carbonate

This factor has been studied over different sodium carbonate quantities ranging from 50 to 500 g/kg ore. 5% of this quantity was sometimes added as sodium fluoride. Other factors were fixed at 5-min sintering time, 700°C temperature, and ore milled to 325 mesh size.

The results given in Table 2 show that the percentage of P_2O_5 leached increased with an increase in the amount of sodium carbonate and that a minimum of about 300 g Na_2CO_3/kg ore appears to be sufficient for the maximum recovery of P_2O_5 (about 80%).

(d) Effect of temperature

Figure 1 shows the effect of sintering temperature on the leaching of the phosphate sample. It is clear that about 75–80% P_2O_5 could dissolve at 700°C after sintering in the presence of 15 g NaF/kg ore as a sintering promoter.

At this low sintering temperature calcium carbonate present as calcareous gangue does not interfere with the sintering reaction.

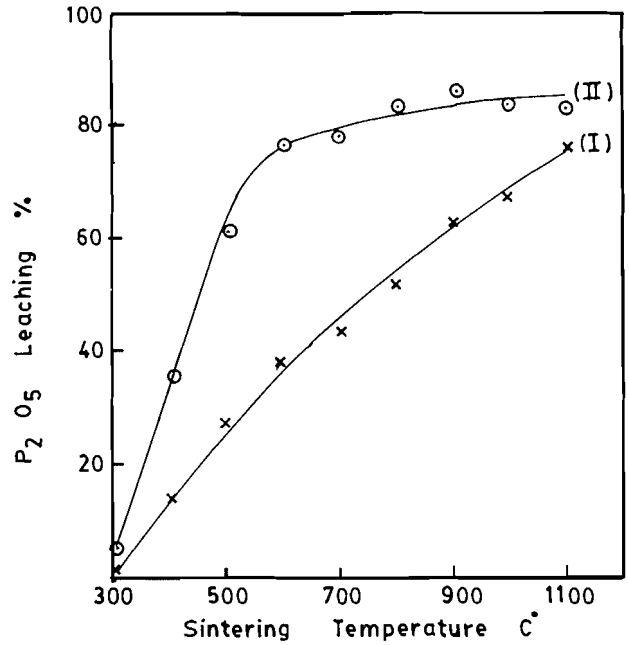

FIG. 1. Leaching efficiency of P_2O_5 versus sintering temperature using Na_2CO_3 (*I*) and Na_2CO_3 + NaF (*II*).

The 80% leachable P_2O_5 could also be obtained by sodium carbonate sintering without calcium fluoride at 1100°C. However, subsequent leaching of uranium from that product proved to be difficult.

Carbonate leaching

The chemistry of the carbonate process is discussed here, and has been fully explained by Merritt (4).

$$2UO_2 + O_2 \rightleftharpoons 2UO_3$$

$$UO_3 + Na_2CO_3 + 2NaHCO_3 \rightleftharpoons Na_4[UO_2(CO_3)_3] + H_2O$$

Bicarbonate is added to the leach solution to react with hydroxyl ion and thereby prevent reprecipitation of part of the dissolved uranium. The hydroxyl ion will form in the absence of bicarbonate by carbonate reaction with uranium as follows:

$$UO_3 + 3Na_2CO_3 + H_2O \rightleftharpoons Na_4UO_2(CO_3)_3 + 2\ NaOH$$

The results of alkaline leaching tests on the sintered ore are summarized in Table 3. In this table sodium carbonate and sodium bicarbonate are given in g/kg ore; however, the two reagents were used in equal proportions with respect to their sodium content. This investigation was carried out at a solid/liquid ratio of 1:1. To take into consideration the fact that alkaline leaching is a slow process, a series of preliminary experiments covering a range of 2 to 28 h agitation time were carried out. On the basis of the data obtained, it may be concluded that 12 h agitation time in atmospheric alkaline leaching and 3 h agitation time in pressure alkaline leaching is quite adequate to bring about the required leaching efficiency.

According to Frank (4), the optimum temperature range appears to be 80–115°C. It was therefore decided to adopt 90°C for uranium alkaline leaching.

Uranium recovery from carbonate leach liquors

The pregnant liquor thus formed can then be subjected to a sodic decomposition step whereby sodium diuranate assaying

Can. J. Chem. Downloaded from www.nrcresearchpress.com by 210.87.254.6 on 09/06/12
For personal use only.

TABLE 3. Results of atmospheric and pressure alkaline leaching

Atmospheric alkaline leaching						Pressure alkaline leaching					
Na_2CO_3 (g/kg)	$NaHCO_3$ (g/kg)	Oxidant air (m^3/kg ore)	Time (h)	Temperature (°C)	%U leached	$NaCO_3$ (g/kg)	$NaHCO_3$ (g/kg)	Oxidant $KMnO_4$ (g/kg)	Time (h)	Temperature (°C)	%U leached
300	475	—	12	90	40.07	300	475	—	3	90	42.05
300	475	0.0071	12	90	70.13	300	475	5	3	90	65.23
300	475	0.0142	12	90	80.00	300	475	10	3	90	81.00

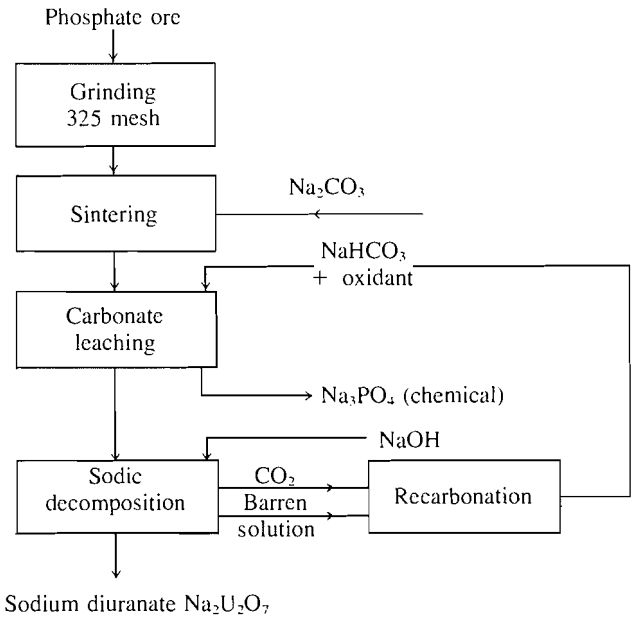

FIG. 2. Process flowsheet for uranium recovery from phosphates.

65% U is produced.

$$2UO_2(CO_3)_3^{4-} + 6OH^- + 2Na^+ \rightarrow Na_2U_2O_{7\downarrow} + 6CO_3^{2-} + 3H_2O$$

Sodium hydroxide neutralizes first the bicarbonate ions and then proceeds to precipitate the uranium at pH 11 (5).

For uranium to precipitate by the above process its concentration should be 3–4 g/L and since the liquor is very dilute, the addition of a primer such as a known amount of uranium to initiate the precipitation is essential. An alternative is to recycle the dilute liquor for further leaching in order to enrich it in uranium before precipitation. Partial evaporation of the dilute liquor could also be employed. Sodium phosphate is recovered from the carbonate liquor by fractional crystallization. A process flowsheet is shown in Fig. 2.

Conclusion

Alkaline sintering at moderate temperature of phosphate ores like the presently studied sample will allow industry to obtain by-product uranium according to local conditions, and to make effective use of a wider variety of ore material including those of low phosphate grade. The idea that alkaline leach methods are ineffective in the dissolution of uranium from phosphate is discredited.

1. W. H. WAGGMAN. Phosphoric acid, phosphates and phosphatic fertilizers. Am. Chem. Soc. Monograph, Reinhold, New York. 1952. Sec. 20.
2. A. GMELINS. Handbuck der anorganischen Chemie. 28(Calcium), Teil B, Liefering 1. 1973. pp. 206–213.
3. A. J. E. J. WELCH. Lean phosphate beneficiation. J. Chem. Soc. 734 (1978).
4. A. J. FRANK. Summary of carbonate leaching of uranium ores, U.S. Atomic Energy Comm., ACCO-48, American Cyanamid Company, Winchester, MA. 1954.
5. R. C. MERRITT. The extractive metallurgy of uranium, Colorado School of Mines Res. Inst., Golden, Colorado, 1971. p. 88.

Can. J. Chem. Downloaded from www.nrcresearchpress.com by 210.87.254.6 on 09/06/12
For personal use only.

Potentiométrie de précision à basse température dans les mélanges eau − éthylène glycol; grandeurs thermodynamiques relatives aux ionisations de l'acide acétique et du solvant mixte

HAMED BAHRI, JEAN-CLAUDE HALLÉ[1] ET ROBERT SCHAAL

Laboratoire de Physicochimie des Solutions, LA CNRS 161, E.N.S.C.P. 11 Rue Pierre et Marie Curie, F75231 Paris Cedex 05, France

Reçu le 3 janvier 1983

HAMED BAHRI, JEAN-CLAUDE HALLÉ et ROBERT SCHAAL. Can. J. Chem. **61**, 2344 (1983).

Des mesures de forces électromotrices de piles sans jonction, comportant une électrode d'hydrogène et une électrode argent − chlorure d'argent, ont permis de déterminer dans les mélanges eau − éthylène glycol contenant 50 et 70% en masse de diol, et pour 14 températures allant de −35 à 30°C, les fonctions thermodynamiques relatives à la dissociation de l'acide acétique d'une part et du solvant mixte d'autre part. Les standards primaires d'acidité de ces mélanges, tamponnés par l'acide acétique ou rendus basiques par la soude sont également donnés.

HAMED BAHRI, JEAN-CLAUDE HALLÉ, and ROBERT SCHAAL. Can. J. Chem. **61**, 2344 (1983).

Electromotive force measurements of cells without liquid-junction containing hydrogen electrodes and silver − silver chloride electrodes have been used to derive the dissociation constants of acetic acid and solvent water − ethylene glycol mixtures (50 and 70 mass % of ethyleneglycol) at 14 temperatures from −35 to 30°C. Primary acidity standards related to these acetic buffered and sodium hydroxide solutions are given.

Can. J. Chem. Downloaded from www.nrcresearchpress.com by 210.87.254.6 on 09/06/12
For personal use only.

Introduction

Au cours des dix dernières années l'utilisation d'agents cryoprotecteurs a considérablement amélioré les conditions de conservation des tissus vivants et en particulier, des organes en attente d'être greffés (1−6). La maîtrise du niveau d'acidité de ces solutions refroidies, obtenues le plus souvent en ajoutant à de l'eau des alcools ou du diméthylsulfoxyde (1, 6−8), s'est vite révélée indispensable pour une meilleure connaissance des réactions cellulaires (2−5, 9−12). A part les standardisations précises très récentes de quelques tampons, réalisées à l'électrode d'hydrogène dans des mélanges eau−DMSO (11) et eau−éthanol (12) les échelles d'acidité établies à ce jour en-dessous de 0°C, ont été construites par potentiométrie à l'électrode de verre (9, 13, 14) et doivent donc être utilisées avec circonspection tant qu'elles n'auront pas été contrôlées par des mesures absolues à l'électrode d'hydrogène (14, 15). Un des buts de ce travail est donc la standardisation jusqu'à −35°C des solutions eau − éthylène glycol (EGOH), contenant respectivement 50 et 70% d'alcool en masse, tamponnées à partir de l'acide acétique et simultanément, nous avons déterminé dans ces milieux refroidis, les fonctions thermodynamiques relatives à la dissociation de cet acide. Le bon fonctionnement de l'électrode d'hydrogène dans ces mélanges hydroorganiques rendus basiques par l'addition d'une base forte a également rendu possible la détermination des niveaux d'alcalinité élevés obtenus, permettant ainsi l'utilisation à basse température de tout le domaine acido-basique accessible.

Résultats et discussion

1. Dissociation de l'acide acétique

La constante d'acidité K_a de l'acide acétique (HAc), relative à l'équilibre d'ionisation:

$$HAc + HS \rightleftharpoons Ac^- + H_2S^+$$

dans les solvant mixte HS, et qui s'exprime par:

$$[1] \quad K_a = a_{H_2S^+} \frac{m_{Ac^-}}{m_{HAc}} \frac{\gamma_{Ac^-}}{\gamma_{HAc}}$$

est reliée à la force électromotrice E_A — ramenée à la pression d'hydrogène d'une atmosphère (15) — de la chaîne électrolytique (A) par l'expression [2]

$$[A] \quad Pt;\ H_2\ (g,\ 1\ atm) \left| \begin{array}{l} HAc\ (m_{HAc}),\ NaAc\ (m_{NaAc}) \\ \\ NaCl\ (m_{NaCl})\ dans\ HS \end{array} \right| AgCl;\ Ag$$

$$[2] \quad pK_a = \frac{E_A - E^0}{(RT \ln 10)/F} + \log_{10} \frac{m_{HAc}\, m_{Cl^-}}{m_{Ac^-}} + \log_{10} \frac{\gamma_{HAc}\, \gamma_{Cl^-}}{\gamma_{Ac^-}}$$

Dans ces expressions a, m et γ désignent respectivement les activité, molalité et coefficient d'activité des différentes espèces (H_2S^+ représente le proton solvaté par l'eau et/ou par le diol) et E^0 le potential standard de l'électrode AgCl, Ag déterminé préalablement (15). La constante diélectrique relativement élevée de ces mélanges (15) rend la dissociation des sels (NaCl et NaAc) totale.

L'expérience montre que le dernier terme de l'expression [2] est une fonction linéaire de la force ionique I du milieu qui, compte tenu des conditions expérimentales ($m_{HAc} = m_{NaAc} = m_{NaCl} = m$), est égale à $2m$. Le pK_a s'obtient donc par extrapolation à force ionique nulle du pK'_a apparent calculé à partir de [3]:

$$[3] \quad pK'_a = \frac{E_A - E^0}{(RT \ln 10)/F} + \log_{10} m = pK_a - \beta I$$

Pour chaque molalité m étudiée, il se trouve que la f.e.m. E_A de la pile (A) est une fonction linéaire de la température centigrade t. Les coefficients a et b représentatifs de cette variation apparaissent dans le tableau 1. L'extrapolation linéaire à dilution infinie de pK'_a (éq. [3]) conduit aux valeurs de pK_a rassemblées dans le tableau 2. Nous avons également reporté dans le tableau 2 les niveaux d'acidité ($pa_H = -\log a_{H_2S^+}$) des solutions tamponnées de molalité 0,01. Ils ont été calculés à partir de la relation [4]:

$$[4] \quad pa_H = pK_a + \log_{10} \frac{m_{Ac^-}}{m_{HAc}} + \log_{10} \frac{\gamma_{Ac^-}}{\gamma_{HAc}}$$

[1]À qui toute correspondance doit être adressée.

Can. J. Chem. Downloaded from www.nrcresearchpress.com by 210.87.254.6 on 09/06/12
For personal use only.

TABLEAU 1. Coefficients a et b représentatifs de l'influence de la température sur la force électromotrice E_A de la pile A: $E_A = a + bt$ dans les milieux EGOH−H_2O contenant 50 et 70% d'éthylène glycol en masse

EGOH−H_2O 50%			EGOH−H_2O 70%		
m	a	$b \times 10^4$	m	a	$b \times 10^4$
0,150245	0,54721	4,58617	0,157055	0,55167	3,51622
0,138384	0,54932	4,75144	0,139111	0,55461	3,57875
0,118684	0,55287	4,88479	0,118603	0,55819	3,77639
0,100315	0,55635	5,08305	0,104737	0,56102	3,99133
0,091136	0,55918	5,18251	0,093225	0,56393	3,94462
0,081085	0,56149	5,27285	0,083713	0,56593	4,19663
0,070931	0,56474	5,46844	0,071907	0,56987	4,41718
0,061807	0,56774	5,68509	0,062645	0,57323	4,40346
0,051789	0,57168	5,70317	0,051728	0,57767	4,55028
0,039946	0,57787	6,02018	0,041059	0,58272	4,88810
0,030005	0,58449	6,25285	0,031325	0,58876	5,07208
0,019474	0,59415	6,65112	0,020555	0,59905	5,39624
0,009768	0,61035	7,36719	0,010627	0,61387	6,09306

TABLEAU 2. Influence de la température sur le pK_a de l'acide acétique (HAc) et sur le pa_H du tampon acétique calculé d'après l'éq. [4] ($m_{HAc} = m_{Ac^-} \simeq 0{,}01$) dans les milieux EGOH−$H_2O$ contenant respectivement 50 et 70% d'éthylène glycol en masse

	EGOH−H_2O 50%		EGOH−H_2O 70%	
t°C	pK_a	pa_H	pK_a	pa_H
30	5,423	5,356	5,815	5,741
25	5,418	5,352	5,813	5,740
20	5,416	5,351(5,25[a])	5,813	5,740
15	5,418	5,354	5,815	5,743
10	5,422	5,358	5,820	5,749
5	5,430	5,367	5,828	5,757
0	5,442	5,380(5,35[a])	5,839	5,769
−5	5,458	5,397	5,854	5,785
−10	5,477	5,416(5,40[a])	5,871	5,802
−15	5,501	5,441	5,892	5,824
−20	5,530	5,470(5,45[a])	5,917	5,850
−25	5,563	5,503	5,946	5,879
−30	5,602	5,542(5,50[a])	5,980	5,914
−35	5,646	5,586	6,017	5,951

[a]Références 14 et 16, échelle molaire ($c_{HAc} = c_{Ac^-} = 0{,}01$).

en identifiant, d'une part le coefficient d'activité de la molécule d'acide acétique à l'unité ($\gamma_{HAc} \simeq 1$) ce qui est raisonnable tant que la molalité reste faible, et d'autre part, le coefficient d'activité de l'anion acétate au coefficient d'activité moyen $\gamma_\pm$ déterminé préalablement (15). Les niveaux d'acidité du même tampon acétique déterminés à l'aide d'une électrode de verre (14, 16) par Douzou et collaborateurs pour l'un des milieux étudiés (référés à l'échelle molaire) apparaissent également dans le tableau 2 (entre parenthèses). Leur conversion dans l'échelle molale n'est pas nécessaire pour conclure à l'excellent accord qui les lie à nos résultats. La majoration qu'il faudrait leur apporter pour les amener dans l'échelle molale, égale au logarithme décimal de la masse volumique (15), reste en effet inférieure à l'incertitude expérimentale des mesures de Douzou: $\Delta p a_H = 0{,}05$.

Parmi les diverses équations proposées pour rendre compte de l'influence de la température sur le pK_a (17), la plus utilisée — éq. [5], (18) — est ici encore celle qui convient le mieux:

$$[5] \quad pK_a = \frac{A}{T} - C + DT$$

Les coefficients A, C et D qui redonnent les valeurs de pK_a expérimentales à 0,001 près valent respectivement 1573,2; 5,3309 et 0,018354 pour le milieu contenant 50% de diol et 1299,3; 2,9845 et 0,014889 pour celui titrant 70% de diol. Ils permettent le calcul des fonctions thermodynamiques usuelles relatives à la dissociation de l'acide acétique soit:

$$[6] \quad \begin{aligned} \Delta G^0 &= R\ (\ln 10)\ (A - CT + DT^2) \\ \Delta S^0 &= R\ (\ln 10)\ (C - 2DT) \\ \Delta H^0 &= R\ (\ln 10)\ (A - DT^2) \\ \Delta C_p{}^0 &= R\ (\ln 10)\ (-2DT) \end{aligned}$$

La mesure au centième de millivolt des forces électromotrices, rend la détermination, par cette méthode, de l'enthalpie libre de dissociation très précise. Si la précision reste bonne après une première dérivation (ΔS^0 et ΔH^0), il faut être conscient que le $\Delta C_p{}^0$ résultant d'une seconde dérivation sera beaucoup moins fiable car il dépendra beaucoup plus de l'expression retenue pour caractériser la dépendance du pK_a avec la température (19). Les $\Delta C_p{}^0$ ainsi obtenus, ont néanmoins été consignés dans le tableau 3 avec les valeurs des autres grandeurs thermodynamiques.

Comme dans beaucoup de solvants, la dissociation de l'acide acétique est maximum au voisinage de 20°C, son ionisation athermique se situant respectivement à 19,6°C et 22,2°C pour les deux mélanges étudiés.

II. Dissociation du solvant

(1) Détermination du produit ionique

Le caractère amphotère des deux constituants du mélange permet de schématiser la réaction d'ionisation du solvant par l'expression suivante:

$$2HS \rightleftharpoons H_2S^+ + S^-$$

où H_2S^+ désigne toujours le proton solvaté sous ses différentes formes ($H_3O^+ + EGOH_2^+$) et où S^- représente la base conjuguée du solvant c'est à dire OH^- et EGO^-. Le produit ionique K_s du milieu mixte défini par:

$$[7] \quad K_s = a_{H_2S^+} a_{S^-}$$

est accessible à partir de la force électromotrice E_B de la pile B

Can. J. Chem. Downloaded from www.nrcresearchpress.com by 210.87.254.6 on 09/06/12
For personal use only.

TABLEAU 3. Fonctions thermodynamiques relatives à la dissociation de l'acide acétique dans les milieux EGOH−H_2O contenant respectivement 50% (*a*) et 70% (*b*) d'éthylène glycol en masse

	ΔG^0 (J mol^{-1})		ΔH^0 (J mol^{-1})		ΔS^0 (J $K^{-1}mol^{-1}$)		ΔC_p^0 (J K^{-1} mol^{-1})	
t°C	(*a*)	(*b*)	(*a*)	(*b*)	(*a*)	(*b*)	(*a*)	(*b*)
30	31473	33753	−2175,7	−1322,7	−111,0	−115,7	−213,1	−172,8
25	30927	33181	−1119,2	−465,7	−107,5	−112,8	−209,5	−170,0
20	30399	32624	−80,3	+377,1	−104,0	−110,0	−206,0	−167,1
15	29888	32081	+941,1	+1205,7	−100,5	−107,1	−202,5	−164,3
10	29394	31553	+1944,8	+2019,9	−96,9	−104,3	−199,0	−161,4
5	28919	31038	+2931,1	+2820,0	−93,4	−101,4	−195,5	−158,6
0	28459	30538	+3899,7	+3605,7	−89,9	−98,6	−192,0	−155,7
−5	28019	30052	+4850,8	+4377,3	−86,4	−95,7	−188,5	−152,9
−10	27596	29581	+5784,3	+5134,5	−82,9	−92,9	−184,9	−150,0
−15	27190	29123	+6700,2	+5877,5	−79,4	−90,0	−181,4	−147,2
−20	26801	28680	+7598,6	+6606,3	−75,9	−87,2	−177,9	−144,3
−25	26430	28251	+8479,4	+7320,8	−72,3	−84,3	−174,4	−141,5
−30	26078	27837	+9342,6	+8021,1	−68,8	−81,5	−170,9	−138,6
−35	25745	27436	+10188,2	+8707,1	−65,3	−78,6	−167,4	−135,8

TABLEAU 4. Coefficients a', b' et c' représentatifs de l'influence de la température sur la force électromotrice E_B de la pile B: $E_B = a' + b't + c't^2$ dans les milieux EGOH−H_2O contenant 50 et 70% d'éthylène glycol en masse

EGOH−H_2O 50%				EGOH−H_2O 70%			
m_{S^-}[a]	a'	$b' \times 10^4$	$c' \times 10^7$	m_{S^-}	a'	$b' \times 10^4$	$c' \times 10^7$
0,016019	0,9847	5,21	−22,3	0,008630[b]	0,97823	4,28	−25,2
0,030123	0,9855	5,50	−19,7	0,016859[b]	0,97872	4,76	−8,19
0,054015	0,9865	5,82	−3,0	0,035280[b]	0,97967	4,74	−3,02
0,059116	0,9867	5,64	−9,2	0,048514[a]	0,9730	4,46	−5,91
0,072582	0,9874	5,95	−8,6	0,051049[b]	0,97944	4,59	−10,04
0,090669	0,9877	5,76	−6,7	0,062006[b]	0,97769	4,55	−5,50
0,104660	0,9874	5,75	−11,1	0,069930[b]	0,98057	4,77	−2,39
0,128282	0,9888	5,76	−10,3	0,091959[b]	0,98070	4,61	−10,22
0,148663	0,9891	5,52	−11,0	0,093308[a]	0,9727	4,35	−4,58
				0,130691[b]	0,98223	4,84	−1,06
				0,169661[b]	0,98227	4,83	+1,43

[a] $\log_{10} m_{Cl^-}/m_{S^-} = 0{,}015$.
[b] $\log_{10} m_{Cl^-}/m_{S^-} = -0{,}081$.

[B] Pt; H_2 (g, 1 atm) | NaS (m_{NaS}), NaCl (m_{NaCl}) / solvant HS | AgCl; Ag

En effet, le pK_s du milieu (éq. [8]) s'obtient par extrapolation à dilution infinie du pK_s' aisément calculable (éq. [9])

$$[8] \quad pK_s = \frac{E_B - E^0}{(RT \ln 10)/F} + \log_{10} \frac{m_{Cl^-}\,\gamma_{Cl^-}}{m_{S^-}\,\gamma_{S^-}}$$

$$[9] \quad pK_s' = \frac{E_B - E^0}{(RT \ln 10)/F} + \log_{10} \frac{m_{CL^-}}{m_{S^-}} = pK_s - \log_{10} \frac{\gamma_{Cl^-}}{\gamma_{S^-}}$$

Un programme de régression polynomiale d'ordre multiple (calculateur Apple II 64K) montre que la force électromotrice E_B (ramenée à la pression d'une atmosphère) est une fonction du second degré en t ($E = a' + b'c + c't^2$), dont les coefficients sont rassemblés dans le tableau 4.

L'expérience montre que pK_s' est une fonction linéaire de la force ionique du milieu ce qui rend aisée et précise la détermination de pK_s (tableau 5). Il ressort du tableau 5, que nos résultats sont en bon accord avec les pK_s antérieurement mesurés au-dessus de 0°C, en utilisant l'électrode de référence argent − bromure d'argent (20).

Les niveaux d'acidité (pa_H) des solutions alcalines peuvent être calculés au moyen de la relation [10].

$$[10] \quad pa_H = pK_s + \log_{10} m_{S^-} + \log_{10} \gamma_{S^-}$$

où le coefficient d'activité de la base γ_{S^-} est identifié au coefficient d'activité moyen $\gamma_\pm$ déjà rapporté (15). Les niveaux d'acidité correspondant aux solutions 0.01 molales en base forte apparaissent dans le tableau 5.

(2) Fonction thermodynamiques

Dans la mesure où la relation [5] s'applique également au pK_s, les fonctions thermodynamiques relatives à la dissociation du solvant sont représentées par les éq. [6] avec pour A, C et D les valeurs 3103,4; −0,20907 et 0,01025 lorsque le milieu contient 50% de diol en masse et 2835,7; −1,8525 et 8,075 $\times 10^{-3}$ lorsqu'il en contient 70%. L'examen du tableau 6, où nous avons reporté quelques valeurs ainsi calculées, montre que le processus de dissociation des solvants mixtes étudiés est essentiellement enthalpique d'une part, et que nos résultats sont en bon accord avec ceux rapportés par Banerjee à 25°C (20) d'autre part.

Nous avons déjà mentionné que, contrairement aux enthalpies libres de dissociation, les fonctions dérivées entropie et

Can. J. Chem. Downloaded from www.nrcresearchpress.com by 210.87.254.6 on 09/06/12
For personal use only.

TABLEAU 5. Influence de la température sur le pK_s des milieux mixtes EGOH−H_2O contenant respectivement 50 et 70% d'éthylène glycol en masse d'une part, et sur le niveau d'acidité (pa_H) des mêmes milieux 0,01 molal en base forte ($m_{S^-} = 0{,}01$)

	EGOH−H_2O 50%		EGOH−H_2O 70%	
t°C	pK_s	pa_H	pK_s	pa_H
45	13,224[a] (13,22)[b]	11,153	13,355[c] (13,40)[b]	11,279
40	13,329[a]	11,259	13,437[c]	11,362
35	13,438[a] (13,43)[b]	11,369	13,543[c] (13,61)[b]	11,468
30	13,553 (13,54)[b]	11,486	13,655 (13,71)[b]	11,581
25	13,673 (13,66)[b]	11,607	13,771 (13,82)[b]	11,698
20	13,799	11,734	13,892	11,819
15	13,933 (13,92)[b]	11,869	14,020 (14,05)[b]	11,948
10	14,071	12,007	14,154	12,083
5	14,216 (14,21)[b]	12,153	14,293 (14,32)[b]	12,222
0	14,370	12,308	14,440	12,370
−5	14,531	12,470	14,593	12,524
−10	14,699	12,638	14,753	12,684
−15	14,876	12,816	14,922	12,854
−20	15,061	13,001	15,098	13,031
−25	15,258	13,198	15,283	13,216
−30	15,464	13,404	15,479	13,413
−35	15,681	13,621	15,682	13,616

[a]Valeurs calculées à partir de l'équation:

$$pK_s = \frac{3103{,}40}{T} + 0{,}20907 + 0{,}01025T$$

[b]Référence 20.
[c]Valeurs calculées à partir de l'équation:

$$pK_s = \frac{2835{,}74}{T} + 1{,}8525 + 0{,}008075T.$$

TABLEAU 6. Fonctions thermodynamiques relatives à la dissociation des milieux EGOH−H_2O contenant respectivement 50% (a) et 70% (b) d'éthylène glycol en masse[a]

	ΔG^0 (J mol^{-1})		ΔH^0 (J mol^{-1})		ΔS^0 (J K^{-1} mol^{-1})	
t°C	(a)	(b)	(a)	(b)	(a)	(b)
30	78664	79245	41380	40073	−123	−129
25	78054	78603	41970[c]	40539[d]	−121[e]	−128[f]
20	77454	77969	42550	40996	−119	−126
15	76863	77342	43120	41446	−117	−125
10	76283	76723	43680	41887	−115	−123
5	75712	76112	44232	42322	−113	−121
−0	75151	75508	44773	42748	−111	−120
−5	74600	74912	45304	43167	−109	−118
−10	74059	74324	45825	43578	−107	−117
−15	73527	73745	46337	43981	−105	−115
−20	73005	73172	46838	44376	−103	−114
−25	72493	72607	47330	44764	−101	−112
−30	71991	72050	47812	45144	−99	−111
−35	70499	71500	48284	45516	−97	−109

[a]Valeurs précédemment déterminées par Banerjee *et al.* (20): 41208 J mol^{-1} (c); 39129 J mol^{-1} (d); −123 J K^{-1} mol^{-1} (e); −133 J K^{-1} mol^{-1} (f).

enthalpie, sont moins précises. Il était donc souhaitable de comparer ces valeurs à celles obtenues par mesure directe. Pour ce faire nous avons déterminé par microcalorimétrie à 25°C, l'enthalpie de dissociation des deux mélanges étudiés. Les ΔH^0 ainsi obtenus et qui valent 44611 et 42102 J mol^{-1} pour les milieux hydroalcooliques contenant respectivement 50 et 70% d'éthylène glycol, sont supérieurs d'environ 5% aux déterminations potentiométriques (Tableau 6). Bien qu'un écart de cet ordre et dans ce sens ait déjà été constaté entre les résultats obtenus par ces deux techniques (21−24) aucune explication n'a été à ce jour proposée et nous ne pensons pas comme l'a suggéré l'un des Referee que la détermination des coefficients d'activité soit responsable des écarts observés.

Partie expérimentale

La purification de l'éthylène glycol (Prolabo Normapur) et les dis-

positifs expérimentaux ont déjà été décrits (15). Il en est de même de la purification de l'acide acétique et de l'acétate de sodium (Prolabo) (25). Le chlorure de sodium a été purifié par trois précipitations successives en ajoutant de l'éthanol à une solution aqueuse saturée en sel. Le produit obtenu, séché sous vide, est alors exempt de bromure (26) anion qui nuirait au bon fonctionnement de l'électrode Ag, AgCl (27). Les solutions basiques ont été obtenues à partir d'une solution mère aqueuse, préparée par dissolution de soude exempte de carbonate (J. T. Baker) dans de l'eau bidistillée soigneusement décarbonatée et standardisée à partir d'une solution chlorhydrique elle-même standardisée par gravimétrie.

Le remplissage de la cellule se fait à l'abri de l'oxygène et sous un courant d'hydrogène qui permet aussi de dégazer les solutions.

Les électrodes sont thermoélectriquement préparées (28) et la cellule potentiométrique, semblable à celle utilisée par Bates (29), a été entourée d'une gaine dans laquelle circule de l'azote gazeux thermorégulé (30). Une coque moulée de polyuréthane de 2 cm d'épaisseur assure une excellente isolation thermique à l'ensemble. L'incertitude sur la température (repérée à l'intérieur de la solution au moyen d'une sonde à résistance de platine) est de l'ordre de 0,05°C et permet d'estimer les f.e.m. à 10^{-5} V près.

Ce dispositif ne permet que très difficilement de stabiliser la température à des valeurs reproductibles pour les différentes solutions. Nous avons donc choisi de déterminer pour chaque molalité, à partir d'une vingtaine de mesures comprises entre 30 et −35°C, les paramètres de l'équation $E = f(t)$ (Tableaux 1 et 4), qui permettent ensuite de calculer les f.e.m. pour les 14 températures entières espacées de 5°.

Les mesures calorimétriques des enthalpies d'ionisation des solvants à 50 et 70% d'alcool en masse ont été réalisées sur un microcalorimètre dynamique Picker à écoulement continu (31) commercialisé en France par Sétaram. L'incertitude sur les valeurs de l'enthalpie mesurées à l'aide de cet appareil est estimée à 1%.

1. P. DOUZOU. Cryobiochemistry. An introduction. Academic Press, London. 1977. Chapt. I.
2. F. S. SOLIMAN et L. VANDEN BERG, Cryobiology, **8**, 73 (1971); **8**, 265 (1971).
3. B. C. ELFORD et C. A. WALTER. Cryobiology, **9**, 82 (1972).
4. D. E. PEGG. J. Chim. Pathol. **29**, 271 (1976).
5. M. J. TAYLOR, C. A. WALTER, et B. C. ELFORD. Cryobiology, **15**, 452 (1978).
6. W. L. REYNOLDS. Dimethylsulfoxide in inorganic chemistry. *Dans* Progress in inorganic chemistry. Vol. 2. *Edité par* S. J. Lippard. Interscience. 1970. p. 1.
7. J. E. LOVELOCK et M. W. H. BISHOP. Nature, London, **183**, 1394 (1959).
8. T. NASH. J.Gen. Physiol. **46**, 167 (1962).
9. G. HUI BON HOA et P. DOUZOU. J. Biol. Chem. **248**, 4649 (1973).
10. Référence 1, chapt. III.
11. M. J. TAYLOR. J. Chem. Eng. Data, (*a*) **23**, 308 (1978); (*b*) **24**, 230 (1979).
12. (*a*) M. SANKAR, J. B. MACASKILL et R. G. BATES. J. Solution Chem. **8**, 887 (1979); (*b*) R. G. BATES, H.P. BENETTO et M. SANKAR. Anal. Chem. **52**, 1598 (1980).
13. Référence 1, Chapt. II.
14. P. MAUREL, G. HUI BON HOA et P. DOUZOU. J. Biol. Chem. **250**, 1376 (1975).
15. H. BAHRI et J. C. HALLE. Bull. Soc. Chim. Fr. 1448 (1981).
16. Référence 1, p. 53.
17. H. S. HARNED et B. B. OWEN. The physical chemistry of electrolytic solutions. 2nd ed. Reinhold Publishing Corp., New York, NY. p. 490.
18. H. S. HARNED et R. A. ROBINSON. Trans. Faraday Soc. **36**, 973 (1940).
19. R. GABORIAUD. Bull. Soc. Chim. Fr. 1605 (1971).
20. S. K. BANERJEE, K. K. KUNDU et M. N. DAS. J. Chem. Soc. (A), 166 (1967).
21. L. AVEDIKIAN. Bull. Soc. Chim. Fr. **8**, 2832 (1971).
22. C. P. BEZBORUAH, M. F. G. F. C. CAMOES, A. K. COVINGTON et J. V. DOBSON. J. Chem. Soc. Faraday Trans. I, **69**, 949 (1973).
23. G. OLOFSSON et I. OLOFSSON. J. Chem. Thermodyn. **5**, 533 (1973).
24. A. K. COVINGTON, M. I. A. FERRA et R. A. ROBINSON. J. Chem. Soc. Faraday Trans. I, **73**, 1721 (1977).
25. J. C. HALLE et R. G. BATES. J. Soln. Chem. **4**, 1033 (1975).
26. W. C. SOMMERVILLE et A. D. CAMPBELL. Microchim. Acta, 991 (1963).
27. G. D. PINCHING et R. G. BATES. J. Res. Natl. Bur. Stand. **37**, 311 (1946).
28. R. G. BATES. Determination of pH theory and practice. 2nd ed. J. Wiley and Sons. 1973.
29. R. G. BATES. Ed. N.B.S. Tech. Note 271, 27 (1965).
30. J. C. HALLE, R. SCHAAL, A. M. KOULKES-PUJO, J. SUTTON et T. H. TRAN THI. J. Chem. Res. (M) 1133 (1979).
31. P. PICKER, P. A. LEDUC, P. R. PHILIP et J. E. DESNOYERS. J. Chem. Thermodyn. **3**, 631 (1971).

Can. J. Chem. Downloaded from www.nrcresearchpress.com by 210.87.254.6 on 09/06/12
For personal use only.

The crystal structure and single crystal polarized spectra of *trans*-bis(trichloroacetato)bis(*N*,*N*-dimethylethylenediamine)cobalt(II)

DAVID B. EVANS AND MARY FRANCES RICHARDSON[1]
Department of Chemistry, Brock University, St. Catharines, Ont., Canada L2S 3A1

PAUL J. MCCARTHY
Department of Chemistry, Canisius College, Buffalo, NY 14208, U.S.A.

AND

A. B. P. LEVER,[1], S. R. PICKENS, AND I. M. WALKER[1]
Department of Chemistry, York University, Downsview, Ont., Canada M3J 1P3

Received January 19, 1983

DAVID B. EVANS, MARY FRANCES RICHARDSON, PAUL J. MCCARTHY, A. B. LEVER, S. R. PICKENS, and I. M. WALKER. Can. J. Chem. **61**, 2349 (1983).

$CO[(CH_3)_2NCH_2CH_2NH_2]_2[CCl_3CO_2]_2$ belongs to the monoclinic crystal system, space group $P2_1/c$ with a = 7.216(1) Å, b = 12.117(3) Å, c = 13.616(4) Å, β = 103.27(2)°, V = 1158.7 Å^3, Z = 2. The structure was solved by the heavy atom method and was refined to R = 0.048, R_w = 0.056 for 1761 reflections with $I \geq 3\sigma(I)$. The complexes lie on crystallographic centers of symmetry. Deviations from regular octahedral coordination are due to steric crowding and chelate ring constraints. The Co—NMe_2 bond is longer than the Co—NH_2 bond (2.258(3) vs. 2.100(3) Å). The Co—O distance is 2.138(3) Å. The chelate rings each contain a disordered carbon atom such that these rings are 54% *gauche* and 46% envelope. There are intramolecular and intermolecular H-bonds between the Me_2en and trichloracetate ligands. The polarized single crystal spectra are interpreted in terms of D_{2h} symmetry for the complex.

DAVID B. EVANS, MARY FRANCES RICHARDSON, PAUL J. MCCARTHY, A. B. P. LEVER, S. R. PICKENS et I. M. WALKER. Can. J. Chem. **61**, 2349 (1983).

Les cristaux de $CO[(CH_3)_2NCH_2CH_2NH_2]_2[CCl_3CO_2]_2$ sont monocliniques et appartiennent au groupe d'espace $P2_1/c$ avec a = 7,216(1) Å, b = 12,117(3) Å, c = 13,616(4) Å, β = 103,27(2)°, V = 1158,7 Å^3, Z = 2. On a résolu la structure par la méthode de l'atome lourd et on l'a affinée jusqu'à des valeurs de R = 0,048 et de R_w = 0,056 pour 1761 réflexions avec $I \geq 3\sigma(I)$. Les complexes se situent sur des centres cristallographiques de symétrie. Les déviations par rapport à une coordination octaédrique régulière sont dues à un encombrement stérique et à des contraintes dans le cycle chélaté. La liaison Co—NMe_2 est plus longue que la liaison Co—NH_2 (2,258(3) contre 2,100(3) Å). La distance Co—O est de 2,138(3) Å. Chaque cycle chélaté contient un atome de carbone déformé de telle sorte que ces cycles sont à 54% *gauche* et à 64% de type enveloppe. Il y a des liaisons hydrogènes inter et intramoléculaires entre les ligands Me_2 en et trichloroacétate. On interprète les spectres polarisés du monocristal en fonction d'une symétrie D_{2h} du complexe.

[Traduit par le journal]

Introduction

The spectra of six-coordinate d^7 and d^8 metal ions in octahedral and tetragonal symmetries have been the subject of numerous studies (1, 2). The splittings of the octahedral T-states into E and A or B states in tetragonal symmetry are well understood. The band splittings are especially well resolved when there are marked differences in the strengths of the in-plane and axial ligand fields.

Systems whose symmetries are less than D_{4h} are very numerous, yet detailed treatments of their spectra are few. The situation is complicated by the large number of possible low symmetry point groups which result from loss of the four-fold axis. Detailed X-ray structural information is essential in order to establish which of the many possible types of distortion actually applies to an individual complex.

In our early explorations of this neglected area, we reported analyses of the electronic spectra of several complexes whose C_{2v} symmetry had been previously demonstrated by detailed X-ray work (3). The reduction in symmetry from D_{4h} to C_{2v} was explored theoretically by means of the Normalised Spherical Hamiltonian (NSH), and Angular Overlap Model (AOM) methods.

More recently, we have studied complexes whose geometry is very nearly D_{2h} due to their all-*trans* nature. We have reported the X-ray structure and crystal spectrum of $Ni((C_2H_5)_2NCH_2CH_2NH_2)_2(NCS)_2$, in which the lowest triplet band is clearly resolved into three well separated peaks (4). The X-ray structure of this complex reveals that the Ni—NEt_2 distance is very much longer than usual for Ni—N distances in complexes. This provides an explanation for the rhombic spectrum in terms of a reduced AOM σ parameter for the dialkylated nitrogen bond vector. We were thus able to extend the work of Bertini *et al.* (5), thereby demonstrating a clear inverse correlation between metal ligand bond length and AOM σ bonding parameters.

As part of an on-going study related to the single crystal spectra of low symmetry transition metal complexes (1–7), we now report the X-ray crystallographic analysis and low temperature electronic spectrum of bis(trichloroacetato)bis(*N*,*N*-dimethylethylenediamine)cobalt(II).

Experimental

Crystals were grown following stoichiometric reaction of cobalt trichloroacetate with *N*,*N*-dimethylethylenediamine under a nitrogen blanket. Analyses were satisfactory.

Many of the crystals were twinned. One rather large red crystal, 0.55 × 0.35 × 0.23 mm, appeared to be single and was chosen for further work. Unit cell parameters were determined from 20 reflections ($10.2° < \theta < 16.9°$) measured on an Enraf-Nonius CAD-4

[1]To whom correspondence should be addressed.

Can. J. Chem. Downloaded from www.nrcresearchpress.com by 210.87.254.6 on 09/06/12
For personal use only.

Can. J. Chem. Downloaded from www.nrcresearchpress.com by 210.87.254.6 on 09/06/12
For personal use only.

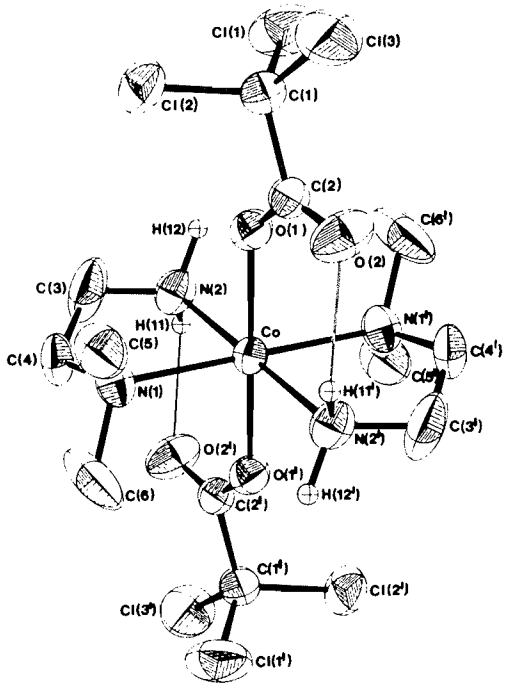

FIG. 1. The *trans*-$[Co(Me_2en)_2(CCl_3CO_2)_2]$ molecule showing the numbering scheme and thermal ellipsoids. The superscript refers to centrosymmetrically related atoms. Hydrogen atoms except those on the $—NH_2$ group have been omitted for clarity.

diffractometer with MoKα radiation (λ = 0.71069 Å). Crystal data are:

$C_{12}H_{24}Cl_6CoN_4O_4$ fw = 560.00

Monoclinic, $P2_1/c$, a = 7.216(1), b = 12.117(3), c = 13.616(4), Å, β = 103.27(2)°, V = 1158.7 Å^3, ρ_o = 1.60 g cm^{-3}, Z = 2, ρ_c = 1.60 g cm^{-3}, $F(000)$ = 570, μ(MoKα) = 14.84 cm^{-1}.

Data collection was carried out at room temperature (23 ± 3°C). The ω−2θ technique was used, with an ω scan width (degrees) of 0.80 + 0.35 tan θ, maximum ω scan speed 10° min^{-1}, maximum scan time 300 s, background counted one quarter of the scan time at each end of the scan. A standard was measured every hour, and the orientation checked every 100 measured reflections. The standard exhibited only minor variations from one measurement to the next. Two quadrants of data (3778 reflections) were measured with $2° < \theta < 25°$. The equivalences ($I_{hkl} = I_{h\bar{k}\bar{l}}$) confirmed the crystal system as monoclinic, and the systematic absences indicated space group $P2_1/c$. Intensities were corrected for background and change in the standard, and converted to structure factors after applying Lorentz and polarization corrections. Equivalent reflections were averaged. No absorption correction was made. A total of 2046 unique reflections was obtained, of which 1760 had $I > 3\sigma(I)$ and were classified as observed.

The structure was solved by the heavy atom method and refined by full-matrix least-squares techniques with the SHELX set of programs (8). Scattering factors for neutral C, H, N, O, Cl, and Co were taken from the International Tables for X-ray Crystallography (9). The function minimized was $\Sigma w\Delta^2$, where $\Delta = |F_o| - |F_c|$ and $w = (\sigma^2(F_o) + 0.0003F_o^2)^{-1}$. One of the dimethylethylenediamine carbon atoms (C(4)) was disordered; an occupancy factor was refined alternately with the temperature factors for the two locations. Peaks attributable to hydrogen atoms appeared on the difference map after a cycle of anisotropic refinement. In the final cycles of refinement, the methyl groups were treated as rigid rotors, the positions of the NH_2 hydrogen atoms (H(11) and H(12)) were refined, and the positions of the remaining hydrogen atoms were calculated. Isotropic thermal parameters were refined for the methyl hydrogens as a group (U = 0.15 Å^2) and for the remaining hydrogens (U = 0.09 Å^2). The final R and R_w were 0.048 and 0.056 for the 1761 observed reflections, and 0.064 and 0.056 for all 2046 reflections. The final difference map had no features larger than 0.7 e Å^{-3} in height. The three largest residual peaks were located near the chlorine atoms.

TABLE 1. Fractional positional parameters and equivalent isotropic thermal parameters for the non-hydrogen atoms; estimated standard deviations in parentheses

Atom	x/a	y/b	z/c	U_{eq}*
Co	0.0000	0.5000	0.5000	0.0333(3)
C(1)	0.4554(6)	0.4726(3)	0.7836(3)	0.0494(16)
C(2)	0.3715(5)	0.5086(3)	0.6722(3)	0.0411(14)
C(3)	−0.1721(9)	0.3094(4)	0.5771(5)	0.0840(30)
C(4)	−0.1081(13)	0.2628(7)	0.4938(8)	0.0572(35)
C(4a)†	−0.0172(13)	0.2604(8)	0.55543(10)	0.0544(40)
C(5)	0.2513(7)	0.2877(4)	0.5049(4)	0.0701(21)
C(6)	0.0040(9)	0.2944(5)	0.3594(5)	0.1041(31)
N(1)	0.0529(5)	0.3214(3)	0.4680(3)	0.0447(13)
N(2)	−0.1914(6)	0.4269(3)	0.5757(3)	0.0501(15)
O(1)	0.2003(4)	0.4837(2)	0.6418(2)	0.0455(11)
O(2)	0.4774(4)	0.5544(3)	0.6273(3)	0.0658(14)
Cl(1)	0.3162(3)	0.5211(1)	0.8644(1)	0.0972(8)
Cl(2)	0.4629(2)	0.3268(1)	0.7898(1)	0.0655(5)
Cl(3)	0.6944(2)	0.5195(1)	0.8282(1)	0.982(7)

*$U_{eq} = \frac{1}{3}\Sigma_i\Sigma_j U_{ij} a_i^* a_j^* \bar{a}_i \cdot \bar{a}_j$.

†The occupancy factor of C(4) is 0.54; that of C(4a) is 0.46.

TABLE 2. Bond distances with estimated standard deviations in parentheses

Bond	Length (Å)	Bond	Length (Å)
Co—N(1)	2.258(3)	C(3)—C(4a)	1.357(11)
Co—N(2)	2.100(4)	C(3)—N(2)	1.431(6)
Co—O(1)	2.138(3)	C(2)—O(1)	1.247(4)
N(1)—C(4)	1.471(9)	C(2)—O(2)	1.217(4)
N(1)—C(4a)	1.579(10)	C(2)—C(1)	1.560(5)
N(1)—C(5)	1.463(5)	C(1)—Cl(1)	1.753(5)
N(1)—C(6)	1.477(6)	C(1)—Cl(2)	1.769(4)
C(3)—C(4)	1.435(10)	C(1)—Cl(3)	1.785(4)
		N(2)—H(11)	0.81(5)
		N(2)—H(12)	0.73(6)

The numbering scheme for the complex and the thermal ellipsoids are shown in Fig. 1, and the molecular packing diagram is given in Fig. 2 (10). Atomic positional parameters are reported in Table 1. Tables 2 and 3 list important bond distances and angles. Anisotropic thermal parameters for the non-hydrogen atoms, the hydrogen atom positional parameters, and a table of observed and calculated structure factors have been placed in the Depository of Unpublished Data.[2]

Results and discussion

X-ray structure determination

The cobalt complexes lie on crystallographic centres of symmetry, with a distorted octahedral environment about the cobalt atom. Four nitrogen atoms from the two chelating Me_2en ligands define a distorted square plane, and two oxygen atoms, one from each of two trichloroacetate ligands, occupy axial positions on the octahedron. The Co—NMe_2 bond length of 2.258(3) Å is significantly longer than the Co—NH_2 bond length of 2.100(4) Å. Similar effects have been noted in other complexes of *N*,*N*-dimethylethylenediamine (12−14), and are

[2]This material is available, at a nominal charge, from the Depository of Unpublished Data, CISTI, National Research Council of Canada, Ottawa, Ont., Canada K1A 0S2.

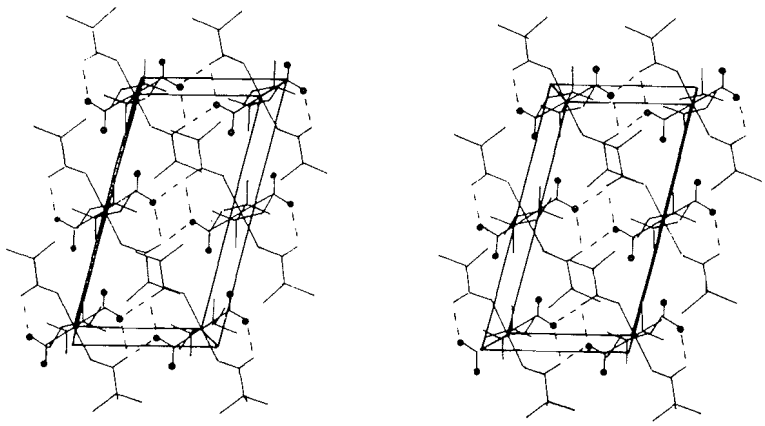

FIG. 2. Packing diagram for *trans*-$[Co(Me_2en)_2(CCl_3CO_2)_2]$. The view is down the *y*-axis with the *x*-axis horizontal. The small circles represent hydrogen atoms; hydrogen bonds are shown as dotted lines.

TABLE 3. Bond angles with estimated standard deviations in parentheses

Bond	Angle (deg)	Bond	Angle (deg)
N(1)—Co—N(2)	81.4(1)	N(2)—C(3)—C(4)	115.4(5)
O(1)—Co—N(1)	88.6(1)	N(2)—C(3)—C(4a)	121.0(5)
O(1)—Co—N(2)	84.4(1)	N(1)—C(4)—C(3)	114.5(6)
Co—N(1)—C(4)	103.8(4)	N(1)—C(4a)—C(3)	112.5(6)
Co—N(1)—C(4a)	101.9(4)	C(2)—O(1)—Co	133.7(3)
Co—N(1)—C(5)	113.4(2)	O(1)—C(2)—O(2)	129.2(4)
Co—N(1)—C(6)	113.2(3)	O(1)—C(2)—C(1)	112.9(3)
Co—N(2)—C(3)	110.7(3)	O(2)—C(2)—C(1)	117.9(3)
C(5)—N(1)—C(6)	105.8(4)	C(2)—C(1)—Cl(1)	111.5(3)
C(4)—N(1)—C(5)	123.2(5)	C(2)—C(1)—Cl(2)	109.1(3)
C(4a)—N(1)—C(5)	93.9(5)	C(2)—C(1)—Cl(3)	111.8(3)
C(4)—N(1)—C(6)	96.4(5)	Cl(1)—C(1)—Cl(2)	108.7(2)
C(4a)—N(1)—C(6)	127.4(5)	Cl(1)—C(1)—Cl(3)	109.1(2)
		Cl(2)—C(1)—Cl(3)	106.5(2)

generally attributed to steric crowding at the substituted nitrogen (13). Recent structure determinations for two octahedral cobalt(II) complexes of *N,N,N',N'*-tetramethylethylenediamine yielded Co—NM_2 bond distances of 2.205–2.239 Å (15).

The Co—O bond length (2.138(3) Å) is slightly longer than observed in other octahedral cobalt(II) complexes with carboxylate ligands. Thus, the Co—O distance is 2.074(2) Å in a monochloroacetate complex (15), and 2.039(4)–2.123(3) Å in cobalt(II) complexes of ethylenediaminetetraacetate and *o*-phenylenediaminetetraacetate (16).

Further deviations of the CoN_4O_2 chromophore from ideal D_{4h} symmetry are evident from the bond angles in the complex. The N(1)—Co—N(2) angle of 81.4(1)° is normal for a five-membered chelate ring, but the O(1)—Co—N(2) angle of 84.4(1)° is surprisingly far removed from the ideal value of 90°. This may be due to the hydrogen bonding contact between O(2) and N(2)' (Fig. 1).

The Me_2en chelate rings exhibit *gauche*:envelope disorder, as shown by the deviations from the Co—N(1)—N(2) plane (Table 4). Atom C(4), with an occupancy factor of 0.54, completes a *gauche*-type ring, whereas atom C(4a), with an occupancy factor of 0.46, completes an envelope-type ring. High correlations between the thermal parameters, occupancy factors, and positional parameters made it difficult to locate C(4) and C(4a) accurately, which accounts for the relatively large deviations from normal values of bond distances and angles involving these atoms.

One of the hydrogen atoms in the NH_2 groups is involved in two short contacts to carboxylate oxygen atoms, one in the same molecule, and one in an adjacent molecule (Figs. 1 and 2; Table 5). These are apparently not strong, as the O...H van der Waals separation is ca. 2.7 Å (17). The other NH_2 hydrogen atom, H(12), is not involved in hydrogen bonding.

Electronic spectra

The electronic spectra of single crystals of the cobalt complex were recorded in polarised light along orthogonal extinction axes of the crystals at room temperature, and at 10 K, using a Displex Cryogenic Refrigerator (11). The marked drop in intensity on cooling indicates that the quartet bands are of vibronic origin, in keeping with the presence of a centre of symmetry at the cobalt. A similar vibronic effect operates in the analogous $Ni(Me_2en)_2(CCl_3CO_2)_2$ complex. The spectrum at 10 K is shown in Fig. 3.

As was observed in the analogous nickel complex (7), splitting of the lowest *T*-state into three well-resolved bands is seen. By analogy with the nickel complex, the splitting of the upper *T*-state would be predicted to be much less (Fig. 3); this is in agreement with experiment.

While the point symmetry at the cobalt is C_i, the spectra are most conveniently fitted to theory using D_{2h} symmetry. Past experience (3) has shown that, provided angular deviations from 90° are small, one can assume angles of 90° with little

Can. J. Chem. Downloaded from www.nrcresearchpress.com by 210.87.254.6 on 09/06/12
For personal use only.

TABLE 4. Least-squares plane and deviations (in Å) atoms with superscript *a* are used in calculating the plane; the plane equation is $-0.5432X + 0.0431Y - 0.8382Z = -4.443$

Atom	Deviation	Atom	Deviation
Co[a]	0.000	C(3)	0.150
N(1)[a]	0.000	C(4)	−0.358
N(2)[a]	0.000	C(4a)	0.579

*X, Y, and Z are orthogonal coordinates, in Å, in a system having X, Y, and Z axes parallel to a^*, b, and c, respectively.

TABLE 5. Hydrogen bond lengths and angles*

Hydrogen bond	N...O, Å	H...O, Å	N—H...O, deg
N(2)—H(11)...O(2)[ii]	3.055(5)	2.44(6)	134(6)
N(2)—H(11)...O(2)[i]	3.060(5)	2.54(6)	123(6)

*Symmetry superscripts: *i*, $(-x, 1-y, 1-z)$; *ii*, $(x-1, y, z)$.

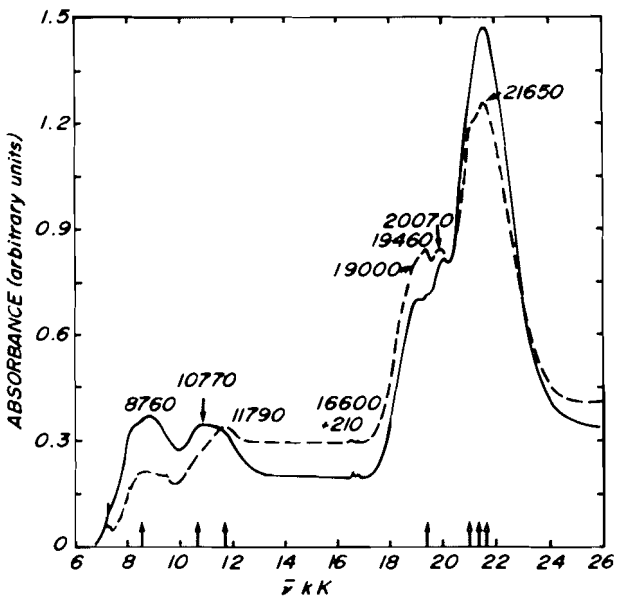

FIG. 3. The single crystal polarized spectra of $Co(Me_2en)_2(CCl_3CO_2)_2$ at 10 K. Two polarizations along orthogonal axes are displayed. The arrows indicate the calculated energies, namely: 8570, 10780, 11785, 19470, 21045, 21360, 21565 cm^{-1}.

attendant error. Major band splitting in rhombic systems of this type arises primarily from two sources: changes in the identity of the ligand atom, and variations in metal−ligand bond distance (4).

The results of our calculations are shown in Table 6, where comparative information on the nickel complex is also included. The angular overlap model (18) was employed using $e_\sigma(N(1))$, $e_\sigma(O)$, $e_\sigma(N(2))$, $e_\pi(O)$, $e_\pi(N(1))$, and B as variables, where N(1) and N(2) refer to the numbering system in Fig. 1. The $e_\pi(N(2))$ is assumed to be zero.

The relationship of the crystal extinction axes used in the spectroscopic study to the molecular axes of the chromophore has not been determined. We therefore adopt the procedure of using extensive past experience on closely related complexes (1) as our guide to the assignment of the spectrum. The association of specific σ and π parameters with specific ligands in

TABLE 6. Parameter sets for rhombic cobalt(II) and nickel(II) complexes*

	Value	
Parameter	$Co(Me_2en)_2(CCl_3CO_2)_2$	$Ni(Me_2en)_2(CCl_3Co_2)_2$
$e_\sigma(N(2))$	4610	4700
$e_\sigma(O)$	3000	2800
$e_\sigma(N(1))$	3690	3675
$e_\pi(O)$	400	460
$e_\pi(N(1))$	−250	120
B	750	880
$10Dq(N(2))$	13830	14100
$10Dq(O)$	7400	6560
$10Dq(N(1))$	12070	10545
DQ†	30520	28600
DS	−1250	−1975
DT	−4300	−4464
DU	2026	1567
DV	−1181	−2385

*Six variables were used to solve the spectra (5 × AOM, + B). Calculated transition energies are shown in the caption to Fig. 3.

†Normalized Spherical Harmonic Hamiltonian parameters (19).

Table 6 therefore follows from our knowledge of how well-defined tetragonal complexes of these ligands behave. Thus, for example, the M—O bond is known to have an $e_\sigma(O)$ value between 2500−3000 cm^{-1}, and an $e_\sigma(N)$ value for a normal length M—N bond should lie between 4000 and 4800 cm^{-1} (for M—Co(II) or Ni(II) (1)). The $e_\sigma(N)$ value for the long N—M—N bond is consistent with previous studies of such systems (1, 4). The remarkably close similarity between the data set necessary to fit the nickel spectra and that necessary to fit the cobalt spectra is noteworthy and must provide confidence in the assignment.

As anticipated, the increase in Co—N bond distance along the Me_2N—Co—NMe_2 bond vector does result in a significant decrease in the σ bonding parameter, relative to a normal length bond. The non-zero π value for this bond is small and probably not significant; it may arise because the bond angles are not strictly 90°, thus small deviations of the model from reality may be reflected in this term. The more positive value associated with the carboxylate O—Co—O bond vector is consistent with the anticipated small π-donation effect of the oxygen atoms with the previous nickel result. However, it too should not be given too much significance.

Acknowledgements

We thank the Natural Sciences and Engineering Research Council of Canada for financial support, and are especially grateful to the Atkinson Charitable Foundation and the J. P. Bickell Foundation for grants towards the purchase of the CAD-4 diffractometer. P.J.M. acknowledges the Research Corporation for funds to purchase the Displex Refrigerator.

1. A. B. P. LEVER. Coord. Chem. Rev. **43**, 63 (1982).
2. A. B. P. LEVER, I. M. WALKER, and P. J. MCCARTHY. Inorg. Chim. Acta, **39**, 81 (1980).
3. A. B. P. LEVER, I. M. WALKER, and P. J. MCCARTHY. Can. J. Chem. **60**, 495 (1982).
4. A. B. P. LEVER, I. M. WALKER, P. J. MCCARTHY, K. B. MERTES, A. JIRCITANO, and R. SHELDON. Inorg. Chem. In press.
5. I. BERTINI, D. GATTESCHI, A. SCOZZAFAVA. Inorg. Chem. **15**, 203 (1976).
6. M. R. BURKE, P. J. MCCARTHY, and M. F. RICHARDSON. J.

Can. J. Chem. Downloaded from www.nrcresearchpress.com by 210.87.254.6 on 09/06/12
For personal use only.

Cryst. Spectrosc. To be published.
7. A. B. P. LEVER, I. M. WALKER, and P. J. MCCARTHY. Inorg. Chim. Acta, **44**, L143 (1980).
8. G. SHELDRICK. SHELX-76 program for crystal structure determination. University of Cambridge, England. 1976.
9. International tables for X-ray crystallography. Vol. IV. The Kynoch Press, Birmingham. 1974.
10. C. JOHNSON. ORTEP-II. A thermal ellipsoid plot program for crystal structure illustrations. Oak Ridge National Laboratory, Oak Ridge, TN. 1976.
11. A. B. P. LEVER, G. LONDON, and P. J. MCCARTHY. Can. J. Chem. **55**, 3172 (1977).
12. M. G. B. DREW, D. M. L. GOODGAME, M. A. HITCHMAN, and D. ROGERS. Proc. Chem. Soc. 363 (1964).
13. D. W. PHELPS, W. H. GOODMAN, and D. J. HODGSON. Inorg. Chem. **15**, 2266 (1976).
14. M. A. BUSH and D. E. FENTON. J. Chem. Soc. A, 2446 (1971).
15. U. TURPEINEN, M. AHLGREN, and R. HAMALAINEN. Acta Crystallogr. B**38**, 1580 (1982).
16. E. F. K. MCCANDLISH, T. K. MICHAEL, J. A. NEAL, E. C. LINGAFELTER, and N. J. ROSE. Inorg. Chem. **17**, 1383 (1978).
17. W. C. HAMILTON and J. A. IBERS. Hydrogen bonding in solids. W. A. Benjamin, Inc., New York. 1968.
18. C. E. SHAFFER. Struct. Bonding. **5**, 68 (1968); **14**, 69 (1973).
19. J. C. DONINI, B. R. HOLLEBONE, and A. B. P. LEVER. Progr. Inorg. Chem. **22**, 225 (1977).

Can. J. Chem. Downloaded from www.nrcresearchpress.com by 210.87.254.6 on 09/06/12
For personal use only.

The synthesis of primary, secondary, and tertiary ferrocenylethylamines

IAN R. BUTLER AND WILLIAM R. CULLEN

Chemistry Department, University of British Columbia, Vancouver, B.C., Canada V6T 1Y6

Received February 8, 1983

IAN R. BUTLER and WILLIAM R. CULLEN. Can. J. Chem. **61**, 2354 (1983).

A simplified procedure for the preparation of α-*N*,*N*-dialkylaminoethylferrocenes R_2NR' (R = Me, C_6H_{11}, $CHMe_2$; R' = $CH(CH_3)C_5H_4FeC_5H_5$) from the alcohol R'OH by treatment with HBr and R_2NH is described. Use of ammonia results in the isolation of $R'NH_2$, R'_2NH (major product) and R'_3N and use of the optically active amine *d*-(+)-$H_2NCH(CH_3)C_6H_5$ gives rise to diastereomers $R'NHCH(CH_3)C_6H_5$ which are separable. When diphenylphosphine is substituted for an amine the oxide $R'P(O)Ph_2$ is obtained in low yield. The secondary amine R'_2NH reacts with *n*-butyllithium and chlorodiphenylphosphine to afford R'_2NPPh_2.

IAN R. BUTLER et WILLIAM R. CULLEN. Can. J. Chem. **61**, 2354 (1983).

On décrit une méthode simplifiée de préparation des α-*N*,*N*-dialkylaminoéthylferrocènes R_2NR' (R = Me, C_6H_{11}, $CHMe_2$; R' = $CH(CH_3)C_5H_4FeC_5H_5$) à partir de l'alcool R'OH que l'on fait réagir avec le HBr et le R_2NH. L'utilisation de l'ammoniac conduit à la formation des composés $R'NH_2$, R'_2NH (produits majoritaires) et R'_3N et l'emploi de l'amine optiquement active *d*-(+)-$H_2NCH(CH_3)C_6H_5$ permet d'obtenir les diastéréoisomères $R'NHCH(CH_3)C_6H_5$ que l'on peut séparer. Si on remplace l'amine par le diphénylphosphine on obtient avec un faible rendement l'oxyde $R'P(O)Ph_2$. L'amine secondaire R'_2NH réagit avec le *n*-butyllithium et le chlorodiphénylphosphine pour donner le composé R'_2NPPh_2.

[Traduit par le journal]

Introduction

Ferrocenylamines have been used for a considerable period as starting compounds for the synthesis of multidentate ferrocenyl ligands. α-*N*,*N*-Dimethylaminoethylferrocene, **1**, which may be prepared readily in its optically active form (1), is probably the most widely used of these. Kumada and co-workers (2, 3), Cullen and co-workers (4, 5), and Ugi and co-workers (6) have synthesised a variety of bidentate ligands which are useful in catalytic asymmetric syntheses from this precursor (Scheme 1). There are presently three major synthetic routes to **1**. The first of these, documented by Hauser and Lindsay (7), involves the conversion of the commercially available ferrocene carboxaldehyde to the aminonitrile derivative **2** which in turn is converted to **1** by methylmagnesium iodide (eq. [1]).

The second route of Ugi and co-workers (8) involves the conversion of α-hydroxyethylferrocene **3** to **1**. This is achieved via the acetylation of the alcohol followed by the reaction of the product ester with a secondary amine (eq. [2]). This route offers a less expensive synthesis starting with the easily accessible **3** (from ferrocene via acetylferrocene).

The third route again pioneered by Ugi and co-workers (9, 10) involves a one-pot method starting from ferrocene as outlined in eq. [3]. The initial reaction is carried out in strong acid solution (trichloroacetic acid/fluorosulfuric acid/acetic acid) and the overall yield of **1** is good (62%).

All three routes can be generalized using different amines, Grignard reagents, and carbonyl compounds. However, the

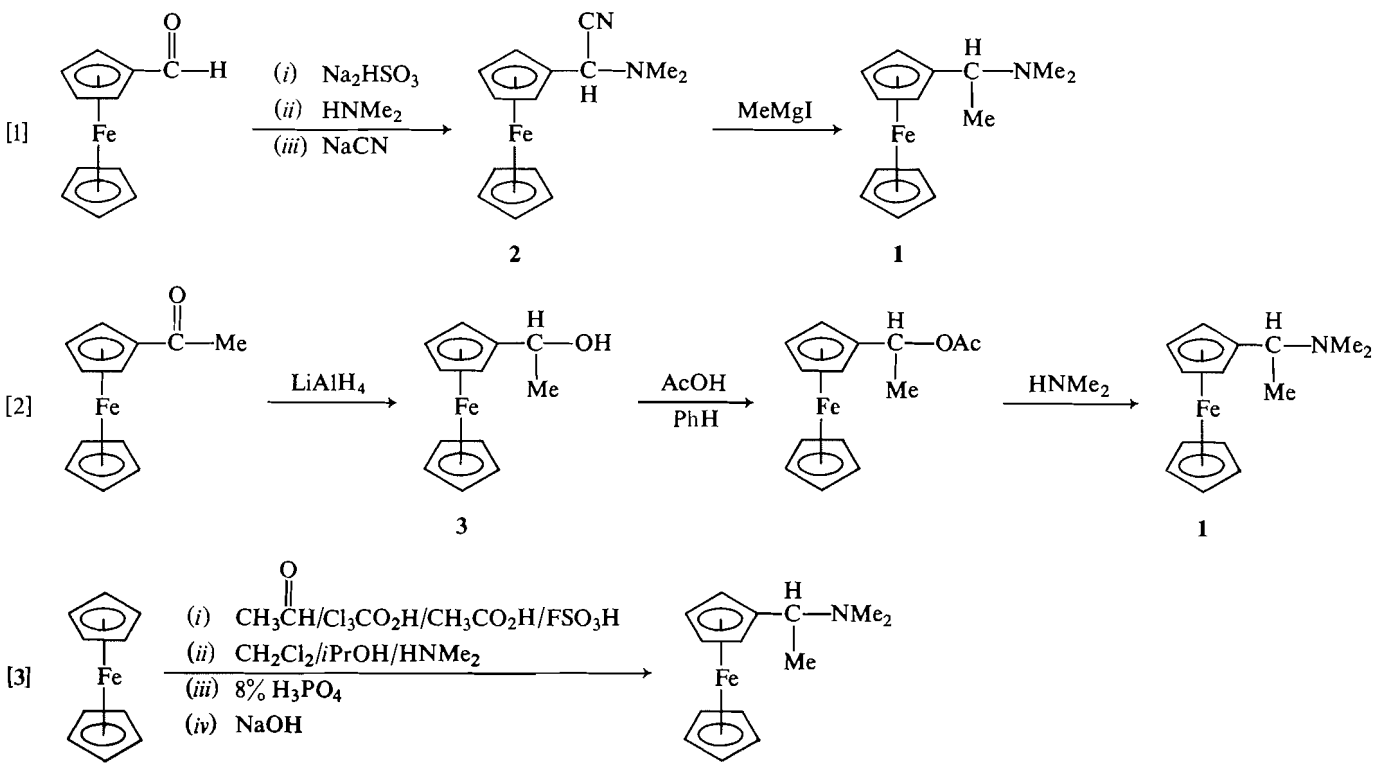

Can. J. Chem. Downloaded from www.nrcresearchpress.com by 210.87.254.40 on 09/06/12
For personal use only.

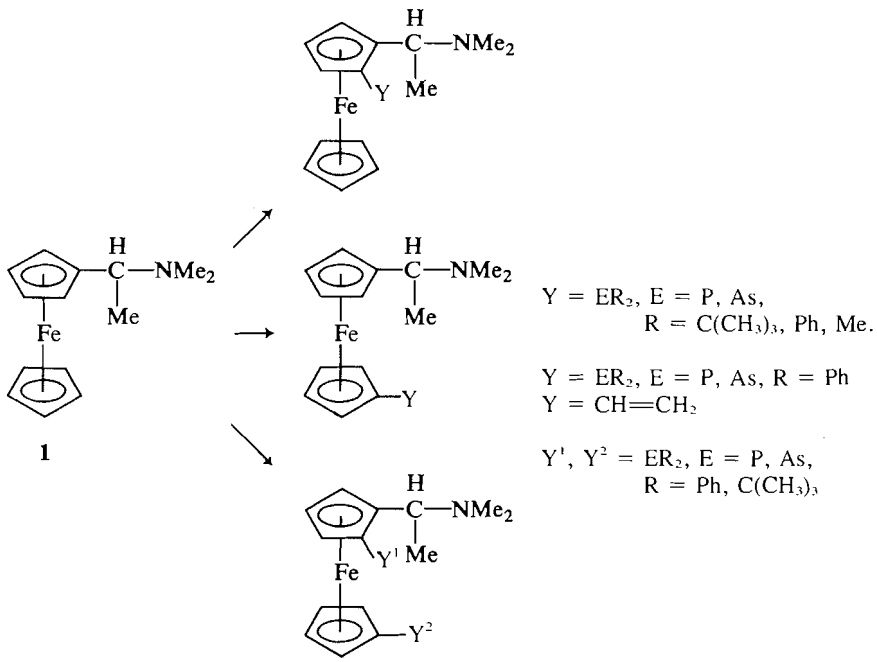

SCHEME 1.

synthesis of the important primary amines by the one-pot procedure results in low yields whilst the other protocols require synthesis of the dimethylamino derivatives first (9, 11).

The direct reaction of 1,1′-bis(α-hydroxyethyl)ferrocene with HBr and HNR_2 to give the corresponding diamines has recently been reported (12). This procedure offers a relatively simple diamine preparation since previous preparations have involved the formation of such diamines from ferric chloride and fulvenes. (Route 2 could not be used because an intramolecular reaction occurs to give a ferrocenophane derivative (13) and route 3 could not be applied because substitution on only one ring is observed (9)). We have now applied this reaction procedure to the synthesis of **1** and some related amines as well as extending it to the synthesis of primary, secondary, and tertiary α-ferrocenylethylamines. These procedures are of interest because of our continuing involvement in catalytic studies utilizing these derivatives as asymmetric ligands and because of our desire to circumvent the necessary resolution step by using a synthetic sequence which involves an asymmetric catalyzed reaction. Only the first two routes meet this requirement in that, in principle, both the Grignard coupling reaction and the ketone reduction can be carried out asymmetrically (14). We hope to use the product ferrocenylamines as ligands in metal catalyzed reactions, which breed their own chirality. (This has already been achieved in a very elegant manner in the case of the ligand (R)-prophos $(C_6H_5)_2PCH(CH_3)CH_2P(C_6H_5)$ (15)). The reaction is further developed to prepare a ferrocenylphosphine derivative but in low yield.

Experimental

All solvents were reagent grade and were used without further purification. α-Hydroxyethylferrocene was prepared by reduction of acetylferrocene using lithium aluminium hydride (16). ^1H nmr spectra were recorded on either a Varian XL-100 or a Bruker WP-80 spectrometer. Elemental analyses were performed by Mr. Peter Borda of this department. Mass spectra were obtained using a Kratos MS-50 instrument. The yields obtained in these reactions are variable because of the nature of the experimental conditions employed, therefore only approximate average yields are given.

1. Reaction of ***3*** *with HBr and* HNR_2*. Preparation of* α*-N,N-dialkylaminoethylferrocenes* ***1****,* $R = CH_3$*;* ***4****a,* $R = CH(CH_3)_2$*;* ***4****b,* $R = C_6H_{11}$

General procedure: Gaseous HBr was bubbled through a well stirred benzene solution of **3** (generally 1 g **3** per 50 mL benzene) until the solution darkened, becoming almost black. Excess of the appropriate amine[1] was then added (the solution colour changed back to yellow). The mixture was hydrolysed (H_2O, equal volume to benzene volume) and the organic layer was separated and dried over anhydrous $MgSO_4$. Following filtration, the solvent volume was reduced to a few mL and the resultant oil chromatographed on neutral alumina (activity grade III) eluting with hexane/diethyl ether, 50/50, v/v. (***4****b* was hexane eluted under these conditions.) The yellow product amine band was isolated (generally the only coloured band present, although some starting material may be present if excess HBr has not been added). The product yields were variable but generally fell in the range of 60–85%. The products were identified by comparison of their nmr spectra with those of authentic samples and by elemental analyses (where appropriate). Elemental analyses and relevant spectral data are given in Tables 1–3.

2. Reaction of ***3*** *with HBr and* NH_3 *solution*

General procedure: The previous experimental procedure (section 1) on a 1.0 g scale of **3** was applied replacing the secondary amine with concentrated ammonia solution. The work up procedure was identical. The crude reaction mixture prior to column chromatography was examined by tlc (hexane/diethyl ether, 80/20 eluant). Column chromatographic separation of the product fractions was achieved on a neutral alumina support (activity in the range III–V), eluting with progressively polar mixtures of hexane, diethyl ether, and chloroform. The product fractions were identified initially by mass spectroscopy. Analytical samples were prepared by crystallisation from hexane, hexane/diethyl ether, or hexane/methanol mixtures. The yields quoted are based on the product weight as obtained from the column following solvent removal (i.e. prior to recrystallisation).

Reaction a: HBr was bubbled through the benzene solution for 1 min (bubble rate ~2 per second using a 5 mm bore gas inlet tube). Tlc examination of the product solution following the general procedure outlined above showed five yellow product bands, two of which were in minor concentration. The three major product bands

[1]Aqueous or anhydrous amine can be used.

Can. J. Chem. Downloaded from www.nrcresearchpress.com by 210.87.254.40 on 09/06/12
For personal use only.

TABLE 1. Elementary analysis data[a]

Compound	Formula	Calcd.			Found		
		C	H	N	C	H	N
4*a*	$C_{18}H_{27}FeN$	69.01	8.69	4.47	69.29	8.75	4.30
4*b*	$C_{24}H_{35}FeN$	73.28	8.97	3.56	73.05	8.83	3.58
5*b*	$C_{24}H_{27}Fe_2N$	65.34	6.17	3.17	65.19	6.13	3.15
6	$C_{20}H_{23}FeN$	72.08	6.96	4.20	72.02	7.20	4.30

[a]**5***a* and **5***c* were characterised by ^{1}H nmr and mass spectroscopy because they always crystallised with incorporation of trace quantities of solvent. Similar problems were encountered with **8**.

TABLE 2. Proton nmr data[a]

Compound	Ferrocenyl protons	Residual protons
4*a*	3.85−4.28(m,10)[b]	3.08(q,1), CH; 1.36(d,3), CH_3; 1.05(d,6), 0.94(d,6), $N(CH_3)_2$
4*b*	3.88−4.28(m,10)[b]	2.30−2.75, 0.80−2.00 (m, 25), $N(C_6H_{11})_2$ + CH_3[d,1.35]
5*a*	4.00−4.22(m,9)	3.80(q,1), CH; 1.68(bs,2), NH_2; 1.34(d,3), CH_3
5*b*	4.00−4.30(m,18)	3.57(q,1), 3.66(q,1), 2 × CH; 1.34−1.42(bs,1), N*H*: 1.34(d,3), 1.92(d,3), CH_3
5*c*	3.75−4.24(m,27)	3.33(m,3), CH; 1.33, 1.40, 1.49, 1.55, (4s,[d]9), 3 × CH_3
6	4.00−4.25(m,9)[b]	7.25−7.40(m,5), Ph; 3.85(2q,1), CH; 3.35(2q,1) CH; 1.52(bs,1); N*H*, removed by D_2O shake; 1.20−1.50 (4d,6), 2 × CH_3
7*c*[c]	3.80−4.30(m,20)[b]	7.00−7.75(m,10), Ph; 1.30−1.75(m,6), 2 × CH_3
8	3.80−4.25(m,9)	1.50, 1.63(2 × d,3) J_{P-H} = 16 Hz, CH_3; 3.52(m,1) CH; 7.30−8.00(m,10), 2 × C_6H_5

[a]$CDCl_3$ is the solvent, bs = broad singlet.
[b]Contains peaks from other neuclei (—C*H*Me—).
[c]Compound readily decomposes to give product with vinylic protons in $CDCl_3$.
[d]These are asymmetric singlets at 80 MHz arising from doublet overlap.

were isolated: the first was identified as the secondary amine **5***b* (hexane eluted), ~40%; the second as starting material **3**, (hexane/ether, 80/20) ~20%; and the third as the primary amine **5***a* (chloroform eluted) ~10%.

Reaction b: HBr bubbled through the solution for 5 min (bubble rate as above). Three major fractions were identified by tlc then isolated: the first **5***c* (hexane eluted) ~5%; the second **5***b* (hexane/ether, 95/5) ~65%; and the third an unidentified product with parent mass ion, *m/e* 530, **8**, (hexane/ether, 50/50 eluted).

Reaction c: The addition of the NH_3 solution to the brominated solution (HBr bubbled for 3 min) was carried out dropwise. Four major fractions were identified by tlc and isolated by column chromatography; **5***c* (hexane eluted) ~5%, **5***b* (hexane/ether, 95/5) ~40%, the unidentified compound with parent mass ion at *m/e* 530 (hexane/ether, 50/50) and an unidentified product with parent mass ion at *m/e* 636 (chloroform eluted) **10**. The last two products were isolated in very low yield.

Reaction d: The reaction was carried out as documented in reaction *b* on a 5 g scale. Five fractions (eluted with solvent mixtures as above) were identified and isolated following column chromatography; **5***c*, ~8%, **5***b*, ~50%, **3** and trace of product with parent mass *m/e* 530, the unidentified product with parent mass of 636 and **5***a*, ~15%).

Crystallisation of 5a−c: **5***a* was crystallised from diethyl ether/hexane, 70/30, **5***b* from hexane, and **5***c* from hexane/methanol; generally the two solvent layers were allowed to diffuse slowly. Elemental analyses and spectral data are given in Tables 1−3. **5***a* and **5***c* were characterised by ^{1}H nmr and mass spectroscopy only because the compounds were difficult to obtain free from solvent.

3. Reaction of **3** *with d-(+)-α-aminoethylbenzene. Preparation of* **6**

The previous experimental procedures were applied to this synthesis replacing the amine solution with *d*-(+)-α-aminoethylbenzene (Aldrich Chemical Co.). The major product isolated following column chromatography was the secondary amine **6** (>60%). This compound was obtained by crystallisation from hexane as a waxy crystalline solid. Small quantities of the tertiary amine were also identified in solution (mass spectroscopy); however, no crystallisation of this compound was attempted. Spectral and analytical data for **6** are given in Tables 1−3.

4. Lithiation of 5b *and reaction with* $ClPPh_2$. *Preparation of* **7**

The following reactions were carried out under an inert atmosphere.

(a) Reaction in ether: To an ethereal solution of **5***b* (1 g, 2.27 mmol in 50 mL) a solution of 1.6 *M n*-butyllithium in *n*-hexane (1.5 mL) was added. The solution was stirred overnight. Chlorodiphenylphosphine (0.5 g, 2.27 mmol) was then added to the chilled solution (−78°C). The solution was warmed to 20°C and stirred for a further 1 h before hydrolysis (H_2O, 20 mL). The ethereal layer was separated, dried over anhydrous $MgSO_4$ and, following filtration, the product mixture was chromatographed on neutral alumina. The red/orange product fraction was isolated and recrystallised from *n*-hexane. ^{1}H nmr and spectroscopic data are given in Tables 1 and 2. The product yield obtained was 18%.

(b) Reaction in hexane: Dropwise addition of *n*-butyllithium (1 mL, 1.6 *M* solution in hexane, excess) to a solution of **5***b* (300 mg, 0.68 mmol) in hexane (50 mL) resulted in the rapid precipitation of the lithium salt of **5***b* as a pale orange powder. The solution was stirred for 5 min before chlorodiphenylphosphine (0.5 g, excess) was added. The resultant mixture was heated to 50°C and was stirred at this temperature for a further 15 min. A deep orange/red colour developed in the reaction mixture with deposition of LiCl. Tlc examination at this stage showed the presence of two products, the first a yellow/orange

Can. J. Chem. Downloaded from www.nrcresearchpress.com by 210.87.254.40 on 09/06/12
For personal use only.

TABLE 3. Mass spectral data

Compound	Mass spectral fragmentation pattern (m/e values, % relative intensities given in parentheses)
4*a*	314(5.59); 313(23.04), $M^{+\cdot}$; 299(3.25); 298(15.97), 256(309); 255(5.56); 214(19.40), 213 (100.00); 212(83.78)
4*b*	394(11.64); 393(40.25), $M^{+\cdot}$; 391(2.65); 379(5.28); 378(19.39); 214(35.73); 213(47.42); 212(100.00); 211(14.83); 181(13.07), 138(83.06)
5*a*	230(26.81); 229(100.00), $M^{+\cdot}$; 228(16.70); 227(17.65); 215(11.42); 214(68.44); 213(38.09); 212(100.00); 210(12.28)
5*b*	443(1.13); 442(6.40); 441(20.86), $M^{+\cdot}$; 440(3.34); 439(10.29); 348(3.17); 229(24.62); 227(12.46); 214(52.99); 213(99.42); 212(100.00)
5*c*	654(1.17); 653(2.45), $M^{+\cdot}$; 570(1.61); 530(1.79); 504(2.99); 464(1.25); 441(11.86); 229(16.64); 213(84.41); 212(100.00)
6	334(5.58); 333(22.88), $M^{+\cdot}$; 318(5.65); 267(2.04); 252(2.46); 214(21.91); 213(36.39); 212(100.00); 186(10.20)
6*a*[a]	543($M^{+\cdot}$) 541, 529, 490, 464, 450, 448, 424, 410, 356, 333, 318
7	625(0.78); $M^{+\cdot}$; 596(2.62); 442(3.72); 428(5.09); 414(5.59); 413(29.57); 412(100.00); 399(18.78); 398(35.39); 347(13.20); 346(41.52)
8	415(28.14); 414(100.00), $M^{+\cdot}$; 350(23.33); 349(99.26); 322(19.79), 257(6.11); 244(3.22); 226(9.16); 214(13.38); 213(88.08); 212(28.47)
9	532(1.33); 531(1.50); 530(3.72); 478(3.51); 465(10.19); 464(29.14); 441(3.22); 424(6.42); 3.98(2.12); 380(1.97); 356(4.04); 332(6.52); 314(5.57); 230(46.08); 212(100.00)
10	637(7.25); 636(16.37); 596(12.97); 530(15.79); 490(17.07); 464(5.78); 424(26.80); 396(5.74); 330(14.00); 229(41.37); 213(54.56); 212(100.00)

[a]This compound was not crystallized; the mass spectrum was obtained from a sample in solution.

compound eluting with hexane and the second a red compound which required polar solvents, e.g., CH_2Cl_2, for elution. The reaction mixture was filtered under an inert atmosphere to give a clear orange solution which was reduced in volume *in vacuo* until precipitation just began. This solution was then set to crystallize overnight. The residual red powder consisting primarily of LiCl was extracted with methylene chloride. The red methylene chloride solution was reduced in volume to ca. 3 mL and a top hexane layer (5 mL) was added. The mixture was then left to crystallize at ~−15°C. The orange/red crystalline product obtained from the latter solution was identified as **7** by mass spectroscopy (Table 3) and the yellow/orange crystalline compound obtained from the former solution was identified as the starting compound **5***b* which crystallized initially as one pure diastereomer. The yield of **7** was 8%.

5. Reaction of 3 with HBr and $HPPh_2$. Preparation of 8

A solution of **3** (1.0 g) in benzene (50 mL) was treated with HBr according to the general procedure. Excess $HPPh_2$ was then added. The solution was then hydrolysed (H_2O, 50 mL) and the organic layer separated and dried over anhydrous $MgSO_4$. Following solvent removal large quantities of phosphine by-products separated. The orange product fraction was repeatedly chromatographed on a neutral alumina support until a pure product fraction was obtained. Spectral details of **8** are given in Tables 2 and 3.

Results and discussion

The synthesis of α-*N*,*N*-dimethylaminoethylferrocene **1** from the alcohol **3** has been achieved by reaction with HBr followed by $HNMe_2$ using the method previously applied to the synthesis of diamines (9). The yields of **1** are variable (60−80%) which compare favourably with the previous syntheses. In common with the second route of Ugi and coworkers (8) the starting compound is easily accessible from ferrocene by acylation followed by reduction with lithium aluminium hydride. This procedure offers an alternative rapid synthesis of **1** with no special handling procedure necessary. Two derivatives of the type $[(\eta^5\text{-}C_5H_5)Fe(\eta^5\text{-}C_5H_4CH(Me)\text{-}NR_2)]$ R = cyclohexyl, isopropyl, **4***a* and **4***b* have also been prepared by this method. **4***b* is not a new compound (2).

The main focus of this work has been the preparation of primary, secondary, and tertiary ferrocenylethylamines of the type $[(\eta^5\text{-}C_5H_5)Fe(\eta^2\text{-}C_5H_4C(H)Me)_xNH_{3-x}]$. The synthesis of these derivatives was conveniently achieved from **3** by the stepwise reaction with HBr and NH_3 (eq. [4]).

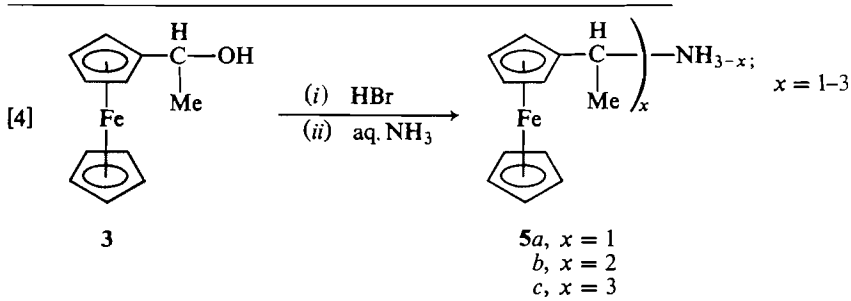

3

5*a*, $x = 1$
b, $x = 2$
c, $x = 3$

Can. J. Chem. Downloaded from www.nrcresearchpress.com by 210.87.254.40 on 09/06/12
For personal use only.

Can. J. Chem. Downloaded from www.nrcresearchpress.com by 210.87.254.40 on 09/06/12
For personal use only.

The experimental conditions were varied since it would be expected that addition of the acidified reaction solution of **3** to the aqueous amine solution would give rise to higher yields of **5***a* while the dropwise addition of the aqueous ammonia solution to the acidified reaction solution would give relatively higher yields of **5***c*. This was found to be the case; however, the combined yields of **5***a* and **5***c* were found to be generally very low under all the experimental conditions employed and that the secondary amine **5***b* predominated. **5***b* is separable by chromatography into its diastereoisomers which show a significant chemical shift in the nmr spectra, Table 2. No attempt was made to separate the isomers of **5***c*. Two unidentified products were obtained in low yield in the preparation, the first with mass ion at *m/e* 530, **9**, and the second at *m/e* 636, **10**. The identity of these compounds was not pursued although their mass spectra are given in Table 3. Addition of HBr to the benzene solution of **3** could give rise to vinylferrocene derivatives by the well documented acid catalysed dehydration of **3**, but by-product formation of this type is apparently minimised under these experimental conditions, since no evidence was found for their existence in significant quantities.

The compound **3** was reacted by an identical procedure to the above with *d*-(+)-α-aminoethylbenzene, a low cost, commercially available chiral amine. The major product isolated was the secondary amine, α-N(α′-ethylphenyl)aminoethylferrocene, **6**, obtained as a mixture of diastereomers which are separable (tlc). Thus a convenient resolution of the carbon α to ferrocene can be achieved. This could be of synthetic utility in chiral ligand preparation.

Lithiation of **5***b* followed by reaction of the product mixture with chlorodiphenylphosphine gave the N—P bonded ligand **7**, as a red/orange solid. The yield obtained, however, was extremely low (~10%) and the product was very air sensitive in solution.

The lithiation of **5***b* has been recently examined using excess *n*-butyllithium. Treatment of the lithiated solution with $ClSiMe_3$ has yielded a series of silylated compounds including ring silylated products (16).

Treatment of **3** with HBr followed by reaction with diphenylphosphine gave the phosphine oxide **8** (the phosphine is oxidised during workup); however, the isolation of this compound was found to be particularly laborious because of the significant quantities of organic solvent soluble phosphine by-products. The formation of these by-products may be minimised by the careful dropwise addition of the phosphine, however, it is difficult to conclude when the optimum quantity of phosphine has been added.

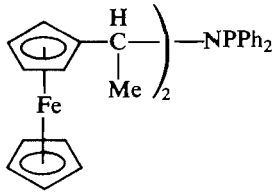

7

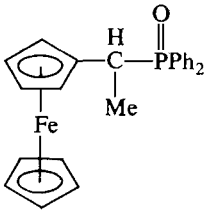

8

In summary, our procedure offers a rapid synthesis of **1** and related compound using essentially no special handling procedures, starting with easily accessible starting materials. The application to the preparation of potentially chiral phosphine derivatives may be somewhat limited, however, because of the extra effort required during the work up procedure necessary to obtain the pure product.

Acknowledgements

An operating grant from N.S.E.R.C. (Canada) to W.R.C. is gratefully acknowledged as is the assistance of the staff of the U.B.C. mass spectroscopy centre.

1. S. W. GOKEL and I. K. UGI. J. Chem. Educ. **49**, 249 (1972).
2. T. HAYASHI, T. MISE, M. FUKUSHIMA, M. KOGATANI, N. NAGASHIMA, Y. HAMADA, A. MATSUMOTO, S. KAWAKAMI, M. KONISHI, K. YAMAMOTO, and M. KUMADA. Bull. Chem. Soc. Jpn. **53**, 1138 (1980).
3. T. HAYASHI, T. MISE, S. MITACHI, K. YAMAMOTO, and M. KUMADA. Tetrahedron Lett. 1133 (1976).
4. W. R. CULLEN and J. D. WOOLINS. Can. J. Chem. **60**, 1793 (1982).
5. I. R. BUTLER and W. R. CULLEN. Can. J. Chem. **61**, 147 (1983).
6. D. MARQUARDING, H. BURGHARD, I. UGI, and R. URBAN. J. Chem. Res. (S) 82 (1977); (M) 0915 (1977).
7. C. R. HAUSER and J. K. LINDSAY. J. Org. Chem. **22**, 906 (1957).
8. G. W. GOKEL and I. K. UGI. J. Chem. Educ. **49**, 292 (1972)
9. R. HERRMAN and I. UGI. Tetrahedron, **37**, 1001 (1981)
10. R. HERRMAN and I. UGI. Angew. Chem. Int. Ed. **18**, 956 (1979).
11. G. EBERLE, I. LAGERLUND, I. UGI, and R. URBAN. Tetrahedron, **34**, 977 (1978).
12. I. R. BUTLER and W. R. CULLEN. Synth. React. Inorg. Met.-Org. Chem. **13**, 321 (1983).
13. E. C. WINSLOW and L. W. BREWSTER. J. Org. Chem. **26**, 2982 (1961).
14. M. KUMADA. Acc. Chem. Res. **15**, 395 (1982).
15. M. D. FRYZUK and B. BOSNICH. J. Am. Chem. Soc. **100**, 5491 (1979).
16. I. R. BUTLER and W. R. CULLEN. Unpublished results.

Réduction électrochimique de γ-nitrocétones. Conditions expérimentales d'accès à des dérivés de la pyrroline et de la pyrrolidine

MICHEL CARIOU, ROLAND HAZARD, MICHEL JUBAULT ET ANDRÉ TALLEC

Laboratoire d'Electrochimie, ERA CNRS 896, Université de Rennes, Campus de Beaulieu, 35042 Rennes Cédex, France

Reçu le 7 avril 1983

MICHEL CARIOU, ROLAND HAZARD, MICHEL JUBAULT et ANDRÉ TALLEC. Can. J. Chem. **61**, 2359 (1983).

Une étude détaillée du comportement électrochimique, sur cathode de mercure et en milieu hydro-alcoolique, de quelques γ-nitrocétones **1** et de leurs produits de réduction permet de définir les conditions d'électrosynthèses de trois types d'hétérocycles azotés.

Les pyrrolines *N*-oxyde **3** sont obtenues par réduction à potentiel peu négatif (cyclisation de l'hydroxylamine); les rendements sont quantitatifs dans le cas des dérivés nitrés tertiaires; dans le cas des dérivés secondaires et primaires, il y a formation parasite de cétones-oximes **6**.

Pour les autres hétérocycles, les conditions de préparation dépendent de la nature du substituant situé en α du carbonyle. Dans le cas d'un substituant méthyle, les pyrrolines **4** peuvent être obtenues par réduction du dérivé nitré **1** ou de la pyrroline *N*-oxyde **3**; les pyrrolidines **5** sont obtenues par réduction de **1** ou également de **3** et **4** dans le cas des dérivés nitrés tertiaires. Dans le cas d'un substituant phényle, les pyrrolines **4** ne peuvent être obtenues que par réduction des hétérocycles **3**, provenant d'un dérivé nitré tertiaire; les pyrrolidines **5** se préparent par réduction de **1** (dérivés primaires et secondaires) ou de **3** et **4** (dérivés tertiaires).

MICHEL CARIOU, ROLAND HAZARD, MICHEL JUBAULT, and ANDRÉ TALLEC. Can. J. Chem. **61**, 2359 (1983).

Optimal conditions for electrosynthesis, at a mercury cathode in hydroalcoholic media, of three classes of nitrogen heterocyclic compounds are set up from an exhaustive study of the electrochemical behaviour of γ-nitroketones **1** and their reduction products.

Pyrroline-*N*-oxides **3** are obtained by cyclization of the hydroxylamine when the nitro compounds are reduced at sufficiently low cathodic potentials. Quantitative yields are achieved in the case of tertiary nitro compounds. In other cases (primary and secondary nitro compounds), simultaneous formation of ketone-oximes **6** occurs.

According to the nature of the α-substituent of the carbonyl, the other heterocyclic derivatives can be prepared as follows. In the case of a methyl substituent, pyrrolines **4** can be obtained by reduction of nitro compounds **1** or of *N*-oxyde pyrrolines **3**. Pyrrolidines **5** are prepared by reduction of **1**, or **3** and **4** in the case of tertiary compounds. In the case of a phenyl substituent, pyrrolines **4** can only be obtained by reduction of compounds **3** arising from a tertiary nitro compound. Pyrrolines **5** are prepared by direct reduction of **1** (primary and secondary nitro compounds) or of **3** and **4** (tertiary nitro compounds).

L'électroréduction de dérivés nitrés aromatiques, substitués en *ortho* par des groupements susceptibles de réagir sur la fonction hydroxylamine, a été largement utilisée pour la préparation d'hétérocycles azotés (1, 2). En série aliphatique par contre, si quelques essais ont été tentés par réduction chimique de γ-nitroesters et de γ-nitrocétones (3), il ne semble pas que la méthode électrochimique ait été mise en oeuvre.

Dans une note préliminaire (4), nous avons indiqué les conditions d'obtention de pyrrolines *N*-oxydes **3**, de pyrrolines **4** et de pyrrolidines **5** (schéma 1), par électrolyse à potentiel contrôlé des γ-nitrocétones **1***a* et **1***b*.

Nous nous proposons ici de montrer comment il est possible, par une étude détaillée du comportement électrochimique des nitrocétones **1** et des hétérocycles qui en dérivent, de déterminer les conditions expérimentales optimales, permettant d'accéder sélectivement aux différents produits de cyclisation. Les rendements des électrosynthèses peuvent être rendus pratiquement quantitatifs, lorsque le groupement nitré est porté par un carbone tertiaire (composés **1***a* et **1***b*). Par contre, des réactions parasites accompagnent la réduction des dérivés nitrés secondaires (**1***c* et **1***e*) et primaires (**1***d* et **1***f*).

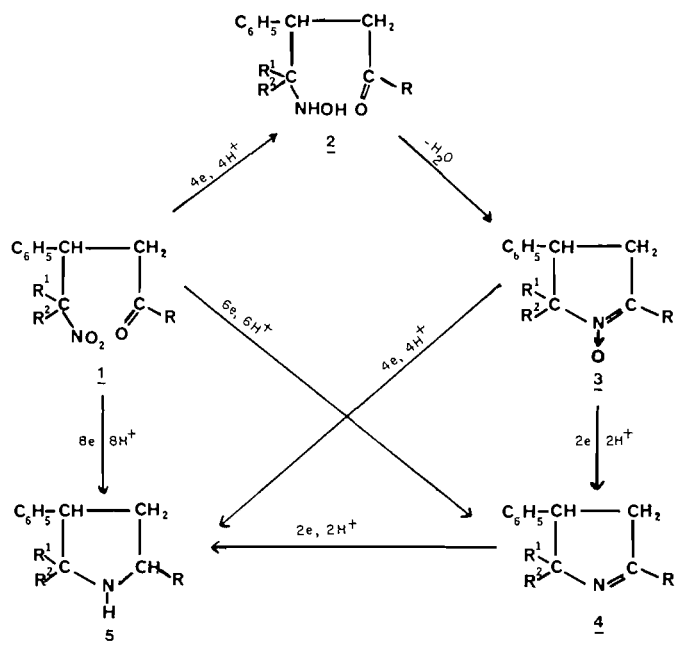

1_a $R^1 = R^2 = CH_3$; $R = C_6H_5$

1_b $R^1 = R^2 = CH_3$; $R = CH_3$

1_c $R^1 = CH_3$, $R^2 = H$; $R = C_6H_5$

1_d $R^1 = R^2 = H$; $R = C_6H_5$

1_e $R^1 = CH_3$, $R^2 = H$; $R = CH_3$

1_f $R^1 = R^2 = H$; $R = CH_3$

SCHÉMA 1

1. Réduction de la nitrocétone 1a

1.1 *Etude polarographique*

Les polarogrammes du dérivé nitré **1***a* et des hétérocycles **3***a* et **4***a* ont été enregistrés à différents pH, dans un milieu tampon B.R. + éthanol (1 pour 1 en volumes). Quelques résultats sont représentés sur la figure 1.

Etude du dérivé nitré ***1***a (fig. 1a)

En milieu très acide, le polarogramme présente une première vague à 4 électrons (vague A), suivie de deux vagues mal

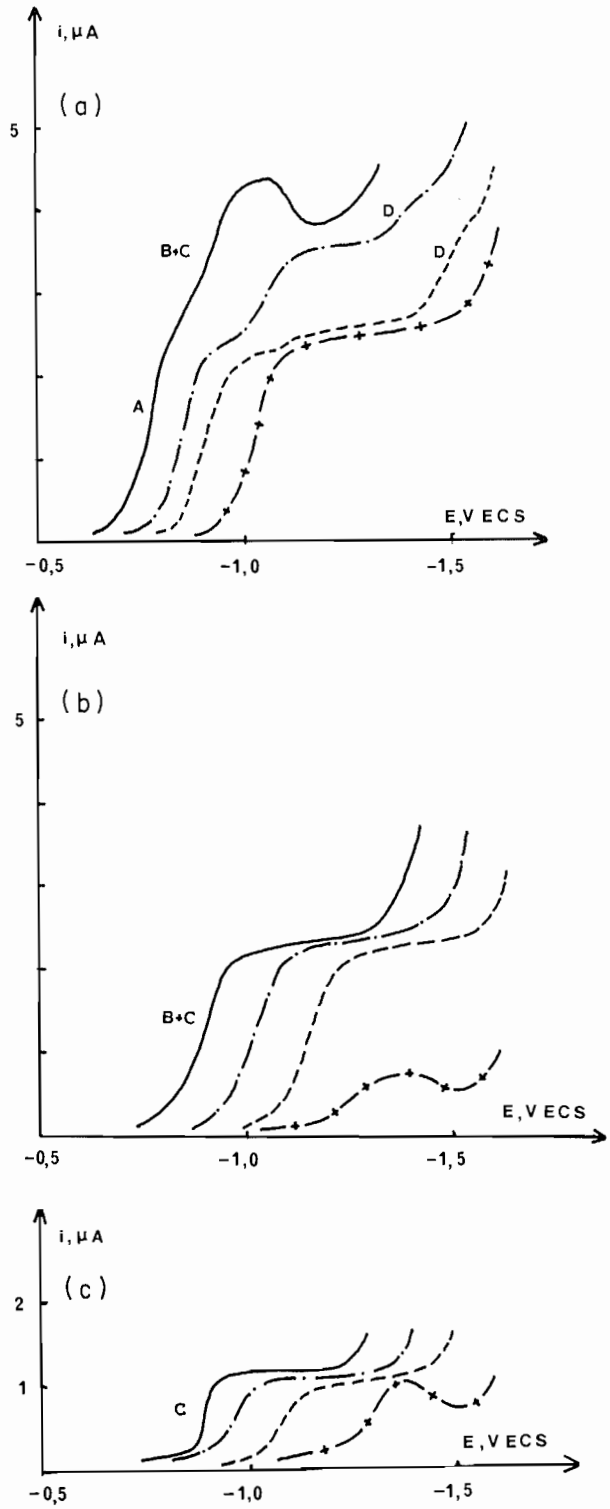

FIG. 1. (a) Polarogrammes de **1***a* en milieu tampon B.R. + éthanol (1 : 1) de pH croissant; de gauche à droite: pH = 2,0; 4,1; 6,0; 8,0. (b) Polarogrammes de **3***a* en milieu tampon B.R. + éthanol (1 : 1) de pH croissant; de gauche à droite: pH = 2,0; 4,0; 6,0; 8,0. (c) Polarogrammes de **4***a* en milieu tampon B.R. + éthanol (1 : 1) de pH croissant; de gauche à droite: pH = 2,0; 4,0; 6,0; 8,0.

séparées (B et C), dont la hauteur totale correspond pratiquement à une réduction à 8 électrons. A potentiel plus négatif, il apparaît un creux, le courant minimum correspondant à une réduction à 6 électrons.

Lorsque le pH augmente, les potentiels de demi-vague se déplacent vers des valeurs cathodiques et l'allure des polarogrammes est modifiée: la vague A est mieux dégagée (déplacement moins prononcé de son $E_{1/2}$); les vagues B et C, dès pH = 4, sont confondues en une vague unique présentant un caractère cinétique marqué: à période de chute constante des gouttes de mercure, l'intensité limite diminue quand le pH augmente (pour $\tau = 2$ s, la vague B + C disparaît pratiquement dès pH = 6); à pH donné, l'intensité diminue avec la période de chute (à pH = 4, la vague est à 4 électrons pour $\tau = 6$ s; pratiquement à 2 électrons pour $\tau = 2$ s et elle n'est plus visible pour $\tau < 0{,}5$ s). Il apparaît à potential très négatif une nouvelle vague D dont la hauteur relative augmente avec le pH; elle correspond à 2 électrons vers pH = 6 (lorsque la vague B + C a pratiquement disparu); mais en milieu basique elle est masquée par la décharge des cations de l'électrolyte-support, de sorte qu'à pH = 8, le polarogramme ne présente que la seule vague A. Cependant, en tampon ammoniacal, la vague D située vers −1,5 V persiste car elle est avancée par la présence des ions NH_4^+.

Etude des hétérocycles **3***a et* **4***a* (figs. 1b et 1c)

En milieu très acide, la pyrroline *N*-oxyde **3***a* présente les vagues B et C mal séparées tandis que seule la vague C (réduction à 2 électrons) apparaît sur le polarogramme de la pyrroline **4***a*.

Lorsque le pH augmente, les vagues B et C de **3***a* se recouvrent. Mais on remarquera que jusqu'à pH = 6, la vague unique B + C présentée par **3***a* (réduction à 4 électrons) et la vague C de **4***a* possèdent des hauteurs constantes. Leur caractère cinétique n'apparaît qu'en milieu basique; il se traduit, dès pH = 8, par l'obtention de vagues en S renversé, dont l'allure est caractéristique de l'intervention de phénomènes de protonation en surface d'électrode (5). Ces vagues disparaissent pour pH > 10.

1.2 *Interprétation*

L'étude qui précède permet l'attribution des vagues A, B, C respectivement:

à la réduction du groupement nitré de **1***a*

$$\text{Vague A}\quad \mathbf{1}a + 4H^+ + 4e \rightarrow \mathbf{2}a + H_2O$$

L'hydroxylamine **2***a* se cyclise plus ou moins rapidement en pyrroline *N*-oxyde **3***a*.

à la réduction du la fonction *N*-oxyde de **3***a*

$$\text{Vague B}\quad \mathbf{3}a + 2H^+ + 2e \rightarrow \mathbf{4}a + H_2O$$

A la réduction de la liaison C=N de **4***a*

$$\text{Vague C}\quad \mathbf{4}a + 2H^+ + 2e \rightarrow \mathbf{5}a$$

A partir de ces conclusions, il est possible d'interpréter les autres phénomènes observés en polarographie.

L'existence du creux qui apparaît un milieu très acide, vers −1,15 V ECS, sur le polarogramme de **1***a* n'est pas due à une modification de l'électroactivité des hétérocycles **3***a* et **4***a* (cf. figs. 1b et c). C'est donc la réduction de la fonction carbonyle du produit de départ qui est responsable de la diminution du courant. Dans la partie descendante du polarogramme, il y a compétition entre la réaction de cyclisation de la cétone sur le groupement hydroxylamine (suivie de la réduction de **3***a* et de **4***a*) et sa réduction en alcool; cette dernière finit par l'emporter à potentiel suffisamment négatif et l'on observe alors un processus de réduction à 6 électrons:

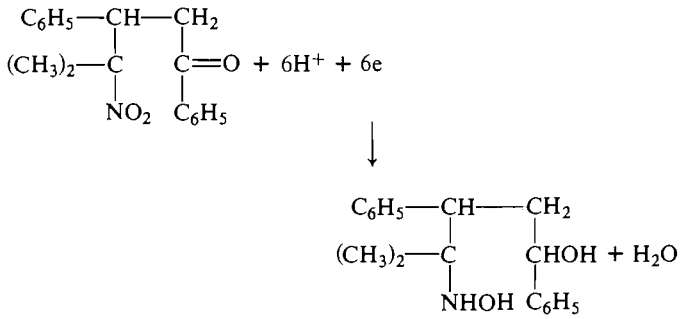

En milieu faiblement acide, les vagues B et C présentent une hauteur normale lorsqu'elles sont enregistrées à partir des hétérocycles. Leur caractère cinétique, qui apparaît sur les polarogrammes de **1***a*, résulte donc du fait que la cyclisation de l'hydroxylamine **2***a* est alors relativement lente, tandis qu'elle est très rapide pour pH < 2.

Cette observation permet d'attribuer la vague D, située à potentiel très négatif, à la réduction du carbonyle, d'autant plus facile à observer que la cyclisation de l'intermédiaire **2***a* est plus lente:

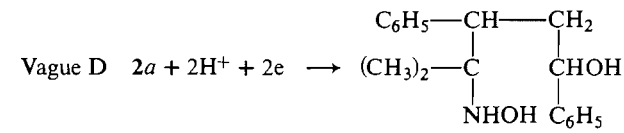

Cette interprétation est confirmée par une étude voltammétrique, réalisée en tampon acétique (fig. 2); à faible vitesse de balayage, on observe trois pics cathodiques: A (réduction de NO_2), B + C (réduction de **3***a* et **4***a*) et D, moins marqué (réduction du carbonyle en alcool); si l'on balaye plus rapidement, la cyclisation de **2***a* n'a plus le temps de s'effectuer et il ne subsiste, sur le voltammogramme, que les pics A et D. On notera le net déplacement du potentiel de pic A, vers les valeurs cathodiques, lorsque la vitesse de balayage augmente: ce phénomène est caractéristique d'un mécanisme EC dans lequel le transfert électronique (E) est suivi d'une réaction chimique lente (C).

Remarque: l'allure de la vague de réduction de **3***a* en milieu basique rappelle celle observée à partir d'oximes (5) et est due à des réactions de protonation, précédant le transfert électronique. Par comparaison avec un travail antérieur (6), nous avons étudié la réduction polarographique du composé **3***a* dans un tampon ammoniacal, fréquemment utilisé pour effectuer les électrolyses préparatives. La vague est alors dédoublée (fig. 3): la hauteur relative de la première vague B_1 est d'autant plus importante que la période de chute est élevée (fig. 3a) ou la proportion d'ions ammonium plus grande (fig. 3b). Cette première vague correspond alors à la réduction de 3*a* après préprotonation, en surface d'électrode, sous l'action de NH_4^+. La seconde vague B_2 (réduction sans protonation de **3***a*) est déplacée vers les potentiels anodiques, par rapport à un tampon B.R. de même pH. En résumé et comme dans le cas des oximes (6), les ions ammonium exercent une double influence: ils sont susceptibles de jouer le rôle d'agent protonant pour l'hétérocycle **3***a* et leur présence dans la double couche facilite la réduction de la forme non-protonée.

1.3 *Détermination des conditions expérimentales pour la préparation des hétérocycles* **3**a, **4**a *et* **5**a

La connaissance du comportement électrochimique de la nitrocétone **1***a* et de ses produits de réduction permet maintenant de choisir les meilleures conditions d'électrolyse (sur cathode de mercure) pour préparer sélectivement les différents hétérocycles.

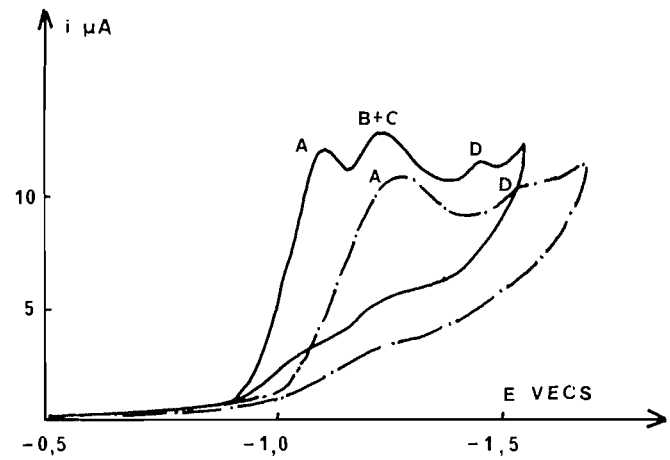

FIG. 2. Voltammogramme de **1***a* ($c = 10^{-3}$ mol L^{-1}) en milieu tampon acétique + éthanol (1:3) sur électrode de mercure, pour différentes vitesses de balayage des potentiels: $v = 0{,}1$ V s^{-1} (——); $v = 10$ V s^{-1} (– · – ·).

Préparation de la pyrroline N-*oxyde* **3**a

Ce composé doit être préparé dans un milieu où la vague A est nettement séparée des vagues B et C; les milieux très acides ne conviennent donc pas. Les électrolyses, contrôlées par coulométrie, ont été effectuées en tampon acétique et en tampon ammoniacal; mais, dans les deux cas, le choix du potentiel de travail est important.

En tampon acétique + éthanol (1:4), il faut éviter la réduction ultérieure de **3***a* et opérer à un potentiel $E_T = -1{,}1$ V ECS, correspondant au début du palier de la vague A (fig. 4); le résultat coulométrique est alors 4,0 faradays par mole et l'enregistrement d'un polarogramme en fin d'électrolyse (fig. 4, courbe 3) montre que le rendement en pyrroline *N*-oxyde formée est supérieure à 90%.

En tampon ammoniacal + éthanol (1:4), l'aspect du polarogramme initial (fig. 5, courbe 1) laisse penser que le choix du potentiel est moins drastique puisque le palier de diffusion s'étend de −1 à −1,5 V ECS. En fait, la vague de réduction de **3***a*, avec préprotonation (B_1), n'apparaît pas sur le polarogramme de la nitrocétone alors qu'elle est visible lorsque l'hétérocycle **3***a* est présent en solution (fig. 5, courbe 2). Cet exemple montre bien la nécessité d'une étude préliminaire complète pour définir les conditions d'électrolyses. Nous avons pu obtenir la pyrroline *N*-oxyde, avec un rendement pratiquement quantitatif, par réduction de **1***a* en tampon ammoniacal, à $E_T = -1{,}15$ V ECS (coulométrie à 4,0 faradays mol^{-1}).

Préparation de la pyrroline **4**a

C'est le composé pour lequel le choix des conditions expérimentales est le plus délicat, puisqu'il faut opérer dans un milieu où la vague B est suffisamment séparée de la vague C; les milieux faiblement acides et basiques sont donc à proscrire. La pyrroline **4***a* peut être préparée par réduction du dérivé *N*-oxyde **3***a*, à $E_T = -0{,}7$ V ECS, dans un milieu H_2SO_4 *N* + éthanol (1:1); on a alors $E_{1/2}$ (B) = −0,7 V ECS et $E_{1/2}$ (C) = −0,83 V ECS. Par contre, le composé **4***a* n'a pu être obtenu par réduction directe de la nitrocétone **1***a*; celle-ci étant

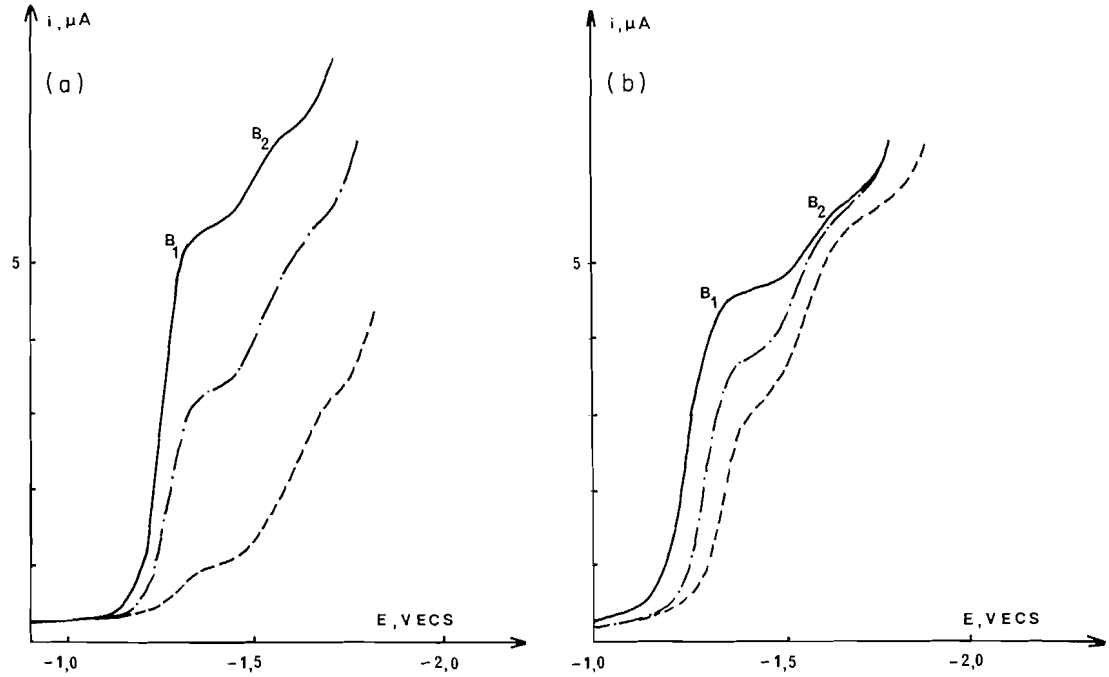

FIG. 3. (a) Polarogrammes de **3***a* en milieu tampon ammoniacal + éthanol (1:1), à différents temps de chute des gouttes de mercure; τ = 8 s (——); 2 s (— · —); 0,1 s (– – –). (b) Polarogrammes de **3***a* en milieu tampon ammoniacal + éthanol (1:1), pour différentes concentrations en ions ammonium NH_4^+. $[NH_4^+]\%$ = 90 (——); 50 (— · —); 20 (– – –).

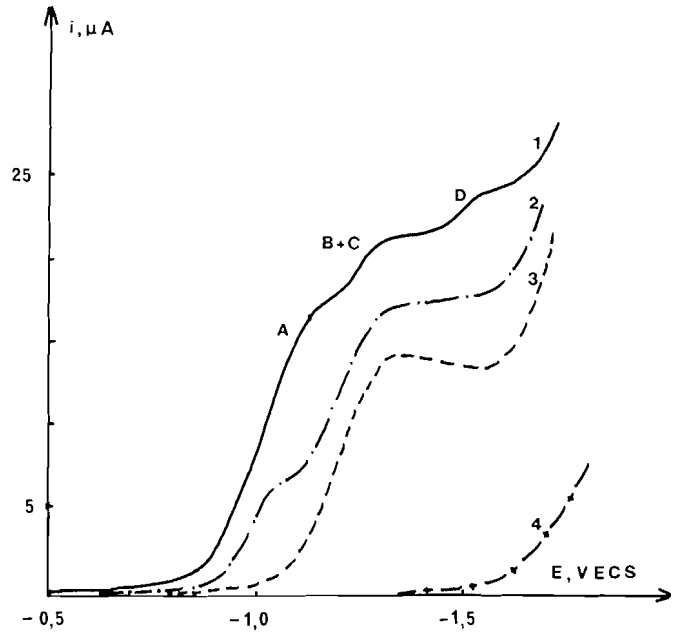

FIG. 4. Evolution des polarogrammes au cours de la réduction de **1***a* (5×10^{-4} mol) dans un mélange tampon acétique (30 cm^3) + éthanol (120 cm^3). 1: avant réduction; 2 et 3: après réduction à E_T = −1,1 V ECS (2: après passages de 2,4 F/mol; 3: après passage de 4 F/mol); 4: après réduction ultérieure à E_T = −1,35 V ECS et passage de 7,6 F/mol de **1***a*.

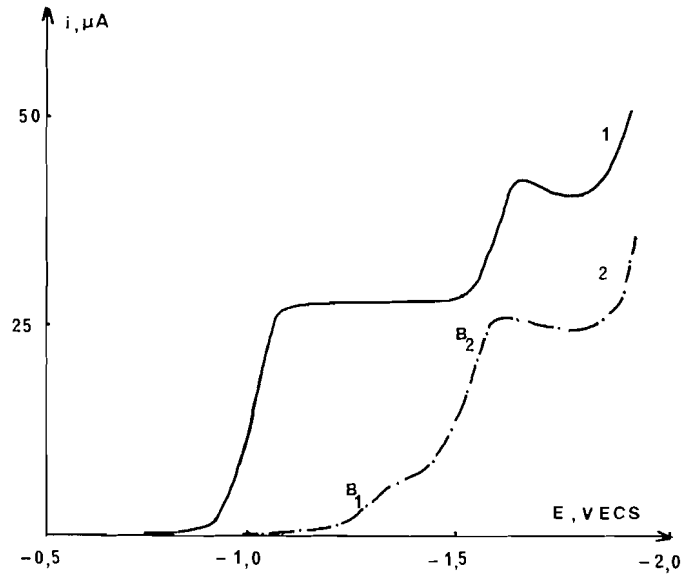

FIG. 5. Evolution des polarogrammes au cours de la réduction de **1***a* (5×10^{-4} mol) dans un mélange tampon ammoniacal (30 cm^3) + éthanol (120 cm^3). 1: avant réduction; 2: après réduction à E_T = −1,15 V ECS et passage de 4F/mol de **1***a*.

beaucoup moins soluble que les dérivés hétérocycliques, l'électrolyse devrait être réalisée dans un milieu H_2SO_4 *N* + éthanol (1:4); mais, dans ces conditions, le dérivé nitré de départ présente une vague unique de réduction à 8 électrons (superposition des vagues A, B et C).

Préparation de la pyrrolidine **5**a

Il existe a priori de nombreuses possibilités pour la préparation électrochimique de ce composé.

On pourrait penser réduire directement (à 8 faradays par mole) la nitrocétone de départ, à un potentiel correspondant au palier de la vague C (ou B + C). Mais d'une part, en milieu très acide, ce palier est mal défini par suite de l'électroactivité du groupement carbonyle et la réduction n'est pas sélective; ainsi, une électrolyse de **1***a*, réalisée à environ −1,15 V ECS dans H_2SO_4 *N* + éthanol (1:4) consomme 7,0 faradays par mole et conduit à un mélange de 50% de pyrrolidine **5***a* et 50% d'hydroxylamino-alcool (correspondant à une réduction à 6 faradays par mole). D'autre part, en milieu moins acide (tam-

pon acétique ou tampon ammoniacal), compte-tenu du caractère cinétique des vages B et C, les réductions sont plus lentes; de plus, elles s'accompagnent d'un déficit coulométrique (*vide infra*).

La meilleure façon de préparer **5***a* consiste à réduire **3***a* (à 4 faradays par mole) ou **4***a* (à 2 faradays par mole). En fait, l'électroréduction de la pyrroline *N*-oxyde **3***a*, en tampon acétique (E_T = −1,25 V ECS) comme en tampon ammoniacal (E_T = −1,50 V ECS) conduit à un résultat coulométrique compris entre 3 et 4 faradays par mole. Le déficit, par rapport aux 4 faradays attendus, provient de la formation d'un produit de duplication, résultant de la réduction à 1 électron, de la pyrroline **4***a*:

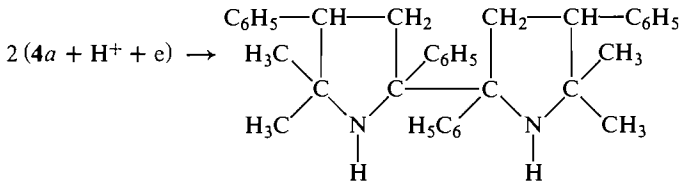

La proportion de produit de duplication formé augmente avec la concentration en substrat et la vitesse d'agitation de la cathode de mercure. Finalement, c'est en milieu H_2SO_4 *N* + éthanol (1 : 1) que la pyrrolidine **5***a* doit être préparée, par réduction de **3***a* ou de **4***a*; les électrolyses, suivies par coulométrie, sont effectuées à −0,95 V ECS et le rendement en **5***a* est alors pratiquement quantitatif.

Remarque: étude stéréochimique de la formation de **5**a

L'examen des spectres rmn de la pyrrolidine **5***a* montre qu'il se forme un mélange d'isomères *cis* et *trans*. Nous avons étudié la variation des pourcentages relatifs des deux stéréoisomères obtenus, d'une part en fonction de la nature du produit soumis à réduction (**3***a* ou **4***a*), d'autre part en fonction des conditions d'électrolyse (nature du milieu, potentiel de travail). Les résultats obtenus sont rassemblés dans le tableau 1.

L'isomère *trans*, thermodynamiquement le plus stable, est toujours majoritaire et on notera que les résultats sont sensiblement les mêmes, que l'on réduise la pyrroline ou la pyrroline *N*-oxyde. Par ailleurs, le pourcentage en isomère *trans* augmente avec le pH: il est probable qu'en milieu très acide la protonation finale s'effectue en partie à la cathode (et conduit alors au dérivé saturé *cis*); au fur et à mesure que l'acidité de la solution diminue, la proportion de carbanion subissant la protonation en solution augmente, entraînant une augmentation du pourcentage en dérivé *trans*. Cependant, en tampon ammoniacal, la proportion en isomère *cis* croît à potentiel très négatif: on peut penser que les ions ammonium s'accumulent alors à la cathode et jouent le rôle d'agent protonant vis-à-vis du carbanion; un effet semblable a déjà été observé lors de la réduction de bromocyclopropanes optiquement actifs (7).

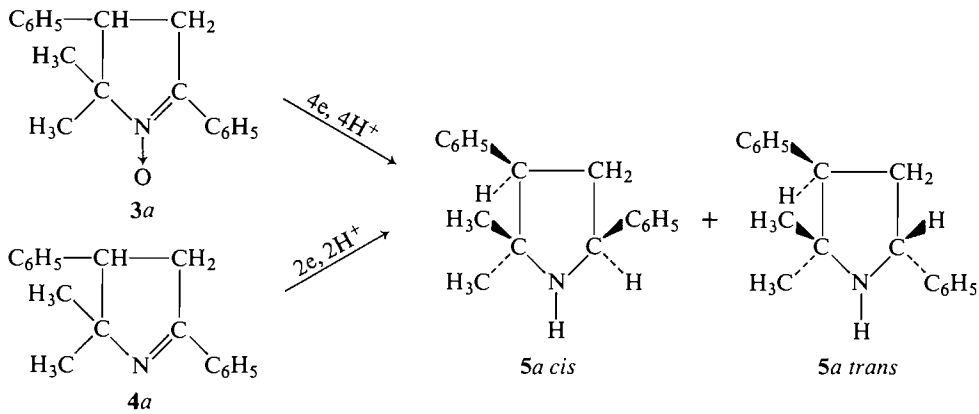

2. Réduction de la nitrocétone 1*b*

Des études analogues à celles qui précèdent ont été réalisées sur la nitrocétone **1***b* et les hétérocycles **3***b* et **4***b*. Nous présenterons brièvement les résultats essentiels, en les analysant par comparaison aux conclusions précédentes, avant de préciser les conditions des électrolyses préparatives.

2.1 *Etude polarographique*

Le polarogramme du *dérivé nitré* **1**b présente, en milieu très acide (pH ≃ 0), deux vagues successives: la première (vague A) est à 4 électrons; la seconde (vague B) est à 2 électrons. Lorsque le pH augmente, ces deux vagues restent bien séparées, mais la hauteur de la seconde croît rapidement pour atteindre 4 électrons (vague B + C) dès pH = 3; elle conserve une hauteur constante jusqu'à pH = 5. A pH plus élevé, elle disparaît, masquée par la décharge des cations de l'électrolyte.

La pyrroline N-*oxyde* **3**b présente une vague unique de réduction à 2 électrons (vague B) à pH ≃ 0. L'intensité de diffusion augmente avec le pH et la vague est à 4 électrons (vague B + C) pour 3 < pH < 5.

TABLEAU 1. Stéréochimie de la pyrrolidine **5***a* obtenue par électroréduction des hétérocycles **3***a* et **4***a*

	Milieu							
	H_2SO_4 *N*		Tampon acétique		Tampon ammoniacal			
Composé réduit	**3***a*	**4***a*	**3***a*	**4***a*	**3***a*	**4***a*	**3***a*	**4***a*
Potentiel E_T (V ECS)	−1,00	−1,00	−1,25	−1,25	−1,35	−1,35	−1,50	−1,50
%trans	63	59	70	65	83	87	67	68

TABLEAU 2. Electroréduction de dérivés nitrés secondaires et primaires à potentiel peu négatif. Milieu: électrolyte-support + éthanol (1:1)

Electrolyte-support (E_T V ECS)	Dérivé nitré	Coulométrie n (F mol^{-1})	Rendement ρ en **3***
H_2SO_4 *N*	**1***e*	3,5	75%
(−0,75)	**1***f*	3,7	85%
Tampon acétique	**1***e*	3,4	70%
(−1,1)	**1***f*	3,5	75%
Tampon ammoniacal	**1***e*	3,7	85%
(−1,2)	**1***f*	3,8	90%

*Calculé à partir du résultat coulométrique ρ% = 50(n − 2).

Enfin, *la pyrroline* **4**b n'est électroactive que pour 3 < pH < 7,5 et présente, dans ce domaine d'acidité, une vague unique de réduction à 2 électrons (vague C).

2.2 *Comparaison avec les composés* **1**a, **3**b, *et* **4**a

Comme précédemment, les trois vagues correspondent respectivement à la réduction du groupement nitré (vague A), de la fonction *N*-oxyde (vague B) et de la double liaison carbone−azote (vague C). Les différences essentielles sont les suivantes. (*i*) En milieu acide, la vague A est mieux séparée de la vague B. (*ii*) La pyrroline **4***b*, contrairement à son homologue **4***a*, n'est pas réductible sur mercure en milieu très acide. (*iii*) Il n'apparaît jamais sur les polarogrammes de vague D (ou de creux) correspondant à la réduction du carbonyle. (*iv*) Enfin, les vagues B ou B + C, enregistrées à partir du dérivé nitré **1***b*, ne présentent pas de caractère cinétique.

Les trois premières observations relèvent de la même interprétation: les hétérocycles **3***b* et **4***b*, substitués par un groupement méthyle sur le carbone lié à l'azote sont plus difficilement réductibles que leurs homologues de la série *a*, substitués par un groupement phényle; de même, la fonction cétone du produit de départ est plus difficile à réduire en série *b*.

Enfin, l'absence de caractère cinétique des vagues de réduction de **3***b* et **4***b* prouve que la cyclisation de l'hydroxylamine **2***b* est plus rapide que celle de **2***a*.

2.3 *Conditions expérimentales de préparation des hétérocycles* **3**b, **4**b *et* **5**b

Le comportement polarographique des composés de la série *b* étant nettement simplifié, les possibilités de préparation électrochimique des hétérocycles sont plus nombreuses et le choix des conditions expérimentales moins draconien.

La pyrroline N-*oxyde* **3**b est préparée, quel que soit le milieu, par réduction au potentiel du palier de la vague A. Les rendements sont quantitatifs (coulométrie à 4,0 faradays mol^{-1}) dans les conditions suivantes: milieu H_2SO_4 *N* + éthanol (1:1), E_T = −0,75 V ECS; tampon acétique + éthanol (1:1), E_T = −1,10 V ECS; tampon ammoniacal + éthanol (1:1), E_T = −1,20 V ECS.

La pyrroline **4**b ne peut être obtenue qu'en milieu H_2SO_4 *N* + éthanol (1:1), par réduction au potentiel de la vague B (E_T = −1,10 V ECS). L'électrolyse peut être effectuée sur l'hétérocycle **3***b* (à 2,0 faradays mol^{-1}) ou directement sur le dérivé nitré **1***b* (à 6,0 faradays mol^{-1}).

La pyrrolidine **5**b peut être préparée, en tampon acétique + éthanol (1:1), par réduction de **1***b* (8,0 faradays mol^{-1}), **3***b* (4,0 faradays mol^{-1}) ou **4***b* (2,0 faradays mol^{-1}), au potentiel E_T = −1,50 V ECS, correspondant au palier de la vague B + C. Contrairement au cas de la série *a*, on n'observe jamais la formation de composé de duplication.

3. Réduction des dérivés nitrés secondaires et primaires

3.1 *Etude polarographique*

Elle apporte peu d'éléments nouveaux. Les composés **1***c* et **1***d*, porteurs d'un groupement COC_6H_5, possèdent un comportement voisin de celui de **1***a*. En milieu très acide, le polarogramme présente les trois vagues A, B et C mal séparées, suivies, à potentiel plus négatif, d'une diminution du courant de diffusion due à la réduction du groupement carbonyle. En milieu peu acide, la vague A reste très proche d'une seconde vague (de type B + C) à caractère cinétique, elle-même suivie d'une vague de type D. Ce n'est qu'en milieu basique (en particulier en tampon ammoniacal) qu'apparaît une vague A bien séparée d'une seconde vague de type D.

Les composés **1***e* et **1***f*, dont la fonction cétone est substituée par un groupement méthyle, se conduisent comme **1***b*. En milieu très acide, il existe deux vagues distinctes A et B. Lorsque le pH augmente, la vague A est suivie jusqu'à pH = 6 d'une vague B + C qui ne présente pas de caractère cinétique.

3.2 *Mesures coulométriques et électrolyses*

Contrairement à ce que l'on observe dans le cas des dérivés nitrés tertiaires, les électrolyses, réalisées au potentiel des vagues A des composés **1***c* à **1***f*, sont caractérisées par un déficit coulométrique par rapport aux 4 faradays attendus (cf. tableau 2). A côté de la pyrroline *N*-oxyde **3**, la solution obtenue contient une oxime-cétone **6**, non électroactive dans les conditions utilisées. Selon Iversen et Lund (8), cette dernière provient de la formation transitoire de dérivé nitroso dont une partie se transpose et l'autre se réduit en hydroxylamine (schéma 2):

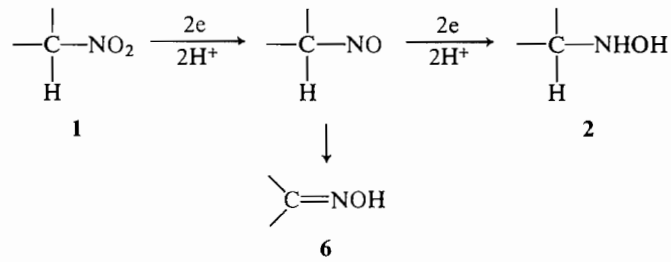

SCHÉMA 2

Il apparaît donc que l'électroréduction de dérivés nitrés primaires ou secondaires ne constitute pas une méthode sélective d'accès aux pyrrolines *N*-oxydes **3**. En conséquence, il n'apparaît pas rentable de chercher à les isoler pour les réduire ultérieurement. Nous avons alors été conduits à rechercher des conditions d'obtention des autres hétérocycles par réduction directe des dérivés nitrés **1***c* à **1***f*; si les pyrrolidines peuvent être ainsi préparées avec des rendements satisfaisants, l'obtention des pyrrolines est plus délicate et seules **4***e* et **4***f* ont pu être caractérisées.

3.21 *Obtention des pyrrolines* N-*oxydes*

Ces composés se forment à côté de la cétone-oxime **6** par réduction à potentiel peu négatif (vague A).

Dans le cas des composés méthylés **1***e* et **1***f*, les électrolyses peuvent être réalisées dans différents milieux. Les résultats coulométriques, rassemblés dans le tableau 1, montrent que les rendements en composés hétérocycliques sont plus faibles en tampon acétique.

Dans le cas des composés phénylés, il est exclu d'opérer en milieu acide, les vagues A et B (ou B + C) étant trop rapprochées. En tampon ammoniacal, on se heurte à la même

difficulté que dans le cas de **3***a*: alors que le polarogramme des nitrocétones **1***c* et **1***d* ne présente que les vagues A et D, en cours d'électrolyse, il apparaît une vague de type B_1, trop proche de A, correspondant à la réduction de la pyrroline *N*-oxyde qui s'est accumulée en solution. Le résultat coulométrique est alors peu reproductible ($3{,}8 < n(F) < 4{,}2$) et l'on obtient un mélange de l'hétérocycle cherché (**3***c* ou **3***d*) et de pyrroline (**4***c* ou **4***d*) en proportions variables selon les conditions d'électrolyse.

3.22 *Obtention des pyrrolines* ***4***

Tous les essais d'obtention des pyrrolines **4***c* et **4***d* se sont soldés par des échecs, comme le laissait prévoir l'étude polarographique.

Les dérivés méthylés **4***e* et **4***f* ont pu être préparés, en milieu sulfurique, par électrolyse au palier de la vague B de réduction de **1***e* ou **1***f* ($E_T = -1{,}0$ V ECS); les résultats coulométriques sont inférieurs aux 6 F attendus et les rendements ne sont pas quantitatifs.

3.23 *Obtention des pyrrolidines* ***5***

La réduction, à 8 faradays par mole, du dérivé nitré doit être réalisée au palier d'une vague B + C.

Pour **1***c* et **1***d*, les électrolyses ne peuvent être effectuées en milieu sulfurique (du fait de la réduction du carbonyle à potentiel très négatif) ni en tampon acétique (déficit coulométrique dû, d'une part à la formation d'oxime lors du passage par le nitroso intermédiaire, d'autre part à la formation d'un produit de duplication, lors du passage pyrroline–pyrrolidine). Ce n'est donc qu'en tampon ammoniacal, au potentiel $E_T = -1{,}45$ V ECS (supérieur au $E_{1/2}$ de la vague D) que nous avons pu préparer **5***c* et **5***d*. Les résultats coulométriques (voisins de 7,8 faradays) indiquent un rendement proche de 95%.

Pour **1***e* et **1***f*, la vague B + C n'apparaît qu'en tampon acétique. Les électrolyses, réalisées dans ce milieu à $E_T = -1{,}5$ V ECS, permettent d'obtenir **4***e* et **4***f* avec de bons rendements.

Partie expérimentale

1. *Techniques électrochimiques*

Les polarogrammes sont enregistrés à l'aide d'un appareil à trois électrodes (enregistreur EPL 2B Tacussel équipé d'un tiroir Tipol). Les coulométries et les électrolyses préparatives sont réalisées à potentiel contrôlé (potentiostat Tacussel 20-2; intégrateur IG 5) dans la cellule décrite par Moinet et Peltier (9). Les essais portent sur 0,1 à 1 g de dérivé nitré; la température est voisine de 20°C.

Les milieux aqueux utilisés comme électrolyte-support sont les suivants.

En polarographie

pH < 2: solutions d'acide sulfurique

$2 <$ pH < 12: tampons Britton-Robinson (notés B.R.) 4×10^{-2} *M* + KNO_3 0,2 *M*. Les polarogrammes sont enregistrés sur des solutions 5×10^{-4} *M* en dérivé nitré dissous dans un mélange électrolyte-support + éthanol (1:1) en volume.

En électrolyse préparative

Milieux tres acides: acide sulfurique normal; milieux peu acides: tampon acétique 0,5 *M* en CH_3CO_2H et 0,5 *M* en CH_3CO_2Na (pH ≃ 4,8); milieux basiques: tampon ammoniacal 0,5 *M* en NH_3 et 0,5 *M* en NH_4Cl ou $NH_4CH_3CO_2$.

Les expériences sont conduites dans des mélanges électrolyte-support + éthanol, en proportions 1:1 ou 1:4 selon la solubilité du substrat. Les produits de réduction sont extraits à l'éther après évaporation de l'éthanol et neutralisation éventuelle de la solution par Na_2CO_3.

2. *Préparation des dérivés nitrés de départ*

Les dérivés γ-nitrés sont généralement obtenus par addition d'un nitroalcane sur un composé éthylénique activé en présence d'un catalyseur basique.

Quelques γ-nitrocétones avaient déjà été préparés antérieurement (3, 10) par condensation du nitrométhane ou du nitro-2 propane sur une benzylidène-cétone, en présence de catalyseurs variés.

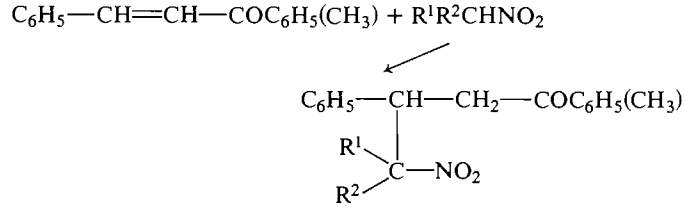

($R^1 = R^2 = H$ ou $R^1 = R^2 = CH_3$)

Nous avons diminué les temps de réaction et amélioré les rendements en utilisant la tétraméthylguanidine comme catalyseur. L'addition se fait alors à température ambiante et conduit, avec de bons rendements aux γ-nitrocétones **1***a* à **1***f*.

1*a*: F = 150°C (3); **1***b*: F = 54°C (3); **1***c*: F = 75°C (mélange de deux diastéréoisomères)

1*d*: F = 99°C (10); **1***e*: $E_{b_{0,5}}$ = 148°C (mélange de deux diastéréoisomères)

1*f*: F = 96–100°C (10).

3. *Préparation et caractéristiques des produits de réduction*

3.1 *Pyrrolines* N-*oxydes*

Les conditions de préparation et les caractéristiques des pyrrolines *N*-oxydes **3***a* et **3***b*, issues de la réduction de **1***a* et **1***b*, sont données dans la note préliminaire (4).

Les hétérocycles **3***c* et **3***d* sont obtenus par réduction de **1***c* et **1***d* en milieu tampon ammoniacal + éthanol (1:4); potentiel de travail $E_T = -1{,}05$ V ECS; résultat coulométrique *n* voisin de 4 F par mole de dérivé nitré; spectres ir (CCl_4) de **3***c* et **3***d* identiques à celui de **3***a*.

Les hétérocycles **3***e* et **3***f* sont préparés par réduction de **1***e* et **1***f* en milieu tampon ammoniacal + éthanol (1:1); $E_T = -1{,}15$ V ECS; n = 3,69 F par mole pour **1***e* et n = 3,80 F par mole pour **1***f*. Spectres ir (CCl_4) de **3***e* et **3***f* identiques à celui de **3***b*.

Remarque: l'hétérocycle **3***f* a également été caractérisé à l'état de picrate: F = 133–135°C (11).

3.2 *Pyrrolines*

Les caractéristiques des pyrrolines **4***a* et **4***b* sont données dans la réf. 4. Pour les raisons invoquées précédemment, les pyrrolines **4***c* et **4***d* n'ont pu être obtenues. Les pyrrolines **4***e* et **4***f* sont préparées par réduction de **1***e* et **1***f* en milieu H_2SO_4 *N* + éthanol (1:1); $E_T = -1{,}0$ V ECS; *n* compris entre 5,8 et 6,0 F par mole pour **1***e* et n = 5,77 F par mole pour **1***f*. Les spectres ir (CCl_4) de **4***e* et **4***f* sont identiques à celui de **4***b*.

3.3 *Pyrrolidines*

Les caractéristiques rmn des pyrrolidines **5***a* et **5***b* sont données dans la réf. 4. Les spectres ir de ces deux composés enregistrés dans CCl_4 sont identiques. Composé **5***a*; ν_{max}: 3370, 3080, 3040, 2970, 2940, 2870, 1950, 1875, 1810, 1605, 1495, 1455, 1425, 1380 cm^{-1}.

Préparation de **5**c: réduction de **1***c* en tampon ammoniacal + éthanol (1:4); $E_T = -1{,}5$ V ECS; *n* voisin de 7,8 F par mole; spectre ir (CCl_4) de **5***c* identique à celui de **5***a*; l'hétérocycle **5***c* a également été caractérisé par son dérivé benzoylé: F = 142°C.

Préparation de **5**d: réduction de **1***d* en tampon ammoniacal + éthanol (1:4); $E_T = -1{,}4$ V ECS; *n* voisin de 7,6 F par mole; spectre ir (CCl_4) de **5***d* identique à ceux de **5***a* et **5***c*; l'hétérocycle **5***d* a également été caractérisé par son dérivé benzoylé: F = 120°C (litt. (10) F = 122°C).

Préparation de **5**e: réduction de **1***e* en tampon acétique + éthanol (1:1); $E_T = -1{,}5$ V ECS; *n* voisin de 7,7 F par mole; spectre ir (CCl_4) de **5***e* identique à celui de **5***b*.

Préparation de **5**f: réduction de **1***f* en tampon acétique + éthanol (1:1); $E_T = -1{,}5$ V ECS; *n* voisin de 7,7 F par mole; spectre ir (CCl_4)

de **5***f* identique à ceux de **5***b* et **5***e*.

3.4 *Les cétones oximes* **6** ont été identifiées à partir de leur spectre ir (CCl_4): ν_{OH} = 3600 cm^{-1}; $\nu_{C=O}$ = 1720 cm^{-1}.

Conclusion

Les résultats obtenus au cours de cette étude montrent que l'électroréduction, à potentiel contrôlé, de γ-nitrocétones est une méthode de choix pour la préparation de pyrrolines *N*-oxydes, de pyrrolines et de pyrrolidines, lorsque le groupement nitré est porté par un carbone tertiaire. Mais, même dans ce cas, le choix des conditions expérimentales, appropriées pour la préparation sélective de chaque hétérocycle, nécessite une étude préalable du comportement électrochimique du dérivé nitré de départ et de ses produits de réduction.

Dans le cas des dérivés nitrés secondaires et primaires, la formation parasite d'une cétone-oxime lors des réductions à potentiel peu négatif, limite les rendements en pyrrolines *N*-oxydes. Si les pyrrolidines peuvent être encore préparées par électrolyse à potentiel très négatif dans un milieu convenablement choisi, la méthode est difficilement applicable à la préparation des pyrrolines.

1. H. LUND. Organic electrochemistry. *Edité par* M. M. Baizer. Marcel Dekker, New York. 1973. p. 563.
2. A. TALLEC. L'actualité chimique. 1977. p. 7.
3. J. B. BAPAT et D. ST. C. BACK. Austr. J. Chem. **21**, 2483 (1968); **21**, 2497 (1968).
4. M. CARIOU, R. HAZARD, M. JUBAULT et A. TALLEC. Tetrahedron Lett. **22**, 3961 (1981).
5. S. G. MAIRANOVSKII. Catalytic and kinetic waves in polarography. Plenum Press, New York. 1968. p. 187.
6. E. RAOULT, M. JUBAULT et D. PELTIER. Electrochim. Acta, **24**, 1219 (1979).
7. R. HAZARD, S. JAOUANNET, E. RAOULT et A. TALLEC. Nouv. J. Chim. **6**, 325 (1982).
8. E. IVERSEN et H. LUND. Tetrahedron Lett. 4027 (1967).
9. C. MOINET et D. PELTIER. Bull. Soc. Chim. Fr. 690 (1969).
10. M. C. KLOETZEL. J. Am. Chem. Soc. **69**, 2271 (1947).
11. R. F. C. BROWN, L. SUBRAHMANYAN et C. P. WHITTLE. Aust. J. Chem. **20**, 339 (1967).

Substituent-induced chemical shifts in 3- and 4-substituted styrenes: factor analysis of the styrene data matrix

WILLIAM F. REYNOLDS, ANABELA GOMES, ANTONINA MARON, DOUGLAS W. MACINTYRE, ROBERT G. MAUNDER, ATES TANIN, AND HECTOR E. WONG

Department of Chemistry, University of Toronto, Toronto, Ont., Canada M5S 1A1

GORDON K. HAMER

Xerox Research Centre of Canada, 2480 Dunwin Drive, Mississauga, Ont., Canada L5L 1J9

AND

IAN R. PEAT

U.S. Industrial Chemicals Ltd., 1275 Section Road, Cincinnati, OH 45237 U.S.A.

Received November 16, 1982

WILLIAM F. REYNOLDS, ANABELA GOMES, ANTONINA MARON, DOUGLAS W. MACINTYRE, ROBERT G. MAUNDER, ATES TANIN, HECTOR E. WONG, GORDON K. HAMER, and IAN R. PEAT. Can. J. Chem. **61**, 2367 (1983).

The techniques of factor analysis are used to investigate a data matrix constructed from magnetic resonance parameters for seventy-five 4-substituted styrenes, α-methylstyrenes, and α-*tert*-butylstyrenes and 3-substituted styrenes and α-methylstyrenes (with fifteen common substituents for each series). Two substituent factors (parameters) are clearly both *necessary* and *sufficient* to predict long-range chemical shifts within experimental uncertainty. Target testing indicates that Taft's σ_I and σ_R^0 constants are appropriate for this purpose. One additional major factor is required for each of *ipso* and *ortho* carbons and a minor factor is apparently required for *meta* carbons.

Conclusions do not appear to be sensitive to the weighting of individual variables and the specific variables included in the data matrix. However, the use of an extensive and well-chosen substituent set is essential.

WILLIAM F. REYNOLDS, ANABELA GOMES, ANTONINA MARON, DOUGLAS W. MACINTYRE, ROBERT G. MAUNDER, ATES TANIN, HECTOR E. WONG, GORDON K HAMER et IAN R. PEAT. Can. J. Chem. **61**, 2367 (1983).

On a utilisé les techniques d'analyse de facteurs pour étudier une matrice de données construite à partir des paramètres de résonance magnétique de soixante-quinze composés comprenant des styrènes substituées en position 4, des α-méthylstyrènes et α-*tert*-butylstyrènes, des styrènes substitués en position 3 et des α-méthylstyrènes (avec 15 substituants communs dans chaque série). Deux facteurs de substituant (paramètres) sont nécessaires et suffisants pour prédire les constantes de couplage à longue distance à l'intérieur des marges d'erreur expérimentale. Les tests cibles indiquent que les constantes σ_I et σ_R^0 de Taft conviennent dans ce cas. On a besoin d'un facteur principal additionnel pour chaque carbone *ipso* et *ortho* et d'un facteur secondaire pour les charbones en *méta*.

La pondération des variables individuelles et des variables spécifiques incluses dans la matrice ne semblent pas avoir d'influence sur les faits observés. Cependant il est essentiel d'utiliser un ensemble de substituants très convenablement choisis.

[Traduit par le journal]

Introduction

Ten years ago, we published the results of nmr investigations of a series of 4-substituted styrenes (**4H**), 4-substituted α-methylstyrenes (**4M**) and 4-substituted α-*tert*-butylstyrenes (**4B**) (1, 2). Nuclear magnetic resonance spectral data were obtained for more than 50 compounds, measured under inert conditions. Our two main conclusions were: (a) that a dual substituent parameter (dsp) treatment was necessary to adequately account for substituent-induced long-range chemical shifts in styrenes, and (b) that the actual chemical shifts reflected a combination of resonance, field, and π inductive (polarization) effects (1, 2). The **4H**, **4M**, and **4B** derivatives were ideal for this purpose since the increasing size of the alkyl groups progressively decreased phenyl−vinyl conjugation, thus altering the ratio of resonance to field/inductive effects in a qualitatively predictable manner (2).

Subsequently, a number of other groups have used our styrene data to test various other models of single and dual substituent parameter scales (3−9). This may be regarded as part of a more general debate concerning the relative merits of these two approaches (10). We were flattered that so many groups were sufficiently impressed by our data set to use it in their investigations, even if we didn't always agree with their conclusions (11, 12). However, we were never entirely happy with the original data set. In particular, both the **4M** and **4B** substituent sets contained only one strong acceptor group (NO_2) (2), thus not fulfilling Taft's recommended minimal substituent set for dsp correlations (13).

Consequently, the appearance of the most recent alternative explanation of our styrene data (9) catalyzed us to expand the substituent set to incorporate a better-balanced set of substituents. At the same time, we decided to synthesize 3-substituted styrenes (**3H**) and 3-substituted α-methylstyrenes (**3M**). This should again alter phenyl-vinyl conjugation by going from a conjugated to a formally unconjugated orientation of the substituent and vinyl groups.

We have now ^{13}C data for 15 common substituents (X = H, $N(CH_3)_2$, NH_2, OCH_3, SCH_3, CH_3, $Si(CH_3)_3$, F, Cl, Br, $COCH_3$, CO_2CH_3, CF_3, CN, and NO_2) in the five styrene series, well in excess of the recommended minimum substituent set (13). In this paper we report the results of factor analysis of this large data set. Factor analysis and the closely related technique of principal components analysis can be used without prior assumptions to determine the number of factors or components necessary to account for any data set (14, 15). Both techniques have recently been applied to the analysis of substituent-induced chemical shifts (9, 16−19). We chose to use factor analysis because a standard program (FACTANAL (20)) was readily available, along with a recent book which provides a very clear description of this technique (14). It was

Can. J. Chem. Downloaded from www.nrcresearchpress.com by 210.87.254.105 on 09/06/12
For personal use only.

TABLE 1. ^{13}C chemical shifts for new 4-substituted styrenes (**4H**), α-methylstyrenes (**4M**), and α-*tert*-butylstyrenes (**4B**) (in ppm relative to internal $(CH_3)_4Si$)

Series	X	$\delta_{C(4)}$[b]	$\delta_{C(3)}$	$\delta_{C(2)}$	$\delta_{C(1)}$	$\delta_{C(\alpha)}$	$\delta_{C(\beta)}$
4H	F[a]	162.40	115.22	127.50	133.57	135.74	113.05
4H	NH_2	145.77	114.47	127.09	138.04	136.58	109.40
4H	CO_2CH_3	129.55	129.76	125.73	141.38	136.19	115.69
4M	NH_2	145.38	114.23	126.22	131.38	142.30	109.08
4M	SCH_3	137.53	126.53	125.55	138.00	142.28	111.67
4M	Br	121.32	131.08	126.83	139.88	141.95	112.79
4M	$COCH_3$	136.25	128.06	125.27	145.15	142.29	114.20
4M	CO_2CH_3	129.19	129.43	125.08	145.14	142.33	114.10
4M	CF_3	129.69	125.02	125.55	144.56	142.01	114.33
4M	CN	111.72	131.67	125.85	145.05	141.65	115.21
4B	NH_2	144.33	113.61	129.49	133.31	159.31	111.16
4B	SCH_3	136.32	126.01	129.11	140.13	158.98	111.65
4B	$Si(CH_3)_3$	137.18	132.03	128.17	143.63	159.39	111.31
4B	$COCH_3$	135.66	127.22	128.80	147.86	158.86	111.89
4B	CO_2CH_3	128.25	128.55	128.61	147.73	158.81	111.81
4B	CF_3	128.98	124.14	128.98	146.77	158.38	112.29
4B	CN	111.38	130.86	129.43	147.70	158.27	112.59

[a]Corrected values (12)
[b]Numbering:

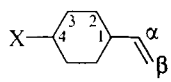

TABLE 2. ^{13}C chemical shifts for 3-substituted styrenes (**3H**) (in ppm relative to internal $(CH_3)_4Si$)

X	$\delta_{C(1)}$[a]	$\delta_{C(2)}$	$\delta_{C(3)}$	$\delta_{C(4)}$	$\delta_{C(5)}$	$\delta_{C(6)}$	$\delta_{C(\alpha)}$	$\delta_{C(\beta)}$
H	137.40	126.00	128.13	127.46	128.13	126.00	136.96	113.20
$N(CH_3)_2$	137.93	110.69	150.39	112.33	128.72	115.07	137.84	112.51
NH_2	138.34	112.38	146.14	114.32	128.98	116.68	137.24	112.81
OCH_3	138.72	111.41	159.76	113.23	128.98	118.65	136.95	113.33
SCH_3	137.89	124.61	138.67	125.98	128.47	122.79	136.50	113.85
CH_3	137.31	126.74	137.03	128.22	128.06	123.26	137.13	112.94
$Si(CH_3)_3$	136.53	131.10	139.80	132.44	127.63	126.28	137.20	113.12
F	139.73	113.09	163.00	114.62	129.51	121.79	135.89	114.39
Cl	139.19	126.13	134.57	127.56	129.28	124.04	135.64	114.82
Br	139.46	129.08	122.74	130.49	129.58	124.48	135.54	114.88
$COCH_3$	137.61	125.81	137.46	127.29	128.18	130.09	136.03	114.62
CO_2CH_3	137.49	127.29	130.55	128.68	128.05	129.87	136.00	114.52
CF_3	138.14	122.84	131.26	124.15	128.43	129.22	135.53	115.38
CN	138.46	129.42	113.52	130.65	128.94	129.63	134.86	116.16
NO_2	139.00	120.67	148.82	122.12	128.94	131.18	134.81	116.57

[a]Numbering:

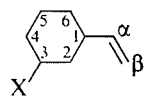

hoped that this investigation might finally resolve the single–dual substituent parameter controversy.

The results are summarized below.

Results

^{13}C data for new **4H**, **4M**, and **4B** derivatives are summarized in Table 1.[1] Data for **3H** derivatives are in Table 2 while **3M** derivatives are in Table 3. Chemical shifts for phenyl carbons were assigned on the basis of intensities and the assumed additivity of ^{13}C chemical shifts. Fortunately styrenes show insignificant deviations from additivity, in contrast to some other di-substituted benzenes (21), thus making assignment straightforward. α and β carbon assignments were generally straightforward. In the case of 3-OCH_3, NH_2 and $N(CH_3)_2$ derivatives, INEPT spectral editing (22) was used to distinguish the β CH_2 from high-field aromatic CH carbons.

Discussion

(a) *Probable experimental errors in data*

Knowledge of the probable experimental errors in the data set is very important in factor analysis since the most obvious choice for the correct number of factors for a particular problem is the number which reproduces the data within experimental uncertainty (14). Fewer factors will result in the loss of potentially useful information while over-parameterization will only complicate the interpretation of the problem.

The data set used in this investigation has been obtained over a period of 15 years on four different nmr spectrometers

[1]Data for other 4-substituted styrenes are listed in refs. 1 and 2.

Can. J. Chem. Downloaded from www.nrcresearchpress.com by 210.87.254.105 on 09/06/12
For personal use only.

TABLE 3. ^{13}C chemical shifts for 3-substituted α-methylstyrenes (**3M**) (in ppm relative to internal $(CH_3)_4Si$)

X	$\delta_{C(1)}$[a]	$\delta_{C(2)}$	$\delta_{C(3)}$	$\delta_{C(4)}$	$\delta_{C(5)}$	$\delta_{C(6)}$	$\delta_{C(\alpha)}$	$\delta_{C(\beta)}$
H	141.07	125.25	127.87	127.05	127.87	125.25	142.97	112.13
$N(CH_3)_2$	141.92	110.06	150.14	111.91	128.39	114.58	143.96	111.57
NH_2	142.11	111.98	145.87	113.82	128.68	115.79	143.28	111.75
OCH_3	142.53	111.35	159.42	112.45	128.68	117.85	143.04	112.23
SCH_3	141.72	124.13	138.32	125.63	128.23	122.24	142.73	112.64
CH_3	141.17	126.08	136.80	127.83	127.83	122.59	143.18	111.89
$Si(CH_3)_3$	140.42	130.01	139.35	132.04	127.31	125.89	143.38	112.14
F	143.53	112.44	162.82	113.96	129.42	120.84	142.05	113.22
Cl	142.99	125.72	134.33	127.20	129.02	123.29	141.92	113.37
Br	143.26	128.60	122.54	130.13	129.28	123.73	141.82	113.44
$COCH_3$	141.45	125.05	137.26	127.03	128.01	129.34	142.32	113.22
CO_2CH_3	141.12	126.56	130.57	127.71	128.30	129.15	142.21	113.07
CF_3	141.87	122.19	130.97	123.86	128.34	128.34	141.96	113.90
CN	142.20	128.84	113.30	130.35	128.65	129.01	141.20	114.43
NO_2	142.65	120.20	148.58	121.88	128.65	130.52	141.10	114.77

[a]Numbering is the same as in Table 2.

(Varian HA-100, XL-100, and XL-200 and Bruker WP-80). Many of the measurements have been repeated at least twice on different spectrometers with different operators, and sometimes at different concentrations. On the basis of these observations, we believe that a conservative estimate of the uncertainty in the ^{13}C data is 0.1 ppm. The use of a constant probe temperature seems particularly important since initial measurements made on the XL-200 spectrometer at 20°C differed by as much as 0.2 ppm from those made on the XL-100 at 32°C. In the case of ^1H data, chemical shifts appear to be reliable within 0.01 ppm and $^1H-^1H$ coupling constants within 0.03 Hz.

(b) *Processing of data for factor analysis*

There appears to be no single agreed "best" method for processing of data for factor analysis (14). Consequently, we will present results obtained from three different methods, in order to demonstrate that our conclusions are not significantly affected by the method of data processing.

Analyses were performed using both actual chemical shifts (including the parent compound (X = H)) and for substituent-induced chemical shifts (expressed relative to the parent compound which is then excluded from the analysis). We prefer the former approach[2] but have included the latter because it is favoured by many investigators of substituent effects (13). It should be noted that the two approaches yield a different number of factors. Expressed as Hammett type relations, the former approach is represented by

$$[1] \quad \delta_x = \delta_0 + \sum^{n} \rho_n \sigma_n$$

while the latter is given by

$$[2] \quad \Delta\delta(\equiv \delta_x - \delta_0) = \sum^{n} \rho_n \sigma_n$$

Thus the first approach requires one additional factor for the intercept.

Another area of choice is the weighting used for individual variables in constructing the data matrix. One obvious approach is to weight all variables so that they have equal experimental uncertainties, facilitating the determination of the correct number of factors (14). In our case, ^{13}C chemical shift data were multiplied by one, ^1H chemical shift data by ten, and $^1H-^1H$ coupling constants by three, yielding a common experimental uncertainty of 0.1. This approach was used in constructing data matrices from both δ and Δδ values. An alternative, commonly used (15, 16), scheme is to adjust the variance of each variable to unity so that each variable covers a similar range. This normalization procedure was used in conjunction with Δδ values. It should be noted that it leads to a different experimental uncertainty for each variable.

(c) *Tests used for determining the correct number of factors*

Of the various tests described by Malinowski and Howery (14), three were chosen. The first and simplest test is that the residual standard deviation (RSD) for the data matrix should be approximately equal to the experimental uncertainty for the correct number of factors. The second, related test is that no individual point should show a deviation more than three times the experimental uncertainty (3σ test). The third is the empirical indicator function (IND) which is defined as

$$[3] \quad \text{IND} = \text{RSD}/(x - n)^2$$

where x is the number of columns or rows (whichever is the lesser) in the data matrix and n is the number of factors. IND should reach a minimum for the correct number of factors (14).

(d) *Factor analysis of long-range substituent-induced chemical shifts*

Our initial focus was on long-range chemical shifts, in order to avoid the known complications associated with short-range effects (1, 23). The main data set incorporated *para* (to the substituent), α, and β carbon chemical shifts for **4H**, **4M**, **4B**, **3H**, and **3B** derivatives as well as β ^1H chemical shifts and $^1H-^1H$ coupling constants for **4H** derivatives. ^1H chemical shifts for other derivatives were omitted since these are very sensitive to variations in ring current effects originating in the phenyl group. These variations are due to minor substituent-induced changes in vinyl group conformation (2). The 15 common substituents listed in the Introduction were used, yielding an 18 × 15 data matrix. A more restricted data matrix incorporating only the six **4H** variables was also tested, to determine

[2]The parent compound data have experimental errors similar to those for the rest of the data set. Consequently, we see no justification in forcing the data to pass through an origin defined by the parent compound, thus giving this point infinite weight.

Can. J. Chem. Downloaded from www.nrcresearchpress.com by 210.87.254.105 on 09/06/12
For personal use only.

TABLE 4. Results of factor analysis of long-range substituent effects in styrene derivatives: (a) 18 variable data set (data for all five series, see text); (b) 6 variable data set (data for **4H** derivatives only)

(a) 18 Variable data set

	δ^a			$\Delta\delta^b$			Normalized $\Delta\delta^c$	
Factors	RSD[d]	3σ[e]	IND[f]	RSD	3σ	IND	RSD	IND
1	2.25	82.8	1.1×10^{-2}	0.82	64.4	2.8×10^{-3}	0.150	8.9×10^{-4}
2	0.44	44.8	2.6×10^{-3}	0.11	0.8	4.4×10^{-4}	0.024	1.6×10^{-4}
3[g]	0.09	0.0	6.5×10^{-4}	0.08	0.0	3.5×10^{-4}	0.016	1.4×10^{-4}
4	0.07	0.0	6.0×10^{-4}	0.07	0.0	3.4×10^{-4}	0.013	1.3×10^{-4}
5	0.07	0.0	6.9×10^{-4}	0.06	0.0	3.4×10^{-4}	0.010	1.3×10^{-4}
6	0.06	0.0	7.5×10^{-4}	0.05	0.0	3.4×10^{-4}	0.008	1.4×10^{-4}

(b) 6 Variable data set

	δ			$\Delta\delta$			Normalized $\Delta\delta$	
Factors	RSD	3σ	IND	RSD	3σ	IND	RSD	IND
1	1.73	63.3	6.9×10^{-2}	0.69	63.1	3.0×10^{-2}	0.139	5.5×10^{-3}
2	0.39	33.0	2.4×10^{-2}	0.09	0.0	5.7×10^{-3}	0.019	1.2×10^{-3}
3	0.07	0.0	8.0×10^{-3}	0.08	0.0	8.8×10^{-3}	0.013	1.5×10^{-3}
4	0.06	0.0	1.6×10^{-2}	0.07	0.0	1.6×10^{-2}	0.011	2.7×10^{-3}
5	0.06	0.0	6.6×10^{-2}	0.06	0.0	5.5×10^{-2}	0.009	9.1×10^{-3}

[a]Actual chemical shifts (see text for weighting of variables).
[b]Chemical shifts relative to parent compound (see text for weighting of variables).
[c]Relative chemical shifts with variance of each variable adjusted to unity.
[d]Residual standard deviation.
[e]Percentage of points with errors more than 3 times the experimental uncertainty.
[f]Empirical indicator function (see eq. [3]).
[g]Tests corresponding to optimum number of factors are underlined. Note that δ analyses require one addition factor for the intercept.

the sensitivity of the results to the number of columns in the data matrix.

Results of the various tests to determine the number of factors are summarized in Table 4. We will first consider the data matrices which have been scaled for a common experimental uncertainty of 0.1 (δ and $\Delta\delta$). In each of the four cases, RSD drops rapidly to ca. 0.1 and then changes much more slowly with increasing numbers of factors. Furthermore, in each case, the number of points with error greater than 3σ drops to zero or almost zero at the same time. In the case of δ, the clear break occurs at three factors (two substituent factors (parameters) plus an intercept; see eq. [1]). For $\Delta\delta$, the break occurs at two factors, again corresponding to two substituent parameters (see eq. [2]). The only difference is that RSD is slightly larger (ca. 0.02) for $\Delta\delta$ than for δ in both cases, reflecting the fact that $\Delta\delta$ values contain not only their own experimental errors but also any errors in δ for the parent compounds. The normalized $\Delta\delta$ values generally show very similar patterns of test results to the $\Delta\delta$ values, suggesting that the weighting of individual variables is not a critical parameter.

The empirical indicator function, IND, does not give as consistent results as the other two tests. For the 6 column data matrix (**4H** data only), IND drops rapidly to a sharp minimum at the point corresponding to the correct number of factors, as expected (14). However, for the full data set, IND gives a very shallow minimum extending over several factors. For the correct number of factors as indicated by the other tests, IND is not at a minimum but rather at a point on the curve corresponding to the onset of the shallow minimum. This difference apparently reflects the sensitivity of eq. [3] to the number of columns in the data matrix. For example, for a 6×15 matrix, $(x - n)^2$ changes from 9 to 4 on going from 3 to 4 factors but only from 144 to 121 for the corresponding number of factors for a 18×15 matrix. Thus for the 6×15 data matrix, IND increases suddenly at the point where RSD begins to level off but for the 18×15 matrix, the change in $(x - n)^2$ is so slow that IND only starts to level off as RSD levels off.

The data in Table 4 strongly support our previous view (12) that a dual substituent parameter treatment is both *necessary* and *sufficient* to account for long-range substituent-induced chemical shifts in aromatic derivatives. Certainly, a single substituent factor is inadequate since this gives residual errors which are four to eight times larger than experimental errors. Equally, the slow decrease in RSD for substituent parameters in excess of two suggests that the additional factors are primarily trying to accommodate experimental error. It is to be hoped that the observations in this section will finally resolve the long-standing controversy concerning single versus dual substituent parameter treatments of nmr data.

Target testing can be used to test possible candidates for the two subtituent factors (14). σ_I and σ_R^0 (13, 24) were used as initial test vectors. Both gave excellent agreement between input and predicted test vectors (see Figs. 1 and 2), suggesting that these are appropriate parameters to use in dsp treatments of aromatic chemical shifts. The F (rms error = 0.082) and R (rms error = 0.054) parameters of Swain and Lupton (25) were poorer test vectors, suggesting that they would be less appropriate. Finally, unity was also an excellent test vector for the data matrix of δ values, as expected for a data matrix incorporating an origin for each variable. The three test vectors can be used in combination to reproduce the data matrix according to eq. [4] (17*b*)

Can. J. Chem. Downloaded from www.nrcresearchpress.com by 210.87.254.105 on 09/06/12
For personal use only.

Can. J. Chem. Downloaded from www.nrcresearchpress.com by 210.87.254.105 on 09/06/12
For personal use only.

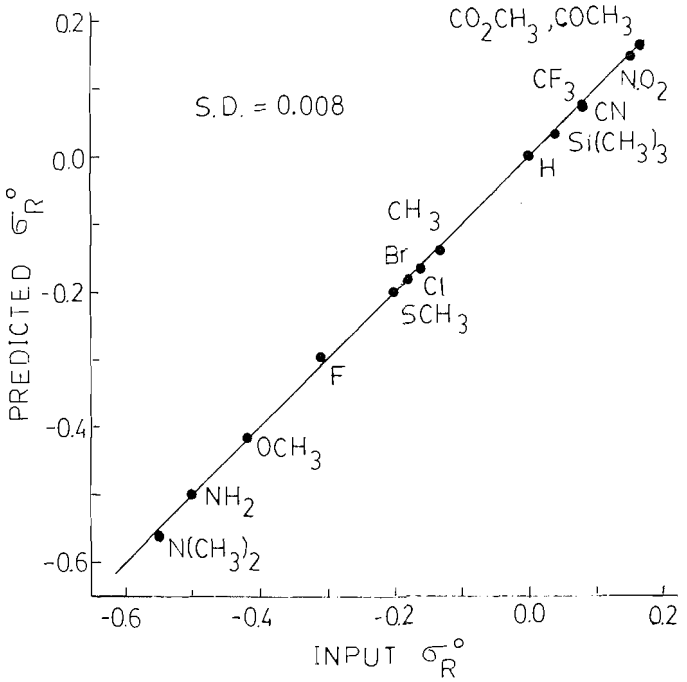

FIG. 1. Plot of input (from refs. 13 and 24) versus predicted (by target testing) σ_R^0 values.

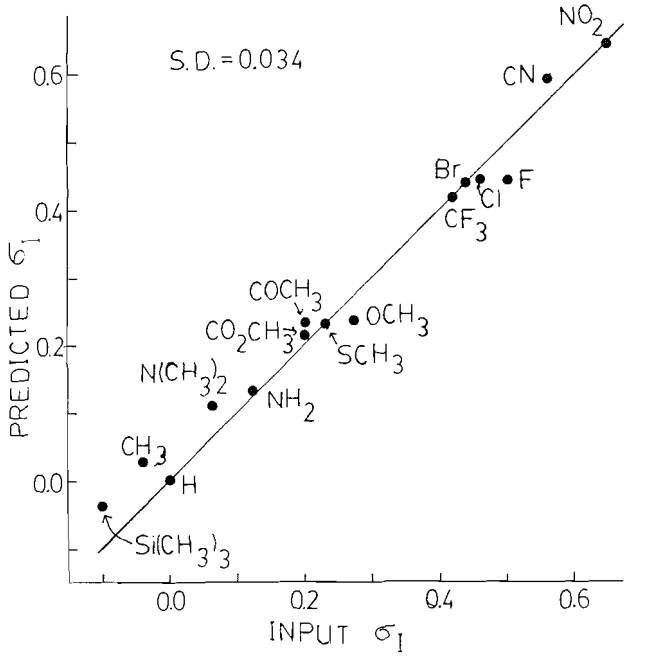

FIG. 2. Plot of input (from refs. 13 and 24) versus predicted (by target testing) σ_I values.

$$[4]\quad \delta_{xk} = a_{x1}b_{1k} - a_{x2}b_{2k} + a_{x3}b_{3k}$$

where a_{xi} are the three substituent factors (parameters) for substituent X (e.g. 1, $\sigma_{I(X)}$, and $\sigma^0_{R(X)}$) and b_{ik} are the cofactors or weighting terms for each variable k ($\delta_{0(k)}$, $\rho_{I(k)}$, and $\rho_{R(k)}$, see eq. [1]). Using the predicted σ_I and σ_R^0 values from Figs. 3 and 4, eq. [4] reproduced the data matrix with an overall rms error of 0.10 (individual variables gave rms errors of 0.05 to 0.16). Furthermore, the predicted δ_0 value for each variable was in excellent agreement with the corresponding chemical shift for the parent compound (X = H). Thus, individual long-range chemical shifts in styrene derivatives are predicted with excellent precision by

$$[5]\quad \delta_{xk} = \delta_{0(k)} + \sigma_{I(k)}\rho_{I(k)} + \sigma^0_{R(X)}\rho_{R(k)}$$

(e) *Comparison with a previous principal components analysis of long-range substituent effects on 4-substituted styrenes*

On the basis of the SIMCA method of principal components analysis (15), Edlund and Wold concluded that a single substituent parameter was sufficient to account for long-range chemical shifts in **4H**, **4M**, and **4B** derivatives (9). This is a most surprising conclusion in view of the results in the previous section. While we earlier felt that their conclusions might be biased by their method of pre-processing the data (12), the results in Table 4 suggest that this may not be of major importance. However, one obvious difference between the two investigations was that they used a much smaller substituent set ($N(CH_3)_2$, OCH_3, CH_3, $C(CH_3)_3$, F, Cl, and NO_2 (9), representing the only common substituents other than H which were available in all three series at that time). Since it is disturbing that two closely related techniques should give very different conclusions, we carried out a factor analysis for the same data matrix which they used, in order to test the effect of the size of the substituent set. Analyses were again carried out using δ, $\Delta\delta$, and normalized $\Delta\delta$ scales. Results for the δ correlations are summarized in Table 5. The other two analyses gave similar patterns of results.

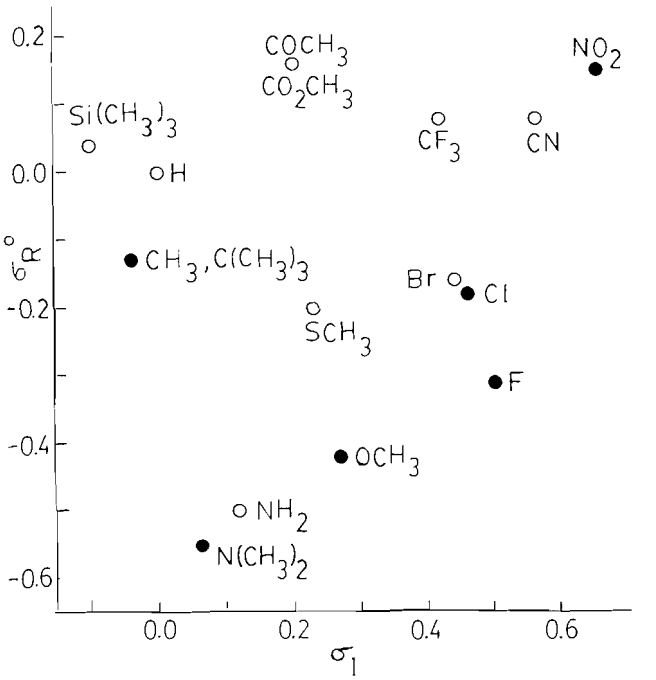

FIG. 3. Plot of σ_I versus σ_R^0 for restricted data set used in ref. 9 (filled circles) plus additional substituents in this investigation (open circles).

Using estimated error as a criterion, the factor analysis for the smaller substituent set again suggests two substituent parameters (plus an intercept). However, the distinction between one and two substituent parameters is not nearly as clear-cut as in the case of the larger substituent parameter set. Edlund and Wold used a different procedure (cross validation (15)) to determine the correct number of principal components. This purely statistical criterion obviously must accept as satisfactory the reasonably good fit given by one component.

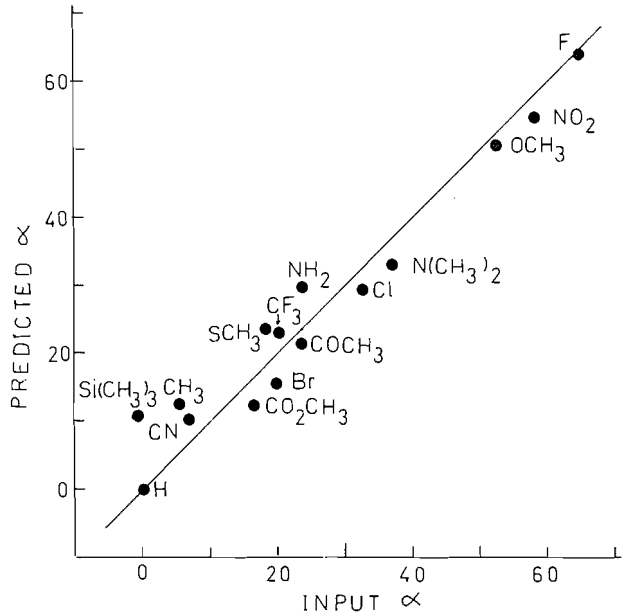

FIG. 4. Plot of input versus predicted α values for *ipso* carbons.

A plot of σ_I versus σ_R^0 for the various substituents (Fig. 3) demonstrates why the limited substituent set does not so clearly distinguish between one and two substituent factors. For five of the seven substituents, σ_I shows a fair linear relationship with σ_R^0, with only the alkyl groups deviating. Thus for the limited substituent set, σ_I and σ_R^0 are not fully independent and consequently one substituent factor provides a reasonable fit. This is not true, however, for our full substituent set where no such relationship exists. This confirms the comments made by Taft and co-workers concerning the necessity of using a well-balanced substituent set in investigations of substituent effects (13).

(f) *Factor analysis incorporating short-range chemical shifts*

Four separate factor analyses were carried out involving short-range chemical shifts. In the first, *ipso* carbon (C(4)) chemical shifts for **4H**, **4M**, and **4B** derivatives were incorporated into a data matrix in conjunction with the eighteen long-range parameters from part (d). In the second, *ortho* carbon (C(3)) chemical shifts were used with the 18 parameter set, while in the third, *meta* (C(2)) chemical shifts were used. Finally, all three variables for the three derivatives were combined with the long-range parameters to product a 27 × 15 data matrix. Results for δ and Δδ analyses are summarized in Table 6 (normalized Δδ analyses gave similar patterns of results).

In the case of C(4), one additional substituent parameter (for a total of three) is clearly required. One also appears sufficient, although a very small percentage of data points give errors greater than 3σ. With C(3), one additional parameter is again obviously needed and in this case it is also obvious that one extra is also sufficient. However, the results for C(2) are ambiguous. The δ values suggest that two substituent factors (plus an intercept) are still adequate. However, the Δδ values suggest a third factor is required. Significantly, if only two factors are used, then the six largest errors all involve C(2) (including at least one from each of **4H**, **4M**, and **4B**). Apparently a third, relatively small, factor is required for C(2). However, because it is small, it can reasonably well be incorporated in the δ analysis by having a δ_0 which differs from δ_H.

The analysis involving C(4), C(3), and C(2) simultaneously confirmed the conclusions given above. In this case four substituent factors were clearly required with a fifth of marginal significance. The only logical conclusion to draw from these results is that the original two factors (σ_I and σ_R^0) are still operative plus one additional significant factor for each of C(4) and C(3) and a minor factor for C(2).

TABLE 5. Comparison of results of factor analysis for the same data set as used in ref. 9 with the results for the 18 parameter set[a]

Factors	RSD[b]	3σ[b]	IND[b]
1	1.16(2.25)[c]	62.5(82.2)[c]	$2.4\times10^{-2}(1.1\times10^{-2})$[c]
2	0.20(0.44)	13.5(44.8)	$6.0\times10^{-3}(2.6\times10^{-3})$
3	0.10(0.09)	0.0(0.0)	$4.2\times10^{-3}(6.5\times10^{-4})$
4	0.04(0.07)	0.0(0.0)	$3.1\times10^{-3}(6.0\times10^{-4})$
5	0.03(0.07)	0.0(0.0)	$4.8\times10^{-3}(6.9\times10^{-4})$

[a]Factor analysis for actual chemical shifts. Δδ and normalized Δδ values gave similar results.
[b]Terms defined in Table 4.
[c]First values are for data set used in ref. 9, while those in brackets are data for 18 variable set from Table 4. Note the much smaller differences between two and three factors (one and two substituent factors) for first values.

Target testing of σ_I and σ_R^0 showed that these were again excellent target vectors for data matrices incorporating short range chemical shifts. As initial target vectors for the short range *ipso* (C(4)) and *ortho* (C(3)) factors, we chose the corresponding α and β chemical shifts in monosubstituted cyclohexanes. The logic was that σ_I and σ_R^0 would represent perturbation of the π electron system by field-induced π polarization and resonance respectively (26), while α and β parameters from cyclohexanes would approximately mirror any substituent-induced changes in the σ system. α turned out to be a reasonable test vector for the *ipso* factor (see Fig. 4). Furthermore, when the predicted α was used in conjunction with σ_I and σ_R^0 to reproduce the data matrix, the co-factors for α were 0.819, 0.822, and 0.824 for C(4) of **4H**, **4M**, and **4B**, respectively, while the next largest co-factor was 0.003. Thus, it is clear that the ipso factor, α, is specific to this position and contributes nothing to the long-range chemical shifts. The *ipso* factor appears to be basically a group electronegativity factor (26), as might be expected for a directly bonded substituent.

Target testing of β was less satisfactory. There are significant differences between input and predicted β values (see Fig. 5). Thus it is entirely possible that the predicted β is not a pure factor but rather some linear combination of the actual *ortho* factor and σ_I and/or σ_R^0. As an alternative, we also tried Schaefer's semi-empirical Q parameter (27), as modified by Smith for use as a predictor of *ortho* ^{13}C chemical shifts (28). There is fairly good agreement between input and predicted Q (see Table 7). However, both the input and particularly the predicted Q parameters are strongly correlated with σ_R^0, suggesting again that Q is not a pure *ortho* parameter but rather a linear combination σ_R^0 and the *ortho* factor. It appears that further work is necessary to correctly identify the true *ortho* factor.

One objective method for testing the validity of individual test vectors is the SPOIL test (14). According to Malinowski, test vectors which give a SPOIL test of 0–3 are acceptable, those with SPOIL from 3 to 6 are moderately acceptable, while those with SPOIL greater than 6 are not acceptable (14). σ_R^0, σ_I, α, β, and Q gave respective SPOIL tests of 1.69, 2.70, 8.50, 12.8, and 39.9. Thus, only σ_I and σ_R^0 are good test vectors, according to the SPOIL test. However, it should be stressed

Can. J. Chem. Downloaded from www.nrcresearchpress.com by 210.87.254.105 on 09/06/12
For personal use only.

TABLE 6. Results of factor analysis of short-range chemical shifts for **4H**, **4M**, and **4B** derivatives in combination with 18 variable long-range chemical shift data set from Table 4

	18 + C(4) data[a]						18 + C(3) data[a]					
	δ[b]			Δδ[b]			δ			Δδ		
Factors	RSD[b]	3σ[b]	IND[b]	RSD	3σ	IND	RSD	3σ	IND	RSD	3σ	IND
1	5.48	90.5	2.8×10^{-2}	2.41	83.0	1.4×10^{-2}	2.93	85.1	7.3×10^{-2}	1.72	82.0	4.2×10^{-2}
2	1.62	76.5	9.6×10^{-3}	0.62	40.8	4.4×10^{-3}	1.49	80.3	4.0×10^{-3}	0.61	37.8	1.7×10^{-3}
3	0.42	37.8	2.9×10^{-3}	0.12	1.7	9.9×10^{-4}[c]	0.38	31.7	1.1×10^{-3}	0.11	0.7	3.3×10^{-4}
4	0.10	0.3	8.2×10^{-4}	0.09	0.7	9.3×10^{-4}	0.09	0.0	3.1×10^{-4}	0.08	0.0	2.6×10^{-4}
5	0.07	0.0	8.0×10^{-4}	0.07	0.0	8.7×10^{-4}	0.07	0.0	2.6×10^{-4}	0.06	0.0	2.5×10^{-4}
6	0.07	0.0	9.1×10^{-4}	0.05	0.0	9.1×10^{-4}	0.06	0.0	2.7×10^{-4}	0.05	0.0	2.4×10^{-4}

	18 + C(2) data[a]						18 + C(4), C(3), and C(2) data[a]					
	δ			Δδ			δ			Δδ		
Factors	RSD	3σ	IND	RSD	3σ	IND	RSD	3σ	IND	RSD	3σ	IND
1	2.24	87.9	1.0×10^{-2}	0.82	63.6	4.8×10^{-3}	5.39	89.4	2.8×10^{-2}	2.49	82.4	1.5×10^{-2}
2	0.47	48.3	4.3×10^{-3}	0.16	4.8	1.1×10^{-3}	1.79	79.0	1.1×10^{-2}	1.15	61.9	8.7×10^{-3}
3	0.12	1.3	9.3×10^{-4}[c]	0.09	0.0	7.2×10^{-4}	1.07	69.3	7.8×10^{-3}	0.60	30.7	5.0×10^{-3}
4	0.08	0.0	8.0×10^{-4}	0.07	0.0	7.7×10^{-4}	0.36	32.0	3.2×10^{-3}	0.15	3.2	1.5×10^{-3}
5	0.08	0.0	8.5×10^{-4}	0.06	0.0	8.2×10^{-4}	0.10	0.0	1.2×10^{-3}	0.08	0.5	1.0×10^{-3}
6	0.07	0.0	9.2×10^{-4}	0.06	0.0	9.1×10^{-4}	0.08	0.0	9.5×10^{-4}	0.07	0.0	1.1×10^{-3}

[a]Extra data for **4H**, **4M**, and **4B** derivatives.
[b]Terms defined in Table 4.
[c]The tests are marginal for 3 factors.

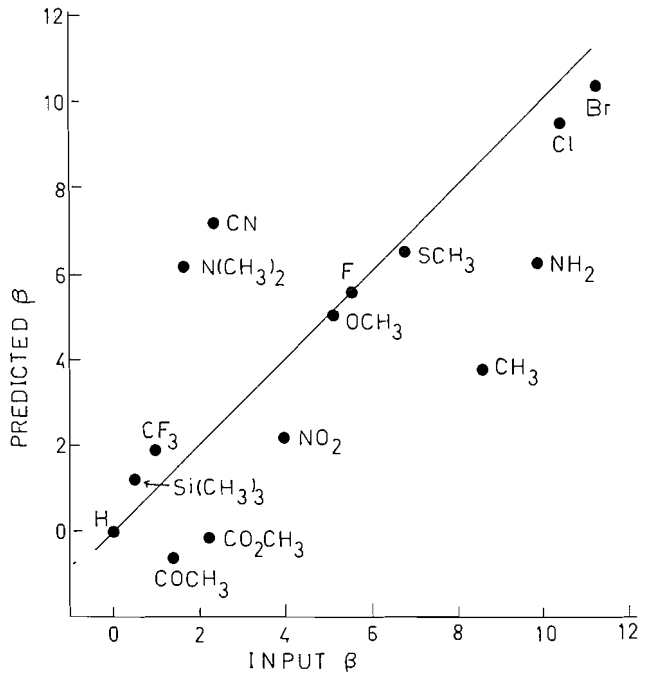

FIG. 5. Plot of input versus predicted β values for *ortho* carbons.

TABLE 7. Target testing of Q as a substituent factor for *ortho* ^{13}C chemical shifts

X	Input ΔQ[a]	Predicted ΔQ[b]	σ_R^0[c,d]
$N(CH_3)_2$	—	−2.66	−0.55
NH_2	−2.95	−2.26	−0.50
OCH_3	−1.74	−2.14	−0.42
SCH_3	—	−0.20	−0.20
CH_3	−0.51	−0.09	−0.13
$Si(CH_3)_3$	—	0.62	0.04
F	−1.24	−1.54	−0.31
Cl	0.27	0.27	−0.18
Br	0.88	0.69	−0.16
$COCH_3$	0.06	0.52	0.20
CO_2CH_3	—	0.67	0.20
CF_3	1.43	0.23	0.08
CN	1.15	1.24	0.08
NO_2	−0.48	0.38	0.15

[a]Data from ref. 28. $\Delta Q = Q_X - Q_H$. ΔQ was used to make it comparable with other substituent factors, i.e. $\Delta Q = 0$ for X = H.
[b]Results of target testing of input ΔQ against data matrix of 18 long-range chemical shift variables plus C(2) from **4H**, **4M**, and **4B**.
[c]σ_R^0 values from ref. 24 or ref. 13 if not included in ref. 24.
[d]A correlation of predicted ΔQ with σ_R^0 gave a correlation coefficient, $r = 0.90$.

that α and β values are not constant, even from one aliphatic series to another (23), and, consequently, significant differences might be expected between aliphatic and aromatic derivatives.

The question of whether predicted α, β, and Q are pure factors or rather linear combinations of σ_I, σ_R^0, and the actual factors is probably best addressed by correlation analysis. This is reported in the subsequent paper (29). There we derive what we believe are the true third *ortho* and *meta* factors and suggest a possible *ipso* factor. The first two are totally independent of σ_I and σ_R^0. This allows us to separate electronic (σ_I and σ_R^0) contributions from other short-range, non-electronic contributions (29).

Comparison with previous interpretations of short-range chemical shifts

Bailey *et al.* (17*b*) have used factor analysis to analyze ^{13}C

Can. J. Chem. Downloaded from www.nrcresearchpress.com by 210.87.254.105 on 09/06/12
For personal use only.

Can. J. Chem. Downloaded from www.nrcresearchpress.com by 210.87.254.105 on 09/06/12
For personal use only.

chemical shifts in a large number of haloaromatic and haloalkene derivatives. They concluded that two major and one minor factor were necessary to account for the chemical shifts, compared to four major and one minor factor according to this investigation. The problem is that the halogens constitute an entirely unsatisfactory substituent set (13). As they acknowledge (17*b*), many different variables are strongly interrelated; e.g., σ_I, σ_R^0, and α are all linearly related to one another for this substituent set. Consequently, the number of factors will inevitably be larger for a correctly chosen substituent set. These observations reinforce our earlier comments about the necessity of using a well-balanced substituent set, as outlined by Taft and co-workers (13).

Smith and Proulx have proposed a general approach for correlation of substituent effects upon aromatic chemical shifts (30). This involves correlation with F, R, and Q. This approach has been strongly criticized on the grounds that it has never been subjected to proper statistical testing (18). The results presented above suggest that it is invalid. To begin, a third substituent parameter is unnecessary for long-range chemical shifts. Furthermore, while a third parameter is undoubtedly necessary for short-range chemical shifts, different parameters are needed for *ipso* and *ortho* positions. Finally, although Q may be an appropriate parameter for *ortho* chemical shifts, it is sufficiently strongly correlated with σ_R^0 (or R) that the weighting coefficients in a multiple linear regression analysis of *ortho* shifts are likely to be of dubious reliability (29).

Conclusions

Factor analysis of long range chemical shifts in 3- and 4-substituted styrene derivatives demonstrates that two substituent factors (parameters) are both *necessary* and *sufficient* to account for substituent-induced chemical shifts. Target testing indicates that σ_I and σ_R^0 are appropriate substituent parameters for this purpose.

σ_I and σ_R^0 are also appropriate parameters for short-range chemical shifts in styrene derivatives. However, one additional factor is needed for each of *ipso* and *ortho* carbon chemical shifts. There also appears to be a *meta* factor but this is of marginal significance. Target testing indicates that α chemical shifts in cyclohexane derivatives provide a fair model for the *ipso* factor which appears to be basically a group electronegativity factor. However, neither β cyclohexane shifts nor the empirical Q parameter appear to be good models for the *ortho* factor. Q in particular is strongly correlated with σ_R^0, suggesting that it may be some linear combination of σ_R^0 and the true *ortho* factor.

These conclusions are in good agreement with what has been observed for Hammett–Taft treatments of aromatic reactivities. For example, many investigators have used different linear combinations of σ_I and σ_R to account for *meta* and *para* reactivities (13), while a third (steric) parameter is used in conjunction with σ_I and σ_R for *ortho* reactivities (10).

The results of factor analysis are not strongly influenced by the techniques used to pre-process the data matrix. However, it is essential to use a well-balanced substituent set. While it is probably not necessary to use as extensive a substituent set as we have used, the recommendations of Taft concerning minimal substituent sets (13) should certainly be followed.

Experimental

The new **3H**, **3M**, and **4M** derivatives were all known compounds and were synthesized by known methods. Most new **4B** derivatives were synthesized by reaction of the corresponding 4-substituted acetophenone with *tert*-butylmagnesium chloride, followed by aqueous acidic work-up to yield the appropriate 2-(4-X-phenyl)-3,3-dimethyl-2-butanol. Catalytic dehydration over activated alumina (2) then yielded the appropriate 4-substituted α-*tert*-butylstyrene (X = SCH_3, $COCH_3$, CF_3, CN). The NH_2 derivative was synthesized from the NO_2 derivative (1) by reduction with Sn/HCl (31). The $Si(CH_3)_3$ and CO_2CH_3 derivatives were synthesized from the corresponding Cl derivative via Grignard routes (2). All **4B** derivatives were produced in low yield at 80–90% purity (typically contaminated with starting acetophenone) and were used without further purification. These compounds were characterized by ^1H and ^{13}C nmr spectroscopy and high resolution mass spectrometry.

^{13}C spectral data were obtained on a Varian XL-200 spectrometer operating at a probe temperature of 32°C under variable temperature control (some preliminary measurements were made on a Brüker WP-80 at 35°C). Spectra were measured for 0.2 *M* solutions in CCl_4 with 8 vol.% C_6D_{12} as internal lock and ca. 0.5% $(CH_3)_4Si$ as internal reference. 10 000 Hz spectral widths were used with 32K real points, a recycle time of 3.2 s, and 30°–40° pulse widths.

Details of calculations

Factor analyses were performed on the program FACTANAL (20), modified to operate on the Department of Chemistry SEL 75 computer. Modifications include sub-routines to calculate RSD, IND, and SPOIL, using equations from ref. 14.

Acknowledgments

Financial support from the Natural Sciences and Engineering Research Council is gratefully acknowledged (W.F.R.).

1. G. K. HAMER, I. R. PEAT, and W. F. REYNOLDS. Can. J. Chem. **51**, 897 (1973).
2. G. K. HAMER, I. R. PEAT, and W. F. REYNOLDS. Can. J. Chem. **51**, 915 (1973).
3. P. J. MITCHELL and L. PHILLIPS. J. Chem. Soc. Perkin Trans. 2, 109 (1974).
4. (*a*) N. INAMOTO, S. MASUDA, K. TOKUMARA, K. TORI, M. YOSHIDA, and Y. YOSHIMURA. Tetrahedron Lett. 3711 (1976); (*b*) N. INAMOTO, S. MASUDA, K. TORI, and Y. YOSHIMURA. Tetrahedron Lett. 737 (1977); (*c*) N. INAMOTO and S. MASUDA. Tetrahedron Lett. 3287 (1977).
5. (*a*) D. A. R. HAPPER, S. A. MCKERROW, and A. L. WILKINSON. Aust. J. Chem. **30**, 1715 (1977); (*b*) D. A. R. HAPPER and G. J. WRIGHT. J. Chem. Soc. Perkin Trans. 2, 769 (1977).
6. M. GODFREY. J. Chem. Soc. Perkin Trans. 2, 769 (1977).
7. J. M. HACHEY. Can. J. Spectrosc. **23**, 147 (1978).
8. H. O. KRABBENHOLT. J. Org. Chem. **43**, 1830 (1978).
9. U. EDLUND and S. WOLD. J. Magn. Reson. **37**, 183 (1980).
10. J. SHORTER. Correlation analysis in organic reactivity with particular reference to multiple regression. Research Studies Press, New York. 1982.
11. D. A. DAWSON and W. F. REYNOLDS. Can. J. Chem. **53**, 373 (1975).
12. W. F. REYNOLDS, P. DAIS, D. W. MACINTYRE, G. K. HAMER, and I. R. PEAT. J. Magn. Reson. **43**, 81 (1981).
13. S. EHRENSON, R. T. C. BROWNLEE, and R. W. TAFT. Prog. Phys. Org. Chem. **10**, 1 (1973).
14. E. R. MALINOWSKI and D. G. HOWERY. Factor analysis in chemistry. Wiley–Interscience, New York. 1980.
15. (*a*) S. WOLD. Pattern Recognition, **8**, 127 (1976); (*b*) S. WOLD and M. SJÖSTRÖM. *In* Chemometrics, theory and practice. *Edited by* B. Kowalski. A.C.S. Symp. Series No. 52. Am. Chem. Soc., Washington, D.C. 1977. p. 243.
16. M. J. SJÖSTRÖM and U. EDLUND. J. Magn. Reson. **25**, 285 (1977).
17. (*a*) K. B. WIBERG, W. PRATT, and E. BAILEY. J. Org. Chem. **45**, 4936 (1980); (*b*) W. F. BAILEY, E. A. CIOFFI, and K. B. WIBERG. J. Org. Chem. **46**, 4219 (1981).

18. B. ELIASSON and U. EDLUND. J. Chem. Soc. Perkin Trans. 2, 403 (1981).
19. G. MUSUMARRA, G. SCARLATA, and S. WOLD. Gazz. Chim. Ital. **3**, 499 (1982).
20. Q.C.P.E. Program #320. Quantum Chemistry Program Exchange, University of Indiana, Bloomington, Indiana.
21. J. BROMILOW, R. T. C. BROWNLEE, V. O. LOPEZ, and R. W. TAFT. J. Org. Chem. **45**, 2429 (1980).
22. G. A. MORRIS. J. Am. Chem. Soc. **102**, 428 (1980).
23. G. MACIEL. *In* Topics in carbon-13 nmr spectroscopy. *Edited by* G. Levy. John Wiley and Sons, New York. 1979.
24. J. BROMILOW, R. T. C. BROWNLEE, V. O. LOPEZ, and R. W. TAFT. **44**, 4766 (1979).
25. C. G. SWAIN and E. P. LUPTON. J. Am. Chem. Soc. **90**, 4328 (1968).
26. W. F. REYNOLDS. Prog. Phys. Org. Chem. **14**, 165 (1983).
27. F. HRUSKA, H. M. HUTTON, and T. P. SCHAEFER. Can. J. Chem. **43**, 2392 (1965).
28. W. B. SMITH, A. M. IHRIG, and J. L. ROARK. J. Phys. Chem. **74**, 812 (1970).
29. W. F. REYNOLDS, ANABELA GOMES, A. MARON, D. W. MACINTYRE, A. TANIN, G. K. HAMER, and I. R. PEAT. Can. J. Chem. **61**, 2376 (1983).
30. W. B. SMITH and T. W. PROULX. Org. Magn. Reson. **8**, 567 (1976).
31. G. K. HAMER. Ph.D. thesis, University of Toronto, 1973.

Can. J. Chem. Downloaded from www.nrcresearchpress.com by 210.87.254.105 on 09/06/12
For personal use only.

Substituent-induced chemical shifts in 3- and 4-substituted styrenes: definition of substituent constants and determination of mechanisms of transmission of substituent effects by iterative multiple linear regression

WILLIAM F. REYNOLDS, ANABELA GOMES, ANTONINA MARON, DOUGLAS W. MACINTYRE, AND ATES TANIN
Department of Chemistry, University of Toronto, Toronto, Ont., Canada M5S 1A1

GORDON K. HAMER
Xerox Research Centre of Canada, 2480 Dunwin Drive, Mississauga, Ont., Canada L5L 1J9

AND

IAN R. PEAT
U.S. Industrial Chemicals Ltd., 1275 Section Road, Cincinnati, OH 45237 U.S.A.

Received November 16, 1982

Can. J. Chem. Downloaded from www.nrcresearchpress.com by 210.87.254.40 on 09/06/12
For personal use only.

WILLIAM F. REYNOLDS, ANABELA GOMES, ANTONINA MARON, DOUGLAS W. MACINTYRE, ATES TANIN, GORDON K. HAMER, and IAN R. PEAT. Can. J. Chem. **61**, 2376 (1983).

Iterative multiple linear regression analysis of substituent-induced chemical shifts in 3- and 4-substituted styrene derivatives is used to redefine σ_F and σ_R^0 substituent constants (with respective standard errors of ca. 0.01 and 0.005). Correlations with the data for various model systems indicate that these substituent constants are applicable to data sets involving both chemical shift and acidity measurements in aprotic media. The approach we have used involving a homogeneous data set with a large number of variables is particularly suited for providing well-defined dual substituent parameter constants for the more common neutral substituents.

Correlations for individual nuclei are entirely consistent with a previously proposed model of substituent effects involving field, resonance, and polarization effects. From these results and the results for other model systems, it is concluded that σ_F and σ_R^0 are respectively pure field and resonance substituent constants. It is pointed out that a combination of detailed statistical testing and chemical modelling is essential for a thorough understanding of aromatic substituent effects.

Parameters for predicting non-electronic contributions to *ortho* and *meta* chemical shifts are derived, thus allowing the patterns of electronic substituent effects for these carbons to be determined. However, only an approximate *ipso* factor can be deduced.

WILLIAM F. REYNOLDS, ANABELA GOMES, ANTONINA MARON, DOUGLAS W. MACINTYRE, ATES TANIN, GORDON K. HAMER et IAN R. PEAT. Can. J. Chem. **61**, 2376 (1983).

On a utilisé l'analyse par régression linéaire multiple itérative des déplacements chimiques induits par un substituant dans les dérivés du styrène substitués en positions 3 et 4 afin de redéfinir les constantes de substituants σ_F et σ_R^0 (avec des erreurs normales respectives de 0,01 et de 0,005). Les corrélations avec les données relatives à divers systèmes modèles indiquent que ces constantes de substituants peuvent s'appliquer à des ensembles de données qui impliquent à la fois le déplacement chimique et les mesures d'acidité en milieu aprotique. Nous avons utilisé une approche qui, faisant intervenir un ensemble de données homogènes avec un grand nombre de variables, est particulièrement adéquat pour fournir des constantes de paramètre de substituant double pour les substituants neutres les plus courants.

Les corrélations avec des noyaux individuels sont tout à fait en accord avec les modèles proposés antérieurement pour des effets de substituants impliquant les effets de champ, de résonance et de polarisation. A partir de ces résultats et à partir d'autres systèmes models, on peut conclure que σ_F et σ_R^0 sont respectivement des constantes de substituant de champ pur et de résonance. On met en évidence qu'une combinaison d'essais statistique, détaillées et de modèles chimiques est essentielle pour une compréhension profonde des effets de substituant aromatique.

On a déduit les paramètres qui permettent de prédire les contributions non électronique aux déplacements chimiques des positions *ortho* et *méta*, ce qui permet ainsi de déterminer les models d'effets électroniques de substituant pour ces carbones. Cependant on ne peut déduitre qu'un facteur *ipso* approximatif.

[Traduit par le journal]

Introduction

In the preceding paper, we used the technique of factor analysis to demonstrate that a dual substituent parameter (dsp) treatment is both necessary and sufficient to account for long-range chemical shifts in 3- and 4-substituted styrene derivatives (1). Furthermore, target testing indicated that Taft's σ_I and σ_R^0 scales (2) were appropriate for that purpose.

In this paper, iterative multiple linear regression analysis of nmr data for almost ninety 4-substituted styrenes (**4H**), α-methylstyrenes (**4M**), and α-*tert*-butylstyrenes (**4B**), as well as 3-substituted styrenes (**3H**) and α-methylstyrenes (**3M**), is used to estimate refined σ_F and σ_R^0 constants for 18 substituents as well as to provide a detailed test of our previously proposed model of mechanism of transmission of substituent effects in styrene derivatives (3, 4). Finally, new **O** and **M** substituent parameters are deduced to account for non-electronic contributions to *ortho* and *meta* chemical shifts.

Results and discussion

^{13}C chemical shifts of previously unreported iodo, *tert*-butyl, and trimethyltin derivatives of styrene are listed in Table 1. All other data used in this investigation have been reported elsewhere (1, 3, 4).

TABLE 1. Additional ^{13}C nuclear magnetic resonance data for previously unreported compounds (in ppm from internal $(CH_3)_4Si$)

Series	X	$\delta_{C(1)}$	$\delta_{C(2)}$	$\delta_{C(3)}$	$\delta_{C(4)}$	$\delta_{C(5)}$	$\delta_{C(6)}$	$\delta_{C(\alpha)}$	$\delta_{C(\beta)}$
4B	$Sn(CH_3)_3$	143.10	128.52	134.45	138.72	134.45	128.52	159.38	111.31
3M	$Sn(CH_3)_3$	140.99[a]	132.42	140.89[a]	134.26	127.84	125.22	143.39	112.11
3H	$C(CH_3)_3$	137.38	123.04[a]	150.44	124.46	127.90	123.08[a]	137.00	112.79
3H	I	139.53	135.07	94.57	136.44	129.79	125.09	135.41	114.83
3M	I	143.45	134.60	95.12	136.10	129.50	124.41	141.80	113.37

[a]Peak assignments could be interchanged.

(a) *Estimation of refined σ_F and σ_R^0 constants by iterative multiple linear regression and comparison with previous dsp scales*

$\sigma_F(\sigma_I)$[1] and σ_R^0 constants have been refined at least twice in recent years (2). We decided to continue this process, using our very extensive styrene data set to redefine σ_F and σ_R^0 constants (with statistically defined uncertainties) by iterative multiple linear regression. This involves two fundamental assumptions. The first is that long-range chemical shifts for styrenes can be predicted, within experimental uncertainty, by only two substituent constants. This has been clearly demonstrated by factor analysis (1). For example, the residual standard deviation (RSD) between predicted and observed long-range chemical shifts decreases from 2.24 ppm for one factor (intercept only) to 0.09 ppm for three factors (intercept plus two substituent parameters). However, four additional factors are required to reduce RSD from 0.09 to 0.05 ppm (1). Thus, it is obvious that the additional factors are attempting to fit random errors rather than additional substituent effects. The second assumption is that the substituent constants for this system are sufficiently close to Taft's σ_I and σ_R^0 constants (2) that they can be reliably estimated by iterative multiple linear regression. Target testing of σ_I and σ_R^0 against the styrene data matrix has demonstrated that this is a valid assumption (2).

We believe that there are three major advantages to the approach which we have used. First, all data are for a closely related series of compounds and are measured in the same laboratory under constant conditions. By contrast, most other dsp scales have been defined using data from different systems measured in different laboratories (2*a*, 6, 7). These scales must inevitably contain artifacts due to the use of heterogeneous data sets. Second, σ_F and σ_R^0 are defined by the solution of a large number (up to 18) of simultaneous equations, providing statistically well-defined substituent constants. Many previous dsp constants have been defined from as few as two experimental points (6, 7). Finally, the individual styrene variables show a wide range of responses to polar and resonance effects ($\lambda(\equiv\rho_R/\rho_I)$ varies from ca. 0 to 5 (see part C), compared to 0.3−1.2 for typical acidity and reactivity data (2*a*)), thus facilitating the accurate definition of σ_F and σ_R^0. For these reasons, we are convinced that iterative multiple linear regression analysis of the styrene data set will provide better defined and more reliable dsp constants than those previously available.

ρ_F and ρ_R values were first estimated by multiple linear regression analysis according to eq. [1], using the most recent values of $\sigma_F(\sigma_I)$ and σ_R^0 (2):

$$[1]\quad \delta_x = \delta_0 + \rho_F\sigma_F + \rho_R\sigma_R^0$$

Fifteen substituents were used in each correlation (X = H, $N(CH_3)_2$, NH_2, OCH_3, SCH_3, CH_3, $Si(CH_3)_3$, F, Cl, Br, $COCH_3$, CO_2CH_3, CF_3, CN, and NO_2). Correlations were carried out for the same 18 variables as used in the factor analysis of long-range chemical shifts (*para*, α, and β carbons for all five series as well as β ^1H chemical shifts and $^1H-^1H$ coupling constants for **4H** derivatives). ^1H chemical shifts were weighted by 10 and $^1H-^1H$ coupling constants by 3 to produce similar experimental uncertainties for all 3 variables (1). Without this weighting, the latter variables would have made negligible contributions in the second state of the iterative process.

In the second stage, the predicted ρ_F and ρ_R values and predicted intercepts, δ_0, from eq. [1] were used in a reverse correlation to solve for σ_F and σ_R^0 constants for individual substituents according to eq. [2]:

$$[2]\quad \delta_x - \delta_0 = \sigma_F\rho_F + \sigma_R^0\rho_R$$

This involves solving 18 simultaneous equations for only two unknowns, σ_F and σ_R^0. The process was then repeated, using the revised σ_F and σ_R^0 constants (but maintaining the standard constraint (2) that $\sigma_F = \sigma_R^0 = 0$ for X = H) as input parameters to eq. [1]. Convergence to constant σ_F, σ_R^0, ρ_F, and ρ_R values was essentially complete after 10 iterative cycles but was allowed to continue for 25 cycles, at which point changes in ρ and σ values between successive cycles was well below 0.001.

The final ρ_F and ρ_R values were also used to estimate σ_F and σ_R^0 constants for I, $C(CH_3)_3$, and $Sn(CH_3)_3$. These were not included in the iteration since data were not available for all five styrene derivatives for these substituents.

The re-determined σ_F and σ_R^0 constants are listed in Tables 2 and 3 along with the 95% confidence limits for the uncertainties in these parameters. Almost all σ_R^0 constants have uncertainties below 0.01 while typical σ_F uncertainties are about 0.02. The corresponding standard errors are ca. 0.004 for σ_R^0 and ca. 0.01 for σ_F. This represents the limits in precision possible for these parameters, given the experimental uncertainty of ca. 0.1 for individual data points (an uncertainty of 0.005 in σ_R^0 corresponds to an uncertainty of 0.1 in *para* carbon chemical shifts, since $\rho_R \sim 20$ for these carbons). The revised constants are in excellent agreement with those obtained by target testing during factor analysis (1), indicating that our iterative procedure is valid. While target testing could also have been used to redefine σ_F and σ_R^0, the approach used here has the advantage of providing a detailed statistical analysis of error.

The revised σ_R^0 values are in excellent agreement with those of Taft (2) (see Table 2). While the revised σ_F constants show somewhat larger deviations from Taft's σ_I scale (see Table 3), the only qualitative differences are for the two alkyl substituents which are predicted to have small positive σ_F values, in contrast to the previously reported small negative values (2, 8).

[1]It has recently been pointed out that σ_I should really be renamed σ_F in view of the strong evidence that it is a field parameter rather than a σ inductive parameter (5). This convention will be adopted subsequently throughout this paper when referring to the scale which we have derived.

Can. J. Chem. Downloaded from www.nrcresearchpress.com by 210.87.254.40 on 09/06/12
For personal use only.

Can. J. Chem. Downloaded from www.nrcresearchpress.com by 210.87.254.40 on 09/06/12
For personal use only.

TABLE 2. σ_R^0 constants estimated by iterative multiple linear regression compared with literature values and those obtained by target testing

X	σ_R^0 [a]	σ_R(lit.)[b]	σ_R^0 (tt)[c]
H	0.000±0.008	0.00	0.000
$N(CH_3)_2$	−0.567±0.013	−0.55	−0.564
NH_2	−0.495±0.008	−0.50	−0.499
OCH_3	−0.417±0.005	−0.42	−0.414
SCH_3	−0.199±0.005	−0.20	−0.200
CH_3	−0.137±0.005	−0.13	−0.141
$Si(CH_3)_3$	0.028±0.005	0.04	0.031
F	−0.297±0.011	−0.31	−0.294
Cl	−0.180±0.005	−0.18	−0.181
Br	−0.157±0.008	−0.16	−0.158
$COCH_3$	0.161±0.007	0.16	0.159
CO_2CH_3	0.162±0.004	0.16	0.157
CF_3	0.077±0.008	0.08	0.078
CN	0.071±0.009	0.08	0.073
NO_2	0.144±0.007	0.15	0.148
$C(CH_3)_3$	−0.145±0.014[d]	—	[e]
$Sn(CH_3)_3$	0.004±0.008[d]	—	[e]
I	−0.119±0.007[d]	−0.14	[e]

[a]This work. Estimated value ± 95% confidence limit.
[b]Reference 2.
[c]Predicted σ_R^0 values from target testing during factor analysis.
[d]These data were not include in the iterative process but rather were estimated by solving eq. [2] using all available data for these compounds (12−15 variables).
[e]No target testing was performed since these compounds were not included in the data matrix which was subject to factor analysis.

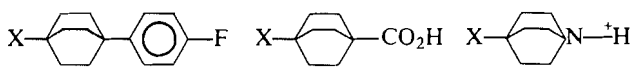

1 2 3

Interestingly, Adcock's ^{19}F chemical shift data for 1-X-4-(*p*-fluorophenyl) bicyclo[2.2.2.]octane derivatives, **1**, also suggested small positive polar constants for alkyl groups (9*a*) (see Table 3). It is possible that the previous negative σ_I values for alkyl groups (which have been estimated mainly from reactivity data) reflect small contributions from alkyl group polarizabilities (10). In any case, σ_F values for alkyl groups are statistically little different from zero, as suggested by Adcock and Abeywickrema (9*b*).

Adcock has very recently used his data for **1** to derive σ_I constants for different solvents (9*b*). His scale for CCl_4 (our solvent system) is reproduced in Table 3. There is generally excellent agreement between σ_F and σ_I scale. Interestingly, for the two substituents where there are significant differences ($COCH_3$ and F), our values are intermediate between those of Taft and Adcock.

Much larger differences are noted between our σ_F scale and the σ_I scales of Grob *et al.* (11) and Charton (6) (see Table 3), both of which are based upon acidity measurements in aqueous solutions. In particular, the latter two scales show markedly enhanced σ_I values for $N(CH_3)_2$, NH_2, OCH_3,SCH_3, $COCH_3$, and CO_2CH_3. Significantly, these are precisely the group of substituents which Taft has claimed will show enhanced polar effects in protic solvents, due to their hydrogen bond acceptor abilities (12, 13). Furthermore, Adcock's σ_I scale for CH_3OH also shows enhanced σ_I constants for several of these substituents (9*b*). This raises the obvious possibility that the σ_F scale which we have defined is best suited for measurements in aprotic media, while the σ_I scales of Grob and Charton are better for measurements in protic (particularly aqueous) media. This possibility will be considered in the following section.

(b) *Concerning the "purity" of* σ_F *and* σ_R^0 *and the range of applicability of these parameters*

The results of both target testing (1) and iterative multiple linear regression (part (a)) clearly demonstrate that σ_F and σ_R^0 are appropriate parameters for predicting chemical shifts in styrene derivatives. σ_F is considered to be a field effect parameter (5) while σ_R^0 is generally regarded as a resonance (π charge transfer) parameter (14). However, our results do not prove that σ_F and σ_R^0 are pure field and resonance substituent constants since they could also be linear combinations of the true parameters (15). In fact, Fadhil and Godfrey have recently argued that the previously defined σ_I scale is not a true (coulombic) field scale (16). If true, this would equally apply to σ_F. No amount of statistical testing alone can resolve this question. However, it can be addressed by considering appropriate model systems. Other questions which can be similarly addressed include whether σ_F and σ_R^0 are applicable to measurements in both protic and aprotic media and whether they are applicable to both spectroscopic and reactivity measurements.

An appropriate model system for addressing the first question is one in which resonance effects have been eliminated, leaving only field effects (6). One obvious choice is Adcock's ^{19}F chemical shift data set for **1** (9). This has the additional advantage that raw chemical shift data have been reported for both protic (CH_3OH) and aprotic (C_6H_{12}, C_6H_6, CH_2Cl_2, and $(CH_3)_2NCHO$ (DMF)) media (9*a*), thus allowing simultaneous consideration of questions 1 and 2. The substituent-induced chemical shifts have been correlated against σ_F and the σ_I scales of Grob (11) and Charton (6). Results are presented in Table 4. It is seen that σ_F gives uniformly excellent correlations for chemical shifts in aprotic media (while the correlation coefficient drops below 0.99 for DMF, the standard deviation of the correlation is comparable to the estimated experimental uncertainty of 0.05 (9*a*)). However, the correlation in CH_3OH is of significantly lower precision. By contrast, the correlation against σ_I scales are consistently poorer in aprotic media but significantly better in CH_3OH.

There is a dearth of good data sets (with a well-balanced range of substituents) for considering the applicability of σ_F to reactivity or acidity measurements in aprotic media. However, recently determined gas phase acidities for 4-substituted bicyclo[2.2.2]octane-1-carboxylic acids, **2**,[2] provide an ideal system in the ultimate aprotic medium. Similarly Grob's aqueous acidity data for 4-substituted quinuclidinium ions, **3** (11), provide a good test of the applicability of σ_F to acidity data in a protic medium. Results of correlations of data for **2** and **3** against σ_F and Charton's σ_I scale are summarized in Table 4. σ_F gives an excellent correlation for **2** but not for **3** while the exact reverse is found for σ_I.

Considering all of the results in Table 4, the obvious conclusion is that σ_F is a pure field parameter which is applicable to both spectroscopic and thermodynamic measurements in aprotic media. Furthermore, σ_F is applicable to measurements in both aromatic and aliphatic systems. Finally, in view of the precise correlations against σ_F for data from various aprotic

[2]R. W. Taft, private communication.

TABLE 3. σ_F constants estimated by iterative multiple linear regression compared with previous values and those obtained by target testing

			σ_I				
X	σ_I[a]	σ_F (tt)[b]	Taft[c]	Adcock[d]	Grob[e]	Charton[f]	Adcock[g]
H	0.000±0.023	0.00	0.00	0.00	0.00	0.00	0.00
$N(CH_3)_2$	0.098±0.037	0.102	0.06	0.12	0.19	0.17	0.28
NH_2	0.135±0.023	0.136	0.12	0.13	0.19	0.17	0.26
OCH_3	0.242±0.015	0.238	0.27	0.21	0.34	0.30	0.30
SCH_3	0.232±0.013	0.232	0.23	—	0.30	0.30	—
CH_3	0.025±0.014	0.028	−0.04	(0.03)	0.02	−0.01	—
$Si(CH_3)_3$	−0.042±0.015	−0.037	−0.10	0.00	—	−0.11	—
F	0.454±0.030	0.446	0.50	0.39	0.47	0.54	0.41
Cl	0.454±0.013	0.449	0.46	0.43	0.46	0.47	0.43
Br	0.450±0.022	0.445	0.44	0.44	0.48	0.47	0.44
$COCH_3$	0.229±0.021	0.233	0.20	0.29	0.31	0.30	0.30
CO_2CH_3	0.210±0.012	0.214	0.20	0.23	0.31	0.32	0.29
CF_3	0.421±0.012	0.419	0.42	0.44	—	0.40	0.42
CN	0.599±0.024	0.594	0.56	0.58	0.56	0.57	0.54
NO_2	0.651±0.021	0.646	0.65	0.66	0.64	0.67	0.62
$C(CH_3)_3$	0.039±0.037[h]	—	(−0.05)	(0.01)	−0.03	−0.01	—
$Sn(CH_3)_3$	−0.042±0.024[h]	—	—	0.00	−0.05	—	—
I	0.425±0.042[h]	—	0.39	0.43	0.43	0.40	0.41

[a]This work. σ_F ± 95% confidence limit.
[b]Predicted value from target testing (1).
[c]Reference 2 (ref. 8 for $C(CH_3)_3$).
[d]Reference 9*b*. This scale is based on chemical shifts for **1** in CCl_4 (CH_3 and $C(CH_3)$ parameters from results in C_6H_{12}).
[e]Reference 11. $\sigma_I(T)$ parameters are divided by 5.5 to place them on the same scale as the other parameters.
[f]Reference 6.
[g]Reference 9*b*, based on chemical shifts in CH_3OH.
[h]Values estimated by solving eq. [2], using all available data for each substituent (12−15 data points).

TABLE 4. Comparison of correlations against σ_F and σ_I for various model systems in which only field effects are anticipated

System	Solvent	Variable	σ	$\rho_F(\rho_I)$[a]	C[a]	r[b]	S.D.[c]	F[d]	N[e]
I	C_6H_{12}	$\Delta\delta_F$	σ_F	2.57±0.10	−0.01	0.9926	0.072	734	13
			σ_I[f]	2.41±0.18	−0.06	0.9721	0.139	189	13
	C_6H_6		σ_F	1.69±0.06	−0.06	0.9930	0.046	777	13
			σ_I[g]	1.60±0.10	0.06	0.9783	0.081	246	13
	CH_2Cl_2		σ_F	2.06±0.07	0.04	0.9939	0.052	890	13
			σ_I[h]	1.96±0.10	0.03	0.9873	0.075	426	13
	DMF		σ_F	1.41±0.08	0.04	0.9821	0.062	299	13
			σ_I[i]	1.35±0.08	0.03	0.9794	0.067	259	13
	CH_3OH		σ_F	1.32±0.18	0.20	0.9275	0.113	55	11
			σ_I[j]	1.57±0.13	0.07	0.9709	0.072	148	11
II	Gas	$-\Delta G^0$	σ_F	13.97±0.66	0.12	0.9933	0.375	443	8
			σ_I[k]	14.29±1.48	0.48	0.9694	0.798	94	8
III	H_2O	$-\Delta pK_a$	σ_F	5.17±0.35	0.24	0.9674	0.295	190	15
			σ_I[l]	5.17±0.18	0.11	0.9922	0.145	822	15

[a]Terms for correlation equation variable = $\rho_F\sigma_F + C$ or $\rho_I\sigma_I + C$.
[b]Correlation coefficient.
[c]Standard deviation of estimate.
[d]*F* test of variance.
[e]Number of substituents included in the correlation. In general, this included all substituents for which data were available and for which σ_F and σ_I were defined in all three scales.
[f]σ_I from ref. 6. Grob's σ_I scale gave r = 0.9706, S.D. = 0.142, F = 179.
[g]σ_I from ref. 6. Grob's σ_I scale gave r = 0.9770, S.D. = 0.083, F = 230.
[h]σ_I from ref. 6. Grob's σ_I scale gave r = 0.9860, S.D. = 0.079, F = 385.
[i]σ_I from ref. 6. Grob's σ_I scale gave r = 0.9776, S.D. = 0.069, F = 237.
[j]σ_I from ref. 11. Charton's σ_I scale gave r = 0.9500, S.D. = 0.094, F = 83.
[k]σ_I from ref. 6. No correlation was performed for Grob's σ_I scale since no σ_I value is defined for CF_3.
[l]σ_I from ref. 6. Since this data set was used to define Grob's σ_I scale, it would give a perfect correlation with that scale.

media, it appears that definition of different polar substituent parameters for different aprotic media (9*b*) is not really necessary, at least at this time. However, there do appear to be sufficient differences between results in aprotic and protic media to justify having a separate σ_F (or σ_I) scale for the latter solutions. Since Charton's σ_I scale has been extensively tested

Can. J. Chem. Downloaded from www.nrcresearchpress.com by 210.87.254.40 on 09/06/12
For personal use only.

TABLE 5. Final results of iterative multiple linear regression analysis of long-range substituent effects in styrene derivatives, using eq. [1] and σ_I and σ_R^0 values from Table 2

Compound	Variable	δ_0[a]	δ_H[b]	ρ_F[c]	ρ_R[d]	r[e]	F[f]	S.D.[g]
4H	C(1)	137.32	137.40	4.33±0.12	19.74±0.11	0.9999	19996	0.095
4H	C(α)	136.82	136.96	−2.59±0.10	−0.25±0.09	0.9915	347	0.082
4H	C(β)	113.27	113.20	5.11±0.14	8.78±0.13	0.9992	3681	0.114
4H	H(B)[h]	5.629	5.629	0.153±0.012	0.464±0.011	0.9974	1140	0.010
4H	H(C)[h]	5.101	5.114	0.290±0.011	0.472±0.010	0.9983	1783	0.009
4H	J_{BC}[i]	1.101	1.09	−0.709±0.030	−0.426±0.027	0.9943	521	0.024
4M	C(1)	140.96	141.07	4.64±0.15	20.48±0.14	0.9998	13833	0.119
4M	C(α)	142.82	142.97	−2.00±0.14	0.32±0.13	0.970	97	0.114
4M	C(β)	112.13	112.13	4.16±0.12	6.93±0.11	0.9991	3290	0.096
4B	C(1)	143.20	143.08	4.81±0.21	21.34±0.19	0.9996	7744	0.165
4B	C(α)	159.36	159.43	−2.09±0.10	−0.37±0.09	0.989	270	0.078
4B	C(β)	111.33	111.39	2.03±0.07	0.86±0.06	0.9952	617	0.057
3H	C(6)	125.94	126.00	3.79±0.10	19.81±0.09	0.9999	27283	0.081
3H	C(α)	137.03	136.96	−3.42±0.17	−1.58±0.15	0.9909	325	0.134
3H	C(β)	113.23	113.20	4.52±0.12	2.27±0.11	0.9976	1243	0.093
3M	C(6)	125.31	125.25	3.53±0.16	19.94±0.14	0.9997	111421	0.125
3M	C(α)	143.16	142.97	−3.07±0.21	−1.38±0.19	0.983	177	0.162
3M	C(β)	112.14	112.13	3.59±0.08	1.76±0.08	0.9976	1252	0.073

[a]Intercept in equation $\delta_i = \delta_0 + \rho_F\sigma_F + \rho_R\sigma_R^0$.
[b]Chemical shift of parent compound.
[c]σ_F ± standard error in ρ_F.
[d]ρ_R ± standard error in ρ_R.
[e]Multiple correlation coefficient.
[f]F test of variance.
[g]Standard deviation between estimated and actual chemical shifts.
[h]Weighted by 10 during iterative multiple linear regression.
[i]Weighted by 3 during iterative multiple linear regression.

using data for protic media (6), it is probably the most appropriate choice for this purpose at the present time.

Before considering the range of applicability of σ_R^0, one must consider the type of system to which it would apply. Historically, σ_R^0 has been considered to be applicable to systems with negligible through-conjugation between the substituent and probe group, e.g. ring-substituted phenylacetic acid derivatives (2*a*). However, more recently it has been considered as applicable to systems with π electron demand almost identical to that in benzene (2*b*, 17, 18).[3] While it is probably impossible to find a model system in which only resonance effects are present, the *para* ^{13}C chemical shifts in monosubstituted benzenes (and styrenes) provide a very good test of σ_R^0, since these chemical shifts are dominated by resonance effects (ref. 2*b*, also see Table 5). In fact, σ_F and σ_R^0 give correlations of outstanding precision for *para* carbon shifts in monosubstituted benzenes (e.g. r = 0.998, F = 13 985, S.D. = 0.12 for chemical shifts in $CDCl_3$ (data from ref. 2*b*)). Comparable correlations are obtained for *para* chemical shifts in styrenes (Table 5). Thus we believe that we have defined σ_R^0 for aprotic media to a very high degree of precision. This is important, since σ_R^0 provides the central anchor point for a proposed bilinear resonance scale (18). It is not yet clear whether a separate σ_R^0 scale will be required for protic media. We intend to investigate this by determining chemical shifts for a number of styrene derivatives in CH_3OH, applying similar statistical techniques to those used in ref. 1 and in this manuscript to determine σ_F and σ_R^0 in a protic medium.

[3]Styrene derivatives satisfy this definition due to the completely amphielectronic nature of the vinyl group (18, 19).

(c) ρ_I and ρ_R values from eq. [1] and mechanisms of transmission of long-range substituent effects in styrene derivatives

ρ_F and ρ_R values determined from eq. [1] in the final cycle of iterative multiple linear regression are given in Table 5, along with various statistical tests of individual correlations. In terms of statistical tests such as the correlation coefficient, r, and F test, the correlations range from good (for the poorest C(α) correlations) to outstanding (for all *para* carbon correlations). However, the most significant observation is that all of the standard deviations are comparable with the estimated experimental uncertainty in these variables (0.1 for ^{13}C chemical shifts, 0.01 for ^1H chemical shifts, and 0.03 for $^1H-^1H$ coupling constants). On this basis, it appears that all of the correlations are of equal validity. It is also noteworthy that the ρ_F and ρ_R values for the **4H** correlations are quite similar to the values obtained previously by simple multiple linear regression, using literature σ_I and σ_R^0 values (20). Thus no anomalies are introduced by the iterative process.

As discussed in part (b), σ_F is considered to be a field parameter while σ_R^0 is regarded as a resonance parameter. Thus ρ_F and ρ_R values for individual nuclei should reflect the relative importance of field (including π inductive) and resonance effects at those positions. Thus they can be used to test our previously proposed model for mechanism of transmission of long-range substituent effects in styrene derivatives (3, 4).

In the case of **4H** derivatives, a specific prediction was made with respect to ^1H chemical shifts. It was assumed that substituent effects which altered the π electron density at C(β) (resonance and π inductive (polarization) effects) would affect H(B) and H(C) equally. On the other hand, field effects should be greater for H(C) than H(B) because the electric field due to the

Can. J. Chem. Downloaded from www.nrcresearchpress.com by 210.87.254.40 on 09/06/12
For personal use only.

TABLE 6. Statistical testing of model for mechanism of transmission of substituent effects to β vinyl protons

	H(B)[a]	H(C)	t^b	P^c
ρ_F	0.1528±0.0123	0.2900	11.2	$<10^{-7}$
ρ_R	0.4639±0.0111	0.4724	0.77	~0.25

[a] ρ_F (or ρ_R) for H(B) ± standard error in ρ_I (or ρ_R).
[b] t test of null hypothesis.
[c] Probability that $\rho_F H(B) = \rho_F H(C)$ or $\rho_R H(B) = \rho_R H(C)$. Probability for one-sided t test for 12 degrees of freedom. $P = 0.25$ corresponds to a 75% confidence limit that $\rho_R H(B) < \rho_R H(C)$.

polar substituent is greater along C(β)—H(C) than along C(β)—H(B) (3). Thus the prediction is $\rho_F H(C) > \rho_F H(B)$ and $\rho_R H(C) \sim \rho_R H(B)$. The ρ_F and ρ_R values for H(B) and H(C) are entirely consistent with this prediction (see Table 3). However, this prediction can be subjected to even more rigorous testing by using the t test of the null hypothesis (20, 21) (see Table 6). This shows only about a 75% probability that $\rho_R H(C) > \rho_R H(B)$ but essentially 100% probability that $\rho_F H(C) > \rho_F H(B)$. Based on the usual 95% confidence limit for null hypothesis testing (11), one can state that the proposed model is clearly statistically justified.

A specific model was also proposed for ^{13}C chemical shifts in **4H**, **4M**, and **4B** derivatives (3, 4). It was assumed that resonance effects in **4H** should mainly affect the conjugated *ortho*, *para*, and β carbons (see **4**). The resonance effect at C(β) should drop off rapidly (by approximately $\cos^2 \phi$, where ϕ is the angle of twist between the phenyl and vinyl groups) from **4H** ($\phi \sim 0°$) to **4M**($\phi \sim 30°$) to **4B** ($\phi \sim 65°$) (4). The predicted field dependence of ^{13}C chemical shifts is more complex. It was suggested that the main field effect was field-induced polarization of the styrene π electron system (π polarization effect) (4). The proposed model involved two components of π polarization: (a) direct (and independent) polarization of phenyl and vinyl groups (see **5**) and (b) polarization of the entire styrene π electron system with π electron transfer from C(β) to the phenyl group (see **6**). The latter effect has recently been given the name extended π polarization (22).

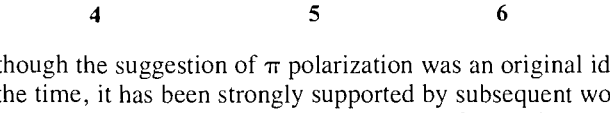

4 **5** **6**

Although the suggestion of π polarization was an original idea at the time, it has been strongly supported by subsequent work by ourselves (23) and several other groups (9, 22, 24). Evidence for π polarization has recently been reviewed (5, 25). Extended π polarization should be particularly important in the planar **4H** derivatives, resulting in a relatively large (positive) ρ_F value for C(β). However, this component should be almost entirely eliminated in **4B** derivatives, leaving a pattern of ρ_F values for the vinyl group similar to that shown in **5**.

The correlations in Table 5 strongly support this model. As expected, ρ_R is much greater for C(β) than C(α) (ρ_R for C(α) is little different from zero in any of the three derivatives). Furthermore, ρ_R for C(β) drops off rapidly from 8.8 (**4H**) to 6.9 (**4M**) to 0.9 (**4B**) as the vinyl group is twisted out of conjugation. It is interesting to note that ρ_R for C(1) increases as ρ_R for C(β) decreases. This could reflect a localization of the resonance effect of the substituent within the phenyl group as conjugation is destroyed. By contrast with ρ_R, ρ_F for C(β) drops off much less rapidly (from 5.1 to 4.2 to 2.0) as conjugation is destroyed. Furthermore, the ρ_F values for C(α) and C(β) are essentially equal and opposite in the case of **4B**. This is consistent with essentially complete elimination of extended π polarization, leaving only the direct polarization contribution (as in **5**). It is interesting to note that ρ_F is greater for C(β) than for C(1) in **4H** (by contrast ρ_R is more than twice as large for C(1) than C(β)). This reflects the relative efficiency of the two component π polarization mechanism in transmitting polar effects to remote positions in planar conjugated derivatives (5).

In the case of 3-substituted styrenes, one would reasonably expect much-reduced resonance effects in the side chain since the vinyl groups and the substituent are no longer formally conjugated. Predictions of π polarization effects are more difficult due to the presence of two non-equivalent conformations (see **7**). However, simple electrostatic calculations suggest a

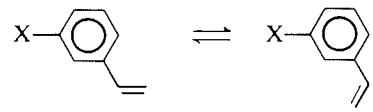

7

ca. 1/3 larger direct π polarization component for either conformer of **3H** than for **4H**. On the other hand, assuming that the magnitude of the extended π polarization component will be determined by the electron deficiency of the phenyl carbon to which the vinyl group is attached (5), this component should be smaller in **3H** than in **4H**. Once again, both the resonance and extended π polarization components should decrease on going from **3H** to **3M**.

The results in Table 3 are entirely consistent with these predictions. ρ_R for C(β) in **3H** is ca. 1/4 of that in **4H** and further decreases from **3H** to **3M**. Interestingly, ρ_R for C(α) shows a significant negative value in **3H** and **3M**, nearly equal to the positive ρ_R values for C(β). It appears that the resonance component in 3-substituted styrenes may be transmitted by a secondary field mechanism in which the large resonance-induced changes in π electron density at C(2) and C(6) set up an electric field which polarizes the vinyl group.

ρ_F values for C(β) in **3H** and **3M** are only slightly smaller than the corresponding values for **4H** and **4M**, while ρ_I values for C(α) show larger negative values than in **4H** and **4M**. If one takes the magnitudes of the ρ_F values for C(α) in the two α-methylstyrenes as approximate indicators of the direct π polarization component while ρ_F values for C(β) reflect the total π polarization effect, then the relative proportions of direct to extended π polarization are ca. 2:3 in **4H** and ca. 3:1.5 in **3H**, consistent with the arguments presented above.

In concluding this section, it should be noted that the fact that we can rationalize ρ_F and ρ_R values for individual substituents in terms of a reasonable model for transmission of substituent effects provides further evidence for the view that σ_F and σ_R^0 are, respectively, pure field and resonance substituent constants. In particular, correlations of $\delta_{H(B)}$ and $\delta_{H(C)}$ for **4H** provide a separation which is in exact agreement with the predicted model of substituent effects. One would not expect such a clear-cut separation of effects if σ_F and σ_R^0 were each some linear combination of two other substituent constants.

(d) *Short-range substituent effects in styrene derivatives*

Factor analysis of the styrene data set indicated that three factors were required to predict *ipso* and *ortho* chemical shifts and that there also appeared to be a minor third factor for *meta*

Can. J. Chem. Downloaded from www.nrcresearchpress.com by 210.87.254.40 on 09/06/12
For personal use only.

Can. J. Chem. Downloaded from www.nrcresearchpress.com by 210.87.254.40 on 09/06/12
For personal use only.

TABLE 7. Results of cross-correlations for various parameters with short-range aromatic substituent parameters[a]

Dependent variable	Independent variable	r	r^2 [b]	$1 - r^2$
σ_I	σ_R^0	0.236	0.055	0.945
α	σ_F, σ_R^0	0.623	0.388	0.612
β	σ_F, σ_R^0	0.800	0.641	0.359
Q	σ_F, σ_R^0	0.898	0.807	0.193
I	σ_F, σ_R^0	0.000	0.000	1.000
O	σ_F, σ_R^0	0.000	0.000	1.000
M	σ_F, σ_R^0	0.000	0.000	1.000

[a]Correlations forced through origin.
[b]r^2 = coefficient of determination, i.e. the fraction of the dependent variable accounted for by the independent variable(s). $1 - r^2$ can be referred to as the coefficient of non-determination and gives the fragment of the variance of the dependent variable *not* accounted for by the independent variable(s).

shifts (1). Target testing revealed that σ_F and σ_R^0 were two of the factors in each case. A possible third *ipso* factor, α, was estimated using cyclohexane *alpha* ^{13}C chemical shifts to provide an input test vector. Similarly cyclohexane *beta* chemical shifts and the semiempirical Q factor of Smith and Proulx (26) were used as test vectors to estimate two possible *ortho* factors, β and Q (1). However, it was pointed out that any or all of α, β, and Q might not be true factors but rather some linear combination(s) of σ_F and/or σ_R^0 and the true factor (obviously β and Q cannot both be true *ortho* factors) (1).

To check this point, α, β, and Q were correlated against σ_F and σ_R^0. Results are summarized in Table 7. Based on the coefficient of determination, Q is a totally unreliable *ortho* parameter since only 19% of its variance is *not* accounted for by σ_F and σ_R^0. β contains a larger, but still minor, component of the actual *ortho* factor while α contains a major component of the true *ipso* factor. One can estimate the actual parameters by an orthogonalization procedure. For example, β appears to be a linear combination of σ_F, σ_R^0, and the missing *ortho* factor, **O**. Consequently, in a correlation of β with σ_F and σ_R^0, the residual error in β for a given substituent X, $\Delta(X)$, should be proportional to **O**(X), i.e.

$$[3]\quad \beta(X) = \rho_F\sigma_F(X) + \rho_R\sigma_R^0(X) + \Delta(X) = \rho_F\sigma_F(X) + \rho_R\sigma_R^0(X) + w\mathbf{O}(X)$$

Similarly, Q should be a different linear combination of σ_F, σ_R^0, and **O**, but the residuals, $\Delta(X)$, should be porportional to the residuals from eq. [3]. In fact, the two sets of differences are precisely linearly related ($r = 0.999$, $F = 49\ 400$), indicating that we have succeeded in isolating from β (or Q) an *ortho* factor which is completely orthogonal to σ_F and σ_R^0 (this is confirmed by a correlation of **O** versus σ_F and σ_R^0, see Table 7). The differences, $\Delta(X)$, have been scaled to produce **O** constants (see Table 8). The scaling factor was chosen so that the weighting factor, w, equals unity in a correlation of **O**, σ_F, and σ_R^0 versus $\delta_{C(3)}$ for **4H** (see Table 8). This correlation is much more precise than one with σ_F and σ_R^0 alone and the ρ_F and ρ_R values are consistent with the expected pattern of substituent effects as shown in **4** and **5**.

A similar approach was used to isolate the *meta* factor. γ

TABLE 8

(a) Results of iterative multiple linear regression analysis of phenyl chemical shifts in **4H** derivatives using σ_I, σ_R^0, and various short-range parameters

Variable	Parameter[a]	δ_0	δ_H	ρ_F	ρ_R	w[b]	r	F	S.D.
C(1)	None	137.32	137.40	4.33	19.74	—	0.9999	19996	0.095
C(2)	None	125.76	126.00	1.65	−2.14	—	0.939	38	0.212
C(2)	**M**	126.01	126.00	1.29	−1.94	1.000	0.9946	338	0.077
C(3)	None	129.46	128.15	−5.20	24.65	—	0.798	10.5	4.71
C(3)	0	128.16	128.15	−3.14	23.57	1.000	0.9999	15702	0.124
C(4)	None	134.19	127.46	−0.14	−31.83	—	0.568	2.86	11.99
C(4)	α	127.49	127.46	−38.95	0.82	1.000	0.9999	16596	0.226
C(4)	**I**	127.49	127.46	13.85	−39.16	1.000	0.9999	16507	0.227

(b) Values of short-range substituent parameters used in the above correlations

X[c]	$N(CH_3)_2$[d]	NH_2[d]	OCH_3[d]	SCH_3[d]	CH_3[d]	$C(CH_3)_3$[e]	$Si(CH_3)_3$[d]	$Sn(CH_3)_3$[e]	F[d]
M	−0.45	−0.07	+0.01	−0.28	−0.26	−0.56	−0.45	−0.28	+0.39
O	−2.20	−1.58	−4.06	+3.98	+3.96	+0.35	+4.14	+7.19	−4.64
α	+27.00	+24.01	+41.46	+19.49	+10.26	+24.21	+9.49	+11.92	+52.72
I	−0.84	−2.91	+12.00	−0.72	+3.46	+16.35	+13.13	+14.30	+16.87

X[c]	Cl[d]	Br[d]	I[e]	$COCH_3$[d]	CO_2CH_3[d]	CF_3[d]	CN[d]	NO_2[d]
M	+0.22	+0.46	+0.90	−0.25	−0.28	−0.20	−0.13	−0.16
O	+5.91	+8.23	+13.34	−2.89	−1.62	−3.29	+4.15	−5.86
α	+23.56	+11.73	−17.84	+18.17	+10.23	+18.83	+7.93	+45.25
I	−7.61	−18.32	−45.04	+12.52	+5.62	−0.32	−20.86	+16.63

[a]Parameter used in combination with σ_F and σ_R^0 for multiple linear regression with the indicated variable. Symbols are defined in the text.
[b]Weighting factor for the indicated parameter. Note that **M**, **O**, α, and **I** are scaled to yield $w = 1.000$ for **4H** derivatives. Other headings are identical to those defined in Table 5.
[c]**M** = **O** = **I** = α = 0.00 for X = H. This equality is assured by forcing the correlation equations (see Table 7) to pass through the origin.
[d]Values defined from eq. [3], as discussed in the text.
[e]Values estimated from three parameter correlations for **4H** and chemical shifts for **4H** derivative.

Can. J. Chem. Downloaded from www.nrcresearchpress.com by 210.87.254.40 on 09/06/12
For personal use only.

cyclohexane chemical shifts were used as an initial target vector (1) and the predicted γ values were used in an equation similar to eq. [3] to predict individual *meta* factors, **M**(X) (see Table 8). These factors are quite small, as previously suggested (1). Nevertheless, the correlation of $\delta_{C(2)}$ for **4H** is significantly improved by the inclusion of **M**. The ρ_F and ρ_R values are once again consistent with the expected pattern of substituent effects in **4** and **5** (see Table 8). Finally, we attempted to isolate an orthogonal *ipso* factor, **I**, from the predicted α values, using the same procedure (see Table 8). However, in this case, a correlation of σ_F, σ_R^0, and **I** versus $\delta_{C(4)}$ for **4H** gives apparently unreasonable ρ_F and ρ_R values. Based upon correlations of *ipso* π electron densities in styrenes with field and resonance substituent parameters (27), we would have expected $\rho_F \simeq -15$ and $\rho_R \simeq -20$ for $\delta_{C(4)}$.[4] Before considering the significance of this last observation, it is useful to consider the assumptions which we have made in this section.

The first assumption is that we can divide short-range substituent effects at a given position into electronic components (predicted by σ_F and σ_R^0) and an orthogonal component (predicted by **M**, **O**, or **I**) which reflects effects other than ground-state electronic effects. The second assumption is that ρ_F and ρ_R values reflect substituent-induced changes in π electron density. We will consider this latter assumption first. While the theoretical origins of linear chemical shift – π electron electron correlations remain obscure (29), there is ample empirical evidence for quite precise linear relationships in the case of long-range aromatic chemical shifts (14, 27, 30). The facts that σ_F and σ_R^0 are factors for short-range chemical shifts, and that reasonable ρ_F and ρ_R values are obtained for *ortho* and *meta* chemical shifts, suggest that these correlations still exist at short range, after non-electronic effects are factored out. With respect to the first assumption, it is significant that β and γ substituent effects in alkyl derivatives are complex and bear no apparent relationship to ground state electronic effects (31). This is also true of **O** and **M** (see Table 8). Thus the assumption of non-electronic components at these positions appears reasonable. However, α chemical shifts in aliphatic derivatives appear to be partially related to substituent group electronegativity (4, 32, 33). This may also be true of the *ipso* factor (1). While group electronegativity is not linearly related to σ_F, it is partially correlated with the latter parameter (33) and perhaps with σ_R^0 as well. The partially correlated component is factored out in deriving **I**. Consequently, when one performs a correlation with σ_F, σ_R^0, and **I**, part of the electronegativity dependence appears in ρ_F and ρ_R, giving misleading values for these parameters. Unfortunately, if the third substituent "effect" is partially electronic in nature, no unique solution exists for the third factor. Comparison of the correlations of $\delta_{C(4)}$ with **I** and α (see Table 8) with the anticipated ρ_F and ρ_R values (see above) suggests that the true *ipso* factor may have a value somewhere between **I** and α (the arithmetic mean of **I** and α gives $\rho_F = -12.6$ and and $\rho_R = -19.2$, close to the anticipated values). However, it is impossible to determine a precise scale.

To summarize this section, we believe that we have succeeded in isolating non-electronic *ortho* (**O**) and *meta* (**M**) factors for *ortho* and *meta* chemical shifts. Short-range electronic effects can be probed by correlating these chemical shifts with σ_F, σ_R^0, and **O** or **M**. However, the third *ipso* factor has not been conclusively identified, although it may fall close to the average of **I** and α.

One final point must be stressed most strongly. If one wishes to carry out a three parameter correlation of this kind, it is essential to have a large and well-balanced substituent set. Taft's minimal substituent set represents an absolute lower limit (2*a*).

Conclusions

Iterative multiple linear regression analysis of the chemical shift data for 3- and 4-substituted styrenes has given highly refined values of σ_F (standard error ~0.01) and σ_R^0 (standard error ~0.005). It is shown that these constants are, respectively, pure field and resonance substituent parameters and that they are applicable to both chemical shift and acidity measurements in aprotic media. The approach which we have adopted is particularly suitable for deriving quite precise dsp constants for most of the common neutral substituents.

The ρ_F and ρ_R values from individual correlations are entirely consistent with a previously proposed model for mechanism of transmission of substituent effects in styrene derivatives involving field, resonance, and π polarization effects. In particular, the results support the model of a two-component π polarization mechanism involving: (1) direct and independent polarization of the phenyl and vinyl groups, and (2) extended polarization of the entire styrene π electron system.

Values for non-electronic *ortho* and *meta* substituent factors have been determined, allowing the reliable estimation of electronic effects at these positions. However, a reliable *ipso* factor has still not been determined, although a possible scale is suggested.

While factor analysis has pointed out the number of substituent parameters required to describe the styrene data matrix and target testing has identified possible substituent parameter scales (particularly σ_F and σ_R^0) (1), no amount of statistical testing alone can prove that these are the actual substituent parameter scales rather than some linear combination of the true scales. It is the observation that correlations involving σ_F and σ_R^0 give chemically reasonable results in this and related systems which allows us to conclude that σ_F and σ_R^0 are pure field and resonance substituent parameter scales. Thus we conclude that in any thorough investigation of substituent effects, it is essential to prove that one's conclusions are *both* statistically valid and make chemical sense. Neither approach alone is sufficient.

Finally, if the approach we have presented for interpreting short-range substituent effects is valid, then it should be applicable to other aromatic derivatives. This will be the topic of a subsequent publication.

Experimental and details of calculations

Full experimental details are given elsewhere (1). Multiple linear regression analyses were performed with a program written for this purpose for mini-computers[5] and subsequently modified by us to allow iterative multiple linear regression. All calculations were performed on the Department of Chemistry Sel 75 Computer.

[4]Consistent with this is the large negative *ipso* shift in $C_6H_5CO^+$ ($\Delta\delta = -40.9$ ppm (28)). Even if one compares with the isoelectronic C_6H_5CN derivative to partially correct for resonance and magnetic anisotropy effects, the residual shift is ca. −25 ppm. This indicates a large negative polar constribution to this *ipso* shift (see **5**) which must outweigh any positive electronegativity contribution.

[5]Private communication from Professor R. J. Leroy (Waterloo) via Professor G. Burns.

Acknowledgments

Financial support from the Natural Sciences and Engineering Research Council of Canada is gratefully acknowledged (W.F.R.)

1. W. F. REYNOLDS, A. GOMES, A. MARON, D. W. MACINTYRE, R. G. MAUNDER, A. TANIN, H. E. WONG, G. K. HAMER, and I. R. PEAT. Can. J. Chem. **61**, 2367 (1983).
2. (*a*) S. EHRENSON, R. T. C. BROWNLEE, and R. W. TAFT. Prog. Phys. Org. Chem. **10**, 1 (1973); (*b*) J. BROMILOW, R. T. C. BROWNLEE, V. O. LOPEZ, and R. W. TAFT. J. Org. Chem. **44**, 4766 (1979).
3. G. K. HAMER, I. R. PEAT, and W. F. REYNOLDS. Can. J. Chem. **51**, 897 (1973).
4. G. K. HAMER, I. R. PEAT, and W. F. REYNOLDS. Can. J. Chem. **51**, 915 (1973).
5. W. F. REYNOLDS. Prog. Phys. Org. Chem. **14**, 165 (1983).
6. M. CHARTON. Prog. Phys. Org. Chem. **13**, 119 (1981).
7. C. G. SWAIN and E. C. LUPTON. J. Am. Chem. Soc. **90**, 4328 (1968).
8. L. S. LEVITT and H. F. WIDING. Prog. Phys. Org. Chem. **12**, 119 (1976).
9. (*a*) W. ADCOCK and T. C. KHOR. J. Am. Chem. Soc. **100**, 7799 (1978); (*b*) W. ADCOCK and A. N. ABEYWICKREMA. J. Org. Chem. **47**, 2957 (1982).
10. J. E. BRAUMAN and J. K. BLAIR. J. Am. Chem. Soc. **90**, 5636 (1968); **90**, 6501 (1968).
11. C. A. GROB, B. SCHAUB, and M. G. SCHLAGETER. Helv. Chim. Acta, **63**, 57 (1980).
12. M. FUJIO, R. T. MCIVER, and R. W. TAFT. J. Am. Chem. Soc. **103**, 4017 (1981).
13. R. W. TAFT. Prog. Phys. Org. Chem. **14**, 247 (1983).
14. W. J. HEHRE, R. W. TAFT, and R. D. TOPSOM. Prog. Phys. Org. Chem. **12**, 159 (1976).
15. E. R. MALINOWSKI and D. G. HOWERY. Factor analysis in chemistry. Wiley–Interscience, New York. 1980.
16. G. F. FADHIL and M. GODFREY. J. Chem. Soc. Perkin Trans. 2, 933 (1982).
17. J. BROMILOW, R. T. C. BROWNLEE, V. O. LOPEZ, and R. W. TAFT. J. Org. Chem. **45**, 2429 (1980).
18. W. F. REYNOLDS, P. DAIS, D. W. MACINTYRE, R. D. TOPSOM, S. MARRIOTT, E. VON NAGY-FELSOBUKI, and R. W. TAFT. J. Am. Chem. Soc. **105**, 378 (1983).
19. W. F. REYNOLDS, T. A. MODRO, P. G. MEZEY, E. SKORUPAWA, and A. MARON. Can. J. Chem. **58**, 412 (1980).
20. W. F. REYNOLDS, P. DAIS, D. W. MACINTYRE, G. K. HAMER, and I. R. PEAT. J. Magn. Reson. **43**, 81 (1981).
21. S. CLEMENTI, F. FRINGUIELLI, P. LINDA, and G. SAVELLI. Gazz. Chim. Ital. **105**, 281 (1975).
22. R. T. C. BROWNLEE and D. J. CRAIK. J. Chem. Soc. Perkin Trans. 2, 760 (1981).
23. W. F. REYNOLDS and G. K. HAMER. J. Am. Chem. Soc. **98**, 7296 (1976).
24. D. F. EWING and K. J. TOYNE. J. CHEM. SOC. PERKIN TRANS. 2, 243 (1979).
25. R. T. C. Brownlee and D. J. CRAIK. Prog. Phys. Org. Chem. **14**, 1 (1983).
26. W. B. SMITH and T. W. PROULX. Org. Magn. Reson. **8**, 567 (1976).
27. W. F. REYNOLDS, P. G. MEZEY, and G. K. HAMER. Can. J. Chem. **55**, 522 (1977).
28. D. F. EWING. Org. Magn. Reson. **12**, 499 (1979).
29. D. J. FARNUM. Adv. Phys. Org. Chem. **11**, 123 (1975).
30. W. F. REYNOLDS, V. C. GIBB, and N. PLAVAC. Can. J. Chem. **58**, 839 (1980).
31. G. MACIEL. *In* Topics in carbon-13 nmr spectroscopy. *Edited by* G. Levy. John Wiley & Sons, New York. 1979.
32. W. F. REYNOLDS. J. Chem. Soc. Perkin Trans. 2, 985 (1980), and references therein.
33. N. INAMOTO and S. MASUDA. Tetrahedron Lett. 3287 (1977).

Can. J. Chem. Downloaded from www.nrcresearchpress.com by 210.87.254.40 on 09/06/12
For personal use only.

Ozonolysis of vinyl chloride in methanol: a convenient entry to methoxymethylhydroperoxide and its chemistry[1]

MARTIN MEISTER, GERHARD ZWICK, AND KARL GRIESBAUM[2]
Engler-Bunte-Institut, Bereich Petrochemie, Universität Karlsruhe (TH), D-7500 Karlsruhe, West Germany

Received February 3, 1983

MARTIN MEISTER, GERHARD ZWICK, and KARL GRIESBAUM. Can. J. Chem. **61**, 2385 (1983).

Ozonolysis of vinyl chloride (**7**) in methanol at −78°C afforded methoxymethylhydroperoxide (**10**) in high yield along with only trace amounts of methyl formate (**14**). The former (**10**) was converted into a mixture of methyl formate (**14**) as the major and dimethylformal (**18**) as the minor product by HCl-catalysis in methanol. Reduction of **10** with dimethylsulfide and subsequent treatment with HCl–methanol gave dimethylformal (**18**). Partial reduction of **10** with a deficient amount of triphenylphosphine gave formaldehyde hemiacetal (**19**) and methoxymethylhydroxymethylperoxide (**20**).

MARTIN MEISTER, GERHARD ZWICK et KARL GRIESBAUM. Can. J. Chem. **61**, 2385 (1968).

L'ozonolyse du chlorure de vinyle (**7**) dans le méthanol à la température de −78°C conduit dans un haut rendement au méthoxyméthylhydroperoxide (**10**) et seulement à des traces de formiate de méthyle (**14**). Le premier, catalysé par le chlorure d'hydrogène dans le méthanol est transformé en formiate de méthyle (**14**), produit principal, et en diméthylacétal de formaldéhyde (**18**), produit secondaire. La réduction de **10** par le sulfure de méthyle, suivi d'un traitement avec le chlorure d'hydrogène dans le méthanol conduit au diméthylacétal de formaldéhyde (**18**). La réduction partielle de **10** avec une quantité insuffisante de triphenylphosphine conduit au méthylhémiacétal du formaldéhyde (**19**) et au méthoxyméthylhydroxyméthylperoxide (**20**).

Introduction

In previous work (1) we have examined the ozonolysis in methanol of a series of olefins (**1**) having monochloro substituted double bonds. It was found that the cleavage occurred in one direction only, such that the chlorinated moiety of the double bond afforded the carbonyl fragment (**3**) and the non-chlorinated moiety afforded the zwitterion fragment (**2**). Both fragments **2** and **3** were immediately trapped by methanol to give methoxyhydroperoxides (**5**) and methyl esters (**4**), respectively, as well as hydrogen chloride as a by-product. The latter, in turn, initiated a spontaneous acid catalyzed conversion of the methoxyhydroperoxides (**5**) into the corresponding methyl esters (**6**).

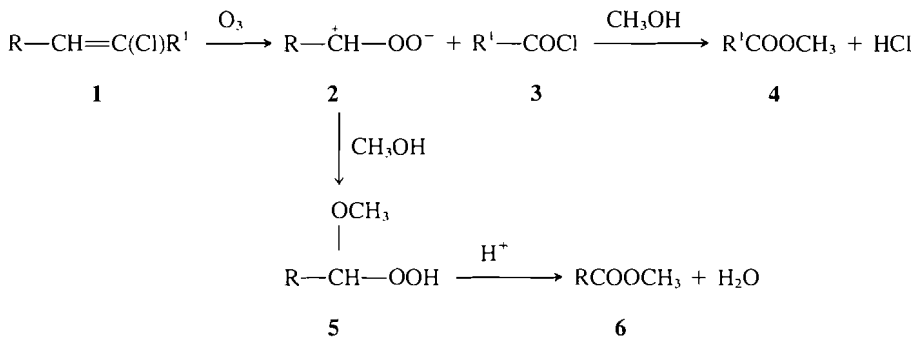

There were, however, two exceptions to this reaction scheme. Thus, chloroolefins (**1**) bearing a CHCl-moiety (i.e. R^1 = H) gave carbon monoxide and not methyl formate and chloroolefins (**1**) bearing a CH_2-moiety (i.e. R = H) gave a more persistent methoxyhydroperoxide which was only slowly converted into methyl formate by the action of hydrochloric acid. It was assumed that this more persistent methoxyhydroperoxide is the methoxymethylhydroperoxide **10**. The latter had been obtained and spectroscopically characterized previously in ozonolysis reactions of methylene-terminated olefins in methanol (2, 3). To our knowledge, however, its elemental analysis has not yet been reported and its chemistry has not been studied to any extent.

The two above-mentioned moieties CHCl and CH_2, which led to the cited exceptional ozonolysis results, are jointly present in the lowest member of the class of chloroolefins, viz. vinyl chloride (**7**), which to our knowledge has not been ozonized under the conditions and aspects which were the basis of our previous investigation (1). In view of this unique structural feature and also in consideration of the potential ecological interest in methods for the destructive oxidation of this compound, we have studied the ozonolysis of vinyl chloride (**7**) in methanol.

Results and discussion

Vinyl chloride (**7**) was ozonized to completion in methanol solution at −78°C. Ozone was not completely consumed and the solution became strongly acidic as the reaction progressed. If the solution was allowed to warm up to room temperature while it was still somewhat acidic, ^{1}H nmr analysis showed the presence of **10** as the major component, along with several unidentified signals. However, if the solution was carefully neutralized by solid sodium bicarbonate at low temperatures and subsequently warmed up to room temperature, the only

[1] Presented in part by Martin Meister at the 64th Canadian Chemical Conference, May 31 to June 3, 1981 at Halifax, N.S., Canada.

[2] Author to whom correspondence should be addressed.

Can. J. Chem. Downloaded from www.nrcresearchpress.com by 210.87.254.40 on 09/06/12
For personal use only.

Can. J. Chem. Downloaded from www.nrcresearchpress.com by 210.87.254.40 on 09/06/12
For personal use only.

detectable products were methoxymethylhydroperoxide (**10**) and trace amounts of methyl formate (**14**). After removal of methanol, methoxymethylhydroperoxide (**10**) was the only product left as the residue. This demonstrates that the expected initial ozonide **8** reacts overwhelmingly in one direction only to form the fragments carbon monoxide, hydrogen chloride, and the zwitterion **9** as a precursor for the major product **10**. The conceivable alternate mode of cleavage of **8** into fragments **11** and **12**, on the other hand, occurs only to a very minor extent, at best. For, formaldehyde (**11**) or products derived from it like dimethylformal (**18**) or trimeric formaldehyde were not detected, and methyl formate (**14**), the end product expected from the zwitterion fragment **12** by the sequence **12** → **13** → **14** (4), was only present in trace amounts. But, as will be shown below, the sequence **8** → **12** → **13** → **14** is not the only possible mode of formation for **14**, since **14** could have also been formed by HCl-catalyzed dehydration of the major product **10** prior to the neutralization step. Hence, cleavage of **8** into fragments **11** and **12** may not have occurred at all.

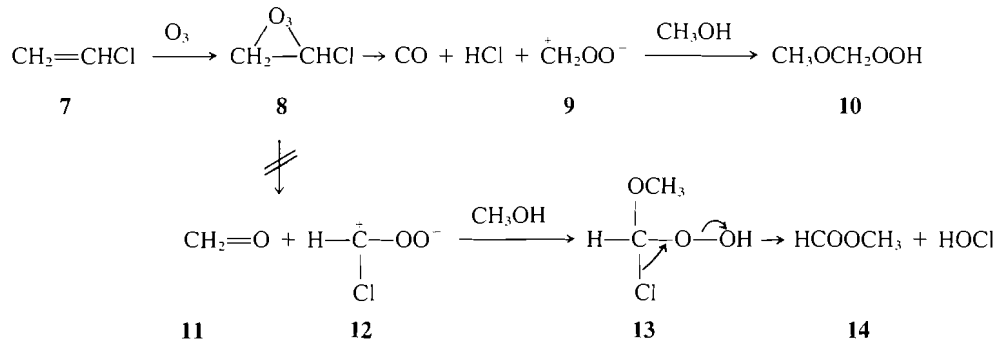

Due to the above-described selective mode of cleavage, the ozonolysis of vinyl chloride (**7**) in methanol opens a convenient method for the preparation of methoxymethylhydroperoxide (**10**) in yields of ca. 70% and in high purity. It is a colorless slightly viscous liquid which, in line with a previous report (3), was found to be sensitive to heat, but also to shock. Thus, a sample of **10** exploded violently when it was hit with a hammer, and at one occasion a sample of **10** which was kept stirring at ambient temperatures exploded, too. Furthermore, an attempt at injecting a sample into the inlet port of a gas-chromatograph led to an explosion, accompanied by the disruption of the syringe and of its needle. Hence, the methoxymethylhydroperoxide **10** has to be handled with extreme care and by applying stringent safety measures.

The structure of **10** has been established by elemental analysis and by its ^{1}H nmr, ir, and chemical ionization ms spectra. This assignment was further substantiated by the results of the reactions of **10** described in the following paragraphs.

Reaction of **10** in a 1:10 mixture of anhydrous hydrogen chloride in methanol at 40°C afforded a mixture of methylformate (**14**) and of dimethylformal (**18**) in 89 and 11% yield, respectively. A similar result was obtained at ambient temperatures, albeit at a considerably slower rate. This result is rationalized by protonation of **10** at the two available oxygen

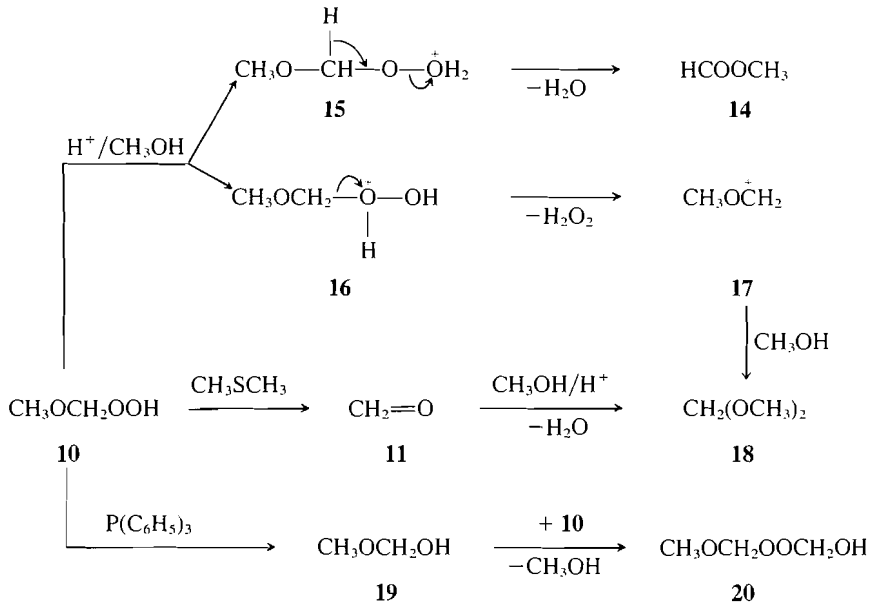

atoms of the hydroperoxide group to give the intermediates **15** and **16**, and subsequent reactions of these intermediates via **15** → **14** and **16** → **17** → **18**, respectively.

Reduction of **10** with dimethyl sulfide at room temperature and subsequent treatment with a 1:10 mixture of anhydrous hydrogen chloride in methanol afforded dimethylformal (**18**) and dimethyl sulfoxide in equimolar amounts. Partial reduction of **10** with a deficient amount of triphenylphosphine in deuteriated trichloromethane, on the other hand, gave a mixture consisting of **19** (17%), **20** (51%), and unreacted **10** (32%).

Can. J. Chem. Downloaded from www.nrcresearchpress.com by 210.87.254.40 on 09/06/12
For personal use only.

The formation of **20** is rationalized by the reaction of unconverted starting material **10** with its reduction product(s) **11** and/or **19**. Similar reactions have been observed by us between other methoxyhydroperoxides and formaldehyde (5) as well as between **10** and other aldehydes.[3]

The hemiperacetal **20** has been isolated as a colorless, slightly viscous liquid. It was identified by elemental analysis as well as by its ir and ^{1}H nmr spectra. The latter exhibited a triplet signal for each of the two CH_2-groups,[4] indicating a coupling across the peroxide bond. Similar couplings have been also observed in the spectra of other peracetals.[3]

Materials and methods

Materials

All chemicals were of commercial grade. Methanol was dried prior to its use by refluxing and subsequent distillation over magnesium shavings. The 1:10 mixtures of hydrogen chloride in methanol were prepared by introducing gaseous anhydrous hydrogen chloride into dried methanol at 0°C and monitoring the HCl content by titration of aliquots with a standard sodium hydroxide solution using phenolphthalein as indicator.

Analytical methods

Gas–liquid chromatographic analyses were carried out on a Shimadzu GC-6A unit with flame ionization detector. Glass columns: 0.3 × 500 cm, 5% Carbowax 20M on Chromosorb G; conditions: 60°C to 160°C at 4°C per min, 30 mL N_2 per min. Nuclear magnetic resonance spectra were recorded on a Bruker WP 60, infrared spectra on a Beckman IR 4260 spectrometer.

Equipment and general procedure of ozonolysis

All ozonolyses were carried out in a calibrated narrow tubular glass reactor which was equipped with a magnetic stirring bar and with an insert containing a dropping funnel, a gas inlet tube which reached to the bottom of the reactor, and a gas outlet line. The reactor was cooled to −78°C and vinyl chloride was transferred from a cylinder via the gas inlet tube and condensed into the reactor. Then a mixture of methanol and dichloromethane was added dropwise and the reactor content was mixed by passing a slow stream of nitrogen through the reactor. Ozonolysis was carried out at −78°C, and the exit gas from the reactor was passed through a buffered aqueous solution of potassium iodide. Ozone treatment was terminated when the reactor content turned blue, and the excess of ozone was removed by flushing the reactor with nitrogen. Then 6.0 g of solid sodium bicarbonate, 6.0 g of solid sodium sulfate, and 10 mL of dichloromethane were added, the insert was replaced by a balloon filled with nitrogen, and the mixture was stirred and allowed to warm up to ca. −20°C. When the mixture had turned neutral it was filtered; the filtrate was warmed up to room temperature and analyzed by ^{1}H nmr spectroscopy. Then the solvents were removed at room temperature and at approximately 20 Torr to leave a slightly viscous, colorless liquid residue. If the latter still contained residual particles of sodium bicarbonate and/or sodium sulfate, a small amount of dichloromethane was added, the solution was removed with a pipette, and the solvent was again removed as described above.

Ozonolysis of vinyl chloride (7) and characterization of methoxymethylhydroperoxide (10)

A solution of 2 mL (ca. 32 mmol) of vinylchloride (**7**) in 7 mL of methanol and 7 mL of dichloromethane was treated with a stream of 3 vol% of ozone in oxygen as described above. Soon after starting, unreacted ozone was detected in the reactor off-gases, as indicated by iodine formation in the potassium iodide solution. The ^{1}H nmr analysis of the filtrate in $CDCl_3$/TMS showed a strong signal for the CH_2-group in **10** at δ 4.95 and very weak signals for the CH- and CH_3O-groups in **14** at δ 3.76 and 8.08, respectively, in addition to the overlapping CH_3O- signals of **10** and of methanol at δ 3.45 and the CH_2-signal of dichloromethane at δ 5.31. After removal of the solvents there remained 1.8 g of virtually pure **10**. For analytical purposes, a sample of the latter was further purified by thin-layer chromatography on silica gel using a 10:1 mixture of dichloromethane and methanol as eluent and by subsequent distillation at room temperature and 2.6 × 10^{-2} millibar.

Methoxymethylhydroperoxide (10)

Colorless, slightly viscous liquid; yield ca. 71%; ir (film): 3310, 2970, 2940, 2840, 1455, 1390, 1212, 1150, 1078, 998, 992, 917 cm^{-1}; ^{1}H nmr ($CDCl_3$, TMS) δ: 3.50 (s, 3H), 4.98 (s, 2H), ca. 9.40 (broad s, 1H); ^{13}C nmr ($CDCl_3$, TMS) δ: 56.42 (q, t, J = 143.0 and 5.0 Hz), 100.79 (t, q, J = 165.0 and 5.0 Hz); ms (chemical ionization with methane, temperature of the ionization source 100°C) m/e (relative intensities): 79 (17) $(M + 1)^+$, 61 (100) $(M - OH)^+$, 47 (14) $(M - CH_3O)^+$. *Anal.* calcd. for $C_2H_6O_3$: C 30.77, H 7.75; found: C 30.66, H 7.81.

HCl-catalyzed reaction of methoxymethylhydroperoxide (10) in methanol

A mixture of 200 mg (2.6 mmol) of **10**, 0.85 mL of CH_3OD, 0.35 mL of a 7.5 molar solution of hydrogen chloride in methanol, and 153 mg (0.91 mmol) of 1,1,2,2-tetrachloroethane (as an internal standard) was kept in a closed flask at 40°C for 24 h. Then the mixture was cooled to 0°C and analyzed; ^{1}H nmr analysis ($CDCl_3$, TMS) showed the signals of **14** at δ 3.76 (d, J = 0.8 Hz, 3H) and 8.08 (q, J = 0.8 Hz, 1H) and of **18** at δ 3.36 (s, 6H) and 4.58 (s, 2H). The assignments are based on the comparison of the above data with those obtained from authentic samples of **14** and **18**. The yields of **14** and of **18** were 89% and 11%, respectively, calculated on the basis of the signal intensities as compared with that of the internal standard 1,1,2,2-tetrachloroethane. The glc analysis showed the peaks of **14** (t_R = 4.0 min; 8%) and of **18** (t_R = 3.8 min; 2%) in addition to those of the solvents. The assignment of these peaks was confirmed by coinjection with authentic samples and by gc–ms analysis, m/e (relative intensities) for **14**: 61 (33) $(M + 1)^+$, 60 (100) M^+, 45 (6) $(M - CH_3)^+$, 44 (11) $(CO_2)^+$; for **18**: 75 (45) $(M - 1)^+$, 45 (100) $(M - OCH_3)^+$.

Reduction of methoxymethylhydroperoxide (10) with dimethylsulfide

To a stirred mixture of 120 mg (1.5 mmol) of **10** in 0.2 mL of dichloromethane was added 0.14 mL (1.9 mmol) of dimethylsulfide at 0°C. The mixture was allowed to warm up to room temperature and was kept there for 6 h. Then 0.1 mL of a 7.5 molar solution of hydrogen chloride in methanol was added and the mixture was kept at room temperature for another 15 h. The ^{1}H nmr analysis ($CDCl_3$, TMS) showed as the sole products **18** (δ 3.36 and 4.58, s, each) and dimethylsulfoxide (δ 2.62, s) in an equimolar ratio. The glc analysis showed the peaks of **14** (t_R = 4.0 min; traces only), of **18** (t_R = 3.8 min), and of dimethylsulfoxide (t_R = 29.7 min). These assignments were confirmed by coinjections with authentic samples and by gc–ms analysis.

Partial reduction of methoxymethylhydroperoxide (10) with triphenylphosphine

To a stirred solution of 700 mg (9.0 mmol) of **10** in 6 mL of deuteriochloroform was added dropwise a solution of 1.0 g (3.8 mmol) of triphenylphosphine in 3 mL of deuteriochloroform at 0°C. The ^{1}H nmr analysis showed the presence of unreacted **10** (32%; δ 4.93 for the CH_2-signal which is shifted by the presence of triphenylphosphineoxide as compared to that of pure **10**), of **19** (17%; δ 4.74 for the CH_2-signal) (5), and of **20** (51%; δ 5.16 for the CH_2-signal). For the isolation of **20**, the reaction mixture was concentrated to a volume of 3 mL by evaporation at ambient temperatures and at reduced pressure. The residue was separated by column chromatography (column 3 × 60 cm; 180 g of silicagel; ether and n-pentane in a volumetric ratio of 5:1) to give 100 mg of a mixture containing 70% of **20** and 30% of **10**. This mixture was distilled at 1

[3] M. Meister, unpublished results.

[4] In some of the spectra these triplets were not well resolved and the signals each appeared as broad singlets.

millibar and at room temperature to remove **10**. Subsequently, the residue was distilled at 1.3×10^{-3} millibar and the distillate (50 mg) was collected in a trap at 0°C. It consisted of pure **20**.

*Methoxymethylhydroxymethylperoxide (**20**)*

Colorless, slightly viscous liquid; ir (film): 3400, 2960, 1450, 1370, 1270, 1205, 1140, 1045, 960, and 910 cm^{-1}; ^1H nmr ($CDCl_3$, TMS) δ: 3.52 (s, 3H), 5.05 (t, J = 0.8 Hz, 2H),[4] 5.16 (t, J = 0.8 Hz, 2H),[4] 3.62 (broad s, 1H); ^{13}C nmr ($CDCl_3$, TMS) δ: 56.68 (q, t, J = 143.2 and 6.0 Hz), 93.14 (t, J = 165.2 Hz), 99.92 (t, q, J = 165.2 and 5.0 Hz). *Anal.* calcd. for $C_3H_8O_4$: C 33.33, H 7.46; found: C 33.16, H 7.22.

1. H. KEUL and K. GRIESBAUM. Can. J. Chem. **58**, 2049 (1980).
2. J. RENARD and S. FLISZÁR. Can. J. Chem. **47**, 3333 (1969).
3. W. P. KEAVENEY, M. G. BERGER, and J. J. PAPPAS. J. Org. Chem. **32**, 1537 (1967).
4. T. S. HUH, J. NEUMEISTER, and K. GRIESBAUM. Can. J. Chem. **59**, 3188 (1981).
5. K. GRIESBAUM, H. KEUL, S. AGARWAL, and G. ZWICK. Chem. Ber. **116**, 409 (1983).

Can. J. Chem. Downloaded from www.nrcresearchpress.com by 210.87.254.40 on 09/06/12
For personal use only.

Synthesis and redox chemistry of octaethylporphyrin complexes of ruthenium(II) and ruthenium(III)

MARK BARLEY, JAMES Y. BECKER,[1] GEORGE DOMAZETIS, DAVID DOLPHIN,[2] AND BRIAN R. JAMES[2]
Department of Chemistry, University of British Columbia, Vancouver, B.C., Canada V6T 1Y6

Received March 9, 1983

MARK BARLEY, JAMES Y. BECKER, GEORGE DOMAZETIS, DAVID DOLPHIN, and BRIAN R. JAMES. Can. J. Chem. **61**, 2389 (1983).

The syntheses and characterization of some new octaethylporphyrin complexes of ruthenium(II) and ruthenium(III) are described; the complexes are $Ru(OEP)(P^nBu_3)_2$, $Ru(OEP)(CO)L$ (L = PPh_3, P^nBu_3), $[Ru(OEP)(P^nBu_3)_2]Br$, and $Ru(OEP)(P^nBu_3)Br$, where OEP is the dianion of octaethylporphyrin. The Ru(OEP)(CO)EtOH complex, **1**, which reversibly loses the ethanol ligand in CH_2Cl_2 solution, undergoes a one-equivalent oxidation at the porphyrin ligand to generate the cation-radical $[Ru(OEP)^{\cdot+}(CO)]^+$; a purple species of $^2A_{2u}$ ground state, produced electrochemically in perchlorate media, can coordinate bromide to generate a green $^2A_{1u}$ ground state species that also results from oxidation of **1** using bromine. Coordination of pyridine to $[Ru(OEP)^{\cdot+}CO]^+$ yields the $Ru(OEP)^{\cdot+}(CO)py$ species that can also be formed by electrochemical oxidation of Ru(OEP)(CO)py. Addition of tertiary phosphines (PR_3) to the cation-radical carbonyl species can lead to formation of $[Ru(OEP)(PR_3)_2]^+$, via an internal electron transfer process from Ru(II) to the $OEP^{\cdot+}$ that appears to be triggered by loss of the CO ligand. A reversible one-electron electrochemical oxidation of $Ru(OEP)(P^nBu_3)_2$ at 0.03 V (vs. Ag/AgCl) in CH_2Cl_2 also gives the ruthenium(III) biphosphine cation, while a further one-electron oxidation at 1.2 V generates $[Ru(OEP)^{\cdot+}(P^nBu_3)_2]^{2+}$, a ruthenium(III) π-cation radical characterized by esr. The $[Ru(OEP)(P^nBu_3)_2]Br$ complex decomposes in the solid state to a mixture of $Ru(OEP)(P^nBu_3)Br$, formed together with free phosphine via an intramolecular ligand exchange, and $Ru(OEP)(P^nBu_3)_2$, formed by reduction of the initial ionic ruthenium(III) cation with the phosphine that appears as $[P^nBu_3Br]Br$.

MARK BARLEY, JAMES Y. BECKER, GEORGE DOMAZETIS, DAVID DOLPHIN et BRIAN R. JAMES. Can. J. Chem. **61**, 2389 (1983).

On décrit la synthèse et la caractérisation de quelques nouveaux complexes d'octaéthylporphyrines du ruthénium(II) et du ruthénium(III); ce sont le $Ru(OEP)(P^nBu_3)_2$, le $Ru(OEP)(CO)L$ (L = PPh_3, P^nBu_3), le $[Ru(OEP)(P^nBu_3)_2]Br$ et le $Ru(OEP)(P^nBu_3)Br$, où OEP est le dianion de l'octaéthylporphyrine. Le complexe Ru(OEP)(CO)EtOH (**1**) qui de façon réversible perd le ligand éthanol en solution dans le CH_2Cl_2 subit une oxydation de 1 équivalent au niveau du ligand porphyrine pour donner le cation radicalaire $[Ru(OEP)^{\cdot+}(CO)]^+$; une espèce pourpre d'état fondamental $^2A_{2u}$; il se produit électrochimiquement dans un milieu contenant du perchlorate et peut coordonner le brome pour donner une espèce verte d'état fondamental $^2A_{1u}$ qui se forme aussi par oxydation du composé **1** par le brome. La coordination de la pyridine au cation $[Ru(OEP)^{\cdot+}(CO)]^+$ donne l'espèce $Ru(OEP)^{\cdot+}(CO)py$ qui peut se former également par oxydation électrochimique du complexe Ru(OEP)(CO)py. L'addition de phosphines tertiaires (PR_3) au cation radicalaire carbonylé conduit à la formation de l'ion $[Ru(OEP)(PR_3)_2]^+$ via un processus de transfert interne d'électron du Ru(II) à l'ion radicalaire $OEP^{\cdot+}$ qui semble se former par perte du ligand CO. Une oxydation électrochimique à un électron réversible du $Ru(OEP)(P^nBu_3)_2$ à 0,03 V (vs. Ag/AgCl) dans du CH_2Cl_2 donne également le cation biphosphine ruthénium(III) tandis qu'une oxydation plus poussée à un électron à 1,2 V génère le cation radicalaire $[Ru(OEP)^{\cdot+}(P^nBu_3)_2]^{2+}$, un cation radicalaire π du ruthénium(III) que l'on a caractérisé par la rpe. Le complexe $[Ru(OEP)(P^nBu_3)_2]Br$ se décompose à l'état solide en un mélange de $Ru(OEP)(P^nBu_3)Br$ et de phosphine libre qui se forme par l'intermédiaire d'un échange intramoléculaire de ligand; le $Ru(OEP)(P^nBu_3)_2$, se forme par réduction du cation initial de ruthénium(III) avec la phosphine sous forme de $[P^nBu_3Br]Br$.

[Traduit par le journal]

Introduction

The use of synthetic porphyrins and metalloporphyrins such as $Fe^{II}(OEP)$ and $Fe^{II}(TPP)$ to model naturally occurring porphyrin systems, which are difficult to study directly, is well established (1). Interest has increased recently in the ruthenium analogues of these compounds because otherwise reactive intermediates are expected to be more stable for the ruthenium complexes than for the iron complexes (2, 3). This is particularly relevant in the study of porphyrin cation radicals which have been suggested as intermediates in a number of natural porphyrin systems such as cytochrome P450 (4) and horseradish peroxidase (5). It was hoped that the slower kinetics at ruthenium centres would allow better characterization of intermediates and products of porphyrin systems at different levels of oxidation.

The redox properties of metalloporphyrins in general have been studied extensively (6), but the studies on ruthenium systems have been limited and concentrated initially on $[Ru^{II}(porp)(CO)L]$ and $[Ru^{II}(porp)L_2]$ complexes: L = py, CH_3CN, THF, and PR_3; (porp) = dianion of octaethylporphyrin (OEP) or *meso*-tetraphenylporphyrin (TPP) (2, 7–9). Oxidation of the L_2 species electrochemically by removal of one electron is thought to give a ruthenium(III) complex as judged by the visible spectrum, and the lack of an esr signal, attributable to a cation radical (2, 9), while oxidation of the carbonyls occurs at the ring to give a π-cation radical species (7, 8).

In this study we describe the redox properties of ruthenium porphyrin complexes and report on an internal electron transfer from the metal atom to the porphyrin ring. A similar transfer has been seen in the system $[Ni^{II}(TPP^{\cdot+})]^+ \rightleftharpoons [Ni^{III}(TPP)]^+$ where it was suggested that axial ligation may trigger the electron transfer (10). The present studies strongly support this hypothesis. We also report on the preparation of two new ruthenium(III) complexes and the formation of a ruthenium(III) cation radical species. Part of this work has been described briefly elsewhere (11).

[1] On leave from Ben-Gurion University, Beer-Sheva, Israel.
[2] Authors to whom all correspondence should be addressed.

Can. J. Chem. Downloaded from www.nrcresearchpress.com by 210.87.254.40 on 09/06/12
For personal use only.

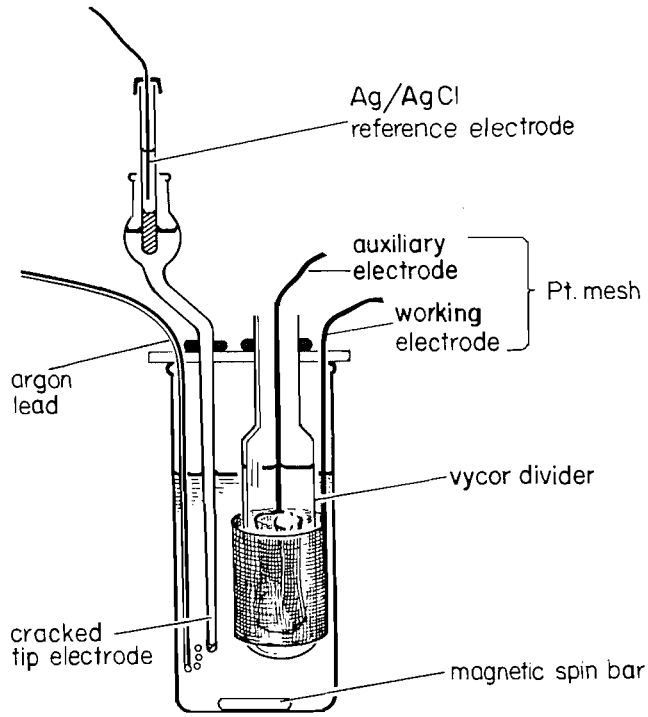

FIG. 1. The apparatus used for bulk electrochemical oxidations.

Experimental section

Materials and methods

Elemental analyses were performed by P. Borda of this department. Mass spectral data were taken on a KRATOS-AEI MS 902, source temperature 220–240°C, direct insertion probe, electron energy 70 eV.

Preparations were conducted under an inert atmosphere. Recrystallizations were carried out under a slow stream of argon which evaporated off the more volatile solvent over a period of days.

Electronic absorption spectra were recorded on a Cary 1756 spectrophotometer. Cyclic voltammograms were recorded using apparatus previously described (9) with the following modifications: the potential was controlled via an EG and G PARC Model 175 Universal Programmer linked to a Model 173 PAR potentiostat. Scan speed was 250 mV/s unless otherwise indicated.

Syntheses of oxidized species by electrochemistry and coulometry were performed using a PAR 173 module with an HDC-371 integrator attachment. The solution to be electrolyzed was placed in a cylindrical glass container. A teflon cap for this container supported a closed tube of Vycor porous glass (Corning 7930) filled with electrolyte solution, and containing the platinum mesh auxiliary electrode. The reference electrode (saturated AgCl/Ag) was held by a cracked tip electrode filled with electrolyte solution. A large platinum mesh electrode (25 cm^2) was wound around the Vycor and immersed in the solution in the glass container which thus formed the working electrode compartment. Argon was bled in via a teflon lead and the solution stirred with a magnetic spin-bar (Fig. 1). The working compartment solution was first pre-electrolyzed at a potential higher than that required for the porphyrin sample. The potential was then brought to zero, the porphyrin added and then electrolyzed at the chosen potential. All potentials are quoted with respect to the saturated AgCl/Ag electrode.

The conductivity results were obtained using a standard electrode set up (cell constant = 0.12 cm^{-1}) in conjunction with a model RCM 15B1 conductivity bridge from Arthur H. Thomas Company.

The magnetic susceptibilities were measured at room temperature on powdered samples, using a Faraday balance that has been described elsewhere (12). The esr spectra were recorded at 77 K on a Varian E-3.

Reagent grade dichloromethane (Fisher), distilled until the uv cut-off was less than 231 nm, was used as a general purpose solvent and also to charge a still over calcium hydride (MC/B). CH_2Cl_2 used for electrochemistry was freshly distilled under argon.

B.D.H. "Omnisolve" acetonitrile was used without further purification. Triphenylphosphine was recrystallized from ethanol before use. Tri-*n*-butylphosphine (MC/B) was distilled at reduced pressure and stored under argon. Tetra-*n*-butylammonium perchlorate, TBAP, (G. Frederick Smith Chemical Company) was recrystallized from Spectro grade acetone (Eastman), dried under vacuum, and stored over P_2O_5. Tetra-*n*-butylammonium tetrafluoroborate, TBATFB, was prepared by the reaction of tetra-*n*-butylammonium bromide and ammonium tetrafluoroborate in aqueous solution. The crude solid was recrystallized from methanol/water, filtered as a solution in dichloromethane and then recrystallized from hot acetone. The crystals were crushed, dried under vacuum, and stored over P_2O_5. Tetra-*n*-propylammonium trifluoromethanesulphonate (13) and tetra-*n*-butylammonium hexafluorophosphate, TBAH (9, 14), were prepared as described in the literature. Tetra-*n*-butylammonium borohydride was kindly provided by B. Tarpey, having been prepared by a method previously described (15). The solid was recrystallized from ethyl acetate, dried under vacuum, and stored over P_2O_5.

Silver tetrafluoroborate (Aldrich) was handled in a glovebag under an argon atmosphere in reduced lighting conditions, and stored under argon.

Ruthenium was available as the trichloride hydrate (42.26% Ru) from Johnson, Matthey Ltd. The dodecacarbonyl, $Ru_3(CO)_{12}$, was obtained from the chloride by a literature procedure (16), as well as commercially from Strem Chemicals. Octaethylporphyrin, H_2(OEP), was prepared by standard procedures (17).

All other solvents and chemicals were reagent grade. The uv/visible spectra of all the isolated and *in situ* species are given in Table 1.

Carbonylethanol(octaethylporphinato)ruthenium(II), (1)

In a modified method of earlier workers (18), 0.8 g of H_2(OEP) (1.5 mmol) was refluxed with 0.8 g of $Ru_3(CO)_{12}$ in toluene (150 mL) for 22 h under argon. When the uv/visible spectrum indicated complete reaction, the solvent was removed by rotary evaporation. The solid was dissolved in 100 mL of 1:1 v/v CH_2Cl_2/EtOH and the solution refluxed under argon for 1 h. Removal of the solvent gave solid Ru(OEP)(CO)EtOH, which was purified on an activity III neutral alumina column (E. Merck) by elution with CH_2Cl_2 – 2% isopropyl alcohol and recrystallization from CH_2Cl_2/EtOH (50 mL of 3:1 v/v). The crystalline product was washed with hexane and dried; yield 0.67 g (63%).

Anal. calcd. for $C_{39}H_{49}N_4O_2Ru$: C 66.24, H 6.99, N 7.93; found: C 66.27, H 7.20, N 7.79. *Mass spec. m/e* 662(10), Ru(OEP)$(CO)^+$; 634(100), Ru(OEP)$^+$; 317(15), Ru(OEP)$^{2+}$. *Nmr* δ_{TMS} ($CDCl_3$): 1.92 (t, 24H, —CH_3), 4.01 (q, 16H, —CH_2—), 9.9 (s, 4H, =CH—).

Carbonyl(octaethylporphinato)(pyridine)ruthenium(II), (2)

This was a gift from P.D. Smith; the method of preparation has already been described (19).

*(Octaethylporphinato)bis(tri-*n*-butylphosphine)ruthenium(II), (3)*

To 400 mg of Ru^{II}(OEP)(CO)EtOH (**1**) (0.56 mmol), dissolved in ~50 mL of CH_2Cl_2 under Ar, was added excess P″Bu_3 (~3 mL) until the initial 393 nm and 408 nm Soret peaks had disappeared. The CH_2Cl_2 was then removed by rotovap and the residue washed several times with acetonitrile prior to recrystallization from 50 mL of 1:1 CH_3CN/CH_2Cl_2 mixture; yield 400 mg (69%).

Anal. calcd. for $C_{60}H_{98}N_4P_2Ru$: C 69.42, H 9.51, N 5.40; found: C 69.26, H 9.60, N 5.60. *Mass spec. m/e* 1038(<0.1), Ru(OEP)(P″$Bu_3)_2^+$; 836(100), Ru(OEP)(P″$Bu_3)^+$; 634 (71), Ru(OEP)$^+$; 418 (21), Ru(OEP)(P″$Bu_3)^{2+}$. The ^{1}H nmr has been reported previously (20).

*(Octaethylporphinato)bis(tri-*n*-butylphosphine)ruthenium(III) bromide, (4)*

A solution of 420 mg of Ru^{II}(OEP)(P″$Bu_3)_2$ (**3**) (0.4 mmol), in CH_2Cl_2 (~50 mL) was titrated with a CH_2Cl_2 solution of bromine

Can. J. Chem. Downloaded from www.nrcresearchpress.com by 210.87.254.40 on 09/06/12
For personal use only.

TABLE 1. Spectroscopic data for the ruthenium porpyhrin complexes

	Complex	λ_{max}/nm (log ϵ)
1	$Ru^{II}(OEP)(CO)EtOH^a$	548(4.53), 515(4.23), 393(5.50)
1a	$Ru^{II}(OEP)(CO)$	547(4.63), 512(4.20), 393(5.40)
2	$Ru^{II}(OEP)(CO)py^b$	549(4.39), 518(4.20), 396(5.37)
3	$Ru^{II}(OEP)(P^nBu_3)_2$	535(4.04), 511(4.20), 428(5.28) 358(4.65)
4	$[Ru^{III}(OEP)(P^nBu_3)_2]^+Br^-$	
9	$[Ru^{III}(OEP)(P^nBu_3)_2]^+ClO_4^-$	790(3.52), 516(3.95), 410(4.65) 363(4.72)
5	$Ru^{II}(OEP)(PPh_3)_2^c$	532(4.08), 518(4.04), 422(5.24)
6	$Ru^{II}(OEP)(CO)PPh_3^c$	555(4.23), 525(4.23), 407(5.28)
7	$[Ru^{II}(OEP)^{+\cdot}(CO)]ClO_4^{-\ d}$	610(3.70), 587(4.00), 535(3.93) 375(5.00)
7a	$[Ru^{II}(OEP)^{+\cdot}(CO)py]ClO_4^-$	610(3.80), 590(3.99), 540(3.90) 376(4.95)
8	$[Ru^{II}(OEP)^{+\cdot}(CO)Br]^d$	630(4.04), 575(3.86), 385(4.85)
10	$[Ru^{III}(OEP)(PPh_3)_2]^+ClO_4^-$	810(3.6), 518(4.0), 410(4.8) 370(4.6)
11	$Ru^{II}(OEP)(CO)P^nBu_3$	555(3.97), 528(4.14), 408(5.23) 387(4.57)
12	$Ru^{III}(OEP)(P^nBu_3)Br$	710(3.04), 512(4.04), 410(4.85) 363(4.65)
13	$[Ru^{III}(OEP)^{+\cdot}(P^nBu_3)_2]^{2+}2ClO_4^-$	510(4.04), 363(4.88)
	$[Ru^{III}(OEP)(MeCN)_2]^+ClO_4^{-\ e}$	530(4.15), 500(4.08), 390(5.00)
	$[Ru^{III}(OEP)(P^nBu_3)(MeCN)]^+ClO_4^{-\ f}$	530(4.02), 515(4.02), 394(5.04) 740(3.34)

[a] Spectrum obtained in the presence of excess EtOH.
[b] Reference 19.
[c] Spectrum obtained in the presence of excess PPh_3.
[d] The extinction coefficients given in ref. 11 were low due to incorrect coefficients for complex (**1**).
[e] Reference 2.
[f] Reference 28.

(standardized spectrophotometrically, λ_{max} at 410 nm, $\epsilon = 210\ M^{-1}\ cm^{-1}$) until the absorption spectrum in the Soret region indicated completion of reaction (approximately 0.5 equiv. of Br_2 per Ru). The solvent was then removed and the solid recrystallized from 50 mL of 1:1 hexane/CH_2Cl_2, followed by hexane washes (5 × ~5 mL) to give a yield of 255 mg (56%). The crystals were dried and analyzed immediately, as the solid slowly decomposes to give a mixture of $Ru^{II}(OEP)(P^nBu_3)_2$ (**3**) and $Ru^{III}(OEP)(P^nBu_3)Br$ (**12**) (see below).

Anal. calcd. for $C_{60}H_{98}N_4P_2BrRu$: C 64.46, H 8.84, N 5.02, Br 7.09, P 5.55; found: C 64.11, H 8.74, N 5.00, Br 6.95, P 5.77. *Mass spec. m/e* 836(100), $Ru(OEP)(P^nBu_3)^+$; 634(75), $Ru(OEP)^+$; 418(20), $Ru(OEP)(P^nBu_3)^{2+}$.

This compound was shown by conductivity studies to be a 1:1 electrolyte in CH_2Cl_2 (Λ = 130 mho $cm^2\ mol^{-1}$), and magnetic studies showed the presence of one unpaired electron (μ ~ 1.9 BM) on the ruthenium atom.

(Octaethylporphinato)bis(triphenylphosphine)ruthenium(II), (5)

This complex, to be described elsewhere (21), was kindly provided by T. Leung.

Carbonyl(octaethylporphinato)(triphenylphosphine)ruthenium(II), (6)

Complex **1** (200 mg, 0.28 mmol) was dissolved in 50 mL of CH_2Cl_2 and refluxed for 3–4 h with 225 mg of PPh_3 (~3 equiv.) under argon. The solution was taken to dryness on a rotary evaporator, and the residue placed on a column of Florisil in hexane. The excess phosphine was eluted off with hexane/toluene, and the product with toluene/CH_2Cl_2.

Anal. calcd. for $C_{55}H_{59}N_4OPRu$: C 71.48, H 6.44, N 6.06; found: C 71.30, H 6.23, N 5.96. *Mass spec. m/e* 895(100), $Ru(OEP)(PPh_3)^+$; 711(2), $Ru(OEP)(Ph)^+$?; 662(4), $Ru(OEP)(CO)^+$; 634(100), $Ru(OEP)^+$. *Infrared* ν(CO) = 1952 cm^{-1}. *Nmr* δ_{TMS} ($CDCl_3$) 1.83 (t, 24H, —CH_3), 3.85 (m, 16H, —CH_2—), 9.45 (s, 4H, =CH—), 6.71 (t, 3H, *p*-H), 6.35 (t, 6H, *m*-H), 3.67 (t, 6H, *o*-H).

*Carbonyl(octaethylporphinato)(tri-*n*-butylphosphine)ruthenium(II), (11)*

Complex **1** dissolved in CH_2Cl_2 (~100 mL) was titrated with a CH_2Cl_2 solution of P^nBu_3 until the Soret absorption indicated complete formation of product (408 nm), prior to any formation of $Ru(OEP)(P^nBu_3)_2$ (**3**) (428 nm). The solution was evaporated to dryness under vacuum to yield 146 mg of crude product. This was purified by chromatography on activity III alumina, the product eluting off in CH_2Cl_2 well ahead of residual complex **1**.

Anal. calcd. for $C_{49}H_{71}N_4OPRu$: C 68.10, H 8.28, N 6.48; found: C 68.20, H 8.25, N 6.30.

The ^1H and ^{31}P nmr data have been reported previously (20).

*Bromo(octaethylporphinato)(tri-*n*-butylphosphine)ruthenium(III), (12)*

To 100 mg of crude $Ru(OEP)(CO)P^nBu_3$ (**11**) dissolved in 100 mL of CH_2Cl_2 was added a slight excess (~5%) of bromine in CH_2Cl_2 (0.5 Br_2/Ru). The reaction was followed by the loss of absorbance at 408 nm. The solvent was then removed under vacuum, and the crude residue (90 mg, yield 85%) was chromatographed on activity III alumina, the product eluting off in 2–4% isopropanol in CH_2Cl_2.

Anal. calcd. for $C_{48}H_{71}N_4BrPRu$: C 62.93, H 7.81, N 6.12, Br 8.72; found: C 62.93, H 7.93, N 6.00, Br 8.55.

Conductivity studies showed this compound to be a non-electrolyte when dissolved in CH_2Cl_2 (Λ = 2.0 mho $cm^2\ mol^{-1}$), showing that the bromide ligand is coordinated. Magnetic studies showed the presence of one unpaired electron (μ ~ 2.0 BM) on the ruthenium atom.

Results and discussion

There has been discussion as to whether the ethanol ligand

Can. J. Chem. Downloaded from www.nrcresearchpress.com by 210.87.254.40 on 09/06/12
For personal use only.

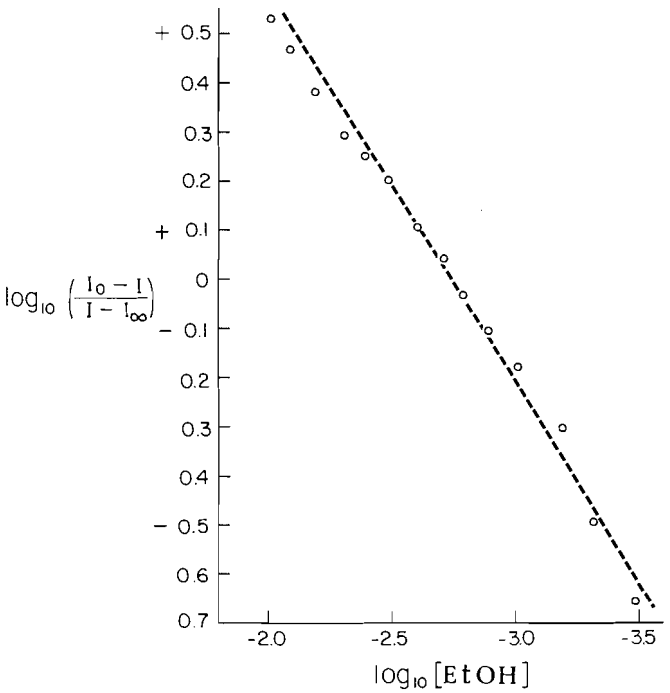

FIG. 2. Plot of $\log_{10}$ {[Ru(OEP)(CO)EtOH]/[Ru(OEP)(CO)]} vs. $\log_{10}$ [EtOH] to obtain the equilibrium constant for eq. [1]. [Ru(OEP)(CO)EtOH] is $\propto (I_0 - I)$, and [Ru(OEP)(CO)] is $\propto (I - I_\infty)$, where I_0 and I_∞ are the absorbances with no added ethanol and high [ethanol] (~1.0 *M*), respectively; I is an intermediate absorbance at a known added [ethanol]. Slope of line = 0.8 ± 0.2 and estimated equilibrium constant = 550 ± 70 M^{-1}.

in complexes of the type Ru(porp)(CO)EtOH, such as **1**, dissociates in dilute solutions of non-complexing solvents (18, 22). We find that the addition of excess EtOH (up to ~1.0 *M*) to (**1**) in CH_2Cl_2 (~5×10^{-5} *M*) causes a change in the visible spectrum in that the intensity ratio of the ~547 and ~512 nm bands decreases from ~2.6 to 2.0; the ratio was unaffected by the addition of more EtOH. This suggests that ethanol at high concentrations coordinates, and implies that an equilibrium exists between, for example, a five-coordinate Ru(OEP)(CO), (**1***a*), species (I_{547}/I_{512} = 2.6) and the six-coordinate ethanol adduct (**1**) (I_{548}/I_{515} = 2.0; compared to **1***a*, the absorptions are slightly shifted to the red):

$$[1] \quad \underset{\mathbf{1}a}{\text{Ru(porp)(CO)}} + \text{EtOH} \overset{K}{\rightleftharpoons} \underset{\mathbf{1}}{\text{Ru(porp)(CO)EtOH}}$$

Spectral changes observed during the addition of ethanol to a dilute solution (~10^{-5} *M*) of **1** in CH_2Cl_2 (presumably present as **1***a*) allows for a plot of $\log_{10}$ {[Ru(OEP)(CO)EtOH]/[Ru(OEP)(CO)]} vs. $\log_{10}$ [EtOH] (Fig. 2). This gives a straight line of slope 0.8 ± 0.2 which agrees reasonably well with the equilibrium shown in eq. [1] and gives an association constant K of 550 ± 70 M^{-1} at room temperature. Such a value shows that in all spectroscopic solutions (<10^{-4} *M*), complex **1** would be greater than 95% dissociated to **1***a*, although more concentrated solutions would show a higher degree of association. The slight decrease in the I_{547}/I_{512} ratio (from ~2.6 to 2.4) seen in samples covering a wider concentration range (up to 5×10^{-4} *M*) is consistent with the estimated K value.

Oxidation of monocarbonyl ruthenium(II) porphyrin complexes occurs at the porphyrin ring to give a π-cation radical species (8). We find that the first oxidation potential of Ru(OEP)(CO) (**1***a*), formed *in situ* from **1** in dichloromethane, is dependent upon the nature of the electrolyte used (Table 2). Of the four electrolytes, perchlorate, hexafluorophosphate, and trifluoromethanesulphonate give about the same potential while fluoroborate averages ~0.1 V higher. This effect of the fluoroborate anion has been noticed before (24), although a satisfactory explanation has not been given.

TABLE 2. Reversible potentials[a] for Ru(OEP)(CO) in CH_2Cl_2, (1.5–2.5) × 10^{-4} *M*, in the presence of 0.05 *M* electrolyte

Electrolyte anion	E_1 (V)	E_2 (V)
BF_4^-	+0.82	+1.30
ClO_4^-	+0.71	+1.19
PF_6^-	+0.70[b]	+1.20[b]
$CF_3SO_3^-$	+0.65	+1.16

[a] E_1 values are formal reduction potentials for the reaction: $[Ru^{II}(OEP)^{\cdot+}(CO)]^+ + e \rightleftharpoons [Ru^{II}(OEP)(CO)]$; E_2 values are in the range expected for reduction of ruthenium(III) π-cation radical species (refs. 7, 23, and present text), for example: $[Ru^{III}(OEP^{\cdot+})(CO)]^{2+} + e \rightleftharpoons [Ru^{II}(OEP^{\cdot+})(CO)]^+$.

[b] Reference 8 gives E_1 and E_2 values of +0.69 and +1.26 V, respectively.

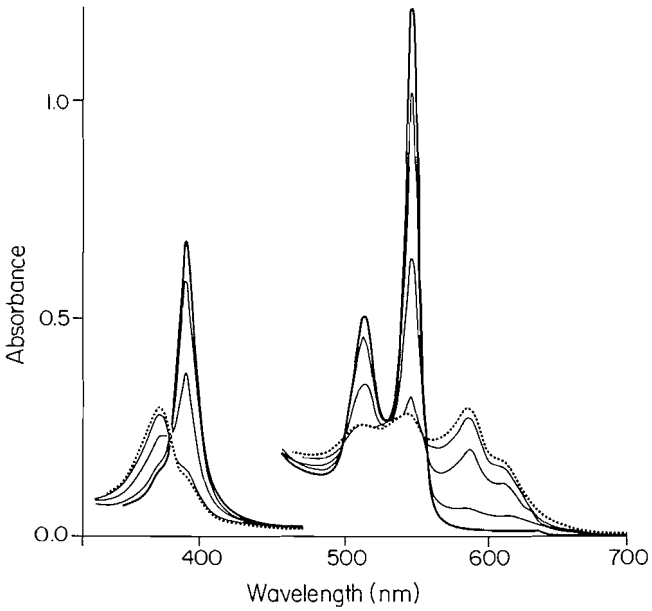

FIG. 3. Optical spectra during the electrochemical oxidation of a solution of Ru(OEP)(CO)EtOH (—) in CH_2Cl_2 (mixture of species (**1**) and (**1***a*)) in the presence of 0.05 *M* $TBA^+ClO_4^-$ to give the cation radical (**7**) (- - -). The absorbance scale refers to the 500–700 nm region; absorbance in the Soret region is reduced by a factor of 10.

Electrolysis in all cases occurred smoothly and gave good isosbestic points when followed spectroscopically (Fig. 3), to form essentially the same deep purple solution (**7**) with a strong sharp esr signal at g = 2.00, typical of an organic radical. The solution could be reconverted, by the action of reducing agents, or electrochemically, back to the pink Ru(OEP)(CO) species (**1***a*).

In contrast, addition of a dilute solution of bromine in CH_2Cl_2 to a solution of Ru(OEP)(CO) (**1***a*) gave a deep green solution (**8**) after the addition of a slight excess of bromine ((1/2)Br_2/Ru). Species **8**, which also gave a strong sharp esr

Can. J. Chem. Downloaded from www.nrcresearchpress.com by 210.87.254.40 on 09/06/12
For personal use only.

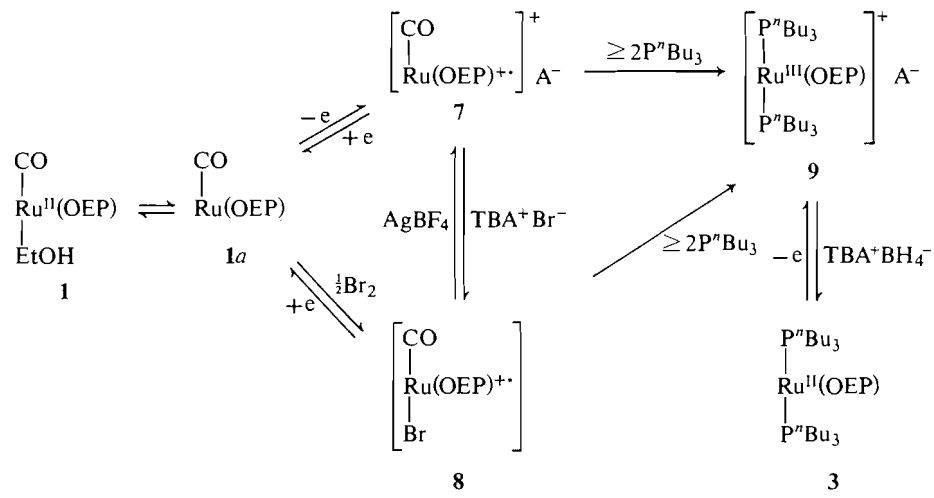

SCHEME I

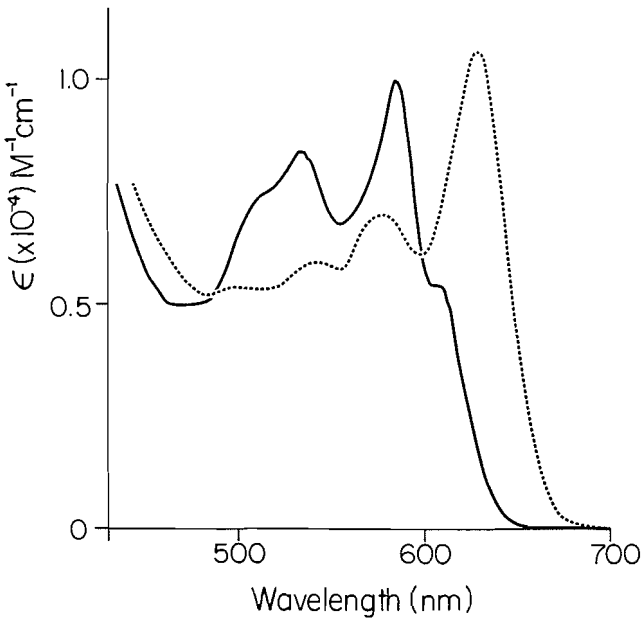

FIG. 4. Optical spectra of the cation radical (**8**) (- - -); $^2A_{1u}$ ground state, and the spectrum of the cation radical (**7**) (—), $^2A_{2u}$, obtained by the addition of $AgBF_4$ to species (**8**).

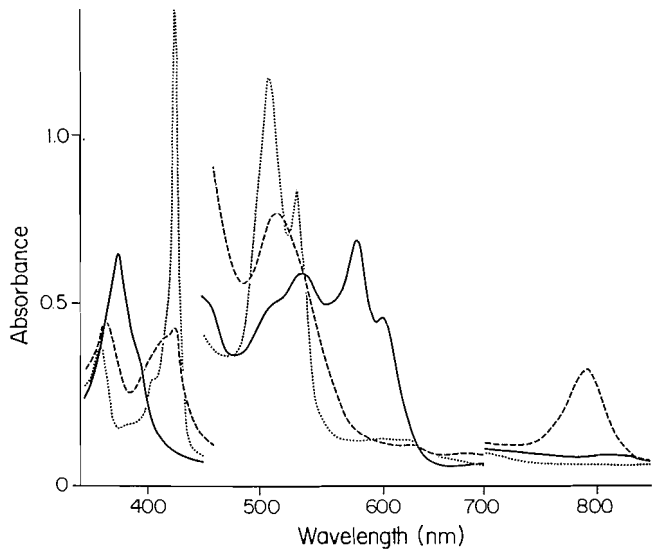

FIG. 5. Optical spectrum of the electrochemically prepared cation radical (**7**) prepared from a CH_2Cl_2 solution of Ru(OEP)(CO)EtOH in the presence of 0.05 *M* $TBA^+ClO_4^-$ (—). The spectrum of species (**9**) formed by the addition of >2 equiv. of P^nBu_3 (– – –), and the spectrum of (**3**) obtained by the reduction of this product (- - -). The absorbance scale refers to the region above 500 nm; absorbance in the Soret region is reduced by a factor of 10.

signal at $g = 2.00$ (attributed to an organic radical) was again easily converted back, chemically or electrochemically, to a species identical by uv/vis spectroscopy with **1***a*.

Addition of 1 equiv. of tetra-*n*-butylammonium bromide to a purple solution of **7** caused conversion to the green species **8**; the reverse reaction could be achieved by adding $AgBF_4$ to a solution of **8**. Scheme 1 summarizes the data including the interconvertibility of the cation radicals, whose uv/vis spectra are shown in Fig. 4.

Similar results have been seen with oxidation of $Co^{II}(OEP)$ systems (5). Electrochemical oxidation of $Co^{II}(OEP)$ in the presence of perchlorate ion gave first $[Co^{III}(OEP)]^+$ and then a cation-radical species $[Co^{III}(OEP)^{+\cdot}]^{2+}2ClO_4^-$, whose optical spectrum was considered, from theoretical calculations and comparison with that of $Zn^{II}(TPP)^{+\cdot}$, to derive from a $^2A_{2u}$ ground state. Bromine oxidation of $Co^{II}(OEP)$ to $Co^{III}(OEP)^{+\cdot}2Br^-$, however, gave a different optical spectrum for the cation-radical and that was considered to have a $^2A_{1u}$ ground state (25). The two cobalt cation-radicals could be interchanged by addition of the appropriate anions as in the ruthenium systems. On the basis of similarity in optical spectra, green species **8** would be assigned a $^2A_{1u}$ ground state and the purple form **7** a $^2A_{2u}$ ground state.

Conductivity studies show that (**8**) is essentially a non-electrolyte in CH_2Cl_2; the molar conductivity ($\Lambda \sim 1.0$ mho $cm^2\ mol^{-1}$) is comparable to that of $Ru^{III}(OEP)(P^nBu_3)Br$ ($\Lambda \sim 2.0$), which is very different to that of the 1:1 electrolyte $[Ru^{III}(OEP)(P^nBu_3)_2]^+Br^-$ ($\Lambda \sim 130$). This suggests that the coordination of bromide causes the molecule to change from a $^2A_{2u}$ to a $^2A_{1u}$ ground state. Such ligand coordination induced ground state transitions were suggested previously for the $Co^{III}(OEP)$ cation radicals (25), and such an explanation is strongly supported by the ruthenium data.

The marked similarity of the spectra of the ruthenium(II) cation radical species with those of the reported cobalt(III) analogues (5, 25) is in line with the general conclusion that such spectra are relatively insensitive to the nature of the cen-

Can. J. Chem. Downloaded from www.nrcresearchpress.com by 210.87.254.40 on 09/06/12
For personal use only.

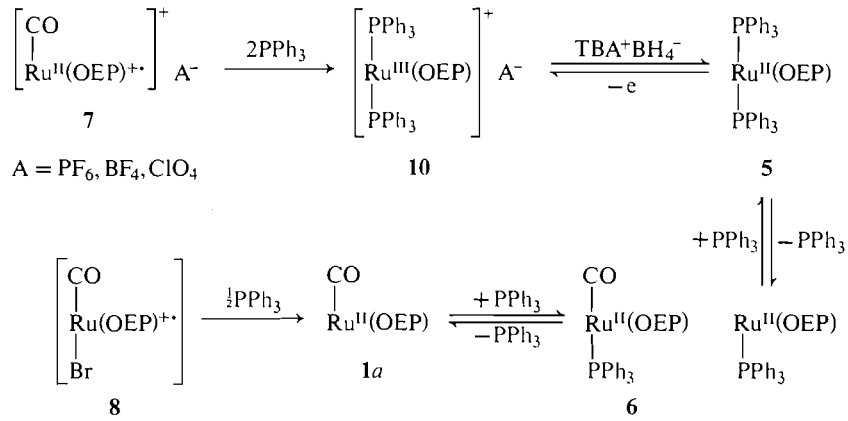

SCHEME 2

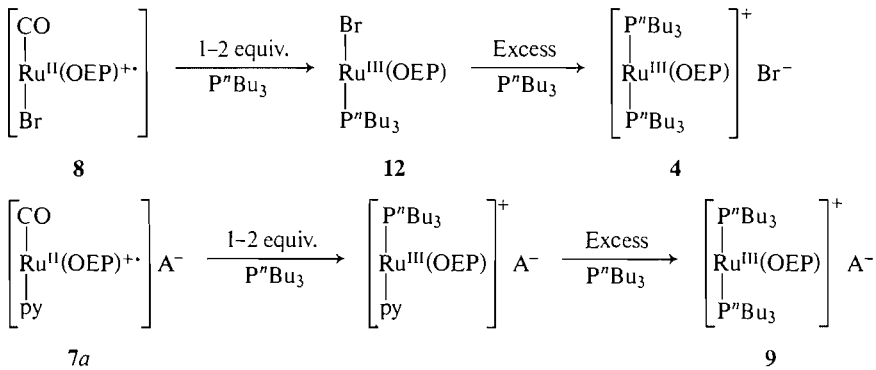

SCHEME 3

tral metal atom, at least, when the metalloporphyrin is diamagnetic (26); this supports the concept of the modelling of heme cation radicals using other metalloporphyrin complexes.

Recent magnetic circular dichroism spectral data on the cobalt π-cation radical species mentioned above and on the compound I derivatives of horseradish peroxidase and catalase (27) have confirmed the iron(IV) π-cation radical nature of the enzyme compound I species (5, 25).

Addition of two or more equivalents of tri-*n*-butylphosphine to a solution of either **7** or **8** produced the bis-phosphine ruthenium(III) cation $[Ru(OEP)(P^nBu_3)_2]^+$ (**9**), as judged by the optical spectrum which was identical with that of the characterized $[Ru^{III}(OEP)(P^nBu_3)_2]^+Br^-$ complex (**4**) (Fig. 5). Reduction of **9** with tetrabutylammonium borohydride gave a solution species identical to $Ru^{II}(OEP)(P^nBu_3)_2$ (**3**). The reversible electrochemical conversion **3** ⇌ **9** could be accomplished in CH_2Cl_2 with TBAP as supporting electrolyte ($E_{1/2} \sim 0.0$ V vs. Ag/AgCl) (Scheme 1); clean spectral changes with several isosbestic points were observed for the electrochemical conversion (cf. Fig. 5), and are consistent with no accompanying ligand exchange reactions. The reduction potential for this Ru(III)/Ru(II) couple is lower than those of related bis(tertiary phosphine) complexes of Ru(TPP) (9), and is consistent with a relative stabilization of Ru(III) by the more basic OEP ligand system.

Addition of triphenylphosphine to a solution of **7** gave a similar result with formation of what is believed to be the bis-(triphenylphosphine)ruthenium(III) cation $[Ru(OEP)(PPh_3)_2]^+$ (**10**), since borohydride reduction gave a species spectrally identical to $Ru^{II}(OEP)(PPh_3)_2$ (**5**) in the presence of excess phosphine. Genuine samples of **5** in dilute solution (Soret at 422 nm) dissociate a phosphine to give an equilibrium mixture with the five-coordinate species $Ru(OEP)(PPh_3)$ that has a Soret band at 396 nm (21); addition of excess phosphine regenerates pure **5** with concomitant loss of the 396 nm peak. Samples of **5** in the absence of excess phosphine could nevertheless be electrochemically oxidized ($E_{1/2} \sim 0.25$ V vs. Ag/AgCl with TBATFB as electrolyte) to generate **10**, Scheme 2.

The reaction of cation-radical **8** with triphenylphosphine was very different and involved a reduction to give Ru(OEP)-(CO)(PPh_3) (**6**), probably via the Ru(OEP)(CO) intermediate. A controlled addition of half a mole of phosphine per Ru to **8** generated a spectrum attributed to Ru(OEP)(CO) (Table 1); further phosphine then generated the spectrum of complex **6** (this appears to dissociate triphenylphosphine in solution, since excess phosphine is necessary to fully generate the typical spectrum of a carbonylphosphine complex (Table 1)). The mechanisms of this and similar reduction reactions of both cation radical ground states are under investigation.

Careful addition of tri-*n*-butylphosphine to a solution of the green cation-radical (**8**) showed the formation of an intermediate requiring a substantial excess of phosphine to convert completely to the final product $[Ru^{III}(OEP)(P^nBu_3)_2]^+Br^-$ (**4**). The intermediate was spectrally identical to a prepared sample of $Ru^{III}(OEP)(P^nBu_3)Br$ (**12**), which also gave **4** on the addition of excess phosphine (Scheme 3).

Electrochemical oxidation of $Ru^{II}(OEP)(CO)py$ (**2**) gave a purple cation radical species (**7***a*) whose spectrum was similar to that of **7** except that the peaks were slightly red shifted, suggesting that the pyridine was still coordinated. Addition of 1 equiv. of pyridine to **7** also generated the spectrum of **7***a*. Addition of tri-*n*-butylphosphine to **7***a* eventually gave the $[Ru^{III}(OEP)(P^nBu_3)_2]^+$ cation (**9**), but an intermediate was

Can. J. Chem. Downloaded from www.nrcresearchpress.com by 210.87.254.40 on 09/06/12
For personal use only.

Can. J. Chem. Downloaded from www.nrcresearchpress.com by 210.87.254.40 on 09/06/12
For personal use only.

detected by monitoring an increase and then a decrease of absorption at 730 nm before the 790 nm peak of **9** was fully formed. The data are consistent with the formation of the mixed phosphine pyridine ruthenium(III) complex (28), $[Ru^{III}(OEP)(P^nBu_3)py]^+$ (Scheme 3).

The mechanism of the intramolecular electron transfer in these reactions is still under investigation. However, the formation of Ru(III) intermediates with only one phosphine coordinated shows that electron transfer occurs before coordination of the second phosphine, implying that the electron transfer is triggered by the loss of the CO group (28).

The cyclic voltammogram of $Ru^{II}(OEP)(P^nBu_3)_2$ (**3**) in CH_2Cl_2 with $TBA^+ClO_4^-$ as supporting electrolyte showed two reversible oxidations at +0.03 V and +1.2 V (vs. AgCl/Ag reference electrode). Electrochemical oxidation at a potential slightly above +0.03 V gave an orange solution of $[Ru^{III}(OEP)(P^nBu_3)_2]^+ClO_4^-$ (**9**) (cf. Fig. 5). The second quasi-reversible wave is attributed to the formation of a ruthenium(III)-π-cation radical, $[Ru^{III}(OEP)^{+\bullet}(P^nBu_3)_2]^{2+}$ (**13**). The cyclic voltammogram of **9** in CH_2Cl_2 with $TBA^+ClO_4^-$ as supporting electrolyte was identical to that of **3** (due to rapid reduction of **9** to **3** in the vicinity of the working electrode at the beginning of the sweep at 0.0 V) under the same conditions. Addition of acetonitrile to the solution of **9** shifted both E_p values to less positive potentials. Addition of too much acetonitrile caused the first wave to become irreversible due to deposition of the insoluble (in CH_3CN) reduced complex $Ru(OEP)(P^nBu_3)_2$ (**3**) on the working electrode. The reductions in E_p values were particularly marked for the second wave (see figure in ref. 11) (+1.2 V in pure CH_2Cl_2 to +1.05 V in acetonitrile). We attribute this to enhanced stabilization of the positively charged species by the more polar acetonitrile; the effect is more marked for the dipositive cation radical species where the delocalized charge allows for more effective solvation. For solutions containing sufficient CH_2Cl_2 to prevent precipitation of **3**, the lack of peak broadening or new waves and an i_{pc}/i_{pa} ratio of unity indicate no ligand exchange on the time scale of the cyclic voltammetry (29).

Electrochemical oxidation of acetonitrile solutions of $[Ru^{III}(OEP)(P^nBu_3)_2]^+ClO_4^-$ (**9**) at +1.2 V gave a magenta-coloured solution of $[Ru^{III}(OEP)^{+\bullet}(P^nBu_3)_2]^{2+}2ClO_4^-$ (**13**) which was easily converted back to **9**, electrochemically or by reducing agents including methanol. Solutions of **13** at 77 K showed a broad esr signal at $g_{ave} = 2.35$ (half peak width 80 G) attributable to low spin ruthenium(III) (30), and a sharp $g_{ave} = 2.008$ cation radical-like signal (peak-to-peak width 10 G). Integration of the two peaks showed approximate equal areas. Thus there appears to be no coupling between the paramagnetic centres of the dication **13**, although on warming the solution to 200 K the broad signal was lost and the narrow signal was weakened considerably.

Solutions of **13** in acetonitrile under argon reverted after a few hours to the mono-cation (**9**) as judged by the uv/vis spectrum. Compound **9** then slowly changed over a few days to a further species, characterized by a peak at 392 nm. The spectrum closely resembled that of $[Ru^{III}(OEP)(MeCN)_2]^+ClO_4^-$ (2) and that of the mixed ligand species $[Ru^{III}(OEP)(P^nBu_3)(MeCN)]^+ClO_4^-$ (28) (Table 1); either product seems plausible. The identity of the final complex could not be determined by isolation after reduction, as this gave $Ru(OEP)(P^nBu_3)_2$ (**3**) as product due to re-coordination of the phosphine. Surprisingly, fresh samples of **9**, prepared electrochemically from **3** in dichloromethane but redissolved in acetonitrile, did not change into the "392 nm product". For this conversion to occur, species **9** had to be formed via the dication **13**. To ensure that the effect was not due to the oxidation of an impurity in the acetonitrile during electrochemical formation of the dication, the dication was prepared by electrolysis of **9** in dichloromethane. The dication **13** again reverted after a few hours to **9**; removal of solvent followed by addition of acetonitrile again gave *in situ* **9** that slowly loses phosphine ligand(s) via solvation. The data suggest that during the second oxidation a trace quantity of some species is formed that catalyzes the substitution reaction.

Samples of freshly prepared $[Ru^{III}(OEP)(P^nBu_3)_2]^+Br^-$ (**4**) slowly deteriorated while being stored as a solid. The decomposition rate depended upon the purity of the solid, cruder samples tending to deteriorate much faster. A sample a few weeks old would typically show in CH_2Cl_2 a weak 428 nm peak due to small quantities of $Ru(OEP)(P^nBu_3)_2$ (**3**). In an attempt to remove this impurity the solid was rinsed with hexane. However, instead of removing the hexane-soluble **3**, up to 50% of the solid dissolved as **3**! Repeated rinses with hexane eventually did remove all of complex **3** present, and the remaining small amount of solid (**4** and **12**, see below) could be dried and stored. The slow deterioration behaviour, however, was again observed. After weeks, the spectrum (in CH_2Cl_2) of the mixture **4** + **12** showed increasing amounts of $Ru^{III}(OEP)(P^nBu_3)Br$ (**12**), which could be very effectively purified from residual **4** by recrystallizing from a dichloromethane/hexane mixture.

Solutions of **4** in dichloromethane sealed under argon were indefinitely stable, showing no tendency to form **3**. Partly degraded samples of **4** showed peaks in the mass spectrum at $m/e = 202$ and 204 (free P^nBu_3), while a sample obtained following extraction by hexane and acetonitrile (to remove **3**) gave intense peaks at $m/e = 281$ and 283 attributable to the $[P^nBu_3Br]^+$ cation.

The slow degradation of **4** is thought to be initiated by the gradual replacement of a coordinated phosphine by a bromide ion to give two neutral molecules (**12** and P^nBu_3), the driving force being the relative instability of lattices containing ions of disparate size (31) (such as **4**). The phosphine is trapped in the crystal lattice, and dissolving such a sample in CH_2Cl_2 will give a typical Ru^{III} type spectrum — a mixture of species **4** and **12** — with little sign of $Ru(OEP)(P^nBu_3)_2$, (**3**) (recognized by a very intense Soret 428 nm). If, however, the sample is rinsed with hexane, some of the trapped phosphine will be released. In hexane both ruthenium(III) species are insoluble but **3** is soluble. Tri-*n*-butylphosphine is known to react readily with free bromine to give the species $P^nBu_3Br_2$ (32). Thus, in hexane both the equilibrium of this reaction (eq. [2]) and that shown in eq. [3] will be shifted to the right.

[2] $P^nBu_3 + Br_2 \rightleftharpoons P^nBu_3Br_2$

[3] $2[Ru^{III}(OEP)(P^nBu_3)_2]^+Br^- + P^nBu_3$

4

$$\xrightleftharpoons[CH_2Cl_2]{\text{hexane}} 2Ru^{II}(OEP)(P^nBu_3)_2 + P^nBu_3Br_2$$

3

[4] $\left[\begin{array}{l} P^nBu_3 \\ | \\ Ru^{III}(OEP) \\ | \\ P^nBu_3 \end{array}\right]^+ Br^- \xrightarrow{\text{slow}} \begin{array}{l} P^nBu_3 \\ | \\ Ru^{III}(OEP) \\ | \\ Br \end{array} + P^nBu_3$

4 **12**

The driving force for reaction [3] is probably the thermodynamic stability of complex **3** coupled with the insolubility of **4** in hexane. Repeated washing with hexane will remove more and more of **3** and eventually leave pure **12** (eq. [4]). While **4** is stable in polar solvents like CH_2Cl_2, attempted recrystallization from CH_2Cl_2/hexane is likely to speed up bromide substitution to give uncharged **12**. The free phosphine could then react rapidly by the above equilibrium (eq. [3]) to give **3**. This could explain how residual **4** is removed from **12** by recrystallization from hexane/CH_2Cl_2. All these processes would be speeded up by residual phosphine trapped in the crystal lattice of **4** from the preparation of **3**. It is very difficult to remove all the free phosphine and so the purity of **3** used to prepare the bromide complex **4** would determine how fast, and in what proportions, the reduced complex **3** and the ruthenium(III) product **12** would be formed.

Conclusions

Our continuing interest in the development of ruthenium porphyrin chemistry has led to isolation of several new tertiary phosphine complexes of ruthenium(II) and ruthenium(III). The latter ones containing bromide may be cationic or neutral and, to our knowledge, are the first well-characterized ruthenium(III) porphyrins with ligated phosphines. Studies on redox chemistry have shown: (*a*) that coordination of a ligand (bromide) to the ruthenium(II) cation-radical species $[Ru(OEP)^{\cdot+}(CO)]^+$ generates a different ground-state porphyrin radical species, (*b*) that replacement of the carbonyl ligand of these π-cation radical species by phosphine may induce an internal electron transfer from the metal to the porphyrin radical, and (*c*) the existence of a ruthenium(III) porphyrin cation-radical. Peripheral redox chemistry at the porphyrin macrocycle is known to be important in several iron enzyme systems, and more detailed studies on the internal electron transfer reactions in the ruthenium complexes are in progress.

Acknowledgements

This is a contribution from the Bioinorganic Chemistry Group. The work was supported by grants from the Natural Sciences and Engineering Research Council of Canada and the United States Institutes of Health (CAM 17989). We thank also Drs. T.W. Leung and R.C. Thompson for the magnetic susceptibility measurements, and Johnson Matthey Ltd. for the loan of $RuCl_3 \cdot 3H_2O$.

1. (*a*) J. W. BUCHLER. *In* The porphyrins. Vol. I. *Edited by* D. Dolphin. Academic Press, New York. 1978. p. 453, and references therein; (*b*) C. H. WELBORN, D. DOLPHIN, and B. R. JAMES. J. Am. Chem. Soc. **103**, 2869 (1981); (*c*) T. MASHIKO, C. A. REED, K. J. HALLER, M. E. KASTNER, and W. R. SCHEIDT. J. Am. Chem. Soc. **103**, 5758 (1981).
2. N. P. FARRELL, D. DOLPHIN, and B. R. JAMES. J. Am. Chem. Soc. **100**, 324 (1978).
3. H. MASUDA, T. TAGA, K. OSAKI, H. SUGIMOTO, M. MORI, and H. OGOSHI. J. Am. Chem. Soc. **103**, 2199 (1981).
4. J. T. GROVES, R. L. HAUSHALTER, M. NAKAMURA, T. E. MEMO, and B. J. EVANS. J. Am. Chem. Soc. **103**, 2884 (1981).
5. D. DOLPHIN, A. FORMAN, D. C. BORG, J. FAJER, and R. H. FELTON. Proc. Natl. Acad. Sci. USA, **68**, 614 (1971).
6. R. H. FELTON. *In* The porphyrins. Vol. V. *Edited by* D. Dolphin. Academic Press, New York. 1978. Chapt. 3.
7. D. P. RILLEMA, J. K. NAGLE, L. F. BARRINGER JR., and T. J. MEYER. J. Am. Chem. Soc. **103**, 56 (1981).
8. G. M. BROWN, F. R. HOPF, J. A. FERGUSON, T. J. MEYER, and D. G. WHITTEN. J. Am. Chem. Soc. **95**, 5939 (1973).
9. D. DOLPHIN, B. R. JAMES, A. J. MURRAY, and J. R. THORNBACK. Can. J. Chem. **58**, 1125 (1980), and references therein.
10. E. C. JOHNSON, T. NIEM, and D. DOLPHIN. Can. J. Chem. **56**, 1381 (1978).
11. M. H. BARLEY, J. Y. BECKER, G. DOMAZETIS, D. DOLPHIN, and B. R. JAMES. J. Chem. Soc. Chem. Commun. 982 (1981).
12. F. G. HERRING, B. LANDA, R. C. THOMPSON, and C. F. SCHWERDTFEGER. J. Chem. Soc. A, 528 (1971).
13. K. ROUSSEAU, G. C. FARRINGTON, and D. DOLPHIN. J. Org. Chem. **37**, 3968 (1972).
14. W. LANGE and E. MÜLLER. Chem. Ber. **63**, 1058 (1930).
15. A. BRANDSTROM, V. JUNGGREN, and B. LAMM. Tetrahedron Lett. **31**, 3173 (1972).
16. A. MANTOVANI and S. CENINI. Inorg. Synth. **16**, 47 (1976).
17. J. B. PAINE III, W. B. KIRSHNER, D. W. MOSKOWITZ, and D. DOLPHIN. J. Org. Chem. **41**, 3857 (1976).
18. M. TSUTSUI, D. OSTFELD, and L. M. HOFFMAN. J. Am. Chem. Soc. **93**, 1820 (1971).
19. A. ANTIPAS, J. W. BUCHLER, M. GOUTERMAN, and P. D. SMITH. J. Am. Chem. Soc. **100**, 3015 (1978).
20. G. DOMAZETIS, B. R. JAMES, and D. DOLPHIN. Inorg. Chim. Acta, **54**, L47 (1981).
21. T. LEUNG, B. R. JAMES, and D. DOLPHIN. Unpublished results.
22. J. T. BONNET, S. S. EATON, G. R. EATON, R. H. HOLM, and J. A. IBERS. J. Am. Chem. Soc. **95**, 2141 (1973).
23. C. J. MALERICH. Inorg. Chim. Acta, **58**, 123 (1982).
24. J. Y. BECKER, D. DOLPHIN, J. B. PAINE, and T. WIJESEKERA. J. Electroanal. Chem. Interfacial Electrochem. Submitted.
25. D. DOLPHIN, Z. MULJIANI, K. ROUSSEAU, D. C. BORG, J. FAJER, and R. H. FELTON. Ann. N.Y. Acad. Sci. **206**, 177 (1973).
26. N. CARNIERI and A. HARRIMAN. Inorg. Chim. Acta, **62**, 103 (1982).
27. W. R. BROWETT and M. J. STILLMAN. Inorg. Chim. Acta, **49**, 69 (1981); Biochim. Biophys. Acta, **623**, 21 (1980).
28. M. H. BARLEY, D. DOLPHIN, and B. R. JAMES. Unpublished results.
29. K. M. KADISH, M. SWEETLAND, and J. S. CHENG. Inorg. Chem. **17**, 2795 (1978).
30. O. K. MEDHI and V. AGARWALA. Inorg. Chem. **19**, 1381 (1980).
31. F. A. COTTON and G. WILKINSON. Advanced inorganic chemistry. 4th ed. Wiley, New York. 1980. Chapt. 1.
32. D. HELLWINKEL. *In* Organic phosphorus compounds. Vol. 3. *Edited by* G. M. Kosolapoff and L. Maier. Wiley, New York. 1972. Chapt. 5B.

Can. J. Chem. Downloaded from www.nrcresearchpress.com by 210.87.254.40 on 09/06/12
For personal use only.

A kinetic and nuclear magnetic resonance study of methylated pyrimidine nucleosides

B. D. ALLORE, A. QUEEN, W. J. BLONSKI, AND F. E. HRUSKA
Department of Chemistry, University of Manitoba, Winnipeg, Man., Canada R3T 2N2

Received April 15, 1983

B. D. ALLORE, A. QUEEN, W. J. BLONSKI, and F. E. HRUSKA. Can. J. Chem. **61**, 2397 (1983).

Alkylated pyrimidine nucleosides are of interest from the viewpoint of mutagenesis and carcinogenesis. ^1H and ^{13}C nmr data are presented for a series of 2′-deoxynucleosides methylated at the O2-, O4-, and N3-positions of the base, and discussed in terms of their physical properties. The pH dependence of the stability of the O2- and O4-methylated 2′-deoxyribosides as well as the corresponding ribosides was examined by ^1H nmr and ultraviolet (uv) spectrophotometric methods.

B. D. ALLORE, A. QUEEN, W. J. BLONSKI et F. E. HRUSKA. Can. J. Chem. **61**, 2397 (1968).

Les nucléosides du type pyrimidine alkylée sont importants du point de vue de la mutagénèse et de la carcinogénèse. On présente les données de la rmn du ^1H et du ^{13}C d'une série de déoxy-2′ nucléosides méthylés en positions O-2, O-4 et N-3 de la base et on en discute en fonction de leurs propriétés physiques. On étudie par la rmn du ^1H et par spectrophotométrie uv, l'influence du pH sur la stabilité des déoxy-2′ ribosides méthylés en positions O-2 et O-4 aussi bien que sur la stabilité des ribosides.

[Traduit par le journal]

Introduction

Alkylation of purine and pyrimidine bases is of interest from the viewpoint of mutagenesis and carcinogenesis (1–9). Following the early interest in N7-alkylation of guanine (10, 11), much attention shifted to O-alkylation when Loveless (12) suggested that the O6 of guanosine in nucleic acids could be alkylated and proposed that atypical base pairing could result. Further interest in O-alkylation was generated by the isolation of O2- and O4-alkylated pyrimidine nucleosides which were overlooked in earlier work because the acid and alkaline conditions used to release the nucleosides from polynucleotides led to their dealkylation or depyrimidination (7).

In an earlier study (13) we reported a ^1H and ^{13}C nmr study of a series of O-methylated pyrimidine ribonucleosides (Fig. 1), and commented on their conformational and hydrogen bonding properties. We have completed the synthesis of an analogous series of 2′-deoxyribosides (m^2dUrd, m^4dUrd, m^2dThd, and m^4dThd; Fig. 1) and report here a similar ^1H and ^{13}C nmr study for these molecules as well as for the N3-methylated analogs m^3dUrd and m^3dThd. In addition, using ^1H nmr and uv spectrophotometry, we have examined the pH dependence of the stability of the O-methylated molecules in both the ribose and 2′-deoxyribose series at 25°C. The pH profiles for the pseudo first-order rate constants for demethylation and depyrimidination are presented, and compared with the work of Singer *et al.* (7) on O-ethylated nucleosides carried out at mainly 100°C. Our data should be useful for appreciating the persistance of O-alkyl groups in polynucleotides (1) and the care to be exercised when handling the fragile O-alkylated nucleosides.

Experimental

Materials

The Urd, dUrd, and dThd (Sigma Chemical Co.) were used without further purification. With Urd, dUrd, or dThd as starting material, the procedure of Robins and Naik (14) was used to prepare the O4-methylated derivatives. Urd was converted to m^2Urd according to Kimura *et al.* (15, 16). The N3-methylated derivatives, m^3dUrd and m^3dThd, were prepared according to Farmer *et al.* (17). To obtain m^2dUrd and m^2dThd, dUrd and dThd were converted to their 3′-acyl derivatives by standard procedures (18) and then to the 2,5′-anhydronucleoside following Secrist (19). Reflux of the anhydronucleoside (1 mmol) in 20 mL of methanolic sodium methoxide (0.11 *M*) afforded the unprotected m^2dUrd and m^2dThd. After neutralization with IRC-50 resin, the nucleosides were purified by paper chromatography with the solvent system n-butanol–ethanol–water (9:1:2 volume ratio). Identification of the molecules was made by comparison of published uv spectral data (7, 20) and consideration of the trends in the ^1H and ^{13}C nmr data (13).

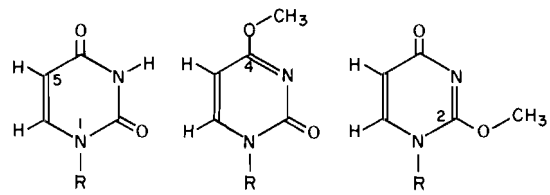

FIG. 1. Structures and abbreviations. Ribosides (R = D-ribose): uridine (Urd), O^4-methyluridine (m^4Urd), O^2-methyluridine (m^2Urd). Corresponding 2′-deoxyribosides (R = 2′-deoxy-D-ribose): dUrd, m^4dUrd, m^2dUrd. The thymine derivatives (5-CH_3): dThd, m^4dThd, m^2dThd. The free bases: uracil (Ura), thymine (Thy), O^4-methyluracil (m^4Ura), and O^2-methyluracil (m^2Ura). The N3-methyl derivatives: m^3dUrd and m^3dThd.

^1H nuclear magnetic resonance experiments

The ^1H nmr spectra were obtained on either a Nicolet NT360 (Purdue University) or a Bruker WH-270 (University of Wisconsin, Madison). All samples were examined in 5 mm (od) tubes at concentrations of 2–5 mg/mL in D_2O containing 0.1 mg/mL of sodium 3′-trimethylsilylpropionate-2,2,3,3-d_4 (TSP) as internal reference. Treatment with dithizone according to Cozzone and Jardetzky (21) removed paramagnetic metal ions. The pH was 7.0 ± 0.2 in each case (uncorrected for the deuterium isotope effect). The temperature was maintained at 25°C (360 MHz data) or at 21°C (270 MHz data). Spectral analysis was carried out using LAME (22) and computer-simulated spectra were generated as a final test of the chemical shifts (δ) and coupling constants (J) (Table 1). The uncertainties in δ and J are estimated to be about ±0.001 ppm and ±0.1 Hz, respectively. For comparison, literature data for dUrd (23) and dThd (24) are included.

^{13}C nuclear magnetic resonance experiments

Proton-decoupled ^{13}C nmr spectra were obtained on a Bruker WH-90DS spectrometer (22.63 MHz), according to described procedures (25). The nucleoside samples were contained in 10 mm (od) tubes at concentrations of 25–50 mg/mL in D_2O, containing 1% dioxane as internal reference. Paramagnetic ions were removed by shaking the

Can. J. Chem. Downloaded from www.nrcresearchpress.com by 210.87.254.6 on 09/06/12
For personal use only.

TABLE 1. ^{1}H chemical shifts (δ) and coupling constants (J) for a series of 2′-deoxyribosides[a,b]

Parameter[c]	dUrd	m^{2}dUrd	m^{4}dUrd	m^{3}dUrd	dThd	m^{2}dThd	m^{4}dThd	m^{3}dThd
δ6	7.87	8.01	8.14	7.85	7.68	7.85	7.90	7.67
5	5.89	6.16	6.25	5.96	1.89	1.95	1.99	1.93
1′	6.29	6.30	6.27	6.30	6.28	6.31	6.28	6.33
2′	2.38	2.42	2.33	2.37	2.39	2.42	2.32	2.37
2″	2.44	2.51	2.53	2.44	2.40	2.48	2.49	2.41
3′	4.47	4.46	4.44	4.46	4.49	4.47	4.46	4.47
4′	4.06	4.09	4.11	4.06	4.04	4.07	4.09	4.04
5′	3.85	3.86	3.87	3.85	3.86	3.87	3.88	3.86
5″	3.77	3.76	3.78	3.76	3.79	3.78	3.79	3.78
O(N)CH$_3$	—	4.04	3.95	3.29	—	4.03	3.97	3.31
J1′2′	6.5	6.4	6.4	6.6	[6.9[d]	6.4	6.5	6.5
1′2″	6.7	6.5	6.4	6.6	6.9]	6.6	6.5	6.7
2′3′	6.8	6.5	6.5	6.8	[5.6[d]	6.6	6.6	6.9
2″3′	3.5	4.4	4.3	4.1	5.6]	4.6	4.3	3.8
3′4′	4.0	4.2	4.1	3.9	3.7	4.2	4.3	4.3
4′5′	3.4	3.5	3.6	3.6	3.6	3.6	3.5	3.5
4′5″	5.1	5.2	5.2	5.2	4.9	5.1	5.1	5.1
56	8.0	7.6	7.5	8.1	1.1	1.1	1.1	1.1

[a] δ (ppm) from TSP. J in Hz. Abbreviations in Fig. 1.
[b] Data at 360 MHz (25°C) (m^{3}dUrd, m^{3}dThd); 270 MHz (21°C) (m^{2}dUrd, m^{4}dUrd, m^{2}dThd, m^{4}dThd); 220 MHz (18°C) (dUrd, dThd). dUrd from ref. 23.
[c] Not included are $J_{2'2''}$ and $J_{5'5''}$ which lie in the range −14.1 ± 0.2 Hz and −12.5 ± 0.1 Hz, respectively.
[d] In dThd δ2′ ≈ δ2″. Hence only the sum of the connected ([ ) J pairs is meaningful.

TABLE 2. ^{13}C chemical shifts for a series of 2′-deoxyribosides in aqueous solution[a]

Parameter	dUrd	m^{2}dUrd	m^{4}dUrd	m^{3}dUrd	dUrd$^-$	dThd	m^{2}dThd	m^{4}dThd	m^{3}dThd	dThd$^-$
δ4	167.4	8.8	6.7	−0.7	10.6	167.7	8.6	5.4	−0.6	9.9
2	152.8	5.5	5.9	0.4	7.8	152.9	4.8	5.8	0.3	7.6
6	143.2	−1.6	1.9	−2.3	−1.6	138.7	−1.1	2.9	−2.1	−1.2
5	103.5	4.8	−5.1	−0.8	0.7	112.7	5.1	−4.1	−1.0	0.3
1′	86.5	1.7	1.4	0.9	0.1	86.3	1.8	1.5	1.0	0.1
2′	40.0	0.7	0.9	0.3	0.1	39.8	0.7	1.0	0.2	0.2
3′	71.8	−0.3	−0.1	−0.1	0.2	71.7	−0.4	−0.2	−0.1	0.3
4′	88.0	0.6	0.3	0.1	−0.4	87.8	0.4	0.3	0.1	−0.4
5′	62.6	−0.2	−0.1	−0.1	0.2	62.5	0.3	0.1	0.0	0.3
C—CH$_3$	—	—	—	—	—	12.8	1.1	−0.3	0.7	1.3
O(N)—CH$_3$	—	57.5	56.1	29.0	—	—	57.4	56.1	29.2	—

[a] Carbon data of dUrd and dThd (24°C) in ppm at 22.63 MHz measured relative to internal dioxane and converted to a TMS scale by δ(TMS) = δ(DIOXANE) +67.86 ppm. The chemical shifts of m^2-, m^4-, and m^{3}dUrd are relative to dUrd; the shifts of m^2-, m^4-, and m^{3}dThd are relative to dThd. The O(N)–CH$_3$ shifts are relative to TMS. A positive number indicates a deshielding relative to the reference molecule. dUrd$^-$ and dThd$^-$ are the anions formed by N3–H ionization (pH = 11.5).

sample with an acetylacetone–toluene mixture (equal volumes) and separating the phases (13). The pH was adjusted to 7.0 ± 0.2 (uncorrected for the deuterium isotope effect). The probe temperature was regulated at 24°C. The ^{13}C chemical shift data (Table 2) are reported in ppm downfield from external TMS by setting internal dioxane equal to 67.86 ppm. The assignments of the ^{1}H and ^{13}C spectra were facilitated by comparison with other nucleosides (13, 26). However, C1′ and C4′ can not be unambiguously assigned without further experiments because their chemical shifts are similar. In each of the 2′-deoxyribosides, C4′ was assigned to the low field resonance. With this assignment the effects of base methylation on their chemical shifts parallel the trends observed for the ribosides i.e., the effect is greater on C1′ than on C4′ (13).

Kinetic studies

We determined the products of hydrolysis for each of the six O-methylated molecules at 32°C by monitoring the time dependence of their ^{1}H nmr spectra under acidic and basic conditions on a Bruker WH-90 DS spectrometer, followed by comparison with the spectra of the parent nucleoside (Urd, etc.) and the free thymine (Thy) and uracil (Ura) bases obtained under identical conditions. Changes in chemical shifts and in the J(5, 6) proton coupling constant (13), the appearance of a methanol resonance at 3.34 ppm, and the appearance of resonances corresponding to the anomeric H1′ of the free 2-deoxyribose sugar (27) (formed in depyrimidinations) were useful diagnostic tests.

In basic solution (pH ≈ 13) the O-methylated molecules were found to undergo dealkylation to methanol and the parent nucleoside; no evidence for any depyrimidination was provided by the ^{1}H nmr spectra. Singer *et al.* (7) noted that at pH = 12.5 (100°C) the corresponding O-ethylated molecules, e^{2}Urd, e^{4}Urd, e^{4}dUrd, and e^{4}dThd also undergo dealkylation with, in the case of e^{2}Urd, some competition from depyrimidination to the 2-deoxyribose sugar and the e^{2}Ura base. However, in contrast with our observations on m^{2}dUrd and m^{2}dThd, e^{2}dUrd and e^{2}dThd were found to undergo mainly depyrimidination yielding the e^{2}Ura and e^{2}Thy bases respectively; dealkylation of e^{2}dUrd and e^{2}dThd was found to occur at a much lower rate. We cannot rationalize now this striking difference in behaviour between the O-methyl and O-ethyl derivatives because of the much higher temperatures (100°C) employed by Singer *et al.* (7).

In line with the study of O-ethylated nucleosides by Singer *et al.* (7), the m^{2}Urd, m^{4}Urd, m^{4}dUrd, and m^{4}dThd were found to dealkylate in acid solution (pH = 1.5) whereas m^{2}dUrd and m^{2}dThd were

Can. J. Chem. Downloaded from www.nrcresearchpress.com by 210.87.254.6 on 09/06/12
For personal use only.

found to undergo an initial depyrimidination to liberate the corresponding O-methylated bases followed by a slower dealkylation of the base to yield the Ura and Thy bases. The ^{1}H nmr spectra revealed that a competitive dealkylation of m^{2}dUrd and m^{2}dThd also occurred to a small extent (≤5%).

The kinetics of the dealkylations were monitored at 25.0 ± 0.02°C in a Beckman DU spectrophotometer modified so that its output could be digitized by a voltmeter (Dana, model 5330) and stored in a Wang 600 calculator (28). Pseudo first-order rate constants (k_0) were calculated automatically by a least-squares method using eq. [1], where A represents absorbance.

$$[1] \quad \ln (A_\infty - A_t) = \ln (A_\infty - A_0) - k_0 t$$

The kinetic data for the depyrimidination of m^{2}dUrd and m^{2}dThd were obtained from the time dependence of the H6 proton nmr intensities obtained at 90 MHz (Bruker WH-90DS). (The nmr rather than spectrophotometric method was necessary because the uv spectra of the O-methylated nucleosides and the released bases are similar, and because of the complicating subsequent demethylation of the base.) The probe was maintained at a higher temperature (32 ± 0.5°C) than in the spectrophotometric experiments to lessen precipitation of the relatively insoluble bases formed in the reactions. Solutions were made up by dilution of stock 2.0 *M* HCl or 2.0 *M* NaOH, with the addition of sufficient NaCl to maintain a constant ionic strength of 2.0 *M*.

Results and discussion

^{1}H nuclear magnetic resonance data

The ^{1}H chemical shifts (δ) and coupling constants (J) of the methylated 2′-deoxyribonucleosides are given in Table 1. The striking similarity in the magnitudes of the corresponding coupling constants across the series of sugar residues indicates that the sugar conformation is little affected by O- or N-methylation of the base. (This contrasts with the shifts towards the 3′*endo* conformation effected by O-methylation in the corresponding ribonucleosides (13).) Estimates based on J(3′,4′) indicate a bias (60%) for the 2′*endo* pucker, as expected for "normal" 2′-deoxyribose sugars (29). Evaluation of the C4′–C5′ orientation according to Haasnoot *et al.* (30) gives the following narrow ranges of populations: g^+ (50 ± 2%); t (37 ± 2%); g^- (12 ± 1%). The bias towards the g^+ rotamer and the minimal contribution from g^- are standard features of normal 2′-deoxyribosides (26).

Like the coupling constants, the proton shifts of the sugar residues show only small variation. For example, δ(H2′) lies in the narrow range 2.3–2.4 ppm. Because H2′ is expected at ≈3.0 ppm in a *syn* 2′-deoxyriboside (31), a preference for the *anti* conformation is apparent. (dUrd and dThd are *anti* in the crystal state (32, 33); of the methylated derivatives only m^{4}Urd has been crystallized and shown to be *anti*.)[1] In the case of m^{2}dUrd and m^{2}dThd, methylation has converted the 2-keto oxygen to a methoxyl whose shielding effects in a *syn* pyrimidine have not been evaluated. However, the overall trends in the ^{1}H chemical shift and coupling constant data suggest the *anti* form for m^{2}dUrd and m^{2}dThd as well.

In line with observations on the ribosides (13), O2- and O4-methylation cause a 0.5 Hz decrease in J(5,6) (Table 1). This effect has been discussed in terms of the tautomeric changes in the ring (13).

^{13}C nuclear magnetic resonance data

Because the trends in the δ(C) data (Table 2) for the most part parallel those observed for the O- and N-methylated ribosides (13), only brief comment is needed here. The effects of methylation upon the sugar carbons are generally less than 1 ppm although O-methylation causes a deshielding of Cl′ of 1.4–1.8 ppm. N3-methylation has a smaller influence on δ(Cl′), in line with the smaller electronic effects associated with this modification. N3-methylation has only a small effect on the C2, C4, and C5 positions (≤1 ppm), but its shielding effect on the most distant carbon (C6) is substantial.

The most interesting observations, which reflect the strong conjugation of the O2–C2–N3–C4–O4 fragment, are that both C2 and C4 are deshielded by methylation of either of the carbonyl groups, and that C4 is more strongly affected than C2 by methylation of O2. Note further that C4 is more strongly deshielded by O4-methylation in the dUrd series than in the dThd series, suggesting some influence of the 5-CH_3 on the electronic changes associated with O4-methylation. Also interesting is that C6 is shielded by O2-methylation and deshielded by O4-methylation, whereas C5 is deshielded by O2-methylation and shielded by O4-methylation. These trends reflect a characteristic, general polarization of the O-methylated bases, but we leave for theory a more explicit discussion of electronic changes. In this regard it is interesting to note that ionization of the N3-H at basic pH to yield the anions dUrd$^-$ and dThd$^-$ has a substantial deshielding effect on C4 (≈10 ppm) and a somewhat smaller effect on C2 (≈8 ppm) (Table 2). Though somewhat larger, these changes parallel those of O-methylation, and suggest that the electronic effects of O-methylation on the O2–C2–N3–C4–O4 fragment may imitate those of base ionization. The remaining carbons are affected very little by ionization (≤0.7 ppm) except for C6 which experiences a shielding effect of 1.2–1.6 ppm.

Nuclear magnetic resonance titrations

To obtain information about the ionization behaviour of the O-methylated molecules, required for understanding their hydrolysis, we obtained the pH dependence of the H6, H5, 5-CH_3, and 2 (or 4)-OCH_3 ^{1}H chemical shifts (Fig. 2). The study focussed on the acid range because the bases have no acidic sites which could undergo ionization in basic solution. However, the ^{1}H nmr spectra reveal sugar hydroxyl ionization at pH 12, as originally noted by Fox and Shugar (34). The study could not be taken much below pH 1 where rapid decomposition occurs (see below).

For all O-methylated molecules except m^{4}dThd, the chemical shifts remain constant in the pH range 2–7 and move abruptly downfield in more acid solution. Unfortunately, a complete sigmoidal titration curve is not observed in the available pH range. Thus, the chemical shifts of the cation formed and its pK_a for ionization cannot be determined. However, the general appearance of the curves suggest pK_a values which are less than about 1.5 in all instances. In m^{4}dThd virtually no change occurs in any of the chemical shifts over the accessible pH range (0.2–7.0), suggesting that the pK_a value of its protonated form is substantially less than that of the other molecules. These trends are in rough correspondence with the pK_a data for the O-ethylated deoxyribosides obtained by Singer *et al.* using uv spectrophotometry (7): e^{2}dUrd (0.92), e^{2}dThd (0.5), e^{4}dUrd (0.66), and e^{4}dThd (−0.32).

Kusmierek and Singer (35) suggested that N3 is the primary protonation site of N1-substituted O-alkylated uracil bases, as is the case in N1-substituted cytosine. Comparison of the nmr titration behaviour of m^{4}Urd and m^{4}dUrd with that of cytidine (Cyd) (36) provides support for this suggestion. Thus, with

[1] R. Brennan and M. Sundaralingam, private communication.

Can. J. Chem. Downloaded from www.nrcresearchpress.com by 210.87.254.6 on 09/06/12
For personal use only.

Can. J. Chem. Downloaded from www.nrcresearchpress.com by 210.87.254.6 on 09/06/12
For personal use only.

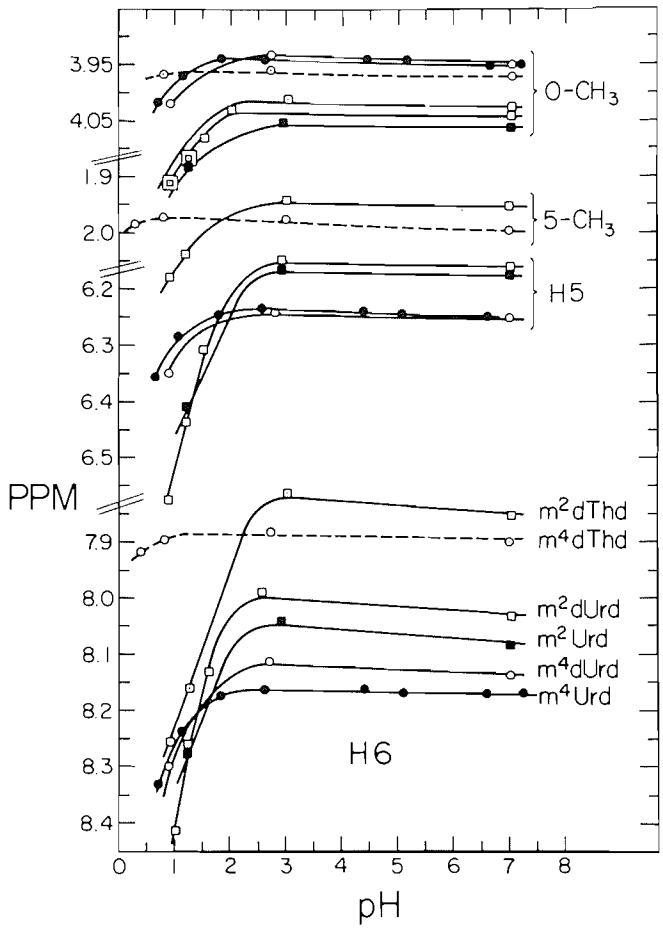

FIG. 2. The pH dependence of the proton chemical shifts of the O-methylated nucleosides. In the discontinuous vertical scale, the various ranges apply as follows: 3.95–4.05 ppm (O—CH_3), 1.9–2.0 ppm (5-CH_3 of thymine derivatives), 6.2–6.5 ppm (H5), and 7.9–8.4 ppm (H6). See Fig. 1 for numbering. The chemical shifts are relative to internal TSP. The pH is the pH-meter reading uncorrected for the deuterium isotope effect.

formation of the cytidine cation by N3 protonation, H6 and H5 move downfield by 0.33 and 0.24 ppm respectively (relative effect H6:H5 = 1.4). In our incomplete titration of m^4Urd we find downfield shifts for H6 (0.18 ppm) and H5 (0.12 ppm) in the most acidic solution (relative effect 1.5). Similarly in m^4dUrd in the most acid solution, H6 and H5 have shifted downfield by 0.19 and 0.11 ppm (relative effect 1.7). The similarity in the relative protonation effects suggests the primary protonation site is the same in Cyd, m^4Urd, and m^4dUrd. It seems likely that N3 is the primary protonation site in the other O-alkylated molecules, although we cannot entirely discount some competing protonation of the carbonyl oxygens.

Singer *et al.* (7) have noted that 5-methylation leads to a large *decrease* in the pK_a of the O4-ethylated pyrimidine base. (Compare pK_a of e^4dUrd (0.66) and of e^4dThd (−0.32)). Our titration curves for m^4dUrd and m^4dThd indicate a similar trend due to a 5-methyl group (Fig. 2). These trends are surprising in view of the finding by Borodavkin *et al.* (37) that 5-alkylation of the cytosine base leads to a small *increase* in its pK_a, suggesting an electron donating role for the 5-alkyl group. Furthermore, 5-alkylation of the uracil base leads to an increase in the pK_a of the N3-H (38, 39). Perhaps the increased acidity of cationic e^4dThd is due in part to a steric effect of the bulky 5-alkyl group which stabilizes the planar, *syn* conformation

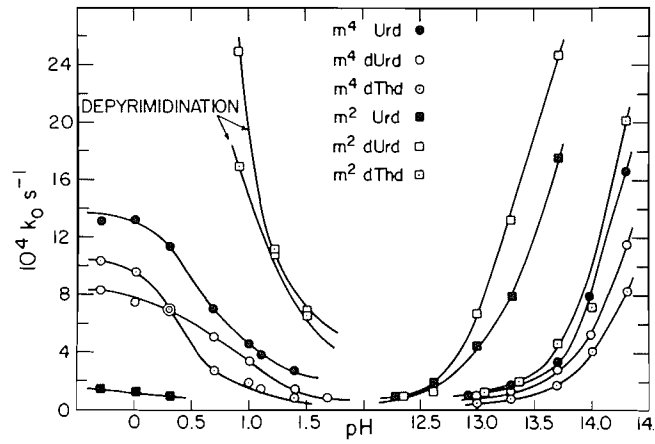

FIG. 3. Plot of the observed pseudo first-order rate constants (k_0, in 10^4 s^{-1}) versus pH, for the decomposition of O-methylated nucleosides in aqueous solution. The data for m^2dUrd and m^2dThd in *acid* solution represent the initial depyrimidination step and were obtained by ^{1}H nmr spectroscopy (32°C in D_2O). The remaining data represent demethylation processes and were obtained by uv spectrophotometry (25°C in H_2O). The pH represents −log [HCl], or 14 − log [NaOH] in basic solution.

about the C4—O4 bond. This conformation places the hydrophobic methoxyl methyl near to the N3 protonation site and should reduce its basicity.

Kinetics of alkaline demethylations

Figure 3 shows the pH dependence of the observed pseudo first-order rate constants (k_0) for the hydrolysis of the O2- and O4-methylated molecules. The m^2dUrd and m^2dThd data in *acid* solution (32°C) represent the initial depyrimidination step and were obtained from the time dependence of the H6 nmr intensities. The remaining data (25°C) represent the demethylation processes.

In the pH range 3–12 all of the nucleosides are relatively stable; at neutral pH no noticeable decomposition occurs after weeks of standing. In more basic solution, rapid demethylation ensues with k_0 increasing exponentially with pH. The plot of k_0 versus the hydroxide ion concentration is linear for each of the O-methylated molecules and passes through the origin. This indicates that the demethylation processes involve a rate determining attack of the OH^- ion, with negligible neutral hydrolysis at this temperature. One mechanism consistent with these observations involves direct S_N2 attack at the methyl group; a second mechanism involves S_NAr attack at the methoxylated ring carbon. We are considering ^{18}O isotope experiments that would provide further mechanistic information. Values of the second-order rate constants for basic hydrolysis, k_{OH}, were obtained from the slopes of the k_0 versus $[OH^-]$ plots and are listed in Table 3.

From the list of k_{OH} (Table 3), we see that the relative ease of demethylation follows the order m^2dUrd > m^2Urd ≫ m^2dThd > m^4Urd > m^4dUrd > m^4dThd. Thus the O2-methylated molecules are more labile to alkaline demethylation than the O4-methylated molecules. (This contrasts with Singer *et al.* (7) who noted at 100°C and pH = 12.5 that e^2Urd is much less readily dealkylated than e^4Urd (approximate half-lives: 4 h and <10 min, respectively).) In the O2-methylated series the deoxyriboside m^2dUrd is more labile than the riboside m^2Urd, whereas in the O4-methylated series the riboside m^4Urd is more labile than m^4dUrd. (Comparison with the work of Singer *et al.*

TABLE 3. Rate constants for the neutral (k_{H_2O}), acid (k_H), and base (k_{OH}) catalyzed hydrolysis of methylated nucleosides. Acid dissociation constants for their conjugated acids (K_a)

Compound	$10^3 k_H$ (s^{-1})	K_a	pK_a	$10^4 k_{H_2O}$ (s^{-1})	$10^4 k_{OH}$ ($1\ m^{-1}\ s^{-1}$)
m^4Urd	1.36±0.13	0.18±0.02	0.8	−0.20±0.29	8.24±0.28
m^4dUrd	0.98±0.14	0.20±0.03	0.7	0.12±0.15	5.63±0.18
m^4dThd	1.29±0.30	0.56±0.15	0.3	−0.05±0.06	4.13±0.06
m^2Urd	0.14±0.01	0.22±0.01	0.7	0.59±0.26	34.3±1.1
m^2dUrd	6.7±5.9	0.27±0.25	0.6	0.69±1.10	49.8±4.5
m^2dThd	3.3±0.3	0.11±0.01	1.0	−0.85±1.03	10.4±1.0

"The data are for demethylation processes (25°C) except k_H for m^2dUrd and m^2dThd in acid solution (32°C) which are for the initial depyrimidinations.

cannot be made because on the one hand e^2dUrd and e^2dThd primarily undergo depyrimidination and on the other hand the half-lives of e^4Urd and e^4dUrd could not be accurately measured at 100°C in basic solution (7)). Thus, our data show that sugar 2′-hydroxyl stabilizes the O2-methylated molecules and destabilizes the O4-methylated molecules to alkaline hydrolysis. Discussion of the effect of the 2′-hydroxyl is complicated because this group undergoes ionization at pH > 12, which is reflected in the ^{1}H nmr spectrum of the sugar. The greater stability of m^2Urd relative to m^2dUrd could be due in part to electron donation of the 2′-hydroxylate (which would destabilize the transition state) and to steric and electrostatic repulsion of the attacking hydroxide ion.

The 5-methyl has a stabilizing effect on both the 2- and 4-methoxyl groups in alkaline solution. This is expected for an electron donating substitutent, but it is surprising that its effect is larger on the more remote 2-methoxyl group. (Compare the m^2dUrd with m^2dThd and m^4dUrd with m^4dThd in Table 3.)

Kinetics of acidic demethylations

At pH < 3, m^2Urd, m^4Urd, m^4dUrd, and m^4dThd undergo rapid demethylation to the parent nucleoside, as was observed for the corresponding O-ethylated molecules (7). The sigmoidal k_0 versus pH profiles (Fig. 3) for m^4Urd, m^4dUrd, and m^4dThd suggest initial protonation (presumably at N3) followed by a rate determining attack by water. (Figure 2 confirms that protonation of the bases occurs at pH < 3.) The protonation could be followed by either S_N2 attack by water on the methyl group or by S_NAr attack at the methoxylated ring carbon (C2 or C4). Isotope studies might allow us to determine which mechanism prevails.

Assuming a two step model, it can be shown that

$$[2]\quad \frac{1}{k_0} = \frac{K_a}{k_H}\frac{1}{[H_3O^+]} + \frac{1}{k_H}$$

where k_H is the pseudo first-order rate constant for the attack by water on the protonated nucleoside and K_a is the acid dissociation constant of this species. In agreement with eq. [2], plots of k_0^{-1} versus $[H_3O^+]^{-1}$ are linear. The values of k_H, K_a, and pK_a obtained from the slopes and intercepts of the linear plots are listed in Table 3.

Given the combined uncertainties, the agreement is reasonable between our kinetically derived pK_a values and those given for the corresponding O-ethylated derivatives by Singer *et al.* (7). Note in particular that m^4dThd exhibits the smallest pK_a (≈0.3), a trend supported by our partial titration curves (Fig. 2).

From the list of k_H values we note that for the *base-protonated* species, m^4Urd is more labile than m^2Urd, in contrast with the situation in basic solution (compare their k_{OH} values, Table 3). The k_H values for m^4dThd and m^4dUrd suggest a small destabilizing effect of the 5-methyl substituent on the 4-methoxy group, although the trend here is not particularly clear because of the uncertainties in the k_H values. This contrasts with the statement by Singer *et al.* that in acid solution the O4-alkyl groups are more stable on dThd than on dUrd. Note, however, that their conclusion was based on pseudo first-order rate constants (expressed as half-lives) measured at pH 1.5. At this acid strength the molecules would exist partly as the neutral species and partly as the more reactive cationic form. Our full titration curves (Fig. 3) reveal that crossovers in the relative stabilities determined by k_0 can occur because of differences in the K_a values for the cationic species. (See curves for m^4dUrd and m^4dThd in Fig. 3.) Thus, some caution is required in interpreting trends if complete titration curves are not available.

Kinetics of acidic depyrimidinations

Figure 3 shows the pH dependence of k_0 for the initial depyrimidination of m^2dUrd and m^2dThd in acid solution. The rate of the reaction is very rapid at pH < 0.5 (4.6 min half-life for m^2dUrd at pH = 0.9). Thus, we could not ascertain whether the dependence of k_0 upon pH is sigmoidal. However, it is likely that the mechanism of depyrimidination is similar to that of 2′-deoxycytidine derivatives (40) in which a reversible protonation (presumably at N3) precedes a rate determining cleavage of the N-glycosyl bond.[2] In such a mechanism eq. [2] will apply. Approximate values of K_a and pK_a of the protonated nucleosides, and the value of k_H for the cleavage of the N-glycosyl bond were obtained from plots of k_0^{-1} versus $[H_3O^+]^{-1}$ (Table 3).

The uncertainties in the quantities limit the conclusions which can be made. The pK_a values for m^2dUrd and m^2dThd are not out of line with those of e^2dUrd and e^2dThd (7) and the nmr titration curves (Fig. 2). The most interesting result is the large labilization of the N-glycosyl link by O^2-methylation in the *deoxy* series; in contrast no depyrimidination of the O^4-methylated molecules was detected. This indicates that, in the cationic forms of the nucleosides, the 2-methoxylated base is the better leaving group, perhaps due to greater localization of positive charge at the N1-nitrogen of the ring.

Acknowledgements

This work was funded by the Natural Sciences and En-

[2] Our ^{1}H nmr spectra also revealed that demethylation of m^2dUrd and m^2dThd also occurs to a small extent (≈5%).

Can. J. Chem. Downloaded from www.nrcresearchpress.com by 210.87.254.6 on 09/06/12
For personal use only.

gineering Research Council of Canada. We acknowledge discussions with Drs. Charlton, Hunter, McKinnon, and Sadana. We are grateful to Dr. J. L. Markley, the Biochemical Magnetic Resonance Laboratory, Purdue University (NIH Grant RR-01077) for the 360 MHz spectra, and Drs. W. A. Gibbons and W. P. Niemczura for the 270 MHz spectra. We thank K. Marat for help in acquiring the ^{13}C nmr data and G. Privé for some ^{1}H spectral analysis. We also thank J. Betts, J. Blonski, and J. Thompson for some preliminary kinetic studies, and R. Brennan and M. Sundaralingam for informing us of the crystal structure of m^4Urd.

1. B. SINGER, S. SPENGLER, and W. J. BODELL. Carcinogenesis, **2**, 1069 (1981).
2. B. SINGER. *In* Carcinogenesis: fundamental mechanisms and environmental effects. *Edited by* P. O. P. Ts'o and H. Gelboin. D. Reidel Publishing Co., Dordrecht, The Netherlands 1980 p. 91.
3. M. F. RAJEWSKY, R. MULLER, J. ADAMKIEWCZ, AND W. DROSDZIOK. *In* Carcinogenesis: fundamental mechanisms and environmental effects. *Edited by* P. O. P. Ts'o and H. Gelboin, D. Reidel Publishing Co., Dordrecht, The Netherlands. 1980. p. 207.
4. B. PULLMAN, D. PERAHIA, and C. DIDIER. Nucleic Acid Res. **6**, 3821 (1979).
5. R. SAFFHILL and P. J. ABBOTT. Nucleic Acid Res. **5**, 1971 (1978).
6. B. SINGER, H. FRAENKEL-CONRAT, and J. T. KUSMIEREK. Proc. Nat. Acad. Sci. U.S.A. **75**, 1722 (1978).
7. B. SINGER, M. KROGER, and M. CARRANO. Biochemistry, **17**, 2346 (1978).
8. C.-G. LEE and C.-J. CHANG. J. Carbohydr. Nucleosides Nucleotides, **5**, 343 (1978).
9. P. J. ABBOTT and R. SAFFHILL. Nucleic Acid Res. **4**, 761 (1977).
10. P. BROOKES and P. D. LAWLEY. Biochem. J. **80**, 489 (1961).
11. H. FRAENKEL-CONRAT. Biochim. Biophys. Acta, **49**, 169 (1961).
12. A. LOVELESS. Nature, London, **223**, 206 (1969).
13. F. E. HRUSKA and W. J. P. BLONSKI. Can. J. Chem. **60**, 3026 (1982).
14. M. J. ROBINS and S. R. NAIK. Biochemistry, **10**, 3591 (1971).
15. J. KIMURA, Y. FUJISAWA, T. SAWADA, and O. MITSUNOBU. Chem. Let. 691 (1974).
16. J. KIMURA, K. YAGI, H. SUZUKI, and O. MITSUNOBU. Bull. Chem. Soc. Jpn. **53**, 3670 (1980).
17. P. B. FARMER, A. B. FOSTER, M. JARMAN, and M. J. TISDALE. Biochem. J. **135**, 203 (1973).
18. V. AMARNATH and A. D. BROOM. Chem. Rev. **77**, 183 (1977).
19. J. A. SECRIST. Carbohydr. Res. **42**, 379 (1975).
20. B. SINGER. Prog. Nucleic Acid Res. Mol. Biol. **15**, 219 (1975).
21. P. J. COZZONE and O. JARDETZKY. Biochemistry, **15**, 4860 (1976).
22. C. W. HAIGH and J. M. WILLIAMS. J. Mol. Spectrosc. **32**, 398 (1969).
23. T. SCHLEICH, B. J. BLACKBURN, R. D. LAPPER, and I. C. P. SMITH. Biochemistry, **11**, 137 (1972).
24. D. J. WOOD, F. E. HRUSKA, and K. K. OGILVIE. Can. J. Chem. **52**, 3353 (1974).
25. W. P. NIEMCZURA and F. E. HRUSKA. Can. J. Chem. **58**, 472 (1980).
26. D. B. DAVIES. Prog. Nucl. Magn. Reson. Spectrosc. **12**, 135 (1978).
27. R. U. LEMIEUX and J. D. STEVENS. Can. J. Chem. **44**, 249 (1966).
28. A. QUEEN, J. L. CHARLTON, E. DAWSON, and W. BUCHANNON. Chem. Instrum. **6**, 153 (1975).
29. C. ALTONA and M. SUNDARALINGAM. J. Am. Chem. Soc. **95**, 2333 (1973).
30. C. A. G. HAASNOOT, F. A. A. M. DE LEEUW, H. P. M. DE LEEUW, and C. ALTONA. Recl. Trav. Chim. Pays-Bas, **98**, 576 (1980).
31. W. P. NIEMCZURA, F. E. HRUSKA, K. L. SADANA, and P. C. LOEWEN. Biopolymers, **20**, 1671 (1981).
32. A. RAHMAN and H. R. WILSON. Acta Crystallogr. Sect. B, **28**, 2260 (1972).
33. D. W. YOUNG, P. TOLLIN and H. R. WILSON. Acta Crystallogr. Sect. B, **25**, 1423 (1969).
34. J. J. FOX and D. SHUGAR. Biochem. Biophys. Acta, **9**, 369 (1952).
35. J. T. KUSMIEREK and B. SINGER. Nucleic Acid Res. **3**, 989 (1976).
36. G. C. Y. LEE, J. H. PRESTEGARD, and S. I. CHAN. J. Amer. Chem. Soc. **94**, 951 (1972).
37. A. V. BORODAVKIN, Y. S. DOLIN, Y. V. MOROZOV, and F. A. SAVIN. Mol. Photochem. **9**, 403 (1979).
38. I. KULAKOWSKA, M. GELLER, B. LESYNG, and K. L. WIERZCHOWSKI. Biochim. Biophys. Acta, **361**, 119 (1974).
39. J. CLAUWAERT and J. STOCKX. Z. Naturforsch. Teil B, **23**, 25 (1968).
40. R. SHAPIRO and M. DANZIG. Biochemistry, **11**, 23 (1972).

Can. J. Chem. Downloaded from www.nrcresearchpress.com by 210.87.254.6 on 09/06/12
For personal use only.

Acid-catalyzed cleavage of 4-halonortricyclanes. Evidence that the 2-norbornyl cation is an unsymmetrical species

NICK HENRY WERSTIUK, DALJIT DHANOA, AND GEORGE TIMMINS
Department of Chemistry, McMaster University, Hamilton, Ont., Canada L8S 4M1

Received July 28, 1982[1]

NICK HENRY WERSTIUK, DALJIT DHANOA, and GEORGE TIMMINS. Can. J. Chem. **61**, 2403 (1983).

Nortricyclanes **4***a*, **4***c*, **4***d*, and **4***e* were prepared and ring opened in D_2SO_4/CD_3COOD. We found that the ratios of *endo*/*exo* deuterium at C(6) were 1.09 ± 0.02, 1.30 ± 0.03, 1.40 ± 0.04, and 1.45 ± 0.05 for cleavage of **4***a*, **4***c*, **4***d*, and **4***e*, respectively. The amount of 6,2-hydride shift decreased from 14.3 ± 1.0% in the case of nortricyclane (**4***a*) to 6.0 ± 1.1%, 6.4 ± 0.5%, and 8.1 ± 0.7% for **4***c*, **4***d*, and **4***e*, respectively. Although four distinct mechanisms involving either nonclassical or rapidly-equilibrating cations are possible, cleavage most probably occurs to generate 6,2-unsymmetrically-bridged norbornyl cations.

NICK HENRY WERSTIUK, DALJIT DHANOA et GEORGE TIMMINS. Can. J. Chem. **61**, 2403 (1983).

On a préparé les nortricyclanes **4***a*, **4***c*, **4***d* et **4***e* et on a ouvert le cycle dans du D_2SO_4/CD_3COOD. Nous avons trouvé que les rapports du deutérium *endo*/*exo* en C(6) sont de 1,09 ± 0,02, 1,30 ± 0,03, 1,40 ± 0,04 et 1,45 ± 0,05 pour le clivage respectif des composés **4***a*, **4***c*, **4***d* et **4***e*. Le taux de glissement 6,2 d'hydrure diminue de 14,3 ± 1,0% dans le cas du nortricyclane (**4***a*) à 6,0 ± 1,1%, 6,4 ± 0,5% et 8,1 ± 0,7% pour les composés **4***c*, **4***d* et **4***e* respectivement. Bien que quatre mécanismes distincts, impliquant soit des cations non classiques ou des cations qui s'équilibrent rapidement soient possibles, le clivage se produit plus probablement de façon à engendrer des cations norbonyles pontés de façon non symétrique en positions 6,2.

[Traduit par le journal]

Introduction

The norbornyl-cation controversy held the attention of physical organic chemists for two and one-half decades (1). We, along with many researchers, were drawn to contribute to the solution of the problem (2–5). The enormous effort which has been expended world-wide to solve the problem has been documented clearly by Brown (1).[2] In our view, the central issue of the controversy is stated simply in the following question. Is the symmetrical norbornonium ion (**1***a*) an intermediate or does it best represent the transition state between rapidly equilibrating unsymmetrical ions represented by **2***a* and **3***a*? By employing classical substituent effect studies to gain structural information on the norbornyl cation, researchers introduced groups on the [2.2.1]-framework and thereby destroyed the symmetry of **1***a* or rendered the equilibrating unsymmetrical ions non-degenerate. Since C(4) is the only site where a single substitution does not destroy symmetry or clutter the front-face of the cation, we reasoned that the critical question (*vide supra*) could be answered by establishing whether or not a substituent at C(4) influenced the chemistry of the 2-norbornyl cation. To that end we prepared and studied the acid-catalyzed ring opening of nortricyclane (**4***a*) and its 4-halo analogs **4***c*, **4***d*, and **4***e*. If cleavage yields symmetrical cations **1***a*–**1***e*, then the stereochemistry of the ring opening, as monitored by the *endo*/*exo* deuterium ratio at C(6), would be unaffected by the substituent. However, if cleavage yields unsymmetrical cations the rate of rearrangement could be affected by the mass of the substituent – a ponderal effect (6) – and/or a polar effect. Consequently, a change in the stereochemistry of the ring-opening would be observed because subsequent reaction of the *endo*-6-*d*-cation, formed by edge-wise attack of D^+ (7, 8), would compete more effectively with rearrangement. If the mass and/or electronegativity of the substituent at C(4) influences the stereochemistry of the ring-opening, then a change in the degree of 6,2-hydride shift would be expected also. In this publication we give a complete account of the ring cleavages of **4***a*, **4***c*, **4***d*, and **4***e* in deuterated medium. Assuming that *exo*-2-norbornyl acetate-*endo*-6-*d* is not formed by concerted termolecular addition of acetic acid, we consider four probable mechanisms for ring-opening: corner deuteronation (protonation) yielding a symmetrical nonclassical cation; edge deuteronation (protonation) yielding an edge-protonated nortricyclane which rearranges to a nonclassical species; edge-wise approach with a corner slide yielding a 6,2-unsymmetrically bridged cation which undergoes Wagner–Meerwein rearrangement; edge deuteronation (protonation) yielding an edge-deuterated nortricyclane that rearranges to a rapidly-equilibrating 6,2-unsymmetrically bridged 2-norbornyl cation. On the basis of the results of this study and our previous work (5) we prefer a route which involves edge deuteronation and yields a 6,2-unsymmetrically bridged ion.

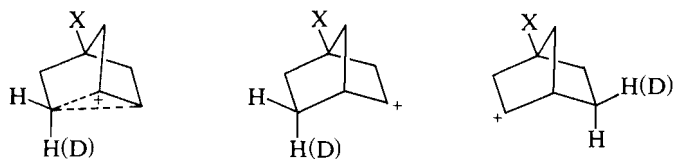

1 2 3

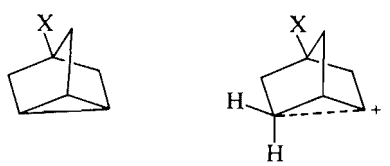

4 5

a X = H
b X = F
c X = Cl
d X = Br
e X = I

[1]Revision received June 1, 1983.
[2]With comments by P. von R. Schleyer.

Can. J. Chem. Downloaded from www.nrcresearchpress.com by 210.87.254.105 on 09/06/12
For personal use only.

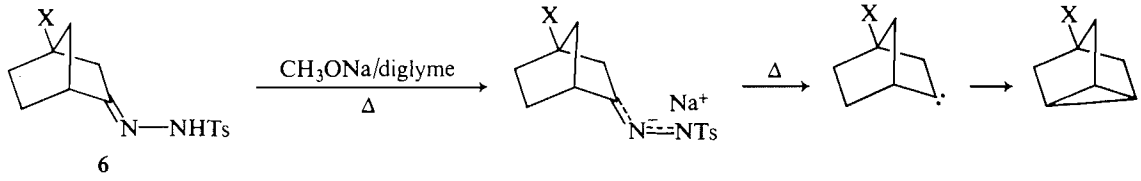

6

a X = H
b X = Cl
c X = Br

SCHEME 1

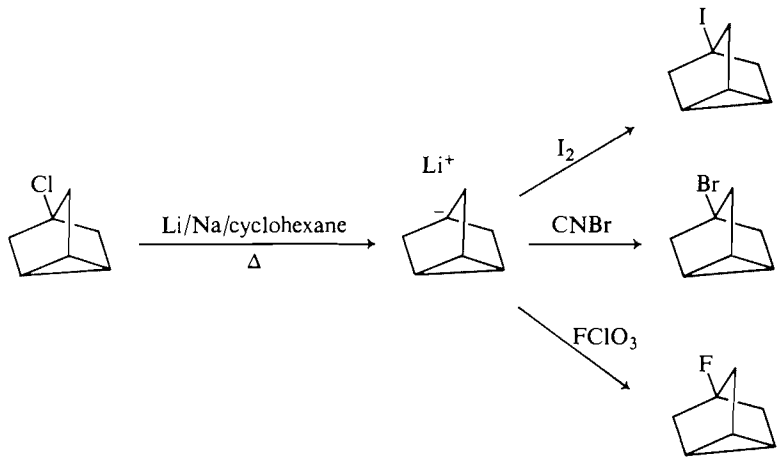

SCHEME 2

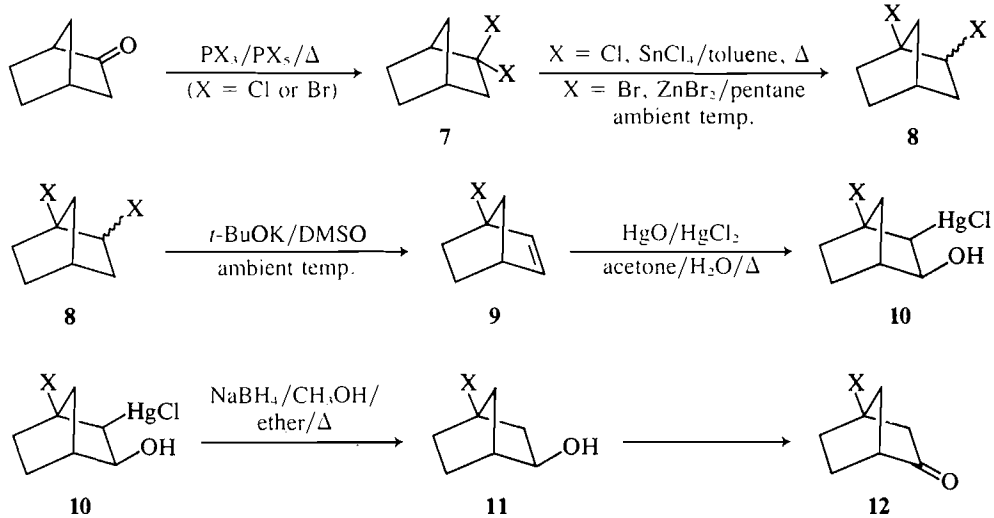

7 8 9 10 10 11 12

a X = Cl
b X = Br

SCHEME 3

Results

Preparation of substrates

Nortricyclanes **4***a*, **4***b*, and **4***c* were prepared by thermal decomposition of the sodium salts of the corresponding *p*-toluenesulfonylhydrazones **6***a*, **6***b*, and **6***c* as shown in Scheme 1 (9). It was established by analytical glpc analysis that the nortricyclanes were >99% pure and contained no norbornenyl impurities. Iodonortricyclane (**4***d*) was prepared by lithiating **4***c* and reacting the anion with I_2 (Scheme 2). We found that oxygen must be scavenged scrupulously from purging argon with benzophenone ketyl and that the rate of lithiation is enhanced markedly by the addition of small amounts of sodium. Attempts to prepare 4-fluoronortricyclane (**4***b*) by reacting the anion with $FClO_3$ resulted in a complex mixture of products, and only a small amount of the fluoride, as determined by ^{19}Fmr, ^{1}Hmr, and ms, was isolated in one case. Bromide **4***d* was prepared also by quenching lithium 4-nortricyclanide with CNBr, but we settled on the synthesis of **4***d* from 2-norbornanone as shown in Scheme 3 because 1-bromonorbornene (**9***a*) could be prepared on a large scale. Furthermore, we wished to use **9***a* as a starting material for the preparation of optically active 4-bromo-*exo*-2-norbornyl brosylate required for future studies of the stereochemistry of solvolysis of optically active 4-substituted norbornyl

Can. J. Chem. Downloaded from www.nrcresearchpress.com by 210.87.254.105 on 09/06/12
For personal use only.

TABLE 1. Proton chemical shifts of nortricyclanes[a]

Substrate	H-1 (2,6)	H-3 (5,7)	H-4
4*a*	0.97	1.18	1.92
4*c*	1.18	1.65	
4*d*	1.11	1.70	
4*e*	0.95	1.71	

[a]Obtained at 90 MHz in CCl_4.

brosylates.

The ^{1}Hmr data on the nortricyclanes are summarized in Table 1. It is interesting to note that while the chemical shifts of the cyclopropyl protons are in the order **4***c* > **4***d* > **4***e* ~ **4***a*, the chemical shifts of methylene protons which are closer to the electron-withdrawing halogens remain essentially constant through the series of halides.

As is shown in Scheme 3, 2-norbornanone was converted into 2,2-dihalides **7***a* and **7***b* that were rearranged to the 1,2-isomers **8***a* and **8***b* by $SnCl_4$ and $ZnBr_2$, respectively. Elimination of HCl and HBr by *t*-BuOK/DMSO gave the corresponding 4-halonorbornenes **9***a* and **9***b* that were oxymercurated by $HgCl_2$/HgO in aqueous acetone (10). $NaBH_4$ reduction of the crude mercurials **10***a* and **10***b* gave the corresponding 4-halo-*exo*-2-norbornanols **11***a* and **11***b* which were oxidized by Brown's reagent to **12***a* and **12***b*, respectively. During the reduction of the mercurials we observed the formation of varying amounts – in some cases up to 70% – of **9***a* and **9***b*, but the norbornenes were recovered and recycled. While the conversion of methoxy mercurials and hydroxy mercurials to starting alkenes has been observed previously, the exact mechanism of their formation remains obscure (11). Is it possible that deoxymercuration occurs by nucleophilic attack of the oxy-anion at mercury to displace chloride, followed by elimination of HgO? That the stereochemistry and regiochemistry of the oxymercuration reactions was that indicated in Scheme 3 was established by ^{1}Hmr analysis of the mercurials and by the fact that the reduction product of **10***a* was identical to 4-chloro-*exo*-2-norbornanol prepared by the silver ion-assisted solvolysis of 1-*exo*-3-dichloronorbornane. The regiochemistry of the oxymercuration of **9***a* and **9***b* is in accord with the regiochemistry of the mercuration of **13** and **14** which yielded **15** and **16** after reduction. We attempted to use the

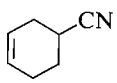

13

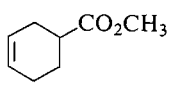

14

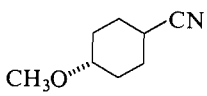

15

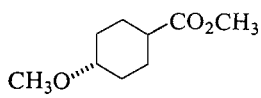

16

solvolysis of the 1,3-dichloride to prepare **11***a* on a large scale, but the addition of gaseous HCl to **9***a* proved to be unreliable. We also attempted to prepare **11***a* by acid-catalyzed hydration of **9***a*, but 2-norbornanone was formed, most probably via a route which involved formation and rearrangement of the 1-chloro-2-norbornyl cation to the 2-chloro-2-cation.

Ring-cleavages of nortricyclanes

Ring-cleavages were carried out in CD_3COOD/0.1 *M* D_2SO_4 rather than in CH_3COOD/D_2SO_4 to avoid dilution of the deuterium pool by exchange of the methyl group. Reduction of the deuterated acetates **17***a*–**17***d* by $LiAlH_4$ in ether gave the corresponding deuterated alcohols **18***a*–**18***d* and **18***b*, **18***c*, and **18***d* that were converted to deuterated *exo*-2-norbornanol by sodium in 2-propanol (Scheme 4). In the case of the reduction of halohydrins **18***b* and **18***c*, an additional product was observed which most likely resulted from a Grob cleavage. Analytical glpc analysis of the deuterated *exo*-norbornanols isolated by preparative glpc established that <1% of the *endo*-alcohol was present in each case. Although ^{2}Hmr showed only four resonances that were assigned to deuterons at C(1), C(2), *exo* and *endo* at C(6), the final analyses were carried out in the presence of $Pr(fod)_3$ to ensure that resonances due to deuterium which might be located at C(3) or C(7) would be shifted and would not interfere with the *endo/exo* analysis. In fact, the halohydrins were reduced to *exo*-norbornanol to insure that the analyses were identical. Figure 1 shows the 60 MHz ^{1}Hmr spectrum of *exo*-2-norbornanol complexed with $Pr(fod)_3$, along with the assignments. Clearly, only resonances due to protons (deuterons) at C(4), C(5), and C(6) appear in the region of interest. Since there are no viable mechanisms for introducing deuterium at C(5) during ring opening, and base-catalyzed deuterium scrambling during reduction should not be significant, the peaks in the region −4 to −5 ppm are due to *exo*- and *endo*-deuterons at C(6). Even if scrambling occurred to a minor extent, ^{2}Hmr analysis would yield a *minimum* C(6)-*endo/exo* deuterium ratio because the D-4 and D-5 resonances overlap with the *exo*-6-D signal. The ^{2}Hmr spectra were subjected to a computerized curve analysis using Lorentzian shapes and the results are reported in Table 2 and Table 3.[3] Figure 2 gives examples of ^{2}Hmr spectra of the deuterated *exo*-2-norbornanols obtained from ring openings of **4***a*, **4***c*, **4***d*, and **4***e* and complexed with $Pr(fod)_3$. Figure 3 provides an example of an actual spectrum, the fitted spectrum, and the resolved spectrum of the deuterated *exo*-norbornanol obtained from **4***a*. The *endo/exo* ratios obtained by averaging the results from at least six curve analyses of ^{2}Hmr spectra from at least two different ring-openings are given in Table 2. The percentages of deuterium at C(1) and C(2) obtained from at least four determinations are listed in Table 3. While there appears to be a distinct difference between the *endo/exo* ratio for **4***a*, **4***c*, and **4***d*, the difference in the ratios for **4***d* and **4***e* may not be significant.

To ensure that the deuterium was not scrambled in the acetates, ring-openings of **4***a* were run for 14 h and 48 h and, for **4***d*, reactions were run for 70 h and 240 h. Within experimental error, the deuterium distributions were identical for each pair of ring-cleavages. That the deuterated 2-norbornanols derived from the ring-openings of **4***c* and **4***d* were composites of 11.3% d_0, 87.3% d_1, 1.4% d_2 and 9.1% d_0, 90.9% d_1 and <0.1% d_2 species, respectively, established that H/D exchange did not occur to a significant extent.

Discussion and conclusions

It is clear from the data in Tables 2 and 3 that the introduction of a halogen substituent at C(4) produces a pronounced increase in the *endo/exo* deuterium ratio at C(6) and a pronounced decrease in the extent of 6,2 (6,1)-hydride shift. The *endo/exo* deuterium ratio of 1.09 ± 0.02 obtained for the ring-opening of **1***a* compares favourably with the ratio of 1.08 ± 0.05

[3]The values listed in Tables 2 and 3 differ slightly from the values reported in our initial publication and include additional analyses which were carried out.

Can. J. Chem. Downloaded from www.nrcresearchpress.com by 210.87.254.105 on 09/06/12
For personal use only.

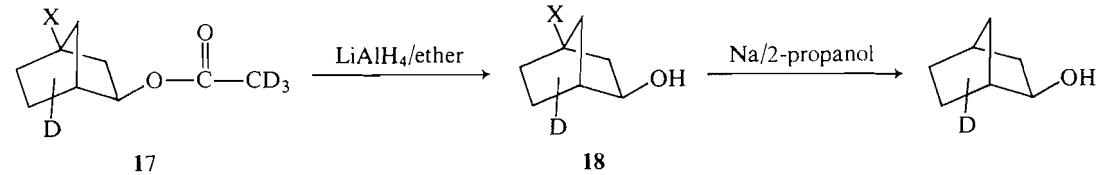

a X = H
b X = Cl
c X = Br
d X = I

SCHEME 4

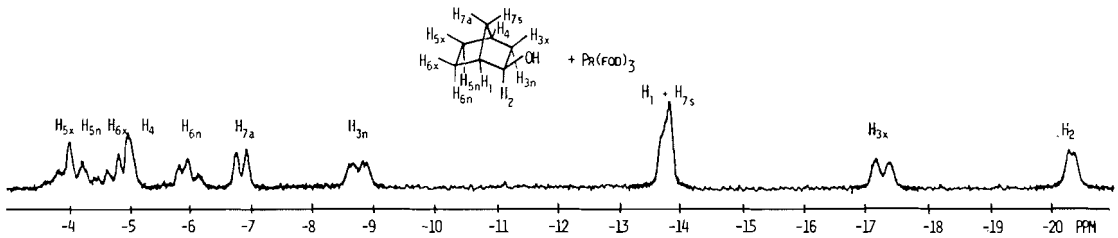

FIG. 1. 60 MHz ^{1}Hmr spectrum of *exo*-2-norbornanol (0.025 g) complexed with Pr(fod)$_3$ (0.100 g) in CCl_4.

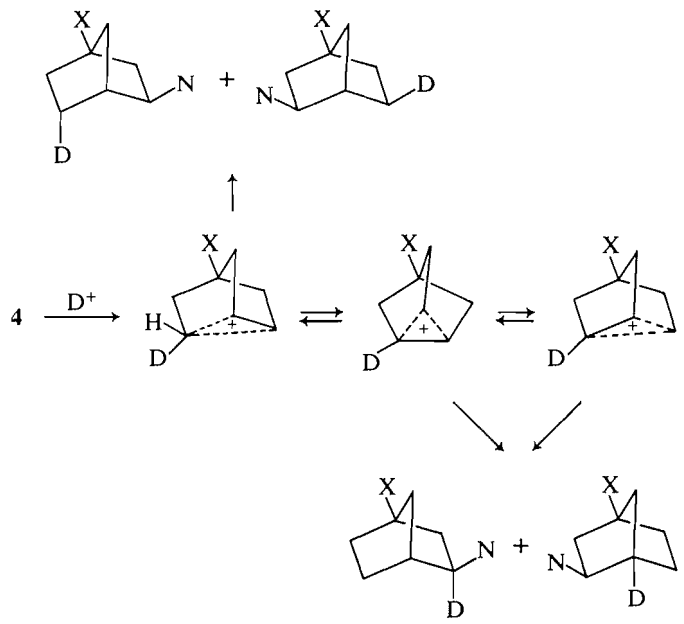

SCHEME 5

TABLE 2. *endo/exo* Deuterium ratios at C(6) of norbornyl acetates[a]

Substrate cleaved	*endo/exo* Deuterium ratio	% Excess *endo-d*
4*a*	1.09±0.02	4.6
4*c*	1.30±0.04	14.9
4*d*	1.40±0.04	21.4
4*e*	1.45±0.05	22.5

[a]Errors are expressed as average deviations from the mean obtained from at least six curve analyses of ^{2}Hmr spectra from at least two ring-openings.

TABLE 3. Percent deuterium at C(1) and C(2) of norbornyl acetates[a]

	Percent deuterium[a]	
Substrate cleaved	C(1)	C(2)
4*a*	7.5±0.6	6.8±0.4
4*c*	2.9±0.5	3.1±0.6
4*d*	3.4±0.4	3.0±0.1
4*e*	3.9±0.4	4.2±0.3

[a]Errors are expressed as average deviations from the mean obtained from at least four curve analyses of ^{2}Hmr spectra.

obtained by Nickon and Hammons (12) using infrared spectroscopy. To establish that the difference in the *endo/exo* ratios observed in the cleavages of **4***a* and the 4-halonortricyclanes was not due to scrambling in the acetates, the results of two ring openings of **4***a* and **4***d* carried out for different reaction periods (*vide supra*) were compared. That the deuterium distributions for both ring-openings of each substrate were identical within experimental error established that scrambling does not occur to a significant extent. This is in accord with Nickon's findings (12) that optically active *exo*-norbornyl acetate does not racemize under the conditions used to ring open **4***a*.

Assuming that *exo*-2-norbornyl acetate-6-*endo-d* is not formed by concerted termolecular addition of acetic acid – concerted bimolecular addition would yield the *endo*-2-acetate – we envisage four probable pathways for acid-catalyzed cleavage of nortricyclanes shown in Schemes 5–8. In pathway 1 (Scheme 5), the nonclassical norbornyl cation is generated by corner deuteronation. While the protio species is symmetrical, the C(6) deuterated nonclassical cation is unsymmetrical and a larger secondary kinetic isotope effect (KIE) for formation of the *exo*-6-*d*-acetate, in principle, could result in a small excess of *endo*-6-*d*-acetate. However, that the *exo*- and *endo*-γ-KIE's for solvolysis of *exo*-norbornyl brosylate are nearly equal[4] es-

[4]The *exo*- and *endo*-6-*d*-KIE's for solvolysis in 80% CH_3CH_2OH/H_2O at 25°C are 1.09 ± 0.03 and 1.11 ± 0.01 (13). In acetic acid at 44°C the KIE's are 1.149 ± 0.016 and 1.097 ± 0.011 (14). The KIE's for solvolysis (80% CH_3CH_2OH/H_2O/25°C) of *syn*-7-chloro-*endo*-6-*d*-, *anti*-7-chloro-*endo*-6-*d*-, *syn*-7-chloro-*exo*,*exo*-5,6-d_2-, and *anti*-7-chloro-*exo*,*exo*-5,6-d_2-*exo*-norbornyl brosylates are 1.125 ± 0.007, 1.120 ± 0.005, 1.119 ± 0.011, and 1.150 ± 0.013, respectively (5).

Can. J. Chem. Downloaded from www.nrcresearchpress.com by 210.87.254.105 on 09/06/12
For personal use only.

Can. J. Chem. Downloaded from www.nrcresearchpress.com by 210.87.254.105 on 09/06/12
For personal use only.

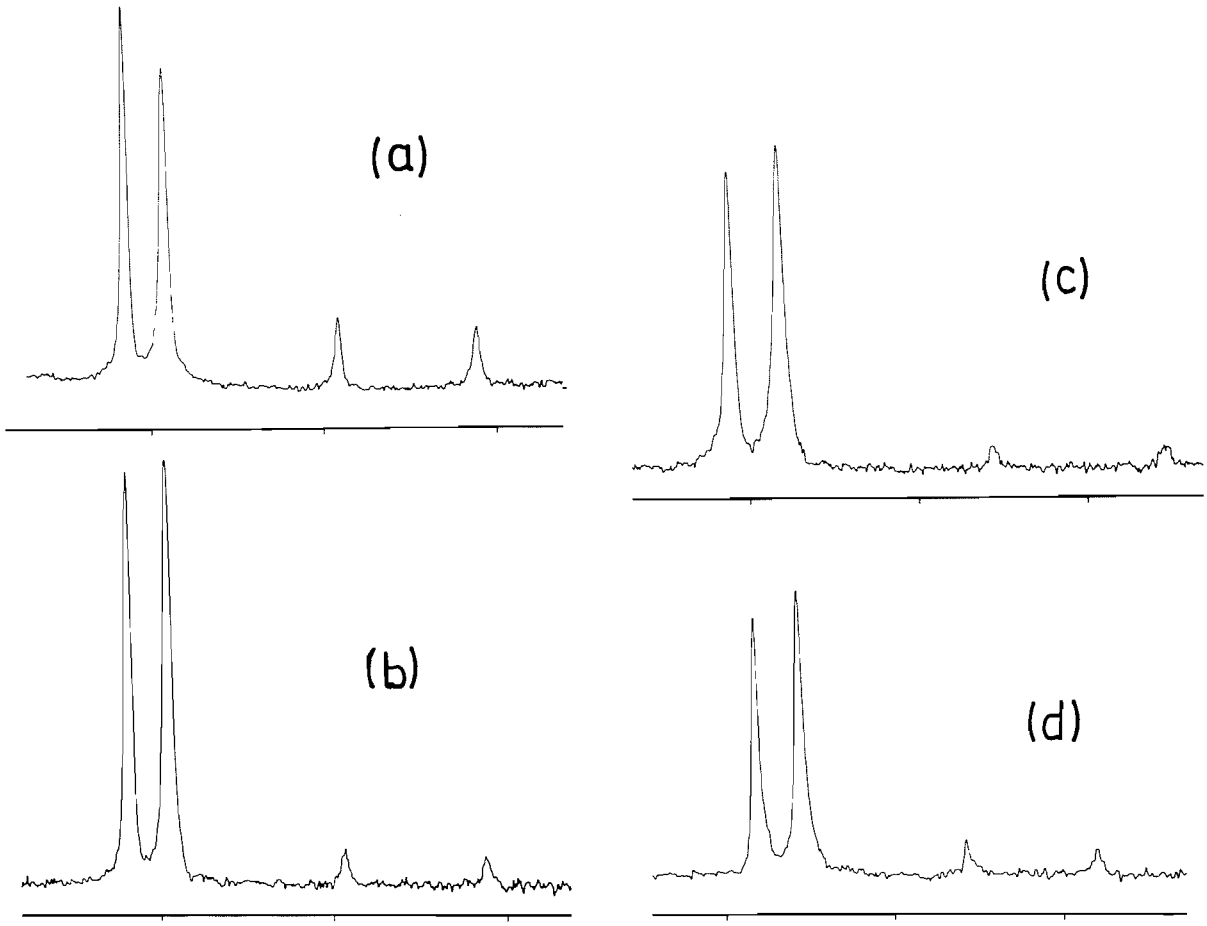

FIG. 2. 13.8 MHz ^{2}Hmr spectra of deuterated *exo*-2-norbornanols in CCl_4; (a) deuterated alcohol (0.0257 g) obtained from **4***a* complexed with $Pr(fod)_3$ (0.0958 g); (b) deuterated alcohol (0.0249 g) obtained from **4***c* complexed with $Pr(fod)_3$ (0.0927 g); (c) deuterated alcohol (0.015 g) obtained from **4***d* complexed with $Pr(fod)_3$ (0.0560 g); (d) deuterated alcohol (0.0090 g) obtained from **4***e* complexed with $Pr(fod)_3$ (0.0340 g).

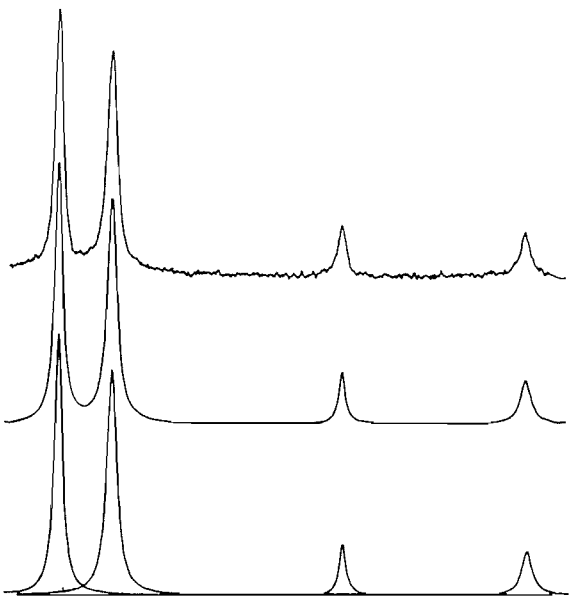

FIG. 3. (a) 13.8 MHz ^{2}Hmr spectrum of deuterated *exo*-2-norbornanol (0.0257 g) obtained from **4***a* complexed with $Pr(fod)_3$ (0.0958 g) in CCl_4; (b) computer-fitted spectrum; (c) resolved spectrum.

tablishes that a differential KIE cannot be invoked to account for the preferential formation of *endo*-6-*d*-acetate. That the γ-KIE's for solvolysis of *syn*- and *anti*-7-chloro-*exo*-brosylate are only slightly larger[4] than the KIE's for the parent brosylates establishes that an electron-withdrawing group at C(7) does not induce a differential in the *exo*- and *endo*-KIE's. We expect the same situation to hold for a halogen located at C(4).

In pathway 2 (Scheme 6) an edge-deuteronated nortricyclane (EDN) is considered as the initial intermediate. The EDN can react with solvent (k_s^{EDN}) or yield a nonclassical cation (NC) via an edge-to-corner deuterium shift. Other deuterated nonclassical species are formed by corner-to-edge-to-corner circumambulations. Assuming the NC's are intermediates in the ring cleavage of **4***a* and that most of the substitution occurs via the NC's (k_s^{NC}), the ratio of C(6) deuterated acetate (85%) to C(1) and C(2) deuterated acetates (15%), including a statistical factor of 2, is approximately equal to the ratio of the rates of substitution and 6,2-H shift, and

$$[1] \quad k_s^{NC}/k_{6,2H} \sim 2.8$$

The value is in good agreement, assuming there is a secondary KIE, with $k_s^{NC}/k_{6,2H}$ ratios of 1.9 ± 0.6 and 1.55 ± 0.35 obtained by Collins and Lietzke through a sophisticated analysis of ^{14}C and ^{3}H scramblings observed in the acetolysis of labelled *exo*-norbornyl brosylates (15). This analysis estab-

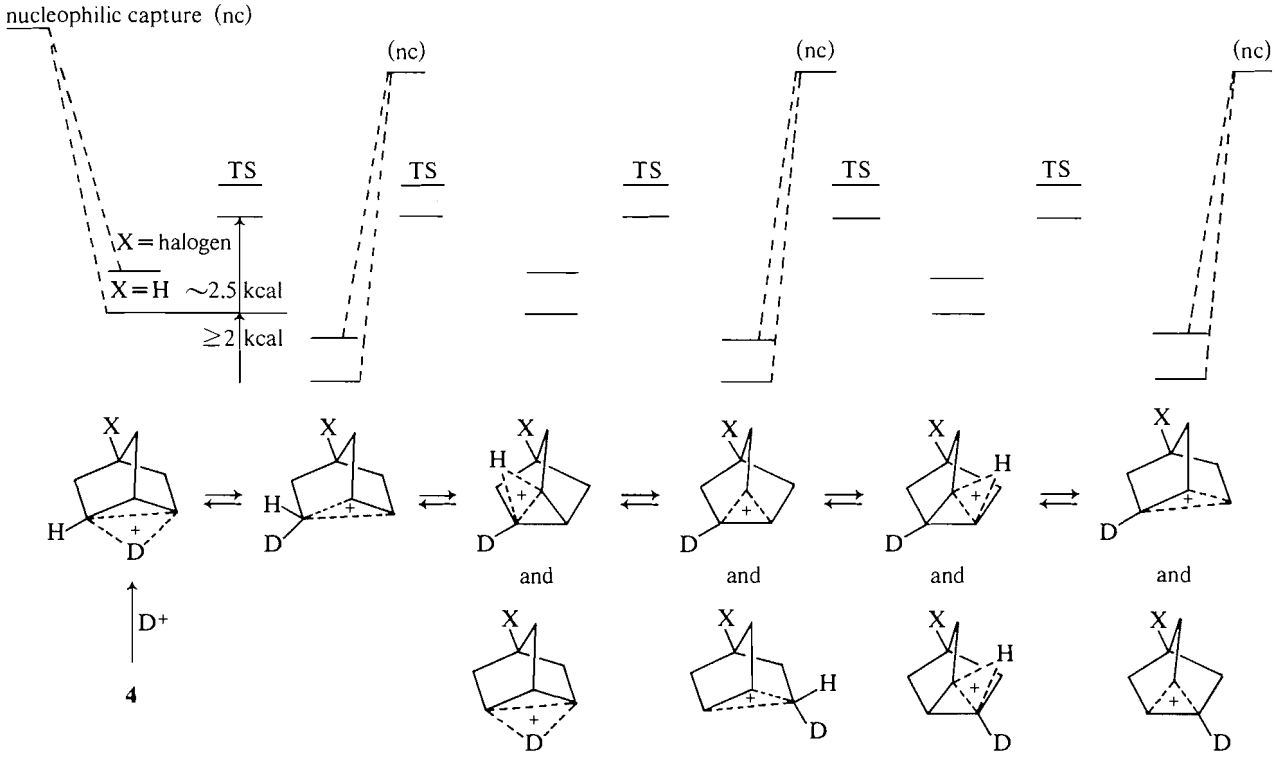

SCHEME 6

lishes that the intermediates, whether they are nonclassical or otherwise, generated by ring opening of norticyclane in acetic acid are the same as the species generated by acetolysis. Assuming that $k_s^{EDN} \sim k_s^{NC}$, not an unreasonable assumption since the charge on the carbon atoms should be similar[5] in both species, then [1] yields

$$[2] \quad k_s^{EDN}/k_{rearr}^{EDN\rightarrow NC} \sim 0.046$$

where 0.046 is the fractional excess (0.044/0.957) of *endo*-6-*d*-acetate formed in the ring opening of **4***a*. Thus [2] yields

$$[3] \quad k_{rearr}^{EDN\rightarrow NC} \sim 2.8 \times k_{6,2H}/0.046$$

and

$$[4] \quad k_{rearr}^{EDN\rightarrow NC} \sim 60 \times k_{6,2H}$$

Since $k_{6,2H} \sim 2.5 \times 10^8$ s^{-1} at 25°C,[6] our analysis establishes that in order for the excess *endo*-6-*d*-acetate to result from reaction of an initially formed EDN with solvent, $k_{rearr}^{EDN\rightarrow NC} \sim 1.5 \times 10^{10}$ s^{-1} and $E_a \sim 2.5$ kcal/mol. Since edge-protonated nortricyclane is not observed down to −141°C even though 6,2-hydride shifts are frozen out, this establishes that EPN (EDN) must be at least 2 kcal higher in energy than the nonclassical ion or a rapidly-equilibrating species. Recent calculations by Goddard *et al.* (18) place EDN ~12.4 kcal/mol higher in energy than classical and nonclassical norbornyl cations. Based on this analysis, E_a for conversion of NC to EPN (EDN) is ≥4.5 kcal. It is interesting to note that E_a for a 6,2-shift has been established at 5.8 kcal/mol (17). If EPN's indeed are intermediates in the ring-openings, they must be involved in solvolysis reactions and 6,2-H(D) shifts most probably occur via EPN's rather than by direct corner-to-corner shifts (19). The approximate energy profiles shown in Scheme 6 can be drawn if isotope effects are neglected. If the mechanism of ring cleavage is as outlined in Scheme 6 and NC's rather than EDN's are the major sources of acetates (*vide supra*), then the amounts of C(1)- and C(2)-deuterated acetates formed, as observed, should be similar.

Based on our previous solvolysis study (5) which pointed to the involvement of unsymmetrically-bridged cations as intermediates, two additional mechanisms can be considered. In pathway 3 (Scheme 7) – the simplest mechanism – an unsymmetrically-2,6-bridged cation (UBC) is generated directly by an edge-wise approach and corner slide of D^+ without formation of an EDN. In this case 6,2-D(H) shifts would occur corner-to-corner (19) via a transition state which resembles an EDN.

In pathway 4 (Scheme 8) edge deuteronation yields an EDN that either reacts with solvent or rearranges to a rapidly-equilibrating UBC. If W−M rearrangement is fast, then the ratio of the rates of solvent capture and 6,2-H shift can be obtained from the ratio of the amounts of acetate with deuterium at C(6) (85%) and acetates with deuterium at C(1) and C(2) (15% total), yielding

$$[5] \quad 2 \times k_s^{UBC}/k_{6,2\text{-}H} \sim 5.7$$

Consequently,

$$[6] \quad k_s^{UBC}/k_{6,2\text{-}H} \sim 2.8$$

in good agreement with $k_s/k_{6,2\text{-}H}$ obtained by Collins and Lietzke (*vide supra*). If excess *endo*-6-*d*-acetate arises from

[5]Dewar *et al.* (16) have calculated that the formal charges at C(1) and C(6) of EDN and at C(1) and C(2) of the NC are 0.176 and 0.142, respectively.

[6]Olah *et al.* (17) have established that the activation energy for a 6,2-shift at −141°C is 5.8 kcal/mol. At 25°C the rate constant is ~2.5 × 10^8 s^{-1}.

Can. J. Chem. Downloaded from www.nrcresearchpress.com by 210.87.254.105 on 09/06/12
For personal use only.

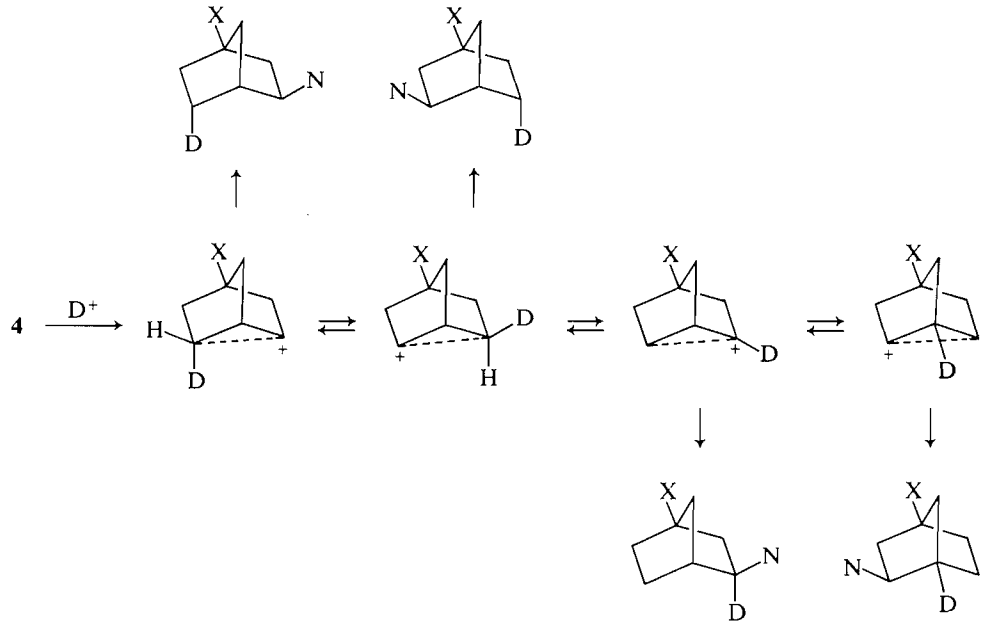

SCHEME 7

reaction of EDN with solvent, then

[7] $$2k_s^{EDN}/k_{rearr}^{EDN\rightarrow UBC} \sim 0.046$$

If the statistical factor reduces the difference in the rates of reaction of UBC and EPN (EDN) expected on the basis of their electrophilicities, then $2k_s^{EDN} \sim k_s^{UBC}$ and

[8] $$k_{rearr}^{EDN\rightarrow UBC} \leq \frac{2.8 \times 2.5 \times 10^8\ s^{-1}}{0.046}$$

since $k_{6,2\text{-H}} \sim 2.5 \times 10^8\ s^{-1}$. Consequently E_a for the rearrangement of EDN to UBC is $\geq$2.5 kcal per mol. That EPN is not observed down to -140°C, while 6,2-shifts are frozen out in the norbornyl cation, establishes that EPN (EDN) must be at least 2 kcal higher in energy than the rapidly equilibrating UBC. In this connection it is interesting to note that Dewar *et al.* (16) have calculated that EPN is 2.8 kcal higher in energy than the classical cation and that the barrier to conversion of EPN to the classical cation is 2.8 kcal/mol. However, recent calculations by Goddard *et al.* (18) place EPN ~12.4 kcal/mol higher in energy than the classical and nonclassical cations. They stated that the 2-norbornyl cation might be best viewed as an unsymmetrically-bridged species. That the acetates with deuterium located at C(1) and C(2) are formed in equivalent amounts, neglecting secondary KIE's, is expected because W–M rearrangement is fast relative to nucleophilic capture by solvent.

Effect of halogen substituents

Since steric interactions of the C(4) substituent with the reaction center are not possible, the substituent, in principle, can influence the chemistry of the 2-norbornyl cation through ponderal and polar effects and by altering solvation.

Ponderal effect

Using a theoretical study of S_N2 reactions of alkyl halides, de la Mare *et al.* (6) defined and quantified a ponderal effect as a nonpolar, nonsteric entropy effect which depends on the mass of a substituent and its position but not on its bulk or charge. Translational, rotational, and vibrational entropies which depend on the mass of a substituent and its position are components of the entropies of the reactants and the transition state and play a major role in determining the magnitude of $\Delta S^{\ddagger}$. By computing the contributions of each type, they showed that the ponderal effect in S_N2 reactions, in general, is rate retarding. While entropy change due to differences in solvation of reactants and transition states is possible also, the authors concluded that this effect would remain essentially constant for a structurally similar series of reactants and transition states, and $\Delta\Delta S^{\ddagger}_{solv} \sim 0$. We expect that the same situation holds for the ring-opening reactions as well. In their analysis of a group of S_N2 reactions (Br^- + RBr; R = methyl, *n*-propyl, isopropyl, *tert*-butyl, neo-pentyl, isobutyl) the translational entropy of activation was obtained as a difference of the terms in eq. [9].

[9] $$\Delta S^{\ddagger}_{trans} = S_t(XRX^-) - S_t(RX) - S_t(X^-)$$

where the translational entropies of the species were evaluated using eq. [10].

[10] $$S_t = 2.303R\,(1.5 \log M + 2.5 \log T) - 2.315$$

For the S_N2 process, because mass (X^-) is added in attaining the transition state, $\Delta S_t^{\ddagger}$ decreases as the mass of R is increased, i.e. $S_t(XRX^-)$ increases more slowly than $S_t(RX)$ because of the logarithm in eq. [10]. If an unsymmetrical ion **2** or **5** is generated in the ring-opening of nortricyclanes, scrambling of the *exo*- and *endo*-hydrogens at C(5) and C(6) would occur by rearrangement of **2** (XR^+) to **3**, or **5** to its enantiomer, via **1** ($XR_{\pm}^+$). Since $S_t(XR_{\pm}^+)$ and $S_t(XR^+)$ must be identical, unlike the case for the S_N2 reactions, $\Delta S^{\ddagger}_{trans} \sim 0$ for the rearrangement and for the conversion of EPN to a nonclassical ion or an unsymmetrical species.

The rotational contribution to the entropy of activation in de la Mare's analysis of S_N2 reactions was given by eq. [11] and the rotational entropies of the species were calculated using eq. [12]. A, B, and C are the principal moments of inertia and

[11] $$\Delta S^{\ddagger}_{rot} = S_r(XRX^-) - S_r(RX)$$

[12] $$S_r = 2.303R\,(0.5 \log ABC - \log \sigma + 1.5 \log T) - 5.384$$

σ is the symmetry factor. According to de la Mare's analysis,

Can. J. Chem. Downloaded from www.nrcresearchpress.com by 210.87.254.105 on 09/06/12
For personal use only.

Can. J. Chem. Downloaded from www.nrcresearchpress.com by 210.87.254.105 on 09/06/12
For personal use only.

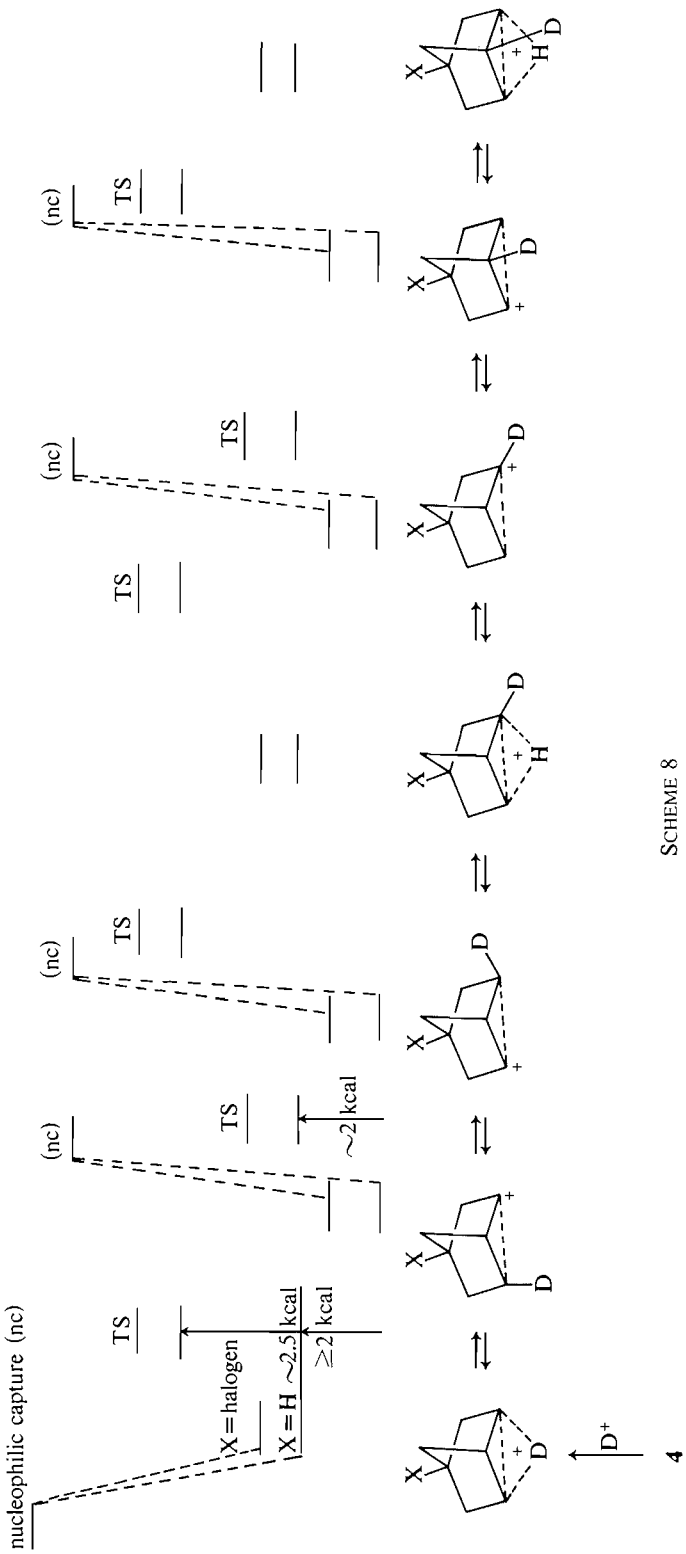

SCHEME 8

an increase in the mass of R will result in an increase or decrease in rotational entropy depending on whether the additional mass is located near or remote from the reaction centre. For the cations generated from **4***a*, **4***c*, **4***d*, and **4***e*, as the mass of X increases there will be a change in the centre of mass, i.e. a shift towards X. While an increase in the ABC term is expected for both $XR_{\pm}^{\ddagger}$ and XR^{+}, whether or not there is a significant decrease in $\Delta S_{rot}^{\ddagger}$ through the series ($\Delta\Delta S^{\ddagger} \neq 0$) is difficult to establish because $XR_{\pm}^{\ddagger}$ and XR^{+} are very similar.

The vibrational entropies of activation $\Delta S_{vib}^{\ddagger}$ for the rearrangement of XR^{+} via transition state $XR_{\pm}^{\ddagger}$ are given by eq. [13].

$$[13] \quad \Delta S_{vib}^{\ddagger} = S_v(XR^{+}) - S_v(XR^{+})$$

when the S_v's are calculated using eq. [14] and $x = 0.00483\ \omega$

$$[14] \quad S_v = \Sigma[-R \ln (1 - e^{-x}) + Rxe^{-x}/(1 - e^{-x})]$$

(ω = vibrational frequency in cm^{-1} at 298K). According to de la Mare, the general effect of added mass would be to lower frequencies and raise vibrational entropies. However, for S_N2 reactions the effect is less pronounced in the transition state than in the initial state because the mass and moments of inertia of the former are larger due to the additions of X^{-}. Thus the changes produced are proportionally smaller. Consequently, for S_N2 processes there is a reduction in $\Delta S_{vib}^{\ddagger}$ as the mass of R is increased and the reaction rate decreases due to the ponderal effect. However, in the rearrangement of cations XR^{+} there is no mass added in the transition state. While the S_v's for the 4-halocations and their corresponding transition states undoubtedly are lower than the S_v's for the unsubstituted species, whether or not $\Delta S_{vib}^{\ddagger}$ decreases or increases as the mass of X increases can only be ascertained by carrying out a complete analysis of the fundamental modes of the cations and the transition states.

Polar effects

The structural changes produced by introducing an EWG at C(4) of the nonclassical cation are difficult to predict with certainty. However, we expect that the dispersal of charge would be unaffected by a halogen at C(4) because it does not destroy the symmetry of the ion. Consequently, if **1** is the sole intermediate in the ring opening it would react as a "symmetrical" species since the γ-secondary KIE's for collapse with solvent should be similar if not identical (*vide supra*). The stereochemistry of the ring-cleavages of **4***c*, **4***d*, and **4***e* in deuterated medium should be unaffected by the halogens at C(4). Consequently, the 4-halonortricyclanes are not cleaved via the mechanism depicted in Scheme 5.

In the case where EDN's and NC's are intermediates (Scheme 6), the increase in the amount of *endo*-6-*d*-acetate obtained upon halogen substitution could result from an increase in the electrophilicity of EDN even though an EWG at C(4), in principle, can affect the rate of EDN-to-NC conversion. A reduction in the amount of "6,2-shift" products could be a consequence of the fact that a halogen-substituted NC reacts faster with solvent, but undergoes a 6,2-shift at a slower rate than the parent NC.

Recently, Grob and co-workers (20, 21) studied the solvolysis of C(6) substituted *exo*-2- and *endo*-2-norbornyl tosylates and concluded that the norbornyl cation is an unsymmetrical 2,6-bridged species **19** in keeping with our previous proposal (5). They found that solvolysis of *exo*-2-norbornyl tosylates bearing EWG's at C(6) yields substantial amounts of *endo*-2-

Can. J. Chem. Downloaded from www.nrcresearchpress.com by 210.87.254.105 on 09/06/12
For personal use only.

norbornanols. The authors concluded that EWG's at C(6) reduce 2,6-bridging and increase the barrier to interconversion of the unsymmetrical ions. If the norbornyl cation is an unsymmetrical species (Schemes 7 and 8), then EWG's at C(4) should produce the same effect as that proposed by Grob: 2,6-bridging should be reduced and the barrier to interconversion should increase. Consequently, solvent capture should compete more effectively with rearrangement and the *endo*/*exo* deuterium ratio at C(6) should increase when a halogen is substituted at C(4). Also, the 4 halogen substituted cations may be more electrophilic than the parent ion and thereby react faster with solvent. The results of our study are in accord with these hypotheses. While a difference in the stereochemistry of the ring-opening of **4***a* and **4***c* is expected on the basis of the electronegativities of H and Cl and is observed, in fact, the difference between **4***c* and the other halonortricyclanes cannot be predicted with certainty. This is so because the values of the substituent constants depend on the mode of derivation. For example, while the field effect parameters F (22) for Cl, Br, and I are 0.690, 0.727, and 0.672, respectively, the σ_I values are 0.47, 0.45, and 0.39 (23). The changes in stereochemistry of the ring-opening of **4***a*, **4***c*, and **4***d* appear to parallel the F values, but the result for iodine appears out of line. Perhaps a ponderal effect is superimposed on the polar effect.

An effect of EWG's at C(4) on 6.2-hydride shifts, E_a ~ 6 kcal/mol, in the [2.2.1]-system should also be expected. An EWG at C(4) would reduce the electron density in the C—H bonds at C(6) and thereby increase the barrier for a 6,2-shift. That a substantial decrease (~50%) in the amount of hydride shift is observed in the ring-opening of halonortricyclanes **4***c*, **4***d*, and **4***e* relative to **4***a* (Table 3) and that there is a rough parallel with substituent constants supports the hypothesis. Thus the simplest mechanism involving only rapidly-equilibrating unsymmetrical cations (Scheme 7) can be invoked to account for the results and the slight excess of *endo*-6-*d*-acetate (4.5%) observed in the cleavage of **4***a* arises from capture of *endo*-6-*d*-UBC before it equilibrates. That the *exo*-acetate obtained from the acetolysis of optically active *exo*-brosylate is racemic, runs counter to our arguments. However, it is conceivable that the brosylate anion shields the UBC and equilibration is essentially complete before solvent intervenes.[7]

In this connection it is interesting to note that addition of protio acids to 2,3-dideuterionorbornene (25) and deuterioacids to norbornene (26–28) yields labelled products which indicate capture of an unsymmetrical cation by nucleophiles. Although the interpretation has been criticized (29) because termolecular processes and 6-membered molecular additions can be involved, it is noteworthy that similar results were obtained using a variety of acids, solvents, and reaction conditions. For example, as shown in Scheme 9, addition of HBr to **20** in aqueous medium yields predominately **21** (25). In this case EPN is not an initial intermediate and a good nucleophile is present. It is difficult to understand why addition should occur via a termolecular process or by a four-centered or 6-membered addition in this case.

If EDN's and UBC's are intermediates (Scheme 8), then the increase in the amount of *endo*-6-*d*-acetate which is observed

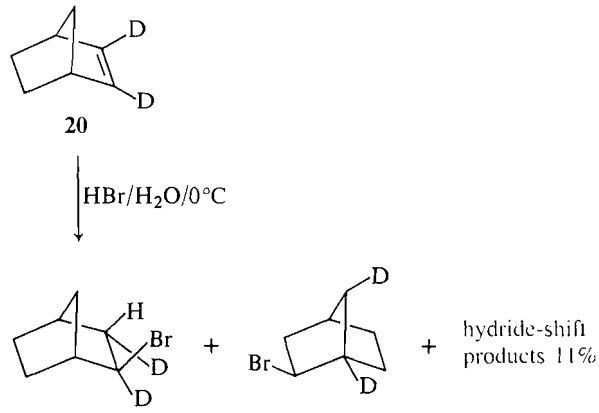

SCHEME 9

upon halogen substitution at C(4) could be due to several factors. It is conceivable that an EWG at C(4) destabilizes the UBC, where charge is localized, more than EPN (EDN), thereby increasing E_a for the EPN(EDN)-to-UBC conversion. Moreover, a halogen at C(4) should increase the electrophilicity of EPN and enhance its rate of reaction with solvent. On this basis, the increase in the amount of *endo*-6-*d*-acetate observed upon halogen substitution could result entirely from reactions of an intermediate EDN. However, an EWG at C(4) could also increase the barrier (*vide supra*) for W—M rearrangement and increase the electrophilicity of the UBC. The net effect would be to increase the rate of capture of *endo*-6-*d*-UBC and consequently decrease the relative amount of 6,2-H shift as well.

Presently, based on the analysis of the results of this study and our previous work (5), we prefer a mechanism which involves formation of rapidly-equilibrating 6,2-bridged norbornyl cations. While edge-protonated norticyclanes can be involved as intermediates, the simplest cleavage mechanism involves edge-wise approach of D^+ to the cyclopropane bond with a corner slide to generate an unsymmetrically 6,2-bridged cation.

Experimental

General

Nuclear magnetic resonance spectra were obtained on Bruker WH-90, Varian EM 390, and Varian T 60 instruments in $CDCl_3$ or CCl_4 with TMS as an internal standard. Deuterium magnetic resonance spectra were obtained at 13.8 MHz. Deuterium analyses were carried out at low voltage (15 eV) on a CEC double-focussing mass spectrometer. Boiling points and melting points are uncorrected. Solutions of organic solvents were dried over anhydrous $MgSO_4$ or Na_2SO_4.

2,2-Dichlorobicyclo[2.2.1]heptane (7a)

2,2-Dichlorobicyclo[2.2.1]heptane (112 g) was prepared from bicyclo[2.2.1]heptan-2-one (101 g) using PCl_3 and PCl_5 according to the method of Wiberg *et al.* (30).

1,2-Dichlorobicyclo[2.2.1]heptane (8a)

1,2-Dichlorobicyclo[2.2.1]heptane (85 g) was obtained by isomerization of 2,2-dichlorobicyclo[2.2.1]heptane (112 g) catalyzed by $SnCl_4$ in toluene using a method similar to the one described by Wilt *et al.* (31).

1-Chlorobicyclo[2.2.1]hept-2-ene (9a)

1,2-Dichlorobicyclo[2.2.1]heptane (85 g, 0.52 mol) was dissolved in dry DMSO (450 mL) and added to *t*-BuOK (84 g, 0.81 mol) in a 1 L flask equipped with a $CaCl_2$ drying tube. The reaction mixture was stirred overnight, added to 1 L of water, and extracted with ether (4 × 250 mL). The combined ether extracts were washed with water (2

[7]That *exo*-brosylate racemizes during acetolysis and only 29% of products are derived from optically active substrate provides support for this possibility (24).

Can. J. Chem. Downloaded from www.nrcresearchpress.com by 210.87.254.105 on 09/06/12
For personal use only.

× 100 mL) and dried. Distillation of the residue after the ether was distilled off yielded 1-chlorononbornene (51 g, bp 135–138°C/atmospheric pressure); ^{1}Hmr ($CDCl_3$) δ: 6.08 (m, 2, vinyl Hs), 2.85 (m, 1, H(4)), 2.2–1.0 (norbornyl envelope).

1,3-Dichlorobicyclo[2.2.1]heptane

1,3-Dichlorobicyclo[2.2.1]heptane (16 g, bp 71.5–73°C/10 Torr) was prepared from 1-chlorobicyclo[2.2.1]hept-2-ene by the addition of HCl in CH_2Cl_2 at −78°C according to the method of Fry and Farnham (32).

*4-Chloro-*exo*-2-bicyclo[2.2.1]heptanol (**11**a)*

To 1,3-dichlorobicyclo[2.2.1]heptane (9.2 g, 0.056 mol) in solution in dioxane (50 mL) was added with stirring $AgNO_3$ (18.6 g, 0.11 mol) in water (50 mL). The solution was refluxed for 39 h and extracted with CH_2Cl_2 (2 × 75 mL). The combined CH_2Cl_2 extracts were washed with water and dried. The solvent was distilled off and the last traces of solvent were removed under vacuum to yield 4.7 g of 4-chloro-*exo*-2-bicyclo[2.2.1]heptan-2-ol; mp 73–79°C; ^{1}Hmr ($CDCl_3$) δ: 3.90 (bd, 1, *endo*-H(2)), 2.40 (s, 1, —OH), 2.4–1.0 (norbornyl envelope).

*Large scale oxymercuration of 1-chlorobicyclo[2.2.1]hept-2-ene (**10**a)*

A solution of **9***a* (141 g, 1.1 mol), yellow mercuric oxide (120 g, 0.56 mol), and mercuric chloride (150 g, 0.56 mol) in 1200 mL of aqueous acetone (50:50) was refluxed for 72 h. Most of the solvent was distilled off and the residue was filtered and dried under vacuum to yield 423 g of organomercurial **10***a*. The dry mercurial was added to 1400 mL of ether–methanol (1:3) in a 2 L flask equipped with a condenser and $NaBH_4$ (92.4 g) was added continuously over a period of 5 h. The mixture was refluxed for 12 h, acidified with 10% aqueous HCl, and extracted with ether (6 × 500 mL). The combined ether layers were washed with saturated aqueous $NaHCO_3$ solution, water, and dried over anhydrous Na_2SO_4. The solvent was distilled off through a 30 cm glass-helices column and glpc analysis of this residue showed that the mixture was composed of ~40% **11***a* and 60% **9***a*. Continuation of the distillation gave 1-chlorononbornene and a viscous residue which crystallized. The remaining traces of alkene were removed under vacuum to yield 42 g of crude 4-chloro-*exo*-2-norbornanol (**11***a*) which was oxidized to **12***a* without further purification.

*1-Chlorobicyclo[2.2.1]heptan-3-one (**12**a)*

The crude chlorohydrin (42 g, 0.29 mol) was dissolved in 200 mL of pre-oxidized ether, 200 mL of Brown's reagent was added carefully with stirring, and the mixture was stirred vigorously for 24 h at ambient temperature. The ether layer was separated and the aqueous layer was extracted with ether (6 × 100 mL). The combined ether extracts were washed with water (150 mL), saturated aqueous sodium bicarbonate (200 mL), water (150 mL), and dried. The ether was distilled off through a 30 cm glass-helices column and the last traces of solvent were removed under vacuum to yield 41 g of **12***a* which was shown to be 90% pure by analytical glpc; ^{1}Hmr ($CDCl_3$) δ: 2.75 (bm, 1, H(1)), 2.55 (bs, 2, *exo*-H(3) and *endo*-H(3)), 2.4–1.0 (norbornyl envelope).

*4-Chlorobicyclo[2.2.1]heptan-2-one tosylhydrazone (**6**b)*

To 43 g 4-chlorobicyclo[2.2.1]heptan-2-one (**12***a*) in 800 mL of absolute ethanol was added *p*-toluenesulfonylhydrazine (56.6 g, 0.30 mol). Concentrated HCl (5 mL) was added and the mixture was heated at reflux for 72 h. The reaction mixture was cooled and the solid that crystallized was filtered off and dried under vacuum to yield 40 g of 4-chloro[2.2.1]heptan-2-one tosylhydrazone (**6***b*), mp 174–176°C.

*4-Chlorotricyclo[2.2.1.0^{2,6}]heptane (**4**c)*

Freshly prepared CH_3ONa (50 g, 0.93 mol) was dissolved in diglyme (575 mL, dried over CaH_2 and distilled), 4-chlorobicyclo-[2.2.1]heptan-2-one tosylhydrazone (35 g, 0.11 mol) was added, and the mixture was heated at reflux for 3 h until nitrogen evolution essentially stopped. The dark-brown reaetion mixture was cooled, poured into water (500 mL), and extracted with ether (6 × 300 mL); the ether extracts were washed with water, dried, and the solvent was removed by distillation through a 30 cm glass-helices column. Since glpc analysis showed that diglyme and **4***c* were present, the residue was dissolved in pentane (500 mL) and the solution was extracted with water (5 × 200 mL), dried, and the pentane was distilled off. The residue was combined with the product of a second reaction of identical scale and 10.5 g of **4***c* (97% pure) were obtained (bp 142–144°C/atmospheric pressure). A second distillation through a 30 cm glass-helices column gave **4***b* which was >99% pure; ^{1}Hmr (CCl_4) δ: 1.65 (s, 6, —CH_2—), 1.18 (s, 3, cyclopropyl H).

*2,2-Dibromobicyclo[2.2.1]heptane (**7**b)*

To norcamphor (43 g, 0.39 mol) in an ice-cooled 3-necked 1 L flask equipped with a magnetic stirrer, a reflux condenser, and drying tube were added PBr_3 (121 g, 0.45 mol) and PBr_5 (191 g, 0.44 mol) with stirring over a period of 2 h. The mixture was warmed to room temperature and stirred for 17 h. The mixture was poured onto ice (800 g), warmed to room temperature with stirring, and extracted with ether (5 × 200 mL). The combined ether extracts were dried and the solvent was distilled off through a 30 cm glass-helices column. The last traces of solvent were removed on the rotatory evaporator to yield 71.5 g of product which was shown by analytical glpc to be composed of two major products (80%) and unreacted norcamphor (15%).

*1,2-Dibromobicyclo[2.2.1]heptane (**8**b)*

The crude 2,2-dibromide (71.5 g) was dissolved in purified pentane (100 mL) and $ZnBr_2$ (40 g) was added. After 1 h the pentane solution was decanted from the sticky mass and fresh $ZnBr_2$ (20 g) was added. The process was repeated once and the solution was agitated with a magnetic stirrer for one week at ambient temperature. The glpc analysis showed that the isomerization was essentially complete and one major product (88%) was present along with ~3% of norcamphor. Distillation yielded 30 g of **8***b* (bp 78–80°C/0.1 Torr) which was shown to be 94% pure by analytical glpc.

*1-Bromobicyclo[2.2.1]heptan-2-ene (**9**b)*

Dibromide **8***b* (30 g, 0.12 mol) was dissolved in purified DMSO (150 mL, stored over NaOH, vacuum distilled, and stored over 4Å molecular sieves), and *t*-BuOK (27 g, 0.24 mol) was added. The mixture was stirred at ambient temperature for 24 h and poured into a separatory funnel containing H_2O (150 mL) and ether (150 mL). The aqueous layer was extracted with ether (6 × 100 mL) and the combined extracts were washed with water (100 mL), saturated aqueous NaCl solution (100 mL), and dried. The solvent was distilled off at atmospheric pressure through a 30 cm glass-helices column and the residue was distilled under aspirator vacuum (~20 Torr) to yield 14.2 g of **9***b*, bp 46–47°C; ^{1}Hmr (CCl_4) δ: 6.05 (m, 2, vinyl H's), 2.75 (m, 1, bridgehead H), 2.2–1.0 (norbornyl envelope).

*Oxymercuration of 1-bromobicyclo[2.2.1]hept-2-ene (**9**b)*

Bromonorbornene **9***b* (5.00 g, 0.029 mol), mercuric oxide (3.13 g, 0.0144 mol), and mercuric chloride (3.92 g, 0.0144 mol) were placed in a 100 mL round-bottomed flask, 50% v/v aqueous acetone (100 mL) was added, and the mixture was refluxed for 72 h with magnetic stirring. The solvent was removed on the rotatory evaporator and the solid was pumped under vacuum while being warmed with a hair dryer to yield 11.9 g (96.7%) of bromomercurial; mp 117–128°C; ^{1}Hmr ($CDCl_3$) δ: 4.00 (bd, 1), 3.55 (dd, 1), 2.50 (d, 1, bridgehead H), 2.4–1.0 (norbornyl evelope and —OH).

*4-Bromobicyclo[2.2.1]heptan-2-one (**12**b)*

To a solution of crude **11***b* (48 g, 0.25 mol, obtained from a large scale oxymercuration of **9***b*) in preoxidized ether (500 mL) in a 1 L flask equipped with a condenser and a magnetic stirrer was added Brown's reagent (126 mL) in small portions. The mixture was stirred vigorously for 46 h at ambient temperature, the ether layer was withdrawn, and the aqueous layer was extracted with ether (5 × 100 mL). The combined ether extracts were washed with aqueous $NaHCO_3$ (2 × 75 mL), water (2 × 100 mL), and dried. The solvent was stripped

Can. J. Chem. Downloaded from www.nrcresearchpress.com by 210.87.254.105 on 09/06/12
For personal use only.

by distillation and the final traces were removed under vacuum to yield 41 g of **12***b*; mp 60–62°C; ^{1}Hmr ($CDCl_3$) δ: 2.55 (m, 1, H(1)), 2.50 (s, 2, *exo*-H(3) and *endo*-H(3)), 2.4–1.4 (norbornyl envelope).

*4-Bromobicyclo[2.2.1]heptan-2-one tosylhydrazone (**6**c)*

To **12***b* (40 g, 0.21 mol) of *p*-toluenesulfonylhydrazine (39.5, 0.21 mol) in 95% ethanol (500 mL) was added concentrated HCl (5 mL) and the mixture was refluxed for 40 h. The reaction mixture was poured into water (800 mL), the solid was isolated by filtration, and the aqueous layer was extracted with CH_2Cl_2 (4 × 250 mL). The combined CH_2Cl_2 layers were washed with water (500 mL), dried, and the solvent was removed by distillation. Recrystallization of the combined solids from 95% ethanol yielded 45.5 g of **6***c*; mp 189.5–190.5°C.

*4-Bromobicyclo[2.2.1.0^{2,6}]heptane (**4**d)*

Tosylhydrazone **6***c* (36 g, 0.1 mol) was added to sodium methoxide (47.5 g, 0.88 mol) in purified diglyme (600 mL), and the mixture was refluxed for 3 h and poured into water (500 mL). The mixture was extracted with ether (10 × 250 mL); the combined ether extracts were washed with water (5 × 250 mL) and dried. The solvent was removed by distillation and the residue was dissolved in pentane (800 mL) and extracted with water (6 × 50 mL). After the pentane solution was dried and concentrated by distillation, **4***d* (7.4 g) was isolated by vacuum distillation (bp 36–37°C/1.8 Torr) and shown to be >99% pure by analytical glpc; ^{1}Hmr (CCl_4) δ: 1.70 (s, 6, —CH_2—), 1.11 (s, 3, cyclopropyl H's).

*4-Iodotricyclo[2.2.1.0^{2,6}]heptane (**4**e)*

Argon, passed through Drierite, bubbled through concentrated H_2SO_4, and passed through a trap, was bubbled through a solution of sodium (2.5 g) and benzophenone (25 g) in toluene (100 mL) in a flask equipped with a condenser and used to flush a two-necked flask equipped with a stopcock at the side and a condenser fitted with a $CaCl_2$ drying tube. The apparatus was charged with purified cyclohexane (25 mL, stored over CaH_2 and distilled), Li (1.0 g, 0.14 mol), and sodium (0.05 g) and the solution was heated at reflux under a constant flow of argon and stirred vigorously with a magnetic stirrer. After a fine Li dispersion formed, **4***c* (2.0 g, 0.016 mol) in cyclohexane (5 mL) was added and the mixture was stirred and refluxed for 7 h and cooled. Freshly sublimed iodine was added through the condenser until a purple color persisted. The solution was washed with water (3 × 25 mL) and the aqueous later was extracted with ether (2 × 20 mL). The combined organic layers were dried and filtered twice and most of the solvent was distilled through a 30 cm helices column. Additional solvent was removed by distillation through a 15 cm helices column and **4***e* (1.9 g) was isolated by preparative glpc using a 1.5 m × 6 mm 15% SE-30 on Chromosorb A column maintained at 175°C. Since the collection efficiency was 92%, the overall yield of the reaction was 58%; ^{1}Hmr (CCl_4) δ: 1.71 (s, 6, —CH_2—), 0.95 (s, 3, cyclopropyl H's).

D_2SO_4-catalyzed ring-opening of trichloro[2.2.1.0^{2,6}]heptanes (nortricyclanes)

A stock solution of D_2SO_4 (0.75 g) in CD_3COOD (75 mL) was prepared and used for the cleavage reactions.

*Tricyclo[2.2.1.0^{2,6}]heptane (**4**a)*

Nortricyclane (**4***a*) (0.23 g, 0.0025 mol) was dissolved in 10.6 mL of CD_3COOD/D_2SO_4 solution and the mixture was stirred at ambient temperature for 14 h. The mixture was added slowly in small portions to saturated aqueous $NaHCO_3$ and the aqueous layer was extracted with ether (6 × 20 mL). The glpc analysis established that the reaction was 98% complete. The combined ether extracts were washed with water, dried, and the solvent was removed by distillation through a 30 cm glass-helices column. The remaining traces of solvent were removed under vacuum to yield 0.35 g of deuterated *exo*-norbornyl acetate.

*4-Chlorotricyclo[2.2.1.0^{2,6}]heptane (**4**c)*

Chloronortricyclane **4***c* (0.36 g, 0.0028 mol) was dissolved in 12 mL of D_2SO_4/CD_3COOD solution and stirred at 49 ± 2°C for 76 h. The reaction was quenched by carefully adding it to saturated aqueous $NaHCO_3$ and extracting the aqueous layer with ether. The glpc analysis showed the reaction to be 90% complete and removal of solvent yielded 0.49 g of deuterated 4-chloronorbornyl acetate.

*4-Bromotricyclo[2.2.1.0^{2,6}]heptane (**4**d)*

Bromonortricyclane (**4***d*) (0.48 g, 0.0028 mol) was dissolved in 12 mL of D_2SO_4/CD_3COOD solution and stirred at 49 ± 2°C for 76 h. The usual work-up and glpc analysis showed that the reaction was 97% complete and evaporation of the final traces of ether under vacuum yielded 0.60 g of deuterated bromoacetate.

*4-Iodo[2.2.1.0^{2,6}]heptane (**4**e)*

Iodonortricyclane **4***e* (0.62 g, 0.0028 mol) was dissolved in 12 mL of deuterated stock acid solution and the solution was stirred at 50 ± 1°C for 90.5 h. The reaction was worked up in the usual manner and glpc analysis showed that the reaction was 97% complete and only the acetate was present. The last traces of solvent were removed under vacuum to yield 0.68 g of deuterated 4-iodonorbornyl acetate.

Lithium aluminium hydride reduction of acetates

Acetate **17***a* (0.35 g) in dry ether (5 mL) was added to a slurry of $LiAlH_4$ (0.35 g) in ether (25 mL) and the mixture was refluxed for 3 h. Water (0.5 mL), 10% aqueous NaOH (0.5 mL), and water (0.5 mL) were added slowly in sequence as the mixture was stirred vigorously. The precipitate was filtered off and washed with ether (25 mL). After the ether solution was dried, most of the solvent was removed by distillation and the deuterated *exo*-2-norbornanol (0.13 g) was isolated by preparative glpc on a 3 m × 6 mm 15% Carbowax on Chromosorb W column maintained at 170°C at a He flow rate of ~20 mL per minute. The alcohol (0.015 g) was complexed with 0.050 g of $Pr(fod)_3$ and a ^{2}Hmr was obtained at 13.8 MHz.

Acetate **17***b* (0.49 g) in dry ether (5 mL) was added to a slurry of $LiAlH_4$ (0.5 g) in dry ether (30 mL) and the mixture was refluxed for 3 h. Water (0.5 mL), 10% NaOH (0.5 mL), and water (0.5 mL) were added sequentially with vigorous stirring and the precipitate was filtered off and washed with ether (25 mL). After the ether solution was dried, the ether was distilled off and the last traces of solvent removed under vacuum to yield 0.31 g of deuterated 4-chloro-*exo*-2-norbornanol. The glpc analysis showed the chlorohydrin to be 98% pure.

Acetate **17***c* (0.60 g) in dry ether (5 mL) was added to a slurry of $LiAlH_4$ (0.5 g) in ether (30 mL) and the mixture was refluxed for 4 h. Work-up in the usual manner, followed by evaporation of the last traces of solvent under vacuum, gave 0.33 g of a solid which was shown by glpc to be comprised of 82% 4-bromo-*exo*-2-norbornanol and 17% of *exo*-2-norbornanol.

Acetate **17***d* (0.68 g) dissolved in ether (5 mL) was added to a slurry of $LiAlH_4$ (0.5 g) in ether (30 mL) and the mixture was refluxed for 3 h. Work-up in the usual manner, followed by removal of the final traces of solvent under vacuum, gave 0.33 g of 4-iodo-*exo*-2-norbornanol, shown to be 99% pure by analytical glpc.

Sodium in 2-propanol reduction of halohydrins

Chlorohydrin **18***a* (0.31 g) was dissolved in reagent-grade 2-propanol (9 mL) in a flask (25 mL) fitted with a condenser and drying tube and the solution was heated to reflux. Sodium (0.5 g) was added in small portions to the refluxing solution over a period of 0.5 h and the mixture was refluxed for 4 h. To the cooled solution was added 15 mL of saturated aqueous NaCL solution and pentane (15 mL). The pentane layer was withdrawn after shaking, the aqueous layer was extracted with additional pentane (3 × 15 mL), the combined extracts were washed with saturated aqueous NaCl solution (2 × 10 mL) and dried. Most of the solvent was removed by distillation through a 30 cm glass-helices column and the deuterated *exo*-2-norbornanol (0.076 g) was isolated by preparative glpc on a 3 mm × 6 mm 15% Carbowax on Chromosorb W column maintained at 170°C. The *exo*-norbornanol (0.013 g) was complexed with $Pr(fod)_3$ (0.113g) in CCl_4 and a 13.8 MHz ^{2}Hmr was obtained.

Bromohydrin **18***b* (0.33 g, 82% bromohydrin and 17% *exo*-norbornanol) was dissolved in 9 mL of 2-propanol, the solution was heated to reflux, 0.5 g of sodium was added in small portions over a period of 0.5 h, and the solution was refluxed for 5.5 h. The glpc analysis of the pentane solution obtained after work-up showed an additional product (~20%) of longer retention time than *exo*-norbornanol. The deuterated *exo*-norbornanol (0.040 g) that was isolated by preparative glpc was shown to be >99% *exo*-alcohol by analytical glpc. The deuterated *exo*-norbornanol (0.024 g) was complexed with $Pr(fod)_3$ (0.090 g) in CCl_4 and a 13.8 MHz ^{2}Hmr was obtained.

Iodohydrin **18***c* (0.45 g) was dissolved in 2-propanol and the solution was heated to reflux. Sodium (0.5 g) was added in small portions over a period of 0.5 h and the mixture was refluxed for 2 h. Analytical glpc analysis of a pentane solution obtained after the usual work-up showed that an additional product (~30%) of longer retention time than *exo*-norbornanol was present. Most of the solvent was removed by distillation and the deuterated *exo*-2-norbornanol (0.080 g) was isolated by preparative glpc as described above. Analytical glpc showed the *exo*-norbornanol to be >99% pure. The deuterated alcohol (0.026 g) was complexed with $Pr(fod)_3$ (0.096 g) and a 13.8 MHz ^{2}Hmr was obtained. The remainder was reinjected on the preparative glpc and the deuterated *exo*-alcohol (0.029 g) was complexed with $Pr(fod)_3$ (0.108 g) in CCl_4 and a 13.8 MHz ^{2}Hmr was obtained.

Acknowledgement

We thank the Natural Sciences and Engineering Research Council of Canada for financial support.

1. H. C. BROWN. *In* The nonclassical ion problem: with comments by P. von R. Schleyer. Plenum, New York. 1977.
2. N. H. WERSTIUK, G. TIMMINS, and F. P. CAPPELLI. Can. J. Chem. **51**, 3473 (1973).
3. S. BANERJEE and N. H. WERSTIUK. Can. J. Chem. **54**, 678 (1976).
4. N. H. WERSTIUK, D. DHANOA, and G. TIMMINS. Can. J. Chem. **57**, 2885 (1979).
5. N. H. WERSTIUK, G. TIMMINS, and F. P. CAPPELLI. Can. J. Chem. **58**, 1738 (1980).
6. P. B. D. DE LA MARE, L. FOWDEN, E. D. HUGHES, C. K. INGOLD, and J. D. H. MACKIE. J. Chem. Soc. 3200 (1955).
7. N. H. WERSTIUK, G. TIMMINS, and F. P. CAPPELLI. Can. J. Chem. **58**, 1709 (1980).
8. N. H. WERSTIUK, G. TIMMINS, and F. P. CAPPELLI. Can. J. Chem. **58**, 1725 (1980).
9. A. NICKON and N. H. WERSTIUK. J. Am. Chem. Soc. **94**, 7081 (1972).
10. T. G. TRAYLOR and A. W. BAKER. J. Am. Chem. Soc. **85**, 2746 (1963).
11. H. B. HENBEST and B. NICHOLLS. J. Chem. Soc. 227 (1959).
12. A. NICKON and J. HAMMONS. J. Am. Chem. Soc. **86**, 3322 (1964).
13. B. L. MURR, A. NICKON, T. D. SCHWARZ, and N. H. WERSTIUK. J. Am. Chem. Soc. **89**, 1730 (1967).
14. J. M. JERKUNICA, S. BORČIĆ, AND D. E. SUNKO. J. Am. Chem. Soc. **89**, 1732 (1967).
15. C. J. COLLINS and M. H. LIETZKE. J. Am. Chem. Soc. **89**, 6565 (1967).
16. M. J. S. DEWAR, R. C. HADDON, A. KOMORNICKI, and H. RZEPA. J. Am. Chem. Soc. **99**, 377 (1977).
17. G. A. OLAH, A. M. WHITE, J. R. DEMEMBER, A. COMMEYRAS, and C. Y. LUI. J. Am. Chem. Soc. **92**, 4627 (1970).
18. J. D. GODDARD, Y. OSAMURA, and H. F. SCHAEFER III. J. Am. Chem. Soc. **104**, 3258 (1982).
19. M. SAUNDERS, P. VOGEL, A. L. HAGEN, and J. ROSENFELD. Acc. Chem. Res. **6**, 53 (1973).
20. W. FISCHER, C. A. GROB, R. HANREICH, G. VON SPRECHER, and A. WALDNER. Helv. Chim. Acta, **64**, 2298 (1981).
21. C. A. GROB, B. GÜNTHER, and R. HANREICH. Helv. Chim. Acta, **64**, 2312 (1981).
22. C. G. SWAIN and E. C. LUPTON. J. Am. Chem. Soc. **90**, 4328 (1968).
23. P. R. WELLS, S. EHRENSON, and R. W. TAFT. Prog. Phys. Org. Chem. **6**, 147 (1968).
24. S. WINSTEIN and D. TRIFAN. J. Am. Chem. Soc. **74**, 1154 (1952).
25. J. K. STILLE and R. D. HUGHES. J. Org. Chem. **36**, 340 (1971).
26. H. C. BROWN, J. H. KAWAKAMI, and K.-T. LIU. J. Am. Chem. Soc. **95**, 2209 (1973).
27. H. C. BROWN and K.-T. LIU. J. Am. Chem. Soc. **97**, 2469 (1975).
28. H. C. BROWN and J. H. KAWAKAMI. J. Am. Chem. Soc. **97**, 5521 (1975).
29. P. VON R. SCHLEYER. *In* The nonclassical ion problem. Plenum, New York. 1977.
30. K. B. WIBERG, B. R. LOWRY, and T. H. COLBY. J. Am. Chem. Soc. **83**, 3998 (1961).
31. J. W. WILT, C. T. PARSONS, C. A. SCHNEIDER, D. G. SCHULTZENOVER, S. J., and W. J. WAGNER. J. Org. Chem. **33**, 694 (1968).
32. A. J. FRY and W. B. FARNHAM. Tetrahedron Lett. **29**, 3345 (1968).

Can. J. Chem. Downloaded from www.nrcresearchpress.com by 210.87.254.105 on 09/06/12
For personal use only.

Pyrrole chemistry. XXVI. A synthesis of porphobilinogen from pyrrole

BASIL J. DEMOPOULOS, HUGH J. ANDERSON,[1] CHARLES E. LOADER, AND KURT FABER
Department of Chemistry, Memorial University of Newfoundland, St. John's, Nfld., Canada A1B 3X7

Received April 13, 1983

BASIL J. DEMOPOULOS, HUGH J. ANDERSON, CHARLES E. LOADER, and KURT FABER. Can. J. Chem. **61**, 2415 (1983).

A synthetic strategy has been developed which enables pyrrole to be used as the starting material for the synthesis of 2,3,4-trisubstituted pyrroles of the type used to construct porphyrins. The total synthesis of porphobilinogen has been accomplished as a demonstration of the applicability of the approach.

BASIL J. DEMOPOULOS, HUGH J. ANDERSON, CHARLES E. LOADER et KURT FABER. Can. J. Chem. **61**, 2415 (1968).

On a mis au point une méthode de synthèse qui permet d'utiliser le pyrrole comme produit de départ dans la synthèse des pyrroles trisubstitués en positions 2,3,4, analogues à ceux que l'on utilise pour synthétiser les porphyrines. On a réalisé la synthèse totale du porphobilinogène dans le but de démontrer la validité de cette méthode.

[Traduit par le journal]

Can. J. Chem. Downloaded from www.nrcresearchpress.com by 210.87.254.40 on 09/06/12
For personal use only.

We have been struck over the years by the fact that the chemists who synthesize the tri- and tetra-substituted pyrroles which are used to assemble porphyrins have invariably chosen to prepare them by ring closure methods (1). It seemed to us that pyrrole itself should be considered as a possible starting material for these substituted pyrroles, and we proposed to demonstrate that a viable route could be developed for a typical example of this type of molecule, given the current state of pyrrole chemistry. In addition to giving an acceptable yield, the new synthetic approach should: (1) be experimentally easy to carry out on a reasonable scale; (2) not make use of large amounts of expensive reagents; (3) be capable of providing isotopically labelled elements in the side chains; (4) be capable of modification to produce related 2,3,4-trisubstituted pyrroles.

The selectivity of the electrophilic substitution reactions of pyrrole derivatives has been shown (2, 3) to be highly dependent on the presence of electron-donating or electron-withdrawing groups. Based on this premise, it was speculated that porphobilinogen, 5-(aminomethyl)-4-(carboxymethyl)-1*H*-pyrrole-3-propanoic acid, **1**, the biological precursor of the porphyrins, chlorophylls, and corrins (4), might be amenable to a total synthesis starting from pyrrole.

Following the isolation and characterization of porphobilinogen by Westall in 1952 (5), and the subsequent structure proof of Cookson and Rimington (6), the first practical synthesis by the Knorr method was carried out by Jackson and MacDonald (7) five years later. This synthesis was improved by Arsenault and MacDonald (8) to give an overall yield of about 1%. Other approaches by Plieninger *et al.* (9) and by Kenner *et al.* (10) increased the yield of the key MacDonald intermediate:

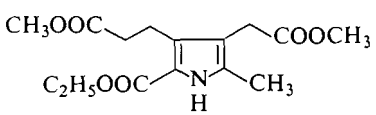

A quite different route was developed by Frydman *et al.* (11) in 1965, extending a pyridine derivative by ring closure to an azaindole which was eventually converted to the porphobilinogen lactam:

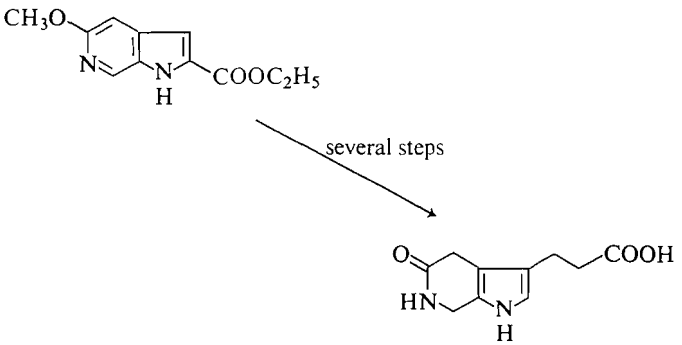

A major improvement to this approach was made by Battersby *et al.* (12), giving an overall yield of about 15% from a commercially available pyridine derivative.

Our extensive investigations of methods for the introduction of the cyano group onto pyrrole and its simple derivatives (13), as well as the behaviour of pyrrole-2-carbonitrile in substitution reactions (14), had led to a consideration of other functionalities derivable from the cyano group. One such reduction product is the aminomethyl group, an interesting grouping which occurs in porphobilinogen.

There is no easy sequence of substitution reactions that enables pyrrole to be converted directly to 2,3- or 2,3,4-substituted derivatives. While it is possible to obtain large amounts of 2-substituted pyrroles of various types, the next group enters position 4 or 5, but not position 3; except for a few special examples. In turn, 2,4-substituted compounds generally do not lead to 2,3,4-substituted products. The only general approach to the 2,3-substitution pattern starts from pyrrole with an electron donor group in position 3 (2).

As a basic synthetic plan, the sequence shown in Scheme 1 was chosen. This involves the stepwise introduction of: (a) the 3-acetate moiety, which it was hoped would behave as an electron donor, (b) the 2-aminomethyl group in the form of an electron-withdrawing functional precursor such as the cyano group, (c) the 4-propanoate moiety, and finally, (d) reduction and hydrolysis to porphobilinogen **1**. Thus pyrrole-3-acetic acid, or its ester, became the initial target molecule. Although structurally simple, no efficient syntheses for pyrrole-3-acetates on a reasonable scale are available. Ethyl pyrrole-3-acetate (**2**) has been shown (15) to form, along with the C-2 isomer, from the reaction of pyrrole with ethyl diazoacetate, but the separation of these two isomers on a preparative scale was not reported.

[1]Author to whom all correspondence should be addressed.

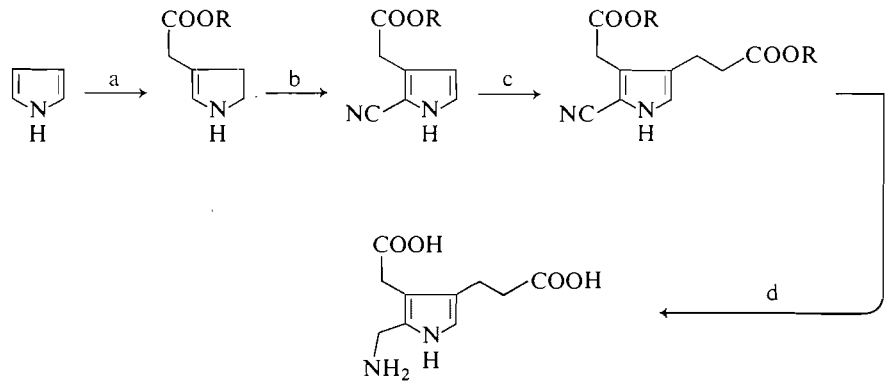

1

SCHEME 1

It is known (16) that the Friedel–Crafts acylation of the Vilsmeier–Haack intermediate **3** of pyrrole is selective, leading to the formation of 4-acylpyrrole-2-carboxaldehydes. In turn, the aldehyde group is easily removed to afford the 3-acylpyrrole. The same approach could be used for a 3-alkylpyrrole synthesis. It is not possible to use haloacetic acid or ester in the Friedel–Crafts synthesis to give the 4-acetic acid (or ester)-2-aldehyde (17). An attempt to use glyoxalic acid in the reductive alkylation procedure (18) on the Vilsmeier–Haack intermediate was unsuccessful. However, 4-acetylpyrrole-2carboxaldehyde was readily available from the acetylation of the Vilsmeier intermediate followed by hydrolytic work-up. It was then subjected to the thallium(III)-catalyzed rearrangement (19). Although that reaction succeeded, the yield of methyl 2-formylpyrrole-3-acetate was low and we were reluctant to proceed with the method because of (1) the large amounts of $Tl(NO_3)_3 \cdot 3H_2O$ needed at this early stage of the synthetic sequence, (2) the consequent cost, and (3) the toxicity of the reagent. On the other hand, the preparation of **4**, its decarbonylation, and the reduction of the glyoxalate **5** were anticipated to provide a facile route to the acetic ester grouping of **2**, free from the C-2 isomer, as shown in Scheme 2. Accordingly, ethyl 2-formylpyrrole-4-glyoxalate (**4**) was synthesized (69% yield) using ethyl oxalyl chloride as the acylating agent on the Vilsmeier–Haack intermediate. Two other possible isomers, **6** and **7**, were also isolated, but in yields of less than 2%.

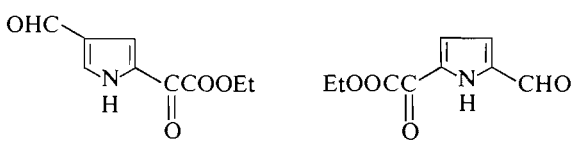

6 **7**

We had hoped that it would be possible to decarbonylate the aldehyde group of **4** and reduce the glyoxalate to the acetic ester in a single operation through the use of Raney nickel. However, although nuclear magnetic resonance spectra showed that this succeeded to some extent, other products were also present. Milder conditions led to the presence of alcohol groups and more vigorous ones reduced some of the aldehyde function to methyl. Consequently we decided to carry out the operations individually. Compound **4** was then smoothly decarbonylated to **5** with palladium on charcoal in refluxing mesitylene (92% yield). Apparently the strong electron-withdrawing effect of the glyoxalate group present on **4** facilitates the reaction. This type of palladium catalyzed decarbonylation has been previously conducted on pyrroles (16) without a solvent at higher temperatures and, although successful here, did not give as good a yield as the solution method.

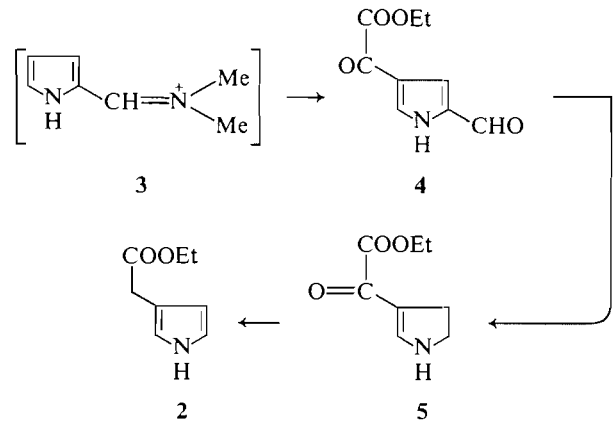

3 **4** **2** **5**

SCHEME 2

The reduction of the glyoxalate **5** to the acetate **2** was troublesome. The apparent tendency of **2** towards self-polymerization in acidic media and the ease of reduction of the pyrrole ring were major obstacles. It has been shown (20) that W-7 Raney Nickel in 50% aqueous ethanol hydrogenolyzes benzylic ketones under virtually neutral conditions. Although **2** was formed under these conditions, tarring and reduction of the pyrrole ring were still major side reactions. On the other hand, a 67% yield of **2** was attained by conducting the reduction with W-7 Raney Nickel in a two phase system consisting of toluene and 50% aqueous ethanol. Under these conditions **2** is effectively removed from the aqueous reduction medium into the toluene layer as soon as it is formed. Thus, the 3-acetic ester may be prepared easily, and on a large scale, in three steps with an overall yield of greater than 40%.

As mentioned earlier, electrophilic substitution on 3-alkylpyrroles has been shown to favor attack at position C-2 over C-5.[2] The Vilsmeier–Haack reaction is an extremely mild and selective reaction which is also very easy to carry out with pyrroles. Thus it was the reaction chosen to test the behaviour of the 3-acetic ester as a directing group. The product was a mixture of 2- and 5- substitution products **8** and **9** in which the desired 2-aldehyde-3-acetic ester was the predominant isomer. We further observed that the distribution of the two isomers

[2] See ref. 3, p. 194; ref. 2, p. 119.

Can. J. Chem. Downloaded from www.nrcresearchpress.com by 210.87.254.40 on 09/06/12
For personal use only.

(C-2 versus C-5) depended on the temperature of the reaction. For instance, lowering the reaction temperature by 20°C (0°C to −20°C) during the Vilsmeier–Haack reaction with **2** resulted in a 17% enrichment of isomer **8** (C-2 attack) over isomer **9** (C-5 attack), based on ^{1}H nmr data.

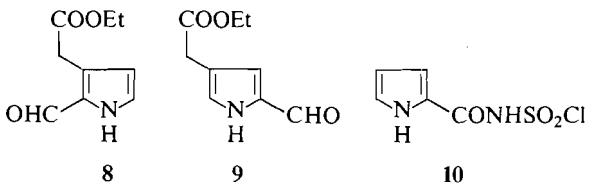

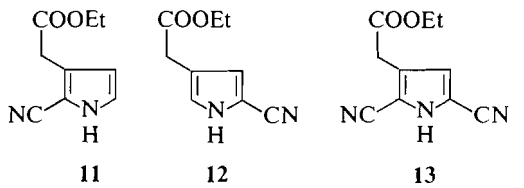

Chlorosulfonyl isocyanate (CSI) has been shown (13*b*) to react smoothly with pyrrole at low temperatures and, further, decomposition of the intermediate **10** so formed with dimethylformamide (DMF) affords pyrrole-2-carbonitrile in excellent yield. In accordance, ethyl pyrrole-3-acetate (**2**) was treated with CSI at −42°C and the intermediate was decomposed with DMF. Medium-pressure liquid chromatography (21) of the crude product afforded **11** (53%), **12** (12%), and **13** (0.8%). Lower reaction temperatures failed to change the ratio of the two monocyano isomers, while at higher reaction temperatures the amount of the disubstituted product **13** was substantially increased. That the product was a mixture, and extremely difficult to separate by column chromatography, led us to consider other pathways which might avoid this problem. One route (shown in Scheme 3) would retain the original aldehyde group, but block it as the acetal **14** formed with 2,2-dimethyl-1,3-propanediol (cf. ref. 22) until after the cyanation step, to be followed by hydrolysis and decarbonylation. Another pathway would use the readily available 2-ester as starting material, as shown in Scheme 4.

It was anticipated that one of these routes would provide an alternative, though longer, approach to the carbonitrile **11**, free from the undesired isomer **12**. Although the 2-acetal-4-glyoxalate ester **14** was readily synthesized from **4**, it resisted all attempts to reduce the keto group selectively. The 2-ester-4-glyoxalate **15** was prepared and reduced in a two-step process (23), first by Pd/charcoal to the hydroxyester **16** and then using triphenylphosphine – triphenylphosphine diiodide to give **17**. Cyanation of **17** then gave **18**, as expected. However, selective cleavage of the methyl ester in **18** under nonhydrolytic (24) conditions was not successful, so we returned to the direct cyanation of the 3-acetic ester **2** as our synthesis of **11**.

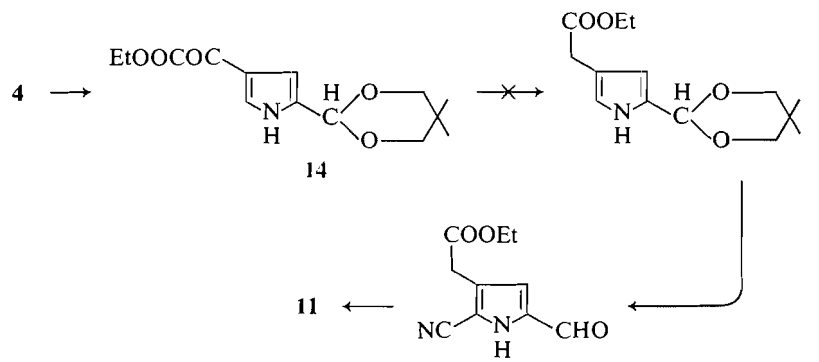

SCHEME 3

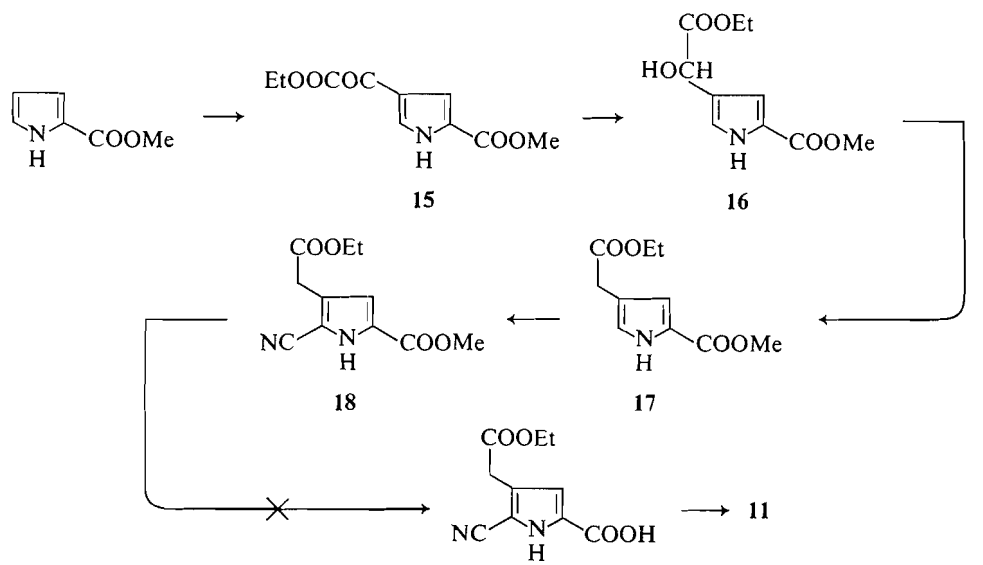

SCHEME 4

Can. J. Chem. Downloaded from www.nrcresearchpress.com by 210.87.254.40 on 09/06/12
For personal use only.

Can. J. Chem. Downloaded from www.nrcresearchpress.com by 210.87.254.40 on 09/06/12
For personal use only.

The well established (14, 25) 4-directing effect of a cyano group at the C-2 position of the pyrrole ring was expected to facilitate the introduction of electrophilic substituents at position C-4 of **11**. Aldehyde **19** or iodide **20** appeared to be suitable precursors for the construction of a 4-acrylate grouping which would be reduced subsequently to the propanoate side chain present on porphobilinogen. Formylation of **11** using a variety of methods (dichloromethyl alkyl ether – Lewis acid (14, 26), Vilsmeier–Haack, trifluoroacetic acid/triethyl orthoformate (27)) was unsuccessful; however, iodination (iodine/iodic acid (28)) proved to be specific and resulted in a

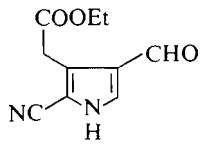

19

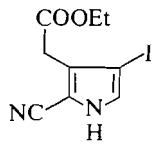

20

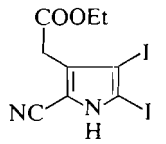

21

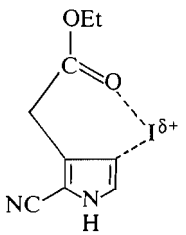

A

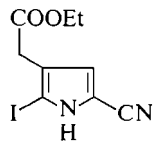

22

97% yield of **20** along with a very small amount (<1%) of the diiodo derivative **21**. It was thought at first that this high degree of selectivity derived from a six-membered transition state **A**, similar to that suggested for the thallium trifluoroacetate substitution (29). This was not the case because it was found that pyrrole-2-carbonitrile was converted selectively to 4-iodopyrrole-2-carbonitrile (67%) under the same reaction conditions.

On a preparative scale, it was now established that the use of liquid chromatography to separate isomers **11** and **12** could be avoided by iodination of that mixture. The desired product, **20**, can then be easily separated in pure form by flash chromatography. The overall yield of **20** from **2** was almost identical to that from the lengthier operation.

It has been shown (30) that acrylates react with aryl iodides in the presence of palladium acetate to form the corresponding cinnamates in high yield. Although **23** was formed from **20** and ethyl acrylate under these conditions, Michael type addition of ethyl acrylate on the pyrrole nitrogen and reduction of the iodo group at position C-4 to give back **11** were major side reactions. Reduction of the iodo group on electron-rich aryl iodides during the palladium acetate catalyzed vinylic arylation of olefins has been previously observed (30*a*, 31). On the other hand, as shown in Scheme 5, the *N*-benzoyl derivative of **20**, **24**, was smoothly converted to **25** (58%), along with an amount of **23**. The latter compound was immediately re-*N*-benzoylated, thus increasing the yield of **25** to 91.5%. The overall yield from pyrrole was 19% at this point.

The conversion of **25** to porphobilinogen **1** could be carried out by one of the two routes shown in Scheme 6. Hydrogenation of **25** over Adams' catalyst in acetic anhydride (32) gave the amide **26**. We had hoped that the acetylation of the aminomethyl group would provide added stability to the reduced product but the acetamide was quite unstable and could not be obtained completely pure. It was characterized by ^{1}H and ^{13}C nmr, infrared, and mass spectra. A competing reaction was the hydrogenation of the pyrrole ring of **26**. Therefore, the reaction had to be closely monitored and stopped before any substantial amount of that by-product was formed. At this point there was always some unreduced carbonitrile **27** present, as well as an unidentified by-product. A major difficulty was the need to remove the solvent and unreduced nitrile from the amide **26** as rapidly as possible. Partial decomposition during work-up could not be avoided despite the variety of techniques used.

Attempts were made to improve the hydrogenation by altering the reaction conditions. With Pd/charcoal (10%) or Pd black the reduction ceased after saturation of the double bond. While PtO_2 appeared to be the best catalyst, it afforded no real

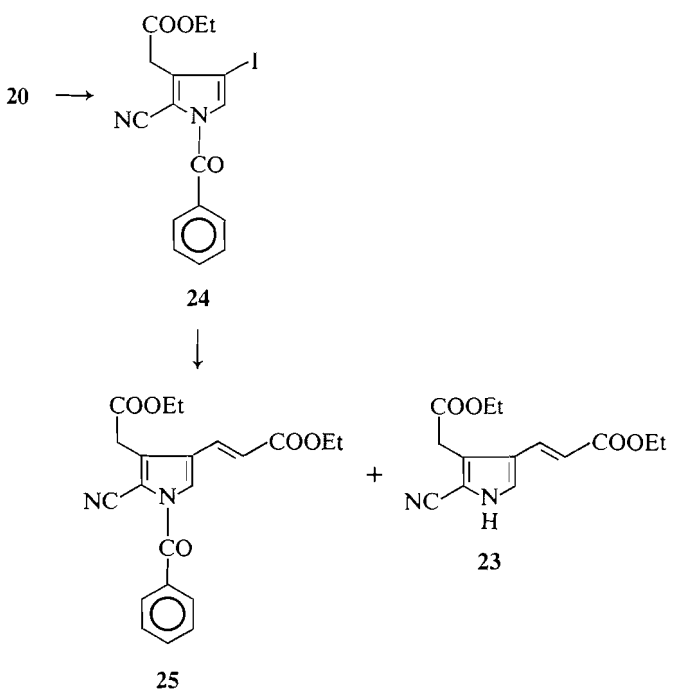

SCHEME 5

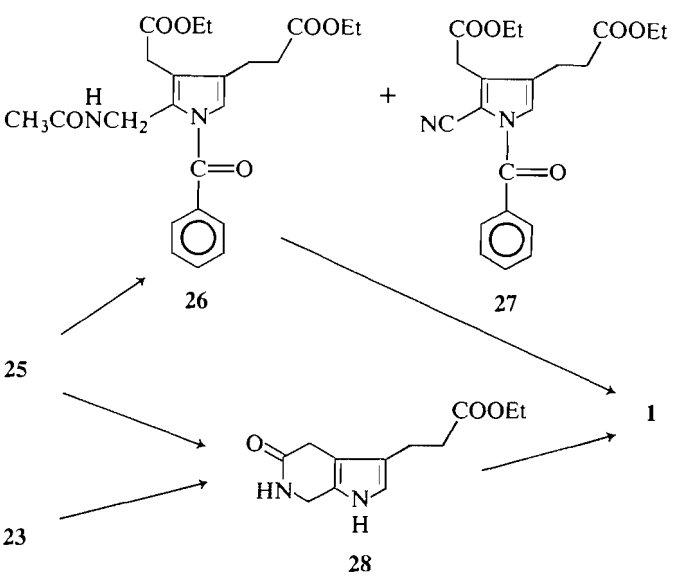

SCHEME 6

Can. J. Chem. Downloaded from www.nrcresearchpress.com by 210.87.254.40 on 09/06/12
For personal use only.

selectivity between the nitrile and the pyrrole ring. Acidic conditions greatly increased the rate of reduction but did not improve the selectivity. The use of cobalt boride catalyst (33) was unsuccessful. It is interesting to note that, where reduction of substituted pyrrole-2-carbonitriles has been successful, there was another electron-withdrawing group present on the ring (7, 34). The 1-benzoyl group does not appear to provide the required effect here.

Finally, the use of Pd black and PtO_2 in ethanol/ammonia, where the ester-amine forms the fairly stable porphobilinogen lactam-ester **28** (8, 37, 38) under the action of the weak base, almost doubled the yield from the hydrogenation. Under the conditions used, the *N*-benzoyl group was solvolytically cleaved to give the 1-*H* lactam ester.

The hydrolysis of **26** or **28** was carried out in a similar way to that of porphobilinogen lactam (11) for 96 h using 2 mol L^{-1} aqueous potassium hydroxide, followed by adjustment of the pH to precipitate porphobilinogen hydrate. It had the correct physical properties (10) and was identical to a commercial sample of authentic material isolated from natural sources. The overall yield of recrystallized porphobilinogen obtained in nine steps from pyrrole was about 6%.

While the preparation of porphobilinogen has been successfully accomplished, it is evident that the nitrile reduction step must be improved or replaced to achieve the maximum benefit from our new approach. We intend to explore the use of the aldoxime group as an alternative. Nevertheless, we feel that the flexibility of pyrrole as a starting material for the preparation of 2,3,4-substituted pyrroles possessing side-chains of interest to the porphyrin chemist has been adequately demonstrated. Most of the steps are extremely easy to carry out, even on a large scale, and yields are all very good aside from the reduction step.

Experimental

Melting points are uncorrected. Elemental analyses were by Atlantic Microlabs, GA, U.S.A. The ir spectra were recorded on a Perkin–Elmer 237B grating spectrophotometer as solutions in $CHCl_3$ unless otherwise stated. The ^1H nmr spectra (nmr) were determined using a Varian EM 360 or a Bruker WP-80 instrument and are expressed in ppm (δ values) relative to tetramethylsilane as internal reference in $CDCl_3$ unless otherwise stated. Mass spectra were recorded on a VG Micromass 7070HS spectrometer. The ^{13}C nmr spectra were determined at 20.122 MHz in $CDCl_3$ on a Bruker WP-80 Fourier transform instrument. All solvents were dried and distilled before use. Throughout, the term "petroleum" refers to the fraction of bp 30–60°C. The term "hexanes" refers to a mixture of isomers bp. 65.8–69.0°C (Fisher Scientific). Flash chromatography (35) was carried out using "Baker Analyzed" silica gel for flash chromatography.

*Ethyl 2-formylpyrrole-4-glyoxalate (**4**)*

The Vilsmeier–Haack iminium chloride **3** of pyrrole was made as previously described (16) from pyrrole (21 g, 0.313 mol), DMF (35 g, 0.48 mol), and oxalyl chloride (43.8 g, 0.34 mol) in 1,2-dichloroethane (700 mL) under nitrogen. The reaction mixture was cooled (ice bath), and $AlCl_3$ (185 g, 1.39 mol) was added. The reaction was allowed to warm to room temperature over 10 min and then nitromethane (56 mL, 1.04 mol) was added. The resulting red solution was cooled (ice bath) and ethyl oxalyl chloride (64 g, 0.47 mol) was added as rapidly as possible. The ice bath was removed and the reaction mixture was stirred vigorously under nitrogen for 4 h. The mixture was then poured into a stirred mixture of ice/water (5 L) and the stirring was continued for an additional 4 h. The aqueous and the organic layers were separated. The aqueous layer was extracted with dichloromethane (3 × 500 mL portions). The combined organic layer and the dichloromethane extracts were washed with saturated aqueous NaCl, dried ($MgSO_4$), and the solvent removed under reduced pressure. The solid residue was recrystallized from dichloromethane/petroleum to afford ethyl 2-formylpyrrole-4-glyoxalate (**4**) (41.32 g, 68%), mp 99–99.5°C. The mother liquors from the recrystallization were evaporated under reduced pressure and the residue was flash chromatographed on silica gel with petroleum – ethyl acetate (10:3 to 10:10) to afford (a) an additional 530 mg of ethyl 2-formylpyrrole-4-glyoxalate, raising the total yield to 41.85 g (69%); ir (Nujol): 1675, 1750, 1845, 3220 cm^{-1}; nmr: 1.4 (3H, t, $—CH_2—CH_3$), 4.38 (2H, q, $—CH_2—CH_3$), 7.64 (1H, m, 3-H), 8.16 (1H, m, 5-H), 9.55 (1H, s, —CHO), $J_{1,3}$ = 2.5, $J_{1,5}$ = 3.4, $J_{3,5}$ = 1.3, $J_{2\text{-CHO}}$ = 1.1 Hz; *m/e*: 195. *Anal.* calcd. for $C_9H_9NO_4$: C 55.38, H 4.64; found: C 55.32, H 4.66; (b) ethyl 2-formylpyrrole-5-glyoxalate (**7**) (639 mg, 1%), mp 57–58°C; ir: 1670, 1730, 3400 cm^{-1}; nmr: 1.4 (3H, t, CH_3, J = 7 Hz), 4.4 (2H, q, CH_2, J = 7 Hz), 6.94 (1H, dd, pyrrole H), 7.34 (1H, dd, pyrrole H), 9.68 (1H, s, —CHO), 10.6 (1H, broad s, NH), $J_{3,4}$ = 4.4, $J_{1,3}$ = 2.6 Hz; *m/e*: 195. *Anal.* calcd. for $C_9H_9NO_4$: C 55.38, H 4.64; found: C 55.43, H 4.65; (c) ethyl 3-formylpyrrole-5-glyoxalate (**6**) (234 mg, 0.4%), mp 85.5–87°C; ir: 1670, 1730, 3400 cm^{-1}; nmr: 1.4 (3H, t, CH_3, J = 7 Hz), 4.4 (2H, q, CH_2, J = 7 Hz), 7.8 (2H, m, 2-H and 4-H), 9.87 (1H, s, —CHO), 10.7 (1H, broad s, NH); *m/e*: 195. *Anal.* calcd. for $C_9H_9NO_4$: C 55.38, H 4.64; found: C 55.44, H 4.69.

*Ethyl pyrrole-3-glyoxalate (**5**)*

A mixture of ethyl 2-formylpyrrole-4-glyoxalate (**4**) (10 g, 0.051 mol) and 5% palladium on charcoal (1.5 g) in mesitylene (100 mL) was refluxed under nitrogen for 6 h. The mixture was then cooled to room temperature, diluted with dichloromethane (300 mL), filtered through Celite, and the catalyst was washed on the filter with several portions of dichloromethane. The dichloromethane solution from the combined filtrate and washings was evaporated under reduced pressure, and the residue was treated with petroleum (200 mL) and then refrigerated for 3 h. The precipitated solid was collected and recrystallized from dichloromethane/petroleum to afford ethyl pyrrole-3-glyoxalate (**5**) (7.885 g, 92%), mp 91–92°C; ir (Nujol): 1665, 1760, 3250 cm^{-1}; nmr: 1.35 (3H, t, CH_3), 4.66 (2H, q, CH_2), 6.62 (2H, m, 4-H and 5-H), 7.72 (1H, dd, 2-H), $J_{2,4}$ = 1.4, $J_{2,5}$ = 2.0, $J_{4,5}$ = 3.0 Hz; *m/e*: 167. *Anal.* calcd. for $C_8H_9NO_3$: C 57.48, H 5.43; found: C 57.30, H 5.54.

*Ethyl pyrrole-3-acetate (**2**)*

A mixture of ethyl pyrrole-3-glyoxalate (**5**) (12 g, 0.072 mol) and seven teaspoons (35 mL) of W7[3] Raney nickel (36), ethanol (200 mL), water (200 mL), and toluene (400 mL) was stirred vigorously at room temperature under nitrogen for 1.5 h. Seven more teaspoons of W7 Raney nickel were then added and the stirring was continued for an additional 3 h. Saturated aqueous NaCl (200 mL) and ether (200 mL) were then added to the mixture. The two layers that formed were separated, the aqueous layer was extracted with ether (2 × 200 mL), and the combined extracts and the organic layer were washed with saturated aqueous NaCl and then dried by filtration through a small plug of $MgSO_4$. Evaporation of the solvent under reduced pressure afforded an oil which was flash chromatographed on silica gel with ether–petroleum (1:2) as the eluent to give ethyl pyrrole-3-acetate (**2**) (7.310 g, 67%).[4] An analytical sample was prepared with some loss of material by a bulb-to-bulb distillation (0.5 Torr, 170°C); ir: 1720, 3380, 3475 cm^{-1}; nmr: 1.24 (3H, t, CH_3, J = 7 Hz), 3.48 (2H, s, CH_2COO), 4.1 (2H, q, CH_2, J = 7 Hz), 6.1 (1H, m, 4-H), 6.6 (2H,

[3] NOTE: Depending on its activity, greater or lesser amounts of the W7 Raney nickel catalyst and longer or shorter reaction times may be required. To obtain the desired activity it was necessary to double the suggested number of washings (36). The progress of the reduction was conveniently followed by thin-layer chromatography (silica gel with ether/petroleum 2:1 as the eluent) using samples taken from the toluene layer.

[4] *Storage*: The compound can be stored for long periods under nitrogen in a refrigerator without decomposition.

Can. J. Chem. Downloaded from www.nrcresearchpress.com by 210.87.254.40 on 09/06/12
For personal use only.

m, 2-H and 5-H), 8.3 (1H, broad s, NH); *m/e*: 153. *Anal.* calcd. for $C_8H_{11}NO_2$: C 62.72, H 7.24, N 9.15; found: C 62.55, H 7.29, N 9.09.

*Ethyl 2-cyanopyrrole-3-acetate (**11**)*

To a well stirred and cooled (−42°C, acetone/solid CO_2 bath) solution of **2** (6 g, 0.039 mol) in acetonitrile (80 mL) and dichloromethane (20 mL), CSI (5.83 g, 3.59 mL, 0.0412 mol) was added dropwise over 30 min under nitrogen. The mixture was then stirred at the same temperature for an additional 2.5 h. DMF (15 mL) was then added rapidly and the reaction mixture was allowed to warm to room temperature over 1.5 h. The volatiles were removed under reduced pressure, the residue was taken up in toluene (400 mL) and washed successively with dilute $NaHCO_3$ solution (1 × 100 mL), water (3 × 100 mL), saturated aqueous NaCl, and then dried ($MgSO_4$). Evaporation of the toluene afforded a crude mixture of the carbonitriles **11**, **12**, and **13**. The mixture was separated using medium pressure liquid chromatography (21) on silica gel (500 g Merck Kieselgel 60, 230–400 mesh) with benzene/petroleum/ethyl acetate (10:10:1.5 rising to 10:10:3) as the eluent. The separation was monitored by a combination of ^1H nmr and tlc. The following products were eluted (in order).

(a) Ethyl 2,5-dicyanopyrrole-3-acetate (**13**) (67 mg, 0.84%), mp 73–73.5°C (from dichloromethane–petroleum); ir: 1725, 2225 cm^{-1}; nmr: 1.3 (3H, t, CH_3, J = 7 Hz), 3.64 (2H, s, CH_2COO), 4.2 (2H, q, CH_2, J = 7 Hz), 6.8 (1H, broad s, pyrrole H), 10.7 (1H, broad s, NH); *m/e*: 203. *Anal.* calcd. for $C_{10}H_9N_3O_2$: C 59.11, H 4.47, N 20.68; found: C 59.15, H 4.47, N 20.64.

(b) Ethyl 2-cyanopyrrole-3-acetate (**11**) (3.716 g, 53%) as an oil. An analytical sample was made by bulb-to-bulb distillation (200°C/0.1 Torr); ir: 1730, 2225, 3300, 3450 cm^{-1}; nmr: 1.28 (3H, t, CH_3, J = 7 Hz), 3.62 (2H, s, CH_2COO), 4.16 (2H, q, CH_2, J = 7 Hz), 6.14 (1H, dd, 4-H), 6.74 (1H, t, 5-H), 9.65 (1H, broad s, NH), $J_{4,5}$ = 2.72, $J_{1,4}$ = 2.2 Hz; *m/e*: 178. *Anal.* calcd. for $C_9H_{10}N_2O_2$: C 60.66, H 5.66, N 15.73; found: C 60.37, H 5.70, N 15.62.

(c) Ethyl 2-cyanopyrrole-4-acetate (**12**) (844 mg, 12%) as an oil. An analytical sample was made by bulb-to-bulb distillation (220°C/0.1 Torr); ir: 1725, 2225, 3300, 3450 cm^{-1}; nmr: 1.28 (3H, t, CH_3, J = 7 Hz), 3.5 (2H, s, CH_2COO), 4.14 (2H, q, CH_2, J = 7 Hz), 6.7 (2H, m, pyrrole H), 9.7 (1H, broad s, NH); *m/e*: 178. *Anal.* calcd. for $C_9H_{10}N_2O_2$: C 60.66, H 5.66, N 15.73; found: C 60.40, H 5.72, N 15.65.

*Ethyl 2-cyano-4-iodopyrrole-3-acetate (**20**)*

I. A mixture of ethyl 2-cyanopyrrole-3-acetate (**11**) (1 g, 5.62 mmol), iodic acid (198 mg, 1.123 mmol), and iodine (570 mg, 2.24 mmol) in carbon tetrachloride (40 mL), water (1.2 mL), acetic acid (2.8 mL), and concentrated sulfuric acid (0.1 mL, about 4 drops) was stirred vigorously at room temperature under nitrogen for 24 h. At this point the coloration due to the iodine had been discharged. The reaction mixture was then diluted with dichloromethane (100 mL) and the two layers formed were separated. The organic layer was washed with saturated sodium thiosulfate solution (1 × 50 mL), 5% $NaHCO_3$ (1 × 50 mL), saturated aqueous NaCl, and dried ($MgSO_4$), and the volatiles removed under reduced pressure. The solid residue was crystallized from CH_2Cl_2/petroleum to afford the product **20** (1.422 g, 83%), mp 118–118.5°C; ir: 1730, 2210, 3400 cm^{-1}; nmr: 1.3 (3H, t, CH_3, J = 7 Hz), 3.6 (2H, s, CH_2COO), 4.2 (2H, q, CH_2, J = 7 Hz), 6.84 (1H, d, 5-H, $J_{1,5}$ = 3 Hz), 9.8 (1H, broad s, NH); *m/e*: 304. *Anal.* calcd. for $C_9H_9N_2O_2I$: C 35.55, H 2.98, N 9.21; found: C 35.63, H 3.01, N 9.19.

The mother liquors from the recrystallization were concentrated and the residue was flash cromatographed on silica gel with petroleum/benzene/ethyl acetate (10:2:2) as the eluent. Thus was obtained: (a) a further 238 mg of **20**, increasing the total yield to 1.660 g (97%), and (b) ethyl 2-cyano-4,5-diiodopyrrole-3-acetate (**21**) (21 mg, 0.1%), mp 118–118.5°C; ir: 1730, 2210, 3400 cm^{-1}; nmr: 1.3 (3H, t, CH_3, J = 7 Hz), 3.64 (2H, s, CH_2COO), 4.18 (2H, q, CH_2, J = 7 Hz), 9.7 (1H, broad s, NH); *m/e*: 430. *Anal.* calcd. for $C_9H_8N_2O_2I_2$: C 25.14, H 1.88, N 6.52; found: C 25.17, H 1.93, N 6.49.

II. On a preparative scale the medium pressure chromatographic separation of **11** and **12** can be avoided by using the isomer mixture without further purification as starting material for the preparation of ethyl 2-cyano-4-iodopyrrole-3-acetate (**20**). Thus the mixture of **11** and **12** (1 g, 5.62 mmol) was treated as in I above. After removal of solvents, the residue was flash chromatographed on silica gel using hexanes/ether (4:1) as the eluent. Thus were obtained in order of elution: (a) ethyl 2-cyano-5-iodopyrrole-4-acetate (**22**). An analytical sample was prepared by bulb-to-bulb distillation (230°C/0.8 Torr) (199 mg, 11.6%), mp 81.5–82°C; ir: 1720, 2200, 3000 (broad), 3400 cm^{-1}; nmr: 1.3 (3H, t, CH_3, J = 7 Hz), 3.45 (2H, s, CH_2COO), 4.2 (2H, q, CH_2, J = 7 Hz), 6.75 (1H, d, 3-H, $J_{1,3}$ = 3 Hz), 10.0 (1H, broad s, NH); *m/e*: 304. *Anal.* calcd. for $C_9H_9N_2O_2I$: C 35.55, H 2.98, N 9.21; found: C 35.46, H 2.99, N 9.13; (b) ethyl 2-cyano-4,5-diiodopyrrole-3-acetate (**21**), (13 mg, 0.53%); (c) ethyl 2-cyano-4-iodopyrrole-3-acetate (**20**), (877 mg, 51.4%).

4-Iodopyrrole-2-carbonitrile

Pyrrole-2-carbonitrile (8.78 g, 0.095 mol) was converted to 4-iodopyrrole-2-carbonitrile according to the method used for the synthesis of **20**. The crude product was recrystallized from dichloromethane/petroleum to afford the product (13.94 g, 67%), mp 105–106°C; ir: 2210, 3400 cm^{-1}; nmr: 6.68 (2H, m, 3-H and 5-H), 9.5 (1H, broad s, NH); *m/e*: 218. *Anal.* calcd. for $C_5H_3N_2I$: C 27.55, H 1.39, N 12.85; found: C 27.51, H 1.44, N 12.83.

*Ethyl 1-benzoyl-2-cyano-4-iodopyrrole-3-acetate (**24**)*

Benzoyl chloride (844 mg, 6 mmol) in dichloromethane (10 mL) was added dropwise over 30 min to a well stirred and cooled (ice bath) mixture of **20** (1.216 g, 4 mmol), powdered NaOH (272 mg, 6.8 mmol), and tetrabutylammonium hydrogen sulfate (68 mg, 0.2 mmol) in dichloromethane (30 mL) under nitrogen. This was then stirred at the same temperature under nitrogen for an additional 2 h. The reaction mixture was filtered through Celite and the precipitate was washed on the filter with several portions of dichloromethane. The combined filtrate and washings were washed with saturated aqueous NaCl and dried ($MgSO_4$). Evaporation of the dichloromethane afforded crude **24** which was flash chromatographed on silica gel with hexanes/ether (2:1) as the eluent to give the pure product **24** (1.623 g, 99.5%), mp 116–117°C; ir: 1730, 2220 cm^{-1}; nmr: 1.34 (3H, t, CH_3, J = 7 Hz), 3.68 (2H, s, CH_2COO), 4.24 (2H, q, CH_2, J = 7 Hz), 7.28 (1H, s, 5-H), 7.6 (5H, m, phenyl H); *m/e*: 408. *Anal.* calcd. for $C_{16}H_{13}N_2O_3I$: C 47.08, H 3.21, N 6.87; found: C 47.01, H 3.23, N 6.84.

*Ethyl 1-benzoyl-2-cyano-4-carbethoxyvinylpyrrole-3-acetate (**25**)*

A mixture of ethyl 1-benzoyl-2-cyano-4-iodopyrrole-3-acetate (**24**) (2.04 g, 5 mmol), triethylamine (850 mg, 8.42 mmol), ethyl acrylate (750 mg, 7.5 mmol), CH_3CN (2 mL), and palladium(II) acetate (25 mg) was placed in a heavy walled Pyrex tube sealed at one end and fitted with a Teflon cap. The tube was flushed out with dry nitrogen. The Teflon cap was then fitted tightly and the tube was inserted into a preheated oil bath controlled within the range 99–100°C. The reaction mixture was then stirred at this temperature for 40 min. The mixture was allowed to cool to room temperature and then dissolved in dichloromethane (200 mL), washed with dilute (0.5 mol L^{-1}) HCl, saturated aqueous NaCl, and dried ($MgSO_4$). Evaporation of the volatiles afforded the crude product which was flash chromatographed on silica gel with hexanes/ether (3:2) as the eluent. Thus were obtained: (a) ethyl 1-benzoyl-2-cyano-4-carbethoxyvinylpyrrole-3-acetate (**25**) (1.103 g, 58%), mp 104–105°C (from dichloromethane/petroleum); ir: 1710, 2225 cm^{-1}; nmr: 1.3 (6H, t, CH_3, J = 7 Hz), 3.8 (2H, s, CH_2COO), 4.18 (4H, q, CH_2, J = 7 Hz), 6.1 (1H, d, CH=C*H*, J = 16 Hz), 7.38 (1H, d, 5-H), 7.4 (1H, d, C*H*=CH, J = 16 Hz), 7.6 (5H, m, phenyl H); *m/e*: 380. *Anal.* calcd. for $C_{21}H_{20}N_2O_5$: C 66.30, H 5.30, N 7.37; found: C 66.24, H 5.34, N 7.34; (b) ethyl 2-cyano-4-carbethoxyvinylpyrrole-3-acetate (**23**), (0.431 g, 31.2%), mp 107–108°C (from dichloromethane/petroleum); ir: 1635, 1710, 2200 cm^{-1}; nmr: 1.29, 1.31 (each 3H, t, CH_3, J = 7 Hz), 3.72 (2H, s, CH_2COO), 4.20 (2H, q, C*H*$_2$—CH_3, J = 7 Hz), 4.22 (2H, q,

Can. J. Chem. Downloaded from www.nrcresearchpress.com by 210.87.254.40 on 09/06/12
For personal use only.

CH_2—CH_3, J = 7 Hz), 6.1 (1H, d, CH=C*H*, J = 16 Hz), 7.1 (1H, d, 5-H, J = 3 Hz), 7.45 (1H, d, C*H*=CH, J = 16 Hz), 10.1 (1H, broad s, N-H). *Anal.* calcd. for $C_{14}H_{16}N_2O_4$: C 60.86, H 5.84, N 10.14; found: C 61.07, H 5.85, N 10.02. The latter compound was rebenzoylated according to the procedure for **24**, raising the overall yield of **25** to 91.5%.

Ethyl 1-benzoyl-2-acetamidomethyl-4-carbethoxyethylpyrrole-3-acetate (26)

A solution of **25** (300 mg, 0.79 mmol) in acetic anhydride (3 mL) was hydrogenated over PtO_2 (100 mg) at atmospheric pressure and room temperature for 6 h.[5] The solution was taken up in ethyl acetate (50 mL) and then filtered through a Celite pad. The Celite pad was washed several times with portions of ethyl acetate and the filtrate and washings were combined and the solvent was removed under reduced pressure. The residue was flash-chromatographed on silica gel with petroleum/benzene/ethyl acetate (10:10:0 to 10:10:10) to afford the crude product (225 mg).[6]

*Ethyl 4,5,6,7-tetrahydro-5-oxo-1*H*-pyrrolo[2,3-c]pyridine-3-propanoate (28) (porphobilinogen lactam ethyl ester)*

Ethyl 1-benzoyl-2-cyano-4-carbethoxyvinylpyrrole-3-acetate (**25**) (304 mg, 0.8 mmol)[7] was dissolved in dry ethanol (30 mL) which was then saturated with dry ammonia. After the addition of Pd black (50 mg) and PtO_2 (120 mg) the mixture was hydrogenated at room temperature and pressure until H_2-takeup ceased at about 2.5 equivalents (about 24 h when thin-layer chromatography showed that all of the starting material had been consumed). The solution was then warmed to about 50°C and filtered from the catalyst through a Celite pad. The Celite pad was washed with several portions of hot dry ethanol and the combined filtrate and washings were evaporated under reduced pressure (bath temperature: 40°C) until the first cloudy precipitate appeared. The mixture was then quickly heated until the precipitate redissolved and the solution was set aside in a refrigerator overnight. The white precipitate that formed was collected and washed with dry ether to give pure **28**. A second crop was obtained by repeating the evaporation and cooling procedure to give a total yield of 102 mg (54%), mp (in a sealed, evacuated capillary, 0.05 Torr) 251°C (lit. (37) mp 261°C; (8) mp 239–244°C); ir: 1580, 1615, 1650, 1725, 2875, 3150 cm^{-1}; nmr (DMSO-d_6): 1.17 (3H, t, CH_2CH_3, J = 7 Hz), 2.50–2.55 (m, propanoate methylenes, obscured by DMSO), 3.14 (2H, t, J = 3.2 Hz, 4-H), 4.04 (2H, q, J = 7 Hz, CH_2CH_3), 4.30 (2H, m, 7-H), 6.45 (1H, d, 2-H, J = 2.3 Hz), 7.66 (1H, broad, lactam NH), 10.3 (1H, broad, pyrrole NH).

Porphobilinogen (1)

I. A mixture of the product from the foregoing reaction **26** (340 mg) in potassium hydroxide (2.5 mL, 2 mol L^{-1}) was stirred in darkness for 96 h under N_2 at room temperature. The pH of this solution was then adjusted to 6–7 with glacial acetic acid, cooled (ice bath), and the flask was scratched to initiate the precipitation of **1**. After 4 h at 0°C the precipitate was collected by filtration and washed quickly with cold water, followed by ether, and then dried for 4 h under high vacuum to give the product (106 mg, 36% from **25**), mp 174–177°C (dec., inserted at 167°C). Recrystallization from 0.7 mol L^{-1} ammonia solution/glacial acetic acid did not change the mp and gave a recovery of 55 mg (19% from **25**). Infrared and Fast Atom Bombardment mass spectra were identical to those of an authentic sample (Sigma Chemical Company) as was the ascending paper chromatogram (8). The chemical shifts in both the ^1H and ^{13}C nmr spectra matched those given in the literature (10).

II. The ethyl ester of porphobilinogen lactam (**28**) (110 mg, 0.47 mmol) was hydrolyzed in the same way to yield **1** (94 mg, 83% from **28**), identical in all respects with the product from I.

Ethyl 2-carbomethoxypyrrole-4-glyoxalate (15)

A mixture of methyl pyrrole-2-carboxylate (400 mg, 3.2 mmol), $AlCl_3$ (1.7 g, 12.8 mmol), and ethyl oxalyl chloride (0.45 g, 4.8 mmol) in dichloromethane (20 mL) containing nitromethane (0.52 mL) was stirred at room temperature under nitrogen for 15 h. This was then poured with stirring into a mixture of water and ice (200 mL) and the two layers were separated. The aqueous layer was extracted with dichloromethane (2 × 50 mL) and the combined organic layer and the extracts were washed with saturated aqueous NaCl, dried ($MgSO_4$), and the volatiles removed under reduced pressure. The residue was flash chromatographed on silica gel with ether/petroleum (2:1) as the eluent to afford the product **15** (323 mg, 45%), mp 109.5–110°C; ir: 1675, 1710, 3400 cm^{-1}; nmr: 1.44 (3H, t, CH_2CH_3, J = 7 Hz), 3.9 (3H, s, CH_3), 4.4 (2H, q, CH_2CH_3, J = 7 Hz), 7.48 (1H, m, 3-H), 7.98 (1H, m, 5-H), 10.5 (1H, broad s, NH), $J_{3,5}$ = 1.6 Hz; *m/e*: 225. *Anal.* calcd. for $C_{10}H_{11}NO_5$: C 53.33, H 4.93, N 6.22; found: C 53.33, H 4.96, N 6.21.

Ethyl 2-carbomethoxypyrrole-4-acetate (17)

Ethyl 2-carbomethoxypyrrole-4-glyoxalate (**15**) (600 mg, 2.67 mmol) in absolute ethanol (120 mL) was hydrogenated over 10% Pd/C (60 mg) in a Parr Shaker apparatus for 17 h with an initial hydrogen pressure of 40 psi. The reaction mixture was then filtered through Celite, the catalyst was washed on the filter with several portions of ethanol, and the combined washings and filtrate were evaporated under reduced pressure to leave a thick oily residue, the ^1H nmr of which indicated complete reduction of **15** to the alcohol **16**.

Triphenylphosphine (1.4 g, 5.34 mmol) was added to a stirred solution of iodine (677 mg, 2.67 mmol) in benzene (30 mL) under nitrogen. After 10 min, crude compound **16** in benzene (20 mL) was added in one portion. The mixture was then refluxed for 2 h under nitrogen. The mixture was filtered through Celite, and the precipitate was washed on the filter with several portions of benzene. The combined filtrate and washings were washed with saturated aqueous NaCl and dried ($MgSO_4$). Evaporation of the benzene under reduced pressure afforded crude material which was flash chromatographed on silica gel with ether/petroleum (1:1) as the eluent to give pure **17** (512 mg, 91%), mp 64–65°C; ir: 1700, 1725, 3420 cm^{-1}; nmr: 1.3 (3H, t, CH_2CH_3, J = 7 Hz), 3.49 (2H, s, CH_2COO), 3.8 (3H, s, CH_3), 4.15 (2H, q, CH_2CH_3, J = 7 Hz), 6.8 (2H, m, 3-H and 5-H), 9.2 (1H, broad s, NH); *m/e*: 211. *Anal.* calcd. for $C_{10}H_{13}NO_4$: C 56.86, H 6.20, N 6.63; found: C 56.79, H 6.23, N 6.60.

Ethyl 2-carbomethoxy-5-cyanopyrrole-4-acetate (18)

To a well stirred and cooled (−23°C, carbon tetrachloride – solid CO_2 bath) solution of **17** (300 mg, 1.42 mmol) in acetonitrile (30 mL), CSI (260 mg, 1.84 mmol) was added in one portion. The mixture was stirred at the same temperature under nitrogen for 2 h. DMF (1 mL) was then added rapidly and the reaction mixture was allowed to warm to room temperature over 2 h. The volatiles were removed under reduced pressure, the residue was taken up in benzene (50 mL) and washed with water (3 × 20 mL), saturated aqueous NaCl, and then dried ($MgSO_4$). Evaporation of the benzene afforded the crude material which was flash chromatographed on silica gel with ether/petroleum (1:2) as the eluent to give **18** (282 mg, 84%), mp 97–99°C; ir: 1725, 2225, 3200, 3400 cm^{-1}; nmr: 1.38 (3H, t, CH_2CH_3, J = 7 Hz), 3.6 (2H, s, CH_2COO), 3.9 (3H, s, CH_3), 4.14 (2H, q, CH_2CH_3, J = 7 Hz), 6.9 (1H, d, 3-H), 10.6 (1H, broad s, NH), $J_{1,3}$ = 1.8 Hz; *m/e*: 236. *Anal.* calcd. for $C_{11}H_{12}N_2O_4$: C 55.79, H 5.12, N 11.82; found: C 55.92, H 5.13, N 11.84.

Ethyl 2-(5,5-dimethyl-1,3-dioxan-2-yl)-pyrrole-4-glyoxalate (14)

Compound **14** was synthesized from **4** (2.0 g, 10.2 mmol) and 3.2 g (30.7 mmol) of 2,2-dimethyl-1,3-propanediol, according to the previously described method (22). The crude product was recrystallized from $CHCl_3$/petroleum to give 2.67 g (93%), mp 120–121°C; ir: 1670, 1740, 3430 cm^{-1}; nmr: 0.78 (3H, s, CH_3), 1.24 (3H, s, CH_3), 1.34 (3H, t, CH_2CH_3), 3.7 (4H, s, OCH_2), 4.3 (2H, q,

[5] The time required for the hydrogenation depended on the amount of reactants used. The reaction must be closely monitored by tlc.

[6] The chromatographed product was contaminated with a by-product which could not be distinguished from **26** by tlc.

[7] Ethyl 2-cyano-4-carbethoxyvinylpyrrole-3-acetate (**23**) (221 mg, 0.8 mmol) can be used instead of **25** without a significant change in the yield of **28**.

CH_2CH_3), 5.38 (1H, s, O—CH—O), 6.74 (1H, m, 3-H), 7.7 (1H, m, 5-H), 9.3 (1H, broad s, NH), $J_{2,3}$ = 1.6 Hz; *m/e*: 281. *Anal.* calcd. for $C_{14}H_{19}NO_5$: C 59.77, H 6.81, N 4.98; found: C 59.83, H 6.87, N 4.99.

Acknowledgements

The authors gratefully acknowledge the financial assistance of the Memorial University of Newfoundland and the Natural Sciences and Engineering Research Council of Canada. They also thank Dr. Brian Gregory for Fast Atom Bombardment (FAB) mass spectra, Mr. Avery Earle for ^{13}C nmr spectra, and Miss Annette Daley for technical assistance.

1. J. B. PAINE III. *In* The porphyrins. Vol. 1A. *Edited by* D. Dolphin. Academic Press, New York, San Francisco, London. 1978. pp. 101–163.
2. A. GOSSAUER. Die Chemie der Pyrrole. Springer-Verlag, New York, Berlin, Heidelberg. 1974. pp. 119–123.
3. R. A. JONES and G. P. BEAN. The chemistry of pyrrole. Academic Press, New York. 1977. pp. 115–207.
4. A. R. BATTERSBY and E. MCDONALD. *In* Porphyrins and metalloporphyrins. *Edited by* K. M. Smith. Elsevier, Amsterdam, Oxford, New York. 1975. p. 62.
5. R. G. WESTALL. Nature, **170**, 614 (1952).
6. G. H. COOKSON and C. RIMINGTON. Biochem. J. **57**, 476 (1954).
7. A. H. JACKSON and S. F. MACDONALD. Can. J. Chem. **35**, 715 (1957).
8. G. P. ARSENAULT AND S. F. MACDONALD. Can. J. Chem. **39**, 2043 (1961).
9. H. PLIENINGER, P. HESS, and J. RUPPERT. Chem. Ber. **101**, 240 (1968).
10. G. W. KENNER, K. M. SMITH, and J. F. UNSWORTH. J. Chem. Soc. Chem. Commun. 43 (1973).
11. B. FRYDMAN, M. E. DESPUY, and H. RAPOPORT. J. Am. Chem. Soc. **87**, 3530 (1965); B. FRYDMAN, S. REIL, M. E. DESPUY, and H., RAPOPORT. J. Am. Chem. Soc. **91**, 2338 (1969).
12. A. R. BATTERSBY, E. MCDONALD, H. K. W. WURZIGER, and K. J. JAMES. J. Chem. Soc. Chem. Commun. 493 (1975).
13. (*a*) G. H. BARNETT, H. J. ANDERSON, and C. E. LOADER. Can. J. Chem. **58**, 409 (1980); (*b*) C. E. LOADER and H. J. ANDERSON. Can. J. Chem. **59**, 2673 (1981); (*c*) C. E. LOADER, G. H. BARNETT, and H. J. ANDERSON. Can. J. Chem. **60**, 383 (1982).
14. H. J. ANDERSON, C. R. RICHE, T. G. COSTELLO, C. E. LOADER, and G. H. BARNETT. Can. J. Chem. **56**, 654 (1978).
15. B. E. MARYANOFF. J. Org. Chem. **44**, 4410 (1979).
16. H. J. ANDERSON, C. E. LOADER, and A. FOSTER. Can. J. Chem. **58**, 2527 (1980).
17. F. A. DRAHOWZAL. *In* Friedel–Crafts and related reactions. Vol. II. *Edited by* G. A. Olah. Wiley–Interscience, New York. 1964. pp. 466–467.
18. B. V. GREGOROVICH, K. S. LIANG, D. M. CLUGSTON, and S. F. MACDONALD. Can. J. Chem. **46**, 3291 (1968).
19. A. MCKILLOP, B. P. SWANN, and E. C. TAYLOR. J. Am. Chem. Soc. **95**, 3340 (1973).
20. R. H. MITCHELL and Y. H. LAI. Tetrahedron Lett. 2637 (1980).
21. A. I. MEYERS, J. SLADE, R. K. SMITH, and E. D. MIHELICH. J. Org. Chem. **44**, 2247 (1979).
22. C. E. LOADER and H. J. ANDERSON. Synthesis, 295 (1978).
23. (*a*) F. BOHLMANN, J. STAFFOLDT, and W. SKUBALLA. Chem. Ber. **109**, 1586 (1976); (*b*) H. CARPIO, E. GALEAZZI, R. GREENHOUSE, A. GUZMÁN, E. VELARDE, Y. ANTONIO, F. FRANCO, A. LEON, V. PERÉZ, R. SALAS, D. VALDÉS, J. ACKRELL, D. CHO, P. GALLEGRA, O. HALPERN, R. KOEHLER, M. L. MADDOX, J. M. MUCHOWSKI, A. PRINCE, D. TEGG, T. C. THURBER, A. R. VAN HORN, and D. WREN. Can. J. Chem. **60**, 2295 (1982).
24. (*a*) P. MULLER and B. SIEGFRIED. Helv. Chim. Acta, **57**, 987 (1974); (*b*) J. MCMURRY. Org. React. **24**, 187 (1976).
25. H. J. ANDERSON and C. W. HUANG. Can. J. Chem. **45**, 897 (1967).
26. A. H. LEWIN, S. R. PARKER, N. B. FLEMING, and F. I. CARROLL. Org. Prep. Proced. Int. **10**, 201 (1978).
27. P. S. CLEZY, C. J. R. FOOKES, and A. J. LIEPA. Aust. J. Chem. **25**, 1979 (1972).
28. M. FARNIER and P. FOURNARI. C. R. Acad. Sci. Ser. C, **273**, 919 (1971); Bull. Soc. Chim. Fr. 351 (1973).
29. E. C. TAYLOR, F. KIENZLE, R. L. ROBEY, A. MCKILLOP, and J. D. HUNT. J. Am. Chem. Soc. **93**, 4845 (1971).
30. (*a*) C. B. ZIEGLER and R. F. HECK. J. Org. Chem. **43**, 2941 (1978); (*b*) J. E. PLEVYAK, J. E. DICKERSON, and R. F. HECK. J. Org. Chem. **44**, 4078 (1979).
31. (*a*) A. J. CHALK and S. A. MAGENNIS. J. Org. Chem. **41**, 1206 (1976); (*b*) N. A. CORTESE, C. B. ZIEGLER, B. J. HRNJEZ, and R. F. HECK. J. Org. Chem. **43**, 2952 (1978).
32. W. H. CAROTHERS and G. A. JONES. J. Am. Chem. Soc. **47**, 3051 (1925).
33. S. W. HEINZMAN and B. GANEM. J. Am. Chem. Soc. **104**, 6801 (1982).
34. A. R. BATTERSBY, E. MCDONALD, J. R. REDFERN, J. STAUNTON, and R. WIGHTMAN. J. Chem. Soc. Perkin. Trans. 1, 266 (1976).
35. W. C. STILL, M. KAHN, and A. MITRA. J. Org. Chem. **43**, 2923 (1978).
36. H. R. BILLICA and H. ADKINS. Org. Synth. Coll. Vol. 3, *Edited by* E. C. Horning. J. Wiley and Sons, Inc., New York. 1955. p. 176.
37. G. UFER, S. S. TJOA, and S. F. MACDONALD. Can. J. Chem. **56**, 2437 (1978).
38. Y. C. KIM. Can. J. Chem. **47**, 3259 (1969).

Can. J. Chem. Downloaded from www.nrcresearchpress.com by 210.87.254.40 on 09/06/12
For personal use only.

A useful method for preparation of carboxylic acids from terminal alkynes[1]

SUZANNE R. ABRAMS

Prairie Regional Laboratory, National Research Council of Canada, Saskatoon, Sask., Canada S7N 0W9

Received April 5, 1983

SUZANNE R. ABRAMS. Can. J. Chem. **61**, 2423 (1983).

Substituted acetic acids can be prepared in good yield (50–80%) from terminal acetylenes of the same chain length. The alkyne is first converted to the thiophenyl ether, which is treated without purification with mercuric sulfate in acetic acid and 2 *N* sulfuric acid affording the carboxylic acid. The method is particularly useful in the synthesis of long chain ω-hydroxyalkanoic acids.

SUZANNE R. ABRAMS. Can. J. Chem. **61**, 2423 (1968).

On peut préparer les acides acétiques substitués avec un bon rendement (50–80%) à partir des acétylènes terminaux dont la chaîne est de la même longueur. On transforme d'abord l'alcyne en éther thiophényle que l'on traite sans aucune purification avec le sulfate mercurique dans de l'acide acétique et l'acide sulfurique 2 *N* pour obtenir l'acide carboxylique. La méthode est particulièrement utile dans la synthèse des acides ω-hydroxyalcanoiques à longue chaîne.

[Traduit par le journal]

In the course of a synthesis of some macrocylic lactones **1** (n = 15, 23, 25), some of which (n = 23, 25) are found in the defence secretion of a species of soldier termite (1), we encountered difficulty obtaining good yields of the substituted acetic acids **2** from the readily available ω-alkyn-1-ols **3** (2) using known methods. A sequence employing Jones oxidation of the alcohol and subsequent hydroboration of the triple bond to the primary alcohol suffered from low yields in the first step (3). The oxidation afforded poorly soluble soap-like acetylenic acids which were difficult to isolate. An alternate plan, in which the triple bond was to be converted to the carboxylic acid, met with limited success. Hydroboration of the non-polar bistrimethylsilyl derivative (4) of **3** gave the α,ω-diol as a major contaminant (50%). We sought to develop an alternative method for the preparation of alkanoic acids from terminal alkynes of the same chain length that would be suitable both for long chain alkynes and other compounds containing terminal triple bonds.

Terminal alkynes can be converted to their thioether derivatives in high yield (5) and it is known that hydration of the latter compounds with or without mercuric ion catalysis results in anti-Markovnikov attack at the terminal carbon (6). We have found that the thiophenyl derivative can be prepared in quantitative yield and treated with mercuric sulfate in 2 *N* sulfuric acid and acetic acid to give the alkanoic acid in good yield. The intermediate thiophenyl derivative does not require purification before hydrolysis.

The sequence is illustrated for 16-hydroxyhexadec-1-yne (Scheme 2). To a solution of the methoxyethoxymethyl (MEM) ether of 16-hydroxyhexadec-1-yne in THF was added n-butyllithium followed by diphenyldisulfide. The crude product **4**, was treated with a solution of mercuric sulfate, 2 *N* H_2SO_4, and acetic acid for a minimum of 4 hours at 80°C. The product. 16-acetoxyhexadecanoic acid **5**, obtained in 80% yield, is formed as the result of several processes: (1) hydration of the triple bond in the desired sense, (2) hydrolysis of the resulting thiophenyl ester, (3) removal of the MEM protecting group, and (4) acetylation of the alcohol. The product is a convenient starting material for preparation of the corresponding iodoacid (from HI and acetic acid) which can be cyclized to the macrocyclic lactone (7).

To show the generality of the procedure, a variety of alkynes

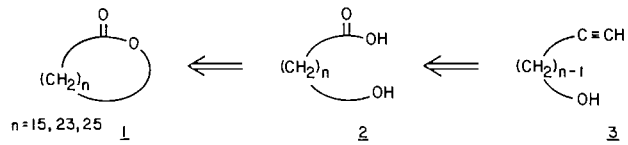

SCHEME 1

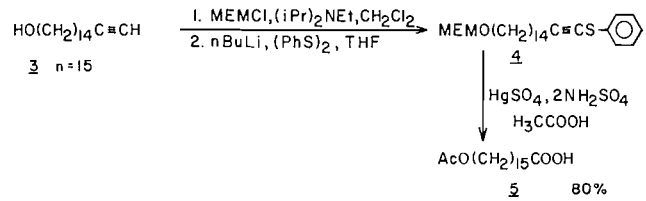

SCHEME 2

have been converted to their acetic acid derivatives (Table 1). The yields are based upon conversion from the alkyne without purification of the intermediate thioether, and are of isolated, pure products. The only exception is 1,7-octadiyne (entry 6); the intermediate monothioether was isolated before hydrolysis. The low yield of myristic acid is probably due to isolation problems.

This method for conversion of terminal alkynes to carboxylic acids of the same chain length compares favorably to those presently available (4, 10, 11). Alk-1-ynes can be converted to 1-chloroalk-1-ynes (12) which, upon treatment with base, afford carboxylic acids, but the yields are moderate (4). A direct method of preparation of carboxylic acids from acetylenes is the oxidation of 1,1-diborylalkanes with *m*-chloroperbenzoic acid, which proceeds in good yield but requires the separation of the desired acid from *m*-chlorobenzoic acid (11).

Experimental

Preparation and hydrolysis of the thiophenylacetylenic ethers was carried out under identical conditions. One experiment is described in full.

Cyclohexylacetic acid

Under a slight positive pressure of dry nitrogen, to a solution of cyclohexylacetylene (Farchan Labs., 2.16 g, 20 mmol) in THF (freshly distilled from benzophenone ketyl, 100 mL) at −70°C was added a solution of n-butyllithium (in hexane, 1.6 *M*, 15.1 mL, 24 mmol). The cooling bath was removed and the solution allowed to

[1] NRCC No. 22418.

Can. J. Chem. Downloaded from www.nrcresearchpress.com by 210.87.254.6 on 09/06/12
For personal use only.

TABLE 1. Carboxylic acids prepared by hydrolysis of the monothiophenyl derivative of some alkynes

Entry	Alkyne	Carboxylic acid	Yield (%)[a]
1	$MEMO(CH_2)_{14}C{\equiv}CH$	$AcO(CH_2)_{15}COOH$	80
2	$C_6H_5C{\equiv}CH$	$C_6H_5CH_2COOH$	70
3	$C_6H_{11}C{\equiv}CH$	$C_6H_{11}CH_2COOH$	64
4	$H_3C(CH_2)_5C{\equiv}CH$	$H_3C(CH_2)_6COOH$	49
5	$H_3C(CH_2)_{11}C{\equiv}CH$	$H_3C(CH_2)_{12}COOH$	32
6[b]	$HC{\equiv}C(CH_2)_4C{\equiv}CH$	$H_3CC(=O)(CH_2)_5COOH$	70

[a] Yields of isolated, pure products. The ^1H nmr and ir spectra and bp or mp were identical with literature values.
[b] The monothiophenyl derivative was isolated.

warm to 0°C, and then cooled again to −70°C prior to the dropwise addition of a solution of diphenyldisulfide (4.8 g, 22 mmol) in THF (25 mL). The solution was stirred and allowed to warm to ambient temperature overnight, then poured into ice water and extracted with ether (3X). The combined ether extracts were washed with NaCl solution, dried over Na_2SO_4, filtered, and the solvent evaporated to afford 4.46 g crude thioether which gave ir (film) ν_{max}: 3300 (absent), 3050 (w), 2910 (s), 2840 (s), 2160 (w), 2050 (absent), 1560 (m); ^1H nmr ($CDCl_3$, 90 MHz) δ: 7.1–7.5 (m, 5H), 2.5–3.0 (m, 1H), 1.1–2.0 (m, 10H).

A mixture of the crude thioether (3.46 g, 15.6 mmol in theory) mercuric sulfate (3.0 g, 10 mmol), 2 *N* sulfuric acid (60 mL), and acetic acid (180 mL) was heated at 80°C, in an oil bath overnight. The mixture was cooled, and extracted with $CHCl_3$ (3X). The combined organic extracts were washed with water, then NaCl solution, dried over Na_2SO_4, filtered, and evaporated. The crude product was taken up in ether and extracted with $NaHCO_3$ solution (3X). The combined basic extracts were acidified with HCl and extracted with $CHCl_3$ (3X). The combined extracts were washed with NaCl solution, dried over Na_2SO_4, filtered and evaporated, and distilled using a kugelrohr apparatus (140–150°C, 10 Torr), affording 1.4 g (64%) cyclohexylacetic acid which solidified on standing: ir (melt) ν_{max}: 3300–2500 (s), 1700 (s), 1440 (m), 1400 (m), and 1300 (m) cm^{-1} (9); ^1H nmr ($CDCl_3$) δ: 2.2 (d, J = 7 Hz, 2H), 0.8–1.9 (m, 11H) (8).

Acknowledgments

The skillful technical assistance of Angela C. Shaw and Gnoc Son Ho are gratefully acknowledged.

1. G. D. PRESTWICH and M. S. COLLINS. Tetrahedron Lett. **22**, 4587 (1981).
2. S. R. MACAULAY. J. Org. Chem. **45**, 734 (1980).
3. S. R. ABRAMS. Chem. Phys. Lipids, **28**, 379 (1981).
4. G. ZWEIFEL and S. J. BACKLUND. J. Am. Chem. Soc. **99**, 3184 (1977).
5. L. BRANDSMA, H. J. T. BOS, and J. F. ARENS. The chemistry of acetylenes. *Edited by* H. G. Viehe. Marcel Dekker Co., New York. 1969. Chapt. XI.
6. H. J. BOONSTRA, L. BRANDSMA, A. M. WIEGMAN, and J. F. ARENS. Recl. Trav. Chim. Pays-Bas, **78**, 252 (1959).
7. W. H. KRUIZINGA and R. M. KELLOGG. J. Am. Chem. Soc. **103**, 5183 (1981); C. GALLI and L. MANDOLINI. Org. Synth. **58**, 98 (1978).
8. C. J. POUCHERT and J. R. CAMPBELL. The Aldrich Library of NMR Spectra. Vol. 2. Aldrich Chemical Co. 1974. 183A.
9. C. J. POUCHERT. The Aldrich Library of IR Spectra. 3rd ed. Aldrich Chemical Co. 1981. 314H.
10. M. JULIA and J.-M. SUZUR. Bull. Soc. Chim. Fr. 1620 (1956); R. TRUCHET. Ann. Chim. **16**, 309 (1931); Chem. Abstr. **26**, 2175 (1932).
11. G. ZWEIFEL and H. ARZOUMANIAN. J. Am. Chem. Soc. **89**, 291 (1967).
12. L. BRANDSMA. Preparative acetylenic chemistry. Elsevier Publishing Co., New York. 1971. p. 97.

Can. J. Chem. Downloaded from www.nrcresearchpress.com by 210.87.254.6 on 09/06/12
For personal use only.

Optically active 1-aminoalkanephosphonic acids. Dibenzoyl-L-tartaric anhydride as an effective agent for the resolution of racemic diphenyl 1-aminoalkanephosphonates

PAWEŁ KAFARSKI AND BARBARA LEJCZAK

Institute of Organic and Physical Chemistry, Technical University of Wrocław, Wybrzeże Wyspiańskiego 27,50-370 Wrocław, Poland

AND

JERZY SZEWCZYK

Department of Organic Chemistry, Technical University of Gdańsk, Majakowskiego 11/12, 80-952 Gdańsk, Poland

Received December 14, 1982

PAWEŁ KAFARSKI, BARBARA LEJCZAK, and JERZY SZEWCZYK. Can. J. Chem. **61**, 2425 (1983).

Optically active phosphonic analogues of alanine, valine, leucine, phenylalanine, and phenylglycine were obtained by resolution of diphenyl 1-aminoalkanephosphonates with dibenzoyl-L-tartaric acid anhydride.

PAWEŁ KAFARSKI, BARBARA LEJCZAK et JERZY SZEWCZYK. Can. J. Chem. **61**, 2425 (1983).

On a obtenu des analogues phosphoniques optiquement actifs de l'alanine, de la valine, de la leucine, de la phénylalanine et de la phénylglycine, par la résolution des dérivés diphenylamino-1-alkanephosphonates avec l'anhydride de l'acide dibenzoyl-L-tartarique.

[Traduit par le journal]

Can. J. Chem. Downloaded from www.nrcresearchpress.com by 210.87.254.5 on 09/06/12
For personal use only.

Phosphonic analogues of important naturally occurring amino acids have received considerable attention in the past ten years in both academic and industrial laboratories.

It is now well established that 1-aminoalkanephosphonic acids act as substrates or inhibitors of several enzymes involved in the metabolism of amino acids (1).

Unfortunately, nearly all the biochemical studies were carried out using racemic 1-aminoalkanephosphonates, and evaluation of their action and of structure–activity relationships is strongly limited. Thus, for biochemical studies, the pure enantiomers of 1-aminoalkanephosphonic acids are desirable.

The optically pure 1-aminoalkanephosphonates described so far include only the analogues of alanine (2), valine (3), phenylglycine (3–5), and phenylalanine (6).

In this work the readily available diphenyl 1-aminoalkanephosphonates **1** (7) have been chosen as substrates for the preparation of the optically pure 1-aminoalkanephosphonic acids. Our attempts to separate diastereomeric salts of **1** with L-malic, L-mandelic, L-lactic, or dibenzoyl-L-tartaric acids were unsuccessful. However, we achieved successful resolution using dibenzoyl-L-tartaric anhydride **2**, which has been recently applied as a resolving agent for amines.[1]

We wish to describe here the use of this approach for the preparation of optically pure 1-aminoalkanephosphonic acids.

Optically active 1-aminealkanephosphonic acids

Reaction of dibenzoyl-L-tartaric anhydride **2** with diphenyl 1-aminoalkanephosphonate **1** leads to the corresponding am-

TABLE 1. Optically active 1-aminoalkanephosphonic acids **4**

R[a]	Configuration of aminophosphonic acids	Melting[b] point (°C)	Yield (%)	$[\alpha]_{578}^{20}$ (*c* 1,1 *N* NaOH)	$[\alpha]_{D}^{20}$ (*c* 1,1 *N* NaOH) from literature	Literature
CH_3	*S*	278–279	70	+17±1°	+16.8°	2
	R	277–278	88	−16±1°	−16.9°	2
$(CH_3)_2CH$	*S*	277–278	78	−0.6±0.2°[c]	−10.0°[d]	3
	R	272–273	59	+0.6±0.2°[c]	+10.0°[d]	3
$(CH_3)_2CHCH_2$	*S*[e,f]	278–280	71	+25±1°[c]	—	
	R[e,f]	288–290	71	−24±1°	—	
C_6H_5	*S*	278–279	85	−20±1°	−19.4°	3, 5
	R	280–282	81	+19±1°	+19.4°	3, 5
$C_6H_5CH_2$	*S*[e,g]	269–270	73	+52±1°	—	
	R[e,g]	267–268	87	−49±1°	—	

[a]The ir, ^1H nmr, and tlc data for enantiomers of 1-aminoalkanephosphonic acids are identical with those obtained for their racemic mixtures.

[b]All the compounds melted with decomposition.

[c]*c* 5,1 N NaOH.

[d]According to the authors statement, the specific rotation value for the valine analogue given in the literature is an apparent error and should be printed as 1.0°.

[e]Tentative configuration.

[f]Elemental analyses calcd. For $C_5H_{14}NO_3P \cdot nH_2O$ for *S*-isomer are (*n* = 1.5): N 7.21%, P 15.97%; found: N 6.90%, P 16.18%, while for *R*-isomer (*n* = 0.5), calcd.: N 7.95%, P 17.61%; found: N 8.22%, P 17.80%.

[g]Elemental analyses calcd. for $C_8H_{12}NO_3P \cdot nH_2O$ for *S*-isomer are (*n* = 1.5): N 6.14%, P 13.59%; found: N 6.13%, P 13.78%. For *R*-isomer (*n* = 1), calcd.: N 6.39%, P 14.16%; found: N 6.64%, P 13.92%.

[1]T. Kolasa and A. Chimiak, private communication.

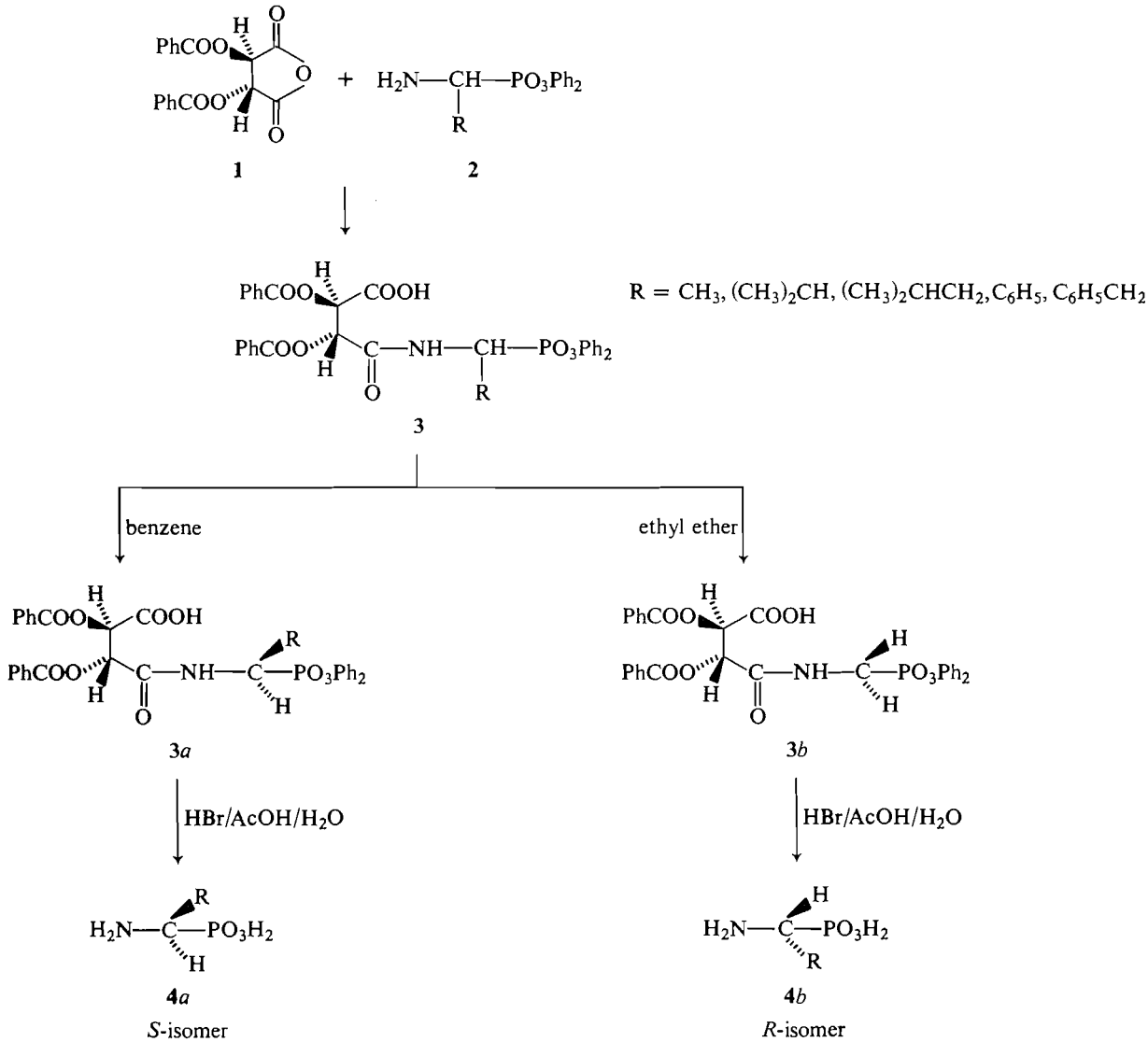

ides **3**, which were easily separated into diastereoisomers **3***a* and **3***b* by crystallization (Table 2).

The procedure is very effective: only one crystallization is sufficient to obtain pure diastereomeric amides **3** of sharp melting point. The purity of diastereoisomers was monitored by ^{31}P nmr and only one peak characteristic for the particular diastereomeric amide appeared in all cases.

Hydrolysis of **3***a* or **3***b* yielded the corresponding enantiomers of 1-aminoalkanephosphonic acids **4***a* and **4***b* in high yields (Table 1). In this manner we obtained enantiomeric phosphonic analogues of alanine, valine, leucine, phenylglycine, and phenylalanine. The absolute configuration of the analogues of alanine (2), valine (3), and phenylglycine (3) are given in the literature. The configurations of the phosphonic analogues of leucine and phenylalanine are tentative and are based on similar physical properties of the respective amides **3***a* and **3***b*.

Conversion of the amides 3 into imides 5

We hoped that the amides **5**, being "phthaloyl-like" molecules, could have been used for the preparation of optically active diphenyl 1-aminoalkanephosphonates. Unfortunately, the decomposition of these molecules under basic conditions (i.e. in the presence of amine, hydrazine, ammonia, or sodium hydroxide in alcohol or dioxane) yielded multicomponent mixtures without production of the desired diphenyl 1-aminoalkanephosphonates.

This part of our work, although unsuccessful in its final outcome, provided new information on the chemical properties of the amides **3** and, particularly, on chemical differences between diastereoisomers **3***a* and **3***b*.

We have noticed that the ring closure reaction rates differ significantly for diastereomeric **3***a* and **3***b*. Thus, reaction of diastereoisomeric mixtures of **3** with slight excess of thionyl chloride in benzene – methylene chloride suspension resulted, at room temperature, in formation of the soluble imide **5***b*, while unreacted amide **3***a* remained insoluble. The transformation of both stereoisomers of **3** into the imides **5** was smoothly accomplished by refluxing **3** in benzene with excess of thionyl chloride for several hours.

However, the separation of diastereomeric imides **5** was much more difficult than the separation of the corresponding amides (Table 3) and it was not recommended as a method for resolution, meaning that it is more convenient to use resolved amides **3***a* and **3***b*, instead of their mixtures, for the preparation of pure diastereoisomers of imides **5**.

*Structure of diastereomeric amides 3*a *and 3*b

Spectral data for the representative amides **3***a* and **3***b* are given in the Experimental section. Some additional comments

Can. J. Chem. Downloaded from www.nrcresearchpress.com by 210.87.254.5 on 09/06/12
For personal use only.

TABLE 2. Optically active amides **3**

R	Aminophosphonate configuration	Yield (%)	Melting point (°C)	$[\alpha]_{578}^{20}$ (*c* 1, acetone)	Elemental analyses %N calcd. / found	Elemental analyses %P calcd. / found	^{31}P nmr (DMSO, 85% H_3PO_4) δ (ppm)
CH_3	*S*	70	176.5–177	−86±1°	2.27 / 2.05	5.02 / 5.20	14.63
	R	100	81–83	−70±1°	2.27 / 2.19	5.02 / 4.75	14.45
$(CH_3)_2CH$	*S*	83	186–186.5	−75±1°	2.17 / 2.28	4.94 / 4.72	18.01
	R	76	82–85	−72±1°	2.17 / 1.93	4.94 / 4.98	17.97
$(CH_3)_2CHCH2$	*S*	90	181–182	−81±1°	2.13 / 2.34	4.70 / 4.35	18.69
	R	93	89–91	−82±1°	2.13 / 2.08	4.70 / 4.44	18.53
C_6H_5	*S*	92	146–148	−48±1°	2.06 / 2.08	4.57 / 4.70	13.40
	R	84	96–98	−53±1°	2.06 / 2.17	4.57 / 4.51	13.09
$C_6H_5CH_2$	*S*	78	160–161.5	−52±1°	2.02 / 1.96	4.47 / 4.13	17.46
	R	86	79–80	−47±1°	2.02 / 2.09	4.47 / 4.29	17.27

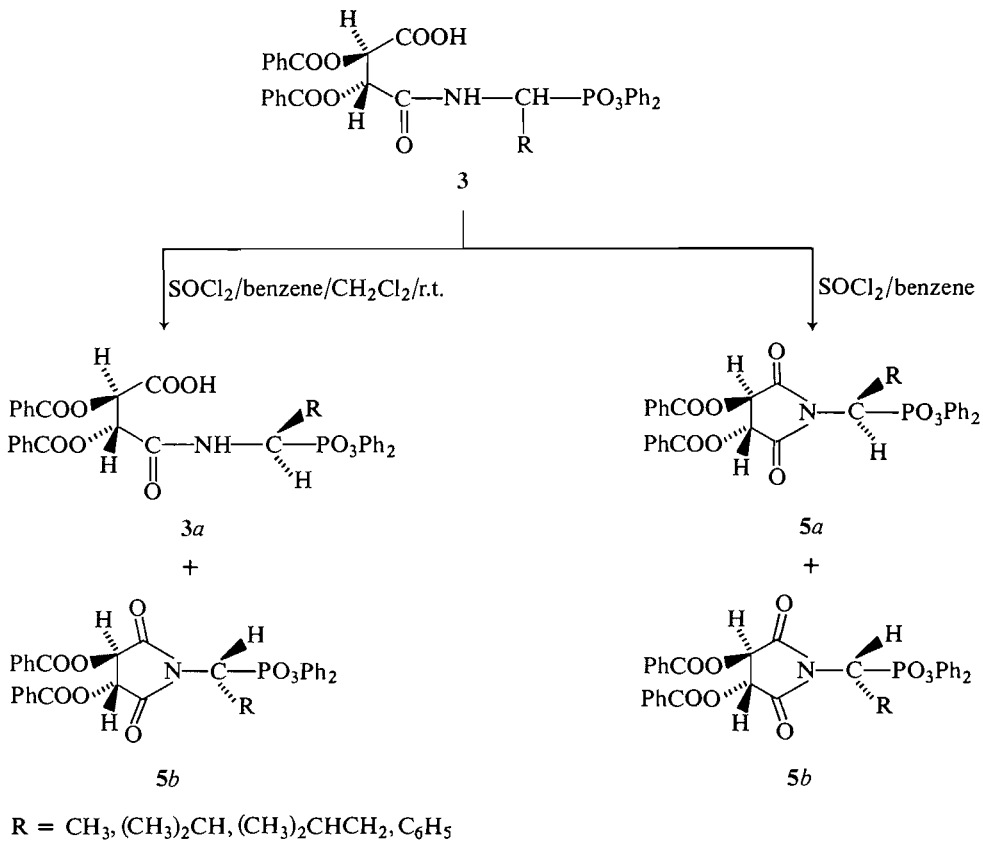

are in order.

The ^{1}H nmr as well as ir spectra of amides **3***a* clearly show the existence of strong hydrogen bonding in the molecule while spectra of **3***b* are tyical for amides. Thus, the spectra of amides **3***a* show N—H stretching frequencies in the range 3330–3360 cm^{-1} (3240–3250 cm^{-1} for **3***b*). It is conspicuous that two P=O stretching frequencies are found in the spectra of **3***a* while only one signal is present in the spectra of **3***b*. The splitting of P=O signals for **3***a* indicates that two non-equivalent phosphonate groups are present and suggests that **3***a* exists as dimer in the solid phase. Similar features were observed in the spectra of methyl esters **6**.

Can. J. Chem. Downloaded from www.nrcresearchpress.com by 210.87.254.5 on 09/06/12
For personal use only.

TABLE 3. Optically active imides **5**

R	Aminophosphonate configuration	Yield (%)	Melting point (°C)	$[\alpha]_{578}^{20}$ (c 1, acetone)	Elemental analyses %N calcd. / found	Elemental analyses %P calcd. / found	^{31}P nmr (DMSO, 85% H_3PO_4) δ (ppm)
CH_3	*S*	45[a]	160–160.5	+91±1°	2.52 / 2.30	5.18 / 5.05	14.25
		85[b]					
	R	44[a]	155–156	+94±1°	2.52 / 2.58	5.18 / 5.05	13.97
		83[b]					
$(CH_3)_2CH$	*S*	52[a]	84–85	+88±1°	2.23 / 2.43	4.94 / 4.66	13.48
		86[b]					
	R	82[a]	123–124	+86±1°	2.23 / 2.53	4.94 / 4.98	13.12
		86[b]					
$(CH_3)_2CHCH2$	*S*	96[b]	45–48	+73±1°	2.19 / 2.01	4.84 / 4.65	13.81
	R	79[b]	84–85	+86±1°	2.19 / 2.35	4.84 / 4.74	13.41
C_6H_5	*S*	92[b]	140.5–141	+69±1°	2.12 / 1.82	4.68 / 4.74	9.61
	R	85[b]	54–55	+93±1°	2.12 / 2.35	4.68 / 4.78	9.61

[a]By separation of diastereomeric **5***a* and **5***b* by crystallization.
[b]By ring closure of amides **3***a* or **3***b*.

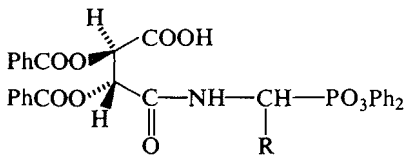

3

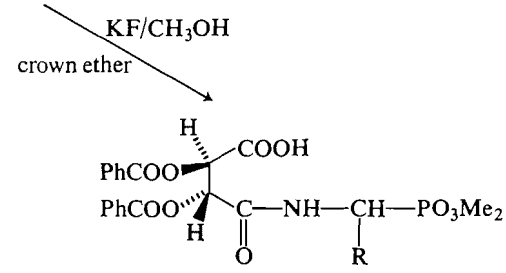

6

To confirm that the hydrogen bond in amides **3***a* is due to the participation of the phosphonic moiety, we synthesized similar amides derived from n-propylamine **7** and diphenyl aminomethanephosphonate **8**. As expected, the spectra of **8** were very close to those obtained for amides **3***a*, while spectra of n-propylamine derivative **7** were similar to those obtained for amides **3***b*.

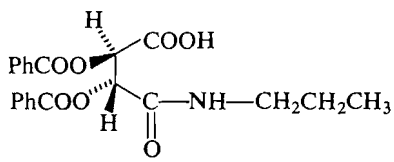

7

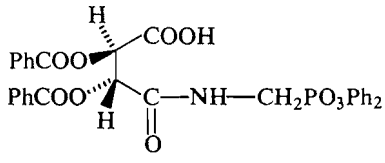

8

The big difference in the structure of diastereomeric amides **3**, revealed by spectroscopy, explains the high effectiveness of the separation process, the reaction with thionyl chloride, as well as the big difference in the melting point values.

Experimental

The melting points were determined on a Koeffler apparatus and are uncorrected. Infrared spectra were taken on a Perkin–Elmer 621 instrument as KBr pellets. Absorptions are given in cm^{-1}. Nuclear magnetic resonance spectra were recorded on a Tesla BS467 instrument in DMSO-d_6 or in $CDCl_3$ solutions. The chemical shifts are reported as δ(ppm), using a capillary tube with hexamethyldisiloxane as standard. The ^{31}P nmr spectra were taken at the Centre of Molecular and Macromolecular Studies, Polish Academy of Sciences, Łódź, using 85% H_3PO_4 as internal standard.

Diphenyl 1-aminoalkanephosphonates **1**

The hydrobromide of **1** (0.06 mol) (7) was suspended in chloroform and an equal volume of 2 *N* sodium hydroxide was added. The mixture was shaken in the separatory funnel until all the solid dissolved. The chloroform layer was separated, washed with brine, and dried over anhydrous magnesium sulphate. Evaporation of the solvent yielded the desired esters in 90–98% yield.

Preparation of amides **3** *and separation of diastereoisomers – general procedure*

Diphenyl 1-aminoalkanephosphonate **1** (0.05 mol) was dissolved in 200 cc of dioxane and 17.0 g (0.05 mol) of dibenzoyl-L-tartaric anhydride **2** were added. The mixture was shaken until all the anhydride dissolved and left for 3 days at room temperature. Then the solvent was evaporated under reduced pressure, 100 cc of benzene were added (warming until all the oil dissolved) and the mixture was left in the refrigerator overnight. The product was collected by filtration and the second crop was obtained by reducing the volume of benzene to 50 cc.

The pure **3***a*, was obtained after crystallization from 75 cc of benzene or toluene.

To obtain **3***b*, the benzene was evaporated from the filtrate and the resulting oil was dissolved in 50 cc of ether. The solution was left

Can. J. Chem. Downloaded from www.nrcresearchpress.com by 210.87.254.5 on 09/06/12
For personal use only.

TABLE 4. Optically active amides **6**

R	Aminophosphonate configuration	Yield (%)	Melting point (°C)	$[\alpha]_{578}^{20}$ (*c* 1, acetone)	Elemental analyses: calcd. / found	calcd. / found
$(CH_3)_2CH$	*S*	69	196–199	−73±1°	2.69 / 2.61	5.95 / 5.80
	R	43	99–102	−81±1°	2.69 / 3.01	5.95 / 5.68
$(CH_3)_2CHCH_2$	*S*	56	179–181	−62±1°	2.62 / 2.63	5.79 / 5.50
	R	86	Oil	−61±1°	2.62 / 2.33	5.79 / 5.51
C_6H_5	*S*	86	162–166	−69±1°	2.52 / 2.69	5.59 / 5.24
	R	72	108–110	−47±1°	2.52 / 2.30	5.59 / 5.44

overnight in the refrigerator and the precipitated **3***b* was collected by filtration. The second crop of the amide **3***b* was obtained by reducing the solvent volume to 25 cc.

The analytical data for the amides obtained, **3***a* and **3***b*, are given in Table 2. Spectroscopic data of the representative pairs of isomers are given below, for those containing the phosphonic analogue of alanine.

Compound **3**a (R = CH_3)

Infrared: 3600–2400, 3340 (NH), 1745, 1715, 1690 (CO), 1530 (NH), 1265, 1236 (PO); ^{1}H nmr (DMSO): 1.33 (dd, J^3_{HH} = 7.5 Hz, J^3_{PH} = 18.5 Hz, 3H, CH_3); 4.0–5.1 (m, J^3_{HH} = 7.5 Hz, 1H, CHP), 6.11 (s, 2H, 2 × COOCH), 5.5–6.1 (m, 1H, COOH), 6.45–8.0 (m, 20H, 4 × C_6H_5), 9.13 (d, J^3_{HH} = 9.0 Hz, 1H, NH); ^{1}H nmr ($CDCl_3$): 1.21 (dd, J^3_{HH} = 7.5 Hz, J^3_{PH} = 18.5 Hz, 3H, CH_3), 4.2–5.1 (m, 1H, CHP), 5.7–6.2 (m, 3H, 2 × COOCH, NH), 6.7–8.1 (m, 21H, 4 × C_6H_5, COOH).

Compound **3**b (R = CH_3)

Infrared: 3600–2400, 3250 (NH), 1760, 1730, 1685 (CO), 1539 (NH), 1250 (PO); ^{1}H nmr (DMSO): 1.22 (dd, J^3_{HH} = 7.5 Hz, J^3_{PH} = 19.0 Hz, 3H, CH_3), 4.2–5.0 (m, 1H, CHP), 5.99 (db, J^3_{HH} = 7.5 Hz, 2H, 2 × COOCH), 5.9–6.3 (m, 1H, COOH), 6.5–8.2 (m, 20H, 4 × C_6H_5), 9.23 (d, J^3_{HH} = 9.0 Hz, 1H, NH); ^{1}H nmr ($CDCl_3$): 1.23 (dd, J^3_{HH} = 7.5 Hz, J^3_{PH} = 19.0 Hz, 3H, CH_3), 4.25–5.2 (m, 1H, CHP), 5.92 (s, 2H, 2 × COOCH), 6.93 and 6.98 (s, 5H, C_6H_5OP), 7.0–8.8 (m, 12H, 2 × C_6H_5COO, COOH, NH). Infrared data for the **3***a* and **3***b* series respectively are very close and nmr data for the fragment common for all the amides containing the defined enantiomer of aminophosphonate are analogous.

Optically active 1-aminoalkanephosphonic acids – general procedure

The amide **3** or **3***b* (0.01 mol) was dissolved in 60 mL of acetic acid and 60 cc of 40% hydrobromic acid were added. The obtained mixture was refluxed for 20 h. After cooling to room temperature, the solvents were removed under reduced pressure, the residue was mixed with 50 cc of water, benzoic acid was filtered out, the solution clarified with charcoal, and applied to the Dowex 50W X8 50–100 mesh column (15 × 300 mm). The column was washed with water and ninhydride-positive fractions were collected. Evaporation of water yielded pure, crystalline enantiomers **4***a* and **4***b* (Table 1).

Preparation of imides **5** *– general procedure*

Amide **3** (0.01 mol) was dissolved (or suspended) in 50 cc of benzene and 2 cc of thionyl chloride were added. The mixture was refluxed for 3–5 hours. The solvent was removed under reduced pressure and the residue crystallized from ether.

The analytical data and yields of the imides obtained, **5***a* and **5***b*, are collected in Table 3. Spectroscopic data of the representative pair of imides are given for those containing the phosphonic analogue of alanine.

Compound **5**a (R = CH_3)

Infrared: 1740, 1720 (CO), 1260 (PO), 1095 (POC); ^{1}H nmr (DMSO): 1.92 (dd, J^3_{HH} = 7.5 Hz, J^3_{PH} = 18.0 Hz, 3H, CH_3), 5.15 (qq, J^3_{HH} = 7.5 Hz, J^2_{PH} = 19.0 Hz, 1H, CHP), 6.43 (bs, 2H, 2 × COOCH), 7.43 and 7.46 (s, 5H, C_6H_5OP), 7.3–8.3 (m, 10H, 2 × C_6H_5COO).

Compound **5**b (R = CH_3)

Infrared: 1740, 1720 (CO), 1265, 1210 (PO), 1100 (POC); ^{1}H nmr (DMSO): 1.72 (dd, J^3_{HH} = 7.5 Hz, J^3_{PH} = 18.0 Hz, 3H, CH_3), 4.95 (qq, J^3_{HH} = 7.5 Hz, J^2_{PH} = 18.5 Hz, 1H, CHP), 6.28 and 6.30 (s, 1H, COOH), 7.27 (bs, 10H, 2 × C_6H_5OP), 7.3–8.1 (m, 10H, 2 × C_6H_5COO).

Transesterification of amides **3** *– general procedure*

Amide **3***a* or **3***b* (2.5 mmol) was dissolved in 50 cc of methanol and 2.0 g of potassium fluoride monohydrate and 10 mg of 18-crown-6 were added. The mixture was heated until all the solid material dissolved and left for two days at room temperature. Then solvent was removed on the rotatory evaporator. The residue was dissolved in 50 cc of water and acidified to about pH 3 with concentrated hydrochloric acid. The mixture was left in the refrigerator overnight and the product was filtered off. The crystallization from ethyl ether yielded the corresponding amides **6***a* and **6***b* (Table 4).

Spectroscopic data of the representative pair of isomers are given below for those containing the phosphonic analogue of phenylglycine.

Compound **6**a (R = C_6H_5)

Infrared: 3600–2200, 3300 (NH), 1735, 1725, 1695 (CO), 1545, 1525 (NH), 1270, 1240 (PO), 1060, 1030 (POC); ^{1}H nmr (DMSO): 2.46 and 2.68 (d, J^3_{PH} = 10.5 Hz, 3H, $POCH_3$), 4.76 (tt, J^3_{HH} = 5.0 Hz, J^2_{PH} = 21.5 Hz, J^3_{HH} = 8.5 Hz, 1H, CHP), 5.33 (s, 2H, 2 × COOCH), 6.5–7.6 (m, 16H, 3 × C_6H_5, COOH), 8.90 (d, J^3_{HH} = 8.5 Hz, 1H, NH).

Compound **6**b (R = C_6H_5)

Infrared: 3600–2200, 3225 (NH), 1720, 1700 (CO), 1530 (NH), 1240 (PO), 1060, 1030 (POC); ^{1}H nmr (DMSO): 2.85 and 3.01 (d, J^3_{PH} = 10.5 Hz, 3H, $POCH_3$), 4.78 (dd, J^2_{PH} = 21.5 Hz, J^3_{HH} = 9.5 Hz, 1H, CHP), 5.40 (bd, J^3_{HH} = 6.0 Hz, 2H, 2 × COOCH), 6.1–7.5 (m, 16H, 3 × C_6H_5, COOH), 9.02 (bd, J^3_{HH} = 9.5 Hz, 1H, NH).

Also, in this case, ir data for the **6***a* and **6***b* series respectively are very close and nmr data for the molecular fragment common for all the amides containing the defined enantiomer of 1-aminoalkanephosphonate are analogous.

Preparation of the amide **7**

As described for the preparation of the amides **3**, starting from n-propylamine. After crystallization from benzene, the product melting at 89–92°C and of $[\alpha]_{578}^{20}$ −82°C (*c* 1, acetone) was obtained in 74% yield; ir: 3650–2300, 3200 (NH), 1730, 1710 (CO), 1540 (NH); ^{1}H nmr (DMSO): 0.80 (t, J^3_{HH} = 6.5 Hz, 3H, CH_3), 1.46 (sex,

Can. J. Chem. Downloaded from www.nrcresearchpress.com by 210.87.254.5 on 09/06/12
For personal use only.

J^3_{HH} = 6.5 Hz, 2H, CH_2CH_3), 3.24 (bq, J^3_{HH} = 6.5 Hz, 2H, $NHCH_2$), 6.05 (s, 2H, 2 × COOCH), 7.4–8.9 (m, 12H, 2 × C_6H_5, COOH, NH). Elemental analyses calcd. for $C_{21}H_{21}NO_7$: N 4.53%; found N 4.68%.

Preparation of the amide **8**

As described for the preparation of **3**, starting from diphenyl aminomethanephosphonate. The product was crystallized from benzene. White crystals melting at 148–150°C and of $[\alpha]^{20}_{578}$ −113°C (*c* 1, acetone) were obtained in 83% yield; ir: 3650–2350, 3250 (NH), 1725, 1690 (CO), 1585 (NH), 1240 (PO); ^{1}H nmr (DMSO): 4.25 (dd, J^3_{HH} = 6.5 Hz, J^2_{PH} = 11.0 Hz, 2H, CH_2P), 6.13 (s, 2H, 2 × COOCH), 7.0–8.5 (m, 21H, 4 × C_6H_5, COOH), 9.43 (bt, J^3_{HH} = 6.5 Hz, 1H, NH). Elemental analyses calcd. for $C_{31}H_{26}NO_{10}P$: N 2.32%, P 5.12%; found: N 2.49%, P 4.97%.

Acknowledgement

This work was supported by grants MR 1.12 and R.1.9.

1. E. NEUZIL and A. CASSAIGNE. Ann. Biochem. Exp. Med. **34**, 165 (1980).
2. R. F. ATHERTON, M. J. HALL, C. H. HASSALL, R. W. LAMBERT, and P. S. RINGROSE. Antimicrob. Agents Chemother. **15**, 677 (1979).
3. T. GŁOWIAK, W. SAWKA-DOBROWOLSKA, J. KOWALIK, P. MASTALERZ, M. SOROKA, and J. ZOŃ. Tetrahedron Lett., 3965 (1977).
4. W. F. GILMORE and M. A. MCBRIDE. J. Am. Chem. Soc. **94**, 4361 (1973).
5. M. HOFFMAN. Pol. J. Chem. **52**, 851 (1978).
6. A. K. KOTYŃSKI and W. J. STEC. J. Chem. Res. (S), 41 (1978).
7. J. OLEKSYSZYN, L. SUBOTKOWSKA, and P. MASTALERZ. Synthesis, 985 (1979).

Can. J. Chem. Downloaded from www.nrcresearchpress.com by 210.87.254.5 on 09/06/12
For personal use only.

A model for estimating ^{59}Co nmr chemical shifts and line widths and its application to cobalt dioxygen complexes

STEVE C. F. AU-YEUNG AND DONALD R. EATON
Department of Chemistry, McMaster University, Hamilton, Ont., Canada L8S 4M1

Received May 4, 1983

STEVE C. F. AU-YEUNG and DONALD R. EATON. Can. J. Chem. **61**, 2431 (1983).

A simple point charge model has been developed for calculating the chemical shifts and line widths obtained from the ^{59}Co nmr spectra of Co(III) complexes. The chemical shift calculations assume the predominance of the paramagnetic term in the Ramsey equation and the relationship of this term to the energies of the $d-d$ electronic transitions. The line width calculations assume the predominance of quadrupolar broadening and use a point charge model to calculate electric field gradients in a manner previously used to interpret Mössbauer spectra. The model is tested by application to some fifty known Co(III) complexes. Most of the ^{59}Co spectra have been remeasured for this purpose. One chemical shift parameter and one line width parameter are required for each different type of ligand. These parameters are related to each other and to the crystal field splitting parameters of the ligands. The calculations can be readily applied to complexes of any symmetry and differentiate between different isomers of the same complex. The calculated chemical shifts cover a range of more than 14 000 ppm and the standard deviation between the calculated and experimental values is 108 ppm. Relative chemical shifts between complexes with similar ligands are calculated with considerably higher accuracy. The agreement between calculated and experimental line widths is only qualitative but the line width calculations provide valuable additional information for making assignments. The model is applied to the assignment of different isomers of cobalt dioxygen compounds and to the identification of products from oxygenation reactions.

STEVE C. F. AU-YEUNG et DONALD R. EATON. Can. J. Chem. **61**, 2431 (1983).

On a mis au point un modèle de charge ponctuelle simple pour calculer les déplacements chimiques et la largeurs des raies obtenues à partir des spectres de rmn du ^{59}Co des complexes de Co(III). Les calculs des déplacements chimiques supposent la prédominance du terme paramagnétique dans l'équation de Ramsey et la relation de ce terme avec les énergies des transitions électroniques $d-d$. Les calculs de la largeur des raies admettent la prédominance de l'élargissement quadrupolaire et utilisent le modèle de charge ponctuelle pour calculer les gradients de champ électrique comme cela a été fait antérieurement pour interpréter les spectres Mössbauer. On a vérifié l'utilité de ce modèle en l'appliquant à quelques 50 complexes connues du Co(III). Dans ce but, on a mesuré de nouveau la plupart des spectres du ^{59}Co. On a besoin d'un paramètre de déplacement chimique et d'un paramètre de largeur de raie pour chaque différent type de ligand. Ces paramètres sont reliés l'un à l'autre et au paramètre de dédoublement de champ du cristal des ligands. On peut facilement appliquer les calculs aux complexes de n'importe quelle symétrie et on peut distinguer les différents isomères du même complexe. Les déplacements chimiques calculés s'étendent sur plus de 14,000 ppm et la déviation normale entre les valeurs calculées et expérimentales est de 108 ppm. On a calculé les déplacements chimique relatifs entre les complexes ayant des ligands semblables avec une précision nettement plus grande. L'accord entre les largeur de raies calculées et expérimentales est seulement qualitatif mais les calculs de la largeur de raies fournissent une information additionnelle valable pour faire des attributions. On applique le modèle à l'identification des différents isomères des composés de cobalt dioxygénés et à l'identification des produits provenant des réactions d'oxygénation.

[Traduit par le journal]

Introduction

The ^{59}Co nmr spectra of a wide variety of Co(III) complexes have been reported (1). The chemical shifts cover a range of more than 10 000 ppm and the line widths vary from a few Hz to more than 10 kHz. Potentially, therefore, the combination of chemical shift and line width data, both of which may be readily obtained with modern multinuclear nmr spectrometers, provides a convenient method for characterizing a given complex. This potential has not been extensively exploited. It is the purpose of the present paper to develop a model which will allow facile estimation of the chemical shift and line width expected for a complex with given ligands arranged in a given geometry, using a minimal number of parameters. We will then proceed to demonstrate the utility of this model for assigning resonances and for identifying isomeric structures. The derived chemical shift and line width parameters for each type of ligand are related to the electronic structures of the ligands.

Chemical shift correlations

^{59}Co chemical shifts are dominated by the paramagnetic term in the Ramsey expression (2) for chemical shifts. The application of this theory to Co nmr was first carried out by Griffith and Orgel (3) and by Freeman, Murray, and Richards (4). Correlation of the chemical shifts with the inverse of the energy of the first spin-allowed $d-d$ transition was predicted and demonstrated to hold experimentally. The theory was further developed by Fujiwara *et al.* (5), who made allowance for variation of the orbital reduction factor k' and radial factor $\langle r^{-3}\rangle$ from complex to complex. Typically this leads to expressions such as:

$$[1]\quad \sigma_{zz} = -4\left(\frac{eh}{2mc}\right)^2\left\langle\frac{1}{r^3}\right\rangle\frac{8(k_1')^2}{\Delta E(^1A_{1g} - {}^1A_{2g})}$$

$$[2]\quad \sigma_{xx} = \sigma_{yy} = -4\left(\frac{eh}{2mc}\right)^2\left\langle\frac{1}{r^3}\right\rangle\frac{8(k_2')^2}{\Delta E(^1A_{1g} - {}^1E_{1g}(^1T_{1g}))}$$

for the components of the chemical shielding tensor for a D_{4h} complex. The nomenclature is that of ref. 5. The isotropic chemical shift can be obtained as the average of these diagonal terms. Juranic *et al.* (6, 7) have applied these results to a variety of Co(III) complexes and have pointed out the necessity of allowing for the anisotropy of the chemical shift and for variations in the orbital reduction factor from compound to compound. Yamasaki, Yajima, and Fujiwara (8) have also cor-

Can. J. Chem. Downloaded from www.nrcresearchpress.com by 210.87.254.6 on 09/06/12
For personal use only.

related ^{59}Co chemical shifts with ligand electronegativities.

The objective in the present case is to derive a set of ligand parameters which will allow facile estimation of the chemical shift for a given complex. Yajima *et al.* (9) have proposed a simple linear correlation

$$\delta = 360x + \sum_{i=1}^{y} \delta_i(L)$$

for complexes of the type $Coen_x(NH_3)_{6-2x-y}L_y$ where $\delta_i(L)$ is a constant for a given ligand L. This type of correlation is not satisfactory for a wider range of complexes.

The isotropic shielding constant is given by

$$\sigma_{iso} = \frac{1}{3}(\sigma_{xx} + \sigma_{yy} + \sigma_{zz})$$

where the components of the chemical shielding tensor are given by expressions of the type of eq. [1] and [2]. It is usual to measure chemical shifts of ^{59}Co relative to the cobalticyanide anion in aqueous solution. Fujiwara *et al.* (5) have estimated the gyromagnetic ratio for ^{59}Co by plotting the chemical shifts of cobalt complexes versus the reciprocals of the energy of the first electronic transition. This estimate leads to an absolute value of 1.10% or 11 000 ppm for the shielding constant of $Co(CN)_6^{3-}$. We may therefore write the chemical shift relative to $Co(CN)_6^{3-}$ as

$$[3] \quad \delta = \frac{1}{3}\left(\frac{1}{\Delta E_x} + \frac{1}{\Delta E_y} + \frac{1}{\Delta E_z}\right) - 11\,000$$

For an octahedral complex the lowest excited state is triply degenerate but this splits into a maximum of three states with energies of E_x, E_y, and E_z as the symmetry is lowered. Ballhausen (10) has pointed out that these energies depend only on the sum of the charges produced by the ligands on the x axis, the y axis, and the z axis, respectively. We may therefore write

$$[4] \quad \delta = \frac{1}{3}\left(\frac{1}{S_1 + S_2} + \frac{1}{S_3 + S_4} + \frac{1}{S_5 + S_6}\right) - 11\,000 \text{ (in ppm)}$$

where S_1 and S_2 are parameters characteristic of the ligands on the x axis, S_3 and S_4 of ligands on the y axis, and S_5 and S_6 of ligands on the z axis. Given a set of parameters S_L for all the different ligands encountered this expression suffices to calculate the chemical shift of any cobalt complex. Yamatera (11) has applied a similar approach to the calculation of the splitting of the $d-d$ electronic bands of *cis* and *trans*, *mer* and *fac* isomers. Wentworth and Piper (12) have made similar calculations. Equation [4] is quite general and may be used for any six-coordinated Co(III) complex.

There are a number of approximations inherent in the use of eq. [4]. The major ones are: (*1*) the correct expressions for the electronic transition energies also include terms involving the inter-electronic repulsion (the Racah parameter) which may vary with the ligand in a different manner to the crystal field splitting parameter D_q; (*2*) the orbital reduction factors (k' of eqs. [1] and [2]) and radial terms $\langle r^{-3} \rangle$ will vary from complex to complex; (*3*) the crystal field splitting and hence the chemical shift parameter S, for a given ligand may depend upon the other ligands present. For these reasons we would expect only limited success in fitting experimental chemical shifts to eq. [4].

Line width correlations

The variation of line widths of Co(III) complexes has not previously been considered in detail. It has been widely recognized that complexes with low symmetry have broader lines than complexes with high symmetry and this has proved a useful generalization in assigning resonances. Yajima *et al.* (9) deduced from simple crystal field considerations that *trans* isomers should show broader lines than *cis* isomers and that for complexes of the stoichiometry CoA_3B_3 the *mer* isomer should have a broad line and the *fac* isomer a narrow line.

^{59}Co has a spin of 7/2 and therefore possesses a quadrupole moment. If quadrupolar relaxation is dominant the line width will be given by

$$[5] \quad \Delta\nu_{1/2} = \frac{\pi}{98} A^2 \tau_c$$

where

$$A^2 = \left(1 + \frac{\eta^2}{3}\right)\left(\frac{e^2qQ}{h}\right)^2$$

with

$$eq = V_{zz} \text{ and } \eta = \frac{V_{xx} - V_{yy}}{V_{zz}}$$

V_{zz}, V_{xx}, and V_{yy} are the principal components of the field gradient tensor, Q is the qudrupole moment of ^{59}Co, and τ_c is a rotational correlation time. If the correlation times for a series of complexes are approximately the same the line width will then depend only on the quadrupole coupling constants (e^2qQ/h) and the asymmetry parameters (η).

There are three approximations inherent in eq. [5]. First the instrumental contribution to the line width is neglected. Since this contribution is no more than a few Hz this is not a significant error. Secondly the contribution of relaxation mechanisms other than quadrupolar is neglected. The other mechanisms of possible importance are those arising from chemical shift anisotropy and from scalar relaxation of the second kind. We have recently shown that chemical shift anisotropy can be important for low symmetry complexes (13). However, the variation of the chemical shift tensor with geometry mathematically parallels that of the field gradient tensor. Spiess, Haas, and Hartman (14) have indeed found that for several complexes the chemical shift anisotropies measured for single crystals of cobalt complexes are directly proportional to the quadrupolar coupling constants. It seems therefore a reasonable procedure to develop line width correlations based on quadrupolar relaxation providing that it is recognized that the derived broadening parameters may contain a contribution from chemical shielding anisotropy which will be field dependent.

Scalar relaxation of the second kind involving coupling to the ^{14}N of amines is important for some complexes with high symmetry and relatively narrow lines. We must therefore expect that the model will be quantitatively poor for complexes with narrow lines. The third approximation of eq. [5] is that the extreme narrowing limit ($\omega^2\tau_c^2 \ll 1$) is assumed. This approximation is probably good for the large majority of the complexes.

A point charge model for quadrupolar coupling has been developed by Bancroft and Platt (15) and has been extensively applied to the interpretation of quadrupole coupling constants derived from Mössbauer spectra. Valiyev and Zripov (16) have presented a similar model. The latter theory has been applied to the ^{93}Nb line width of niobium halides by Tarasov *et al.* (17) and the ^{27}Al line widths of aluminum halide complexes by Wehrli and Wehrli (18). The components of the electric field

Can. J. Chem. Downloaded from www.nrcresearchpress.com by 210.87.254.6 on 09/06/12
For personal use only.

TABLE 1. Line width formula for complexes derived from the point charge model

Structural type[a]	η	Line width formula
MA_6	0	0
(a,bcdef)-MAB_5	0	$4(\gamma_A - \gamma_B)^2$
cis-(be,acdf)-MA_2B_4	0	$4(\gamma_B - \gamma_A)^2$
trans-(af,bcde)-MA_2B_4	0	$16(\gamma_A - \gamma_B)^2$
fac-(bef,acd)-MA_3B_3	0	0
mer-(abf,cde)-MA_3B_3	≠0	$9(\gamma_A - \gamma_B)^2 + 3(\gamma_B - \gamma_A)^2$
cis-(b,acdf,e)-MAB_4C	≠0	$(2\gamma_B - \gamma_A - \gamma_C)^2 + 3(\gamma_C - \gamma_A)^2$
trans-(a,bcde,f)-MAB_4C	0	$4(\gamma_A + \gamma_C - 2\gamma_B)^2$
fac-(b,acd,ef)-MAB_3C_2	0	$4(\gamma_C - \gamma_A)^2$
mer,trans-(b,adf,ce)-MAB_3C_2	≠0	$(3\gamma_B - 2\gamma_C - \gamma_A)^2 + 3(2\gamma_C - \gamma_B - \gamma_A)^2$
mer,cis-(b,aef,cd)-MAB_3C_2	≠0	$(3\gamma_B - 2\gamma_C - \gamma_A)^2 + 3(\gamma_B - \gamma_A)^2$
cis,cis,cis-(be,ad,cf)-$MA_2B_2C_2$	≠0	$(\gamma_B + \gamma_C - 2\gamma_A)^2 + 3(\gamma_C - \gamma_B)^2$
trans,cis,cis-(af,be,cd)-$MA_2B_2C_2$	0	$4(2\gamma_A - \gamma_B - \gamma_C)^2$
trans,trans,trans-(bd,af,ce)-$MA_2B_2C_2$	≠0	$4(3\gamma_B - \gamma_C - \gamma_A)^2 + 12(\gamma_C - \gamma_A)^2$
fac-(b,ade,c,f)-MAB_3CD	≠0	$(-\gamma_A - \gamma_C + 2\gamma_D)^2 + 3(-\gamma_A + \gamma_C)^2$
mer-(b,acf,d,e)-MAB_3CD	≠0	$(2\gamma_B - \gamma_A - \gamma_C - \gamma_D)^2 + 3(\gamma_B + \gamma_D - \gamma_A - \gamma_C)^2$
mer-(b,adf,c,e)-MAB_3CD	≠0	$(3\gamma_B - \gamma_A - \gamma_C - \gamma_D)^2 + 3(\gamma_C + \gamma_D - \gamma_A - \gamma_B)^2$
trans,cis-(b,af,de,c)-MAB_2C_2D	≠0	$(4\gamma_B - 2\gamma_C - \gamma_A - \gamma_D)^2 + 3(\gamma_D - \gamma_A)^2$
cis,cis-(b,ae,cf,d)-MAB_2C_2D	≠0	$4(\gamma_B + \gamma_C - \gamma_A - \gamma_D)^2$
trans,cis-(b,ce,ad,f)-MAB_2C_2D	≠0	$(2\gamma_D - \gamma_C - 2\gamma_B - \gamma_A)^2 + 3(2\gamma_B - \gamma_A - \gamma_C)^2$
cis,cis-(b,ae,cd,f)-MAB_2C_2D	≠0	$(2\gamma_D + \gamma_B - 2\gamma_C - \gamma_A)^2 + 3(\gamma_B - \gamma_A)^2$
cis,cis-(b,ad,ef,c)-MAB_2C_2D	≠0	$(\gamma_B + \gamma_C - \gamma_A - \gamma_D)^2 + 3(\gamma_D + \gamma_C - \gamma_A - \gamma_B)^2$
trans,trans-(b,ce,af,d)-MAB_2C_2D	≠0	$(4\gamma_C - 2\gamma_B - \gamma_D - \gamma_A)^2 + 3(2\gamma_B - \gamma_A - \gamma_D)^2$

[a]The ligating atoms are arranged as indicated by the IUPAC convention (Commission on the Nomenclature of Inorganic Chemistry. Pure Appl. Chem. **28**, 1 (1971)).

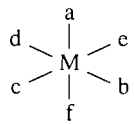

gradient tensor are expressed in terms of the partial quadrupole splitting parameters for the individual ligands. Thus a single ligand gives rise to the field gradient

$$[6]\quad \begin{aligned} V_{xx} &= Zer^{-3}(3\sin^2\theta\cos^2\phi - 1)\\ V_{yy} &= Zer^{-3}(3\sin^2\theta\sin^2\phi - 1)\\ V_{zz} &= Zer^{-3}(3\cos^2\theta - 1)\end{aligned}$$

where Z is the charge on the ligand, e the charge of an electron, and r, θ, and ϕ are the polar coordinates of the ligand. The field gradient for a complex is obtained by summing the contributions to V_{xx}, V_{yy}, and V_{zz} from all six ligands with the θ and ϕ values being determined by the position of each ligand in the complex. On this model different ligands have different values of Zr^{-3}. Combination of eqs. [5] and [6] results in expressions for the line widths in terms of parameters for the individual ligands. Thus for example in the case of a *trans*-CoA_4B_2 complex:

$$\begin{aligned} V_{xx}' = V_{yy} &= [-2(Zr^{-3})_A + 2(Zr^{-3})_B]e\\ V_{zz} &= [4(Zr^{-3})_A - 4(Zr^{-3})_B]e\end{aligned}$$

where the subscripts A and B correspond to the appropriate ligands. Substitution in eq. [5] gives $\eta = 0$ and

$$\begin{aligned}\Delta\nu_{1/2} &= \frac{\pi}{98}\frac{Q^2e^4}{h}[4(Zr^{-3})_A - 4(Zr^{-3})_B]^2\tau_c\\ &= [4\gamma_A - 4\gamma_B]^2\end{aligned}$$

where

$$\gamma_A = \frac{\pi}{98}\frac{Q^2e^4}{h^2}(Zr^{-3})_A\tau_c$$

and γ_B is analogous.

In Table 1 expressions for the line widths in terms of the broadening parameters γ_A, γ_B etc. are given. The expressions of Table 1 agree with those given by Bancroft and Platt (15) for all cases where direct comparison is possible. A few of the numerical factors differ from those given by Tarasov *et al.* (17). In deriving the line broadening parameters from line width data, only the differences are obtained and there is an ambiguity in sign since they appear as squares. It will be shown that absolute values can be obtained by comparison with Mössbauer data.

Experimental

^{59}Co nmr spectra were obtained at 21.252 MHz using a Bruker WH90 FT spectrometer. The probe temperature was 24°C. A few spectra were also obtained at 94 MHz using a Bruker WH400 spectrometer. Aqueous samples were contained in 10 mm (e.d.) round bottomed tubes purchased from Wilmod Glass Co. The pH of the solutions was 5–6 except for the tetraethylene pentamine oxygen complexes which have pH values in the 6–7 range. Line widths were measured as the full width at half height of the absorption signal. Chemical shifts are reported relative to $Co(CN)_6^{3-}$ and were obtained by direct frequency measurements. Susceptibility corrections are of the order of 1–2 ppm and were neglected. ^{59}Co nmr data have been reported previously for most but not all of the complexes discussed below. Many have been remeasured since the line widths in particular vary considerably in the older literature reports. In cases where the spectra have been remeasured or are reported for the first time, appropriate synthetic references are given in the tables. Data fitting was carried out using an Osborne I microcomputer using BASIC programming. The "Supercalc" software was also used and is particularly convenient for optimizing the least-squares fit of a large amount of experimental data with variation of the chemical shift and line broad-

Can. J. Chem. Downloaded from www.nrcresearchpress.com by 210.87.254.6 on 09/06/12
For personal use only.

TABLE 2. ^{59}Co chemical shift and line widths of cobalt (III) complexes

Complex	δ/ppm Exp.[a]	δ/ppm Calcd.	$\Delta\nu_{1/2}$/Hz Exp.	$\Delta\nu_{1/2}$/Hz Calcd.	Synthetic reference
		CoA_6			
$Co(CN)_6^{3-}$	0	246	5± 2 (—)	0	—
$Coen_3^{3+}$	7146± 5 (7110)	7149	90± 10 (87−120)	0	25
$Co(NH_3)_6^{3+}$	8175± 5 (8160)	8172	172± 10 (87−350)	0	26
$Co(N_3)_6^{3-}$	12532± 5 (—)	12530	207± 20 (—)	0	This work
$Co(CO_3)_3^{3-}$/satd. $KHCO_3$	14070± 5 (13975)	13789	513± 20 (437)	0	27
		CoA_5B			
$Co(NH_3)_5F^{2+}$	— (9520)	9520	— (1750)	10816	—
$Co(NH_3)_5Cl^{2+}$	8887± 5 (8850)	8925	1460± 100 (1750)	1311	28
$Co(NH_3)_5Br^{2+}$	8823± 5 (8820)	8820	1317± 100 (1750)	1032	29
$Co(NH_3)_5I^{2+}$	— (8760)	8760	— (2100)	484	—
$Co(NH_3)_5CO_3^{+}$	9062± 15 (9000)	8988	1947± 150 (—)	1089	30
$Co(NH_3)_5N_3^{+}$	8821± 5 (8680)	8823	396± 30 (350)	324	31
$Co(NH_3)_5NCS^{2+}$	8328± 10 (8200)	8328	1317± 100 (—)	196	32
$Co(NH_3)_5SCN^{2+}$	8600± 10 (8760)	8545	1538± 100 (—)	784	32
$Co(NH_3)_5H_2O^{3+}$	9147± 10 (9170)	9143	4018± 200 (5248)	4196	26
		cis,trans-*CoA_4B_2*			
cis-$Coen_2Cl_2^{+}$	8974± 30 (8970)	8901	5126± 100 (7870)	2150	33,34
trans-$Coen_2Cl_2^{+}$	9333± 50 (8970)	9198	8597± 300 (14000)	8601	33,34
cis-$Coen_2Br_2^{+}$	8764± 30 (8960)	8708	5420± 300 (5250)	1788	35
trans-$Coen_2Br_2^{+}$	8982± 50 (8960)	8939	7453± 300 (9620)	7152	35
cis-$Co(NH_3)_4Cl_2^{+}$	9630± 20 (9810)	9618	3400± 150 (3500)	1311	36
trans-$Co(NH_3)_4Cl_2^{+}$	9808± 20 (9810)	9880	5857± 200 (7000)	5243	36
cis-$Co(CO_3)_2(NH_3)_2^{-}$	11626± 20 (11647)	11678	820± 100 (—)	1089	37
trans-$Co(CO_3)_2(NH_3)_2^{-}$	11933± 20 (—)	11917	4274± 100 (—)	4356	37
cis-$Coen_2(N_3)_2^{+}$	8763± 10 (8400)	8711	986± 100 (875)	793	38
trans-$Coen_2(N_3)_2^{+}$	9092± 15 (—)	8942	3500± 100 (—)	3172	38
cis-$Co(NH_3)_4(N_3)_2^{+}$	9448± 5 (9400)	9476	385± 20 (525)	324	39
trans-$Co(NH_3)_4(N_3)_2^{+}$	— (9170)	9624	— (875)	1296	—
cis-$Coen_2(NH_3)_2^{3+}$	— (7400)	7480	— (350)	103	—
trans-$Coen_2(NH_3)_2^{3+}$	— (7510)	7490	— (700)	413	—
cae,bfd-$Co(dien)_2^{3+}$	6968± 5 (—)	7003	395± 30 (—)	30	This work
bae,cfd-$Co(dien)_2^{3+}$	6836± 5 (—)	6856	425± 30 (—)	135	This work
cis-$Coen(NH_3)_4^{3+}$	7843± 5 (7790)	7822	325± 30 (—)	103	40
cis-$Co(NH_3)_4CO_3^{+}$	9732± 20 (9735)	9805	3291± 300 (1925)	1089	34
cis-$Coen_2CO_3^{+}$	8888± 20 (8880)	9020	2968± 200 (3325)	1862	34
		$Co(CN)_{6-x}(NH_3)_x$			
$Co(NH_3)_5CN^{2+}$	6675± 10 (6695)	6507	2370± 200 (3005)	3025	—
cis-$Co(NH_3)_4(CN)_2^{+}$	5132± 10 (5665)	4842	2489± 200 (2804)	3025	42,43
trans-$Co(NH_3)_4(CN)_2^{+}$	5498±100 (6045)	5530	14810±2000 (4006)	12100	42,43
fac-$Co(NH_3)_3(CN)_3$	3314± 5 (3325)	3176	618± 50 (1002)	0	42,43
mer-$Co(NH_3)_3(CN)_3$	3991± 10 (4045)	3865	4542± 500 (2503)	9075	42,43
cis-$Co(NH_3)_2(CN)_4^{-}$ [b]	2457±100 (—)	2200	2673± 500 (—)	3025	—
trans-$Co(NH_3)_2(CN)_4^{-}$ [b]	2744±200 (—)	2888	13096±2000 (—)	12100	—
$Co(NH_3)(CN)_5^{2-}$	1168± 20 (—)	1223	3131± 300 (—)	3025	44
		$Co(CN)_{6-2x}(en)_x$			
cis-$Coen_2(CN)_2^{+}$	4379± 30 (—)	4308	3700± 300 (—)	2010	43
trans-$Coen_2(CN)_2^{+}$	4727± 50 (—)	4848	8089± 600 (—)	8043	43
cis-Coen $(CN)_4^{-}$	2006± 30 (—)	2026	5410± 300 (—)	2010	43,45

[a]Values in parentheses obtained from ref. 1, Chapt. 8, and references therein.
[b]Observed as transient in a saturated solution of $Co(NH_3)_5H_2O^{3+}$ containing 1 *M* KCN.

ening parameters. For complex spectra, a non-linear least-square program was developed. The spectrum is fitted to a sum of Lorenztians with a sixth order polynomial baseline function. The criteria for best fit is determined by the value of χ^2/df (~1.0). The standard errors were calculated in the usual way from the estimated variance-covariance matrix of the fitted parameters (19).

Results

Table 2 contains chemical shifts and line widths for 44 Co(III) complexes. The complexes reported in this table are all well characterized compounds of the types CoA_6, CoA_5B, *cis*- and *trans*-CoA_4B_2, and *mer*- and *fac*-CoA_3B_3. These data will be used to test the models for calculating chemical shifts and line widths described above. Data taken from literature sources are given in parentheses. ^{59}Co nmr spectra for eleven of these compounds have not been reported previously. Of the remainder all but five have been remeasured. Agreement with the literature chemical shift values is generally good with the ex-

Can. J. Chem. Downloaded from www.nrcresearchpress.com by 210.87.254.6 on 09/06/12
For personal use only.

TABLE 3. ^{59}Co chemical shift and line width for low symmetry cobalt(III) complexes

Complex[a]	δ/ppm Exp.	δ/ppm Calcd.	$\Delta\nu_{1/2}$/Hz Exp.	$\Delta\nu_{1/2}$/Hz Calcd.	Synthetic reference
cis,*cis*,*cis*-Coen$(NH_3)_2Cl_2^+$	— (9320)	9285	— (5342)	1783	—
cis,*cis*,*trans*-Coen$(NH_3)_2Br_2^+$	— (9310)	9270	— (8548)	5537	—
cis-Coen$_2(NH_3)Cl^{2+}$	— (8050)	8191	— (4375)	1782	—
cis-Coen$_2(NH_3)Br^{2+}$	— (8040)	8094	— (3500)	1462	—
df,abe,c-CoendienCl^{2+}	7758±30 (—)	7875	2787±100 (—)	2454	46
de,abf,c-CoendienCl^{2+}	7964±40 (—)	7951	3194±200 (—)	2290	46
mer-Coen$(NH_3)_3Br^{2+}$	— (8390)	8435	— (4375)	809	—
mer-Co(dien)Cl_3	9988± 5 (—)	9977	2080±200 (—)	6464	47
fac-Co$(NH_3)_3(N_3)_3$	9917± 2 (9970)[b]	9911	250± 10 (297)[b]	0	48

[a]See footnote *a*, Table 2.
[b]In dimethylsulfoxide.

ception of some of the values for the *cis*- and *trans*-CoA_4B_2 isomers. Some of the older studies using broad line nmr instruments did not distinguish between the isomers. The present results give distinct chemical shifts for the different isomers in all cases. There is considerable variation in the line widths reported in the literature. In one or two cases the present line widths do not agree with literature values obtained from broad line instruments. The ligands chosen range from the strong field CN^- to the weak field CO_3^{2-}. The total range of chemical shifts is more than 14 000 ppm which is close to the maximum observed for Co(III) complexes. These data should therefore provide a fair and adequate test for the model.

Table 3 gives chemical shift and line width data for ten low symmetry Co(III) complexes. All of these complexes have three different ligands and offer a variety of isomeric possibilities. Most, but not all, of these data have been taken from the literature. None of these data were used in the calculation of the ligand parameters and they therefore provide a further more rigorous test for the model. Table 4 gives ^{59}Co nmr data for a series of bridged cobalt complexes. Some of these data have been briefly reported in a communication (20). They will be used to provide illustrative examples of the application of the chemical shift and line width models.

Table 5 lists the chemical shift parameters (S_A, S_B, ...) and line width parameters (γ_A, γ_B, ...) which have been defined above. Tables 2, 3, and 4 include the chemical shifts and line widths calculated from these parameters.

The derivation of the chemical shift parameters of Table 5 is straightforward. For example, $S(NH_3)$ can be obtained directly from the chemical shift of $Co(NH_3)_6^{3+}$ and then used to find S(Cl) from the chemical shift of $Co(NH_3)_5Cl^{2+}$. An initial set of parameters obtained in this manner was then adjusted to optimize the fit of the data in Table 2.

The calculation of the partial broadening parameters of Table 5 is a little more complex. According to the definition proposed above the square root of the line width of a given complex, e.g., $Co(NH_3)_5Cl^{2+}$ gives the difference ($\gamma_{NH_3} - \gamma_{Cl^-}$). The signs of these differences were obtained by comparison with the analogous ^{57}Fe Mössbauer partial quadrupole coupling constants given by Bancroft and Platt (15). A plot of the differences in partial broadening constants versus the differences in ^{57}Fe partial quadrupole splitting constants is shown in Fig. 1. There is a linear relationship with a correlation coefficient of 0.988. Since the absolute values of the quadrupole splitting constants are known, the absolute values of the partial broadening constants can be obtained from the slope of this plot. This leads to a set of γ values which were then adjusted to give the best fit to the line widths of Table 2. The assumption implicit in this treatment is that since the Co(III) complexes and the Fe(II) complexes are isostructural and isoelectronic there will be proportionality between the electric field gradient produced by a given ligand at the Co nucleus and the electric field gradient produced by the same ligand at the Fe nucleus. The approximation involved in this assumption is probably less than the errors arising from assuming constant correlation times and neglecting relaxation mechanisms other than quadrupolar. For the monomeric complexes of Table 2 the variation in the correlation times may be estimated from the ionic radii to be around 20%. Bridged complexes such as those containing the peroxy ion will have significantly longer correlation times and hence the lines are likely to be significantly broader than calculated by the above simple procedure.

Discussion

A. Evaluation of the model

Of the 44 complexes in Table 2, five of the type $Co(NH_3)_5X^{2+}$ where X = F^-, I^-, NCS^-, SCN^-, and H_2O have been included to provide the corresponding *X* parameters. These ligands are only present in one compound and so the calculated shifts provide no test for the validity of the model. The remaining 39 complexes contain eight different ligands (NH_3, en, CN^-, Cl^-, Br^-, CO_3^{2-}, N_3^-, and dien). The terminal NH_2 of the dien ligand has been assigned the same parameters as the NH_2 of en. Two different parameters have been used for the central NH of dien depending on whether the three coordination positions are planar or at right angles. The same parameters will be used below for the trien and tetraen ligands. The same parameters have been used for both monodentate and bidentate CO_3^{2-}. A total of nine parameters have therefore been used to fit the 39 chemical shifts and a similar number to calculate the line widths. The standard deviation of the calculated from the experimental shifts is 108 ppm. The total range of the shifts is 14 070 ppm. As might be anticipated the fit is worst at the extreme ends of the chemical shift range. Of the four complexes for which the differences between observed and calculated are greater than 200 ppm, three are cyanide compounds (including $Co(CN)_6^{3-}$) and the fourth is the tris-carbonato complex. It is reasonable that the approximation of assuming a constant orbital reduction factor will be least applicable for these compounds. The calculations predict that *trans* isomers will have a greater shift than *cis* isomers and *mer* isomers a larger shift than *fac* isomers. The experimental data

Can. J. Chem. Downloaded from www.nrcresearchpress.com by 210.87.254.6 on 09/06/12
For personal use only.

Can. J. Chem. Downloaded from www.nrcresearchpress.com by 210.87.254.6 on 09/06/12
For personal use only.

TABLE 4. ^{59}Co chemical shift and linewidth of cobalt dioxygen complexes

Complex assignment	21.252 MHz		59.035 MHz		94.457 MHz		Calculated
	δ/ppm	$\Delta\nu_{1/2}$/Hz	δ/ppm	$\Delta\nu_{1/2}$/Hz	δ/ppm	$\Delta\nu_{1/2}$/Hz	δ/ppm ($\Delta\nu_{1/2}$/Hz)
$(Co(NH_3)_5)_2O_2^{4+}$/6 *M* NH_4OH	8759± 5	1172± 25					8758(228)
sym[a]-e,c(adf),b-$(CO(NH_3)(trien))_2O_2^{4+}$/pH = 10.5	7655± 10	1913± 50					7680(888)
" /pH = 4.75	7672± 10	1766± 50					
sym-$(Co(salen))_2O_2(DMSO)_2$[b]	8369±100	12854±1500			8367±50	13287±1000	
sym-$(Co(salen))_2O_2(DMF)_2$[b]	8375±100	13624±2000					
sym-$((Co(salen))_2O_2(H_2O))_2$	8365±100	13249±1500			8381±50	13158±2000	
sym-edf,ac,b-$(Co(dien)(en))_2O_2^{4+}$	7555± 5	760± 30	7552± 5	846± 20	7554±10	1282±50	7681(379)
sym-def,ac,b-$(Co(dien)(en))_2O_2^{4+}$	7572± 5	850± 50	7569±10	924± 20	7568±20	1661±50	7718(819)
sym-aef,cd,b-$(Co(dien)(en))_2O_2^{4+}$	7652± 10	1453± 50	7654±20	2231± 50	7650±20	3560±100	7795(718)
sym-edacf,b-$(Co(tetraen))_2O_2^{4+}$	7447± 5	777± 50	7456± 2	967± 50	7455±1	958±30	7458(572)
sym-aedcf,b-$(Co(tetraen))_2O_2^{4+}$	7484± 2	364	7483± 1	553± 50	7483±1	667±30	7484(408)
sym-deacf,b-$(Co(tetraen))_2O_2^{4+}$	7569± 10	1311± 50	7560		7576±2	2386±250	7575(985)
(dfcaa′,ed′e′b′f′),bc′-$(Co(tetraen))_2O_2^{4+}$ [c]	7516± 10	970± 100	7515± 5	1721± 200	7518±1	1621±50	7502(1113), 7556(772)
					7552±1	3858±400	
(fcdaa′,f′bcde′),bc′-$(Co(tetraen))_2O_2^{4+}$ [c]	7408± 50	2354± 200	7417±50	8500±1000	—	—	7381(638), 7556(772)
(cfed′e′,f′b′a′ad),bc′-$(Co(tetraen))_2O_2^{4+}$ [c,d]					7494±1[d]	801±140	7498(1061), 7575(985)
					7594±3[d]	3932±600	
(acff′b′,a′e′d′ed),bc′-$(Co(tetraen))_2O_2^{4+}$ [c,d]	7614± 30	2985± 200	7632±30	4200± 800	7640±2	6386±400	7612(960), 7458(572)

[a]Symmetric with respect to peroxo-bridge.

[b]^{1}H nmr indicated that DMSO, DMF is replaced by H_2O followed by dimerization to form *sym*-$(Co(salen))_2O_2(H_2O))_2$. Solution molecular weight studies support this assignment and the resonance is best assigned to the Cobalt center of the inner dimeric pair. The terminal Co(salen) group do not conform to $Co^{III}O_2^{2-}Co^{III}$ formalism (49). This is supported by kinetic results which will be published elsewhere.

[c]

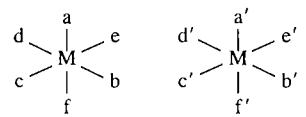

[d]Assignment is less certain.

TABLE 5. ^{59}Co chemical shift (S_L) and broadening (γ_L) parameters for cobalt(III) complexes

Ligand[f]	S_L (10^{-5} ppm^{-1})	γ_L(Hz$^{1/2}$)	f-factor[e]
*CN^-	4.446	79.500	~1.7
*$N(CH_2CH_2NH_2)_3$	3.087	65.958	—
*$NH(CH_2CH_2NH_2)_2$[a]	2.895	59.985	1.29
*NH_2CH	2.858	59.210	1.30
$NH(CH_2CH_2NH_2)_2$[b]	2.823	58.488	1.29
*$NH_2CH_2CH_2NH_2$	2.755[c]	57.080[c]	1.28
*NH_3	2.608	52.000	1.25
*NCS^-	2.476	45.000	1.02
*SCN^-	2.320	38.000	0.73
*O_2^{2-}	2.169[c]	44.446[c]	—
*I^-	2.168	41.000	—
*N_3^-	2.125	43.000	0.83
*Br^-	2.125	35.938	0.72
*Cl^-	2.058	33.895	0.78
*CO_3^{2-}[d]	2.017	35.500	—
*OH^-	1.930	19.658	—
*H_2O	1.920	19.613	1.00

[a]Terminal amine groups arranged 90° to each other.
[b]Terminal amine groups arranged 180° to each other.
[c]Per ligating atom.
[d]Same value for bidentate and monodentate carbonate.
[e]Reference 50.
[f]Asterisk indicates ligating atom.

Can. J. Chem. Downloaded from www.nrcresearchpress.com by 210.87.254.6 on 09/06/12
For personal use only.

support these predictions in all cases.

The agreement between observed and calculated line widths is only qualitative but is nevertheless useful for making assignments as will be illustrated below. Thus it is predicted that *trans*-CoA_4B_2 isomers will be broader than *cis* by a factor of four. In all cases the *trans* lines are indeed broader but the factor is generally less than four. We attribute this mainly to broadening due to chemical shift anisotropy as has been discussed elsewhere (13). Similarly *mer* isomers always show broader lines than *fac* isomers as predicted. The calculated quadrupolar broadening for the *fac* isomers is zero and the residual width of a few hundred Hz probably arises from scalar relaxation with the nitrogen ligands. The correct prediction of trends in the line widths may be illustrated with the series of *cis*-$Coen_2X_2^+$ complexes with X = Cl^-, Br^-, CN^-, CO_3^{2-}, N_3^-, and NH_3. The experimental widths are 5126, 5420, 3700, 2968, 986, and 350 Hz, respectively and the calculated widths 2150, 1788, 2010, 1862, 793, and 103 Hz, respectively. The trend is correctly predicted but the widths of the broader lines are underestimated.

Table 3 illustrates the results of calculating chemical shifts and line widths for complexes of low symmetry. For the ten compounds in this table the standard deviation between observed and calculated chemical shifts is 66 ppm. None of these data were used in deriving the parameters. Most of the data are from the literature and were obtained on a broad line instrument which does not provide shift and line widths of the accuracy expected from a modern F.T. instrument. Nevertheless the model can clearly be used to predict the spectral parameters for complexes with several different ligands.

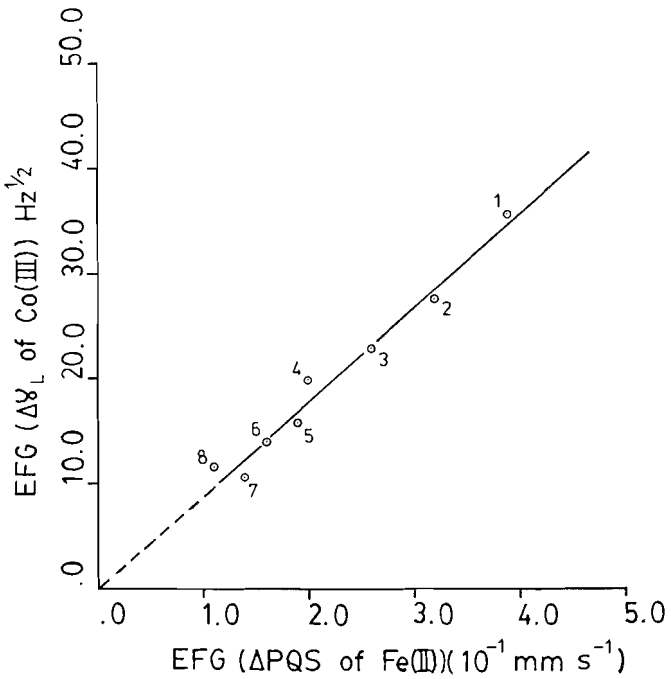

FIG. 1. A plot of the differences in partial broadening factor ($\Delta\gamma_L$) versus the corresponding differences in the isoelectronic Fe(II) partial quadrupole splitting values for various ligand pairs. *1*, CN^- − H_2O; *2*, CN^- − NH_3; *3*, en − Br^-; *4*, NH_3 − Cl^-; *5*, en − N_3^-; *6*, en − NO_2^-; *7*, NH_3 − N_3^-; *8*, NO_2^- − NH_3.

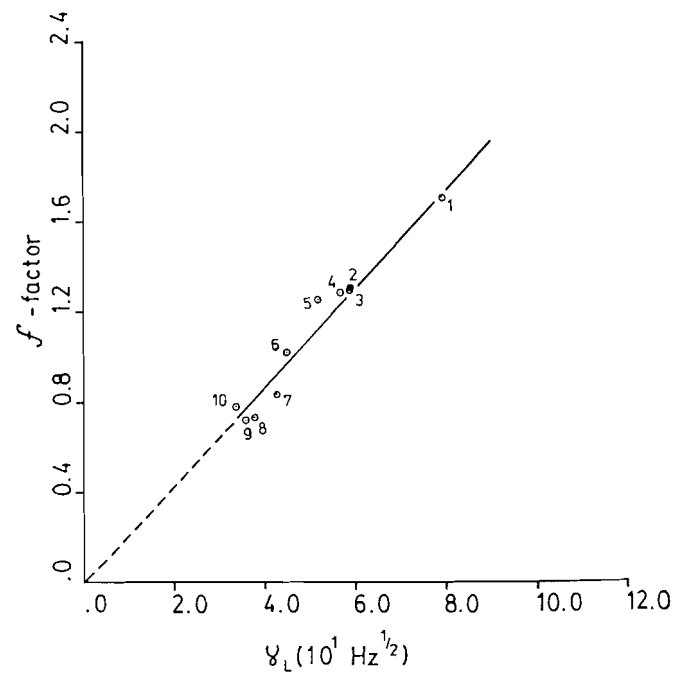

FIG. 2. A plot of the ligand field factor f versus the partial broadening factor γ_L. *1*, CN^-; *2*, $NH(CH_2CH_2NH_2)_2$; *3*, NH_2OH; *4*, $NH_2(CH_2)_2NH_2$; *5*, NH_3; *6*, NCS^-; *7*, N_3^-; *8*, SCN^-; *9*, Br^-; *10*, Cl^-.

B. Application to cobalt dioxygen complexes

The point charge model used to calculate the line width parameters uses precisely the same assumptions as the familiar crystal field theory used to obtain the crystal field splitting parameters, D_q, from electronic spectra. Jørgensen (21) has expressed D_q in terms of ligand contributions and metal ion

Can. J. Chem. Downloaded from www.nrcresearchpress.com by 210.87.254.6 on 09/06/12
For personal use only.

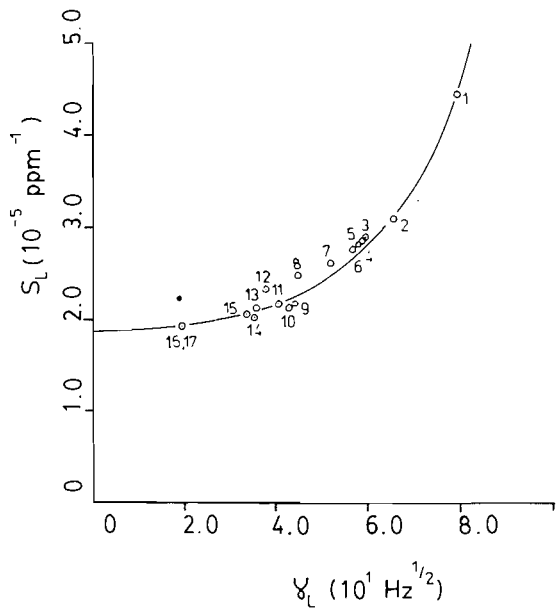

FIG. 3. A plot of the shift parameter S_L versus the partial broadening factor γ_L. *1*, CN^-; *2*, $N(CH_2CH_2NH_2)_3$; *3*, $NH(CH_2CH_2NH_2)_2$ (see footnotes *a* and *b* of Table 5); *4*, NH_2OH; *5*, $NH(CH_2CH_2NH_2)_2$; *6*, $NH_2(CH_2)_2NH_2$ (see footnotes *a* and *b* of Table 5); *7*, NH_3; *8*, NCS^-; *9*, SCN^-; *10*, O_2^{2-}; *11*, I^-; *12*, N_3^-; *13*, Br^-; *14*, Cl^-; *15*, CO_3^{2-}; *16*, OH^-; *17*, H_2O.

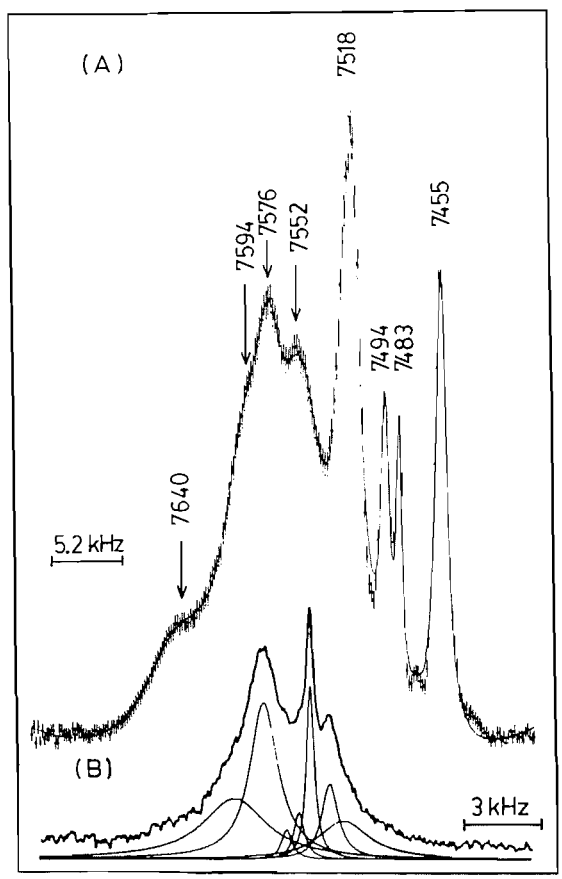

FIG. 4. ^{59}Co nmr spectrum of $(Co(tetraen))_2O_2(ClO_4)_4$ in aqueous solution (*A*) 94.457 MHz (9.395T), (*B*) 21.252 MHz (2.1139T). In (*A*) the continuous line is the stimulated spectrum.

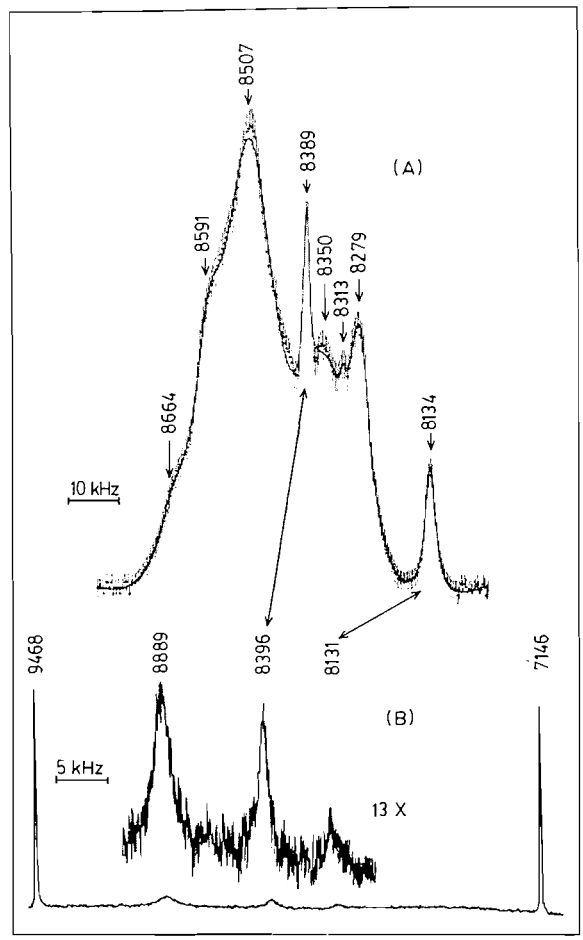

FIG. 5. ^{59}Co nmr spectrum of the oxygenation reaction of $Co(SCN)_2 + 2en + 4KSCN \xrightarrow{O_2}$ product. (*A*) 94.457 MHz (9.395T) spectrum obtained after 15 min; (*B*) 21.252 MHz (2.1139T) spectrum obtained after 1 h. In *A* the continuous line is the simulated spectrum.

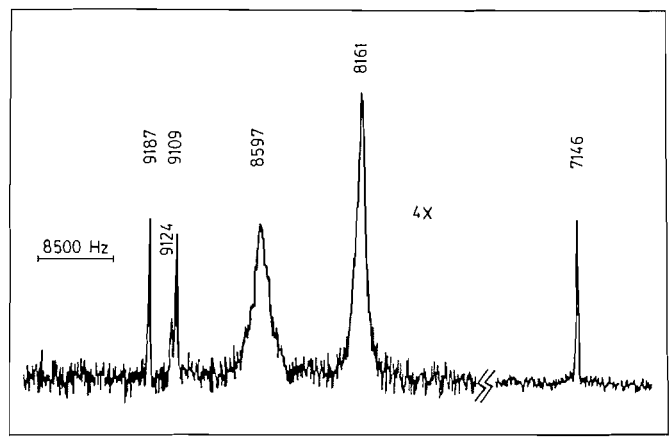

FIG. 6. 21.252 MHz (2.1139T) ^{59}Co nmr spectrum of the oxygenation reaction described by Fig. 5 after 2 h, showing the final products of the reaction.

contributions, i.e.,

$$10D_q = f_{\text{ligand}} \times g_{\text{ion}}$$

and has evaluated f values for a variety of ligands. These f factors are given in Table 5. Figure 2 shows a plot of the f-values versus the line broadening parameters γ for the same

TABLE 6.
(*a*) Species observed after 15 min (94.475 MHz ^{59}Co) and after 1 h (21.252 MHz ^{59}Co) for the reaction $Co(SCN)_2 + 2en + 4KSCN \xrightarrow{O_2}$ products

Complex assignment	Experimental 21.252 MHz δ/ppm	Experimental 21.252 MHz $\Delta\nu_{1/2}$/Hz	Experimental 94.457 MHz δ/ppm	Experimental 94.457 MHz $\Delta\nu_{1/2}$/Hz	Calculated δ/ppm	Calculated $\Delta\nu_{1/2}$/Hz
$Coen_3^{3+}$	7146±2	97± 10	7146±1	100± 5	7146	0
sym[a]-ad,cf,e,b-$(Coen_2NCS)_2O_2^{2+}$	8131±2	839±150	8134±1	2522± 213	8190	612
sym-ae,cf,d,b-$(Coen_2NCS)_2O_2^{2+}$	—	—	8279±1	4964± 517	8275	2443
sym-ad,bc,f,e-$(Coen_2(NCS)_2SCN)_2en$	—	—	8313±1	871± 128	8313	196
sym-cd,af,b,e-$(Coen(NCS)_2SCN)_2en$	—	—	8350±5	12064±2257	8349	1947
sym-ad,cf,e,b-$(Coen_2SCN)_2O_2^{2+}$	8396±5	1230±100	8389±1	1400± 226	8387	1130
sym-ae,cf,d,b-$(Coen_2SCN)_2O_2^{2+}$	—	—	8501±1	13646±1003	8525	4023
sym-ac,df,e,b-$(Coen(NCS)_2)_2(en)(O_2)$	—	—	8591±3	6951±1132	8598	1833
sym-ad,c,f,e,b-$(Coen(NCS)(SCN))_2(en)(O_2)$	—	—	8664±5	7023±1266	8710	182
sym-cd,(a,e,f),b-$(Coen(NCS)_3)_2O_2^{2-}$	8889±5	2084±200	—	—	8873	558
sym-cf,(d,a,e),b-$(Coen(NCS)_3)_2O_2^{2-}$					8921	638
sym-(a,c,d,e,f),b-$(Co(NCS)_5)_2O_2^{6-}$	9468±2	219±20	—	—	9413	196

[a]See footnote of Table 4.

(*b*) Species observed after 2 h for the reaction $Co^{II}(SCN) + 2en + 4KSCN \xrightarrow{O_2}$ product

Complex assignment	Experimental 21.252 MHz δ/ppm	Experimental 21.252 MHz $\Delta\nu_{1/2}$/Hz	Calculated δ/ppm	Calculated $\Delta\nu_{1/2}$/Hz
$Coen_3^{3+}$	7146± 1	100± 10	7146	0
ad,cf,b,e-$Coen_2(SCN)_2^+$	8161± 2	1144±100	8186	1456
sym-ac,df,c,b-$(Coen(NCS)_2)_2en(O_2)$	8597±20	1742±150	8598	1833
sym-bcde,a,f-$(Co(NCS)_4(SCN))_2en^{4-}$	9101± 2	180± 10	9031	103
sym-acdf,b,e-$(Co(NCS)_4(SCN))_2en^{4-}$			9054	1117
cd,abe,f-$(Coen(SCN)_3NCS)^-$	9124± 2	302± 20	9087	584
cd,aef,f-$(Coen(SCN)_3NCS)^-$			9124	2186
$Co(NCS)_6^{3-}$	9187± 2	158± 10	9194	0

ligands. There is an excellent linear correlation ($\gamma = 0.98$) with the plot passing through the origin. A plot of the shift parameters S versus the line width parameter γ is shown in Fig. 3. There is again a smooth correlation but the plot is not linear. This reflects the fact that E, and hence S, depends on both D_q and the Nephelauxetic parameter β and that, particularly for the strong field ligands, changes in the orbital reduction factor cannot be neglected. Both the line width parameter and the shift parameter are therefore indicative of the position of a ligand in the spectrochemical series. ^{59}Co nmr spectra may therefore be used to obtain this information in cases where charge transfer or other transitions complicate the interpretation of the $d-d$ electronic spectra.

The compounds formed by the reaction of molecular oxygen with Co(II) complexes (22) fall in this class. Table 4 contains the ^{59}Co nmr data for a variety of compounds with 2:1 $Co:O_2$ stoichiometries. These compounds are usually regarded as complexes of Co(III) with bridging peroxide ligands but it has been suggested on the basis of their ligand lability, that the oxidation state of the cobalt is intermediate between 2+ and 3+ (23). The nmr data indicate that they are normal Co(III) complexes. The broadening parameter (44.446 $Hz^{1/2}$) and shift parameter (2.17×10^{-5} ppm^{-1}) given in Table 5 have been used to obtain the calculated shifts and line widths of Table 4. For the shifts the agreement is good, giving a standard deviation of 9 ppm for 10 compounds. The line widths are again in qualitative agreement. For these dimeric compounds the assumption of a constant correlation time is questionable. The shift and line width parameters would place the O_2^{2-} bridging ion close to N_3^- and I^- in the spectrochemical series with an f-value of 0.95.

In many of these complexes there are extensive possibilities for isomerism. Thus in the case of the complex $(Co(dien)(en))_2O_2^{4+}$ consideration of the arrangements of the ligands bonded to the Co predicts three different isomers. The 94 MHz ^{59}Co spectra (20) clearly show three resonances for this complex. The possibility of *cis*/*trans* isomerism about the bridging oxygen is neglected. The calculated chemical shifts for these isomers are all 130–140 ppm higher than the experimental values but the relative shifts are well predicted, i.e., a low field line 77 ppm from the central line (observed 80 ppm) and a high field line 37 ppm from the central line (observed 17 ppm). The calculations also correctly predict that the highest field line will have the smallest width. On this basis the lines are given the assignments shown in Table 4. We note that application of this model has led to a change in the assignments previously given (20) which were derived by direct analogy with higher symmetry *cis* and *trans* isomers. We have some kinetic evidence that the rates of reaction of the different isomers are different so the assignments are a matter of some significance.

The complex $(Co(tetraen))_2O_2^{4+}$ has more extensive isomeric possibilities (tetraen ≡ tetraethylene pentamine). There are four possible arrangements of the pentadentate amine and the peroxide about an octahedral Co^{3+} ion. The 21 MHz and 94

Can. J. Chem. Downloaded from www.nrcresearchpress.com by 210.87.254.6 on 09/06/12
For personal use only.

Can. J. Chem. Downloaded from www.nrcresearchpress.com by 210.87.254.6 on 09/06/12
For personal use only.

MHz ^{59}Co spectra of this compound are shown in Fig. 4. This spectrum shows a minimum of seven lines and computer fitting shows that eight lines are required to obtain a satisfactory fit. A fit of the spectrum using eight lines is shown in the figure. Three of the four predicted isomers have calculated shifts of 7445, 7460, and 7550 ppm and calculated widths of 571, 408, and 985 Hz. These fit well with the observed lines at 7455, 7484, and 7569 ppm with widths of 777, 304, and 1311 Hz. The fourth isomer is predicted at 7381 ppm but not observed. Crawford *et al.* (24) have demonstrated the formation of μ-ethylenediamine-μ-peroxy complexes by the oxygenation of cobalt amine solutions. We tentatively assign the remaining resonances to complexes of this type. The calculated chemical shifts are consistent with such an assignment and are given in Table 4. The chemical shifts observed can only be associated with compounds containing five coordinated amine groups and a peroxide. Aquated species are therefore unlikely.

A final example involves an experiment in which a mixture in the ratio of 1 mol of $Co(SCN)_2$, 2 mol of ethylenediamine, and 4 mol of potassium thiocyanate was oxygenated. The initial ^{59}Co spectrum obtained is shown in Fig. 5. Parts of this spectrum were also run at 94 MHz and are shown on an expanded scale to illustrate the additional structure present. After standing for 2 h the mixture gave the ^{59}Co spectrum shown in Fig. 6. We note that it takes approximately 1 h to obtain a spectrum on the WH90 instrument. The WM400 spectrum was obtained in 15 min. The intermediate species therefore appear more strongly in the high field spectrum. Only the line at 7146 ppm (line width 97 Hz) is common to the spectra of Figs. 5 and 6. This line clearly arises from $Coen_3^{3+}$ which is formed rapidly. The remaining resonances of Fig. 5 are assigned as dioxygen complexes formed as intermediates in the oxidation of Co^{2+} to Co^{3+}. The assignments, together with those of the final Co^{3+} complexes, are given in Table 6. Most of the oxygen complexes found were of the types $(Coen_2NCS)_2O_2^{2+}$, μ-ethylenediamine-μ-O_2-$(Coen(NCS)_2)_2$, $(Coen(NCS)_3)_2O_2^{2-}$, and $(Co(NCS)_5)_2O_2^{6-}$, i.e., the ethylenediamine isothiocyanato complex series predominates and there are no thiocyanato/isothiocyanato mixed ligand complexes. The final product shows a mixture of $Coen_3^{3+}$, $Coen_2(SCN)_2$ (*cis*-isomer), and $Co(NCS)_6^{3-}$. We note that the latter complex can be assigned with some confidence to the line at 9194 ppm (line width 158 Hz) on the basis of the calculated shift of 9187 ppm (line width 0 Hz). This simple complex has apparently yet to be isolated. In addition to the above, the product mixture shows resonances at 9124 and 9101 ppm. These resonances can be assigned to the *mer* and *fac* isomers of $Coen(SCN)_3(NCS)^-$ on the basis of chemical shifts. The agreement between experimental and calculated line widths is poor, the observed line widths being too small. An alternative to these assignments involves bridged ethylenediamine complexes with four isothiocyanato and one thiocyanate ligands. These data are collected in Table 6. The assignments for the latter two resonances (i.e., 9124 and 9101 ppm) must be regarded as tentative. The occurrence of the dibridged μ-ethylenediamine, μ-O_2-$(Coen(NCS)_2)_2$ complex in the final product mixture is consistent with the known stability of μ-ligand, μ-peroxo bridged cobalt dioxygen complex (22).

The above examples are illustrative of the potential utility of the simple point charge model for calculating ^{59}Co chemical shifts and line widths. The model has clear limitations, especially in its application to line width calculations, but provides at least a reasonable starting point for assigning complex spectra of the types shown in Figs. 4, 5, and 6. With the increasing availability of high field nmr instruments, spectra of this type are likely to be encountered frequently, and to provide valuable structural and mechanistic information in the area of Co(III) chemistry.

Acknowledgements

We are indebted to the Natural Sciences and Engineering Research Council of Canada for financial support of this research and to the South West Ontario High Field NMR centre for providing access to the WM400 NMR instrument. The assistance of Dr. G. Dénès of CNRS, France, in the computer simulation of spectra is also gratefully acknowledged.

1. R. G. KIDD and B. J. GOODFELLOW. *In* NMR and the Periodic Table. *Edited by* B. K. Harris and B. E. Mann. Academic Press, New York. 1978.
2. N. F. RAMSEY. Phys. Rev. **77**, 567 (1950); **78**, 699 (1950); **83**, 540 (1951).
3. J. S. GRIFFITH and L. E. ORGEL. Trans. Faraday Soc. **53**, 601 (1957).
4. R. FREEMAN, G. R. MURRAY, and R. E. RICHARDS. Proc. R. Soc. London, A**242**, 455 (1957).
5. S. FUJIWARA, F. YAJIMA, and A. YAMASAKI. J. Magn. Reson. **1**, 203 (1969).
6. N. JURANIC, M. B. CELAP, D. VUČELIĆ, M. J. MALINAR, and P. N. RADIVOJSA. J. Magn. Reson. **35**, 319 (1979).
7. N. JURANIC, M. B. CELAP, D. VUČELIĆ, M. J. MALINAR, and P. N. RADIVOJSA. Spectrochim. Acta, **35A**, 997 (1979).
8. A. YAMASAKI, F. YAJIMA, and S. FUJIWARA. Inorg. Chim. Acta, **2**, 39 (1968).
9. F. YAJIMA, Y. KOIKE, A. YAMASAKI, and S. FUJIWARA. Bull. Chem. Soc. Jpn. **17**, 1442 (1974).
10. C. J. BALLHAUSEN. Introduction to ligand field theory. McGraw-Hill, New York. 1962. p. 107.
11. H. YAMATERA. Bull. Chem. Soc. Jpn. **37**, 95 (1958).
12. R. A. D. WENTWORTH and T. S. PIPER. Inorg. Chem. **4**, 709 (1965).
13. S. C. F. AU-YEUNG and D. R. EATON. J. Magn. Reson. In press.
14. H. W. SPIESS, H. HAAS, and H. HARTMANN. J. Chem. Phys. **50**, 3057 (1969).
15. G. M. BANCROFT and R. H. PLATT. Adv. Inorg. Radio Chem. **15**, 59 (1972); G. M. BANCROFT. Coord. Chem. Rev. **11**, 247 (1973).
16. K. A. VALIYEV and M. M. ZRIPOV. Zh. Struckt. Khim. **7**, 494 (1966).
17. V. P. TARASOV, V. I. PRIVALOV, and YU. A. BUSLAEV. Mol. Phys. **35**, 1047 (1978).
18. F. W. WEHRLI and S. WEHRLI. J. Magn. Reson. **44**, 197 (1981).
19. T. K. KEIPERT and D. W. MARQUARDT. J. Magn. Reson. **24**, 181 (1976).
20. S. C. F. AU-YEUNG and D. R. EATON. Inorg. Chim. Acta Lett. **76**, L141 (1983).
21. C. K. JØRGENSEN. Absorption spectra and chemical bonding in complexes. Pergamon Press, New York. 1962; Oxidation numbers and oxidation states. Springer, New York. 1969.
22. G. MCLENDON and A. E. MARTELL. Coord. Chem. Rev. **19**, 1 (1976).
23. T. SHIBAHARI and M. MORI. Bull. Chem. Soc. Jpn. **45**, 1433 (1972).
24. M. CRAWFORD, S. A. BEDELL, R. I. PATEL, L. W. YOUNG, and R. NAKON. Inorg. Chem. **18**, 2075 (1979).
25. J. B. WORK. Inorg. Synth. **2**, 221 (1946).
26. R. D. LINDHOLM. Inorg. Synth. **18**, 67 (1978).
27. H. F. BAUER and W. C. DRINKLAND. Inorg. Synth. **8**, 202 (1966).
28. G. G. SCHLESSINGER. Inorg. Synth. **9**, 160 (1967).
29. H. DIEHL, H. CLARK, and H. H. WILLARD. Inorg. Synth. **6**, 186 (1939).

30. F. BASOLO and R. K. MURMANN. Inorg. Synth. **4**, 171 (1953).
31. M. LINHARD and H. FLYGARE. Z. Anorg. Alleg. Chem. **262**, 328 (1950).
32. M. LINHARD and H. BIEBERT. Z. Anorg. Alleg. Chem. **278**, 287 (1955).
33. J. C. BAILER JR. Inorg. Synth. **2**, 222 (1946).
34. J. SPRINGBØRG and C. E. SCHAFFER. Inorg. Synth. **14**, 63 (1973).
35. W. G. JACKSON and C. M. BEGBIE. Inorg. Synth. **21**, 119 (1982).
36. A. WERNER. Lieb. Ann. **386**, 103 (1912).
37. M. MORI, M. SHIBATA, and E. KYUNO. Bull. Chem. Soc. Jpn. **29**(8), 883 (1956).
38. W. STRECKER and H. OXENIUS. Z. Anorg. Alleg. Chem. **218**, 151 (1934).
39. M. LINHARD, M. WEIGEL, and H. FLYGARE. Z. Anorg. Alleg. Chem. **263**, 233 (1950).
40. M. SHIBATA. Chem. Chem. Ind. **20**(9), 116 (1967).
41. H. SIEBERT. Z. Anorg. Alleg. Chem. **327**, 63 (1964).
42. M. SHIBATA. J. Jpn. Chem. (Kagaku No Ryoiki), **90**, 9 (1970).
43. K. KONYA, H. NISHIKAWA, and M. SHIBATA. Inorg. Chem. **7**(6), 1165 (1968).
44. A. HAIM and W. K. WILMARTH. Inorg. Chem. **1**, 573 (1962).
45. K. OHKAWA, J. FUJITA, and Y. SHIMURA. Bull. Chem. Soc. Jpn. **38**(1), 66 (1965).
46. D. A. HOUSE and D. A. GAINSFORD. Inorg. Chim. Acta, **3**(3), 367 (1969).
47. D. H. CRAYTON. Inorg. Synth. **7**, 207 (1963).
48. M. LINHARD and M. WEIGEL. Z. Anorg. Alleg. Chem. **263**, 245 (1950).
49. B.-C. WANG and W. P. SCHAFFER. Science, **166**, 1404 (1969).
50. C. K. JØRGENSEN. Oxidation numbers and oxidation states. Springer, New York. 1969. pp. 84–85.

Can. J. Chem. Downloaded from www.nrcresearchpress.com by 210.87.254.6 on 09/06/12
For personal use only.

COMMUNICATION

On the synthesis of cardioactive steroid glycosides. On cardioactive steroids. XI[1]

HAOLUN JIN, THOMAS Y. R. TSAI, AND KAREL WIESNER
Natural Products Research Centre, University of New Brunswick, Fredericton, N.B., Canada E3B 6E2

Received July 7, 1983

HAOLUN JIN, THOMAS Y. R. TSAI, and KAREL WIESNER. Can. J. Chem. **61**, 2442 (1983).

A stereoselective β-glycosidation of digitoxose and digitoxigenin involving a 1−3 participation of a urethane group is described. The conversion of digitoxin (**10**) to its furyl derivative **11** and the reoxidation of **11** to digitoxin and isodigitoxin (**12**), respectively, in high yield is reported for the first time. This is of fundamental importance for the use of the new glycosidation method in the total synthesis of digitoxin and its analogues.

HAOLUN JIN, THOMAS Y. R. TSAI et KAREL WIESNER. Can. J. Chem. **61**, 2442 (1983).

On décrit une β-glycosidation stéréosélective de la digitoxose et de la digitoxigénine qui implique une participation 1−3 d'un groupe uréthane. On rapporte pour la première fois la transformation de la digitonine (**10**) en son dérivé furyle (**11**) et la réoxydation de ce dérivé en digitonine et en isodigitonine (**12**) respectivement avec un rendement élevé. Cette réaction est très importante pour l'application de la nouvelle méthode de glycosidation dans la synthèse totale de la digitonine et de ses analogues.

[Traduit par le journal]

In previous communications of this series we have disclosed a simple and efficient methodology for the synthesis of cardenolides and bufadienolides and their analogues. As a result of this novel technique, we have succeeded in synthesizing several derivatives which, when tested in the form of glucosides, have shown a high level of inotropic activity and a margin of safety one or two orders of magnitude greater than the precariously narrow margin displayed by the natural digitalis glycosides used in therapy.[2] As our studies progressed it gradually became clear that glucosides invariably have a duration of action too short to be of practical use. Consequently, it became imperative to work out methods for the attachment of the natural glycosidic chain of digitoxin to our synthetic steroids.

A stereoselective β-glycosidation of 2-desoxyhexoses is unknown and specifically in the case of digitoxigenin and digitoxose the ß-glycoside was obtained in a yield of 4.5% in mixture with 5.4% of the corresponding α-glycoside (2). At this point we have noticed a paper by Hanessian *et al.* (3) in which 1,2,3-trideoxy-4,6-di-*O*-*p*-nitrobenzoyl-3-trifluoroacetamido-L-arabino-hex-1-enopyranose yielded on acid catalysis stereospecifically the α-glycoside with daunomicinone. It seemed to us that this process must operate via the intermediate **1** (cf. also ref. 4). We have first attempted with no success to control the glycosidation of digitoxose derivatives by 1−3 participation of a variety of esters. Finally, we decided to try a urethane group which is very similar to an acetamide by its electronic properties. We have prepared by a straightforward process starting from the known compound **2** (5) both anomers of **3** (6). (β-anomer mp 130−131°C; ir ($CHCl_3$): 3475 (NH), 1720 (C=O), 1610 cm^{-1} (aromatic); pmr ($CDCl_3$): δ = 3.87 (s, 3H, aromatic OCH_3), 3.52 (s, 3H, 1-OCH_3), 2.74 (d, J = 5 Hz, N—CH_3), 1.30 (d, J = 6 Hz, 6-CH_3); $[\alpha]_D^{22}$ = +59.18 ($CHCl_3$).)

The β-anomer **3** was hydrolysed with aqueous acetic acid at 110°C for 40 min to the foamy anomeric mixture **4**. Compound **4** was reconverted with high stereoselectivity to the β-anomer **3** with methanol under the conditions described below for a digitoxigenin derivative.

The furyl derivative of digitoxigenin (7) was coupled with 2 mol of **4** and 0.2 mol of *p*-toluenesulfonic acid in CH_2Cl_2−benzene (1:1) for 45 min at room temperature. The anomeric mixture **5** was obtained besides some starting material in a yield of 83% on the basis of starting material consumed. A small amount of the cyclic urethane **8** (mp 146−148°C; ir ($CHCl_3$): 1700 (C=O), 1610 cm^{-1} (aromatic); pmr ($CDCl_3$): δ = 3.88 (s, 3H, aromatic OCH_3), 3.12 (s, 3H, NCH_3), 1.31 (d, J = 6 Hz, 3H, 6-CH_3); $[\alpha]_D^{22}$ = +159.93 ($CHCl_3$)) was also found in this experiment. Compound **8** may be obtained quantitatively from **3** or **4** on prolonged reflux with aqueous acetic acid. Its utilization for a second method of stereospecific β-glycosidation of digitoxose is being studied. For the separation of the anomers **5**, it is necessary to deblock R_1 or both R_1 and R_2.

The anomeric mixture **5** was reduced with $LiAlH_4$ and the anomers **6** were easily separated by chromatography on silicic acid.The ratio β:α was found to be 7:1. (The α-anomer mp 173−175°C; pmr ($CDCl_3$): δ = 7.34 (br. s, 1H, 23-H), 7.24 (br. s, 1H, 21-H), 6.50 (br. s, 1H, 22-H), 5.03 (d, J = 4 Hz, 1H, 1′-H), 3.16 (m, 1H, 5′-H), 0.95 (s, 3H, 19-CH_3), 0.72 (s, 3H, 18-CH_3); $[\alpha]_D^{22}$ = +73.79 ($CHCl_3$). The major β-anomer mp 189−191°C; pmr ($CDCl_3$): δ = 7.34 (br. s, 1H, 23-H), 7.24 (br. s, 1H, 21-H), 6.49 (br. s, 1H, 22-H), 4.91 (d, J = 10 Hz, 1H, 1′-H), 3.35 (m, 1H, 5′-H), 0.92 (s, 3H, 19-CH_3), 0.72 (s, 3H, 18-CH_3); $[\alpha]_D^{22}$ = −10.51 ($CHCl_3$).)

The major β-anomer **6** was oxidized as described previously (7, 8) and yielded the known β-digitoxoside **7** (2). We believe that the intermediate responsable for the steric control observed is not the urethane **8** but the charged species **9**.

In order to find out if the methodology described is of potential use for the synthesis of digitoxin and its analogues it was necessary to ascertain whether the lactone, furan, isolactone interconversions (cf. 7, 8) are possible on the level of the

[1]For Part X, see ref. 1.

[2]All the pharmacology of our compounds was performed and will gradually be reported by Professor Rafael Mendez, Departamento de Farmacologia, Instituto Nacional de Cardiologia, Juan Badiano #1, Mexico 22, D. F., Mexico and his collaborators.

Can. J. Chem. Downloaded from www.nrcresearchpress.com by 210.87.254.6 on 09/06/12
For personal use only.

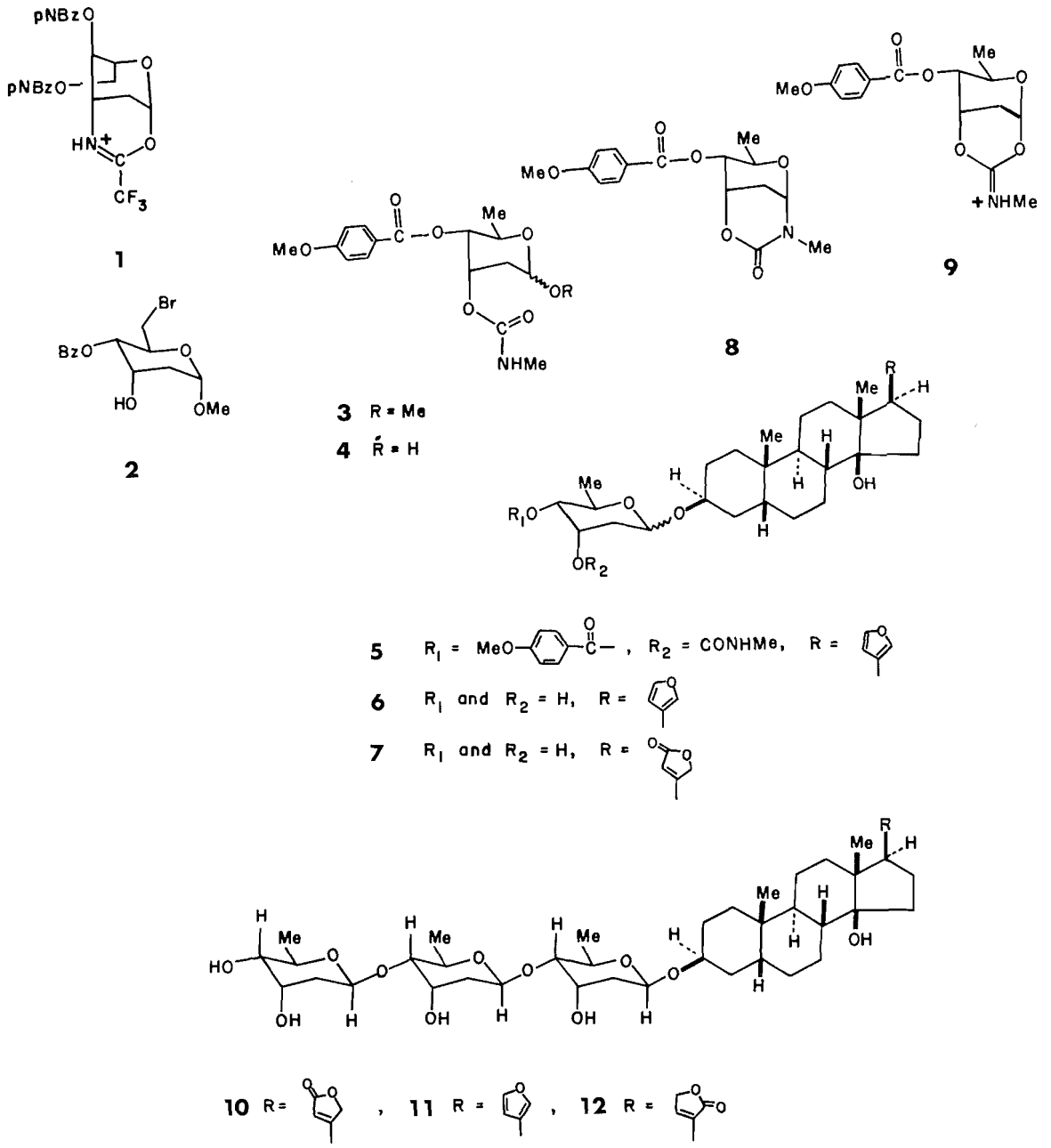

triglycosides. We have now finally succeeded in carrying out the conversion of digitoxin (**10**) to the furan derivative **11** and the oxidation of this material back to digitoxin (**10**) and to the isolactone **12** (cf. 7, 8).

Compund **11** was obtained from digitoxin (**10**) in a yield of 86%. (mp 240–241°C; pmr ($CDCl_3$): δ: = 7.34, 7.23, 6.49 (br. s, 1H each, furan), 4.91 (m, $W_{1/2}$ = 20 Hz, 3H, 3 anomeric H, 1.31 (d, J = 6 Hz, 3H, 1 glycosidic-CH_3), 1.25 (d, J = 6 Hz, 6H, 2 glycosidic-CH_3), 0.92 (s, 3H, 19-CH_3), 0.72 (s, 3H, 18-CH_3); $[\alpha]_D^{22}$ = +12.05.) Oxidation of **11** with peracid followed by reduction with $NaBH_4$ (8) gave digitoxin (**10**) in a yield of 75%.

The conversion of **11** to isodigitoxin (**12**) was performed as described (8) and the product was obtained in a yield of 65% after chromatography on silicic acid (mp 149–150°C; ir ($CHCl_3$); 3590, 3500 (OH), 1740 cm^{-1} (C=O); pmr ($CDCl_3$): δ = 7.30 (br. s, 1H, H-22), 4.91 (m, $W_{1/2}$ = 20 Hz, 3H, 3 anomeric H), 4.81 (d, J = 2 Hz, 2H, H-23), 1.31 (d, J = 6 Hz, 3H, 1 glycosidic-CH_3), 1.25 (d, J = 6 Hz, 6H, 2 glycosidic-CH_3), 0.92 (s, 3H, 19-CH_3), 0.82 (s, 3H, 18-CH_3); $[\alpha]_D^{22}$ = +8.68 ($CHCl_3$).)

Thus a synthesis of **11** will represent not only a total synthesis of digitoxin but also a synthesis of the pharmacologically very interesting isodigitoxin (**12**) (1). Our attention has been drawn by a referee to a report in which participation in the glycosidation by a urethane group in the 2-position of a glucose derivative has been previously reported (9).

Acknowledgements

We wish to thank the Natural Sciences and Engineering Research Council of Canada, the Canadian Heart Foundation, and Advance Biofactures Corporation, New York, for the support of this work.

1. A. SEN, F. J. JÄGGI, T. Y. R. TSAI, and K. WIESNER. Chem. Commun. 1214 (1982).

Can. J. Chem. Downloaded from www.nrcresearchpress.com by 210.87.254.6 on 09/06/12
For personal use only.

2. W. W. ZORBACH, N. HENDERSON, and S. SAEKI. J. Org. Chem. **29**, 2016 (1964).
3. F. ARCAMONE, A. BARGIOTTI, G. CASSINELLI, S. REDAELLI, S. HANESSIAN, A. DI MARCO, A. M. CASASZA, T. DASDIA, A. NECCO, P. REGGIANI, and R. SUPINO. J. Med. Chem. **19**, 733 (1976).
4. P. J. L. DANIELS, A. K. MALLAMS, and J. J. WRIGHT. Chem. Commun. 675 (1973).
5. S. HANESSIAN and N. R. PLESSAS. J. Org. Chem. **34**, 1045 (1969).
6. HAOLUN JIN. Ph.D. Thesis, University of New Brunswick. In preparation.
7. J. M. FERLAND, Y. LEFEBVRE, R. DEGHENGHI, and K. WIESNER. Tetrahedron Lett. **30**, 3617 (1966).
8. T. Y. R. TSAI, A. MINTA, and K. WIESNER. Heterocycles, **12**, 1397 (1979).
9. R. ELY and C. SCHUERCH. Carbohydr. Res. **27**, 63 (1973).

Can. J. Chem. Downloaded from www.nrcresearchpress.com by 210.87.254.6 on 09/06/12
For personal use only.

^{15}N and ^{199}Hg magnetic resonance spectral investigation of inosine protonation and diamagnetic metal ion complexation

G. W. BUCHANAN AND M. J. BELL

Ottawa–Carleton Institute for Research and Graduate Studies in Chemistry, Department of Chemistry, Carleton University, Ottawa, Ont., Canada K1S 5B6

Received December 28, 1982

G. W. BUCHANAN and M. J. BELL. Can. J. Chem. **61**, 2445 (1983).

On the basis of complexation induced ^{15}N chemical shift changes, the nucleoside inosine is shown to protonate preferentially at the N-7 site. This nitrogen is also favoured by Zn^{+2} and Hg^{+2} ions. ^{199}Hg shifts support the notion that the binding of the first equivalent of Hg^{+2} is site selective.

G. W. BUCHANAN et M. J. BELL. Can. J. Chem. **61**, 2445 (1983).

Basé sur les changements des déplacements chimiques dan l'rmn de l'azote-15 pour le nucléoside inosine, on a montré que la protonation arrive sur N-7. Ce site est aussi favourisé par les ions Zn^{+2} et Hg^{+2}. Les déplacements chimiques dans l'rmn du ^{199}Hg sont en accord avec l'idée que la complexation du premier équivalent de l'ion metallique est selective pour un site.

Can. J. Chem. Downloaded from www.nrcresearchpress.com by 210.87.254.6 on 09/06/12
For personal use only.

Introduction

The nature of the interactions between nucleic acid components and metal ions is of intense interest because these phenomena are related to the toxic properties of some metal ion complexes (1) and the antitumour activity of others (2, 3). There appears to be a tendency for "soft" metal ions such as Pt^{2+}, Pd^{2+}, Hg^{2+}, and CH_3Hg^+ to favour nitrogenous sites for complexation, although the kinetically and thermodynamically favoured sites may not coincide (4, 5). Metals such as Zn^{2+}, which are less "soft", may prefer different nitrogenous sites of the nucleoside bases (6, 7) whereas "hard" metal ions, such as Na^+, Mg^{2+}, Ca^{2+}, Ba^{2+}, and Mn^{2+}, appear to complex preferentially at oxygenated sites.

Recent results from this laboratory (7) indicate that ^{15}N nmr chemical shift changes provide a powerful method for the study of nitrogen site-selectivity in binding of diamagnetic metal ions to the nucleosides adenosine, cytidine, and guanosine in DMSO solutions. We now wish to report on our investigation of this selectivity in the binding of Ba^{2+}, Hg^{2+}, and Zn^{2+} ions to the nucleoside inosine which contains the rare base hypoxanthine. This base occurs primarily as part of the anticodon triplet in a number of t-RNA species. For comparison with the metal ion studies, the inosine sites preferred by protons have been elucidated, whereas for the Hg^{2+} complexes, ^{199}Hg chemical shifts are reported.

As in our previous work (7), dimethyl sulfoxide has been used as solvent because relatively high concentrations of metal ions and nucleosides can be achieved in this medium. The metal ions Ba^{2+}, Zn^{2+} and Hg^{2+} were selected as examples of "hard", "intermediate", and "soft" respectively, according to the well-known classification of Lewis acid strength (8).

Although for physiological reasons water would have been a preferable solvent, work to date (9) indicates that metal binding sites on nucleosides are similar in DMSO and H_2O, except that binding sites which require deprotonation are not normally observed in DMSO solutions (4). Another factor in the choice of DMSO as solvent is the enhanced stability of metal ion – nucleoside complexes in DMSO vs. H_2O, presumably due to the lower degree of solvation of nucleoside lone pairs by DMSO than by H_2O.

Results and discussion

The structure and numbering scheme for inosine **1** is shown below. The molecule is shown in the *anti* conformation about the glycosidic bond.

TABLE 1. ^{15}N chemical shifts of inosine (δ_N from NH_3) $\pm 0.1^a$

Concn.	N-1	N-3	N-7	N-9
1.15 M^b	176.8	216.3	250.5	176.8
0.5–1.0 M^c	175.1	214.6	249.1	175.1

[a] DMSO-d_6 solutions.
[b] Present work.
[c] Reference 10.

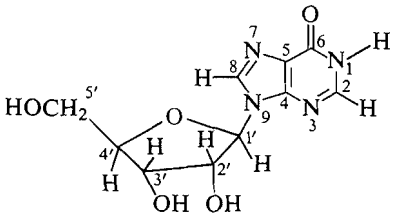

1

(a) *^{15}N nuclear magnetic resonance studies*

The ^{15}N chemical shifts of **1** in DMSO have been reported previously (10) and our results (Table 1) are in good accord with the earlier work. Results in Fig. 1 show that upon addition of $HgCl_2$, the N-7 resonance is most affected, there being a 4.8 ppm *upfield* shift upon addition of 0.75 molar equivalents of the mercuric salt. Above this concentration of $HgCl_2$, the N-7 signal cannot be observed, perhaps due to broadening caused by trace amounts of paramagnetic impurities although care was taken to remove these. (See experimental section.) The N-9 resonance of **1** moves downfield, whereas the N-1 and N-3 resonances are essentially unaffected.

Although the N-1 and N-9 resonances of **1** overlap in the absence of $HgCl_2$, they become separate when 0.2 molar equivalents of salt are added, and they can easily be distinguished via the INEPT experiment (11, 12), in which the N-1 resonance is considerably enhanced in intensity relative to N-9, due to the transfer of polarization from the directly bonded proton on N-1 to the nitrogen.

Upon addition of $Zn(NO_3)_2$ similar trends are noted in the induced ^{15}N shifts for **1** (Fig. 2) although the upfield shift for N-7 is considerably larger than in the case of $HgCl_2$ addition.

Can. J. Chem. Downloaded from www.nrcresearchpress.com by 210.87.254.6 on 09/06/12
For personal use only.

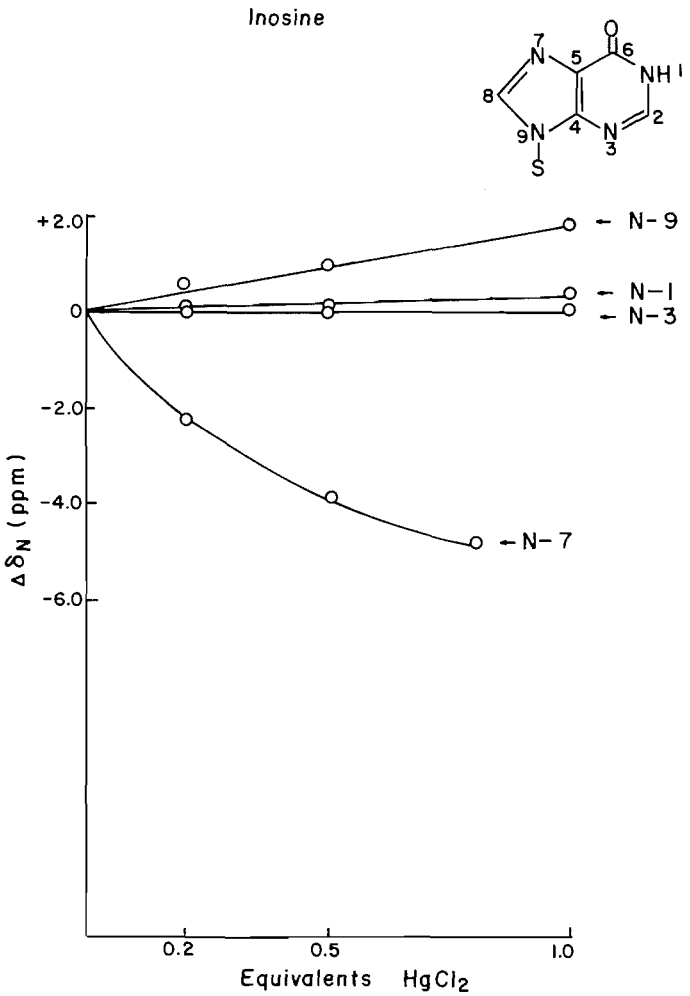

FIG. 1. ^{15}N chemical shift changes as a function of added metal ion: + sign denotes increased δ value (downfield shift); − sign denotes decreased δ value (upfield shift). **1** + $HgCl_2$.

By contrast, addition of $BaNO_3$ causes no detectable changes in the ^{15}N resonance positions for any of the nitrogens of **1**, suggesting that any binding of the "hard" metal in Ba^{2+} does not involve primarily the nitrogenous sites.

It is of interest to compare the present ^{15}N results with those for the structually similar nucleoside guanosine **2** studied earlier in this laboratory (7).

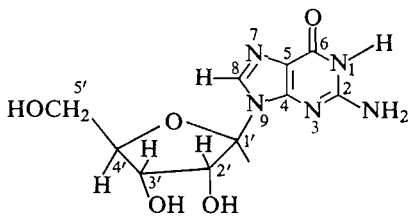

2

For **2**, the N-7 resonance was also shifted considerably upfield by addition of either $HgCl_2$ or $Zn(NO_3)_2$, whereas N-9 moved downfield, but to a lesser extent. Resonances for NH_2, N-1, and N-3 were affected to a very minor extent. These results were interpreted in terms of N-7 being involved in the primary binding site for these metal ions, in agreement with predictions based on electron density calculations (13).

The similarity of the ^{15}N results for **1** and **2** support the notion

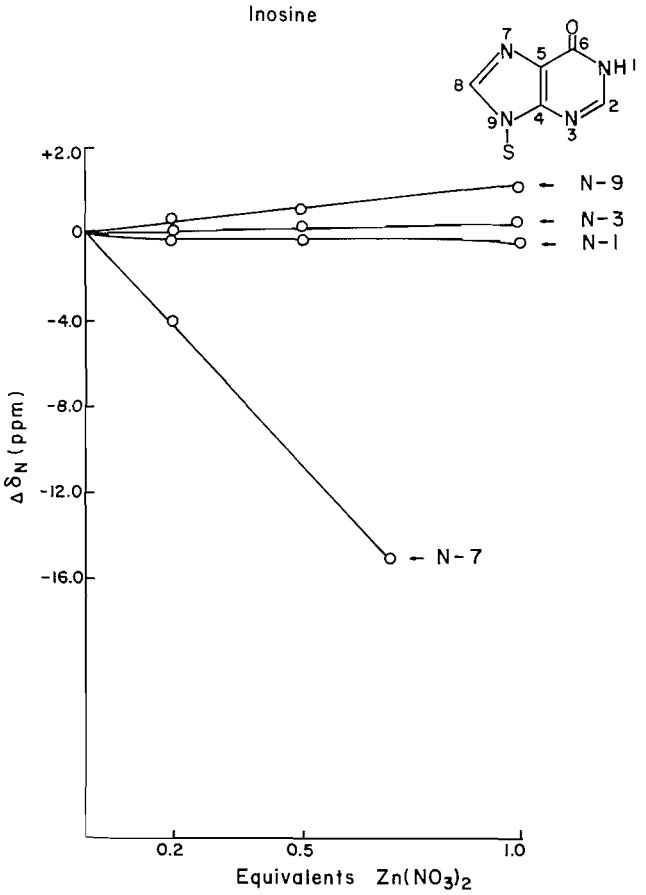

FIG. 2. **1** + $ZnNO_3$.

that N-7 is the preferred site of "soft" and "intermediate" metal ion complexation for both these nucleosides in DMSO solution. Findings of a recent ^{13}C nmr study of these interactions (4) are in accord with our conclusions.

It is useful to compare the metallation induced shifts of **1** with those caused by protonation. In their early work (10), Roberts *et al.* studied the ^{15}N spectra of protonated adenosine, cytidine, guanosine, and ATP in DMSO solutions, the protonating agent being trifluoroacetic acid (TFA).

For inosine our results are depicted in Fig. 3. The upfield shift of ca. 13 ppm for N-7 on addition of 1 molar equivalent of TFA suggests preferred protonation at this site (10). For the structurally similar guanosine nucleoside, Roberts *et al.* (10) found that N-7 was shifted upfield by ca. 40 ppm on addition of 1 molar equivalent of TFA whereas N-3 showed a minor upfield shift (ca. 1 ppm), N-9 was shifted downfield by ca. 3 ppm, and N-1 showed a very small downfield shift. Thus, the shift trends for each nitrogen resonance of inosine upon protonation are qualitatively similar to those found for guanosine. Furthermore, the directions of the protonation induced ^{15}N shift of **1** are the same as those induced by complexation with Zn^{2+} and Hg^{2+} ions. Recently, Nee and Roberts have noted the same trends for platinum complexation with nucleosides (14).

(b) *^{199}Hg nuclear magnetic resonance studies*

To study the binding of Hg^{2+} to nucleic acid components, ^{199}Hg nmr presents an interesting complement to the ^{15}N work because the range of chemical shifts for ^{199}Hg is very large and it is a relatively easy nucleus to observe experimentally (15, 16).

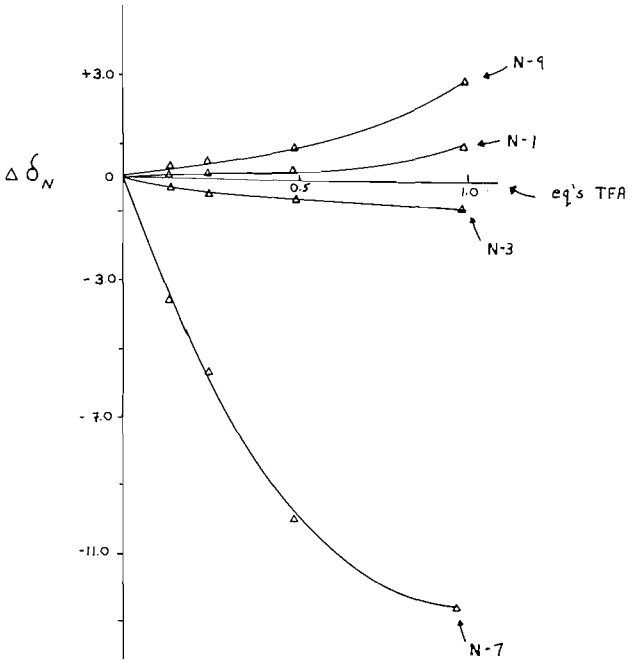

FIG. 3. ^{15}N chemical shift changes as a function of added trifluoroacetic acid (TFA).

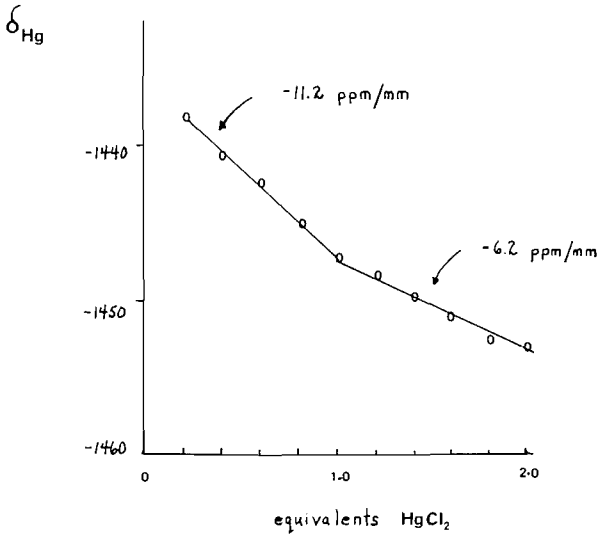

FIG. 4. ^{199}Hg chemical shifts for $HgCl_2$ as a function of added Hg^{2+} in a 0.55 *M* solution of **1** in DMSO-d_6; − sign denotes decreased δ value (upfield shift).

In the present work, we started with a fixed concentration of inosine (0.55 *M*) in DMSO-d_6 and aliquots of $HgCl_2$ were added until a ratio of 2:1 (metal/nucleoside molar equivalents) was reached. Results are shown in Fig. 4. Clearly the slope changes at 1.0 equivalents. We interpret this result in terms of selective complexation of the first metal ion equivalent (presumably at N-7) of **1**. After this site is metallated, others no doubt become complexed to varying degrees.

Unfortunately, due to solubility problems and the need for high concentrations of nucleoside for ^{15}N studies, we were not able to carry out ^{15}N studies above 1.0 equivalents of $HgCl_2$ to determine which nitrogen is metallated after N-7. It was found that $HgCl_2$ shows a marked concentration dependence (in DMSO-d_6) for the chemical shift in the absence of nucleoside, the slope being −18.7 ppm mm^{-1} $HgCl_2$ added.[1] Extrapolation to infinite dilution gives a chemical shift for $HgCl_2$ of −1464.4 ppm relative to neat $(CH_3)_2Hg$, in agreement with the literature (16).

For both ^{199}Hg and ^{15}N data, the chemical shifts of the metal–nucleoside solutions represent an average of the free and complexed shifts, the rate of metal exchange being fast on the nmr timescale. In no cases were ^{15}N–^{199}Hg couplings observed.

To conclude, this study shows the utility of ^{15}N and ^{199}Hg nmr for studying selective protonation and metallation of inosine. The N-7 site is protonated preferentially and favoured by Zn^{2+} and Hg^{2+} ions. The ^{199}Hg shifts indicate site-selective binding of the first equivalent of Hg^{2+}.

Experimental

(a) *Materials*

Inosine was obtained from the Sigma Chemical Company, St. Louis, MO 63178, U.S.A. and was used without further purification. Mercuric chloride, barium nitrate, and zinc nitrate were Fisher Certified ACS grade and were vacuum sublimed before use in an effort to remove paramagnetic impurities. Dimethylsulfoxide-d_6 was purchased from Stohler Isotope Chemicals, Montreal 101, Quebec, Canada. It was dried over molecular sieves before use and no aqueous impurity was detected by ^1H Fourier transform nmr.

(b) *Spectra*

^{15}N spectra were recorded on a Varian XL-200 spectrometer at 20.27 MHz. Routinely, the nOe. suppressed spectra were recorded using a pulse angle of 90° and a delay time of 40 s. Typical spectral width was 10 000 Hz, and satisfactory signal-to-noise ratios for 1.0 *M* inosine solutions (in 10 mm tubes) were normally obtained after ca. 1000 transients. Acquisition time was 1.6 s and 32 K data points were employed.

For the ^{15}N INEPT spectra, the refocussed sequence (11, 12) was used. Employing $^1J_{NH}$ = 90 Hz, the delays were τ = 2.78 ms (1/4*J*) and Δ = 4.17 ms (3/8*J*). The 90° pulses were 24 μs for ^{15}N and 48 μs for ^1H respectively, with a recycle time of 2 s. Chemical shifts were measured relative to external saturated aqueous NH_4Cl and then converted to the ^{15}N scale in ppm relative to NH_3 using a conversion constant of +27.3 ppm (17).

The ^{199}Hg spectra were recorded at 35.8 MHz on the Varian XL-200 spectrometer, using 10 mm sample tubes. Typical spectra width was 30 000 Hz, with a 60° pulse width, 0.53 s acquisition time (32 K data points), and a pulse repetition rate of 2 s. Chemical shifts were referenced to an external capillary of 0.5 *M* $HgCl_2$ in DMSO-d_6 and then converted to the ppm scale relative to $(CH_3)_2Hg$ (15).

Acknowledgements

We thank the Natural Sciences and Engineering Research Council of Canada for financial support in the form of operating grants (GWB) and postgraduate scholarships (MJB).

1. C. MATTHEW and Z. AL-DOORI. Mutat. Res. **40**, 31 (1976).
2. B. ROSENBURG. Cancer Chemother. Rep. **59**, 539 (1975).
3. F. K. V. LEH and W. WOLF. J. Pharm. Sci. **65**, 315 (1976).
4. L. G. MARZILLI, B. DE CASTRO, and C. SOLORZANO. J. Am. Chem. Soc. **104**, 461 (1982).
5. P. I. VESTUES and R. B. MARTIN. J. Am. Chem. Soc. **103**, 806 (1981).
6. L. G. MARZILLI, B. DE CASTRO, J. P. CARADONNA, R. C. STEWART, and C. P. VANVUUREN. J. Am. Chem. Soc. **102**, 916 (1980).

[1] The $HgCl_2$ concentration range for the DMSO-d_6 solutions is 0.13–0.45 *M*, whereas for the inosine containing DMSO-d_6 solutions it is 0.11–1.10 *M*.

Can. J. Chem. Downloaded from www.nrcresearchpress.com by 210.87.254.6 on 09/06/12
For personal use only.

7. G. W. BUCHANAN and J. B. STOTHERS. Can. J. Chem. **60**, 787 (1982).
8. F. BASOLO and R. G. PEARSON. Mechanisms of inorganic reactions. 2nd ed. Wiley Interscience, New York, NY. 1967.
9. L. G. MARZILLI. Adv. Inorg. Biochem. **3**, 47 (1981).
10. V. MARKOWSKI, G. R. SULLIVAN, and J. D. ROBERTS. J. Am. Chem. Soc. **99**, 714 (1977).
11. G. A. MORRIS and R. FREEMAN. J. Am. Chem. Soc. **101**, 760 (1979).
12. G. A. MORRIS. J. Am. Chem. Soc. **102**, 428 (1980).
13. D. PERATHIA, A. PULLMAN, and B. PULLMAN. Theor. Chim. Acta, **43**, 207 (1977).
14. M. NEE and J. D. ROBERTS. Biochemistry, **21**, 4920 (1982).
15. R. G. KIDD. Ann. Rep. NMR Spectrosc. **10A**, 1 (1980).
16. R. G. KIDD and R. J. GOODFELLOW. *In* NMR and the periodic table. *Edited by* R. K. Harris and B. E. Mann. Academic Press, New York, NY. 1978. Chapt. 8.
17. G. C. LEVY and R. L. LICHTER. Nitrogen-15 nuclear magnetic resonance spectroscopy. Wiley-Interscience, New York, NY. 1979. p. 32.

Can. J. Chem. Downloaded from www.nrcresearchpress.com by 210.87.254.6 on 09/06/12
For personal use only.

Base mediated dimerization of 2-tetradecynoic acid[1]

SUZANNE R. ABRAMS[2]
Prairie Regional Laboratory, National Research Council of Canada, Saskatoon, Sask., Canada S7N 0W9
J. WILSON QUAIL
Department of Chemistry, University of Saskatchewan, Saskatoon, Sask., Canada S7N 0W0
AND
LOUIS T. J. DELBAERE
Department of Biochemistry, University of Saskatchewan, Saskatoon, Sask., Canada S7N 0W0

Received February 2, 1983

SUZANNE R. ABRAMS, J. WILSON QUAIL, and LOUIS T. J. DELBAERE. Can. J. Chem. **61**, 2449 (1983).

Under the influence of the very strong base, the sodium salt of 1,2-diaminoethane in 1,2-diaminoethane, 2-tetradecynoic acid is converted to 3-tetradecynoic acid (35%) and a novel dimer **3**. Compound **3** ((*Z*)-2-(1-dodecynyl)-3-undecyl-pent-2-en-1,5-dioic diacid) is isolated as the monomethyl ester **1** after treatment of the crude product with methanolic HCl. The structures of **1** and **3** are deduced from an X-ray crystallographic analysis of the dimethyl ester **2** obtained by reaction of **1** with diazomethane. The dimer **3** is thought to arise from Michael addition of the dianion **4** of 3-tetradecynoic acid with the sodium salt of 2-tetradecynoic acid.

SUZANNE R. ABRAMS, J. WILSON QUAIL et LOUIS T. J. DELBAERE. Can. J. Chem. **61**, 2449 (1983).

Sous l'influence d'une base très forte, le sel de sodium du diamino-1,2 éthane dans le diamino-1,2 éthane transforme l'acide tétradécyne-2 oique en acide tétradécyne-3 oique (35%) et en un nouveau dimère (**3**). On a isolé le composé **3**, le diacide (*Z*)-dodécyne-1 yl-2 undécyl-3 pentène-2 dioique-1,5, sous forme de monoester méthylique (**1**) après avoir fait réagir le produit brut avec du HCl méthanolique. L'analyse par cristallographie de rayons-x de l'ester diméthylique **2**, obtenu par réaction de **1** avec le diazométhane, a permis de déterminer les structures des composés **1** et **3**. On pense que le dimère **3** provient d'une addition de Michael du dianion **4** de l'acide tétradécyne-3 oique sur le sel de sodium de l'acide tétradécyne-2 oique.

[Traduit par le journal]

Can. J. Chem. Downloaded from www.nrcresearchpress.com by 210.87.254.6 on 09/06/12
For personal use only.

Introduction

One of us recently reported the rearrangement of a series of isomeric tetradecynoic acid (2-, 3-, 5-, 7-, 9-, 11-) mediated by the very strong base, the sodium salt of 1,2-diaminoethane in 1,2-diaminoethane (1). The principal products were (*E,E*)- and (*E,Z*)-3,5-tetradecadienoic acids; the latter is the sex pheromone of the black carpent beetle (*Attagenus megatomia*). 2-Tetradecynoic acid was shown to be isomerized first as expected (2) to 3-tetradecynoic acid which, in turn, was rearranged to the isomeric dienoic acids. The conversion of 2- to 3-tetradecynoic acid was poor. Isolation by treatment with methanolic hydrochloric acid followed by chromatography of the crude reaction mixture afforded methyl 3-tetradecynoate in 35% yield. Unexpectedly, a polar by-product **1** (mp 104–105°C) was isolated in 24% yield. Treatment of **1** with diazomethane gave a second product **2** (mp 63–64°C) which was less polar. Spectral data indicated that the new compounds were formally methylated dimers of 2-tetradecynoic acid, but these data could not be interpreted unambiguously to permit elucidation of the structures.

We were able to find no literature precedent for a base mediated rearrangement–dimerization of a 2-alkynoic acid, and were intrigued by the apparent simplicity of the spectral data, and by the fact that the two esterification procedures gave different compounds. We thus undertook to determine the structure of these unexpected products by an X-ray analysis of the second compound **2**. The structures of the original dimeric acid **3** and the monomethylated compound **1** have been assigned by comparison of the spectral data of **1** and **2**. A mechanism is proposed to account for the transformation of 2-tetradecynoic acid to **3**.

[1] NRCC No. 22443.

[2] Author to whom correspondence may be addressed.

Results and discussion

2-Tetradecynoic acid was isomerized with 4.5 equivalents of the sodium salt of 1,2-diaminoethane for 5 minutes at 60°C. Tetradecanoic acid was used as an internal standard. Analysis by glc indicated a 35% conversion to 3-tetradecynoic acid, and complete consumption of the starting material. Esterification with methanolic HCl and subsequent chromatography over silica gel gave methyl 3-tetradecynoate (34%), followed by **1** (24%, mp 104–105°C from hexane). Treatment of either the crude product followed by chromatography, or of **1**, with diazomethane afforded **2** (mp 63–64°C from methanol), upon which an X-ray crystallographic analysis was performed.

An ORTEP (3) diagram of **2**, including the numbering system which we adopted is shown in Fig. 1. Table 1 contains the positional parameters and average temperature factors for the non-hydrogen atoms of dimer **2**. Bond lengths and angles of the functionalized portion of **2** are given in Tables 2 and 3. The molecule consists of two linear fourteen-carbon chains with a double bond occurring between the second carbon atom of one chain and the third carbon atom of the other chain, and the two hydrocarbon chains are in a *cis* configuration. The IUPAC name for **2** is dimethyl (*Z*)-2-(1-dodecynyl)-3-undecylpent-2-endioate. The enyne system shows two (of the three) bonds with lengths very close to values predicted by Dewar and Schmeising (4*a*). The double bond between C(2) and C(3) is of normal length (d = 1.34(1) Å) (cf. 1.338 Å (4*a*)). A linear triple bond (d = 1.22(2) Å) joins C(6) and C(7) (cf. 1.205 Å (4*a*)). The bond between C(2) and C(6), which joins the double to triple bond, has a length of 1.37(2) Å. This length is shorter than 1.432 Å predicted by Dewar and Scheising (4*a*), but is similar to the value (1.376(6) Å) observed in a related system by Smith and Luss (4*b*). In addition, Smith and Luss also observed a triple bond length of 1.212(6) Å and a double bond

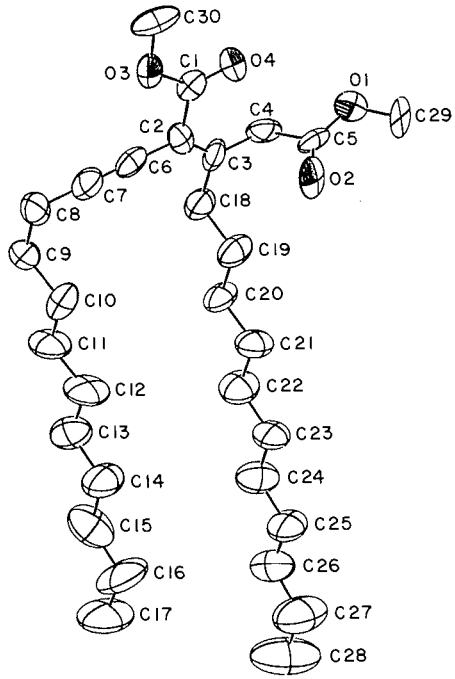

FIG. 1. ORTEP perspective drawing of dimer **2**. Hydrogens are omitted for clarity.

TABLE 1. Positional parameters and average temperature factors for dimer **2**

Atom	x/a	y/b	z/c	U_{eq} (Å^2)
O(1)	0.858(2)	0.4356(2)	0.851(1)	0.073
O(2)	0.530(2)	0.3951(3)	0.784(1)	0.075
O(3)	0.316(3)	0.4550(2)	0.297(1)	0.082
O(4)	0.557(3)	0.4611(3)	0.514(1)	0.088
C(1)	0.479(3)	0.4438(3)	0.408(1)	0.047
C(2)	0.547(3)	0.4038(3)	0.392(1)	0.055
C(3)	0.743(–)	0.3878(3)	0.485(–)	0.055
C(4)	0.894(3)	0.4068(3)	0.613(2)	0.064
C(5)	0.740(3)	0.4112(3)	0.765(1)	0.051
C(6)	0.420(3)	0.3852(3)	0.271(2)	0.060
C(7)	0.289(4)	0.3708(3)	0.165(2)	0.081
C(8)	0.126(4)	0.3522(4)	0.033(2)	0.074
C(9)	0.231(4)	0.3144(4)	0.011(2)	0.082
C(10)	0.180(4)	0.2887(4)	0.140(2)	0.089
C(11)	0.272(4)	0.2506(4)	0.112(2)	0.089
C(12)	0.211(5)	0.2249(4)	0.237(2)	0.103
C(13)	0.283(4)	0.1877(4)	0.208(2)	0.098
C(14)	0.213(5)	0.1606(4)	0.326(2)	0.117
C(15)	0.288(5)	0.1219(5)	0.304(3)	0.132
C(16)	0.214(6)	0.0943(6)	0.417(3)	0.159
C(17)	0.311(7)	0.0569(4)	0.382(3)	0.180
C(18)	0.809(4)	0.3492(4)	0.462(2)	0.084
C(19)	0.717(4)	0.3238(4)	0.587(2)	0.081
C(20)	0.792(4)	0.2853(4)	0.563(2)	0.085
C(21)	0.703(4)	0.2595(4)	0.684(2)	0.088
C(22)	0.783(5)	0.2218(4)	0.660(2)	0.103
C(23)	0.693(4)	0.1948(4)	0.776(2)	0.092
C(24)	0.778(4)	0.1568(4)	0.750(2)	0.105
C(25)	0.706(5)	0.1290(4)	0.862(2)	0.125
C(26)	0.794(5)	0.0922(4)	0.836(2)	0.116
C(27)	0.718(6)	0.0637(6)	0.941(3)	0.181
C(28)	0.805(7)	0.0265(5)	0.907(4)	0.233
C(29)	0.734(4)	0.4399(4)	1.001(2)	0.084
C(30)	0.221(4)	0.4935(4)	0.303(2)	0.083

$U_{eq} = (U_{11} + U_{22} + U_{33})/3$.

TABLE 2. Selected bond lengths (Å) for dimer **2**

Bond	Length
O(1)—C(5)	1.29(2)
O(1)—C(29)	1.47(2)
O(2)—C(5)	1.18(2)
O(3)—C(1)	1.28(2)
O(3)—C(30)	1.51(2)
O(4)—C(1)	1.17(2)
C(1)—C(2)	1.53(2)
C(2)—C(3)	1.34(1)
C(2)—C(6)	1.37(2)
C(3)—C(4)	1.48(2)
C(3)—C(18)	1.49(2)
C(4)—C(5)	1.55(2)
C(6)—C(7)	1.22(2)
C(7)—C(8)	1.51(2)

TABLE 3. Selected bond angles (°) for dimer **2**

Bond	Angle
C(5)—O(1)—C(29)	115(1)
C(1)—O(3)—C(30)	117(1)
O(3)—C(1)—O(4)	125(1)
O(3)—C(1)—C(2)	112(1)
O(4)—C(1)—C(2)	123(1)
C(1)—C(2)—C(3)	121(1)
C(1)—C(2)—C(6)	118(1)
C(3)—C(2)—C(6)	120(1)
C(2)—C(3)—C(4)	122(1)
C(2)—C(3)—C(18)	120(1)
C(4)—C(3)—C(18)	118(1)
C(3)—C(4)—C(5)	119(1)
O(1)—C(5)—O(2)	128(1)
O(1)—C(5)—C(4)	112(1)
O(2)—C(5)—C(4)	120(1)
C(2)—C(6)—C(7)	175(2)
C(6)—C(7)—C(8)	179(1)

length of 1.386(6) Å. The enyne system (C(1), C(2), C(3), C(4), C(6), C(7), C(8), and C(18)) is planar within 0.03 Å of the least-squares plane between these atoms. The angles between the plane of the enyne system and the planes of the carboxyl groups on C(1) and C(5) are 8 and 88 degrees, respectively. The near coplanarity of the carboxyl group on C(1) and the enyne system is favorable for π electron overlap between these two groups and the ir bands at 1740 cm^{-1} and 1720 cm^{-1} (see Experimental) indicate the presence of both a saturated and an α,β-unsaturated ester. However, the bond between C(1) and C(2) (d = 1.53(2) Å) is normal in length for a single bond and shows no shortening due to conjugation between the enyne system and the carboxyl group. In addition, the 1.17(2) Å bond length of the carbonyl group on C(1) is not significantly different from the length of the C(5)—O(2) bond (1.18(2) Å) in the other carboxyl group.

An ORTEP diagram of the packing in the crystal is shown in Fig. 2. The molecules pack with the ester groups of different molecules in close proximity to each other. The hydrocarbon tails of neightboring molecules interact with each other in a manner similar to that found for the lipid hydrocarbon chains of biological membranes (5). The molecules are aligned approximately along the b axis of the unit cell. The attractive

Can. J. Chem. Downloaded from www.nrcresearchpress.com by 210.87.254.6 on 09/06/12
For personal use only.

Can. J. Chem. Downloaded from www.nrcresearchpress.com by 210.87.254.6 on 09/06/12
For personal use only.

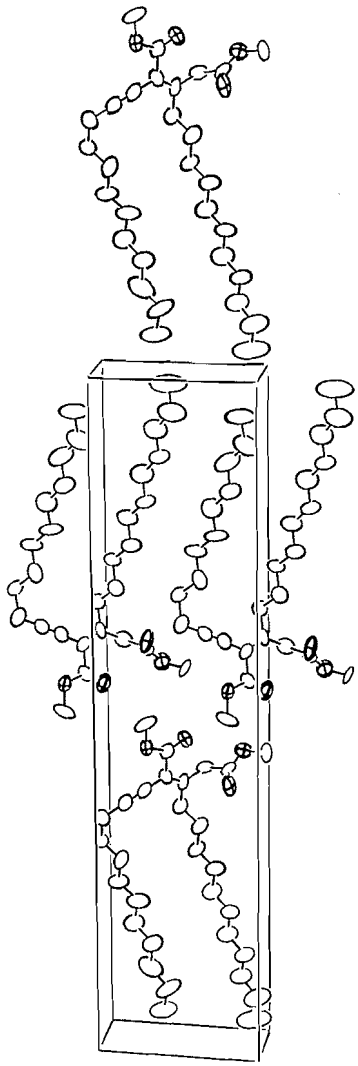

FIG. 2. Projection of the crystal structure looking approximately down the *a* axis of the unit cell of **2**.

forces between the termini of the aliphatic chains of different molecules would be very weak; consequently, the crystals grow very slowly along the *b* axis, producing soft, very thin crystal ribbons.

Detailed spectroscopic data are given in the experimental section; the highlights of the mass, ^{13}C and ^{1}H nmr spectra are presented here.

The 400 MHz ^{1}H nmr spectra of dimers **1** and **2** have the signals expected for the $COOCH_3$ and for the $=CCH_2(CH_2)_9CH_3$ and $\equiv CCH_2(CH_2)_8CH_3$ units in which only the sets of allylic and propargylic protons have different chemical shifts. The protons at C(4) of dimer **1** appear as a two proton singlet (δ 3.68), just resolved from the $COOCH_3$ singlet (δ 3.66). A similar singlet appears in the spectrum of dimer **2** at δ 3.61. Kagan *et al.* (6) reported similar shifts (δ 3.65, 3.61) for the C(4) protons of the corresponding mono- and di-esterified (Z)-2-methylpent-2-en-1,5-dioic acids.

While there have been thorough systematic studies of assignments of ^{13}C nmr signals of simple alkenoic and alkynoic acids and esters (7), data are lacking for extensively substituted conjugated systems such as those encountered here. Assignments of the ^{13}C signals of **1** and **2** (Table 4) have been made by extrapolation of available literature data and thus are tentative.

TABLE 4. ^{13}C chemical shifts of **1** and **2**[a]

Carbon	Shift		Analogs[b–e]
	Dimer **1**	Dimer **2**	
1	169.68	165.91	167.00[b]
2	114.95	115.36	119.25[b]
3	159.03	156.50	151.05[b]
4	38.73*	38.54*	38.7[c]
5	170.45	170.64	172.08[d]
6	75.77	76.06	72.95[e]
7	97.31	96.66	90.00[e]
8	19.70	19.74	18.70[e]
9	27.17	27.18	27.60[f]
10–14,19–25	28.74–29.71	28.78–29.75	
15,26	31.99	31.99	31.85[f]
16,27	22.75	22.74	22.70[f]
17,28	14.16	14.15	14.05[f]
18	38.63*	38.21*	
29	52.05	52.12**	
30	—	51.98**	

[a] In ppm relative to $(CH_3)_4Si$; in $CDCl_3$; * ambiguous pair; ** ambiguous pair.
[b] OOCC=C of methyl-2-Z-undecenoate (5).
[c] $OOCCH_2C{=}C{-}C{=}C{-}$ (1).
[d] $OOCCH_2C{\equiv}C$ of methyl 3-octadecynoate (5).
[e] $OOCC{\equiv}CCH_2CH_2$ of methyl 2-undecynoate (5).
[f] $H_3CCH_2CH_2{-}$ of methyl 2-undecynoate (5).

Particularly confusing, before the X-ray structure was obtained, were the chemical shifts of the pairs of olefinic and acetylenic carbon atoms, both of which appeared to be next to a carboxyl group. As well as the chemical shifts of the carbons, the chemical shift difference between two alkyne carbons is usually diagnostic for proximity to the carboxyl group (Δ2, 20 ppm; Δ3, 13 ppm; Δ4, 3 ppm).

The mass spectra gave the exact masses of the molecular ions, but revealed little structural information. Dimer **2**, particularly, gave only two intense fragments with *m/z* greater than 200. With the disclaimer that multiple unsaturated long chain compounds are notorious for suffering rearrangement upon electron impact, a scheme is proposed that accounts for the two extremely stable fragments observed. The base peak (*m/z* 444, 100%) corresponds to the loss of methanol from the molecular ion (*m/z* 476, 11%). The base peak can arise by two different pathways involving an intramolecular hydrogen abstraction (Scheme 1). Both yield stabilized radicals which could lose $\cdot C_9H_{19}$ with facility to give the second large fragment (*m/z* 317, 65%). There are two lesser peaks with *m/z* greater than 200. One (*m/z* 350, 7%) probably is the product of a McLafferty rearrangement of the molecular ion ejecting C_9H_{18}; the other (*m/z* 331, 12%) may correspond to the loss of $\cdot C_8H_{17}$ from the base peak.

The fragmentation pattern of the monomethyl ester **1** is slightly more complicated. The fragmentation pattern of **2** is repeated, except that ions arise from loss of water (*m/z* 444, 93%) and from loss of methanol (*m/z* 430, 41%). The base peak (*m/z* 317, 100%) is due to expulsion of $\cdot C_9H_{19}$ from the ion with *m/z* 444. The other major fragment comes from loss of the same unit from the ion with *m/z* 430 to give an ion with *m/z* 303, 47%. While the cleavage patterns are similar in the two dimers, **1** is susceptible to more extensive fragmentation.

The carbon skeleton of the dimers is made up of two fourteen-carbon units with a double bond between C(2) of one chain and C(3) of the other. This linkage could arise from

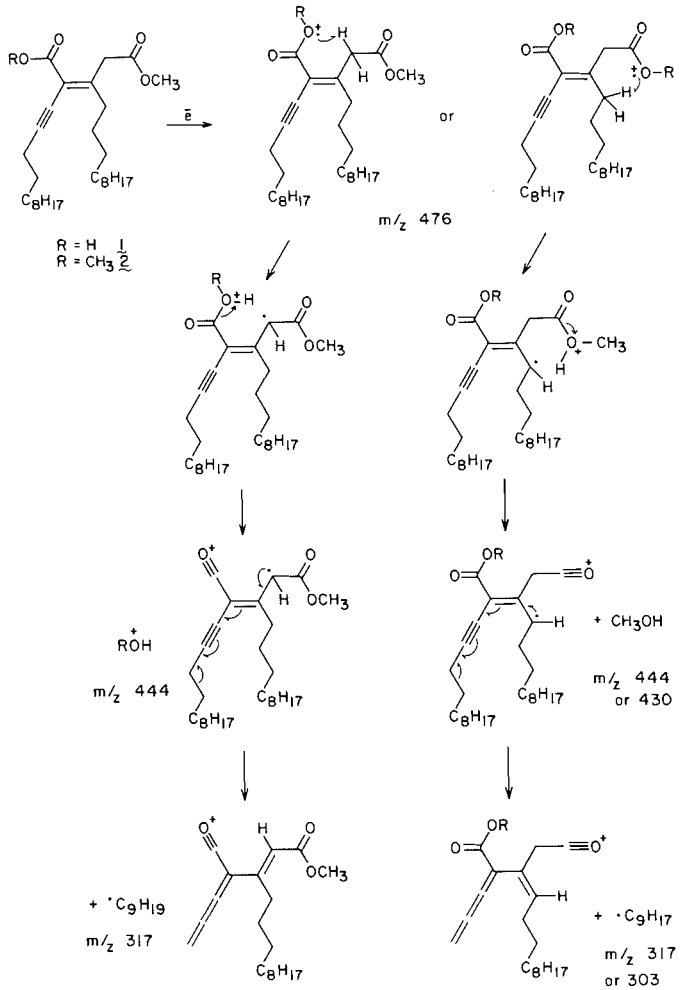

SCHEME 1

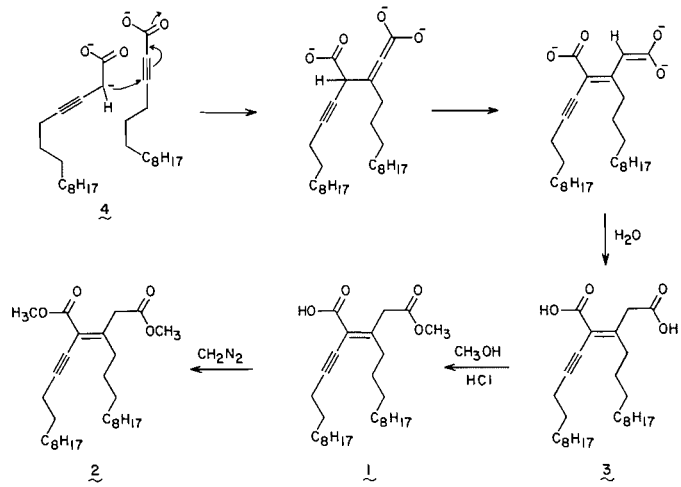

SCHEME 2

Michael addition of a dianion **4** of 3-tetradecynoic acid (the major product isolated from the reaction) to the starting 2-tetradecynoic acid (Scheme 2). The adduct could undergo a 1,3-proton shift giving a stabilized extensively delocalized trianion. The same postulated intermediate could arise from protonation of C(4) and subsequent deprotonation of C(2). Protonation of the trianion on work-up would afford the dimeric diacid **3**.

Stabilized propargylic anions such as **4** are postulated intermediates in base mediated isomerizations of acetylenic acids (2, 8). There are a limited number of examples in the literature of reactions of dianions of acetylenic acids. The alkylation of propynoic, butynoic, and pentynoic acids has been investigated. The dianion of 2-butynoic acid affords on alkylation both 4-alkyl-2-butynoic acid (γ attack) and 2-alkyl-2,3--butadienic acid (α attack) (9, 10). The dianion of 3-butynoic acid, a special case in which the stable terminal acetylide salt is formed, is silylated exclusively at C-4 (11). Treatment of 2-pentynoic acid with three equivalents of lithium diisopropylamide followed by chlorotrimethylsilane affords a product silylated at both C-2 and C-4 (12). The authors attribute this result to isomerization during anion formation. No direct analogy to the present case, in which a longer chain acetylenic acid undergoes isomerization prior to alkylation, has been found.

There is, however, a report of a dianion of a carboxylic acid attacking the salt of an α,β-unsaturated acid. The dilithium salt of propanoic acid is found to add to lithium methacrylate in a Michael type reaction affording 2,4-dimethylglutaric acid in 67% yield (9).

The stereochemistry about the double bond may be due to several factors. Perhaps in the polar reaction medium there is a lipophilic attraction between the two methylene chains of **4** and the anion of 2-tetradecynoic acid. Perhaps a counter-ion stabilizes the intermediate trianionic diacid.

The formation of the monomethyl ester upon treatment with methanolic HCl occurs at the less hindered carboxyl group, while the carboxyl group on the double bond survives the treatment. Kagan *et al.* (6) reported that reaction of 2-methyl-Z-pent-2-en-1,5-dioic acid with concentrated sulfuric acid, followed by quenching with methanol, afforded the analogous monomethyl ester. The ir data of dimer **1** are consistent with the β,γ-unsaturated acid being esterified first.

Either the diacid **3** or dimer **1** would be expected to give dimer **2** on treatment with diazomethane.

Conclusion

Although isomerizations of alkynes have been studied extensively (8, 13), we have found no report of a rearrangement reaction such as that observed in this work.

Analogous reactions may prove useful in organic synthesis. A functionalized structure is produced that contains two carboxyl groups with different reactivities, and an unusual enyne system.

Experimental

Ultraviolet spectra were recorded on a Beckman DU-8 spectrophotometer. Infrared spectra were obtained on a Perkin–Elmer 237-B instrument. Band intensities are reported using the following abbreviations: s strong, w weak, br broad. Gas chromatographic separations were carried out on a Varian 3700 instrument with an SP2100 capillary column (J and W Scientific, 30 m) with a flame ionization detector, and were run isothermally at 160°C. Mass spectra were obtained with an MS902S instrument with VG console update at the Psychiatric Research Unit, University of Saskatchewan. Accurate masses were obtained at 1500 resolution and 3 s/decade using accurate mass – low resolution software with PFTBA internal standard. Mass spectra are reported in mass-to-charge units (m/z) with the relative intensities as percentages of the base peak. Only fragments with $m/z > 200$ are given. Proton nmr spectra were recorded on a Bruker WH 400 spectrometer using deuterochloroform with internal $(CH_3)_4Si$ as reference.

Can. J. Chem. Downloaded from www.nrcresearchpress.com by 210.87.254.6 on 09/06/12
For personal use only.

Can. J. Chem. Downloaded from www.nrcresearchpress.com by 210.87.254.6 on 09/06/12
For personal use only.

Assignments of protons are reported using the number of the carbon to which they are attached. Carbon nmr spectra were recorded on a Varian XL-100-15 instrument in the Fourier Transform mode at 25.16 MHz with proton noise decoupling. Deuterochloroform was used as solvent and also provided the internal deuterium lock. Elemental analyses were performed by Spang Microanalytical Laboratory, Eagle Harbour, Michigan, U.S.A.

The preparations of 2- and 3-tetradecynoic acids are reported in a previous paper (1).

Isomerization of 2-tetradecynoic acid

Under nitrogen, to a solution of the sodium salt of 1,2-diaminoethane at 60°C (prepared by reaction of sodium hydride, 57% in mineral oil, 380 mg, 9.2 mmol, washed free of oil with hexane, and 1,2-diaminoethane, 5.0 mL (previously distilled from BaO and stored over activated 4 Å sieves) at 60°C for 1.0 h) was added a solution of 2-tetradecynoic acid (450 mg, 2.0 mmol) and tetradecanoic acid (45 mg, 0.2 mmol) in 1,2-diaminoethane (5.0 mL). After 5 min the reaction was quenched by pouring into ice water. The mixture was acidifed with HCl and extracted with ether 3 times. The combined ethereal extracts were washed with water, then NaCl solution, dried over Na_2SO_4, filtered, and the solvent evaporated to give 533 mg of crude product. A small sample was treated with diazomethane. Analysis by glc gave peaks corresponding to methyl tetradecanoate (22%), methyl 3-tetradecynoate (69%), but no peak for methyl 2-tetradecynoate, indicating 35% conversion of 2- to 3-tetradecynoic acid. A portion of the crude product (479 mg, 90%) was dissolved in methanol (25 mL) and 3 drops of concentrated HCl added. The solution was refluxed for 2.5 h. The methanol was evaporated at reduced pressure and the residue partitioned between ether and water. The ether layer was washed successively with $NaHCO_3$ solution and NaCl solution, dried over Na_2SO_4, filtered, and the solvent removed to yield 500 mg product. This material was chromatographed over a column of silica gel (BioRad 200–400 mesh) made up in ether/hexane (20:80), eluting with 20% ether first, then 50% ether/hexane. First to elute was residual mineral oil, then methyl tetradecanoate, followed by methyl 3-tetradecynoate (140 mg, 34%). The dimer **1** was obtained last (100 mg, 24%) and gave mp 104–105°C (hexane); tlc R_f 1 (20% ether/80% hexane); uv λ_{max} 251 nm (6500) in methanol; ir ν_{max} (CCl_4): 3400–2500 (s, br), 2200 (w), 1740 (s), and 1685 (s) cm^{-1}; ^1H nmr δ: 3.68 (s, 2H, H(4)), 3.66 (s, 3H, H(29)), 2.54 (dd, J = 8.0, 7.9 Hz, 2H, H(8) or H(18)), 2.41 (t, J = 7.5 Hz, 2H, H(8) or H(18)), 1.59 (m, 2H, H(9) or H(19)), 1.46 (m, 2H, H(9) or H(19)), 1.26 (m, 34H, H(10) to H(16) and H(20) to H(27)), 0.89 (t, J = 7 Hz, 6H, H(17) and H(28)); mass spectrum: 462 (7), 445 (27), 444 (93), 431 (16), 430 (41), 385 (10), 331 (20), 319 (12), 318 (36), 317 (100), 304 (29), 303 (47), 290 (20), 277 (20), and 275 (17); molecular ion *Exact Mass* calcd.: 462.3758; found: 462.3702. *Anal.* calcd. for $C_{29}H_{50}O_4$: C 75.28, H 10.89; found: C 75.57, H 10.93.

Treatment of **1** with diazomethane gave, after work-up, dimer **2** which gave mp 63–63.5°C from methanol: tlc R_f 4 (20% ether/80% hexane); uv λ_{max} 261 (7700) in methanol; ir ν_{max} (CCl_4): 2200 (w), 1740 (s), 1720 (s) cm^{-1}; ^1H nmr δ 3.73 (s, 3H, H(30)), 3.67 (s, 3H, H(29)), 3.61 (s, 2H, H(4)), 2.50 (dd, J = 8.0, 7.9 Hz, 2H, H(8) or H(18)), 2.39 (t, J = 7.5 Hz, 2H, H(8) or H(18)), 1.57 (m, 2H, H(9) or H(19)), 1.45 (m, 2H, H(9) or H(19)), 1.26 (m, 34H, H(10) to H(16) and H(20) to H(27)), 0.88 (t, J = 7.0 Hz, 6H, H(17) and H(28)); mass spectrum: 476 (11), 445 (37), 444 (100), 350 (8), 331 (12), 318 (22), 317 (65); molecular ion *Exact Mass* calcd.: 476.3905; found 476.3884. *Anal.* calcd. for $C_{30}H_{52}O_4$: C 75.58, H 11.00; found: C 75.65, H 10.94.

Crystallographic analysis

Data collection

Dimethyl (*Z*)-2-(1-dodecynyl)-3-undecylpent-2-endioate crystallized as very thin {010} ribbons, with a tendency to curl, on slow evaporation of a methanol solution. A crystal was cut from a ribbon with a razor blade. Precession photographs showed the crystal to be monoclinic, and from the systematic absences of reflections $h0l$, l = $2n + 1$ the space group was determined to be either Pc or $P2/c$. The molecular formula was known to be $C_{30}H_{52}O_4$ from the mass spectrum. From the carbon-13 nmr it was known that all of the carbons were non-equivalent. There was sufficient space in the unit cell for only 2 molecules. Since the centrosymmetric space group $P2/c$ would require molecular symmetry, the acentric space group Pc (No. 7) (13) was chosen for the crystal, and this choice was confirmed by the successful refinement of the structure. The crystal data were the following:

$C_{30}H_{52}O_4$ mw = 476.72

Monoclinic, space group Pc, a = 4.699(2) Å, b = 37.288(12) Å, c = 8.743(2) Å, β = 92.95(2) Å, V = 1529.9 Å^3, Z = 2, ρ_o = 1.06 g cm^{-3}, ρ_c = 1.04 g cm^{-3}, $F(000)$ = 528e, radiation Ni-filtered Cu $K_{\bar{\alpha}}$, λ = 1.5418 Å, $2\theta_{max}$ = 120°, crystal dimensions (mm) 0.7 × 0.04 × 0.6, max decay correction 1.12, temp. 14°C.

The single crystal was mounted about the c^* axis on an Enraf–Nonius CAD4F diffractometer and data were collected with an $\omega/2\theta$ scan. A total of 1584 reflections (of 2282 total) had net $I > 2\sigma(I)$ and these reflections were used in the analysis. The data were corrected for Lorentz and polarization effects. Intensity data were corrected for absorption using the Gaussian integration method (14). Observational weights (15) for the reflections were derived from the formula: $W = (2I)^2/|F_o|^2\ (T + (0.02\ I)^2 + r^2B)$, where I is the net intensity, F_o is the observed structure amplitude, T is the total peak count, B is the sum of the background counts, and r is the ratio of the peak-scan time to the total background-counting time (r = 2 for this data).

MULTAN 80 (16) was used to generate starting sets of phases. Five sets of phases had similar combined figures of merit (2.6–2.2) and R_{Karle} (17) values of 0.18. The fifth best solution was selected because it showed chains of atoms (the reactant was a linear molecule) and the atoms occupied most of the volume of the repeating unit. Least-squares refinement on 26 atoms from the MULTAN solution, using unit weights, gave an R of 0.306. Additional atoms were located from difference Fourier maps. After 34 atoms had been located, the four oxygens were identified from the stereochemistry and the lower temperature factors. Refinement of atomic parameters was carried out by blocked-matrix least-squares techniques using anisotropic temperature factors and unit weights. A difference Fourier map at this point did not locate the hydrogens. Forty hydrogens (all except those on the four methyl groups) were positioned from the stereochemistry. These hydrocarbons were assigned isotropic temperature factors equal to those of the attached carbons. These forty hydrogens were not refined. Refinement was carried out using observational weights and including an extinction coefficient (18, 19).[3] The final agreement factors were $R = 0.112$ ($R = \sum_{hkl} \| |F_o| - |F_c| \| / \sum_{hkl} |F_o|$) and $R_w = 0.121$ ($R_w = (\sum_{hkl} w\Delta^2 / \sum_{hkl} w|F_o|^2)^{1/2}$). In the last least-squares cycle, the largest and average shifts in any parameter were 0.88 and 0.055 times the estimated standard deviation, respectively. Crystallographic computations were carried out using the XRAY 76 System (19) on the DEC 2060 computer at the University of Saskatchewan.[4]

Refinement based on counting statistics was chosen for the final report rather than refinement based on unit weights, because of the poor fit of about 20 intense reflections at θ values between 3 degrees and 12 degrees. When unit weights were used, these reflections dominated the refinement. Re-collection of these strong reflections some weeks after the data set was complete showed that a few of the strong reflections actually had increased in intensity (max. increase 35%).

Acknowledgements

The authors would like to thank Dr. Tom Nakashima, Department of Chemistry, University of Alberta, for the

[3] The XRAY 76 computer program package was used in this analysis.

[4] Tables of atomic parameters, bond lengths and angles, and structure factors are available, at nominal charge, from the Depository of Unpublished Data, CISTI, National Research Council of Canada, Ottawa, Ont., Canada K1A 0S2.

400 MHz nmr spectra, Dr. G. D. Abrams for helpful discussions, and the Medical Research Council of Canada for research fund support to L.T.J.D.

1. S. R. ABRAMS. Can. J. Chem. **60**, 1238 (1982).
2. (*a*) R. J. BUSHBY and G. H. WHITHAM. J. Chem. Soc. (B) 67 (1969); (*b*) J. C. CRAIG and M. MOYLE. J. Chem. Soc. 4402 (1963).
3. C. K. JOHNSON. OR TEP-II. Report ORNL-5138: A fortran thermal-ellipsoid plot program for crystal structure illustrations. Oak Ridge National Laboratory, Oak Ridge, TN. (1976).
4. (*a*) M. J. S. DEWAR and H. N. SCHMEISING. Tetrahedron, **11**, 96 (1960); (*b*) D. L. SMITH and H. R. LUSS. Acta Crystallogr. Sect. B, **31**, 402 (1975).
5. L. STRYER. Biochemistry. 2nd ed. W.H. Freeman and Company, San Francisco. 1981. p. 213.
6. J. KAGAN, L. TOLENTINO, and M. G. ETTLINGER. J. Org. Chem. **40**, 3085 (1975).
7. (*a*) J. BUS, I. SIES, and M. S. F. LIE KEN JIE. Chem. Phys. Lipids **17**, 501 (1976); (*b*) **18**, 130 (1977); (*c*) F. D. GUNSTONE, M. R. POLLARD, C. M. SCRIMGEOUR, and H. S. VEDANAYAGAM. Chem. Phys. Lipids, **18**, 115 (1977); (*d*) F. D. GUNSTONE, M. R. POLLARD, and C. M. SCRIMGEOUR. Chem. Phys. Lipids, **17**, 1 (1976).
8. R. J. BUSHYBY. Q. Rev. Chem. Soc. **24**, 585 (1970).
9. N. PETRAGNANI and M. YONASHIRO. Synthesis, 521 (1982).
10. B. S. PITZELE, J. S. BARAN, and D. H. STEINMAN. J. Org. Chem. **40**, 269 (1975).
11. C. C. SHEN and C. AINSWORTH. Tetrahedron Lett. 93 (1979).
12. C. C. SHEN and C. AINSWORTH. Tetrahedron Lett. 87 (1979).
13. F. THÉRON, M. VERNY, and R. VESSIÈRE. *In* The chemistry of the carbon–carbon triple bond. *Edited by* S. Patai. John Wiley and Sons, Toronto. 1978. Chapt. 10.
14. P. COPPENS, L. LEISEROWITZ, and D. RABINOVICH. Acta Crystallogr. **18**, 1035 (1965).
15. F. R. AHMED, S. R. HALL, M. E. PIPPY, and C. P. HUBER. N.R.C. crystallographic programs for the IBM/360 system. Accession Nos. 133–147. *In*: J. Appl. Crystallogr. **6**, 309 (1973).
16. P. MAIN, S. J. FISKE, S. E. HULL, L. LESSINGER, G. GERMAIN, J-P. DECLERCQ, and M. M. WOOLFSON. MULTAN 80. A system of computer programs for the automatic solution of crystal structures from X-ray diffraction data. University of York, England. 1980.
17. J. KARLE and I. L. KARLE. Acta Crystallogr. **21**, 849 (1966).
18. A. C. LARSON. Acta Crystallogr. **23**, 664 (1967).
19. J. M. STEWART. The X-ray system of crystallographic computer programs. Computer Science Center, University of Maryland, College Park, MD. 1976.

Can. J. Chem. Downloaded from www.nrcresearchpress.com by 210.87.254.6 on 09/06/12
For personal use only.

A kinetic study of the H_2O_2-accelerated formation of *o*-nitrophenol from *o*-dinitrobenzene

RAYMOND A. HELLER, MARILYN FEWSTER,[1] AND TAYLER LAMBERT[2]
Department of Chemistry, Wilfrid Laurier University, Waterloo, Ont., Canada N2L 3C5

Received April 4, 1983

RAYMOND A. HELLER, MARILYN FEWSTER, and TAYLER LAMBERT. Can. J. Chem. **61**, 2455 (1983).

At 30°C in 50% v/v dioxane in water, the reaction of *o*-dinitrobenzene with hydroxide ion to form *o*-nitrophenolate anion is very slow but it proceeds much more rapidly when H_2O_2 is also present. Although the phenolate product absorbs strongly in the visible region, standard kinetic analysis of the spectral data fails for both the peroxide-free and the peroxide-accelerated reactions. A more thorough examination of the spectral evidence reveals that, for the peroxide-accelerated reaction, a reasonably stable intermediate is first formed so that the overall reaction is in fact a two-step sequence. We have used a computer modelling technique to determine rate constants for the two steps and we find that both rate constants are dependent on $[H_2O_2]$. Several possible structures for the intermediate are discussed, with the radical anion being preferred.

RAYMOND A. HELLER, MARILYN FEWSTER et TAYLER LAMBERT. Can. J. Chem. **61**, 2455 (1983).

A 30°C dans un mélange dioxanne-eau 50% v/v, la réaction du *o*-dinitrobenzène avec l'ion hydroxyde qui conduit à l'anion *o*-nitrophénolate est très lente mais elle est beaucoup plus rapide lorsqu'on ajoute du H_2O_2. Bien que le phénolate obtenu absorbe fortement dans la région visible, l'analyse cinétique normale des données spectrales fait défaut dans le cas des réaction sans peroxyde et des réactions accélérées par le peroxyde. Une étude soignée des preuves spectrales révèle que pour la réaction accélérée par le peroxyde, un intermédiaire raisonnablement stable se forme le premier de telle sorte que la réaction globale est en fait une séquence à deux étapes. Nous avons utilisé la technique du modèle par ordinateur pour déterminer les constantes de vitesse des deux étapes et nous avons trouvé que les deux constantes dépendent de $[H_2O_2]$. On discute des diverses structures possibles de l'intermédiaire avec une préférence pour l'anion-radicalaire.

[Traduit par le journal]

Can. J. Chem. Downloaded from www.nrcresearchpress.com by 210.87.254.42 on 09/06/12
For personal use only.

It has long been known that appropriately substituted nitroaromatic systems are subject to attack by powerful basic species resulting in the displacement of nitrite ion. Some time ago, Tommila and Murto published (1) the results of their kinetic investigations into the reactions of *ortho*- and *para*-dinitrobenzene with hydroxide and alkoxide ions in both pure and mixed solvents. In the majority of these cases they observed clean second-order kinetic behaviour corresponding to reactions [1] and [2]:

$$[1]\quad ArNO_2 + HO^- \rightarrow ArOH + NO_2^-$$

$$[2]\quad ArNO_2 + RO^- \rightarrow ArOR + NO_2^-$$

However, as a minor part of their studies on *p*-dinitrobenzene (*p*DNB), they reported that ". . . . with dioxane–water mixtures, it was difficult to obtain a good constancy for *k*. In these runs *k* in general gradually decreased as the reaction proceeded." By a simple extension of Tommila and Murto's work, we were able to determine that *o*-dinitrobenzene (*o*DNB) exhibits similar irregular behaviour. Intrigued by the anomalous kinetics of the dinitrobenzenes in dioxane–water, we decided to attempt a thorough rate study, focussing on the *ortho* isomer. Early in the course of our investigation we happened to use some impure dioxane and thus made the surprising discovery that hydroperoxides have a strong accelerating effect on the DNB – hydroxide ion reaction. We have investigated this phenomenon in some detail and our results are presented in this paper.

While there are many literature reports describing the use of peroxides, especially hydrogen peroxide, in the production of phenols, the great majority of these deal with acidic conditions. We have found only two publications detailing the effect of H_2O_2 in aromatic substitution under basic conditions. Vainshtein *et al.* (2) have reported that the reaction between *p*-nitrobenzenesulfonic acid and hydroxide ion to give *p*-nitrophenol occurs much more rapidly in the presence of hydrogen peroxide. More recently, Ivanova and Shein (3) found that the reaction of 2,4-dinitrochlorobenzene with triethylamine in dimethylformamide is accelerated both by hydrogen peroxide and benzoyl peroxide, but it is not clear from their report whether the presence of peroxide leads to the same product mix.

Experimental

Commercial *o*-dinitrobenzene was recrystallized from benezene, mp 119–121°C (uncorrected; lit. (16) mp 118.5°C). *o*DNB stock solutions of approximately 5×10^{-4} *M* concentration were prepared by dissolving carefully weighed quantities of the crystals in peroxide-free, redistilled 1,4-dioxane. The *o*DNB concentration could be readily confirmed by diluting a measured amount of the stock solution to a specified volume with strong NaOH, sealing the mixture in a vial, and heating overnight at 70–80°C, thereby ensuring total conversion of the *o*DNB to *o*-nitrophenolate anion, the concentration of which could be measured spectrophotometrically, λ_{max} 424 nm (ϵ = 5200 M^{-1} cm^{-1}).

Hydrogen peroxide stock solutions were prepared by appropriate dilution of 30% commercial H_2O_2. Sodium hydroxide stock solutions were prepared by diluting portions of a saturated (carbonate-free) NaOH solution. For our kinetic runs, the H_2O_2 and NaOH concentrations were selected on the basis of the following considerations: (*a*) the desire to have H_2O_2 and NaOH concentrations much higher than the *o*DNB concentration so the psuedo first-order kinetics might prevail; (*b*) the observation that, when the NaOH concentration in 50% v/v dioxane in water is greater than 0.5 *M*, precipitation usually occurs; (*c*) the observation that the phenol product was not completely ionized when H_2O_2 concentration was approximately equal to, or greater than, the NaOH concentration, presumably because of competitive ionization of the H_2O_2.

For a typical kinetic run, 10 mL of *o*DNB stock solution, 40 mL of freshly distilled dioxane, and 2 mL of H_2O_2 stock solution were placed in a 100-mL volumetric flask. This mixture and a separate container of the NaOH stock solution were brought to temperature equilibrium

[1] WLU Undergraduate Summer Research Assistant, 1976.
[2] WLU Undergraduate Summer Research Assistant, 1977.

Can. J. Chem. Downloaded from www.nrcresearchpress.com by 210.87.254.42 on 09/06/12
For personal use only.

in a 30.0°C bath. To initiate the reaction, NaOH stock solution was added to the dioxane, bringing the total volume to 100 mL. After rapid mixing, the kinetic solution was poured into a uv cell which was placed in the thermostatted (30.0°C) cell compartment of a Beckman DB-G spectrophotometer. The reference solution was prepared similarly, substituting 10 mL of dioxane for the *o*-DNB stock solution.

All kinetic runs were carried out in duplicate. Early in each run, two aliquots of the kinetic solution were titrated with standard $KMnO_4$ to determine the hydrogen peroxide concentration, and two additional aliquots were titrated with standard acid to obtain the exact NaOH concentration.

Results

When a dilute solution of *o*DNB in dioxane is added to strong aqueous NaOH and the resulting mixture is maintained at 30.0°C, a yellow color very slowly develops. The progress of the reaction may be monitored by periodic scanning of the 250–500 nm spectral region, thus establishing that the adsorption peak originates and remains at 424 nm, which is characteristic of *o*-nitrophenolate anion. A plot of A_{424} vs. time yields a smooth, continuous line of negative curvature, asymptotically approaching a maximum value which corresponds to total conversion of the starting material to phenolate product. However, if these data are subjected to conventional first- or second-order kinetic analysis, no linear relationship is obtained.

The addition of hydrogen peroxide to the *o*DNB–NaOH reaction mixture causes the yellow color to develop much more rapidly. For example, at 30.0°C with no peroxide present and [NaOH] = 0.22 *M*, the time required for A_{424} to reach one-half of its "infinity" value is about 4500 min. If the same solution also contains 0.075 *M* H_2O_2, the corresponding time period drops to 80 min. The final absorption curves are identical in magnitude, shape, and position whether or not H_2O_2 is present, thereby indicating that the same product is formed in each case. Furthermore, if the reaction is done on a large scale with peroxide added, *o*-nitrophenol (*o*NP) may be isolated in abundance with no evidence of other products. Kinetically, the absorbance data (424 nm) for the peroxide-accelerated reaction again fail to conform to standard mathematical analysis, thus paralleling the behaviour of the peroxide-free reaction.

In the absence of NaOH, a solution containing *o*DNB and H_2O_2 is stable for many days, showing only absorbance due to *o*DNB itself; this observation establishes HO_2^- as the species responsible for the increased reaction rate.

Although we have examined only the hydrogen peroxide effect, it is worth repeating that our preliminary findings with impure dioxane strongly indicate a similar rate enhancement due to organic hydroperoxides; in contrast, we have determined that benzoyl peroxide (and presumably other organic peroxides) is not effective in this regard.

A second interesting aspect of the peroxide-accelerated system becomes apparent when the progress of the reaction is followed by regularly scanning the 300–500 nm region. In the earliest stages of the reaction, a distinct peak is observable at approximately 385 nm, but as time progresses the peak shifts to higher wavelength and increases in size until it ultimately assumes the position and magnitude corresponding to 100% formation of the *o*-nitrophenolate anion. The series of spectra shown in Fig. 1 illustrates the sequential changes for a typical reaction. Because this finding inevitably suggests the formation of an intermediate with a reasonable life-time, we are led to the conclusion that the peroxide-accelerated reaction must take place in at least two well-defined steps (see [3]) having rate

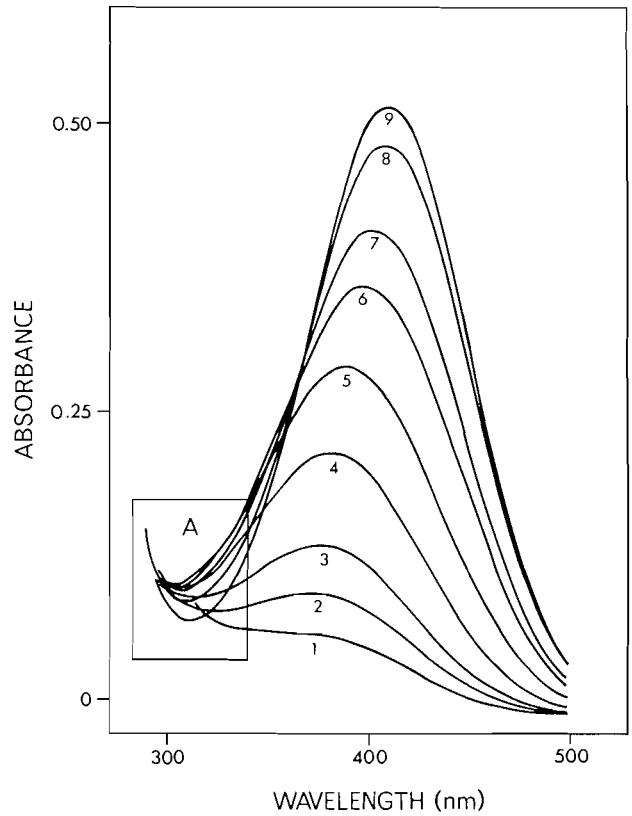

FIG. 1. Conversion of *o*-dinitrobenzene to *o*-nitrophenol anion. Spectral changes during the course of the reaction (30.0°C; 50% v/v dioxane in water; $[o\text{DNB}]_0 = 1 \times 10^{-4}$ *M*; $[\text{NaOH}]_0 = 0.449$ *M*; $[H_2O_2]_0 = 0.0805$ *M*). Spectral scans started at: 1, 8.25 min; 2, 15.5 min; 3, 25.25 min; 4, 50.5 min; 5, 84.5 min; 6, 125 min; 7, 150 min; 8, 240 min; 9, 1300 min.

$$[3] \quad o\text{DNB} \xrightarrow{k_1} (\text{intermediate}) \xrightarrow{k_2} o\text{NP anion}$$

constants of comparable magnitude, and thus we have an explanation for the nonlinear kinetic pattern.

Kinetic analysis

The elucidation of the kinetic picture for the *o*DNB–$NaOH$–H_2O_2 reaction is rather difficult, primarily because the absorbance peaks of the intermediate and the product overlap extensively and there is no direct means available for obtaining an extinction coefficient value for the intermediate. In addition, there are two other, although minor, complicating features of our reaction system. First, the initial mixing of aqueous base with dioxane produces a slight warming effect which must result in a faster reaction rate for the first few minutes. Second, there is slow but measurable decomposition of the hydrogen peroxide (typically about 5%) during the course of the *o*DNB reaction.

We have attempted to solve the kinetic problem by constructing a computer model which reproduces on a relative scale the experimental absorbance readings as a function of time. Briefly, our approach has been to assume a value for the extinction coefficient of the intermediate at 424 nm and derive from this (via an initial rate treatment) a reasonable value for k_1 which then, in conjunction with a knowledge of the time, t_{max}, corresponding to maximum concentration of the intermediate, enables k_2 to be reasonably estimated. This method

TABLE 1. Conversion of *o*-dinitrobenzene (*o*DNB) to *o*-nitrophenol (*o*NP) anion. Calculated and observed absorbance (424 nm) as a function of time

Time (min)	Calculated[a] relative concentrations			Relative absorbance at 424 nm	
	*o*DNB	Intermediate	*o*NP anion	calcd.[b]	obsv'd[c]
0	1.000	0.000	0.000	0	—
10	0.787	0.195	0.019	0.112	0.152
20	0.619	0.316	0.066	0.217	0.251
30	0.487	0.384	0.129	0.314	0.339
40	0.383	0.415	0.202	0.401	0.412
50	0.301	0.422	0.277	0.480	0.482
60	0.237	0.411	0.352	0.550	0.548
70	0.186	0.389	0.424	0.612	0.608
80	0.147	0.361	0.492	0.666	0.662
90	0.115	0.330	0.554	0.713	0.717
100	0.091	0.298	0.611	0.754	0.763
110	0.071	0.267	0.662	0.790	0.799
120	0.056	0.237	0.707	0.821	0.835
130	0.044	0.209	0.747	0.847	0.862
140	0.035	0.183	0.782	0.870	0.887
150	0.027	0.160	0.813	0.890	0.908
160	0.022	0.139	0.840	0.907	0.926
170	0.017	0.120	0.863	0.921	0.937
180	0.013	0.103	0.883	0.933	0.947
190	0.010	0.089	0.901	0.943	0.957
200	0.008	0.076	0.915	0.952	0.967

[a] Assuming reaction [3] and using $k_1 = 4.0 \times 10^{-4}$ s^{-1} and $k_2 = 3.0 \times 10^{-4}$ s^{-1}.

[b] Using $\epsilon_{424}^{INT} = 2500\ M^{-1}\ cm^{-1}$ and $\epsilon_{424}^{oNP} = 5200\ M^{-1}\ cm^{-1}$.

[c] 50% v/v dioxane in water; $[o\text{DNB}]_0 = 9.9 \times 10^{-5}\ M$; $[\text{NaOH}]_0 = 0.453\ M$; $[H_2O_2]_0 = 0.144\ M$; 30.0°C.

requires a great deal of trial-and-error computer calculation and may appear somewhat arbitrary. However, we have found that most combinations of ϵ_{424}^{INT}, k_1, and k_2 completely fail to reproduce the experimental data and we therefore have some confidence that the numerical results which produce a good match do, in fact, reflect the realities of the reacting system. At the same time it must be acknowledged that our computer analysis, while quite extensive, is not exhaustive and the results may possibly be further refined.

In more detail, we consistently find that for the first few minutes of our kinetic runs, a plot of A_{424} vs. time yields an excellent straight line. During this early time period [*o*DNB] may be taken to be the known initial concentration $[o\text{DNB}]_0$. It is similarly reasonable to assign [*o*NP] = 0.0 *M*, leaving the intermediate as the only absorbing species at 424 nm. If one then assumes a value for the extinction coefficient of the intermediate at that wavelength, it is possible to apply an "initial rate" approach and calculate k_1. Our wide-ranging attempts indicate that the value $\epsilon_{424}^{INT} = 2500\ M^{-1}\ cm^{-1}$, together with the subsequently derived k_1 and k_2, leads to the best fit between calculated and observed absorbances over the entire course of the reaction.

With a value for k_1 in hand, it is possible to evaluate k_2 by making use of the information obtainable from the 325–340 nm segments (region "A" of Fig. 1) of the spectra recorded at various time intervals during the kinetic run. In the early part of the reaction this absorption valley slowly increases in height, then reaches a maximum, and subsequently decreases. Similar behaviour has been observed for the reaction of NaOH with

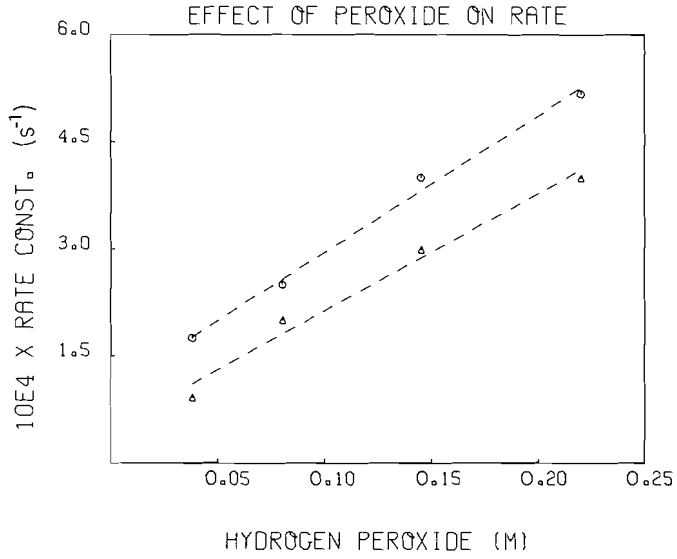

FIG. 2. Variation of rate constants with H_2O_2 concentration [NaOH] = 0.45 *M*, 30.0°C; ○ k_1, $r = 0.996$; △ k_2, $r = 0.990$.

*o*DNB in 4% v/v water in DMSO (4). Such behaviour may logically be associated with the increase of the intermediate to some maximum concentration followed by a decrease to zero. Standard equations are available (5) for relating k_1 and k_2 to the time, t_{max}, required for the concentration of the intermediate to reach a maximum, and therefore k_2 is accessible.

The derived rate constants, k_1 and k_2, may then be substituted into the appropriate integrated rate equations (ref. 5, pp. 153–154) and the relative concentrations of *o*DNB, intermediate, and *o*NP calculated as a function of time. Using the 424 nm extinction coefficients of the two absorbing species, the relative absorbances can also be evaluated and compared with the actual experimental findings. A typical set of results is shown in Table 1. (The correlation between "calculated" and "observed" absorbance is rather poor during the first 20–30 min. We believe this may be explained by the heating effect which takes place when the aqueous NaOH is mixed with the dioxane solution to begin the reaction. Thus, during the early stages, the real reaction would be somewhat faster than calculated.)

By this method we were able to obtain pairs of rate constants for a set of kinetic runs in which NaOH concentration was held constant while the hydrogen peroxide concentration was varied. The resulting k_1 and k_2 values both yield excellent linear correlations when plotted against $[H_2O_2]$, as shown in Fig. 2.

A parallel attempt to determine k_1 and k_2 as functions of NaOH concentration gave results which were less clear-cut but which unambiguously established that the two steps of the reaction are minimally affected by changes in [NaOH] so long as $[\text{NaOH}] > [H_2O_2]$.

Our overall analysis therefore indicates that k_1 is slightly greater than k_2 for any given kinetic run. We have also determined that in each case it is possible to find an alternate pair of rate constants, with $k_1 < k_2$, which also give a reasonable match. We reject these as possible solutions on the following grounds: (*a*) the alternate *k* values shown no linearity when plotted against H_2O_2 concentration; and (*b*) the t_{max} calculated from the alternate values is grossly different from the observed t_{max}.

Can. J. Chem. Downloaded from www.nrcresearchpress.com by 210.87.254.42 on 09/06/12
For personal use only.

Can. J. Chem. Downloaded from www.nrcresearchpress.com by 210.87.254.42 on 09/06/12
For personal use only.

We have not ignored the possibility that the first step of [3] is reversible, in which case a "k_{-1}" term must be introduced into our considerations. In fact, starting with a given pair of k_1 and k_2 values, we can achieve an equally good time–absorbance fit by keeping k_2 constant, increasing k_1 slightly, and setting $k_{-1} = 0.1\ k_1$. More extensive changes to k_1, k_{-1}, and k_2 result in much poorer numerical matches. Because the k_1 and k_2 values do not change appreciably when k_{-1} is included, we have opted in favour of simplicity, assuming that the first step is essentially irreversible.

Somewhat surprisingly then, our overall results establish that *both* steps of the reaction sequence are dependent on $[H_2O_2]$. Specifically, the linear plots indicate that the empirically derived psuedo first-order rate constants, k_1 and k_2, may be written as:

$$[4a] \quad k_1 = k_1^0 + k_1' [H_2O_2]$$

$$[4b] \quad k_2 = k_2^0 + k_2' [H_2O_2]$$

where the intercept, k^0, represents the rate of reaction in the absence of H_2O_2 and the slope, k^1, may be taken as the second-order rate constant for the hydrogen peroxide reaction. Equations [4*a*] and [4*b*] apply at constant $[HO^-]$ and therefore each may be rewritten in the general form:

$$[5] \quad k = k^{00} [HO^-] + k'' [HO^-] [H_2O_2]$$

Our observation that a mixture of *o*DNB and H_2O_2 undergoes no spectral change in the absence of NaOH proves that at least the first step of the reaction must be a function of $[HO_2^-]$ rather than $[H_2O_2]$. We may explicitly introduce the $[HO_2^-]$ term into the equations by taking into account the ionization of H_2O_2 in base:

$$[6] \quad H_2O_2 + HO^- \rightleftharpoons HO_2^- + H_2O$$

Reaction [6] would have an equilibrium constant $K_A = K_{H_2O_2}/K_W$ and thus we may rewrite eq. [5] in the kinetically equivalent form:

$$[7] \quad k = k^{00} [HO^-] + k'' (1/K_A) [H_2O] [HO_2^-]$$

Equation [7] would have significance if the numerical value of K_A were known, but $K_{H_2O_2}$ and K_W are not available for 50% v/v dioxane in water.

Nature of the intermediate and possible mechanisms

Given our experimental findings, we are faced with the problem of identifying an intermediate which is formed through the action of hydrogen peroxide anion and which then undergoes 100% conversion to the phenol product, with the two steps occurring much more rapidly than the simple attack of HO^- on the nitroaromatic ring. A number of possibilities must be considered.

Classical $S_{N_{Ar}}2$ mechanism

If it is assumed that the attack of HO^- on *o*DNB proceeds by the traditional sigma (σ) complex mechanism (eq. [8], R = H), it is logical to suspect that hydroperoxide ion behaves in the

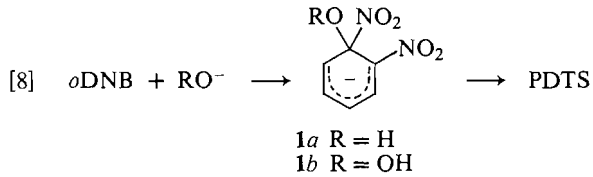

1*a* R = H
1*b* R = OH

same fashion, giving structure **1***b* as the intermediate. At first glance this possibility is attractive in that it apparently constitutes another example of the well-known "alpha (α) effect" (6), a phenomenon typified by the observation that HO_2^- is about 200 times better than HO^- as a nucleophile in attack on carbonyl carbon and tetrahedral phosphorus. Furthermore, **1***b* might be expected to have an absorbance spectrum extending into the visible region (see, for example, ref. 7).

However, strong arguments against **1***b* arise from a consideration of its probable fate. Upon elimination of NO_2^-, **1***b* would be transformed into the aryl hydroperoxide, **2**, which must also be rejected as the intermediate of interest because

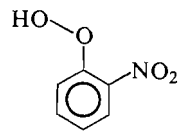

2

neither its ionized nor its unionized form would have the requisite spectral characteristics. More importantly, how would the aryl hydroperoxide be rapidly converted to the corresponding phenol? The only apparent pathway requires displacement by RO^- on peroxide oxygen as in eq. [9], and reactions of this type are extremely slow (ref. 6*a*, p. 20, and ref. 8). Additionally,

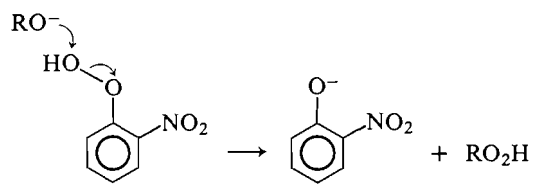

if R = H, eq. [9] fails to account for the peroxide dependence of k_2. On the other hand, if the attacking group in eq. [9] is the more powerful nucleophile, HO_2^-, the k_2 peroxide dependence is satisfied[3] although the secondary product would then be the unusual chemical species H_2O_3. Reaction [9] would also seem to demand that the aryl hydroperoxide be in the unionized form, but the anionic form would predominate under our reaction conditions. Thus, it is difficult to understand how a normal $S_{N_{Ar}}2$ mechanism could provide the explanation for our fast reaction sequence.

Oxidative elimination from the σ complex

Again assuming that **1***b* accumulates in detectable quantities, an alternative fate for it is suggested by the previously mentioned report (2) dealing with the conversion of *p*-nitrobenzenesulfonic acid to *p*-nitrophenol. These workers report that when the peroxide-accelerated reaction is carried out in $H_2^{18}O$, no ^{18}O is found in the phenol product. On this basis they suggest a mechanism involving the elimination of SO_4^{2-} rather than SO_3^{2-} as shown in reaction [10]:

[3] We thank one of the referees for bringing this possibility to our attention.

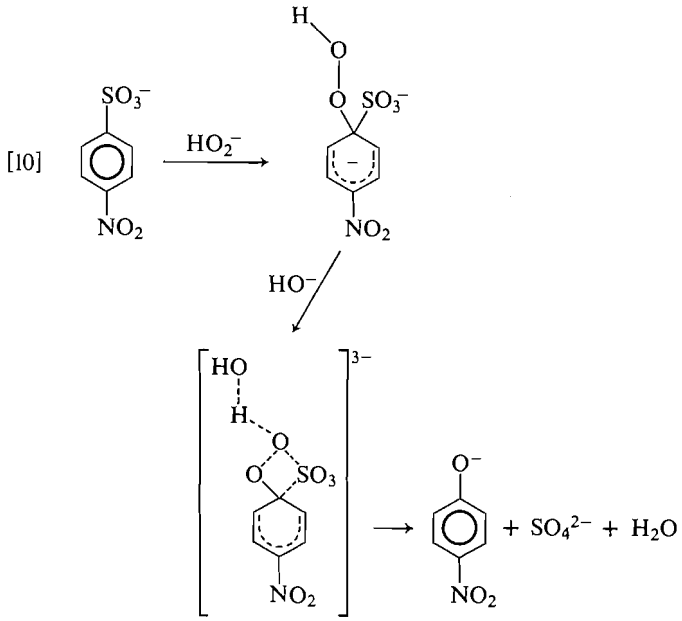

A parallel sequence for our reaction would proceed via intermediate **1***b* to transition state **3** and result in the formation of NO_3^- instead of NO_2^-. We have ruled out this interesting

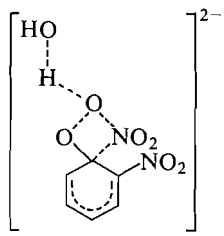

3

possibility by analyzing[4] for nitrite ion during the course of the reaction. Specifically, at the time when the spectral data show $[o\text{NP}] = 0.75\,[o\text{DNB}]_0$, we find that $[NO_2^-] = 0.63\,[o\text{DNB}]_0$, thus accounting for (0.63/0.75) = 84% of the theoretical amount of NO_2^-. The remaining nitrite may have been oxidized to nitrate by slow reaction with H_2O_2 (ref. 8, p. 106).

Radical anion intermediate

There is a growing school of thought which argues that many reactions which have traditionally been interpreted in terms of ionic mechanisms are, in fact, radical in nature. Eberson has recently published a comprehensive and persuasive review presenting the case for one-electron mechanisms as alternatives to two-electron processes (9). A more limited survey of radical-like intermediates in organic reactions has also been carried out by Guthrie (10).

More directly pertinent to our work are reports regarding the formation of nitroaromatic radical anions under basic conditions (ref. 7, pp. 213–214). In particular, there have been several papers claiming proof of the presence of dinitrobenzene radical anions in DMSO solutions containing hydroxide ion and *o*DNB (4) or pDNB (11, 12). Abe and Ikegami (11) believe that the radical anions are intermediates in the nucleophilic substitution sequence rather than irrelevant structures reversibly formed in side reactions. Their position has theoretical backing from Nagakura and Tanaka (13) who have suggested that nucleophilic aromatic substitution reactions in general are initiated by a one-electron transfer.

Thus, as outlined in reaction [11], Abe and Ikegami suggest

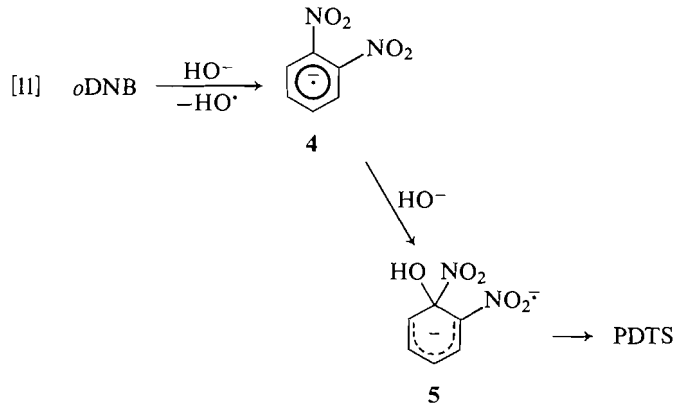

an electron transfer from hydroxide to DNB, producing hydroxyl radical and a reasonably stable DNB radical anion. They argue that HO$^\cdot$ would be rapidly destroyed by reaction with DMSO and that the DNB radical anion, **4**, undergoes attack by a second hydroxide ion to form structure **5**. For the conversion of **5** to nitrophenol they postulate two possible mechanisms, the first requiring the elimination of the radical dianion, $NO_2^{2-\cdot}$, and the other involving electron transfer from nitrophenol radical anion to unreacted DNB.

The *o*DNB radical anion identified by Abe and Ikegami is an attractive candidate for the intermediate formed in our peroxide system. A comparison of the effectiveness of HO^- and HO_2^- as electron donors (eqs. [12] and [13]) is instructive in this connection. Interestingly, the aqueous E_0 values (14) for the

[12] *o*DNB + HO^- → **4** + HO$^\cdot$

[13] *o*DNB + HO_2^- → **4** + $HO_2^\cdot$

$HO_2^\cdot/HO_2^-$ (0.8 V) and HO$^\cdot$/HO^- (1.9 V) couples lead via Marcus' Theory to the expectation[5] that [13] should be much faster than [12] even when allowance is made for the altered solvent conditions. Our confidence in the Marcus treatment is somewhat undermined by the associated prediction that [12] should be so slow as to fall into the "no reaction" category, in contrast to Abe and Ikagami's apparently firm evidence that the reaction does occur at measurable rates.

In any case, we suggest that the rapid rate of [13] accounts for the peroxide acceleration of the first step in [3].

If **4** is indeed the intermediate formed in our system, it may proceed to product via reaction with hydroxide ion as suggested by Abe and Ikegami. However, this interpretation again fails to explain the H_2O_2 dependence of k_2. A possible alternative is reaction of **4** with HO$^\cdot$, a species which might be present in relatively high concentration in the hydrogen peroxide solution, but we have no real evidence to support this view.

Additional remarks

Rather than a formal radical anion intermediate, it is possible that we are dealing with a charge transfer complex such as **6**.

[4] We thank Dr. D. Peirson of the Department of Biology, Wilfrid Laurier University, for performing these analyses.

[5] We thank one of the referees for drawing our attention both to the E_0 data and the derived rate constant values.

Can. J. Chem. Downloaded from www.nrcresearchpress.com by 210.87.254.42 on 09/06/12
For personal use only.

TABLE 2. Comparison of k^0 values

	Peroxide-free computer match	Figure 2 intercept
$10^5 k_1^0$ (s^{-1})	4.7	10.0
$10^5 k_2^0$ (s^{-1})	3.0	4.8

Electron spin reasonance studies (15) have indicated that the interaction between an electron donor and a nitroaromatic

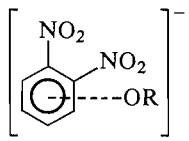

6*a* R = H
6*b* R = OH

acceptor may be extremely close. Therefore, although we have assumed that there is a common intermediate, **4**, formed whether or not peroxide is present, we must admit to the possibility that there may be two distinct species, **6***a* and **6***b*, with different spectral characteristics and different rates of conversion to the phenol. We are undertaking nmr and esr studies in the hope of obtaining a more precise understanding of the structure of the intermediate.

We have also established that the parallel reaction of *p*DNB with hydroxide ion is similarly affected by the addition of hydrogen peroxide (greatly enhanced rate; spectrophotometrically detectable intermediate) and we are investigating the wider generality of this peroxide effect.

Because the peroxide-free reaction of *o*DNB with HO^- does not conform to orthodox kinetic treatment, we suspect that it also takes place in two well-defined steps although no intermediate is detectable in the spectrum. This may be explained by the presence of a different intermediate (e.g., **6***a* in place of **6***b*) with minimal absorbance in the 350–450 nm region.

We have attempted to analyze the peroxide-free reaction, assuming that the same intermediate, **4**, ($\epsilon_{424}^{INT} = 2500\ M^{-1}\ cm^{-1}$) is formed, but we have been unable to find a pair of k_1^0 and k_2^0 values which result in a good match. However, if we introduce "k_{-1}" under the assumption that the first step is reversible or that **4** decays by some equivalent process to regenerate *o*DNB, a good match can be obtained. It is particularly interesting to compare the k_1^0 and k_2^0 values derived in this way with those obtained as the intercepts of the plots shown in Fig. 2. As Table 2 shows, the k^0 values obtained by the two methods are roughly comparable.

Acknowledgements

We thank the Research Office of Wilfrid Laurier University for financial support of this project. We also thank Mrs. A. Kinastowski for her generous help in all stages of the experimental work. The assistance of the staff of the WLU Computing Centre and helpful discussions with Dr. R. Elliott and Dr. S. Stack of the Department of Mathematics, WLU, are gratefully acknowledged.

1. E. TOMMILA and J. MURTO. Acta Chem. Scand. **16**, 53 (1962).
2. M. VAINSHTEIN *et al.* Zh. Org. Khim. **3**, 1654 (1967); Chem. Abstr. **68**, 2135g (1968).
3. T. M. IVANOVA and S. M. SHEIN. Zh. Org. Khim. **16**, 1221 (1980).
4. T. ABE and Y. IKEGAMI. Bull. Chem. Soc. Jpn. **49**, 3227 (1976).
5. A. A. FROST and R. G. PEARSON. Kinetics and mechanism. John Wiley and Sons, Inc., New York. 1953. p. 155.
6. (*a*) J. O. EDWARDS and R. B. PEARSON. J. Am. Chem. Soc. **84**, 16 (1962); (*b*) S. L. JOHNSON. Adv. Phys. Org. Chem. **5**, 284 (1967).
7. M. R. CRAMPTON. Adv. Phys. Org. Chem. **7**, 211 (1969), and references cited therein.
8. E. J. BEHRMAN and J. O. EDWARDS. Progr. Phys. Org. Chem. **4**, 93 (1967).
9. L. EBERSON. Adv. Phys. Org. Chem. **18**, 79 (1982).
10. R. D. GUTHRIE. *In* Comprehensive carbanion chemistry. *Edited by* E. Buncel and T. Durst. Elsevier, Amsterdam. 1980.
11. T. ABE and Y. IKEGAMI. Bull. Chem. Soc. Jpn. **51**, 196 (1978).
12. I. BIL'KIS and S. SHEIN. Izv. Akad. Nauk SSR Ser. Khim. 961 (1973); Chem. Abstr. **79**, 52546k (1973).
13. S. NAGAKURA and J. TANAKA. Bull. Chem. Soc. Jpn. **32**, 734 (1959).
14. V. M. BERDNIKOV and N. M. BAZHIN. Russ. J. Phys. Chem. **44**, 395 (1970).
15. R. O. C. NORMAN and B. C. GILBERT. Adv. Phys. Org. Chem. **5**, 54 (1969).
16. R. C. WEAST (Editor). Handbook of chemistry and physics. 57th ed. CRC Press, Cleveland. 1976. p. C-163.

Can. J. Chem. Downloaded from www.nrcresearchpress.com by 210.87.254.42 on 09/06/12
For personal use only.

Synthesis of coleon B tetramethyl ether

ROBERT H. BURNELL, MICHEL JEAN, AND SYLVAIN SAVARD
Département de chimie, Université Laval, Québec (Qué.), Canada G1K 7P4

Received April 25, 1983

ROBERT H. BURNELL, MICHEL JEAN, and SYLVAIN SAVARD. Can. J. Chem. **61**, 2461 (1983).

Using a simple model available from podocarpic acid, a method to synthesize the Ring A and B chromophore of coleon B (**6***b*) was elaborated. When applied to the correctly substituted starting ketone **8**, this reaction sequence afforded the first synthesis of coleon B, as the tetra-*O*-methyl ether **15***a*.

ROBERT H. BURNELL, MICHEL JEAN et SYLVAIN SAVARD. Can. J. Chem. **61**, 2461 (1983).

A partir de modèles simples obtenus de l'acide podocarpique, nous avons réussi à élaborer une méthode de synthèse des cycles A et B afin d'obtenir un chromophore analogue à celui de la coléone B (**6***b*). Mettant à profit ces résultats et en les appliquant à la cétone **8** qui a le cycle C correctement substitué, nous avons réalisé la première synthèse de la coléone B sous forme de dérivé tétra-*O*-méthylé **15***a*.

Can. J. Chem. Downloaded from www.nrcresearchpress.com by 210.87.254.105 on 09/06/12
For personal use only.

In planning synthetic approaches to several classes of diterpenes from podocarpic acid (**1***a*), we felt that the introduction of a functionality in the A ring could be a critical step. Reactions involving "remote" mechanisms might succeed but, at least as a first approach, we chose to try to extend a series of conjugated functions from the aromatic ring around the perimeter. To do this one of the two groups at C.4 must be expelled and naturally the more susceptible would be the ester function.

The α,β-unsaturated ketone **2***a* is available from methyl *O*-methyl podocarpate **1***b* in one step using DDQ (1) and it is also known (2*a*, *b*) that heating this enone with 3-quinuclidinol (or other bases such as DBN, DBU, or BBN) provokes demethoxycarbonylation to give **3***a*. Extending the conjugation should be easy and, in fact, when the enone **3***a* was treated with *N*-bromosuccinimide the major product (70%) isolated was the dienone **5***a*. The intermediate bromide suffers spontaneous elimination. The minor product (14%) was the less stable isomer **4***a* in which the newly introduced double bond is exocyclic to ring A but, by acid catalysis, this was quantitatively converted to the endocyclic compound **5***a*. When subjected to Ratcliffe–Rodehorst oxidation conditions (3) the latter afforded a useful yield of the diene-dione **6***a*, the chromophore of which is reminiscent of that of coleon B (4*a*) (**15***b*) with, however, the vital difference, the hydroxyl at C.6.

It was tempting to try the same sequence of reactions on the hydroxyl containing analogue **2***b* to see if the enol double bond would behave similarly to that of the enone **2***a*. The ketone **1***c* was obtained from methyl *O*-methyl podocarpate by chromic oxidation and when shaken with oxygen in the presence of strong base (*t*-BuOK in *t*-BuOH) was converted to the enolic α-diketone **2***b* (89%) along with a trace (4%) of the over-oxidized and extremely polar product **7**. The demethoxycarbonylation reaction (quinuclidinol in refluxing *o*-xylene) proved even more rewarding in this case because the isolated product had been oxidized directly to the enolic enedione **5***b*, thus shortening the sequence by one step. The enolic hydroxyl was protected as the *O*-methyl ether (**5***c*) and then oxidation led to the C.2 ketone **6***b* as in the simpler model.

These exploratory results showed that coleon B should be accessible from the correct starting ketone **8** which happens to be one of the end products of our model experiments (5*a*) which led to the synthesis of coleon U (5*b*) and coleon C (5*c*). When ketone **8** was stirred under oxygen in strong base the C.6 position was oxidized to give the diosphenol as in numerous previous cases but, surprisingly, the ester residue was also hydrolysed and the major product was the acid **10***a*. Repeating this reaction on a larger scale confirmed this unusual result and we also isolated minor quantities of the diosphenol ester **10***b*, the enone **9**, and the lactone **11**. Both the ester **10***b* and the acid

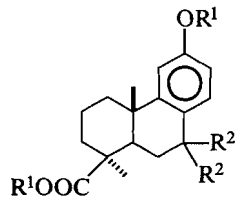

1*a* R¹ = R² = H
1*b* R¹ = Me, R² = H
1*c* R¹ = Me, R²/R² = O

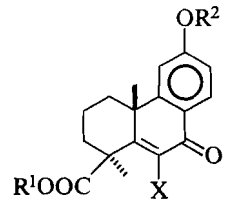

2*a* R¹ = R² = Me, X = H
2*b* R¹ = R² = Me, X = OH
2*c* R¹ = H, R² = Me, X = OH

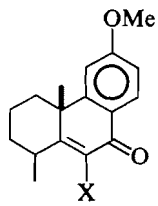

3*a* X = H
3*b* X = OH
3*c* X = OMe

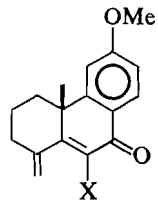

4*a* X = H
4*b* X = OH

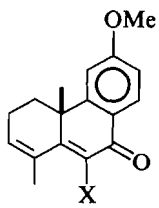

5*a* X = H
5*b* X = OH
5*c* X = OMe

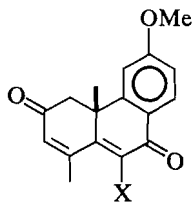

6*a* X = H
6*b* X = OMe

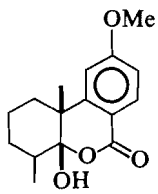

7

Can. J. Chem. Downloaded from www.nrcresearchpress.com by 210.87.254.105 on 09/06/12
For personal use only.

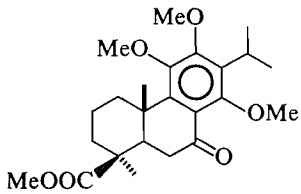

8

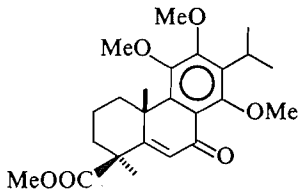

9

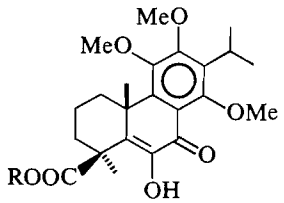

10*a* R = H
10*b* R = Me

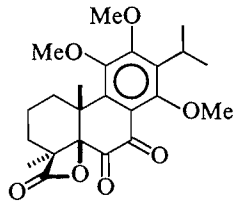

11

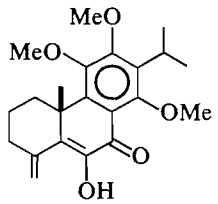

12

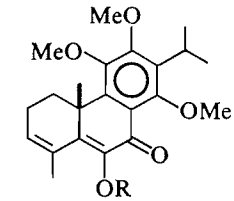

13*a* R = H
13*b* R = Me

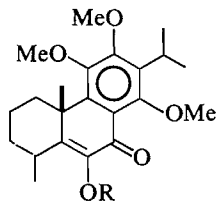

14*a* R = H
14*b* R = Me

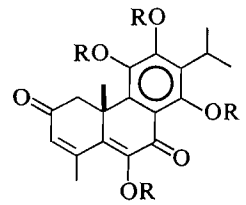

15*a* R = Me
15*b* R = H

10*a* were converted to the enedione **13***a* by refluxing in *o*-xylene containing quinuclidinol; later we found that merely refluxing the acid **10***a* in benzene also effected the oxidative decarboxylation, but in this case the major product **12** contained an exocyclic double bond. The latter reaction involved some decarboxylation to give the enolic α-diketone **14***a* (17%) but we were unable to isolate this product in pure form except after *O*-methylation which afforded **14***b*. Since the exocyclic compound **12** readily isomerizes to the more stable transoid endocyclic system **13***a*, this milder two-step sequence proved advantageous since the product from the quinuclidinol reaction was invariably difficult to purify. In fact, the unoxidized diosphenol **14***a* was also present in the quinuclidinol reaction mixture and proved extremely difficult to separate from **13***a*, whereas it was easily removed from **12**. To complete the synthesis, the enedione **13***a* was *O*-methylated to the enol ether **13***b* and the latter afforded coleon B tetra-O-methyl ether **15***a* by chromium trioxide oxidation. Comparison with an authentic sample of this derivative, most kindly provided by Professor Eugster, Zürich, who first described coleon B in the literature (4*b*), showed our synthetic material to be identical with that obtained from nature.

Curiosity forced us to repeat the formation of the model diosphenol **2***b* several times (O_2, *t*-BuOH, *t*-BuOK) but the acid **2***c* never represented more than a minor product. Eventually we did prepare the acid by refluxing the ester **2***b* in ethanolic potassium hydroxide (1 hour). As in the more complex example, refluxing in benzene was sufficient to decarboxylate the acid to the exocyclic enedione **4***b* which also isomerized readily to the endocyclic compound **5***b*.

The assignment of structures to the compounds mentioned in the text was greatly helped by the ^{13}Cmr spectral results which are given in Table 1. The attribution of the resonances was inspired by the authoritative paper of Enzell and co-workers (6) concerning diterpenes.

A very recent synthesis of a Ring A and Ring B analog of Coleon B is described by Matsumoto *et al.* (7). The route employed is completely different from ours and the final product is comparable to **15***a* but with no methoxyl groups on the C ring.

Experimental

Unless otherwise stated the conditions and instruments used to characterize the products were: melting points, Electrothermal, uncorrected; ultraviolet spectra, ethanol solutions (log ε in parenthesis), Hewlett–Packard 8450 A; infrared spectra, carbon tetrachloride solutions, Beckman 4250 and Perkin–Elmer 457; proton magnetic resonance spectra, deuteriochloroform solutions, TMS internal standard (multiplicity, integrated peak areas, coupling constants, and assignments in parenthesis), Bruker HX 90; carbon-13 magnetic resonance spectra, deuteriochloroform solutions, TMS internal standard, Bruker WP 80; mass spectra, Hewlett Packard 5992. Elemental analyses were by Galbraith Laboratories, Knoxville. The high resolution mass spectra were recorded on an A.E.I. MS-30. Unless otherwise stated, dry column chromatography implies the use of Merck Kieselgel 60F (70–230 mesh) and elution with hexane – ethyl acetate (proportions determined by prior thin-layer chromatography using Machery–Nagel Polygram pre-coated plastic sheets).

Dienones **4***a and* **5***a*

Methyl *O*-methyl podocarpate was converted to the enone **2***a* as described by Findlay and Turner (1). The demethoxycarbonylation of **2***a* was effected following Miles' method (2*b*) which involves refluxing in *o*-xylene in the presence of 3-quinuclidinol. The product **3***a* crystallized after chromatography, mp 122–123°C (lit (2) mp 122.5–123.5°C); the spectral properties were as described. *Anal.* calcd. for $C_{17}H_{20}O_2$: C 79.65, H 7.86; found: C 79.45, H 8.07.

To a refluxing solution of the enone **3***a* (2.2 g) in CCl_4 (180 mL) was added *N*-bromosuccinimide (1.67 g). A photoflood lamp was used as a source of both light and heat. After 10 min the cooled solution was filtered from the floating succinimide and the crude product obtained by evaporation was chromatographed (dry column) over silica gel. The major product (1.52 g; 70%) was *9-oxo-6-methoxy-1,4a(β)-dimethyl-3,4,4a,9-tetrahydrophenanthrene* (**5***a*): mp 91–93°C (from hexane); uv: 233(3.87), 253(3.74), 292(3.96), and 321(3.83) nm; ir (film): 1645 cm^{-1}; ^{1}H nmr δ: 1.34 (s, CH_3—C.10), 1.96 (s, CH_3—C.4), 3.84 (s, CH_3O), 5.97 (m, C.3—H), 6.29 (s, C.6—H), 6.86 (dd, J = 8 and 2.5 Hz, C.13—H), 6.94 (d, J = 2.5 Hz, C.11—H), and 8.10 (d, J = 8 Hz, C.14—H); *m/e*: 254 (M^+).

The other product (315 mg; 14%) was *9-oxo-6-methoxy-1-methylene-4a(β)-methyl-1,2,3,4,4a,9-hexahydrophenanthrene* (**4***a*): colourless oil; uv: 238(3.62) and 310(3.63) nm; ir: 3070, 1650, and 890 cm^{-1}; ^{1}H nmr δ: 1.38 (s, CH_3—C.10), 3.89 (s, CH_3O), 5.00 and 5.13 (2t, J = 1.5 Hz, C.19—H_2), 6.33 (s, C.6—H), 6.95 (dd, J = 2.5 and 9 Hz, C.13—H), 6.98 (d, J = 2.5 Hz, C.11—H), and 8.18 (d, J = 9 Hz, C.14—H).

Refluxing a benzene solution of **4***a* containing catalytic amounts of *p*-toluene sulfonic acid effected the isomerization to **5***a* in almost quantitative yield.

Can. J. Chem. Downloaded from www.nrcresearchpress.com by 210.87.254.105 on 09/06/12
For personal use only.

TABLE 1. ^{13}C nuclear magnetic resonance spectral data[a]

	Compound																				
Carbon	**2***a*	**3***a*	**5***a*	**4***a*	**6***a*	**2***b*	**7**	**5***b*	**2***c*	**4***b*	**3***b*	**3***c*	**8**	**10***a*	**10***b*	**14***b*	**11**	**12**	**13***a*	**13***b*	**15***a*
1	37.3	37.0	32.9	38.5	49.1	49.1	37.2	34.5	32.6	39.4	37.3	37.4	38.9	29.1	29.3	30.1	35.8	36.4	31.6	31.8	47.9
2	19.2	22.0	23.5	22.1	196.8	16.6	21.2	23.8	16.5	22.4	22.4	22.2	19.8	16.5	16.5	22.0	20.3	22.4	23.9	24.0	197.7
3	40.2	41.2	132.9	35.1	130.0	31.6	31.9	129.7	32.3	35.7	41.7	41.7	37.5	31.2	31.5	36.7	41.3	35.9	130.2	131.8	130.4
4	48.0	34.1	131.6	147.1	152.0	46.8	32.5	131.7	46.8	133.5	34.7	34.8	43.8	46.7	46.8	31.3	50.7	133.7	131.8	131.4	149.9
5	164.6	170.3	160.9	166.0	156.5	134.5	110.6	130.7	134.6	140.6	136.4	148.1	50.8	134.0	134.3	144.3	98.0	140.0	130.8	142.8	138.9
6	126.5	121.2	121.4	122.7	127.1	143.9	—	142.7	144.1	141.0	142.1	151.8	37.2	143.1	143.1	148.3	206.9	141.4	141.4	147.0	155.0
7	184.3	184.2	184.8	184.6	183.7	179.6	164.8	179.7	179.7	179.9	180.1	181.0	197.4	178.9	179.0	180.1	190.8	179.4	179.6	180.8	179.9
8	123.9	124.0	124.7	124.5	123.9	121.4	132.7	121.8	121.5	121.5	121.5	112.8	121.8	117.4	117.6	120.9	120.8	118.0	118.0	120.9	120.4
9	154.8	154.8	153.1	153.6	152.2	155.8	148.5	154.5	156.1	155.0	156.0	154.0	148.5	148.0	148.2	151.4	147.6	144.7	144.4	144.2	140.6
10	42.1	41.5	38.5	41.3	41.6	40.4	43.6	40.4	40.3	40.7	41.7	42.7	41.6	40.3	40.5	41.8	45.4	41.0	39.0	39.8	43.0
11	116.8	110.8	110.4	110.8	110.0	110.6	110.6	111.0	110.6	110.9	111.1	110.9	145.6	145.6	145.6	147.7	146.4	148.4	148.4	147.9	147.7
12	163.6	163.2	163.3	163.3	164.2	164.0	163.8	164.0	164.0	163.8	163.6	163.3	156.3	155.4	155.6	155.0	154.7	155.8	155.6	155.2	155.0
13	113.0	113.0	112.7	112.8	114.1	113.3	111.8	113.5	113.2	113.4	113.4	113.3	135.1	135.7	135.8	135.4	136.5	136.0	136.0	135.8	136.8
14	128.7	128.6	128.7	129.1	129.7	129.4	133.3	129.3	129.5	129.5	129.2	129.1	158.0	158.2	158.3	157.2	160.4	158.0	158.0	157.1	155.5
15	—	—	—	—	—	—	—	—	—	—	—	—	25.3	25.2	25.3	25.3	25.7	25.3	25.3	25.3	25.4
16	—	—	—	—	—	—	—	—	—	—	—	—	21.9	21.9	22.0	22.0	21.7	22.0	22.0	22.0	21.9
17	—	—	—	—	—	—	—	—	—	—	—	—	21.9	21.9	22.0	22.0	21.7	22.0	22.0	22.0	21.9
18	27.8	—	—	—	—	24.9	—	—	24.4	—	—	—	28.5	26.5	26.4	—	24.4	—	—	—	—
19	175.6	18.3	19.8	112.9	32.0	177.0	13.6	21.0	181.6	116.2	20.9	20.9	177.4	182.1	177.3	21.0	174.9	115.9	23.2	23.4	23.9
20	27.3	26.9	29.2	28.2	20.3	32.9	25.5	27.9	32.3	28.1	27.1	27.5	16.5	23.6	24.1	19.5	16.2	23.7	22.9	22.6	25.4
MeO 6	—	—	—	—	—	—	—	—	—	—	—	60.6	—	—	—	59.8	—	—	—	59.8	60.0
MeO 11	—	—	—	—	—	—	—	—	—	—	—	—	59.9	60.0	60.1	60.0	60.4	59.9	59.9	59.8	60.0
MeO 12	55.5	55.4	55.5	55.5	55.7	55.5	55.5	55.5	55.5	55.5	55.5	55.5	59.9	59.8	60.1	59.8	60.6	60.1	60.0	59.8	60.0
MeO 14	—	—	—	—	—	—	—	—	—	—	—	—	62.8	62.3	62.5	62.6	62.6	62.4	62.4	62.5	62.6
COOMe	52.0	—	—	—	—	52.0	—	—	—	—	—	—	51.4	—	52.3	—	—	—	—	—	—

[a]In ppm from TMS.

Can. J. Chem. Downloaded from www.nrcresearchpress.com by 210.87.254.105 on 09/06/12
For personal use only.

Diene-dione **6**a

To pyridine (1.5 mL) in anhydrous CH_2Cl_2 (25 mL) was added CrO_3 (900 mg) in small portions. After stirring under nitrogen for 2 h the dienone **5***a* (300 mg) was added and stirring continued 70 min. The crude product was isolated in the usual manner and then dry column chromatography (silica gel; benzene – ethyl acetate 80:20) gave some starting material (90 mg; 30%) and the diene-dione **6***a* (105 mg; 33%), *3,9-dioxo-6-methoxy-1,4a(β)-dimethyl-3,4,4a,9-tetrahydrophenanthrene:* mp 116–117°C (from hexane–ether); uv: 252(4.18), 289(4.16), 301 (sh, 4.07), and 331(3.77) nm; ir: 3040 and 1645 cm^{-1}; ^1H nmr δ: 1.53 (s, CH_3—C.10), 2.27 (d, J = 1 Hz, CH_3—C.4), 3.89 (s, CH_3O), 6.18 (q, J = 1 Hz, C.3—H), 6.73 (s, C.6—H), 6.94 (d, J = 2.0 Hz, C.11—H), 7.01 (dd, J = 8.0 and 2.0 Hz, C.13—H), and 8.19 (d, J = 8.0 Hz, C.14—H); *m/e*: 268 (M^+). *Anal.* calcd. for $C_{17}H_{16}O_3$: C 76.10, H 6.01; found: C 75.96, H 6.12.

Formation of the enolic α-diketone **2**b

The aromatic ketone **1***c* (8) (1.46 g) dissolved in *t*-BuOH (30 mL) was added to the previously prepared solution resulting from dissolving potassium (1.6 g) in *t*-BuOH (40 mL). The solution was stirred vigorously for 1 h in an atmosphere of oxygen and then the product isolated in the usual manner. Dry column chromatography gave the diosphenol **2***b* (1.40 g; 89%), *1(β)-methoxycarbonyl-9-oxo-10-hydroxy-6-methoxy-1(α),4a(β)-dimethyl-1,2,3,4,4a,9-hexahydrophenanthrene:* colourless glass, ir: 3350, 1732, 1640, and 1612 cm^{-1}; ^1H nmr δ: 1.50 and 1.65 (2s, 2 × CH_3—C), 3.72 (s, $COOCH_3$), 3.91 (s, CH_3O), 6.94 (dd, J = 2.0 and 8.5 Hz, C.13—H), 7.03 (d, J = 2.0 Hz, C.11—H), 7.11 (br s, OH, D_2O !), and 8.17 (d, J = 8.5 Hz, C.14—H). *Anal.* calcd. for $C_{19}H_{22}O_5$: C 69.07, H 6.71; found: C 68.85, H 6.74.

A much more polar compound **7** (50 mg; 4%) was also obtained (*9-oxo-6-methoxy-1a-hydroxy-1(α),4a(β)dimethyl-1,1a,2,3,4,4a,9,10-octahydro-10-oxaphenanthrene*): pale yellow oil, uv: 209(4.22) and 267(4.16) nm; ir: 3370, 1680 cm^{-1}; ^1H nmr δ: 1.03 (d, J = 7 Hz, CH_3—CH), 1.28 (s, CH_3—C), 3.91 (s, CH_3O), 3.94 (br s, OH, D_2O !), 6.87 (dd, J = 2.0 and 9.0 Hz, C.13—H), 6.89 (d, J = 2 Hz, C.11—H), and 8.11 (d, J = 9 Hz, C.14—H); *m/e*: 276 (M^+).

Oxidative demethoxycarbonylation of **2**b *to* **5**b

To the enolic diketone **2***b* (500 mg) in *o*-xylene (14 mL) was added quinuclidinol (970 mg) and the mixture refluxed for 6 h. After cooling, benzene was added and the solution washed with 5% HCl and then the crude product was chromatographed (dry column) to give the enedione **5***b* (215 mg; 52%). For properties see later.

Hydrolysis of ester **2**b *(→ acid* **2**c*)*

The ester **2***b* (2.0 g) was dissolved in EtOH (40 mL), aqueous KOH (30 mL of 30%) was added, and the mixture refluxed for 1 h. Extraction gave a solid which crystallized from ether–hexane (1.70 g; 89%) *(1(β)-carboxy-9-oxo-6-methoxy-10-hydroxy-1(α),4a(β)-dimethyl-1,2,3,4,4a,9-hexahydrophenanthrene)*: mp 120°C (dec.); uv: 238(3.85), 288(3.98), and 323(3.97) nm; ir: 3400, 1700, and 1630 cm^{-1}; ^1H nmr δ: 1.54 and 1.64 (2s, 2 CH_3—C), 3.87 (s, CH_3O), 6.92 (dd, J = 2.5 and 8.5 Hz, C.13—H), 7.01 (d, J = 2.5 Hz, C.11—H), 7.18 (br s, OH, D_2O !), 8.13 (d, J = 8.5 Hz, C.14—H), and 11.07 (s, COOH); *m/e*: 316 (M^+). *Anal.* calcd. for $C_{18}H_{20}O_5$: C 68.34, H 6.89; found: C 68.93, H 6.37. (*Note:* this compound is fragile and even recrystallization causes some decarboxylation.)

Decarboxylation of the acid **2**c

The acid (1.7 g) was refluxed in benzene (200 mL) for 3 h. Evaporation of the solvent gave an oil which was purified by dry column chromatography affording the compound **4***b* as a colourless glass *(9-oxo-6-methoxy-10-hydroxy-1-methylene-4a(β)-methyl-1,2,3,4,4a,9-hexahydrophenanthrene*, 910 mg; 62%): uv: 222(4.10) and 277(4.01) nm; ir: 3390, 1625, and 890 cm^{-1}; ^1H nmr δ: 1.40 (s, CH_3—C), 3.89 (s, CH_3O), 5.30 and 5.43 (2m, exocyclic methylene), 6.95 (s, OH, D_2O !), 6.95 (dd, J = 2.5 and 9.0 Hz, C.13—H), 7.00 (d, J = 2 Hz, C.11—H), and 8.20 (d, J = 9.0 Hz, C.14—H).

The decarboxylation product **3***b* was also obtained (glass, 392 mg; 27%; *9-oxo-6-methoxy-10-hydroxy-1(β),4a(β)-dimethyl-1,2,3,4,4a,9-hexahydrophenanthrene*): uv: 245(3.82), 272(4.00), and 323(3.90) nm; ir: 3370, 1650, and 1625 cm^{-1}; ^1H nmr δ: 1.52 (s, CH_3—C), 1.56 (d, J = 7.0 Hz, CH_3—CH), 3.89 (s, CH_3O), 6.97 (dd, J = 2.0 and 8.5 Hz, C.13—H), 7.03 (d, J = 2 Hz, C.11—H), 7.07 (s, OH, D_2O !), and 8.19 (d, J = 8.5 Hz, C.14—H); *m/e*: 272 (M^+). *Anal.* calcd. for $C_{17}H_{20}O_3$: C 74.97, H 7.40; found: C 74.69, H 7.40.

Methylation of the diosphenol **3**b *to* **3**c

The enol **3***b* (500 mg) was methylated in aqueous ethanol using NaOH (10 mL of 30%) and dimethyl sulfate (6 mL) at room temp for 24 h. The pure di-*O*-methyl ether **3***c* (425 mg; 81%) was obtained by dry column chromatography as a yellow oil; uv: 239(4.02), 265(4.03), and 303(4.10) nm; ir: 1630 and 1585 cm^{-1}; ^1H nmr δ: 1.47 (d, J = 5 Hz, CH_3—CH), 1.53 (s, CH_3—C), 3.74 and 3.88 (2s, 2 CH_3O), 6.91 (dd, J = 2.0 and 9.0 Hz, C.13—H), 6.94 (d, J = 2.0 Hz, C.11—H), and 8.15 (d, J = 9.0 Hz, C.14—H); *m/e*: 286 (M^+).

Isomerization of **4**b *to* **5**b

To the enedione **4***b* (1.1 g) in benzene (100 mL) was added *p*-toluene sulfonic acid (50 mg) and the mixture was refluxed for 30 min. The cooled solution was washed with water, dried, evaporated, and the residue chromatographed (dry column) to afford the isomerized product **5***b* (glass, 850 mg; 77%; *9-oxo-6-methoxy-10-hydroxy-1,4a(β)-dimethyl-3,4,4a,9-tetrahydrophenanthrene*): uv: 279(4.17) and 326(4.11) nm; ir: 3370 and 1615 cm^{-1}; ^1H nmr δ: 1.40 (s, CH_3—C), 2.27 (m, CH_3—C.4), 3.91 (s, CH_3O), 5.78 (m, C.3—H), 6.95 (dd, J = 8.0 and 2.5 Hz, C.13—H), 7.03 (d, J = 2.5 Hz, C.11—H), 7.27 (s, OH, D_2O !), and 8.18 (d, J = 8.0 Hz, C.14—H); *m/e*: 270 (M^+).

Methylation of the enol **5**b *to* **5**c *and oxidation to* **6**b

The enol **5***b* (300 mg) was dissolved in ethanol (5 mL) and water (5 mL) and methylated by the addition of 30% NaOH (6 mL) followed by dimethyl sulfate (3.6 mL). After 24 h the product obtained by extraction was chromatographed (dry column) affording the *O*-methyl ether **5***c* (oil, 232 mg; 74%); ^1H nmr δ: 1.38 (s, CH_3—C.10), 2.18 (m, CH_3—C.4), 3.83 and 3.86 (2s, 2 CH_3O), and 5.73 (br s, H—C.3).

The ether **5***c* (200 mg) was oxidized as described above to prepare diene-dione **6***a*. Dry column chromatography gave the "dione" **6***b* (*3,9-dioxo-6,10-dimethoxy-1,4a(β)-dimethyl-3,4,4a,9-tetrahydrophenanthrene*, 84 mg; 40%): mp 102–104°C (from hexane); uv: 260(3.95) and 310(3.99) nm; ir: 1660 and 1610 cm^{-1}; ^1H nmr δ: 1.54 (s, CH_3—C.10), 2.41 (d, J = 1 Hz, CH_3—C.4), 2.74 (AB q, J = 16 Hz, —C(1)H_2—), 3.83 and 3.86 (2s, CH_3O), 5.99 (br s, C.3—H), 6.81 (d, J = 2 Hz, C.11—H); 6.89 (dd, J = 8 and 2 Hz, C.13—H), and 8.07 (d, J = 8 Hz, C.14—H; high resolution *m/e*, calcd. for $C_{18}H_{18}O_4$: 298.1205; found: 298.1208. *Anal.* calcd. for $C_{18}H_{18}O_4$: C 72.46, H 6.08; found: C 72.35, H 6.20.

Reaction of ketone **8** *with oxygen in strong base*

The ketone **8** (2.0 g, prepared as in our earlier study (4)) in *t*-BuOH (30 mL) was added to a solution prepared by dissolving potassium (1.7 g) in *t*-BuOH (40 mL). This mixture was vigorously stirred under oxygen at atmospheric pressure for 1 h. The crude oil obtained by acidification, extraction, etc. was chromatographed (dry column) to give four products.

Acid **10**a (1.5 g; 75%; *7-oxo-11,12,14-trimethoxy-6-hydroxyabieta-5,8,11,13-tetraen-19-oic acid*): mp 148–149°C (from ether); uv: 247(3.95), 278(3.92), and 332(3.96) nm; ir: 3360, 1695, and 1615 cm^{-1}; ^1H nmr δ: 1.33 and 1.36 (2d, J = 7 Hz, isoPr methyls), 1.64 and 1.72 (2s, CH_3—C), 3.60 (sept, J = 7 Hz, $CH(CH_3)_2$), 3.78, 3.87, and 3.88 (3s, CH_3O), 7.30 (br s, OH, D_2O !), and 10.90 (br, COOH); *m/e*: 418 (M^+). *Anal.* calcd. for $C_{23}H_{30}O_7$: C 66.01, H 7.23; found: C 65.88, H 7.35.

Ester **10**b (400 mg; 19%; *methyl 7-oxo-11,12,14-trimethoxy-6-hydroxyabieta-5,8,11,13-tetraen-19-oate*): mp 124–125°C (from ether–hexane); ir: 3360, 1720, and 1620 cm^{-1}; ^1H nmr δ: 1.34 and 1.36 (2d, J = 7 Hz, isoPr methyls), 1.63 and 1.68 (2s, CH_3—C), 3.60 (sept, J = 7 Hz, isoPr CH), 3.37, 3.78, 3.88, and 3.89 (4s, CH_3O), and 7.23 (s, OH, D_2O !); *m/e*: 432 (M^+). *Anal.* calcd. for $C_{24}H_{32}O_7$: C 66.50, H 7.46; found: C 66.49, H 7.62.

Can. J. Chem. Downloaded from www.nrcresearchpress.com by 210.87.254.105 on 09/06/12
For personal use only.

Enone **9** (50 mg; 2.5%; *methyl 7-oxo-11,12,14-trimethoxyabieta-5,8,11,13-tetraen-19-oate*): mp 152–153°C (from hexane); uv: 216(4.28), 248(4.19), 288(3.96), and 326(3.66) nm; ir: 1718, 1648, and 1620 cm^{-1}; ^1H nmr δ: 1.33 (d, J = 7 Hz, isoPr methyls), 1.41 and 1.46 (2s, CH_3—C), 3.58 (sept, J = 7 Hz, isoPr CH), 3.64, 3.77, and 3.83 (3s, CH_3O), and 6.46 (s, =CH—); m/e: 416 (M^+). *Anal.* calcd. for $C_{24}H_{32}O_6$: C 69.21, H 7.74; found: C 69.48, H 7.78.

Lactone **11** (glass, 60 mg; 3%); uv: 215(4.40), 280(4.12), and 327(3.59) nm; ir: 1798 (lactone), 1752, and 1712 cm^{-1}; ^1H nmr δ: 1.31 (s, CH_3—C.4), 1.33 (d, J = 7 Hz, isoPr methyls), 1.41 (s, CH_3—C.10), 3.52 (sept, J = 7 Hz, isoPr CH), 3.84 (s, CH_3O at C.14), and 3.91 (s, 6H, CH_3O at C.11 and C.12); m/e: 416 (M^+).

Decarboxylation of acid ***10****a*

The acid **10***a* (290 mg) was dissolved in benzene (100 mL) and refluxed for 3 h. Evaporation of the solvent afforded the pure diene **12** (200 mg; 77%; *11,12,14-trimethoxy-6-hydroxy-19-norabieta-4(18),5,8,11,13-pentaen-7-one*): mp 132–134°C (from hexane–ether); uv: 249(3.99), 280(3.91), and 336(4.02) nm; ir: 3350, 1670, and 1612 cm^{-1}; ^1H nmr δ: 1.36 (d, J = 7 Hz, isoPr methyls), 1.53 (s, CH_3—C), 3.62 (sept, isoPr CH), 3.79, 3.86, and 3.89 (3s, CH_3O), 5.26 (t, J = 2.0 Hz) and 5.43 (t, J = 1.5 Hz, C=CH_2), and 7.21 (s, OH, D_2O !); m/e: 372 (M^+). *Anal.* calcd. for $C_{22}H_{28}O_5$: C 70.94, H 7.58; found: C 70.81, H 7.31.

The mother liquors yielded a second product **14***a* (50 mg; 17%) which proved very difficult to rid of traces of impurities but was characterized after *O*-methylation in aqueous EtOH (15 mL of 50%), NaOH (5 mL of 30%), and dimethyl sulfate (3 mL, added after stirring for 20 min). After 36 h the product was isolated by extraction. The tetramethyl ether **14***b* (*6,11,12,14-tetramethoxy-18-norabieta-5,8,11,13-tetraen-7-one*) crystallized on standing (40 mg; 77%), mp 145–148°C; uv: 247(3.91), 268(3.87), 294(3.82), and 325(3.65) nm; ir: 1658 and 1560 cm^{-1}; ^1H nmr δ: 1.31 (d, J = 6 Hz, CH_3—C.4), 1.33 (d, 6H, J = 7 Hz, isoPr methyls), 1.59 (s, CH_3—C.10), 3.57 (sept, J = 7 Hz, isoPr CH), 3.76(3H), 3.77(3H), and 3.83(6H) (CH_3O groups at C.6, C.14, C.11, and C.12); m/e: 388 (M^+).

Isomerization of ***12*** *to* ***13****a*

A solution of the enedione **12** (450 mg) in benzene (60 mL) containing *p*-TsOH (60 mg) was refluxed for 1 h. After cooling, the solution was washed with water, dried, and evaporated to afford the endocyclic isomer **13***a* (430 mg; 96%; *11,12,14-trimethoxy-6-hydroxy-19-nor-abieta-3,5,8,11,13-pentaen-7-one*): mp 109–111°C (from hexane–ether); uv: 249(4.09), 284(3.83), and 358(4.03) nm; ir: 3320, 1610, and 1560 cm^{-1}; ^1H nmr δ: 1.36, 1.37 (2d, J = 7 Hz, isoPr methyls), 1.54 (s, CH_3—C.10), 2.26 (m, CH_3—C.4), 3.63 (sept, J = 7 Hz, isoPr CH), 3.79, 3.89, and 3.90 (CH_3O at C.14, C.12, and C.11), 5.79 (m, 1H, =CH—), and 7.54 (s, OH); m/e: 372 (M^+). *Anal.* calcd. for $C_{22}H_{28}O_5$: C 70.94, H 7.50; found: C 70.70, H 7.79.

Methylation of ***13****a* (→ ***13****b*)

Sodium hydroxide (5 mL of 30%) was added to a solution of **13***a* (130 mg) in EtOH (10 mL) and water (5 mL). After stirring for 20 min, dimethyl sulfate (3 mL) was added and stirring continued overnight. Normal extraction and washing afforded the tetra-*O*-methyl ether **13***b* (125 mg; 93%; *6,11,12,14-tetramethoxy-19-norabieta-3,5,8,11,13-pentaen-7-one*) as a pale yellow solid, mp 150–151°C; uv: 250(sh 3.94), 259(sh 3.89), 286(3.94), and 327(4.02) nm; ir: 1625 and 1550 cm^{-1}; ^1H nmr δ: 1.38 (d, J = 7 Hz, 6H, isoPr methyls), 1.56 (s, CH_3—C.10), 2.19 (m, CH_3—C.4), 3.63 (sept, J = 7 Hz, isoPr CH), 3.77(3H), 3.82(3H), and 3.89(6H) (CH_3O groups at C.14, C.6, C.11, and C.12), and 5.83 (m, =CH—); m/e: 386 (M^+). *Anal.* calcd. for $C_{23}H_{30}O_5$: C 71.48, H 7.82; found: C 71.53, H 7.88.

Allylic oxidation to coleon B tetra-O-methyl ether ***15****a*

To a solution of pyridine (1.5 mL) in dichloromethane (50 mL) was added chromium trioxide (0.9 g in small portions). After stirring for 2 h, the tetra-*O*-methyl ether **13***b* (200 mg) was added and the flask was stoppered and stirring continued at room temp for 48 h. After the usual extraction, the crude product was chromatographed (silica gel, dry column, EtOAc–benzene 1:4) to give the pure coleon B derivative **15***a* (55 mg; 27%; *6,11,12,14-tetramethoxy-19-norabieta-3,5,8,11,13-pentaen-2,7-dione*): mp 117–118°C (lit. (4*b*) mp 119–120°C); uv: 213(4.52), 283(4.16), and 326(4.02) nm; ir($CHCl_3$): 1648; ir(CCl_4): 1661 cm^{-1}; ^1H nmr δ: 1.35, 1.36 (2d, J = 7 Hz, isoPr methyls), 1.66 (s, CH_3—C.10), 2.38 (d, 1H, J = 17 Hz, C.1—H), 2.42 (d, 3H, J = 1.5 Hz, CH_3—C.4), 3.60 (sept, J = 7 Hz, isoPr CH), 3.81 (s, CH_3O at C.6), 3.84 (d, 1H, J = 17 Hz, C.1—H), 3.86, 3.87, and 3.88 (3s, CH_3O at C.14, C.12, and C.11), and 6.10 (q, 1H, J = 1.5 Hz, C.3—H); high resolution m/e, calcd. for $C_{23}H_{28}O_6$: 400.1868; found: 400.1886.

Comparison with an authentic sample (mixture mp and tlc in several solvent systems) showed this material to be identical with that described by Prof. C. H. Eugster (Zürich) (4*b*) who kindly provided the sample.

Acknowledgments

We thank the Natural Sciences and Engineering Research Council of Canada and the Ministère de l'Education du Québec for their financial assistance.

1. J. W. A. Findlay and A. B. Turner. J. Chem. Soc. (C), 547 (1971).
2. (*a*) E. J. Parish, B. S. Huang, and D. H. Miles. Synth. Commun. 341 (1975); (*b*) D. H. Miles and B. S. Huang. J. Org. Chem. **41**, 208 (1976).
3. R. Ratcliffe and R. Rodehorst. J. Org. Chem. **35**, 4000 (1970).
4. (*a*) M. Ribi, A. Chang Sin-Ren, H. P. Küng, and C. H. Eugster. Helv. Chim. Acta, **52**, 1685 (1969); (*b*) C. H. Eugster, H. P. Küng, H. Kühnis, and P. Karrer. Helv. Chim. Acta, **46**, 530 (1963).
5. (*a*) A. Andersen, M. Néron-Desbiens, S. Savard, and R. H. Burnell. Synth. Commun. **10**, 183 (1980); (*b*) R. H. Burnell, A. Andersen, M. Néron-Desbiens and S. Savard. Can. J. Chem. **59**, 2820 (1981); (*c*) R. H. Burnell, M. Néron-Desbiens, and S. Savard. Synth. Commun. **12**, 11 (1982).
6. T. Nishida, I. Wahlberg, and C. R. Enzell. Org. Magn. Reson. **9**, 203 (1977).
7. T. Matsumoto, K. Iyo, and S. Miuchi. Bull. Chem. Soc. Jpn. **55**, 3831 (1982).
8. E. Wenkert, P. Beak, R. W. J. Carney, J. W. Chamberlin, D. B. R. Johnston, C. D. Roth, and A. Tahara. Can. J. Chem. **41**, 1924 (1963).

Enamines of 2,2-bis(ethylthio)ethanal: a convenient route to γ-keto crotonate derivatives[1]

GORDON S. BATES[2] AND S. RAMASWAMY

Department of Chemistry, University of British Columbia, Vancouver, B.C., Canada V6T 1Y6

Received March 9, 1983

GORDON S. BATES and S. RAMASWAMY. Can. J. Chem. **61**, 2466 (1983).

A new α-oxoaldehyde reagent, 2,2-bis(ethylthio)ethanal **1**, has been prepared in high yield from ethanedial. Alkylation of the potassium salt of the enamines of **1** with various alkylating agents followed by *in situ* hydrolysis of the intermediate imine afforded high yields of the alkylation products of **1**. This new reagent was used in the synthesis of a chiral potential precursor of the macrocyclic fragment of cytochalasins A, B, and F, as well as in the syntheses of the physiologically active diolides pyrenophorin and norpyrenophorin.

GORDON S. BATES et S. RAMASWAMY. Can. J. Chem. **61**, 2466 (1983).

On a préparé, avec un excellent rendement, un nouveau réactif α-oxoaldéhyde, le bis(éthylthio)-2,2 éthanal (**1**) en partant de l'éthanedial. L'alkylation du sel de potassium de l'énamine du composé **1** avec divers agents alkylants, suivie de l'hydrolyse *in situ* de l'émine intermédiaire, donne avec des rendements élevés les produits d'alkylation du composé **1**. On a utilisé ce nouveau réactif dans la synthèse d'un précurseur potentiel chiral du fragment macrocyclique des cytochalasines A, B et F ainsi que dans la synthèse des diolides physiologiquement actifs: la pyrénophorine et la norpyrénophorine.

[Traduit par le journal]

Can. J. Chem. Downloaded from www.nrcresearchpress.com by 210.87.254.40 on 09/06/12
For personal use only.

An important structural feature of many natural products (e.g. cytochalasin A, and the diolides pyrenophorin, norpyrenophorin, and vermiculin) is the presence of a γ-keto crotonate moiety. In addition, other natural products (e.g. brefeldin A, cytochalasins B and F) contain a partially reduced variation of the above structural unit, i.e. a γ-hydroxy crotonate, which is readily accessible from the above systems.

As part of a programme to develop efficient synthetic methods which are based on inexpensive and readily available reagents, it appeared that ethanedial should be a suitable precursor for **1**. This compound has synthetic potential for entry into the desired functional group array.[3]

Accordingly **1** was prepared in yields of 70−85% by shaking an aqueous ethanedial solution with two equivalents of ethanethiol in the presence of a catalytic amount of hydrochloric acid.[4]

Aldehyde **1** can in principle be elaborated to **5**, a derivative of the desired γ-keto crotonate moiety, in at least two ways. (A) Wittig−Horner or equivalent elaboration of aldehyde **1** may give either **2** or **3**. Deprotonation of either **2** or **3** will generate the same anion. Alkylation of this anion could provide **5**. (B) Alkylation of aldehyde **1** to provide **4** followed by a Wittig-Horner or equivalent elaboration could also lead to compound **5**.

The former route would require a regioselective alkylation of **2** or **3**. Considerable work on such regiocontrol in similar systems (3) has shown that the necessary control is not yet complete. Preliminary experiments in our laboratory confirmed that the anion stabilizing effect of the dithioacetal in the anion derived from **2**/**3** was not sufficient to overcome the predominant regioselectivity (α-alkylation) observed in the alkylation of these systems.

Efforts to alkylate various salts of **1** with simple alkyl halides were unsuccessful. However, the lithio derivative of the aldehyde reacted with 1-bromo-3-methyl-2-butene to provide a 70% yield of the S_N2' alkylation product **7**. This result is analogous to the observation with 2-formyl-1,3-dithiane reported by Wilson and Mathew (4). The formation of **7** may be rationalized by assuming an initial *S*-alkylation of **1** followed by a thermally allowed [2,3]-sigmatropic rearrangement of the resulting sulphonium ylide **6**.[5] It appears likely that the failure to achieve simple alkylation of the anion of **1** was due to preferential attack of the alkylating agent on sulphur rather than on carbon. The resulting stable ylide was then presumably lost in the aqueous phase upon work-up of the reaction mixture.

The pioneering work of Stork and Rowd (5) had established that, whereas aldehyde enolates themselves usually do not alkylate well, the corresponding metallo enamines undergo facile alkylation. Therefore various imine derivatives of **1** were prepared and the ease of alkylation of the corresponding salts was studied.

Various primary amines were condensed with aldehyde **1**. In every case reaction proceeded smoothly. The product was found to be exclusively the enamine tautomer and no detectable amount of the imine form was present in the product as inferred from the ^{1}H nmr spectrum of the product. The formation of the enamine tautomer in the reaction is not unusual in light of the fact that a dithioketal carbon appears to prefer to be sp^2 hydridized if possible (6).

Studies of the ease of alkylation of various salts of enamines **8***a*−*d* using bromethane showed that all of the enamines, excluding that derived from aniline, showed essentially identical reactivity. The alkylations were very regioselective. Alkylation occurred exclusively on carbon for compounds **8***a*−*c*. However, the anion of **8***d* was found to alkylate completely on nitrogen. Hydrolysis of the alkylated imines to the corresponding aldehydes was investigated (Table 1).

The results of these initial alkylation and hydrolysis studies indicated that either the cyclohexyl or 2-methyl-2-propyl enamines **8***a* or **8***b* would be suitable for further investigation. Due to its better storage properties, the cyclohexyl enamine **8***a* was used in subsequent work.

[1]Portions of this work have appeared as a preliminary communication (1).

[2]Author to whom correspondence should be addressed.

[3]For previous approaches to γ-keto crotonate derivatives, see ref. 2.

[4]Attempts to adapt this method to provide the corresponding 2-formyl-1,3-dithiane resulted in the formation of an insoluble, presumably polymeric material.

[5]γ-Alkylation of **2** also has been achieved with allylic halides, presumably via a similar rearrangement.

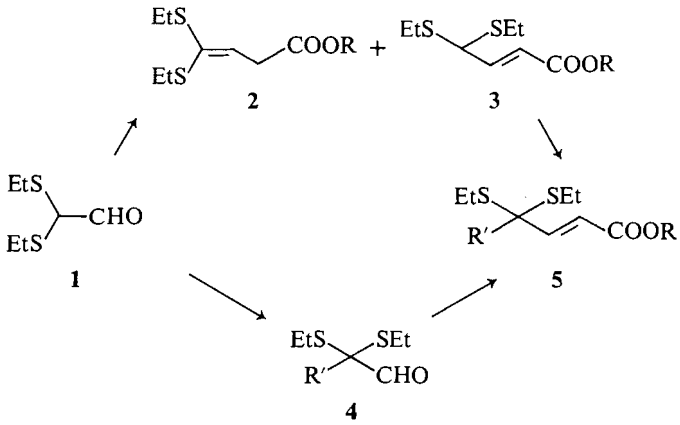

FIG. 1.

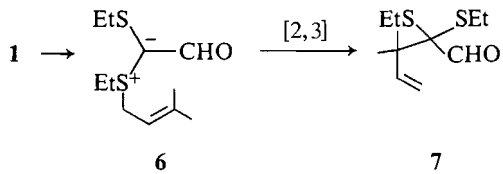

FIG. 2.

Alkylation studies using bromoethane and the cyclohexyl enamine **8***a* showed that either tetrahydrofuran or 1,2-dimethoxyethane was a suitable solvent for the alkylation reactions. However, hydrolysis of the alkylation products was much faster in tetrahydrofuran (ca. 1.5 hours) than in 1,2-dimethoxyethane (incomplete even after 6 hours). Therefore tetrahydrofuran was used as the reaction solvent in most of the subsequent alkylation studies.

A systematic study of the effect of the gegenion on the rate of the alkylation of the enamine anion then was made. The lithium salt generated by the action of lithium diisopropylamide (no significant deprotonation occurred with lithium hydride) on **8***a* was found to be unreactive towards bromoethane. Similarly the corresponding magnesium salt obtained by deprotonation of the enamine with ethyl magnesium bromide exhibited little tendency to react with either bromoethane or iodoethane even after prolonged reaction in refluxing tetrahydrofuran. Moderate yields of the desired alkylation product were obtained with bromoethane and the sodium salt of the enamine derived by deprotonation of the enamine with sodium bis(trimethylsilyl)-amide in tetrahydrofuran (attempted deprotonation with sodium hydride was unsuccessful). However, the potassium salt generated by stirring the enamine with a suspension of potassium hydride underwent smooth alkylation providing a high yield of the desired product. The results of these gegenion variation studies are summarized in Table 2.

The bright yellow potassium salt of the enamine was generated by adding the enamine to a stirred suspension of 1.1 equivalents of mineral oil-free potassium hydride in dry tetrahydrofuran. Alkylations then were carried out with a wide variety of substrates (Table 3). The reaction time for alkylation varied from 15 min at room temperature for allylic halides to 18 h at 50°C for cyclohexyl and cyclopentyl *p*-toluenesulphonates. The alkylated enamine was hydrolyzed *in situ* by stirring the product with dilute aqueous ethanedioic acid for two hours at room temperature.

The relatively low yields of alkylation products obtained

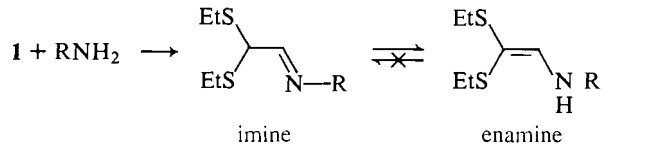

8*a* R = cyclohexyl
8*b* R = 2-methyl-2-propyl
8*c* R = 2-propyl
8*d* R = phenyl

FIG. 3.

TABLE 1. Hydrolysis of imines

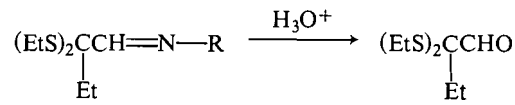

R	Reaction time (h)
Cyclohexyl	1.5
2-Methyl-2-propyl	1.5
2-Propyl	>20

TABLE 2.* Enamine anion akylation: gegenion variation

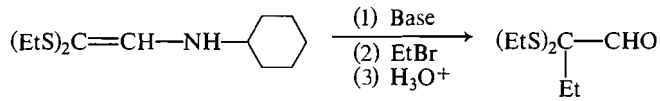

Base	Time (h)	Temperature (°C)	Yield (%)
1. LDA†	2	25	0
2. EtMgBr‡	2	25	0
	20	66	0
3. LiH	2	25	0
4. NaH	2	25	0
5. $(Me_3Si)_2NNa$	2	25	60
6. KH	2	25	75

*All reactions 0.2 *M* in tetrahydrofuran.
†LDA=lithium diisopropylamide.
‡EtI used for reaction at 66°C.

with the highly reactive alkylating agents, iodomethane and methyl bromoacetate, are presumably due to a competing *S*-alkylation pathway followed by hydrolysis of the sulphonium salt during work-up to regenerate water-soluble products. With 2-bromopropane, this expected β-elimination reaction appears to compete with the desired alkylation as reflected by the low yield of the alkylation product. However, a significant increase in the amount of alkylation was observed with 2-propyl *p*-toluenesulphonate. This observation is in agreement with previous observations that *p*-toluenesulphonate esters give better yields of the corresponding substitution products under conditions in which bromides predominantly undergo elimination (7). Good yields of akylation products were obtained even with the elimination-prone cyclohexyl and cyclopentyl *p*-toluenesulphonates.

Interestingly, the reaction of the enamine anion with allylic halides in which regioselective alkylation is possible (entries 13–15) yields, as the sole products, those compounds which result from a formal S_N2 alkylation. For example, the reaction with 1-bromo-3-methyl-2-butene yields compound **9**. This result is strikingly different from the corresponding reaction

Can. J. Chem. Downloaded from www.nrcresearchpress.com by 210.87.254.40 on 09/06/12
For personal use only.

TABLE 3. Alkylation of the cyclohexyl enamine anion

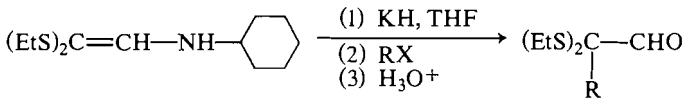

RX	Time (h)	Yield (%)
1. MeI	0.5	35
2. MeOBs	0.5	50
3. EtI	2.0	75
4. EtBr	2.0	75
5. EtOTs	2.0	81
6. *n*-BuBr	4.0	75
7. *n*-BuOTs	4.0	77
8. 2-PrBr	6.0	45
9. 2-PrOTs	18.0	76
10.*c-C_6H_{11}OTs	18.0	67
11.*c-C_5H_9OTs	18.0	63
12. CH_2=CH—CH_2Br	0.25	85
13.† Me_2C=CH—CH_2Br	0.25	90
14.† CH_3CH=$CHCH_2$Br	0.25	88
15.† PhCH=$CHCH_2$Br	0.25	95
16. $PhCH_2$Br	1.0	75
17.‡ $BrCH_2COOMe$	1.0	50

*Reaction carried out at 50°C.
†S_N2 product.
‡Reaction carried out in 1,2-dimethoxyethane. The solvent was exchanged for tetrahydrofuran prior to hydrolysis. Lithium diisopropylamide was used as the base for this reaction.

with the anion of aldehyde **1** (*vide supra*) which yielded compound **7**.

The formation of the S_N2 displacement product **9** can be visualized either as a direct displacement on the halide or via intermediacy of compound **10** arising either by an S_N2' displacement on the halide by the enamine nitrogen or by an internal displacement on an intermediate sulphonium salt (Scheme 1).

To check the validity of these possible pathways involving an aza Cope type of reaction, compound **11** was synthesized by the reaction of *N*-(2-propenyl)cyclohexanamine with aldehyde **1**. The rearrangement of **11** to yield product **12** could not be effected even at the reflux temperature of toluene. This result tends to preclude the intermediacy of compounds similar to **10** in the previous alkylation reactions. Hence it was concluded that the products of entries 12–15 result from a direct displacement on the allylic halide by the imine anion. Reaction of the lithium salt[6] of enamine **8***a* with 2-cyclohexenone afforded a 28% yield of the conjugate addition product **13**. No detectable amount of the 1,2-addition product was observed. The poor yield of the 1,4-addition product is presumably due to the reversibility of the reaction.

An attempted aldol condensation with benzaldehyde, an acylation with benzyl chloride, and an epoxide cleavage with the enamine anion were all unsuccessful.

The scope of a new synthetic method is best demonstrated through its use in a total synthesis. Accordingly, the diolides pyrenophorin and norpyrenophorin, as well as a chiral potential precursor of the macrocyclic fragments of cytochalasins A, B, and F were prepared using the alkylation of enamine **8***a* as a key step in each of the syntheses.

[6]The potassium salt of the enamine in tetrahydrofuran gave an even lower yield of the conjugate addition product.

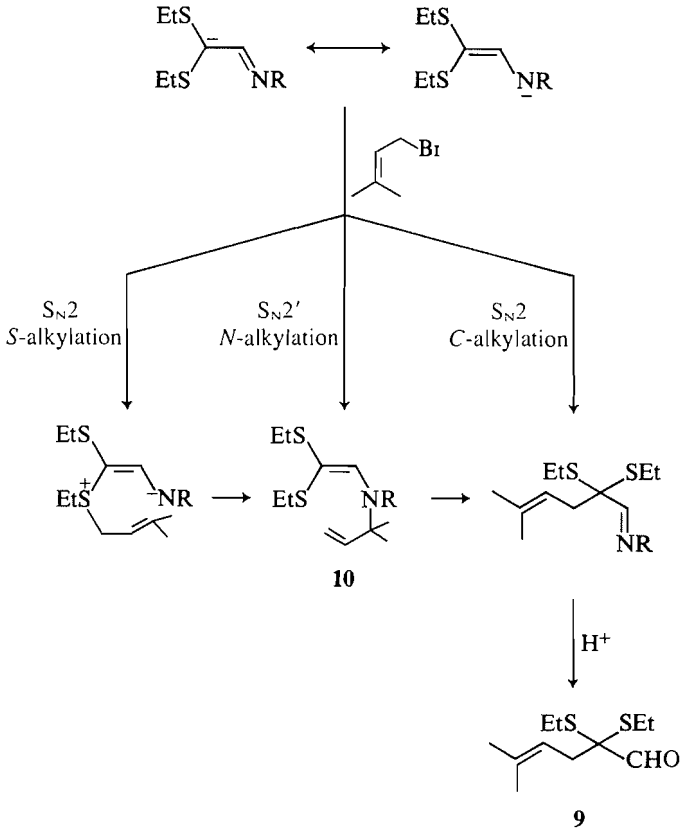

SCHEME 1. Possible pathways for the formation of **9** by the reaction of the enamine anion with 1-bromo-3-methyl-2-butene.

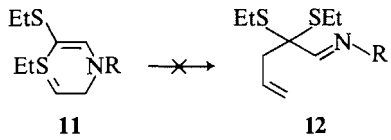

R = cyclohexyl

FIG. 4.

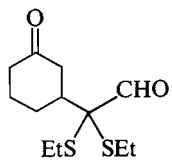

FIG. 5.

Pyrenophorin 20

This 16-membered diolide was first isolated by Ishibashi (8) from culture filtrates of *Pyrenophora avenae*, a pathogen of oats, and was found to possess antifungal and cytostatic properties.

The starting material for the present synthesis[7] of pyrenophorin was 1,3-butanediol. Compound **14** was prepared by regioselective sulphonation of the primary hydroxyl group of 1,3-butanediol, followed by silylation of the secondary alcohol group. Alkylation of the potassium salt of cyclohexyl enamine **8***a* with **14** followed by an *in situ* hydrolysis yielded aldehyde

[7]For previous syntheses, see ref. 9 and references therein.

Can. J. Chem. Downloaded from www.nrcresearchpress.com by 210.87.254.40 on 09/06/12
For personal use only.

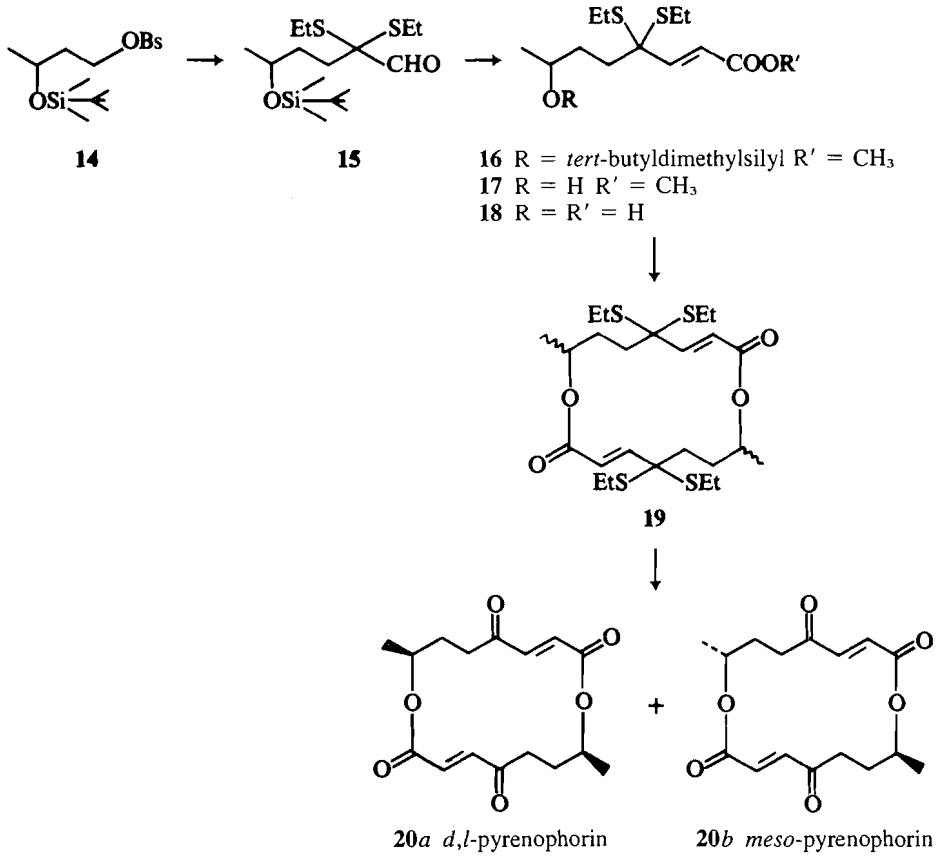

SCHEME 2. Synthesis of pyrenophorin.

15 in 82% yield from **14**. A Wittig–Horner reaction with trimethyl phosphonoacetate afforded ester **16** in 85% yield.

Attempted hydrolysis of the ester functionality in **16** prior to deprotection of the silyl ether resulted in an intractable material. Hence it was necessary to remove the silyl group before ester hydrolysis by stirring **16** with 5 *N* hydrochloric acid for two hours. The crude hydroxy ester **17** was directly saponified in 1 *M* aqueous potassium hydroxide at 60°C for three hours to provide **18** in 81% yield.

A dimerizing lactonization of hydroxy acid **18** was effected using the diethyl azodicarboxylate/triphenylphosphine method of Mitsunobu and co-workers (10) to provide a mixture of *d,l* and *meso* dimers **19** along with some cyclic trimer in ca. 20% total yield. The crude reaction mixture was purified by chromatography on a Florisil column. Although the dimeric precursor to pyrenophorin showed only one homogeneous spot by thin-layer chromatographic analysis, oxidative hydrolysis of **19** using the mercuric oxide and boron trifluoride etherate procedure (11) yielded a mixture which could be resolved into the crystalline *d,l* and *meso* isomers of pyrenophorin by thin-layer chromatography. The faster moving, less polar band was assigned as *d,l*-pyrenophorin **20***a* and the more polar band as the *meso* isomer **20***b*, by comparison with the published thin-layer chromatographic behaviour of these compounds (12).

Norpyrenophorin 26

This didemethyl derivative of pyrenophorin is not a natural product but has been shown to exhibit biological properties similar to those of pyrenophorin.

Although the synthesis of norpyrenophorin, in principle, could be accomplished by subjecting **21** to an identical sequence of reactions as described above for the synthesis of pyrenophorin, it was decided to demonstrate the compatibility of the 2,2-bis(ethylthio)ethanal enamine system to different functional group transformations. Thus, a different synthetic strategy was followed.

Alkylation of the anion of cyclohexyl enamine **8***a* with 3-bromopropene followed by hydrolysis of the resulting imine provided aldehyde **22** in 85% yield. A Wittig–Horner chain elaboration of aldehyde **22** with trimethyl phosphonoacetate afforded unsaturated ester **23** in 93% yield. The crystalline-hydroxy acid **24** was obtained in 70% yield from **23** by a sequence of hydroboration using 9-borabicyclo[3·3·1]nonane with a subsequent oxidative work-up with trimethylamine oxide (13) followed by an alkaline hydrolysis.

Dimerizing lactonization again was effected by the Mitsunobu procedure to provide compound **25**. The crude reaction mixture was chromatographed on a Florisil column to afford the pure crystalline product in 65% yield. Finally, the dithioketals present in **25** were oxidatively hydrolyzed (60%) to provide crystalline norpyrenophorin in an overall yield of over 20% from the cyclohexyl enamine **8***a*.

Cytochalasin macrocycle

The cytochalasins are a group of highly biologically active mould metabolites.[8] Cytochalasin A contains a γ-keto crotonate moiety and the related cytochalasins B and F contain the reduced γ-hydroxy crotonate.

[8]For reviews of (a) the chemistry, (b) the biological activity, and (c) the biosynthesis of the cytochalasins, see ref. 14.

Can. J. Chem. Downloaded from www.nrcresearchpress.com by 210.87.254.40 on 09/06/12
For personal use only.

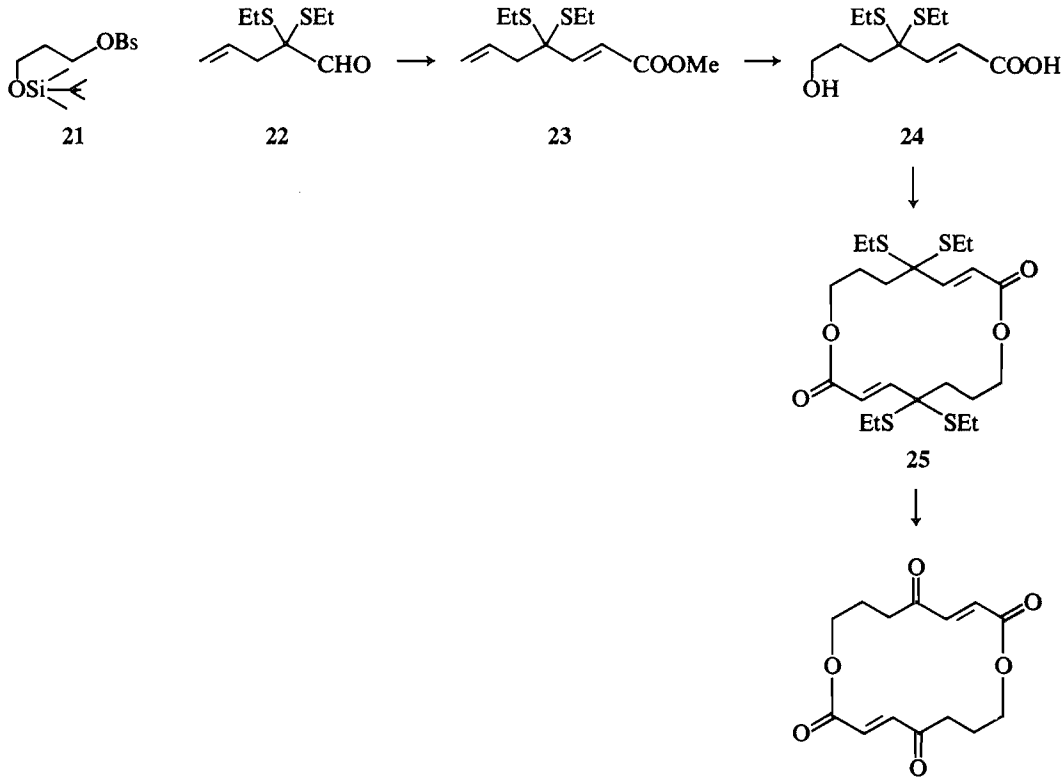

SCHEME 3. Synthesis of norpyrenophorin.

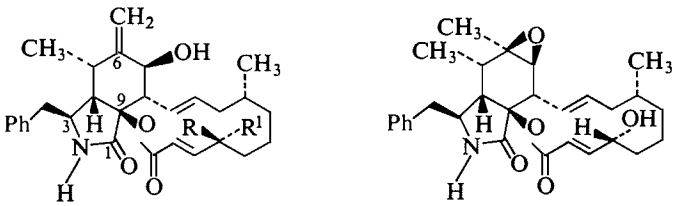

FIG. 6.

In connection with a total synthesis[9] of these microbial metabolites, an efficient preparation of a chiral precursor to the macrocylic fragment was desired. A key step in this synthesis would be the reaction of the salt of **8***a* with an alkylating agent derived from (+)-citronellol.

Initially, the acetate and benzoate esters were used to protect the hydroxyl group of (+)-citronellol. When alkylation of the enamine anion with either benzenesulphonate **27***a* or **27***b* was attempted, both sulphonates underwent a β-elimination reaction, as evidenced by the appearance of a terminal olefinic pattern in the ^{1}H nmr spectrum of the product. This result was surprising since other aliphatic benzenesulphonates clearly alkylated the same enamine anion (see Table 3). This observation may be rationalized in terms of an initial reversible attack on the carbonyl group of the ester followed by an internal alkoxide promoted elimination and a subsequent regeneration of the ester. Eventually the *tert*-butyldimethylsilyl group was found to be a suitable protecting group. Accordingly, compound **27***d* was prepared from (+)-citronellol in 78% overall yield. Alkylation of the potassium salt of **8***a* with sulphonate **27***d* was effected under the standard conditions to provide aldehyde **28** in 82% yield. A Wittig–Horner chain elaboration of **28** subsequently afforded the unsaturated ester **29** in 85% yield. This compound thus has been prepared in 54% overall yield from (+)-citronellol and is a suitable chiral precursor for the desired macrocyclic portion of the cytochalasin target molecules.

Further work on the cytochalasin synthesis is continuing and will be reported in due course.

[9]For other synthetic approaches, see ref. 15.

Experimental

General

All reactions were carried out under a nitrogen atmosphere. Stirring was accomplished using Teflon-coated magnetic stirring bars. Tetrahydrofuran and 1,2-dimethoxyethane were freshly distilled from sodium benzophenone ketyl under a nitrogen atmosphere. Potassium hydride was obtained as a 25% dispersion in mineral oil from Alpha Division, Ventron Corporation. All other reagents were obtained from the Aldrich Chemical Company, Inc. and were used without further purification. The arylsulphonate esters were prepared by reaction of an excess of the appropriate alcohol for 12 hours at 0°C with the required sulphonyl chloride in pyridine, followed by a standard work-up. All extraction and chromatography solvents were distilled before use.

All temperatures are stated in degrees Celsius. Molecular distillations were performed by means of a Buchi Kugelrohr apparatus. Proton magnetic resonance (^{1}H nmr) spectra were obtained on the following instruments: Varian Associates T-60, EM-360L, and HA-100. Spectra were run in deuterochloroform or carbon tetrachloride solution with tetramethylsilane as an internal reference. Chemical shifts are reported on the δ scale. The multiplicity, integrated peak area, and coupling constants in Hertz (Hz) (if observable) are indicated in parentheses after each signal. Infrared spectra were recorded as liquid films using a Perkin–Elmer 700 spectrometer, and were cali-

Can. J. Chem. Downloaded from www.nrcresearchpress.com by 210.87.254.40 on 09/06/12
For personal use only.

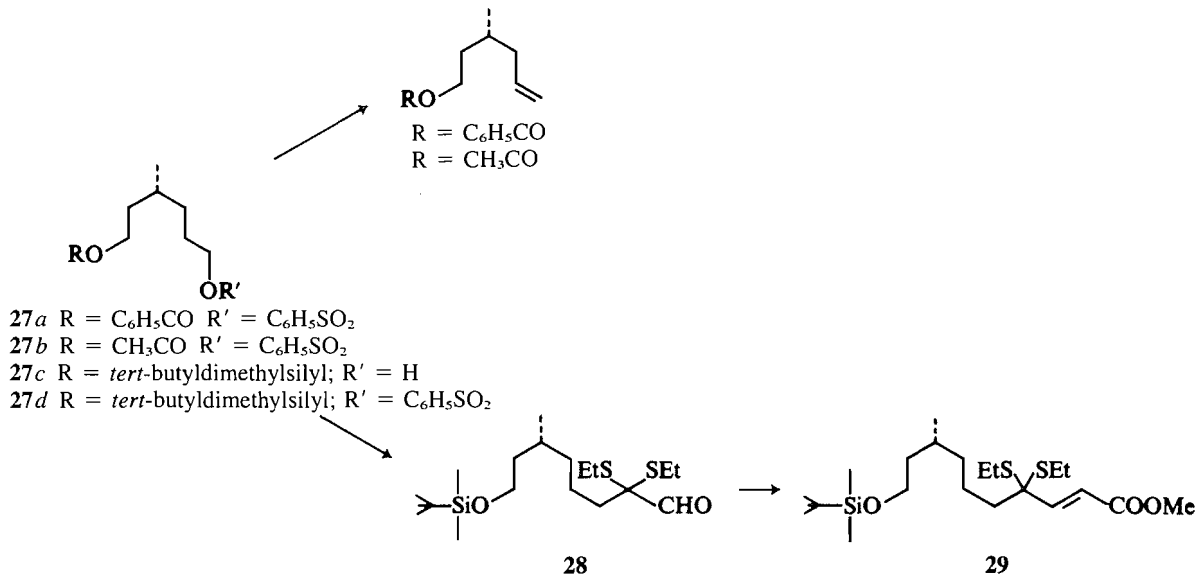

SCHEME 4. Synthesis of a precursor for the macrocyclic portion of cytochalasins A, B, and F.

brated with the 1601 cm^{-1} band of polystyrene. High resolution mass spectra were obtained using an AEI ME-50 mass spectrometer. Elemental analyses were performed at the Microanalytical Laboratory, University of British Columbia.

Merck pre-coated tlc sheets Silica Gel 60F-254 were used for analytical thin-layer chromatography. Florisil (100–200 mesh) supplied by the J. T. Baker Chemical Company and Merck Silica Gel 60 (230–400 mesh) were used for column chromatography. Analytical gas chromatography was carried out on a Hewlett–Packard Model 5830-A chromatograph equipped with 1.8 × 0.3 cm columns packed with 3% OV-101 or 5% Carbowax.

The following abbreviations are used in the description of the multiplicity of each signal in the ^1H nmr spectrum: s = singlet, d = doublet, t = triplet, q = quartet, sept = septet, m = multiplet, dd = doublet of doublets, dt = doublet of triplets, dm = doublet of multiplets, b = broad.

2,2-Bis(ethylthio)ethanal **1**

A mixture of 58 g of an aqueous 40% solution of ethanedial (ca. 400 mmol of ethanedial), 60 mL of ethanethiol (800 mmol), and 5 mL of aqueous 2 *N* HCl was shaken vigorously overnight. The reaction mixture was transferred to a separatory funnel and the heavier organic phase separated. The aqueous phase was extracted once with 50 mL of dichloromethane and the organic phases were combined. The organic phase then was washed once with aqueous dilute Na_2CO_3 and the organic layer filtered through a loose cotton plug. The bulk of the solvent was removed by distillation at atmospheric pressure. The distillation flask was allowed to cool to room temperature and then 50 mL of 30–60 petroleum ether was added to the flask and distillation resumed to ensure that the residual oil in the flask was free from noxious ethanethiol. The residual oil then was distilled under reduced pressure to afford 50.6 g (77%) of 2,2-bis(ethylthio)ethanal as a pale yellow liquid; bp 55–60°C/0.1 Torr (lit. (16) bp 67°C/0.3 Torr); ir: 2708, 1715 cm^{-1}; ^1H nmr (CCl_4) δ: 1.25 (t, 6, J = 7), 2.57 (q, 4, J = 7), 4.12 (d, 1, J = 4.5), 9.08 (d, 1, J = 4.5). *Anal.* calcd. for $C_6H_{12}OS_2$ (164.29): C 43.86, H 7.63, S 39.03; found: C 43.85, H 7.50, S 38.80. *Mol. Wt.* calcd. for $C_6H_{12}OS_2$: 164.0329; found: 164.0325.

Standard procedure for the preparation of the enamines **8**a–**8**d

To a solution of 1.64 g (10 mmol) of 2,2-bis(ethylthio)ethanal in 10 mL of dichloromethane cooled to −15°C was added 11.0 mmol of RNH_2 (R = cyclohexyl, 2-propyl, 2-methyl-2-propyl, or phenyl). The reaction mixture was maintained at −15°C for 6 h. The reaction mixture was filtered through a loose cotton plug to remove the bulk water and the solvent was evaporated under reduced pressure. Molecular distillation of the residual oil afforded the enamine as a yellow oil.

Cyclohexyl enamine **8**a: bp (molecular distillation) 90–100°C/0.1 Torr; ir: 3350, 1665, 1600 cm^{-1}; ^1H nmr ($CDCl_3$) δ: 1.13 (t, 3, J = 7), 1.16 (t, 3, J = 7), 0.95–2.05 (m, 10), 2.51 (q, 2, J = 7), 2.61 (q, 2, J = 7), 2.94 (m, 1), 4.62 (m, 1), 6.83 (d, 1, J = 13). *Mol. Wt.* calcd. for $C_{12}H_{23}NS_2$: 245.1272; found: 245.1280.

2-Methyl-2-propyl enamine **8**b: bp (molecular distillation) 70°C/0.1 Torr; ir: 3300, 1680, 1600 cm^{-1}; ^1H nmr ($CDCl_3$) δ: 1.13 (t, 3, J = 7), 1.17 (t, 3, J = 7), 1.18 (s, 9), 2.47 (q, 2, J = 7), 2.57 (q, 2, J = 7), 4.61 (m, 1), 6.79 (d, 1, J = 13). *Mol. Wt.* calcd. for $C_{10}H_{21}NS_2$: 219.1115; found: 219.1117.

2-Propyl enamine **8**c: bp (molecular distillation) 60°C/0.1 Torr; ir: 3350, 1680, 1605 cm^{-1}; ^1H nmr ($CDCl_3$) δ: 1.1 (t, 3, J = 7), 1.13 (t, 3, J = 7), 1.1 (d, 6, J = 6), 2.43 (q, 2, J = 7), 2.55 (q, 2, J = 7), 3.28 (m, 1), 4.38 (m, 1), 6.68 (d, 1, J = 13). *Mol. Wt.* calcd. for $C_9H_{19}NS_2$: 205.0959; found: 205.0956.

Phenyl enamine **8**d: bp (molecular distillation) 85°C/0.1 Torr; ir: 3370, 1620, 1600, 1505 cm^{-1}; ^1H nmr ($CDCl_3$) δ: 1.16 (t, 3, J = 7), 1.2 (t, 3, J = 7), 2.55 (q, 2, J = 7), 2.67 (q, 2, J = 7), 6.64–7.24 (m, 5), 7.32 (d, 1, J = 12.5). *Mol. Wt.* calcd. for $C_{12}H_{17}NS_2$: 239.0802; found: 239.0803.

N-*(2-propenyl)cyclohexyl enamine* **11**

To a solution of 0.164 g (1 mmol) of 2,2-bis(ethylthio)ethanal in 1 mL of dichloromethane cooled to −15°C was added 0.14 g (1 mmol) of *N*-(2-propenyl)cyclohexanamine. The reaction mixture was maintained at −15°C overnight. The reaction mixture was filtered through a loose cotton plug to remove the bulk water and the solvent evaporated under reduced pressure to afford 0.28 g (100%) of **11** as a pale yellow oil. Infrared: 1605, 1580 cm^{-1}; ^1H nmr ($CDCl_3$) δ: 1.3 (t, 3, J = 7), 1.34 (t, 3, J = 7), 0.9–1.9 (m, 10), 2.59 (q, 2, J = 7), 2.69 (q, 2, J = 7), 3.18 (m, 1), 4.15 (dm, 2), 5.02–5.3 (m, 2), 5.9 (m, 1), 6.85 (s, 1). *Mol. Wt.* calcd. for $C_{15}H_{27}NS_2$: 285.1584; found: 285.1590.

Thermolysis of **11**

A solution of 0.57 g (0.2 mmol) of **11** in 10 mL of toluene was refluxed overnight. The reaction flask was allowed to cool to room temperature. Evaporation of the solvent under reduced pressure afforded a quantitative yield of the unchanged starting material.

Standard procedure for the alkylation of cyclohexyl enamine **8**a

A suspension of 0.160 g (1 mmol) of 25% KH in mineral oil was washed free of oil by stirring with 3 × 5 mL portions of pentane

Can. J. Chem. Downloaded from www.nrcresearchpress.com by 210.87.254.40 on 09/06/12
For personal use only.

Can. J. Chem. Downloaded from www.nrcresearchpress.com by 210.87.254.40 on 09/06/12
For personal use only.

under a N_2 atmosphere. The oil-free KH was suspended in 5 mL of tetrahydrofuran and 0.245 g (1 mmol) of cyclohexyl enamine **8***a* in 0.5 mL of tetrahydrofuran was added. An immediate evolution of H_2 gas was observed and a bright yellow suspension of the potassium salt of the enamine resulted. To this suspension was added 1.05 mmol of the alkylating agent and the reaction mixture was stirred for 0.25–6 h at room temperature (18 h at 50°C for cyclopentyl and cyclohexyl *p*-toluenesulphonates). The resulting imine was hydrolyzed *in situ* by the addition of 0.126 g (1 mmol) of ethanedioic acid dihydrate in 2 mL of H_2O. After 2 h the reaction mixture was diluted with 40 mL of ethyl ether, washed with 5 mL of H_2O, and dried ($MgSO_4$). The solvent was evaporated under reduced pressure to afford the alkylated aldehyde. The trace of pale yellow colour in the product could be conveniently removed by filtration of the product through a small column of Florisil using 1–2% ethyl acetate in 30–60 petroleum ether (v/v) as the eluting solvent.

2,2-Bis(ethylthio)propanal: bp (molecular distillation) 60°C/0.1 Torr; ir: 1705 cm^{-1}; ^1H nmr (CCl_4) δ: 1.25 (t, 6, J = 7), 1.62 (s, 3), 2.57 (q, 4), 9.11 (s, 1). *Anal.* calcd. for $C_7H_{14}OS_2$ (178.318): C 47.15, H 7.91, S 35.76; found: C 47.21, H 8.11, S 35.88. *Mol. Wt.* calcd. for $C_7H_{14}OS_2$: 178.0486; found 178.0471.

2,2-Bis(ethylthio)butanal: bp (molecular distillation) 65°C/0.1 Torr; ir: 1705 cm^{-1}; ^1H nmr ($CDCl_3$) δ: 1.04 (t, 3, J = 6), 1.18 (t, 6, J = 7), 1.81 (q, 2, J = 6), 2.43 (q, 4, J = 7), 8.96 (s, 1). *Anal.* calcd. for $C_8H_{16}OS_2$ (192.345): C 49.96, H 8.38, S 33.34; found: C 50.13, H 8.31, S 33.52. *Mol. Wt.* calcd. for $C_8H_{16}OS_2$: 192.0642; found: 192.0648.

2,2-Bis(ethylthio)-3-methylbutanal: bp (molecular distillation) 65°C/0.1 Torr; ir: 1710 cm^{-1}; ^1H nmr (CCl_4) δ: 1.05 (d, 6, J = 6.5), 1.18 (t, 6, J = 7), 2.24 (sept, 1, J = 6.5), 2.49 (q, 4, J = 7), 9.05 (s, 1). *Anal.* calcd. for $C_9H_{18}OS_2$ (206.370): C 52.38, H 8.79, S 31.07; found: C 52.24, H 8.92, S 31.21. *Mol. Wt.* calcd. for $C_9H_{18}OS_2$: 206.0799; found: 206.0793.

2,2-Bis(ethylthio)hexanal: bp (molecular distillation) 65–70°C/0.1 Torr; ir: 1710 cm^{-1}; ^1H nmr (CCl_4) δ: 0.94 (t, 3, J = 6), 1.18 (t, 6, J = 7), 1.1–1.9 (m, 6), 2.43 (q, 4, J = 7), 8.94 (s, 1). *Anal.* calcd. for $C_{10}H_{20}OS_2$ (220.398): C 54.50, H 9.15, S 29.10; found: C 54.25, H 9.13, S 28.78. *Mol. Wt.* calcd. for $C_{10}H_{20}OS_2$: 220.0955; found: 220.0956.

2,2-Bis(ethylthio)-2-cyclopentylethanal: bp (molecular distillation) 85°C/0.1 Torr; ir: 1710 cm^{-1}; ^1H nmr ($CDCl_3$) δ: 1.18 (t, 6, J = 7), 1.4–2 (m, 9), 2.25 (q, 4, J = 7), 9.05 (s, 1). *Anal.* calcd. for $C_{11}H_{20}OS_2$ (232.410): C 56.85, H 8.67, S 27.59; found: C 56.65, H 8.80, S 27.38. *Mol. Wt.* calcd. for $C_{11}H_{20}OS_2$: 232.0956; found: 232.0957.

2,2-Bis(ethylthio)-2-cyclohexylethanal: bp (molecular distillation) 90°C/0.1 Torr; ir: 1710 cm^{-1}; ^1H nmr (CCl_4) δ: 1.17 (t, 6, J = 7), 1.6–2 (m, 11), 2.47 (q, 4, J = 7), 9.04 (s, 1). *Anal.* calcd. for $C_{12}H_{22}OS_2$ (246.436): C 58.49, H 9.00, S 26.02; found: C 58.49, H 8.97, S 26.02. *Mol. Wt.* calcd. for $C_{12}H_{22}OS_2$: 246.1112; found: 246.1111.

2,2-Bis(ethylthio)pent-4-enal ***22***: bp (molecular distillation) 60°C/0.1 Torr; ir: 1710 cm^{-1}; ^1H nmr (CCl_4) δ: 1.18 (t, 6, J = 7), 2.46 (q, 4, J = 7), 2.56 (dm, 2), 5.0–5.22 (m, 2), 5.87 (m, 1), 8.97 (s, 1). *Anal.* calcd. for $C_9H_{16}OS_2$ (204.356): C 52.90, H 7.89, S 31.38; found: C 52.76, H 7.78, S 31.31. *Mol. Wt.* calcd. for $C_9H_{16}OS_2$: 204.0643; found: 204.0645.

2,2-Bis(ethylthio)-3-phenylpropanal: bp (molecular distillation) 85°C/0.1 Torr; ir: 1710 cm^{-1}; ^1H nmr ($CDCl_3$) δ: 1.16 (t, 6, J = 7), 2.47 (q, 4, J = 7), 3.19 (s, 2), 7.2 (s, 5), 9.19 (s, 1). *Anal.* calcd. for $C_{13}H_{18}OS_2$ (254.416): C 61.37, H 7.13, S 25.20; found: C 61.56, H 7.23, S 25.00. *Mol. Wt.* calcd. for $C_{13}H_{18}OS_2$: 254.0799; found: 254.0799.

2,2-Bis(ethylthio)hex-4-enal: bp (molecular distillation) 70°C/0.1 Torr; ir: 1710 cm^{-1}; ^1H nmr ($CDCl_3$) δ: 1.21 (t, 6, J = 7), 1.66 (d, 3, J = 3), 2.5 (q, 4, J = 7), 2.4–2.6 (m, 2), 5.4–5.7 (m. 2), 9.05 (s, 1). *Anal.* calcd. for $C_{10}H_{18}OS_2$ (218.382): C 55.00, H 8.31, S 29.36; found: C 54.89, H 8.46, S 29.19. *Mol. Wt.* calcd. for $C_{10}H_{18}OS_2$: 218.0800; found: 218.0796.

2,2-Bis(ethylthio)-5-methylhex-4-enal ***9***: bp (molecular distillation) 80°C/0.1 Torr; ir: 1705 cm^{-1}; ^1H nmr ($CDCl_3$) δ: 1.18 (t, 6, J = 7), 1.65 (s, 3), 1.75 (d, 3, J = 1.5), 2.50 (q, 4, J = 7), 2.58 (d, 2, J = 7), 5.30 (tq, 1, J = 7, 1.5), 9.10 (s, 1). *Anal.* calcd. for $C_{11}H_{20}OS_2$ (232.410): C 56.85, H 8.67, S 27.59; found: C 56.96, H 8.81, S 27.40. *Mol. Wt.* calcd. for $C_{11}H_{20}OS_2$: 232.0956; found: 232.0956.

2,2-Bis(ethylthio)-5-phenylpent-4-enal: bp (molecular distillation) 100°C/0.1 Torr; ir: 1710 cm^{-1}; ^1H nmr ($CDCl_3$) δ: 1.24 (t, 6, J = 7), 2.56 (q, 4, J = 7), 2.82 (d, 2, J = 6), 6.35 (dt, 1, J = 16, 6), 6.51 (d, 1, J = 16), 7.22–7.9 (m, 5), 9.15 (s, 1). *Anal.* calcd. for $C_{15}H_{20}OS_2$ (280.454): C 64.24, H 7.19, S 22.87; found: C 64.33, H 7.21, S 22.84. *Mol. Wt.* calcd. for $C_{15}H_{20}OS_2$: 280.0955; found: 280.0954.

Methyl 3,3-bis(ethylthio)-4-oxobutanoate

To a stirred solution of 0.145 mL (1.05 mmol) of diisopropylamine in 2 mL of 1,2-dimethoxyethane cooled to −78°C under a N_2 atmosphere was added 0.8 mL (1 mmol) of 1.25 *M* *n*-butyllithium. After 5 min, 0.245 g (1 mmol) of cyclohexyl enamine **8***a* was added and the reaction mixture stirred for a further 15 min. To the golden yellow solution of the lithium salt of the enamine was added 0.153 g (1 mmol) of methyl bromoacetate in one portion. An immediate precipitate appeared. The reaction mixture was allowed to warm to room temperature over 1.5 h and then 0.126 g (1 mmol) of ethanedioic acid dihydrate in 2 mL of H_2O was added. The bulk of the 1,2-dimethoxyethane was evaporated under reduced pressure and then 2 mL of tetrahydrofuran was added. After 2 h, the reaction mixture was diluted with 50 mL of ethyl ether, washed with 2 × 2 mL of aqueous 2 *N* NaOH, 2 mL of H_2O, and dried ($MgSO_4$). The solvent was evaporated under reduced pressure to afford 0.228 g of crude product which was chromatographed on a 20 g column of Florisil using 2–5% ethyl acetate in 30–60 petroleum ether (v/v) as the eluting solvent. Molecular distillation of the chromatographed product yielded 0.118 g (50%) of the title compound; bp (molecular distillation) 90°C/0.1 Torr; ir: 1735, 1710 cm^{-1}; ^1H nmr (CCl_4) δ: 1.15 (t, 6, J = 7), 2.82 (s, 2), 2.55 (q, 4, J = 7), 3.68 (s, 3), 8.97 (s, 1). *Mol. Wt.* calcd. for $C_9H_{16}O_3S_2$: 236.0541; found: 236.0538.

2,2-Bis(ethylthio)-2-(3-oxocyclohexyl)ethanal ***13***

To a stirred solution of 0.145 mL (1.05 mmol) of diisopropylamine in 2 mL of 1,2-dimethoxyethane cooled to −78°C under a N_2 atmosphere was added 0.8 mL (1 mmol) of 1.25 *M* *n*-butyllithium. After 5 min, 0.245 g (1 mmol) of cyclohexyl enamine **8***a* was added and the reaction mixture stirred for a further 15 min. To the golden yellow solution of the lithium salt of the enamine was added 0.098 mL (1 mmol) of 2-cyclohexenone, the reaction mixture was allowed to warm to room temperature over 2 h, and then 0.126 g (1 mmol) of ethanedioic acid dihydrate in 2 mL of H_2O was added. The bulk of the 1,2-dimethoxyethane was evaporated under reduced pressure and then 2 mL of tetrahydrofuran was added. After 2 h the reaction mixture was diluted with 50 mL of ethyl ether, washed with 2 × 2 mL of aqueous 2 − NaOH, 2 mL of H_2O, and dried ($MgSO_4$). The solvent was evaporated under reduced pressure to afford a crude product which was chromatographed on a 20 g column of Florisil using 2–5% ethyl acetate in 30–60 petroleum ether (v/v) as the eluting solvent. Molecular distillation of the chromatographed product afforded 0.071 g (28%) of **13**; bp (molecular distillation) 110°C/0.1 Torr; ir: 1715, 1705 cm^{-1}; ^1H nmr (CCl_4) δ: 1.20 (t, 3, J = 7), 1.22 (t, 3, J = 7), 1.5–2.8 (m, 9), 2.6 (q, 4, J = 7), 9.05 (s, 1). *Mol. Wt.* calcd. for $C_{12}H_{20}O_2S_2$: 260.0905; found: 260.0902.

*3-(*tert*-Butyldimethylsiloxy)butyl benzenesulphonate* ***14***

To a stirred solution of 3.6 g (40 mmol) of 1,3-butanediol, 3 mL of triethylamine, and 0.060 g (ca. 0.5 mmol) of 4-*N*,*N*-dimethylaminopyridine in 10 mL of dichloromethane cooled to 0°C was added 1.2 mL (10.6 mmol) of benzenesulphonyl chloride over 0.5 h. The reaction mixture was stirred for a further 0.5 h at 0°C, diluted with 60 mL of ethyl ether, and washed successively with 10 mL of H_2O,

Can. J. Chem. Downloaded from www.nrcresearchpress.com by 210.87.254.40 on 09/06/12
For personal use only.

2 × 5 mL of aqueous 2 *N* HCl, 5 mL of aqueous 2 *N* NaOH, and 5 mL of H_2O. The organic phase was dried ($MgSO_4$) and the solvent evaporated under reduced pressure to afford 2.2 g (95%) of a colourless oil which was pure enough for use in the subsequent reaction. Infrared: 3650−3200, 1355, 1185, 1175 cm^{-1}; ^1H nmr ($CDCl_3$) δ: 1.18 (d, 3, J = 6), 1.8 (m, 2), 2.1 (bs, 1), 4.1 (m, 3), 7.76 (m, 5). *Mol. Wt.* calcd. for $C_{10}H_{14}O_4S$: 230.0613; found: 230.0611.

To a stirred solution of 1.15 g (5 mol) of the above alcohol sulphonate, 0.75 g (7.5 mmol) of triethylamine, and 0.05 g (ca. 0.03 mmol) of 4-*N*,*N*-dimethylaminopyridine in 5 mL of dichloromethane cooled to 0°C was added a solution of 0.75 g (ca. 5 mmol) of *tert*-butyldimethylchlorosilane in 1 mL of dichloromethane. The reaction mixture was stirred for 2 h at room temperature, diluted with 100 mL of ethyl ether, and washed successively with 5 mL of aqueous 2 *N* HCl, 5 mL of aqueous saturated $NaHCO_3$, and 5 mL of H_2O. The organic phase was dried ($MgSO_4$) and the solvent was evaporated under reduced pressure. The residual oil was filtered through 10 g of Woelm neutral activity grade I alumina using 2% ethyl acetate in 30−60 petroleum ether (v/v) as the eluting solvent to give 1.5 g (90%) of **14** as a colourless oil. Infrared: 1365, 1190, 1180, 1100 cm^{-1}; ^1H nmr ($CDCl_3$) δ: −0.04 (s, 3), 0.00 (s, 3), 0.8 (s, 9), 1.08 (d, 3, J = 6), 1.73 (m, 2), 3.9 (m, 1), 4.13 (t, 2, J = 6.5), 7.75 (m, 5). *Mol. Wt.* calcd. for $C_{15}H_{25}O_4SSi$: 329.1243; found 329.1252.

*2,2-Bis(ethylthio)-5-(*tert*-butyldimethylsiloxy)hexanal **15***

Alkylation of the potassium salt of cyclohexyl enamine **8***a* was carried out with 0.658 g (2 mmol) of benzenesulphonate **14** using the general procedure outlined above. Aldehyde **15** was obtained in 82% yield; bp (molecular distillation) 90°C/0.1 Torr; ir: 1715 cm^{-1}; ^1H nmr ($CDCl_3$) δ: 0.02 (s, 6), 0.91 (s, 9), 1.25 (t, 6, J = 7), 1.82 (m, 4), 2.53 (q, 4, J = 7), 3.86 (m, 1), 9.12 (s, 1). *Mol. Wt.* calcd. for $C_{15}H_{31}O_2S_2Si$ (M − 15 (CH_3)): 335.1535; found: 335.1530.

*(2*E*)-Methyl 4,4-bis(ethylthio)-7-(*tert*-butyldimethylsiloxy)-2-octenoate **16***

A suspension of 0.250 g (5 mmol) of NaH in mineral oil was washed free of oil by stirring wth 3 × 5 mL portions of pentane under a N_2 atmosphere. The oil-free NaH was then suspended in 5 mL of tetrahydrofuran and the mixture cooled to 0°C. A mixture of 1.618 g (4.38 mmol) of aldehyde **15** and 0.82 g (4.5 mmol) of trimethyl phosphonoacetate in 2 mL of tetrahydrofuran was added to the NaH suspension over 2 min. The cooling bath was removed and the reaction mixture stirred for an additional 2 h at room temperature. The reaction mixture was diluted with 100 mL of ethyl ether, washed with 2 × 10 mL of H_2O, and dried ($MgSO_4$). The solvent was evaporated under reduced pressure to afford 1.68 g (94%) of **16** as a pale yellow oil which was pure enough for use in the subsequent reaction. Infrared: 1730, 1645 cm^{-1}; ^1H nmr ($CDCl_3$) δ: 0.01 (s, 6), 0.85 (s, 9), 1.1 (d, 3, J = 6), 1.18 (t, 3, J = 7), 1.2 (t, 3, J = 7), 1.4−2.0 (m, 4), 2.48 (q, 4, J = 7), 3.72 (s, 3), 3.75 (m, 1), 5.9 (d, 1, J = 16), 6.84 (d, 1, J = 16). *Mol. Wt.* calcd. for $C_{19}H_{38}O_3S_2Si$: 406.2032; found: 406.2048.

*(2*E*)-Methyl 4,4-bis(ethylthio)-7-hydroxy-2-octenoate **17***

To 0.744 g (1.83 mmol) of silyl ether **16** in 2 mL of tetrahydrofuran was added 2 mL of aqueous 5 *N* HCl. The reaction mixture was stirred for 3 h and was diluted with 60 mL of ethyl ether, washed with 3 × 5 mL of H_2O, and dried ($MgSO_4$). The solvent was evaporated under reduced pressure and the residual oil was chromatographed on 40 g of Florisil using 10−30% ethyl acetate in 30−60 petroleum ether (v/v) as the eluting solvent to afford 0.512 g (96%) of **17** as a colourless oil. Infrared: 3470, 1725, 1643 cm^{-1}; ^1H nmr ($CDCl_3$) δ: 1.21 (d, 3, J = 6), 1.24 (t, 3, J = 7), 1.26 (t, 3, J = 7), 1.5−2.1 (m, 5), 2.55 (q, 4, J = 7), 3.78 (s, 3), 3.85 (m, 1), 5.96 (d, 1, J = 16), 6.9 (d, 1, J = 16). *Anal.* calcd. for $C_{13}H_{24}O_3S_2$ (292.464): C 53.39, H 8.27, S 21.92; found: C 53.31, H 8.48, S 21.70. *Mol. Wt.* calcd. for $C_{13}H_{24}O_3S_2$: 292.1167; found: 292.1165.

*(2*E*)-4,4-Bis(ethylthio)-7-hydroxy-2-octenoic acid **18***

To 0.438 g (1.5 mmol) of hydroxy ester **17** was added 3 mL of aqueous 1 *N* KOH. The reaction mixture was maintained at 60°C for 3 h. The reaction mixture was allowed to cool to room temperature and then was transferred to a separatory funnel and washed with 2 × 10 mL of ethyl ether. The aqueous phase was acidified with aqueous 2 *N* HCl and extracted with 2 × 25 mL of dichloromethane. The organic phase was dried ($MgSO_4$) and the solvent evaporated under reduced pressure to afford a pale yellow oil. The acid was purified by chromatography on a Sephadex LH-20 column (15 g). Initial elution was performed with chloroform. A final elution of the column using methanol provided the desired product. Evaporation of the solvent afforded 0.358 g (88%) of hydroxy acid **18** as a pale yellow oil. Infrared: 3600−2400, 1705, 1645 cm^{-1}; ^1H nmr ($CDCl_3$) δ: 1.20 (t, 6, J = 7), 1.20 (d, 3, J = 6), 1.4−2.2 (m, 4), 2.53 (q, 4, J = 7), 3.8 (m, 1), 5.9 (d, 1, J = 16), 6.96 (d, 1, J = 16), 7.2 (bs, 1). *Anal.* calcd. for $C_{12}H_{22}O_3S_2$ (278.437): C 51.77, H 7.96, S 23.03; found: C 52.00, H 7.80, S 22.70. *Mol. Wt.* calcd. for $C_{12}H_{22}O_3S_2$: 278.1010; found: 278.1021.

*Dimerizing lactonization of **18**: preparation of **19***

To a solution of 0.278 g (1 mmol) of hydroxy acid **18** and 0.524 g (2 mmol) of triphenylphosphine in 200 mL of toluene cooled to −40°C was added 0.250 g (1.5 mmol) of diethyl azodicarboxylate over 2 min. The reaction flask was stoppered and stored at −30°C for 24 h, at −15°C for 24 h, and finally at room temperature for 6 h. The solvent was evaporated under reduced pressure and the residue chromatographed on 20 g of Florisil using 2−10% ethyl acetate in 30−60 petroleum ether (v/v) as the eluting solvent to afford 0.072 g of an oil. Upon trituration of this oil with ethyl ether, 0.017 g of colourless crystals of dimeric material **19** was obtained. The mother liquor was evaporated and used without further purification for subsequent reactions; mp 171−172.5°C (ethyl ether); ir ($CHCl_3$): 1710 cm^{-1}; ^1H nmr ($CDCl_3$) δ: 1.22 (d, 6, J = 6), 1.26 (t, 12, J = 7), 1.56−1.95 (m, 8), 2.34−2.71 (m, 8), 4.95 (m, 2), 5.91 (d, 2, J = 16), 6.72 (d, 2, J = 16). *Anal.* calcd. for $C_{24}H_{40}O_4S_4$ (520.843): C 55.35, H 7.76, S 24.62; found: C 55.53, H 7.70, S 24.39. *Mol. Wt.* calcd. for $C_{24}H_{40}O_4S_4$: 520.1810; found: 520.1819.

d,l *and* meso-*Pyrenophorin **20**a and **20**b*

To a stirred suspension of 0.108 g (0.5 mmol) of red HgO and 0.07 g of boron trifluoride etherate in 4 mL of tetrahydrofuran and 1 mL of H_2O was added 0.040 g (0.077 mmol) of the crystalline dimeric material **19** in 0.5 mL of tetrahydrofuran. The reaction mixture was stirred for a further 0.5 h, by which time the red colour of the HgO had disappeared. The reaction mixture was diluted with ethyl ether and then centrifuged. The clear organic phase was washed with 5 mL of aqueous dilute NH_4OH and dried ($MgSO_4$). The solvent was removed under reduced pressure to afford a mixture of products which were separated by preparative thin-layer chromatography on silica using 30% ethyl acetate in 30−60 petroleum ether (v/v) as the eluting solvent.

By comparison with the literature (12) data, the more polar band (0.0075 g) and the less polar band (0.008 g) were identified as the *meso* and the *d,l* isomers of pyrenophorin, respectively

d,l-*Pyrenophorin **20**a*: mp 129−131°C (ethyl ether − 30−60 petroleum ether);[10] ir ($CHCl_3$): 1730, 1700, 1680, 1640 cm^{-1}; ^1H nmr ($CDCl_3$) δ: 1.3 (d, 6, J = 6), 2.1 (m, 4), 2.63 (m, 4), 5.06 (m, 2), 6.49 (d, 2, J = 16), 6.95 (d, 2, J = 16). *Mol. Wt.* calcd. for $C_{10}H_{20}O_6$: 308.1260; found: 308.1264.

[10]Although purified by thin-layer chromatography and the product twice crystallized, the *d,l*-pyrenophorin showed a significantly lower melting point than the highest value reported in the literature (139−140°C (17)). Traces (<5%) of a structurally related impurity, observed in the ^1H nmr spectrum (400 MHz) of the compound, were undoubtedly causing the lowering of melting point. A third recrystallization was not attempted as the sample size was too small. The *meso*-pyrenophorin had a melting point significantly higher than others reported in the literature (118−119°C (12), 126−127.5°C (17*a*), 128−128.5°C (17*b*)).

Can. J. Chem. Downloaded from www.nrcresearchpress.com by 210.87.254.40 on 09/06/12
For personal use only.

meso-*Pyrenophorin* ***20***b: mp 148.5–149°C (ethyl ether – 30–60 petroleum ether);[10] ir ($CHCl_3$): 1725, 1700, 1685, 1620 cm^{-1}; ^1H nmr ($CDCl_3$) δ: 1.29 (d, 6, J = 6), 2.1 (m, 4), 2.6 (m, 4), 5.07 (m, 2), 6.53 (d, 2, J = 16), 6.93 (d, 2, J = 16). *Mol. Wt.* calcd. for $C_{16}H_{20}O_6$: 308.1260; found: 308.1260.

Oxidative hydrolysis of the mother liquor

The mother liquor from the recrystallization of the dimer **19** was evaporated under reduced pressure to afford 0.053 g of oily residue. This material was oxidatively hydrolyzed using the procedure described above to afford a mixture of products which was separated by preparative thin-layer chromatography (silica). The two more polar bands were identified as the *d,l* (0.016 g) and the *meso* (0.012 g) isomers of pyrenophorin. The least polar substance (0.0053 g) was assigned as a cyclic trimeric species based on its spectroscopic properties; mp 148–150°C (ethyl ether – 30–60 petroleum ether; ir ($CHCl_3$): 1720, 1705, 1690, 1650, 1635 cm^{-1}; ^1H nmr ($CDCl_3$) δ: 1.341, 1.342 (d, 9, J = 6), 1.9, 2.08 (m, 6), 2.73 (m, 6), 5.1 (m, 3). 6.62 (dm, 3), 7.02 (dm, 3). *Mol. Wt.* calcd. for $C_{24}H_{30}O_9$: 462.1895; found 462.1892.

*2(*E*)-Methyl 4,4-bis(ethylthio)hepta-2,6-dienoate* ***23***

A 1.35 g (6.61 mmol) sample of aldehyde **22** was reacted with the sodium salt of trimethyl phosphonoacetate using the procedure described above. Molecular distillation of the product yielded 1.61 g (93%) of the unsaturated ester **23**; bp (molecular distillation) 80–90°C/0.1 Torr; ir: 1720, 1640 cm^{-1}; ^1H nmr ($CDCl_3$) δ: 1.22 (t, 6, J = 7), 2.53 (q, 4, J = 7), 2.55, (d, 2, J = 6.5), 3.7 (s, 3), 5.06 (m, 1), 5.2 (m, 1), 5.89 (m, 1) 5.86 (d, 1, J = 16), 6.72 (d, 1, J = 16). *Anal.* calcd. for $C_{12}H_{20}O_2S_2$ (260.421): C 55.35, H 7.74, S 24.62; found: C 55.45, H 7.68, S 24.44. *Mol. Wt.* calcd. for $C_{12}H_{20}O_2S_2$: 260.0923; found: 260.0920.

*2(*E*)-4,4-Bis(ethylthio)-7-hydroxy-2-heptenoic acid* ***24***

To a stirred solution of 1.3 g (5 mmol) of unsaturated ester **23** in 10 mL of tetrahydrofuran was added 1.22 g (10 mmol) of 9-borabicyclo[3·3·1]nonane dimer and the reaction mixture was stirred overnight at room temperature. The solvent was evaporated under reduced pressure and the residue was dissolved in 10 mL of toluene. Then 3.3 g (30 mmol)) of trimethylamine oxide dihydrate were added and the reaction mixture was refluxed for 6 h. The reaction mixture was allowed to cool to room temperature and then was diluted with 50 mL of ethyl ether, and washed with 3 × 10 mL of aqueous saturated NaCl. The solvents were removed under reduced pressure and the crude reaction product was stirred with 10 mL of aqueous 1 *N* KOH at 60°C for 12 h. The reaction mixture was allowed to cool to room temperature and then was extracted with 2 × 10 mL of ethyl ether. The aqueous phase was acidified with aqueous 2 *N* HCl and extracted with 3 × 10 mL of chloroform. The organic phase was dried ($MgSO_4$) and the solvent evaporated under reduced pressure to afford 1.12 g of a yellow oil. The acid was purified by chromatography on a Sephadex LH-20 column (20 g). Initial elution was performed with a mixture of 50% dichloromethane in 30–60 petroleum ether (v/v). A final elution of the column with ethanol afforded 0.92 g (70%) of the desired hydroxy acid **24** as a pale yellow solid; mp 86–87°C (ethyl ether – 30–60 petroleum ether); ir ($CHCl_3$): 3300–2500, 1685, 1635 cm^{-1}; ^1H nmr ($CDCl_3$) δ: 1.18 (t, 6, J = 7), 1.6–2.1 (m, 4), 2.48 (q, 4, J = 7), 3.64 (bt, 2), 5.88 (d, 1, J = 16), 6.9 (d, 1, J = 16), 6.9–7.2 (bs, 2). *Anal.* calcd. for $C_{11}H_{20}O_3S_2$ (264.408): C 49.92, H 7.62, S 24.25; found: C 50.25, H 7.71, S 24.44. *Mol. Wt.* calcd. for $C_{11}H_{20}O_3S_2$: 264.0854; found: 264.0845.

Dimerizing lactonization of ***24****: preparation of* ***25***

A 0.300 g (1.14 mmol) sample of hydroxy acid **24** was dimerized using the triphenylphosphine/diethyl azodicarboxylate method described above. The reaction product was chromatographed on 40 g of Florisil using 2–10% ethyl acetate in 30–60 petroleum ether (v/v) as the eluting solvent to afford 0.18 g (65%) of dimer **25**. The chromatographed product was pure enough to use in subsequent reactions; mp 85–86.5°C (30–60 petroleum ether); ir ($CHCl_3$): 1710, 1635 cm^{-1}; ^1H nmr ($CDCl_3$) δ: 1.25 (t, 12, J = 7), 1.8 (m, 4), 2.08 (m, 4), 2.58 (q, 8), 4.18 (t, 4, J = 5), 5.96 (d, 2, J = 16), 6.82 (d, 2, J = 16). *Anal.* calcd. for $C_{22}H_{36}O_4S_4$ (492.786): C 53.62, H 7.36, S 26.03; found: C 53.87, H 7.46, S 26.12. *Mol. Wt.* calcd. for $C_{22}H_{36}O_4S_4$: 492.1496; found: 492.1492.

Norpyrenophorin ***26***

A 0.98 (0.2 mmol) sample of crystalline dimer **25** was oxidatively hydrolyzed using the HgO/boron trifluoride etherate method described above. The reaction product was recrystallized to afford 0.038 g (68%) of norpyrenophorin as a colourless solid; mp 132–133°C (ethyl ether – 30–60 petroleum ether) (lit. (18) mp 132°C); ir ($CHCl_3$): 1735, 1705, 1690, 1650 cm^{-1}; ^1H nmr ($CDCl_3$) δ: 2.2 (m, 4), 2.61 (t, 4, J = 6), 4.33 (t, 4, J = 5), 6.6 (d, 2, J = 16), 7.04 (d, 2, J = 16). *Mol. Wt.* calcd. for $C_{14}H_{16}O_6$: 280.0947; found: 280.0953.

R-(+)-*4-Methyl-6-(*tert*-butyldimethylsiloxy)-1-hexanol* ***27***c

To a stirred solution of 3.12 g (20 mmol) of (+)-citronellol (19), 3.0 g (ca. 30 mmol) of triethylamine, and 0.061 g (0.5 mmol) of 4-*N*,*N*-dimethylaminopyridine in 20 mL of dichloromethane cooled to 0°C was added a solution of 3.0 g (20 mmol) of *tert*-butyldimethylchlorosilane in 2 mL of dichloromethane. The reaction mixture was stirred for 2 h at room temperature, diluted with 100 mL of ethyl ether, and washed successively with 5 mL of aqueous 2 *N* HCl, 5 mL of aqueous saturated $NaHCO_3$ and dried ($MgSO_4$). The solvent was evaporated under reduced pressure to afford 5.4 g (100%) of the silyl ether as a colourless oil which was pure enough for use in subsequent reactions. Infrared: 1100 cm^{-1}; $[\alpha]_D^{25}$ + 2.75° (*c* 0.625, $CHCl_3$); ^1H nmr ($CDCl_3$) δ: 0.01 (s, 6), 0.85 (d, 3), 0.86 (s, 9), 1.1–1.7 (m, 5), 1.57 (bs, 3), 1.65 (d, 3, J = 1), 1.94 (m, 2), 3.63 (t, 2, J = 6), 5.1 (tm, 1). *Anal.* calcd. for $C_{16}H_{34}OSi$ (270.535): C 71.04, H 12.67; found: C 71.37, H 12.66. *Mol. Wt.* calcd. for $C_{16}H_{34}OSi$: 270.2379; found: 270.2381.

An ozone stream was passed through a solution of 2.7 g (10 mmol) of the above silyl ether in 5 mL of dichloromethane and 5 mL of methanol cooled to −78°C until the solution turned blue. A solution of 0.75 g (ca. 20 mmol) of $NaBH_4$ in 10 mL of methanol was added to the ozonide at −78°C and the reaction mixture was stirred at −78°C for 1 h. Another 0.75 g (ca. 20 mmol) of $NaBH_4$ in 10 mL of methanol was added and the reaction mixture allowed to warm to room temperature over 2 h. The bulk of the solvent was evaporated under reduced pressure and then 40 mL of aqueous 2 *N* NaOH was added to the reaction mixture. The aqueous phase was extracted with 3 × 25 mL of ethyl ether and the organic extract dried ($MgSO_4$). The solvent was evaporated under reduced pressure and the residue was chromatographed on a 50 g column of Florisil using 10–30% ethyl acetate in 30–60 petroleum ether (v/v) as the eluting solvent to afford 1.92 g (78%) of alcohol **27***c* as a colourless oil; bp (molecular distillation) 70°C/0.1 Torr; ir: 3350, 1100 cm^{-1}; $[\alpha]_D^{25}$ +1.17° (*c* 0.27, $CHCl_3$); ^1H nmr ($CDCl_3$) δ: 0.00 (s, 6), 0.84 (d, 3, J = 6), 0.85 (s, 9), 1–1.7 (m, 7), 1.8 (s, 1), 3.59 (t, 2, J = 6), 3.61 (t, 2, J = 6). *Mol. Wt.* calcd. for $C_{12}H_{27}O_2Si$: (M − 15(CH_3)): 231.1780; found: 231.1807.

R-(+)-*4-Methyl-6-(*tert*-butyldimethylsiloxy)-1-hexyl benzenesulphonate* ***27***d

To a stirred solution of 1.48 g (6 mmol) of alcohol **27***c*, 1.2 g (12 mmol) of triethylamine, and 0.040 g (ca. 0.3 mmol) of 4-*N*,*N*-dimethylaminopyridine in 10 mL of dichloromethane cooled to 0°C was added 1.1 g (6.3 mmol) of benzenesulphonyl chloride over a period of 2 min. The reaction mixture was stirred for 3 h at room temperature and then diluted with 60 mL of ethyl ether, washed successively with 10 mL of aqueous 2 *N* HCl, 10 mL of aqueous saturated Na_2CO_3, 10 mL of H_2O, and dried ($MgSO_4$). The solvent was evaporated under reduced pressure to afford 2.28 g (100%) of benzenesulphonate **27***d* which was pure enough for use in subsequent reactions. Infrared: 1360, 1190, 1095 cm^{-1}; $[\alpha]_D^{25}$ +2.0° (*c* 2.45, $CHCl_3$); ^1H nmr ($CDCl_3$) δ: 0.025 (s, 6), 0.88 (s, 9), 0.89 (d, 3, J = 10), 1.48 (m, 7), 3.58 (t, 2, J = 6), 4.04 (t, 2, J = 6), 1.94 (m, 5). *Mol. Wt.* calcd. for $C_{18}H_{31}O_4SSi$ (M − 15(CH_3)): 371.1712;

found: 371.1720.

R-*(+)-2,2-Bis(ethylthio)-6-methyl-8-(*tert*-butyldimethylsiloxy) octanal* ***28***

Alkylation of the potassium salt of cyclohexyl enamine *8a* was carried out with 0.371 g (1 mmol) of benzenesulphonate **27***d* using the general procedure outlined above. Aldehyde **28** was obtained in 82% yield as a colourless oil; bp (molecular distillation) 93°C/0.2 Torr; ir: 1705, 1095 cm^{-1}; $[\alpha]_D^{25}$ +2.67° (*c* 1.0, $CHCl_3$); ^1H nmr ($CDCl_3$) δ: 0.00 (s, 6), 0.83 (d, 3, J = 6), 0.85 (s, 9), 1.18 (t, 6, J = 7), 1−1.9 (m, 9), 2.46 (q, 4, J = 7), 3.6 (t, 2, J = 6), 9.03 (s, 1). *Mol. Wt.* calcd. for $C_{18}H_{37}O_2S_2Si$ (M − 15(CH_3)): 363.2211; found: 363.2241.

R−*(+)-Methyl 4,4-bis(ethylthio)-8-methyl-10-(*tert*-butyldimethyl-siloxy)-2-decenoate* ***29***

A 0.378 g (1 mmol) sample of aldehyde **28** was reacted with the sodium salt of trimethyl phosphonoacetate using the procedure described above. Chromatography of the product yielded 85% yield of the unsaturated ester **29** as a colourless oil; bp (molecular distillation) 105°C/0.1 Torr; ir: 1730, 1640, 1090 cm^{-1}; $[\alpha]_D^{25}$ +3.38° (*c* 1.5, $CHCl_3$); ^1H nmr ($CDCl_3$) δ: 0.00 (s, 6), 0.84 (d, 3, J = 8), 0.85 (s, 9), 1.18 (t, 6, J = 7), 1.05−1.8 (m, 9), 2.48 (q, 4, J = 7), 3.6 (t, 2, J = 6), 3.71 (s, 3), 5.9 (d, 1, J = 16), 6.85 (d, 2, J = 16). *Anal.* calcd. for $C_{22}H_{44}O_3S_2Si$ (448.810): C 58.88, H 9.88, S 14.29; found: C 59.04, H 10.02, S 14.50. *Mol. Wt.* calcd. for $C_{21}H_{41}O_3S_2Si$ (M − 15(CH_3)): 433.2266; found: 433.2243.

Acknowledgements

This work was supported by the Natural Sciences and Engineering Research Council of Canada and in part by a Cottrell Research Grant provided by the Research Corporation.

1. G. S. Bates and S. Ramaswamy. J. Chem. Soc. Chem. Commun. 904 (1980).
2. (*a*) W. G. Overend, L. M. Turton, and L. F. Wiggins. J. Chem. Soc. 3500 (1950); (*b*) H. M. Walton. J. Org. Chem. **22**, 308 (1957); (*c*) M. Kuchar, B. Kamac, and O. Nemacek. Collect. Czech. Chem. Commun. **37**, 3950 (1972); (*d*) P. L. Stoller and J. B. Eppner. Tetrahedron Lett. 2417 (1973); (*e*) P. A. Bartlett. J. Am. Chem. Soc. **98**, 3305 (1976); (*f*) P. Bakuzis, M. L. F. Bakuzis, and T. F. Weingartner. Tetrahedron Lett. 2371 (1978); (*g*) A. E. Greene, C. LeDrian, and P. Crabbe. J. Org. Chem. **45**, 2713 (1980).
3. (*a*) J. A. Katzenellenbogen and A. L. Crumrine. J. Am. Chem. Soc. **96**, 5662 (1974); (*b*) J. A. Katzenellenbogen and A. L. Crumrine. J. Am. Chem. Soc. **98**, 4925 (1976).
4. S. R. Wilson and J. Mathew. Synthesis, 625 (1980).
5. G. Stork and S. R. Rowd. J. Am. Chem Soc. **85**, 2178 (1963).
6. (*a*) A. I. Meyers and R. C. Strideland. J. Org Chem. **37**, 2579 (1972); (*b*) E. Rothstein. J. Chem. Soc. 1550 (1940); 1553 (1940).
7. P. Veeravagu, R. T. Arnold, and E. W. Eigenmann. J. Am. Chem. Soc. **86**, 3072 (1964).
8. (*a*) K. Ishibashi. J. Agric. Chem. Soc. Jpn. **35**, 257 (1971); (*b*) J. Antibiot. Ser. A, **15**, 166 (1962).
9. R. S. Mali, M. Pohmakotr, B. Weidmann, and D. Seebach. Justus Liebigs Ann. Chem. 2272 (1981).
10. T. Kurihara, Y. Nakajima, and O. Mitsunobu. Tetrahedron Lett. 2455 (1976).
11. E. Vedejs and P. L. Fuchs. J. Org. Chem. **36**, 366 (1971).
12. E. W. Colvin, T. A. Purcell, and R. A. Raphael. J. Chem. Soc. Perkin Trans. 1, 1718 (1976).
13. G. W. Kabalka and H. C. Hedgecock, Jr., J. Org. Chem. **40**, 1776 (1975).
14. (*a*) M. Binder and Ch. Tamm. Angew. Chem. Int. Ed. Engl. **12**, 370 (1973); (*b*) S. B. Carter. Endeavour, **113**, 77 (1972); S. W. Tanenbaum (*Editor*). Cytochalasins, biochemical and cell biological aspects. North-Holland, Amsterdam. 1978; (*c*) P. S. Steyn (*Editor*). The biosynthesis of mycotoxins. Academic Press, New York. 1980. Chapt. 8.
15. (*a*) G. Stork, Y. Nakahara, Y. Nakahara and W. J. Greenlee. J. Am. Chem. Soc. **100**, 7775 (1978); (*b*) J. Auerbach and S. M. Weinreb. J. Org. Chem. **40**, 3311 (1975); (*c*) R. Brettle and D. P. CUmming. J. Chem. Soc. Perkin Trans. 1, 2385 (1977); (*d*) S. Masamune, Y. Hayase, W. Schilling, W-K. Chan, and G. S. Bates. J. Am. Chem. Soc. **99**, 6756 (1977); (*e*) E. Vedejs and R. C. Gadwood. J. Am. Chem. Soc. **100**, 376 (1978); (*f*) S. J. Bailey, E. J. Thomas, W. B. Turner, and J. A. J. Jarvis. Chem. Commun. 474 (1978); (*g*) C. Owens and R. A. Raphael. J. Chem. Soc. Perkin Trans. 1, 1504, (1978); (*h*) T. Schmidlin and Ch. Tamm. Helv. Chim. Acta, **61**, 2096 (1978); (*i*) M. Y. Kim and S. M. Weinreb. Tetrahedron Lett. 579 (1979); (*j*) D. A. Clark and P. L. Fuchs. J. Am. Chem. Soc. **101**, 3567 (1979); (*k*) M. Y. Kim, J. E. Starrett, Jr., and S. M. Weinreb. J. Org. Chem. **46**, 5383 (1981).
16. N. Nakane and C. R. Hutchinson. J. Org. Chem. **43**, 3922 (1978).
17. (*a*) H. Gerlach, H. Oertle, and A. Thalmann. Helv. Chim. Acta, **60**, 2860 (1977); (*b*) M. Asaoka, T. Mukuta, and H. Takei. Tetrahedron Lett. **22**, 735 (1981).
18. B. Seuring and D. Seebach. Justus Liebigs Ann. Chem. 2044 (1978).
19. J. Plesek. Collect. Czech. Chem. Commun. **22**, 644 (1957).

Can. J. Chem. Downloaded from www.nrcresearchpress.com by 210.87.254.40 on 09/06/12
For personal use only.

Dérivés allyliques de la colonne IV-A, de type $R_3ECH_2CH{=}CH{-}CH_3$ et $R_3ECH(CH_3)CH{=}CH_2$. Approche des effets électroniques par résonance magnétique nucléaire ^{13}C et ^1H [1]

E. MATARASSO-TCHIROUKHINE ET P. CADIOT

Laboratoire de Recherches de Chimie Organique de l'E.N.S.C.P., 11, rue P. et M. Curie, 75231 Paris Cedex 05, France

Reçu le 16 juillet, 1982[2]

E. MATARASSO-TCHIROUKHINE et P. CADIOT. Can. J. Chem. **61**, 2476 (1983).

Un travail spectroscopique d'ensemble, de caractère comparatif a été réalisé en rmn du carbone ^{13}C et du proton ^1H sur les dérivés allyliques de type $R_3ECH_2CH{=}CH{-}CH_3$, **1***E*, *Z* et $R_3ECH(CH_3)CH{=}CH_2$, **2**; R = $-CH_3$, $-C_6H_5$; E = C, Si, Ge, Sn, Pb. La première partie de ce travail, limitée au fragment allylique, est consacrée à l'étude des déplacements chimiques du carbone, $\delta^{13}C$, du proton, δ^1H, et à l'étude des couplages homonucléaires J(H—H) et hétéronucléaires $^1J(^{13}C{-}H)$, $^nJ(^{13}C{-}E)$, n = 1 à 4 et ^nJ(E—C—H), n = 2 et 5; afin d'éclairer l'influence des effets inductifs des substituants $-ER_3$, une échelle cohérente d'électronégativité a été dressée pour les groupements G(E) = $-E(C_6H_5)_3$; il apparaît que les groupements G(E) possèdent des électronégativités intrinsèques très voisines qui satisfont au classement suivant:

$$\chi^{int}_{G(Pb)} > \chi^{int}_{G(Ge)} \approx \chi^{int}_{G(C)} \approx \chi^{int}_{G(Sn)} > \chi^{int}_{G(Si)}$$

L'étude comparative des spectres dans les séries respectives **1***E*, *Z* et **2** conduit à interpréter les déplacements chimiques des noyaux éthyléniques ainsi que les valeurs élevées des couplages hétéronucléaires ^2J(E—C—H) (CH_2), ^5J(E—C—H) et $^4J(E{-}^{13}C)$, dans le cas des dérivés de l'étain et du plomb, en termes d'hyperconjugaison $\sigma \rightarrow \pi$ de la liaison C—E et de la liaison π-allylique. Des facteurs appartenant en propre à l'élément E contrôlent les déplacements chimiques des noyaux du fragment allylique, en α de cet élément; les couplages $^1J(^{13}C_\alpha{-}H_\alpha)$ semblent dominés par le caractère *s* de la liaison $C_\alpha{-}H_\alpha$ sans que celui-ci puisse être relié de façon précise à une métallohyperconjugaison.

E. MATARASSO-TCHIROUKHINE and P. CADIOT. Can. J. Chem. **61**, 2476 (1983).

A comparative ^1H and ^{13}C nmr study of allylic derivatives of the IV-A group elements, of the type $R_3ECH_2CH{=}CH{-}CH_3$, **1***E*, *Z* and $R_3ECH(CH_3)CH{=}CH_2$, **2**, was performed (R = $-C_6H_5$, $-CH_3$, E = C, Si, Ge, Sn, Pb). The present paper dealing with the allylic moiety concerns both the chemical shifts, δ^1H and $\delta^{13}C$, and the homonuclear J(H—H) and heteronuclear couplings $^1J(^{13}C{-}H)$, $^nJ(^{13}C{-}E)$, n = 1 to 4, ^nJ(E—C—H), n = 2 and 5. The spectra are consistent with a σ-allylic structure. In order to obtain an inductive order for the groups G(E) = $-E(C_6H_5)_3$, a coherent group electronegativity scale was established. The intrinsic group electronegativities, without appreciable change, obey the following sequence:

$$\chi^{int}_{G(Pb)} > \chi^{int}_{G(Ge)} \approx \chi^{int}_{G(C)} \approx \chi^{int}_{G(Sn)} > \chi^{int}_{G(Si)}$$

Both the changes along the series, in spectroscopic parameters, δ^1H, $\delta^{13}C$, and the unusually large heteronuclear couplings, ^2J(E—C—H), ^5J(E—C—H), $^4J(E{-}^{13}C)$ (E = Sn, Pb), are interpreted in terms of an electronic mesomeric donating effect for the substituent σ, R_3ECH_2— and $R_3ECH(CH_3)$—, by $\sigma{-}\pi$ hyperconjugation. Factors intrinsic to the main-group element control the chemical shifts δ^1H_α and $\delta^{13}C_\alpha$. The *s*-character of the bond $C_\alpha{-}H_\alpha$ appears to control the $^1J(^{13}C_\alpha{-}H_\alpha)$ couplings; no correlation with a $\sigma \rightarrow \pi$ hyperconjugation could be established.

Introduction

Nous nous proposons de présenter une approche physicochimique de la structure électronique des dérivés allyliques des éléments de la colonne IV-A de type $R_3ECH_2{-}CH{=}CH{-}CH_3$ **1***E*, *Z* et $R_3ECH(CH_3)CH{=}CH_2$ **2**. Elle a été réalisée en mettant en oeuvre une étude comparative des spectres de rmn ^{13}C et ^1H dans les séries respectives **1***E*, *Z* et **2**. Cette étude a permis d'interpréter les spectres de rmn en termes d'effets électroniques du substituant $-ER_3$.

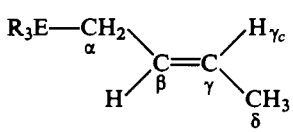

1*E*

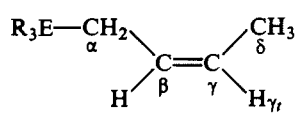

1*Z*

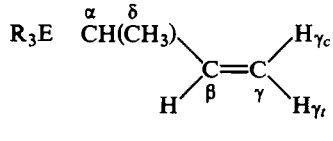

2

R = C_6H_5, CH_3 E = C, Si, Ge, Sn, Pb

A notre connaissance, un tel travail d'ensemble de caractère comparatif sur la totalité de la colonne IV-A n'apparaît point dans la littérature, bien que les dérivés allyliques des éléments de la colonne IV-A, aient fait l'objet de travaux plus ponctuels, notamment en spectroscopie électronique et en spectroscopie de résonance magnétique nucléaire (1 à 13).

Cette première publication portera sur des développements théoriques basés sur l'étude des déplacements chimiques $\delta^{13}C$ et δ^1H, et sur l'étude des couplages homonucléaires, J(H—H), et hétéronucléaires, $^1J(^{13}C{-}H)$, $^nJ(^{13}C{-}E)$, n = 1 à 4 et ^nJ(E—C—H), n = 2 et 5, du fragment allylique des composés **1***E*, *Z* et **2**.

Afin d'interpréter les spectres obtenus en termes d'effets électroniques, il nous a paru indispensable d'établir, en tout premier lieu, une base de comparaison des effets inductifs des groupements $-ER_3$. Dans ce but nous avons dressé une

[1] En accord avec l'usage en vigueur en Amérique du Nord, la nomenclature suivante a été adoptée dans cet article: groupe IV-A = C, Si, Ge, Sn, Pb; bien que, d'après les règles de nomenclature de Chimie Inorganique de l'UICPA les Ge, Sn, Pb constituent le groupe IV-B et les éléments de transition le groupe IV-A.

[2] Revision reçue le 4 janvier, 1983.

Can. J. Chem. Downloaded from www.nrcresearchpress.com by 210.87.254.6 on 09/06/12
For personal use only.

TABLEAU 1. Echelle cohérente d'électronégativité, unités Mulliken, des groupements $-E(C_6H_5)_3$; $\chi_G = a_G + b_G\delta_G$

G	E	$\chi^{int}a_G$	b_G	δ_G	$i\%$	$\chi^{eq.}$
$E(C_6H_5)_3$	C	$8{,}028_5$	$0{,}391_4$	$-0{,}27_2$	27,2	$7{,}921_9$
	Si	$7{,}998_8$	$0{,}386_1$	$-0{,}25_4$	25,4	$\overline{7{,}900_6}$
	Ge	$8{,}032_2$	$0{,}380_8$	$-0{,}27_7$	27,6	$\overline{7{,}926_9}$
	Sn	$8{,}02_0$	$0{,}373_3$	$-0{,}27_0$	27,0	$\underline{7{,}919_4}$
$CH_2CH{=}CHCH_3$		$7{,}597_9$	$1{,}189_4$			

échelle cohérente d'électronégativité pour les groupements $-E(C_6H_5)_3$, celle des groupements $-E(CH_3)_3$ ayant été déterminée par ailleurs (14*a*).

Résultats et discussion

1. *Echelle d'électronégativité cohérente des groupements* $-ER_3$

Il convient ici d'ouvrir une parenthèse et de rappeler brièvement que l'électronégativité des éléments de la colonne IV-A a été sujette à de très nombreuses études et controverses et a suscité des discussions passionnées (15, 16).

Une échelle cohérente d'électronégativité au sens de Hinze et Jaffe (17) a été calculée pour les groupements $-E(C_6H_5)_3$ par la méthode de Huheey (14).

Il convient de rappeler (17) que l'électronégativité χ d'un atome est exprimée en fonction de la charge partielle δ, résultant de la perte ou du gain d'électrons au cours de la formation de la liaison, par la relation:

$$\chi = a + b\delta$$

a = électronégativité intrinsèque; b: coefficient de charge; a et b sont fonction du potentiel d'ionisation et de l'énergie d'affinité électronique de l'atome à l'état de valence.

L'électronégativité d'un groupe sera celle de l'atome liant perturbée par les substituants.

En appliquant le principe d'égalisation des électronégativités (17) de deux orbitales liantes, si deux groupes G_1 et G_2 sont en équilibre dans une molécule et si nous désignons par $\chi^*_{G_1}$ et $\chi^*_{G_2}$ les électronégativités des orbitales liantes à l'équilibre et par $\delta^*_{G_1}$ et $\delta^*_{G_2}$ les quantités de transfert de charge, on peut écrire:

$$\chi^*_{G_1} = \chi^*_{G_2} = a_1 + b_1\delta^*_{G_1} = a_2 + b_2\delta^*_{G_2}$$

En remarquant que pour une liaison neutre $\delta^*_{G_1} + \delta^*_{G_2} = 0$ la quantité de transfert de charge sera exprimé par:

$$\delta^*_{G_1} = -\delta^*_{G_2}\frac{a_{G2} - a_{G1}}{b_{G_1} + b_{G_2}}$$

Sur la base de ces données, l'électronégativité χ_G d'un groupe $G = -w\begin{smallmatrix}x\\y\\z\end{smallmatrix}$ peut être exprimée en fonction des électronégativités intrinsèques a et des coefficients de charge b des substituants, dans le cas général, par la formule [1] (14*a*):

$$[1]\quad \chi_G = \frac{a_w b_x b_y b_z + a_x b_w b_y b_z + a_y b_w b_x b_z + a_z b_w b_x b_y + b_w b_x b_y b_z \delta^*_G}{b_x b_y b_w + b_x b_z b_w + b_x b_y b_z + b_y b_z b_w}$$

Cette méthode, bien que mettant en jeu des approximations importantes, par ex.: assimilation d'un groupement à un atome perturbé $\chi^{int}_G = a_G$ = const., or a_G dépend, pour un groupe, du groupement antagoniste (17, 18), égalisation totale des électronégativités à l'équilibre etc. ..., permet d'obtenir pour les électronégativités de groupe des ordres de grandeur et de calculer une échelle cohérente d'électronégativité. Dans le cas présent les calculs ont été faits en appliquant la formule [2] cas particulier de la formule générale.

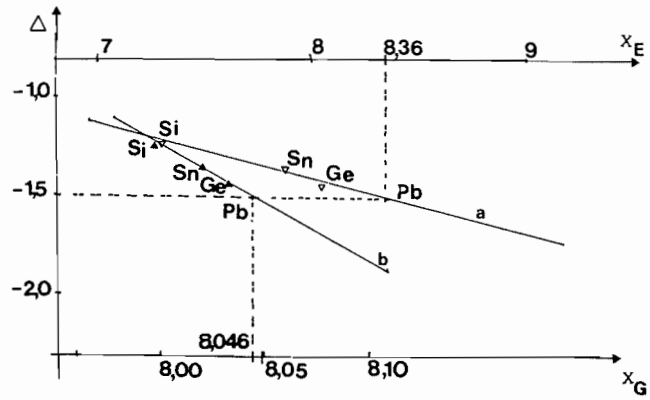

FIG. 1. Déplacement chimique interne $\Delta = \delta^1H(CH_3) - \delta^1H(CH)_\alpha$ composés **2** en fonction (a) de l'électronégativité (unités Mulliken) χ_E de l'élément E; (b) de l'électronégativité χ_G du groupe $G = -E(C_6H_5)_3$.

$$[2]\quad \chi_{G(E)} = \frac{a_E b_\phi + 3b_E a_\phi + b_E b_\phi \delta^*_G}{3b_E + b_\phi};\ G(E) = -E(C_6H_5)_3$$

où a_E et $b_E = a_{C_6H_5}$ et $b_{C_6H_5}$ (14).

Le tableau 1 donne les résultats des calculs concernant les électronégativités à l'équilibre χ^{eq}, les électronégativités intrinsèques $\chi^{int} = a$ et les coefficients de charge b pour les groupes $-E(C_6H_5)_3$, E = C, Si, Ge, Sn à l'état sp^3. L'examen de ce tableau montre que les électronégativités des groupes $-E(C_6H_5)_3$ (E = C à Si, sp^3) sont extrêmement voisines, ce qui correspond aux conclusions de Traylor et coll.: "The inductive effects of metallic groups, MR_3, in the $-CH_2MR_n$ group are negligibly small" (19) (M: élément IV-A, entre autres). Elles satisfont à l'ordre suivant:

$$\chi^{int}_{G(Ge)} \approx \chi^{int}_{G(C)} \approx \chi^{int}_{G(Sn)} > \chi^{int}_{G(Si)}$$

L'électronégativité du groupe $-Pb(C_6H_5)_3$ n'a pu être calculée par cette méthode faute de données, concernant l'électronégativité du plomb sp^3, dans la littérature. Cependant un *ordre de grandeur* pour χ_{Pb} et $\chi_{Pb(C_6H_5)_3}$ peut être obtenu, dans l'échelle d'électronégativité adoptée, en considérant le déplacement chimique interne, $\Delta = \delta^1H(CH_3) - \delta^1H(CH)$, du composé $(C_6H_5)_3PbCH(CH_3)CH{=}CH_2$ **2**; en effet, comme on peut l'observer sur la figure 1 pour les composés **2** étudiés, les déplacements chimiques internes, $\Delta = \delta^1H(CH_3) - \delta^1H(CH)_\alpha$ varient linéairement en fonction de l'électronégativité χ_E (14) de l'élément E, d'une part, et de l'électronégativité $\chi_{G(E)}$ du groupe

Can. J. Chem. Downloaded from www.nrcresearchpress.com by 210.87.254.6 on 09/06/12
For personal use only.

Can. J. Chem. Downloaded from www.nrcresearchpress.com by 210.87.254.6 on 09/06/12
For personal use only.

TABLEAU 2(*a*). Déplacements chimiques du proton, δ^1H; composés **1***E*, *Z*, **2**; R = C_6H_5; fragment allylique

		δ^1H, ppm[a]					
	E	α	β	γ_c	γ_t	γ_c, γ_t	δ
	Si	2,30					$1,53_5$
	Ge	$2,38_5$	5,56	5,34			$1,52_5$
1*E*	Sn	2,36	5,68	5,38			1,55
	Pb	$2,87_5$	5,78	5,35			1,63
	C	3,35					$1,42_5$
	Si	2,33	5,56		5,34		$1,37_5$
1*Z*	Ge	2,43	5,60		5,33		1,39
	Sn	2,39	5,74		5,25		1,46
	Pb	2,90	5,85		5,17		1,57
	Si	2,50	6,06[b]			4,90[b]	1,27
	Ge	2,78	$6,09_5$			4,89	$1,34_5$
2	Sn	2,85	6,27			4,88	1,51
	Pb	3,31	6,36			4,80	1,81
	C	4,1					0,91

[a]Conditions expérimentales; Varian XL 100; solvant: $CDCl_3$; TMS interne.
[b]Centre du multiplet.

G = —E(C_6H_5)$_3$ de l'autre. La connaissance de Δ pour le dérivé **2** du plomb (à partir des données du Tableau 2a) permet de déduire les électronégativités χ_{Pb} et $\chi_{G(Pb)}$ et de les classer comme suit

$$\chi_{Pb(sp^3)} > \chi_{Ge(sp^3)};\ \chi_{G(Pb)} > \chi_{G(Ge)}$$

ce qui est compatible avec des résultats obtenus par ailleurs (20, 21).

II. *Déplacements chimiques* δ^1H *et* $\delta^{13}C$

1. *Spectres du proton (Tableaux 2 à 4)*

L'allure générale du spectre de protons des composés **1***E*, *Z* et **2** correspond à une structure σ-allylique et permet d'écarter un équilibre ionique ou une structure π-allylique. Dans le cas des dérivés primaires, **1***E*, *Z*, la résolution de la région éthylénique du spectre, $H_{\beta,\gamma}$, a été ramenée par double irradiation du groupement —CH_2— à la résolution de la partie AB d'un spectre ABX_3.

En toute rigueur cette partie devrait être traitée en tant que spectre du second ordre, comme on peut le déduire du tableau 4. Cependant $\delta^1H_{\beta,\gamma}$ ont pu être déterminés, comme suit, avec une approximation raisonnable, dans la plupart des cas. *Pour les composés* **1***Z et* **1***E* (E = Pb, Sn, Ge) les quadruplets correspondants aux noyaux A et B (H_β et H_γ) ne sont pas trop déformés et sont relativement aisés à attribuer; ils permettent, avec une approximation raisonnable, de déterminer en faisant leur moyenne la position du spectre pour AB et, de là, calculer

TABLEAU 2(*b*). Déplacements chimiques du proton, δ^1H; composés **1***E*, *Z*, **2**; R = CH_3; fragment allylique

		δ^1H, ppm[a]				
E		CH_3 α′	$\alpha^{b,c}$	$\delta^{b,c}$	$\beta^{b,d}$	$\gamma^{b,d}$
	1*E*	0,09$_2$	[m]: 1,8		[m]: 5,5	
Sn	**1***Z*	0,114	[m]: 1,7		[m]: 5,4	
	2	0,08	2,21	1,41	[m]: 6,0	[m]: 4,7

[a]Conditions expérimentales: Varian XL-100; liquide pur; réf.: benzène interne. Les déplacements chimiques sont donnés par rapport au TMS, en prenant pour le benzène δH_Φ = 7,27 ppm.
[b][m]: centre du multiplet.
[c]Pour les composés **1***E* et **1***Z* les protons α et δ donnent des multiplets confondus, on donne le centre du multiplet commun.
[d]Comme *c*, pour β et γ.

JAB, δAB = $\nu_A - \nu_B$, *JAB*/$\nu_A - \nu_B$ (Tableau 4). En revanche pour le dérivé **1***E* du silicium le couplage des noyaux H_β et H_γ est suffisamment important pour perturber de façon notable les parties ABX_3 du spectre (Fig. 2). De façon générale, il ressort de l'examen du tableau 4 que l'approximation est d'autant meilleure que l'on a affaire aux composés *Z* et que la période à laquelle appartient l'élément *E* est plus élevée.

Pour *les dérivés secondaires* **2**, la résolution de la région éthylénique du spectre se ramène à la résolution de celle, fortement perturbée, d'un spectre de second ordre ABCX. Seuls les centres m des multiplets correspondants aux protons H_β, d'une part, et H_γ, de l'autre, ont été déterminés (Tableau 2a). A titre d'information la partie éthylénique du spectre du dérivé deutérié (C_6H_5)$_3$SnCD$_2$CH=CH$_2$ a été résolue en la traitant, en première approximation, comme un spectre ABX (Tableau 3).

2. *Spectres du carbone* ^{13}C *(Tableau 5)*

L'identification des déplacements chimiques δ^{13}C a été faite en confrontant les spectres de rmn obtenus dans les conditions suivantes: (a) absence totale de découplage; (b) découplage sélectif et (c) découplage total des protons hors résonance. Dans le cas des dérivés de l'étain l'attribution des déplacements chimiques, faite sur la base de l'irradiation sélective des protons, a été confirmée par les valeurs des couplages hétéronucléaires à longue distance, $J(^{117,119}Sn—^{13}C)$ pour lesquels $^1J > {}^3J > {}^2J$ (11).

Pour les dérivés du plomb les attributions des déplacements chimiques des carbones éthyléniques, faites sur la base des couplages $J(^{207}Pb—^{13}C)$, par analogie avec les dérivés de l'étain, et également par comparaison dans la série, ont été confirmées par un enregistrement supplémentaire de spectres rmn à 250 MHz (dérivé **1***E*).

TABLEAU 3. Paramètres de résonance magnétique nucléaire ^{1}H pour le composé

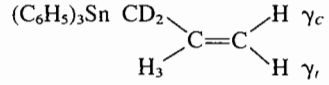

δ^1H, ppm			|J(H—H)|, Hz					
						$J\gamma_c\beta$	$J\gamma_t\beta$	$J\gamma_c\gamma_t$
β	γ_c	γ_t	$J\gamma_c\beta$	$J\gamma_t\beta$	$J\gamma_c\gamma_t$	$\nu_\beta - \nu_{\gamma_c}$	$\nu_\beta - \nu_{\gamma_t}$	$\nu_{\gamma_c} - \nu_{\gamma_t}$
5,92	4,92	4,75	17,33	9,66	2	0,29	0,14	0,20

Conditions expérimentales: Varian XL-100; solvant: $CDCl_3$, TMS interne.

Can. J. Chem. Downloaded from www.nrcresearchpress.com by 210.87.254.6 on 09/06/12
For personal use only.

TABLEAU 4. Déplacements chimiques internes, $\nu_\beta - \nu_\gamma$, des protons éthyléniques H_β, H_γ et couplages $J_{\beta,\gamma}$; composés **1***E*, *Z*; R = C_6H_5

	E	$\nu_\beta - \nu_\gamma$ (Hz)	$\lvert J_{\beta\gamma}\rvert$ (Hz)	$\dfrac{\lvert J_{\beta\gamma}\rvert}{\nu_\beta - \nu_\gamma}$	Période
1*E*	Ge	21,84	15	0,69	4
	Sn	30,39	15,25	0,50	5
	Pb	42,60	15	0,35	6
1*Z*	Si	19,95	10,25	0,51	3
	Ge	27,57	10,5	0,38	4
	Sn	48,63	10,5	0,22	5
	Pb	67,58	10,25	$0,15_5$	6

III. *Interprétation des déplacements chimiques, $\delta^{13}C$ et δ^1H*

L'analyse, au long de la colonne IV-A, des paramètres $\delta^{13}C$ et δ^1H permet de conclure à une structure σ-allylique pour les composés **1***E*, *Z* et **2** et, en tenant compte de l'échelle d'électronégativité, de mettre au jour l'existence d'une hyperconjugaison σ−π de la liaison C—E et de la liaison π allylique, reflétée par les déplacements chimiques des noyaux sp^2, $\delta^{13}C$ $(^1H)_{\beta,\gamma}$, l'effet électronique prédominant sur les noyaux en α de l'hétéroélément étant déterminé par la *nature* même de l'hétéroélément; ces résultats se trouvent corroborés par l'examen des couplages.

Il convient de rappeler ici que, de façon générale pour un noyau A, la constante d'écran σ^A peut être exprimée (22, 23) par la formule [3]

$$[3]\quad \sigma^A = \sigma_d^{AA} + \sigma_p^{AA} + \sum_{A\neq B} [\sigma^{AB} + \sigma^{A,deloc}]$$

δ^1H sera déterminé par le terme diamagnétique σ_d^{AA} et (ou) le terme $\sum_{A\neq B} [\sigma^{AB} + \sigma^{A,deloc}]$, donc (a) par la densité électronique sur le proton ou, indirectement, par la charge portée par le carbone vicinal; (b) par la circulation des électrons sur les noyaux avoisinants; en effet, le terme paramagnétique σ_p^{AA}, est négligeable par rapport aux autres termes de l'équation [3] dans la mesure où les orbitales atomiques 2*p* n'ont pas à être prises en considération (23*b*).

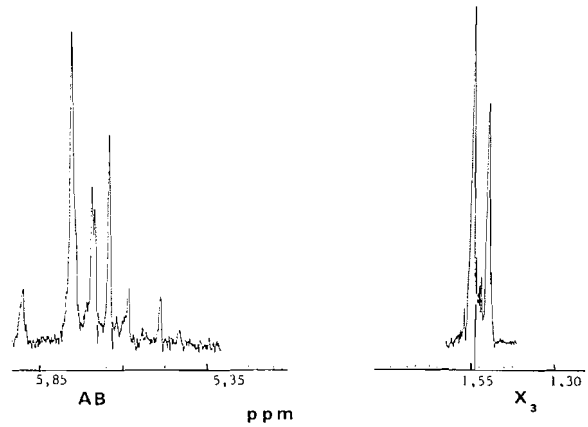

FIG. 2. Déformation d'un spectre ABX_3, par un couplage important des protons AB: partie ABX_3 du spectre de protons du composé A B X_3 $(C_6H_5)_3SiCH_2CH{=}CH{-}CH_3$, obtenue par double irradiation du groupement $-CH_2-$.

$\delta^{13}C$, du fait de l'existance d'états excités de plus basse énergie, est gouverné par le terme σ_p^{AA}; celui-ci est proportionnel à la charge effective du noyau, aux ordres de liaison et inversement proportionnel à l'énergie moyenne d'excitation de la molécule (24, 25).

De façon générale, on remarque un parallélisme entre les variations des déplacements chimiques $\delta^{13}C$ et les paramètres δ^1H des protons vicinaux correspondants, lorsqu'on se déplace le long de la colonne IV-A (Figs. 3 et 4).

Paramètres $\delta^1H_{\beta,\gamma}$ et $\delta^{13}C_{\beta,\gamma}$

Un même facteur, selon toute vraisemblance la charge portée par le carbone, dans le cas de dérivés éthyléniques alkylés, les déplacements chimiques des carbones éthyléniques sont proportionnels aux charges portées par ces atomes (26), contrôle les déplacements chimiques des carbones sp^2, et des protons correspondants; en revanche, l'effet d'anisotropie magnétique voisine, due aux groupements $-ER_3$, se manifeste de façon plus importante sur $\delta^1H_{\gamma_c}$, en position *cis* (Fig. 3). Le choix

TABLEAU 5. Déplacements chimiques du carbone, $\delta^{13}C$, composés **1***E*, *Z*, **2**; fragment allylique

R	E		$\delta^{13}C$ ppm C_α	C_β	C_γ	C_δ	$C_{\alpha'}$	$\Delta = \delta C_\beta - \delta C_\gamma$
C_6H_5	Si	**1***E*	19,16	125,47	125,47	17,97		0
		1*Z*	14,55	124,80	123,31	12,61		1,49
		2	25,08	140,54	112,29	14,05		28,25
	Ge	**1***E*	19,40	126,4	124,9	17,86		1,5
		1*Z*	14,83	125,57	123,0	12,60		2,57
		2	27,62	141,0	111,54	14,81		29,49
	Sn	**1***E*	15,98	127,73	123,04	17,76		4,69
		1*Z*	11,97	126,82	120,96	12,57		5,86
		2	27,81	142,37	109,05	16,07		33,32
CH_3 α′	Sn	**1***E*	15,94	129,32	120,35	17,82	−10,41	8,87
		1*Z*	11,99	128,52	118,39	12,37	−9,99	10,13
		2	25,53	143,47	106,44	15,24	−11,42	37,03
C_6H_5	Pb	**1***E*	27,56	129,17	123,81	17,58		5,36
		1*Z*	23,37	127,95	121,70	12,54		6,25
		2	41,80	142,95	109,30	17,91		33,65
	C	**1***E*	44,39	128,08 ou 127,82	128,08 ou 127,82	18,0		

Can. J. Chem. Downloaded from www.nrcresearchpress.com by 210.87.254.6 on 09/06/12
For personal use only.

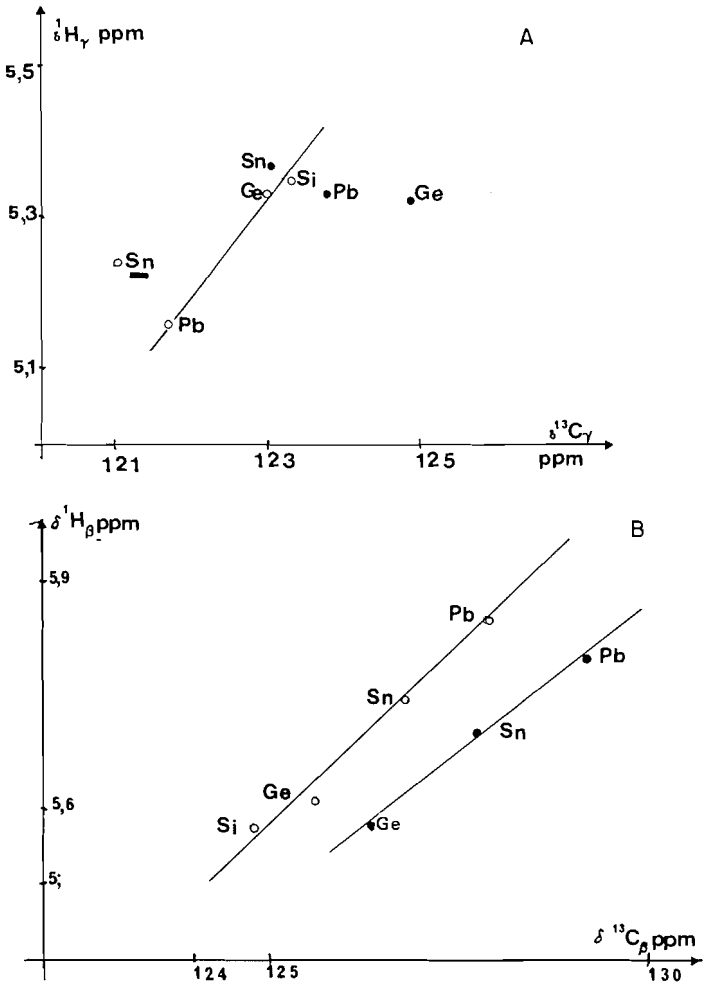

FIG. 3. Déplacement chimique du proton éthylénique ^1H en fonction du déplacement chimique du carbone ^{13}C vicinal, positions β et γ, pour les isomères $(C_6H_5)_3ECH_2CH{=}CH{-}CH_3$ **1***E*, *Z*; $\rho = \Delta\delta^{13}C/\Delta\delta^1H$; (A) position γ: **1***E* −●−; **1***Z* −○−; $\rho\mathbf{1}Z$ = 7,5; (B) position β: **1***E* −●−; **1***Z* −○−; $\rho\mathbf{1}E$ = 13,3; $\rho\mathbf{1}Z$ = 10.

de l'alignement des points pour Si, Ge et Pb, qui laisse un blindage "hors série" pour l'étain, est justifié par l'examen des figures 5 (A) et (B), qui donnent les déplacements chimiques des noyaux éthyléniques N (^{13}C et ^1H) en fonction du numéro atomique Z_E de l'élément E−IV-A.

Le tableau 5 met au jour pour les dérivés des hétéroéléments (E = Si à Pb) une polarisation de la liaison π de la façon

$$\overset{\delta^+}{R_3ECH_2CH}{=}\overset{\delta^-}{CH}{-}CH_3$$

suivante: $R_3ECH_2CH{=}CH{-}CH_3$; elle est pratiquement inexistante lorsque E appartient à la 2de période, E = C. Après avoir remarqué, (a) qu'un substituant σ agit sur la distribution des électrons d'un système π en donnant lieu (α) à une redistribution de la densité électronique du système (effet inductif Iπ, effet de champ F) liée à l'électronégativité du substituant et (ou) (β) à un transfert de charge entre le substituant σ et le système π (effet mésomère R) et (b) que, conformément aux électronégativités calculées Iπ et F, dûs aux groupements $-E(C_6H_5)_3$, doivent être extrêmement faibles, sinon négligeables (l'effet de champ ne joue pas un rôle prédominant sur la polarisation de la liaison π, car dans ce cas (27) un accroissement de l'électronégativité du substituant aurait pour conséquence un déplacement diamagnétique du carbone β, à l'opposé du phénomène observé), nous interpréterons la variation de

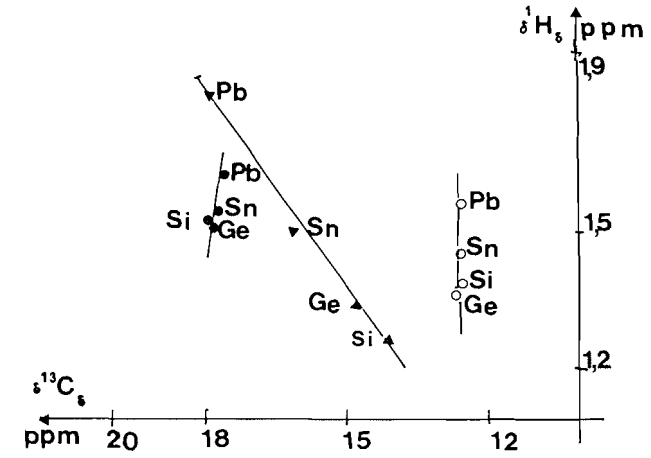

FIG. 4. Déplacement chimique du proton ^1H en fonction du déplacement chimique du carbone ^{13}C vicinal, position δ, pour les isomères $(C_6H_5)_3ECH_2CH{=}CH{-}CH_3$ **1***E* −●−, **1***Z* −○− et $(C_6H_5)_3ECH(CH_3)CH{=}CH_2$ **2** −▼−.

la polarisation de la liaison π, traduite par les spectres de rmn des composés **1***E*, *Z* et **2** (systèmes σ−π de type $R_3E\underset{\sigma}{-}CH_2\underset{\pi}{-}CH{=}CH{-}CH_3$ et $R_3E\underset{\sigma}{-}CH(CH_3)\underset{\pi}{-}CH{=}CH_2$) en termes d'effets électroniques mésomères donneurs des substituants σ (E = Si à Pb) par hyperconjugaison $\sigma \rightarrow \pi$. Des conclusions similaires, basées sur la spectroscopie électronique, ont été faites (19) à propos des dérivés benzyliques correspondants, $(C_6H_5)_3ECH_2C_6H_5$.

Le déplacement chimique interne $\Delta_E = \delta N_\beta - \delta N_\gamma$ (N = ^1H, ^{13}C) est fonction croissante (mais non pas monotone) de la (3ème à la 6ème) période à laquelle appartient l'élément E (Tableaux 3 à 5). Si l'on admet que les déplacements chimiques des carbones éthyléniques sont proportionnels aux charges portées par ces atomes, $\Delta_E = \delta C_\beta - \delta C_\gamma$ sera proportionnelle à la polarisation de la liaison éthylénique $\diagdown C{=}C \diagup$ et traduira l'effet donneur mésomère, du groupement $(C_6H_5)_3E{-}CH_2{-}$, en fonction de l'élément E. Le tableau 5 montre que $\Delta_{Ge} - \Delta_{Si}$ est de l'ordre de l'unité, $\Delta_{Pb} - \Delta_{Sn}$ de l'ordre de 0,5, en revanche $\Delta_{Sn} - \Delta_{Ge}$ est de l'ordre de 3,5, ce qui permet de classer les éléments E, dans l'ordre d'effet donneur mésomère pour les substituants $R_3ECH_2{-}$ et $R_3ECH(CH_3){-}$:

$$Pb \approx Sn \gg Ge > Si$$

Les résultats expérimentaux obtenus, ne sont pas incompatibles avec l'existence (28), d'ailleurs discutée (29), d'un effet $(p-d)\pi$ pour les dérivés du silicium et du germanium, ce qui aurait pour effet une polarisation inverse de la liaison éthylénique par effet accepteur du substituant:

$$R_3E \longleftarrow \underset{CH_2}{\diagup\diagdown} CH{=}CH{-}CH_3$$

Dans ce cas la polarisation observée expérimentalement serait la résultante de deux effets contraires.

Pour les dérivés du plomb et de l'étain les effets mésomères donneurs du substituant σ sont comparables; ce résultat s'interprète en admettant que le groupement $-Pb(C_6H_5)_3$ est plus électronégatif que $-Sn(C_6H_5)_3$. En effet, l'hyperconjugaison de deux systèmes σ et π est sous le contrôle (30) de (a) la différentielle d'énergie $E = E(\sigma) - E(\pi)$; (b) l'intégrale de perturbation $P(\sigma\pi)$; (c) la densité électronique $a^2(\sigma)$ et $a^2(\pi)$

Can. J. Chem. Downloaded from www.nrcresearchpress.com by 210.87.254.6 on 09/06/12
For personal use only.

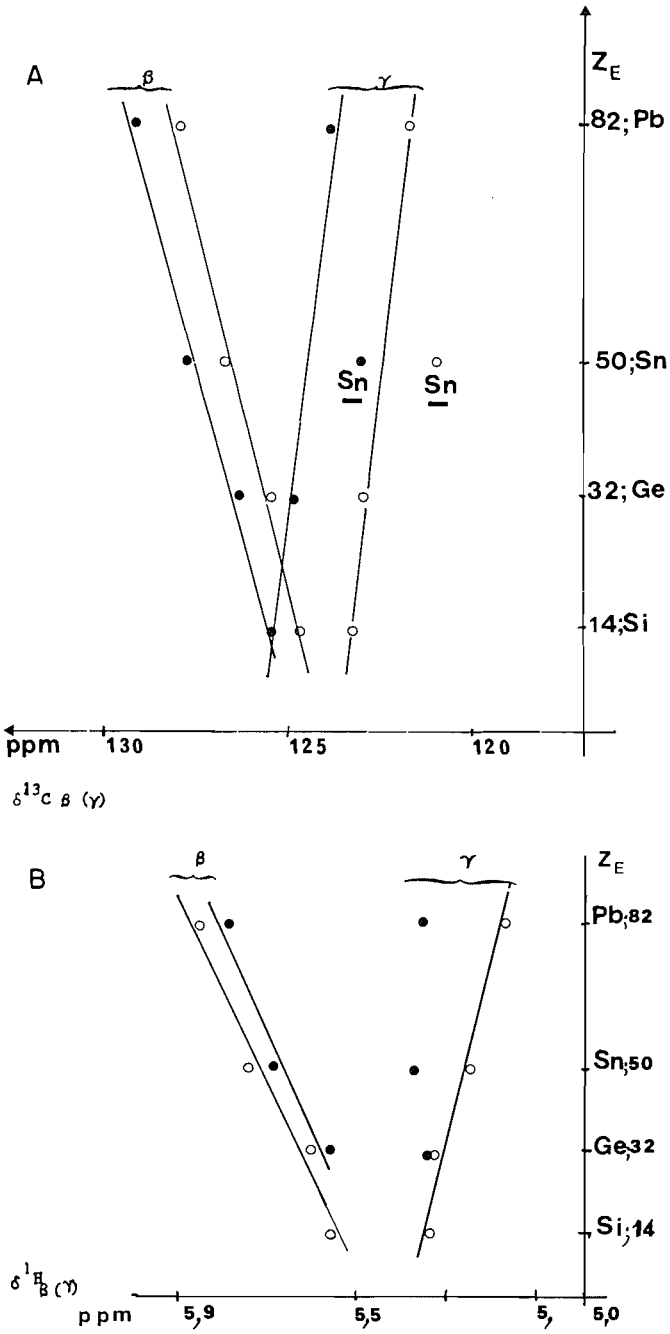

FIG. 5. Déplacements chimiques des noyaux éthyléniques N (^{13}C et ^1H), positions β et γ, en fonction du numéro atomique Z_E de l'élément E—IVA; isomères $(C_6H_5)_3ECH_2CH{=}CH{-}CH_3$, *1E* —●— et *1Z* —○—; (A) N = ^{13}C; (B) N = ^1H. On notera le blindage inattendu des carbones C_γ dans le cas des dérivés de l'étain.

dans les orbitales *p* des atomes reliant les systèmes σ et π; elle est favorisée par une différentielle d'énergie ΔE, faible, et des densités électroniques $a^2(\sigma)$, $a^2(\pi)$, élevées. Pour les systèmes envisagés $(C_6H_5)_3ECH_2CH{=}CH{-}CH_3$ *E*, *Z* et $(C_6H_5)_3ECH(CH_3)CH{=}CH_2$, l'effet donneur observé sera essentiellement sous le contrôle de $R(\sigma)$ et de $a^2(\sigma)$; en effet, $E(\pi)a^2(\pi)$, restent invariant et l'influence de $P(\sigma\pi)$ est faible (30). Comme la différentielle d'énergie, ΔE, décroît de Si à Pb (30, 31), les résultats expérimentaux obtenus impliquent que $a^2(\sigma)_{Pb} < a^2(\sigma)_{Sn}$, c'est-à-dire, que le groupement $-Pb(C_6H_5)_3$ soit plus électronégatif que $-Sn(C_6H_5)_3$, ce qui est en accord avec les résultats présentés antérieurement et comparable aux résultats obtenus par ailleurs (31) pour les systèmes benzyliques correspondants. On ne peut rien conclure quant aux électronégativités respectives des groupements $-Ge(C_6H_5)_3$ et $-Si(C_6H_5)_3$, car l'effet $(p \rightarrow d)\pi$ décroît du dérivé du silicium au dérivé du germanium. L'effet d'hyperconjugaison, traduit par la polarisation de la liaison éthylénique, proportionnelle à $\Delta_E = \delta C_\beta - \delta C_\gamma$, est nettement plus important pour $R = CH_3$ que pour $R = C_6H_5$ (Tableau 5); ce qui est en accord avec l'effet de la taille du substituant R_3E ainsi qu'avec une polarisation plus importante de la liaison $CH_2{-}Sn(CH_3)$ par rapport à $CH_2{-}Sn(C_6H_5)_3$; de plus $Sn(CH_3)_3$ possède un effet donneur par induction tandis que $Sn(C_6H_5)_3$ a une effet accepteur par induction; en effet:

$$\chi^{int}_{Sn(C_6H_5)_3} = 8{,}020 > \chi^{int}_{-CH_2CH=CH-CH_3} = 7{,}597 > \chi^{int}_{Sn(CH_3)_3} = 7{,}47$$

Nous notons, en revanche, une influence négligeable sur les déplacements chimiques δN_α et δN_β (N = ^1H, ^{13}C) du substituant à l'hétéroatome.

Il convient de souligner l'existence d'une corrélation linéaire entre les déplacements chimiques des carbones éthyléniques et le numéro atomique Z_E de l'hétéroatome (Fig. 5A). La même figure fait apparaître un blindage exceptionnel de C dans le cas des dérivés de l'étain; il peut être interprété en termes d'effet stérique γ, lequel pourrait être favorisé pour E = Sn.

Paramètres δ^1H_α, $\delta^{13}C_\alpha$

Ces paramètres sont soumis, en particulier, à l'influence de l'hétéroatome et de la double liaison allylique.

Afin d'éclairer l'influence sur ces variations de la double liaison allylique (métallohyperconjugaison, liaison $(p{-}d)\pi$...) nous avons comparé les données obtenues pour les dérivés *1E*, *Z*, **2** à celles correspondantes extraites de la littérature (32) pour les composés $E(CH_3)_4$. Cette étude comparative met au jour pour ces deux groupes de composés une similitude en ce qui concerne les paramètres δ^1H_α et $\delta^{13}C_\alpha$ (Tableau 6) et, tout particulièrement *un blindage de* $\delta^{13}C_\alpha$, *inattendu à priori, pour les dérivés de l'étain*, que l'effet inductif des groupements $-SnR_3$ (R = CH_3, C_6H_5) ne suffit pas à justifier, ce qui met au jour une solution de continuité dans la série au niveau de l'étain. Par ailleurs (33), les variations des énergies de liaison pour les composés EF_4 le long de la colonne IV-A sont similaires à celles observées pour les paramètres $\delta^{13}C_\alpha$ et δ^1H_α. De même, les courbes $\delta^{13}C_\alpha = f(\delta^1H_\alpha)$, établies pour les deux groupes de composés *1E*, *Z*, **2** et $E(CH_3)_4$ (Fig. 6*a*, *b*, *c*), présentent des analogies importantes. Ces résultats témoignent en faveur du fait que les paramètres δ^1H_α et $\delta^{13}C_\alpha$ ne se trouvent pas sous le contrôle du système π-allylique et qu'ils sont régis par des *facteurs inhérents à la nature même de l'hétéroélément*, tels que l'apparition des orbitales *d* à partir de la 3ième période (E = Si à Pb), la contraction des métaux de transition (4ème période) et la contraction des lanthanides (6^e période), ces deux derniers phénomènes ayant pour effet de rendre plus compacts le germanium et le plomb par rapport aux éléments (Si et Sn) qui les précédent respectivement; de même, dans le cas de éléments des 4ième et 6ièmes périodes, le remplissage des orbitales 3*d* et 4*f*, relativement diffuses, conduit à un blindage de la charge nucléaire moins efficace, ce qui a pour conséquence une attraction plus forte des électrons 4*s* et 6*s*.

Les remarques suivantes peuvent être faites en ce qui concerne les paramètres $\delta^{13}C_\delta$ *et* δ^1H_δ

Pour le composé **2** on observe l'existence d'une corrélation

TABLEAU 6. Données comparatives des paramètres $\delta^{13}C_\alpha$, δ^1H_α et $^1J(^{13}C—H)$ pour les composés **1***E*, *Z* ($R = C_6H_5$) et $E(CH_3)_4$

$(C_6H_5)_3E\underset{\alpha}{CH_2}\underset{\beta}{CH}=\underset{\gamma}{CH}—\underset{\delta}{CH_3}$ **1***E*, *Z*

E	$\delta^{13}C_\alpha$ (ppm)[a] **1***E*	**1***Z*	δ^1H_α (ppm) **1***E*	**1***Z*	$^1J(^{13}C—H)_\alpha$ (Hz)	$E(CH_3)_4$ $\delta^{13}C$ (ppm)	δ^1H (ppm)	$^1J(^{13}C—H)$ (Hz)
C	+44,39		+3,35		127	+31,7	+0,958	124
Si	+19,16	+14,55	+2,30	+2,33	120,6	0	0	119
Ge	+19,40	+14,83	$+2,38_5$	+2,43		−1,4	+0,133	126
Sn	+15,90	+11,97	+2,36	+2,39	131,1	−8,6	+0,033	128
Pb	+27,56	+23,27	$+2,87_5$	+2,90	139,2	−2,6	+0,7	133

[a]Les déplacements chimiques sont donnés par rapport au TMS; un signe positif correspond à un déplacement vers les champs faibles.

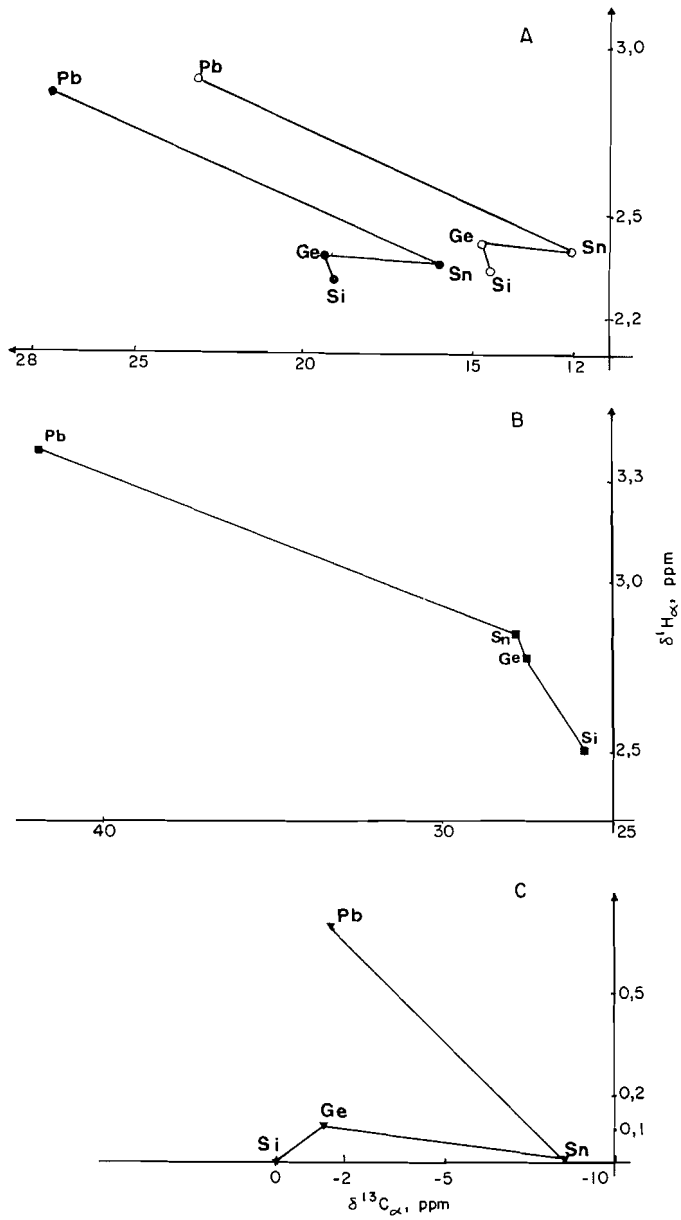

FIG. 6. Déplacement chimique du proton ^1H en fonction du déplacement chimique du carbone vicinal ^{13}C, position α, pour (A): les isomères $(C_6H_5)_3ECH_2CH=CH—CH_3$, **1***E* −●− et **1***Z* −○−; (B): l'isomère $(C_6H_5)_3ECH(CH_3)CH=CH_2$ **2** et (C): les composés $E(CH_3)_4$, données de la littérature (32).

TABLEAU 7. Couplages des protons éthyléniques H_β, H_γ; composés **1***E*, *Z*; $R = C_6H_5$

E	Composé	$J(H_\beta—H_\gamma)$ (Hz)
Si	**1***E*	—
	1*Z*	10,25
Ge	**1***E*	15
	1*Z*	10,5
Sn	**1***E*	15,25
	1*Z*	10,5
Pb	**1***E*	15
	1*Z*	10,25

linéaire entre ces deux paramètres, tandis que pour les composés **1***E*, *Z* $\delta^{13}C$ = const. (Fig. 4); ceci suggère que, dans le premier cas, un même facteur contrôle les deux paramètres tandis que, dans le second, les déplacements chimiques légèrement paramagnétiques du proton sont contrôlés par l'effet d'anisotropie magnétique voisine, dûe aux groupements $—E(C_6H_5)_3$.

IV. *Couplages*

Dans tout ce qui suit seront envisagées les *valeurs absolues* des couplages. L'étude des couplages homonucléaires $J(H—H)$ (Tableau 7), $^1J(^{13}C—H)$ (Tableau 8) $^nJ(E—C—H)$ (Tableaux 9 et 10) et $^nJ(E—^{13}C)$ (Tableau 11) corrobore les conclusions qui se dégagent de l'étude des déplacements chimiques δ^1H et $\delta^{13}C$.

1. *Couplages homonucléaires* $J(H_\beta—H_\gamma)$ *(Tableau 7)*

Les couplages $J(H_\beta—H_\gamma)$ sont de l'ordre de 15 Hz (**1***E*) et de 10 Hz (**1***Z*) (valeurs classiques pour des protons éthyléniques respectivement *trans* et *cis*); ils confirment une structure σ allylique pour les composés **1***E*, *Z*. Pour les dérivés secondaires **2** ces valeurs n'ont pu être déterminées aisément à partir des spectres, les protons H_β et H_γ étant trop fortement couplés. Cependant $J(H_\beta—H_\gamma)$ (*Z*) = 9,66 Hz et $J(H_\beta—H_\gamma)$ (*E*) = 17,33 Hz ont pu être calculés pour le dérivé deutérié $(C_6H_5)_3SnCD_2CH=CH_2$.

2. *Couplages hétéronucléaires*

Avant de discuter les résultats expérimentaux obtenus, il convient d'ouvrir une parenthèse et de rappeler que les constantes de couplage $^1J(^{13}C—H)$, $^1J(E—^{13}C)$ et $^2J(E—C—H)$ sont gouvernées par le terme de contact de Fermi (34−36) et que, si de façon générale nous désignons par N et N′ les deux noyaux couplés, les constantes de couplage envisagées seront données par l'expression [4].

Can. J. Chem. Downloaded from www.nrcresearchpress.com by 210.87.254.6 on 09/06/12
For personal use only.

Can. J. Chem. Downloaded from www.nrcresearchpress.com by 210.87.254.6 on 09/06/12
For personal use only.

TABLEAU 8. Couplages $^1J(^{13}C—H)$; composé **1***E*; R = C_6H_5; fragment allylique

	$^1J(^{13}C—H)$ (Hz)			
E	C_α	C_β	C_γ	C_δ
C	127,6	157,9	158,9	125,6
Si	120,6	151,2	151,6	125,4
Sn	131,1	158,9	150,2	125,2
Pb	139,2	159	148,5	125,6

[4] $J_{NN'} = (C/\Delta E)\,\alpha_N^2\,\alpha_{N'}^2\,\psi^2(0)\mathrm{ns}(N)\,\psi^2(0)\mathrm{ns}(N')$

où α^2: caractère *s* des orbitales formant la liaison; $\psi^2(0)$: densité des électrons *s* des noyaux couplés; ΔE: énergie moyenne d'excitation singulet−triplet; C = ensemble de constantes.

$^1J(^{13}C_\alpha—H_\alpha)$ (Tableau 8)

On observe une variation non monotone du couplage $^1J(^{13}C—H)$ lorsque E varie de la seconde (n = 2) à la sixième période (n = 6) en passant par un minimum $^1J(^{13}C—H)$ = 120,6 cps, E = Si, inférieur à la valeur attribuée à un carbone sp^3, soit 125 Hz.

Conformément à l'équation [4], une interprétation possible de l'accroissement de $^1J(^{13}C—H)$ serait d'envisager un accroissement du caractère *s*, $\alpha^2(C)$, de l'orbitale hybride du carbone formant la liaison $C_\alpha—H_\alpha$ et, de façon hâtive, d'en attribuer l'origine à une hyperconjugaison σ−π. Cependant, une analyse plus poussée montre que l'hyperconjugaison, bien que compatible avec un accroissement du caractère *s* de l'orbitale du carbone formant la liaison C—H, n'est pas l'unique promoteur de celui-ci; en effet, les variations des couplages $^1J(^{13}C—H)$ observées, de même que pour les paramètres δ^1H et $\delta^{13}C_\alpha$, sont en tous points comparables à celles observées pour les dérivés tétramethylés correspondants, $E(CH_3)_4$ (32) (Tableau 6), pour lesquels un accroissement du caractère *s* de l'orbitale du carbone vers l'hydrogène et une diminution de ce caractère vers l'élément IV-A, lorsque E varie de la 3ième à la 6ième période, donc indépendemment de l'existence d'une métallohyperconjugaison, a été mis en évidence (37).

$^1J(^{13}C_\gamma—H_\gamma)$ est fonction décroissante (Tableau 8) de la période de l'élément IV-A. Ce résultat peut être interprété en termes d'une diminution du caractère *s* de l'orbitale hybride du carbone formant la liaison $C_\gamma—H_\gamma$ ou (et) en termes d'une augmentation de la charge portée par le carbone C_γ (l'énergie moyenne d'excitation ΔE, décroît de Si à Pb), ce qui témoigne en faveur de l'existence d'une hyperconjugaison σ−π de la liaison C—E et de la double liaison allylique).

Couplages $^2J(E—C—H)$ (Tableaux 9 et 10)

Si (Tableau 10) nous comparons les constantes de couplages

TABLEAU 9. Couplages $^nJ(E—C—H)$, n = 2, 3, 5; composés **1***E*, *Z*, **2**; E = Sn, Pb; fragment allylique

			$^nJ(E—C—H)$ (Hz)			
R	Composé	E	^2J	$^3J_\delta$	^5J	$^2J_{CH_3}$
C_6H_5	**1***E*	Sn	68		26	
		Pb	86		63	
	1*Z*	Sn			20	
		Pb			51	
	2	Sn		72; 75		
		Pb		158		
CH_3	**1***E*					50,8; 53,6
	1*Z*	Sn				49,6; 53,6
	2			66; 68		49,5

hétéronucléaires $^2J(E—C—H)$ des composés **1***E*, **3**, **4**, **5**, **6** et **7**, il apparait que l'on peut grouper ces composés en *2 groupes distincts: les composés **3**, **4** et **5**, d'une part*, pour lesquels $^2J(E—C—H)$ (CH_3 ou CH_2) se situe entre 50 et 55 Hz (E = Sn) ou 61 à 68,5 Hz (E = Pb) et *les composés allyliques **1** et benzyliques **6**, **7**, de l'autre*, pour lesquels $^2J(E—C—H)$ (CH_2) est nettement plus élevé: 68 Hz (E = Sn); 86 Hz (E = Pb). En outre, l'examen des couplages $^2J(E—C—H)$ (CH_3) pour les composés **1***E*, *Z*, **2** (Tableau 9) et **7** (Tableau 10) montre que celui-ci reste voisin de 50 Hz, donc de la valeur caractéristique pour la liaison $Sn(sp^3)—C(sp^3)$. Ces faits témoignent pour les dérivés allyliques **1** ainsi que pour les dérivés benzyliques **6**, **7** de l'existence d'une contribution importante d'un type particulier au mécanisme de couplage $^2J(E—C—H)$ (CH_2). En effet, la rehybridation de l'hétéroélément est insuffisante pour expliquer a elle seule une différence aussi importante des couplages observés; il paraît raisonnable d'attribuer cette valeur élevée à une contribution importante des électrons π au mécanisme de couplage, accrue par un accès direct aux électrons *s* de l'hétéroélément, ayant pour origine l'hyperconjugaison σ−π de la liaison C—E et de la liaison σ allylique; l'existence de cette dernière a été établie pour les composés **6** et **7** sur la base de la spectroscopie électronique (44) et de la rmn du carbone ^{13}C (45, 46).

$^5J(E—C—H)$ (Tableau 9) et $^nJ(E—^{13}C)$, n = 2−4 (Tableau 11)

Les valeurs élevées des *couplages hétéronucléaires à longue distance*: $^5J(E—C—H)$, $^4J(E—^{13}C)$, $^2J(E—^{13}C_\beta)$ témoignent d'une contribution importante des électrons π au mécanisme de couplage; en accord avec ce qui précède nous l'attribuons à l'hyperconjugaison σ−π.

Des valeurs de $^nJ(Sn—^{13}C)$, n = 2−4 et $^5J(Sn—C—H)$ (CH_3), en fonction du mécanisme de couplage (mécanisme σ avec plus ou moins de contribution des électrons π) sont don-

TABLEAU 10. Comparaison des constantes de couplage hétéronucléaires $^2J(E—C—H)$

		$^2J(E—C—H_\alpha)$ (Hz)	
Composé		$^{117,119}Sn$	^{207}Pb
$(C_6H_5)_3EC\mathit{H}_2CH=CHCH_3$	**1***E*	68	86
$(C_6H_5)_3EC\mathit{H}_3$	**3**	54,4; 56,6 (38)	68,5 (41)
$(C_6H_5)_3EC\mathit{H}_2CH_3$	**4**	56,5 (43)	
$(C\mathit{H}_3)_4E$	**5**	52,0; 54,3 (38)	61,0 (41)
$(C_6H_5)_3EC\mathit{H}_2C_6H_5$	**6**	64,8; 67,0 (42)	
$(C\mathit{H}_3)_3EC\mathit{H}_2C_6H_5$ (38)	**7**	CH_2: 60,4; 62,7; CH_3: 51,0; 53,4	

TABLEAU 11. Couplages $^nJ(E—^{13}C)$, E = Sn, Pb; composés **1***E*, *Z*, **2**; fragment allylique

			$^nJ(E—^{13}C)$ (Hz)					
			^1J		^2J		^3J	^4J
R	E		C_α	C_{CH_3}	C_β	C_δ	C_γ	C_δ
CH_3	Sn	**1***E*	318,7; 304,9	322,7; 308,9	48,5		52	13,5
		1*Z*	302,6; 290,2	322,5; 307,1	49,6		50	13,2
		2	329,9; 316,0	314,9; 301,0	41,5	18,4	48,2	
C_6H_5	Sn	**1***E*	357,1; 340,1		49		56,7	14,0
		1*Z*			52,2		53,6	
		2	364,8; 349,5		44,9	21,7	53,3	
C_6H_5	Pb	**1***E*	334,7		97,3		118,8	32,5
		1*Z*	311,7		100,0		115	
		2			83,6		103,8	

TABLEAU 12. Des valeurs de $^nJ(Sn—C)$ (n = 2–4) et $^5J(Sn—C—H)$ (CH_3) en fonction du mécanisme de couplage

	$^nJ(^{117:119}Sn—C)$ (Hz)			$J(^{117:119}Sn—H)$ (Hz)
Composé	^2J	^3J	^4J	^5J
$R_3SnCH_2CH=CHCH_3$ **1***E*	48,5 49	52 56,7	13,5 14,0	26 a b
$R_3SnCH_2CH=CHCH_3$ **1***Z*	49,6	50	13,2	20 a
$R_3SnCH(CH_3)CH=CH_2$ **2** (δ β γ)	44,9 β 21,7 δ	53,3 γ		
$Sn(CH_2CH_2CH_2CH_3)_4$ **8** (12)	19,6	52	≃0	
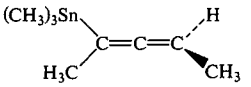 **9** (12)	24,1	51,5	28,2	
o-$CH_3BzSn(CH_3)_3$ **10** (47)				5,2
2,3$(CH_3)_2C_6H_3Sn(CH_3)_3$ **11** (40)	32,4 (40)	41,0	7,4 — CH_3 10,7 Ar	6,4 — CH_3
$Bz(Sn(CH_3)_3$ **12** (11)	36,6	22,6	12,0	
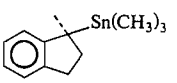 **13** (45)	32,0	22,0		
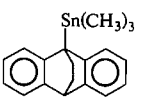 **14** (45)	5,9	34,1		

(a) R = —C_6H_5; (b) R = —CH_3.

nées dans le tableau 12. On remarque, pour $^nJ(Sn—^{13}C)$, que lorsque le mécanisme est de type σ (**8**, **2**(C_δ) et **14**) l'inégalité $^2J < {}^3J$ se trouve vérifiée et que les valeurs des couplages ^2J et ^4J sont, entre autres, fonctions croissantes de la contribution des électrons π au mécanisme de couplage, en effet (Tableau 12) lorsque les électrons π participent au mécanisme de couplage $^2J > {}^3J$ (**12**, **13**) ou $^2J \approx {}^3J$ (**1***E*, *Z*, **2**(C_β), de même ^4J(**8**; σ) < ^4J(**1***E*, *Z*; σ−π) < ^4J(**9**). L'examen des constantes de couplage $^1J(^{13}C—E)$ (E = Sn, Pb) (Tableau 11) qui sont déterminées par le terme de contact de Fermi et données par l'expression [4] ne permet, dans l'état actuel des connaissances, aucune conclusion quant à l'existence d'une hyperconjugaison mettant en jeu la liaison C—E.

Nous terminerons par quelques mots sur la structure géométrique des dérivés étudiés, suggérée par les résultats obtenus au cours de cette étude.

L'hyperconjugaison σ−π entraine la coplanarité de la liaison σ et de l'axe de l'orbital π déficient en électrons. Aussi bien, nous proposons pour les composés étudiés une structure intermédiaire (Fig. 7) entre les formes *gauches* pour lesquelles ϕ = 60° et 120°.

Les conformères *cis* et *trans* sont, en général, évincés au profit des formes *gauches* lorsque la taille de X croît (48), ainsi, pour les halogénures d'allylmercure seules les formes *gauches* existent (29,49). Les valeurs élevées observées pour les couplages $^5J(E—C—H)$ et $^4J(E—^{13}C)$ E = Sn, Pb qui sont fonctions, en particulier, de l'angle dièdre ϕ des plans $SnC_\alpha C_\beta$ et $C_\alpha C_\beta C_\gamma$ (Fig. 7), s'accordent avec l'extrusion de la liaison C—E hors du plan nodal de l'orbitale π allylique favorisant le recouvrement de l'orbital π et de l'orbitale *ns* de l'élément E. Il est possible qu'en cas de demande d'électrons, la liaison σ fasse un angle voisin de 90°, avec le plan nodal de la double liaison allylique, et que, comme pour le bromure d'allymercure (29) dans la configuration d'énergie minimum, la liaison C—E soit perpendiculaire au plan nodal du système oléfinique.

Can. J. Chem. Downloaded from www.nrcresearchpress.com by 210.87.254.6 on 09/06/12
For personal use only.

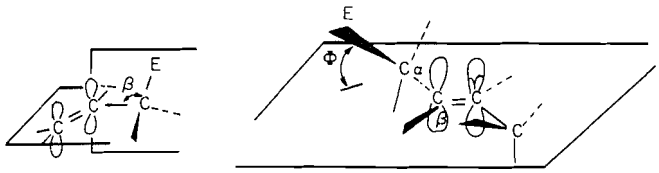

FIG. 7. Structure proposée pour les composés 1*E*, *Z* et **2**.

Partie expérimentale

I. *Synthèse des dérivés 1*E, *Z et 2*

Les synthèses des dérivés primaires $R_3ECH_2CH{=}CH{-}CH_3$ 1*E*, *Z* (E = C, Si, à Pb) (50*a*) et des dérivés secondaires $R_3ECH(CH_3)CH{=}CH_2$ **2** (E = Si à Sn) (50*b*) ont été décrites par ailleurs. Le dérivé secondaire du plomb est obtenu mélangé à du dérivé primaire (**2**: 70%; 1*E*, 1*Z*: 30%) en opérant de la même façon que pour les dérivés de l'étain, mais en effectuant toutes les opérations *rigoureusement sous argon*.

II. *Spectres de résonance magnétique nucléaire du carbone ^{13}C et du proton ^{1}H*

Les spectres de rmn ont été enregistrés sur spectrographe Varian XL-100 (100 MHz) pour le proton et Varian XL-100 (25, 15 MHz) pour le carbone-13, en utilisant la technique de transformée de Fourier; le deutérochloroforme a été utilisé comme solvant et le TMS comme étalon interne.

Remerciements

Nous remercions Madame M.-J. Pouet du laboratoire de RMN de l'E.N.S.C.P., dirigé par Madame M.-P. Simonnin pour l'enregistrement des spectres à 60 et 100 Mz; les spectres à 250 Mz ont été enregistrés au laboratoire de l'E.N.S., dirigé par Monsieur J.-Y. Lallemand, que nous remercions.

1. V. A. PETUKHOV, V. F. MIRONOV et P. P. SHORYGIN. Izv. Akad. Nauk SSSR Ser. Khim. 2203 (1964).
2. A. N. EGOROCHKIN, M. L. KHIDEKEL, G. A. RAZUVAEV, G. G. PETUKHOV et V. F. MIRONOV. Izv. Akad. Nauk SSSR Ser. Khim, 1521 (1964).
3. D. J. BLEARS, S. S. DANYLUCK et S. CAWLEY. J. Organomet. Chem. **6**, 284 (1966).
4. A. N. EGOROCHKIN, A. I. BUROV, V. F. MIRONOV, T. K. GAR et N. S. VYAZANKIN. Izv. Akad. Nauk SSSR Ser. Khim. 51 (1969).
5. A. N. EGOROCHKIN, A. I. BUROV, V. F. MIRONOV, T. K. GAR et N. S. VYAZANKIN. Izv. Akad. Nauk SSSR Ser. Khim. 775 (1969).
6. A. N. EGOROCHKIN, S. YA. KHORCHEV, N. S. VYAZANKIN et E. N. GLADYSHEV. Izv. Akad. Nauk SSSR Ser. Khim. 1863 (1969).
7. K. KAWAKAMI et H. G. KUIVILA. J. Org. Chem. **34**, 1502 (1969).
8. N. M. SERGEYEV, YU. K. GRISHIN, YU. N. LUSIKOV et YU. A. USTYNYUK. J. Organomet. Chem. **38**, C1 (1972).
9. YU. K. GRISHIN, N. M. SERGEYEV et YU. A. USTYNYUK. Org. Magn. Reson. Rev. **4**, 377 (1972).
10. G. C. LEVY, D. M. WHITE et J. D. CARGIOLI. J. Magn. Reson. **8**, 280 (1972).
11. D. DODDRELL, M. L. BULLPITT, C. J. MOORE, C. W. FONG, W. KITCHING, W. ADCOCK et B. D. GUPTA. Tetrahedron Lett. 665 (1973).
12. H. G. KUIVILA, J. L. CONSIDINE, R. J. MYNOTT et R. H. SARMA. J. Organomet. Chem. **55**, C11–C14 (1973).
13. G. DUMARTIN, J.-P. QUINTARD et M. PEREYRE. J. Organomet. Chem. **185**, C34 (1980).
14. J. E. HUHEEY. (*a*) J. Phys. Chem. **69**, 3284 (1965); (*b*) **70**, 2086 (1966).
15. A. L. ALLRED et E. G. ROCHOW. (*a*) J. Inorg. Nucl. Chem. **5**, 264 (1958); **5**, 269 (1958); (*b*) **20**, 167 (1961).
16. R. S. DRAGO. J. Inorg. Nucl. Chem. **15**, 237 (1960).
17. J. HINZE et H. H. JAFFE. (*a*) J. Am. Chem. Soc. **84**, 540 (1962); (*b*) **85**, 148 (1963); (*c*) Can. J. Chem. **41**, 1315 (1963).
18. N. C. BAIRD et M. A. WHITEHEAD. Theor. Chim. Acta, **6**, 178 (1966).
19. W. H. HANSTEIN, H. J. BERWIN et T. G. TRAYLOR. J. Am. Chem. Soc. **92**, 7476 (1970).
20. A. L. ALLRED. J. Inorg. Nucl. Chem. **17**, 215 (1961).
21. P. T. NARASIMHAN et M. T. ROGERS. J. Am. Chem. Soc. **81**, 5983 (1960), et réfs. citées.
22. D. G. FARNUM. Adv. Phys. Org. Chem. **11**, 124 (1976).
23. J. A. POPLE. (*a*) J. Chem. Phys. **37**, 53 (1962); (*b*) Proc. R. Soc. London Ser. A, **239**, 541 (1957).
24. M. KARPLUS et J. A. POPLE. J.Chem. Phys. **38**, 280 (1963).
25. W. J. HEHRE, R. W. TAFT et R. D. TOPSOM. Prog. Phys. Org. Chem. **12**, 173 (1976).
26. H. HENRY et S. FLISZAR. J. Am. Chem. Soc. **100**, 3312 (1978).
27. T. YONEMOTO. J. Magn. Reson. (*a*) **12**, 93 (1973); (*b*) **13**, 153 (1974).
28. J. NAGY et J. REFFY. (*a*) J. Organomet. Chem. **22**, 565 (1970); (*b*) **23**, 79 (1970); (*c*) the 1st Symp. on Org. Chem. of Ge, Sn, Pb (France), Marseille. 1974.
29. R. D. BACH et P. A. SCHERR. J. Am.Chem. Soc. **94**, 220 (1972).
30. C. G. PITT. J. Organomet. Chem. **61**, 49 (1973).
31. W. ADCOCK, D. P. COX et W. KITCHING. J. Organomet. Chem. **133**, 393 (1977).
32. H. SPIESECKE et W. G. SCHNEIDER. J. Chem. Phys. **35**, 722 (1961).
33. A. J. DOWNS et C. J. ADAMS. *Dans* Comprehensive inorganic chemistry. Vol. 2. Pergamon Press, Oxford. 1973, p. 1259; selon K. Seppelt. Angew. Chem. Int. Ed. Engl. **18**, 186 (1979).
34. C. JUAN et H. S. GUTOWSKY. J. Chem. Phys. **37**, 2198 (1962).
35. G. W. SMITH. J. Chem. Phys. **42**, 435 (1965).
36. F. J. WEIGERT, M. WINOKUR, J. D. ROBERTS. J. Am. Chem. Soc., **90**, 1566 (1968).
37. G. W. SMITH. J. Chem. Phys. **39**, 2031 (1963).
38. K. SISIDO, T. MIYANISI, K. NABIKA et S. KOZIMA. J. Organomet. Chem. **11**, 281 (1968).
39. G. BARBIERI et F. TADDEI. J. Chem. Soc. Perkin Trans. 2, 1323 (1972).
40. C. D. SCHAEFFER, JR. et J. J. ZUCKERMAN. J.Organomet. Chem. **99**, 407 (1975).
41. D. DE VOS. J. Organomet. Chem. **104**, 193 (1976).
42. M. GIELEN, M. DE CLERQ et B. DE POORTER. J. Organomet. Chem. **34**, 305 (1972).
43. L. VERDONCK et G. P. VAN DER KELEN. (*a*) Bull. Soc. Chim. Belg. **76**, 258 (1967); (*b*) Ber. Bunsenges. Phys. Chem. **69**, 478 (1965).
44. A. HOSOMI et T. G. TRAYLOR. J. Am. Chem. Soc. **97**, 3682 (1975).
45. W. ADCOCK, B. D. GUPTA, W. KITCHING, D. DODDRELL et M. GECKLE. J. Am. Chem. Soc. **96**, 7360 (1974).
46. W. ADCOCK, B. D. GUPTA, W. KITCHING et D. DODDRELL. J.Organomet. Chem. **102**, 297 (1975).
47. M. DONADILLE, M. A. DELMAS, J. C. MAIRE et T. N. SRIVASTAVA. J. Organomet. Chem. **15**, 244 (1968).
48. A. A. BOTHNER-BY et H. GUNTHER. Disc. Faraday Soc. **34**, 127 (1962).
49. J. MINK et Y. A. PENTIN. J. Organomet. Chem. **23**, 293 (1970).
50. E. MATARASSO-TCHIROUKHINE et P. CADIOT. (*a*) J. Organomet. Chem. **121**, 155 (1976); (*b*) **121**, 169 (1976).

Can. J. Chem. Downloaded from www.nrcresearchpress.com by 210.87.254.6 on 09/06/12
For personal use only.

Two channel competitive photodecomposition reaction of gaseous bromoethane at 193.1 nm

KYUNG-HOON JUNG,[1] CHONG MOK LEE, AND HEE SOO YOO

Department of Chemistry, Korea Advanced Institute of Science and Technology, P.O. Box 150 Chongyangni, Seoul 131, Korea

Received February 28, 1983

KYUNG-HOON JUNG, CHONG MOK LEE, and HEE SOO YOO. Can. J. Chem. **61**, 2486 (1983).

The vacuum ultraviolet photolysis of gas phase bromoethane at 193.1 nm (6.42 eV) was studied over the pressure range of 1.1−303.2 Torr at room temperature using a carbon atom lamp. The pressure effect with and without inert gas, i.e., He or N_2, was investigated. A scavenger effect of the reaction was also observed by adding NO as a radical scavenger. The principal reaction products were C_2H_6, C_2H_4, 1,1-$C_2H_4Br_2$, and *n*-C_4H_{10}. The quantum yields of C_2H_4 and C_2H_6 were found to increase slightly with the reactant pressure. When the pressure of He or N_2 was varied at a constant pressure of C_2H_5Br, however, the quantum yields of C_2H_4 and C_2H_6 were found to be pressure independent. Addition of NO completely suppressed the formation of C_2H_6, $C_2H_4Br_2$, and C_4H_{10}, and partially reduced that of C_2H_4. These results were interpreted in terms of two channel competition between the molecular elimination and the formation of radicals. Two different decomposition modes were 82% radical reaction and 18% molecular elimination.

KYUNG-HOON JUNG, CHONG MOK LEE et HEE SOO YOO. Can. J. Chem. **61**, 2486 (1983).

On a étudié la photolyse sous vide dans l'ultraviolet du bromoéthane gazeux à 193,1 nm (6,42 eV) dans un intervalle de pression allant de 1,1 à 303,2 Torr à la température ambiante en utilisant une lampe au carbone. On a étudié l'effet de la pression, avec ou sans gaz inerte, par exemple le He ou le N_2. On a également observé un effet de piège de la réaction en ajoutant du NO comme piège à radical. Les principaux produits de la réaction sont: le C_2H_6, le C_2H_4, le $C_2H_4Br_2$-1,1 et le *n*-C_4H_{10}. En augmentant la pression du réactif, on a trouvé que les rendements quantiques en C_2H_4 et C_2H_6 augmentent légèrement. Cependant quand on fait varier la pression de He ou de N_2 tout en maintenant la pression du C_2H_5Br constante, on a trouvé que les rendements quantiques en C_2H_4 et C_2H_6 sont indépendants de la pression. L'addition de NO ne supprime pas complètement la formation de C_2H_6, de $C_2H_4Br_2$ et de C_4H_{10}, elle réduit partiellement celle de C_2H_4. On interprète ces résultats en fonction de deux voies compétitives; l'élimination moléculaire et la formation des radicaux. Les différents modes de décomposition sont à 82% de type réaction radicalaire et à 18% de type élimination moléculaire.

[Traduit par le journal]

Introduction

In this study, the vacuum ultraviolet photochemical investigation of the gas phase unimolecular decomposition of bromoethane at 193.1 nm was carried out using a carbon atom lamp. Its objective is to elucidate the primary photodissociation process.

The photochemistry of C_2H_5Br in the 210−313 nm region (1), where only the valence shell transition is possible, proceeds mainly by radical reaction via the C−Br bond fission. On the other hand, Tschuikow-Roux and co-workers reported the molecular elimination as the major primary process in the photolyses of haloethanes at 147 nm (2). Thus it is generally accepted that the modes of photochemical decomposition of the alkyl halides are wavelength dependent (3).

Our recent studies on the photodissociation of C_2H_5Br at 104.8−106.7 nm and 123.6 nm (4) and preliminary experiments of C_2H_5Br at 147 nm, 163.3 nm, and 174.3−174.5 nm also indicate that the primary photochemical decomposition modes of bromoethane are wavelength dependent. Compared with other previous works, our studies have some interesting aspects: the sequential change with wavelength of the relative importance of the two competitive decomposition modes, i.e., radical and molecular processes. The ratios of HBr elimination to C—Br bond fission of C_2H_5Br are 4.0, 1.5, 1.0, 0.47, and 0.25 at 104.8−106.7 nm, 123.6 nm, 147 nm, 163.3 nm, and 174.3−174.5 nm, respectively. In the vacuum ultraviolet and ultraviolet regions, the electronic transition of C_2H_5Br is termed $n \rightarrow \sigma^*$ and its broad maximum appears at about 200 nm. The shorter wavelength side of this absorption frequently extends into the vacuum ultraviolet region where it may overlap the absorption associated with Rydberg type transitions, viz., B band (177 nm) (5). Therefore 193.1 nm, which is between these two strikingly different reaction modes and which lies between the A and B bands, should be the key wavelength to observe the two channel competitive reactions.

Experimental

Photolyses were carried out at room temperature in a static system using a 340 cm^3 borosilicate glass reaction vessel with a CaF_2 window and with an all-glass circulating pump. Total conversions were kept less than 0.5% of the reactant. The light source was a carbon atom lamp (6) equipped with a 1 mm thickness Suprasil quartz window (7*a*) and operated by a microwave generator, KIVA Instrument, Inc., Model MPG-4M. The purity of the light source was routinely checked with a 0.3 m GCA/McPherson 218 VUV monochromator. Without an air filter, the emission spectrum up to 210 nm showed two lines at 165.7 and 193.1 nm. However, with an air filter, only the 193.1 nm line appeared since the 165.7 nm line was absorbed by oxygen in the air (7*b*). Our measurements of the absorption spectrum in this region (Cary 17 spectrophotometer) yielded an extinction coefficient at 193.1 nm in complete agreement with that cited in ref. 3, p. 523. Since carbon deposition on the window originating from the decomposition of CH_4 could not be removed, the percent transmission of the window decreased with prolonged operation of the lamp (8). The intensity fluctuation, i.e., 2×10^{13} to 5×10^{12} photons/s, was averaged by repeating the actinometry readings twice before and after each run. Chemical actinometry was based on the production of acetylene in the photolysis of ethylene, and the quantum yield of 0.40 (9) at 193.1 nm was assumed. Product analysis was done by Hewlett-Packard 5840A GC with twin FID. 1/8″ × 3 m s.s Chromosorb 108 was used to analyze C_2H_4, C_2H_6, and C_4H_{10} and 1/8″ × 3 m Nickel 20% Silicon DC 550/Chromosorb P for $C_2H_4Br_2$ and $C_4H_8Br_2$. C_2H_5Br, Eastman Kodak, was purified until the residual impurities were not detected by gas chromatography.

[1]To whom all correspondence should be addressed.

Can. J. Chem. Downloaded from www.nrcresearchpress.com by 210.87.254.105 on 09/06/12
For personal use only.

TABLE 1. Product quantum yield of photolysis of C_2H_5Br at 193.1 nm

Run No.	$P_{C_2H_5Br}$ (Torr)	Additives (Torr)	Quantum yield C_2H_4	C_2H_6	C_2H_4/C_2H_6	$It/N\times10^4$*
1	1.1		0.16	0.53	0.30	42.94
2	3.0		0.16	0.63	0.25	13.03
3	3.1		0.17	0.69	0.25	10.40
4	4.1		0.20	0.65	0.31	8.14
5	6.3		0.19	0.66	0.29	3.58
6	9.0		0.22	0.76	0.29	3.26
7	10.4		0.21	0.76	0.28	3.51
8	10.6		0.22	0.77	0.29	2.36
9	17.1		0.22	0.75	0.29	1.54
10	20.4		0.23	0.78	0.29	1.63
11	26.0		0.24	0.72	0.33	1.50
12	29.8		0.24	0.74	0.32	0.83
13	35.7		0.21	0.74	0.28	1.47
14	40.6		0.23	0.76	0.30	1.04
15	49.6		0.21	0.74	0.28	0.71
16	49.6		0.24	0.86	0.28	0.83
17	109.4		0.21	0.78	0.27	0.34
18	112.5		0.20	0.79	0.25	0.30
19	235.0		0.23	0.92	0.25	0.15
20	303.2		0.27	0.96	0.28	0.10
21	1.3	NO 1.6	0.15	0.00		38.03
22	3.2	NO 1.3	0.15	0.00		8.85
23	9.1	NO 3.8	0.18	0.00		2.67
24	20.2	NO 0.2	0.17	0.00		1.28
25	29.9	NO 10.0	0.15	0.00		1.46
26	48.8	NO 1.7	0.18	0.00		0.51
27	3.0	He 6.4	0.17	0.59	0.29	10.70
28	3.0	He 12.8	0.13	0.61	0.21	10.70
29	3.0	He 15.4	0.15	0.63	0.24	11.59
30	3.1	He 21.8	0.14	0.59	0.24	10.85
31	3.0	He 30.4	0.16	0.63	0.25	9.70
32	3.0	He 44.2	0.15	0.60	0.25	9.46
33	3.1	N_2 5.4	0.15	0.60	0.25	9.42
34	3.0	N_2 12.0	0.15	0.60	0.25	9.73
35	3.0	N_2 21.2	0.15	0.60	0.25	9.75
36	3.1	N_2 33.9	0.16	0.62	0.26	9.08

*I, number of photons per unit time; t, irradiation time; N, total number of reactant molecule.

Results

The principal reaction products are C_2H_6 and C_2H_4 (Table 1). In Table 1, run Nos. 1–20 represent the pressure effect of C_2H_5Br, where $\phi_{C_2H_6}$ increases from 0.53 to 0.96 and $\phi_{C_2H_4}$ also shows a small increase from 0.16 to 0.27. Run Nos. 21–26 are the results of the scavenger study, where the average $\phi_{C_2H_4}$ is 0.16 while C_2H_6 is not detected. Run Nos. 27–32 and 33–36 show the pressure effects with the addition of He and N_2, respectively, where the average quantum yield for C_2H_6 or C_2H_4 coincides in each case, i.e., $\phi_{C_2H_6}$ and $\phi_{C_2H_4}$ are 0.61 and 0.15, respectively. In addition, we observed the secondary products, $C_2H_4Br_2$ and C_4H_{10}, in a very long photolysis run for each product, i.e., $\phi_{CH_3CHBr_2} \sim 0.078$ while $\phi_{BrCH_2CH_2Br}$ is negligible at 7.2 Torr and $\phi_{C_4H_{10}}$ 0.082 at 48.5 Torr of C_2H_5Br pressure. However, these products are not detected in the presence of NO. The amounts of 2,3-dibromobutane were too small to measure.

Discussion

The discernible decrease of $\phi_{C_2H_4}$, i.e., ca. 0.05, in the presence of NO (Table 1, run Nos. 21–26), indicates the existence of some radical precursor for C_2H_4. Like the scavengeable portion of C_2H_4, the other scavengeable products, i.e., C_2H_6, $C_2H_4Br_2$, and n-C_4H_{10}, may be derived from an ethyl radical which is formed by C—Br bond fission of an electronically excited C_2H_5Br. However, the nonscavengeable portion of C_2H_4 would appear to be formed by a molecular elimination of HBr. Therefore, it is reasonable to assume that C_2H_5Br must be photolyzed by two channel competition. In the photolysis of C_2H_5Cl at 147 nm (2*b*), Tschuikow-Roux and co-workers interpret the results in terms of the initial formation of one and possibly two electronically excited states which decompose by molecular elimination and this state (or these states) is collisionally induced to cross over to an electronically excited state which decomposes by the C—Cl bond fission as the pressure is increased. In the present case, the quantum yield ratios of C_2H_4 and C_2H_6 are independent of the variation of the pressure and the product quantum yields are unaffected by the inert gases (Table 1). From these observations, it may be deduced that one electronically excited state is not converted to another by a collisionally induced process. Since the B and C bands of the Rydberg transitions are very diffuse (10), the $n \rightarrow \sigma^*$ transition absorption band and Rydberg transition absorption bands may overlap, which makes it plausible that the excitation

Can. J. Chem. Downloaded from www.nrcresearchpress.com by 210.87.254.105 on 09/06/12
For personal use only.

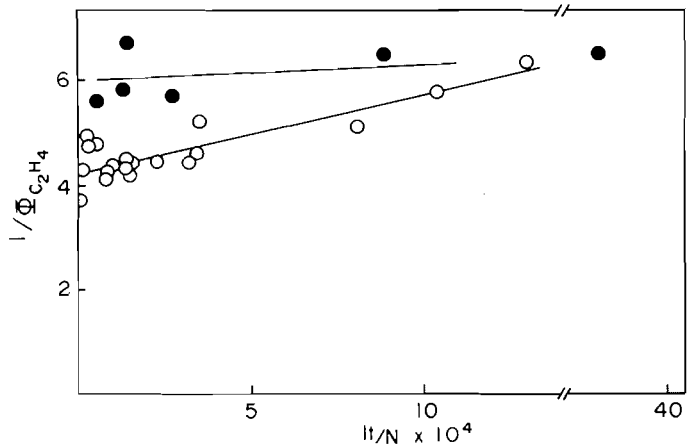

FIG. 1. Reciprocal of product quantum yields of C_2H_4 vs. It/N. ○, experiment without NO; ●, experiment with NO.

by monochromatic radiation results in two different excited states.

[1a] $C_2H_5Br + h\nu \rightarrow C_2H_5Br\dagger^{(1)}$

[1b] $\rightarrow C_2H_5Br\dagger^{(2)}$

[2] $C_2H_5Br\dagger^{(1)} \rightarrow C_2H_5 + Br$

[3] $C_2H_5Br\dagger^{(2)} \rightarrow C_2H_4 + HBr$

where the number dagger denotes an electronically excited state.

Since the photon energy at 193.1 nm is 148.1 kcal/mol and ΔH for [3] is 18.6 kcal/mol (11a), there are still 129.5 kcal/mol of energy remaining to be distributed between C_2H_4 and HBr. If the C_2H_4 molecule takes a large amount of the excess energy, it will be decomposed to C_2H_2, i.e., $C_2H_4^* \rightarrow C_2H_2 + H_2$, where the activation energy is 80 kcal/mol (12). However, the failure to observe C_2H_2 as a final product eliminates the possibility of this proposition. The number of internal degrees of freedom is larger in C_2H_4 than in HBr. Hence the C_2H_4 molecule must have a larger portion of the excess energy than the HBr molecule. Furthermore, the H—Br bond energy is 87.5 kcal/mol (11a) and the total quantum yields does not exceed unity until 100 Torr as shown in Table 1 (run Nos. 1–17). Thus it would not be likely that HBr undergo subsequent dissociation in this study.

From the tendency that $1/\phi_{C_2H_4}$ increases with increasing conversion, It/N (2), as shown in Fig. 1, one may suggest that C_2H_4 decreases by the reverse reaction of [3] and/or through some pathway to produce any other product as follows:

[4] $C_2H_4 + HBr \rightarrow C_2H_5Br$

[5] $C_2H_4 + Br \rightarrow C_2H_4Br$

[6] $C_2H_4 + C_2H_5 \rightarrow C_4H_9$

As $1/\phi_{C_2H_4}$ is almost constant with increasing It/N in the experiments with NO, the possibility of [4] can be eliminated. Since we have observed C_4H_{10} as our final product, it appears that the C_4H_9 radical formed by [6] may abstract a H atom from C_2H_5Br to produce C_4H_{10}.

[7] $C_4H_9 + C_2H_5Br \rightarrow C_4H_{10} + C_2H_4Br$

C_2H_5 radicals abstract H atoms from C_2H_5Br to produce most of the C_2H_6.

[8a] $C_2H_5 + C_2H_5Br \rightarrow C_2H_6 + CH_3CHBr$

[8b] $C_2H_6 + CH_2CH_2Br$

A possible mechanism for the scavengeable portion of the C_2H_4 can be written as:

[9] $C_2H_5 \rightarrow C_2H_4 + H$

[−5] $CH_2CH_2Br \rightarrow C_2H_4 + Br$

[10a] $2C_2H_5 \rightarrow C_2H_4 + C_2H_6$

[10b] $\rightarrow C_4H_{10}$

where the negative sign denotes the reverse reaction. ΔH of [9] is 38.1 kcal/mol (11a) whereas [8] is exothermic. Thus [9] is not plausible. Considering the ratio of [10a] to [10b] (13) and the C_2H_5 radical concentration, the contribution of [10a] is minor. Since the ΔH of [−5] is small, i.e., 8.1 kcal/mol (2c), compared with the excess energy of the bromoalkyl radical, [−5] may contribute to the major portion of scavengeable C_2H_4.

From the structural identity, the CH_3CHBr radical formed in [8a] must be the precursor of the CH_3CHBr_2. Failure to observe the 1,2-isomer (CH_2BrCH_2Br) shows that CH_3CHBr is the "wrong" radical and CH_2CH_2Br is the "right" radical which is formed in [8b] (11b)

[11] $CH_3CHBr + Br \rightarrow CH_3CHBr_2$

Since the product quantum yield of CH_3CHBr_2 is less than expected, one can propose additional termination processes as follows:

[12] $2CH_3CHBr \rightarrow C_4H_8Br_2$

[13] $2Br + M \rightarrow Br_2 + M$

The trace amount of 2,3-dibromobutane observed by GC analysis may be explained by [12].

Finally, this study makes it clear that the major mode of the primary process shifts to the radical reaction from molecular elimination sequentially with increasing wavelength of the light source in the uv/vuv region. Our ratios of $\phi_{C_2H_4}/\phi_{C_2H_6}$ extrapolate to 0.22 at zero pressure of C_2H_5Br which indicates a ratio of molecular elimination to radical decomposition of 18/82 at 193.1 nm. In addition, the importance of this study may be enhanced by the fact that the wavelength of the carbon atom lamp which has been scarcely used for photolysis work coincides with that of the ArF excimer laser and the findings of this study should be used as a key observation for a comparative study between the single photon and the multiphoton processes.

Acknowledgement

The continued support of the Korea Science and Engineering Foundation is gratefully acknowledged.

1. (*a*) J. G. ROOF and F. DANIELS. J. Am. Chem. Soc. **62**, 2912 (1940); (*b*) H. L. FRIEDMAN, R. B. BERNSTEIN, and H. E. GUNNING. J. Chem. Phys. **26**, 528 (1957); (*c*) R. BARKER and A. MACCOLL. J. Chem. Soc. 2839 (1963); (*d*) A. J. FRANK and R. J. HANRAHAN. J. Phys. Chem. **82**, 2194 (1978).
2. (*a*) S. C. CHAN, Y. INEL, and E. TSCHUIKOW-ROUX. Can. J. Chem. **50**, 1443 (1972); (*b*) T. ICHIMURA, A. W. KIRK, G. KRAMER, and E. TSCHUIKOW-ROUX. J. Photochem. **6**, 77 (1976/77); (*c*) T. YANO and E. TSCHUIKOW-ROUX. J. Phys. Chem. **83**, 2572 (1979); (*d*) T. YANO, K.-H. JUNG, and E. TSCHUIKOW-ROUX. J. Phys. Chem. **84**, 2146 (1980).

Can. J. Chem. Downloaded from www.nrcresearchpress.com by 210.87.254.105 on 09/06/12
For personal use only.

3. J. G. CALVERT and J. N. PITTS, JR. Photochemistry. Wiley, New York. 1967. pp. 522–527.
4. (*a*) H. L. KIM, H. S. YOO, and K.-H. JUNG. Bull. Korean Chem. Soc. **2**, 71 (1981); (*b*) H. S. YOO and K.-H. JUNG. Bull. Korean Chem. Soc. **1**, 35 (1980).
5. M. B. ROBIN. Higher excited states of polyatomic molecules. Vol. 1. Academic Press, New York. 1974. pp. 155–172.
6. D. DAVIS and W. BRAUN. Appl. Opt. **7**, 2071 (1968).
7. H. OKABE. Photochemistry of small molecules. John Wiley and Sons, Inc., New York. 1978 (*a*) pp. 107–113; (*b*) p. 178.
8. N. WASHIDA, H. AKIMOTO, and I. TANAKA. Appl. Opt. **9**, 1711 (1970).
9. P. POTZINGER, L. C. GLASGOW, and G. VON BÜNAU. Z. Naturforsch. **27**a, 628 (1972).
10. W. C. PRICE. J. Chem. Phys. **4**, 547 (1936).
11. S. W. BENSON. Thermochemical kinetics. 2nd ed. John Wiley and Sons. 1976 (*a*) pp. 288–299; (*b*) p. 236.
12. A. W. KIRK and E. TSCHUIKOW-ROUX. J. Chem. Phys. **51**, 2247 (1969).
13. D. P. DINGLEDY and J. G. CALVERT. J. Am. Chem. Soc. **85**, 856 (1963).

Can. J. Chem. Downloaded from www.nrcresearchpress.com by 210.87.254.105 on 09/06/12
For personal use only.

Reactions of elemental sulfur with tetrakis(triphenylphosphine)platinum(0). Formation of a complex containing very nucleophilic bridging sulfido ligands

RAVI R. GUKATHASAN, ROBERT H. MORRIS,[1] AND ALAN WALKER[1]

Department of Chemistry, Scarborough College, University of Toronto, Scarborough, Ont., Canada M1C 1A4

Received March 25, 1983

RAVI R. GUKATHASAN, ROBERT H. MORRIS, and ALAN WALKER. Can. J. Chem. **61**, 2490 (1983).

The reactions of $Pt(PPh_3)_4$ with elemental sulfur in ratios S/Pt = 3, 4, 5, and 6 give a mixture of compounds identified as $[PtS(PPh_3)_2]_2$ and $PtS_4(PPh_3)_2$; $PtS_2(PPh_3)_2$ is not detected. The dimeric complex also forms on reaction of $PtS_4(PPh_3)_2$ with 3 mol of $Pt(C_2H_4)(PPh_3)_2$. It is alkylated at one bridging sulfido ligand by CH_2Cl_2 and $CHCl_3$ to give cations $[Pt_2(\mu\text{-}S)(\mu\text{-}SR)(PPh_3)_4]^+$, R = CH_2Cl and $CHCl_2$, respectively, which are characterized as their hexafluorophosphate salts. The cations give extreme AA'BB'X ^{31}Pmr spectra since their *cis*-phosphorus atoms (A,B) have very similar chemical shifts but different coupling constants to ^{195}Pt(X); spectral features are broadened by thiolate inversion processes. Reactions of bridging sulfido ligands with other electrophiles are discussed.

RAVI R. GUKATHASAN, ROBERT H. MORRIS et ALAN WALKER. Can. J. Chem. **61**, 2490 (1983).

Le composé $Pt(PPh_3)_4$ réagit avec le soufre élémentaire dans des rapports de S/Pt = 3, 4, 5 et 6 pour donner un mélange de composés identifiés comme étant le $[PtS(PPh_3)_2]_2$ et le $PtS_4(PPh_3)_2$; on n'a pas décelé la présence du composé $PtS_2(PPh_3)_2$. Il se forme également ce complexe dimère lorsque le composé $PtS_4(PPh_3)_2$ réagit avec trois moles de $Pt(C_2H_4)(PPh_3)_2$. Ce complexe est alkylé au niveau d'un ligand sulfido en position de pont par le CH_2Cl_2 et le $CHCl_3$ pour donner les cations $[Pt_2(\mu\text{-}S)(\mu\text{-}SR)(PPh_3)_4]^+$, R = CH_2Cl et $CHCl_2$ respectivement, que l'on a caractérisés sous forme de leurs sels hexafluorophosphates. Les cations donnent des spectres en rmn du ^{31}P qui à la limite sont du type AA'BB'X puisque leurs atomes de phosphore *cis*(A,B) ont des déplacements chimiques très semblables mais les constantes de couplage avec le ^{195}Pt(X) sont différentes; les caractéristiques spectrales sont élargies par les réactions d'inversion du thiolate. On discute des réactions des ligands sulfure en position de pont avec d'autres électrophiles.

[Traduit par le journal]

Can. J. Chem. Downloaded from www.nrcresearchpress.com by 210.87.254.42 on 09/06/12
For personal use only.

Introduction

Several recent studies have demonstrated that sulfide (S^{2-}) ligands that bridge between two electron-rich transition metal centres are reactive toward a variety of electrophiles. They undergo addition reactions with alkynes (1), isonitriles (2), transition metals (3), and alkyl halides (3). Even dihydrogen can add to sulfide ligands in certain organometallic molybdenum complexes that catalyze the reduction of acetylene to ethylene (1, 4).

Initial studies of sulfido-bridged complexes of platinum conducted by Ugo *et al.* (5) and Chatt and Mingos (6) demonstrated that these complexes also contain nucleophilic sulfido bridges and we have reinvestigated these systems, our results being the subject of this paper. The complex $[Pt(\mu\text{-}S)(PPh_3)_2]_n$, **1** (5), was reported to be dimeric in $CHCl_3$ and to react with alkyl halides RX = $PhCH_2Br$ and CH_3I to afford unstable complexes formulated on the basis of elemental analyses (5) as $[Pt_2(\mu\text{-}SR)_2(PPh_3)_4]X_2$, **2**, whereas the dimer $[Pt(\mu\text{-}S)(PMe_2Ph)_2]_2$, **3**, was reported to combine with benzyl bromide to give the monocation $[Pt_2(\mu\text{-}S)(\mu\text{-}SCH_2Ph)(PMe_2Ph)_4]Br$, **4**, and with excess methyl bromide in $CHCl_3$ to yield only $PtBr_2(PMe_2Ph)_2$ (6). We find that the sulfur ligands in complex **1** are so nucleophilic that even the very mild alkylating agents chloroform and dichloromethane react with **1** in seconds to give monocations similar in structure to **4**; no evidence of dications like **2** was found. This paper reinterprets the findings of the earlier studies in light of these observations.

Experimental

The literature method was used to prepare $[PtCl_2(PPh_3)_2]$ (7), $[Pt(PPh_3)_4]$ (7), and $[Pt(C_2H_4)(PPh_3)_2]$ (7). The ^{1}Hmr spectra were recorded on a Varian XL-200 spectrometer. The ^{31}Pmr spectra were obtained at 81 MHz on this instrument or at 32.3 MHz using a Bruker WP-80 spectrometer and were referenced to trimethylphosphite in C_6D_6 (δ140 ppm from 85% H_3PO_4) in a coaxial tube. Chemical shifts (^{31}P) are reported relative to 85% H_3PO_4. Infrared spectra from samples as KBr disks were recorded using a Beckman IR 12 spectrophotometer. Conductivity measurements were made in nitromethane at 25°C using a Beckman Model RC-18A conductivity bridge. Elemental analyses were performed by the Analytiche Laboratorien, Engelskirchen, and the Canadian Microanalytical Laboratory, Vancouver.

Reactions of sulfur with $Pt(PPh_3)_4$

The variation of product distribution for this reaction was examined for the molar ratios of sulfur to platinum given in Table 1. A representative procedure is given here for the ratio S/Pt = 4.0. To a frozen, degassed suspension of sulfur (0.21 g, 6.5 mmol) in 20 mL benzene was added $Pt(PPh_3)_4$ (2.0 g, 1.6 mmol) under nitrogen. The mixture thawed to give a clear red solution which then deposited an orange solid as it was stirred for 5 h. The solid (1.1 g) was washed with 5 mL benzene and 40 mL hexane and air dried. It analyzed as a mixture of 33% $PtS_4(PPh_3)_2$, **5** (6), and 66% $[PtS(PPh_3)_2]_n$, **1**.

Anal. calcd. for $PtS_2P_2C_{36}H_{30}$: C 55.16, H 3.86, S 8.18; found: C 54.57, H 3.97, S 8.32. This solid is only soluble in chlorinated solvents from which two components, **5** and **6** using CH_2Cl_2 and **5** and **7** using $CHCl_3$, can be separated (see below). Addition of hexane to the benzene filtrate produces in variable yield a brown material containing triphenylphosphine sulfide (^{31}Pmr δ41.5) and a mixture of platinum phosphine species (δ11 to 20, broad multiplets).

*Isolation of $PtS_4(PPh_3)_2$, **5***

Dichloromethane solutions of the orange solids from the reactions above were filtered, treated with ethanol, and vacuum concentrated until orange crystals of **5** precipitated as a CH_2Cl_2 solvate. The product was recrystallized from CH_2Cl_2/EtOH and vacuum dried.

Anal. calcd. for $PtP_2C_{36}H_{30}S_4 \cdot 0.25\ CH_2Cl_2$: C 50.09, H 3.54, S 14.76; found: C 49.73, H 3.61, S 14.78. Mp 147–150°C (lit. (6) 138–140°C). ^{31}Pmr (CH_2Cl_2) δ: 15.09, J^1(Pt—P) = 2967 Hz.

*Isolation of $[Pt_2(\mu\text{-}S)(\mu\text{-}SCH_2Cl)(PPh_3)_4](PF_6)$, **6***

After **5** is isolated, the alcoholic mother liquor is treated with a filtered solution of excess $NaPF_6$ in ethanol to yield yellow crystals which are filtered off, washed with ether, and dried *in vacuo*. Typi-

[1] To whom correspondence should be addressed.

TABLE 1. Variation in product distribution with the molar ratio of the reactants — elemental sulfur to $Pt(PPh_3)_4$

Reactant ratio, S/Pt	Yield of products[a]	
	$[PtS(PPh_3)_2]_n$, **1**	$PtS_4(PPh_3)_2$, **5**
1[b]	65[b]	—
3	75–85	18–12
4	60	30
4.8	32	40
6.3	2–10	40[c]

[a] Compound **1** is taken as $PtS(PPh_3)_2$ for these calculations. Yields of $SPPh_3$ and brown soluble materials also produced could not be determined.
[b] Reference 5.
[c] We have been unable to obtain the 96% yield reported for this reaction (6).

cally, 85% of the compound **1** in the starting mixture of solids can be recovered as **6**.

Anal. calcd. for $Pt_2P_5C_{73}H_{62}S_2ClF_6$: C 51.64, H 3.68, S 3.78, Cl 2.09; found: C 50.93, H 3.79, S 3.84, Cl 2.18. Mp 188–192°C. Λ (CH_3NO_2): 74 mho cm^2 mol^{-1} at 1.0×10^{-3} *M* (1:1 electrolyte). ir (KBr) ν_{max}: 840, 560 (s, PF_6^-). ^{1}Hmr (CD_2Cl_2) δ: 6.8–8.0 (m, 60H, PPh_3), 4.1 (1:8:18:8:1 quintet of broad singlets, J^3(Pt—H) = 34 Hz, 2H, SCH_2Cl). ^{31}Pmr (CH_2Cl_2): $\delta_A \sim \delta_B$ = 22.7 (AA'BB'X, X = ^{195}Pt, J^1(A—X) = 3405, J^1(B—X) = 2631, J^2(A—B) = 20, J^4(A—B', *trans*) = J^4(A'—B, *trans*) = 20 Hz; similar parameters are obtained from the 81 and 32 MHz spectra).

Preparation of [$Pt_2(\mu$-S)(μ-SCHCl$_2$)(PPh_3)$_4$](PF$_6$), 7

Mixtures of **1** and **5** can also be separated using chloroform instead of dichloromethane as above. The yellow crystals of the product are precipitated from ethanol solutions using $NaPF_6$ and recrystallized from $CHCl_3$/ethanol.

Anal. calcd. for $Pt_2P_5C_{73}H_{61}S_2Cl_2F_6$: C 50.61, H 3.55, Cl 4.09; found: C 49.37, H 3.38, Cl 4.02. Mp 202–204°C. Λ (CH_3NO_2) 86 mho cm^2 mol^{-1} at 1.0×10^{-3} *M*. ^{31}Pmr ($CHCl_3$) δ: $\delta_A \sim \delta_B$ = 21.1 (s, br, width at base = 90 Hz, plus ^{195}Pt(X) satellites (broad multiplets) in an ABX spin system, J(A—X) = 2730, J(B—X) = 3570 Hz). Couplings J^4 were not observed.

Preparations of [$PtS(PPh_3)_2$]$_n$, 1

Method 1. According to ref. 5. A suspension of anhydrous lithium sulfide (0.93 g, 20 mmol) and $PtCl_2(PPh_3)_2$ (1.0 g, 1.3 mmol) was stirred in 20 mL benzene under N_2 for 80 h and then heated to reflux for 5 h. The orange product was filtered, washed with water and ethanol, and dried in air. The ^{31}Pmr spectrum of the orange solid (mp 246°C) in CH_2Cl_2 indicated the presence of **6** (50%) and $PtCl_2(PPh_3)_2$ (50%), ^{31}Pmr (CH_2Cl_2) δ: 13.3, J^1(Pt—P) = 3682 Hz. Sodium sulfide gave similar results.

Method 2. The mixtures of **1** and **5** obtained as above can be converted to pure **1** by reacting 3 mol of $Pt(C_2H_4)(PPh_3)_2$ per mol of **5** in the mixture: 0.09 mmol **5** and 0.17 mmol **1** (0.2 g of mixture) were reacted with 0.26 mmol $Pt(C_2H_4)(PPh_3)_2$ in 20 mL degassed benzene under nitrogen. The orange product (0.16 g, 0.21 mmol, 41%) was filtered off after 60 h stirring.

Anal. calcd. for $Pt_2S_2P_4C_{72}H_{60}$: C 57.52, H 4.02, S 4.27; found: C 56.64, H 4.41, S 3.84. Mp 245–247°C (lit. (5) 246°C). Complex **1** is also obtained in 43% yield if pure **5** (0.06 mmol) is reacted with 0.18 mmol of $Pt(C_2H_4)(PPh_3)_2$ in 20 mL benzene.

Discussion

Complex **1** was originally prepared by the reaction of *cyclo*-octasulfur with solutions of $Pt(PPh_3)_x$, x = 2 or 3 although the stoichiometry of the reaction was not precisely defined (5). We have studied the reaction of elemental sulfur with $Pt(PPh_3)_4$ in the stoichiometric ratios listed in Table 1 and find that the main product in each case is an orange, benzene-insoluble precipitate consisting of mixtures of $[PtS(PPh_3)_2]_n$, **1**, and the sulfur metallocycle $PtS_4(PPh_3)_2$, **5** (reaction [1]).

[1] $Pt(PPh_3)_4 + xS_8 \rightarrow$ **1** + **5** + $SPPh_3$

Since both compounds are sparingly soluble in common organic solvents but **1** dissolves with reaction in chlorinated solvents, the mixture can be separated using dichloromethane as in reaction [2], where **1** is converted to an ionic compound **6** whose properties are consistent with structure **I** with a chloride counterion.

[2] **1** + **5** $\xrightarrow[CH_2Cl_2]{}$ **6** + **5**

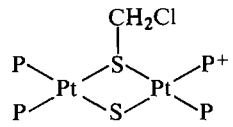

I, 6

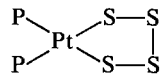

II, 5

Complex **5** is precipitated with ethanol and then **6** is isolated as the hexafluorophosphate salt. The ^{31}Pmr spectrum of complex **5**, which is stable in CH_2Cl_2 for at least 10 h, shows a singlet at δ 15.1 ppm due to equivalent phosphorus atoms (structure **II**, the X-ray structure has been reported (8)) and a platinum-195 coupling of 2967 Hz.

Elemental analyses, conductivity, and nmr measurements indicate that **6** has the structure **I**. The central three resonances of the 1:8:18:8:1 quintet expected for the methylene protons of the alkylated sulfur are observed in the ^{1}Hmr as broad singlets. The broadening may be due to a dynamic inversion of the thiolate sulfur also noticed in the ^{1}H resonance of the benzyl group in compound **4** which also has this structure (6). A CH_2Cl_2 solution of **6** gives the remarkable ^{31}Pmr spectrum shown in Fig. 1. It can be explained by assuming that the *cis*-triphenylphosphine ligands have almost identical chemical shifts of approximately 22.7 ppm but different coupling constants J^1(Pt—P) = 3405 and 2631 Hz. The central line of the spectrum is a broad singlet composed of an AB quartet with additional J^3(P—Pt) and J^4(P—P) couplings, all of which are unresolved. A similar broad centre peak is observed in the ^{31}Pmr spectrum of $[Pt_2(\mu\text{-SMe})H_2(DPPM)_2]^+$ where inversion at the thiolate sulfur can also occur (9). The ^{195}Pt satellites can be analyzed as an AA'BB'X spin system with a *cis*-phosphine coupling constant J^2(A—B) = 20 Hz and a chemical shift difference $\delta_A - \delta_B$ which is too small to be detected. In this spin system the appearance of the ^{195}Pt satellites as pseudo triplets can be explained by invoking a coupling J^4(P—P, *trans*) ~ 20 Hz whilst J^4(P—P, *cis*) is too small to be observed. Complex **1** prepared using the sodium sulfide or lithium sulfide method (5) gives an identical spectrum apart from impurity peaks due to $PtCl_2(PPh_3)_2$. Complex **6** decomposes in CH_2Cl_2 at 30°C ($t_{1/2}$ = 10 h) to several products including $SPPh_3$. The other phosphorus-containing species have not been identified. The decomposition may be initiated by the alkylation of the bridging sulfide ligand in **6**.

A ^{31}Pmr spectrum of the amber benzene solution resulting from the reaction depicted in [1], x = 0.5, gave no evidence for the existence of $Pt(S_2)(PPh_3)_2$ which would have been signalled by a simple singlet with satellites. Such a complex might well have been formed using this stoichiometry by analogy to the reported syntheses of disulfur complexes of other group VIII

Can. J. Chem. Downloaded from www.nrcresearchpress.com by 210.87.254.42 on 09/06/12
For personal use only.

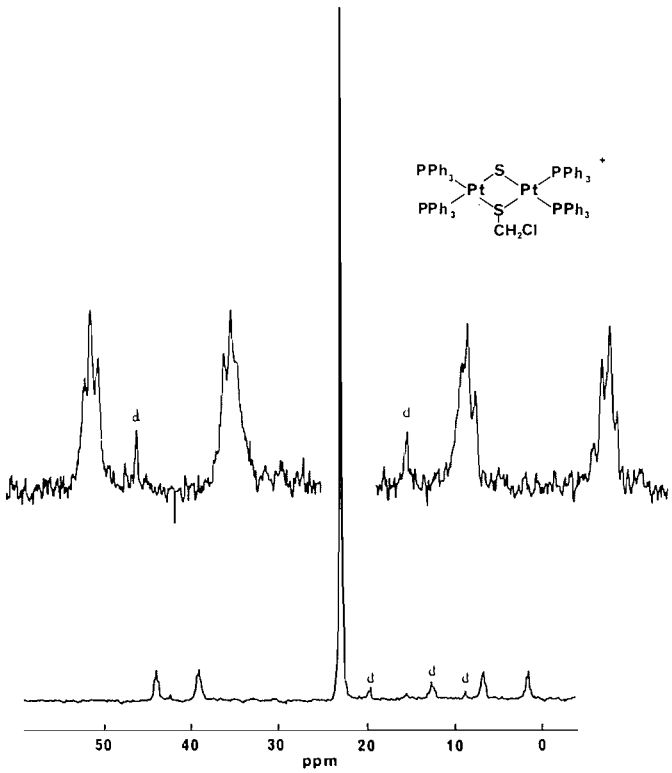

FIG. 1. The ^{31}Pmr spectrum at 81 MHz of $[Pt_2(S)(SCH_2Cl)(PPh_3)_4]PF_6$, **6**, in CH_2Cl_2. Inset are expansions of the ^{195}Pt satellites of the resonances at 22.75 ppm. The peaks labelled with d are decomposition products that formed during the hour of data collection (the probe temperature was 34°C).

metals (10, 11). This compound may form in the reaction but Ginsberg's work (10) suggests that it would be consumed rapidly as in reaction [3].

[3] $Pt(S_2)(PPh_3)_2 + Pt(PPh_3)_4 \rightarrow \mathbf{1} + 2\ PPh_3$

The disulfur ligand in rhodium and iridium complexes was abstracted by $Pt(PPh_3)_4$ to give **1** (10). We have found that even $PtS_4(PPh_3)_2$, **5**, is attacked by the zero valent platinum from $Pt(C_2H_4)(PPh_3)_2$ in benzene so that mixtures of **1** and **5** are converted to pure **1** plus unidentified benzene soluble species.

There is now strong albeit indirect evidence that **1** contains dimeric units with very nucleophilic bridging sulfur groups. Its insolubility can be explained by strong intermolecular attractions between neighbouring phenyl groups. The related ethyldiphenylphosphine derivative has been shown to be dimeric (10). The reaction products from **1** are also dimeric: the SO_2 adduct (5) and complex **6**.

The reaction of sulfur dioxide with **1** gives $[PtS(SO_2)(PPh_3)_2]_2$, **8** (5). We suggest that this Lewis acid reversibly coordinates to the basic sulfur ligands rather than the platinum atoms (5) in complex **8** since the frequencies $\nu(SO) = 1060$ and 1210 cm^{-1} fall in the ranges now recognized as characteristic of a pyramidal O_2S-S system (12). Consistent with this view, complex **8** does not react with oxygen to give sulfates (5, 8).

The "dichloroform adduct" of **1** reported by Ugo *et al.* (5) must now be formulated as $[Pt_2S(SCHCl_2)(PPh_3)_4]Cl \cdot CHCl_3$, a monoalkylated derivative of **1** with 1 mol of chloroform of solvation to explain the analytical results reported. In fact, we have isolated this complex as the hexafluorophosphate salt, **7**, and find that its properties agree with this formulation and a structure analogous to **6**. We also propose that on the basis of the conductivity data given for complexes **2**, the reactions of **1** with other alkyl halides give products alkylated at only one sulfur atom instead of two as was proposed (5). Conductivity data for complexes **2** in nitrobenzene are 22 and 16 mho cm^2 mol^{-1} (5), which match the value of 18 for the monoalkylated complex **4** reported in ref. 6. Ion pairing in solutions of these complexes could explain why these values fall below the range typical of 1:1 electrolytes: 25–30 mho cm^2 mol^{-1}; see ref. 13.

Acknowledgements

This work was funded by grants to R.H.M. by the Atkinson Charitable Foundation and the Natural Sciences and Engineering Research Council of Canada and by support to A.W. from the University of Toronto.

1. M. RAKOWSKI DUBOIS, R. C. HALTIWANGER, D. J. MILLER, and G. GLATZMAIER. J. Am. Chem. Soc. **101**, 5245 (1979).
2. D. J. MILLER and M. RAKOWSKI DUBOIS. J. Am. Chem. Soc. **102**, 4925 (1980).
3. D. SEYFERTH, R. S. HENDERSON, and M. K. GALLAGHER. J. Organomet. Chem. **193**, C75 (1980) and references therein.
4. M. RAKOWSKI DUBOIS, M. C. VAN DERVEER, D. L. DUBOIS, R. C. HALTIWANGER, and W. K. MILLER. J. Am. Chem. Soc. **102**, 7456 (1980).
5. R. UGO, G. LA MONICA, S. CENINI, A. SEGRE, and F. CONTI. J. Chem. Soc. A, 522 (1971).
6. J. CHATT and D. M. P. MINGOS. J. Chem. Soc. A, 1243 (1970).
7. F. R. HARTLEY. The chemistry of platinum and palladium. John Wiley and Sons, New York. 1973. pp. 452–457.
8. D. DUDIS and J. P. FACKLER, JR. Inorg. Chem. **21**, 3577 (1982).
9. M. P. BROWN, J. R. FISHER, R. J. PUDDEPHATT, and K. R. SEDDON. Inorg. Chem. **18**, 2808 (1979).
10. A. P. GINSBERG, W. E. LINDSELL, C. R. SPRINKLE, K. W. WEST, and R. L. COHEN. Inorg. Chem. **21**, 3666 (1982).
11. D. H. FARRAR, K. R. GRUNDY, N. C. PAYNE, W. R. ROPER, and A. WALKER. J. Am. Chem. Soc. **101**, 6577 (1979).
12. G. J. KUBAS. Inorg. Chem. **18**, 182 (1979).
13. W. J. GEARY. Coord. Chem. Rev. **7**, 81 (1971).

Can. J. Chem. Downloaded from www.nrcresearchpress.com by 210.87.254.42 on 09/06/12
For personal use only.

Structural studies of organoboron compounds. XVIII.[1] Crystal and molecular structures of 2,2-diphenyl-1,3-dioxa-3*a*-azonia-2-borataindan and 4-cyclohexyl-6-methyl-2,2-diphenyl-1,3-dioxa-3*a*-azonia-2-borataindan

W. KLIEGEL AND D. NANNINGA

Institut für Pharmazeutische Chemie, der Technischen Universität Braunschweig, 3300 Braunschweig, Beethovenstraße 55, Bundesrepublik Deutschland

AND

STEVEN J. RETTIG AND JAMES TROTTER

Department of Chemistry, University of British Columbia, 2036 Main Mall, Vancouver, B.C., Canada V6T 1Y6

Received May 24, 1983

W. KLIEGEL, D. NANNINGA, STEVEN J. RETTIG, and JAMES TROTTER. Can. J. Chem. **61**, 2493 (1983).

The crystal structures of 2,2-diphenyl-1,3-dioxa-3*a*-azonia-2-borataindan, **6***a*, and 4-cyclohexyl-6-methyl-2,2-diphenyl-1,3-dioxa-3*a*-azonia-2-borataindan, **6***b*, reported here represent the first crystallographic examples of coordination complexes of the anionic ligand derived from 2-hydroxypyridine *N*-oxide. Crystals of **6***a* are monoclinic, a = 11.5210(13), b = 10.2860(8), c = 12.7354(15) Å, β = 101.878(5)°, Z = 4, space group $P2_1/c$; and those of **6***b* are monoclinic, a = 8.5047(8), b = 15.6603(14), c = 16.0501(18) Å, β = 104.776(5)°, Z = 4, space group $P2_1/n$. Both structures were solved by direct methods and were refined by full-matrix least-squares procedures to final R values of 0.039 and 0.042 for 1440 and 1750 reflections with $I \geq 3\sigma(I)$, respectively. Both molecules feature tetrahedrally coordinated boron atoms incorporated into five-membered OBOCN chelate rings which have B-envelope conformations. The observed molecular geometries indicate that the ligand may be classed as a hybrid of the 2-hydroxypyridine *N*-oxide and 1-hydroxy-2-pyridinone tautomers of the parent alcohol. Important bond lengths (corrected for libration) are: O—B = 1.557(3)–1.580(3), mean C—B = 1.600(4), C—O = 1.316(3), and N—O = 1.389(3) Å.

W. KLIEGEL, D. NANNINGA, STEVEN J. RETTIG et JAMES TROTTER. Can. J. Chem. **61**, 2493 (1983).

La structure du cristal de diphényl-2,2 dioxa-1,3 azonia-3*a* borata-2 indane (**6***a*) et celle du cristal de cyclohexyl-4 méthyl-6 diphényl-2,2 dioxa-1,3 azonia-3*a* borata-2 indane (**6***b*) représentent les premiers exemples en cristallographie de complexes de coordination du ligand anionique provenant de la hydroxy-2 pyridine-*N*-oxyde. Les cristaux du composé **6***a* sont monocliniques et appartiennent au groupe d'espace $P2_1/c$ avec a = 11,5210(13), b = 10,2860(8), c = 12,7345(15) Å, β = 101,878(5)°, Z = 4; et ceux du composé **6***b* appartiennent au groupe d'espace monoclinique $P2_1/n$ avec a = 8,5047(8), b = 15,6603(14), c = 16,0501(18) Å, β = 104,776(5)°, Z = 4. On a résolu les deux structures par des méthodes directes et on les a affinées par la méthode des moindres carrés (matrice entière) jusqu'à des valeurs respectives de R de 0,039 et 0,042 pour 1440 et 1750 réflexions avec $I \geq 3\sigma(I)$. Les deux molécules ont des atomes de bore coordonnés de façon tétraédrique et incorporés dans des noyaux chélates à cinq chainons OBOCN qui ont des conformations de type enveloppe B. Les géométries moléculaires observées indiquent que le ligand peut être classé comme un hybride des tautomères de l'hydroxy-2 pyridine *N*-oxyde et de l'hydroxy-1 pyridinone-2 de l'alcool apparenté. Les longueurs importantes de liaison (corrigées pour la libration) sont: O—B = 1,557(3)–1,580(3), C—B (moyenne) = 1,600(4), C—O = 1,316(3) et N—O = 1,389(3) Å.

[Traduit par le journal]

Introduction

2-Hydroxypyridine *N*-oxide[2] can be classed with the cyclic hydroxamic acids or *N*-hydroxy lactams (1) which are derived from heteroaromatic compounds such as pyridine, quinoline, and related ring systems. For the structural description, different canonical forms, **1** ↔ **2** of the lactam (**1**) or **3** ↔ **4** of the lactim (**3**) tautomers can be written (2–6).

On the virtue of a strong intramolecular hydrogen bond (2, 4), one can proceed on the assumption that the proton is "chelated" as in **5** which summarizes the tautomeric equilibrium as well as the individual resonance forms **1**–**4**. Replacement of this "chelated" proton by metal ions has already been demonstrated in connection with the synthesis of 2-hydroxypyridine *N*-oxide (7), which was reported to form chelates with Cu(II) and Fe(II) ions. Many examples of such metal complexes have subsequently been reported (4, 6, 8–12). Among the ligands employed during our earlier investigations of boron chelates of hydroxamic acid derivatives (13–15) were 2-hydroxypyridine *N*-oxide (**5**, $R^1 = R^2 = H$) and a substituted derivative thereof, "ciclopirox" (**5**, $R^1 = C_6H_{11}$, $R^2 = CH_3$),[3] which is known as a very effective antimycotic (16). The exchange of the "chelated" proton in **5** for the diphenylborenium ion (Ph_2B^+) led to the diphenylboron

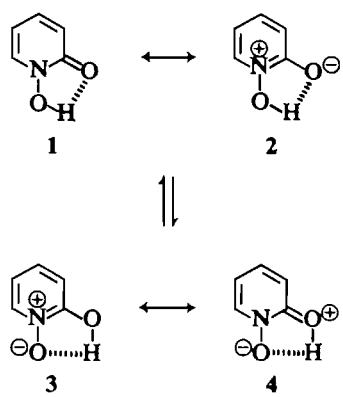

1 **2** **3** **4**

[1] Part XVII: W. Kliegel, D. Nanninga, S. J. Rettig, and J. Trotter. Can. J. Chem. (submitted for publication).

[2] Also referred to in the literature as: 2-pyridinol *N*-oxide, *N*-oxopyridin-2-ol, 1-hydroxypyridine-2-one, 1-hydroxy-2-pyridone, and 1-hydroxy-2(1*H*)-pyridinone.

[3] 6-Cyclohexyl-1-hydroxy-4-methyl-2(1H)-pyridinone, its 2-hydroxyethylammonium salt being named: "ciclopiroxolamine", Hoe 296, Batrafen®.

Can. J. Chem. Downloaded from www.nrcresearchpress.com by 210.87.254.40 on 09/06/12
For personal use only.

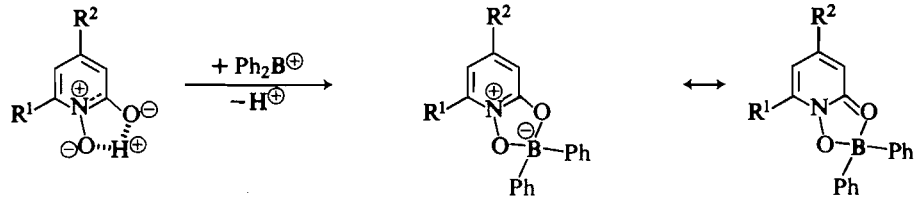

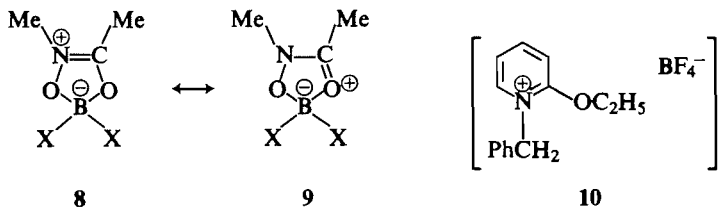

chelate **6** (17). In view of the *B,N*-betaine formulation **8** of open-chain hydroxamic acid boron complexes, which has been verified by X-ray crystallographic analyses of the boron chelates **8** (X = F, Ph) of *N*-methylacethydroxamic acid (13, 14), it was of special interest to determine which of the resonance structures **6**/**7** is the major contributor to the resonance hybrid. The best description for the resonance hybrid **8** ↔ **9** appeared to be the betaine form **8**, based on the analysis of the bond distances which indicate an approximate contribution of 75% by the resonance structure **8** (13, 14).

No X-ray structure analyses have yet been reported for 2-hydroxypyridine *N*-oxide or for complexes of this ligand (6). The structure of an antibiotic with a comparable ring system[4] has been reported (18), but no bond lengths or angles were

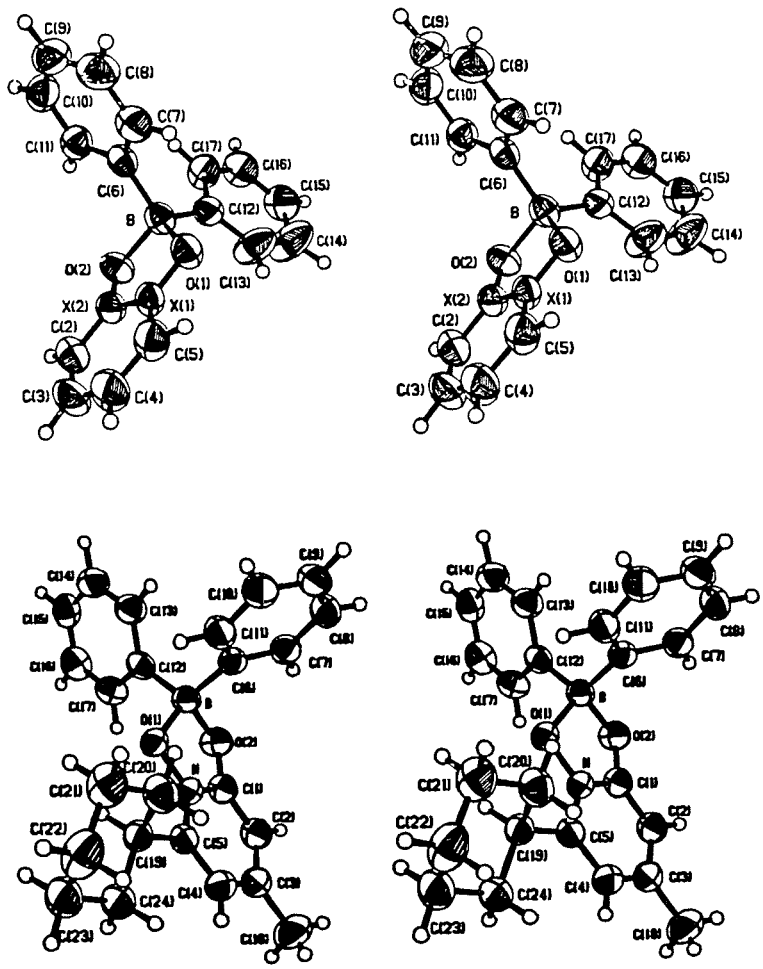

FIG. 1. Stereoscopic views of **6***a* (top) and **6***b* (bottom). 50% probability thermal ellipsoids are shown for the non-hydrogen atoms; hydrogen atoms have been assigned arbitrarily small thermal parameters for the sake of clarity.

[4] 5-Methoxy-6-methyl-1-hydroxy-2(1*H*)-pyridinone.

Can. J. Chem. Downloaded from www.nrcresearchpress.com by 210.87.254.40 on 09/06/12
For personal use only.

TABLE 1. Final positional (fractional) and isotropic thermal parameters ($U \times 10^3$ Å^2) with estimated standard deviations in parentheses

Atom	x	y	z	U^*_{eq}/U_{iso}	Atom	x	y	z	U^*_{eq}/U_{iso}
				6*a* ($\times 10^5$, H $\times 10^4$)					
O(1)	58958(12)	61668(13)	27264(11)	58	C(16)	87068(26)	39287(27)	56694(20)	77
O(2)	62675(12)	39949(12)	22823(11)	56	C(17)	84158(20)	43220(25)	46101(18)	67
X(1)	50565(15)	56941(19)	19349(13)	50	B	69390(21)	51790(22)	29130(19)	51
X(2)	52643(16)	44552(20)	17017(13)	52	H(2)	4665(17)	2941(21)	848(15)	51(6)
C(2)	44664(22)	37856(26)	9507(17)	62	H(3)	2884(23)	3989(23)	−57(21)	91(8)
C(3)	34596(22)	44150(32)	4465(20)	76	H(4)	2604(24)	6153(25)	330(22)	96(9)
C(4)	32753(24)	56873(33)	6768(19)	79	H(5)	4050(22)	7274(28)	1655(19)	98(8)
C(5)	40655(21)	63348(28)	14331(17)	68	H(7)	7710(20)	7599(23)	2422(17)	74(7)
C(6)	79491(17)	56595(20)	23218(15)	50	H(8)	9120(23)	8321(32)	1458(19)	104(9)
C(7)	81506(23)	69666(24)	21467(19)	66	H(9)	10232(23)	6785(26)	802(20)	96(9)
C(8)	90060(26)	73674(31)	16014(21)	80	H(10)	9970(22)	4511(27)	1166(19)	90(9)
C(9)	96997(26)	64809(33)	12242(21)	80	H(11)	8560(18)	3844(23)	2064(16)	69(7)
C(10)	95470(23)	51863(32)	13949(19)	72	H(13)	5847(29)	5229(29)	4593(24)	114(11)
C(11)	86822(21)	47827(25)	19352(17)	59	H(14)	6251(27)	4762(31)	6285(26)	135(12)
C(12)	73067(18)	47992(20)	41523(16)	53	H(15)	8088(21)	3736(22)	7011(21)	85(8)
C(13)	65311(24)	48824(36)	48295(23)	95	H(16)	9461(25)	3616(24)	5932(21)	96(9)
C(14)	68182(27)	44912(43)	58882(22)	113	H(17)	9014(22)	4305(25)	4187(19)	88(8)
C(15)	79091(25)	40072(27)	63006(22)	79					
				6*b* ($\times 10^4$, H $\times 10^3$)					
O(1)	3341(2)	4854(1)	2109(1)	48	B	3452(4)	5664(2)	2685(2)	46
O(2)	2122(2)	5421(1)	3149(1)	53	H(2)	−91(3)	488(2)	311(2)	65(9)
N	1767(3)	4568(1)	2024(1)	43	H(4)	−102(4)	335(2)	106(2)	62(9)
C(1)	1128(4)	4887(2)	2644(2)	48	H(7)	147(3)	700(2)	282(2)	61(9)
C(2)	−401(4)	4621(2)	2684(2)	56	H(8)	91(3)	829(2)	203(2)	63(9)
C(3)	−1212(4)	4032(2)	2087(2)	57	H(9)	195(4)	854(2)	85(2)	82(11)
C(4)	−468(4)	3724(2)	1474(2)	56	H(10)	361(4)	749(2)	44(2)	87(11)
C(5)	1058(3)	3976(2)	1430(2)	45	H(11)	408(4)	620(2)	120(2)	72(10)
C(6)	2887(3)	6491(2)	2104(2)	44	H(13)	613(4)	674(2)	281(2)	83(11)
C(7)	1907(4)	7121(2)	2316(2)	53	H(14)	875(4)	676(2)	373(2)	79(10)
C(8)	1559(4)	7875(2)	1853(2)	62	H(15)	948(3)	578(2)	487(2)	55(8)
C(9)	2159(4)	8009(3)	1152(2)	64	H(16)	744(4)	473(2)	503(2)	91(12)
C(10)	3106(4)	7392(2)	907(2)	64	H(17)	499(4)	469(2)	409(2)	75(11)
C(11)	3438(4)	6645(2)	1375(2)	57	H(18a)	−348(6)	360(3)	157(3)	142(22)
C(12)	5228(3)	5703(2)	3333(2)	47	H(18b)	−346(7)	410(4)	222(3)	166(28)
C(13)	6376(4)	6309(2)	3258(2)	59	H(18c)	−283(8)	321(5)	245(4)	218(35)
C(14)	7913(4)	6337(2)	3814(2)	66	H(19)	316(3)	361(1)	116(1)	36(6)
C(15)	8359(4)	5763(2)	4478(2)	65	H(20a)	84(4)	440(2)	−23(2)	62(9)
C(16)	7249(5)	5156(3)	4573(2)	65	H(20b)	238(4)	489(2)	37(2)	80(11)
C(17)	5725(4)	5126(2)	4010(2)	59	H(21a)	420(4)	400(2)	−10(2)	75(11)
C(18)	−2884(6)	3732(4)	2115(4)	91	H(21b)	311(4)	448(2)	−92(2)	97(12)
C(19)	1990(4)	3677(2)	810(2)	48	H(22a)	136(4)	327(2)	−126(2)	82(11)
C(20)	2023(5)	4348(2)	123(2)	62	H(22b)	322(3)	303(2)	−125(2)	72(9)
C(21)	3066(5)	4054(3)	−464(3)	73	H(23a)	358(4)	244(2)	16(2)	63(9)
C(22)	2505(5)	3196(3)	−873(2)	79	H(23b)	198(4)	200(2)	−50(2)	106(13)
C(23)	2425(5)	2535(3)	−199(3)	74	H(24a)	27(4)	290(2)	2(2)	63(9)
C(24)	1386(4)	2824(2)	391(2)	61	H(24b)	129(4)	239(2)	85(2)	78(10)

* U_{eq} = (1/3) trace U_{diag}.

given. In view of the controversy regarding the structural formulations of 2-hydroxypyridine *N*-oxide and its complexes, an X-ray crystallographic study of the diphenylboron chelate of this ligand has been undertaken. During the course of this investigation it was discovered that there was disorder between the oxygen-bearing N and C atoms of the pyridine ring of **6*a***. In order to resolve this problem (which also occurs in the case of **8** (X = Ph) (14)), the structure of the substituted derivative **6*b*** has also been determined.

Experimental

2,2-Diphenyl-1,3-dioxa-3a-azonia-2-borataindan, **6*a***

The compound was prepared by the literature method (17). Crystals suitable for X-ray analysis were obtained by recrystallization from cyclohexane/chloroform or from *n*-hexane/dioxane mixtures, mp 123–124°C. A crystal bounded by the nine faces (followed by their distances in mm from a common origin): ±(−1 1 1), 0.13, ±(1 0 0), 0.16, ±(−5 1 1), 0.15, ±(0 1 −1), 0.21, (−1 −1 1), 0.28 was mounted in a general orientation. Unit-cell parameters were refined by least-squares on 2 sin θ/λ values for 25 reflections (2θ = 35–42°) measured on a diffractometer with Mo-Kα$_1$ radiation (λ = 0.70930 Å). Crystal data at 22°C are:

$C_{17}H_{14}BNO_2$ fw = 275.11

Monoclinic, a = 11.5210(13), b = 10.2860(8), c = 12.7354(15) Å, β = 101.878(5)°, V = 1479.0(3) Å^3, Z = 4, ρ_c = 1.236 gcm^{-3}, $F(000)$ = 576, μ(Mo-Kα) = 0.75 cm^{-1}. Absent reflections: $h0l$, l odd, and $0k0$, k odd, uniquely indicate the space group $P2_1/c$ (C^5_{2h},

Can. J. Chem. Downloaded from www.nrcresearchpress.com by 210.87.254.40 on 09/06/12
For personal use only.

Can. J. Chem. Downloaded from www.nrcresearchpress.com by 210.87.254.40 on 09/06/12
For personal use only.

TABLE 3. Bond lengths (Å) with estimated standard deviations in parentheses

Bond	Length Uncorr.	Length Corr.	Bond	Length Uncorr.	Length Corr.
			6a		
O(1)—X(1)	1.337(2)	1.343	C(6)—B	1.590(3)	1.595
O(1)—B	1.554(3)	1.563	C(7)—C(8)	1.381(4)	1.386
O(2)—X(2)	1.325(2)	1.331	C(8)—C(9)	1.364(4)	1.371
O(2)—B	1.572(3)	1.580	C(9)—C(10)	1.367(4)	1.376
X(1)—X(2)	1.341(3)	1.351	C(10)—C(11)	1.387(3)	1.392
X(1)—C(5)	1.359(3)	1.365	C(12)—C(13)	1.367(3)	1.391
X(2)—C(2)	1.369(3)	1.375	C(12)—C(17)	1.381(3)	1.398
C(2)—C(3)	1.368(3)	1.374	C(12)—B	1.598(3)	1.602
C(3)—C(4)	1.367(4)	1.377	C(13)—C(14)	1.382(4)	1.384
C(4)—C(5)	1.357(4)	1.362	C(14)—C(15)	1.354(4)	1.369
C(6)—C(7)	1.390(3)	1.400	C(15)—C(16)	1.343(4)	1.368
C(6)—C(11)	1.393(3)	1.401	C(16)—C(17)	1.384(3)	1.387
			6b		
O(1)—N	1.385(3)	1.389	C(8)—C(9)	1.366(4)	1.373
O(1)—B	1.559(4)	1.560	C(9)—C(10)	1.378(4)	1.387
O(2)—C(1)	1.312(3)	1.316	C(10)—C(11)	1.379(4)	1.383
O(2)—B	1.553(3)	1.557	C(12)—C(13)	1.389(4)	1.398
N —C(1)	1.346(3)	1.349	C(12)—C(17)	1.393(4)	1.401
N —C(5)	1.356(3)	1.361	C(12)—B	1.602(4)	1.604
C(1)—C(2)	1.382(4)	1.387	C(13)—C(14)	1.382(4)	1.385
C(2)—C(3)	1.381(4)	1.385	C(14)—C(15)	1.371(5)	1.379
C(3)—C(4)	1.386(4)	1.390	C(15)—C(16)	1.376(5)	1.385
C(3)—C(18)	1.509(5)	1.512	C(16)—C(17)	1.379(4)	1.382
C(4)—C(5)	1.376(4)	1.381	C(19)—C(20)	1.529(4)	1.539
C(5)—C(19)	1.496(4)	1.500	C(19)—C(24)	1.525(4)	1.534
C(6)—C(7)	1.389(4)	1.398	C(20)—C(21)	1.522(4)	1.526
C(6)—C(11)	1.388(4)	1.396	C(21)—C(22)	1.517(5)	1.527
C(6)—B	1.597(4)	1.600	C(22)—C(23)	1.512(5)	1.522
C(7)—C(8)	1.385(4)	1.389	C(23)—C(24)	1.519(5)	1.523

No. 14).

Intensities were measured with graphite-monochromated Mo-Kα radiation (λ = 0.71073 Å) on an Enraf-Nonius CAD4-F diffractometer. An ω-2θ scan at 0.87–10.06° min^{-1} over a range of (0.55 + 0.35 tan θ) degrees in ω (extended by 25% on both sides for background measurement) was employed. Data were measured to 2θ = 55°. The intensities of three check reflections, measured every 3600 s throughout the data collection, remained constant to within ±3%. Of the 3387 independent reflections measured and processed,[5] 1440 (42.5%) had intensities greater than $3\sigma(I)$ above background where $\sigma^2(I) = S + 2B + (0.04(S - B))^2$ with S = scan count and B = normalized background count.

The structure was solved by direct methods, the coordinates of all non-hydrogen atoms being determined from an E-map. After full-matrix least-squares refinement of the non-hydrogen atoms with anisotropic thermal parameters to $R = 0.085$, a difference map revealed the positions of all 14 hydrogen atoms which were refined with isotropic thermal parameters in subsequent cycles of refinement. It became obvious from the derived thermal parameters that the positions X(1) and X(2) were each occupied by both N and C. Refinement of the structure with either of these sites occupied by nitrogen and the other by carbon resulted in $R = 0.044$ and $R_w = 0.050$ with unbalanced thermal parameters. In the final stages of refinement the X positions were assumed to be 50% N and 50% C, this assumption being justified both by the lower residuals and by the near equality of the resulting thermal parameters. The scattering factors of ref. 19 were used for non-hydrogen atoms and those of ref. 20 for hydrogen atoms. The weighting scheme, $w = 1/\sigma^2(F)$ where $\sigma^2(F)$ is derived from the previously defined $\sigma^2(I)$, gave uniform average values of $w(|F_o| - |F_c|)^2$ over ranges of both $|F_o|$ and $\sin\theta/\lambda$ and was employed in the final stages of refinement. Convergence was reached at $R = 0.039$ and $R_w = 0.043$ for 1440 reflections with $I \geq 3\sigma(I)$. For all 3387 reflections $R = 0.130$. The function minimized was $\Sigma w(|F_o| - |F_c|)^2$, $R = \Sigma||F_o| - |F_c||/\Sigma|F_o|$ and $R_w = (\Sigma w(|F_o| - |F_c|)^2/\Sigma w|F_o|^2)^{1/2}$.

On the final cycle of refinement the mean and maximum parameter shifts corresponded to 0.007 and 0.08σ, respectively. The mean error in an observation of unit weight was 1.910. A final difference map was essentially featureless, the largest residual density being +0.156 e $Å^{-3}$ near oxygen. The final positional and thermal parameters appear in Tables 1 and 2[6] respectively. Measured and calculated structure factors have been placed in the Depository of Unpublished Data.[6]

4-Cyclohexyl-6-methyl-2,2-diphenyl-1,3-dioxa-3a-azonia-2-borataindan, ***6b***

Experimental details are as above except where noted. The compound was prepared according to the literature method (17). Crystals were obtained by recrystallization from ethanol, mp 150–152°C, that

[5] The computer programs used include locally written programs for data processing and locally modified versions of the following: MULTAN 80, multisolution program by P. Main, S. J. Fiske, S. E. Hull, L. Lessinger, G. Germain, J. P. Declercq, and M. M. Woolfson; ORFLS, full-matrix least-squares, and ORFFE, function and errors, by W. R. Busing, K. O. Martin and H. A. Levy; FORDAP, Patterson and Fourier syntheses, by A. Zalkin; ORTEP II, illustrations, by C. K. Johnson.

[6] The structure factor table, Table 2 (anisotropic thermal parameters) and other material mentioned in the text are available, at a nominal charge, from the Depository of Unpublished Data, CISTI, National Research Council of Canada, Ottawa, Ont., Canada K1A 0S2.

TABLE 4. Bond angles (deg) with estimated standard deviations in parentheses

Bonds	Angle (deg)	Bonds	Angle (deg)
		6a	
X(1)—O(1)—B	107.10(14)	C(8)—C(9)—C(10)	119.4(3)
X(2)—O(2)—B	106.84(14)	C(9)—C(10)—C(11)	120.0(3)
O(1)—X(1)—X(2)	112.23(14)	C(6)—C(11)—C(10)	122.1(2)
O(1)—X(1)—C(5)	125.9(2)	C(13)—C(12)—C(17)	115.0(2)
X(2)—X(1)—C(5)	121.8(2)	C(13)—C(12)—B	122.3(2)
O(2)—X(2)—X(1)	113.0(2)	C(17)—C(12)—B	122.6(2)
O(2)—X(2)—C(2)	126.4(2)	C(12)—C(13)—C(14)	122.9(3)
X(1)—X(2)—C(2)	120.5(2)	C(13)—C(14)—C(15)	120.2(3)
X(2)—C(2)—C(3)	118.2(2)	C(14)—C(15)—C(16)	119.0(3)
C(2)—C(3)—C(4)	120.4(3)	C(15)—C(16)—C(17)	120.6(3)
C(3)—C(4)—C(5)	120.8(3)	C(12)—C(17)—C(16)	122.3(2)
X(1)—C(5)—C(4)	118.2(3)	O(1)—B —O(2)	98.31(15)
C(7)—C(6)—C(11)	115.8(2)	O(1)—B —C(6)	110.0(2)
C(7)—C(6)—B	122.7(2)	O(1)—B —C(12)	110.5(2)
C(11)—C(6)—B	121.5(2)	O(2)—B —C(6)	109.2(2)
C(6)—C(7)—C(8)	122.0(3)	O(2)—B —C(12)	108.6(2)
C(7)—C(8)—C(9)	120.6(3)	C(6)—B —C(12)	118.3(2)
		6b	
N —O(1)—B	103.5(2)	C(6)—C(11)—C(10)	122.6(3)
C(1)—O(2)—B	107.1(2)	C(13)—C(12)—C(17)	115.5(3)
O(1)—N —C(1)	111.7(2)	C(13)—C(12)—B	122.5(3)
O(1)—N —C(5)	122.4(2)	C(17)—C(12)—B	122.0(3)
C(1)—N —C(5)	125.6(2)	C(12)—C(13)—C(14)	122.3(3)
O(2)—C(1)—N	112.1(2)	C(13)—C(14)—C(15)	120.7(4)
O(2)—C(1)—C(2)	128.9(3)	C(14)—C(15)—C(16)	118.5(3)
N —C(1)—C(2)	119.0(3)	C(15)—C(16)—C(17)	120.5(4)
C(1)—C(2)—C(3)	118.6(3)	C(12)—C(17)—C(16)	122.5(4)
C(2)—C(3)—C(4)	119.2(3)	C(5)—C(19)—C(20)	112.0(2)
C(2)—C(3)—C(18)	119.7(4)	C(5)—C(19)—C(24)	113.1(3)
C(4)—C(3)—C(18)	121.1(4)	C(20)—C(19)—C(24)	110.5(3)
C(3)—C(4)—C(5)	123.0(3)	C(19)—C(20)—C(21)	111.0(3)
N —C(5)—C(4)	114.6(3)	C(20)—C(21)—C(22)	111.5(3)
N —C(5)—C(19)	117.7(2)	C(21)—C(22)—C(23)	111.3(3)
C(4)—C(5)—C(19)	127.7(3)	C(22)—C(23)—C(24)	112.4(3)
C(7)—C(6)—C(11)	115.9(3)	C(19)—C(24)—C(23)	110.6(3)
C(7)—C(6)—B	122.9(2)	O(1)—B —O(2)	98.2(2)
C(11)—C(6)—B	121.1(3)	O(1)—B —C(6)	110.5(2)
C(6)—C(7)—C(8)	122.2(3)	O(1)—B —C(12)	108.7(2)
C(7)—C(8)—C(9)	119.9(4)	O(2)—B —C(6)	109.4(2)
C(8)—C(9)—C(10)	119.7(4)	O(2)—B —C(12)	112.3(2)
C(9)—C(10)—C(11)	119.6(3)	C(6)—B —C(12)	116.3(2)

Can. J. Chem. Downloaded from www.nrcresearchpress.com by 210.87.254.40 on 09/06/12
For personal use only.

employed for the data collection being bounded by the faces (followed by their distances in mm from a common origin): ±(0 1 −1), 0.15, ±(0 1 0), 0.13, ±(0 1 1), 0.16, ±(2 0 −1), 0.28. Crystal data: $C_{24}H_{26}BNO_2$ fw = 371.29 Monoclinic, a = 8.5047(8), b = 15.6603(14), c = 16.0501(18) Å, β = 104.776(5)°, V = 2066.9(4) Å^3, Z = 4, ρ_c = 1.193 g cm^{-3}, $F(000)$ = 792, μ(Mo-Kα) = 0.70 cm^{-1}. Absent reflections: $h0l$, $h + l$ odd, and $0k0$, k odd, uniquely indicate the space group $P2_1/n$ (non-standard setting of $P2_1/c$, equivalent positions: ±(x, y, z; 1/2 − x, 1/2 + y, 1/2 − z)).

An ω–2θ scan at 1.44–10.06° min^{-1} over a range of (0.65 + 0.35 tan θ)° in ω was employed. Of 3604 independent reflections measured (to 2θ = 50°), 1750 (48.6%) had intensities greater than 3σ(I) above background. The intensities of the three standard reflections (chosen to be approximately orthogonal to one another) exhibited severe and somewhat variable decay during the course of the data collection (intensities falling off by 39, 33, and 33%). A correction for anisotropic decay was made (21).

The structure was solved by direct methods, the non-hydrogen atoms being positioned from an E-map and hydrogen atoms from a difference map after refinement of the non-hydrogen atoms with anisotropic thermal parameters to R = 0.097. Hydrogen atoms were refined with isotropic thermal parameters in subsequent least-squares cycles. The structure was refined to R = 0.042 and R_w = 0.046 for 1750 observed reflections; for all 3604 reflections R = 0.119. The mean and maximum parameter shifts on the final cycle of refinement corresponded to 0.05 and 0.80σ respectively, the maximum shift being associated with the y coordinate of H(18c). The mean error in an observation of unit weight was 1.844 and the largest peak on the final difference map was +0.17 e Å^{-3} in the vicinity of oxygen.

Analysis of thermal motion

The thermal motion in both structures (Fig. 1) has been analysed in terms of the rigid-body modes of translation, libration, and screw-motion (22). The rms errors in the U_{ij} (derived from the least-squares analyses) are 0.0015 and 0.0020 Å^2, respectively, for **6***a* and **6***b*. In each case analysis of the entire molecules indicated significant independent motion of various molecular fragments which were then separately analysed (rms ΔU_{ij} = 0.0017–0.0038 Å^2). The appropriate bond distances have been corrected for libration (22, 23), using shape parameters q^2 of 0.08 for all atoms involved. Corrected bond lengths appear in Table 3 along with the uncorrected values; corrected bond

TABLE 5. Intra-annular torsion angles (deg) standard deviations in parentheses

Atoms	Value (deg)
6*a*	
B —O(1)—X(1)—X(2)	11.8(2)
O(1)—X(1)—X(2)—O(2)	−1.9(2)
B —O(2)—X(2)—X(1)	−8.7(2)
X(2)—O(2)—B —O(1)	14.0(2)
X(1)—O(1)—B —O(2)	−15.0(2)
6*b*	
B —O(1)—N —C(1)	−19.6(3)
O(1)—N —C(1)—O(2)	3.2(3)
B —O(2)—C(1)—N	15.1(3)
C(1)—O(2)—B —O(1)	−24.7(3)
N —O(1)—B —O(2)	25.4(2)
C(24)—C(19)—C(20)—C(21)	−56.7(4)
C(19)—C(20)—C(21)—C(22)	55.6(5)
C(20)—C(21)—C(22)—C(23)	−54.1(5)
C(21)—C(22)—C(23)—C(24)	54.3(4)
C(22)—C(23)—C(24)—C(19)	−55.5(4)
C(20)—C(19)—C(24)—C(23)	56.2(4)

angles do not differ by more than 1σ from the uncorrected values given in Table 4. Intra-annular torsion angles defining the conformations of chelate and cyclohexane rings are listed in Table 5. Bond lengths and angles involving hydrogen and a complete listing of torsion angles (Tables 6–8) are included as supplementary material.

Results and discussion

The crystal structure of **6*a*** consists of molecules each linked to two others by a system of weak C—H···O hydrogen bonds (C(5)—H(5)···O(2) ($1 - x$, $1/2 + y$, $1/2 - z$), C···O = 3.251(3), H···O = 2.30(3) Å, C—H···O = 156(2)°) to form continuous spirals about the twofold screw axis. The structure of the substituted derivative **6*b*** consists of discrete molecules separated by normal van der Waals distances.

The central feature of each molecule is the 1,3-dioxa-3*a*-azonia-2-borataindan ring system. The pyridine rings are both slightly, but significantly, non-planar (χ^2 = 50.0 and 48.5, maximum deviation from C_5N mean planes, 0.011(3) and 0.012(2) Å, respectively, for **6*a*** and **6*b***). With the exception of the C(18) methyl substituent in **6*b*** (displacement = 0.008(7) Å), all substituents of the pyridine rings are significantly displaced from the mean plane of the ring in the same direction (displacements range from 0.013(1) Å for O(2) in **6*a*** to 0.083(2) Å for the same atom in **6*b***, mean 0.049 Å). Unlike the planar five-membered OBONC rings in the closely related molecules **8** (13, 14), the analogous rings in **6*a*** and **6*b*** both exhibit non-planar B-envelope conformations, the deviation from planarity being greater in the case of **6*b*** (see Table 5). In view of the chemical similarities between **6** and **8**, the non-planarity of the five-membered rings in the present structures is most likely a result of packing forces since intramolecular steric interactions are minimal.

The N—C(1) (X(1)—X(2)) bond lengths in **6*a*** and **6*b*** are 1.351(3) and 1.349(3) Å, respectively. These distances are significantly shorter than those observed (1.410(10) (24), 1.373(4) (25), and 1.400(5) Å (26)) and calculated (1.408 Å (27) and 1.390 Å (28)) for 2-pyridones; slightly longer than those found (1.341(3) (29) and 1.338(4) Å (25)) or calculated (1.311 Å (28)) for 2-hydroxypyridines; and similar to those observed in *N*-alkylpyridinium salts such as **10** (26) (1.358(7) Å) or in certain substituted pyridine *N*-oxides such as 2-hydroxymethylpyridine *N*-oxide (30) (1.349 and 1.358 Å). The C(1)—O(2) bond distance of 1.316(3) Å in **6*b*** is significantly longer than those observed (1.236(10) (24), 1.262(4) (25), 1.224(3) (26), and 1.250(7) Å (31)) and calculated (1.264 Å (27) and 1.221 Å (28)) for 2-pyridones; slightly shorter than those observed (1.321(3) (29) and 1.330(5) Å (25)) and calculated (1.358 Å (28)) for 2-hydroxypyridines; and equal within experimental error to that observed in **10** (26) (1.317(7) Å). The N—O(1) distance of 1.389(3) Å in **6*b*** is longer than the mean N—O distance of 1.35 Å for a number of pyridine *N*-oxides and their coordination complexes or salts (32), the only comparable distance being that of 1.39 Å reported for *N*-oxopyridinium trichloroacetate (33). Bond lengths in the pyridine ring of **6*b*** (mean[7] N—C = 1.355(6), mean C—C = 1.386(4) Å) indicate a uniform delocalization of electron density. These data indicate that both **6** and **7** (along with related canonical forms) are important contributors to the overall structures of the diphenylboron chelates, the former being dominant. In a closely related Zn(II) complex of the thio analog 2-mercaptopyridine *N*-oxide (34), where N—C(S) = 1.37(1)–1.38(2) and N—O = 1.33(1)–1.37(1) Å, a more substantial contribution of the sulphone form (analogous to **7**) to the overall structure is indicated.

The O(2)—B bond in **6*a***, 1.580(3) Å, is significantly longer than the mean, 1.560(3) Å, of the three other equivalent O—B bonds in **6*a*** and **6*b***. By analogy with a nearly identical situation observed in the structure of *rac*-bis[(salicylaldoximato(2−)) phenylboron] (35), this lengthening of the O—B bond may be ascribed to the participation of the oxygen atom in the C—H···O hydrogen bond. The B—C bonds are essentially equal in the two structures, mean B—C = 1.600(4) Å. These distances are in good agreement with those observed for other resonance-stabilized five-membered *O,O*-chelates of diphenylboron (in **8** (X = Ph) O—B = 1.548(2) and 1.552(2), B—C = 1.609(2), and in (tropolonato)diphenylboron (36) O—B = 1.544(2) and 1.565(2), B—C = 1.599(2) and 1.611(3) Å) and similar to those in the two crystalline forms of (acetylacetonato)diphenylboron (36) which contains a six-membered chelate ring (O—B = 1.530(2)–1.547(2) Å and B—C = 1.601(2)–1.610(3) Å). In the related diphenylboron chelate of *N*-hydroxymethyldimethylamine *N*-oxide (37) (one of the best known donors for the diphenylborenium cation), a saturated derivative of **8** (X = Ph), (N)O—B = 1.556(8), (C)O—B = 1.506(8), and mean B—C = 1.632(7) Å.

The equatorially substituted cyclohexane ring has a regular chair conformation and normal geometry (mean C—C = 1.529(7) Å, mean C—C—C = 111.2(7)°). Of the four B-phenyl rings in the two structures, three are slightly but significantly non-planar while the other (C(12) ring in **6*b***) is planar within experimental error (χ^2 = 32.5, 35.0, 55.4, and 5.7, maximum deviation from the mean plane 0.015(2) Å). The substituent-induced geometrical distortions of the B-substituted phenyl rings are as expected (38).

Acknowledgments

We thank the Natural Sciences and Engineering Research Council of Canada and the Fonds der Chemischen Industrie, Frankfurt am Main, for financial support and the University of British Columbia Computing Centre for assistance.

[7] Here and elsewhere in this report mean values refer to weighted means with rms deviations from the mean in parentheses.

Can. J. Chem. Downloaded from www.nrcresearchpress.com by 210.87.254.40 on 09/06/12
For personal use only.

1. (*a*) R. T. COUTTS. Can. J. Pharm. Sci. **2**, 27 (1967); (*b*) J. B. BAPAT, D. ST. BLACK, and R. F. C. BROWN. Adv. Heterocycl. Chem. **10**, 199 (1969); (*c*) H. MAEHR. Pure Appl. Chem. **28**, 603 (1971).
2. D. V. IOFFE and L. S. EFROS. Usp. Khim. **30**, 1325 (1961); Russ. Chem. Rev. **30**, 569 (1961).
3. E. OCHIAI. Aromatic amine oxides. Elsevier, Amsterdam. 1967. p. 404.
4. A. R. KATRITZKY and J. M. LAGOWSKI. Chemistry of the heterocyclic *N*-oxides. Academic Press, London. 1971. pp. 152, 407.
5. R. S. BROWN, A. TSE, and J. C. VEDERAS. J. Am. Chem. Soc. **102**, 1174 (1980).
6. A. E. LANDERS and D. J. PHILLIPS. Inorg. Chim. Acta, **51**, 109 (1981).
7. (*a*) G. T. NEWBOLD and F. S. SPRING. J. Chem. Soc. 1864 (1948); (*b*) E. SHAW. J. Am. Chem. Soc. **71**, 67 (1949).
8. A. ALBERT, C. W. REES, and A. J. H. TOMLINSON. Rec. Trav. Chim. Pays-Bas, **75**, 819 (1956).
9. P.-J. SUN, Q. FERNANDO, and H. FREISER. Anal. Chem. **36**, 2485 (1964).
10. R. G. GARVEY, J. H. NELSON, and R. O. RAGSDALE. Coord. Chem. Rev. **3**, 375 (1968).
11. N. M. KARAYANNIS, L. P. PYTLEWSKI, and C. M. MIKULSKI. Coord. Chem. Rev. **11**, 93 (1973).
12. D. HUBBARD, G. R. EATON, and S. S. EATON. Inorg. Nucl. Chem. Lett. **15**, 225 (1979).
13. S. J. RETTIG, J. TROTTER, W. KLIEGEL, and D. NANNINGA. Can. J. Chem. **55**, 1 (1977).
14. S. J. RETTIG, J. TROTTER, W. KLIEGEL, and D. NANNINGA. Can. J. Chem. **56**, 1676 (1978).
15. W. KLIEGEL and D. NANNINGA. Chem. Ber. In preparation.
16. G. LOHAUS and W. DITTMAR. Arzneimittelforsch, **31**, 1311 (1981).
17. W. KLIEGEL and D. NANNINGA. Pharmazie, **38**, 131 (1983).
18. J. ITOH, S. AMANO, Y. OGAWA, Y. KODAMA, N. EZAKI, and Y. YAMADA. J. Antibiot. **33**, 1311 (1980).
19. D. T. CROMER and J. B. MANN. Acta Crystallogr. Sect. A, **24**, 321 (1968).
20. R. F. STEWART, E. R. DAVIDSON, and W. T. SIMPSON. J. Chem. Phys. **42**, 3175 (1965).
21. J. A. IBERS. Acta Crystallogr. Sect. B, **25**, 1667 (1969).
22. V. SCHOMAKER and K. N. TRUEBLOOD. Acta Crystallogr. Sect. B, **24**, 63 (1968).
23. D. W. J. CRUICKSHANK. Acta Crystallogr. **9**, 747 (1956); **9**, 754 (1956); **14**, 896 (1961).
24. B. R. PENFOLD. Acta Crystallogr. **6**, 591 (1953).
25. J. ALMLOF, A. KVICK, and I. OLOVSSON. Acta Crystallogr. Sect. B, **27**, 1201 (1971).
26. G. L. WHEELER and H. L. AMMON. Acta Crystallogr. Sect. B, **30**, 680 (1974).
27. N. BODOR, M. J. S. DEWAR, and H. J. HARGET. J. Am. Chem. Soc. **92**, 2929 (1970).
28. H. B. SCHLEGEL, P. GUND, and E. M. FLUDER. J. Am. Chem. Soc. **104**, 5347 (1982).
29. A. KVICK and I. OLOVSSON. Ark. Kem. **30**, 71 (1968).
30. R. DESIDERATO and J. C. TERRY. J. Heterocycl. Chem. **8**, 617 (1971).
31. E. EGERT, H. J. LINDNER, W. HILLEN, and H. G. GASSEN. Acta Crystallogr. Sect. B, **33**, 3704 (1977).
32. D. ULKU, B. P. HUDDLE, and J. C. MORROW. Acta Crystallogr. Sect. B, **27**, 432 (1971).
33. L. GOLIC, D. HADZI, and F. LAZARINI. J. Chem. Soc. Chem. Commun. 860 (1971).
34. B. L. BARNETT, H. C. KRETSCHMAR, and F. A. HARTMAN. Inorg. Chem. **16**, 1834 (1977).
35. S. J. RETTIG and J. TROTTER. Can. J. Chem. **61**, 206 (1983).
36. S. J. RETTIG and J. TROTTER. Can. J. Chem. **60**, 2957 (1982).
37. S. J. RETTIG, J. TROTTER, and W. KLIEGEL. Can. J. Chem. **52**, 2531 (1974).
38. A. DOMENICANO, A. VACIAGO, and C. A. COULSON. Acta Crystallogr. Sect. B, **31**, 221 (1975); **31**, 1630 (1975).

Can. J. Chem. Downloaded from www.nrcresearchpress.com by 210.87.254.40 on 09/06/12
For personal use only.

An *ab initio* study of the $A^2A'-X^2A''$ vibronic transition in the free radical HNF

MILJENKO PERIĆ
Faculty of Science, Institute of Physical Chemistry, University of Belgrade, 11001 Beograd, Yugoslavia

SIGRID D. PEYERIMHOFF
Lehrstuhl für Theoretische Chemie, Universität Bonn, Wegelerstraße 12, D-5300 Bonn 1, West Germany

AND

ROBERT J. BUENKER
Lehrstuhl für Theoretische Chemie, Universität-Gesamthochschule Wuppertal, Gaußstraße 20, D-5600 Wuppertal 1, West Germany

Received March 18, 1983

MILJENKO PERIĆ, SIGRID D. PEYERIMHOFF, and ROBERT J. BUENKER. Can. J. Chem. **61**, 2500 (1983).

Potential energy curves for the two lowest electronic states X^2A'' and A^2A' ($^2\Pi$ in linear geometry) of HNF are calculated employing configuration interaction. A vibrational analysis of the $A^2A'-X^2A''$ transition is undertaken; stretching and bending modes are treated separately but vibronic coupling and large-angle bending is taken into consideration explicitly. The various vibronic levels including their K-type structure are compared with measured data wherever available and the results indicate that the prediction of vibronic spectra in small molecules on the basis of purely *ab initio* data is now within reach.

MILJENKO PERIĆ, SIGRID D. PEYERIMHOFF et ROBERT J. BUENKER. Can. J. Chem. **61**, 2500 (1983).

Utilisant des interactions de configuration, on a calculé les courbes d'énergie potentielle des états électroniques les plus bas X^2A'' et A^2A' ($^2\Pi$ en géométrie linéaire) de HNF. On a effectué une analyse vibrationnelle de la transition $A^2A'-X^2A''$. On a traité séparément les modes d'élongation et de déformation, mais on prend explicitement en considération le couplage vibronique et la déformation de grand angle. On a comparé les divers niveaux vibroniques, y compris leur structure de type K, avec les mesures disponibles et les résultats indiquent que l'on peut maintenant prédire les spectres vibroniques des petites molécules en se basant purement sur des données *ab initio*.

[Traduit par le journal]

Can. J. Chem. Downloaded from www.nrcresearchpress.com by 210.87.254.42 on 09/06/12
For personal use only.

Introduction

The absorption spectrum of the free radical HNF was first observed by Goodfriend and Woods (1) who obtained several bands in the region of 4000–5000 Å by flash photolysing difluoroamine HNF_2. They attributed the spectrum to a bending progression of the $^2A' \leftarrow {}^2A''$ transition in HNF, with an upper state vibrational frequency of about 1035 cm^{-1}. However, the resolution was not high enough to enable a detailed analysis of the K-type structure.

Jacox and Milligan (2) have produced HNF and DNF in an argon matrix by the reaction of photolytically produced atomic fluorine with NH. On the basis of the observed ir spectrum they obtained values for two vibrational fundamentals, 1432 and 1000 cm^{-1}, and attributed them to the bending and N—F stretching, respectively; no N—H stretching frequency has been found. The equilibrium geometry for the ground state of HNF has then been estimated as NH = 1.026 Å, NF = 1.400 Å and ∠HNF = 105°. Electronic transitions in HNF have also been recorded. By employing a value of 1033 cm^{-1} for the excited state (ES) bending frequency (obtained by averaging over five observed band separations) and assuming the stretching frequences to be equal in the ground and excited electronic states, one obtains T_e values of 20 431 cm^{-1} and 20 358 cm^{-1} for HNF and DNF, respectively.

A thorough high-resolution analysis of the HNF absorption spectrum has been carried out by Woodman (3). Seven members of a progression in the upper state bending mode have been observed and the K structure has been analyzed. Several perturbations in the spectrum indicate a coupling between the ν_2 and ν_3 vibrations. A progression in the stretching modes has not been found, however. The equilibrium angles and NF distances in both electronic states have been determined as ∠HNF = 125°, NF = 1.34 Å for the first excited state. The NH distances have been estimated to be 1.06 and 1.03 Å for the ground and excited state, respectively. For the excited state bending and NF stretching vibrations the values of 1070 and 1120 cm^{-1} have been obtained, while the NH stretching vibrational frequency has been estimated to be 2800 cm^{-1}. A T_e value of 20 141.3 cm^{-1} results from this analysis.

The emission spectrum of HNF has been obtained by Lindsay *et al.* (4) as a consequence of the chemiluminiscent reaction $N_2H_4 + F_2$. The transition from the vibrationless excited state to the lowest four bending levels of the ground state, as well as the (010) → (010) excitation have thus far been recorded. The value for the ground state bending vibrational frequency determined from the first electronic transition ($\nu_2'' = 1441.1$ cm^{-1}) is close to that obtained by Jacox and Milligan (2). These authors have also pointed out the large differences which exist between the spectrum of HNF and its isoelectronic analogue HOO.

To our knowledge the only theoretical (*ab initio*) study of the HNF molecule has been reported by Brotchie and Thomson (5). These authors have used the restricted Hartree–Fock scheme with three different basis sets of gaussian orbitals. With the largest set of effectively double-ζ quality, the equilibrium geometry has been calculated to be in good agreement with what has been inferred experimentally. The energy difference between the two lowest-lying electronic states has also been calculated (20 800 cm^{-1}), but altogether this study does not allow more than a rough interpretation of the main features in the HNF spectrum. It is thus the goal of the present work to obtain potential energy curves for this system by means of large-scale CI calculations and on the basis of these results to carry out a detailed vibronic analysis of the first spectral band.

Can. J. Chem. Downloaded from www.nrcresearchpress.com by 210.87.254.42 on 09/06/12
For personal use only.

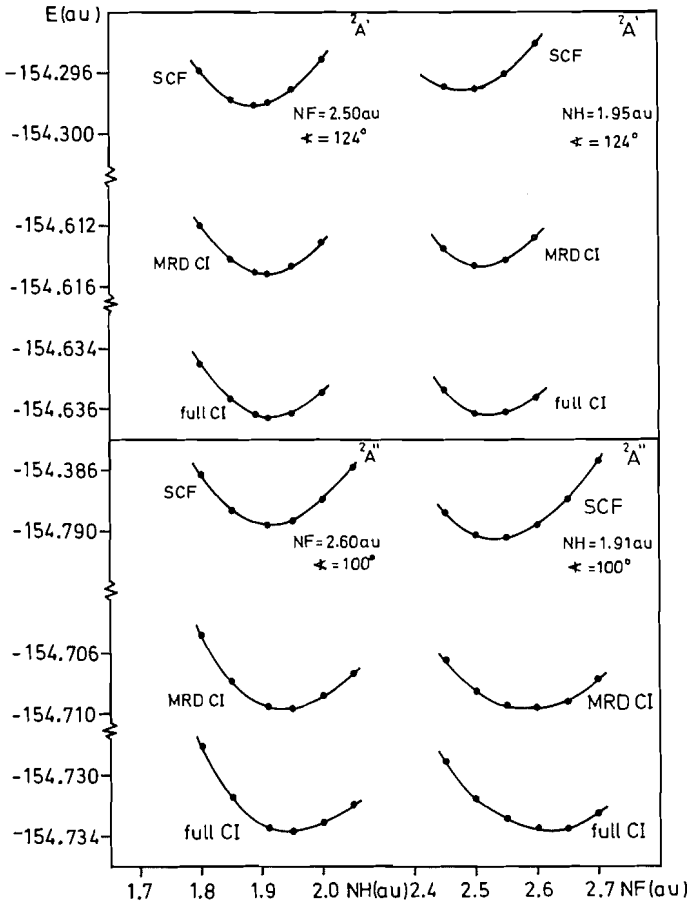

FIG. 1. Calculated potential energy curves for stretching vibrations in the lowest $^2A''$ and $^2A'$ electronic states of HNF.

Technical details of the treatment

In the present work the AO basis proposed by Huzinaga (6*a*) and Dunning (6*b*) is employed. It consists of nine *s* and five *p* functions (6*a*) in the [4*s*, 2*p*] contraction (6*b*) for the N and F atoms, respectively, and two *s* (scaling factor $\eta^2 = 2.3$ relative to the expansion given by J. L Whitten (quoted in ref. 7)) and one *p* group ($\alpha = 0.8462$) for the hydrogen atom. In addition, two sets of cartesian *d* functions are added: the first with the exponent $\alpha(d) = 0.95$ on nitrogen, the second ($\alpha(d) = 1.62$) on fluorine.

The configuration interaction treatment is of the standard MRD-CI type with configuration selection and energy extrapolation (8, 9). A core of two MO's corresponding to the 1*s* shells of N and F is kept doubly occupied in all configurations, while the corresponding two complementary MO's with highest orbital energy are excluded from consideration entirely; all other MO's are allowed variable occupation. Two reference configurations are employed for each state in order to generate the single- and double-excitation space. These are $\ldots 7a'^2\,1a''^2\,2a''$ and $\ldots 7a'^2\,1a''\,2a''^2$ for the X^2A'' ground state and $\ldots 6a'^2\,7a'\,1a''^2\,2a''^2$ and $6a'\,7a''^2\,1a''^2\,2a''^2$ for the $^2A'$ excited state. In this way a configuration space of approximately 30 000 symmetry-adapted functions is obtained, while the sizes of the secular equations actually diagonalized (corresponding to a selection threshold of $T = 10$ μhartree) is in the order of 3400–5400. For each electronic state, the respective SCF orbitals are used as the MO basis. The energy contribution of higher than double-excitation configurations is also estimated in analogy to the formula (10) $\Delta E = (1 - c_0^2) \times (E_{SCF} - E_{CI})$, which upon addition to the corresponding CI result is referred to as the full CI limit in the ensuing discussion; in the present case the SCF energy is replaced by the energy of the 2 × 2 reference set and the SCF coefficient c_0 by the respective sum of the two contributions (approximately 92%).

Since the two lowest lying states of HNF correspond at the linear geometry of the molecule to the same (orbitally) degenerate $^2\Pi$ electronic state (Renner-Teller effect), the Born–Oppenheimer approximation is not capable of yielding a suitably accurate calculation of the vibrational levels. Instead, the total wavefunction must be taken in the form of a linear combination including the electronic and nuclear coordinates of both electronic states. The vibronic energies and wavefunctions can be obtained according to the method proposed by Buenker (11), for which more details are described elsewhere (12, 13), by diagonalizing the Hamiltonian for the electronic and bending motion including rotation about the *a*-axis (coinciding at the linear geometry with the molecular axis):

$$[1]\quad H = -\frac{1}{2}\sum_i^n \Delta_i - \sum_{i,a}^{n,N}\frac{Z_a}{r_{ia}} + \sum_{i<j}^{n}\frac{1}{r_{ij}} + \sum_{a<b}^{N}\frac{Z_a Z_b}{r_{ab}}$$
$$-\frac{1}{2}\left[T_1(\rho)\frac{\partial^2}{\partial\rho^2} + T_2(\rho)\frac{\partial}{\partial\rho} + T_3(\rho)\frac{\partial^2}{\partial\phi^2} + T_4(\rho)\right]$$
$$\equiv H_e - \frac{1}{2}\left[T_1(\rho)\frac{\partial^2}{\partial\rho^2} + T_2(\rho)\frac{\partial}{\partial\rho} + T_3(\rho)\frac{\partial^2}{\partial\phi^2} + T_4(\rho)\right]$$

in a basis consisting of the products of the electronic wavefunctions Ψ^-, Ψ^+ (or linear combinations thereof (12, 13), as actually employed in the present work) calculated in the Born–Oppenheimer approximation with the nuclear functions $\Phi_i(\rho, \phi)$. The symbol ρ denotes the bending coordinate ($\rho = \pi - \angle\mathrm{HNF}$) and φ defines the rotation about the *a* axis. It is assumed that the stretching vibrations and rotations about the axes perpendicular to *a* can be treated separately (a part of the bend–stretch interaction can be included into Hamiltonian (1) (14, 15)). In order to incorporate the coupling between the electronic and bending vibrational motion exactly, the first and the second derivatives of the electronic CI functions with respect to the nuclear coordinates must be calculated (12, 16). In the present study, however, the exact dependence of these derivatives on the rotational angle φ has been replaced by their asymptotic forms $\pm\Lambda$ and $-\Lambda^2$, whereby their ρ dependence has been neglected entirely with the consequence that the secular problem becomes very similar to that in the more conventional approach (17), differing from it only in the form of the potentials (calculated pointwise by the CI method in the present case and expanded in polynomial series in ρ) and the kinetic energy operator.

The coefficients $T_i(\rho)$ ($i = 1, \ldots 4$) in the expression for the kinetic energy operator for the bending vibrations and rotations about the *a* axis are generally functions of the bending coordinate ρ (and also of the internuclear distances for some forms of the bending Hamiltonian (15)) and become constants only for infinitesimal vibrations. Their actual form depends on the Hamiltonian chosen; in the present paper the Hamiltonian developed by Hougen, Bunker, and Johns (18) is used:

$$[2]\quad T'' \equiv H_b^0 + H_{rot}^z - V_0(\rho) = -\frac{1}{2I_{\rho\rho}^0}\frac{\partial^2}{\partial\rho^2} - \frac{1}{2}$$
$$\times\left(\frac{\partial}{\partial\rho}\frac{1}{I_{\rho\rho}^0}\right)\frac{\partial}{\partial\rho} - \frac{1}{2}(\mu^0)^{1/4}\left\{\frac{\partial}{\partial\rho}\frac{1}{I_{\rho\rho}^0}(\mu^0)^{-1/2}\left[\frac{\partial}{\partial\rho}(\mu^0)^{1/4}\right]\right\}$$

TABLE 1. Calculated equilibrium data for the ground and first excited state of HNF (DNF)

	$2A''$ (GS)				$2A'$ (ES)			
Parameter	MRD-CI[b]	MRD-CI	Full CI	Exptl[c]	MRD-CI[b]	MRD-CI	Full CI	Exptl[c]
N—H(au)	1.935	1.94	1.95	2.00(1.06 Å)[a] (3)	1.91	1.91	1.92	1.946(1.03 Å) (3)
N—F(au)	2.56	2.59	2.62	2.59(1.37 Å) (3)	2.51	2.51	2.53	2.53(1.34 Å) (3)
∠HNF(deg)	100	101.1		105(3)	122	123.2		125(3)
E_{min}(au)	−154.70968	−154.7097	−154.7336		−154.61513	−154.6152	−154.6386	
ω^1_{HNF}(cm^{-1})			3200				3600	
ω^2_{HNF}(cm^{-1})		1430		1432(2) 1441.1(4)		1176		1081(2) 1074.1(3)
ω^3_{HNF}(cm^{-1})			1000	1000(2)			1260	
ω^1_{DNF}(cm^{-1})			2330				2600	
ω^2_{DNF}(cm^{-1})		1047		1069(2)		889		
ω^3_{DNF}(cm^{-1})			985	1000(2)			1240	
A_{HNF}(cm^{-1})	18.049			17.688(3)	26.319			27.570(3)
B_{HNF}(cm^{-1})	1.070			1.0389(3)	1.057			1.0329(3)
C_{HNF}(cm^{-1})	1.010			0.9777(3)	1.016			0.9920(3)
A_{DNF}(cm^{-1})	9.896				15.049			
B_{DNF}(cm^{-1})	1.006				0.9521			
C_{DNF}(cm^{-1})	0.9130				0.8955			

[a]Assumed.
[b]The values in this column are obtained from a fit to the original data points generated, while the data in the next two columns result from the polynomial fits with the aid of additional spline points (see text).
[c]Reference number in parentheses.

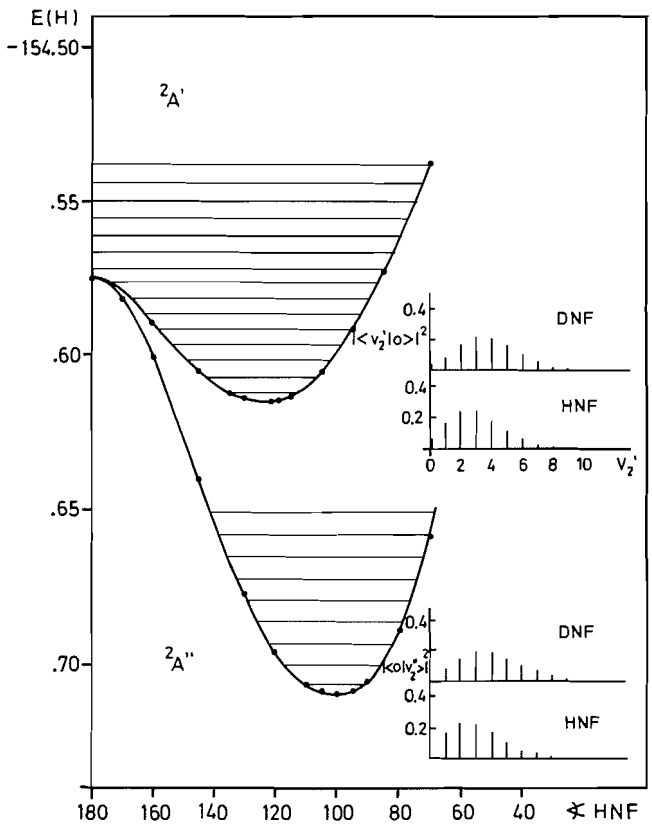

FIG. 2. Calculated MRD-CI bending potential curves and corresponding $K = 0$ vibronic levels for the two lowest electronic states of HNF. Franck–Condon factors for the transitions from $v_2'' = 0$ to various v_2' levels and from $v_2' = 0$ to v_2'' are also given.

This operator corresponds to the integration element $d\rho$. An appropriate form of the kinetic energy operator can be obtained by applying the transformation $\rho^{-1/2}\, T''\, \rho^{1/2}$ to the expression [2] and results in:

$$[3]\quad T = -\frac{1}{2I^0_{\rho\rho}}\frac{\partial^2}{\partial\rho^2} - \frac{1}{2}\left[\frac{1}{I^0_{\rho\rho}\rho} + \frac{\partial}{\partial\rho}\left(\frac{1}{I^0_{\rho\rho}}\right)\right]\frac{\partial}{\partial\rho} + \frac{1}{8I^0_{\rho\rho}\rho^2} - \frac{1}{4\rho}\frac{\partial}{\partial\rho}\left(\frac{1}{I^0_{\rho\rho}}\right) + \frac{1}{8}\mu^0\left\{\frac{\partial}{\partial\rho}\left(\frac{1}{I^0_{\rho\rho}}\right)\frac{\partial}{\partial\rho}\left(\frac{1}{\mu^0}\right) + \frac{1}{I^0_{\rho\rho}}\frac{\partial^2}{\partial\rho^2}\left(\frac{1}{\mu^0}\right) - \frac{3}{4}\frac{\mu^0}{I^0_{\rho\rho}}\left[\frac{\partial}{\partial\rho}\left(\frac{1}{\mu^0}\right)\right]^2\right\} - \frac{m[u_1\cos^2(\rho-\epsilon) + u_3\cos^2\epsilon + 2u_{13}\cos\epsilon\cos(\rho-\epsilon)]}{2(u_1u_3 - u_{13}^2)\sin^2\rho}\frac{\partial^2}{\partial\phi^2}$$

which coorresponds to the integration element $\rho d\rho d\phi$ and thus enables the use of the polar coordinate system. If the internuclear distances are assumed to be constant, it follows from eqs. [37] and [38] of ref. 18 that:

$$[4]\quad I^0_{\rho\rho} = \frac{u_1u_3 - u_{13}^2\cos^2\rho}{m(u_1 + u_3 + 2u_{13}\cos\rho)}$$

and

$$[5]\quad I^0_{yy}I^0_{zz} - I^0_{yz}I^0_{yz} = \frac{(u_1u_3 - u_{13}^2)\sin^2\rho}{m^2}$$

so that

$$[6]\quad \mu^0 = \left[\frac{\sin^2\rho}{m^4}(u_1u_3 - u_{13}^2\cos^2\rho)(u_1u_3 - u_{13}^2)\right]^{-1}$$

In explicit calculations the total Hamiltonian operator is written as

$$[7]\quad H = H_0 + H'$$

with

$$[8]\quad H_0 = \lim_{\rho\to 0} H = T_0 + \frac{1}{2}k\rho^2$$

Can. J. Chem. Downloaded from www.nrcresearchpress.com by 210.87.254.42 on 09/06/12
For personal use only.

Can. J. Chem. Downloaded from www.nrcresearchpress.com by 210.87.254.42 on 09/06/12
For personal use only.

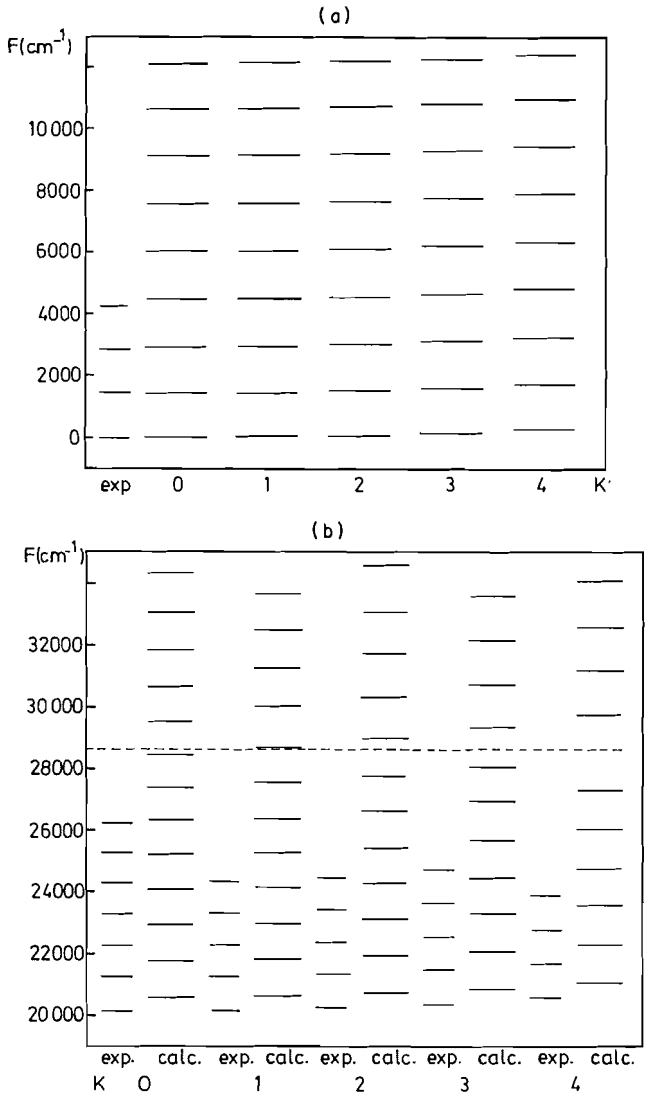

FIG. 3. Calculated $K = 0-4$ vibronic levels of the ground state X^2A'' (a) and excited state $^2A'$ (b) of HNF. Experimentally obtained term values (3, 4) are also shown.

and

$$[9] \quad T_0 = \lim_{\rho \to 0} T = -\frac{1}{2\mu}\left[\frac{\partial^2}{\partial\rho^2} + \frac{1}{\rho}\frac{\partial}{\partial\rho} - \frac{(K \pm \Lambda)^2}{\rho^2}\right]$$

whereby

$$[10] \quad \mu = \frac{u_1 u_3 - u_{13}^2}{m(u_1 + u_3 + 2u_{13})}$$

It should be noted that the force constant k in eq. [8] in general does not have any real physical meaning and can be chosen rather arbitrarily (19). The Hamiltonian [7] is diagonalized in the basis consisting of the eigenfunctions $R_{v,K\pm\Lambda}(\rho, \phi)$ of the two-dimensional harmonic oscillator H_0. The anharmonic part of the potential and the coefficients T_1', ..., T_4' ($T_i'(\rho) = T_i(\rho) - T_i^0$) are calculated for a number of ρ values ($\rho = 0°$, 1°, 2° ... 160°, for example) and the data points obtained are fitted in a power series expansion. The corresponding matrix elements are calculated in the manner described in refs. 19–21.

The Schrödinger equation for the stretching vibrations is solved with the help of the variational method, involving expansion of the vibrational wavefunctions in one-dimensional harmonic oscillator eigenfunctions and employing a polynomial fit for the electronic potential as described elsewhere (19). It has been assumed thereby that the two stretching vibrational modes are independent of one another; furthermore, the very simple form of the kinetic energy operators (diagonal elements of the G^{-1} matrix) is employed. Finally, by the calculations of rotational levels HNF have been treated as an asymmetric top, with the energies having been obtained by diagonalizing the corresponding operator in a basis of symmetric-top eigenfunctions (22).

Results and discussion

The first series of calculations were carried to determine the equilibrium geometries for the two lowest-lying states ($1^2A''$ and $1^2A'$) of HNF. A portion of the results of these calculations is presented in Fig. 1; the potential curves corresponding to the changes of the N—H and N—F distances at the H—N—F angle values of 100° (ground state GS) and 124° (excited state ES) are given. The energy values obtained at various levels of the treatment (SCF, MRD-CI, and estimated full CI) are presented and show large differences between the SCF and CI results in spite of the basically single-configuration nature of each of the two states. The calculated equilibrium data (obtained by means of a least-squares fit) are given in Table 1 and compared with the corresponding values obtained experimentally.

Having found the optimal interatomic distances for both electronic states, the calculation of the bending potential curves was carried out. For the ground state the N—H distance was kept constant at 1.935 au and N—F at 2.56 au; for the excited state the angular potential curve was calculated at N—H = 1.91 au and N—F = 2.51 au. The potential surfaces (MRD-CI values) obtained are presented in Fig. 2. The set of energy points calculated directly was augmented by a number of points generated by means of the cubic spline procedure and after that the potential surfaces have been fitted with the polynomials of the twentieth order in ρ. The $T_i(\rho)$ coefficients are thereby represented by polynomials of the sixteenth order of ρ. The vibronic energy levels are calculated with the help of the method described above, with 2×40 vibrational basis functions for each K value. The $K = 0$ levels are also indicated in Fig. 2. For the bending frequency the values of 1430 cm^{-1} for GS and 1176 cm^{-1} for ES are calculated, both results being obtained by taking the differences between the respective $v_2 = 1$ and $v_2 = 0$ term values. The computed vibronic levels for $K = 0, \ldots, 4$ are presented in Fig. 3 a and b together with the experimentally obtained term values. All calculated vibrational frequencies are collected in Table 1. For T_{00} a value of 20 600 cm^{-1} (compared to exp. 20 141 cm^{-1}) is obtained.

Very close agreement between the calculated and experimental values is not to be expected, in particular not for the stretching vibrational frequencies because of the rather unrealistic assumption of mutual independence of the various vibrational modes. It can also be noted (Fig. 3 a, b) that the agreement between the calculated and observed vibronic energy levels becomes progressively worse with higher quantum numbers, suggesting that the calculated potential curves are too steep; this effect is at least partially caused by the calculation of the bending curves at the constant internuclear distances, i.e. optimal for the equilibrium angles, but not for other values of this variable. Nevertheless, the overall vibronic structure based solely on the *ab initio* results gives a realistic picture of the spectrum.

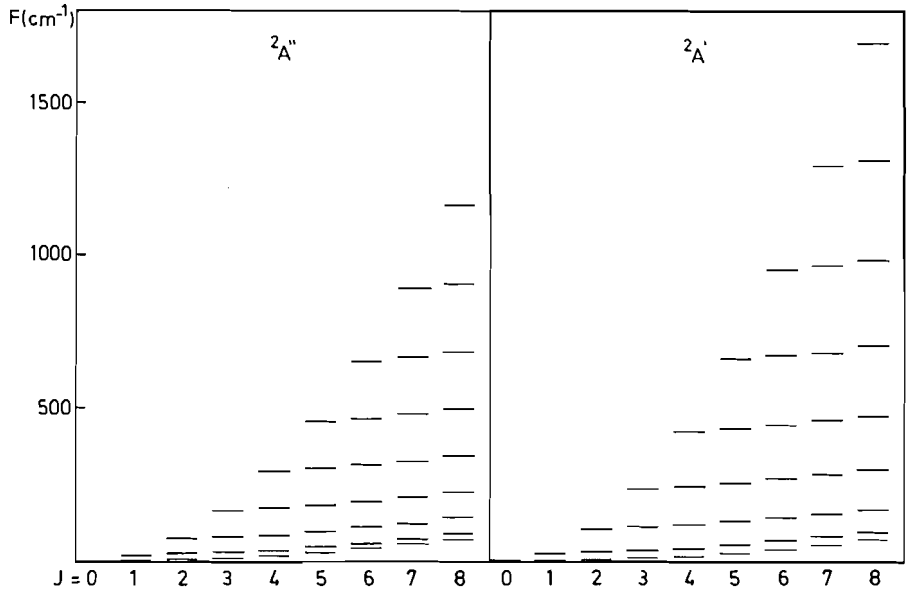

FIG. 4. Calculated rotational levels in the $^2A''$ and $^2A'$ electronic states of HNF.

The Franck–Condon factors for the transitions from the first bending vibrational level of the GS to various $K = 0$ levels of the ES are also shown in Fig. 2 for HNF and DNF. On the basis of the present calculations the strongest bands in the absorption spectrum should be those corresponding to $v_2' = 2$ and 3, whereas Woodman (3) observed the highest intensity in the second ($v_2' = 1$) and the third bands ($v_2' = 2$). The reason for this discrepancy is not clear since on the basis of the potentials themselves (Fig. 2), the vertical transition occurs to the third or fourth excited level rather than the second and direct inclusion of the electronic transition moment (zero at $\angle$HNF = 180° and increasing for smaller angles) into the intensity calculation is not likely to cause a shift relative to the Franck-Condon factors in this case.

In the emission spectrum the most intense bands should correspond to the transition from $v_2' = 0$ to $v_2'' -, 3$, again in some disagreement with the results of Lindsay *et al.* (4) who find $\Delta v_2 = 1$ transitions to be strongest and $\Delta v = 2$ bands to be appreciably weaker. The most intense bands in the stretching progression should definitely correspond to transitions between vibrationless states; the corresponding FC factors are 0.9963, 0.0003, and 0.0010 for $v_1' = 0, 1, 2$, (N—H vibrations) and 0.8538, 0.1230, and 0.0181 for $v_3' = 0, 1, 2$ (N—F vibrations) in the absorption spectrum of HNF.

In Fig. 4 the calculated rotational levels for both electronic states are presented. The corresponding rotational constants are given in Table 1. All the levels except the lowest ones appear practically in pairs; the very small J_τ splitting (which cannot be resolved in the scale used in Fig. 4) reflects the fact that HNF is nearly a symmetric top.

Summary

The present MRD-CI potential curves for the two lowest states of the HNF radical calculated in a standard AO basis (including some polarization functions) allow the geometrical parameters of the molecule to be computed within errors of less than 0.03 bohr and 4° from experimentally determined values. The calculated energy difference between the two states is $T_{00} = 20\,600$ cm^{-1}, compared to the most recent measured value of 20 141 cm^{-1}. Reduction of these discrepancies in the main requires larger AO basis sets, beyond that which has been employed in the present work.

The resulting potential energy curves have then been employed as the basis for a vibronic treatment of the $^2A'-X^2A''$ transition. The rather weak assumption of mutually independent vibrational stretching and bending modes is made. The coupling of the electronic wavefunction with the rotation and bending vibration (Renner–Teller effect) is described via a diagonalization procedure in which the coupling matrix elements (derivatives of the electronic wavefunction with respect to the azimuthal angle) are taken to be independent of the bending angle; the functional basis used thereby consists of two-dimensional harmonic oscillator functions and the corresponding Hamiltonian takes into account large-angle bending by multiplying the differential operators with bending-angle dependent coefficients represented as polynomials. The results, i.e. the K-structure of the transition, compare generally quite well with the measured data. Small discrepancies in the intensity distribution cannot be explained whereby qualitative arguments would seem to support the calculated results rather than those inferred experimentally. Deviations in the energy pattern relative to the observed data seem to result from simplifications made in the theoretical vibrational treatment. In general the present case study supports the position that standard CI calculations combined with a treatment of the Schrödinger equation for nuclear motion (employing a Hamiltonian which accounts for large-amplitude motion and vibronic coupling, if necessary) are capable of predicting to a quite useful level of accuracy the vibronic and rotational structure of electronic transitions in small molecules. These results in turn should be very helpful in interpreting and/or designing experiments from which more highly accurate details of the system under study can then be extracted.

Acknowledgements

The financial support given to part of this work by the SFB 42 is gratefully acknowledged. The services and computer time made available by the University of Bonn Computer Center and the SFB 42 Minicomputer PE 3242 of the University of Wuppertal have been essential to the present study.

Can. J. Chem. Downloaded from www.nrcresearchpress.com by 210.87.254.42 on 09/06/12
For personal use only.

1. P. L. GOODFRIEND and H. P. WOODS. J. Mol. Spectrosc. **20**, 258 (1966).
2. M. E. JACOX and D. E. MILLIGAN. J. Chem. Phys. **46**, 184 (1967).
3. C. M. WOODMAN. J. Mol. Spectrosc. **33**, 311 (1970).
4. D. M. LINDSAY, J. L. GOLE, and J. R. LOMBARDI. Chem. Phys. **37**, 333 (1979).
5. D. A. BROTCHIE and C. THOMSON. Chem. Phys. Lett. **22**, 338 (1973).
6. (*a*) S. HUZINAGA. J. Chem. Phys. **42**, 1293 (1965); (*b*) T. H. DUNNING JR. J. Chem. Phys. **53**, 2823 (1970).
7. S. D. PEYERIMHOFF, R. J. BUENKER, and L. C. ALLEN. J. Chem. Phys. **45**, 734 (1966).
8. R. J. BUENKER and S. D. PEYERIMHOFF. Theoret. Chim. Acta, **39**, 217 (1975); **35**, 33 (1)974).
9. R. J. BUENKER, S. D. PEYERIMHOFF, and W. BUTSCHER. Mol. Phys. **35**, 771 (1978).
10. S. R. LANGHOFF and E. R. DAVIDSON. Int. J. Quantum. Chem. **8**, 61 (1974).
11. R. J. BUENKER. Gazz. Chim. Ital. **108**, 245 (1978).
12. M. PERIĆ, R. J. BUENKER, and S. D. PEYERIMHOFF. Mol. Phys. **49**, 379 (1983).
13. M. PERIĆ, M. MLADENOVIĆ, J. FEJZO, C. M. MARIAN, and P. J. BRUNA. Chem. Phys. Lett. **88**, 547 (1982).
14. T. BARROW, R. N. DIXON, and G. DUXBURY. Mol. Phys. **27**, 1217 (1974).
15. P. R. BUNKER and B. M. LANDSBERG. J. Mol. Spectrosc. **67**, 374 (1977).
16. R. J. BUENKER, M. PERIĆ, S. D. PEYERIMHOFF, and R. MARIAN. Mol. Phys. **43** 987 (1981).
17. R. RENNER. Z. Phys. **92**, 172 (1934).
18. J. T. HOUGEN, P. R. BUNKER, and J. W. C. JOHNS. J. Mol. Spectrosc. **34**, 136 (1970).
19. M. PERIĆ, R. RUNAU, J. RÖMELT, S. D. PEYERIMHOFF, and R. J. BUENKER. J. Mol. Spectrosc. **78**, 309 (1979).
20. M. PERIĆ and J. RADIĆ-PERIĆ. Chem. Phys. Lett. **67**, 138 (1979).
21. M. PERIĆ. Chem. Phys. Lett. **76**, 573 (1980).
22. L. D. LANDAU and E. M. LIFSHITZ. Quantum mechanics. Pergamon Press, London 1958.

Can. J. Chem. Downloaded from www.nrcresearchpress.com by 210.87.254.42 on 09/06/12
For personal use only.

1,3,8-Trimethylxanthine complexes of Cu(II), Zn(II), Cd(II), and Hg(II)

E. COLACIO-RODRIGUEZ
Department of Inorganic Chemistry, Faculty of Sciences, University of Granada, Spain

J. D. LOPEZ-GONZALEZ
Universidad Nacional de educacion a Distancia, Madrid, Spain

AND

J. M. SALAS-PEREGRIN[1]
Department of Inorganic Chemistry, Faculty of Sciences, University of Granda, Spain

Received March 7, 1983

E. COLACIO-RODRIGUEZ, J. D. LOPEZ-GONZALEZ, AND J. M. SALAS-PEREGRIN. Can. J. Chem. **61**, 2506 (1983).

New 1,3,8-trimethylxanthine complexes of Cu(II), Zn(II), Cd(II), and Hg(II) were prepared and studied by ir, H-nmr, magnetic measurements, TG, and DSC techniques. In the Cu(II), Zn(II), and Cd(II) complexes, the 1,3,8-trimethylxanthine is present in anionic form and the coordination to metal ion occurs probably through N_7 atom. In the mercury complex, coordination to metal ion is realized via the N_9 atom of neutral TMH.

E. COLACIO-RODRIGUEZ, J. D. LOPEZ-GONZALEZ et J. M. SALAS-PEREGRIN. Can. J. Chem. **61**, 2506 (1983).

On a préparé de nouveaux complexes triméthyl-1,3,8 xanthine de Cu(II), de Zn(II), de Cd(II) et de Hg(II) et on les a étudiés en faisant appel à la spectroscopie IR, la rmn du ^1H, les mesures magnétiques et les techniques de TG et de DSC. Dans les complexes de Cu(II), de Zn(II) et de Cd(II) la triméthyl-1,3,8 xanthine est sous forme anionique et la coordination à l'ion metallique s'établit probablement par l'intermédiaire de l'atome d'azote en position 7. Dans le cas du complexe de mercure la coordination à l'ion métallique s'établit par l'intermédiaire de l'atome d'azote en position 9 de la THM sous forme neutre.
[Traduit par le joural]

Introduction

The biological importance of purine bases (constituents of the nucleic acids) is well known. The interaction of metal ions with nucleic acids, nucleosides, and nucleotides has been an active area of inorganic and structural chemistry during the last few years and there exist a number of recent reviews on the subject (1, 2). Studies of the reaction of metal ions with the purine bases are important in establishing the sites of binding of the heterocyclic aromatic moiety and the stereochemistry of the compound formed. In this work the interaction of 1,3,8-trimethylxanthine with the metal ions Cu(II), Zn(II), Cd(II), and Hg(II) is studied.

Experimental

Materials

1,3,8-Trimethylxanthine (TMH) was synthesized according to the method described by Speer (3). The suitably formed isolated product was purified and characterized (melting point from its DSC curve is 329.4°C). The results obtained were in agreement with its molecular structure. All the organic salts used were of analytical reagent grade.

Methods

Infrared spectra in the region 4000−200 cm^{-1} of samples in KBr pellets were recorded using a Beckman-4250 spectrophotometer; similarly, spectra in the 600−200 cm^{-1} region of samples in polyethylene pellets were recorded.

Magnetic susceptibilities for copper complex were determined as a function of temperature (293 K, 206 K, 151 K, and 77 K) on a Bruker B-M4 apparatus. Weight changes were obtained from a Sartorius electrobalance. The temperature was controlled using an automatic temperature regulator and mercury tetrathiocyanato cobaltate was used as a standard.

The TG studies were made in static atmosphere of air (in the case of the mercury compound, a flow of 100 mL min^{-1} of pure air was used) on a Mettler TG-50 thermobalance, using a 6.5−9.4 mg sample and a heating rate of 10°C min^{-1}. On the other hand, DSC curves were obtained in a Mettler DSC-20 differential scanning calorimeter using a heating rate of 5°C min^{-1}.

The ^1H-nmr spectra were recorded of a R-600 Hitachi Perkin Elmer, FT-NMR spectrometer, using dimethyl sulfoxide-d_6 as solvent and TMS as standard reference. After which the bands of the NH_3 molecules were removed by the addition of a small amount of D_2O to the DMSO-d_6 solutions.

The microanalyses of C, H, and N were performed using a Carlo Erba 1106 microanalyzer. Metal determination were realized by atomic absorption, using a Perkin-Elmer model 290 spectrophotometer.

Preparation of the complexes

Reactions between TMH and Cu(II), Zn(II), Cd(II), and Hg(II) were carried out in neutral and basic conditions.

In neutral solution only the mercury complex is formed, whereas for Cu(II), Zn(II), and Cd(II), the reactions were not successful due to the precipitation of the ligand.

For the preparation of the complexes in basic medium, we have utilized NH_4OH solutions to preclude metal hydroxide precipitation. In this condition Hg(II) is precipitated as mercury ammine compounds.

Preparation of the $M(TM)_2(NH_3)_2$ compounds

A solution of 3 mmol of $M(NO_3)_2$ (M = Cu, Zn, or Cd), in 50 mL of 7 *M* NH_4OH was added to 6 mmol of 1,3,8-trimethylxanthine dissolved in 50 mL of 7 *M* NH_4OH. In the first hour, the clear solution was heated at 70°C with continuous stirring, and was then allowed to cool slowly to room temperature. The solid complexes precipitated in crystalline form and were filtered, washed consecutively with water, ethanol, and ether, and dried in air.

Preparation of $M(TMH)Cl_2$

A solution of 3 mmol of $HgCl_2$ in 50 mL of hot water was added to a solution of 6 mmol of 1,3,8-trimethylxanthine in 50 mL of hot water. The resulting clear solution was allowed to cool slowly to room temperature. After 1 h, colorless needles appeared, and were filtered, washed consecutively with water, ethanol, and ether, and dried in air.

The analytical data and color of the isolated compounds are: *Anal.* calcd. for $Cu(TM)_2(NH_3)_2$ (brown): C 39.71, H 4.96, N 28.96, Cu

[1]To whom all correspondence should be addressed.

Can. J. Chem. Downloaded from www.nrcresearchpress.com by 210.87.254.105 on 09/06/12
For personal use only.

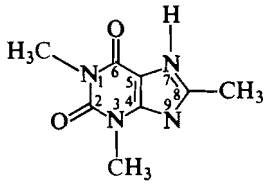

FIG. 1. Structure of 1,3,8-trimethylxanthine (TMH).

13.13; found: C 39.97, H 4.93, N 27.54, Cu 13.07. *Anal.* calcd. for $Zn(TM)_2(NH_3)_2$ (white): C 39.55, H 4.94, N 28.84, Zn 13.47; found: C 39.16, H 4.38, N 28.43, Zn 13.50. *Anal.* calcd. for $Cd(TM)_2(NH_3)_2$ (white): C 36.06, H 4.51, N 26.30, Cd 21.11; found: C 35.31, H 4.49, N 25.52, Cd 20.93. *Anal.* calcd. for $Hg(TMH)Cl_2$ (white): C 20.61, H 2.15, N 12.03; found: C 21.21, H 2.30, N 12.16.

Results and discussion

TMH may exist in two tautomeric forms, with a hydrogen atom localized in N_7 or N_9 atoms. However, in the crystal structure of theophylline (4, 5), analogous to TMH, the imidazole proton was found to be on N(7) rather than on N(9), and we believe that the N_7 tautomeric form in TMH is probably of lower energy.

From the structure of TMH, only N_7 and N_9 positions are available for coordination to metal ions.

The infrared spectrum of TMH shows characteristic absorptions at 3180 cm^{-1} $\nu(N_7—H)$ (this band has been corroborated by deuteration ($\nu(N_7—D)$ = 2380 cm^{-1}), 2940, 2820 cm^{-1} $\nu(CH_3)$, 1710 cm^{-1} $\nu(C_2=O)$ and 1630 cm^{-1} $\nu(C_6=O)$. The low frequency of $\nu(C_6=O)$ suggests the presence of a hydrogen-bond between $O_6—H_7$ atoms, which also occurs in other xanthine derivatives (6).

^{1}H-nmr spectrum of TMH in DMSO-d_6 shows three proton signals at 2.4 ppm ($C_8—CH_3$), 3.3− ppm ($N_1—CH_3$), and 3.5 ppm ($N_3—CH_3$). The corresponding signal to ($N_7—H$) has been not observed. The assignments of these signals are in accordance with the bibliographic data for other methylxanthine derivatives (7, 8).

TG studies on the compounds $Cu(TM)_2(NH_3)_2$ (**I**), $Zn(TM)_2(NH_3)_2$ (**II**), and $Cd(TM)_2(NH_3)_2$ (**III**) show that two molecules of ammonia are present in all cases. Theoretic loss weight percentages (**I** = 7.03, **II** = 7.00, and **III** = 6.39) for the elimination of ammonia molecules are in good agreement with experimental values (**I** = 7.3; **II** = 6.7; **III** = 6.8). The endothermic effects associated with the elimination of these ammonia molecules have been observed in DSC curves at the same temperature. Likewise, TG and DSC studies on the $Hg(TMH)Cl_2$ (**IV**) show the anhydrous nature of this compound.

The presence of coordinated ammonia to Cu(II), Zn(II), and Cd(II) in the corresponding complexes, can be suggested by the following bands: copper complex: 3310 cm^{-1} and 3210 cm^{-1} $\nu(N—H)$; 1125 cm^{-1} $\delta_s(H—N—H)$; 695 cm^{-1} $\rho(NH)$; 460 cm^{-1} $\nu(Cu—NH_3)$; zinc complex: 3350 and 3160 cm^{-1} $\nu(NH)$; 1170 cm^{-1} $\delta_s(H—N—H)$; 395 cm^{-1} $\nu(Zn—NH_3)$; cadmium complex: 3380 and 3250 cm^{-1} $\nu(N—H)$; 1115 cm^{-1} $\delta_s(H—N—H)$, 680 cm^{-1} $\rho(NH_3)$; 445 cm^{-1} $\nu(Cd—NH_3)$.

The second band assigned to $\nu(N—H)$, in the zinc complex (3160 cm^{-1}) is due to coordinated ammonia since under our experimental conditions (pH = 9.7), TMH will be in anionic form.

The assignment of these bands are in agreement with the bibliographic data of ammonia complexes (9).

Complexes **I**, **II**, and **III** did not show the band corresponding to $\nu(N_7—H)$, which in infrared spectrum of free TMH occurs at 3180 cm^{-1}. This observation suggests that coordination of TMH to metal ions takes place in anionic form through N_7 or N_9 atoms. Another marked difference between the TMH and its complexes is the displacement of stretching vibrations corresponding to carbonyl groups, 1680 and 1660 cm^{-1} (**I**), 1680 and 1630 cm^{-1} (**II**), 1695 and 1630 cm^{-1} (**III**), may be indicative of possible hydrogen bond interactions between oxygen atoms of TMH and ammonia molecules.

The infrared spectrum of mercury complex **IV** shows a band at 3160 cm^{-1}, corresponding to $\nu(N—H)$ (this band appears at 3180 cm^{-1} in free TMH). The presence of this band suggests that, in this case, coordination of TMH to Hg(II) takes place through the N_9 atom. In this complex $\nu(C=O)$ appears at 1702 cm^{-1} and 1645 cm^{-1}. The band at 240 cm^{-1} has been assigned to $\nu(Hg—Cl)$.

Chemical shifts and the assignment of the individual ^{1}H-resonance of the prepared compounds in DMSO-d_6 are listed in Table 1.

The upfield shifts of signals corresponding to methyl protons at C_8 in $Zn(TM)_2(NH_3)_2$ and $Cd(TM)_2(NH_3)_2$ indicates, according to the literature (10, 11), the anionic coordination of TMH through N_7 or N_9 atoms. The $N_1—CH_3$ and $N_3—CH_3$ signals practically are not shifted, since charge densities are generally affected more at the atom which is closest to the binding site. The NH_3 peaks resonances are removed when D_2O is added to DMSO-d_6 solutions of complexes **II** and **III**.

In the ^{1}H-nmr spectrum of $(TMH)HgCl_2$ there is no shift of the $C_8—CH_3$ signal. This fact could probably be explained assuming the break of metal—N_9 bonding under our experimental conditions (strong heating due to low solubility in DMSO-d_6 of the complex).

In Table 2 are summarized the found values for the molar magnetic susceptibility and μ_{eff} of $Cu(TM)_2(NH_3)_2$. The room temperature magnetic moment of the new metal complex is normal for high-spin $3d^9$ configuration (12). A small decrease of the magnetic moment (0.16 BM) was observed when the temperature was lowered from 293 K to 77 K. Plot of $1/\chi_M$ vs. T shows that the Curie−Weiss law is obeyed in 293−77 K range, and the Weiss constant corresponding to the plot is −24°. Additional magnetic studies covering the 77−4.2 K

TABLE 1. ^{1}H-nmr shifts (δ, ppm) of TMH and its complexes

Compounds	$N_1—CH_3$	$N_3—CH_3$	$C_8—CH_3$	NH_3	$N_7—H$
TMH	3.30[a]	3.50	2.40	—	[b]
$Zn(TM)_2(NH_3)_2$	3.25	3.45	2.10	3.45	—
$Cd(TM)_2(NH_3)_2$	3.22	3.42	2.15	3.38	—
$Hg(TMH)Cl_2$	3.22	3.42	2.40	—	[b]

[a]All signals are singlets.
[b]Not observed.

Can. J. Chem. Downloaded from www.nrcresearchpress.com by 210.87.254.105 on 09/06/12
For personal use only.

TABLE 2. Values of the magnetic susceptibility for $Cu(TM)_2(NH_3)_2$

T (K)	$\chi_g \cdot 10^6$ (ucgs g^{-1})	$\chi_M \cdot 10^4$ (ucgs mol^{-1})	μ_{eff} (BM)
293	2.7	15.04	1.88
206	3.8	20.59	1.84
151	5.1	26.29	1.80
77	9.5	47.97	1.72

region would be necessary to reveal the possible spin–spin interactions. These studies are planned for the near future. The magnetic evidence available (μ_{eff} decreases with temperature, negative θ) is in favor of bi- or polynuclear rather than monomeric configuration for this compound (13, 14) although due to the small decrease of μ_{eff}, the type of configuration is not clear.

On the basis of experimental results for complexes **I**, **II**, and **III**, two structure assignments are possible: a distorted tetrahedral or a polymeric octahedral with purine bridging (N_7 and N_9 bonds). The second structure type (although the available magnetic data are in agreement with it) has not been found in the xanthine complexes described in the literature; in these complexes, xanthine derivatives ligands use, in anionic form only, a coordination position (normally N_7 (15, 16). Thus the tetrahedral structure is the more probable structure for these complexes (the solubility of the metal complexes in organic media also favors the tetrahedral structure over the polymeric structure).

1. D. J. HODGSON. Prog. Inorg. Chem. **23**, 211 (1977).
2. L. G. MARZILLI. Prog. Inorg. Chem. **23**, 255 (1977).
3. J. H. SPEER and A. RAYMOND. J. Am. Chem. Soc. **75**, 114 (1953).
4. E. SHEFTER. J. Pharm. Sci. **58**, 710 (1969).
5. D. J. SUTOR. Acta Crystallogr. **11**, 83 (1958).
6. A. T. TU and J. A. REINOSA. Biochemistry, **5**, 3375 (1966).
7. D. LICHTENBERG, F. BERGMAN, and Z. NEIMAN. J. Chem. Soc. (C), **10**, 1939 (1971).
8. L-MING TWANMOH, H. B. WOOD, JR., and J. S. DRISCOLL. J. Heterocycl. Chem. **10**(2), 187 (1973).
9. J. R. FERRARO. Low-frequency vibrations of inorganic and coordination compounds. Plenum Press, New York. 1971. pp. 197–198.
10. W. M. BECK, J. C. CALABRESE, and N. KOTTMAIR. Inorg. Chem. **18**, 176 (1979).
11. E. H. GRIFFITH and E. L. AMMA. J. Chem. Soc. Chem. Commun. 324 (1979).
12. B. N. FIGGIS and J. LEWIS. Prog. Inorg. Chem. **6**, 37 (1964).
13. M. LYNCH, K. E. HYDE, P. L. BOCKO, and G. F. KOKOSZKA. Inorg. Chem. **16**, 562 (1977).
14. C. M. MIKULSKI, R. D. PRINCE, T. B. TRAN, and N. M. KARAYANNIS. Inorg. Chim. Acta, **56**, 27 (1981).
15. T. J. KISTENMACHER, D. J. SZALDA, and L. G. MARZILLI. Inorg. Chem. **14**, 1686 (1975).
16. T. SORRELL, L. G. MARZILLI, and T. J. KISTENMACHER. J. Am. Chem. Soc. **98**, 2181 (1976).

Can. J. Chem. Downloaded from www.nrcresearchpress.com by 210.87.254.105 on 09/06/12
For personal use only.

Thermodynamics of aqueous carbon dioxide and sulfur dioxide: heat capacities, volumes, and the temperature dependence of ionization[1]

JOSÉ A. BARBERO[2]
Departamento Química de Reactores, Comisión Nacional de Energía Atómica, Avda del Libertador 8250, 1429 Buenos Aires, Argentina

LOREN G. HEPLER AND KEITH G. MCCURDY[2]
Department of Chemistry, University of Lethbridge, Lethbridge, Alta., Canada T1K 3M4

AND

PETER R. TREMAINE
Oil Sands Research Department, Alberta Research Council, 11315 – 87 Avenue, Edmonton, Alta., Canada T6G 2C2

Received March 1, 1983

JOSÉ A. BARBERO, LOREN G. HEPLER, KEITH G. MCCURDY, and PETER R. TREMAINE. Can. J. Chem. **61**, 2509 (1983).

A flow microcalorimeter and vibrating tube densimeter were used at 25°C to obtain apparent molar heat capacities and volumes of aqueous $NaHCO_3$, $KHCO_3$, $NaHSO_3$, and $KHSO_3$ from 0.1 to 1.0 mol kg^{-1}, aqueous CO_2 from 0.01 to 0.10 mol kg^{-1} and aqueous SO_2 from 0.045 to 2.0 mol kg^{-1}. The contribution of "chemical relaxation" (changes in equilibrium state and enthalpy due to change in temperature) to the experimental heat capacities of aqueous SO_2 required special attention, leading to the derivation of a new equation for calculating this effect. Standard state values for the heat capacities and volumes of aqueous CO_2, SO_2, HCO_3^-, and HSO_3^- were obtained from the apparent molar properties by extrapolation to infinite dilution. Combining these results with other thermodynamic data from the literature gave estimates of $\log K_1^b$, the equilibrium constant for the first neutralization of CO_2 and SO_2, at high temperatures. The results for CO_2 reproduce very accurate literature values to within 0.2 at 200°C. The expression for the reaction $SO_2 + OH^- \rightleftarrows HSO_3^-$, $\log K_1^b = 22.771 + 2776.0/T - 8.058 \log T$, is consistent with the sparse and limited experimental data.

JOSÉ A. BARBERO, LOREN G. HEPLER, KEITH G. MCCURDY et PETER R. TREMAINE. Can. J. Chem. **61**, 2509 (1983).

On a utilisé un microcalorimètre à écoulement et un densimètre à tube vibrant à 25°C pour obtenir les capacités calorifiques molaires apparentes et les volumes de $NaHCO_3$, de $KHCO_3$ et de $KHSO_3$ aqueux de 0,1 à 1,0 mol kg^{-1}, de CO_2 aqueux de 0,01 à 0,10 mol kg^{-1} et de SO_2 aqueux de 0,045 à 2,0 mol kg^{-1}. La contribution de la "relaxation chimique" (variations de l'état d'équilibre et d'enthalpie due à une variation de température) aux capacités calorifiques expérimentales du SO_2 aqueux requiert une attention spéciale et conduit à dériver une nouvelle équation pour calculer cet effet. On a obtenu les valeurs normales des capacités calorifiques et les volumes de CO_2, SO_2, HCO_3^- et HSO_3^- aqueux à partir des propriétés molaires apparentes par extrapolation à dilution infinie. La combinaison de ces résultats avec les autres données thermodynamiques relevées dans la littérature donne des évaluations de $\log K_1^b$, la constante d'équilibre de première neutralisation de CO_2 et de SO_2 à haute température. Les résultats relatifs à CO_2 reproduisent de façon très précise les valeurs de la littérature avec une précision de 0,2 à 200°C. L'expression $\log K_1^b = 22,771 + 2776,0/T - 8,058 \log T$ pour la réaction $SO_2 + OH^- \rightleftarrows HSO_3^-$, est en accord avec les données expérimentales peu nombreuses et limitées.

[Traduit par le journal]

Introduction

Thermodynamic properties of aqueous carbon dioxide and sulfur dioxide and their ionization products are required over a range of temperature to model steam injection and combustion processes for the *in situ* extraction of bitumen and heavy oil. These same thermodynamic properties are also important in connection with such varied problems as wet oxidation boilers, geothermal water systems, water–mineral and water–scale interactions, chemical wood-pulping processes, various pollution control problems, and certain aspects of the chemistry of seawater and blood.

Vapour pressure data and ionization constants have now been reported for aqueous CO_2 over a wide range of temperature (1–5) and for aqueous SO_2 at lower temperatures only (1, 6–12). Standard state enthalpies of solution and ionization for both acid gases (13–17), and partial molar heat capacities for the hydrogen carbonate (18–20) and hydrogen sulfite ions (21) at 25°C are also known. However, the apparent molar heat capacities of aqueous CO_2, SO_2, and indeed most other dissolved gases, have not been measured directly. The purpose of the present investigation has been to measure these heat capacities at 25°C and to use them with other thermodynamic data at 25°C to estimate various equilibrium constants over wide ranges of temperature. Comparisons of these calculated equilibrium constants with those that have been directly measured at high temperature and pressure help to establish the range of validity of the various methods for performing such extrapolations. In cases where the experimental measurements are sparse, the extrapolated equilibrium constants provide tentative values for use until accurate data are available.

Experimental

The heat capacity and density of each solution were measured relative to water using a commercial Picker flow microcalorimeter (22), vibrating tube densimeter (23), and the injection system reported in our earlier, similar study on aqueous H_2S (24). Values cited by Kell (25) for the specific heat capacity and density of pure water at 25°C, $c_{p1}^0 = 4.1793$ J K^{-1} g^{-1} and $d_1^0 = 0.997045$ g cm^{-3}, were used in the calculations. The average of the apparent molar heat capacities from the two calorimeter cells was multiplied by the mean heat leak correction factor $f = 1.009 \pm 0.003$, which we obtained by calibration with aqueous NaCl in the usual way (19).

The preparation and handling of chemicals was similar to that in our

[1]ARC contribution number 1224.

[2]Visiting scientist at the Oil Sands Research Department, Alberta Research Council, 1981–1982.

Can. J. Chem. Downloaded from www.nrcresearchpress.com by 210.87.254.5 on 09/06/12
For personal use only.

Can. J. Chem. Downloaded from www.nrcresearchpress.com by 210.87.254.5 on 09/06/12
For personal use only.

TABLE 1. Experimental apparent molar properties of the aqueous hydrogen carbonate and hydrogen sulfite salts, and carbon dioxide

m	V_ϕ	$C_{p\phi}$	m	V_ϕ	$C_{p\phi}$
mol kg^{-1}	cm^3 mol^{-1}	J K^{-1} mol^{-1}	mol kg^{-1}	cm^3 mol^{-1}	J K^{-1} mol^{-1}
	$NaHCO_3$			$KHCO_3$	
0.0527	24.13	6.2	0.0881	34.49	−30.1
0.2647	24.87	19.0	0.1014	34.85	−26.9
0.3311	25.06	22.4	0.1767	34.86	−22.8
0.4427	25.44	29.7	0.2549	35.37	−15.8
0.5331	25.61	33.6	0.3331	35.26	−13.6
0.6681	25.94	40.4	0.5139	35.90	−5.4
0.8055	26.22	46.4	0.6745	36.11	0.1
0.8963	26.45	50.2	0.7805	36.82	6.9
1.0824	26.88	57.7	0.9072	36.62	8.3
			1.0495	37.28	15.1
	$NaHSO_3$, prepared *in situ*			$NaHSO_3$, from the salt	
0.3217	33.77	60.7	0.0828	32.55	44.1
0.6491	34.25	75.0	0.1427	33.28	50.4
0.9864	34.95	87.8	0.1664	33.15	50.3
			0.1870	32.63	45.6
	$KHSO_3$, prepared *in situ*		0.2367	33.30	55.9
0.2390	43.70	18.6	0.2783	33.61	59.6
0.3308	44.24	24.2	0.3776	33.20	60.5
0.4808	44.10	28.8	0.4790	34.28	70.9
0.5343	44.89	34.9	0.5637	34.22	72.8
0.6718	44.88	37.8	0.5681	33.45	68.6
0.7386	45.35	41.8	0.7234	34.45	78.7
0.8816	45.02	43.3	0.8566	34.97	84.9
0.9915	45.53	47.4	0.9813	35.49	90.4
	CO_2				
0.0122	33.75	239.6			
0.0440	32.10	251.6			
0.0444	33.34	250.9			
0.0534	31.76	227.9			
0.0581	31.20	239.7			
0.0601	32.30	242.8			
0.0746	35.00	246.1			
0.0824	34.27	242.8			
0.0878	33.39	245.6			
0.1014	33.73	243.6			

previous study (24). Distilled water was passed through a Milli-Q reagent grade mixed bed ion exchange and activated carbon system, then vigorously purged with helium immediately before use (final conductivity 1 μS cm^{-1} or less). Fisher Certified ACS anhydrous potassium hydrogen carbonate and sodium hydrogen carbonate, B.D.H. AnalaR potassium hydrogen carbonate and Mallinckrodt Analytical Reagent sodium hydrogen carbonate were dried and then used without further purification. Stock solutions were prepared by mass, then used to prepare more dilute solutions by volumetric dilution. Some of these were also titrated with HCl using bromocresol green indicator. Fisher standardized HCl solutions were checked by titration against Fisher "primary standard" tris(hydroxymethyl)aminomethane.

Stock solutions of sodium and potassium hydrogen sulfite were initially prepared from the Baker Analyzed and Fisher Certified ACS products taken from freshly opened bottles, then standardized by adding an excess of iodine and back titrating with thiosulfate solution. Since aqueous hydrogen sulfite ion is very easily oxidized, we also prepared stock solutions *in situ* by bubbling sulphur dioxide through water in a closed, oxygen-free system, while maintaining the pH in the range 3.5 to 4.5 by dripping in aqueous NaOH or KOH that had been purged with helium. The rather irreproducible heat capacity results from solutions of the commercial crystals were more negative by 5 to 25 J K^{-1} mol^{-1} than those prepared from SO_2 and KOH, probably because of contamination by sulfate or thiosulfate, both of which have very negative heat capacities (26). The presence of sulfate was confirmed by testing with a few drops of aqueous barium hydroxide and, consequently, no data from solutions of the crystals are reported in this study. Some of the $NaHSO_3$ solutions prepared from commercial crystals reacted only slightly to the barium hydroxide test and yielded heat capacity results in good agreement with solutions prepared from SO_2 and aqueous NaOH. These results were considered to be reliable.

Anhydrous CO_2 and SO_2 were obtained from Canadian Liquid Air and Matheson, respectively. The SO_2 was analyzed by gas chromatography and contained less than 0.1% N_2 and CO_2 and no detectable amounts of H_2S, COS, or hydrocarbon impurities (<0.05%). Solutions of aqueous CO_2 and SO_2 were prepared by bubbling the gas into water in a closed pressure bottle, which allowed overpressures of up to 300 kPa. As in our previous investigation of H_2S (24), both the bottle containing the gas solution and that containing the pure water reference liquid were connected to the same cylinder of ultra high purity nitrogen so that manipulating a three-way stopcock allowed either to be pressurized. A second three-way stopcock allowed either solution to be forced into the calorimeter or densimeter by the overpressure of nitrogen and a needle valve downstream of the instruments controlled the flow rate. The CO_2 solutions were standardized by diverting the tubing from the exit so that the solutions flowed under the surface of a known weight of standardized $Ba(OH)_2$ solution, contained in a small bottle, with a few drops of carbonate-free phenolphthalein indicator added. The indicator allowed the flow of the CO_2

Can. J. Chem. Downloaded from www.nrcresearchpress.com by 210.87.254.5 on 09/06/12
For personal use only.

TABLE 2. Apparent molar properties and heat capacity relaxation correction data for aqueous SO_2

Experimental results			Speciation and relaxation contribution values							Values for SO_2 aqueous species		
$m(SO_2, aq)$ / mol kg^{-1}	V_ϕ^{exp} / cm^3 mol^{-1}	$C_{p\phi}^{exp}$ / J K^{-1} mol^{-1}	α	$\gamma_\pm/\gamma_u^{1/2}$	$\frac{1}{m}\left(\frac{\partial \ln \gamma_\pm/\gamma_u^{1/2}}{\partial \alpha}\right)_m$	$L_{\phi 2}$ / J mol^{-1}	$2L_{\phi\pm}$ / J mol^{-1}	$2L_\pm$ / J mol^{-1}	$\Delta H\left(\frac{\partial \alpha}{\partial T}\right)_m$ / J K^{-1} mol^{-1}	$V_\phi(SO_2^0, aq)$ / cm^3 mol^{-1}	$C_{p\phi}^{sp}$ / J K^{-1} mol^{-1}	$C_{p\phi}(SO_2^0, aq)$ / J K^{-1} mol^{-1}
0.04581	—	126.2	0.4567	0.8826	−2.056	9846.6	256.7	378.6	67.4	—	58.8	176.3
0.08529	32.13	160.1	0.3676	0.8671	−1.395	11405.5	311.4	460.8	59.3	41.64	100.8	205.9
0.09881	31.27	153.4	0.3481	0.8636	−1.264	11742.4	325.6	482.3	57.1	39.45	96.4	190.5
0.1111	32.48	162.7	0.3331	0.8609	−1.167	11999.8	337.3	500.1	55.2	40.82	107.4	200.8
0.1955	32.33	160.4	0.2671	0.8486	−0.762	13099.6	398.7	594.3	46.1	38.32	114.3	184.5
0.2002	32.16	161.2	0.2645	0.8481	−0.747	13140.8	401.5	598.6	45.7	38.02	115.5	189.2
0.2382	33.24	165.2	0.2464	0.8448	−0.643	13430.7	422.4	630.8	42.9	38.91	122.3	187.8
0.2979	33.13	163.3	0.2246	0.8408	−0.521	13765.6	450.7	674.5	39.3	38.12	124.0	182.4
0.3356	32.00	173.1	0.2136	0.8388	−0.461	13917.1	466.4	698.8	37.5	36.36	135.6	193.4
0.4184	33.71	166.5	0.1944	0.8355	−0.358	14100.5	496.8	745.7	33.9	37.99	132.6	183.1
0.4231	33.90	165.6	0.1935	0.8353	−0.353	14104.6	498.3	748.1	33.7	38.20	131.9	181.9
0.4514	32.73	174.2	0.1881	0.8345	−0.325	14114.3	507.6	762.4	32.6	36.61	141.6	192.1
0.4974	34.01	168.4	0.1803	0.8333	−0.284	14072.0	521.8	784.3	30.9	37.97	137.4	192.1
0.5018	33.72	165.2	0.1796	0.8332	−0.280	14064.1	523.1	786.3	30.8	37.60	134.5	184.4
0.5462	34.23	167.6	0.1731	0.8322	−0.246	13942.5	535.7	805.8	29.1	38.04	138.5	183.4
0.5889	33.79		0.1674	0.8314						37.36		
0.7733	34.44		0.1481	0.8291						37.63		
0.8051	34.57		0.1455	0.8290						37.72		
1.1134	34.90		0.1253	0.8280						37.59		
1.3862	34.80		0.1130	0.8283						37.17		
1.6546	34.85		0.1039	0.8293						37.01		
2.3995	34.97		0.08665	0.8334						36.74		

TABLE 3. Standard partial molar functions and concentration parameters at 25°C *†

Solute	$C_{p\phi}^{\infty}$ J K^{-1} mol^{-1}	B_C J K^{-1} mol^{-2} kg	V_ϕ^{∞} cm^3 mol^{-1}	B_V cm^3 mol^{-2} kg
$NaHCO_3$	−2.6±0.4	28.2±0.7	23.62±0.02	1.19±0.03
$KHCO_3$	−38.5±0.8	23.1±1.4	33.9 ±0.1	1.2 ±0.2
CO_2^0(aq)	243.2±6.7	0	32.8 ±1.2	0
$NaHSO_3$	34.0±1.2	27.4±2.1	32.02±0.16	1.27±0.29
$KHSO_3$	1.4±1.6	18.2±2.5	42.69±0.26	0.99±0.40
SO_2^0(aq)	195 ±6	−115 ±85	38.47±0.36	−8±3
H_2O	75.290	0	18.068	0

* $Y_\phi = Y_\phi^{\infty} + A_Y(d_1^0 m)^{1/2} + B_Y m$. Debye–Hückel limiting slopes for the electrolytes are $A_C(d_1^0)^{1/2}$ = 28.945 J kg$^{1/2}$ K^{-1} mol^{-1} and $A_V(d_1^0)^{1/2}$ = 1.865 cm^3 kg$^{1/2}$ mol^{-1}. For SO_2^0(aq) and CO_2^0(aq), A_Y = 0. Parameters for SO_2^0(aq) refer to ionic strength, αm, rather than bulk molality. The values for $NaHCO_3$ and $KHCO_3$ contain a very small contribution from disproportionation to CO_2^0(aq) + H_2O + CO_3^{2-}.

† The stated ± values are the standard deviations in Y_ϕ^{∞} and B_Y from the least squares fits, and are a measure of the precision of the fit.

solution to be stopped while excess $Ba(OH)_2$ was present, so that the concentration of CO_2 in the solution could be determined from the weight gain and a back titration of the excess hydroxide with HCl. The exact same procedure was used for handling and analyzing the aqueous SO_2, except that it was trapped in a weighed aliquot of iodine solution and the back titration of excess iodine was done using thiosulfate solution.

Experimental results and analysis of data

Aqueous salts and carbon dioxide

Apparent molar heat capacities, $C_{p\phi}$, and volumes, V_ϕ, are defined by the expression

$$[1] \quad Y_\phi = (Y - n_1 Y_1^0)/n_2$$

where Y is the extensive property of the aqueous solution, Y_1^0 is the property of one mole of pure solvent, and n_1 and n_2 are the number of moles of water and solute respectively so that, if n_1 = 55.509, n_2 is equal to the molality, m. The experimental apparent molar data for the aqueous hydrogen carbonate and hydrogen sulfite salts and aqueous carbon dioxide are tabulated in Table 1. These data are not complicated by any significant degree of ionization or association and can be analyzed in a straightforward fashion using the methods presented below. Heat capacity data for aqueous sulfur dioxide are more difficult to assess because of ionization effects. The experimental results are listed in Table 2, along with other data that will be used to treat these results later in the paper.

Following Roux *et al.* (27) we used the least squares method to fit expressions of the form

$$[2] \quad Y_\phi = Y_\phi^{\infty} + A_Y(d_1^0 m)^{1/2} + B_Y m$$

to the $C_{p\phi}$ and V_ϕ data for the aqueous electrolytes. Here, Y_ϕ^{∞} is the value of Y_ϕ at infinite dilution, $A_Y(d_1^0)^{1/2}$ is the Debye–Hückel limiting slope at the temperature in question on the molality scale, and B_Y is an adjustable parameter.

The values of $C_{p\phi}^{\infty}$, B_C, V_ϕ^{∞}, and B_V that were obtained for $NaHCO_3$, $KHCO_3$, $NaHSO_3$, and $KHSO_3$, are listed in Table 3 along with the Debye–Hückel terms (28) used in the fit. The experimental and fitted values of $C_{p\phi}$ and V_ϕ are plotted in Figs. 1 and 2. The precision can be estimated from the standard deviations of Y_ϕ^{∞} and B, which are included in Table 3. The values for $NaHCO_3$ and $KHCO_3$ include a very small contribution from the disproportionation of HCO_3^- to aqueous CO_2 and CO_3^{2-}, which is discussed in detail later in this paper.

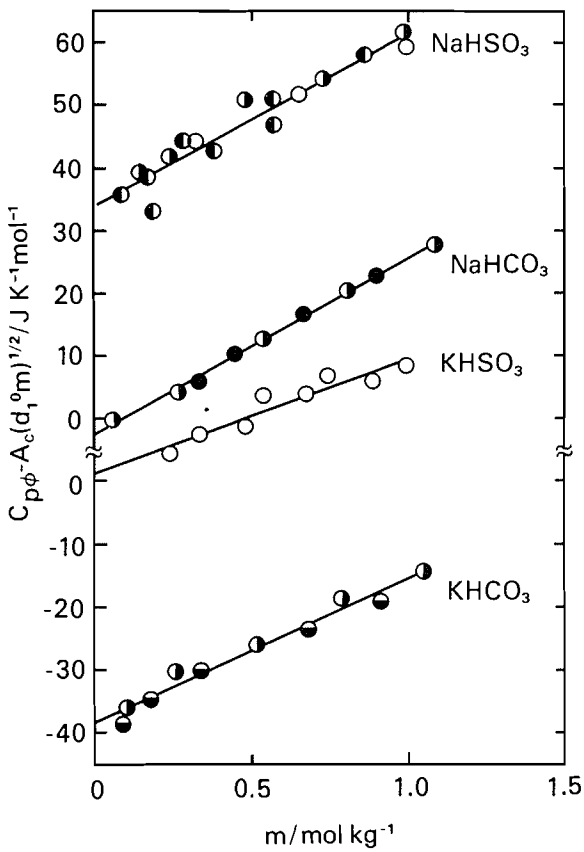

FIG. 1. Apparent molar heat capacities of aqueous hydrogen sulfite and hydrogen carbonate salts at 25°C after subtracting the Debye–Hückel limiting term: ○, synthesized *in situ* from the gas; ◑, ◐, ◒, ●, from salts. The lines are least squares fits.

The apparent molar properties for aqueous CO_2 in Table 1 were obtained at molalities below 0.1 mol kg^{-1} where CO_2 is known to be described by Henry's law (1), and are plotted in Fig. 3. Since no appreciable fraction ionizes under these conditions (3), the measured values were taken to be those at infinite dilution, $Y_\phi^{\infty} = Y^0$, corresponding to the equilibrium mixture of unhydrated CO_2 and H_2CO_3, which we define as CO_2^0 (aq). Averaging the results yields $C_p^0(CO_2^0, aq)$ = 243 J K^{-1} mol^{-1}

Can. J. Chem. Downloaded from www.nrcresearchpress.com by 210.87.254.5 on 09/06/12
For personal use only.

Can. J. Chem. Downloaded from www.nrcresearchpress.com by 210.87.254.5 on 09/06/12
For personal use only.

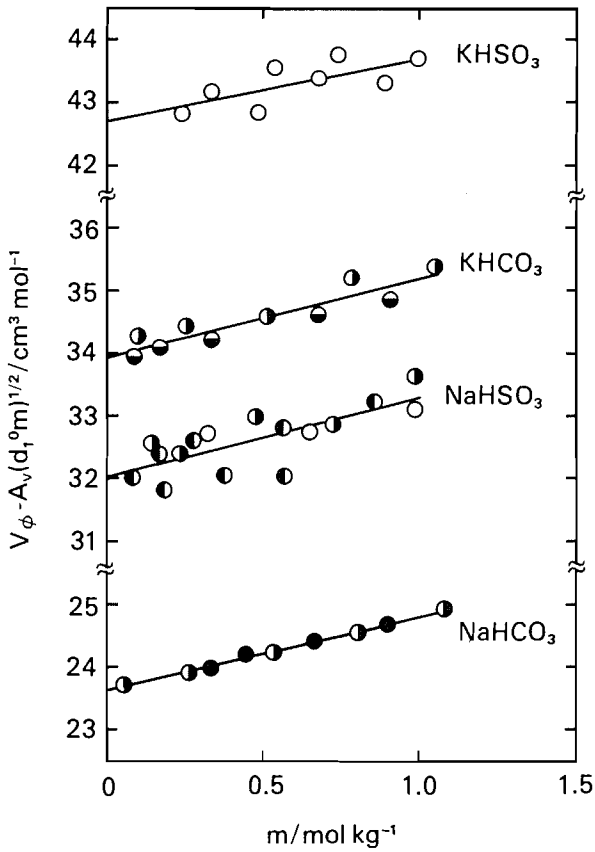

FIG. 2. Apparent molar volumes of aqueous hydrogen sulfite and hydrogen carbonate salts at 25°C after subtracting the Debye–Hückel limiting term: ○, synthesized *in situ* from the gas; ◑, ◐, ◒, ●, from salts. The lines are least squares fits.

and $V^0(CO_2^0, aq) = 32.8\ cm^3\ mol^{-1}$, with standard deviations of 7 J K^{-1} mol^{-1} and 1.2 cm^3 mol^{-1}, respectively.

Aqueous sulfur dioxide

Aqueous solutions of sulfur dioxide are acidic because of the equilibrium represented by

[3] $$SO_2^0(aq) + H_2O(l) \rightleftarrows H^+(aq) + HSO_3^-(aq)$$

At 25°C, the neutral species $SO_2^0(aq)$ and the dissociated, ionic species $HSO_3^-(aq)$ are both present in significant amounts but equilibria involving other species such as $S_2O_5^{2-}$ and SO_3^{2-} are not important at the concentrations studied here. In the discussions that follow, we distinguish between the neutral *species* $SO_2^0(aq)$, and *stoichiometric solutions* of SO_2 which are written as $SO_2(aq)$ without the superscript, and which include the equilibrium proportions of the species $SO_2^0(aq)$ and $HSO_3^-(aq)$. The experimental apparent molar volumes and heat capacities in Table 2, $V_\phi^{exp}(SO_2, aq)$ and $C_{p\phi}^{exp}(SO_2, aq)$, refer to the stoichiometric solutions. With proper attention to detail, the apparent molar properties of each of the species can be calculated from these experimental values. We first consider the volumetric results, then the more complicated analysis of heat capacities.

The experimental apparent molar volumes in Table 2 are considered to result from an appropriate sum of contributions of the species in solution, as expressed by

[4] $$V_\phi^{exp}(SO_2, aq) = (1 - \alpha)\, V_\phi(SO_2^0, aq) + \alpha\, V_\phi(H^+ + HSO_3^-, aq) - \alpha V(H_2O)$$

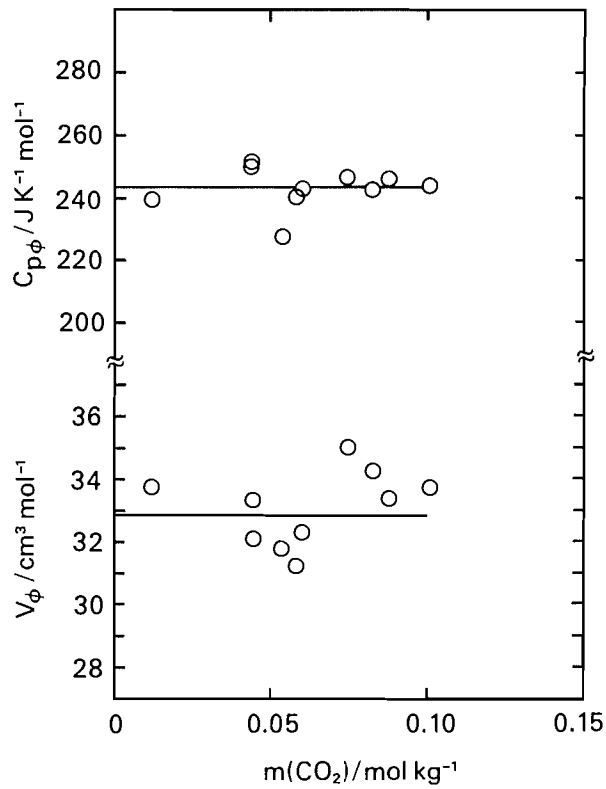

FIG. 3. Apparent molar heat capacities and volumes for aqueous CO_2.

Here, α represents the fraction of stoichiometric sulfur dioxide converted to $H^+(aq) + HSO_3^-(aq)$. For purposes of calculating $V^0(SO_2^0, aq)$, we assume that $V(H_2O) = V^0(H_2O)$ at these small molalities, and that the presence of aqueous SO_2 does not affect the ionic strength dependence of $V_\phi(H^+ + HSO_3^-, aq)$ as described by eq. [2]. Applying these assumptions yields the expression

[5] $$V_\phi(SO_2^0, aq) = \frac{1}{1-\alpha}\{V_\phi^{exp}(SO_2, aq) - \alpha\,[V^0(H^+ + HSO_3^-, aq) + A_V(d_1^0)^{1/2}\,(\alpha m)^{1/2} + B_V(H^+ + HSO_3^-, aq)\,\alpha m] + \alpha V^0(H_2O)\}$$

The degree of dissociation, α, can be calculated from the equilibrium constant for reaction [3],

[6] $$K_1 = m(H^+, aq)\, m(HSO_3^-, aq)\, \gamma_\pm^2 / m(SO_2^0, aq)\gamma_u$$

where $\gamma_\pm$ and γ_u are the activity coefficients of the ionic and undissociated, electrically neutral species, respectively. Literature values for this equilibrium constant have been reviewed by Hepler and Hopkins (29) and by Sadiq and Lindsay (30). We chose Huss and Eckert's recent results (6), $K_1 = 0.0139 \pm 0.0002$ and converted their activity coefficient expression from molarities to molalities to obtain

[7] $$\log(\gamma_\pm/\gamma_u^{1/2}) = \frac{-0.5107 m_i^{1/2}}{1 + 1.643 m_i^{1/2}} + 0.260 m_i$$

in which m_i refers to the molality of ions in a dilute aqueous solution at 25°C.

The values calculated for α are included in Table 2. Because the degree of dissociation decreases with increasing molality, the ionic strength of the solutions, αm, remains quite low. As

Can. J. Chem. Downloaded from www.nrcresearchpress.com by 210.87.254.5 on 09/06/12
For personal use only.

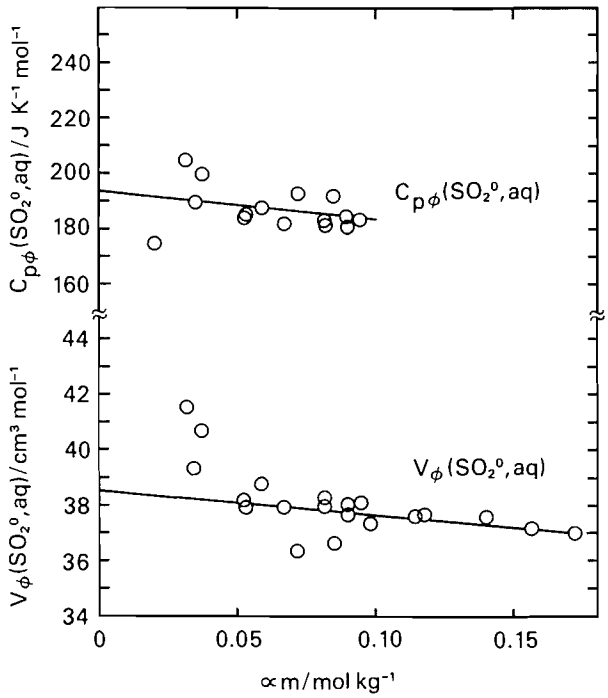

FIG. 4. Apparent molar heat capacities and volumes for the unionized aqueous species $SO_2^0(aq)$, as a function of the ionic strength due to the equilibrium concentration of HSO_3^-. The lines are least squares fits.

a result, the concentration dependence of $V_\phi(H^+ + HSO_3^-, aq)$ is described well by the Debye–Hückel limiting law, and the B_V term in eq. [5] makes only a minor contribution. An approximate value for $B_V(H^+ + HSO_3^-, aq)$ was estimated by assuming that the ionic contributions determined from pure systems are approximately additive, so that

$$B_V(H^+ + HSO_3^-, aq) \approx B_V(NaHSO_3, aq) - B_V(NaCl, aq) + B_V(HCl, aq) = 0.2 \text{ cm}^3 \text{ mol}^{-2} \text{ kg}$$

based on B_V values from ref. 31 and Table 2. The value $V^0(H^+ + HSO_3^-, aq) = 33.5$ cm^3 mol^{-1} was obtained from a similar additivity scheme, described later in the discussion of "best" standard state values.

Apparent molar volumes for undissociated SO_2 calculated from the data and equations outlined above are listed in Table 2 and plotted in Fig. 4 as a function of αm. The ionic strength dependence of $V_\phi(SO_2^0, aq)$ undoubtedly results from some combination of salting out effects (probably small), the approximations inherent in the method, and uncertainties in the degree of dissociation. We chose to calculate the infinite dilution value, $V_\phi^\infty(SO_2^0, aq) = 38.5$ cm^3 mol^{-1}, by fitting a least squares linear function in αm to the data for ionic strengths above 0.05 m. The coefficients and standard deviations are included in Table 3.

Before we can analyze the heat capacities of sulfur dioxide solutions in terms of contributions from the various species present, as in eq. [4] for volumes, it is necessary to recognize that the heat capacity is a sum of contributions from the chemical species plus a contribution due to "relaxation" of the temperature dependent equilibrium represented by [3]. This effect is caused by a shift in the degree of dissociation due to the temperature increment imposed by the calorimeter in the course of measuring the heat capacity. Thus we write

$$[8] \quad C_{p\phi}^{exp} = C_{p\phi}^{sp} + C_{p\phi}^{rel}$$

in which superscripts exp, sp, and rel refer to total experimental apparent molar heat capacity and contributions from chemical species and relaxation, respectively. It has been shown (32–34) that

$$[9] \quad C_{p\phi}^{rel} = \Delta H(\partial\alpha/\partial T)_m$$

Here, ΔH is the enthalpy of reaction at the molality of the solution and $(\partial\alpha/\partial T)_m$ is the shift in the degree of dissociation in the solution with temperature. Combining [8] and [9] gives

$$[10] \quad C_{p\phi}^{sp} = C_{p\phi}^{exp} - \Delta H(\partial\alpha/\partial T)_m$$

Analytic expressions for calculating $\Delta H(\partial\alpha/\partial T)_m$ have been derived for simple ionization or association reactions (32, 33). Some of the simplifying assumptions in these derivations cannot be used when the equilibrium concentrations of all the reactants and products are of the same order of magnitude. Peiper and Pitzer (14) have reported accurate numerical methods for making this calculation. Our method is based on an analytic equation whose derivation is described in Appendix I along with our sources for the necessary enthalpy data. Unfortunately, these enthalpy data only extend up to 0.55 m. The values for $\Delta H(\partial\alpha/\partial T)_m$ from our treatment are listed in Table 2. These were subtracted from $C_{p\phi}^{exp}(SO_2, aq)$ to yield the values for the equilibrium mixture of species in each stoichiometric solution, $C_{p\phi}^{sp}(SO_2, aq)$, also included in the table.

The apparent molar heat capacities of the neutral species $SO_2^0(aq)$ were then evaluated using an expression exactly analogous to that for the volume calculation:

$$[11] \quad C_{p\phi}(SO_2^0, aq) = \frac{1}{1-\alpha}\{C_{p\phi}^{sp}(SO_2, aq) - \alpha[C_p^0(H^+ + HSO_3^-, aq) + A_C(d_l^0)^{1/2}(\alpha m)^{1/2} + B_C(H^+ + HSO_3^-, aq)\,\alpha m] + \alpha C_p^0(H_2O)\}$$

Again, the B_C and C_p^0 terms for the salt were estimated assuming ionic additivity. From data for the sodium salts in ref. 31 and Table 3, $B_C(H^+ + HSO_3^-, aq) \approx 5$ J K^{-1} mol^{-2} kg and, from the scheme described later in this paper, $C_p^0(H^+ + HSO_3^-, aq) = -10$ J K^{-1} mol^{-1}. The resulting values for $C_{p\phi}(SO_2^0, aq)$ are included in Table 2 and plotted in Fig. 4. The infinite dilution value, $C_{p\phi}^\infty(SO_2^0, aq) = 195$ J K^{-1} mol^{-1}, was obtained by a linear least squares fit to all the data, in the manner used for the volumes. The standard deviations and other fitted parameters are listed in Table 3.

Discussion

Standard state properties

The limiting values $C_{p\phi}^\infty$ and V_ϕ^∞ can be shown to be equal to the standard state properties, C_p^0 and V^0. The purpose of this section is to critically compare the results in Table 3 with those of other workers to arrive at "best" values, then to separate these into anionic and cationic contributions according to the conventional scale $[C_p^0(H^+) \equiv 0,\ V^0(H^+) \equiv 0]$. This calculation was based on C_p^0 and V^0 values for $Na^+(aq)$, $K^+(aq)$, and $OH^-(aq)$ listed in Table 4, from Desnoyers *et al.* (19), Roux *et al.* (27), and Millero (35). A detailed examination of all recently published heat capacity values, recently carried out in our laboratories, confirmed these assignments for ionic heat capacities to within 1 J K^{-1} mol^{-1}.

Our experimental values for $C_{p\phi}(NaHCO_3, aq)$ agree well

Can. J. Chem. Downloaded from www.nrcresearchpress.com by 210.87.254.5 on 09/06/12
For personal use only.

TABLE 4. Critically evaluated standard state functions at 25°C*

Ion	C_p^0/J K^{-1} mol^{-1}	V^0/cm^3 mol^{-1}
Na^+(aq)	43	−1.26
K^+(aq)	13	9.0
Cl^-(aq)	−126	18.1
OH^-(aq)	−138	−4.2
HCO_3^-(aq)	−53±4	24.9 ±0.1
HSO_3^-(aq)	−10±4	33.5 ±0.4
CO_2^0(aq)	243±10	32.8 ±2
SO_2^0(aq)	195±10	38.5 ±2

*Ionic values are based on $C_p^0(H^+) = 0$ and $V^0(H^+) = 0$. Values for Na^+, K^+, Cl^-, and OH^- are from Desnoyers *et al.* (19), Roux *et al.* (27), and Millero (35). Here the stated ± values are our estimates of the overall accuracy of the results, as discussed in the text.

with those of Desnoyers *et al.* (18, 19) after their results were corrected for heat leaks (19). Their measurements were taken with a Picker calorimeter similar to ours and are systematically more negative by about 3 J K^{-1} mol^{-1}. As we noted above, aqueous HCO_3^- disproportionates to form CO_2 and HCO_3^-, and both sets of data must be corrected for this effect. Peiper and Pitzer (14) have calculated this correction in a rigorous way, based on the assumption that the equilibrium concentration of CO_2 gas formed during the course of each calorimetric measurement. They estimate that disproportionation caused Desnoyer's value for $C_p^0(HCO_3^-, aq)$ to be too positive by 4 J K^{-1} mol^{-1}. For the calculations in this paper, we assumed that CO_2 formed by disproportionation to the aqueous species, but did not nucleate as the gas. In this case, the degree of dissociation of HCO_3^- is nearly independent of molality, and the correction to $C_{p\phi}^{\infty}(HCO_3^-, aq)$ due to chemical relaxation can be calculated by taking $C_{p\phi}^{rel} \approx (\Delta H^0)^2\alpha/2RT^2$ (see Appendix or ref. 32). Using free energy and enthalpy data from Berg and Vanderzee (13), we calculate the degree of disproportionation to be 0.0205 in dilute solutions and the relaxation effect to be 0.43 J K^{-1} mol^{-1}. The net correction to $C_{p\phi}^{\infty}(HCO_3^-, aq)$, from equations analogous to [10] and [11], is −1.5 J K^{-1} mol^{-1}.

The corrected values for $C_{p\phi}^{\infty}(NaHCO_3, aq)$, −4.1 J K^{-1} mol^{-1} from this work, and −8.7 J K^{-1} mol^{-1} from Desnoyers *et al.* (18, 19) compare to the value −11.6 J K^{-1} mol^{-1} reported by Larson *et al.* (20). The spread between our result and Larson's is about double the usually accepted accuracy of 4 J K^{-1} mol^{-1}, for such measurements (27). Larson's result was obtained from $NaHCO_3/Na_2CO_3$ buffer solutions as part of a study to obtain data for the carbonate ion, and required a method to separate the contribution of the two mixed electrolytes, which may have slightly affected the accuracy. Our own data did not extend to the very low molalities studied by Desnoyers *et al.* and thus our limiting value may be less accurate. Combining Desnoyer's result with $C_p^0(Na^+, aq)$ from Table 4 yields $C_p^0(HCO_3^-, aq) = -52$ J K^{-1} mol^{-1}. A similar calculation based on our corrected value for the potassium salt, $C_{p\phi}^{\infty}(KHCO_3, aq) = -40.0$ J K^{-1} mol^{-1}, gives $C_p^0(HCO_3^-, aq) = -53$ J K^{-1} mol^{-1}. We propose that the value −53 J K^{-1} mol^{-1} be taken as the "best" value for $C_p^0(HCO_3^-, aq)$ and assign it an uncertainty of ±4 J K^{-1} mol^{-1} based on the scatter of the sodium results and the uncertainty in the correction for disproportionation.

Our value $V_\phi^{\infty}(NaHCO_3, aq) = 23.62$ cm^3 mol^{-1} agrees with the values 23.45 and 23.6 cm^3 mol^{-1} reported by Perron *et al.* (18) and Larson *et al.* (20), respectively. Millero (35) cited the values $V_\phi^{\infty}(KHCO_3, aq) = 32.7$ and 30.7 cm^3 mol^{-1} from reviews of work done before 1940. These are slightly less positive than our value, 33.9 cm^3 mol^{-1}. The contribution from the disporportionation reaction to all these results is less than 0.03 cm^3 mol^{-1}. Our values for the sodium and potassium salts in Table 3 lead to the identical single ion value, $V^0(HCO_3^-, aq) = 24.9$ cm^3 mol^{-1}.

The present volumetric result for $NaHSO_3$, $V_\phi^{\infty}(NaHSO_3, aq) = 32.02$ cm^3 mol^{-1}, is lower than the value 33.2 cm^3 mol^{-1}, measured by Allred, Larson, and Hepler (21). Our value and the limiting volume for the potassium salt, $V_\phi^{\infty}(KHSO_3, aq) = 42.69$ cm^3 mol^{-1}, lead to $V^0(HSO_3^-, aq) = 33.3$ and 33.7 cm^3 mol^{-1}, respectively, for the standard state volume of the hydrogen sulfite ion. Averaging these yields the result $V^0(HSO_3^-, aq) = 33.5 \pm 0.4$ cm^3 mol^{-1}. The difference between our limiting heat capacity $C_{p\phi}^{\infty}(NaHSO_3, aq) = 34.0$ J K^{-1} mol^{-1} and Allred's value of 42.2 J K^{-1} mol^{-1} lies only barely within the combined experimental uncertainty. The experimental procedures were different in that Allred *et al.* used buffer solutions prepared from the salts. Our value for the potassium salt, $C_{p\phi}^{\infty}(KHSO_3, aq) = 1.4$ J K^{-1} mol^{-1} is consistent with the sodium result in Table 3 since the derived ionic values are $C_p^0(HSO_3^-, aq) = -12$ and −9 J K^{-1} mol^{-1} respectively, and we tabulate the average, $C_p^0(HSO_3^-, aq) = -10 \pm 4$ J K^{-1} mol^{-1} in Table 4, as the best ionic value for use in calculations described later in this paper.

There are few published heat capacity or volume data for aqueous CO_2^0 and none for SO_2^0. Moore *et al.* (36) and Enns, Scholander, and Bradstreet (37) obtained $V^0(CO_2^0, aq) = 33.9 \pm 0.4$ cm^3 mol^{-1} and 34.8 ± 1.0 cm^3 mol^{-1} from density measurements and the pressure dependence of CO_2 solubility, respectively. Both are in excellent agreement with our result, 32.8 cm^3 mol^{-1}. $C_p^0(CO_2^0, aq)$ has not previously been obtained from calorimetric measurements but can be calculated by twice differentiating very accurate gas solubility data with respect to temperature. Wilhelm, Battino, and Wilcock (1) have critically evaluated literature solubility data. The parameters from their fit to the data give $[C_p^0(aq) - C_p^0(g)] = 175$ J K^{-1} mol^{-1}, probably with a large uncertainty (2). Combining this with McBride and Gordon's value $C_p^0(CO_2, g) = 37.12$ J K^{-1} mol^{-1} (38) yields $C_p^0(CO_2^0, aq) = 212$ J K^{-1} mol^{-1}, in surprisingly good agreement with the result from our direct measurement, $C_p^0(CO_2^0, aq) = 243$ J K^{-1} mol^{-1}.

Ionization equilibria versus temperature and pressure

A major objective of this work was to use the room temperature heat capacities to extrapolate the ionization constants of CO_2^0(aq) and SO_2^0(aq) to high temperatures. The relevant thermodynamic relationships are the following:

$$[12] \quad (\partial \ln K/\partial T)_p = \Delta H^0/RT^2$$

$$[13] \quad (\partial \Delta H_R^0/\partial T)_p = \Delta C_p^0$$

$$[14] \quad (\partial \ln K/\partial P)_T = -\Delta V^0/RT$$

The pressure dependence of the first ionization equilibria of both acid gases has been measured at low temperatures. Values for $\Delta V_1^0(CO_2^0, aq)$ in the range −25.4 to −27.6 cm^3 mol^{-1} have been reported by several workers (4, 39, 40) who applied eq. [14] to their pressure-dependent ionization constant data. These compare favorably with the result calculated from our direct densimetry measurements (Table 4), $\Delta V^0(CO_2^0, aq) =$

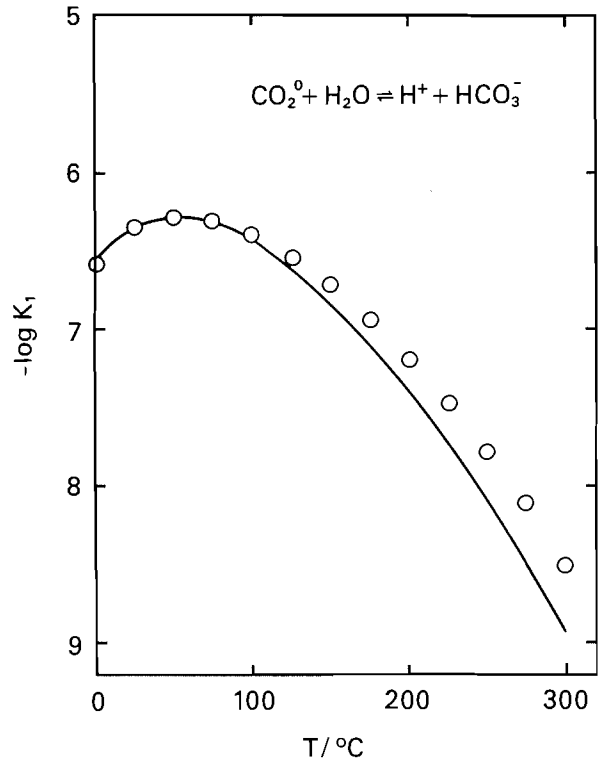

FIG. 5. The temperature dependence of the first ionization constant of aqueous CO_2. Data points are from Patterson *et al.* (3). The curve corresponds to eq. [18].

-26.0 ± 2 cm^3 mol^{-1}. Our result for $\Delta V^0(SO_2^0, aq)$, -23.1 ± 2 cm^3 mol^{-1}, is slightly more negative than Ellis and Anderson's result (12), -19.7 cm^3 mol^{-1}. Standard state volume changes of this magnitude, or even the somewhat more negative values reported at high temperatures (3, 4), would not cause ln K to be significantly affected by the saturation pressure of steam below about 300°C.

Because ΔC_p^0 is related to the second derivative of ln K with respect to temperature and because the pressure effects are so small, even a poor estimate of the temperature dependence of ΔC_p^0 can yield quite accurate values of ln K to rather high temperatures along the steam saturation curve of water, providing that ln K and ΔH^0 are known accurately at 25°C. Lindsay (41) and Murray and Cobble (42) have noted that the temperature dependence of C_p^0 for strong electrolytes is such that ΔC_p^0 changes very little over a wide range of temperatures if the reaction is "isocoulombic", that is if the products and reactants in the reactions are symmetric with respect to the number of ions in each charge type. They suggest that the temperature dependence of ln K for such reactions can therefore be estimated by assuming that ΔC_p^0 (25°C) is independent of temperature. Here, we wish to extrapolate $K_{1,b}$, the equilibrium constant for the isocoulombic neutralization reactions

[15] $CO_2^0(aq) + OH^-(aq) \rightleftarrows HCO_3^-(aq)$

and

[16] $SO_2^0(aq) + OH^-(aq) \rightleftarrows HSO_3^-(aq)$

Integrating eqs. [12] and [13] at constant pressure yields the formula:

TABLE 5. Equilibrium constants for SO_2 neutralization and dissociation from eq. [19]

t/°C	log $K_{1,b}$	log K_w*	log K_1
0	13.30 ±0.049	−14.948	−1.647±0.049
25	12.143†	−13.999	−1.856
50	11.141±0.034	−13.276	−2.135±0.034
75	10.26 ±0.08	−12.711	−2.45 ±0.08
100	9.49 ±0.12	−12.266	−2.78 ±0.12
125	8.79 ±0.18	−11.916	−3.12 ±0.18
150	8.17 ±0.23	−11.644	−3.48 ±0.23
175	7.60 ±0.29	−11.441	−3.84 ±0.29
200	7.08 ±0.35	−11.302	−4.22 ±0.35
225	6.61 ±0.41	−11.222	−4.61 ±0.41
250	6.17 ±0.48	−11.196	−5.02 ±0.48

*From Olofsson and Hepler (43).

†The ± values do not include uncertainties in log $K_{1,b}$ at 25°C, which we estimate to be ±0.01.

$$[17] \quad \ln K_{1,b}(T) \approx \ln K_{1,b}(25°C) - [\Delta H_b^0(25°C)/R - 298.15\ \Delta C_{p,b}^0(25°C)/R]\left[\frac{1}{T} - \frac{1}{298.15}\right] + [\Delta C_{p,b}^0(25°C)/R] \ln (T/298.15)$$

By combining Olofsson and Hepler's (43) compiled results for the dissociation of water with data for the ionization of aqueous CO_2 (13) and SO_2 (6, 29, 44, 48), we obtain the following values for the equilibrium constants and standard enthalpy changes of reactions [15] and [16] at 25°C: log $K_{1,b}(CO_2) = 7.649 \pm 0.005$, $\Delta H_b^0(CO_2) = -46.66 \pm 0.063$ kJ mol^{-1}, log $K_{1,b}(SO_2) = 12.143 \pm 0.010$, $\Delta H_b^0(SO_2) = -73.22 \pm 1.0$ kJ mol^{-1}. The uncertainty assigned to log $K_{1,b}(SO_2)$ includes Huss and Eckert's error estimate (6) and the results of some other workers cited in ref. 30, which are in close agreement. From Table 4, $\Delta C_{p,b}^0(CO_2) = -158 \pm 10$ J K^{-1} mol^{-1} and $\Delta C_{p,b}^0(SO_2) = -67 \pm 10$ J K^{-1} mol^{-1}. These values can be used in eq. [17] to obtain the following expressions for the temperature dependence of log $K_{1,b}$

$$[18] \quad \log K_{1,b}(CO_2, T) = 54.748 - 23/T - 19.003 \log T$$

$$[19] \quad \log K_{1,b}(SO_2, T) = 22.771 + 2776.0/T - 8.058 \log T$$

Values for the first dissociation constant of aqueous CO_2, K_1, are now quite accurately known up to 300°C and provide an excellent test for the accuracy of the extrapolation procedure. Figure 5 shows a comparison between the very detailed results of Patterson *et al.* (3) and those calculated from eq. [18] using the expression

$$\log K_1 = \log K_{1,b} - \log K_w$$

The cumulative error in the extrapolated value for log K_1 is only 0.13 at 150°C, 0.25 at 200°C, and 0.50 at 300°C, consistent with the detailed error analysis presented in our earlier study on H_2S ionization (24).

The dissociation constant of SO_2 above 50°C is much less reliably established and the extrapolated values are of considerably more practical use. These are tabulated in Table 5. The error limits were taken to be the propagated random error due to the uncertainty in ΔH_b^0 in eq. [17] plus the systematic error caused by neglecting the temperature dependence of $\Delta C_{p,b}^0$. The systematic error in the SO_2 extrapolation was simply assumed to be equal to the difference between the experimental

Can. J. Chem. Downloaded from www.nrcresearchpress.com by 210.87.254.5 on 09/06/12
For personal use only.

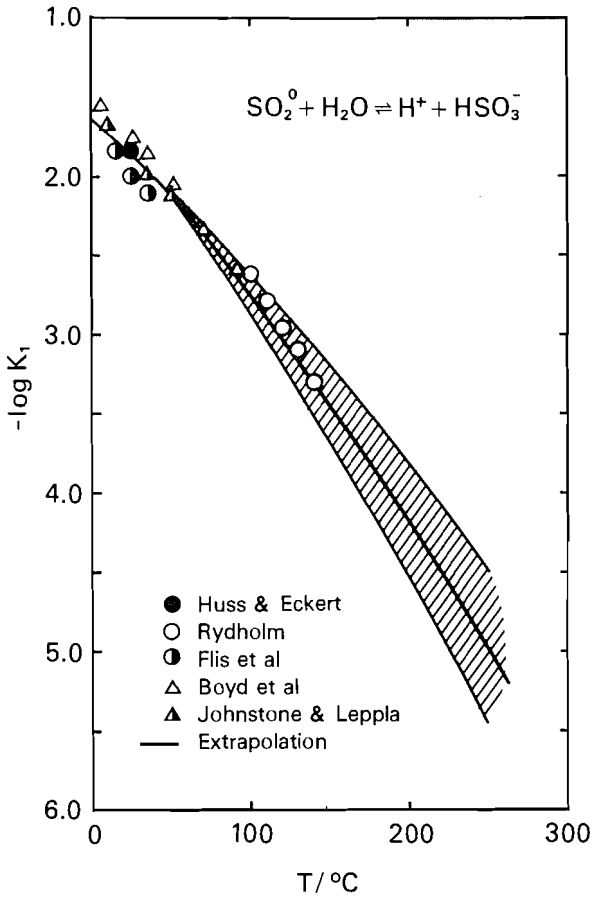

FIG. 6. The temperature dependence of the first ionization constant of aqueous SO_2. The shaded area represents the combined uncertainty in the extrapolation, from Table 5.

and extrapolated results for CO_2 (Fig. 5).

The dissociation of SO_2 has been studied by Campbell and Maass (8) from 0 to 90°C, by Flis *et al.* (7) from 10 to 35°C, and by Kaufman (9) to 130°C. Some of these results have been recalculated by Rydholm (11) and Johnstone and Leppla (10). The high temperature work was done some time ago using conductance methods and may be complicated by decomposition of the hydrogen sulfite ion, which is very easily oxidized (45, 46). These experimental data are plotted in Fig. 6 along with our estimate of the uncertainty due to the extrapolation procedure. The extrapolated results from eq. [19] agree with those of Campbell and Maass (8) and with Rydholm's tabulation of Kaufman's data to well within our estimated error. Because of the experimental problems in working with aqueous SO_2 above 100°C, the calculated K values may well be more accurate than Kaufman's measured K values.

Recently Cobble *et al.* (47) evaluated these same high temperature data using an estimated value for ΔC_p^0 and concluded that the literature values for ΔH^0 used here might be in error by more than 6 kJ mol^{-1}. The calculations outlined above suggest that the discrepancy noted in ref. 47 is due instead to the estimated value for ΔC_p^0, which is more negative than our measured value by 38 J K^{-1} mol^{-1}. Recent work at the University of Lethbridge (48) has confirmed the literature value for ΔH^0.

Acknowledgements

We are grateful to Dr. G. Mains for detailed discussions on the derivation of the heat capacity relaxation formula, to Mrs. K. Sway and Mr. L. Holloway for assistance in preparing and analyzing the solutions, and to the Comisión Nacional de Energía Atómica of Argentina for awarding a CNEA scholarship to J. A. Barbero. Funds for the project were provided by the Alberta Research Council (ARC) and the Alberta Oil Sands Technology and Research Authority, and the experimental work was done in the ARC Oil Sands Research Department.

1. E. WILHELM, R. BATTINO, and R. J. WILCOCK. Chem. Rev. **77**, 219 (1977).
2. L. N. PLUMMER and E. BUSENBERG. Geochim. Cosmochim. Acta, **46**, 1011 (1982).
3. C. S. PATTERSON, G. H. SLOCUM, R. H. BUSEY, and R. E. MESMER. Geochim. Cosmochim. Acta, **46**, 1653 (1982).
4. A. J. READ. J. Solution Chem. **4**, 53 (1975).
5. B. N. RYZHENKO. Geochem. Int. 151 (1963).
6. A. HUSS, JR. and C. A. ECKERT. J. Phys. Chem. **81**, 2268 (1977).
7. I. E. FLIS, G. P. ARKHIPOVA, and K. P. MISHCHENKO. J. Appl. Chem. USSR, **38**, 1466 (1965).
8. W. B. CAMPBELL and O. MAASS. Can. J. Res. **2**, 42 (1930).
9. Z. KAUFMANN. Thesis. Eidg. Techn. Hochschule, Zurich. 1951. Data cited in ref. 11.
10. H. F. JOHNSTONE and P. W. LEPPLA. J. Am. Chem. Soc. **56**, 2233 (1934).
11. S. RYDHOLM. Svensk Paperst. **58**, 273 (1955).
12. A. J. ELLIS and D. W. ANDERSON. J. Chem. Soc. 1765 (1961).
13. (*a*) R. L. BERG and C. E. VANDERZEE. J. Chem. Thermodyn. **10**, 1049 (1978); (*b*) R. L. BERG and C. E. VANDERZEE. J. Chem. Thermodyn. **10**, 1113 (1978).
14. J. C. PEIPER and K. S. PITZER. J. Chem. Thermodyn. **14**, 613 (1982).
15. W. H. JOHNSON and S. SUNNER. Acta Chem. Scand. **17**, 1917 (1963).
16. A. G. STILES and W. A. FELSING. J. Am. Chem. Soc. **48**, 1543 (1926).
17. W. A. ROTH and H. ZEUMER. Z. Elektrochem. **38**, 164 (1932).
18. G. PERRON, J. E. DESNOYERS, and F. J. MILLERO. Can. J. Chem. **53**, 1134 (1979).
19. J. E. DESNOYERS, C. DE VISSER, G. PERRON, and P. PICKER. J. Solution Chem. **5**, 605 (1976).
20. J. W. LARSON, K. G. ZEEB, and L. G. HEPLER. Can. J. Chem. **60**, 2141 (1982).
21. G. C. ALLRED, J. W. LARSON, and L. G. HEPLER. Can. J. Chem. **59**, 1068 (1981).
22. P. PICKER, P.-A. LEDUC, P. R. PHILIP, and J. E. DESNOYERS. J. Chem. Thermodyn. **3**, 631 (1971).
23. P. PICKER, E. TREMBLAY, and C. JOLICOEUR. J. Solution Chem. **3**, 377 (1974).
24. J. A. BARBERO, K. G. MCCURDY, and P. R. TREMAINE. Can. J. Chem. **60**, 1872 (1982).
25. G. S. KELL. *In* Water – a comprehensive treatise. Vol. 1. *Edited by* F. Franks. Plenum Press, New York. 1972.
26. I. V. OLOFSSON, J. J. SPITZER, and L. G. HEPLER. Can. J. Chem. **56**, 1871 (1978).
27. A. ROUX, G. M. MUSBALLY, G. PERRON, J. E. DESNOYERS, P. P. SINGH, E. M. WOOLLEY, and L. G. HEPLER. Can. J. Chem. **56**, 24 (1978).
28. G. PERRON, N. DESROSIERS, and J. E. DESNOYERS. Can. J. Chem. **54**, 2163 (1976).
29. L. G. HEPLER and H. P. HOPKINS, JR. Rev. Inorg. Chem. **1**, 303 (1979).
30. M. SADIQ and W. L. LINDSAY. Selection of standard free energies of formation for use in soil chemistry. Colorado State University Tech. Bull. **134**, 1979.
31. G. C. ALLRED and E. M. WOOLLEY. J. Chem. Thermodyn. **13**, 147 (1981).

Can. J. Chem. Downloaded from www.nrcresearchpress.com by 210.87.254.5 on 09/06/12
For personal use only.

32. E. M. WOOLLEY and L. G. HEPLER. Can. J. Chem. **55**, 158 (1976).
33. C. JOLICOEUR, L.-L. LEMELIN, and R. LAPALME. J. Phys. Chem. **83**, 2806 (1979).
34. G. J. MAINS, J. W. LARSON, and L. G. HEPLER. J. Phys. Chem. In press.
35. F. J. MILLERO. *In* Water and aqueous solutions; structure, thermodynamics, and transport properties. *Edited by* R. A. Horne. Wiley-Interscience, New York, NY. 1972. Chapt. 13.
36. J. C. MOORE, R. BATTINO, T. R. RETTICH, Y. P. HANDA, and E. WILHELM. J. Chem. Eng. Data, **27**, 22 (1982).
37. T. ENNS, P. F. SCHOLANDER, and I. D. BRADSTREET. J. Phys. Chem. **69**, 389 (1965).
38. B. J. MCBRIDE and S. GORDON. J. Chem. Phys. **35**, 2198 (1961).
39. A. J. ELLIS. J. Chem. Soc. 3689 (1959).
40. A. DISTÈCHE and S. DISTÈCHE. J. Electrochem. Soc. **114**, 330 (1967).
41. W. T. LINDSAY, JR. Proc. 41st. International Water Conf. Eng. Soc. Western Penn. Pittsburg, PA. 1980. pp. 284–294.
42. R. C. MURRAY and J. W. COBBLE. Proc. 41st. International Water Conf. Eng. Soc. Western Penn. Pittsburg PA. 1980. pp. 295–310.
43. G. OLOFSSON and L. G. HEPLER. J. Solution Chem. **4**, 127 (1975).
44. D. D. WAGMAN, W. G. EVANS, V. B. PARKER, I. HALOW, S. M. BAILEY, and R. G. SCHUMM. Selected values of chemical thermodynamic properties. U.S. Natl. Bur. Stand. Tech. Note 270-3. 1968.
45. M. AVRAHAMI and R. M. GOLDING. J. Chem. Soc. A, 647 (1968).
46. W. F. GIGGENBACH. Inorg. Chem. **13**, 1724 (1974).
47. J. W. COBBLE, H. P. STEPHENS, I. R. MCKINNON, and E. F. WESTRUM, JR. Inorg. Chem. **11**, 1669 (1972).
48. C. DOBROGOWSKA and L. G. HEPLER. J. Solution Chem. **12**, 153 (1983).

Appendix I

Heat capacity relaxation corrections for partially dissociated solutes

Consider an equilibrium of general type

[I-1] $MX(aq,undiss) \rightleftarrows M^+(aq) + X^-(aq)$

for which the thermodynamic equilibrium constant is

[I-2] $K = \alpha^2 m\gamma_\pm^2/(1 - \alpha)\gamma_u$

and in which symbols have the following meanings: α is the fraction of stoichiometric MX that is dissociated or ionized; m is the stoichiometric molality of MX; $\gamma_\pm$ is the mean activity coefficient of the ions in solution; and γ_u is the activity coefficient of the undissociated or un-ionized MX.

In the main part of this paper (eqs. [8] to [10]), we noted that the temperature increment imposed by any specific heat calorimeter causes a shift in α and that the contribution of this "relaxation" effect is described by the expression (32–34)

[I-3] $C_{p\phi}^{rel} = \Delta H(\partial\alpha/\partial T)_m$

where ΔH is the enthalpy of reaction at molality m.

Our first task is to evaluate $(\partial\alpha/\partial T)_m$ from eq. [I-2]. For this purpose it is convenient to define

[I-4] $F = \alpha^2/(1 - \alpha) = K\gamma_u/m\gamma_\pm^2$

Application of the quadratic equation to [I-4] gives

[I-5] $2\alpha = -F + (F^2 + 4F)^{1/2}$

Differentiation of [I-5] with respect to temperature at constant molality, followed by some algebraic manipulation, gives

[I-6] $$(\partial\alpha/\partial T)_m = \frac{(1 - \alpha)\alpha}{2 - \alpha}\left(\frac{\partial \ln F}{\partial T}\right)_m$$

from which we obtain

[I-7] $$(\partial\alpha/\partial T)_m = \frac{(1 - \alpha)\alpha}{2 - \alpha}[(\partial \ln K/\partial T)_p + (\partial \ln \gamma_u/\partial T)_m - 2(\partial \ln \gamma_\pm/\partial T)_m]$$

The first term within the brackets is easily calculated from the van't Hoff equation,

[I-8] $(\partial \ln K/\partial T)_p = \Delta H^0/RT^2$

The second term requires more care because we require the temperature dependence of $\gamma_\pm$ and γ_u in a solution of a weak electrolyte, for which the molality of ions depends on α as well as m. The temperature dependence of the activity coefficient of any non-reacting solute is given by the expression $(\partial \ln \gamma/\partial T)_m = -L/RT^2$ in which L represents the relative partial molar enthalpy of the solute. We defer, for the moment, the problem of estimating actual values $L_\pm$ and L_u in these weak electrolyte solutions and write

[I-9] $(\partial \ln \gamma_\pm/\partial T)_{\alpha m} = -L_\pm/RT^2$

and

[I-10] $(\partial \ln \gamma_u/\partial T)_{\alpha m} = -L_u/RT^2$

To relate these to [I-7], we write the total differential of $\ln \gamma_\pm$ as

[I-11] $$d \ln \gamma_\pm = (\partial \ln \gamma_\pm/\partial T)_{\alpha m}\, dT + (\partial \ln \gamma_\pm/\partial\alpha)_{T,m}\, d\alpha + (\partial \ln \gamma_\pm/\partial m)_{T,\alpha}\, dm$$

In any one experiment m is constant so that eq. [I-11] becomes

[I-12] $$(\partial \ln \gamma_\pm/\partial T)_m = (\partial \ln \gamma_\pm/\partial T)_{\alpha m} + (\partial \ln \gamma_\pm/\partial\alpha)_{T,m}(\partial\alpha/\partial T)_m$$

Combining [I-12] and the analogous equation for $(\partial \ln \gamma_u/\partial T)_m$ with eqs. [I-7] to [I-10] gives the desired equation for calculating the relaxation correction:

[I-13] $$(\partial\alpha/\partial T)_m = \frac{(1 - \alpha)\alpha}{RT^2(2 - \alpha)} \times \left\{\frac{\Delta H^0 - \bar{L}_u + 2\bar{L}_\pm}{1 + \frac{\alpha(1 - \alpha)}{2 - \alpha}\left(\frac{\partial \ln \gamma_\pm^2/\gamma_u}{\partial\alpha}\right)_{T,m}}\right\}$$

At the low ionic strengths of interest here, the activity coefficient of the undissociated species is taken to be unity and also to be temperature independent so that $\bar{L}_u = 0$. Equation [I-13] then reduces to

[I-14] $$(\partial\alpha/\partial T)_m = \frac{(1 - \alpha)\alpha}{RT^2(2 - \alpha)} \times \left\{\frac{\Delta H^0 + 2\bar{L}_\pm}{1 + \frac{2\alpha(1 - \alpha)}{2 - \alpha}\left(\frac{\partial \ln \gamma_\pm}{\partial\alpha}\right)_{T,m}}\right\}$$

To apply eq. [I-14], we calculated values of α and $(\partial \ln \gamma_\pm/$

Can. J. Chem. Downloaded from www.nrcresearchpress.com by 210.87.254.5 on 09/06/12
For personal use only.

$\partial\alpha)_m = m(\partial \ln \gamma_\pm/\partial\alpha m)_m$ using Huss and Eckert's expression for K_1 and $\ln \gamma_\pm/\gamma_u^{1/2}$, eqs. [6] and [7] in the main text. The standard enthalpy of ionization of aqueous sulphur dioxide was taken to be $\Delta H^0 = -17.4$ kJ mol^{-1} from the National Bureau of Standards compilation by Wagman *et al.* (44). This value is consistent with several earlier investigations (7, 15–17) and with recent results obtained at the University of Lethbridge (48).

An expression for the experimental apparent relative enthalpy of the equilibrium mixture of SO_2^0 and HSO_3^- was obtained by a least squares fit to the tabulated heat of dilution data (44),

$$[\text{I-15}]\quad L_{\phi 2}/\text{J mol}^{-1} = 75224m^{1/2} - 177916m + 216208m^{3/2} - 106428m^2$$

Because the calorimetric enthalpies of dilution of aqueous sulphur dioxide include contributions from the shift in equilibrium as well as dilution of the ions, there are no model-free values of $\bar{L}_\pm$. We have therefore approximated the unknown values of $\bar{L}_\pm$ by taking them to be equal to the mean ionic values for a typical strong electrolyte, hydrochloric acid, at the same molality of ions. Fitting an expression for L_ϕ(HCl) to tabulated data from ref. 44 yielded the result

$$[\text{I-16}]\quad L_\phi(\text{HCl})/\text{J mol}^{-1} = 1972.1m_i^{1/2} - 2315.5m_i + 8139.6m_i^{3/2} - 11542.8m_i^2 + 5417.4m_i^{5/2}$$

The relative partial molal enthalpy, $\bar{L} = L_\phi + m_i(\partial L_\phi/\partial m_i)$, is therefore

$$[\text{I-17}]\quad \bar{L}(\text{HCl})/\text{J mol}^{-1} = 2958.2m_i^{1/2} - 4631.0m_i + 20348.9m_i^{3/2} - 34628.5m_i^2 + 18961.1m_i^{5/2}$$

Here, the first term is defined by the Debye–Hückel limiting slope and m_i refers to the molality of the dissociated acid. In the partially ionized SO_2 solutions m_i equals αm and, according to our assumption, $2L_{\phi\pm} = L_\phi$(HCl) and $2\bar{L}_\pm = \bar{L}$(HCl).

Finally, the enthalpy of ionization at the experimental molality, ΔH, can be calculated from the bulk heat of dilution, $-L_{\phi 2}$, and the estimated contribution of the ions. From the thermodynamic cycles used by Woolley and Hepler (32),

$$[\text{I-18}]\quad \Delta H = \Delta H^0 + 2L_{\phi\pm} - L_{\phi u}$$

and

$$[\text{I-19}]\quad L_{\phi 2} = -(1-\alpha)\Delta H_R{}^0 + (1-\alpha)L_{\phi u} + 2\alpha L_{\phi\pm}$$

Solving these expressions to eliminate the contribution of the undissociated species yields

$$[\text{I-20}]\quad \Delta H = \frac{2L_{\phi\pm} - L_{\phi 2}}{1-\alpha}$$

The enthalpy of reaction at infinite dilution calculated from this scheme agrees with the result for ΔH^0 in ref. 44 to within 0.2 kJ mol^{-1}.

Can. J. Chem. Downloaded from www.nrcresearchpress.com by 210.87.254.5 on 09/06/12
For personal use only.

Spectroscopic and electrochemical studies on linkage isomerism in iron(II) complexes of benzotriazole, a corrosion inhibitor

HENRIQUE E. TOMA, ERNESTO GIESBRECHT, AND RAMÓN L. ESPINOZA ROJAS
Instituto de Química, Universidade de São Paulo, Caixa Postal 20780, São Paulo, SP, Brazil

Received December 16, 1982

HENRIQUE E. TOMA, ERNESTO GIESBRECHT, and RAMÓN L. ESPINOZA ROJAS. Can. J. Chem. **61**, 2520 (1983).

Benzotriazole reacts with the aquapentacyanoferrate(II) complex, at pH 4.5, producing a mixture of N-coordinated isomers. Characterization based on ^1H and ^{13}C nmr spectroscopy yielded an equilibrium constant $K = 1.9 \pm 0.3$, favoring the less symmetric N1-isomer. Two reversible peaks of oxidation, corresponding to the N1 and N2 isomers, were observed in the cyclic voltammograms at high scan rates, with $E_{1/2} = 0.43$ and 0.53 V versus NHE, respectively. The cyclic voltammograms at intermediate scan rates were successfully analysed in terms of an isomerization reaction preceding reversible charge-transfer. The kinetic constants of isomerization, k_f and k_b, were 1.5 and 0.65 s^{-1}, respectively. The limiting dissociative rates, $k_{-L} = 5.3 \times 10^{-3}$ s^{-1}, measured in the presence of dimethyl sulfoxide, support an intramolecular mechanism for the isomerization reaction.

HENRIQUE E. TOMA, ERNESTO GIESBRECHT et RAMÓN L. ESPINOZA ROJAS. Can. J. Chem. **61**, 2520 (1983).

Le benzotriazole réagit avec le complexe $Fe(CN)_5H_2O^{3-}$ à pH 4,5, en produçant une mélange des isomères coordonnés au Nitrogène. L'equilibre de cette réaction, avec $K = 1,9 \pm 0,3$ en faveur de le N1-isomère, a été montrée par la Spectroscopique ^1H et ^{13}C nmr, dans D_2O. Il est possible de voir deux pics correspondents a la oxydation des N1 et N2 isomères, avec $E_{1/2} = 0,43$ et 0,53 V versus ENH, dans les voltamogrammes cycliques à vélocités de balayage plus vite. L'examen théorique des voltamogrammes cycliques dans conditions de velocité de balayage intermèdes, a montrée une réaction de isomèritation précédent le transfèrement reversible des electrons. Les constants cinétiques de la isomèritation, k_f et k_b, ont été calculées comme 1,5 et 0,65 s^{-1}, respectivement. Les constants de substitution limite, $k_{-L} = 5.3 \times 10^{-3}$ s^{-1}, obtenus dans la présence de diméthyl sulfoxyde, permettent proposer un mechanisme intramoléculaire pour la réaction de isomèritation.

Introduction

Benzotriazole ($C_6H_5N_3$ or Bt) is an interesting ligand for transition metal ions, displaying remarkable efficiency as a corrosion inhibitor, particularly for copper and its alloys (1). The protective action has been associated to a compact film of a copper benzotriazole complex, produced on the metal or metal-oxide surface. The pK_a of neutral and protonated benzotriazole is 8.57 and 1.6, respectively (2). In mildly acidic or neutral solutions, there are two nitrogen atoms available for coordination with transition metal ions. Although isomeric mononuclear complexes are possible, no evidence of linkage isomerism in benzotriazole complexes has ever been published in the literature.

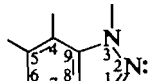

In this article, we report a study on the chemistry of pentacyanoferrate(II) complexes of benzotriazole in aqueous solution. The $Fe(CN)_5^{3-}$ ion can coordinate only one additional ligand, forming stable complexes with aromatic bases like pyridine (3), pyrazine (3), and imidazole (4). Therefore, in the presence of an excess of benzotriazole, two isomeric pentacyanoferrate(II) complexes can result in equilibrium, as a function of their relative stability constants. The characterization of the linkage isomerism in the pentacyanoferrate(II)–benzotriazole system constitutes the subject of this paper.

Experimental

The complex $Na_3Fe(CN)_5NH_3 \cdot 3H_2O$ was prepared from sodium nitroprusside (Carlo Erba) as described in the literature (5). Benzotriazole, dimethyl sulfoxide, and other reagent grade chemicals were used as supplied. The benzotriazole complex was prepared in aqueous solution from the amminepentacyanoferrate(II) complex, in the presence of a large excess of the free ligand at pH 4.5 (acetate buffer).

The electronic spectra of the complexes in the visible and uv region were recorded on a Cary 14 or 17 spectrophotometer fitted with thermostatted cell compartments. The measurements were carried out under argon, in the presence of an excess of benzotriazole to prevent the dissociation of the complex.

The kinetics of formation of the benzotriazole complex were investigated with a Durrum model D-110 stopped-flow apparatus, equipped with a Kel-F flow system. The aquapentacyanoferrate(II) complex was generated at concentrations smaller than 10^{-4} M, by dissolving the appropriate amount of $Na_3Fe(CN)_5NH_3 \cdot 3H_2O$ in argon saturated water. The ligand solutions containing 0.18 M potassium chloride and 0.02 M acetate buffer were always freshly prepared under argon atmosphere.

Cyclic voltammetry measurements were carried out with a Princeton Applied Research instrument, consisting of a 173 potentiostat and a 174 universal programmer. A platinum electrode was employed for the measurements, using the conventional Luggin capillary with the Ag/AgCl (1 M KCl) reference electrode in a non-isothermic arrangement. A platinum wire was used as the auxiliary electrode.

Nuclear magnetic resonance spectra were recorded on a Varian T-60 (^1H) or FT 80A (^{13}C) spectrometer, at a probe temperature of 33°C. Solutions of the pentacyanoferrate(II) complexes (0.9 M) were prepared in D_2O, under argon atmosphere, using stoichiometric amounts of $Na_3Fe(CN)_5NH_3 \cdot 3H_2O$, benzotriazole, and hydrochloric acid. The nmr spectra of benzotriazole were obtained with the sample dissolved in CD_3OD.

Results and discussion

The aquapentacyanoferrate(II) ion reacts with benzotriazole, under argon atmosphere, producing a yellow substituted complex. The electronic spectrum of the product, shown in Fig. 1, has a strong absorption band at 383 nm ($\epsilon = 4.1 \times 10^3$ M^{-1} cm^{-1}) which was assigned to a $d_\pi - p_\pi^*$ charge transfer transition, in analogy with the pentacyanoferrate(II) complexes of aromatic N-heterocycles (3). The complex can be oxidized reversibly, with mild oxidizing agents, to a violet–blue product absorbing at 570 nm ($\epsilon = 1.2 \times 10^3$ M^{-1} cm^{-1}).

Can. J. Chem. Downloaded from www.nrcresearchpress.com by 210.87.254.6 on 09/06/12
For personal use only.

Can. J. Chem. Downloaded from www.nrcresearchpress.com by 210.87.254.6 on 09/06/12
For personal use only.

TABLE 1. Observed rate constants of formation and dissociation of the benzotriazolepentacyanoferrate(II) complex

T (K)	[Bt] (M)	k_{obsd} (s^{-1})
285.7	5.0×10^{-3}	0.56[a]
289.0	5.0×10^{-3}	0.77
289.4	5.0×10^{-3}	0.82
298.2	2.5×10^{-3}	0.81
298.2	5.0×10^{-3}	1.68
298.2	7.5×10^{-3}	2.40
305.0	5.0×10^{-3}	2.65
278.2	4.8×10^{-2}	2.6×10^{-4}[b]
288.2	4.8×10^{-2}	8.3×10^{-4}
298.2	4.8×10^{-2}	5.3×10^{-3}
305.2	4.8×10^{-2}	9.2×10^{-2}

[a] k_{obsd} given by eq. [2], at $\mu = 0.100\ M$ KCl, $[Fe(CN)_5H_2O^{3-}] = 3 \times 10^{-5}\ M$.
[b] k_{obsd} given by eq. [8]; measured in the presence of 0.35 M dimethyl sulfoxide, at $\mu = 0.100\ M$ KCl, $[Fe(CN)_5Bt^{3-}] = 1.2 \times 10^{-3}\ M$.

The kinetics of formation of the benzotriazole complex (reaction [1]) were investigated by the stopped-flow technique under pseudo first order conditions. The results are shown in Table 1. A linear dependence of the observed rate constants, k_{obsd}, with respect to the concentration of the benzotriazole ligand was found according to eq. [2].

$$[1]\quad Fe(CN)_5H_2O^{3-} + Bt \xrightarrow{k_f} Fe(CN)_5Bt^{3-} + H_2O$$

$$[2]\quad k_{obsd} = k_f[Bt], \text{ where } k_f = 330\ M^{-1}\ s^{-1}$$

The specific rates and the activation parameters, $\Delta H^{\ddagger} = 60$ kJ mol^{-1}, $\Delta S^{\ddagger} = 6$ J mol^{-1} deg^{-1}, are consistent with the substitution kinetics previously reported in the literature (4, 6) for the $Fe(CN)_5H_2O^{3-}$ ion. It has been shown that the kinetics are practically independent on the nature of the attacking ligand, in agreement with a dissociative D, or D–IP mechanism. According to these mechanisms, two isomeric forms of the benzotriazole complex, N1 and N2, should be formed simultaneously. However, the stopped-flow kinetics monitored at several wavelengths, and the electronic spectra of the products recorded at several temperatures (Fig. 1) provided little evidence for the isomers in solution.

In the ^{13}C nmr spectrum of benzotriazole there are three peaks at 139.96, 126.93, and 115.93 ppm, which can be assigned to the C8,9, C5,6, and C4,7 atoms, respectively, in comparison with the literature assignment for benzoimidazole (10). Seven intense peaks and two shoulders are observed in the ^{13}C nmr spectra of the benzotriazolepentacyanoferrate(II) complexes (Fig. 2), in addition to broad peaks at 175 ppm, associated to the cyanide ligands.

For symmetry reasons, three ^{13}C nmr peaks are expected for the N2-isomer, and six for the N1-isomer. Therefore, one can see that the ^{13}C nmr spectrum of the complexes is consistent with a mixture of isomers (reaction [3]).

[3] 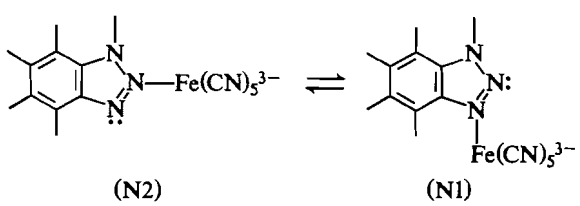

(N2) (N1)

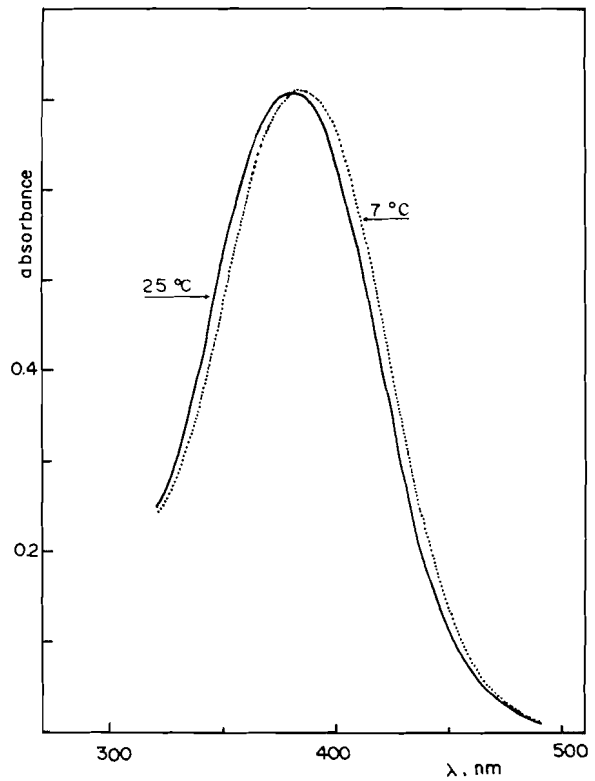

FIG. 1. Electronic spectra of the $Fe(CN)_5$ (benzotriazole)$^{3-}$ complex, $1.5 \times 10^{-4}\ M$, recorded in the presence of free ligand, $5 \times 10^{-3}\ M$, pH 4.5 (acetate buffer).

Previous studies on the ^{13}C nmr spectra of pentacyanoferrate(II) complexes of aromatic N-heterocycles have shown that the $Fe(CN)_5^{3-}$ moiety produces upfield shifts on the remote and carbon atoms, and downfield shifts on the carbon atoms close to the coordinating site. Therefore, in the less symmetric isomer B, the C6, C7, and C8 peaks are shifted downfield with respect to the corresponding C5, C4, and C9 peaks. Based on this argument, we have tentatively assigned the peaks at 126.09, 121.47, and 114.15 ppm to the C8,9, C5,6, and C4,7 atoms, respectively, of the N2-isomer. The corresponding peaks for the N1-isomer are observed at 126.30 (sh, C8), 123.76 (C9), 122.08 (C6), 121.3 (sh, C5), 115.39 (C7), and 113.34 ppm (C4), respectively. Because of strong overlap in the C5,6 and C8,9 peaks, the relative amounts of the isomers were evaluated from the intensities of the C4,7 peaks. The calculated value of K was 1.8 ± 0.4 at 33°C.

As one can see in Fig. 2, there are two groups of peaks at 8.92 and 7.57 ppm in the ^1H nmr spectrum of the benzotriazole complex, shifted downfield and upfield, respectively, from the resonance peaks of the free ligand. Their relative intensities (1.3/6.7) are indicative of a mixture of isomers. The typical A_2B_2 pattern observed for the free ligand is expected to be preserved in the case of the N2-isomer; however, a more complicated pattern is predicted for the less symmetric N1-isomer.

According to several systematic studies on ^1H nmr spectra of pentacyanoferrate(II) complexes of aromatic N-heterocyclic ligands (7–9), the signals of the protons close to the $Fe(CN)_5^{3-}$ group are shifted downfield by the magnetic anisotropy of the metal ion and of the cyanide ligands. In contrast, the peaks of remote protons in the ligand are shifted upfield by π-backbonding interactions with the metal ion. Based on molecular models, we assigned the peaks at 8.92 ppm to the

Can. J. Chem. Downloaded from www.nrcresearchpress.com by 210.87.254.6 on 09/06/12
For personal use only.

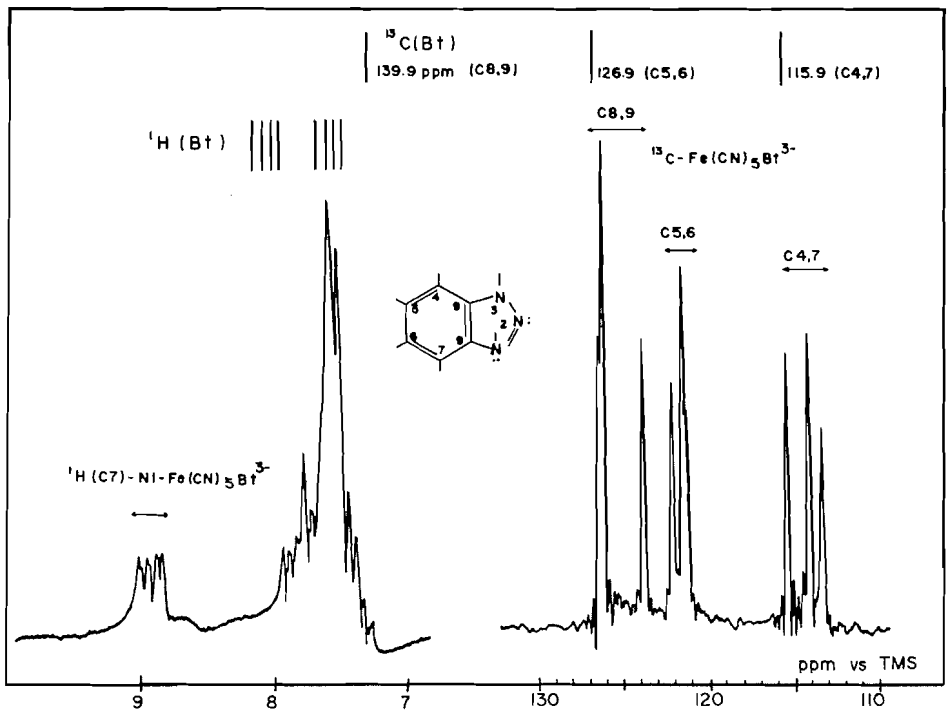

FIG. 2. ^{1}H and ^{13}C nmr spectra of Fe(CN)$_5$ (benzotriazole)$^{3-}$ complexes (0.9 *M*), in D_2O, pH 5, 33°C. The nmr spectra of benzotriazole in CD_3OD are represented by the lines in the figure.

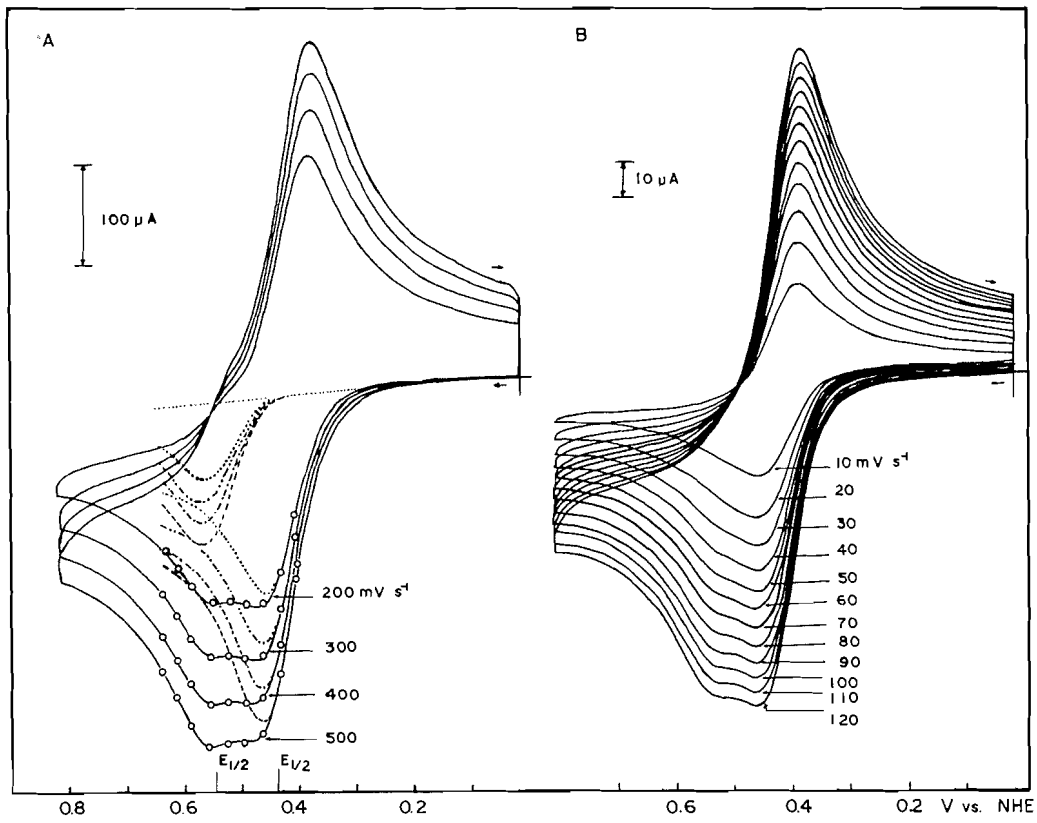

FIG. 3. Cyclic voltammograms of Fe(CN)$_5$ (benzotriazole)$^{3-}$ complexes, 2.0×10^{-3} (*A*) and 1.0×10^{-3} *M* (*B*) in the presence of free ligand, 4.8×10^{-2} *M*, pH 4.5 (acetate buffer), $\mu = 0.100$ *M* KCl, at several potential scan rates. The dotted waves refer to the analysis in terms of two reversible monoelectronic processes. The circles represent the theoretical cyclic voltammograms.

proton at C7 in the N1-isomer. This atom is located perpendicularly to the cyanide ligands, in a region where the deshielding effect is maximum. The splittings are similar to those observed for the C2-proton of quinoline, and consistent with an ABX system. Analogous assignment can be excluded for the N2-isomer, since the protons are quite remote from the

TABLE 2. Isomerization constants and electrochemical parameters for the pentacyanoferrate(II)–benzotriazole system[a] at several temperatures

T (K)	$E^{N1}_{1/2}$ (V vs. NHE)	$E^{N2}_{1/2}$ (V vs. NHE)	K^b	k_{21} (s^{-1})	k_{12} (s^{-1})	k_{-N2}[c] (s^{-1})	k_{-N1}[c] (s^{-1})
278.2	0.45	0.56	2.6	0.51	0.19	4.7×10^{-4}	1.8×10^{-4}
288.2	0.44	0.55	2.5	0.86	0.34	1.5×10^{-3}	5.8×10^{-3}
298.2	0.43	0.53	2.4	1.55	0.65	9.0×10^{-3}	3.7×10^{-3}
305.2	0.42	0.52	2.3	2.6	1.12	1.5×10^{-3}	6.6×10^{-3}

[a] In the presence of an excess of benzotriazole (4.8×10^{-2} *M*), pH 4.5 (acetate buffer), $\mu = 0.100$ *M* KCl.
[b] Isomerization constant for the iron(II) complexes.
[c] Dissociation rate constants expressed by eq. [8], at $\mu = 0.100$ *M* KCl, in the presence of 0.35 *M* dimethyl sulfoxide.

$Fe(CN)_5^{3-}$ group.

The several peaks around 7.57 ppm were ascribed to the other protons in the mixture of isomers. Assuming that the contribution of the N1-isomer to the integrated intensity at 7.57 ppm is three times the value measured at 8.92 ppm, the calculated value for the isomerization constant K is 1.9 ± 0.3 at 33°C, in agreement with the results from ^{13}C nmr.

The electrochemical behavior of the benzotriazole complexes was investigated using cyclic voltammetry. The measurements were carried out in aqueous solutions at pH 4.5 (10^{-2} *M* acetate buffer) in the presence of 0.100 *M* KCl, and at least ten times excess of free ligand to prevent the dissociation of the complexes. Typical cyclic voltammograms of the benzotriazole complexes are shown in Fig. 3.

At low scan rates, e.g., 10 mV s^{-1}, a single peak is observed, exhibiting reversible characteristics, with $E_{1/2}$ = 0.434 V versus NHE and $D = 4.3 \times 10^{-6}$ cm^2 s^{-1}. These voltammograms can be fitted by eq. [4], using the work functions χ previously described in the literature (11),

$$[4] \quad i = nFAC\,(\chi Da)^{1/2}$$

where $a = nFv/RT$, v = scan rate (V s^{-1}), and the other terms have the conventional meaning.

Two peaks of oxidation, separated by 100 mV, were detected in the cyclic voltammograms at high potential scan rates. Theoretical analysis in terms of eq. [4] provided very good fittings, as shown in Fig. 3, indicating that the two oxidation waves are electrochemically reversible. Based on their relative intensities, the oxidation waves with $E_{1/2}$ = 0.43 and 0.53 V versus NHE were assigned to the N1 and N2 isomers, respectively. The equilibrium constants of isomerization evaluated from the cyclic voltammograms at 200, 300, 400, and 500 mV s^{-1}, were respectively, 2.39, 2.40, 2.44, and 2.35 at 25°C. These results are practically identical. Therefore, we conclude that the equilibrium measurements are not affected by the potential scan rates above 200 mV s^{-1}.

The pattern observed at intermediate scan rates, e.g. 50 mV s^{-1}, is characteristic of a reversible electrochemical process preceded by a reversible chemical reaction, as in reaction [5]. In this case, the relaxation time of the chemical system is close to the potential scan rates, and the measurements become dependent on these two variables. At very low potential scan rates, as the N1 isomer is oxidized, the equilibrium is reestablished rapidly enough, so that a single wave is observed.

$$[5] \quad (CN)_5FeBt^{3-}\ (N2) \underset{k_{12}}{\overset{k_{21}}{\rightleftharpoons}} (CN)_5FeBt^{3-}\ (N1)$$

$$(CN)_5FeBt^{3-}\ (N1) \xrightarrow{\text{fast}} (CN)_5FeBt^{2-} + e^-$$

In order to evaluate the kinetic constants of isomerization we have employed eq. [6], previously proposed by Shain and Nicholson (11) for the case of a reversible electrochemical process preceded by a chemical reaction.

$$[6] \quad \frac{i_d}{i} = 1.02 + \frac{0.471}{K}\left[\frac{a}{(k_{12} + k_{21})}\right]^{1/2}$$

In eq. [6], i is the observed current, and i_d is the diffusion controlled current calculated from the data in the absence of chemical reactions, or at low scan rates.

Because the N2-isomer is electrochemically active, the calculations were carried out at the half wave potential of the N1-isomer. Theoretical analysis has shown that the contribution of the N2-isomer to the currents measured at 0.43 V versus NHE is practically zero. Typical results for $k_{12} + k_{21}$, obtained at 20, 30, 40, 50, 60, 70, 80, 90, 100, 110, and 120 mV s^{-1}, were 2.20, 1.99, 2.46, 2.49, 1.95, 1.98, 2.00, 2.15, 2.08, 2.21, and 2.03 s^{-1}, respectively, with an average of 2.14 ± 0.18 s^{-1}. Similar calculations were carried out at several concentrations of the complexes, with identical results. From the values of $k_{21} + k_{12}$ and $K = k_{21}/k_{12}$, we obtained the isomerization constants shown in Table 2.

In order to elucidate the mechanisms involved in the isomerization reaction, we investigated the substitution processes in the benzotriazole complexes. For convenience, the kinetics were carried out using cyclic voltammetry, under identical conditions of the electrochemical study. Dimethyl sulfoxide was chosen as the attacking ligand because it forms a very stable complex with the pentacyanoferrate(II) ion (12), having $E_{1/2}$ = 0.89 V. Thus it does not interfere in the cyclic voltammograms of the starting complex.

The decay of the benzotriazole complexes in the presence of dimethyl sulfoxide is illustrated in Fig. 4. The logarithmic plots of peak currents against time were linear for at least three half lives. The first order rate constants are shown in Table 1. At 25°C, $k_{obsd} = 5.3 \times 10^{-3}$ s^{-1}.

It has been shown (3, 5) that the typical mechanism of substitution in pentacyanoferrate(II) complexes is given by eqs. [7]–[9].

$$[7] \quad Fe(CN)_5L^{3-} \underset{k_L}{\overset{k_{-L}}{\rightleftharpoons}} Fe(CN)_5^{3-} + L$$

$$[8] \quad Fe(CN)_5^{3-} + H_2O \overset{K}{\rightleftharpoons} Fe(CN)_5H_2O^{3-}$$

Can. J. Chem. Downloaded from www.nrcresearchpress.com by 210.87.254.6 on 09/06/12
For personal use only.

Can. J. Chem. Downloaded from www.nrcresearchpress.com by 210.87.254.6 on 09/06/12
For personal use only.

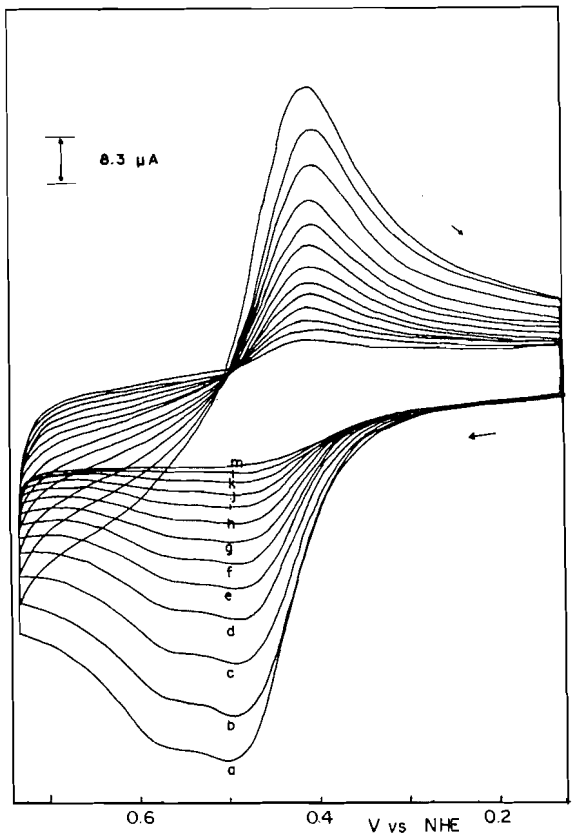

FIG. 4. Decay of the $Fe(CN)_5$ (benzotriazole)$^{3-}$ complexes, 1.2×10^{-3} *M*, followed by cyclic voltammetry, in the presence of 0.35 *M* dmso, 0.048 *M* Bt, 0.100 *M* KCl, at 25°C, 100 mV s^{-1}, from zero time (*a*) to 630 s (m).

$$[9]\quad Fe(CN)_5^{3-} + X \xrightarrow{k_X} Fe(CN)_5X^{3-}$$

In this mechanism, the dissociation of the ligand L constitutes the rate determining step. The observed rate constant follows a saturation behavior with respect to the concentration of the attacking ligand, so that, in the presence of a high excess of X, $k_{obsd} = k_{-L}$.

Because of the isomerization equilibrium, the substitution reactions can take place in two parallel ways, represented by k_{-N1} and k_{-N2}, respectively, in reactions [10]–[12].

$$[10]\quad Fe(CN)_5Bt^{3-}\ (N2) \overset{K}{\rightleftharpoons} Fe(CN)_5Bt^{3-}\ (N1)$$

$$[11]\quad Fe(CN)_5Bt^{3-}\ (N2) \xrightarrow{k_{-N2}} Fe(CN)_5dmso^{3-} + Bt$$

$$[12]\quad Fe(CN)_5Bt^{3-}\ (N1) \xrightarrow{k_{-N1}} Fe(CN)_5dmso^{3-} + Bt$$

In the presence of a high excess of dimethyl sulfoxide, the limiting rate constant is given by eq. [13].

$$[13]\quad k_{obsd} = \frac{k_{-N2} + k_{-N1}K}{1 + K}$$

From the isomerization constants K (Table 2), and k_{obsd} (Table 1), it is possible to calculate the dissociation rate constants k_{-N1} and k_{-N2}. The results at 25°C were 3.7×10^{-3} and 9.0×10^{-3} s^{-1}, respectively. In comparison with the isomerization rates shown in Table 2, one can see that the dissociation of the benzotriazole ligand from the complex is slower by a factor of two orders of magnitude. *Therefore, we conclude that the isomerization mechanism is essentially intramolecular.* Possibly, the mechanism involves π-intermediate complexes, with the $Fe(CN)_5^{3-}$ moiety coordinated to the N=N group.

TABLE 3. Kinetic and thermodynamic parameters for the pentacyanoferrate–benzotriazole system[a]

Parameter	Value	
	N2-isomer	N1-isomer
k_f (M^{-1} s^{-1})	330	330
$\Delta H_f^{\ddagger}$ (kJ mol^{-1})	60	60
$\Delta S_f^{\ddagger}$ (J mol^{-1} deg^{-1})	6	6
k_{-L} (s^{-1})	9.0×10^{-3}	3.7×10^{-3}
$\Delta H_{-L}^{\ddagger}$ (kJ mol^{-1})	89	93
$\Delta S_{-L}^{\ddagger}$ (J mol^{-1} deg^{-1})	11	19
$K_{II} = k_f/k_{-L}$ (M^{-1})	3.7×10^4	8.8×10^4
ΔH_{II} (kJ mol^{-1})	−29	−33
ΔS_{II} (J mol^{-1} deg^{-1})	−5	−13
K_{III} (M^{-1})	67	7.8×10^3

[a] 25°C, μ = 0.100 *M* KCl, pH 4.5 acetate buffer (10^{-2} *M*).

The activation and thermodynamic parameters calculated for the two isomers, based on temperature variation studies, can be seen in Table 3.

In spite of some possible steric hindrance at the N1 atom of benzotriazole, this isomer is more stable thermodynamically than the N2-isomer. The difference is essentially enthalpic, indicating a stronger $d_\pi - p_\pi^*$ interaction in the N1-isomer, in agreement with previous CNDO calculations for the benzotriazole molecule (13).

Because the diffusion coefficients of the oxidized and reduced complexes are similar, the half wave potentials can be considered identical to the formal redox potentials, E^0. Therefore, starting from the E^0 values and the equilibrium constants for the iron(II) complexes, K_{II}, one can calculate the corresponding constants for the oxidized complexes, using eq. [14].

$$[14]\quad K_{III} = K_{II} \exp\left[(E^0_{H_2O} - E^0_{Bt})/RT\right]$$

$E^0_{H_2O}$ is the reduction potential of the $Fe(CN)_5H_2O^{2-}$ complex, equal 0.368 V versus NHE at μ = 0.100 and 25°C.

The calculated value of K_{III} are shown in Table 3. It should be noted that the oxidized form of the N1-isomer is much more stable than the oxidized form of the N2 analog. The ratio of the stability constants defines an isomerization constant $K' = 115$, favoring the N1-isomer.

Returning to the cyclic voltammograms of Fig. 3, one can see that the cathodic response at high or intermediate scan rates has a much greater contribution of the isomer N1 than it would be expected if the relative ratio of the two isomers were constant, i.e., $K = 2.4$. Analysing the cathodic part of the cyclic voltammograms, we observed that the plots of peak currents versus $v^{1/2}$ are linear up to $v = 100$ mV s^{-1}. The peak currents are consistent with a complete conversion of the N2-isomer to the N1-isomer. Above 200 mV s^{-1}, we noted increasing negative deviations from the linear behavior, indicating incomplete relaxation of the oxidized system in the time scale of the cyclic

voltammetry. At the same time, the cathodic wave corresponding to the N2-isomer became more evident in the cyclic voltammograms (see Fig. 3).

In order to estimate the kinetic constants for the oxidized complexes, we considered that the relative distribution of the N1 and N2 isomers at zero time was 71% over 29%, based on $K = 2.4$. The time interval from the oxidation to the reduction of the two isomers was measured directly from the cyclic voltammograms. If the differences from the expected peak currents for the N1-isomer correspond to the amounts of the N2-isomer in solution, then the calculated distribution of the N1 and N2 isomers becomes 86/14, 87/13, 89/11, and 94/6, after 1.4, 1.7, 2.3, and 3.5 s, respectively. These results are consistent with a relaxation constant of $0.45 \pm 0.08\ s^{-1}$, for the oxidized complexes. The elementary constants, k'_{21} and k'_{12} are 0.44 and $0.004\ s^{-1}$, respectively, at 25°C.

The results obtained in this work are summarized in reaction [15].

$$[15]\quad (CN)_5FeBt^{2-}\ (N2) \underset{4\times10^{-3}\ s^{-1}}{\overset{0.44\ s^{-1}}{\rightleftharpoons}} (CN)_5FeBt^{2-}\ (N1)$$

$$\Big\Uparrow\Big\Downarrow 0.53\ V \qquad\qquad \Big\Uparrow\Big\Downarrow 0.43\ V$$

$$(CN)_5FeBt^{3-}\ (N2) \underset{0.65\ s^{-1}}{\overset{1.55\ s^{-1}}{\rightleftharpoons}} (CN)_5FeBt^{3-}\ (N1)$$

$$330\ M^{-1}\ s^{-1} \Big\Uparrow\Big\Downarrow 9.0\times10^{-3}\ s^{-1} \quad 3.7\times10^{-3}\ s^{-1} \Big\Uparrow\Big\Downarrow 330\ M^{-1}\ s^{-1}$$

$$\searrow \qquad Fe(CN)_5H_2O^{3-} + Bt$$

These data provide definite evidence of coordination mobility in a typical benzotriazole complex. A similar case of intramolecular isomerization has been reported by Armor and Taube (14) in the $Ru(NH_3)_5N_2^{2+}$ complex. This kind of mechanism is particularly important in catalytic processes involving π-systems. Following this line, we are investigating the fluxional properties of several ruthenium(II)–benzotriazole complexes.

Acknowledgment

A fellowship from CNPq (R.L.E.R.) is gratefully acknowledged.

1. R. WALKER. J. Chem. Ed. **57**, 789 (1980).
2. A. ALBERT, R. GOULDANE, and J. PHILLIPS. J. Chem. Soc. 2240 (1948).
3. H. E. TOMA and J. M. MALIN. Inorg. Chem. **12**, 1039 (1973).
4. H. E. TOMA, J. M. MARTINS, and E. GIESBRECHT. J. Chem. Soc. Dalton, 1610 (1978).
5. G. BRAUER. Handbook of preparative inorganic chemistry. Vol. II. 2nd ed. Academic Press. 1965. p. 1511.
6. H. E. TOMA and J. M. MALIN. Inorg. Chem. **12**, 2080 (1973).
7. H. E. Toma, J. M. Malin, and C. F. SCHMIDT. Inorg. Chem. **14**, 2924 (1975).
8. J. E. FIGARD, J. V. PAUKSTELIS, E. F. BYRNE, and J. D. PETERSEN. J. Am. Chem. Soc. **99**, 8417 (1977).
9. H. E. TOMA, J. A. VANIN, and J. M. MALIN. Inorg. Chim. Acta, **33**, L157 (1979).
10. R. J. PUGMIRE and D. M. GRANT. J. Am. Chem. Soc. **93**, 1880 (1971).
11. R. S. NICHOLSON and I. SHAIN. Anal. Chem. **36**, 706 (1964).
12. H. E. TOMA, J. M. MALIN, and E. GIESBRECHT. Inorg. Chem. **12**, 2084 (1973).
13. P. A. ESCANDE, J. LAPASSET, R. FAURE, E. J. VINCENT, and J. ELGUERO. Tetrahedron, **30**, 2903 (1974).
14. J. N. ARMOR and H. TAUBE. J. Am. Chem. Soc. **92**, 2561 (1970).

Can. J. Chem. Downloaded from www.nrcresearchpress.com by 210.87.254.6 on 09/06/12
For personal use only.

The alkaloids of *Senecio triangularis* Hook.

H. RÜEGER AND M. H. BENN
Department of Chemistry, The University, Calgary, Alta., Canada T2N 1N4

Received May 2, 1983

H. RÜEGER and M. H. BENN. Can. J. Chem. **61**, 2526 (1983).

Pyrrolizidine alkaloids were isolated from *Senecio triangularis* Hook. growing in Alberta, and identified as 7-angelylretronecine, 7-senecioylretronecine, 7-angelyl-9-sarracinylretronecine, and 7-senecioyl-9-sarracinylretronecine, the last three of which appear to be new natural products.

H. RÜEGER et M. H. BENN. Can. J. Chem. **61**, 2526 (1983).

On a isolé les alcaloides du type pyrrolizidine du *Senecio triangularis* de Hook croissant en Alberta et que l'on a identifiés comme étant l'angélyl-7 rétronécine, la sénécioyl-7 rétronécine, l'angélyl-7 sarracinyl-9 rétronécine et la sénécioyl-7 sarracinyl-9 rétronécine; les trois derniers composés semblent être des nouveaux produits naturels.

[Traduit par le journal]

Can. J. Chem. Downloaded from www.nrcresearchpress.com by 210.87.254.6 on 09/06/12
For personal use only.

Senecio triangularis Hook. is often found growing in cool wet habitats throughout the Rocky Mountains; the Cheyenne Indians are said to have used the plant as a medicinal: to prepare a tea used as a sedative, and to treat chest-pains (1).

In connection with another project, we were faced with the need of a specimen of senecionine (**1**), and knowing that this was the major alkaloid of *S. triangularis* collected around the Arrowhead – Big Bear Lake region of the San Bernadino mountains in S. California (2),[1] we decided to isolate the compound from Albertan plants. To our surprise, *S. triangularis* collected in Kananaskis Country yielded no senecionine, but instead a mixture of four other alkaloids: A – D. We report here the results of our investigations of the structures of these alkaloids.

An initial gc–ms analysis of the mixture of bases suggested that alkaloids A (ca. 60%) and B (ca. 5%), and C (ca. 20%) and D (ca. 15%) were isomeric, with molecular weights of 237 and 335 respectively. Given that the *Senecio* are a rich source of pyrrolizidine alkaloids (2), it seemed very probable that our alkaloids belonged to this class of natural products, and were therefore likely to be ester derivatives of the C_8N skeleton characteristic of most of those compounds. Plausible possibilities for the molecular compositions were then $C_{13}H_{19}NO_3$ (A and B) and $C_{18}H_{25}NO_5$ (C and D).

Alkaloids A, C, and D were individually isolated by chromatographic procedures, detailed in the Experimental, and characterized spectroscopically. The ^1H and ^{13}C nmr data for these compounds are summarized in Tables 1 and 2, and it is apparent that the carbon and proton counts are in accord with the tentative molecular formulae deduced from the gc–ms results.

If alkaloid A is a $C_{13}H_{19}NO_3$ compound, the structure must contain the equivalent of 5 rings/double bonds. Inspection of its ^{13}C nmr spectrum revealed four olefinic carbons and an ester carbonyl carbon. The remaining two units of unsaturation therefore correspond to two rings as expected for a pyrrolizidine. Since the ir spectrum of A contained strong absorptions attributable to hydroxyl as well as ester functions, we suspected that we were dealing with a C_5-monoester of the commonly encountered necine system **2**. The location of the ester followed from a scrutiny of the ^1H nmr spectrum of the alkaloid: the chemical shifts of the almost magnetically equivalent H-9 protons (δ 4.18), as well as of the H-7 proton (δ 5.42), are consistent with the esterified hydroxyl being that at C-7, and not at C-9 (2, 3).

The identity of the C_5-acid component, which must be one of the mono-olefinic $C_5H_8O_2$ possibilities, also followed from the ^1H nmr spectrum of A: the absorptions at δ 1.81, 1.96, and 6.08 define an angelate (*Z*-2-methyl-2-butenoate) unit (2, 4, 5). (These shifts unambiguously exclude the tiglate (*E*-2-methyl-2-butenoate) and senecioate (3-methyl-2-butenoate) alternatives.)

There remained the stereochemistry of the necine moiety: whether the C-7 functionality is *exo*, as in a 7β,8α retronecine system, or *endo*, as in a 7α,8α heliotridine situation. Fortunately, both 7-O-angelylretronecine and 7-O-angelylheliotridine are known compounds, and their cd spectra have been recorded and found to be very different (6). The cd spectrum of alkaloid A corresponded with that reported for 7-O-angelylretronecine, and the mp of the picrate salt of our base was also the same as that given for that compound. Thus alkaloid A is **3**.

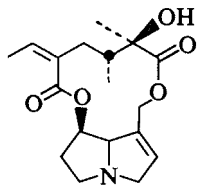

1

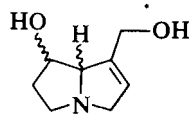

2

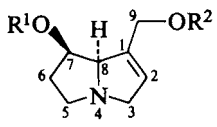

3 R^1 = (*Z*)-$CH_3CH{=}C(CH_3)CO$ (5′-CH_3) R^2 = H

5 R^1 = (*Z*)-$CH_3CH{=}C(CH_3)CO$ (5′-CH_3) R^2 = (*Z*)-$CH_3CH{=}C(CH_2OH)CO$ (5″-CH_2OH)

6 R^1 = $CH_3C{=}CHCO$ (5′-CH_3) R^2 = (*Z*)-$CH_3CH{=}C(CH_2OH)CO$ (5″-CH_2OH)

[1]One of us (M.H.B.) collected *S. triangularis*, in blossom, in the San Bernadino Mountains, with Prof. T. A. Geissman, in Sept. 1960, and isolated senecionine from these plants.

FOR ERRATA SEE
v.62 #12 1984 p.2948

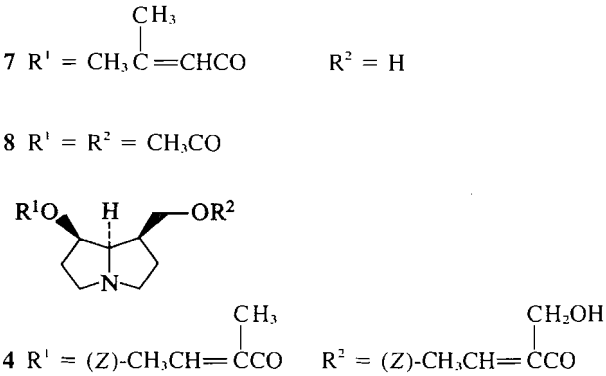

The identities of the other alkaloids proved to be more interesting. By an analysis of the spectroscopic data similar to that described for alkaloid A, C was recognized to be an acyclic diester of **2**. In particular, note that the ^{13}C nmr spectrum of C contained signals due to six olefinic carbons and two ester carbonyl carbons. Comparison of the data with that for alkaloid A revealed the presence of one angelyl unit, and another C_5-alkenoic acid. This second acid differed from angelic acid in having one of the methyl groups converted to hydroxymethyl. That this acid was in fact sarracinic acid (*Z*-2-(hydroxymethyl)-2-butenoic acid) was deduced from the ^1H nmr spectra: the CH_2OH signal contained no vicinal coupling, whereas the methyl signal did, and the *Z*-stereochemistry could be inferred, with reasonable confidence, from the shift of the vinylic proton (δ 6.38) (5). Further comparison of the ^{13}C nmr data wth that for the alkaloid sarracine (**4**) showed an excellent agreement between the signals for its sarracinic acid moiety and these ascribed to that unit in the spectra of alkaloid C (see Table 1).

The close correspondence of the ^{13}C nmr signals for the pyrrolizidine portion of alkaloid C with those recorded for 7,9-diesters of retronecine (as contrasted with 7,9-diesters of heliotridine) (7–9) indicated the nature of the necine. The location of the individual esterifying acids was originally deduced from the ms. Alkaloid C had a base-peak ion at *m/z* 220 corresponding to the loss of 115 mass units, which we ascribed to the typical fragmentation at the allylic site. The loss corresponds to $C_5H_7O_3$, i.e., the loss of the sarracinyl unit. Other independent evidence supporting this conclusion followed from the controlled-hydrolysis studies described later. We therefore formulated our base C as 7-*O*-angelyl-9-*O*-sarracinylretronecine (1,2-didehydrosarracine) (**5**), an apparently previously undescribed alkaloid. The ord/cd data were in accord (6) with the absolute stereochemistry shown in **5**.

Similar inspection of the data collected from alkaloid D revealed that it differed from C only in the nature of the esterifying acid at position 7, this now being senecioic acid (note the absence of a $J^{vic}_{H,H}$ coupling in the methyl signals for this C_5-unit, and the shift of the vinylic proton), i.e. alkaloid D is 7-senecionyl-9-sarracinylretronecine (**6**). Esterification with senecioic acid has rarely been reported in the pyrrolizidine akaloids,[2] and, like C, alkaloid D appears to be a new alkaloid.

We were unable to isolate enough of alkaloid B to characterize it completely. However its ms was consistent with this alkaloid being 7-*O*-senecioylretronecine (**7**), a compound which also does not apear to have been described before, as a natural product.

TABLE 1. ^{13}C nuclear magnetic resonance data for alkaloids A (**3**), C (**5**), D (**6**), and some model systems

Carbon	**2** (9)	**3**	**4**	**5**	**6**	**8** (9)
1	137.9	139.2	40.2	133.8	133.8	133.8
2	127.1	123.8	28.8	127.6	127.5	127.7
3	58.7	60.0	55.2*	60.9	61.1	61.2
4	54.2	53.6	53.6*	59.8	53.7	53.7
6	35.3	34.6	35.1	34.6	34.4	34.4
7	71.1	74.0	68.9	68.9	73.1	74.0
8	79.5	75.9	75.2	75.9	75.7	75.8
9	61.9	63.0	64.1	62.8	62.6	62.9
1′		167.2	166.8	166.8*	165.8*	171.0
2′		127.5	127.1	127.5	115.9	20.8
3′		139.1	139.6	139.2	157.6	
4′		20.5	20.8	20.5	27.5	
5′		15.7	15.7	15.8	20.6	
1″			166.8	166.6*	166.5*	171.0
2″			131.9	131.6	131.6	20.8
3″			140.4	141.2	141.4	
4″			15.7	15.8	15.8	
5″			64.9	65.0	65.1	

Assignments marked in any column may be interchanged.

It will be observed that alkaloids A and C, and B and D are related as pairs of 7,9-diester and 7-ester derivaties of retronecine, in which the 9-ester was sarracinyl. This prompts the thought that the monoesters may be arising from the diesters during the isolation procedures. Controlled saponification of a mixture of alkaloids C and D did generate a mixture of A and B (as determined by gc–ms). But, under the conditions employed for their isolation, alkaloids C and D seemed to be quite stable. Since relatively large amounts of alkaloid A were obtained from the plant, we conclude that it cannot all be an artefact of the isolation procedure, i.e. that A, like C and D, is a genuine alkaloid of Albertan *S. triangularis*. We cannot be as confident about alkaloid B, since it was only present in very small amounts. However, given the authenticity of the monoester A as a natural product, it appears reasonable to accept B as one too.

Apart from the novelty of 7-*O*-angelyl-9-*O*-sarracinylretronecine, 7-senecioyl-9-*O*-sarracinylretronecine, and 7-senecioylretronecine as additions to the already long list of pyrrolizidine alkaloids, their isolation, together with 7-*O*-angelylretronecine, from a plant elsewhere known to produce senecionine is noteworthy. Qualitative, as well as quantitative, intraspecific variations in alkaloid production by plants are well established, and a fairly recent essay has discussed possible genetic control mechanisms (11). In the particular case of *S. triangularis*, our findings recall an apparently unpublished idea of the late Professor Geissman: that macrocylic diester pyrrolizidine alkaloids may be biosynthesized from acylic diesters, i.e. the appearance of 7-*O*-angelyl-9-*O*-sarracinylretronecine in the Albertan plants might reflect the absence of an ability possessed by those in S. California to effect a $C_5 + C_5$ cyclization needed to construct senecionine.

As a final comment, the reputed medicinal use of *S. triangularis*, to which we alluded at the start, would seem to have been hazardous: the toxicological properties of 9-*O*-esters of retronecine and the macrocyclic diesters are well established (2, 12).

[2]See ref. 10 for a recent list of more than 200 pyrrolizidine alkaloids, of which fewer than 2% were esters of senecioic acid.

Can. J. Chem. Downloaded from www.nrcresearchpress.com by 210.87.254.6 on 09/06/12
For personal use only.

TABLE 2. ^{1}H nuclear magnetic resonance data for alkaloids A (**3**), C (**5**), and D (**6**)

Proton	3	5	6
2	5.63 s*	5.80 s*	5.79 s*
3	3.38 m, 3.96 d; J_{AB} = 15 Hz	3.40 d, 3.95 d; J_{AB} = 16 Hz	3.40 d, 3.94 d; J_{AB} = 15 Hz
5	2.71 q J = 8 Hz	2.65 q J = 8 Hz	2.66 q J = 8 Hz
	3.38 m	3.35 m	3.35 m
6	2.14 m	1.9–2.1 m	1.8–2.2 m
7	5.42 br,s*	5.39 br,s*	5.35 m
8	4.40 br,s	4.35 br,s	4.36 m
9	4.18 br,s†	4.69 d, 4.82 d; J_{AB} = 16 Hz	4.68 d, 4.80 d; J_{AB} = 16 Hz
2′			5.59 s*
3′	6.08 q J = 7 Hz	6.09 q* J = 7Hz	
4′	1.96 d* J = 7 Hz	1.96 d* J = 7 Hz	2.13 s*
5′	1.81 s*	1.80 s*	1.81 s*
3″		6.38 q J = 7 Hz	6.37 q J = 7 Hz
4″		2.05 d J = 7 Hz	2.05 d J = 7 Hz
5″		4.22 s†	4.22 s†
OH	3.17 br,s	2.34 br,s	1.8–2.5 v br,s

Signals marked showed additional fine-structure, due to $J \leq 2$ Hz.
†An almost coalesced AB system.

Experimental

The gc–ms analyses were carried out on an HP 5992A instrument using a 2 m × 4 mm glass column packed with 3% OV-1™ on Chromosorb W (80–100 mesh), programmed from 220–250°C at 16°/min, and a He flow of ca. 20 mL/min; hplc separations were done on a Varian Vista instrument.

Other instrumental methods were as described previously (13). Sarracine was obtained from a sample of the hydrogen tartrate salt originally provided by Professor T. A. Geissman.

Isolation of the alkaloids

Blossoming *S. triangularis* plants, incuding the roots, were collected along side-stream banks to the East of Elbow Lake, Kananaskis Country. A voucher specimen of these plants is deposited in the Herbarium, Biology Department, University of Calgary. The air-dried plant material (1.05 kg) was macerated in two portions (Waring Blendor) in ethanol (96%, 4 L) and then filtered. This process was repeated (5×) until the filtrates were pale yellow in colour. The combined filtrates were then concentrated (t < 40°C) to ca. 300 mL, 0.5 M aqueous H_2SO_4 (600 mL) was added, and the mixture was then extracted with $CHCl_3$ (4 × 400 mL). The brownish aqueous phase was brought to ca. 1 M with concentrated H_2SO_4 and then stirred, at room temperature, for 3.5 h with zinc dust (10 g) in order to reduce any N-oxides to the free bases (2). The mixture was filtered, ice added, and then brought to pH ca. 9 (indicator paper) with concentrated NH_4OH. After extraction with $CHCl_3$ (5 × 150 mL), the aqueous phase was made strongly alkaline (pH ca. 14) with aqueous NaOH and reextracted with $CHCl_3$ (5 × 100 mL). Evaporation of these two sets of $CHCl_3$ extracts (dried over $MgSO_4$) gave 2.25 g and 0.45 g of brown oils, respectively. A tlc analysis ($CHCL_3$–MeOH, 4:1) revealed these oils to be similar in composition, showing four Dragendorff-positive components. They were therefore combined and partitioned between $CHCl_3$ (50 mL) and 1 M aqueous H_2SO_4 (20 mL). The aqueous phase was washed with more $CHCl_3$ (2 × 50 mL), and the combined $CHCl_3$ extracts were then backwashed with H_2O (20 mL). The aqueous acid phase and the H_2O-wash were then combined, basified with saturated aqueous K_2CO_3 while kept at ca. 0°C with ice, and extracted with $CHCl_3$ (4 × 50 mL). The combined $CHCl_3$ extracts were then dried ($MgSO_4$) and the solvent removed under reduced pressure to leave the alkaloids as a pale brown oil (2.21 g, 0.21% wt./dry wt. plant).

Thin-layer chromatographic analysis of the alkaloids, as before, revealed 4 components: R_f 0.32, 0.28, 0.13, 0.11. Under the same conditions senecionine had R_f 0.40.

A preliminary fractionation of the mixture was achieved by chromatography on silicic acid (200 g, first washed with $CHCl_3$–MeOH–NH_4OH 9:1:0.3 v/v until the eluate was basic to indicator paper, and then equilibrated with $CHCl_3$–MeOH 95:5 v/v). The alkaloid mixture (2.2 g) was applied to the column in $CHCl_3$–MeOH (95:5 v/v) and then eluted with $CHCl_3$–MeOH–NH_4OH (95:5:0), 500 mL; 90:9:1, 500 mL; 80:18:2, 500 mL; 3:2:1, 300 mL; and 0:10:1, 300 mL), fractions of ca. 50 mL being collected. Fractions 4–11 very largely contained the alkaloids of R_f 0.32 (C) and 0.28 (D), while fractions 12–27 were similarly enriched in the slow-moving pair (A and B). The recovery of alkaloids was ca. 80%.

The gc–ms of 4–11 revealed the following 4 components: A, R_T 2.2 min (ca. 5%), m/z: 237 (17), 219 (24), 218 (10), 193 (17), 154 (43), 138 (66), 137 (100), 136 (62), 126 (17), 124 (38), 117 (15), 111 (42), 108 (10), 107 (11), 106 (41), 94 (49), 93 (70), 83 (12), 81 (10), 80 (73), 55 (32), 53 (18), and 41 (16); B, R_T 2.4 min (ca. 3%), m/z: 237 (22), 219 (4), 193 (37), 155 (37), 154 (39), 138 (37), 137 (100), 136 (60), 126 (17), 124 (47), 117 (32), 111 (50), 106 (46), 94 (41), 93 (65), 83 (29), 80 (73), 55 (22), 53 (16), 43 (10), and 41 (15); C, R_T 9.0 min (ca. 45%), m/z: 335 (3), 237 (46), 236 (15), 221 (15), 220 (100), 219 (58), 136 (72), 121 (17), 120 (44), 119 (20), 94 (32), 93 (34), 83 (21), 80 (11), 55 (26), 53 (16), and 41 (16); and D, R_T 9.9 min (ca. 40%), m/z: 335 (3), 237 (35), 220 (54), 219 (23), 154 (12), 137 (12), 136 (100), 121 (17), 120 (38), 119 (27), 118 (11), 94 (33), 93 (38), 83 (38), 55 (15), 53 (14), and 41 (14).

Similar analysis of fractions 12–27 revealed components with the same R_T and ms as A (ca. 90%), and B (ca. 10%).

A portion (100 mg) of fractions 4–11 was then fractionated by hplc (Varian Micropak MCH-10-N-cap, 24 cm × 8 mm ϕ) using CH_3CN–MeOH 7:3 → 3:7 v/v as eluant, and monitoring the uv absorption of the eluant at 254 nm. By these means we were able to isolate samples of C (39 mg) and D (19 mg) that were homogeneous by tlc analysis (the balance of the alkaloids (32 mg) was recovered as an unresolved mixture). Similar fractionation of part (100 mg) of fractions 12–27 yielded alkaloid A (69 mg) and a mixture of A and B (ca. 30 mg).

Properties of the individual alkaloids (See Tables 1 and 2 for nmr data)

(i) *Alkaloid A (7-O-angelylretronecine)*, (**3**), mp 74°C; ir ($CHCl_3$) ν_{max}: 3400 (w), 3020 (w), 2980 (m), 2860 (m), 2830 (w), 1710 (s), 1640 (m), 1480 (w), 1450 (m), 1435 (m), 1385 (m), 1360 (m), 1260 (m), 1235 (s), 1215 (s), 1155 (s), 1130 (m), 1080 (m), 1045 (s), 1010 (m), 850 (m), and 820 (w) cm^{-1};

Can. J. Chem. Downloaded from www.nrcresearchpress.com by 210.87.254.6 on 09/06/12
For personal use only.

$[\alpha]_D^{25}$ + 43.6° (*c* 1, MeOH); cd: $[\theta]_{223}$ + 9.76 (MeOH). Picrate salt, mp 179–180°C. (*Anal.* calcd. for $C_{19}H_{22}N_4O_{10}$: C 48.93, H 4.76, N 12.01; found: C 49.09, H 4.87, N 11.90. Hydrochloride salt, mp 134–136°C (lit. (2) mp 76–77°C); $[\alpha]_D$ +49° (*c* 1.38, EtOH); cd: $[\theta]_{223}$ + 7.9 (MeOH) (6). *Anal.* calcd. for $C_{13}H_{20}ClNO_3$: C 57.03, H 7.36, N 5.12; found: C 56.59, H 7.30, N 4.87. Picrate salt, mp 179–180°C (14).

(ii) *Alkaloid C (7-O-angelyl-9-O-sarracinylretronecine)*, (**5**) was obtained as a colourless gum; ir ν_{max} ($CHCl_3$): 3400 (m br), 3020 (w), 2990 (s), 2880 (m), 2860 (m), 2830 (m), 1715 (s), 1700 (sh), 1645 (m), 1455 (m), 1440 (m), 1375 (m), 1360 (m), 1255 (sh), 1235 (s), 1215 (sh), 1155 (s), 1085 (m), 1040 (m), 1010 (m), 855 (m), and 830 (w) cm^{-1}; $[\alpha]_D^{25}$ +6.1° (*c* 1.7, MeOH); cd: $[\theta]_{221}$ + 5.68 (MeOH). Picrate salt, mp 139–140°C *Anal.* calcd. for $C_{24}H_{28}N_4O_{12}$:C 51.07, H 5.00, N 9.93; found: C. 50.99, H 5.16, N 9.64.

(iii) *Alkaloid D (7-O-senecioyl-9-O-sarracinylretronecine)*, (**6**), was also obtained as a colourless gum; ir ν_{max} ($CHCl_3$): 3400 (m), 3010 (w), 2990 (s), 2860 (s), 2830 (s), 1715 (s), 1700) (sh), 1455 (m), 1440 (m), 1370 (m), 1210–1230 (s), 1145 (s), 1080 (m), 1010 (m), and 8150 (w) cm^{-1}; $[\alpha]_D^{25}$ +11° (*c* 1.0, MeOH); cd: $[\theta]_{217}$ +5.72 (MeOH). Salt with (+)-tartaric acid, mp 112–113°C. *Anal.* calcd. for $C_{22}H_{31}NO_{11}\cdot 1H_2O$: C 52.48, H 6.61, N 2.79; found: C 52.45, H 6.24, N 2.61.

The controlled saponification of alkaloids C and D

A mixture of alklaoids C and D (11 mg, 33 μmol) was dissolved in aqueous 1,4-dioxane (1:1 v/v, 0.6 mL) containing K_2CO_3 (4.5 mg, 33 μmol). After this reaction mixture had been kept at 20°C for 30 min, gc–ms analysis showed no significant saponification had occurred. The mixture was therefore warmed, first to 50°C for 30 min, and then to 70°C, at which temperature it was held for a further 2.5 h Both gc–ms and tlc revealed that saponification was already appreciable after the 30 min at 50°C, and that it increased further at 70°C. At the end of the experiment similar analyses showed that small amounts of C and D remained, and some retronecine was also detected, but the major products were alkaloids A and B, present in about the same ratio (ca. 5:4) as that of C/D in the starting material.

Acknowledgements

Financial assistance from the Natural Sciences and Engineering Research Council of Canada (grant-in-aid to M.H.B.) and the Alberta Heritage Foundation for Medical Research (scholarship to H.R.) is acknowledged with gratitude. We thank Ms. N. Duke for assistance with the plant collection, and Drs. R. Yamdagni and W.-S Lin for help with instrumental analyses. This paper is dedicated to the memory of the late Professor Ted Geissman, from whom one of us (M.H.B.) learned much during a post-doctoral year (1960–61).

1. M. SHEMLUCK. J. Ethnopharmacol. **5**, 303 (1982).
2. L. B. BULL, C. C. J. CULVENOR, and A. T. DICK. The pyrrolizidine alkaloids. North-Holland Publishing Co., Amsterdam. 1968.
3. C. C. J. CULVENOR and W. G. WOODS. Aust. J. Chem. **18**, 1625 (1965).
4. H. BROUWER and J. B. STOTHERS. Can. J. Chem. **50**, 601 (1972).
5. U. E. MATTER, C. PASCUAL, E. PRETSCH, A. PROSS, W. SIMON, and S. STERNHELL.. Tetrahedron, **25**, 691 (1969).
6. C. C. J. CULVENOR, D. H. G. CROUT, W. KLYNE, W. P. MOSE, J. D. RENWICK, and P. M. SCOPES. J. Chem. Soc (C) 3653 (1971).
7. A. J. JONES, C. C. J. CULVENOR, and L. W. SMITH. Aust. J. Chem. **35**, 1173 (1982).
8. N. V. MODY. R. S. SAWHNEY, and S. W. PELLETIER. J. Nat. Prod. **42**, 417 (1979).
9. L. H. ZALKOW, S. BONETTI, L. GELBAUM, M. M. GORDON, B. B. PATIL, A. SHANI, and D. VAN DERVER. J. Nat. Prod. **42**, 603 (1979).
10. D. J. ROBINS. Fortschr. Chem. Org. Naturst. **41**, 115 (1982).
11. G. R. WALLER and E. K. NOWACKI. Alkaloid biology and metabolism in plants. Plenum Press, New York. 1978. p. 48 *et seq*.
12. G. W. WOGAN and W. F. BUSHBY JR. *In* Toxic constituents of plant foodstuffs. 2nd. ed. *Edited by* E. Leiner. Academic Press, New York. 1980. p. 329, and references therein.
13. H. RÜEGER and M. H. BENN. Can. J. Chem. **60**, 2918 (1982).
14. H. C. CROWLEY and C. C. J. CULVENOR. Aust. J. Chem. **15**, 139 (1962).

Can. J. Chem. Downloaded from www.nrcresearchpress.com by 210.87.254.6 on 09/06/12
For personal use only.

Synthesis of (±)-trixagol by an electrophilic cyclization of an allylsilane

ROSEMARY J. ARMSTRONG AND LARRY WEILER[1]

Department of Chemistry, University of British Columbia, Vancouver, B.C., Canada V6T 1Y6

Received April 18, 1983

ROSEMARY J. ARMSTRONG and LARRY WEILER. Can. J. Chem. **61**, 2530 (1983).

1,5-Dienes containing an allylsilane are cyclized by Lewis acids to methylenecyclohexanes. The trimethylsilyl group exerts a strong activating and directing influence on the regioselectivity of this cyclization. The monocyclic compound **10** was converted into the diterpene, (±)-trixagol (**3**).

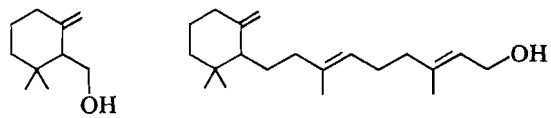

10 **3**

ROSEMARY J. ARMSTRONG et LARRY WEILER. Can. J. Chem. **61**, 2530 (1983).

Les acides de Lewis permettent de cycliser les diènes-1,5 contenant un silane allylique en méthylènecyclohexanes. Le groupe triméthylsilyle agit fortement et influence la régiosélectivité de cette cyclisation. On transforme le composé monocyclique **10** en diterpène, le (±)-trixagol (**3**).

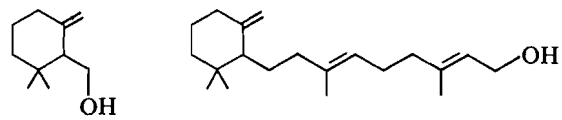

10 **3**

[Traduit par le journal]

In 1955 Stork and Burgstahler (1) and Eschenmoser *et al.* (2) independently proposed the hypothesis that many isoprenoid natural products are biosynthesized via a polyolefinic electrophilic cyclization. Since then this concept has been applied in many natural product syntheses, and has been expanded to include a variety of initiating and terminating groups which yield specific functionalities in the cyclized product. In 1976 Fleming *et al.* (3) showed that the trimethylsilyl moiety in **1** controlled the cyclization (eq. [1]) to regioselectively yield the exocyclic olefin **2**. The allyl silane has been used as an effective terminating unit in electrophilic cyclizations by a number of groups since that time (4). We recently demonstrated the use of allylsilanes in polyolefinic cyclizations of esters and acids (5) and here we report a synthesis of (±)-trixagol (**3**) using an electrophilic cyclization of a polyolefin allylsilane.

[1] 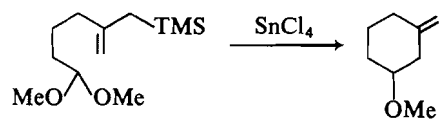

1 **2**

Recently de Pascual Teresa *et al.* isolated a hydroxylated diterpene from the hemiparasite plant *Bellardia trixago* (6). The diterpene was named trixagol and was shown to have the structure **3**, which contains a cyclohexane moiety with an exocyclic methylene and an olefinic side chain. We envisioned a synthesis of **3** via a convergent route which involved joining the two appropriately functionalized subunits A and B.

The sulphone **14** served as the synthetic equivalent of subunit A and a synthesis of **14** is shown in Scheme 1. The dianion of

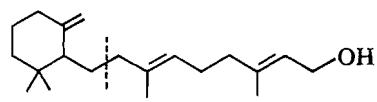

A B

3

methyl acetoacetate (**4**) was alkylated (7) with γ,γ-dimethylallyl bromide to give the β-keto ester **5**, which was then converted to the *Z*-enol phosphate **6** in 82% yield from methyl acetoacetate (7*b*). The enol phosphate was coupled with trimethylsilylmethylmagnesium chloride in the presence of nickel(II) bisacetylacetonate (5, 8) to give the *Z*-allylsilane **7** in 75% yield. No *E*-isomer was detected in either the enol phosphate **6** or the allylsilane **7**. Cyclization of **7** was performed with a series of reagents under a number of different reaction conditions, and the results of this study are shown in Table 1. The ratio of the regioisomers **8**/**9** was determined by 80 MHz ^{1}H nmr. The olefinic protons of **8** resonate at δ 4.75 and 4.86 whereas the olefinic proton of **9** resonates at δ 5.70. First it can be seen that cyclization is only achieved in the presence of a Lewis acid (runs 1–3). Either stannic chloride or boron trifluoride etherate will effect cyclization, but in the latter case at least one equivalent of acetic acid must be used in order to obtain **8** and **9** uncontaminated with by-products (runs 4–6). Interestingly, the presence of acetic acid reduces the amount of exocyclic isomer obtained when stannic chloride is used (runs 7–9). In fact, the *endo* isomer was the sole product obtained (70% yield) with the reaction conditions listed in run 9. The effect of solvent was examined with both boron trifluoride etherate/ acetic acid (runs 6 and 10) and with stannic chloride (runs 7, 11, and 12). There was no change in isomer ratio with either methylene chloride or toluene, but when the solvent was changed to methylene chloride which had been saturated with

[1]Author to whom correspondence may be addressed.

Can. J. Chem. Downloaded from www.nrcresearchpress.com by 210.87.254.6 on 09/06/12
For personal use only.

Can. J. Chem. Downloaded from www.nrcresearchpress.com by 210.87.254.6 on 09/06/12
For personal use only.

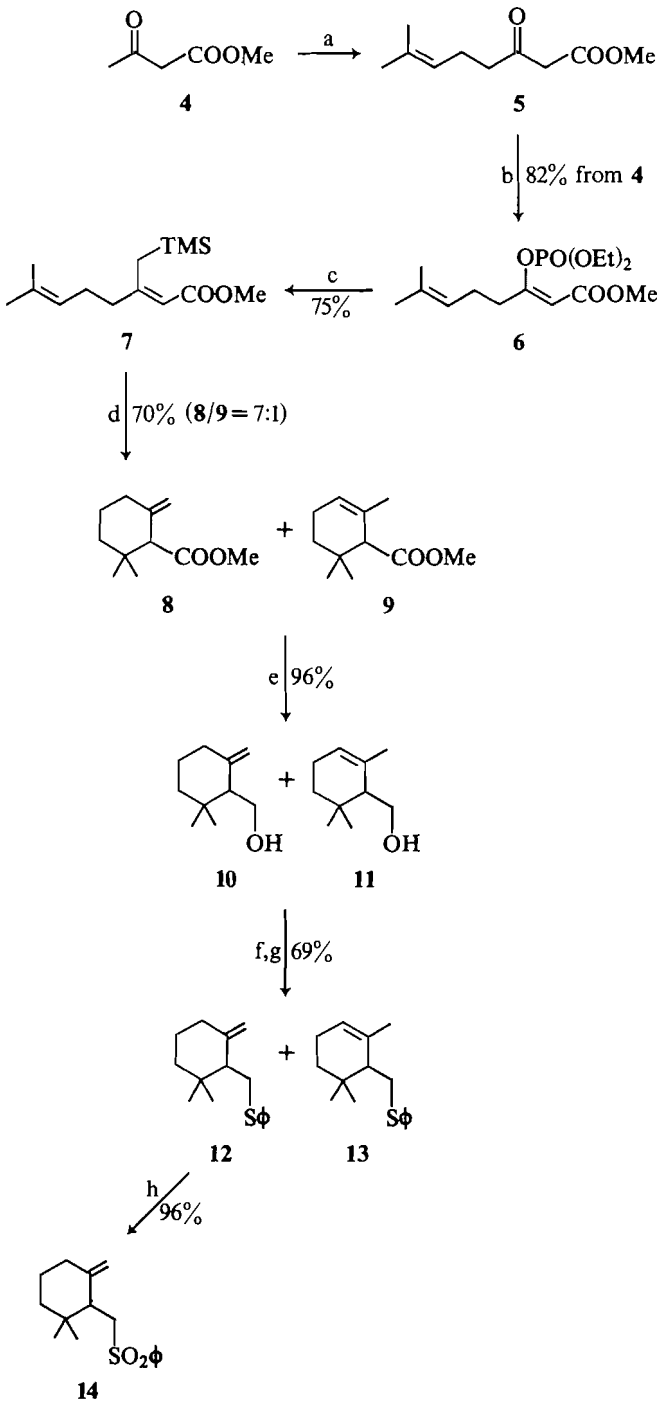

(a) NaH, *n*-BuLi, Me_2CCHCH_2Br; (b) NaH, $ClPO(OEt)_2$; (c) Me_3SiCH_2MgCl, $Ni(acac)_2$; (d) $SnCl_4$; (e) $LiAlH_4$; (f) *p*TsCl, py; (g) ϕSH, KH; (h) MCPBA

SCHEME 1. Synthesis of sulphone **14**

water (run 12) a significant improvement in the ratio of **8**/**9** was observed. Finally a study was performed on the quantity of Lewis acid, the temperature, and the reaction time. At low temperature (run 13) a mixture of endocyclic product, exocyclic product, and also an acyclic chloride **17** was obtained; the yield of the latter was 15%. A similar ratio of **8**/**9** could be obtained by treatment of the allylsilane in wet methylene chloride at 0°C for 2 hours, or at room temperature for 1 hour (runs 14, 15). Higher reaction temperatures gave increasing amounts of the endocyclic isomer and polymeric material. The reaction time could be shortened to 30 min by increasing the amount of stannic chloride (run 16), but the optimum reaction conditions were found to be 5 equivalents of stannic chloride in wet methylene chloride at 0°C for 1 hour (run 12, **8**/**9** = 7:1, 70% yield). It should be noted that the reaction must be performed under dilute conditions (0.08 *M*) in order to obtain this regioselectivity. In addition, it was found that the reaction gave a poorer regioselectivity when it was scaled up to more than 10 mmol of allylsilane. The crude yield of the cyclization step invariably was nearly quantitative.

It is interesting to speculate on the mechanism of the cyclization, but at this stage we merely note that at least one equivalent of Lewis acid is necessary to achieve conversion (run 17). The efficiency of the reaction in the presence of a proton source such as water or acetic acid suggests that the cyclization is initiated by a proton attack on the terminal olefin of **7** (eq. [2]) to give **8** which is subsequently isomerized to **9**.

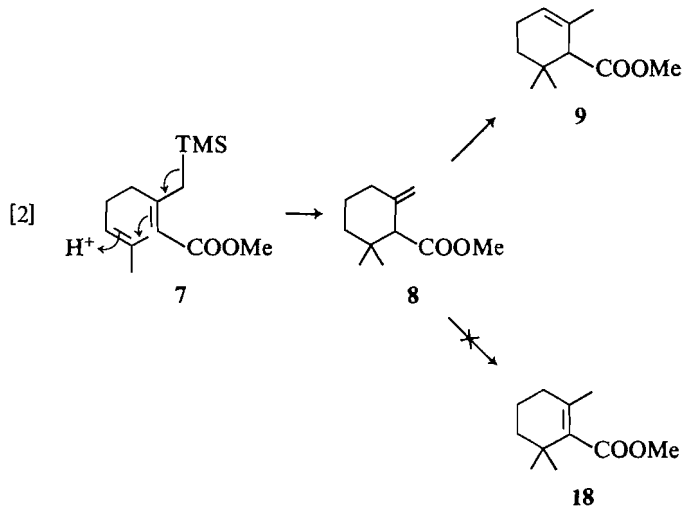

No α,β-unsaturated ester **18** was observed in any cyclization, presumably because of the severe steric hindrance encountered around the tetrasubstituted olefin. The ability of the trimethylsilyl group to control the regioselectivity of the olefin is seen very clearly when one compares the cyclization of **7** with that of methyl geranate (**19**) (eq. [3]). Kurbanov *et al.* (9) were able to cyclize **19** with either sulphuric acid or fluorosulphonic acid, both very strong protonic acid sources. In each case the endocyclic isomer **9** was the major product obtained, presumably via the carbocyclic carbonium ion **20**.

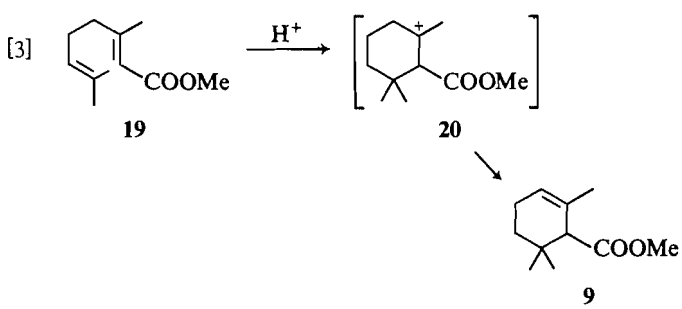

We were unsuccessful in isomerizing the endocyclic isomer **9** to the exocyclic olefin. The mixture of esters **8** and **9** was converted without separation into the alcohols **10** and **11**, and then to the corresponding tosylates in near quantitative yield

TABLE 1. Cyclization of allylsilyl ester **7**

Run	Acid (equiv.)		Solvent	Temperature (°C)	Time (h)	**8/9/7**[a]	Other products
1	Camphorsulphonic acid (1)		CH_2Cl_2	25	72	0:0:1	
2	Trifluoroacetic acid (1)		CH_2Cl_2	25	24	0:0:0	**15**[c]
3	AcOH (5)		CH_2Cl_2	25	3	0:0:1	
4	$BF_3 \cdot Et_2O$ (10)		Toluene	25	24	0:0:1	
5	$BF_3 \cdot Et_2O$ (5)	AcOH (trace)	CH_2Cl_2	25	3	1:1:1	**16**[d] (10%)
6	$BF_3 \cdot Et_2O$ (4)	AcOH (2)	CH_2Cl_2	0	48	3:1:0	
7	$SnCl_4$ (2)		CH_2Cl_2	25	8	2:1:0	
8	$SnCl_4$ (5)	AcOH (trace)	CH_2Cl_2	25	2	1.5:1:0	
9	$SnCl_4$ (5)	AcOH (1)	CH_2Cl_2	25	1	0:1:0	
10	$BF_3 \cdot Et_2O$ (4)	AcOH (2)	Toluene	0	60	3:1:0	
11	$SnCl_4$ (1)		Toluene	0–25	24	2:1:0	
12	$SnCl_4$ (5)		CH_2Cl_2[b]	0	1	7:1:0	
13	$SnCl_4$ (5)		CH_2Cl_2[b]	−23	2	4:1:0	**17**[e] (15%)
14	$SnCl_4$ (1)		CH_2Cl_2[b]	0	2	3:1:0	
15	$SnCl_4$ (1)		CH_2Cl_2[b]	25	1	3:1:0	
16	$SnCl_4$ (10)		CH_2Cl_2[b]	0	0.5	5:1:0	
17	$SnCl_4$ (0.05)		CH_2Cl_2[b]	25	4	0:0:1	

[a]Ratios were determined by ^1H nmr.
[b]Methylene chloride saturated with water.

[c] **15** =

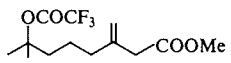

15

[d] **16** =

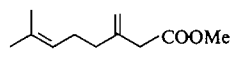

16

[e] **17** =

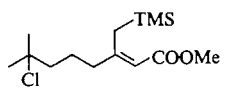

17

using standard procedures. At this point it is pertinent to mention the severe steric hindrance of the hydroxymethyl group in the exocyclic isomer **10**. All attempts to convert the alcohol to a halide were unsuccessful, and this is undoubtedly due to the severe steric crowding around the hydroxymethyl in **10** flanked by the quaternary carbon and the exocyclic double bond (A (1, 3) strain (ref. 10)). Consistent with this analysis was the observation that conversion of the cyclohexenyl alcohol **11** to the tosylate could be performed in 24 h, whereas the alcohol in **10** required 72 h for complete conversion to the tosylate. The sulphides **12** and **13** were obtained in 74% yield from their respective tosylates using the highly nucleophilic thiophenolate anion (11) in ethanol under reflux for 16 h. Sulphides **12** and **13** were separated by flash chromatography (12). Sulphone **14** was readily obtained from **12** in 96% yield via oxidation using *m*-chloroperoxybenzoic acid.

A second approach to subunit A was studied using the carbocyclic acid **24** as shown in Scheme 2. Diketene (**21**) was treated with trimethylsilylmethylmagnesium chloride via the method of Itoh and co-workers (13, 14) but with some modifications. Alkenoic acid **22** was then alkylated in the γ-position (13, 15) with γ,γ-dimethylallyl bromide to give the silyl acid **23** in 70% yield. No α-alkylation was observed. Although this alkylation is regioselective, it is not stereoselective, and a mixture of *E* and *Z* isomers of **23** was obtained (*E*/*Z* = 7:3). A variety of reaction conditions and reagents were studied in the cyclization of the silyl acid **23**, and these results are shown in Table 2. Similarly to the ester cyclizations, the ratio of the regioisomers **24**/**25** was determined by integration of the resonances due to the olefinic protons in the ^1H nmr (**24**, δ 4.85, δ 4.91; and **25**, δ 5.65). It was found that titanium tetrachloride gave a very poor isomer ratio regardless of the temperature employed (runs 1 and 2). However, both stannic chloride and boron trifluoride etherate gave similar product ratios. The addition of acetic acid with boron trifluoride etherate had no effect on the ratio of **24**/**25**, but the yield of the reaction was improved (runs 3–5). Toluene was found to be the solvent of choice over both methylene chloride and benzene when using boron trifluoride etherate as the Lewis acid. However, when stannic chloride was employed the cyclization seemed to be solvent independent (runs 3, and 6–9). The optimum temperature with stannic chloride appeared to be quite low (−50°C), but higher temperatures were required for cyclization to proceed when using boron trifluoride etherate/acetic acid (runs 5, 10, and 11). However, increasing the temperature above ambient temperature did not improve the isomer ratio. Run 12 shows that a very poor ratio of **24**/**25** was obtained with wet methylene chloride under the conditions found to be the best for the

Can. J. Chem. Downloaded from www.nrcresearchpress.com by 210.87.254.6 on 09/06/12
For personal use only.

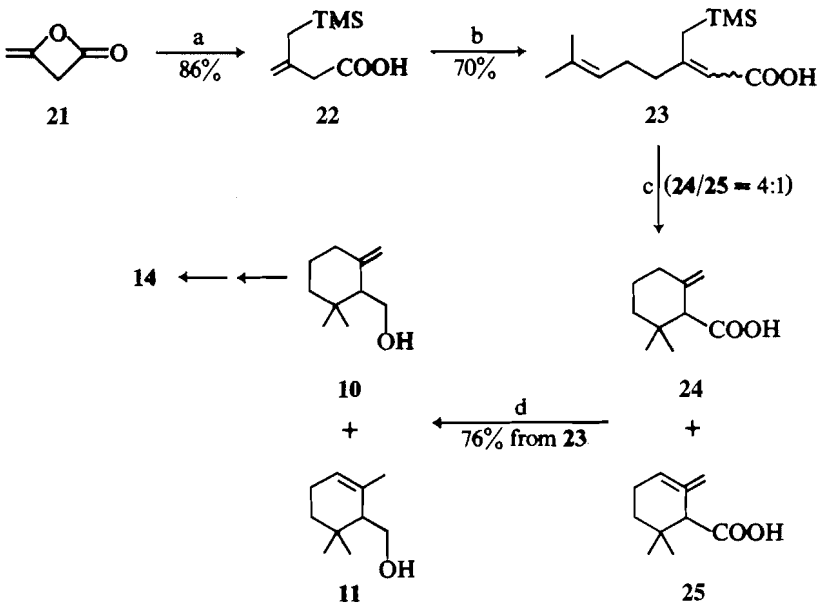

(a) Me_3SiCH_2MgCl, $NiCl_2 \cdot 6H_2O$; (b) LDA (2 equiv.), CuI, Me_2CCHCH_2Br; (c) $BF_3 \cdot Et_2O$, AcOH; (d) $LiAlH_4$

SCHEME 2. Synthesis of cyclohexylcarboxylic acid **24**

TABLE 2. Cyclization of allylsilyl acid **23**

Run	Acid (equiv.)		Solvent	Temperature (°C)	Time (h)	24/25/23[a,b]
1	$TiCl_4$ (1)		CH_2Cl_2	0	4	1:8:0
2	$TiCl_4$ (1)		CH_2Cl_2	−50	14	0:1:6[c]
3	$SnCl_4$ (1)		CH_2Cl_2	−50	15	3:1:0
4	$BF_3 \cdot Et_2O$ (10)		Toluene	0–25	1.5	4:1:0[d]
5	$BF_3 \cdot Et_2O$ (5)	AcOH (1)	Toluene	0–25	2.5	4:1:0[e]
6	$SnCl_4$ (1)		Toluene	−50	24	3:1:0
7	$BF_3 \cdot Et_2O$ (2)	AcOH (2)	CH_2Cl_2	0	4	1.5:1:0
8	$BF_3 \cdot Et_2O$ (10)	AcOH (5)	Benzene	5	48	1.5:1:0
9	$BF_3 \cdot Et_2O$ (10)	AcOH (5)	Toluene	5	48	3:1:0
10	$BF_3 \cdot Et_2O$ (10)	AcOH (5)	Toluene	−23	8	0:0:1
11	$BF_3 \cdot Et_2O$ (8)	AcOH (4)	Toluene	−7	12	3:1:0
12	$SnCl_4$ (5)		CH_2Cl_2[f]	25	2	1:4:0

[a] Ratios were determined by ^1H nmr.
[b] Crude yields of all runs were nearly quantitative.
[c] Some acyclic product with no trimethylsilyl residue was also obtained.
[d] 40% purified yield of **24** and **25**.
[e] 76% purified yield of **24** and **25** after conversion to alcohols **10** and **11**.
[f] Methylene chloride saturated with water.

cyclization of the silyl ester **7**.

The optimum cyclization conditions for the silyl acid **23** are those shown in run 5 (**24**/**25** = 4:1) and, after reduction to the alcohols **10** and **11**, the yield for the two steps was 76%, or 61% for the conversion of **23** into pure exocyclic alcohol **10**. However, the cyclization of ester **7** was the preferred route because of the higher ratio of the exocyclic to endocyclic products.

The protected hydroxy bromide **30** is the synthetic equivalent of unit B, and a synthesis of **30** is shown in Scheme 3. Geraniol (**26**) was protected as its benzoate ester **27** in quantitative yield. Oxidation of **27** was performed with selenium dioxide and 70% *tert*-butyl hydroperoxide using a modification (*7b*) of the method of Umbreit and Sharpless (16). The desired alcohol **28** was isolated in 50% yield, in additon to recovered starting material **27** (40%) and aldehyde **29** (5%). It was found that if the reaction temperature was allowed to warm above 10°C a higher proportion of the undesired aldehyde was obtained. Conversion of alcohol **28** to the bromide **30** was performed in 97% yield using phosphorus tribromide and pyridine.

With subunits A and B in hand, the synthesis of trixagol was effected as shown in Scheme 4. Sulphone **14** was deprotonated, using *n*-butyllithium, and coupled to bromide **30** in the presence of hexamethylphosphoramide to give a mixture of diastereomers **31** in a nine-to-one ratio (as determined by ^1H nmr). The alcohol was deprotected by removal of the benzoate ester using diisobutylaluminium hydride to give hydroxy sulphone **32** in 64% yield from the coupling reaction. Unreacted

Can. J. Chem. Downloaded from www.nrcresearchpress.com by 210.87.254.6 on 09/06/12
For personal use only.

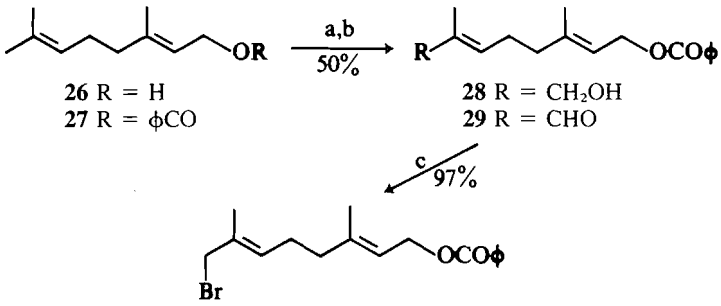

30

(a) φCOCl, py, DMAP; (b) SeO_2, 70% *t*-BuOOH; (c) PBr_3, py

SCHEME 3. Synthesis of bromobenzoate **30**

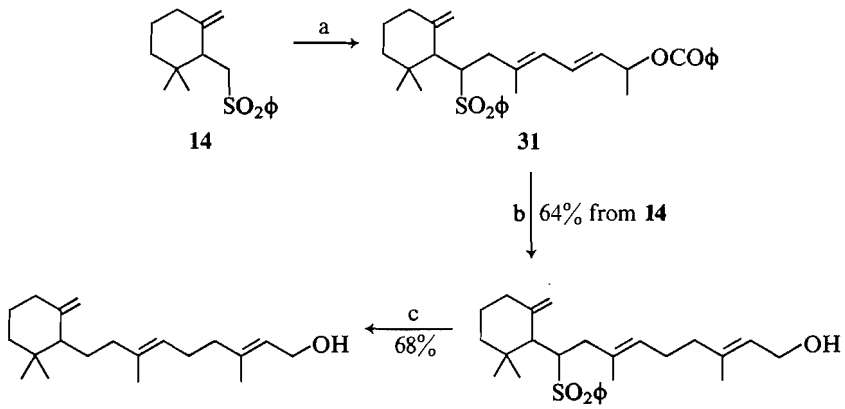

(a) *n*-BuLi, THF–HMPA, **30**; (b) DIBAL; (c) 6% Na–Hg, Na_2HPO_4

SCHEME 4. Synthesis of (±)-trixagol

sulphone **14** (36%) was also recovered during purification. We had attempted several other methods without success to form the C—C bond between subunits A and B. The hydroxymethyl group in **10** and related derivatives is severely hindered towards nucleophilic substitution. We were unable to add any carbon nucleophiles to this centre. There are three possible conformations for such a nucleophilic substitution, *X*, *Y*, and *Z*.

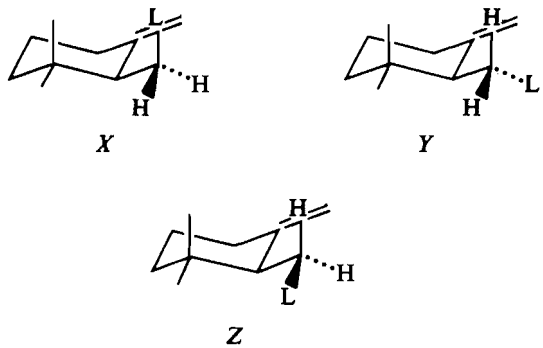

The conformation *X* has a serious 1,3-interaction between a methyl and the leaving group L, making this conformation rather inaccessible. In conformations *Y* and *Z* the backside of the C—L bond is effectively blocked by the *gem* dimethyl group or the exocyclic methylene, respectively. Kocienski (17*a*) has reported similar problems and in his synthesis of diumycinol (**34**) the next higher homologue of **10**, namely the alcohol **33**, was used to overcome the problems associated with the lack of reactivity in **10** and its derivatives (17*b*).

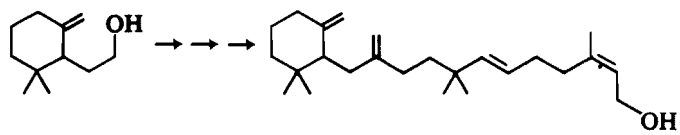

33 34

The final step in our synthesis was achieved by hydrogenolysis of the sulphone moiety with 6% sodium amalgam in a method analogous to that of Trost *et al.* (18). Once again some difficulties were encountered in this reaction due to the steric hindrance of functionalities attached to the carbon α to the ring. Trost *et al.* achieved cleavage of model sulphones with temperatures from −20°C to room temperature, and reaction times ranging from 7 min to 1 hour. However it was necessary to heat sulphone **32** in boiling ethanol for 16 h before cleavage could be effected (68% yield). The ir, ^1H nmr, and gas chromatographic data of the synthetic racemic trixagol were identical with that of the natural compound (6).

From these results and others (3–5) it is clear that the trimethylsilyl group is exceedingly effective in activating an alkene in an electrophilic cyclization and in controlling the regiochemistry of the resulting alkene. This methodology is particularly useful in generating exocyclic alkenes which are

Can. J. Chem. Downloaded from www.nrcresearchpress.com by 210.87.254.6 on 09/06/12
For personal use only.

isomerized to the endocyclic isomers under more vigorous conditions.

Experimental

General

Unless otherwise stated the following are implied.

Melting points (mp) were determined on a Kofler micro heating stage and are uncorrected. Kugelrohr distillations were performed by means of a Büchi Kugelrohr thermostat. The 80 MHz nuclear magnetic resonance spectra were recorded on a Bruker WP 80. Chemical shifts in ppm are reported using the δ scale with tetramethylsilane (TMS) as internal reference. Signal multiplicity, coupling constants, and integrated areas are indicated in parentheses. Infrared spectra were recorded on a Perkin–Elmer model 710B spectrophotometer. Solution spectra were performed using a sodium chloride solution cell of 0.2 mm thickness. Absorption positions are given in cm^{-1} and are calibrated by means of the 1601 cm^{-1} band of polystyrene. Low resolution mass spectra were determined on either a Varian MAT model CH4B or a Kratos-AEI model MS50 mass spectrometer. Spectra are quoted as *m/e* values. The major ion fragmentations are reported as percentages of the base peak. High resolution mass measurements were determined using a Kratos-AEI model MS50 mass spectrometer. Gas–liquid chromatography was performed on a Hewlett–Packard Model 5830A gas chromatograph using a 6 ft × 1/8 in. column of 10% Carbowax C-20M and nitrogen as the carrier gas. The flow rate was 30 mL/min. Microanalyses were performed by Mr. P. Borda, Microanalytical Laboratory, University of British Columbia, Vancouver.

Silica gel $PF_{254+366}$ supplied by E. Merck Co. was used for preparative thin layer chromatography (tlc). The plates were approximately 1 mm in thickness and were visualized under long and short wavelength ultraviolet radiation, iodine vapour staining and/or 3 *M* sulphuric acid spray, then heating. Flash chromatography (12) was performed using silica gel 60, 230–400 mesh ASTM, supplied by E. Merck Co.

The petroleum ether used was of boiling range ca. 30–60°C. Dry ethyl ether (ether) and tetrahydrofuran (THF) were obtained by distillation from lithium aluminium hydride. Methylene chloride (CH_2Cl_2) was dried by distilling from phosphorus pentoxide. Wet methylene chloride was obtained by shaking with water and using the saturated methylene chloride layer. Anhydrous hexamethylphosphoramide (HMPA), pyridine (py), toluene, and diisopropylamine were obtained by distillation from calcium hydride. Ethanol was dried by distillation from magnesium ethoxide. Sodium hydride was weighed as a 50% or 60% dispersion in mineral oil and was washed with dry ether to remove the oil prior to use.

Diisobutylaluminium hydride (in hexane) (DIBAL) and *n*-butyllithium (in hexane) were obtained from Aldrich Chemical Company, Inc. The alkyllithium solution was standardized by titration against 1.0 *M* *tert*-butanol in benzene using 1,10-phenanthroline as indicator.

All reactions involving air or moisture sensitive reagents were performed under an atmosphere of dry nitrogen using either oven or flame-dried glassware.

Methyl 7-methyl-3-oxo-6-octenoate (5)

This compound was prepared using a method analogous to that of Sum and Weiler (7).

Methyl Z-3-(diethylphosphoryloxy)-7-methyl-2,6-octadienoate (6)

To a stirred suspension of 10.6 g (0.22 mol) of sodium hydride (50% in oil) in ether at 0°C was slowly added 39.5 g of the crude β-keto ester **5** as a solution in ether. After 10 min at 0°C, 31.7 mL (0.22 mol) of diethyl chorophosphate was quickly added and the reaction mixture was stirred for 2 h while allowing it to warm to room temperature. The reaction was quenched with 1 *M* HCl and diluted with ether. The ethereal layer was washed twice with saturated $NaHCO_3$, twice with saturated NaCl, dried ($MgSO_4$), and concentrated. The orange oil was then distilled (bp 144–148°C/0.25 Torr) to give 52.7 g (82% from methyl acetoacetate) of enol phosphate **6** as a yellow oil. Preparative tlc of a small amount of this material using petroleum ether – ethyl acetate (2:1) gave **6** as a colourless liquid; ir ($CHCl_3$): 1730, 1670, 1280, and 1030 cm^{-1}; ^1H nmr ($CDCl_3$) δ: 1.35 (dt, $J_{CH_2CH_3}$ = 7 Hz, $J_{POCH_2CH_3}$ = 1 Hz, 6H), 1.60 (s, 3H), 1.70 (s, 3H), 2.15–2.60 (m, 4H), 3.68 (s, 3H), 4.30 (dq, $J_{CH_2CH_3}$ = 7 Hz, J_{POCH_2} = 8 Hz, 4H), 5.00–5.20 (m, 1H), and 5.35 (s, 1H); mass spectrum, *m/e*: 320(18), 289(11), 252(23), 220(31), 192(23), 176(17), 174(19), 155(100), 150(10), 135(18), 134(63), 127(41), 119(13), 107(26), 106(28), 105(15), 98(57), 91(25), 81(18), 79(12), and 69(31). *Anal.* calcd. for $C_{14}H_{25}O_6P$: C 52.50, H 7.87; found: C 52.49, H 7.92.

Methyl Z-3-(trimethylsilylmethyl)-7-methyl-2,6-octadienoate (7)

The Grignard reagent was prepared from 1.82 g (0.075 mol) of magnesium turnings and 11.8 mL (0.085 mol) of trimethylsilylmethyl chloride in ether at room temperature, and to this stirred solution was added 0.32–0.64 g (2.5–5.0 mmol) of anhydrous nickel(II) bis-acetylacetonate (8). The dark-brown mixture which resulted was stirred for 5 min at room temperature and a solution of 16.0 g (0.050 mol) of enol phosphate **6** in ether was slowly added (exothermic reaction). The reaction mixture was heated to reflux for 16 h and further portions of 0.32–0.64 g (2.5–5.0 mmol) of nickel(II) bis-acetylacetonate were added after ½ h, 1½ h, 2½ h, and 4 h. The reaction mixture was cooled to room temperature, quenched by the careful addition of 1 *M* HCl (until acidic to litmus paper), and diluted with ether. The organic layer was washed once with saturated $NaHCO_3$, twice with saturated NaCl, dried ($MgSO_4$), and concentrated to give 12.7 g of crude product. Purification by flash chromatography using petroleum ether – ethyl acetate (40:1) as eluant gave 9.5 g (75%) of **7** as a yellow oil. Preparative tlc of a small amount of this material using petroleum ether – ethyl acetate (20:1) gave **7** as a colourless liquid; bp (Kugelrohr distillation) 90°C/0.1 Torr; ir ($CHCl_3$): 1705, 1620, 1435, 1250, 1155, and 850 cm^{-1}; ^1H nmr ($CDCl_3$) δ: 0.05 (s, 9H), 1.60 (s, 3H), 1.70 (s, 3H), 2.05–2.20 (m, 4H), 2.43 (s, 2H), 3.65 (s, 3H), 4.95–5.25 (m, 1H), and 5.55 (s, 1H); mass spectrum, *m/e*: 255(4), 254(18), 239(32), 223(13), 186(19), 150(30), 135(22), 107(63), 89(28), 82(60), 80(20), 73(100), 69(33), and 59(22). *Anal.* calcd. for $C_{14}H_{26}O_2Si$: C 66.07, H 10.32; found: C 65.89, H 10.24.

Methyl 2,2-dimethyl-6-methylenecyclohexanecarboxylate (8)

To a solution of 2.54 g (0.010 mol) of the trimethylsilyl ester **7** in 110 mL of CH_2Cl_2 saturated with water at 0°C was slowly added a solution of 5.85 mL (0.050 mol) of $SnCl_4$ in 15 mL of wet CH_2Cl_2. The reaction mixture was stirred for 1 h at 0°C, then quenched with an aqueous solution of KF at 0°C. The organic layer was diluted with ether, washed four times with aqueous KF, twice with saturated $NaHCO_3$, once with saturated NaCl, dried ($MgSO_4$), and the solvent removed to give 2.0 g of a mixture of **8** and the *endo* isomer **9** (**8**/**9** = 7:1, as determined by ^1H nmr and gc (*T* = 100°C)). Purification by flash chromatography using petroleum ether – ethyl acetate (40:1) as eluant gave 1.27 g (70%) of **8** and **9** (7:1), and this mixture was used without further purification in the preparation of alcohol **10**. Preparative tlc of a small amount of this material using petroleum ether – ethyl acetate (10:1) gave **8** as a colourless liquid; bp 130°C/760 Torr; ir ($CHCl_3$): 1730, 1645, and 1155 cm^{-1}; ^1H nmr ($CDCl_3$) δ: 0.95 (s, 3H), 1.02 (s, 3H), 1.10–2.55 (m, 6H), 2.90 (s, 1H), 3.67 (s, 3H), 4.75 (bs, 1H), and 4.86 (bs, 1H); mass spectrum, *m/e*: 182(46), 167(29), 125(31), 123(65), 122(77), 114(42), 107(41), 83(22), 82(31), 81(31), 79(20), 59(100), and 57(21). *Anal.* calcd. for $C_{11}H_{18}O_2$: C 72.49, H 9.95; found: C 72.36, H 10.05. The *endo* isomer **9** was prepared as shown below.

Methyl 2,6,6-trimethylcyclohex-2-enecarboxylate (9)

To a solution of 2.54 g (0.010 mol) of the trimethylsilyl ester **7** in 110 mL of CH_2Cl_2 saturated with water was added a solution of 0.58 mL (0.010 mol) of acetic acid at room temperature. A solution of 5.85 mL (0.050 mol) of $SnCl_4$ in 20 mL of wet CH_2Cl_2 was added slowly, and the reaction mixture was stirred at room temperature for 2 h. The solution was quenched with an aqueous solution of KF, diluted with ether, and the organic layer washed four times with aqueous KF and

Can. J. Chem. Downloaded from www.nrcresearchpress.com by 210.87.254.6 on 09/06/12
For personal use only.

Can. J. Chem. Downloaded from www.nrcresearchpress.com by 210.87.254.6 on 09/06/12
For personal use only.

once with saturated NaCl. The solution was dried ($MgSO_4$) and the solvent removed to give 1.64 g of crude ester **9**. Purification by flash chromatography using petroleum ether – ethyl acetate (19:1) as eluant gave 1.28 g (70%) of **9**[2] as a colourless liquid; bp (Kugelrohr distillation) 80°C/0.8 Torr; ir ($CHCl_3$): 1730, 1440, and 1160 cm^{-1}; ^1H nmr ($CDCl_3$) δ: 0.97 (s, 6H), 1.10–2.25 (m, 4H), 1.67 (s, 3H), 2.64 (s, 1H), 3.71 (s, 3H), and 5.70 (bs, 1H).

*2,2-Dimethyl-6-methylenecyclohexanemethanol (**10**)*

A slurry of 0.59 g (0.015 mol) of $LiAlH_4$ in dry ether was stirred at 0°C, and 2.81 g (0.015 mol) of a mixture of esters **8** and **9** in dry ether was slowly added to the slurry. The reaction mixture was heated to reflux for 2 h, then cooled to room temperature and quenched with 1 *M* HCl. The ethereal layer was washed once with 1 *M* HCl, twice with saturated NaCl, dried ($MgSO_4$), and concentrated to give 2.22 g (96%) of alcohol **10** and 2,6,6-trimethylcyclohex-2-ene methanol **11** (**10**/**11** = 7:1) as determined by ^1H nmr and gc (T = 130°C). This material was used without further purification in the preparation of the corresponding tosylates. Purification of a small amount of this material by flash chromatography using petroleum ether – ethyl acetate (9:1) as eluant gave **10**[3] as a colourless liquid; bp (Kugelrohr distillation) 80–86°C/2.0 Torr; ir ($CHCl_3$): 3600, 3400, 1245, and 850 cm^{-1}; ^1H nmr ($CDCl_3$) δ: 0.88 (s, 3H), 0.97 (s, 3H), 1.20–1.80 (m, 4H), 1.70 (bs, 1H, exchangeable with D_2O), 1.90–2.25 (m, 3H), 3.58–3.80 (m, 2H), 4.75 (bs, 1H), and 4.95 (bs, 1H).

The *endo* isomer **11** was prepared in a similar manner using 0.19 g (0.005 mol) of $LiAlH_4$ and 0.91 g (0.005 mol) of ester **9**. Work-up of the reaction mixture as above gave 0.76 g (99%) of crude **11** which was purified by flash chromatography using petroleum ether – ethyl acetate (9:1) as eluant to give **11** as a colourless liquid; bp (Kugelrohr distillation) 95°C/0.8 Torr. The spectral data are in good agreement with the literature values (21); ir ($CHCl_3$): 3450, 1450, 1390, 1370, and 1025 cm^{-1}; ^1H nmr ($CDCl_3$) δ: 0.92 (s, 3H), 1.06 (s, 3H), 1.25–2.10 (m, 5H), 1.40 (bs, 1H, exchangeable with D_2O), 1.78 (bs, 3H), 3.86 (d, 2H), and 5.62 (bs, 1H).

p-*Toluenesulphonyloxy-2,2-dimethyl-6-methylenecyclohexanemethanol*

To a solution of 2.22 g (0.014 mol) of a mixture of alcohols **10** and **11** in ether at 0°C was added 4.85 mL (0.060 mol) of pyridine. The reaction mixture was stirred at 0°C for 5 min, then 2.86 g (0.015 mol) of *p*-toluenesulphonyl chloride (22*a*) was added and the mixture was refrigerated at 0°C for 72 h. The reaction was quenched with iced water, diluted with ether, and the organic phase washed twice with 1 *M* HCl, twice with saturated $NaHCO_3$, once with saturated NaCl, and dried ($MgSO_4$). The solvent was removed to yield 4.30 g (97%) of a mixture of two tosylates which was used without purification in the preparation of sulphide **12**. Flash chromatography of a small amount of this material using petroleum ether – ethyl acetate (15:1) gave pure exocyclic tosylate from **10** as a colourless oil; ir ($CHCl_3$): 1650, 1600, 1360, 1175, 1100, and 960 cm^{-1}; ^1H nmr ($CDCl_3$) δ: 0.84 (s, 3H), 0.98 (s, 3H), 1.25–2.30 (m, 7H), 2.50 (s, 3H), 4.00–4.40 (eight-line ABX, J_{AB} = 9 Hz, J_{AX} = 6 Hz, J_{BX} = 5 Hz, 2H), 4.58 (bs, 1H), 4.84 (bs, 1H), and 7.30–7.90 (AA′XX′, $\delta_A = \delta_{A'}$ = 7.38, $\delta_X = \delta_{X'}$ = 7.82; J_{AX} = 8 Hz, 4H); mass spectrum, *m/e*: 308(0.1), 173(2), 155(11), 137(17), 136(100), 122(54), 108(16), 107(30), 81(20), 80(16), 79(18), 69(22), 68(20), 57(17), 55(74), 53(46), and 41(65).

*2,2-Dimethyl-6-methylene-1-phenylthiomethylcyclohexane (**12**)*

A slurry of 4.96 g (0.031 mol) of KH (25% in oil) in dry ethanol was stirred at room temperature and 3.14 mL (0.031 mol) of thiophenol (11) was added to the slurry. After 10 min a solution of 4.71 g (0.015 mol) of the above tosylates in ethanol was added to the mixture and the reaction was heated to reflux for 16 h. The ethanol was removed under reduced pressure and the residue was dissolved in ether and saturated NaCl. The two phases were acidified with 1 *M* HCl, and the organic layer was washed twice with saturated NaCl, dried ($MgSO_4$), and concentrated. The crude product was purified by flash chromatography using petroleum ether as eluant, and performing three successive chromatographic separations on the mixture of isomers. The following compounds were obtained in order of elution: (a) diphenyl disulphide: R_f 0.7; ir ($CHCl_3$): 3050, 2950, 1580, 1480, 1440, and 1025 cm^{-1}; ^1H nmr ($CDCl_3$) δ 7.25–7.60; (b) 0.35 g (9%) of 2,6,6-trimethyl-1-phenylthiomethylcyclohex-2-ene (**13**) as a colourless oil; R_f 0.6; bp (Kugelrohr distillation) 110°C/0.5 Torr; ir ($CHCl_3$): 1585, 1480, and 1440 cm^{-1}; ^1H nmr ($CDCl_3$) δ: 0.88 (s, 6H), 1.20–2.40 (m, 5H), 1.62 (bs, 3H), 2.79–3.12 (m, 2H), 5.45 (bs, 1H), and 7.15–7.40 (bm, 5H); mass spectrum, *m/e*: 247(12), 246(62), 231(7), 137(32), 136(30), 123(100), 121(36), 109(13), 107(20), 95(27), 93(20), 91(12), 81(57), 79(20), 77(17), 69(14), 67(16), and 55(17). *Exact Mass* calcd. for $C_{16}H_{22}S$: 246.1443; found (ms): 246.1438; (c) 2.40 g (65%) of thioether **12** as a colourless oil: R_f 0.5; bp (Kugelrohr distillation) 100°C/0.5 Torr; ir ($CHCl_3$): 3180, 1640, 1580, 1480, 1440, 1390, 1370, 1095, 1025, and 900 cm^{-1}; ^1H nmr ($CDCl_3$) δ: 0.92 (s, 3H), 1.01 (s, 3H), 1.25–1.75 (m, 4H), 1.98–2.27 (m, 3H), 2.86–3.34 (eight-line ABX, J_{AB} = 11 Hz, J_{AX} = 10 Hz, J_{BX} = 5 Hz, 2H), 4.70 (bs, 1H), 4.90 (bs, 1H), and 7.15–7.42 (bm, 5H); mass spectrum, *m/e*: 247(7), 246(29), 137(25), 136(61), 124(15), 123(100), 121(21), 107(16), 95(18), 93(30), 92(15), 81(47), 79(20), 77(16), 69(24), 67(22), 55(18), 45(16), 41(36), and 37(79). *Anal.* calcd. for $C_{16}H_{22}S$: C 77.99, H 9.00, S 13.01; found: C 77.83, H 8.94, S 12.80.

*2,2-Dimethyl-6-methylene-1-phenylsulphonylmethylcyclohexane (**14**)*

To a solution of 1.01 g (4.1 mmol) of thioether **12** in CH_2Cl_2 at 0°C was slowly added 1.78 g (0.010 mol) of MCPBA (22*b*). The ice bath was removed from the reaction mixture and the reaction was stirred for 3 h and allowed to warm to room temperature. The reaction was quenched with saturated $NaHCO_3$ and diluted with ether. The organic phase was washed three times with saturated $NaHCO_3$, once with saturated NaCl, dried ($MgSO_4$), and concentrated to give 1.2 g of crude **14**. Purification by flash chromatography using petroleum ether – ethyl acetate (9:2) as eluant gave 1.09 g (96%) of sulphone **14** as a viscous oil. Preparative tlc of a small amount of this material using petroleum ether – ethyl acetate (9:2) gave **14** as a colourless oil; bp (Kugelrohr distillation) 150°C/0.5 Torr; ir ($CHCl_3$): 1445, 1300, 1140, and 1080 cm^{-1}; ^1H nmr ($CDCl_3$) δ: 0.80 (s, 3H), 0.91 (s, 3H), 1.20–1.60 (m, 4H), 1.90–2.12 (m, 2H), 2.45 (dd, J = 7 Hz, 4 Hz, 1H), 3.25–3.40 (m, 2H), 4.58 (bs, 1H), 4.74 (bs, 1H), and 7.40–8.00 (m, 5H); mass spectrum, *m/e*: 278(0.05), 143(17), 138(26), 137(81), 136(100), 121(36), 95(31), 94(30), 93(54), 82(22), 81(66), 79(23), 77(29), 69(70), 67(21), 55(25), and 41(58). *Anal.* calcd. for $C_{16}H_{22}O_2S$: C 69.03, H 7.97, S 11.52; found: C 68.90, H 8.06, S 11.33.

*3-Trimethylsilylmethyl-3-butenoic acid (**22**)*

This compound was prepared using a method analogous to that of Itoh and co-workers (13, 14). The Grignard reagent was prepared from 5.35 g (0.22 mol) of magnesium turnings and 27.8 mL (0.20 mol) of trimethylsilylmethyl chloride in dry THF, and to this stirred suspension was added 0.48 g (2.0 mmol) of nickel(II) chloride (8) at 0°C. The brown mixture was stirred for 10 min at room temperature, cooled to 0°C, and a solution of 15.6 mL (0.20 mol) of diketene in THF was added. The resulting green reaction mixture was stirred for 5 h and allowed to warm to room temperature. The reaction mixture was quenched with 1 *M* HCl and diluted with ether. The aqueous layer was separated, extracted twice with ether, and the combined organic layers washed twice with saturated NaCl, dried ($MgSO_4$), and concentrated. The crude material was diluted with 200 mL of hexane, stirred for 10 min, decanted from an insoluble gum, and the solvent was removed under reduced pressure to give 29.7 g of **22** (86%) as an orange oil. Preparative tlc of a small amount of this material using petroleum ether – ethyl acetate – acetic acid (93:5:2) gave **22** as a colourless liquid; R_f 0.4; bp (Kugelrohr distillation) 53°C/0.01 Torr. The spec-

[2] Spectral information on compound **9** was kindly provided by Professor Joseph Wolinsky, Purdue University (19).

[3] A ^1H nmr spectrum of alcohol **10** was kindly provided by Professor Paul A. Grieco, Indiana University (20).

Can. J. Chem. Downloaded from www.nrcresearchpress.com by 210.87.254.6 on 09/06/12
For personal use only.

tral data are in good agreement with the literature values (13); ir ($CHCl_3$): 1710, 1635, and 850 cm^{-1}; ^1H nmr ($CDCl_3$) δ: 0.10 (s, 9H), 1.62 (d, J = 1 Hz, 2H), 2.98 (d, J = 1 Hz, 2H), 4.70–4.80 (m, 2H), and 11.35 (bs, 1H); mass spectrum, *m/e*: 172(0.5), 157(5), 117(5), 82(5), 75(30), 74(10), 73(100), and 53(14). *Anal.* calcd. for $C_8H_{16}O_2Si$: C 55.77, H 9.36; found: C 56.00, H 9.44.

*3-Trimethylsilylmethyl-7-methyl-2,6-octadienoic acid (**23**)*

This compound was prepared using a method analogous to that of Itoh and co-workers (13) and Katzenellenbogen and Crumrine (15). To 9.23 mL (0.066 mol) of a solution of diisopropylamine in dry THF at 0°C was added 42.6 mL (0.066 mol) of a 1.55 *M* solution of *n*-butyllithium in hexane. The pale yellow solution was stirred for 30 min and a solution of 5.16 g (0.030 mol) of **22** in dry THF was added slowly. The mixture was stirred for 30 min at 0°C, forming an orange solution, cooled to −78°C, and 5.72 g (0.030 mol) of freshly purified cuprous iodide (23) was added. The slurry was stirred for 1 h at −78°C and 3.49 mL (0.030 mol) of freshly distilled 1-bromo-3-methyl-2-butene was quickly added to the bright yellow slurry. The reaction was stirred overnight while allowing it to warm to room temperature. The reaction mixture was quenched with 1 *M* HCl, diluted with ether, and filtered through a Celite pad. The aqueous layer was extracted four times with ethyl acetate, and the combined organic layers were washed twice with saturated NaCl, dried ($MgSO_4$), and concentrated. The crude material was diluted with hexane, stirred for 10 min, decanted from an insoluble gum, and the solvent was removed under reduced pressure to give 23 as a yellow oil. Purification by flash chromatography using chloroform as eluant gave 5.05 g (70%) of **23** as a pale yellow oil. Preparative tlc of a small amount of this material using petroleum ether – ethyl acetate – acetic acid (93:5:2) gave a mixture of *E*- and *Z*-isomers of **23** as a colourless liquid (*E*/*Z* = 7:3); R_f 0.6; bp (Kugelrohr distillation) 105°C/0.20 Torr; ir ($CHCl_3$): 2960, 1680, 1608, and 850 cm^{-1}; ^1H nmr ($CDCl_3$) δ: 0.05 (s, 9H), 1.60 (s, 3H), 1.67 (s, 3H), 1.80 (s, 1.4H), 2.05–2.75 (m, 4H), 2.45 (s, 0.6H), 4.90–5.30 (m, 1H), 5.48 and 5.58 (2s, 0.7H and 0.3H), and 12.85 (bs, 1H); mass spectrum, *m/e*: 240(3), 225(7), 157(14), 156(11), 122(13), 107(17), 82(36), 75(40), 73(100), 69(59), and 45(20). *Anal.* calcd. for $C_{13}H_{24}O_2Si$: C 64.95, H 10.06; found: C 65.23, H 10.17.

*2,2-Dimethyl-6-methylenecyclohexanecarboxylic acid (**24**)*

To a solution of 4.80 g (0.020 mol) of the trimethylsilyl acid **23** in 150 mL of toluene was added 1.15 mL (0.020 mol) of acetic acid at 0°C. A solution of 12.3 mL (0.10 mol) of $BF_3 \cdot Et_2O$ in 25 mL of toluene was added slowly, and the reaction mixture was stirred for 2.5 h while allowing it to warm to room temperature. The solution was quenched with saturated NaCl, diluted with ether, and washed four times with saturated NaCl. The organic layer was dried ($MgSO_4$) and concentrated to give 4.30 g of a mixture of **24** and the *endo* isomer **25** (**24**/**25** = 4:1, as determined by ^1H nmr). The crude mixture was used without further purification in the preparation of alcohol **10**. Preparative tlc of 310 mg of acids **24** and **25** using petroleum ether – ethyl acetate – acetic acid (93:5:2) gave the following components: (a) 140 mg of **24** as a colourless oil (bp 75°C/0.20 Torr, Kugelrohr distillation) which crystallized on standing; R_f 0.3; mp 43–48°C; ir ($CHCl_3$): 2950, 1705, 1645, and 900 cm^{-1}; ^1H nmr ($CDCl_3$) δ: 0.96 (s, 3H), 1.07 (s, 3H), 1.10–2.70 (m, 6H), 2.90 (s, 1H), 4.85 (bs, 1H), 4.91 (bs, 1H), and 10.50 (bs, 1H); mass spectrum, *m/e*: 169(4), 168(38), 153(21), 125(19), 123(22), 111(19), 100(24), 82(18), 81(15), and 69(100). *Anal.* calcd. for $C_{10}H_{16}O_2$: C 71.39, H 9.59; found: C 71.60, H 9.66; (b) 40 mg of 2,6,6-trimethylcyclohex-2-enecarboxylic acid (**25**) as a colourless oil (bp 90°C/0.10 Torr, Kugelrohr distillation) which crystallized on standing; R_f 0.15; mp 101–103°C (lit. (24) mp 104°C); ir ($CHCl_3$): 2950, 1705 cm^{-1}; ^1H nmr δ: 1.00 (s, 3H), 1.07 (s, 3H), 1.20–2.30 (m, 4H), 1.75 (d, J = 1 Hz, 1H), 2.64 (bs, 1H), 5.65 (bs, 1H), and 9.50 (bs, 1H).

*2,2-Dimethyl-6-methylenecyclohexanemethanol (**10**)*

A mixture of 4.30 g of the crude acids **24** and **25** in dry ether was slowly added to a slurry of 0.76 g (0.02 mol) of $LiAlH_4$ in dry ether at 0°C. The reaction mixture was heated to reflux for 2.5 h, then cooled to room temperature. The reaction mixture was quenched with 1 *M* HCl, diluted with ether, and the organic phase was washed once with 1 *M* HCl, twice with saturated NaCl, dried ($MgSO_4$), and concentrated to give a mixture of alcohols **10** and **11**. Purification by flash chromatography using petroleum ether – ethyl acetate (9:1) as eluant gave 2.34 g of **10** and **11** (**10**/**11** = 4:1; 76% from **23**). The spectral data of the mixture of alcohols was in good agreement with that obtained previously.

*(E)-3,7-Dimethyl-2,6-octadienyl benzoate (**27**)*

A mixture of 17.3 mL (0.10 mol) of geraniol, 16.2 mL (0.20 mol) of pyridine, and a catalytic amount of 4-dimethylaminopyridine was stirred in dry ether at room temperature. A solution of 12.8 mL (0.11 mol) of benzoyl chloride in ether was added to the mixture and the reaction was stirred for 2 h at room temperature. The reaction mixture was washed three times with saturated $NaHCO_3$, three times with 1 *M* HCl, twice with saturated NaCl, dried ($MgSO_4$), and concentrated to give 27.4 g (quantitative yield) of ester **27**. This material was used without purification in the preparation of alcohol **28**: ir ($CHCl_3$): 1710, 1450, 1270, and 1010 cm^{-1}; ^1H nmr ($CDCl_3$) δ: 1.64 (s, 3H), 1.71 (s, 3H), 1.80 (s, 3H), 2.07–2.25 (m, 4H), 4.86 (d, J = 7 Hz, 2H), 5.14 (bs, 1H), 5.52 (t, J = 7 Hz, 1H), 7.25–7.66 (m, 3H), and 8.00–8.20 (m, 2H).

*(E,E)-8-Hydroxy-3,7-dimethyl-2,6-octadienyl benzoate (**28**)*

A suspension of 1.90 g (0.017 mol) of freshly sublimed selenium dioxide and 9.4 mL (0.069 mol) of 70% *tert*-butylhydroperoxide (Aldrich) in CH_2Cl_2 was stirred for 30 min at room temperature in the dark (7, 16). To the resulting solution was added 8.90 g (0.034 mol) of diene **27** at 10°C and the mixture was stirred for 5 h at 10°C, then quenched with saturated $NaHCO_3$. The organic phase was diluted with ether, washed three times with saturated $NaHCO_3$, once with saturated NaCl, dried ($MgSO_4$), and concentrated. The crude material was purified by flash chromatography using petroleum ether – ethyl acetate (4:1) as eluant to give the following compounds in order of elution: (a) starting material **27** (3.50 g, 40%); R_f 0.85; (b) 0.46 g (5%) of (*E,E*)-3,7-dimethyl-8-oxo-2,6-octadienyl benzoate (**29**) as a colourless oil: R_f 0.6; bp (Kugelrohr distillation) 112°C/0.15 Torr; ir ($CHCl_3$): 1710, 1460, 1280, and 1110 cm^{-1}; ^1H nmr ($CDCl_3$) δ: 1.78 (s, 3H), 1.83 (s, 3H), 2.20–2.65 (m, 4H), 4.87 (d, J = 7 Hz, 2H), 5.55 (t, J = 7 Hz, 1H), 6.50 (t, J = 7 Hz, 1H), 7.30–7.70 (m, 3H), 8.00–8.17 (m, 2H), and 9.42 (s, 1H); mass spectrum, *m/e*: 272(0.1), 214(1), 150(25), 121(15), 106(11), 105(100), 96(12), 95(12), 94(12), 93(12), 84(20), 82(19), 81(10), 77(25), 68(13), 67(13), 55(23), 53(14), and 51(16). *Anal.* calcd. for $C_{17}H_{20}O_3$: C 74.97, H. 7.40; found: C 75.05, H 7.41; (c) 4.66 g (50%) of alcohol **28** as a viscous oil; R_f 0.4; bp (Kugelrohr distillation) 140°C/0.15 Torr; ir ($CHCl_3$): 3600, 3450, 1715, 1455, 1280, and 1115 cm^{-1}; ^1H nmr ($CDCl_3$) δ: 1.67 (s, 3H), 1.78 (s, 3H), 2.05–2.26 (m, 4H), 2.55 (s, 1H, exchangeable with D_2O), 3.99 (s, 2H), 4.85 (d, J = 6 Hz, 2H), 5.25–5.60 (m, 2H), 7.27–7.70 (m, 3H), and 7.98–8.19 (m, 2H); mass spectrum, *m/e*: 274(0.01), 257(0.1), 152(5), 134(24), 121(6), 119(7), 106(9), 105(100), 95(5), 94(13), 93(8), 84(31), 81(5), 80(7), 79(7), 77(32), 69(5), 68(22), and 67(7). *Exact Mass* calcd. for $C_{17}H_{22}O_3$: 274.1569; found (ms): 274.1564.

*(E,E)-8-Bromo-3,7-dimethyl-2,6-octadienyl benzoate (**30**)*

To a stirred solution of 1.10 g (4.0 mmol) of alcohol **28** and 0.016 mL (0.20 mmol) of pyridine in dry ether at 0°C was slowly added 0.15 mL (1.6 mmol) of phosphorus tribromide in ether. The reaction mixture was stirred at 0°C for 5 h, then quenched with iced water. The organic phase was diluted with ether, washed 3 times with saturated $NaHCO_3$, once with saturated NaCl, dried ($MgSO_4$), and concentrated to give 1.31 g (97%) of bromide **30** which was used without further purification in the preparation of compound **31**. Preparative tlc of a small amount of this material using petroleum ether – ethyl acetate (10:1) gave **30** as a colourless oil which decomposed upon distillation; ir ($CHCl_3$): 1710, 1455, 1275, and 1105 cm^{-1}; ^1H nmr ($CDCl_3$) δ: 1.79 (s, 6H), 2.12–2.40 (m, 4H), 3.97 (s, 2H), 4.86 (d, J = 7 Hz,

Can. J. Chem. Downloaded from www.nrcresearchpress.com by 210.87.254.6 on 09/06/12
For personal use only.

2H), 5.39–5.71 (m, 2H), 7.27–7.70 (m, 3H), and 8.00–8.20 (m, 2H); mass spectrum, *m/e*: 257(8), 136(8), 135(62), 134(6), 107(24), 106(30), 105(100), 93(34), 91(10), 81(10), 79(13), 77(47), 68(39), 67(38), 55(13), 53(20), 51(14), and 41(29). *Anal.* calcd. for $C_{17}H_{21}BrO_2$: C 60.54, H 6.28, Br 23.69; found: C 60.67, H 6.48, Br 23.50.

(E,E)-9-(2',2'-Dimethyl-6'-methylenecyclohexanyl)-3,7-dimethyl-9-phenylsulphonyl-2-6-nonadienyl benzoate (31)

To a stirred solution of 0.22 g (0.80 mmol) of sulphone **14** in 8 mL of THF and 0.8 mL of HMPA at 0°C was added 0.70 mL (1.2 mmol) of a 1.7 *M* solution of *n*-butyllithium in hexane. After 1 h a solution of 0.30 g (0.88 mmol) of halide **30** in 3 mL of THF (pre-dried by stirring over CaH_2) was added at 0°C and the reaction mixture was stirred overnight, while allowing it to warm to room temperature. The reaction mixture was quenched with 1 *M* HCl, diluted with ether and petroleum ether, the organic phase washed once with 1 *M* HCl, and four times with saturated NaCl. It was dried ($MgSO_4$) and the solvent removed to give 0.44 g of crude coupled product **31** which was used without further purification in the preparation of alcohol **32**. Preparative tlc of a small amount of this material using petroleum ether – ethyl acetate (6:1) gave both diastereomers of **31** (≈9:1 as determined by ^{1}H nmr) as a viscous oil which decomposed upon distillation; ir ($CHCl_3$): 1705, 1445, 1300, 1275, and 1145 cm^{-1}; ^{1}H nmr ($CDCl_3$) δ: 0.76 (s, 0.3H), 0.87 (s, 0.3H), 0.96 (s, 2.7H), 1.10 (s, 2.7H), 1.30–2.75 (m, 13H), 1.76 (s, 6H), 3.40–3.70 (m, 1H), 4.79 (bs, 1H), 4.82 (d, J = 6 Hz, 2H), 5.05 (bs, 1H), 5.25–5.40 (m, 1H), 5.47 (t, J = 6 Hz, 1H), and 7.38–8.17 (m, 10H); mass spectrum, *m/e*: 534(0.5), 413(2), 412(5), 272(17), 271(65), 270(31), 255(12), 215(12), 203(21), 202(12), 201(14), 187(13), 177(17), 175(22), 163(11), 161(15), 159(16), 149(19), 148(18), 147(66), 146(23), 145(16), 135(25), 133(32), 123(38), 122(59), 121(40), 120(35), 119(38), 109(42), 107(42), 105(100), 95(39), 93(52), 91(30), 81(67), 79(33), 77(59), 69(48), 67(24), and 55(37). *Exact Mass* calcd. for $C_{33}H_{42}O_4S$: 534.2804; found (ms): 534.2789.

(E,E)-9-(2',2'-Dimethyl-6'-methylenecyclohexanyl)-3,7-dimethyl-9-phenylsulphonyl-2-6-nonadien-1-ol (32)

To a stirred solution of 0.44 g of crude benzoic ester **31** in dry ether at 0°C was added 2.4 mL (2.4 mmol) of a 1 *M* solution of DIBAL in hexane. The reaction was stirred for 2 h and allowed to warm to room temperature, then cooled to 0°C and quenched with 1 *M* HCl until both layers were clear. The mixture was stirred for 15 min, then diluted with ether, the organic phase washed twice with saturated $NaCl_3$, dried ($MgSO_4$), and the solvent removed. The crude product was purified by flash chromatography using petroleum ether – ethyl acetate (7:2) as eluant to give the following compounds in order of elution: (a) sulphone **14** (0.083 g, 36% from coupling reaction); R_f 0.80; (b) 0.219 g (64% from coupling reaction) of both diastereomers of alcohol **32** (≈9:1 as determined by ^{1}H nmr), as an extremely viscous oil which rearranged upon distillation; R_f 0.40; ir ($CHCl_3$): 3600, 3500, 1450, 1305, 1150, and 1090 cm^{-1}; ^{1}H nmr ($CDCl_3$) δ: 0.98 (s, 2.7H), 1.10 (s, 2.7H), 1.19 (s, 0.3H), 1.24 (s, 0.3H), 1.30–2.80 (m, 13H), 1.65 (s, 6H), 1.90 (bs, 1H, exchangeable with D_2O), 3.45–3.90 (m, 1H), 4.12 (d, J = 7 Hz, 2H), 4.76 (bs, ~0.9H), 5.04 (bs, ~1.1H), 5.10–5.25 (m, 1H), 5.40 (t, J = 7 Hz, 1H), and 7.40–7.95 (m, 5H); mass spectrum, *m/e*: 430(1.5), 289(14), 288(17), 272(12), 271(43), 270(21), 255(13), 203(34), 162(20), 149(25), 147(54), 135(30), 133(32), 123(55), 122(36), 121(45), 120(20), 119(33), 109(55), 107(52), 105(52), 95(52), 93(60), 91(38), 81(100), 80(20), 79(52), 77(34), 69(92), 67(39), 57(26), 55(78), and 53(22). *Anal.* calcd. for $C_{26}H_{38}O_3S$: C 72.52, H 8.89, S 7.45; found: C 72.26, H 8.80, S 7.31.

(E,E)-9-(2',2'-Dimethyl-6'-methylenecyclohexanyl)-3,7-dimethyl-2,6-nonadien-1-ol (trixagol) (3)

To a stirred solution of 0.151 g (0.35 mmol) of sulphone **32** in dry ethanol was added 0.20 g (1.4 mmol) of disodium hydrogen phosphate, then 0.54 g (1.4 mmol) of freshly ground 6% sodium amalgam (18, 25). The reaction mixture was heated to reflux for 16 h, then cooled to room temperature, quenched with 1 *M* HCl, diluted with ether, and decanted from the mercury. The organic phase was washed once with 1 *M* HCl, twice with saturated $NaHCO_3$, twice with saturated NaCl, dried ($MgSO_4$), and the solvent removed. The crude product was purified by flash chromatography using petroleum ether – ethyl acetate (5:1) as eluant to give 0.069 g (68%) of alcohol **3**[4] as a colourless oil whose spectral data are in good agreement with the literature values (6*a*); ir ($CHCl_3$): 3600, 3450, 1645, 1450, 1385, 990, and 800 cm^{-1}; ^{1}H nmr ($CDCl_3$) δ: 0.85 (s, 3H), 0.91 (s, 3H), 1.15–2.20 (m, 15H), 1.20 (bs, 1H, exchangeable with D_2O), 1.60 (s, 3H), 1.70 (s, 3H), 4.17 (d, J = 7 Hz, 2H), 4.54 (m, 1H), 4.75 (m, 1H), 4.95–5.20 (m, 1H), and 5.45 (t, J = 7 Hz, 1H), mass spectrum, *m/e*: 290(1.5), 288(3), 257(6), 204(7), 203(6), 177(20), 175(26), 137(28), 136(42), 135(23), 123(29), 121(36), 109(45), 107(36), 105(24), 95(45), 93(57), 81(100), 79(27), 69(71), 67(28), and 55(37). *Exact Mass* calcd. for $C_{20}H_{34}O$: 290.2610; found (ms): 290.2610.

Acknowledgements

We are grateful to Professors Wolinsky, Grieco, and Joaquin de Pascual Teresa for spectral data and comparison samples, and to the Natural Sciences and Engineering Research Council of Canada for financial support. Once of us (R.J.A.) is grateful to the Canadian Commonwealth Scholarship and Fellowship Plan for the award of a graduate scholarship.

1. G. STORK and A. W. BURGSTAHLER. J. Am. Chem. Soc. **77**, 5068 (1955).
2. A. ESCHENMOSER, L. RUZICKA, O. JEGER, and D. ARIGONI. Helv. Chim. Acta, **38**, 1890 (1955).
3. I. FLEMING, A. PEARCE, and R. L. SNOWDEN. J. Chem. Soc. Chem. Commun. 182 (1976).
4. (*a*) T. K. SARKAR and N. H. ANDERSEN. Tetrahedron Lett. 3513 (1978); (*b*) L. R. HUGHES, R. SCHMID, and W. S. JOHNSON. Bioorg. Chem. **8**, 513 (1979); (*c*) I. FLEMING and A. PEARCE. J. Chem. Soc. Perkin Trans. 1, 251 (1981).
5. R. J. ARMSTRONG, F. L. HARRIS, and L. WEILER. Can. J. Chem. **60**, 673 (1982).
6. (*a*) J. DE PASCUAL TERESA, E. CABALLERO, C. CABALLERO, M. MEDARDE, A. F. BARRERO, and M. GRANDE. Tetrahedron Lett. **37**, 3491 (1978); (*b*) Tetrahedron, **38**, 1837 (1982).
7. (*a*) S. N. HUCKIN and L. WEILER. J. Am. Chem. Soc. **96**, 1082 (1974); (*b*) F. W. SUM and L. WEILER. Tetrahedron, **37**, Supplement 1, 303 (1981).
8. T. HAYASHI, Y. KATSURO, and M. KUMADA. Tetrahedron Lett. **21**, 3915 (1980).
9. M. KURBANOV, A. V. SEMENOVSKII, and V. A. SMIT. Bull. Acad. Sci. USSR, Div. Chem. Sci. 370 (1973).
10. F. JOHNSON. Chem. Rev. **68**, 375 (1968).
11. T. MUKAIYAMA and N. IWASAMA. Chem. Lett. 29 (1981).
12. W. C. STILL, M. KAHN, and A. MITRA. J. Org. Chem. **43**, 2923 (1978).
13. (*a*) K. ITOH, T. YOGO, and Y. ISHII. Chem. Lett. 103 (1977); (*b*) H. NISHIYAMA, K. ITAGAKI, K. TAKAHASHI, and K. ITOH. Tetrahedron Lett. **22**, 1691 (1981).
14. K. ITOH, M. FUKUI, and Y. KURACHI. J. Chem. Soc. Chem. Commun. 500 (1977).
15. J. A. KATZENELLENBOGEN and A. L. CRUMRINE. J. Am. Chem. Soc. **98**, 4925 (1976).
16. M. A. UMBREIT and K. B. SHARPLESS. J. Am. Chem. Soc. **99**, 5526 (1977).
17. (*a*) P. J. KOCIENSKI. 65th Canadian Chemical Conference, Toronto, June 1982. Abstr. OR15-2; (*b*) P. KOCIENSKI and M. TODD. J. Chem. Soc. Chem. Commun. 1078 (1982).

[4] Spectral information and a sample of trixagol were kindly provided by Professor Joaquin de Pascual Teresa, Salamanca University, Spain (6*a*).

18. B. M. TROST, H. C. ARNDT, P. E. STREGE, and T. R. VERHOEVEN. Tetrahedron Lett. 3477 (1976).
19. R. H. BEDOUKIAN and J. WOLINSKY. J. Org. Chem. **40**, 2154 (1975).
20. P. A. GRIECO, Y. MASAKI, and D. BOXLER. J. Org. Chem. **40**, 2261 (1975).
21. D. V. BANTHORPE and P. A. BOULLIER. J. Chem. Soc. Perkin Trans. 1, 1637 (1974).
22. (*a*) L. F. FIESER and M. FIESER. Reagents for organic synthesis. Vol. I. John Wiley and Sons, New York, NY. 1967 p. 1179; (*b*) p. 135.
23. G. B. KAUFFMAN and L. A. TETER. Inorg. Synth. **7**, 9 (1963).
24. D. J. BENNETT, G. R. RAMAGE, and J. L. SIMONSEN. J. Chem. Soc. 418 (1940).
25. R. N. MCDONALD and C. E. REINEKE. Org. Synth. **50**, 50 (1970); V. DEULOFEU and T. J. GUERRERO. Org. Synth. **22**, 89 (1942).

Can. J. Chem. Downloaded from www.nrcresearchpress.com by 210.87.254.6 on 09/06/12
For personal use only.

Synthesis of spin-labeled analogues of drug molecules with potential action on neuroreceptors

H. DUGAS, C. SPINO, AND M. OUELLETTE

Department of Chemistry, Université de Montréal, C.P. 6210, Montreal, P.Q., Canada H3C 3V1

Received February 17, 1983

H. DUGAS, C. SPINO, and M. OUELLETTE. Can. J. Chem. **61**, 2540 (1983).

The syntheses of novel spin-labeled analogues of butaclamol, a spin-labeled phenylaziridinium and two amino derivatives of butaclamol, are presented. Preliminary results of in vitro activity of these compounds on dopaminergic, serotoninergic, and adrenergic receptors correlate with the importance of the previously proposed lipophilic accessory binding site in CNS dopamine receptor.

H. DUGAS, C. SPINO et M. OUELLETTE. Can. J. Chem. **61**, 2540 (1983).

L'article présente la synthèse de nouveaux analogues marqueurs de spin de butaclamol, d'un marqueur de spin du type phénylaziridinium et de deux dérivés aminés du butaclamol. Les résultats préliminaires d'activité in vitro de ces produits sur les récepteurs dopaminergique, sérotoninergique et adrénergique sont en accord avec l'hypothèse d'un site auxiliaire lipophilique pour le récepteur de dopamine au système nerveux central.

Can. J. Chem. Downloaded from www.nrcresearchpress.com by 210.87.254.42 on 09/06/12
For personal use only.

Introduction

Spin-labeled (SL) drugs have become in the past ten years important molecular probes in studies of drug mechanisms at a molecular level. For example, a large number of drug analogues containing the nitroxide moiety have been synthesized and used to study the topography of specific binding sites in receptor macromolecules. The most representative efforts toward this goal include the preparation of SL-analogues of acetylcholine (1–3), SL-quaternary ammonium ligands (4, 5), SL-propranolol (6, 7), SL-narcotics (8), SL-steroids (9–11), SL-phenytoin (12), SL-penicillin (13), and a SL-analogue of *N*,*N*-dimethyl-2-phenylaziridinium (14).

The antipsychotic agent butaclamol **1** and related compounds are rigid dopamine antagonists and may thus be very helpful probes in receptor mapping. Furthermore, the fact that the dopamine receptor is highly stereoselective for the (+)-isomer of butaclamol derivatives (15–17), in both in vivo and in vitro experiments, renders the preparation of SL-analogues even more attractive as molecular monitors for the mapping of the dopamine receptor.

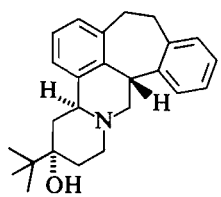

1

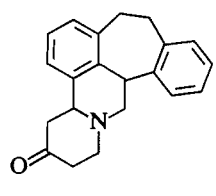

2

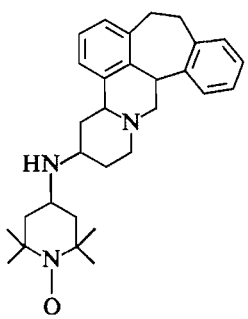

3

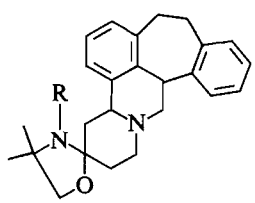

4*a* R = H
b R = O

In this report, we describe for the first time the synthesis of such SL-analogues, a new SL-analogue of phenylaziridinium as well as two amino derivatives of butaclamol. Preliminary biochemical tests on these compounds are also disclosed.

Results and discussion

Chemistry

The ketone precursor **2** (15) was treated with 4-amino-2,2,6,6,-tetramethylpiperidinyl-1-oxyl in the presence of $NaBH_3CN$ to give **3** in 53% yield. In the presence of 2-methyl-2-amino-1-propanol and *p*-TsOH, **2** was converted to the oxazolidine **4***a* in 65% yield. Unfortunately, all attempts to obtain the corresponding nitroxide **4***b* using the procedure of Waggoner *et al.* (18), or variations thereof, were unsuccessful. This is probably due to the presence in the molecule of another nitrogen atom which may also be partially oxidized during the process, resulting only in decomposition products.

The SL-ester **5** was obtained in 17% yield by heating (+)-butaclamol with the acid chloride of 2,2,5,5-tetramethylpyrrolidinyl-1-oxyl-3-carboxylic acid in the presence of AgCN (19). The methylamino compound **6***a* and the isobutylamino compound **6***b* were prepared by treatment of the ketone **2** with the corresponding amine in the presence of $NaBH_3CN$ and were obtained in 32% and 57% yield respectively.

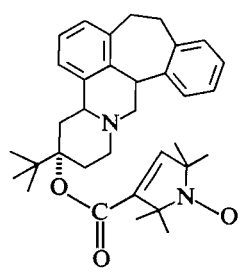

5

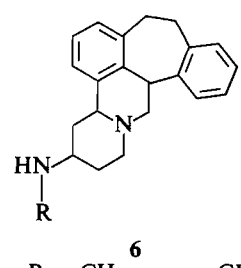

6
a R = CH_3
b R = CH_2—$CH(CH_3)_2$

The preparation of the 2-phenylaziridinium precursor **10***b* is illustrated in Scheme 1. Epoxystyrene **9** and *N*-methyl-4-amino-2,2,6,6-tetramethylpiperidinyl-1-oxyl **8**, prepared from tampone **7** according to the procedure of Rosen (20), were used as starting materials. The compounds were coupled in the pres-

TABLE 1. Receptor binding assays[a]

Compounds	^{3}H-Spiroperidol (dopamine)	^{3}H-LSD (serotonin)	^{3}H-WB4101 (α_1-adrenergic)
3	50%, 1.5×10^{-7} *M*[b]	—	—
4*a*	20%, 10^{-6} *M*	—	—
5[d]	21%, 10^{-6} *M*	—	—
6*a*	22%, 10^{-6} *M*	—	—
6*b*	64%, 10^{-6} *M*	—	—
10*b*	2%, 10^{-6} *M*	6%, 10^{-6} *M*	7%, 10^{-6} *M*
11	2%, 10^{-6} *M*	7%, 10^{-6} *M*	0%, 10^{-6} *M*
(±)-Butaclamol	IC_{50}, 5×10^{-9} *M*[c]		
Methysergide		IC_{50}, 1.6×10^{-8} *M*[c]	
Prazosin			IC_{50}, 2×10^{-9} *M*[c]

[a] The in vitro tests were performed on rat striatum (23) (dopamine), cortex (24) (serotonin), and forebrain (25) (α_1-adrenergic). Although at Ayerst spiroperidol is used routinely, Lazareno and Nahorski (26) have shown recently that ^{3}H-domperidone would be a much better ligand to label dopamine receptors.

[b] The concentration corresponds to the amount of drug-analogue used in the test and the percentage represents the amount of radioactive tracer displaced.

[c] These standards are included for comparative purposes.

[d] With the exception of **5**, all compounds are racemic mixtures.

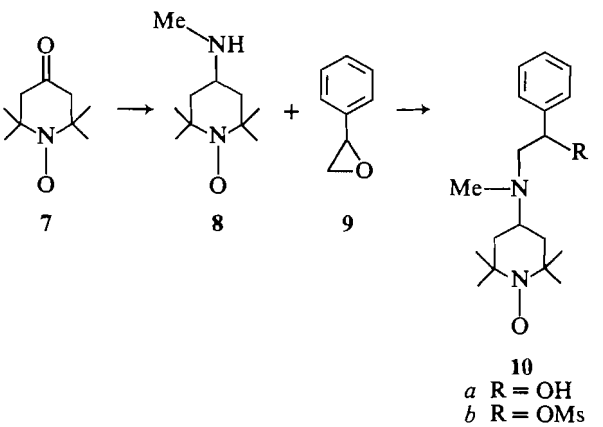

SCHEME 1

ence of water to give **10***a* as the ring-opening product in 98% yield. Treatment of **10***a* with mesyl chloride in dry benzene followed by a trace of HCl gave the expected hydrochloride salt of the SL-mesyl amine **10***b* in 49% yield. The compound gives a typical three-line epr signal with a_N = 17.2 G in water. This salt is expected to cyclize instantaneously to the aziridinium chloride salt in aqueous buffer above pH 7 (21).

The synthesis of a similar molecule **11**, but with the nitroxide function in a different position, has already been reported (14). Originally the synthesis of the SL-amine **11** was developed with the objective of probing the geometry of the anionic site of acetylcholinesterase since the corresponding *N*,*N*-dimethyl-2-phenylaziridinium chloride has been shown to be a potent anionic-site-directed irreversible inhibitor (21, 22).

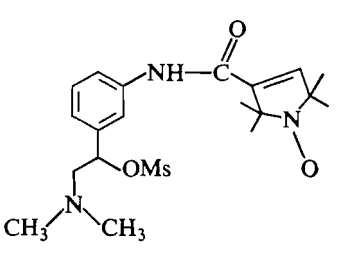

11

However, the product turned out to be only a poor competitive inhibitor (K_i = 2.1 × 10^{-3} *M*) of bovine erythocyte acetylcholinesterase (14). The reason probably lies in the presence of a bulky spin label group on the aromatic ring. To overcome this problem, the synthesis of the *N*-SL analogue **10***b* was envisaged.

Biochemistry

The compounds cited in this article were tested on rat striatal membranes for dopaminergic activity (23), as well as rat cortex for serotoninergic (24) and rat forebrain for α_1-adrenergic (25) activities, for compounds **10***b* and **11**. The results are presented in Table 1. Generally, binding studies are not sufficient on their own to demonstrate the interaction of compounds with receptors, especially if only one concentration is used. Nevertheless, a general trend can be observed from these preliminary results even though the dopaminergic activity, represented in percentage of inhibition of ^{3}H-spiroperidol binding, is low. It seems that a bulky substituent at position 3 of butaclamol enhances the activity since the activity found is **6***b* ≈ **3** > **6***a*. On the other hand, the presence of a chemical group in the axial orientation reduces considerably the activity, as in **4***a* and **5**. This observation is in agreement with the hypothesis of a lipophilic accessory binding site for the *tert*-butyl group of butaclamol, as proposed previously by Humber and co-workers (16).

As for compounds **10***b* and **11**, both are inactive in all three assays and thus further investigations of the covalent binding of these compounds to receptor macromolecules, using the present spin-labeling approach, is unwarranted.

In conclusion, only the spin-label analogue **3** shows some promise for the study of its interaction with membrane systems in an attempt to ascertain the mode of action of this class of drugs. In particular, the molecule should allow monitoring of both dynamical and structural perturbations of the dopamine receptor macromolecules by neuroleptic agents at specific binding sites. Work is also in progress to bind covalently **6***a* and **6***b* to Sepharose gel for the eventual purification of solubilized dopaminergic D_2 receptor by affinity chromatography.

Experimental

Melting points were obtained with a Reichert micro hotstage apparatus and are uncorrected. Elemental analytical results were performed

Can. J. Chem. Downloaded from www.nrcresearchpress.com by 210.87.254.42 on 09/06/12
For personal use only.

Can. J. Chem. Downloaded from www.nrcresearchpress.com by 210.87.254.42 on 09/06/12
For personal use only.

by H. Seguin of the National Research Council of Canada, Ottawa and at the Microanalysis Center, Université Louis Pasteur, Strasbourg. Infrared (ir) spectra were recorded on a Perkin–Elmer 710A spectrometer as films on NaCl or in solution in $CHCl_3$. The ^1H nmr spectra were recorded using a Varian Associates EM-360A or a Bruker-WH90 spectrometer in $CDCl_3$, using Me_4Si as the internal standard. Mass spectra (ms) were obtained using a Hitachi–Perkin–Elmer model RMU 6-D. For tlc, commercial plates of silica gel (Eastman or Mancherey–Nagel) were used. Nitroxide group gives white spots on a blue background with molybdenum (Zinzadze) reagent. Nitroxide starting materials were purchased from Aldrich and Frinton Laboratories.

(4a,13b-trans*)-2,3,4,4a,8,9,13b,14-Octahydro-1*H*-benzo[6,7]-cyclohepta[1,2,3,*d,e*]-pyrido[2,1,*a*]-isoquinolin-3-[4'-amino-2',2',6',6'-tetramethylpiperidinyloxyl] (**3**)*

The ketone **2** (Ayerst) (300 mg, 0.99 mmol) was dissolved in tetrahydrofuran (15 mL) and added to a solution of 4-amino-2,2,6,6-tetramethylpiperidinyloxyl (168 mg, 0.99 mmol) and sodium cyanoborohydride (Aldrich) (62 mg, 0.99 mmol) in methanol (30 mL). The reaction mixture was stirred at room temperature in the dark for 48 h. The solution was then evaporated to dryness under reduced pressure, dissolved in chloroform, and washed four times with cold water. The chloroformic solution was dried over magnesium sulfate and evaporated under reduced pressure to give a crude orange oil. The crude product was chromatographed on an alumina (activity 1) column and the desired product was eluted with a mixture of benzene and acetone to give 167 mg (53%) of **3** as salmon colored crystalline needles; mp 75°–76°C; ir cm^{-1}: 3600–3400 (N—H), 2950–2850 (Boltzman's band), 1600, 1475 (aromatic); epr ($CHCl_3$) 3 lines, a_N = 14.5 G; ms *m/e*: 459 (M^+), 304, 287. *Anal.* calcd. for $C_{30}H_{40}N_3O$: C 78.57, H 8.89, N 9.16; found: C 77.42, H 8.81, N 8.35.

(4a,13b-trans*)-2,3,4,4a,8,9,13b,14-Octahydro-1*H*-benzo[6,7]-cyclohepta[1,2,3,*d,e*]-pyrido[2,1,*a*]-isoquinolin-3-[2',2'-dimethyloxazolidine] (**4**a)*

Toluene (80 mL), *p*-toluenesulfonic acid (25 mg), and 2-methyl-2-amino-1-propanol (Aldrich) (724 mg, 8.1 mmol) were refluxed for 15 min with a Dean–Stark trap to remove the water. Then the ketone **2** (400 mg, 1.3 mmol) was added and the mixture left under reflux for 48 h in the dark. The solution was filtered, washed four times with a saturated solution of $NaHCO_3$ (15 mL), once with cold water, dried over $MgSO_4$, and evaporated to dryness to give 324 mg (65%) of the crystalline yellow product **4***a*, mp 61°–62°C; ir cm^{-1}: 3600–3400 (N—H), 2950–2850 (Boltzman's band), 1600, 1475 (aromatic); ^1H nmr ($CDCl_3$) δ: 1.35 (s, 6H), 3.70 (s, 2H), 4.5 (s, 1H), 7.4 to 6.9 (m, 7H). *Anal.* calcd. for $C_{24}H_{30}NO_2$: C 79.51, H 8.34, N 7.73; found: C 78.55, H 7.99, N 7.41.

(4a,13b-trans*)-2,3,4,4a,8,9,13b,14-Octahydro-1*H*-benzo[6,7]-cyclohepta[1,2,3,*d,e*]-pyrido[2,1,*a*]-isoquinolin-3-*tert*-butyl-3-[2',2',5',5'-tetramethylpyrrolidinyloxyl-3'-carboxyl]ester (**5**)*

(+)-Butaclamol·HCl (Ayerst) was converted to the free base by passing a methanolic solution on an ion exchange resin AG1-X8, OH^- form (Bio-Rad). Butaclamol (200 mg, 0.552 mmol) was dissolved in 4 mL of anhydrous benzene and freshly prepared AgCN (19) (268 mg, 0.552 mmol) was added with vigorous stirring. To this was added the acid chloride (108 mg) of 2,2,5,5-tetramethylpyrrolidinyloxyl-3-carboxylic acid (from $SOCl_2$ in $CHCl_3$) and the mixture was refluxed for 18 h. The reaction mixture was diluted with 20 mL of pentane, filtered over Fuller's earth, washed with 10% $NaHCO_3$, water, then dried (Na_2SO_4) and evaporated to dryness to give 73 mg of a yellow oily crude product. Preparative tlc (Macherey–Nagel) silica gel G-100, UV_{254} with benzene–$CHCl_3$ (1:1) was used to purify the product and gave 42 mg (17%) of a yellow oil, homogenous on tlc; ir cm^{-1}: 1715 (ester), 1600 (aromatic), 1290 (C—O); epr ($CHCl_3$) 3 lines, a_N = 14.0 G. The ^1H nmr ($CDCl_3$) was taken on 7 mg of material in the presence of a microdroplet of phenylhydrazine to reduce the nitroxide function; δ: 0.9 (s, 9H, *tert*-butyl), 1.15 (d, 12H, tetramethyl), 6.8 to 7.3 (m, 7H, aromatic).

N-*methyl-(4a,13b*-trans*)-2,3,4,4a,8,9,13b,14-octahydro-1*H*-benzo[6,7]cyclohepta[1,2,3,*d,e*]pyrido[2,1,*a*]isoquinolin-3-amine (**6**a)*

To a solution of the ketone **2** (300 mg, 0.99 mmol) in 15 mL anhydrous THF were added an excess of methylamine·HCl (Anachemia) (100 mg) and 61 mg (0.99 mmol) of $NaBH_3CN$ (Aldrich) dissolved in 40 mL MeOH.

The mixture was stirred at ambiant temperature for 48 h. The solution was evaporated and the residue redissolved in $CHCl_3$, washed four times with 10 mL water, dried (Na_2SO_4), filtered, and evaporated to dryness. The resulting oil was chromatographed on an alumina column (activity 1) with $CHCl_3$ as eluant and 105 mg (32%) of a pale yellow crystalline material was obtained, mp 65°–66°C; ^1H nmr ($CDCl_3$) δ: 2.43 (s, 3H), 6.8 to 7.4 (m, 7H). For analysis, the compound was converted to its hydrochloride salt (HCl–Et_2O). *Anal.* calcd. for $C_{22}H_{28}N_2Cl_2$: C 67.51, H 7.21, N 7.16, Cl 18.12; found: C 67.98, H 7.46, N 7.45, Cl 17.11.

N-*isobutyl-(4a,13b*-trans*)-2,3,4,4a,8,9,13b,14-octahydro-1*H*-benzo[6,7]cyclohepta[1,2,3,*d,e*]pyrido[2,1,*a*]isoquinolin-3-amine (**6**b)*

The methodology was the same as above. From 100 mg (0.33 mmol) of ketone **2**, 68 mg (57%) of the desired product was obtained, after preparative tlc (silica gel), as an oil; ^1H nmr ($CDCl_3$) δ: 0.8 (d, 6H), 2.0 to 3.5 (m, 2H), 6.7 to 7.4 (m, 7H).

N-*methyl*-N'-*4'-(2',2',6',6'-tetramethylpiperidinyloxyl)-2-hydroxy-1-aminoethylbenzene (**10**a)*

N-methyl-4-amino-(2,2,6,6-tetramethylpiperidinyloxyl) **8** (20) (254 mg, 1.39 mmol) was dissolved in 3 mL of distilled water (33 % by weight) and epoxystyrene **3** (Eastman) (166 mg, 1.39 mmol) was added. The reaction mixture was left at room temperature in the dark for five days. At the end of this period, more than 95% of the products were coupled as judged by tlc. The solution was evaporated under reduced pressure to give 418 mg (98%) of an orange oil which was directly used for the next step; ir cm^{-1}: 3600–3200 (OH), 1240–1200 (C—O).

N-*methyl*-N'-*4'-(2',2',6',6'-tetramethylpiperidinyloxyl)-2-methylsulfonyloxy-1-aminoethylbenzene hydrochloride salt (**10**b)*

The alcohol nitroxide **10***a* (418 mg, 1.38 mmol) was dissolved in 6 mL of dry benzene and mesyl chloride (157 mg, 1.38 mmol) was added dropwise over a period of 10 min at room temperature under argon atmosphere in the dark. After 2 h of stirring, 2 drops of concentrated HCl were added to precipitate the product in its hydrochloride form. The solvent was removed to yield 257 mg (49%) of the yellow crystalline compound **10***b* and 168 mg of an orange oily substance that can easily be separated. The compound is rather hygroscopic and melts at 145°–153°C; ^1H nmr ($CDCl_3$), in the presence of phenylhydrazine to reduce the nitroxide group, δ: 1.4 (s, 12H), 2.35 (s, 3H, N—CH_3), 3.0 (s, 3H, CH_3SO_2—), 7.5 (bs, 5H); ms *m/e*: 419. *Anal.* calcd. for $C_{19}H_{32}N_2O_4Cl\cdot 2H_2O$: C 50.48, H 8.02, N 6.21; found: C 50.48, H 8.22, N 6.84.

Acknowledgments

The authors would like to express their gratitude to Dr. L. Humber and Ayerst Research Laboratories for a generous supply of (+)-butaclamol·HCl and the ketone precursor **2** and to Dr. M. Stern, Ayerst Research Laboratories, for conducting the receptor binding studies. Financial support from the Natural Sciences and Engineering Research Council of Canada (NSERC) is also acknowledged.

1. C. F. Chignell, D. K. Starkweather, and R. H. Erlich. J. Med. Chem. **15**, 876 (1972).
2. M. B. Abou-Donia, G. M. Rosen, and J. Paxton. Int. J. Biochem. **7**, 371 (1976).

3. M. B. ABOU-DONIA and G. M. ROSEN. Biophys. Chem. **6**, 15 (1977).
4. V. T. WEE, B. K. SINHA, P. W. TAYLOR, and C. F. CHIGNELL. Mol. Pharmacol. **12**, 667 (1976).
5. B. K. SINHA and C. F. CHIGNELL. J. Med. Chem. **18**, 669 (1975).
6. G. J. RAUCKMAN, G. M. ROSEN, and R. J. LEFKOWITZ. J. Med. Chem. **19**, 1254 (1976).
7. L. E. G. ERIKSSON and J. WESTMAN. Biophys. Chem. **13**, 253 (1981).
8. W. Y. WU, L. G. ABOOD, M. GATES, and R. W. KREILICK. Mol. Pharmacol. **13**, 766 (1977).
9. T. L. KIRLEY, E. D. SPRAGUE, and H. D. HALSALL. Biophys. Chem. **15**, 209 (1982).
10. H. O. MANKOVSZKY, K. HIDIG, and L. LEX. Synthesis, 914 (1980).
11. G. DEFAYE, M. BASSET, N. MONNIER, and E. M. CHAMBAZ. Biochem. Biophys. Acta, **623**, 280 (1980).
12. D. CHOU, C. F. POLNASZEK, Y. YOST, I. E. LIPPIK, and J. M. HOLTZMAN. Mol. Pharmacol. **20**, 674 (1981).
13. D. COOKSON and R. J. P. WILLIAMS. J. Inorg. Nucl. Chem. **41**, 1089 (1979).
14. C. KAVANAGH-CARON, M. CARON, N. BRISSON, and H. DUGAS. Can. J. Chem. **54**, 3545 (1976).
15. L. G. HUMBER, F. T. BRUDERLEIN, A. H. PHILIPP, and M. GÖTZ. J. Med. Chem. **22**, 761 (1979).
16. A. H. PHILIPP, L. G. HUMBER, and K. VOITH. J. Med. Chem. **22**, 765 (1979).
17. P. SEEMAN, K. WESTMAN, M. PROTIVA, J. JILEK, P. C. TAIN, A. K. SAXENA, N. ANAD, L. HUMBER, and A. H. PHILIPP. Eur. J. Pharmacol. **56**, 247 (1979).
18. A. S. WAGGONER, T. J. KINGZETT, S. ROTTSCHEAFFER, O. H. GRIFFITH, and A. D. KEITH. Chem. Phys. Lipids, **3**, 245 (1969).
19. S. TAKIMOTO, J. INANAGA, T. KATSUKI, and M. YAMAGUCHI. Bull. Chem. Soc. Jpn. **49**, 2335 (1976).
20. G. M. ROSEN. J. Med. Chem. **17**, 358 (1974).
21. B. BELLEAU and H. TANI. Mol. Pharmacol. **2**, 411 (1966).
22. B. BELLEAU and H. TANI. Can. J. Pharmacol. Sci. **4**, 14 (1969).
23. I. CREESE, D. R. BURT, and S. H. SNYDER. Life Sci. **17**, 993 (1976).
24. J. P. BENNETT, JR. and S. H. SNYDER. Mol. Pharmacol. **12**, 373 (1976).
25. D. A. GREENBERG, D. C. U'PRICHARD, and S. H. SNYDER. Life Sci. **19**, 69 (1976).
26. S. LAZARENO and S. R. NAHORSKI. Eur. J. Pharmacol. **81**, 273 (1982).

Can. J. Chem. Downloaded from www.nrcresearchpress.com by 210.87.254.42 on 09/06/12
For personal use only.

Hydride transfer reactions. Substituent effects in oxidation of *N*-benzylacridans by π acceptors

ALLAN K. COLTER, CHARLES C. LAI, TERRY W. WILLIAMSON, AND RAYMOND E. BERRY
Guelph–Waterloo Centre for Graduate Work in Chemistry, University of Guelph, Guelph, Ont., Canada N1G 2W1

Received January 6, 1983

ALLAN K. COLTER, CHARLES C. LAI, TERRY W. WILLIAMSON, and RAYMOND E. BERRY. Can. J. Chem. **61**, 2544 (1983).

The kinetics of oxidation of a series of eight *N*-(substituted benzyl)acridans (**3**, NBA's) by 1,4-benzoquinone (BQ), *p*-chloranil (CA), 2,3-dicyano-1,4-benzoquinone (DCBQ), 7,7,8,8-tetracyanoquinodimethane (TCNQ), and tetracyanoethylene (TCNE) in acetonitrile (AN) and by BQ in 50:50 (v/v) AN-water were measured at 25°C. Equilibrium constants for pseudobase formation, K_{R^+}, from the corresponding acridinium ions (**4**) were measured in water at 25°C. Hammett correlations of the second-order rate constants for reaction of the NBA's without *ortho* substitutents (**3***a*–*e*) led to ρ values of −0.29 (BQ, AN), −0.55 (CA), −0.56 (DCBQ), −0.64 (TCNQ), −0.41 (TCNE), and −0.47 (BQ, 50:50 AN–water). The second-order rate constants for **3***a*–*e* also give good linear free energy correlations with the pK_{R^+} values of **4***a*–*e*. These correlations and the pK_{R^+} values for the *ortho*-substituted acridinium ions (**4***f*, *g*, *h*) are used to calculate rate constants for oxidation of the corresponding *ortho*-substituted NBA's (**3***f*, *g*, *h*). The rate constants calculated in this way are 4.7 to 6.6 times and 6.4 to 12 times larger, respectively, than the observed rate constants for *N*-(2,4,6-trimethylbenzyl) and *N*-(2,6-dichlorobenzyl)acridan (**3***g* and *h*). The variations in ρ values are attributed mainly to differences in the amount of electrostatic stabilization in the transition state resulting from differences in the separation of donor and acceptor and the degree of delocalization of the negative charge. The rate retarding effect of a pair of *ortho* substituents is attributed to steric effects in a preferred face-to-face transition state.

ALLAN K. COLTER, CHARLES C. LAI, TERRY W. WILLIAMSON et RAYMOND E. BERRY. Can. J. Chem. **61**, 2544 (1983).

On a étudié les cinétiques d'oxydation d'une série de 8 acridanes ayant un substituant benzyle sur l'azote (**3**, NBA) par la benzoquinone-1,4 (BQ), par le *p*-chloranil (CA), par la dicyano-2,3 benzoquinone-1,4 (DCBQ), par le tétracyano-7,7,8,8 quinodiméthane (TCNQ) et par le tétracyanoéthylène (TCNE) dans l'acétonitrile (AN) et par la BQ dans un mélange 50:50 (v/v) de AN–eau, à 25°C. On a mesuré, dans l'eau à 25°C, la constante d'équilibre de formation de la pseudobase pK_{R^+} à partir des ions acridinium (**4**). Les corrélations de Hammett relatives à la constante de vitesse d'ordre deux de la réaction des NBA sans substituant en position *ortho* (**3***a*–*e*) conduisent à des valeurs de ρ de: −0,29 (BQ, AN), de −0,55 (CA), de −0,56 (DCBQ), de −0,64 (TCNQ), de −0,41 (TCNE) et de −0,47 (BQ, 50:50 AN–eau). La constante de vitesse du deuxième ordre des composés **3***a*–*e* donne également de bonnes corrélations linéaires de l'énergie libre avec les valeurs de pK_{R^+} des composés **4***a*–*e*. On a utilisé ces corrélations et les valeurs du pK_{R^+} des ions acridinium substitués en position *ortho* (**4***f*, *g*, *h*) pour calculer la constante de vitesse d'oxydation des composés NBA (**3***f*, *g*, *h*) correspondants substitués en position *ortho*. Les constantes de vitesse calculées de la sorte sont respectivement de 4,7 à 6,6 fois et de 6,4 à 12 fois plus grandes que les constantes de vitesse observées pour les *N*-(trimethyl-2,4,6 benzyl) et *N(dichloro-2,6)benzylacridane* (**3***g* et *h*). On attribue les variations des valeurs de ρ principalement aux différences dans le taux de stabilisation électrostatique de l'état transition résultant des différences de séparation du donneur et de l'accepteur ainsi qu'au degré de délocalisation de la charge négative. On attribue l'effet retardant de vitesse d'une paire de substituants en position *ortho* aux effets stériques dans une conformation face à face privilégiée de l'état de transition.

[Traduit par le journal]

Introduction

Oxidation of *N*-methylacridan (**1**, NMA) to *N*-methylacridinium ion (**2**) by π acceptors has been investigated (1, 2) as a model for biological redox reactions involving the nicotinamide coenzymes (3, 4) and as a common type of reaction between π donors and π acceptors (5). The net result of this and similar oxidations of dihydropyridines and dihydropyridine benzologues is transfer of a hydride ion from a hydride donor

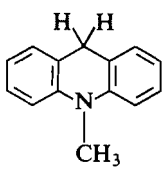

1, NMA

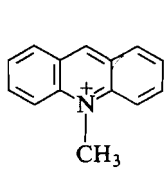

2

such as **1** to a suitable hydride acceptor. In theory, the formal transfer of hydride could occur in a single step or by any of several mechanisms involving transfer of an electron and a hydrogen atom in two steps or two electrons and a proton in three steps. Stepwise mechanisms with an electron transfer as the first step have been suggested for particular hydride transfer reactions on the basis of spin-trapping experiments (2), hydrogen/deuterium isotope effects (6–11), detection of radical products (12), isotopic exchange with solvent (13–15), and substituent effects on the degree of asymmetric induction in reductions by chiral dihydronicotinamides (16). However, there remains considerable disagreement about the interpretation of many of these results. Recently, for example, it has been shown that some of the discrepancies between deuterium isotope effects measured by product and kinetic studies are due to the formation of a covalent adduct intermediate rather than an intermediate formed by electron transfer (17). For most hydride transfers it remains difficult to specify the mechanism with any certainty.

We have previously reported the kinetics and kinetic isotope effects in oxidation of NMA by a series of quinone and cyanomethylene acceptors spanning a greater than 10^7-fold range of reactivity. The present study was initiated with the hope that a change in mechanism or significant changes in transition state structure might be revealed by kinetic substituent effects if studied for a sufficiently wide range of acceptor strengths.

We report here an investigation of substituent effects in the oxidation of a series of *N*-(substituted benzyl)acridans (**3**, NBA's) with a series of 3 benzoquinone and 2 cyanomethylene acceptors (**5**–**9**), eq. [1]. The substituents in compounds **3***a*–*e*

Can. J. Chem. Downloaded from www.nrcresearchpress.com by 210.87.254.40 on 09/06/12
For personal use only.

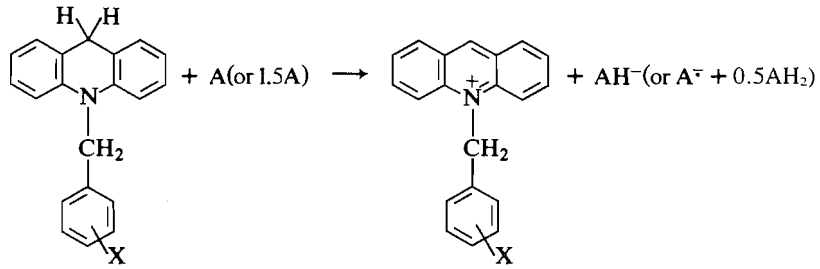

[1]

3

a X = 4-OCH_3
b X = 4-CH_3
c X = H
d X = 4-CN
e X = 4-NO_2

4

f X = 2-CH_3
g X = 2,4,6-$(CH_3)_3$
h X = 2,6-Cl_2

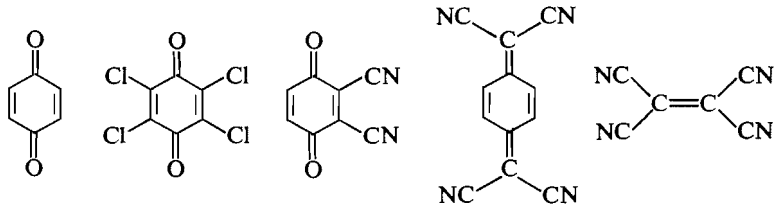

5, BQ **6**, CA **7**, DCBQ **8**, TCNQ **9**, TCNE

are sufficiently remote and insulated from the reaction site so that they are not likely to have any significant effect on the mechanism as compared to that for NMA. Compounds **3***f*, *g*, *h* were included with the hope of learning something about transition state geometry through steric effects of *ortho* substituents.

Results

The product of oxidation of **3** by the five acceptors **5**–**9** is in every case the corresponding *n*-benzylacridinium ion **4**, identified by spectral examination of reaction mixtures and, in selected reactions, by isolation as the perchlorate or chloride salt. The corresponding reduction product of each acceptor, A, is identical to that produced in oxidation of NMA (1, 18), namely AH_2 from BQ + acetic acid, $A^{\cdot-}$ + 0.5 AH_2 from DCBQ, TCNQ, and TCNE, and a mixture of $A^{\cdot-}$, AH^-, and AH_2 from CA. As emphasized earlier (1), the radical anions of **6**–**9** are known to form very rapidly by reaction of AH^- (the product of hydride transfer) with unreacted acceptor ($2AH + A \rightarrow 2A^{\cdot-} + AH_2$), consequently the formation of $A^{\cdot-}$ in these reactions sheds no light on the mechanism of hydride transfer.

All rate measurements were carried out under pseudo first-order conditions using a 30-fold or greater excess of acceptor and following the progress of the reaction as previously described (1). The kinetics followed a first-order rate law through more than 3 half-lives, with pseudo first-order rate constants proportional to acceptor concentration within experimental error. The kinetic results for the NBA's without *ortho* substituents are summarized in Table 1, together with rate constants for NMA included for comparison.

The second-order rate constants in Table 1 are well-correlated by eq. [2] using normal σ values. Best fit slopes (ρ) and intercepts are listed in Table 2.

$$[2] \quad \log k = \rho\sigma + A$$

In order to obtain a measure of the electronic effects of substitution in the *ortho*-substituted NBA's, **3***f*, *g*, and *h*, equilibrium constants for pseudobase formation (20), eq. [3] were measured for all of the *N*-benzylacridium salts (**4**). The results

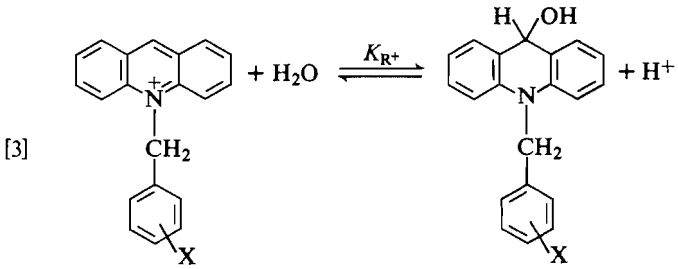

[3]

are summarized in Table 3. The pK_{R^+} values for **4***a*–*e* are also well correlated by Hammett σ values (eq. [4]).

$$[4] \quad pK_{R^+} = -0.794(\text{s.d. } 0.010)\sigma + 8.925(\text{s.d. } 0.005)$$

(corr. coeff. = 0.9996)

The correlations [2] and [4] require a correlation between log *k* for **3***a*–*e* and pK_{R^+} for **4***a*–*e*. This relationship (eq. [5]) is obtained by combination of [2] and [4] with elimination of σ.

$$[5] \quad \log k = \rho \frac{(8.925 - pK_{R^+})}{0.794} + A$$

Lacking appropriate σ values for the *ortho* substituents, the pK_{R^+} values for **4***f*, *g*, and *h* can now be used with eq. [5] to calculate the second-order rate constants for oxidation of **3***f*, *g*, and *h* under the 5 sets of conditions studied. These values are listed in Table 4, together with the observed rate constants for **3***f*, *g*, and *h*, and the ratio of the two values. This comparison is just a way of examining how well the rate constants for oxidation of the *N*-benzylacridans with one or two *ortho* substituents fit the correlation [5] between log *k* and pK_{R^+} defined by the NBA's without *ortho* substituents.

Discussion

Because of the similarity in the reactivities of the NBA's and

Can. J. Chem. Downloaded from www.nrcresearchpress.com by 210.87.254.40 on 09/06/12
For personal use only.

TABLE 1. Rates of oxidation of *N*-(4-substituted benzyl)acridans with π acceptors[a]

Acceptor	[Acceptor], *M*	k (M^{-1} s^{-1})[b] 4-OCH_3 (**4***a*)	4-CH_3 (**4***b*)	4-H (**4***c*)	4-CN (**4***d*)	4-NO_2 (**4***e*)	NMA[c]
BQ[d]	$(1.4-5.8)\times10^{-2}$	3.23×10^{-2}	2.84×10^{-2}	2.35×10^{-2}	1.17×10^{-2}	1.02×10^{-2}	2.54×10^{-2}
BQ[e]	$(0.94-1.9)\times10^{-1}$	7.08×10^{-4}	6.86×10^{-4}	6.25×10^{-4}	3.93×10^{-4}	3.53×10^{-4}	5.79×10^{-4}
TCNQ	$(0.43-1.4)\times10^{-2}$	2.84×10^{-1}	2.65×10^{-1}	2.22×10^{-1}	7.60×10^{-2}	6.59×10^{-2}	2.32×10^{-1}
CA	$(1.8-1.9)\times10^{-3}$	1.20×10	1.08×10	8.60	3.82	3.17	1.17×10
TCNE	4.3×10^{-3}	7.56×10	7.17×10	5.88×10	3.11×10	2.88×10	1.01×10^{2}
DCBQ	$(2.93-3.0)\times10^{-3}$	8.04×10^{3}	7.83×10^{3}	6.07×10^{3}	2.78×10^{3}	2.07×10^{3}	8.67×10^{3}

[a]Temperature 25.0°C. Solvent acetonitrile unless otherwise specified; [*N*-benzylacridan] = $2-7\times10^{-5}$ *M*.
[b]Psuedo first-order rate constant ÷ [acceptor]. Reproducibilities ±2% with BQ and CA, ± 3% with TCNE and DCBQ, and ±5% with TCNQ.
[c]Reference 1. Acceptor concentrations are those in ref. 1.
[d]50:50 (v/v) acetonitrile − water containing 0.01 *M* acetic acid.
[e]0.01 *M* acetic acid added.

TABLE 2. Hammett correlations for reaction of *N*-(4-substituted benzyl)acridans with π acceptors[a]

Acceptor	ρ ± std. dev.[b]	Intercept, *A* ± std. dev.	Correlation coefficient
BQ[c]	−0.47±0.01	−1.624±0.002	0.9998
BQ	−0.29±0.01	−3.216±0.004	0.998
TCNQ	−0.64±0.02	−0.689±0.010	0.997
CA	−0.55±0.01	0.936±0.003	0.9997
TCNE	−0.41±0.01	1.774±0.004	0.999
DCBQ	−0.56±0.02	3.780±0.012	0.995

[a]Least-squares slope and intercept of plot of log k vs. σ (taken from ref. 19).
[b]Estimated uncertainties in p: ±0.04 for TCNQ, ±0.02 for all others.
[c]50:50 (v/v) acetonitrile − water.

NMA under the same conditions (Table 1), we assume in the discussion which follows that earlier mechanistic conclusions based on solvent effects (1), deuterium labelling experiments (1), and spin-trapping experiments (2) are equally valid for oxidation of an NBA under the same conditions.

Before discussing the substantial differences in ρ values we note first that the results are consistent with a transition state having a partial positive charge on the hydride donor (NBA) for all of the reactions studied. The ρ value for the pK_{R^+} correlation (−0.79) can be taken as a measure of the sensitivity to substitution in the phenyl ring expected for development of a full positive charge, well separated from the negative charge on the acceptor, in aqueous solution. In AN the absolute value of ρ, i.e., |ρ|, is expected to be somewhat larger than 0.79. Bunting *et al.* (22) have compared ρ values for oxidation of *N*-(substituted benzyl)dihydronicotinamides by three quaternary heterocyclic cations in 20% AN − 80% water, with ρ values for dissociation of the cyanide adduct of the corresponding pyridinium ion oxidation product in the same solvent. Based on the assumption that |ρ| is proportional to charge development, these comparisons led to estimates of 0.7 to 0.8 of a full positive charge on the hydride donor in the transition state. If valid, these estimates exclude a mechanism involving reversible electron transfer followed by rate-determining hydrogen atom transfer in which the donor would bear a full positive charge in the rate-determining transition state. Our results strongly point to a similar conclusion for the hydride transfers studied in this work. However, as discussed later, in reaction of an uncharged donor with an uncharged acceptor the |ρ| value could be significantly reduced if the developing positive and negative charges are in close proximity.

TABLE 3. pK_{R^+} values for *N*-(substituted benzyl)acridinium ions (**5**)[a]

Substituted	pK_{R^+} ± std. dev.[b]
4-OCH_3 (**5***a*)	9.139±0.022
4-CH_3 (**5***b*)	9.061±0.025
None (**5***c*)	8.923±0.030
4-CN (**5***d*)	8.384±0.007
4-NO_2 (**5***e*)	8.322±0.014
2-CH_3 (**5***f*)	8.878±0.025
2,4,6-$(CH_3)_3$	8.880±0.010
2,6-Cl_2	8.357±0.032
NMA	9.999±0.021[c]

[a]Temperature 25.0°C. Corrected to zero ionic strength in aqueous solution (see Experimental).
[b]Averages of 7 or more values measured over a range of 1.0−1.3 pH units.
[c]Literature (21) 9.86 ± 0.06 (uncorrected for ionic strength).

In considering possible reasons for the substantial differences in the |ρ| values in Table 2 it is instructive to first consider the changes in transition state structure expected on changing from a relatively unreactive hydride acceptor and weak electron acceptor such as BQ (E^0_{red} in AN = −0.51 V vs. SCE (23)) to DCBQ, which is 10^7 times as reactive in oxidation of NMA and which is a much stronger electron acceptor (E^0_{red} in AN = 0.31 V vs. SCE (24)). The results of our earlier studies with NMA (1, 2) as well as those of the present studies with NBA's are equally compatible with a one-step hydride transfer mechanism [6] or with a three-step electron−proton−electron mechanism [7] in which the proton transfer step is rate-determining.

[6] $DH + A \rightarrow D^+ + AH^-$

[7] $DH + A \underset{k_{-1}}{\overset{k_1}{\rightleftharpoons}} DH^+ A^- \xrightarrow[k_2]{\text{slow}} D\,AH^{\cdot} \xrightarrow{\text{fast}} D^+ + AH^-$

(DH represents hydride donor (NMA or NBA) and A the hydride (or π) acceptor.)

Following an argument first presented by Verhoeven and co-workers (25), we can now ask whether the radical cation − radical anion pair intermediate, DH^+A^-, of [7] is energetically accessible in the reactions investigated in this work. The standard free energy change accompanying formation of DH^+A^- from DH + A in AN is given by (25, 26):

[8] $\Delta G^0 = E^0_{ox}(DH/DH^+) - E^0_{red}(A/A^-) - C$

where $E^0_{ox}(DH/DH^+)$ is the standard one-electron oxidation

Can. J. Chem. Downloaded from www.nrcresearchpress.com by 210.87.254.40 on 09/06/12
For personal use only.

TABLE 4. Comparison of measured and calculated rates of oxidation of *N*-(*ortho*-substituted benzyl)acridans[a]

Acceptor	k (M^{-1} s^{-1}), obsd.	k (M^{-1} s^{-1}), calcd.[b]	k_{obsd}/k_{calcd}[c]
	2-CH_3 (**4***f*)		
BQ[d]	2.49×10^{-2}	2.23×10^{-2}	1.12±0.13
BQ	7.06×10^{-4}	5.84×10^{-4}	1.21±0.11
TCNQ	2.79×10^{-1}	1.88×10^{-1}	1.49±0.26
CA	1.07×10	8.01	1.34±0.17
TCNE	6.92×10	5.62×10	1.23±0.13
DCBQ	7.35×10^{3}	5.58×10^{3}	1.32±0.16
	2,4,6-$(CH_3)_3$ (**4***g*)		
BQ[d]	3.82×10^{-3}	2.24×10^{-2}	$1.71\pm0.18 \times 10^{-1}$
BQ	1.24×10^{-4}	5.85×10^{-4}	$2.12\pm0.18 \times 10^{-1}$
TCNQ	3.82×10^{-2}	1.89×10^{-1}	$2.02\pm0.33 \times 10^{-1}$
CA	1.34	8.03	$1.63\pm0.19 \times 10^{-1}$
TCNE	1.01×10	5.63×10	$1.79\pm0.18 \times 10^{-1}$
DCBQ	8.49×10^{2}	5.60×10^{3}	$1.52\pm0.17 \times 10^{-1}$
	2,6-Cl_2		
BQ[d]	9.43×10^{-4}	1.10×10^{-2}	$0.86\pm0.13 \times 10^{-1}$
BQ	4.44×10^{-5}	3.75×10^{-4}	$1.18\pm0.13 \times 10^{-1}$
TCNQ	8.40×10^{-3}	7.21×10^{-2}	$1.17\pm0.26 \times 10^{-1}$
CA	3.01×10^{-1}	3.50	$0.86\pm0.14 \times 10^{-1}$
TCNE	4.07	3.01×10	$1.35\pm0.19 \times 10^{-1}$
DCBQ	3.78×10^{2}	2.41×10^{3}	$1.57\pm0.26 \times 10^{-1}$

[a]25.0°C, other conditions as in Table 1.
[b]Calculated using eq. [5] together with appropriate values of ρ (Table 2) and pK_{ROH} (Table 3).
[c]Experimental uncertainties from propagation of errors calculations using the estimated uncertainties in rate constants (footnote to Table 1) and ρ (footnote to Table 2), and standard deviations in pK_{ROH} (Table 3).
[d]50:50 (v/v) AN–water containing 0.01 *M* acid.

potential of the donor, $E^0_{red}(A/A^{\cdot-})$ the standard reduction potential of A (vs. the same reference), and C is the coulombic stabilization of the $DH^{+}A^{\cdot-}$ ion pair (about 0.06 eV in AN (26)). For strongly endothermic electron transfer the standard free energy of activation, $\Delta G^{\ddagger}$, can be approximated by ΔG^0, and the rate constant for electron transfer calculated from eq. [9] (27).

$$[9] \quad k_{ET} = 10^{11}\, e^{-\Delta G^{\ddagger}/RT}\, M^{-1}\, s^{-1}$$

The value of E^0 (DH/DH^{+}) cannot be measured precisely electrochemically because of the irreversibility of the one-electron oxidation on the time scale of the electrochemical measurements. However, from CV measurements on a series of acridans (28) a value of about 0.78 V (vs. SCE) can be estimated for NMA. Using this value, eqs. [8] and [9] lead to a value of 1.2×10^{-10} M^{-1} s^{-1} for k_{ET} from NMA to BQ. This value is 3×10^6 times smaller than the observed rate constant for oxidation of NMA by BQ, hence the radical ion pair $NMA^{+}BQ^{\cdot-}$ would appear to be an unlikely reaction intermediate. However, this discrepancy decreases with increasing reduction potential among the quinone oxidants studied and with DCBQ the calculated k_{ET} is 1.3 times the observed rate of oxidation of NMA by DCBQ. Successful trapping of the *N*-methyl-9-acridanyl radical (D˙) in this hydride transfer is evidence that a three-step mechanism is followed at least in part. With the cyanomethylene acceptors TCNQ (E^0_{red} vs. SCE = 0.19 V (29)) and TCNE (E^0_{red} vs. SCE = 0.24 V (29)) the calculated values of k_{ET} are 6×10^2 and 9 times larger, respectively, than their measured rate constants for oxidation of NMA, suggesting that mechanism [7] is at least possible in these reactions.

Application of the Hammond postulate to either of the mechanisms [6] or [7] leads to the prediction that |ρ| for a series of structurally-related acceptors should decrease with increasing acceptor reactivity. With the one-step mechanism [6], increasing acceptor reactivity is predicted to result in a more reactant-like transition state with less charge development. In the e^-, H^+, e^- mechanism [7] the charges in the radical ion pair intermediate are partially neutralized in the slow proton transfer (k_2) step. For the quinone acceptors the basicity of $A^{\cdot-}$ decreases with increasing acceptor reduction potential (30), hence k_2 should decrease at the same time, leading to a more product-like transition state with more complete charge neutralization. The same conclusion concerning the k_2 step in [7] is required by the observation (1)[1] that the observed rate constant for oxidation of NMA with quinones increases more slowly with increasing reduction potential than would the ratio k_1/k_{-1}.

Clearly, the observed ρ values, except those for TCNQ (−0.64) and TCNE (−0.41) are not in accord with these predictions. Furthermore, the two cyanomethylene acceptors are the most likely to react via a stepwise mechanism, yet their |ρ| values are the highest and second lowest, respectively. The ρ values alone therefore do not provide any clear evidence for a change in mechanism.

The observation that the rates of oxidation by BQ, the least reactive acceptor, are the least sensitive to substitution was unexpected. It is possible that the substituents in CA and TCNQ, as well as the greater delocalization of negative charge with these acceptors results in a transition state with greater charge separation and consequently less electrostatic stabilization of the developing positive charge.

The increase in |ρ| accompanying the change from AN to AN–water solvent is also unexpected. If the most important effect of water cosolvent is more effective solvation of the

[1]G. Saito. Unpublished results.

Can. J. Chem. Downloaded from www.nrcresearchpress.com by 210.87.254.40 on 09/06/12
For personal use only.

TABLE 5. Physical data for *N*-benzylacridinium salts

Benzyl substituent	Anion	Melting point (°C)[a]	Mass spectrum (*m/e*)	^{1}H nmr, ppm[b]			
				Benzyl H[c]	Phenyl H	Acridine H	Substituent
4-Methoxy	Cl^-	188–190	300(M^+),299,180,179,121	6.7	7.2 (s, 4H)	7.8–8.6[d] 9.9[e]	4.0 (s, 3H)
4-Methyl	Br^-	233–235	285,284(M^+),180,179,105	6.7	7.3 (s, 4H)	7.8–8.6[d] 10.0[e]	2.4 (s, 3H)
None	Br^-	203–207	271,270(M^+),180,179,91	6.7	6.8–7.4 (m, 5H)	7.8–8.6[d] 9.9[e]	—
4-Cyano	Br^-	182–186	295(M^+),294,180,179,116	6.8	7.4(AA′BB′q, 4H)	7.8–8.6[d] 10.0[e]	—
4-Nitro	Br^-	280–295	315(M^+),314,179	6.9	7.3–7.7 (m, 4H)	7.8–8.6[d] 9.9[e]	—
2-Methyl	Br^-	170–205	285,284(M^+),180,179,105	6.5	6.8–7.5 (m, 4H)	7.8–8.6[d] 9.9[e]	2.8 (s, 3H)
2,4,6-Trimethyl	ClO_4^-	240–246	313(M^++1),180,179,133	6.57	6.83 (s, 2H)	7.8–8.6[d] 9.8[e]	1.84 (s, 6H) 2.24 (s, 3H)
2,6-Dichloro	Br^-	245–270	341,339(M^+),180,179,161,159	6.7	7.5 (s, 3H)	7.8–8.6[d] 9.9[e]	—

[a]All melted with decomposition with darkening around 150°C.
[b]Trifluoroacetic acid solvent.
[c]s, 2H.
[d]m, 8H.
[e]s, 1H, acridinium 9-H.

developing negative charge on the acceptor, an increased separation of charge in the transition state with consequent decreased stabilization of the developing positive charge, and a larger $|\rho|$ value, could result.

The ρ value for pseudobase formation (−0.79) is to be compared with values of −1.32 and −1.14 for pseudobase formation from *N*-(substituted benzyl)-5-nitroquinolinium and 5-nitroisoquinolinium ions, respectively (31). The difference must reflect more extensive charge delocalization in the acridinium ions.

A single *ortho* methyl group in the *N*-benzylacridinium ions has an acidifying effect of 0.045 pK_a units, while the acidifying effect of two *ortho* methyl groups (**4***g* vs. **4***b*) is 0.181 pK units. No earlier examples of reversal of the normal effect of methyl substitution are known in pseudobase formation; however, numerous analogies are known with Brönsted acids. For example, the pK_a's of substituted benzylammonium ions fall in the order 4-methyl- > unsubstituted > 2-methyl (32). The usual explanation is steric inhibition of solvation (33).

As noted above, the rate constants for oxidation of **3***g* and *h* are 4.7 to 6.6 and 6.4 to 12 times smaller, respectively, than predicted by [5] from the pK_{R^+} values of **4***g* and *h*. Molecular models indicate that NBA's having two *ortho* substituents are forced to adopt a conformation in which the phenyl and heterocyclic rings are perpendicular and in which the nitrogen atom is shielded from both sides by the two *ortho* substituents. The perpendicular conformation is supported by nmr studies on *ortho*-substituted *N*-benzylpyridinium ions (34) and by nmr and dipole moment measurements and force field calculations on substituted diphenylmethanes (35). The *ortho* substituents in a conformation of this kind prevent an ideal face-to-face transition state in which electrostatic attraction between the positive and negative charges and π−π charge transfer interaction are maximized. The discrepancies between the calculated and observed rate constants for **3***g* and *h* therefore provide strong evidence for a face-to-face relationship between the donor and acceptor in the transition state. Given the differing steric requirements of the different acceptors and the differing degrees of charge delocalization, both of which will affect the degree of stabilization to be gained from an ideal face-to-face arrangement, it is perhaps surprising that the discrepancies between the calculated and observed rate constants for **3***g* and *h* are so similar.

Using eq. [5] and the pK_R- value for **2** it is also possible to predict a rate constant for NMA in each of the oxidations studied in this work. The rate constants calculated in this way are uniformly greater than the measured rate constants for NMA, the discrepancies varying from a factor of 2.6 (BQ in AN) to 6.4 (TCNQ). Speculation on the origin of these differences must await a more extensive investigation of substituent effects.

Experimental

Melting points were measured in open capillary tubes and are uncorrected. Proton nmr spectra were measured using Varian T60 or A60 spectrometers. Chemical shifts are reported in δ units, with tetramethylsilane as internal standard. Ultraviolet–visible spectra were obtained using Unicam SP800, Beckman 24, or Cary 118C spectrophotometers. Mass spectra were measured with a Varian Mat CH7 mass spectrometer. Elemental microanalyses were performed by Guelph Chemical Laboratories, Guelph, Ontario, or by MHW Laboratories, Phoenix, Arizona.

Reagents and solvents

BQ, CA, DCBQ, TCNE, and TCNQ were obtained and purified as previously described (1). Borax buffers (pH 8.00–9.40) were prepared from Fisher Scientific sodium hydroxide and hydrochloric acid solutions, and sodium tetraborate (Fisher, reagent) following Bates (36). Reagent grade acetonitrile was purified as described previously (1).

N-*Benzylacridinium salts* (**4**)

Six of the *N*-benzylacridinium bromides (all except **4***g* and *h*) were prepared by alkylation of acridine. Acridine (1.79 g, 0.010 mol) was heated with 0.015 mol of the appropriate benzyl bromide at 120°C (oil bath) for 24 h in a stoppered flask. (All of the bromides were commercially available except for *p*-methoxybenzyl bromide, which was prepared from the corresponding alcohol (37).) The resulting black solids were washed with large portions of ether until the washings were

Can. J. Chem. Downloaded from www.nrcresearchpress.com by 210.87.254.40 on 09/06/12
For personal use only.

TABLE 6. Physical data for *N*-benzylacridans

Benzyl substituent	Melting point (°C)	Mass spectrum (*m/e*)	^{1}H nmr, ppm[a] Benzyl H[b]	Acridan methylene[b]	Aromatic H	Substituent
4-Methoxy	133–135	301(M^+),180,179,121	4.99	4.01	6.6–7.4 (m, 12H)	3.73 (s, 3H)
4-Methyl	106.5–108	285(M^+),180,179,105	5.12	4.10	6.6–7.3 (m, 12H)	2.33 (s, 3H)
None	113–115	217(M^+),180,179,91	5.10	4.07	6.7–7.4 (m, 13H)	—
4-Cyano	163–163.5	296(M^+),180,179,116	5.15	4.05	6.4–7.6 (m, 12H) 6.5–7.6 (m, 10H)	—
4-Nitro	173–175	316(M^+),180,179	5.20	4.08	8.2 (d, 2H)	—
2-Methyl	150–152	285(M^+),180,179,105	5.01	4.11	6.4–7.2 (m, 12H)	2.44 (s, 3H) 2.20 (s, 3H)
2,4,6-Trimethyl	136–138	313(M^+),180,179,133	5.00	3.92	6.6–7.4 (m, 10H)	2.32 (s, 6H)
2,6-Dichloro	177–178	342,340,(M^+),180,179,161,159	5.31	3.88	6.8–7.4 (m, 11H)	—

[a]$CDCl_3$ solvent.
[b]s, 2H.

TABLE 7. Analytical data for *N*-benzylacridans

Benzyl substituent	C calcd.	C found	H calcd.	H found	N calcd.	N found
4-Methoxy	83.69	83.73	6.35	6.44	4.65	4.66
4-Methyl	88.38	88.49	6.71	6.74	4.91	4.75
None	88.52	88.79	6.31	6.21	5.16	5.35
4-Cyano	85.11	85.41	5.44	5.12	9.45	9.10
4-Nitro	75.93	75.88	5.10	4.91	8.85	8.61
2-Methyl	88.38	88.33	6.71	6.41	4.91	5.01
2,4,6-Trimethyl	88.14	88.13	7.40	7.22	4.47	4.76
2,6-Dichloro	Cl calcd. 20.84			Cl found 20.57		

almost colourless. The crude products were dissolved in the minimum amount of hot ethanol and precipitated by addition of ether at 0°C. The greenish powders were vacuum dried for 12 h at 78°C. Yields of salts prepared in this way were around 40%, and they were often contaminated by varying amounts of acridinium bromide. All attempts to obtain **4***g* and *h* in this way were unsuccessful.

Higher purity *N*-benzylacridinium salts were obtained by oxidation of the corresponding NBA's (below) with 2,3-dichloro-5,6-dicyano-1,4-benzoquinone (DDQ) and isolation as the chloride or perchlorate. In a typical oxidation a solution of 0.85 g (3.7×10^{-3} mol) of DDQ in 125 mL of ether was added dropwise to a stirred solution of 3.5×10^{-3} mol of the NBA in 25 mL of ether at room temperature. Hydrogen chloride gas was passed through the black suspension until the solution turned clear, and the precipitated chloride salt isolated in essentially quantitative yield by filtration. Alternatively, the perchlorate salt could be isolated by addition of 3.0 mL of 70% $HClO_4$, instead of HCl gas, to the initial ether suspension. The crude product was purified by repeated solution in 10 mL of methanol followed by precipitation by addition of 50 mL of ether. The *N*-benzylacridinium salts melted with decomposition with darkening around 150°C. Their uv–visible spectra were all similar to that of *N*-methylacridinium cation (38) with characteristic maxima at 342, 358, 400, 420, and 440 nm in 0.01 mol dm^{-3} aqueous HCl solution. The *N*-benzylacridinium salts were further characterized by their ^{1}H nmr and mass spectra (Table 5) as well as by reduction to the corresponding NBA's (below). The mass spectra showed characteristic peaks at *m/e* corresponding to the cation of the salt (M^+) and often $M^+ + 1$, 179 and/or 180 (acridine and acridine + H) and (except for **4***e*) $M^+ - 179$, corresponding to a substituted benzyl cation. Similar results with quaternary pyridinium salts have been interpreted as arising from thermal reduction to the corresponding dihydro derivative (in this work, NBA's) prior to evaporation (39).

*N-Benzylacridans (**3**, NBA's)*

The NBA's were prepared by sodium borohydride reduction of the corresponding *N*-benzylacridinium salts as described earlier for *N*-methylacridinium salts (1). Yields were quantitative. All of the NBA's except **4***e* were also prepared by reaction of the lithium salt of acridan with the appropriate benzyl bromide. The following procedure for **4***d* is typical. To a stirred solution of 1.5 g (8.3×10^{-3} mol) of acridan in dry tetrahydrofuran (THF) under a nitrogen atmosphere and connected to a mercury bubbler was added 10 mL of 1.6 *M* butyllithium in hexane. The solution immediately turned purple with evolution of butane. After addition of gas stopped (ca. 5 min), a solution of 1.7 g (8.7×10^{-3} mol) of 4-cyanobenzyl bromide in 25 mL of THF was added. The solution turned a clear straw color after a few seconds. The THF was distilled off to a volume of about 15 mL and 85 mL of ether added. The ether solution was washed with water, dried over $MgSO_4$, filtered, and evaporated to yield a pale yellow solid which was crystallized from ethanol to yield 1.0 g (41% of theory) of white needles, mp 163–163.5°C. The NBA's were characterized by their ^{1}H nmr and mass spectra and by elemental analysis (Tables 6 and 7).

Kinetic measurements

Kinetic measurements were carried out spectrophotometrically as previously described for NMA (1). Measurements were carried out under pseudo first-order conditions using a 30-fold or greater excess of acceptor. The progress of the reaction was followed at the acridinium ion absorption maxima at 357.5–359 nm (BQ, CA, TCNE) or 420 nm (DCBQ), or the acceptor radical anion absorption at 680 or 725 nm (TCNQ). First-order plots were linear through at least 3 half-lives.

Final absorbances were constant for at least 20 half-lives in all rates except those involving oxidation of **3***a–f* with BQ in AN, where optical densities decreased very slowly after 7 to 10 half-lives. The uv–visible spectra of solutions of the *N*-benzylacridinium perchlorates, **4** ClO_4^-, in AN or 50:50 AN–water showed no detectable change over the periods of time involved in the rate measurements.

With BQ in 50:50 AN–water, CA, TCNE, and DCBQ infinite time absorbances (after subtraction of the absorbance due to the radical anion reduction products) agreed within ±5% of the values predicted from independently measured absorbances of **4** ClO_4^- in AN or AN–water. The final absorbances in the rates with BQ in AN were approximately 75% of the expected value with all donors. The reason for this discrepancy is not clear; however no product other than the *N*-benzylacridinium ion could be detected by uv–visible spectroscopy and **4***c* ClO_4^- was isolated in 88% yield in oxidation of **3***c* with BQ in AN (below). The absorbance due to **4** is masked in the TCNQ rates; however, uv–visible spectroscopy showed that the theoretical amount of $TCNQ^-$ was produced.

To further confirm that the NBA's are cleanly oxidized to the corresponding *N*-benzylacridinium ion, the products of oxidation of **3***c* and/or **3***d* by all acceptors in AN and by BQ in 50:50 AN–water

Can. J. Chem. Downloaded from www.nrcresearchpress.com by 210.87.254.40 on 09/06/12
For personal use only.

Can. J. Chem. Downloaded from www.nrcresearchpress.com by 210.87.254.40 on 09/06/12
For personal use only.

were isolated as the perchlorate salt. The following procedure is typical. A mixture of 0.0970 g (3.57×10^{-4} mol) of **3***c* and 0.0470 g (4.35×10^{-4} mol) of BQ was dissolved in 2 mL of AN containing 20 μL of anhydrous acetic acid. After 40 h at room temperature (correspondingly shorter times with 50:50 AN–water solvent and with the more reactive acceptors), the mixture was transferred to 50 mL of ether and 1 mL of 60% aqueous $HClO_4$ added. Filtration yielded 0.1165 g (88.1%) of **4** ClO_4^-, shown to be pure by quantitative uv–visible spectroscopy. Yields of 80–90% were obtained in the other product isolations.

pK_a measurements

The pK_a values were determined as described by Albert and Serjeant (40). Optical densities were measurd using a Guilford model 200 spectrophotometer with the cell compartment maintained at 25.00 ± 0.05°C, and were reproducible to ±0.002. pH measurements were carried out with a Beckman Research model pH meter equipped with a Sargent model DS-30072-15 combination glass–thallium amalgam electrode, in a jacketted cell mainained at 25.00 ± 0.05°C. A 0.01 *M* sodium tetraborate solution (pH = 9.180 at 25.0°C) was used as the primary pH standard. The pH readings were stable for at least 1 h and were reproducible to ±0.002 pH units. Solutions were prepared by dilution of 5.00 mL aliquots of a 10^{-4} *M* stock solution of the chloride or bromide salt to 50.00 mL with 0.01 *M* hydrochloric acid and 0.01 *M* sodium hydroxide solutions. Spectra were recorded from 300–500 nm in order to ensure stability of the acridinium ion and pseudobase. All of the salts had an adsorption maximum near 358 nm ($\epsilon \sim 2.6 \times 10^4$) where the pseudobase had no measurable absorbance at these concentrations. The position of this maximum was chosen as the analytical wavelength. A series of 7 or 8 solutions covering a pH range of at least 1.0 between 10% and 90% pseudobase formation was then prepared by dilution of the stock solution with borax buffers, and the pH and optical density (1 cm cell) at the analytical wavelength measured for each solution. With **4***h*, precipitation of pseudobase occured at 10^{-5} *M* concentrations necessitating further dilution to about 2×10^{-6} *M* and use of a 10-cm cell. Following each pH measurement the pH meter was rechecked with standard buffer to confirm instrumental stability during the measurements.

The aqueous stock solutions and the solutions of salts in 0.01 *M* hydrochloric acid showed no detectable change in absorbance after 48 h. The more basic buffer solutions faded slowly, particularly those of **4***a* and **4***g* which showed a detectable decrease after about 20 min. Absorbance readings were taken between 5 and 15 min of preparation of the solutions, during which no detectable change in absorbance occurred. The reaction responsible for the decrease in absorbance was not investigated.

A "mixed" pK_a value, pK_a^M (40) was calculated from each set of measurements using the equation

$$[10] \quad pK_a^M = pH + \log\frac{[OD - OD_{base}]}{OD_{acid} - OD}$$

where OD, OD_{base}, and OD_{acid} are the optical densities of the solution prepared from buffer, NaOH, and HCl solutions. Each "mixed" constant so obtained was corrected to zero ionic strength by means of the expression (40)

$$[11] \quad pK_a = pK_a^M - \frac{0.507\, I^{1/2}}{1 + 1.6\, I^{1/2}}$$

where I is the ionic strength for the particular buffer (36). Corrections varied from −0.048 to −0.067.

Acknowledgements

Financial support from the Natural Sciences and Engineering Research Council of Canada is gratefully acknowledged.

1. A. K. COLTER, G. SAITO, and F. J. SHAROM. Can. J. Chem. **55**, 2741 (1977).
2. C. C. LAI and A. K. COLTER. J. Chem. Soc. Chem. Commun. 1115 (1980).
3. R. J. KILL and D. A. WIDDOWSON. *In* Bioorganic chemistry. Vol. IV. *Edited by* E. E. van Tamelen. Academic Press, New York. 1978. p. 239.
4. D. S. SIGMAN, J. HAJDU, and D. S. CREIGHTON. *In* Bioorganic chemistry. Vol. IV. *Edited by* E. E. van Tamelen. Academic Press, New York. 1978. p. 385.
5. A. K. COLTER and M. R. J. DACK. *In* Molecular complexes. Vol. 2. *Edited by* R. Foster. Crane Russak, New York. 1974. p. 1.
6. J. J. STEFFENS and D. M. CHIPMAN. J. Am. Chem. Soc. **93**, 6694 (1971).
7. D. J. CREIGHTON, J. HAJDU, G. MOOSER, and D. S. SIGMAN. J. Am. Chem. Soc. **95**, 6855 (1973).
8. D. J. CREIGHTON, J. HAJDU, and D. S. SIGMAN. J. Am. Chem. Soc. **98**, 4619 (1976).
9. P. VAN EIKEREN and D. L. GRIER. J. Am. Chem. Soc. **99**, 8057 (1977).
10. (a) A. OHNO, H. YAMAMOTO, and S. OKA. J. Am. Chem. Soc. **103**, 2041 (1981); (*b*) A. OHNO, T. SHIO, H. YAMAMOTO, and S. OKA. J. Am. Chem. Soc. **103**, 2045 (1981).
11. S. SHINKAI, T. TSUNO, and O. MANABE. CHEM. LETT. 1203 (1981).
12. A. OHNO and N. KITO. Chem. Lett. 369 (1972).
13. P. VAN EIKEREN, P. KENNEY, and R. TOKMAKIAN. J. Am. Chem. Soc. **101**, 7402 (1979).
14. S. YASUI, K. NAKAMURA, A. OHNO, and S. OKA. Bull. Chem. Soc. Jpn. **55**, 196 (1982).
15. S. SHINKAI, T. TSUNO, and O. MANABE. J. Chem. Soc. Chem. Commun. 592 (1982).
16. A. OHNO, J. NAKAI, K. NAKAMURA, T. GOTO, and S. OKA. Bull. Chem. Soc. Jpn. **54**, 3486 (1981).
17. D. M. CHIPMAN, R. YANIV, and P. VAN EIKEREN. J. Am. Chem. Soc. **102**, 3244 (1980).
18. G. SAITO and A. K. COLTER. Tetrahedron Lett. **38**, 3325 (1977).
19. D. H. MCDANIEL and H. C. BROWN. J. Org. Chem. **23**, 420 (1958).
20. J. W. BUNTING. *In* Advances in heterocyclic chemistry. Vol. 25. *Edited by* A. R. Katritzky and A. J. Boulton. Academic Press, New York. 1979. p. 1.
21. J. W. BUNTING and W. G. MEATHREL. Can. J. Chem. **50**, 917 (1972).
22. (*a*) J. W. BUNTING and S. SINDHUATMADJA. J. Org. Chem. **46**, 4211 (1981); (*b*) J. W. BUNTING, V. S. F. CHEW and G. CHU. J. Org. Chem. **47**, 2308 (1982).
23. M. E. PEOVER. J. Chem. Soc. 4540 (1962).
24. R. M. SCRIBNER. J. Org. Chem. **31**, 3671 (1966).
25. F. M. MARTENS, J. W. VERHOEVEN, R. A. GASE, U. K. PANDIT, and TH. J. DE BOER. Tetrahedron, **34**, 443 (1978).
26. D. REHM and A. WELLER. Ber. Bunsenges. Phys. Chem. **73**, 834 (1969).
27. B. A. KOWERT, L. MARCOUX, and A. J. BARD. J. Am. Chem. Soc. **94**, 5538 (1972).
28. E. STURM. H. KIESELE, and E. DALTROZZO. Chem. Ber. **111**, 227 (1978).
29. M. E. PEOVER. Trans. Faraday Soc. **58**, 2370 (1962).
30. (*a*) E. HAYON and M. SIMIC. Acc. Chem. Res. **7**, 114 (1974); (*b*) P. S. RAO and E. HAYON. J. Phys. Chem. **77**, 2274 (1973).
31. J. W. BUNTING and D. J. NORRIS. J. Am. Chem. Soc. **99**, 1189 (1977).
32. W. H. CAROTHERS, C. F. BICKFORD, and G. J. HURWITZ. J. Am. Chem. Soc. **49**, 2908 (1927).
33. J. HINE. Structural effects on equilibria in organic chemistry. Wiley–Interscience, New York. 1975. p. 168.
34. G. MONTAUDO, G. KRUK, and J. W. VERHOEVEN. Tetrahedron Lett. 1841 (1974).
35. (*a*) G. MONTAUDO, S. CACCAMESE, and P. FINOCCHIARO. J. Am. Chem. Soc. **93**, 4202 (1971); (*b*) G. MONTAUDO and P.

FINOCCHIARO. J. Am. Chem. Soc. **94**, 6745 (1972).
36. R. G. BATES. Determination of pH. 2nd ed. John Wiley and Sons, New York, NY. 1972. p. 462.
37. R. C. COOKSON and S. R. WALLIS. J. Chem. Soc. B, 1245 (1966).
38. J. W. BUNTING and W. G. MEATHREL. Can. J. Chem. **52**, 981 (1974).
39. (*a*) P. ELLINGSEN, G. HVISTENDAHL, and K. UNDHEIM. Org. Mass Spectrom. **13**, 455 (1978); (*b*) E. LARSEN, H. EGSGAARD, and H. HOLMEN. Org. Mass Spectrom. **13**, 417 (1978).
40. A. ALBERT and E. P. SERJEANT. The determination of ionization constants. Chapman and Hall Ltd., London 1971. p. 44.

Can. J. Chem. Downloaded from www.nrcresearchpress.com by 210.87.254.40 on 09/06/12
For personal use only.

A constrained configuration interaction method

G. D. ZEISS and M. A. WHITEHEAD

Chemistry Department, McGill University, 801 Sherbrooke Street West, Montreal, P.Q., Canada H3A 2K6

Received February 21, 1983

G. D. ZEISS and M. A. WHITEHEAD. Can. J. Chem. **61**, 2552 (1983).

Constrained configuration interaction (CI) wavefunctions (CVM-CI) were determined using the modified perturbation–iteration (MPI) method, two approximate versions of the MPI method, and the secant-parameterization method. The results of constrained CI calculations on CO using a 25 configuration wavefunction showed that the MPI method converged rapidly, and that the secant-parameterization method was computationally more economical.

G. D. ZEISS et M. A. WHITEHEAD. Can. J. Chem. **61**, 2552 (1983).

On a déterminé les fonctions d'onde (CVN-IC) d'interaction de configuration (IC) contrainte en utilisant la méthode modifiée de perturbation–itération (MPI), deux versions approximatives de la méthode MPI ainsi que la méthode de paramétrisation séquentielle. Les résultats des calculs de IC contrainte, effectués sur le CO en utilisant une fonction d'onde à 25 configurations, montrent que la méthode MPI converge rapidement et que la méthode de paramétrisation séquentielle est, du point de vue du temps de calcul, plus économique.

[Traduit par le journal]

Can. J. Chem. Downloaded from www.nrcresearchpress.com by 210.87.254.105 on 09/06/12
For personal use only.

Introduction

The variational problem of minimizing the energy of the trial wavefunction which is constrained to give a known theoretical or experimental expectation value of an operator is well known, and becomes even more difficult when the trial wavefunction is a configuration interaction expansion.

An earlier attempt (1, 4*a*) to solve constrained secular equations for configuration interaction calculations, the modified perturbation–iteration method, MPI, needed an initially fully diagonalized Hamiltonian matrix, which is a serious computational disadvantage, because for large CI expansions, the time required to fully diagonalize the Hamiltonian is formidable. Therefore two approximate MPI methods which use a partially diagonalized Hamiltonian matrix and the secant-parameterization procedure which does not require the Hamiltonian matrix to be diagonal will be developed and their results compared to those from the MPI method using a diagonalized Hamiltonian matrix. The test molecule is CO with a 25 configuration CI wavefunction on which the constrained calculations are performed. The relative accuracies and computational efficiencies of the methods will be compared.

The constrained configuration interaction equations

The general form of a CI wavefunction (2, 3) is

$$[1] \quad \psi_{CI} = \sum_i c_i \Phi_i$$

The Φ_i are orthogonal, symmetry-adapted linear combinations of Slater determinants D_k,

$$[2] \quad \Phi_i = \sum_k a_k D_k$$

the a_k are determined by requiring each configuration Φ_i to have the correct spatial and spin symmetry. The constrained CI equations are suitable to solve by the parameterization (4*b*) or iterative–perturbation procedures (4*b*) and the variational principle (5) to give

$$[3] \quad \sum_j (H'_{ij} - E\,\delta_{ij})\, c_j = 0$$

where

$$H' = H + \lambda[M - \mu]$$

and

$$[4] \quad \sum_{ij} c_i (M_{ij} - \mu\delta_{ij})\, c_j = 0$$

where H'_{ij} and M_{ij} are matrix elements of the Hamiltonian H' and the property operator, M', is the known expectation value of the operator M which constrains the Hamiltonian

$$[5a] \quad H'_{ij} = \langle \phi_i | H' | \phi_j \rangle = \langle \phi_i | H + \lambda[M - \mu] | \phi_j \rangle$$

and

$$[5b] \quad M_{ij} = \langle \phi_i | M | \phi_j \rangle$$

Only single constraints μ are explicitly considered. Generalization of [3] and [4] to multiple constraints μ, ν etc. is straightforward.

Procedures for solving the constrained CI equations

The secant-parameterization (6) and a modified perturbation–iteration method are considered (6).

The secant-parameterization procedure is easily adapted to constrained CI calculations. Instead of solving the constrained RHF equation (6)

$$\sum_j^m F'_{ij} C_{iv} = \sum_j^m S_{ij} C_{jv} \epsilon'_v$$

for each new estimate of λ, the constrained CI equation [3] is solved. The ground state CI wavefunction for each new estimate of λ is found; they are very rapid procedures to calculate one or more eigenvectors of large matrices (7–11).

The perturbation–iteration method (12, 13) is iterative; a new λ is obtained in each iteration using the perturbation expression (1, 4). The perturbation energy coefficients $E^{(n)}$ are evaluated using sum-over-states expressions involving eigenvalues and matrix elements between eigenfunctions of a zeroeth order Hamiltonian (14). The zeroeth order eigenvalues and eigenfunctions are chosen to be the eigenvalues and eigenfunctions of H' from the previous iteration; thus, H' is diagonalized completely for each new λ. When the CI expansion eq. [1] involves more than a few terms, the time to repeatedly fully diagonalize H' becomes prohibitive.

The modified perturbation–iteration (MPI) method (1) diagonalizes the unperturbed Hamiltonian H, uses the eigenvalues and eigenfunctions to calculate a set of perturbation energies

Can. J. Chem. Downloaded from www.nrcresearchpress.com by 210.87.254.105 on 09/06/12
For personal use only.

TABLE 1. CO, x_n, dipole moment,[d] constrained CI calculations using the MPI,[a] SEMPI,[b] and RHFMPI[c] procedures; the Lagrange multiplier λ and remaining error in the constrained property are given for each iteration

	MPI		SEMPI		RHFMPI	
Iteration	$\lambda^{(i)}$	$\Delta^{(i)}$	$\lambda^{(i)}$	$\Delta^{(i)}$	$\lambda^{(i)}$	$\Delta^{(i)}$
0	0.0	−0.46975	0.0	−0.24615	0.0	−0.24615
1	−0.079647	−0.00031	−0.025293	−0.33023	−0.021162	−0.35356
2	−0.079694	-5×10^{-8}	−0.063363	−0.10384	−0.054915	−0.15593
3			−0.076830	−0.01851	−0.071839	−0.05046
4			−0.079330	−0.00236	−0.077691	−0.01296
5			−0.079651	−0.00028	−0.079228	−0.00302
6			−0.079689	−0.00003	−0.079589	−0.00069
7					−0.079671	−0.00015

[a]Modified perturbation iteration method, refs. 1 and 4.
[b]Approximate MPI method in which approximate zeroeth order eigenvalues and eigenfunctions are obtained in the singly excited CI or Tamm−Dancoff approximation (20).
[c]RHF ground and singly excited configurations and the corresponding diagonal H elements give approximate zeroeth order eigenvalues and eigenfunctions.
[d]The dipole moment, $ea_0 = 2.54158 \times 10^{-18}$ esu cm = 2.54158 debye.

TABLE 2. CO: the $-\theta_n^c$, molecular quadrupole moment[a] constrained CI calculations using the MPI, SEMPI, and RHFMPI procedures; the Lagrange multiplier λ and remaining error in the constrained property are given for each iteration

	MPI		SEMPI		RHFMPI	
Iteration	$\lambda^{(i)}$	$\Delta^{(i)}$	$\lambda^{(i)}$	$\Delta^{(i)}$	$\lambda^{(i)}$	$\Delta^{(i)}$
0	0.0	0.82494	0.0	0.89982	0.0	0.89982
1	0.059910	0.00091	0.060803	−0.01315	0.060773	−0.01268
2			0.060005	−0.00088	0.060002	−0.00083

[a]Molecular quadrupole moment, esu cm^2 (expt), au (theory); au = ea_0^2 (proton charge and Bohr radius from ref. 26) = 1.34492×10^{-2} esu cm^2.

TABLE 3. CO: the r_n^2, diamagnetic contribution to the diamagnetic susceptibility,[a] constrained CI calculations using the MPI, SEMPI, and RHFMPI procedures; the Lagrange multiplier λ and remaining error in the constrained property $\Delta^{(i)}$, are given for each iteration

	MPI		SEMPI		RHFMPI	
Iteration	$\lambda^{(i)}$	$\Delta^{(i)}$	$\lambda^{(i)}$	$\Delta^{(i)}$	$\lambda^{(i)}$	$\Delta^{(i)}$
0	0.0	−1.3809	0.0	−1.5430	0.0	−1.5430
1	−0.19629	−0.0261	−0.14504	−0.3519	−0.12699	−0.4662
2	−0.20000	−0.0021	−0.18064	−0.1265	−0.17217	−0.1804
3	−0.20028	−0.0002	−0.19094	−0.0605	−0.18587	−0.0930
4			−0.19537	−0.0318	−0.19200	−0.0536
5			−0.19759	−0.0174	−0.19527	−0.0324
6			−0.19877	−0.0097	−0.19716	−0.0201
7			−0.19942	−0.0055	−0.19832	−0.0127
8			−0.19978	−0.0031	−0.19903	−0.0081
9			−0.19999	−0.0018	−0.19947	−0.0051
10			−0.20011	−0.0010	−0.19976	−0.0033

[a]Diamagnetic contribution to the diamagnetic susceptibility, au; au = $N_0 a_0^3$ (Avogadros Number and Bohr radius from ref. 26) = 8.92394×10^{-2} cm mol^{-1}.

$E^{(n)}$ that are used throughout the iterative procedure. After the first iteration only the eigenfunction corresponding to the lowest eigenvalue is needed; this is a very rapid process (7−11).

For elaborate CI wavefunctions it is computationally unfeasible to fully diagonalize the Hamiltonian matrix, and *approximate* zeroeth order eigenfunctions and eigenvalues are used to evaluate the perturbation energies $E^{(n)}$ by partially diagonalizing the Hamiltonian. This is equivalent to solving the CI eq. [3] for a truncated CI expansion eq. [1] obtained by including only the most important configurations, depending on the particular constraint, and the method to construct the configurations Φ_i. If one configuration, Φ_0, is expected to be the dominant term, i.e. $c_0 \gg c_i$ for $i > 0$, then one criterion for choosing the configurations to be included in the truncated expansion is that $|M_{0j}|^2/|H_{00} - H_{jj}|$ be large.

For a closed shell system the configuraion Φ_i in eq. [1] is the RHF wavefunction and the excited RHF symmetry adapted configurations are obtained by exciting one or more electrons into virtual RHF orbitals (15). The RHF wavefunction is the dominant term in the CI expansion for the ground state wave-

TABLE 4. CO: constrained CI calculations using the secant-parameterization procedure; the Lagrange multiplier λ and remaining error in the constrained property $\Delta^{(i)}$ are given for each iteration

	Constrained property					
	x_n[a]		$-\theta_n^e$[b]		r_n^2[c]	
Iteration	$\lambda^{(i)}$	$\Delta^{(i)}$	$\lambda^{(i)}$	$\Delta^{(i)}$	$\lambda^{(i)}$	$\Delta^{(i)}$
0	0.0	−0.46975	0.0	0.82492	0.0	−1.3809
1	−0.087504	0.05111	0.068966	−0.14011	−0.15922	−0.2624
2	−0.078918	−0.00503	0.058955	0.01521	−0.19659	−0.0239
3	−0.079687	−0.00005	0.059936	0.00018	−0.20033	0.0004
4	−0.079694	4×10^{-8}				

[a]The dipole moment, $ea_0 = 2.54158 \times 10^{-18}$ esu cm = 2.54158 debye.
[b]The molecular quadrupole moment.
[c]The diamagnetic contribution to the diamagnetic susceptibility.

TABLE 5. Constrained X_n, the dipole moment, ea_0 calculations on CO; comparison of SDECI, SECI, and UCRHF I perturbation energies $E^{(n)}$, estimates of $\lambda^{(n)}$ obtained using second ($n = 2$) and seventh ($n = 7$) order perturbation expansions, and the remaining error in the constrained property for $\lambda = \lambda^{(7)}$

	Value		
Parameter[a]	SDECI	SECI	UCRHF I
$E^{(1)}$	−0.46975	−0.24615	−0.24615
$E^{(2)}$	−2.6839	−5.0381	−5.9882
$E^{(3)}$	1.8039	−3.9537	−4.5675
$E^{(4)}$	−4.7283	19.436	31.922
$E^{(5)}$	−7.3913	63.255	87.895
$E^{(6)}$	21.853	−107.62	−289.06
$E^{(7)}$	−43.498	985.20	−1718.9
$\lambda^{(2)}$	−0.087512	−0.024429	−0.020556
$\lambda^{(7)}$	−0.079647	−0.025293	−0.021162
$\Delta^{(7)}$	−0.00031	−0.33023	−0.35356

[a]$E^{(n)}$ in hartrees.

TABLE 6. Molecular quadrupole $-\theta_n^e$ constrained calculations on CO; comparison of SDECI, SECI, and UCRHF I perturbation energies $E^{(n)}$, estimates of $\lambda^{(n)}$ obtained using second ($n = 2$) and seventh ($n = 7$) order perturbation expansions, and the remaining error in the constrained property for $\lambda = \lambda^{(7)}$

	Value		
Parameter[a]	SDECI	SECI	UCRHF I
$E^{(1)}$	0.82494	0.89982	0.89982
$E^{(2)}$	−5.9765	−6.2355	−6.2617
$E^{(3)}$	−10.708	−13.737	−13.587
$E^{(4)}$	2.2534	1.8918	3.1014
$E^{(5)}$	78.581	157.24	155.57
$E^{(6)}$	141.93	538.73	496.08
$E^{(7)}$	−648.40	−482.97	−599.43
$\lambda^{(2)}$	0.069016	0.072153	0.071869
$\lambda^{(7)}$	0.059910	0.060803	0.060773
$\Delta^{(7)}$	0.00091	−0.01315	−0.01268

[a]E's in hartrees.

function (16). For a one-electron operator M, the matrix element M_{0j} remains only for the singly excited configurations. Therefore an appropriate choice of configurations in the truncated expansion is the ground state and singly excited RHF configurations: the eigenvalues and eigenfunctions[1] from solving the CI eq. [3] are the singly excited state energies and wavefunctions in the Tamm–Dancoff approximation (20) and represent reasonable approximations to the eigenvalues and eigenfunctions of the full Hamiltonian matrix, which make the largest contributions to $E^{(n)}$.

Another choice of approximate zeroeth order wavefunctions and energies is the RHF ground and singly excited configurations and the corresponding diagonal elements of the Hamiltonian matrix, which is equivalent to the uncoupled RHF, UCRHF, method I approximate RHF perturbation theory (4, 6).

Constrained CI calculations on CO: comparison of the secant-parameterization and modified perturbation–iteration methods

Singly constrained calculations using the dipole moment, x_n, molecular quadrupole moment $-\theta_n^e$, and the diamagnetic contribution to the diamagnetic susceptibility, r_n^2, as constraints were performed on CO using a minimum basis set of STO-4G (21) functions with Slater exponents (22). The CI wavefunction was expanded in $25\,^1\Sigma^+$ configurations (78 Slater determinants), including the RHF ground state and all singly and doubly excited RHF configurations (SDECI) except doubly excited configurations involving excitations from the 1σ and 2σ core orbitals and a small number of doubly excited configurations that contributed negligibly to the unperturbed ground state CI wavefunction. Eigenfunctions of the S^2 spin operator were obtained by the diagonalization method (23–25). The lowest eigenvalue of the unperturbed CI Hamiltonian matrix was calculated to be −134.6760 hartree, 0.1282 hartree below the minimum basis set RHF energy. The increase in the total energy due to each constraint was x_n, 0.0193, $-\theta_n^e$, 0.0257, and T_n^2, 0.1314 hartree. The results of the constrained CI calculations are reported in Tables 1 through 3. The MPI procedure converges very rapidly, requiring from one to three iterations. The SEMPI and RHFMPI procedures converge to the correct value much more slowly. Comparing the perturbation–iteration and secant-parameterization procedure results, Table 4 shows the latter procedure requires a few more iterations for convergence than the MPI method. However, the computation time to fully diagonalize the initial unperturbed Hamiltonian matrix outweighs the advantages of the better rate of conver-

[1]Brillouin's theorem (17–19) requires that Hamiltonian matrix elements between the ground state RHF wavefunction and singly excited RHF configurations vanish. Therefore the ground state wavefunction in the single excitation CI approximation is just the RHF ground state wavefunction.

Can. J. Chem. Downloaded from www.nrcresearchpress.com by 210.87.254.105 on 09/06/12
For personal use only.

TABLE 7. Constrained r_n^2, diamagnetic contribution to the diamagnetic susceptibility, Na_0^3, calculations on CO; comparison of SDECI, SECI, and UCRHF I perturbation energies $E^{(n)}$, estimates of $\lambda^{(n)}$ obtained using second ($n = 2$) and seventh ($n = 7$) order perturbation expansions, and the remaining error in the constrained property for $\lambda' = \lambda^{(7)}$

Parameter[a]	Value		
	SDECI	SECI	UCRHF I
$E^{(1)}$	−1.3809	−1.5430	−1.5430
$E^{(2)}$	−4.3359	−6.2379	−7.2388
$E^{(3)}$	−5.7273	−1.6607	−2.7593
$E^{(4)}$	−12.605	10.423	22.312
$E^{(5)}$	−11.939	−49.950	−23.978
$E^{(6)}$	−9.8446	−47.965	−156.43
$E^{(7)}$	50.972	1145.4	1051.7
$\lambda^{(2)}$	−0.15924	−0.12368	−0.10657
$\lambda^{(7)}$	−0.19629	−0.14504	−0.12699
$\Delta^{(7)}$	−0.0261	−0.3519	−0.4662

[a] $E^{(n)}$ in hartrees.

gence using the MPI procedure. The secant-parameterization procedure usually converges much more rapidly than the approximate MPI procedures.

Values of the perturbation energies $E^{(n)}$ and perturbation estimates of λ calculated using the SDECI, SECI, and UCRHF I ground and excited wavefunctions are reported in Tables 5 thorough 7. Except the values of $E^{(2)}$ through $E^{(4)}$ obtained when $-\theta_n^c$ is the constrained property, the SECI and UCRHF I values of the $E^{(n)}$ agree poorly with the SDECI results, accounting for the poor rate of convergence obtained with the approximate MPI procedures. The SECI and UCRHF I results agree well. The difference between the SECI and UCRHF I second and seventh order estimates of λ, $\lambda^{(2)}$, and $\lambda^{(7)}$ respectively is small compared to the error in the quantities due to the choice of zeroeth-order eigenvalues and eigenfunctions. Therefore there appears to be little value in carrying the perturbation expansion beyond second order.

Conclusion

The results of the constrained CI calculations on CO show that the secant-parameterization procedure is computationally a more economical constraint procedure than the MPI or approximate MPI methods because, in contrast to the MPI methods, *it is not necessary* to fully diagonalize the Hamiltonian matrix initially, a very important advantage in large CI calculations. The secant-parameterization procedure is easily extended to multiple constraint calculations, whereas for multiple constraints the MPI method is unwieldly.

Acknowledgement

This research was supported by the Natural Sciences and Engineering Research Council of Canada.

1. D. P. CHONG. Theoret. Chim. Acta, **12**, 337 (1968).
2. E. A. HYLLERAAS. Z. Physik. **48**, 469 (1928).
3. S. F. BOYS. Proc. R. Soc. A**200**, 542 (1950).
4. G. D. ZEISS. Ph.D. Thesis, McGill University. 1976. (*a*) Appendix F; (*b*) Chapt. 1.
5. W. BYERS BROWN. J. Chem. Phys. **45**, 392 (1966).
6. G. D. ZEISS and M. A. WHITEHEAD. Int. J. Quantum Chem. In press; Can. J. Chem. **61**, 128 (1983); Can. J. Chem. **61**, 675 (1983).
7. J. L. B. COOPER. Q. Appl. Math. **6**, 179 (1948).
8. R. K. NESBET. J. Chem. Phys. **43**, 311 (1965).
9. I. SHAVITT. J. Comput. Phys. **6**, 124 (1970).
10. I. SHAVITT, C. F. BENDER, A. PIPANO, and R. P. HOSTENY. J. Comput. Phys. **11**, 90 (1973).
11. E. R. DAVIDSON. J. Comput. Phys. **17**, 87 (1975).
12. Y. RASIEL and D. R. WHITMAN. J. Chem. Phys. **42**, 2124 (1965).
13. N. BJØRNA. Mol. Phys. **24**, 1 (1972).
14. R. HUBY. Proc. Phys. Soc. **78**, 529 (1961).
15. H. F. SCHAEFER, III. The electronic structure of atoms and molecules. Addison-Wesley. 1972. p. 37.
16. E. R. DAVIDSON. *In* The world of quantum chemistry. Proc. First Intl. Cong. Quantum Chem. *Edited by* R. Daudel and B. Pullman. Reidel 1974. p. 17.
17. L. BRILLOUIN. Act. Sci. Ind. Nos. 71, 159, 160 (1933–34).
18. C. MØLLER and M. S. PLESSET. Phys. Rev. **46,** 618 (1934).
19. D. J. THOULESS. The quantum mechanics of many-body systems. Academic Press, Inc., New York. 1961.
20. T. H. DUNNING and V. MCKOY. J. Chem. Phys. **47**, 1735 (1967).
21. W. J. HEHRE, R. F. STEWART, and J. A. POPLE. J. Chem. Phys. **51**, 2657 (1969).
22. J. C. SLATER. Phys. Rev. **36**, 51 (1930); Quantum theory of atomic structure. Vol. 1. McGraw-Hill. 1960 p. 368.
23. M. H. JOHNSON. Phys. Rev. **39**, 197 (1932).
24. H. F. SCHAEFER, III, and F. E. HARRIS. J. Comput. Phys. **3**, 217 (1968).
25. H. F. SCHAEFER, III. J. Comput. Phys. **6**, 142 (1970).
26. E. R. COHEN. Res. Dev. **25**, 32 (1974).

Can. J. Chem. Downloaded from www.nrcresearchpress.com by 210.87.254.105 on 09/06/12
For personal use only.

Kinetics and mechanism of the bromination of 4-pyridone and related derivatives in aqueous solution

OSWALD S. TEE[1] AND MARTINO PAVENTI

Department of Chemistry, Sir George Williams Campus, Concordia University, Montreal, P.Q., Canada H3G 1M8

Received May 9, 1983

OSWALD S. TEE and MARTINO PAVENTI. Can. J. Chem. **61**, 2556 (1983).

The kinetics of bromination of 4-pyridone and selected derivatives have been measured in aqueous solutions in the pH range 0–9, at 25°C. The tautomerie system 4-pyridone ⇄ 4-hydroxypyridine (**1***a* ⇄ **2***a*) reaets with bromine via the predominant (pyridone) tautomer at pH < 6 and via the conjugate anion at pH > 6. 3-Bromo-4-pyridone behaves similarly. The kinetics also reveal that the facile dibromination of 4-pyridone occurs because at most pH's the monobromo derivative is actually more reactive towards bromine by virtue of its lower pK_a values. From the point of view of reactivity the 4-pyridones and their anions behave as substituted phenoxide ions. 4-Methoxypyridine does not undergo bromination under comparable conditions, but rather forms a complex with bromine.

OSWALD S. TEE et MARTINO PAVENTI. Can. J. Chem. **61**, 2556 (1983).

On a mesuré les cinétiques de la bromation de la pyridone-4 et de quelques dérivés en solutions aqueuses et dans un intervalle de pH allant de 0 à 9, à 25°C. Le système tautomère pyridone-4 ⇄ hydroxy-4 pyridine (**1***a* ⇄ **2***a*) réagit avec le brome par l'intermédiaire du tautomère prédominant (pyridone) à un pH < 6 et par l'intermédiaire de l'anion conjugué à un pH > 6. La bromo-3 pyridone-4 se comporte de la même façon. La cinétique révèle également que la débromation facile de la pyridone-4 se produit parce qu'à plusieurs pH le dérivé monobromé est actuellement plus réactif vis-à-vis du brome en raison de ses pK_a's plus faibles. Du point de vue de la réactivité, les pyridones-4 et leurs anions se comportent comme des ions phénoxydes substitués. La méthoxy-4 pyridine, dans des conditions comparables, n'est pas bromé, mais elle forme de préférence un complexe avec le brome.

[Traduit par le journal]

Introduction

Pyridones react readily with halogens or halogenating agents in various media (1). The reactions are so facile that 3,5-disubstitution is almost always observed, and useful clean monohalogenation has rarely been reported (1, 2). We recently showed that monobromination of 2-pyridone can be achieved in aqueous solution by controlling the pH of the medium (3). This was made possible by a kinetic study of the bromination of 2-pyridone and selected derivatives over a wide range of pH. We ascertained the reactive forms of 2-pyridone and the relative reactivities of its monobromo derivatives and their reactive forms. This information enables the choice of conditions such that the second bromination is slow relative to the first (3).

The present paper reports an analogous study of the aqueous bromination of 4-pyridone (**1***a*). In it we likewise ascertain the reactive forms of the substrate and probe the origins of its facile dihalogenation. As a result, we show how its monobromination can be carried out relatively easily. In contrast, other routes to 3-bromo-4-pyridone are long and give poor overall yields.

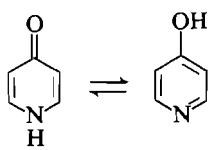

1*a* **2***a*

In the vapour phase and in dilute nonpolar solution the tautomeric equilibrium **1***a* ⇄ **2***a* favours 4-hydroxypyridine (**2***a*). However, in aqueous solution the pyridone tautomer **1***a* predominates by a factor of ~2000:1 (4). Nevertheless, in principle the aqueous bromination of 4-pyridone could take place upon the minor tautomer if this was sufficiently reactive. Therefore, in order to find out which of the tautomers is the reactive form we have studied the bromination of the tautomeric system **1***a* ⇄ **2***a*, and of the methyl derivatives, 1-methyl-4-pyridone (**1***b*) and 4-methoxypyridine (**2***b*).

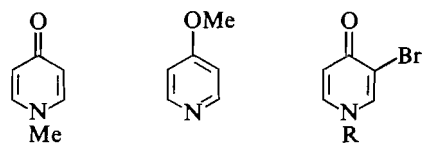

1*b* **2***b* **3***a*, R = H
3*b*, R = Me

To gain insight into the facile dihalogenation of 4-pyridone we have also studied the bromination of 3-bromo-4-pyridones **3***a* and **3***b*. As with our previous study, the speed of the reactions rules out conventional means of following the kinetics, and so we have used stopped-flow uv spectrophotometry (3, 5).

Results

All of the substrates studied react fairly quickly with bromine in water and undergo bromination, with the exception of 4-methoxypyridine, **2***b*. This substrate reacts to form a 1:1 complex with bromine which impedes normal electrophilic bromination of **2***b* (see Experimental).

Kinetic studies

The four remaining substrates (**1***a*, **1***b*, **3***a*, **3***b*) were studied in reaction with bromine in aqueous media in the pH range 0–9 using the same methods as earlier (3, 5). For the most part a large excess of substrate over bromine was employed, and under these conditions the disappearance of bromine was cleanly first-order. Rate constants (k_1^{obs}) obtained from analysis of the absorbance data increased linearly with substrate concentration, but were independent of the initial bromine concentration. Thus we conclude that at any given pH the reaction of

[1]Author to whom correspondence should be addressed.

Can. J. Chem. Downloaded from www.nrcresearchpress.com by 210.87.254.6 on 09/06/12
For personal use only.

Can. J. Chem. Downloaded from www.nrcresearchpress.com by 210.87.254.6 on 09/06/12
For personal use only.

TABLE 1. Rate constants for reactions of bromine with 4-pyridones in 1 *M* KBr at 25°C

S	pH	$[S] \times 10^4$, (*M*)	$[Br_2] \times 10^5$, (*M*)	k_1^{obs}, (s^{-1})	k_2^{obs}, ($M^{-1}\ s^{-1}$)
1*a*[a]	1.12[b]	15.29	5.0	—	44.8
	1.45	20.0	5.0	0.0102	88.5
	2.08[b]	1.529	5.0	—	397
		3.824	5.0	—	426
		7.647	5.0	—	400
	2.35[b]	7.647	5.0	—	844
	3.17[b]	7.647	5.0	—	3720
	3.30	20.0	5.0	0.410	3580
	3.80	10.0	5.0	0.371	6630
	4.90	10.0	5.0	0.614	11000
	5.52	10.0	5.0	0.683	12200
	5.56	10.0	5.0	0.852	15200
	6.24	10.0	5.0	2.06	36800
	6.50	10.0	5.0	2.14	38300
	6.93	10.0	5.0	6.27	113000
	7.40	20.0	5.0	33.1	293000
	7.92	10.0	5.0	39.1	738000
	8.74	5.0	5.0	0.113	6710000
1*b*[c]	1.10	25.0	5.0	0.00598	41.5
	2.25	5.0	5.0	—	597
		12.5	5.0	—	597
	3.12	5.0	5.0	0.0888	3360
	3.31	5.0	5.0	0.113	4280
	3.96	5.0	5.0	0.243	9560
	4.96	5.0	5.0	0.308	11600
	5.97	5.0	5.0	—	13300
		7.5	5.0	—	13200
	6.92	5.0	5.0	—	12800
3*a*	0.08	10.0	2.5	0.00171	29.9
	0.66	5.0	2.5	0.00262	93.9
	1.90	5.0	2.5	0.0130	465
	2.37	2.5	2.5	0.00784	592
	3.00	5.0	2.5	0.0224	802
	3.41	2.5	2.5	0.0121	914
	4.03	2.5	2.5	0.0184	1390
	4.75	1.25	2.5	0.0145	2470
	5.26	2.5	2.5	—	7560
		5.0	2.5	—	7860
	5.95	2.5	2.5	0.295	22300
	6.25	2.5	2.5	0.508	38300
	7.18	1.25	2.5	3.05	522000
		2.5	2.5	6.66	507000
	7.61	2.5	2.5	15.2	1170000
	8.00	2.5	2.5	35.7	2850000
3*b*	0.50	20.0	5.0	0.00389	43.9[d]
	1.00	20.0	5.0	0.0119	114 [d]
	1.50	8.0	5.0	0.0106	240
	2.00	12.0	5.0	0.0250	369
		20.0	5.0	0.0449	391
		28.0	5.0	0.0618	382
	3.34	20.0	5.0	0.0567	494
	4.91	20.0	5.0	0.0658	573
	6.28	20.0	5.0	0.0644	562
	7.32	8.0	5.0	0.0263	602
	8.50	20.0	5.0	0.0476	537

[a]Introduced as HNO_3 salt.
[b]Introduced as sodium salt dihydrate.
[c]Introduced as HBr salt.
[d]Correction for Br^- includes contribution from KBr + HBr.

bromine with the substrates follows a second-order rate law. Accordingly, the observed values of k_1^{obs} were converted to

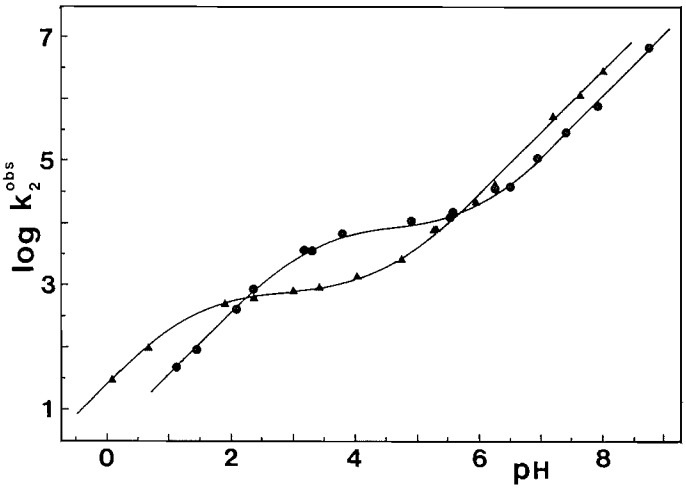

FIG. 1. pH–rate profiles for reaction of aqueous bromine with 4-pyridone **1***a* (circles) and 3-bromo-4-pyridone **3***a* (triangles) at 25°C, I = 1.0 *M* (KBr).

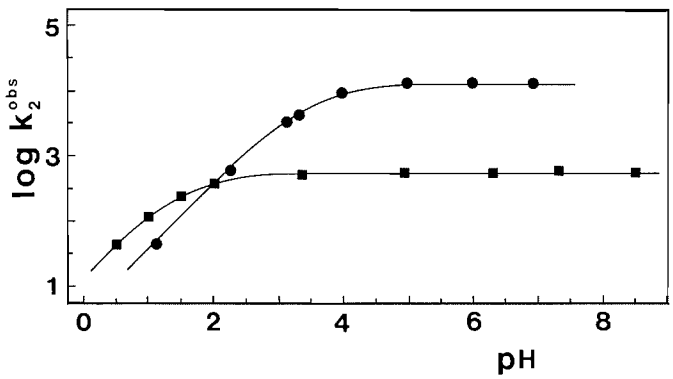

FIG. 2. pH–rate profiles for reaction of aqueous bromine with 1-methyl-4-pyridone **1***b* (circles) and 3-bromo-1-methyl-4-pyridone **3***b* (squares) at 25°C, I = 1.0 *M* (KBr).

second-order rate constants (k_2^{obs}), taking into account the substrate concentration and the depletion of free bromine due to the formation of tribromide ion, hypobromous acid, and its anion (see Experimental).

The observed rate constants are collected in Table 1, and displayed in Figs. 1 and 2. In many cases the absorbance data were also analyzed directly for second-order behaviour (5*c*). The rate constants (k_2^{obs}, after correction for the free bromine concentration) thus obtained were generally in good agreement with those derived from k_1^{obs} values. In Table 1, where no entry is given for k_1^{obs}, the value of k_2^{obs} was obtained solely from second-order analysis (5*c*).

The observed pH–rate profiles (Figs. 1 and 2) are very similar to those obtained earlier for the analogous 2-pyridones (3). The *N*-methyl derivatives **1***b* and **3***b* show profiles (Fig. 2) appropriate for reaction upon their free base forms, since the literature protonation pK for **1***b* is 3.33 (6) and that for **3***b* we have measured to be 1.52. For such behaviour (eq. [1]) the appropriate form of the observed rate constant is given by

$$[1]\quad SH^+ \overset{K_1}{\rightleftharpoons} S \xrightarrow[Br_2]{k_2} \text{products}$$

$$[2]\quad k_2^{obs} = k_2K_1/(K_1 + [H^+])$$

eq. [2]. The calculated curves in Fig. 2 were generated from eq. [2] using the values of k_2 and K_1 (expressed as pK_1) given

TABLE 2. Constants for reaction of bromine with 4-pyridones in aqueous solution (25°C, I = 1.0 M (KBr))

Substrate	pK_1 meas.	pK_1 fitted	pK_2	k_2 (M^{-1} s^{-1})	$k_2'K_2$ (s^{-1})	k_2' (M^{-1} s^{-1})
1*a*	3.27[a]	3.46	11.09[a]	10100	0.0110	1.35×10^9
1*b*	3.33[a]	3.58	—	12800	—	—
3*a*	1.37[b]	1.53	9.46[c]	791	0.0287	8.28×10^7
3*b*	1.52[b]	1.58	—	549	—	—

[a]At 20°C, from ref. 6.
[b]This work, at 25°C, and I = 0.15 M ($HClO_4$ + $NaClO_4$).
[c]This work, at 25°C, and I = 0.1 M (KBr).

in Table 2. The fitted values of pK_1 (3.58 and 1.58) are in good agreement with the measured values (3.33 and 1.52).

The data for 4-pyridone **1***a* and its 3-bromo derivative **3***a*, which are shown in Fig. 1, cannot be solely explained by eqs. [1] and [2]. Clearly in each case another process takes over at the higher pH's which we believe to be reaction upon the conjugate anions of the substrates. Such behaviour was observed earlier for 2-pyridones (3). For this situation (eq. [3]) the expected variation of k_2^{obs} with acidity is given by eq. [4].

[3] $$SH_2^+ \overset{K_1}{\rightleftharpoons} SH \overset{K_2}{\rightleftharpoons} S^-$$
$$k_2 \downarrow Br_2 \qquad k_2' \downarrow Br_2$$
$$\rightarrow \text{products} \leftarrow$$

[4] $$k_2^{obs} = \frac{k_2K_1}{(K_1 + [H^+])} + \frac{k_2'K_2}{[H^+]}$$

The simplicity of the second term in this equation is warranted at the pH's employed, since for 4-pyridone pK_2 = 11.09 (6) and for 3-bromo-4-pyridone we have measured pK_2 = 9.46.

From Fig. 1 and the calculated curves shown therein, it is clear that eq. [4] gives an excellent representation of the data for the substrates **1***a* and **3***a*. The appropriate parameters are again collected in Table 2.

In summary, the reaction of bromine with the 4-pyridones **1***a*, **1***b*, **3***a*, and **3***b* over the pH range 0–9 apparently involves attack upon the free base form and upon the conjugate anions of **1***a* and **3***a* at higher pH (see Fig. 1).

Product studies

As noted above, and detailed in the experimental section, 4-methoxypyridine **2***b* does not undergo normal electrophilic bromination, but rather forms a relatively stable complex with bromine. This complex is obtained whether the solvent is water, ethanol, or chloroform. It brominates acetone in chloroform and **2***b* is recoverable as its hydrobromide salt.

Attempted bromination of 4-pyridone **1***a* in concentrated hydrobromic acid gave a 73% yield (based on bromine) of 3,5-dibromo-4-pyridone **4***a*. Proton magnetic resonance analysis of the mother liquor revealed a 2:5 ratio of **3***a*/**1***a*. Likewise, bromination of **1***a* in unbuffered 1 M aqueous KBr gave a 67% yield of **4***a*. When this reaction was repeated in the presence of one equivalent (to **1***a*) of KOH the yield of **4***a* was 86%. In all cases, 3-bromo-4-pyridone **3***a* was only a minor product of reaction.

We also carried out various other bromination reactions employing different reagents and solvents. In all cases the dibromo derivative **4***a* was the major product, with yields of 60–72% (see Experimental).

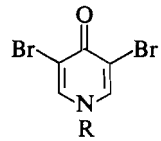

4*a*, R = H
4*b*, R = Me

After we had obtained the kinetic data shown in Fig. 1 it seemed likely that the best chance of monobrominating 4-pyridone was in aqueous solution buffered in the region pH 3–5, the only region where the rate profile of **1***a* rises above that of **3***a*. Accordingly, bromine in aqueous KBr was slowly added to an equivalent amount of 4-pyridone in water buffered with sodium acetate/acetic acid to pH 4.2–4.4. From solution there precipitated a 26.2% yield of the dibromo compound **4***a*, but the mother liquor contained **3***a* (73.8%) and the appropriate amount of **1***a* (26.2%). After purification and recrystallization we obtained a 28% yield of the desired 3-bromo-4-pyridone, **3***a*. No optimization was attempted, but probably with stronger buffering and improved separation of the product mixture a higher isolated yield of **3***a* could be obtained.

Other routes to **3**a

At the outset various attempts were made to synthesize **3***a* unambiguously using routes based directly or indirectly on literature precedents. With one exception they were unsuccessful due to reactions giving no product or an undesired product. The successful exception involves a multistep route in which the last step gave a very poor yield of the desired product. 3-Bromopyridine (7) was converted to its *N*-oxide (8) which was then nitrated to 3-bromo-4-nitropyridine-*N*-oxide by a modification of literature procedures (9, 10). Simultaneous reduction of the nitro group and the *N*-oxide moiety by iron and acetic acid (11) gave 3-bromo-4-aminopyridine. After several attempts, hydrolysis of this product by diazotization (12) produced only 3% of the desired 3-bromo-4-pyridone, **3***a*.

3-Bromo-4-nitropyridine was made by deoxygenation (13) of its *N*-oxide (*vide supra*). An attempt to hydrolyse it to **3***a* with aqueous barium hydroxide (14) failed. Hydrolysis in refluxing aqueous sulphuric acid gave material which had some of the characteristics of **3***a*, but the melting point was 125° too low!

Bromination of 4-hydroxypyridine-*N*-oxide, according to the procedure of Hayashi (15), gave the 3,5-dibromo derivative and not the desired 3-bromo product, as reported (15). Likewise, attempted monobromination of chelidamic acid (4-pyridone-2,6-dicarboxylic acid) gave the undesired dibromo derivative.

Can. J. Chem. Downloaded from www.nrcresearchpress.com by 210.87.254.6 on 09/06/12
For personal use only.

Can. J. Chem. Downloaded from www.nrcresearchpress.com by 210.87.254.6 on 09/06/12
For personal use only.

Monobrominations of 4-aminopyridine and of 4-dimethylaminopyridine were also not successful due to the formation of complexes with the halogen (16).

Clearly, on the basis of our experience, the best approach to 3-bromo-4-pyridone **3***a* is to use direct bromination of 4-pyridone in an aqueous medium strongly buffered at pH 4.

Discussion

Reactive forms

Over the pH range 0–5 the rate profiles of 4-pyridone **1***a* and its *N*-methyl derivative **1***b* are virtually superimposable. This is reflected in Table 2 by their very similar values of k_2. In contrast, the *O*-methyl derivative **2***b* shows quite different behaviour towards bromine. Given that the pyridone tautomer **1***a* greatly predominates in aqueous solution (4), our results provide compelling evidence that 4-pyridone **1***a* reacts with bromine as its major tautomer and not via the minor hydroxy tautomer **2***a*, at pH < 6. At higher pH the rate of bromination of **1***a* increases in a manner appropriate for reaction upon its conjugate anion (eq. [4], Fig. 1).

In the same way, the reactivity of the monobromo derivatives **3***a* and **3***b* are very similar at low pH, consistent with **3***a* reacting as such. Above pH > 3.5, **3***a* apparently reacts with bromine via its anion.

Our results complement those of Katritzky and co-workers for the nitration in strong acid and the deuterium exchange of 4-pyridone at high temperatures (17, 18). Nitration takes place upon the free base pyridone tautomer except at higher acidities where the conjugate acid reacts (17). Hydrogen isotope exchange apparently only involves the free base form (18).

Reactivities

For 2-pyridones and their anions we showed that they react with bromine at rates expected for substituted phenoxide ions (3). This correlation is rationalized by consideration of the dipolar valence-bond structures which contribute to a pyridone. In the case of the 4-pyridones **1**, there must be significant contributions from the structures **1′** and **1″**, as Acheson emphasizes (19). They can account for various properties of **1***a* (19),

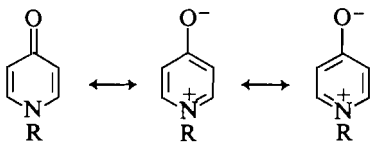

1 **1′** **1″**

including the solvent dependence of its tautomerism (4) and its reactivity in deuterium exchange (18). The structures **1′** and **1″** suggest that 4-pyridone can be considered as phenoxide ion bearing a *para* azonium nitrogen (=$\overset{+}{N}$H—) as substituent. Of course, the anion of **1***a* is phenoxide ion with a *para* aza nitrogen (=N—).

Using literature values of σ_m^+ for azonium nitrogen (2.00), aza nitrogen (0.54), and bromine (0.41) (3, 20, 21) the rate data for **1***a*, **3***a*, and their respective anions give a good correlation (r = 0.9987) with $\rho^+ = -3.43$. This is similar to the value of −3.83 for 2-pyridones and their anions (3) and the value of −3.5 for phenoxide ions estimated by Kulic and Vecera (22). It adds further weight to the idea that, with respect to reactivity, pyridones and their anions behave as substituted phenoxides.

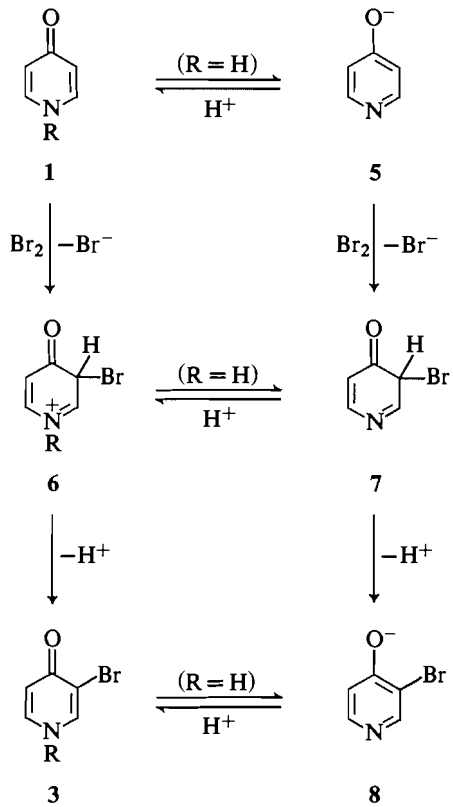

SCHEME 1

Mechanism

Our data can be explained by the simple pathways set out in Scheme 1. In acidic solution **1** (*a* or *b*), in equilibrium with its protonated form, is attacked by bromine to give the transient cation **6** which is deprotonated to form the product **3**. In the case where R = H the cation **6***a* may also deprotonate to the neutral azacyclohexadienone **7**. However, we see no evidence of the build-up of any intermediates during the reaction.[2] Therefore we surmise that acid- or base-catalyzed tautomerization of **7** to **3***a* is relatively fast.[3]

At higher pH 4-pyridone **1***a* reacts via its anion **5** to give directly the azacyclohexadienone **7**. Again, tautomerization of this intermediate (**7** → **8** → **3**) is presumed to be fast.[3] This pathway is analogous to that followed by phenols which react via their anions, except at high acidities (22, 23).

The brominations of **3***a* and **3***b* show similar rate profiles to those of **1***a* and **1***b*. Therefore we propose that they occur by mechanisms analogous to those set out in Scheme 1.

[2]We have observed the formation of relatively long-lived intermediates during the bromination of pyrimidones, uracils, and cytosines (5).

[3]Available evidence in the literature suggests that cyclohexadienones are not observable in the aqueous bromination of phenols. Kulic and Vecera found that bromine decrease and product increase occur at the same rate for various *para* substituted phenols (22). However, we have recently shown that 4-bromo-2,5-cyclohexadienones are observable in the aqueous bromination of simple phenols. On the other hand, we cannot detect any intermediates from phenols bearing electron-withdrawing groups or the cyclohexadienones derived from *ortho* bromine attack. In these cases tautomerization to the aromatic product is almost certainly too fast (39).

Can. J. Chem. Downloaded from www.nrcresearchpress.com by 210.87.254.6 on 09/06/12
For personal use only.

The principal active electrophile in the brominations of **1** and **3** is almost certainly molecular bromine, as depicted in Scheme 1. Tribromide ion is present in significant concentration under the conditions used. However, it is a much weaker electrophile in general (24), and for highly reactive phenoxide ions its reactivity is only about 1% of that of bromine (23). It is probable, therefore, that Br_3^- only makes a contribution where 4-pyridone is reacting via its anion **5**.

Other potential electrophiles are hypobromous acid (HOBr) and its protonated form (H_2OBr^+) (24). The former is much less reactive than bromine and its concentration is very low under our conditions, excepts at the higher pH's. Moreover, the observed pH dependences are inconsistent with its involvement. The concentration of the much more reactive electrophile H_2OBr^+ must be extremely low, given the low concentration of HOBr. For it to be involved in the reaction of the anions of **1***a* and **3***a* would required rate constants above diffusion-controlled (25).

Disubstitution

The reasons behind the facile dibromination of 4-pyridone **1***a* are easily seen by referring to Fig. 1 and Table 2. Except for the relatively small range of pH 2.5−5.5, 3-bromo-4-pyridone **3***a* is effectively more reactive than **1***a* (Fig. 1). This apparently anomalous situation arises because of the relationships between the values of k_2K_1 and k_2K_2 for the two substrates.

At pH < 2, where both **1***a* and **3***a* are significantly protonated, the difference in reactivity of **1***a* and **3***a* (factor of 12) is more than offset by the difference in K_1 values (factor of 85). Likewise at pH > 5.5, where reaction upon the conjugate anions predominates, the higher reactivity of the anion of 4-pyridone is more than compensated for by the larger value of K_2 for **3***a*.

Even at pH 4, where the rate profile for **1***a* is significantly above that for **3***a*, reaction upon **1***a* is only favored by a factor of about 6.3 (Fig. 1). Therefore, in a 1:1 reaction of bromine with 4-pyridone **1***a*, by the time of 86% reaction the product **3***a* effectively competes with **1***a* for bromine, and a significant amount of dibromo product **4***a* will result. Seen in this light, our 26% yield of **4***a* from a reaction buffered around pH 4.3 is not surprising.

The literature contains a preparative iodination of 4-pyridone, carried out with iodine in aqueous potassium iodide (26). This procedure leads to a 50% yield of the 3-iodo derivative, as well as 21% of the 3,5-diiodo compound. Presumably similar factors are involved here as in the bromination reaction, and so one can anticipate similar rate profiles. A higher yield of the monoiodo product might be obtained by using a medium buffered around pH 4.

Experimental

Kinetic methods

The stopped-flow apparatus, data acquisition, and data analysis were as in other recent work (3, 5). All kinetics solutions were 1.0 *M* in potassium bromide and, except for the highest acidities, I = 1.0 *M*. For pH > 1 a "universal buffer" was used as before (3). Reactions were followed as bromine disappearance by monitoring the tribromide ion band near 265 nm. Temperature control was obtained by circulation of water from a Lauda constant temperature bath kept at 25.0 ± 0.1°C.

The second-order rate constants (k_2^{obs}) given in the main text have been corrected for the actual free concentration of bromine. This is less than the total concentration of bromine due to the formation of tribromide ion and, at higher pH, of hypobromous acid (5*a*). In the present work, since higher pH's were employed than earlier, it was also necessary to correct for the ionization of HOBr.

The relevant equilibria are:

$$Br_3^- \overset{K_1}{\rightleftharpoons} Br^- + Br_2$$

$$Br_2 + H_2O \overset{K_2}{\rightleftharpoons} H^+ + Br^- + HOBr$$

$$HOBr \overset{K_3}{\rightleftharpoons} H^+ + {}^-OBr$$

From $[Br_2]_t = [Br_2] + [Br_3^-] + [HOBr] + [{}^-OBr]$ and the definition of K_1, K_2, and K_3 one can easily derive the equation for the correction factor, as given below in eq. [5].

$$[5] \quad \frac{[Br_2]_t}{[Br_2]} = 1 + \frac{[Br^-]}{K_1} + \frac{K_2}{[H^+][Br^-]} + \frac{K_2K_3}{[H^+]^2[Br^-]}$$

The appropriate values of the constants are K_1 = 0.0625 *M* (27), $K_2 = 9.6 \times 10^{-9}$ M^2 (28), and $K_3 = 2.06 \times 10^{-9}$ *M* (29). Apparent second-order rate constants, either from direct analysis or from pseudo first-order rate constants, were multiplied by the factor in eq. [5] to give values of k_2^{obs}. Those given in the text are averages of 3−5 runs. The validity of the corrections for HOBr and OBr^- is supported by the lack of systematic deviations in the rate profiles at the higher pH's.

*p*K *measurements*

These were made by the normal spectrophotometric method (30), at 25°C. For **3***a* we obtained pK_1 = 1.37 ± 0.01, pK_2 = 9.46 ± 0.02, and for **3***b* we found pK_1 = 1.52 ± 0.02. Ionic strength was 0.1 *M* or 0.15 *M*, as given in Table 2. For future use we also measured pK_1 = 7.14 ± 0.02 (I = 0.1 *M*) for 4-amino-3-bromopyridine.

Substrates and products

The compounds used in this study are known from the literature. Accordingly, in the following we provide details only for those procedures which differed from the literature either in execution or in outcome. Elemental analyses were performed by Galbraith Labs. Inc., Knoxville, Tennessee.

*4-Pyridone (1*a*)*

This substance is difficult to purify and to keep pure. Therefore we made use of salts, since this approach worked well in earlier work (3).

Compound **1***a* (Aldrich, technical grade) was dissolved in ethanol and decolourized with charcoal. To the clear filtrate was added one equivalent of sodium ethoxide, and the *sodium salt* was precipitated with acetone. Three recrystallizations from 10:1 CH_3CN/EtOH gave white needles, mp 96−97°C. Spinner and White (31, 32) reported this compound but gave no melting point. Proton magnetic resonance in D_2O and in DMSO-d_6 suggested two waters of crystallization, but the elemental analysis was poor. *Anal.* calcd. for $C_5H_4NONa \cdot 1.25\ H_2O$: C 43.14, H 4.71, N 10.06; found: C 43.42, H 5.76, N 10.15.

Initial kinetic studies were carried out with the above material. However, the *nitrate salt* proved to be a superior alternative which was used for the remainder of the kinetic work. It was initially produced by accident during an attempted nitration following Albert and Barlin (33). 4-Hydroxypyridinium nitrate was extracted from the salts with ethanol, decolourized with charcoal, and twice recrystallized from water, mp 198−200°C (dec). *Anal.* calcd. for $C_5H_6N_2O_4$: C 37.98, H 3.82, N 17.72; found: C 37.94, H 3.95, N 17.58. The same nitrate salt was more conveniently prepared by acidifying a concentrated aqueous solution of **1***a* with nitric acid to pH 1. After standing, the material which crystallized out was treated as above. It gave an identical ir spectrum and mp.

*1-Methyl-4-pyridone (1*b*) hydrobromide salt*

Compound **1***a* (practical grade) was partially dehydrated and purified by heating with two equivalents of hexamethyldisilazane in chloroform. Solid material was filtered off and the filtrate was reduced to half its original volume. Addition of ether gave white flakes of a hydrate of **1***a*, mp 66−67°C (sublimed **1***a* has mp 148−149°C) (18).

To this hydrate (7.6 g, 68 mmol) and sodium methoxide (3.7 g, 68.5 mmol) in 10 mL methanol was added, with stirring, dimethyl

Can. J. Chem. Downloaded from www.nrcresearchpress.com by 210.87.254.6 on 09/06/12
For personal use only.

sulphate (8.83 g, 70 mmol) in 10 mL methanol. The solution was heated for 15 min and then the pH was adjusted to 7–8 with sodium bicarbonate. Repeated addition and evaporation with 1:1 acetone/chloroform precipitated the salts which were filtered off. The filtrate was reduced to give an oil which was dissolved in acetone containing a slight excess of concentrated hydrobromic acid. Evaporation of the solvent gave the hydrobromide salt (6 g, 46%), recrystallized from methanol/ether, mp 175–177°C (when dried at 110°C for 1 hour). *Anal.* calcd. for C_6H_8BrNO: C 37.92, H 4.24, N 7.37, Br 42.05; found: C 37.80, H 4.16, N 7.22, Br 41.95.

*4-Methoxypyridine (2*b*)*

To 4-methoxypyridine-*N*-oxide (Aldrich) was slowly added 2 equivalents of phosphorus trichloride and a vigorous reaction ensued. The solution was stirred for 20 min and then made slightly alkaline with concentrated aqueous ammonia. The resultant solution was extracted 3 × 100 mL of chloroform and the dried extracts (Na_2SO_4) were evaporated to give an 85% yield of **2***b*. The proton nmr agreed with the literature (34).

4-Methoxypyridine: bromine complex

Addition of bromine to **2***b* in water, ethanol, or in chloroform precipitated a complex. From water the complex was yellow, mp 120–121°C; from chloroform it was red, mp 117–119°C. The proton nmr spectra of these materials were similar to that of **2***b*.

The complex brominated acetone in chloroform and gave back **2***b* as its HBr salt. Its ir spectrum was identical to that of the hydrochloride salt (34). Upon heating the bromine complex in water, bromine vapour was evolved and no bromination of **2***b* was detected.

*3-Bromo-4-pyridone (3*a*)*

(a) *From 4-amino-3-bromopyridine* (see below)

Diazotization of this compound employing the procedure of Talik (12) gave only a 3% yield after several attempts.

(b) *From bromination of 4-pyridone (1*a*)*

4-Pyridone (0.95 g, 10 mmol) was dissolved in 50 mL water containing sodium acetate (1 g, 12 mmol) and the pH was adjusted to 4.2–4.4 with acetic acid. This solution was cooled in ice, and bromine (1.6 g, 10 mmol) in 50 mL 1 *M* aqueous KBr was added, with stirring, over 45 min. A precipitate of dibromo compound **4***a* (0.33 g, 26.2% based on bromine) was filtered off and the filtrate was evaporated to dryness. The residue, containing inorganic salts and organics, was extracted with ethanol and the extract was evaporated. The solid residue contained a 4:1 mixture of **3***a* and **1***a*, from its ^{1}Hmr spectrum. To effect further separation from salts the residue was treated with boiling acetone. The hot solution was filtered and reduced to dryness to give 1.55 g of solid which contained 80% 3-bromo-4-pyridone **3***a* (73.8%, based on bromine) and 20% unreacted 4-pyridone **1***a*. Decolourization with charcoal and recrystallization from boiling water gave **3***a* (0.48 g, 28% isolated yield), mp 229–231°C (lit. (9) mp 228–230°C).

No optimization was attempted. Doubling the concentrations of the reactants caused a 1.6-fold increase in the percent formation of the undesired dibromo product **4***a*.

Attempted brominations of 4-pyridone

(a) *In acid*

To 4-pyridone (0.95 g, 10 mmol) in 25 mL of concentrated HBr was added, with stirring, an equivalent amount of bromine in 25 mL of the same acid, over 30 min. Ice was added and the pH brought to 3 with sodium carbonate. The solution was reduced in volume on a water bath and, upon cooling, 0.923 g of 3,5-dibromo-4-pyridone (**4***a*) crystallized out (73% yield, based on bromine). Its ir spectrum matched that in the literature (35). The ^{1}Hmr analysis of the solid from evaporating the filtrate showed a 2:5 mixture of **3***a* and unreacted **1***a*.

(b) *In 1* M *aqueous KBr*

The above procedure again yielded **4***a* (0.842 g, 67%).

(c) *In base*

The same procedure in 1 *M* aqueous KBr containing 1 equivalent of KOH precipitated **4***a* (1.08 g, 86%). Both here and in (b) **3***a* was a minor product.

(d) *In dioxane*

"Dioxane dibromide" is considered a mild brominating agent (36). However, mixing equimolar quantities of bromine and **1***a*, each in dioxane, slowly precipitated **4***a* (60% yield).

(e) *Pyridinium hydrobromide perbromide* (37) and **1***a* in $CHCl_3$ gave **4***a* (72%).

(f) *2,4,4,6-Tetrabromo-2,5-cyclohexadienone* is another mild brominating agent (38). From a 1:1 reaction with **1***a* in $CHCl_3$ at 0°C we again obtained **4***a* (65%).

*Other routes to 3*a

Various other attempts to make **3***a* were unsuccessful, as outlined in the text. These failed either because of a recalcitrant hydrolysis step, or due to attempted monobromination again giving undesired dibromination.

4-Amino-3-bromopyridine

3-Bromopyridine was obtained from Aldrich and by diazotization of 3-aminopyridine (74% yield) (7). It was oxidized in 90–93% yield (8), and the *N*-oxide was nitrated as follows.

3-Bromopyridine-*N*-oxide hydrochloride (8) (35 g, 0.166 mmol) dissolved in 35 mL concentrated H_2SO_4 was poured into a mixture of KNO_3 (32 g), concentrated HNO_3 (54 mL), concentrated H_2SO_4 (42 mL), and 20% oleum (28 mL). The solution was heated slowly to 100°C and held there for 21 h. The cooled solution was treated with ice and sodium carbonate, and finally brought to pH 7–8 with aqueous ammonia. After cooling in ice for 20 min the solid from the mixture was filtered off and dried in air. The desired 3-bromo-4-nitropyridine-*N*-oxide (25.1 g, 70%) was extracted from the solid with boiling $CHCl_3$ and was recrystallized from benzene, mp 150–152°C (lit. (8) mp 152–152.5°C, 58%).

The above product was reduced by a procedure modified from the literature (11). 3-Bromo-4-nitropyridine-*N*-oxide (5.0 g, 22.8 mmol) was dissolved in 100 mL acetic acid containing iron powder (8.33 g) in apparatus fitted with fast mechanical stirring. Gentle heat was applied to bring the temperature to 80°C. After 10 min the exothermic reaction brought the temperature to 110°C and the heat source was temporarily removed until it fell back to 80°C. After 90 min at this temperature the solution was cooled and brought to pH 8 with sodium bicarbonate and then ammonium hydroxide. Extraction with ether (3 × 300 mL) and evaporation of the extract gave 4-amino-3-bromopyridine (3.42 g, 86.7%), mp 66–68°C from light petroleum (lit. (11) mp 66–68°C),

This compound has a protonation p*K* of 7.14 ± 0.02 (*vide supra*).

*3-Bromo-1-methyl-4-pyridone (3*b*)*

To **3***a* (1.5 g, 8.6 mmol) in 30 mL MeOH containing KOH (0.48 g) was added dimethyl sulphate (1.6 mL, 18 mmol), and the mixture was refluxed for 2 h. The cooled solution was made basic with sodium methoxide. Addition of acetone (200 mL) and ether (10 mL) precipitated salts. Further removal of salts was achieved by repeated treatment with chloroform/acetone. After solvent removal the residual oil was dissolved in $CHCl_3$, filtered, and the filtrate was evaporated. The resulting oil was dissolved in acetone and addition of a slight excess of concentrated HBr precipitated **3***b*, as *the hydrobromide salt* (1.57 g, 68%). Recrystallization from acetonitrile (1 g/300 mL) gave transparent needles, mp 253–255°C; ^{1}Hmr (D_2O/DSS) δ: 4.23 (s, 3), 7.13 (d, 1, $J_{5,6}$ = 7.0 Hz), 8.23 (q, 1, $J_{2,6}$ = 2.4 Hz), 8.64 (d, 1). *Anal.* calcd. for $C_6H_7NOBr_2$: C 26.80, H 2.62, N 5.21, Br 59.42; found: C 27.08, H 2.69, N 5.23, Br 59.48.

Acknowledgement

The authors thank the Natural Sciences and Engineering Research Council of Canada for operating grants to O.S.T. and a postgraduate scholarship to M.P.

1. R. A. ABRAMOVITCH and J. G. SAHA. Adv. Heterocycl. Chem. **6**, 229 (1966).

2. H. MEISLICH. Pyridine and its derivatives. Part III. Wiley–Interscience, New York. 1962. Chapt. 12; H. Tieckelmann. *In* Pyridine and its derivatives. Supplement. Part III. *Edited by* R. A. Abramovitch. Interscience, New York. 1974. Chapt. XII, p. 800.
3. O. S. TEE and M. PAVENTI. J. Am. Chem. Soc. **104**, 4142 (1982).
4. P. BEAK, F. S. FRY, JR., J. LEE, and F. STEELE. J. Am. Chem. Soc. **98**, 171 (1976); P. Beak. Acc. Chem. Res. **10**, 186 (1977), and references therein.
5. (*a*) O. S. TEE and C. G. BERKS. J. Org. Chem. **45**, 830 (1980); (*b*) O. S. TEE and M. PAVENTI. J. Org. Chem. **45**, 2072 (1980); (*c*) J. Org. Chem. **46**: 4172 (1981); (*d*) O. S. TEE, M. J. KORNBLATT, and C. G. BERKS. J. Org. Chem. **47**, 1018 (1982).
6. A. ALBERT and J. N. PHILLIPS. J. Chem. Soc. 1294 (1962).
7. T. TALIK, Z. TALIK, and H. BAN-OGANOWSKA. Synthesis, 293 (1974).
8. E. MATSUMURA and M. ARIGA. Bull. Chem. Soc. Jpn. **46**, 3144 (1973).
9. T. TALIK and Z. TALIK. Rocz. Chem. **36**, 539 (1962); Chem. Abstr. **57**, 12421a (1962).
10. R. JUJO. Yakugaku Zasshi, **66** (B), 49 (1946).
11. H. J. DEN HERTOG and J. OVERHOFF. Recl. Trav. Chim. Pays-Bas, **69**, 468 (1950).
12. T. TALIK. Rocz. Chem. **36**, 1049 (1962); Chem. Abstr. **58**, 7480f (1963).
13. M. HAMANA. J. Pharm. Soc. Jpn. **71**, 263 (1951).
14. T. TALIK. Rocz. Chem. **37**, 69 (1963); Chem. Abstr. **59**, 8697f (1963).
15. E. HAYASHI. J. Pharm. Soc. Jpn. **71**, 213 (1951).
16. G. ALOISI, G. CAUZZO, and U. MAZZUCATO. Trans. Faraday Soc. **63**, 1858 (1967).
17. P. J. BRIGNELL, A. R. KATRITZKY, and H. O. TARHAN. J. Chem. Soc. (B), 1477 (1967).
18. P. BELLINGHAM, C. D. JOHNSON, and A. R. KATRITZKY. J. Chem. Soc. (B), 1226 (1967); 866 (1968).
19. R. M. ACHESON. An introduction to the chemistry of heterocyclic compounds. 2nd ed. Interscience, New York. 1967. Chapt. 5.
20. P. TOMASIK and C. D. JOHNSON. Adv. Heterocycl. Chem. **20**, 1 (1976).
21. J. MARCH. Advanced organic chemistry. McGraw–Hill, New York. 1968. p. 241.
22. J. KULIC and M. VECERA. Collect. Czech. Chem. Commun. **39**, 71 (1974).
23. R. P. BELL and D. J. RAWLINSON. J. Chem. Soc. 63 (1961).
24. P. B. D. DE LA MARE. Electrophilic halogenation. Cambridge University Press, London. 1976.
25. J. H. RIDD. Adv. Phys. Org. Chem. **16**, 1 (1973).
26. F. W. BROEKMAN and H. J. C. TENDELOO. Recl. Trav. Chim. Pays-Bas, **81**, 107 (1962).
27. G. JONES and S. BAECKSTROM. J. Am. Chem. Soc. **56**, 1517 (1934).
28. J. M. PINK. Can. J. Chem. **48**, 1169 (1970).
29. R. C. WEAST (*Editor*). Handbook of chemistry and physics. 55th ed. C.R.C. Press, Cleveland, Ohio. 1974. p. D-130.
30. A. ALBERT and E. P. SERJEANT. Ionization constants of acids and bases. Methuen, London. 1962.
31. (*a*) E. SPINNER and J. C. B. WHITE. J. Chem. Soc. (B), 991 (1966); (*b*) 996 (1966).
32. E. SPINNER. J. Chem. Soc. 1232 (1960).
33. A. ALBERT and G. B. BARLIN. J. Chem. Soc. 5156 (1963).
34. E. SPINNER and J. C. B. WHITE. J. Chem. Soc. 3115 (1962).
35. B. D. BATTS and E. SPINNER. Aust. J. Chem. **22**, 2581 (1969).
36. A. P. TERENTYEV, L. I. BELENKY, and L. A. YANAVSKAYA. J. Gen. Chem. U.S.S.R. **24**, 1251 (1954).
37. L. F. FIESER. Organic experiments. 2nd ed. Raytheon Education Co., Lexington, MA. 1968. p. 70.
38. G. J. FOX and G. HALLAS. Org. Synth. **55**, 20 (1976).
39. O. S. TEE, N. R. IYENGAR, and M. PAVENTI. J. Org. Chem. **48**, 759 (1983).

Can. J. Chem. Downloaded from www.nrcresearchpress.com by 210.87.254.6 on 09/06/12
For personal use only.

Hydrazines et hydrazones hétérocycliques. IV. Synthèses de dérivés de l'hydrazine dans la série des imidazo[4,5-*d*] pyridazinones-4

MARTINE BELJEAN-LEYMARIE ET MICHEL PAYS
U. E. R. des Sciences Pharmaceutiques, 1, rue Vaubénard, 14032 Caen Cédex, France

ET

JEAN-CLAUDE RICHER
Département de Chimie, Université de Montréal, B.P. 6210, Montréal (Qué.), Canada H3C 3V1

Reçu le 21 avril 1981[1]

MARTINE BELJEAN-LEYMARIE, MICHEL PAYS et JEAN-CLAUDE RICHER. Can. J. Chem. **61**, 2563 (1983).

On rapporte les synthèses d'alkyl ou d'aryl-5 dihydro-3,5 (ou 1,5) imidazo-[4,5-*d*] pyridazinones-4 effectuées à partir des diaminopyridazinones correspondantes. La méthylation d'alkyl ou d'aryl-5 mercapto-2 dihydro-3,5 (ou 1,5) imidazo-[4,5-*d*] pyridazinones-4 conduit à des mélanges d'alkyl ou d'aryl-5 méthyl-1 méthylthio-2 dihydro-3,5 (ou 1,5) imidazo-[4,5-*d*] pyridazinones-4 et d'alkyl ou d'aryl-5 méthyl-3 méthylthio-2 dihydro-3,5 (ou 1,5) imidazo-[4,5-*d*] pyridazinones-4 dont les structures ont pu être établies par effet Overhauser. Ces imidazo-[4,5-*d*] pyridazinones-4 sont utilisées pour les synthèses d'hydrazines et d'hydrazones. Les spectres de masse de quelques intermédiaires clés sont rapportés et discutés.

MARTINE BELJEAN-LEYMARIE, MICHEL PAYS, and JEAN-CLAUDE RICHER. Can. J. Chem. **61**, 2563 (1983).

We report the syntheses of 5-alkyl or 5-aryl-3,5-dihydro[4,5-*d*]imidazo-4-pyridazinones (or the 1,5-dihydro derivatives) from the corresponding diaminopyridazinones. The methylation of 5-alkyl or 5-aryl-2-mercapto-3,5 (or 1,5)-dihydro [4,5-*d*]imidazo-4-pyridazinones leads to mixtures of 5-alkyl or 5-aryl-1methyl-2-methylthio-3,5 (1,5)-dihydro[4,5-*d*]imidazo-4-pyridazinones and 5-alkyl or 5-aryl-3-methyl-2-methylthio-3,5 (or 1,5)-dihydro[4,5-*d*]imidazo-4-pyridazinones whose structures have been established by the Overhauser effect. These [4,5-*d*]imidazo-4-pyridazinones are used for the syntheses of hydrazines and hydrozones. The mass spectra of several key intermediates are presented and discussed.

[Journal translation]

Introduction

Dans le cadre de nos études sur les propriétés, en chimie analytique, d'hydrazines et d'hydrazones de composés hétérocycliques, nous avons entrepris la synthèse et la caractérisation d'alkyl ou d'aryl-5 dihydro-3,5 (ou 1,5) imidazo-[4,5-*d*] pyridazinones-4 isostères d'alkyl ou d'aryl-6 dihydro-2,3 6*H*-thiazolo[4,5-*d*] pyridazinones-7 précédemment décrites (1). Ce sont les résultats obtenus au cours de ces études qui font l'objet du présent travail.

En raison de leur analogie de structure avec les bases puriques, les imidazo-[4,5-*d*] pyridazines sont fait l'objet d'études nombreuses de la part de différents auteurs (2−7). Par contre, les alkyl ou les aryl-5 dihydro-3,5 (ou 1,5) imidazo-[4,5-*d*] pyridazinones-4 n'avaient pas été synthétisées à l'exception de la mercapto-2 phényl-5 dihydro-3,5 imidazo-[4,5-*d*] pyridazinone-4 qui a été signalée comme produit secondaire d'une réaction (8) avant d'être synthétisée pour fins d'identification par condensation de la thiourée sur la diamino-4,5 phényl-1 pyridazinone-6.

Résultats et discussion

Les synthèses que nous avons mises en oeuvre utilisent les diaminopyridazinones (**4**) correspondantes, soit la diamino-4,5 méthyl-1 pyridazinone-6 (**4***a*) et la diamino-4,5 phényl-1 pyridazinone-6 (**4***b*). Les essais d'utilisation des dihydro-3,5 imidazo-[4,5-*d*] pyridazinones-4 n'ont pas abouti. Dans le but d'obtenir des composés substitués en 2, les diaminopyridazinones (**4**) ont été condensées avec le sulfure de carbone. Les alkyl ou les aryl-5 mercapto-2 dihydro-3,5 (ou 1,5) imidazo-[4,5-*d*] pyridazinones-4 (**5**) ainsi obtenues conduisent ensuite à des thioéthers méthyliques (**6** et **7**), puis à des hydrazines (**10** et **11**) ou à l'hydrazone (14).

I. *Méthodes de synthèse*

Les alkyl ou les aryl-2 diamino-4,5 pyridazinones-3 (**4**) sont synthétisées à partir des composés dichlorés-4,5 correspondants (**1**) selon les procédés de Reicheneder et Dury (9−11) par l'intermédiaire de dérivés nitroaminés (**3**) (cf. Schéma 1). A la méthode classique de réduction de **3** par hydrogénation catalytique en présence de platine utilisée par ces auteurs (11) et même plus récemment par Yanai *et al.* (12), nous avons préféré le procédé de Kuhn (13), plus simple et plus rapide, qui consiste en un reflux dans l'éthanol en présence d'hydrazine et de charbon palladié.

La synthèse d'alkyl ou d'aryl-5 mercapto-2 dihydro-3,5 (ou 1,5) imidazo-[4,5-*d*] pyridazinones-4 (**5**) à partir d'alkyl ou d'aryl-2 diamino-4,5 pyridazinones-3 correspondantes (**4**) peut s'effectuer selon les deux procédés habituels: cyclisation avec le sulfure de carbone en milieu pyridinique ou condensation à sec avec la thiourée en utilisant la technique décrite par Elion (14). Contrairement aux résultats rapportés par Itai et Suzuki (5) avec la diamino-4,5 diméthoxy-3,6 pyridazine, la condensation à sec avec la thiourée ne conduit aux mercapto-2 imidazo-[4,5-*d*] pyridazinones désirées qu'avec des rendements variables. Le rendement de la cyclisation de nos dérivés diaminés avec le sulfure de carbone s'est révélé constant et supérieur aux 30% décrit(5); nous avons donc préféré ce procédé.

Mis en solution aqueuse de soude à 10%, à température ambiante et en présence d'iodure de méthyle, les composés **5** conduisent aux composés mono S-méthylés (**8**). Dans des conditions plus drastiques, soit une solution aqueuse de soude à 10% en présence d'iodure de méthyle à 80°C ou une solution de sodium dans le méthoxy-2 éthanol à froid en présence d'un excès de CH_3I, les dérivés **5** conduisent à des mélanges des composés N et S-méthylés **6** et **7**, en proportions variables selon les séries *a* et *b*: environ 5% de **6***a* et 95% de **7***a*; environ 25% de **6***b* et 75% de **7***b*. Facilement mis en évidence par chromatographie en couche mince, les composés ont pu être

[1]Revision reçue le 3 juin 1983.

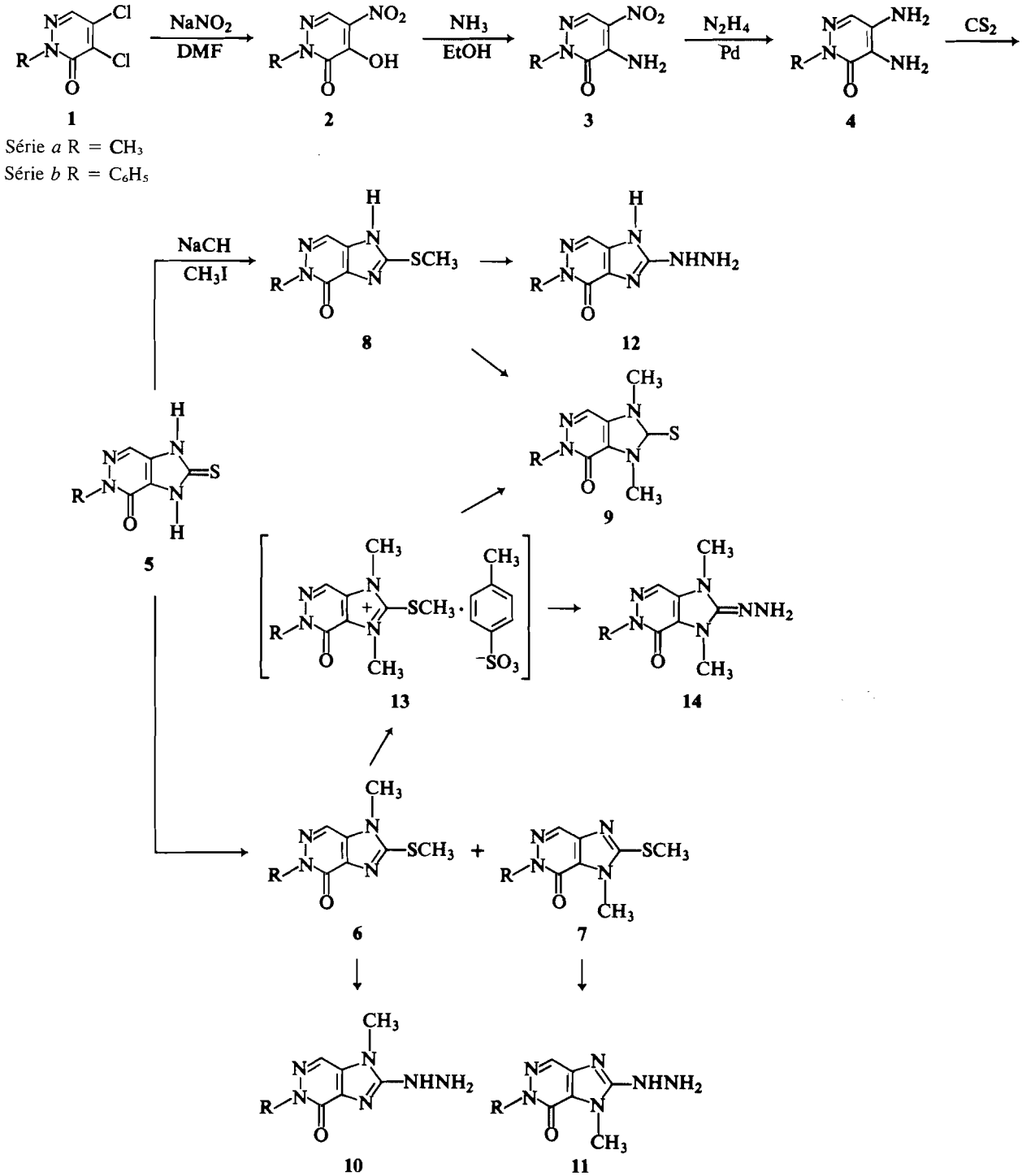

SCHÉMA 1. Synthèses d'hydrazino-2 ou hydrazono-2 alkyl- ou aryl-5 dihydro-3,5 (ou 1,5) imidazo 4,5-*d* pyridazinones-4.

isolés par chromatographie sur colonne de gel de silice. Dans des conditions encore plus fortes (méthoxy-2 éthanol et sodium à chaud en présence d'un excès de CH_3I, **5***b* conduit encore au même mélange 25:75 de **6***b* et **7***b*. Par contre, **5***a* conduit à un nouveau composé, soit le dérivé N_1, N_3 diméthylé (**9***a*). Ce composé **9***a* ne se forme qu'à chaud en solution dans le méthoxyéthanolate de sodium et en présence d'un grand excès d'iodure de méthyle. En effet, **5***a* porté au reflux dans ce milieu en présence de 2 équivalents d'iodure de méthyle conduit au mélange de **6***a* et de **7***a*; par contre, en présence d'une quantité d'iodure de méthyle supérieure à 3 équivalents **5***a* donne **9***a*.

De plus, **9***a* porté à reflux dans le méthoxy-2 d'éthanolate de sodium avec une quantité d'iodure de méthyle légèrement supérieure à 2 équivalents conduit également à **8***a*. Par contre, le composé **9***b* mis dans les mêmes conditions conduit au mélange de **6***b* et de **7***b*. Il semble donc possible d'envisager un mécanisme de formation de **8***a* impliquant la formation d'un dérivé quaternaire intermédiaire instable à la chaleur et représenté dans le schéma 2.

D'ailleurs ce phénomène de déquaternisation par la chaleur

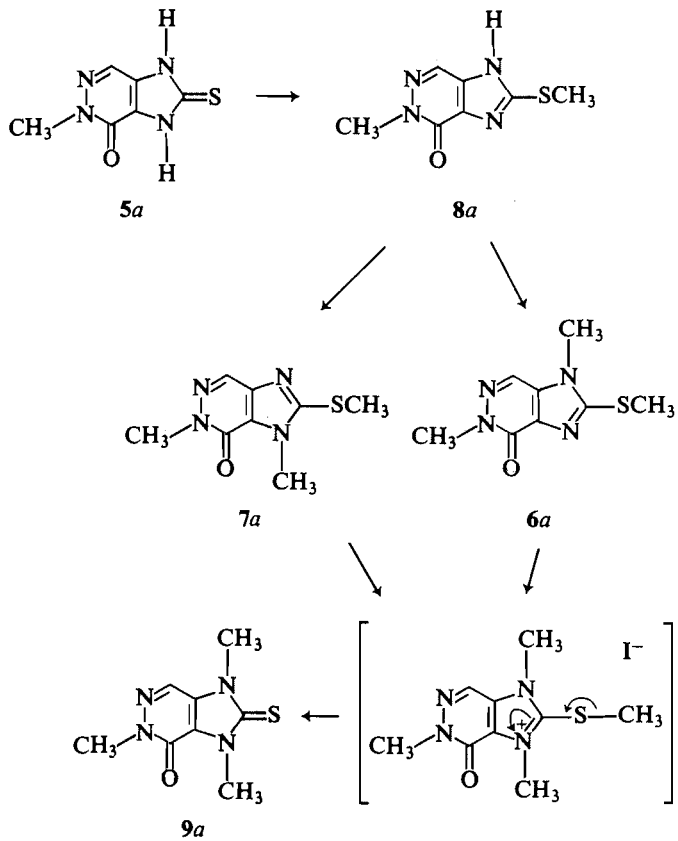

SCHÉMA 2. Rationalisation de la formation de **9***a* à partir de **5***a*, **6***a*, **7***a* ou **8***a*.

a été également décrit auparavant pour les sels de benzimidazolium (15). Les synthèses des dérivés hydrazino-2 (**10**, **11**, et **12**) ont été effectuées à partir des dérivés méthylthio-2 correspondants (**6**, **7** et **8**) alors que la synthèse des hydrazino-2 diméthyl-1,3 alkyl ou aryl-5 dihydro-3,5 imidazo-[4,5-*d*] pyridazinone-4 (**14**) peut être effectuée à partir des composés **6** et **7** selon le procédé classique décrit en la série thiazolique (1, 16), soit la formation d'un sel immonium par réaction à chaud avec le *p*-toluènesulfonate de méthyle suivi d'une décomposition par l'hydrazine; la synthèse de l'hydrazino-2 triméthyl-1,3,5 dihydro-3,5 imidazo-[4,5-*d*] pyridazinone-4 (**14**) doit toutefois être menée avec précaution car un chauffage trop prolongé de **13***a* entraine sa déquaternisation en **9***a* (voir plus haut).

II. *Détermination des structures des composés 6 et 7*

L'attribution des structures des composés **6** et **7** dans les séries *a* ainsi que *b* est basée sur des mesures en rmn du ^1H, d'effet Overhauser obtenu par irradiation de la fréquence de résonance des groupes N—CH_3. On a enregistré l'intensité du signal du proton pyridazinique situé à 8,3 ppm pour les composés *b*, en appliquant successivement une irradiation de puissance modérée à la fréquence de résonance du N—CH_3 (4,1 ppm) et à 500 Hz de cette fréquence. Dans le cas du composé **7***b* (F = 150°C), l'irradiation provoque une augmentation relative de l'intensité du signal qui est inférieure à 5% pour les dix intégrations effectuées tandis que l'on note une augmentation moyenne de 32% pour les dix mesures dans le cas du composé **6***b* (F = 230°C). Ce composé possède donc la structure pour laquelle le proton pyridazinique se trouve dans l'environnement du N—CH_3 (cf. Schéma 1).

III. *Spectres de masse des produits et de quelques-uns de leurs intermédiaires*

Les principales fragmentations observées lors de la spectrométrie de masse sous impact électronique, des dérivés **5***a* et **5***b*, **6***a* et **6***b*, **7***a* et **7***b*, **8***a* et **8***b* ainsi que **9***a* sont rapportées dans la partie expérimentale. Une comparaison des résultats obtenus permet de réaliser que les substituants R qui différencient les séries *a* et *b* n'ont qu'une influence négligeable sur le cours des fragmentations; on n'a pas observé de fragmentations importantes de la liaison N—R.

Par ailleurs, les groupements méthyles attachés au soufre sous forme de S—CH_3 n'ont pas tendance à se dissocier; on observe plutôt des pertes de SCH_3. Dans les séries examinées, l'expulsion d'un groupe méthyle est une caractéristique des composés portant au moins un CH_3 attaché aux azotes de l'imidazo. Cette propriété pourrait s'avérer utile au point de vue analytique.

Dans les composés isomères **6** et **7**, les groupes méthyles des composés **7** qui sont soumis à des interactions stériques plus grandes que ceux des composés **6** sont expulsés plus facilement que ceux des composés **6** (35 vs. 15 et 23 vs. 13%). Il est peut-être possible de relier cette sélectivité accrue dans un processus primaire de fragmentation des composés **7** avec le fait que l'on observe un plus grand nombre de pics d'intensité > 5% dans les composés **6** par rapport aux composés **7**.

Finalement, on doit noter la stabilité remarquable des composés **5** sous impact électronique; leur fragmentation est minimale.

Partie expérimentale

Les points de fusion ont été mesurés sur un banc Kofler. Les spectres ir ont été enregistrés à l'aide d'un spectrophotomètre Perkin–Elmer.

Les spectres de résonance magnétique nucléaire ont été déterminés sur un spectromètre modèle T-60 de la compagnie Varian pour des solutions dans le DMSO-d_6 (à moins d'indication contraire).

Les spectres de masse à haute résolution ont été déterminés à l'aide d'un spectromètre AEI MS–902 relié à un ordinateur PDP-8; toutes les masses moléculaires expérimentales déterminées correspondent à ±0,0015 unités de masse aux valeurs calculées.

L'effet Overhauser nucléaire à été mesuré à 302 K sur des échantillons rigoureusement dégazés, par plusieurs cycles de pompage sous vide et de refroidissement à l'azote liquide, au moyen du spectrographe Varian XL 100-12 du Centre Régional de Mesures Physico-Chimique de l'Ouest (Nantes).

Synthèse des alkyl-1 ou aryl-1 diamino-4,5 pyridazinones-6 (4)

Une solution de 50 g d'alkyl ou aryl-1 amino-4 nitro-5 pyridazinone-6 (**3**) obtenue selon Reicheneder et Dury (10) dans 500 mL d'éthanol contenant 50 mL d'hydrate d'hydrazine et 1 g de charbon palladié à 10% est portée au reflux pendant 4 heures. Par refroidissement, les dérivés diaminés précipitent et on les obtient sous forme de poudre blanche avec un rendement de 80% après recristallisation dans l'éthanol.

Composé **4***a*: pf = 212°C; spectres ir et rmn rapportés antérieurement (1). *Anal.* calc. pour $C_5H_8N_4O$: C 42,85, H 5,75, N 39,98; trouvé: C = 43,05, H = 6,0, N = 39,77.

Composé **4***b*: pf = 200°C *Anal.* calc. pour $C_{10}H_{10}N_4O$: C 59,39, H 4,98, N 27,71; trouvé: C 59,07, H 4,95; N 27,84.

Synthèse des méthyl ou phényl-5 mercapto-2 dihydro-3,5 imidazo-[4,5-d] pyridazinones-4 (5)

On porte 0,075 mol de **4** à reflux 2 heures dans 200 mL de pyridine en présence de 0,15 mol (6 g) de soude caustique et de 150 mL de CS_2. Par concentration, les composés **5** précipitent avec un rendement de 70%.

Composé **5***a*: pf > 260°C; ir (KBR cm^{-1}): 3410 f, 1670 f, 1592 tf,

1510 f, 1210 f, 975 f, 827 f; rmn: 3,92 (N—CH_3), 8,00 (H-7). Masse, *m/e* (intensité): 182 (100), 154 (12, −H, −HCN), 111 (12, $C_4H_3N_2S$). *Anal.* calc. pour $C_6H_6N_4OS$: C 39,56, H 3,30, N 30,75; trouvé: C 39,42, H 3,29, N 30,62.

Composé **5***b*: pf > 260°C ir (KBR cm^{-1}): 1672 f, 1658 tf, 1480 f, 1450 f, 1190 f, 690 f, 635 f; rmn: 7,56 (C_6H_5) et 8,25 (H-7). Masse: 244 (100), 243 (31), 111 (6, $C_4H_3N_2S$). *Anal.* calc. pour $C_{11}H_8N_4OS$: C 54,10, H 3,30, N 22,94; trouvé: C 54,24, H 3,26, N 22,80.

Synthèse des composés ***6*** *et* ***7***

A 2,5 g de sodium dissous dans 80 mL de carbitol, on ajoute 15 g de **5** et 10 mL d'iodure de méthyle. On agite une heure. On isole un produit blanc formé par un mélange de deux isomères **6** et **7**. Par chromatographie sur colonne de gel de silice, on sépare les deux isomères à l'aide d'un mélange éluant benzène−méthanol (95:5 v/v).

Composé **6***a*: pf = 230°C; ir (KBr cm^{-1}): 1648 tf, 1550 f, 1039 f, 960 f, 698 f, rmn ($CDCl_3$): 2,79 (s, CH_3), 3,84 et 4,02 (N—CH_3), et 8,19 (H-7). Masse: 210 (100), 209 (12), 195 (15, $-CH_3$), 182 (6, −HCN), 177 (14, −SH), 163 (12, $-SCH_3$). *Anal.* calc. pour $C_8H_{10}N_4OS$: C 45,71, H 4,80, N 26,66, S 15,47; trouvé: C 46,02, H 4,75, N 26,45, S 15,60.

Composé **6***b*: pf = 230°C; ir (KBr cm^{-1}): 1660 tf, 1555 f, 1120 f, 755 f, 685 f. rmn: 2,78 (SCH_3), 3,62 (N—CH_3), 8,0 (H-7). Masse: 272 (100), 271 (44), 257 (13, $-CH_3$), 225 (13, $-SCH_3$), 180 (14, $-C_6H_5NH$), 179 (8, $-C_6H_5NH_2$). *Anal.* calc. pour $C_{13}H_{12}N_4OS$: C 57,35, H 4,44, N 20,58; trouvé: C 57,36, H 4,40, N 20,52.

Composé **7***a*: pf = 150°C; ir (KBr cm^{-1}): (1680−1650) tf, 1370 f, 948 f, 870 f, 830 f, 660 f, 560 f. Masse 210 (100), 209 (11), 195 (35, $-CH_3$), 182 (5, −H, −HCN), 177 (25, −SH), 163 (5, $-SCH_3$). *Anal.* calc. pour $C_8H_{10}N_4OS$: C 45,71, H 4,80, N 26,66, S 15,41; trouvé: C 45,83, H 5,00, N 26,66, S 15,22.

Composé **7***b*: pf = 150°C; ir (KBr cm^{-1}): 1665 tf, 1545 f, 1370 f, 1310 f, 925 f, 748 f, 685 f; rmn: 2,68 (SCH_3), 3,89 (NCH_3), 7,32 (C_6H_5), 8,18 (H-7). Masse: 272 (100), 271 (22), 257 (23, $-CH_3$), 225 (11, $-SCH_3$), 180 (7, $-C_6H_5$ − NH), 179 (23, $-C_6H_5NH_2$). *Anal.* calc. pour $C_{13}H_{12}N_4OS$: C 57,35, H 4,44, N 20,58; trouvé: C 57,32, H 4,46, N 20,43.

Synthèse des composés ***8***

A une solution alcaline saturée du composé **5**, on ajoute 1,5 équivalent de CH_3I. On maintient le mélange à la température ambiante. Les composés **8** précipitent et on les obtient avec un rendement de 90% après les avoir essorés et recristallisés.

Composé **8***a*: pf > 260°C; ir (KBr cm^{-1}): 1650 tf, 1540 f, 1430 f, 1375 f, 827 f; rmn: 2,70 (SCH_3), 3,74 (NCH_3), 8,34 (H−7). Masse: 196 (100), 195 (16), 168 (6, −H, −HCN), 167 (6, −H, −CO), 163 (12, −SH). *Anal.* calc. pour $C_7H_8N_4OS$: C 42,86, H 4,1, N 28,56, S 16,31; trouvé: C 42,71, H 4,09, N 28,32, S 16,15.

Composé **8***b*: pf = 280°C; ir (KBr cm^{-1}): 1650 tf, 1545 f, 1490 f, 1420 f, 1390 f, 1300 f, 675 f; rmn: 2,73 (SCH_3), 7,55 (C_6H_5), 8,68 (H-7). Masse: 258 (100), 257 (32), 229 (5, −H, −CO), 225 (8, −SH). *Anal.* calc. pour $C_{12}H_{10}N_4OS$: C 55,81; H 3,90, N 21,70, S 12,39; trouvé: C 55,41, H 3,99 N 21,67, S 12,55.

Synthèse du composé ***9***a

A une solution de 3 g de sodium dans 100 mL de méthoxyéthanol, on ajoute 9 g de **5***a* et 12 mL de CH_3I. On maintient ce mélange au reflux pendant 4 heures alors que le produit **9***a* précipite. Le produit filtré et recristallisé dans l'éthanol présente les caractéristiques suivantes: pf = 238°C; ir (KBr cm^{-1}): 1670 tf, 1580 f, 1350 tf, 1025 f, 982 f, 888 f, 782 f; rmn: 3,70, 3,74 et 3,89 (N—CH_3) et 8,60 (H-7). Masse: 210 (100), 209 (6), 195 (37, $-CH_3$), 182 (10), −H, −HCN). *Anal.* calc. pour $C_8H_{10}N_4OS$: C 45,71, H 4,8, N 26,66, S 15,41; trouvé: C 45,92, H 5,0, N 26,24, S 15,27.

Synthèse des composés ***10***, ***11*** *ou* ***12***

On porte respectivement à reflux pendant 6 heures des solutions de **6**, **7** ou **8** dans le méthoxyéthanol en présence de 1,5 équivalents d'hydrate d'hydrazine. Après concentration, on obtient avec des rendements de 90% les composés **10**, **11** ou **12** que l'on purifie par recristallisation dans le méthoxy-2 éthanol (à moins d'indication contraire).

Composé **10***b*: pf > 260°C; (recristallisation dans l'éthanol); ir (KBr cm^{-1}): (1680−1660) tf, 1480 f, 1392 f, 1345 f, 1034 f, 760 f, 700 f; rmn: 3,68 (N—CH_3), 7,53 (C_6H_5), 8,57 (H-7). *Anal.* calc. pour $C_{12}H_{12}N_6O$: C 56,24, H 4,72, N 32,80; trouvé: C 56.13, H 5,03, N 32,55.

Composé **11***a*: pf = 244°C; ir (KBr cm^{-1}): 3300 f, 1640 tf, 1570 f; rmn: 3,69 et 3,75 (N—CH_3), 8,1 (H-7). *Anal.* calc. pour $C_7H_{10}N_6O$: C 43,29, H 5,19, N 43,28; trouvé: C 43,29, H 5,16, N 43,07.

Composé **11***b*: pf = 242°C (recristallisation dans l'éthanol); ir (KBr cm^{-1}): 3295 f, (1660−1650 tf), 1563 f, 1385 f, 755 f, 690 f; rmn: 3,75 (N—CH_3), 7,47 (C_6H_5), 8,28 (H-7). *Anal.* calc. pour $C_{12}H_{12}N_6O$: C 56,24, H 4,72, N 32,82; trouvé: C 56,00, H 5,00 N 32,43.

Composé **12***a*: pf > 260°C. *Anal.* calc. pour $C_6H_8N_6O$: C 40,00, H 4,48, N 46,65; trouvé: C 40,15, H 4,43, N 46,51.

Composé **12***b*: pf > 260°C; rmn: 7,48 (C_6H_5), 8,15 (H-7). *Anal.* calc. pour $C_{11}H_{10}N_6O$: C 54,54, H 4,16, N 34,70; trouvé: C 54,40, H 4,25, N 34,55.

Synthèse des composés ***14***

On porte respectivement les composés **6** ou **7** (isolés ou en mélange) au bain d'huile à 180°C en présence d'une quantité équivalente de *p*-toluènesulfonate de méthyle, pendant 5 min; on refroidit et isole le sel grâce à un mélange d'éthanol et d'éther. Après avoir dissous le sel dans l'eau, on ajoute deux équivalents d'hydrate d'hydrazine à la température ambiante. Après avoir laissé le mélange au repos pour une heure, on extrait au chloroforme. Les produits sont obtenus avec un rendement de 60% après recristallisation dans l'acétate d'éthyle.

Composé ***14b***: pf = 174°C (recristallisation dans l'éthanol); ir (KBr cm^{-1}): 3380 f, (1680−1650) tf, 1555 f, 995, 760 f, 685 f. *Anal.* calc. pour $C_{13}H_{14}N_6O$: C 57,76, H 5,22, N 31,10, trouvé: C 57,92, H 5,12, N 31,18.

Remerciements

Les auteurs remercient vivement le Conseil national de recherches Canada et les autorités chargées d'administrer les accords franco-québécois pour l'aide apportée sous forme d'octroi et de frais de mission. Les auteurs tiennent aussi à exprimer leur gratitude au Dr. G. J. Martin et son équipe pour la détermination des effets Overhauser nucléaires ainsi qu'au Dr. A. Martineau et Mademoiselle Marie-Thérèse Delair pour l'aide technique apportée.

1. M. Beljean et M. Pays. Bull. Soc. Chim. Fr. 3324 (1973).
2. R. N. Castle et W. S. Seese. J. Org. Chem. **23**, 1534 (1958).
3. J. A. Carbon. J. Am. Chem. Soc. **80**, 6083 (1958).
4. J. Druey. Angew. Chem. **70**, 5 (1958).
5. T. Itai et S. Suzuki. Chem. Pharm. Bull. **8**, 999 (1960).
6. G. A. Gerhardt, D. L. Aldous et R. N. Castle. J. Heterocycl. Chem. **2**, 247 (1965).
7. S. F. Martin et R. N. Castle. J. Heterocycl. Chem. **6**, 93 (1969).
8. N. B. Galstukhova, G. S. Predvoditeleva, I. M. Berzina, T. V. Kartsiva, T. N. Zyhova, M. N. Shukina et G. N. Perkin. Khim. Farm. Zh. **3**, 7 (1969); Chem. Abstr. **71**, 61312 r (1969).
9. F. Reicheneder et K. Dury. Brevet Français 384.304 (4 janvier 1965); Chem. Abstr. **62**, 16.265b (1965).
10. F. Reicheneder et K. Dury. Brevet Belge, 660,637 (6 septembre 1965); Chem. Abstr. **64**, 5.108d (1966).
11. F. Reicheneder et K. Dury. Brevet Belge, 655,648 (12 mai 1965); Chem. Abstr. **65**, 2.277 g (1966).
12. M. Yanai, T. Kinoshita, S. Taheda, H. Sadahi et H. Watanabe. Chem. Pharm. Bull. **18**, 1680 (1970).
13. L. P. Kuhn. U. S. Patent 2,768, 209 (23 octobre 1956).
14. G. B. Elion, I. Goodman, W. Lange et G. H. Hitchings. J. Am. Chem. Soc. **81**, 1898 (1959).
15. B. H. Klanderman. J. Org. Chem. **30**, 2469 (1965).
16. M. Beljean et M. Pays. Bull. Soc. Chim. Fr. 3044 (1973).

Skeletal isomerization of cyclohexene on $AlPO_4$ catalysts

J. M. CAMPELO,[1] A. GARCIA, J. M. GUTIERREZ, D. LUNA, AND J. M. MARINAS
Department of Organic Chemistry, Faculty of Sciencies, Córdoba University, Cordoba-5, Spain

Received November 17, 1982[2]

J. M. CAMPELO, A. GARCIA, J. M. GUTIERREZ, D. LUNA, and J. M. MARINAS. Can. J. Chem. **61**, 2567 (1983).

The skeletal isomerization of cyclohexene, in a microcatalytic pulse reactor, was investigated by using aluminium orthophosphates (Al/P = 1) as catalysts. An attempt has been made to correlate the isomerization activity with the acid properties of the solids, measured by means of the irreversible adsorption of different organic bases in cyclohexane, at 298 K, using a spectrophotometric method.

Apparent rate constants were calculated in terms of the kinetic model of Bassett and Habgood. Selectivity studies led to the conclusion that 1-MCP and 3-MCP were competitive products. Correlation between the kinetic selectivity factor, σ, and the number of strong acid sites has been sought.

A possible parallel reaction pathway is proposed, which agrees with both the observed rates and selectivities.

J. M. CAMPELO, A. GARCIA, J. M. GUTIERREZ, D. LUNA et J. M. MARINAS. Can. J. Chem. **61**, 2567 (1983).

On a étudié l'isomérisation du cyclohexène dans un réacteur microcatalytique à impulsion en utilisant les orthophosphates d'aluminium (Al/P = 1) comme catalyseur. On a essayé d'établir une corrélation entre l'activité d'isomérisation et les propriétés acides du solide mesurées au moyen de l'adsorption irréversible des différentes bases organiques dans le cyclohexane à 298 K en faisant appel à la méthode spectrophotométrique.

On a calculé les constantes de vitesse apparentes en fonction du modèle cinétique de Bassett et Habgood. Des études sélectives portent à conclure que le MPC-1 et le MPC-3 sont des produits de compétition. On a établi une corrélation entre le facteur de sélectivité σ et le nombre de sites d'acide fort.

On propose un chemin réactionnel possible qui est en accord avec les vitesses et les sélectivités observées.

[Traduit par le journal]

Introduction

The catalytic activity of many surfaces has been linked strongly with the presence of acid sites. Not only the number of acid sites, but also their strength, is important in many catalytic conversions. Thus, it is well known that the isomerization of olefins readily proceeds in the presence of acidic catalysts and that, for skeletal isomerization, acidic sites of high strength are necessary (1–3). Isomerization of CH to 1- and 3-MCP is sometimes even used as a model reaction for testing catalyst acidity.

The use of amorphous aluminium orthophosphates as catalysts in various organic reactions, viz. dehydration, isomerization, alkylation, cracking, etc., has been summarized in a recent review (4). The fact that the $AlPO_4$ surface possesses acid sites capable of taking part in the catalytic process has been shown in several ways (3, 5). Thus, the catalytic activity of $AlPO_4$ is affected by two main factors: the chemical nature of the surface (number and strength of acid sites) and the texture of the solid.

In previous papers (6, 7) we have shown the applicability of a spectrophotometric method in determing the acid properties of $AlPO_4$, $AlPO_4-Al_2O_3$, and $AlPO_4-SiO_2$ catalysts by means of the adsorption of different organic bases. The use of compounds with different pK_a enables us to obtain information on the strength distribution of acid sites.

The present paper deals with the study of the catalytic properties of several aluminium orthophosphates (Al/P = 1) in comparison to their surface acidity, measured by a spectrophotometric method developed by Marinas *et al.* (6) in the skeletal isomerization of CH, carried out in a microcatalytic pulse reactor using the Bassett–Habgood kinetic model (8). This model is applied to the first order processes in which the surface reaction is the controlling step and the partial pressure of the reactant is low.

[1]Author to whom correspondence should be addressed.

[2]Revision received May 19, 1983.

Experimental

Catalysts

Three $AlPO_4$ samples were studied in this investigation: sample F was prepared by precipitation from aluminium chloride and phosphoric acid (aqueous solutions), using ammonium hydroxide solution. Samples B and BP were precipitated using ethylene and propylene oxide, respectively. The three parent $AlPO_4$ samples received the same thermal treatment, namely, drying at 393 K for 24 h and calcination at 923 K for 3 h in a muffle furnace. In all cases, the composition was Al/P = 1.

Physico-chemical properties

The physico-chemical properties of the solids have already been researched. Thus, the surface area, accumulated pore volume, and main pore diameter were determined by the BET method (9) from the adsorption–desorption nitrogen isotherms at liquid nitrogen temperature (10, 11). The porosity detection was carried out by means of the Lecloux method (12) using n_3 due to the monolayer value. Pore size analysis was made using the "corrected modelless" method developed for the analysis of mesopores (13) using cylindrical idealization.

The surface acidity was determined by titration with cyclohexylamine (pK_a = 10.6), pyridine (pK_a = 5.3), and aniline (pK_a = 4.6) from cyclohexane solutions (spectroscopic grade, Merck) at 298 K using a spectrophotometric method described elsewhere (6).

In each experiment, a freshly prepared titrant agent solution (10 mL) is pipetted into a cylindrical glass tube that previously was loaded with the solid (about 0.1 g). The tube is fitted with a ground glass stopper, shaken for 1 h at constant temperature, 298 K, and the concentration of the organic base is determined spectrophotometrically.

Sorption experiments are developed at the wavelength of the maximum absorption (λ_{max}, nm) and between the titrant concentration were the Lambert–Beer law is fitted. The time required for the system to reach the equilibrium at constant temperature was checked for each solid and it was never more than 45 minutes.

The chemical interaction adsorbate–surface may be accomplished by applying the linear transformed Langmuir adsorption isotherm:

$$[1] \quad c/x = 1\,b\,x_m + c/x_m$$

The monolayer coverage, which corresponds to the theoretical

Can. J. Chem. Downloaded from www.nrcresearchpress.com by 210.87.254.40 on 09/06/12
For personal use only.

TABLE 1. Textural properties and surface acidity of $AlPO_4$ catalysts

Catalyst	S (m^2/g)	V (mL/g)	D (nm)	Surface acidity (μmol/g) CY	PY	AN
BP	210	0.42	2.5	732	380	125
B	256	0.60	4.5	789	320	86
F	181	0.40	3.6	1042	260	75

amount of solute adsorbed by 1.0 g of solid system if all sites are covered, must be assumed as a measure of the acid sites corresponding to a pK_a equal to or greater than that of the base.

Thus, the irreversible adsorption of bases with different pK_a's allows us to obtain the strength distribution of acid sites.

This method lets us determine the surface acidity of white, as well as deeply coloured, porous solids. The bases used as titrants were high purity materials from various commercial suppliers and were used without additional purification.

Apparatus and procedure

The CH isomerization was carried out in a microcatalytic pulse reactor. The pulse system consisted of a 5830 Hewlett–Packard gas chromatograph modified by the introduction of a microreactor between the sample inlet and the analytical column. The catalyst (100–150 mg, ≤0.07 mm) was held by small plugs of Pyrex glass wool in the 4 mm diameter reactor tube. The carrier gas was ultrapure nitrogen (40–60 mL min^{-1}). The experiments were conducted at temperatures between 573 and 673 K, and the hydrocarbon pulse was in the range 0.2–1.0 L.

Before each run, samples of the catalyst were standardized in a stream of 40 mL min^{-1} of dehydrated and deoxygenated nitrogen at 573 K for 1 h. The reproducibility for different samples was checked experimentally, and the measurements were repeated 2–3 times. The relative error was approximately 7%.

The products were analyzed on a 3 m stainless-steel column of 2 mm diameter, filled with 5% squalane on Chromosorb G AW-DMCS 80/100. A Hewlett–Packard electronic digital integrator was connected to the gas chromatograph. The temperature of the column was 338 K. Response factors were equal for all alkenes (CH, 1-MCP, and 3-MCP). The column gave the following order of elution: 3-MCP, 1-MCP, CH.

Results and discussion

Textural and acid properties

The adsorption isotherms are type II of Brunauer's classification, and pronounced hysteresis loops are exhibited for the three parent $AlPO_4$. The hysteresis loops close at some intermediate relative pressure.

For the pore size analysis, using the "corrected modelless" method developed for the analysis of mesopores, the cylindrical idealization could fit the criteria of corrected analysis, including the agreement between the total pore volume (the saturation point of the isotherm) and the cumulative pore volume.

The surface area, pore volume, and the main pore diameter for the $AlPO_4$ samples are collected in Table 1. Also, in Table 1, the surface acidity values are presented.

The reproducibility of the spectrophotometric method was checked experimentally, and the measurements were repeated 2–3 times. The relative error was approximately 6%.

Since the amount required to cover the surface of the solid with a monolayer was assumed as the acidity of the sample, corresponding to a specific pK_a of the titrant used, the chemisorption of CY was greater than that of the any other base. Thus, because of its high pK_a, by definition, CY measures the total acidity of these surfaces. The sequence obtained, in all cases, is:

TABLE 2. Catalytic isomerization in the CH isomerization on BP

Catalyst	W (mg)	Q (mL/min)	Total conversion 573 K	623 K	673 K
BP	100	40	0.019	0.043	0.060
		50	0.015	0.034	0.056
		60	0.012	0.029	0.043
	148	40	0.021	0.057	0.082
		50	0.017	0.042	0.078
		60	0.014	0.036	0.059
	183	40	0.028	0.081	0.099
		50	0.022	0.054	0.082
		60	0.020	0.049	0.072

$$CY > PY > AN$$

On the other hand, the differences between the values for CY and the other bases (PY and AN) are a measure of the number of weaker acid sites. Thus, sample F has the highest number of acid sites, though of moderate strength. B and BP samples exhibit a lower number of acid sites, although their strength is greater.

Aluminium orthophosphate BP shows the highest concentration of strong acid sites (vs. PY and AN) of all phosphates studied. The sequence obtained for the number of stronger acid sites (vs. AN) is:

$$BP > B > F$$

Thus, the number and strength of acid sites of phosphates depend on the method of precipitation, independent of the identical value of Al/P ratio and the results provide strong evidence for the existence of a heterogeneous distribution of surface acid sites of different acid strengths.

Catalytic activity

The operating variables, space velocity and particle size, were so chosen as to eliminate diffusion control on the reaction rate. On the other had, the thermal process without catalyst is negligible.

In the catalytic studies, CH isomerization was maintained at low conversion levels, ranging approximately from 0.1 to 8–10%.

The skeletal isomerization process of CH yields a mixture of 1- and 3-MCP. The 4-MCP isomer was not detected among the reaction products as a result of the short contact time in the reaction process.

The isomerization activity was expressed by the total conversion to 1-MCP and 3-MCP at different flow rates of the carrier gas in the reaction (mL min^{-1}), which only is exact for conversions below 10–20%, where the equilibrium reaction can be neglected.

In Table 2 the conversion values are listed at different temperatures and catalyst weights on BP catalyst. All values were reproducible to within about 7%.

The experimental results are adjusted to the Bassett–Habgood eq. [2] (8) as may be seen in Fig. 1.

$$[2] \quad \ln (1/1 - X) = RT \cdot kK (W/Q)$$

Thus, the skeletal isomerization of CH is a first order kinetic process, where the fractional conversion of reactants to products is independent of the pressure, and the rate of adsorption is faster than the rate of surface reaction, the latter being the

Can. J. Chem. Downloaded from www.nrcresearchpress.com by 210.87.254.40 on 09/06/12
For personal use only.

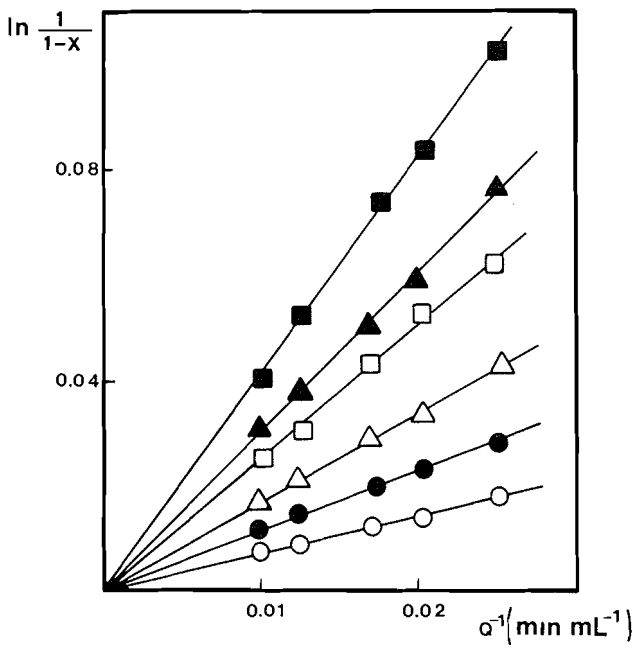

FIG. 1. Test of first order rate law for cyclohexene isomerization on BP catalyst. 100 mg (○) 573 K; (△) 623 K; (□) 673 K. 182 mg (●) 573 K; (▲) 623 K; (■) 673 K.

TABLE 3. Apparent rate constants and apparent activation energies for CH isomerization on $AlPO_4$

Catalyst	T (K)	kK 10^6 (mol/atm g s)	E_a (kJ/mol)	
BP	573	2.28±0.16		
	623	5.31±0.37	43.3	3.9
	673	7.06±0.49		
B	573	0.27±0.02		
	623	0.68±0.05	50.5	4.5
	673	1.06±0.07		
F	573	0.11±0.01		
	623	0.24±0.02	42.3	3.8
	673	0.34±0.02		

rate determining step.

[3] $r = kP_{CH}$

In our experimental conditions the catalytic activity of sample F is negligible and, therefore, more data are reported on B and BP samples, especially the latter.

From eq. [2] it is possible to obtain the apparent rate constant, kK, at a fixed temperature, by plotting $\ln (1/1 - X)$ vs. $1/Q$. The apparent activation energy is obtained in each case by plotting $\ln [\ln (1/1 - X)]$ vs. $1/T$. The results are summarized in Table 3.

The apparent activation energies are practically constant for all $AlPO_4$ studied. This, together with the fact that we are dealing with first order kinetics, seems to indicate that the transition state is of the same type for all catalysts.

On the other hand, the total conversion of CH increases with both temperature and catalyst charges and the concentration of 1-MCP was always higher than of 3-MCP, as may be seen in Tables 4 and 5.

To determine if the above mentioned products are really competitors, we employ the kinetic selectivity factor (σ) of

TABLE 4. CH isomerization to 1-MCP and 3-MCP on BP sample

Catalyst	W (mg)	Q (mL/min)	T (K)	X_1	X_3
BP	100	40	573	0.014	0.005
		50		0.010	0.004
		60		0.008	0.003
	148	40		0.016	0.006
		50		0.012	0.005
		60		0.010	0.004
	100	40	623	0.031	0.012
		50		0.025	0.009
		60		0.020	0.008
	148	40		0.042	0.016
		50		0.030	0.012
		60		0.026	0.010
	100	40	673	0.044	0.017
		50		0.039	0.015
		60		0.031	0.012
	148	40		0.058	0.023
		50		0.056	0.020
		60		0.043	0.016

TABLE 5. CH isomerization to 1-MCP and 3-MCP on B and F samples

Catalyst	W (mg)	Q (mL/min)	T (K)	$X_1 \times 10^3$	$X_3 \times 10^3$
B	151	40	573	1.75	1.18
		50		1.40	0.98
		60		1.20	0.90
		40	623	4.60	3.12
		50		3.95	2.95
		60		3.65	2.50
		40	673	7.55	5.38
		50		6.75	4.93
		60		6.30	4.55
F	100	40	573	0.41	0.34
			623	0.98	0.84
			673	1.52	1.28
	151	40	573	0.61	0.53
			623	1.49	1.27
			673	2.29	1.95

Wheeler (14), viz., that for a process such as is outlined:

[4] $\mathrm{CH} \xrightarrow{k_1} \text{1-MCP}$, $\mathrm{CH} \xrightarrow{k_3} \text{3-MCP}$

when a first order kinetics is followed, can be written

[5] $\sigma = k_1/k_3 = X_1/X_3$

The application of this criterion allows us to draw the conclusion that 1-MCP and 3-MCP are competitive products with a first order kinetics (Fig. 2). This also occurs when the isomerization is carried out with traditional solid acids as catalysts (1, 15).

A least-squares regression analysis shows correlation coefficients above 0.99. A "t-test" of significance, performed on the coefficients of regression, shows that these are significant at a level better than 1%. This is a measure of accuracy of fit of the data, in all experimental conditions, by the linear plots of Fig. 2.

Since Fig. 2 contains points at all temperatures, the apparent

Can. J. Chem. Downloaded from www.nrcresearchpress.com by 210.87.254.40 on 09/06/12
For personal use only.

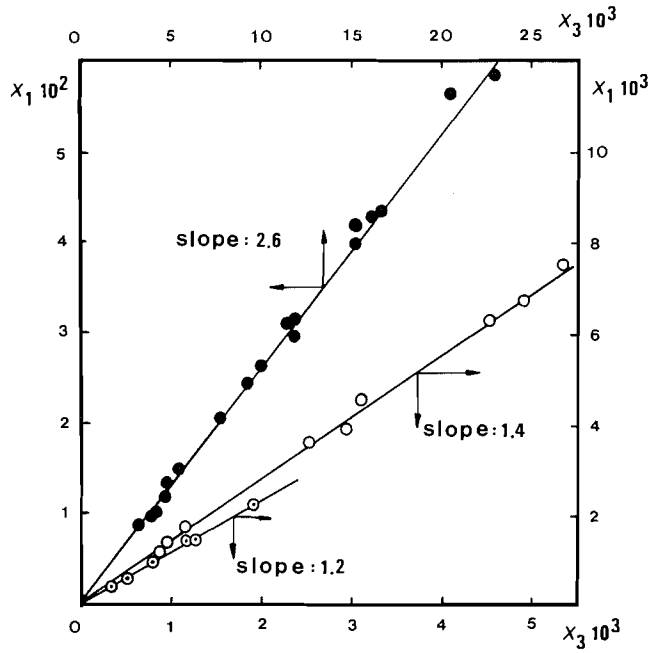

FIG. 2. Selectivity factors X_1 vs. X_3 on BP (●), B (○), and F (⊙) catalysts (data at every temperature).

activation energies for K_1 and K_3 are identical on each catalyst.

On the other hand, the selectivity to 1-MCP clearly increases in the order:

$$BP > B > F$$

This sequence is the same as that which was found for the number of strongest acid sites. Thus, if on each catalyst K_1 and K_3 have identical apparent activation energies, σ can be expressed by

$$[6] \quad \sigma = \frac{A_1 \exp(-E_{a_1}/RT)}{A_3 \exp(-E_{a_3}/RT)} = \frac{A_1}{A_3}$$

and, since the preexponential factor is a function of the number of active sites that is different on each catalyst, the selectivities on the three $AlPO_4$ samples are different. Therefore, the different σ values on each catalyst are due to different A_1/A_3 ratios.

Furthermore, by plotting the selectivity factors, σ, vs. the acidity of the catalysts (vs. AN, Fig. 3) it can be seen that the selectivity of 1-MCp formation increases with an increase of the catalyst acidity, and that its variation is linear.

Thus, it seems that the sites with higher acid strength (vs. AN) are those mainly responsible for the skeletal isomerization of CH, the sample BP being the most active catalyst in this series of samples. As well, the apparent rate constant, Kk, also increases when the number of strongest acid sites is increased, and this variation is linear (vs. AN) with a correlation coefficient of 0.99.

Conclusions

From the results obtained, it seems that the acidity of the catalyst is the main variable to be considered, and that the stronger acid sites are necessary for the CH isomerization to 1- and 3-MCP on $AlPO_4$ catalyst. Thus, the $AlPO_4$ obtained by precipitation with propylene oxide has the highest number of acid sites of high strength and, therefore, exhibits the highest isomerization activity and selectivity to 1-MCP.

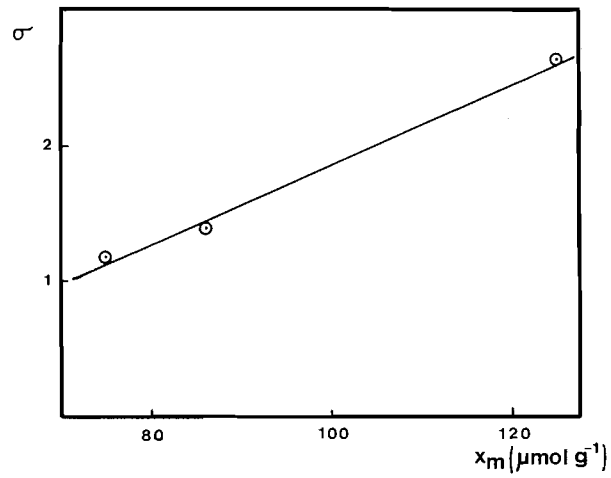

FIG. 3. Selectivity factors, σ, vs. acidity measured by titration with aniline.

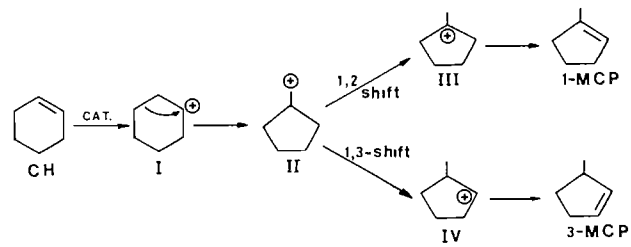

SCHEME 1

The isomerization products are obtained by parallel reactions according to a carbocationic mechanism with rearrangement of intermediates (3, 11, 15–19).

The mechanism proposed below agrees with the experimental results and is an attempt to explain how both reaction products could be formed. The first step would imply the chemisorption of CH on the acid sites of the catalyst resulting in the formation of a carbenium ion (I), which suffers skeletal isomerization (Wagner–Meerwein rearrangement) involving a less stable primary carbenium ion (II), which rearranges to a more stable tertiary carbenium ion (III) by 1,2-hydride shift. This then desorbs as 1-MCP. A 1,3-hydride shift changes the carbenium ion I to a secondary ion (IV). The desorption of this intermediate gives rise to 3-MCP.

The fact that the 1,3-hydride shift is not so easy as the 1,2-hydride shift, and that the stability of intermediate III is greater than II, accounts for the lower concentration of 3-MCP. Thus, an increase in the acid strength of catalyst produces intermediates with a more developed carbocationic character and, therefore, increases the conversion of both substrates (1- and 3-MCP) with a rise in the selectivity factor, σ, since a 1,2-hydride shift is easier.

Furthermore, the results seem to confirm the applicability of the spectrophotometric method in determining the acid site distribution of heterogeneous catalysts by the adsorption of bases with different pK_a.

1. H. PINES and J. MANASSEN. Adv. Catal. **16**, 49 (1960).
2. B. OZIMEK and B. RADOMYSKI. React. Kinet. Catal. Lett. **15**, 407 (1980).
3. J. M. CAMPELO, J. M. MARINAS, and R. PEREZ-OSSORIO. An. Quim. **74**, 86 (1978).
4. M. A. ARAMENDIA, J. M. CAMPELO, S. ESTEBAN, C. JIMENEZ, J. M. MARINAS, and J. V. SINISTERRA. Rev. Mex. Petrol. **12**, 3 (1980).

Can. J. Chem. Downloaded from www.nrcresearchpress.com by 210.87.254.40 on 09/06/12
For personal use only.

5. J. M. CAMPELO and J. M. MARINAS, Afinidad, **38**, 333 (1981).
6. J. M. MARINAS, C. JIMENEZ, J. M. CAMPELO, M. A. ARAMENDIA, V. BORAU, and D. LUNA. Proc. 7th Symp. Iberoamerican Catal. La Plata, 1980. p. 79.
7. J. M. CAMPELO, A. GARCIA, D. LUNA, and J. M. MARINAS. Afinidad, **39**, 61 (1982).
8. D. BASSETT and H. W. HABGOOD. J. Phys. Chem. **64**, 769 (1960).
9. S. BRUNAUER, P. H. EMMETT, and E. TELLER. J. Am. Chem. Soc. **77**, 5860 (1930).
10. J. M. CAMPELO, J. M. MARINAS, and R. PEREZ-OSSORIO. An. Quim. **72**, 698 (1976).
11. J. M. CAMPELO, J. M. MARINAS, and R. PEREZ-OSSORIO. Proc. 5th Symp. Iberoamerican Catal. Vol. 1. Lisbon, 1976. p. 84.
12. A. LECLOUX and J. P. PIRARD. J. Colloid Interface Sci. **70**, 265 (1979).
13. S. BRUNAUER, R. SH. MIKHAIL, and E. BODOR. J. Colloid Interface Sci. **24**, 541 (1967).
14. A. WHEELER. Adv. Catal. **3**, 250 (1951).
15. J. E. GERMAIN and M. BLANCHARD. Bull. Soc. Chim. Fr. 958 (1958); 1000 (1958).
16. D. A. BEST and W. WOJCIECHOWSKI. J. Catal. **47**, 343 (1977).
17. G. SAITO, K. SATO, and N. ABE. Bull. Chem. Soc. Jpn. **36**, 1064 (1978).
18. M. G. MITICHENKO, H. M. A. SHENAVI and A. A. KUBASOV. Zh. Prkil. Kim. **45**, 455 (1972).
19. V. KRISHNASAMY and P. RATNASAMY. J. Indian Chem. Soc. **49**, 839 (1982).

Nomenclature

A: preexponential factor of Arrhenius equation
AN: aniline (λ_{max}: 232 nm)
b: constant of Langmuir (L mol^{-1})
c: concentration of titrant agent in solution at equilibrium with the adsorbate on the surface acid sites (mol L^{-1}).
CH: cyclohexene
CY: cyclohexylamine (λ_{max}: 225 nm)
E_a: apparent activation energy (kJ mol^{-1})
k: rate constant of the surface process (s^{-1})
K: adsorption constant of the CH on the catalyst (mol atm^{-1} g^{-1})
MCP: methylcyclopentene
P_{CH}: cyclohexene pressure (atm)
PY: pyridine (λ_{max}: 252 nm)
Q: flow rate of the carrier gas (mL s^{-1})
r: reaction rate
R: gas constant (atm 1 mol^{-1} K^{-1})
S: surface area (BET method, m^2g^{-1})
T: reaction temperature (K)
V: pore volume (mL g^{-1})
x: amount of titrant agent adsorbed on the acid sites (mol g^{-1})
x_m: saturation concentration; the theoretical amount of titrant agent that may be chemically adsorbed by 1.0 g of solid system (mol g^{-1})
X: molar fractionary conversion
σ: kinetic selectivity factor
λ: wavelength of the maximum absorption (nm)

Subscripts: 1: 1-MCP; 3: 3-MCP

Can. J. Chem. Downloaded from www.nrcresearchpress.com by 210.87.254.40 on 09/06/12
For personal use only.

Conformational analysis of chiral hindered amides

ARVI RAUK, DONALD F. TAVARES,[1] MOHSIN A. KHAN,[2] AMY J. BORKENT,[3] AND JOHN F. OLSON[3]
Department of Chemistry, University of Calgary, Calgary, Alta., Canada T2N 1N4

Received April 29, 1983

ARVI RAUK, DONALD F. TAVARES, MOHSIN A. KHAN, AMY J. BORKENT, and JOHN F. OLSON. Can. J. Chem. **61**, 2572 (1983).

The static and dynamic structures of the amide derivatives of racemic and (*R*)-(+)-2-methoxy-2-phenyl-3,3,3-trifluoropropanoic acid (MPTA) with diisopropyl amine (**1**), *meso*-2,6-dimethylpiperidine (**2**), (*R*)-(−)- and (*S*)-(+)-2-methylpiperidine (**3** and **4**, respectively) were investigated by proton nmr spectroscopy. The piperidine rings adopt a single dominant conformation in which the substituent methyl groups occupy axial positions. One of the isopropyl groups of **1** is oriented in the same way as the corresponding side of the piperidine ring of **2**−**4** but the other (*syn* to carbonyl oxygen) is turned so that the methyl groups are toward the carbonyl oxygen and the oxygen lies in the plane bisecting the C—C—C angle. Rotation about the amide C(O)—N bond of **1** is accompanied by concurrent rotation about each of the N—*i*Pr single bonds. The free energies of activation of the hindered rotation about the C(O)—N bond in **1**−**4**, 81 kJ/mol, 77 kJ/mol, 77kJ/mol, and 79kJ/mol, respectively, are higher than found in most other hindered amides, suggesting that buttressing due to the steric crowding around the amide functionality is felt throughout the rotational pathway.

ARVI RAUK, DONALD F. TAVARES, MOHSIN A. KHAN, AMY J. BORKENT et JOHN F. OLSON. Can. J. Chem. **61**, 2572 (1983).

Faisant appel à la spectroscopie de rmn du proton, on a étudié les structures statique et dynamique des amides provenant de la réaction des acides racémique et (*R*)-(+) méthoxy-2 phényl-2 trifluoro-3,3,3 propanoiques (MPTA) avec la diisopropylamine (**1**), la *méso*-diméthyl-2,6 pipéridine (**2**), les (*R*)-(−) et (*S*)-(+) méthyl-2 pipéridine (**3** et **4** respectivement). Le cycle pipéridine adopte une conformation simple dominante dans laquelle les groupes méthyles occupent des positions axiales. L'un des groupes isopropyle du composé **1** s'oriente de la même manière que le côté correspondant du cycle pipéridine des composés **2**−**4** mais l'autre face (*syn* par rapport à l'oxygène du carbonyle) se tourne de telle sorte que les groupes méthyles soient vis-à-vis de l'oxygène du carbonyle et l'oxygène se trouve dans le plan bisecteur de l'angle C—C—C. La rotation autour de la liaison C(O)—N de l'amide s'accompagne d'une rotation de même sens autour de chaque liaison simple N—*i*Pr. Les énergies libres d'activation de la rotation empêchée autour de la liaison C(O)—N dans les composés **1** à **4** sont respectivement de 81, de 77, de 77 et de 79 kJ/mol. Elles sont plus élevées que celles de la plupart des autres amides encombrées, ce qui suggère un effet de compression, du à l'encombrement stérique autour de la liaison amide, qui se manifeste entièrement dans la rotation.

[Traduit par le journal]

Introduction

In a previous communication, we reported the results of an investigation by ^{19}F nmr spectroscopy, on hindered rotation about a carbon−carbon single bond to a trifluoromethyl group in a series of derivatives of 2-methoxy-2-phenyl-3,3,3-trifluoropropanoic acid (MPTA), including several hindered chiral amides (1). As an extension of that work, we wish to report the observations on the static and dynamic stereochemistry associated with severe steric crowding about the nitrogen atom of the amide functionality. The presence in our system of a chiral centre of known absolute configuration enables the unambiguous assignment of the stereochemistry associated with groups on the nitrogen atom. The large magnetic anisotropy of the phenyl group as well as of the carbonyl bond in the amide group greatly assists in the assignments. All of the molecules involved in the present study are amide derivatives of racemic or (*R*)-(+)-MPTA (2) with the amines diisopropyl amine, *cis*-2,6-dimethylpiperidine, and (*R*)-(−)- and (*S*)-(+)-2-methylpiperidine (3), i.e. compounds **1**−**4**, respectively.

Crystallographic (4−7) and nmr (6−14) investigations of 2-methyl- and 2,6-dimethylpiperidyl derivatives have established that steric constraints force the methyl groups to adopt axial positions when the substituent on nitrogen conjugates sufficiently well with the nitrogen lone pair to impose a planar or near planar geometry (Structure A). This is the case with amides (X=Y = RCO) and *N*-nitroso (X=Y = N=O)

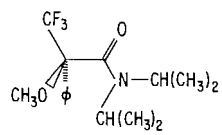

1

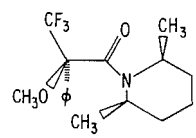

2

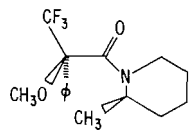

3

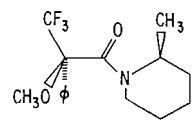

4

compounds. The structurally related hydrazones (X=Y = N=CR_1R_2) adopt a conformation in which the average plane of the ring is perpendicular to the plane of the N substituents (15) (Structure B). Amidines (X=Y = RC=NR) represent an intermediate case and both structures have been found by Lunazzi *et al.* (6). Even with bulky acyl substituents, amides (X=Y = CO*t*Bu) adopt the planar A ground state structure, the equilibrium structure being destabilized by buttressing effects by an amount roughly equivalent to the $A^{(1,3)}$ strain (11). The results presented below on **2**, **3**, and **4** require a different interpretation, as do the results for **1**.

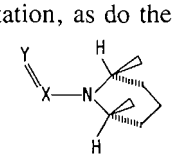

A X=Y = COR
= N=O
= N=NR

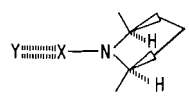

B X=Y = N=CC_1C_2

[1]Author to whom correspondence should be addressed.
[2]Present address: Department of Chemistry, University of Karachi, Karachi-32, Pakistan.
[3]NSERC Summer Undergraduate Research Assistant.

Can. J. Chem. Downloaded from www.nrcresearchpress.com by 210.87.254.42 on 09/06/12
For personal use only.

Can. J. Chem. Downloaded from www.nrcresearchpress.com by 210.87.254.42 on 09/06/12
For personal use only.

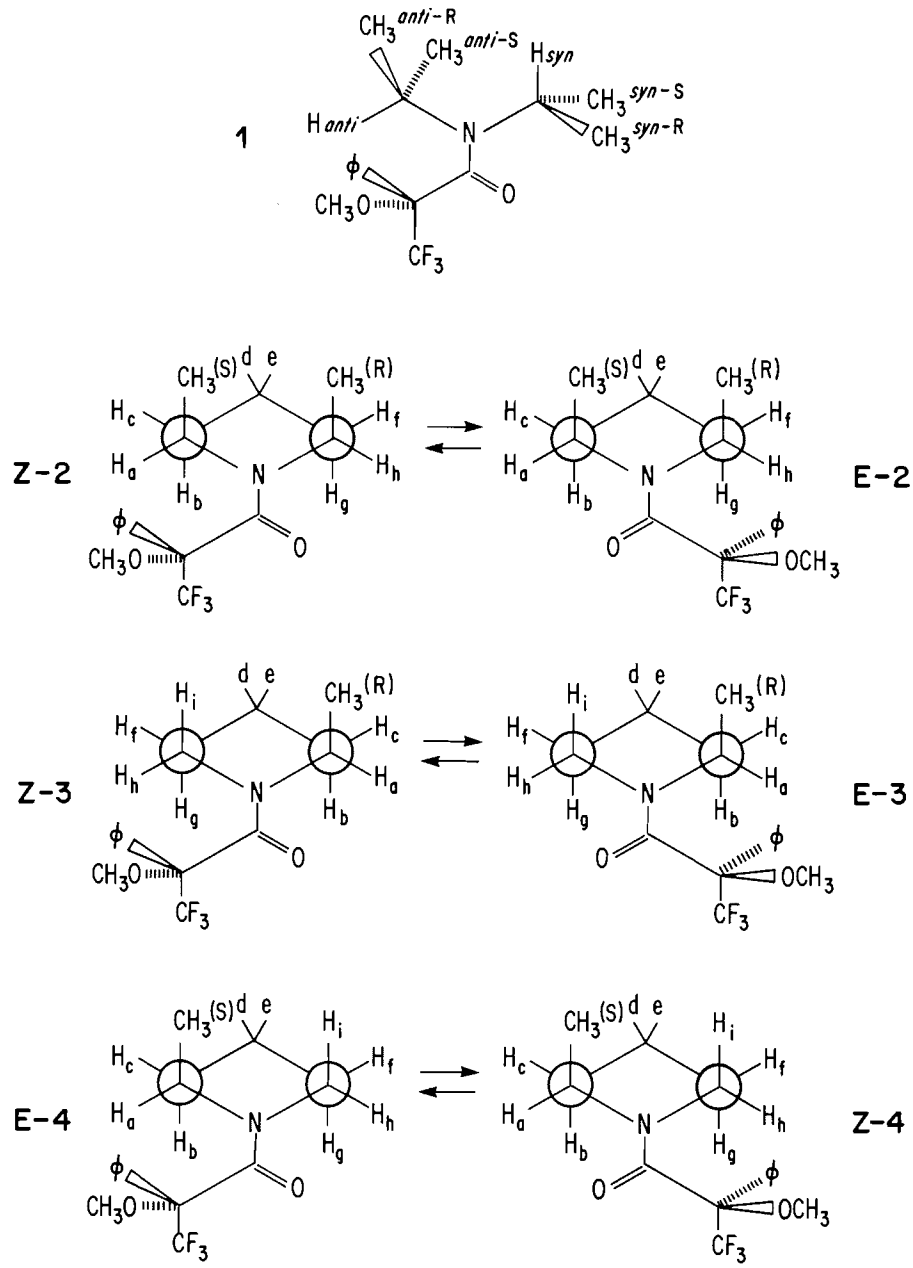

FIG. 1. Structures **1**–**4**, identifying protons discussed in the text.

The structures of the systems of the present study are shown in Fig. 1. Amides **2**–**4** are capable of rotational isomerism about the C(O)—N bond. The resulting structures are distinguished by the stereochemical labels, *Z* and *E*, and are defined in Fig. 1. Each of **2**–**4** is presented as having axial methyl groups. For clarity, the structures are drawn as Newman projections and all the protons which could be assigned by decoupling experiments are explicitly labelled. The α-methyl groups of **2**–**4** are labelled *R* or *S* according to the absolute configuration of the carbon atom to which they are attached. The methyl groups of **1** are labelled in a similar manner according to whether the isopropyl group (*syn* or *anti* to carbonyl oxygen) would gain the *R* or *S* configuration, respectively, if the priority of the methyl carbon were increased by isotopic substitution.

Rotation about the C(O)—N bond in most amides is hindered by barriers in the range 67–92 kJ/mol (4, 11, 16). The higher values are found for relatively unhindered amides (for example, $HC(O)N(CH_3)_2$: 88 kJ/mol (4)). Since the six-atom amide unit is essentially coplanar, increasing the steric size of either the acyl moiety or the nitrogen substituents is expected to destabilize the crowded planar ground state configuration (Structure A) compared to the relatively less crowded perpendicular geometry (4) (Structure B) which should resemble the transition state for C(O)—N bond rotation. Thus the rotation barrier for the highly crowded benzamide of 2,6-dimethylpiperidine (A, X=Y = $C(O)C_6H_5$) is abnormally low, namely 52 kJ/mol (11). If the acyl group is sufficiently large to "lock" the substituents on nitrogen into a planar configuration, much higher values are found (4). For example, a barrier of 125 kJ/mol has been estimated for 2,4,6-(tBu)$_3C_6H_2C(O)NMe_2$ (17). Electronic effects also influence the magnitudes of barriers to rotation about the C(O)—N bond, electron withdrawing substituents on the acyl moiety tending to increase the height of the barrier (18). The latter two effects will be seen to contribute to the magnitudes of the rotation barriers of amides **1**–**4**.

Can. J. Chem. Downloaded from www.nrcresearchpress.com by 210.87.254.42 on 09/06/12
For personal use only.

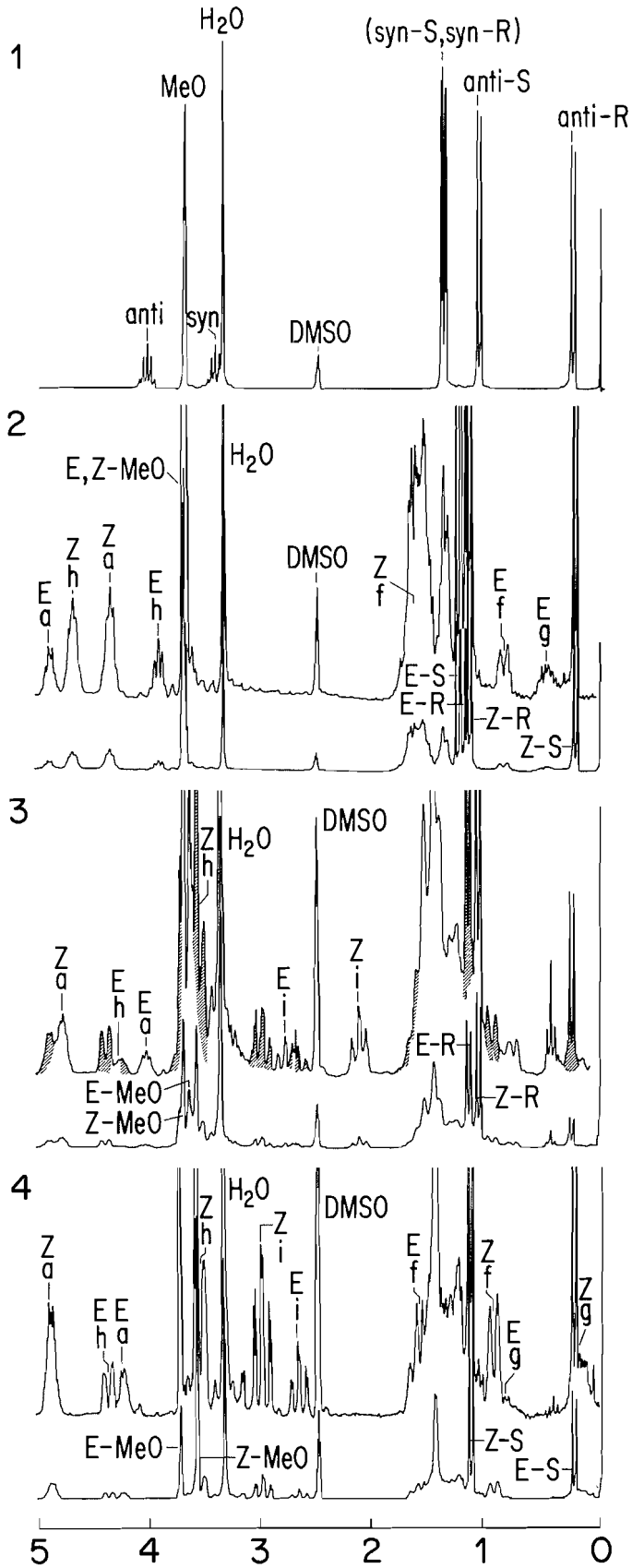

FIG. 2. Proton nmr spectra of **1**–**4** in DMSO-d_6 at 22°C. The sample of **3** is contaminated by 43% admixture of **4** (shaded peaks). All of the spectra have absorptions due to water and incompletely deuterated DMSO. Prominent proton absorptions are identified according to the convention adopted (refer to Figs. 1 and 3).

Results

Ambient temperature nuclear magnetic resonance spectra of 1–4

The ^{1}H nmr spectra of amides **1**–**4** in DMSO-d_6 at 22°C are shown in Fig. 2.[4] Chemical shift data are presented in Table 1. As discussed in the Introduction, compounds **2**–**4** are capable of geometric isomerism due to hindered rotation about the C(O)—N bond. The spectra of **1**, **2**, and **4** exhibit unusually high field methyl absorptions. at 0.30 ppm, 0.21 ppm, and 0.25 ppm, respectively. The positions of the remaining methyl absorptions of the four amides fall into the narrow range 1.07–1.17 ppm downfield from TMS. The only exceptions are the absorptions due to two of the methyl groups of **1**, which occur at 1.45 and 1.46 ppm. The significance of this result is discussed below.

Variable temperature nuclear magnetic resonance spectra of 1–4

The nmr spectra of **1**–**4** were determined in the temperature range −90°C to 180°C. For the low temperature study, the samples were dissolved in $CDCl_3$/acetone-d_6 (50:50). The high temperature spectra were determined for solutions in DMSO-d_6. At low temperatures, all of the samples showed general line broadening which seems most likely to be due to viscosity broadening. Only one dynamic intramolecular process is slowed in this temperature range, rotation about the C—CF_3 bond, which manifests itself in the collapse of the methoxy methyl quartet and its recovery as a doublet. Previous work has demonstrated a stereospecific long range H—F coupling of the methyl to a single fluorine atom of the trifluoromethyl group (1).

All of the compounds **1**–**4** exhibit temperature dependent phenomena at elevated temperatures. The temperature dependent proton nmr spectrum of **1** is shown in Fig. 4. The variation of the nmr spectra of **2** and **4** with temperature is shown in Figs. 5 and 6, respectively. The corresponding spectra for **3** are not shown since this compound was not prepared free of **4**.

Activation parameters for rotation about the C(O)—N bond were estimated as described below. The results are shown in Table 2 and Fig. 7.

Discussion

Equilibrium geometries of 1–4

Structures **1**–**4** have a number of conformational options available as a consequence of rotation about the single bonds to the chiral centre of the MPTA moiety, rotation about the amide C(O)—N bond, and chair–chair inversion of the six-membered piperidine ring. In fact, we will argue that the results of the present study are consistent with a very limited subset of the possible conformations. Inspection of the nmr spectra shown in Fig. 2 reveals that **1** appears to have only a single dominant conformation, and **2**, **3**, and **4** seem to exist as a mixture of only two conformations present in unequal proportions. Although an X-ray structure of MPTA or any of its derivatives has not been reported, numerous applications of chiral amide and ester derivatives of MPTA for the determination of absolute configurations and optical purities by nmr spectroscopy after the work of Mosher and co-workers (19), as well as CD studies (20), are consistent with the CF_3 group

[4]The ^{1}H nmr spectrum of **3** is contaminated by 43% admixture of **4**.

TABLE 1. Chemical shifts (ppm in DMSO-d_6 at 22°C)[a]

Compound	MeO	Me (*R*)	Me (*S*)	H (a)	H (f)	H (g)	H (h)	H (i)
1	3.75	1.45 or 1.46[b]	0.30[c]	4.01[d]	1.14[e]	1.46 or 1.45[f]	3.48[g]	—
(*Z*)-**2**[h]	3.72	1.07	0.21	4.35	1.68	[i]	4.68	—
(*E*)-**2**	3.72	1.22	1.27	4.89	0.85	0.44	3.92	—
(*Z*)-**3**[h]	3.72	1.08	—	4.78	[i]	[i]	3.6	2.15
(*E*)-**3**	3.67	1.17	—	4.04	[i]	[i]	4.38	2.79
(*Z*)-**4**[h]	3.61	—	1.17	4.88	0.97	0.20	3.55	3.01
(*E*)-**4**	3.75	—	0.25	4.24	1.6–1.7[i]	0.86	4.38	2.69

[a]Refer to Fig. 1 for assignment of protons. The phenyl absorptions are at (ppm): **1**, 7.47; *Z*-**2**, 7.49; *E*-**2**, 7.47; **3**, 7.49; **4**, 7.50.
[b]*syn-R*-methyl.
[c]*anti-R* methyl.
[d]*anti* Methine proton.
[e]*anti-S* methyl.
[f]*syn-S* methyl.
[h]Major conformer.
[i]Not assigned.

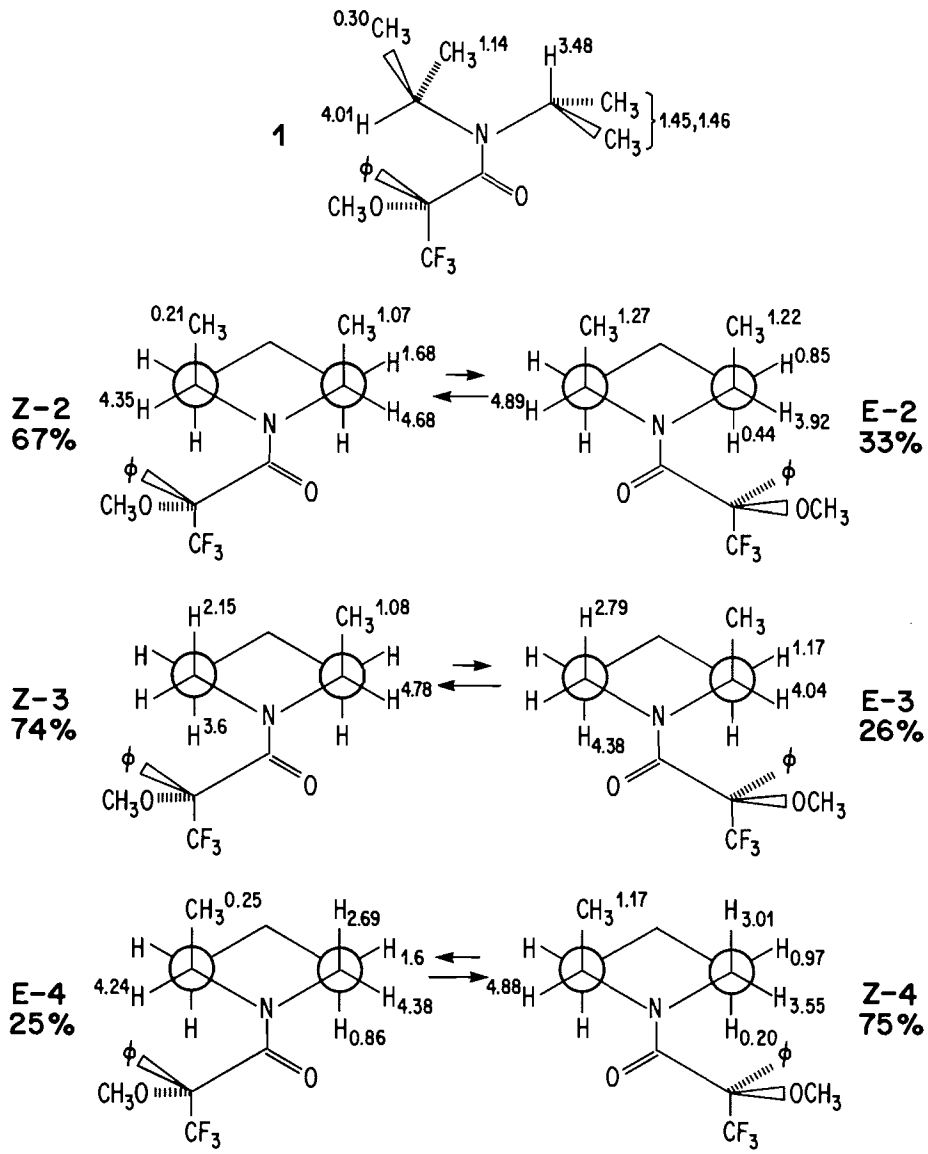

FIG. 3. Structures **1**–**4**. Chemical shifts in ppm relative to internal TMS and the fractional populations at 22°C in DMSO-d_6 are shown (refer to Figs. 1 and 2).

Can. J. Chem. Downloaded from www.nrcresearchpress.com by 210.87.254.42 on 09/06/12
For personal use only.

Can. J. Chem. Downloaded from www.nrcresearchpress.com by 210.87.254.42 on 09/06/12
For personal use only.

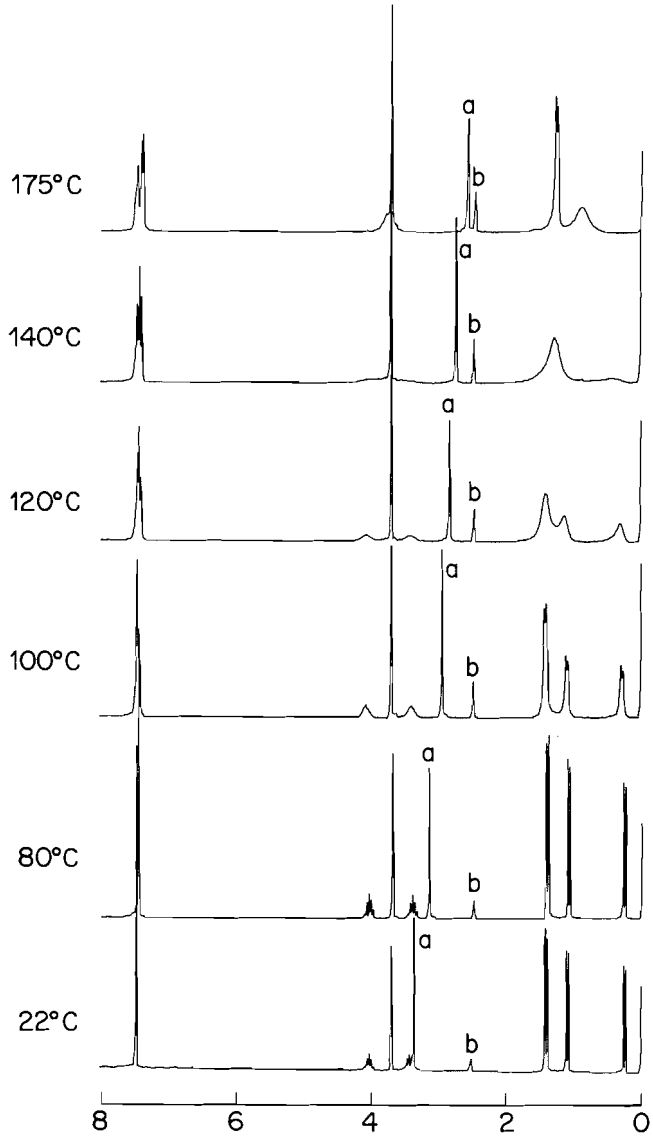

FIG. 4. Temperature dependent nmr spectrum of **1** in DMSO-d_6. The water (a) and incompletely deuterated DMSO (b) peaks are marked.

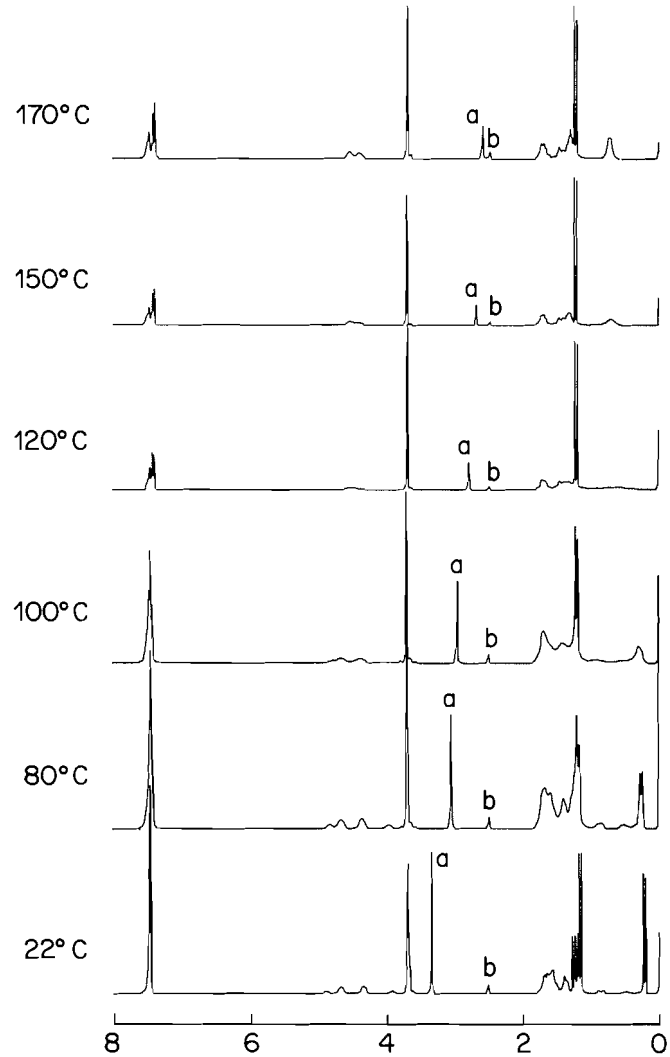

FIG. 5. Temperature dependent nmr spectrum of **2** in DMSO-d_6. The water (a) and incompletely deuterated DMSO (b) peaks are marked.

being eclipsed to the carbonyl double bond. Limited geometry optimization of the structure of the dimethylamide of MPTA by MNDO calculations also showed that the C—CF_3 and C=O bonds are eclipsed (1).[5] As a result, the position of the phenyl group on one side of the mean plane of the amide functionality serves as an internal probe for the positions of other groups in the molecule, on the nitrogen atom in the present case.

It has previously been shown by nmr (6–8, 11) studies that amides of 2-methylpiperidine and 2,6-dimethylpiperidine adopt the chair form of the piperidyl ring which has the α-methyl substituents in the axial positions. The structures in solution are deduced from chemical shifts and coupling constants, as well as thermodynamic activation parameters for the hindered rotation about the C(O)—N bond (11). The spectra of compounds **3** and **4** (Fig. 2) are consistent with axial methyl groups in each of the diastereomeric rotamers. Inspection of molecular models, in which the CF_3 group is eclipsed to the carbonyl bond, reveals that in each of compounds **1**, **2**, and **4** there is a methyl group positioned directly over the phenyl ring, in the shielding region of the ring magnetic anisotropy. This is not the case for amide **3**. Assuming a distance of 3.7 Å (measured from Dreiding models) between the plane of the phenyl group and the methyl carbon atom, and using an average value of 1.17 ppm for the chemical shift of an axial α-methyl group, one sees that *a methyl group situated 3.7 Å above a phenyl ring is shifted upfield by about 0.92 ppm*. This value is in accord with that predicted by the free electron model of long range shielding associated with the benzene ring, as proposed by Johnson and Bovey (21).

The low field positions of the α methine proton absorptions, H_h in *Z*-**2** (4.68 ppm), H_a in *E*-**2** (4.89 ppm), H_a in *Z*-**3** (4.78 ppm), and H_a in *Z*-**4** (4.88 ppm) can be taken as representative of the position of an equatorial methine proton approximately in the plane of the amide carbonyl. The average value is 4.81 ppm. The other equatorial α methine protons, H_a of *Z*-**2** (4.35 ppm), H_h of *E*-**2** (3.92 ppm), H_a of *E*-**3** (4.04 ppm) and H_a of *E*-**4** (4.24 ppm) yield an average value 4.14 ppm as reference. While this may not be typical of equatorial

[5]One cannot determine from the present results whether or not rotation about the C(O)—C bond is slow on the nmr time scale. However, the results strongly suggest a single dominant conformation in which C—CF_3 is eclipsed to C=O.

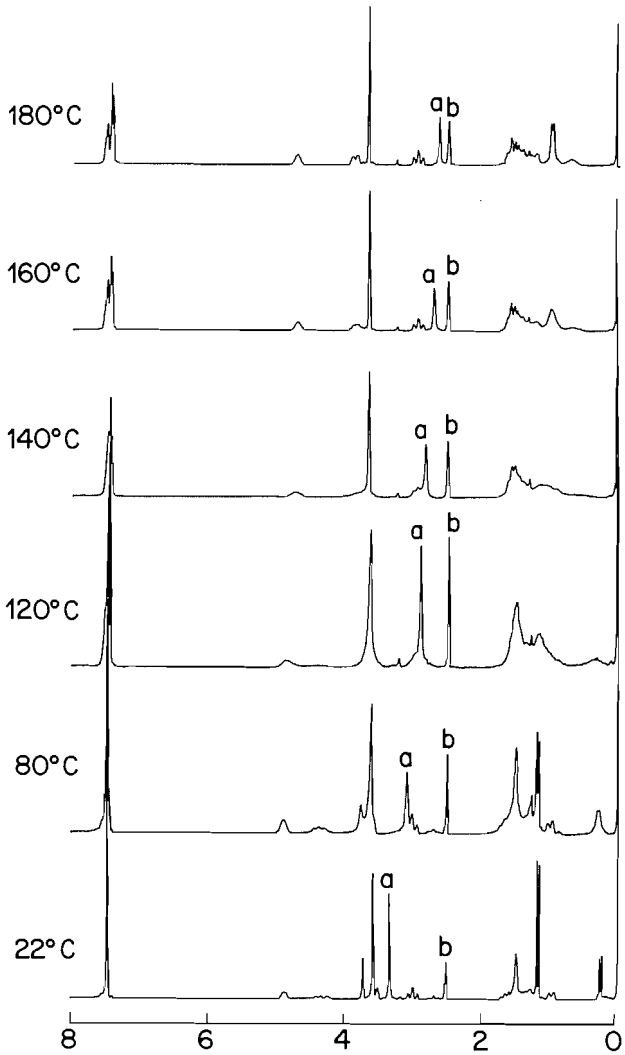

FIG. 6. Temperature dependent nmr spectrum of **4** in DMSO-d_6. The water (a) and incompletely deuterated DMSO (b) peaks are marked.

α-methine protons because of the atypical grouping of substituents on the saturated carbon atom, the difference, 0.67 ppm, serves as a measure of the deshielding effect of the amide carbonyl at a distance of 2.9 Å (measured from Dreiding models). A similar comparison of the equatorial α-methylene protons deshielded by carbonyl (H_h of *E*-**3** (4.38 ppm) and H_h of *E*-**4** (4.38 ppm)) and not deshielded by the carbonyl (H_h of *Z*-**3** (3.6 ppm) and H_h of *Z*-**4** (3.55 ppm)) yields a somewhat higher value of 0.80 ppm for the deshielding effect of the amide carbonyl at about the same distance.

It is apparent from the nmr spectrum of **1** (see Figs. 1 and 2 and Table 1) that the isopropyl group which is *syn* to the chiral centre is oriented in the same way as the corresponding side of the six membered ring in **2** and **4**. The *anti*-(*R*) methyl group is highly shielded (0.30 ppm), the other has a normal chemical shift (1.14 ppm), and the methine proton has a chemical shift (4.01 ppm) close to the average value (4.14 ppm) for corresponding equatorial methine protons of **2**–**4**. On the other hand, the isopropyl group *syn* to oxygen must be oriented differently from the corresponding side of the six membered ring in **2** and **3**. The two methyl groups are nearly isochronous and are deshielded by 0.3 ppm relative to all of the other methyl groups which are not in the shielding region of the phenyl group. In addition, the chemical shift of the methine proton (3.48 ppm) suggests that this proton is oriented in a different fashion than any of the others. Thus structure **5** cannot correspond to the most stable conformation of **1**.

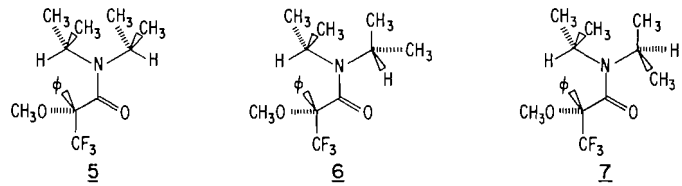

5 **6** **7**

Mechanism of conformational interchange

Although the diisopropyl amide, **1**, could exist in many conformations that can be generated by torsional motions about the single bonds, in actuality very few of the possible structures are available to it because of steric interactions. As discussed above, the amide unit is essentially planar and the chiral centre is oriented so that the trifluoromethyl group is eclipsed with the carbonyl group. The group attached to the nitrogen which is *syn* to the chiral centre must be oriented in such a way as to present a hydrogen atom toward the chiral centre. The isopropyl group *syn* to the chiral centre thus has no rotational flexibility. At first glance, there does not appear to be as great an impediment preventing the isopropyl group *anti* to the chiral centre from adopting any of several staggered conformations, such as **6**, **7**,

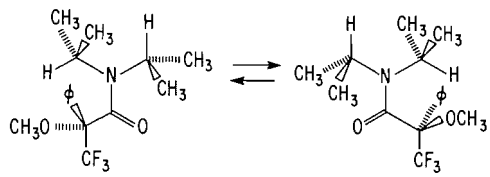

8a **8b**

or **8**. Indeed, the small difference in the chemical shift, 0.01 ppm, may be due to residual diastereotopism after rapid rotational averaging among structures **6**, **7**, and **8** (for example). Evidence that this is unlikely to be the case for **1** is the observation that the nmr spectrum of **1** remains unchanged as the temperature of a solution of **1** in $CDCl_3$/acetone-d_6 is lowered to −90°C with the exception that the methoxy peak becomes a doublet (as a result of slowing the CF_3 rotation (1)) and there is a general broadening of all of the signals, probably due to increased viscosity of the medium. The positions of the absorptions remain at 1.45 and 1.46 ppm. Raising the temperature of a solution of **1** in DMSO-d_6, Fig. 4, brings about exchange coalescence of the (*S*)-methyls (at 1.14 and 1.45/6 ppm), of the (*R*)-methyls (at 0.30 and 1.46/5 ppm), and of the methine septets. The temperatures of maximum broadening of the signals occur at approximately 130°C, 145°C, and 140°C, respectively. Rates of exchange, k, at these temperatures were determined by comparison of computed lineshapes[6] with the experimentally obtained nmr spectra. Application of the Eyring equation [1]

$$[1] \quad k = \left(\frac{k_B}{h}T\right)e^{-\Delta G^*/RT}$$

[6]Lineshapes were calculated for various rates of exchange from equation [15] of Binsch (22*a*). Linewidths in the absence of exchange were assumed to be 1 Hz, measured from the room temperature spectrum. A full lineshape analysis could not be performed to extract enthalpies and entropies of activation for amides **2**–**4** because of the complexity of the spectra.

Can. J. Chem. Downloaded from www.nrcresearchpress.com by 210.87.254.42 on 09/06/12
For personal use only.

TABLE 2. Activation parameters for hindered rotation[a]

Compound	Observed exchange $Z \rightleftarrows E$ ppm		Temperature[b] °C	Rate[c] s^{-1}	Barrier[d] kJ/mol
1[e]	Me(R)	1.45−0.30	145	1100	79
	Me(S)	1.46−1.14	128	250	81
	CH	3.48−4.01	140	830	81
2	Me(S)	0.21−1.27	130	1000	77
	H(a)	4.35−4.89	110[f]	530	75
	H(f)	1.68−0.85	110[f]	750	74
	H(h)	4.68−3.92	110[f]	700	74
3	H(a)	4.78−4.04	125	730	77
4	Me	1.17−0.25	135	940	79
	H(a)	4.24−4.48	125	560	78
	H(g)	0.20−0.86	140[f]	590	80
	H(h)	3.55−4.38	140[f]	660	80
	H(i)	3.01−2.69	110[f]	250	77

[a]Refer to Figs. 1−3 for assignment of protons.
[b]Temperature at which maximum broadening is judged to occur.
[c]Reference 23.
[d]$\Delta G^{\ddagger}$, estimated using eq. [1].
[e]Z and E refer to the isopropyl groups which are *syn* and *anti* to the carbonyl oxygen, respectively. From lineshape analysis, $\Delta H^{\ddagger} = 83 \pm 2$ kJ/mol, $\Delta S^{\ddagger} = 5 \pm 4$ J/mol deg, $\Delta G^{\ddagger} = 80.56 \pm 0.04$ kJ/mol.
[f]Approximate values; see text for discussion.

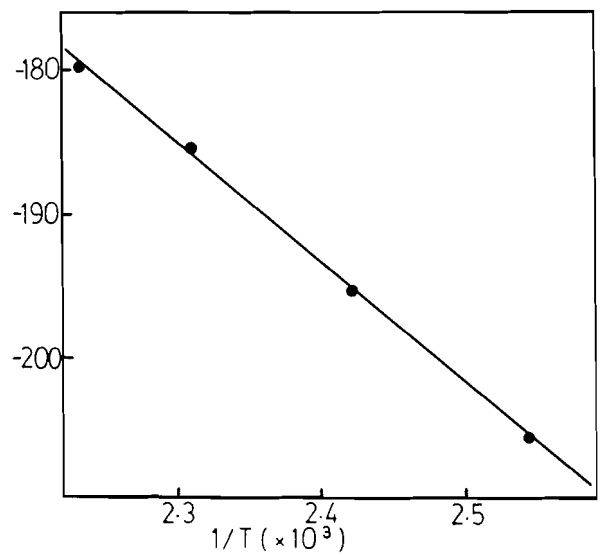

FIG. 7. Plot of ln (k/T) vs. T^{-1} for **1** from lineshape fitting of the 0−2 ppm region of the nmr spectrum (see Fig. 4). The ordinate is R ln (hk/k_BT) in units of J/deg mol. The data are: 155 s^{-1}, 120°C; 550 s^{-1}, 140°C; 1900 s^{-1}, 160°C; 3800 s^{-1}, 175°C.

yields three independent estimates of the free energy of activation, $\Delta G^{\ddagger}$, for the conformational process, 81 kJ/mol, 79 kJ/mol, and 81 kJ/mol, respectively, at the above-mentioned temperatures. Details are given in Table 2. Rate constants at four temperatures spanning the range 120°C−175°C were obtained by lineshape analysis of the methyl region of **1**. A plot of ln (k/T) vs. T^{-1} (Fig. 7) yields the results: $\Delta H^{\ddagger} = 83 \pm 2$ kJ/mol; $\Delta S^{\ddagger} = 5 \pm 4$ J/mol deg. From the values for $\Delta H^{\ddagger}$ and $\Delta S^{\ddagger}$, a more accurate value for $\Delta G^{\ddagger}$ may be calculated: $\Delta G^{\ddagger} = 80.6 \pm 0.04$ kJ/mol (22*b*) at 145°C. The error in $\Delta G^{\ddagger}$ was computed from the least-squares errors for $\Delta H^{\ddagger}$ and $\Delta S^{\ddagger}$ by the method of Binsch and Kessler (22*b*).

The insensitivity of the chemical shifts of the two methyls of the isopropyl group *syn* to the carbonyl oxygen over a wide temperature range (−90°C to +120°C) renders it probable that only a single conformation of **1** is significantly populated. We shall assume that that conformation is **8**. The data in Table 2 are interpreted as corresponding to the conformational exchange process **8***a* ⇌ **8***b*. Rotation through 180° about the C(O)—N bond involves simultaneous rotations about both N—*i*Pr single bonds. Thus, the methyl groups which exchange their environments are on the same side of the amide plane.

Amides **2**, **3**, and **4** exist as equilibrating mixtures of Z and E diastereomeric forms. The free energy differences, estimated (by integration) from the populations at 22°C are 1.7 kJ/mol, 2.6 kJ/mol, and 2.7 kJ/mol, respectively. The process which interconnects the Z and E forms may be regarded as simple rotation about the C(O)—N bond. While the piperidine ring may undergo chair−chair inversion during the course of the rotation, thus placing the methyl group(s) into equatorial position(s), the population of such forms as **9***a* and **9***b* must be too

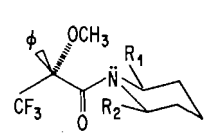

9a

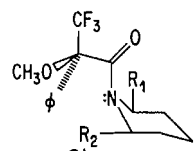

9b

small to have consequences to the temperature dependence of the nmr spectra in the accessible temperature range. Thus the interpretation of the temperature dependent nmr spectra of **2** (Fig. 5), **3**, and **4** (Fig. 6) is most appropriate in terms of the equilibrium between Z and E pairs as shown in Figs. 1 or 3 in which rotation through 180° has taken place about the C(O)—N bond and the piperidine ring remains in the same chair form with the substituents in the axial positions.

Free energies of activation for the rotation about the C(O)—N bond of **2**, **3**, and **4** were determined in the same way as described above for **1** (22), taking into account the variation of population with temperature, and assuming that entropy differences between the conformers are zero. The data are

Can. J. Chem. Downloaded from www.nrcresearchpress.com by 210.87.254.42 on 09/06/12
For personal use only.

Can. J. Chem. Downloaded from www.nrcresearchpress.com by 210.87.254.42 on 09/06/12
For personal use only.

collected in Table 2. As can be seen in Figs. 2, 5, or 6, the spectra are more complicated and, in the instances noted in Table 2, it was not possible to determine very accurately the temperature of maximum line broadening for some of the exchanging protons. We believe the values of $\Delta G^{\ddagger}$ obtained, though approximate, for the independently observed exchange processes are similar enough to reinforce the hypothesis that the piperidine rings of **3** and **4** are "frozen" into a single chair conformation. That this also appears to be true for **2** is somewhat surprising since the $A^{(1,3)}$ strain for diaxial methyls, 20 kJ/mol (11) is close to the energy of a "twist boat" conformation, 23 kJ/mol for cyclohexane (23). From inspection of models, it does not appear that the chemical shifts of the methyl and methine protons of **2** in the chair and "twist boat" forms should differ appreciably. As the expected barrier to interconversion of the two forms, 24 kJ/mol, is too low to have been detected in the present study, the question of the dynamics of the 2,6-dimethylpiperidine ring system remains unresolved.

The observed magnitudes of the rotation barriers are larger than barriers found in a previous investigation on related systems (11). We attribute this result to a combination of two factors, both of which have the effect of raising the barrier to rotation about an amide bond. An electron withdrawing group on the acyl carbon atom has the effect of increasing the electronic demand of that centre and thus of increasing the involvement of the nitrogen lone pair in bonding to it (18). In the present case, the acyl carbon is substituted by a carbon containing a trifluoromethyl and a methoxy group. Second, and probably more important in view of the above discussion, is the very large steric bulk of the acyl group. It is evident that buttressing effects due to the acyl group are manifest throughout the rotational motion, the transition state being destabilized approximately as much as the ground state (4).

Finally, we note that the phenyl absorptions of all of the present systems also undergo significant changes in appearance as the temperature is raised (see Figs. 4, 5, and 6). In all cases the phenyl absorption is sharp at ambient temperature and broadens, revealing considerable structure, as the temperature is changed. The nature of the temperature dependence is not suggestive of an exchange process, but rather of a differential temperature dependence of the chemical shifts of the aromatic protons, probably due to changing solvation.[7]

Experimental

Materials

Diisopropyl amine, 2,6-dimethylpiperidine, and 2-methylpiperidine were commercial reagent grade (Aldrich Chemical Co.) and were redistilled before use, and their purity was checked by glc (Porapak Q). The 2,6-dimethylpiperidine was shown to be exlusively the *cis*- or (*R*,*S*)-isomer by ^{13}C nmr spectroscopy (24). The 2-methylpiperidine was resolved as described below.

(R)-(−)- and (S)-(+)-2-methylpiperidine

2-Methylpiperidine was resolved as reported by Craig and Pinder (25), using (*R*)-(−)-mandelic acid (Sigma Chemical Co.). After two recrystallizations from anhydrous methanol−ether (1:4), the mandelate salt, $[\alpha]_D$ −59.8° (*c* 2.5%, methanol) was converted to the free base, to give (*S*)-(+)-2-methylpiperidine, $[\alpha]_D$ +33.1° (neat), after distillation; lit (26) $[\alpha]_D$ +31.2° (neat). This material was shown to be optically pure (*S*)-(+)-isomer (3) by preparation of the amide, **4**, from (*R*)-(+)-MPTA (see below). No trace of the other diastereomer, **3**, could be detected by ^{19}F nmr spectroscopy (18). Concentration of the solvent from which the aforementioned mandelate salt was isolated gave a syrupy residue. Conversion of this residue to the free base gave material enriched in the (*R*)-(−)-enantiomer, $[\alpha]_D$ −5.75° (neat), after distillation. From the optical rotation, it can be estimated that the composition was 58.7% (*R*)-(−)-2-methylpiperidine mixed with 41.3% of the (*S*)-(+)-enantiomer. The composition estimated by integration of the ^{19}F absorptions due to amides **3** and **4** from this material confirmed this (19*a* and footnote 4).

Racemic and (R)-(+)-2-methoxy-2-phenyl-3,3,3-trifluoropropanoyl chloride

These acid chlorides were prepared from racemic or (+)-α-methoxy-α-trifluoromethylphenylacetic acid (Aldrich Chemical Co.) by a modification of the published procedure (19), using a catalytic amount of dimethylformamide (27).

Preparation of racemic and optically active 2-methoxy-2-phenyl-3,3,3-trifluoropropanamides

Racemic or (*R*)-(+)-2-methoxy-2-phenyl-3,3,3-trifluoropropanoyl chloride (2) was heated (reflux) for about 12 h with a four- to eightfold excess of amine, followed by standing at room temperature for 18−20 h. Acidification with concentrated hydrochloric acid, followed by extraction with ether, gave the crude amides, after evaporation of the ether.

N,N-*Diisopropyl-(R,S)-2-methoxy-2-phenyl-3,3,3-trifluoropropanamide* **1**, recrystallized from hexane. Sublimation *in vacuo* afforded an analytical sample, mp 94−96°C (uncorrected). *Anal.* calcd. for $C_{16}H_{22}O_2NF_3$: C 60.56, H 6.99, N 4.41; found: C 60.74, H 6.83, N 4.74. Specific details concerning the ^1H nmr spectrum of **1** are given in Table 1.

(R,S)-2,6-Dimethylpiperidinyl-(R,S)-2-methoxy-2-phenyl-3,3,3-trifluoropropanamide **2**, recrystallized from hexane. Sublimation *in vacuo* afforded an analytical sample, mp 83−87°C (uncorrected). *Anal.* calcd. for $C_{17}H_{22}O_2NF_3$: C 61.99, H 6.73, N 4.25; found: C 62.10, H 6.65, N 4.17. Specific details concerning the ^1H nmr spectrum of **2** are given in Table 1.

(R,S)-2-Methylpiperidinyl-(R,S)-2-methoxy-2-phenyl-3,3,3-trifluoropropanamide **3/4**, recrystallized from cyclohexane.[8] Sublimation *in vacuo* afforded an analytical sample, mp 61−64°C (uncorrected). *Anal.* calcd. for $C_{16}H_{20}O_2NF_3$: C 60.99, H 6.39, N 4.44; found: C 60.83, H 6.41, N 4.62. Specific details concerning the ^1H nmr spectra of **3** and **4** are given in Table 1.

(+)-(S)-2-Methylpiperidyl-(R)-2-methoxy-2-phenyl-3,3,3-trifluoropropanamide **4**

(*S*)-(+)-2-Methylpiperidine (see above), dissolved in triethylamine, was added to an equimolar amount of (*R*)-(+)-2-methoxy-2-phenyl-3,3,3-trifluoropropanoyl chloride and heated at reflux for 7 h. The crude amide was recrystallized from methanol−water,[8] mp 80−84°C (uncorrected), $[\alpha]_D$ +92.4 (*c* 2.4%, methanol). Specific details of the ^1H nmr spectrum of **4** are given in Table 1.

(59% 3/41% 4) **3**

The mixture of amines enriched in the (*R*)-(−)-enantiomer (see above) was added to (*R*)-(+)-2-methoxy-2-phenyl-3,3,3,-trifluoropropanoyl chloride, as described above. The crude product was subjected to ^{19}F and ^1H nmr analysis without further purification by recrystallization.[8] The composition of the mixture was confirmed by integration of the CF_3 signals in DMSO-d_6 at 80°C; found: 57% **3**, 43% **4**. Specific details of the ^1H nmr spectrum are given in Table 1.[4]

Recrystallization from methanol−water[8] afforded a sample of composition 47.3% **3**/52.7% **4**, $[\alpha]_D$ +75.5 (*c* 1.0%, methanol), from which the specific rotation of optically pure **3** could be calculated; $[\alpha]_D$ +57°.

[7]Solvent dependence of aromatic protons is well established (ref. 28). This is observed in the present systems as well. As an example, the nmr spectrum of a solution of **1** in $CDCl_3$ shows the phenyl absorption to be split into two groups of peaks, at 7.49 ppm (2H) and 7.34 ppm (3H), respectively.

[8]Recrystallization of **3** (*RR* and/or *SS*)/**4** (*RS* and/or *SR*) from methanol−water leads to enrichment of the sample in **4** (*RS* and/or *SR*).

^{1}H nuclear magnetic resonance experiments

The ^{1}H nmr spectra were obtained on a Varian XL-200 spectrometer, equipped with a variable temperature controller (accurate to ± 1°C). For the high temperature measurements (22°C to 180°C), samples were dissolved in DMSO-d_6; for the low temperature measurements (−90°C to 22°C), samples were dissolved in $CDCl_3$/acetone-d_6 (50:50). Chemical shift data (δ) are presented in Table 1, relative to tetramethylsilane (δ = 0) as internal reference.

Acknowledgments

We wish to thank R. Yamdagni for running the nmr spectra and T. S. Sorensen for valuable discussions. The financial support of the Natural Sciences and Engineering Research Council of Canada is gratefully appreciated.

1. M. A. KHAN, D. F. TAVARES, and A. RAUK. Can. J. Chem. **60**, 2451 (1982).
2. W. H. PIRKLE and S. D. BEARE. Tetrahedron Lett. 2579 (1968).
3. W. KLYNE and J. BUCKINGHAM. Atlas of stereochemistry. Absolute configurations of organic molecules. Vol. 1. Oxford University Press, New York, NY. 1974. p. 14.
4. H. KESSLER. Angew. Chem. Int. Ed. Engl. **9**, 219 (1970).
5. E. ARTE, J. FERRAN-DUPONT, J. P. DECLERQ, G. GERMAIN, and M. VAN DER MEERSCHE. Cryst. Struct. Commun. **6**, 773 (1973).
6. L. LUNAZZI, D. MACCIANTELLI, D. TASSI, and A. DONDONI. J. Chem. Soc. Perkin Trans. 2, 717 (1980).
7. L. LUNAZZI, G. CERIONI, E. FORESTI, and D. MACCIANTELLI. J. Chem. Soc. Perkin Trans. 2, 686 (1978).
8. L. LUNAZZI, G. CERIONI, and K. U. INGOLD. J. Am. Chem. Soc. **98**, 7484 (1976).
9. T. P. FORREST, D. L. HOOPER, and S. RAY. J. Am. Chem. Soc. **96**, 4286 (1974).
10. R. R. FRASER and T. B. GRINDLEY. Can. J. Chem. **53**, 2465 (1975).
11. Y. L. CHOW, C. J. COLON, and J. N. S. TAM. Can. J. Chem. **46**, 2821 (1968).
12. G. E. ELLIS, R. G. JONES, and M. G. PAPADOPOULOS. J. Chem. Soc. Perkin Trans 2, 1381 (1974).
13. R. R. FRASER and T. B. GRINDLEY. Tetrahedron Lett. 4169 (1974).
14. R. K. HARRIS and R. A. SPRAGG. J. Mol. Spectrosc. **23**, 158 (1967).
15. L. LUNAZZI and G. CERIONI. J. Chem. Soc. Perkin Trans 2, 1666 (1977).
16. (*a*) M. T. ROGERS and J. C. WOODBREY. J. Phys. Chem. **66**, 540 (1962); (*b*) A. GREENVILLE WITTAKER and S. SIEGEL. J. Chem. Phys. **43**, 1575 (1965); (*c*) F. CONTI and W. VON PHILIPSON. Helv. Chim. Acta, **50**, 603 (1967); (*d*) A. MONTAUDO, P. MARAVIGNA, S. CACCAMESE, and V. LIBRANDO. J. Org. Chem. **39**, 2806 (1974).
17. H. A. STAUB and D. LAUER. Chem. Ber. **101**, 864 (1968).
18. M. D. WUNDERLICH, L. K. LEUNG, J. A. SANDBERG, K. D. MEYER, and C. H. YODER. J. Am. Chem. Soc. **100**, 1500 (1978).
19. (*a*) J. A. DALE, D. L. DULL, and H. S. MOSHER. J. Org. Chem. **34**, 2543 (1969); (*b*) G. R. SULLIVAN, J. A. DALE, and H. S. MOSHER. J. Org. Chem. S **38**, 2143 (1973); (*c*) J. A. DALE and H. S. MOSHER. J. Am. Chem. Soc. **95**, 512 (1973).
20. A. GARTH, W. VOELTER, H. S. MOSHER, E. BUNNENBERG, and C. R. DJERASSI. J. Am. Chem. Soc. **92**, 875 (1970).
21. C. E. JOHNSON, JR. and F. A. BOVEY. J. Chem. Phys. **29**, 1012 (1958).
22. (*a*) G. BINSCH. Topics in Stereochemistry. Vol. 3. *Edited by* E. L. Eliel and N. L. Allinger. Wiley Interscience Pub., 1968. p. 106; (*b*) G. BINSCH and H. KESSLER. Angew. Chem. Int. Ed. Engl. **19**, 411 (1980).
23. M. SQUILLACOTE, R. S. SHERIDAN, O. L. CHAPMAN, and F. A. L. ANET. J. Am. Chem. Soc. **97**, 3244 (1975).
24. D. WENDISCH, H. FELTKAMP, and U. SCHEIDEGGER. Org. Magn. Reson. **5**, 129 (1972).
25. J. C. CRAIG and A. R. PINDER. J. Org. Chem. **36**, 3648 (1971).
26. W. LEITHE. Monatsh. **50**, 40 (1928).
27. Y. EGAWA, M. SUZUKI, and T. OKUDA. Chem. Pharm. Bull. **11**, 589 (1963).
28. L. M. JACKMAN and S. STERNHELL. Applications of nuclear magnetic resonance spectroscopy in organic chemistry. 2nd ed. Pergamon Press, Toronto. 1969. pp. 104–113.

Can. J. Chem. Downloaded from www.nrcresearchpress.com by 210.87.254.42 on 09/06/12
For personal use only.

Réaction entre solvant et espèces intermédiaires apparues lors de l'électroréduction–acylation de la fluorènone et de la fluorènone-anil dans l'acétonitrile

CHANTAL DEGRAND[1]
Laboratoire de Synthèse et d'Electrosynthèse Organométalliques, associé au CNRS (LA 33), Faculté des Sciences Gabriel, 21100 Dijon, France

GERARD BELOT
University of Petroleum and Minerals, Chemistry Department, Dhahran, Saudi Arabia

ET

PAUL-LOUIS COMPAGNON ET FRANÇOISE GASQUEZ
Laboratoire de Chimie Organique, Faculté de Pharmacie, Bd Jeanne d'Arc, 21100 Dijon, France

Reçu le 8 avril 1983

CHANTAL DEGRAND, GERARD BELOT, PAUL-LOUIS COMPAGNON et FRANÇOISE GASQUEZ. Can. J. Chem. **61**, 2581 (1983).

Dans l'acétonitrile, les anions $^-CH_2CN$ électrogénérés provoquent la régression de divers composés de réduction–acylation de la fluorènone **1***a* et de son anil **1***b* vers **1***a* et **1***b*; cette évolution est contrôlée par l'introduction fortuite d'oxygène moléculaire. Les anions $^-CH_2CN$ catalysent alors la transformation de **1***a* et **1***b* en fluorènylidèneacétonitrile FlC=CHCN **17**, dont dérivent les nitriles FlC=CHC(CN)=C(NH$_2$)CH$_3$ **8**, FlC=C(CN)CHFl **10** et FlC=C(CN)CH$_2$CN **11**. Ces résultats permettent d'interpréter l'évolution de la nature des produits apparus pendant l'électrolyse de la fluorènone dans l'acétonitrile, en présence d'un équivalent de chlorure ou d'anhydride d'acide ω-chloré. Apparaissent successivement les dérivés de réduction–acylation, puis les nitriles FlC(OH)CH$_2$CH$_2$CN **3***a*, **10**, FlC(OH)CH$_2$CN **24** et des polymères. Grâce à sa basicité, le radical-anion de la fluorènone est le promoteur des réactions avec le solvant, l'oléfine **17** étant un intermédiaire privilégié. Le bis-fluorènol, le fluorènol, enfin le fluorène accompagnent **1***a* et les produits ci-dessus.

CHANTAL DEGRAND, GERARD BELOT, PAUL-LOUIS COMPAGNON, and FRANÇOISE GASQUEZ. Can. J. Chem. **61**, 2581 (1983).

The electrogenerated anions $^-CH_2CN$ induce the conversion of the various reduction–acylation products of fluorenone **1***a* and its anil **1***b* in acetonitrile into **1***a* and **1***b*; this phenomenon is controlled by the fortuitous introduction of molecular oxygen. The $^-CH_2CN$ anions catalyse the transformation of **1***a* and **1***b* into fluorenylideneacetonitrile (FlC=CHCN) **17**, convertible into the nitriles FlC=CHC(CN)=C(NH$_2$)CH$_3$ **8**, FlC=C(CN)CHFl **10**, and FlC=C(CN)CH$_2$CN **11**. These observations allow us to interpret the formation of the products appearing during the electrolysis of fluorenone in acetonitrile in the presence of an equivalent of chloride or anhydride of ω-chloro acid. The products of reduction–acylation appear successively, followed by the nitriles, FlC(OH)CH$_2$CH$_2$CN **3***a*, **10**, FlC(OH)CH$_2$CN **24**, and polymers. Because of its basicity the fluorenone radical anion promotes reactions with the solvent, olefin **17** being a preferred intermediate. Bis-fluorenol, fluorenol, and finally fluorene are found with **1***a* and the above products.

[Journal translation]

Introduction

Au cours d'électroréductions effectuées dans l'acétonitrile, divers exemples de cyanométhylation ont été signalés (1–11). L'acidité de ce solvant est telle que de nombreuses formes réduites (dianions, monoanions, voire même radicaux-anions) sont suffisamment basiques pour le déprotoner. Les anions $^-CH_2CN$ ainsi formés réagissent avec diverses espèces présentes au sein du catholyte pour livrer une grande variété de nitriles.

Nous avons pour notre part (12) observé que la réduction acylante de la fluorènone **1***a* et de sa base de Schiff **1***b* dans l'acétonitrile en présence du chlorure d'acide **2***a* conduit, entre autres, à la formation de produits mineurs inattendus, les propionitriles **3***a* et **3***b*. En cours d'électrolyse, nous avions observé une évolution des formes réduites acylées **4***a*, *b* et **5***a*, *b* de la fluorènone; la nature de cette évolution n'avait pas été établie, celle-ci fait l'objet de ce travail.

Dans la partie A, nous étudions le comportement des composés **4***a–c*, **5***b*, **6***a*, *b*, **7***a*, *b* vis-à-vis des anions $^-CH_2CN$ électrogénérés par réduction de l'azobenzène en son dianion au sein de l'acétonitrile (2, 6, 13). Ces composés sont obtenus par électroréduction–acylation de la fluorènone **1***a* ou de son anil

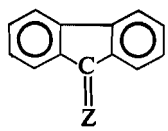

1*a*: Z = O
1*b*: Z = NPh

RCOX

2*a*: R = $(CH_2)_3Cl$, X = Cl
2*b*: R = $(CH_2)_3Cl$, X = $OCO(CH_2)_3Cl$
2*c*: R = CH_3 , X = $OCOCH_3$

FlC(ZH)CH$_2$CH$_2$CN

3*a*: ZH = OH
3*b*: ZH = NHPh

FlCHOCOR

4*a*: R = cycloPr
4*b*: R = $(CH_2)_3Cl$
4*c*: R = CH_3

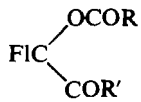

5*a*: R = R′ = cycloPr
5*b*: R = $(CH_2)_3Cl$, R′ = cycloPr
5*c*: R = R′ = $(CH_2)_3Cl$

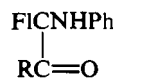

6*a*: R = cycloPr
6*b*: R = CH_3

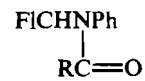

7*a*: R = cycloPr
7*b*: R = CH_3

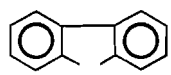

Fl

[1]Auteur à qui adresser la correspondance.

Can. J. Chem. Downloaded from www.nrcresearchpress.com by 210.87.254.105 on 09/06/12
For personal use only.

TABLEAU 1. Rendements en produits isolés après addition de $^-CH_2CN$ (2 équivalents) aux différents substrats

Expérience	Substrat	Conc. (m*M*)	Rendements en nitriles (%) 8	9*a*	10	11	Rendements en composés divers (%)
1	**4***a*	1,0	30	10	11	3	
2	**4***b*	0,85	25,5	19	40,5		**1***a* (9)
3	**4***c*	1,0	59				
4	**5***b*	1,0	7	48	45		**1***a* (traces)
5	**6***a*	0,7	52	35			**1***b* (10)
6	**6***b*	1,7	26			30	**1***b* (6), FlCHNHPh (3)
7	**7***a*	0,5	Traces				**7***a*[a]
8	**7***b*	1,6	Traces				**7***b* (50)
9	**17**	1,0	43			23	

[a] Produit principal, rendement non calculé.

1*b*, les agents acylants étant le chlorure et l'anhydride d'acide ω-chloré **2***a* et **2***b* (12) et l'anhydride acétique **2***c*.

Dans la partie B, nous examinerons en détail l'électroréduction de la fluorènone conduite dans l'acétonitrile, en présence d'un équivalent d'agent acylant **2***a* ou **2***b*. L'évolution de la nature des produits en fonction du degré d'avancement de l'électrolyse est interprétée compte tenu des résultats de la première partie.

Résultats et discussion

A. *Stabilité des formes réduites acylées de la fluorènone ou de sa base de Schiff vis-à-vis d'anions $^-CH_2CN$ électrogénérés*

L'addition de deux équivalents de $^-CH_2CN$ aux diverses formes réduites acylées étudiées conduit à l'obtention des nitriles **8**, **9***a*, **10** et **11**. Les rendements obtenus après purification par chromatographie sont indiqués dans le Tableau 1 (expériences 1 à 8).

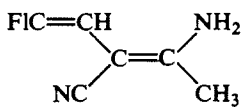

8

$RCOC(CN)=C(NH_2)CH_3$

9*a*: R = cycloPr
9*b*: R = $(CH_2)_3Cl$
9*c*: R = CH_3

$FlC=C(CN)CHFl$

10

$FlC=C(CN)CH_2CN$

11

Les résultats des expériences 1 à 8 du Tableau 1 conduisent aux conclusions suivantes.

(*i*) Dans la moitié des expériences, la fluorènone ou sa base de Schiff est isolée en faible quantité.

(*ii*) Dans toutes les expériences, on obtient le dièmaminonitrile **8**. Nous avons montré récemment (14) que l'attaque par $^-CH_2CN$ de la fluorènone et de ses bases de Schiff conduit également à **8**, à l'abri de l'air. En présence de traces d'oxygène, la formation de **8** est en compétition avec celle de **11** (15).

(*iii*) L'attaque par $^-CH_2CN$ des formes réduites N-acylées **7***a* et **7***b* est lente puisque le substrat est en grande partie récupéré après les temps de contact choisis (expériences 7 et 8).

(*iv*) L'énaminonitrile cyclopropylé **9***a* est isolé dans toutes les expériences où le substrat possède un reste cyclopropyle préexistant ou potentiel ($CO(CH_2)_3Cl$) sauf dans l'expérience 7 pour la raison précédente.

(*v*) A partir des dérivés de la fluorènone, on obtient le produit de couplage **10** (16*a*), exception faite de l'expérience 3 où, en revanche, le rendement en **8** est élevé.

La formation de fluorènone ou de son anil se conçoit comme résultat de l'action conjointe des anions $^-CH_2CN$ électrogénérés dans un premier temps et de traces d'oxygène qui peuvent s'introduire de façon aléatoire dans la seconde phase non-électrochimique.

TABLEAU 2. Valeurs des pK_a dans le DMSO de divers composés à H mobile

	CH_3CN	$FlCH_2$	FlCHOH	$FlCHOCH_3$
pK_a	31,3[a]	22,6[b]	16[c]	16[c]
	$PhCOCH_2CN$	H_2O	$CH_3CHOHCH_3$	$PhNH_2$
pK_a	10,2[a]	31,4[d]	30,2[d]	30,7[e]

[a] Voir réf. 31.
[b] Voir réf. 32.
[c] Voir réf. 33.
[d] Voir réf. 34.
[e] Voir réf. 35.

Le tableau 2 rassemble les pK_a dans le DMSO de quelques molécules afin de montrer que $^-CH_2CN$ peut générer leurs anions et provoquer les réarrangements évoqués ci-dessous. Le DMSO est retenu comme solvant de référence pour son caractère dipolaire non-hydroxylé ("aprotique") qui est celui de MeCN.

Esters de fluorènol **4**a–c

Ils doivent se cliver en premier lieu selon [1].

L'alcoolate libéré se réarrange spontanément en carbanion **12** (17). Ce carbanion est très sensible aux traces d'oxygène puisque par voltamétrie cyclique dans le DMF, on observe son potentiel de pic d'oxydation E_{pa} à −1,21 V/ECS (17) tandis que l'oxygène se réduit vers −0,7 V. La fluorènone est régénérée dans le milieu basique selon le processus catalytique [3]–[6]: la formation de la fluorènone provient de la rupture du bis-fluorènol intermédiaire par une base B^- telle que l'anion **12** (21). L'ion superoxyde constitue éventuellement une autre base; il évolue probablement vers la formation d'eau oxygénée. L'ènol de la réaction [1] conduit à l'anion correspondant **13** selon [7].

Can. J. Chem. Downloaded from www.nrcresearchpress.com by 210.87.254.105 on 09/06/12
For personal use only.

Can. J. Chem. Downloaded from www.nrcresearchpress.com by 210.87.254.105 on 09/06/12
For personal use only.

[1] 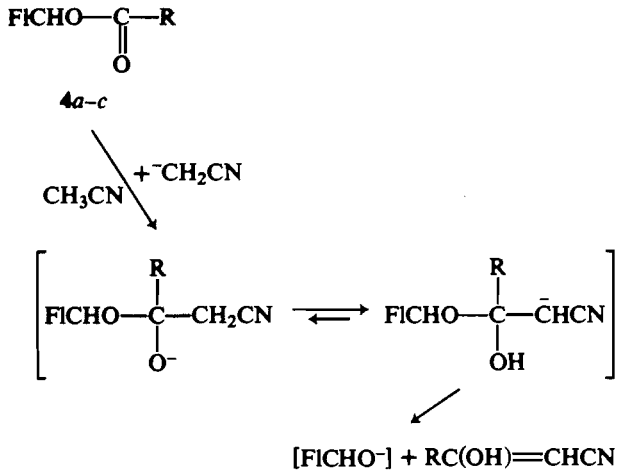

[2] 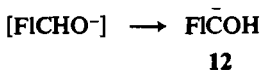

[3] 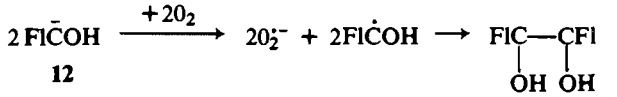

[4] 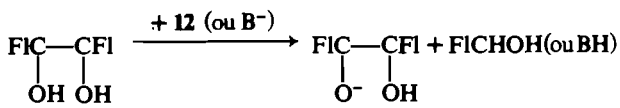

[5] 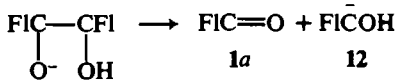

[6] 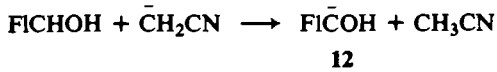

[7] 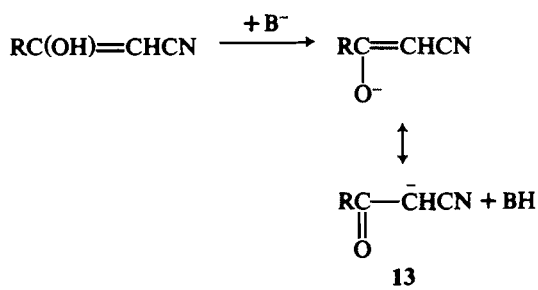

Dérivé diacylé **5**b

Il conduit aussi à la fluorènone puisque le dérivé acylé **4***b* se forme intermédiairement.

[8] 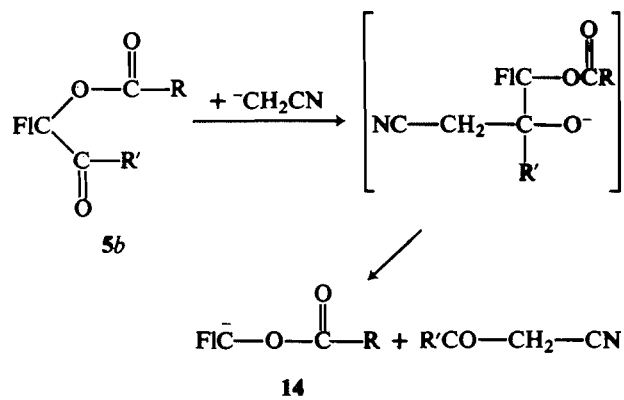

[9] 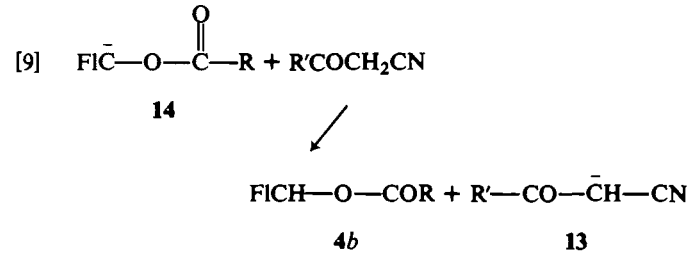

Dérivés C-acylés **6**a, b

Après libération de l'anion **15**, un processus d'oxydation par O_2 conduit à la base de Schiff **1***b* selon [11]–[13]. Le mécanisme proposé tient compte des observations suivantes. L'anion **15** est facilement oxydable par l'oxygène [11] puisqu'on observe son oxydation à $E_{pa} = -0{,}93$ V/ECS par voltamétrie cyclique dans le DMF (18). Les bases fortes B^- déprotonent le radical apparu (18). Le radical-anion de la base de Schiff s'oxyde, lui aussi très facilement, à $-1{,}4$ V (12); en conséquence, il réduit instantanément les traces d'oxygène. On peut également envisager[2] que le radical apparu dans [11] se dimérise selon [13] avant de livrer la base de Schiff **1***b*.

[10] 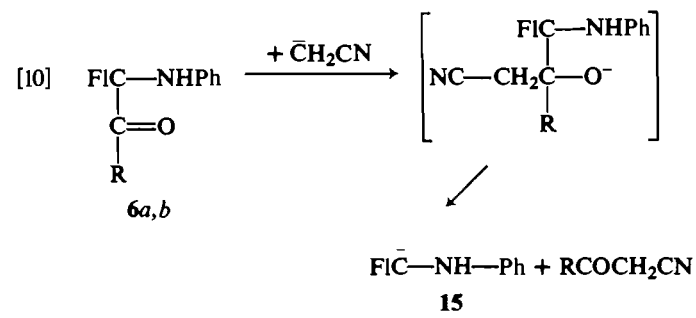

[11] 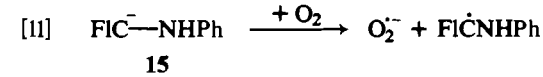

[12] 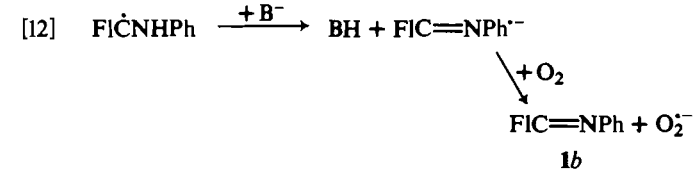

[13] 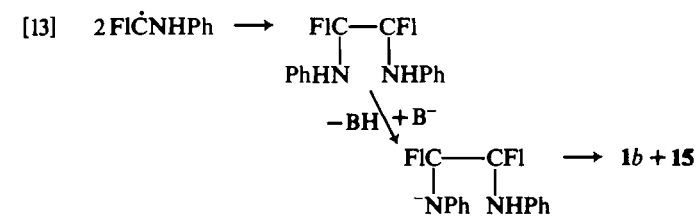

Dérivés N-acylés **7**a, b

La déprotonation de **7***a, b* est certainement plus rapide que l'addition nucléophile au carbonyle de **6***a, b*. On observe cependant que l'anion **16** ainsi formé [14] évolue difficilement: le produit principal est le produit initial. L'anion **16** est plus stable et moins facilement oxydable que l'anion **15**; ceci justifie la lenteur d'évolution des composés **7***a, b*.

[2] Suggestion de l'un des examinateurs.

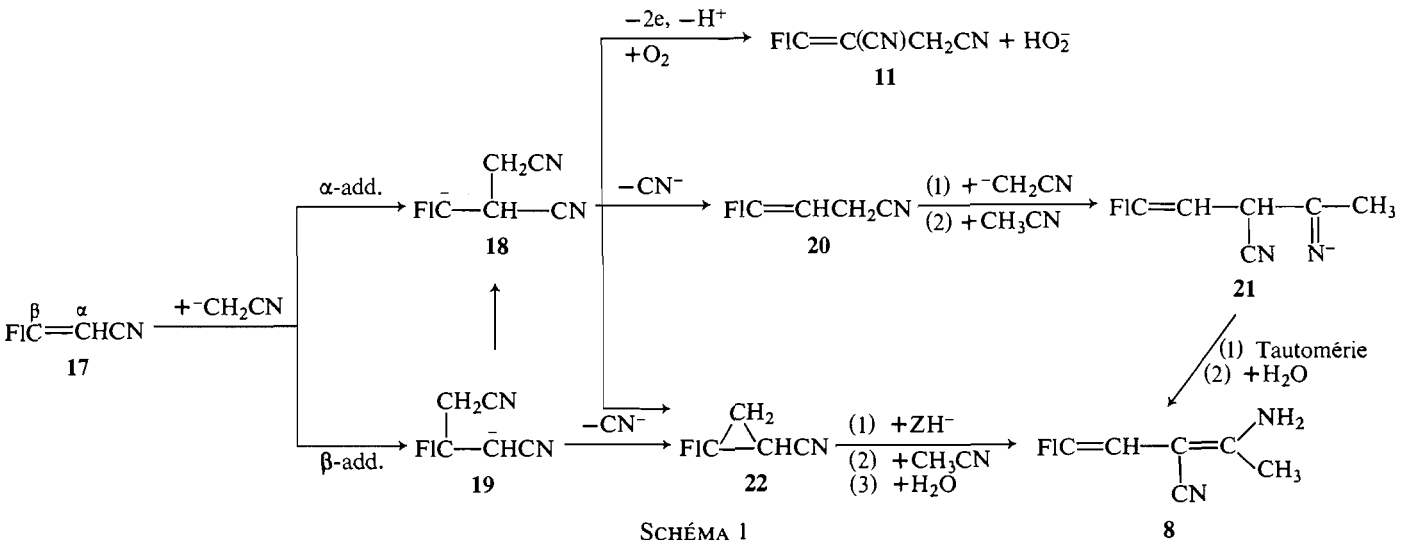

SCHÉMA 1

[14] $FlCH{-}NPh \xrightarrow{+{}^-CH_2CN} Fl\bar{C}{-}NPh$ (RC=O)

7*a*,*b* 16

Les anions **13**, issus des β-cétonitriles $RCOCH_2CN$, se comportent comme de bons nucléophiles. Leur condensation avec l'acétonitrile-solvant conduit aux ènaminonitriles **9***a*–*c*. Que

[15] $RCO\bar{C}HCN \xrightarrow{+CH_3CN} RCOCH{-}C(CN){=}N^-$ (CN, CH_3)

13

$RCO\bar{C}{-}C{=}NH \leftrightarrow RCOC(CN){=}C(NH^-)CH_3$

$\xrightarrow{+H_2O}$ $RCOC(CN){=}C(NH_2)CH_3$

9*a*–*c*

l'on parte de **4***a*, **6***a*, ou de **4***b*, **5***b*, seul **9***a* est isolé; dans le cas de **4***b*, **5***b*, la basicité du milieu induit la cyclisation de **9***b* en **9***a*. En revanche, l'homologue méthylé **9***c* n'a pu être isolé à partir de **4***c*, **6***b*, et **7***c*. L'étude spectroscopique de **9**a montre un équilibre tautomère entre les formes ènamine et imine.

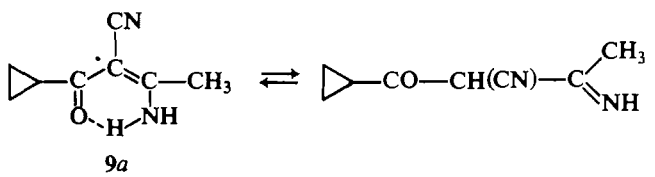

9*a*

La fluorènone **1***a* et son anil **1***b* régénérés à partir des divers substrats sont eux-mêmes sensibles à l'attaque nucléophile des anions $^-CH_2CN$ (14): il en résulte un nitrile α,β-éthylénique **17** très électrophile [16]. En quelques étapes (Schéma 1), on accède aux nitriles **8** et **11** à partir du promoteur **17** (14, 15). Les résultats de l'expérience 9 (Tableau 1) confirment que ces deux nitriles dérivent bien de **17**. Le dinitrile **11** résulte de l'oxydation de l'anion **18** par l'oxygène moléculaire (15). Le potentiel d'oxydation de **18** n'est pas connu, mais il est voisin de celui des anions fluorènyles $FlCH^-$, $E_0 = -0{,}67$ V/ECS dans le DMF (19) et $Fl\bar{C}CH_3$, $E_0 = -0{,}78$ V/ECS dans le DMF (17). Le dièneaminonitrile **8** provient de l'oléfine **20** et/ou du dérivé cyclopropylé **22** (14), dont l'ouverture résulte de l'attaque de bases telles HO^-, $PhNH^-$ (ZH^- accompagne la formation de **17**). L'attaque du dérivé cyclopropyle **22** par les bases HO^- et $PhNH^-$ permet également d'accéder aux propionitriles **3***a*, *b* [17] qui sont apparus lors de l'électroréduction–acylation de la fluorènone (12).

[16] $FlC{=}Z \xrightarrow{+{}^-CH_2CN} FlC{=}CHCN + ZH^-$

1*a*: Z = O
1*b*: Z = NPh

17

[17] $FlC(CH_2){-}CH{-}CN \xrightarrow{+ZH^-} FlC(ZH){-}CH_2{-}\bar{C}H{-}CN$

22

(ZH^-: HO^-, $PhNH^-$)

$\xrightarrow{+H^+}$ **3***a*,*b*

L'attaque nucléophile du nitrile α,β-éthylènique **17** par les anions $^-CH_2CN$ implique une régiosélectivité particulière. L'attaque du C-β conduirait à un produit classique d'addition-1,4, avec formation de l'anion intermédiaire **19**. La protonation de **19** par le solvant ou lors du traitement final par l'eau livrerait le dinitrile $FlC(CH_2CN)_2$ que nous n'avons pas isolé. Des nitriles analogues, les glutaronitriles $PhRC(CH_2CN)_2$ ont été obtenus par électroréduction de PhCOR et d'oléfines activées $PhRC{=}CHCN$ dans l'acétonitrile; seule intervient alors la β-addition d'anions $^-CH_2CN$ électrogénérés (1, 2, 6, 9–11). Dans notre cas, l'attaque du C-α livre l'anion fluorènyle **18** beaucoup plus stable. L'anion **19** est donc peu compétitif vis-à-vis de **18**; s'il apparaît, il s'isomérise plutôt en anion **18**.

L'attaque du C-α du nitrile **17** est aussi sensible à d'autres nucléophiles tels les anions **14** $Fl\bar{C}OCOR$ issus de **5***b* [8] ou de **4***a*–*c*. On obtient alors un anion très délocalisé **23** dont le traitement final par l'eau livre le nitrile **10**. Le pK_a dans le DMSO du fluorènylidèneméthyl-9 fluorène est évalué à 14,2

Can. J. Chem. Downloaded from www.nrcresearchpress.com by 210.87.254.105 on 09/06/12
For personal use only.

TABLEAU 3. Potentiel de demi-vague $E_{1/2}$ ou de pic E_{pc} de formes réduites acylées de **1***a* et de **1***b* et des nitriles insaturés **8**, **10**, **11** et **17**

		Substrats				Nitriles insaturés			
	Solvant	**4***a*	**4***b*	**5***a*	**6***a*	**8**	**10**	**11**	**17**
$E_{1/2}$ ou E_{pc}* (V)	MeCN	−2,30	−2,30	−2,12		−1,86*	−1,42*	−1,22*	−1,35*
	DMF	−2,21		−2,06	−2,25	−1,90		−1,18	

(16*b*), celui de **10** est inférieur à 14 grâce à l'effet −I du groupe cyano.

[18]

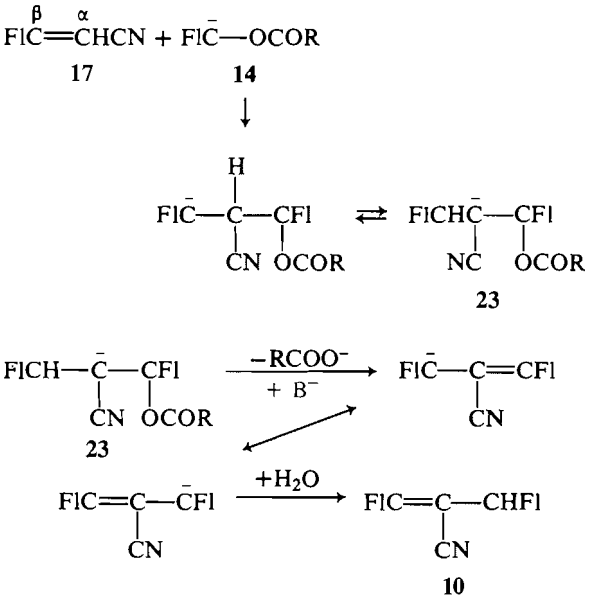

Une grande dispersion caractérise les rendements exposés au tableau 1. Le taux de récupération du noyau fluorène varie de 44 à 66% (en moyenne 55%) car la formation de polymères est fréquente. En ce qui concerne l'acyl-ènaminonitrile **9***a*, son instabilité lors de l'hydrolyse est sans doute cause des variations de rendement observées. Par ailleurs, si la formation d'un composé dépend de la concentration aléatoire en oxygène moléculaire résiduel, il faut s'attendre à des fluctuations de son rendement. Ainsi le nitrile **11**, résultat du processus oxydatif de l'anion **18** (Schéma 1), a un rendement variant de 0 à 30% selon l'électrolyse. Si ce processus est limité, la formation de **8** est favorisée. Enfin, les nitriles **8** et **10** sont en compétition à partir de l'oléfine **17** (Schéma 1 et [18]). Dans le meilleur cas, **10** atteint un rendement de 45% au lieu des 1 à 5% de la référence 16*a*; la méthode électrochimique constitue donc une bonne voie d'accès à cette molécule.

Pour aborder la deuxième partie de notre étude, il est nécessaire de déterminer les propriétés électroréductrices (potentiel de demi-vague $E_{1/2}$ sur électrode à gouttes de mercure ou potentiel de pic E_{pc} sur électrode stationnaire de carbone vitreux) de quelques dérivés acylés des types **4**, **5** et **6** et des divers nitriles insaturés préparés. Ces données sont rassemblées dans le tableau 3. La réduction de tous les dérivés acylés survient au-delà de −2 V. Elle provoque la rupture des composés **4***a*, *c* libérant l'anion fluorènyle $FlCH^-$ rouge intense qui, après traitement, livre du fluorène et de la fluorènone. L'anion $Fl\bar{C}H$ est, en effet, très sensible aux traces d'oxygène, et donne de la fluorènone (20). Par exemple, une électroréduction préparative à partir de **4***c*, à −2,2 V dans l'acétonitrile conduit à un mélange de fluorène, de fluorènone **1***a* et d'alcool **24** en proportions relatives de 24, 40 et 36%. Ce dernier apparaît également lors de la réduction de **1***a* (voir partie B). Les nitriles insaturés

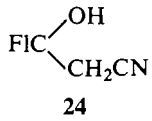

24

8, **10**, **11** et **17** sont plus faciles à réduire. Le premier stade de réduction correspond à la fixation d'un électron. La voltamétrie cyclique indique que les radicaux-anions obtenus ont des stabilités différentes: le plus stable est issu de **10**. Dans ce cas, le catholyte devient bleu intense; de plus cette coloration persiste malgré un barbotage d'oxygène. Nous suggérons que le radical-anion conduit à deux espèces très stables: l'anion délocalisé bleu **23** et le radical encombré **25**. Le mécanisme [19] fera l'objet d'une étude ultérieure.

[19]

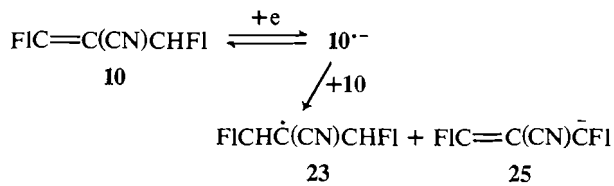

Une électroréduction préparative de **17** conduit à une solution vert bronze. Après passage de 1 F, on note à côté d'oléfine résiduelle **17**, la présence principale de polymères.

B. *Electroréduction acylante de la fluorènone dans l'acétonitrile liée à la présence d'un équivalent de chlorure ou d'anhydride d'acide* **2**a *ou* **2**b

Une série d'électrolyses préparatives sur nappe de mercure a été effectuée à des potentiels contrôlés E_c qui correspondent à la formation initiale du radical-anion de la fluorènone (E_c = −1,35 ± 0,15 V); un équivalent de **2***a* ou **2***b* est initialement présent. Ces expériences sont résumées dans le Tableau 4 (électrolyses 1–4). Elles correspondent à divers degrés d'avancement de l'électrolyse, le nombre *n* de faradays consommés variant de 1,7 à 3,2. Les rendements indiqués sont calculés après purification par chromatographie sur colonne.

Le degré d'avancement de l'électrolyse se traduit par une évolution de la couleur du catholyte, ce qui permet de distinguer six étapes successives. Le Tableau 5 rassemble ces données ainsi que la nature des produits identifiés à chaque étape par chromatographie en couche mince. Ces deux tableaux révèlent la complexité des réactions qui se produisent au sein du catholyte. Cette complexité se retrouve dans l'évolution du courant faradaïque présentée par la Fig. 1. Après une décroissance normale, on note deux reprises successives de l'électrolyse quand *n* = 1,6 F et *n* = 2,4 F.

Can. J. Chem. Downloaded from www.nrcresearchpress.com by 210.87.254.105 on 09/06/12
For personal use only.

TABLEAU 4. Electroréduction préparative de **1***a* en présence (électrolyses 1–4) ou en l'absence (électrolyse 5) d'un équivalent de **2***a* ou **2***b*. Influence du nombre *n* de F consommés sur la nature et les rendements des produits isolés

					Rendements (%)										
								Dérivés acylés				Dérivés nitriles			
Electrolyse	**1***a* (m*M*)	Agent acylant	*n*	Etape[a]	Fluorènone	Fluorènol	Fluorène	**4***a*	**4***b*	**5***a*	**5***b*	**3***a*	**10**	**17**	**24**
1	11	**2***a*	1,70[b]	IV	15	11			3,5	8	17	5			
2	2,8	**2***b*	2,36	V	30		4	28		7					11
3	3,3	**2***b*	2,60[c]	V	16		13	14,5		2		4	8		8
4	11	**2***a*	3,20[c]	VI	20		16						4,5		
5	2,6		1,04[c]		26									8	31

[a] L'étape est définie en fonction de *n* et de la couleur du catholyte dans le Tableau 5.
[b] Voir la référence 12.
[c] Des substances polymériques non identifiées sont également isolées.

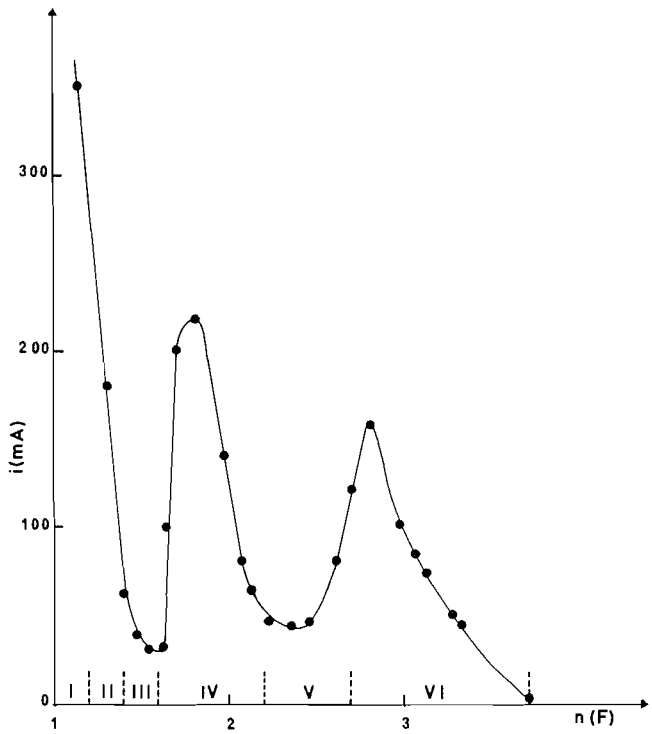

FIG. 1. Electroréduction préparative à −1,4 V de **1***a* en présence d'un équivalent de **2***a*. Les conditions sont celles du Tableau 5. Influence du nombre *n* de F consommés sur l'intensité du courant faradaïque. Les nombres romains indiquent les étapes successives définies dans le Tableau 5, à partir de la couleur du catholyte.

Les électrolyses conduisent aux remarques suivantes.

(*i*) La présence de fluorènone est constante. Son taux oscille autour de 20% de façon aléatoire: lorsque l'électrolyse progresse, il peut augmenter ou diminuer.

(*ii*) L'évolution de l'électrolyse ne semble pas corrélée à la nature de l'agent acylant. L'utilisation du chlorure d'acide **2***a* favorise cependant la formation des formes réduites diacylées aux dépens des formes monoacylées.

(*iii*) Le bis-fluorènol et le fluorènol se forment dès l'origine, mais le premier disparaît plus précocement que le second.

(*iv*) Le fluorène apparaît tardivement avec l'étape V.

(*v*) Les dérivés acylés disparaissent en fin d'électrolyse.

(*vi*) Les étapes finales se caractérisent surtout par l'apparition des nitriles **3***a*, **10** et **24**.

Etape I

Elle correspond à la réduction acylante de la fluorènone; l'excès originel d'agent acylant autorise à partir de l'anion **14**, la formation du diacylé **5***c*. La rapidité des acylations cause la disparition immédiate du radical-anion **26** rouge et de l'anion **14**. Le catholyte reste jaune même au voisinage immédiat de la nappe de mercure. Le dérivé diacylé **5***c* disparaît dès cette étape en détruisant **26**. La chromatographie sur couche mince (Tableau 5) révèle déjà **5***b*, à côté du bisfluorènol, de l'ester **4***b* et du fluorènol qui proviennent du traitement par l'eau des anions **14** et **12** respectivement.

[20] $\underset{\mathbf{1}a}{FlC{=}O} \overset{+e}{\rightleftharpoons} \underset{\mathbf{26}}{Fl\dot{C}{-}O^-}$

$\underset{\mathbf{26}}{Fl\dot{C}{-}O^-} \xrightarrow{+2a,b,\ +e} \underset{\mathbf{14}}{Fl\bar{C}{-}OCOR} \xrightarrow{+2a,b} \underset{\mathbf{5}c}{FlC(COR)OCOR}$

[21] $\underset{\mathbf{5}c}{5c} + \underset{\mathbf{26}}{Fl\dot{C}{-}O^-} \rightarrow 5b + Cl^- + Fl\dot{C}{-}OH \xrightarrow{+e} \underset{\mathbf{12}}{Fl\bar{C}{-}OH}$

$Fl\dot{C}{-}OH \rightarrow \tfrac{1}{2}FlC(OH)C(OH)CFl$

Etape II

Avec la progression de l'électrolyse, les concentrations relatives de **2***a*, *b* diminuent: le radical-anion **26** réagit avec le dérivé diacylé **5***c* dont la cyclisation progresse de **5***b* vers **5***a*. La coloration rouge du catholyte au voisinage de la nappe de mercure montre l'accumulation du radical-anion **26**. En conséquence, la cyclisation **5***b* → **5***a*, sous l'influence de **26**, est relativement lente.

Etape III

Elle s'achève avec la réduction totale de la fluorènone et la formation des esters **4***b*, **5***a*, *b*, de fluorènol et de bis-fluorènol. Le courant faradaïque devient négligeable et le catholyte incolore.

Etape IV

Elle correspond à la reprise du courant faradaïque et à une nouvelle coloration en rouge du catholyte; des radicaux anions **26** réapparaissent tandis que le bis-fluorènol disparaît. Les esters **4***b* et **5***a*, *b* n'étant pas réductibles au potentiel utilisé (Tableau 3), la formation de radicaux-anions **26** est liée à la réapparition de fluorènone au sein du catholyte. La régénéra-

Can. J. Chem. Downloaded from www.nrcresearchpress.com by 210.87.254.105 on 09/06/12
For personal use only.

Can. J. Chem. Downloaded from www.nrcresearchpress.com by 210.87.254.105 on 09/06/12
For personal use only.

tion de la cétone est provoquée par la présence de bases telles que FlC̄OH qui catalysent la transformation du bis-fluorènol en fluorènone (21) (voir partie A, [4] à [6]).

Les radicaux-anions **26** à nouveau apparus sont suffisamment basiques pour déprotoner le solvant. Ceci est démontré par l'électrolyse 5 du tableau 4, effectuée *sans agent acylant*. Les résultats de cette électrolyse annexe sont intéressants car, nous le verrons, ils entrent en ligne de compte dans l'interprétation du cours de cette étape et des suivantes. L'électrolyse 5 montre une intervention des anions $^{-}CH_2CN$ puisqu'elle conduit à la formation des nitriles **17** et **24** selon [22] à [26]. La transformation de la fluorènone en oléfine **17** est un processus catalytique (séquence [23]–[25]) en raison de la basicité de l'ion HO^{-} dans l'acétonitrile (cf. les pK_a du tableau 2).

[22] $FlC{=}O \underset{}{\overset{+e}{\rightleftharpoons}} Fl\dot{C}{-}O^{-}$ (**26**)

$Fl\dot{C}{-}O^{-} + CH_3CN \rightarrow Fl\dot{C}{-}OH + {}^{-}CH_2CN$

[23] ${}^{-}CH_2CN + FlC{=}O \rightarrow FlC(O^{-}){-}CH_2CN \rightleftharpoons FlC(OH)\bar{C}HCN$

[24] $FlC(OH)\bar{C}HCN \rightarrow HO^{-} + FlC{=}CHCN$ (**17**)

[25] $HO^{-} + CH_3CN \rightleftarrows HOH + \bar{C}H_2CN$

[26] $FlC(OH)\bar{C}HCN \xrightarrow{+H_3O^{+}} FlC(OH)CH_2CN$ (**24**)

Compte tenu des résultats de cette électrolyse, on conçoit que dans l'étape IV, les radicaux anions **26** à nouveau apparus, livrent l'oléfine **17** selon [22] à [24]. Dans cette étape, la formation de polymères est induite à partir de **17** selon [27] et celle du nitrile **3***a* s'effectue probablement selon [28] (cf. partie A, Schéma 1 et [17]). La consommation continuelle et rapide de la fluorènone provoque la chute du courant faradaïque.

[27] $FlC{=}CHCN$ (**17**) $\xrightarrow{+Fl\dot{C}OH}$ polymères

[28] $FlC{=}CHCN$ (**17**) $\xrightarrow{\text{Schéma 1}}$ $FlC(CH_2){-}CHCN$

$FlC(CH_2){-}CHCN \xrightarrow{+HO^{-}} FlC(OH)CH_2\bar{C}HCN \xrightarrow{\text{hydrolyse}} \mathbf{3}a$

Etape V

Elle débute quand **5***b* est totalement cyclisé en **5***a*. Les bases fortes présentes ($Fl\dot{C}{-}O^{-}$, HO^{-}, $^{-}CH_2CN$) entraînent la cyclisation de **4***b* en **4***a*. L'oléfine activée **17** formée dès l'étape IV constitue toujours un piège pour d'éventuels radicaux $Fl\dot{C}OH$, d'où l'apparition de polymères [27]. Par ailleurs, **17** est elle-même réductible en polymères au potentiel appliqué (Tableau 3).

TABLEAU 5. Electroréduction préparative de **1***a* en présence d'un équivalent de **2***a*. Au total, 3,72 F sont consommés (cf. Fig. 1). Influence du degré d'avancement de l'électrolyse sur la couleur du catholyte et sur la nature des produits apparus en cours d'expérience. Ces produits sont identifiés par chromatographie sur couche mince

			Temps d'électrolyse[a]					Dérivés acylés				Dérivés nitriles		
Etape	Couleur	n^a	(min)	Fluorènone	Bisfluorènol	Fluorènol	Fluorène	**4***a*	**4***b*	**5***a*	**5***b*	**3***a*	**10**	**24**
I	Jaune	1,2	70	+	+	+			+		+			
II	Jaune en solution	1,4	90	+	+	+			+	+	+			
	Rouge au contact de la nappe													
III	Incolore	1,6	210	+	+	+			+	+	+			
IV	Rouge	2,2	300	+	+	+			+	+	+	+		+
V	Bleu foncé	2,7	470	+	+		+	+		+		+	+	
VI	Violet	3,7	1400	+			+						+	

[a] Fin de l'étape.

Le nitrile **24** se forme, lors de l'extraction, selon [23] et [26]. Le nitrile insaturé **10** FlC=C(CN)CHFl dérive de **17** à la suite de deux types d'addition. Nous avons montré dans la partie A, que l'addition à **17** des anions **14** issus du dérivé monoacylé **4***a*, conduit à **10** [18]; on note en conséquence une disparition progressive de **4***a*. L'anion du fluorènol FlC̄OH peut lui aussi se condenser avec **17** [29] entraînant la disparition du fluorènol à cette étape. La présence de l'anion **23** issu de **10** provoque la coloration bleu foncé du catholyte. Du fluorène est identifié dont l'origine est discutée ci-dessous.

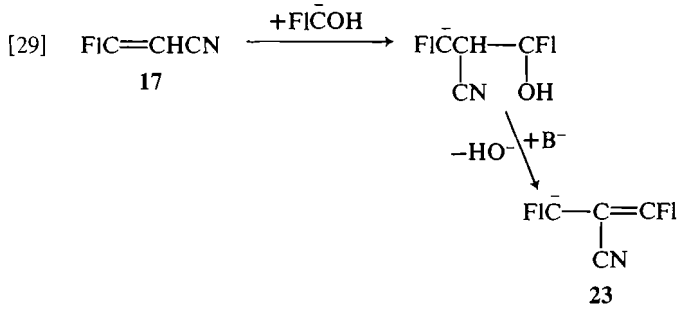

Etape VI

Elle est caractérisée par la reprise d'un courant faradaïque de faible intensité, suggérant la réapparition de traces de fluorènone. La couleur violette du catholyte résulte du mélange d'anions bleus **23** du nitrile **10** et du radical-anion **26** de la fluorènone. Du fluorène et de la fluorènone sont encore identifiés dans cette étape. Enfin, le dérivé diacylé **5***a* disparaît à son tour. Dans la partie A, nous avons montré que la présence de traces d'oxygène est favorable à une décomposition de **4***a*, *b* et **5***a*, *b* en fluorènone; nous avons aussi rappelé que l'anion fluorènyle livre de la fluorènone en présence de O_2 (20).

Les bases fortes présentes (HO^- et $^-CH_2CN$) provoquent également la rupture de **5***a* selon [30] et [31]. L'anion **14***a* libéré est piégé par **17**, donnant l'anion bleu **23** [18]. Le

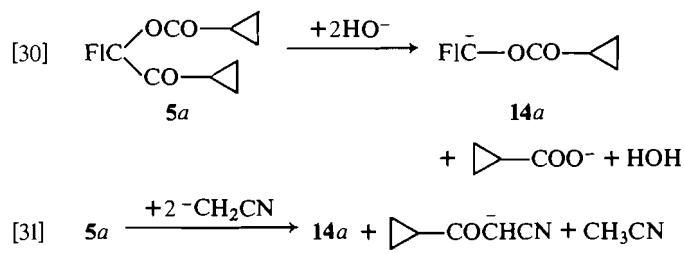

fluorène, déjà trouvé à l'étape V, est le stade final de réduction de **1***a*. Plusieurs composés formés pendant l'électrolyse se réduisent en fluorène, mais au-delà de −2 V: le fluorènol et ses éthers se rompent entre C et O (17, 22–24); de même, les esters **4***a*, *b* se réduisent avec coupure à −2,3 V (Tableau 3). Le bis-fluorènol dont le stade final de réduction est aussi le fluorène, est réduit dans une première étape en fluorènol (réfs. 17 et 22). Ici, le potentiel d'électrolyse ne dépasse pas −1,5 V. La réduction d'un intermédiaire instable non identifié peut conduire au fluorène; mais nous émettons également l'hypothèse suivante, en raison de la nature hyperbasique du catholyte (25). Le pouvoir réducteur des électrons serait exalté par le milieu hyperbasique, à l'image de l'accroissement considérable du pouvoir réducteur de HNa par les alcoolates RONa (26) découverts par Caubère et coll. Selon Bordwell et Clemens (27), plus un carbanion est basique, plus grande est la probabilité qu'il réagisse selon un processus de transfert (mono) électronique plutôt que par un processus S_N2. Cet accroissement du pouvoir de transfert expliquerait la réduction finale en fluorène.

Conclusion

Nos résultats montrent que l'évolution de l'électroréduction–acylation de la fluorènone est orientée par la réaction du solvant, l'acétonitrile, avec les intermédiaires apparus, en particulier le radical-anion de la fluorènone.

Partie expérimentale

Un potentiostat Amel-552 et un intégrateur Tacussel IG5-N sont utilisés pour l'électrosynthèse; une unité Tacussel UAP 4 et un générateur de fonctions Tacussel GST pour les expériences en voltamétrie. Les voltamogrammes sont enregistrés sur un appareil Ifelec 2025 CX-Y. Les spectres de rmn ^1H sont tracés sur un spectromètre Perkin–Elmer R-24, les spectres de masse sur un spectromètre Finnigan 3003 (introduction directe; 70 eV), les spectres ir sur un spectromètre Beckman IR-8. Les points de fusion sont déterminés sur un banc de Köfler. Les chromatographies sur colonne sont conduites sur gel de silice Kieselgel 70, 70–230 mesh, Merck 7734 et celles en couche mince sur plaques de Kieselgel 60F 254 Merck 5554 (éluant: acétone/hexane 3:7).

Les solvants (MeCN et DMF) de pureté analytique sont soigneusement séchés sur tamis moléculaire 4 Å, puis sur alumine neutre.

Tous les potentiels indiqués se réfèrent à l'électrode au calomel saturé (ECS).

L'électrosynthèse des dérivés acylés **4***a*, **4***b*, **5***a*, **5***b*, **6***a* et **7***a* est déjà décrite (12). L'électroréduction de la fluorènone dans l'acétonitrile en présence d'un équivalent d'anhydride acétique, a permis l'obtention de **4***c*. Les composés **6***b* et **7***b* sont obtenus électrochimiquement à partir de l'anil **1***b*. Ils sont identiques à ceux décrits dans la littérature: **4***c* (28), **6***b* (29) et **7***b* (30).

Les anions $^-CH_2CN$ (2 équivalents) sont électrogénérés par réduction de l'azobenzène dans l'acétonitrile selon la procédure décrite dans la référence 14. L'électroréduction de la fluorènone en présence d'un équivalent de **2***a* ou **2***b* est effectuée selon la méthode B de la référence 12.

Les nitriles sont séparés par chromatographie dans l'ordre d'élution suivant: **10** (16*b*), **11** (15), **9***a* et **8** (14).

Amino-3 cyano-2 cyclopropyl-1 butène-2 one-1 **9***a*

Cristaux beiges, F = 141°C (éther diéthylique – hexane); ir (KBr) cm^{-1}, ν_{NH_2} et ν_{NH}: 3320 (épaulements à 3400, 3300, 3250) et 3140, $\nu_{C=C-C\equiv N}$: 2230, $\nu_{C=C-C=O}$: 1700, $\nu_{C=C}$ ou $\nu_{C=N}$: 1645, 1530, 1400, 1320, 1200, 940; rmn ^1H ($CDCl_3$, référence interne TMS) δ ppm: 0,7–1,2 (m, 4H, cyclopropyle), 1,3–1,7 (m, 1H, cyclopropyle), 2,20 (s, 3H, CH_3), 6,40 (s, 1H, H—C-2), 7,85 (large s, 1H, NH); spectre de masse *m/e* (intensité relative %): 151 (11), 150 ($M^{\cdot+}$, 100), 149 (4), 122 (M − 1 − HCN, 12), 82 (16), 70 (15). En raison de son instabilité, l'analyse centésimale de **9***a* n'a pu être effectuée.

Fluorènyl-9 fluorènylidène-9' acétonitrile ***10***

Aiguilles jaunes, solution bleue dans l'acétone, F = 264–267°C (heptane) (litt. (16*b*) F = 218°C); ir (KBr) cm^{-1}, $\nu_{C=C-C\equiv N}$: 2200, 1440; rmn ^1H ($CDCl_3$) δ ppm: 6,0 (s, 1H), 7,15–7,95 (m, 14H), 8,10–8,35 (m, 1H), 8,35–8,70 (m, 1H); spectre de masse *m/e* (intensité relative %): 368 (13), 367 (M^+, 37), 340 (M − HCN, 16), 339 (M − 1 − HCN, 22), 201 (18), 176 (13), 175 (19), 166 (14), 165 (100, cation fluorènylium), 164 (41), 163 (35), 139 (14). *Anal.* calc. pour CHN: C 91,52, H 4,66, N 3,81; trouvé: C 90,6, H 5,30, N 3,86.

1. E. M. Abbot, A. J. Bellamy et J. B. Kerr. Chem. Ind. (London) 828 (1974).
2. A. J. Bellamy. J. Chem. Soc. Chem. Commun. 944 (1975).
3. Y. Takahashi, M. Tokuda, M. Itoh et A. Susuki. Chem. Lett. 523 (1975).
4. B. F. Becker et H. P. Fritz. Justus Liebigs Ann. Chem. 1015 (1976).

Can. J. Chem. Downloaded from www.nrcresearchpress.com by 210.87.254.105 on 09/06/12
For personal use only.

5. W. J. M. VAN TILBORG, C. J. SMIT et J. J. SCHEELE. Tetrahedron Lett. 2113 (1977).
6. A. J. BELLAMY, G. HOWAT et I. S. MAC KIRDY. J. Chem. Soc. Perkin Trans. 2, 786 (1978).
7. G. C. BARRETT et T. J. GRATTAN. Tetrahedron Lett. 4237 (1979).
8. L. KISTENBRÜGGER, P. MISCHKE, J. VOSS et G. WIEGAND. Justus Liebigs Ann. Chem. 461 (1980).
9. A. J. BELLAMY et I. S. MAC KIRDY. J. Chem. Soc. Perkin Trans. 2, 1093 (1981).
10. A. J. BELLAMY, J. B. KERR, C. J. MCGREGOR et I. S. MAC KIRDY. J. Chem. Soc. Perkin Trans. 2, 161 (1982).
11. E. M. ABBOT, A. J. BELLAMY, J. B. KERR et I. S. MAC KIRDY. J. Chem. Soc. Perkin Trans. 2, 425 (1982).
12. G. BELOT, C. DEGRAND et P. L. COMPAGNON. J. Org. Chem. **47**, 325 (1982).
13. K. G. BOTO et F. G. THOMAS. Aust. J. Chem. **26**, 1251 (1973).
14. C. DEGRAND, P. L. COMPAGNON et F. GASQUEZ. J. Org. Chem. **47**, 4586 (1982).
15. C. DEGRAND, P. L. COMPAGNON et F. GASQUEZ. J. Chem. Soc. Chem. Commun. 383 (1983).
16. (*a*) H. BAUER, C. MOERLER et D. REWICKI. Chem. Ber. **112**, 1473 (1979); (*b*) R. KUHN et D. REWICKI. Angew. Chem. **79**, 648 (1967); Ann. Chem. **706**, 250 (1967).
17. C. NUNTNARUMIT et M. D. HAWLEY. J. Electroanal. Chem. **133**, 57 (1982).
18. J. H. BARNES, F. M. TRIEBE et M. D. HAWLEY. J. Electroanal. Chem. **139**, 395 (1982).
19. K. J. BORHANI et M. D. HAWLEY. J. Electroanal. Chem. **101**, 407 (1979).
20. R. DIETZ et H. LUND. *Dans* Organic electrochemistry. *Edité par* M. M. BAIZER. Marcel Dekker, New York. 1973. Chap. 24. p. 831.
21. C. NUNTNARUMIT, F. M. TRIEBE et M. D. HAWLEY. J. Electroanal. Chem. **126**, 145 (1981).
22. H. LUND, H. DOUPEUX, M. A. MICHEL, G. MOUSSET et J. SIMONET. Electrochim. Acta, **19**, 629 (1974).
23. E. SANTIAGO et J. SIMONET. Electrochim. Acta, **20**, 853 (1975).
24. M. A. MICHEL, G. MOUSSET et J. SIMONET. Electrochim. Acta, **20**, 143 (1975).
25. P. CAUBERE. Acc. Chem. Res. **7**, 301 (1974) et références citées.
26. J. MOREAU et P. CAUBERE. Tetrahedron, **27**, 5741 (1971) et références citées.
27. F. G. BORDWELL et A. H. CLEMENS. J. Org. Chem. **46**, 1035 (1981).
28. J. SCHMIDT et R. MEZGER. Chem. Ber. **39**, 3895 (1906).
29. M. MASAKI et M. OHTA. Bull. Chem. Soc. Jpn. **34**, 1257 (1961).
30. A. J. HAILWOOD et R. ROBINSON. J. Chem. Soc. 1292 (1932).
31. F. G. BORDWELL et H. E. FRIED. J. Org. Chem. **46**, 4327 (1981).
32. F. G. BORDWELL, G. E. DRUCKER et H. E. FRIED. J. Org. Chem. **46**, 632 (1981).
33. M. NOVAK et T. C. BRUICE. J. Am. Chem. Soc. **99**, 8079 (1977).
34. W. N. OLMSTEAD, Z. MARGOLIN et F. G. BORDWELL. J. Org. Chem. **45**, 3295 (1980).
35. F. G. BORDWELL, D. ALGRIM et N. R. VANIER. J. Org. Chem. **42**, 1817 (1977).

Can. J. Chem. Downloaded from www.nrcresearchpress.com by 210.87.254.105 on 09/06/12
For personal use only.

Vibrations of the scissile C—O bond in an acyl-chymotrypsin observed by resonance Raman spectroscopy[1]

P. R. CAREY[2]

Division of Biological Sciences, National Research Council of Canada, Ottawa, Ont., Canada K1A 0R6

AND

D. J. PHELPS

Bristol Laboratories, P.O. Box 657, Syracuse, NY 13201, U.S.A.

Received May 16, 1983

P. R. CAREY and D. J. PHELPS. Can. J. Chem. **61**, 2590 (1983).

5-Methylthienylacryloyl chymotrypsin has been prepared with ^{13}C at the carbonyl and, separately, at the α carbon atoms of the acyl moiety. The isotopically labelled species confirm the assignments of several of the bands in the resonance Raman (RR) spectrum of the acyl-enzyme and show that the feature occurring near 1260 cm^{-1} involves the motion of the carbonyl carbon atom. It is likely that the 1260 cm^{-1} band is associated with the stretching vibration of the C—O bond in the =C—C(=O)—O— chymotrypsin moiety, i.e. the vibration of the bond being cleaved in the active site. A moderately intense 1260 cm^{-1} feature occurs only in the RR spectrum of the native acyl-enzyme and possible reasons are given for its appearance. The labelled species also confirm that the bands appearing near 1715 cm^{-1} in the RR spectrum of the acyl-enzyme are associated with the stretching mode of the acyl carbonyl, $\nu_{C=O}$. This frequency is that expected for an unperturbed α,β-unsaturated ester. Additionally, RR data are presented for 5-methylthienylacrylic acid in its —COOH and —COO^- forms labelled with ^{13}C at the C=O and α carbon positions.

P. R. CAREY et D. J. PHELPS. Can. J. Chem. **61**, 2590 (1983).

On a préparé la méthyl-5 thiénylacryloyl chymotrypsine avec un ^{13}C au niveau du carbonyl et séparément avec un ^{13}C au niveau des atomes de carbone en α du groupe acyle. Les espèces marquées confirment les attributions de plusieurs bandes qui apparaissent dans le spectre de résonance Raman (RR) de l'enzyme acylé et montrent que la particularité observé près de 1260 cm^{-1} implique le mouvement de l'atome de carbone du carbonyle. Il est probable que la bande à 1260 cm^{-1} est communément associée à la vibration d'élongation de la liaison C—O de l'unité =C—C(=O)—O— chymotropsine, c'est-à-dire de la vibration de la liaison qui se clive dans le site actif. Une caractéristique modérément intense à 1260 cm^{-1} apparaît uniquement dans le spectre de RR de l'enzyme acylé naturel et on donne les raisons possibles de son aspect. Les espèces marquées confirment également que les bandes qui apparaissent près de 1715 cm^{-1} dans le spectre de RR de l'enzyme acylé sont associées avec le mode d'élongation du carbonyle de l'acyle, $\nu_{C=O}$. Cette fréquence est celle attendue pour un ester α,β insaturé non perturbé. On présente de plus des données de RR pour l'acide méthyl-5 thiényl-acrylique dans ses formes —COOH et —COO^- marqués au ^{13}C au niveau du C=O et au niveau des carbones en α.

[Traduit par le journal]

Can. J. Chem. Downloaded from www.nrcresearchpress.com by 210.87.254.40 on 09/06/12
For personal use only.

Introduction

A detailed description of the chemical events occurring in an enzyme's active site during the catalytic process is a major goal of enzymological studies. Although no single technique can provide a complete picture of the process at the molecular level it is becoming increasingly apparent that resonance Raman (RR) spectroscopy is capable of delineating structural and conformational events in an enzyme-bound substrate (1, 2). The spectroscopic data obtained is a property of the vibrational motions of the molecules and since these are sensitive to effects, such as hydrogen bonding, the disposition of charges and dipoles and conformational strain, which are of interest in mechanistic analysis, the RR spectrum provides an ideal probe of the catalytic process (3). There are, moreover, two other factors which strengthen the RR approach. Firstly, joint Raman and X-ray crystallographic studies on single crystals of suitable model compounds permit us to set up precise spectra–structure correlations which go a long way towards eliminating the problems of spectral interpretation. Secondly, using multiplex detection (4) it is possible to obtain the RR data for the enzyme substrate complex in a short time span, which, of course, renders the technique suitable for the characterisation of transient species.

Due to the availability of suitable laser excitation wavelengths the first RR studies of enzyme–substrate complexes (5) utilised substrates which were derivatives of cinnamic acid esters and which gave rise to an electronic absorption band in the 450 nm region. As reliable laser sources became available in the 350 nm spectral range it was possible to extend the work to include substrates based on furylacryloyl and thienylacryloyl derivatives undergoing transformation by chymotrypsin (6, 7), papain (8), and glyceraldehyde-3-phosphate dehydrogenase (9). Some of the intermediates in these reactions have been the subject of pioneering studies principally by Bernhard and coworkers (10, and references therein). These workers characterised the intermediates by absorption spectroscopy and with the higher information content of RR spectroscopy it is now possible to build on and refine their findings.

The impetus for the present work came from two sources. In recent papers concerning some furylacryloyl- and thienylacryloyl chymotrypsins (6, 7) we observed a feature which occurred only in the RR spectra of the native acyl-enzymes. To investigate further the origins of this curious, and possibly important, band we have synthesised two ^{13}C substituted derivatives of 5-methylthienylacryloyl chymotrypsin. The second stimulus for synthesising the isotopically substituted derivatives relates to the absorption studies on substrates with extended π-electron system mentioned above. The absorption maximum, λ_{max}, of the enzyme-bound acyl group shows a characteristic red shift compared to λ_{max} of various model compounds (10). A possible explanation of the red shift seen for the

[1] NRCC No. 22511.

[2] To whom all correspondence should be addressed.

Can. J. Chem. Downloaded from www.nrcresearchpress.com by 210.87.254.40 on 09/06/12
For personal use only.

acyl group in an acyl chymotrypsin such as furylacryloyl chymotrypsin is that the ester group linking the acyl group to the enzyme moiety becomes ketone-like due to the alkoxy oxygen atom being forced out of the plane defined by the C=C—C=O atoms (10). Since the RR spectral signatures of $\nu_{C=O}$ from α,β-unsaturated esters and ketones are characteristic and different, we may use the RR spectrum to test the "ketone" hypothesis. Previously, we assigned bands near 1720 cm^{-1} in the RR spectra of the acyl enzymes to $\nu_{C=O}$ of an ester function (6) and now it is necessary to confirm this assignment by ^{13}C substitution to either support or refute the analysis based on the early absorption studies.

Experimental procedures

Synthesis

The ^{13}C-labelled substrates were synthesized in two steps from malonic acid-2 ^{13}C or malonic acid-1,3 $^{13}C_2$ (Merck, Sharp and Dohme) and 5-methyl-2-thiophenecarboxaldehyde (Aldrich) as reported by MacClement *et al.* (6). Products were crystallized and identified by comparison to authentic unlabelled samples.

Preparation of acyl-enzymes and Raman measurements

The acyl-enzymes were prepared and the RR spectra recorded in the manner described in MacClement *et al.* (6).

Results and discussion

The acyl-enzyme 5-methylthienylacryloyl chymotrypsin is formed by reacting an excess of the corresponding acylimidazole with the enzyme near neutral pH. After approximately half a minute the pH of the reaction mixture is reduced to 3.0 by adding 1 *N* HCl. At this pH the acyl-enzyme is completely stable and may be purified by dialysis or column chromatography (6). The pure stable acyl-enzyme is the subject of discussion here. The 350.7 nm excited RR spectra of the 5-methylthienylacryloyl chromophore, unlabelled and substituted in the C=^{13}C—C=O and C=C—^{13}C=O positions are shown in Figs. 1–3. The spectra in Fig. 1 are for the acyl-enzymes at pH 3.0, while the spectra in Figs. 2 and 3 are of the ionised and unionised acid derivatives, respectively. In every instance the solvent is water, with, in the case of the acids, a small amount of CH_3CN being present to aid solubility. Before proceeding to a discussion of the isotope shifts and related assignments in Figs. 1–3 it is necessary to briefly summarise the state of our knowledge regarding the conformations of thienylacryloyl-like molecules in solution and bound to the active site of chymotrypsin.

For the acids in solution it is likely that the thienylacryloyl skeleton is essentially planar and predominantly *s-trans* about the single bond linking the ring and the ethylenic double bond. However, the enthalpy difference of the *s-cis* and *s-trans* forms is probably <1 kcal/mol (11, 12) and it is likely that there are significant amounts of both forms in solution. Furthermore, the position of the proton in the —COOH group is another source of conformational heterogeneity. Therefore, the ethylenic stretch, $\nu_{C=C}$, probably contains unresolved components, with each component due to one of two or several rotamers and reflecting the spectral signature and population of that rotamer. In recognition of the composite nature of such features we call the measured value $\langle\nu_{C=C}\rangle$, the fences standing for weighted mean. Support for this concept comes from the spectrum of the =^{13}C—COOH molecule obtained at higher resolution (~4 cm^{-1} spectral slit) where the 1599 cm^{-1} band seen in Fig. 3 (bottom) could be partially resolved into two features (data not shown). For the unlabelled acyl-chymotrypsin the appearance of two features in the carbonyl stretching region between 1700 and 1725 cm^{-1} is taken as evidence for the presence of two conformational states for the enzyme-bound acyl group (6). This finding is consistent with kinetic (13) and nmr (14) studies on other acyl-chymotrypsins. In the RR spectrum the sharp feature occurring near 1725 cm^{-1} is assigned to a carbonyl in a hydrophobic environment and for which the acryloyl moiety is essentially planar and possibly *s-cis* about the =C—C=O single bond. The broader $\nu_{C=O}$ occurring near 1700 cm^{-1} in the RR spectrum is assigned to a strongly H-bonded carbonyl attached to an essentially planar acryloyl moiety which is *s-trans* about the =C—C=O single bond. Again, the intense ethylenic feature near 1612 cm^{-1} is made up of contributions from both conformers.

Isotope shifts and band assignments

In general, for either the acids or the acyl-chymotrypsin the effects of isotopic substitution are seen only in a few features. For the unionised acid, the band at 1617 cm^{-1} moves to 1610 and 1599 cm^{-1} in the =C—^{13}C=O and =^{13}C—C=O derivatives, respectively (Fig. 3). In the ionised acid the corresponding band shifts from 1627 cm^{-1} to 1625 and 1606.5 cm^{-1} (Fig. 2). For the acyl-enzyme, the intense band at 1612.5 cm^{-1} is unshifted in the =C—^{13}C=O derivative but moves to 1594.5 cm^{-1} in the =^{13}C—C=O compound (Fig. 1). In each case the results support the assignment of the intense band in the 1615 cm^{-1} region to $\langle\nu_{C=C}\rangle$. The shift of $\langle\nu_{C=C}\rangle$ by only ~20 cm^{-1} in the —C=^{13}C—C=O compounds is not unexpected for a conjugated ethylenic linkage and emphasises the fact that the —C=C— group cannot be regarded as a simple diatomic oscillator. The differences in position of $\langle\nu_{C=C}\rangle$ for the acids and the acyl-enzyme can be understood in terms of the electron polarisation theory (3, 15). According to this theory, the RR and absorption spectral properties are explained by changes in the distribution of the electrons in the chromophore's extended π-electron chain. The changes may be caused intramolecularly by factors such as the addition of electron donating or accepting groups, or caused intermolecularly by, for example, protein H-bonds or charges when the chromophore is enzyme bound.

The ^{13}C derivatives also confirm the assignment of the weak bands near 1700 cm^{-1} to $\nu_{C=O}$. The broad band near 1680 cm^{-1} in the unlabelled and ^{13}C=C—COOH form of the acid is not resolved in the —^{13}COOH derivative (Fig. 3, although it may appear as a shoulder on the 1610 cm^{-1} feature) and thus the 1680 cm^{-1} feature is assigned to $\nu_{C=O}$ for the —COOH acid, which is broadened by hydrogen bonding to solvent. For the —COO^- acid the band at 1342.5 cm^{-1}, which appears to shift to 1323 and 1339 cm^{-1} in the =C—$^{13}COO^-$ and =^{13}C—COO^- molecules, respectively (Fig. 2), is assigned to the symmetric stretching motion of the —COO^- moiety. For the acyl-chymotrypsin the ^{13}C results confirm the important assignment of the profile centred about 1710 cm^{-1} to $\nu_{C=O}$ modes (6). In the case of the =C—^{13}C=O derivative, both the broad band at 1700 cm^{-1} and the sharper feature at 1725 cm^{-1} shift to lower wavenumbers, while for the =^{13}C—C=O derivative the 1710 cm^{-1} region appears to be unchanged (Fig. 1). The normal mode origins of the bands seen in the unlabelled —COO^- molecule at 1428 and 1546 cm^{-1}, and which are sensitive to isotopic substitution are not understood. However, the isotopic substitutions do cast light on the nature of the band appearing near 1260 cm^{-1} in the acyl-enzyme. This feature is unusual in that it appears only in the native 5-methyl-

Can. J. Chem. Downloaded from www.nrcresearchpress.com by 210.87.254.40 on 09/06/12
For personal use only.

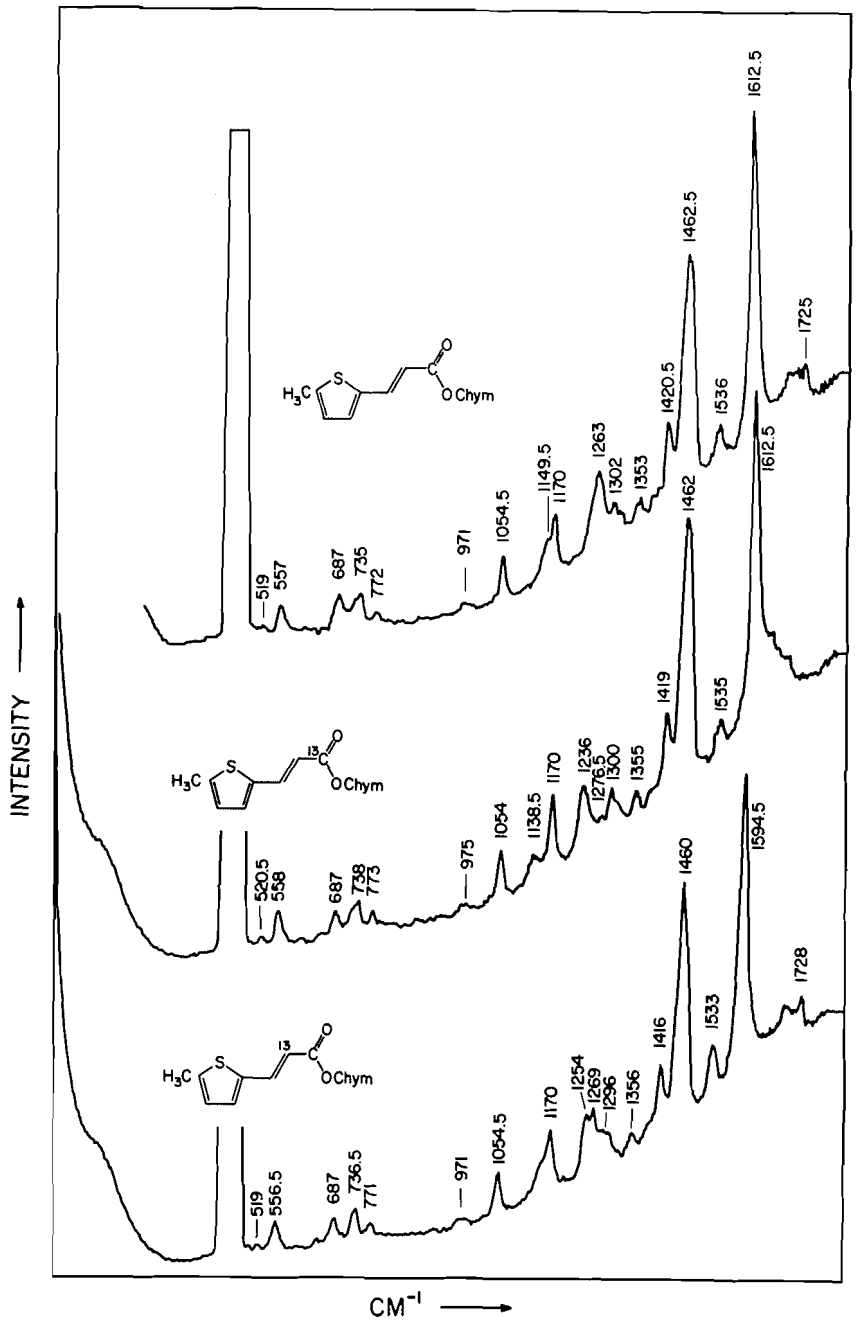

FIG. 1. Resonance Raman spectra of unlabelled and ^{13}C substituted 5-methylthienylacryloyl chymotrypsin. Enzyme ~4×10^{-4} M, approximately 75% acylated. Laser excitation ~100 mW, 350.7 nm; 8 cm^{-1} spectral slit.

thienylacryloyl chymotrypsin. A band of comparable intensity is absent in the SDS denatured complex (6) and in the RR spectra of any of the other 5-methylthienylacryloyl derivatives examined. Substitution in the $=^{13}C-C=O$ position seems to have little effect on the 1260 cm^{-1} mode (Fig. 1) but upon substitution in the $=C-^{13}C=O$ position the band shifts to 1236 cm^{-1}. At the same time the shoulder at 1149.5 cm^{-1} is unshifted in the $=^{13}C-C=O$ form but moves to 1138.5 cm^{-1} in the $=C-^{13}C=O$ derivative (Fig. 1). It is believed that both the 1260 and 1150 cm^{-1} features are associated with C—O stretching motions. The infrared studies of Thompson and coworkers (16) drew attention to two fairly intense bands in the 1000–1200 cm^{-1} range which are associated with the C—O and O—C bonds. Later investigations (17) found that α,β-unsaturated esters show two strong IR bands in the 1300–1100 cm^{-1} region. These findings, taken with the present ^{13}C substitutions, strongly favour the assignment of the 1260 and 1150 cm^{-1} bands to motions involving the C—O atoms. The large shift of the 1260 cm^{-1} peak, in particular, upon $=C-^{13}C=O$ substitution suggests a major contribution of the C—O stretching motion to this feature.

Consequences for the structure of the enzyme-bound acyl group

For the acyl-enzyme, the results of ^{13}C substitution presented here confirm the assignments made earlier (6) of the intense RR band at 1612.5 cm^{-1} and the profile around 1710 cm^{-1} to modes associated with the C=C and C=O moieties (Fig. 1), respectively. There does not appear to be extensive vibrational coupling between the two, since substitution at $=C-^{13}C=O$ does not perturb $\langle \nu_{C=C} \rangle$ and substitution at $=^{13}C-C=O$ does

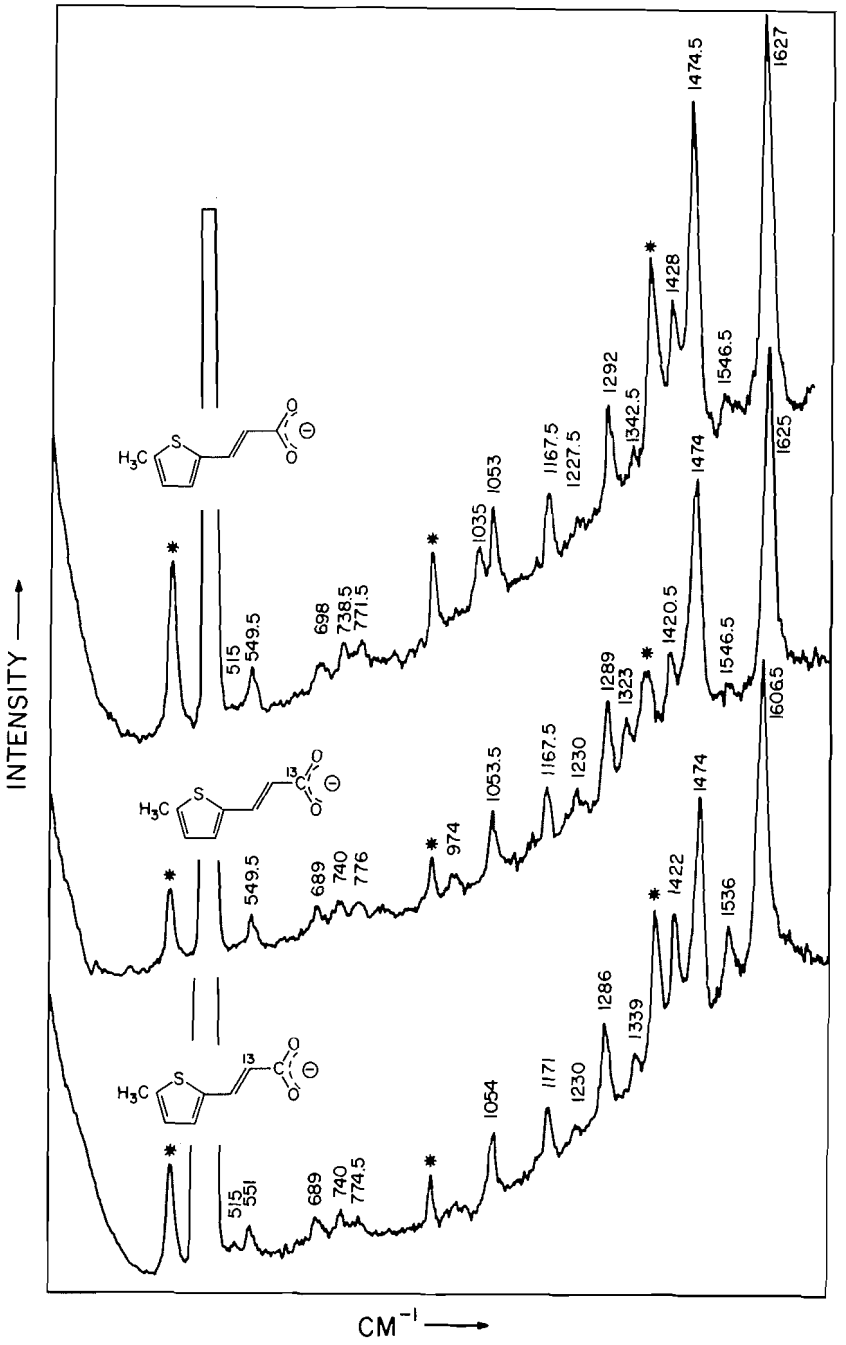

FIG. 2. Resonance Raman spectra of $\sim 2 \times 10^{-4}$ *M* unlabelled and ^{13}C substituted 5-methylthienylacrylic acid near neutral pH and thus in the ionised form. Approximately 15% of CH_3CN is present to aid solubility, CH_3CN peaks marked with an asterisk. Laser excitation ~100 mW, 350.7 nm; 8 cm^{-1} spectral slit.

not perturb the $\nu_{C=O}$ profile. Thus, the model given earlier (6) for the bound acyl group still holds. There are two conformers in the active site, neither of which is grossly distorted from planarity. One form has strong, sterically well-defined hydrogen bonds to the carbonyl and is *s-trans* about the =C—C=O single bond, while the second conformer probably binds *s-cis* about this linkage and has its carbonyl in a hydrophobic non-hydrogen bonding environment. The presence of the first conformer is consistent with crystallographic (18) and chemical evidence (19) for the formation of a strong hydrogen bond to the ester carbonyl.

Confirmation by the present studies of the $\nu_{C=O}$ assignments enables us to eliminate certain mechanisms which have been proposed to account for the absorption spectral properties of acyl-enzymes such as cinnamoyl- and furylacryloyl-chymotrypsins (10). In one of these mechanisms, the alkoxy oxygen atom (contributed by Ser-195) of the acyl-enzyme is brought out of the plane of the —C=C—C=O group. The resulting loss of conjugation renders the carbonyl aldehyde- or ketone-like and Bernhard and co-workers (10) have noted the striking similarity between the absorption spectra of the chromophoric acyl-enzymes and their corresponding aldehydes and ketones. However, $\nu_{C=O}$ for α,β-unsaturated ketones or aldehydes occurs near 1680 cm^{-1} (e.g. at 1679 cm^{-1} in the RR spectrum of 3-(2-furyl)acrolein in CH_3CN, unpublished work from this laboratory). The 1700 and 1725 cm^{-1} $\nu_{C=O}$ features

Can. J. Chem. Downloaded from www.nrcresearchpress.com by 210.87.254.40 on 09/06/12
For personal use only.

Can. J. Chem. Downloaded from www.nrcresearchpress.com by 210.87.254.40 on 09/06/12
For personal use only.

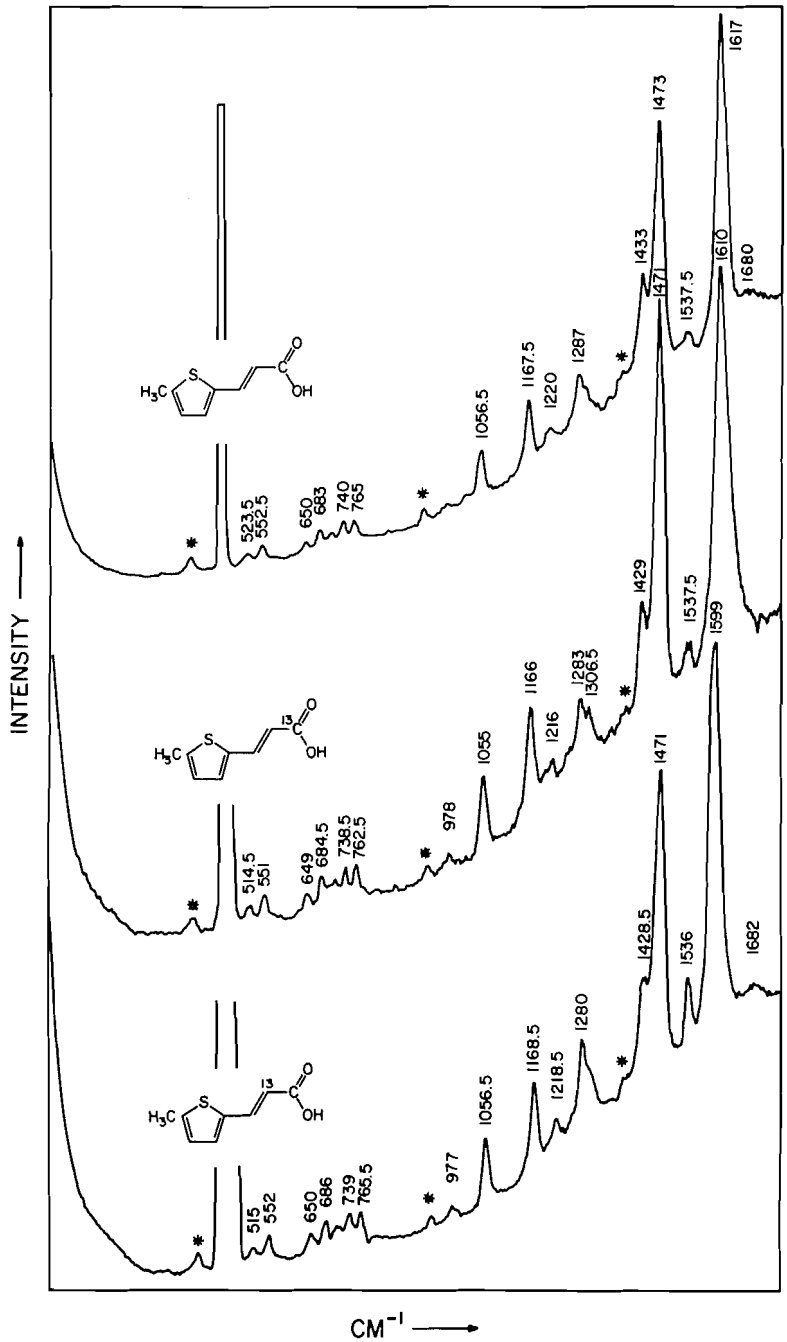

FIG. 3. Resonance Raman spectra of $\sim 2 \times 10^{-4}$ *M* unlabelled and ^{13}C substituted 5-methylthienylacrylic acid in the —COOH form, pH ~2.5. Approximately 5% of CH_3CN is present to aid solubility, CH_3CN peaks marked with an asterisk. Laser excitation ~100 mW, 350.7 nm; 8 cm^{-1} spectral slit.

seen for the acyl-enzymes are characteristic of α,β-unsaturated esters. Indeed, a $\nu_{C=O}$ feature is seen near 1720 cm^{-1} for the esters of 5-methyl- and 5-ethyl furylacrylic acid in CCl_4 (6). The observation of the $\nu_{C=O}$'s near 1715 cm^{-1} also rules out the possibility that the carbonyl group has become protonated. The cause of the spectral red shift seen in chromophoric acyl-chymotrypsins has been discussed in detail before (3, 6, 15). The red shift is due to the polarisation of the π electrons throughout the entire π-electron chain. In turn, the polarisation is caused by one or more of a number of possible effects such as well-defined hydrogen bonding to the ester C=O group, the conformation about the =C—C=O single bond and local protein dipoles (6). The correspondence between the absorption maxima of an acyl-enzyme and its aldehyde or ketone analog is, in all likelihood, coincidental.

The assignment of the 1260 cm^{-1} band in the RR spectrum of the acyl-enzyme (Fig. 1) raises several interesting questions. The mode involves the carbonyl carbon atom and is probably ascribable, in part, to the stretching motion of the C—O single bond. Since this is the bond being cleaved during the hydrolysis of the acyl-enzyme, it might be expected to offer insight into the special chemical nature, if any, of this linkage in the enzyme's active site. However, the appearance of the 1260 cm^{-1} band appears to be related to subtle stereochemical factors which are not correlated with chemical reactivity. The important observations regarding the 1260 cm^{-1} feature are as

Can. J. Chem. Downloaded from www.nrcresearchpress.com by 210.87.254.40 on 09/06/12
For personal use only.

follows: (*1*), it is observed for only certain furylacryloyl- or thienylacryloyl-based acyl-enzymes (6); (*2*), there appears to be no correlation between the appearance of the 1260 cm^{-1} band and the appearance of the $\nu_{C=O}$ profile or the deacylation rate (6, 7); (*3*), a band of comparable intensity has not been observed in the RR spectra of any model compounds or the SDS denatured acyl-enzymes; (*4*), it is unaffected by raising pH and forming the catalytically active acyl-enzyme (7); and (*5*), it is unchanged in D_2O solvent compared to H_2O.

In connection with (*3*) above we have examined the 647.1 nm excited Raman spectra of the methyl esters of furylacrylic acid and its 5-methyl- and 5-ethyl-derivatives in CH_3CN solution and as solids. The rationale for these experiments was to search for a Raman mode which occurs in the 1200 cm^{-1} region in the spectra of the solid forms but which might appear with reduced intensity or disappear altogether in the solvated species. The appearance in the solid would then have been ascribed to the formation of a single "locked" conformation, and its disappearance in solution to the formation of a population of rotamers and their non-planar, torsionally excited states. However, for the three esters studied, the Raman spectra of the solution and solid forms appeared to be identical in the 1000–1350 cm^{-1} region. In an additional experiment, we synthesised and examined the RR spectra of the ethyl ester of 5-methylthienylacrylic acid. This was to investigate the effect on the RR spectrum of attaching a C—C moiety to the alkoxy atom and thereby producing a heavy atom skeleton more closely resembling that seen in the acyl-serine moiety. The ethyl ester was examined in H_2O (containing 5% CH_3CN) and in CCl_4 with 324 and 350.6 nm excitation. In CCl_4 solution a band was detected at 1269 cm^{-1} but it was of low relative intensity; it could not be associated with reasonable probability with the 1260 cm^{-1} band seen in the RR spectrum of the native acyl-enzyme.

Taking these data together it seems that the appearance of the 1260 cm^{-1} C—O stretch in the RR spectrum of a thienyl- or furylacryloyl based acyl-enzyme occurs by chance. It probably relies on the active site of the enzyme selecting out a particular, but presently unknown, conformation about the ester bonds. This selection is determined, in turn, by enzyme contacts about the furyl or thienyl ring and, given the variation among the substituted rings, the process must be subtle. Additionally, the 1260 cm^{-1} feature may require the process of electron polarisation producing, within the selected conformer, a higher degree of RR intensity enhancement for modes associated with the C—O linkage. Acyl groups such as thienylacryloyl and furylacryloyl are, of course, quite far removed from natural, specific substrates. The former do provide good probes for the physical forces operating in the active site and one can obtain detailed data on the structure of the non-specific acyl group bound to the active site. But facts such that 5-methylthienylacryloyl chymotrypsin gives a fairly intense 1260 cm^{-1} band, whereas the 5-methylfurylacryloyl analog does not, suggest that considerable care must be exercised in drawing conclusions on the catalytic mechanisms for specific substrates from the spectroscopic results on non-specific substrates. This situation is not without its positive aspects, since, by using non-specific substrates, we may be able to probe key processes which would not be observable using specific substrates. For example, the phenomenon of electron polarisation is now well established for non-specific substrates with delocalised π-electron systems (3, 5–9, 15). We may speculate that the forces that give rise to these effects in the ground state of the non-specific acyl-enzymes would not be observed at all for the specific intermediates. Instead, for the latter, precise stereochemical factors might ensure that the electrical forces are used solely in the transition state to stabilise the build up of charge (20).

Acknowledgement

The authors are grateful to Mr. R. G. Carriere for his help in obtaining the RR spectra.

1. Y. Ozaki, D. H. Pliura, P. R. Carey, and A. C. Storer. Biochemistry, **21**, 3102 (1982).
2. C. P. Huber, Y. Ozaki, D. H. Pliura, A. C. Storer, and P. R. Carey. Biochemistry, **21**, 3109 (1982).
3. P. R. Carey. Biochemical applications of Raman and resonance Raman spectroscopies. Academic Press, New York. 1982. Chapt. 6.
4. (*a*) M. Bridoux and M. Delhaye. Adv. Infrared Raman Spectrosc. **2**, 140 (1976); (*b*) P. R. Carey and L. R. Sans Cartier. J. Raman Spectrosc. In press.
5. P. R. Carey and H. Schneider. Acc. Chem. Res. **11**, 122 (1978).
6. B. A. E. MacClement, R. G. Carriere, D. J. Phelps, and P. R. Carey. Biochemistry, **20**, 3438 (1981).
7. D. J. Phelps, H. Schneider, and P. R. Carey. Biochemistry, **20**, 3447 (1981).
8. P. R. Carey, R. G. Carriere, D. J. Phelps, and H. Schneider. Biochemistry, **17**, 1081 (1978).
9. A. C. Storer, D. J. Phelps, and P. R. Carey. Biochemistry, **20**, 3454 (1981).
10. S. A. Bernhard and S.-J. Lau. Cold Spring Harbor Symp. Quant. Biol. **36**, 75 (1972).
11. A. J. Bowles, W. O. George and D. B. Cunliffe-Jones. J. Chem. Soc. B, 1070 (1970).
12. W. J. E. Parr, R. E. Wasylishen, and T. Schaeffer. Can. J. Chem. **54**, 3216 (1976).
13. J. E. Baggott and M. H. Klapper. Biochemistry, **15**, 1473 (1976).
14. M. L. Maddox, D. C. Roe, and J. T. Gerig. J. Chem. Soc. Chem. Commun. 902 (1975).
15. P. R. Carey. Can. J. Spectrosc. **26**, 134 (1981).
16. H. W. Thompson and P. Torkington. J. Chem. Soc. 640 (1945). R. A. Russell and H. W. Thompson. J. Chem. Soc. 479 (1955).
17. L. J. Bellamy. The infrared spectra of complex molecules. Vol. 1. 3rd Ed. Chapman and Hall. 1975. p. 215.
18. R. Henderson. J. Mol. Biol. **54**, 341 (1970).
19. S. A. Bernhard, E. Herschberger, and J. Keizer. Biochemistry, **5**, 4120 (1966).
20. A. Warshel. Acc. Chem. Res. **14**, 284 (1981).

Ab initio molecular orbital studies on thiirene and its isomeric structures

RATNAKAR K. GOSAVI AND OTTO P. STRAUSZ
Department of Chemistry, University of Alberta, Edmonton, Alta., Canada T6G 2G2

Received March 3, 1983

This article is dedicated to Professor Harry E. Gunning on the occasion of his 65th birthday

RATNAKAR K. GOSAVI and OTTO P. STRAUSZ. Can. J. Chem. **61**, 2596 (1983).

Ab initio molecular orbital calculations have been carried out on the lowest closed shell singlet states of six isomeric forms of C_2H_2S at the SCF and CI levels using STO-3G and 6-31G* basis sets. Molecular geometries of the isomers and the activated complexes for their isomerization reactions were optimized by the energy gradient method at the SCF level and the CI calculations were performed at these geometries. In addition, the lowest singlet and triplet states of the ·SCHĊH diradical were also studied and their geometries optimized by the Restricted Hartree Fock method.

The computed stabilities follow the order

$$H_2C{=}C{=}S\ (S_0) > HC{\equiv}CSH\ (S_0) > \text{ 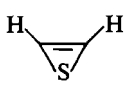 }\ (S_0) > \cdot SCH\dot{C}H\ (T_0) \approx \cdot SCH\dot{C}H\ (S_1) > \text{}\ (S_0) >$$

$$\text{ 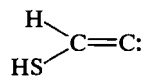 }\ (S_0) > H\ddot{C}{-}\text{ 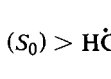 }\ (S_2)$$

The pseudo antiaromatic character of the 4n-π electron thiirene is manifested by its drastically reduced C—S bond energy, ~15 kcal mol^{-1} as compared to the value of >40 kcal mol^{-1} estimated for its 2n-π electron analog, thiirane. This explains why thiirenes can be stabilized in inert matrices at 8 K but decompose readily at higher temperatures. In agreement with experimental results the lowest energy path for the unimolecular decomposition of thiirene leads to thioketene via the lowest singlet (or triplet) state of thioformylmethylene.

The ir frequencies calculated for thiirene from *ab initio* mo theory using 6-31G + polarization functions on the sulfur show reasonably good agreement with the experimental frequencies, confirming the earlier assignments of the ir spectrum of thiirene.

RATNAKAR K. GOSAVI et OTTO P. STRAUSZ. Can. J. Chem. **61**, 2596 (1983).

On a effectué des calculs *ab initio* d'orbitales moléculaires sur l'état singulet ayant la couche électronique complète de plus bas niveau d'énergie de six formes isomères du C_2H_2S aux niveaux SCF et CI en utilisant les ensembles de bases STO-3G et 6-31G*. On a optimisé les géométries moléculaires des isomères et des complèxes activés de leurs réactions d'isomérisation, en utilisant la méthode de gradient d'énergie au niveau SCF et on a effectué les calculs de CI sur ces géométries. De plus on a étudié les états singulets et triplets de plus bas niveau d'énergie de diradical ·SCHĊH et on a optimisé leurs géométries par le méthode restreinte de Hartree–Fock.

Les stabilités calculées sont dans l'ordre suivant:

$$H_2C{=}C{=}S\ (S_0) > HC{\equiv}CSH\ (S_0) > \text{ 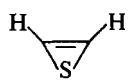 }\ (S_0) > \cdot SCH\dot{C}H\ (T_0) \approx \cdot SCH\dot{C}H\ (S_1) > \text{}\ (S_0) >$$

$$\text{ 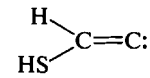 }\ (S_0) > H\ddot{C}{-}\text{ 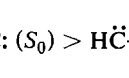 }\ (S_2)$$

Le caractère pseudo antiaromatique de l'électron 4n-π du thiirène se manifeste par la réduction drastique de son énergie de liaison C—S de ≃ 15 kcal mol^{-1} telle que comparée à la valeur supérieure à 40 kcal mol^{-1} évaluée pour l'électron 2n-π analogue du thiirane. Ceci explique pourquoi on peut stabiliser les thiirènes dans des matrices inertes à 8 K mais ils se décomposent rapidement à des températures plus élevées. En accord avec les résultats expérimentaux, la voie de plus faible énergie pour la décomposition unimoléculaire du thiirène conduit au thiocétène via l'état singulet (ou triplet) le plus bas du thioformylène.

Les fréquences ir calculées pour le thiirène à partir de la théorie *ab initio* des OM utilisant la base 6-31G + les fonctions de polarisation du soufre montrent un accord raisonnablement bon avec les fréquences expérimentales confirmant ainsi les attributions antérieures du spectre ir du thiirène.

[Traduit par le journal]

Introduction

The intervention of thiirene, **1**, as a reactive intermediate in a reaction mechanism was first suggested for the $S(^1D_2) + C_2H_2$ system and the photochemical decomposition of 1,2,3-thiadiazole, **2**, in 1967 (1) and since then a series of thiirenes, including the parent compound, have been isolated and characterized in the low temperature argon-matrix photolysis of **2** and its derivatives (2, 3), and of vinylene trithiocarbonate (4). In the Pyrex filter photolysis of **2** only two principal products, the thioketene, **3**, and the ethynylthiol, **4**, have been isolated and identified by ir spectroscopy (2). Isotopic labelling studies, however, indicated that ethynylthiol was formed mainly via the intermediacy of thiirene (2). In the λ = 215 or 265 nm photolysis, however, in addition to **3** and **4** another product appeared which was identified by ir spectroscopy as being the thiirene (2, 3). On further photolysis of

Can. J. Chem. Downloaded from www.nrcresearchpress.com by 210.87.254.105 on 09/06/12
For personal use only.

Can. J. Chem. Downloaded from www.nrcresearchpress.com by 210.87.254.105 on 09/06/12
For personal use only.

the photolyzate with λ = 330–370 nm light, thiirene could readily be converted to **3** and **4**. Spectral assignments of the vibrational frequencies of **1** have been made (5–8) and several substituted thiirenes have subsequently been synthesized (2–4, 9, 10).

Of the six valence isomers of formula C_2H_2S, all of which may be implicated in the photodecomposition sequence of 1,2,3-thiadiazole, three (**1**, **3**, **4**) have bond order of six and the other three (**5**–**7**) five:

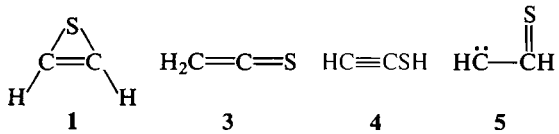

1 **3** **4** **5**

6 **7**

Of these, only the molecular species thiirene, **1**, thioketene, **3**, and ethynylthiol, **4**, have been isolated to date. *Ab initio* molecular orbital calculations on the relative stabilities of these isomers at the SCF level using the STO-4G basis set predicted the following order and energy separations (kcal mol^{-1}) (10, 11) for the lowest singlet state:

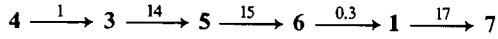

In the photolysis of 1,2,3-thiadiazole, **2**, thioformylmethylene, **5**, is generated, probably in a higher excited singlet state:

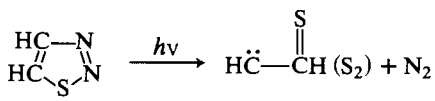

2 **5**

and undergoes rapid internal conversion to give the vibrationally excited S_1 state.

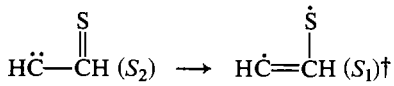

Earlier theoretical calculations also predicted a triplet ground state for **5** with a small T_0–S_1 energy separation of the order of −9 kcal mol^{-1} (11). The isolation of thioformylmethylene has not been achieved to date, but its diphenyl derivative, thiobenzoylphenylmethylene, has recently been isolated in the low temperature photolysis of 4,5-diphenyl-1,2,3-thiadiazole and identified by esr spectroscopy (12).

On the basis of experimental observations and in analogy with the well documented Wolff rearrangement of ketocarbenes (10, 13–15) the subsequent reactions of the vibrationally hot S_1 state **5** would be:

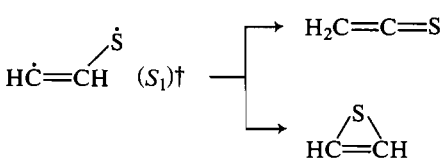

Photolysis of ^2H and ^{13}C labelled **2** affords completely randomized ethynylthiol, but the bulk (~80%) of the thioketene retains the original skeleton of the precursor (2). This requires the intermediacy in the conversion of thiirene to ethynylthiol of some structure(s) which features complete carbon and hydrogen equivalences. For this, thiiranylidine, **6**, (16) and the zwitter ion (9, 10)

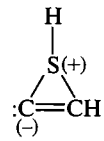

have been considered.

In order to get a better understanding of the thermodynamic stabilities of the C_2H_2S isomers and their interconnecting reaction surfaces we have carried out a more detailed molecular orbital computational study of these systems.

Method

It is known that SCF geometry predictions using split valence or double ζ basis sets for molecules containing H, C, N, and O usually yield bond lengths within ~0.02 Å and bond angles within 2° of the experimental values (17); however, for molecules containing heavier atoms such as S, little is known concerning the effects of the basis set size on SCF structural predictions (18–21).

Therefore, for comparison purposes, we carried out SCF geometry optimizations of the ground state singlet using STO-3G (for S, ref. 22*a*; for C and H, ref. 22*b*), STO-3G* (18), 6-31G (21)[1], and 6-31G* basis sets for the molecules: hydrogen sulfide, methanethiol, thiirane, thioformaldehyde, and thioketene, for which the experimental geometries are known (23–25).

On the basis of these results, we then reoptimized the geometries of all six C_2H_2S isomers at the SCF level and studied the reaction paths for their interconversions at the CI level to include the correlation energy.

All the molecular calculations were performed with the MONSTERGAUSS Program (26). Five 3*d* polarization functions (on S, α = 0.5874) for the 6-31G* basis set were optimized for the thioketene molecule at the experimental geometry (25) using the Davidon (27, 28) method, and used in all the subsequent 6-31G* calculations. All geometries were fully optimized at the SCF level by the energy gradient method (29, 30). STO-3G, STO-3G*, 6-31G, and 6-31G* basis sets were used for the geometry optimization of the six C_2H_2S isomers. Reaction path transition states were optimized with STO-3G and 6-31G* basis sets using the VAO5AD optimization method (31). Configuration interaction calculations include all singly and doubly excited configurations (CISD) with respect to the closed shell SCF configuration, and were done using the direct CI method (32) at the SCF level optimized geometry. Davidson's formula (33) was applied to the CI results to estimate the correction for the quadruple excitations (CISDQ). The lowest seven orbitals, corresponding to carbon 1*s* and sulfur 1*s*, 2*s*, 2*p* core orbitals, were kept doubly occupied and frozen, and the top ten virtual orbitals in the 6-31G* basis set calculations were kept frozen in the CI calculations. All calculations were carried out on an AMDAHL 470 V/7 computer at the University of Alberta.

[1] For S, ref. 21*a*; for C, ref. 21*b*; for H, ref. 21*c*.

Can. J. Chem. Downloaded from www.nrcresearchpress.com by 210.87.254.105 on 09/06/12
For personal use only.

TABLE 1. Effect of basis set size on the singlet ground state optimized molecular geometry of H_2S, CH_3SH, C_2H_4S, CH_2S, and H_2C_2S

Parameter	Value				
	STO-3G	STO-3G*	6-31G	6-31G*	Experimental[a]
$H_2S(^1A_1)$					
R(S—H) Å	1.3287	1.3182	1.3541	1.3297	1.328
∠HSH	92.53°	91.72°	96.12°	94.23°	92.2°
E (hartree)	−394.311630	−394.344435	−398.628512	−398.667701	
$H_3C—SH(^1A')$					
R(C—S) Å	1.7991	1.7839	1.8821	1.8252	1.819
R(C—H) Å	1.0861	1.0885	1.0772	1.0795	1.091
R(S—H) Å	1.3304	1.3197	1.3552	1.3295	1.336
∠HCH	107.94°	107.79°	110.14°	109.15°	109.8°
∠CSH	94.92°	94.48°	97.71°	97.11°	96.5°
E (hartree)	−432.895798	−432.929478	−437.648146	−437.683675	
$C_2H_4S(^1A_1)$					
R(C—C) Å	1.5070	1.5161	1.4592	1.4815	1.492
R(C—S) Å	1.7737	1.7442	1.9167	1.8226	1.819
R(C—H) Å	1.0833	1.0856	1.0703	1.0718	1.078
∠HCH	112.78°	112.49°	115.34°	114.40°	116.00°
Out-of-plane ∠HCHC	146.80°	145.43°	155.28°	151.32°	151.70°
E (hartree)	−470.276760	−470.318291	−475.479015	−475.509110	
$H_2C{=}S(^1A_1)$					
R(C—S) Å	1.5740	1.5514	1.6439	1.6048	1.6108[b]
R(C—H) Å	1.0900	1.0931	1.0734	1.0756	1.0925
∠HCH	112.00°	111.68°	116.40°	115.60°	116.87°
E (hartree)	−431.671367	−431.708746	−436.458079	−436.489588	
$H_2C{=}C{=}S(^1A_1)$					
R(C—C) Å	1.2953	1.3010	1.2945	1.2998	1.314[c]
R(C—S) Å	1.5370	1.5115	1.6082	1.5620	1.554
R(C—H) Å	1.0801	1.0785	1.0730	1.0726	1.090
∠HCH	117.03°	117.27°	118.40°	118.32°	120.3°
E (hartree)	−469.047855	−469.088727	−474.290769	−474.326113	

[a] Reference 23.
[b] Reference 24.
[c] Reference 25.

Results

The optimized and experimental geometries of the model molecules H_2S, CH_3SH, C_2H_4S, CH_2S, and C_2H_2S are summarized in Table 1. For the five molecules the geometries optimized by the minimal STO-3G basis set are in better agreement with the experimental values than the significantly extended (s,p) basis set (6-31G). Addition of polarization functions ($3d$) on the sulfur atom to the extended 6-31G basis (6-31G*) improved the geometry and the optimized geometries are in very good agreement with the experimental values.

For the C_2H_2S isomers the optimized geometries and total SCF energies with STO-3G, STO-3G*, 6-31G, and 6-31G* basis sets are summarized in Table 2. CI calculations were performed at the optimized geometries with STO-3G and 6-31G* basis sets and the total energies for the lowest closed shell singlet states are tabulated in Table 3, while the relative energies with respect to thioketene are given in Table 4.

Experimental values of the geometrical parameters are known only for thioketene (25) and the optimized values of the STO-3G and 6-31G* basis sets are in good agreement. The C—S bond distance in thiirene (1.812 Å, STO-3G and 1.861 Å, 6-31G*) appears to be reasonable, in comparison with the experimental value of the C—S bond distance in thiirane (1.819 Å) (23). The C=C distance (1.266 Å) is similar to the experimental value of 1.300 Å for cyclopropene (23) and the calculated values for oxirene (1.270 Å) (14) and 2-azirine (1.265 Å) (34). The effect of polarization functions and correlation energy on the relative energies varies with structure. Inclusion of polarization functions decreases the relative energies for all the isomers with the exception of thioformylmethylene and thiirene (Fig. 1). The inclusion of correlation energy increases the relative energies of thioformylmethylene and thiovinylidene, and decreases them in thiirene and ethynylthiol (Fig. 1).

The present results (Table 4) predict thioketene **3** to be the most stable C_2H_2S isomer, closely followed (7.8 kcal mol^{-1}) by ethynylthiol **4**. Thiirene **1** is 35.1 kcal mol^{-1} higher in energy than thioketene. All three carbenoid structures **5**, **6**, **7**, have higher energies than the molecular species **1**, **3**, **4**. Of the three carbenes thioformylmethylene **5** is the least stable and the cyclic thiiranylidene **6** is the most stable.

Thioformylmethylene lies 31.6 kcal mol^{-1} higher in energy than thiirene.

TABLE 2. Optimized geometries of the six C_2H_2S isomers

Parameter	Value			
	STO-3G	STO-3G*	6-31G	6-31G*
Thiirene ($^1A_1$)				
R(C—C) Å	1.2668	1.2775	1.2537	1.2662
R(C—S) Å	1.8119	1.7717	1.9725	1.8605
R(C—H) Å	1.0761	1.0781	1.0579	1.0599
∠HCC	149.31°	147.68°	155.41°	152.20°
E_{SCF} (hartree)	−468.996100	−469.043589	−474.232240	−474.260050
Thioketene ($^1A_1$)				
R(C—C) Å	1.2953	1.3010	1.2945	1.2998 (1.314)[a]
R(C—S) Å	1.5370	1.5115	1.6082	1.5620 (1.554)
R(C—H) Å	1.0801	1.0785	1.0730	1.0726 (1.090)
∠HCH	117.03°	117.27°	118.40°	118.32° (120.3°)
E_{SCF} (hartree)	−469.047855	−469.088727	−474.290769	−474.326113
Ethynylthiol ($^1A'$)				
R(C—C) Å	1.1717	1.1753	1.1943	1.1963
R(C—S) Å	1.7177	1.6947	1.7589	1.7050
R(C—H) Å	1.0641	1.0639	1.0498	1.0531
R(S—H) Å	1.3348	1.3235	1.3550	1.3299
∠CCH	180.00°	180.00°	179.59°	180.30°
∠CCS	177.97°	177.34°	176.38°	176.70°
∠HSC	95.26°	95.12°	97.68°	97.36°
E_{SCF} (hartree)	−469.044954	−469.084640	−474.258932	−474.302137
Thioformylmethylene (^1A)				
$R(C_1—C_3)$ Å	1.4793	1.4950	1.3355	1.3592
$R(C_1—S_2)$ Å	1.5893	1.5618	1.7413	1.6753
$R(C_1—H_4)$ Å	1.0983	1.1010	1.0796	1.0781
$R(C_3—H_5)$ Å	1.1212	1.1222	1.0737	1.0765
$\angle C_3C_1S_2$	127.39°	127.00°	122.40°	117.11°
$\angle C_3C_1H_4$	108.99°	109.05°	117.40°	119.98°
$\angle C_1C_3H_5$	107.75°	106.42°	132.99°	129.19°
Out-of-plane				
$\angle S_2C_3C_1H_4$	174.59°	175.42°	174.94°	174.31°
$\angle S_2C_1C_3H_5$ (*trans* to H_4)	93.22°	92.82°	89.72°	83.84°
E_{SCF} (hartree)	−468.932935	−468.968463	−474.200479	−474.223862
Thiiranylidene ($^1A'$)				
$R(C_1—C_3)$ Å	1.5302	1.5529	1.4547	1.4925
$R(C_1—S_2)$ Å	1.7696	1.7291	1.9130	1.8137
$R(C_3—S_2)$ Å	1.7333	1.6658	1.8622	1.7348
$R(C_1—H)$ Å	1.0845	1.0866	1.0730	1.0734
$\angle C_3C_1S_2$	62.88°	60.72°	65.50°	62.41°
$\angle C_1C_3S_2$	65.33°	64.88°	69.20°	67.91°
$\angle HC_1H$	112.62°	112.64°	115.02°	114.32°
Out-of-plane				
$\angle HHC_1C_3$	147.29°	147.07°	152.34°	150.23°
E_{SCF} (hartree)	−468.996701	−469.052019	−474.197589	−474.236624
Thiolvinylidene (^1A)				
$R(C_1—C_3)$ Å	1.2907	1.3034	1.3045	1.3064
$R(C_1—S_2)$ Å	1.8011	1.7408	1.8403	1.7882
$R(C_1—H_4)$ Å	1.0720	1.0731	1.0707	1.0725
$R(S_2—H_5)$ Å	1.3375	1.3347	1.3563	1.3304
$\angle C_3C_1S_2$	89.06°	78.46°	116.22°	115.75°
$\angle C_3C_1H_4$	145.40°	150.82°	124.18°	123.26°
$\angle C_1S_2H_5$	97.45°	100.95°	98.05°	97.75°
Out-of-plane				
$\angle C_3S_2C_1H_4$	178.44°	178.76°	176.55°	177.00°
$\angle C_3C_1S_2H_5$ (*trans* to H_4)	94.91°	94.35°	98.69°	98.96°
E_{SCF} (hartree)	−468.969191	−469.024984	−474.201861	−474.240373

[a] Experimental geometry ref. 25.

Can. J. Chem. Downloaded from www.nrcresearchpress.com by 210.87.254.105 on 09/06/12
For personal use only.

TABLE 3. Total energies (hartree) of the six C_2H_2S isomers at the SCF optimized geometries with STO-3G and 6-31G* basis sets

Molecule	Symmetry	Basis set	Total energy SCF	CISD	CISDQ
Thiirene **1** ($^1A_1$)	C_{2v}	STO-3G	−468.996100	−469.172435	−469.190645
		6-31G*	−474.260050	−474.439758	−474.458096
Thioketene **3** ($^1A_1$)	C_{2v}	STO-3G	−469.047855	−469.227276	−469.246488
		6-31G*	−474.326113	−474.496559	−474.514039
Ethynylthiol **4** ($^1A'$)	C_s	STO-3G	−469.044954	−469.218528	−469.234772
		6-31G*	−474.302137	−474.483437	−474.501672
Thioformylmethylene **5** (^1A)	C_1	STO-3G	−468.932935	−469.090692	−469.108211
		6-31G*	−474.223862	−474.387705	−474.407686
Thiiranylidene **6** ($^1A'$)	C_s	STO-3G	−468.996701	−469.157882	−469.175147
		6-31G*	−474.236624	−474.407629	−474.425532
Thiolvinylidene **7** (^1A)	C_1	STO-3G	−468.969191	−469.128103	−469.143701
		6-31G*	−474.240373	−474.396868	−474.412592

TABLE 4. Relative energies (kcal mol^{-1}) of the C_2H_2S isomers with respect to thioketene at the optimized geometries

Molecule	Relative energy STO-3G SCF	CISD	CISDQ	6-31G* SCF	CISD	CISDQ
Thiirene **1**	32.48	34.41	35.04	41.46	35.64	35.10
Thioketene **3**	0.0	0.0	0.0	0.0	0.0	0.0
Ethynylthiol **4**	1.82	5.49	7.35	15.05	8.23	7.76
Thioformylmethylene **5**	72.11	85.71	86.77	64.16	68.31	66.74
Thiiranylidene **6**	32.10	43.55	44.77	56.16	55.80	55.54
Thiolvinylidene **7**	49.36	62.23	64.50	53.80	62.56	63.66

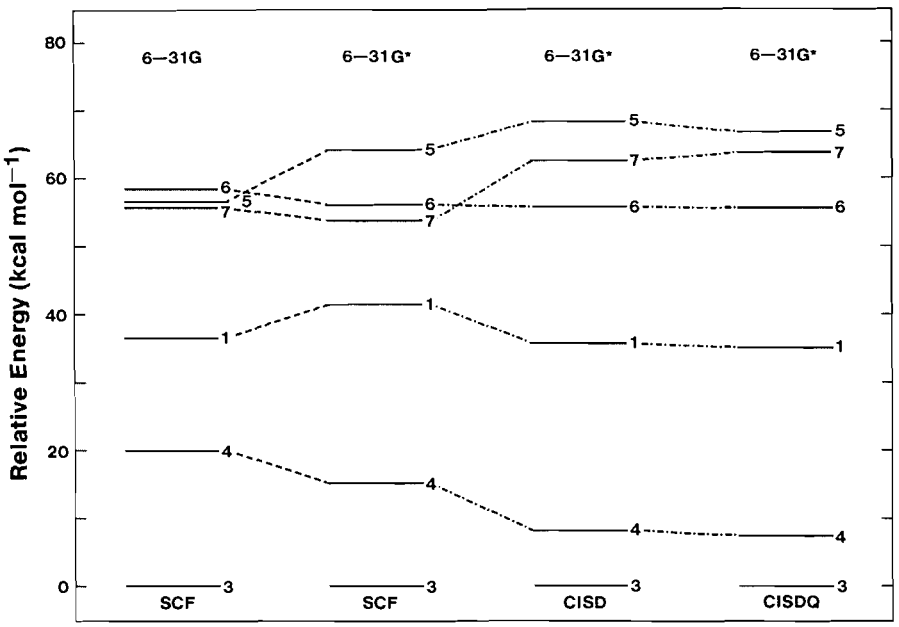

FIG. 1. Relative energies (kcal mol^{-1}) and effect of polarization (- - -) and correlation energy (-·-·-) on relative energies of C_2H_2S isomers with 6-31G and 6-31G* basis sets.

Thioformylmethylene

Thioformylmethylene **5** can also be written as a 1,3-diradical structure:

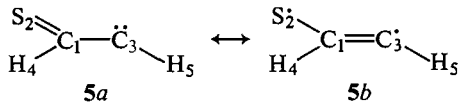

5*a* **5***b*

In the earlier report by Strausz *et al.* (11), the energy for the optimized geometry of the 1,3-diradical structure was calculated by using the UHF-SCF method with STO-4G basis set. We have now optimized the geometries for the *cis*, *trans*, and linear configurations of the $^1A''$, $^1A'$, $^3A''$, and $^3A'$ states of the diradical structure (**5***b*) with the open shell Restricted Hartree Fock (RHF) SCF method using both STO-3G and 6-31G* basis

Can. J. Chem. Downloaded from www.nrcresearchpress.com by 210.87.254.105 on 09/06/12
For personal use only.

Can. J. Chem. Downloaded from www.nrcresearchpress.com by 210.87.254.105 on 09/06/12
For personal use only.

TABLE 5. Optimized geometries of the 1,3-diradical configuration of thioformylmethylene (C_s) (**5***b*) for the open shell lowest singlet and triplet states (bond distances are in Å and bond angles in deg)

Parameter		Value											
		STO-3G						6-31G*					
		Singlet, $^1A''$, $^1A'$			Triplet, $^3A''$, $^3A'$			Singlet, $^1A''$, $^1A'$			Triplet, $^3A''$, $^3A'$		
		cis	Linear	*trans*	*cis*	Linear	*trans*	*cis*	Linear	*trans*	*cis*	Linear	*trans*
$R(C_1—C_3)$	A''	1.3033	1.2902	1.3031	1.3050	1.2882	1.3051	1.3151	1.3073	1.3150	1.3198	1.3081	1.3204
	A'	1.3012	1.2849	1.3003	1.2981	1.2797	1.2968	1.3107	1.2995	1.3097	1.3081	1.2951	1.3066
$R(C_1—S_2)$	A''	1.7716	1.7766	1.7733	1.7547	1.7693	1.7573	1.7699	1.7760	1.7742	1.7449	1.7618	1.7478
	A'	1.7635	1.7742	1.7651	1.7614	1.7745	1.7657	1.7714	1.7826	1.7758	1.7695	1.7854	1.7778
$R(C_1—H_4)$	A''	1.0887	1.0915	1.0866	1.0883	1.0907	1.0866	1.0758	1.0759	1.0726	1.0758	1.0753	1.0728
	A'	1.0876	1.0912	1.0870	1.0882	1.0919	1.0875	1.0782	1.0794	1.0767	1.0790	1.0802	1.0773
$R(C_3—H_5)$	A''	1.0864	1.0672	1.0860	1.0860	1.0673	1.0864	1.0703	1.0562	1.0693	1.0702	1.0563	1.0697
	A'	1.0831	1.0637	1.0829	1.0822	1.0638	1.0824	1.0685	1.0542	1.0679	1.0676	1.0544	1.0674
$\angle C_3C_1S_2$	A''	123.67°	124.46°	123.78°	123.14°	123.77°	123.29°	122.49°	123.07°	122.12°	122.05°	122.45°	121.66°
	A'	126.07°	127.31°	127.88°	125.84°	127.34°	128.08°	126.24°	127.27°	127.81°	125.96°	127.17°	127.82°
$\angle C_3C_1H_4$	A''	118.77°	119.30°	118.62°	119.07°	120.02°	118.81°	120.58°	121.08°	120.80°	120.57°	121.44°	120.63°
	A'	119.89°	120.37°	118.71°	120.19°	120.84°	118.91°	120.90°	121.40°	120.00°	121.13°	121.86°	120.29°
$\angle C_1C_3H_5$	A''	132.67°	180.00°	132.68°	132.84°	180.00°	132.15°	135.60°	180.00°	136.16°	135.39°	180.00°	135.06°
	A'	131.37°	180.00°	132.85°	132.44°	180.00°	132.72°	134.62°	180.00°	137.25°	135.60°	180.00°	137.99°

Can. J. Chem. Downloaded from www.nrcresearchpress.com by 210.87.254.105 on 09/06/12
For personal use only.

TABLE 6. Total energies (hartree) of the 1,3-diradical configuration (C_s) of thioformylmethylene (**5***b*) for the lowest singlet and triplet states at SCF optimized geometry

Geometry		Total energy SCF	CISD	CISDQ
		STO-3G basis set		
Singlet				
cis	$^1A''$	−468.996969	—	—
	$^1A'$	−469.000070	—	—
Linear	$^1A''$	−468.979442	—	—
	$^1A'$	−468.981036	—	—
trans	$^1A''$	−468.997171	—	—
	$^1A'$	−468.999539	—	—
Triplet				
cis	$^3A''$	−469.003995	−469.149075	−469.164712
	$^3A'$	−469.002779	−469.145510	−469.159388
Linear	$^3A''$	−468.986712	−469.135037	−469.150989
	$^3A'$	−468.986552	−469.132581	−469.147007
trans	$^3A''$	−469.005211	−469.152003	−469.167992
	$^3A'$	−469.003510	−469.147117	−469.161246
		6-31G basis set*		
Singlet				
cis	$^1A''$	−474.259806	—	—
	$^1A'$	−474.256311	—	—
Linear	$^1A''$	−474.247967	—	—
	$^1A'$	−474.243839	—	—
trans	$^1A''$	−474.260372	—	—
	$^1A'$	−474.255591	—	—
Triplet				
cis	$^3A''$	−474.267241	−474.418390	−474.434291
	$^3A'$	−474.258818	−474.406274	−474.420482
Linear	$^3A''$	−474.255596	−474.412058	−474.428610
	$^3A'$	−474.248147	−474.401502	−474.416514
trans	$^3A''$	−474.269447	−474.421843	−474.438040
	$^3A'$	−474.259028	−474.407934	−474.422442

sets. The results are presented in Table 5. Due to technical difficulties, CI calculations on the open shell singlet were not performed. SCF and CI energies for the triplet states and SCF energy for the singlet states of the 1,3-diradical are summarized in Table 6. The C—C bond distance in the 1,3-diradical is close to the C—C double bond distance and the C—S bond distance is close to the single bond C—S distance.

The energy difference for the $^1A''$ and $^1A'$ states is about 2–3 kcal mol^{-1} at the SCF level with 6-31G* basis and ~5–7 kcal mol^{-1} at the SCF level and ~8–10 kcal mol^{-1} at the CISDQ level for the $^3A''$ and $^3A'$ states. The *trans* and *cis* structures have almost the same stability; slightly favouring the trans configuration in $^1A''$, $^3A''$, and $^3A'$, and the *cis* in $^1A'$. The barrier for the *trans* → *cis* in plane isomerization in the $^1A''$ state and *cis* → *trans* in the $^1A'$ state, both are 7.8 kcal mol^{-1}. The barrier for the *trans*–*cis* in plane isomerization in the $^3A''$ and $^3A'$ states are 8.7 and 6.8 kcal mol^{-1} at the SCF level and 5.9 and 3.7 kcal mol^{-1} at the CISDQ level, respectively. The triplet singlet separation (ΔT_0–S_1) at the SCF level is very small (−5.7 kcal mol^{-1} for the *trans* A'' state) (Table 5) and the singlet ($^1A''$) 1,3-diradical has almost the same total energy as thiirene.

The complications in geometry optimizations for 3-center, 3-electron π networks have recently been discussed by Baird *et al.* (35). They and others (36, 37) have shown that the RHF SCF geometry optimization for open shell molecules containing multiple bond(s) tends to over-estimate the stability of the extreme, localized structures. SCF-CI optimization gives a completely delocalized structure with a global minimum lying below either of the local minima in the SCF hypersurface. On this basis it would be expected that both the singlet and triplet state energies of 1,3-diradicals would decrease somewhat in energy on reoptimization with inclusion of CI. The main consequence of this in the present context would be a decrease in the computed bond dissociation energy of thiirene (*vide infra*).

Although the correlation energy for the singlet diradical structure could not be calculated, a reasonably close estimate of it can be made from the averages of the computed correlation energies, Table 7, which have the values of 0.1696 hartree for the various isomers of the triplet state diradical, 0.1809 hartree for the closed shell singlet carbenoid structures (**5**, **6**, **7**) and 0.1952 hartree for the singlet state molecular species (**1**, **3**, **4**). The variation is small and the trend lies in the direction expected. The correlation energy for the singlet diradical should lie between the values for the triplet diradical and closed shell singlet carbenoids. These differ by only 0.0114 hartree and their mean value is 0.1752 hartree. The CISDQ energy of the *trans*, $^1A''$, singlet diradical is then computed to be −474.2604 + −0.1752 = −474.4356 hartree and the T_0–S_1 splitting ($^3A''$–$^1A''$) for the *trans*-1,3-diradical is ca. −1.5 kcal mol^{-1}.

Geometry optimizations for the lowest closed shell singlet state of the carbene structure (**5***a*) were carried out for the planar *cis*, *trans*, and linear configurations and the results with the total energies are summarized in Table 8. The *cis* and *trans* configurations have almost the same stability although the *trans* configuration is slightly favoured. Both configurations appear as first order saddle points on the energy hypersurface with critical point order of 1. The optimized C—C bond distance is close to the normal C—C single bond, and the C—S bond distance is close to the C—S double bond distance. In contrast, the linear configuration has a C—C bond distance which is much shorter than the normal single bond and slightly longer than the double bond distance. The C—S bond distance is slightly longer than the normal C=S distance, probably due to the contribution from the open shell, 1,3-diradical singlet configuration (**5***b*). On relaxing the planarity, the hydrogen (H_5) on the carbene carbon (C_3) moves out of the plane and converges to the thioformylmethylene structure (**5**). Both the linear (**5***a*) and perpendicular (**5**) structures have a critical point order of 0 corresponding to minima on the potential energy surface. The linear structure is only 5.4 kcal mol^{-1} higher in energy than the thioformylmethylene perpendicular (**5**) structure. Thus, the present optimized geometry (Table 2) for the lowest closed shell singlet state of the carbene structure **5** predicts that the hydrogen (H_5) on the carbene carbon (C_3) is in the plane perpendicular to the CCS plane, similar to the case of formylmethylene (13–15).

These results are in agreement with the small value of the zero field splitting parameter, D = 0.0318 cm^{-1}, obtained for thiobenzoyl phenylmethylene (12) which points to a high degree of delocalization of the unpaired electron on sulfur. Also the decay of the triplet spectrum followed a first order kinetics in the temperature range of 77–106 K with an activation energy of 5.4 kcal mol^{-1} which may correspond to the triplet–singlet energy separation.

Reaction path for the isomerization of C_2H_2S isomers

Transition state geometries for the isomerization reactions were optimized at the SCF level by the VA05AD gradient optimization method (31) for the closed shell singlet with both

TABLE 7. Correlation energy (hartree) at the CISDQ level with 6-31G* basis set

For closed shell singlet				For open shell triplet	
Molecular species		Carbene species		1,3-diradicals	
Thiirene ($^1A_1$)	0.198046	Thiiranylidene ($^1A'$)	0.188908	**5***b*, *cis* ($^3A''$)	0.167050
Thioketene ($^1A_1$)	0.187926	Thiolvinylidene (^1A)	0.172219	**5***b*, *trans* ($^3A''$)	0.168593
Ethynylthiol ($^1A'$)	0.199535	Thioformylmethylene		**5***b*, linear ($^3A''$)	0.173014
		5, (^1A)	0.183824		
		5*a*, *cis* ($^1A'$)	0.178656		
		5*a*, *trans* ($^1A'$)	0.182186		
		5*a*, linear ($^1A'$)	0.179698		
Mean	0.195169		0.180915		0.169552

TABLE 8. Optimized geometry and total energy (hartree) of the carbene planar (C_s) configuration of thioformylmethylene (**5***a*) for the closed shell lowest singlet ($^1A'$) state (bond distances are in Å and bond angles in deg)

	Value					
	STO-3G			6-31G*		
Parameter	*cis*	Linear	*trans*	*cis*	Linear	*trans*
$R(C_1—C_3)$	1.5078	1.3397	1.5157	1.4954	1.2992	1.4998
$R(C_1—S_2)$	1.5949	1.6425	1.5946	1.6099	1.7204	1.6130
$R(C_1—H_4)$	1.0919	1.1030	1.0900	1.0786	1.0886	1.0742
$R(C_3—H_5)$	1.1209	1.0769	1.1212	1.0997	1.0603	1.0951
$\angle C_3C_1S_2$	120.94°	126.54°	125.59°	120.28°	128.51°	125.11°
$\angle C_3C_1H_4$	119.13°	109.77°	114.18°	121.30°	111.75°	115.80°
$\angle C_1C_3H_5$	104.35°	180.00°	103.69°	108.09°	180.00°	107.81°
E_{SCF}	−468.923467	−468.897777	−468.923733	−474.195752	−474.219422	−474.198954
E_{CISD}	−469.081969	−469.054809	−469.083245	−474.357483	−474.381313	−474.363793
E_{CISDQ}	−469.099589	−469.077950	−469.101116	−474.374408	−474.399120	−474.381140

STO-3G and 6-31G* basis sets. Optimized geometries are shown in Fig. 2 and total energies are summarized in Table 9. All possible reaction paths for the isomerization reactions were studied by STO-3G basis set and the important ones were repeated with the 6-31G* basis set, mainly due to economical reasons. The activation energies calculated for the various possible interconversions are summarized in Table 10 and illustrated schematically in Figs. 3, 4, and 5.

Thioformylmethylene **5** can isomerize to thioketene **3** with no activation energy (with STO-3G) or with a very small activation energy of 1.8 kcal mol^{-1} (with 6-31G*) (Figs. 3 and 5). Direct isomerization to thiirene **1** is predicted to have no activation energy. STO-3G basis set geometry optimization of transition state **8** (Fig. 2) at SCF level predicts a very small (3.5 kcal mol^{-1}) activation energy; however, 6-31G* basis set geometry optimization did not predict any transition state. If we assume the *cis* configuration of thioformylmethylene to be the transition state between thioformylmethylene **5** and thiirene **1**, then the activation energy is 20.9 kcal mol^{-1} with 6-31G* basis set and 5.4 kcal mol^{-1} with STO-3G basis set. The ring closure of *cis* thioformylmethylene to thiirene does not show any activation energy. All the other possible rearrangements, i.e., to ethynylthiol **4**, thiiranylidene **6**, or thiolvinylidene **7**, feature substantial energy requirements (Table 10 and Figs. 3 and 5) and are not likely to occur thermally in low temperature matrices.

The lowest energy reaction path on the lowest closed shell singlet surface for the isomerization of thiirene **1** is to thiolvinylidene **7** with E_a = 43.5 kcal mol^{-1} (Figs. 4 and 5, Table 10). The next lowest energy reaction path is the C—S ring cleavage of **1** to produce thioformylmethylene **5** via the *cis* thioformylmethylene intermediate with 52.5 kcal mol^{-1} activation energy. Thus, the transformation of thiirene to thioketene is more favorable via the sequence **1** → **5** → **3** than via the direct route **1** → **3** involving the activated complex **13** for which E_a = 68.7 kcal mol^{-1}. In spite of the fact that thiiranylidene **6** is thermodynamically more stable than **5** or **7**, the rearrangement **1** → **6** appears to have prohibitively high energy requirements. Similarly, interconversion of **1** to **3** and **4** via the activated complexes **13** and **14**, respectively, are extremely high energy processes (Fig. 4 and Table 10).

Isomerization of thiiranylidene **6** to thioketene **3** requires an activation energy of 21.3 kcal mol^{-1}, to ethynylthiol **4** via migration of one H from C_1 to S_2 and opening of the $C_1—S_2$ bond (**18***a*, Fig. 2); and via simultaneous migration of both hydrogens from C_1: one to S_2 and the other to C_3, and opening of the $S_2—C_3$ bond (**18***b*, Fig. 2), both requiring 70–75 kcal mol^{-1} (Fig. 5, and Table 10). Similarly, isomerization to **7** also requires about 79 kcal mol^{-1} (Fig. 4 and Table 10).

Two reaction paths were also considered for the isomerization of thiolvinylidene **7** to ethynylthiol **4**: (*1*) migration of H_4 from C_1 to C_3 with accompanying changes in the $S_2C_1C_3$ angle (**20***a*, Fig. 2); and (*2*) maintaining H_4 on C_1 and varying the $S_2C_3C_1$ angle (**20***b*, Fig. 2), i.e., the migration of SH from C_1 to C_3. In both cases, the computed activation energies are low, 8.5 and 7.3 kcal mol^{-1}, respectively.

The thioketene ethynylthiol rearrangement in the singlet ground state possesses an intrinsic energy barrier of about 94.7 kcal mol^{-1} (Fig. 4).

Next the isomerization reactions of the 1,3-diradicals were explored in some detail. Geometry optimized total energies were calculated at various CCS bond angles en route to the

Can. J. Chem. Downloaded from www.nrcresearchpress.com by 210.87.254.105 on 09/06/12
For personal use only.

Can. J. Chem. Downloaded from www.nrcresearchpress.com by 210.87.254.105 on 09/06/12
For personal use only.

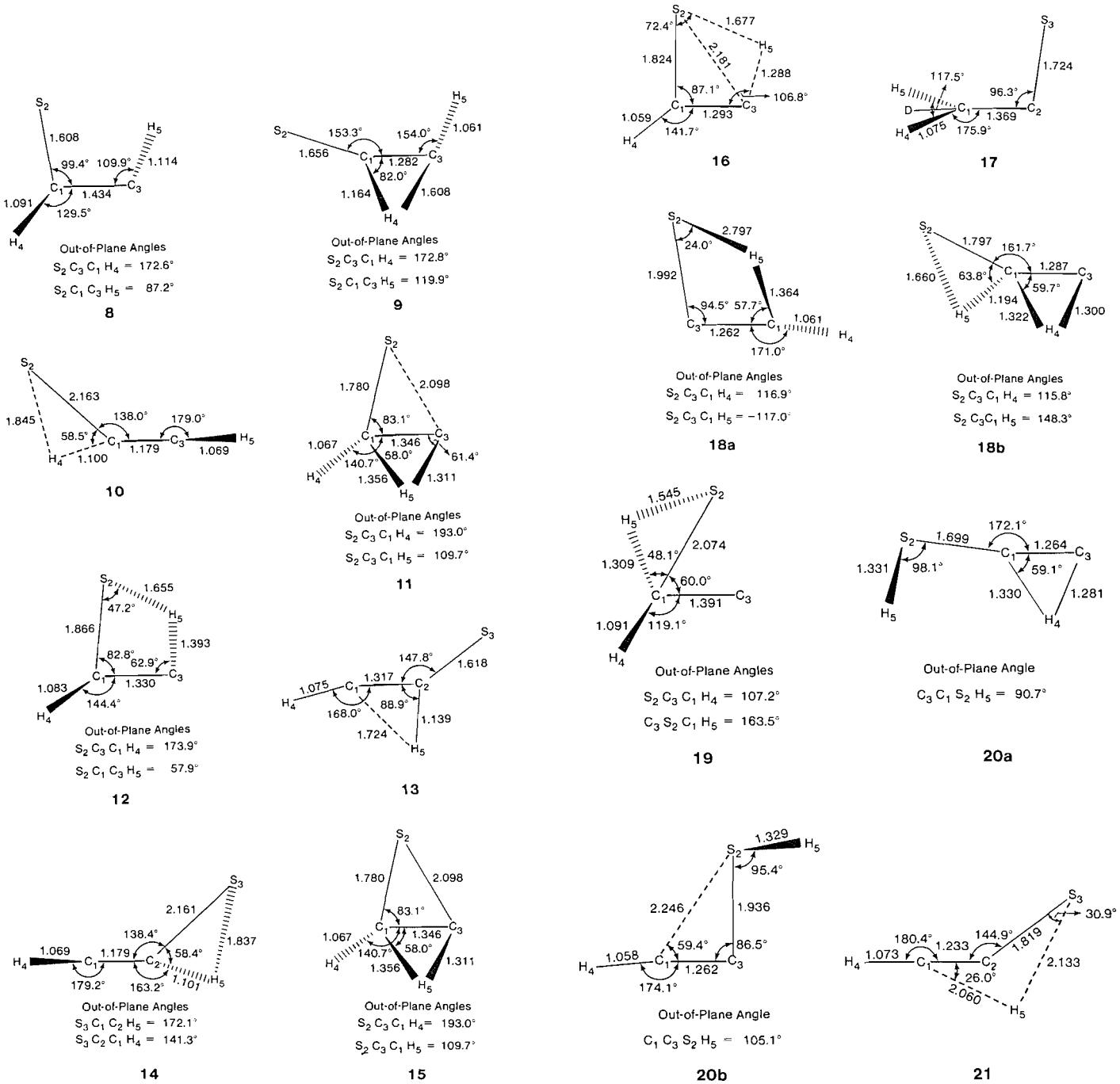

FIG. 2. Optimized geometries of the lowest closed shell singlet transition states for the C_2H_2S isomerizations with 6-31G* basis set except for **8**, **10**, **12**, **13**, **14**, **19**, and **21** for which values are of STO-3G basis set. Bond lengths are in Å and bond angles in deg.

thiirene geometry for the triplet and singlet *cis* $^3A''$, $^3A'$, $^1A''$, and $^1A'$ diradicals at the SCF level using the 6-31G* basis. Similarly, total energies were calculated for the ring opening of thiirene en route to the diradical structures (Fig. 6). The crossing points are assumed to represent the transition states with activation energies for the 1,3-diradical → thiirene rearrangement ranging between 14.8 and 17.3 kcal mol^{-1} (Table 11). For the lowest lying crossing point ($^3A''$) the geometry was reoptimized keeping the CCS angle fixed at 95.5°, at the SCF level and the CI calculation was then performed at the SCF optimized geometry. This gave E_a = 12.7 kcal mol^{-1} (at CISDQ) for the *cis*-1,3-diradical ($^3A''$) → thiirene step which may be viewed as an upper limit (and may be a factor of three too high) because CI calculations on the entire curve would have had the effect of lowering the thiirene curve relative to the curves of the diradicals (cf. Table 7).

The results of analogous calculations for the triplet ($^3A''$) and singlet ($^1A''$) *trans*-1,3-diradical ↔ thiolvinylidene (Fig. 7 and Table 12), and the singlet ($^1A'$) *cis*-1,3-diradical ↔ ethynylthiol rearrangement (Fig. 8 and Table 13) yielded intrinsic activation energies of 17.1 and 17.9 kcal mol^{-1} and 39.9 kcal mol^{-1}, respectively.

Finally we computed the ir frequencies of the thiirene molecule using the 6-31G* basis set on the 6-31G* optimized geometry of the molecule. HONDO 76 (IBM version) (38) program was used for vibrational frequencies calculations. The results

TABLE 9. Total energies for the isomerization path transition states

Isomerization (transition state)	Total energy					
	STO-3G			6-31G*		
	SCF	CISD	CISDQ	SCF	CISD	CISDQ
5 → **1** (**8**)	−468.927415	−469.099259	−469.123364	—	—	—
5 → **1** (**5***a cis*)	−468.923467	−469.081969	−469.099589	−474.195752	−474.357483	−474.374408
5 → **3** (**9**)	−468.916407	−469.088332	−469.108303	−474.213166	−474.385211	−474.404877
5 → **4** (**10**)	−468.886121	−469.055907	−469.073443	—	—	—
5 → **6** (**11**)	−468.883457	−469.053240	−469.071370	−474.154439	−474.330721	−474.349095
5 → **7** (**12**)	−468.811680	−468.989978	−469.010447	—	—	—
1 → **3** (**13**)	−468.896617	−469.058809	−469.081244	—	—	—
1 → **4** (**14**)	−468.886057	−469.056021	−469.073595	—	—	—
1 → **6** (**15**)	−468.883456	−469.053240	−469.071370	−474.154439	−474.330721	−474.349095
1 → **7** (**16**)	−468.908516	−469.103715	−469.129105	−474.173926	−474.365949	−474.388849
6 → **3** (**17**)	−468.897720	−469.085515	−469.113794	−474.203486	−474.371239	−474.391594
6 → **4** (**18***a*)	−468.792824	−468.956880	−468.976164	−474.115747	−474.293847	−474.314063
6 → **4** (**18***b*)	−468.789284	−468.964331	−468.990904	−474.105579	−474.284184	−474.305325
6 → **7** (**19**)	−468.864920	−469.030948	−469.049601	—	—	—
7 → **4** (**20***a*)	−468.940106	−469.104563	−469.120823	−474.210099	−474.381640	−474.399020
7 → **4** (**20***b*)	−468.931745	−469.103595	−469.125248	−474.202834	−474.380782	−474.400960
3 → **4** (**21**)	−468.875008	−469.059056	−469.095602	—	—	—

TABLE 10. Calculated activation energies (kcal mol^{-1}) for the isomerization of thioformylmethylene **5**, thiirene **1**, thiirenylidene **6**, and thiolvinylidene **7**

Isomerization	Activation energy					
	STO-3G			6-31G*		
	SCF	CISD	CISDQ	SCF	CISD	CISDQ
5 $\xrightarrow{8}$ **1**	3.46	−5.38	−9.51	—	—	—
5 $\xrightarrow{5a\ cis}$ **1**	5.94	5.47	5.41	17.64	18.96	20.88
5 $\xrightarrow{9}$ **3**	10.37	1.48	−0.06	6.71	1.57	1.76
5 $\xrightarrow{10}$ **4**	29.38	21.83	21.82	—	—	—
5 $\xrightarrow{11}$ **6**	31.05	23.50	23.12	43.56	35.76	36.77
5 $\xrightarrow{12}$ **7**	76.09	63.20	61.35	—	—	—
1 $\xrightarrow{13}$ **3**	62.52	71.30	68.65	—	—	—
1 $\xrightarrow{14}$ **4**	69.05	73.05	73.45	—	—	—
1 $\xrightarrow{5a\ cis}$ **5**	45.58	56.77	57.14	40.35	51.63	52.52
1 $\xrightarrow{15}$ **6**	70.68	74.80	74.85	66.27	68.42	68.40
1 $\xrightarrow{16}$ **7**	54.96	43.12	38.62	54.04	46.32	43.45
6 $\xrightarrow{17}$ **3**	62.11	45.41	38.50	20.79	22.84	21.30
6 $\xrightarrow{18a}$ **4**	127.93	126.13	124.86	75.85	71.40	69.95
6 $\xrightarrow{18b}$ **4**	130.16	121.46	115.61	82.23	77.46	75.43
6 $\xrightarrow{19}$ **7**	82.69	79.65	78.78	—	—	—
7 $\xrightarrow{20a}$ **4**	18.25	14.77	14.36	19.00	9.56	8.52
7 $\xrightarrow{20b}$ **4**	23.50	15.38	11.58	23.56	10.09	7.30
3 $\xrightarrow{21}$ **4**	108.46	105.56	94.68	—	—	—

along with earlier literature data on the experimental and computed frequencies from *ab initio* mo calculations with 4-31G basis set and from normal coordinate analyses are presented in Table 14.

Can. J. Chem. Downloaded from www.nrcresearchpress.com by 210.87.254.105 on 09/06/12
For personal use only.

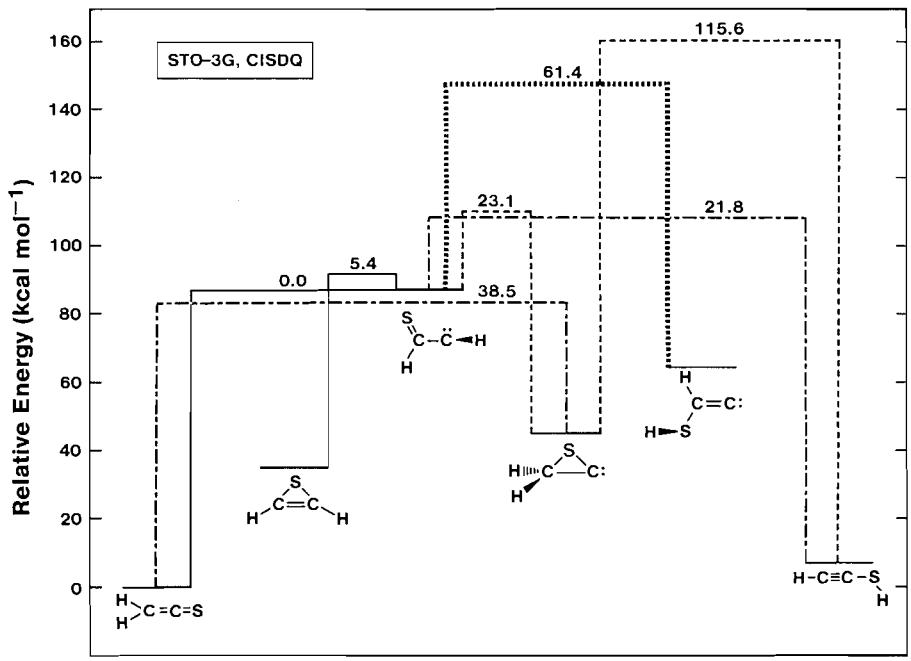

FIG. 3. Activation energies (kcal mol^{-1}) at CISDQ level for the possible isomerization reactions of thioformylmethylene (**5**) in the lowest singlet state with STO-3G basis set.

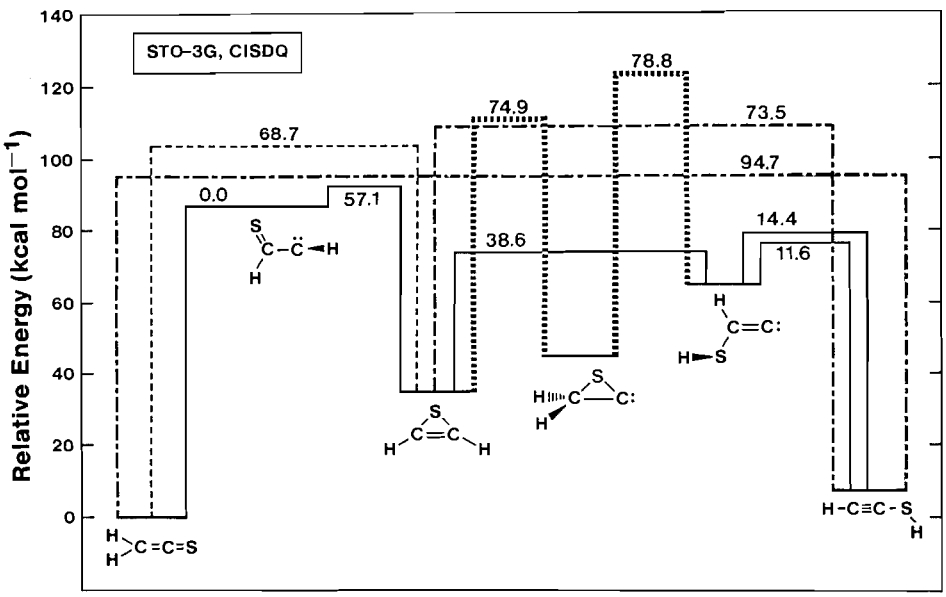

FIG. 4. Activation energies (kcal mol^{-1}) at CISDQ level for the possible isomerization reactions of thiirene in the ground singlet state with STO-3G basis set.

Discussion

The great theoretical interest in the stability, structure, and chemistry of thiirene is partly related to its 4n-π electron system which by definition implies an antiaromatic character for this molecule.

The low thermal stability of thiirene and its derivatives along with the results of an earlier *ab initio* mo calculation with STO-4G basis set and the unrestricted Hartree Fock method for the calculation of its ring opened structure, the 1,3-diradical form of thioformylmethylene predicting a lower thermodynamic stability of the ring structure (9–11) appeared to lend support to the antiaromaticity of thiirene. The results of the present, more refined calculations, however, appear to suggest otherwise.

At all levels of calculation the ground state of thioformylmethylene is the triplet ($^3A''$) 1,3-diradical which is nearly isoenergetic with the lowest singlet ($^1A''$) state, also corresponding to the 1,3-diradical structure. The T_0–S_1 (*trans* A'') energy separation at the 6-31G* CISDQ level is estimated to be ca. -1.5 kcal mol^{-1}. The S_2 state corresponds to the closed shell thioformylmethylene carbene with $E(T_0$ — *trans* $^3A'') - E(S_2)$ = 19.0 kcal mol^{-1} and 16.7 kcal mol^{-1} with *cis* $^3A''$ (6-31G* CISDQ). The T_0(*trans* $^3A''$) diradical at the SCF level lies 5.9 kcal mol^{-1} and *cis* $^3A''$, 4.5 kcal mol^{-1} below thiirene, however, when the correlation energy is included at CI level, it has the effect of lowering the energy of thiirene below that of the $T_0(^3A'')$ state of the diradical. At the 6-31G* CISDQ level $E(T_0(^3A''$ *cis*) − diradical) − $E(S_0$ − thiirene ($^1A_1$)) = 14.9 kcal

Can. J. Chem. Downloaded from www.nrcresearchpress.com by 210.87.254.105 on 09/06/12
For personal use only.

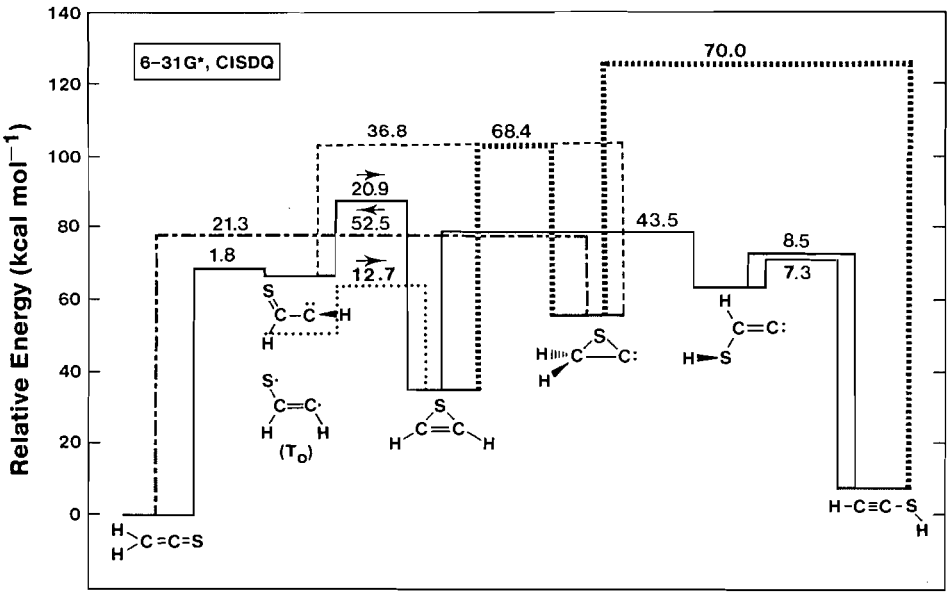

FIG. 5. Activation energies (kcal mol^{-1}) at CISDQ level for the C_2H_2S isomerization reactions with 6-31G* basis set.

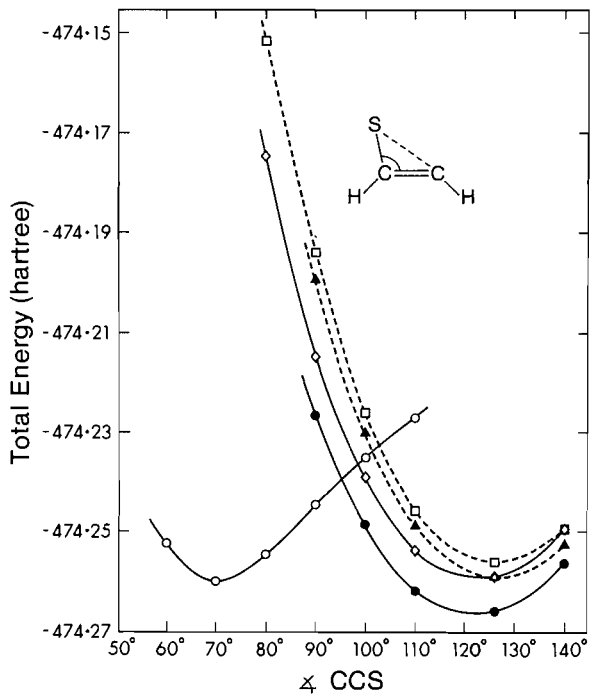

FIG. 6. Potential energy surfaces of triplet and singlet state *cis*-1,3-diradical-thioformylmethylene ↔ lowest singlet state thiirene at SCF level with 6-31G* basis set. ○ ground state singlet thiirene, ● lowest triplet (T_0) 1,3-diradical ($^3A''$), ▲ ($^3A'$), ◇ lowest singlet (S_1) 1,3-diradical ($^1A''$), □ ($^1A'$).

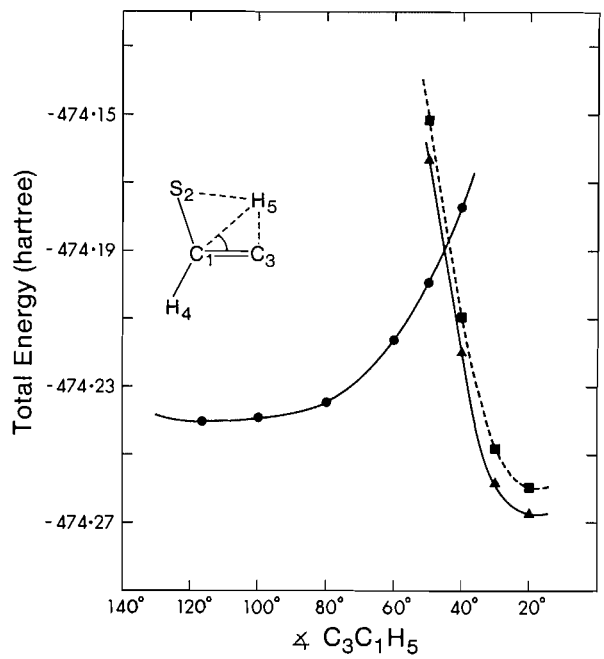

FIG. 7. Potential energy surface of lowest triplet and singlet state *trans*-1,3-diradical-thioformylmethylene ↔ lowest singlet thiolvinylidene at SCF level with 6-31G* basis set. ● lowest singlet thiolvinylidene, ▲ lowest triplet $^3A''$, 1,3-diradical, ■ lowest singlet $^1A''$, 1,3-diradical.

mol^{-1} and consequently, in spite of its low thermal stability, thiirene is not strictly antiaromatic. On the other hand, the cyclic electron delocalization in thiirene has a marked lowering effect on its C—S bond energy ~15 kcal mol^{-1} as compared to its 2n-π electron analog, the thiirane molecule, where the corresponding value is >40 kcal mol^{-1} (39). Thus, while the effect of electron destabilization is clearly evident, it is not sufficient to thermodynamically destabilize the ring structure with respect to the open structure. The phenomenon may be termed "pseudo" antiaromaticity and the thiirene molecule a pseudo antiaromatic molecule. It should be noted at this point that the decrease in stability of the thiirene versus the thiirane ring may be partly due to increased angular strain (as in the case of the cyclopropene versus cyclopropane ring) which, however, may be offset by the relief of the eclipsing strain present in thiirane as in cyclopropane (40).

Thiirene is also thermodynamically more stable than its other two closed shell carbenoid isomers, the thiiranylidene and thiolvinylidene (Tables 3 and 4) and its rearrangement on the lowest closed shell singlet surface appears to be prohibited by large energy barriers (Figs. 4 and 5). The lowest energy reaction channel which may be accessible at low thermal energies is isomerization to the thioketene via the T_0 or S_1 diradical

Can. J. Chem. Downloaded from www.nrcresearchpress.com by 210.87.254.105 on 09/06/12
For personal use only.

TABLE 11. Total energies[a] and activation energy for the crossing points on the *cis*-1,3-diradical → thiirene potential energy surfaces

	Triplet		Singlet	
	$^3A''$	$^3A'$	$^1A''$	$^1A'$
∠CCS	95.5°	101.25°	98.75°	103.00°
Total energy (hartree)	−474.23975[b]	−474.23400	−474.23625	−474.23250
Activation energy (kcal mol^{-1})	17.25	15.57	14.78	14.94

[a] Values are taken from the potential energy plots.
[b] Complete geometry optimization at ∠CCS 95.5° was done for the open shell triplet ($^3A''$) and CI calculation was carried out at this optimized geometry. For triplet diradical E_{SCF} = −474.239784, E_{CISD} = −474.397064, E_{CISDQ} = −474.414044, and E_a = 17.23 kcal mol^{-1} at SCF and 12.71 kcal mol^{-1} at CISDQ.

TABLE 12. Total energies and activation energy for the crossing points on the *trans* ($^3A''$ and $^1A''$) 1,3-diradical → thiolvinylidene potential energy surface

Parameter	Value	
	Triplet $^3A''$	Singlet $^1A''$
$\angle C_3C_1H_5$	45.0°[a]	43.7°[b]
Total energy (hartree) from the plot	−474.1895	−474.1870
Activation energy (kcal mol^{-1})	50.17	46.04
Total energy (hartree) at complete optimized geometry		
E_{SCF}	−474.192151	−474.189194
E_{CISD}	−474.353173	
E_{CISDQ}	−474.371634	
Activation energy (kcal mol^{-1})		
SCF	48.50	44.66
CISDQ	41.67	

[a] With closed shell singlet optimized geometry, E_{SCF} = −474.187674, E_{CISD} = −474.365993, E_{CISDQ} = −474.385303, E_a for thiolvinylidene → triplet ($^3A''$) 1,3-diradical (*trans*) = 33.07 kcal mol^{-1} at SCF and 17.12 kcal mol^{-1} at CISDQ.
[b] With closed shell singlet optimized geometry, E_{SCF} = −474.184679, E_{CISD} = −474.364429, E_{CISDQ} = −474.384042, E_a for thiolvinylidene → singlet ($^1A''$) 1,3-diradical (*trans*) = 34.95 kcal mol^{-1} at SCF and 17.92 kcal mol^{-1} at CISDQ.

intermediate with computed activation energies of E_a (via T_0 (*cis* $^3A''$)) ≈ 28 and E_a (via S_1) ≈ 29 kcal mol^{-1}. These values, were they correct, should endow the thiirene molecule with considerable stability even at room temperature where the lifetime for unimolecular isomerization would be in the order of tens of minutes. The actual activation energies are the sum of the enthalpy changes and intrinsic activation energies. The computed values of the latter, $E_a(T_0) \approx 12.7$ and $E_a(S_1) \approx 14.8$ kcal mol^{-1}, are probably too high by as much as a factor of three because of the inadequate representation of correlation energies (*vide supra*). An overall activation energy of about 20 kcal mol^{-1} would be more realistic and in better agreement with the observed stability of thiirene and its derivatives in low temperature inert matrices, although no quantitative kinetic measurements have been reported to date on the thermal isomerization of thiirene. The only relevant piece of information that exists comes from the low temperature kinetic study of triplet ground state diphenyl substituted thioketocarbene, thiobenzoylphenylmethylene (12), which isomerizes to the thioketene structure in a first order process with an activation

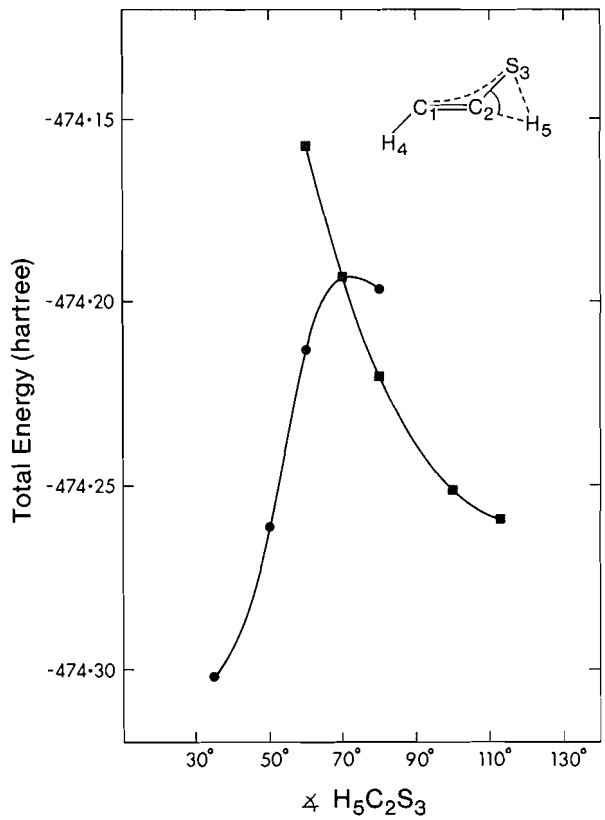

FIG. 8. Lowest singlet potential energy surface of *cis* 1,3-diradical-thioformylmethylene ↔ ethynylthiol. ● lowest singlet ethynylthiol, ■ singlet $^1A'$, 1,3-diradical.

TABLE 13. Total energy and activation energy for the crossing points on the *cis* ($^1A'$) singlet 1,3-diradical → ethynylthiol potential energy surface

Parameter	Value
$\angle H_5C_2S_3$	70.0°
Total energy[a] (hartree) at SCF	−474.192686
Activation energy (kcal mol^{-1})	39.93

[a] With optimized geometry at SCF level.

energy of 5.4 kcal mol^{-1} and an A factor of 1.2×10^{-9} s^{-1}. The activation energy for the process was assigned to the T_0–S_1 energy separation.

The existence of a substantial activation energy for the isomerization of thiirenes are also in agreement with the results of

Can. J. Chem. Downloaded from www.nrcresearchpress.com by 210.87.254.105 on 09/06/12
For personal use only.

TABLE 14. Observed and calculated vibrational frequencies (cm^{-1}) of thiirene

		Vibrational frequency				
			Calculated			
			Normal coordinate	*Ab initio*		
Symmetry	Assignment	Observed[a]	analysis[a]	4-31G[b]	6-31G*[c]	Δ[d]
a_1	C—H stretch	3208	3222	3645	3571	11
	C=C stretch	1660	1683	1935	1857	12
	C—H bend, in-plane	—	951	939	1011	—
	Ring deformation sym.	657	674	509	671	2
a_2	C—H bend, out-of-plane	—	647	934	942	—
b_1	C—H bend, out-of-plane	563	566	808	743	32
b_2	C—H stretch	3169 3165	3183	3548	3505	11
	C—H bend, in-plane	912 910	882	996	1090	20
	Ring deformation asym.	—	489	448	562	—

[a] References 5, 6.
[b] Reference 8.
[c] Present work.
[d] $\Delta = (\nu_{cal} - \nu_{obs})/\nu_{obs} \times 100$.

gas phase studies (1). The lifetime of thiirenes

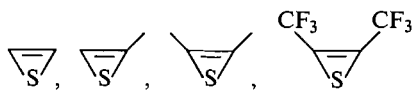

produced in the gas phase addition of $S(^1D_2)$ atoms to acetylenes have been estimated to lie in the tenths to few seconds range at low pressures. Also the ready scavengability of thiirene in the gas phase by perfluorobutyne-2 requires a substantial lifetime for these molecules.

In contrast, the oxygen analog of thiirene, oxirene computed to be antiaromatic even at *ab initio* double ζ basis SCF level (13–15): it lies higher in energy than any of its ring opened diradical or carbenoid isomers and its ring opening reaction features a small activation energy, 2–6 kcal mol^{-1}. In line with the computed low stability of oxirene all previous attempts for its isolation have failed, although recently we have succeeded in isolating an intermediate, in low yields, to which the structure of bis(trifluoromethyl)oxirene has been assigned (41). The chemical scavenging of oxirenes has not been achieved on account of its short lifetime, in spite of the fact that its intermediacy in the reactions of many diazoketones and diazoesters have been known for over fifteen years (10).

The present computational result that the lowest energy reaction channel for thiirene is conversion to the thioketene is in agreement with the experimental observation that thiirene thermally converts only to thioketene (42–44). The appearance of ethynylthiol among the low temperature argon-matrix photolysis products of 1,2,3-thiadiazoles can be ascribed to the secondary photolysis of thiirene. This has been demonstrated experimentally: photolysis of matrix isolated thiirene at 10 K with λ > 330 nm radiation resulted in its conversion to ethynylthiol, and to thioketene in smaller yields. The photochemical path involves the lowest excited singlet state of thiirene with an excitation energy of about 85 kcal mol^{-1} which could then energetically readily convert to ethynylthiol via the intermediacy of thiiranylidene, or vinylidenethiol which can result in isotopic scrambling when isotopically labelled thiirene is used:

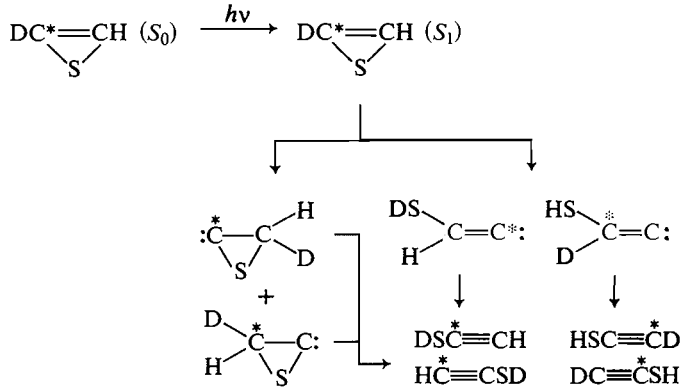

The computed relatively high stability of thiirene is also in accord with its computed geometry, in particular, with the magnitude of the C—S bond length which at the 6-31G* SCF level is only 0.04 Å larger than the experimental value in the 2n-π electron analog, thiirane. Calculations using the 6-31G basis set without the polarization function tend to give about 0.1 Å larger bond length (Tables 1 and 2).

The ir spectra of argon-matrix isolated thiirene, d_1- and d_2-thiirenes have been analyzed previously with the aid of normal coordinate calculations (5, 6) and *ab initio* SCF mo calculations using the 4-31G basis set (8). From the data summarized in Table 14 it is seen that the present 6-31G* basis set calculations gave ir frequencies which are from 2% to 31% larger than the experimental values. In comparing them to the frequencies computed with the 4-31G basis set we note that, with one exception, the 6-31G* computed frequencies are closer to the experimental values. The most notable discrepancies exist for the ring deformation frequencies, the values of which are underestimated by the 4-31G calculation probably because this basis set gives incorrect molecular geometries and too large C—S bond lengths.

Can. J. Chem. Downloaded from www.nrcresearchpress.com by 210.87.254.105 on 09/06/12
For personal use only.

After submission of the present article we came across a paper by Siegbahn, Yoshimine, and Pacansky (45) dealing with the *ab initio* theoretical study of the lowest singlet and triplet states of the C_2H_2S isomers. Our results are in good agreement with their findings.

Further studies are in progress.

Acknowledgment

The authors thank the Natural Sciences and Engineering Research Council of Canada for continuing financial support.

1. (*a*) O. P. STRAUSZ, J. FONT, E. L. DEDIO, P. KEBARLE, and H. E. GUNNING. J. Am. Chem. Soc. **89**, 4805 (1967); (*b*) O. P. STRAUSZ. Pure Appl. Chem. **4**, 165 (1971); (*c*) J. FONT, M. TORRES, H. E. GUNNING, and O. P. STRAUSZ. J. Org. Chem. **43**, 2487 (1978).
2. (*a*) A. KRANTZ and J. LAURENI. J. Am. Chem. Soc. **96**, 6768 (1974); (*b*) J. LAURENI, A. KRANTZ, and R. A. HAJDU. J. Am. Chem. Soc. **98**, 7872 (1976); (*c*) A. KRANTZ and J. LAURENI. J. Am. Chem. Soc. **99**, 4842 (1977); Ber. Bunsenges. Phys. Chem. **82**, 13 (1978).
3. M. TORRES, A. CLEMENT, J. E. BERTIE, H. E. GUNNING, and O. P. STRAUSZ. J. Org. Chem. **43**, 2490 (1978).
4. M. TORRES, A. CLEMENT, H. E. GUNNING, and O. P. STRAUSZ. Nouv. J. Chim. **3**, 149 (1979).
5. M. TORRES, I. SAFARIK, A. CLEMENT, J. E. BERTIE, and O. P. STRAUSZ. Nouv. J. Chim. **3**, 365 (1979).
6. I. SAFARIK, M. TORRES, and O. P. STRAUSZ. Chem. Phys. Lett. **72**, 388 (1980).
7. A. KRANTZ and J. LAURENI. J. Org. Chem. **44**, 2730 (1979).
8. B. A. HESS, JR., L. J. SCHAAD, and C. S. EWIG. J. Am. Chem. Soc. **102**, 2507 (1980).
9. M. TORRES, E. M. LOWN, and O. P. STRAUSZ. Heterocycles, **11**, 697 (1978).
10. M. TORRES, E. M. LOWN, H. E. GUNNING, and O. P. STRAUSZ. Pure Appl. Chem. **52**, 1623 (1980).
11. O. P. STRAUSZ, R. K. GOSAVI, F. BERNARDI, P. G. MEZEY, J .D. GODDARD, and I. G. CSIZMADIA. Chem. Phys. Lett. **53**, 211 (1978).
12. H. MURAI, M. TORRES, and O. P. STRAUSZ. J. Am. Chem. Soc. **101**, 3976 (1979).
13. O. P. STRAUSZ, R. K. GOSAVI, and H. E. GUNNING. Chem. Phys. Lett. **54**, 510 (1978).
14. (*a*) K. TANAKA and M. YOSHIMINE. J. Am. Chem. Soc. **102**, 7655 (1980); (*b*) J. BARGON, K. TANAKA, and M. YOSHIMINE. *In* Computational methods in chemistry. *Edited by* J. Bargon. Plenum Press, New York. 1980. p. 239.
15. W. J. BOUMA, R. H. NOBES, L. RADOM, and C. E. WOODWARD. J. Org. Chem. **47**, 1869 (1982).
16. A. KRANTZ and J. LAURENI. J. Am. Chem. Soc. **103**, 486 (1981).
17. J. A. POPLE. *In* Modern theoretical chemistry. Vol. 4. *Edited by* H. F. Schaefer. Plenum Press, New York. 1977. p. 1.
18. J. B. COLLINS, P. VON RAGUE SCHLEYER, J. S. BINKLEY, and J. A. POPLE. J. Chem. Phys. **64**, 5142 (1976).
19. Y. SAKAI, H. TATEWAKI, and S. HUZINAGA. J. Comput. Chem. **2**, 108 (1981).
20. J. D. GODDARD. Can. J. Chem. **59**, 3200 (1981).
21. (*a*) R. A. POIRIER, R. DAUDEL, P. G. MEZEY, and I. G. CSIZMADIA. Int. J. Quantum Chem. **21**, 799 (1982); (*b*) W. J. HEHRE, R. DITCHFIELD, and J. A. POPLE. J. Chem. Phys. **56**, 2257 (1972); (*c*) R. DITCHFIELD, W. J. HEHRE, and J. A. POPLE. J. Chem. Phys. **54**, 724 (1971).
22. (*a*) W. J. HEHRE, R. DITCHFIELD, R. F. STEWART, and J. A. POPLE. J. Chem. Phys. **52**, 2769 (1970); (*b*) W. J. HEHRE, R. F. STEWART, and J. A. POPLE. J. Chem. Phys. **51**, 2657 (1969).
23. L. E. SUTTON. Tables of interatomic distances and configuration in molecules and ions. The Chemical Society, London. 1965.
24. D. R. JOHNSON, F. X. POWELL, and W. H. KIRCHHOFF. J. Mol. Spectrosc. **39**, 136 (1971).
25. K. GEORGIOU, H. W. KROTO, and B. M. LANDSBERG. J. Mol. Spectrosc. **77**, 365 (1979).
26. M. R. PETERSON and R. A. POIRIER. MONSTERGAUSS 81, Department of Chemistry, University of Toronto, Toronto, Ont., Canada. 1981.
27. W. C. DAVIDON. Math Programming, **9**, 1 (1975).
28. W. C. DAVIDON and L. NAZARETH. Technical Memos 303 and 306, Argonne National Laboratory, Argonne, IL 60439, U.S.A.
29. P. PULAY. Mol. Phys. **17**, 197 (1969); **18**, 473 (1970); *In* Modern theoretical chemistry. Vol. 4. *Edited by* H. F. Schaefer. Plenum Press, New York. 1977. p. 153.
30. (*a*) H. B. SCHLEGEL. Ph.D. Thesis. Queen's University, Kingston, Ont. 1975; (*b*) H. B. SCHLEGEL, S. WOLF, and F. BERNARDI. J. Chem. Phys. **63**, 3632 (1975).
31. M. J. D. POWELL. VAO5AD, Harwell Subroutine Library, Atomic Energy Research Establishment, Harwell, U.K.
32. N. C. HANDY, J. D. GODDARD, and H. F. SCHAEFER. J. Chem. Phys. **71**, 426 (1979).
33. S. R. LANGHOFF and E. R. DAVIDSON. Int. J. Quantum Chem. **8**, 61 (1974).
34. A. C. HOPKINSON, M. H. LIEN, K. YATES, and I. G. CSIZMADIA. Int. J. Quantum Chem. **12**, 355 (1977).
35. N. C. BAIRD, R. R. GUPTA, and K. F. TAYLOR. J. Am. Chem. Soc. **101**, 4531 (1979).
36. J. F. HARRISON, A. DENDRAMIS, and G. E. LEROI. J. Am. Chem. Soc. **100**, 4352 (1978).
37. E. R. DAVIDSON and W. T. BORDEN. J. Am. Chem. Soc. **99**, 2053 (1977).
38. M. DUPUIS, J. RYS, and H. F. KING. HONDO 76 (IBM Version), QCPE Program No. 338, Quantum Chemistry Program Exchange, Indiana University, Bloomington, IN 47401, U.S.A.
39. E. M. LOWN, K. S. SIDHU, A. W. JACKSON, A. JODHAN, M. GREEN, and O. P. STRAUSZ. J. Phys. Chem. **85**, 1089 (1981).
40. J. MARCH. Advanced organic chemistry. 2nd ed. McGraw Hill Book Company, New York. 1977. p. 146.
41. M. TORRES, J. L. BOURDELANDE, A. CLEMENT, and O. P. STRAUSZ. J. Am. Chem. Soc. **105**, 1698 (1983).
42. B. BAK, O. J. NIELSEN, H. SVANHOLT, A. HOLM, N. H. TOUBRO, A. KRANTZ, and J. LAURENI. Acta Chim. Scand. A**33**, 161 (1979).
43. H. BOCK, B. SOLOUKI, G. BERT, and P. ROSMUS. J. Am. Chem. Soc. **99**, 1663 (1977).
44. M. TORRES and O. P. STRAUSZ. Unpublished results.
45. P. E. M. SIEGBAHN, M. YOSHIMINE, and J. PACANSKY. J. Chem. Phys. **78**, 1384 (1983).

Can. J. Chem. Downloaded from www.nrcresearchpress.com by 210.87.254.105 on 09/06/12
For personal use only.

The crystal structure of bis(triphenyltin)telluride and the interpretation of the ^{119}Sn Mössbauer and nuclear magnetic resonance data of the bis(triphenyltin) and bis(trimethyltin) chalcogenides

F. W. B. EINSTEIN, C. H. W. JONES, T. JONES, AND R. D. SHARMA
Department of Chemistry, Simon Fraser University, Burnaby, B.C., Canada V5A 1S6

Received March 10, 1983

F. W. B. EINSTEIN, C. H. W. JONES, T. JONES, and R. D. SHARMA. Can. J. Chem. **61**, 2611 (1983).

The structure of $(Ph_3Sn)_2Te$ has been determined by X-ray crystallography. The compound crystallizes in the space group $C2/c$ with a = 18.578(3) Å, b = 7.731(1) Å, c = 25.272(4) Å, β = 117.17(1)°, ρ_c = 1.702 g cm^{-3}, $\rho_o(CHCl_3/CH_2I_2)$ = 1.69 g cm^{-3}, and Z = 4. Intensities were measured for 2853 independent reflections ($2\theta \leq 50°$) of which 2044 were observed ($I \leq 2.3\sigma(I)$) and used in subsequent refinement (final R values were R = 0.034 and R_w = 0.045). The $(Ph_3Sn)_2Te$ molecule exhibits a "bent" structure in which Sn—Te—Sn = 103.68(2)° and Te—Sn = 2.7266(6) Å and in which the Te atom lies on a crystallographic two-fold axis. Comparison of the present structure with corresponding selenide and sulphide analogues indicates that in all three cases the environment about tin corresponds to that of sp^3 hybridisation. The ^{119}Sn Mössbauer quadrupole splittings of $(Ph_3Sn)_3E$ and $(Me_3Sn)_2E$, where E = S, Se, or Te, show a correlation with the ^{119}Sn solution nmr chemical shifts and this correlation is discussed.

F. W. B. EINSTEIN, C. H. W. JONES, T. JONES et R. D. SHARMA. Can. J. Chem. **61**, 2611 (1983).

On a déterminé, par cristallographie de rayons X, la structure du cristal de $(Ph_3Sn)_2Te$. Le composé cristallise dans le groupe d'espace C_2/c avec a = 18,578(3) Å, b = 7,731(1) Å, c = 25,272(4) Å, β = 117,17(1)°, ρ_c = 1,702 g cm^{-3}, $\rho_o(CHCl_3/CH_2I_2)$ = 1,69 g cm^{-3} et Z = 4. On a mesuré les intensités pour 2853 réflexions indépendantes ($2\theta \leq 50°$) et 2044 de ces réflexions sont observées ($I \leq 2{,}3\sigma(I)$); on les a utilisées dans les améliorations subséquentes jusqu'à des valeurs de R = 0,034 et de R_w = 0,045. La molécule de $(Ph_3Sn)_2Te$ a une structure déformée dans laquelle l'angle Sn—Te—Sn = 103,68(2)° et la liaison Te—Sn = 2,7266(6) Å et où l'atome de Te se trouve sur un axe cristallographique binaire. La comparaison de cette structure avec celle de séleniure correspondant et des sulfures analogues indique que dans les trois cas, l'environnement autour de l'étain correspond à celui d'une hybridation sp^3. Les découplages quadrupolaires de Mössbauer du ^{119}Sn des composés $(Ph_3Sn)_3E$ et $(Me_3Sn)_2E$ où E = S, Se ou Te montrent une corrélation avec les déplacements chimiques dans la rmn du ^{119}Sn en solution. On discute de cette corrélation.

[Traduit par le journal]

Can. J. Chem. Downloaded from www.nrcresearchpress.com by 210.87.254.40 on 09/06/12
For personal use only.

Introduction

As part of a detailed ^{119}Sn and ^{125}Te Mössbauer and nmr study of the compounds $(R_3M)_2E$ where M = C, Si, Ge, Sn, and Pb, E = S, Se, and Te, it was relevant to determine the crystal structure of $(Ph_3Sn)_2Te$. The crystal structures of the compounds $(Ph_3Sn)_2S$ and $(Ph_3Sn)_2Se$ have previously been reported and it was of interest to establish how the coordination about the tin in $(Ph_3Sn)_2Te$ compared with the sulphur and selenium derivatives, since this might allow conclusions to be drawn about the ^{119}Sn Mössbauer and ^{119}Sn solution nmr data.

The X-ray crystal structure of $(Ph_3Sn)_2Te$ has been determined and the ^{119}Sn Mössbauer and solution nmr spectra of $(Ph_3Sn)_2E$, E = Se and Te, and $(Me_3Sn)_2E$, E = S, Se, Te, measured. The Mössbauer (1) and nmr (2) data for $(Ph_3Sn)_2S$ have previously been reported. The trends in the Mössbauer and nmr data for $(Ph_3Sn)_2E$ and $(Me_3Sn)_2E$ are discussed briefly.

Experimental

The preparation of compounds

The compounds $(Ph_3Sn)_2E$, E = Se and Te, were synthesised in 80–85% yield in the following way. Sodium hydrogen selenide (telluride) was prepared by reacting selenium (tellurium) with $NaBH_4$ in a water/ethanol mixture. A benzene solution of Ph_3SnCl was then added drop-wise. The benzene layer containing $(Ph_3Sn)_2E$ was separated off and evaporated to dryness and the resulting residue was then recrystallised several times from a diethyl ether/hexane mixture. *Anal.* calcd. for $(Ph_3Sn)_2Se$: C 55.51, H 3.88; found: C 55.40, H 3.86; mp 150°C (lit. (3) 148°C). *Anal.* calcd. for $(Ph_3Sn)_2Te$: C 52.25, H 3.65; found: C 52.40, H 3.62; mp 150°C (lit. (3) 149–150°C).

This one-pot synthesis proved a much more direct way of preparing $(Ph_3Sn)_2E$ than the literature method (3) and gave much better yields. The latter is a multi-step synthesis involving the preparation $Ph_3Sn^-Li^+$, its reaction with selenium (tellurium) to give Ph_3SnELi and finally the reaction of Ph_3SnELi with Ph_3SnCl to yield $(Ph_3Sn)_2E$.

The bis(trimethyltin) selenide and telluride were synthesised using the method of ref. 4, appropriately adapted to tin rather than silicon chemistry. Bis(trimethyltin) sulphide was prepared by reacting trimethyltin chloride with sodium sulphide in water. These three compounds are all liquids at room temperature and it was not possible to obtain consistent chemical analyses for them. They were characterised by their proton nmr spectra and by their ^{119}Sn nmr spectra, which were in agreement with the literature values.

Spectroscopic studies

The ^{119}Sn Mössbauer spectra were recorded with the source and absorbers at liquid nitrogen temperature using a conventional constant acceleration drive. A $Ba^{119m}SnO_3$ (New England Nuclear) source was used and the Mössbauer γ-ray monitored using a NaI(Tl) scintillation counter. The spectra were computer fitted to Lorentzians.

^{119}Sn nmr spectra were obtained on a Bruker WM400 spectrometer at 149 MHz operating at ambient temperature. Resonances were found by utilizing 100–150 kHz sweep widths, 10 μs (25°) pulse widths, and a 0.05 s delay between acquisitions. Final spectra were obtained at the appropriate frequency generally using a 5 kHz sweep width and 90° pulse widths with no delay. No broadband decoupling was employed. Data acquisitions consisted of 16K data points which were zero filled to 32K data points for the Fourier transform. Linewidths were in the range of 5 to 15 Hz. Samples were prepared in $CDCl_3$ for field shimming. Where the deuterium lock was insensitive to the shim coils, the homogeneity was adjusted by monitoring the FID.

Structure determination

Crystal data are

$C_{36}H_{30}Sn_2Te$ fw = 827.62

Monoclinic, a = 18.578(3) Å, b = 7.731(1) Å, c = 25.272(4) Å, β = 117.17(1)°, V = 3229.21 Å^3, ρ_c = 1.702 g cm^{-3},

TABLE 1. Atomic coordinates[a] for $Ph_3SnTeSnPh_3$

Atom	X	Y	Z	B_{iso}[b]
Te	0	0.15018 (7)	1/4	6.27 (3)
Sn	−0.03770 (2)	−0.06773 (5)	0.15617 (1)	4.13 (2)
C(1)	0.0591 (3)	−0.2373 (7)	0.16721 (21)	4.1 (2)
C(2)	0.1394 (3)	−0.1893 (7)	0.1972 (3)	5.6 (3)
C(3)	0.2002 (3)	−0.3021 (9)	0.2028 (3)	6.8 (3)
C(4)	0.1819 (4)	−0.4650 (9)	0.1786 (3)	6.4 (3)
C(5)	0.1028 (4)	−0.5143 (9)	0.1500 (3)	6.9 (3)
C(6)	0.0422 (3)	−0.4022 (8)	0.1442 (3)	5.6 (3)
C(7)	−0.0652 (3)	0.1140 (7)	0.0855 (2)	4.4 (2)
C(8)	−0.0230 (4)	0.1210 (8)	0.0538 (3)	5.8 (3)
C(9)	−0.0427 (4)	0.2477 (9)	0.0079 (3)	7.4 (4)
C(10)	−0.1055 (4)	0.3591 (8)	−0.0037 (3)	6.9 (3)
C(11)	−0.1463 (4)	0.3544 (8)	0.0289 (3)	6.3 (3)
C(12)	−0.1279 (3)	0.2353 (8)	0.0730 (3)	5.3 (3)
C(13)	−0.1410 (3)	−0.2267 (7)	0.1359 (2)	4.6 (2)
C(14)	−0.1361 (4)	−0.3649 (9)	0.1724 (3)	6.7 (3)
C(15)	−0.2014 (5)	−0.4721 (11)	0.1568 (3)	9.4 (5)
C(16)	−0.2730 (4)	−0.4441 (9)	0.1069 (4)	8.5 (4)
C(17)	−0.2783 (4)	−0.3095 (10)	0.0714 (3)	8.0 (4)
C(18)	−0.2130 (3)	−0.1993 (9)	0.0855 (3)	6.5 (3)

[a]Estimated standard deviations refer to the last digit printed.
[b]For anisotropic atoms (all non-hydrogen atoms) $B_{iso} = 8\pi^2(U_{11} + U_{22} + U_{33})/3$.

$\rho_o(CHCl_3/CH_2I_2)$ = 1.69 g cm^{-3}, Z = 4, μ = 24.96 cm^{-1}, λ(Mo-K$_{\alpha 1}$) = 0.70926 Å, $F(000)$ = 1591.8.

A crystal suitable for data collection (0.25 × 0.25 × 0.13 mm) was mounted in a Lindemann glass capillary tube. Weissenberg and precession photographs were used to determine approximate cell dimensions and to define the space group as Cc or $C2/c$ (systematic absences: hkl, $h + k = 2n$; $h0l$, $l = 2n$). Accurate cell dimensions were determined by least-squares refinement of 20 accurately centred reflections (2θ = 27−36°). Data were collected using an automatic Picker FACS-I four-circle diffractometer with a graphite monochromator and a scintillation counter with pulse height discrimination. The take-off angle was 3° and a symmetrical θ−2θ scan (2°/min) of (1.3 + 0.692 tan θ)° was used. Stationary-crystal, stationary-counter background counts of 10% of the scan time were taken at each side of the scan. The peak profile of each reflection was analysed and used to derive its intensity and associated error (5). Intensity measurement of two standards every 40 reflections showed no evidence of crystal deterioration, however, there did appear to be a cyclical variation in their intensity (±5%) during data collection which was corrected appropriately.

Intensities were measured for 2853 independent reflections (2θ ≤ 50°), of which 2044 were classed observed ($I \leq 2.3\sigma(I)$). The data have been corrected for Lorentz, polarisation, and absorption effects (transmission coefficients varied from 0.536−0.738). The structure was solved using conventional Patterson and Fourier methods. The Te atom was found to lie on a crystallographic two-fold axis. Hydrogen atoms were included as fixed contributions in their calculated positions and given isotropic temperature factors derived from their parent carbon atoms. Block diagonal least-squares refinement with anisotropic temperature factors for all non-hydrogen atoms gave final agreement factors of $R = 0.034$ ($R = \Sigma||F_o| - |F_c||\Sigma|F_o|$) and $R_w = 0.045$ ($R_w = (\Sigma w(|F_o| - |F_c|)^2/\Sigma w|F_o|^2)^{1/2}$) for 177 variables. A weighting scheme of the form $w = 1/\sigma^2(F_o) + (kF_o)^2$ has been applied (where $k = 0.03$) (Table 1).

The final difference map was very clean (<0.3 e/Å^3) apart from five positive peaks (0.4−0.7 e/Å^3) and two negative peaks (1.2 e/Å^3) close to the Te and Sn atoms. To account for this electron density the possibility of alternative models involving (*a*) disorder or (*b*) an asymmetric Ph_3Sn—Te—$SnPh_3$ unit with approximate two-fold symmetry in space group Cc were considered. However, in view of the good agreement achieved with the present model and the well behaved nature of the phenyl rings, pursuit of these other alternatives was not deemed worthwhile.

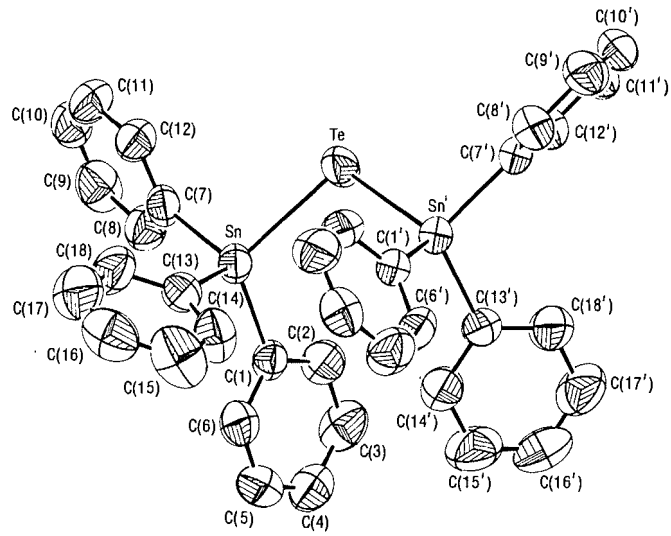

FIG. 1. ORTEP[8] diagram and numbering scheme for the $(Ph_3Sn)_2Te$ molecule. Atoms are represented by 50% thermal ellipsoids. (Hydrogen atoms have not been included for clarity.)

Atomic scattering factors including anomalous dispersion were taken from ref. 6. The computer programs used are those from ref. 7. Final positional parameters are listed in Table 2.[1]

Discussion

An ORTEP (8) diagram and numbering scheme for the $(Ph_3Sn)_2Te$ molecule is given in Fig. 1. Bond parameters are given in Table 2. The molecule possesses a crystallographic two-fold symmetry axis which runs through the central Te

[1]Complete set of structure factor listings, anisotropic temperature factors, and hydrogen atom parameters are available at a nominal charge, upon request, from the Depository of Unpublished Data, CISTI, National Research Council of Canada, Ottawa, Ont., Canada K1A 0S2.

Can. J. Chem. Downloaded from www.nrcresearchpress.com by 210.87.254.40 on 09/06/12
For personal use only.

TABLE 2. Bond parameters for $Ph_3Sn—Te—SnPh_3$

Bond	Distance (Å)	Bond	Distance (Å)
Te—Sn	2.7266(6)	C(8)—C(9)	1.431(9)
Sn—C(1)	2.138(5)	C(9)—C(10)	1.370(10)
Sn—C(7)	2.143(5)	C(10)—C(11)	1.353(10)
Sn—C(13)	2.134(5)	C(11)—C(12)	1.362(8)
C(1)—C(2)	1.381(7)	C(12)—C(7)	1.415(8)
C(2)—C(3)	1.382(9)	C(13)—C(14)	1.388(8)
C(3)—C(4)	1.373(10)	C(14)—C(15)	1.370(9)
C(4)—C(5)	1.363(9)	C(15)—C(16)	1.368(11)
C(5)—C(6)	1.374(9)	C(16)—C(17)	1.349(12)
C(6)—C(1)	1.376(8)	C(17)—C(18)	1.390(9)
C(7)—C(8)	1.354(8)	C(18)—C(13)	1.379(8)
Bonds	**Angle (deg)**	**Bonds**	**Angle (deg)**
Sn—Te—Sn	103.68(2)	Sn—C(7)—C(8)	122.6(4)
Te—Sn—C(1)	113.5(1)	Sn—C(7)—C(12)	118.7(4)
Te—Sn—C(7)	100.9(1)	C(8)—C(7)—C(12)	118.8(5)
Te—Sn—C(13)	114.2(1)	C(7)—C(8)—C(9)	120.2(6)
C(1)—Sn—C(7)	112.1(2)	C(8)—C(9)—C(10)	118.9(6)
C(1)—Sn—C(13)	106.8(2)	C(9)—C(10)—C(11)	120.8(5)
C(7)—Sn—C(13)	109.4(2)	C(10)—C(11)—C(12)	121.0(6)
		C(11)—C(12)—C(7)	120.3(6)
Sn—C(1)—C(2)	122.7(4)	Sn—C(13)—C(14)	120.4(4)
Sn—C(1)—C(6)	119.8(4)	Sn—C(13)—C(18)	121.4(4)
C(2)—C(1)—C(6)	117.4(5)	C(14)—C(13)—C(18)	118.3(5)
C(1)—C(2)—C(3)	121.0(5)	C(13)—C(14)—C(15)	119.6(6)
C(2)—C(3)—C(4)	120.5(5)	C(14)—C(15)—C(16)	122.1(7)
C(3)—C(4)—C(5)	118.7(6)	C(15)—C(16)—C(17)	118.7(6)
C(4)—C(5)—C(6)	120.8(6)	C(16)—C(17)—C(18)	120.8(6)
C(5)—C(6)—C(1)	121.5(5)	C(17)—C(18)—C(13)	120.6(6)

TABLE 3. Summary of important bond parameters in $(Ph_3Sn)_2E$ (where E = S, Se or Te)

Compound	Bond lengths[a]		Bond angles[b]		
	Sn—E	Sn—C	Sn—E—Sn	E—Sn—C	C—Sn—C
$(Ph_3Sn)_2S$	2.370(4), 2.403(4)	2.12(1)–2.15(1)	107.4(1)	99.1(3)–116.3(3)	110.3(ave)[c]
$(Ph_3Sn)_2Se$[d] (*i*)	2.521(3), 2.522(3)	2.109(12)–2.168(16)	103.4(1)	104.3(5)–112.5(4) 109.8(ave)	106.8(8)–113.4(8) 109.1(ave)
(*ii*)	2.538(3), 2.523(3)	2.107(16)–2.159(17)	105.2	104.4(4)–114.8(4) 109.5(ave)	107.4(8)–110.6(8) 109.4(ave)
$(Ph_3Sn)_2Te$[e]	2.7266(6)	2.134(5)–2.143(5)	103.68(2)	100.9(1)–114.2(1) 109.5(ave)	106.8(2)–112.1(2) 109.4(ave)

[a]Bond lengths in Å.
[b]Angles in deg.
[c]The error in an individual C—Sn—C angle was 0.4°.
[d]There are two independent molecules in the asymmetric unit.
[e]The Te atom lies on a crystallographic two-fold axis; consequently both halves of the molecule are equivalent.

atom. As expected the "bent" structure found for the present compound, $(Ph_3Sn)_2E$, where E = Te, is very similar to those found for the analogous compounds where E = S (9) and Se (10). Important bond parameters for all three compounds are summarized in Table 3. The coordination about tin is essentially tetrahedral in each case. Indeed, while a range of bond angles is observed about tin in each compound, the average E—Sn—C and C—Sn—C bond angles all approach the tetrahedral value of 109.5°. As might have been predicted, the Sn—E—Sn angle contracts on moving from S → Se → Te, corresponding to an increase in Te—E distance in the same order. There were no unusual intermolecular distances found for $(Ph_3Sn)_2Te$.

The fact that the coordination about the tin is essentially tetrahedral in all the triphenyltin chalcogenides is of some importance in interpreting the Mössbauer and nmr spectroscopic data for these compounds.

The ^{119}Sn Mössbauer quadrupole splittings (Table 4) for $(Ph_3Sn)_2E$ and for $(Me_3Sn)_2E$ show a trend to smaller values as the electronegativity of the chalcogen decreases. This is readily understood in terms of an increased donation of electron density from the chalcogen to the tin as the chalcogen electronegativity decreases, since this would lead to a decrease in the *p*-orbital imbalance about the tin and hence a smaller quadrupole splitting. The very small increase in the Mössbauer isomer shifts with decreasing electronegativity of the chalcogen corre-

Can. J. Chem. Downloaded from www.nrcresearchpress.com by 210.87.254.40 on 09/06/12
For personal use only.

TABLE 4. Mössbauer and nmr data

Compound	Mössbauer data δ[a] (mm s^{-1})	Mössbauer data Δ (mm s^{-1})	NMR data Chemical shift[b] ppm	Ref.[c]
$(Ph_3Sn)_2S$	1.20	1.46	−48.7 (neat)	2
$(Ph_3Sn)_2Se$	1.32(2)	1.40(2)	−76 ($CDCl_3$)	
$(Ph_3Sn)_2Te$	1.33(2)	1.23(2)	−143.2 ($CDCl_3$)	
$(Me_3Sn)_2S$	1.26(2)	1.68(2)	+93.9 ($CDCl_3$)	
			+84.9 (neat)	13
$(Me_3Sn)_2Se$	1.29(2)	1.59(2)	+50.7 ($CDCl_3$)	
			+44.5 (neat)	13
$(Me_3Sn)_2Te$	1.32(2)	1.49(2)	−59.3 ($CDCl_3$)	
			−66.8 (CH_2Cl_2)	13

[a] ^{119}Sn Mössbauer isomer shift with respect to $BaSnO_3$; the Mössbauer data for $(Ph_3Sn)_2S$ are taken from ref. 1. The data for the other compounds are this work with the source and absorbers at 77 K and the errors are shown in parentheses.

[b] ^{119}Sn nmr chemical shifts relative to Me_4Sn; up-field shifts are negative.

[c] References to the literature values for the nmr data are as shown. The measurements made in $CDCl_3$ solution are this work.

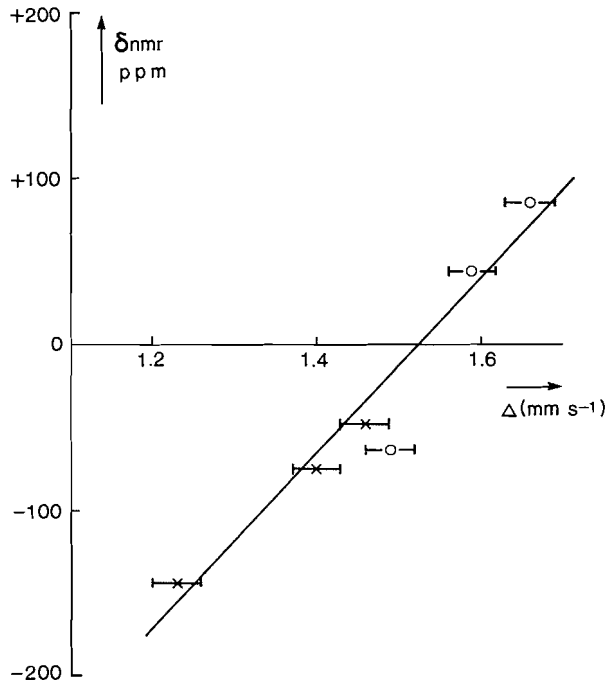

FIG. 2. A plot of the ^{119}Sn Mössbauer quadrupole splittings against the ^{119}Sn nmr chemical shifts for ×, $(Ph_3Sn)_2E$ and ○, $(Me_3Sn)_2E$ where E = S, Se, or Te.

sponds to the increased donation from the chalcogen into an sp^3 hybrid orbital on the tin and a small net increase in the *s*-electron density at the nucleus.

It can also be seen that the quadrupole splittings for the trimethyltin compounds are consistently greater than those of the triphenyltin analogues. This is consistent with the phenyl group having a greater electronegativity than the methyl group in these compounds.

In contrast with the ^{119}Sn Mössbauer data in the solid state, the ^{119}Sn solution nmr chemical shifts exhibit a wide range of values (Table 4). The chemical shifts of the heavier nuclei, such as tin, are generally assumed to be dominated by the Ramsey paramagnetic term (11−14) which may be written approximately as:

$$\sigma^p \propto \frac{-1}{\Delta E}\left(\langle r^{-3}\rangle_{5p}P + \langle r^{-3}\rangle_{5d}D\right)$$

where ΔE is the mean electronic excitation term, the $\langle r^{-3}\rangle$ terms are the mean inverse cubes of the $5p$ and $5d$ electron−nuclear distances, and the P and D terms reflect the imbalance of the $5p$ and $5d$ orbitals. Within a closely related series of compounds the ΔE terms may be taken as comparable and, if the D term can be neglected, then the chemical shifts should show a dependence on the P term. As the electronegativity of the chalcogen bonded to tin decreases in the $(R_3Sn)_2E$ compounds, then P should decrease, the nucleus should become increasingly shielded, and the chemical shift should become more negative, as is indeed observed, both for the triphenyl and the trimethyl compounds. While there are many other factors which may also influence the nmr chemical shifts (12), the above argument provides a qualitative explanation for the observed trends.

The preceding discussion suggests that in these compounds, assuming that the chemical environment about the tin in these molecules is similar in solution to that in the solid state, the ^{119}Sn Mössbauer quadrupole splitting and the ^{119}Sn nmr chemical shift should be correlated. As is illustrated in Fig. 2 this would appear to be the case. The fact that in Fig. 2 the triphenyltin and trimethyltin compounds all appear to lie on a straight line may be fortuitous since the parent species, Ph_4Sn and Me_4Sn, do not themselves have the same chemical shift. It should also be noted that for selenium, and more particularly for tellurium, the so-called (12) "bulky atom effect" may also influence the chemical shifts. Nevertheless, it can be seen the correlation between the nmr chemical shifts and Mössbauer quadrupole splittings is the same for both the triphenyltin and the trimethyltin compounds.

It must be emphasised that such correlations between the Mössbauer and nmr data can only be anticipated within a series of compounds of similar structure and where the environment about the tin is similar throughout the series in both the solid state and in solution. The present crystal structure data confirms that the environment about the tin in the telluride is indeed similar to that in the selenide and sulphide. Moreover, since this environment is very close to tetrahedral in the solid state, with the absence of any significant intermolecular inter-

Can. J. Chem. Downloaded from www.nrcresearchpress.com by 210.87.254.40 on 09/06/12
For personal use only.

actions, it would be expected that a similar geometry would prevail in solution. Crystal structure data for the $(Me_3Sn)_2E$ compounds are not currently available.

Acknowledgements

Grants from the Natural Sciences and Engineering Research Council of Canada in support of this research are gratefully acknowledged by F. W. B. Einstein and C. H. W. Jones. The assistance of Dr. A. S. Tracey in measuring the ^{119}Sn nmr spectra is also acknowledged.

1. R. H. HERBER, H. A. STÖCKLER, and W. T. REICHLE. J. Chem. Phys. **42**, 2447 (1965).
2. B. K. HUNTER and L. W. REEVES. Can. J. Chem. **46**, 1399 (1968).
3. H. SCHUMANN, K. F. THOM, and M. SCHMIDT. J. Organomet. Chem. **2**, 361 (1964).
4. M. R. DETTY and M. D. SEIDLER. J. Org. Chem. **47**, 1354 (1982).
5. D. F. GRANT and E. J. GABE. J. Appl. Crystallogr. **11**, 114 (1977).
6. D. T. CROMER and J. T. WABER. International tables for X-ray crystallography. Vol. IV. Kynoch Press, Birmingham, England. 1974.
7. A. C. LARSON and E. J. GABE. Computing in crystallography. *Edited by* H. Schenk *et al*. Delft University Press, Holland. 1978. p. 81.
8. C. K. JOHNSON. ORTEP. Report ORNL-5138, Oak Ridge National Laboratory, TN. 1976.
9. O. A. D'YACHENKO, A. B. ZOLOTOI, L. O. ATOVMYAN, R. G. MIRSKOV, and M. G. VORONKOV. Dokl. Akad. Nauk SSSR, **237**, 1142 (1977).
10. B. KREBS and H.-J. JACOBSEN. J. Organomet. Chem. **178**, 301 (1978).
11. J. D. KENNEDY and W. MCFARLANE. J. Organomet. Chem. **94**, 7 (1975).
12. R. K. HARRIS, J. D. KENNEDY, and W. MCFARLANE. NMR and the periodic table. *Edited by* R. K. Harris and B. E. Mann. Academic Press, New York. 1978. pp. 342–366.
13. P. J. SMITH and A. P. TUPCIAUSKAS. Ann. Rep. NMR Spectrosc. **8**, 291 (1978).
14. R. HANI and R. A. GEANANGEL. Co-ord. Chem. Rev. **44**, 229 (1982).

Can. J. Chem. Downloaded from www.nrcresearchpress.com by 210.87.254.40 on 09/06/12
For personal use only.

The use of shift reagents and ^{13}C nuclear magnetic resonance for assignment of stereochemistry to oximes[1]

ROBERT R. FRASER AND RAJ CAPOOR
Ottawa–Carleton Institute for Research and Graduate Studies in Chemistry, University of Ottawa, Ottawa, Ont., Canada K1N 9G4

AND

JOHN W. BOVENKAMP, BENOIT V. LACROIX, AND JACK PAGOTTO
Defence Research Establishment Ottawa, Ottawa, Ont., Canada K1A 0Z4

Received March 23, 1983

ROBERT R. FRASER, RAJ CAPOOR, JOHN W. BOVENKAMP, BENOIT V. LACROIX, and JACK PAGOTTO. Can. J. Chem. **61**, 2616 (1984).

The effects of the shift reagents $Eu(dpm)_3$ and $Eu(fod)_3$ on the ^1H and ^{13}C nmr spectra of twelve oximes of diverse structure were examined. The proton data show that the use of proton shifts to assign oxime stereochemistry, as has been done in the past, is unreliable. In contrast, $Eu(dpm)_3$ causes LIS values for the ^{13}C signals of α carbons which are strongly dependent on stereochemistry. Signals for all α carbons *anti* to the oxime oxygen experience large downfield shifts while all *syn* carbons are either unaffected or shifted upfield. Thus the effects of $Eu(dpm)_3$ on these ^{13}C signals provides an unambiguous method of configurational assignment to oximes. The effects of $Eu(fod)_3$, though similar to $Eu(dpm)_3$, were less consistent and thus less promising for making configurational assignments.

ROBERT R. FRASER, RAJ CAPOOR, JOHN W. BOVENKAMP, BENOIT V. LACROIX et JACK PAGOTTO. Can. J. Chem. **61**, 2616 (1984).

On a étudié les effets des réactifs de contact $Eu(dpm)_3$ et $Eu(fod)_3$ sur les spectres de rmn du ^1H et du ^{13}C de douze oximes ayant diverses structures. Les données de la rmn du proton révèlent que l'utilisation des réactifs de contact pour attribuer la stéréochimie d'oximes n'est pas rigoureuse. Le $Eu(dpm)_3$ au contraire provoque des déplacements des signaux du ^{13}C des carbones en position α qui dépendent beaucoup de la stéréochimie. Les signaux de tous les carbones α en position *anti* par rapport à l'oxime-oxygène subissent de forts déplacements vers les champs faibles tandis que tous les carbones en position *syn* ou bien ne bougent pas ou alors se déplacent vers les champs forts. Ainsi l'effet du $Eu(dpm)_3$ sur ces signaux du ^{13}C fournit une méthode non équivoque d'attribution de configuration des oximes. Les effets du $Eu(fod)_3$, quoiqu'identiques à ceux du $Eu(dpm)_3$, sont moins cohérents et par conséquent peu sûrs pour faire des attributions de configuration.

[Traduit par le journal]

Can. J. Chem. Downloaded from www.nrcresearchpress.com by 210.87.254.42 on 09/06/12
For personal use only.

The effect of the addition of the shift reagent, $Eu(dpm)_3$[2] on the proton spectra of oximes has been the subject of some controversy and of considerable misunderstanding. The first study by Wolkowski (1) described the observation of a dependence of the observed downfield shifts on the proton to oxime oxygen distance. In the same year, a paper by Berlin and Rengaraju (2) described a study of the effect of adding $Eu(dpm)_3$ to a mixture of *E* and *Z* 2-butanone oximes. The conclusion of this paper, based on the observation of larger lanthanide induced shifts (LIS values) for all of the protons in the *Z* isomer, was that complexation occurred at the nitrogen atom. Concurrently, a third paper by Tronchet *et al.* (3) described a study of LIS values for pairs of isomeric aldoximes. For this class of oximes the *Z* isomers were also observed to give much larger downfield shifts, indicative of coordination at nitrogen. Subsequently, the proposed distance relation of Wolkowski was employed in assigning configuration to pairs of oximes. In one paper the assignment on this basis (4) turned out to be in error (5), while a second utilization of the dependence on distance from oxygen actually gave the correct assignment as it was unambiguously confirmed by subsequent Beckmann rearrangements (6). Interestingly, a comparable number of later papers chose to interpret Berlin's data as indicating that protons closer to the lone pair on nitrogen should show larger LIS values (by assuming a distance dependent correlation). Both of these papers (5, 7) in fact, gave correct assignments as subsequently validated by Beckmann rearrangements. In view of such conflicting results, we hesitated in using any shift reagent data to aid us in assessing the configurations of oximes of unknown stereochemistry. We therefore decided to undertake a more thorough examination of the effects of stereochemistry on proton LIS values obtained using both $Eu(dpm)_3$ and the more popular $Eu(fod)_3$ with a variety of ketoximes. We have extended the study to include the comparison of all ^{13}C spectral changes as well. The results clearly show ^1H nmr to be an unreliable probe for the correlation of LIS values with configurational assignments. In contrast, ^{13}C nmr provides a strikingly clear relationship between LIS values and the stereochemistry of oximes.

Scope of studies

We have examined the effects of the addition of the two most commonly used shift reagents, $Eu(dpm)_3$ and $Eu(fod)_3$, on both the ^1H and ^{13}C spectra of twelve ketoximes, including four symmetrical oximes, and four pairs of *E* and *Z* stereoisomers. The resultant proton data are reported in Fig. 1, and the ^{13}C data appear in Fig. 2.

Results of proton spectral studies

The first observation of interest is the very good agreement (<5% difference in all LIS) between our proton data for **2** and **3** and that reported earlier under identical conditions (in $CDCl_3$) by Berlin and Rengaraju (2). In contrast, the values reported by Wolkowski (1) differ widely (in one case, three-fold) from the results obtained by us under his conditions (in CCl_4). His

[1]DREO Report No. 879.

[2]$Eu(dpm)_3$ is the abbreviation for tris(2,2,6,6-tetramethylheptane-3,5-dionato)europium, $Eu(fod)_3$ for tris(1,1,1,2,2,3,3-heptafluoro-7,7-dimethyloctane-4,6-dionato)europium.

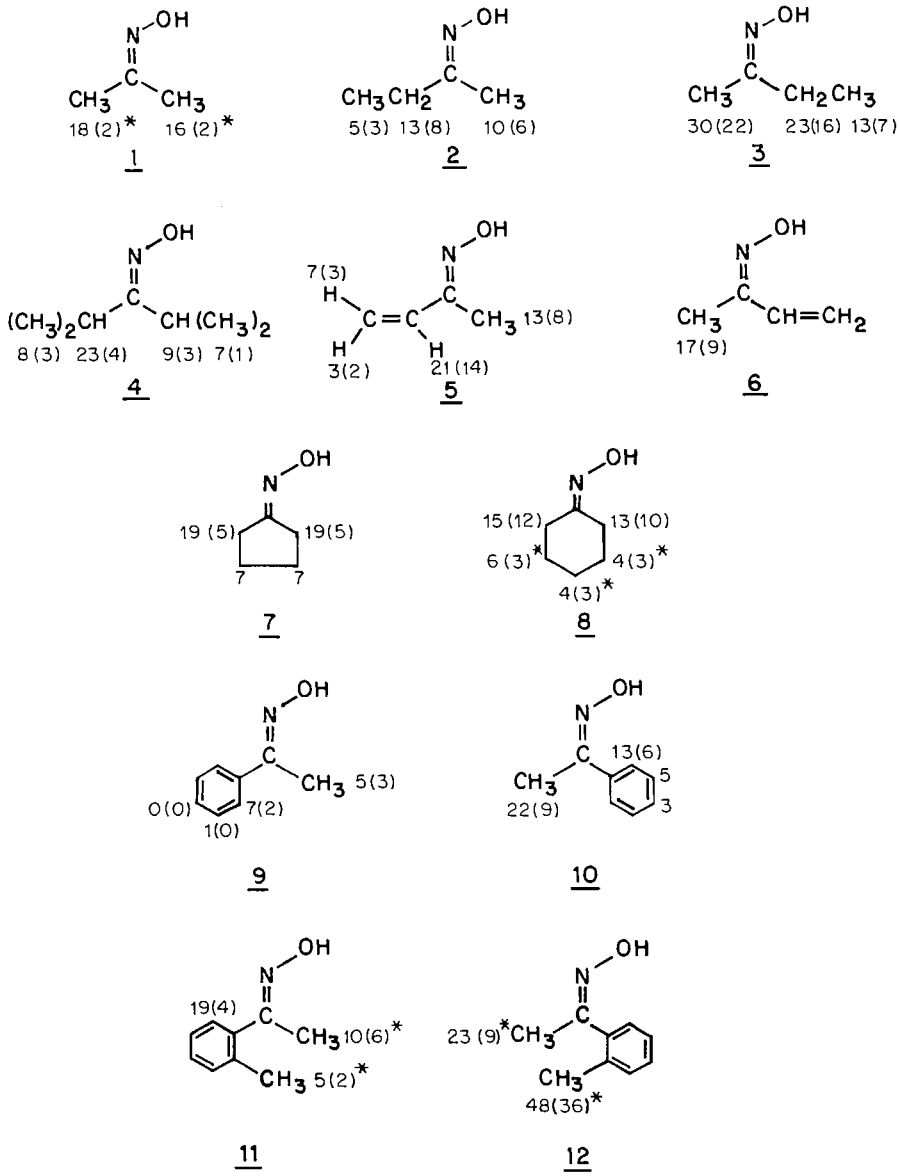

FIG. 1. The downfield shifts (LIS values) are given for individual protons, as induced by the addition of 0.1 equivalent of shift reagent to 0.5 *M* solutions, in $CDCl_3$, of oximes **1** to **12**. The figures represent the effects of $Eu(dpm)_3$ and (in brackets) $Eu(fod)_3$ after extrapolation to one equivalent. Those shifts which might reasonably be interchanged are indicated with an asterisk.

reported LIS values for acetone oxime and methyl vinyl ketoxime also differ from those we report in Fig. 1. Furthermore, Wolkowski's values for the *Z* and *E* isomers of acetaldoxime were reported to be in error in the paper by Tronchet *et al.* (3). It is therefore clear, though for reasons not apparent, that the data reported in ref. 1 are not reliable. The other results in Fig. 1 further support this contention in that the purported relationship between the magnitude of the LIS value of a proton and its distance from the oxime oxygen cannot be seen.

For all pairs of oximes, **2** and **3**, **5** and **6**, **9** and **10**, and **11** and **12** there is a consistent pattern in that the *Z* isomer having the methyl *syn* to the lone pair on nitrogen always exhibits larger LIS values for all its proton signals than for those of the *E* isomer, a result consistent with greater binding of the *Z* isomer at nitrogen.[3] Another feature of the ^1H data is the complete lack of any relationship between the LIS values and distance between the proton and the nitrogen binding site (see, for example, data on **1**, **7**, and **8**). The lack of any distance dependence may arise from a number of factors including a variation in binding site. The most likely complication is a significant contribution from the angular term (8) which would cause protons *syn* to the binding site at nitrogen to be much less influenced by the shift reagent than those *anti* but further away. The presence of a contact shift which can occur with both aliphatic and aromatic amines (8) would further obscure any distance dependence. A recent review (9) discusses these and several other factors which are widely recognized contributors to the complication of LIS data. The net result is the failure of the data in Fig. 1 to provide a general method of configurational assignment. However, it can be said that for a pair of ketoximes of recognizable differences in steric access to the oxime nitrogen an assignment could be made on the basis of relative binding strengths, as was seen for aldoximes (7). Finally, it should be pointed out that the LIS data for $Eu(fod)_3$

[3]This does not preclude the possibility of some binding of the *Z* isomer at oxygen, or of a larger amount of binding at oxygen by the *E* isomer.

Can. J. Chem. Downloaded from www.nrcresearchpress.com by 210.87.254.42 on 09/06/12
For personal use only.

Can. J. Chem. Downloaded from www.nrcresearchpress.com by 210.87.254.42 on 09/06/12
For personal use only.

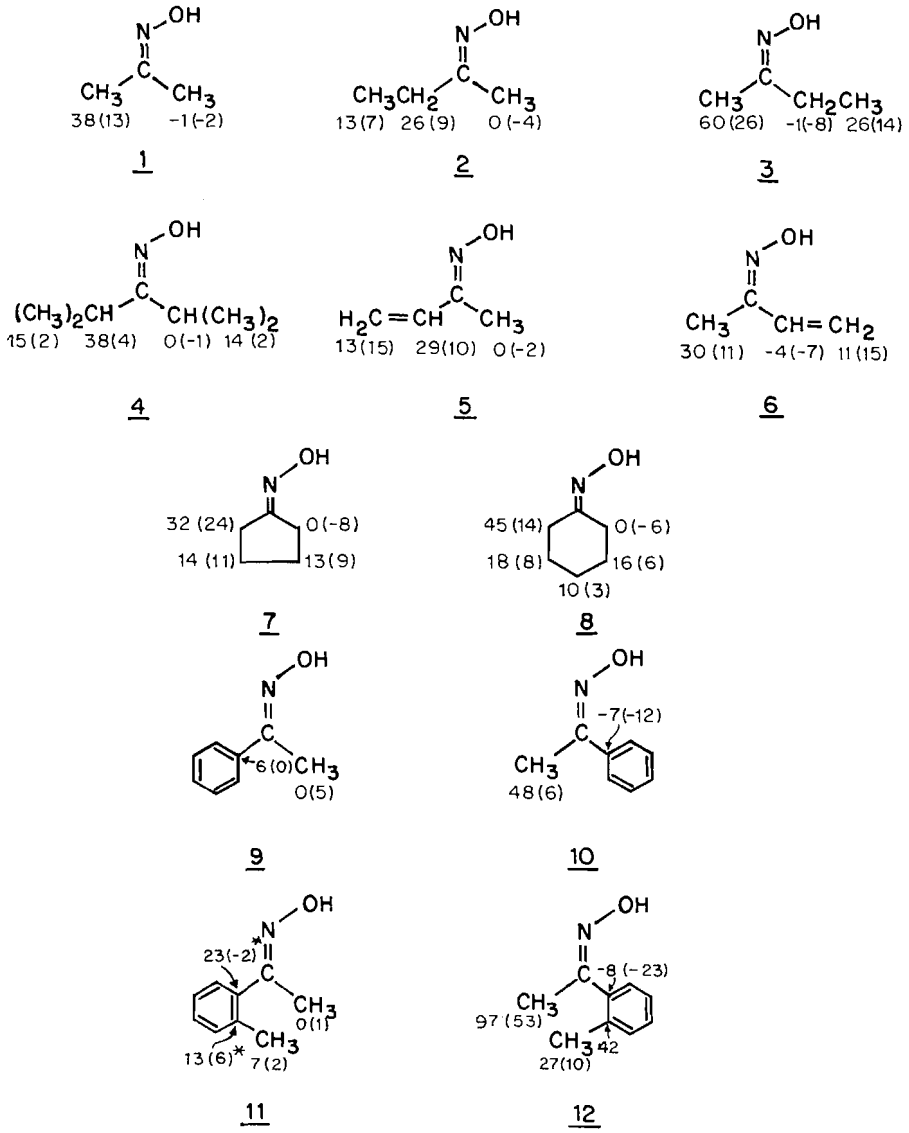

FIG. 2. The LIS values are given for the ^{13}C nuclei, induced by the addition of 0.1 equivalent of shift reagent to 0.5 *M* solutions, in $CDCl_3$ of oximes **1** to **12**. The figures, extrapolated to 1 equivalent, represent the effects of $Eu(dpm)_3$ and (in brackets) $Eu(fod)_3$. Negative values indicate upfield shifts.

is notable only in the sense that the induced shifts are consistently much smaller. This is an effect opposite to that normally seen (8) although there is precedent in the literature (10).

A special comment is required regarding some of the data in Fig. 1 and also Fig. 2. The data for **2** and **3**, for **5** and **6**, and for **11** and **12** were obtained from a mixture of both components (see Experimental for compositions). As a result of the greater binding ability of the *Z* isomer, there is a bias to larger LIS values for each *Z* isomer and concomitantly a depression of the figures for the *E* isomers. The data for **9** and **10** were obtained using the pure compounds.

Results of ^{13}C spectral studies

(a) *Effects of Eu(dpm)$_3$*

The ^{13}C data in Fig. 2 show a remarkably clear pattern of stereochemical influence on the shifts caused by the addition of this shift reagent. The α carbon *syn* to the lone pair on nitrogen is always shifted downfield more than any other carbon and the carbon *anti* to the lone pair on nitrogen is either shifted upfield or unaffected. Such a marked difference in LIS behaviour provides an unmistakable method for the assignment of configuration to ketoximes. The compounds studied include α carbons which are aliphatic, olefinic, and aromatic and so structural variation has not affected their LIS values. The reason for the strikingly different results for *syn* and *anti* α carbons is undoubtedly the intrusion of a stereochemically dependent contact shift. Studies of the effect of nickel(II) acetylacetonate have clearly shown that its complex formation with amines causes contact shifts of the ^{13}C nuclei whose magnitudes depend on both stereochemistry and the number of intervening bonds. A β carbon *trans* to the lone pair site of complexation experiences a two to threefold larger contact shift than when *gauche* or *cis* (11, 12). There is also ample evidence that ^{13}C shifts are much more susceptible than protons to contact shifts when complexed to a europium tris diketonate (13, 14). In one study, the proportion of contact to pseudo-contact (normal) mechanism contributing to the LIS of ^{13}C nuclei using $Eu(fod)_3$ has been shown to be of approximately the same magnitude for picoline and for octylamine (15). Thus, the LIS values in Fig. 2 for $Eu(dpm)_3$ reflect a downfield shift

Can. J. Chem. Downloaded from www.nrcresearchpress.com by 210.87.254.42 on 09/06/12
For personal use only.

resulting from dominance of the pseudocontact mechanism for all carbons except those *anti* to the lone pair on nitrogen. In the latter case, the contact mechanism causes an upfield shift equal to or greater than the pseudocontact contribution and the resultant zero or upfield movement of the carbon signal. Shifts for the other carbons can, in principle, receive finite but smaller contact contributions whose signs sometimes alternate with distance. The magnitude of such contributions to the observed carbon shifts cannot be properly assessed.

Regardless of the limitations to our rationalization of these results, as we also must bear in mind the caveats of ref. 9, the ^{13}C LIS values induced by $Eu(dpm)_3$ provide an unambiguous method for the assignment of configuration to oximes. Indeed the differences in behaviour of *E* and *Z* isomers is sufficiently great that a reliable assignment should be possible even in a case where only one isomer is available. The same does not appear to apply to previous methods involving proton shifts (16–18). Additionally, $Eu(dpm)_3$ provides a method of signal assignment in symmetrical ketoximes.

(b) *Effects of $Eu(fod)_3$*

There are several notable features seen in the effects of $Eu(fod)_3$ on the ^{13}C spectra of **1** to **12**. In general, the induced shifts are algebraically more negative than those produced by $Eu(dpm)_3$. This very likely reflects a weaker binding of $Eu(fod)_3$ as is evident by the much smaller LIS values at the β carbons. There also appears to be a larger contact shift at the α carbons *anti* to the lone pair on nitrogen. The striking exception, **9**, shows a significantly more positive LIS caused by $Eu(fod)_3$ at the carbon *anti* to the lone pair on nitrogen. A possible explanation for this deviant behaviour is a decrease in the strength of binding at nitrogen due to interference by the bulky phenyl group, which thereby decreases the contact shift and allows the effect of binding at oxygen to be seen. As a consequence of this lesser consistency in the effects of $Eu(fod)_3$ on ^{13}C shifts, we recommend that only $Eu(dpm)_3$ be used, in conjunction with ^{13}C, as a reliable method of making configurational assignments to oximes.

Spectral assignments

Most of the oximes in this paper have been the subject of earlier ^{13}C studies (19–22). One of the signal assignments, specifically that made for the α carbon *syn* to the oxime function in **8**, (19, 20) must be altered. The signal appearing at δ 24.4, previously assigned to C–4, is the peak whose LIS in the presence of $Eu(dpm)_3$ is zero and thus represents C-2 (*syn* to the oxime oxygen). The low field peaks at δ 25.6, 25.8, and 26.9 are best assigned to C-3, C-4, and C-5 respectively, also on the basis of the LIS data.

Those oximes whose ^{13}C spectra have not yet been described, **6**, **11**, and **12**, presented little difficulty in signal assignment. For **6**, present as a minor component with **5** in a mixture of stereoisomers, the configurations were assigned utilizing the general rule that the upfield methyl signal belongs to the *E* isomer (19, 20, 23). In **11** and **12**, it was first necessary to establish the methyl assignments by measuring the fully coupled spectrum of each isomer. The signal for the α methyl in the *Z* isomer (δ 21.9) appeared as a sharp quartet while the *ortho* methyl (δ 19.4) gave a quartet consisting of four peaks broadened substantially by unresolved coupling with the *ortho* (and *para*) protons on the aromatic ring. The methyl assignments for the *E* isomer were similarly determined. The complete shift data for **6**, **11**, and **12** appears in the Experimental.

The proton data given in Fig. 1 are ambiguous in certain cases due to uncertain proton assignments. Specifically, in **1** and **7** the LIS shifts for the α protons were so similar that there was no need to make a rigorous assignment. To indicate where the possibility of a reversal of assignment exists, as in **1**, the LIS value is given an asterisk. For **4**, the proton assignments were proven by selective decoupling of the peaks for the α ^{13}C signals and are given in the Experimental. For **8**, the previous literature assignments (24) were confirmed by selective decoupling.

Experimental

The oximes **1**, **7**, **8**, and **9** were obtained commercially. The oximes of 2-butanone (**2** and **3**), synthesized by the method of Pearson and Bruton (25), were produced in a 76:24 ratio respectively (determined from the proton nmr spectrum of 50 mg of the oxime mixture and 60 mg of $Eu(fod)_3$ in 0.5 mL carbon tetrachloride). Berlin and Rengaraju (2) reported a similar ratio of 72:28. Ketoxime **4**, obtained by the method of Pearson and Bruton (25), had a bp of 89°C/20 Torr (lit. (26) bp 91°C/21 Torr); nmr in $CDCl_3$, δ: 1.13, 1.16 (CH_3's), 2.5 (CH *anti* to oxime), 3.2 (CH *syn* to oxime). Oximes **5** and **6** were obtained as an 85:15 mixture by reacting methyl vinyl ketone with hydroxylamine hydrochloride in the presence of sodium acetate (27). An identical ratio was obtained by Buczkowski and Plenkiewicz (28). The pure *Z*-isomer of α bromoacetophenone oxime was prepared using the method Blumbergs *et al.* (29) and then converted to **10** as described by Smith and Kaiser (30) (mp 82–83°C (lit. (30) mp 81–83°C).

A mixture of **11** and **12** was obtained by the oximation of 2-methylacetophenone (31). The ratio of **11** to **12** in the semi-solid product was shown to be 67:33, as determined by hplc (Waters Associates model ALC/GPC 201, uBondapak C18 column (7.8 mm × 30 cm), water/methanol 50:50).

All ^1H nmr spectra were measured on a Varian T-60 nmr spectrometer. The LIS values reported in Fig. 1 were obtained from spectra run in the presence of 0.05 and 0.1 mmol of shift reagent added to 0.5 mL of 0.5 *M* solution of the oxime in $CDCl_3$. The LIS values for **2** and **3** in CCl_4 under the conditions of Wolkowski (1) were for **2**: 12(C-1), 16(C-3), and 6(C-4), and for **3**: 40(C-1), 35(C-3), and 17(C-4). All ^{13}C spectra were measured on a Varian FT-80 nmr spectrometer. The LIS values reported in Fig. 2 were obtained from spectra run in the presence of 0.05 and 0.1 mmol of shift reagent added to 2.0 mL of 0.5 *M* solution of the oxime in $CDCl_3$. Selective decoupling of the α protons in **4** and **8** during measurement of the ^{13}C spectra were performed on a Varian XL-200.

^{13}C chemical shifts

The ^{13}C spectra of oximes **6**, **11**, and **12** have not been reported previously. For the major isomer of methyl vinyl ketoxime, **5**, shifts were measured on the neat liquid (22). Our shifts (δ in ppm from TMS) measured on 0.5 *M* solutions of **5**, **6**, **11**, and **12** and assigned as discussed earlier are, for *E*-1-buten-3-one oxime, C-1 (118.7), C-2(134.2), C-3(156.6), C-4(9.0), and *Z*-1-buten-3-one oxime, C-1(122.2), C-2(125.9), C-3(163.9), C-4(16.2); and for *E-ortho*-methylacetophenone oxime, C_α(15.9), C=N(157.9), *o*-CH_3(20.0), C-1—C-6(137.4 and 135.7, quaternary carbons; 125.8, 128.2, 128.6, 130.7, tertiary carbons) and *Z-ortho*-methylacetophenone oxime, C_α(21.9), C=N(156.5), *o*-CH_3(19.4), C-1 and C-2(135.5 and 134.6), C-3—C-6 unidentified.

Acknowledgements

We wish to thank Dr. G. W. Buchanan of Carleton University for performing the selective decoupling experiments. RRF and RC thank the Department of National Defence and NSERCC for financial assistance.

1. Z. W. WOLKOWSKI. Tetrahedron Lett. 825 (1971).
2. K. D. BERLIN and S. RENGARAJU. J. Org. Chem. **36**, 2912 (1971).
3. J. M. J. TRONCHET, F. BARBALAT-REY, and N. LEHONG. Helv. Chim. Acta, **54**, 2615 (1971).
4. R. K. HILL and D. A. CULLISON. J. Am. Chem. Soc. **95**, 2923 (1973).
5. C. A. GROB and J. IDE. Helv. Chim. Acta, **57**, 2562 (1974).
6. S. R. WILSON and R. A. SAWICKI. J. Org. Chem. **44**, 330 (1979).
7. T. SASAKI, S. EGUCHI, and O. HIROAKI. J. Org. Chem. **41**, 1803 (1976).
8. O. HOFER. Top. Stereochem. **9**, 111 (1976).
9. F. INAGAKI and T. MIYAZAWA. Prog. Nucl. Magn. Reson. Spectrosc. **14**, 67 (1980).
10. B. L. SHAPIRO, M. D. JOHNSTON, JR., A. D. GODWIN, T. W. PROULX, and M. J. SHAPIRO. Tetrahedron Lett. 3233 (1972).
11. I. MORISHIMA, K. OKADA, T. YONEZAWA, and K. GOTO. J. Am. Chem. Soc. **93**, 3922 (1971).
12. I. MORISHIMA, K. OKADA, and T. YONEZAWA. J. Am. Chem. Soc. **94**, 1425 (1972).
13. G. E. HAWKES, C. MARZIN, S. R. JOHNS, and J. D. ROBERTS. J. Am. Chem. Soc. **95**, 1661 (1973).
14. O. A. GANSOW, P. A. LOEFFLER, R. E. DAVIS, M. R. WILCOTT III, and R. E. LENKINSKI. J. Am. Chem. Soc. **95**, 3389 (1973).
15. K. AJISAKA and M. KAINOSHO. J. Am. Chem. Soc. **97**, 330 (1975).
16. G. J. KARABATSOS and R. A. TALLER. Tetrahedron, **24**, 3347 (1968).
17. G. G. KLEINSPEHN, J. A. JUNG, and S. A. STUDNIARZ. J. Org. Chem. **32**, 460 (1967).
18. J. P. GUETTÉ, J. ARNEAUD, and L. LACOMBE. C. R. Acad. Sci. Paris Ser. C, **264**, 1509 (1967).
19. G. E. HAWKES, K. HERWIG, and J. D. ROBERTS. J. Org. Chem. **39**, 1017 (1974).
20. P. GENESTE, R. DURAND, J. M. KAMENKA, H. BEIERBECK, R. MARTINO, and J. K. SAUNDERS. Can. J. Chem. **56**, 1940 (1978).
21. G. W. BUCHANAN and B. A. DAWSON. Can. J. Chem. **55**, 1437 (1977).
22. Z. W. WOLKOWSKI, E. VAUTHIER, B. GONBEAU, and H. SAUVAITRE. Tetrahedron Lett. 565 (1972).
23. G. C. LEVY and G. L. NELSON. J. Am. Chem. Soc. **94**, 4897 (1972).
24. W. F. TRAGER and A. C. HUITRIC. Tetrahedron Lett. 825 (1966).
25. D. E. PEARSON and J. D. BRUTON. J. Org. Chem. **19**, 957 (1954).
26. P. T. SCOTT, D. E. PEARSON, and L. J. BIRCHER. J. Org. Chem. **19**, 1815 (1954).
27. M. BENDER, Z. BUCZKOWSKI, and J. PLENKIEWICZ. Bull. Acad. Pol. Sci. Ser. Sci. Chem. **17**, 643 (1969).
28. Z. BUCZKOWSKI and J. PLENKIEWICZ. Bull. Acad. Pol. Sci. Ser. Sci. Chim. **18**, 647 (1970).
29. P. BLUMBERGS, C. B. THANNAWALLA, and A. B. ASH. J. Org. Chem. **36**, 2023 (1971).
30. J. H. SMITH and E. T. KAISER. J. Org. Chem. **39**, 728 (1974).
31. D. E. PEARSON and W. E. COLE. J. Org. Chem. **20**, 488 (1955).

Can. J. Chem. Downloaded from www.nrcresearchpress.com by 210.87.254.42 on 09/06/12
For personal use only.

The retroaldol reaction of chalcone

J. Peter Guthrie,[1] John Cossar, Patricia A. Cullimore, Nayyer Monshizadeh Kamkar, and Kathleen F. Taylor

Department of Chemistry, University of Western Ontario, London, Ont., Canada N6A 5B7

Received April 7, 1983

J. Peter Guthrie, John Cossar, Patricia A. Cullimore, Nayyer Monshizadeh Kamkar, and Kathleen F. Taylor. Can. J. Chem. **61**, 2621 (1983).

All four rate constants required to describe the hydration and aldolization/dealdolization reactions of chalcone (1,3-diphenyl-2-propen-1-one) have been determined in aqueous sodium hydroxide solutions. Kinetics were studied starting with chalcone, with its hydrate, 1,3-diphenyl-3-hydroxy-1-propanone, and with benzaldehyde in the presence of excess acetophenone. The rate constants for hydroxide catalyzed reactions, defined in terms of eq. [1] are: $k_{12} = 10.5 \pm 0.5 \times 10^{-4}\ M^{-1}\ s^{-1}$; $k_{21} = 0.026 \pm 0.002\ M^{-1}\ s^{-1}$; $k_{23} = 0.194 \pm 0.017\ M^{-1}\ s^{-1}$; and $k_{32} = 0.84 \pm 0.12\ M^{-2}\ s^{-1}$ (all at ionic strength 0.1). The corresponding equilibrium constants for aldol adduct formation and dehydration are 4.3 M^{-1} and 25.

J. Peter Guthrie, John Cossar, Patricia A. Cullimore, Nayyer Monshizadeh Kamkar et Kathleen F. Taylor. Can. J. Chem. **61**, 2621 (1983).

On a déterminé, dans des solutions aqueuses d'hydroxyde de sodium, les quatre constantes de vitesse requises pour décrire l'hydratation et les réactions d'aldolisation/désaldolisation de la chalcone (diphényl-1,3 propène-2 one-1). On a étudié les cinétiques en partant de la chalcone, de son hydrate, la diphényl-1,3 hydroxy-3 propanone-1 et du benzaldéhyde en présence d'un excès d'acétophénone. Les constantes de vitesse des réactions catalysées par l'hydroxyde, définies selon l'équation [1], sont de $k_{12} = 10{,}5 \pm 0{,}5 \times 10^{-4}\ M^{-1}\ s^{-1}$, $k_{21} = 0{,}026 \pm 0{,}002\ M^{-1}\ s^{-1}$, $k_{23} = 0{,}194 \pm 0{,}017\ M^{-1}\ s^{-1}$ et $k_{32} = 0{,}84 \pm 0{,}12\ M^{-2}\ s^{-1}$ (le tout à une force ionique de 0,1). Les constantes d'équilibre correspondantes de la formation de l'adduit aldolique et de la déshydratation sont de 4,3 M^{-1} et de 25.

[Traduit par le journal]

Introduction

We have reported a study (1) of the equilibrium constants for aldol condensation reactions. Since we consider it important to have a reliable set of rate and equilibrium constants for a set of simple aldol reactions and need such data for an examination of rate–equilibrum correlations for the aldol reaction, we have undertaken the investigation of the kinetics of various aldol reactions (2–4), studying them in the reverse sense to avoid the difficulties of side reactions which often plague the kinetics of aldol reactions in the forward sense. Very few other aldol reactions had been subjected to kinetic study when we began this investigation (5–21). The case of chalcone is of interest because, despite a number of studies by various research groups, no detailed kinetic analysis for reactions in aqueous solution has been reported. There have been previous studies of the formation and breakdown of chalcone in alcohol (16, 18, 19) and in acetic acid (17, 18), and there has been a qualitative kinetic study using polarographic analysis in aqueous ethanol (21). More recently there has been an investigation of the cleavage of a series of substituted chalcones in aqueous alkali (20). Although three of the four rate constants have been reported for alcoholic solution (18), there was no consideration of the possible addition of ethanol to chalcone as a confusing side reaction. There are literature methods for preparing the ketol corresponding to chalcone, i.e. 3-hydroxy-1,3-diphenyl-1-propanone (18, 22). This compound proved essential to the investigation, because the equilibrium constant for dehydration to chalcone is quite large and cannot be measured directly by studying the hydration of chalcone, yet must be known to sort out the kinetics. By measuring the rates of formation of chalcone from benzaldehyde in the presence of excess acetophenone we have been able to determine the overall equilibrium constant for chalcone formation in aqueous solution.

[1]E. W. R. Steacie Memorial Fellow, 1980–82. Author to whom correspondence may be addressed.

Results and discussion

The retroaldol reaction of chalcone can be followed spectrophotometrically; when chalcone, as a solution in acetonitrile, is injected into aqueous sodium hydroxide solution there is a smooth disappearance of the absorbance at 312 nm, which follows a simple first order rate law. Thus one can see no sign of the two stages which are believed to be essential for this reaction as shown in eq. [1].

$$[1]\quad \mathrm{Ph{-}Ch{=}CH{-}CO{-}Ph} \underset{k_{21}}{\overset{k_{12}}{\rightleftharpoons}} \mathrm{Ph{-}CHOH{-}CH_2{-}CO{-}Ph}$$

$$\mathrm{Ph{-}CHOH{-}CH_2{-}CO{-}Ph} \underset{k_{32}}{\overset{k_{23}}{\rightleftharpoons}} \mathrm{Ph{-}CHO + CH_3{-}CO{-}Ph}$$

The two phases of the reaction are quite apparent when the ketol, 3-hydroxy-1,3-diphenyl-1-propanone, is injected into aqueous sodium hydroxide solution; the absorbance at 312 nm first rises and then, about 250 times more slowly, falls again; see Fig. 1. The rate of the slow fall in absorbance is essentially identical to the rate of disappearance of the absorbance of chalcone when the latter is used to initiate reaction. Analysis of the two-phase kinetics data permits evaluation of the rate constants. For the system of interest, where a low concentration of ketol product undergoes retroaldol cleavage, the rate of the second order ketol formation process, k_{32}, is negligible. A rigorous solution of the kinetics equations is possible following the procedure described in Moore and Pearson (23), but leads to a cumbersome equation of the form [2]:

$$[2]\quad A = A_B + \alpha \exp(-\lambda_2 t) + \beta \exp(-\lambda_3 t)$$

where A = absorbance and $\lambda_{2,3}$ = the apparent rate constants. In the present case, the two exponential terms correspond to

Can. J. Chem. Downloaded from www.nrcresearchpress.com by 210.87.254.6 on 09/06/12
For personal use only.

Can. J. Chem. Downloaded from www.nrcresearchpress.com by 210.87.254.6 on 09/06/12
For personal use only.

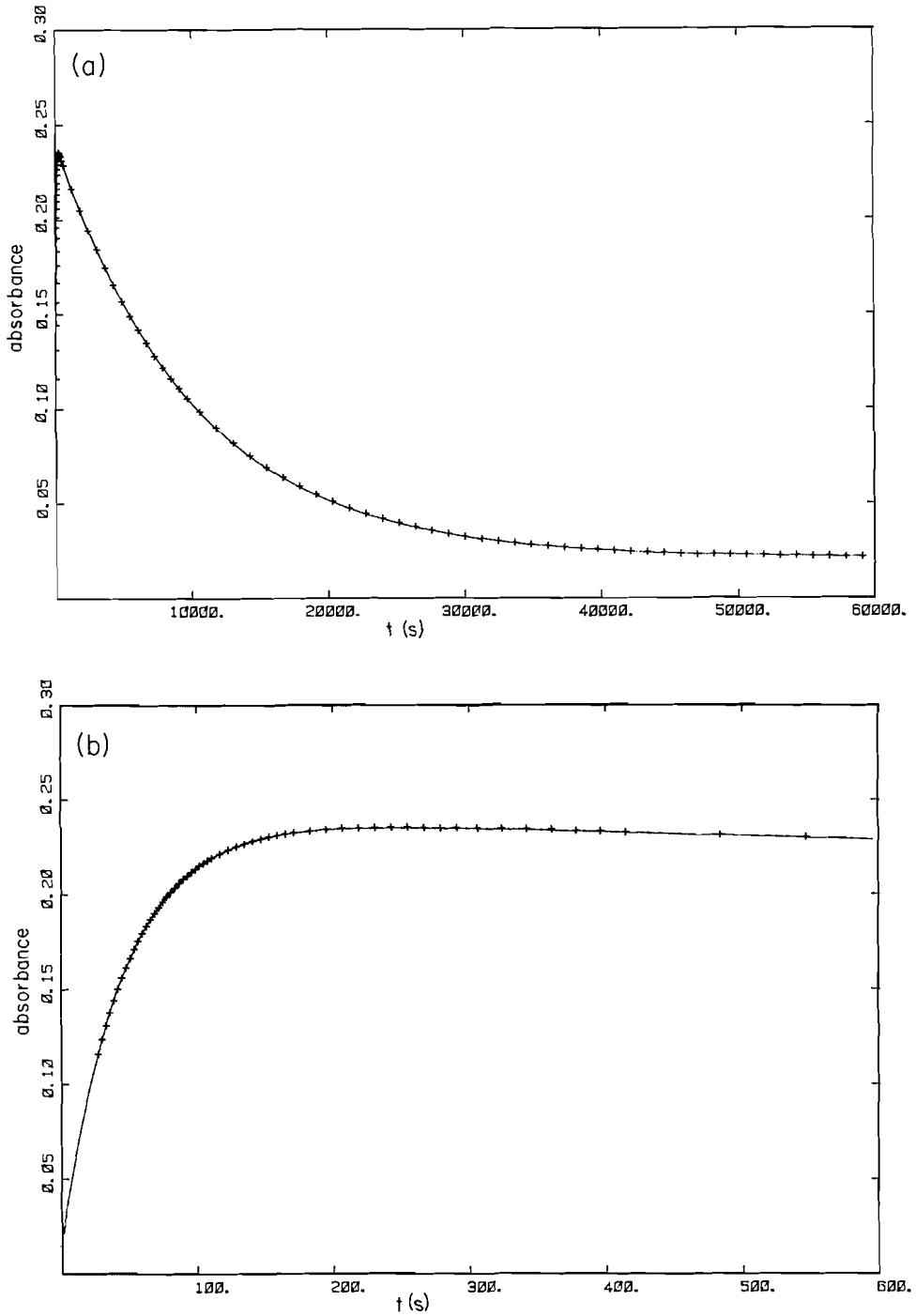

FIG. 1. Biphasic kinetics for the reaction of 3-hydroxy-1,3-diphenyl-1-propanone. Initial concentrations of starting materials was 8.5×10^{-6} *M*, in 0.1 *N* NaOH at 25°C.

very different time scales, so that it is practical to use an approximation treating the two stages separately. The fast reaction, breakdown of the ketol to enone or benzaldehyde plus acetophenone, has rate constant $\lambda_2 \simeq k_{21} + k_{23}$, and an absorbance change governed by the fraction of the ketol which goes to enone, i.e.

$$|\alpha| \simeq C_2^0 \epsilon_1 k_{21}/(k_{21} + k_{23})$$

where C_2^0 is the initial concentration of ketol, and the extinction coefficients are ϵ_i: i = 1, chalcone; 2, ketol; 3, acetophenone + benzaldehyde. The slow reaction is the hydrolysis of the enone so formed, with the ketol as a steady state intermediate, with $\lambda_3 \simeq k_{12}/(1 + k_{21}/k_{23})$. These equations may also be derived from the rigorously correct general solution, by imposing the conditions $\epsilon_1 \gg \epsilon_2$, ϵ_3 and $\lambda_2 \gg \lambda_3$.

The equations used to calculate the rate constants are:

$$k_{21} = |\alpha|\lambda_2/C_2^0\epsilon_1$$

[3] $$k_{23} = \lambda_2 - k_{21}$$

$$k_{12} = \lambda_3(1 + k_{21}/k_{23})$$

Table 1 shows the results of applying this analysis to the experimental data for chalcone and the corresponding ketol. We used $\epsilon_1 = 2.1 \pm 0.02 \times 10^4$; see Experimental. The

TABLE 1. Kinetic results for the retroaldol reaction of chalcone[a]

(a) Reactions starting with 3-hydroxy-1,3-diphenyl-1-propanone[b]

[NaOH]	α	$10^2 \times \lambda_2$	β	$10^5 \times \lambda_3$ or $10^6 \times d$	$10^3 \times k_{21}$	$10^2 \times k_{23}$	k_{21}/k_{23}
0.1[c]	−0.2265±0.0005	2.20±0.005	0.2203±0.0001	9.89±0.01	2.70±0.13	1.93±0.01	0.140±0.008
0.1[d,e]	−0.0236±0.001	2.37±0.11	0.0262±0.0001	7.76±0.1	3.47±0.22	2.02±0.09	0.171±0.009
0.0590	−0.2297±0.0001	1.27±0.001		−12.6±0.06	1.63±0.077	1.11±0.077	0.148±0.0080
0.0291	−0.2247±0.0001	0.630±0.0006		−6.39±0.04	0.793±0.037	0.551±0.0038	0.144±0.0077
0.0038	−0.2246±0.0001	0.0663±0.0001		−0.85±0.01	0.0834±0.0039	0.0580±0.0004	0.144±0.0077

(b) Reactions starting with chalcone

[NaOH]	μ	$10^6 \times C_1^0$	β	$10^5 \times \lambda_3$	$10^4 \times k_{12}$
1.0	1.0	7.80	1.655±0.006	108.0±0.3	9.41±0.048
0.6	1.0	7.81	1.713±0.004	59.6±0.1	5.19±0.024
0.3	1.0	5.20	1.098±0.003	24.5±0.1	2.13±0.013
0.1	1.0	5.20	1.099±0.005	8.43±0.04	0.734±0.0047
0.1	0.1	5.20	1.103±0.004	8.90±0.04	0.775±0.0048

[a]In aqueous solution at 25°C, ionic strength 0.1 *M* (KCl) unless otherwise noted; all rate constants in s^{-1}.
[b]Initial concentration 8.5×10^{-6} *M* unless otherwise stated.
[c]$k_{12} = 11.3 \pm 0.076 \times 10^{-5}\ s^{-1}$.
[d]Initial concentration was 8.5×10^{-7} *M*.
[e]$k_{12} = 9.10 \pm 0.14 \times 10^{-5}\ s^{-1}$.

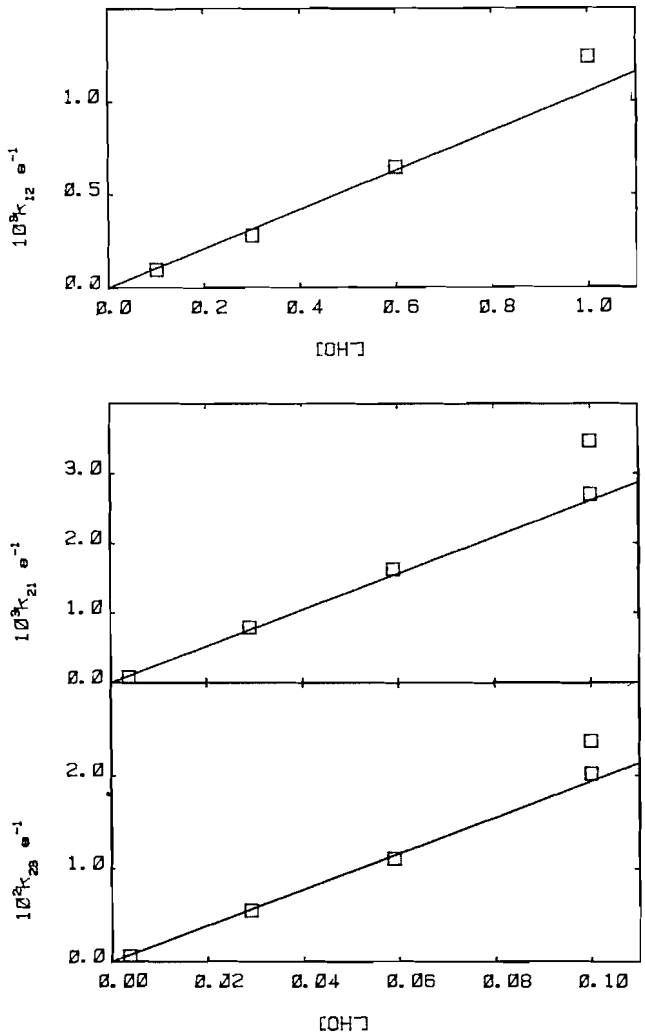

FIG. 2. Hydroxide dependence of the rate constants for each step of the aldol reaction; k_{12} at μ = 1.0; k_{21} and k_{23} at μ = 0.1.

TABLE 2. Second order rate constants for formation and retroaldol cleavage of chalcone

Rate constant	Value[a] ($M^{-1}\ s^{-1}$)		Value in aqueous ethanol ($M^{-1}\ s^{-1}$)
$10^4 \times k_{12}'$	10.5±0.7[b]	11.96[f]	0.19[c], 5.2[d]
	10.5±0.5		
$10^2 \times k_{21}'$	2.61±0.17		6.25[e]
$10^2 \times k_{23}'$	19.4±1.7		24.2[e]
k_{32}'	1.20±0.09[b]		0.21,[c] 0.18[e]
	0.84±0.12		

[a]This work; aqueous solution at 25°C, ionic strength 0.1 *M* (KCl) unless otherwise noted.
[b]Ionic strength 1.0 *M*.
[c]In 95% ethanol at 25°C (16); calculated from the apparent rate constants using eq. [3] and a value of k_{21}/k_{23} based on results in 90% ethanol (18).
[d]Corrected for the difference in water concentration between aqueous solution and constant boiling ethanol; see text.
[e]In 90% ethanol with 0.02 *N* NaOH at 26°C (18).
[f]Calculated from the apparent rate constant of ref. 20 using our value for k_{21}/k_{23}.

individual rate constants show the expected first order dependence upon the hydroxide concentration; see Fig. 2. For reactions starting with the ketol, the maximum absorbance corresponds to about 12% conversion to chalcone, which then undergoes slow cleavage.

Table 2 shows the second order rate constants for the individual steps evaluated in this work, and compares them with literature values for aqueous ethanol, and the results of studies of the overall retroaldol reaction in aqueous solution. It is interesting that k_{21} and k_{23} are quite similar in water and 90% aqueous ethanol, whereas k_{12} in constant boiling aqueous ethanol is different by a factor of about 60 from the value in water. This difference is in large measure attributable to the lowered concentration of water in the mixed solvent; constant boiling aqueous ethanol is 4.4% or 1.96 *M* water. If the concentration of hydroxide ion in aqueous ethanol containing a fixed concen-

Can. J. Chem. Downloaded from www.nrcresearchpress.com by 210.87.254.6 on 09/06/12
For personal use only.

TABLE 3. Kinetic results for chalcone formation[a]

$[OH^-]$ M	$[PhCOCH_3]$ M	[PhCHO] $10^4\ M$	A_∞	$A_\infty - A_0$	k_{app} $10^3\ s^{-1}$
0.966	0.0199[b]	1.03	3.682±0.003	1.600±0.004	4.56±0.03
0.996	0.0095[b]	1.03	1.826±0.002	0.835±0.003	3.04±0.03
0.966	0.00303	1.03	0.787±0.0001	0.507±0.001	1.52±0.003
0.0987	0.0214[b]	1.03	3.658±0.001	1.280±0.004	0.380±0.003
0.0987	0.00949	1.03	2.249±0.0008	1.055±0.0008	0.195±0.0004
0.0987	0.00340	1.03	0.838±0.0002	0.527±0.0002	0.139±0.0001

[a]In aqueous solution at 25°C.
[b]Final solution was cloudy.

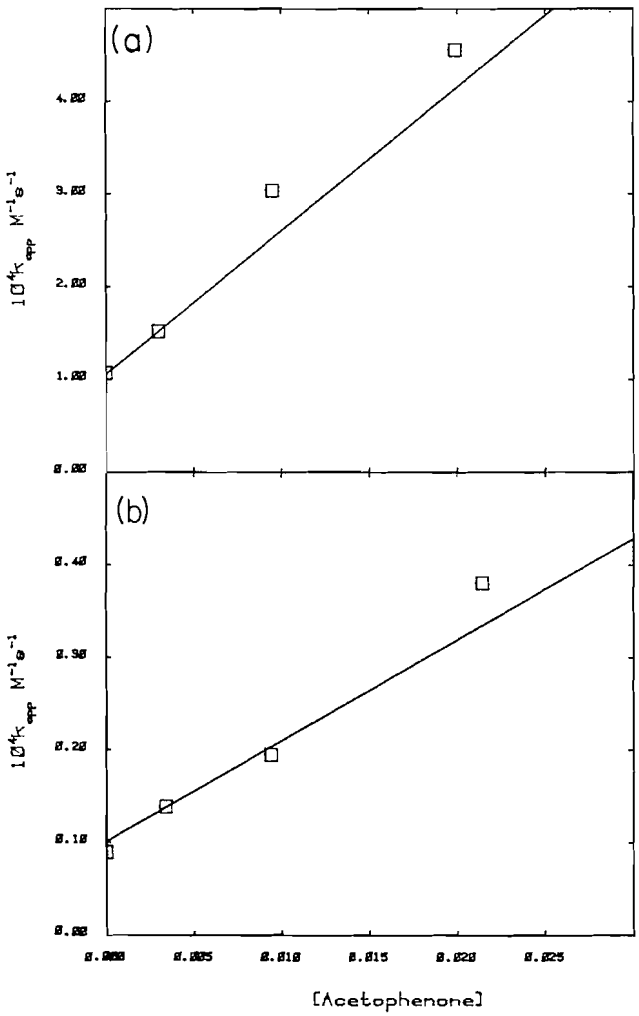

FIG. 3. Dependence of the apparent second order rate constants for chalcone formation on the acetophenone concentration. (a) [NaOH] = 1.0 M; (b) [NaOH] = 0.1 M.

tration of sodium hydroxide/ethoxide is proportional to the water concentration (which will not be exactly true, but should be a rough approximation) then the rate of productive lyate ion additions to chalcone will be decreased by 55.5/1.96 or 28-fold in constant boiling aqueous ethanol. Applying this correction to the k_{12} value estimated from the data in ref. 16 leads to a value within a factor of two of that observed in this work for water. The remaining difference can reasonably be ascribed to solvent effects upon the rate constant, and/or imperfections in our approximation. It should be noted that the unknown amount of addition of ethoxide ion to chalcone leads to an unproductive adduct which cannot react further, and will not accumulate because the equilibrium constant for addition is unfavorable.

The equilibrium constant for aldol dehydration (k_{21}/k_{12}) calculated from the rate constants determined in this work is 25, which differs significantly from the value of 87 which we estimated previously (1) from the rate constants in aqueous ethanol. The previous estimate was indirect, requiring the overall equilibrium constant and the equilibrium constant for the aldol addition, both in aqueous ethanol. We had, therefore, to consider the possibility that this estimated value for the overall equilibrium constant was in error, and accordingly studied the kinetics of the formation of chalcone in order to determine the equilibrium constant in water.

These experiments were done with excess acetophenone to give pseudo first order conditions; acetophenone does not react in the presence of base at rates which would give difficulties, either with itself or with oxygen. Since the equilibrium constant is not strongly favorable it was necessary to use acetophenone concentrations of 0.003−0.02 M in order to get satisfactory amounts of conversion. This has as an unavoidable consequence a large background absorption due to the acetophenone, and necessarily limits the precision of our kinetics. Furthermore, cloudiness was noticeable for the final solutions from the runs at the two highest concentrations of acetophenone in 1.0 M NaOH, and for the run at the highest concentration of acetophenone in 0.1 M NaOH. At either ionic strength good first order behavior was seen for 2−3 half-lives at the two highest acetophenone concentrations and for 7 half-lives at the lowest concentration. We are clearly at the solubility limit for chalcone, yet to lower the benzaldehyde concentration would result in a small change in absorbance superimposed on the unavoidable high background absorbance from the acetophenone. The acetophenone concentrations could not be lowered if the forward reaction were to make a major contribution to the observed rate of approach to equilibrium. Our kinetics results are given in Table 3. When the apparent second order rate constants for approach to equilibrium (first order in benzaldehyde, first order in hydroxide) were plotted as a function of acetophenone concentration, Fig. 3, the data at either ionic strength could be fitted to a straight line, and the intercepts matched the apparent rate constants obtained starting with chalcone cleavage under the same conditions.

In these experiments, the observed rate constants reflect the rate of approach to equilibrium, and will be the sum of the rate constants for chalcone formation and cleavage. From the previous experiments studying cleavage we know that no intermediates will accumulate. Necessarily, the rate of cleavage of chalcone must be the same for a given set of conditions, wheth-

Can. J. Chem. Downloaded from www.nrcresearchpress.com by 210.87.254.6 on 09/06/12
For personal use only.

er it is measured in the cleavage for formation direction.

$$[4]\quad PhCHO + PhCOCH_3 \underset{k_r[OH^-]}{\overset{k_f[OH^-]}{\rightleftharpoons}} Ph—CH=CH—CO—Ph$$

$$k_{obs}/[OH^-] = k_f[PhCOCH_3] + k_r$$

Thus we expect k_r, the intercept of a plot of $k_{obs}/[OH^-]$, to be identical to $\lambda_3/[OH^-]$ from cleavage experiments. In fact, when the appropriate values of $\lambda_3/[OH^-]$ were included in the plots of $k_{obs}/[OH^-]$ vs. $[PhCOCH_3]$ they were in excellent agreement. Figure 3 shows these plots; the fit is by weighted least squares, using weights based on the errors estimated by the least-squares fit to the kinetic data (24). The rate constants for runs at high acetophenone concentration, which are known to be less reliable because the final solutions were turbid, had larger errors, and so were allowed to deviate more by the least-squares calculations. Using the slopes and intercepts of these lines we obtain overall equilibrium constants $K = 148 \pm 4\ M^{-1}$ at 1 M ionic strength, and $K = 108 \pm 20\ M^{-1}$ at 0.1 M ionic strength. These values are very similar, as one would expect for an equilibrium involving neutral moelcules. These values are disturbingly different from the value of $K = 66\ M^{-1}$ which we estimated (1) on the basis of data in aqueous ethanol (16, 18). Clearly our attempts to correct for the change in solvent were imperfect, although the difference in free energy terms is still small enough (0.5 kcal/mol) that it makes little difference to the overall arguments in ref. 1.

We may calculate a value for k_{32} from the apparent third order rate constant for chalcone formation, noting that

$$k_{app} = k_{32}/(1 + k_{23}/k_{21})$$

and consequently that $k_{32} = k_{app}(1 + k_{23}/k_{21})$. In this way we obtain $k_{32} = 1.20 \pm 0.09\ M^{-2}\ s^{-1}$ at 1.0 M ionic strength and $0.84 \pm 0.12\ M^{-2}\ s^{-1}$ at 0.1 M ionic strength.

These values differ by a factor of 5 or more from the values estimated from data in aqueous ethanol. No obvious rationalization for what is, after all, a rather small solvent effect has presented itself.

With directly measured values now in hand we can compare the equilibrium constants for condensation of acetone and acetophenone with benzaldehyde. The equilibrium constants are much more similar than previously estimated: for the aldol addition to benzaldehyde, $K_1 = 8.5\ M^{-1}$ for acetone and 4.3 M^{-1} for acetophenone, while $K_2 = 31$ for acetone and 25 for acetophenone. This agreement is in fact quite reasonable because the varying substituent, methyl or phenyl, is isolated from the reaction center by the carbonyl.

Experimental

Materials

3-Hydroxy-1,3-diphenyl-1-propanone was prepared by directed aldol condensation. To a reaction flask containing 20 mL dry tetrahydrofuran (THF) (distilled from $LiAlH_4$) at −70°C under a nitrogen atmosphere was added 6 mL n-butyllithium solution (2.2 M in hexane) and then 1.7 mL diisopropylamine dissolved in 10 mL dry THF; the solution was stirred for 10 min. Acetophenone (1.3 mL) in dry THF (10 mL) was added and the solution stirred for 20 min. Benzaldehyde (1.3 mL) in dry THF (10 mL) was added and the solution was stirred for 30 min. Acetic acid (0.7 mL) in water (10 mL) was added to quench the reaction and the entire solution was poured into 60 mL ice water and then extracted using ethyl acetate (3 × 30 mL); the combined organic layers were washed with saturated $NaHCO_3$, water, and saturated NaCl, dried over anhydrous Na_2SO_4, and evaporated. The resulting oil was purified by medium pressure chromatography on silica (Merck PF 254) using Glenco apparatus with a continuous gradient from petroleum ether (30−60) to 60% ethyl acetate − 40% petroleum ether to elute the product. Crystallization from petroleum ether gave material of mp 51.7−52.3°C (lit. (18) mp 49.7−50.7°C). Chalcone (Aldrich) was purified by recrystallization from petroleum ether; mp 55.5−56.5°C (lit. (25) mp 57−58°C). Acetophenone and benzaldehyde were redistilled immediately before use in kinetics.

Methods

We had immense difficulty in this project because of irreproducible kinetic behavior which was finally ascribed to impurities in the tetrahydrofuran which we used for stock solutions of the substrates. The THF was always purified, starting from reagent or spectrophotometric grade solvent or even Caledon "distilled in glass" grade, at least by passage through alumina, and sometimes by distillation from sodium benzophenone ketyl. In all cases there were impurity peaks at about 313 nm (smaller in the solvent from Caledon), and rate constants were not accurately reproducible. These problems ceased when we began to use spectrophotometric grade acetonitrile to make up the stock solutions. Calculations showed that consumption of OH^- by hydrolysis of the acetonitrile would be negligible over the course of a kinetics experiment.

Weighed amounts of acetophenone were dissolved in aqueous sodium hydroxide solutions. A stock solution of benzaldehyde in spectrophotometric grade acetonitrile was used; reaction was initiated by adding 30 μL of a 0.0104 M solution to 3.0 mL of acetophenone − sodium hydroxide solution. Stock solutions of chalcone and ketol were prepared in spectrophotometric grade acetonitrile and were used to initiate kinetics; all reactions were followed at 310 nm. The procedure for kinetics was as previously described (4). All reactions were carried out in 10 cm cells holding 25 mL of solution. The extinction coefficient of chalcone was measured by adding measured amounts (Hamilton syringe) of a stock solution in acetonitrile (two different stock solutions were used) to 25 mL of pH 10 carbonate buffer, μ = 1.0 (KCl). The value so obtained was $2.10 \pm 0.02 \times 10^4\ M^{-1}\ cm^{-1}$. This is in good agreement with the value calculated from the absorbance changes for reactions where chalcone was injected into sodium hydroxide solutions: $\epsilon = 2.13 \pm 0.04 \times 10^4\ M^{-1}\ cm^{-1}$.

1. J. P. GUTHRIE. Can. J. Chem. **56**, 962 (1978).
2. J. P. GUTHRIE. Can. J. Chem. **52**, 2037 (1974).
3. J. P. GUTHRIE. Can. J. Chem. **59**, 45 (1981).
4. J. P. GUTHRIE and B. A. DAWSON. Can. J. Chem. **61**, 171 (1983).
5. Y. OGATA, A. KAWASAKI, and K. YOKOI. J. Chem. Soc. (B), 1013 (1967).
6. J. E. VIK. Acta Chem. Scand. **26**, 3165 (1972).
7. K. KOELICHEN. Z. Phys. Chem. **33**, 129 (1900).
8. G. AKERLOF. J. Am. Chem. Soc. **48**, 3046 (1926).
9. C. C. FRENCH. J. Am. Chem. Soc. **51**, 3215 (1929).
10. G. M. MURPHY. J. Am. Chem. Soc. **53**, 977 (1931).
11. V. K. LA MER and M. L. MILLER. J. Am. Chem. Soc. **57**, 2676 (1935).
12. J. M. STURTEVANT. J. Am. Chem. Soc. **59**, 1528 (1937).
13. R. P. BELL. J. Chem. Soc. 1637 (1937); R. P. BELL and M. J. SMITH. J. Chem. Soc. 1691 (1958).
14. F. GRONLUND and B. ANDERSEN. Acta Chem. Scand. Ser. A, **33**, 329 (1979).
15. D. S. NOYCE and W. L. REED. J. Am. Chem. Soc. **81**, .624 (1959).
16. E. COOMBS and D. P. EVANS. J. Chem. Soc. 1295 (1940).
17. D. S. NOYCE and W. A. PRYOR. J. Am. Chem. Soc. **77**, 1397 (1955).
18. D. S. NOYCE, W. A. PRYOR, and A. H. BOTTINI. J. Am. Chem.

Can. J. Chem. Downloaded from www.nrcresearchpress.com by 210.87.254.6 on 09/06/12
For personal use only.

Soc. **77**, 1402 (1955).
19. E. A. WALKER and J. R. YOUNG. J. Chem. Soc. 2045 (1957).
20. A. DE BLIC and P. MARONI. Bull. Soc. Chim. Fr. 512 (1975).
21. P. CARSKY, P. ZUMAN, and V. HORAK. Collect. Czech. Chem. Commun. **30**, 4316 (1965).
22. C. SCHOPF and K. THIERFELDER. Ann. **518**, 127 (1935).
23. J. W. MOORE and R. G. PEARSON. Kinetics and mechanism, 3rd ed. Wiley, New York. 1981. p. 296.
24. P. R. BEVINGTON. Data reduction and error analysis for the physical sciences. McGraw–Hill, New York. 1969.
25. M. WINDHOLZ (*Editor*). The Merck Index, 9th ed. Merck and Co., Rahway, NJ. 1976.

Can. J. Chem. Downloaded from www.nrcresearchpress.com by 210.87.254.6 on 09/06/12
For personal use only.

Hydrogen isotope exchange between fluoroform (CF_3H) and water. 4. Catalysis by NaOH and anionic resin above 100°C as an alternative to DMSO addition for rate enhancement[1]

E. Allan Symons, J. Douglas Bonnett, and M. de Lurdes Martins

Physical Chemistry Branch, Chalk River Nuclear Laboratories, Atomic Energy of Canada Limited, Research Company, Chalk River, Ont., Canada K0J 1J0

Received March 18, 1983

E. Allan Symons, J. Douglas Bonnett, and M. de Lurdes Martins. Can. J. Chem. **61**, 2627 (1983).

Measurement of rate constants for NaOH-catalyzed CF_3D/H_2O isotopic exchange has been extended from 80 to 140°C. Corresponding CF_3H solubility data were obtained for water and 1.0 mol/L NaOH solution up to 120°C. Above 120°C, the NaOH solution provides sufficient catalytic activity to be considered as a simple alternative to the use of aqueous DMSO systems containing NaOH for a CF_3H redeuteration process.

Tests done with both Ionac A-935 and regular types of anion exchange resin in the hydroxide ion form indicate that these resins, although initially quite effective for deuterium exchange catalysis, lose their reactivity when employed above 100°C. The thermal instability of this type of supported ^-OH catalyst makes it unsuitable for use (as a substitute for NaOH) at elevated temperatures in packed towers in a commercial process.

E. Allan Symons, J. Douglas Bonnett et M. de Lurdes Martins. Can. J. Chem. **61**, 2627 (1983).

On a mesuré les constantes de vitesse de l'échange isotopique CF_3D/H_2O catalysé par du NaOH dans un intervalle de température allant de 80 à 140°C. On a obtenu les données relatives à la solubilité du CF_3H dans l'eau et dans une solution de NaOH 1 mol/L jusqu'à 120°C. Au-dessus de 120°C, la solution de NaOH a suffisamment d'activité catalytique pour être considérée comme une alternative à l'utilisation du système DMSO aqueux contenant du NaOH dans le processus de redeutération du CF_3H.

Des essais effectués sur une résine échangeuse d'anion, sous forme d'ions hydroxydes, de type Ionac A-935 et de type régulier, indiquent que ces résines, au départ tout à fait efficaces pour catalyser l'échange de deutérium, perdent leur activité au-dessus de 100°C. L'instabilité thermique de ce type de catalyseur empêche de l'utiliser (comme substitut au NaOH) à des températures élevées dans les colonnes à remplissage des procédés industriels.

[Traduit par le journal]

Introduction

Efficient catalysis of deuterium transfer to gaseous fluoroform from a natural deuterium source like liquid water will be a vital part of any heavy water production process based on laser-induced multiphoton dissociation of CF_3D in the presence of excess CF_3H (1, 2). The effectiveness of a variety of both homogeneous and heterogeneous catalysts for exchange with water has been studied (3–5). Although none were found to be very active in the temperature range 25 to 80°C, hydroxide ion, when used in the presence of dimethyl sulfoxide (DMSO) as co-solvent with water, provided in-solution deuterium exchange rates that would be suitably fast for an industrial process at 60–70°C (1, 4).[2] Unfortunately, the cost of DMSO addition to and recovery from large process water streams is likely to be prohibitive.[2]

The Arrhenius activation energy for NaOH catalysis of CF_3D-H_2O exchange is quite large over the temperature range 50 to 80°C, being 125 kJ/mol (29.9 kcal/mol) (corrected value, slightly lower than that given in ref. 3). Kinetic measurements have now been extended up to 140°C, to determine how high a reaction temperature would be needed to achieve rates comparable to the fastest values possible for the DMSO–water system at 70°C. In addition, as an extension of a parallel study based on catalysis by anion exchange resins (5), the exchange reactivity and thermal stability of a "high temperature" resin, Ionac A-935, have been examined at temperatures from 90 to 140°C. These results obtained for both NaOH and A-935 catalysis are given in this paper.

Experimental

CF_3D was prepared in batches by NaOD-catalyzed reaction of CF_3H with D_2O as already described (4). Stock NaOH solutions were prepared by diluting Fisher Scientific concentrates with deionized distilled water. The Ionac Chemical Company's A-935 resin (Aquacare Services Ltd., Huntsville, Ontario) was converted to the hydroxide form and analyzed for base strength by standard column techniques (6). This strong base resin is recommended for continuous use up to 100°C (Ionac literature). Analysis of two separate preparative batches (treated only with NaOH) gave loadings of 1.53 and 1.57 mmol $^-OH/g$ dried resin. However, the values are well below the Ionac specification of 3.5 (for Cl^-). With a recommended Na_2SO_4 solution rinse of the Cl^- form resin prior to NaOH treatment, only a slight increase to 1.69 mmol $^-OH/g$ was achieved. Even if the remaining Cl^- sites could be converted to ^-OH, these ions would probably be in locations less accessible for catalysis.

For deuterium exchange kinetic runs at up to 90°C one of our glass, stirred gas/liquid reactors (3) was employed. Because of high water vapour pressure above 90°C, a metal shell reactor of similar design (nickel bottom half for corrosion resistance and aluminum top half for magnetic stirring from above) was constructed for these runs. Fluoroform sample analysis and data treatment methods were the same as used previously (3).

For calculation of in-solution exchange rate constants from the measured rate constant data, the solubility of fluoroform in the catalyst solutions as a function of temperature is required. Measurements of CF_3H solubility in water, 1.0 mol L^{-1} NaOH solution, and A-935 resin slurry between 80 and 120°C were carried out with the same gas chromatographic method used to obtain the solubility data at lower temperature (3, 5). The metal stirred reactor, modified to take a long syringe needle mounted along the inside wall, was substituted for the glass flask system to permit gas–liquid equilibration and solution sampling at the higher total pressures.

The rate of CF_3H hydrolysis below 80°C had been determined to be low (3). The extent of such reaction at higher temperatures was studied by analyzing solutions for $[F^-]$ after exchange runs, using the same specific fluoride ion electrode technique (3).

[1]AECL Report 8144.

[2]A. I. Miller and J. R. Lebenhaft, Chemical Engineering Branch, Chalk River Nuclear Laboratories, Atomic Energy of Canada Limited, personal communication.

Can. J. Chem. Downloaded from www.nrcresearchpress.com by 210.87.254.5 on 09/06/12
For personal use only.

Can. J. Chem. Downloaded from www.nrcresearchpress.com by 210.87.254.5 on 09/06/12
For personal use only.

Results

CF_3H solubility in H_2O and NaOH solution

In both water and 1 mol/L NaOH solution the solubility of CF_3H decreases, but progressively more slowly, over the temperature range 20 to 70°C (3). Between 90 and 130°C the solubility has become practically independent of temperature; the values are $0.89 \pm 0.03 \times 10^{-4}$ and $0.55 \pm 0.03 \times 10^{-4}$ mol fraction for the water and NaOH solution, respectively. There may be a shallow minimum in this region; such behaviour has been observed for other inert gases like H_2 dissolved in water (7).

CF_3D-H_2O exchange

The temperature dependence of the calculated in-solution/slurry rate constants is shown in Fig. 1. The deviation from linearity seen for both solid-line ln k versus $1/T$ plots at higher temperatures arises most likely from mass transfer limitation. Data could not be obtained independent of stirring rate above ~100°C (max. ~800 r/min) in the sealed metal reactor, so that points on the curved sections are minimum values. From the linear sections, Arrhenius activation energies of 129 and 112 ± 4 kJ/mol (30.8 and 26.7 ± 1 kcal/mol) were calculated for NaOH and A-935 resin catalysis, respectively.

Even the "high temperature" Ionac A-935 resin was found to be thermally unstable above 100°C, where its initial ^-OH activity would be acceptable. For example, catalytic reactivity declined by 30% after 19 h at 108°C and by a factor of seven after 22 h at 136°C. A slight curvature was seen in most kinetic plots for the resin runs, an indication of the gradual loss of ^-OH groups.

The greater catalytic activity for resin-bound ^-OH groups compared to solution NaOH and the temperature dependence of this effect, seen in Fig. 1, were also noted for Rexyn 201 (OH) resin (5). In each case E_a (NaOH) is larger than E_a (resin ^-OH) by ~10–15 kJ/mol. Possible reasons for this behaviour, including changes in fluoroform solubility and ^-OH ion solvation, have been discussed elsewhere (5).

Fluoroform hydrolysis

As expected, hydrolysis of the fluoroform in 1 mol/L hydroxide solution becomes more significant with increasing temperature. Although variation in fluoride ion concentration for identical or similar reaction conditions was sometimes as great as a factor of five (measured $[F^-]$ range 1×10^{-5} to 4×10^{-2} mol/L), the trend is clear. After 24 h in the stirred reactor the following approximate percentages of the fluoroform charge had been hydrolyzed: 0.008% at 98°C, 0.2% at 108°C, 4% at 117°C, and 15% at 126°C.

Discussion

Recorded in Table 1 are the calculated in-solution half-lives for CF_3D exchange in 1.0 mol/L NaOH solution from 100 to 140°C. The two sets of data are derived from the experimental curved plot in this region and the extrapolated straight line plot in Fig. 1; the latter set will be valid if the mass transfer effect can be eliminated by more efficient gas/liquid mixing. For comparison, some data are included for representative aqueous DMSO systems near the solubility-limited, maximum NaOH concentrations (4). Because the exchange reaction is first order in ^-OH (3), the higher [NaOH] possible in pure water will give shorter reaction half-lives (3). However, proportionately higher *rates* of deuterium exchange would not be fully realized, because of greater salting out of solution of the fluoroform gas with increasing NaOH concentration (3).

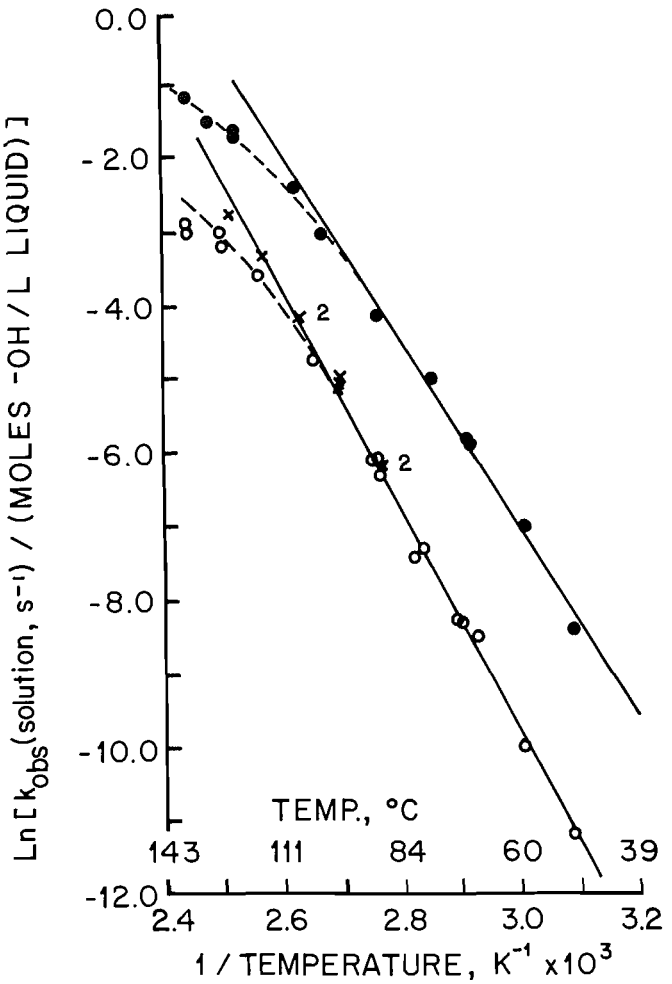

FIG. 1. Temperature dependence of CF_3D/H_2O isotope exchange rate constant for catalysis by (○) 60 mL 1.0 mol/L NaOH solution, and (●) 5 g dried Ionac A-935 resin slurried in 50 mL H_2O, 1.53 mmol ^-OH/g; molar NaOH/resin ^-OH ratio = 7.8. (Points (×) added in press, obtained for 8000 r/min runs in high speed stirred reactor equipped with ferrofluidic rotary feedthrough; mass transfer limitation suppressed.)

TABLE 1. Temperature dependence of in-solution reaction half-life for CF_3D-H_2O exchange in 1.0 mol L/NaOH[a]

Temperature °C	$t_{1/2}$, s (exper.)[b]	$t_{1/2}$, s (extrap.)[c]
100	106	90
110	43	30
120	21	11
130	13	4.1
140	9	1.6

[a]For comparison, the following aqueous DMSO solutions produce similar exchange reactivities: 25 mol% DMSO with 1.0 mol/L NaOH at 68°C, 40 s; 50 mol% DMSO with 0.1 mol/L NaOH at 68°C, 7 s. DMSO thermal stability in alkaline solution may be a problem at higher temperature.

[b]Experimental NaOH line in Fig. 1, including curved section.

[c]Extrapolated straight line for NaOH data in Fig. 1.

We have confirmed that by simply raising the temperature of aqueous solution to about 120°C, fluoroform–water exchange

rate constants comparable to those measured for, e.g., 50 mol% (80 vol%!) DMSO in water at 70°C (4) can be achieved. From an industrial point of view, the expense of handling large volumes of DMSO and of recovering this co-solvent from the effluent water stream can thus be avoided. However, the advantage of higher fluoroform solubility in the aqueous DMSO systems (4) would be lost.

In general, the results of this study look encouraging for the use of aqueous NaOH solution (no DMSO) above ~120°C for a CF_3H redeuteration step.[2] The physical advantage of utilizing *supported* ^-OH groups under packed tower conditions is offset, unfortunately, by the poor thermal stability of commercial anion exchange resins at the temperatures necessary for effective deuterium exchange catalysis. Alternative types of supported basic catalysts are under investigation. Hydrolysis of fluoroform should not be a significant problem.

Acknowledgements

The authors wish to thank Mr. B. H. McGilvray for construction of the metal stirred gas/liquid reactor. The test sample of A-935 resin provided by Ionac Chemical Company/Aquacare Services Ltd. is gratefully acknowledged.

1. J. B. MARLING, I. P. HERMAN, and S. C. THOMAS. J. Chem. Phys. **72**, 5603 (1980).
2. D. K. EVANS, R. D. MCALPINE, and H. M. ADAMS. J. Chem. Phys. **77**, 3551 (1982).
3. E. A. SYMONS and M. J. CLERMONT. J. Am. Chem. Soc. **103**, 3127 (1981).
4. E. A. SYMONS, M. J. CLERMONT, and L. A. CODERRE. J. Am. Chem. Soc. **103**, 3131 (1981).
5. E. A. SYMONS, J. H. ROLSTON, L. A. BALDISERA, J. C. G. DROVER, and J. D. BONNETT. Can. J. Chem. **61**, 1301 (1983).
6. Duolite Ion-Exchange Manual, Diamond Shamrock Chemical Co., Redwood City, Calif. 1969.
7. C. L. YOUNG (*Editor*). Hydrogen and deuterium. Solubility Data Series, Volume 5/6, Pergamon Press, New York, NY. 1981.

Can. J. Chem. Downloaded from www.nrcresearchpress.com by 210.87.254.5 on 09/06/12
For personal use only.

COMMUNICATION

Structure of the principal antineoplastic glycosides of *Phyllanthus acuminatus* Vahl[1]

GEORGE R. PETTIT, GORDON M. CRAGG, MARGARET L. NIVEN,[2] AND LUIGI R. NASSIMBENI[3]
Cancer Research Institute and Department of Chemistry, Arizona State University, Tempe, AZ 85287, U.S.A.

Received June 20, 1983

GEORGE R. PETTIT, GORDON M. CRAGG, MARGARET L. NIVEN, and LUIGI R. NASSIMBENI. Can. J. Chem. **61**, 2630 (1983).

A series of degradative and X-ray crystallographic studies has led to unequivocal evidence for the structure (**3***a*) assigned to the unique disaccharide phyllanthose. In turn, the X-ray crystal structure of phyllanthose confirms structures previously assigned to the potentially important antineoplastic plant glycosides phyllanthostatins 1 and 2 (**1***a*, *c*) and phyllanthoside (**1***b*). The chemical degradation and crystallographic analyses allowed assignment of structure **2***a* to phyllanthostatin 3.

GEORGE R. PETTIT, GORDON M. CRAGG, MARGARET L. NIVEN et LUIGI R. NASSIMBENI. Can. J. Chem. **61**, 2630 (1983).

Une série d'études impliquant des dégradations et des diffractions de rayons-X a permis d'établir la structure du disaccharide phyllanthose (**3***a*). Cette démonstration de la structure du phyllanthose permet de confirmer les structures attribuées antérieurement aux glycosides phyllanthostatines 1 et 2 (**1***a* et **1***c*) et phyllanthoside (**1***b*), des produits antinéoplastiques potentiellement importants extraits de plantes. Les dégradations chimiques et les analyses cristallographiques permettent d'attribuer la structure **2***a* à la phyllanthostatine 3.

[Traduit par le journal]

Can. J. Chem. Downloaded from www.nrcresearchpress.com by 210.87.254.6 on 09/06/12
For personal use only.

While only a relatively small number (<5%) of higher plants have received even a superficial examination for anticancer constituents, a series of such promising candidates bearing novel structures is beginning to reach clinical trial in the U.S. National Cancer Institutes (NCI) programs. Several are already established drugs for human cancer treatment (1). Analogous chemical and medical progress continues to be made with lower plant biosynthetic products for cancer chemotherapy. New advances in the chemistry of both higher (2) and lower (3) plant antineoplastic components combined with increasing successes in the total syntheses (4, 5) of these very important substances provide an instructive overview.

Recently we summarized the isolation and antineoplastic activity of phyllanthostatins 1–3 (**1***a*, *c*, **2***a*) and phyllanthoside (**1***b*) from roots of the Central American tree *Phyllanthus acuminatus* Vahl (2*a*, *b*). Glycosides **1***a* and **1***b* are two of the higher plant constituents presently being considered by the NCI for eventual clinical trial. The structural assignments for these principal *P. acuminatus* glycosides were based upon detailed interpretation of their high resolution (400 MHz) ^{1}H nmr, ^{13}C nmr, and mass spectra. Assignment (2*a*) of the aglycone unit of glycosides **1***a*–*c* resided upon an earlier X-ray crystallographic study of phyllanthocin (**1***d*) (6), but the unique

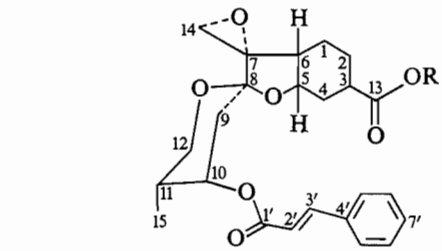

1, R = 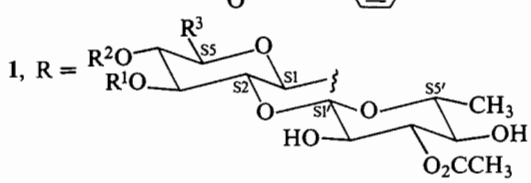

a, $R^1 = H$; $R^2 = COCH_3$; $R^3 = CH_3$
b, $R^1 = COCH_3$; $R^2 = H$; $R^3 = CH_3$
c, $R^1 = COCH_3$; $R^2 = H$; $R^3 = CH_2OH$
d, R = CH_3

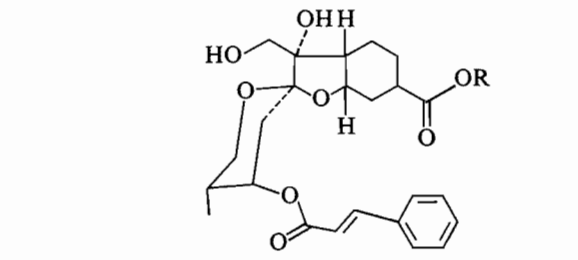

2*a*, R = CH_3CO_2-

2*b*, R = CH_3

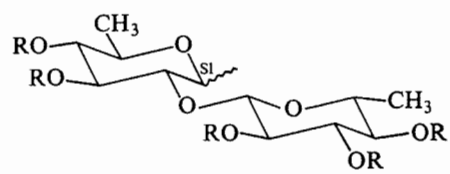

3*a*, = H
b, = $COCH_3$, Slα

$1 \rightarrow 2$ linked disaccharide (**3***a*) herein named phyllanthose, as well as definition of the phyllanthostatin 3 (**2***a*) stereochemistry at position C-7, could not be established with absolute certainty. We now report that further chemical degradation, and X-ray crystallographic studies, have culminated in unequivocal

[1]Component 94 of Antineoplastic Agents; for the preceding part, see ref. 8.

[2]Author to whom correspondence should be directed.

[3]Department of Physical Chemistry, University of Cape Town, Rondebosch 7700, South Africa.

Can. J. Chem. Downloaded from www.nrcresearchpress.com by 210.87.254.6 on 09/06/12
For personal use only.

evidence for the structure (**3***a*) previously assigned phyllanthose and thereby for the very important glycosides **1***a*–*c*. We also report completion of the phyllanthostatin 3 (**2***a*) assignments by determining the crystal structure of an aglycone segment termed phyllanthocindiol methyl ester (**2***b*).

Selective methanolysis (0.1 *N* sodium methoxide in methanol, 30 min, room temperature) of phyllanthostatin 3 (**2***a*) afforded the aglycone methyl ester **2***b*: crystals from acetone–hexane, mp 127–128°C; $[\alpha]_D^{25}$ +2.45° (*c* 1.63, chloroform).[4] The neutralized (1 *N* hydrochloric acid) aqueous fraction from isolation of ester **2***b* was treated with Amberlite MB-3 and lyophilized to yield phyllanthose (**3***a*) (6); mp 225–229°C; $[\alpha]_D^{26}$ −3.3°; FAB ms *m/e*: 333 $(M + Na)^+$.[4] Phyllanthose (**3***a*) was found identical (ir in KBr, tlc) with the disaccharide (**3***a*) obtained by methanolysis of phyllanthostatin 1 (**1***a*) and phyllanthoside (**1***b*). Peracetylation (acetic anhydride – pyridine, 1:1, room temperature, 2 days) of phyllanthose yielded 2-*O*-(6-deoxy-β-D-glucopyranosyl)-6-deoxy-α-D-glucopyranose hexaacetate (**3***b*) as crystals from acetone–hexane; mp 224–226°C; $[\alpha]_D^{26}$ +71.1° (*c* 0.83, chloroform); and EI ms *m/e*: 562 (M^+), 561 $(M^+ - H)$ and 503 $(M^+ - O_2CCH_3)$.[4]

A single crystal (0.75 × 0.5 × 0.5 mm) of phyllanthocindiol methyl ester (**2***b*) recrystallized from acetone–hexane was analyzed using a Philips PW1100 four-circle diffractometer with CuKα radiation (λ = 1.5418 Å). The crystals were found to exhibit monoclinic space group $P2_1$ with cell constants a = 9.891 (5), b = 24.84 (1), and c = 9.687 (5) Å; β = 94.82 (2) Å by least squares from the setting of 25 high-order reflections. Intensities were collected in the range $8 < 2\theta < 136$ by the $\omega-2\theta$ scan technique and were corrected for Lorentz polarization but not for absorption. Of the 4011 reflections obtained, 3692 (with $I_{rel} > 2\sigma I_{rel}$) were employed in the solution. The crystal density (ρ = 1.21 Mg m^{-3}) gave $Z = 4$ corresponding to two molecules of $C_{25}H_{32}O_8$, M_r = 460.52, per asymetric unit.

The structure (**2***b*) was solved by direct methods using the multisolution tangent refinement procedures of the program SHELX (7). A starting set of eight reflections (with three used for origin definition) generated 256 permutation. Twelve *E*-maps were obtained and the first (reliability index $R_A = 0.138$), which gave 36 of the 66 non-hydrogen atoms, yielded sufficient phase information to locate all the non-hydrogen atoms in subsequent weighted difference syntheses. The hydrogens of CH_2 and CH units were placed at 1.00 Å from their parent carbons and their positions were dictated by the geometry of the molecule. Methyl hydrogens were treated as rigid groups. Hydroxyl hydrogens (on 07 and 014) were not revealed in the final difference maps, and are not included in the final model. However, there is strong evidence for both intra- and intermolecular H-bonding involving the 07 and 014 atoms. Because of the large number of independent atoms, final refinements were accomplished using the blocked-matrix technique with the non-hydrogen atoms treated anisotropically and the hydrogen atoms isotropically to provide a final $R = 0.072$ (R_w = 0.085, $w = (\sigma^2 F + 0.002F^2)^{-1}$.

By the same general X-ray crystallographic techniques, a single crystal (0.15 × 0.25 × 0.50 mm) of phyllanthose peracetate (**3***b*) led to the following summary data: space group $P2_1$ with a = 13.077 (7), b = 9.306 (5), and c = 12.009 (6) Å with β = 92.33 (2) Å. As above, intensities were collected in the range $10° < 2\theta < 120°$ by the $\omega-2\theta$ scan technique. A total of 2299 reflections was obtained and 1930 (with $I_{rel} > 2\sigma I_{rel}$) were employed in the solution. Density (ρ = 1.24 Mg m^{-3}) of the crystal gave $Z = 2$, allowing one molecule of $C_{24}H_{34}O_{15}$ with M_r = 562.52 for each asymmetric unit.

The program SHELX (7) was employed as outlined above, using a starting set of eleven reflections to generate 256 permutations. Of the twelve *E*-maps obtained, the fifth (reliability index $R_A = 0.129$) gave, as a recognizable molecular fragment, 21 of the 39 non-hydrogen atoms in the asymmetric unit. Weighted difference syntheses yielded the remaining non-hydrogen atoms. Hydrogen atoms were placed at 1.00 Å from their respective carbon atoms and their positions were based on the geometry of the molecule. Again, methyl hydrogens were handled as rigid groups. Because of the large number of independent atoms, final refinements were performed using the blocked-matrix technique with the non-hydrogen atoms treated anisotropically and the hydrogen atoms isotropically to yield $R = 0.053$ (unit weights).

Completion of the X-ray crystal structure determinations of phyllanthocindiol methyl ester (**2***b*) and phyllanthose acetate (**3***b*) clearly substantiates the assignment of structure **2***a* to phyllanthostatin 3 and confirms the previous (**2***a*, *b*) assignments of phyllanthostatins 1 and 2 (**1***a*, *c*) and of phyllanthoside (**1***b*). Presently, the results of these structural elucidations are being employed in establishing structures for related glycosides in this potentially important series of biosynthetic products.

Acknowledgments

We are pleased to record that the necessary financial assistance was provided by Mary Dell Pritzlaff, the Olin Foundation (Spencer T. and Ann W.) the Fannie E. Rippel Foundation, Eleanor W. Libby, the Donald Ware Waddell Foundation, the Flinn Foundation, Jack W. Whiteman, Pearl Spear, Robert B. Dalton, and Contract NO1-CM-97297 with the Division of Cancer Treatment, NCI, National Institutes of Health, DHHS. The UCT chemists received financial assistance from the University of Cape Town and the C.S.I.R., Pretoria. We also wish to thank Drs. M. I. Suffness and D. Gust for other helpful assistance.

1. G. R. PETTIT. J. Nat. Prod. In preparation. M. SUFFNESS and J. DOUROS. J. Nat. Prod. **45**, 1 (1982); J. M. CASSADY and J. D. DOUROS (*Editor*). Anticancer agents based on natural products models. Academic Press, New York. 1980; G. R. PETTIT. Biosynthetic products for cancer chemotherapy. Vol. 1. Plenum Publishing Corp., New York. 1977.
2. (*a*) G. R. PETTIT, G. M. CRAGG, D. GUST, and P. BROWN. Can. J. Chem. **60**, 544 (1982). (*b*) G. R. PETTIT, G. M. CRAGG, D. GUST, P. BROWN, and J. M. SCHMIDT. Can. J. Chem. **60**, 939 (1982); (*c*) R. G. POWELL, D. WEISLEDER, C. R. SMITH, JR., J. KOZLOWSKI, and W. K. ROHWEDDER. J. Am. Chem. Soc. **104**, 4929 (1982); (*d*) V. LUKAČOVA, J. POLONSKY, C. MORETTI, G. R. PETTIT, and J. M. SCHMIDT. J. Nat. Prod. **45**, 288 (1982); (*e*) C. MORETTI, J. POLONSKY, M. VUILHORGNE, and T. PRANGE. Tetrahedron Lett. **23**, 647 (1982); (*f*) S. D. JOLAD, J. J. HOFFMANN, K. H. SCHRAM, J. R. COLE, M. S. TEMPESTA, G. R. KRIEK, and R. B. BATES. J. Org. Chem. **47**, 3151 (1982); (*g*) Y. NAGAO, N. ITO, T. KOHNO, H. KURODA, and E. FUJITA. Chem. Pharm. Bull. **30**, 727 (1982); (*h*) S. MUKHOPADHYAY, G. A. HANDY, S. FUNAYAMA, and G. A. CORDELL. J. Nat. Prod. **44**, 696 (1981).
3. K. KOMIYAMA, K.-I. EDANAMI, H. YAMAMOTO, and I. UME-

[4]Elemental microanalytical and other (ir, ^1H and ^{13}C nmr spectral) data were consistent with the assigned structures and will be presented in a future complete manuscript.

ZAWA. J. Antibiot. **35**, 703 (1982); H. NAKANO, M. YOSHIDA, K. SHIRAHATA, S. ISHII, Y. ARAI, M. MORIMOTO, and F. TOMITA. J. Antibiot. **35**, 760 (1982); K. SHIMIZU, S. OHKUBO, M. MORIMOTO, and F. TOMITA. J. Antibiot. **35**, 87 (1982); R. MISRA, R. C. PANDEY, and J. V. SILVERTON. J. Am. Chem. Soc. **104**, 4478 (1982); D. M. BALITZ, F. A. O'HERRON, J. BUSH, D. M. VYAS, D. E. NETTLETON, R. E. GRULICH, W. T. BRADNER, T. W. DOYLE, E. ARNOLD, and J. CLARDY. J. Antibiot. **34**, 1544 (1981); T. TAKEUCHI, H. IINUMA, S. KUNIMOTO, T. MASUDA, M. ISHIZUKA, M.TAKEUCHI, M. HAMADA, H. NAGANAWA, S. KONDO, and H. UMEZAWA. J. Antibiot. **34**, 1619 (1981); C. G. CHIDESTER, W. C. KRUEGER, S. A. MIZSAK, D. J. DUCHAMP, and D. G. MARTIN. J. Am. Chem. Soc. **103**, 7629 (1981).

4. M. ISOBE, M. KITAMURA, and T. GOTO. J. Am. Chem. Soc. **104**, 4997 (1982). P. A. GRIECO, G. F. MAJETICH, and Y. OHFUNE. J. Am. Chem. Soc. **104**, 4226 (1982); E. E. VAN TAMELEN and T. M. LEIDEN. J. Am. Chem. Soc. **104**, 1785 (1982).
5. Y. AOYAGI, H. SUGUNA, N. MURUGESAN, G. M. EHRENFELD, L.-H. CHANG, T. OHGI, M. S. SHEKHANI, M. P. KIRKUP, and S. M. HECHT. J. Am. Chem. Soc. **104**, 5237 (1982); T. FUKUYAMA and R. A. SACHLEBEN. J. Am. Chem. Soc. **104**, 4957 (1982); S. M. WEINREB, F. Z. BASHA, S. HIBINO, N. S. KHATRI, D. KIM, W. E. PYE, and T.-T. WU. J. Am. Chem. Soc. **104**, 536 (1982).
6. S. M. KUPCHAN, E. J. LAVOIE, A. R. BRANFMAN, B. Y. FEI, W. M. BRIGHT, and R. F. BRYAN. J. Am. Chem. Soc. **99**, 3199 (1977).
7. G. M. SELDRICK. SHELX in computing in crystallography. *Edited by* H. Schenk, R. Olthof-Hazekamp, H. van Koningsveld, and G. C. Bassi. Delft University Press, pp. 34–42.
8. G. R. PETTIT, C. L. HERALD, and Y. KAMANO. J. Org. Chem. In press.

Can. J. Chem. Downloaded from www.nrcresearchpress.com by 210.87.254.6 on 09/06/12
For personal use only.

Glycosides from *Muscari comosum*. 4.[1] Structure of muscaroside A[2]

M. ADINOLFI, G. BARONE, R. LANZETTA, G. LAONIGRO, L. MANGONI, AND M. PARRILLI[3]

Istituto di Chimica Organica e Biologica della Università di Napoli, Via Mezzocannone 16, 80134 Napoli, Italy

Received March 9, 1983

M. ADINOLFI, G. BARONE, R. LANZETTA, G. LAONIGRO, L. MANGONI, and M. PARRILLI. Can. J. Chem. **61**, 2633 (1983).

The less polar component of the glycoside mixture extracted from the bulbs of *Muscari comosum* has been completely characterized. This glycoside, **5**, possesses an α-L-rhamnopyranosyl(1→2)-β-D-glucopyranosyl(1→2)-α-L-arabinopyranosyl-(1→6)-β-D-glucopyranosyl chain linked at the C-3 position of eucosterol **1**.

M. ADINOLFI, G. BARONE, R. LANZETTA, G. LAONIGRO, L. MANGONI et M. PARRILLI. Can. J. Chem. **61**, 2633 (1983).

On a identifié complètement le composé le moins polaire du mélange de glycosides extrait des bulbes du *Muscari comosum*. Ce glycoside, **5**, possède une chaîne de α-L-rhamnopyrannosyl(1→2)-β-D glucopyrannosyl(1→2)-α-L-arabinopyrannosyl-(1→6)-β-D glucopyrannosyle, liée au carbone en position 3 de l'eucostérol (**1**).

[Traduit par le journal]

Muscari comosum Mill. is a plant widely distributed in the Mediterranean area. Its aqueous extracts have been reported (1) to display antitumoral activity. Recently we have isolated from the bulbs of the plant a complex glycoside mixture and identified aglycone moieties **1**−**4** (2−4). Compounds **1**−**4** possess a 27-norlanostane skeleton and are characterized by the unique structural feature constituted by a tetrahydrofuran ring spirofused at the C-17 position. In continuation of our study on this subject, we report now the isolation and the structural elucidation of muscaroside A, **5**, the less polar component of the glycoside mixture. It possesses an α-L-rhamnopyranosyl-(1→2)-β-D-glucopyranosyl(1→2)-α-L-arabinopyranosyl(1→6)-β-D-glucopyranosyl chain as its sugar moiety linked at the C-3 position of eucosterol **1**.

Column chromatography (silica gel) of the crude glycoside mixture extracted (4) from the bulbs afforded four main fractions. High performance liquid chromatography (hplc) of the less polar one yielded muscaroside A. This was shown to be homogeneous by spectroscopy (^{13}C and ^{1}H nmr, Tables 1 and 2, respectively) and by degradative experiments (see below). Muscaroside A is levorotatory, $[\alpha]_D$ −20°, and melts at ca. 205°C with decomposition. Chemical analysis gave $C_{52}H_{82}O_{23}$, according to the pseudo-molecular ion peak (MH^+ 1075) in the FAB mass spectrum. On enzymatic hydrolysis, it yielded eucosterol **1** as aglycone, identified by comparison (tlc, mp, ^{13}C and ^{1}H nmr) with an authentic sample.

The acid hydrolysis (7% H_2SO_4) of muscaroside A gave rhamnose, arabinose, and glucose, identified by tlc. In the ^{1}H nmr spectrum (DMSO-d_6) of this monose mixture the signals of the anomeric protons of rhamnopyranose, glucopyranose, arabinopyranose, and arabinofuranose were identified through a comparison with the signals displayed by equilibrated authentic samples of the monoses and attributed on the basis of the displayed shifts and coupling constants (5). The integration of the anomeric proton signals established the 1:2:1 molar ratio of rhamnose, glucose, and arabinose. The monoses were identified also by hplc analysis of the hydrolysate, and calibration of the peak integrated areas against known concentrations confirmed that molar ratio. Isolation of the three monoses from the hydrolysate by hplc and determination of their rotations established the absolute D-configuration of glucose and the L-configuration of arabinose and rhamnose. The L-configuration of arabinose was confirmed by the positive response of a D-galactose dehydrogenase test (6, 7).

Permethylation (DMF/NaH/MeI) (8) of muscaroside A and subsequent acid hydrolysis (2 *N* HCl/dioxane) afforded, after column chromatography, 2,3,4-tri-*O*-methyl-L-rhamnopyranose, 3,4,6-tri-*O*-methyl-D-glucopyranose, 2,3,4-tri-*O*-methyl-D-glucopyranose, and 3,4-di-*O*-methyl-L-arabinopyranose, identified by comparison (tlc, ^{1}H nmr) with authentic samples. Methanolysis (anhydrous HCl/MeOH) of the permethylated muscaroside A followed by column chromatography gave methyl 3,4,6-tri-*O*-methyl-α-D-glucopyranoside, methyl 2,3,4-tri-*O*-methyl-α-D-glucopyranoside, and methyl 3,4-di-*O*-methyl-α-L-arabinopyranoside, identified by comparison (tlc, ^{1}H nmr) with authentic samples. We were not able to isolate the permethylation−methanolysis product of the rhamnose unit in a pure form. However, all these data safely establish the interglycosidic linkages in muscaroside A and the sugar-ring size; more precisely, L-rhamnopyranose is the terminal sugar unit, L-arabinopyranose is linked at position 2, one D-glucopyranose is linked at position 2, and the other at position 6.

The configuration at the anomeric centres of the monose units of muscaroside A was suggested by consideration of molecular rotation values in the light of Klyne's rule (9). Calculation (Table 3) led to the conclusion that α-configuration of the anomeric centres of the rhamnose and arabinose units and β-configuration of the anomeric centres of the two glucose units may be assumed.

The ^{13}C and ^{1}H nmr spectra of muscaroside A agreed with all above conclusions and also indicated the attachment position of the sugar chain to the aglycone moiety.

The significant (+9.0) downfield shift observed for the C-3 of the aglycone unit clearly indicates (10−13) that this carbon bears the sugar chain. Furthermore, deshielding of G′-6 and G″-2 and shielding of the adjacent carbons G′-5, G″-1, and G″-3 fully accord (10−13) with the above established interglycosidic linkages involving the glucose units. Given the size of the coupling constants (14) (Table 1), the signals at δ 102.0 and δ 101.2 in the ^{13}C-spectrum in Py-d_6 may be attributed to R-1 and A-1 respectively. However, the unchanged shifts of the other carbons of the rhamnose unit, as compared to those of methyl α-L-rhamnopyranoside, agreed with the terminal location of rhamnose. Furthermore, the line of A-1 is shifted

[1]Part 3: ref. 3.

[2]Preliminary communication: 13th International Symposium on the Chemistry of Natural Products, Pretoria, South Africa, August 1982.

[3]Author to whom correspondence should be addressed.

Can. J. Chem. Downloaded from www.nrcresearchpress.com by 210.87.254.40 on 09/06/12
For personal use only.

TABLE 1. ^{13}C nuclear magnetic resonance shifts of muscaroside A, **5**, and reference substances (glycosylation shift, $J^{1}_{C\text{-}1,H\text{-}1}$)[a]

Carbon		Reference substances[b,c]		**5**[c,d]	**5**[c,f]	Carbon	Reference substances[b,c]		**5**[c,d]	**5**[c,f]
	G′-1	A	105.4	106.1 (*158*)	106.1	1	D	35.9	35.7	36.6
	G′-2		74.8	75.4	75.7	2		29.0	27.4	28.0
-6)-β-D-Glu*p*-(1-	G′-3		78.1	78.2	78.1	3		80.0	89.0 (+9.0)	90.5
	G′-4		71.4	71.5	71.9	4		43.2	44.4	44.9
	G′-5		78.1	75.5 (−2.6)	76.1	5		51.3	51.4	52.5
	G′-6		62.5	68.7 (+6.2)	69.5	6		18.9	18.7	19.5
						7		27.3	27.4	27.9
	A-1	B	105.9	101.2 (−4.7, *166*)	102.4	8		133.1	133.2	134.1
	A-2		72.2	79.3 (+7.1)	79.2	9		136.4	136.6	137.7
-2)-α-L-Ara*p*-(1-	A-3		74.4	72.3 (−2.1)	72.0	10		37.7	37.3	38.2
	A-4		69.1	66.5	67.8	11		20.9	20.8	21.7
	A-5		66.6	64.2	64.0	12		23.3	23.3	24.4
						13		47.6	47.7	[g]
	G″-1	A	105.4	103.1 (−2.3, *154*)	103.0	14		58.0	58.0	59.4
	G″-2		74.8	78.3 (+3.5)	79.2	15		215.2	215.2	218.5
-2)-β-D-Glu*p*-(1-	G″-3		78.1	77.7 (−0.4)	78.0	16		52.0	52.0	52.7
	G″-4		71.4	71.5	72.2	17		91.3	91.3	92.5
	G″-5		78.1	78.3	78.1	18		20.4	20.5	21.0
	G″-6		62.5	62.7	62.7	19		20.0	19.4	19.8
						20		43.4	43.4	44.6
	R-1	C	102.4	102.0 (*171*)	102.2	21		17.2	17.1	17.6
	R-2		71.9	72.7	72.3	22		36.9	36.9	37.8
α-L-Rha*p*-(1-	R-3		72.5	72.7	72.5	23		81.9	81.9	82.9
	R-4		73.6	74.3	74.2	24		211.9	211.7	214.3
	R-5		69.4	69.5	70.0	25		32.4	32.3	33.2
	R-6		18.4	18.7	18.2	26		7.6	7.6	7.7
						30		23.4	23.2	23.1
						31		64.4	62.3	63.5
						32		24.1	24.1	24.6

[a]Assignment of signals with very close chemical shifts may be interchanged.
[b]Reference substances: A, methyl β-D-glucopyranoside (21); B, methyl α-L-arabinopyranoside (21); C, methyl α-L-rhamnopyranoside (21); D, eucosterol **1** (2).
[c]Measured in pyridine-d_5.
[d]Assignment is based on comparison with the reference substances; see also text.
[e]Measured in methanol-d_4.
[f]Assignment is based on comparison with the spectrum in pyridine-d_5; see also text.
[g]Obscured by methanol signal.

TABLE 2. ^{1}H nuclear magnetic resonance chemical shifts (δ) of muscaroside A, **5**, in methanol-d_4

18-H_3 } 19-H_3 }	0.97 s, 0.98 s
26-H_3	1.03 t, $J_{25,26}$ = 7.4 Hz
21-H_3	1.13 d, $J_{20,21}$ = 6.6 Hz
30-H_3	1.22 s
R-6-H_3	1.27 d, $J_{5,6}$ = 6.3 Hz
32-H_3	1.38 s
25-H_2	2.51 q, $J_{25,26}$ = 7.4 Hz
16-H_2	2.29 and 2.74, ABq, J_{AB} = 19.1 Hz
23-H	4.75 m
G′-1-H	4.42 d, $J_{1,2}$ = 7.7 Hz
	(4.98 d, $J_{1,2}$ = 7.5 Hz)[a]
A-1-H	4.63 d, $J_{1,2}$ = 4.4 Hz
	(5.37 d, $J_{1,2}$ = 3.3 Hz)[a]
G″-1-H	4.69 d, $J_{1,2}$ = 7.4 Hz
	(5.18 d, $J_{1,2}$ = 6.8 Hz)[a]
R-1-H	5.25 d, $J_{1,2}$ = 1.5 Hz
	(6.36 d, $J_{1,2}$ = 2.0 Hz)[a]

[a]In pyridine-d_5.

upfield as compared to that of the reference compound and this, besides the downfield shift of A-2, indicates that arabinose is linked at this latter position.

TABLE 3. Calculated and observed contribution of the sugar chain to the $[M]_D$ of muscaroside A, **5**[a]

Chain	$[M]_D$
Methyl α-D-glucopyranoside	+309°
Methyl β-D-glucopyranoside	−66°
Methyl α-L-arabinopyranoside	+17°
Methyl β-L-arabinopyranoside	+245°
Methyl α-L-rhamnopyranoside	−111°
Methyl β-L-rhamnopyranoside	+170°
β-D-glu*p* + α-L-ara*p* + β-D-glu*p* + α-L-rha*p*	−225°[b]
$[M]_{D_{muscaroside\ A}} - [M]_{D_{eucosterol\ 1}}$	−304°

[a]$[M]_D$ values of methyl glycosides are taken from ref. 23.
[b]All other possible combinations give much more positive values.

The anomeric proton signals (methanol-d_4) at δ 4.42 and 4.69 may be attributed to G′-1-H and G″-1-H, respectively, as they were correlated to the signals (methanol-d_4) of G′-1 and G″-1, respectively, by pertinent heteronuclear selective decoupling experiments. The $J^{3}_{H\text{-}1,H\text{-}2}$ coupling constant values (~7 Hz) are compatible only with β-configuration at these centres (5). Accordingly (14), the values 158 and 154 Hz were observed for the $J^{1}_{C\text{-}1,H\text{-}1}$ of G′-1 and G″-1 in the spectrum in Py-d_5. The α-configuration of the L-rhamnose anomeric centre

Can. J. Chem. Downloaded from www.nrcresearchpress.com by 210.87.254.40 on 09/06/12
For personal use only.

Can. J. Chem. Downloaded from www.nrcresearchpress.com by 210.87.254.40 on 09/06/12
For personal use only.

was confirmed by the good agreement in the R-3 and R-5 peaks (δ 72.7 and δ 69.5, respectively, in Py-d_5) with the values given for methyl α-L-rhamnopyranoside (δ 72.5 and δ 69.4, respectively), the values for the β-anomer being instead δ 75.3 and δ 73.4, respectively (15).

No further support for the α-configuration of the L-arabinose unit could be drawn from the nmr data. In the ^{1}H nmr spectrum of muscaroside A in methanol-d_4 the signal at δ 4.63, J = 4.4 Hz, may be attributed to the anomeric proton of the arabinose unit, as the remaining anomeric signal (δ 5.25, J = 1.5 Hz) fits the R-1-H proton well (15, 16). The 4.4 Hz value for $J^3_{H\text{-}1,H\text{-}2}$ of the arabinose unit falls in a range which has often been taken as an indication of α-configuration (17, 18). More recently, however, the value of this coupling constant, as well as $J^1_{C\text{-}1,H\text{-}1}$, has been reported (19) not to be diagnostic on its own, owing to the high conformational mobility of arabinopyranosides ($^4C_1 \rightleftarrows {}^1C_4$) (20). Finally, shift values (δ 66.5 and δ 64.2) attributed (Table 1, Py-d_5) to A-4 and A-5, respectively, accorded neither with the corresponding values (δ 69.1 and δ 66.6, respectively) given for reference methyl α-L-arabinopyranoside nor with the values (δ 70.8 and δ 63.9, respectively) given (21) for methyl β-L-arabinopyranoside. However, we have found shifts similar to those reported (19) for carbons 4 and 5 of the 2-linked α-arabinopyranose units of a series of glycosides. In conclusion, α-configuration of the arabinose unit in muscaroside A rests only on the evidence afforded by the application of Klyne's rule. This indication, however, appears to be particularly sound, as the alternative combination β-D-glu*p* + β-L-ara*p* + β-D-glu*p* + α-L-rha*p* implies (Table 3) a contribution of +2° to the $[M]_D$ of **5**, much further indeed from the observed value (−304°).

Sequence of the monose units in muscaroside A was readily arrived at as follows. Rhamnose having been established as the terminal unit, the small value (+4.5) of the glycosylation shift of G″-2 indicates (22) that the glucose unit linked at position 2 is glycosylated by rhamnose. Furthermore, a significant Overhauser effect was measured for the signal at δ 4.42 (in methanol-d_4) of the anomeric G′-1-H of the other glucose unit upon irradiation of the 30-H_3 protons of muscaroside A. This result indicates spatial proximity between the G′-1-H and the 30-H_3 protons and established that the glucose unit substituted at position 6 is directly linked to the C-3 carbon of the aglycone moiety. The location of the arabinose unit between the two glucose units necessarily follows.

Experimental[4]

General

Melting points were determined with a Kofler block. The ^{1}H (270 MHz) and ^{13}C nmr (67.88 MHz) spectra were taken on a Fourier transform Bruker instrument WH 270 (TMS as internal reference) with an Aspect 2000 computer with 48 K memory (32 K data). Nuclear Overhauser enhancement effects were obtained in the difference mode as reported in ref. 3. Mass spectra were recorded with a Kratos 902 instrument equipped with a FAB source. Rotations were determined on a Perkin–Elmer 141 polarimeter. The hplc was performed with a Varian 5020 instrument using a differential refractometer Waters R 401 as the detector. The tlc was carried out on precoated silica gel layers (0.25 mm, Merck F_{254}). Silica gel 0.05–0.20 (Merck) was used for column chromatography. Sugars and methylated sugars were detected with aniline phtalate or *p*-anisaldehyde, glycosides and aglycone with chromium oxide/sulphuric acid.

[4]With the assistance of Italo Giudicianni.

Reference methylated sugars

These were obtained by permethylation (NaH/DMF/MeI, see below) followed by acid hydrolysis (1:1 2 *N* HCl/dioxane, 4 h, reflux) or methanolysis (anhydrous 3% HCl/MeOH, 3 h, 90°C) from starting material indicated below and were purified by preparative tlc (97:3 or 9:1 chloroform–methanol).

Methyl 2,3,4-tri-*O*-methyl-β-L-rhamnopyranoside was obtained by permethylation of L-rhamnose. Acid hydrolysis of the former gave 2,3,4-tri-*O*-methyl-L-rhamnopyranose. 3,4,6-Tri-*O*-methyl-D-glucopyranose was prepared by permethylation and acid hydrolysis from naringin (Fluka AG). Methyl 3,4,6-tri-*O*-methyl-α-D-glucopyranose was prepared by permethylation and acid methanolysis from naringin. 2,3,4-Tri-*O*-methyl-D-glucopyranose was prepared by permethylation and acid hydrolysis from rutin (Fluka AG). Methyl 2,3,4-tri-*O*-methyl-α-D-glucopyranoside was prepared by permethylation and acid methanolysis from rutin. Methyl 3,4-di-*O*-methyl-L-arabinopyranosides were prepared as in ref. 24. Their acid hydrolysis gave 3,4-di-*O*-methyl-L-arabinopyranose.

The ^{1}H nmr data of methylated sugars are summarized in Table 4.

Isolation of muscaroside A

The glycoside mixture (9 g), extracted from sliced fresh bulbs (1 kg) of the plant as reported in ref. 4, was chromatographed on a silica gel (200 g) column with a Chromatospac Prep. 10 apparatus (Jobin Yvon). Elution with 3:2 chloroform–methanol afforded four main fractions: *a* (1.4 g), *b* (2 g), *c* (1.5 g), and *d* (1 g) (decreasing R_f order).

Fraction *a* was subjected to semi-preparative hplc (Lichrosorb RP-18 (7 μm) column, 75:25 methanol–water, 5 mL min^{-1}, 75 mg in 1 mL of 75:25 methanol–water) to give muscaroside A (215 mg); mp (from ethanol) 205°C dec.; $[\alpha]_D$ −20° (methanol, *c* 0.6); FAB-ms: 1074 *m/e*. Elemental analysis: C 57.9, H 7.6 ($C_{52}H_{82}O_{23}$ requires C 58.1, H 7.7%). The ^{1}H and ^{13}C nmr data are given in Tables 2 and 1, respectively.

Enzymatic hydrolysis of muscaroside A

To a solution of muscaroside A (30 mg) in water (10 mL), digestive juice of *Helix pomatia* (0.1 mL, Industrie Biologique Française) was added. The solution was stirred for 40 days at room temperature and then extracted with chloroform. Evaporation of the chloroform extract gave a solid (8 mg). Preparative tlc (4:1 chloroform – ethyl acetate, 2 runs) yielded eucosterol **1** (6 mg), identical (mp, ms, ^{1}H nmr) to an authentic sample (4, 25).

Acid hydrolysis of muscaroside A

A solution of muscaroside A (50 mg) in 7% H_2SO_4 (5 mL) was heated at 90°C for 3 h. The solution was cooled and washed with chloroform. The aqueous layer was filtered through an Amberlite IR-4B (OH) (2 g) column and the eluate was freeze-dried to give a solid (28 mg, monose mixture).

A sample was dissolved in water and analyzed by tlc (silica gel layers, 14:6:1 chloroform–methanol–water and silica gel layers treated with 0.2 *N* sodium acetate, 24:12:64 isopropanol–water – ethyl acetate); the presence of rhamnose, glucose, and arabinose was established by comparison with authentic samples.

Anomeric proton signals in the ^{1}H nmr spectrum (DMSO-d_6) δ: 4.84 d, J = 1.7 Hz and 4.56 bs (α- and β-anomer, respectively, of rhamnopyranose); 4.23 d, J = 7.7 Hz and 4.92 d, J = 3.4 Hz (β- and α-anomer, respectively, of glucopyranose); 4.23 d, J = 6.5 Hz and 4.87 d, J = 3.0 Hz (α- and β-anomer, respectively, arabinopyranose); 4.92 d, J = 3.0 Hz and 5.01 d, J = 3.9 Hz (α- and β-anomer, resp. of arabinofuranose). The integration of these signals established the molar ratio 1:2:1 rhamnose/glucose/arabinose.

A sample of the monose mixture was analyzed at hplc (Lichrosorb NH_2 (10 μm); 4:1 acetonitrile–water; 0.5 mL min^{-1}). Glucose (t_r 18.3 min), arabinose (t_r 13.7 min), and rhamnose (t_r 10.4 min) were identified by comparison with authentic samples. The areas of the peaks were in the same ratio as those of a 2:1:1 mixture of authentic glucose, rhamnose, and arabinose.

Semi-preparative hplc with the same column (1.5 mg per 200 μL, 4:1 acetonitrile–water) allowed separation of D-glucose ($[\alpha]_D$ +58°

TABLE 4. ^{1}H nuclear magnetic resonance ($CDCl_3$) shifts (δ) of reference methylated sugars

	Anomeric protons		Methoxyl protons	
	α	β	α	β
2,3,4-Tri-*O*-methyl-L-rhamnopyranose[a]	5.26 bs	4.64 bs	3.51 (6H), 3.56	3.54 3.56, 3.67
Methyl 2,3,4-tri-*O*-methyl-β-L-rhamnopyranoside[b]		4.27 s		3.49 3.51 3.56 3.64
3,4-Di-*O*-methyl-L-arabinopyranose	4.62 d *J* = 7.4 Hz	5.29 d *J* = 3.7 Hz	3.47, 3.47, 3.51, 3.54,	
Methyl 3,4-di-*O*-methyl-L-arabinopyranoside	4.13 d *J* = 7.4 Hz	4.80 d *J* = 3.7 Hz	3.47, 3.51 3.55	3.50, 3.47 3.45
3,4,6-Tri-*O*-methyl-D-glucopyranose	5.26 d *J* = 4.0 Hz	4.57 d *J* = 7.7 Hz	3.49, 3.54 (6H), 3.56, 3.66, 3.67	
Methyl 3,4,6-tri-*O*-methyl-α-D-glucopyranoside	4.76 d *J* = 4.5 Hz		3.42 (6H), 3.53, 3.66	
2,3,4-Tri-*O*-methyl-D-glucopyranose	5.32 d *J* = 3.7 Hz	4.61 d *J* = 7.4 Hz	3.53, 3.54, 3.56, 3.63, 3.63 (6H)	
Methyl 2,3,4-tri-*O*-methyl-α-D-glucopyranoside	4.81 d *J* = 3.3 Hz		3.41, 3.52, 3.58, 3.63,	

[a]Chemical shifts of —CH_3 at C-5: 1.29 (d, *J* = 6.6 Hz, α-anomer), 1.33 (d, *J* = 6.6 Hz, β-anomer).
[b]Chemical shift of —CH_3 at C-5: 1.36 (d, *J* = 6.6 Hz).

(final, H_2O), lit. (26*a*) +53° (final)); L-arabinose ($[\alpha]_D$ +102° (final, H_2O), lit. (26*b*) +105° (final)); and L-rhamnose ($[\alpha]_D$ +10° (final, H_2O), lit. (26*c*) +8° (final)). The L-arabinose sample obtained produced the expected response with the D-galactose dehydrogenase system in an assay for determination of L-arabinose as described in ref. 7 and in the information sheet from Boehringer Mannheim GMBH.

Permethylation of muscaroside A

To a solution of **5** (100 mg) in anhydrous dimethylformamide (20 mL), NaH (400 mg) was added and the mixture was stirred in an ice bath for 15 min. Methyl iodide (15 mL) was added and the mixture was stirred for 10 min in the ice bath and for 12 h at room temperature. The excess of sodium hydride was destroyed by adding methanol (2 mL). After evaporation at reduced pressure, the residue was treated with water and chloroform. The chloroform layer was evaporated. The residue (120 mg) is a complex mixture since the aglycone moiety undergoes changes in the alkaline medium of reaction (25). However, the occurrence of a complete permethylation was confirmed by the ir spectrum which showed no —OH absorption. Conclusive evidence was furnished by the fact that attempts at further methylation (with $NaH/CH_3I/DMF$) or acetylation (Ac_2O/Py) left the sample totally unchanged (tlc, ir, nmr).

Acid hydrolysis of permethylated muscaroside A

Permethylated muscaroside A (60 mg) was hydrolyzed with 1:1 dioxane − 2 *N* HCl (10 mL) by refluxing for 6 h. The cooled mixture was neutralized with solid Na_2CO_3 and evaporated. The residue was extracted with chloroform and the chloroform extract was evaporated. The residue (60 mg) was chromatographed on a column of silica gel (8 g). Elution with chloroform containing increasing percentages of ethyl acetate afforded pure 2,3,4-tri-*O*-methyl-L-rhamnopyranose (9 mg), 3,4,6-tri-*O*-methyl-D-glucopyranose (10 mg), 2,3,4-tri-*O*-methyl-D-glucopyranose (10 mg), and 3,4-di-*O*-methyl-L-arabinose (8 mg) which were identified by comparison (tlc, 1:9 methanol−water, 1 run; ^{1}H nmr: see Table 4) with authentic samples.

Acid methanolysis of permethylated muscaroside A

Permethylated muscaroside A (60 mg) was heated in anhydrous HCl/methanol (3%, 5 mL) at 90°C for 3 h. After cooling, the mixture was neutralized with Ag_2CO_3, filtered, and evaporated. The residue (60 mg) was chromatographed on a column of silica gel (12 g). Elution with chloroform containing increasing percentages of ethyl acetate yielded pure methyl 3,4,6-tri-*O*-methyl-α-D-glucopyranoside, methyl 2,3,4-tri-*O*-methyl-α-D-glucopyranoside, and methyl 3,4-di-*O*-methyl-α-L-arabinopyranoside which were identified by comparison (tlc, 3:97 methanol−chloroform, 1 run; ^{1}H nmr: see Table 4) with authentic samples.

Acknowledgments

Thanks are due to Mr Ron Self (Food Research Institute, Norwich, U.K.) for FAB mass spectra. This investigation was supported by CNR (Consiglio Nazionale delle Ricerche, Rome).

1. B. PRESCOTT AND G. CALDES. Proc. Soc. Exp. Biol. Med. **129**, 190 (1969).
2. M. PARRILLI, M. ADINOLFI, and L. MANGONI. Gazz. Chim. Ital. **109**, 611 (1979).
3. M. PARRILLI, R. LANZETTA, M. ADINOLFI, and L. MANGONI. Tetrahedron, **36**, 3591 (1980).
4. M. PARRILLI, R. LANZETTA, V. DOVINOLA, M. ADINOLFI, and L. MANGONI. Can. J. Chem. **59**, 2261 (1981).
5. T. D. INCH. Nuclear magnetic resonance spectroscopy in the study of carbohydrates and related compounds. *In* Annual Reports on NMR Spectroscopy. *Edited by* E. F. Money. Academic Press, London. 1972. p. 305; and references therein.
6. O. OLSEN, K. W. RASMUSSEN, and H. SORENSEN. Phytochemistry, **20**, 1857 (1981).
7. E. O. BLACHNITZKY, F. WENGENMAYER, and G. KURZ. Eur. J. Biochem. **47**, 235 (1974).
8. H. WAGNER and O. SELIGMANN. Tetrahedron, **29**, 3029 (1973).
9. W. KLYNE. Biochem. J. **47**, 4 (1950).
10. K. YAMASAKY, H. KOHDA, T. KOBAYASHI, R. KASAI, and O. TANAKA. Tetrahedron Lett. 1005 (1976).
11. R. KASAI, M. SUZUO, J. T. ARAKAWA, and O. TANAKA. Tetrahedron Lett. 175 (1977).
12. K. TORI, Y. YOSHIMURA, S. SEO, K. SAKURAWI, Y. TOMITA, and H. ISHII. Tetrahedron Lett. 4163 (1976); 4167 (1976).
13. K. TOSI, S. SEO, Y. YOSHIMURA, H. ARITA, and Y. TOMITA. Tetrahedron Lett. 179 (1977).
14. K. BOCK and C. PEDERSEN. J. Chem. Soc. Perkin Trans. 2, 293 (1974).

Can. J. Chem. Downloaded from www.nrcresearchpress.com by 210.87.254.40 on 09/06/12
For personal use only.

15. R. KASAI, J. OKIHARA, K. ASAKAWA, I. MITZUTANI, and O. TANAKA. Tetrahedron, **35**, 1427 (1979).
16. H. W. LIU and K. NAKANISHI. Tetrahedron, **38**, 513 (1982).
17. T. KONOSHIMA, H. FUKUSHIMA, H. INUI, K. SATO, and T. SAWADA. Phytochemistry, **20**, 139 (1981).
18. S. B. SINGH, R. S. THAKUR, and H. R. SCHULTEN. Phytochemistry, **21**, 2079 (1982).
19. H. ISHII, I. KITAGAWA, K. MATSUSHITA, K. SHIRAKAWA, K. TORI, T. TOZYO, M. YOSHIKAWA, and Y. YOSHIMURA. Tetrahedron Lett. 1529 (1981).
20. D. E. DORMAN and J. D. ROBERTS. J. Am. Chem. Soc. **92**, 1355 (1970).
21. S. SEO, Y. TOMITA, K. TORI, and Y. TOSHIMURA. J. Am. Chem. Soc. **100**, 3331 (1978).
22. S. B. MAHATO, N. P. SAHU, A. N. GANGULY, R. KASAI, and O. TANAKA. Phytochemistry, **19**, 2017 (1980).
23. H. OTSUKA, T. AKIYAMA, K. KAWAI, S. SHIBATA, O. INONE, and Y. OGIHARA. Phytochemistry, **17**, 1349 (1978).
24. P. A. MIED and Y. C. LEE. Anal. Biochem. **49**, 534 (1972).
25. R. ZIEGLER and C. TAMM. Helv. Chim. Acta, **59**, 1997 (1976).
26. L. HOUGH and A. C. RICHARDSON. *In* Rodd's Chemistry of Carbon Compounds. Vol. 1, 2nd ed. *Edited by* S. Coffey. Elsevier, Amsterdam. 1967, Part F. (*a*) p. 237; (*b*) p. 229; (*c*) p. 521.

Can. J. Chem. Downloaded from www.nrcresearchpress.com by 210.87.254.40 on 09/06/12
For personal use only.

The intercalation of bromine fluorosulfates into graphite

S. KARUNANITHY and F. AUBKE

Department of Chemistry, The University of British Columbia, Vancounver, B.C., Canada, V6T 1Y6

Received April 8, 1983

S. KARUNANITHY and F. AUBKE. Can. J. Chem. **61**, 2638 (1983).

The action of bromine(I)fluorosulfate on graphite has led to the synthesis of several novel intercalation compounds. The intercalation of bromine(I)fluorosulfate at room temperature results in a first stage compound, $C_{12}BrSO_3F$, while at higher temperatures (~110°C) $C_{20}BrF(SO_3F)_2$ forms instead. Oxidation of $C_{12}BrSO_3F$ with $S_2O_6F_2$ yields $C_{16}Br(SO_3F)_3$ and this reaction can be reversed by reacting the latter with an excess of Br_2.

Graphite trifluoromethylsulfate $C_{12}SO_3CF_3$ is formed in the solvolysis of $C_{12}BrSO_3F$ with an excess of trifluoromethylsulfuric acid. First stage nature of these compounds has been confirmed by the X-ray identity period along *C* axis and $\nu_{E_{2g}}$ vibrational lattice mode in the Raman spectra. The use of ^{19}F nmr in identifying the chemical species in the inter-lamellar space has been demonstrated. The planar electrical conductivity of these compounds has been observed to be three to six times higher than that of graphite.

S. KARUNANITHY et F. AUBKE. Can. J. Chem. **61**, 2638 (1983).

L'action du fluorosulfate de brome(I) sur le graphite conduit à la synthèse de plusieurs noveaux composés d'insertion. L'insertion du fluorosulfate de brome(I) à la température ambiante conduit dans un premier temps au composé $C_{12}BrSO_3F$ tandis qu'à des températures plus élevées (~110°C) il se forme de préférence le composé $C_{20}BrF(SO_3F)_2$. L'oxydation du composé $C_{12}BrSO_3F$ par le $S_2O_6F_2$ donne le composé $C_{16}Br(SO_3F)_3$ et on peut inverser cette réaction en faisant réagir le produit obtenu avec un excès de Br_2.

La solvolyse du $C_{12}BrSO_3F$ dans de l'acide trifluorométhylsulfurique en excès conduit à la formation du trifluorométhylsulfate de graphite $C_{12}SO_3CF_3$. On a confirmé la nature du premier stade de ces composés, par la période d'identité aux rayons X le long de l'axe *C* et par le mode de réseau vibrationnel $\nu_{E_{2g}}$ des spectres Raman. On met en évidence l'utilisation de la rmn du ^{19}F pour identifier les espèces chimiques dans l'espace interlamellaire. On a observé que la conductivité électrique planaire de ces composés est de 3 à 6 fois plus élevées que celle du graphite.

[Traduit par le journal]

1. Introduction

The intercalation of a rather wide range of elements and molecular compounds into the layer lattice of graphite is well documented and a large number of lamellar compounds of graphite have been synthesized and extensively studied over the years (1, 2). Recent interest in intercalation compounds of graphite has focussed in particular on those compounds where molecular intercalants are capable of acting as electron acceptors, giving rise to intriguing electronic properties and reactivities (3), with a wide range of possible applications (4).

Two examples, both germane to our study, may serve as illustrations. Intercalation of bromine was first observed in 1933 (5), with the highest degree of saturation found for a second stage compound of the stoichiometry C_8Br (6). The mechanism of intercalation by Br_2 and the nature of the resulting materials, in particular the extent of electron transfer from graphite to intercalant, have all been the subject of numerous studies (1, 2).

The oxidative intercalation of bis(fluorosulfuryl)peroxide, $S_2O_6F_2$, on the other hand, was first reported in 1978 (7) with the highest saturation found in first stage compounds of the stoichiometry C_nSO_3F with *n* between 7 and 8 (8, 9). The electron transfer appeared to be complete and formulation of the product as graphite salt $C_n^+SO_3F^-$ seemed justified in this case.

We became interested in attempting the intercalation of bromine(I)fluorosulfate for a number of reasons.

(*i*) $BrSO_3F$ is obtained by the reaction of Br_2 with $S_2O_6F_2$ according to reaction [1] (10,11):

$$[1]\quad Br_2(l) + S_2O_6F_2(l) \rightarrow 2\ BrSO_3F(l)$$

Since both "parent molecules" Br_2 and $S_2O_6F_2$ intercalate, the chance that $BrSO_3F$ would intercalate as well appeared rather high, even though no previous intercalation by any halogen oxyacid derivative (12) seemed to have been undertaken.

(*ii*) The physical properties of bromine(I)fluorosulfate (11) suggested possible intercalation with $BrSO_3F$ either in the gas or the liquid phase. Its chemical behavior as "pseudohalogen" with positively polarized bromine should facilitate charge transfer and formation of an acceptor intercalation compound.

(*iii*) Two typical chemical reactions of $BrSO_3F$, the further oxidation of bromine(I)fluorosulfate (10):

$$[2]\quad BrSO_3F + S_2O_6F_2 \rightarrow Br(SO_3F)_3$$

and its complex formation with metal fluorosulfates (13), e.g.

$$[3]\quad CsSO_3F + BrSO_3F \rightarrow Cs[Br(SO_3F)_2]$$

could possibly be extended to intercalated systems. Again very little reaction chemistry of intercalants in the graphite lattice seemed to have been studied so far and it became a challenge to see to what extent reactivity is affected by intercalation.

2. Experimental

(a) Chemicals

One type of natural graphite (Ticonderoga mines, New York) and two synthetic Graphites, powdereus SP 1 (Union Carbide) and HOPG (highly oriented pyrolytic graphite) in plate and powder form were used in this study. All graphite samples were dried *in vacuo* at 150°C over a period of 24 h, immediately prior to use. Bis-(fluorosulfuryl)peroxide, $S_2O_6F_2$ (14), and bromine(I)fluorosulfate, $BrSO_3F$ (11), were synthesized according to published methods. All other chemicals were obtained from commercial sources in the highest grade of purity available.

(b) Instrumentation

A Spex Ramalog 5 Spectrometer, equipped with an Ar^+ laser (Spectra Physics 164) with the 514.5 nm line was used for excitation. A back scattering geometry was used similar to the one described in the literature (15). The sample was contained in a Teflon sample holder,

Can. J. Chem. Downloaded from www.nrcresearchpress.com by 210.87.254.40 on 09/06/12
For personal use only.

Can. J. Chem. Downloaded from www.nrcresearchpress.com by 210.87.254.40 on 09/06/12
For personal use only.

fitted with circular quartz windows. Spectra were recorded on low laser output power to prevent de-intercalation. X-ray powder photographs were obtained using a Phillips powder camera of 57 mm radius and a Cu source. Samples were sealed in 0.5 mm od Lindemann glass capillaries.

Room temperature ^{19}F solid state nmr spectra were taken at 188 MHz with a Brucker CXP-200 Fourier Transform-NMR spectrometer using a high power ^{19}F probe. Samples were contained in nmr tubes of 30 mm length with a 5 mm od. Electrical conductivity measurements were made at room temperature, employing a contactless radio frequency technique (16). The ferrite core system was used at an induction frequency of 16.8 kHz. Samples of a thickness of 0.2 to 0.4 mm were used for both calibration and measurements.

The conductivity σ was evaluated from the relationship $\Delta V = Kts^2\sigma$, where ΔV = voltage change observed in the sensory coil (using a Keithley 148 Nano voltmeter), t = thickness of the sample (measured with a tool makers micrometer), and s = area of plate (measured with a travelling microscope). The system was calibrated with samples of known resistivity (e.g. Cu, Al, brass, and Pb) in order to obtain K. The resistivity of these samples was checked by means of the four point method (17).

Microanalysis for sulfur bromine and fluorine contents was performed by Analytische Laboratorien, Gummersbach, West Germany. Chemical analysis for carbon and hydrogen was carried out by Mr. P. Borda of this department. A Carbo Erba Model 1106 analyser employing a flash oxidation technique was used and CuO was added to samples. Details of the method were similar to those given in a recently published report (18).

Standard vacuumline techniques were used for the transfer of volatile materials. Solids were manipulated in a Vacuum Atmosphere Corp. "Dri lab", Model HE-43-2, filled with purified dry nitrogen and equipped with a "Dri-Train" Model No. He-93-B circulating unit. Reactions, oxidative intercalation, as well as solvolysis were performed in Pyrex reaction vials fitted with Teflon stem valves (Kontes Glasware). All reactions were followed by recording weight changes.

(c) Synthesis and chemical analysis

(i) The reaction of $BrSO_3F$ with graphite at ambient temperature

In a typical reaction 0.5237 g of vacuum dried graphite powder (SP-1) was allowed to react with ~20 mL of freshly prepared $BrSO_3F$ for a period of 48 h, with the suspension vigorously stirred magnetically. The reddish-brown colour of pure $BrSO_3F$ persisted in the liquid phase throughout the reaction and no evidence for bromine formation could be detected.

Excess $BrSO_3F$ was removed in a dynamic vacuum. Since intercalated $BrSO_3F$ gives a ^{19}F nmr signal at 9.3 ppm relative to $CFCl_3$ and surface adsorbed material resonates at about 35 ppm, ^{19}F nmr could be used to monitor the evaporation process. The signal at 9.3 ppm was found to persist even after prolonged pumping, while the 35 ppm signal eventually disappeared. The resulting solid showed a deep blue luster. Gravimetry gave slightly varying compositions depending on the type of graphite used. Natural graphite flakes: $C_{12.14}BrSO_3F$, HOPG plates: $C_{12.6}BrSO_3F$ and SP-1 powder: $C_{12.03}BrSO_3F$. The SP-1 sample had an interlayer separation $I_c = 7.75 \pm 0.03$ Å. *Anal.* calcd. for $C_{12}BrSO_3F$: C 44.59, S 9.91, Br 24.74, F 5.88; found: C 44.47, S 10.22, Br 24.48, F 5.75. Higher stage compounds used for electrical conductance studies are more conveniently prepared inside the conductance cell by gas phase intercalation. The composition of these samples was determined gravimetrically after prolonged pumping.

(ii) The reaction of $BrSO_3F$ with graphite at 105 to 110°C

In a typical reaction 0.1776 g of graphite powder was heated to 105 to 110°C together with about 20 mL of freshly prepared $BrSO_3F$ for a period of about 48 h. Bromine released during the reaction was evident in the gas phase. Volatile materials were removed *in vacuo* until constant weight of 0.4038 g was reached and a black–blue solid was obtained. *Anal.* calcd. for $C_{20}BrF(SO_3F)_2$: C 44.71, Br 14.87, S 11.93, F 10.61; found: C 44.50, Br 14.90, S 12.08, F 10.55. Interlayer separation. $I_c = 7.76 \pm 0.03$ Å.

(iii) The reaction of $C_{12}BrSO_3F$ with $S_2O_6F_2$

In a typical reaction 0.2785 g of graphite powder were converted quantitatively into $C_{12}BrSO_3F$ following the procedure described above. The composition of the product was determined gravimetrically and an excess of $S_2O_6F_2$ was distilled onto the black–blue solid and the suspension was stirred magnetically for 48 h at room temperature. Removal of all volatiles over several days in a dynamic vacuum to constant weight yielded 0.8291 g of final product. Gravimetry suggested a composition $C_{15.9}Br(SO_3F)_3$, while microanalysis agrees well with $C_{16.5}Br(SO_3F)_3$. *Anal.* calcd.: C 34.43, Br 13.91, F 9.91; found: C 34.48, Br 14.04, F 10.01. Interlayer separation = 7.92 Å.

(iv) The reactionof C_7SO_3F with $BrSO_3F$

In a typical reaction 0.3045 g of C_7SO_3F, prepared from the interaction of SP-1 graphite powder with an excess of $S_2O_6F_2$, was allowed to react with an excess of $BrSO_3F$ for 48 h. The excess of $BrSO_3F$ was subsequently removed *in vacuo*. Initially samples exhibiting two broad ^{19}F nmr signals at 11 and 32 ppm respectively were obtained but continued pumping produced a sample with a single line at 10.16 ppm and small shoulders at 22.4 and 25.3 ppm respectively. The interlayer separation of the product was 7.86 ± 0.03 Å and microanalysis gave C 45.45, Br 1.88.

(v) The reaction of $C_{16}Br(SO_3F)_3$ with Br_2

In a typical reaction 0.1550 g of graphite were first converted to $C_{12}BrSO_3F$ and then to $C_{16}Br(SO_3F)_3$ as described above. Reaction of $C_{16}Br(SO_3F)_3$ with an excess of bromine at room temperature for 24 h and removal of all volatiles yielded 0.3481 g of $C_{12}BrSO_3F$. *Anal.* calcd. for $C_{11.98}BrSO_3F$: C 44.52; found C 44.77.

(vi) The reaction of $C_{12}BrSO_3F$ with HSO_3CF_3

As described before 0.2749 g of graphite was converted to 0.6166 g of $C_{12}BrSO_3F$, which was subsequently reacted with about 10 mL of freshly distilled HSO_3CF_3 for 48 h. Evolution of Br_2 was noted during the reaction and 0.5873 g of the composition ~$C_{12}SO_3CF_3$ were obtained and identified by an interlayer separation of 8.08 ± 0.03 Å, in good agreement with the published value (9). *Anal.* calcd.: C 51.24; found C 51.01.

Results and discussion

The intercalation of bromine(I)fluorosulfate into graphite proceeds smoothly and efficiently at room temperature over a period of 48 h to give a deep blue intercalation compound of the limiting composition $C_{12}BrSO_3F$, according to:

[4] $12C + BrSO_3F \rightarrow C_{12}BrSO_3F$

Small variations in the composition of the final product depend on the type of graphite used and may be due to differences in flake size and the degree of order found in the lattice. No Br_2 seems to be formed during the reaction, which argues against a mere fluorosulfonation reaction of the type:

[5] $14C + 2BrSO_3F \rightarrow 2C_7SO_3F + Br_2$

Microanalysis and the observed ratio of Br:F:S of 1:1.012:1.04 are very consistent with our formulation as $C_{12}BrSO_3F$.

Identification of $C_{12}BrSO_3F$ as a first stage intercalation compound is based on the observed interlayer separation of 7.75 ± 0.03 Å and the shift of the Raman active E_{2g} lattice vibration of graphite to 1641 cm^{-1} in agreement with published observations for other first stage compounds (19, 20).

That the intercalant is packed rather tightly may be deduced in the following manner: the interlayer separation of 7.75 Å, allowing 3.35 Å for the carbon layer, suggests a gallery volume of 11.4 $Å^3$ per C atom. The reported density of $BrSO_3F$ (11) at 25°C is 2.238 g/cm^3 which leads to a molecular volume

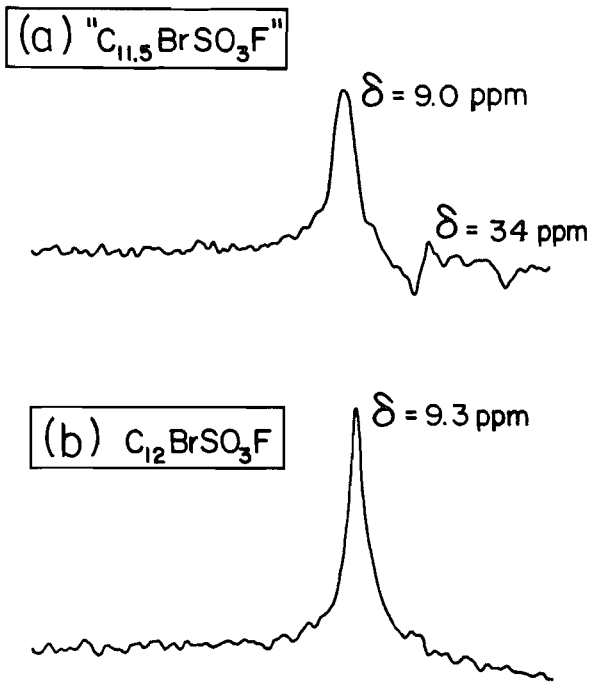

FIG. 1. The ^{19}F nmr spectrum of C_nBrSO_3F.

of about 133 Å^3. This would then suggest an "ideal" composition of $C_{11.67}BrSO_3F$, in reasonable agreement with our experimental finding, with molecular association found in the liquid to persist on intercalation.

While no vibrational modes due to the intercalant are observable in the Raman spectrum, the ^{19}F nmr spectrum shows a single resonance at 9.3 ppm relative to $CFCl_3$ shifted upfield from 34.6 ppm in liquid $BrSO_3F$ (see Fig. 1*a*). ^{19}F nmr spectra are also rather useful in testing for the complete removal of non intercalated $BrSO_3F$. As illustrated in Fig. 1, a weak signal at 34 ppm found in a product of the composition $C_{11.5}BrSO_3F$ appears to be due to surface adsorbed $BrSO_3F$. This signal will disappear on prolonged pumping, the resulting composition will then be close to $C_{12}BrSO_3F$ and the single resonance shown in Fig. 1*b* is observed.

Even though $C_{12}BrSO_3F$ is stable at 25°C *in vacuo*, heating to 100°C results in some decomposition. Both Br_2 and $BrSO_3F$ are detected in the volatile fraction by Raman spectroscopy. Since $BrSO_3F$ is reported to be thermally stable up to 150°C (11), the formation of bromine at 100°C prompted us to study the intercalation at about this temperature using an excess of $BrSO_3F$. Evolution of Br_2 is instantaneous and after a reaction time of 48 h and removal of all volatiles *in vacuo*, a product of the composition $C_{20}BrF(SO_3F)_2$ is obtained. Microanalysis indicates a ratio of Br:S:F of 1:2.02:2.98. Again an interlayer separation of 7.76 ± 0.03 Å and a frequency shift of the E_{2g} band to 1645 cm^{-1} suggest a first stage intercalation compound with the composition indicative of the large size of the intercalant.

^{19}F nmr provides information on the nature of the intercalant: two single, broad resonances at +9.7 ppm (assigned to fluorine attached to sulfur) and at −84.1 ppm are observed of the approximate intensity ratio of 2:1 (see Fig. 2). This second resonance is attributed to fluorine attached to bromine.

The proposed assignment is aided by a ^{19}F nmr study of the system BrF_3–$Br(SO_3F)_3$ (21). It appears that both BrF_3 and $Br(SO_3F)_3$ are miscible over the entire composition range to

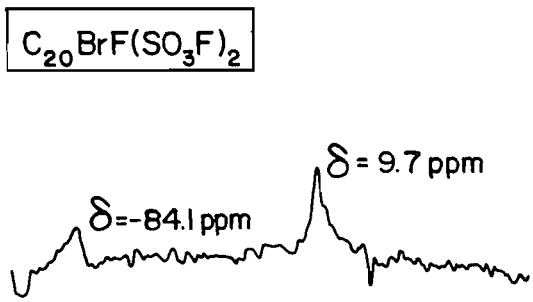

FIG. 2. The ^{19}F nmr spectrum of $C_{20}BrF(SO_3F)_2$.

give viscous liquids of the general composition $BrF_x(SO_3F)_{3-x}$, with x ranging from 0 to 3. Rapid ligand exchange produces two single broad resonances with the chemical shift depending on the composition. For $BrF(SO_3F)_2$ resonances at −46.5 ppm (Br−F group) and about 40 ppm (F attached to S) would be expected. A substantial upfield shift of both resonances appears to occur on intercalation, similar to the one found for $C_{12}BrSO_3F$.

Formation of $BrF(SO_3F)_2$ on intercalation of $BrSO_3F$ at elevated temperature may be rationalized in the following manner: Initial disproportionation of $BrSO_3F$ according to

[6] $3\ BrSO_3F \rightarrow Br_2 + Br(SO_3F)_3$

is followed by partial decomposition

[7] $Br(SO_3F)_3 \rightarrow BrF(SO_3F)_2 + SO_3$

during the intercalation process. It must be emphasized, however, that the proposed disproportionation is well known for BrF (22), but hitherto not observed for $BrSO_3F$ in its pure state (12). Likewise the proposed decomposition is a very plausible reaction for fluorosulfates (23), but again has not been observed for $Br(SO_3F)_3$ (12).

The oxidation of $C_{12}BrSO_3F$ with an excess of $S_2O_6F_2$ leads to a black–blue product of the composition $C_{16.5}Br(SO_3F)_3$. The interlayer separation of 7.92 Å and a Raman band at 1646 cm^{-1} agree well with expectations for a first stage intercalation compound, however, it is very unlikely that all $Br(SO_3F)_3$ is intercalated for the following reason:

Since all three graphite intercalation compounds of bromine fluorosulfate derivatives discussed so far are first stage compounds with all galleries filled, their overall composition should reflect the intercalant size, with the highest carbon:bromine ratio expected for $Br(SO_3F)_3$ as intercalant. It is therefore not unexpected that the ^{19}F nmr spectrum of $C_{16.5}Br(SO_3F)_3$ has two rather broad resonances (see Fig. 3): one of these at 38.3 ppm is quite close to the literature value of free $Br(SO_3F)_3$ of 39.0 ppm (21), while a second, approximately three times more intense line at 10.6 ppm is attributed to intercalated $Br(SO_3F)_3$. It appears then that oxidation of $C_{12}BrSO_3F$ occurs under extrusion of some $BrSO_3F$ from the lattice, followed by oxidation to give "free" $Br(SO_3F)_3$. While some of this material is removed with the excess $S_2O_6F_2$, some of the bromine(III)fluorosulfate, a solid at room temperature, remains mixed in with the intercalation compound. We have so far failed to affect a complete separation of the two reaction products. Nevertheless, the experiment confirms that intercalant oxidation is possible, leading to a first stage compound. Supporting evidence for the formulation of intercalated $Br(SO_3F)_3$ in the previous reaction may also be obtained from the successful reduction with an excess of Br_2 according to

Can. J. Chem. Downloaded from www.nrcresearchpress.com by 210.87.254.40 on 09/06/12
For personal use only.

TABLE 1. Some physical properties of selected graphite intercalation compounds

Compound	Physical properties of the intercalation compounds			Chemical shift of intercalant		Electrical conductance data			
	I_c (Å)	$\nu_{E_{2g}}$ (cm^{-1})	δ^a (ppm)	δ^a (ppm)	Ref.	σ (ohm^{-1} cm^{-1})	$\sigma/\sigma_g{}^d$	$t/t_0{}^e$	$k/k_g{}^f$
$C_{12}BrSO_3F$	7.75	1641	9.3	34.6	11	7.3×10^4	3.2	2.8	9.0
$C_{20}BrF(SO_3F)_2$	7.76	1645	9.7	40.0					
					21				
			-84.1^b	-46.5^b					
$C_{16}Br(SO_3F)_3$	7.92	1646	10.6	39.0	10	7.7×10^4	3.3	2.6	7.0
C_7SO_3F	7.81	1635	14.7	38.5[c]		4.8×10^4	2.1	2.7	5.8
$C_{12}SO_3CF_3$	8.12	1634	−71.1	Center of broad peak at −56.0[c]		14.0×10^4	6.1	2.5	15.8

[a]Relative to ext. $CFCl_3$.
[b]Due to F attached to bromine.
[c]This study, solid state data obtained on KSO_3F and $AgSO_3CF_3$.
[d]σ_g = conductivity of H.O.P.G. = 2.3×10^4 ohm^{-1} cm^{-1}.
[e]t/t_0 = relative increase in thickness on intercalation.
[f]k denotes specific conductivity per plane of graphite, $k/k_G = \Delta V/\Delta V_G$.

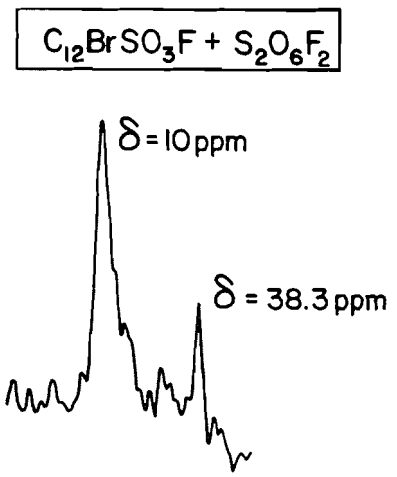

FIG. 3. The ^{19}F nmr spectrum of the product of the reaction of $C_{12}BrSO_3F$ with $S_2O_6F_2$.

[8] $3C_{16}Br(SO_3F)_3 + 3Br_2 \rightarrow 4C_{12}BrSO_3F + 5BrSO_3F$

with the resulting product identified by gravimetry and microanalysis.

The attempted complex formation of C_7SO_3F with $BrSO_3F$ to form intercalated $[Br(SO_3F)_2]^-$ was, however, less successful. There appears to be a small change in the interlayer separation, but the bromine contents of 1.88% and the ^{19}F nmr resonance at 32 ppm suggest rather surface adsorption than intercalation to occur.

Another attempted reaction also did not yield the expected product. We reacted $C_{12}BrSO_3F$ with an excess of trifluoromethyl sulfuric acid in the hope to produce $C_nBrSO_3CF_3$, in analogy to the previously reported (9) successful conversion of C_7SO_3F into $C_{12}SO_3CF_3$. Evolution of Br_2 from the reaction mixture indicated a reaction. The isolated solid, however,was free of bromine and analysed as $C_{12}SO_3CF_3$, suggesting the overall reaction:

[9] $2C_{12}BrSO_3F + 2HSO_3CF_3 \rightarrow 2C_{12}SO_3CF_3 + Br_2 + 2HSO_3F$

with HSO_3F reacting further with HSO_3CF_3 (9). Our inability to convert intercalated bromine(I)fluorosulfate into the trifluoromethyl sulfate analogue is not unexpected since $BrSO_3CF_3$ is not thermally stable above 0°C (24).

The reactions described here allow a few, general conclusions, concerning the reaction chemistry of graphite intercalation compounds. Where the initial intercalant is attacked and, during the course of the reaction, consumed, as in the reaction of $C_{12}BrSO_3F$ with HSO_3CF_3, oxidized, as in the reaction of $C_{12}BrSO_3F$ with $S_2O_6F_2$, or reduced as in reaction [8], conversion of one intercalation compound into another one is observed. The previously reported conversions of C_7SO_3F into $C_{12}SO_3CF_3$ (9) or into C_8SbF_6 (25) by solvolysis in HSO_3CF_3 or SbF_5 respectively belong to the same reaction type.

On the other hand, the attempted complexation of C_7SO_3F, where all galleries in the graphite layer lattice are completely filled, with an excess of $BrSO_3F$ would require an extrusion of some SO_3F^- to enable complexation to take place. Our evidence suggests surface adsorbtion rather than a complexation takes place. We have noted a similar lack of reactivity of C_7SO_3F towards HSO_3F, where previously known (26) acid salts of the type $C_n(SO_3F)_x(HSO_3F)_y$ had been expected (9).

The high temperature intercalation reaction with $BrSO_3F$ illustrates a third point. Here the presence of graphite leads to a disproportionation of $BrSO_3F$, which, though not totally unexpected, had not been observed before for neat $BrSO_3F$. There appear to be no precedents for this reaction, when interhalogen compounds are intercalated (1, 27).

The identification of all new graphite intercalation compounds as first stage compounds had been based on the interlayer separation I_c, the shift in frequency for the Raman active E_{2g} lattice vibration, the ^{19}F nmr spectra and last but not least the chemical analysis.The physical data for the new intercalation compounds as well as pertinent data for C_7SO_3F and $C_{12}SO_3CF_3$ (9) are summarized in Table 1. The measured ^{19}F nmr chemical shift data are compared to literature data for the pure intercalants. Also tabulated are the results of our electrical conductance studies for first stage compounds only.

All interlayer separations for the fluorosulfates fall well below 8.0 Å, suggesting tightly packed structures with electron transfer from graphite to intercalant causing Coulomb attraction between the carbon and the intercalant layer. Considering the rather large size of $Br(SO_3F)_3$ the small value of 7.92 Å seems surprising, but if one assumes that the planar coordination around bromine suggested for $Br(SO_3F)_3$ (26) is retained on intercalation the observed separation becomes plausible. Unfortunately we were unable to observe any vibrational

Can. J. Chem. Downloaded from www.nrcresearchpress.com by 210.87.254.40 on 09/06/12
For personal use only.

bands, due to the intercalants, which would have provided more definitive information on the structure of the various intercalants in these compounds.

Additional evidence for the intercalants acting as electron acceptors may be found in the other data tabulated. The strong shift of the Raman active E_{2g} lattice vibration is consistent with reports (19, 20) for other first stage acceptor compounds of graphite. The ^{19}F nmr chemical shifts appear all shifted to higher fields relative to the position for the neat intercalants. Fluorine attached to sulfur in the fluorosulfates studied here appears to be shifted by about 25 ppm upon intercalation, while an even larger shift is found for fluorine attached to bromine.

Because of this shift it is possible, as demonstrated in the preparation of $C_{12}BrSO_3F$, to differentiate between intercalated and surface adsorbed $BrSO_3F$.

The increased electrical conductivities for all compounds studied, with σ/σ_g values of approximately 3, point again to extensive electron transfer from graphite to the intercalant. Even greater enhancements of basal plane electrical conductivities are found in the higher stage intercalation compounds formed by $BrSO_3F$, and details of our conductance studies on this and related systems will be published shortly (27).

While sufficient evidence has been presented for the action of $BrSO_3F$ and $Br(SO_3F)_3$ as acceptors of electronic charge, two points still remain unsolved: (*a*) the exact extent of charge transfer, commonly expressed in terms of f, the carrier density parameter (28), and (*b*) the anions formed in the intercalant layer on charge transfer. Both $Br(SO_3F)_2^-$ (13) and $Br(SO_3F)_4^-$ (26) are well established in the form of alkali salts but others like $Br_2SO_3F^-$ may be possible as well.

Acknowledgements

Financial support by the Natural Sciences and Engineering Research Council of Canada is gratefully acknowledged, as well as the award of a University Graduate Fellowship to one of us (S.K.).

1. (*a*) W. RÜDORFF. Adv. Inorg. Chem. Radiochem. **1**, 233 (1959). (*b*) H. SELIG and L. B. EBERT. Adv. Inor. Chem. Radiochem. **23**, 281 (1980).
2. (*a*) N. BARTLETT and B. W. MCQUILLAN. *In* Intercalation chemistry. *Edited by* M. S. Wittingham and A. J. Jacobson. Academic Press. 1982. p. 19; (*b*) W. C. FORSMAN, T. DZIEMIANOWICZ, K. LEONG, and D. CARL. Synth. Met. **5**, 77 (1983).
3. J. E. FISCHER. *In* Intercalated layered materials. *Edited by* F. Lévy. D. Reidel Publishing Co., Dordrecht, Holland. 1979. p. 481
4. M. S. WITTINGHAM and L. S. EBERT. *In* Intercalated layer materials. *Edited by* F. Lévy. D. Reidel Publishing Co., Dordrecht, Holland. 1979 p. 533.
5. A. FRENZEL. Dissertation, Technische Hochschule, Berlin. 1933.
6. W. RÜDORFF. Z. Anorg. Allg. Chem. **245**, 383 (1941).
7. N. BARTLETT, R. N. BIAGIONI, B. W. MCQUILLAN, A. S. ROBERTSON, and A. C. THOMPSON. J. Chem. Soc. Chem. Commun. 200 (1978).
8. R. N. BIAGIONI. Ph.D. thesis, Lawrence Berkeley Laboratory, University of California. 1980.
9. S. KARUNANITHY and F. AUBKE. Carbon, **20**, 237 (1982).
10. J. E. ROBERTS and G. H. CADY. J. Am. Chem. Soc. **82**, 352 (1960).
11. F. AUBKE and R. J. GILLESPIE. Inorg. Chem. **7**, 599 (1968).
12. F. AUBKE and D. D. DESMARTEAU. *In* Fluorine chemistry reviews. Vol. 8. *Edited by* P. Tarrant. Marcel Dekker Inc., New York. 1977. p. 73.
13. C. CHUNG and G. H. CADY. Z. Anorg. Allg. Chem. **385**, 18 (1971).
14. G. H. CADY and J. M. SHREEVE. Inorg. Synth. **7**, 124 (1963).
15. P. C. EKLUND, N. KAMBE, G. DRESSELHAUS, and M. S. DRESSELHAUS. Phys. Rev. **B18** 7069 (1978).
16. C. ZELLER, A. DENENSTEIN, and G. M. T. FOLEY. Rev. Sci. Instr. **50**, 602 (1979).
17. C. ZELLER, G. M. T. FOLEY, E. R. FALARDEAU, and F. L. VOGEL. Mat. Sci. Eng. **31**, 255 (1977), and references therein.
18. P. BORDA and P. LEGZDINS. Anal. Chem. **52**, 1777 (1980).
19. M. S. DRESSELHAUS, G. DRESSELHAUS, P. C. EKLUND, and D. D. L. CHUNG. Mat. Sci. Eng. **31**, 141 (1977).
20. P. C. EKLUND, E. R. FALLARDEAU, and J. E. FISCHER. Solid State Commun. **32**, 631 (1979).
21. W. P. GILBREATH and G. H. CADY. Inorg. Chem. **2**, 496 (1963).
22. L. STEIN. *In* Halogen chemistry. Vol. 1, *Edited by* V. Gutmann. Academic Press, London 1967. p. 133.
23. A. A. WOOLF. *In* New pathways in inorganic chemistry, Cambridge Univ. Press. 1968. p. 327.
24. Y. KATSUHARA and D. D. DESMARTEAU. J. Fluor. Chem. **16**, 257 (1980).
25. S. KARUNANITHY and F. AUBKE. J. Fluor. Chem. In press.
26. H. A. CARTER, S. P. L. JONES, and F. AUBKE. Inorg. Chem. **9**, 2485 (1970).
27. S. KARUNANITHY and F. AUBKE. Mater. Sci. Eng. In press.
28. F. R. HANLON, E. R. FALARDEAU, and J. E. FISCHER. Solid State Commun. **24**, 377 (2977).

Can. J. Chem. Downloaded from www.nrcresearchpress.com by 210.87.254.40 on 09/06/12
For personal use only.

Détermination cinétique de la nature du conformère réactif dans l'hydrolyse des orthoesters[1]

GÉRARD LAMATY, CLAUDE MOREAU ET ZÉPHIRIN MOULOUNGUI
Laboratoire de Chimie Organique Physique, Université des Sciences et Techniques du Languedoc, Place Eugène Bataillon, 34060 Montpellier Cédex, France

Reçu le 17 mars 1983

GÉRARD LAMATY, CLAUDE MOREAU et ZÉPHIRIN MOULOUNGUI. Can. J. Chem. **61**, 2643 (1983).

Les vitesses d'hydrolyse des orthoesters diéthoxy-1,1 dihydro-3,4 benzopyrannes-2 substitués en position 6 ou 7 (R = 6-MeO, H, 7-MeO, 7-NO_2 et 6-NO_2) ont été déterminées à 27°C dans le solvant eau/dioxanne 2:1 en volumes. Les constantes de vitesse et les constantes ρ de Hammett montrent que l'étape limitante est la formation d'un ion carboxonium cyclique. Ces résultats constituent une preuve cinétique quant à la nature du conformère réactif dans l'hydrolyse des orthoesters dialkoxy-2,2 tétrahydropyrannes.

GÉRARD LAMATY, CLAUDE MOREAU, and ZÉPHIRIN MOULOUNGUI. Can. J. Chem. **61**, 2643 (1983).

The rates of hydrolysis of the following orthoesters, 6 or 7-substituted 1,1-diethoxy 3,4-dihydrobenzo-2-pyrans (R = 6-MeO, H, 7-MeO, 7-NO_2 and 6-NO_2) were determined at 27°C in water/dioxan (2:1 by volume). The catalytic rate constants as well as the Hammett ρ constants show that the rate-determining step is the formation of a cyclic carboxonium ion intermediate and constitute a kinetic piece of evidence for the determination of the nature of the reactive conformer in hydrolysis of 2,2-dialkoxy tetrahydropyran orthoesters.

Can. J. Chem. Downloaded from www.nrcresearchpress.com by 210.87.254.42 on 09/06/12
For personal use only.

Introduction

Les intermédiaires tétraédriques, dans lesquels un atome de carbone est lié à trois hétéroatomes, jouent un rôle de premier plan dans un grand nombre de réactions tant organiques que bioorganiques, catalysées ou non par les enzymes. L'étude de la réactivité de systèmes mettant en jeu ce type d'intermédiaires est donc nécessaire pour contribuer à l'élucidation des mécanismes biologiques.

Un progrès très important a été réalisé dans ce sens avec l'élaboration d'une théorie stéréoélectronique qui implique une relation très étroite entre la conformation et la réactivité d'un intermédiaire tétraédrique (2).

Les orthoesters constituent un modèle chimique de ce type d'intermédiaires et il nous a paru intéressant de revenir sur un point particulier concernant la nature du conformère réactif dans l'hydrolyse des orthoesters diéthoxy-2,2 tétrahydropyrannes.

Ce problème a déjà été abordé par Deslongchamps *et al.* (3) en utilisant une méthode analytique basée sur l'analyse des produits de la réaction. Une telle méthode implique que l'intermédiaire hémiorthoester conserve la configuration et la conformation du produit de départ et, par conséquent, ne constitue pas une preuve absolue quant à la conformation de ce produit de départ; en effet, si l'on considère le mécanisme de l'hydrolyse des dialkoxy-2,2 tétrahydropyrannes (4), il existe deux étapes faisant intervenir la coupure d'une liaison C—O tout en respectant les règles stéréoélectroniques (schéma 1): (1) la formation de l'ion carboxonium intermédiaire, étape cinétique de la réaction (eq. [1]); (2) la décomposition de l'intermédiaire tétraédrique hémiorthoester, laquelle décomposition détermine la nature du ou des produit(s) de la réaction (eq. [3]).

Nous souhaitons rapporter dans le présent travail les résultats cinétiques obtenus au cours de la première étape du processus d'hydrolyse, résultats qui permettent de trancher définitivement sur la nature du conformère réactif.

Parmi les neuf conformères possibles représentant un orthoester diéthoxy-2,2 tétrahydropyranne, Deslongchamps *et al.* avaient retenu deux conformères réactifs seulement, équivalents du point de vue stéréoélectronique de surcroît: *A* et *F* (Fig. 1).

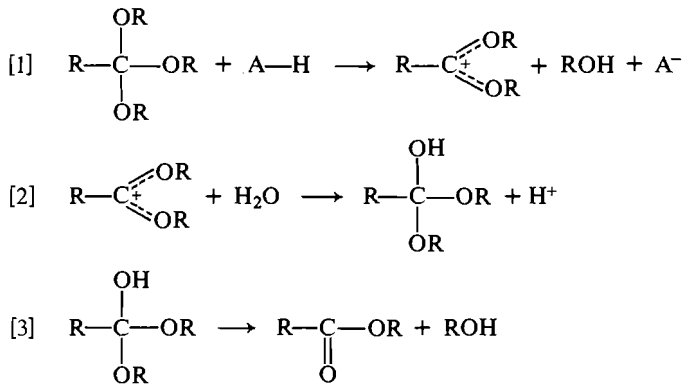

SCHÉMA 1

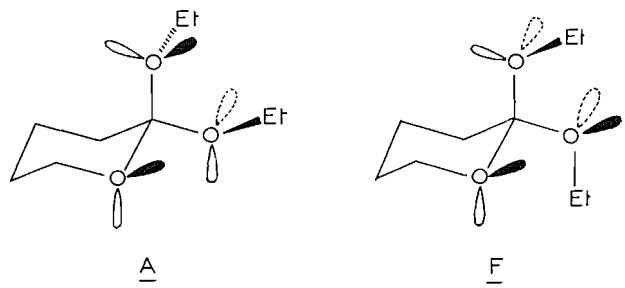

A F

FIG. 1.

En se basant sur l'analyse des produits de la réaction d'hydrolyse, les auteurs avaient conclu que le conformère *A*, plutôt que *F*, était le conformère réagissant (2, 3).

On pouvait espérer obtenir d'autres arguments, en particulier cinétiques, puisque l'hydrolyse des conformères *A* et *F* fait intervenir deux sortes d'ions carboxoniums intermédiaires, un ion cyclique dans le cas de *A* et un ion non cyclique dans le cas de *F* (Schéma 2).

La différenciation entre les deux modes de rupture de la liaison C—O, exocyclique (*A*) ou endocylique (*F*), nous apparaissait possible a priori. En effet, Kresge et coll. ont montré

[1]Ce travail a été présenté à la VI° Conférence I.U.P.A.C. de Chimie Organique Physique, Louvain la Neuve, Belgique, Juillet 1982 (1).

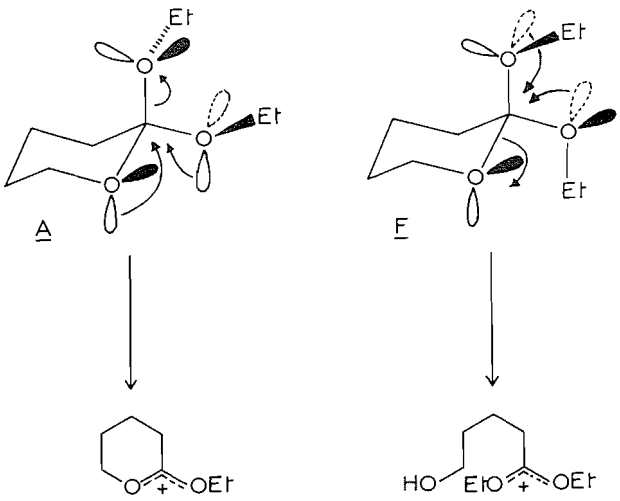

SCHÉMA 2

qu'il existait un empêchement stérique à la conjugaison dans l'ion carboxonium issu de l'hydrolyse de l'orthobenzoate de méthyle, empêchement stérique qui n'existe plus dans l'ion carboxonium issu de l'hydrolyse du méthoxy-2 phényl-2 dioxolanne-1,3 (5); dans le premier cas, l'ion carboxonium n'est pas cyclique alors que cet ion est cyclique dans le second cas. Cet empêchement stérique à la conjugaison se traduit par des différences à la fois dans les vitesses d'hydrolyse ($k_{cycle}/k_{non\ cycle} \simeq 100$) et dans les constantes ρ de Hammett ($\rho_{cycle} = -1{,}60$; $\rho_{non\ cycle} = -1{,}12$) (6); ces deux points seront repris dans la discussion.

Pour concilier dans une même molécule la réactivité d'un système orthobenzoate et la conformation d'un diéthoxy-2,2 tétrahydropyranne, nous avons, dans un premier temps, synthétisé une série d'orthoesters dérivés de la dihydro-3,4 isocoumarine (Fig. 2) et, dans un deuxième temps, nous avons étudié l'hydrolyse acido-catalysée de ces produits.

Résultats expérimentaux

I. *Synthèse*

Les orthoesters **1** à **5** ont été préparés à partir des lactones convenablement substituées selon la procédure générale décrite par Deslongchamps *et al.* (3). Les propriétés physicochimiques des nouveaux produits sont données en détail dans la partie expérimentale.

II. *Analyse des produits de la réaction*

L'analyse des produits de la réaction d'hydrolyse peut apporter des renseignements utiles sur le sens d'ouverture des orthoesters: l'hydrolyse des composés **1** à **5** peut conduire à deux couples de produits suivant la rupture, endocyclique ou exocyclique, de la liaison C—O tout en respectant les règles stéréoélectroniques: lactone + 2EtOH ou bien hydroxyester + EtOH (Schéma 3). Expérimentalement, l'hydrolyse des orthoesters **1** à **5** conduit à des mélanges lactone + hydroxyester. Cet aspect sera développé plus en détail dans la partie discussion.

III. *Résultats cinétiques*

L'hydrolyse acido-catalysée des diéthoxy-1,1 dihydro-3,4 benzopyrannes-2 substitués en position 6 ou 7 a été effectuée dans le solvant eau/dioxanne 2:1 en volumes à 27°C. Les couples acide/base utilisés pour tamponner le milieu sont acide formique/formiate de sodium, acide acétique/acétate de

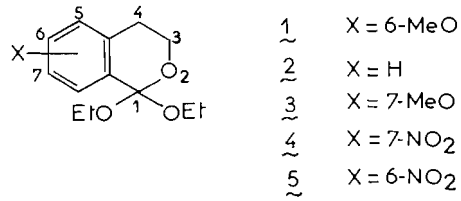

FIG. 2.

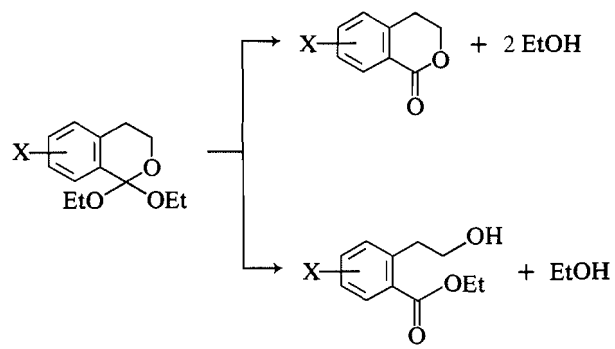

SCHÉMA 3

TABLEAU 1. Hydrolyse des orthoesters **2** à **5** dans le mélange tampon acide formique/formiate de sodium: constantes de vitesse k_{obs} exprimées en s^{-1} à 27,0°C et à force ionique égale à 0,1 *M* (KCl)

Tampon formique	[HCOOH]/[HCOONa] = 0,25; $pH_{réel}$ = 5,22		
	$k_{obs} \times 10^2$		
[HCOOH] × $10^3(M)$	**2** X = H	**3** X = 7-MeO	**4** X = 7-NO_2
9,9	10,6	6,39	5,18
4,55	9.78	—	4,75
2,22	9,17	5,45	4,61
1,23	8,82	5,21	4,51
Tampon formique	[HCOOH]/[HCOONa] = 1; $pH_{réel}$ = 4,48		
	$k_{obs} \times 10^2$		
[HCOOH] × $10^3(M)$	**4** X = 7-NO_2		**5** X = 6-NO_2
8,3	2,55		2,46
4,1	2,28		—
2,0	2,17		2,03
1,02	2,07		1,99

sodium et acide cacodylique/cacodylate de sodium. La force ionique a été maintenue constante et égale à 0,1 *M* par addition de chlorure de potassium Les résultats cinétiques sont donnés dans les tableaux 1, 2 et 3; la reproductibilité moyenne sur les constantes de vitesse observées est de ±3%. Les constantes catalytiques $k_{H_3O^+}$, k_{HCOOH}, k_{CH_3COOH}, $k_{(CH_3)_2AsOOH}$ et k_{H_2O} (corrections faites de l'effet de solvant et de l'activité du milieu[2]) ont été obtenues en exploitant les résultats des tableaux 1, 2 et 3; ces constantes catalytiques sont rassemblées dans le tableau 4.

Interprétation des résultats expérimentaux

L'examen des tableaux 1 à 3 montre que l'hydrolyse des

[2]L'influence de la composition du solvant et de l'activité du milieu sur les pK_a des acides catalyseurs et sur le calcul des constantes catalytiques est détaillée dans la partie expérimentale.

Can. J. Chem. Downloaded from www.nrcresearchpress.com by 210.87.254.42 on 09/06/12
For personal use only.

TABLEAU 2. Hydrolyse des orthoesters **1** à **5** dans le mélange tampon acide acétique/acétate de sodium: constantes de vitesse k_{obs} exprimées en s^{-1} à 27,0°C et à force ionique égale à 0,1 *M* (KCl)

Tampon acétique	$[CH_3COOH]/CH_3COONa] = 1$; $pH_{réel} = 5,58$				
	$k_{obs} \times 10^2$				
$[CH_3COOH] \times 10^3$(M)	**1** X = 6-MeO	**2** X = H	**3** X = 7-MeO	**4** X = 7-NO_2	**5** X = 6-NO_2
8,55	—	4,24	3,01	2,14	2,12
4,27	7,60	3,73	2,62	1,81	1,85
2,06	6,73	3,47	2,33	1,73	1,68
1,11	6,24	3,17	2,09	1,56	1,64

TABLEAU 3. Hydrolyse des orthoesters **1** à **5** dans le mélange tampon acide cacodylique/cacodylate de sodium: constantes de vitesse k_{obs} exprimées en s^{-1} à 27,0°C et à force ionique égale à 0,1 *M* (KCl)

Tampon cacodylique	$[(CH_3)_2AsOOH]/(CH_3)_2AsOONa] = 1$; $pH_{réel} = 6,96$				
	$k_{obs} \times 10^3$				
$[(CH_3)_2AsOOH] \times 10^2$(M)	**1** X = 6-MeO	**2** X = H	**3** X = 7-MeO	**4** X = 7-NO_2	**5** X = 6-NO_2
9,1	6,31	2,80	1,78	1,09	1,20
4,625	4,96	2,21	1,33	0,89	1,03
2,30	3,88	1,89	1,27	—	—
1,164	3,48	1,74	1,12	0,70	0,79

TABLEAU 4. Hydrolyse des orthoesters **1** à **5**: constantes catalytiques exprimées en $M^{-1}\,s^{-1}$ à 27,0°C et à force ionique égale à 0,1 *M* (KCl)

	Constantes catalytiques				
	$k_{obs} \times 10^2$				
Catalyseur	**1** X = 6-MeO	**2** X = H	**3** X = 7-MeO	**4** X = 7-NO_2	**5** X = 6-NO_2
H_3O^+	$1,44 \cdot 10^4$	$7,72 \cdot 10^3$	$5,07 \cdot 10^3$	$3,81 \cdot 10^2$	$3,88 \cdot 10^2$
HCOOH	—	1,99	1,31	$6,45 \cdot 10^{-2}$	$6,59 \cdot 10^{-2}$
CH_3COOH	$4,23 \cdot 10^{-1}$	$1,35 \cdot 10^{-1}$	$1,18 \cdot 10^{-1}$	$7,23 \cdot 10^{-3}$	$6,58 \cdot 10^{-3}$
$(CH_3)_2AsOOH$	$3,59 \cdot 10^{-2}$	$1,34 \cdot 10^2$	$7,95 \cdot 10^{-3}$	$4,93 \cdot 10^{-4}$	$5,04 \cdot 10^{-4}$
H_2O[a]	$1,9 \cdot 10^{-5}$	$8,1 \cdot 10^{-6}$	$4,9 \cdot 10^{-6}$	$3,5 \cdot 10^{-7}$	$3,0 \cdot 10^{-7}$

[a]Les constantes k_{H_2O} ont été évaluées à partir des ordonnées à l'origine des graphes k_{obs} en fonction de AH; l'erreur sur ces constantes est de l'ordre de 50%.

diéthoxy-1,1 dihydro-3,4 benzopyrannes-2 substitués en position 6 ou 7 est soumise à une catalyse acide générale; ce type de catalyse est courant dans l'hydrolyse des orthoesters et nous avons montré par ailleurs qu'il était compatible avec le concept de contrôle stéréoélectronique qui implique que la rupture d'une liaison C—O est favorisée si les deux autres atomes d'oxygène ont chacun une paire d'électrons libres orientée de manière antipériplanaire par rapport à la liaison C—O qui se coupe (4).

Par ailleurs, les résultats expérimentaux sont en accord avec un mécanisme dans lequel l'étape déterminant la vitesse de réaction est la formation d'un ion carboxonium (7, 8). Les constantes ρ de Hammett, mesurant l'influence des substituants polaires en position 6 ou 7 sur le mécanisme de la réaction, sont obtenues en portant log k_{AH} en fonction des constantes de substituants σ (Fig. 3). Les constantes ρ ont été calculées ainsi que les écart-types correspondants et sont rassemblés dans le tableau 5.

Les constantes ρ sont négatives quel que soit le catalyseur et sont compatibles avec l'apparition d'une charge positive dans l'état de transition, la diminution de la densité électronique sur le carbone réactionnel étant favorisée par des groupements donneurs d'électrons et, à l'inverse, défavorisée par des groupements attracteurs d'électrons.

Si l'on associe les constantes ρ de Hammett à la position de l'état de transition le long du chemin réactionnel, les valeurs trouvées (−1,62 à −2,02) indiquent que l'état de transition possède un caractère ion carboxonium peu accentué comparativement à la valeur de ρ = −3,3 déterminée dans l'hydrolyse des acétals où l'état de transition est proche de l'ion carboxonium (9). Le faible avancement de la réaction a été démontré par ailleurs (7, 8).

Discussion

Trois points importants se dégagent des résultats expérimentaux en vue de discuter de la nature des conformères réac-

Can. J. Chem. Downloaded from www.nrcresearchpress.com by 210.87.254.42 on 09/06/12
For personal use only.

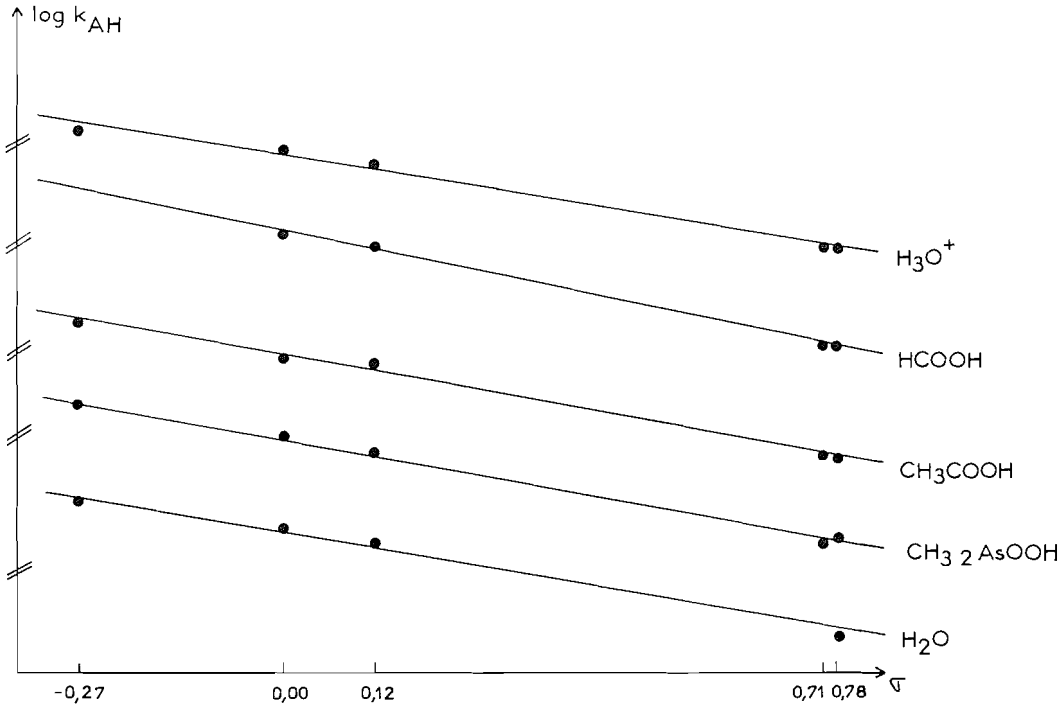

FIG. 3. Hydrolyse des orthoesters **1** à **5**: graphe de Hammett pour les différents acides catalyseurs.

TABLEAU 5. Hydrolyse des orthoesters **1** à **5**: constantes ρ de Hammett, coefficients de corrélation et écart-types correspondants, pour les différents acides catalyseurs

Catalyseur	ρ	Coeff. corrélation	Ecart-type
H_3O^+	−1,62	0,993	0,09
HCOOH	−2,02	0,997	0,08
CH_3COOH	−1,77	0,996	0,07
$(CH_3)_2AsOOH$	−1,86	0,998	0,06
H_2O	−1,78[a]	0,998	0,08

[a]Etant donné l'erreur importante sur les constantes k_{H_2O}, la valeur de ρ_{H_2O} n'est pas absolument significative.

tifs, *A* ou *F*: (1) l'analyse des produits de la réaction, (2) l'examen des constantes de vitesse d'hydrolyse et (3) l'influence des substituants polaires sur la réactivité.

Analyse des produits de la réaction

Nous avons déjà mentionné que la nature des produits de la réaction d'hydrolyse ne constituait pas une preuve formelle quant à la conformation du produit de départ; il est cependant intéressant de considérer le chemin suivi par chacun des deux conformères *A* et *F* (Schéma 4)[3] puisque l'hydrolyse des orthoesters **1** à **5** peut s'effectuer par rupture d'une liaison C—O exocyclique (conformère *A*) ou bien par rupture d'un liaison C—O endocyclique (conformère *F*), tout en respectant les règles stéréoélectroniques.

(a) *Rupture d'une liaison C—O exocyclique (conformère A)*

La rupture d'une liaison C—OEt exocyclique conduit à l'ion carboxonium cyclique A^+; l'addition de l'eau sur cet ion conduit préférentiellement à l'intermédiaire tétraédrique IT_1 qui, s'il ne subit pas de mouvements conformationnels, se décompose avec assistance stéréoélectronique par rupture de la liaison C—O endocyclique pour donner l'hydroxyester.

S'il existe une possibilité d'inversion de cycle, c'est-à-dire si le temps de demi-vie de l'intermédiaire IT_1 est suffisamment long, le nouvel intermédiaire résultant de l'inversion du cycle, IT_2, pourra se décomposer avec assistance stéréoélectronique par rupture d'une liaison C—O exocyclique ou endocyclique pour donner la lactone ou (et) l'hydroxy-ester.

(b) *Rupture de la liaison C—O endocyclique (conformère F)*

La rupture de la liaison C—O endocyclique conduit à l'ion carboxonium non cyclique F^+; l'addition de l'eau sur l'une ou l'autre face de cet ion conduit à deux intermédiaires tétraédriques lesquels se décomposent avec assistance stéréoélectronique pour donner uniquement l'hydroxy-ester.

En suivant la cinétique de disparition de l'orthoester par rmn ^1H on observe des quantités variables d'hydroxy-ester et de lactone selon le substituant X (Tableau 6).

La lactone observée au cours de l'hydrolyse peut être soit le résultat cinétique de la réaction, soit le résultat de la transestérification de l'hydroxy-ester. La vitesse de transestérification a été obtenue avec le dérivé non substitué; dans les conditions expérimentales utilisées (D_2O/acétone-d_6 20:80, pD = 1,74) la constante de vitesse bimoléculaire de transestérification est voisine de $10^{-4}\ M^{-1}\ s^{-1}$; cette constante est du même ordre de grandeur que celle reportée dans la littérature par McClelland dans le cas d'un système similaire au nôtre, le diéthoxy-1,1 dihydro-1,3 isobenzofuranne ($1{,}4 \times 10^{-3}\ M^{-1}\ s^{-1}$) (10) et bien inférieure à la constante de vitesse d'hydrolyse ($7{,}7 \times 10^{3}\ M^{-1}\ s^{-1}$). La lactone ne peut donc pas provenir de la transestérification de l'hydroxy-ester; elle provient par conséquent du chemin réactionnel qui met en jeu l'ion carboxonium cyclique, l'intermédiaire IT_1 ayant un temps de demi-vie suffisamment long pour que l'équilibre $IT_1 \rightleftarrows IT_2$ puisse s'établir; cette hypothèse est vraisemblable au vu des travaux récents de McClelland et Alibhai (10).

[3]Par souci de clarté dans le schéma 4, les cycles aromatiques n'ont pas été représentés sur les dessins en trois dimensions; l'examen des modèles moléculaires montre cependant que l'orientation relative des liaisons C—O et des paires d'électrons libres est la même dans les orthoesters **1** à **5** que dans le diéthoxy-2,2 tétrahydropyranne.

Can. J. Chem. Downloaded from www.nrcresearchpress.com by 210.87.254.42 on 09/06/12
For personal use only.

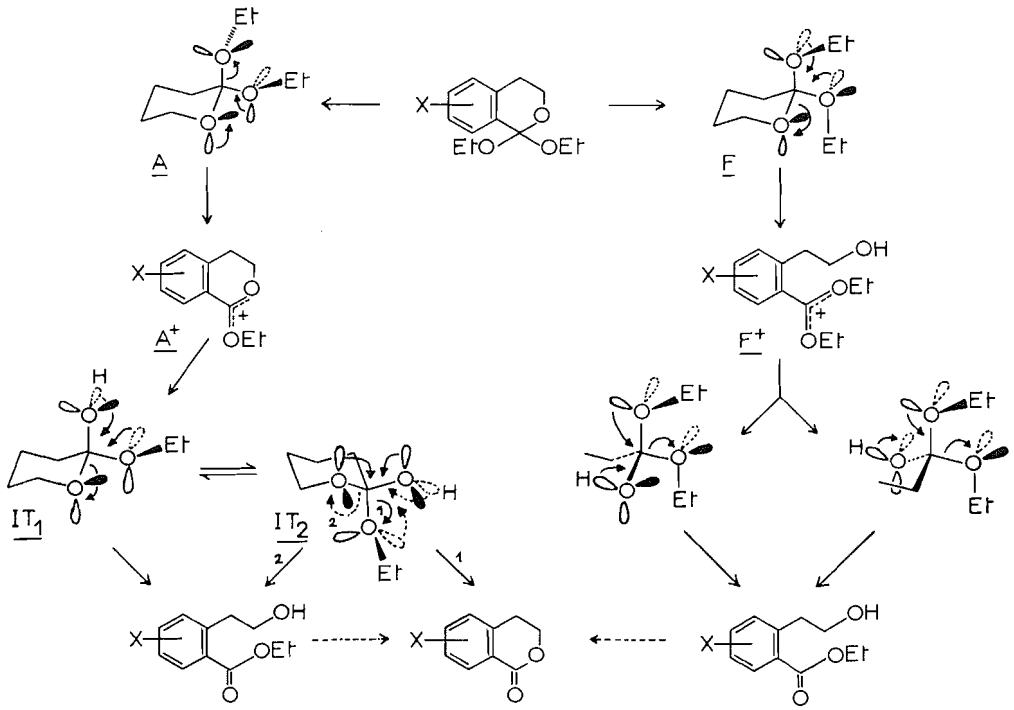

SCHÉMA 4

TABLEAU 6. Pourcentage des produits formés au cours de l'hydrolyse des orthoesters **1** à **5** en suivant la disparition de l'orthoester par rmn ^1H

Orthoesters	% Lactone	%Hydroxyester
1 X = 6-MeO	50	50
2 X = H	60	40
3 X = 7-MeO	75	25
4 X = 7-NO_2	100	Non détectable
5 X = 6-NO_2	100	Non détectable

La variation du pourcentage de produits d'hydrolyse en fonction du substituant X peut résulter d'une compétition entre la voie cinétique (formation de lactone + alcool) et la voie thermodynamique (formation de l'hydroxy-ester, ester transoïde plus stable que la lactone, ester cisoïde (2)), les substituants donneurs d'électrons orientant la décomposition de l'intermédiaire tétraédrique vers le produit le plus stable et inversement avec des substituants attracteurs.

Même si la nature des produits d'hydrolyse ne se détermine qu'après l'étape cinétique du processus réactionnel, la présence de lactone est une bonne indication en faveur du conformère *A*.

Analyse des constantes de vitesse d'hydrolyse

Les constantes de vitesse d'hydrolyse peuvent apporter les éléments cinétiques permettant de déterminer la nature du conformère réactif. Kresge et coll. (11) ont montré qu'il existait un empêchement stérique à la conjugaison dans l'ion carboxonium issu de l'hydrolyse de l'orthobenzoate de méthyle, empêchement stérique qui n'existe plus dans l'ion carboxonium issu de l'hydrolyse du méthoxy-2 phényl-2 dioxolanne-1,3; cet empêchement stérique se traduit par une vitesse d'hydrolyse beaucoup plus faible dans le cas d'un ion carboxonium non cyclique comparativement à un ion carboxonium cyclique (Tableau 7).

Si l'on compare nos résultats expérimentaux avec ceux de la littérature (Tableau 7), on s'aperçoit que les trois systèmes qui conduisent au cours de l'étape cinétique à un ion carboxonium

TABLEAU 7. Tableau comparatif des constantes de vitesse $k_{H_3O^+}$ obtenues dans l'hydrolyse des différents systèmes orthobenzoates

Produits	$k_{H_3O^+}(M^{-1}\ s^{-1})$	Réf.
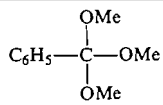	69,7 à 25°C	5
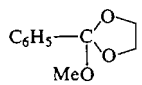	$7{,}37 \cdot 10^3$ à 25°C	5
	$5{,}4 \cdot 10^3$ à 25°C	11
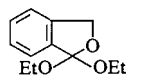	$3{,}1 \cdot 10^3$ à 25°C	10
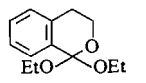	$7{,}72 \cdot 10^3$ à 27°C	Ce travail

cyclique ont des vitesses d'hydrolyse du même ordre de grandeur et très différentes, par un facteur 50 à 100, de celles d'une système non cyclique.

Effets de substituants

Nous avons montré dans un précédent travail que la substitution d'un groupe phényle par un groupe méthyle se traduisait, dans l'hydrolyse d'orthoesters cycliques, par un rapport $k_{C_6H_5}/k_{CH_3} \simeq 0{,}4$ à 1,4 (12). En comparant la réactivité de l'orthoester non substitué **2** à celle du diéthoxy-2,2 tétrahydropyranne (Schéma 5) (4) on obtient un rapport $k_{C_6H_5}/k_{CH_3}$ égal à 0,35.

Donc aussi bien l'analyse des constantes de vitesse proprement dites que les effets de substituants constituent un premier argument cinétique en faveur du conformère *A*.

Influence des substituants polaires sur le réactivité

L'empêchement stérique à la résonance invoqué lors de la

Can. J. Chem. Downloaded from www.nrcresearchpress.com by 210.87.254.42 on 09/06/12
For personal use only.

TABLEAU 8. Tableau comparatif des constantes ρ de Hammett obtenues dans l'hydrolyse de différents systèmes orthobenzoates

Produits	Catalyseur	ρ (écart-type)	Coefficient de corrélation	Réf.
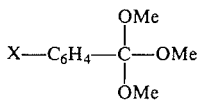	H_3O^+	−1,12 (0,03)	0,998	13
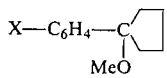	H_3O^+	−1,60 (0,03)	0,999	6
	$H_2PO_4^-$	−1,88 (0,15)	0,987	
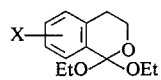	H_3O^+	−1,62 (0,09)	0,993	Ce travail
	HCOOH	−2,02 (0,08)	0,997	
	CH_3COOH	−1,77 (0,07)	0,996	
	$(CH_3)_2AsOOH$	−1,86 (0,06)	0,998	
	H_2O	−1,78 (0,08)	0,998	

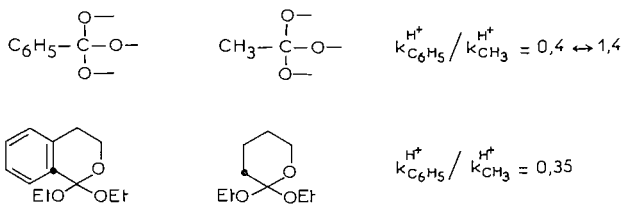

SCHÉMA 5

discussion des constantes de vitesse a également des conséquences sur les constantes ρ de Hammett: plus l'état de transition sera conjugué (systèmes cycliques), plus la constante ρ sera négative et réciproquement pour les systèmes non cycliques. C'est en effet ce qu'il ressort de l'examen du tableau 8; il existe un parallélisme assez fidèle entre les constantes ρ déterminées dans l'hydrolyse de nos composés et l'hydrolyse des méthoxy-2 phényl-2 dioxolannes-1,3: les constantes $\rho_{H_3O^+}$ sont sensiblement les mêmes et légèrement inférieures aux constantes ρ déterminées pour les autres catalyseurs acides. Si l'on tient compte des écart-types associés aux constantes ρ, cette tendance ne paraît pas absolument significative (14). Par contre, dans la réaction catalysée par H_3O^+, les différences dans les constantes ρ entre le système non cyclique (ρ = −1,12) et les deux systèmes cycliques (ρ = −1,60 et −1,62) sont, elles, significatives.

Donc, dans le cas des systèmes que nous avons étudiés, la détermination des constantes ρ de Hammett constitue un deuxième argument cinétique en faveur du conformère *A*.

Conclusion

Dans le travail que nous avons présenté, nous avons voulu reconsidérer d'un point de vue quantitatif la nature du conformère réactif dans l'hydrolyse des orthoesters diéthoxy-2,2 tétrahydropyrannes, aspect qui avait été abordé antérieurement par Deslongchamps d'un point de vue qualitatif.

En faisant appel à des composés ayant la réactivité d'un système orthobenzoate et la conformation d'un diéthoxy-2,2 tétrahydropyranne, nous avons pu apporter les éléments cinétiques qui manquaient; ces éléments cinétiques confirment ce qui avait été observé à partir de l'analyse des produits de la réaction d'hydrolyse, à savoir que le conformère réactif, dans l'hydrolyse des orthoesters diéthoxy-2,2 tétrahydropyrannes, est le conformère *A*.

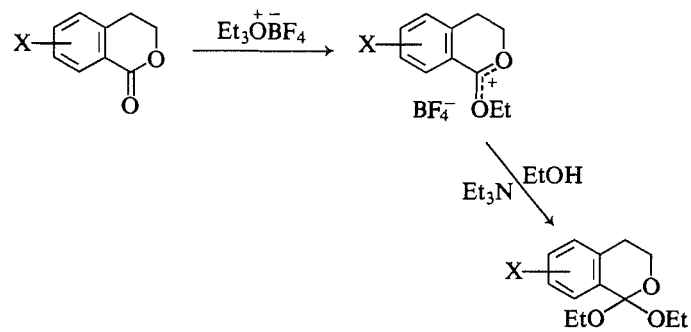

SCHÉMA 6

Partie expérimentale

Produits

Les orthoesters **1** à **5** ont été préparés à partir des lactones convenablement substitués selon le schéma 6.

(1) *Synthèse des lactones*

Les dihydro-3,4 isocoumarines substituées en position 6 ou 7 ont été synthétisées par les voies décrites dans la littérature: méthoxy-6 (15, 16), non substituée (17), méthoxy-7 (18) et nitro-7 (19); la nitro-6 dihydro-3,4 isocoumarine a été synthétisée à partir de l'acide nitro-4 homophtalique (20) en adaptant la procédure décrite dans la littérature pour le composé méthoxy-6 (15, 16) (Schéma 7).

Nitro-6 dihydro-3,4 isocoumarine: F: 162−164°C (MeOH); rendement à partir de l'acide nitro-4 homophtalique: 47%; ir ($CHCl_3$) $\nu_{c=o}$: 1725 cm^{-1}; rmn ^1H ($CDCl_3$) 3,22 δ: (2H, triplet, *J* = 6 Hz, méthylène sur C_4), 4,62 (2H, triplet, *J* = 6 Hz, méthylène sur C_3), 8,22 (3H, multiplet, protons aromatiques). *Anal.* ($C_9H_7NO_4$): calc. (%): C 55,96, H 3,65, N 7,25; tr. (%): C 55,84, H 3,81, N 7,07.

(2) *Mise au point de la synthèse des ions lactonium (X = H)*

Les sels de lactonium sont extrêment hygroscopiques et la synthèse s'effectue en boîte à gants sous atmosphère anhydre.

552 mg (3,73 mmol) de dihydro-3,4 isocoumarine sont ajoutés à une solution de 850 mg (4,47 mmol) de tétrafluoroborate de triéthyloxonium dans 10 mL de dichlorométhane séché sur tamis moléculaire

Can. J. Chem. Downloaded from www.nrcresearchpress.com by 210.87.254.42 on 09/06/12
For personal use only.

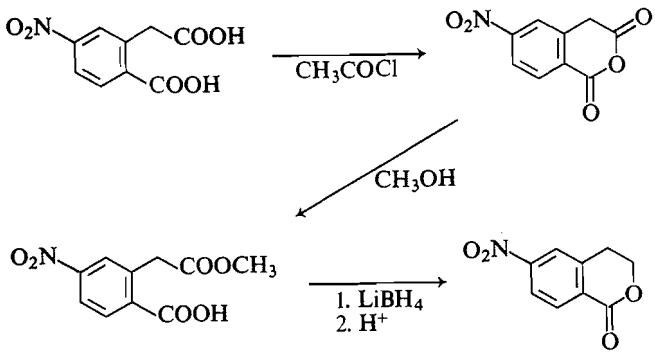

SCHÉMA 7

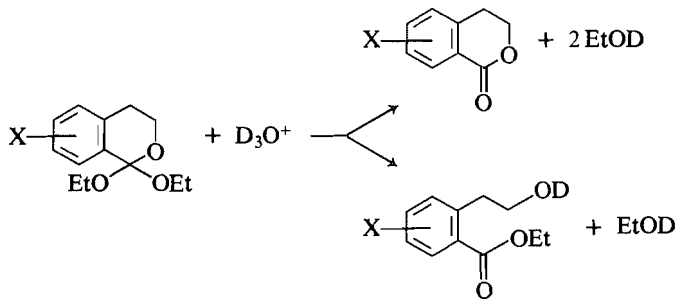

SCHÉMA 8

4 Å. Après 24 h à température ambiante, l'ion lactonium précipite sous forme d'un solide marron. Le solide est rapidement filtré et dissous dans du nitrométhane deutérié (1 mL); la fin de la réaction est contrôlée par rmn ^{1}H δ: 1,66 (3H, triplet, J = 7,5 Hz, $\overset{+}{O}CH_2CH_3$), 3,50 (2H, triplet, J = 6 Hz, méthylène sur C_4), 5,07 (2H, quadruplet, $\overset{+}{O}CH_2CH_3$), 5,31 (2H, triplet, J = 6 Hz, méthylène sur C_3), 7,20 à 8,60 (4H, protons aromatiques).

La même procédure expérimentale a été suivie pour les autres substituants au facteur temps de réaction près: 48 h pour les méthoxy-6 et méthoxy-7, 96 h pour les nitro-6 et nitro-7.

(3) *Préparation* in situ *des orthoesters 1 à 5 (procédure générale)*

La suspension d'ion lactonium est ajoutée lentement, sous atmosphère d'azote, à une solution refroidie à −64°C. (chloroforme − azote liquide) de deux équivalents d'éthanol anhydre et trois équivalents de triéthylamine dans 20 mL de dichlorométhane anhydre. L'agitation est maintenue pendant 2 heures à −64°C. Après avoir laissé le mélange réactionnel revenir à température ambiante, on ajoute 20 mL d'une solution aqueuse saturée de carbonate de sodium. Après décantation et réextraction de la phase aqueuse avec du dichlorométhane, la phase organique est séchée sur carbonate de potassium anhydre et évaporée.

Par rmn ^{1}H, on observe la présence de traces de lactone. Les orthoesters bruts sont repris avec de la soude 4 *N* pendant 24 h à température ambiante et extraits comme précédemment.

Identification des orthoesters

1 (6-MeO): résidu cristallin blanchâtre; rendement: 97%; rmn ^{1}H ($CDCl_3$) δ: 1,17 (6H, triplet, J = 7,5 Hz, O—CH_2—CH_3), 2,83 (2H, triplet, J = 6 Hz, méthylène sur C_4), 3,26 à 3,96 (4H, 2 octuplets,[4] O—CH_2—CH_3), 3,80 (3H, singulet, —OCH_3), 4,12 (2H, triplet, J = 6 Hz, méthylène sur C_3), 6,66 (1H, quadruplet, $J_{méta}$ = 3 Hz, H_5), 6,87 (1H, quadruplet, J_{ortho} = 9 Hz, $J_{méta}$ = 9 Hz, H_8).

2 (H): résidu cristallin blanchâtre; rendement: 74%; rmn ^{1}H ($CDCl_3$) δ: 1,17 (6H, triplet, J = 7,5 Hz, O—CH_2—CH_3), 2,78 (2H, triplet, J = 6 Hz, méthylène sur C_4), 3,23 à 3,93 (4H, deux octuplets,[4] O—CH_2—CH_3), 4,08 (2H, triplet, J = 6 Hz, méthylène sur C_3), 6,93 à 7,60 (4H, massif, protons aromatiques).

3 (7-MeO): huile jaune; rendement: 41%; rmn ^{1}H ($CDCl_3$) δ: 1,13 (6H, triplet, J = 7,5 Hz, O—CH_2—CH_3), 2,78 (2H, triplet, J = 6 Hz, méthylène sur C_4), 3,13 à 3,93 (4H, deux octuplets,[4] O—CH_2—CH_3), 3,77 (3H, singulet, O—CH_3), 4,07 (2H, triplet, J = 6 Hz, méthylène sur C_3); 6,67 à 7,20 (3H, massif, protons aromatiques).

4 (7-NO_2): liquide qui cristallise; rendement: 69%; rmn ^{1}H ($CDCl_3$) δ: 1,17 (6H, triplet, J = 6 Hz, O—CH_2—CH_3), 2,93 (2H, triplet, J = 6 Hz, méthylène sur C_4), 3,23 à 3,97 (4H, deux octuplets,[5] O—CH_2—CH_3), 4,15 (2H, triplet, J = 6 Hz, méthylène sur C_3), 7,3 (1H, doublet, J_{ortho} = 9 Hz, H_5), 8,10 (1H, quadruplet, J_{ortho} = 9 Hz, $J_{méta}$ = 3 Hz, H_6), 8,33 (1H, doublet, $J_{méta}$ = 3 Hz, H_8).

5 (6-NO_2): liquide qui cristallise; rendement: 60%; rmn ^{1}H ($CDCl_3$) δ: 1,13 (6H, triplet, J = 7 Hz, O—CH_2—CH_3), 2,93 (2H, triplet, J = 6 Hz, méthylène sur C_4), 3,25 à 3,95 (4H, deux octuplets,[5] O—CH_2—CH_3), 4,13 (2H, triplet, J = 6 Hz, méthylène sur C_3), 7,55 à 8,13 (3H, massif, protons aromatiques).

Analyse des produits d'hydrolyse

Les produits de la réaction d'hydrolyse des orthoesters **1** à **5** ont été analysés par rmn ^{1}H de la façon suivante: 50 mg d'orthoester sont dissous dans 600 μL d'acétone-d_6 et 100 μL de D_2O; 2 à 5 μL d'une solution de DCl dans D_2O (≈0,1 *M*) sont ajoutés dans le tube rmn; dans ces conditions, on peut suivre la disparition de l'orthoester ainsi que l'apparition du ou des produits d'hydrolyse (Schéma 8).

Les intensités relatives des protons méthyléniques sur le carbone C_3 de la lactone (triplet, J = 6 Hz, δ ≃ 4,6 ppm) et des protons méthyléniques de la fonction ester de l'hydroxy-ester (quadruplet, J = 7 Hz, δ ≃ 4,40 ppm) permettent de déterminer la proportion des produits formés dans les conditions cinétiques (cf. Tableau 6).

Lactonisation de l'hydroxy-ester

Une estimation de la vitesse de la lactonisation en milieu acide de l'hydroxy-ester a été obtenue avec le composé non substitué (X = H) de la façon suivante: après disparition de l'orthoester dans les conditions cinétiques (cf. ci-dessus) la composition des produits de la réaction est 60% de lactone et 40% d'hydroxy-ester; on ajoute dans le tube rmn 2 μL de DCl 20% dans D_2O et on enregistre les spectres rmn à des intervalles de temps réguliers; au bout de 3 jours, la composition des produits est 80% de lactone et 20% d'hydroxy-ester, ce qui confirme l'extrême lenteur de la réaction de lactonisation déjà observée par McClelland sur un composé voisin de ceux que nous avons étudiés (10).

Méthodes cinétiques

Les réactions d'hydrolyse sont suivies par spectrophotométrie uv (Gilford 250 équipé d'un passeur automatique de cuves) en mesurant l'augmentation de la densité optique due à l'apparition des produits. Les longueurs d'onde utilisées sont les suivantes: 240 nm (**1**), 235 nm (**2**), 235 nm (**3**), 232 nm (**4**) et 267 nm (**5**). Les cuves en quartz contiennent 2 mL de solution tampon à la température désirée et 20 μL de solutions 10^{-2} *M* d'orthoester dans le dioxanne pur.

Après agitation, la densité optique est enregistrée en fonction du temps. Les constantes de vitesse k_{obs} sont obtenues en traitant l'exponentielle $D = D_\infty + (D_\infty - D_0)e^{-kt}$ par la méthode des moindres carrés ou bien en portant $\ln (D_\infty - D)/(D_\infty - D_0)$ en fonction du temps. Les concentrations en orthoester sont choisies de façon à avoir une variation convenable de densité optique (0,2 à 0,8).

Influence de la composition du solvant et de l'activité du milieu sur les pK_a des acides catalyseurs et sur le calcul des constantes catalytiques

(1) *pH réels, pK_a réels*

Les valeurs des pH et des pK_a dans un solvant mixte peuvent être déterminées directement en utilisant un pH-mètre conventionnel qui a

[4]Les protons méthyléniques ne sont pas équivalents; ils sont diastéréotopes et se présentent sous la forme d'un système ABX: $J_{AX} = J_{BX} \simeq 7$ Hz, $J_{AB} \simeq 10 - 11$ Hz.

[5]cf. Note 4.

Can. J. Chem. Downloaded from www.nrcresearchpress.com by 210.87.254.42 on 09/06/12
For personal use only.

TABLEAU 9. Variation des pK_a des acides formique, acétique et cacodylique en fonction de la composition du solvant

Acides	pK_a réels $\mu = 0{,}1\ M$ Eau/dioxanne 2:1	pK_a $\mu = 0$ H_2O	ΔpK_a	Correction
Formique	4,48	3,75	0,73	0,9
Acétique	5,58	4,76	0,82	1,0
Cacodylique	6,96	6,19	0,77	(0,95)

été standardisé à l'aide de tampons dans le même solvant (21).

Une méthode approchée de détermination des pH réels est également possible si le pH-mètre est standardisé à l'aide de tampons aqueux; la lecture (pH lu), obtenue dans un solvant mixte, diffère par une quantité δ de la lecture (pH réel) qui est obtenue lorsque le pH-mètre est standardisé à l'aide de tampons dans ce solvant mixte.

$$\text{pH réel} = \text{pH lu} - \delta \qquad pK_a \text{ réel} = pK_a \text{ lu} - \delta$$

Ainsi, une valeur approchée de pH peut être obtenue si les valeurs de δ sont connues. Dans le cas du solvant que nous avons utilisé, eau/dioxanne 2:1 en volumes, le terme δ est égal à $-0{,}08$ (22).

(2) *pK_a des acides formique, acétique et cacoadylique dans le solvant eau/dioxanne 2:1 en volumes*

L'influence de la composition du solvant sur le pK_a des acides catalyseurs est connue pour les acides formique et acétique (23):

$$\text{HCOOH: } pK_a \text{ (eau/dioxanne 2:1)} = pK_a \text{ (eau)} + 0{,}9 = 4{,}65$$

$$CH_3COOH: pK_a \text{ (eau/dioxanne 2:1)} = pK_a \text{ (eau)} + 1{,}0 = 5{,}76$$

Le pK_a de l'acide cacodylique dans l'eau/dioxanne 2:1 à force ionique nulle peut être estimé à partir des différences ΔpK_a observées entre les pK_a réels (égaux aux pH réels lorsque $[AH] = [A^-]$) déterminés dans l'eau/dioxanne 2:1 à force ionique égale à 0,1 *M* et les pK_a correspondants connus dans l'eau à force ionique nulle (Tableau 9).

La valeur ΔpK_a obtenue pour l'acide cacodylique est intermédiaire entre celles calculées pour les acides acétique et formique. Nous pouvons donc raisonnablement penser que la correction de pK_a à apporter sera, selle aussi, comprise entre les corrections apportées aux acides formique et acétique à force ionique nulle.

Le pK_a de l'acide cacodylique dans l'eau/dioxanne 2:1 en volumes et à force ionique nulle peut donc être estimé à 6,19 + 0,95 = 7,14.

(3) *pK_a de H_3O^+ et H_2O dans le solvant eau/dioxanne 2:1 en volumes*

Les values de pK_a de H_3O^+ et H_2O peuvent être calculées à partir des données de la littérature (23):

$$H_3O^+: pK_a = -1{,}57 \qquad H_2O: pK_a = 16{,}67$$

(4) *Calcul des constantes catalytiques* k_{AH}, $k_{H_3O^+}$ et k_{H_2O}

Le calcul des différentes constantes catalytiques nécessite la connaissance de la concentration en proton pour chaque acide dans le milieu eau/dioxanne 2:1 en volumes et à force ionique égale à 0,1 *M*. La concentration en proton est calculée au moyen de la formule ci-dessous (24):

$$[H^+] = K_a \frac{[AH]}{[A^-]} \times \frac{1}{\gamma_\pm^2} \quad \text{avec} \quad \begin{matrix} [AH] = [AH]_0 - [H^+] \\ [A^-] = [A^-]_0 - [H^+] \end{matrix}$$

Le coefficient d'activité $\gamma_\pm$ peut être déterminé par extrapolation des valeurs de $\gamma_\pm$ reportées dans la littérature (ref. 23, p. 717); pour un mélange eau/dioxanne 2:1 en volumes et à force ionique égale à 0,1 *M*, $\gamma_\pm = 0{,}66$.

La résolution du système d'équation ci-dessus conduit aux concentrations en proton suivantes.

Acide formique $[AH]_0/[A^-]_0 = 0{,}25$ $[H^+] = 1{,}28 \times 10^{-5}\ M$

Acide formique $[AH]_0/[A^-]_0 = 1$ $[H^+] = 5{,}13 \times 10^{-5}\ M$

Acide acétique $[AH]_0/[A^-]_0 = 1$ $[H^+] = 3{,}99 \times 10^{-6}\ M$

Acide cacodylique $[AH]_0/[A^-]_0 = 1$ $[H^+] = 1{,}28 \times 10^{-5}\ M$

La concentration en proton est négligeable devant la concentration en acide non dissocié [AH]; on peut donc assimiler [AH] et $[AH]_0$. En portant k_{obs} en fonction de $[AH]_0$ # [AH], on obtient ainsi les constantes catalytiques k_{AH}.

Les constantes catalytiques $k_{H_3O^+}$ et k_{H_2O}, difficiles à déterminer directement, sont obtenues en résolvant le système d'équations des ordonnées à l'origine des graphe $k_{obs} = f([AH])$ pour les acides acétique et cacodylique.

1. G. LAMATY, C. MOREAU et Z. MOULOUNGUI. Bull. Soc. Chim. Belg. **91**, 389 (1982).
2. P. DESLONGCHAMPS. Heterocycles, **7**, 1271 (1977) et références citées.
3. P. DESLONGCHAMPS, R. CHENEVERT, R. J. TAILLEFER, C. MOREAU et J. K. SAUNDERS. Can. J. Chem. **53**, 1601 (1975).
4. O. BOUAB, C. MOREAU et M. ZEH AKO. Tetrahedron Lett. 61 (1978).
5. Y. CHIANG, A. J. KRESGE, P. SALOMAA et C. I. YOUNG. J. Am. Chem. Soc. **96**, 4494 (1974).
6. Y. CHIANG, A. J. KRESGE et C. I. YOUNG. Finn. Chem. Lett. 13 (1978).
7. T. H. FIFE. Acc. Chem. Res. **5**, 264 (1972).
8. E. H. CORDES et H. G. BULL. Chem. Rev. **74**, 581 (1974).
9. R. B. DUNLAP, G. A. GHANIN et E. H. CORDES. J. Phys. Chem. **73**, 1898 (1969).
10. R. A. MCCLELLAND et M. ALIBHAI. Can. J. Chem. **59**, 1169 (1981).
11. M. AHMAD, R. G. BERGSTROM, M. J. CASHEN, Y. CHIANG, A. J. KRESGE, R. A. MCCLELLAND et M. F. POWELL. J. Am. Chem. Soc. **101**, 2669 (1979).
12. O. BOUAB, G. LAMATY, C. MOREAU et O. POMARES. Nouv. J. Chim. **5**, 175 (1981).
13. H. G. BULL, K. KOEHLER, T. C. PLETCHER, J. J. ORTIZ et E. H. CORDES. J. Am. Chem. Soc. **93**, 3002 (1971).
14. P. D. LARK, B. R. CRAVEN et R. C. L. BOSWORTH. The handling of chemical data. Pergamon Press, New York. 1968. p. 136.
15. N. K. BOSE et D. N. CHAUDHURY. J. Indian Chem. Soc. **46**, 854 (1969).
16. N. S. NARASHIMAHAN et ET B. H. BIDE. Tetrahedron, **27**, 6171 (1971).
17. J. COLONGE et P. BOISDE. Bull. Soc. Chim. Fr. 1337 (1956).
18. N. K. BOSE et D. N. CHAUDHURY. J. Indian Chem. Soc. **41**, 103 (1964).
19. G. ODASSO et G. WINTERS. Farmaco Ed. Sci. **33**, 148 (1978).
20. A. BRUGGINK et A. MCKILLOP. Tetrahedron, **31**, 2607 (1975).
21. D. D. PERRIN et B. DEMPSEY. Buffers for pH and metal ion control. Chapman et Hall, London. 1974. p. 77.
22. G. DOUHERET. Bull. Soc. Chim. Fr. 1412 (1967).
23. H. S. HARNED et B. B. OWEN. The physical chemistry of electrolytic solutions, 3° éd. Chapman et Hall, London. 1958. pp. 662 et 756.
24. S. R. WANN et M. M. KREEVOY. J. Org. Chem. **46**, 419 (1981).

Can. J. Chem. Downloaded from www.nrcresearchpress.com by 210.87.254.42 on 09/06/12
For personal use only.

Effet de groupe partant dans l'hydrolyse d'orthoesters cycliques: changement de conformère réactif dans l'hydrolyse des diéthoxy-2,2 tétrahydropyrannes[1]

GÉRARD LAMATY, PHILIPPE LORENTE ET CLAUDE MOREAU

Laboratoire de Chimie Organique Physique, Université des Sciences et Techniques du Languedoc, Place Eugène Bataillon, 34060 Montpellier Cédex, France

Reçu le 17 mars 1983

GÉRARD LAMATY, PHILIPPE LORENTE et CLAUDE MOREAU. Can. J. Chem. **61**, 2651 (1983).

Les vitesses d'hydrolyse des orthoesters diéthoxy-2,2 dihydro-3,4 benzopyrannes-1 substitués en position 6 (X = OMe, Me, H et Cl) ont été déterminées à deux températures dans le solvant eau/dioxanne 2:1 en volumes. Le changement de signe observé dans les constantes ρ de Hammett ($\rho_{H_3O^+} = -0{,}8$; $\rho_{AH} = +0{,}7$) est caractéristique du départ d'un groupe phénolate, c'est-à-dire de la rupture de la liaison C—O endocyclique dans les systèmes étudiés ici; ces résultats indiquent un changement du conformère réactif dans l'hydrolyse des diéthoxy-2,2 tétrahydropyrannes.

GÉRARD LAMATY, PHILIPPE LORENTE, and CLAUDE MOREAU. Can. J. Chem. **61**, 2651 (1983).

The rates of hydrolysis of 6-substituted 2,2-diethoxy 3,4-dihydro benzo-1-pyrans (X = MeO, Me, H and Cl) were determined at two temperatures in water/dioxane 2:1 by volume. The observed change of sign of the Hammett ρ constants ($\rho_{H_3O^+} = -0.8$; $\rho_{AH} = +0.7$) is characteristic of a phenolate leaving group, i.e. of the rate-determining cleavage of the endocyclic C—O bond in the systems here studied; these results clearly indicate a change in the nature of the reactive conformer in hydrolysis of 2,2-diethoxy tetrahydropyrans.

Introduction

De nombreuses réactions rencontrées en biochimie font intervenir des intermédiaires tétraédriques dans lesquels trois hétéroatomes sont fixés sur l'atome de carbone siège de la réaction.

L'étude de ces intermédiaires a connu un regain d'intérêt avec l'élaboration d'une théorie stéréoélectronique qui permet d'expliquer et de prévoir la formation et la décomposition d'intermédiaires tétraédriques et qui s'énonce comme suit (2): "la coupure spécifique d'une liaison carbone−hétéroatome n'intervient que si les deux autres hétéroatomes ont chacun une paire d'électrons libres anticoplanaire à la liaison carbone−hétéroatome qui va se couper".

Pour étayer cette théorie, de nombreuses réactions chimiques ont été étudiées, en particulier la réaction d'hydrolyse des orthoesters qui fait intervenir des intermédiaires tétraédriques hémiorthoesters. Les travaux effectués ont clairement montré, qu'au cours de la réaction d'hydrolyse, interviennent des coupures spécifiques de liaisons C—OR en accord avec la théorie stéréoélectronique.

La spécificité observée ne peut être expliquée qu'en postulant une différence entre les énergies libres d'activation pour les réactions de coupure des différentes liaisons C—OR; c'est ainsi que dans un précédent travail (3), nous avons montré à partir de résultats cinétiques que l'hydrolyse des diéthoxy-2,2 tétrahydropyrannes s'effectuait par l'intermédiaire du conformère *A* et non par l'intermédiaire du conformère *F* (Schéma 1), hypothèse déjà retenue à partir de l'analyse des produits de réactions (4).

L'hydrolyse préférentielle par l'intermédiaire du conformère *A* réside très vraisemblablement dans le facteur entropique qui défavorise l'ouverture du cycle tétrahydropyranne dans le conformère *F*. Pour essayer de déterminer la réactivité du conformère *F*, il faut favoriser la rupture de la liaison C—O endocyclique; en adjoignant un cycle benzénique au cycle tétrahydropyranne, on obtient l'équivalent d'un groupement phénolate connu pour être un meilleur groupe partant qu'un groupement alcoolate (5), situation que l'on rencontre dans les orthoesters dérivés de la dihydro-3,4 coumarine (Fig. 1).

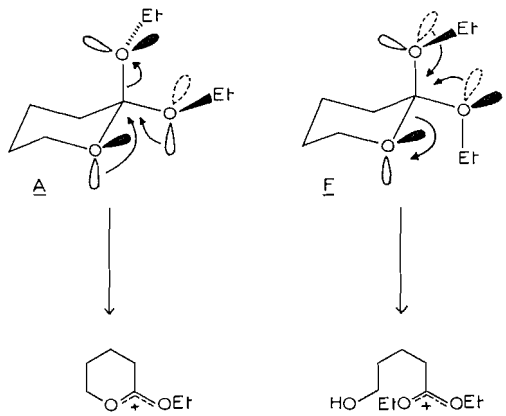

SCHÉMA 1

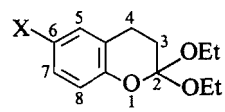

1 X = OMe
2 X = Me
3 X = H
4 X = Cl

FIG. 1

La synthèse des orthoesters **1** à **4** a donc été effectuée dans un premier temps; dans un deuxième temps, nous avons étudié l'hydrolyse de ces composés, du point de vue qualitatif (analyse des produits d'hydrolyse) et du point de vue quantitatif (constantes de vitesse d'hydrolyse, type de catalyse, grandeurs d'activation).

Résultats expérimentaux

I. *Synthèse*

Les composés étudiés ont été synthétisés à partir des lactones convenablement substituées selon la procédure générale décrite par Deslongchamps *et al.* (2, 4). Les propriétés physicochimiques des nouveaux produits sont donnés en détail dans la partie expérimentale.

II. *Analyse des produits de la réaction*

L'analyse des produits de la réaction d'hydrolyse peut ap-

[1]Ce travail a été présenté en partie à la VI° Conférence I.U.P.A.C. de Chimie Organique Physique, Louvain la Neuve, Belgique, juillet 1982 (1).

Can. J. Chem. Downloaded from www.nrcresearchpress.com by 210.87.254.6 on 09/06/12
For personal use only.

Can. J. Chem. Downloaded from www.nrcresearchpress.com by 210.87.254.6 on 09/06/12
For personal use only.

TABLEAU 1. Hydrolyse du méthoxy-6 diéthoxy-2,2 benzopyranne-1 (**1**) dans l'eau/dioxanne 2:1 en volumes, à force ionique égale à 0,0686 *M* (KCl) et à 25,2°C

Acide chlorhydrique					
$[HCl] \times 10^4$ *M*	6,03	5,63	2,51		
$k_{obs} \times 10^2$ s^{-1}	9,81	9,50	4,48		
Acide chloracétique/chloracétate de sodium					
$[ClCH_2COOH]/[ClCH_2COONa] = 1$; pH* = 3,67					
$[ClCH_2COOH] \times 10^2$ *M*	7,5	5,75	3,75	1,98	0,94
$k_{obs} \times 10^2$ s^{-1}	5,55	4,89	4,85	4,11	3,83
Acide formique/formiate de sodium					
[HCOOH]/[HCOONa] = 1, pH* = 4,39					
$[HCOOH] \times 10^2$ *M*	6,86	4,99	3,55	1,79	0,87
$k_{obs} \times 10^2$ s^{-1}	1,14	1,06	0,98	0,84	0,78
Acide acétique/acétate de sodium					
$[CH_3COOH]/[CH_3COONa] = 1$; pH* = 5,58					
$[CH_3COOH] \times 10^2$ *M*	3,75	1,88	0,90		
$k_{obs} \times 10^4$ s^{-1}	9,23	7,96	6,46		

*pH réels: pH réel = pH lu + 0,08.

TABLEAU 2. Hydrolyse du méthyl-6 diéthoxy-2,2 benzopyranne-1 (**2**) dans l'eau/dioxanne 2:1 en volumes, à force ionique égale à 0,0686 *M* (KCl) et à 25,2°C

Acide chlorhydrique					
$[HCl] \times 10^4$ *M*	6,03	5,63	2,51		
$k_{obs} \times 10^2$ s^{-1}	9,76	8,88	4,08		
Acide chloracétique/chloracétate de sodium					
$[ClCH_2COOH]/[ClCH_2COONa] = 1$, pH* = 3,67					
$[ClCH_2COOH] \times 10^2$ *M*	7,5	5,75	3,75	1,98	0,94
$k_{obs} \times 10^2$ s^{-1}	5,31	4,56	4,40	3,79	3,42
Acide formique/formiate de sodium					
[HCOOH]/[HCOONa] = 1; pH* = 4,39					
$[HCOOH] \times 10^2$ *M*	6,86	4,99	3,55	1,79	0,87
$k_{obs} \times 10^2$ s^{-1}	1,27	1,14	1,01	0,85	0,78
Acide acétique/acétate de sodium					
$[CH_3COOH]/[CH_3COONa] = 1$; pH* = 5,58					
$[CH_3COOH] \times 10^2$ *M*	3,75	1,88	0,90		
$k_{obs} \times 10^4$ s^{-1}	9,61	7,58	6,35		

*pH réels: pH réel = pH lu + 0,08.

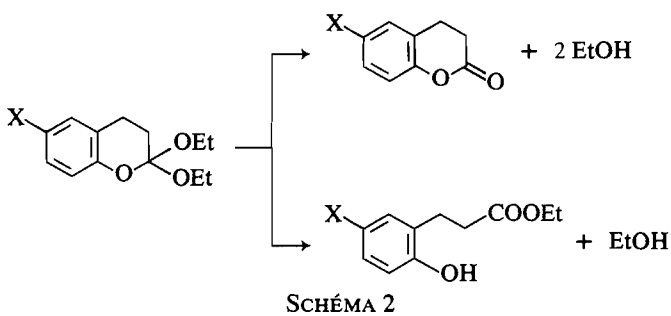

SCHÉMA 2

porter des renseignements utiles sur le sens d'ouverture des orthoesters: l'hydrolyse des composés **1** à **4** peut conduire à deux couples de produits suivant la rupture – endocyclique ou exocyclique – de la liaison C—O, tout en respectant les règles stéréoélectroniques: lactone + 2EtOH ou hydroxy-ester + EtOH (Schéma 2). Expérimentalement, l'hydrolyse des orthoesters **1** à **4** conduit essentiellement à l'hydroxy-ester. Ce point sera repris plus en détail dans la partie discussion.

III. *Résultats cinétiques*

L'hydrolyse acido-catalysée des diéthoxy-2,2 benzopyrannes-1 substitués en position 6 a été effectuée dans le solvant eau/dioxanne 2:1 en volumes. Les couples acide/base utilisés pour tamponner le milieu sont acide monochloracétique/monochloracétate de sodium, acide formique/formiate de sodium et acide acétique/acétate de sodium. La force ionique a été maintenue constante à 0,0686 *M* par addition de chlorure de potassium. Les résultats cinétiques obtenus dans l'eau/dioxanne 2:1 en volumes sont rassemblés dans les tableaux 1 à 4. Les constantes catalytiques k_{H^+}, k_{ClCH_2COOH}, k_{HCOOH} et k_{CH_3COOH} (corrections faites de l'effet de solvant et de l'activité du milieu)[2] ont été obtenues en exploitant les résultats des tableaux 1 à 4;[3] ces constantes sont rassemblées dans le tableau 5.

[2]L'influence de la composition du solvant et de l'activité du milieu sur les pK_a des acides catalyseurs et sur le calcul des constantes catalytiques est donnée en détail dans l'article précédant directement celui-ci (3).

[3]Le graphe obtenu en portant la constante de vitesse observée en fonction de la concentration en acide faible, pour un pH donné, n'est pas linéaire. Un comportement semblable a déjà été observé par d'autres auteurs (5, 6) et aucune analyse approfondie du phénomène n'a été faite jusqu'à présent. Les constantes catalytiques reportées dans le tableau 5 ont été déterminées en effectuant les régressions linéaires pour les valeurs de k_{obs} aux trois plus faibles concentrations.

TABLEAU 3. Hydrolyse du diéthoxy-2,2 benzopyranne-1 (**3**) dans l'eau/dioxanne 2:1 en volumes, à force ionique égale à 0,0686 *M* (KCl) et à 25,2°C

Acide chlorhydrique					
$[HCl] \times 10^4$ *M*	6,03	5,63	2,51		
$k_{obs} \times 10^2$ s^{-1}	7,27	7,38	3,40		
Acide chloracétique/chloracétate de sodium					
$[ClCH_2COOH]/[ClCH_2COONa] = 1$; pH* = 3,67					
$[ClCH_2COOH] \times 10^2$ *M*	7,5	5,75	3,75	1,98	0,94
$k_{obs} \times 10^2$ s^{-1}	5,87	5,55	4,60	3,45	3,18
Acide formique/formiate de sodium					
[HCOOH]/[HCOONa] = 1; pH* = 4,39					
$[HCOOH] \times 10^2$ *M*	6,86	4,99	3,55	1,79	0,87
$k_{obs} \times 10^2$ s^{-1}	1,32	1,22	1,02	0,82	0,67
Acide acétique/acétate de sodium					
$[CH_2COOH]/[CH_3COONa] = 1$; pH* = 5,58					
$[CH_3COOH] \times 10^2$ *M*	3,75	1,88	0,90		
$k_{obs} \times 10^3$ s^{-1}	1,12	0,93	0,71		

*pH réels: pH réel = pH lu + 0,08.

TABLEAU 4. Hydrolyse du chloro-6 diéthoxy-2,2 benzopyranne-1 (**4**) dans l'eau/dioxanne 2:1 en volumes, à force ionique égale à 0,0686 *M* (KCl) et à 25,2°C

Acide chlorhydrique					
$[HCl] \times 10^4$ *M*	6,03	5,63	2,51		
$k_{obs} \times 10^2$ s^{-1}	4,29	3,98	1,89		
Acide chloracétique/chloracétate de sodium					
$[ClCH_2COOH]/[ClCH_2COONa] = 1$; pH* = 3,67					
$[ClCH_2COOH] \times 10^2$ *M*	7,5	5,75	3,75	1,98	0,94
$k_{obs} \times 10^2$ s^{-1}	5,63	4,78	4,18	3,08	2,33
Acide formique/formiate de sodium					
[HCOOH]/[HCOONa] = 1; pH* = 4,39					
$[HCOOH] \times 10^2$ *M*	6,86	4,99	3,55	1,79	0,87
$k_{obs} \times 10^2$ s^{-1}	1,34	1,22	0,88	0,76	0,56

*pH réels: pH réel = pH lu + 0,08.

TABLEAU 5. Hydrolyse des orthoesters **1** à **4**: constantes catalytiques (M^{-1} s^{-1}) et constantes ρ de Hammett à 25,2°C dans l'eau/dioxanne 2:1 en volumes et à force ionique égale à 0,0686 *M* (KCl)

	X					
Constante	OMe	Me	H	Cl	ρ	Écart-type sur ρ
k_{H^+}	166	160	126	71	−0,76	0,05
k_{ClCH_2COOH}	0,368	0,349	0,519	0,654	+0,57	0,08
k_{HCOOH}	0,070	0,088	0,128	0,153	+0,65	0,08
k_{CH_3COOH}	0,0098	0,0114	0,0136	—	+0,52	0,07

Interprétation des résultats expérimentaux et discussion

Les composés que nous avons étudiés peuvent théoriquement s'hydrolyser par rupture d'une liaison C—OEt exocyclique ou bien par rupture de la liaison C—O endocyclique (Schéma 3)[4] au cours de l'étape limitante. Deux points importants sont donc à élucider: le premier est de savoir quelle est la nature de la liaison C—O qui se coupe au cours de l'étape cinétique et le second point est de savoir quelle est la nature du conformère réactif. Ces deux points seront abordés successivement.

I. *Nature de la liaison C—O qui se coupe*

La nature de la liaison C—O qui se coupe peut être déterminée à partir des résultats obtenus dans le solvant eau/dioxanne 2:1 en volumes: l'examen des tableaux 1 à 4 montre que l'hydrolyse des composés étudiés est soumise à une catalyse acide générale; ce type de catalyse est généralement celui qui est observé dans l'hydrolyse des orthoesters (7, 8) et est compatible avec le concept de contrôle stéréoélectronique (9).

Analyse des produits d'hydrolyse

Dans le cas d'une rupture de la liaison C—O endocyclique (Schéma 3, conformère *F*) le produit d'hydrolyse normalement attendu est l'hydroxy-ester. Par contre dans le cas d'une rupture

[4]Par souci de clarté dans le schéma 3, les cycles aromatiques n'ont pas été représentés sur les dessins en trois dimensions; l'examen des modèles moléculaires montre que l'orientation relative des liaisons C—O et des paires d'électrons libres est la même dans les orthoesters **1** à **4** que dans le diéthoxy-2,2 tétrahydropyranne lui-même. La position du groupe phényle est symbolisée par la liaison en trait épais.

Can. J. Chem. Downloaded from www.nrcresearchpress.com by 210.87.254.6 on 09/06/12
For personal use only.

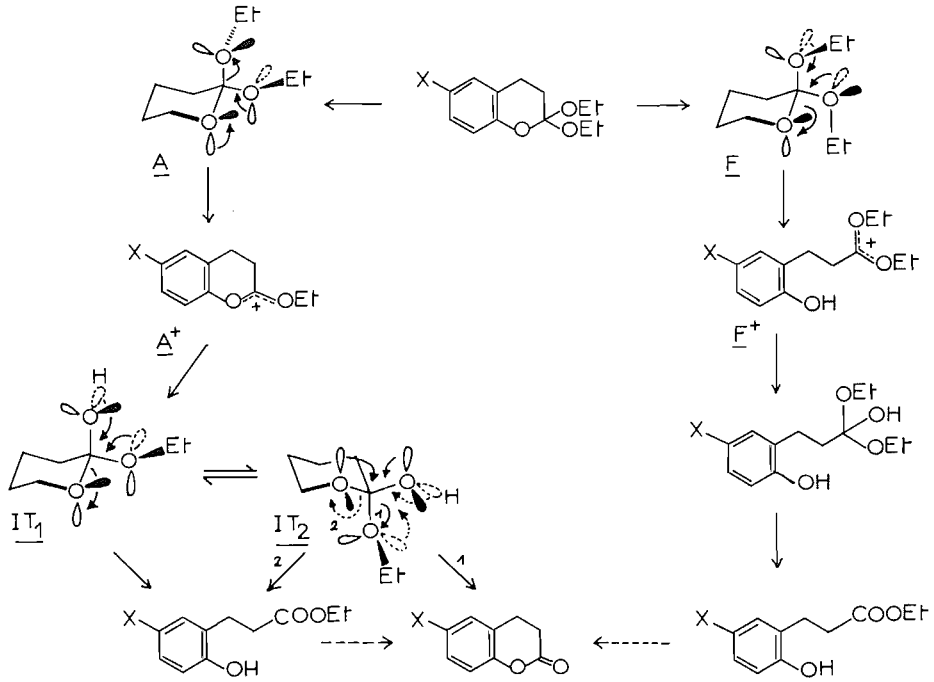

SCHÉMA 3

TABLEAU 6. Hydrolyse des orthoesters **1** à **4**: constantes catalytiques k_{H^+} (M^{-1} s^{-1}) à deux températures et paramètres d'activation donnés à 25,0°C

X	k_{H^+} à 12,0°C	k_{H^+} à 25,2°C	$\Delta H^{\neq}$ kcal/mol	$\Delta S^{\neq}$ ue
OMe	74	166	9,7	−16
Me	70	160	9,9	−15
H	56	126	9,7	−16
Cl	32	71	9,5	−18

de la liaison C—O exocyclique (Schéma 3, conformère *A*) deux produits peuvent être présents, la lactone et l'hydroxy-ester, tout en respectant les règles stéréoélectroniques. La lactone ne peut se former que si le temps de demi-vie de l'intermédiaire tétraédrique est suffisamment long pour permettre l'équilibre $IT_1 \leftrightarrows IT_2$ (Schéma 3). Capon et Grieve (10) ont montré que l'hydrolyse du diéthoxy-2,2 tétrahydropyranne lui-même conduisait à 30% de lactone. La présence d'un caractère double liaison dans le cycle tétrahydropyrannyle des systèmes que nous avons étudiés devrait donc favoriser l'équilibre $IT_1 \leftrightarrows IT_2$, et par conséquent, accroître le pourcentage de lactone. Expérimentalement, nous n'observons qu'un faible pourcentage de lactone, environ 4%, ce qui laisse penser que le chemin *F* serait favorisé, en l'occurrence la rupture de la liaison C—O serait endocyclique.

Analyse des constantes ρ de Hammett

L'examen des constantes ρ de Hammett calculées pour l'hydrolyse de nos composés (Tableau 5) amène deux remarques intéressantes: (1) la constante ρ, en valeur absolue, est de faible amplitude et (2) la constante ρ change de signe lorsque le catalyseur passe d'un acide fort ($\rho_{H_3O^+} < 0$) à un acide faible ($\rho_{AH} > 0$).

Ces résultats montrent que l'étape cinétique est la rupture de la liaison C—O endocyclique:

(1) Le pouvoir électroattracteur du groupe phénolate a pour conséquence deux effets d'influence contraire: d'une part il favorise la coupure de la liaison C—O et d'autre part il défavorise la protonation. La superposition de ces deux effets entraîne un nivellement de la différence de réactivité en fonction du substituant, et donc, des valeurs de la constante ρ de faible amplitude. Ce résultat a déjà été observé dans l'hydrolyse d'acétals faisant intervenir le départ d'un groupe phénolate (5, 11, 12).

(2) Le changement de signe de la constante ρ lorsque le catalyseur passe d'un acide faible à un acide fort a également été observé dans l'hydrolyse d'acétals faisant intervenir le départ d'un groupe phénolate (7, 12) et est donc caractéristique d'un effet de groupe partant, c'est-à-dire dans le cas des orthoesters étudiés dans ce travail, d'une rupture de la liaision C—O endocyclique, équivalente à une liaison C—Oϕ. Ce changement de signe de la constante ρ de Hammett a été interprété de la façon suivante: en milieu acide faible, l'élongation de la liaison C—O est plus importante que la protonation du groupe phénolate, ce qui entraîne une augmentation de la densité électronique sur l'atome réactionnel, dans ce cas l'atome d'oxygène, donc une valeur de ρ positive.

En milieu acide fort, à l'inverse, la protonation du groupe phénolate est plus importante que l'élongation de la liaison C—O. L'atome d'oxygène réactionnel voit donc sa densité électronique diminuer, conduisant ainsi à une constante ρ négative.

Analyse des entropies d'activation

Les grandeurs d'activation déterminées pour les composés **1** à **4** font apparaître des valeurs fortement négatives pour les entropies d'activation dans l'hydrolyse catalysée par le proton (Tableau 6). Ces valeurs négatives peuvent résulter de deux choses: (1) du remplacement d'un groupe éthylate par un groupe phénolate (Tableau 7) comme cela a été montré dans l'hydrolyse des éthoxy-2 et phénoxy-2 tétrahydropyrannes (11); (2) du passage d'un système non cyclique à un système cyclique comme on peut le voir dans le tableau 8 à partie des résultats obtenus dans l'hydrolyse des acétals dérivés de l'éthanol ou de l'éthylèneglycol et du formaldéhyde ou du benzaldéhyde (13, 14).

Can. J. Chem. Downloaded from www.nrcresearchpress.com by 210.87.254.6 on 09/06/12
For personal use only.

TABLEAU 7. Hydrolyse des éthoxy-2 et phénoxy-2 tétrahydropyrannes: grandeurs d'activation dans la réaction catalysée par le proton (11)

	R	$\Delta H^{\neq}$ (kcal/mol)	$\Delta S^{\neq}$ (ue)
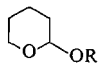	C_2H_5	22,2	+8
	C_6H_5	17,9	−3

TABLEAU 8. Hydrolyse des acétals dérivés de l'éthanol et de l'éthylèneglycol avec le formaldéhyde et le benzaldéhyde: grandeurs d'activation dans la réaction catalysée par le proton (13, 14)

	R	$\Delta H^{\neq}$ (kcal/mol)	$\Delta S^{\neq}$ (ue)
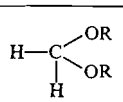	C_2H_5	24,9	+7
	Dioxolanne-1,3	24,9	−1
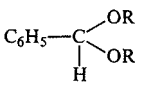	C_2H_5	16,5	+1
	Dioxolanne-1,3	15,5	−9

Que ce soit donc l'analyse des produits d'hydrolyse, l'analyse des constantes ρ de Hammett ou bien l'analyse des entropies d'activation, ces trois points permettent de conclure sans ambiguité que l'étape cinétique de la réaction d'hydrolyse des orthoesters étudiés ici est la rupture de la liaison C—O endocyclique.

II. *Nature du conformère réactif*

Il a été montré que dans l'hydrolyse des orthoesters diéthoxy-2,2 tétrahydropyrannes, aussi bien à partir de la nature des produits d'hydrolyse (2, 4) qu'à partir de résultats cinétiques (3) le conformère réactif était, dans le cas d'une rupture de liaison C—O exocyclique, le conformère *A* et non *F* (Schéma 1).

Dans le cas de nos composés, nous venons de montrer que c'est la liaison C—O endocyclique qui se coupe au cours du processus cinétique. Si l'on considère les orientations relatives des liaisons C—O et des paires d'électrons libres dans chacun des conformères, le conformère réactif serait le conformère *F*.

La réactivité du conformère *F* peut être évaluée d'une façon approchée à partir des valeurs des grandeurs d'activation obtenues pour le conformère *A* qui s'hydrolyse par rupture de la liaison C—OEt axiale. Il suffit, ensuite, d'ajouter algébriquement les incréments spécifiques à nos produits, incréments qui rendent compte de l'ouverture d'un cycle et du remplacement d'un groupe éthylate par un groupe phénolate; le système d'équations suivant peut donc être posé:

$$\Delta H_F^{\neq} = \Delta H_A^{\neq} + \Delta H^{\neq}_{\text{groupe partant}} + \Delta H^{\neq}_{\text{cycle}}$$

$$\Delta S_F^{\neq} = \Delta S_A^{\neq} + \Delta S^{\neq}_{\text{groupe partant}} + \Delta S^{\neq}_{\text{cycle}}$$

D'après les tableaux 7 et 8, les grandeurs d'activation pour le groupe partant sont:

$$\Delta H^{\neq}_{\text{groupe partant}} = -4{,}3 \text{ kcal/mol et } \Delta S^{\neq}_{\text{groupe partant}} = -11 \text{ ue;}$$

pour l'ouverture d'un cycle, les valeurs sont:

$$\Delta H^{\neq}_{\text{cycle}} = -0{,}5 \text{ kcal/mol et } \Delta S^{\neq}_{\text{cycle}} = -9 \text{ ue.}$$

Ces valeurs peuvent être considérées comme extrêmes puisqu'empruntées à l'hydrolyse des acétals où l'état de transition est très avancé le long du chemin réactionnel. Pour tenir compte de l'avancement moindre de l'état de transition dans l'hydrolyse des orthoesters ces valeurs peuvent être raisonnablement réduites de moitié. Sachant que $\Delta H_A^{\neq} = 11$ kcal/mol et $\Delta S_A^{\neq} = -3$ ue (15) il est possible de calculer les grandeurs d'activation pour le conformère *F*: $\Delta H_F^{\neq} = 11{,}1 - 4{,}3/2 - 0{,}5/2 = 8{,}7$ kcal/mol et $\Delta S_F^{\neq} = -3 - 11/2 - 9/2 = -13$ ue, valeurs très proches des valeurs expérimentales (9,7 kcal/mol et −16 ue).

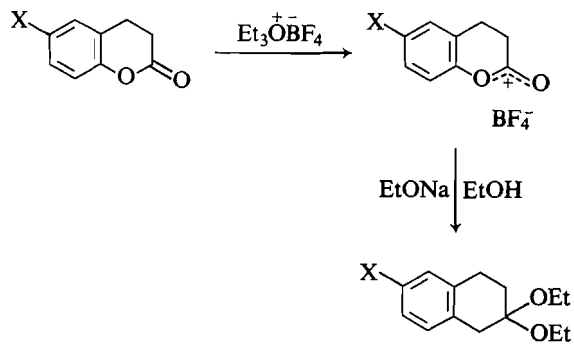

SCHÉMA 4

Conclusion

Dans le travail que nous avons présenté ici, il a donc été possible de montrer, par des mesures cinétiques, que des changements conformationnels peuvent s'opérer afin de respecter les règles stéréoélectroniques.

Il a été également possible d'évaluer la différence d'énergie d'activation entre les conformères *A* et *F*, différence égale à 2,5 kcal/mol qui favorise largement le conformère *A* sur le conformère *F* en l'absence d'effets particuliers.

Partie expérimentale

I. *Synthèse*

Les orthoesters ont été préparés à partir des lactones correspondantes, selon la procédure décrite par Deslongchamps *et al.* (4) (Schéma 4).

La lactone non substituée (X = H) est un produit commercial. La synthèse des lactones substituées (X = OMe, X = Me et X = Cl) a été effectuée selon la procédure décrite dans la littérature (16). Les rendements indiqués n'ont cependant jamais été atteints. Avant d'effectuer la synthèse des orthoesters, une vérification de la formation de l'ion lactonium a été faite pour les composés **2** (X = Me) et **3** (X = Cl).

Formation de l'ion lactonium

0,5 mmol de lactone et 0,5 mmol de tétrafluoroborate de triéthyloxonium sont dissous dans 1 mL de dichlorométhane deutérié. Le mélange est agité à température ambiante. La quantité approximative des produits présents dans le milieu est déterminée à partir des intensités relatives des différents signaux rmn observés.

X = H t = 5 h: lactonium
X = Me t = 24 h: lactonium (34%) + lactone (49%) + hydroxyester (17%)
t = 48 h: lactonium (29%) + lactone (55%) + hydroxyester (22%)

Le temps de réaction utilisé pour la formation des ions lactonium est de 24 h.

Les spectrres rmn ^{1}H ont été enregistrés sur un appareil Varian EM 390 (solvant: CD_2Cl_2; référence interne: TMS).

X = H; rmn, ^{1}H δ: 1,60 (3H, triplet, J = 7 Hz, OCH_2CH_3), 2,60 à 3,10 (4H, massif, méthylène sur C3 et C4), 4,80 (2H, quadruplet, J = 7 Hz, $\overset{+}{O}CH_2CH_3$), 6,90 à 7,40 (4H, massif, H aromatiques).

X = Me: rmn, ^{1}H δ: 1,60 (3H, triplet, J = 7 Hz, OCH_2CH_3), 2,35

Can. J. Chem. Downloaded from www.nrcresearchpress.com by 210.87.254.6 on 09/06/12
For personal use only.

(3H, singulet, CH_3 sur C6), 3,10 à 3,50 (4H, multiplet, méthylènes sur C3 et C4), 5,20 (2H, quadruplet, J = 7 Hz, $\overset{+}{O}CH_2CH_3$), 7,10 à 7,40 (3H, massif, H aromatiques).

Pour la suite de la synthèse des orthoesters, nous avons reproduit la procédure décrite dans la littérature (4).

Caractérisation des orthoesters

Une première caractérisation des produits formés est donnée par les spectres rmn ^1H (solvant: $CDCl_3$, référence interne: TMS).

Des analyses élémentaires, constituant une seconde caractérisation, ont ensuite été effectués pour les produits distillés, par le Service Central de Microanalyse de Vernaison.

1 – Rendement brut: 35%; rmn ^1H δ: 1,15 (6H, triplet, J = 7 Hz, OCH_2CH_3), 2,02 (2H, triplet, J = 6,5 Hz, méthylène sur C3), 2,80 (2H, triplet, J = 6,5 Hz, méthylène sur C4), 3,68 (4H, quadruplet, J = 7 Hz, OCH_2CH_3), 3,70 (3H, singulet, OCH_3), 6,50 à 6,88 (3H, massif, H aromatiques).

2 – Rendement brut: 27%; Eb. = 99°C/0,28 Torr; rmn ^1H δ: 1,15 (6H, triplet, J = 7 Hz, OCH_2CH_3), 2,08 (2H, triplet, J = 6,5 Hz, méthylène sur C3), 2,25 (3H, singulet, CH_3 sur C6), 2,82 (2H, triplet, J = 6,5, méthylène sur C4), 3,70 (4H, quadruplet, J = 7 Hz, OCH_2CH_3), 6,70 à 7,10 (3H, massif, H aromatiques). *Anal.* calc. (%) pour $C_{14}H_{20}O_3$: C 71,19, H 8,47, O 20,34; tr. (%): C 71,86, H 7,70, O 19,33.

3 – Rendement brut: 23%; Eb. = 66°C/0,1 Torr; rmn ^1H δ: 1,16 (6H, triplet, J = 7 Hz, OCH_2CH_3), 2,08 (2H, triplet, J = 6,5 Hz, méthylène sur C3), 2,82 (2H, triplet, J = 6,5 Hz, méthylène sur C4), 3,70 (4H, quadruplet, J = 7 Hz, OCH_2CH_3), 6,70 à 7,20 (4H, massif, H aromatiques). *Anal.* calc. (%) pour $C_{13}H_{18}O_3$: C 70,25, H 8,16, O 21,59; tr. (%): C 70,30, H 8,25, O 21,40.

4 – Rendement brut: 6%; rmn ^1H δ: 1,15 (6H, triplet, J = 7 Hz, OCH_2CH_3), 2,04 (2H, triplet, J = 6,5 Hz, méthylène sur C3), 2,80 (2H, triplet, J = 6,5 Hz, méthylène sur C4), 3,70 (4H, quadruplet, J = 7 Hz, OCH_2CH_3), 6,76 (1H, doublet, J = 9 Hz, H8), 6,90 à 7,20 (2H, massif, H5, H7).

II. *Identification des produits d'hydrolyse*

Cette identification a été faite avec le composé non substitué **3**. La procédure employée est la suivante: 20 μL de solution d'HCl 0,1 *N* sont ajoutés à 400 mg d'orthoester (1,8 mmol) dissous dans 2 mL de solvant MeOH/H_2O 80:20 en volumes. Le mélange est agité à température ambiante pendant 5 min, puis versé en refroidissant dans un mélange contenant 10 mL d'anhydride acétique et 10 mL de pyridine anhydre.

L'agitation à température ambiante est maintenue pendant 24 h, le mélange est ensuite évaporé à sec.

Le spectre rmn ^1H ($CDCl_3$) permet de connaître la composition du produit, par comparaison des intensités des différents signaux: lactone: 4%, acétoxyester: 96%.

III. *Cinétiques*

Les cinétiques d'hydrolyse ont été suivies par spectrophotométrie uv (Gilford 250). Une procédure détaillée concernant la mise en oeuvre des cinétiques ainsi que le mode de calcul des constantes catalytiques a été décrite par ailleurs (3). Les longueurs d'onde permettant de faire notre étude sont les suivantes: λ = 240 nm (**1**), 234 nm (**2**), 274 nm (**3**) et 290 nm (**4**). La reproductibilité sur les constantes de vitesse observées est de ±3%.

1. G. LAMATY, P. LORENTE et C. MOREAU. Bull. Soc. Chim. Belg. **91**, 390 (1982).
2. P. DESLONGCHAMPS. Heterocycles, **7**, 1271 (1977) et références citées.
3. G. LAMATY, C. MOREAU et Z. MOULOUNGUI. Can. J. Chem. **61**, 2643 (1983).
4. P. DESLONGCHAMPS, R. CHENEVERT, R. J. TAILLEFER, C. MOREAU et J. K. SAUNDERS. Can. J. Chem. **53**, 1601 (1975).
5. B. CAPON et K. NIMMO. J. Chem. Soc. Perkin Trans. 2, 1113 (1975).
6. E. S. HAND et W. P. JENCKS. J. Am. Chem. Soc. **97**, 6221 (1975).
7. T. H. FIFE. Acc. Chem. Res. **5**, 264 (1972).
8. E. H. CORDES et H. G. BULL. Chem. Rev. **74**, 581 (1974).
9. O. BOUAB, C. MOREAU et M. ZEH AKO. Tetrahedron Lett. 61 (1978).
10. B. CAPON et D. McL. A. GRIEVE. Tetrahedron Lett. **23**, 4823 (1982).
11. T. H. FIFE et L. K. JAO. J. Am. Chem. Soc. **90**, 4081 (1968).
12. C. MENUT. Thèse de Doctorat d'Etat, Montpellier (1982).
13. T. H. FIFE et L. K. JAO. J. Org. Chem. **30**, 1492 (1965).
14. E. H. CORDES. Prog. Phys. Org. Chem. **4**, 1 (1967).
15. O. BOUAB. Thèse de Doctorat d'Etat, Montpellier (1981).
16. K. SATO, T. AMAKASU et S. ABE. J. org. Chem. **29**, 2971 (1964).

Can. J. Chem. Downloaded from www.nrcresearchpress.com by 210.87.254.6 on 09/06/12
For personal use only.

Reaction of γ-carboxyglutamic acid with aldehydes

RENATO CAPASSO AND GIACOMINO RANDAZZO
Institute of Organic and Biological Chemistry, Universiy of Naples, Via Mezzocannone, 16 80134-Naples, Italy
AND
LAURA PECCI
Institute of Biological Chemistry, University of Rome, Piazzale Aldo Moro, 00100-Rome, Italy

Received February 17, 1983

RENATO CAPASSO, GIACOMINO RANDAZZO, and LAURA PECCI. Can. J. Chem. **61**, 2657 (1983).

The DL-γ-carboxyglutamic acid (Gla) reacts quantitatively with formaldehyde to give 4,4-dicarboxyproline and with other aldehydes to give the racemic diastereoisomers of the 5-substituted 4,4-dicarboxyprolines. The pH-dependent reaction rate and the stereochemical behaviour suggest an intramolecular Mannich mechanism.

After heating at 100°C for 30 min, the 4,4-dicarboxyproline and the 5-substituted 4,4-dicarboxyprolines lose a carboxyl group from C4 to give the racemic diastereoisomers of the cyclic analogs of glutamic acid.

RENATO CAPASSO, GIACOMINO RANDAZZO et LAURA PECCI. Can. J. Chem. **61**, 2657 (1983).

L'acide DL-γ-carboxyglutamique (Gla) réagit quantitativement avec le formaldéhyde pour donner la dicarboxy-4,4 proline tandis qu'avec d'autres aldéhydes, on obtient les diastéréoisomères racémiques des dicarboxy-4,4 prolines substitués en position 5. La vitesse de la réaction qui dépend du pH et le comportement stéréochimique fait penser à un mécanisme de Mannich intramoléculaire.

Par chauffage à 100°C pendant 30 minutes, la dicarboxy-4,4 proline et les dicarboxy-4,4 prolines substituées en position 5 perdent le groupe carboxyle du carbone en position 4 en donnant les diastéréoisomères des analogues cycliques de l'acide glutamique.

[Traduit par le journal]

Can. J. Chem. Downloaded from www.nrcresearchpress.com by 210.87.254.6 on 09/06/12
For personal use only.

Introduction

γ-Carboxyglutamic acid (Gla) was found in the N-terminal calcium binding region of vitamin K-dependent coagulation factors II, VII, IX, and X (1, 2). Gla-containing proteins were identified also in calcified tissues such as the organic matrix of bone (3), renal stones (4), and atherosclerotic plaque (5). Free Gla was found in human urine (6) as a metabolite of the catabolism of Gla-containing proteins (6, 7). In pharmacological therapy with warfarin (8) and in pathological cases such as osteoporosis (9), abnormal levels of Gla were found in urine. The determination of Gla levels in urine may assume an important role as a diagnostic parameter.

In a recent paper (10), a method for the quantitative determination of Gla, based on the reaction with acetaldehyde, has been described. Here, we discuss the mechanism (Scheme 1) and products **1**–**7** (Fig. 1) obtained by the reaction of Gla with aldehydes. We also report the nature of the derivatives produced by heating compounds **1**–**7** at 100°C.

Experimental

The DL-γ-carboxyglutamic acid was a gift of Dr. S. Dupré, University of L'Aquila, Italy. The aldehydes were provided by commercial sources. The amino acid analysis was performed on a LKB 4400 Amino Acid Analyzer. The proton ^{1}H nmr spectra were run on a Bruker 270 spectrometer, using (unless otherwise noted) deuterated water as solvent and *tert*-butyl alcohol as internal reference (1.23 ppm); all the chemical shifts are reported in ppm from TMS. The mass spectrum was recorded on an AEI-902 spectrometer at 70 eV. The uv spectra were recorded in water on a Cary-118 spectrophotomer and the ir spectra were run in chloroform or in Nujol. Electrophoresis was run on a silica gel plate (20 × 20 cm, Kieselgel Merck 0.25 mm) in 0.5% pyridine and 5% acetic acid buffer, pH 3.5, at 500 volt for one hour. Thin-layer chromatography (tlc) was performed on silica gel plates (Kieselgel 60 F_{254} 0.25 mm, chloroform–isopropanol, 90:10, as eluent) and on cellulose plates (F 0.1 mm, n-butanol – acetic acid – water 60:15:25, as eluent); the spots were developed by spraying with ninhydrin and heating at 110°C for 10 min. Dowex-50 (Fluka AG) and DEAE-cellulose (Whatman DE 52) were used for chromatographic separations.

The reaction rate of Gla with aldehydes as a function of pH was monitored by tlc of 10^{-2} *M* Gla and 5 *M* aldehyde solutions in 0.3 *M* pyridine acetate buffers of pH values ranging from 2 to 8.

4,4-Dicarboxyproline ***1***

DL-Gla (35 mg) is dissolved in 4.5 mL of 35% aqueous formaldehyde. The reaction is completed after 16 h, as shown on tlc by the appearance of a new yellow spot with R_f higher than Gla. The mixture is chromatographed on a DEAE-cellulose column (1.2 × 55 cm) equilibrated and eluted with 0.3 *M* pyridine acetate buffer, pH 4.75. The fractions are analyzed by tlc and those giving the yellow spot with ninhydrin are pooled and lyophilized. The residue, redissolved and lyophilized at least three times, is a white crystalline solid (25 mg); mp 120–130°C, with full transformation to **8**, as shown by tlc control; electrophoresis: at pH 3.5, **1** shows a yellow spot with a higher anodic mobility than glutamic acid and aspartic acid; automatic aminoacid analysis: **1** shows a single peak eluted 5 min after sample loading or 16.5 min before proline; ir (Nujol) ν_{max}: 3500, 3150, 1730, and 1630 cm^{-1}; ^{1}H nmr and uv data are summarized in Table 1 and Fig. 2.

Trimethylester of 4,4-dicarboxyproline ***1***a

Compound **1** (5 mg) is dissolved in methanol (2 mL) and treated with diazomethane in an ice bath under stirring until the yellow colour of mixture persists. After tlc control (chloroform–isopropanol, 90:10, ninhydrin), which shows a single yellow spot, the solution is evaporated under reduced pressure; the residue is an amorphous solid (5 mg); ir($CHCl_3$), ν_{max}: 3400 and 1730 cm^{-1}; ^{1}H nmr ($CDCl_3$): 3.71, 3.72, and 3.73 (3s, 3 × 3H, 3-COOMe); ms, m/z: 244(M^+ – H), 214 (M^+ – OMe), 186(M^+ – COOMe), 68(M^+ – 3COOMe).

4,4-Dicarboxy-5-methylproline ***2*** *and -5-ethylproline* ***3***

To a solution of DL-Gla (5.7 mg) in water (0.6 mL) freshly distilled acetaldehyde (150 μL) (propionaldehyde, 150 μL) is added. The reaction is carried out at room temperature and monitored by tlc as for **1**. After two hours, the acetaldehyde (propionaldehyde) in excess is carried off under a nitrogen stream and the solution is lyophilized. The residue is crystalline (6.7 mg for **2**, 7 mg for **3**). The ^{1}H nmr and uv

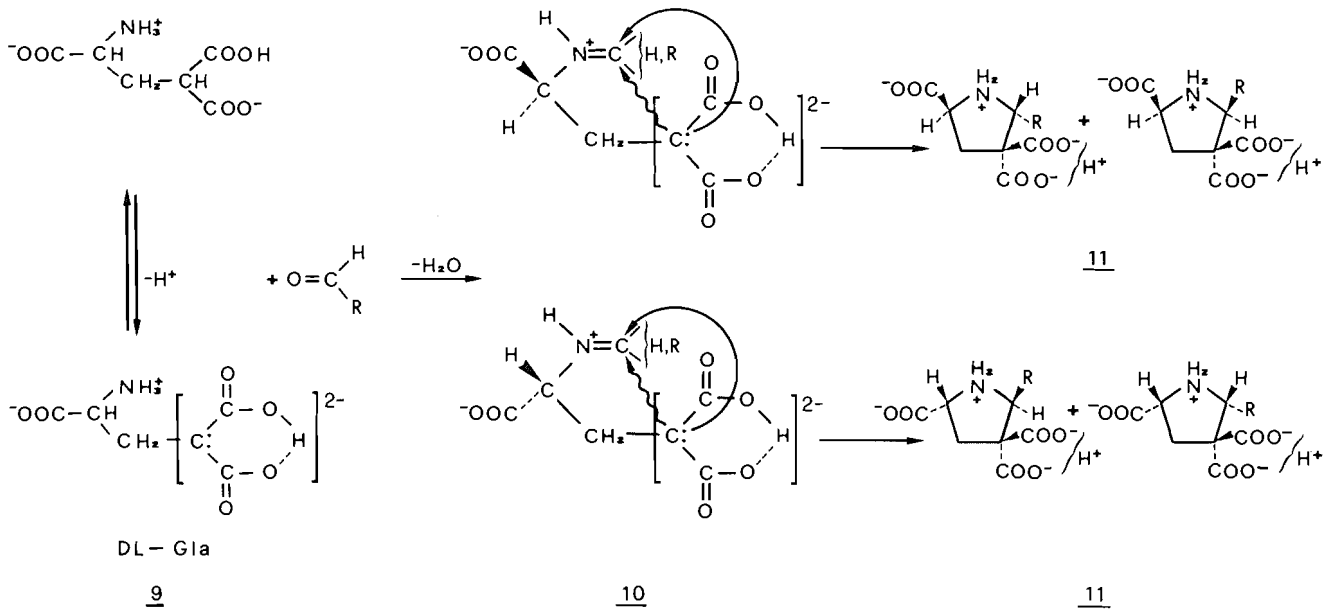

SCHEME. 1. Mannich reaction mechanism of Gla with aldehydes.

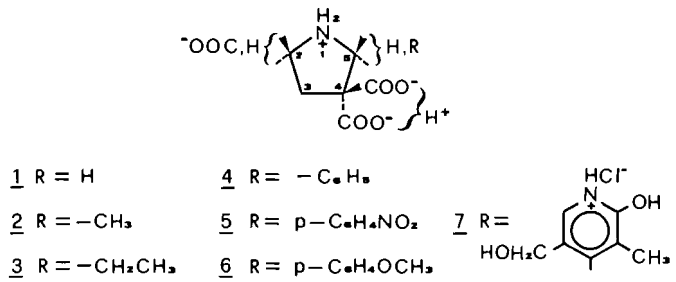

FIG. 1. Reaction products of Gla with aldehydes.

data are summarized in Table 1. As an example, the nmr spectrum of **2** is reported in Fig. 3(*a*).

4,4-Dicarboxy-5-phenylproline **4**, *-5-(*p*-NO_2-phenyl)proline* **5**, *and -5-(*p*-OCH_3-phenyl)proline* **6**

DL-Gla (6 mg) is dissolved in a mixture of water (3 mL) and methanol (3 mL). To this solution, benzaldehyde (0.6 mL) (*p*-NO_2-benzaldehyde, 300 mg, for **5**, *p*-OCH_3-benzaldehyde, 0.7 mL, for **6**) is added. The reaction is left overnight at room temperature and monitored as described above. Methanol is evaporated from the mixture under reduced pressure. The remaining aqueous phase is washed with methylene chloride (3 × 3 mL). When the solid *p*-NO_2-benzaldehyde is used, the mixture is filtered before washing. The lyophilized residue is crystalline (8 mg for **4**, 8.6 mg for **5**, and 8.3 mg for **6**). The ^{1}H nmr and uv data are summarized in Table 1. As an example, the nmr spectrum of **4** is reported in Fig. 3(*b*).

4,4-Dicarboxy-5-pyridoxylproline hydrochloride **7**

DL-Gla (10 mg) is dissolved in water (5 mL). To the solution, three aliquots of pyridoxal hydrochloride (50 mg) are added every two hours. After the last addition, the solution is left overnight at room temperature, then monitored by tlc. A yellow spot with R_f 0.5 appears after spraying with ninhydrin in the usual chromatographic system. The solution is then chromatographed on a Dowex-50 column (2 × 10 cm), equilibrated, and eluted with ammonium formate buffer 0.1 *M*, pH 4. The fractions which give yellow spots with ninhdydrin are pooled and lyophilized. The residue, redissolved and lyophilized at least three times, is a white crystalline solid (16 mg). The ^{1}H nmr and uv data are summarized in Table 1.

4-Carboxy-4-deuteroproline **8**

Compound **1** (5 mg) is dissolved in D_2O (0.5 mL) in an ^{1}H nmr tube. The solution is heated for 30 min at 100°C and cooled to room temperature. The solution is analyzed by ^{1}H nmr (Fig. 4 and Table 1). The amino acid analysis of **8** shows two peaks with elution times 12 min and 13.2 min respectively (9.9 min and 8.7 min before proline).

4-Carboxy-4-deuteroprolines, 5-substituted

Compounds **2**–**7** are treated as **8** and analyzed by ^{1}H nmr.

Results and discussion

The structure **1** has been suggested for the product of reaction between Gla and formaldehyde (11). We have confirmed the structure **1** mainly by ^{1}H nmr spectrum (Fig. 2 and Table 1) and by the spectroscopic analysis of its trimethylester derivative **1***a*. The ^{1}H nmr spectrum (Fig. 2) displays a typical ABX system, where the AB part consists of H_A— and H_B—C3, each resonating as a quartet centred at 3.08 δ and 2.80 δ respectively (J_{AB} = 15 Hz, J_{AX} = J_{BX} = 7.5 Hz), while the X part consists of H_X—C2, resonating as a triplet centered at 4.70 δ (J_{AX} = J_{BX} = 7.5 Hz). Finally, two doublets centered at 4.22 δ and 4.12 δ (J_{AB} = 12.75 Hz) appear, corresponding to H_A— and H_B—C5, respectively.

When the Gla is left to react with other aldehydes, the products are 5-substituted 4,4-dicarboxyprolines **2**–**7** (Fig. 1), as shown mainly by ^{1}H nmr data (Table 1). The ^{1}H nmr spectra of **2** and **4** (Figs. 3(*a*) and (*b*)), reported as examples, display the same characteristic signals of an ABX system as **1**, but doubled, while the signals related to C5 are modified as compared to **1**. The double signals, which are of similar intensity, are attributed to racemic diastereoisomers formed by the introduction of a new racemic center (C5) in the pyrrolidinic ring (Scheme 1). The reaction rate has been studied as a function of pH. The reaction takes place at pH values ranging from 3 to 6.5; its rate depends on pH and on the solubility of the aldehydes in water. Our data are consistent with the curve reported for the reaction of Gla with pyridoxal phosphate (11); in this case it has been shown that the proline derivative is formed only when the iminium ion is present as intermediate. In the above pH range Gla is present as polyanion as the C-γ proton is able to dissociate at slightly acidic pH values giving rise to the exocyclic planar carbanion **9** (13). In fact, as shown

Can. J. Chem. Downloaded from www.nrcresearchpress.com by 210.87.254.6 on 09/06/12
For personal use only.

Can. J. Chem. Downloaded from www.nrcresearchpress.com by 210.87.254.6 on 09/06/12
For personal use only.

TABLE 1. Proton shifts[a] and ultraviolet absorptions of **1–8**

	H_X—C2	H_A—C3	H_B—C3	H—C5	R—C5	λ_{max} (nm)
1	4.70t $J_{AX} = J_{BX} = 7.50$ Hz	3.08q $J_{AB} = 15$ Hz $J_{AX} = 7.50$ Hz	2.80q $J_{AB} = 15$ Hz $J_{BX} = 7.50$ Hz	4.22d(H_A) $J_{AB} = 12.75$ Hz	4.12d(H_B) $J_{AB} = 12.75$ Hz	End absorption
2	4.70q $J_{AX} = 10.39$ Hz $J_{BX} = 7.35$ Hz	3.12q $J_{AB} = 15$ Hz $J_{AX} = 10.39$ Hz	2.60q $J_{AB} = 15$ Hz $J_{BX} = 7.35$ Hz	4.45q $J_{H,Me} = 6.52$ Hz	1.44 (Me) $J_{Me,H} = 6.52$ Hz	
	4.56q $J_{AX} = 10.39$ Hz $J_{BX} = 7.35$ Hz	2.99q $J_{AB} = 15$ Hz $J_{AX} = 10.39$ Hz	2.83q $J_{AB} = 15$ Hz $J_{BX} = 7.35$ Hz	4.45q $J_{H,Me} = 6.52$ Hz	1.44 (Me) $J_{Me} = 6.52$ Hz	End absorption
3	4.72q $J_{AX} = 10.19$ Hz $J_{BX} = 7.20$ Hz	3.14q $J_{AB} = 15$ Hz $J_{AX} = 10.19$ Hz	2.63q $J_{AB} = 15$ Hz $J_{BX} = 7.20$ Hz	4.50t $J_{H,Et} = 6.52$ Hz	2.03m and 1.10t (Et)	
	4.58q $J_{AX} = 10.19$ Hz $J_{BX} = 7.20$ Hz	3.02q $J_{AB} = 15$ Hz $J_{AX} = 10.19$ Hz	2.85q $J_{AB} = 15$ Hz $J_{BX} = 7.20$ Hz	4.50t $J_{H,Et} = 6.52$ Hz	2.03m and 1.10t (Et)	End absorption
4	4.42t $J_{AX} = J_{BX} = 10$ Hz	2.90 two $J_{AB} = 14$ Hz $J_{AX} = J_{BX} = 10$ Hz	Superimposed	5.37s	7.44m (Ph)	
	4.60q $J_{AX} = 10$ Hz $J_{BX} = 6$ Hz	3.15q $J_{AB} = 14$ Hz $J_{AX} = 10$ Hz	2.71q $J_{AB} = 14$ Hz $J_{BX} = 6$ Hz	5.34s	7.46m (Ph)	254
5	4.38t $J_{AX} = J_{BX} = 9$ Hz	2.87 two $J_{AB} = 15$ Hz $J_{AX} = J_{BX} = 9$ Hz	Superimposed	5.51 (5.45)s	7.65m and 8.27m ($PhNO_2$)	
	4.63q $J_{AX} = 9$ Hz $J_{BX} = 6.75$ Hz	3.17q $J_{AB} = 15.75$ Hz $J_{AX} = 9$ Hz	2.66q $J_{AB} = 15.75$ Hz $J_{BX} = 6.75$ Hz	5.45 (5.51)s	7.65m and 8.27m ($PhNO_2$)	270
6	4.29t $J_{AX} = J_{BX} = 9$ Hz	2.83 two $J_{AB} = 15.75$ Hz $J_{AX} = J_{BX} = 9$ Hz	Superimposed	5.32 (5.25)s	3.78s (OMe) 7d and 7.33t (PhOMe)	
	4.55q $J_{AX} = 9$ Hz $J_{BX} = 6.75$ Hz	3.15q $J_{AB} = 15.75$ Hz $J_{AX} = 9$ Hz	2.60q $J_{AB} = 15.75$ Hz $J_{BX} = 6.75$ Hz	5.25 (5.32)s	3.78s (OMe) 7d and 7.33t (PhOMe)	272
7	3.72q $J_{AX} = 4$ Hz $J_{BX} = 8.5$ Hz	2.34q $J_{AB} = 13.50$ Hz $J_{AX} = 4$ Hz	2.16q $J_{AB} = 13.50$ Hz $J_{BX} = 8.50$ Hz	5.97s	4.70s ($HOCH_2Py$) 2.43s (MePy) 7.59s (Py)	
	4.01q $J_{AX} = 13.50$ Hz $J_{BX} = 5.5$ Hz	3.03t $J_{AB} = 13.50$ Hz $J_{AX} = 13.50$ Hz	2.77q $J_{AB} = 13.50$ Hz $J_{BX} = 5.5$ Hz	5.97s	4.70s ($HOCH_2Py$) 2.43s (MePy) 7.59s (Py)	325
8	4.20t $J_{AX} = J_{BX} = 8.26$ Hz	2.70q $J_{AB} = 14.40$ Hz $J_{AX} = 8.26$ Hz	2.25q $J_{AB} = 14.40$ Hz $J_{BX} = 8.26$ Hz		3.60m(H_2—C_5)	
	4.25t $J_{AX} = J_{BX} = 8.26$ Hz	2.53q $J_{AB} = 14.40$ Hz $J_{AX} = 8.26$ Hz	2.40q $J_{AB} = 14.40$ Hz $J_{BX} = 8.26$ Hz		3.60m(H_2—C_5)	

[a]The double values of δ for **2–8** have been assigned by ^{1}H nmdr and have to be attributed to racemic diastereoisomers of **2–8**.

Can. J. Chem. Downloaded from www.nrcresearchpress.com by 210.87.254.6 on 09/06/12
For personal use only.

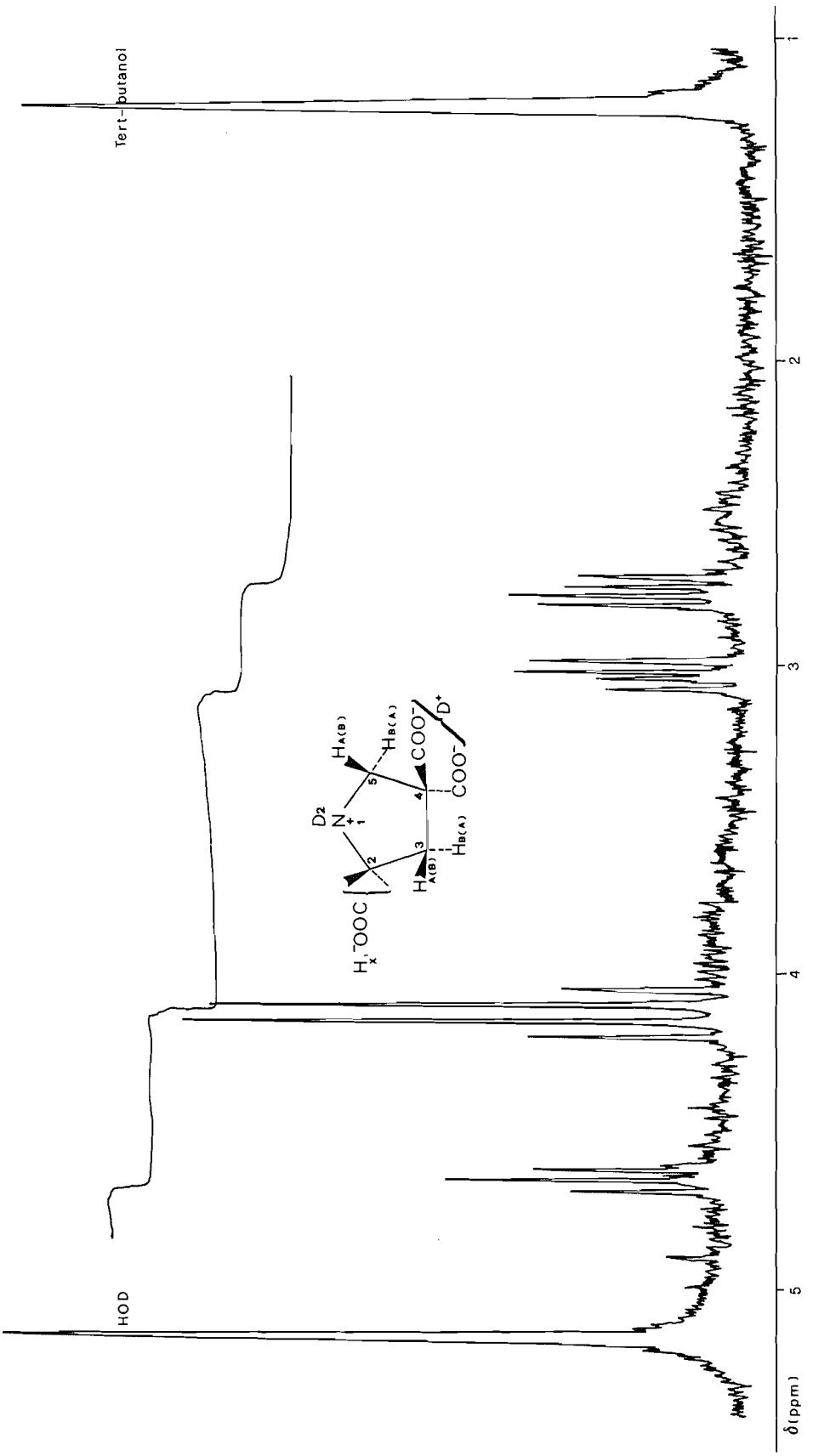

FIG. 2. The ^1H nmr spectrum of **1**.

Can. J. Chem. Downloaded from www.nrcresearchpress.com by 210.87.254.6 on 09/06/12
For personal use only.

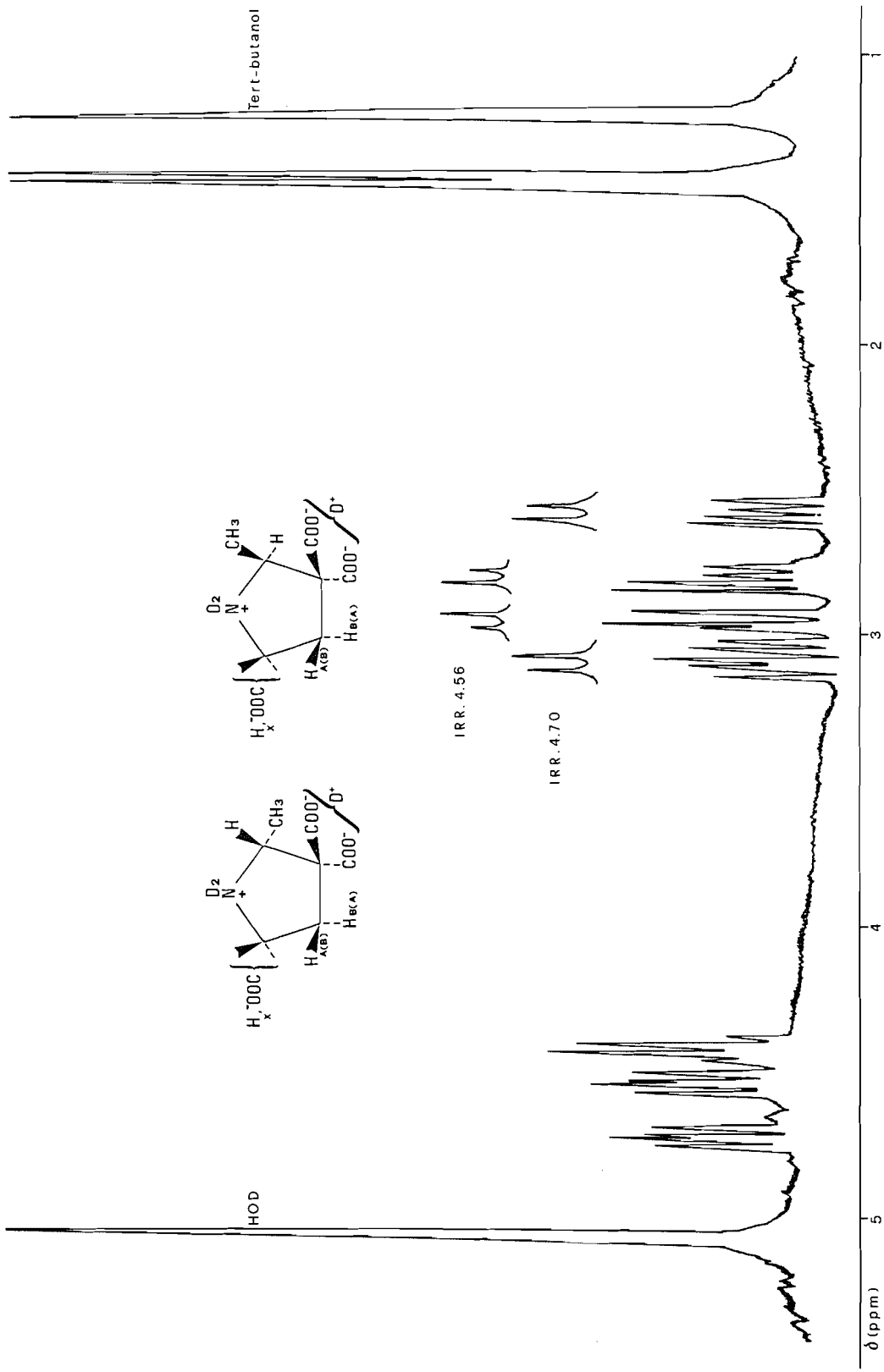

FIG. 3(*a*). The ^{1}H nmr spectrum of **2**.

Can. J. Chem. Downloaded from www.nrcresearchpress.com by 210.87.254.6 on 09/06/12
For personal use only.

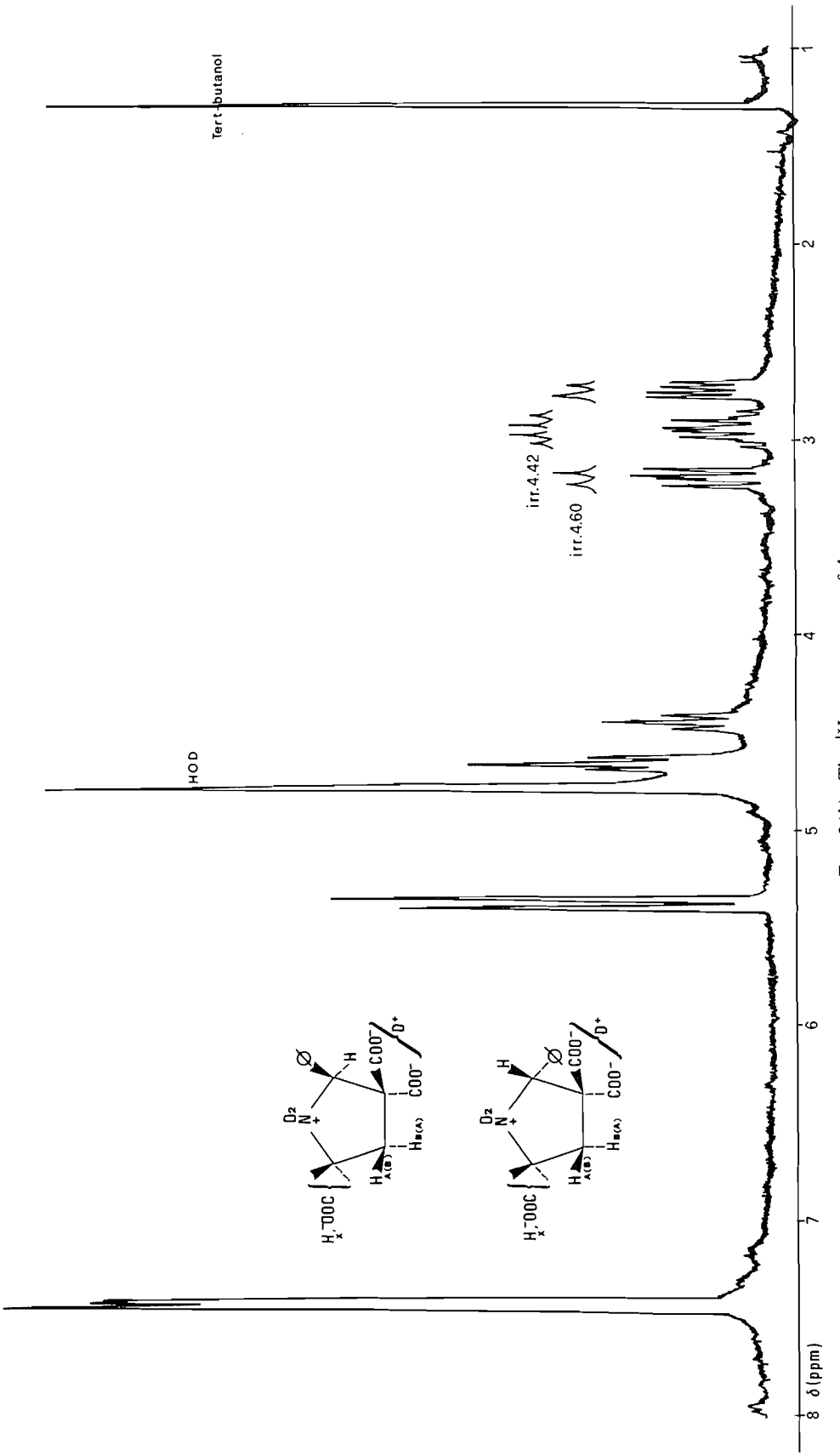

FIG. 3(*b*). The ^{1}H nmr spectrum of **4**.

Can. J. Chem. Downloaded from www.nrcresearchpress.com by 210.87.254.6 on 09/06/12
For personal use only.

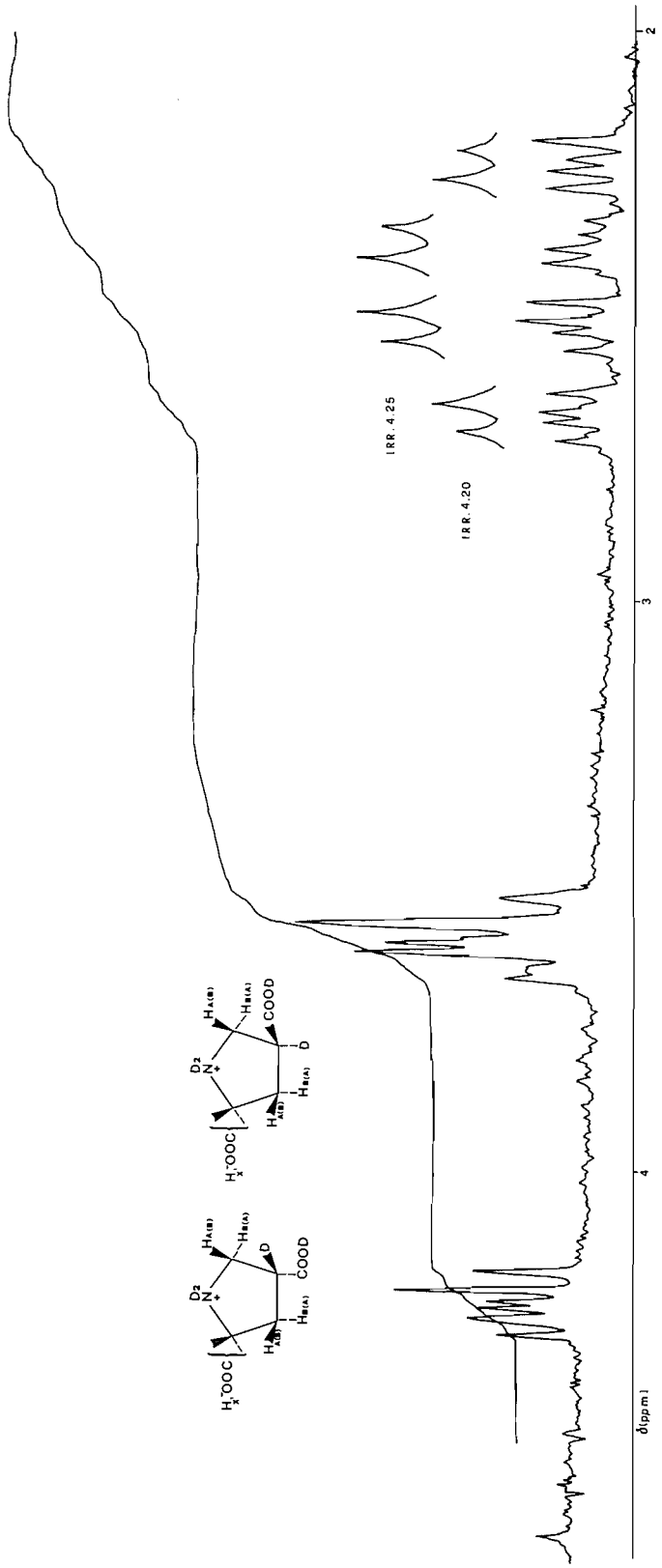

FIG. 4. The ^1H nmr spectrum of **8** in D_2O, using as internal reference *tert*-butyl alcohol (1.23 ppm).

by Price *et al.* (13), the C-γ proton of Gla easily exchanges in the acidic pH range with maximal rate at about pH 3.1 and the nmr spectrum of Gla in D_2O does not show any C-γ proton chemical shift. Therefore, these data allow us to formulate the Mannich mechanism in Scheme 1 for the reaction of Gla with aldehydes and to exclude three alternative possibilities (12): (a) formation of the Mannich base at alkaline pH by a S_N2 mechanism between the methylol derivative and the carbanion; (b) reaction at acidic pH, by a S_E2 mechanism, between the Schiff base and the compound containing the activated hydrogen; (c) formation, from the activated-hydrogen compound and the aldehyde, of an intermediate adduct which, in turn, reacts with the amino group. In fact, the iminium ion in **10** (the protonated Schiff base (11), Scheme 1) gives an intramolecular ion−ion reaction with the C-γ carbanion of amino acid **9** (Scheme 1); at pH > 6.5, the formation of the prolinic ring is not observed, because the C-γ hydrogen does not dissociate; the two carboxyl groups of the side chain of **9** are fully ionized ($pK_1 = 2.03$ and $pK = 4.37$) (13) and the Schiff base in **10** deprotonates. At pH < 3, the reaction is not observed, due to loss of nucleophilicity of the ammonium ion of Gla (Scheme 1). Finally, the attack of C-γ of the adduct **10** on both faces of the iminium ion of **10** occurs statistically to give both possible stereoisomers **11** (Scheme 1). According to the Curtin−Hammett principle (14), this result means that the relative energy levels of the transition states by which the stereoisomers are formed are very similar.

We will now discuss the behaviour of **1**−**7** upon heating in D_2O for 30 min at 100°C. In particular, the ^1H nmr spectrum of the product of heating **1**−**8**, (Fig. 4 and Table 1) shows double signals with the same intensity, shifted upfield, in comparison to the ^1H nmr spectrum of **1**. These signals are attributed to the racemic diastereoisomers of **8** (Fig. 4), produced by the introduction of a new chiral racemic center in C4 of **1**, as a consequence of the statistical replacement of one carboxyl group with deuterium. The appearance of two peaks in the amino acid chromatogram indicates that the two diastereoisomers have different acid properties, due to the possibility of hydrogen bonding between the two *syn* carboxyl groups. A similar behaviour is shown by the **2**−**7** derivatives, whose ^1H nmr spectra are not reported here. The described treatment leads to the formation of many different cyclic analogs of glutamic acid which could possess biological activity (15).

In conclusion, the quantitative and rapid reaction of Gla with aldehydes suggests the possibility of applying this reaction for analytical purposes, by using a coloured or fluorescent aldehyde for quantitative determination of Gla in the serum.

Acknowledgment

The authors are indebted to Professor V. Buonocore for helpful discussion.

1. J. STENFLO and J. W. SUTTIE. Ann. Rev. Biochem. **46**, 157 (1977).
2. J. W. SUTTIE. Crit. Rev. Biochem. **8**, 191 (1980).
3. P. V. HAUSCHKA, J. B. LIAN, and P. M. GALLOP. Proc. Natl. Acad. Sci. U.S.A. **72**, 3925 (1975).
4. J. B. LIAN, E. L. PRIEN JR., M. J. GLIENCHER, and P. M. GALLOP. J. Clin. Invest. **59**, 1151 (1977).
5. J. B. LIAN, W. STURMER, M. J. GLIENCHER, and P. M. GALLOP. Biochem. Biophys. Res. Commun. **73**, 349 (1975).
6. P. FERNLUND. Clin. Chim. Acta, **72**, 147 (1976).
7. D. V. SHAM, J. K. TEWIS, A. E. HARPER, and J. W. SUTTIE. Biochem. Biophys. Acta, **539**, 209 (1978).
8. R. G. LEVY and J. B. LIAN. Clin. Pharmacol. Ther. **25**, 562 (1979).
9. R. G. LEVY, J. B. LIAN, C. GUNDBERG, and P. M. GALLOP. *In* Vitamin K metabolism and vitamin K-dependent proteins. *Edited by* J. W. Suttie. Univ. Park Press, Baltimore. 1980. p. 375.
10. L. PECCI and D. CAVALLINI. Anal. Biochem. **118**, 70 (1981).
11. L. PECCI. S. DUPRÉ, A. ANTONUCCI, and D. CAVALLINI. Experientia, **36**, 910 (1980).
12. TH. F. CUMMINGS and J. R. SHELTON. J. Org. Chem. **25**, 419 (1960).
13. P. A. PRICE, M. K. WILLIAMSON, and D. J. EPSTEIN. J. Biol. Chem. **256**, 1172 (1981).
14. D. Y. CURTIN. Rec. Chem. Prog. **15**, 111 (1954).
15. H. GERSON and A. SCALA. J. Org. Chem. **26**, 2347 (1961).

Can. J. Chem. Downloaded from www.nrcresearchpress.com by 210.87.254.6 on 09/06/12
For personal use only.

Effect of metal ions in organic synthesis. Part XV. Reaction of (arylazo) alkenes and copper(II) chloride in dienophiles or acetone. Synthesis of some *N*-(α-chlorobenzylidene)-*N'*-arylhydrazines

ORAZIO ATTANASI

Cattedra di Chimica Organica della Facoltà di Scienze, Università di Urbino, Piazza Rinascimento, 6, 61029 Urbino, Italia

AND

PAOLO BATTISTONI AND GABRIELE FAVA

Dipartimento di Scienze dei Materiali e della Terra, Università di Ancona, Via della Montagnola, 30, 60100 Ancona, Italia

Received January 7, 1983

ORAZIO ATTANASI, PAOLO BATTISTONI, and GABRIELE FAVA. Can. J. Chem. **61**, 2665 (1983).

The reaction of (phenylazo) stilbene and copper(II) chloride wih some dienophiles produced benzaldehyde and *N*-(α-chlorobenzylidene)-*N'*-phenylhydrazine, instead of the expected (4+2)-cycloaddition products. By reaction of some (arylazo) alkenes and copper(II) chloride in acetone at 0°C, the relative *N*-(α-chlorobenzylidene)-*N'*-arylhydrazine derivatives were successfully obtained in high yields.

ORAZIO ATTANASI, PAOLO BATTISTONI et GABRIELE FAVA. Can. J. Chem. **61**, 2665 (1983).

Le (phénylazo) stilbène et le chlorure de cuivre(II) réagissent avec quelques diénophiles en donnant le benzaldéhyde et le *N*-(α-chlorobenzylidène)*N'*-phénylhydrazine au lieu des produits de cycloaddition (4+2) attendus. On a obtenu, avec des rendements élevés, les dérivés *N*-(α-chlorobenzylidène)*N'*-arylhydrazine apparentés en faisant réagir quelques (arylazo)alcènes et le chlorure de cuivre(II) dans l'acétone, à 0°C.

[Traduit par le journal]

Can. J. Chem. Downloaded from www.nrcresearchpress.com by 210.87.254.42 on 09/06/12
For personal use only.

It is known that the conjugated azo-ene system of aliphatic and aromatic azoalkenes, with or without electron-withdrawing groups on the azo group, frequently have a reactivity analogous to that of other conjugated double bonds. In fact, several of these compounds are known to undergo (2+2)- and (4+2)-type cycloadditions with some carbon–carbon dienophiles and heterodienophiles, providing interesting heterocyclic compounds (1). Furthermore, some azoalkene derivatives are known to give 1,4-additions (Michael-type) with a variety of nucleophiles, producing the respective hydrazone derivatives and simultaneous C-functionalization which may be of great usefulness in organic synthesis (2–6). In particular, some (arylazo) alkenes are demonstrated to undergo 1,4 conjugate addition of activated methylene compounds (3, 6). However, several of the above-mentioned reactions cannot always be so immediately extended and generalized to all azoalkene derivatives known, mainly because of their different degree of stability and reactivity. In fact, some of these compounds may not be sufficiently stable and may be difficult to preserve, while others are fairly stable and easily available products (2–7). Furthermore, a lot of these compounds are in general rather reactive, while others are much less reactive. For these reasons, the activation by metal ions of some azoalkenes in certain 1,4-addition reactions was studied and reported in our previous papers (2, 3). On the basis of these investigations and considering that several (4+2)-type cycloadditions may be promoted by metal ions, and especially by copper ions (8), we undertook the study of the reaction between some (arylazo) alkenes (**1**) and copper(II) chloride dihydrate (**3**) in the presence of some dienophiles (**2**).

Results and discussion

While in the absence of **3** no reaction was observed, in the presence of this inorganic salt (phenylazo) stilbene **1***a* in tetrahydrofuran (THF) and **2** (acrylonitrile, tetracyanoethylene, *N*-phenylmaleimide) react, sometimes completely, providing benzaldehyde (**4**), *N*-(α-chlorobenzylidene)-*N'*-phenylhydrazine (**5***a*), and traces of benzoic acid, instead of the expected (4+2)-cycloaddition products (Scheme 1).

In Table 1 are reported the percentages of unreacted **1***a*, and **4** and **5***a* produced (detected by hplc).

The results (Table 1) do not allow elucidation of the reaction pathway or the role played by copper(II) chloride and dienophiles. For this reason, we examined the reaction of **1***a* with **2** in THF and tetracyanoethylene **6** in particular (Table 2).

This investigation demonstrated that **6** did not behave as a dienophile with **1***a* and suggested **3** to have a reactive rather than a catalytic role, as suggested in our previous papers (2, 3). All the experimental evidence supports the hypothesis that two different and concomitant pathways for reaction of **1***a* may be operative. Route A: probable adduct between **1***a*, **6**, and **3** would promote the 1,4-addition of water to **1***a*, producing the benzoin phenylhydrazone intermediate that provides at first **4** and benzaldehyde phenylhydrazone **7**. This latter compound affords a further molecule of **4** by copper(II) ion-promoted hydrolysis, in accordance with previous investigations (2).

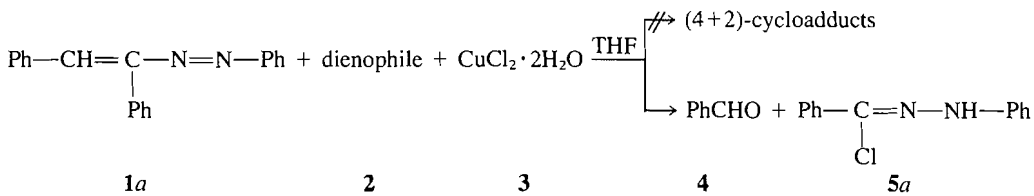

SCHEME 1

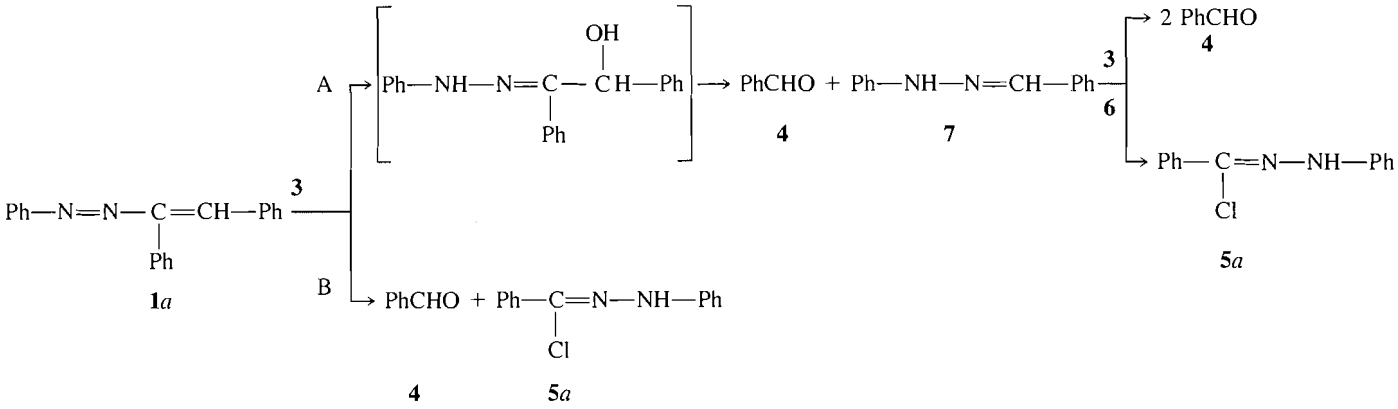

SCHEME 2

TABLE 1. Percentages of unreacted **1***a*, and **4** and **5***a* provided by varying the molecular ratios in the reactions between **1***a*, **2**, and **3** (reaction time 48 h)

2	1a/2/3	1a res %	4 %[a]	5a %
Acrylonitrile	1:1:1	20	90	28
	1:1:4		120	32
Tetracyanoethylene	1:1:1	3	35	27
	1:1:4		130	30
N-phenylmaleimide	1:1:1	40	30	14
	1:1:4	35	56	15

[a]Yields of **4** provided were calculated assuming that one molecule arises from each molecule of **1***a*.

TABLE 2. Percentages of unreacted **1***a*, and **4**, **5***a*, and benzaldehyde phenylhydrazone produced by varying the molecular ratios in the reactions between **1***a*, **6**, and **3** (reaction time 21 h)

1a/6/3	1a res %	4 %[a]	5a %	7 %
1:1:0.1	90	5		6
1:4:0.1	90	5		6
1:1:1	3	35	27	4
1:1:2		50	26	
1:0.1:1		35	28	3
1:0.1:2		50	31	
1:0.1:3		100	29	
1:0.1:4		130	30	

[a]Yields of **4** produced were calculated assuming that one molecule arises from each molecule of **1***a*.

Route B: the same adduct would also activate the chlorination of **1***a*, producing **4** and **5***a*. This hypothesis is supported by some previous findings on this matter (9). On the other hand, **7**, **3**, and excess **6** provide only **4**, but not **5***a* (Scheme 2), in spite of its good stability in the reaction medium.

This compound **5***a* represents a very important intermediate in the chemistry of the 1,3-dipolar cycloadditions, where its basic treatment (generally triethylamine) easily generates, by 1,3-elimination of hydrogen chloride, diphenylnitrilimine ($Ph—\overset{+}{C}=N—\bar{N}—Ph \leftrightarrow Ph—C\equiv\overset{+}{N}—\bar{N}—Ph$). Furthermore, if produced *in situ*, it readily reacts with several 1,3-dipolarophile reagents, providing very interesting heterocyclic compounds (10, 11). Our attention was then focused on finding the best reaction conditions for synthesis of **5***a*. Considering that this compound arises from chlorination of **1***a*, and since under several reaction conditions no substantial increase of **5***a* to more than 30% yields was observed, a tentative experiment using acetone instead of dienophile was performed. In fact, it is known that acetone, as well as several other ketones, promotes the chlorine transfer from copper(II) chloride by chloro-acetone intermediate formation, coming from chlorocopper(II) – acetone precursor complexes (9, 12).

By a detailed experiment it was found that formation of **5***a*, due to the chlorination of **1***a* by **3**, occurs faster and with highest yields in pure acetone and when the molecular ratio between **1***a* and **3** is 1:2, respectively. Under the same reaction conditions **7** gave **4** as the main reaction product, while **5***a* was detected only in traces. This observation is in accordance with the reaction pathway shown in Scheme 2.

In view of the synthetic usefulness of *N*-(α-chlorobenzylidene)-*N'*- arylhydrazine derivatives, the reaction discussed above was successfully extended to [(*p*-chlorophenyl)azo] stilbene **1***b* and (*p*-tolylazo)stilbene **1***c* (Scheme 3). According to our preliminary paper (11), treatment of these compounds with **3** in acetone at 0°C readily affords **5***a–c* in high yields (90–95% by hplc, 80–85% after column chromatography and crystallization).

These derivatives appear not to be easily synthesizable by other known methods (10, 11, 13). Furthermore, **5***a–c* prepared with our method can be utilized without complicated procedures for their isolation and purification. In fact, the reaction mixture, after extraction with benzene and aqueous hydrogen chloride, affords **5***a–c* in good purity. These latter products, without further purification, were successfully utilized by us in some typical 1,3-dipolar cycloadditions. This possibility is also noteworthy in consideration of the fact that these compounds are seriously irritant and the occasional contact with contaminated articles causes severe dermatitis.

For these reasons, the procedure reported here represents a mild, simple, and convenient method for the synthesis and use in organic synthesis of the mentioned *N*-(α-chlorobenzylidene)-*N'*-arylhydrazine derivatives.

In order to make the present method even more convenient, the procedure previously reported (11) for the synthesis in high yields of (phenylazo) stilbene **1***a* was successfully applied to the synthesis of the other unknown (arylazo) alkene derivatives **1***b–c* considered in this work (see Experimental section).

Experimental

(Arylazo) alkenes **1**a–c

These compounds were synthesized according to the procedure previously reported in detail for the synthesis of (phenylazo) stilbene,

Can. J. Chem. Downloaded from www.nrcresearchpress.com by 210.87.254.42 on 09/06/12
For personal use only.

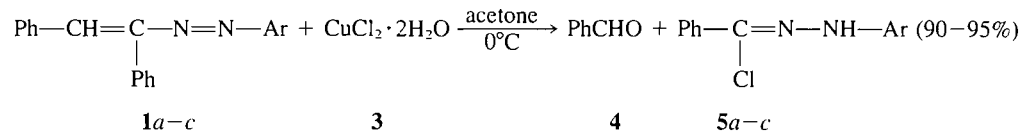

1*a*–*c* 3 4 5*a*–*c*

a Ar = C_6H_5
b Ar = *p*-ClC_6H_4
c Ar = *p*-$CH_3C_6H_4$

SCHEME 3

and were used as mixtures of two isomers (*EE* and *ZE*) (11). The analytical data of compound **1***a* were described in detail by Bonini *et al.* (1) and Brodka and Simon (5).

*[(*p*-Chlorophenyl)azo] stilbene* **1**b: yield 83%; red crystals from n-pentane (or petroleum ether 40–60°C); mp 100–104°C with decomposition (uncorrected); ir (Nujol) and ^{1}H nmr ($CDCl_3$, Me_4Si) spectra show no particular features. *Anal.* calcd. for $C_{20}H_{15}N_2Cl$: C 75.35, H 4.74, N 8.79; found: C 75.71, H 4.69, N 8.85.

*(*p*-Tolylazo) stilbene* **1**c: yield 78%; red crystals from n-petane (or petroleum ether 40–60°C); mp 112–116°C with decomposition (uncorrected); ir (Nujol) spectrum shows no particular features; ^{1}H nmr ($CDCl_3$, Me_4Si) δ: 2.25 (3H, s), 7–8 (15H, m). *Anal.* calcd. for $C_{21}H_{18}N_2$: C 84.53, H 6.08, N 9.39; found: C 85.02, H 5.99, N 9.43.

Reaction of **1**a *and* **3** *in* **2**. *General procedure*

A solution of an appropriate amount of **2** (see Tables 1 and 2) in THF (20 mL) was added dropwise at room temperature to a stirred solution of **1***a* (0.70 mmol) and an appropriate amount of **3** (see Tables 1 and 2) in THF (20 mL). The mixture was stirred magnetically at room temperature during 21 or 48 h. THF was then evaporated under reduced pressure, the residue was dissolved in ether and washed several times with water. The organic layer was dried with anhydrous sodium sulphate and concentrated under reduced pressure. The reaction mixtures were examined by hplc. Alternatively, the reaction components were isolated by chromatography on a silica gel column (at first elution with cyclohexane and then with cyclohexane–benzene mixtures, gradually increasing the amount of benzene to a 60:40 (v/v) ratio).

Reaction of (arylazo) alkenes **1**a–c *and* **3** *in acetone. General procedure for the synthesis of* **5**a–c *derivatives*

A solution of (arylazo) alkenes **1***a*–*c* (0.07 mmol) in acetone (50 mL) was added dropwise to a stirred solution of **3** (1.4 mmol) in acetone (50 mL), cooled in an ice bath. The mixture was stirred magnetically at 0°C during 1 h until the reaction was completed (monitored by silica gel tlc). Acetone was then evaporated under reduced pressure, the residue was dissolved in benzene and washed several times with 5% aqueous hydrogen chloride and then with water. The organic layer was dried with anhydrous magnesium sulphate and concentrated under reduced pressure. The crude **5***a*–*c* derivatives obtained in good purity can be further purified by chromatography on a silica gel column (at first elution with cyclohexane and then with cyclohexane–benzene mixtures, gradually increasing the amount of benzene to a 60:40 (v/v) ratio). Alternatively, the crude products may be successfully used for 1,3-cycloaddition reactions, without further purification.

N-(α-Chlorobenzylidene)-N′-phenylhydrazine **5**a: yield 95% by hplc, yield 85% of isolated product by chromatography on a silica gel column; white crystals from acetonitrile–acetone; mp 129–131°C (uncorrected) (lit. (11) mp 129.5–130.5 or 128–131°C); ir (Nujol): 3305 (NH), 1600 (aromatic) cm^{-1}; ^{1}H nmr (CCl_4, Me_4Si) spectrum shows no particular features. *Anal.* calcd. for $C_{13}H_{11}N_2Cl$: C 67.68, H 4.81, N 12.14; found: C 67.79, H 4.85, N 12.09.

N-(α-Chlorobenzylidene)-N′-p-chlorophenylhydrazine **5**b: yield 92% by hplc, yield 83% of isolated product by chromatography on a silica gel column; white crystals from acetonitrile–acetone; mp 105–107°C (uncorrected); ir (Nujol): 3320 (NH), 1600 (aromatic) cm^{-1}; ^{1}H nmr (CCl_4, Me_4Si) spectrum shows no particular features. *Anal.* calcd. for $C_{13}H_{10}N_2Cl_2$: C 58.89, H 3.80, N 10.57; found: C 58.99, H 3.76, N 10.62.

N-(α-Chlorobenzylidene)-N′-p-tolylhydrazine **5**c: yield 90% by hplc, yield 80% of isolated product by chromatography on a silica gel column; white crystals from acetonitrile–acetone; mp 118–121°C (uncorrected); ir (Nujol): 3320 (NH), 1610 (aromatic) cm^{-1}; ^{1}H nmr (CCl_4, Me_4Si) δ: 2.30 (3H, s), 7–8 (10H, m). *Anal.* calcd. for $C_{14}H_{13}N_2Cl$: C 68.71, H 5.35, N 11.45; found: C 68.85, H 5.29, N 11.52.

1. W. BARBIERI, L. BERNARDI, P. MASI, L. CAGLIOTI, and G. ROSINI. Tetrahedron Lett. 1343 (1970); L. CAGLIOTI, E. FORESTI, and L. RIVA DI SANSEVERINO. Tetrahedron Lett. 1347 (1970); L. CAGLIOTI, G. ROSINI, P. TUNDO, and A. VIGEVANI. Tetradedron Lett. 2349 (1970); W. BARBIERI, L. BERNARDI, P. MASI, A. VIGEVANI, L. CAGLIOTI, and G. ROSINI. Tetrahedron, **27**, 5505 (1971); K. L. ZELENIN, V. A. NIKITIN, N. M. ANODINA, and Z. M. MATVEEDA. Zh. Org. Khim. **8**, 1438 (1972); Chem. Abstr. **77**, 139384 (1972); P. DE MARIA, F. GASPARRINI, L. CAGLIOTI, and M. GHEDINI. J. Chem. Soc. Perkin Trans. 2, 1922 (1973); S. SOMMER. Tetrahedron Lett. 117 (1977); Angew. Chem. Int. Ed. Engl. **16**, 58 (1977); Synthesis, 305 (1977); Angew. Chem. Int. Ed. Engl. **18**, 695 (1979); **18**, 696 (1979); B. F. BONINI, G. MACCAGNI, G. MAZZANTI, G. ROSINI, and E. FORESTI. J. Chem. Soc. Perkin Trans. 1, 2322 (1981); and references cited therein.
2. O. ATTANASI. Studi Urbinati Fac. Farm. **17**, 123 (1975); O. ATTANASI, P. BATTISTONI, and G. FAVA. Synth. Commun. **9**, 465 (1979); O. ATTANASI. Studi Urbinati Fac. Farm. **22**, 135 (1980); O. ATTANASI, P. BATTISTONI, and G. FAVA. J. Org. Chem. **46**, 447 (1981).
3. O. ATTANASI, P. BONIFAZI, E. FORESTI, and G. PRADELLA. J. Org. Chem. **47**, 684 (1982); O. ATTANASI, P. BONIFAZI, and F. BUIANI. J. Heterocycl. Chem. In press; O. ATTANASI and S. SANTEUSANIO. Synthesis. In press.
4. S. BOZZINI, S. GRATTON, A. RISALITI, A. STENER, M. CALLIGARIS, and G. NARDIN. J. Chem. Soc. Perkin Trans. 1, 1377 (1977); S. BOZZINI, S. GRATTON, G. PELLIZER, A. RISALITI, and A. STENER. J. Chem. Soc. Perkin Trans. 1, 869 (1979); S. BOZZINI, B. COVA, S. GRATTON, A. LISINI, and A. RISALITI. J. Chem. Soc. Perkin Trans. 1, 240 (1980); S. BOZZINI, S. GRATTON, A. LISINI, G. PELLIZER, and A. RISALITI. Tetrahedron, **38**, 1459 (1982); and references cited therein.
5. L. CAGLIOTI, P. GRASSELLI, F. MORLACCHI, and G. ROSINI. Chem. Ind. (London), 25 (1968); L. CAGLIOTI, A. DONDONI, and G. ROSINI. Chem. Ind. (Milano), **50**, 122 (1968); A. DONDONI, G. ROSINI, G. MOSSA, and L. CAGLIOTI. J. Chem. Soc. (B), 1404 (1968); L. CAGLIOTI and G. ROSINI. Chem. Ind. (London), 1093 (1969); S. BRODKA and H. SIMON. Chem. Ber. **102**, 3647 (1969); P. M. COLLINS, D. GARDINER, S. KUMAR, and W. G. OVEREND. J. Chem. Soc. Chem. Commun. 1433 (1970); C. E. SACKS and P. L. FUCHS. J. Am. Chem. Soc. **97**, 7372 (1975); S. CACCHI, F. LA TORRE, and D. MISITI. Chem. Ind. (Milano), **60**, 715 (1978); G. S. HAJIVARNAVA, W. G. OVEREND, and N. R. WILLIAMS. J. Chem. Soc. Perkin Trans 1, 205 (1982); J. G. SCHANTL, P. KARPELLUS, and M. PREAN. Tetrahedron, **38**,

Can. J. Chem. Downloaded from www.nrcresearchpress.com by 210.87.254.42 on 09/06/12
For personal use only.

2643 (1982); and references cited therein.
6. L. BERNARDI, P. MASI, and G. ROSINI. Ann. Chim. (Roma), **63**, 601 (1973); S. BRODKA and H. SIMON. Justus Liebigs Ann. Chem. **745**, 193 (1971); S. CACCHI, D. MISITI, and M. FELICI. Synthesis, 147 (1980).
7. L. CAGLIOTI and A. G. GIUMANINI. Bull. Chem. Soc. Jpn. **44**, 1048 (1971); G. ROSINI and R. RANZA. J. Org. Chem. **36**, 1915 (1971); G. ROSINI and S. CACCHI. J. Org. Chem. **37**, 1856 (1972); L. CAGLIOTI, F. GASPARRINI, G. PAOLUCCI, G. ROSINI, and P. MASI. J. Org. Chem. **38**, 920 (1973); G. ROSINI and G. BACCOLINI. J. Org. Chem. **39**, 826 (1974); and references cited therein.
8. E. J. COREY, N. M. WEINSHENKER, T. K. SCHAAF, and W. HUBER. J. Am. Chem. Soc. **91**, 5675 (1969); S. MIYATA. Japan Kokai 73 39, 469. Chem. Abstr. **79**, 91684w (1973); A. I. MOGILYANSKII, O. N. TEMKIN, R. M. FLID, L. M. KOGAN, I. E. BONDARENKO, and L. S. KULESHOV. Uch. Zap. Mosk. Inst. Tonkoi Khim. Tekhnol. **1**, 10 (1970); Chem. Abstr. **77**, 74448p (1972); J. Th. M. Evers and A. MACKOR. Tetradhedron Lett. 2317 (1978); K. NAGAI, S. MACHIDA, and T. MONAKA. J. Polym. Sci. Polym. Chem. Ed. **19**, 773 (1981); J. T. FITZPATRICK and E. MARCUS. U. S. Patent 3,072,706; Chem. Abstr. **58**, 13816f (1963); R. ROBINSON and G. I. FRAY. U.S. Patent 3,067,244; Chem. Abstr. **58**, 13816h (1963).
9. F. MINISCI and U. PALLINI. Gazz. Chim. Ital. **90**, 1318 (1960); F. MINISCI, R. GALLI, and M. CECERE. Gazz. Chim. Ital. **95**, 751 (1965); M. BOLTE and J. LEMARIE. Nouv. J. Chem. **4**, 461 (1980).
10. R. HUISGEN. Angew. Chem. Int. Ed. Engl. **2**, 565 (1963); **2**, 633 (1963); J. Org. Chem. **41**, 403 (1976); H. ULRICH. The chemistry of imidoil halides. Plenum Press, New York. 1968; and references cited therein.
11. O. ATTANASI, P. BATTISTONI, and G. FAVA. Org. Prep. Proced. Int. **15**, 1 (1983).
12. E. HORVATH, J. SYKORA, E. HULINOVA, and J. GAZO. 7th Conference Coordination Chemistry. September 11–14, 1978. Bratislava.
13. R. HUISGEN, J. SAUER, and M. SEIDEL. Chem. Ber. **94**, 2503 (1961); R. HUISGEN, M. SEIDEL, G. WALLBILLICH, and H. KNUPFER. Tetrahedron, **17**, 3 (1962); R. HUISGEN, R. GRASHEY, H. KNUPFER, R. KUNZ, and M. SEIDEL. Chem. Ber. **97**, 1085 (1964); R. HUISGEN, H. KNUPFER, R. SUSTMANN, G. WALLBILLICH, and V. WEBERNDORFER. Chem. Ber. **100**, 1580 (1967); P. WOLKOFF. Can. J. Chem. **53**, 1333 (1975).

Can. J. Chem. Downloaded from www.nrcresearchpress.com by 210.87.254.42 on 09/06/12
For personal use only.

High resolution HeI and HeII photoelectron spectra of the thallium halides: valence bands and Tl 5*d* ligand field splittings

G. M. BANCROFT[1] AND D. J. BRISTOW[2]

Department of Chemistry, University of Western Ontario, London, Ont., Canada N6A 5B7

Received January 17, 1983

G. M. BANCROFT and D. J. BRISTOW. Can. J. Chem. **61**, 2669 (1983).

We report high resolution photoelectron spectra of both the valence bands and Tl 5*d* levels of the thallium halides (TlX; X = Cl, Br, I) in the gas phase. A transition state Xα-SW calculation on TlCl agrees with previous valence band assignments, although our calculated orbital characters are quite different from those reported previously. The calculated spin–orbit splitting of the $2^2\Pi$ state in TlI is in good agreement with the observed value of 0.83 eV. Line width variations are rationalized considering the increase in covalency from TlCl to TlI, and variations in the slope of the excited state potential curve.

Ligand field splitting of the Tl 5*d* level has been resolved in all three compounds. The observed values of the non-cubic part of the crystal field (C_2^0) are: −0.0210 eV (TlCl), −0.0233 eV (TlBr), and −0.0258 eV (TlI). The above trend is due to the increasing covalency from TlCl to TlI, with a concomitant increase in the Tl 6*p* orbital population. Calculated C_2^0 values are in good agreement with those observed. The configuration interaction structure in the Tl 5*d* region is explained qualitatively using Xα-SW calculations of two-hole valence band energies in TlCl.

G. M. BANCROFT et D. J. BRISTOW. Can. J. Chem. **61**, 2669 (1983).

Nous rapportons les spectres photoélectroniques à haute résolution des bandes de valence ainsi que des niveaux de 5*d* du Tl des halogènures de thallium (TlX; X = Cl, Br, I) en phase gazeuse. Un calcul de l'état de transition Xα-SW du TlCl s'accorde avec les attributions antérieures des bandes de valence, quoique notre calcul des caractères d'orbitale soit tout à fait différent de ceux rapportés antérieurement. Le découplage spin–orbite calculé de l'état $2^2\Pi$ du TlI est en accord avec la valeur de 0,83 eV observée. On rationalise les variations de la largeur des raies en considérant l'augmentation de la covalence à partir du TlCl au TlI et les variations de la pente de la courbe d'énergie potentielle de l'état excité.

On a résolu le découplage de champ du ligand du niveau 5*d* du Tl dans les trois composés. Les valeurs observées pour la partie non cubique du champ du cristal (C_2^0) sont de: −0,0210 eV (TlCl), −0,0233 eV (TlBr) et de −0,0258 eV (TlI). Cette tendance est due à l'augmentation de la covalence de TlCl à TlI avec une augmentation concomitante de la population de l'orbitale 6*p* du Tl. Les valeurs de C_2^0 calculées sont en bon accord avec celles observées. On explique de façon qualitative la structure de l'interaction de configuration dans la région 5*d* du Tl en utilisant les calculs Xα-SW des énergies de la bande de valence à deux trous du TlCl.

[Traduit par le journal]

Introduction

During the last ten years, there has been a number of uv photoelectron studies on the thallium halides in the gas phase (1–5). In fact, the pioneering work with high temperature vapours involved these compounds (1). The focus of these previous studies has centred both on the assignment of the valence bonds (1, 2, 4), and the interpretation of the Tl 5*d* spectra (2–5). Like the Zn 3*d* and Cd 4*d* spectra of the Zn and Cd dihalides (ref. 6 and references therein), the Tl 5*d* spectra exhibit final state effects such as ligand field splitting and configuration interaction. However, in the previous studies, the resolution of the Tl 5*d* spectra was not sufficient to resolve and characterize the ligand field splittings and configuration interaction. As a result, derived ligand field parameters in two studies (3, 4) were not in good agreement; and in one study (4), the unexpected increase in ligand field splitting from TlI to TlCl and TlBr was rationalized using the spectrochemical series (7).

In this paper, we report high resolution HeI valence band and HeII Tl 5*d* photoelectron spectra of the thallium halides. With the aid of our higher resolution and an Xα-SW calculation on TlCl, we are able to characterize further the valence band spectra. Of greater interest, we have been able to resolve more fully the ligand field splitting and configuration interaction peaks on the Tl 5*d* levels. Our calculations of the major crystal field parameter C_2^0 are in surprisingly good agreement with the values obtained from the spectra.

Experimental

The experimental details for our high temperature spectra have been reported in two previous papers (8, 9). All spectra were obtained on our McPherson ESCA-36 photoelectron spectrometer using a hollow cathode He lamp (10). The spectra have been computer fitted to Lorentzian–Gaussian line shapes (11). The compounds were heated up to within about 30°C of their literature melting points (≥400°C) to obtain sufficient vapour pressure.

Results and discussion

(a) Valence bands

The HeI spectra of the valence bands of the thallium halides are presented in Fig. 1. The general features are similar to those published previously (1–4). However, higher resolution in the present work has enabled further analysis. Our assignments binding energies, relative areas, and half widths are given in Table 1.

For the assignment of these spectra, we follow the original assignment (1). The results of extended Hückel calculations were used to determine the orbital character associated with each band (1). Taking TlCl as an example, the highest occupied orbital was found to be predominantly Tl 6*s* (62%) in character. This fact was used to explain the sharpness of the low binding energy peak (A, Fig. 1) in the photoelectron spectrum. It was rationalized that removal of an electron from a predominantly metal centre should increase the Coulombic attraction only slightly between the metal and halogen (12). Conversely, the broadness of the second band (B) results from a significant disruption of the ionic bond via removal of an electron from a lone pair *p* orbital centred on the negative halogen. The 3σ orbital (C) was found to be about 65% Cl $3p_\sigma$ and 20% Tl 6*s* (1).

[1]To whom all correspondence should be addressed.

[2]Present address: Research Department, Imperial Oil Limited, Sarnia, Ont., Canada N7T 7M1.

Can. J. Chem. Downloaded from www.nrcresearchpress.com by 210.87.254.42 on 09/06/12
For personal use only.

Can. J. Chem. Downloaded from www.nrcresearchpress.com by 210.87.254.42 on 09/06/12
For personal use only.

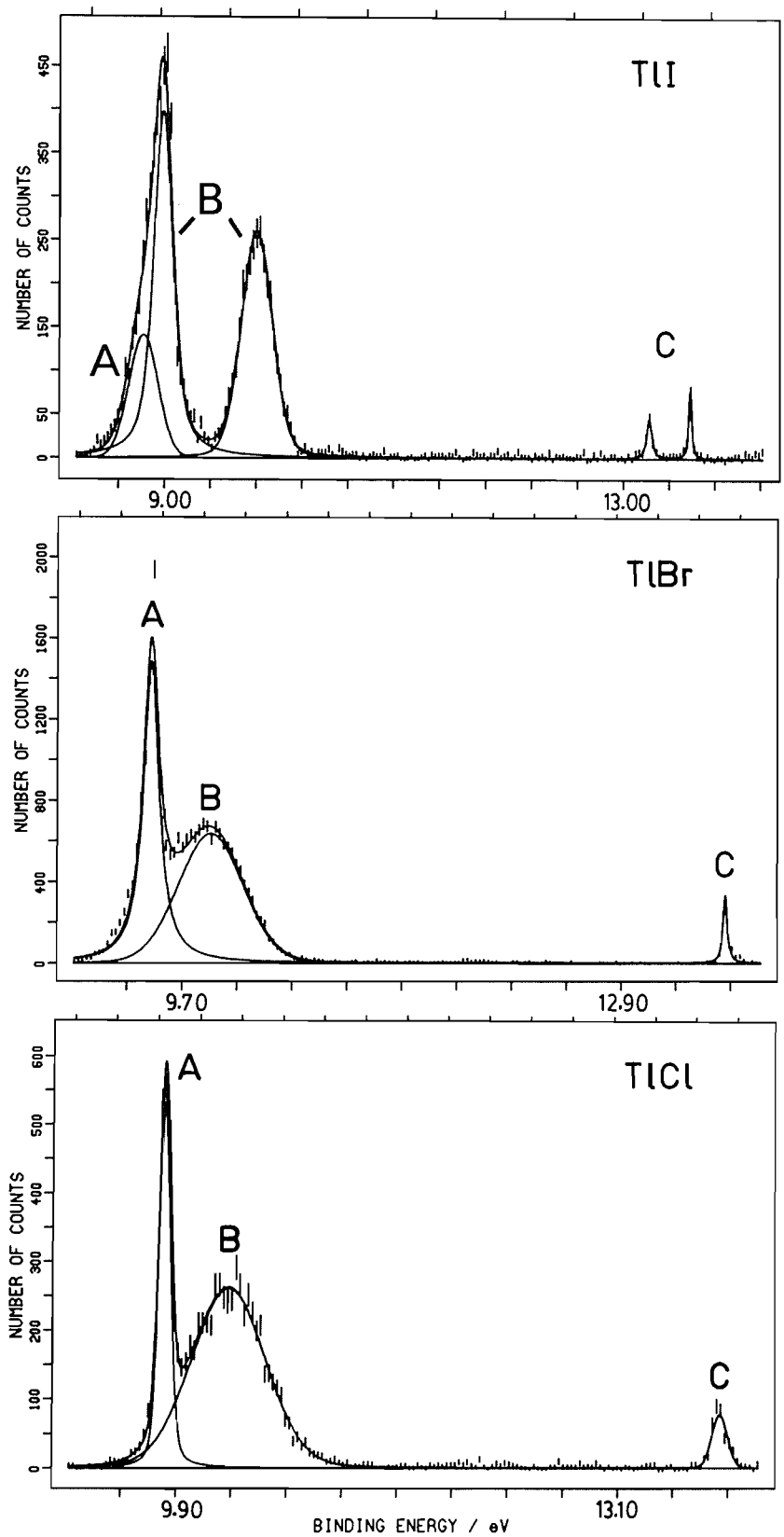

FIG. 1. HeI valence band spectra of the Tl halides.

We have undertaken a non-relativistic Xα-SW calculation on TlCl and the Xα parameters appear in Table 4. The calculated binding energies based on the HOMO transition state and the percentage orbital character for the ground state are presented in Table 5. By use of Stater's transition state concept (13), quantitative agreement has been obtained between observed and calculated optical transition energies in many molecules. Schwarz's α_{HF} values (14) were used for the atomic exchange parameters. For the extramolecular and intersphere regions, a weighted average (weighting factors proportional to the num-

TABLE 1. Valence and Tl 5*d* binding energies for TlCl

Peak	State	Binding energy (eV) Exp.	Theor.[a]	Relative area	FWHM (eV)
A	$4^2\Sigma_{1/2}$	9.885	8.64	0.239	0.099
B	$2^2\Pi_{3/2,1/2}$	10.346	10.54	0.699	0.629
C	$3^2\Sigma_{1/2}$	13.906	11.86	0.0625	0.134
D	CI1	20.257	—	—	0.101
E	CI2	20.663	—	—	0.320
$5d_{5/2}$	$2^2\Sigma_{1/2}$	20.986	20.999	—	0.112
F	CI3	21.102	—	—	0.0819
$5d_{5/2}$	$1^2\Pi_{3/2}$	21.199	21.212	—	0.0698
	$1^2\Delta_{5/2}$	21.283	21.262	—	0.0852
G	CI4	21.499	—	—	0.174
$5d_{3/2}$	$1^2\Pi_{1/2}$	23.286	23.363	—	0.150
	$1^2\Delta_{3/2}$	23.505	23.530	—	0.103

[a]The values for peaks A, B, and C are from the Xα-SW calculation; while the other values are calculated using the derived C_2^0 and C_4^0 values (Table 6) and the crystal field Hamiltonian, refs. 17–19.

ber of valence electrons in Cl(7) and Tl(3)) of the values in the atomic region was used. Norman's nonempirical procedure (15) was used to obtain the ratio of sphere radii. The intersphere charge, which in the valence region comprises ~20% of the total, has not been assigned specific character. Partitioning of the intersphere charges into atomic spheres is proportional to the percentage atomic character (16).

It is immediately evident that the Xα-SW calculation implies considerably more mixing between the Tl 6*s* and Cl 3*p* orbitals in both the 4σ and 3σ molecular levels than was the case with the extended Hückel calculation. These results imply that the first photoelectron peak (A) results from ionization of a slightly antibonding Tl—Cl level rather than a predominantly Tl 6*s* orbital. The 3σ orbital represents the bonding part of this combination while the 2π orbital is essentially 100% lone pair Cl 3*p* in character. Removal of an electron from a slightly antibonding (4σ) level should not disrupt the bond greatly. Hence the experimentally observed narrow peak (A) is consistent with the present calculation.

This conclusion is substantiated by a recent DV-Xα calculation on TlCl (17). The DV-Xα calculation indicates 25% and 67% Tl 6*s* participation in the 4σ and 3σ orbitals, respectively. This division of bond character is essentially the reverse of the extended Hückel calculations.

As with the Zn and Cd dibromide and diodide spectra (9), we expect to be able to resolve the spin–orbit splitting in the 2π state for TlBr and TlI. In the TlBr spectrum, peak B is too broad to resolve the expected spin–orbit splitting of about 0.3 eV (9). However, in the TlI spectrum, a distinct asymmetry is seen on the low binding energy band, and the band is readily resolved into two peaks (Fig. 1). Previous spectra (1, 3, 4) were not of sufficient resolution to allow determination of accurate binding energies for these two peaks. We assign the low binding energy peak (peak A) to the $4\Sigma_{1/2}$ state. This leaves us with a $2^2\Pi$ spin–orbit splitting of 0.82 eV, considerably larger than the expected two thirds of the atomic splitting (9, 18). This increase in spin–orbit splitting results from mixing and repulsion between the $2^2\Pi_{1/2}$ and $4^2\Sigma_{1/2}$ states. Using the method (18) outlined in our previous paper (9), the predicted splitting is 0.83 eV, in good agreement with that observed. The $2^2\Pi_{1/2}$ peak is broader and less intense than the $2^2\Pi_{3/2}$ peak, presumably because of mixing between the $2^2\Pi_{1/2}$ and $4^2\Sigma_{1/2}$ states.

The variation in peak widths from TlCl to TlI is also of some interest. For example, for peaks A and B, the linewidths increase and decrease respectively on going from TlCl to TlI. Both trends can be rationalized by the increasing importance of covalency from TlCl to TlI as suggested by Berkowitz for peak A (1). In the more covalent TlI, peaks B are much narrower than in TlCl and TlBr, as expected for ionization from a nonbonding halogen orbital in a covalent molecule.

The width of the $3^2\Sigma_{1/2}$ peak(s) decreases markedly in going from TlCl to TlBr and TlI. Indeed, these peak widths for TlBr and TlI are rather close to our instrumental resolution of ≤30 meV, and appear as very sharp spikes. These narrow widths for the TlI doublet make it possible to comment further on the origin of this splitting. It was originally proposed (1) that the splitting arose from Franck–Condon transitions from higher vibrational levels of the ground state. In a subsequent publication on the indium halides (12) it was pointed out that the splitting could be due to a double minimum in the hole state curve in the Franck–Condon region. It has been shown that the width of a photoelectron peak can be related to the slope of the hole state potential energy (19). This correlation arises from the fact that a steep slope in the Franck–Condon region provides overlap with a large number of vibrational states, leading to a broad peak (e.g. peaks B in our spectra). The large reduction in half width of the $3^2\Sigma_{1/2}$ peak on going from TlCl to TlBr and TlI implies a corresponding reduction in the slope of the hole state potential energy curve. For TlI, the double minimum explanation is reasonable, because such a phenomenon is more easily envisioned in a potential region exhibiting little slope. Also, as was pointed out previously (1), the ground vibrational frequency in TlBr (192 cm^{-1}) is not a great deal larger than that in TlI (~152 cm^{-1}), and a bimodal ground state distribution should split the $3^2\Sigma_{1/2}$ peak in TlBr as well as in TlI.

*(b) Ligand field splitting on the Tl 5*d *orbitals*

Our primary interest in this work was the investigation of the ligand field splitting of the Tl 5*d* level. The HeII spectra of these levels are presented in Figs. 2 to 4. A broader scan of the TlCl $5d_{5/2}$ region has been included (Fig. 4) because of additional structure at the low binding energy end of the spectrum. Due to the relatively large spin–orbit coupling value in this orbital we collected the $5d_{5/2}$ and $5d_{3/2}$ regions in separate spectra. This was done in order to maintain high resolution during the short scans of each region. Individual scans were later added together on a computer with a provision for shifting spectra to eliminate differential charging effects. Since the two regions were of necessity collected for different periods of time and on different days it is not possible to obtain $^2D_{5/2}/^2D_{3/2}$ ratios.

The binding energies, relative areas, and widths are summarized in Tables 1–3. Many of the widths are ~100 meV — probably very close to the lifetime values for the Tl 5*d* level. As a result, we have been able to resolve a number of additional peaks in these spectra from those reported previously, and in all three cases, we have resolved the five Tl 5*d* peaks due to ligand field splitting. The peaks due to configuration interaction are labelled with letters (D, E, F, etc) and will be discussed later. The additional peaks are crucial to the assignment, interpretation, and trends. However, our assignment of the *ordering*

Can. J. Chem. Downloaded from www.nrcresearchpress.com by 210.87.254.42 on 09/06/12
For personal use only.

Can. J. Chem. Downloaded from www.nrcresearchpress.com by 210.87.254.42 on 09/06/12
For personal use only.

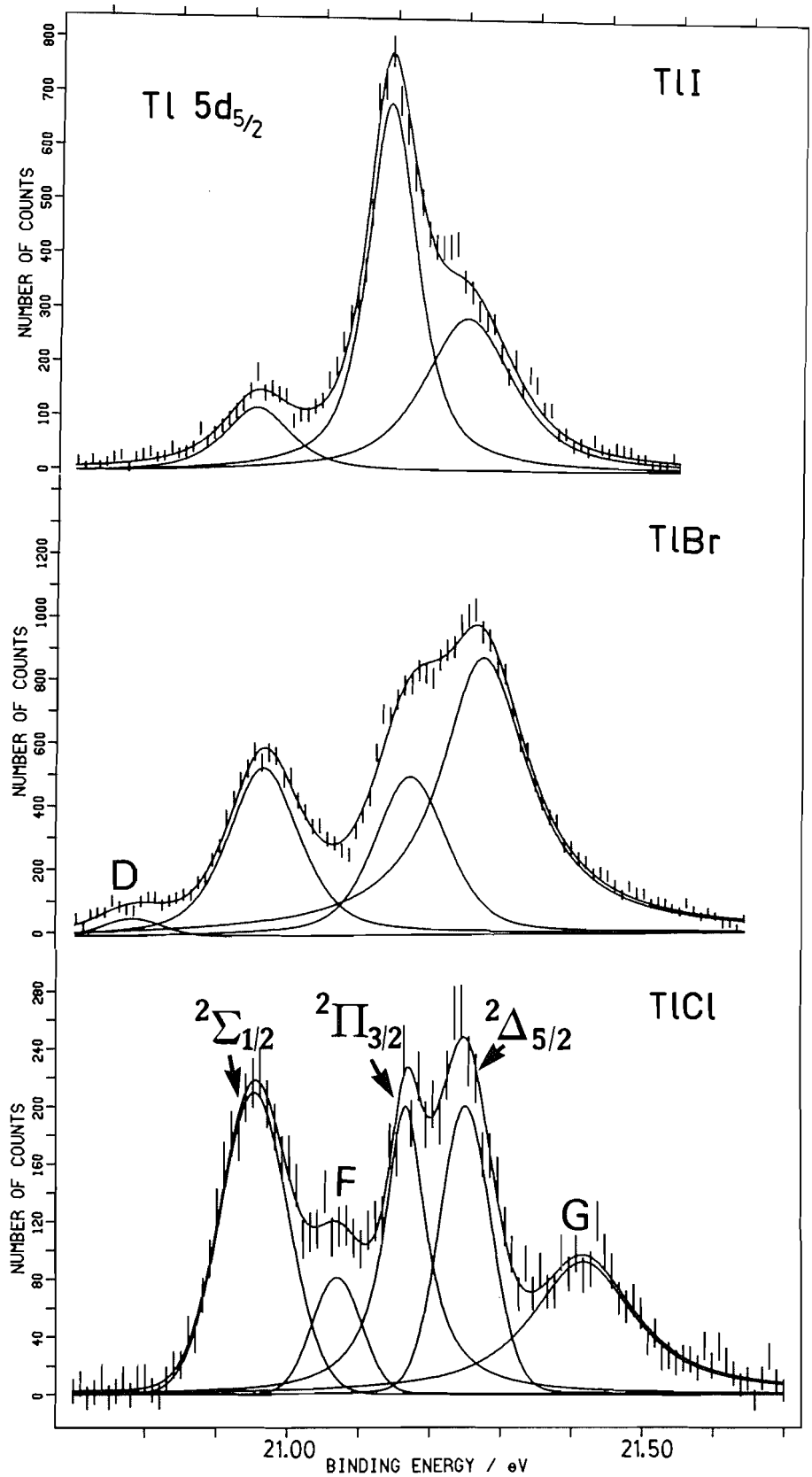

FIG. 2. HeII spectra of the Tl $5d_{5/2}$ region in the Tl halides. The $2^2\Sigma_{1/2}$ peaks at low binding energy are at the same apparent binding energy to facilitate comparison of the spectra.

of the ligand field states is the electrostatic order assumed previously (3, 4):

$$^2\Sigma_{1/2} < {}^2\Pi_{3/2} < {}^2\Delta_{5/2} < {}^2\Pi_{1/2} < {}^2\Delta_{3/2}$$

Also, where peaks were resolved in the previous studies, previous binding energies are in good agreement with ours.

The rich structure in the Tl $5d_{5/2}$ region in the TlCl spectrum presented an initial problem, which is readily clarified when the

Can. J. Chem. Downloaded from www.nrcresearchpress.com by 210.87.254.42 on 09/06/12
For personal use only.

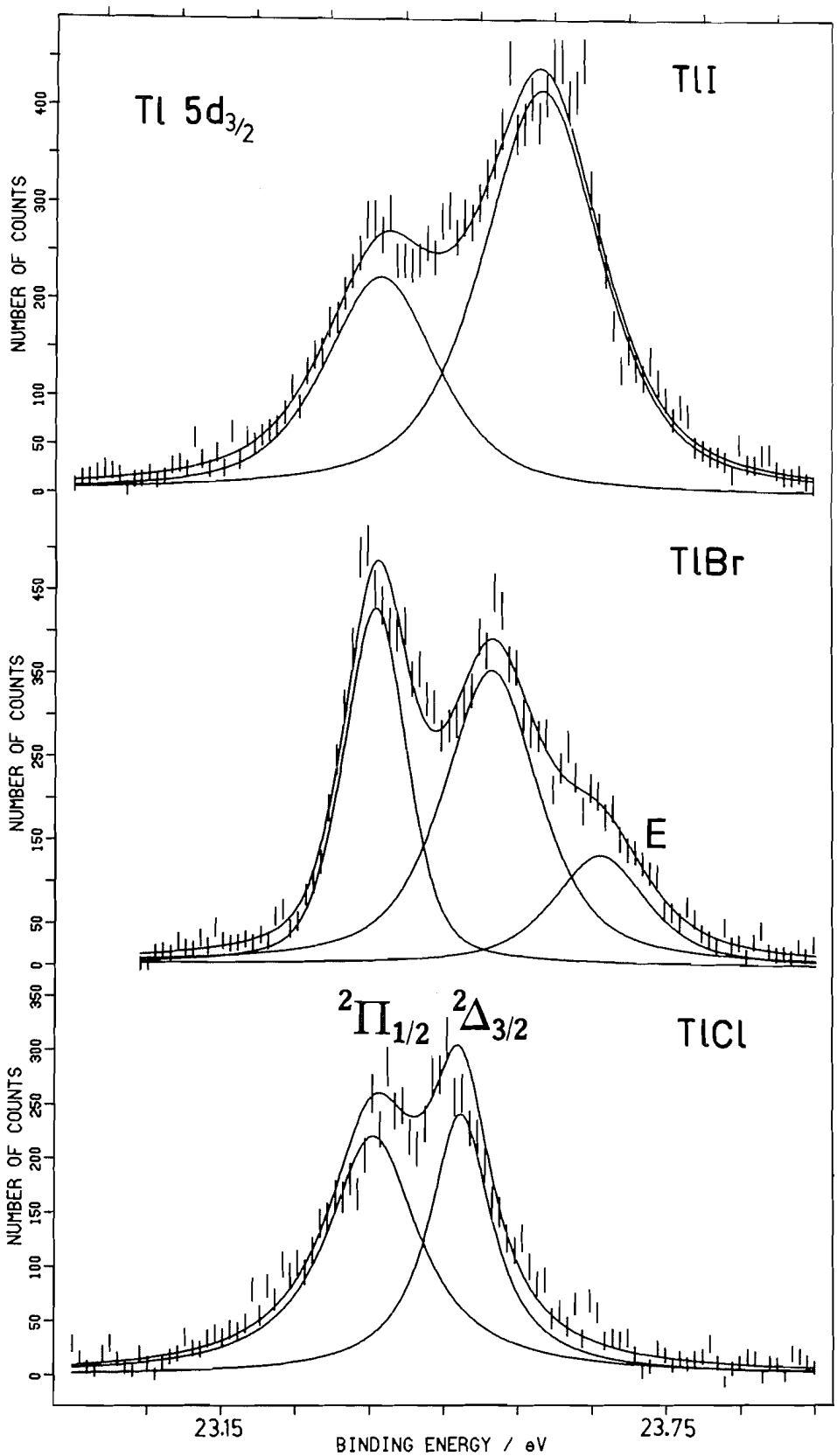

FIG. 3. HeII spectra of the Tl $5d_{3/2}$ region in the Tl halides. The $1^2\Pi_{1/2}$ peaks at low binding energy are at the same apparent binding energy.

$5d_{5/2}$ spectra for all three compounds are directly compared (Fig. 2). The third and fourth peaks from the left in TlCl are most logically assigned to the $^2\Pi_{3/2}$ and $^2\Delta_{5/2}$ levels respectively, since they line up rather well with the corresponding peaks in the bromide and iodide. In both the Tl $5d_{5/2}$ and $5d_{3/2}$ regions, the splitting increases in the order Cl < Br < I, although the increase in splitting is much more pronounced in the $5d_{3/2}$ region. In previous spectra (2–4), peaks

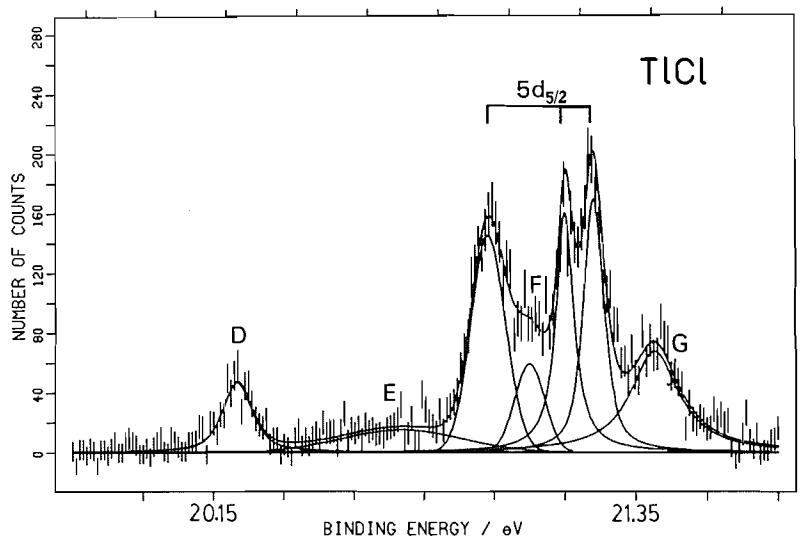

FIG. 4. Expanded HeII spectrum of the Tl $5d_{5/2}$ region in TlCl.

TABLE 2. Valence and Tl $5d$ binding energies for TlBr

Peak	State	Binding energy (eV) Exp.	Theor.[a]	Relative area	FWHM
A	$4^2\Sigma_{1/2}$	9.488	—	0.428	0.137
B	$2^2\Pi_{3/2,1/2}$	9.923	—	0.531	0.555
C	$3^2\Sigma_{1/2}$	13.676	—	0.0404	0.0368
D	Cl1	20.663	—	—	0.109
$5d_{5/2}$	$2^2\Sigma_{1/2}$	20.849	20.859	—	0.118
	$1^2\Pi_{3/2}$	21.056	21.061	—	0.120
	$1^2\Delta_{5/2}$	21.161	21.142	—	0.149
$5d_{3/2}$	$1^2\Pi_{1/2}$	23.088	23.073	—	0.101
	$1^2\Delta_{3/2}$	23.245	23.261	—	0.154
E	Cl2	23.393	—	—	0.153

[a]Calculated using the derived C_2^0 and C_4^0 values (Table 6) and the crystal field Hamiltonian, refs. 17–19.

TABLE 3. Valence and Tl $5d$ binding energies for TlI

Peak	State	Binding energy (eV) Exp.	Theor.[a]	Relative area	FWHM
A	$4^2\Sigma_{1/2}$	8.728	—	0.172	0.300
B	$2^2\Pi_{3/2}$	8.897	—	0.410	0.200
	$2^2\Pi_{1/2}$	9.712	—	0.374	0.318
C	$3^2\Sigma_{1/2}$	13.136	—	0.0211	0.0543
	$3^2\Sigma_{1/2}$	13.495	—	0.0221	0.0312
$5d_{5/2}$	$2^2\Sigma_{1/2}$	20.550	20.544	—	0.113
	$1^2\Pi_{3/2}$	20.741	20.743	—	0.0836
	$1^2\Delta_{5/2}$	20.848	20.850	—	0.150
$5d_{3/2}$	$1^2\Pi_{1/2}$	22.809	22.814	—	0.183
	$1^2\Delta_{3/2}$	23.027	23.024	—	0.191

due to $^2\Pi_{3/2}$ and $^2\Delta_{5/2}$ levels were not resolved in any of the spectra, and in one case (4), peak G in TlCl was assigned to the $\Delta_{5/2}$ state.

As in our previous papers (6, 20–22), we use the crystal field Hamiltonian for a d^9 state in a $D_{\infty h}$ or $C_{\infty v}$ crystal field to analyze the ligand field splitting. The five energies for the d levels yield the chemical shifts, spin–orbit splittings, and axial and cubic components (C_2^0 and C_4^0 respectively) of the crystal field. These are summarized in Table 6. Using these values, the peak positions are generally reproduced to within 0.02 eV (Tables 1–3). The parameter of greatest interest — the C_2^0 value — increases steadily from TlCl to TlI. This is the same trend as in the zinc and cadmium halide series (6), and corresponds to an increasing $6p$ orbital population on Tl from chloride to iodide expected from covalency considerations. The order is not that of the spectrochemical series (4). The chemical shifts are in good agreement with those reported earlier (3, 4). The spin–orbit coupling values are all fairly close to the atomic value (2.25 eV), implying that the $5d$ level is essentially atomic in nature. The fact that the TlCl value (2.28 eV) is within 2% of the atomic splitting is more evidence that our assignment of the $5d_{5/2}$ levels is correct.

TABLE 4. Parameters used in the Xα-SW TlCl calculation

Region	X	Y	Z	R	α
Outer	0.0	0.0	0.0	5.1658	0.69289
Tl	0.0	0.0	−1.8715	2.8077	0.72323
Cl	0.0	0.0	2.8166	2.3492	0.71413

In order to determine the relative magnitudes of the crystal field and valence contributions to the observed C_2^0 term, we have calculated C_2^0 values using our previous theoretical approach (6, 22) (Table 6). It is immediately obvious that the crystal field contribution ($C_2^0{}_{C.F.}$) is considerably smaller than the valence contribution ($C_2^0{}_{Val}$), and that $C_2^0{}_{Val}$ is in remarkably good agreement with the derived experimental values. In the Zn and Cd halides, $C_2^0{}_{C.F.}$ was larger than $C_2^0{}_{Val}$, although $C_2^0{}_{Val}$ was probably underestimated (6). There are at least two reasons for this difference between Tl and Zn, Cd compounds. First, there is only one negatively charged ligand in the Tl compounds which, assuming the same ligand charge as in the Zn and Cd analogs, would immediately halve $C_2^0{}_{C.F.}$. In fact, the ligand charges calculated from the chemical shifts using the normal treatment (23) are smaller than in the Zn and Cd series, leading to an expected C_2^0 value for Tl of well under one half that for the Zn and Cd analogs. Using Pauling's electro-

Can. J. Chem. Downloaded from www.nrcresearchpress.com by 210.87.254.42 on 09/06/12
For personal use only.

TABLE 5. Xα-SW calculated binding energies and charge distribution (%) for TlCl

Orbital	Binding energy[a] (eV)	Tl%				Cl%				Outer%[b]	Inter%[b]
		s	*p*	*d*	*f*	*s*	*p*	*d*	*f*		
4σ	8.64	33.76	6.25	1.03	0.33	0.31	26.36	0.11	—	9.58(*s*)	22.26
2π	10.54	—	0.73	0.38	0.19	—	75.35	—	—	2.94(*p*)	20.40
3σ	11.86	26.07	2.66	0.91	0.29	0.81	47.11	0.28	—	4.39(*p*)	17.46
2σ	21.62	0.20	0.18	67.97	—	26.95	0.53	—	—	0.62	3.33
1π	22.15	—	—	98.13	—	—	—	—	—	3.46(*d*)	1.63
1δ	22.15	—	—	98.26	—	—	—	—	—	—	1.70
1σ	23.02	0.56	0.62	29.87	—	61.99	0.47	—	—	0.78	5.39

[a]Calculated using the 4σ* transition state.
[b]Only the majority contribution (*s*, *p*, etc.) to the total character is indicated.

TABLE 6. Experimental and theoretical C_K^0 parameters (eV)

Compound	Experimental					Theoretical					
						Crystal field			Valence		
	E_{nd}	C_2^0	C_4^0	C_2^0/C_4^0	5/2λ	q^a	$C_{2\,C.F.}^{0\,b}$	$C_{4\,C.F.}^{0\,b}$	$\Delta\rho^c$	$C_{2\,Val}^{0\,d}$	5/2λ
TlCl	22.05	−0.0210	−0.0021	9.95	2.28	0.206	−0.0051	−0.00013	0.794	−0.0216	2.25
TlBr	21.86	−0.0233	−0.0018	12.8	2.14	0.140	−0.0029	−0.00007	0.860	−0.0234	2.25
TlI	21.58	−0.0258	−0.0016	15.5	2.20	0.0571	−0.0009	−0.00002	0.94	−0.0257	2.25

[a]Calculated using the experimental chemical shifts and the usual treatment (20). Bond lengths are from ref. 27: TlCl, 4.69; TlBr, 5.07; TlI, 5.43 (au).
[b]Calculated using the following values for Tl^+: $\langle r^2\rangle$ = 1.960 au, $\langle r^4\rangle$ = 6.313 au.
[c]$\Delta\rho = 1 - q$.
[d]Calculated using the following values: $F^2(dp)$ = 0.0977 Ryd; $G^1(dp)$ = 0.0310 Ryd; $G^3(dp)$ = 0.0274 Ryd.

negativity expression (24, 25):

$$q \times 100 = |\chi_A - \chi_B| + 3.5|\chi_A - \chi_B|^2$$

where χ_A and χ_B are the electronegativities of the two atoms, we obtain q values which are in qualitative agreement with those obtained from the chemical shifts in Table 6: 0.223, 0.177, and 0.113 for TlCl, TlBr, and TlI, respectively. Second, $C_2^0{}_{val}$ for the Tl compounds is much larger for the Zn and Cd analogs, because Δρ (Δρ = $n_{pz} - (1/2)(n_{px} + n_{py})$) is much larger for Tl than for Zn or Cd. This difference can be related, at least to a first approximation, to the electronic structure of these atoms. Zinc and cadmium both have two valence electrons (ns^2) and thallium has three ($6s^26p$). In the ionic limit, zinc and cadmium lose both outer *s* electrons while thallium loses the 6*p* electron. As these atoms form covalent bonds, the halide ligands donate charge to the outer *s* and *p* orbitals of zinc and cadmium, but primarily to the 6*p* orbital in Tl. In fact, the Xα calculation in our previous paper (9) indicates that the majority of charge in Zn and Cd compounds is located in the outer *s* orbital which does not contribute to Δρ. If we consider that Tl^+ has the electronic configuration $6s^2$, donation of charge in the halides will be to the Tl 6*p* orbital, and we can take Δρ = 1 − *q*. Our Xα calculation (Table 5) shows that this simple approximation will undoubtedly lead to an overestimate of Δρ.

To test our theory further, we use the combined crystal field and valence matrix elements (6, 22) to calculate the relative positions of the Tl 5*d* levels. These results appear in Table 7, and show that the agreement between experiment and theory is relatively good. It is interesting to note that the separation of the $2^2\Sigma_{1/2}$ level from the $1^2\Delta_{5/2}$ is consistently underestimated throughout the series. This may be indicative of a slight interaction with the halogen localized *s* orbital as was observed in the Zn and Cd series (6). The steady reduction in relative intensity of the $^2\Sigma_{1/2}$ level from TlCl to TlI (Fig. 2) may suggest that such an interaction exists, although other effects may be responsible for these changes (6).

TABLE 7. Relative theoretical Tl $5d^{-1}$ hole state binding energies

Compound	State	Relative energies	
		Experimental	Theoretical[a]
TlCl	$2^2\Sigma_{1/2}$	−0.297	−0.228
	$1^2\Pi_{3/2}$	−0.0840	−0.146
	$1^2\Delta_{5/2}$	0.0	0.0
	$1^2\Pi_{1/2}$	2.10	2.04
	$1^2\Delta_{3/2}$	2.22	2.21
TlBr	$2^2\Sigma_{1/2}$	−0.312	−0.215
	$1^2\Pi_{3/2}$	−0.105	−0.143
	$1^2\Delta_{5/2}$	0.0	0.0
	$1^2\Pi_{1/2}$	1.91	2.05
	$1^2\Delta_{3/2}$	2.08	2.22
TlI	$2^2\Sigma_{1/2}$	−0.306	−0.214
	$1^2\Pi_{3/2}$	−0.107	−0.114
	$1^2\Delta_{5/2}$	0.0	0.0
	$1^2\Pi_{1/2}$	1.96	2.05
	$1^2\Delta_{3/2}$	2.17	2.21

[a]Calculated using the parameters in Table 6, and the matrix elements in refs. 6 and 19.

A good correlation between $C_2^0{}_{Exp.}$ and the chemical shift of the Tl 5*d* orbital has been obtained and is presented in Fig. 5. The chemical shifts have been taken relative to the metal (4). The $C_2^0{}_{Val}$ term is essentially colinear with the experimental values while the crystal field term is considerably smaller and of course has the opposite slope. These results again indicate a

Can. J. Chem. Downloaded from www.nrcresearchpress.com by 210.87.254.42 on 09/06/12
For personal use only.

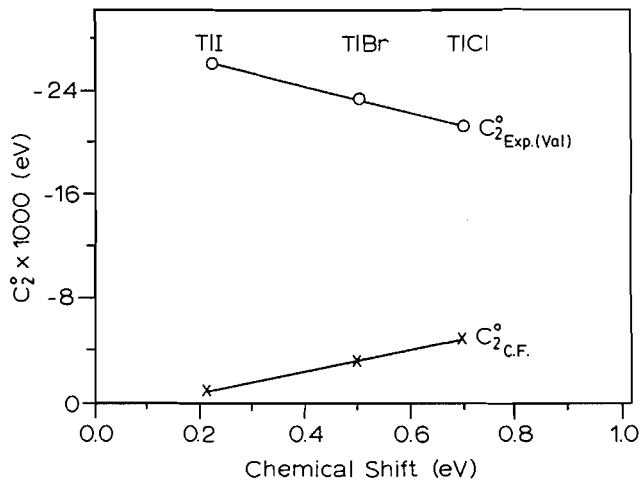

FIG. 5. Plot of C_2^0 versus the Tl $5d$ chemical shift for the Tl halides. The chemical shifts are given relative to Tl metal (4).

predominantly valence contribution to the C_2^0 asymmetric potential felt by the Tl $5d$ orbital.

(c) Configuration interaction

The additional structure in the Tl $5d$ region of TlCl and TlBr is of some interest. The structure in TlCl is associated with the $5d_{5/2}$ level (Fig. 4, peaks D, E, F, G), while that in TlBr can be seen in both the $5d_{5/2}$ (Fig. 2, peak D) and $5d_{3/2}$ (Fig. 3, peak E) regions. We also observed the additional weak peak observed by other workers (3, 4) at an ionization potential of 18.55 eV. The two primary effects which could be responsible for this additional structure are initial state configuration interaction (ISCI) and final ionized state configuration interaction (FISCI). Since the additional peaks are associated with the localized Tl $5d$ orbital, it would seem reasonable to investigate initially the atomic Tl $5d$ spectrum (26–29) which has rich CI structure. This system is immediately complicated, of course, by the unpaired electron in the Tl atom ground state ($5d^{10}6s^26p^1$). Ignoring further effects, this will produce a doublet for both the $5d_{5/2}$ and $5d_{3/2}$ components of the spin–orbit pair due to coupling to the unpaired $6p$ electron. Two peaks are in fact observed for the $5d_{5/2}$ ionization, but six peaks arise with $5d_{3/2}$ ionization (27). There are fundamentally two different types of processes responsible for the structure, both of which are attributed to FISCI. An example of the first of these can be illustrated schematically as (27):

$$(5d_{3/2})^3(5d_{5/2})^6(6s)^2(6p_{1/2})^1(6p_{3/2})^0 \leftrightarrow (5d_{3/2})^4(5d_{5/2})^5(6s)^2(6p_{1/2})^0(6p_{3/2})^1$$

This then is a two electron process in which an electron has fallen from the $5d_{5/2}$ manifold into the $5d_{3/2}$ at the same time as the $6p_{1/2}$ electron jumps up to the $6p_{3/2}$ level. This process (one electron up, one electron down) is only available for the deeper lying $5d_{3/2}$ level. The other type of two electron process contributing to the structure but which maintains the full complement of $5d$ electrons derives from final states such as $5d^{10}6s^17p^1_{3/2,1/2}$ (26, 27). It seems clear that the first type of process involving the $5d^9$ hole and $6p$ electron is not possible for the halides: all the valence orbitals are full and electrons paired. The second type is possible, the only restriction being that the final state have the same designation as the one electron $5d$ ionization and close to the same total energy. In general, it has been found that this type of CI occurs where there is an appropriate orbital at approximately half the binding energy of the primary hole (30–32).

Looking at TlCl first, this prerequisite is met by the $4^2\Sigma_{1/2}$ and $1^2\Pi_{3/2,1/2}$ states (Table 1). We see from the Xα calculation that the majority of the Tl $6s$ character (47%) is located in the 4σ orbital, and this could be viewed as a prime candidate for CI. One possibility for interacting configurations is

$$1\sigma^21\delta^41\pi^42\sigma^13\sigma^22\pi^44\sigma^2 \leftrightarrow 1\sigma^21\delta^41\pi^42\sigma^23\sigma^22\pi^44\sigma^0n\sigma^{*1}$$

where the orbital numbering begins with Cl $3s$ level. The left hand side is the one electron 2σ ($5d$) ionization while that on the right is a two electron process involving simultaneous photo ejection and excitation from the 4σ (HOMO) orbital. The designation of both final states would be $^2\Sigma_{1/2}$.

We have used our Xα calculation on TlCl to obtain the "binding" energies for two electron processes such as the one just described and present the results in Table 8. The results included in this table are for monopole transitions only such as $\sigma \rightarrow \sigma^*$ and $\pi \rightarrow \pi^*$. The various final states possible have been included in the left hand column of the table. These calculations have been performed by initially removing one electron from the valence orbital involved (4σ, 2π, or 3σ) and obtaining the corresponding converged potential. Using this potential then, a second electron from the same orbital is transferred to one of the virtual levels and the final converged potential is obtained. The total energy involved in this process is simply the difference between the total ground state molecular energy. These values have been listed in the column labelled energy of Table 8. It is immediately clear that a number of the final states represent energies in the range of the Tl $5d$ ionizations (~20 eV). The calculation itself, however, provides no indication of the relative probability associated with the various transitions. Since the $5d$ orbital is localized on thallium, valence and virtual orbitals exhibiting a significant population on thallium and close to the same final state energy as the $5d$ ionization might be expected to be the most likely for configuration interaction. Both the 4σ and 3σ valence orbitals possess a considerable thallium contribution. The $5\sigma^*$ virtual level is also predominantly thallium in character, but the higher virtual levels are associated primarily with the outer sphere region. In these cases, transitions to virtual orbitals with a high percentage of s-character in the outer sphere region such as the $6\sigma^*$ and $8\sigma^*$ are likely as the valence character of the 4σ and 3σ levels on thallium is primarily Tl $6s$. Based on these arguments then, the $4\sigma \rightarrow n\sigma^*$ (n = 5, 6, 8) and $3\sigma \rightarrow 5\sigma^*$ transitions would all appear to be possible candidates for final state configuration interaction. Of these possibilities the $4\sigma \rightarrow 8\sigma^*$ and $3\sigma \rightarrow 5\sigma^*$ at 19.63 eV and 23.18 eV, respectively, are energetically the most favourable as their final energies are closest to the $5d$ ionization energies. The $2\pi \rightarrow n\pi^*$ are not as likely since the valence 2π orbital is localized almost entirely on chlorine. It is not possible to unequivocally assign the CI structure because of the numerous transitions available (Table 8) and the lack of information concerning their cross-sections.

It is interesting to note that simple monopole transitions cannot give rise to $^2\Delta$ type final states. The $^2\Delta$ final state is strictly inaccessible from valence σ-orbitals because of the selection rule $\Delta\lambda = 0, \pm 1$. However, if we assume that conjugate shakeup (33, 34) represents a significant configuration interaction mechanism, then a transition such as $2\pi \rightarrow n\sigma^*$ involving the excited electron would produce a $^2\Delta$ final state. In support of this conjecture, work on Ne (33) concludes that at low photon energies, up to 25% of the shakeup intensity

Can. J. Chem. Downloaded from www.nrcresearchpress.com by 210.87.254.42 on 09/06/12
For personal use only.

TABLE 8. "Binding energies" for two electron processes distributions (%) for monopole excitations in TlCl

Transition (final states)	Orbital	Centre	Energy (eV)	% Orbital character				Inter %
				s	*p*	*d*	*f*	
$4\sigma \rightarrow n\sigma^*$		Tl		33.76	6.25	1.03	0.33	
($^2\Sigma$)	4σ	Cl	—	0.31	26.36	0.11	—	22.26
		Outer		—	2.53	0.88	0.64	
		Tl		—	22.57	1.18	0.56	
	$5\sigma^*$	Cl	15.09	2.84	4.60	0.41	—	40.36
		Outer		5.59	13.63	7.38	0.82	
		Tl		5.94	12.69	—	—	
	$6\sigma^*$	Cl	16.67	—	3.02	6.66	0.14	24.30
		Outer		41.42	0.60	1.26	3.64	
		Tl		1.81	1.33	0.54	—	15.65
	$7\sigma^*$	Cl	18.75	1.18	0.41	0.53	—	
		Outer		1.72	56.36	11.62	8.63	
		Tl		—	2.02	0.41	0.42	
	$8\sigma^*$	Cl	19.63	—	0.21	4.55		5.87
		Outer		64.36	0.68	18.83	2.57	
		Tl		0.14	0.98	—	0.30	
	$9\sigma^*$	Cl	20.23	0.77	0.12	0.18	—	5.58
		Outer		4.68	38.66	45.46	2.98	
$2\pi \rightarrow n\pi^*$		Tl		—	0.73	0.38	0.19	
($^2\Pi$, $^2\Phi$)	2π	Cl	—	—	75.35	—	—	20.40
		Outer		—	1.40	—	—	
		Tl		—	27.66	—	—	
	$3\pi^*$	Cl	20.97	—	1.16	2.06	—	51.16
		Outer			14.25	3.43	—	
		Tl		—	6.82	0.44	—	
	$4\pi^*$	Cl	25.212	—	1.84	0.49	—	25.67
		Outer			34.73	27.80	2.13	
		Tl		—	0.37	3.28	0.54	
	$5\pi^*$	Cl	26.23	—	0.21	20.69	2.86	21.99
		Outer		—	32.07	8.08	11.28	
$3\sigma \rightarrow 5\sigma^*$		Tl		26.07	2.66	0.91	0.29	
($^2\Sigma$)	3σ	Cl	—	0.81	47.11	0.28	—	17.46
		Outer		7.20	1.27	2.82	0.15	
		Tl		0.35	20.47	0.65	0.35	
	$5\sigma^*$	Cl	23.18	2.68	1.87	0.15	—	43.37
		Outer		5.85	15.28	8.45	0.38	

TABLE 9. "Binding energies" for dipole excitations in TlCl

Transition	Final states	Energy (eV)
$2\pi \rightarrow 5\sigma^*$	$^2\Sigma$, $^2\Delta$	22.56
$2\pi \rightarrow 6\sigma^*$		23.78
$2\pi \rightarrow 7\sigma^*$		25.93
$2\pi \rightarrow 8\sigma^*$		26.53
$4\pi \rightarrow 3\sigma^*$	$^2\Pi$	13.09
$4\pi \rightarrow 4\sigma^*$		17.95
$4\pi \rightarrow 5\sigma^*$		19.46

could be due to "conjugate" shakeup. Also, 20% of the $^2P_{3/2,1/2}$ intensity observed in the spectra of atomic mercury (34) is due to the "conjugate" shakeup mechanism.

We have calculated a number of transitions in which the dipole process now involves the electron undergoing excitation ("conjugate" shakeup) and present the results in Table 9. The percent orbital character of all the levels appears in Table 8. While this calculation has been performed on TlCl, the small difference in binding energies for the TlBr orbitals (Table 2) suggests that the energy involved in TlBr CI will be quite similar to TlCl. Thus a transition such as

$$2\pi^4 \rightarrow 2\pi^2 6\sigma^{1*}\ (^2\Delta) + e$$

which requires 23.8 eV (Table 9) could be responsible for peak E in the $5d_{3/2}$ region of TlBr (Fig. 2) which has an ionization energy of 23.4 eV (Table 2). This peak (E) is apparently associated with the $1^2\Delta_{3/2}$ state as was the case for the $3d$ orbital of $ZnBr_2$.

Conclusion

Tl $5d$ core level ligand field splittings have been completely resolved in the photoelectron spectra of the main group thallium halides. The splitting is mainly due to the non-cubic (C_2^0)

Can. J. Chem. Downloaded from www.nrcresearchpress.com by 210.87.254.42 on 09/06/12
For personal use only.

part of the crystal field. For the first time, our calculated C_2^0 values are in very good agreement with the observed values, and we show that the valence part of the C_2^0 term, $C_2^0{}_{val}$, is the dominating contribution to C_2^0. We have also advanced the understanding of the Tl $5d$ configuration interaction structure and the valence bonds with the aid of our higher resolution and transition state Xα-SW calculation.

Acknowledgements

We are very grateful to NSERC for financial assistance, Dr. J. S. Tse for helpful discussions, and Drs. E. Pellach and L. L. Coatsworth for technical assistance.

1. J. BERKOWITZ. J. Chem. Phys. **56**, 2766 (1972).
2. A. W. POTTS and W. C. PRICE. Phys. Script. **16**, 191 (1977).
3. A. W. POTTS and M. O. LYUS. J. Electron Spectrosc. **13**, 327 (1978).
4. R. G. EGDELL and A. F. ORCHARD. Trans. Faraday Soc. **74**, 1179 (1978).
5. S. SÜZER. Chem. Phys. Lett. **69**, 230 (1980).
6. G. M. BANCROFT, D. J. BRISTOW, and J. S. TSE. Chem. Phys. **75**, 277 (1983).
7. C. J. BALLHAUSEN. Ligand field theory. McGraw-Hill. 1962.
8. G. M. BANCROFT, D. J. BRISTOW, and L. L. COATSWORTH. Chem. Phys.Lett. **82**, 344 (1981).
9. D. J. BRISTOW, G. M. BANCROFT, and J. S. TSE. Chem. Phys. **75**, 263 (1983).
10. L. L. COATSWORTH, G. M. BANCROFT, D. K. CREBER, R. LAZIER, and P. W. M. JACOBS. J. Electron. Spectrosc. **13**, 395 (1978).
11. G. M. BANCROFT, I. ADAMS, L. L. COATSWORTH, C. D. BENNEWITZ, J. D. BROWN, and W. D. WESTWOOD. Anal. Chem. **47**, 586 (1975).
12. J. BERKOWITZ and J. L. DEHMER. J. Chem. Phys. **57**, 3194 (1972).
13. J. C. SLATER. The self consistent field for molecules and solids. Vol. 4. McGraw-Hill, New York. 1974.
14. K. SCHWARZ. Phys. Rev. B**5**, 2466 (1972).
15. J. G. NORMAN, JR. J. Chem. Phys. **61**, 4630 (1974).
16. J. TSE, D. J. BRISTOW, G. M. BANCROFT, and G. SCHROBILGEN. Inorg. Chem. **18**, 1766 (1979).
17. J. S. TSE. Ph.D. Thesis, University of Western Ontario, London, Ont. 1979.
18. K. WITTEL. Chem. Phys. Lett. **15**, 555 (1972).
19. O. GOSCINSKI, J. MULLER, E. POULAIN, and H. SIEGBAHN. Chem. Phys. Lett. **55**, 407 (1978).
20. G. M. BANCROFT, D. K. CREBER, and H. BASCH. J. Chem. Phys. **67**, 6891 (1977).
21. D. K. CREBER and G. M. BANCROFT. Inorg. Chem. **19**, 643 (1980).
22. R. P. GUPTA, J. S. TSE, and G. M. BANCROFT. Phil. Trans. R. Soc. London, **293**A, 535 (1980).
23. J. BERKOWITZ. J. Chem. Phys. **61**, 407 (1974).
24. F. A. COTTON and G. WILKINSON. Advanced inorganic chemistry. 3rd. ed. Interscience. 1972.
25. C. A. COULSON. Valence. Clarendon. 1952.
26. E. P. F. LEE and A. W. POTTS. J. Electron Spectrosc. **19**, 65 (1980).
27. L. E. SUTTON (*Editor*). Tables of interatomic distances and configurations in molecules and ions. 1958.
28. D. M. P. HOLLAND and K. CODLING. J. Phys. B, **13**, L745 (1980).
29. W. H. E. SCHWARTZ. J. Electron Spectrosc. **21**, 257 (1980).
30. G. K. WERTHEIM and A. ROSENCWAIG. Phys. Rev. Lett. **26**, 1179 (1971).
31. S. P. KOWALCZYK, L. LEY, R. A. POLLAK, F. R. MCFEELY, and D. A. SHIRLEY. Phys. Rev. B, **7**, 4009 (1973).
32. G. M. BANCROFT, T. K. SHAM, and S. LARSSON. Chem. Phys. Lett. **46**, 551 (1977).
33. F. WUILLEUMIER and M. O. KRAUSE. Phys. Rev. A**10**, 242 (1974).
34. J. BERKOWITZ, J. L. DEHMER, Y. K. KIM, and J. P. DESCLAUX. J. Chem. Phys. **61**, 2556 (1974).

Can. J. Chem. Downloaded from www.nrcresearchpress.com by 210.87.254.42 on 09/06/12
For personal use only.

Charge distributions and chemical effects. XXXII. Energies of multiple carbon–carbon bonds

S. FLISZÁR

Department of Chemistry, University of Montreal, Montreal, P.Q., Canada H3C 3V1

Received April 11, 1983

S. FLISZÁR. Can. J. Chem. **61**, 2679 (1983).

Bond energies are derived from total (nuclear–electronic and nuclear–nuclear) potential energies involving the individual nuclei of a molecule. It appears that the carbon–carbon bond energies in ethane, ethylene, allene, acetylene, and benzene are in a ratio of 1:2:1.9:2.9:1.6. This result enables a rapid estimate of approximate atomization energies of unsaturated hydrocarbons from those of their corresponding saturated parent compounds and, more importantly, shows the links relating to one another the various classes of saturated and unsaturated hydrocarbons in a unifying fashion.

S. FLISZÁR. Can. J. Chem. **61**, 2679 (1983).

Les énergies de liens sont déduites à partir des énergies potentielles noyau–électron et noyau–noyau impliquant les noyaux individuels d'une molécule. Les énergies de liens carbone–carbone de l'éthane, de l'éthylène, de l'allène, de l'acétylène et du benzène sont dans un rapport de 1:2:1.9:2.9:1.6. Cette information permet une évaluation rapide des énergies d'atomisation de composés insaturés à partir de leurs précurseurs saturés et, primordialement, illustre les liens de parenté reliant entre elles les différentes classes d'hydrocarbures saturés et insaturés.

Can. J. Chem. Downloaded from www.nrcresearchpress.com by 210.87.254.6 on 09/06/12
For personal use only.

Introduction

The concept of a chemical bond is central in the understanding of many aspects of molecular structure and thermochemical stability. The present study considers the problem for molecules taken in their hypothetical vibrationless state, at 0 K. Attention is primarily directed toward the conceptual aspects surrounding the energy partitioning among chemical bonds, in order to put in a clear perspective what type of approximations are involved in the derivation of theoretical bond energies and what causes them to differ from the usual ones, retrieved from empirical correlations. Unlike empirical bond energies, the present theoretical results create a clear link between the different types (single, double, etc.) of carbon–carbon bonding and offer a simple unifying view encompassing both saturated and unsaturated hydrocarbons.

Atoms in a molecule

The difference between a molecule as we know it and the corresponding collection of isolated atoms is a relatively minor one, from the energetic point of view. In this sense, it is fair to say that the largest part, by far, of the molecular energy is already partitioned in a quite natural way, in terms of atomic contributions. What really remains to be partitioned is the difference

$$[1]\quad \Delta E_a^* = \Sigma_i E_i^{\text{atom}} - E^{\text{molecule}}$$

between the energy of the isolated atoms making up a molecule and that of the molecule itself. Viewing the latter as a collection of "atoms" with energies E_i^{mol} differing from those of their isolated counterparts, let

$$[2]\quad \Delta E_i = E_i^{\text{atom}} - E_i^{\text{mol}}$$

describe this energy difference for atom i. The atomization energy ΔE_a^*, which measures chemical binding, is then $\Delta E_a^* = \Sigma_i \Delta E_i$. The advantage offered by this type of description resides in the fact that nonrelativistic atomic and molecular ground-state energies can be expressed in terms of the electrostatic potentials at the nuclei, the molecular energy thus being given as a sum of atomiclike terms (1).

For the isolated, viz. bonded, atom i, we can write (2–4)

$$[3]\quad E_i^{\text{atom}} = K_i^{\text{at}} V_{\text{ne}}(\text{atom } i)$$

$$[4]\quad E_i^{\text{mol}} = K_i^{\text{mol}} V(i, \text{mol})$$

where (in conventional notation)

$$V_{\text{ne}}(\text{atom } i) = -Z_i \int \frac{\rho(\boldsymbol{r})}{|\boldsymbol{r} - \boldsymbol{r}_i|}\, d\boldsymbol{r}$$

is the nuclear–electronic potential energy of the isolated atom i and

$$V(i, \text{mol}) = -Z_i \int \frac{\rho(\boldsymbol{r})}{|\boldsymbol{r} - \boldsymbol{r}_i|}\, d\boldsymbol{r} + Z_i \sum_{k \neq i} Z_k / r_{ki}$$

is the total potential energy involving nucleus i, due to all the electrons and nuclei other than i in the molecule. In eq. [3], K_i^{at} is necessarily a constant for each individual atom. For hydrogen, $K_{\text{H}}^{\text{at}} = 1/2$ (because of the virial theorem); $K_i^{\text{at}} \simeq 3/7$ for atoms other than H is predicted by the Thomas–Fermi model (5–7) as well as by approaches (1, 8) rooted in density functional theory (9). Selected K_i^{at} values, deduced from SCF calculations, are (2–4) 0.4276 (C), 0.4239 (N), and 0.4201 (O). The K_i^{mol} coefficient introduced by Politzer (2) in writing eq. [4] appears to behave as a constant for each atomic species, as indicated by a host of SCF calculations (2–4), but this is not an exact result. Selected K_i^{mol} values are: 1/2 (H), 0.4287 (C), 0.4260 (N), and 0.4213 (O). Constancy of these K_i^{mol} coefficients is assumed in the present work. In this approximation, the binding contributed by atom i is

$$[5]\quad \Delta E_i = K_i^{\text{at}} V_{\text{ne}}(\text{atom } i) - K_i^{\text{mol}} V(i, \text{mol})$$

This energy partitioning involves no distinction between bonded and nonbonded atoms in a molecule. Unfortunately, ΔE_i is not what one is usually looking for, as important arguments in the understanding of chemistry still remain linked to the concept of chemical bonds. This concept shall now be examined, taking eq. [5] as a starting point.

The chemical bond

Before entering the world of chemical bonds, let us briefly consider atom pairs (in a molecule) which are not bonded in the usual chemical sense. In σ systems, their interactions can be estimated using Del Re's approximation (10)

$$E(\text{nonbonded}) = \tfrac{1}{2} \sum_{k,l} q_k q_l / r_{kl}$$

Can. J. Chem. Downloaded from www.nrcresearchpress.com by 210.87.254.6 on 09/06/12
For personal use only.

which is simply the Coulomb energy between net (i.e., nuclear minus electronic) charges of nonbonded atoms at a distance r_{kl}. These interactions are not only minor (typically 0.02−0.05% of ΔE_a^*) but often exhibit the wrong trend in comparisons between structural isomers (3). (For example, the difference in nonbonded energy between normal pentane and neopentane is only ~0.1 kcal mol^{-1} favoring, as expected, the normal isomer, whereas neopentane is actually the more stable form by ~4 kcal mol^{-1} (3)). Temporarily neglecting nonbonded contributions, it is therefore defendable to assimilate the bonded part of ΔE_a^* to ΔE_a^* itself, i.e.,

$$[6] \quad \Delta E_a^{*\text{bonded}} \simeq \Delta E_a^*$$

In this approximation, we write

$$[7] \quad \Delta E_a^* \simeq \Sigma \epsilon_{ij}$$

where ϵ_{ij} is the contribution of the bond formed by atoms i and j to the total atomization energy. Note that for any bonded atom pair we speak in all cases of *one* bond only, whether this bond is a single one (in conventional language), like the CC bond in ethane, or a multiple bond (like the CC bonds in ethylene, acetylene, benzene, etc.). Also note that the ϵ_{ij} bond contributions under scrutiny are dictated by the actual bond properties in the molecule (internuclear distance and local charge density): they should not be mistaken for the energy required for breaking these bonds. Indeed, bond dissociation energies depend also on electronic rearrangements (like making sure that a neutral H atom is formed during the cleavage of a CH bond in methane, in which hydrogen carries a partial charge) and on structural changes in the fragments (like that of a CH_3 radical formed during a CH bond cleavage in methane).

The derivation of the equation describing ϵ_{ij} involves the following steps. From eq. [1], written (in conventional notation) as

$$\Delta E_a^* = \Sigma_i \langle \psi_i^{at} | H_i^{at} | \psi_i^{at} \rangle - \langle \psi^{mol} | H^{mol} | \psi^{mol} \rangle$$

one obtains by means of the Hellmann−Feynman theorem that (3)

$$Z_i(\partial \Delta E_a^*/\partial Z_i) = V_{ne}(\text{atom } i) - V(i, \text{mol})$$

which is an exact equation for molecules at equilibrium. On the other hand, it follows from eq. [7] that

$$\partial \Delta E_a^*/\partial Z_i \simeq \Sigma_j(\partial \epsilon_{ij}/\partial Z_i)$$

where the j atoms are bonded to atom i. Consequently, it results that

$$[8] \quad Z_i \Sigma_j(\partial \epsilon_{ij}/\partial Z_i) \simeq V_{ne}(\text{atom } i) - V(i, \text{mol})$$

and, from eq. [5],

$$[9] \quad \Delta E_i \simeq K_i^{mol} Z_i \Sigma_j(\partial \epsilon_{ij}/\partial Z_i) + (K_i^{at} - K_i^{mol}) V_{ne}(\text{atom } i)$$

What has happened here can be described as follows. With the calculation of $Z_i(\partial \Delta E_a^*/\partial Z_i)$ from eq. [1], we have reduced the quantum chemical problem to a purely electrostatic one, with a solution for each individual atom i. Then, introducing the concept of chemical bonds by means of eq. [7], we have obtained an energy formula, eq. [9], for the binding of each atom in the molecule, featuring the role of the bonds it forms. The point is that eq. [9] expresses most appropriately that part of the "true" ΔE_i which depends specifically on bond formation, i.e., precisely what is required for deducing ϵ_{ij}. Indeed, the "extraction" from the host molecule of an atom i forming v_i bonds requires an energy $(K_i^{at} - K_i^{mol}) V_{ne}(\text{atom } i)/v_i$ for each bond, meaning that this type of contribution must be counted once for both the i and j atoms of the ij bond. In addition, this "atomization" requires an energy $K_i^{mol} Z_i(\partial \epsilon_{ij}/\partial Z_i)$ for each bond formed by i, meaning that the suppression of an ij bond involves this type of contribution for each bonded partner. Consequently, it follows from this partitioning that (3)

$$[10] \quad \epsilon_{ij} = K_i^{mol} Z_i(\partial \epsilon_{ij}/\partial Z_i) + K_j^{mol} Z_j(\partial \epsilon_{ij}/\partial Z_j) + (K_i^{at} - K_i^{mol}) V_{ne}(\text{atom } i)/v_i + (K_j^{at} - K_j^{mol}) V_{ne}(\text{atom } j)/v_j$$

Numerical applications of eq. [10] are presented below. These calculations involve two assumptions. Firstly, the K_i^{mol}'s are treated as constants — an assumption which is supported by Hartree-Fock results (2−4). Secondly, it is regarded that nonbonded interactions are sufficiently small as to permit a reasonable evaluation of $\Sigma_j(\partial \epsilon_{ij}/\partial Z_i)$ from Hartree−Fock applications of eq. [8]. These working hypotheses are tested in comparisons involving experimental energies, which is a severe way of assessing their validity. Unfortunately, it is by no means an easy task to estimate the $\partial \epsilon_{ij}/\partial Z_i$ derivatives at the level of experimental accuracy. It has been done in a few cases (3, 11), e.g., for the ethane CC and CH bonds and for the ethylene CC double bond. However, this type of calculation needs to be done only once for each type of chemical bond, for reasons given below. Selecting ethane as the reference compound for the definition of reference bond energies ϵ_{ij}^0, it is found (3) from eq. [10] that $\epsilon_{CC}^0 = 69.633$ and $\epsilon_{CH}^0 = 106.806$ kcal mol^{-1}. (For ethylene (11), $\epsilon_{C=C}^0 = 139.27$ kcal mol^{-1}). Here we wish to show that the reference bond energies ϵ_{CC}^0 and ϵ_{CH}^0 indicated above for ethane and the use of eqs. [8] and [10] suffice for describing both saturated and unsaturated hydrocarbons (e.g., benzene) at a level reasonably close to experimental accuracy. In this manner, it becomes possible to show that eq. [10] provides a unifying picture for the thermochemical stability of hydrocarbons belonging to well diversified classes as regards their molecular and electronic structure. This approach is thus markedly different from the usual bond additivity schemes which require separate parametrizations for single, double, etc. bonds, developed on an empirical basis for satisfying observed thermochemical properties.

There is a point of utmost importance which requires immediate attention. The derivatives $\partial \epsilon_{ij}/\partial Z_i$ are bound to the conditions set by the present use of the Hellmann−Feynman theorem in that they are carried out leaving the internuclear distances and number of electrons unchanged, as they are in the molecule under study. A transfer of the corresponding ϵ_{ij}'s (like the ϵ_{CC}^0 and ϵ_{CH}^0 energies deduced for ethane) from one molecule to another implies the transfer of the bond-forming atoms as they are in the molecule for which they were derived. Such a transfer, involving invariant "local" electron populations, cannot (as a rule) describe an electroneutral molecule (3). For example, if the ethane C and H net charges are 0.0351 and −0.0117 e (3), respectively, a methane "molecule" constructed from these "atoms" would carry a negative charge of −0.0117 e. Clearly, the simple transfer of selected "reference" bond energies ϵ_{ij}^0 would not satisfy the requirement for molecular electroneutrality. The appropriate charge renormalization accompanying the use of "reference" bond energies ϵ_{ij}^0 leads to a description of ϵ_{ij}, eq. [11], featuring the effects due to changes in net atomic charges (Δq_i and Δq_j) with respect to the charges of the atoms forming the reference bonds (3).

Can. J. Chem. Downloaded from www.nrcresearchpress.com by 210.87.254.6 on 09/06/12
For personal use only.

$$[11] \quad \epsilon_{ij} = \epsilon^0_{ij} + a_{ij}\Delta q_i + a_{ji}\Delta q_j$$

The a_{ij} parameters are derived from theory (3). Typical values are, for alkanes, $a_{CC} = -0.777$, $a_{CH} = -0.394$, and $a_{HC} = -1.007$ au. Note that the sum of all the ϵ_{ij}'s yields the bonded part of ΔE^*_a, i.e.,

$$[12] \quad \Delta E^*_a \simeq \Sigma\epsilon^0_{ij} + \Sigma_i\Sigma_j a_{ij}\Delta q_i$$

Equation [12] offers a detailed insight into charge effects governing bond energies and has been applied to a body of over 120 molecules, with an accuracy which is well within experimental uncertainties (3, 11, 12). The point made here is that only a few ϵ^0_{ij}'s need now be calculated by means of eq. [10]. (The new problem, of course, is one of calculating charges — a task which is aided by correlations involving nuclear magnetic resonance shifts (3, 13)).

So far we have dealt with theoretical energies defined by eqs. [10] and [11]. Let us briefly examine the nature of their empirical counterparts. Saturated hydrocarbons $C_nH_{2n+2-2m}$ containing m (≥ 0) cycles serve as a simple typical example. For these compounds, the expansion of eq. [12] yields (3)

$$[13] \quad \Sigma\epsilon_{ij} = (n + m - 1)(\epsilon^0_{CC} - a_{HC}q^0_C/2) + (2n + 2 - 2m)(\epsilon^0_{CH} - a_{HC}q^0_H/4) + \lambda_1\Sigma N_{CC}\Delta q_C + \lambda_2\Sigma\Delta q_C$$

where the Δq_C's are the increments in net charge at the carbon atoms, relative to that of ethane, whose net charge is q^0_C (= 0.0351 e), with $q^0_H = -q^0_C/3$ = hydrogen net charge. $\lambda_1 = a_{CC} - a_{CH}$, $\lambda_2 = 4a_{CH} - a_{HC}$; N_{CC} = number of CC bonds a C atom is engaged in. Note that $(n + m - 1)$ and $(2n + 2 - 2m)$ are the numbers of CC and CH bonds in the molecule, respectively. If all Δq_C's are set equal to 0, eq. [13] reduces formally to a simple bond additivity scheme with no explicit charge effects. Indeed, in this manner we achieve a token charge renormalization by assuming constant atomic charges for the carbon atoms and letting the hydrogen atoms pick up whatever is necessary to ensure electroneutrality. The "apparent" CC and CH bond contributions are then

$$\epsilon^{apparent}_{CC} = \epsilon^0_{CC} - a_{HC}q^0_C/2 = 80.723 \text{ kcal mol}^{-1}$$

$$\epsilon^{apparent}_{CH} = \epsilon^0_{CH} - a_{HC}q^0_H/4 = 104.958 \text{ kcal mol}^{-1}$$

Clearly, these quantities are not true CC and CH bond energies. This aspect is important because it explains the origin of this sort of numerical values obtained from empirical correlations and the fallacy underlying them. Of course, empirical schemes also incorporate part of the $\lambda_1\Sigma N_{CC}\Delta q_C + \lambda_2\Sigma\Delta q_C$ term in "apparent" bond energies and account, in one way or another, for the remaining part in terms of "steric effects". (For example, Allen's scheme (14), which is successful in its own right, gives 82.31 and 104.73 kcal mol^{-1} for the CC and CH bonds of ethane, respectively.) The fact remains that "apparent" bond energies, like those retrieved from empirical correlations, should not be mistaken for true bond properties.

We can now proceed with an examination of the merits of bond energies expressed by eq. [10].

A unifying description of hydrocarbons

Detailed charge analyses are not yet available for a number of classes of compounds (e.g., dienes, allenes, alkynes, and benzene), thus precluding temporarily the evaluation of the $\Sigma_i\Sigma_j a_{ij}\Delta q_i$ terms which are required in any accurate calculation of atomization energies. However, it is still possible to gain some insight into the major factors governing their thermochemical stabilities by taking advantage of an approximation as regards the role of the $\Sigma_i\Sigma_j a_{ij}\Delta q_i$ part. In doing so, we lose the fine-tuning offered by this term which differentiates isomers from one another and introduce an uncertainty of a few kcal mol^{-1} in ΔE^*_a, but this is a small price to pay for the possibility of presenting a general view on the thermochemical stabilities of hydrocarbons in terms of eq. [10].

TABLE 1. Selected $\Sigma_i\Sigma_j a_{ij}\Delta q_i$ values of saturated hydrocarbons and monoolefins (kcal mol^{-1})[a]

Alkane	$\Sigma_i\Sigma_j a_{ij}\Delta q_i$	Alkene	$\Sigma_i\Sigma_j a_{ij}\Delta q_i$
Ethane	0	Ethene	−4.27
Propane	10.38	Propene	8.90
Butane	20.82	1-Butene	19.57
		(Z)2-Butene	20.84
		(E)2-Butene	22.01
Pentane	31.25	1-Pentene	30.18
		(Z)2-Pentene	31.65
		(E)2-Pentene	32.49
Hexane	41.69	1-Hexene	40.28
		(Z)2-Hexene	42.12
		(E)2-Hexene	43.09
		(Z)3-Hexene	42.38
		(E)3-Hexene	43.10

[a]Results extracted from refs. 3 and 11 for the saturated and unsaturated compounds, respectively. A systematic error in Table 3 of ref. 11 indicates $\Sigma_i\Sigma_j a_{ij}\Delta q_i$ values which are too low by 2.13 kcal mol^{-1} and $\Sigma\epsilon^0_{ij}$'s too large by the same amount — an error which is of no consequence as regards the final ΔE^*_a results given for the olefins.

This approach is rooted in two conclusions derived from the detailed energy analyses of alkanes (3) and simple olefins C_nH_{2n} (11). Firstly, it has appeared from eq. [10] that the energy contribution of the carbon−carbon double bond in ethylene (139.27 kcal mol^{-1}) is virtually twice that of the simple bond in ethane (69.633 kcal mol^{-1}) although, admittedly, minor uncertainties subsist as regards the precision of the $\epsilon^0_{C=C}$ term. It is clear that this result departs markedly from the usual understanding of a double vs. a single CC bond which is based on empirical bond energies. In the following, we shall assume that, indeed, $\epsilon^0_{C=C} = 2\epsilon^0_{CC}$ and see what happens. Secondly, it is observed that the $\Sigma_i\Sigma_j a_{ij}\Delta q_i$ terms are quite similar for the alkanes and the alkenes having the same number of carbon atoms. (This information is easily extracted from the results given in Table 1.) Hence, the argument focusses now on the $\Sigma\epsilon^0_{ij}$ part of ΔE^*_a: if we decide not to be too critical about discrepancies of a few kcal mol^{-1} when examining the major trends in hydrocarbon chemistry, it appears that the difference in ΔE^*_a energy between a C_nH_{2n+2} and a C_nH_{2n} hydrocarbon is roughly due to the removal of two CH bonds (2 × 106.81 kcal mol^{-1}) and their replacement by a CC bond (69.63 kcal mol^{-1}), representing a decrease of ~144.0 kcal mol^{-1} in chemical binding energy. Table 2 offers this type of rough estimates using, where appropriate, the averages of the various alkene isomers (e.g., the average ΔE^*_a of *cis*- and *trans*-2-butene, in the comparison with butane). These estimates, whose theoretical validity rests on the similarity in the $\Sigma_i\Sigma_j a_{ij}\Delta q_i$ values for alkanes and alkenes with the same number of carbon atoms, certainly support the result that $\epsilon^0_{C=C} = 2\epsilon^0_{CC}$ given by eq. [10]. No traditional (empirical) bond energies could provide this sort of simple link between saturated and unsaturated hydro-

Can. J. Chem. Downloaded from www.nrcresearchpress.com by 210.87.254.6 on 09/06/12
For personal use only.

TABLE 2. Alkene atomization energies estimated from the parent alkanes (kcal mol^{-1})[a]

Alkane/alkene	ΔE_a^*, alkene Estd.	Exptl.
1 Ethane/ethylene	566.5	562.2
2 Propane/propene	860.1	858.6
3 Butane/butene	1154.2	1154.5
4 Pentane/pentene	1448.2	1447.6
5 Hexane/hexene	1742.0	1741.9
6 Butane/1,3-butadiene	1010.2	1010.2
7 Cyclohexane/cyclohexene	1616.8	1616.1
8 Methylcyclohexane/1-methylcyclohexene	1913.1	1913.2
9 Ethylcyclohexane/1-ethylcyclohexene	2206.3	2207.6
10 Cyclohexane/1,4-cyclohexadiene	1472.8	1472.8

[a]The experimental ΔE_a^* values are from refs. 3 and 12 for the saturated hydrocarbons and ref. 11 for the olefins **1**–**5**. The ΔE_a^* of cyclohexene was deduced from ΔH_f^0(298.15, gas) = −0.84 (15) and ZPE + $H_T - H_0$ = 92.70 kcal mol^{-1}, from data given in ref. 16. For 1-methylcyclohexene, ΔH_f^0(298.15, gas) = −10.0 (15) and ZPE + $H_T - H_0$ = 110.57 kcal mol^{-1} were used, following the rules given by Fliszár and Cantara (12). For 1-ethylcyclohexene, ΔH_f^0(298.15, gas) = −15.0 (15) and ZPE + $H_T - H_0$ = 128.8 kcal mol^{-1} (estimated from 1 methylcyclohexene, using the rules indicated in ref. 12) were used. For 1,4-cyclohexadiene, ΔH_f^0(298.15, gas) = 26.3 (15) and ZPE + $H_T - H_0$ = 77.8 kcal mol^{-1} were used (estimated from the difference between cyclohexane and cyclohexene (14.84 kcal mol^{-1}) which is subtracted from the value of cyclohexene). The ΔE_a^* of butadiene was deduced from ΔH_f^0(298.15, gas) = 26.33 (15), $H_T - H_0$ = 3.63 (17) and ZPE = 51.56 kcal mol^{-1}, from data given in ref. 18.

carbons.

Of course, these results trigger the question about allenic double bonds, triple bonds, and the CC bonding in benzene. In order to gain an insight into these problems, we go back to the fundamental equations [8] and [10] and calculate the appropriate bond energies from the total potential energies $V(i, \text{mol})$ at the atomic nuclei. The following results (Table 3) are derived from SCF calculations at the $(9s5p/6s) \rightarrow [5s3p/3s]$ level. Although this basis cannot match experimental accuracy, it remains that comparisons on a relative scale can be reasonably regarded as being meaningful.

While the result $\epsilon_{C=C}^0 \simeq 2\epsilon_{CC}^0$ is clearly confirmed, it also appears that the carbon–carbon triple bond in acetylene is not far from being the triple of a single bond contribution. It remains, however, that the 2.9 factor (instead of 3) is significant. Indeed, by subtracting four CH bond contributions from butane and adding $1.9\epsilon_{CC}^0$ (i.e., by subtracting ~295 kcal mol^{-1} from the ΔE_a^* of butane) we obtain, in this rough estimate, ΔE_a^* (2–butyne) ≃ 1003.1 kcal mol^{-1}. Under these circumstances, the agreement with the experimental value,[1] ΔE_a^* = 1001.5 kcal mol^{-1}, is certainly satisfactory. On the other hand, taking now propane as model compound in order to evaluate allene, we replace four CH bonds by two CC bonds using the 128.5/66.7 ratio given by *ab initio* calculations (Table 3). The value estimated for allene, $\Delta E_a^* \simeq$ 705.9 kcal mol^{-1}, is reasonably close to its thermochemical counterpart,[2] ~701.9 kcal mol^{-1}. Similarly, the atomization energy of 2,3-pentadiene, 1294.0 kcal mol^{-1}, deduced from normal pentane compares favorably with its experimental counterpart,[3] 1293.3 kcal mol^{-1}. Finally, using now the 1.6 factor deduced from benzene, we estimate its atomization energy from that of cyclohexane by removing six CH bonds and adding six times $0.6\epsilon_{CC}^0$. This estimate leads to ΔE_a^*(benzene) ≃ 1370.6 kcal mol^{-1}, still in acceptable agreement with its experimental value,[4] ΔE_a^* = 1366.51 kcal mol^{-1}. Obviously, it is not everyday chemistry to deduce the energy of benzene from that of cyclohexane in a simple way, with the aid of eq. [10]. Needless to say, conventional empirical bond energies would not have permitted us to see the simple link between these molecules. There is another point worth mentioning. Had we taken the benzene CC bond contribution as the average of single and double bond energies (i.e., the factor 1.5 instead of 1.6) as if there were 3 single and 3 double bonds in the cycle, the estimated energy would be 1328.9 kcal mol^{-1}, leaving us with the problem of explaining why benzene is 37.6 kcal mol^{-1} more stable than the prediction based on this model. The traditional answer, of course, is "resonance energy." This question now seems somewhat artificial since eq. [10] (and the SCF results which are used in its application) clearly lead to a result which, under the present circumstances, is sufficiently close to the experimental value as to kill the problem before it arises.

TABLE 3. SCF calculations of selected bond energy contributions, eqs. [8] and [10], using the contracted $[5s3p/3s]$ basis set[a]

Molecule	V(C, mol), au	ϵ_{CC}, kcal mol^{-1}	Ratio relative to 66.7
Ethane	−88.4670	66.7	1.00
Ethylene	−88.4168	133.7	2.00
Acetylene	−88.3345	193.6	2.90
Benzene	−88.3391	108.1	1.62
Allene	−88.3582 (C-1) −88.2815 (C-2)	128.5	1.93

[a]The following SCF values were used for atomic carbon: E(C, at) = −37.5995 and V_{ne}(C, at) = −87.9315 au, as well as $\partial\epsilon_{CH}/\partial Z_C \simeq 0.026$ au.

Conclusions

The chemical binding of a molecule is conveniently expressed by a sum, $\sum\epsilon_{ij}^0$, of appropriately selected reference bond energies plus a term, $\sum_i\sum_j a_{ij}\Delta q_i$, which ensures molecular electroneutrality, on one hand, and provides an accurate fine-tuning of molecular energies, on the other. The dehydrogenation of a saturated hydrocarbon to give a monoolefin is shown (in a first approximation) not to affect the $\sum_i\sum_j a_{ij}\Delta q_i$ term, thus suggesting the reasonable expectation that, in similar manner, the dehydrogenation of a monoolefin to give a diolefin also leaves $\sum_i\sum_j a_{ij}\Delta q_i$ practically unchanged, an uncertainty of a few (say, 5) kcal mol^{-1} being regarded acceptable in this approximation. It turns out that this rough approach is also valid when dehydrogenation is carried further, e.g., in the series cyclohexane, cyclohexene, cyclohexadiene and, finally,

[1]This value was deduced from ΔH_f^0(298.15, gas) = 34.97 (15), $H_T - H_0$ = 3.96 (17), and ZPE = 51.21 kcal mol^{-1}, from data given in ref. 19.

[2]Deduced from ΔH_f^0(298.15, gas) = 45.92 kcal mol^{-1} (15). The ZPE + $H_T - H_0$ = 37.2 kcal mol^{-1} value is estimated from the difference between propane (20) and propene (11) (i.e. 14.38 kcal mol^{-1}) which is subtracted from the value of propene.

[3]ΔH_f^0(298.15, gas) = 31.79 kcal mol^{-1} (15). The value for ZPE + $H_T - H_0$ = 73.15 kcal mol^{-1} is estimated from the difference between *n*-pentane (20) and pentene (11) (i.e., 14.84 kcal mol^{-1}) which is subtracted from the value of pentene.

[4]ΔH_f^0(298.15, gas) = 19.82 kcal mol^{-1} (15). ZPE + $H_T - H_0$ = 66.22 kcal mol^{-1}, from data given in ref. 19.

benzene, as well as in the formation of allenic and triple CC bonds.

The $\sum_i \sum_j a_{ij} \Delta q_i$ term being practically invariant in dehydrogenations, the change in energy is primarily reflected in the $\sum \epsilon_{ij}^0$ sum. Equation [10] and the appropriate Hartree–Fock potential energies yield (on the basis of $\epsilon_{CC}^0 = 69.633$ for the CC single bond) the following results for CC bonds: 139.27 (ethylene), 201.9 (triple bond), 134.2 (allenic double bond), and 111.4 kcal mol^{-1} (benzene). These theoretical energies enable a simple description of energy changes in dehydrogenations, quite unlike their empirical counterparts which already include part of the $\sum_i \sum_j a_{ij} \Delta q_i$ term. No claim for accuracy can be made for this sort of brute force approach. It remains, however, that a clear link is created in this manner between typical saturated, olefinic, acetylenic, and aromatic compounds. Of course, a host of details has to be worked out, a task which looks promising. The present results should certainly encourage us to do some more thinking about possible further applications of eq. [10].

Acknowledgement

Financial assistance by the National Research Council of Canada is gratefully acknowledged.

1. P. POLITZER and R. G. PARR. J. Chem. Phys. **61**, 4258 (1974).
2. P. POLITZER. J. Chem. Phys. **70**, 1067 (1979).
3. S. FLISZÁR. J. Am. Chem. Soc. **102**, 6946 (1980).
4. S. FLISZÁR, M. FOUCRAULT, M.-T. BÉRALDIN, and J. BRIDET. Can. J. Chem. **59**, 1074 (1981); S. FLISZÁR and M.-T. BÉRALDIN. J. Chem. Phys. **72**, 1013 (1980).
5. L. H. THOMAS. Proc. Camb. Philos. Soc. **23**, 542 (1926).
6. E. FERMI. Z. Physik **48**, 73 (1928).
7. N. H. MARCH. Self-consistent fields in atoms. Pergamon Press Ltd., Oxford, U.K. 1975.
8. J. A. ALONSO, D. J. GONZÁLEZ, and L. C. BALBÁS. Int. J. Quantum Chem. **22**, 989 (1982); N. H. MARCH. *In* Theoretical Chemistry, A Specialist Periodical Report, **4**, 92 (1981), The Royal Society of Chemistry, Burlington House, London W1V 0BN.
9. P. HOHENBERG and W. KOHN. Phys. Rev. **136**, B864 (1964).
10. G. DEL RE. Gazz. Chim. Ital. **102**, 929 (1972).
11. M.-T. BÉRALDIN and S. FLISZÁR. Can. J. Chem. **61**, 197 (1983).
12. S. FLISZÁR and M.-T. BÉRALDIN. Can. J. Chem. **60**, 792 (1982); J. K. CHOI, M. J. JONCICH, Y. LAMBERT, P. DESLONGCHAMPS, and S. FLISZÁR. J. Mol. Struct. (Theochem.) **89**, 115 (1982); S. FLISZÁR and J.-L. CANTARA. Can. J. Chem. **59**, 1381 (1981).
13. S. FLISZÁR, G. CARDINAL, and M.-T. BÉRALDIN. J. Am. Chem. Soc. **104**, 5287 (1982); M.-T. BÉRALDIN, E. VAUTHIER, and S. FLISZÁR. Can. J. Chem. **60**, 106 (1982); H. HENRY and S. FLISZÁR. J. Am. Chem. Soc. **100**, 3312 (1978); S. FLISZÁR. Can. J. Chem. **54**, 2839 (1976); S. FLISZÁR, A. GOURSOT, and H. DUGAS. J. Am. Chem. Soc. **96**, 4358 (1974).
14. T. L. ALLEN. J. Chem. Phys. **31**, 1039 (1959).
15. S. W. BENSON, F. R. CRUICKSHANK, D. M. GOLDEN, G. R. HAUGEN, H. E. O'NEIL, A. S. RODGERS, R. SHAW, and R. WALSH. Chem. Rev. **69**, 279 (1969).
16. N. NETO, C. DILAURO, E. CASTELLUCCI, and S. CALIFANO. Spectrochim. Acta, **23**A, 1763 (1967).
17. F. D. ROSSINI, K. S. PITZER, R. L. ARNETT, R. M. BRAUN, and G. C. PIMENTEL. Selected values of physical and thermodynamic properties of hydrocarbons and related compounds. American Petroleum Institute, Carnegie Press, Pittsburgh, PA. 1953.
18. YU. N. PANCHENKO. Spectrochim. Acta, **31**A, 1201 (1975).
19. G. HERZBERG. Molecular spectra and molecular structure. II. Infrared and Raman spectra of polyatomic molecules. D. Van Nostrand Co. Inc., Princeton, NJ. 1968.
20. H. HENRY, G. KEAN, and S. FLISZÁR. J. Am. Chem. Soc. **99**, 5889 (1977).

Can. J. Chem. Downloaded from www.nrcresearchpress.com by 210.87.254.6 on 09/06/12
For personal use only.

Deuterium isotope effects on the partial molal volumes of cyclohexane, acetone, and acetonitrile in carbon tetrachloride

G. RONALD BROWN, JULIAN K. EDWARD, AND JOHN T. EDWARD

Department of Chemistry, McGill University, 801 Sherbrooke St. W., Montreal, (P.Q.), Canada H3A 2K6

Received March 2, 1983

G. RONALD BROWN, JULIAN K. EDWARD, and JOHN T. EDWARD. Can. J. Chem. **61**, 2684 (1983).

At 25°C both molar volumes V and partial molal volumes $\bar{V}^0_{CCl_4}$ in carbon tetrachloride of cyclohexane-d_{12} and of acetone-d_6 are smaller than V and $\bar{V}^0_{CCl_4}$ of the corresponding protio compounds. However, both V and $\bar{V}^0_{CCl_4}$ of acetonitrile-d_3 are larger than V and $\bar{V}^0_{CCl_4}$ of acetonitrile-h_3, and in solvent cyclohexane $\bar{V}^0_{C_6H_{12}}$ of acetone-d_6 and of acetone-h_6 are approximately equal. Apparently deuteration has not only a steric effect, but (in polar compounds) a counter-balancing effect, which may be polar.

G. RONALD BROWN, JULIAN K. EDWARD et JOHN T. EDWARD. Can. J. Chem. **61**, 2684 (1983).

A 25°C, les volumes molaires V et les volumes molaires partiels $\bar{V}^0_{CCl_4}$ du cyclohexane-d_{12} et de l'acétone-d_6 dans le tétrachlorure de carbone sont plus faibles que V et $\bar{V}^0_{CCl_4}$ des composés non deutérés correspondants. Cependant, les valeurs de V et de $\bar{V}^0_{CCl_4}$ de l'acétonitrile-d_3 sont plus grandes que les valeurs correspondantes pour l'acétonitrile non deutéré; dans le cyclohexane comme solvant, les valeurs de $\bar{V}^0_{C_6H_{12}}$ de l'acétone-d_6 et de l'acétone-h_6 sont à peu près égales. Apparemment, la deutération n'a pas seulement un effet stérique, mais (dans les composés polaires) un effet contre balançant qui peut être polaire.

[Traduit par le journal]

A large number of examples of secondary deuterium isotope effects on reaction rates (reviewed in refs. 1–3) has been observed. One explanation which accounts for many results depends on the idea that protio-alkyl groups (such as CH_3) occupy a slightly larger volume than the corresponding deuteroalkyl groups (such as CD_3), because of the greater amplitude of the zero-point vibration of the C—H as compared with the C—D bond. This idea finds support in the studies of Baldry and Robinson (4) on the conformational equilibrium of *trans*-1-methyl-d_3-3-methylcyclohexane, which showed the conformation having CD_3 axial favoured by 11 cal mol^{-1} over the conformation having CH_3 axial; in optical rotatory dispersion studies of Djerassi and co-workers (5); and in studies of steric effects of H and D on ^1H and ^{13}C chemical shifts by Anet and Dekmezian (6).

However, the most direct indication of this volume difference might be expected to come from measurements of molar volumes. Indeed, at the triple point (7) and at the critical temperature (8) the molar volume V of CH_4 is greater than that of CD_4. Similarly, at ordinary temperatures the molar volumes of benzene (9–11), cyclohexane (16), and toluene (11) are greater than the volumes of their deuterated forms. However, Rabinovich (11) reported that the molar volumes of $CDCl_3$, CD_3NO_2, $PhND_2$, CH_3OD, CH_3CH_2OD, $CH_3CH_2CH_2OD$, $(CH_3)_2CHOD$, $CH_3CH_2CH_2CH_2OD$, $CH_2OD—CH_2OD$, $CH_2OD—CHOD—CH_2OD$, and $(CH_3)_3CCO_2D$ were greater than the volumes of the corresponding protio compounds.

This last result pointed to a curious difference between hydrocarbons and more polar organic molecules which we thought worth confirming, particularly since it was based on density measurements made with pyknometers, which are probably less accurate than the direct-reading density meters now available. Furthermore, measurements of partial molal volumes $\bar{V}^0$ in a single solvent should be preferable to measurements of molar volumes of the neat liquids in revealing differences in intrinsic volumes of molecules. Liquids differ in internal pressure (12) and cohesive energy density (13), factors which might be expected to change on deuteration and to affect V. We have chosen carbon tetrachloride as our solvent for $\bar{V}$; it is probably the favoured solvent for partial molal volume determinations because it is reasonably non-polar and yet has fairly good solvent properties. We have also made a few measurements using cyclohexane as solvent.

Experimental

Materials

Perdeuterated solvents were obtained from Merck, Sharp and Dohme Inc., and are reported to be >99% isotopically pure. They were used without further purification. Cyclohexane, acetone, and acetonitrile were spectrograde solvents and were also used without purification. All of these solvents showed only one peak in vapour phase chromatography. Carbon tetrachloride was purified as reported previously (14), but results using this purified material did not differ appreciably from results using Fisher Scientific Company spectrograde material, and so the latter was used as solvent in later experiments.

Measurements

Density measurements were carried out at 25.0°C using a Paar digital precision density meter, Model DMA 02C. A water bath thermostat (12 L) was used to control the temperature of the density meter. The temperature was monitored continuously using an HP Quartz Thermometer (Model 2804A) and was kept constant at 25.00 ± 0.01°C. Apparent molar volumes ϕ_v of solutes were calculated from

$$\phi_v = M \frac{1/d - w_1/d^0}{w_2}$$

where M is the molecular weight of the solute, w_2 its concentration expressed as a weight fraction, w_1 the weight fraction of the solvent (carbon tetrachloride or cyclohexane), and d and d^0 the density of solution and of solvent, respectively. Solutions were made up by weight. The chief source of error in w_2 was found to be the loss of solvent when a flask was unstoppered to allow the addition of very small amounts of solute; this was prevented by the use of serum caps impermeable to the vapors of carbon tetrachloride or cyclohexane.

Results

Results are given in Table 1 and shown graphically in Figs. 1 and 2. Agreement with data in the literature, where available, is good, as shown by footnotes in Table 1 and, more convincingly, by the points from literature data for cyclohexane and acetone plotted in Fig. 1.

Values of apparent molal volumes in carbon tetrachloride ϕ_v plotted against concentration expressed as mole fraction fitted

Can. J. Chem. Downloaded from www.nrcresearchpress.com by 210.87.254.5 on 09/06/12
For personal use only.

TABLE 1. Molar volumes, V, and partial molal volumes in carbon tetrachloride $\bar{V}^0_{CCl_4}$ (both at 25.00°C)

Compound	V (mL mol^{-1})	Δ_1* (mL mol^{-1})	$\bar{V}^0_{CCl_4}$ (mL mol^{-1})	Δ_2† (mL mol^{-1})
Cyclohexane	108.995‡	0.463	109.63	0.52
Cyclohexane-d_{12}	108.532§		109.11	
Acetonitrile	52.796	−0.082	52.54	−0.15
Acetonitrile-d_3	52.878		52.69	
Acetone	73.987	0.132	74.15	0.15
Acetone-d_6	73.865		74.00	

* $\Delta_1 = V$ (protio compound) − V (deutero compound).
† $\Delta_2 = \bar{V}^0_{CCl_4}$ (protio compound) − $\bar{V}^0_{CCl_4}$ (deutero compound).
‡ From the data of Dixon and Schiessler (10), it may be calculated that at 25.0°C, V = 108.75 mL mol^{-1}.
§ V = 108.42 from the data in ref. 10.

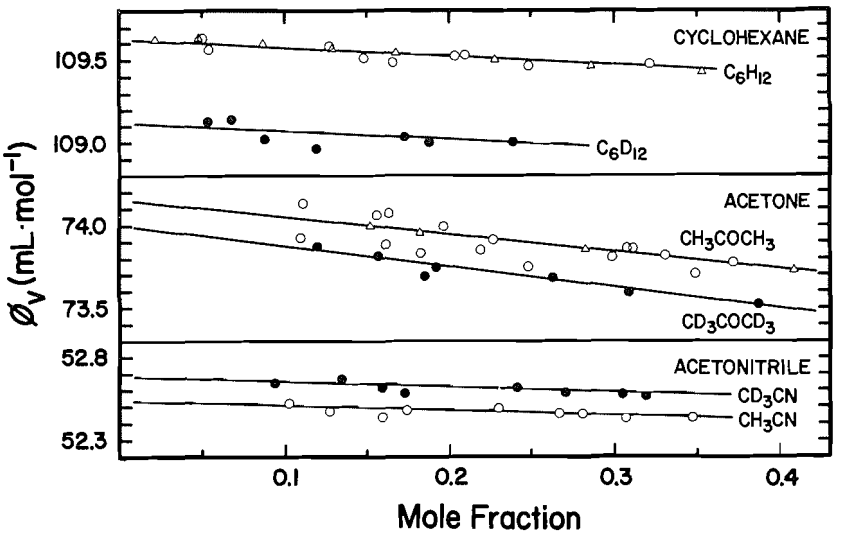

FIG. 1. Plots of apparent molal volume ϕ_v of cyclohexane, acetone, and acetonitrile (open circles), and of cyclohexane-d_{12}, acetone-d_6, and acetonitrile-d_3 (filled circles) against concentration of solute in carbon tetrachloride. Straight lines show least-squares fit to data. Values calculated from excess volumes of cyclohexane + carbon tetrachloride (ref. 15) and of acetone + carbon tetrachloride (ref. 16) in the literature are shown as triangles, and not included in least-squares calculations.

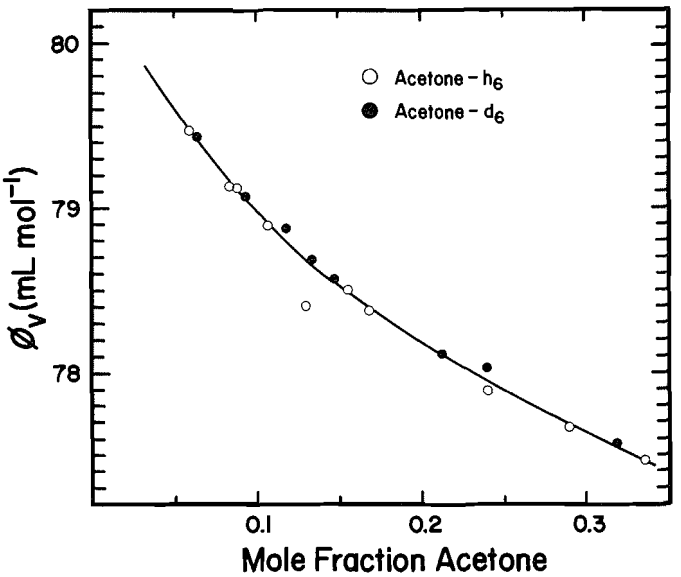

FIG. 2. Plots of apparent molal volumes ϕ_v of acetone (open circles) and of acetone-d_6 (filled circles) in cyclohexane as solvent. (Notice that scale for y-axis is the same as in Fig. 1.)

straight lines of negative slope, as is generally found for solutions in this solvent, and $\bar{V}^0_{CCl_4}$ values were obtained by extrapolation to zero concentration. Although the points show some scatter, the differences between $\bar{V}^0_{CCl_4}$ of protio- and deutero-compounds are too great to be dismissed as experimental error. Furthermore, as seen in Table 1, the differences Δ_2 between $\bar{V}^0_{CCl_4}$ values are not greatly different from the differences Δ_1 between V values. The latter are obtained from densities of the neat liquids, without the errors introduced by making up solutions of known concentration, and hence V values are likely to be very accurate.

Discussion

Cyclohexane and cyclohexane-d_{12}

It is evident from Table 1 that replacing the protium atoms of C_6H_{12} by deuterium to give C_6D_{12} results in a contraction of about 0.5 mL mol^{-1} in both V and $\bar{V}^0_{CCl_4}$.

The volume occupied by a mole of cyclohexane, either as the neat liquid (V), or at infinite dilution in carbon tetrachloride ($\bar{V}^0_{CCl_4}$), is made up of the van der Waals volume V_w ($\equiv Nv_w$) of Avogadro's number N of molecules, each having a van der Waals volume v_w (17, 18), plus the empty volume V_e ($\equiv Nv_e$) require to pack the molecules into the pure liquid or into the

Can. J. Chem. Downloaded from www.nrcresearchpress.com by 210.87.254.5 on 09/06/12
For personal use only.

Can. J. Chem. Downloaded from www.nrcresearchpress.com by 210.87.254.5 on 09/06/12
For personal use only.

carbon tetrachloride solvent (18, 19).

Cyclohexane C_6H_{12} has $V_w = 61.4$ mL mol^{-1}, and hence V_e makes a contribution of 47.6 mL mol^{-1} to V and 48.2 mL mol^{-1} to $\bar{V}^0_{CCl_4}$, i.e. about 44% to each volume. V_e decreases with decreasing V_w (20). We shall consider first the decrease in V_w, and then the decrease in V_e, to be expected on replacing H by D.

In ethane the bond length of C—H is 1.112 ± 0.001 Å, as determined by electron diffraction; this is reduced to 1.107 ± 0.001 Å for C—D (ref. 2, p. 59). This shortening of the bond will (according to the method of calculation described in ref. 22) result in v_w of D attached to aliphatic carbon being smaller by 0.021 Å^3 than H attached to aliphatic carbon, or v_w of C_6D_{12} being 0.25 Å^3 smaller than v_w of C_6H_{12}, i.e. in V_w for C_6D_{12} being 0.15 mL mol^{-1} smaller than V_w for C_6H_{12}.

Going along with a smaller V_w will be a smaller V_e. While $v_w \propto r_w^3$, very roughly $v_e \propto r_w^2$ (20, 23), and so one may expect V_e for C_6D_{12} to be about 0.16% smaller than V_e for C_6H_{12}, or 48.1 mL mol^{-1} in $\bar{V}^0_{CCl_4}$. Consequently, a total reduction of 0.15 + 0.10 = 0.25 mL mol^{-1} is to be expected in $\bar{V}^0_{CCl_4}$ in going from C_6H_{12} to C_6D_{12}.

This is about half the reduction observed. It seems likely that because of the closer approach of solvent CCl_4 molecules to the skeletal carbon atoms of C_6D_{12}, the time-averaged attraction will be greater and the empty volume will be reduced more than calculated above. (The calculations above assume V_e to be determined solely by geometric factors, and attractive forces to be the same for protio- and deutero-compounds). More accurate data (e.g. by excess volume measurements by dilatometry) would be desirable to check this idea.

Acetone and acetone-d_6

A molecule of acetone has half the number of hydrogen atoms of a molecule of cyclohexane, and so the reduction in V and $\bar{V}^0_{CCl_4}$ of acetone on replacing H by D might be expected to be half as great as the reduction in V and $\bar{V}^0_{CCl_4}$ of cyclohexane for this change. In fact, it was only about one-third as great in both cases. It has been shown that the proportion of empty volume in $\bar{V}^0_{CCl_4}$ of acetone is smaller than in $\bar{V}^0_{CCl_4}$ of a hydrocarbon of equal v_w (23), presumably because of the attractive effect of the dipolar carbonyl group on the polarizable CCl_4 molecule. If, indeed, deuteration affects volume largely by changes in v_e surrounding the solute molecules, then its effect might be expected to be diminished as v_e is diminished.

Similar considerations might be expected to apply to V of acetone, v_e being diminished by the dipole–dipole attractions of the molecules of the liquid. Consequently, it was thought that greater volume differences would show up if the solvent were changed from carbon tetrachloride to the less polarizable cyclohexane, in which v_e surrounding the solute acetone molecules should become greater (24).

These expectations were not realized, as shown by the ϕ_v values of acetone-h_6 and acetone-d_6 plotted in Fig. 2: although there is some indication that ϕ_v of the deutero compound at a given mole fraction is slightly *greater* than ϕ_v of the protio compound, the differences are within experimental error. The plots are no longer straight lines, making extrapolation to zero concentration to get $\bar{V}^0_{C_6H_{12}}$ difficult, but it is apparent that $\bar{V}^0_{C_6H_{12}}$ is essentially the same for the two compounds.

The curvature of the plots and the steepness of the slopes in Fig. 2 probably result from solute–solute interactions, which can be expected to be much greater in cyclohexane than in carbon tetrachloride. A comparison of the results for acetone in CCl_4 in Fig. 1 and in cyclohexane in Fig. 2 shows why carbon tetrachloride is preferred as solvent in volumetric studies of polar organic molecules.

Acetonitrile and acetonitrile-d_3

The same arguments which led us to expect a small reduction in $\bar{V}^0_{CCl_4}$ of acetone in carbon tetrachloride on replacing H by D lead us to expect a yet smaller decrease in $\bar{V}^0_{CCl_4}$ of acetonitrile on replacing H by D. However, an increase and not a decrease in $\bar{V}^0_{CCl_4}$ is now observed.[1] This, like the abolition of the expected decrease in volume in $\bar{V}^0_{C_6H_{12}}$ on going from acetone to acetone-d_6, indicates that some second effect is at work in polar compounds which can more than offset the simple steric effect observed with hydrocarbon solutes. The nature of this second effect remains unclear. The smaller polarizability of C—D bonds (10) might be expected to cause polar molecules such as CD_3CN to have slightly lower dipole moments that their protio analogues and hence to attract solvent CCl_4 molecules less strongly, leading to larger $\bar{V}^0_{CCl_4}$ values. This agrees with the view of Buckingham (25), who has asserted that deuterium compounds have lower dipole moments than the corresponding protium compounds. However, majority opinion at present supports the opposite viewpoint (21), and further investigations are required.

Acknowledgments

We are grateful to the Natural Sciences and Engineering Research Council of Canada for financial support, and to Prof. D. Patterson and Dr. J. McGarrity for advice and discussion.

1. P. Lazlo and Z. Welvart. Bull. Soc. Chim. Fr. 2412 (1966).
2. C. J. Collins and N. S. Bowman (*Editors*). Isotope effects in chemical reactions. Van Nostrand-Reinhold, New York. 1971. pp. 46, 56–63, 176, 234, 235.
3. L. Melander and R. E. Carter. Advances in physical organic chemistry. Vol. 10. *Edited by* V. Gold and D. Bethell. Academic Press, London. 1974. p. 1.
4. K. W. Baldry and M. J. T. Robinson. Tetrahedron, **33**, 1663 (1977).
5. S.-F. Lee, G. Barth, and C. Djerassi. J. Am. Chem. Soc. **103**, 295 (1981).
6. F. A. L. Anet and A. H. Dekmezian. J. Am. Chem. Soc. **101**, 5449 (1979).
7. K. Clusius and K. Weigand. Z. Physik. Chem. B**46**, 1 (1940).
8. A. F. Grigor and W. A. Steele. J. Chem. Phys. **48**, 1032 (1968).
9. C. K. Ingold, C. G. Raisin, C. L. Wilson, C. R. Bailey, and B. Topley. J. Chem. Soc. 915 (1936). L. H. P. Weldon and C. L. Wilson. J. Chem. Soc. 235 (1946).
10. J. A. Dixon and R. W. Schiessler. J. Am. Chem. Soc. **76**, 2197 (1954).
11. I. B. Rabinovich. Influence of isotopy on the physicochemical properties of liquids. Consultants Bureau, New York. 1970. p. 124.
12. J. H. Hildebrand and R. L. Scott. Solubility of nonelectrolytes. 3rd ed. Reinhold, New York. 1950. Chapt. V.
13. M. R. J. Dack. Chem. Soc. Rev. **4**, 211 (1975).
14. J. T. Edward, P. G. Farrell, and F. Shahidi. J. Phys. Chem. **82**, 2310 (1978).
15. O. Kiyohara and G. C. Benson. J. Chem. Thermodyn. **9**, 807 (1977).
16. R. K. Nigam, B. S. Mahl, and P. P. Singh. J. Chem. Thermodyn. **4**, 41 (1972).

[1]Acetonitrile is not miscible enough in cyclohexane for ϕ_v determinations (cf. Fig. 2) in this solvent.

17. A. BONDI. J. Phys. Chem. **68**, 441 (1964).
18. J. T. EDWARD. J. Chem. Educ. **47**, 261 (1970).
19. A. BONDI. J. Phys. Chem. **58**, 929 (1954).
20. J. T. EDWARD and P. G. FARRELL. Can. J. Chem. **53**, 2965 (1975).
21. E. A. HALEVI. *In* Progress in physical organic chemistry. Vol. 1. *Edited by* S. G. Cohen, A. Streitwieser, and R. W. Taft. Interscience, New York. 1963. pp. 114–121.
22. J. T. EDWARD. Chem. Ind. London, 774 (1956).
23. J. T. EDWARD, P. G. FARRELL, and F. SHAHIDI. Can. J. Chem. **57**, 2585 (1978).
24. J. T. EDWARD, P. G. FARRELL, and F. SHAHIDI. Can. J. Chem. **57**, 2887 (1978).
25. A. D. BUCKINGHAM. Personal communication, quoted in ref. 21.

Can. J. Chem. Downloaded from www.nrcresearchpress.com by 210.87.254.5 on 09/06/12
For personal use only.

A reversal in the order of H-6$_R$ and H-6$_S$ chemical shifts of some aldohexopyranose derivatives, associated with the acetylation of OH-4 and OH-6 groups. A distinction between 3- and 4-linked D-glucose residues in disaccharides

VANGA S. RAO AND ARTHUR S. PERLIN
Department of Chemistry, McGill University, Montreal, P.Q., Canada H3A 2A7

Received April 11, 1983

VANGA S. RAO and ARTHUR S. PERLIN. Can. J. Chem. **61**, 2688 (1983).

On peracetylation of methyl α- or β-D-glucopyranoside, there is a reversal in the order of the chemical shifts of the 6,6′-methylene protons, i.e., whereas the H-6$_S$ signal appears downfield of H-6$_R$ in the spectra of the glucosides, their relative locations in the spectra of the tetraacetates are interchanged. Evidence is presented from comparative data for a wide range of regioselectively acetylated D-glucose derivatives, showing that the reversal in chemical shifts of the methylene protons occurs only when *both* O-4 and O-6 are acetylated. Consequently, in the disaccharide series, shift reversal is *not* observed with glucose residues that are bonded glycosidically through O-4, whereas the reversal occurs when the linkage is through O-3. A conformational model offered to account for these effects suggests that the 4- and 6-*O*-acetyl substituents are oriented by means of a weak, mutual, interaction in such a way that the magnetic anisotropy of the carbonyl group of the 6-*O*-acetyl substituent can induce selective deshielding of H-6$_R$. The comparable influences of *O*-benzoyl and *O*-(4-nitro)benzoyl substituents on chemical shift are consistent with this proposal. D-Mannopyranosides exhibit characteristics analogous to those of their D-*gluco* epimers, whereas D-galactopyranosides give a different, more complex, chemical shift pattern.

VANGA S. RAO et ARTHUR S. PERLIN. Can. J. Chem. **61**, 2688 (1983).

La peracétylation de l'α ou du β-D-glucopyrannoside de méthyle provoque une inversion dans l'ordre des déplacements chimiques des protons du méthylène en 6,6′; par exemple, alors que le signal du H-6$_S$ sort à champ faible par rapport à celui du H-6$_R$ dans les spectres des glucosides, leurs positions relatives sont interchangées dans les spectres des tétraacétates. A partir de données comparatives se rapportant à un grand nombre de dérivés du D-glucose acétylé de façon régiosélective, on montre que l'inversion des déplacements chimiques des protons du méthylène se produit uniquement lorsque les deux oxygènes en positions 4 et 6 sont acétylés. Par conséquent, dans la série des disaccharides, on n'observe pas d'inversion dans les déplacements chimiques lorsque les unités de glucose sont liées de façon glycosidique par l'intermédiaire de l'oxygène en position 4 cependant l'inversion se produit lorsque cette liaison s'établit par l'intermédiaire de l'oxygène en position 3. Un modèle conformationnel utilisé pour tenir compte de ces effets suggère que les substituants O-4 et O-6 acétylés sont orientés par une interaction mutuelle faible de telle sorte que l'anisotropie magnétique du groupe carbonyle du substituant acétyle peut induire un déblindage sélectif de H-6$_R$. Les influences comparables des substituants *O*-benzoyle et *O*-(nitro-4)benzoyle sur les déplacements chimiques sont en accord avec cette suggestion. Les D-mannopyrannosides présentent des caractéristiques semblables à celle de leurs épimères D-gluco, tandis que les D-galactopyrannosides ont des déplacements chimiques différents et plus complexes.

[Traduit par le journal]

Introduction

Of the two anisochronous 6,6′-methylene proton nmr signals of methyl 2,3,4,6-tetra-*O*-acetyl-α-D-glucopyranoside (**2**), that at lower field (δ 4.25, $J_{H\text{-}5,H\text{-}6}$ = 4.6 Hz) has been unambiguously assigned (1) to the *pro-R* hydrogen, and the higher field resonance (δ 4.08, $J_{H\text{-}5,H\text{-}6}$ = 2.4 Hz) to the *pro-S* nucleus. From the magnitude of proton coupling, it has been estimated (1) that *RHS* and *RCS* represent the major rotamers about the C-5,C-6 bond; little or no contribution would be expected from the *ROS* rotamer, because of an unfavorable *quasi-syn-axial* interaction between the 4- and 6-*O*-acetyl group. The corresponding data (2) for the methylene protons of methyl α-D-glucopyranoside (**1**) differ from those of **2** in that the smaller coupling (2.2 Hz) is exhibited by the downfield H-6 resonance of **1** (δ 3.85), and the larger value (5.4 Hz) by that at higher field (δ 3.75). Consequently, when compound **1** is peracetylated there appears to be a reversal either in the order of the chemical shifts of H-6$_R$ and H-6$_S$, or else in the magnitude of their couplings with H-5. Although a change in coupling appeared to be less likely, because it would entail a major contribution from the *contra* thermodynamic rotamer (*ROS*) as well as from the *RHS* rotamer, a more definitive answer to the question was warranted.

Results and discussion

A choice between the two possibilities represented by the apparent change in the coupling or chemical shift pattern was readily provided by reference to the ^{1}H nmr spectra of methyl α-D-glucopyranoside, partially monodeuterated at C-6 (**3**), and its tetraacetate (**4**) (3). This showed that *chemical shift reversal* occurs: i.e., the more downfield of the methylene resonances was produced by H-6$_S$ of **3**, and by H-6$_R$ of **4** (Fig. 1).[1] Clearly, also, the rotamer population about the C-5,C-6 bond of methyl α-D-glucopyranoside (**1**) must be closely similar to that in tetraacetate **2**, because the appropriate couplings are of virtually the same size in both spectra.

Considering the orientations of the methylene protons in major rotamers *RHS* and *RCS* leads to the expectation that H-6$_R$ should resonate at higher field than H-6$_S$, according to the "*syn*-up" rule (2). That is, H-6$_R$ is *syn* with respect to C-4 in both rotamers and also to O-5 in *RCS*, whereas H-6$_S$ experiences only two *syn* relationships – with respect to O-5 in *RHS* and to C-4 in *RCS*. Consequently, although the "*syn*-up" rule is applicable with **1**, it fails with **2**.[2] As shown later, this difference can be attributed to the replacement of OH-4 and

[1] Each spectrum consists (3) of overlapping signals produced by a mixture of molecules in which either H-6$_R$ or H-6$_S$ is replaced by deuterium, together with molecules in which C-6 is not deuterated. Consequently, the upfield values of δ correspond to deuterium isotope shielding increments of 0.014–0.02 ppm.

[2] However, the data used in formulating the "*syn*-up" rule (2) did not include those for *O*-acyl derivatives.

Can. J. Chem. Downloaded from www.nrcresearchpress.com by 210.87.254.105 on 09/06/12
For personal use only.

Can. J. Chem. Downloaded from www.nrcresearchpress.com by 210.87.254.105 on 09/06/12
For personal use only.

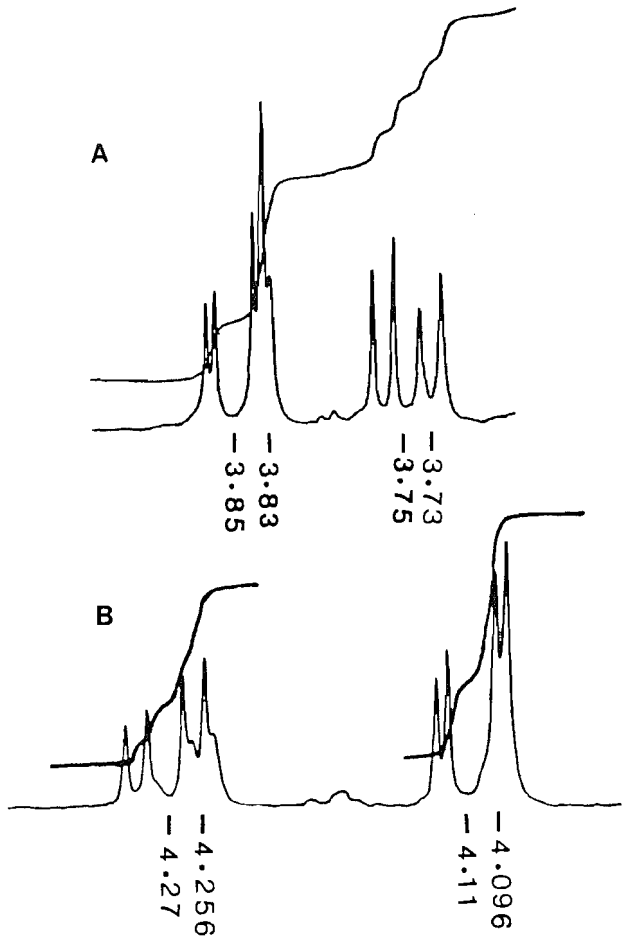

FIG. 1. Partial ^1H nmr spectra (400 MHz) of methyl α-D-glucopyranoside partially deuterated at C-6 (**3**, in D_2O) and its 2,3,4,6-tetraacetate (**4** in $CDCl_3$), A: resonance signals of H-6_S (downfield) and H-6_R of **3**; B: resonance signals of H-6_R (downfield) and H-6_S of **4**.

OH-6 by *O*-acetyl groups, and the associated changes in magnetic anisotropy in the vicinity of C-6.

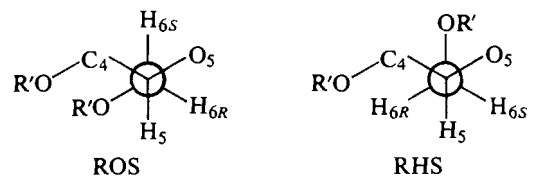

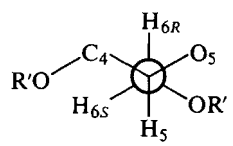

RCS

R′ = H, Ac

Analogous reversals in the order of methylene ^1H-chemical shifts were inferred for a number of glucopyranoside derivatives assuming, on the basis of the observed coupling patterns, that the population of rotamers is essentially the same in these instances as in **1** and **2**. Thus, in the spectra of methyl 2-*O*-benzyl- (**5**), 3-*O*-benzyl- (**7**), 2,3-di-*O*-benzyl- (**9**), and 2,3,4-tri-*O*-benzyl- (**11**) β-D-glucopyranosides, available from a previous study (4), the lower field signal consistently showed weaker coupling with H-5 (2.7–3.6 Hz) than did the upfield multiplet (4.6–5.0 Hz) (Table 1). For acetylated compounds **6**, **8**, and **10**, as well as for their α-anomers (**15**, **17**, and **19**), the order was reversed, as the downfield signal always was characterized by the larger coupling with H-5 (4.4–5.0 Hz vs. 2.0–2.4 Hz) (Table 1). By analogy with monodeuterated **3** and **4**, H-6_S is taken to be the less shielded proton within the non-acetylated series, and the more shielded nucleus within the series of *O*-acetyl derivatives.

An exception was found, nevertheless, in the relationship between methyl 2,3,4-tri-*O*-benzyl-β-D-glucoside (**11**) and its 6-acetate (**12**). Hence, the downfield H-6 signal for both compounds exhibited the smaller coupling with H-5, suggesting that there was no reversal in the methylene chemical shifts when OH-6 was converted into OAc-6. The most obvious way in which **11** and **12** differ from the other pairs of compounds is in having an ether substituent at O-4, which prevents the introduction of an *O*-acetyl group at that position. This indicated that a 4-*O*-acetyl substituent must be present if the order of the chemical shifts is to be reversed, although it was not clear that a 6-*O*-acetyl group is a prerequisite as well. Consequently, several other derivatives were chosen to examine systematically the effect of different combinations of substitution at O-4 and O-6. The data they afforded (Table 2) clearly indicate that both a 4-*O*-acetyl and a 6-*O*-acetyl group, as in **23** (or **24**), are essential for the interchange in the methylene chemical shifts to be observed. Hence, **23** and **24** exhibited an interchange, whereas when there was an acetyl group solely at O-4 (**22**, **25**), or only at O-6 (**12** (Table 1), **21**), or when other types of substituents were present at position-6 (**26**–**28**), the combined pattern of chemical shifts and couplings paralleled that of the unsubstituted glycoside (**20**): i.e., the smaller of the H-5,H-6 couplings (1.6–2.8 Hz vs. 3.6–6.7 Hz), was consistently observed in the downfield multiplet.

O-*Acetyl derivatives of* D-*glucose disaccharides*

If the phenomenon just described is a general one, it should also be evident with more complex types of structures. For example, the methylene protons of the reducing end residue of a D-glucose disaccharide linked through O-4 or O-6 should, upon acetylation, exhibit neither a reversal in chemical shift nor a change in coupling pattern. Accordingly, H-6_S would be expected to show a smaller coupling than H-6_R with H-5, in both the free sugar and its peracetate. However, if the glycosidic bond were (1 → 3) or/and (1 → 2), then the signal position of the methylene protons of the acetate should be interchanged and, by analogy with **2**, the signal at lower field should exhibit the larger coupling with H-5.

A comparison of the appropriate data for the β-(1 → 4) linked disaccharide, cellobiose (**33**) (5), and acetylated cellobioside **34** (6) (Table 3) shows that the chemical shifts of H-6_R and H-6_S of the reducing end residue retain the same relative order (based on the observed couplings with H-5) whether *O*-acetyl groups are present, or not. By contrast, the two C-6 protons of the non-reducing group do exhibit the expected shift reversal (Table 3), as the broader signal (J = 4.4 Hz) is located more upfield in the spectrum of **33**, and downfield in that of **34**. Strictly analogous results were found (Table 3) with the α-(1 → 4) linked isomer, i.e., in comparing maltose (**35**) with heptaacetate **36**. Consequently, although unequivocal assignments for the methylene protons of **36** were not available (whereas those of **34** were (6)), we propose that they are now established by the present findings. Noteworthy also is the

Can. J. Chem. Downloaded from www.nrcresearchpress.com by 210.87.254.105 on 09/06/12
For personal use only.

TABLE 1. Chemical shift and coupling data[a] for the 6,6′-methylene protons of *O*-benzyl derivatives of D-glucopyranosides, and their peracetates

Compound	H-6 δ	H-6′ δ	$J_{5,6}$	$J_{5,6'}$	$J_{6,6'}$	OCH_3 δ	$OCOCH_3$ δ
Methyl 2-*O*-benzyl-β-D-glucopyranoside (**5**)	3.89	3.81	3.3	4.7	11.8	3.56	
3,4,6-triacetate (**6**)	4.22	4.04	4.8	2.4	12.0	3.52	2.01, 1.93, 1.84
Methyl 3-*O*-benzyl-β-D-glucopyranoside (**7**)	3.90	3.79	3.6	4.9	11.8	3.56	
2,4,6-triacetate (**8**)	4.24	4.13	4.8	2.4	12.0	3.49	2.08, 2.01, 1.96
Methyl 2,3-di-*O*-benzyl-β-D-glucopyranoside (**9**)	3.88	3.77	3.6	5.0	11.8	3.58	
4,6-diacetate (**10**)	4.24	4.08	4.9	2.4	12.2	3.58	2.07, 1.92
Methyl 2,3,4-tri-*O*-benzyl-β-D-glucopyranoside (**11**)	3.87	3.71	2.7	4.6	12.0	3.56	
6-acetate (**12**)	4.34	4.23	1.6	4.2	12.4	3.56	2.03
6-*O*-trityl (**13**)	3.62	3.27	2.0	3.6	10.0	3.69	
Methyl 2-*O*-benzyl-α-D-glucopyranoside (**14**)	3.84–3.52		2.2	4.8	12.0	3.33	
3,4,6-triacetate (**15**)	4.30	4.07	4.4	2.0	12.4	3.42	2.09, 2.03, 2.01
Methyl 3-*O*-benzyl-α-D-glucopyranoside (**16**)	3.90–3.75		—	—	—	3.46	
2,4,6-triacetate (**17**)	4.16	4.03	4.8	2.4	12.4	3.35	2.04, 2.01, 1.88
Methyl 2,3-di-*O*-benzyl-α-D-glucopyranoside (**18**)	3.86–3.77		—	—	—	3.40	
4,6-diacetate (**19**)	4.21	4.00	5.0	2.2	12.3	3.39	2.06, 1.91

[a] In $CDCl_3$.

TABLE 2. Chemical shift and coupling data[a] for the 6,6′-methylene protons of *O*-acyl derivatives of methyl β-D-glucopyranoside

Compound	H-6 δ	H-6′ δ	$J_{5,6}$	$J_{5,6'}$	$J_{6,6'}$	OCH_3 δ	$OCOCH_3$ δ
Methyl β-D-glucopyranoside (D_2O) (**20**)	3.72	3.51	2.0	5.8	12.3	3.37	
6-acetate (D_2O) (**21**)	4.24	4.11	2.3	4.9	12.3	3.37	1.95
4-acetate (D_2O) (**22**)	3.69	3.49	2.2	5.9	12.5	3.34	
4-acetate ($CDCl_3$) (**22**)	3.75	3.59	2.1	3.6	12.5	3.56	2.13
4,6-diacetate (D_2O) (**23**)	4.16	3.98	3.8	2.1	12.6	3.38	1.97, 1.94
2,3,4,6-tetraacetate ($CDCl_3$) (**24**)	4.29	4.15	4.6	2.5	12.3	3.51	2.09, 2.06, 2.03, 2.01
2,3,4-triacetate ($CDCl_3$) (**25**)	3.76	3.67	2.0	4.6	12.0	3.52	2.05(2×), 2.01
4-*O*-acetyl-6-*O*-trityl ($CDCl_3$) (**26**)	3.24	3.11	2.1	5.1	10.3	3.63	1.81
2,3-di-*O*-benzyl-4-*O*-acetyl-6-*O*-trityl ($CDCl_3$) (**27**)	3.16	3.09	2.1	4.9	10.3	3.66	1.63
2,3,4-tri-*O*-acetyl-6-iodo ($CDCl_3$) (**28**)	3.64	3.57	2.8	6.7	12.0	3.54	2.06(2×), 2.01
2,3,4,6-tetrabenzoate ($CDCl_3$) (**29**)	4.66	4.51	3.3	4.6	12.1	3.55	
2,3,4-tri-*O*-acetyl-6-*O*-benzoyl ($CDCl_3$) (**30**)	4.55	4.37	3.1	4.6	12.1	3.51	2.05, 2.01(2×)
2,3,4-tri-*O*-benzoyl-6-*O*-acetyl ($CDCl_3$) (**31**)	4.35	4.29	4.6	3.1	12.2	3.56	2.05
2,3,4,6-tetra-*O*-(4-nitro)benzoate ($CDCl_3$) (**32**)	4.74	4.60	2.5	4.5	12.6	3.59	

[a] In solvent indicated (in parenthesis).

close correspondence between the data for **36** (reducing end residue) and cyclohexaamylose peracetate (**37**) (Table 3), in that H-6 of the latter (δ 4.74) exhibits the smaller coupling with H-5 (J = 2.1 Hz) as compared with H-6′ (δ 4.69, J = 4.2 Hz).

In complete accord with the foregoing considerations, it is found (Table 3) that the data for a (1 → 3) linked disaccharide

TABLE 3. Chemical shift and coupling data[a] for the 6,6′-methylene protons of D-glucopyranoside residues of disaccharides, and their peracetylated analogs

Compound	Reducing residue (non-reducing end)				
	H-6 δ	H-6′ δ	$J_{5,6}$	$J_{5,6'}$	$J_{6,6'}$
β-Cellobiose (D_2O) (**33**)[b]	3.97	3.82	2.0	5.6	12.0
	(3.92)	(3.75)	(2.0)	(4.4)	(12.0)
2-Chlorophenyl β-cellobioside heptaacetate ($CDCl_3$) (**34**)	4.57	4.15	1.5	5.6	12.0
	(4.39)	(4.07)	(4.4)	(1.6)	(12.4)
β-Maltose (D_2O) (**35**)[b]	3.92	3.77	2.0	5.0	12.0
	(3.86)	(3.77)	(2.0)	(5.0)	(12.0)
4-Chlorophenyl β-maltoside heptaacetate ($CDCl_3$) (**36**)	4.48	4.26	2.0	5.1	12.0
	(4.26)	(~4.06)	(4.6)	(2.0)	(12.0)
Cyclohexaamylose peracetate (C_6D_6) (**37**)	4.74	4.69	2.1	4.2	12.2
Cyclohexaamylose peracetate ($CDCl_3$) (**37**)	~4.4	~4.4	—	—	—
β-Laminaribiose (D_2O) (**38**)[b]	3.90	3.74	2.0	5.0	12.0
	(3.93)	(3.73)	(2.0)	(5.4)	(12.0)
β-Laminaribiose octaacetate ($CDCl_3$) (**39**)[c]	4.22	4.13	4.2	1.6	12.2
	(4.38)	(4.06)	(4.8)	(2.2)	(12.3)
β-Isomaltose (D_2O) (**40**)[b]	4.02	3.71	4.0	2.0	11.4
	(3.85)	(3.77)	(~2.0)	(~4.8)	(12.0)
β-Isomaltose octaacetate ($CDCl_3$) (**41**)	3.72	3.66	4.1	2.9	11.3
	(4.23)	(4.04)	(4.5)	(2.1)	(12.4)

[a] In solvent indicated (in parenthesis).
[b] Data from ref. 5.
[c] Data for reducing and non-reducing residues may be interchanged.

(**38**) and its octaacetate (**39**) amount to an interchange in the order of H-6_R and H-6_S chemical shifts for both the reducing and non-reducing moieties. Consequently, with OH-4 and OH-6 of each residue accessible to acetylation, chemical shift reversal must occur as the coupling patterns observed for the two pairs of methylene protons are analogous to those of **1** and **2**, respectively.

A departure from this consistent series of observations is found with 6-*O*-α-D-glucopyranosyl-D-glucose (isomaltose, **40**). That is, the more downfield H-6 signal of the reducing end residue is broader (J = 4.0 Hz) than the upfield one (J = 2.0 Hz) (Table 3), which is the converse of what is observed when O-6 is not glycosidically bonded. According to Rees and Scott (7), the average orientation of the C-1′—O′—C-6—C-5 sequence of bonds in **40** is approximately *anti*, and the rotamer population about the C-6—C-5 bond contains major contributors analogous to *RHS* and *RCS*. Within this conformation of **40**, as depicted for the *RCS* rotamer in Fig. 2, H-6_R (reducing end) appears to be much nearer to O-5 and O-6 than is H-6_S, and hence could experience additional deshielding by the oxygen atoms.[3] As this possibility does not apply for any of the other compounds mentioned, it may account for the apparent discrepancy in chemical shifts exhibited by the methylene protons of **40**. With peracetylated isomaltose (**41**), nevertheless, the chemical shift and coupling pattern are consistent with expectation (Table 3), in that H-6 and H-6′ of the non-reducing end unit undergo chemical shift reversal whereas those of the reducing end residue do not.

Inasmuch as both a 4-*O*-acetyl and 6-*O*-acetyl group are essential for these alterations in signal position to occur, it appears probable that the orientations of the two substituents are strongly interdependent. Moreover, their net conformational preferences, determined by the interaction between them, must lead to disparate shielding influences on H-6_R and H-6_S of the acetylated D-glucose residue. One conformational possibility is depicted in Fig. 3 for the *RHS* rotamer; under these circumstances, the C=O functions are positioned so that minimum energy orientations of the *O*-acetyl groups are favored by a weak polar interaction or, perhaps, a π-stacking type of interaction between the two π bonds. The carbonyl oxygen of the 6-*O*-acetyl group may then be close enough to H-6_R to induce deshielding in the acetylated species sufficient for a reversal in chemical shift.

O-*Benzoyl derivatives of* D-*glucopyranosides*

The reversal in chemical shift observed for 6,6′-methylenic protons upon acetylation of O-4 and O-6 does not occur when these oxygen atoms are benzoylated. Hence, the patterns of chemical shift and coupling with H-5 are analogous for both methyl β-D-glucopyranoside (**20**) and its 2,3,4,6-tetrabenzoate (**29**), in that the more downfield H-6 resonance (attributed accordingly to H-6_S) exhibits the smaller coupling in each instance (Table 2). As envisaged in Fig. 3*a*, selective deshielding of H-6_R is attributed to the magnetic anisotropy of the carbonyl function of the 6-*O*-acetyl substituent, which is appropriately oriented through a weak interaction between the latter and the 4-*O*-acetyl substituent. By analogy, the fact that the deshielding is not observed in the presence of *O*-benzoyl substituents implies a reduction in the anisotropy effect of the 6-benzoate, or of the interaction between the 4- and 6-substituents, or both. Charge delocalization by the phenyl group, in contrast to methyl, may account for these differences by altering the polarization of the C=O bond and its effect on the anisotropy of the carbonyl group.

Consistent with these possibilities are the ^{1}H nmr characteristics of other derivatives, chosen specifically in order to examine the influence of various combinations of *O*-acyl substituents at the 4- and 6-positions (Table 2). Thus, in the spectrum of methyl 2,3,4-tri-*O*-acetyl-6-*O*-benzoyl-β-D-gluco-

[3] However, we are unable to assess the magnitude of deshielding by neighboring oxygen atoms in a mobile system of this kind.

Can. J. Chem. Downloaded from www.nrcresearchpress.com by 210.87.254.105 on 09/06/12
For personal use only.

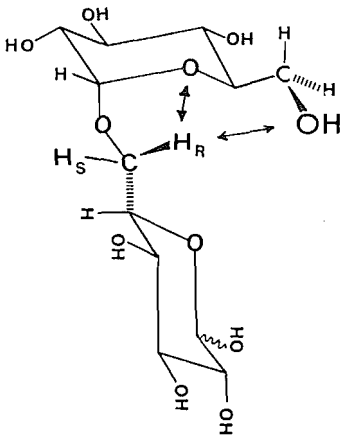

FIG. 2. Representation of 6-*O*-α-D-glucopyranosyl-D-glucose (isomaltose, **40**) in a favored conformation (7), showing the close proximity of H-6_R of the reducing end residue to oxygen atoms of the non-reducing end group.

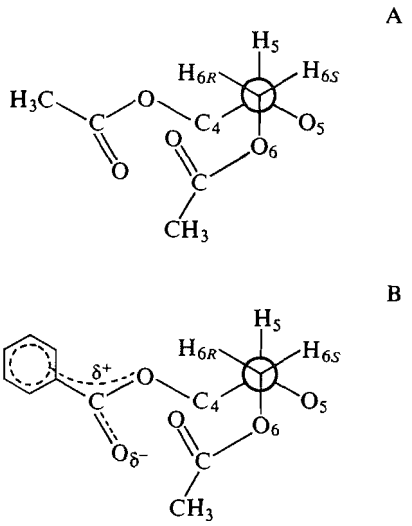

FIG. 3. Conformational representation of the C-4,C-5,C-6 segment of (A): a 4,6-di-*O*-acetyl aldopyranose derivative, or (B): a 6-*O*-acetyl-4-*O*-benzoyl aldopyranose derivative, showing possible orientations of the *O*-acyl substituents.

pyranoside (**30**) the 6,6′-protons display a pattern closely similar to that of the tetrabenzoate (**29**). By contrast, a chemical shift reversal is indeed observed for the methylene protons of methyl 2,3,4-tri-*O*-benzoyl-6-*O*-acetyl-β-D-glucopyranoside (**31**). Consequently, irrespective of the nature of the 4-*O*-acyl substituent, a 6-*O*-benzoyl group (in **29** or **30**) does not deshield H-6_R sufficiently to cause it to resonate downfield of H-6_S, whereas a 6-*O*-acetyl group does. When, as in **31**, there is a combination of 4-*O*-benzoyl and 6-*O*-acetyl substituents, it appears that the former substituent is adequate for the maintenance of an (presumably, essential) anchoring interaction between the two carbonyl groups, so as to enable the acetyl group on O-6 to exert its anisotropic effect on H-6_R. Nevertheless, the chemical shift difference between the methylene protons of **31** is only about one-half (0.06 ppm) of that observed (0.14 ppm) with the peracetylated derivative, which may reflect a lower degree of interaction between the 4-*O*-benzoyl and 6-*O*-acetyl substituents, and the extent to which they influence each other's conformational preference.

The *O*-(4-nitro)benzoyl substituent also was introduced to see if the change expected in the polarization of the C=O group, as compared with that of *O*-benzoyl, would alter the anisotropic influence upon H-6_R. For methyl 2,3,4,6-tetra-*O*-(4-nitro)benzoyl-β-D-glucopyranoside (**32**), no chemical shift reversal was observed, as the downfield H-6 signal (δ 4.74) had the smaller coupling (2.5 Hz) (Table 2). Moreover, the chemical shifts of H-6 and H-6′ of **32** differed by about the same amount (0.08 ppm) as found with the tetrabenzoate (**29**). This close similarity suggested that in neither of these two compounds does the 6-*O*-acyl substituent exert an appreciable anisotropic deshielding effect, because the C=O bond polarization[4] difference should then be evident. Consequently, as already implied for **29** and **30**, the 4- and 6-*O*-acyl substituents of **32** may not interact sufficiently to ensure that the C-6 carbonyl function is oriented suitably for inducing enhanced deshielding of H-6_R. These findings are taken as additional support, therefore, for the present proposals about the orientations favored by the 4- and 6-*O*-acetyl substituents of D-glucopyranosides.

Derivatives of D-*mannopyranose and* D-*galactopyranose*

The resonance characteristics of the C-6 protons of methyl α-D-mannopyranoside (**42**) and its tetraacetate (**43**) are only slightly different from those described for their *gluco* (C-2) epimers. As shown in Table 4, the more downfield H-6 signal has the smaller spacing (J = 1.7 Hz) in the spectrum of **42**, whereas in the spectrum of **43** it is the broader signal (J = 5.4 Hz). Assuming that the rotamer population about the C-5,C-6 bond is essentially the same in both compounds (and similar to that in the *gluco* series), these data represent an additional example of an interchange in the order of the H-6_R and H-6_S chemical shifts upon acetylation of both OH-4 and OH-6.

The presence of an axial 4-hydroxyl group in compounds of the D-*galacto* configuration is regarded (2) as the source of a rotamer population about the C-5—C-6 bond differing from those of the *gluco* and *manno* diastereomers, based on coupling between H-5 and the 6,6′-methylene protons. Rotamer ROS has been designated (2) as a major contributor in methyl β-D-galactopyranoside (**44**), and this has been confirmed by the examination of a specimen of **44** stereoselectively deuterated at C-6 (9). That is, the observed values (Table 4) of $J_{5,6_S}$ = 8.00 Hz and $J_{5,6_R}$ = 4.3 Hz, while consistent with a high population of rotamer ROS, show that the contribution of rotamer RCS must be minimal. As to chemical shift, the H-6_S signal of **44** is slightly downfield of that of H-6_R (Table 4), which is opposite to that found in the spectrum of the 2,3,4,6-tetraacetate (**45**) (9). However, the two couplings with H-5 in **45** are almost equal (Table 4). Consequently, the acetylation of **44** does not induce a reversal in chemical shift, although there is an accompanying change in the rotamer population. Both of these characteristics add to the distinctiveness of the *galacto* isomer, when compared with the *gluco* and *manno* isomers.

Experimental

General methods

Solutions were evaporated below 40°C under diminished pressure.

[4] For a detailed study of "localized" and "extended" π-polarization effects on carbonyl ^{13}C chemical shifts in a wide range of *meta*- and *para*-substituted benzoyl derivatives of the type XC_6H_4COZ, see ref. 8.

Can. J. Chem. Downloaded from www.nrcresearchpress.com by 210.87.254.105 on 09/06/12
For personal use only.

TABLE 4. Chemical shift and coupling data[a] for the 6,6′-methylene protons of D-manno- and D-galactopyranosides, and their tetraacetates

Compound	H-6 δ	H-6′ δ	$J_{5,6}$	$J_{5,6'}$	$J_{6,6'}$	OCH_3	$OCOCH_3$
Methyl α-D-mannopyranoside (D_2O) (**42**)	3.70	3.54	1.7	5.6	12.0	3.20	
-2,3,4,6-tetraacetate ($CDCl_3$) (**43**)	4.30	4.12	4.5	2.4	12.2	3.41	2.16, 2.11, 2.05, 2.00
Methyl β-D-galactopyranoside (D_2O) (**44**)	3.53	3.49	8.00	4.3	11.5	3.33	
-2,3,4,6-tetraacetate ($CDCl_3$) (**45**)	4.20	4.14	6.5	7.2	11.5	3.53	2.17, 2.08, 2.07, 2.00

[a] In solvent indicated (in parenthesis).

Eastman Chromagram sheets of silica gel with fluorescent indicator were used for thin-layer chromatography. Proton magnetic resonance spectra were recorded with a Varian XL-200, or a Bruker WH-400, with the aid of homonuclear decoupling. Chemical shifts (δ) are reported with reference to tetramethylsilane with $CDCl_3$ as solvent, and *HOD* (δ 4.61) with D_2O as solvent. Elemental analyses were obtained from Guelph Chemical Laboratories, Guelph, Ont. Compounds **5** to **19** were available from an earlier study (4) although the complete proton nmr data for **12** were not given therein.

Methyl 6-O-acetyl-β-D-glucopyranoside (21)

The title compound was obtained, as a 3:1 mixture with its 4-*O*-acetyl isomer, by catalytic transfer hydrogenolysis of the *O*-benzyl groups of methyl 2,3,4-tri-*O*-benzyl-6-*O*-acetyl-β-D-glucopyranoside (**12**) using 10% Pd–C/formic acid/ methanol, as described earlier (10). The ^1H nmr data for **12** ($CDCl_3$, δ: 7.5–7.2 (m, 15H, $3C_6H_5$), 4.94 and 4.81 (AB, 2H, OCH_2, J_{gem} = 10.9 Hz), 4.90 and 4.72 (AB, 2H, OCH_2, J_{gem} = 11.0 Hz), 4.85 and 4.56 (AB, 2H, OCH_2, J_{gem} = 10.8 Hz), 4.31 (d, H-1, $J_{1,2}$ = 7.7 Hz), 3.74–3.38 (m, H-3, 4, 5), 3.56 (s, 3H, OCH_3), 3.43 (dd, H-2, $J_{2,3}$ = 8.8 Hz), 2.03 (s, 3H, CH_3); other data are given in Table 2. The ^1H nmr data for **21** (D_2O), δ: 4.22 (d, H-1, $J_{1,2}$ = 7.9 Hz), 3.09 (dd, H-2, $J_{2,3}$ = 9.4 Hz), 3.37 (s, 3H, OCH_3), 3.30 (m, overlapping, H-3), ~3.5 (m, overlapping, H-5), 1.95 (s, 3H, CH_3); other data are given in Table 2.

Methyl 4-O-acetyl-β-D-glucopyranoside (22)

Methyl 2,3-di-*O*-benzyl-β-D-glucopyranoside was tritylated with trityl chloride in dry pyridine. The reaction mixture,[5] after work-up, was chromatographed on silica gel (packed in chloroform under pressure) by gradient elution with chloroform – ethyl acetate which readily separated the unreacted material (R_f 0.63, EtOAc) from the product, methyl 2,3-di-*O*-benzyl-6-*O*-trityl-β-D-glucopyranoside (R_f 0.34, EtOAc). The ^1H nmr data ($CDCl_3$; D_2O exchanged), δ: 7.5–7.2 (m, 25H, phenyl), 4.93 and 4.71 (AB, 2H, OCH_2, J_{gem} = 11.0 Hz), 4.90 and 4.74 (AB, 2H, OCH_2, J_{gem} = 11.0 Hz), 4.34 (d, H-1, $J_{1,2}$ = 7.3 Hz), 3.64 (t, H-4, $J_{3,4} = J_{4,5}$ = 9.0 Hz), 3.60 (s, 3H, OCH_3), 3.45 (t, H-3, $J_{2,3}$ = 9.0 Hz), 3.42 (H-2), 3.35–3.44 (m, overlapping, 3H, H-5, 6 and 6′). *Anal.* calcd. for $C_{40}H_{40}O_6$: C 77.92, H 6.49; found: C 78.02, H 6.61.

The product was acetylated with Ac_2O/pyridine to give methyl 2,3-di-*O*-benzyl-4-*O*-acetyl-6-*O*-trityl-β-D-glucopyranoside (**27**). The ^1H nmr data for **27** ($CDCl_3$), δ: 7.5–7.2 (m, 25H, phenyl), 5.07 (m, combination transition, H-4), 4.94 and 4.71 (AB, 2H, OCH_2, J_{gem} = 11.0 Hz), 4.80 and 4.58 (AB, 2H, OCH_2, J_{gem} = 11.6 Hz), 4.37 (m, combination transition, H-1, $J_{1,2}$ = 7.6 Hz), 3.66 (s, 3H, OCH_3), 3.59–3.52 (m, overlapping, H-2 and 3), 3.42 (m, H-5), 1.63 (s, 3H, CH_3); other data are given in Table 2. *Anal.* calcd. for $C_{42}H_{42}O_7$: C 76.59; H 6.38; found: C 76.58, H 6.28.

A solution of **27** (0.17 g) in a mixture of formic acid (98%, 1 mL), methanol (9 mL), and tetrahydrofuran (5 mL) was added to a stirred suspension of 10% Pd–C (1 g) in formic acid (98%, 1 mL) and methanol (9 mL), under nitrogen. After 20 h, when tlc showed that the reaction was complete, the catalyst was filtered off, washed with chloroform, tetrahydrofuran, and water, and the combined filtrate was evaporated, affording methyl 4-*O*-acetyl-6-*O*-trityl-β-D-glucopyranoside (**26**) (0.1 g; R_f 0.33 (EtOAc)). The ^1H nmr data for **26** ($CDCl_3$), δ: 7.5–7.2 (m, 15H, C_6H_5), 4.98 (t, H-4, $J_{3,4} = J_{4,5}$ = 9.4 Hz), 4.25 (d, H-1, $J_{1,2}$ = 7.4 Hz), 3.63 (s, 3H, OCH_3), 3.60 (t, H-3), 3.50 (dd, H-2), ~3.5 (m, H-5), 1.81 (s, 3H, CH_3); other data are given in Table 2.

Removal of the 6-*O*-trityl group from 26 under catalytic transfer hydrogenolysis conditions with 10% Pd–C/formic acid/methanol (10) gave a 1:3 mixture of methyl 4-*O*-acetyl (**22**) and 6-*O*-acetyl (**21**)-β-D-glucopyranosides, consistent with the reported (11) acyl migration from O-4 to O-6 under acid catalysis conditions. The ^1H nmr data for **22** ($CDCl_3$, sparingly soluble), δ: 4.89 (t, H-4, $J_{3,4} = J_{4,5}$ = 9.3 Hz), 4.25 (d, H-1, $J_{1,2}$ = 7.8 Hz), 3.75 (dd, H-6, $J_{5,6}$ = 2.1, $J_{6,6'}$ = 12.5 Hz), 3.7 (t, H-3, $J_{2,3} = J_{3,4}$ = 9.3 Hz), 3.59 (dd, H-6′, $J_{5,6'}$ = 3.6 Hz), 3.56 (s, 3H, OCH_3), 3.45 (dd, H-2), ~3.45 (m, H-5), 2.13 (s, 3H, CH_3); other data, obtained with D_2O as solvent, are given in Table 2.

Methyl 4,6-di-O-acetyl-β-D-glucopyranoside (23)

Methyl 2,3-di-*O*-benzyl-β-D-glucopyranoside was acetylated with acetic anhydride in pyridine to the corresponding 4,6-di-*O*-acetyl derivative which was then de-*O*-benzylated under catalytic transfer hydrogenation conditions, as already described, to afford the title compound. The ^1H nmr data for **23** (D_2O), δ: 4.68 (dd, H-4, $J_{3,4}$ = 9.3 Hz, $J_{4,5}$ = 9.5 Hz), 4.27 (d, H-1, $J_{1,2}$ = 7.8 Hz), 3.69 (m, H-5), 3.55 (t, H-3, $J_{2,3} = J_{3,4}$ = 9.3 Hz), 3.38 (s, 3H, OCH_3), 1.97, 1.94 (s, 2 × 3H, CH_3); other data are given in Table 2.

Methyl 2,3,4-tri-O-acetyl-β-D-glucopyranoside (25)

Methyl β-D-glucopyranoside was 6-*O*-tritylated with trityl chloride in pyridine, followed by acetylation with acetic anhydride – pyridine. Subsequent de-*O*-tritylation under catalytic transfer hydrogenation conditions, as above, gave the title compound as the sole product. The ^1H nmr data for **25** ($CDCl_3$), δ: 5.26 (t, H-3, $J_{2,3} = J_{3,4}$ = 9.6 Hz), 5.04 (t, H-4, $J_{4,5}$ = 9.6 Hz), 4.97 (dd, H-2, $J_{1,2}$ = 8.0 Hz), 4.46 (d, H-1), ~3.54 (m, H-5), 3.52 (s, 3H, OCH_3), 2.05 (s, 2 × 3H, CH_3), 2.01 (s, 3H, CH_3); other data are given in Table 2.

Methyl 2,3,4-tri-O-benzoyl-6-O-acetyl-β-D-glucopyranoside (31)

Methyl β-D-glucopyranoside was 6-*O*-tritylated, as above, followed by benzoylation with benzoyl chloride in pyridine, the progress

[5] The tlc examination (ethyl acetate) showed that, even after 8 days, the reaction was incomplete. In a separate experiment, the addition of the trityl chloride over a period of several days did not improve the yield of product.

Can. J. Chem. Downloaded from www.nrcresearchpress.com by 210.87.254.105 on 09/06/12
For personal use only.

of the reaction being monitored by tlc. (R_f 0.55, 7:4 petroleum ether – EtOAc). The ^{1}H nmr data ($CDCl_3$), δ: 8.2–7.1 (phenyl), 5.81 (t, H-3, $J_{2,3} = J_{3,4} = 9.6$ Hz), 5.65 (t, H-4, $J_{4,5} = 9.6$ Hz), 5.55 (dd, H-2, $J_{1,2} = 7.7$ Hz), 4.74 (d, H-1), 3.86 (m, H-5), 3.62 (s, 3H, OCH_3), 3.37 (dd, H-6, $J_{5,6} = 2.5$ Hz, $J_{6,6'} = 10.5$ Hz), 3.28 (dd, H-6′, $J_{5,6'} = 4.7$ Hz).

The product was de-*O*-tritylated by catalytic transfer hydrogenation, as above, to give methyl 2,3,4-tri-*O*-benzoyl-β-D-glucopyranoside after chromatography on silica gel (packed in petroleum ether under pressure) by gradient elution with petroleum ether and ethylacetate (R_f 0.13, 7:4 petroleum ether – EtOAc). The ^{1}H nmr data ($CDCl_3$), δ: 8.15 – 7.24 (phenyl), 5.95 (t, H-3, $J_{2,3} = J_{3,4} = 9.7$ Hz), 5.51 (dd, H-2, $J_{1,2} = 7.9$ Hz), 5.50 (t, H-4, $J_{4,5} = 9.7$ Hz), 3.93–3.72 (m, 3H, H-5, 6 and 6′, $J_{5,6'} = 4.0$ Hz), 3.57 (s, 3H, OCH_3). Acetylation of the product with acetic anhydride – pyridine gave the title compound as a syrup. The ^{1}H nmr data for **31** ($CDCl_3$), δ: 8.00–7.80 (m, 6H, phenyl-*ortho*), 7.6–7.2 (m, 9H, phenyl-*meta, para*), 5.88 (t, H-3, $J_{2,3} = J_{3,4} = 9.7$ Hz), 5.60 (t, H-4, $J_{4,5} = 9.7$ Hz), 5.50 (dd, H-2, $J_{1,2} = 7.8$ Hz), 4.74 (d, H-1), 4.02 (m, H-5); the other data are given in Table 2.

Methyl 2,3,4,6-tetra-O-(4-nitro)benzoyl-β-D-glucopyranoside (32)

A solution of methyl β-D-glucopyranoside (0.25 g) and 4-nitrobenzoyl chloride (3.0 g, 12 equiv.) in pyridine was stirred for 48 h, and then poured onto ice. The precipitated material was recovered, suspended in chloroform (50 mL), and the chloroform extract was washed with sodium hydrogen carbonate solution and water, dried over anhydrous sodium sulfate, and evaporated. The ^{1}H nmr data for **32** ($CDCl_3$), δ: 8.44–7.98 (phenyl), 5.93 (t, H-3, $J_{2,3} = J_{3,4} = 9.6$ Hz), 5.74 (t, H-4, $J_{4,5} = 9.6$ Hz), 5.57 (dd, H-2, $J_{1,2} = 7.8$ Hz), 4.84 (d, H-1), 4.24 (m, H-5); the other data are given in Table 2.

Acknowledgments

The authors gratefully acknowledge generous support by the Natural Sciences and Engineering Research Council of Canada. Compound **3** was provided by F. Balza, and compounds **28–30** by A. Maradufu. F. Sauriol kindly assisted in the recording of the 200 MHz spectra, and the 400 MHz spectra were obtained at Laboratoire Regional de RMN à Haut Champ, Université de Montréal.

1. D. Gagnaire, D. Horton, and F. R. Taravel. Carbohydr. Res. **27**, 363 (1973).
2. A. de Bruyn and M. Anteunis. Carbohydr. Res. **47**, 311 (1976); R. U. Lemieux and J. D. Stevens. Can. J. Chem. **43**, 2059 (1965).
3. F. Balza and A. S. Perlin. Carbohydr. Res. **107**, 270 (1982).
4. V. S. Rao and A. S. Perlin. Can. J. Chem. **61**, 652 (1983).
5. A. de Bruyn, M. Anteunis, and G. Verhegge. Bull. Soc. Chim. Belg. **84**, 721 (1975).
6. J. Dunand, D. Gagnaire, L. Odier, and M. Vincendon. Org. Magn. Reson. **4**, 523 (1972).
7. D. A. Rees and W. E. Scott. J. Chem. Soc. (*B*), 469 (1971).
8. (*a*) J. Bromilow, R. T. C. Brownlee, D. J. Craik, P. R. Fiske, J. E. Rowe, and M. Sadek. J. Chem. Soc. Perkin Trans. 2, 753 (1981); (*b*) R. T. C. Brownlee and D. J. Craik. J. Chem. Soc. Perkin Trans. 2, 760 (1981); J. Am. Chem. Soc. **105**, 872 (1983), and references cited.
9. A. Maradufu, G. M. Cree, and A. S. Perlin. Can. J. Chem. **49**, 3429 (1971).
10. V. S. Rao and A. S. Perlin. Carbohydr. Res. **83**, 175 (1980).
11. Y. Tsuda and K. Yoshimoto. Carbohydr. Res. **87**, C1 (1981), and references cited therein.

Can. J. Chem. Downloaded from www.nrcresearchpress.com by 210.87.254.105 on 09/06/12
For personal use only.

Hydrogen bonded interactions of methanol and water with purines and pyrimidines

J. N. SPENCER, S. W. BARTON, K. A. SMITH, W. S. WOLBACH, J. F. POWELL, M. R. KIRSHENBAUM, D. W. FIRTH, E. M. HARRIS, AND T. A. JUDGE

Department of Chemistry, Franklin and Marshall College, Lancaster, PA, 17604, U.S.A.

Received October 13, 1982[1]

J. N. SPENCER, S. W. BARTON, K. A. SMITH, W. S. WOLBACH, J. F. POWELL, M. R. KIRSHENBAUM, D. W. FIRTH, E. M. HARRIS, and T. A. JUDGE. Can. J. Chem. **61**, 2695 (1983).

The solvation of benzimidazole, 4-azabenzimidazole, purine, adenine, uracil, thymine, and cytosine in water and methanol was determined by a combination of calorimetric and spectral analysis. Specific enthalpies have been assigned to each interaction site in the first solvation shell. Calculations, based on the enthalpies of hydrogen bond formation with water, and estimates for intermolecular hydrogen bond enthalpies, show that the self-association of purine and adenine in water through hydrogen bonded interactions is enthalpically possible.

J. N. SPENCER, S. W. BARTON, K. A. SMITH, W. S. WOLBACH, J. F. POWELL, M. R. KIRSHENBAUM, D. W. FIRTH, E. M. HARRIS et T. A. JUDGE. Can. J. Chem. **61**, 2695 (1983).

Faisant appel à l'analyse spectrale combinée à l'analyse calorimétrique, on a déterminé le solvatation du benzimidazole, de l'aza-4 benzimidazole, de la purine, de l'adénine, de l'uracile, de la thymine et de la cytosine dans l'eau et dans le méthanol. On a attribué les enthalpies spécifiques à chaque site d'interaction dans la première couche de solvatation. Les calculs, basés sur les enthalpies de formation de la liaison hydrogène avec l'eau et les évaluations des enthalpies de liaison hydrogène intermoléculaire, montrent que l'autoassociation de la purine et de l'adénine dans l'eau par l'intermédiaire des interactions liées d'hydrogène est possible du point de vue de l'enthalpie.

[Traduit par le journal]

Can. J. Chem. Downloaded from www.nrcresearchpress.com by 210.87.254.5 on 09/06/12
For personal use only.

Introduction

The calculation of hydration schemes for the bases of the nucleic acids have been the object of several theoretical studies (1–3). These studies have generally been concerned with the first hydration shell and have dealt with preferred orientations of water molecules for hydrogen bonded interactions. Teplitsky *et al.* (4) have used enthalpies of sublimation and solution to calculate the overall hydration of uracil, thymine, and their derivatives. From a study of the temperature dependence of the enthalpy of solution of thymine in water and ethanol, Alvarez and Biltonen (5) have concluded that nucleic acid bases do not make all possible hydrogen bonds in the vicinity of room temperature. Gill, Downing, and Sheats (6) determined the enthalpy of self association of purine derivatives in water and attributed the association to base stacking interactions. D'Albis, Wickens, and Gratzer (7) investigated the association of derivatives of uracil and adenine in $CHCl_3$ in the presence of dissolved water. They conclude that the extent of association is unchanged by the presence of water and that little or no competition occurs between the formation of base pairs through hydrogen bonds and bonding of water to the bases.

The object of the present study was to make reasonable estimates of the hydrogen bonding of water to purines and pyrimidines in the first hydration shell and to estimate the overall hydration enthalpy. Solvation schemes in methanol were also determined and transfer enthalpies were used to assess the relative hydrogen bonded interactions in water and methanol.

Experimental

The calorimetric methods used have been previously described as have the purifications of water and methanol (8). Aldrich tech. grade benzimidazole and Aldrich 98% 4-azabenzimidazole were vacuum sublimed. Aldrich 99% purine was vacuum dried and used without further purification. 1-Methyl-2-pyridone and 4(3*H*)-pyrimidone were supplied by Aldrich and were distilled under nitrogen atmosphere. Successive injections of solute were used to identify any concentration dependence of the enthalpy of solution. Concentrations of solutes ranged from 0.003 to 0.015 *M*.

Calculation and discussion

The assignment of enthalpies due to interactions at each site of the first solvation shell made use of calorimetric and near ir spectroscopic data. For adenine, the interaction at the amino group was considered to be the formation of two hydrogen bonds by the solvent, either methanol or water, to the N6 protons. These interactions were taken to be the same as those found from pure base calorimetric analysis for the amino group interaction of 2-aminopyridine with methanol and water, −3.5 and −2.8 kcal mol^{-1}, respectively (8). Previous studies of pyrrole, imidazole, the diazines (9), and the aminopyridines showed that an interaction by methanol at the nitrogen of amino groups and at the nitrogen of N—H ring groups was responsible for the greater enthalpic stability of the aminopyridines, pyrrole, and imidazole in methanol relative to water (Table 1). The methanol interaction at N6 of adenine was assumed to be that previously assigned to the interaction between methanol and the amino group nitrogen of 2-aminopyridine, −1.7 kcal mol^{-1}. No similar interaction was found for water at these nitrogen sites for pyrrole, imidazole, or the aminopyridines.

The interaction at the imidazole moiety of benzimidazole, 4-azabenzimidazole, purine, and adenine was taken to be the same as that for the corresponding nitrogen in imidazole. The aza nitrogen of 4-azabenzimidazole was modeled by the pyridine nitrogen interaction (9).

The interactions at N1 and N3 of purine and adenine were determined from a plot of pK versus enthalpies of interaction for the diazines (9). pK values at N3 for purine and adenine were obtained from a relationship between pK and the sum of particular coulomb integrals for the purine and pyrimidine bases (10).

Interactions by the N—H of the imidazole moiety of these compounds were calculated from a two-parameter equation

[1]Revision received June 16, 1983.

TABLE 1. Enthalpies of solution (kcal mol^{-1}, 298 K)

Solute	Enthalpy of solution in H_2O	Enthalpy of solution in CH_3OH	ΔH_{tr} $H_2O \rightarrow CH_3OH$
Benzimidazole	+4.85±0.21	+2.53±0.20	−2.32
4-Azabenzimidazole	+4.14±0.13	+2.89±0.18	−1.25
Purine	+4.48±0.23	+4.85±0.10	+0.37
Adenine	+8.00±0.24[a]	+5.16±0.22[b]	−2.84
Pyridine[c]	−2.30	−0.96±0.04	+1.34
Imidazole[c]	+3.09±0.01	+1.77±0.2	−1.32
Pyrimidine[c]	−2.33±0.03	+0.30±0.02	+2.63
2-Aminopyridine[d]	+3.61±0.18	+2.60±0.17	−1.01
1-Methyl-2-pyridone	−3.30±0.07	−0.39±0.14	+2.91
4(3*H*)-Pyrimidone	+4.09±0.15	+5.13±0.14	+1.04

[a]Reference 17.
[b]Reference 18.
[c]Reference 9.
[d]Reference 8.

developed by Rider (11):

$$\Delta H = bxc$$

b is a measure of the relative proton donating abilities of a series of acids with a given base and is considered to be related to the corresponding frequency shifts. The parameter c represents the proton accepting abilities of the base, which is constant, if the base remains the same. Rider (11) has determined these constants for methanol and water. By using enthalpy changes found for pyrrole and imidazole with water and methanol (9) along with Rider's values for c, the parameter b was calculated for imidazole and pyrrole. Then, frequency shifts for imidazole and pyrrole with *N*,*N*-dimethylformamide (DMF) in CCl_4 solvent were used to establish a relation between b and these frequency shifts. The b value for benzimidazole was then determined from the derived relation between b and the frequency shift. The frequency shift for benzimidazole is 192 cm^{-1}, compared to 176 cm^{-1} for imidazole, and 135 cm^{-1} for pyrrole. Thus benzimidazole is a better proton donor than either imidazole or pyrrole. The previously determined enthalpies of hydrogen bond formation of pyrrole and imidazole with methanol were −3.0 and −3.8 kcal mol^{-1}, respectively (9). The assigned interaction enthalpy of the N—H of benzimidazole with methanol is −4.1 kcal mol^{-1}. In water, the corresponding N—H interaction enthalpies for pyrrole (9), imidazole (9), and benzimidazole are −2.3, −2.7, and −2.9 kcal mol^{-1}, respectively.

Due to low solubility, frequency shifts for purine could not be determined in CCl_4 solvent. Mixtures of DMF and CCl_4 were used as a solvent and the frequency shift data were extrapolated to infinite dilution in DMF. The frequency shift found for purine was nearly the same as that found for benzimidazole. Thus the enthalpies due to interactions at the purine N9—H were taken to be the same as for benzimidazole. It was also assumed that the same interactions occurred with 4-azabenzimidazole and adenine. The last interaction remaining to be assigned is that of the nitrogen of the imidazole N—H group with methanol.

The enthalpy of N—H hydrogen bonding for pyrrole to methanol is −3.0 kcal mol^{-1} (9). The interaction enthalpy at the nitrogen is −0.4 kcal mol^{-1} (8). The N_1—H hydrogen bond enthalpy of imidazole hydrogen bonding to methanol is −3.8 kcal mol^{-1} and the N_1 interaction enthalpy is −1.2 kcal mol^{-1} (8). The interaction enthalpy at the nitrogen thus increases directly with the N—H bond enthalpy in almost a one-to-one correspondence. Similar results are found for corresponding interactions with 2- and 3-aminopyridine (8). The N—H_2 enthalpies for these two compounds are −3.5 and −3.7 kcal mol^{-1}, respectively, and the amino nitrogen–methanol interactions are −1.7 and −1.9 kcal mol^{-1}, respectively. This allowed the assignment of the interactions at the imidazole nitrogen given in Table 2.

Gonnella and Roberts (12) report that in water solvent, the purine N7H and N9H tautomers are present in nearly equal amounts. Similar observations were made for adenine. Thus the tautomers of purine and those of adenine must undergo similar interactions with water since neither is preferred. It was assumed that the same would be true for methanol solvent.

The transfer enthalpies from water to methanol given in Table 1 indicate that benzimidazole, 4-azabenzimidazole, and adenine are enthalpically stabilized by methanol relative to water. Only purine is more strongly solvated by water than by methanol. In addition to the hydrogen bonding to the ring nitrogens and amino group by water and methanol, interactions at the π clouds are possible. The factors which contribute to the enthalpic stability of these solutes in methanol and water can be determined from an analysis of the transfer enthalpies.

That part of the transfer enthalpy due to the making and breaking of hydrogen bonds to the ring nitrogens and amino group can be estimated from the enthalpies given in Table 2. The cavity and interaction terms of the remainder of the molecule can be estimated by choosing an appropriate model compound. Benzimidazole was chosen to model 4-azabenzimidazole, purine, and adenine. The transfer enthalpy from water to methanol for benzimidazole is −2.3 kcal mol^{-1}. The N_1—H and N_3 hyrogen bonded interactions in methanol and water contribute −1.4 kcal mol^{-1} to the transfer enthalpy. Thus −0.9 kcal mol^{-1} must be due to differences in cavity and interaction terms for the ring system in methanol and water.

By using the interaction enthalpies given in Table 2 and the transfer enthalpy just found for the cavity and interaction terms, the transfer enthalpies for 4-azabenzimidazole, purine, and adenine may be calculated. The results of this calculation are given in Table 3.

The transfer enthalpy for benzene from water to methanol is −0.1 kcal mol^{-1} (9) and that for the imidazole ring, when hydrogen bonded interactions by N1H and N3 are taken into account, is −0.4 kcal mol^{-1}. Previous studies of the amino-

Can. J. Chem. Downloaded from www.nrcresearchpress.com by 210.87.254.5 on 09/06/12
For personal use only.

TABLE 2. Enthalpies due to interactions (kcal mol^{-1})

Solute		$-\Delta H$ H_2O	$-\Delta H$ CH_3OH
Benzimidazole	N1—H	2.9	4.1
	N1		1.6
	N3	4.3	2.9
4-Azabenzimidazole	N1—H	2.9	4.1
	N1		1.6
	N3	4.3	2.9
	N4	4.3	2.9
Purine	N1	4.2	2.9
	N3	3.2	1.8
	N7	4.3	2.9
	N9—H	2.9	4.1
	N9		1.6
Adenine	N1	5.8	4.6
	N3	5.1	3.8
	N6—H_2	2.8	3.5
	N6		1.7
	N7	4.3	2.9
	N9—H	2.9	4.1
	N9		1.6
1-Methyl-2-pyridone	N		0.4
	—CH_3	1.6	0.8
	=O	5.9	3.4
4(3*H*)-Pyrimidone	N_1	5.8	4.6
	N_3—H	2.9	4.1
	N_3		1.6
	=O	5.9	3.4
Uracil (thymine)	N_1H	2.9	4.1
	N_1		1.6
	N_3H	2.9	4.1
	N_3		1.6
	$=O_2$	4.5	2.0
	$=O_4$	5.9	3.4
	(—CH_3)[a]	1.6	0.8
Cytosine	N_1—H	2.9	4.1
	N_1		1.6
	=O	5.9	3.4
	N_3	5.8	4.6
	NH_2	3.2	4.0
	C_4—N		3.0

[a]Thymine interaction enthalpies are taken to be the same as those for uracil. The contribution of the methyl group is added to the uracil interaction terms.

pyridines have shown that the transfer enthalpy from water to methanol could be accounted for if only the making and breaking of hydrogen bonds in the two solvents were considered. Thus, any cavity or interactions terms due to the benzene ring or imidazole ring are not of overriding significance in determining the transfer enthalpy. The sum of the transfers of the appropriate six-member ring and imidazole compounds should give the transfer enthalpy for the compound formed from the fusion of these two compounds if only the making and breaking of hydrogen bonds is important. The sum of the transfer enthalpies for pyrimidine and imidazole should approximate the transfer enthalpy of purine; benzene and imidazole transfers should approximate that of benzimidazole; pyridine and imidazole serve as models for the transfer of 4-azabenzimidazole; and the sum of transfers of imidazole, 2-aminopyridine, and pyridine should give the transfer enthalpy of adenine. The sums

TABLE 3. Calculated and experimental transfer enthalpies (kcal mol^{-1}) for purines[a]

Solute	ΔH_{tr}[b] HB	ΔH_{tr}[c] C, i	ΔH_{tr}[d] calcd.	ΔH_{tr}[e] exptl.	ΔH_{tr}[f] sum
Benzimidazole	−1.4	−0.9	(−2.3)	−2.3	−1.4
4-Azabenzimidazole	0	−0.9	−0.9	−1.3	0
Purine	+1.3	−0.9	+0.4	+0.4	+1.3
Adenine	−1.3	−0.9	−2.2	−2.8	−1.0

[a]All transfers are from water to methanol.
[b]Calculated from the interaction enthalpies given in Table 2.
[c]Cavity and interaction terms for the transfer of benzimidazole.
[d]Transfer enthalpy calculated from columns 2 and 3.
[e]Experimental transfer enthalpies.
[f]Calculated from the appropriate sum of the transfer enthalpies of pyridine, pyrimidine, 2-aminopyridine, and imidazole.

of these transfers are given in Table 3. These summed transfers agree very closely with the transfers calculated on the basis of the assigned interaction enthalpies (column 2, Table 3). If only making and breaking of hydrogen bonds are significant for the transfer enthalpies, exactly such an agreement would be expected. However, the experimental transfer enthalpies for the solutes of this work are all about 1 kcal mol^{-1} more negative than the summed transfer enthalpies or those transfer enthalpies calculated from assigned specific interactions. It would appear that when ring systems such as pyrimidine and imidazole are fused, the cavity and interaction terms for the fused compound may be quite different than for the separate components. The transfer enthalpy of benzene from water to methanol is −0.1 kcal mol^{-1}, the same transfer for biphenyl is −3.0 kcal mol^{-1} and that for naphthalene is −2.5 kcal mol^{-1} (13, 14).

D'Albis *et al.* (7) have suggested that nucleic acid bases in water solvent may self-associate through hydrogen bonding. An estimate of the enthalpy change for the formation of a hydrogen bonded self-association complex of purine in water may be made by using the enthalpies given in Table 2. If a cyclic dimer is formed by hydrogen bonding from N9H of one purine molecule to N_3 of another, water molecules must be cleared from both sites; this requires 6.1 kcal mol^{-1}. The resulting N—H···N hydrogen bond releases about 4.3 kcal mol^{-1} (15). The water molecules cleared from N9H and N_3 reform hydrogen bonds to other water molecules. The water−water hydrogen bond is estimated to be 5.1 kcal mol^{-1}. For the dimerization,

$$2w - \text{pur-2} = (\text{pur})_2 + 2ww$$

the enthalpy change is +12.2 − 8.6 − 10.2 = −6.6 kcal mol^{-1}.

A similar analysis allows the assignment of the first solvation shell hydrogen bond enthalpies for uracil, thymine, and cytosine. The model compound 1-methyl-2-pyridone and previously determined interaction enthalpies were used to make these assignments (8, 9).

The transfer enthalpy from water to methanol, +2.9 kcal mol^{-1}, for 1-methylpyridone was considered to be the sum of the transfers of the methyl group, the carbonyl group, and the nitrogen atom. The cavity and interaction terms for the benzene moiety are insignificant. The transfer enthalpy, water to methanol, is +0.8 kcal mol^{-1} for the methyl group (9) and −0.4 kcal mol^{-1} for the nitrogen (8, 9). Thus the transfer enthalpy for the carbonyl group is +2.5 kcal mol^{-1}. If DMA is used as a model for the carbonyl group, the interaction enthalpy previously determined (16) for the carbonyl−water hydrogen

Can. J. Chem. Downloaded from www.nrcresearchpress.com by 210.87.254.5 on 09/06/12
For personal use only.

TABLE 4. Calculated and experimental transfer enthalpies for pyrimidines

Solute	$\overline{\Delta H_s}$ (kcal mol^{-1}) CH_3OH	$\overline{\Delta H_s}$ (kcal mol^{-1}) H_2O	ΔH_{tr} $H_2O \rightarrow CH_3OH$ Exptl.	ΔH_{tr} $H_2O \rightarrow CH_3OH$ Calcd.
Uracil	6.37[a]	6.70[a]	−0.3	−0.6
		7.00[b]	−0.6	
		7.05[c]	−0.7	
Thymine	5.9[d]	5.4[d]	+0.5	+0.2
		5.8[e]	+0.1	
		5.5[c]	+0.4	
Cytosine	4.2[a]	7.7[a]	−3.5	−2.9
		6.5[f]	−2.3	
4(3*H*)-Pyrimidone	5.1	4.1	+1.0	+0.9
1-Methyl-2-pyridone	−0.4	−3.3	+2.9	(+2.9)

[a]Reference 19.
[b]Reference 20.
[c]Reference 21.
[d]Reference 22, ethanol solvent.
[e]Reference 23.
[f]Reference 24.

bond, −5.9 kcal mol^{-1}, may be used to assign the hydrogen bond enthalpy for the carbonyl−methanol hydrogen bond as −3.4 kcal mol^{-1}.

The transfer enthalpy of 4(3*H*)-pyrimidone is then considered to involve the transfer of the ring nitrogen (pyridine is the model compound) (9), the carbonyl group, and the N—H group. The N—H enthalpies are taken to be the same as those determined for adenine.

For uracil and thymine O_2 and O_4 are not equivalent (15) and consequently previously determined interactions for these groups hydrogen bonding to water have been used (16). The hydrogen bonded interactions with methanol were taken to be less than those to water by the transfer enthalpy of 2.5 kcal mol^{-1}. For cytosine, 4-aminopyridine was used to model the amino group interactions (8). These interaction enthalpies, given in Table 2, may be used to calculate the transfer enthalpies. The results of these calculations are given in Table 4.

The transfer enthalpies given in Table 4 show that 4(3*H*)-pyrimidone and 1-methyl-2-pyridone are enthalpically more stable in water than in methanol. The interaction enthalpies indicate that water stabilizes these two compounds relative to methanol because the proton donating ability of water is greater than that for methanol. The order of enthalpic stability is reversed for uracil and cytosine with methanol being the better solvent. This is due to the two proton donating groups on these compounds and the superior proton accepting ability of methanol over water. Thymine is slightly more stable in water than in methanol. The methyl group of thymine is 0.8 kcal mol^{-1} more stabilized by water than methanol due to the structuring of water molecules about this non-polar group. Hydrophobic hydration of the methyl group is thus seen to be the reason for the greater enthalpic stability of thymine in water relative to methanol.

Acknowledgments

This research was partially supported by the National Science Foundation under Grant No. PRM-8102879. Additional support was provided by Research Corporation through the Cottrell College Science Grants Program and by Franklin and Marshall College.

1. B. PULLMAN, M. STANISLAV, and D. PERAHIA. Theoret. Chim. Acta, Berlin, **50**, 317 (1979).
2. A. PULLMAN. Structure and conformation of nucleic acids and protein − nucleic acid interactions. *Edited by* M. Sundaralingam and S. T. Rao. University Park Press, Baltimore. 1975. p. 457.
3. E. CLEMENTI and G. CORONGIV. J. Chem. Phys. **72**, 3979 (1980).
4. A. B. TEPLITSKY, I. K. YANSON, O. T. GLUKHOVA, A. ZIELENKIEWICZ, W. ZIELENKIEWICZ, and K. L. WIERZCHOWSKI. Biophys. Chem. **11**, 17 (1980).
5. J. ALVAREZ and R. BILTONEN. Biopolymers, **12**, 1815 (1973).
6. S. J. GILL, M. DOWNING, and G. F. SHEATS. Biochemistry, **6**, 272 (1967).
7. A. D'ALBIS, M. P. WICKENS, and W. B. GRATZER. Biopolymers, **14**, 1423 (1975).
8. J. N. SPENCER, S. W. BARTON, K. A. SMITH, W. S. WOLBACH, J. F. POWELL, M. R. KIRSHENBAUM, and D. W. FIRTH. Can. J. Chem. **61**, 194 (1983).
9. J. N. SPENCER, E. S. HOLMBOE, M. R. KIRSHENBAUM, S. W. BARTON, K. A. SMITH, W. S. WOLBACH, J. F. POWELL, and C. CHORAZY. Can. J. Chem. **60**, 1183 (1982).
10. B. PULLMAN and A. PULLMAN. Quantum biochemistry. Interscience Publishers, New York. 1963. pp. 232−233.
11. P. E. RIDER. J. Appl. Polymer Sci. **25**, 2975 (1980).
12. N. C. GONNELLA and J. D. ROBERTS. J. Am. Chem. Soc. **104**, 3162 (1982).
13. R. F. BOHON and W. F. CLAUSSEN. J. Am. Chem. Soc. **73**, 1571 (1951).
14. R. FUCHS, L. L. COLE, and R. F. RODEWALD. J. Am. Chem. Soc. **94**, 8645 (1972).
15. J. N. SPENCER, J. E. GLEIM, C.H. BLEVINS, R. C. GARRETT, F. J. MAYER, J. E. MERKLE, S. L. SMITH, and M. L. HACKMAN. J. Phys. Chem. **83**, 2615 (1979).
16. J. N. SPENCER, S. K. BERGER, C. R. POWELL, B. D. HENNING, G. S. FURMAN, W. M. LOFFREDO, E. M. RYDBERG, R. A. NEUBERT, C. E. SHOOP, and D. N. BLAUCH. J. Phys. Chem. **85**, 1236 (1981).
17. M. V. KILDAY. J. Res. Natl. Bur. Stand. **83**, 347 (1978).
18. M. V. KILDAY. J. Res. Natl. Bur. Stand. **84**, 231 (1979).
19. R. L. SCRUGGS, E. A. ACHTER, and P. D. ROSS. Biopolymers, **11**, 1961 (1972).
20. M. V. KILDAY. J. Res. Natl. Bur. Stand. **83**, 547 (1978).
21. J. K. AHMED, G. A. W. DERWISH, and F. I. KANBOUR. J. Soln. Chem. **10**, 343 (1981).
22. J. ALVAREZ, and R. BILTONEN. Biopolymers, **12**, 1815 (1973).
23. M. V. KILDAY. J. Res. Natl. Bur. Stand. **83**, 529 (1978).
24. M. V. KILDAY. J. Res. Natl. Bur. Stand. **83**, 539 (1978).

Can. J. Chem. Downloaded from www.nrcresearchpress.com by 210.87.254.5 on 09/06/12
For personal use only.

Étude polarographique du niobium dans les mélanges eau − fluorure d'hydrogène

H. MÉNARD et R. BEAUDOIN

Département de chimie, Faculté des sciences, Université de Sherbrooke, Sherbrooke (Qué.), Canada J1K 2R1

Récu le 8 mars 1983

H. MÉNARD et R. BEAUDOIN. Can. J. Chem. **61**, 2699 (1983).

L'analyse de certains minerais requiert leur solubilisation dans le fluorure d'hydrogène. Nous avons élaboré une méthode d'analyse directement applicable aux mélanges eau − fluorure d'hydrogène.

Cependant, dans l'acide fluorhydrique 50% le niobium est soluble sous la forme du complexe NbF_6^- qui est réductible à l'électrode polarographique à un potentiel de −0,880 volt vs. ECS. Pour des concentrations inférieures à 45% en HF, le complexe du niobium s'hydrate pour donner l'ion $NbOF_5^{-2}$ non réductible.

H. MÉNARD and R. BEAUDOIN. Can. J. Chem. **61**, 2699 (1983).

Solubilization in hydrogen fluoride is required for the analysis of some minerals. A method of analysis directly applicable to water − hydrogen fluoride mixtures was worked out.

However, in 50% hydrofluoric acid niobium is soluble as NbF_6^- complex, which can be reduced with a polarographic electrode at a potential of −0.880 V vs. E.C.S. For concentrations lower than 45% in HF, the niobium complex is hydrated and exists as a non-reducible ion $NbOF_5^{-2}$.

[Journal translation]

Can. J. Chem. Downloaded from www.nrcresearchpress.com by 210.87.254.105 on 09/06/12
For personal use only.

Introduction

La polarographie du niobium peut s'effectuer dans un grand nombre de milieux (1), pour autant que les éléments interférents soient absents au facilement éliminables. Le minerai de niobium contient généralement du tantale. Il est donc important de pouvoir analyser le mélange de ces deux métaux doués de propriétés similaires. Quoique le tantale ne donne que rarement une vague polarographique (2), il peut toutefois interférer dans certains milieux en formant un complexe contenant à la fois le tantale et le niobium. Ces complexes diffusent plus lentement à cause de leur taille accrue, ce qui contribue à la diminution du courant de diffusion lié à la réduction du niobium. Il existe quelques études polarographiques de la réduction du niobium dans divers solvants et électrolytes supports (1, 3−6).

Les solutions sont généralement préparées par fusion de l'oxyde de niobium dans le carbonate de potassium, suivie de la dissolution du mélange dans le milieu choisi.

La réduction dans l'acide chlorhydrique dilué est impossible à cause de l'instabilité de la solution. Selon Henrion et Alder (7) et Elving et Olson (8), la vague présente son amplitude maximale pour une concentration de 11 mol/L en HCl. Aux concentrations plus faibles, il y a formation hydrolytique d'acide niobique. McCullough et Meites (9, 10) ont étudié en détail le mécanisme du transfert d'électrons. Ils arrivent à la conclusion que le transfert monoélectronique est suivi par une disproportion du type suivant:

$$[1] \quad Nb^{+5} + é \rightarrow Nb^{+4}$$

$$[2] \quad 2Nb^{+4} \rightarrow Nb^{+5} + Nb^{+3}$$

la contribution de la réaction [2] étant relativement négligeable.

L'oxyde de niobium est très soluble dans les mélanges eau − fluorure d'hydrogène à partir de faibles concentrations en HF. La polarographie dans ce milieu permet donc d'éliminer l'étape de la fusion alcaline suivie de la redissolution dans le milieu désiré. De plus le tantale ne donne pas de vague de réduction et n'interfère pas sur celle du niobium dans ce milieu; il n'est donc pas nécessaire d'éliminer le tantale de la solution avant la détermination du niobium. La présence des complexes NbF_6^- et $NbOF_5^{-2}$ peut aussi être mise en évidence, l'ion $NbOF_5^{-2}$ n'étant pas électroactif. Plusieurs auteurs (11−14) ont étudié les complexes du niobium dans les mélanges eau − fluorure d'hydrogène. Pour des solutions contenant plus de 35% en HF, le complexe prédominant est NbF_6^-, alors que pour une concentration inférieure à 25% en HF, l'espèce prépondérante devient $NbOF_5^{-2}$.

Partie expérimentale

La cellule polarographique est constitutée d'un bécher en polyméthylpentane d'une capacité de 50 mL surmonté d'un couvercle de Teflon qui sert à maintenir les électrodes. L'électrode de référence au calomel saturé est munie d'une double jonction séparée de la solution par une gaine de Teflon et un disque de polyéthylène poreux. L'électrode auxiliaire est un fil de platine. L'électrode de travail est un capillaire polarographique Sargent−Welch S-2418 recouvert de polyéthylène (15) et dont la période de chute est contrôlée par un dispositif électronique réalisé dans nos ateliers. Tous les potentiels se réfèrent à l'électrode de calomel saturé. L'analyseur polarographique PAR est le modèle 364. La table traçante est une techneurop, Sefram T.G.M. 101.

Les produits utilisés sont: niobium métallique en poudre de Pfaltz and Bauer; Nb_2O_5 99,9% de Alfa Product et HF 49% de Baker.

Le niobium métallique n'est soluble que dans un mélange d'acide nitrique et fluorhydrique. Pour faire une mesure polarographique, il suffit d'évaporer à sec pour éliminer l'acide nitrique et redissoudre dans l'acide fluorhydrique. Le résidu obtenu après évaporation dans un bain d'huile est un fluorure de niobium qui peut être redissous en un temps très court.

La mise en solution du minerai s'effectue en pesant environ 0,25 g dans un erlenmeyer de polyéthylène auquel au ajoute 10 mL d'acide fluorhydrique à 49% puis 5 mL d'acide nitrique concentré. Le mélange est agité et évaporé à sec sur bain d'huile. Le résidu est redissous dans HF 49% et jaugé à 100 mL. Le polarogramme peut être pris directement ou en diluant à la concentration requise.

Pour l'analyse des minerais bruts dont la teneur en niobium se situe entre 0 et 1%, il est préférable d'utiliser la méthode des ajouts dosés. La technique consiste à peser des échantillons du minerai (soit un gramme) auxquels on additionne des quantités croissantes de Nb_2O_5. Après resolubilisation, les polarogrammes sont enregistrés et la concentration de niobium dans le minerai est déduite par extrapolation.

Résultats

Dans l'acide fluorhydrique, on observe une vague de réduction de niobium. La figure 1 montre la vague obtenue par rapport au courant résiduel du HF 49%. Quoiqu'assez près du

Can. J. Chem. Downloaded from www.nrcresearchpress.com by 210.87.254.105 on 09/06/12
For personal use only.

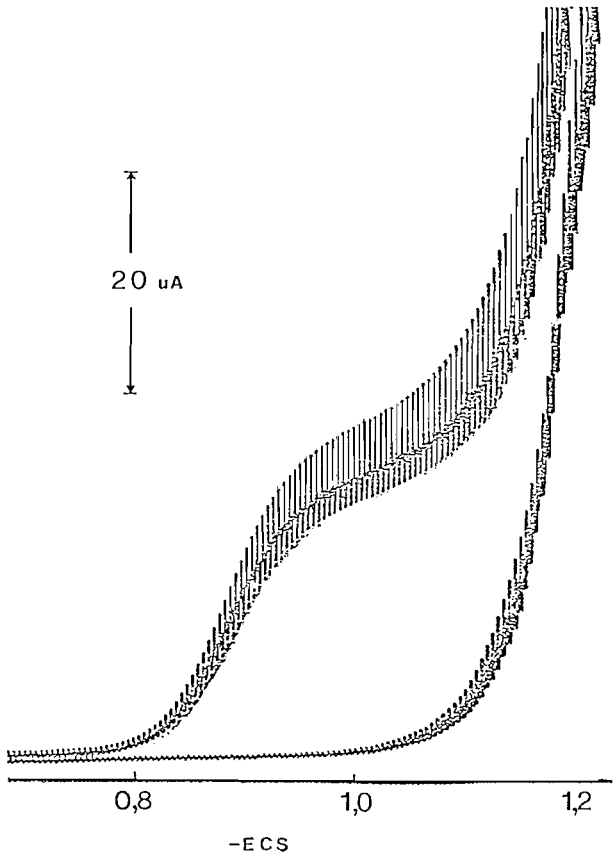

FIG. 1. Polarogramme du niobium dans HF 49,1%.

mur de réduction de l'hydrogène la vague est suffisamment bien résolue. Le potentiel de demi-vague est de −0,880 V.

La réversibilité de la vague a été vérifiée à partir de différentes techniques polarographiques: le graphique du potentiel en fonction du log $i/(id-i)$ présente une droite dont la pente est de 59 mV; le potentiel de demi-vague obtenu par polarographie impulsionnelle est le même que celui obtenu par polarographie classique; le pic que l'on obtient par polarographie impulsionnelle différentielle est situé à la valeur de potentiel prévue par Parry et Osteryoung (16), plus positive de 25 mV que la valeur obtenue par polarographie classique, dans le cas d'une impulsion de 50 mV.

A partir de l'équation du courant en polarographie impulsionnelle différentielle:

$$[3] \quad \delta i = \frac{nFAD^{1/2}C_0^*}{\Pi^{1/2}(\tau - \tau')^{1/2}} \left| \frac{P_A(1-\sigma^2)}{(\sigma + P_A)(1 + P_A\sigma)} \right|$$

où τ' est le temps immédiatement avant l'impulsion et τ est le temps juste avant la fin de l'impulsion,

$$[4] \quad P_A = \left(\frac{D_0}{D_R}\right) \exp\left[\frac{nF}{RT}\left(E + \frac{\Delta E}{2} - E^{0\prime}\right)\right]$$

et

$$[5] \quad \sigma = \exp\frac{nF}{RT}\frac{\Delta E}{2}$$

où ΔE est le saut de potentiel.

On démontre facilement par dérivation $d(\delta i)/dP_A$ que δi est maximum pour $P_A = 1$.

Dès lors:

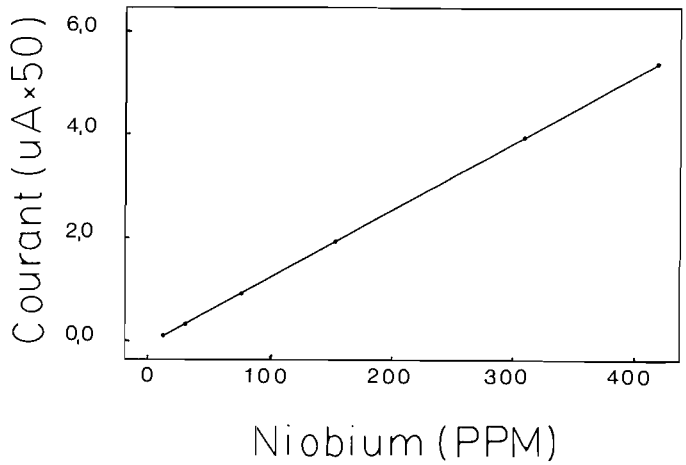

FIG. 2. Courbe d'étalonnage pour la détermination quantitative du niobium en milieu HF 49%, en régime polarographie impulsionnelle différentielle.

$$[6] \quad E_{max} = E_{1/2} - \frac{\Delta E}{2}$$

La largeur du pic à mi-hauteur augmente avec l'amplitude de l'impulsion imposée (17); elle est de 100 mV pour une amplitude de 50 mV.

Ces mesures confirment le caractère réversible et monoélectronique de la réaction.

$$[7] \quad Nb^{+5} + e^- \rightleftarrows Nb^{+4}$$

Cette conclusion peut être correlée au fait que Senderoff et Mellors (17) ont établi que la réduction du niobium V au niobium IV est également une réaction réversible en milieu fluorure fondu.

Les résultats polarographiques permettent de calculer le coefficient de diffusion du niobium dans HF commercial à 49% à partir de l'équation d'Ilkovic. La valeur est de $9{,}1 \times 10^{-6}$ cm^2/s.

Du point de vue analytique, il est préférable d'utiliser la polarographie impulsionnelle différentielle. Le niobium présente un pic à un potentiel de −0,855 V pour une hauteur d'impulsion de 50 mV et une vitesse de balayage de 2 mV par seconde, le temps de chute de la goutte de mercure étant de 1.00 s.

La hauteur du pic est proportionnelle à la concentration. La figure 2 montre une courbe d'étalonnage à laquelle correspond une limite de détection de l'ordre de 15 ppm. Cette valeur est essentiellement déterminée par l'interférence entre le mur de réduction de l'hydrogène et le pic de réduction du niobium.

Il est à remarquer que la concentration minimale détectable ne varie pas en fonction du vieillissement des solutions de niobium dans le fluorure d'hydrogène.

Le tableau 1 montre les résultats obtenus pour des échantillons de minerais concentrés ayant une teneur en niobium de l'ordre de 60%. Ces résultats sont reproductibles à environ 1%.

Lorsque l'on diminue la concentration en HF, la hauteur de la vague de niobium décroît et finit par disparaître complètement pour un pourcentage en HF de 22% (Fig. 3). Le potentiel de demi-vague n'étant pas déplacé, on peut conclure à la simple disparition de l'espèce électroactive. L'observation de la solution ne montre aucun signe de précipitation, la décroissance de l'onde polarographique étant due à la formation d'un nouveau complexe, selon

TABLEAU 1. Analyse de minerais

Echantillon	% Nb_2O_5	% Moyen	% Fluorescence X*
1	60,4		
	61,4	61,5	60,5
	62,7		
2	63,6		
	63,4	64,0	64,0
	64,1		
3	63,7		
	63,1	63,0	61,6
	62,2		
4	55,9		
	55,8	55,7	56,2
	55,4		

*Valeurs fournies par la compagnie Niobec.

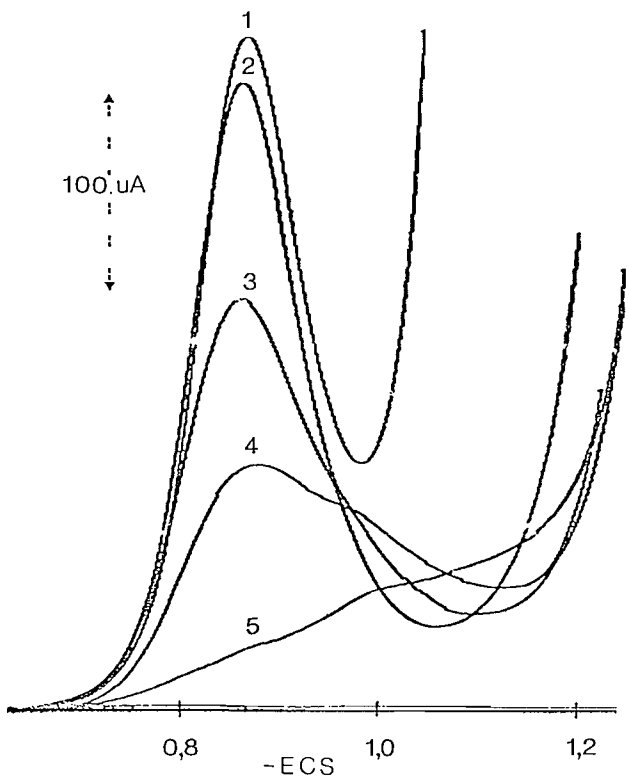

FIG. 3. Polarogrammes en régime impulsionnel différentiel du niobium dans des solutions de HF à: (1) 49,1%; (2) 39,3%, (3) 29,5%; (4) 25,5%; (5) 19,6%.

[8] $HNbF_6 + H_2O \rightleftarrows H_2NbOF_5 + HF$

Les espèces $HNbF_6$ et H_2NbOF_5 étant les espèces ioniques fortement solvatées, l'équilibre est essentiellement contrôlé par l'activé du HF et de H_2O en solution. Les activités sont calculées selon Vaillant (18) à partir des valeurs de pression partielle de l'eau, P_{H_2O} et de HF, P_{HF} publiés par Munter *et al.* (19). L'activité de l'eau est calculée à l'aide de la loi de Raoult (état de référence: eau pure):

[9] $P_{H_2O} = a_{H_2O} P^0_{H_2O}$

L'activité du fluorure d'hydrogène est calculée à partir de la

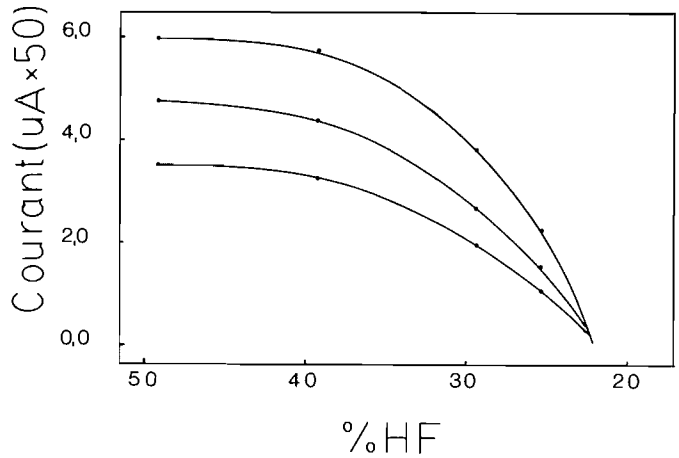

FIG. 4. Influence de la concentration en HF sur le courant de pic aux concentrations suivantes en niobium: (1) $2{,}21 \times 10^{-3}$ mol/L; (2) $1{,}67 \times 10^{-3}$ mol/L; (3) $1{,}23 \times 10^{-3}$ mol/L.

loi de Henry (référence: solution infiniment diluée de HF dans l'eau):

[10] $\text{fugacité}_{HF} = a_{HF} K_{HF}$

Le coefficient de Henry, K_{HF}, est déterminé à partir de la courbe de variation de P_{HF} en fonction de la concentration (en molarité).

La constante d'équilibre peut être calculée si on fait l'approximation que l'activité des complexes du niobium est égale à leur concentration. A la concentration en HF où le courant est la moitié de sa valeur maximale (HF à 50%), la valeur est de $0{,}7 \times 10^2$.

[11] $$K = \frac{[NbF_6^-]\, a_{HF}}{[NbOF_5^{-2}]\, a_{H_2O}}$$

Le complexe $NbOF_5^{-2}$ n'est pas réductible à l'électrode polarographique et il est responsable de la disparition de la vague de réduction. La figure 4 montre les courbes obtenues pour trois concentrations de niobium en fonction de la concentration en HF. Le point de convergence pour la disparition complète de la vague du niobium est le même dans les trois cas, soit 22% en HF.

Keller (13) puis Howell et Moss (15) ont démontré par spectroscopie que la totalité du niobium se retrouve sous la forme de NbF_6^- dans HF 50% et sous forme $NbOF_5^{-2}$ dans une solution contenant moins de 20% en HF. A partir des données polarographiques, confirmées par spectroscopie, il est aisé de calculer le pourcentage de chacun des deux complexes en fonction de la concentration en HF (Tableau 2). L'accord entre les données spectroscopiques et électrochimiques démontre que la réaction d'interconversion est très lente, à l'échelle de la période de chute de l'électrode à goutte.

Keller et Chetham-Strode (20) ont comparé le comportement du niobium et du tantale dans les mélanges eau − fluorure d'hydrogène. Le niobium a tendance à s'hydrater lorsque la concentration en HF diminue (11). En milieu chlorhydrique, on observe la précipitation d'acide niobique à acidité décroissante (7). Dans l'acide fluorhydrique, le complexe $NbOF_5^{-2}$ très stable s'observe pour des concentrations inférieures à 40% en HF. Le tantale forme également un complexe oxyfluorure mais celui-ci disparaît à une concentration de 0,1 mol/L en HF pour faire place au complexe heptafluoré (18). Les complexes heptafluorés étant généralement instables, le niobium ne donne le

Can. J. Chem. Downloaded from www.nrcresearchpress.com by 210.87.254.105 on 09/06/12
For personal use only.

TABLEAU 2. Pourcentage des deux complexes fluorés du niobium en fonction du pourcentage en fluorure d'hydrogène

Polarographie			Bandes infrarouge actives* (cm^{-1})	
% HF	NbF_6^-	$NbOF_5^{-2}$	NbF_6^-	$\%NbOF_5^{-2}$
50	~100	~0	685 (forte)	—
40	93	7	685 (forte)	—
35	78	22	686 (moyenne)	935 (fabile)
30	60	40	685 (moyenne)	935 (faible)
25	36	64	685 (faible)	935 (moyenne)
22	~0	~100	—	930 (moyenne)

*Selon réf. (12).

complexe NbF_7^{-2} qu'en sel fondu (21) où la concentration en fluorure libre est très élevée par rapport aux mélanges eau − fluorure d'hydrogène.

Conclusions

Nous avons étudié le comportement polarographique du niobium dans les mélanges eau − fluorure d'hydrogène jusqu'à 50%. Dans les mélanges à 50%, on observe une réduction monoélectronique réversible dont le potentiel de demi-vague est de −0,880 V.

Du point de vue analytique, il est possible de déterminer la concentration de niobium contenue dans un minerai avec une limite de détection de 15 ppm, même en présence de tantale.

Pour des concentrations en HF inférieures à 45% il y a formation du complexe $NbOF_5^{-2}$ non réductible, qui devient prépondérant aux concentrations en HF inférieures à 25%.

Remerciements

Nous remercions le Ministère de l'Education du Québec et le Conseil de Recherches en Sciences naturelles et en Génie du Canada pour leur support financier. Nous remercions aussi la compagnie NIOBEC pour nous avoir fourni des échantillons de minerais analysés par fluorescence des rayons X.

1. P. PASCAL. Nouveau traité de chimie minérale. Tome VI. Masson et Cie, Paris (1961).
2. A. A. VLCEK. Chem. Listy, **49**, 260 (1955).
3. E. I. KRYLOV, V. S. KOLEVATOVA et U. A. SAMARINA. Zh. Anal. Khim. **11**, 144 (1965).
4. J. H. KENNEDY. Anal. Chem. **33**, 943 (1961).
5. J. D. FERRETT et G. W. C. MILNER. J. Chem. Soc. London, 1186 (1956).
6. G. POPA, R. LERCH et I. C. CAZACU. An. Univ. Bucuresti Chim. **19**, 9 (1970).
7. G. HENRION et F. ALDER. Z. Chem. **15**, 321 (1975).
8. P. J. ELVING et E. C. OLSON. Anal. Chem. **28**, 338 (1956).
9. J. G. MCCULLOUGH et L. MEITES. J. Electroanal. Chem. Interfacial Electrochem. **18**, 123 (1968).
10. J. G. MCCULLOUGH et L. MEITES. J. Electroanal. Chem. Interfacial Electrochem. **19**, 111 (1968).
11. N. S. NIKOLAEV et YU. A. BUSLAEV. Russ. J. Inorg. Chem. **4**, 84 (1959).
12. O. L. KELLER. Inorg. Chem. **2**, 783 (1963).
13. K. J. PARKER et E. L. MUETTERTIES. J. Am. Chem. Soc. **85**, 3035 (1963).
14. J. A. S. HOWELL et K. C. MOSS. J. Chem. Soc. A, 2481 (1971).
15. H. MENARD et F. LEBOND-ROUTHIER. Anal. Chem. **50**, 687 (1978).
16. E. P. PARRY et R. A. OSTERYOUNG. Anal. Chem. **37**, 1634 (1965).
17. S. SENDEROFF et G. W. MELLORS. J. Electrochem. Soc. **113**, 66 (1966).
18. A. VAILLANT. Thèse de troisième cycle. Université Paris 6 (1976).
19. M. E. MUNTER, P. AEPLI et H. G. KOSSATY. Ind. Eng. Chem. **41**, 1504 (1949).
20. O. L. KELLER et A. CHETHAM-STRODE. Inorg. Chem. **5**, 367 (1966).
21. J. S. FORDYCE et R. L. BAUM. Abstract, 150th National Meeting of the American Chemical Society, Atlantic City, NJ, Sept. 13−17, 1965.

Can. J. Chem. Downloaded from www.nrcresearchpress.com by 210.87.254.105 on 09/06/12
For personal use only.

State-resolved quantum yields of the reactions of metastable Ca(^3P, ^1D) with NO_2 and N_2O

HUI WANG[1] AND MICHAEL MENZINGER

Department of Chemistry, University of Toronto, Toronto, Ont., Canada M5S 1A1

Received January 4, 1983

HUI WANG and MICHAEL MENZINGER. Can. J. Chem. **61**, 2703 (1983).

Absolute chemiluminescence and quenching (beam attenuation) cross sections were measured for the title reactions in a beam/gas experiment. In the Ca* + NO_2 system, both quantities are about twice as large as in the N_2O reaction. The chemiluminescence quantum yields, corrected for infrared emission from the $A\,^1\Sigma^+$ and $A'\,^1\Pi$ states, are of similar magnitude $Y_{CL}(Ca^* + N_2O) = 7.2 \pm 1.1\%$ and $Y_{CL}(Ca^* + N_2O) = 8.0 \pm 0.9\%$. The quenching cross sections are $\sigma_T(Ca^* + N_2O) = 153 \pm 32$ Å^2 and $\sigma_T(Ca^* + N_2O) = 73.2 \pm 5.7$ Å^2, consistent with a long-range harpooning process in the former and an electron transfer at closer range for the latter system. The partial resolution of CL spectra was aided by lifetime-separated spectroscopy. The principal emitter in both systems is the long-lived CaO($A'\,^1\Pi$), next to minor yields of CaO in the short-lived $A\,^1\Sigma^+$, $B\,^1\Pi$, and "orange and green arc band" states. The results are discussed in light of adiabatic correlations. The arc states are argued to arise in nearly coplanar collisions from the rearrangement of an excited intermediate. An information theoretical analysis reveals considerable dynamical bias in the form of non-linear surprisal plots.

HUI WANG et MICHAEL MENZINGER. Can. J. Chem. **61**, 2703 (1983).

On a mesuré les sections droites de chimiluminescence et d'extinction (attenuation de faisceau) des réactions mentionnées dans le titre dans une expérience de faiseau/gas. Dans le système Ca* + NO_2 les deux quantités sont environ deux fois plus élevées que dans la réaction du N_2O. Les rendements quantiques de chimiluminescence, corrigés pour l'émission infrarouge à partir des états $A\,^1\Sigma^+$ et $A'\,^1\Pi$, sont du même ordre de grandeur $Y_{CL}(Ca^* + N_2O) = 7{,}2 \pm 1{,}1\%$ et $Y_{CL}(Ca^* + N_2O) = 8{,}0 \pm 0{,}9\%$. Les sections droites d'extinction sont de: $\sigma_T(Ca^* + N_2O) = 153 \pm 32$ Å^2 et $\sigma_T(Ca^* + N_2O) = 73{,}2 \pm 5{,}7$ Å^2 et elles sont en accord avec un processus d'harponnage à longue distance dans le premier transfert d'électron à un intervalle plus rapproché que celui du dernier système. La spectroscopie de temps de vie séparé aide à résoudre partiellement les spectres du CL. Le principal émetteur dans les deux systèmes est le CaO ($A'\,^1\Pi$) de longue période de vie après $B\,^1\Pi$ et "la bande d'arc orange et vert". On discute des résultats en fonction des corrélations adiabatiques. On pense que les états d'arc proviennent de collisions quasi coplanaires à partir de la transposition d'un intermédiaire excité. Une information d'analyse théorique révèle une déviation dynamique considérable dans la forme non linéaire surprenante des courbes.

[Traduit par le journal]

Introduction

Since the first studies, more than a decade ago (1), on the chemiluminescence from alkaline earth metal atoms M with oxidizers N_2O and NO_2, much progress has been made in understanding their rich spectroscopy and dynamics (2). The complexity of these seemingly innocuous reactions becomes first evident in the spectroscopy of the metal oxides (3), which has made the determination of the primary product state distribution a non-trivial and still ongoing task (4). The dramatic rise of photon yield with pressure (5) and the entire issue of dark (or reservoir) states have made the Ba + N_2O system a cause celèbre (2) and a paradigm for similar systems reflecting the importance of energy transfer following the primary reaction step. The involvement and the high quantum yields of the metastable M(^3P, ^1D) metal atoms reacting with N_2O were first noted in ternary flames (6) in the presence of CO. It was subsequently shown (7) that the metastable reactions lend themselves readily to measuring absolute chemiluminescence and quenching cross sections σ_{CL}, σ_T, without the need for tedious and inherently inaccurate absolute calibrations (5). The present work was undertaken to shed light on the multi-potential energy surface dynamics through its key-witness, the partitioning of electronic energy. We concern ourselves only with the primary reaction yields and hence have confined the measurements to gas pressures below 1.4 mTorr. Dagdigian and co-workers have already studied the Ca* + N_2O system both under single collision (8) and multiple collision conditions (8) and have reported state-resolved quantum yields. The purpose of the present work is to study comparatively the NO_2 as well as the N_2O reactions under single collision conditions and to further develop the resolution of product states (8).

The assignment and "carving up" of the CL spectra relies greatly on indirect inference based on lifetime-separated spectroscopy (9). By this technique the long-lived CaO($A'\,^1\Pi$) state can be shown to be the principal emitter, while ($A\,^1\Sigma^+$), ($B\,^1\Pi$), and the "orange and green arc band" emitters are relatively minor products for the NO_2 and N_2O reactions alike. Possible dark products are CaO($X\,^1\Sigma^+$, $^3\Sigma^+$, $a^3\Pi$, $b^3\Pi$) (26).

This paper concludes with an interpretation of the observed distributions in terms of two limiting points of view: adiabatic correlations (10) provide a classification of the observed channels into diabatic and adiabatic, as well as an appreciation of the high degree of departure of the present reactions from simple expectations based on the Born–Oppenheimer approximation (the conservation of spin and symmetry). An opposite, statistical viewpoint is taken in an information theoretical analysis. Given the failure of state correlations in providing a reliable predictive tool, one may ask whether and to what extent dynamics matters at all. Again we find substantial departures from prior expectation and conspicuously non-linear surprisal plots, indicating electronic energy partitioning that cannot be explained by presently available simplified models.

The experiments

Standard metastable metal chemiluminescence measurements (7, 8) were modified to obtain lifetime-separated spectral information. To this end two types of detection geometry were employed: the first type (mode V) saw only those short-lived emitters radiating directly from the collision zone. The second type (mode H) viewed a bigger detection volume that includes those long-lived products that had drifted

[1]On leave from the Institute of Physical Chemistry, Chinese Academy of Sciences, Dalien, People's Republic of China.

Can. J. Chem. Downloaded from www.nrcresearchpress.com by 210.87.254.42 on 09/06/12
For personal use only.

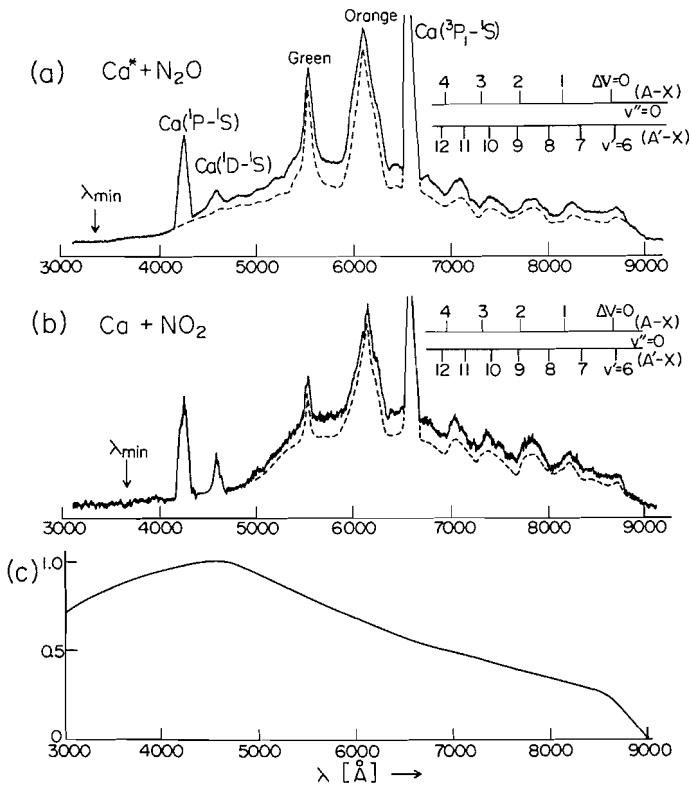

FIG. 1. Chemiluminescence spectra $S(\lambda)$ for (a) Ca* + N_2O and (b) Ca* + NO_2. The solid line S_H represents measurements in the H-mode and the dashed line in the V-mode. Both are normalized to equal arc band intensity. (c) Spectral response $D(\lambda)$ of the detection system.

out of the collision volume prior to radiative decay.

A metastable $Ca(^3P,^1D)$ beam, generated by a low-voltage discharge at the exit orifice of an effusive beam oven (8, 12) was, after deflection of charged particles, shot into a 4 × 4 × 6 cm scattering chamber. The latter was blackened with soot and carried a Wood's horn at the beam-exit orifice for reducing stray light from the discharge. The pressure in the scattering chamber was directly measured by a capacitance manometer (MKS Baratron 77H3) connected to the chamber by a 25 cm long, 2 cm diameter tube. The pressure dependence of the metastable decay lines $Ca(^3P_1-{}^1S_0$, $^1D_2-{}^1S_0)$ and of the chemiluminescence were monitored by a 30 cm monochromator and an RCA C31034 multiplier, and analyzed as described below (7, 8). The wavelength response $D(\lambda)$ of the detector (Fig. 1c) was obtained with a standard tungsten lamp. The observation zone was confined by a mask on the scattering chamber window to a horizontal slit (mask: 0.36 cm high, 3 cm wide; both the mask and the viewing direction are at right angles to the metal beam), located at a distance $l = 2.2 \pm 0.18$ cm (the scattering path length) downstream from the (0.25 cm diameter) beam entrance orifice. Two quartz lenses (overall magnification $M = 0.51$) sharply focussed the reaction zone onto the 2.0 × 0.2 cm monochromator slit.

The monochromator was operated with its slit either vertical (normal, mode V) or horizontal (mode H). In mode V the detection volume was 0.36 × 0.4 cm, formed by the intersection of the horizontal mask with the vertical slit. Short-lived emitters are seen preferentially in this mode. In mode H the 0.36 × 3.0 cm detection volume coexistent with the horizontal mask contained those long-lived emitters (with radiative lifetime $\tau_R = 10^{-5}-10^{-6}$ s) that had drifted out of the metal beam prior to their decay and also the elastically scattered metastable atoms.

From the fluorescence spectra of the pure metal beam and the known radiative lifetimes $\tau_R(Ca^3P) = 5.0 \pm 0.4 \times 10^{-4}$ s (13, 14) and $\tau_R(Ca^1D_2) = 2.3 \pm 0.5 \times 10^{-3}$ s (14), the $^1D/^3P$ density ratio was found (14b) to be 0.03 ± 0.005 under typical discharge conditions.

Results and discussion

1. Chemiluminescence spectra and assignment

Chemiluminescence overview spectra $S(\lambda)$ are presented in Fig. 1a, b for Ca* + N_2O and NO_2, respectively. Their independence from pressure ($p < 1.4$ mTorr) indicates that single collision conditions prevail. Measurements with vertical and horizontal monochromator slits (V- and H-modes) are represented by dotted and full curves, respectively. They are normalized to equal arc band intensity since the short-lived arc band emitters ($\tau_R = 42 \pm 2$ and 33 ± 3 ns for the green and orange systems) (8) are considered a measure of the rate of formation of nascent products.

Both systems yield qualitatively similar spectra in either of the (H, V) detection modes. Superimposed on a broad quasi-continuum extending from 3250 Å and 3650 Å for N_2O and NO_2 respectively to the detection limit at 9000 Å, one discerns the atomic lines $Ca(^1P_1-{}^1S_0)$ at 4228 Å, $(^1D_1-{}^1S_0)$ at 4577 Å, and $(^3P_1-{}^1S_0)$ at 6575 Å; the following clearly structured molecular band systems: the green and the orange "arc band" systems at 5440−5670 Å and 5913−6345 Å, respectively (32); and to the red side of the orange band where one expects the $CaO(A'^1\Pi-X^1\Sigma^+)$ and $(A^1\Sigma^+-X^1\Sigma^+)$ emission to occur, a series of bands peaking at 6040, 6450, 6900, 7400, 7780, 8220, and 8720 Å. Since the detector cuts off at 9000 Å (see Fig. 1c), the emission continues most likely into the infrared, as discussed below. None of the latter bands could be unambiguously assigned to the $A'-X$ and $A-X$ systems, respectively, due to their inherent complexity (overlapping sequences) and to low spectral resolution, but their relative contributions were determined by lifetime-separated spectroscopy.

The principal differences of the N_2O and NO_2 spectra are (*1*) the more rapid fall-off of the continuum in the less exothermic NO_2 reaction (short wavelength limits $\lambda_{min}(N_2O) = 3250$ Å and $\lambda_{min}(NO_2) = 3650$ Å, corresponding to the exothermicities $\Delta E(N_2O) = -429$ kJ/mol and $\Delta E(NO_2) = -292$ kJ/mol), (*2*) the decreased relative intensities of both arc bands in the NO_2 reaction, and (*3*) the decreased (green/orange) arc band ratio in the NO_2 system. The shapes and the intensities of the $A-X$ and $A'-X$ bands in the 6700−9000 Å range are surprisingly similar in both cases. The two detection modes have qualitatively similar effects in both systems: the continuum emission and the "red" bands are reduced by ca. 30% in the V-mode, relative to the H-mode. The loss of continuum and "red" band emitters from the V-mode detection volume due to drift constitutes proof of their long radiative lifetime. The $CaO(A'^1\Pi)$ state has both a suitably long radiative lifetime[2] $\tau_R = 10^{-5}$s and an assigned emission spectrum in the 5490−7520 Å range (unassigned bands at $\lambda > 4864$ Å) resembling closely our unresolved "continuum" emission (19). In agreement with Irvin *et al.* (8) we therefore ascribe this feature primarily to the $A'^1\Pi-X^1\Sigma^+$ band system although other contributors cannot be excluded. A similar analysis has led to the assignment of $BaO(A'^1\Pi-X^1\Sigma^+)$ as the primary emitter in the Ba + N_2O reaction (3a, 9).

To analyze more closely the V- and H-mode spectra (Fig. 1a, b), we have plotted the ratios of the normalized signals:

[2]The radiative lifetime $\tau(A'^1\Pi)$ was estimated analogously to $BaO(A'^1\Pi)$ in ref. 8.

Can. J. Chem. Downloaded from www.nrcresearchpress.com by 210.87.254.42 on 09/06/12
For personal use only.

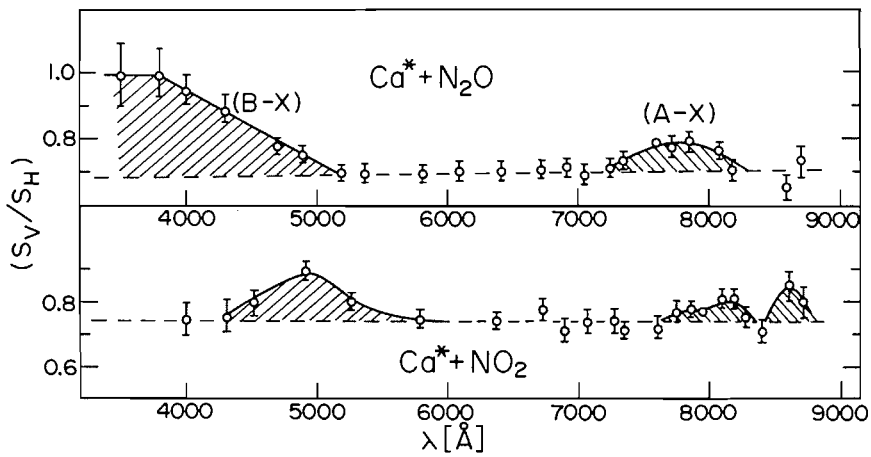

FIG. 2. Ratio $R(\lambda) = S_V/S_H$ of CL signals measured with vertical and horizontal slit. A low value of $R(\lambda)$ indicates a long-lived emitter that has drifted out of the collision zone. The shaded areas above the dashed lines are interpreted as the relative contributions of the short-lived $A\,^1\Sigma^+$ and $B\,^1\Pi$ emitters.

TABLE 1. Absolute cross sections (in Å^2) for beam attenuation $\sigma_T^{Ca^*}$, σ_T^{CL} and for total CL production σ_{CL} and quantum yields Y_{CL} (in %)[e]

	Value			
	Ca* + NO_2		Ca* + N_2O	
Parameter	Ca(^3P)	Ca(^1D)	Ca(^3P)	Ca(^1D)
$\sigma_T^{Ca^*}$	153±32[H] 218[d]	216±30[H] 816[d]	73.2±5.7[H] 89.5±8.7[V] 66.9±3.3[a]	73±8[H] 69.5±6[a]
σ_T^{CL}	168.6±19[H]	n.d.	65.3±7[H]	n.d.
σ_{CL}^{vis}	9.11±1.2[H,b]	n.d.	4.77±0.45[H,b] 4.8±1.5[a,b]	n.d. 3.6±1.9[a,b]
σ_{CL}^{tot}	11.38±1.38[c]	n.d.	5.77±0.64[c]	n.d.
Y_{CL}^{vis}	5.95±1.3[H,b]	n.d.	6.5±0.6[H,b] 7.2±2.6[a,b]	n.d. 5.1±3.2[a,b]
Y_{CL}^{tot}	7.47±1.11[c]	n.d.	7.98±0.87[c]	n.d.

[a]From Irvin and Dagdigian (ref. 8).
[b]For "visible" emission $3000 < \lambda < 9000$ Å.
[c]Corrected for ir emission.
[d]Calculated harpooning cross section, assuming $E_A(NO_2) = 2.5$ eV.
[e]Error bars, 2σ; n.d., not determined; superscript H, H-mode (monochromator slit horizontal); superscript V, V-mode (monochromator slit vertical): upper limit due to non-reactive scattering contribution.

[1] $R(\lambda) = S_V(\lambda)/S_H(\lambda)$

as a function of wavelength in Fig. 2*a*, *b*.

For N_2O (Fig. 2*a*), the constant and low value of $R = 0.7$ at $5200 < \lambda < 7200$ Å is taken as evidence for CaO($A'-X$) emission alone. The rise of R at either side of this range reflects the participation of shorter lifetime emitters. The CaO($B\,^1\Pi-X\,^1\Sigma^+$) system (20) appears as the most obvious, *known* source of the R-enhancement at $\lambda < 5200$ Å, since most higher states emitting to $X\,^1\Sigma^+$ in this region (see Table 4) are expected to be long-lived with respect to emission to $X\,^1\Sigma^+$ on the basis of spin and symmetry restrictions. The absence of an identifiable ($B-X$) structure is not surprising, considering the known (20*b*) complexity of the $B-X$ spectrum and the low resolution and population. The enhanced collection efficiency R in the $7250 < \lambda < 8200$ Å range is ascribed to the ($A\,^1\Sigma^+-X\,^1\Sigma^+$) band system (20). Quantitative estimates of the $B\,^1\Pi$ and $A\,^1\Sigma^+$ contributions are obtained by taking the areas above the $R = 0.7$ asymptote relative to the total area under the curve as the fractions of the $B\,^1\Pi$ and $A\,^1\Sigma^+$ states emitting in the corresponding spectral regions. The formation of the short-lived emitter of blue light which we assign here to CaO($B\,^1\Pi$) has escaped the attention of previous workers (8).

The NO_2 system (Fig. 2*b*) exhibits similar $R(\lambda)$ structure as N_2O: the flat portion occurs at $R = 0.75$, probably reflecting the lower exothermicity and lower recoil velocity of the emitter and hence its enhanced collection efficiency. The short wavelength feature in $R(\lambda)$ is much less pronounced than in N_2O, reflecting a lower $B\,^1\Pi$ population, while the $A\,^1\Sigma^+$ feature is of about equal integrated intensity.

2. *Chemiluminescence branching ratios*

Having assigned the $A'\,^1\Pi$, $A\,^1\Sigma^+$, $B\,^1\Pi$, "green and orange arc band" emitters, their relative populations are obtained from the wavelength-corrected spectra $S(\lambda)/D(\lambda)$ as the relative areas under the corresponding spectral features. The A and B state contributions were obtained as described above. These fractions for visible emission f_i^{vis} are listed in Tables 2 and 3 for

Can. J. Chem. Downloaded from www.nrcresearchpress.com by 210.87.254.42 on 09/06/12
For personal use only.

TABLE 2. State-resolved chemiluminescence cross sections and quantum yields for $Ca(^3P) + NO_2$[c,f]

		Visible		Visible + infrared	
Emitter i	f_i^{vis}	$\sigma_{CL}^{vis}(i)$[d]	$Y_{CL}^{vis}(i)$[c]	$\sigma_{CL}^{tot}(i)$	$Y_{CL}^{tot}(i)$
$A'^1\Pi$	0.89±0.12	8.13±1.1	5.3±1.5	10.2±1.4	6.67±0.90
$A^1\Sigma^+$	0.039±0.01	0.36±0.11	0.24±0.1	0.44±0.13	0.29±0.08
$B^1\Pi$	0.01±0.01	0.09±0.09 (2.7±2.7)[f]	0.06±0.06 (2.0±2.0)[f]	0.09±0.09	0.06±0.06
Orange arc	0.051±0.005	0.58±0.06 (17.4±1.8)[f]	0.30±0.08 (11.4±2.6)[f]	0.58±0.06	0.4±0.06
Green arc	0.008±0.001	0.07±0.01 (2.1±0.3)[f]	0.05±0.02 (1.0±0.2)[f]	0.07±0.01	0.05±0.02
Total	1.00	9.11±1.4[a]	5.95±1.8[a]	11.38±1.7	7.47±1.11

[a,c,d,e,f] See footnotes in Table 3.

TABLE 3. State-resolved chemiluminescence cross sections and quantum yields for $Ca(^3P) + N_2O$[c,f]

		Visible		Visible + infrared	
Emitter i	$f_{(i)}^{vis}$	$\sigma_{CL}^{vis}(i)$[d]	$Y_{CL}^{vis}(i)$[c]	$\sigma_{CL}^{tot}(i)$	$Y_{CL}^{tot}(i)$[c]
$A'^1\Pi$	0.82±0.10	3.91±0.37	5.34±0.9	4.91±0.46	6.8±0.63
$A^1\Sigma^+$	0.021±0.1	0.10±0.05	0.14±0.08	0.12±0.06	0.16±0.08
$B^1\Pi$	0.024±0.1	0.11±0.06 (3.3±1.8)[f]	0.15±0.09 (4.5±2.7)[f]	0.11±0.06	0.15±0.08
Orange arc	0.097±0.008	0.46±0.04 (13.8±1.2)[f]	0.63±0.10 (18.9±4.0)[f]	0.46±0.04	0.63±0.05
Green arc	0.035±0.004	0.17±0.02 (5.1±0.6)[f]	0.23±0.040 (7.0±1.0)[f]	0.17±0.02	0.23±0.03
Total	1.000	4.75±0.54[a] (4.8±1.5)[b]	6.5±1.6[a] (7.2±2.6)[b]	5.77±0.64	7.98±0.87

[a] The different error limits from those in Table 1 arise from uncertainties of fractions $f_{(i)}^{vis}$.
[b] From Irving and Dagdigian (8).
[c] Units of Y_{CL} in %.
[d] Monochromator slit horizontal (H-mode).
[e] σ_{CL}, Y_{CL} evaluated under assumption that all CL stems from $Ca(^3P)$.
[f] The values for the B and arc states, quoted in parentheses are calculated assuming exclusive formation by $Ca(^1D)$.

N_2O and NO_2, respectively.

To obtain the total CL emission one has to correct for the loss of the long-lived and rapidly recoiling $A'^1\Pi$ emitters from the observation zone, and for emission of $A'^1\Pi$ and $A^1\Sigma^+$ in the infrared $\lambda > 9000$ Å, beyond the detector cutoff. The former effect can be shown to be small (<10%), assuming a forward peaked angular distribution with 25% translational energy release, and a radiative lifetime of $\tau(A'^1\Pi) = 10^{-5}$ s (8, 18), particularly since losses from the observation zone are nearly balanced by a corresponding gain of emitters formed upstream.

The correction for emission in the infrared is obtained as follows. The fraction $F(v')$ emitted in the visible ($\lambda < 9000$ Å) from the vibrational level v' is taken to be the ratio of the Einstein emission coefficients

$$[2] \quad F^{vis}(v') = \sum_{v''=0}^{v''_{max}} q_{v',v''}\nu^3 \Big/ \sum_{v''=0}^{v''} q_{v',v''}\nu^3$$

where $q_{v',v''}$ is the Franck–Condon Factor, ν is the wavenumber of the v',v'' band origin, and v_{max}'' is the highest vibrational level of the $X^1\Sigma^+$ state for which emission still occurs below 9000 Å. Rotational broadening of the vibrational bands has been neglected. Franck–Condon factors for the $(A-X)$ and $(A'-X)$ band systems were kindly calculated for us by Telle (21) from literature spectroscopic constants (20) for $v',v'' < 50$. To assess the influence of molecular rotation on $F^{vis}(v')$, the FCF calculations were performed both for rotationless as well as for $J' = J'' = 75$ molecules. Although some *FCF*'s depend markedly on J', the total fractions F^{vis} (eq. [3]) are independent of J' within 1%.

The fraction of the total chemiluminescence in the visible F^{vis}, regardless of the upper vibrational state is

$$[3] \quad F^{vis} = \sum_{v'} F^{vis}(v')P(v')$$

where $P(v')$ is the (unknown) normalized vibrational distribution in the upper state. It is approximated by

$$[4] \quad F^{vis} = \sum_{v'} F^{vis}(v')/v_{max}'$$

assuming for simplicity a uniform vibrational distribution for both NO_2 and N_2O systems, and is proportional to the area under the $F^{vis}(v')$ curves, Fig. 3. According to this analysis,

Can. J. Chem. Downloaded from www.nrcresearchpress.com by 210.87.254.42 on 09/06/12
For personal use only.

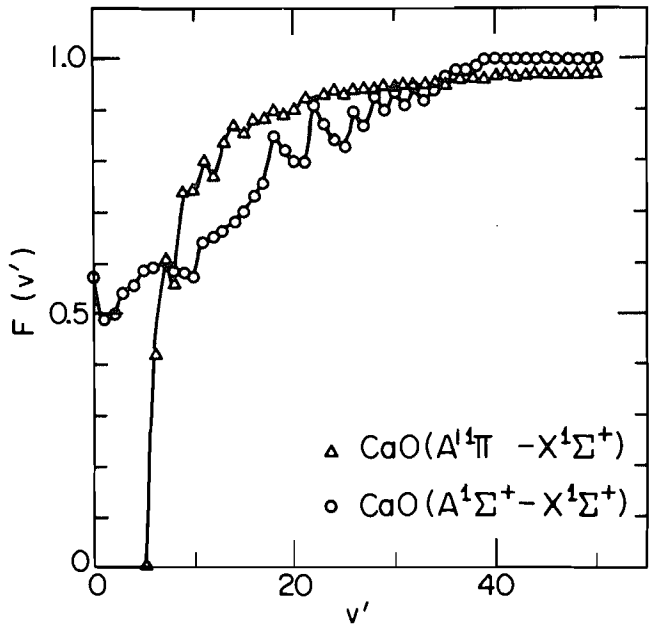

FIG. 3. Fractions $F^{vis}(v')$ of CaO($A\,^1\Sigma^+$) and ($A'\,^1\Pi$) that radiate in the part of the spectrum visible to the detector ($\lambda < 9000$ Å) as a function of vibrational state v' (eq. [2]). The areas under the curves are the total relative fractions F^{vis} emitting in the visible for a uniform distribution $P(v')$.

our experiments "see" only $F^{vis} = 79.7\%$ and 82.6% of the $A'-X$ and $A-X$ emission, respectively. The cross sections for total emitter production

$$[5] \quad \sigma_{CL}{}^{tot} = \sigma_{CL}{}^{vis}/F^{vis}$$

are summarized in Tables 2 and 3.

3. $Ca(^3P_J)$ and $Ca(^1D_J)$ attenuation cross sections σ_T

These were determined from Beer's law attenuation of the metastable emission signal as a function of scattering gas density (7, 8):

$$[6] \quad \ln (I_{Ca^*}) = \text{constant} - nl\,\sigma_T{}^{Ca^*}$$

via linear least square fits of the $\ln (I_{Ca^*})$ vs. n data. This yielded well reproducible results for $Ca(^3P_1)$, while the $Ca(^1D_1)$ results are of poorer quality, due to the much weaker $Ca(^1D_1)$ line and the relatively intense CL background (see Table 1).

The alternate chemiluminescence attenuation cross sections $\sigma^{CL}{}_T$, obtained from a linear plot of the CL signal (7*b*)

$$[7] \quad \ln (I_{CL}/n) = \text{constant} - nl\,\sigma_T{}^{CL}$$

against the scattering gas number density n is given in the second column. Its agreement with the metastable attenuation cross section $\sigma_T{}^{Ca^*}$ shows that the bulk of the chemiluminescence arises from the $Ca(^3P_1)$ state. For $Ca(^3P) + N_2O$, the first and second entries in Table 1 were taken with horizontal and vertical detector slits. The increased V-mode cross section with its higher angular resolution reflects a 22% contribution from elastic scattering. Hence the H-mode attenuation cross sections represent a more realistic upper limit of the total reaction cross section. In the N_2O reaction the attenuation cross sections for $Ca(^3P)$ and (^1D) are practically equal, while for NO_2 the (^1D) value is significantly higher. In the NO_2 reaction the agreement of $\sigma_T{}^{CL}$ with $\sigma_T{}^{Ca(^3P)}$ rather than with $\sigma_T{}^{Ca(^1D)}$ confirms $Ca(^3P)$ as the principal CL precursor. The high attenuation cross sections in the NO_2 system compared with N_2O are evidence for a long-range electron transfer as the rate determining step. Harpooning cross sections calculated for NO_2 are included in Table 1. Although they reproduce the general trend, they overestimate the experimental data, particularly for the (^1D) state. The failings of the simple harpoon model due to "reactive" electron affinities, diabatic effects, dynamical constraints, and lastly due to the fact that not all states that correlate with the metastable reactants do harpoon due to symmetry constraints, are well known (23). The Ca* + N_2O reaction is likewise thought to be initiated by an electron transfer, albeit at closer range than in the NO_2 case due to the negative electron affinity (15, 33) of the target molecule, as has been established elsewhere (15) for the Ba + N_2O system.

4. Absolute chemiluminescence cross sections σ_{CL} and quantum yields γ_{CL}

The theory and practice of absolute σ_{CL} measurements has been amply discussed (7, 8). We first present the cross section $\sigma_{CL}{}^{vis}$ for total CL production in the visible and compare them with published values (7). In applying the working formula (7)

$$[8] \quad I_{CL}/I_{Ca^3P} = \sigma_{CL}{}^{vis}\,\langle v\rangle\,\tau_R\,[n]/f_{J=1}$$

where $\langle v\rangle$ is the average relative velocity (15), τ_R the radiative lifetime of the ^3P state, $f_{J=1}$ the fraction in the emitting $^3P_1$ state, and $[n]$ the gas density. The measurement reduces to determining $[n]$ at the point where the ratio of the carefully normalized intensities is unity: $I_{CL}/I_{Ca^3P} = 1$. The results, given in Tables 2, 3 along with the corresponding quantum yields $Y_{CL} = 100(\sigma_{CL}/\sigma_T{}^{Ca^*})$, represent averages over five runs. It was implicitly assumed that all CL stems from Ca^3P and that the ^1D contribution was negligible. The N_2O cross section $\sigma_{CL}{}^{vis} = 4.75 \pm 0.45$ Å^2 agrees excellently with published data (8). The NO_2 cross section $\sigma_{CL}{}^{vis} = 9.11 \pm 1.2$ Å^2 is nearly twice this value, but due to the likewise enhanced σ_T, the NO_2 quantum yield is of the same order and slightly less than that for N_2O.

5. State-resolved (visible + ir) CL cross sections $\sigma_{CL}{}^{tot}$ (i)

These were obtained by partitioning the total visible $\sigma_{CL}{}^{vis}$ (Table 1) into the contributions from the individual emitters i, using the relative contributions f_i^{vis} to the visible spectra (Fig. 1, Tables 2, 3), and subsequently correcting the cross sections for ir emission from the $A'\,^1\Pi$ and $A\,^1\Sigma^+$ states by $(1/F^{vis})$. The resulting cross sections and quantum yields are summarized in Tables 2, 3. Compared to the data on the Ca* $+N_2O$ reaction reported elsewhere (8), the $B-X$ emission has been assigned tentatively and the total CL yield $Y_{CL}{}^{tot}$ is enhanced through the ir contribution.

6. Discussion

To interpret the results of Tables 2 and 3 we have at our disposal simple classification schemes such as spin- and symmetry-correlation rules (10) as well as statistical and information theoretical methods (11). The conceptual machinery of full dynamical calculations on more than one potential energy surface (24) is too complex to be of practical use, and there is little middle ground between these extremes. In using state correlation diagrams as devices for rationalizing the observed distributions and as a means for classifying processes, one searches for the point group of lowest symmetry which is statistically acceptable, and for an angular momentum coupling scheme that is appropriate to both reagents and products, for which adiabatic pathways in favour of the major products (24) exist. In the absence of such correlations, an observed channel

Can. J. Chem. Downloaded from www.nrcresearchpress.com by 210.87.254.42 on 09/06/12
For personal use only.

Can. J. Chem. Downloaded from www.nrcresearchpress.com by 210.87.254.42 on 09/06/12
For personal use only.

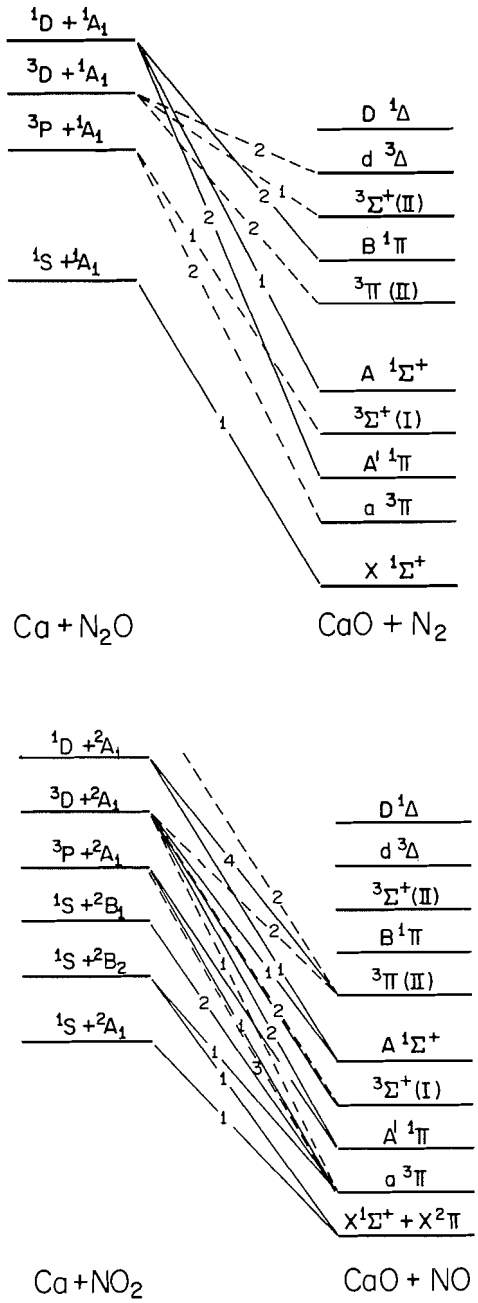

FIG. 4. Adiabatic state correlation diagrams in C_1 point group. Energies are not to scale. The numbers represent the degeneracies of the surfaces; top, Ca* + N_2O. Solid lines: singlet states, dashed lines: triplet states; bottom, Ca + NO_2. Solid lines: doublets, dashed lines: quartets.

is classified as diabatic. Furthermore, one expects correlation rules to provide some guidance regarding the distribution of the dark states (in our cases $X\,^1\Sigma^+$, $^3\Sigma^+$, and $a\,^3\Pi$) which account for the bulk (>90%) of the products.

The *adiabatic state correlation diagrams* shown in Figs. 4*a*, *b* are drawn for the point group C_1, assuming $L-S$ coupling. Going to C_s, C_{2v}, and $C_{\infty v}$ point groups does not change the following conclusions: in the *Ca* + N_2O system* there is no adiabatic pathway to the principal $A'\,^1\Pi$ product. Instead, the reactants correlate with the lowest $a\,^3\Pi$ and $^3\Sigma^+$ states (25). For this reason this reaction is a good candidate for the search for this $b\,^3\Pi^+$ state which has so far not been observed. In BaO it has been identified by laser-induced fluorescence (25). In the J-coupling representation (10), the intersection of the latter triplet surface correlating with CaO($^3\Sigma^+$) with the singlet surface connecting Ca(^3P) with CaO($A'\,^1\Pi$) provides an adiabatic avenue to the main product. Hence CaO($A'\,^1\Pi$) formation can be explained by a spin–orbit mechanism similar to the one responsible for the quenching of O(^1D) by N_2 via a long-lived complex and the multiple passage through the coupling region (27). While none of the minor products are adiabatically accessible from Ca(^3P), the $A'\,^1\Pi$, $A\,^1\Sigma^+$, and $B\,^1\Pi$ states correlate with the minor beam constituent Ca(^1D). Indeed the yields of A and B states are not inconsistent with ^1D as the parent. According to Irvin *et al.* (8), ^1D produces the arc band emitters ca. 10 times more efficiently than Ca(^3P), a reasonable finding if one considers the great number of surface-hops required for their formation from Ca(^3P).

An electron jump, albeit at closer range than in the NO_2 system, has been shown to be the initial rate determining step in the Ba(^1S) + N_2O reaction (15), and is thought to operate also in the present metastable Ca(^3P) + N_2O reaction. It is accompanied and facilitated by N_2O bending which lowers the energy of the accepting (10*a*) LUMO (15).

The *Ca + NO_2 correlation diagram* (Fig. 4*b*) is more complex than that for N_2O due to the radical character of both NO_2 and NO and the low lying NO_2 ($^2B_2$ and $^2B_1$) states. The reactants give rise to three doublet and quartet surfaces of which the former correlate adiabatically with the principal product CaO($A'\,^1\Pi$) and with CaO($a\,^3\Pi$). The statistical weights would favor the triplet over the singlet state 3:1. A long-range electron transfer (harpooning) in the entrance channel is a virtual certainty for the NO_2 reaction, considering the Ca(^3P) ionization potential (4.22 eV) and the NO_2 electron affinity (ca. 2.5 eV (22)). This is confirmed by the agreement of attenuation and calculated harpooning cross sections (Table 1).

In both reactions, the ion-pair intermediates appear to rearrange with equal ease into the principal $A'\,^1\Pi$ product, regardless of the absence (NO_2) or presence (N_2O) of spin restrictions. Arguments based on adiabatic correlations appear to be of little predictive value in these systems.

Formation of the high-lying (arc band and $B\,^1\Pi$) emitters can be understood by a mechanism which emphasizes the transitions between electron configurations, similar to that discussed by Brinkmann *et al.* (17, 29): For nearly coplanar (C_s) collisions in which the $p(a'')$ orbital of Ca*(^3P) is oriented perpendicular to the molecular plane, transfer of the electron from this orbital into the LUMO's of both NO_2 (a') and N_2O(a') (30, 31) is symmetry forbidden. Consequently the subjacent Ca($4s(a')$) electron is transferred, resulting in an excited ionic intermediate which eventually rearranges smoothly into products with Ca($4p\pi$)O($2p\sigma^1 2p\pi^4$) configuration, from which the $B\,^1\Pi$ state and the arc states derive (8, 16, 17, 26, 32). The decreased yield of arc state emitters in the NO_2 reaction relative to the N_2O system is consistent with the decreased probability of such coplanar collisions due to the non-linearity of the NO_2 molecule.

An information theoretic analysis has been performed as follows (11, 17). The surprisal I_i of product state i is

$$[9] \quad I_i = \ln (p_i{}^0/p_i)$$

in terms of the branching ratio $p_i = Y_{CL}(i)/100$. The prior branching ratio is normalized to unity

$$[10] \quad P_i{}^0 = g_i\rho_i(E_i')/\sum_j g_j\rho_j(E_j')$$

where g_j is the statistical weight (spin multiplicity times orbital

Can. J. Chem. Downloaded from www.nrcresearchpress.com by 210.87.254.42 on 09/06/12
For personal use only.

TABLE 4. Surprisal analysis for $Ca(^3P) + N_2O$ and $Ca(^1D) + N_2O$

Product state i[a]	$Ca(^3P) + N_2O$				$Ca(^1D) + N_2O$			
	E_i'[b]	p_i^0	p_i[c]	$-I_i$[d]	E_i'[b]	p_i^0	p_i[c]	$-I_i$[d]
$X^1\Sigma^+$	429.4	0.226	0.92	+1.40[e]	508.5	0.181		
$a^3\Pi$	330.0	0.415		+0.79[f]	408.5	0.406		
$A'^1\Pi$	328.5	0.135	0.068	−0.686	407.7	0.134		
$^3\Sigma$	314.1	0.166			393.2	0.171		
$A^1\Sigma^+$	291.4	0.0395	1.6(−3)	−3.21	370.5	0.0436	0.048	+0.096
$^3\Pi$	119.7	4.32(−3)			198.8	0.0159		
$B^1\Pi$	118.7	1.42(−3)	1.5(−3)	+0.055	197.8	5.18(−3)	0.045	+2.16
$^3\Sigma^+$	103.3	1.11(−3)			182.4	5.39(−3)	0.189 orange	+1.78
$d^3\Delta$	99.3	2.80(−3)	6.3(−3) orange	+0.49	178.5	1.47(−2)		
$D^1\Delta$	98.4	8.95(−4) 6.0(−3)[g]	[5.1(−3)][h]		177.5	4.77(−3) 3.18(−2)[g]		
$^{1,3}\Sigma^-$	95.5	1.04(−3)	2.3(−3) green	−0.96	174.6	5.91(−3)	0.07 green	+0.79
$C^1\Sigma^+$	84.0	1.46(−4)	1.3(−3)[h]		163.1	1.09(−3)		
Reactants	12.1	1.44(−7)	n.d.		12.1	5.38(−8)	n.d.	
$Ca(^1S)$	194.4	6.39(−3)	n.d.		273.5	1.11(−2)	n.d.	

[a]Observed states from ref. (20), others are calculated (26).
[b]Total energy available to products in state i; units, kJ/mol; computed using D_0^0 (CaO) = 397.5 kJ/mol from Irvin and Dagdigian (8).
[c]The experimental reaction probabilities are given by $p_i = Y_i/100$.
[d]Negative surprisals $-I_i$ are recorded. A positive value of $-I_i$ corresponds to overpopulation, etc.
[e]Assuming that no $a^3\Pi$ is formed.
[f]Assuming that no $X^1\Sigma^+$ is formed.
[g]The average prior was used for the arc states.
[h]From Irvin and Dagdigian (8).
[i]The principal products (dark products and $A'^1\Pi$) cannot derive mainly from $Ca(^1D)$, otherwise $p_i > 1$.

TABLE 5. Surprisal analysis for $Ca(^3P) + NO_2$ and $Ca(^1D) + NO_2$

Product state i^a	$Ca(^3P) + NO_2$				$Ca(^1D) + NO_2$			
	$E_i'^b$	p_i^0	p_i^c	$-I_i^d$	$E_i'^b$	p_i^0	p_i^c	$-I_i^d$
$X^1\Sigma$	291.8	0.380	0.928	+0.893[e]	371.5	0.487		
$a^3\Pi$	192.5	0.355		+0.961[f]	272.1	0.120		
$A'^1\Pi$	191.0	0.114	0.067	−0.532	270.2	0.116	[i]	[i]
$^3\Sigma$	176.6	0.121			255.7	0.0907		
$A^1\Sigma^+$	153.9	0.022	2.9(3)	−2.03	233.5	0.0603	0.087	+0.367
$^3\Pi$	−17.8				61.8	1.52(−4)		
$B^1\Pi$	−18.8		6.0(−4)		60.8	1.42(−4)	0.013	+4.51
$^3\Pi$	−34.2		4.0(−3) orange arc		45.4	3.8(−5)	0.08 orange arc	+6.63
$d^3\Delta$	−38.1				41.5	2.5(−5)		
$D^1\Delta$	−39.1		5.0(−4) green arc		40.5	2.3(−5)	1.05(−4)[g] 0.017 green arc	+5.09
$^{1,3}\Sigma^-$	−42.0				37.6	1.6(−5)		
$C^1\Sigma^+$	−53.5				25.5	2.8(−6)		
Reactants	13.0	1.03(−4)	n.d.		13.0	1.37(−7)	n.d.	
$Ca(^1S)$	195.4	20.38	n.d.		274.5	0.125	n.d.	

[a–i] See footnotes in Table 4.

degeneracy) of the product state j. It was calculated from the rigid rotor harmonic oscillator (RRHO) approximation of the diatomic product state densities (28):

$$[11] \quad \rho_j(E_j') = k\,\mu'^{3/2}\,(\omega_{\gamma j}\omega_\delta B_{\gamma j};\, B_\delta)^{-1}(E_i')^{4.5}$$

Here k is a collection of constants, μ' is the product reduced mass, ω and B are the vibrational and rotational constants of the products $\gamma = CaO(j)$, and $\delta = N_2$, NO, and E_j' is the total energy excluding the electronic excitation of product j. Although this simplest form of the prior disregards the cutoff angular momentum for complex formation, and treats all degrees of freedom classically, it is known to agree quite well with more detailed treatments (11*b*, 30). For non-reactive (elastic and electronic quenching) scattering the atom-triatom state density is

$$[12] \quad \rho_j(E_j') = k\mu'^{3/2}A(E_j')^n$$

where $n = 5$ and 5.5 for non-linear (NO_2) and linear (N_2O) reactants, respectively, and $A^{-1} = (\omega_1\omega_2\omega_3(A_0B_0C_0)^{1/2})$ for nonlinear and $A^{-1} = B(\omega_1\omega_2^2\omega_3)$ for linear (N_2O) reactants. The ω_1, ω_2, ω_3 are vibrational constants (10). The translational−vibrational−rotational product energies E_j' are given by energy conservation

$$[13] \quad E_j' = E_{trans} + E_{v,J} + \Delta D_0 + E_{el}(Ca^*) - E_{el}'(CaO(j))$$

The reactant energies E_{trans} and $E_{v,J}$ are thermal averages appropriate to the experimental conditions (15), dissociation energies were taken from Irvin *et al.* (8) and from standard tables (20*a*), and the electronic term energies of CaO were the observed (20*a*) and *ab initio* calculated (26) values for observed and hitherto unobserved states respectively.

Since the dark state distribution is unknown, we computed the surprisals for the two assumptions of exclusive $X^1\Sigma^+$ and of exclusive $a^3\Pi$ formation. The results for both reactions are summarized in Tables 4, 5. They include also the energetics of the elastic and electronic quenching channels, for which experimental data are however lacking.

In neither of the two reactions do the branching ratios decrease monotonically with excitation energy, suggesting already qualitatively some measure of non-statistical behaviour. While the primary products (dark products and $A'^1\Pi$) are formed mainly from $Ca(^3P)$, since the reaction probability P_i calculated for ^1D exclusively would exceed unity for these products, there is some ambiguity regarding the precursor of the minor products. Surprisals were therefore calculated under the assumptions that they are formed from either reactant state. The surprisals are all non-zero, non-linear, and erratic, indicating definite dynamical bias.

In the $Ca(^3P) + NO_2$ case the high energy channels comprising the $B^1\Pi$ and arc states are energetically inaccessible: hence $Ca(^1D)$ is necessarily their precursor. A similar conclusion has been reached by Irvin *et al.* (8) for the $Ca + N_2O$ system, where the corresponding ($Ca(^3P) + N_2O \rightarrow$ arc state) reaction, in spite of being energetically feasible, appears to be dynamically disfavoured relative to the $Ca(^1D)$ reaction. This finding is in agreement with the correlation diagrams, Figs. 4*a*, *b*, which demonstrate that the diabatic formation of arc states from $Ca(^1D)$ requires fewer surface-hops than if $Ca(^3P)$ were the reactant.

In both reactions, the principal CL channel $A'^1\Pi$ is characterized by relatively low surprisal. Phase space theory serves as a reasonable first approximation to their dynamics. The $A^1\Sigma^+$ channels, on the other hand, exhibit substantial surprisals (underpopulation) if $Ca(^3P)$ is assumed to be the reactant, but a nearly statistical population if $Ca(^1D)$ is the precursor. In the N_2O reaction the surprisal of the high energy channels, particularly those of the $B^1\Pi$ and "orange arc states" are moderate but non-negligible. The surprisals of the corresponding states in the NO_2 reaction are very substantial and correspond to overpopulations from 90 (for $B^1\Pi$) to 757 (for the "orange arc state").

Conclusion

Some comments are in order regarding the information theoretical analysis. The surprisals are erratic albeit small and within the accuracy of the analysis non-linear in the state energy E_i'. This is in contrast to what has become an established amenity in many examples of reactive and non-reactive vibrational and rotational energy disposal (11). Monotonic (e.g. linear) surprisal plots are prevalent in systems where the product levels form a smooth sequence of hierarchically equivalent states: in vibrational disposal, for instance, there is no qual-

Can. J. Chem. Downloaded from www.nrcresearchpress.com by 210.87.254.42 on 09/06/12
For personal use only.

itative difference between the formation of products in states v' and in $v' + 1$.

In contrast, the present systems as well as the better documented Mg, Ca(^3P) + X_2 reactions (34) are characterized by conspicuously non-monotonic surprisals, which probably reflect the specific nature of the electronic transitions between pairs of potential energy surfaces that are generally localized in different regions of configuration space. This and the coupling mechanisms and strengths that may differ greatly between pairs of surfaces due to symmetry, spin, energy, and geometric restrictions, lend a high degree of individuality to each transition. Indeed, it is puzzling that these reactions exhibit as little surprisal as they do: product phase space considerations seem to take care of the bulk of electronic energy disposal. A well documented and even more striking example for this behaviour are the well-known reactions between alkali dimers and halogen atoms, the source of luminescence in alkali diffusion flames (35). They have yielded a puzzlingly statistical product M*-state distribution.

Is statistics then all, or most of what there is to electronic energy disposal? The results of the present study and previous ones (34) show clearly that this is not the case. Yet it is the tendency toward statisticity which has prevented specific energy disposal and electronic inversions from occurring in the great number of chemiluminescent reactions that have been studied during the past decade (36) in the course of searches for electronic transition lasers (18).

Can. J. Chem. Downloaded from www.nrcresearchpress.com by 210.87.254.42 on 09/06/12
For personal use only.

Acknowledgements

H. W. acknowledges support by the Chinese government that has made his stay at this institution possible. Dr. H. Telle has kindly calculated for us the Franck–Condon factors on which part of our analysis is based.

1. (*a*) CH. OTTINGER and R. N. ZARE. Chem. Phys. Lett. **5**, 243 (1970); (*b*) C. D. JONAH, R. N. ZARE, and CH. OTTINGER. J. Chem. Phys. **56**, 263 (1972).
2. R. W. FIELD. *In* Molecular spectroscopy: modern research. Vol. 2. *Edited by* K. N. Rao. 1976. p. 261.
3. (*a*) R. W. FIELD, R. A. GOTTSCHO, J. G. PRUETT, and J. J. REUTHER. Barium oxide: the question unanswered. *In* Proceedings of 14th International Conference on Free Radicals. Sauda, Japan. 1979; (*b*) R. W. FIELD. J. Chem. Phys. **60**, 2400 (1974); (*c*) R. A. GOTTSCHO, P. S. WEISS, and R. W. FIELD. J. Mol. Spectrosc. **82**, 283 (1980); (*d*) R. A. GOTTSCHO, J. B. KOFFEND, and R. W. FIELD. J. Mol. Spectrosc. **82**, 310 (1980).
4. A. TORRES-FILHO and J. G. PRUETT. J. Chem. Phys. **70**, 1427 (1979).
5. (*a*) C. R. JONES and H. P. BROIDA. J. Chem. Phys. **59**, 6677 (1973); (*b*) C. J. HSU, W. D. KRUGH, and H. B. PALMER. J. Chem. Phys. **60**, 5118 (1974); (*c*) C. R. DICKSON, S. M. GEORGE, and R. N. ZARE. J. Chem. Phys. **67**, 1024 (1976).
6. (*a*) D. J. BENARD, W. D. SLAFER, and H. P. LEE. J. Chem. Phys. **43**, 69 (1976); (*b*) D. J. BENARD, W. D. SLAFER, and J. HECHT. J. Chem. Phys. **66**, 1013 (1977); (*c*) D. J. BENARD and W. D. SLAFER. Appl. Opt. **66**, 1017 (1977); (*d*) D. J. BENARD, W. D. SLAFER, and H. P. LEE. Appl. Opt. **16**, 2108 (1977).
7. (*a*) P. J. DAGDIGIAN. Chem. Phys. Lett. **55**, 239 (1978); (*b*) H. TELLE and U. BRINKMANN. Mol. Phys. **39**, 361 (1970); (*c*) B. E. WILCOMB and P. J. DAGDIGIAN. J. Chem. Phys. **69**, 1779 (1978).
8. J. A. IRVIN and P. J. DAGDIGIAN. J. Chem. Phys. **74**, 6178 (1981).
9. A. SIEGEL and A. SCHULTZ. Chem. Phys. **28**, 265 (1978).
10. G. HERZBERG. Electronic spectra of polyatomic molecules. Van Nostrand, Princeton. 1967.
11. (*a*) R. B. BERNSTEIN and R. D. LEVINE. Adv. At. Mol. Phys. **11**, 216 (1975); (*b*) M. B. FAIST and R. D. LEVINE. Chem. Phys. Lett. **47**, 5 (1977).
12. U. BRINKMANN, A. STEUDEL, and H. WALTHER. Z. Angew. Phys. **22**, 223 (1967).
13. (*a*) G. GIUSFERDI, P. MINGUZZI, F. STRUMIA, and M. IONELLI. Z. Phys. A**274**, 279 (1975); (*b*) P. S. FURCINETTI, L. C. BALLING, and J. J. WRIGHT. Phys. Lett. **534**, 75 (1975); (*c*) E. LUC-KOENIG. J. Phys. B**7**, 1052 (1974).
14. (*a*) L. PASTERNACK, D. M. SILVER, D. R. YARKONY, and P. J. DAGDIGIAN. J. Phys. B, **13**, 2231 (1980); (*b*) R. N. DIFFENDERFER, P. J. DAGDIGIAN, and D. R. YARKONY. J. Phys. B**14**, 21 (1981).
15. D. J. WREN and M. MENZINGER. Faraday Discuss. Chem. Soc. **67**, 97 (1979).
16. L. PASTERNACK and P. J. DAGDIGIAN. Chem. Phys. **33**, 1 (1978).
17. M. ALEXANDER and P. J. DAGDIGIAN. Chem. Phys. **33**, 13 (1978).
18. J. I. STEINFELD (*Editor*). Electronic transition lasers. M.I.T. Press, Cambridge, MA. 1976.
19. R. W. FIELD, G. A. CAPELLE, and C. R. JONES. J. Mol. Spectrosc. **54**, 156 (1975).
20. (*a*) K. P. HUBER and G. HERZBERG. Constants of diatomic molecules. Van Nostrand, Reinhold, New York. 1979; (*b*) S. N. SUCHARD. Spectroscopic constants for selected hetero-nuclear diatomic molecules. Report TR0074(4641)-6. The Aerospace Corporation. 1974; (*c*) M. HULTIN and A. LAGERQVIST. Ark. Fysik, **2**, 471 (1951); (*d*) A. LAGERQVIST. Ark. Fysik, **8**, 83 (1954).
21. H. TELLE. To be published.
22. B. K. JANOUSEK and J. I. BRAUMANN. *In* Gas phase ion chemistry. Vol. 2, 53 (1979).
23. J. LOS and A. W. KLEYN. *In* Alkali halide vapors. *Edited by* P. Davidovits and D. L. McFadden. Academic Press, New York. 1979.
24. (*a*) T. CARRINGTON. *In* Chemiluminescence and bioluminescence. *Edited by* M. J. Cormier, D. M. Hercules, and J. Lee. Plenum Press, New York. 1973; (*b*) G. VAN VOLCKENBURGH, T. CARRINGTON, and R. A. YOUNG. J. Chem. Phys. **59**, 6035 (1973).
25. R. A. GOTTSCHO. J. Chem. Phys. **70**, 3554 (1979).
26. C. W. BAUSCHLICHER and D. R. YARKONY. Chem. Phys. **68**, 3990 (1978).
27. (*a*) J. C. TULLY. J. Chem. Phys. **61**, 61 (1974); (*b*) G. P. SCHMID and R. N. ZARE. J. Am. Chem. Soc. **97**, 1985 (1975); (*c*) G. P. SCHMID and R. N. ZARE. J. Am. Chem. Soc. **98**, 294 (1976).
28. M. BULLITT, M. FISCHER, and J. L. KINSEY. J. Chem. Phys. **60**, 479 (1974).
29. H. TELLE and U. BRINKMANN. J. Phys. B, **39**, 361 (1980).
30. G. V. PFEIFFER and L. C. ALLEN. J. Chem. Phys. **51**, 190 (1969).
31. D. G. HOPPER, N. C. WAHL, R. C. WU, and T. O. TIERNAN. J. Chem. Phys. **65**, 2733 (1971).
32. R. F. MARKS, H. S. SCHWEDA, R. A. GOTTSCHO, and R. W. FIELD. J. Chem. Phys. **76**, 4689 (1982).
33. S. FRANKLIN and P. W. HARLAND. Ann. Rev. Phys. Chem. **25**, 485 (1974).
34. (*a*) A. KOWALSKI and M. MENZINGER. Chem. Phys. Lett. **78**, 461 (1981); (*b*) A. KOWALSKI and M. MENZINGER. J. Chem. Phys. **78**, 5612 (1983); (*c*) A. KOWALSKI and M. MENZINGER. J. Chem. Phys. To be published.
35. W. S. STRUVE, J. R. KRENOS, D. L. MCFADDEN, and D. R. HERSHBACH. J. Chem. Phys. **62**, 404 (1975).
36. M. MENZINGER. Adv. Chem. Phys. **42**, 1 (1980).

Studies of silyl and germyl Group VI species. Part VII. The substituent effects of the vinyl group in 1,3-divinyltetramethyldisilyl chalcogenides[1]

JOHN E. DRAKE AND ANKIN VAHRADIAN

Department of Chemistry, University of Windsor, Windsor, Ont., Canada N9B 3P4

AND

BORIS M. GLAVINCEVSKI[2]

Fuels and Lubricants Laboratory, Division of Mechanical Engineering, National Research Council of Canada, Ottawa, Ont., Canada K1A 0R6

Received April 14, 1983

JOHN E. DRAKE, ANKIN VAHRADIAN, and BORIS M. GLAVINCEVSKI. Can. J. Chem. **61**, 2712 (1983).

Symmetrically substituted 1,3-divinyltetramethyldisilyl chalcogenides $(CH_2{=}CHSiMe_2)_2E$, where E = O, S, Se, and Te have been prepared and characterized by their ir, Raman, ^1H and ^{13}C nmr spectra. Reactions of the sulfide and selenide with anhydrous H_2S and H_2Se, respectively, are discussed.

JOHN E. DRAKE, ANKIN VAHRADIAN et BORIS M. GLAVINCEVSKI. Can. J. Chem. **61**, 2712 (1983).

On a préparé des divinyl-1,3 tétraméthyldiselylchalcogénures $(CH_2{=}CHSiMe_2)_2$ E, où E = O, S, Se et Te, et on les a caractérisé à partir de leurs spectres ir, Raman et de rmn du ^1H et du ^{13}C. On discute des réactions respectives du sulfure et du séléniure avec le H_2S et le H_2Se anhydres.

[Traduit par le journal]

Introduction

The effect of substituents on the spectroscopic features and structure–reactivity relationships of silyl species has been a concern for many years, particularly the substituent effects of halogens, chalcogens, hydrogen, phenyl and methyl groups (1). However, the effect of the vinyl group on the ^1H, ^{13}C, and ^{29}Si nmr (2–8, 13), vibrational (9–11), photoelectron (12, 13), and mass (13–15) spectra of various silyl compounds has been the subject of much discussion. We report on the synthesis and characterization of some new 1,3-divinyltetramethyldisilyl chalcogenides, $(CH_2{=}CHSiMe_2)_2E$ where E = O, S, Se, and Te and draw comparisons with the related species $(Me_nH_{3-n}Si)_2E$ (16, 17).

Experimental

All preparative manipulations were conducted using a conventional high-vacuum system fitted with greaseless stopcocks. The allied spectroscopic techniques were as described previously (16, 17). Details of the preparation of Li_2E (E = S, Se, Te) have been given elsewhere (18). Hydrogen sulfide and selenide were obtained by hydrolysis of the respective Al_2E_3 (19) and were dried by passing through $CaCl_2$ and P_4O_{10}. Peroxide-free diethyl ether was distilled in a vacuum system from fresh $Li[AlH_4]$ and stored *in vacuo*. Chlorovinyldimethylsilane was obtained commercially (Petrarch Systems) and the purity was confirmed by its ir/Raman (20) and nmr (6) spectra. The new compounds, $(CH_2{=}CHSiMe_2)_2E$, were synthesised in essentially the same manner as in the published procedures (16) for related compounds.

Reactions of 1,3-divinyltetramethyldisilyl chalcogenides with hydrogen halides

Typically, $(CH_2{=}CHSiMe_2)_2S$ (0.16 mmol), anhydrous HCl (0.38 mmol), and traces of TMS were condensed into a semi-micro nmr tube which was then sealed and allowed to warm to room temperature. After ca. 30 min the ^1H nmr spectrum showed the resonances expected for $CH_2{=}CHSiMe_2Cl$ (6) and H_2S (δ(SH) 0.82 ppm).

Reactions of $(CH_2{=}CHSiMe_2)_2E$ with H_2E where E = S and Se

The sulfide, $(CH_2{=}CHSiMe_2)_2S$ (0.0306 g, 0.15 mmol), and an excess of anhydrous H_2S (0.5 mmol) were sealed in a semi-micro nmr tube with some TMS. The ^1H nmr spectrum of the reaction was recorded after 10 min and disclosed only the resonances of the starting materials $(CH_2{=}CHSiMe_2)_2S$ (δ(Me) 0.38 ppm and δ(H_2S) 0.82 ppm). After a longer reaction time (ca. 14 days) there was still essentially no change in the ^1H nmr spectrum.

In an analogous manner, the selenide $(CH_2{=}CHSiMe_2)_2Se$ (0.083 g, 0.39 mmol) and an excess of H_2Se (1.13 mmol) were sealed in a semi-micro nmr tube. The ^1H nmr spectrum of the reaction was recorded after 16 h and revealed resonances centred at ca. 2.68, ca. 1.50, ca. 1.29, ca. 0.48, ca. −0.83, and a very weak peak at ca. −2.82 ppm. assignable to $(HSeCH_2CH_2SiMe_2)_2Se$ and presumably traces of $HSeCH_2CH_2SiMe_2SeH$.

Results and discussion

Metathesis reactions between Group IV halides and dilithium salts have been demonstrated previously for the synthesis of a number of disilyl and digermyl chalcogenides (16, 18, 21). In this study the method was extended to the synthesis of otherwise inaccessible vinyl-containing species, i.e.

$$[1]\quad 2CH_2{=}CHSiMe_2Cl + Li_2E \xrightarrow{Et_2O} (CH_2{=}CHSiMe_2)_2E + 2LiCl \quad (E = S, Se, Te)$$

The yields are high (ca. 80–90%) and the only significant loss of material arose because of the susceptible nature of the Si—Cl and Si—E bond to hydrolysis. The formation of disilazane $(CH_2{=}CHSiMe_2)_2NH$ was often observed in cases where the dilithium salt contained ammonia, $Li_2E \cdot nNH_3$. The use of a slight excess of chalcogen and removal of the solvated ammonia from Li_2E resulted in complete conversion of the chloride into the corresponding Si—E species. The oxide, $(CH_2{=}CHSiMe_2)_2O$, was readily obtained by the hydrolysis of the chloride. The other Si—E (E = S, Se, Te) species are all unstable to air and moisture. With the exception of the siloxane linkage Si—O—Si, these bonds are readily cleaved by HCl with formation of $CH_2{=}CHSiMe_2Cl$ and the corresponding H_2E, i.e.

$$[2]\quad (CH_2{=}CHSiMe_2)_2Se + 2HCl \rightarrow 2CH_2{=}CHSiMe_2Cl + H_2Se$$

[1] NRCC No. 22512.

[2] To whom all correspondence should be addressed.

Can. J. Chem. Downloaded from www.nrcresearchpress.com by 210.87.254.5 on 09/06/12
For personal use only.

TABLE 1. Chemical shifts and coupling constants of $(CH_2{=}CHSiMe_2)_2E$ species

	$(CH_2{=}CHSiMe_2)_2E$				
E	$^1H\delta$(Me)	$^{13}C\delta$(Me)	$^{13}C\delta(CH_2)$	$^{13}C\delta$(CH)	$\lvert J_{^{13}CH}\rvert$ (Me)
O	0.12	−0.44	130.85	138.83	118.0
S	0.36	2.28	131.92	139.09	119.6
Se	0.45	2.67	132.12	139.16	120.7
Te	0.60	3.58	132.14	139.35	121.5

Analogous reactions with H_2Se gave addition across the double bond with anti-Markownikoff orientation, i.e.

[3] $(CH_2{=}CHSiMe_2)_2Se + H_2Se$ (excess)
$\rightarrow (HSeCH_2CH_2SiMe_2)_2Se$

The reaction of the sulfide, $(CH_2{=}CHSiMe_2)_2S$, with hydrogen sulfide did not lead to the addition of H_2S to the vinyl group or cleavage of the Si—S—Si linkage. These reactions demonstrate the resistance of the Si—E—Si linkage (where E = S, Se, Te) to attack in these compounds in contrast to the species $(H_{n-3}SiMe_n)_2E$ (16).

(i) The ^1H and ^{13}C nmr spectra

The observed methyl proton and carbon-13 parameters are given in Table 1. The values of the proton chemical shifts of the methyl group $^1H\delta$(Me) fall generally between the values of those obtained for $(HSiMe_2)_2E$ and $(SiMe_3)_2E$ (16).

The largest deviation in the magnitude of $^1H\delta$(Me) is shown between the selenides ($(CH_2{=}CHSiMe_2)_2Se$ (0.45 ppm) and $(HSiMe_2)_2Se$ (0.51 ppm)) and oxides ($(CH_2{=}CHSiMe_2)_2O$ (0.12 ppm) and $(SiMe_3)_2O$ (0.06 ppm)) with chemical shift differences of 0.06 ppm. While the shift of $^1H\delta$(Me) values from 0.06 → 0.12 → 0.14 ppm in the series

$$(SiMe_3)_2O \rightarrow (CH_2{=}CHSiMe_2)_2O \rightarrow (HSiMe_2)_2O$$

implies weakening of the oxygen–silicon ($p \rightarrow d$) π bonding, the magnitude of $^1H\delta$(Me) values for the selenides

$$(SiMe_3)_2Se\ (0.42) \rightarrow (CH_2{=}CHSiMe_2)_2Se\ (0.45) \rightarrow (HSiMe_2)_2Se\ (0.51)\ \text{ppm}$$

suggest that the vinyl group has a similar effect as does a methyl group even though the electro-negativity of the vinyl group has been inferred to be comparable to that of a hydridic hydrogen atom (22). However, the effect of the introduction of the vinyl group on the carbon-13 chemical shifts is large, so that the trend of shielding parallels only that of $(SiMe_3)_2E$ (17). The magnitude of the values indicates that the methyl carbons in the vinyl-containing species are more shielded and the shielding increases as it does for the protons in the series

$$Te(3.58) \rightarrow Se(2.67) \rightarrow S(2.28) \rightarrow O(-0.44)\ \text{ppm}$$

Apparently, there is a linear relationship between the ^{13}C and ^1H chemical shifts which suggests that similar factors are responsible for the observed trends.

The carbon-13 resonances of the sp^2 carbons appear considerably down-field relative to those of the sp^3 carbon. The shielding of the sp^3 carbons is much more sensitive to substituent changes than the sp^2 carbons. Thus as the chalcogen changes from oxygen to tellurium there is a slight successive down-field shift in the ^{13}C (sp^2) resonances matching a larger similar shift in the sp^3 resonances. The effect of chalcogen change is markedly attenuated on $\delta^{13}C(sp^2)$ such that the values of $\delta(C_\beta)$ and $\delta(C_\alpha)$ are relatively small between the selenide and telluride (Δ = 0.02 ppm), and the sulfide and selenide (0.07 ppm), respectively. In contrast to the successive down-field shift of the $^{13}C(sp^2)$ resonances from oxygen to tellurium, the internal chemical shift $\Delta = \delta(C_\alpha) - \delta(C_\beta)$ increases from

$$Se\ (7.04) \rightarrow S\ (7.17) \rightarrow Te\ (7.21) \rightarrow O\ (7.98)\ \text{ppm}$$

It has been suggested (23) that the internal chemical shift is a measure of a double bond polarization

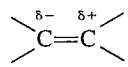

and if other effects remain constant, increased polarization should increase the Δ value. Nevertheless, the deshielding or the chemical shift of the C_β is presumably controlled by the π-electron density and that of the C_α by σ-electron density, though other effects may also contribute.

The trends in the values of the ^{13}CH coupling constants parallel those for $^1H\delta$(Me), in that they fall between those for $(SiMe_3)_2E$ and $(HSiMe_2)_2E$ (16). The effect of the chalcogen is substantial and leads to an increase in the ^{13}CH coupling constants along the series

$$O(118.0) \rightarrow S(119.6) \rightarrow Se(120.7) \rightarrow Te(121.5)\ \text{Hz}$$

This increase suggests that the *s*-hypothesis (the Fermi contract term) might not dominate the coupling mechanism between carbon and hydrogen.

(ii) Vibrational spectra

The assignment of spectral features (Table 2) is based on comparisons within the $(CH_2{=}CHSiMe_2)_2E$ series (E = O → S → Se → Te) and on the spectra of the known species $(CH_2{=}CHSiMe_2)_2O$ (24), $CH_2{=}CHSiMe_2Cl$ (11), $(CH_2{=}CH)_4Si$ and $(CH_2{=}CH)SiH_3$ (9, 10). The three Raman bands at ca. 3053 ($\nu_a(CH_2)$), ca. 3008 (ν(CH)), and ca. 2969 cm^{-1} ($\nu_s(CH_2)$) with corresponding ir absorptions can be assigned to the vinyl CH and CH_2 stretches. Except for the oxide, the $\nu_s(CH_2)$ stretching frequency is indistinguishable from the $\nu_a(CH_3)$ mode. The latter mode is observed as a very strong polarized band at ca. 2902 cm^{-1} with a weak ir counterpart. The C=C stretching vibration gives rise to the band at ca. 1592 cm^{-1}.

The CH_2 scissors and δ(CH) vibrations are obscured by $\delta_a(CH_3)$ at 1404 cm^{-1} and the ν(Si—O) mode at 510 cm^{-1}, respectively. The $\delta(CH_2)$ vibration is assigned at somewhat higher frequency at ca. 1440 cm^{-1} as a very weak absorption. The remaining bands appearing at ca. 1264, 1000, 947, and 1242 cm^{-1} are assigned to ρ(CH), δ_{tw}(CH), $\delta_{wag}(CH_2)$, and $\delta_s(CH_3)$ in agreement with previous reports (9, 11, 12, 25), as are the C_3Si skeletal vibrations between ca. 787 and ca. 574 cm^{-1}. The Si—E—Si stretching vibrations at 1049 and 542 (O), 448 (S), 398 (Se), and 297 cm^{-1} (Te) are the most characteristic of the new chalcogenides. The large splitting between the asymmetric and symmetric mode for the oxide is as expected for a Si—O—Si angle greater than 120°, whereas the negligible splitting for the other species is as expected if the Si—E—Si angles are close to 90°. The marked decrease in the values of (Si—E) are greater than that expected purely on the

Can. J. Chem. Downloaded from www.nrcresearchpress.com by 210.87.254.5 on 09/06/12
For personal use only.

Can. J. Chem. Downloaded from www.nrcresearchpress.com by 210.87.254.5 on 09/06/12
For personal use only.

TABLE 2. The ir and Raman spectra (cm^{-1}) of the 1,3-divinyltetramethyldisilyl chalcogenides[a]

Tentative assignment	$(CH_2{=}CHSiMe_2)_2O$		$(CH_2{=}CHSiMe_2)_2S$		$(CH_2{=}CHSiMe_2)_2Se$		$(CH_2{=}CHSiMe_2)_2Te$	
	Infrared	Raman	Infrared	Raman	Infrared	Raman	Infrared	Raman
$\nu_a(CH_2{=})$	3045m	3054m, dp	3040m	3051m, dp	3031m	3055m, dp	3033m	3053m, dp
$\nu(=CH-)$	3005w	3013wsh, p	2998w	3008wsh	2990w	3008wsh, p	2988w	3005wsh, p
$\nu_a(CH_3)$, $(CH_2{=})$	2951s	2969vs, p	2948m	2967vs, p	2939m	2972vs, p	2936m	2968vs, p
$\nu_s(CH_3)$	2891wsh	2902vs, p	2888w	2898vs, p	2878	2902vs, p	2875	2896vs, p
$\nu(C{=}C)$	1585m	1596s, p	1585m	1589s, p	1580m	1594vs, p	1580m	1589s, p
$\delta_a(CH_2{=})$	1440brsh	ca. 1469vvw		ca. 1478vvw	1435vw	ca. 1471vvw	1435vvw	ca. 1469vvw
$\delta_a(CH_3)$, $\delta_{sc}(CH_2)$	1397s	1408ms, p	1393s	1404msp	1391s	1405s, p	1391s	1405ms, p
$\rho(=CH-)$	1260wsh	1273ms, p		1269ms, p		1269s, p		1269ms, p
$\delta_s(CH_3)$	1242vs	1253vvw	1241vs	1247wsh, dp	1246vs	1248wsh, dp	1245vs	ca. 1247vvw
$\delta_{tw}(=CH-)$	997s	1008w, dp	996s	1005vvw, dp	992s	1006w, dp	992s	1003vw
$\delta_{wag}(CH_2{=})$	947s	955vw, dp	945s	954vw, dp	940s	957vw, dp	940s	ca. 940vvw
$\rho(CH_3)$	830vs	854vw, dp	832vs	830vw, dp	830vs	825w, p	830vs	818w, p
$\nu_a(SiC)$	787vs	783w, dp	791vs	778w, dp	788vs	780w, dp	788vs	777w, dp
	775vs		769s	754w	764s	756wsh	762s	ca. 754vvw
$\nu_s(SiC)$	693ms	706m, p	692ms	702m, p	690ms	701m, p	690ms	697w, p
	680vwsh	686wd, p	680vwsh	ca. 686wd, p	680vwsh			
	643w	656w, p		632s, p		627s, p	645vvw	620m, p
	600m	608w, p	610ms	ca. 601vwsh	600ms	ca. 581vw	600ms	574m, p
$\delta(=CH-)$	510ms[b]	512sh, p	515m,[b] p	530m,[b] p	509m[b]	528m, p[b]	510mw[b]	
$\nu(Si-E)$ a	1049vs		478ms	487sh	390ms			
$\nu(Si-E)$ s	510ms[b]	542vs, p	441w	448vs, p		398s, p		297vs, p
skel. def.	391w	388wbr, p		390vw	ca. 365wsh	370w, p		378m, p
	367vw	358wbr, p		345m, p	ca. 340wbr			325sh
	315wbr	316wsh, p		ca. 319vwsh	ca. 315wbr	313vs, p		ca. 306
	ca. 210vwbr	210wsh		224sh	205vw	202wsh		192s, p
		172m, dp		169m, dp		170m, dp		165sh
						ca. 73vwsh		

[a] Spectra recorded at room temperature; v, very; b, broad; sh, shoulder; s, strong; m, medium; ms, moderately strong; w, weak; p, polarized; dp, depolarized.
[b] Coincident with $\nu(Si-O)$.

basis of the increasing reduced mass. Similar trends of decreasing Si—E stretching frequencies have been observed in related silyl species (16). The remaining vibrational degrees of freedom involve only the deformations of the

C=C—Si—E—Si—C=C

skeletal frame and they appear in the low-frequency region. The frequency of the Si—E—Si deformations decreases as expected, but less rapidly than the frequency of the skeletal stretching.

The force constants (26) of the Si—E bonds were calculated by making the naive assumption that in the 1,3-divinyltetramethyldisilyl chalcogenides the Si—E bond can be treated as a diatomic molecule, the average values of the ν_a(Si—E) and ν_s(Si—E) stretches were taken as the stretching vibrations of the assumed diatomics. The Si—E bond "force constants" so calculated give the values 3.8, 1.9, and 1.2×10^5 dyn/cm^{-1} for Si—O, Si—S, Si—Se, and Si—Te, respectively. Despite the exaggerated approximation these values disclose the expected trend where the force constant of Si—O is very much greater than that of the other Si–chalcogen bonds, which suggests a much greater rigidity for the Si—O bond. This is, of course, in keeping with the general stability of compounds containing Si—O bonds where a degree of Si—O π-bonding has been invoked. Given the gross approximation, the calculated values still suggest a bond of similar rigidity in the case of Si—S and Si—Se but a weaker one for Si—Te.

1. E. A. V. EBSWORTH. Volatile silicon compounds. Pergamon Press Inc., New York. 1963; B. J. AYLETT. Silicon hydrides and their derivatives. Adv. Inorg. Chem. Radiochem. *Edited by* H. J. Emeleus and A. G. Sharpe. Academic Press, New York. 1968; E. A. EBSWORTH. *In* Organometalic compounds of the Group IV elements. *Edited by* A. G. MacDiarmid. Marcel Dekker, Inc., New York. 1968.
2. R. T. HOBGOOD, J. H. GOLDSTEIN, and G. S. REDDY. J. Chem. Phys. **35**, 2038 (1961); R. T. HOBGOOD, JR. and J. H. GOLDSTEIN. Spectrochim. Acta, **19**, 321 (1963).
3. R. SUMMITT, J. J. EISCH, J. T. TRAINOR, and M. T. ROGERS. J. Phys. Chem. **67**, 2362 (1963).
4. S. COWLEY and S. DANYLUK. Can. J. Chem. **46**, 2373 (1968).
5. T. SCHRAML, V. CHVALOVSKY, M. MAGI, and E. LIPPMAA. Coll. Czech. Chem. Commun. **42**, 306 (1977).
6. J. SCHRAML and V. CHVALOVSKY. Coll. Czech. Chem. Commun. **31**, 503, (1966).
7. J. SOUČEK, G. ENGELHARDT, K. STRANSKY, and J. SCHRAML. Coll. Czech. Chem. Commun. **41**, 234 (1976).
8. P. E. RAKITA and L. S. WORSHAM. J. Organomet. Chem. **139**, 135 (1977).
9. S. G. FRANKISS. Spectrochim. Acta, **22**, 295 (1966); G. DAVIDSON. Spectrochim. Acta, **27A**, 1161 (1971).
10. G. MASETTI and G. ZERBI. Spectrochim. Acta, **26A**, 1891 (1970).
11. R. RERICHA, J. ŠTOKR, M. JAKOUBKOVA, P. SVOBODA, and V. CHVALOVSKY. Coll. Czech. Chem. Commun. **39**, 1303 (1974).
12. U. WEIDNER and A. SCHWEIG. J. Organomet. Chem. **39**, 261 (1972).
13. V. P. YURIEV, A. A. PANASENKO, V. I. KHVOSTENKO, L. M. KHALILOV, YA. B. YASMAN, M. M. TIMOSHENKO, YU. V. CHIZHOV, B. G. ZYKOV, I. I. FURLEI, and S. R. RAFIKOV. J. Organomet. Chem. **166**, 169 (1979).
14. J. TAMAS, K. UJSZASZY, and GY. BUJTAS. Acta Chem. Acad. Sci. Hung. **64**, 305 (1970).
15. A. N. POLIVANOV, T. F. SLYUSARENKO, V. I. ZHUN', V. N. BOCHKAREV, and V. D. SHELUDYAKOV. Zh. Obshch. Khim. **49**, 1311 (1979).
16. J. E. DRAKE, B. M. GLAVINCEVSKI, and R. T. HEMMINGS. Can. J. Chem. **58**, 2161 (1980).
17. J. E. DRAKE, B. M. GLAVINCEVSKI, R. E. HUMPHRIES, and A. MAJID. Can. J. Chem. **57**, 3253 (1979).
18. J. E. DRAKE, B. M. GLAVINCEVSKI, R. T. HEMMINGS, and H. E. HENDERSON. Inorg. Synth. **20**, 171 (1980).
19. G. R. WAITKINS and R. SHUTT. Inorg. Synth. **2**, 183 (1946); A. TIAN and S. AUBANEL. Compt. Rend. Trav. Faculté Sci., Marselle, **1**, 97 (1942).
20. V. F. MIRONOV and N. A. CHUMAEVSKII. Dokl. Akad. Nauk. SSSR, **146**, 1117 (1962).
21. J. E. DRAKE, B. M. GLAVINCEVSKI, R. T. HEMMINGS, and H. E. HENDERSON. Can. J. Chem. **56**, 465 (1978).
22. T. A. ZAKOMOLDINA, P. G. SENNIKOV, V. A. KUZNETSOV, A. N. EGOROCHKIN, and V. O. REIKHSFELD. Zh. Obshch. Khim. **50**, 898 (1980).
23. R. W. HOFFMAN and H. KURZ. Chem. Ber. **108**, 119 (1975).
24. VON G. ENGELHARDT and H. KREIEGSMANN. Z. Anorg. Allg. Chem. **328**, 194 (1964).
25. J. D. ODOM, L. W. HALL, S. RIETHMILLER, and J. R. DURIG. Inorg. Chem. **13**, 170 (1974).
26. G. M. BARROW. The structure of molecules. W. A. Benjamin Inc., New York, Amsterdam. 1963; A. VAHRADIAN. M.Sc. Thesis. University of Windsor, Windsor, Ont. 1981.

Can. J. Chem. Downloaded from www.nrcresearchpress.com by 210.87.254.5 on 09/06/12
For personal use only.

The reactions of $O(^3P)$ with the butanols

JOHN M. ROSCOE
Department of Chemistry, Acadia University, Wolfville, N.S., Canada B0P 1X0

Received April 26, 1983

JOHN M. ROSCOE. Can. J. Chem. **61**, 2716 (1983).

The reactions of $O(^3P)$ with the butanols were studied kinetically as a function of temperature and substrate concentration. The absolute rate constants for the gas phase reactions, in the units M^{-1} s^{-1}, obey the following relations.

O + 1-butanol: $\ln k = 24.12 \pm 0.16 - (1.78 \pm 0.19) \times 10^3/T$
O + 2-butanol: $\ln k = 22.22 \pm 0.16 - (1.19 \pm 0.19) \times 10^3/T$
O + 2-methyl-1-propranol: $\ln k = 22.02 \pm 0.13 - (1.10 \pm 0.15) \times 10^3/T$
O + 2-methyl-2-propranol: $\ln k = 22.33 \pm 0.20 - (2.19 \pm 0.27) \times 10^3/T$

The results suggest that although the α-CH bond in these alcohols is the most reactive one, reaction of $O(^3P)$ with other CH bonds in the alcohols is also appreciable. The kinetic data for these and other alcohols are separated into contributions from the different types of CH bonds and the results are discussed in terms of linear free energy relations.

JOHN M. ROSCOE. Can. J. Chem. **61**, 2716 (1983).

On a étudié la cinétique en fonction de la température et de la concentration de substrat, des réactions de $O(^3P)$ avec les butanols. Les constantes absolues de vitesse des réactions en phase gazeuse ayant pour unités M^{-1} s^{-1} obéissent aux relations suivantes:

O + butanol-1: $\ln k = 24.12 \pm 0.16 - (1.78 \pm 0.19) \times 10^3/T$
O + butanol-2: $\ln k = 22.22 \pm 0.16 - (1.19 \pm 0.19) \times 10^3/T$
O + methyl-2 propanol-1: $\ln k = 22.02 \pm 0.13 - (1.10 \pm 0.15) \times 10^3/T$
O + methyl-2 propanol-2: $\ln k = 22.33 \pm 0.20 - (2.19 \pm 0.27) \times 10^3/T$

Ces résultats suggèrent qu'en dépit du fait que la liaison CH-α de ces alcools soit la plus réactive, $O(^3P)$ réagit avec les autres liaisons de façon appréciable. On a séparé les données cinétiques de ces alcools et celles relatives à d'autres alcools en des contributions provenant de différents types de liaison CH et on discute des résultats en fonction des relations linéaires d'énergie libre.

[Traduit par le journal]

Can. J. Chem. Downloaded from www.nrcresearchpress.com by 210.87.254.105 on 09/06/12
For personal use only.

Introduction

The general features of the reactions of $O(^3P)$ with alcohols have been thoroughly documented (1–4). The primary reaction path is thought to be abstraction of the hydrogen atom α- to the OH, although the reactivity of other CH bonds in the alcohols does not seem to have been evaluated directly. The overall reaction is generally discussed in terms of the following general mechanism under conditions of large excess of the alcohol.

[1] $O + R{-}\underset{\displaystyle R'}{\underset{|}{C}}HOH \rightarrow R{-}\underset{\displaystyle R'}{\underset{|}{C}}OH + OH$ (R and R′ = H or alkyl)

[2] $OH + R{-}\underset{\displaystyle R}{\underset{|}{C}}HOH \rightarrow R{-}\underset{\displaystyle R'}{\underset{|}{C}}OH + H_2O$

[3] $2R{-}\underset{\displaystyle R'}{\underset{|}{C}}OH \rightarrow R{-}\overset{\displaystyle OH}{\overset{|}{\underset{\displaystyle R'}{\underset{|}{C}}}}{-}\overset{\displaystyle OH}{\overset{|}{\underset{\displaystyle R'}{\underset{|}{C}}}}{-}R$

[4] $2R{-}\underset{\displaystyle R'}{\underset{|}{C}}OH \rightarrow R{-}\underset{\displaystyle R'}{\underset{|}{C}}HOH + RC\overset{\displaystyle O}{\overset{\|}{}}R'$

When $O(^3P)$ is in excess, or when the alcohol is not in sufficient excess, reactions [2] to [4] become less important and one must include reactions such as (4, 5)

[5] $O + OH \rightarrow O_2 + H$

[6] $O + R{-}\underset{\displaystyle R'}{\underset{|}{C}}OH \rightarrow RC\overset{\displaystyle O}{\overset{\|}{}}{-}R' + OH$

The reactions of $O(^3P)$ with the butanols were studied for several reasons. 2-Methyl-2-propanol is the simplest alcohol lacking α-CH bonds. Its reactivity toward $O(^3P)$ would indicate whether corrections should be applied in the reactions of $O(^3P)$ with other alcohols to compensate for the reactivity of CH bonds that are not α- to OH. The other butanols include two primary alcohols, one of which is branched, as well as a secondary alcohol. Kinetic data for their reactions with $O(^3P)$ might be combined with other work in the literature to assess correlations of reactivity with structure. This might be useful in predicting the reactivity of other alcohols with $O(^3P)$.

Experimental

The experimental methods and apparatus used in this work have been described in detail elsewhere (4, 6). The reactions were studied in a conventional flow system at pressures from 0.7 to 1.2 Torr. Oxygen atoms were formed by titrating $N(^4S)$ atoms with NO in order to prevent interference from O_2 (4, 5). $N(^4S)$ was produced by dissociating purified N_2 with a microwave discharge. The concentration of $O(^3P)$ produced in this way was kept small by passing only a small part of the total nitrogen flow through the discharge, the remainder of the nitrogen mixing with the products of the discharge upstream from the NO inlet. This arrangement made it possible to achieve as much as 500-fold excess of alcohol, thereby avoiding interference from the

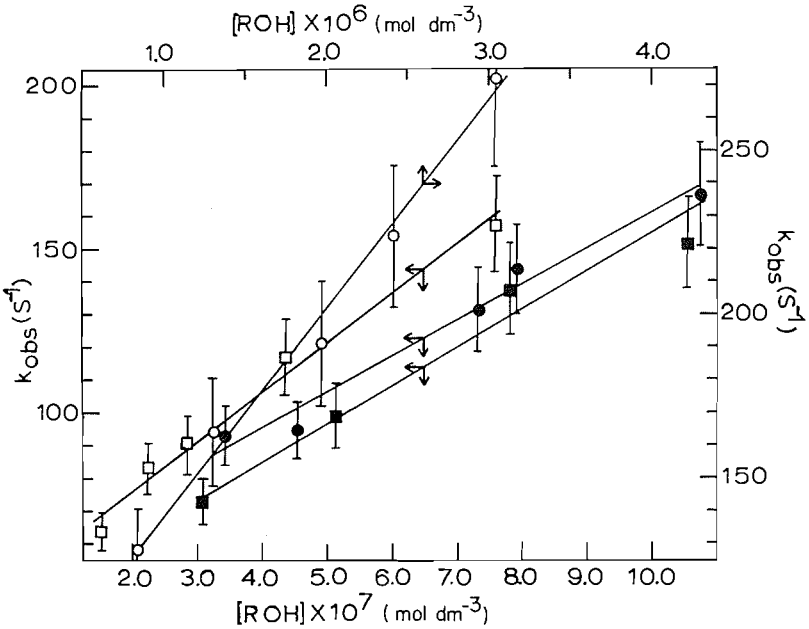

FIG. 1. Dependence of pseudo first order rate constant on alcohol concentration ○, O + 2-methyl-2-propanol, 461 K; □, O + 1-butanol, 320 K; ●, O + 2-methyl-1-propanol, 357 K; ■, O + 2-butanol, 303 K.

secondary reactions of $O(^3P)$ referred to in the Introduction. The concentration of $O(^3P)$ was determined by measuring the intensity of the emission from electronically excited NO_2 produced by adding a small amount of NO in excess of that required to completely consume the $N(^4S)$. The rate constants obtained in this way were independent of the amount of excess NO used.

The alcohols (Fisher, Certified) were purified by repeated fractional distillation until no impurities could be detected by gas chromatography. Their purity was estimated on this basis to be better than 99.999%. Gas chromatographic analysis of both starting materials and reaction products was done on an 8-foot column packed with Porapak Q, using a F and M model 700 gas chromatograph equipped with both a flame ionization detector and a thermal conductivity detector. The former detector was used for analysis of starting materials while the latter was used for analysis of reaction products because of the need to detect water. The reaction products were trapped at liquid nitrogen temperature, warmed to room temperature, and then removed from the flow system for injection into the gas chromatograph. Because of the large excess of alcohol used in these experiments, the alcohol could be used as an internal standard for the determination of other products.

The method of data analysis differed somewhat from that used in earlier work (4, 6). This was necessary because of a complicating first order loss route for $O(^3P)$ which was independent of both the alcohol and NO concentrations, was insensitive to temperature, and was only observed after the alcohol had been admitted to the reaction vessel. It seems probable that this loss route represents a heterogeneous process due to efficient adsorption of a reactant or product on the walls of the reactor. As indicated in Fig. 1, this behaviour is adequately represented by

$$[7] \quad k_{obs} = k_0 + k_R[ROH]$$

At each temperature, first order rate constants (k_{obs}) were plotted as in Fig. 1 to yield a straight line whose slope was k_R at that temperature. It is assumed that k_R is the rate constant for the homogeneous reaction between $O(^3P)$ and the alcohol and that k_0 refers to the extraneous first order loss route for $O(^3P)$. Both the first order rate constants (k_{obs}) and the Arrhenius parameters obtained from them were calculated by weighted least squares with weights $y^2/\sigma^2(y)$ where $y = k_R$ in the Arrhenius expression and $y = O(^3P)$ signal in the pseudo first order analysis of $O(^3P)$ decay. Data for both the rate constant determinations and the Arrhenius expressions were within two standard deviations of the regression line.

Results and discussion[1]

Gas chromatographic analysis of the reaction products indicated that the yield of water was equivalent to the consumption of O atoms. This suggests that the mechanism outlined in the Introduction adequately describes the reactions of the primary and secondary butanols with $O(^3P)$ under our experimental conditions. The reaction of $O(^3P)$ with 2-methyl-2-propanol would then be described by reactions analogous to [1], [2], and [3] but involving β-CH bonds. This would be consistent with other work (1, 2, 4–6) and would mean that k_R is the absolute rate constant for reaction [1].

No products other than water could be detected by gas chromatography. This could result if the organic radical formed in reactions [1] and [2] underwent recombination in preference to disproportionation. The glycols that would be formed would be expected to adhere to the glass tubing between the reaction vessel and the cold trap and would be lost to analysis. Moreover, the chromatographic column used gives poor results for high molecular weight glycols. Similar behaviour was experienced in our earlier work with the propanols (6) in which pinacol was detected, but could not be quantified and the glycol produced by the reaction of $O(^3P)$ with 1-propanol could not be detected. This is also consistent with our experience that recombination products predominated over disproportionation products in the reactions of $O(^3P)$ with methanol and ethanol under similar experimental conditions (4). These results suggest that reaction [6] does not occur to any appreciable extent with the large alcohol/$O(^3P)$ ratios used in this work.

Pseudo first order loss of $O(^3P)$ was observed for alcohol/atom concentration ratios ranging from about 50 to nearly 500 and for temperatures ranging from 300 K to 600 K. The temperature dependence of the homogeneous rate constants for the reactions of $O(^3P)$ with the butanols is summarized in Table 1 and Fig. 2. As anticipated, the rate

[1]Complete set of raw data may be obtained, at a nominal charge, from the Depository of Unpublished Data, CISTI, National Research Council of Canada, Ottawa, Ont., Canada K1A 0S2.

Can. J. Chem. Downloaded from www.nrcresearchpress.com by 210.87.254.105 on 09/06/12
For personal use only.

TABLE 1. Summary of Arrhenius parameters for reactions of $O(^3P)$ with alcohols

Alcohol	$A\times10^{-9}$ (M^{-1} s^{-1})	ΔE_a (kJ mol^{-1})	$A_\alpha\times10^{-9}$ (M^{-1} s^{-1})	ΔE_α (kJ mol^{-1})	Reference
CH_3OH[a]	1.70±0.66	11±2	0.57±0.22	11±2	3
CH_3OH	1.44±0.12	13±1	0.48±0.04	13±1	4
CH_3OH	9.79±2.71	18.8±0.9	3.26±0.90	18.8±0.9	9
CH_3OH	34±11	22.9±1.2	11.3±3.6	22.9±1.2	10
CH_3OH	16.3±3.0	21.0±0.7	5.4±1.0	21.0±0.7	11
C_2H_5OH[a]	0.67±0.08	6.3±1.7	0.26±0.03	5.4±2.2	4
n-C_4H_9OH	29.9±4.8	14.8±1.6	13.5±3.9	14.6±4.2	This work
iso-C_4H_9OH	3.66±0.48	9.1±1.3	1.39±1.8	8.4±2.4	This work
sec-C_4H_9OH	4.47±0.71	9.9±1.6	3.06±0.49	9.0±2.4	This work
tert-C_4H_9OH	4.99±1.00	18.2±2.4	—	—	This work
n-C_3H_7OH[b]	0.792±0.071	12.5±1.4	—	—	6
sec-C_3H_7OH[b]	0.319±0.022	9.1±1.2	—	—	6

[a]Several kinetic studies have given values which deviate markedly from the results tabulated here and from the predictions of correlations such as those of ref. 12. These values have been omitted from this table but may be found in refs. 13 to 16 inclusive.

[b]While the preexponential factors for these reactions are evidently too small and calculation of the components due to the α-CH bonds is not possible, these values are included because the activation energies correlate well with the other reactions.

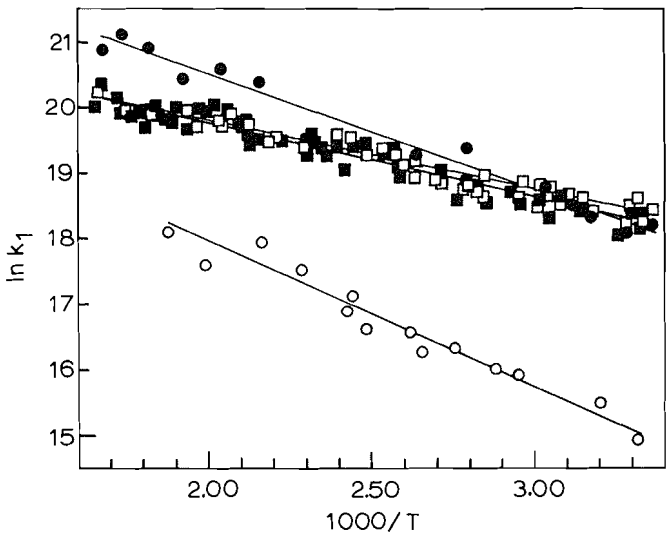

FIG. 2. Arrhenius plots for the reaction of O atoms with the butanols. Absolute uncertainty in ln k is 0.16. ○, O + 2-methyl-2-propanol; ●, O + 1-butanol; □, O + 2-methyl-1-propanol; ■, O + 2-butanol.

constants for the reaction of O atoms with 2-methyl-2-propanol were much smaller, at a given temperature, than those for the corresponding reactions of the other alcohols. This is primarily due to the relatively large activation energy for the reaction with 2-methyl-2-propanol and confirms the earlier suggestion (1−3, 6) that $O(^3P)$ reacts with alcohols primarily by abstracting the H atom α- to the OH group.

While good Arrhenius behaviour was observed for all the reactions studied, it is evident that abstraction of hydrogens that are not α- to OH can be a significant reaction path for $O(^3P)$. Moreover, the comparatively large activation energy for this path makes it increasingly important as the temperature increases. This situation may be described by

$$[8]\quad k = k_\alpha + k' = n_\alpha A_\alpha \exp(-\Delta E_\alpha/RT) + n'A' \exp(-\Delta E'/RT)$$

where n_α and n' are the number of CH bonds α- and not α- to OH, A_α and A' are the corresponding Arrhenius preexponential factors per CH bond, and ΔE_α and $\Delta E'$ are the activation energies characteristic of abstraction of the two kinds of hydrogen atom. Equation [8] could be further refined by writing the last term on the right as a sum of contributions by primary, secondary, and tertiary CH bonds that are not α- to OH. This approach has been applied to the reactions of $O(^3P)$ with alkanes (7), but the smaller activation energies for the reactions of $O(^3P)$ with the alcohols made this impractical. It has also been assumed that abstraction of the OH hydrogen is of negligible importance. While there is no direct proof that this is valid, it seems reasonable in view of the relatively small reactivity of CH bonds which are not α- to OH. It is also relevant that product analysis in reactions of $O(^3P)$ with alcohols has not detected products which could be unambiguously attributed to radicals formed by abstracting the OH hydrogen from the alcohol (1−3, 6).

If eq. [8] is to be applied to existing data, it is necessary to assume that all CH hydrogens not α- to OH have the same Arrhenius parameters and that these may be estimated from the data for the reaction of $O(^3P)$ with 2-methyl-2-propanol. This is likely to be an oversimplification since, by analogy with the reactions of $O(^3P)$ with the alkanes, the activation energy should decrease in the order primary CH > secondary CH > tertiary CH (7). However, since 2-methyl-2-propanol contains only primary CH hydrogens and the contribution per CH is small in our temperature range, this approximation will at worst underestimate the contribution of hydrogens not α- to OH. The availability of kinetic data for a more extensive range of tertiary alcohols would clearly improve the accuracy of this analysis, particularly at the high temperatures typical of combustion where such contributions would be substantial.

The Arrhenius parameters for abstraction of the α-hydrogen atoms, calculated from eq. [8], are given in Table 1. In making these calculations, the contribution of non-α CH bonds ($n'A' \exp(-\Delta E'/RT)$) was calculated from the data for 2-methyl-2-propanol and subtracted from the measured absolute rate constant for each set of experimental conditions. The resulting rate constants (k_α) were then fitted to the Arrhenius equation by y-weighted least squares as described in the Experimental section. The resulting slope and intercept gave values of $-\Delta E_\alpha$ and $n_\alpha A_\alpha$ in the usual way. Also found in Table 1 are Arrhenius

Can. J. Chem. Downloaded from www.nrcresearchpress.com by 210.87.254.105 on 09/06/12
For personal use only.

Can. J. Chem. Downloaded from www.nrcresearchpress.com by 210.87.254.105 on 09/06/12
For personal use only.

parameters for other alcohols as reported in the literature and the corresponding values of the parameters for abstraction of the α-CH hydrogens calculated as above. As with the lower alcohols, the preexponential factors are some 10 to 100 times smaller than those obtained for the reactions of $O(^3P)$ with the alkanes (3, 4, 7). However, no clear relation between the preexponential factor and molecular structure is evident other than a purely statistical dependence on the number of α-CH bonds. Our earlier results for the reactions of the propanols with $O(^3P)$ (6) give preexponential factors which are much too small in comparison with the results for the other alcohols. This problem was referred to in our earlier work although no explanation could be offered.

The activation energy for abstraction of the α-hydrogen by $O(^3P)$ also shows little variation among the alcohols. The value for ethanol seems smaller than for the other primary alcohols, but this may be accidental as a result of the limited temperature range used in that work and the relatively large uncertainty reported for the activation energy. The activation energies for the reactions of $O(^3P)$ with 2-propanol and 2-butanol are similar and are smaller than the values obtained with the primary alcohols, as might be expected due to the somewhat weakened α-CH bond in the secondary alcohols.

It is useful to compare the activation energies for the reactions of $O(^3P)$ with alcohols to those for the corresponding reactions of alkanes. In so doing, one must allow for the differences in reactivity of primary, secondary, and tertiary CH bonds referred to earlier. Since primary alcohols except methanol have secondary CH bonds, primary alcohols should be compared with alkane secondary CH bonds and secondary alcohols should be compared with alkane tertiary CH bonds. With this in mind, the ratio of activation energies for α-hydrogen abstraction from primary and secondary alcohols is about the same as the ratio of activation energies for abstraction of secondary and tertiary hydrogens in the alkanes. However, the activation energies for the reactions of $O(^3P)$ with the alcohols are some two to four times smaller than those for the alkane reactions as a result of the inductive effect of the alcohol oxygen atom. This makes differences in activation energy for different kinds of CH bonds in the alcohols more difficult to measure than in the alkane reactions. It is also of interest that the activation energy for the reaction of $O(^3P)$ with 2-methyl-2-propanol is comparable to that for abstraction of a secondary CH hydrogen from an alkane. Since 2-methyl-2-propanol contains only primary CH bonds this implies that the inductive effect of OH is significant more than one carbon atom into the aliphatic chain.

Useful qualitative information may often be obtained by correlating relative rate constants with functional group parameters through a linear free energy relation. An appropriate correlation of this type is the Taft equation (8) which estimates the sensitivity of a reaction to inductive donation of electron density at the reactive site. A comparison of some abstraction reactions of $O(^3P)$ and of OH radicals is provided in Table 2 and in Fig. 3.

The Taft polar reaction coefficient, ρ*, is negative for all the reactions tested, indicating that $O(^3P)$ is an electrophile as expected (12). The steric sensitivity parameter, δ, is negligibly small for all the reactions, suggesting that structural variation within a given class of compound does not significantly alter the steric constraints on oxygen atom attack at the reactive site. This would not preclude the existence of some constant steric feature such as the postulated preferential collision of the elec-

TABLE 2. Summary of data for Taft correlations[a]

Reaction	k_{298}[b] (M^{-1} s^{-1})	σ*	E_s	Reference
$O+CH_3OH$	2.53×10^6	0.49	1.24	4
$O+CH_3OH$	1.65×10^6	0.49	1.24	9
$O+CH_3OH$	1.09×10^6	0.49	1.24	10
$O+CH_3OH$	1.13×10^6	0.49	1.24	11
$O+C_2H_5OH$	4.3×10^7	0.00	0.00	1
$O+C_2H_5OH$	2.94×10^7	0.00	0.00	4
$O+n\text{-}C_3H_7OH$	2.25×10^{7b}	−0.10	−0.07	12
$O+n\text{-}C_4H_9OH$	4.22×10^{7b}	−0.115	−0.36	12
$O+n\text{-}C_4H_9OH$	3.72×10^7	−0.115	−0.36	This work
$O+iso\text{-}C_4H_9OH$	4.68×10^7	−0.19	−0.47	This work
ρ* = −2.37	δ = 0.01	Standard deviation = 0.17		
$OH+CH_3OH$	6.4×10^8	0.49	1.24	17
$OH+C_2H_5OH$	2.4×10^9	0.00	0.00	17
$OH+n\text{-}C_3H_7OH$	3.21×10^9	−0.10	−0.07	17
$OH+n\text{-}C_4H_9OH$	4.57×10^9	−0.115	−0.36	12
ρ = −1.31	δ = 0.01	Standard deviation = 0.06		
$O+CH_4$	1.02×10^4	0.49	1.24	12
$O+C_2H_6$	5.48×10^5	0.00	0.00	12
$O+neo\text{-}C_5H_{12}$	3.31×10^6	−0.30	−1.54	12
ρ = −4.48	δ = 0.37	Standard deviation = 0		
$OH+CH_4$	4.82×10^6	0.49	1.24	12
$OH+C_2H_6$	1.69×10^8	0.00	0.00	12
$OH+neo\text{-}C_5H_{12}$	5.60×10^8	−0.30	−1.54	12
ρ* = −4.55	δ = 0.55	Standard deviation = 0		
$O+HC(=O)$	9.03×10^7	0.49	1.24	12
$O+CH_3C(=O)$	2.77×10^8	0.00	0.00	12
$O+C_2H_5C(=O)$	4.22×10^8	−0.10	−0.07	12
$O+n\text{-}C_3H_7C(=O)$	5.75×10^8	−0.12	−0.36	12
$O+iso\text{-}C_3H_7C(=O)$	7.24×10^8	−0.19	−0.47	12
ρ* = −1.29	δ = 0.01	Standard deviation = 0.08		
$OH+HC(=O)$	5.66×10^9	0.49	1.24	12
$OH+CH_3C(=O)$	9.03×10^9	0.00	0.00	12
$OH+C_2H_5C(=O)$	1.57×10^{10}	−0.10	−0.07	12
$OH+n\text{-}C_3H_7C(=O)$	1.82×10^{10c}	−0.12	−0.36	12
$OH+iso\text{-}C_3H_7C(=O)$	2.14×10^{10c}	−0.19	−0.47	12
ρ* = −0.82	δ = 0.01	Standard deviation = 0.09		

[a]In all cases the reference compound is the one for which $\sigma^* = E_s = 0.00$ by definition.

[b]Rate constants for the reactions of $O(^3P)$ with the alcohols were calculated for abstraction of hydrogen from a single α-C—H bond.

[c]Calculated in ref. 12 from linear free energy correlations with other reactions.

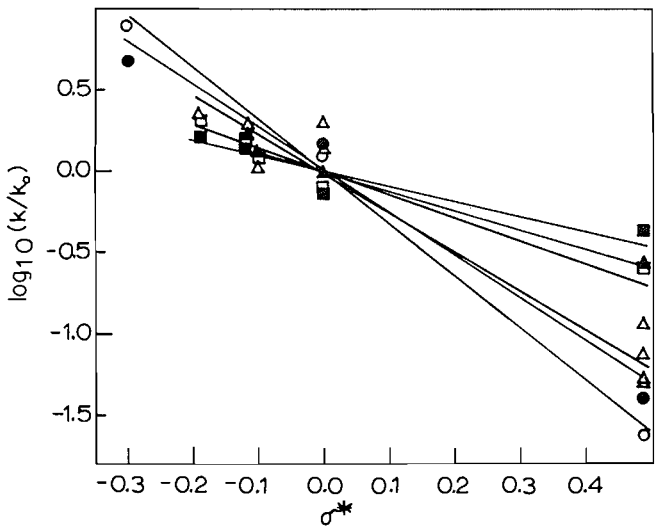

FIG. 3. Taft plots for ○, O + alkanes containing only primary C—H bonds; ●, OH + alkanes containing only primary C—H bonds; □, O + aldehydes; ■, OH + aldehydes; △, O + primary alcohols; ▲, OH + primary alcohols.

trophyllic $O(^3P)$ with the OH group of an alcohol (3), which is unreactive and could lead to an unusually small Arrhenius preexponential factor for all the reactions in an homologous series of alcohols.

The values of ρ* become less negative as the strength of the reactive CH bond decreases. This is in agreement with the theoretical result (18) that the absolute value of the selectivity parameter (ρ* in the Taft equation) should become smaller as the general reactivity increases. The sensitivity to polar effects also appears somewhat greater for reactions of $O(^3P)$ than for the corresponding reactions of OH. This is consistent with the linear free energy correlation of Gaffney and Levine (12) in which the slope (1.364) of their correlation of log $k_{(O(^3P))}$ with log $k_{(OH)}$ for hydrogen atom abstraction can be identified as $\rho^*_{(O(^3P))}/\rho^*_{(OH)}$ in the Taft analysis.

Acknowledgment

Financial support for this work was provided by the Natural Sciences and Engineering Research Council of Canada.

1. A. KATO and R. J. CVETANOVIĆ. Can. J. Chem. **45**, 1845 (1967).
2. A. KATO and R. J. CVETANOVIĆ. Can. J. Chem. **46**, 235 (1968).
3. H. F. LEFEVRE, J. F. MEAGHER, and R. B. TIMMONS. Int. J. Chem. Kinet. **4**, 103 (1972).
4. C. M. OWENS and J. M. ROSCOE. Can. J. Chem. **54**, 984 (1976).
5. N. WASHIDA. J. Chem. Phys. **75**, 2715 (1981).
6. A. L. AYUB and J. M. ROSCOE. Can. J. Chem. **57**, 1269 (1979).
7. J. T. HERRON and R. E. HUIE. J. Phys. Chem. **73**, 3327 (1969).
8. N. B. CHAPMAN and J. SHORTER. Advances in linear free energy relationships. Plenum, London. 1972.
9. R. L. FAILES, D. L. SINGLETON, G. PARASKEVOPOULOS, and R. S. IRWIN. Int. J. Chem. Kinet. **14**, 371 (1982).
10. H. H. GROTHEER and TH. JUST. Chem. Phys. Lett. **78**, 71 (1981).
11. D. G. KEIL, T. TANZAWA, E. G. SKOLNIK, R. B. KLEMM, and J. V. MICHAEL. J. Chem. Phys. **75**, 2693 (1981).
12. J. S. GAFFNEY and S. Z. LEVINE. Int. J. Chem. Kinet. **11**, 1197 (1979).
13. L. I. AVRAMENKO, R. V. KOLESNIKOVA, and N. L. KUZNETSOVA. Izv. Akad. Nauk SSSR, Otd. Khim. 599 (1961).
14. V. YA. BASEVICH, S. M. KOGARKO, and G. A. FURMAN. Izv. Akad. Nauk SSSR, Ser. Khim. 1035 (1975).
15. C. LALO and C. VERMEIL. J. Chem. Phys. **77**, 131 (1980).
16. L. I. AVRAMENKO, R. V. KOLESNIKOVA, and G. I. SAVINOVA. Izv. Akad. Nauk SSSR, Ser. Khim. 22 (1967).
17. R. OVEREND and G. PARASKEVOPOULOS. J. Phys. Chem. **82**, 1329 (1978).
18. J. E. LEFFLER and E. GRUNWALD. Rates and equilibria of organic reactions. Wiley, New York. 1963.

Can. J. Chem. Downloaded from www.nrcresearchpress.com by 210.87.254.105 on 09/06/12
For personal use only.

Pictet–Spengler reaction of biogenic amines with carbohydrates. Synthesis of novel *C*-nucleosides[1]

IAN M. PIPER AND DAVID B. MACLEAN[2]
Department of Chemistry, McMaster University, Hamilton, Ont., Canada L8S 4M1

AND

INGEMAR KVARNSTRÖM AND WALTER A. SZAREK[2]
Department of Chemistry, Queen's University, Kingston, Ont., Canada K7L 3N6

Received May 6, 1983

IAN M. PIPER, DAVID B. MACLEAN, INGEMAR KVARNSTRÖM, and WALTER A. SZAREK. Can. J. Chem. **61**, 2721 (1983).

Several novel *C*-nucleosides have been prepared by Pictet–Spengler condensations between biogenic amines and carbohydrates. Dopamine hydrochloride reacted with D-glucose to give 6,7-dihydroxy-1(*R*)- and -1(*S*)-(D-*gluco*-pentitol-1′-yl)-1,2,3,4-tetrahydroisoquinoline hydrochlorides, and with 2,5-anhydro-D-mannose to give 1(*R*)- and 1(*S*)-(α-D-arabinofuranosyl)-6,7-dihydroxy-1,2,3,4-tetrahydroisoquinoline hydrochlorides. Tryptamine hydrochloride and histamine did not react with D-glucose, but with 2,5-anhydro-D-mannose gave 1(*R*)- and 1(*S*)-(α-D-arabinofuranosyl)-1,2,3,4-tetrahydro-β-carboline and 4-(α-D-arabinofuranosyl)-imidazo[4,5-*c*]-4,5,6,7-tetrahydropyridine, respectively. The structures of the compounds have been established by nmr experiments and by mass spectrometry.

IAN M. PIPER, DAVID B. MACLEAN, INGEMAR KVARNSTRÖM et WALTER B. SZAREK. Can. J. Chem. **61**, 2721 (1983).

On a préparé plusieurs nouveaux *C*-nucléosides par des condensations de Pictet–Spengler entre des amines biogènes et des hydrates de carbone. Le chlorhydrate de dopamine réagit avec D-glucose pour conduire aux chlorhydrates des dihydroxy-6,7 (D-*gluco* pentitolyl-1)-1(*R*) et -1(*S*) tétrahydro-1,2,3,4 isoquinoléines et avec l'anhydro-2,5 D-mannose pour conduire aux (α-D-arabinofurannosyl)-1(*R*) et -1(*S*) dihydroxy-6,7 tétrahydro-1,2,3,4 isoquinoléines. Le chlorohydrate de tryptamine et l'histamine ne réagissent pas avec le D-glucose, mais avec l'anhydro-2,5 D-mannose, ils donnent respectivement les (α-D-arabinofurannosyl)-1(*R*) et -1(*S*) tétrahydro-1,2,3,4 β-carbolines et la (α-D-arabinofurannosyl)-4 imidazo[4,5-*c*] tétrahydro-4,5,6,7 pyridine. On a déterminé les structures par spectroscopie rmn et par spectrométrie de masse.

[Traduit par le journal]

Introduction

The Pictet–Spengler reaction has been widely employed in the synthesis of isoquinolines and related heterocyclic systems (1–3). However, to our knowledge, reactions of this type have not been reported between biogenic amines and sugars or sugar derivatives. The synthesis of pyridindolol by Cook and co-workers (4), by the condensation of tryptophan with glyceraldehyde, represents a related example. In an earlier report, Severin and Heidenhain (5) obtained 1-(1,2-dihydroxyethyl)-1,2,3,4-tetrahydro-β-carboline-3-carboxylic acid and 1-(1,2,-dihydroxyethyl)-1,2,3,4-tetrahydro-β-carboline from the reaction of glyceraldehyde with tryptophan and tryptamine respectively. Severin and Bräutigam (6) have also reported the production, in low yields, of a variety of compounds containing the β-carboline skeleton from the reaction of tryptophan or tryptamine with xylose or glucose. However, the condensation reactions in each case were accompanied by extensive elimination and rearrangement processes. Almost all reported reactions involving the amino group of the amines and the carbonyl function of sugars have dealt with the Amadori rearrangement (7) or the Maillard (browning) reaction (8). It seemed likely to us that a Pictet–Spengler reaction, between a biogenic amine and a sugar, (or sugar derivative containing a carbonyl group), might be used to prepare *C*-glycosides, or to provide useful intermediates for isoquinoline alkaloid synthesis. Furthermore, it was hoped that use of the asymmetric sugar moieties would encourage stereoselectivity in the formation of the new chiral centre of the product heterocycle.

Results and discussion

Heating at reflux temperature of dopamine hydrochloride (**1**) with D-glucose in aqueous solution gave, after work-up and chromatography, 6,7-dihydroxy-1(*R*)- and -1(*S*)-(D-*gluco*-pentitol-1′-yl)-1,2,3,4-tetrahydroisoquinoline hydrochlorides (**2**), in excellent yield (Scheme 1). In a similar fashion, dopamine hydrochloride (**1**) reacted with 2,5-anhydro-D-mannose (**3**), prepared from 2-amino-2-deoxy-D-glucose by a modification of the method of Horton and Philips (9), to give a mixture of 1(*R*)- and 1(*S*)-(α-D-arabinofuranosyl)-6,7-dihydroxy-1,2,3,4-tetrahydroisoquinoline hydrochlorides (**4**), and tryptamine hydrochloride (**5**) reacted with **3** to give 1(*R*)- and 1(*S*)-(α-D-arabinofuranosyl)-1,2,3,4-tetrahydro-β-carboline (**6**). 3,4-Dimethoxyphenylethylamine hydrochloride gave no appreciable reaction with either D-glucose or **3**, presumably because of the known (10) lower activation of *para*-methoxyl groups compared with hydroxyl groups in electrophilic substitution reactions. Additionally, no products could be detected in the reaction between tryptamine hydrochloride and D-glucose after heating at reflux temperature in water or ethanol for 48 hours; the starting materials were recovered in each case.

Histamine dihydrochloride gave no observable reaction with **3**, probably because protonation of the imidazole ring discourages electrophilic attack at the C-4 of imidazole. However, reaction of histamine (**7**) with **3** in slightly alkaline aqueous solution (see ref. 11) gave 4-(α-D-arabinofuranosyl)-imidazo[4,5-*c*]-4,5,6,7-tetrahydropyridine (**8**) in moderate yield and high purity (Scheme 2). No reaction was obtained with D-glucose.

With the exception of the product of condensation between histamine (**7**) and **3**, all of the products were obtained as mixtures of isomers at C-1. In the case of **6** the mixture of isomers

[1]A preliminary account of this work has appeared in J. Chem. Soc. Chem. Commun., 601–602 (1983).

[2]Authors to whom correspondence may be addressed.

Can. J. Chem. Downloaded from www.nrcresearchpress.com by 210.87.254.40 on 09/06/12
For personal use only.

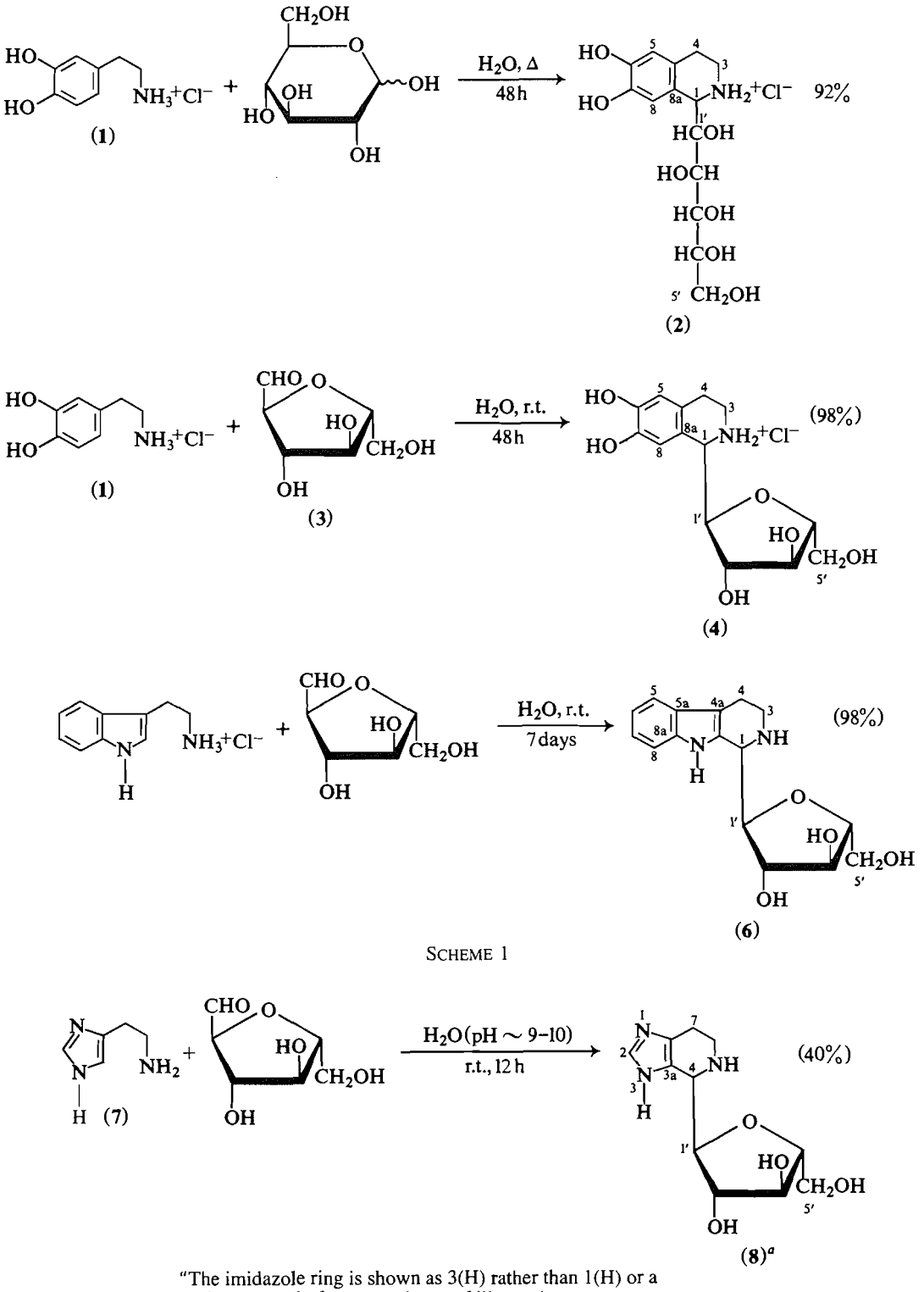

SCHEME 1

"The imidazole ring is shown as 3(H) rather than 1(H) or a mixture purely for convenience of illustration

SCHEME 2

was resolved by column chromatography, but in the cases of **2** and **4** conversion into their peracetyl derivatives was necessary to effect separation. One interesting point is that while **2** and **4** were isolated as the hydrochlorides, **6** (prepared by the same method) was found to be a free base. The titration curve confirmed this observation, and showed that the product had $pK_a \sim 6.7$, but the result was still rather surprising. One possibility is that internal hydrogen bonding may lessen the availability of the lone pair on N-2 of the tetrahydro-β-carboline ring, thus reducing basicity.

The structures assigned to the compounds were supported by their ^1H- and ^{13}C-spectra. The assignments of the signals in the spectra were made by comparison with those of model compounds, and by off-resonance ^{13}C and homonuclear ^1H decoupling experiments. For the products derived from dopamine, the model compounds for the amine portion were dopamine hydro-

Can. J. Chem. Downloaded from www.nrcresearchpress.com by 210.87.254.40 on 09/06/12
For personal use only.

TABLE 1. Selected signals in the ^{13}C nmr spectra of **12**, **4**, **6**, and **8**

Compound	Isomer ratio	Selected ^{13}C resonances[a] and splittings on off-resonance decoupling[b]		
		C_a and C_b[c]	C_c	C_d
12	4:1	C-4a and C-8a, 131.1 and 133.7, (s)	C-1, 50.8, (d)	C-1′, 73.9, (d)
4	4:1	C-4a and C-8a, 120.9 and 126.1 (s)	C-1, 56.5 (d)	C-1′, 78.5 (d)
6	60:40	C-1a and C-4a, 109.1 and 127.2, (s)	C-1, 51.9 (d)	C-1′, 76.9 (d)
8		C-3a and C-7a, 127.7 and 130.3, (s)	C-4, 53.4 (d)	C-1′, 76.6 (d)

[a]Key to resonances:

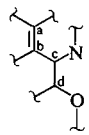

[b]s = singlet (no protons attached), d = doublet (>CH—)
[c]No attempt is made to assign carbons C_a and C_b separately.

chloride (**1**) and 6,7-dimethoxy-1,2,3,4-tetrahydroisoquinoline (**9**) (12). For the product **6**, derived from tryptamine, comparison was made with tryptamine hydrochloride and with 2-methyl-1,2,3,4-tetrahydro-β-carboline (**10**) (13), while for compound **8** the model compound was histamine (**7**). For the sugar portions of the compounds derived from 2,5-anhydro-D-mannose, assignments in the cases of **6** and **8** were confirmed by ^1H homonuclear decoupling experiments, and in the case of **4** assignment was by analogy with these results. For compound **2**, derived from D-glucose, the model compound was D-glucitol (**11**) (14). It was important to establish that cyclization had occurred and to demonstrate that the product was not a Schiff base. For each compound (**2**, **4**, **6**, and **8**) this aspect was apparent from both ^1H- and ^{13}C-spectra. In each of the compounds examined there was one fewer aromatic proton signal than in the spectrum of the corresponding amine. Secondly, no signal was visible in the ^1H nmr spectrum corresponding to an iminium proton ($CH{=}\overset{+}{N}$, ~9−10 ppm), expected of a Schiff base. Finally, in the ^{13}C nmr spectrum, off-resonance decoupling clearly showed that the carbon atom to which cyclization should occur did not bear any hydrogen (Table 1).

Mass spectral analysis of the condensation products (**2**, **4**, **6**, and **8**) gave unsatisfactory spectra because of their involatility. The use of a variety of protecting groups was examined, the most satisfactory one being the acetyl group.

Under electron impact conditions the molecular ions of the peracetylated compounds were either very weak or not observable. Instead, the base peak of the spectrum in each case corresponded to a fragment arising from C-1—C-1′ fission (or C-4—C-1′ fission in the case of the imidazo[4,5-*c*]tetrahydropyridine derivative (**15**)) (Schemes 3−6), thus confirming that cyclization had taken place. Other major peaks observed were those due to successive losses of ketene (15) from this fragment. As a result, little evidence was obtained for the existence of the sugar portion of the compounds. Various other derivatives, in particular alkyl silyl ethers, were prepared in the hope of obtaining prominent ions containing the sugar portion (16), but with little success. More satisfactory results were obtained by use of chemical ionization on the peracetylated compounds. In each case, the expected $(M + 1)^+$ ion was observed as the base peak; additionally, the peak corresponding to C-1—C-1′ (or C-4—C-1′) fission was observable. In several cases, other peaks could be assigned to successive losses of acetic acid from the sugar portions of the molecules (15) (Schemes 3−6). High resolution mass spectrometry was used (under electron impact conditions) to measure masses of major ions; accurate mass measurement of the molecular ion was possible only in two cases (**14** and **15**) since the molecular ion was not observable in other cases. Likely fragmentation patterns for the compounds prepared are summarized in Schemes 3−6. Ions whose compositions were confirmed by high resolution measurements are indicated by a dagger symbol (†). These data are shown in Table 2.

The compounds above represent a new group of organic compounds of potential value as pharmaceuticals and as synthons in enantioselective synthesis of alkaloids and other natural products. It is well known that the tetrahydroisoquinolines, tetrahydro-β-carbolines, and imidazo[4,5-*c*]tetrahydropyridines resulting from analogous condensations involving simple aldehydes show a variety of pharmacological activities (17). The condensation products can also be viewed as a novel class of *C*-nucleosides; such compounds are of great interest because of their demonstrated antibiotic and antitumor activities (8). A biological evaluation of the new compounds is in progress and the results will be reported separately.

Experimental

The nmr spectra were run on a Varian EM390 (90 MHz), a Bruker WP80 (80 MHz), or a Bruker WM250 (250 MHz) spectrometer. Chemical shifts are reported in ppm (δ) from tetramethylsilane. The symbols, s (singlet), d (doublet), t (triplet), q (quartet), and b (broad) are used to report the multiplicity and shape of signals. Coupling constants are accurate within ±0.5 Hz. Mass spectra were recorded on a VG Micromass 7070F mass spectrometer at an ionizing voltage of 70 eV and a source temperature of 120°C (for C.I. (CH_4)) or 200°C (for E.I.), and are reported as m/z values with relative intensities in brackets. Natural abundance ^{13}C nmr spectra were recorded on a Bruker WP80 Fourier transform spectrometer at 20.1 MHz, or on a Bruker WM250 spectrometer at 62.9 MHz. Melting points are uncorrected. Silica gel G/UV-254 (Merck) was used for tlc analysis,

Can. J. Chem. Downloaded from www.nrcresearchpress.com by 210.87.254.40 on 09/06/12
For personal use only.

(a) Electron impact

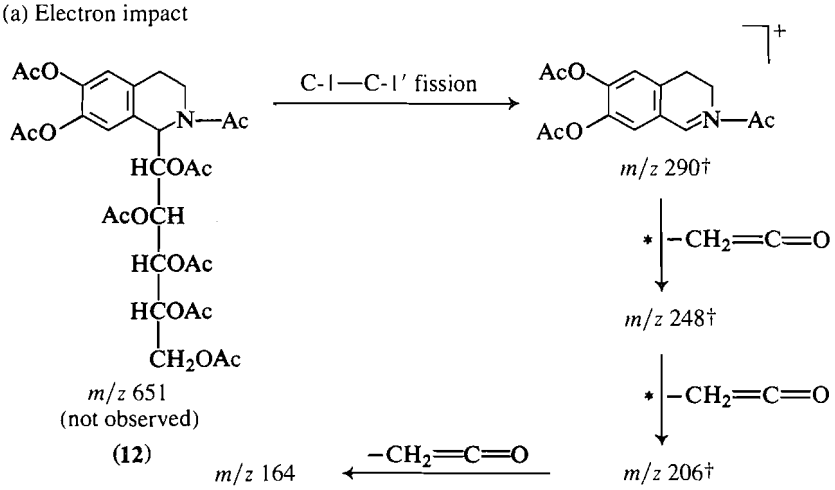

Notes: The symbol * indicates that a metastable ion for the fragmentation was observed; the symbol † is used to denote an ion on which high resolution measurements were made

(b) Chemical ionization

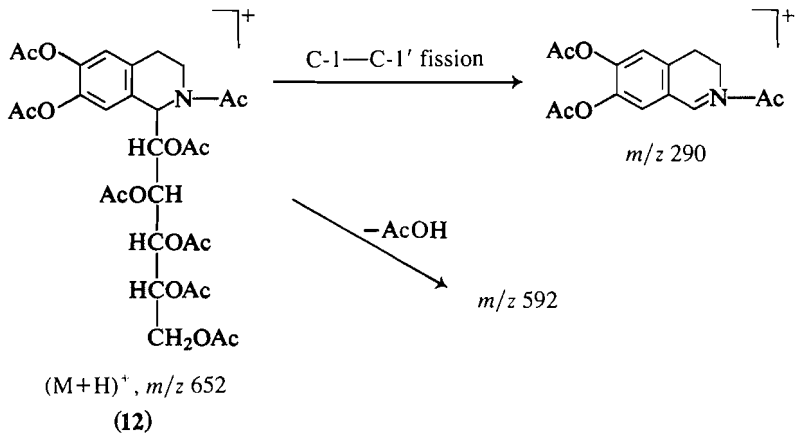

Note: In this and subsequent chemical ionization schemes the position of the hydrogen in the $(M + H)^+$ ion is not indicated

SCHEME 3. Likely mass spectral fragmentations for **12**.

silica gel 60 (Merck, 70–230 mesh) for column chromatography, and silica gel 60 (Merck, 230-400 mesh) for flash chromatography (19).

Acetylation of condensation products: general procedure

The compound to be acetylated (5 mg) was taken up in dry pyridine (0.3 mL) and acetic anhydride (0.3 mL) was added. The mixture was stirred for 24 h at room temperature. The resulting solution was analysed directly by probe ms. Alternatively, on a preparative scale, the compound (~0.5 g) was treated for 24 h with dry pyridine (5 mL) and acetic anhydride (5 mL). The resulting solution was poured into chloroform (75 mL) and washed with water (3 × 25 mL). The chloroform solution was dried over $MgSO_4$ and the solvents removed, finally under high vacuum, to yield a yellow-brown foam (70%–85%). The product was purified by column chromatography or flash chromatography on silica gel, using a variety of solvents.

2,5-Anhydro-D-mannose

2-Amino-2-deoxy-D-glucose hydrochloride (1.08 g, 5 mmol) was dissolved in water (10 mL), and the solution was cooled to 0°C. Sodium nitrite (0.69 g, 10 mmol) was added in one batch, followed by cation-exchange resin (Amberlite IR-120, (H^+), 7 g) in portions with stirring, the temperature being maintained at 0°C–5°C during the addition. The mixture was stirred vigorously for 1 h while it warmed to room temperature. The resin was filtered, and the filtrate was neutralized by addition of anion-exchange resin (Amberlite IRA-400, (−OH)). The mixture was filtered and the filtrate concentrated to a small volume by rotary evaporation without heating. The solution was used directly in the condensation reactions described below. In a separate experiment, complete removal of solvent gave a hygroscopic, yellow-white solid (0.77 g, 95%); $[\alpha]_D^{20}$ +30.2 (*c* 1.26, H_2O); ^1H nmr (D_2O): 4.04–4.24 (3H, m, H's at C-5 and C-6),4.27–4.39 (1H, m, H at C-2), 4.46 (1H, t, H at C-3, J = 5 Hz), 4.59 (1H, t, H at C-4, J = 5 Hz), 5.50 (1H, d, H at C-1, J = 5 Hz) ppm; ^{13}C nmr (D_2O): 62.1 (C-6), 77.9, 78.4, 84.1, 85.4 (C-2, C-3, C-4, and C-5), 90.6 (C-1) ppm; ms: 133 ($(M - 28)^+$, 24), 126 (18), 113 (38), 97 (100).

Reaction of dopamine hydrochloride with D-glucose

Dopamine hydrochloride (1.33 g, 7 mmol) and D-glucose (5.05 g, 28 mmol) were dissolved in water (30 mL), and the solution was boiled under reflux for 48 h, then cooled and filtered. The resulting dark brown solution was stirred for 1 h with cation-exchange resin (Amberlite IR-120, (H^+), 15 g), and filtered. The resin was washed with water to remove non-basic impurities (150 mL), and then with HCl solution (2 *M*, 500 mL). The acidic filtrate was evaporated to give a yellow-brown powder (3.0 g). This was purified on a short column of silica gel (25 g) using acetonitrile/water (9:1), to give the product

Can. J. Chem. Downloaded from www.nrcresearchpress.com by 210.87.254.40 on 09/06/12
For personal use only.

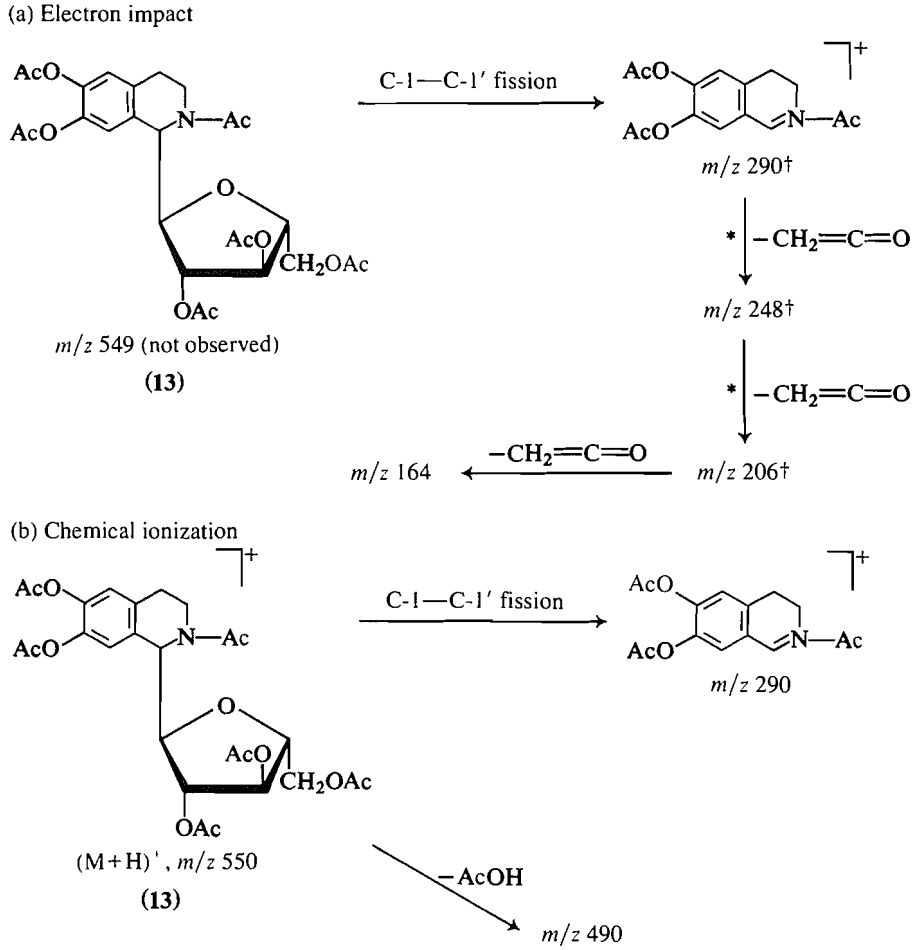

SCHEME 4. Likely mass spectral fragmentations for **13**.

as a yellow hygroscopic solid (2.3 g, 92%). The ^{1}H and ^{13}C nmr spectra indicated that the product was a mixture of two isomers, in the approximate ratio of 4:1. The chemical shifts for the minor isomer are given in square brackets where observed; ^{1}H nmr (D_2O): 2.88–3.13 (2H, m, H's at C-4), 3.60–3.93 (6H, m, H's at C-3, C-3′, C-4′, and C-5′), 4.16 (1H, t, H at C-2′, J = 2 Hz), 4.37 (1H, dd, H at C-1′, J = 4.5 Hz and J = 2 Hz), 4.71 (1H, d, H at C-1, J = 4.5 Hz) [4.61 (1H, d, J = 4.5 Hz)], 6.80 (1H, s) [6.77 (1H, s)], and 6.87 (1H, s) [6.84 (1H, s)] (H's at C-5 and C-8) ppm; ^{13}C nmr (D_2O): 24.7 [25.6] (C-4), 40.4 [42.1] (C-3), 57.9 [59.9] (C-1), 63.6 (C-5′), 70.5 [69.9], 72.3, 73.4 (C-1′, C-2′, C-3′, and C-4′), 115.3 [114.5] and 117.0 (C-5 and C-8), 121.7 [120.8] and 126.4 (C-4a and C-8a), 144.0 and 145.3 (C-6 and C-7) ppm.

The condensation product was peracetylated by the method described and a partial separation of the isomers effected by column chromatography using ethyl acetate (R_f (major isomer) = 0.23, R_f (minor isomer) = 0.25). The major isomer was obtained pure, as a pale yellow syrup; $[\alpha]_D^{20}$ +12.8, (c 1.71, $CHCl_3$); ^{1}H nmr ($CDCl_3$): 1.83 (3H, s, $(CO)CH_3$), 2.08, (9H, s, 3 × $(CO)CH_3$), 2.23, 2.24, 2.27, 2.30 (12H, 4 × s, 4 × $(CO)CH_3$), 2.78–3.02 (2H, m, C-4), 3.80–4.01 (2H, m, C-3), 4.22–4.37 (2H, m, H's at C-5′), 4.89–5.53 (4H, m, H's at C-1′, C-2′, C-3′, and C-4′), 5.80 (1H, d, C-1, J = 9 Hz), 7.03 (1H, s) and 7.07 (1H, s) (H's at C-5 and C-8) ppm; ^{13}C nmr ($CDCl_3$): 20.5 ($(CO)CH_3$), 21.5 ($(CO)CH_3$), 28.2 (C-4), 42.1 (C-3), 50.8 (C-1), 62.0 (C-5′), 68.8 (C-2′, C-3′, and C-4′), 73.9 (C-1′), 122.4 and 123.2 (C-5 and C-8), 131.1 and 133.7 (C-4a and C-8a), 140.8 and 141.4 (C-6 and C-7), 167.8 and 170.1 ($CO CH_3$) ppm; ms (C.I.): 652 ($(M + 1)^+$, 100), 592 (37), 290 (59); ms (E.I.): 290 (96), 248 (100), 206 (30), 164 (27).

Reaction of dopamine hydrochloride with 2,5-anhydro-D-mannose

Dopamine hydrochloride (1.33 g, 7.0 mmol) was added to an aqueous solution (ca. 10 mL) containing 2,5-anhydro-D-mannose (prepared as described above from 2-amino-2-deoxy-D-glucose hydrochloride (3.23 g, 15 mmol)). The resulting solution was kept at room temperature for 48 h, then evaporated to dryness, to give a brown solid (3.5 g). Chromatography on a short column of silica gel (25 g), using acetonitrile/water (9:1), gave the product as a pale yellow hygroscopic powder, (2.30 g, 98%); ^{1}H nmr (D_2O): 2.99–3.17 (2H, m, H's at C-4), 3.58–3.91 (4H, H's at C-3 and C-5′), 4.13 (1H, m, H at C-4′), 4.19 (1H, t, H at C-2′, J = 5 Hz), 4.28 (1H, dd, H at C-1′, J = 5 Hz, J = 7.5 Hz), 4.41 (1H, t, H at C-3′, J = 5 Hz), 4.71 (1H, d, H at C-1, J = 7.5 Hz), 6.83 (1H, s) and 6.89 (1H, s) (H's at C-5 and C-8) ppm. The ^{13}C nmr spectrum showed 2 isomers to be present, in the approximate ratio of 4:1. The chemical shifts for the minor isomer are shown in square brackets where observed; ^{13}C nmr (D_2O): 24.6 [25.0] (C-4), 39.9 [41.5] (C-3), 56.5 (C-1), 62.4 (C-5′), 78.5 [77.2], 79.2, 83.2 [84.0], 84.9 [85.6] (C-1′, C-2′, C-3′, and C-4′), 115.5 and 117.1 (C-5 and C-8), 120.9 [120.2] and 126.1 (C-4a and C-8a), 143.9 and 145.5 (C-6 and C-7) ppm.

The compound was peracetylated and a partial separation of the isomers effected by chromatography as described above, using ethyl acetate (R_f (major isomer) = 0.19, R_f (minor isomer) = 0.24). For the major isomer, the following data were obtained: $[\alpha]_D^{20}$ −19.6 (c 2.56, $CHCl_3$); ^{1}H nmr ($CDCl_3$): 2.08, (6H, s, 2 × $(CO)CH_3$), 2.11, 2.20, 2.30, 2.31 (12H, 4 × s, 4 × $(CO)CH_3$), 2.96 (2H, m, H's at C-4), 3.87 (2H, m, H's at C-3), 4.19–4.35 (3H, m, H's at C-4′ and C-5′), 4.46 (1H, t, H at C-1′, J = 5 Hz), 5.17 (1H, t, H at C-3′, J = 3 Hz), 5.37 (1H, dd, H at C-2′, J = 5 Hz, J = 3 Hz), 5.95 (1H, d, H at C-1,

Can. J. Chem. Downloaded from www.nrcresearchpress.com by 210.87.254.40 on 09/06/12
For personal use only.

Can. J. Chem. Downloaded from www.nrcresearchpress.com by 210.87.254.40 on 09/06/12
For personal use only.

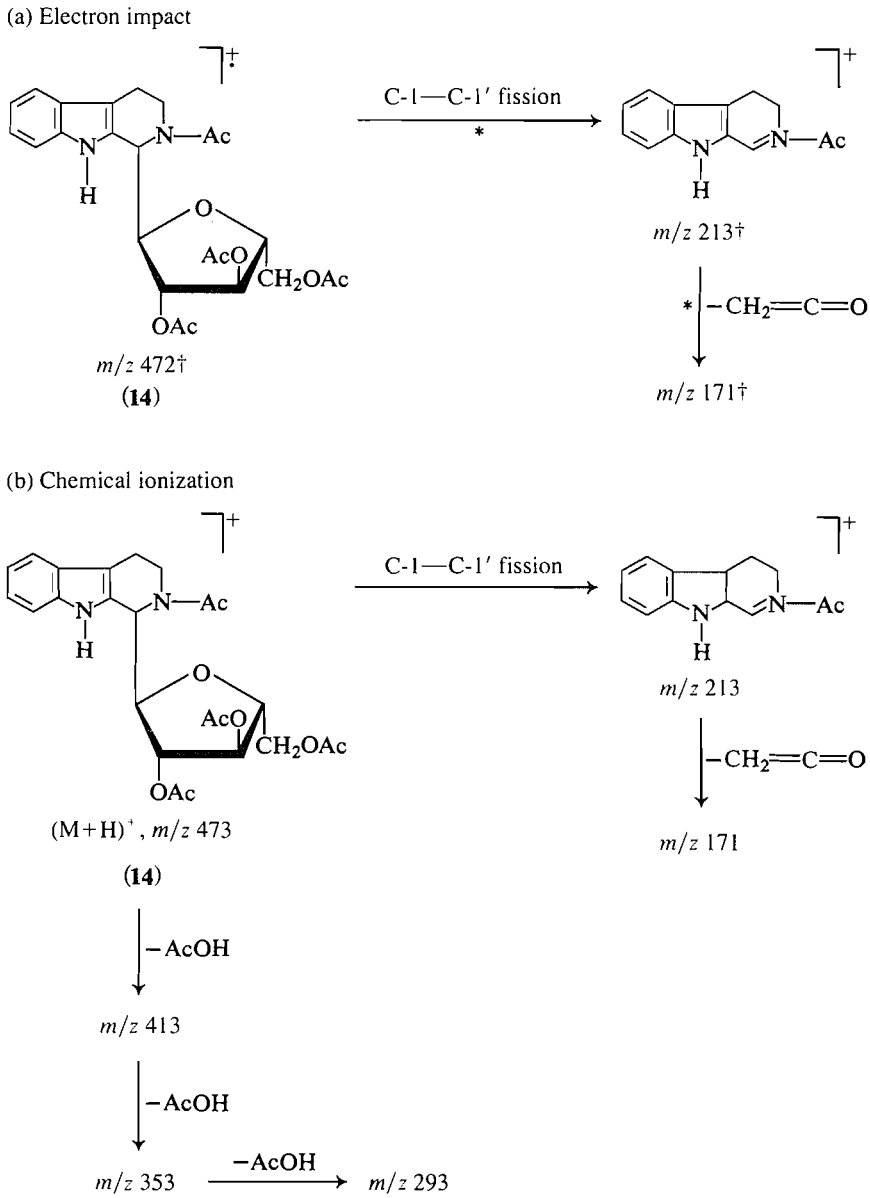

SCHEME 5. Likely mass spectral fragmentations for **14**.

J = 5 Hz), 7.09 (1H, s) and 7.17 (1H, s) (H's at C-5 and C-8) ppm; ^{13}C nmr ($CDCl_3$): 20.6 ((CO)CH_3), 21.7 ((CO)CH_3), 28.4 (C-4), 42.1 (C-3), 52.0 (C-1), 62.9 (C-5′), 78.7, 80.9, 85.5 (C-1′, C-2′, C-3′, and C-4′), 122.5 and 123.4 (C-5 and C-8), 132.3 and 133.2 (C-4a and C-8a), 141.0 and 141.6 (C-6 and C-7), 168.0 and 170.3 (COCH$_3$) ppm; ms (C.I.): 550 ((M + 1)$^+$, 100), 490 (14), 290 (28), 248 (8); ms (E.I.): 290 (100), 248 (95), 206 (29), 164 (36).

Reaction of tryptamine hydrochloride with 2,5-anhydro-D-mannose

Tryptamine hydrochloride (1.38 g, 7.0 mmol) was added to an aqueous solution (ca. 20 mL) containing 2,5-anhydro-D-mannose (prepared as described above from 2-amino-2-deoxy-D-glucose hydrochloride (3.23 g, 15 mmol)). The mixture was warmed gently (to ~40°C) until all material had dissolved, and the solution was kept at room temperature for 7 days. Evaporation gave an amorphous brown solid (3.5 g), which was purified on a short column of silica gel (25 g) using acetonitrile/water (9:1), giving the product as a yellow-brown powder (2.35 g, 98%). The product was found to be a mixture of two isomers in the approximate ratio of 40:60. These were partly separated by chromatography on silica gel using ethyl acetate/methanol/water (85:10:5) (R_f (major isomer) = 0.07, R_f (minor isomer) = 0.12). Each isomer crystallized as fine white needles from methanol, mp 228°C–230°C (dec.) for each isomer. Mixture mp 216°C–218°C (dec.); $[\alpha]_D^{20}$ (major isomer) +51.0 (c 0.6, 0.1 M HCl); $[\alpha]_D^{20}$ (minor isomer) +21.9 (c 0.54, 0.1 M HCl). *Anal.* calcd. for $C_{16}H_{20}N_2O_4$: C 63.15, H 6.62, N 9.20; found (major isomer): C 63.18, H 6.66, N 9.39%; found (minor isomer): C 63.11, H 6.71, N 9.04%.

Minor isomer

^{1}H nmr (DMSO-d_6 + D_2O): 2.95 (2H, m, H's at C-4), 3.26 (2H, m, H's at C-3), 3.57 (2H, dd, H's at C-5′, J = 5.1 Hz, J = 6.8 Hz), 3.78 (1H, t, H at C-2′, J = 3.5 Hz), 3.90 (1H, t, H at C-3′, J = 3.1 Hz), *3.96 (1H, m, H at C-4′), 4.18 (2H, s, H's at C-1 and C-1′), 6.99 (1H, t, J = 7.5 Hz) and 7.08 (1H, t, J = 7.5 Hz) (H's at C-6 and C-7), 7.38 (1H, d, J = 7.9 Hz) and 7.44 (1H, d, J = 7.9 Hz) (H's at C-5 and C-8) ppm; ^{13}C nmr (DMSO-d_6 + D_2O): 22.0 (C-4), 42.0 (C-3), 54.2 (C-1), 62.2 (C-5′), 77.8, 79.2, 86.8 (C-1′, C-2′, C-3′, and

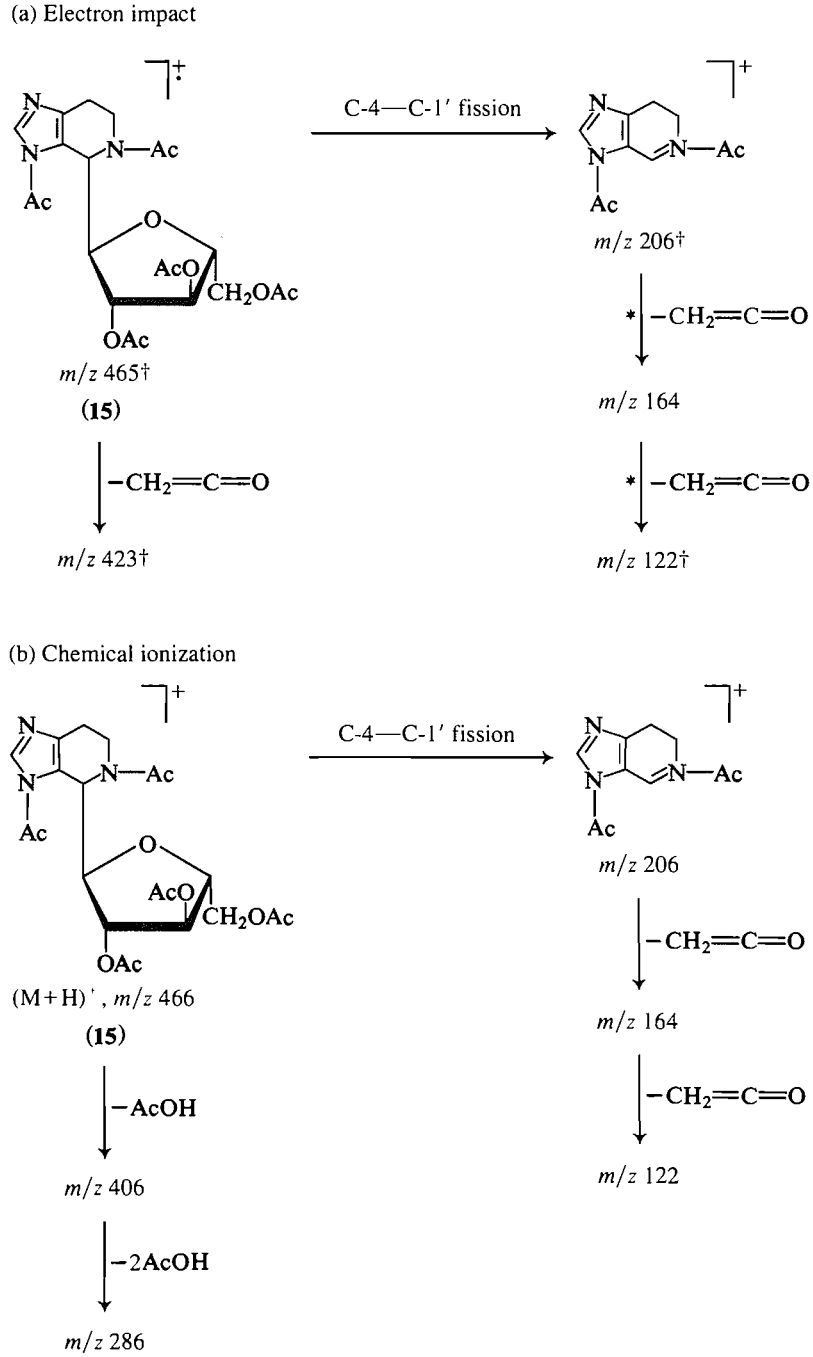

SCHEME 6. Likely mass spectral fragmentations for **15**.

C-4′), 107.9 and 126.7 (C-1a and C-4a), 111.2 and 117.6 (C-5 and C-8), 118.3 and 120.6 (C-6 and C-7), 134.0 and 135.8 (C-8a and C-5a) ppm.

Major isomer

^{1}H nmr (DMSO-d_6 + D_2O): 2.96 (2H, m, H's at C-4), 3.25 (2H, m, H's at C-3), *3.46 (2H, d of AB q, H's at C-5′, $J_{5'a-5'b}$ = 11.6 Hz, $J_{5'a-4'}$ = 3.8 Hz, $J_{5'b-4'}$ = 5.2 Hz), 3.77 (1H, q, b, H at C-4′, $J_{4'-5'a}$ = 3.8 Hz, $J_{4'-5'b}$ = 5.2 Hz), *3.86 (1H, t, H at C-3′, J = 5.1 Hz), *4.07 (1H, s, b, H at C-1), *4.19 (1H, t, H at C-2′, $J_{2'-1'}$ = 5.8 Hz), *4.27 (1H, dd, H at C-1′, $J_{1'-2'}$ = 5.8 Hz, $J_{1'-1}$ = 1.9 Hz), 6.99 (1H, t, J_{6-7} = 7.3 Hz) and 7.07 (1H, t, J_{6-7} = 7.4 Hz) (H's at C-6 and C-7), 7.34 (1H, d, $J_{5-6\text{ or }7-8}$ = 7.9 Hz) and 7.41 (1H, d, $J_{5-6\text{ or }7-8}$ = 7.5 Hz) (H's at C-5 and C-8) ppm; ^{13}C nmr (DMSO−d_6 + D_2O): 22.3 (C-4), 51.9 (C-1), 62.8 (C-5′), 76.9, 77.9, 84.9, 85.5 (C-1′, C-2′, C-3′, and C-4′), 109.1 and 127.2 (C-1a and C-4a), 111.1 and 117.5 (C-5 and C-8), 118.4 and 120.7 (C-6 and C-7), 134.5 and 135.8 (C-5a and C-8a) ppm. The signal for C-3 was obscured by DMSO peaks in the range of 36.5−41.7 ppm. Assignment of signals marked with an asterisk is supported by homonuclear decoupling experiments.

For ms analysis, the compound was peracetylated by the usual procedure; ms (C.I.): 473 ((M + 1)$^+$, 100), 413 (68), 353 (16), 293 (11), 213 (78), 171 (14); ms (E.I.): 472 (M$^+$, 7), 213 (100), 171 (36).

Reaction of histamine with 2,5-anhydro-D-mannose

Histamine dihydrochloride (1.84 g, 10 mmol) and potassium hydroxide (1.18 g, 21 mmol) were dissolved in water (5 mL), and a solution of 2,5-anhydro-D-mannose (1.78 g, 10.5 mmol) in water (5 mL) was added. The resulting colourless solution was stirred over-

Can. J. Chem. Downloaded from www.nrcresearchpress.com by 210.87.254.40 on 09/06/12
For personal use only.

TABLE 2. Accurate masses of selected ions in the mass spectra of **12**, **13**, **14**, and **15**

Compound	Peak	Composition	Accurate mass observed	Accurate mass calcd.
	290	$C_{15}H_{16}NO_5$	290.105	290.103
12	248	$C_{13}H_{14}NO_4$	248.096	248.092
	206	$C_{11}H_{12}NO_3$	206.080	206.082
	290	$C_{15}H_{16}NO_5$	290.105	290.103
13	248	$C_{13}H_{14}NO_4$	248.090	248.092
	206	$C_{11}H_{12}NO_3$	206.078	206.082
	472	$C_{24}H_{28}N_2O_8$	472.185	472.185
14	213	$C_{13}H_{13}N_2O$	213.102	213.103
	171	$C_{11}H_{11}N_2$	171.091	171.092
	465	$C_{21}H_{27}N_3O_9$	465.174	465.175
	423	$C_{19}H_{25}N_3O_8$	423.160	423.164
15	206	$C_{10}H_{12}N_3O_2$	206.092	206.093
	164	$C_8H_{10}N_3O$	164.083	164.082
	122	$C_6H_8N_3$	122.071	122.072

night. The colourless solution was concentrated to ~5 mL, the white solid was removed by filtration and washed with a little ice-cold water. The solid was recrystallized from water, to give the product as white crystals (1.1 g, 40%), mp 234°C−236°C; $[\alpha]_D^{20}$ +50.2 (*c* 2.65, 0.1 *M* HCl); ^{1}H nmr (D_2O): *2.50 (2H, q, b, H's at C-7, J_{7-6} = 5.2 Hz), *2.77 (1H, m) and *3.10 (1H, m) (H's at C-6), *3.56 (2H, d of AB q, H's at C-5′, $J_{5'a-5'b}$ = 12.4 Hz, $J_{5'a-4'}$ = 5.2 Hz, $J_{5'b-4'}$ = 3.6 Hz), *3.77 (1H, q, b, H at C-4′, $J_{4'-5'a}$ = 5.2 Hz, $J_{4'-5'b}$ = 3.6 Hz, $J_{4'-3'}$ = 6.0 Hz), *3.90 (1H, d, b, H at C-4, $J_{4-1'}$ = 4.6 Hz), *3.98 (1H, t, H at C-3′, $J_{3'-4'}$ = 6.0 Hz, $J_{3'-2'}$ = 6.6 Hz), *4.03 (1H, t, H at C-2′, $J_{2'-3'}$ = 6.6 Hz, $J_{2'-1'}$ = 5.2 Hz), *4.21 (1H, t, H at C-1′, $J_{1'-2'}$ = 5.2 Hz, $J_{1'-4}$ = 4.6 Hz), 7.48 (1H, s, H at C-2) ppm; ^{13}C nmr (D_2O): 22.0 (C-7), 40.8 (C-6), 53.4 (C-4), 61.4 (C-5′), 76.6, 77.4, 82.9, 82.9 (C-1′, C-2′, C-3′, and C-4′), 127.7 (C-7a), 130.3 (C-3a), 135.1 (C-2) ppm. Assignment of signals marked * is supported by homonuclear decoupling experiments. *Anal.* calcd. for $C_{11}H_{17}N_3O_4$: C 51.76, H 6.67, N 16.47; found: C 51.76, H 7.00, N 16.39%.

Acknowledgements

We thank the Natural Sciences and Engineering Research Council of Canada for financial support of this work in the form of grants to DBM and WAS.

1. W. M. WHALEY and T. R. GOVINDACHARI. Org. React. **6**, 151 (1951).
2. T. HUDLICKY, T. M. KUTCHAN, G. SHEN, V. E. SUTLIFF, and C. J. COSCIA. J. Org. Chem. **46**, 1738 (1981).
3. H. A. BATES. J. Org. Chem. **46**, 4931 (1981).
4. D. SOERENS, J. SANDRIN, F. UNGEMACH, P. MOKRY, G. S. WU, E. YAMANAKA, L. HUTCHINS, M. DIPIERRO, and J. M. COOK. J. Org. Chem. **44**, 535 (1979).
5. T. SEVERIN and B. HEIDENHAIN. Z. Lebensm. Unters. Forsch. **132**, 65 (1966).
6. (*a*) T. SEVERIN and K.-H. BRÄUTIGAM. Chem. Ber. **106**, 2943 (1973); (*b*) T. SEVERIN and K.-H. BRÄUTIGAM. Z. Lebensm. Unters. Forsch. **154**, 80 (1974).
7. J. E. HODGE. Adv. Carbohydr. Chem. **10**, 169 (1955).
8. G. P. ELLIS. Adv. Carbohydr. Chem. **14**, 63 (1959).
9. D. HORTON and K. D. PHILIPS. Methods Carbohydr. Chem. **7**, 68 (1976).
10. M. SHAMMA and J. L. MONIOT. Isoquinoline alkaloids research 1972−1977. Plenum Press, New York. 1978. p. 4.
11. (*a*) D. HEYL, E. LUZ, S. A. HARRIS, and K. FOLKERS. J. Am. Chem. Soc. **70**, 3669 (1948); (*b*) **74**, 414 (1952); (*c*) E. KITA, D. KIERSKA, and C. MAŚLIŃSKI. Rocz. Chem. **51**, 1741 (1977); (*d*) L. CASELLA and M. GULLOTTI. J. Am. Chem. Soc. **103**, 6338 (1981).
12. D. W. HUGHES, H. L. HOLLAND, and D. B. MACLEAN. Can. J. Chem. **54**, 2252 (1976).
13. C. POUPAT, A. AHOND, and T. SÉVENET. Phytochemistry, **15**, 2019 (1976).
14. G. W. SCHNARR, D. M. VYAS, and W. A. SZAREK. J. Chem. Soc. Perkin Trans. 1, 496 (1979).
15. H. BUDZIKIEWICZ, C. DJERASSI, and D. H. WILLIAMS. Structure elucidation of natural products by mass spectrometry. Vol. II. Holden-Day Inc., San Francisco. 1964. pp. 204−216.
16. DANIEL R. KNAPP. Handbook of analytical derivatisation reactions. Wiley−Interscience, New York. 1979. pp. 599−615.
17. (*a*) R. DEITRICH and V. ERWIN. Ann. Rev. Toxicol. **20**, 55 (1980); (*b*) G. COHEN, C. MYTILINEOU, and R. E. BARRETT. Science, **175**, 1269 (1972); (*c*) G. ARCARI, L. BERNARDI, G. FALCONI, F. LUINI, G. PALAMIDESSI, and U. SCARPONI. Ger. Patent No. 2,700,012, July 21, 1977; (*d*) G. C. HABERMEHL and W. ECSY. Heterocycles, **5**, 127 (1976).
18. J. G. MOFFATT, H. P. ALBRECHT, G. H. JONES, D. B. REPKE, G. TRUMMLITZ, H. OHRUI, and C. M. GUPTA. *In* Chemistry and biology of nucleosides and nucleotides. *Edited by* R. E. Harmon, R. K. Robins, and L. B. Townsend. Academic Press, Inc., New York, NY. 1978. p. 359.
19. W. C. STILL, M. KAHN, and A. MITRA. J. Org. Chem. **43**, 2923 (1978).

Can. J. Chem. Downloaded from www.nrcresearchpress.com by 210.87.254.40 on 09/06/12
For personal use only.

Acidity measurements in THF. III. Aldimines and ketimines[1]

ROBERT R. FRASER, MONIQUE BRESSE, AND NOEMI CHUAQUI-OFFERMANNS
Ottawa-Carleton Institute for Graduate Studies and Research in Chemistry, University of Ottawa, Ottawa, Ont., Canada KIN 9B4

AND

K. N. HOUK AND N. G. RONDAN
Department of Chemistry, University of Pittsburgh, Pittsburgh, PA 15260, U.S.A.

Received June 1, 1983

ROBERT R. FRASER, MONIQUE BRESSE, NOEMI CHUAQUI-OFFERMANNS, K. N. HOUK, and N. G. RONDAN. Can. J. Chem. **61**, 2729 (1983).

The relative acidities of fiteen aldimines and ketimines have been measured in THF using either ^{13}C nmr spectroscopy or trapping experiments with methyl iodide. The pK_A's are found to vary over a range of more than four pK units. The effects of structure on acidity indicate the acid-weakening effect of alkyl substitution in ketimines to be due to steric effects. This interpretation is supported by the results of *ab initio* calculations. The data also permit a quantitative estimation of the preference for the *syn* configuration of lithiated imines to be at least four kcal/mol. The *anti* selectivity previously reported for the lithiation of endocyclic imines can be accounted for by angular constraints, as indicated by both *ab initio* calculations and pK_a data on this class of imine.

ROBERT R. FRASER, MONIQUE BRESSE, NOEMI CHUAQUI-OFFERMANNS, K. N. HOUK et N. G. RONDAN. Can. J. Chem. **61**, 2729 (1983).

On a mesuré les acidités relatives de quinze aldimines et cétimines dans le THF en faisant appel soit à la spectroscopie rmn du ^{13}C ou à des expériences de trappage avec l'iodure de méthyle. On a trouvé que les pK_a varient sur plus de quatre unités de pK. Les effets de structure sur l'acidité indiquent que l'abaissement de l'acidité lors de la substitution alkyle dans les cétémines serait dû à des effets stériques. Cette interprétation est en accord avec les résultats de calculs *ab initio*. Les données permettent aussi d'évaluer quantitativement, à au moins 4 kcal/mol, la préférence pour la configuration *syn* des imines lithiés. On peut expliquer la sélectivité *anti* rapportée antérieurement lors de la lithiation d'imines endocycliques en faisant appel à des contraintes angulaires qui sont suggérées à la fois par les calculs *ab initio* et les données de pK_a sur cette classe de composés.
[Traduit par le journal]

Can. J. Chem. Downloaded from www.nrcresearchpress.com by 210.87.254.6 on 09/06/12
For personal use only.

During the course of our investigations on the chemistry of lithiated aldimines (1) and ketimines (2) a number of unusual results were encountered for which satisfactory explanations required further experimental support. For example, with but two exceptions the lithiation of aldimines and ketimines gave exclusively anions having the *syn* configuration, the main exception being the endocyclic imines **9** to **12** which formed *anti* lithio derivatives only (3).[2] A second striking feature of the lithiation of ketimines concerns the regioselectivity of the reaction. Just as had been observed earlier for ketone oximes (4), oxime ethers (5), and hydrazones (6), lithiation is markedly favored at a primary vs. secondary carbon atom (7) or at a secondary vs. a tertiary one (2, 8). This is anomalous too, in the sense that the stability differences at primary, secondary, and tertiary carbons are normally small and in the reverse order when a change of sp^3 to sp^2 hybridization is involved (9, 10).

As a potential aid to our understanding these results, we set out to obtain quantitative information on the deprotonation reaction, that is, to measure the relative acidities of a variety of imines on a common scale of pK's. As will be shown later, the pK's obtained not only fulfilled our original aim, but provided information on the magnitude of steric effects in aldimine lithiation which permits us to estimate more acurately the magnitude of the "*syn* effect" (11) in imine lithiations.

Measurements of pK's

The development of an acidity scale for weak carbon acids has been a continuously evolving area of research. The MSAD scale was assembled by Cram (12) from the works of many chemists, mainly W. K. McEwen, A. Streitwieser, Jr., D. E. Applequist, and R. E. Dessy and covered a total range in pK's of 18.5 (9-phenylfluorene was chosen as the standard having this pK) to 40 in a variety of solvents.

Two newer scales have been developed which extend the coverage to include much weaker acids. One scale, developed and expanded by Bordwell and co-workers (13) uses pure DMSO as solvent and, from rates of proton abstractions, uses Brønsted correlations to estimate acidities. The second one, developed by Streitwieser and co-workers, has been termed an "ion-pair acidity scale" to indicate the nature of the ionic solutes in his chosen solvent, cyclohexylamine (14). Two special techniques have also provided additional useful data on pK's. Breslow and co-workers have been able to determine the pK's of extremely weak acids using an electrochemical technique (15) and Arnett and Venkatasubramanian have recently described estimates of pK's from measurements on the enthalpies of deprotonation (16). Remarkably good agreement has been achieved for those measurements common to the three different solvents in spite of the known dependence of pK on solvent (17). For example, the pK_a of toluene is assessed at 41.2 (18) in cyclohexylamine, 42 (19) in DMSO, and 45 (15) in THF containing hexamethylphosphoramide.

Most recently, we have initiated studies of pK_a's in THF using lithium diisopropylamide (LDA) as the proton abstraction reagent. We have found that there is a sufficiently slow rate of proton transfer between LDA and diisopropylamine, as well as between both of these and weak carbon acids and their anions, to allow direct observation of an equilibrium mixture of two anions and their conjugate acids using ^{13}C nmr at room

[1]This is the third in a series of papers describing acidity measurements in tetrahydrofuran (THF). Parts I and II are ascribed to the refs. 20 and 21 respectively.

[2]The other exception recently reported a striking solvent effect of HMPA on lithiated propionaldimine (25).

TABLE 1. Relative pK's from alkylation reactions[a]

Entry	Compound	Reference compound	K (eq. [1])	ΔpK	Assigned pK[b,c]
1	$CH_3CH_2(CH_3)C{=}NCH_2\phi$ (**2**)	**1**	2	0.3	0.3
2	$CH_3CH_2(CH_3)C{=}NCH_2\phi$ (**2**)	**2** (CH_3 protons)	81	1.9	2.0
3	$(CH_3CH_2)_2C{=}NCH_2\phi$ (**3**)	**2** (CH_3 protons)	182	2.3	2.4
4	$(CH_3CH_2)_2C{=}NCH(CH_3)_2$ (**4**)	**3**	67	1.8	4.2
5	$(CH_3CH_2)_2C{=}NCH(CH_3)\phi$ (**5**)	**4**	0.62	−0.2	4.0
6	$(CH_3)_2C{=}NCH(CH_3)_2$ (**6**)	**4**	0.0059	−2.2	2.2 (2.5)[d]
7	$CH_3CH{=}NCH(CH_3)\phi$ (**7**)	**2**	2.3	0.3	0.6
8	$CH_3CH_2CH_2CH{=}NCH(CH_3)\phi$ (**8**)	**7**	1.2	0.1	0.7
9	(**9**)	**7**	9	1.0	1.6
10	(**10**)	**4**	0.02	−1.7	2.5
11	(**11**)	**4**	0.25	−0.6	3.6
12	(**12**)	**11**	0.04	−1.4	2.2

[a]All K's determined at −78°C.
[b]Statistically corrected (7) for number of hydrogens.
[c]$(CH_3)_2C{=}NCH_2\phi$, **1**, is assigned a pK = 0.
[d]The weighted average of entries 6 and 15.

TABLE 2. Relative pK's from ^{13}C intensity measurements[a]

Entry	Compound	Reference compound	K	ΔpK	Assigned pK[b,c]
13	$(CH_3)_2CHCH{=}NCH(CH_3)\phi$ (**13**)	**3**	4	0.6	2.7
14	$(CH_3)_2CHCH{=}NCH(CH_3)\phi$ (**13**)	**5**	0.125	−0.9	2.8
15	$(CH_3)_2C{=}NCH(CH_3)_2$ (**6**)	**3**	1.6	0.2	2.6 (2.5)[d]
16	$(CH_3)_2CH(CH_3)C{=}NCH(CH_3)_2$ (**14**)	**6**	18	1.3	3.8
17	$(CH_2)_5C{=}NCH(CH_3)_2$ (**15**)	**6**	1.14	0.1	2.4

[a]All measurements at 298 K.
[b]Statistically corrected for number of hydrogens.
[c]Relative to **1**, pK = 0.
[d]The weighted average of entries 6 and 15.

temperature. This provides a value for K for the equilibrium [1]

[1] $HA_1 + A_2^- \rightarrow A_1^- + HA_2$

where $K = K_1/K_2$ and thus yields a $\Delta pK = -\log K = pK_1 - pK_2$.[3] Using this technique we have determined an increasing order of acidities for tetramethylpiperidine, diisopropylamine, and *cis*-2,6-dimethylpiperidine (20) (relative pK_a's being 2.1, 0.5, and 0). We have subsequently utilized the lithio derivatives of these amines to measure the relative pK's of fifteen weak carbon acids (21). One of the most notable facts emerging from these preliminary studies is a very different order of acidities in THF compared to cyclohexylamine. Since the most common synthetic method for the generation of anions utilizes LDA in THF, additional quantitative data in this medium should prove of widespread use in furthering our understanding of anion reactions. Towards our goal of elucidation of the chemical properties of lithiated imines in THF, we have employed this method in conjunction with a second to measure their relative acidities. The latter involves the trapping of a mixture of anions by alkylation with methyl iodide at −78°C. This approach is somewhat more complex to use, since all the alkylation products are formed initially in the *syn* configuration, but isomerize at varying rates to the *anti* form in the case of aldimines or to a *syn*−*anti* mixture in the case of ketimines. In some cases, spectra could be obtained before isomerization intervened, and in other alkylations, spectra were measured only after equilibrium had been reached. The observation of each of the four species in eq. [1] at equilibrium at room temperature is quite remarkable in the sense that the lithium−hydrogen interchange is sufficiently slow, on the nmr time scale, to permit the direct measurement of signal intensities for all species. For this to be possible, the barrier to interconversion can be calculated to have a minimum value of 16 kcal/mol.[4] There is, however, a limitation to the use of either method, particularly the direct method at room temperature. On certain occasions, reaction of an anion and an imine can occur, usually with compounds of low molecular weight. For example, we were unable to measure the pK_a of $CH_3CH{=}NCH_2\phi$ vs. **7** due to a destructive reaction even at −78°C.

A total of fifteen imines have been subjected to pK measurements using the two methods. Table 1 presents the results of competitive alkylation studies and Table 2 gives the results of direct measurements of ΔpK. All of the data are presented in the Summary of results using acetone *N*-benzylimine as the reference (pK = 0) since it is the strongest acid of all the imines studied herein. It would be desirable to anchor the scale to a known standard and work is proceeding to this end. We can put some estimates on the pK of the least acidic imine; since it is completely deprotonated by LDA (pK_a = 35.7) (21) it must have a maximum for its pK_a of 33. The fact that DMSO-d_6

[3]Reference 10, Chapt. 1. In converting our data into pK units, we adopt the common assumption that activity coefficients may be assumed to have unit value.

[4]We have determined the barrier to lithium−hydrogen exchange between LDA and tetramethylpiperidine to be 16.8 kcal/mol. (20).

Can. J. Chem. Downloaded from www.nrcresearchpress.com by 210.87.254.6 on 09/06/12
For personal use only.

Can. J. Chem. Downloaded from www.nrcresearchpress.com by 210.87.254.6 on 09/06/12
For personal use only.

Summary of results

Aldimines

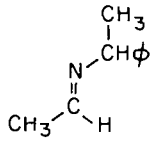

7 (0.6)

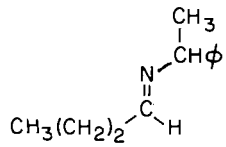

8 (0.7)

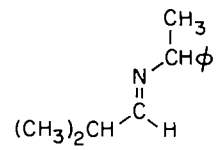

13 (2.8)

An Exocyclic Ketimine

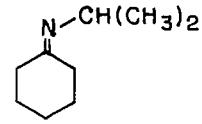

15 (2.4)

Acyclic Ketimines

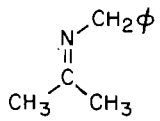

1 (0)

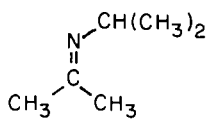

6 (2.5)

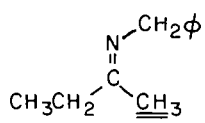

2 (0.3)

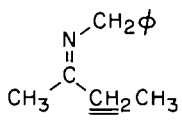

2 (2.0)

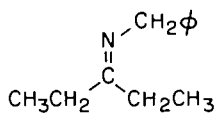

3 (2.4)

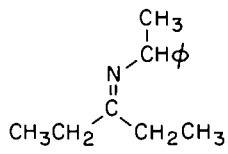

5 (4.0)

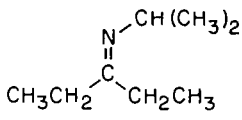

4 (4.2)

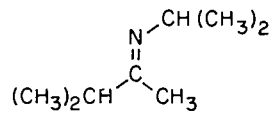

14 (3.8)

Endocyclic Ketimines

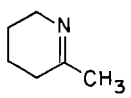

9 (1.6)

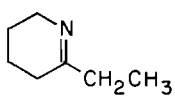

10 (2.5)

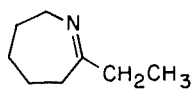

11 (3.6)

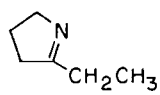

12 (2.2)

exchanges its deuterium with acetone imine in the presence of *tert*-butoxide (2) allows an estimate for its minimum to be around 30 on the DMSO scale, near enough to the pK of DMSO, (35 on Bordwell's scale (13)) to permit facile exchange.

There is some risk in comparing the pK's from method (a) measured at −78°C with those obtained at room temperature by method (b), as it requires the assumption of a constant ΔS for all equilibria. This assumption has previously been tested and found valid by Jaun *et al.* (15) for acids in THF containing 20% HMPA. Furthermore, there is an established internal consistency in our results which indicates the assumption to be valid for our imines. For example, using method (b), the acidity of **13** was established in relation to both **3** and **5** as being 2.8 and 2.7 respectively on the chosen scale. This agreement is particularly satisfying when one considers the acidities of **3** and **5** were each established relative to **4** using method (a). Method (a) was also proven consistent in the determinations of the pK for **6** by comparison with **3** (pK = 2.6) and with **4** (pK = 2.2). The former value will be the more accurate since K for the pair **6** and **3** is close to unity, in which instance a 5% error in peak intensities gives the smallest error in pK (<0.1 units). Thus we have assigned a weighted average pK values of 2.5 to **6**.

The accuracy of both our methods is limited primarily by the accuracy of the intensity measurements. While we have adopted operating conditions for spectral acquisition which nullify the effects of differing relaxation times on peak intensities (see Experimental), there is nevertheless a limit in accuracy of ±5% for each peak intensity measurement. This alone introduces an uncertainty in K of 20% and in each ΔpK of ±0.1. Including all operational and systematic errors, we estimate a maximum error in pK's of ±0.3 units.

Results and discussion

The data in Table 1 provide a value for the ΔpK between various pairs of imines. Since we have assigned a pK = 0 to the imine **1**, we must make a statistical correction for each ΔpK measurement in which a different number of acidic hydrogens in the two imines is involved. Since $\Delta pK = \log K = \Delta G/2.3RT$ and this statistical contribution to ΔG will be a $T\Delta S$ term equal to $2.3RT \log (N_1/N_2)$, the correction term for ΔpK will be $\log (N_1/N_2)$, i.e., log 3/2, log 3/1, or log 2 as the case

Can. J. Chem. Downloaded from www.nrcresearchpress.com by 210.87.254.6 on 09/06/12
For personal use only.

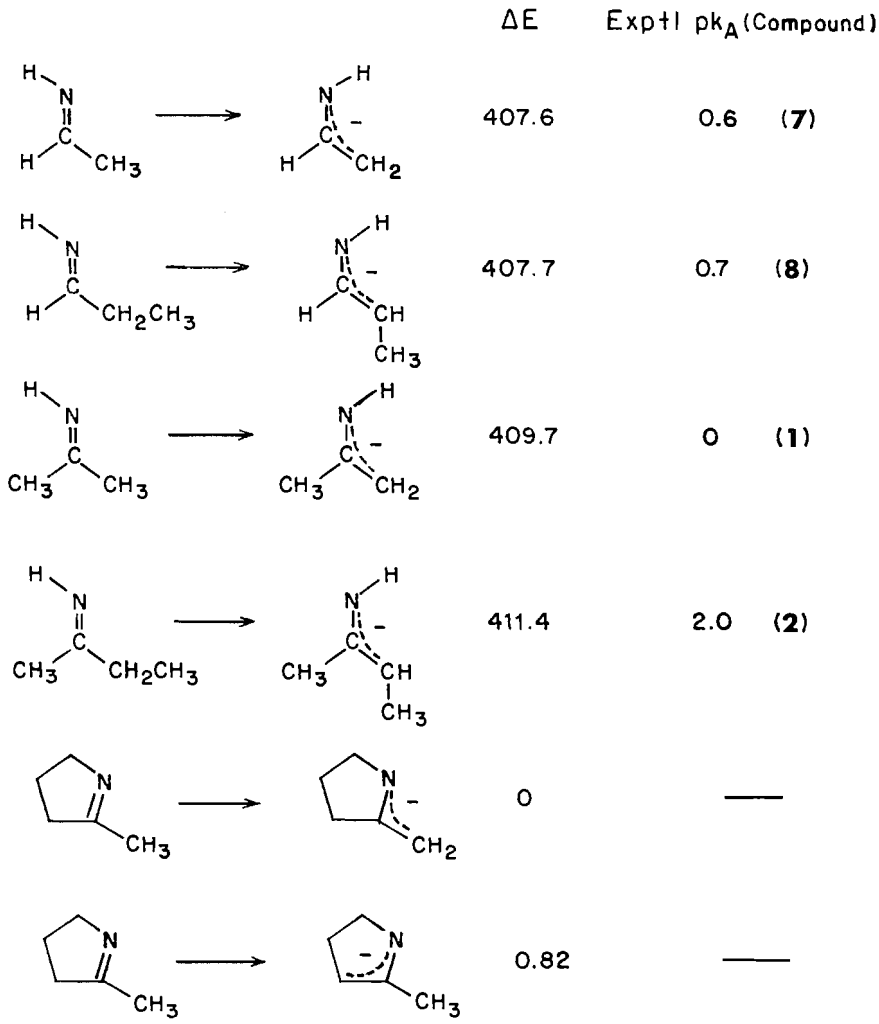

FIG. 1. A comparison of the deprotonation energies obtained by *ab initio* calculations with the experimental values for pK_a.

may be.

Several interesting effects of structure on acidity are revealed by the pK's in the Summary. A most informative feature is the relative insensitivity of pK to a change from a primary to a secondary α carbon as in **7** vs. **8**. This contrasts with 2 pK unit increase for the same structural change in ketimines **2** (at the CH_2) or **3** vs. **1**. The latter change is completely consistent with the well-documented behaviour observed for the lithiation of ketimines (2, 7, 8).[5] A comparison of **7** with **8** shows that the electronic effect of an alkyl substituent is negligible as expected (9, 10). It would seem likely that the large effect of the methyl substituent in ketimines **2** (or **3**) versus **1** arises from another source, most probably steric in origin. Specifically, lithiation of **8** produces **8**-Li which possesses no steric problems in the *E* configuration (see the structure (*E*) **8**-Li); in contrast, **3**-Li will suffer a destabilizing influence at the methyl on the lithiation site in either the *E* or *Z* configurations. Further support for this explanation is seen in the pK value for **15**.

The data for the endocyclic ketimines, **9** to **12**, support our earlier contention that the lithiation occurs in the *anti* position effectively by default, since *syn* lithiation would produce an anion whose internal C═C═N bond angle is highly strained when unable to attain the optimum value of 133°. Comparison of **9** with **1** shows that the endocyclic imine is considerably less acidic, though not as much as anticipated on the basis of the completely selective *syn* deprotonation of **1** versus *anti* deprotonation of **9**. Perhaps there is also a stabilizing effect of the cyclic structure on **9**-Li, conceivably in making the optimum C—C—N bond angle of 127° easier to achieve than in **1**.

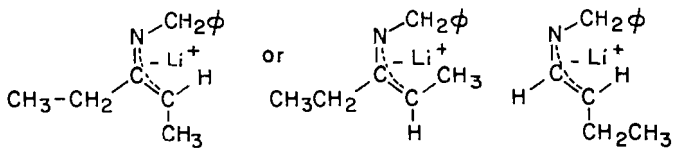

(E) **3**-Li (Z) **3**-Li (E) **8**-Li

Since we have been continuing our theoretical studies (3) on imines and their lithio derivatives, we have available the results of our *ab initio* calculations for the effect of a methyl group on the deprotonation of aldimines versus ketimines for comparison with experiments. The deprotonation energies, obtained from optimization of all structures at the 4-31G level (23), appear in Fig. 1. Since the calculations refer to the free anions in the gas

[5]Very recently, a complete reversal of regioselectivity was reported to be attainable by changing the lithiation agent from LDA to an alkyllithium; see ref. 22. There is additional evidence (D. E. Bergbreiter, private communication) that the reason for the reversal is that totally *anti* deprotonation yields the high proportion of most substituted carbanion which reflects the ratio of *syn*—*anti* isomeric imines.

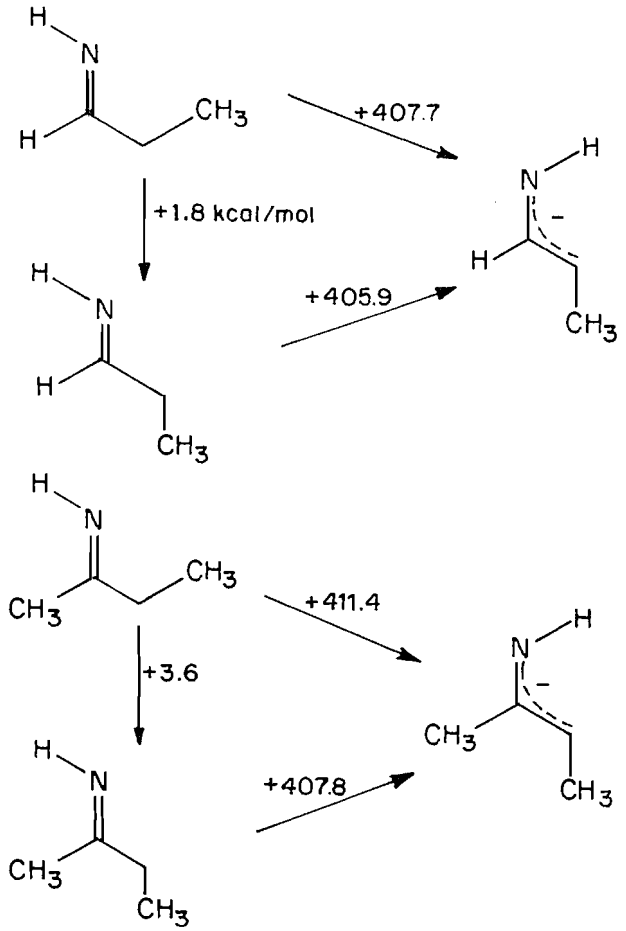

FIG. 2. A comparison of the calculated deprotonation energies of propionaldimine and 2-butanone imine with the inclusion of conformational effects in the neutral imine.

phase, the close agreement between computations and experiment suggests that lithium coordination of the anions, and aggregation and solvation of the resulting ion pairs, must occur with equal exothermicity, or with exothermicity approximately linearly related to anion stabilities. Figure 1 also presents the difference in deprotonation energies for abstraction of the endocyclic versus exocyclic proton in 2-methylpyrroline. Here there is a qualitative accord with experiment, the observed exclusivity in *exo* abstraction being much more than that suggested by either the calculations (done at the STO-3G level for these two reactions) or the pK_a data.

The large difference in the acidity of **4** and **15**, and the similarity between the acidities of **15** and **6** can be understood with the aid of calculations. The preferred conformations of propionaldimine and of methyl ethyl ketimine, each having the allylic methyl group eclipsed with the CN double bond, are shown in Fig. 2. Also shown are higher energy conformations of each in which the N—C—C—C fragment has the same planar arrangement as in the most stable (*E*) conformations of their corresponding anions (25).[6] The energy for deprotonation of the ketimine is calculated to be 3.7 kcal/mol more endothermic than for the aldimine and appears to be due, in part, to the energetically more demanding change in conformation of the ketimine. Compound **15**, which is already constrained to the same conformation as that of the most stable anion, is therefore more easily deprotonated than **4** (by an amount which the calculations for methyl ethyl ketimine indicate to be 3.6 kcal/mol).

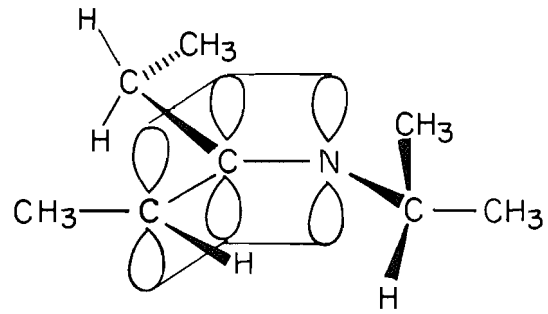

4-Li

The pK value for the isobutyraldimine **13** provides valuable information regarding the magnitude of the "*syn* effect" (11), that factor responsible for complete *syn* lithiation. We had earlier estimated it to be in excess of 4 kcal/mol (1). We have established the stereochemistry of the anion **13**-Li to be entirely *syn* in THF through variable-temperature ^{13}C studies (26), indicating the *syn* **13**-Li anion to be at least 2 kcal/mol more stable than its *anti* form (assuming we would be capable of detecting 4% of *anti*). Since *syn* **13**-Li is strained by 2 kcal/mol as indicated by the pK value for **13** being 2.1 units higher than for **8**, yet exists solely in the *syn* configuration, we can assess a minimum value of 4 kcal/mol to the "*syn* effect."

Experimental

All ^{13}C spectra were recorded on a Varian TF-80 nmr spectrometer. In order to obtain accurate quantitative results, it was necessary to ensure that effects due to differential T_1's were negligible. For this reason the signals chosen to measure $[HA_1]$ versus $[HA_2]$ and $[A_1^-]$ versus $[A_2^-]$ or their alkylation products had similar structures. For example, a pair of methyl, methylene, or methine groups would be selected and quarternary carbons were not used. Furthermore, the repetition rate and pulse angle were varied to test for a variation in intensity ratios. It was found that use of a pulse angle of 26° and a one-second repetition rate gave intensity ratios which were not altered (±5%) by a further decrease in pulse angle or increase in delay time between acquisitions.

All alkylation reactions were carried out under the atmosphere of nitrogen and all reagents added by syringe.

Method (a): measurement of ΔpK by competitive alkylation

A typical procedure is as follows: to a septum-capped flask under an atmosphere of nitrogen was added 0.46 mL (3 mmol) of diisopropylamine in 4 mL of dry THF. To this stirred solution at −20°C was added 1.4 mL (3 mmol) of n-butyllithium in hexane. After 10 min, 3 mmol of **4** and 3 mmol of **6** were added. The flask was then warmed to 0°C and stirring continued for 1 hour. After cooling the mixture to −78°C, 0.39 mL (3.1 mmol) of benzyl bromide was added and stirring continued for 1 hour. The solution was concentrated at −20°C and 3 mL of deuterochloroform was added. The solution gave a ^{13}C nmr spectrum which indicated the presence of **4** and **6** and their alkylation products. By recording the spectrum immediately over a 17 minute period it was possible to obtain a spectrum in which only the presence of *syn* benzyl derivatives could be detected. Even in the case

[6]In this paper, the *E* configuration has been observed for lithiated *N*-cyclohexyl propionaldimine and lithiated *N*-*tert*-butyl propionaldimine (as indicated by J_{H-H} = 15 Hz for the attached vicinal protons). The extra ethyl group in **4**-Li would not affect the stability of this configuration on the basis of previously observed *cis* preference in butenyllithiums (27). The same paper reports partial isomerization of the *E* to *Z* isomer when hexamethylphosphoramide is added.

Can. J. Chem. Downloaded from www.nrcresearchpress.com by 210.87.254.6 on 09/06/12
For personal use only.

of the alkylations of aldimines **7** and **8** this rapid work-up and spectral acquisition avoided complication by the presence of *anti* isomers.

Method (b): direct measurement of equilibrium position

In a typical experiment, 2 mmol of lithium diisopropylamide were prepared by the addition of 0.95 mL (2 mmol) of butyllithium in hexane to 0.28 mL (2 mmol) of diisopropylamine in 2 mL THF. A mixture of two imines (2 mmol of each) was then added and the solution stirred for 30 min. The solution was then transferred under argon to an nmr tube filled with argon. The tube was capped, wrapped with Parafilm, and subjected to ^{13}C nmr analysis. Typically, 3 to 5 thousand transients gave a spectrum having sufficiently low signal-to-noise to allow accurate intensity measurements.

Theoretical calculations

The *ab initio* calculations were performed using the GAUSSIAN 80 program by J. S. Binkley, R. A. Whiteside, R. Krishnan, R. Seeger, D. J. DeFrees, H. B. Schlegel, S. Topiol, L. R. Kahn, and J. A. Pople, QCPE 406, Quantum Chemistry Program Exchange, Indiana University, Bloomington, IN. The program was modified for Harris 800 and DEC 1099 computers by Dr. John H. Yates.

Acknowledgement

The authors thank the Natural Sciences and Engineering Research Council of Canada for financial support.

1. R. R. FRASER and J. BANVILLE. J. Chem. Soc. Chem. Commun. 47 (1979).
2. R. R. FRASER, J. BANVILLE, and K. L. DHAWAN. J. Am. Chem. Soc. **100**, 7999 (1978).
3. K. N. HOUK, R. W. STROZIER, N. G. RONDAN, R. R. FRASER, and N. CHUAQUI-OFFERMANNS. J. Am. Chem. Soc. **102**, 1426 (1980).
4. W. G. KOFRON and M.-K. YEH. J. Org. Chem. **41**, 439 (1976).
5. R. R. FRASER and K. L. DHAWAN. J. Chem. Soc. Chem. Commun. 674 (1976).
6. E. J. COREY and D. ENDERS. Chem. Ber. **111**, 1337 (1978), and references therein.
7. T. CUVIGNY, M. LARCHEVÊQUE, and H. NORMANT. Tetrahedron Lett. 1237 (1974).
8. A. I. MEYERS, D. R. WILLIAMS, G. W. ERICKSON, S. WHITE, and M. DRUELINGER. J. Am. Chem. Soc. **103**, 3081 (1981).
9. A. STREITWIESER. Equilibrium carbon acidities in solution. *In* Comprehensive carbanion chemistry. Part I. *Edited by* E. Buncel and T. Durst. Elsevier/North Holland, 1980.
10. J. HINE. Structure effects on equilibria in organic chemistry. Wiley–Interscience, New York. 1975. p. 183.
11. ROBERT R. FRASER. The *syn* effect and the use of enolate equivalents in synthesis. *In* Comprehensive carbanion chemistry. Part 2. *Edited by* E. Buncel and T. Durst. Elsevier/North Holland. 1983.
12. D. J. CRAM. Fundamentals of carbanion chemistry. Academic Press, New York. 1965. p. 19.
13. W. N. OLMSTEAD, Z. MARGOLIN, and F. G. BORDWELL. J. Org. Chem. **45**, 3295 (1980), and references therein.
14. D. W. BOERTH and A. STREITWIESER. J. Am. Chem. Soc. **103**, 6443 (1981), and references therein.
15. B. JAUN, J. SCHWARTZ, and R. BRESLOW. J. Am. Chem. Soc. **102**, 5741 (1980), and references therein.
16. E. M. ARNETT and K. G. VENKATASUBRAMANIAN. Tetrahedron Lett. 987 (1981).
17. C. D. RITCHIE. *In* Solute–solvent interactions. *Edited by* J. F. Coetzee and C. D. Ritchie. Marcel Dekker, New York. 1969. Chapt. 4.
18. A. STREITWIESER and F. GUIBÉ. J. Am. Chem. Soc. **100**, 4532 (1978).
19. D. ALGRIM, J. E. BARES, J. C. BRANCA, and F. G. BORDWELL. J. Org. Chem. **43**, 5024 (1978).
20. R. R. FRASER, A. BAIGNÉE, M. BRESSE, and K. HATA. Tetrahedron Lett. 4195 (1982).
21. R. R. FRASER, M. BRESSE, and T. S. MANSOUR. Chem. Commun. 620 (1983).
22. A. HOSOMI, Y. ARAKI, and H. SAKURAI. J. Am. Chem. Soc. **104**, 2081 (1982).
23. R. DITCHFIELD, W. J. HEHRE, and J. A. POPLE. J. Chem. Phys. **54**, 724 (1971).
24. W. J. HEHRE, R. F. STEWART, and J. A. POPLE. J. Chem. Phys. **51**, 2627 (1969).
25. J. Y. LEE, T. J. LYNCH, D. T. MAO, D. E. BERGBREITER, and M. NEWCOMB. J. Am. Chem. Soc. **103**, 6215 (1981).
26. R. R. FRASER and M. BRESSE. In preparation.
27. M. SCHLOSSER and J. HARTMANN. J. Am. Chem. Soc. **98**, 4674 (1976).

Can. J. Chem. Downloaded from www.nrcresearchpress.com by 210.87.254.6 on 09/06/12
For personal use only.

The crystal structure of potassium 1-(*N*,*N*-diphenylhydrazono)-2,4,6-trinitrobenzenide[1]

RAMANATHAN GOPAL AND BEVERLY E. ROBERTSON[2]
Department of Physics and Astronomy, University of Regina, Regina, Sask., Canada S4S 0A2

AND

JOHN A. WEIL
Department of Chemistry, University of Saskatchewan, Saskatoon, Sask., Canada S7N 0W0

Received March 9, 1983

RAMANATHAN GOPAL, BEVERLY E. ROBERTSON, and JOHN A. WEIL. Can. J. Chem. **61**, 2735 (1983).

Crystals of potassium 1-(*N*,*N*-diphenylhydrazono)-2,4,6-trinitrobenzenide, $C_{18}H_{12}N_5O_6K$, are monoclinic, $P2_1/c$, a = 9.871(2), b = 12.940(3), c = 16.754(4) Å, β = 118.31(1)°, Z = 4, T = 22°C. Diffraction data were collected on a modified Picker FASC-1 diffractometer. The structure was solved by direct methods and refined by full-matrix least-squares to $R = R_w = 0.056$ using the 2627 independent reflections with $|F_o| > \sigma(|F_o|)$. The benzenide ring shows a significant puckering toward the boat conformation. Some important canonical structures contributing to the average geometry of the molecule are discussed. The bonding sphere of the K^+ cation contains all of the oxygen atoms and the hydrazine nitrogen atom bonded to the trinitrobenzenide group. Two phenyl carbon atoms also have short contact distances to the cation.

RAMANATHAN GOPAL, BEVERLY E. ROBERTSON et JOHN A. WEIL. Can. J. Chem. **61**, 2735 (1983).

Les cristaux du (*N*,*N*-diphénylhydrazono)-1 trinitro-2,4,6 benzéniure de potassium, $C_{18}H_{12}N_5O_6K$, sont monocliniques et appartiennent au groupe d'espace $P2_1/c$ avec a = 9,871(2), b = 12,940(3), c = 16,754(4) Å, β = 118,31(1)°, Z = 4, T = 22°C. On a recueilli les données de diffraction à l'aide d'un diffractomètre modifié de Picker FASC-1. On a résolu la structure par des méthodes directes et on l'a affiné par la méthode des moindres carrés (matrice entière) jusqu'à des valeurs de $R = R_w$ = 0,056 pour 2627 réflexions indépendantes avec $|F_o| > \sigma(|F_o|)$. Le cycle benzéniure montre un gauchissement significatif vers la conformation bateau. On discute de quelques structures canoniques importantes qui contribuent à la géométrie moyenne de la molécule. La sphère de liaison du cation K^+ contient tous les atomes d'oxygène et l'atome d'azote de l'hydrazine liés au groupe trinitrobenzéniure. Deux atomes de carbone du phényle sont également très près du cation.

[Traduit par le journal]

Introduction

It has long been known that the addition of bases to solutions of 2,2-diphenyl-1-picrylhydrazine produces a dark colour and the reaction has been assumed to involve the removal of the hydrazine proton (1). Isolation and characterization of salts produced by the reaction was reported by Weil and Janusonis (2) in 1962. Their nmr results indicated that the 1-(*N*,*N*-diphenylhydrazono)-2,4,6-trinitrobenzenide ion was indeed formed. Optical spectroscopic studies showed that the primary peak responsible for the intense colour occurs at 424 nm and is independent of the cationic species present (2). The transitions giving rise to the colour were therefore assumed to be internal to the anion, probably involving quinoid and nitronic canonical structures. A knowledge of the important canonical structures contributing to the ground state of the anion is therefore of interest. This might be inferred both from the precise geometry of the molecule and from the nature of the association between it and the cation.

The present structure determination was therefore undertaken to (*i*) establish unambiguously the existence of the 1-(*N*,*N*-diphenylhydrazono)-2,4,6-trinitrobenzenide ion, (*ii*) determine the nature of the association between the anion and the cation, (*iii*) determine the exact geometry of the anion, and therefore (*iv*) provide information which might lead to a better understanding of the optical transition.

Experimental

$C_{18}H_{12}N_5O_6K$ fw = 433.42
Monoclinic, $P2_1/c$, a = 9.871(2), b = 12.940(3), c = 16.754(4) Å, β = 118.31(2)°, Z = 4, V = 1884.0 Å^3, T = 22(1)°, D_x = 1.528 g cm^{-3}, μ(MoKα) = 3.33 cm^{-1}, F(000) = 867, λ(MoK$\bar{\alpha}$) = 0.71069 Å.

Black crystals of the title compound were prepared by the method described previously by Weil and Janusonis (2), with crystallization from an acetone/petroleum ether mixed solvent. A crystal with dimensions 0.06 × 0.06 × 0.04 cm was selected for data collection. Lattice constants were determined and the Laue group and systematic absences ($h0l$, $l = 2n + 1$; $0k0$, $k = 2n + 1$) indicated space group $P2_1/c$. Data were collected using MoKα radiation in $\theta-2\theta$ scan mode, 2.65° minimum base width, 40 s background counts at the limits of the scan, a scan rate of 1° min^{-1} and a graphite monochromator, up to 2θ values of 50°. Data were collected in the hkl and $\bar{h}kl$ octants. The intensities of three standard reflections were collected after each set of 51 reflections were recorded and were observed to decrease by 7% over the period of the data collection. The intensities of the 3340 independent reflections were compensated for this variation and reduced to observed structure factors using standard procedures. The standard deviation was calculated as $1.0 + 0.01|F| + \sigma$ where σ represents counting statistics. No corrections were made for absorption or extinction effects. Scattering factors for the potassium ion, and carbon, oxygen, and nitrogen atoms were taken from those given by Cromer and Mann and for hydrogen from Stewart *et al.* (3). Corrections for anomalous absorption were not made. The 300 reflections with $E > 1.8$ were used in the multiple solution, logical symbolic addition method of Germain and Woolfson (4). The E map calculated from the best non-trivial solution gave the positions of all of the non-hydrogen atoms. After anisotropic refinement hydrogen atoms were found from a difference map. The largest peaks in the difference map used to locate the hydrogen atoms were those corresponding to the hydrogen atoms themselves.

The structure was refined by the full-matrix least-squares method using isotropic temperature factors for the hydrogen atoms, with the Busing, Martin, and Levy program ORFLS (5). The weighting scheme used in the final cycles of least-squares was given by $w^{-1/2} = 1.065 - 0.0183|F_o| + 0.00032|F_o|^2$. This weighting scheme is based on the assumption that the best estimate of $\sigma(|F_o|)$ in a range of $|F_o|$

[1]These results were reported in partial form, Program and Abstracts, American Crystallographic Association, Series 2, Vol. 6, 72 (1979).

[2]To whom all correspondence should be addressed.

Can. J. Chem. Downloaded from www.nrcresearchpress.com by 210.87.254.5 on 09/06/12
For personal use only.

is the average value of $||F_o| - |F_c||$. The final values of $R = [\Sigma||F_o| - |F_c||]/\Sigma|F_o|$ and $R_w = \{[\Sigma w(|F_o| - |F_c|)^2]/\Sigma w|F_o|^2\}^{1/2}$ for 2627 reflections with $|F_o| > \sigma(|F_o|)$ were both 0.056. Using all reflections, the corresponding values were 0.083 and 0.057, respectively. Observed and calculated structure factors, individual anisotropic temperature factors, and equations of the planes of the molecule have been placed in the Depository of Unpublished Data.[3]

Results and discussion

Final atomic positional parameters and U or U_{eq} for non-hydrogen atoms or hydrogen atoms respectively are given in Table 1. The atom numbering scheme as well as the bond lengths and bond angles, with esd's are given in Fig. 1 for the anion, whose existence is confirmed by the results of this structural study.

There are seven oxygen atoms lying within 2.875(3)–3.174(3) Å of the potassium ion; all six independent oxygen atoms are involved at least once and one, O(1), is involved twice. These distances are within the expected range for ionic bonds. The atom N(4) of the hydrazine linkage is also ionically bonded to potassium. As is shown in Fig. 2, these atoms occupy roughly one half of a sphere about the K^+ ion. The other half of the sphere contains a phenyl ring with two short K—C distances.

This unusual coordination about potassium and the short K—C distances are not solely a consequence of the need to coordinate to the atom N(4), because N(4) can be approached without bringing the potassium ion so near one of the phenyl rings. More general packing considerations might explain the geometry of the coordination sphere, but the nature of the short K—C interactions remains of interest. The relevant contact distances to the K^+ ion are given in Table 2. The angles between the planes of the molecule, as defined in Fig. 3, are given in Table 3. The torsional angles of rotation about the C—N bonds to the nitro groups are also given in Fig. 3.

In Fig. 3, plane *10* contains atoms C(7) to C(12) and is closest to the nitro group containing N(2). The dihedral angle between the planes of these groups is forced by steric requirements to be relatively small, at 34.7°. Atoms O(3) and O(1) are only 3.004(4) and 2.709(4) Å from atom N(4). Atom O(1) not only enters into the coordination sphere of two cations but it also forms the two shortest K—O distances. Its N—O distance is also the longest, at 1.242(3) Å. We note that the K^+ ion contains in its coordination sphere atoms N(4) and O(1) of the same anion, forming the equivalent intramolecular linkage as that which might be formed by an intramolecular hydrogen bond in 2,2-diphenyl-1-picrylhydrazyl.

Various important canonical structures contributing to the average geometry of the molecule are shown in Fig. 4. Forms **1**, **2**, and **4** have a multiplicity of 2, to give a total of eight. The 0.067(6) Å shortening of [C(4)—C(5)] over [C(2)—C(3)] and of [C(5)—C(6)] over [C(2)—C(1)] is contributed by some combination of one each of **2** and **4**. The additional 0.030(6) Å shortening of [C(3)—C(4)] over [C(2)—C(3)], and of [C(1)—C(6)] over [C(2)—C(1)], is contributed by **3** and **5** and one of **2** and **4**. We assume that a combination of **2** and **4** is an important contributor to the average structure of the molecule

TABLE 1. Fractional atomic coordinates (× 10^4) and isotropic or equivalent isotropic temperature factors (× 10^3) for potassium 1-(*N*,*N*-diphenylhydrazono)-2,4,6-trinitrobenzenide (esd's in parentheses)

Atom	x	y	z	U/U_{eq}
K	1038.8(9)	4950.0(2)	1409.2(5)	51.7(4)
O(1)	1424(2)	6114(2)	69(2)	56(1)
O(2)	3607(3)	5454(2)	1022(2)	57(1)
O(3)	1534(3)	8555(2)	−2120(2)	77(2)
O(4)	3399(4)	8571(3)	−2444(2)	91(2)
O(5)	8120(3)	5986(2)	771(2)	67(2)
O(6)	8019(3)	6756(3)	−403(2)	80(2)
N(1)	2809(3)	5944(2)	3260(2)	45(1)
N(2)	2748(4)	8204(3)	−2038(2)	61(2)
N(3)	7401(3)	6456(3)	47(2)	58(2)
N(4)	1146(3)	6395(2)	−1605(2)	45(1)
N(5)	439(3)	6607(2)	−2543(2)	49(1)
C(1)	3494(3)	6336(3)	−205(2)	39(1)
C(2)	2552(4)	6726(3)	−1126(2)	41(2)
C(3)	3464(4)	7362(3)	−1411(2)	46(2)
C(4)	5018(4)	7264(3)	−1048(3)	52(2)
C(5)	5804(4)	6637(3)	−286(2)	46(2)
C(6)	5054(4)	6244(3)	172(2)	43(2)
C(7)	1091(4)	6194(3)	−3071(2)	49(2)
C(8)	753(5)	6669(4)	−3883(3)	65(2)
C(9)	1295(6)	6257(5)	−4437(3)	84(3)
C(10)	2203(7)	5401(6)	−4177(5)	95(4)
C(11)	2595(8)	4954(5)	−3353(5)	105(4)
C(12)	2017(6)	5339(4)	−2807(4)	77(3)
C(13)	−1190(4)	6660(3)	−2910(2)	49(2)
C(14)	−1783(5)	7271(4)	−2475(3)	66(2)
C(15)	−3349(6)	7284(5)	−2783(4)	81(3)
C(16)	−4323(6)	6727(5)	−3506(4)	91(3)
C(17)	−3756(6)	6136(5)	−3952(4)	94(3)
C(18)	−2172(5)	6100(4)	−3659(3)	70(2)
H(4)	5502(39)	7673(28)	−1286(23)	56(11)
H(6)	5624(39)	5914(28)	762(25)	57(10)
H(8)	132(51)	7218(36)	−4057(30)	80(16)
H(9)	1037(53)	6605(38)	−5003(33)	125(16)
H(10)	2523(59)	5136(42)	−4566(37)	126(19)
H(11)	3219(68)	4365(50)	−3163(40)	137(24)
H(12)	2226(56)	5040(39)	−2272(34)	98(17)
H(14)	−997(49)	7678(34)	−1944(29)	74(14)
H(15)	−3707(56)	7688(40)	−2506(33)	88(18)
H(16)	−5367(55)	6714(35)	−3711(29)	100(15)
H(17)	−4316(58)	5690(41)	−4443(34)	119(18)
H(18)	−1811(64)	5594(48)	−3922(39)	86(23)

but that a combination of **3** and **5** is less important. However, **5** also decreases [N(3)—C(5)] over [N(2)—C(3)] and [N(1)—C(1)] by 0.022 Å which suggests that **5** is important. These observations and the nature of the coordination sphere of the cation suggest that all forms in Fig. 4 play an appreciable role.

The contribution of canonical structures involving the substituents allows significant puckering of the trinitrobenzenide ring. The least-squares plane fitted to the six atoms of the ring shows the atoms C(1) and C(3) to be approximately 0.10 Å below the plane, the atoms C(4) and C(6) also to be 0.03 Å below, and the atoms C(2) and C(5) are 0.15 and 0.10 Å respectively above the plane. The conformation is clearly *boat*. However, in order to describe the ring in quantitative terms we use the analysis of Cremer and Pople (6). We find for the benzenide ring, in terms of their pseudorotation parameters for six-membered rings, $\theta = 71.9°$, $\phi = 62.3°$, and $Q = 0.23$

[3]Tables of observed and calculated structure factor amplitudes, anisotropic temperature factors and the equations of the planes of this anion are available, at a nominal charge, from the Depository of Unpublished Data, CISTI, National Research Council of Canada, Ottawa, Ont., Canada K1A 0S2.

Can. J. Chem. Downloaded from www.nrcresearchpress.com by 210.87.254.5 on 09/06/12
For personal use only.

Can. J. Chem. Downloaded from www.nrcresearchpress.com by 210.87.254.5 on 09/06/12
For personal use only.

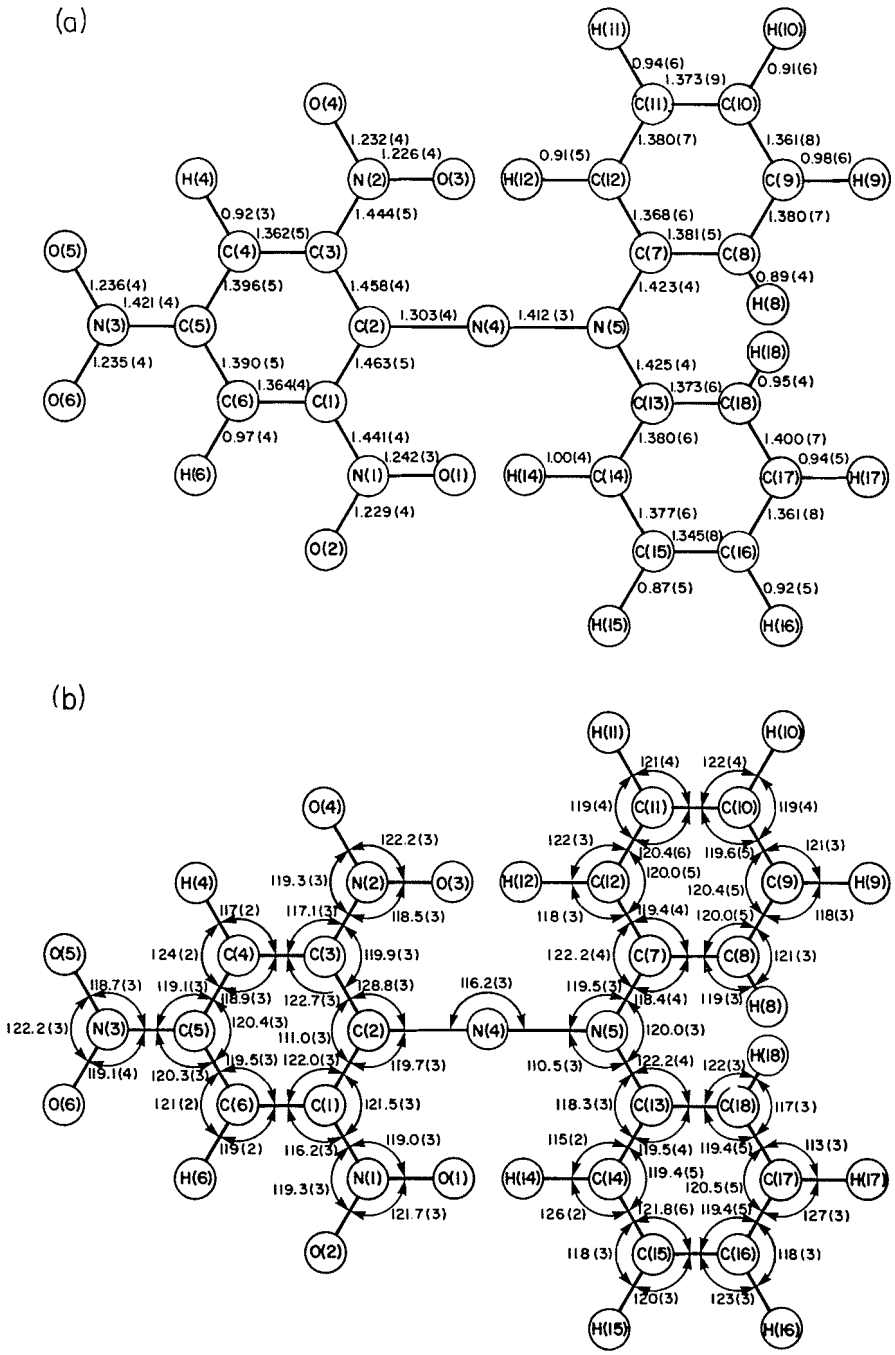

FIG. 1. (*a*) Atom labelling and bond lengths with esd's for the anion. (*b*) Bond angles with esd's for the anion.

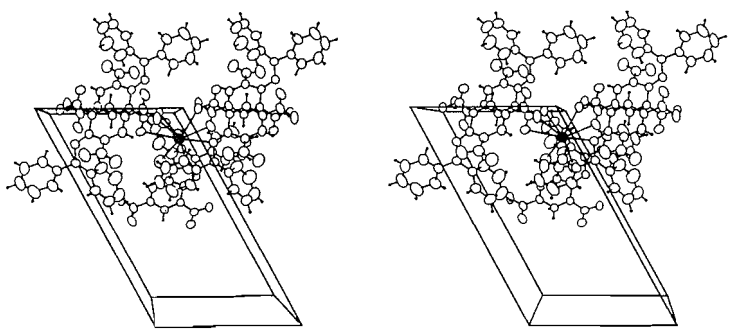

FIG. 2. Stereoscopic view of the packing of the molecules and the coordination to the cation. ***a*** points to the right, ***b*** is into the plane of the paper, and ***c*** is towards the upper left. The cation is shaded.

TABLE 2. Distances from potassium to near neighbours*

Bond	Distance (Å)
K—O(1)	2.875(3)
K—O(2)	2.972(3)
K—(1)[a]	2.868(3)
K—O(3)[b]	2.985(3)
K—O(4)[b]	2.992(3)
K—O(5)[c]	2.884(3)
K—O(6)[d]	3.174(3)
K—N(4)[a]	2.908(4)
K—C(13)[a]	3.213(5)
K—C(14)[a]	3.279(5)

*Symmetry operators: *a*, $-x$, $1-y$, $-z$; *b*, $-x$, $\frac{1}{2}-y$, $\frac{1}{2}+z$; *c*, $-1+x$, y, z; *d*, $1-x$, $1-y$, $-z$.

TABLE 3. Dihedral angles (deg) between planes

Planes*	Angle
1–2	8.5
1–3	20.0
1–4	8.2
1–5	25.7
2–6	6.2
3–7	12.6
7–8	61.5
7–9	26.8
8–10	22.0
9–11	50.7
5–10	34.7
5–3	44.8
10–11	70.6

*See Fig. 3.

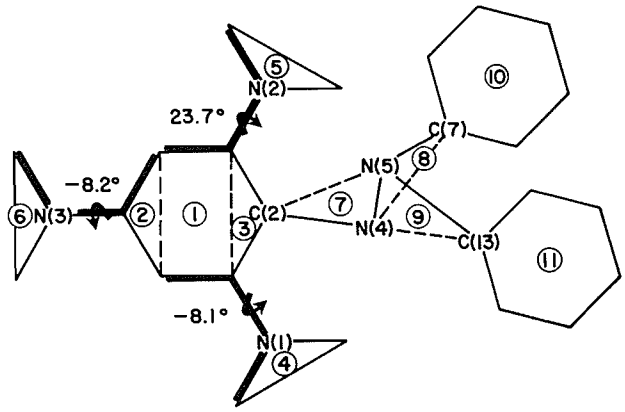

FIG. 3. Designation of the molecular planes of the anion.

(Q is a measure of the magnitude of the puckering). The ϕ angle is nearly an even multiple of 30° which indicates that the ring would have the *boat* conformation if θ were 90°. However, the two folds of the molecule, which correspond to the dihedral angles between planes *1* and *2* and between planes *1* and *3*, are 8.5° and 20.0°, respectively. If these dihedral angles were equal, the parameters describing the conformation of the molecule would approach much more closely to those of the *boat* conformation.

The hydrazine linkage to the trinitrobenzenide group (plane *7*) is nearly coplanar with that part of the trinitrobenzenide group to which it is bonded (plane *3*). The nitro group at C(3) is rotated 25.7° from the plane of the central part of the benzenide ring (plane *1*) and 44.8° from plane *3*. This rotation is much greater than that of the other nitro groups but it has not significantly affected the C—N bond length relative to the other C—N bonds to nitro groups although all show evidence of some double bond character.

We now compare the geometry of the 1-(*N*,*N*-diphenyl-

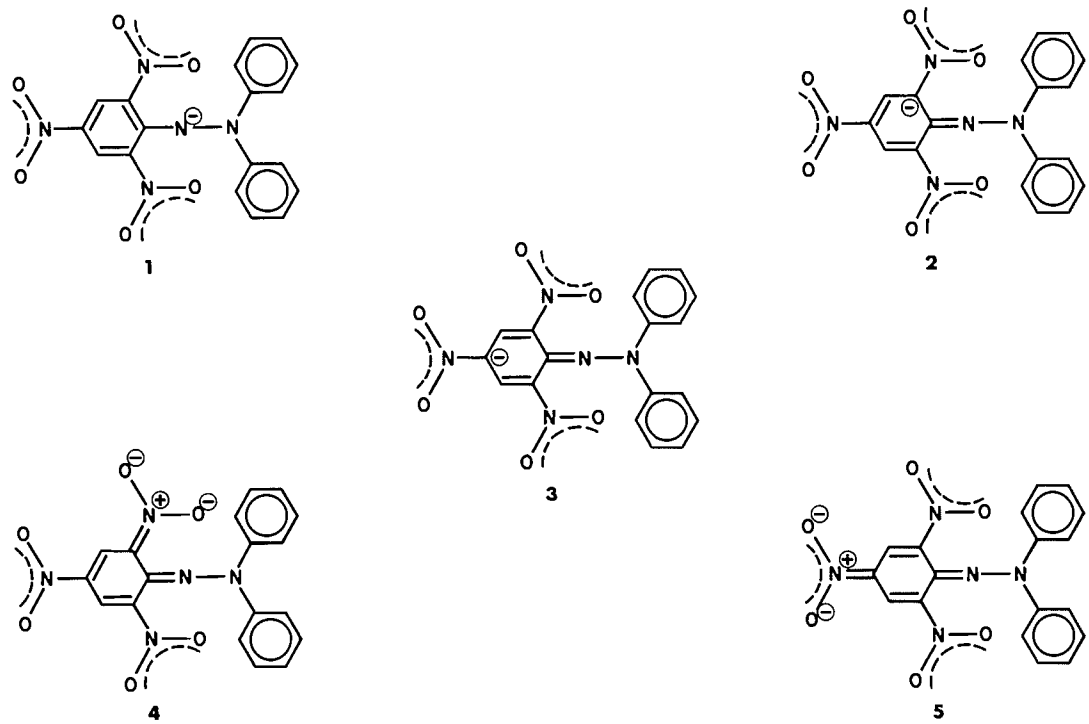

FIG. 4. Important canonical structures of the trinitrobenzenide ring contributing to the anion in its ground state.

Can. J. Chem. Downloaded from www.nrcresearchpress.com by 210.87.254.5 on 09/06/12
For personal use only.

hydrazone)−2,4,6-trinitrobenzenide with that of the related free radical 2,2-diphenyl-1-picrylhydrazyl. The molecule exists in several crystalline forms but the more precise structural determination is that of Kiers *et al.* (7). The N—N bond length in the anion, 1.412(3) Å, is 0.076 longer than the average value for the N—N bonds in the two independent molecules of the free radical, as found in the aforementioned structure determination. Similarly, the C(2)—N(4) bond length, 1.303(4) Å, is 0.061 Å shorter than in the free radical, clearly demonstrating the influence of the canonical structures shown in Fig. 4. The N—N bond length found here compares with the single N—N bond length of 1.390(8) Å in the room temperature structures of tetraphenylhydrazine (8) (the value at −160°C is 1.406(4) Å). The C(2)—N(4) bond length compares with the C—N double bond length of 1.287(4) Å, as determined in *N*-(diphenylmethane) aniline at −160°C (9).

The trinitrobenzenide ring in the free radical is nearly planar. As a result, the two *ortho nitro* groups are rotated through large angles to avoid close contacts between nitro oxygen atoms and N(4). In particular, the nitro groups analogous to O(1)—N(1)—O(2) in the ion are rotated 60.6 and 57.1° from coplanarity with the trinitrobenzenide ring in the two independent molecules of the free radical. The *boat* conformation in the ion obviates the need for much of this rotation.

The two phenyl rings are oriented similarly in the ion and in the free radical. The dihedral angle between the planes of the two rings in the anion is 70.6°, compared to 62° and 65° in the free radical. However, the geometry of the central moiety of the molecule containing the hydrazine linkage and the atoms C(7) and C(13) are quite dissimilar. In the free radical these four atoms are nearly coplanar. In the ion, atoms C(7) and C(13) are 0.71 and 0.76 Å removed from planes *9* and *8* respectively.

Acknowledgements

The authors acknowledge the support of the Natural Sciences and Engineering Research Council of Canada in the form of operating grants to B. E. Robertson and J. A. Weil, and thank K. Wolbaum for assistance with the manuscript.

1. S. GOLDSCHMIDT and K. RENN. Ber. **55**, 628 (1922); R. H. POIRIER, E. J. KAHLER, and F. BENINGTON. J. Org. Chem. **17**, 1437 (1952); A. T. BALABAN, P. T. FRANGOPOL, M. MARCULESCU, and J. BALLY. Tetrahedron, **13**, 258 (1961).
2. J. A. WEIL and G. A. JANUSONIS. J. Org. Chem. **27**, 1248 (1962).
3. D. T. CROMER and J. B. MANN. Acta Crystallogr. A**24**, 321 (1968); R. F. STEWART, E. R. DAVIDSON, and W. T. SIMPSON. J. Chem. Phys. **42**, 3175 (1965).
4. G. GERMAIN and M. M. WOOLFSON. Acta Crystallogr. B**24**, 91 (1968).
5. W. R. BUSING, K. O. MARTIN, and H. A. LEVY. ORFLS, Report ORNL-TM-305. Oak Ridge National Laboratory, Oak Ridge, TN. 1965.
6. D. CREMER and J. A. POPLE. J. Am. Chem. Soc. **97**, 1354 (1975).
7. C. TH. KIERS, J. L. DE BOER, R. OLTHOF, and A. L. SPEK. Acta Crystallogr. B**32**, 2297 (1976).
8. A. HOEKSTRA, A. VOS, P. B. BRAUN, and J. HORNSTRA. Acta Crystallogr. B**31**, 1708 (1975).
9. P. A. TUCKER, A. HOEKSTRA, J. M. TEN CATE, and A. VOS. Acta Crystallogr. B**31**, 733 (1975).

Can. J. Chem. Downloaded from www.nrcresearchpress.com by 210.87.254.5 on 09/06/12
For personal use only.

New multidentate ligands. XXI. Synthesis, proton, and metal ion binding affinities of *N,N′,N″*-tris[2-(*N*-hydroxycarbamoyl)ethyl]-1,3,5-benzenetricarboxamide (BAMTPH)

ISAO YOSHIDA, ICHIRO MURASE, RAMUNAS J. MOTEKAITIS, AND ARTHUR E. MARTELL[1]
Department of Chemistry, Texas A&M University, College Station, TX 77843, U.S.A.

Received February 22, 1983

ISAO YOSHIDA, ICHIRO MURASE, RAMUNAS J. MOTEKAITIS, and ARTHUR E. MARTELL. Can. J. Chem. **61**, 2740 (1983).

Synthesis of a new tris-bidentate multidentate ligand, *N, N′, N″*-tris[2-(*N*-hydroxycarbamoyl)ethyl]-1,3,5-benzenetricarboxamide (BAMTPH), designed for the binding of trivalent metal ions such as Fe(III), Ga(III), and Al(III), is described. Its cation binding affinities for hydrogen ion and for Fe(III), Co(II), Ni(II), Cu(II), Zn(II), Ga(III), and Al(III) ions are described, and the equilibrium data are compared with those of analogous ligands. The binding constants of trivalent metal ions with the ligand do not show a chelate effect relative to the binding to individual bidentate hydroxamic acids.

ISAO YOSHIDA, ICHIRO MURASE, RAMUNAS J. MOTEKAITIS et ARTHUR E. MARTELL. Can. J. Chem. **61**, 2740 (1983).

On décrit la synthèse d'un nouveau ligand bis tridentate multidentate, *N,N′,N″*-tris[(*N*-hydroxycarbamoyl)-2 éthyl]benzène-tricarboxamide-1,3,5 (BAMTPH) conçu pour se lier aux ions métalliques trivalents comme le Fe(III), le Ga(III) et le Al(III). On décrit les affinités de liaison de ce ligand pour les ions hydrogènes et pour les ions Fe(III), Co(II), Ni(II), Cu(II), Zn(II), Ga(III) et Al(III) et on compare les données d'équilibre avec celle de ligands analogues. Les constantes de liaison des ions métalliques trivalents avec le ligand ne montrent aucun effet de chélation par rapport à la liaison avec des acides hydroxamiques qui sont des bidentates individuels.

[Traduit par le journal]

Introduction

A major group of the numerous microbial ligands for the complexation of iron(III) are hydroxamic acids such as the ligands in ferrichromes and the ferrioxamines (1). Ferrichrome in particular has a large polypeptide macrocyclic structure holding three side chains, each containing a hydroxamate group in sterically favorable configuration for formation of a stable macrocyclic complex of iron(III), gallium(III), and other trivalent ions. The ligand described in the present paper is analogous to the natural iron(III) carriers in that it contains three hydroxamic acid groups bound to the 1,3,5-positions of a benzene ring. These donor groups are sterically arranged in positions that allow facile binding to a single metal ion. This paper describes the synthesis of this ligand, *N,N′,N″*-tris-[2-(*N*-hydroxycarbamoyl)ethyl]-1,3,5-benzenetricarboxamide (BAMTPH), **1**, and a potentiometric and spectrophotometric study of its affinity for iron(III) and representative trivalent and divalent metal ions.

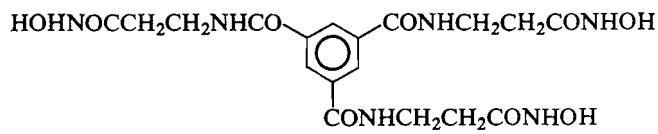

1

Experimental

N,N′,N″-Tris(2-carboxyethyl)-1,3,5-benzenetricarboxamide

An ether solution (200 mL) of 1,3,5-benzenetricarbonyl chloride (27 g, 0.1 mol) was added dropwise at 5–10°C with vigorous stirring to an aqueous solution (250 mL) of β-alanine (36 g, 0.4 mol) and potassium hydroxide (46 g, 0.8 mol). The mixture was stirred further at room temperature for 2 h. The aqueous layer was acidified with 3 *M* sulfuric acid and the resulting precipitate was collected by filtration. Yield 36 g (86%). The sample was recrystallized from boiling water and dried at 60°C under vacuum, mp 257–258°C (decomp). ^{1}H nmr (D_2O + NaOD) δ 2.6 (t, J = 7.5 Hz, 6, CH_2), 3.66 (t, J = 7 Hz, 6, CH_2), 8.25 (s, 3, ArH). Ir (KBr) 1722 (s, COOH), 1640 (s, amide I), 1540 (s, amide II). *Anal.* calcd. for $C_{18}H_{21}N_3O_9$: C 51.06, H 5.01, N 9.93; found: C 50.91, H 5.08, N 9.89.

[1]To whom all correspondence should be addressed.

N,N′,N″-Tris(2-ethoxycarbonylethyl)-1,3,5-benzenetricarboxamide

A suspension of the acid (18 g, 0.043 mol) in absolute ethanol (200 mL) containing 0.50 g of *p*-toluenesulfonic acid was refluxed for 48 h and a clear solution was obtained. Ethanol (100 mL) was removed by distillation, absolute ethanol (100 mL) was added, and the solution was refluxed further for 24 h. The solvent was removed by distillation under reduced pressure to give an oily residue which solidified upon standing. It was treated with ether, filtered, and dried under vacuum. Yield 21 g (96%). The sample was recrystallized from dilute ethanol, mp 110–111°C. Ir (KBr) 1727, 1710 (s, ester C=O), 1670, 1638 (s, amide I), 1522 (s, amide II). *Anal.* calcd. for $C_{24}H_{33}N_3O_9$: C 56.78, H 6.57, N 8.28; found: C 56.24, H 6.49, N 8.17.

N,N′,N″-Tris[2-(N-hydroxycarbamoyl)ethyl]-1,3,5-benzenetricarboxamide

An alkaline solution of hydroxylamine was prepared by mixing hydroxylamine hydrochloride (8.4 g, 0.12 mol) in methanol (50 mL) and potassium hydroxide (11.8 g, 0.20 mol) in methanol (30 mL) at a temperature below 30°C, followed by filtration of the resulting potassium chloride. To the filtrate was added a methanol solution (30 mL) of the ester (10.1 g, 0.02 mol) and the mixture was stirred for 3 days at room temperature. A potassium salt of the hydroxamic acid was obtained as an insoluble precipitate. It was suspended in methanol (150 mL) and an excess of acetic acid was added to give a clear solution. It soon became turbid and a colorless precipitate was obtained after standing 1 h in a refrigerator. The product was collected by filtration and recrystallized from 90% methanol. Yield 5.2 g (55%), mp 139–140°C. Ir (KBr) 1650, 1638 (s, amide I), 1543, 1530 (s, amide II). *Anal.* calcd. for $C_{18}H_{24}N_6O_9$: C 46.14, H 5.17, N 17.94; found: C 46.13, H 5.27, N 17.76.

Apparatus

The equipment employed consisted of a Cary Model 14 vis–uv spectrophotometer, a Corning Model 130 pH meter equipped with extension calomel reference and high pH glass electrodes, a Metrohm 10-mL piston burette, a Haake refrigerated constant temperature bath set at 25.0°C, an all-glass jacketed, stirred, and sealed 50 mL reaction vessel, and a Varian EM 390 NMR spectrophotometer.

Reagents

The ferric salt, $Fe(NO_3)_3 \cdot 9H_2O$, was obtained as reagent grade material from Baker Chemical Co. The gallium employed was the pure metal. Other materials used were: $Al(NO_3)_3 \cdot 9H_2O$ (Baker); $Co(NO_3)_2 \cdot 6H_2O$, $Ni(NO_3)_2 \cdot 6H_2O$, $Zn(NO_3)_2 \cdot 6H_2O$ (MCB); KOH, 0.100 *M*, CO_2-free Dilut-It^R (Baker); and doubly distilled water.

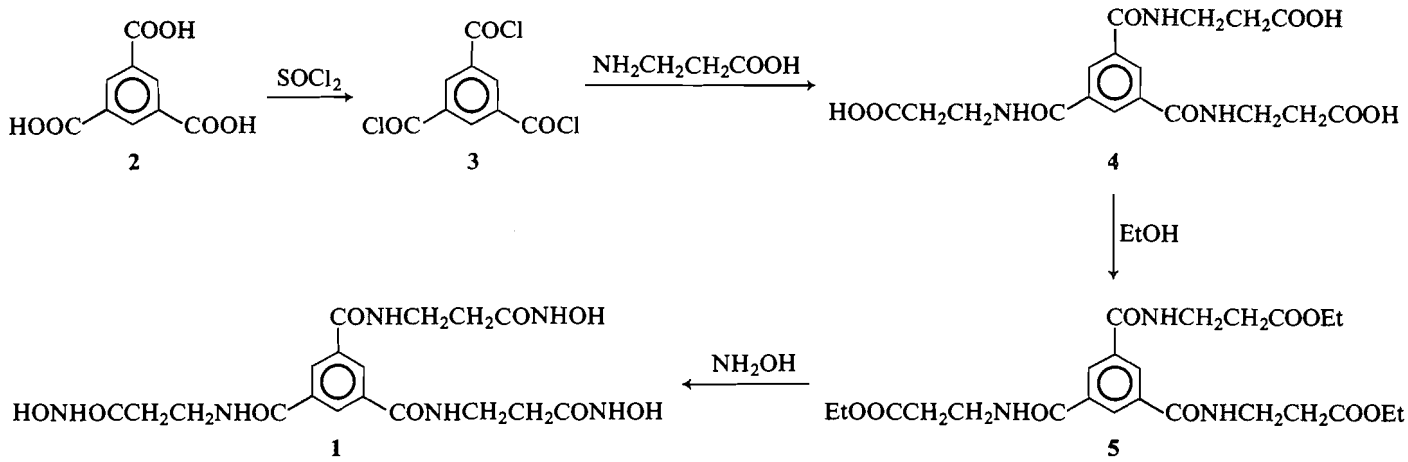

Experimental solutions

Stock solutions of metal salts were prepared by dissolving the appropriate compound and determining the metal ion concentrations by EDTA titration procedures found in Welcher (2) or Schwarzenbach (3). Standard gallium chloride solution was prepared by dissolving a weighed amount of gallium metal in 1 mL of concentrated HCl with heating followed by quantitative dilution. Excess mineral acid in the iron(III) solutions was determined potentiometrically, taking into account the hydrolysis constant for the ferric ion (4). For the gallium solution, Gran's method (5) was employed.

Experimental procedures

Potentiometric equilibrium measurements were made with a Corning research pH meter calibrated to read $-\log [H^+]$ directly by using solutions containing standard 0.01–0.0001 *M* HCl with KNO_3 added to maintain $\mu = 0.100$ *M* at 25.0°C. The basic region was standardized in a similar manner with standard KOH solution. The calibration was checked after each experiment. For each metal ion – ligand system, as well as for the ligand alone, the pH profile was determined from pH 2 to pH 11. The detailed procedure has been described in previous publications (6, 7). Care was taken to exclude carbon dioxide and other contaminants and to obtain the best quality data possible.

Computations

Protonation constants were computed with the FORTRAN program PKAS (8) while the stability constants were in general computed using the FORTRAN program BEST (9). The Fe(III) binding constant was computed from spectrophotometric data taken over a moderately to strongly acid pH range by treating ϵ_{FeL} as an adjustable parameter to minimize the discrepancies between the constants computed as the ratio of iron/ligand was varied. The computers employed were a PDP 11/44 and a VAX 11/780.

Results

Synthesis and characterization

The new ligand **1** was synthesized from commercially available benzene-1,3,5-tricarboxylic acid **2**. This compound was converted to the acid chloride **3**, which upon treatment with β-alanine was converted to **4**. **4** was then converted to the ester **5** which on treatment with hydroxylamine gave the crystalline ligand **1**. With space-filling CPK molecular models it was shown that the three hydroxamic acid groups may simultaneously coordinate to a central metal ion. This property is made possible by the length of the chains and their inherent flexibility. The purity of the compound was determined by elemental analysis and nmr spectra as shown in the Experimental section and by potentiometric titration.

Proton – metal ion – ligand interactions

Protonation reactions. The trihydroxamic acid, **1**, is an

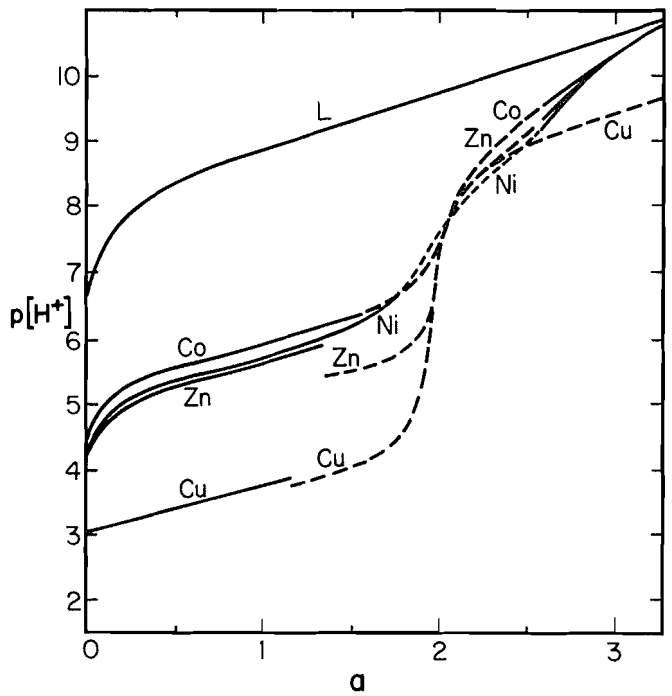

FIG. 1. Potentiometric equilibrium curves for BAMTPH, H_3L, in terms of $-\log [H^+]$ as a function of added base (a = mol KOH/mol ligand) for ligand alone, and for 1:1 molar ratios of ligand to metal ion. In all cases $T_L = 1.058 \times 10^{-3}$ *M*, $T_M = 1.028 \times 10^{-3}$ *M*, $t = 25.0$°C, $\mu = 0.100$ *M* KNO_3.

H_3L-type compound, implying that it has three dissociable hydrogen ions per molecule. The potentiometric equilibrium profile of pH vs. a (a = mol of KOH added/mol ligand present), shown as the upper curve in Fig. 1, has a long high pH buffer zone starting at $a = 0$, and with no break at $a = 3$ because of the high pH of the system. The successive protonation constants calculated for these equilibria are 10.04, 9.33, and 8.48 log units respectively. These values were rounded to two decimals, but the computer-refined constants provided an excellent recalculation of the entire titration curve with a value of $\sigma = 0.0012$ log $[H^+]$. A discussion of the nature and significance of σ values has been published (8). The differences (0.71, 0.85) between the successive protonation constants indicate essentially statistical behavior with negligible intergroup interaction in the absence of metal ions. These values also compare well with acetohydroxamic acid which has

TABLE 1. Proton – metal ion – ligand interactions at $\mu = 0.100\ M\ KNO_3$, $t = 25.0°C$ ligand H_3L)

Quotient, Q	log Q^f							
	H[e]	Cu^{2+}	Ni^{2+}	Co^{2+}	Zn^{2+}	Fe^{3+}	Ga^{3+}	Al^{3+}
$\frac{[HL]}{[H][L]}$	10.04	—	—	—	—	—	—	—
$\frac{[H_2L]}{[H][HL]}$	9.33	—	—	—	—	—	—	—
$\frac{[H_3L]}{[H][H_2L]}$	8.48	—	—	—	—	—	—	—
$\frac{[ML]}{[M][L]}$	—	[a]	10.55	9.95	10.40	26.32[c,g,h]	[c]	21.85
$\frac{[MHL]}{[ML][H]}$	—	[d]	8.81	8.95	9.17	[b]	[b]	[b]
$\frac{[MH_2L]}{[MHL][H]}$	—	3.48	5.06	5.20	4.77	[b]	[b]	[b]

[a] $M(OH)_2$ separated from solution.
[b] Species absent.
[c] ML separated from solution.
[d] $\log \beta_{MHL} = 23.48$.
[e] σ (log units) = 0.001 for recomputation of curve.
[f] $\sigma \leqq 0.01$ (log units) for recomputation of curve.
[g] Determined spectrophotometrically.
[h] $\sigma = 0.08$.

a protonation constant of 9.36 (10). This comparison indicates the absence of inductive interactions through the connecting amide groups because of the insulating methylene groups on each side chain.

Divalent metal ion interactions. The potentiometric behavior of the divalent ions investigated was found to be similar near neutral pH, but markedly different for Cu(II) at pH ~7–10. As shown in Fig. 1, each divalent ion produces a two-proton displacement buffer region, part of which is obscured by precipitation. In the cases of Co(II), Ni(II), Cu(II), and Zn(II) these precipitates are the neutral MHL species, and form at a values of 1.5, 1.8, 1.1, and 1.5 respectively. Accurate stability constant computations were found to be possible in each soluble region and the calculated results are listed in Table 1. The formation equilibria at low pH were therefore found to be:

$$[1]\quad M^{2+} + H_3L \rightleftharpoons MH_2L^+ + H^+$$

$$[2]\quad MH_2L^+ \rightleftharpoons MHL^0 + H^+$$

Beyond $a = 2$ the highly insoluble MHL^0 species dissolved in proportion to the amount of base added, and with the exception of Cu(II), each system cleared up when the neutralization value reached $a \cong 2.5$ to give a completely clear solution. Equation [3] expresses the reaction that occurs in this buffer region.

$$[3]\quad MHL \rightleftharpoons ML^- + H^+$$

The corresponding chelate protonation constants are listed in Table 1. It should be borne in mind that they were computed at pH values near those at which precipitation occurred. The high pH curve at $a > 2$ for Cu(II) indicates that $Cu(OH)_2$ forms and that the ligand is not able to keep divalent copper ion in solution at these pH values, perhaps because the ligand is not able to conform sterically to the well-known square planar coordination tendency of the metal ion.

Trivalent ions. When Fe(III) and H_3L solutions were mixed

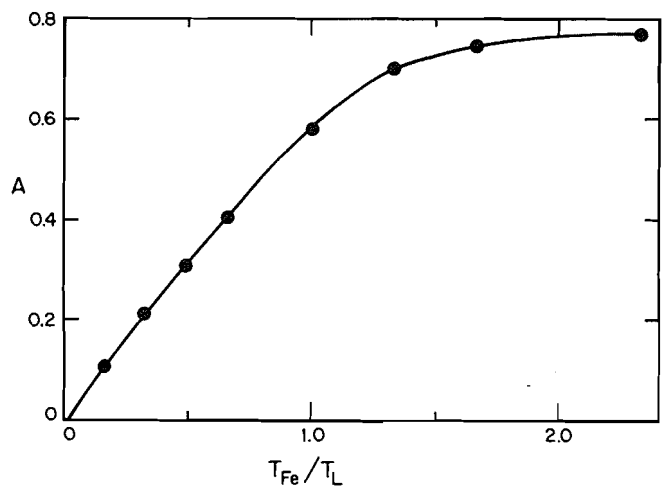

FIG. 2. Absorbance vs. molar ratio of total iron(III)/total ligand measured at 463 nm. $T_L = 3.00 \times 10^{-4}\ M$; $T_{Fe} = 5.00 \times 10^{-5}$ to $7.00 \times 10^{-4}\ M$, $t = 25.0°C$, $\mu = 0.100\ M\ KNO_3$, $-\log [H^+] = 1.80$.

a red precipitate formed immediately from a red solution. Addition of base revealed a strong acid behavior with a break from the acid to the alkaline region at $a = 3$. The total conversion to the products indicated in reaction [4] apparently took place

$$[4]\quad Fe^{3+} + H_3L \rightleftharpoons FeL^0\downarrow + 3H^+$$

at the beginning of the potentiometric determination. In the presence of excess acid, however, achieved by lowering the pH to 1.80 and dilution of the reaction mixture, it was found to be possible to compute the equilibrium constant corresponding to reaction [4] from spectrophotometric data. Figure 2 shows the variation of absorbance with the ratio of a T_{Fe}/T_{H_3L} where T represents the total analytical concentrations of the species involved. The non-limiting slope and the curvature of the plot

indicate the presence of an equilibrium situation. From the data in Fig. 2, the value of log K_{ML} was then computed to be 26.32 ± 0.08 (ϵ_{FeL} = 3324 at 463 nm).

The titration curve of the 1:1 Ga(III)/H_3L solution also provided a strong acid titration, indicating very strong metal ion coordination. After the break at a = 3, there is an indication that Ga(III) may be converted to $Ga(OH)_4^-$, but this matter was not pursued further since equilibrium analysis in the presence of solid phases is difficult. Since Ga(III) is colorless, the stability constant could not be obtained from spectrophotometric measurements.

The equilibrium measurements made on aluminum(III) resulted in the formation of a white precipitate (probably ML) at a = 0.5, beyond which the measurement of useful potentiometric data was not possible. However, an approximate formation constant was calculated directly and was found to be log K_{ML} = 21.85 ± 0.01.

Discussion

The results demonstrate that it is possible to utilize basic principles for the design and synthesis of chelating agents possessing desirable properties. It is disappointing in this particular case, however, that the neutral species CoHL, NiHL, ZnHL, CuHL, and GaL, FeL, and AlL are insoluble. On the other hand, it is obvious now that the use of appropriate solubilizing groups would convert the ligand and its chelates to more soluble compounds without the loss of metal ion affinity, and that such compounds should be the subject for further investigations.

Both internal comparisons and comparisons with published data reveal interesting structural information for the probable arrangements of coordination linkages around each metal ion.

The most obvious difference between the metal chelates investigated is the approximately ten orders of magnitude between the stabilities of the di- and trivalent metal chelates. Also, the absence of protonated complexes of the Fe(III), Ga(III), and Al(III) chelates indicates the participation of all three hydroxamate groups in complex formation even at very low pH when these trivalent metal ions combine with the ligand.

The fact that the protonation constant of the ML species for the Ni(II), Co(II), and Zn(II) complexes is 8.8−9.2 strongly supports the conclusion that in the divalent systems, only two arms of the ligand are utilized for coordination while the third probably is extended away from the metal center, and exhibits little or no apparent interaction with the metal ion. In dramatic contrast, the log $K^{H}_{MH_2L}$ values for these metals range from 5.2−4.8 (values much smaller than ~9) indicating a strong tendency for the participation of two hydroxamic acid moieties in complex formation. Thus divalent metal chelates can be represented schematically by the general formula **7** while the trivalent metal chelates are given by **6**.

The stability constant for the formation of a 1:1 chelate between Fe^{3+} and acetohydroxamic acid is $10^{11.42}$ (12). Comparison of this value with the results of this work (26.32) indicates that more than two hydroxamates are bound in the complex formed from the trishydroxamate ligand. In addition, when one compares the overall reactions of 3-acetohydroxamates with Fe^{3+} (log β_3 = 28.3) (12), it is seen that the stability of the latter is just ~2 log units higher than the iron binding constant found in the present work. This comparison shows a substantial lack of any additional stabilization resulting from the fact that the hydroxamate groups are bound to the benzene ring. In fact, it was pointed out by Schwarzenbach (13) that the Fe^{3+} binding constant to desferrichrome (log K_{ML} = 29.1) does not indicate the presence of a chelate effect, or of stabilization through the attachment of the hydroxamate groups to a macrocycle.

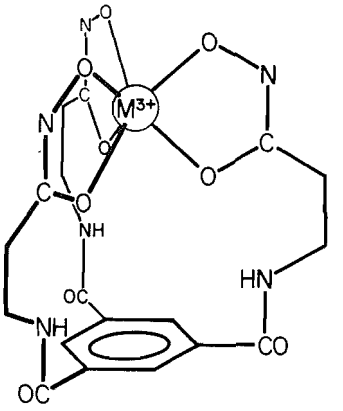

6, BAMTPH complex of a trivalent metal ion (formal charges and some H atoms omitted for clarity)

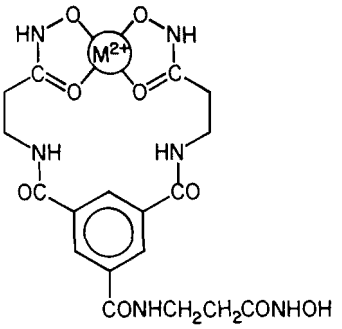

7, BAMTPH complex of a divalent metal ion (formal charges and some H atoms omitted for clarity)

Similar comparisons can be made for tris-acetohydroxamate of Al^{3+} (log β_3 = 21.47) (12) with the value found for K_{ML} in this work (log β = 21.85). This result points to the same conclusion concerning the lack of a chelate effect as was reached in the case of Fe(III), discussed above. A similar conclusion had been reached for a "rhodotorulate" determination of the Fe(III) binding constant (14). Rhodotorulate is a natural bis-hydroxamic acid of bacterial origin.

The log K_{ML} values for the Ni(II), Co(II), and Zn(II) chelates of BAMTPH are only 1.0 log unit larger than that of the bis-acetohydroxamates (12) of these metals. Thus the divalent ions also indicate negligible additional stabilization resulting from attachment of the bidentate moieties of BAMTPH to a benzene ring. The lack of appreciable chelate effects in these systems, previously pointed out by Schwarzenbach (13) and Raymond (14), is reaffirmed by the results of the present paper. This result is no doubt due to the long bridges between the bidentate pairs in the sexadentate and quadridentate ligands, which therefore function essentially independently, and result in the formation of very large chelate rings.

Acknowledgement

This research was supported by a grant No. CA22464 from the National Cancer Institute.

1. J. B. NEILANDS. Struct. Bonding, **1**, 59 (1966).
2. F. J. WELCHER and F. JOHNSON. The analytical uses of ethylene-

diaminetetraacetic acid. Van Nostrand, Princeton, NJ. 1958.
3. G. SCHWARZENBACH. Complexometric titrations. Interscience, New York. 1957.
4. A. E. MARTELL and R. M. SMITH. Critical stability constants. Vol. 4. Plenum, New York. 1976.
5. F. J. C. ROSSOTTI and H. ROSSOTTI. J. Chem. Ed. **42**, 375 (1965).
6. R. J. MOTEKAITIS and A. E. MARTELL. Inorg. Chem. **19**, 1646 (1980).
7. C. Y. NG, R. J. MOTEKAITIS, and A. E. MARTELL. Inorg. Chem. **18**, 2982 (1979).
8. R. J. MOTEKAITIS and A. E. MARTELL. Can. J. Chem. **60**, 168 (1982).
9. R. J. MOTEKAITIS and A. E. MARTELL. Can. J. Chem. **60**, 2403 (1982).
10. A. E. MARTELL and R. M. SMITH. Critical stability constants. Vol. 5. Plenum, New York. 1982.
11. A. E. MARTELL. Development of iron chelators for clinical use. Elsevier North Holland, New York. 1981. pp. 67–104.
12. A. E. MARTELL and R. M. SMITH. Critical stability constants. Vol. 3. Plenum, New York. 1975.
13. G. SCHWARZENBACH and K. SCHWARZENBACH. Helv. Chim. Acta, **46**, 1390 (1963).
14. C. J. CARRANO, S. R. COOPER, and K. N. RAYMOND. J. Am. Chem. Soc. **101**, 599 (1979).

Evans holes in the infrared spectra of some transition metal formate dihydrates

G. D. TEWARI, D. P. KHANDELWAL, AND H. D. BIST
Department of Physics, Indian Institute of Technology, Kanpur, 208016, India

AND

V. P. TAYAL
Department of Physics, H. B. Technological Institute, Kanpur, 208002, India

Received March 22, 1983

G. D. TEWARI, D. P. KHANDELWAL, H. D. BIST, and V. P. TAYAL. Can. J. Chem. **61**, 2745 (1983).

Evans holes have been identified in OH(OD) stretching regions in the ir spectra of $M(HCOO)_2.2X_2O$ (M = Mn, Co, Ni and Zn; X = H, D) and attributed to Fermi interaction between the stretching mode and an overtone of the bending mode of water.

G. D. TEWARI, D. P. KHANDELWAL, H. D. BIST et V. P. TAYAL. Can. J. Chem. **61**, 2745 (1983).

On a identifié les trous d'Evans dans les régions d'élongation du OH(OD) des spectres IR du $M(HCOO)_2.2X_2O$ (M = Mn, Co, Ni et Zn; X = H, D) et on les a attribué à l'interactions de Fermi entre le mode d'élongation et une harmonique de mode de déformation de l'eau.

[Traduit par le journal]

Can. J. Chem. Downloaded from www.nrcresearchpress.com by 210.87.254.40 on 09/06/12
For personal use only.

Evans and Wright (1) have shown that a sharp and weak absorption band X, falling within the energy range of a strong and broad band Y, may create a transmission window (hole) in its position due to Fermi interactions. Such holes have been observed in the ir spectra of crystal hydrates by Othen *et al.* (2) and are important in interpreting the shape of the OH stretching profiles (3). In the present paper the presence of Evans holes in the OH stretching region of water is shown in eight samples of formates $M(HCOO)_2.2X_2O$ (M = Mn, Co, Ni and Zn; X = H, D).

The methods of preparation of samples and recording of ir and Raman spectra have been described elsewhere (4). The accuracy in the measurement of band positions is ± 4 cm^{-1}, while the estimated half-widths and relative intensities are dependable within 20% for the OH stretching region.

The isomorphous compounds $M(HCOO)_2.2H_2O$ belong to the monoclinic space group C_{2h}^5 ($Z = 4$) with two inequivalent C_1 sites for each of the species M^{2+}, $HCOO^-$, and H_2O (5). The structural data (6) of $Zn(HCOO)_2.2H_2O$, a representative of the series, indicate that the hydrogen bonding effects are stronger in H_2O(I) than in H_2O(II).

The ir spectra of the samples in the OH and OD stretching regions at 300 K and 93 K are shown in Fig. 1(*A*).The corresponding Raman spectra at 300 K are shown in Fig. 2. The observed band positions along with their relative intensities and half-widths are given in Table 1.

In general the ν_1 mode is stronger than ν_3 mode in the Raman spectra, therefore two very weak bands (e.g. at 3420 and 3120 cm^{-1} in Mn salt) and two very strong bands (e.g. at 3360 and 3268 cm^{-1} in the same salt) in Raman spectra (cf. Table 1) are assigned to the ν_3 and ν_1 modes of water, respectively. A fifth band (at 3218 cm^{-1} in Mn salt) is assigned to the combination mode of different factor group components of ν_2 modes of water ($\nu_2^u + \nu_2^g$). The bands pertaining to H_2O(I) and H_2O(II) are distinguished considering the relative strengths of hydrogen bonding in the two types of water molecules. The lower and higher set of ν_3 and ν_1 bands are obviously assignable to H_2O(I) and H_2O(II), respectively (6).

The ν_2 bands of water are identified by their shifts on deuteration, and are assigned to H_2O(I) and H_2O(II) such that the $\nu_2^u + \nu_2^g$ falls close to the corresponding ν_1 mode of water. Interpretation of the low temperature spectra justifies these choices.

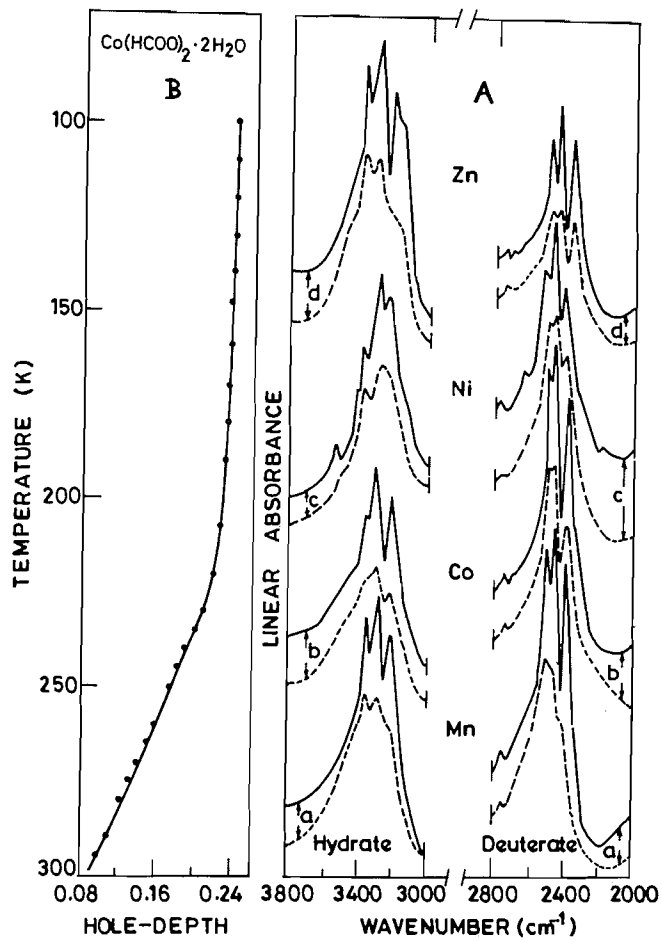

FIG. 1.(*A*) IR spectra of the hydrated and the deuterated formate dihydrates of (*a*) Mn, (*b*) Co, (*c*) Ni, and (*d*) Zn, recorded in linear absorbance mode. The continuous and broken curves in each case represent the spectra at 93 K and 300 K respectively. (*B*) Temperature dependence of hole-depth in $Co(HCOO)_2.2H_2O$. The depth is given in absorbance unit.

In going to 93 K a sharp dip appears between the ν_1 and $\nu_2^u + \nu_2^g$ modes of H_2O(I). This feature is common to all the compounds of the two isotopic series studied, and gets satisfactory explanation on the basis of Evans holes. In the deu-

Can. J. Chem. Downloaded from www.nrcresearchpress.com by 210.87.254.40 on 09/06/12
For personal use only.

TABLE 1. Peak positions of the stretching modes of water in $M(HCOO)_2.2X_2O$ (M = Mn, Co, Ni, Zn; X = H, D)[a]

	Hydrate			Deuterate			
	Infrared		Raman	Infrared		Raman	
Compounds	300 K	93 K	300 K	300 K	93 K	300 K	Assignments
Mn	3430(0.24×200)	3424(0.30×180)	3420 w	2600(0.20×150)	2590(0.25×120)		ν_3H_2O(II)
	3356(0.30×100)	3350(0.40×60)	3360(3×120)	2500(0.25×60)	2496(0.35×50)	2494(3×120)	ν_1H_2O(II)
		3300(0.20×50)				—	$2\nu_2H_2O$(II)
	3280(0.28×90)	3285(0.45×60)	3268(3×140)	2455(0.20×90)	2448(0.40×60)	2458(3×140)	ν_1H_2O(I)
	3220(0.10×60)	3210(0.15×40)	3218(2×100)	2395(0.10×70)	2382(0.22×50)	2400(2×100)	$2\nu_2H_2I$(I)
	3130(0.25×200)	3124(0.30×150)	3120 w	2315 sh	2300 sh	—	ν_3H_2O(I)
Co[b]	3430(0.10×200)	3420(0.14×180)	3420 w	2600(0.10×150)	2580(0.15×130)	—	ν_3H_2O(II)
	3355(0.15×100)	3350(0.20×60)	3356(2×100)	2485(0.20×60)	2475(0.30×40)	—	ν_1H_2O(II)
	3300(0.21×80)	3290(0.30×60)	3292(2×110)	2460(0.30×80)	2450(0.50×60)	—	ν_1H_2O(I)
	3220(0.18×80)	3200(0.20×50)	3212(1×80)	2385(0.25×50)	2370(0.35×40)	—	$2\nu_2H_2O$(I)
	3140(0.10×150)	3120(0.20×130)		2320 sh	2310(0.15×120)	—	ν_3H_2O(I)
Ni	3530(0.10×100)	3530(0.12×40)					comb.
		3395(0.15×40)	3420 sh	2620(0.10×140)	2620(0.13×110)		ν_3H_2O(II)
	3360(0.25×100)	3358(0.35×60)	3360(3×120)	2500(0.21×80)	2500(0.30×70)	2494(4×100)	ν_1H_2O(II)
		3310(0.17×60)					$2\nu_2H_2O$(II)
	3270(0.35×120)	3268(0.45×100)	3250(4×150)	2460(0.30×80)	2450(0.50×60)	2448(5×100)	ν_1H_2O(I)
	3225(0.05×100)	3230(0.10×70)	3200 wsh	2392(0.24×40)	2390(0.32×30)	2385(2×80)	$2\nu_2H_2O$(I)
	3140(0.05×150)	3120(0.10×100)	3110 wsh	2310 sh	2305 sh	—	ν_3H_2O(I)
Zn	3430(0.30×150)	3420(0.33×100)	3415 w	2600(0.10×100)	2592(0.20×60)	—	ν_3H_2O(II)
	3360(0.43×100)	3350(0.60×50)	3355(3×80)	2500(0.28×60)	2498(0.37×40)	2494(5×60)	ν_1H_2O(II)
		3300(0.37×70)					$2\nu_2H_2O$(II)
	3280(0.40×80)	3264(0.70×60)	3272(2×100)	2450(0.42×50)	2445(0.47×40)	2443(6×60)	ν_1H_2O(I)
		3185(0.47×40)		2375(0.35×40)	2370(0.40×30)	2376(7×40)	$2\nu_2H_2O$(I)
	3200(0.30×180)		3215(2×100)				
		3140(0.5×90)		2310(0.15×120)	2300(0.20×80)		ν_3H_2O(I)

[a]The data in parentheses are relative intensities and half-widths.
[b]Raman bands could not be accurately identified in the Raman spectra due to high fluorescence background in the deuterated salt of Co.

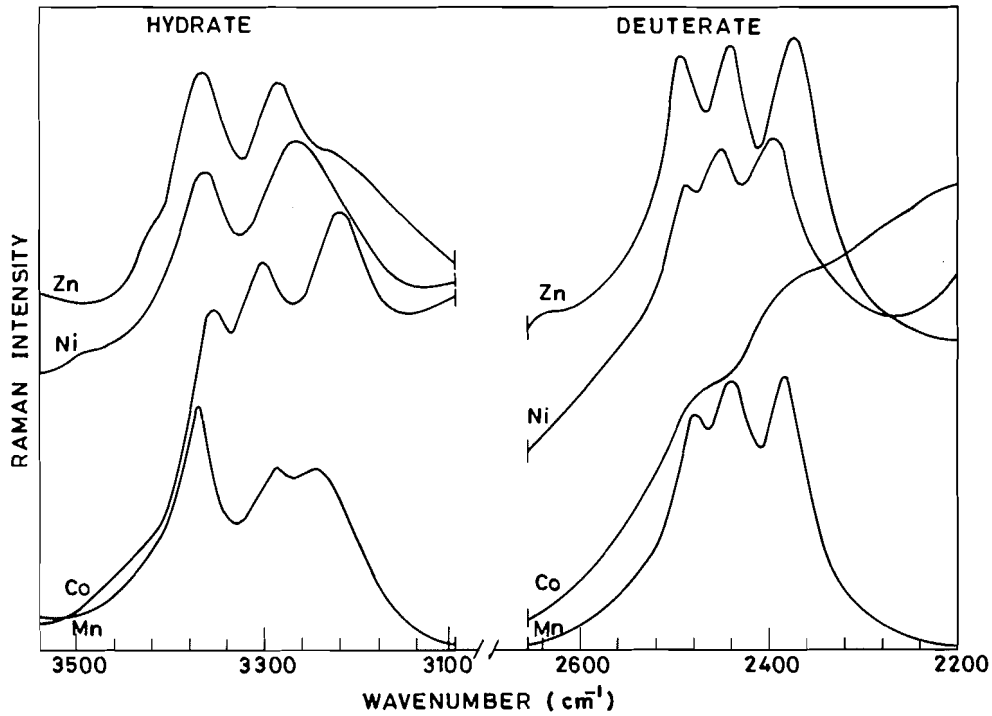

FIG. 2. Raman spectra of the hydrated and the deuterated formate dihydrates of Mn, Co, Ni, and Zn and 300 K (the Co salt shows background fluorescence on 514.5 nm excitation).

TABLE 2. The positions (cm^{-1}) of Evans holes (dips) (ν_h) and bending modes (peaks) (ν_2) in the ir spectra and their shifts in going from 300 K to 93 K ($\Delta\nu_h$ and $\Delta\nu_2$ respectively) in $M(HCOO)_2.2X_2O$ (M = Mn, Co, Ni, and Zn; X = H and D)

	Mn		Co		Ni		Zn		
T(K)	H_2O	D_2O	H_2O	D_2O	H_2O	D_2O	H_2O	D_2O	Description
300	—	2404	3240	2406	—	2410	—	2400	ν_h
93	3244	2411	3248	2413	3250	2418	3222	2408	ν_h
	—	+7	+8	+7	—	+8	—	+8	$\Delta\nu_h$
300	1622	1210	1628	1214	1634	1215	1620	1205	ν_2
93	1630	1213	1632	1216	1640	1220	1625	1208	ν_2
	+8	+3	+4	+2	+6	+5	+5	+3	$\Delta\nu_2$

terated salts the hole appears weakly even at 300 K, and gets considerably enhanced in going to 93 K. To study the temperature dependence of the depth of the holes, Co salt was chosen which shows the hole at 300 K in the ir spectrum of its hydrate (cf. Fig. 1(*B*)). The hole-depth increases linearly till the temperature falls to 220 K and thereafter becomes almost constant. In contrast, the hydrated Ni salt shows a weak hole even at 93 K (cf. Fig. 1*A*(*c*)).

The positions of the dip of Evans holes and ν_2 peaks are given in Table 2 along with their shifts ($\Delta\nu_h$ and $\Delta\nu_2$ respectively) in going from 300 K to 93 K. It is observed that the effect of the temperature on the peak of the bending fundamental (shifts towards higher frequencies) broadly agrees in direction and magnitude with the effect of the temperature on the position of the holes (the shifts $\Delta\nu_h$ are approximately twice of $\Delta\nu_2$ within the experimental errors).

The ir-active components of the ν_1 mode of H_2O(I) belong to A_u, B_u species. Suitable combinations of ν_2 mode such as $\nu_2^u + \nu_2^g$ also belong to A_u, B_u species and may thus show strong Fermi interaction with ν_1. Assuming such interactions, the unperturbed frequencies of the interacting bands are obtained from the relation (1, 3):

$$[1] \quad \frac{I_1}{I_2} = \frac{\Delta - \delta}{\Delta + \delta}$$

where I_1 and I_2 are the observed intensities of the weak and the strong bands respectively, Δ is their perturbed (observed) separation, and δ is the unperturbed separation. In the Zn salt the unperturbed position of $\nu_2^u + \nu_2^g$ comes to 3224 cm^{-1}, and we note that this is in close agreement with the position of the hole (3222 cm^{-1}). Such close agreement is an essential characteristic of Evans holes. The observed and the calculated data on Evans holes are given in Table 3, which shows that such agreement holds in all the eight samples studied.

Since the ν_2^g mode expected in Raman spectrum does not show up in our spectra, we use $2\nu_2^u$ as a close approximation to the expected $\nu_2^u + \nu_2^g$, and get 3250 cm^{-1} for H_2O(I) as compared to 3224 cm^{-1} deduced from Fermi interaction formula. Anharmonicity of this order (26 cm^{-1}) is reasonable. Considerable enhancement of the interaction on lowering of temperature is because the downward shift of ν_1 and upward shift of $\nu_2^u + \nu_2^g$ brings them closer at 93 K than at 300 K.

The strength of the interaction between the two levels can be determined by the magnitude of the Fermi-interaction energy,

Can. J. Chem. Downloaded from www.nrcresearchpress.com by 210.87.254.40 on 09/06/12
For personal use only.

TABLE 3. Infrared data on Evans holes[a] in $M(HCOO)_2.2X_2O$ (M = Mn, Co, Ni and Zn; X = H and D) at 93 K

Details of data	Mn		Co		Ni		Zn	
	H_2O	D_2O	H_2O	D_2O	H_2O	D_2O	H_2O	D_2O
ν_1 (observed)	3285	2448	3290	2450	3268	2450	3264	2445
$\nu_2^u + \nu_2^g$ (observed)	3210	2382	3200	2370	3230	2390	3185	2370
ν_{hole} (observed)	3244	2411	3248	2413	3250	2418	3222	2408
$\nu_2^u + \nu_2^g$ (unperturbed)[b]	3245	2415	3247	2414	3249	2419	3224	2407
ν_1 (unperturbed)[b]	3279	2427	3267	2435	3264	2435	3254	2423
$\nu_2^u + \nu_2^g$ (calculated)[c]	3260	2424	3264	2428	3280	2440	3250	2416
W_{12}	33	32	43	39	17	28	36	36

[a]All the data are in cm^{-1}.
[b]Calculated from the Fermi interaction formula.
[c]Double of the observed ν_2 frequency.

W_{12}, given by (3)

$$[2] \quad W_{12} = \frac{(\Delta^2 - \delta^2)^{1/2}}{2}$$

where Δ and δ are the perturbed and unperturbed separations as in eq. [1]. The calculated values of W_{12} are also given in Table 3. The lower value of W_{12} in the hydrated Ni salt as compared to those in the other salts explains the observance of a relatively weaker hole in this salt; though the calculated values of W_{12} correspond to the case of weak Fermi-resonance interactions in all these compounds (3).

Acknowledgement

Thanks are due to Department of Science and Technology (India) for financial assistance.

1. J. C. EVANS and N. WRIGHT. Spectrochim. Acta, **16**, 353 (1960); **16**, 994 (1960); **18**, 507 (1962).
2. D. A. OTHEN, O. KNOP, and M. FALK. Can. J. Chem. **53**, 3837 (1975).
3. J. R. SCHERER. The vibrational spectroscopy of water, advances in infrared and Raman spectroscopy. Vol. V. *Edited by* R. J. H. Clark and R. E. Hester. Heyden, London. 1978. p. 149.
4. G. D. TEWARI, V. P. TAYAL, D. P. KHANDELWAL, and H. D. BIST. Appl. Spectrosc. **36**, 441 (1982).
5. G. WEBER. Acta Crystallogr. B**36**, 3107 (1980).
6. N. BURGER and H. FUESS. Z. Kristallgr. **145**, 346 (1977).

Can. J. Chem. Downloaded from www.nrcresearchpress.com by 210.87.254.40 on 09/06/12
For personal use only.

Studies of the dihedral angle of a crowded diselenide by X-ray crystallography and ultraviolet spectroscopy

THOMAS G. BACK[1] AND PENELOPE W. CODDING
Department of Chemistry, University of Calgary, Calgary, Alta., Canada T2N 1N4

Received April 25, 1983

THOMAS G. BACK and PENELOPE W. CODDING. Can. J. Chem. **61**, 2749 (1983).

Bis(di-*tert*-butylmethyl) diselenide (**4**) is the first example of a diselenide with an abnormal obtuse dihedral angle resulting from steric crowding. Its value was determined to be 112.1(3)° by X-ray crystallography, as compared with typical dihedral angles of 74–87° for other diselenides. The uv spectrum of **4** supports a similar conformation in solution.

THOMAS G. BACK et PENELOPE W. CODDING. Can. J. Chem. **61**, 2749 (1983).

Le diséléniure **4** est le premier exemple d'un tel composé qui possède un angle dièdre abnormalment étendu à cause de la congestion stérique. Sa valeur de 112.1(3)° était determinée par la crystallographie à rayons X. Par comparaison, les diséléniures typiques ont les angles dièdres entre 74° et 87°. Le spectre uv de **4** est en accord avec une conformation similaire en solution.

Can. J. Chem. Downloaded from www.nrcresearchpress.com by 210.87.254.5 on 09/06/12
For personal use only.

The crystal structures of a considerable number of organoselenium compounds have been determined (1). The range of observed values for parameters such as bond angles and bond lengths is well defined for many selenium-containing functionalities and often shows relatively little variation between members of that class. In the case of diselenides **1** (2–6), the C—Se bond lengths typically fall within the range of 1.91–1.97 Å, while the diselenide linkage (Se—Se) has values of 2.285–2.33 Å. These compounds show a consistent preference for conformations where the dihedral angle (C—Se—Se/Se—Se—C) (Fig. 1) is acute and lies within the range of 74°–87°, except when constrained by the imposition of a cyclic structure. Thus, the cyclic diselenide **2** displays a dihedral angle of only 56° (7).

The effects of very bulky substituents on the conformations of diselenides have not been investigated by crystallographic methods. To our knowledge, even the most hindered diselenide with a known crystal structure, bis(diphenylmethyl) diselenide (**3**), exhibits a normal, acute dihedral angle of 82° (2). More recently, Barton and co-workers (8) reported the preparation of bis(di-*tert*-butylmethyl) diselenide (**4**), a stable, crystalline substance. An examination of a model of this compound indicated that steric interactions might be severe enough to result in significant departure from the usual preferred diselenide geometry. Steric congestion could be relieved either through an increase in the dihedral angle or by lengthening of the bonds in the C—Se—Se—C moiety. It is also interesting to note that the analogous triselenide **5**, whose crystal structure has been reported (9), displays normal C—Se and Se—Se bond lengths and moderate extension of the two C—Se—Se/Se—Se—Se dihedral angles to 100.6° and 86.9°. It is evident, however, that any steric effects resulting from the interaction of the bulky terminal substituents are greatly reduced in the triselenide by

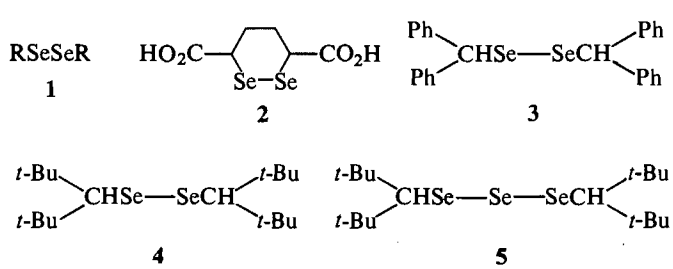

[1]Author to whom correspondence should be addressed.

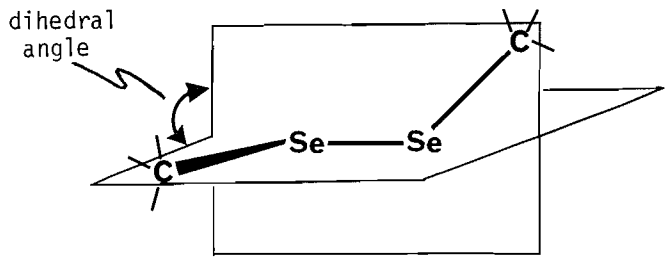

FIG. 1. Conformation of a typical diselenide.

the interposition of the third contiguous selenium atom. To ascertain the extent of such effects in diselenide **4**, we undertook its X-ray crystallographic structure determination. We now report the first example of a diselenide with an obtuse dihedral angle.

Since molecular conformations may differ in the solid state and in solution, we also endeavoured to confirm that diselenide **4** has an abnormal dihedral angle in solution. Compression of the dihedral angle from the preferred value of 74–87° raises the energy of the ground state of a diselenide but has little effect on the excited state (10). Thus, cyclic diselenides such as **2** exhibit strong bathochromic shifts as a result of the lowered excitation energy (11). A similar phenomenon might be expected in the case of a diselenide in which destabilization of the ground state results from the enlargement rather than the compression of the dihedral angle, although such an effect has not yet been documented. We believe that diselenide **4** constitutes the first such example, as it displays a marked bathochromic shift compared to other, less crowded acyclic diselenides.

Experimental

Bis(di-*tert*-butylmethyl) diselenide (**4**) was prepared by the method of Barton and co-workers (8) and was crystallized from hexane–methanol by slow evaporation of the solvent at room temperature. The uv spectrum was recorded on a Varian–Cary 219 Spectrometer in 95% ethanol solution and had λ_{max} = 324 nm (ϵ = 310).

Crystal structure analysis

A yellow plate-like crystal was used for the data collection on an Enraf Nonius CAD4F diffractometer. The crystal data are in Table 1. The procedures for the alignment, space group determination, and intensity data measurements were as described previously (12). Systematic absences of (hkl), $h + k = 2n + 1$; ($h0l$), $l = 2n + 1$; and the symmetry of the diffracted intensities identified the space group as $C2/c$. The intensities were converted to structure factors by the appli-

Can. J. Chem. Downloaded from www.nrcresearchpress.com by 210.87.254.5 on 09/06/12
For personal use only.

TABLE 1. Crystal data for bis(di-*tert*-butylmethyl) diselenide

Formula	$C_{18}H_{38}Se_2$
FW	412.4
Space group	$C2/c$
a (Å)	24.795(4)
b (Å)	7.7324(5)
c (Å)	22.207(4)
β (°)	98.546(8)
V (Å^3)	4210(1)
Z	8
ρ_c (g cm^{-3})	1.30
Crystal dimensions (mm)	0.25 × 0.10 × 0.25
Radiation	CuKα (1.54178 Å) Ni filter
θ_{max}(°)	50
Scan range	$\Delta\omega = 1.54\ (0.52 + 0.14 \tan\theta)$
Unique reflections	2378
No. included in refinement	1800
$R = (\Sigma\|\|F_o\| - \|F_c\|\|/\Sigma\|F_o\|)$	0.044
R (for excluded reflections)	0.21
$R_w = [\Sigma w(\|F_o\| - \|F_c\|)^2/\Sigma w(F_o)^2]^{1/2}$	0.057
μ (cm^{-1})	48.7

TABLE 2. Atomic coordinates (× 10^5 for Se and × 10^4 for C) and U_{eq}(× 10^3) for Se and C atoms in bis(di-*tert*-butylmethyl) diselenide

Atom	x/z	y/b	z/c	U_{eq}
Se1	57140(3)	28199(11)	20488(3)	59
Se2	65543(3)	37318(11)	25424(3)	64
C1	5924(2)	1101(8)	1444(3)	49
C2	6556(3)	2748(9)	3380(3)	49
C11	5544(3)	−526(10)	1476(3)	65
C12	5989(3)	1991(10)	834(3)	61
C21	7091(3)	1637(10)	3527(3)	64
C22	6393(3)	4150(10)	3824(3)	63
C111	4941(3)	−57(11)	1411(4)	81
C112	5624(4)	−1898(12)	999(5)	100
C113	5711(4)	−1430(11)	2085(4)	92
C121	6379(4)	3534(12)	963(4)	88
C122	5449(4)	2726(12)	498(4)	93
C123	6253(4)	854(14)	410(4)	110
C211	7616(3)	2607(13)	3435(5)	105
C212	7040(3)	55(12)	3102(4)	91
C213	7187(4)	913(14)	4176(4)	103
C221	6830(4)	5529(11)	3984(4)	102
C222	6249(4)	3334(12)	4404(3)	82
C223	5862(4)	5005(11)	3525(4)	90

cation of Lorentz and polarization corrections; no absorption correction was applied. E-values were calculated by applying a K-curve.

The structure was solved using the program MULTAN 78 (13). All of the Se and C atoms were located in the first E-map. After nonlinear least-squares refinement of the atomic positions and thermal parameters (isotropic parameters for the carbon atoms and anisotropic parameters for the Se atoms), a difference Fourier synthesis revealed the positions of at least one hydrogen atom on each methyl carbon atom. This allowed calculation of the position of all the hydrogen atoms; they were included in the model at ideal positions, were assigned an isotropic thermal parameter which was 20% greater than that of the appropriate methyl carbon atom, and were not refined. The positions and anisotropic thermal parameters of the carbon and selenium atoms were refined along with an isotropic extinction correction using the 1444 reflections with $I > 3\sigma(I)$ and the 356 reflections with $I_{calc} > 3 \times \sigma(I_{obs})$. The final cycle had a maximum shift/error of 0.021 and the standard deviation of an observation of unit weight was 0.87. A final difference Fourier synthesis contained four peaks of 0.6 e/Å^3 which were diffraction ripples near the two Se positions; all other peaks were

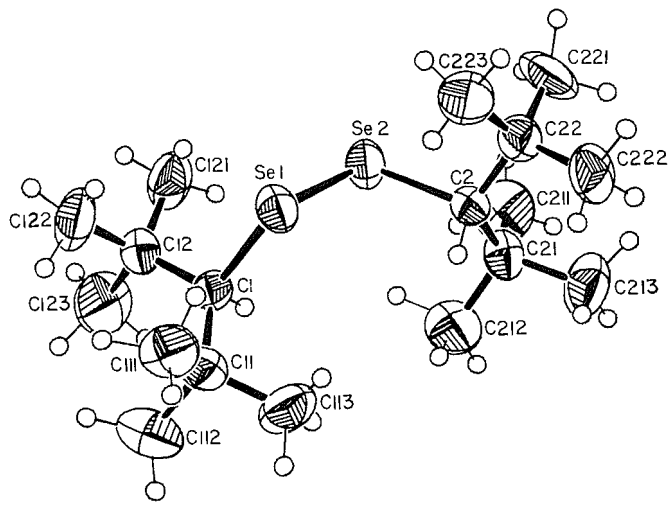

FIG. 2. The conformation and atomic labeling scheme for bis(di-*tert*-butylmethyl) diselenide. The drawing was made with the computer program ORTEP (19), the thermal ellipsoids are drawn at the 50% probability level for Se and C, while the H atoms are represented as spheroids of radius 0.1 Å.

less than 0.3 e/Å^3. The weights were defined as $\omega = 1/(\sigma^2(F_o) + 0.005\ F_o^2)$. The value of g, the isotropic extinction factor, was 4.0(1) × 10^{-3} where the treatment of g followed that of Larson (14). Atomic coordinates[2] for Se and C are given in Table 2 with the atoms labeled as shown in Fig. 2.

All computations were done using the XRAY 76 system of programs (15) on a Honeywell computer with a Multics operating system. The scattering factors were those of Cromer and Mann (16).

Results and discussion

The bond lengths and bond angles in diselenide **4** are shown in Table 3 and an illustration of the structure, including the labeling scheme employed, is shown in Fig. 2. The average C—Se and the Se—Se bond lengths of 2.010(6) Å and

[2] The anisotropic thermal parameters, hydrogen atom parameters, and the observed and calculated structure factor amplitudes are available at a nominal charge from the Depository of Unpublished Data. CISTI, National Research Council of Canada, Ottawa, Ont., Canada, K1A 0S2.

TABLE 3. Bond distances and bond angles for the selenium and carbon atoms

Atoms	Distance (Å)	Atoms	Angle (°)
Se1—Se2	2.315(1)	Se2—Se1—C1	102.3(2)
Se1—C1	2.013(6)	Se1—Se2—C2	101.6(2)
Se2—C2	2.008(6)		
C1—C11	1.580(10)	Se1—C1—C11	106.2(4)
C1—C12	1.549(10)	Se1—C1—C12	111.2(4)
		C11—C1—C12	122.3(5)
C11—C111	1.53(1)	C111—C11—C112	108.9(6)
C11—C112	1.53(1)	C111—C11—C113	109.0(7)
C11—C113	1.52(1)	C112—C11—C113	104.5(7)
		C1—C11—C111	113.0(6)
		C1—C11—C112	112.4(6)
		C1—C11—C113	108.7(6)
C12—C121	1.53(1)	C121—C12—C122	106.4(6)
C12—C122	1.54(1)	C121—C12—C123	104.6(7)
C12—C123	1.51(1)	C122—C12—C123	109.8(6)
		C1—C12—C121	109.0(5)
		C1—C12—C122	113.0(6)
		C1—C12—C123	113.5(6)
C2—C21	1.572(10)	Se2—C2—C21	106.6(4)
C2—C22	1.559(10)	Se2—C2—C22	110.9(4)
		C21—C2—C22	122.6(5)
C21—C211	1.54(1)	C211—C21—C212	107.4(7)
C21—C212	1.54(1)	C211—C21—C213	106.6(6)
C21—C213	1.53(1)	C212—C21—C213	105.9(7)
		C2—C21—C211	114.1(6)
		C2—C21—C212	108.5(5)
		C2—C21—C213	113.8(6)
C22—C221	1.52(1)	C221—C22—C222	109.8(6)
C22—C222	1.52(1)	C221—C22—C223	109.6(7)
C22—C223	1.53(1)	C222—C22—C223	104.5(7)
		C2—C22—C221	113.0(7)
		C2—C22—C222	111.3(6)
		C2—C22—C223	108.3(6)

2.315(1) Å, respectively, are only slightly longer than normal values for an aliphatic diselenide. The corresponding values for diselenide **3** are 1.97(1) Å and 2.285(5) Å (2). The bond angles C(1)—Se(1)—Se(2) and C(2)—Se(2)—Se(1) are 102.3(2)° and 101.6(2)°, respectively, and show little variation from those in triselenide **5** (9). Similarly, bond lengths and bond angles in the di-*tert*-butylmethyl residues resemble those of the triselenide, as expected.

The chief steric interactions in **4** involve the selenium atoms and the nearest methyl groups on both the distant and adjacent alkyl residues. The Se2 to C121 distance is 3.472(8) Å and Se1 to C223 is 3.657(9) Å (see Fig. 2); the sum of the van der Waals radii for a selenium atom and a methyl group is 4.0 Å (17). Also, C223 is closest to Se2 at 3.129(9) Å and C121 is closest to Se1 at 3.164(9) Å. All other intramolecular selenium-to-methyl group distances are greater than 4.2 Å when the methyl groups are part of the distant alkyl residue, and greater than 3.4 Å when they are in the adjacent alkyl moiety. The contact between the methyl groups at C212 and C113 is 3.88 Å, again slightly shorter than the sum of the van der Waals radii. The most striking feature in **4** is the abnormally large dihedral angle C1—Se1—Se2—C2 of 112.1(3)°. The crystal structure clearly demonstrates that the principal means for relieving congestion in this crowded molecule is by torsion about the Se1—Se2 bond rather than through the lengthening of bonds C1—Se1, Se1—Se2, or Se2—C2.

The closest intermolecular contacts are between methyl groups; C123 to C222 at $(x, -y, z - 1/2)$ is 3.93(1) Å and C122 to C111 at $(1 - x, -y, -z)$ is 3.99(1) Å. The shortest Se atom to methyl group intermolecular contact is between Se2 and C212 at $(3/2 - x, 1/2 + y, 1/2 - z)$ and is 4.090(9) Å. All other intermolecular contacts are greater than 4.2 Å.

Typical acyclic dialkyl diselenides have uv absorption maxima in the range 286–316 nm, the precise wavelength being determined by three effects: inductive, hyperconjugative, and torsional (or steric) (10–11, 18). Since inductive effects are comparable for different alkyl groups, they will play a relatively minor role in the absence of polar substituents. Hyperconjugation lowers the energy of the electronic transition. Hence, diselenides which contain more α-hydrogens display bathochromic shifts relative to those with fewer or none (18). For example, this phenomenon is chiefly responsible for the difference in the uv spectra of di-*tert*-butyl diselenide, which has no α-hydrogens (λ_{max} = 286 nm), and dimethyl diselenide which has six (λ_{max} = 316 nm). A valid comparison can be made between diisopropyl diselenide and compound **4**, as each has two α-hydrogens. The former compound has λ_{max} = 305 nm (18) whereas we observed λ_{max} of diselenide **4** at 324 nm. If we rule out differences in inductive and hyperconjugative effects, the bathochromic shift of 19 nm for the more hindered diselenide must be attributed to the torsional effect. We therefore conclude that bis(di-*tert*-butylmethyl) diselenide (**4**) exhibits an abnormally large dihedral angle in solution as well as in the solid state.[3,4]

Acknowledgements

We thank the Natural Sciences and Engineering Research Council for financial support to T.G.B. and the Alberta Heritage Foundation for Medical Research for a Scholarship and Establishment Grant to P.W.C. We also thank Joanita Jakana for technical assistance and K.A. Kerr for use of the diffractometer.

1. I. L. KARLE and J. KARLE. *In* Organic selenium compounds: their chemistry and biology. *Edited by* D. L. Klayman and W. H. H. Günther. Wiley–Interscience, New York. 1973. Chapt. 15H.
2. H. T. PALMER and R. A. PALMER. Acta Crystallogr. Sect B, **25**, 1090 (1969).
3. R. E. MARSH. Acta Crystallogr. **5**, 458 (1952).
4. F. H. KRUSE, R. E. MARSH, and J. D. MCCULLOUGH. Acta Crystallogr. **10**, 201 (1957).
5. C. M. WOODWARD, D. S. BROWN, J. D. LEE, and A. G. MASSEY. J. Organomet. Chem. **121**, 333 (1976).
6. G. LLABRES, M. BAIWIR, and J. L. PIETTE. J. Appl. Crystallogr. **7**, 299 (1974).
7. O. FOSS, K. JOHNSEN, and T. REISTAD. Acta. Chem. Scand. **18**, 2345 (1964).
8. T. G. BACK, D. H. R. BARTON, M. R. BRITTEN-KELLY, and F. S. GUZIEC JR. J. Chem. Soc. Perkin Trans. 1, 2079 (1976).
9. B. J. MCKINNON, P. DE MAYO, N. C. PAYNE, and B. RUGE. Nouv. J. Chim. **2**, 91 (1978).

[3] The study of conformational effects in hindered diselenides in solution by nmr spectroscopy may provide an interesting subject for future work.

[4] In response to a referee's suggestion, we attempted to obtain a solid state diffuse reflectance spectrum of diselenide **4** in Nujol and observed the same λ_{max} = 324 nm. However, we suspect that a significant amount of the diselenide dissolves in Nujol under these conditions. A KBr disc transmission absorption spectrum of **4** produced a very broad, flat absorption from which a reliable value of λ_{max} could not be determined.

Can. J. Chem. Downloaded from www.nrcresearchpress.com by 210.87.254.5 on 09/06/12
For personal use only.

10. J. E. KUDER. *In* Organic selenium compounds: their chemistry and biology. *Edited by* D. L. Klayman and W. H. H. Günther. Wiley–Interscience, New York. 1973. Chapt. 15B.
11. G. BERGSON, G. CLAESON, and L. SCHOTTE. Acta Chem. Scand. **16**, 1159 (1962).
12. P. W. CODDING. Can. J. Chem. **61**, 529 (1983).
13. G. GERMAIN, P. MAIN, and M. M. WOOLFSON. Acta Crystallogr. Sect A, **27**, 368 (1971).
14. A. C. LARSON. Acta Crystallogr. **23**, 664 (1967).
15. J. M. STEWART. The X-ray system of crystallographic programs. Computer Science Center, University of Maryland, College Park, MD. 1976.
16. D. T. CROMER and J. B. MANN. Acta Crystallogr. Sect A, **24**, 321 (1968).
17. L. PAULING. *In* The nature of the chemical bond. 3rd ed. Cornell University Press, Ithaca, NY. 1960. p. 260.
18. G. BERGSON. Ark. Kemi, **13**, 11 (1958).
19. C. K. JOHNSON. ORTEP Report ORNL-3794 (2nd ed.). Oak Ridge National Laboratory, Oak Ridge, TN. 1970.

Can. J. Chem. Downloaded from www.nrcresearchpress.com by 210.87.254.5 on 09/06/12
For personal use only.

The reaction of chrysotile asbestos with titanium(III) chloride. Characterization of the reaction products

DANIEL COZAK,[1] CLAUDE BARBEAU, FRANÇOIS GAUVIN, JEAN-PIERRE BARRY, CHRISTIAN DEBLOIS, and ROBERT DEWOLF

Département de chimie, Université Laval, Québec (Qué.), Canada G1K 7P4

AND

FRANK KIMMERLE

Programme de recherche sur l'amiante de l'Université de Sherbrooke (PRAUS), Département de chimie, Université de Sherbrooke, Sherbrooke (Qué.), Canada J1K 2R1

Received December 22, 1983

DANIEL COZAK, CLAUDE BARBEAU, FRANÇOIS GAUVIN, JEAN-PIERRE BARRY, CHRISTIAN DEBLOIS, ROBERT DEWOLF, and FRANK KIMMERLE. Can. J. Chem. **61**, 2753 (1983).

The reaction products of chrysotile asbestos with titanium trichloride in organic and aqueous media are described. The titanium(III) acidity in H_2O solution is sufficiently strong to cause fiber lixiviation and unrollment. The reaction product of the water reacted fiber is an amorphous titanium containing silicate. A series of reactions with $TiCl_3$ in THF were carried out. The results show that the titanium bonded species is a $Ti^{III}Cl_n$ group with $n \leq 2$. In some experiments as much as 3 wt% titanium was fixed to the fiber without destroying the fiber structure of chrysotile. All the reaction products discussed were characterized by sem X-ray analysis, ir, esr, dta, and elemental microanalysis.

DANIEL COZAK, CLAUDE BARBEAU, FRANÇOIS GAUVIN, JEAN-PIERRE BARRY, CHRISTIAN DEBLOIS, ROBERT DEWOLF et FRANK KIMMERLE. Can. J. Chem. **61**, 2753 (1983).

Nous avons fait réagir l'amiante chrysotile avec le trichlorure de titane. Les produits de réaction en milieu organique et en milieu aqueux sont ici caractérisés. En milieu aqueux on constate que l'acidité du titane(III) est suffisamment forte pour causer la lixiviation du chrysotile. Le produit de réaction est un silicate amorphe contenant du titane. Pour les réactions en milieu tetrahydrofurane, la structure fibreuse du chrysotile est préservée. Les essais que nous avons fait en milieu organique indiquent que l'espèce $Ti^{III}Cl_n$, $n \leq 2$ se trouve chimiquement lié à la fibre. Dans les cas extrêmes nous avons réussis a fixer jusqu'à 3% (p/p) de titane à la fibre sans détruire la structure fibreuse. Les produits de réactions ont été caractérisés par analyse thermogravimétrique différentielle, microscopie électronique (morphologie et rayon-X), infrarouge, résonance paramagnétique électronique et microanalyse élémentaire.

Can. J. Chem. Downloaded from www.nrcresearchpress.com by 210.87.254.42 on 09/06/12
For personal use only.

Introduction

Asbestos fibers are used as filler in the industrial fabrication of several materials having widespread fields of application such as concrete cement, plastics, paper, etc. (1). For these applications the most important fiber property is its good mechanical performance, which makes it an interesting filling material, for example, in the reinforcement of plastics or for the armature of concrete cement. Studies have shown that the mechanical characteristics of these new composites are related to the physico-chemical interaction at the fiber–matrix interface (2, 3). Hence, in the chemical treatment of fibers, conditioning is an important step aimed at improving chemical interaction between the silicate mineral and the host material without changing the fibers' mechanical properties.

The exact composition of asbestos varies significantly, depending on its origin and history (4, 5). The Quebec 4-T-30 asbestos samples used in this work are known to contain 80–90% chrysotile fibers (5, 6). Chrysotile has the formula $Mg_3(Si_2O_5)(OH)_4$ and is the only known member of its type with a cylindrical structure (7). A detailed atomic structure is given in Fig. 1*A*, showing the hexagonal close packing arrangement of the oxygen and hydroxyl groups forming the $(SiO_4)^{2-}$ tetrahedrons of the silicate layer and the brucite –Mg(OH) octahedrons. The fiber can also be represented, Fig. 1*B*, as a hollow tube with its external surface covered with hydroxyl groups (brucite layer) and the inner hollow center made up of bridging oxygen atoms (silicate layer).

In aqueous media chrysotile has a positively charged surface (55 $\mu C/cm^2$ at pH 7 (8)] and gradually dissociates water until an acid–base equilibrium is reached. To explain this behaviour, chemical and thermodynamical considerations led Ahmed (8) to propose, among others, a reaction scheme in which the freed protons coagulate on the fibers' surface between ca. pH 6 and 10, while the released hydroxyl groups contribute to the solution's basicity. Depending on the fibers' condition, the zero point charge is reached between pH = 10–12. Furthermore, under acidic conditions (pH < 6), rapid decomposition of the fiber is observed due to acidic attack of the brucite layer, Fig. 1*B*. Similarly, in highly basic media (pH > 10) dissolution of the silicate also causes unrollment of the fiber.

Moreover, chemical treatment of asbestos is an important avenue currently being explored for the development of less pathogenic chrysotile fibers (9). Work on the chemical properties of asbestos will give, we believe, more insight into the physiological interaction of silicate minerals in living organisms (10). The biological tests performed on short fiber chrysotile asbestos show a net decrease in the cytotoxic and hemolytic properties for the titanium modified fibers (11). Furthermore, binding of the known carcinogen benzopyrene drops significantly for the titanium treated fibers (in THF) discussed in this work (12). The property of chrysotile to concentrate carcinogenic agents has been linked with the unusually high lung cancer incidence observed in asbestos workers who smoked (10).

In the following sections, the products of reaction of short fiber chrysotile asbestos with $TiCl_3$ in water and in tetrahydrofuran are described. Our main concern in this work was to verify the fibers' condition after reaction and to characterize the resulting titanium species. Titanium treated fibers have in the

[1]To whom all correspondence should be addressed.

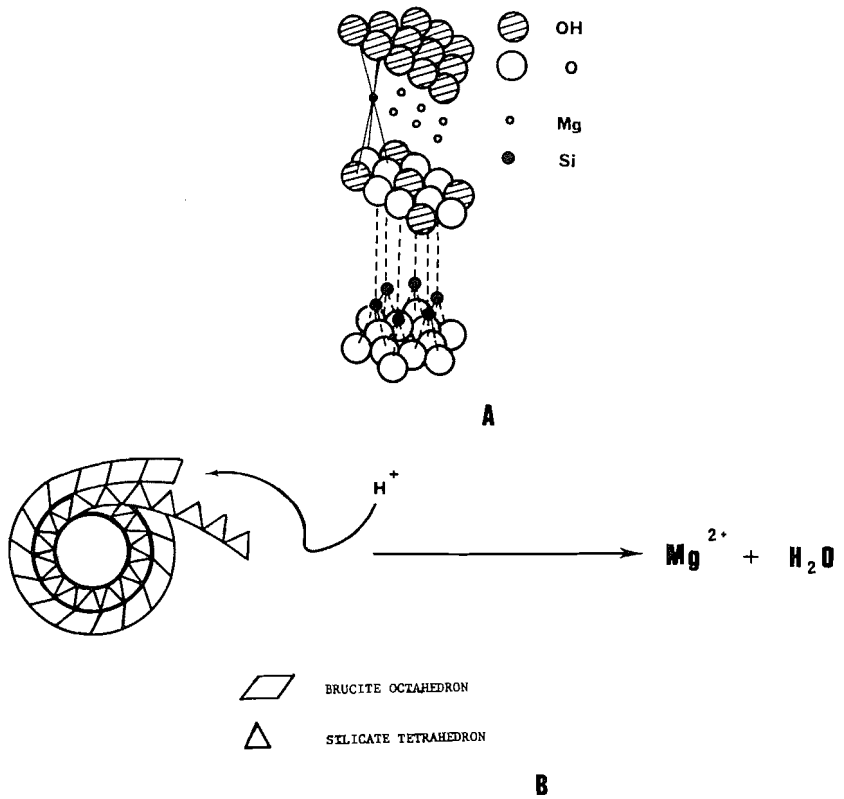

FIG. 1. *A*, Blown-up view of the chrysotile mineral structure, $Mg_3(Si_2O_5)(OH)_4$. *B*, acid lixiviation reaction showing unrollment of the chrysotile fiber.

past been used as paint pigment (13) and filling material in Ziegler-Natta prepared polymers (14). In the latter case, repeated reaction with the pure $TiCl_4$ liquid yielded a maximum titanium concentration in the fiber of 0.28 wt%. To the best of our knowledge no attempts as yet have been made to isolate and identify reaction products of chrysotile asbestos with titanium(III) or (IV) compounds.

Experimental

All the chemical reactions, together with microanalytical analyses, ir, nmr, and esr spectroscopy, were done under anaerobic conditions using Schlenk type vessels and argon filled glove bags. Exceptions are sample preparation for scanning electron microscopy (sem), differential thermogravimetric analysis (dta) experiments, and certain titanium analysis, which were carried out in the open air. Also chemical reactions were repeated at least twice to insure reproducibility of the results.

The argon gas used was first circulated through a copper catalyst, BASF-R3-11 (Badische Anilin und Soda-Fabrik AG, 6700 Ludwigshafen, W. Germany), at 200°C and then on molecular sieve, type 4A, to remove oxygen and water contained in the commercial argon. Titanium trichloride, $TiCl_3$ 98%, purchased from Ventron-Thiokol-Alfa, was stocked under argon and used without any further purification. Tetrahydrofuran (THF) was distilled under argon after refluxing for 30 min over a benzophenone–sodium drying mixture. Aqueous solutions were deoxygenated by distillation under argon. Asbestos fibers classified 4-T-30 from Johns Manville Ltd. (Thetford mines, Quebec) were generously supplied to us by the Asbestos Mining Association of Quebec (AMAQ).[2]

The elemental Mg, Si, and Ti microanalyses were done by atomic flame absorption using a Perkin Elmer model 305 spectrometer (λ = 285.2, 251.6, and 276.8 nm, respectively). Because of the methodology followed, the Mg analysis is reproducible only to ±1 wt% due to dilution factors of the mother solution prepared for all three elements analysed. The C, H, N, and Cl analyses were carried out by Schwarzkopf Microanalytical Laboratory, New York, U.S.A. and by us on a Hewlett Packard 185 CHN analyser. Electron spin resonance (esr) spectra were recorded on a Varian E-9 (9.3 GHz) spectrometer and proton nuclear magnetic resonance (^{1}H-nmr) on a Bruker WP-80-FT spectrometer. Infrared (ir) spectra were recorded in KBr pellets on a Beckman IR-4250 spectrometer and calibrated against a polystyrene film (±3 cm^{-1}) or on a Digilab FTS-11 Fourier transform ir spectrometer. Fiber morphology was checked using an Itec Auto Scan scanning electron microscope (sem) equipped with a Quantex-7000 Kevex energy dispersive (ed) X-ray analyser with which the spectra were recorded. Samples for sem-ed analysis were prepared in the following manner. A thick layer of fibers is formed by syringing through a millipore filter (0.4 μm pores,13 mm diameter), 1 mL containing ca. 0.6 mg fiber from an aqueous solution. The samples were then mounted on a metal stub, dried over night in a vacuum desiccator, and sputtered with gold. Sem morphology verifications were performed on more dilute samples and using Nuclepore filters. Reproducibility of the elemental peak intensity ratios for a given fiber was found to be satisfactory. Variations from one sample preparation to another for the same reacted fibers did not exceed ±5% for $Si/Mg(K_\alpha)$ and $Ti/Mg(K_\alpha)$ ratios under the same spectroscopic conditions. Also, irregular distribution of the fibers on the filter and possibly composition heterogeneity in the fibers themselves is believed to be the prime source of error for the intensity ratios, especially in fibers with more than 2 wt% titanium. Therefore, in all cases discussed hereafter reproducibility of the sem-ed analysis results are compatible with the mean ratio variation averaged for three spectra (covering 1 μm^2 area) taken from the same experiment, i.e., maximum observed variation ±3% and ±12% for Si/Mg and Ti/Mg respectively as indicated in Table 2. Differential thermogravimetric

[2]The designation 4-T-30 is a commercial grading code for medium length asbestos. The fibers of this category are mainly (~80%) 1–4 mm long.

Can. J. Chem. Downloaded from www.nrcresearchpress.com by 210.87.254.42 on 09/06/12
For personal use only.

TABLE 1. Microanalytical data for chrysotile asbestos fibers

Chrysotile fibers		Weight percent (wt%) C	H	Si	Mg	Ti	Cl	Total wt%
$Mg_3(Si_2O_5)(OH)_4$	calculated	0.00	1.44	20.27	26.31	0.00	0.00	48.02
	found[a]	0.25	1.67	18.89	24.71	<0.05	<0.3[b]	45.52
$TiCl_3$–THF reacted fibers (method A)		1.62	1.51	17.03	22.86	2.02	1.21	46.25
$TiCl_3$–H_2O reacted fibers (method B)		—	—	14.59	19.28	3.97	7.27	45.11
$TiCl_3$–H_2O with buffer		0.56	1.65	17.40	12.50	4.90	[c]	37.36
Reacted fibers following method A, after soxhlet extraction		1.16	1.66	17.44	23.08	2.04	<0.3	45.38

[a]Analysis for short fiber chrysotile. Also found Fe = 3.58 wt%.
[b]When NaCl was used as electrolyte in the sedimentation of the short fibers, 2–3 wt% chlorine was detected.
[c]Value found for another sample from a different experiment; Cl = 7.27 wt%.

TABLE 2. Analytical results for the series of $TiCl_3$–THF reacted (method A) chrysotile asbestos

Reaction	Reactant ratio Ti/Mg(surf.)	Sem-energy dispersion analysis[a] Si/Mg	Ti/Mg[b]	Microanalysis, wt% Ti	Mg[c]	Si	Cl
[A]	0.0	1.2 (0.02)	0.00	<0.05	21.98		0.00
[B]	0.1	1.3 (0.01)	0.04 (0.005)	0.59	23.58 (0.38)	17.59	0.81
				0.58	23.91		
[C]	0.2	1.3 (0.03)	0.01 (0.002)	0.33	27.00[d]		
[D]	0.4	1.3 (0.01)	0.09 (0.02)	1.38	23.39 (0.64)		
[E]	0.7	1.4 (0.06)	0.12 (0.02)	2.02[e]	22.86 (1.32)	17.03	1.21
		1.5 (0.04)	0.11 (0.02)[f]				
[F]	1.4	1.3 (0.007)	0.12 (0.01)	2.30	25.88 (1.40)		
[G]	2.3	1.3 (0.01)	0.09 (0.01)	1.18	17.06		
		1.3 (0.03)	0.08 (0.01)	2.04	23.08	17.44	1.41[f]
[H]	5.0	1.3 (0.04)	0.13 (0.03)	2.48	24.50 (1.13)		
[I]	28.2	1.4 (0.14)	0.15 (0.03)	3.23	21.98 (0.87)	16.20	2.10
				3.45	23.22		

[a]The standard deviations are given in parentheses and are calculated from three different spectra of the same experiment (area = 1 μm^2; acquisition time = 300 s).
[b]Fe/Mg = 0.046 (0.001) for the reaction [A] fibers. This value decreased monotonously with increase titanium ratio in reactions [B]–[I].
[c]In parentheses is the magnesium content found in the reaction filtrates expressed as the wt% fiber loss.
[d]Analyses from other experiments gave lower values, e.g. Mg = 23.20 wt%.
[e]Analysis performed on a different sample of the same experiment gave Ti = 1.73 wt% and Mg = 23.01 wt%.
[f]Analysis performed on a different sample of the same experiment.

experiments were carried out in a nitrogen atmosphere on ca. 20 mg oxidized fiber samples using a Perkin Elmer thermal data system model TGS-2 equipped with a TADS computer. During the experiments the temperature was varied from 50 to 1000°C at a rate of 20°/min.

Sedimentation of short fiber chrysotile

Short fiber chrysotile can be separated from the commercial product in the following way. A glass column measuring 120 cm long and 9 cm wide was filled with 6 L of distilled water to which 60 to 80 g of 4-T-30 asbestos fibers were added in loose bundles. The column was then turned over several times until the fibers were well suspended in the tube. On standing for 1 h, the longer fibers deposited at the bottom and the milky white solution was transferred to a second identical column equipped with a 6 mm stop-cock at the bottom. Coagulation of the short fibers was then triggered by adding 5 g NaBr (ca. 10 m*M*) to the white suspension.[3] Within 10 min the sedimentation was over and the product was recovered through the stop-cock, filtered, and washed with distilled water until the washings were free of bromide (AgBr test). Following this the fibers were predried over P_4O_{10} in a vacuum desiccator, transferred to a Schlenk tube, and further dried for 20 h at 250°C, 10^{-2} Torr. The fibers were stored under argon.

Using this method, two successive separations on a 60.90 g batch of asbestos yielded, respectively, 4.40 and 1.73 g of short fiber chrysotile asbestos for a total yield of 10%. Since chrysotile is very sensitive to pH conditions (5, 8) care was taken to avoid exposing the fibers needlessly to water for long periods.

Reaction of short fiber chrysotile with $TiCl_3$ in THF (method A)

In a typical reaction 0.493 g (3.19 mmol) $TiCl_3$ were mixed together with 1.821 g (6.58 mmol) fibers in a 250 mL Schlenk tube. Freshly distilled THF, 150 mL, was added and the suspension was refluxed under a positive argon pressure. After 20 h, the solution was cooled and the fibers were collected on a fritted disk while the blue THF filtrate was discarded. The fibers were then rinsed with two 50 mL portions of THF and dried on the fritted disk under vacuum for 2 h at ambient temperature. Weight of the dry fibers, 1.647 g. The microanalytical data are given in Table 1. Analyses of the reaction filtrate indicated only slight amounts of magnesium, cf. Table 2.

[3]When NaCl was used as coagulating electrolyte instead of NaBr, a significant amount of halogen (e.g. 2 wt%) was detected in the fiber. Care was taken to make sure that no halogen was left in order to avoid false Cl/Ti atomic ratios in the microanalytic data of the reacted fibers.

Can. J. Chem. Downloaded from www.nrcresearchpress.com by 210.87.254.42 on 09/06/12
For personal use only.

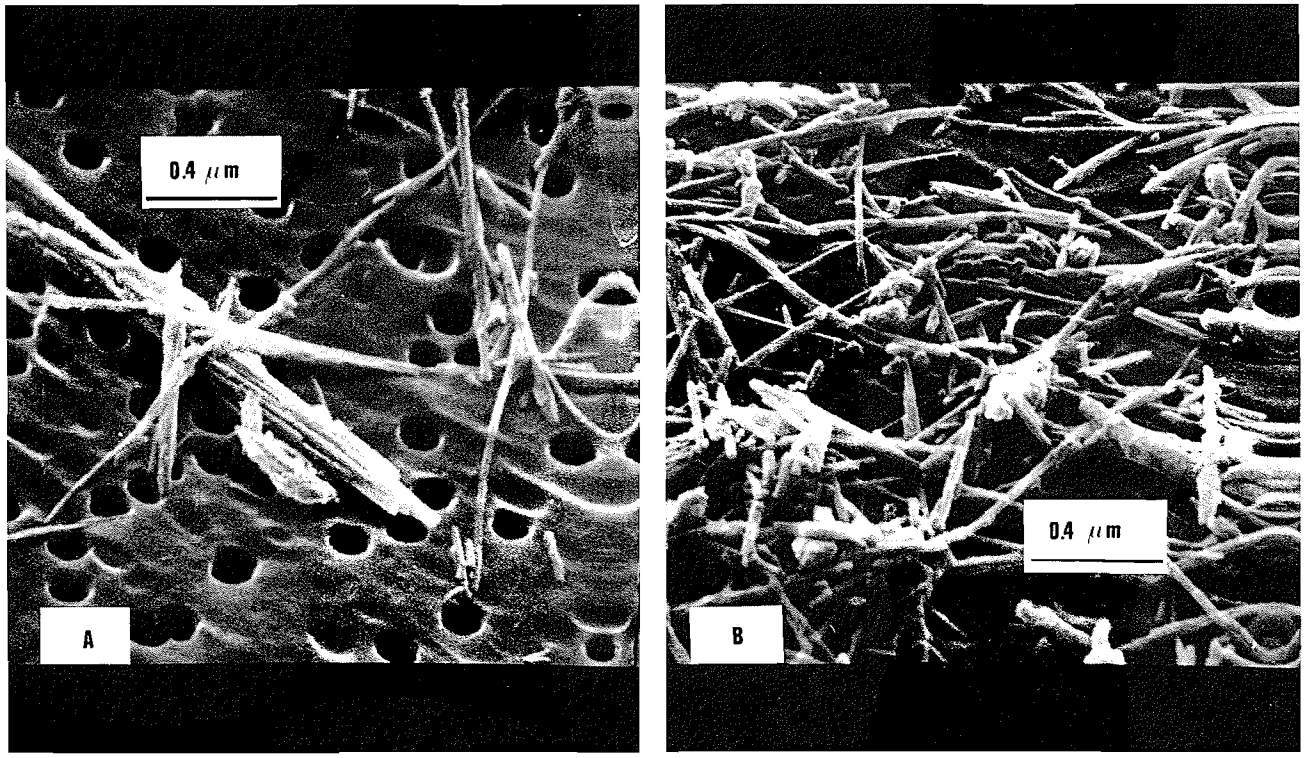

FIG. 2. Scanning electron micrographs (20 000×) of *A*, 4-T-30 asbestos chrysotile showing long fibers and fiber bundles; *B*, $TiCl_3$–THF reacted short fiber chrysotile (reaction [I], Table 2). This micrograph is representative of the monofibril morphology observed after reaction of the sedimented short fibers.

In some reactions a pale blue prismatic air sensitive compound crystallized from the solution upon cooling.This compound analyzed as $TiCl_2(OH)\cdot 2(C_4H_8O)$. *Anal.* calcd.: C 34.31, H 6.12, Ti 17.11, Cl 25.31; found: C 33.46, H 6.15, Ti 17.36, Cl 25.06. Furthermore, ^{1}H-nmr of this compound in D_2O shows two broad featureless resonances at 1.48 and −0.48 ppm (half height width, $H_{1/2}$ = 23 Hz), in acetone-d_6 the resonances are at 1.41 and −0.17 ppm ($H_{1/2}$ = 40 Hz). These values are significantly upfield from those of the free uncomplexed THF, 3.71 and 1.83 ppm (AA′BB′ spin coupled multiplets). No proton nmr signal for the hydroxyl group was observed in the spectra. Nuclei adjacent to a paramagnetic transition metal center such as that found here for Ti—OH are generally hard to detect due to excessive signal broadening.

Reaction of short fiber chrysotile with $TiCl_3$ in H_2O (method B)

The same procedure as in method A was followed using this time 0.890 g (5.76 mmol) $TiCl_3$, 1.060 g (3.82 mmol) fibers, and 100 mL H_2O instead of THF. The mixture was then refluxed for 2 h. From this reaction 0.790 g of air sensitive blue solid was recovered. Microanalysis data of the reaction product are given in Table 1.

Results and discussion

The short fibers reported in our work were separated from the commercial asbestos by the sedimentation–flocculation method (15). Short monofibril chrysotile isolated, as described in the Experimental section, are highly homogeneous in size and are relatively free of amorphous material. For example, the corrected stoichiometry found for these fibers, $2.94MgO\cdot 1.94SiO_2\cdot 2.42H_2O$, is very close to the ideal formula for chrysotile asbestos, $3MgO\cdot 2SiO_2\cdot 2H_2O$.[4] The sem micrographs (20 000×) of the separated fibers show monofibrils which are in most part 1.5–2.0 μm in length, cf. Fig. 2. These results are in good agreement with a more detailed characterization reported by Jolicoeur *et al.* in which they report 90% of the separated short fibers to be less than or equal to 2 μm long. Moreover, the X-ray sem-ed spectrum, Fig. 3A ($Si(K_\alpha)$ = 1.7 keV, $Mg(K_\alpha)$ = 1.3 keV, and Si/Mg(intensity) = 1.3) is in good agreement with the previously reported data for chrysotile (16, 17).

Aqueous reaction of the fibers

The reaction of chrysotile with $TiCl_3$ in H_2O affords a blue solid product. The sem reveals that this product has neither the morphology nor the chemical composition of chrysotile. In addition, analysis of the reaction filtrate for different reactions indicates that 80 to 100% of the chrysotiles magnesium is leached out of the fiber during reaction, depending on the reaction times. Accordingly, the ν(Mg—OH) bands usually visible at 3685 and 3640 cm^{-1} in the ir spectrum are absent. Also, the ir spectra for all the $TiCl_3$—H_2O reacted chrysotile experiments showed changes in the ν(Si—O) vibration intensities at 1075, 1015, and 950 cm^{-1}, and the appearance of a new absorption at 795 cm^{-1}. This is characteristic of acid lixiviated and unrolled fibers (5, 11).

Lixiviation or leaching of chrysotile by organic and mineral acids is well known (5). The present results indicate that the Lewis acid property of $TiCl_3$ is responsible for the observed reaction of chrysotile in water. The following hydrolysis equilibrium is known to be the main chemical process for titanium(III) ions in H_2O (18–20),

$$[Ti(H_2O)_6]^{3+} \rightleftharpoons [Ti(H_2O)_5(OH)]^{2+} + H^+$$

The resulting decrease in pH when $TiCl_3$ dissolves is sufficient

[4]A correction of 4 wt% was made on the total weighed analytical mass due to impurities; iron (3.58 wt%), carbon (0.25 wt%) and other undetermined but small quantities of; sodium, potassium, calcium, manganese, chrome, nickel, and aluminium, usually found in Quebec asbestos. See refs. 1, 5, and 6.

Can. J. Chem. Downloaded from www.nrcresearchpress.com by 210.87.254.42 on 09/06/12
For personal use only.

Can. J. Chem. Downloaded from www.nrcresearchpress.com by 210.87.254.42 on 09/06/12
For personal use only.

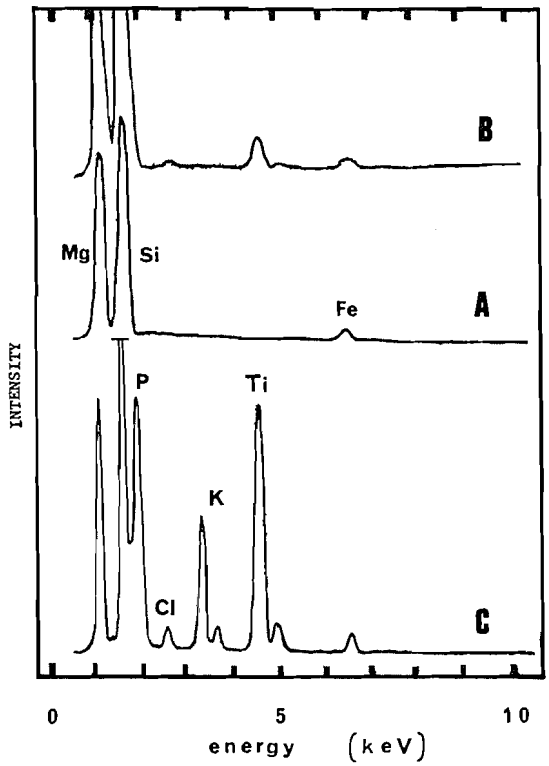

FIG. 3. Scanning electron microscope X-ray spectra of *A*, short fiber chrysotile asbestos; *B*, $TiCl_3$–THF reacted fibers (method A); and *C*, $TiCl_3$–H_2O reacted fibers (method B) with phosphate buffer (pH = 7).

to cause acid lixiviation of the chrysotiles –MgOH layer.[5]

In an attempt to control the pH a phosphate buffer (KH_2PO_4) solution was used as reaction media. Microanalysis (cf. Table 1), ir and sem-ed X-ray spectroscopy (cf. Fig. 3*C*) were used to characterize the blue solid reaction product. The analytical data confirm the previously reported chemical reactivity of chrysotile towards phosphate compounds (e.g. NaH_2PO_4, Cl_3PO, etc.) (22). Invariably most buffers have good coordinating anions capable of complexation with either titanium or magnesium.[6] Hence, the use of an aprotic solvent seemed to be a more convenient way of loading significant amounts of titanium on to the fiber without destroying it.

Tetrahydrofuran reacted fibers

The reactivity of the chrysotile–$TiCl_3$–THF system is very different from the aqueous analogue. Titanium(III) chlorides are in general good Lewis acids. In the presence of THF the following acid-base pair is formed (18)

$$TiCl_3 + nC_4H_8O \rightarrow TiCl_3 \cdot n(C_4H_8O) \qquad n = 3$$

When the $TiCl_3$ reaction concentration exceeded 0.04 *M*, a blue crystalline solid was observed in addition to the fibers. Microanalysis of these crystals is consistent with the formulation of the THF addition compound, $TiCl_2(OH) \cdot 2(C_4H_8O)$. This result is in agreement with the above reaction assuming $n = 2$ and that one chlorine atom has been replaced by one hydroxyl group from the fiber.

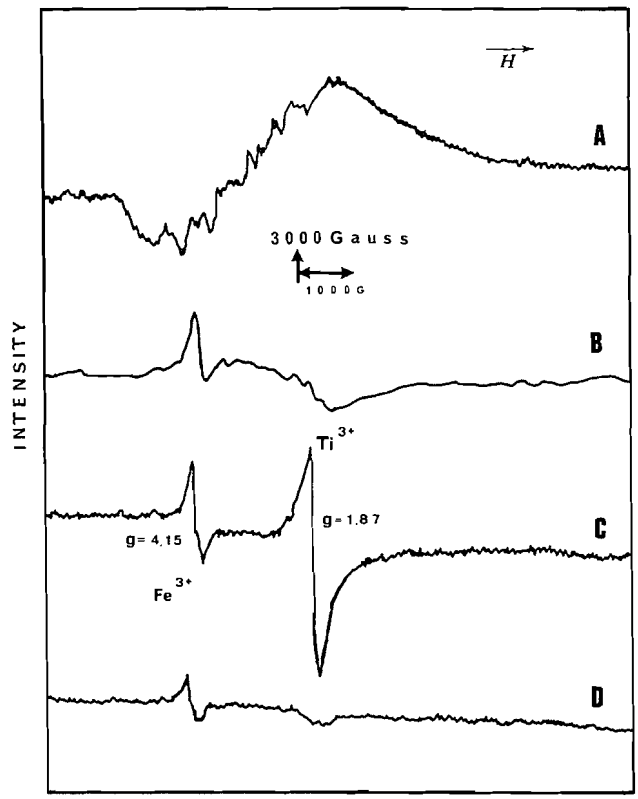

FIG. 4. Room temperature esr spectra of *A*, short fiber chrysotile; *B*, $TiCl_3$–THF reacted fibers (method A); *C*, $TiCl_3$–H_2O reacted fibers (method B); and *D*, same sample as *C* but 20 min after opening the cell to air.

In a series of experiments short fiber chrysotile was reacted under the same conditions. In order to study the influence of the reactants concentration on the titanium fixation to the fiber, the $TiCl_3$ to chrysotile ratio was varied. Moreover, since 7% of the total brucite is estimated to be at the fiber surface (2), the concentrations in Table 2 are expressed as the titanium to surface-magnesium ratio, Ti/Mg(surf.). The solvent volume was kept constant throughout the experiments.

The blue reacted fibers obtained were characterized by dta, elemental microanalysis, sem, esr, and ir spectroscopy. The esr spectrum of the THF reacted chrysotile is somewhat different from that of the product obtained from the reaction in water, Fig. 4. Nevertheless, a broad resonance at $g = 1.87$ indicates the presence of Ti(III). The possible interference from Mn(II) impurities ($g = 2.05$, sextet), contained in the fibers, is improbable due to the experimental conditions used here (i.e. T = 25°C) (23). The signal observed in all spectra at $g = 4.15$ is attributable to the presence of Fe(III) impurities. Identical spectra, for the reacted fibers, were observed at lower temperatures, 25 to –196°C.

The presence of titanium and chloride in the fibers was confirmed by microanalysis, Tables 1 and 2, and by sem-ed analysis, Fig. 3. The X-ray emission at 2.6 keV indicates only slight amounts of chlorine in the air exposed fibers. Under these conditions, oxidation of the titanium(III) chloride is expected to give a titanium(IV) product and HCl (18). In accord with this is the color change from blue to white when the reacted fibers are exposed to air. Moreover, the transformation of paramagnetic titanium(III) to diamagnetic titanium(IV) was followed by esr. Figure 4*D* shows the final spectrum of the

[5]In this case the acidity of $TiCl_3$, $pK_a = 3.9$, is comparable to that of acetic acid, $pK_a = 4.8$. This acid is a well known leaching agent for chrysotile.

[6]In the latter case solubilisation of the brucite layer through uncontrolled complexation rather than acid attack will also cause fiber unrollment.

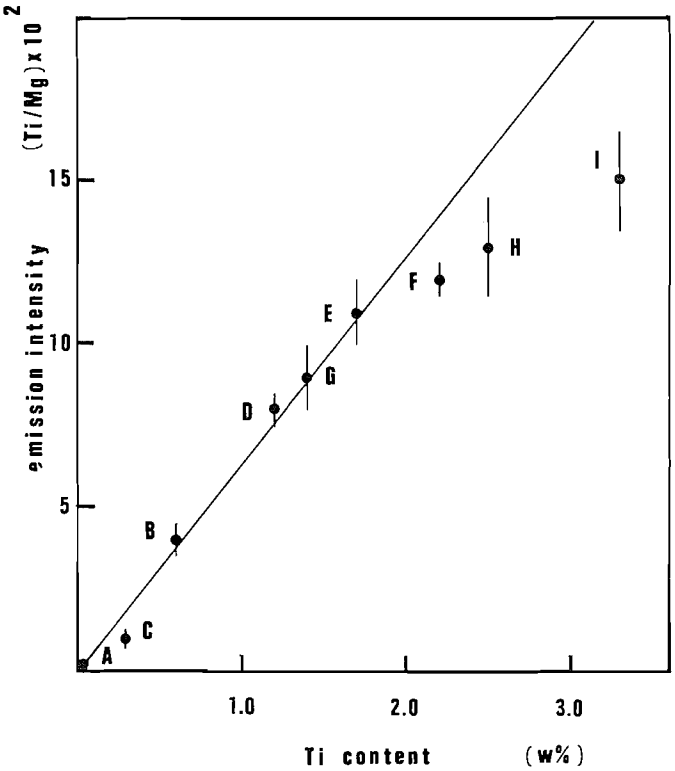

FIG. 5. Graph showing the titanium sem-ed X-ray emission intensity, Ti/Mg(K_α) versus the total titanium content (microanalysis) for a series of reacted fibers. The letters correspond to the reactions in Table 2. The vertical lines show the mean standard deviation for three spectra.

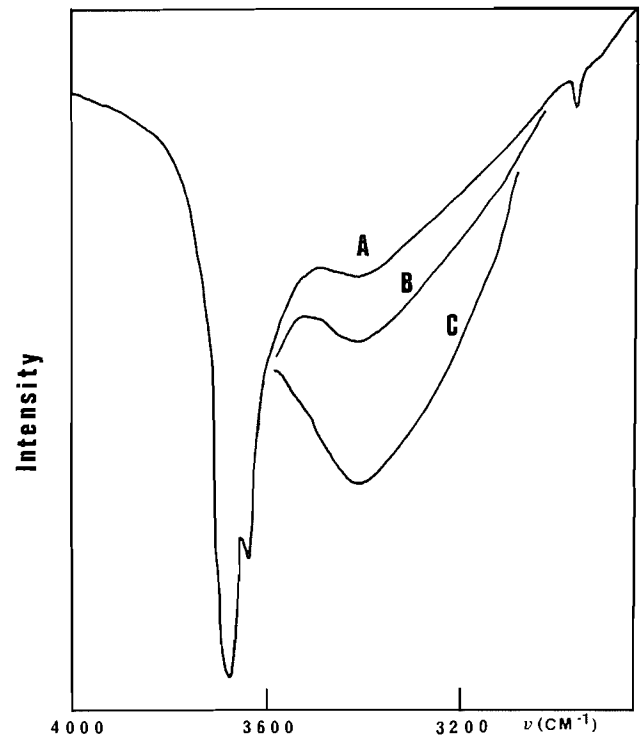

FIG. 6. Infrared spectra of the ν(OH) region of $TiCl_3$–THF reacted chrysotile; *A*, before heating (solvent evaporated, 25°C/10^{-2} Torr), and fibers heated in vacuum for (125°C, 10^{-2} Torr) *B*, 2 h; *C*, 14 h.

$TiCl_3$–H_2O reacted fiber when the seal of the esr cell is broken and air slowly diffuses in. The main change observed is the disappearance of the $g = 1.87$ resonance assigned to titanium(III). This oxidation was also observed for the THF reacted fibers, but oxidation is not as rapid.

Varying the reactants Ti/Mg (surf.) ratio over a 100-fold concentration does not affect significantly the Si/Mg ratio of the sem-ed spectra, Table 2. Also, microanalytical data for the series of reaction products in this table show no appreciable changes in the magnesium and silicon composition of the reacted fibers (for reactions [C] and [G] in Table 2, the offset Mg wt% analysis is given for coherency with the sem-ed results. A more complete analysis, also given, is more consistent with this affirmation). Furthermore, unlike the water reacted fibers the sem micrographs (20 000×) show a cylindrical monofibril morphology for the THF reacted fibers, identical to the original fibers, Fig. 2*B*.

Figure 5 gives the plot of the sem-ed X-ray intensity for titanium, Ti/Mg, as a function of the total microanalytical concentration of this element in the treated fibers. This relation is linear for concentrations below ca. 2 wt%. The weaker emission observed for the concentrations above this value can be due to either sample absorption or to binding of the titanium elsewhere than on the surface of the fiber. Moreover, the graph shows that there is a good correlation between the two analytical methods and as expected the amount of reacted titanium increases with the reactants Ti/Mg(surf.) ratio. However, this increase is not regular. For example, the amount of titanium found in the fibers of reaction [B] is greater than in reaction [C], though the titanium chloride concentration used in the latter reaction is greater. Hence, in Fig. 5, points B and C are inverted on the graph, as well as points corresponding to reactions [E], [F], and [G]. As we will see further, the amount of reacted titanium depends on the heating rate of the reaction.

All the elemental analyses for the THF reacted fibers invariably gave Cl/Ti ratios equal to or smaller than 2, depending on the experiment. For example, the fibers from reactions [B] and [I] give atomic ratios of 1.86 and 0.88, respectively. Thus it seems that the titanium attached species, (fiber)–$TiCl_n$, is a mixture of $n \leq 2$ species.

Moreover, the ir spectrum of the $TiCl_3$–THF treated fiber contained more water after reaction judging from the stronger H_2O bands at ca. 3400 and 1625 cm^{-1}. Figure 6 shows the high frequency ν(OH) water band for THF reacted fibers (reaction [H], Table 2). After reaction the intensity of this band is already stronger relative to the chrysotile spectrum when compared to the original unreacted fibers. Heating the treated fibers under vacuum caused the set of water bands to grow as shown for the ν(OH) band at 3400 cm^{-1} in spectra [B] and [C]. Concomitantly, new bands at 2960, 1260, and 795 cm^{-1} for the reacted fibers were also affected in the same way. Goni *et al.* (21) have studied the ir spectra of acid lixiviated chrysotile. Especially interesting is the absorption band, here at 795 cm^{-1}, which they assign to the presence of amorphous silicate and is taken to be symptomatic for open or unrolled fibers. Early thermal decomposition of the chrysotile can be ruled out to explain the observed ir changes on the basis of previously reported ir results on the thermal degradation of asbestos (24). The thermally induced lixiviation observed here is consistent with the proposed reaction scheme in Fig. 7.

The differential thermogravimetric analysis curves for the reacted and unreacted fibers were found to be identical. Both curves show weight loss caused by residual water at 100 and

Can. J. Chem. Downloaded from www.nrcresearchpress.com by 210.87.254.42 on 09/06/12
For personal use only.

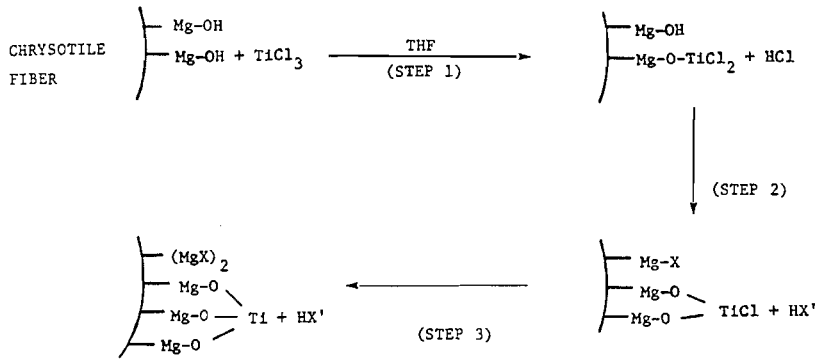

FIG. 7. Proposed reaction scheme for chrysotile asbestos with $TiCl_3$ in THF; X = OH or Cl, X′ = Cl or OH.

111°C, and dehydroxylation of chrysotile at 658 (−11.7 wt%) and 676°C (−11.4 wt%), respectively. From the recorded weight loss, the amount of water contained in the reacted fibers is 2.1 wt% compared to less than 0.1 wt% before reaction. Furthermore, the weight loss usually observed at 370−400°C(1) due to dehydroxylation of amorphous brucite, often present with asbestos minerals, was negligible (<0.1 wt%) for the short fibers and was not observed for the reacted fibers.

In one experiment, THF reacted fibers were washed for 24 h with THF in a soxhlet under positive argon pressure. The only change in the composition of the resulting white chrysotile, cf. microanalysis in Table 1, is the disappearance of chlorine. Furthermore, the sem spectroscopic results corroborate the presence of titanium and the fibrous structure of the product. The absence of chloride in these fibers can be accounted for by the reaction scheme discussed below.

The reaction scheme in Fig. 7 summarizes the observed chemical behavior of $TiCl_3$−THF treated asbestos chrysotile. For example, the analytical data for the soxhlet extracted fiber are consistent with the reaction product of step 3, X = OH and X′ = Cl. In summary, this scheme is applicable in any case where reacted fibers are either directly or indirectly submitted to heat treatment such as in a reaction or soxhlet extraction. Therefore, when X′ = Cl the freed hydrogen chloride can, in the presence of trace amounts of H_2O, lixiviate the fiber, steps 1, 2 and 3. On the other hand, if X′ = OH water is directly produced. In either case, the reaction scheme accounts well for the observed experimental data of $TiCl_3$−THF reacted fibers; i.e. increased water and decreased chloride content of the fibers as $TiCl_3$ reacts with chrysotile.

These results lend support to our belief that the titanium chloride is chemically bonded to chrysotile and not chemisorbed. Attempts to isolate characteristic titanium vibrations (e.g. ν (Ti—O), ν(Ti—Cl), etc.) between 1000 and 200 cm^{-1} in the ir were unsuccessful owing to strong silicate and brucite vibration modes in this region. We are currently seeking more information on the titanium binding mode to the fiber using Auger, esca, and uv spectroscopic techniques.

Acknowledgements

The authors are especially grateful to the "Institut de recherche et de développement sur l'amiante (IRDA)", as well as to the Quebec "Formation de chercheurs et d'action concertée (FCAC)" foundation program and to the Natural Sciences and Engineering Research Council of Canada (NSERC) for their financial support. Moreover, two of us (R.D. and C.D.) are indebted to the "Institut de recherche en santé et sécurité au travail (IRSST)" for their contribution of a summer stipend during the course of this work.

1. P.-C. AITCIN, and F. KIMMERLE (*Editors*). L'Amiante chrysotile. Université de Sherbrooke. Sherbrooke, P.Q., Canada. 1981. Chapt. 5.
2. H. EDWARDS. J. Appl. Chem. **20**, 76 (1970).
3. R. F. GOULD. (*Editor*). Adv. Chem. **134**, 16 (1974); D. F. HERMAN, A. L. RESNICK, and D. SIMONE. U.S. Pat. No. 3 265 644 (1966); J. C. BOLGER. U.S. Pat. No. 3 519 593 (1970); A. SHERMAN MICHAELS. U.S. Pat. No. 3 519 594 (1970).
4. M. S. BADOLLET and J. P. MCGOURTY. *In* Asbestos: a symposium of articles. *Edited by* M. S. Badollet. The Canadian Mining and Metallurgical Bulletin. 1961. p. 44.
5. P.-C. AITCIN and F. KIMMERLE. (*Editors*). L'Amiante chrysotile. Université de Sherbrooke. Sherbrooke, P.Q., Canada. 1981. Chapt. 8.
6. M. S. BADOLLET. *In* Asbestos: a symposium of articles. *Edited by* M. S. Badollet. The Canadian Mining and Metallurgical Bulletin. 1961. p. 30.
7. K. YADA. Acta Crystallogr. **23** 704 (1967).
8. S. M. AHMED. Adsorption from aqueous solutions. *Edited by* P. H. Tewari. Plenum Press, New York, U.S.A. 1981. p. 213.
9. J. DUNNIGAN, D. NADEAU, D. PARADIS, J.-P. PELÉ, R. CALVERT, J.-M. LALANCETTE, and M. COSSETTE. Fourth International Conference on Asbestos. Torino, Italy. May 1980. M. V. Marshal, D. L. McLemore, D. L. Feuerbacher, and A. C. Griffin. Proc. Am. Asso. Cancer Res. **22**, 72 (1981).
10. S. SHUGAR. Les effets de l'amiante dans l'environnement au Canada. National Research Council of Canada publication No. 16453 (1980). Ottawa, Canada; E. T. DEGENS, W. A. P. LUCK, and D. D. PERRIN. Topics in current chemistry. Inorganic biochemistry. Vol. 64, Springer-Verlag, Berlin, W. Germany. 1976. p. 3.
11. D. COZAK, M. PAGÉ, G. HARVEY, L. DUMAS, and M. FONTAINE. Second International Conference on Clinical Chemistry and Chemical Toxicology of Metals. Montreal, Canada. July 1983. L. DUMAS, M. PAGÉ et M. SENNEVILLE. Hémolyse et cytotoxicité des fibres d'amiante *in vitro*. Cinquantième congrès de l'association canadienne française pour l'avancement des sciences (ACFAS). Montréal, Canada. May 1982.
12. GUY HARVEY. M. Sc. thesis. Université Laval, Laval. September 1982.
13. J. L. MYERS, R. W. LASHER, and R. D. JAMES. U.S. Pat. No. 3 947 286 (1970); Chem. Abstr. **85**: 99046*j*.
14. R. DECHENNE and P. DECROLE. Ger. Pat. No. 2 130 677 (1971); Chem. Abstr. **76**: 114154 (1972).
15. C. JOLICOEUR, P. ROBERGE, and J.-L. FORTIER. Can. J. Chem. **59**, 1140 (1981).
16. E. S. CRAWFORD, D. A. JEFFERSON, J. M. THOMAS, and A. C. BISHOP. J. Chem. Soc. Chem. Commun. 986 (1978).

Can. J. Chem. Downloaded from www.nrcresearchpress.com by 210.87.254.42 on 09/06/12
For personal use only.

17. M. SUZUKI, S. AITA, and H. HAYASHI. Jeol News, **13**, 7 (1975).
18. F. A. COTTON and G. WILKINSON. Advanced inorganic chemistry. John Wiley and Sons. 4th ed. New York, U.S.A. 1980. p. 702.
19. M. ORHANOVIC and J. E. EARLEY. Inorg. Chem. **14**, 1478 (1975).
20. B. S. BRUNSCHWIG and N. SUTIN. Inorg. Chem. **18**, 1731 (1979) and references therein.
21. Z. JOHAN, J. GONI, C. SARCIA, G. BONNAUD, and J. BIGNON. Advances in organic geochemistry. Proceedings of the Sixth International Meeting on Organic Geochemistry. Rueil-Malmaison, France. September 1973. *Edited by* B. Tissot and F. Bienner. Edition Technip. Paris, France. 1973.
22. M. FREDERICK, JR. U.S. Pat. No. 3 957 571 (1976); Chem. Abstr. **85**: 112187*c* (1976); J. DUNNIGAN. Can. Pat. Deposit. No. 375388. April (1981).
23. P. SHARROCK. Geochim. Cosmochimi. Acta, **46**, 1311 (1982).
24. C. JOLICOEUR and D. DUCHESNE. Can. J. Chem. **59**, 1521 (1981).

Can. J. Chem. Downloaded from www.nrcresearchpress.com by 210.87.254.42 on 09/06/12
For personal use only.

Picosecond excited state absorption studies of isothiocyanato complexes of Cr(III) in solution[1,2]

R. LE SAGE, K. L. SALA,[3] AND R. W. YIP
Division of Chemistry, National Research Council of Canada, Ottawa, Ont., Canada K1A 0R6

AND

C. H. LANGFORD
Department of Chemistry, Concordia University, Montreal, P.Q., Canada H3G 1M8

Received May 19, 1983

R. LE SAGE, K. L. SALA, R. W. YIP, and C. H. LANGFORD. Can. J. Chem. **61**, 2761 (1983).

The spectra and risetimes for the doublet excited state absorption (ESA) of *t*-$[Cr(NH_3)_2(NCS)_4]^-$ (Reineckate ion), $[Cr(NCS)_6]^{3-}$, and *t*-$[Cr(en)_2(NCS)_2]^+$ have been measured at picosecond times in several solvents. The ESA spectra observed after approximately one half the risetimes showed no measurable change with time. The result is consistent with vibrational relaxation times which are comparable to or faster than the risetimes. The ESA risetimes for Reineckate ion and *t*-$[Cr(en)_2(NCS)_2]^+$ were found to be fastest in hydroxylic solvents and slowest in non-hydroxylic solvents. No such solvent trend was found for $[Cr(NCS)_6]^{3-}$. Possible photophysical models to account for the observed solvent-dependent risetimes are discussed. Kinetic simulations based on a quasi four-level model which explicitly includes the pump pulse function are reported.

R. LE SAGE, K. L. SALA, R. W. YIP et C. H. LANGFORD. Can. J. Chem. **61**, 2761 (1983).

On a mesuré les spectres et les temps d'apparition de l'absorption de l'état excité du doublet (AEE) de *t*-$[Cr(NH_3)_2(NCS)_4]^-$ (ion de Reineckate), de $[Cr(NCS)_6]^{3-}$ et de *t*-$[Cr(en)_2(NCS)_2]$ dans des temps de l'ordre de la picoseconde et dans plusieurs solvants. Les spectres observés pour l'AEE après approximativement la moitié du temps d'apparition ne révèlent pas de changements mesurables avec le temps. Le résultat est en accord avec des temps de relaxation vibrationnelle qui sont comparables ou plus élevés que les temps d'apparition. On a trouvé que les temps d'apparition de l'AEE de l'ion de Reineckate et du *t*-$[Cr(en)_2(NCS)_2]$ sont plus rapides dans les solvants hydroxyliques et plus lents dans les solvants non hydroxyliques. On n'a pas trouvé une telle tendance avec le $[Cr(NCS)_6]^{3-}$. On discute des modèles photophysiques susceptibles d'expliquer l'influence du solvant sur les temps d'apparition. On rapporte les simulations cinétiques basées sur le quasi modèle à 4 niveaux qui comprend explicitement la fonction de pompe à pulsation.

[Traduit par le journal]

1. Introduction

In O_h symmetry Cr(III) complexes, the photochemistry and photophysics are associated with two close-lying states: a $^4T_{2g}$ and a ^2E_g state, the former being "distorted" with respect to the ground state. The spin-forbidden ^2E_g state, which is usually the lowest energy and the emitting state, has been extensively studied (1–4). However, owing to the close but unquantified proximity of the two excited states, the respective roles of the quartet and doublet states in photoreactions and in the decay of the doublet state has not yet been unambiquously delineated for most systems (3–8).

Although the vibrationally relaxed doublet state of Cr(III) complexes is well characterized, data at early times leading to the formation of the relaxed doublet are sparse. Notable exceptions are the picosecond excited state absorption (ESA) studies by Windsor and co-workers (9, 10). Doublet risetimes of 16–22 ps for three Cr(III) isothiocyanato complexes in H_2O were reported. It was suggested that the risetime may reflect a combination of intersystem crossing and relaxation within the doublet manifold.

The influence of solvent on the primary photophysical/photochemical rates following population of the Franck–Condon quartet state is unclear. Provided that intersystem crossing occurs after substantial quartet relaxation, significant change from the Franck–Condon geometry and solvent reorganization can occur. The role of solvent in the relaxation process might involve a non-specific property such as viscosity or a specific solvent–ligand interaction such as hydrogen bonding.

To gain further understanding of the primary processes involved in Cr(III) complexes, we have measured the doublet ESA spectra and risetimes of $[Cr(NCS)_6]^{3-}$, *t*-$[Cr(NH_3)_2(NCS)_4]^-$ (Reineckate ion, R^-), and *t*-$[Cr(en)_2(NCS)_2]^+$ in a variety of solvents and analyzed these results in terms of the rate constants associated with the quartet and doublet states. Kinetic simulations in terms of a quasi four-level model are reported.

2. Experimental

The Nd/glass picosecond absorption apparatus used (11) was similar to that reported earlier (12) but has been significantly improved. The 5 cm D_2O cell used to produce the 1.06 u superbroadened picosecond probe beam (13, 14) was reduced to 2.0 cm. This reduction in cell length resulted in a probe beam with a reduced chirp (measured 6 ps) (15) and which was spectrally more uniform and reproducible across the echelon. The equally stepped echelon used previously was replaced with a quartz 5-step echelon having relative step differentials of 50, 5, 5, 20, and 50 mm (= 81.3, 8.13, 8.13, 32.5, and 81.3 ps at 5300 Å). The first step provided a "$-\infty$" time spectrum in advance of the 5300 Å pump pulse and the last step a "$+\infty$" long time continuum reference spectrum. The spectra were recorded on Royal Pan-X sheet film which was pushed-developed (in HC-110B) to yield an effective ASA of 3000, with a measured γ of 0.64 and a linear density range of 0.4–1.4. The film containing a set of six spectra was scanned by a microprocessor-controlled sampling microdensitometer (16). The data were smoothed by a series of Fast Fourier transform based algorithms (11) to yield a sequence of related density spectra. A selected

[1]NRCC No. 22596.

[2]Taken, in part, from the Ph.D. Thesis of R.L.S., Carleton University, Ottawa, Canada.

[3]NRCC Research Associate, 1980–1983.

Can. J. Chem. Downloaded from www.nrcresearchpress.com by 210.87.254.42 on 09/06/12
For personal use only.

Can. J. Chem. Downloaded from www.nrcresearchpress.com by 210.87.254.42 on 09/06/12
For personal use only.

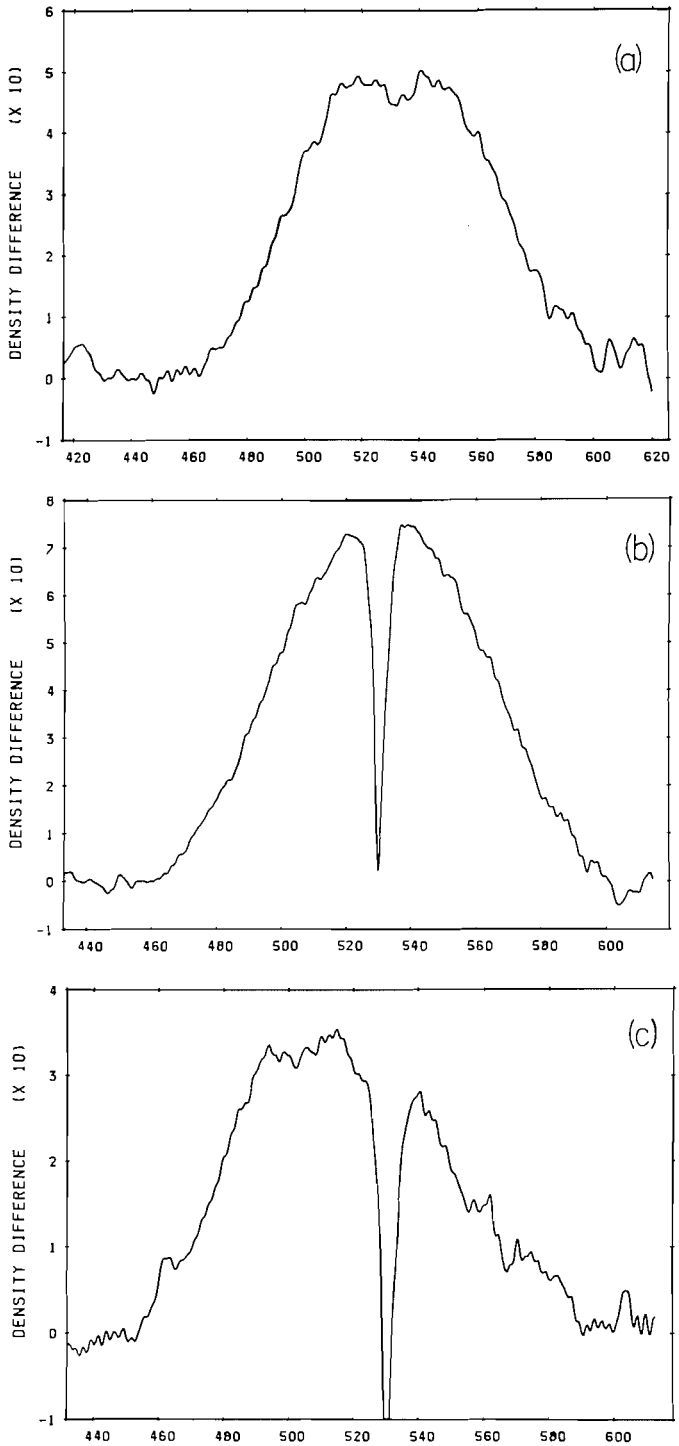

FIG. 1. Transient absorption spectra of R^- in (*a*) in DMF at 51 ps; (*b*) in acetone at 160 ps; and (*c*) H_2O at 57 ps.

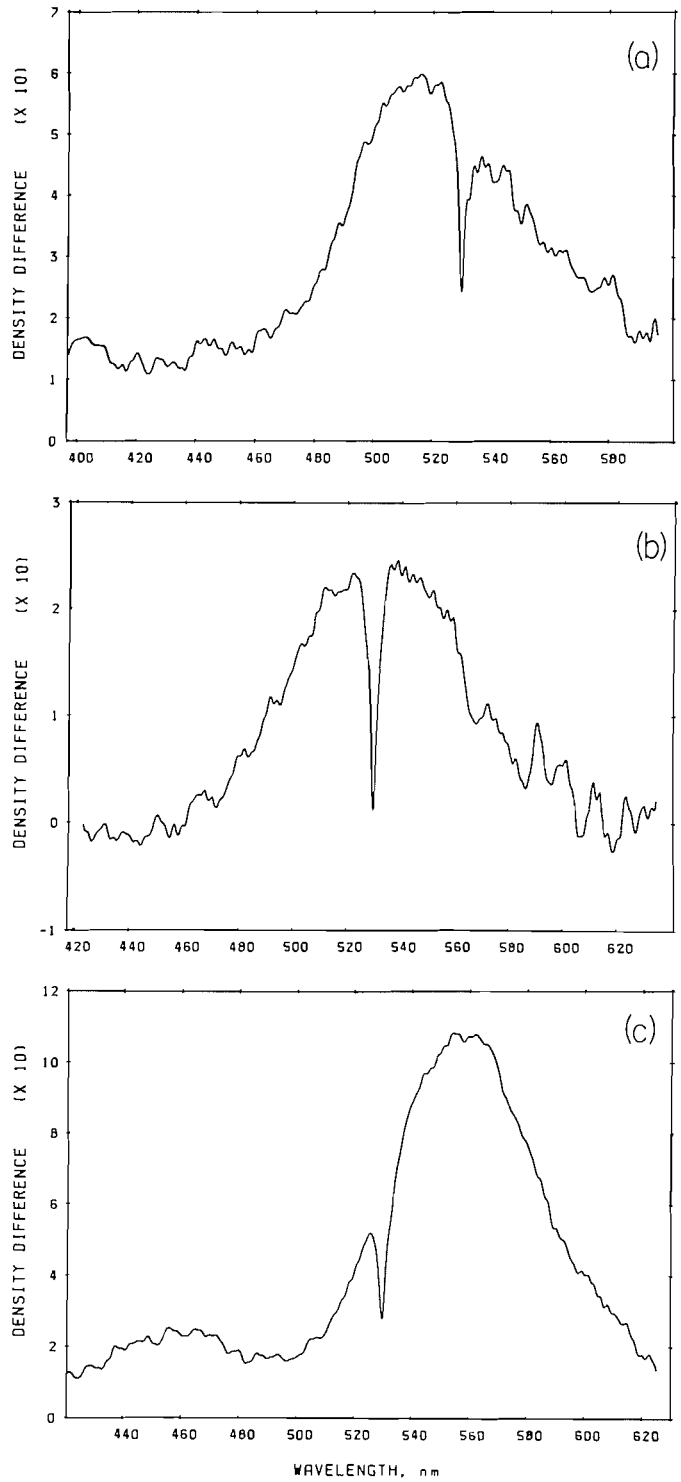

FIG. 2. Transient absorption spectra of some isothiocyanato Cr(III) complexes in acetonitrile solution. (*a*) $[Cr(NCS)_6]^{3-}$ at 47 ps; (*b*) R^- at 71 ps; and (*c*) $[Cr(en)_2(NCS)_2]^+$ at 43 ps.

wavelength range of the transient absorption spectra was integrated and used for kinetics. The relative timing of the excitation and probe pulse was determined to within 3 ps by a sensitive zero-background null method based on the Kerr gating of the continuum pulse (15).

3. Results

Transient absorption spectra were observed when $[Cr(NCS)_6]^{3-}$, R^-, and *t*-$[Cr(en)_2(NCS)_2]^+$ in various solvents were excited by picosecond laser pulses at 530 nm. Typical spectra recorded at probe delay times of less than 100 ps are shown in Figs. 1 and 2, and the transient absorption maxima recorded in Table 1. The transient absorption band observed for both R^- and *t*-$[Cr(en)_2(NCS)_2]^+$ showed a noticeable solvent dependence (shifted towards the blue in water), whereas the symmetric complex $[Cr(NCS)_6]^{3-}$ did not. The intensities of the transient absorption bands for R^- and $[Cr(NCS)_6]^{3-}$ were comparable, independent of solvent, and approximately two times less intense than that for *t*-$[Cr(en)_2(NCS)_2]^+$. We were

TABLE 1. Absorption maxima of transient[a]

Complex	Solvent	$\lambda_{max,nm}$
R^-	CH_3CN	533, (525)[b]
	DMF	531
	CH_3COCH_3	530
	CH_3CH_2OH	530
	D_2O	510
	H_2O	510
	CH_3CN/H_2O (X_{H_2O}=0.84)	(521)[c]
t-$[Cr(en)_2(NCS)_2]^+$	CH_3CN	558, 456
	H_2O	530
$[Cr(NCS)_6]^{3-}$	CH_3CN	516
	DMF	520
	H_2O	520
	Glycerol/H_2O (65% by wt.)	516
	Alcohol glass (100 K)	(538)[d]
	EPA (77 K)	(542)[e]

[a]Figures in parentheses are the literature values for the doublet excited state.
[b]Reference 20.
[c]Reference 19.
[d]Reference 17.
[e]Reference 18.

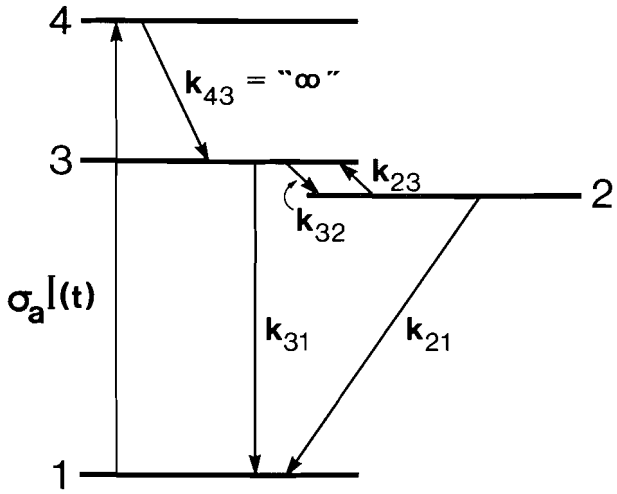

FIG. 3. Schematic of a quasi four-level system.

unable to detect a change in any of the transient absorption spectra with time. Any change was therefore either small or very rapid ($t < 1/2$ risetime), or both.

Buildup of the transient absorption for the complexes varied from a few picoseconds to tens of picosecond depending upon the complex and solvent. During the excitation pulse, formation of the transient population will be integral functions of the excitation pulse. Therefore, for those transients rising within one or two laser pulse widths (6–12 ps), the pump pulse function cannot be ignored in any kinetic analysis. For a quasi four-level system (Fig. 3), we have for the populations of the three states:

$$[1] \quad \dot{n}_1 = -\sigma_a I(t) n_1 + k_{31} n_3 + k_{21} n_2$$

$$[2] \quad \dot{n}_2 = k_{32} n_3 - (k_{23} + k_{21}) n_2$$

$$[3] \quad \dot{n}_3 = \sigma_a I(t) n_1 + k_{23} n_2 - (k_{31} + k_{32}) n_3$$

where σ_a is the absorption cross section (see Fig. 3). Empirically, a satisfactory fit of the data was obtained with the function

$$[4] \quad n_2(t) = 1/2(T\sqrt{\pi} I_0 \sigma_a n_1) \{\exp(-k_{32}t + k_{32}^2 T^2/4) \times [1 + \text{erf}(t/T - k_{32}T/2)] - [1 + \text{erf}(t/T)]\}$$

which can also be derived from the three coupled differential equations for the conditions in which $\dot{n}_1 = 0$; $k_{31} = k_{21} = k_{23} = 0$; and for the Gaussian pulse

$$[5] \quad I(t) = I_0[\exp(-t^2/T^2)]$$

where I_0 is the peak photon flux of the pump pulse. The data were fitted to eq. [4] by trial values of the parameter T and k_{32} to find the smallest value of the sum of squares of the residuals between the calculated and observed values of n_2 for the set of data. The parameter T in the Gaussian pulse is related to τ, the full-width at half-maximum (FWHM) by $T = \tau/2\sqrt{\ln 2}$. The kinetics for formation of the transient from R^- in D_2O and acetone are shown in Figs. 4 and 5. The solid curves are calculated from eq. [4]. Risetime results are recorded in Table 2. The most significant variations in the risetimes were found for R^- which varied from less than 6 ps in H_2O to 29 ps in DMF. The risetimes of R^- in H_2O appeared to be faster than

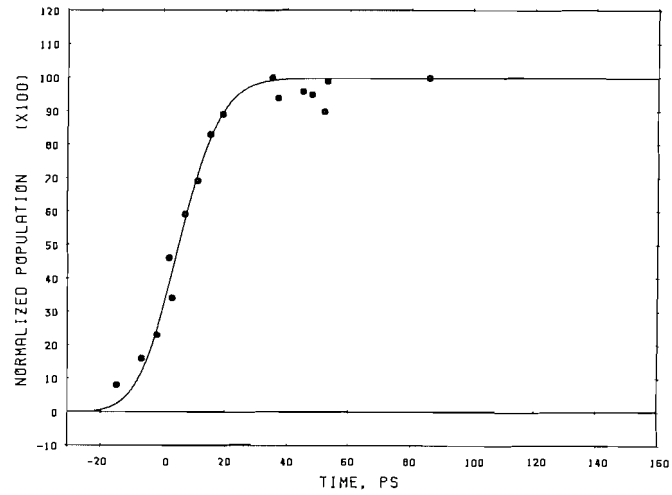

FIG. 4. Transient ESA buildup for R^- in D_2O. The solid curve was calculated from eq. [4] (see text).

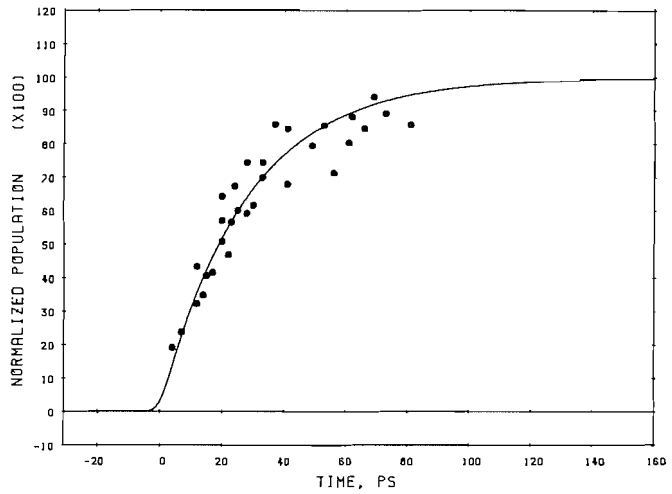

FIG. 5. Transient ESA buildup for R^- in acetone. The solid curve was calculated from eq. [4] (see text).

Can. J. Chem. Downloaded from www.nrcresearchpress.com by 210.87.254.42 on 09/06/12
For personal use only.

Can. J. Chem. Downloaded from www.nrcresearchpress.com by 210.87.254.42 on 09/06/12
For personal use only.

TABLE 2. Risetime of transient[a]

Complex	Solvent	τ, ps
R^-	CH_3CN	18
	DMF	29
	CH_3COCH_3	27
	CH_3CH_2OH	8
	D_2O	6 (11)[b]
	H_2O	<6 (22)[b] (<5)[c]
t-$[Cr(en)_2(NCS)_2]^+$	CH_3CN	15
	H_2O	9 (16)[b]
$[Cr(NCS)_6]^{3-}$	CH_3CN	5
	DMF	10
	H_2O	11 (16)[b]
	Glycerol/H_2O (65% by wt.)	6

[a]Figures in parentheses are literature values.
[b]Reference 10.
[c]Reference 9.

D_2O but both risetimes are fast and close to the temporal width of the laser pulse. While it is possible to obtain reliable risetimes to within a fraction of the laser pulse width using our data fitting procedure, the requirement of low jitter in the width of the pulse from shot to shot is presently one of the main, though not insurmountable, difficulty towards realizing a shorter time resolution.

4. Discussion

The transients observed for the three chromium complexes have been assigned to excited state absorption from the doublet state on the basis of the agreement between the transient absorption and phosphorescence lifetimes (7−10, 17−21). The ESA risetime for R^- and *t*-$[Cr(en)_2(NCS)_2]^+$ were found to be fastest in hydroxylic solvents and slowest in non-hydroxylic less polar solvents. No such solvent trend was found for the symmetric $[Cr(NCS)_6]^{3-}$. The risetime in glycerol/water was not significantly different from the less viscous solvents. This observation could be interpreted in two ways: either (*1*) bulk viscosity does not correlate with the difficulty of solvation shell rearrangement because of the presence of few glycerol molecules in the solvent sphere of the complex ion, or (*2*) solvent-restricted quartet relaxation for $[Cr(NCS)_6]^{3-}$ is unimportant in the photophysics.

The absence of observable time dependent changes in the ESA spectra after approximately one half the risetimes is consistent with vibrational relaxation times which are comparable to or faster than the risetimes. Absorption from vibrationally unrelaxed states of the doublet appears as "hot band" absorption. In the case of very fast crossing the unrelaxed doublet followed by slow vibrational relaxation to the zero level of the doublet, the shift is given by the difference in energy between the pump wavelength and 0−0 transition between the doublet and the ground state. The shift is substantial for the present complexes. In the case of reduced hot band population due to substantial vibrational relaxation, the shift is less evident. Another caveat to the above conclusion is the remote possibility of the effects of vibrational relaxation being masked by compensating time-dependent solvation effects.

The simplest interpretation of the observed solvent-dependent ESA risetimes is to assume that the risetime is governed by the rate of intersystem crossing from the quartet manifold. An intersystem crossing model involving "prompt" crossing from the unrelaxed quartet levels and a slower crossing rate is expected to give a risetime with a slow and fast regime. We found no kinetic evidence for this. In the case of R^- in water, buildup of the doublet was complete after less than 20 ps; a slower component, which would be noticeable, was not observed.

A possible explanation for a solvent-dependent intersystem crossing in non-symmetrically substituted complexes such as the R^- ion (D_{4h} symmetry) was suggested by Orlandi and Siebrand (22). The model assumes rapid vibrational relaxation and redistribution and that the solvent dependent electrostatic field of the ligand influences the energies of the quartet states. Because of a lowering in symmetry for O_h to D_{4h} because of the unequal ligands, $^4T_{2g}$ splits into $^4E + {}^4B_{2g}$. The splitting, ϵ, is assumed to be solvent dependent. On the basis of symmetry arguments, the coupling between the ^4E and ^2E is zero but coupling between the $^4B_{2g}$ and ^2E is non-zero. For the case in which the ^4E is lower in energy than the ^4B state, the relative population of the $^4B_2$ and ^4E states differ by the Boltzmann factor $\exp(-\epsilon/kT)$, so that the rate of intersystem crossing

$$[6] \quad k_{isc} = 2\pi/\hbar|\langle {}^2E|H_{so}|{}^4B_2\rangle|^2 \exp(-\epsilon/kT)\rho_E$$

is solvent dependent through ϵ. For R^-, owing to solvation of the charged NCS groups, ϵ is expected to be smaller in polar than non-polar solvents. For the symmetric $[Cr(NCS)_6]^{3-}$ complex, no solvent effect is predicted. For the cationic *t*-$[Cr(en)_2(NCS)_2]^+$ complex where the relative energies of the $^4B_{2g}$ and ^4E states would be the opposite that of R^-, no solvent effect is predicted. The Orlandi−Siebrand model correctly predicts the trend of the results for R^- and $[Cr(NCS)_6]^{3-}$ but not for *t*-$[Cr(en)_2(NCS)_2]^+$, where a small solvent effect is observed. In the case of the *t*-$[Cr(en)_2NCSF]^+$, differential quenching and quantum yield evidence does indeed suggest the participation of two quartet states (23).

Hollebone and co-workers (24) have described a model in which photochemistry and intersystem crossing competes with vibrational relaxation and redistribution. In this model, population and decay on a specific nuclear coordinate governs the photophysical and photochemical behaviour. Solvents which hydrogen bond to the ligands could couple to vibrational coordinates active in intersystem crossing. The present data are consistent with the view that hydrogen-bonding is an important influence on the rate of intersystem crossing.

Thus far, we have assumed that the risetime is governed only by the rate constant for intersystem crossing, k_{32}. To investigate the sensitivity of the *form* of the normalized risetime function to other rate constants, numerical simulations were carried out based on the quasi four-level system (Fig. 3). The system can be characterized by the equations:

$$[7a] \quad \dot{n}_2(x) = R_5[n_3 - (R_2 + R_3)n_2]$$

$$[7b] \quad \dot{n}_3(x) = R_5[R_4F(x)(1 - n_2 - n_3) + R_3n_2 - (1 + R_1)n_3]$$

$$[8] \quad n_1 + n_2 + n_3 = 1$$

and the five dimensionless parameters:

$$[9a] \quad R_1 = k_{31}/k_{32}$$

$$[9b] \quad R_2 = k_{21}/k_{32}$$

$$[9c] \quad R_3 = k_{23}/k_{32}$$

$$[9d] \quad R_4 = \sigma_a I_0/k_{32}$$

$$[9e] \quad R_5 = \tau k_{32}$$

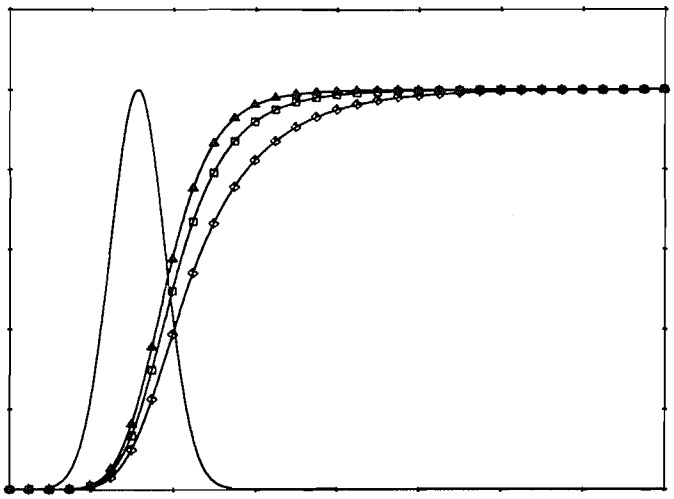

FIG. 6. Calculated normalized $n_2(x)$ vs. x from numerical simulation (see text). $R_2 = 0, R_3 = 0, R_4 = 0, R_5 = 1.0$. (△) $R_1 = 0$; (□) $R_1 = 0.5$; (◇) $R_1 = 1.0$. The curve without symbol is the Gaussian pump function $F(x)$ vs x.

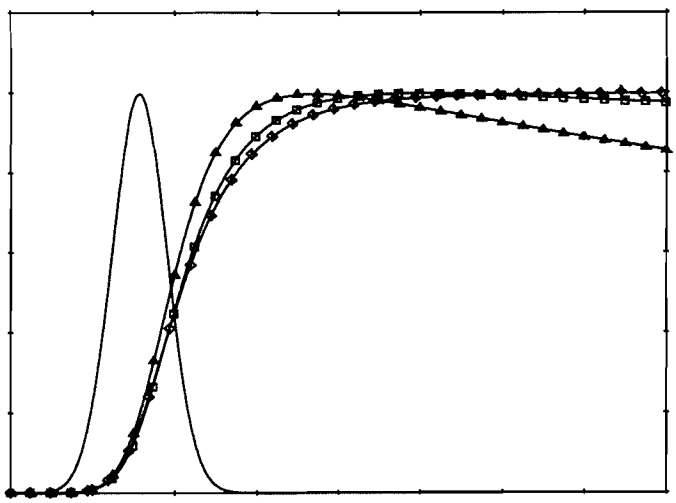

FIG. 7. Calculated normalized $n_2(x)$ vs. x from numerical simulation (see text). $R_2 = 0, R_3 = 0.1, R_4 = 0, R_5 = 1.0$. (△) $R_1 = 0$; (□) $R_1 = 0.1$; (◇) $R_1 = 0.5$. The curve without symbol is the pump pulse function $F(x)$ vs. x.

where τ is the full-width at half-maximum of the pump pulse, and I_0 is the maximum intensity of the pump pulse $I(t) = I_0F(x)$, $(0 < F(x) < 1$ for $\tau > 0)$, and $x = t/\tau$. The coupled first-order differential equations, [7*a*] and [7*b*], which explicitly include the pump function, were solved using Hamming's modified predictor-corrector method (25). The time-dependent population of level 2, $n_2(t)$, was calculated for a Gaussian pump pulse and for the parameter $R_2 = 0$, since decay of the doublet state is known to be negligible over the range of the dimensionless time variable $x = t/\tau$ of the simulation. Details of a general treatment of the quasi four-level system, driven by an arbitrary laser pulse, will be reported in a future publication. The normalized population of level 2 together with the laser pulse function is shown in Figs. 6–8. The simulation shows that: (*1*) For no reverse reaction ($k_{23}/k_{32} = 0$), level 2 builds up more rapidly as k_{31} is increased. (*2*) The rate of buildup of level 2 is also increased when the reverse reaction is included ($k_{23}/k_{32} > 0$). In this case, the effect of k_{31} is to cause a decay in the population of level 2 after the maximum population is reached.

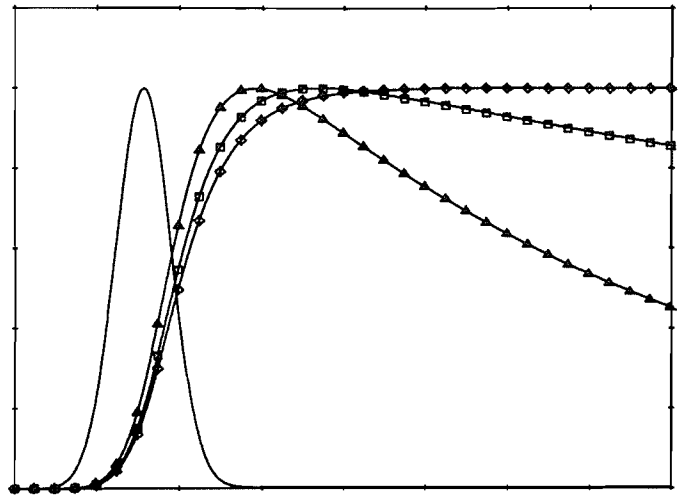

FIG. 8. Calculated normalized $n_2(x)$ vs. x from numerical simulation. $R_2 = 0, R_3 = 0.5, R_4 = 0, R_5 = 1.0$. (△) $R_1 = 0$; (□) $R_1 = 0.1$; and (◇) $R_1 = 0.5$. The curve without symbol is the pump pulse function $F(x)$ vs. x.

In the present study, no doublet state decay has been observed over the range of time studied. Therefore the rate of back intersystem crossing from the initially formed vibrationally excited doublet state appears to be significantly slower than the rate of intersystem crossing or vibrational relaxation. The simulation suggests that the conditions $k_{23}/k_{32} > 0.1$ and $k_{31}/k_{32} > 0.1$ cannot be both true. Less can be said about the relative rates of decay and intersystem crossing of the quartet state. There are two consequences of quartet decay in competition with intersystem crossing: the yield of doublet, and the form of the doublet population vs. time function (especially in the rising part) are affected. If the rate constant for intersystem crossing (k_{isc}) is much greater than other quartet decay channels (k_Q), then the doublet yield will not be very sensitive to changes in k_Q. Current data on the relative doublet yield in various solvents are consistent with this condition, although we cannot exclude the possibility on the basis of doublet yield alone, that both k_Q and k_{isc} are affected by solvent.

As the simulation shows, the precise form of the doublet population function is sensitive to five kinetic parameters R_1–R_5. Of the five, R_4 is constant and R_5 can be controlled. The parameter R_2, which measures decay directly from the doublet state, is known to be small compared with R_1 and R_3. With sufficiently accurate data, it is thus possible to obtain the rate constants for quartet decay and back intersystem crossing relative to that for intersystem crossing by fitting the data with the exact form of the population function. The realization of this goal awaits the obtention of highly accurate kinetic data which requires close control of the laser parameters and possibly signal averaging.

Acknowledgements

We thank W. Siebrand (NRCC), B. R. Hollebone (Carleton University), and G. Orlandi (University of Bologna) for stimulating discussion.

1. A. W. ADAMSON and P. D. FLEISCHAUER (*Editors*). Concepts in inorganic photochemistry. Wiley, New York. 1975.
2. V. BALZANI and V. CARASSITI. Photochemistry of coordination

Can. J. Chem. Downloaded from www.nrcresearchpress.com by 210.87.254.42 on 09/06/12
For personal use only.

compounds. Academic Press, London. 1970.
3. A. D. KIRK. Coord. Chem. Rev. **39**, 225 (1981).
4. N. J. SHIPLEY and R. G. LINCK. J. Phys. Chem. **84**, 2492 (1980).
5. L. S. FORSTER, and F. CASTELLI. J. Phys. Chem. **84**, 2492 (1980).
6. N. J. LINCK, S. J. BERENS, D. MAGDE, and R. G. LINCK. J. Phys. Chem. **87**, 1733 (1983).
7. S. R. ALLSOPP, A. COX, T. J. KEMP, W. J. REED, S. SOSTERO, and O. TRAVERSO. J. Chem. Soc. Faraday I, **76**, 162 (1980).
8. A. D. KIRK and G. B. PORTER. J. Phys. Chem. **84**, 887 (1980).
9. A. D. KIRK, P. E. HOGGARD, G. B. PORTER, M. G. ROCKLEY, and M. W. WINDSOR. Chem. Phys. Lett. **37**, 199 (1976).
10. S. C. PYKE and M. W. WINDSOR. J. Am. Chem. Soc. **100**, 6518 (1978).
11. K. L. SALA, R. W. YIP, and R. LESAGE. Appl. Spectrosc. **37**, 273 (1983).
12. J. M. GRZYBOWSKI, S. E. SUGAMORI, D. F. WILLIAMS, and R. W. YIP. Chem. Phys. Lett. **65**, 456 (1979).
13. D. K. SHARMA, R. W. YIP, D. F. WILLIAMS, and S. E. SUGAMORI. Chem. Phys. Lett. **41**, 460 (1976).
14. D. K. SHARMA and R. W. YIP. Opt. Commun. **30**, 113 (1979).
15. K. L. SALA, R. LESAGE, and R. W. YIP. Appl. Spectrosc. In press.
16. K. L. SALA, R. LESAGE, and R. W. YIP. Rev. Sci. Instr. **53**, 1682 (1982).
17. R. A. KRAUSE, I. TRABJERG, and C. J. BALLAHUSEN. Chem. Phys. Lett. **3**, 197 (1969).
18. T. OHNO and S. KATO. Bull. Chem. Soc. Jpn. **43**, 8 (1970); **46**, 1602 (1973).
19. S. C. PYKE, M. OGASAWARA, L. KEVAN, and J. F. ENDICOTT. J. Phys. Chem. **82**, 902 (1978).
20. A. R. GUTIERREZ and A. W. ADAMSON. J. Phys. Chem. **82**, 902 (1978).
21. Y. S. KANG, F. CASTELLI, and L. S. FORSTER. J. Phys. Chem. **83**, 2368 (1979).
22. G. ORLANDI and W. SIEBRAND. Private communications.
23. A. D. KIRK, L. A. FREDERICK, and S. G. GLOVER. J. Am. Chem. **102**, 7120 (1980).
24. B. R. HOLLEBONE, C. H. LANGFORD, and N. SERPONE. Coord. Chem. Rev. **39**, 181 (1981).
25. A. RALSTON and H. S. WILF. Mathematical methods for digital computers. Wiley, New York. 1960. pp. 95–109.

Can. J. Chem. Downloaded from www.nrcresearchpress.com by 210.87.254.42 on 09/06/12
For personal use only.

Nitric oxide and oxygen reactions with 1-butene over manganese(III) oxide

ROBERT ANDERSON ROSS[1] AND CRAIG FAIRBRIDGE[2]

Department of Chemistry, Lakehead University, Thunder Bay, Ont., Canada P7B 5E1

Received April 15, 1983

ROBERT ANDERSON ROSS and CRAIG FAIRBRIDGE. Can. J. Chem. **61**, 2767 (1983).

Reactions of 1-butene with nitric oxide from 623 to 723 K and with oxygen from 433 to 573 K have been studied in a differential flow system over manganese(III) oxide. Nitrous oxide was formed in the reaction of the hydrocarbon with nitric oxide along with products of complete combustion. The apparent activation energies were respectively 69 ± 4, 78 ± 4, and 30 ± 4 kJ mol^{-1} for nitrogen, carbon dioxide, and nitrous oxide reaction rates. The corresponding pre-exponential factors were 1.72×10^{-1} and 1.16 $mol^{0.5}\ L^{-0.5}\ m^2\ g^{-1}$, and 1.99×10^{-2} $mol^{-0.35}\ L^{0.35}\ m^2\ g^{-1}$. In the reaction with oxygen, apparent activation energies of 183 ± 4, 523 to 503 K, and 88 ± 4 kJ mol^{-1}, 503 to 433 K, were determined with pre-exponential factors 1.74×10^{15} and 2.94×10^5 $mol^{0.3}\ m^{-2}\ g^{-1}$. During catalysis the oxide underwent a partial phase change from α to γ in both reactions. Additionally, nitrate species were present on the surface after oxidation with nitric oxide. Kinetic expressions have been derived and mechanisms proposed for both reactions which may occur in emission control systems requiring the removal of NO_x and unburned hydrocarbons.

ROBERT ANDERSON ROSS et CRAIG FAIRBRIDGE. Can. J. Chem. **61**, 2767 (1983).

On a étudié les réactions du butène-1 avec l'oxyde nitrique à des températures allant de 623 à 723 K et avec l'oxygène dans l'intervalle de température allant de 433 à 573 K, dans un système à écoulement différentiel sur l'oxyde de manganèse(III). Il se forme de l'oxyde nitreux ainsi que des produits de combustion complète dans la réaction avec l'oxyde nitrique. Les énergies apparentes d'activation sont respectivement de 69 ± 4, 78 ± 4 et de 30 ± 4 kJ mol^{-1} pour les vitesses de réaction de l'azote, du dioxyde de carbone et de l'oxyde nitreux. Les facteurs pré exponentiels correspondants sont respectivement 1,72 $\times 10^{-1}$ et 1,16 $mol^{-0.5}\ L^{-0.5}\ m^2\ g^{-1}$ et $1{,}99 \times 10^{-2}$ $mol^{-0.35}\ L^{0.35}\ m^2\ g^{-1}$. Dans le cas de la réaction avec l'oxygène les énergies apparentes d'activation sont: 183 ± 4 de 523 à 503 K et de 88 ± 4 de 503 à 433 K avec des facteurs pré exponentiels de 1,74 $\times 10^{15}$ et de $2{,}94 \times 10^5$ $mol^{0.3}\ m^{-2}\ g^{-1}$. Au cours de la réaction, l'oxyde subit un changement partiel de phase d'α à γ dans les deux réactions. De plus, on constate la présence d'espèces nitrates sur la surface après l'oxydation par l'oxyde nitrique. On a déduit des expressions cinétiques et on propose des mécanismes pour les deux réactions qui peuvent se produire dans les systèmes de contrôle d'émission nécessitant l'élimination de NO_x et des hydrocarbures qui n'ont pas brûlés.

[Traduit par le journal]

Introduction

Currently the combination of the reduction of oxides of nitrogen and the complete oxidation of hydrocarbons is of practical significance because of the impact of such gases on urban environments. A major source is the automobile exhaust where components from both groups of compounds occur along with oxygen and several pollutants. Catalytic processes may be applied as one way of removing the noxious gases and these processes continue to receive acute attention.

The main problem in finding a suitable catalyst (1) lies probably in obtaining a high activity for hydrocarbon oxidation at low temperatures in tandem with high stability and, thus, an acceptable lifetime. Generally, unsaturated hydrocarbons are more reactive towards oxygen than are saturated hydrocarbons and therefore they react over "milder" catalysts with better selectivity. The reaction rates and selectivities vary with the position of the double bond and the nature of substituent groups (2).

The present work considers the catalysed reaction of 1-butene with nitric oxide and with oxygen in a link to recent studies of the oxidation of ethane by nitrous (3) and nitric oxides (4) over Mn_2O_3.

Experimental

Materials

Oxygen (99.99%), nitric oxide (99.0%), and 1-butene (99.0%) were supplied by Matheson of Canada Limited. All other gases were at least 99.5% pure and were obtained from Canadian Liquid Air Limited. Manganese(III) oxide was prepared and analysed as described elsewhere (5).

Procedure and apparatus

Helium was the carrier gas in the quartz reactor flow system (6) and in the Hewlett–Packard Research Chromatograph, Model 5754B. Gases were analysed by a thermal conductivity bridge from stainless steel analytical columns packed with "Poropak Q" (4). A Beckman 951 NO/NO_x analyser was used in series with the gas chromatograph.

Kinetic measurements were conducted at a total flow rate of 350 mL min^{-1} (NTP) on 1 g catalyst samples, <37 μm maximum diameter with surface area 15.5 $m^2\ g^{-1}$, and were recorded as the rate of carbon dioxide, nitrous oxide, or nitrogen production after attaining the steady level at less than 15% total conversion to products. The temperature regions were defined by the maximum of 15% conversion at the high end and at the low end by the reasonable limits of detection of nitrogen and carbon dioxide, $>10^{-4}$ mol L^{-1}. The experimental conditions were chosen after the usual preliminary tests to ascertain the regime in which reaction rates were not influenced by external or internal diffusion (3).

Infrared spectra were measured with a Beckman IR-12 spectrophotometer (3). A Vacuum Generator ESCA-3 instrument was used for XPS determinations.

Results

The nitric oxide/1-butene reaction

When the catalyst was exposed to 3.06 kPa nitric oxide and 2.32 kPa 1-butene at 673 K, the initial rates of nitrogen (r_1) and carbon dioxide (r_2) formation were very high, Fig. 1. These rates quickly decreased to steady values in approximately 5 h. The rate of nitrous oxide production (r_3) increased in the first hour then decreased to reach a constant value after 5 h. Under these experimental conditions, the rate of reaction remained

[1] Present address: Alcan International Limited, Kingston Laboratories, Box 8400, Kingston, Ont., Canada K7L 4Z4.

[2] Present address: Energy Research Laboratories, Energy, Mines and Resources Canada, 555 Booth Street, Ottawa, Ont., Canada K1A 0G1.

Can. J. Chem. Downloaded from www.nrcresearchpress.com by 210.87.254.40 on 09/06/12
For personal use only.

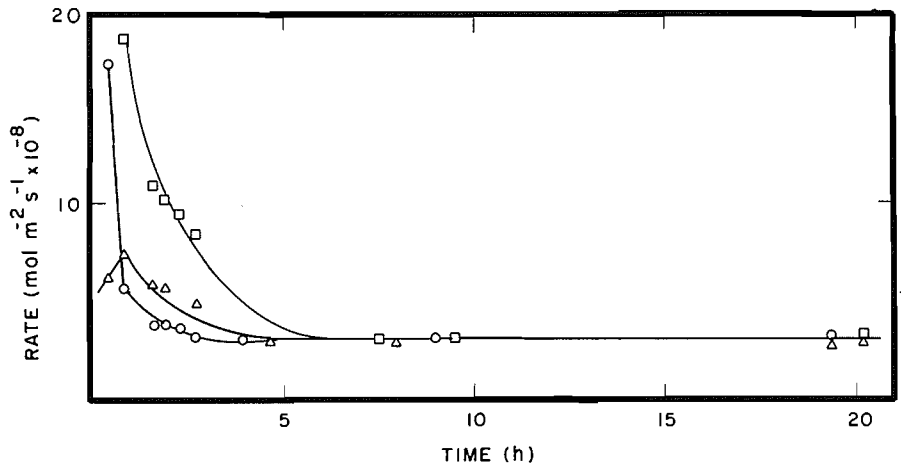

FIG. 1. The effect of exposure time on the NO/C_4H_8 reaction; □, r_1 (nitrogen); ○, r_2 (carbon dioxide); △, r_3 (nitrous oxide).

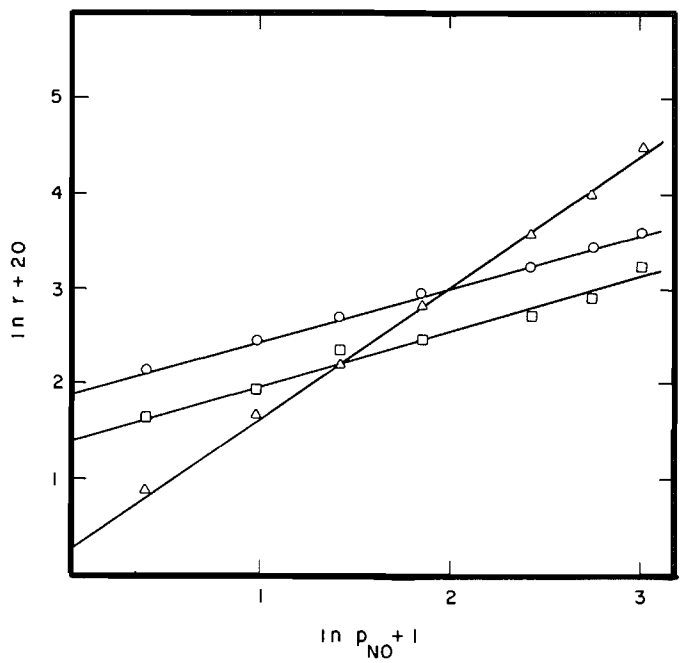

FIG. 2. The effect of variation in nitric oxide partial pressure on the NO/C_4H_8 reaction; □, r_1; ○, r_2; △, r_3.

constant for up to 48 h and the conversion of 1-butene reached 13% at 723 K.

Rate orders were determined at 673 K after catalyst pretreatment under standard conditions of 2.89 kPa nitric oxide and 2.35 kPa 1-butene for 12 h.

Nitric oxide

The partial pressure of nitric oxide was adjusted from 0.17 to 8.17 kPa with 1-butene maintained at 2.60 kPa. A reaction rate order of 0.5 with respect to nitric oxide partial pressure was found from logarithmic plots of nitrogen and carbon dioxide experimental rates, Fig. 2. For the rate of nitrous oxide formation, a rate order of 1.35 with respect to nitric oxide partial pressure was calculated.

1-Butene

A zero order rate dependency with respect to 1-butene partial pressure variations from 0.92 to 7.49 kPa was observed, Table 1, with the partial pressure of nitric oxide constant at 3.05 kPa.

TABLE 1. The effects of component partial pressures on the NO/C_4H_8 reaction over Mn_2O_3

$P_{C_4H_8}$ (kPa)	$r_1 \times 10^{-8}$ (mol m^{-2} s^{-1})	$r_2 \times 10^{-8}$ (mol m^{-2} s^{-1})	$r_3 \times 10^{-8}$ (mol m^{-2} s^{-1})
0.92	3.39	3.00	2.55
1.32	3.26	2.68	2.93
1.44	3.39	2.48	3.19
1.63	3.39	2.74	2.90
2.77	3.26	3.16	3.16
2.84	3.29	3.55	2.81
3.22	2.87	2.80	3.19
3.72	3.10	2.81	2.90
5.50	3.26	2.81	2.58
6.09	3.26	2.74	3.12
7.49	3.19	2.95	2.68
P_{NO} (kPa)	$r_1 \times 10^{-8}$ (mol m^{-2} s^{-1})	$r_2 \times 10^{-8}$ (mol m^{-2} s^{-1})	$r_3 \times 10^{-8}$ (mol m^{-2} s^{-1})
0.17	0.56	0.98	0.07
0.55	1.08	1.78	0.49
0.98	1.43	2.40	1.11
1.52	2.19	3.03	1.84
2.34	2.41	3.94	3.53
4.15	3.00	5.23	7.54
5.75	3.78	6.30	11.25
8.17	5.26	7.54	18.55

Nitrogen

With the partial pressures of nitric oxide and 1-butene maintained at 2.41 and 2.57 kPa, respectively, the nitrogen partial pressure was altered from 0.55 to 6.94 kPa. This had no effect on the rate of reaction, r_2 or r_3, and therefore the rate order was zero with respect to nitrogen concentration.

Carbon dioxide

Variations in the carbon dioxide partial pressure from 0.82 to 7.15 kPa had no effect on the rate of nitrogen or nitrous oxide formation. The reaction was zero order with respect to carbon dioxide concentration wih nitric oxide and 1-butene partial pressures maintained at 2.41 and 2.57 kPa, respectively.

Water vapour

The reactant partial pressures were held constant as described above while the water vapour concentration was altered from 0.07 to 2.41 kPa. This had no effect on the experimental

Can. J. Chem. Downloaded from www.nrcresearchpress.com by 210.87.254.40 on 09/06/12
For personal use only.

Can. J. Chem. Downloaded from www.nrcresearchpress.com by 210.87.254.40 on 09/06/12
For personal use only.

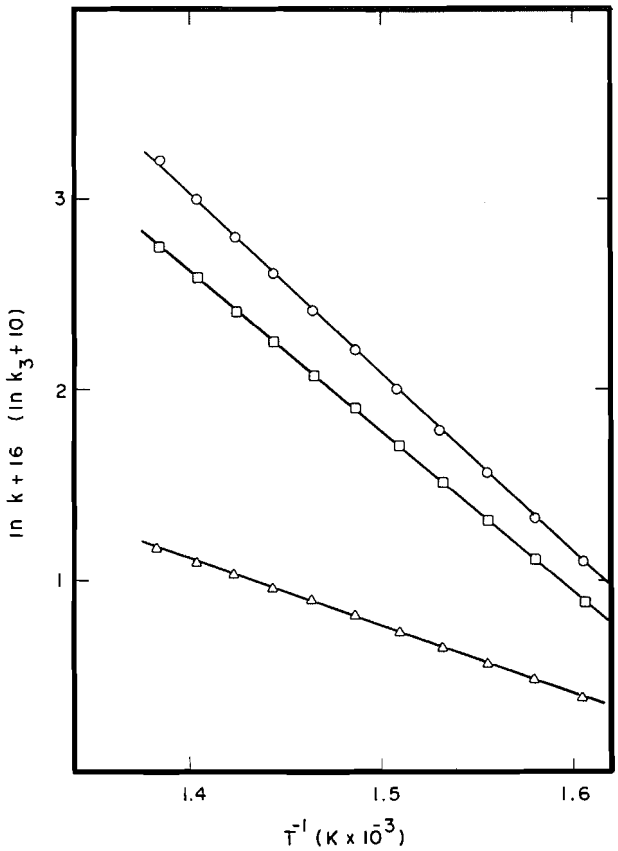

FIG. 3. Arrhenius plots for the NO/C_4H_8 reaction; □, k_1; ○, k_2; △, k_3.

rates of reaction and thus the reaction was zero order with respect to water vapour partial pressure.

From the preceding results, the experimental rate of reaction was given by:

[1] $r = kP_{NO}^{0.5}$

for r_1 and r_2 and

[2] $r_3 = k_3 P_{NO}^{1.35}$

Temperature/time effects

Specific rate constants were calculated from the integrated forms of eqs. [1] and [2] with respect to concentration at temperatures from 723 to 623 K. The catalyst was pretreated with 2.89 kPa nitric oxide and 2.35 kPa 1-butene for 12 h. Apparent activation energies, determined from Arrhenius plots, Fig. 3, were 69 ± 4, 78 ± 4, and 30 ± 4 kJ mol^{-1} from nitrogen, carbon dioxide, and nitrous oxide rates, respectively. The corresponding pre-exponential factors were 1.72×10^{-1} and 1.16 $mol^{0.5}\ L^{-0.5}\ m^2\ g^{-1}$, and $1.99 \times 10^{-2}\ mol^{-0.35}\ L^{0.35}\ m^2\ g^{-1}$.

After 48 h exposure to 3.06 kPa nitric oxide and 2.32 kPa 1-butene at 673 K, the catalyst surface area remained 15.5 $m^2\ g^{-1}$. Under the scanning electron microscope, catalyst particles exhibited a separate crystalline phase on parts of the surface similar to that previously observed in studies of the reaction of ethane with nitric oxide over manganese(III) oxide (4). The infrared spectrum of the oxide after catalysis was also similar to that obtained after the C_2H_6/NO reaction and included absorption bands at 1630, 1390, and 845 cm^{-1} indicative of a nitrate species, along with bands at 615, 490, 425, and 350 cm^{-1}.

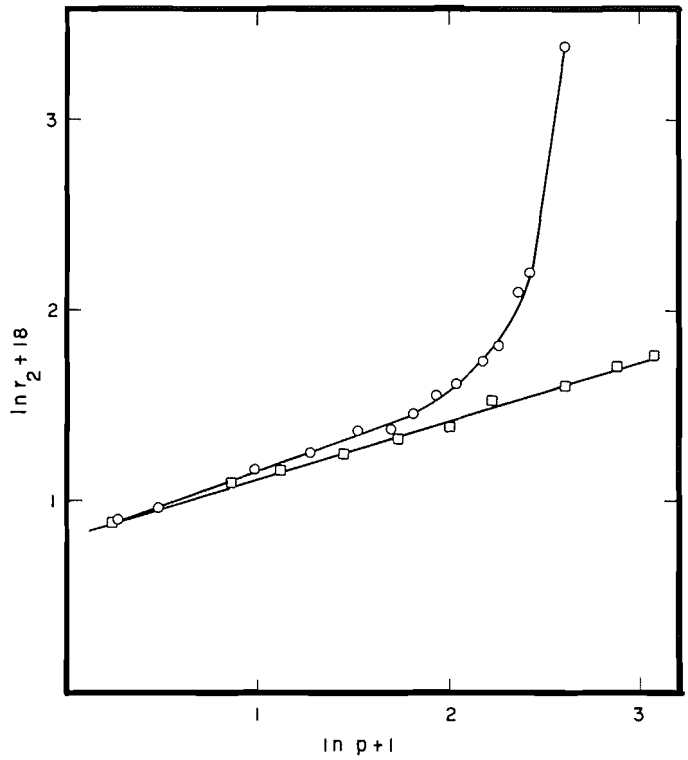

FIG. 4. Effect of component partial pressures on the rate of the O_2/C_4H_8 reaction; P_{O_2}, ○, r_2; $P_{C_4H_8}$, □, r_2.

Chemical analysis indicated 69.0% w/w manganese in the used catalyst which remained black in colour. X-ray powder diffraction produced *d*-spacings corresponding to γ manganese(III) oxide; 2.48, 2.74, 3.08, 1.54, 1.56, 1.81, and 2.06 Å.

The oxygen/1-butene reaction

With 2.12 kPa oxygen and 2.35 kPa 1-butene, the catalytic reaction rate increased slightly for the first 30 min of reaction and then remained constant for at least 24 h at 523 K where the conversion of 1-butene was 13%. Prior to subsequent experiments the catalyst was pretreated under these conditions for 3 h.

Reaction rate orders were evaluated at 473 K.

Oxygen

The partial pressure of oxygen was altered from 0.48 to 4.95 kPa with that of 1-butene maintained at 2.77 kPa. For oxygen partial pressures <2.20 kPa, the rate order with respect to oxygen was 0.4, Fig. 4. The rate order increased with an increase in partial pressure above this point.

1-Butene

With oxygen partial pressure maintained at 2.18 kPa, the rate order was 0.3 with respect to 1-butene from 0.46 to 7.88 kPa, Fig. 4.

Carbon dioxide

Variations in the partial pressure of carbon dioxide from 0.55 to 6.45 kPa had no effect on experimental reaction rates with oxygen and 1-butene partial pressures held constant at 2.16 and 2.71 kPa, respectively. Hence the rate order with respect to carbon dioxide concentration was zero.

Water vapour

With the partial pressures of oxygen and 1-butene main-

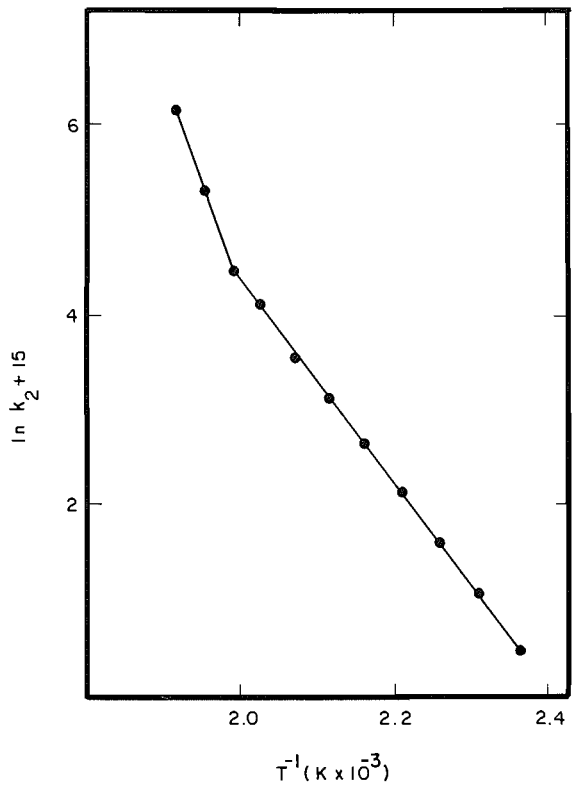

FIG. 5. Arrhenius plot for the O_2/C_4H_8 reaction.

tained at 2.16 and 2.71 kPa, respectively, the rate order was zero with respect to water vapour partial pressure from 0.08 to 2.33 kPa.

On the basis of these results, the catalytic rate of reaction was expressed as:

$$[3] \quad r_2 = kP_{O_2}^{0.4} P_{C_4H_8}^{0.4}$$

for $0.48 < P_{O_2} < 2.20$ kPa.

The effects of temperature and reaction conditions

Rate constants were calculated from the integrated form of eq. [3] from 523 to 433 K. When plotted as ln k versus T^{-1}, Fig. 5, two linear regions were observed which gave apparent activation energies of 183 ± 4 and 88 ± 4 kJ mol^{-1} for the ranges 523 to 503 K and 503 to 433 K. The corresponding pre-exponential factors were 1.74×10^{15} and 2.94×10^5 $mol^{0.3}$ $L^{-0.3}$ m^2 g^{-1}.

The oxide surface area remained 15.5 m^2 g^{-1} after reaction at 523 K for 24 h and the infrared spectrum, with absorption bands at 615, 490, 425, and 350 cm^{-1}, was similar to that described above. Chemical analyses yielded 69.3% w/w manganese and the *d*-spacings were 2.48, 2.74, 3.08, 1.54, 1.56, 1.80, and 2.08 Å as determined by X-ray diffraction.

X-ray photoelectron spectra of the catalysts used in both reactions were corrected for charging by reference to the C(1*s*) line at 285.0 eV. The Mn($2p_{3/2}$) spectrum gave a binding energy of 642.0 eV for all samples in comparison with 640.7 eV for unreacted managanese(III) oxide. The O(1*s*) spectrum of the latter gave a binding energy of 528.7 eV which became 528.8 eV after the O_2/C_4H_8 reaction and split to 530.0 and 533.0 eV after the NO/C_4H_8 reaction. Catalysts used in the nitric oxide work gave a N(1*s*) spectrum with a binding energy 406.2 eV.

The atomic percentages were 26.4 carbon, 18.1 and 37.3 oxygen, 8.7 manganese, and 9.5 nitrogen for catalysts from the nitric oxide/1-butene reaction and 19.3 carbon, 60.1 oxygen, and 20.6 manganese for those from the oxygen/1-butene reaction.

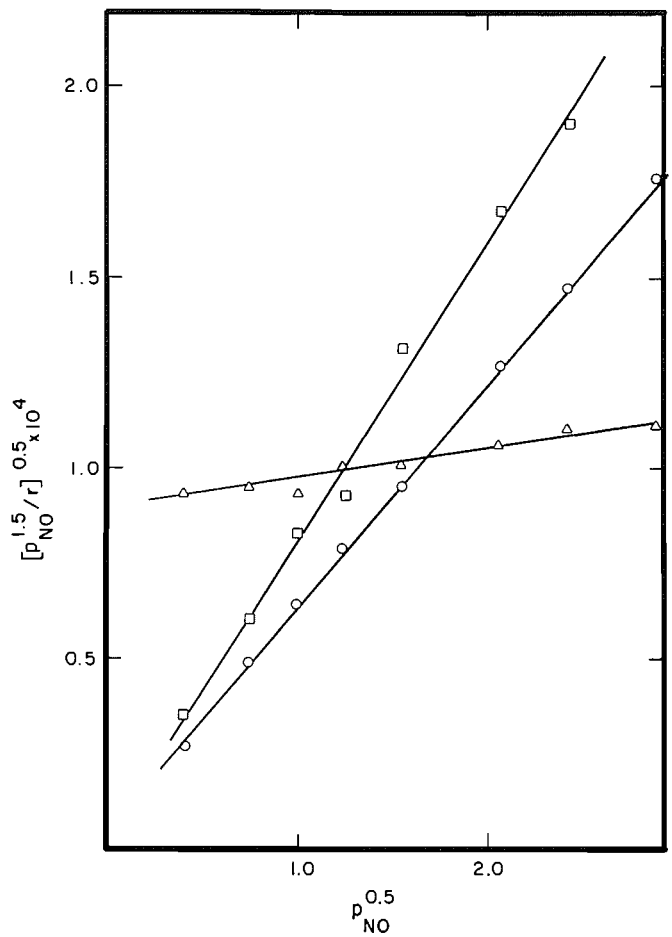

FIG. 6. Reduced plots corresponding to eq. [4] for the NO/C_4H_8 reaction at 673 K; □, r_1; ○, r_2; △, r_3.

Discussion

The nitric oxide/1-butene reaction

Various kinetic expressions mainly of the Langmuir–Hinshelwood type (7–10) were surveyed and tested. The equation which gave the best statistical correlation coefficient for all of the rate order data was then adopted. As shown by the linear plots of $P_{NO}^{0.5}$ against $(P_{NO}^{1.5}/r)^{0.5}$, Fig. 6, only one expression accommodated the nitric oxide rate order results:

$$[4] \quad r = \frac{kaP_{NO}^{0.5}}{(1 + aP_{NO}^{0.5})^2} \times P_{NO}$$

The square-root relationship with the partial pressure of nitric oxide suggests that this species adsorbs and reacts on two surface sites while the zero order rate dependency on 1-butene concentration indicates that adsorption and reaction of 1-butene is very rapid compared to the reactions of nitric oxide.

A surface mechanism consistent with the experimental results may be formulated:

$$[5] \quad C_4H_{8(g)} \rightleftharpoons C_4H_{8(ads)}$$

$$[6] \quad NO + S + C_4H_{8(ads)} \rightarrow C_4H_{7(ads)} + HNO_{(ads)}$$

$$[7] \quad 2HNO_{(ads)} \rightarrow N_2O_{(ads)} + H_2O_{(ads)}$$

Can. J. Chem. Downloaded from www.nrcresearchpress.com by 210.87.254.40 on 09/06/12
For personal use only.

Can. J. Chem. Downloaded from www.nrcresearchpress.com by 210.87.254.40 on 09/06/12
For personal use only.

where S is a surface site. These reactions account for the formation of nitrous oxide. Further reactions involve nitric oxide as indicated by the P_{NO} term in eq. [4] and, overall, these might be represented by:

[8] $2C_4H_{7(ads)} + 22NO + [O] \rightarrow 8CO_2 + 7H_2O + 11N_2$

As was observed in the nitric oxide/ethane reaction (4), the rate of nitrogen production was less than that of carbon dioxide which suggests that disproportionation may occur between two nitric oxide molecules to give nitrous oxide and an oxygen ion (11, 12) as previously suggested for the nitric oxide/methane reaction over platinum (13).

The apparent activation energies were similar to those found in the nitric oxide/ethane reaction over the same catalyst (4) and to the nitric oxide/propane (14, 15) and nitric oxide/propylene (16) reactions over various catalysts. In the propane reaction (15) over bismuth phosphomolybdate, the activation energy was 92 kJ mol^{-1} for nitrogen formation and 55 kJ mol^{-1} for nitrous oxide while the corresponding values in the present work were 69 and 30 kJ mol^{-1}.

Infrared spectra showed the presence of a nitrate species with absorption bands at 1630, 1390, and 845 cm^{-1}. The catalyst appeared to have undergone a phase change from α to γ manganese(III) oxide. The extent of this change is not known, although the fact that it occurs indicates that surface oxygen ions are actively involved in reaction.

Nitric oxide has been shown to exist as $(NO)_2$ or as a nitro species on different surfaces (17–19) and this species may be involved in the disproportionation reaction. The nitrous oxide thus produced may also take part in the oxidation of 1-butene, although in the nitric oxide/methane reaction in a static system (13), methane oxidation by nitrous oxide only occurred when all of the nitric oxide was consumed. It seems more likely that the oxygen ion produced by disproportionation would be involved in 1-butene oxidation.

The oxygen/1-butene reaction

A number of kinetic expressions were examined and the best correlations were obtained with the equation:

$$[9] \quad r = \frac{kaP_{O_2}^{0.5} bP_{C_4H_8}^{0.5}}{(1 + aP_{O_2}^{0.5} + bP_{C_4H_8}^{0.5})^2} \times (P_{O_2} P_{C_4H_8})$$

The reduced plots are shown in Fig. 7.

The equation suggests that an irreversible bimolecular reaction occurs between adsorbed species (20), and each species is adsorbed on two surface sites as indicated by the one-half order exponents. Additional reactions involve both oxygen and 1-butene as indicated by the $(P_{O_2} P_{C_4H_8})$ term. With eq. [9] as a general guide, a plausible surface mechanism was developed:

[10] $C_4H_{8(g)} + 2S \rightleftharpoons C_4H_{8(ads)}$

[11] $O_2 + [\ ] + C_4H_{8(ads)} \rightarrow C_4H_{7(ads)} + [OOH]$

[12] $C_4H_8 + S + [OOH] \rightarrow C_4H_{7(ads)} + [O] + H_2O$

and additional reactions summarized by:

[13] $2C_4H_{7(ads)} + 11O_2 + [O] \rightarrow 8CO_2 + 7H_2O + [\ ] + 4S$

The square-root relationships in eq. [9] with respect to 1-butene and oxygen are rationalized in steps [10] and [11], respectively.

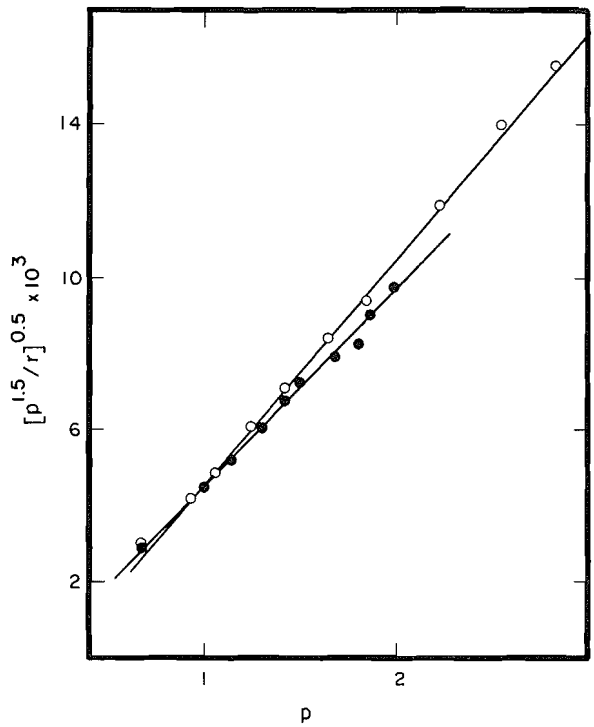

FIG. 7. Reduced plots corresponding to eq. [9] for the O_2/C_4H_8 reaction at 473 K; ○, r_2 for $P_{C_4H_8}$; ●, r_2 for P_{O_2}.

The change in apparent activation energy from 88 kJ mol^{-1}, 433 to 503 K, to 183 kJ mol^{-1}, 503 to 523 K, occurs at the temperature at which the conversion of oxygen exceeds 15%. As the temperature is increased above 503 K, the conversion of oxygen increases rapidly compared to 1-butene as expected from the overall stoichiometry:

[14] $2C_4H_8 + 12O_2 \rightarrow 8CO_2 + 8H_2O$

The lower value for activation energy corresponds closely to that found in the complete oxidation of ethane on palladium (21) or nickel(II) oxide and to that for propane oxidation on manganese(IV) oxide (22). The rate-determining step may involve C—H bond rupture as in eqs. [11] and [12].

Although the kinetic parameters for the oxygen/1-butene reaction correspond closely to those for the reaction of nitric oxide with ethane (3), the rate with respect to the oxidizing gas increased with partial pressures >2.6 kPa for the unsaturated hydrocarbon. The rate-limiting step would then be the adsorption and reaction of the oxidizing gas, eq. [11].

XPS showed two O(1*s*) binding energy values in catalysts used in the NO/C_4H_8 reaction. This indicates that two surface oxygen species are present. The lower energy of 530.0 eV is close to that expected for chemisorbed oxygen in metal oxides while the higher value of 533.0 eV characterizes the presence of a molecular oxygen species (23). Elsewhere, it has been proposed that in hydrocarbon oxidation reactions, oxygen is activated and adsorbed on the catalyst surface as O^- or O_2^- species which may result in the formation of epoxy or peroxy intermediates (24).

Conclusions

Products of complete oxidation only were observed in the reaction of 1-butene with oxygen over manganese(III) oxide. When nitric oxide was the oxidant, nitrous oxide was also

present in the effluent. These reactions may all occur in emission control systems which require the removal of NO_x and unburned hydrocarbons.

Manganese(III) oxide underwent a partial phase change from α to γ during catalysis indicating that the involvement of active surface centres in the reactions had some effect on lattice stability. Nitrate species were present on the surface after oxidation of 1-butene by nitric oxide.

Both reactions appear to initiate via an irreversible bimolecular reaction between adsorbed species on the catalyst surface which may involve C—H bond rupture.

1. C. KEMBALL and W. R. PATTERSON. Proc. R. Soc. A, **270**, 219 (1962).
2. H. V. VOGE and C. R. ADAMS. Adv. Catal. **17**, 151 (1967).
3. C. FAIRBRIDGE and R. A. ROSS. Can. J. Chem. **60**, 893 (1982).
4. R. A. ROSS and C. FAIRBRIDGE. Can. J. Chem. **59**, 2232 (1981).
5. E. F. MCCAFFREY, D. G. KLISSURSKI, and R. A. ROSS. J. Catal. **26**, 380 (1972).
6. D. V. FIKIS, W. J. MURPHY, and R. A. ROSS. Can. J. Chem. **56**, 2530 (1978).
7. O. A. HOUGEN and K. M. WATSON. Chemical process principles. Part III, John Wiley and Sons, New York. 1966.
8. A. CLARK. The theory of adsorption and catalysis. Academic Press, New York. 1970.
9. S. W. WELLER. Chemical reaction engineering reviews. *Edited by* H. M. Hulbert. Am. Chem. Soc. Washington, D.C. 1975.
10. B. W. KRUPAY and R. A. ROSS. J. Catal. **50**, 220 (1977).
11. I. S. SAZANOVA, G. M. ALIKINA, G. V. GLAZOREVE, N. P. KEIER, N. E. BOGDANCHIKOVA, and V. G. DEVYATOV. Kinet. Katal. **18**, 44 (1977).
12. K. OTTO and M. SHELEF. Paper No. 16, Proc. 5th Int. Cong. Catal. *Edited by* J. W. Hightower. North-Holland, Amsterdam. 1973.
13. I. HU, D. VAN-LINSBURG, and J. W. HIGHTOWER. Kinet. Katal. **18**, 545 (1977).
14. J. W. AULT and R. J. AYEN. AIChE J. **17**, 265 (1971).
15. T. J. STELLEY and J. B. BUTT. Ind. Eng. Chem. Prod. Res. Devel. **11**, 397 (1972).
16. M. W. CHIEN and K. NOBE. Am. Chem. Soc., Div. Water, Air, Waste Chem. Preprints, **11**, 71 (1971).
17. G. BLYHOLDER and M. C. ALLEN. J. Phys. Chem. **65**, 3998 (1965).
18. D. V. POZDNYAKOV and V. N. FILLIMONOV. Adv. Mol. Relax. Proc. **5**, 55 (1973).
19. B. A. MORROW and L. E. MORAN. J. Catal. **62**, 294 (1980).
20. P. H. EMMETT. Catalysis. Vol. 5. *Edited by* P. H. Emmett. Reinhold, New York. 1954.
21. C. F. CULLIS and T. G. NEVELL. Proc. R. Soc. A, **349**, 523 (1976).
22. O. S. ZANEVSKAYA, V. YA. VOL'FSON, and O. T. CHUGAEVA. Kinet. Katal. **10**, 8 (1973).
23. M. W. ROBERTS. Adv. Catal. **29**, 55 (1980).
24. J. HABER and M. WITKO. Acc. Chem. Res. **14**, 1 (1981).

Can. J. Chem. Downloaded from www.nrcresearchpress.com by 210.87.254.40 on 09/06/12
For personal use only.

The spin–spin coupling mechanism for ^5J(C-4, CH_α) in toluene derivatives and its conformational applications

TED SCHAEFER, JAMES PEELING,[1] AND GLENN H. PENNER
Department of Chemistry, University of Manitoba, Winnipeg, Man., Canada R3T 2N2

Received May 10, 1982

TED SCHAEFER, JAMES PEELING, and GLENN H. PENNER. Can. J. Chem. **61**, 2773 (1983).

It is shown that the spin–spin coupling over five formal bonds between carbon 4 and the α protons in toluene and its ring or sidechain substituted derivatives is transmitted by a σ–π mechanism. As such it varies as $\sin^2\theta$, where θ is the angle by which the α C—H bond twists out of the benzene plane, and can be used to determine the conformational preference and the barrier to internal rotation about the exocyclic sp^2–sp^3 carbon–carbon bond. The coupling is remarkably insensitive to ring substituents, even to those at carbon 4. Two measurements suggest that the coupling over six formal bonds between a β carbon nucleus and a *para* proton also represents a σ–π interaction

TED SCHAEFER, JAMES PEELING et GLENN H. PENNER. Can. J. Chem. **61**, 2773 (1983).

On démontre que le couplage spin–spin à travers cinq liaisons formelles entre les protons du carbone 4 et ceux en α du toluène se transmet par un mécanisme σ–π; cette conclusion est aussi vraie pour les dérivés du toluène substitués que le cycle ou sur la chaîne latérale. L'intensité de ce couplage varie donc en fonction de $\sin^2\theta$, où θ est l'angle formé par la α liaison C—H et le plan du noyau benzénique; elle peut donc être utilisée pour déterminer la préférence conformationnelle et la barrière à la rotation interne autour de la liaison carbone–carbone sp^2–sp^3 exocyclique. Cette constante de couplage est peu sensible aux substituants du cycle, même ceux en position 4. Deux mesures suggèrent que le couplage à travers six liaison formelles entre un noyau de carbone en β et un proton en *para* représente aussi une interaction σ–π.

[Traduit par le journal]

Can. J. Chem. Downloaded from www.nrcresearchpress.com by 210.87.254.6 on 09/06/12
For personal use only.

Introduction

The σ–π electron coupling mechanism of $^6J_p^{H,CH_3}$ in toluene is well established, entails a $\sin^2\theta$ dependence (1, 2) in **1**, and

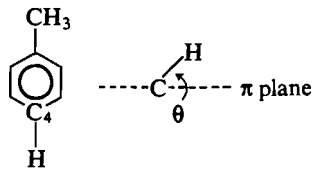

1

via an appropriate averaging procedure can be used to determine the preferred conformations and barriers to internal rotation about the C_{sp^2}—C_{sp^3} bonds in toluene derivatives (3). One simply uses eq. [1], in which $^6J_{90}$ is the H,H coupling constant

$$[1]\quad {}^6J_p^{H,CH} = {}^6J_{90}\,\langle\sin^2\theta\rangle$$

over six bonds between the sidechain and ring protons at θ = 90° and $\langle\sin^2\theta\rangle$ is the expectation value of $\sin^2\theta$ as determined by the preferred conformation, the magnitude of the internal rotational barrier, and the temperature. The latter determines the populations of the hindered rotor states.

It has been suggested (4, 5) that $^5J_p^{C,CH}$ in toluene is also dominated by a π electron mechanism. In this paper its coupling mechanism is investigated and its use in conformational applications is indicated.

Experimental

Most of the compounds were available commercially. The 3,5-dibromo derivatives of ethyl and isopropylbenzene were prepared in the obvious way from the 4-amino derivatives. The 2,6-dichloro derivative of ethyl benzene was obtained by hydrogenation of the corresponding styrene (6).

The ^{13}C nmr spectra were recorded at 22.63 MHz on a WH90 Bruker spectrometer. For reasons of sensitivity, the INEPT sequence was used (7). For C-4 in 4-fluorotoluene this sequence involved transfer of polarization from ^{19}F to ^{13}C. The 90° pulse for ^{19}F was of 50 μs duration while that for ^{13}C was 12 μs. A spectral width of 400 Hz was studied, 2600 acquisitions into 32 K being summed during a time of 20.48 s for each free induction decay.

Samples were prepared in solvents as indicated in Table 1 and were transferred to 10-mm od nmr sample tubes. The solutions were degassed by a number of freeze–pump–thaw cycles and the tubes were flame-sealed.

INDO MO FPT calculations (8) were performed on an Amdahl 470/V7 system.

Results and discussion

1. *Spectral analysis*

The proton-coupled spectra of C-4 were analyzed with the computer program LAME (9, 10). The initial assignments were facilitated by knowledge of the proton chemical shifts and of the proton–proton coupling constants. The C,H couplings could be estimated from data for toluene (4) and the monosubstituted benzenes (5). Iteration then yielded the data in Table 1. An example of the analysis is that for *p*-fluorotoluene. Of the 205 calculated transitions in the C-4 region, 166 transitions were assigned to 92 observed peaks. The calculated and observed spectra are shown in Fig. 1. The important parameters, ^5J(C-4, H) ≡ $^5J_p^{C,CH}$ ≡ ^5J is 0.948 ± 0.009 Hz, where the standard deviation from the analysis is multiplied by three.

Substantial data sets were also obtained for C,H couplings involving C-2, C-3, C-α, and C-β. Most of them (but see below) do not contribute to the point of this paper nor are they properly understood in terms of coupling mechanisms or their conformational or substituent dependence. These data sets are not reproduced here, but will be published if and when their conformational behaviour becomes clear.

2. *The mechanism for* ^{5}J *in toluene*

(i) *INDO MO FPT calculations*

Calculations of ^5J(C-4, H) ≡ ^5J have been performed previously (5). So as to obtain some hints as to the perturbations of ^5J caused by ring or sidechain substituents, INDO MO FPT

[1]On sabbatical leave from the University of Petroleum and Minerals, Saudi Arabia.

TABLE 1. Spin–spin coupling constants to C-4 in some toluene derivatives in Hz at 305 K

Compound	^1J(C,H)	^2J(C,H)	^3J(C,H)	^5J(C,H)
Toluene[a]	158.8	1.07	7.54	0.84±0.03
4-F[b]	−241.434(6)[g]	−4.810(5)	10.706(5)	0.948(3)
2,6-DiCl[c]	164.863(9)	0.627(6)	—	0.893(5)
3,5-DiCl[c]	171.008(9)	—	5.379(6)	0.883(5)
3,5-DiBr-α-CH_3[d]	172.585(3)	—	5.707(2)	0.680(2)
3,5-DiBr-α,α-diCH_3[b]	172.739(18)	—	5.694(8)	0.368(2)
2,6-DiCl-α-CH_3[e]	164.173(7)	0.619(5)	—	0.353(5)
2,6-DiCl-α,α-diCl[f]	166.865(17)	0.419(34)	—	0.0
2,6-DiCl-α-Br[c]	165.638(8)	0.556(6)	—	0.276(6)
2,6-DiCl-α-Cl[c]	165.499(13)	0.578(9)	—	0.278(9)
2,6-DiCl-α-OH[c]	164.961(17)	0.583(12)	—	0.282(12)

[a]From ref. 4, 64% v/v in acetone-d_6 (18% v/v), 18% v/v CS_2, and ca. 0.5% v/v TMS.
[b]50% v/v in acetone-d_6.
[c]20% v/v in benzene-d_6 containing 20% v/v acetone-d_6.
[d]25% v/v in benzene-d_6.
[e]35% v/v in benzene-d_6.
[f]40% v/v in benzene-d_6.
[g]This is ^1J(C,F).

calculations were done for toluene, ethylbenzene, *p*-fluorotoluene, benzyl fluoride, *p*-fluorobenzyl fluoride, 2,3,5,6-tetrafluorobenzyl fluoride, benzal fluoride, *p*-fluorobenzal fluoride, and 2,3,5,6-tetrafluorobenzal fluoride. Some of the calculated couplings are given in Table 2.

For toluene the numbers agree well with previous data (5) and can be reproduced by the equation $^5J = 0.20 + 3.89 \sin^2 \theta$ where θ is the angle by which the C—H bond of the methyl group twists out of the ring plane. For reasons given below the value of 0.20 Hz at $\theta = 0$ is most likely an artefact of the calculation. Substraction of 0.20 Hz from each calculated number in Table 2 gives a set related by $^5J = 3.89 \sin^2 \theta$. Consequently, these calculations can be taken (1, 3) to imply a σ−π electron mechanism for ^5J(C-4, H) in toluene.

Very similar numbers are computed for ethyl benzene in Table 2 and suggest a similar equation for ^5J. In *p*-fluorotoluene the same computed behaviour appears with the proviso that $^5J_{90}$ increases slightly to 4.02 Hz from the 3.89 Hz in toluene.

Substitution of fluorine into the sidechain reduces the calculated couplings by about 15%. An asymmetry is introduced into the θ dependence of ^5J in that the values at 30° and 150° are no longer equal (see Table 2). However, the averages of the values at θ and 180° − θ still follow closely a $\sin^2 \theta$ relationship. Of course, an observed ^5J involves both methylene protons and is the average of the couplings at θ and 180° − θ.

Substitution of a second flourine into the methyl group causes a further reduction of about 20% in the calculated ^5J numbers (about 30% relative to toluene), but does not change the θ dependence of ^5J.

In summary, the INDO MO FPT computations are consistent with a $\sin^2 \theta$ dependence of $^5J_p^{C,CH}$ in toluene, a small increase caused by ring substituents more electronegative than hydrogen, and a somewhat larger decrease entailed by electronegative α-substituents.

(ii) *Experimental verification of the σ−π mechanism for* $^5J_p^{C,CH}$

In toluene, $^5J_p = 0.84 \pm 0.03$ Hz (3). In 2,6-dichlorotoluene it is 0.893 ± 0.015 Hz, where the error is taken as three times the standard deviation (Table 1). In 3,5-dichlorotoluene the coupling is 0.883 ± 0.015 Hz (the analysis for C-4 in these two compounds is rather less complex than for toluene itself). It appears that substitution at sites along the coupling path does not perturb ^5J significantly, just as for $^6J_p^{H,CH}$ (3, 11). The expectation value of $\sin^2 \theta$ is 0.5 for 3,5-dichlorotoluene. Therefore write

$$[2] \quad {}^5J = {}^5J_{90} \langle \sin^2 \theta \rangle = 1.77 \langle \sin^2 \theta \rangle$$

In *p*-fluorotoluene, $^5J = 0.948 \pm 0.009$ Hz, implying a 7% increase in $^5J_{90}$ when the highly electronegative fluorine substituent is introduced at one end of the coupling path. This rather small increase is in qualitative agreement with the computed numbers in Table 2.

If eq. [2] represents ^5J correctly, then in 3,5-dibromoethylbenzene $\langle \sin^2 \theta \rangle$ should be 0.385 as deduced originally (3, 12) from $^6J_p^{H,CH}$. Indeed, ^5J in this compound is 0.680 ± 0.006 Hz (Table 1) yielding $\langle \sin^2 \theta \rangle$ as 0.680/1.77 = 0.384. In view of the possible measurement errors, the agreement is probably too good. It does imply that eq. [2] is good and that ^5J is dominated by a σ−π mechanism. Furthermore, the computed numbers in Table 2 are clearly overestimated and the nonvanishing values at $\theta = 0$ should very likely be ignored.

Another test of eq. [2] is provided by the value of 0.368 ± 0.006 Hz in 3,5-dibromoisopropylbenzene in Table 1. Hence, $\langle \sin^2 \theta \rangle$ is 0.368/1.77 or 0.208, again as deduced (13) from the σ−π coupling, $^6J_p^{H,CH}$, which yielded 0.204. In both of these examples it is assumed that the CH_3 substituents do not appreciably perturb ^5J, as is also suggested by the theoretical numbers in Table 2.

In Table 2 the computed ^5J values for benzal fluoride indicate a substantial decrease relative to toluene. In 2,6-dichlorobenzal chloride, in which the C_α—H bond prefers the ring plane to the extent of about 57 kJ/mol (14), ^5J was too small to observe. Because the calculated value at $\theta = 0°$ is now also smaller (fluorine simulates chlorine) than in toluene, this experiment does not prove that ^5J vanishes, although it is consistent with this condition implied by an equation of type [2].

3. *The 2,6-dichloro derivatives*

As discussed above, ^5J is 0.89 Hz in 2,6-dichlorotoluene, in line with a rather small perturbation of the coupling mechanism by the chlorine substituents. In the corresponding ethyl benzene, $^6J_p^{H,CH}$ is −0.29 ± 0.02 Hz (6), approximating to the

Can. J. Chem. Downloaded from www.nrcresearchpress.com by 210.87.254.6 on 09/06/12
For personal use only.

Can. J. Chem. Downloaded from www.nrcresearchpress.com by 210.87.254.6 on 09/06/12
For personal use only.

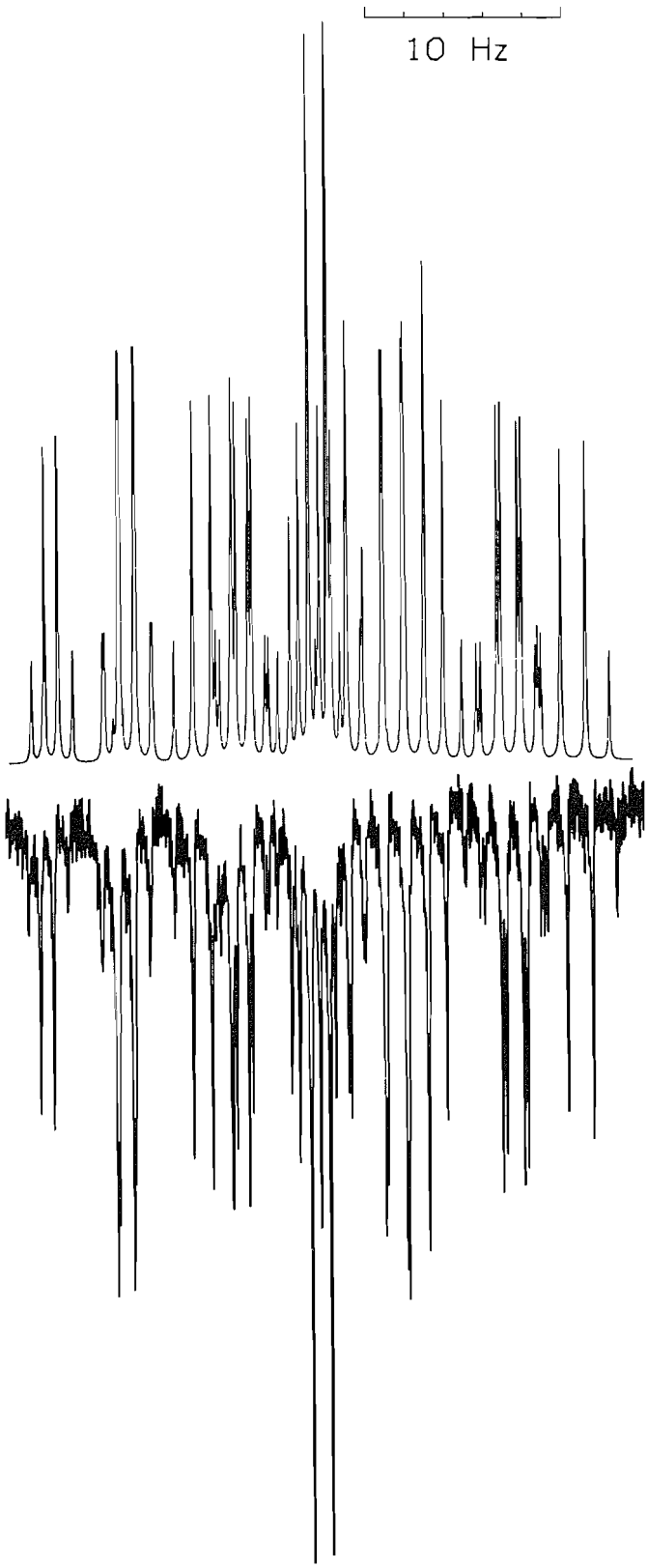

FIG. 1. The low-field part of the C-4 nmr spectrum of a 50% v/v solution of *p*-fluorotoluene in acetone-d_6 recorded at 22.63 MHz and 305 K. Polarization was transferred to ^{13}C from ^{19}F by the INEPT pulse sequence. The spectrum was acquired into 32 K using 20.48 s of acquisition time for each of 2600 scans and a spectral width of 400 Hz. The calculated spectrum assumed a linewidth at half-height of 0.08 Hz.

TABLE 2. INDO MO FPT values for ^5J(C-4, H) in toluene and some derivatives in Hz

θ/deg[a]	Toluene[b]	α-CH_3	*p*-F	α-F	α,α-F_2[c]
0	0.20	0.19	0.21	0.22	0.07
7.5	0.27	—	0.27	—	—
15	0.46	0.50	0.59	0.22(0.67)[d]	0.24
30	1.17	1.21	1.22	0.66(1.45)	0.77
45	2.15	2.18	2.21	1.46(2.35)	1.48
60	3.12	3.15	3.20	2.37(3.13)	2.20
75	3.83	3.88	3.94	3.15(3.58)	2.72
90	4.09	4.14	4.23	3.59	2.89

[a]The angle θ is zero when the C—H bond of the methyl group lies in the benzene plane.

[b]These numbers for ^5J(C-4, H) ≡ $^5J^{C,CH}$ ≡ ^5J in Hz may be compared with those given in ref. 5.

[c]The calculations did not converge for θ = 0° and 90°. Therefore 5° should be added to the θ value tabulated as 0° and subtracted at θ = 90°. The value at θ = 90° must be very near 2.91 Hz.

[d]The asymmetry introduced by the highly electronegative α-substituent entails values tabulated for θ between 0 and 180°. For a given pair of numbers the one in parentheses corresponds to 180° − θ.

−0.31 Hz expected for a *very* large twofold barrier to rotation about the C_{sp^2}—C_{sp^3} bond. Consequently, the lower limit of $^5J_p^{C,CH}$ in 2,6-dichloroethyl benzene, in which θ = 30° as in **2**,

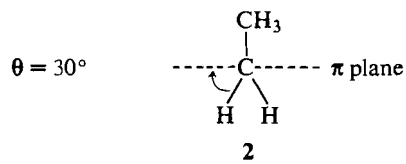

2

should be 1.77 $\langle \sin^2 \theta \rangle$ = 0.44 Hz. The observed value is 0.353(15) Hz, corresponding to a θ value of 27°. A similar discrepancy exists for the benzyl halide and benzyl alcohol derivatives in Table 1, where the numbers would suggest a θ value of 23°. These are numbers for a *rigid* conformation of structure type **2**. Now, the σ−π parameter[2] for the methylene protons depends somewhat on the electronegativity of the substituent (3), decreasing as the electronegativity increases. Part of the discrepancy arises from this perturbation. The theoretical numbers in Table 1 indicate a reduction in ^5J in the presence of an electronegative α substituent, but not to the extent suggested by the experimental data for the 2,6-disubstituted derivatives in Table 2. However, the methyl group is not very much more electronegative than a hydrogen substituent. The possibility of a distortion of the sidechain geometry has been previously discussed in detail (15) and it is possible that an effective $\langle \theta \rangle$ of less than 30° can occur for the 2,6-dichoro derivatives. Yet the molecular orbital calculations in ref. 15 gave ambiguous support to this hypothesis (depending on the level of the calculations).[3] Again, a cosine potential might suffer a distortion in these *ortho*-substituted compounds and could possibly account for the anomalous observations. Nevertheless, it should be noted that the V_2 value derived from the *J* method for ethyl benzene agrees exactly with the latest thermodynamic results

[2]In 2,6-dichloro-4-methylbenzyl bromide $^7J_p^{H,H}$ is +0.204 Hz (unpublished work in this laboratory), compared to a value of −0.21(2) Hz for $^6J_p^{H,H}$ in 2,6-dichlorobenzyl bromide (6). The anomalous numbers are therefore still σ−π couplings.

[3]A detailed structure determination would be of interest for compounds of this kind.

(16) and is possibly more precise than conclusions based on electron diffraction data (17).

$^6J_p^{H,C\text{-}\beta}$ in 2,6-dichloroethyl benzene

This coupling changes the relevant preferred θ value to 90° (see structure **2**). Its magnitude is 0.618 ± 0.016 Hz (the coupled spectra are rather complex, causing a substantial error). In the 3,5-dibromo derivative this coupling between the *para* proton and the methyl ^{13}C nucleus is 0.432 ± 0.005 Hz (standard deviations being given in both instances). If 0.618 Hz represents the magnitude of $^6J_p^{H,C}$ at θ = 90°, then $\langle \sin^2 \theta \rangle$ becomes (0.432 ± 0.005)/(0.618 ± 0.016) or 0.699 ± 0.027 for the 3,5-dibromo compound. The relationship between $\langle \sin^2 \theta \rangle$ for the methyl carbon data and $\langle \sin^2 \theta \rangle$ for the methylene protons is $\langle \sin^2 \theta \rangle^C = 1.5 - 2\langle \sin^2 \theta \rangle^H$. When V_2 is zero both expectations are 0.5, whereas they are unity and 0.25 when V_2 is infinite. Thus one has (see previous sections) 0.699 ± 0.027 = 1.5 − 2 (0.384 ± 0.010) = 0.732 ± 0.020. This agreement is taken as confirmation of the σ−π mechanism[4] for $^6J_p^{H,C}$.

4. *Conformational analysis*

The σ−π mechanism for $^5J_p^{C,CH}$ and its $\sin^2 \theta$ dependence implies its use in the determination of preferred conformations and barriers to internal rotation. An advantage of $^5J_p^{C,CH}$ over $^6J_p^{H,CH}$ is that substituents other than hydrogen are allowed at C-4. Note that even a polar fluorine substituent at this position causes only a small change in ^5J. Of course, a substituent which gives rise to very short T_1 or T_2 values for C-4 would cause line broadening and would interfere with the measurement of ^5J; although if it shortened T_2 only, then enrichment of ^{13}C at C-4 would circumvent the difficulty because the coupling would be obtainable from the ^1H nmr spectrum. A wider variety of molecules has therefore become amenable to studies by the *J* method (3). A sensible procedure would involve the measurement of $^5J_p^{C,CH}$ in the toluene substituted at C-4 followed by study of the corresponding benzyl or benzal compound.

[4]The sign of $^6J_p^{H,C}$ is most likely negative, by analogy to the σ−π coupling, $^6J_p^{H,CH_3}$ in toluene; its sign could not be determined because the INEPT sequences were necessary for reasons of sensitivity.

Acknowledgments

We are grateful to Kirk Marat for setting up the INEPT sequences for the transfer of polarization to ^{13}C from ^1H and ^{19}F and to the Natural Sciences and Engineering Research Council of Canada and the University of Petroleum and Minerals for financial assistance.

1. R. WASYLISHEN and T. SCHAEFER. Can. J. Chem. **50**, 1852 (1972).
2. C. J. MACDONALD and W. F. REYNOLDS. Can. J. Chem. **48**, 1002 (1970).
3. W. J. E. PARR and T. SCHAEFER. Acc. Chem. Res. **13**, 400 (1980), and references therein.
4. M. HANSEN and H. J. JAKOBSEN. J. Magn. Reson. **20**, 520 (1975).
5. L. ERNST, V. WRAY, V. A. CHERTKOV, and N. M. SERGEYEV. J. Magn. Reson. **25**, 123 (1977).
6. A. F. JANZEN and T. SCHAEFER. Can. J. Chem. **49**, 1818 (1971).
7. G. A. MORRIS and R. J. FREEMAN. J. Am. Chem. Soc. **101**, 760 (1979).
8. P. A. DOBOSH. Quantum Chemistry Program Exchange, **11**, 1414 (1979).
9. S. CASTELLANO and A. A. BOTHNER-BY. J. Chem. Phys. **41**, 3863 (1964).
10. C. W. HAIGH. Annu. Rep. Nucl. Magn. Reson. Spectrosc. **4**, 311 (1971).
11. T. SCHAEFER, R. SEBASTIAN, R. P. VEREGIN, and R. LAATIKAINEN. Can. J. Chem. **61**, 29 (1983).
12. T. SCHAEFER, L. KRUCZYNSKI, and W. NIEMCZURA. Chem. Phys. Lett. **38**, 498 (1976).
13. T. SCHAEFER, W. J. E. PARR, and W. DANCHURA. J. Magn. Reson. **25**, 167 (1977).
14. H. G. GYULAI, B. J. FUHR, H. M. HUTTON, and T. SCHAEFER. Can. J. Chem. **48**, 3877 (1970).
15. T. SCHAEFER, J. B. ROWBOTHAM, W. J. E. PARR, K. MARAT, and A. F. JANZEN. Can. J. Chem. **54**, 1322 (1976).
16. A. MILLER and D. W. SCOTT. J. Chem. Phys. **68**, 1317 (1978).
17. P. SCHARFENBERG, B. ROZSONDAI, and I. HARGITTAI. Z. Naturforsh. Teil A, **35**, 431 (1980).

Can. J. Chem. Downloaded from www.nrcresearchpress.com by 210.87.254.6 on 09/06/12
For personal use only.

A relationship between some long-range $^2H/^1H$ isotope shifts in ^{13}C nuclear magnetic resonance and long-range spin–spin coupling constants for toluene, ethylbenzene, and isopropylbenzene

TED SCHAEFER, JAMES PEELING,[1] AND TIMOTHY A. WILDMAN
Department of Chemistry, University of Manitoba, Winnipeg, Man., Canada R3T 2N2

Received May 25, 1983

TED SCHAEFER, JAMES PEELING, and TIMOTHY A. WILDMAN. Can. J. Chem. **61**, 2777 (1983).

A very good correlation exists between long-range spin–spin coupling constants involving the α-protons in toluene, ethylbenzene, and cumene, and the changes in the chemical shifts of the *para* and α carbons caused by deuterium substitution at the α carbon. The coupling constants depend on $\sin^2\theta$, where θ is the angle by which the α C—H bond twists out of the ring plane, and can be used to find the expectation value of $\sin^2\theta$. Consequently the observed correlation provides quantitative support for the hyperconjugative model employed by Wesener and Günther.

TED SCHAEFER, JAMES PEELING et TIMOTHY A. WILDMAN. Can. J. Chem. **61**, 2777 (1983).

Il existe une très bonne corrélation entre les constantes de couplage à longue distance impliquant les protons en α du toluène, de l'éthylebenzène et du cumène et les variations, provoquées par l'introduction d'un deutérium sur le carbone α, des déplacements chimiques des carbones en position *para* et α. Les constantes de couplage dépendent de $\sin^2\theta$, où θ est l'angle de déformation hors du plan de la liaison C—H en position a; elles peuvent être utilisées pour trouver la valeur probable de $\sin^2\theta$. Par conséquent, les corrélations observées appuient de façon quantitative le modèle d'hyperconjugaison utilisé par Wesener et Günther.

[Traduit par le journal]

Can. J. Chem. Downloaded from www.nrcresearchpress.com by 210.87.254.5 on 09/06/12
For personal use only.

Introduction

Although all $^2H/^1H$ isotope effects, $^n\Delta$, on ^{13}C chemical shifts originate in vibrational/rotational perturbations (1, 2), a simple hyperconjugative model (3) has had some success (4) in the rationalization of some observed $^n\Delta$ values (*n* counts the number of formal bonds between ^2H and ^{13}C sites). In particular, Wesener and Günther (5) indicate that in the title compounds the lesser hyperconjugative electron-donating ability of an α C—D bond relative to a C—H bond, combined with the preferred conformations **1** and **2**, accounts for the magnitudes

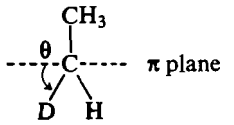

1

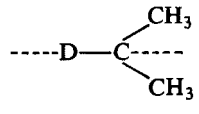

2

of the negative $^5\Delta$ at C-4 (downfield shifts caused by ^2H substitution). These authors suggest further investigations as to whether these isotope shifts can serve as probes for hyperconjugation.

A quantitative hyperconjugative model for $^5\Delta$

Indeed, if the hyperconjugative interaction has a $\sin^2\theta$ dependence (6, 7), where θ is measured from the π plane as in **1**, then a quantitative test of such a model becomes possible. The *J* method (8), as applied to the title molecules, relates $^6J_p^{H,CH}$, the spin–spin coupling constant between the *para* proton and the α-protons, to the preferred conformations and to the internal barrier to rotation about the C_{sp^2}—C_{sp^3} bond. In other words, the observed ^6J_p allows a derivation of $\langle\sin^2\theta\rangle$ (angular brackets indicate the expectation value), which in turn is related via a hindered rotor model to the internal barrier, taken as twofold for ethylbenzene and isopropylbenzene. One has eq. [1]

$$[1]\quad {}^6J_p^{H,CH}\,(\text{Hz}) = {}^6J_{90}\,\langle\sin^2\theta\rangle$$

in which $^6J_{90}$ is the coupling when θ is 90° (see **1**).

Therefore, hypothesize eq. [2],

$$[2]\quad {}^n\Delta(\text{ppb}) = a\langle\sin^2\theta\rangle + b$$

implying a linear relationship between ^6J_p and $^5\Delta$, where $^5\Delta$ is the value observed for C-4 in these compounds. In fact, the data in Table 1 yield eq. [3] in which, because $^6J_p^{H,CH}$ is negative, the magnitude of the latter is employed. In this way the

$$[3]\quad {}^5\Delta(\text{ppb}) = -10.6|{}^6J_p^{H,CH}| + 2.69, \qquad r = -1.0000$$

negative $^5\Delta$ is emphasized. Furthermore, *a* and *b* in eq. [2] are found as in eq. [4]. For toluene, $\langle\sin^2\theta\rangle$ is 0.5 because the

$$[4]\quad {}^5\Delta(\text{ppb}) = -13.5\,\langle\sin^2\theta\rangle + 2.9$$

barrier to internal rotation is only 59 J/mol (9). Because successive deuteration of the methyl group in toluene produces additive changes in $^5\Delta$, the present treatment is consistent with the assumption that any conformational preferences introduced by C—D bonds are insignificant. The $\langle\sin^2\theta\rangle$ values in Table 1 for ethylbenzene and cumene are those derived by the *J* method (8) and correspond to twofold internal barriers of 5.0 and 8.2 kJ/mol, respectively.

In as yet unpublished work, we show that $^5J_p^{C,CH}$, the coupling between C-4 and α-protons, is transmitted by the same kind of mechanism as $^6J_p^{H,CH}$ and therefore also depends on $\langle\sin^2\theta\rangle$. The data in Table 1 follow eq. [5]. It is interesting that

$$[5]\quad {}^5\Delta(\text{ppb}) = -7.50\,{}^5J_p^{C,CH} + 2.83, \qquad r = 0.9970$$

the constants of 2.8 ± 0.1 ppb in eqs. [3] to [5] are positive. Presumably this number does not have a hyperconjugative origin and is plausibly assigned to an angle-independent inductive shift (7), it being known that C—D bond is *more* inductively electron-donating than a C—H bond.

If the model is adequate, then two predictions are possible. First, in the presence of *ortho* substituents which raise the internal barrier substantially and therefore tend to stabilize conformations **1** and **2**, $^5\Delta$ should approach −0.4 ppb in the ethylbenzene derivative ($\langle\sin^2\theta\rangle \sim 0.25$). Second, $^5\Delta$ should be as

[1]On sabbatical leave from the University of Petroleum and Minerals, Saudia Arabia.

TABLE 1. Some long-range spin–spin coupling constants and changes in ^{13}C chemical shifts caused by deuteration in toluene, ethylbenzene, and cumene

	$^6J_p^{H,CH}$(Hz)	$^5J_p^{C,CH}$(Hz)	$^5\Delta$(ppb)[f]	$^1\Delta$(ppb)[f]	$\langle\sin^2\theta\rangle$[g]
Toluene-α-d_1	−0.62[a]	0.88_3[d]	−3.9	275.5	0.500
Ethylbenzene-α-d_1	−0.45[b]	0.68_0[e]	−2.1	349.1	0.385
Cumene-α-d_1	-0.25_3[c]	0.36_8[e]	0	434.4	0.204

[a]See ref. 13. All these couplings are for undeuterated compounds, ±0.01 to 0.02 Hz.
[b]W. E. Hull, to be published; for a $CDCl_3$ solution.
[c]For the 3,5-dibromo derivative; see ref. 14.
[d]For the 3,5-dichloro derivative in a mixture of benzene-d_6 and acetone-d_6.
[e]For the 3,5-dibromo derivative and as in [b].
[f]From ref. 5, ±0.4 ppb (parts per billion).
[g]From ref. 8. These are H values (see text).

large as 2.9 ppb for the cumene derivative ($\langle\sin^2\theta\rangle \sim 0$). These measurements cannot be made in this laboratory.

Concerning $^1\Delta$

While the discussion above supports the suggestions of Wesener and Günther (5), it is notable that $^1\Delta$ also correlates with $^6J_p^{H,CH}$ and $^5J_p^{C,CH}$ as in eqs. [6] and [7]. These *upfield* shifts

$$[6] \quad {}^1\Delta(\text{ppb}) = 433.0\ {}^6J_p^{H,CH} + 543.9 \qquad r = 1.000$$

$$[7] \quad {}^1\Delta(\text{ppb}) = -305.6\ {}^5J_p^{C,CH} + 549.7 \qquad r = 0.9969$$

increase as the hyperconjugative release to the π system decreases. Thus, if $^6J_p^{H,CH}$ were zero – no hyperconjugation – then $^1\Delta$ would be 543.9 ppb or, alternatively, would be 549.7 ppb if $^5J_p^{C,CH}$ were to vanish. Again, if the barrier to internal rotational in toluene-α-d_1 is negligibly different from 59 J/mol, as in toluene, then $\langle\sin^2\theta\rangle$ is 0.5, so that 275.5 × 2 = 551 ppb would represent $^1\Delta$ in the absence of hyperconjugation, where 275.5 ppb is the shift observed in toluene-α-d_1. In other words, the three different estimates suggest 548 ± 4 ppb for $^1\Delta$ in the absence of hyperconjugation. This value contrasts with a $^1\Delta$ of only 187 ppb in CH_3D (10). In the latter one expects a rather different potential energy surface than in toluene, of course. In any event, we take eqs. [6] and [7] as confirmation that both $^1\Delta$ and $^5\Delta$ originate in isotopic perturbations of the vibrational/rotational potential energy surface.

Other $^n\Delta$ values

An insignificant correlation, $r = 0.964$, exists between $^3\Delta$ at C-2 and $^4J_4^{H,CH}$ for these three compounds. The data are therefore not reproduced here, although it should be noted that an angle-dependence of $^3\Delta$ can occur in saturated systems (11). No $^4\Delta$ at C-3 is observed in the title compounds, perhaps because substituents in benzene perturb only slightly the shielding of *meta* carbon nuclei.

In ethylbenzene-β-d_3, $^6\Delta$ at C-4 is +12.6 ppb (5). A tentative observation holds that the C—C bond hyperconjugates, perhaps better than a C—H bond (12), and that deuteration of the group enhances this interaction, being an inductive donor to the C—C bond region. This line of argument implies two consequences. The $^6\Delta$ value should increase as substitution at the *ortho* positions stabilizes **1**. Furthermore, a single CD_3 group in cumene should cause a smaller $^6\Delta$ than in ethylbenzene. This result follows from the $\langle\sin^2\theta\rangle$ numbers in Table 1 because $\langle\sin^2\theta\rangle^C = 1.5 - 2\langle\sin^2\theta\rangle^H$ for ethylbenzene and for cumene one has $\langle\sin^2\theta\rangle^C = 0.75 - 0.5\langle\sin^2\theta\rangle^H$.

In summary, the present discussion provides evidence in favour of the approach used by Wesener and Günther and suggests further quantitative tests of $^2H/^1H$ isotope shifts of ^{13}C as a hyperconjugative probe.

Acknowledgments

We thank the Natural Sciences and Engineering Research Council of Canada and the University of Petroleum and Minerals for financial assistance.

1. H. BATIZ-HERNANDEZ and R. A. BERNHEIM. Prog. Nucl. Magn. Reson. Spectrosc. **3**, 63 (1967).
2. C. J. JAMESON. J. Chem. Phys. **66**, 4983 (1977); and in Spec. Per. Rep. R. Soc. Chem. Nucl. Magn. Reson. **10**, 11 (1980).
3. E. A. HALEVI. Prog. Phys. Org. Chem. **1**, 109 (1963).
4. L. ERNST, S. ELTAMANY, and H. HOPF. J. Am. Chem. Soc. **104**, 299 (1982), and references therein.
5. J. R. WESENER and H. GÜNTHER. Tetrahedron Lett. **23**, 2845 (1982).
6. D. E. SUNKO, I. SZELE, and W. J. HEHRE. J. Am. Chem. Soc. **99**, 5000 (1977).
7. D. J. DEFREES, W. J. HEHRE, and D. E. SUNKO. J. Am. Chem. Soc. **101**, 2323 (1979).
8. W. J. E. PARR and T. SCHAEFER. Acc. Chem. Res. **13**, 400 (1980).
9. H. D. RUDOLPH, H. DREIZLER, A. JAESCHKE, and P. WENDLING. Z. Naturforsch. Teil A, **22**, 940 (1967).
10. M. ALEI and W. E. WAGEMAN. J. Chem. Phys. **68**, 783 (1978).
11. J. L. JURLINA and J. B. STOTHERS. J. Am. Chem. Soc. **104**, 4677 (1982).
12. R. HOFFMANN, L. RADOM, J. A. POPLE, P. V. R. SCHLEYER, W. J. HEHRE, and L. SALEM. J. Am. Chem. Soc. **94**, 6221 (1972).
13. M. P. WILLIAMSON, R. KOSTELNICK, and S. M. CASTELLANO. J. Chem. Phys. **49**, 2218 (1968).
14. T. SCHAEFER, W. J. E. PARR, and W. DANCHURA. J. Magn. Reson. **25**, 167 (1977).

Can. J. Chem. Downloaded from www.nrcresearchpress.com by 210.87.254.5 on 09/06/12
For personal use only.

Signs and mechanisms of ^{13}C, ^{19}F spin–spin coupling constants in benzotrifluoride and its derivatives

TED SCHAEFER, KIRK MARAT, JAMES PEELING,[1] and RICHARD P. VEREGIN
Department of Chemistry, University of Manitoba, Winnipeg, Man., Canada R3T 2N2

Received May 2, 1983

TED SCHAEFER, KIRK MARAT, JAMES PEELING, and RICHARD P. VEREGIN. Can. J. Chem. **61**, 2779 (1983).

The magnitudes of ^nJ(C, F) for n = 3, 4, 5 bonds are remeasured for benzotrifluoride. The signs of ^2J(C, F) and ^3J(C, F) are determined for 4-chloro-3,5-dinitrobenzotrifluoride and that of ^5J(C, F) for 2-amino-3,5-dibromobenzotrifluoride. ^4J(C, F) is not observable in these compounds. The contact contributions to ^nJ(C, F) are calculated for benzotrifluoride by INDO MO FPT. The long-range coupling constants are discussed in terms of the mechanisms which transmit nuclear spin state information. It seems that ^5J(C, F) is a $\sigma-\pi$ coupling, ^4J(C, F) is a composite of σ and $\sigma-\pi$ components of opposite sign, and that ^3J(C, F) has a Karplus behaviour modified by a $\sigma-\pi$ contribution.

TED SCHAEFER, KIRK MARAT, JAMES PEELING et RICHARD P. VEREGIN. Can. J. Chem. **61**, 2779 (1983).

On a mesuré de nouveau les valeurs ^nJ(C, F) pour n = 3, 4, 5 liaisons du benzotrifluorure. On a déterminé les signes de ^2J(C, F) et de ^3J(C, F) du chloro-4 dinitro-3,5 benzotrifluorure et ceux de ^5J(C, F) de l'amino-2 dibromo-3,5 benzotrifluorure. Dans ces composés, on n'a pas observé de ^4J(C, F). On a calculé les contributions de contact à ^nJ(C, F) du benzotrifluorure en faisant appel aux méthodes INDO OM FTP. On discute des constantes de couplage à longue distance en fonction du mécanisme qui transmet l'information de l'état de spin nucléaire. Il semble que ^5J(C, F) est un couplage $\sigma-\pi$, ^4J(C, F) est un mélange de contributions α et $\sigma-\pi$ de signes opposés et que ^3J(C, F) a un comportement de Karplus modifié par une contribution $\sigma-\pi$.

[Traduit par le journal]

Can. J. Chem. Downloaded from www.nrcresearchpress.com by 210.87.254.40 on 09/06/12
For personal use only.

Introduction

INDO MO FPT calculations give a decent account of the signs and magnitudes of the long-range spin–spin coupling constants, $^nJ(H, CH_3)$, between methyl and ring protons in toluene (1). Similar calculations (2) for couplings (3) between methyl protons and ring carbon nuclei in toluene agree rather less well with experiment, yet they do provide information about the conformational dependence of these coupling parameters.

The electronic interactions of the CF_3 group with the phenyl moiety in benzotrifluoride are rather different (4) from the analogous interactions in toluene. Nevertheless, the magnitudes and signs of $^nJ(H, CF_3)$ in benzotrifluoride are not strikingly different from $^nJ(H, CH_3)$ in toluene (5). $^nJ(F, CH_3)$ and $^nJ(F, CF_3)$ in fluorine derivatives of toluene and benzotrifluoride, respectively, have also been discussed in some detail in terms of composite coupling mechanisms (6, 7).

The magnitudes of ^nJ(C, F) are available for many benzotrifluoride derivatives (8–10). In 2-fluorobenzotrifluoride $^1J(C, F_3)$ is negative and $^3J(C\text{-}2, F)$ is positive (11). Sign determinations for all ^nJ(C, F) in benzotrifluoride itself, as was done for toluene (3), would be ideal but would also require much more effort than is necessary. The magnitudes of ^nJ(C, F) are not very sensitive to substitution. Accordingly we remeasured the magnitudes of ^nJ(C, F), for n = 3, 4, 5, in benzotrifluoride, **1**, and determined the signs of ^nJ(C, F), for n = 2, 3, 5 employing 4-chloro-3,5-dinitrobenzotrifluoride, **2**, and 2-amino-3,5-dibromobenzotrifluoride, **3**, in double resonance experiments. These results are reported here, as are INDO MO FPT calculations for **1**, and ^nJ(C, F) for n = 3, 4, 5 are discussed in terms of coupling mechanisms.

Experimental

Compounds **1** and **2** came from Pierce Chemical Company and **3** was prepared from 2-aminobenzotrifluoride (Aldrich) by bromination. A 7.8 mol% solution of **2** in acetone-d_6 (nearly saturated) and a 38 mol% solution of **3** in the same solvent were degassed by a number of freeze–pump–thaw cycles and were flame-sealed into 10-mm od nmr sample tubes. A 50% v/v solution of **1** in acetone-d_6 was not degassed but simply transferred to a 10-mm od nmr tube.

The ^{13}C, ^{19}F, and ^1H nmr spectra were accumulated on a WH-90 spectrometer at a probe temperature of 305 K and at transmitter frequencies of 22.63, 84.70, and 90.02 MHz, respectively. The spectrometer employs a Bruker magnet and console, except that it uses a 293 A′ pulse programmer and an 1180 data system and associated software from Nicolet Technology Corporation. The B_1 fields for multiple resonance experiments were calibrated with off-resonance techniques and could be controlled in 1-dB steps. Details of the instrumental modifications for such experiments have been mentioned (12, 13). A typical experiment on **3** involved 256 scans over a period of 96 minutes with 32 K data points devoted to a spectral width of 800 Hz, yielding ^{13}C multiplets of the kind displayed in Fig. 1. Experiments on the dilute solution of **2** involved as many as 3152 transients to obtain a coupled ^{13}C nmr spectrum. The proton-decoupled ^{13}C nmr spectrum of **1** could be obtained relatively easily and displayed linewidths at half-height of ≤0.2 Hz.

INDO MO FPT calculations (14) of ^nJ(C, F) in benzotrifluoride employed an Amdahl 470/V7 system and were based on the recent electron diffraction geometry (15).

Results and discussion

1. *Signs of* $^nJ(C, F)$ *in 2 and 3*

The coupling data for **2**, relevant to the present discussion, are given in Table 1. The sign of $^3J(C\text{-}2, F)$ in **2** was determined by double resonance experiments (16) on the nmr spectra of the isotopomer, **4**. Irradiation of the appropriate ^{19}F peaks

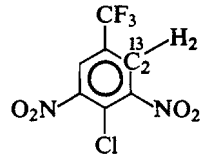

4

and observation of the connected transitions in the H-2 nmr spectrum showed that $^3J(C\text{-}2, F)/^1J(C, H) > 0$. Therefore (17)

[1]On sabbatical leave from the University of Petroleum and Minerals, Saudi Arabia.

Can. J. Chem. Downloaded from www.nrcresearchpress.com by 210.87.254.40 on 09/06/12
For personal use only.

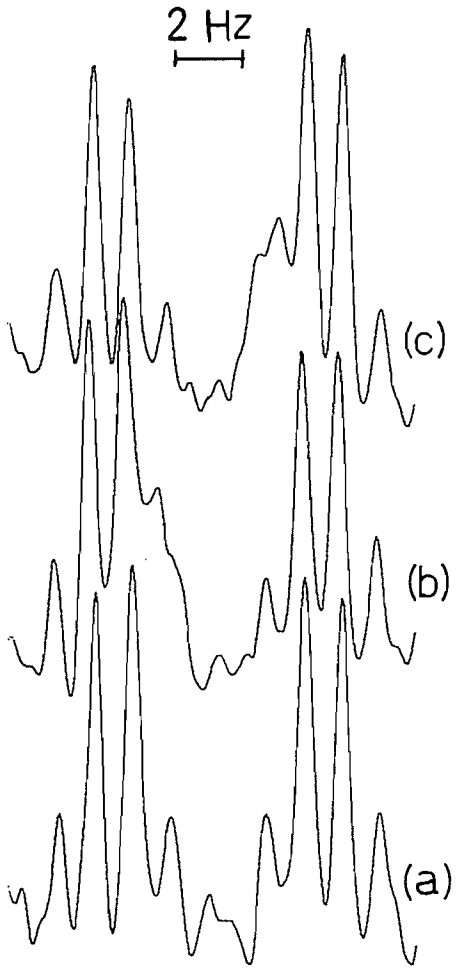

FIG. 1. In (a), the C-4 resonance at 22.63 MHz of 2-amino-3,5-dibromobenzotrifluoride, **3**, in acetone-d_6 solution is shown for one spin state of H-4 and both spin states of H-6. The pair of quartets is separated by ^3J(H-6, C-4). The quartet splitting represents ^5J(F, C-4). In (b), the same quartets are displayed under conditions where one peak in an H-4 quartet is irradiated corresponding to selected spin states of H-6 and CF_3. In (c), a peak of H-4 is irradiated with spin states of H-6 and CF_3 opposite to those in (b). The experiments show that ^5J(F, C-4)/^6J(F, H-4) < 0. Therefore ^5J(F, C-4) is positive. In these experiments it is useful to remember that one finds the ratio of the signs of the coupling constants to a third nucleus from the observed nucleus-one and irradiated nucleus-two. For example, half of the H-4 signal consists of a pair of quartets, separated by ^3J(H-6, H-4). This coupling is small enough so that the quartets due to ^6J(F, H-4) overlap. However, the lowest field peak corresponds to a single spin state of each of H-6 and of the F nuclei. Irradiation of only this peak causes the high-field peak of the low-field quartet in (b) to be split. This shows that the ^{19}F nuclei couple to C-4 with an interaction of opposite sign to their coupling to H-4. The latter is negative. Furthermore, this experiment also shows that ^3J(H-3, H-4) and ^3J(C-4, H-6) have the same sign.

^3J(C-2, F) = +3.75 Hz in **2** and no doubt +3.9 Hz in **1** (10). This sign agrees with the +2.6 Hz found by ^{19}F {^{19}F} double resonance experiments in 2-fluorobenzotrifluoride (11).

That ^2J(C-1, F)/^2J(C-1, H) < 0 was ascertained from irradiation of the appropriate transitions of H-2,6 in the molecule **5** and observation of the ^{19}F nmr peaks. The sequence of ^2J(C-1, H) in C_6H_5X compounds is +1.1, +0.5, −2.5, −3.4, −3.6, −4.9 Hz for X = H, CH_3, I, Cl, NO_2, F, respectively (2, 3, 18), and shows a very rough correlation with the electronegativity of X. The electronegativity of the CF_3 group is at least as large as that of the iodine substituent (19), so that ^2J(C-1, H) is no doubt negative in benzotrifluoride itself. Furthermore, a chlorine substituent on benzene causes a decrease in ^2J(C-4, H) of 0.25 Hz, whereas a nitro group increases ^2J(C-3, H-4) by 0.35 Hz and decreases ^2J(C-3, H-2) by 1.4 Hz. Accordingly, it seems certain that ^2J(C-1, H-2) is −1.9 Hz in **5** (see Table 1). Therefore ^2J(C-1, F) is +36.0 Hz in **2** and no doubt +32.2 Hz in **1** (20).

TABLE 1. Summary of coupling constant data for 4-chloro-3,5-dinitrobenzotrifluoride,[a] **2**

Parameter	Value	Parameter	Value
^1J(C, F)	−272.82(1)	^3J(C-2, H)	7.03(1)
^1J(C, H)	174.83(4)	^3J(C-4, H)	7.76(6)
^2J(C-1, F)	+36.01(2)[b]	^4J(F, H)	−2.68(2)
^2J(C-1, H)	−1.9(1)[b]	^4J(H, H)	2.11(2)
^3J(C_α, H)	4.53(4)	^5J(C-4, F)	+1.11(5)[c]
^3J(C-2, F)	+3.75(1)[d]	^4J(C-3, F) ^4J(C-5, F)	not seen[e]

[a]For a 7.8 mol% solution in acetone-d_6 and 305 K, values in Hz.
[b]If ^2J(C-1, H) is negative, as is almost certain, then ^2J(C-1, F) is positive. See text.
[c]Assumed to be of the same sign as the +1.10(2) Hz determined for ^5J(C-4, F) in 2-amino-3,5-dibromobenzotrifluoride (see text and Fig. 1).
[d]Sign is relative to ^1J(C, H) and is the same as the +2.6 Hz determined for ^3J(C-2, F) in 2-fluorobenzotrifluoride (11).
[e]For the 50% v/v solution of benzotrifluoride in acetone-d_6, repeated measurements gave ^4J(C-3, F) < 0.1 Hz, the linewidth at half height being 0.2 Hz for C-4 and other carbons; ^3J(C-2, F) = 3.92 ± 0.05 Hz, ^5J(C-4, F) = 1.39 + 0.03 Hz.

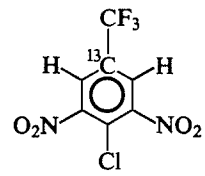

5

Multiple resonance experiments designed to determine the sign of ^5J(C-4, F) in **2** were unsuccessful. Even weak irradiation of ^{1}H nmr peaks caused large polarizations of the C-4 populations, leading to large negative and positive enhancements of those C-4 peaks corresponding to +1 and −1 spin states of the H-2,6 triplet. These phenomena can be traced back to the rather long relaxation time of C-4 and are interesting here only insofar as they obscured the relative sign information inherent in the experiment.

Consequently, the sign of ^5J(C-4, F) was determined for structure **6** of compound **3**.

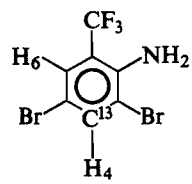

6

This molecule also gives rise to spectra for which double resonance experiments are unequivocal in that the spectra do not deviate greatly from first order. Figure 1 displays one-half of the C-4 multiplets of **6** and shows how they are perturbed by

Can. J. Chem. Downloaded from www.nrcresearchpress.com by 210.87.254.40 on 09/06/12
For personal use only.

TABLE 2. Some nmr spectral parameters for 2-amino-3,5-dibromobenzotrifluoride[a] **3**

Parameter	Value	Parameter	Value
δ_1	116.0[b]	^2J(C, F)	30.99(5)
δ_2	142.1_5	^3J(C-6, F)	5.61(2)
δ_3	107.4	^3J(C-2, F)	1.3(2)
δ_4	140.7	^3J(C-4, H-6)	6.25(4)
δ_5	111.4	^3J(C-6, H-4)	6.03(2)
δ_6	128.8	^4J(H, H)	2.26(1)
δ_{CF_3}	123.9	^4J(H, F)	−0.591(4)
^1J(C, F)	(−)272.9(1)	^6J(H, F)	−0.625(8)
^1J(C-4, H)	170.95(2)	^5J(C-4, F)	+1.10(2)
^1J(C-6, H)	168.17(3)	^4J(C-3, F)	Not
		^4J(C-5, F)	seen

[a]For a 38 mol% solution in acetone-d_6 at 305 K.
[b]In ppm corrected to internal TMS by adding 29.8 ppm to the shifts, which were measured relative to acetone solvent. The C-3 and C-5 shifts are assigned on the basis of additivity of substituent induced shifts and could possibly be reversed.

irradiation of peaks from H-4 which correspond to selected spin states of H-6 and ^{19}F. The experiment gives ^5J(C-4, F)/^6J(F, H-4) < 0 and therefore (5) ^5J(C-4, F) = +1.10 Hz. Undoubtedly this coupling is then +1.11 Hz in **2** and +1.39 Hz in **1**. Because ^{13}C nmr data are not documented for **3**, Table 2 collects our spectral data for this compound.

2. *The C, F, spin–spin coupling mechanisms*

(i) *Preliminary considerations*

In toluene, $^6J(H, CH)$ is −0.62 Hz (21) and is transmitted via a σ−π electron spin polarization mechanism (1, 22). As such, it is expected and calculated to follow the relationship $^6J = {}^6J_{90} \sin^2 \theta$, where θ is the angle by which the C—H bond of the methyl group twists out of the benzene plane (1). $^6J_{90}$ is the value of ^6J when θ is 90°. The INDO MO FPT calculations agree quantitatively with experiment, indicating that the σ−π parameters for the methyl group and the ring C—H bond are correctly reproduced by the INDO parameterization.

Similarly, $^6J(H, CF)$ in benzotrifluoride is −0.64 Hz (5), suggesting that the σ−π parameters for the CH_3 and CF_3 groups are nearly the same, in line with the hyperfine parameters for the neutral $CF_3CH_2\cdot$ and $CH_3CH_2\cdot$ radicals (23, 24). In contrast to $^6J(H, CH)$ in toluene derivatives (7), $^6J(H, CF)$ is somewhat substituent dependent ranging from −0.58 to −0.68 Hz (6, 25). It has been suggested that this coupling contains a σ electron contribution of 0.15 ± 0.05 Hz (6), although it seems reasonable that the σ−π parameter of the CF_3 group be somewhat more sensitive to the presence of ring substituents than is the CH_3 moiety, so that a σ electron contribution is not certain.[2] Certainly, INDO MO FPT computations of $^6J(H, CF)$ indicate (26) a precise $\sin^2 \theta$ dependence, i.e., a σ−π mechanism (1), but yield $^6J_{90}$ as −2.40 Hz instead of the −1.28 Hz expected from experiment. The barrier to internal rotation in benzotrifluoride (27) is only 40 J/mol; hence the average value of $\sin^2 \theta$ is 0.5. Therefore $^6J(H, CF)$ should be $-1.28 \langle \sin^2 \theta \rangle$ or −0.64 Hz. It appears that the INDO calculations overestimate the σ−π parameter for the CF_3 group by a factor of 1.87_5. Note that the toluene data indicate a correct INDO value for the σ−π parameter of the *para* C—H bond.

TABLE 3. INDO MO FPT values for C, F couplings in benzotrifluoride in Hz[a]

θ[b]	^1J	^2J	^3J	^4J	^5J
0	—	—	10.72	−0.20	0.15
3	−171.0	7.82	10.67	−0.23	0.19
7.5	−171.1	7.75	10.51	−0.32	0.30
15	−170.8	7.44	10.13	−0.63	0.66
30	−169.8	6.36	8.98	−1.76	2.00
45	−169.0	4.93	7.81	−3.25	3.85
60	−169.2	3.59	7.17	−4.65	5.71
75	−170.0	2.68	7.34	−5.50	7.10
90	−170.6	2.38	8.34	−5.53	7.61
105	—	—	9.86	−4.72	—
120	—	—	11.60	−3.20	—
135	—	—	13.46	−1.23	—
150	—	—	15.39	0.81	—
165	—	—	16.98	2.39	—
172.5	—	—	17.44	2.84	—
177	—	—	17.54	2.96	—
180	—	—	17.60	3.10	—

[a]Using the electron diffraction geometry (15).
[b]The value of θ is zero degrees when the C—F bond lies in the benzene plane and is *cis* to the carbon atom for ^3J and ^4J. See, for example, Fig. 2.

Of course, the present discussion imples that a discussion of the coupling mechanism in terms of σ and of π electrons is useful. As developed below, such a model can rationalize ^4J(C-3, F) in benzotrifluoride.

(ii) $^5J(C\text{-}4, F)$ *in benzotrifluoride as a* σ−π *coupling*

The INDO values for this coupling in Table 3 closely follow a $\sin^2 \theta$ relationship if the value at θ = 0°, 0.15 Hz, is subtracted from each entry. The theoretical coupling obeys eq. [1]

[1] $^5J(C\text{-}4, F) = 0.15 + 7.46 \sin^2 \theta$

to within an average deviation of 0.01_5 Hz. The number, 0.15 Hz, can be considered as an angle independent (σ) term or as an artifact of the calculation.

However, $7.46 = {}^5J_{90}$ is clearly much too large. In benzotrifluoride, ^5J(C-4, F) is 1.39(3) Hz (Table 1). The present study finds it as +1.11(5) Hz in 4-chloro-3,5-dinitrobenzotrifluoride and as +1.10(2) Hz in 2-amino-3,5-dibromobenzotrifluoride. Assuming 1.3_9 Hz as the proper value, and remembering the overestimate of the σ−π parameter for the CF_3 group above (1.87_5), one has $7.46/(1.87_5 \times 2 \times 1.39)$ or 1.43 as the overestimate of the σ−π parameter for the *para* carbon atom. In other words, *if* ^5J(C-4, F) is indeed a σ−π coupling, then it can be written as eq. [2]

[2] $^5J(C\text{-}4, F) = A + (2.78 - A) \sin^2 \theta$

This discussion describes ^5J(C-4, F) as predominantly a σ−π coupling. Then the substituent-induced variations in this coupling arise from a perturbation of one or both of the σ−π parameters at the ends of the coupling fragment.[3] If the present approach has value, then it should rationalize the unobservably small ^4J(C-3, F) in benzotrifluoride and its derivatives.

[2]Such a contribution can only be established by a lengthy and systematic study of a large number of benzotrifluoride derivatives, similar to the one recently described for 2-fluorotoluene and its derivatives (7), and is in progress.

[3]The σ−π parameter at C-4, which might be writtten as Q^C_{CX}(28), no doubt consists of a number of terms (29) and would need to be established for each type of sidechain at C-1. The σ−π parameter will be sensitive to the spin densities at the neighbouring carbon atoms, for example.

Can. J. Chem. Downloaded from www.nrcresearchpress.com by 210.87.254.40 on 09/06/12
For personal use only.

(iii) *^4J(C-3, F) as a composite σ and σ−π coupling*

It has been suggested (8) that this coupling apparently vanishes because of σ and σ−π electron contributions of opposite sign. INDO calculations of $^5J(F, CF_3)$ in 3-fluorotoluene are indeed compatible with such a situation for the very small *substituent-independent* coupling of ca. +0.25 Hz (7, 30). Furthermore, $^5J(H, SH)$ and $^5J(H, CH_3)$ in thiophenol (31) and toluene (1) can be rationalized as additive contributions of σ and σ−π mechanisms of the same sign. Indeed, in thiophenol and some of its derivatives, $^5J(H, SH)$ can be written as (31) eq. [3],

$$[3] \quad {}^5J = A \sin^2(\theta/2) + B \sin^2\theta$$

where the first term represents the σ electron part of ^5J.

Now, the INDO numbers of ^4J(C-3, F) in Table 3 are approximately reproduced by a closely related eq.[4]

$$[4] \quad {}^4J(\text{C-3, F}) = -0.20 + 3.10 \sin^2(\theta/2) - 6.88 \sin^2\theta$$

with an average absolute deviation of 0.07 Hz. It can be argued that the constant term is contrary to the implied coupling mechanism and that it should be eliminated. It is small, however, and any adjustment to eq. [4] would be somewhat arbitrary. Because the rotational averages of $\sin^2\theta$ and of $\sin^2(\theta/2)$ are both 0.5 (31), the calculated value of ^4J(C-3, F) becomes −2.89 Hz. Of course, the composite σ−π parameters are incorrect and, as estimated above for ^5J(C-4, F), should be reduced by a factor of 2.67 = 1.43 × 1.87. Therefore, the rotationally averaged ^4J(C-3, F) becomes +0.06 Hz, indeed compatible with an experimentally vanishing coupling.

This argument implies that the σ electron contribution to ^4J(C-3, F) is calculated correctly by the theory. The σ−π contribution is negative because of electron correlation. The spin correlation function for atoms belonging to different classes is negative (28), so that if positive σ−π components occur at C-2 and C-4, the component at C-3 is expected to be negative.

(iv) *The vicinal coupling, ^{3}J(C-2, F)*

The vicinal coupling ^3J(C-2, F), calculated in Table 3, displays a distorted Karplus behaviour in that the minimum lies nearer 60° than 90°. A reasonable fit to an equation of the form $^3J = A + B\cos\theta + C\cos 2\theta$ is not possible. Furthermore, the value of 10.72 Hz at θ = 0° is very small relative to that of 17.60 Hz at θ = 180° when compared to other theoretical and experimental vicinal couplings (32), e.g. ^3J(H, C). The reason for the small $^3J(\theta = 0°)$ is very likely related to large negative couplings to ^{19}F, calculated by INDO MO FPT when the other nucleus lies near ^{19}F. For example, in benzotrifluoride large negative ^4J(F, H-2) numbers are computed for θ < 45° (26). Again in 2-fluorotoluene similar negative $^4J(F, CH_3)$ values arise for θ values which bring the methyl hydrogen atoms and the fluorine atom into proximity (26). In fact, $^4J(F, CH_3)$ is +0.5 Hz for θ ~ 0° (7), not −3.2 Hz, as calculated (26). Similar remarks apply to $^5J(CHO, CF_3)$ in 2-trifluoromethylbenzaldehyde (33).

We suggest that the calculated ^3J(C-2, F) parameters in Table 3 suffer from such distortions. The normal Karplus curve displays a minimum nearer 90°. The calculated data in Table 3 are easily adjusted to meet these requirements and yield the Karplus eq. [5]. This equation gives 11.51 Hz as the average

$$[5] \quad {}^3J = 11.51 - 2.28\cos\theta + 3.81\cos 2\theta$$

^3J, whereas the observed average is 3.92 ± 0.05 Hz. Of course, a positive σ−π contribution to ^3J of the form $D \sin^2\theta$ is also expected. Because $2\sin^2\theta = 1 - \cos 2\theta$, eq. [5] contains this contribution. It enters as $A + D/2$ and $C - D/2$, where A and C are the σ electron terms. Available data (1, 26) indicate that its *calculated* magnitude will be comparable to the σ−π contribution to the *para* position (cf. eqs. [1] and [4]). A brief speculation then proposes eq. [6]

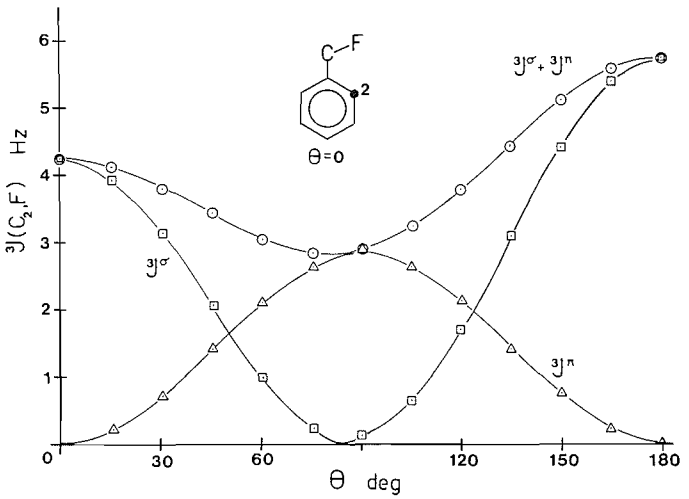

FIG. 2. ^3J(C-2, F) in benzotrifluoride is plotted versus the dihedral angle θ. The circles represent the equation $^3J(\text{C-2, F}) = 2.52 - 0.74\cos\theta + 2.44\cos^2\theta + 2.79\sin^2\theta$. The π electron contribution is given by the last term of this equation and is also plotted in the figure, as is the σ electron component given by the first three terms of the equation. See text for a discussion.

$$[6] \quad {}^3J = 7.78 - 2.28\cos\theta + 7.54\cos 2\theta + 7.46\sin^2\theta$$

where the σ−π contribution is written explicitly. Now, 7.46 $\sin^2\theta$, the σ−π term, is too large by a factor of 2.67 (see above). Furthermore, to obtain agreement with experiment, divide the σ terms in eq. [6] by an arbitrary factor of 3.08 and obtain eq. [7].

$$[7] \quad {}^3J(\text{C-2, F}) = 2.52 - 0.74\cos\theta + 2.44\cos 2\theta + 2.79\sin^2\theta$$

In eq. [7] the average over essentially free rotation is now 3.92 Hz, as observed (note that $\langle\cos\theta\rangle = \langle\cos 2\theta\rangle = 0$ and $\langle\sin^2\theta\rangle = 0.5$). This equation is plotted in Fig. 2 and may represent the experiment in a reasonable way. Of course, for a CF_3 group with its threefold local symmetry, this equation predicts the same *average* ^3J(C-2, F) value for any θ, so that it could be tested only for a situation where reorientation about the C_{sp^2}—C_{sp^3} bond were slow enough to cause the differences in observable chemical shifts among the ^{19}F nuclei of the CF_3 group. Note that *meta* or *para* substitution with up to three substituents in benzotrifluoride causes very little change (9) in ^3J(C-2, F). A 2-X substituent decreases ^3J(C-2, F) and increases ^3J(C-6, F), as can be seen for **3**. In view of the properties of eq. [7], such changes reflect intrinsic substituent perturbations of ^3J(C, F) and not conformational preferences of the CF_3 group. Some support for the presence of a σ−π contribution to ^3J(C, F) can be garnered from the data on 2-trifluoromethylnaphthalene (8). In this compound, ^3J(C-3, F) is 3.2 Hz and ^3J(C-1, F) is 4.5 Hz, whereas ^3J(C-2, F) in benzotrifluoride is 3.9 Hz. The double-bond character of the C-1, C-2 bond in naphthalene is larger than that in benzene, while that of the C-2, C-3 bond is smaller. The σ−π contribu-

Can. J. Chem. Downloaded from www.nrcresearchpress.com by 210.87.254.40 on 09/06/12
For personal use only.

tion should therefore be larger to ^3J(C-1, F) in the naphthalene derivative than to ^3J(C, F) in benzotrifluoride and should be less to ^5J(C-3, F), as is observed.

(v) ^2J(C-1, F) *and* ^1J(C, F)

The discussions of ^nJ(C, F) for $n = 3$, 4, 5 above are couched in terms of σ and $\sigma-\pi$ components, and are based on experiment and on hints from the INDO computations. The latter are based on the contact term only. Neglect of other than contact terms for ^1J(C, F) is not justified and ^2J(C, F) very likely also contains such terms. It may be noted that the θ dependence of ^2J(C-1, F) in Table 3 is qualitatively similar to that computed for ^2J(C-1, CH_3) in toluene (3), but is too *small* (compare ^nJ(C, F) for $n = 3$, 4, 5 in Table 3 where the calculated values are too *large*) by a factor of about seven. This result can be taken as a hint that other than contact terms are significant.

(vi) *Concerning non-contact contributions to* ^{n}J(C, F)

As a referee points out, the possible presence of non-contact mechanisms for ^nJ(C, F) must be considered. Beginning with ^1J(C, F) early calculations (34) noted the disagreement between the INDO MO FPT contact contributions and experiment. Non-contact contributions to ^1J(C, F) were mentioned as one possible reason for the disagreement. Indeed, their presence was confirmed by Blizzard and Santry (35). Other calculations have been reviewed (36–39). Computations of ^2J(C, F) are more equivocal as to the relative contributions of non-contact mechanisms (37–40), but their presence seems likely, particularly in fluorobenzene (39–43). In the latter compound ^3J(C, F) and ^4J(C, F) are also calculated to have non-contact contributions.

However, it has been shown experimentally and theoretically, as reviewed by Wray (44), that ^3J(C, F) in saturated acyclic and cyclic fluorine derivatives is dominated by the contact mechanism and that other mechanisms are not important in determining its conformational behaviour. The CF_3 group in benzotrifluoride is to first order a saturated group and the C—F bonds interact only in a second order manner with the aromatic ring. In that sense, the approach taken in this paper to ^3J(C, F) may have validity.

Turning to ^5J(C-4, F), the contact contributions in Table 3 yield a $\sigma-\pi$ mechanism, but are too large by a factor of 2.7. Similar calculations (45) for ^5J(C-4, H) in toluene suggest a $\sigma-\pi$ mechanism, yet are again too large by a factor of 2.4. In a recent extensive theoretical and experimental investigation, we have shown that ^5J(C-4, H) is indeed a $\sigma-\pi$ coupling (46). The overestimate of its magnitude and that of ^nJ(C-4, F) by INDO MO FPT methods is very likely traceable to the theoretical, effective $\sigma-\pi$ parameter at C-4 in these compounds. It seems unlikely that the theoretical overestimates are an indication of other than contact mechanisms for ^5J(C-4, F) and ^5J(C-4, H).

As to ^4J(C, F) we have presented a rationalization of its absence in benzotrifluoride but cannot prove that non-contact mechanisms are negligible. A full theoretical approach is indicated, now that all the signs of ^nJ(C, F) in benzotrifluoride are known.

Conclusions

The long-range coupling ^5J(C-4, F), in benzotrifluoride can be interpreted as a π electron-mediated interaction, while ^4J(C-3, F) is a composite of mutually cancelling σ and π electron components of opposite sign. Any substituent perturbations of these components must also compensate one another. ^3J(C-2, F) very likely consists of a σ electron contribution, obeying a Karplus dependence on the conformational angle θ, and a π electron contribution which, obeying a $\sin^2\theta$ law, can be absorbed into a Karplus equation.

Acknowledgements

We are grateful to the Natural Sciences and Engineering Research Council of Canada and to the University of Petroleum and Minerals for support. The referees are thanked for very helpful criticism.

1. R. WASYLISHEN and T. SCHAEFER. Can. J. Chem. **50**, 1852 (1972).
2. L. ERNST, V. WRAY, V.A. CHERTKOV, and N. M. SERGEYEV. J. Magn. Reson. **25**, 123 (1977).
3. M. HANSEN and H. J. JAKOBSEN. J. Magn. Reson. **20**, 520 (1975).
4. L. M. STOCK and M. R. WASIELEWSKI. Prog. Phys. Org. Chem. **13**, 253 (1981).
5. R. J. KOSTELNIK, M. P. WILLIAMSON, D. E. WISNOSKY, and S. M. CASTELLANO. Can. J. Chem. **47**, 3313 (1969).
6. T. SCHAEFER, W. NIEMCZURA, C. M. WONG, and K. MARAT. Can. J. Chem. **57**, 807 (1979), and references therein.
7. T. SCHAEFER, R. SEBASTIAN, R. P. VEREGIN, and R. LAATIKAINEN. Can. J. Chem. **61**, 29 (1983), and references therein.
8. D. DODDRELL, M. BARFIELD, W. ADCOCK, M. AURANGZEB, and D. JORDAN. J. Chem. Soc. Perkin Trans. **2**, 402 (1976).
9. R. A. NEWMARK and J. R. HILL. Org. Magn. Reson. **9**, 589 (1977).
10. F. J. WEIGERT and J. D. ROBERTS. J. Am. Chem. Soc. **93**, 2361 (1971).
11. S. L. MANATT and M. A. COOPER. J. Am. Chem. Soc. **99**, 4561 (1977).
12. T. SCHAEFER and K. MARAT. Org. Magn. Reson. **15**, 294 (1981).
13. T. SCHAEFER, K. MARAT, A. LEMIRE, and A. F. JANZEN. Org. Magn. Reson. **18**, 90 (1982).
14. P. A. DOBOSH. Quantum Chemistry Program Exchange, **11**, 1414 (1979).
15. G. SCHULTZ, I. HARGITTAI, and R. SEIP. Z. Naturforsch. Teil A, **36**, 669 (1981).
16. R. FREEMAN and W. A. ANDERSON. J. Chem. Phys. **37**, 2053 (1962).
17. R. FREEMAN. J. Chem, Phys. **43**, 3087 (1965).
18. A. R. TARPLEY, JR. and J. H. GOLDSTEIN. J. Phys. Chem. **76**, 515 (1972).
19. J. E. HUHEEY. J. Phys. Chem. **69**, 3284 (1965).
20. L. F. JOHNSON and W. C. JANKOWSKI. Carbon-13 N.M.R. spectra. Wiley, New York. 1972.
21. M. P. WILLIAMSON, R. KOSTELNIK, and S. M. CASTELLANO. J. Chem. Phys. **49**, 2218 (1968).
22. C. J. MACDONALD and W. F. REYNOLDS. Can. J. Chem. **48**, 1002 (1970).
23. M. JINGUCHI, K. C. LIN, C. A. MCDOWELL, and P. RAGHUNATHAN. J. Chem. Phys. **65**, 3910 (1976).
24. R. W. FESSENDEN and R. H. SCHULER. J. Chem. Phys. **39**, 2147 (1963).
25. T. SCHAEFER and J. B. ROWBOTHAM. Can. J. Chem. **54**, 2243 (1976).
26. R. E. WASYLISHEN and M. BARFIELD. J. Am. Chem. Soc. **97**, 4545 (1975).
27. T. OGATA and A. P. COX. J. Mol. Spectrosc. **61**, 265 (1976).
28. H. M. MCCONNELL. J. Chem. Phys. **30**, 126 (1959).
29. M. KARPLUS and G. K. FRAENKEL. J. Chem. Phys. **35**, 1312 (1961).
30. T. SCHAEFER, W. DANCHURA, and W. NIEMCZURA. Can. J. Chem. **56**, 2233 (1978).
31. T. SCHAEFER, T. A. WILDMAN, and R. SEBASTIAN. Can. J.

Chem. **60**, 1924 (1982).
32. R. WASYLISHEN and T. SCHAEFER. Can. J. Chem. **51**, 961 (1973), and references therein.
33. T. SCHAEFER, S. R. SALMAN, and T. A. WILDMAN. Can. J. Chem. **58**, 2364 (1980)
34. G. E. MACIEL, J. W. MCIVER, JR., N. S. OSTLUND, and J. A. POPLE. J. Am. Chem. Soc. **92**, 11 (1970).
35. A. C. BLIZZARD and D. P. SANTRY. J. Chem. Phys. **55**, 950 (1971); **58**, 4714 (1973).
36. J. B. STOTHERS. Carbon-13 nuclear magnetic resonance spectroscopy. Academic Press, New York. 1972.
37. J. W. EMSLEY, L. PHILLIPS, and V. WRAY. Prog. Nucl. Magn. Reson. Spectrosc. **10**, 85 (1977).
38. R. E. WASYLISHEN. Annu. Rep. NMR Spectrosc. **7**, 245 (1977).
39. J. KOWALEWSKI. Annu. Rep. NMR Spectrosc. **12**, 82 (1982).
40. H. JENSEN and K. SCHAUMBURG. Mol. Phys. **22**, 1041 (1971).
41. V. GALASSO. Org. Magn. Reson. **12**, 318 (1979).
42. P. E. HENSEN, A. BERG, H. J. JAKOBSEN, A. P. MANZARA, and J. MICHL. Org. Magn. Reson. **10**, 179 (1977).
43. S. DUANGTHAI and G. A. WEBB. Org. Magn. Reson. **12**, 98 (1979).
44. V. WRAY. J. Am. Chem. Soc. **103**, 2503 (1981).
45. L. ERNST, V. WRAY, V. A. CHERTKOV, and N. M. SERGEYEV. J. Magn. Reson. **25**, 123 (1977).
46. T. SCHAEFER, J. PEELING, and G. H. PENNER. Can. J. Chem. **61**, 2773 (1983).

Can. J. Chem. Downloaded from www.nrcresearchpress.com by 210.87.254.40 on 09/06/12
For personal use only.

Concerning the mechanism of $^5J_m^{H,CH_3}$ in toluene and its derivatives

TED SCHAEFER AND REINO LAATIKAINEN[1]

Department of Chemistry, University of Manitoba, Winnipeg, Manitoba, Canada R3T 2N2

Received June 7, 1983

TED SCHAEFER and REINO LAATIKAINEN. Can. J. Chem. **61**, 2785 (1983).

On the basis of the observed five-bond spin–spin coupling constants between the α protons and the *meta* ring protons in the 2,6-difluoro derivatives of toluene, ethylbenzene, and cumene, it is argued that $^5J_m^{H,CH_3}$ in toluene can be written as $A\langle\sin^2\theta\rangle + B\langle\sin^2(\theta/2)\rangle$. A and B are of the same sign and of very similar magnitude. In consequence, $^5J_m^{H,CH_3}$ cannot be used to measure the conformational preference of the methyl group. However, $^5J_m^{H,CH_2}$ and $^5J_m^{H,CH}$ in α-substituted toluene derivatives will be useful in conformational studies. $^5J_m^{H,CH_3}$ in toluene derivatives varies between 0.30 and 0.46 Hz and some patterns in its ring substituent dependence can be gleaned from some fifty precise values.

TED SCHAEFER et REINO LAATIKAINEN. Can. J. Chem. **61**, 2785 (1983).

En se basant sur les constantes de couplage spin–spin à travers cinq liaisons que l'on a observées entre les protons α et les protons en position *meta* du cycle dans les difluoro-2,6 toluène, ethylbenzène et cumène, on suggère que $^5J_m^{H,CH_3}$ dans le toluène peut être représentée par l'équation $A\langle\sin^2\theta\rangle + B\langle\sin^2(\theta/2)\rangle$. Les constantes A et B ont le même signe et sont de valeurs semblables. En conséquence, on ne peut pas utiliser $^5J_m^{H,CH_3}$ pour mesurer la préférence conformationnelle du groupe methyle. Toutefois, $^5J_m^{H,CH_2}$ et $^5J_m^{H,CH}$ dans les dérivés du toluène substitués en α peuvent être utiles dans des études conformationnelles. Les valeurs de $^5J_m^{H,CH_3}$ dans les dérivés du toluène varient entre 0.30 et 0.46 Hz et quelques patrons de leur dépendance avec les substituants du cycles peuvent être glanés à partir de cinquante valeurs précises.

[Traduit par le journal]

Can. J. Chem. Downloaded from www.nrcresearchpress.com by 210.87.254.6 on 09/06/12
For personal use only.

Introduction

The long-range spin–spin coupling constants between nuclei in the benzene ring and those in sidechains are of interest in the theory of the transmission of nuclear spin state information via electronic interactions, as well as in their applications to conformational problems. For example, the coupling over six bonds between α and ring protons, $^6J_p^{H,CH_3}$, in toluene is proportional to $\sin^2\theta$ (see **1**). $^6J_p^{H,CH_3}$ is therefore understood as a

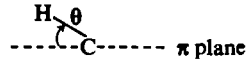

1

σ–π coupling mechanism (1), in which the π electrons transmit the spin information and a σ–π spin polarization acts at both ends of the coupling path to complete the interaction between the protons in the σ electron framework. The θ dependence implies the use of $^6J_p^{H,CH_3}$ in conformational studies which, in fact, can yield quantitative information about the orientational preferences and the small internal barriers to rotation about the exocyclic bonds in molecules such as ethylbenzene (1, 2). The somewhat more complex angle dependence of $^4J_o^{H,CH_3}$ has recently been discussed in detail (3), and discussions of $^5J_{o,m,p}^{F,CH_3}$ are also available (4–7).

For couplings over five formal bonds, two mechanisms must be considered. A σ–π contribution no doubt exists. It is very likely that a σ contribution is also present. The latter will have its largest magnitude when the nucleus in the sidechain lies in the plane of the benzene ring, as in **2**. When the sidechains are

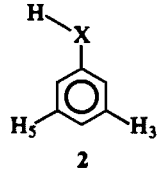

2

aldehydic or hydroxyl groups, for which the stereochemistry of **2** is strongly preferred, many studies have shown the coupling to H-3 to be large (θ = 180°) and that to H-5 (θ = 0°) to be very small or, more often, undetectable (8–14).

The behaviour of ^5J for θ values other than 0° or 180°, that is for nonplanar conformations, has received much less attention. A detailed INDO MO FPT approach to toluene and the xylenes suggested that $^5J_m^{H,CH_3}$ was a composite of σ–π and σ electron interactions (15). The former varied as $\sin^2\theta$ and the latter perhaps as $\sin^2(\theta/2)$. There exists some evidence for the σ–π component (16–19) from the methyl group replacement technique (20), in which the coupling over six formal bonds between the methyl groups in *m*-xylene is taken as the negative of the σ–π component of $^5J_m^{H,CH_3}$.

More recently, a σ component of $^5J_m^{H,SH}$ varying as $\sin^2(\theta/2)$ was plausibly deduced for thiophenol and its *para*-substituted derivatives (21). In such molecules $\langle\sin^2(\theta/2)\rangle$ (brackets indicate expectation values) is necessarily 0.5 whatever the twofold barrier to rotation about the C—S bond, whereas $\langle\sin^2\theta\rangle$ varies with the twofold barrier, allowing a decomposition of the observed couplings into their two components.

For methyl groups, with their local threefold symmetry, the properties of $\sin^2\theta$ and $\sin^2(\theta/2)$ make such a decomposition rather more difficult. In addition, substituents placed along the coupling path may alter the magnitudes of the two components. Nevertheless, a sizeable number of $^5J_m^{H,CH}$ values are available in this laboratory and the most precise of these allow a test of the hypothesis in eq. [1]. In this equation, $^5J_{90}^{\pi} \equiv {}^5J^{\pi}$ is the magnitude of the σ–π component for θ = 90° and $^5J_{180}^{\sigma} \equiv {}^5J^{\sigma}$

$$[1]\quad {}^5J_m^{H,CH_3} = {}^5J_{90}^{\pi}\langle\sin^2\theta\rangle + {}^5J_{180}^{\sigma}\langle\sin^2(\theta/2)\rangle$$

is the magnitude of the σ component for θ = 180°, or planar zig-zag bond arrangement. $^5J^{\pi}$ vanishes for conformations in which the α C—H bond lies in the molecular plane and $^5J^{\sigma}$ vanishes only at θ = 0°.

Discussion

Whatever the preferred orientation of the methyl group, for example as in **3** for an *ortho* substituted toluene, both $\sin^2\theta$ and

[1] Present address: Department of Chemistry, University of Kuopio, Kuopio 10, Finland.

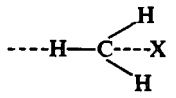

3

$\sin^2(\theta/2)$ yield 0.5 when averaged over the three protons. Of course, a rigid conformation **3** does not exist. Thus, in 2-fluorotoluene the microwave spectra demonstrate **3** as the most stable and that the threefold rotation barrier lies near 3 kJ/mol (22). Nevertheless, the implied torsional motions will still leave $\langle\sin^2\theta\rangle$ and $\langle\sin^2(\theta/2)\rangle$ as 0.5. In other words, any orientation of the methyl group yields the same value of these quantities, simply because of the threefold symmetry of the methyl group (this is not true for sidechains like SH or CHO, for example).

A disentanglement of the σ and $\sigma-\pi$ components of $^5J_m^{H,CH_3}$ requires a lower symmetry in the sidechain. This situation is achieved by substitution at the methyl site, preferably with substituents which do not significantly alter the coupling mechanisms nor their magnitude. Such substituents may well be methyl groups (1). Furthermore, a range of $\langle\sin^2\theta\rangle$ and $\langle\sin^2(\theta/2)\rangle$ values is needed in order to have a set of well-conditioned equations of type [1]. This need is met by the introduction of *ortho* substituents to give conformations as in **4** and **5**. In the 2,6-difluoro derivatives of toluene, ethylbenzene,

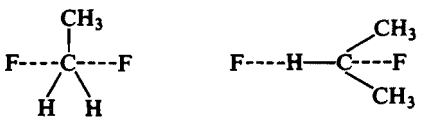

4 5

4, and cumene, **5**, one has (4, 23) $^5J_m^{H,CH}$ as 0.438(2), 0.363(2), and 0.292(3) Hz, respectively. Also, the values of $\langle\sin^2\theta\rangle$ are 0.5, 0.277, and 0.074 in the same order (23), as deduced from $^6J^{H,CH}$, whereas $\langle\sin^2(\theta/2)\rangle$ is 0.5 for each molecule because of the twofold nature of the barriers involved (21). Hence one has eq. [2] to [4], which yield $^5J_{90}^{\pi}$ as 0.336 Hz and $^5J_{180}^{\sigma}$ as

$$[2]\quad 0.438 = 0.5\,J_{90}^{\pi} + 0.5\,J_{180}^{\sigma}$$

$$[3]\quad 0.363 = 0.277\,J_{90}^{\pi} + 0.5\,J_{180}^{\sigma}$$

$$[4]\quad 0.292 = 0.074\,J_{90}^{\pi} + 0.5\,J_{180}^{\sigma}$$

0.540 Hz. In view of the possible errors, the exact agreement among the three equations is surprising. Nevertheless, they are consistent with a composite of σ and $\sigma-\pi$ mechanisms. The $^5J_{90}^{\pi}$ value of 0.336 Hz compares with the 0.38 ± 0.04 Hz implied by $^6J_m^{CH_3,CH_3}$ in a *m*-xylene derivative (16). The $^5J_{180}^{\sigma}$ number of 0.540 Hz can be compared with the 0.54 ± 0.02 Hz measured (24) in rigid **6** (no coupling to H-5),

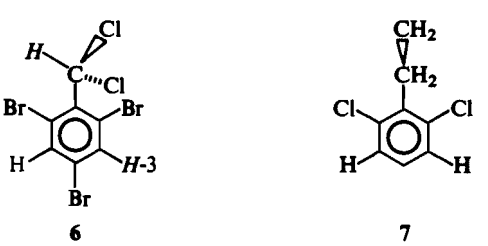

6 7

and similar compounds (25).

In **7** the ^5J numbers from eqs. [2] to [4] predict $^5J_m^{H,CH_2}$ as 0.354 Hz if $\langle\sin^2\theta\rangle$ is taken as 0.25, approximately correct for a very large twofold barrier. In ethylbenzene itself one has a twofold barrier of 5 kJ/mol (2) and in **4** it is ca. 25 kJ/mol (23), corresponding to a $\langle\sin^2\theta\rangle$ of 0.277. In **7**, $^5J_m^{H,CH_2}$ is 0.36(3) Hz (26).

Intrinsic perturbations of $^5J_m^{H,CH_3}$ *by ring substituents*

In toluene, $^5J_m^{H,CH_3}$ is 0.356(6) Hz (27) and is 0.438(2) Hz in 2,6-difluorotoluene (see Table 1). From the discussion above it appears that the major part of the increase on *ortho* substitution arises from an increase in the σ electron contribution, that is, in $^5J^{\sigma}$. The relative insensitivity of $^5J^{\pi}$ to ring substitution (16, 17, 28) as measured by $^5J_m^{CH_3,CH_3}$ and, indeed, to replacement of a ring carbon by nitrogen as in some dimethyl pyridine derivatives (19), is consistent with the invariance of $^6J_p^{H,CH_3}$ in toluene derivatives (1, 4). The latter is a pure $\sigma-\pi$ coupling, as far as can be discovered.

If $^5J^{\pi}$ is 0.336 Hz, then in toluene itself $^5J_{180}^{\sigma}$ follows as 0.376 Hz, yielding $^5J_m^{H,CH_3}$ as 0.5(0.336) + 0.5(0.376) = 0.356 Hz. Allowing for experimental error, it seems that the σ and $\sigma-\pi$ components of $^5J_m^{H,CH_3}$ in toluene are roughly equal in magnitude and of the same sign.

In the following paragraphs, 52 precise values of $^5J_m^{H,CH_3} \equiv {}^5J$ are surveyed and are given in Table 1. Most of these numbers are unpublished results from this laboratory. Their standard deviations as determined from least-squares analyses are typically less than 0.005 Hz, so that an error of rather less than 0.02 Hz may probably be assumed. The values range from 0.300(1) to 0.464(4) Hz. At the very least, this data set provides hints as to the initial guess at ^5J in an interative analysis of the spectrum of a toluene derivative.

There exist some patterns in the substituent perturbations of ^5J in Table 1. For example, examine ^5J(Hz) in the sequence **8**

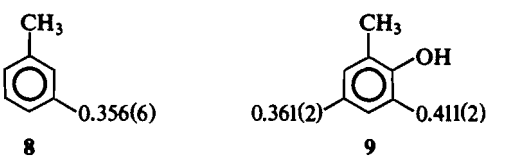

8 9

10 11

to **11**, in which the numbers in parentheses are standard deviations and were obtained for solutions in CCl_4 at the same concentrations, at the same temperature, and by experienced analysts employing the same calibration and spectral analytical procedures. The 2-OH substituent increases $^5J_3$ (to H-3) by 0.05_5 Hz, but does not alter $^5J_5$ (to H-5) significantly, suggesting that the perturbation occurs, not in the methyl group orbitals but in the orbitals involved in the coupling path in the ring (see **2**). Now, addition of a chlorine substituent at position 3 to give **10** causes a decrease of 0.03_9 Hz in $^5J_5$, whereas a remote chlorine substituent at position 5, giving **11**, decreases $^5J_3$ by 0.03_5 Hz. This pattern is general. A substituent *meta* to the methyl group in toluene derivatives decreases the (single) ^5J (a possible exception is 2-fluoro-*m*-xylene in Table 1, where the 3-CH_3 substituent does not appear to cause a decrease in $^5J_5$ from its value in 2-fluorotoluene). Whether these decreases in ^5J arise from a perturbation at the CH_3 site or in the ring path cannot be said, although it is interesting that a *meta* fluorine

Can. J. Chem. Downloaded from www.nrcresearchpress.com by 210.87.254.6 on 09/06/12
For personal use only.

TABLE 1. Values of $^5J_m^{H,CH_3}$ (Hz) in a number of toluene derivatives[a] at 305 K

Compound	$^5J_m^{H,CH_3}$	Compound	$^5J_m^{H,CH_3}$	Compound	$^5J_m^{H,CH_3}$
1. Toluene	0.356(6)[b,c]	19. 2-F-5-NO_2	0.389(2)	28. 2-F-6-NO_2	0.439(4)
2. 4-F	0.341(3)[d]	20. 2-F	0.401(2)	H-5	0.369(3)
3. 4-SO_2F	0.337(4)[e]	H-5	0.352(2)	29. 2-F-6-NH_2	0.424(2)
5. 4-NH_2	0.320(10)[f]	21. 2-OH	0.411(2)[l,o]	H-5	0.429(3)
6. 4-CH_2Br	0.349(1)[g]	H-5	0.361(2)	30. 2-F-6-Cl	0.452(2)
7. 3-F	0.300(1)[h]	22. 2-CHO	0.367(2)[i]	H-5	0.402(2)
8. 3-F-6-Cl	0.355(3)[h]	H-5	0.349(2)	31. 2,6-DiF	0.438(2)
9. 2-CH_3-3-F	0.301(2)	23. 2-F-4-NO_2	0.411(3)	32. 2-F-6-CH_3	0.440(2)
10. 2-F-3-CH_3	0.353(2)	H-5	0.396(3)	H-5	0.455(2)
11. 2-CFO-5-Cl	0.353(3)[j]	24. 2-F-4-NH_2	0.380(3)	33. 2,6-DiCl-4-CH_2F	0.454(2)[q]
12. 2-CFO-3-CH_3	0.343(1)[j]	H-5	0.349(3)	34. 2-F-4,5-diNO_2	0.409(5)
13. 2-OH-3-Cl	0.322(2)[k]	25. 2-F-4-CFO	0.428(2)	35. 2-F-4,6-diNO_2	0.443(5)
14. 2-OH-5-Cl	0.376(2)[l]	H-5	0.388(2)	H-5	0.443(5)
15. 2-OH-3-allyl	0.316(1)[m]	26. 2-F-4-I	0.414(2)	36. 2-F-4,6-diBr	0.464(4)
16. 2-F-5-Br	0.377(2)	H-5	0.388(2)	H-5	0.414(4)
17. 2-Br-5-SH	0.368(3)[n]	27. 2-NO_2-4-Cl	0.368(5)[p]	37. 2-F-4,6-diI-5-NH_2	0.429(1)
18. 2-F-F-NH_2	0.387(3)	H-5	0.373(4)	38. 2-F-4-I-5-NH_2	0.394(2)

[a] Solvent and concentration conditions for 2-fluorotoluene derivatives are given in ref. 4, the usual solvent being CS_2.
[b] Reference 27, neat compound.
[c] Numbers in parentheses are standard deviations.
[d] Reference 5, acetone-d_6 solution.
[e] Measured in $CDCl_3$ solution under conditions given in ref. 36.
[f] In $CDCl_3$, unpublished from this laboratory.
[g] In acetone-d_6, from ref. 37.
[h] Reference 6, CS_2 solution.
[i] Reference 12, CCl_4 solution.
[j] Reference 38, CS_2 solution.
[k] Reference 39, 4.7 mol% in CCl_4.
[l] Reference 40, 5.0 mol% in CCl_4 but ^5J is not reported in this reference.
[m] Reference 9, CCl_4 solution.
[n] In CCl_4 solution, unpublished work in this laboratory.
[o] 5.0 mol% in CCl_4. In a 5 mol% solution in benzene-d_6 the values are 0.408(2) and, to H-5, 0.354(2) Hz.
[p] In CS_2 solution, unpublished work in this laboratory.
[q] Reference 41, in CS_2 solution.

substituent causes only a slight change (0.8 ± 0.6 Hz) in ^1J (^{13}C, H) of CH_3, whereas ^1J (^{13}C, H) increases by 1.7_5 ± 0.6 Hz in the presence of a *meta* nitro group (29–31). In Table 1, nitro and amino groups in the *meta* position cause the same (small) reduction of ^5J.

A lone *para* substituent apparently causes a very small reduction in ^5J (F, SO_2F, SH, NH_2, CH_2, Br). Two *ortho* substituents induce relatively large increases in ^5J (although a single *ortho* CHO group does not). Thus, for 2-F-6-Y toluenes one has $^5J_5 + {}^5J_3$ as 0.753, 0.808, 0.853, 0.854, 0.876, 0.895 Hz for Y = H, NO_2, NH_2 Cl, F, CH_3, respectively. For toluene this sum is 0.712 Hz. For 2-F-4-Y toluene derivatives, the sum is 0.753, 0.807, 0.729, 0.816, 0.802 Hz for Y = H, NO_2, NH_2, CFO, I, respectively. In more heavily substituted toluene derivatives, ^5J is largest.

As stated above, eqs. [2] to [4] and the methyl group replacement technique suggest that $^5J^{\pi}$ is relatively insensitive to ring substitution. INDO MO FPT calculations of $^5J_{180}$ for toluene yield 0.831 Hz, an overestimate as has been discussed (15). For 3-fluorotoluene, this number is computed as 0.758 Hz, in *qualitative* agreement with the observed reduction of 0.05_6 Hz in $^5J_m^{H,CH_3}$. The theoretical value is (0.831 − 0.758)/2 (average of $\sin^2(\theta/2)$ is 0.5) or 0.037 Hz. For 4-fluorotoluene, $^5J_{180}$ is calculated as 0.798 Hz, indicating a decrease of 0.033/2 Hz, again in qualitative agreement with the *apparent* experimental decrease of 0.015 Hz. In 2-fluorotoluene INDO MO FPT finds $^5J_{180}$ to H-3 as 0.858 Hz and to H-5 as 0.819 Hz, the changes from toluene being also in very rough agreement with experiment. Similar calculations on nitro and amino derivatives of 2-fluorotoluene gave mixed results, only $^5J_{180}$ for the 5-nitro derivative agreeing with experimental trends.

Furthermore, although in 3-fluorotoluene the average of $^5J_m^{H,CH_3}$ over 13 values of θ (15° intervals) is indeed computed to be 0.03 lower than in toluene (observed reduction is 0.05_6 Hz), and can reasonably be attributed to a change in the σ component, similar averages for the two couplings in 2-fluorotoluene yield changes which are the reverse of the observed ones. It must be concluded that the theoretical computations provide ambiguous evidence as to the nature of the small perturbations induced in $^5J_m^{H,CH_3}$ by ring substituents. Accordingly the large theoretical data set is not reproduced here.

A more systematic and extensive experimental study of $^5J_m^{H,CH_3}$ would be necessary in order to establish a clear separation between σ and σ−π substituent perturbations. However, because the changes in ^5J are so small and because the first section of this paper suggests the infeasibility of $^5J_m^{H,CH_3}$ as a conformational indicator, such an expenditure of effort is not recommended. Note, however, that this recommendation does *not* apply to α-substituted toluenes, for which $^5J_m^{H,CH_2}$ and $^5J_m^{H,CH}$ can provide detailed conformational information.

Conclusions

In toluene the coupling over five bonds between the methyl and ring protons consists of roughly equal σ−π and σ electron contributions. The former varies as $\sin^2\theta$, where θ is the angle by which the α C—H bond twists out of the nodal plane of the π electrons. The latter is proportional to $\sin^2(\theta/2)$. The same

Can. J. Chem. Downloaded from www.nrcresearchpress.com by 210.87.254.6 on 09/06/12
For personal use only.

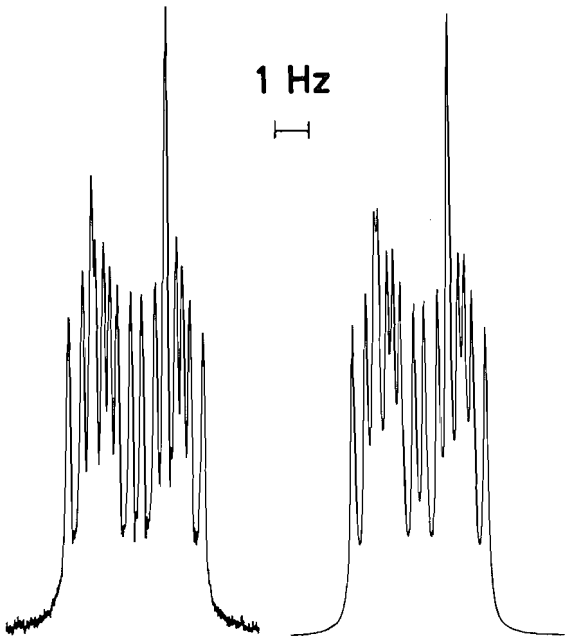

FIG. 1. The observed and calculated ^{1}H nmr spectra of the methyl protons for a 4.5 mol% solution of 2-fluoro-5-aminotoluene in CCl_4 at 305 K and 100.001 MHz (centerband). The calculated spectrum assumes a linewidth at half-height of 0.14 Hz and the parameters from a full analysis of the experimental spectrum from seven spins. It should be noted that the analysis is one of the *least* satisfactory for the molecules in Table 1, the rms deviation between calculated and observed transtions amounting to 0.024 Hz. Of 220 calculated transitions in the proton region, 201 were assigned. The ^{19}F nmr spectrum was not analyzed. $^5J_m^{H,CH_3}$ is 0.387(3) Hz.

behaviour has been previously noted for $^5J_m^{H,SH}$ in thiophenol, suggesting a similar dependence for ^5J in other molecules like benzaldehyde and phenol.

An important consequence for toluene derivatives is that $^5J_m^{H,CH_3}$ *cannot* be used as a indicator of the conformational preferences of the methyl group. However, in the presence of substituents on the methyl group this restriction is lifted and encourages the use of $^5J^{H,CH_2}$ and $^5J^{H,CH}$ in conformational analysis.

The ring-substituent dependence of $^5J_m^{H,CH_3}$ is generally such that a *meta* substituent causes a decrease, while *ortho* substituents cause an increase, in its magnitude.

Finally, it may be noted that partially restricted molecular orbitals, designed to estimate the $\sigma-\pi$ component of $^5J_m^{H,CH_3}$, appear to overestimate its magnitude substantially (32).

Experimental

The data in Table 1 (except for toluene) were accumulated in this laboratory during the last dozen years and are the results of careful analyses and spectral calibrations (33) using an HA100 nmr spectrometer at a probe temperature of 305 K. The solvents were usually CCl_4 or CS_2 but acetone-d_6, chloroform-d, or benzene-d_6 were employed for a few of the analyses. The footnotes to Table 1 may be consulted for further information, particularly footnote *o* where analyses for two different solvents are compared. Some 16 of the 52 values of $^5J_m^{H,CH_3}$ in Table 1 have been published previously, but not discussed.

In Fig. 1 the calculated and observed spectra of the methyl protons in 2-fluoro-5-aminotoluene are depicted. The figure caption points out that the analysis of the seven-spin spectrum was among the least satisfactory obtained for the examples in Table 1. Indeed, small deviations between the observed and calculated spectra are noticeable, parts of which arise from the finite sweep rate of the spectrometer.

INDO MO FPT computations (34) of $^5J_m^{H,CH_3}$ were performed on an Amdahl 470/V7 system, employing standard geometries (35) for the most part, but for 2-fluorotoluene some partially optimized (4) geometries were also used for purposes of comparison. No alteration in relative trends of $^5J_m^{H,CH_3}$ were found.

Acknowledgements

We are grateful to a number of co-workers, named in the references, for the spin–spin coupling data. The Natural Sciences and Engineering Research Council of Canada and the Research Council for the Natural Sciences of the Academy of Finland are thanked for financial support.

1. W. J. E. PARR and T. SCHAEFER. Acc. Chem. Res. **13**, 400 (1980), and references therein.
2. T. SCHAEFER, L. KRUCZYNSKI, and W. NIEMCZURA. Chem. Phys. Lett. **38**, 498 (1976).
3. M. BARFIELD, C. J. FALLICK, K. HATA, S. STERNHELL, and P. W. WESTERMAN. J. Am. Chem. Soc. **105**, 2178 (1983).
4. T. SCHAEFER, R. SEBASTIAN, R. P. VEREGIN, and R. LAATIKAINEN. Can. J. Chem. **61**, 29 (1983).
5. R. WASYLISHEN and T. SCHAEFER. Can. J. Chem. **49**, 94 (1971).
6. T. SCHAEFER, W. DANCHURA, and W. NIEMCZURA. Can. J. Chem. **56**, 2233 (1978).
7. R. E. WASYLISHEN and M. BARFIELD. J. Am. Chem. Soc. **97**, 4545 (1975).
8. T. SCHAEFER, R. SEBASTIAN, and T. A. WILDMAN. Can. J. Chem. **59**, 3021 (1981).
9. T. SCHAEFER, R. SEBASTIAN, and T. A. WILDMAN. Can. J. Chem. **57**, 3005 (1979).
10. R. FREEMAN. Mol. Phys. **6**, 535 (1963).
11. S. FORSÉN and R. A. HOFFMAN. J. Mol. Spectrosc. **20**, 168 (1966).
12. T. SCHAEFER, S. R. SALMAN, and T. A. WILDMAN. Can. J. Chem. **58**, 2364 (1980).
13. S. FORSÉN, B. AKERMARK, and T. ALM. Acta Chim. Scand. **18**, 2313 (1964).
14. G. J. KARABATSOS and F. M. VANE. J. Am. Chem. Soc. **85**, 3886 (1963).
15. R. WASYLISHEN and T. SCHAEFER. Can. J. Chem. **50**, 1852 (1972).
16. C. J. MACDONALD and W. F. REYNOLDS. Can. J. Chem. **48**, 1002 (1970).
17. J. B. ROWBOTHAM and T. SCHAEFER. Can. J. Chem. **52**, 489 (1974).
18. W. J. E. PARR and T. SCHAEFER. Can. J. Chem. **54**, 3564 (1976).
19. J. B. ROWBOTHAM and T. SCHAEFER. Can. J. Chem. **50**, 2344 (1972).
20. R. A. HOFFMAN. Mol. Phys. **1**, 326 (1958).
21. T. SCHAEFER, T. A. WILDMAN, and R. SEBASTIAN. **60**, 1924 (1982).
22. D. SCHWOCH and H. D. RUDOLPH. J. Mol. Spectrosc. **57**, 47 (1975).
23. T. SCHAEFER, R. P. VEREGIN, R. LAATIKAINEN, R. SEBASTIAN, K. MARAT, and J. L. CHARLTON. Can. J. Chem. **60**, 2611 (1982).
24. J. PEELING, T. SCHAEFER, and C. M. WONG. Can. J. Chem. **48**, 2839 (1970).
25. J. PEELING, L. ERNST, and T. SCHAEFER. Can. J. Chem. **52**, 849 (1974).
26. A. F. JANZEN and T. SCHAEFER. Can. J. Chem. **49**, 1818 (1971).
27. M. P. WILLIAMSON, R. KOSTELNIK, and S. M. CASTELLANO. J. Chem. Phys. **49**, 2218 (1968).
28. W. J. E. PARR and T. SCHAEFER. Can. J. Chem. **54**, 3564 (1976).
29. C. H. YODER, R. H. TUCK, and R. E. HESS. J. Am. Chem. Soc. **91**, 539 (1969).
30. R. E. HESS, C. D. SCHAEFFER, JR., and C. H. YODER. J. Org.

Can. J. Chem. Downloaded from www.nrcresearchpress.com by 210.87.254.6 on 09/06/12
For personal use only.

Chem. **36**, 2201 (1971).
31. C. H. YODER, F. K. SHEFFY, R. HOWELL, R. E. HESS, L. PACALA, C. D. SCHAEFFER, JR., and J. J. ZUCKERMAN. J. Org. Chem. **41**, 1511 (1976).
32. A. R. ENGLEMAN, R. H. CONTRERAS, and J. C. FACELLI. Theor. Chim. Acta (Berl.) **59**, 17 (1981).
33. T. SCHAEFER and R. SEBASTIAN. J. Magn. Reson. **41**, 395 (1980).
34. P. A. DOBOSH. Quantum Chemistry Program Exchange, **11**, 1414 (1979).
35. J. A. POPLE and M. S. GORDON. J. Am. Chem. Soc. **89**, 4253 (1967).
36. T. SCHAEFER and W. J. E. PARR. Can. J. Chem. **56**, 1717 (1978).
37. K. CHUM, J. B. ROWBOTHAM, and T. SCHAEFER. Can. J. Chem. **52**, 3489 (1974).
38. T. SCHAEFER, K. CHUM, K. MARAT, and R. E. WASYLISHEN. Can. J. Chem. **54**, 800 (1976).
39. T. A. WILDMAN. M.Sc. Thesis, University of Manitoba, 1978.
40. T. SCHAEFER and K. CHUM. Can. J. Chem. **56**, 1788 (1978).
41. T. SCHAEFER, W. P. NIEMCZURA, R. SEBASTIAN, L. J. KRUCZYNSKI, and W. DANCHURA. Can. J. Chem. **58**, 1178 (1980).

Can. J. Chem. Downloaded from www.nrcresearchpress.com by 210.87.254.6 on 09/06/12
For personal use only.

The thermal and photochemical decompositions of succinic anhydride and 2,3-dimethyl succinic anhydride in the gas phase[1]

S. YAMAMOTO[2] AND R. A. BACK

Division of Chemistry, National Research Council of Canada, 100 Sussex Drive, Ottawa, Ont., Canada K1A 0R6

Received March 4, 1983

S. YAMAMOTO and R. A. BACK. Can. J. Chem. **61**, 2790 (1983).

The absorption spectrum of succinic anhydride shows a broad maximum near 220 nm, attributed to the lowest π^*-n^- transition. Photolysis in this region (220–270 nm) gives CO_2, CO, and C_2H_4, but not in the equimolar quantities expected from a simple molecular dissociation. Production of CO also shows a time dependence, increasing with time, and a free-radical mechanism is tentatively suggested to account for this. The thermal decomposition of succinic anhydride at 625–775 K yields the same products, but is more complex, with larger deviations from the simple stoichiometry, and product formation non-linear with time and pressure. At short times, production of CO, the most abundant product, is described by first-order Arrhenius parameters of log A (s^{-1}) = 11.6 and E = 53 kcal/mol, apparently independent of surface.

The photolysis of the *cis* and *trans* isomers of 2,3-dimethylsuccinic anhydride at 250 and 230 nm is simpler than that of succinic anhydride, giving equimolar CO and CO_2, but with butene-2 still falling short of a stoichiometric yield by from 10 to 40%. Both *cis*- and *trans*-butene-2 were produced, with the latter always in excess and with no retention of the configuration of the original anhydride. The thermal decomposition of 2,3-dimethylsuccinic anhydride is more complex than the photolysis, with much less butene-2 produced (again with no retention of *cis–trans* configuration) and methane an important product. Activation energies for CO formation were about 48 and 45 kcal/mol and log A (s^{-1}) was 10.4 and 9.5 for the *cis* and *trans* isomers, respectively.

S. YAMAMOTO et R. A. BACK. Can. J. Chem. **61**, 2790 (1983).

Le spectre d'absorption de l'anhydride succinique révèle un large maximum près de 220 nm que l'on attribue à la plus faible transition π^*-n^-. La photolyse à cette longueur d'onde (220–270 nm) donne du CO_2, du CO et du C_2H_4 mais pas selon les quantités équimoléculaires attendues pour une simple dissociation moléculaire. La formation de CO montre également une influence du temps augmentant avec le temps et on essaie d'expliquer ce fait en faisant intervenir un mécanisme par radical libre. La décomposition thermique de l'anhydride succinique donne les mêmes produits, mais elle est plus complexe avec de plus grandes différences par rapport aux quantités stoechiométriques et la formation des produits ne varie pas de façon linéraire avec le temps et la pression. A des temps courts, on décrit la production de CO le produit le plus abondant avec les paramètres d'Arrhenius de premier ordre: log A (s^{-1}) = 11,6 et E = 53 kcal/mol qui sont apparemment indépendants des surfaces.

La photolyse des isomères *cis* et *trans* de l'anhydride diméthyl-2,3 succinique à 250 et 230 nm est plus simple que celle de l'anhydride succinique et donne des quantités équimolaires de CO et de CO_2 mais avec le butène-2, là encore l'on s'écarte des rendements stoechiométriques de 10 à 40%. On obtient les butènes-2 *cis* et *trans* avec le produit *trans* toujours en excès et sans rétention de la configuration de l'anhydride original. La décomposition thermique de l'anhydride diméthyl-2,3 succinique est plus complexe que la photolyse avec beaucoup moins de butène-2 produit (encore sans rétention de la configuration *cis–trans*) et le méthane comme produit majoritaires. Les énergies d'activation de la formation du CO sont de 48 et de 45 kcal/mol environ et les valeurs de log A (s^{-1}) sont respectivement 10,4 et 9,5 pour les isomères *cis* et *trans*.

[Traduit par le journal]

Can. J. Chem. Downloaded from www.nrcresearchpress.com by 210.87.254.40 on 09/06/12
For personal use only.

Introduction

There have been few quantitative studies of the decomposition of simple cyclic anhydrides in the gas phase. Recent work in this laboratory on maleic anhydride showed a simple unimolecular decomposition into C_2H_2, CO_2, and CO in both the thermal and photochemical reactions, with the former at least apparently following a concerted path rather than a biradical one (1). Watkins and Whittle found a similar simple decomposition in the photolysis of perfluorosuccinic anhydride (2). The present study was undertaken to see whether other simple cyclic anhydrides show similar behaviour.

Experimental

Apparatus and techniques were similar to those used earlier (1). The light source was a 1000 W Hg–Xe arc with matching monochromator. Analysis of products was by simple fractionation at 77, 195, and 273 K, measurement by gas burette, and by gas chromatography.

Succinic anhydride was obtained from Aldrich and used after simple degassing and sublimation. The *cis* and *trans* isomers of 2,3-dimethylsuccinic anhydride were prepared by dehydration of the appropriate acids from Aldrich, by treatment with excess acetic anhydride or acetyl chloride. *Meso*-2,3-dimethylsuccinic acid yielded *meso-cis*-2,3-dimethyl-succinic anhydride (mp 37°C), while a racemic mixture of the D- and L-acids gave the mixed D- and L-*trans*-anhydride.

Absorption spectra were measured in a double-beam spectrophotometer fitted with a 4 m heated absorption cell.

Results and discussion

Succinic anhydride

The absorption spectrum (Fig. 1) shows a broad maximum at about 220 nm, with absorption on the long-wavelength side extending to at least 300 nm. Weak vibrational features are evident on the long-wavelength shoulder, with an average separation of about 1200 cm^{-1}, probably corresponding to excitation of a carbonyl stertching vibration in the excited state. The photoelectron spectrum of succinic anhydride, supported by calculations (3, 4), indicates that the n^-, the out-of-phase combination of the two carbonyl lone-pair orbitals, is the highest occupied orbital. The extinction coefficient of about 25 M^{-1} cm^{-1} estimated at 220 nm is reasonable for a weakly allowed π^*-n^- transition.

The photolysis was studied at wavelengths of 220, 230, 252, and 270 nm, and pressures of anhydride from about 3 to

[1]NRCC No. 22589.

[2]NRCC Research Associate, 1981–1983.

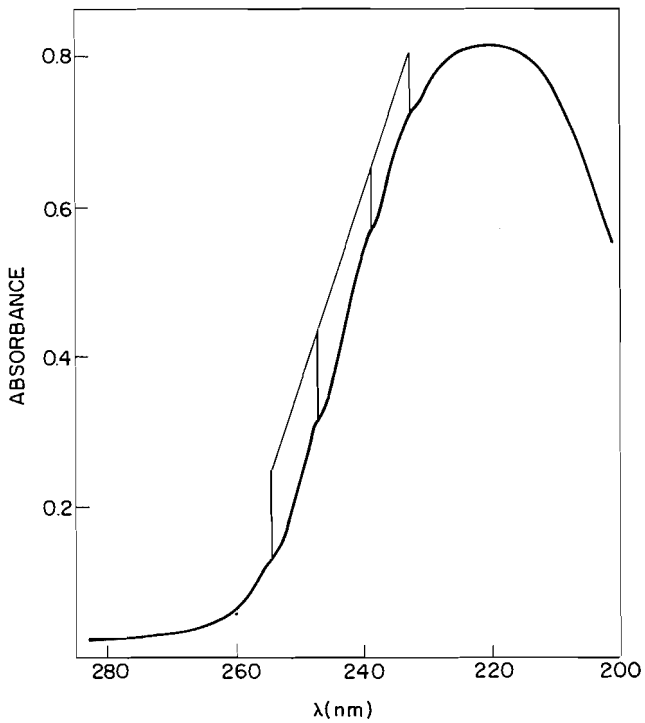

FIG. 1. Absorption spectrum of succinic anhydride measured at pressures of about 2 Torr.

15 Torr, all at a temperature of about 400 K. The major volatile products of the photolysis were CO_2, C_2H_4, and CO, but these were not produced in the equimolar quantities expected from a simple fragmentation as observed with maleic anhydride (1). Production of CO_2 and of C_2H_4 were linear with time, and the ratio C_2H_4/CO_2 was consistently about 0.9 (±0.05), independent of reaction time, wavelength, and pressure of succinic anhydride. The formation of CO was not linear with time, and the ratio CO/CO_2 increased from about 0.5 at the shortest times observed to about 1.0 at the longest. This time dependence varied with pressure and wavelength, but when variation in light intensity and absorption were taken into account by plotting CO/CO_2 against CO_2 (Fig. 2), a common simple dependence on the amount of reaction (measured by CO_2), independent of pressure and wavelength, was shown.

It is clear from these observations that the photolysis of succinic anhydride does not proceed simply by a direct fragmentation into CO_2, C_2H_4, and CO, although as much as about half of the products *may* have been formed in this way. The delayed appearance of at least half of the CO, but not of the other products is difficult to explain by any simple mechanism; one that can be suggested involves the initial formation of CO_2 and acrolein, perhaps following ring opening,

[1] $C_4H_4O_3 + h\nu \rightarrow C_4H_4O_3^* \rightarrow CO.CH_2CH_2CO.O \rightarrow CO_2 + CH_2{=}CH{-}CH.O^{\ddagger}$

This reaction releases 98 kcal/mol at 270 nm and 122 kcal/mol at 220 nm, and the acrolein could be formed with enough energy to dissociate[3]

[2] $CH_2{=}CH{-}CH.O^{\ddagger} \rightarrow C_2H_3 + HCO$

Abstractions by vinyl and formyl radicals would follow,

[3] $C_2H_3 + C_4H_4O_3 \rightarrow C_2H_4 + C_4H_3O_3$

[4] $HCO + C_4H_4O_3 \rightarrow H_2CO + C_4H_3O_3$

These reactions account for the initial formation of CO_2 and C_2H_4, and as formaldehyde built up in the system, attack by free radicals such as vinyl, HCO, and $C_4H_3O_3$ on the weakly bound hydrogen could lead to formation of CO;

[5] $R + H_2CO \rightarrow RH + HCO$

[6] $R + HCO \rightarrow RH + CO$

Some loss of C_2H_3 by combination or disproportionation with other radicals could account for the observed deficit of C_2H_4 relative to CO_2, and the detection of small amounts of C_2H_2, 1,3-butadiene, and acrolein, products of such reactions, lends some support to this mechanism. Formaldehyde, which should have been present as an intermediate in amounts equal to the CO deficit, could not be detected, but the small amounts may well have been lost in the analysis. In one experiment, 260 Torr of N_2 was added to the photolysis at 230 nm, with no effect on the C_2H_4/CO_2 ratio. This suggests that the excited acrolein formed in reaction [1] must have decomposed quantitatively even under these conditions, not unreasonable considering the excess energy at this wavelength. An alternative, probably less likely, mechanism for the photolysis involves formation of a CO – succinic anhydride adduct, of unspecified structure,

[7] $C_4H_4O_3 + h\nu \rightarrow C_4H_4O_3^* \xrightarrow{+C_4H_4O_3} CO_2 + C_2H_4 + C_5H_4O_4$

which subsequently decomposes to CO and succinic anhydride.

The thermal decomposition of succinic anhydride was studied at pressures from about 4 to 20 Torr and temperatures from 625 to 775 K. The main products observed were CO, CO_2, and C_2H_4, and again these products expected from simple fragmentation were not produced in equimolar quantities, with the reaction apparently even more complex than the photolysis. While CO_2 and C_2H_4 production were approximately linear with time (with perhaps some upward curvature in CO_2), the production of CO was strongly time dependent, with the yield increasing sharply to a value more than ten times that of CO_2 (Fig. 3). As in the photolysis, trace quantities of C_2H_2, 1,3-butadiene, and acrolein were detected. The CO yield also rose sharply, with respect to CO_2 and C_2H_4, with increasing anhydride pressure (Fig. 4).

In the early stages of the reaction, CO production is approximately described by a first-order rate constant given by $\log k\ (s^{-1}) = 11.6 - 53000/4.58T$, which was found to be unchanged when the surface/volume ratio was increased by a factor of 4 by packing the reaction vessel with tubing. Production of CO_2, on the other hand, while again approximately first order, showed much lower Arrhenius parameters ($\log A\ (s^{-1}) = 5.5$, $E = 34$ kcal/mol) and was markedly increased in the packed vessel.

The mechanism of the thermal decomposition is clearly complex, and no quantitative conclusions can be drawn about its thermochemistry. There may be some simple unimolecular decomposition into CO, CO_2, and C_2H_4, but the activation energy for CO formation is much too low for biradical formation by opening of the almost strain-free anhydride ring. The sharply accelerating production of CO in amounts greatly exceeding CO_2 and C_2H_4, and its sharp increase with pressure, suggest an autocatalytic free-radical chain reaction, or perhaps formation of an unstable intermediate that begins to eliminate CO thermally as it accumulates. In either case, CO_2 and C_2H_4 must

[3]Based on ΔH_f^0 of −125 and −23 kcal/mol for succinic anhydride and acrolein, respectively, calculated from heats of combustion (5).

Can. J. Chem. Downloaded from www.nrcresearchpress.com by 210.87.254.40 on 09/06/12
For personal use only.

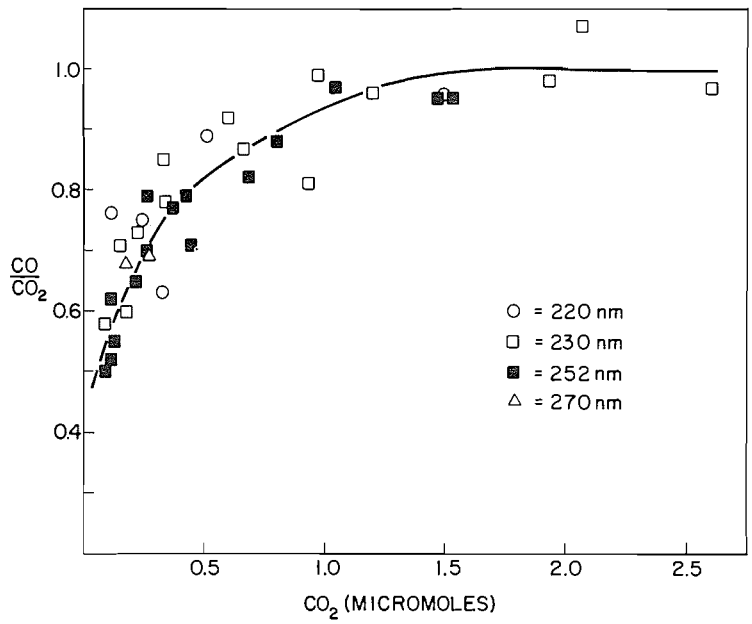

FIG. 2. The product ratio, CO/CO_2, for the photolysis of succinic anhydride, vs. yield of CO_2.

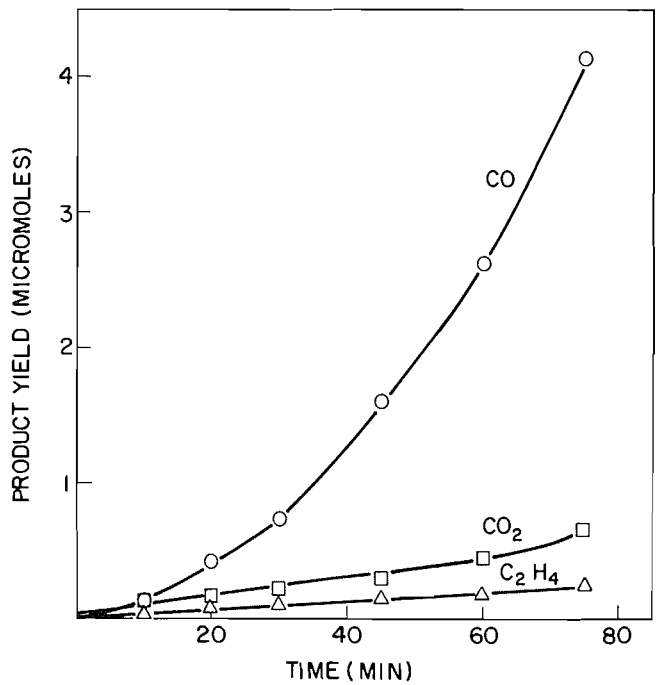

FIG. 3. Time dependence of products in the thermal decomposition of succinic anhydride at 722 K and a pressure of 10 Torr.

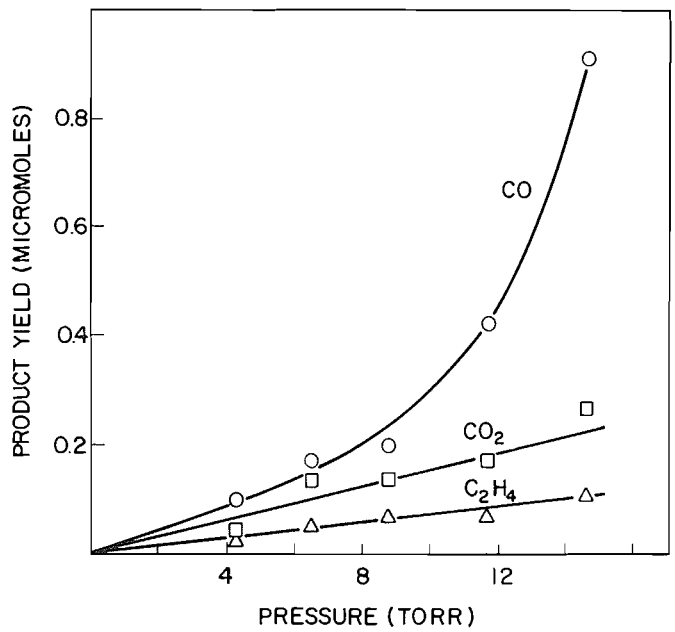

FIG. 4. Pressure dependence of products in the thermal decomposition of succinic anhydride at 722 K and a reaction time of 20 min.

remain tied up in non-volatile products. Brown and Ritchie (6) proposed a ketene acid, O=C=CH—CH_2CO.OH as an intermediate in the "hot tube" pyrolysis of succinic anhydride at 773 K, and its decomposition to CO and acrylic acid (which they observed as a product) could account for our CO formation if the acrylic acid were lost by polymerization or other reaction. Rice and Murphy (7), on the other hand, observed almost stoichiometric formation of CO, CO_2, and C_2H_4 in a single experiment at much higher temperature (1170 K). This could indicate that a simple fragmentation, having a high activation energy, becomes predominant at high temperature. In the present experiments, the decomposition is certainly not simple, and further speculation about mechanism is unwarranted.

2,3-Dimethylsuccinic anhydride

The spectra of *cis*- and *trans*-dimethylsuccinic anhydride were similar to that of succinic anhydride, with similar extinction coefficients, but with the maxima red-shifted to about 230 and 225 nm, respectively. No vibrational structure was evident.

The photolysis of both *cis* and *trans* isomers was studied at 250 and 230 nm, at pressures of about 10 Torr and a temperature of 400 K. Products volatile at room temperature were CO_2 and CO, formed in equal amounts in all experiments, and butene-2, which was always appreciably less than stoichiometric. With the *trans* isomer at both wavelengths and the *cis* isomer at 250 nm, the amounts of these products were always proportional to the photolysis time. With the *cis* isomer at 230 nm, formation of all products showed a distinct acceler-

Can. J. Chem. Downloaded from www.nrcresearchpress.com by 210.87.254.40 on 09/06/12
For personal use only.

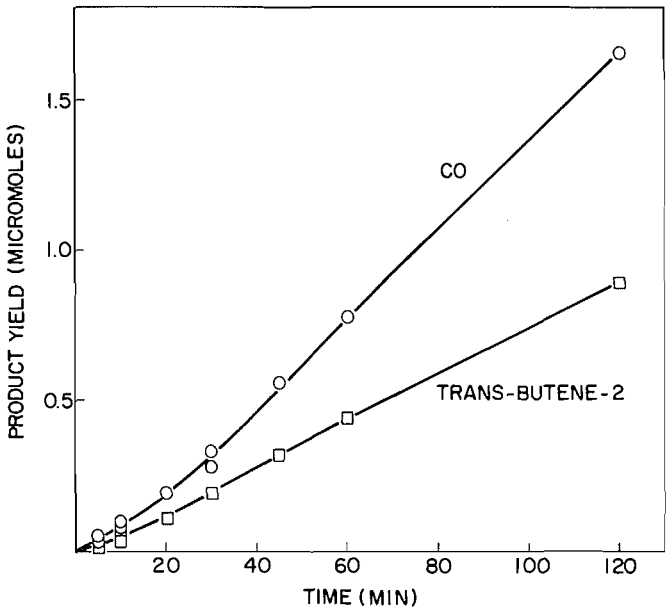

FIG. 5. Time dependence of products from the photolysis of *cis*-dimethylsuccinic anhydride at 230 nm.

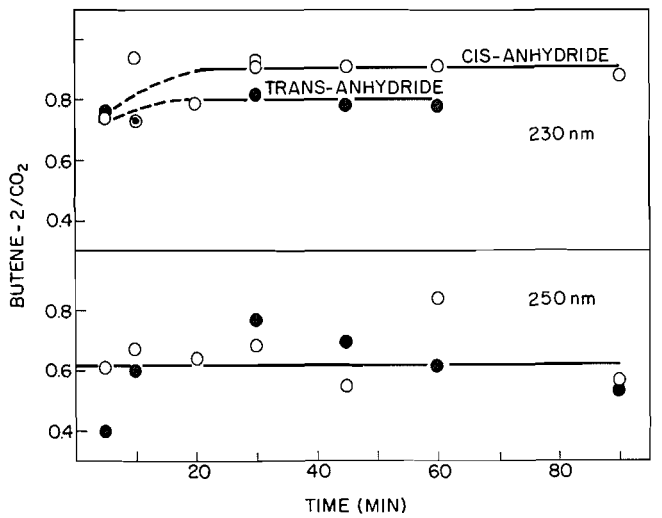

FIG. 6. Time dependence of product ratios from the photolysis of *cis*-dimethylsuccinic anhydride (○) and *trans*-dimethylsuccinic anhydride (●).

ation with increasing time, reaching a constant rate after about 20 min (Fig. 5). The ratio butene-2/CO_2, (Fig. 6) and CO/CO_2 were effectively independent of photolysis time. Both *cis*- and *trans*-butene-2 were produced in the photolysis, and ratios of the two isomers are shown in Fig. 7.

The photolysis of 2,3-dimethylsuccinic anhydride appears to be a much cleaner and simpler decomposition than that of succinic anhydride itself. Yields of CO and CO_2 are always equal, with stoichiometric deficits of butene-2 of 40% at 250 nm and about 10% at 230 nm. No other C_4 or lighter hydrocarbons were detected, and the missing butene-2 must be accounted for by higher, non-volatile products or polymer.

There appears to be a complete loss of *cis*–*trans* configuration of the methyl groups in the photolysis. At 250 nm, the *cis*-anhydride in fact gave a slightly higher ratio of *trans*-butene-2/*cis*-butene-2 than does the *trans* anhydride (Fig. 7), while at 230 nm, the ratio of butene isomers from the two

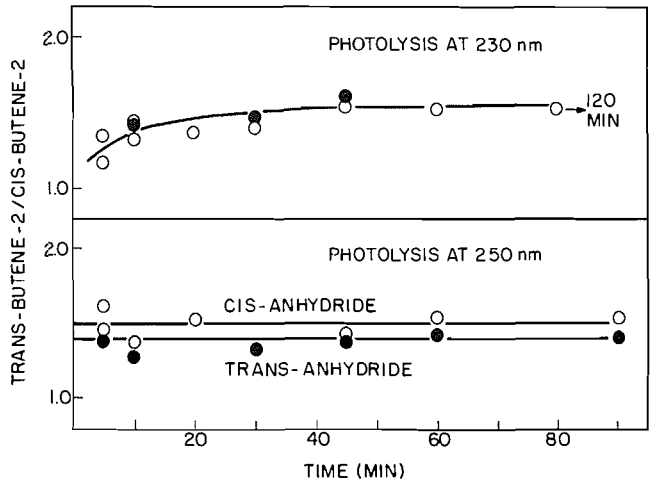

FIG. 7. Ratio of *trans*-butene-2/*cis*-butene-2 from the photolysis of the *cis* (○) and *trans* (●) isomers of dimethylsuccinic anhydride.

anhydrides was the same. The lack of retention of the *cis*–*trans* configuration, and the deficit of butene-2, both argue strongly against a direct molecular dissociation into CO_2, CO, and butene, and suggest instead ring-opening to form a biradical which successively loses CO_2 and CO, leaving a C_4H_8 biradical that can be stabilized as butene-2 by hydrogen transfer or can react to form higher products. Rotation about the C—C bond leading to loss of the *cis*–*trans* configuration may occur in the primary biradical or in those formed by successive loss of CO_2 and CO. The preferred formation of *trans*–butene-2 is not surprising, and can be attributed to repulsion of the methyl groups in the transition state finally leading to butene formation.

While this simple picture of the photolysis is attractive, there is clear evidence that at least at 230 nm, the system is more complex. The partial induction period observed with the *cis*-anhydride (Fig. 5) suggests that there is an intermediate which is decomposed by secondary photolysis to form the final products. The time dependence of the product yields is paralleled by a change in the *trans*-butene-2/*cis*-butene-2 ratio (Fig. 7) and perhaps by a change in the butene-2/CO_2 ratio (Fig. 6). The fact that the ratio of butene-2 isomers at long reaction times from the *cis*-anhydride rises to the same value observed with the *trans*-anhydride suggests that the same intermediate may be present in the photolysis of the latter, but is decomposed more rapidly (perhaps because of a shift in the absorption spectrum) so that its presence was not evident at the shortest times used in the present experiments.

The thermal decomposition of *cis*- and *trans*-dimethylsuccinic anhydride was studied from about 630 to 770 K at pressures from 4 to 13 Torr. Products observed were CO, CO_2, butene-2, and CH_4, all formed linearly with time (conversions were below 10%). The product with the highest yield was CO; CO_2 was less, with CO_2/CO ratios varying from about 0.25 at the highest temperature to 0.75 at the lowest. The ratio CH_4/CO varied from about 0.15 at the highest temperature to almost unity at the lowest. Yields of butene-2 were about 10% of the CO, independent of temperature, and all product ratios were about the same for the two anhydride isomers.

First-order rate constants for production of CO gave reasonable Arrhenius plots (Fig. 8) with values for the *cis* isomer consistently higher than for the *trans*. Arrhenius parameters were E = 47.6 kcal/mol and log A (s^{-1}) = 10.4 for the

Can. J. Chem. Downloaded from www.nrcresearchpress.com by 210.87.254.40 on 09/06/12
For personal use only.

cis-anhydride, and $E = 45.3$ and $\log A = 9.55$ in the same units for the *trans*-anhydride. Packing the reaction vessel with tubing to increase the surface/volume ratio by a factor of 4 had no significant effect, and the production of CO is apparently a gas-phase process. Production of CO_2, on the other hand, had an appreciably lower activation energy and *A*-factor for both isomers (E = ~42 kcal/mol, log A (s^{-1}) = ~8.2), and was much higher in the packed vessel, while the formation of CH_4 was also enhanced by the increase in surface.

Both *cis*- and *trans*-butene-2 were formed in the decompositions, with a *trans*/*cis* ratio of about 2.6 for both anhydride isomers, independent of reaction temperature, time, and S/V ratio. Blank experiments with butene-2 showed that there was negligible thermal *cis-trans* isomerization. Thus, as in the photolysis, there is complete loss of configuration of the methyl groups in the decomposition to form butene-2. The observed activation energies, however, are much too low to permit direct opening of the anhydride ring to form a biradical, so that rotation of the methyl groups must occur in some other way. (This raises the possibility that biradicals are not necessarily involved in the photolysis either, although there is more than enough energy for their formation).

The Arrhenius parameters for CO formation may correspond to a simple unimolecular process, perhaps elimination of CO concerted with H-atom transfer, or perhaps an isomerization to a ketene acid as suggested by Brown and Ritchie (6).

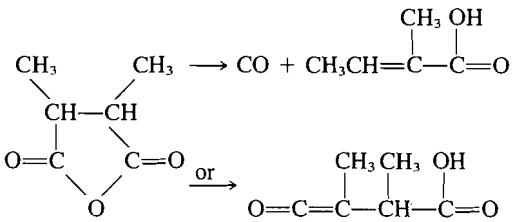

The linear rate of formation of all products with time indicates that, whatever the intermediate, it must have decomposed or reacted rapidly to yield the ultimate products observed. The surface dependence of CO_2 and CH_4 formation must then arise from some surface-dependent stoichiometry in this decomposition. The system is obviously complicated and further discussion of mechanism is not justified.

Conclusions

Neither the photochemical nor the thermal decomposition of succinic anhydride and its 2,3-dimethyl derivative follows a simple unimolecular dissociation as apparently observed with maleic anhydride (1) and perfluorosuccinic anhydride (2). The main products in all cases were those expected from such a dissociation, CO_2, CO, and an olefin, and *part* of each decomposition may proceed in a simple way, but products are not formed in stoichiometric ratios. The photolyses were simpler than the thermal reactions, probably reflecting the higher energy content of the decomposing molecules in the former, but in both systems there was evidence for unstable intermediates and higher, non-volatile products, and complex mechanisms are indicated. Complete loss of *cis*–*trans* configuration of the methyl groups in the photolysis of 2,3-dimethylsuccinic anhydride suggests a biradical intermediate, but this also occurred in the thermal decomposition in which the activation energy is too low to permit biradical formation. The more complex behaviour of these anhydrides compared with maleic anhydride may reflect a more easy intramolecular transfer of hydrogen atoms in the saturated ring than in the stiffer conjugated structure of maleic anhydride with the hydrogens in the molecular plane. It is interesting that the photolysis and the thermal decomposition of succinimide vapor, studied in this laboratory (8), showed a similar behaviour, with both a simple decomposition into HNCO, CO, and C_2H_4, together with several more complex channels involving internal hydrogen transfer.

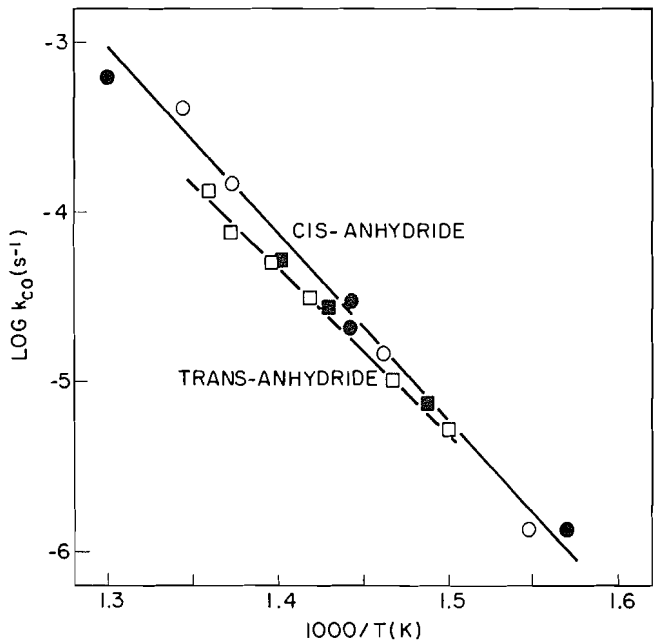

FIG. 8. Arrhenius plots of first-order rate constants for CO production from the thermal decomposition of the dimethylsuccinic anhydride isomers. Filled points correspond to experiments in the packed reaction vessel.

1. R. A. BACK and J. M. PARSONS. Can. J. Chem. **59**, 1342 (1981).
2. P. E. WATKINS and E. WHITTLE. J. Chem. Soc. Faraday I, **76**, 503 (1980).
3. M. ALMEMARK, J. E. BACKVALL, C. MOBERG, and B. AKERMARK. Tetrahedron, **30**, 2503 (1974).
4. D. DOUGHERTY, P. BRINT, and S. P. MCGLYNN. J. Am. Chem. Soc. **100**, 5597 (1978).
5. Handbook of chemistry and physics. 62nd ed. CRC Press Inc. Boca Raton, Florida. 1981–82. Heats of combustion, vaporization and fusion of organic compounds.
6. A. L. BROWN and P. D. RITCHIE. J. Chem. Soc. C, 2007 (1968).
7. F. O. RICE and M. T. MURPHY. J. Am. Chem. Soc. **64**, 896 (1942).
8. G. CHOUDHARY, A. M. CAMERON, and R. A. BACK. J. Phys. Chem. **72**, 2289 (1968).

Can. J. Chem. Downloaded from www.nrcresearchpress.com by 210.87.254.40 on 09/06/12
For personal use only.

Thallimetric oxidations. Part II. Titrimetric and spectrophotometric methods for the determination of oxalate

S. R. SAGI, K. APPA RAO, AND M. S. PRASADA RAO
Inorganic Chemistry Laboratories, Andhra University, Waltair-530 003, India

Received January 13, 1983

S. R. SAGI, K. APPA RAO, and M. S. PRASADA RAO. Can. J. Chem. **61**, 2795 (1983).

Titrimetric and spectrophotometric methods are developed for the estimation of oxalate at mmole and micromole ranges, respectively. In these methods thallium(III) is used as the oxidant and the reduced thallium(I) is determined oxidimetrically by potassium bromate in the titrimetric method and by measuring the optical density of thallium(III) at 260 nm in the presence of 0.1 *M* HCl and 1 *M* $HClO_4$ in the spectrophotometric method. A series of photochemical and thermal redox methods are described for the estimation of oxalate in the presence of a number of carboxylic acids.

S. R. SAGI, K. APPA RAO et M. S. PRASADA RAO. Can. J. Chem. **61**, 2795 (1983).

On a mis au point des méthodes titrimétriques et spectrophotométriques pour évaluer l'oxalate en mmole et en micromole respectivement. Dans ces méthodes, on utilise le thallium(III) comme oxydant et on détermine le thallium réduit(I) par oxydimétrie à l'aide du bromate de potassium dans la méthode titrimétrique et en mesurant la densité optique du thallium(III) à 260 nm en présence de HCl 0,1 *M* et de $HClO_4$ 1 *M* dans la méthode spectrophotométrique. On décrit une série de méthodes photochimiques et redox pour évaluer l'oxalate en présence d'un certain nombre d'acides carboxyliques.
[Traduit par le journal]

Can. J. Chem. Downloaded from www.nrcresearchpress.com by 210.87.254.105 on 09/06/12
For personal use only.

Introduction

The unique properties like acidity, reducing capacity, and chelating ability of oxalic acid and oxalates made them a very useful class of compounds in industry as well as in analytical chemistry. Oxalates occur widely in many biological systems. The various spectrophotometric, solubility, kinetic, ion exchange, solvent extraction, potentiometric, polarographic, and other methods for the determination of oxalates were reviewed by Murty and Harris (1). Rao and Aravamudan (2) have surveyed the available methods for the determination of oxalic acid and described a new method utilising the photochemical reaction between iron(III) and oxalic acid, titrating the iron(II) formed by sodium vanadate. The advantages claimed by the authors over other methods are (*i*) no heating is required and (*ii*) formic acid will not interfere in the method. Riggs and Bricker (3) have extended the same idea and estimated oxalic acid at mg level by titrating the iron(II) formed using potassium dichromate stating that its interference with organic substances is tolerable. However, they pointed out that an inert atmosphere is necessary to avoid the air oxidation of iron(II) formed during the reaction; about this Rao and Aravamudan have not mentioned anything. Rao *et al.* (4) avoided the use of dichromate because of the induced oxidation of oxalic acid in the presence of iron(II), they preferred sodium vanadate as the oxidant.

Riggs and Bricker followed the progress of the reaction with the time of irradiation by estimating iron(II) formed with dichromate. If the view expressed by Rao *et al.* regarding the induced oxidation of oxalic acid by dichromate was correct the values reported by these authors were prone to error especially in reporting the interferences.

Using the same photochemical reaction Cooley and Kratochvil (5) have described a method for the determination of oxalate using a CO_2 electrode detector. Later using the same reaction they described another method (6) using a gas chromatographic technique for measuring CO_2, and claimed that this method is less expensive and rapid and also subject to fewer interferences compared to their first method. They reported obtaining values with an accuracy of about 2%.

In the light of the above reports the present authors have attempted to suggest simple and convenient methods for the estimation of oxalic acid in the presence of other organic acids both at mg and μg levels.

A consideration of the redox potentials of the thallium(III)/thallium(I) couple in perchloric and sulphuric acid media, and the special photochemical properties associated with the thallium species have led the present authors to investigate the use of thallium(III) for the estimation of oxalic acid.

Experimental

Thallium(III) solution was prepared and standardised as reported earlier (7, 8). All the other reagents are of AR grade. Though the photochemical reactions described take place much faster under direct sun light, in view of its variable intensity all the investigative work described here was done using a Phillips high pressure mercury vapour lamp (200/250 V − 125 W) as the light source. The photochemical reactions were carried out by exposing the solutions in colourless glass containers, kept a constant distance of 6 in. from the light source.

A Shimadzu, U.V. 140 double beam spectrophotometer is used for the optical density measurements.

Results and discussion

The photochemical reduction of thallium(III) with oxalic acid in the presence of halides as catalysts has been reported (8). Studies on photochemical oxidation of oxalic acid with thallium(III) show that the stoichiometry of the reaction may be represented by the equation

$$Tl(III) + H_2C_2O_4 \rightarrow Tl(I) + 2CO_2 + 2H^+$$

A minimum of double the amount of thallium(III) with respect to oxalic acid is necessary for a rapid reaction to take place and any ratio of thallium(III) to oxalate above 2:1 will not very much increase the rate of the reaction. Hence, keeping the concentration of thallium(III) double that of oxalic acid, the effect of acid, chloride, and bromide concentration on the speed of the reaction is studied in perchloric acid medium and the results are represented in Figs. 1 and 2. The relative mean deviation of the values recorded is 2%. The progress of the reaction is followed by monitoring the thallium(I) formed by oxidimetric titration with potassium bromate.

From Figs. 1 and 2 it is clear that the time required for completion of the reaction is minimum when the chloride concentration is double or the bromide concentration is half that of

Can. J. Chem. Downloaded from www.nrcresearchpress.com by 210.87.254.105 on 09/06/12
For personal use only.

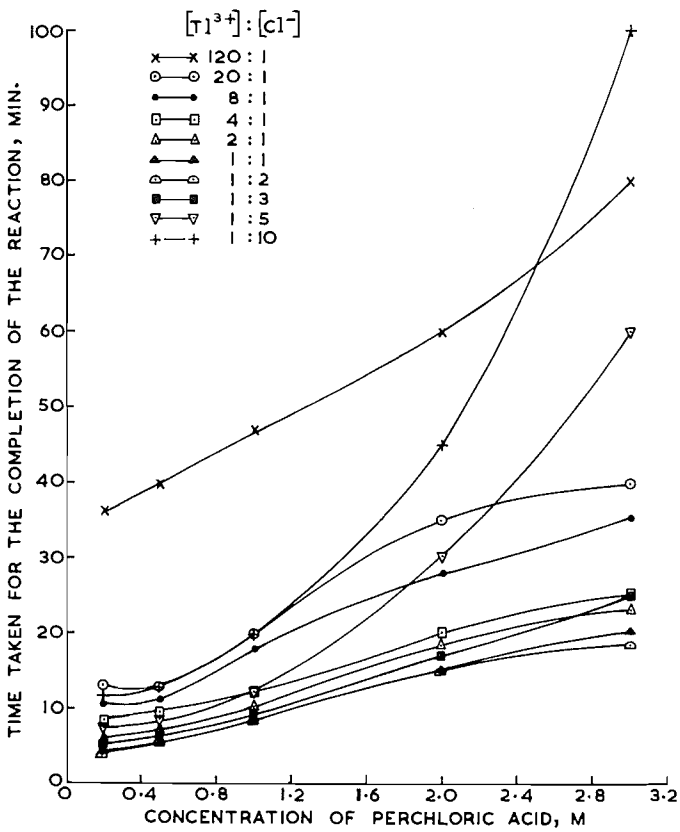

FIG. 1. Effect of $[H^+]$ and $[Cl^-]$ on the rate of photochemical oxidation of oxalate by thallium(III). Volume of the reaction mixture, 100 mL; amount of thallium(III), 0.25 mmol; amount of oxalate, 0.125 mmol.

TABLE 1. Estimation of oxalate (titrimetric method)

Oxalate (mmol)		
Taken	Found	% Error
	Photochemical	
0.0500	0.050_0	Nil
0.0550	0.055_0	Nil
0.1250	0.125_5	0.4
0.2000	0.199_5	0.3
0.2500*	0.250_0	Nil
0.4500	0.450_0	Nil
0.5000	0.500_0	Nil
	Thermal	
0.0500	0.050_0	Nil
0.1000	0.100_5	0.5
0.1250	0.125_5	0.4
0.2500†	0.250_0	Nil
0.3000	0.301_5	0.5
0.4500	0.449_0	0.2
0.5000	0.499_0	0.2

*Relative mean deviation is 0.2%.
†Relative mean deviation is 0.16%.

thallium(III). The reaction is fast even when the Tl(III)-to-Cl^- ratio is in the range of 10:1 to 1:10 and Tl(III)-to-Br^- ratio is in the range of 10:1 to 1:1. Under these conditions thallium(III) is known to exist as $TlCl^{2+}$, $TlCl_2^+$, $TlBr^{2+}$ (9, 10), which are likely to be photochemically active and hence give the fast rate of the reaction.

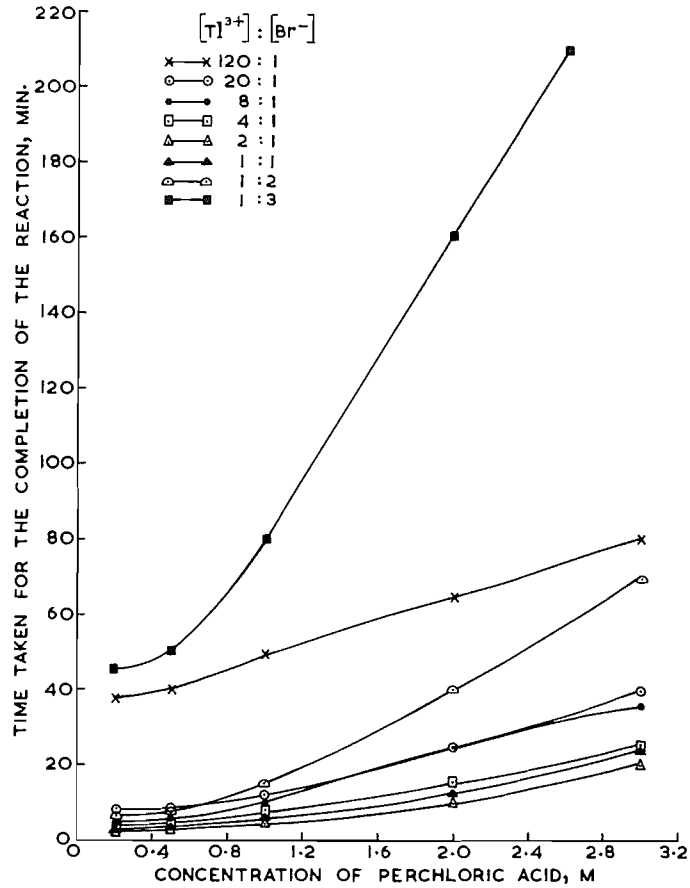

FIG. 2. Effect of $[H^+]$ and $[Br^-]$ on the rate of photochemical oxidation of oxalate by thallium(III). Volume of the reaction mixture, 100 mL; amount of thallium(III), 0.25 mmol; amount of oxalate, 0.125 mmol.

TABLE 2. Estimation of oxalate (μmol range, spectrophotometric method)

Oxalate (μmol)		
Taken	Found	% Error
	Photochemical	
0.01000	0.0097_5	2.5
0.02000	0.0197_5	1.2
0.03000	0.0305_0	1.7
0.04000	0.0405_0	1.3
0.05000*	0.0505_0	1.0
0.07000	0.0705_0	0.7
0.09000	0.0890_0	1.1
	Thermal	
0.01000	0.0097_5	2.5
0.03000	0.0300_0	Nil
0.05000†	0.0495_0	1.0
0.07000	0.0690_0	1.4
0.09000	0.0907_5	0.8
0.10000	0.1000_0	Nil
0.13000	0.1313_0	1.0

*Relative mean deviation is 1.7%.
†Relative mean deviationis 1.4%.

An increase in acid concentration has a retarding effect on the rate of the reaction. The acid concentration has less effect on the chloride ion catalysis than on the bromide ion catalysis.

TABLE 3. Interferences*

Name of carboxylic acid studied	Ratio of oxalate to carboxylic acid	Titrimetric method: Photochemical Cl^- catalysis	Titrimetric method: Photochemical Br^- catalysis	Titrimetric method: Thermal	Spectrophotometric method: Photochemical, Cl^- catalysis	Spectrophotometric method: Thermal
Formic acid	1:1	/	×	×	/	×
	1:10	/	×	×	/	×
	1:100	×	×	×	×	×
Acetic acid	1:1	/	×	/	/	/
	1:10	/	×	/	/	/
	1:100	/	×	/	/	/
Propionic acid	1:1	/	×	/	/	/
	1:10	RRR	×	/	RRR	/
	1:100	RRR	×	/	RRR	/
Malonic acid	1:1	RRR	×	×	RRR	×
Succinic acid	1:1	/	×	/	/	/
	1:10	/	×	/	/	/
	1:100	RRR	×	/	RRR	/
Glutaric acid	1:1	/	×	/	/	/
	1:10	RRR	×	/	RRR	/
	1:100	RRR	×	/	RRR	/
Adipic acid	1:1	/	×	/	/	/
	1:10	RRR	×	/	RRR	/
	1:100	RRR	×	/	RRR	/
Pimelic acid	1:1	/	×	/	/	/
	1:10	RRR	×	/	RRR	/
	1:100	RRR	×	/	RRR	/
Lactic acid	1:1	/	×	×	/	/
	1:10	×	×	×	×	×
Malic acid	1:1	×	×	×	×	×
Tartaric acid	1:1	×	×	×	×	×
Citric acid	1:1	×	×	×	×	×

* / = do not interfere, × = interfere, RRR = reaction rate reduced (this drawback can be avoided by suitably increasing the time of exposure to light).

Recommended procedure (photochemical method, mmol range)

To an aliquot containing 0.05 to 0.5 mmol of sodium oxalate in a 200 mL beaker add 20 mL of 1 *M* perchloric acid, 2 mmol of chloride (or 0.5 mmol of bromide), 1 mmol of thallium(III), and dilute to 100 mL. Stir the solution and expose to the light from a high pressure mercury vapour lamp for 10 min. Add 25 mL of concentrated hydrochloric acid, 0.1 mL of 0.1% methyl orange or brilliant ponceaux 5R indicator, heat to 60°C, and titrate with 0.05 *N* potassium bromate (1.392 g/L) until the indicator is destroyed. The method is applicable in sulphuric acid medium also.

Thermal method

The thermal reaction between thallium(III) and oxalic acid is quantitative even in the presence of stoichiometrically equal amounts of oxalic acid and thallium(III). To an aliquot containing 0.05 to 0.5 mmol of sodium oxalate in a 200 mL beaker add 10 mL of perchloric acid (or 10 mL of 5 *M* sulphuric acid), 1 mmol of thallium(III), dilute to 100 mL, and heat on a boiling water bath for 5 min (or heat just to boiling). The reduced thallium(I) is titrated with potassium bromate under the conditions already described.

In the thermal method chloride or bromide will not interfere if the concentration is half or one fourth that of thallium(III) respectively. But further increase in chloride concentration decreases the rate of the reaction, and bromide gives erroneous results. Typical results are summarized in Table 1.

Spectrophotometric method for the estimation of microquantities of oxalate

The absorption spectra (11) of thallium(I) and thallium(III) separately in a medium containing 1 *M* perchloric acid and 0.1 *M* hydrochloric acid show that at 260 nm thallium(III) has considerable molar absorptivity ($\epsilon \approx 9150$) while thallium(I) has no absorbance. At 260 nm thallium(III) species obey Beers law under the above conditions. In this method excess of thallium(III) is allowed to react with oxalic acid either photochemically (using chloride as catalyst) or thermally. The amount of oxalate corresponds to the amount of thallium(III) reduced to thallium(I), which can be computed from a calibration curve (Table 2).

Recommended procedures

1. Photochemical: To an aliquot containing 0.01 to 0.12 μmol of sodium oxalate add 1 mL of 5 *M* perchloric acid, 0.5 μmol of sodium chloride, 5 mL of 5×10^{-4} *M* thallium(III), and expose it to the light of mercury vapour lamp for

Can. J. Chem. Downloaded from www.nrcresearchpress.com by 210.87.254.105 on 09/06/12
For personal use only.

10 min. Transfer the solution to a 50 mL volumetric flask, add 8 mL of 5 *M* perchloric acid, and 5 mL of 1 *M* hydrochloric acid, and dilute to volume (I). Prepare another solution in a 50 mL flask by mixing all the above solutions except oxalate (II). Shake well and wait 60 min. Adjusting the optical density of I to zero measure the optical density of II (which corresponds to the thallium(III) reacted). The concentration of thallium thus reacted is read from a calibration curve. The oxalate concentration corresponds to the thallium(III) reacted.

2. Thermal method: To an aliquot containing 0.01 to 0.13 μmol of sodium oxalate add 9 mL of 5 *M* perchloric acid, 5 mL of 5×10^{-4} *M* of thallium(III) in 1.0 *M* perchloric acid, and boil for 2 min. Cool and transfer to a 50 mL volumetric flask. Add 5 mL of 1 *M* hydrochloric acid and dilute to volume (I). Adopting the same procedure in the absence of oxalate prepare another solution and dilute to volume (II). The amount of oxalate is computed as before.

Interferences: Sodium oxalate (0.125 mmol) is used for the study of interferences in the titrimetric method; while 0.05 μmol is used in the spectrophotometric method. The results of the study of the interferences of some organic acids is given in Table 3.

From the data in Table 3 it is clear that by suitably selecting the method, oxalate in the mmole to micromole range can be determined even in the presence of other carboxylic acids (except in the presence of malic, tartaric, and citric acids).

If the sample contains Cl^- or Br^-, their content has to be taken into account in maintaining the proper ratio of thallium(III) to halide in the photochemical determination. In these methods the use of an inert atmosphere is not necessary, the possibility of induced reactions is completely excluded and the methods do not need cumbersome apparatus. Of the common reagents used in these methods, potassium bromate is a primary standard and thallium(III) perchlorate is very stable.

1. K. V. K. MURTY and G. M. HARRIS. Chem. Rev. **61**, 213 (1961).
2. G. G. RAO and G. ARAVAMUDAN. Anal. Chim. Acta, **13**, 415 (1955).
3. W. M. RIGGS and C. E. BRICKER. Anal. Chem. **38**, 897 (1966).
4. G. G. RAO, G. ARAVAMUDAN, and N. C. VENKATAMMA. Z. Anal. Chem. **146**, 161 (1955).
5. J. M. COOLEY and B. KRATOCHVIL. Can. J. Chem. **56**, 2452 (1978).
6. J. M. COOLEY and B. KRATOCHVIL. Can. J. Chem. **58**, 627 (1980).
7. S. R. SAGI and K. V. RAMANA. Talanta, **16**, 1217 (1969).
8. S. R. SAGI, G. S. PRAKASA RAJU, K. APPA RAO, and M. S. PRASADA RAO. Talanta, **29**, 413 (1982).
9. S. GILKS, T. E. ROGERS, and G. M. WAIND. Trans. Faraday Soc. **57**, 1371 (1961).
10. T. G. SPIRO. Inorg. Chem. **4**, 731 (1965).
11. L. B. MONSTED, O. MONSTED, and G. NORD. Trans. Faraday Soc. **66**, 936 (1970).

Can. J. Chem. Downloaded from www.nrcresearchpress.com by 210.87.254.105 on 09/06/12
For personal use only.

A photoconductivity study of trapped electrons in γ-irradiated hydrocarbon glasses at 77 K

NAOTO OKABE, TOYOAKI KIMURA,[1] AND KENJI FUEKI

Department of Synthetic Chemistry, Faculty of Engineering, Nagoya University, Furo-cho, Chikusa-ku, Nagoya 464, Japan

Received May 3, 1983

NAOTO OKABE, TOYOAKI KIMURA, and KENJI FUEKI. Can. J. Chem. **61**, 2799 (1983).

Photoconductivity spectra of trapped electrons in γ-irradiated 3-methylpentane, 2-methylpentane, 3-methylheptane, and 3-methylpentane–methylcyclohexane (1:9 volume ratio) glasses at 77 K were measured. From the comparison of photoconductivity and optical absorption spectra in these systems we have obtained relative values of quantum efficiencies for a trapped electron in the ground state to be excited to the conduction band by photo-induced transition. For electrons stably trapped, we have measured the ranges of trap depths from the shallowest to the deepest in these systems.

NAOTO OKABE, TOYOAKI KIMURA et KENJI FUEKI. Can. J. Chem. **61**, 2799 (1983).

On a mesuré à 77 K les spectres de photoconductivité des électrons piégés dans des verres de méthyl-3 pentène, de méthyl-2 pentène, de méthyl-3 heptane et de méthyl-3 pentane-méthylcyclohexane (rapport de volume 1:9) irradiés aux rayons γ. A partir de la comparaison des spectres de photoconductivité et d'absorption optique de ces systèmes, on a obtenu les valeurs relatives des efficacités quantiques de l'électron piégé dans l'état fondamental et qui doit être excité à la bande de conduction par une transition photoinduite. Par rapport à la profondeur des pièges à électron dans lesquels les électrons sont piégés de façon stable, on a trouvé que la profondeur des pièges va du piège le moins profond au piège le plus profond dans ces systèmes.
[Traduit par le journal]

Can. J. Chem. Downloaded from www.nrcresearchpress.com by 210.87.254.6 on 09/06/12
For personal use only.

Introduction

Ionizing radiations produce trapped electrons in various frozen matrices and many studies of these trapped electrons have been reported (1). Light irradiation to trapped electrons under an applied field gives photocurrents when the photon energy is higher than the binding energy of trapped electrons. Thus comparison of optical absorption and photoconductivity spectra is expected to provide information on the energy level structure of trapped electrons. For trapped electrons in polar glasses several photoconductivity studies have been made (2–9) and theoretical approaches have been attempted to interpret these experimental results (10, 11). On the other hand, only a few photoconductivity studies have been done for trapped electrons in nonpolar organic glasses (12, 13).

In the present work we have measured optical absorption and photoconductivity spectra of trapped electrons in γ-irradiated 3-methylpentane (3MP), 2-methylpentane (2MP), 3-methylheptane (3MHp), and a mixture of 3MP and methylcyclohexane (3MP–MCH) in 1:9 volume ratio. We have set up an apparatus for the photoconductivity measurement with a time constant of 30 ms for a current rise (0 ~ 90%) in order to observe photocurrents induced by monochromatic light at shorter times than in the previously reported work (12). Using this apparatus we have investigated in some detail the wavelength and light intensity dependence of photocurrents in the γ-irradiated hydrocarbon glass at 77 K. From comparison of photoconductivity spectra with optical absorption spectra we have deduced some significant information on the energy level structure of trapped electrons in these hydrocarbon matrices.

Experimental

3-Methylpentane and 2-methylpentane were standard pure (99% up) from Tokyo Kagaku Seiki. 3-Methylheptane was of special grade from Wako Pure Chemicals. Methylcyclohexane was standard pure (99.9%) from Tokyo Kagaku Seiki. The hydrocarbons were degassed on a vacuum line, vacuum-distilled into glass bulbs containing molecular sieves 13X pellets, heated at 280–300°C for 10 h *in vacuo* before use, and stored overnight in the dark. The purification with molecular sieves 13X was repeated three times. The purified hydrocarbons were then vacuum-distilled into photoconductivity cells and sealed off from the vacuum line. The photoconductivity cell was made of Supracil quartz and consisted of a Teflon spacer and electrodes (whose spacing was 0.6 and 1.1 mm) made of Supracil quartz coated with In–Sn. The design of the photoconductivity cell was described previously (14). In the case of 3MP, the conductivity cell with stainless mesh electrodes (whose spacing was 1 mm) was used. Both types of cells were also used for optical absorption measurements.

^{60}Co γ-rays were used for irradiation and the dose was 9.4×10^4 rad. Samples were kept in the dark at 77 K during γ-irradiations and photoconductivity or optical absorption measurements. When the samples were transferred from the γ-irradiation to the measuring Dewar, a bucket made of copper foil was used in order to keep the main part of the cell immersing in liquid nitrogen during the transfer.

The scheme of the photoconductivity measurement was given in ref. 14. A dc voltage (8 kV/cm) was supplied to the electrodes with a Watanabe PH-8A power supply. By opening a mechanical shutter, light from a xenon lamp (Xebex UXL-1000D-0) passed through a Ritsu MC-10N monochromator and an optical filter, generating a photocurrent in a γ-irradiated sample, which was amplified by a Keithley 427 current amplifier and stored in a Nicolet 2090-204 digital oscilloscope. In order to eliminate electrical noise, both the photoconductivity cell in a liquid nitrogen Dewar and the amplifier were set in a copper box which was connected to the ground. BNC connectors and coaxial cables were used and they were further shielded by mesh wires when necessary. The window through which the light passed was made of Supracil quartz coated with In–Sn which was stuck to a copper box with an electrical conductive paint.

In addition to electrical noise, there was also noise generated by mechanical vibrations. To avoid the latter the copper box was set on a polystyrene foam.

Toshiba glass filters UV-39, VR-69, and IR-D1A, which cut off the light shorter than 390, 690, and 900 nm, respectively, were used for the monochromatic light irradiation over the wavelength region of 500 ~ 700, 700 ~ 1000, and 1000 ~1600 nm, respectively. A silicone filter was used for the light of 1600 ~ 2200 nm. The actual band widths were <30 nm and ~60 nm for the visible and ir light, respectively. The intensity of monochromatic light was measured by a YSI Model 65A radiometer.

Optical absorption spectra were measured on a Hitachi model 323 spectrophotometer.

[1] To whom correspondence should be addressed.

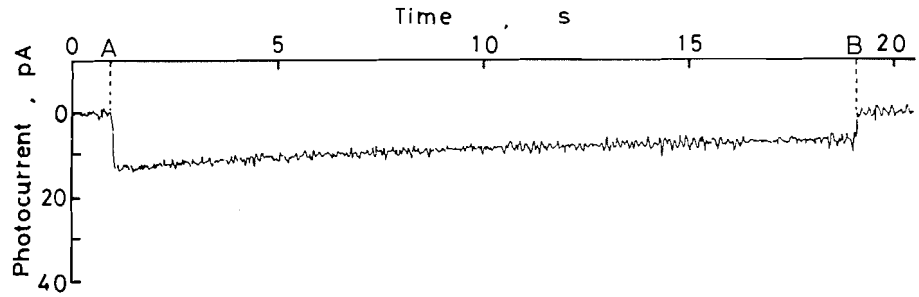

FIG. 1. Time profile of photocurrent in 3MP–MCH system. *A*: shutter opened; *B*: shutter closed.

Results and discussion

1. Time profile of photocurrents

The time constant (30 ms) in the present work is fast enough to make measurements on a time scale of second. In every case throughout this work, photocurrent was generated instantaneously when the shutter was opened; it then decayed very slowly during the light irradiation and fell to zero instantaneously when the shutter was closed. A typical example is shown in Fig. 1. A large decrease in photocurrent such as that reported in ref. 12 for the case of 3-methylhexane (3MHx) was not observed for 3MP, 2MP, 3MHp, and 3MP–MCH systems studied here. However, we have reconfirmed the large decrease in photocurrent, irrespective of the incident photon energy, for the 3MHx systems.[2] Except in the case of 3MHx, a flat time profile such as that shown in Fig. 1 appears to be a general feature of photocurrents in hydrocarbon glasses at 77 K. Trapped electrons cannot be considerably bleached out on a time scale of seconds by monochromatic light, intensity of which is at most 10^{15} photon/s. Thus, the time profile of such flat shape as shown in Fig. 1 is readily understandable because the concentration of trapped electrons remaining changes only slightly with irradiation time.

Photocurrents are related to the drift mobility of mobile electrons along the direction of the applied electric field. The mobile electron alternates between the conduction state in which the mobility is high and the localized state in which the mobility is negligibly small (15). This localized state corresponds to very shallow trapping sites and should be differentiated from deep trapping sites in which electrons can be stably trapped to form the so-called trapped electrons. Deeply trapped electrons cannot be detrapped unless photoexcited.

The magnitude of photocurrents depends on the equilibrium between the rates of production and depletion of mobile electrons. The depletion of mobile electrons results from their retrapping in the matrix or reactions with radicals, positive ions, and impurities, etc. The fact that time profiles of photocurrents are flat indicates that the major process for depletion of mobile electrons is retrapping on the time scale studied, otherwise such flat profiles would not be observable. Therefore, photocurrents are observed as a result of repetition of the production and depletion of mobile electrons in the matrix: trapped electrons are mobilized by absorbing photons, retrapped in the matrix, mobilized again, and so on.

2. Photoconductivity and optical absorption spectra of trapped electrons

As was described already we have obtained the relationship between the magnitude of photocurrent and the intensity of incident photon for each photon energy and for each system. Examples of a linear or nonlinear relation between the magnitude of photocurrent and the intensity of incident photon are shown for 3MP in Fig. 2. Nonlinear relationship, as shown in Fig. 2(*b*), was frequently observed in the experiments on 3MHx.[2] However, this nonlinear relationship was not observed for 2MP, 3MHp, and 3MP–MCH systems. Thus 3MP is in between 3MHx and the group of 2MP, 3MHp, and 3MP–MCH in the photocurrent – light intensity relationship.

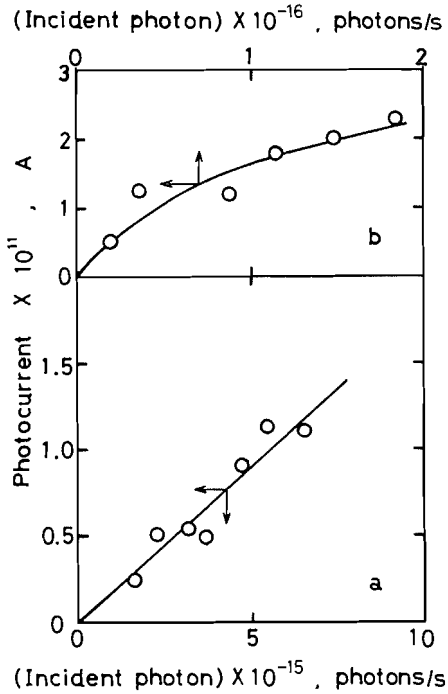

FIG. 2. Photocurrent vs. intensity of incident photon in 3MP system. *a*: wavelength of incident light, 1300 nm; *b*: wavelength of incident light, 1000 nm.

Photocurrents per incident photon for the 3MP, 2MP, 3MHp, and 3MP–MCH systems are plotted, together with the optical densities of trapped electrons, in Figs. 3, 4, 5, and 6, respectively. When the photocurrent is nonlinearly dependent on the incident photon intensity as shown in Fig. 2(*b*), the initial slope is taken as the value of photocurrent per incident photon. The unit of the ordinate in the photoconductivity spectra is expressed as A/(photon per s) which is equal to C/photon. Thus we will use C/photon for the ordinate of the photoconductivity spectra. Optical absorption spectra shown in Figs. 3–6 are normalized so that the magnitude of their maxima is equal to that of the maxima of the corresponding photoconductivity spectra. The tails of the optical absorption spectra on the low energy side cannot be fully given because of the high

[2] N. Okabe, T. Kimura, and K. Fueki. Unpublished results.

Can. J. Chem. Downloaded from www.nrcresearchpress.com by 210.87.254.6 on 09/06/12
For personal use only.

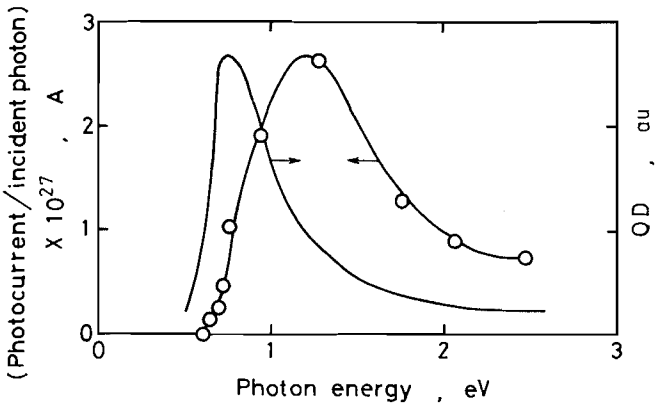

FIG. 3. Photocurrent per incident photon and optical density of trapped electrons in 3MP system vs. photon energy.

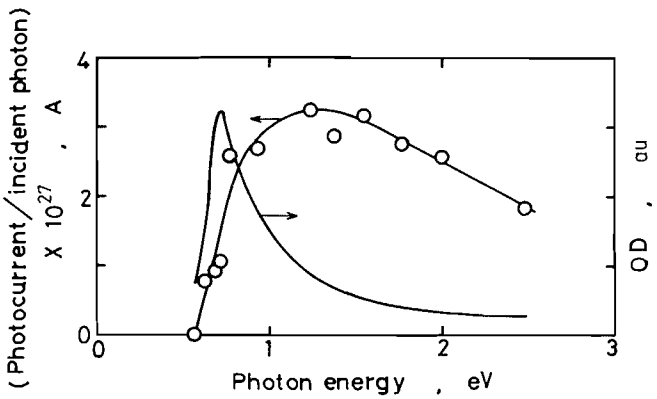

FIG. 4. Photocurrent per incident photon and optical density of trapped electrons in 2MP system vs. photon energy.

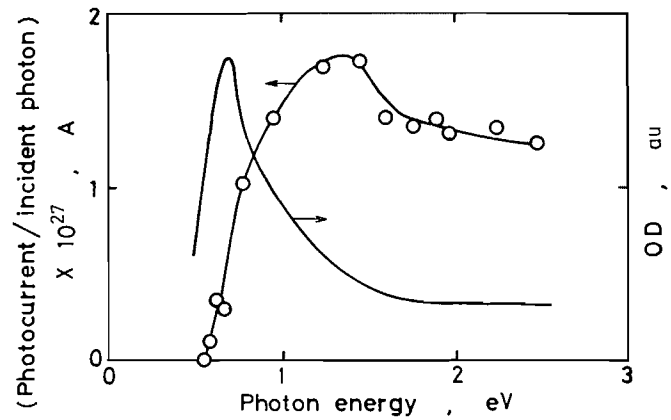

FIG. 5. Photocurrent per incident photon and optical density of trapped electrons in 3MHp system vs. photon energy.

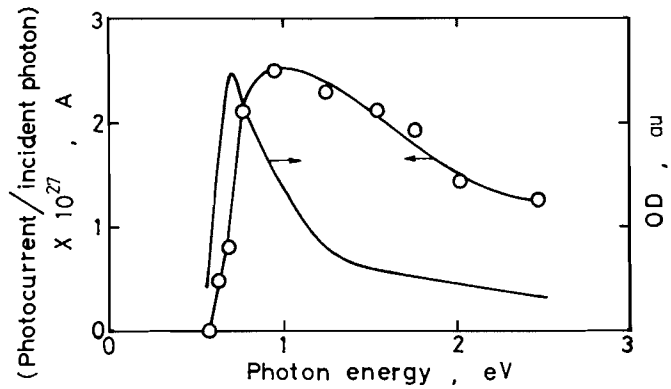

FIG. 6. Photocurrent per incident photon and optical density of trapped electrons in 3MP–MCH system vs. photon energy.

absorbance of the matrix itself.

There is no doubt that the photoconductivity spectra represent the transition probabilities from the ground state to the conduction state (bound–free transitions) vs. incident photon energy. However, the optical absorption spectra represent the transition probabilities from the ground state to the bound excited states (bound–bound transitions) and/or the conduction state vs. incident photon energy. Some experimental evidence by which optical absorption spectra can be assigned to bound–bound and bound–free transitions has been reported (2–5, 7, 12), but this is not conclusive because the photoconductivity thresholds are not given in these studies. Recent work has determined the photoconductivity thresholds for trapped electrons in amine and alcohol glasses at 77 K (16). On the other hand, some workers have assigned the entire spectrum of trapped electrons in a hydrocarbon glass to the bound–free transition alone (17). However, we have shown from the measurement of photoconductivity threshold that the optical absorption spectrum of trapped electrons in 3MP can be assigned to the bound–bound and bound–free transitions (13). The present results on 2MP, 3MHp, and 3MP–MCH systems also support the conclusion given in ref. 13. In all of Figs. 3–6, the photoconductivity thresholds appear at the photon energies at which the corresponding optical absorption is still finite. This indicates that optical absorption at photon energies less than the photoconductivity threshold, E_{th}^{ph}, must be attributed to bound–bound transitions alone. In the photon energy range between E_{th}^{ph} and the energy, E_{max}^{ab}, at which the optical absorption spectrum is maximum, bound–bound, and bound–free transition coexist but the former is predominant. In the photon energy range between E_{max}^{ab} and the energy, E_{max}^{ph}, at which the photoconductivity spectrum is maximum, both bound–bound and bound–free transitions exist to a significant extent. At photon energies higher than E_{max}^{ph} the bound–free transition is predominant.

The results in Figs. 3–6 are similar to each other, but the photoconductivity spectra on the high energy side differ slightly among each other. The photoconductivity spectrum for 3MP is the lowest in its intensity on the high energy side. The energy separation between E_{max}^{ab} and E_{max}^{ph} is similar among 3MP, 2MP, and 3MHp. However, in the 3MP–MCH system the photoconductivity maximum is closer to the optical absorption maximum.

3. Relative quantum efficiency for the bound–free transition

Photocurrent, i, can be given by eq. [1].

$$[1] \quad i = \frac{e\mu V}{d} 10^{-3} [e_m^-] N_0 S$$

where e is the charge on an electron, μ is the drift mobility of the mobile electron, V is the applied voltage, $[e_m^-]$ is the concentration of mobile electrons in units of M, N_0 is Avogadro's number, S is the surface area of electrodes, and d is the separation distance between electrodes. Since the time profiles of photocurrents observed are nearly flat as was already described, we can assume a steady-state for the production and depletion of mobile electrons:

Can. J. Chem. Downloaded from www.nrcresearchpress.com by 210.87.254.6 on 09/06/12
For personal use only.

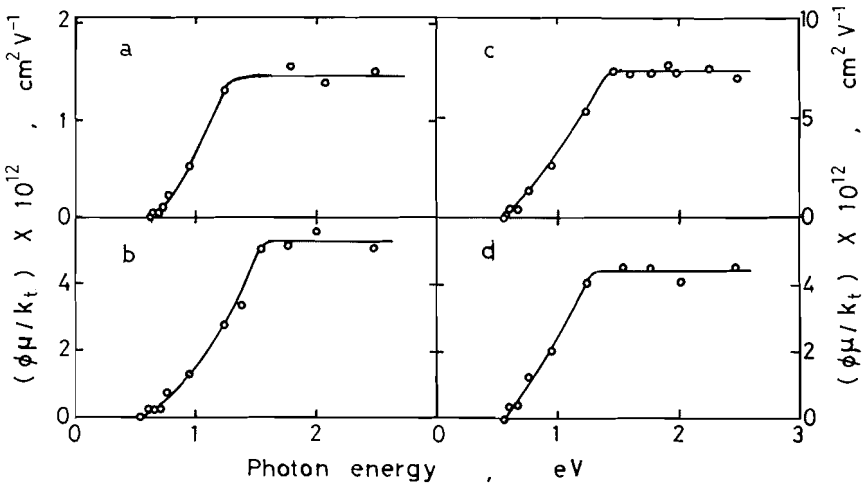

FIG. 7. $\phi\mu/k_t$ vs. photon energy. *a*: 3MP; *b*: 2MP; *c*: 3MHp; *d*: 3MP–MCH.

$$[2]\quad \frac{d[e_m^-]}{dt} = \phi I_0(1-10^{-OD})/(10^{-3}N_0 d) - k_t[e_m^-] = 0$$

where I_0 is the number of incident photons per unit time (s) per unit area (cm^2), OD is the optical density of trapped electrons at a specified photon energy, and ϕ and k_t are the quantum efficiency for the bound–free transition and the rate constant for the depletion of mobile electrons by trapping, respectively. Then the steady-state concentration of mobile electrons are derived as eq. [3] from eq. [2].

$$[3]\quad [e_m^-] = \frac{10^3 \phi I_0}{N_0 d k_t}(1-10^{-OD})$$

From eqs. [1] and [3] we obtain,

$$[4]\quad \frac{\phi\mu}{k_t} = \frac{id^2}{I_0(1-10^{-OD})SeV}$$

It should be noted that all the quantities on the right hand side of eq. [4] are observable or known. We assume here that μ/k_t is independent of the photon energy. This assumption is valid when the hot electron relaxation time is short compared with the measurement time. This condition is satisfied under our experimental conditions. If this assumption is accepted, the value of the right-hand side of eq. [4] gives the relative value of ϕ. The values of $\phi\mu/k_t$ for 3MP, 2MP, 3MHp, and 3MP–MCH systems are plotted as a function of photon energy in Fig. 7. It should be noted that for all four systems, the values of $\phi\mu/k_t$ are constant when the photon energy is greater than a certain value, E_c^{ph}. These critical photon energies, E_c^{ph}, are slightly different for the four systems. The values of $\phi\mu/k_t$ decrease monotonically with decreasing photon energy below E_c^{ph} and fall to zero at the photon energies which correspond to the photoconductivity thresholds, E_{th}^{ph}. Based upon the above assumption, all the results in Fig. 7 are satisfactorily explained as follows. We consider that electrons are stably localized in matrix traps whose depths have a certain distribution. Here we define the trap depth as the difference in energy between the bottom of the conduction state and the ground state. When the photon energy is lower than the value corresponding to the depth of the shallowest trap,[3] no bound–free transition occurs

[3] This is the shallowest trap relevant to stably trapped electrons, but not to mobile electrons.

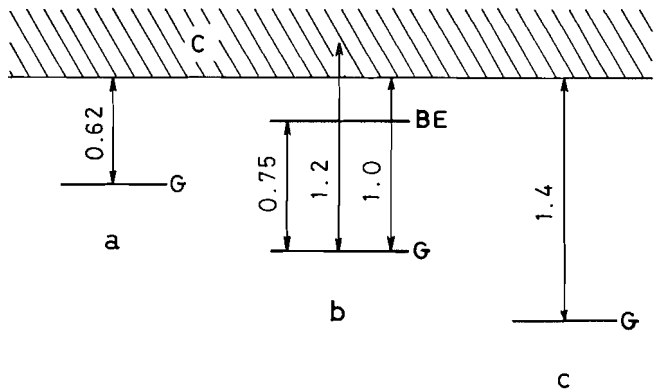

FIG. 8. Energy diagram for trapped electrons in 3MP at 77 K. G, BE, and C denote the ground, bound-excited, and conduction states, respectively, and arrows show the difference between the two energy levels in units of eV. *a*: the shallowest trap; *b*: the average trap, *c*: the deepest trap.

and ϕ is zero. In the photon energy range between those corresponding to the shallowest and deepest traps, photon absorption by trapped electrons, whose trap depths are less than the photon energy, results in bound–free transitions, but photon absorption by trapped electrons, whose trap depths are greater than the photon energy, does not. Thus it is expected that a fraction of the bound–free transition, i.e., ϕ, increases with increasing photon energy in this range. When the photon energy exceeds the energy value corresponding to the deepest trap, photon absorption results in only bound–free transitions, i.e., $\phi = 1$, independent of photon energy. Assuming that the depths of the shallowest and deepest traps correspond to E_{th}^{ph} and E_c^{ph}, respectively, we see that the experimental results shown in Fig. 7 can be well accounted for: the relative values of ϕ are zero for the photon energy $< E_{th}^{ph}$, increase with increasing photon energy between E_{th}^{ph} and E_c^{ph} and are constant when the photon energy $> E_c^{ph}$.

The values of the shallowest and deepest trap depths obtained as E_{th}^{ph} and E_c^{ph} from Fig. 7 are listed in Table 1 together with the energies, E_{max}^{ab} and E_{max}^{ph}, corresponding to the optical absorption and photoconductivity maxima, respectively. Taking 3MP as an example, the shallowest and deepest trap depths are 0.6 and 1.4 eV, respectively. If it is assumed that the optical absorption and photoconductivity maxima correspond to the

Can. J. Chem. Downloaded from www.nrcresearchpress.com by 210.87.254.6 on 09/06/12
For personal use only.

TABLE 1. The energy, E^{ab}_{max}, at the optical absorption maximum, the energy, E^{ph}_{max}, at the photoconductivity maximum, and the shallowest and deepest trap depths for trapped electrons in the hydrocarbon matrices at 77 K, determined by photoconductivity and optical absorption measurements

Glass	E^{ab}_{max}, eV	E^{ph}_{max}, eV	Shallowest trap depth, eV	Deepest trap depth, eV
3MP	0.75	1.2	0.62	1.4
2MP	0.72	1.2	0.56	1.6
3MHp	0.70	1.4	0.56	1.5
3MP–MCH	0.71	0.95	0.56	1.3

most probable excitation energies for bound–bound and bound–free transitions, the average energy level of the bound excited state lies above that of the ground state by 0.75 eV and the most probable bound–free transition occurs at 1.2 eV above the average energy level of the ground state. The energy level to which the most probable bound–free transition occurs is higher by 0.2 eV than the bottom of the conduction state. The energy level diagram for trapped electrons in 3MP is schematically shown in Fig. 8.

Since two types of conductivity cells were used in the present work, we do not intend to compare the absolute values of $\phi\mu/k_t$ among the hydrocarbon systems studied here. $\phi\mu/k_t$ in the present work corresponds to $\langle\phi\mu\tau\rangle$ in refs. 5 and 6. The reported values of $\langle\phi\mu\tau\rangle$ in polar aqueous and alcoholic glasses and aqueous LiCl glass are $10^{-15} \sim 10^{-13}$ and 10^{-12} cm^2 V^{-1}, respectively. The constant values of $\phi\mu/k_t$ for the photon energy $> E^{ph}_c$ are of the order of 10^{-12} cm^2 V^{-1}. If we use a $(1/k_t)$ value of $\sim 10^{-10}$ s (18) and a μ value of $\sim 10^{-2}$ cm^2 V^{-1} s^{-1} (19–21),[4] then ϕ becomes the order of 1.

Steen and Moan have stated that photobleaching of trapped electrons occurs by photoexcitation from the ground to a superexcited state which lies above the bottom of the conduction state and then the superexcited state autoionizes to give conduction electrons (22). The present results do not discriminate whether trapped electrons are mobilized by direct transitions from the ground to conduction states or by transitions to superexcited states and subsequent autoionization. If we take the latter process into consideration, the depths of the shallowest and deepest traps may be somewhat lower than the values listed in Table 1, since it is stated that the probability of autoionization relative to deactivation of superexcited states increases rapidly with increasing excitation energy (22).

As described above, we have shown the existence of the range of trap depths based on the assumption that μ/k_t is independent of photon energy. Figure 7 shows that the values of $\phi\mu/k_t$ are constant in the higher photon energy region. Since it is expected that ϕ is constant when photon energy exceeds a certain value, μ/k_t could be constant in the higher photon energy region. In the lower photon energy region, however, we might suppose that μ/k_t may not be independent of photon energy. If a bound–free transition takes place at an energy only slightly above the threshold, the electron formed may have so little energy that it can be thermalized and be attracted back to the trap very quickly without ever being able to escape from the locale of the trap. If so, this would be reflected as a decrease in ϕ in the present experimental system, because we have observed photocurrents in the time scale of seconds. Then, ϕ would increase from zero (photon energy = threshold) with increasing photon energy. An alternative explanation for the increase in $\phi\mu/k_t$ with increasing photon energy in Fig. 7 may be as follows: depth of electron traps is uniform and ϕ increases from zero (photon energy = threshold) with increasing photon energy (uniform trap depth model). However, the fact that the most probable bound–bound transition occurs at a photon energy higher than E^{ph}_{th} cannot be explained by the uniform trap depth model. Even if there exists a range of trap depths, ϕ may increase with increasing photon energy for electrons trapped in a specified depth of trap. If this is true, the depths of the deepest traps would be somewhat lower than those listed in Table 1.

[4] The reported electron mobilities in organic glasses at 77 K are 0.1 (19) and 0.055 (20) cm^2 V^{-1} s^{-1} for 3MP and MTHF, respectively. However, Kevan and Rice have suggested later that the lower limit of electron mobility in MTHF at 77 K is 0.005 cm^2 V^{-1} s^{-1} (21). Thus we may say that electron mobility in organic glasses at 77 K is of the order of 10^{-2} V^{-1} s^{-1}.

1. L. KEVAN. Advances in radiation chemistry. Vol. 4. *Edited by* M. Burton and J. L. Magee. Wiley-Interscience, New York. 1974. p. 181.
2. K. F. BAVERSTOCK and P. J. DYNE. Can. J. Chem. **48**, 2128 (1970).
3. T. HUANG, I. EISELE, D. P. LIN, and L. KEVAN. J. Chem. Phys. **56**, 4702 (1972).
4. S. NODA and L. KEVAN. J. Phys. Chem. **78**, 2454 (1974).
5. S. A. RICE and L. KEVAN. J. Phys. Chem. **81**, 847 (1977).
6. S. A. RICE, G. DOLIVO, and L. KEVAN. J. Chem. Phys. **68**, 4864 (1978).
7. S. A. RICE, G. DOLIVO, and L. KEVAN. J. Chem. Phys. **70**, 18 (1979).
8. M. MIEŃSKA-TOMCZYK. Radiochem. Radioanal. Lett. **36**, 275 (1978).
9. N. KATO, K. AKIYAMA, and K. FUEKI. J. Phys. Chem. **85**, 3087 (1981).
10. T. SHIDA, S. IWATA, and T. WATANABE. J. Phys. Chem. **76**, 3683 (1972).
11. K. FUEKI, D.-F. FENG, and L. KEVAN. J. Chem. Phys. **59**, 6201 (1973).
12. T. HUANG and L. KEVAN. J. Am. Chem. Soc. **95**, 3122 (1973).
13. T. FUNABASHI, N. OKABE, T. KIMURA, and K. FUEKI. J. Chem. Phys. **75**, 1576 (1981).
14. T. KIMURA, K. HIRAO, N. OKABE and K. FUEKI. Can. J. Chem. To be published.
15. A. O. ALLEN, T. E. GANGWER, and R. A. HOLROYD. J. Phys. Chem. **79**, 25 (1975).
16. N. KATO, S. TAKAGI, and K. FUEKI. J. Phys. Chem. **85**, 2684 (1981).
17. T. ICHIKAWA and H. YOSHIDA. J. Chem. Phys. **73**, 1540 (1980).
18. N. KATO, T. KIMURA, and K. FUEKI. Can. J. Chem. **55**, 3973 (1977).
19. Y. MARUYAMA and K. FUNABASHI. J. Chem. Phys. **56**, 2342 (1972).
20. T. HUANG and L. KEVAN. J. Chem. Phys. **61**, 4660 (1974).
21. S. A. RICE and L. KEVAN. Radiat. Phys. Chem. **15**, 353 (1980).
22. H. B. STEEN and J. MOAN. J. Phys. Chem. **76**, 3366 (1972).

Can. J. Chem. Downloaded from www.nrcresearchpress.com by 210.87.254.6 on 09/06/12
For personal use only.

III. Order–disorder transitions and electrical conductivity studies in Na_2SO_4 – Ag_2SO_4 system

M. SUNITHA KUMARI and ETALO A. SECCO[1]

Chemistry Department, St. Francis Xavier University, Antigonish, N.S. Canada B2G 1C0

Received May 20, 1983

M. SUNITHA KUMARI and ETALO A. SECCO. Can. J. Chem. **61**, 2804 (1983).

The physico-chemical aspects of the order–disorder phase transitions occurring in the Na_2SO_4–Ag_2SO_4 system were investigated by thermal analyses, X-ray diffraction, and electrical conductivity techniques. Electrical conductivity data on pure and doped compositions reveal high conductivity values in the high temperature phase.

The lower conductivity of Ag_2SO_4 with Na^+ presence relative to pure Ag_2SO_4 is attributed to lattice contraction effecting lower mobility of ions.

M. SUNITHA KUMARI et ETALO A. SECCO. Can. J. Chem. **61**, 2804 (1983).

On a étudié les aspects physico-chimiques de l'ordre et du désordre des transitions de phase qui se produisent dans le système Na_2SO_4–Ag_2SO_4 en faisant appel à l'analyse thermique, aux techniques de diffraction des rayons-X et à la conductivité électrique. Les données de conductivité électrique des compositions à l'état pur et à l'état dopé révèlent des valeurs élevées de conductivité dans la phase à haute température.

On attribue la plus faible conductivité du Ag_2SO_4 en présence de Na^+ par rapport à celle du Ag_2SO_4 à l'état pur à une contraction du réseau qui provoque une plus faible mobilité des ions.

[Traduit par le journal]

Can. J. Chem. Downloaded from www.nrcresearchpress.com by 210.87.254.105 on 09/06/12
For personal use only.

Introduction

Recently, we reported on the order–disorder phase transitions occurring in the Na_2SO_4–K_2SO_4 system (1) and on the high ionic conductivity values observed in the high temperature phase of undoped and doped $KNaSO_4$ and $K_3Na(SO_4)_2$ (2). Binary sulfates containing monovalent cations are members of a group of compounds which exhibit fast-ion or super-ionic conductivity in the high-temperature phase (3). The mechanism of fast-ion conduction is not completely understood although proposed models involve basically two structural types, viz. (*i*) layer structure as in β-alumina and (*ii*) channel structure as in NASICON where an open network or skeleton framework of anions facilitate cation mobility (3).

The low temperature form of Ag_2SO_4, I-Ag_2SO_4 (β), orthorhombic and space group *Fddd* with unit cell dimensions a_0 = 5.82 Å, b_0 = 12.70 Å, c_0 = 10.27 Å, is isomorphic with the low temperature form of Na_2SO_4, V-$NaSO_4$, with unit cell dimensions a_0 = 5.80 Å, b_0 = 12.30 Å, c_0 = 9.82 Å (4). Furthermore, the high temperature forms of Ag_2SO_4, II-Ag_2SO_4(α), and of Na_2SO_4, I-Na_2SO_4, are isostructural hexagonal with space groups $P6_3/mmc$ and $P6_3/mc$, respectively. With their lattice constants differing by <4%, Ag_2SO_4 and Na_2SO_4 are expected to form a continuous solid solution over the entire composition range with only one single solid phase present.

The early paper of Nacken (5) reporting on the Na_2SO_4–Ag_2SO_4 phase diagram was followed by the study of Burmistrova *et al.* (6) wherein solid solutions and solid–solid phase transitions are shown to exist over the complete composition range. Since Ag_2SO_4 exhibited high cationic conductivity in the high temperature phase (7, 8), the prospect of higher cationic conductivity with smaller radius and lower mass Na^+, r_{Na^+} = 96 pm versus r_{Ag^+} = 126 pm, in the Ag_2SO_4 structure prompted us to probe the nature of the solid–solid phase transitions in the Na_2SO_4–Ag_2SO_4 system and to explore its potential for enhanced fast-ion conduction using thermal analyses, DSC, electroconductivity, and X-ray diffractometry techniques.

[1]To whom all correspondence should be addressed.

Experimental

Anhydrous Na_2SO_4 was from two sources, Fisher Certified and Alfa Products ultrapure grade. Anhydrous Ag_2SO_4 was Alfa Products ultrapure grade. Although there was no discernible difference in the measured physico-chemical and thermal properties of Na_2SO_4–Ag_2SO_4 samples using Na_2SO_4 from both sources, the electrical conductivity measurements revealed parallel but distinct plots. Only ultrapure Na_2SO_4–Ag_2SO_4 results are reported here. The $CdSO_4$ was Fisher Certified grade and $Gd_2(SO_4)_3$ was Alfa Ventron Corp. of stated purity 99.9%.

Na_2SO_4–Ag_2SO_4 samples, undoped and doped (Cd^{2+}, Gd^{3+}), were prepared by fusing the requisite composition mixture, previously well ground manually, of the respective sulfates in a Pt crucible.

DTA traces were recorded on a duPont 990 Thermal Analyzer in a flowing N_2 (ultrapure) atmosphere using ignited Al_2O_3 as reference material. The precision of a melting temperature measurement was ±5°C whereas the transition temperature measurement was within ±2°C. The enthalpies and heat capacities of transformation were evaluated with the DSC accessory to the 990 DTA module using the heats of fusion for In, Sn, and Zn as references; samples were encapsulated in Al containers — identical results within experimental error were obtained using Au containers.

X-ray diffraction patterns were obtained using a Norelco diffractometer with CuK_α radiation. Diffraction patterns at elevated temperatures were recorded with a Model X-86-N high temperature accessory (Materials Research Corp.) attached to the Norelco unit (9).

Electrical conductivity measurements were made on compressed polycrystalline sample in a stainless steel conductivity cell following the procedure described earlier (2, 10). The sample was in the form of a disc, 1 mm thick and 100 mm^2 in surface area, for Na_2SO_4 and Ag_2SO_4. All other compositions were 1 mm thick and ~30–50 mm^2 in surface area whose shape ranged from a semi-circle to a sector — it was the crack-free portion recovered from the compressed disc.

Results and discussion

Phase diagram

The transition temperatures recorded on DTA traces and plotted versus composition in Fig. 1. Figure 1*a* represents the solid–solid phase diagram and Fig. 1*b* represents the solid–liquid phase diagram. The cool mode plot, filled circles, in Fig. 1*a* and *b* are in general agreement with the reports of Nacken (5) and Burmistrova *et al.* (6). Figure 2 gives the enthalpy change, ΔH_t, dependence on composition for the solid–solid

Can. J. Chem. Downloaded from www.nrcresearchpress.com by 210.87.254.105 on 09/06/12
For personal use only.

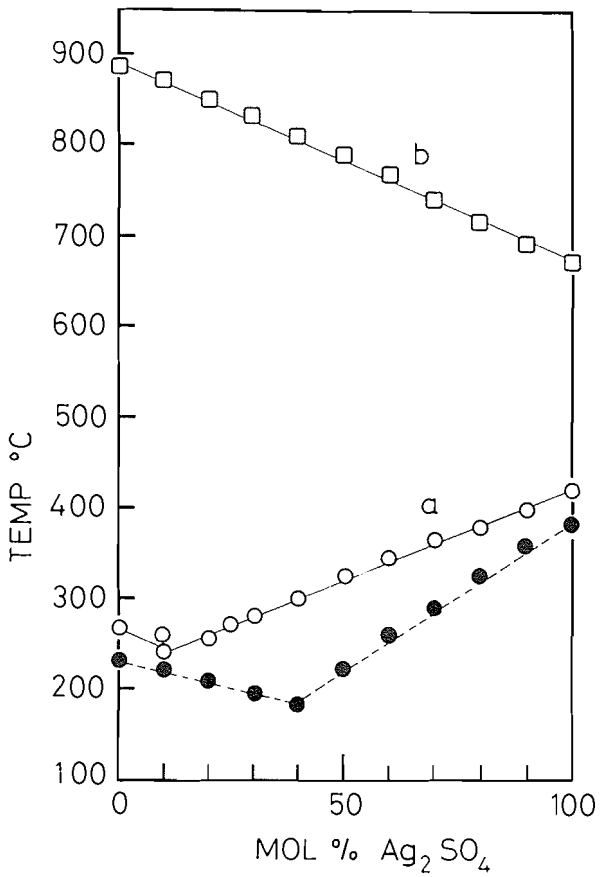

FIG. 1. (*a*) Solid–solid phase diagram Na_2SO_4–Ag_2SO_4 system; ○, heat mode; ●, cool mode. (*b*) Solid–liquid phase diagram Na_2SO_4–Ag_2SO_4 system, heat mode.

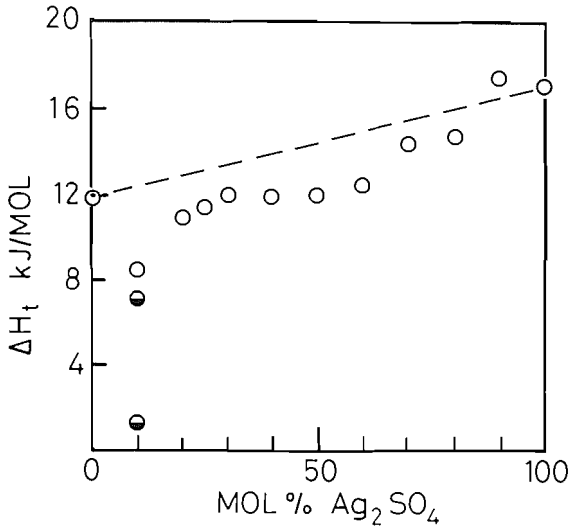

FIG. 2. Plot of enthalpy change for solid–solid phase transitions versus composition in Na_2SO_4–Ag_2SO_4 system; ◒, two endotherms; and ○, their sum.

transition and Fig. 3 presents the heat capacity C_p dependence on temperature for the solid–solid transition of 40 mol% and 20 mol% Ag_2SO_4 compositions, trace *b* and trace *a*, respectively, and Fig. 4 plots the property of strain energy $\sim\Delta T\Delta S$ versus composition.

(i) Solid–liquid

The solid–liquid diagram exhibits the solid solution behav-

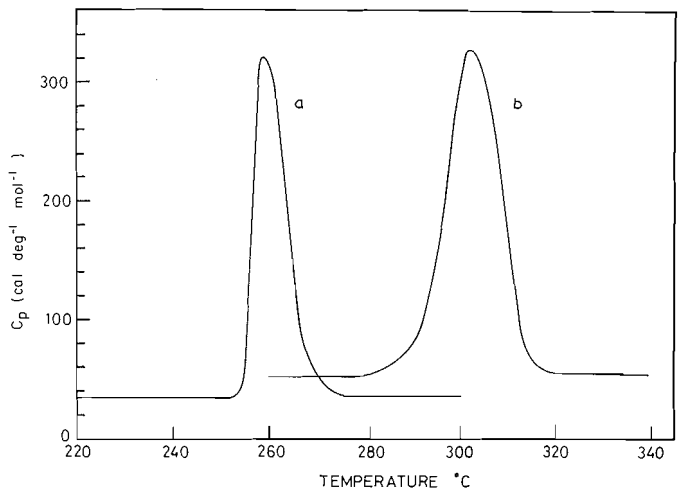

FIG. 3. Plots of C_P versus temperature. (*a*) 20 mol% Ag_2SO_4; (*b*) 40 mol% Ag_2SO_4.

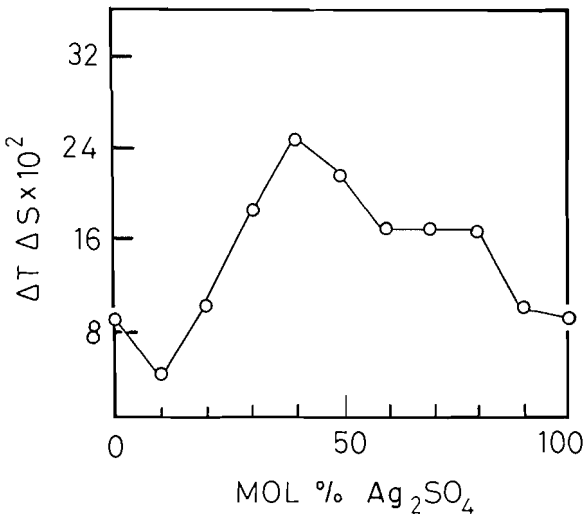

FIG. 4. Plot of $\Delta T\Delta S$ versus composition.

ior expected for isomorphic binary systems with conspicuous absence of the solidus curve. Reisman (11) has done theoretical analyses of solid solutions using computer-derived models incorporating the ΔH_f^0, heat of fusion, and T_0, the melting temperature for each component. The Na_2SO_4–Ag_2SO_4 binary system with ΔH_f^0 = 5.8 kcal/mol, T_0 = 1153 K and ΔH_f^0 = 4.3 kcal/mol, T_0 = 954 K, respectively is expected to show a linear liquidus curve with a slightly convex solidus separation. No solidus curve was discernible in our data but there is evidence of slight concavity among the data although we chose a straight line plot.

(ii) Solid–solid

The solid phase diagram displays a simple linear dependence of the transition temperature on composition from 10 mol% to pure Ag_2SO_4 in the heat mode. The higher transition temperature at 10 mol% represents the shoulder of the endotherm, Fig. 5*a*. Figure 5 presents traces *a*, *b*, and *c* in the heat mode for 10, 20, and 30 mol% Ag_2SO_4. The upper trace is for the sample within 24 h after fusion and cooled abruptly by sample withdrawal from furnace to room temperature. The lower trace is for the same sample after 15–21 days storage at room temperature in open air or on second heating after slow cooling in the DTA cell. The DTA cool traces of these compositions

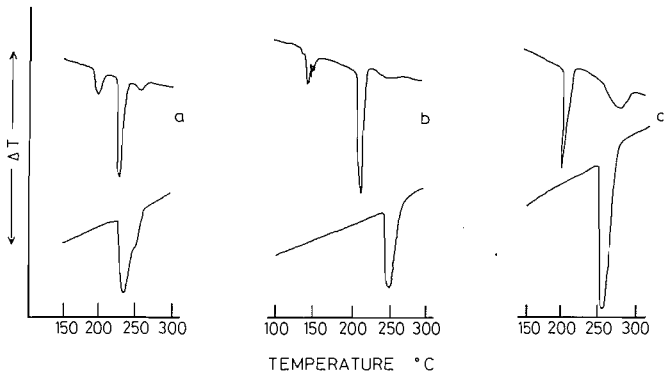

FIG. 5. DTA heat mode traces of fused $Na_2SO_4-Ag_2SO_4$ samples: upper trace, cooled abruptly to room temperature and 24 h after fusion; lower trace, after 15–21 days storage at room temperature or on second heating after slow cooling in DTA cell. (*a*) 10 mol% Ag_2SO_4; (*b*) 20 mol% Ag_2SO_4; (*c*) 30 mol% Ag_2SO_4.

showed only one exotherm, indicating the stabilization to a single phase after slow cooling or storage. Figures 1*a* and 1*b* and Figs. 2, 3, and 4 are for samples after 15–21 days storage.

The irregular behavior of the 10 mol% composition throughout the study most likely originates with the polymorphism of Na_2SO_4 where four phases have been confirmed (12). That is, two kinds of $Ag_2SO_4-Na_2SO_4$ solid solutions exist where Ag_2SO_4 is distributed between two structural forms of Na_2SO_4 – a novel effect where a solute is distributed between two immiscible solid phases of the same compound.

The cool mode data display appreciable hysteresis effects relative to the heat mode data, with the minimum at 40 mol%, which are consistent with the diagram from Nacken (5). Our T_t of 422°C for Ag_2SO_4 is closer to value of 420°C from Burmistrova *et al.* (6) than the values of 412°C and 430°C of Nacken (5) and Hedvall *et al.* (13) respectively. Thermal hysteresis effect, $\Delta T = T_p^f - T_p^r$, where T_p^f refers to the peak temperature on heating and T_p^r the peak temperature on cooling, has been linked (14) to a necessary consequence of the coexistence mechanism of continuous transformations with the main factor controlling the hysteresis being the strain energy E_s. Thermodynamic considerations relate strain energy to $\Delta T\Delta S$, i.e. $E_s \propto \Delta T\Delta S$ where ΔS is the entropy change for the transformation. Figure 4 shows a maximum strain energy at 40 mol% whereas the pure components, Na_2SO_4 and Ag_2SO_4, possess the same strain energy. Another basis for the hysteresis effect may be the disorder → order direction which imposes a configurational requirement of "long-range" order with the ordered migration of ions from one set of sites to another. The largest hysteresis may imply the highest order-to-disorder ratio resulting from the existence of predetermined and specifically crystallographically identified sites for each ionic species. Guthrie and McCullough (15) expressed this approach by the relation $\Delta S = R \ln Q$, where Q is the ratio of the numbers of disordered states in the two phases, and ΔS is the entropy of transformation. Using this equation for the 40 mol% ΔS_t of 20.5 J mol^{-1} K^{-1} and subtracting a correction for the librational entropy of 3 J mol^{-1} K^{-1} and assuming no cation disorder, a disorder ratio of $Q = 11$ is found in good agreement with the value of $Q = 10$ for model substances of pure compounds. However, Fig. 2 reveals an essentially constant ΔH_t or ΔS_t value up to 60 mol%, excepting 10 mol%, suggesting that the order-to-disorder ratio is also constant. But this inference ignores the binding energy between like pairs and unlike pairs,

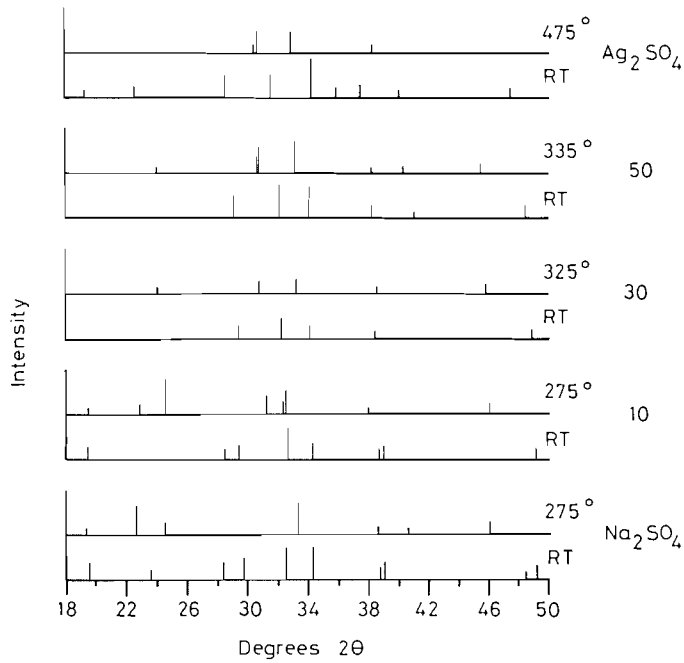

FIG. 6. X-ray diffraction line patterns, converted from diffractogram peaks, of relative intensity versus angle 2θ for Na_2SO_4, 10, 30, 50 mol% Ag_2SO_4, and Ag_2SO_4 at room temperature (RT) and transition temperatures in °C.

i.e. Na^+ and Ag^+, in the lattice where a change in binding energy may be compensated by the enthalpy of mixing. The dashed linear relation in Fig. 2 represents the physical mixture of Na_2SO_4 and Ag_2SO_4 where the difference between this value and the observed solid solution value is taken as the net binding energy – enthalpy of mixing contribution. This latter topic is planned as a further study.

X-ray diffraction

X-ray diffraction patterns at room temperature and above the transition temperature for Na_2SO_4, Ag_2SO_4, 10 mol% Ag_2SO_4, 30 mol% Ag_2SO_4, and 50 mol% Ag_2SO_4 are presented in Fig. 6. The patterns confirm the solid phase structural transformation. Na_2SO_4 and Ag_2SO_4 correlate with their reported patterns (4). The room temperature 10 mol% pattern, except for minor displacements and intensity differences, resembles the Na_2SO_4 pattern at room temperature; distinct differences appear, however, above the transition temperature (275°C) for the two samples. While the room temperature patterns of 30 and 50 mol% Ag_2SO_4 show strong resemblance to each other and are simpler than the room temperature patterns of Na_2SO_4 and Ag_2SO_4, their high temperature patterns closely resemble the Ag_2SO_4 high temperature pattern. These patterns imply that the low temperature structure of a $Na_2SO_4-Ag_2SO_4$ solid solution undergoes a phase transformation resembling the II-Ag_2SO_4 (α) form at high temperature with ΔH_t equal to that value for Na_2SO_4.

Electrical conductivity

The temperature dependence of the ionic conductivity, σ, is interpreted in terms of the Arrhenius-type equation.

$$\sigma = (\sigma_0/T) \exp(-Q_c/RT)$$

where σ_0 represents a composite constant $(ne^2\lambda^2\nu/k)$; n, the number of ions per unit volume; e, the ionic charge; λ, the distance between two jump positions; ν, the jump frequency; k,

Can. J. Chem. Downloaded from www.nrcresearchpress.com by 210.87.254.105 on 09/06/12
For personal use only.

Can. J. Chem. Downloaded from www.nrcresearchpress.com by 210.87.254.105 on 09/06/12
For personal use only.

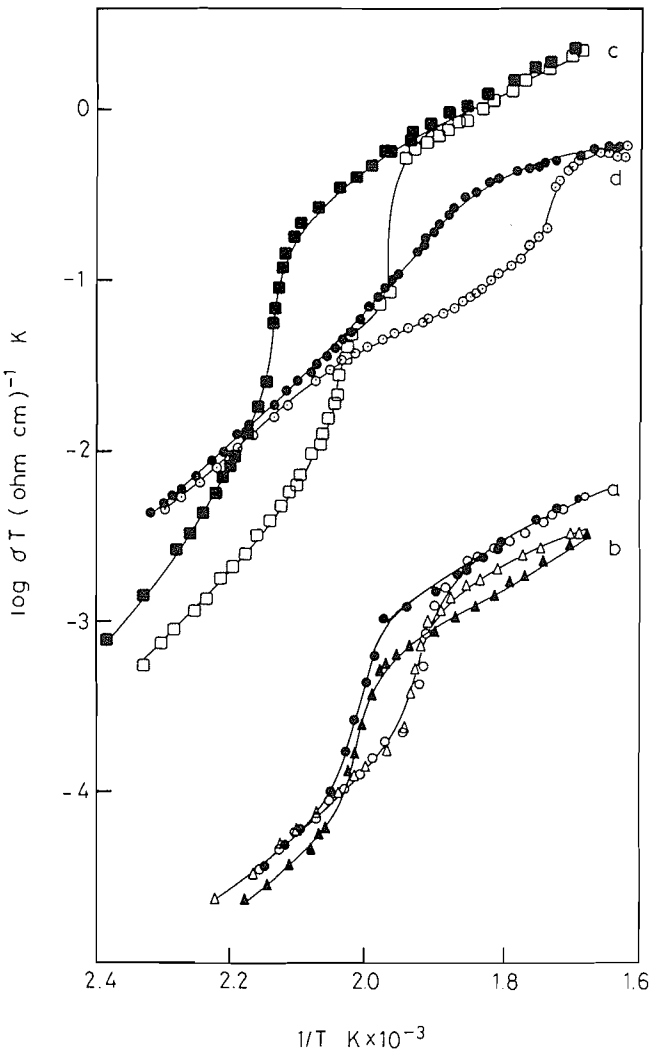

FIG. 7. Plots of log σT versus $1/T$: (*a*) Na_2SO_4, Fisher Certified, ○, ● heat and cool modes, respectively; (*b*) Na_2SO_4, Alfa ultrapure, △, ▲ heat and cool modes, respectively; (*c*) 5 mol% Cd^{2+} in Na_2SO_4, □, ■ heat and cool modes, respectively; (*d*) 5 mol% Gd^{3+} in Na_2SO_4, ○, ● heat and cool modes, respectively.

the Boltzmann constant; and Q_c is the activation energy for ionic motion, assuming the conductivity to be effectively ionic with negligible electronic or hole conductivity.

Plots of log (σT) vs. $1/T$ K for pure and doped Na_2SO_4, pure Ag_2SO_4, and doped and undoped 40 mol% Ag_2SO_4 are presented in Figs. 7 and 8, respectively. The two samples of undoped Na_2SO_4, curves *a* and *b* in Fig. 7, from different sources display the same behavior on the heat mode within limits of experimental error, but show a distinct difference on the cool mode. The doped samples, curves *c* and *d* in Fig. 7, were with Alfa Products Na_2SO_4. Na_2SO_4 doped with 5 mol% $CdSO_4$ showed higher σ values above the transition temperature than Na_2SO_4 doped with 5 mol% $Gd_2(SO_4)_3$. The reduced transition effect, temperature dependence and σ value for 5 mol% $Gd_2(SO_4)_3$ is consistent with vacancy-cation cluster formation analogous to that proposed for anion conductors (16). These plots show the expected phase transition and hysteresis effects consistent with DTA traces.

The conductivity plots in Fig. 8 reveal pronounced hysteresis effects for the 40 mol% Ag_2SO_4 composition consistent with the DTA result, Fig. 1*a*, whereas a minor hysteresis effect

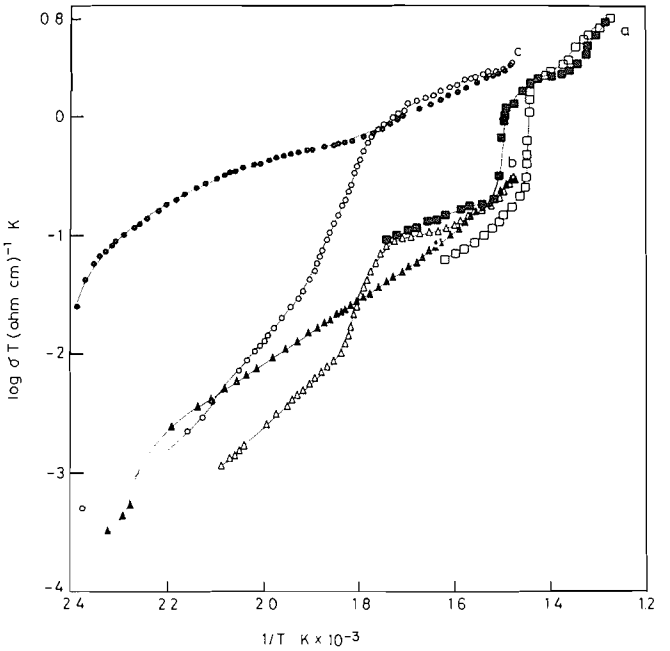

FIG. 8. Plots of log σT versus $1/T$: (*a*) Ag_2SO_4, □, ■ heat and cool modes, respectively; (*b*) 40 mol% Ag_2SO_4, △, ▲ heat and cool modes, respectively; (*c*) 4 mol% Cd^{2+} in 40 mol% Ag_2SO_4, ○, ● heat and cool modes, respectively.

appears for Ag_2SO_4. While the 4 mol% $CdSO_4$ doped sample possesses a higher conductivity than the undoped sample, the undoped sample conductivity is lower than the Ag_2SO_4 value and furthermore the sharper transition of Ag_2SO_4 is evident. The predicted enhanced conductivity of Na^+ incorporated in the Ag_2SO_4 structure did not materialize. A lattice contraction with Na^+ in the Ag_2SO_4 structure, as suggested by X-ray diffraction patterns, would effect a lower mobility of Na^+ and Ag^+ ions. The presence of 4 mol% $CdSO_4$ in the lattice provides vacant sites, on the basis of electroneutrality requirement, and greater freedom for mobility of Na^+ and Ag^+ ions.

The activation energy Q_c for the phase transition of the undoped 40 mol% Ag_2SO_4 of 163 ± 15 kJ/mol and 177 ± 20 kJ/mol for the 4 mol% $CdSO_4$ doped sample indicates a common conductivity mechanism. However, the higher conductivity of the doped sample must originate with the higher number of mobile charge carriers. That is, the kinetic mechanism remains the same but the concentration factor, *n*, is increased by Cd^{2+} presence. The Q_c values for the post transition region of the 4 mol% doped 40 mol% Ag_2SO_4, the 5 mol% doped Na_2SO_4, and pure Na_2SO_4 are 37 ± 5, 45 ± 5, and 50 ± 5 kJ/mol, respectively. The Q_c values suggest the major charge carrier to be Na^+ ion and the number of mobile ions per unit volume to be approximately the same in the first two samples whereas a much lower *n* appears in pure Na_2SO_4.

Acknowledgement

The authors gratefully acknowledge the financial support from the Natural Sciences and Engineering Research Council of Canada.

1. M. S. KUMARI and E. A. SECCO. Can. J. Chem. **61**, 594 (1983).
2. M. S. KUMARI and E. A. SECCO. Can. J. Chem. **61**, 599 (1983).
3. P. VASHISTA, J. N. MUNDY, and G. K. SHENOY. (*Editors*). Fast ion transport in solids. Elsevier North-Holland Inc., New York. 1979.

4. ASTM File Nos. 7-203 and 5-0631.
5. R. NACKEN. Neues Jahrb. Mineral. Geol. **24**, 55 (1907).
6. N. P. BURMISTROVA, E. G. VOLOZHANINA, and L. N. MARKOVA. Zhur. Neorg. Khim. **12**, 784 (1967) (Russ. J. Inorg. Chem. **12**, 411 (1967)).
7. A. HOOPER, P. MCGEEHIN, K. T. HARRISON, and B. C. TOFIELD. J. Solid State Chem. **24**, 265 (1978).
8. K. HAUFFE and D. HOEFFGEN. Zeit. Physik. Chem. Neue Folge **49**, 94 (1966).
9. E. A. SECCO. Can. J. Chem. **42**, 2143 (1964).
10. M. NATARAJAN and E. A. SECCO. Can. J. Chem. **52**, 712 (1974).
11. A. REISMAN. Phase equilibria. Academic Press, New York. 1970 Chapt. 28.
12. R. MACL. MURRAY and E. A. SECCO. Can. J. Chem. **56**, 2616 (1978).
13. J. A. HEDVALL, R. LINDNER, and N. HARTLER. Acta Chem. Scand. **4**, 1099 (1950).
14. C. N. R. RAO and K. J. RAO. Prog. Solid State Chem. **4**, 131 (1967).
15. G. B. GUTHRIE and J. P. MCCULLOUGH. J. Phys. Chem. Solids, **18**, 53 (1961).
16. H. SCHMALZRIED. Z. Phys. Chem. **105**, 47 (1977).

Can. J. Chem. Downloaded from www.nrcresearchpress.com by 210.87.254.105 on 09/06/12
For personal use only.

The crystal and molecular structure of di-μ-phenylthiolatobis[trichloro(dimethyl sulfide) tungsten(IV) (W—W)]

P. MICHAEL BOORMAN,[1] JOANNE M. BALL, KELLY J. MOYNIHAN, VIKRAM D. PATEL, AND JOHN F. RICHARDSON
Department of Chemistry, University of Calgary, Calgary, Alta., Canada T2N 1N4

Received May 30, 1983

P. MICHAEL BOORMAN, JOANNE M. BALL, KELLY J. MOYNIHAN, VIKRAM D. PATEL, and JOHN F. RICHARDSON. Can. J. Chem. **61**, 2809 (1983).

The complex $(Me_2S)Cl_3W(\mu\text{-}SPh)_2WCl_3(SMe_2)$, **1**, has been isolated as one product of the 1:1 reaction between $WCl_4(Me_2S)_2$ and $SiMe_3(SPh)$ in CH_2Cl_2 solution. A single crystal X-ray diffraction study shows that the molecule has the relatively unusual edge-shared bioctahedral structure, with a W—W bond length of 2.759(1) Å. The dimethyl sulfide ligands occupy positions *trans* to one another in the equatorial mean plane of the molecule, which has two-fold symmetry imposed on it. The structure was solved by the heavy atom method and refined to $R = 0.044$ and $R_w = 0.058$ for 2001 reflections. Crystals of **1** are monoclinic, space group $C2/c$, with $a = 17.445(4)$, $b = 12.594(2)$, $c = 11.509(3)$ Å, $\beta = 91.22(1)°$, and $Z = 4$.

P. MICHAEL BOORMAN, JOANNE M. BALL, KELLY J. MOYNIHAN, VIKRAM D. PATEL et JOHN F. RICHARDSON. Can. J. Chem. **61**, 2809 (1983).

On a isolé le complexe $(Me_2S)Cl_3W(\mu\text{-}SPh)_2WCl_3(SMe_2)$, **1**, lors de la réaction 1:1 entre le $WCl_4(Me_2S)_2$ et le $SiMe_3(SPh)$ dans une solution de CH_2Cl_2. Une étude de diffraction sur un monocristal indique que la molécule a une structure inhabituelle bioctaédrique à arête séparée avec une longueur de liaison W—W de 2,759(1) Å. Les ligands sulfure de diméthyle sont en position *trans* l'un par rapport à l'autre dans le plans équatorial moyen de la molécule qui a un axe de symétrie binaire. On a résolu la structure par la méthode de l'atome lourd et on l'a affinée jusqu'à des valeurs de $R = 0{,}044$ et de $R_w = 0{,}058$ pour 2001 réflexions. Les cristaux du composé **1** sont monocliniques et appartiennent au groupe d'espace $C2/c$ avec $a = 17{,}445(4)$, $b = 12{,}594(2)$, $c = 11{,}509(3)$ Å, $\beta = 91{,}22(1)°$ et $Z = 4$.

[Traduit par le journal]

Can. J. Chem. Downloaded from www.nrcresearchpress.com by 210.87.254.5 on 09/06/12
For personal use only.

There is intense current interest in the chemistry of metal thiolates, due largely, no doubt, to the biological importance of such complexes (see for example, ref. 1). Recent studies in our laboratory have shown that the W—SR group in complexes of tungsten(IV) is unstable as a terminal entity (2–5). By metathesis of WCl_4L_2 (L = Me_2S; C_4H_8S) with $SiMe_3(SR)$ (R = alkyl, aryl), the intermediates $WCl_{4-n}(SR)_nL_2$, **2**, have been prepared via the equation:

$$WCl_4L_2 + nSiMe_3(SR) \rightarrow WCl_{4-n}(SR)_nL_2 + nSiMe_3Cl$$

2 can undergo degradation by one of two observed pathways, depending on the stoichiometry (i.e. the value of n) and the nature of R. When $n > 1$, reductive elimination of R_2S_2 is predominant, yielding complexes with lower oxidation state metal centres. On the other hand, monothiolato-complexes of the type $WCl_3(SR)L_2$ are prone to degrade via the elimination of RCl. In both instances we have observed a pronounced tendency for the dimerization of the intermediates to yield confacial bioctahedral complexes such as $LCl_2W(\mu\text{-}S)(\mu\text{-}SR)_2WCl_2L$ (W—W), **3** (3, 5), and $LCl_2W(\mu\text{-}SR)_3WCl_2L$ (W—W), **4** (4). The inherent stability of thiolato-bridged, metal–metal bonded confacial bioctahedral complexes of tungsten(III)/(IV) has been a prominent feature of this synthetic program, along with the apparent instability of complexes of the type $WCl_3(SR)L_2$ or any species containing terminal thiolate groups.

Recently, we have been studying the reaction between $WCl_4(Me_2S)_2$ and $SiMe_3(SPh)$. In the light of earlier work (2) we anticipated that the loss of PhCl would be unlikely and that the reductive elimination of Ph_2S_2 would probably occur. So it transpired (6), since the major product isolated was the mixed oxidation state confacial bioctahedral dimer, $(Me_2S)Cl_2W(\mu\text{-}Cl)(\mu\text{-}SPh)_2WCl_2(SMe_2)$, **5**. Since **4** is also a compound of this type, this seems to be a useful synthetic route to these relatively unusual mixed oxidation state dimers.

We have subsequently isolated and characterized a second species from the 1:1 reaction between $WCl_4(Me_2S)_2$ and $SiMe_3(SPh)$, namely, the title compound, $(Me_2S)Cl_3W(\mu\text{-}SPh)_2WCl_3(SMe_2)$, **1**. This compound contains the hitherto elusive species "$WCl_3(SR)$", but in a dimeric, thiolato-bridged edge-sharing bioctahedron rather than in a monomeric molecule containing a terminal thiolate.

Experimental

Synthesis of **1** was achieved by the reaction of $WCl_4(Me_2S)_2$ with $SiMe_3(SPh)$ as follows. A one molar equivalent of $SiMe_3(SPh)$ in dry CH_2Cl_2 was added to a stirred solution of 2.56 g (56.9 mmol) of $WCl_4(Me_2S)_2$ in ~40 mL of CH_2Cl_2 under an atmosphere of dry nitrogen. The solution color changed from orange–brown to red–brown immediately upon the addition of the $SiMe_3(SPh)$. After stirring for 20 h at room temperature a brown precipitate was filtered off, which we have recently reported as the mixed oxidation state W(III)/W(IV) dimer, $(Me_2S)Cl_2W(\mu\text{-}Cl)(\mu\text{-}SPh)_2WCl_2(SMe_2)$. Concentration of the red–brown filtrate by removal of ~10 mL of solvent *in vacuo* allowed the growth of small red crystals of $(Me_2S)Cl_3W(\mu\text{-}SPh)_2WCl_3(SMe_2)$, **1**. Yield: 13%, based on $WCl_4(Me_2S)_2$. *Anal.* calcd. for $W_2Cl_6(SPh)_2(Me_2S)_2$: C 20.8, H 2.40; found: C 20.9, H 2.38. The starting materials were obtained as previously described (5).

X-ray analysis

A needle-shaped crystal of the title complex, **1**, which had been coated with epoxy resin to minimize aerial decomposition, was mounted on an Enraf Nonius CAD4F automated diffractometer. The unit cell was identified as C-centred monoclinic using the indexing routines of the instrument. Examination of the intensities measured during the data collection confirmed this lattice assignment and systematic absences of (hkl), $h + k = 2n + 1$; $(h0l)$, $l = 2n + 1$ identified the space group as either Cc or $C2/c$. $C2/c$ was the final choice based on the centric distribution of E values and the successful solution of the structure. With four formula units per unit cell, site

[1]To whom all correspondence should be addressed.

Can. J. Chem. Downloaded from www.nrcresearchpress.com by 210.87.254.5 on 09/06/12
For personal use only.

TABLE 1. Crystal data

Formula	$C_{16}H_{22}Cl_6S_4W_2$
fw	923.03
Space group	$C2/c$
Z	4
a (Å)	17.445(4)
b (Å)	12.594(2)
c (Å)	11.509(3)
β (deg)	91.22(1)
V (Å^3)	2527.9(9)
D_c (g cm^{-1})	2.42
μ(Mo-K$_\alpha$) (cm^{-1})	105.1
Crystal dimensions (mm)	0.08 × 0.09 × 0.19
Radiation	Mo-K$_\alpha$ = 0.71069 Å graphite monochromator
Temperature	295(2) K
2θ range for 25 reflections used in least squares cell	25−42°
Scan speed	5° min^{-1}, ranging to 1/2° min^{-1}
Scan width	$\Delta\omega = 1.5(0.6 + 0.347 \tan\theta)°$
Intensity standards	$(\bar{7}1\bar{3}, 71\bar{1}, 1\bar{5}\bar{5})$
Frequency of standard measurement	Every 2000 s of exposure time
Decomposition	± 3%
Data collection range	$2° \leq \theta \leq 27°$
No. unique reflections	2762
No. with $I > 3\sigma(I)$	1269

symmetry 2 is imposed on the molecule. The crystal data and crystallographic experimental conditions are summarized in Table 1.

Data were collected at room temperature using an ω/2θ scan of 96 steps, of which the central 64 steps were taken as the peak, P, and the first and last 16 steps were taken as backgrounds, $B1$ and $B2$, so that $I = [P - 2(B1 + B2)]Q$, where Q was the scan rate. The standard deviation of the intensity was defined as $\sigma(I) = [P + 4(B1 + B2)]^{1/2}Q$. Lorentz and polarization corrections were applied and E values were calculated using a K-curve. After the data collection was complete, the crystal was measured for an absorption correction. Eight faces of the forms {111} and {11−1} were identified. The data were corrected for absorption effects using the Gaussian method[2] with a 16 × 10 × 10 grid. Transmission coefficients were found to vary from 0.213 to 0.439.

The coordinates of the unique W atom were located from a three-dimensional Patterson synthesis. Structure factor and difference Fourier calculations revealed the positions of the remaining unique non-hydrogen atoms. Refinement of atomic parameters was carried out by full-matrix least-squares techniques based on F, minimizing the function $\Sigma w(|F_o| - |F_c|)^2$, where the weight w was defined as $[\sigma^2(F_o) + 0.002(F_o^2)]^{-1}$ in the final cycles. All computations were done using the XRAY 76 system of programs[3] implemented on a Honeywell computer with a Multics operating system. Scattering factors were those of Cromer and Mann (9).

The 11 unique hydrogen atoms were readily located from a difference Fourier map and were included in idealized positions (sp^2 or sp^3 hybridization at C, C—H, 0.95 and 1.00 Å, respectively), but not refined. For the final cycles, positional and anisotropic thermal parameters were refined for all non-hydrogen atoms, an isotropic extinction correction was refined, and the H atom positions were recalculated after each cycle. The model converged for 2001 reflections (observed reflections plus those for which $I_c > 3\sigma(I_o)$) and 128 variables with the agreement factors $R = \Sigma(||F_o| - |F_c||)/\Sigma|F_o| = 0.044$ and $R_w = [\Sigma w(|F_o| - |F_c|)^2/\Sigma w|F_o|^2]^{1/2} = 0.058$. In the final cycle, the maximum shift/error was 0.04, the goodness of fit value was 0.85, and the isotropic extinction parameter was 2.4(9) × 10^{-4}. The highest peak in the final difference Fourier map was approximately 2.5 e Å^{-3}, and this peak was associated with the W atom. Final atomic positional parameters for the non-hydrogen atoms are presented in Table 2. Anisotropic thermal parameters, H atom parameters, and a table of observed and calculated structure amplitudes have been deposited.[4]

TABLE 2. Atomic coordinates (W, S, Cl × 10^4; C × 10^3) and U_{eq} (× 10^3) for the non-hydrogen atoms of $(Me_2S)Cl_3W(\mu\text{-}SPh)_2WCl_3(SMe_2)$; standard deviations are given in parentheses

Atom	x/a	y/b	z/c	U_{eq}*
W	501.2(3)	2257.6(6)	6588.9(5)	27
S(1)	861(2)	2007(3)	8575(3)	32
S(2)	382(2)	2153(4)	4286(4)	41
Cl(1)	575(2)	423(4)	6340(4)	44
Cl(2)	378(2)	4052(4)	6274(4)	42
Cl(3)	1844(2)	2446(4)	6250(4)	47
C(1)	112(1)	134(2)	378(2)	50
C(2)	69(1)	335(2)	368(1)	81
C(11)	140(1)	301(2)	931(2)	46
C(12)	158(1)	281(2)	1043(1)	53
C(13)	201(1)	355(2)	1110(2)	66
C(14)	227(1)	443(2)	1059(2)	72
C(15)	210(1)	463(2)	946(2)	68
C(16)	166(1)	394(2)	877(2)	62

*U_{eq} is $(1/3)\Sigma_i U_{ii}$ of the diagonalized U_{ij} matrix.

Results and discussion

The structure of **1** is shown in Fig. 1, with only the unique atoms labelled and hydrogen atoms omitted for clarity. The packing diagram (Fig. 2) displays the molecule as viewed approximately down the metal−metal vector. It can be seen that

[2]The absorption correction was performed using the program CADABS, a local modification of ref. 7.

[3]Computing was performed at the University of Calgary using the XRAY-76 package of crystallographic programs (8).

[4]Anisotropic thermal parameters, H atom parameters, and observed and calculated structure amplitudes are available at a nominal charge from the Depository of Unpublished Data, CISTI, National Research Council of Canada, Ottawa, Ontario, Canada, K1A 0S2.

TABLE 3. Bond distances (Å) and angles (deg) for $(Me_2S)Cl_3W(\mu\text{-}SPh)_2WCl_3(SMe_2)$

Bond	Distance	Bond	Distance
W—W′	2.759(1)	S(2)—C(2)	1.76(2)
W—S(1)	2.379(4)	S(1)—C(11)	1.77(2)
W—S(1)′	2.401(4)	C(11)—C(12)	1.35(2)
W—S(2)	2.658(4)	C(12)—C(13)	1.41(3)
W—Cl(1)	2.332(5)	C(13)—C(14)	1.34(3)
W—Cl(2)	2.298(5)	C(14)—C(15)	1.35(4)
W—Cl(3)	2.394(4)	C(15)—C(16)	1.40(3)
S(2)—C(1)	1.76(2)	C(16)—C(11)	1.42(3)

Atoms	Angle	Atoms	Angle
S(1)—W—W′	55.13(9)	W′—W—Cl(1)	97.5(1)
S(1)′—W—W′	54.4(1)	W′—W—Cl(2)	93.5(1)
S(1)—W—S(1)′	107.4(1)	W′—W—Cl(3)	139.6(1)
S(1)—W—S(2)	164.9(1)	W′—W—S(2)	136.11(9)
S(1)—W—Cl(1)	88.4(1)	W—S(1)—C(11)	119.5(6)
S(1)—W—Cl(2)	107.7(1)	W′—S(1)—C(11)	116.9(6)
S(1)—W—Cl(3)	86.0(1)	W—S(1)—W′	70.5(1)
S(1)′—W—S(2)	81.9(1)	S(1)—C(11)—C(12)	116(2)
S(1)′—W—Cl(1)	85.3(1)	S(1)—C(11)—C(16)	123(1)
S(1)′—W—Cl(2)	91.6(1)	C(16)—C(11)—C(12)	120(2)
S(1)′—W—Cl(3)	166.0(1)	C(11)—C(12)—C(13)	120(2)
S(2)—W—Cl(1)	80.3(2)	C(12)—C(13)—C(14)	120(2)
S(2)—W—Cl(2)	83.5(2)	C(13)—C(14)—C(15)	120(2)
S(2)—W—Cl(3)	84.2(1)	C(14)—C(15)—C(16)	122(2)
Cl(1)—W—Cl(2)	163.7(2)	C(15)—C(16)—C(11)	116(2)
Cl(1)—W—Cl(3)	91.2(2)	C(1)—S(2)—C(2)	98(1)
Cl(2)—W—Cl(3)	88.0(2)		

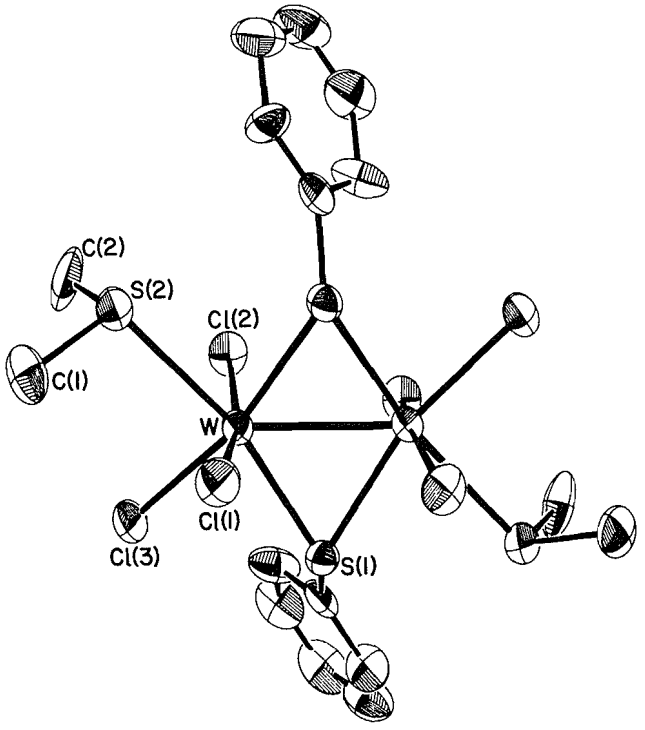

FIG. 1. ORTEP view of the structure of $(Me_2S)Cl_3W(\mu\text{-}SPh)_2WCl_3(SMe_2)$ showing the atomic numbering scheme. Thermal ellipsoids are drawn at the 50% probability level.

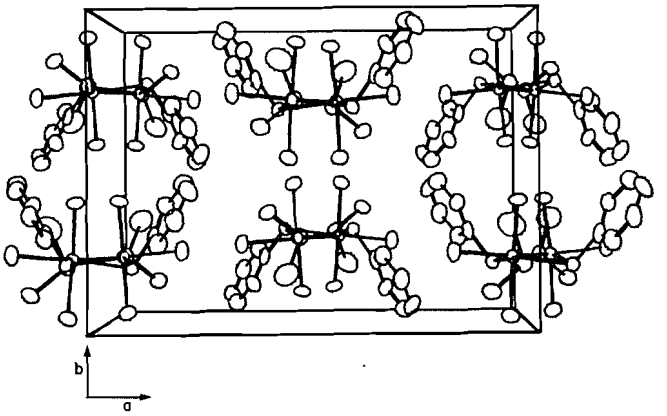

FIG. 2. Crystal packing of the compound $(Me_2S)Cl_3W(\mu\text{-}SPh)_2WCl_3(SMe_2)$.

the molecule possesses an edge-sharing bioctahedral structure, with the phenylthiolato groups occupying the bridging positions. The phenyl groups lie in *syn*–*syn* configurations. A crystallographic two-fold axis perpendicular to the mean $W—S_{br}—W—S_{br}$ plane imposes the observed symmetry on the molecule. Thus the two terminal Me_2S ligands are *trans* to one another, in the equatorial plane.

The structural data for **1** are presented in Table 3. There is strong evidence for the presence of metal–metal bonding in this diamagnetic d^2–d^2 species, in which a formal double bond could occur (**10**). A search for related structures contained in the literature reveals a surprising dearth of edge-sharing bioctahedral molecules of tungsten(IV) which contain formal metal–metal double bonds (10). Furthermore, there seems to be no precedent for such bonds to be longer than ca. 2.55 Å. The alkoxo-bridged ditungsten(IV,IV) complexes $W_2Cl_4(OR)_4(ROH)_2$ (R = Me, Et) possess W—W bond lengths of 2.481–2.483(1) Å (11), for which calculations showed the existence of a σ- and a π-bond. Similarly, in

Can. J. Chem. Downloaded from www.nrcresearchpress.com by 210.87.254.5 on 09/06/12
For personal use only.

comparing the complexes $W_2(\mu\text{-}S)_2(Et_2NCS_2)_2(\mu\text{-}Et_2NCS_2)_2$, (W(IV),W(IV)), and $W_2(\mu\text{-}S)_2(Et_2NCS_2)_2(CH_3O)_4$, (W(V), W(V)), bond lengths of 2.530(2) and 2.791(1) Å were concluded to be consistent with the presence of double and single bonds respectively (12). Only rarely have pairs of related structures such as these been available to justify such conclusions. Thus in the case of **1**, on the basis of bond length alone a single W—W bond might have been diagnosed. However, the nature of the bridging ligands has been shown both theoretically (13, 14) and experimentally (15) to have a profound influence on the metal–metal separation in dinuclear complexes. The terminal ligands can also play a role in this matter (14). Previous work in our laboratory has indicated some similarity in the structures of thiolato-bridged and chloro-bridged confacial bioctahedral structures. We have therefore extended the present comparison to chloro-bridged, edge-sharing bioctahedral structures of ditungsten(III), (IV), and (V), and ditantalum(III) complexes, since the latter are isoelectronic with ditungsten(IV).

The structure of W_2Cl_{10} is a classical case of a molecule in which no metal–metal bond exists, even though the two d^1 centres are potentially capable of forming a single bond (16). The W···W separation, 3.813(1) Å, and the related distortions of the entity **I**,

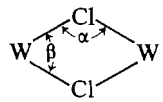

I

all indicate repulsion between the metal atoms. The angles α, 98.5(1)°, have opened up from the 90° required for a pure edge-shared bioctahedron while β undergoes a contraction from 90° to 81.5(1)° (16).

Jackson and Streib (17) described the structure of $W_2Cl_6py_4$, which is shown schematically as **II**:

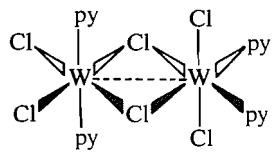

II

This ditungsten(III) complex has been interpreted as containing a single W—W bond, since the 6*d* electrons are believed to adopt a $\sigma^2\pi^2\delta^{*2}$ configuration (10, 13).

The structure **II** appears to be particularly stable for $M_2Cl_6L_4$ complexes. For example, the ditantalum(III) species, $Ta_2Cl_6(R_3P)_4$ (R = Me, Et), have been reported by Sattelberger and co-workers. The formal Ta=Ta double bond in $Ta_2Cl_6(Me_3P)_4$ is 2.721(1) Å in length, and the angles subtended at the μ-Cl atom (equivalent to α in **I**) are very acute (67.4(1)°) (18).

This latter structure is very similar to that of **1** as far as the

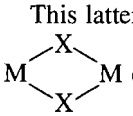

entity is concerned. In **1**, the formal W=W bond length (2.759(1) Å) and the W—(μ-S)—W angles (70.5(1)° ≡ α in **I**) and the (μ-S)—W—(μ-S) angles (107.4(1)° ≡ β in **I**) strongly support the existence of metal–metal bonding, rather than repulsion as in W_2Cl_{10}. Also, as can be seen in Fig. 1, the axial ligands are tipped away from the metal–metal vector. The terminal thioether ligands possess very long W—S bonds while the μ-S atoms to which they are *trans* have relatively short W—S bonds. This, of course, introduces a further distortion from the pure bioctahedral stereochemistry.

Thus the structure of **1** possesses a number of interesting features which will enhance the available data on ditungsten(IV) species.

Acknowledgements

We thank the Natural Sciences and Engineering Research Council of Canada for financial support (to P.M.B., J.M.B., and K.J.M.) and Dr. K. A. Kerr for the use of the diffractometer.

1. R. H. HOLM. Chem. Soc. Rev. **10**, 455 (1981).
2. P. M. BOORMAN and B. D. O'DELL. J. Chem. Soc. Dalton Trans. 257 (1980).
3. P. M. BOORMAN, P. W. CODDING, K. A. KERR, K. J. MOYNIHAN, and V. D. PATEL. Can. J. Chem. **60**, 1333 (1982).
4. P. M. BOORMAN, V. D. PATEL, K. A. KERR, P. W. CODDING, and P. VAN ROEY. Inorg. Chem. **19**, 3508 (1980).
5. P. M. BOORMAN, K. A. KERR, and V. D. PATEL. J. Chem. Soc. Dalton Trans. 506 (1981).
6. J. M. BALL, P. M. BOORMAN, K. J. MOYNIHAN, V. D. PATEL, J. F. RICHARDSON, D. COLLISON, and F. E. MABBS. J. Chem. Soc. Dalton Trans. In press.
7. P. COPPENS *et al.* Crystallographic computing programs. State University of New York at Buffalo; Acta Crystallogr. **18**, 1035 (1965).
8. J. M. STEWART (*Editor*). Technical Report TR-446. Computer Science Centre. University of Maryland. 1976.
9. D. T. CROMER and J. B. MANN. Acta Crystallogr. Sect. A, **24**, 321 (1968).
10. F. A. COTTON and R. A. WALTON. Multiple bonds between metal atoms. John Wiley and Sons Inc., New York. 1982.
11. L. B. ANDERSON, F. A. COTTON, D. DEMARCO, A. FANG, W. H. ILSLEY, B. W. S. KOLTHAMMER, and R. A. WALTON. J. Am. Chem. Soc. **103**, 3078 (1981).
12. A. BINO, F. A. COTTON, Z. DORI, and J. C. SEKUTOWSKI. Inorg. Chem. **17**, 2946 (1978).
13. S. SHAIK, R. HOFFMANN, C. R. FISEL, and R. H. SUMMERVILLE. J. Am. Chem. Soc. **102**, 4555 (1980).
14. R. H. SUMMERVILLE and R. HOFFMANN. J. Am. Chem. Soc. **101**, 3821 (1979).
15. P. M. BOORMAN, K. J. MOYNIHAN, and R. T. OAKLEY. J. Chem. Soc. Chem. Commun. 899 (1982).
16. F. A. COTTON and C. E. RICE. Acta Crystallogr. Sect. B, **34**, 2833 (1978).
17. R. B. JACKSON and W. E. STREIB. Inorg. Chem. **10**, 1760 (1971).
18. A. P. SATTELBERGER, R. B. WILSON, and J. C. HUFFMAN. Inorg. Chem. **21**, 2392 (1982).

Can. J. Chem. Downloaded from www.nrcresearchpress.com by 210.87.254.5 on 09/06/12
For personal use only.

The synthesis of Nauclea indole-pyridine alkaloids. 3,4-Disubstituted and 3,4,5-trisubstituted pyridines as synthetic intermediates; a total synthesis of (±)-decarbomethoxy-3α- and -3β-nauclechine

AZIM SHARIFF[1] AND STEWART MCLEAN

Department of Chemistry, University of Toronto, Toronto, Ont., Canada M5S 1A1

Received April 29, 1983

AZIM SHARIFF and STEWART MCLEAN. Can. J. Chem. **61**, 2813 (1983).

Synthetic routes to a number of 3,4-disubstituted and 3,4,5-trisubstituted pyridines have been explored. These pyridines, designed to be used in the synthesis of Nauclea indole-pyridine alkaloids, are potentially useful intermediates in a number of syntheses. Particular attention has been paid to more highly substituted derivatives of 4-pyridineacetic acid, and the experimental limitations associated with their synthesis and use in subsequent reactions such as the Bischler–Napieralski cyclization have been described and explained. A synthesis of decarbomethoxynauclechine from 4-methylnicotinaldehyde avoiding these difficulties was then designed and executed. Both diastereoisomers, (±)-decarbomethoxy-3α-nauclechine and (±)-decarbomethoxy-3β-nauclechine, were obtained; the structure and stereochemistry of each was rigorously established, but it was not possible to demonstrate which corresponded to the natural alkaloid, decarbomethoxynauclechine, reported previously.

AZIM SHARIFF et STEWART MCLEAN. Can. J. Chem. **61**, 2813 (1983).

On a exploré diverses voies de synthèse de pyridines disubstituées en 3,4 ou trisubstituées en 3,4,5. Ces pyridines, qui pourraient être utilisées dans la synthèse d'alcaloïdes indole-pyridine de la famille Nauclea, sont des intermédiaires qui pourraient s'avérer utiles dans plusieurs synthèses. On a fait particulièrement attention aux dérivés plus substitués de l'acide pyridineacétique-4 et aux limitations expérimentales associées avec leur synthèse; de plus, on décrit et on explique leur utilisation dans des réactions subséquentes comme les cyclisations de Bischler–Napieralski. On a proposé et réalisé une synthèse de la décarbométhoxynaucléchine à partir de la méthyl-4 nicotinaldéhyde qui évite ces difficultés. On a obtenu les deux diastéréoisomères, les (±)-décarbométhoxy-3α (et -3β) nauclechine; on a établi d'une façon rigoureuse la structure et la stéréochimie de chacun des composés mais il n'a pas été possible de démontrer lequel correspond à l'alcaloïde naturel, decarbomethoxynaucléchin, rapportée antérieurement.

[Traduit par le journal]

Can. J. Chem. Downloaded from www.nrcresearchpress.com by 210.87.254.5 on 09/06/12
For personal use only.

As part of our program concerned with the synthesis of Nauclea alkaloids we have turned our attention to those such as nauclechine (**1***a*) (2) and decarbomethoxynauclechine (**1***b*) (3) that can, in a retrosynthetic manner, be readily dissected into a tryptamine unit and a 3,4-disubstituted or 3,4,5-trisubstituted pyridine (**2**), but have not been synthesized previously. The nature of the substituents on the precursor **2** can be specified more precisely: the nature of R obviously depends on whether the target is **1***a* or **1***b*; in principle, X could be any substituent that would allow **2** to be used in a Pictet–Spengler or Bischler–Napieralski reaction with tryptamine, but the nature of X is very much more restricted in practice by the requirement that **2** should not undergo ready decarboxylation or decarbonylation; Y is a hydroxyl group, actual or latent, and Z is a function that can be used in the formation of the C—N bond with the tryptamine unit. Our first task was the synthesis of suitable intermediates corresponding to **2**.

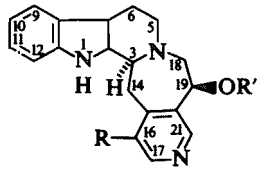

1 *a* R = COOMe; R′ = H
b R = H; R′ = H
c R = H; R′ = Ac

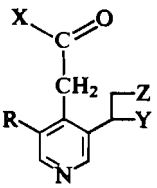

2

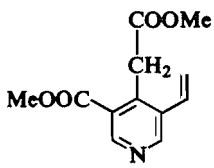

3

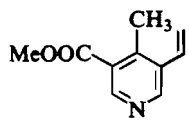

4

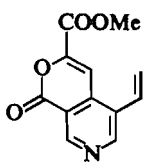

5

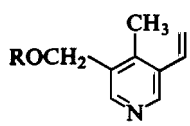

6 *a* R = H
b R = TBDMS

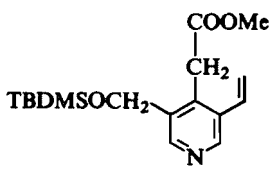

7

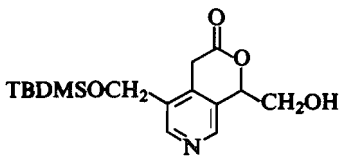

8

3,4,5-Trisubstituted pyridines

Compound **3** was an attractive sub-target for the synthesis of **2** (R = COOMe); a useful synthesis of precursor **4** has been reported (4), there is ample precedent for the carboalkoxylation of a γ-picoline, and the vinyl side chain could be used to incorporate several variations of the functionality (Y, Z) required for **2**. Consequently, **4** was prepared from 2-acetylbutyrolactone and cyanoacetamide in seven steps, and then subjected to reaction conditions normally used for carbomethoxylation. In related studies we have generally found that the most satisfactory procedure for carboalkoxylating a γ-picoline has been that described by Uskoković *et al.* (5), in which the picolyl anion is formed at low temperature (−78°C)

[1]Taken from the Ph.D. thesis of A.S. (University of Toronto, 1982). Part of this work has appeared in preliminary form (1).

Can. J. Chem. Downloaded from www.nrcresearchpress.com by 210.87.254.5 on 09/06/12
For personal use only.

by the action of lithium diisopropylamide (LDA); the dialkyl carbonate is then introduced, and the temperature is kept low until the reaction is complete. However, **4** did not undergo carbomethoxylation by this method, and was recovered unchanged. That the picolyl anion had formed was clear from the deep color of the reaction mixture and from the demonstration that deuterium was incorporated into recovered **4** when the reaction mixture was treated with D_2O. Attempts were made to carry out the carbomethoxylation step at higher temperatures, but even at −15°C there was no significant improvement, and raising the temperature further led to intractable products, probably polymeric. In the best case, a 4% yield of **3** was isolated, and 7% of **4** was recovered. Numerous variations of the carboalkoxylation process were attempted, using other strong bases and other acylating agents (simple esters, oxalates, chloroformates, dimethylformamide, etc.), but only the method described by Wenkert *et al.* (6), using potassium *tert*-butoxide as base and dimethyl oxalate as acylating agent, gave a satisfactory yield of product. The product isolated (in 72% yield) was the lactone **5**, the analog of Wenkert's product; very similar results have been reported by Kametani *et al.* (4). However, the vinyl side chain made **5** unsuitable for conversion to **3** by a continuation of Wenkert's procedure, which required hydrolysis and peroxide-induced decarbonylation of the intermediate.

The reluctance of the picolyl anion derived from **4** to undergo acylation can be attributed to the additional stabilizing effect of the carbomethoxyl group, resulting from charge delocalization and from chelation, especially when the counter ion is lithium. In order to mask the carbomethoxyl group, **4** was reduced to the alcohol **6***a* by lithium aluminum hydride; the reaction was clean and the yield was high (93%). The alcohol was protected as its *tert*-butyldimethylsilyl (TBDMS) ether (**6***b*), which now underwent carbomethoxylation by the Uskoković procedure without difficulty, and the ester **7** was isolated in 68% yield.

In a brief investigation of selective oxidations of the vinyl group of **7**, it was found that, although dihydroxylation could not be effected using catalytic osmium tetraoxide systems, osmylation was successful when stoichiometric amounts of the reagent were used, and the lactonized product **8** was isolated in 47% yield after treatment of the osmylated intermediate with aqueous sodium bisulfite. This product comes close to meeting the requirements specified for the intermediate **2** in the proposed synthesis of **1***a*. However, a considerable amount of exploration of the remaining steps of the proposed route was still needed, and the preparation of the intermediate **8** had already involved a lengthy sequence of reactions. Consequently, we decided to investigate first the remainder of the route with a simpler intermediate, **2** (R = H), the precursor of **1***b*.

3,4-Disubstituted pyridines

Two known 3,4-disubstituted pyridines appeared to be especially promising starting materials, and the conversion of each to useful synthetic intermediates was investigated. The first, 4-methyl-3-vinylpyridine (**9***a*), the analog of **4**, was prepared by established procedures (4, 7) and converted to the ester **9***b* in 57% yield by Uskoković's carbomethoxylation procedure (5). The reaction of **9***b* with tryptamine provided the amide **10***a* in 77% yield. Dihydroxylation of **10***a* produced the glycol **10***b* in 50% yield; as was the case with **7**, the method employing a stoichiometric amount of osmium tetraoxide had to be used for this conversion. This intermediate satisfied the criteria defined for **2** (R = H).

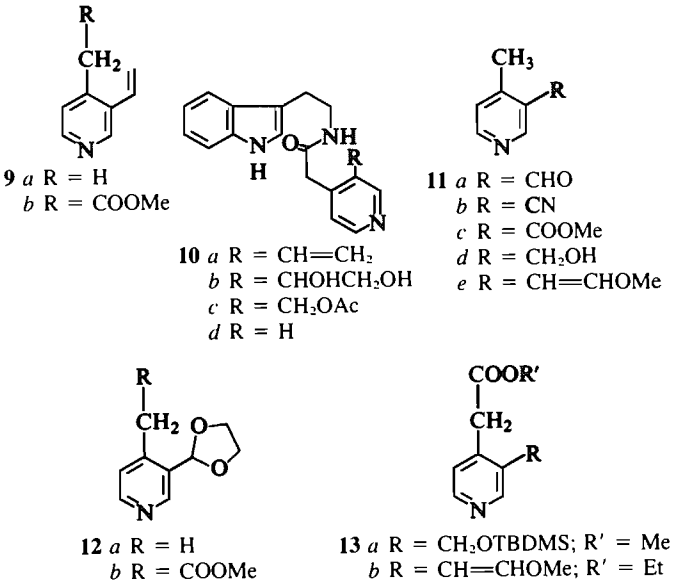

The aldehyde **11***a* is another known 3,4-disubstituted pyridine that is an attractive starting material for the projected synthesis. We prepared **11***a* by the method of Bobbitt and Scola (8) with a few minor modifications: the conversion of the nitrile intermediate **11***b* to the ester **11***c* was carried out in 84% yield by the action of methanolic sulfuric acid (9), and the alcohol **11***d*, obtained on reduction of **11***c*, was cleanly and efficiently oxidized to the aldehyde **11***a* (85% yield) by activated manganese dioxide at room temperature (10). The aldehyde was then protected as its acetal **12***a*, a conversion that Bobbitt and Scola (8) had been unable to take to completion; we found that when **11***a* was treated with ethylene glycol and *p*-toluenesulfonic acid in refluxing benzene for 48 hours, no aldehyde remained, and **12***a* was isolated in 65% yield. Carbomethoxylation of **12***a* by the Uskoković procedure provided **12***b* in a very disappointing yield (19%); the poor yield in this case appears to be caused by degradation of the product during isolation and purification. The attractiveness of this route was further diminished when we discovered that we could not regenerate the aldehyde function from **12***b* by the usual acid-catalyzed hydrolysis, and more vigorous conditions caused the ester to undergo hydrolysis and decarboxylation. The resistance of this acetal to hydrolysis is attributed to the difficulty of cleaving a carbon–oxygen bond after O-protonation since this would lead to the development of positive charge at the picolyl position of a pryidine that is also N-protonated. The difficulty observed in preparing the acetal **12***a* from the aldehyde **11***a* provides support for this explanation.

Under these circumstances we decided to explore an approach which retained the C-3 substituent at the oxidation level of an alcohol, leaving the oxidation and further elaboration of the side chain to a later stage in the synthesis, and carry out the carbomethoxylation on **11***d* after it had been protected as its TBDMS ether. This sequence worked well, and the carbomethoxylation step, using the Uskoković procedure, provided ester **13***a* in 48% yield. Deprotection of the alcohol, either by acid or by tetrabutylammonium fluoride, led to lactonization. Consequently, **13***a* was converted to an amide by reaction with tryptamine in methanol containing sodium methoxide; the silyl

Can. J. Chem. Downloaded from www.nrcresearchpress.com by 210.87.254.5 on 09/06/12
For personal use only.

ether was cleaved in this process, so the crude product was treated with acetic anhydride and isolated as the acetate **10***c* in 73% yield from **13***a*.

The most serious defect in compound **13***a* with respect to the criteria defined for a key intermediate of form **2** (R = H) is that it carries a one-carbon substituent in place of the bifunctional two-carbon substituent required. The aldehyde **11***a* remained the most promising intermediate for development of all of the required functionality. Its homologation through the Wittig product **11***e* appeared to offer a useful route that also had the advantages that carboalkoxylation of **11***e* should take place without difficulty and procedures for converting the methoxyvinyl substituent of **11***e* to the required bifunctional side chain are easily recognized. In practice, the Wittig reaction converted **11***a* to **11***e* (88% yield of a 3:2 mixture of *E* and *Z* isomers) and carboethoxylation converted **11***e* to **13***b* (62% yield) without difficulty. Unfortunately, attempts to oxidize **13***b* with osmium tetraoxide failed to give recognizable products, and simple acidic hydrolysis led to a product that was extremely unstable; the ^{1}Hmr spectrum of freshly isolated product showed signals corresponding to the required aldehyde, but the spectrum rapidly became more complex. It appeared, therefore, that this type of aldehyde is inherently unstable.

We turned, therefore, to a strategy that converted **11***a* to a derivative having, in effect, a masked α-hydroxy aldehyde as the C-3 substituent. The aldehyde **11***a* was converted by treatment with vinylmagnesium bromide to the allyl alcohol **14***a*, which was then protected as its TBDMS ether, **14***b* (54% yield from **11***a*). Carbomethoxylation of **14***b* by the Uskoković procedure provided the ester **15***a* in 64% yield. The vinyl substituent served as a masked aldehyde which could be revealed by ozonolysis; treatment of a solution of **15***a* in a dichloromethane–methanol mixture with ozone at −40°C and then dimethyl sulfuide (11) generated **15***b* which, although unstable, showed the expected signals in the ^{1}Hmr spectrum, of which the doublet, J = 2 Hz, at δ 9.53 was the most significant. This aldehyde was normally not isolated; instead the reaction mixture, after treatment with dimethyl sulfide, was washed with brine and dried with anhydrous sodium sulfate; tryptamine was added to couple with the aldehyde and the product was subsequently reduced with sodium borohydride. By this sequence, **15***a* was converted to the amino ester **16** in 50% yield. Conversion of **16** to the lactam **17** was carried out by heating **16** for 20 hours in refluxing methanol containing anhydrous potassium carbonate; the yield was disappointing (40%), but the alternative methods tried either failed to cause lactamization or else led to a considerable amount of degradation.

Decarbomethoxynauclechine

Among the intermediates we have described are tryptamides (**10***a*–*c*) that appeared to provide access through a Bischler–Napieralski cyclization to the corresponding dihydro-β-carbolines. We have previously used this process to cyclize tryptamides derived from pyridinecarboxylic acids (12) and a 3-pyridineacetic acid (13), but we found, in accord with earlier reports, that yields are variable and it is critically important to find the optimal reaction conditions in order to obtain acceptable yields. However, with tryptamides of general formula **10** no such conditions could be found; the simplest member of the series, **10***d*, was prepared for model studies, but no reaction conditions were found that gave more than an unacceptably low yield of a dihydro-β-carboline. We are led,

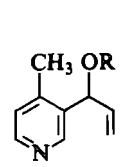

14 *a* R = H
b R = TBDMS

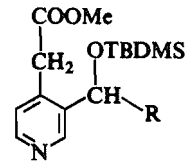

15 *a* R = CH=CH$_2$
b R = CHO

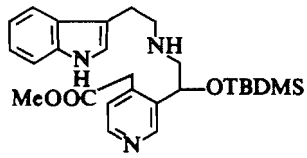

16

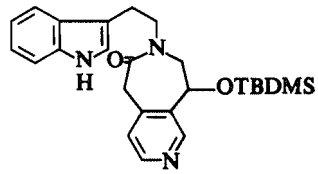

17

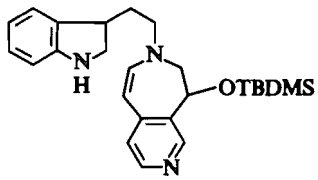

18

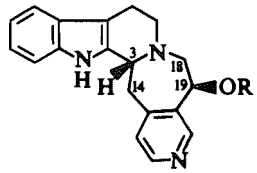

19 *a* R = TBDMS
b R = H
c R = Ac

consequently, to the conclusion that tryptamides **10** are inherently unsuitable for Bischler–Napieralski cyclization, and we feel that an explanation can be found by recognizing that a 4-picolyl unit, especially when N-protonated, can act as a good leaving group (as in the facile decarboxylation of 4-pyridineacetic acid). The detailed mechanism of the Bischler–Napieralski reaction continues to be a subject of discussion (14), but it is clear that at an early stage the tryptamide is converted into an intermediate that normally undergoes an elimination to form an iminium species, and we suggest that it is at this stage that the intermediate derived from **10** can eliminate a 4-picolyl unit, leading to a destructive fragmentation in competition with the desired reaction. In the case of the 3-pyridineacetic acid derivative previously cited (13), we obtained the dihydro-β-carboline in 38% yield, and we note the analogy that 3-pyridineacetic acid undergoes decarboxylation much less readily than 4-pyridineacetic acid.

Under these circumstances it was deemed unwise to subject our most advanced intermediate, the tryptamide **17**, to Bischler–Napieralski conditions. However, as a tertiary amide, **17** appears ideally suited to the procedure described by Takano *et al.* (15) which transforms the cyclization into a Pictet–Spengler process. We reduced **17** by the action of excess diisobutylaluminum hydride at −78°C; the best results were obtained with four equivalents of the hydride, but even then nearly half of the starting material (**17**) was recovered and could be recycled. It appears that, in a competitive reaction, a proton is removed from the unusually acidic 4-picolyl site, preventing reduction but allowing **17** to be recovered on work-up. The reduction product, obtained in 84% yield based on unrecovered **17**, was shown to be the enamine **18**; the material could not be completely characterized because of its instability, but it provided a ^{1}Hmr spectrum completely in accord with the assigned structure, the one-proton doublets, J = 10 Hz, at δ 6.23 and 4.88 assigned to vinyl protons being of special significance since they show that the reduction product in this case is

TABLE 1. Nuclear magnetic resonance data for the acetates of synthetic decarbomethoxy-3α- and -3β-nauclechine[a]

3α Isomer **1c**			3β Isomer **19c**	
Chemical shift (δ)	Multiplicity; coupling constants (Hz)	Proton[b]	Multiplicity; coupling constants (Hz)	Chemical shift (δ)
8.50 8.50	s d, $J_{16,17} = 5$	21 17	Unresolved	8.50
8.16	s	1	s	7.93
7.51	d, $J_{9,10} = 8$	9	d, $J_{9,10} = 8$	7.50
7.34	d, $J_{11,12} = 8$	12	d, $J_{11,12} = 8$	7.35
7.22–7.08	Unresolved (3H)	10, 11 and 16	Unresolved (3H)	7.20–7.05
5.91	dd $J_{18a,19} = 6$, $J_{18b,19} = 2$	19	dd $J_{18b,19} = 9$, $J_{18a,19} = 1.5$	6.34
4.04	d, $J_{3,14a} = 10$	3	d, $J_{3,14a} = 10$	3.93
3.73	dd $J_{14a,14b} = 15$, $J_{3,14a} = 10$	14a	dd $J_{14a,14b} = 15$, $J_{3,14a} = 10$	3.48
3.55	dd $J_{18a,18b} = 14$, $J_{18a,19} = 6$	18a	dd $J_{18a,18b} = 13$, $J_{18a,19} = 1.5$	3.33
3.38	m	5 or 6	m	3.38
3.17	dd $J_{18a,18b} = 14$, $J_{18b,19} = 2$	18b	dd $J_{18a,18b} = 13$, $J_{18b,19} = 9$	3.12
2.98	d, $J_{14a,14b} = 15$	14b	d, $J_{14a,14b} = 15$	3.02
2.98 2.90 2.73	m m m	5 and 6	m m m	3.02 2.93 2.78
2.06	s (3H)	OAc	s (3H)	2.26

[a] Spectra at 400 MHz. Solutions in $CDCl_3$.

[b] Numbering system shown in structural formula **1**; descriptors a and b are used arbitrarily to distinguish between two hydrogens on the same carbon atom.

an enamine rather than a hemiaminal (15). Since we had previously found 90% formic acid to be a particularly effective reagent in a Pictet–Spengler cyclization (16), a solution of **18** in 90% formic acid was stirred overnight at room temperature. A mixture of two main components was obtained, and the major product, shown subsequently to be **19***a*, was isolated in 63% yield by chromatography; the second component could not be obtained free from a contaminant by this procedure, but its spectroscopic characteristics indicated it to be a diastereoisomer of **19***a*. The TBDMS group of **19***a* proved to be unusually resistant to acidic hydrolysis and the best experimental procedure for isolating the deprotected materials was to treat the mixture of cyclized products obtained from the Pictet–Spengler reaction with tetrabutylammonium fluoride in tetrahydrofuran at room temperature. Chromatography then provided both diastereoisomers, **19***b* and **1***b*, in pure form in a ratio of about 3:1 (yield > 95%). When the Pictet–Spengler cyclization was carried out by treating **18** with methanolic hydrogen chloride at room temperature overnight, a mixture of cyclized products was again obtained; in this case most of the product had been desilylated, but some retained the TBDMS substituent. On work-up, both **19***b* and **1***b* were obtained (65% yield), but in this case, **1***b* was the dominant isomer by a factor of 5:1. Both isomers were obtained crystalline, both darkened on standing in air, and neither was appreciably soluble in chloroform; each formed a chloroform-soluble acetate, but neither acetate was obtained crystalline.

The diastereoisomers **1***b* and **19***b* showed, predictably, very similar spectroscopic characteristics, as did their acetates **1***c* and **19***c*. Only the 400 MHz ^{1}Hmr spectra of **1***c* and **19***c* showed significant differences (see Table 1), and these were essentially confined to the characteristics associated with protons on the seven-membered ring; even here the chemical shifts of the protons at C-3 and C-14 showed only small differences between the two compounds and the coupling constants $J_{3,14a} = 10$, $J_{3,14b} = 0$, $J_{14a,14b} = 15$ Hz were the same in both compounds, indicating that the conformational relationships on this side of the ring are the same in both isomers. Only the protons on the other side of the ring led to distinctive differences in the spectra; in **1***c*, the chemical shifts of the protons designated H-19, H-18a, and H-18b were δ 5.91, 3.55, and 3.17 respectively, and the coupling constants were $J_{18a,19} = 6$, $J_{18b,19} = 2$, and $J_{18a,18b} = 14$ Hz, while the corresponding values for the protons of **19***c* were δ 6.34, 3.33, and 3.12 and 1.5, 9, and 13 Hz. These differences are clearly of stereochemical origin, but we could not use them with confidence to make configurational assignments to the flexible seven-membered rings incorporating a pyramidal nitrogen atom and two sp^2 carbon atoms. Consequently, the structure and stereochemistry of the synthetic alcohols **1***b* and **19***b* were determined to be as shown

Can. J. Chem. Downloaded from www.nrcresearchpress.com by 210.87.254.5 on 09/06/12
For personal use only.

Can. J. Chem. Downloaded from www.nrcresearchpress.com by 210.87.254.5 on 09/06/12
For personal use only.

by single-crystal X-ray crystal structure analysis;[2] the configurational assignments for all of the cyclized products obtained from **18** were made on the basis of their chemical relationship to **1***b* and **19***b*.

The synthesis has thus provided both diastereoisomers, **1***b* and **19***b*. Why the Pictet–Spengler cyclization of **18** by the action of methanolic hydrogen chloride gave **1***b* as the dominant isomer while formic acid led to the other isomer remains an intriguing question. It is tempting to suggest that it is the nature of the substituent at C-19 that governs the stereochemistry of the process: in formic acid the silyl ether survives the reaction and the substituent is undoubtedly OTBDMS while the C-3 stereochemistry is being established, while it is possible that the substituent has already become OH by this stage in methanolic hydrogen chloride. However, the chronology of the latter process is by no means certain, and further study is required to establish it; we note that some silyl ether survives the conditions used, and the silyl ether in **19***a* is unusually difficult to hydrolyze in acid, but we have no direct information concerning its ease of hydrolysis in the precursor **18**.

Even with both **1***b* and **19***b* in hand in racemic form we were unable to complete the task of establishing which corresponded to the *Nauclea latifolia* alkaloid described by Pousset and coworkers (3). Only a very small quantity (1 mg) of the natural alkaloid was isolated, and very few physical data were determined. Crystals, mp 222°C, were obtained from ethyl acetate; the alkaloid can be expected to be optically active, but this was not established. When recrystallized from ethyl acetate, synthetic **1***b* formed crystals, mp 218–221°C (prior phase change at 213°C), and **19***b* formed crystals mp 219–220°C (dec.). Only the mass spectrum of the natural alkaloid was available for spectroscopic comparison. The mass spectra of **1***b* and **19***b*, obtained on our spectrometer, were virtually identical; the mass spectrum of the natural material, obtained previously on a different spectrometer and kindly provided by Professor Pousset, resembled our spectra, the main points of difference being in the relative intensities of the strongest peaks. Consequently, it is not possible to identify either of the synthetic products as the racemic form of a natural alkaloid. In order to avoid possible confusion in the future, and because of the obvious analogy with the dihydrocadambines (13, 16, 17), we shall refer to **1***b* as decarbomethoxy-3α-nauclechine and to **19***b* as decarbomethoxy-3β-nauclechine, anticipating that both may eventually be isolated from natural sources.

Experimental

Melting points were determined on a calibrated Thomas–Kofler micro hot stage. Infrared spectra were measured on a Perkin–Elmer 137 spectrometer; the wavelengths (μ) of selected absorptions of solutions in chloroform are reported. Unless otherwise indicated, ^{1}Hmr spectra of solutions in $CDCl_3$ were recorded at 60 MHz on a Varian T-60 spectrometer, and chemical shifts (δ scale) are reported followed in parentheses with a description of the multiplicity (initial letter), coupling constants, if measurable, and number of protons associated with the signal; a Bruker WH-400 spectrometer was used for spectra at 400 MHz. Mass spectra were measured at 70 eV on a Bell and Howell CEC 21-490 mass spectrometer, and *m/z* values for significant ions are reported followed in parentheses by the relative peak height; exact mass measurements were made on an AEI MS 902 mass spectrometer.

[2] The X-ray analyses were carried out by Dr. Jeffery F. Sawyer of this Department, whom we thank. A detailed account of this work will be published.

*3-Hydroxymethyl-4-methyl-5-vinylpyridine (**6**a) and its derivatives*

A solution of 3-carbomethoxy-4-methyl-5-vinylpyridine (4) (9.30 g; 52.5 mmol) in 250 mL of dry ether was added over 50 min to a stirred suspension of lithium aluminum hydride (2.40 g; 63.2 mmol) in 100 mL of ether under nitrogen, and stirring was continued for a further 30 min. After the reaction mixture had been treated with sodium sulfate decahydrate and worked up, the alcohol **6***a* was isolated as an oil (7.30 g; 50.0 mmol); recrystallization from ether provided white crystals, mp 50–51°C; ir: 2.78, 6.20, 6.30; ^{1}Hmr: 8.33 (s, 1), 8.20 (s, 1), 6.81 (dd, *J* = 11, 17; 1), 5.56 (dd, *J* = 2, 17; 1), 5.36 (dd, *J* = 2, 11; 1), 4.92 (s, 1, D_2O removed), 4.67 (s, 2), 2.33 (s, 3); ms: 149 (100), 131 (53), 130 (49), 120 (57). *Anal.* calcd. for $C_9H_{11}NO$: C 72.45, H 7.43, N 9.39; found: C 72.13, H 7.48, N 9.40.

The tert*-butyldimethylsilyl ether **6***b* was prepared by treating a solution of **6***a* (6.74 g; 45.2 mmol) in 35 mL of dry dimethylformamide under nitrogen with imidazole (8.1 g; 120 mmol) and *tert*-butyldimethylsilyl chloride (8.9 g; 60 mmol). The reaction mixture was stirred for 18 h at room temperature, the solvent was removed under reduced pressure, and the residue was treated with 100 mL of water and extracted with chloroform. The extract afforded a dark oil that was distilled under vacuum, and **6***b* was obtained as a clear liquid (8.88 g; 33.8 mmol), bp 84–86°C (0.01 Torr); ir: 6.10, 6.30; ^{1}Hmr: 8.48 (s, 1), 8.38 (s, 1), 6.87 (dd, *J* = 11, 17; 1), 5.61 (dd, *J* = 2, 17; 1), 5.36 (dd, *J* = 2, 11;1), 4.71 (s, 2), 2.28 (s, 3), 0.98 (s, 9), 0.10 (s, 6); ms: 264 (3), 206 (100), 176 (26), 132 (35). *Anal.* calcd. for $C_{15}H_{25}NOSi$: C 68.39, H 9.56, N 5.32; found: C 68.71, H 9.52, N 5.73.

Carbomethoxylation product 7

A solution of **6***b* (8.0 g; 30.4 mmol) in 80 mL of dry tetrahydrofuran was added dropwise over 20 min to a stirred solution in 80 mL of tetrahydrofuran, under nitrogen and cooled in an acetone – Dry Ice bath, of lithium diisopropylamide prepared from butyllithium (90 mmol in hexane) and diisopropylamine (110 mmol). The red solution was stirred for 15 min further, and dimethyl carbonate (110 mmol) in 30 mL of tetrahydrofuran was added over 10 min. The solution was stirred at −78°C for 30 min, and then the cooling bath was removed. When the reaction mixture had reached room temperature, it was treated with 50 mL of saturated aqueous sodium bicarbonate; the aqueous layer was separated and extracted with dichloromethane, and the extract was combined with the organic layer. The organic solvents were removed by evaporation and the dark oil that remained was chromatographed (silica gel; 2:8 ethyl acetate – hexane); a small amount of **6***b* (0.67 g; 2.5 mmol) was recovered unchanged, and **7** (6.11 g; 19.0 mmol) was isolated as an oil, bp 90–95°C (0.005 Torr); ir: 5.77, 6.14, 6.31; ^{1}Hmr: 8.55 (s, 1), 8.41 (s, 1), 6.85 (dd, *J* = 11, 17; 1), 5.62 (dd, *J* = 2, 17;1), 5.41 (dd, *J* = 2, 11; 1), 4.73 (s, 2), 3.83 (s, 2), 3.67 (s, 3), 0.93 (s, 9), 0.10 (s, 6); ms: 265 (57), 264 (100), 232 (21), 131 (45), 130 (77), 103 (35). *Anal.* calcd. for $C_{17}H_{27}NO_3Si$: C 63.51, H 8.47, N 4.36; found: C 63.17, H 8.52, N 4.44.

Dihydroxylation product 8

A solution of **7** (1.26 g; 3.9 mmol) and osmium tetraoxide (1.0 g; 3.9 mmol) in 15 mL of distilled pyridine was stirred at room temperature for 3 h. A solution of sodium bisulfite (1.8 g) in 30 mL of water and 20 mL of pyridine was added and stirring was continued overnight. Extraction with dichloromethane provided the product which was purified by chromatography (silica gel; 9:1 ethyl acetate – hexane) and isolated as a white amorphous solid (0.61 g; 1.9 mmol); ir: 2.77, 5.73, 6.29; ^{1}Hmr: 8.55 (s, 1), 8.38 (s, 1), 5.50 (m, 1), 4.72 (s, 2), 4.10 (m, 2), 3.81 (s, 2), 2.93 (broad, 1, D_2O removed), 0.93 (s, 9), 0.10 (s, 6); ms: 266 (64), 146 (80), 108 (57), 75 (100), 73 (33). *Exact Mass* calcd. for $C_{12}H_{16}NO_4Si$ (M − *t*-Bu): 266.0848; found: 266.0852.

*4-Methoxycarbonylmethyl-3-vinylpyridine (**9**b) and its derivatives*

4-Methyl-3-vinylpyridine (**9***a*) was prepared by the method of Stevens *et al.* (7), except that Kametani's procedure (4) was used in the final step to effect quantitative dehydrochlorination. A solution of **9***a* (5.80 g; 48.7 mmol) was carbomethoxylated by the Uskoković pro-

Can. J. Chem. Downloaded from www.nrcresearchpress.com by 210.87.254.5 on 09/06/12
For personal use only.

cedure (5) described above for **7**. When the reaction mixture had reached room temperature, 80 mL of benzene and 80 mL of saturated aqueous sodium sulfate were added and, after a short period, excess anhydrous sodium sulfate was added. After filtration, the solvent was removed by distillation, the residue was dissolved in benzene, and the solution was extracted with 5% hydrochloric acid. The acidic solution was made basic with aqueous ammonia and extracted with dichloromethane. This extract afforded the product, which was purified by Kugelrohr distillation at 70°C (0.01 Torr), and **9***b* (4.90 g; 27.6 mmol) was isolated as a clear oil; ir: 5.75, 6.13, 6.27; ^{1}Hmr: 8.60 (s, 1), 8.38 (d, J = 5; 1), 7.09 (d, J = 5; 1), 6.83 (dd, J = 11, 17; 1), 5.66 (dd, J = 2, 17; 1), 5.40 (dd, J = 2, 11; 1), 3.71 (s, 5); ms: 177 (85), 162 (22), 120 (23), 119 (37), 118 (89), 117 (100), 91 (43), 85 (42), 83 (69), 65 (24), 59 (29), 51 (21) *Exact Mass* calcd. for $C_{10}H_{11}NO_2$: 177.0790; found: 177.0794; also characterized as its dihydro derivative (catalytic hydrogenation) described previously by Uskoković (5): ir and ^{1}Hmr data identical, hydrochloride mp 163–164°C (lit. (5) mp 167–168°C).

The tryptamide **10***a* was prepared by refluxing a solution of **9***b* (5.00 g; 28.2 mmol), tryptamine (4.55 g; 28.4 mmol), and sodium methoxide (30 mmol) in 100 mL of dry methanol under argon for 17 h. The solution was cooled, 100 mL of water and 100 mL of brine were added sequentially, and the mixture was extracted with dichloromethane. The material (7.85 g) obtained from the extract was purified by flash chromatography (18) (93:7 chloroform–methanol) to provide **10***a* (6.59 g; 21.61 mmol) as an amorphous solid; ir: 2.91, 5.98, 6.28; ^{1}Hmr: 8.53 (s, 1), 8.5 (broad, 1, D_2O removed), 8.28 (d, J = 5; 1), 7.55–6.67 (complex, 7), 5.6 (broad, 1, D_2O removed), 5.52 (dd, J = 2, 17; 1), 5.29 (dd, J = 2, 11; 1), 3.52 (s, 2), 3.52 (m, 2), 2.88 (m, 2); ms: 305 (10), 143 (100), 130 (53). *Exact Mass* calcd. for $C_{19}H_{19}N_3O$: 305.1528; found 305.1518.

Dihydroxylation product **10***b* was prepared by treatment of **10***a* (487 mg; 1.60 mmol) with osmium tetraoxide (411 mg; 1.62 mmol) in 6 mL of pyridine in the manner described for **8** above. The product (385 mg) was purified by flash chromatography (18) (8:2 dichloromethane–methanol) and **10***b* (272 mg; 0.80 mmol) was isolated as a white amorphous solid, insoluble in chloroform. This material was treated with acetic anhydride in pyridine to obtain its diacetate as an amorphous solid; ir: 2.84, 5.73, 5.96, 6.24; ^{1}Hmr: 8.55 (s, 1), 8.39 (d, J = 5, 1), 8.1 (broad, 1, D_2O removed), 7.57–6.80 (complex, 6), 6.12 (m, J = 6; 1) 6.1 (broad, 1, D_2O removed), 4.15 (d, J = 5; 2), 3.60 (s, 2), 3.55 (m, 2), 2.95 (m, 2), 2.03 (s, 3), 2.00 (s, 3); ms: 423 (5), 281 (15), 144 (18), 143 (100), 130 (44). *Exact Mass* calcd. for $C_{23}H_{25}N_3O_5$; 423.1794; found: 423.1796.

*4-Methylnicotinaldehyde (**11**a) and its derivatives*

The preparation of **11***a* followed the procedures described by Bobbitt and Scola (8) with the following modifications. The nitrile **11***b* was heated to 130°C with 75% sulfuric acid (20 mL/g of **11***b*) under nitrogen for 20 h; the mixture was allowed to cool, methanol (40 mL) was added, and the solution was heated to reflux for 4 h. The ester **11***c* (84%) was isolated by standard procedures (9). Reduction of **11***c* by lithium aluminum hydride (8) provided the alcohol **11***d* nearly quantitatively. The alcohol was stirred with freshly activated manganese dioxide (10) (6.7 g/g of **11***d*) in dichloromethane (100 mL) under argon for 24 h. After filtration, evaporation of the solvent, and distillation under reduced pressure, **11***a* (8) was isolated as a clear liquid (85% yield). The acetal (**12***a*) was prepared in 65% yield by the method described previously (8), except that reflux in benzene was continued for 48 h.

*3-(β-Methoxyvinyl)-4-methylpyridine (**11**e)*

A solution of **11***a* (300 mg; 3.3 mmol) in 4 mL of dry dimethyl sulfoxide was added over 2 min to the Wittig reagent prepared (19) from (methoxymethyl)triphenylphosphonium chloride (2.82 g; 8.2 mmol) in 10 mL of dimethyl sulfoxide and sodium hydride (8.4 mmol) in 4 mL of dimethyl sulfoxide under nitrogen. The reaction mixture was stirred at room temperature for 14 h, treated with excess saturated aqueous sodium bicarbonate, and extracted with ether. The extract afforded a solid which was subjected to Kugelrohr distillation at 95°C (0.005 Torr) and **11***e* (433 mg; 2.91 mmol) was obtained as an oily mixture of stereoisomers; ir: 6.1, 6.27; ^{1}Hmr (combined areas for E and Z isomers shown as 1H, etc.): 8.97 (s) and 8.40 (s) (1H), 8.23 (d, J = 5) and 8.19 (d, J = 5) (1H), 7.00 (d, J = 5; 1H), 6.85 (d, J = 13) and 6.22 (d, J = 7) (1H), 5.75 (d, J = 13) and 5.22 (d, J = 7) (1H), 3.75 (s) and 3.72 (s) (3H), 2.27 (s, 3H); ms: 149 (100), 134 (40), 117 (22), 106 (33), 77 (20). *Exact Mass* calcd. for $C_9H_{11}NO$: 149.0841; found 149.0824.

*Carbomethoxylation product **12**b*

The procedure described above for the carbomethoxylation of **9***a* was employed, using acetal **12***a* (1.0 g; 6.2 mmol) in 5 mL of tetrahydrofuran, lithium diisopropylamide (13 mmol) in 10 mL of tetrahydrofuran, and dimethyl carbonate (15 mmol) in 5 mL of tetrahydrofuran, with the modification that stirring at −78°C was continued for 2 h. The oily product (930 mg) was purified by bulb-to-bulb distillation at 130°C (0.05 Torr), and **12***b* (266 mg; 1.2 mmol) was isolated as a yellow oil; ir: 5.76, 6.25; ^{1}Hmr: 8.70 (s, 1), 8.57 (d, J = 5; 1), 7.20 (d, J = 5; 1), 5.93 (s, 1), 4.08 (broad, 4), 3.82 (s, 2), 3.70 (s, 3); ms: 223 (1), 222 (5), 150 (100), 120 (22), 92 (20), 73 (49). *Exact Mass* calcd. for $C_{11}H_{13}NO_4$: 223.0845; found: 223.0855.

*Carbomethoxylation product **13**a*

The alcohol **11***d* (6.10 g; 49.2 mmol) in 30 mL of dry dimethylformamide at 35°C under nitrogen was treated with imidazole (8.8 g; 130 mmol) and *tert*-butyldimethylsilyl chloride (9.4 g; 62 mmol) and the mixture was stirred for 1.5 h. Volatile materials were removed under vacuum at room temperature, the oily residue was treated with 200 mL of water and thoroughly extracted with ether. The extract afforded the TBDMS ether of **11***d* which was distilled and obtained as a colorless oil (10.5 g; 44.2 mmol), bp 84–85°C (0.05 Torr); ir: 6.23; ^{1}Hmr: 8.47 (s, 1), 8.33 (d, J = 5; 1), 6.99 (d, J = 5; 1), 4.70 (s, 2), 2.28 (s, 3), 0.93 (s, 9), 0.10 (s, 6); ms: 180 (100), 150 (26), 106 (52), 75 (22). *Anal.* calcd. for $C_{13}H_{23}NOSi$: C 65.77, H 9.76, N 5.90; found: C 65.71, H 9.66, N 5.64.

The TBDMS ether (8.0 g; 33.8 mmol) in 80 mL of dry tetrahydrofuran was added to lithium diisopropylamide (72 mmol) and treated with dimethyl carbonate (95 mmol) in the manner described above for **7**; in the work-up, 100 mL of saturated aqueous ammonium chloride was used (in place of sodium bicarbonate). The oily product was chromatographed (silica gel; 4:5 ethyl acetate – hexane) to provide **13***a* (4.80 g; 16.3 mmol), bp 95°C (0.005 Torr); ir: 5.76, 6.25; ^{1}Hmr: 8.52 (s, 1), 8.41 (d, J = 5; 1), 7.11 (d, J = 5; 1), 4.73 (s, 2), 3.72 (s, 2), 3.67 (s, 3), 0.92 (s, 9), 0.08 (s, 6); ms: 239 (100), 207 (20), 132 (75), 104 (45), 89 (44). *Anal.* calcd. for $C_{15}H_{25}NO_3Si$: C 60.97, H 8.52, N 4.74; found: C 61.18, H 8.93, N 4.89.

*The carboethoxylation product **13**b*

The mixture of stereoisomers **11***e* (355 mg; 2.38 mmol) was treated with lithium diisopropylamide (5.6 mmol) and diethyl carbonate (5.9 mmol) by the procedure described above for **7**. The crude product was dissolved in benzene and extracted with cold 10% hydrochloric acid; the acidic extract was made basic with ammonia and extracted with dichloromethane. This extract afforded **13***b* which was obtained as an oily mixture of stereoisomers (329 mg; 1.49 mmol) after Kugelrohr distillation at 110°C (0.025 Torr); ir: 5.77, 6.10, 6.29; ^{1}Hmr (combined areas for E and Z isomers shown as 1H, etc.): 8.97 (s) and 8.48 (s) (1H), 8.34 (d, J = 5) and 8.29 (d, J = 5) (1H), 7.09 (d, J = 5; 1H), 6.88 (d, J = 13) and 6.24 (d, J = 7) (1H), 5.80 (d, J = 13) and 5.24 (d, J = 7) (1H), 4.16 (q, J = 7; 2H), 3.76 (s) and 3.73 (s) (3H), 3.47 (s, 2H), 1.23 (t, J = 7, 3H); ms: 221 (100), 176 (22), 148 (26), 133 (53), 132 (22), 118 (27), 117 (63), 105 (24), 104 (20). *Exact Mass* calcd. for $C_{12}H_{15}NO_3$: 221.1052; found: 221.1050.

The tryptamide **10***c* was prepared by refluxing a solution of the ester **13***a* (3.50 g; 11.8 mmol), tryptamine (2.0 g; 12.5 mmol), and sodium methoxide (12.4 mmol) in 50 mL of dry methanol under nitrogen for 13 h. The methanol was removed under reduced pressure, and the residual oil was treated with brine and extracted with chloroform. The extract afforded a product (3.27 g) that was acetylated with acetic anhydride in pyridine. The crude product was purified by chromatography (silica gel; 9:1 chloroform–methanol) and **10***c* (3.04 g;

Can. J. Chem. Downloaded from www.nrcresearchpress.com by 210.87.254.5 on 09/06/12
For personal use only.

8.7 mmol) was isolated as a pale yellow amorphous solid; ir: 5.74, 5.99, 6.24; ^{1}Hmr: 8.88 (broad, 1, D_2O removed), 8.42 (broad, 2), 7.56–6.73 (complex, 6), 6.13 (m, 1, D_2O removed), 5.03 (s, 2), 3.55 (m, 2), 3.50 (s, 2), 2.90 (m, 2), 1.93 (s, 3); ms: 351 (7), 143 (100), 130 (98). *Exact Mass* calcd. for $C_{20}H_{21}N_3O_3$: 351.1583; found: 351.1584.

*3-(3-Hydroxy-3-propenyl)-4-methylpyridine (**14**a) and its derivatives*

A solution of the aldehyde **11***a* (1.22 g; 10.0 mmol) in 5 mL of dry tetrahydrofuran was added over 20 min to a solution of vinylmagnesium bromide (12 mmol) in 6 mL of tetrahydrofuran (20), and the mixture was refluxed for 30 min. The mixture was cooled, treated with 2 mL of saturated aqueous ammonium chloride, and worked up by standard procedures. The product was isolated as a viscous oil (1.10 g; 7.4 mmol); a sample of **14***a* was purified by molecular distillation at 80°C (0.005 Torr) and isolated as a clear colorless oil; ir: 2.85, 6.10, 6.23; ^{1}Hmr: 8.47 (s, 1), 8.22 (d, J = 5; 1), 7.00 (d, J = 5; 1), 6.0 (m, 1), 5.4–5.1 (complex, 3), 4.35 (broad, 1, D_2O removed), 2.33 (s, 3); ms: 149 (28), 148 (37), 132 (21), 131 (70), 130 (28), 122 (40), 120 (100), 106 (20), 94 (51), 93 (40), 92 (60), 65 (30). *Exact Mass* calcd. for $C_9H_{11}NO$: 149.0841; found: 149.0853.

Undistilled **14***a* (2.95 g; 19.8 mmol) in 12 mL of dry dimethylformamide under argon was treated with imidazole (3.24 g; 47.6 mmol) and *tert*-butyldimethylsilyl chloride (3.58 g; 23.8 mmol), and the mixture was stirred for 15 h at room temperature. Volatile materials were removed under vacuum at room temperature, the residue was treated with 100 mL of water, and extracted with ether. The extract afforded **14***b* as an oil (4.64 g), which was purified by Kugelrohr distillation at 100°C (0.005 Torr) and obtained as a clear colorless liquid (3.28 g; 14.5 mmol); ir: 6.23; ^{1}Hmr: 8.53 (s, 1), 8.32 (d, J = 5; 1), 6.97 (d, J = 5; 1), 6.0 (m, 1), 5.4–5.0 (complex, 3), 2.33 (s, 3), 0.95 (s, 9), 0.10 (s, 3), 0.03 (s, 3); ms: 263 (1), 206 (100), 132 (71), 75 (35). *Exact Mass* calcd. for $C_{11}H_{16}NOSi$ (M − *t*-Bu): 206.1001; found: 206.1002.

The carbomethoxylation product **15***a* was prepared from **14***b* (3.5 g, 13.3 mmol) by the procedure used to prepare **13***a*. The product was purified by chromatography (silica gel; 7:3 hexane – ethyl acetate) and **15***a* was obtained as a pale yellow oil (2.71 g; 8.4 mmol); a sample, purified by molecular distillation at 90°C (0.005 Torr), was obtained as a colorless oil; ir: 5.75, 6.24; ^{1}Hmr: 8.52 (s, 1), 8.37 (d, J = 5; 1), 7.07 (d, J = 5; 1), 6.0 (m, 1), 5.4–5.0 (complex, 3), 3.75 (s, 2), 3.65 (s, 3), 0.90 (s, 9), 0.08 (s, 3), 0.00 (s, 3); ms: 264 (100), 232 (29), 158 (22), 130 (66), 93 (40), 89 (33), 85 (39), 83 (60), 77 (37), 75 (91), 73 (27). *Exact Mass* calcd. for $C_{13}H_{18}NO_3Si$ (M − *t*-Bu): 264.1055; found: 264.1055.

*The tryptamine derivative **16***

A solution of **15***a* (548 mg; 1.7 mmol) in 15 mL of 95:5 dichloromethane–methanol was cooled to −40°C and saturated with ozonized oxygen. The system was flushed with argon and 1 mL of dimethyl sulfide was added to the stirred reaction mixture which was then allowed to warm slowly (3 h) to room temperature. The solution was diluted with 50 mL of dichloromethane and washed with brine. The organic solution was stirred with an excess of anhydrous sulfate while tryptamine (546 mg; 3.4 mmol) was added. After 1.5 h the solution was filtered, the solvent was removed under reduced pressure and replaced with 50 mL of dry benzene, which was then removed in the same way; the residue was dried further in a vacuum system and then dissolved in 20 mL of dry methanol. To the stirred solution, placed under argon and cooled in an ice bath, sodium borohydride (137 mg; 2.6 mmol) was added in small portions. The ice bath was removed, stirring was continued for 17 h, and 25 mL of brine and 5 drops of acetic acid were then added. The mixture was thoroughly extracted with dichloromethane, and the material (966 mg) recovered from the extract was chromatographed (silica gel; 95:5 dichloromethane–methanol). The product **16** (365 mg; 0.78 mmol) was isolated as a white amorphous solid that darkened on standing; ir: 2.86, 2.99, 5.71, 5.90, 6.24; ^{1}Hmr: 8.55 (s, 1), 8.32 (d, J = 5; 1), 8.03 (broad, 1, D_2O removed), 7.7–7.0 (complex, 5), 6.99 (d, J = 5; 1), 4.97 (m, 1), 3.8–3.6 (complex, 5), 2.92 (s, 4), 2.9 (m, 2), 2.02 (broad, 1, D_2O removed), 0.77 (s, 9), 0.00 (s, 3), −0.15 (s, 3); ms: 467 (1), 452 (1), 410 (5), 337 (6), 297 (7), 296 (24), 295 (100), 237 (4), 223 (9), 205 (10), 173 (7), 144 (29), 130 (29). *Exact Mass* calcd. for $C_{22}H_{28}N_3O_3Si$ (M − *t*-Bu): 410.1900; found: 410.1891.

*The lactam **17***

A solution of the amino ester **16** (322 mg; 0.69 mmol) in 15 mL of dry methanol under argon was stirred with anhydrous potassium carbonate (103 mg; 0.75 mmol) and refluxed for 20 h. The methanol was removed under reduced pressure, the residue was dissolved in dichloromethane, and the solution was washed with brine. The product (283 mg) isolated from the organic solution was purified by flash chromatography (96:4 dichloromethane–methanol) (18), and **17** (111 mg; 0.26 mmol) was isolated as a white amorphous solid; ir: 2.87, 6.00, 6.25; ^{1}Hmr: 8.62 (broad, 1, D_2O removed), 8.4–8.2 (complex, 2), 7.7–6.8 (complex, 5), 6.75 (d, J = 2; 1), 4.4 (m, 1), 4.1–2.9 (complex, 8), 0.83 (s, 9), 0.03 (s, 3), −0.07 (s, 3); ms: 436 (2), 435 (6), 296 (4), 293 (15), 145 (6), 144 (19), 143 (100), 130 (16), 117 (5). *Exact Mass* calcd. for $C_{25}H_{33}N_3O_2Si$: 435.2342; found: 435.2359.

*The enamine **18***

Diisobutylaluminum hydride (0.84 mmol; 25% solution in toluene) was added over 7 min to a stirred solution of lactam **17** (93 mg; 0.21 mmol) in 2 mL of dry tetrahydrofuran at −65°C under argon. Stirring was continued for 1 h further, and saturated aqueous ammonium chloride (250 μL) was then added. The reaction mixture was allowed to warm to room temperature, the solvent was removed under reduced pressure, replaced with toluene, which was then removed in the same way, and then the residue was stirred in chloroform with anhydrous sodium sulfate. The chloroform solution, after filtration, was evaporated and the residue (92 mg) was subjected to flash chromatography (9:1 dichloromethane–methanol). Unchanged **17** (40 mg; 0.092 mmol) was recovered, and **18** (43 mg; 0.10 mmol) was isolated as an unstable amorphous solid; ir: 2.86, 6.13, 6.29; ^{1}Hmr: 8.73 (broad, 1, D_2O removed), 8.37 (s, 1), 8.18 (d, J = 5; 1), 7.7–7.0 (complex, 4), 6.95 (d, J = 2; 1), 6.84 (d, J = 5; 1), 6.23 (d, J = 10; 1), 4.9 (m, 1), 4.88 (d, J = 10; 1), 3.8–2.9 (complex, 6), 0.92 (s, 9), 0.13 (s, 3), −0.03 (s, 3).

The decarbomethoxynauclechines

Formic acid procedure

A solution of enamine **18** (71 mg; 0.17 mmol) in 1.5 mL of 90% formic acid was stirred at room temperature under argon for 18 h. The resulting solution was added dropwise to 20 mL of aqueous sodium carbonate, and the mixture was thoroughly extracted with chloroform. Drying (Na_2SO_4) and evaporation of the extract provided a yellow residue (73 mg) that was subjected to flash chromatography (18) (93:7 dichloromethane–methanol). The major component, **19***a* (45 mg; 0.11 mmol), was isolated as an amorphous yellow solid; ir: 2.89, 3.55, 3.61, 6.25; ^{1}Hmr: 9.00 (s, 1, D_2O removed), 8.77 (s, 1), 8.37 (d, J = 5; 1), 7.5–6.9 (complex, 5), 5.22 (d, J = 8; 1), 3.8–2.6 (complex, 9), 0.98 (s, 9), 0.20 (s, 3), 0.03 (s, 3); ms: 421 (8), 420 (34), 419 (100), 418 (55), 286 (21), 272 (12), 250 (23), 245 (26), 184 (41), 183 (69), 170 (38), 169 (36), 156 (20), 143 (25). Another fraction (14 mg) appeared to be a mixture of at least two components, but these could not be separated by further chromatography.

When the mixture of products before flash chromatography was stirred with 2 equivalents of tetrabutylammonium fluoride in dry tetrahydrofuran at room temperature under argon for 1 h, desilylated products were obtained. A minimum of water was added, solvent was removed under reduced pressure, and the residue was dried. By flash chromatography (9:1 dichloromethane–methanol) of the residue, **1***b* (see below) was isolated (25% yield for the desilylation step) in early fractions, and decarbomethoxy-3β-nauchlechine (**19***b*) was isolated (73%) as a white amorphous solid that rapidly became yellow; recrystallization from ethyl acetate provided pale yellow crystals, mp 219–220°C (dec.); ms: 306 (21), 305 (100), 304 (76), 288 (33), 274 (23), 245 (16), 184 (44), 183 (33), 170 (32), 169 (44), 156 (26), 144 (22), 143 (23). *Exact Mass* calcd. for $C_{19}H_{19}N_3O$: 305.1528; found: 305.1524. Acetylation of **19***b* with acetic anhydride in pyridine pro-

vided a product that was purified by flash chromatography (95:5 dichloromethane–methanol) and **19***c* was isolated as an amorphous solid; ir: 2.88, 5.75, 6.25; ^{1}Hmr: see Table 1 (400 MHz spectrum).

Hydrogen chloride procedure

A solution of enamine **18** (188 mg; 0.45 mmol) in 6 mL of 10% methanolic hydrogen chloride was allowed to stand under argon for 14 h. The solution was neutralized with anhydrous sodium carbonate added in small portions, filtered, and evaporated to dryness. The residue was thoroughly triturated with acetone, and the solution obtained was evaporated to dryness. The residue (117 mg) was subjected to flash chromatography (as described above), and **1***b* (38 mg; 0.12 mmol) was isolated as a white amorphous solid that turned yellow on standing; recrystallization from ethyl acetate provided colorless crystals, mp 218–221°C (prior phase change at 213°C); ms: 306 (21), 305 (100), 304 (77), 288 (33), 274 (16), 245 (13), 184 (25), 170 (17), 169 (26), 156 (11), 144 (10), 143 (15). *Exact Mass* calcd. for $C_{19}H_{19}N_3O$: 305.1528; found: 305.1530. Acetate **1***c* was prepared (see preparation of **19***c*) and obtained as an amorphous solid; ir: 2.89, 5.74, 6.25; ^{1}Hmr: see Table 1 (400 MHz spectrum). Later fractions provided **19***b* (8 mg; 0.026 mmol) and a middle fraction contained both **1***b* and **19***b* (25 mg; 0.08 mmol); one fraction afforded undesilylated cyclized material (see **19***a*) (37 mg; 0.09 mmol).

Acknowledgements

We thank Professor J.-L. Pousset, University of Dakar, for unpublished information regarding natural decarbomethoxynauclechine. This research received financial support from the Natural Sciences and Engineering Research Council of Canada.

1. A. SHARIFF and S. MCLEAN. Tetrahedron Lett. **23**, 4895 (1982).
2. D. G. MURRAY, A. SZAKOLCAI, and S. MCLEAN. Can. J. Chem. **50**, 1486 (1972).
3. F. HOTELLIER, P. DELAVEAU, R. BESSELIÈVRE, and J.-L. POUSSET. C.R. Acad. Sci. Ser. C, **282**, 595 (1976).
4. T. KAMETANI, M. TAKESHITA, M. IHARA, and K. FUKUMOTO. J. Org. Chem. **41**, 2542 (1976).
5. M. R. USKOKOVIĆ, T. HENDERSON, C. REESE, H. L. LEE, G. GRETHE, and J. GUTZWILLER. J. Am. Chem. Soc. **100**, 571 (1978).
6. E. WENKERT, K. G. DAVE, and F. HAGLID. J. Am. Chem. Soc. **87**, 5461 (1965).
7. J. R. STEVENS, R. H. BEUTEL, and E. CHAMBERLIN. J. Am. Chem. Soc. **64**, 1093 (1942).
8. J. M. BOBBITT and D. A. SCOLA. J. Org. Chem. **25**, 560 (1960).
9. M. LOUNASMAA and C.-J. JOHANSSON. Tetrahedron, **33**, 113 (1977).
10. A. FATIADI. Synthesis, **65**, 133 (1976).
11. P. L. STOTTER and J. B. EPPNER. Tetrahedron Lett. 2417 (1973).
12. D. G. MURRAY, A. SZAKOLCAI, and S. MCLEAN. Can. J. Chem. **50**, 1486 (1972).
13. S. MCLEAN, G. I. DMITRIENKO, and A. SZAKOLCAI. Can. J. Chem. **54**, 1262 (1976).
14. G. FODOR and S. NAGUBANDI. Tetrahedron, **36**, 1279 (1980).
15. S. TAKANO, N. TAMURA, and K. OGASAWARA. J. Chem. Soc. Chem. Commun. 1155 (1981).
16. G. N. SAUNDERS, R. G. HAMILTON, and S. MCLEAN. Tetrahedron Lett. **23**, 2359 (1982); R. G. HAMILTON, G. N. SAUNDERS, and S. MCLEAN. Can. J. Chem. **61**, 284 (1983).
17. R. T. BROWN and S. B. FRASER. Tetrahedron Lett. 1957 (1974); R. T. BROWN and C. L. CHAPPLE. Tetrahedron Lett. 2723 (1976).
18. W. C. STILL, M. KAHN, and A. MITRA. J. Org. Chem. **43**, 2923 (1978).
19. R. GREENWALD, M. CHAYKOVSKY, and E. J. COREY. J. Org. Chem. **28**, 1128 (1963).
20. D. SEYFERTH. Org. Synth. Coll. Vol. **4**, 258 (1963).

Can. J. Chem. Downloaded from www.nrcresearchpress.com by 210.87.254.5 on 09/06/12
For personal use only.

Discreteness-of-charge effects in electrode kinetics. II. The electroreduction of hexamminocobalt(III) cation in the presence of specifically adsorbed nitrate anions

W. RONALD FAWCETT AND KVETA MARKUŠOVÁ[1]

Guelph–Waterloo Centre for Graduate Work in Chemistry (Guelph Campus), Department of Chemistry, University of Guelph, Guelph, Ont., Canada N1G 2W1

Received February 28, 1983

W. RONALD FAWCETT and KVETA MARKUŠOVÁ. Can. J. Chem. **61**, 2821 (1983).

The kinetics of electroreduction of the hexamminocobalt(III) cation have been studied at a Hg electrode in aqueous solutions of $NaNO_3$ + NaF and KNO_3 + KF with an ionic strength of 0.2 *M*. The rate of reaction was observed to increase with increasing nitrate ion concentration but was independent of the cation nature. Analysis of the double layer effect for this system indicates that ion pairs formed between the reacting cation and anions of the base electrolyte also participate in the electrode reaction, and that attractive interactions between the reactant and adsorbed anions have a significant influence on the interfacial kinetics.

W. RONALD FAWCETT et KVETA MARKUŠOVÁ. Can. J. Chem. **61**, 2821 (1983).

On a étudié la cinétique de l'électroréduction du cation hexamminocobalt(III) utilisant une électrode au Hg dans des solutions aqueuses de $NaNO_3$ + NaF et de KNO_3 + KF avec une force ionique de 0,2 *M*. On a noté que la vitesse de la réaction augmente avec la concentration en ions nitrates, mais elle ne dépend pas de la nature du cation. L'analyse de l'effet de couche double dans ce système, indique que les paires d'ions formées entre le cation réagissant et les anions de l'électrolyte de base participent également à la réaction d'électrode et que les interactions attractives entre le réactif et les anions absorbés ont une influence significative sur la cinétique à l'interface.

[Traduit par le journal]

Introduction

In reviewing the literature concerned with discreteness-of-charge effects in interfacial electrochemistry, one finds considerable interest in the effects of specifically adsorbed ions on the kinetics of simple electrode reactions (1–4). A large fraction of the experimental work has been directed to studies of the effects of specifically adsorbed non-reacting anions on the electroreduction of a second anion; an example of such a system, which has been studied in some detail (5–7), is the electroreduction of tetrathionate anion at mercury in the presence of specifically adsorbed iodide anions. In this case, significant deceleration of the reaction rate is observed due to the increase in the electric field at the interface in the negative direction with increasing anion adsorption. The opposite occurs in the case of the electroreduction of a cation; the reaction rate increases with increasing anion adsorption. However, because of the attractive interactions between the reacting cation and adsorbed anion, local ion pairing effects involving the adsorbed species are also possible in the latter system (8–10).

Double layer effects on the electroreduction of a variety of Co(III) ammine complexes were recently studied by Satterberg and Weaver (11). They showed that the increase in the logarithm of the apparent rate constant at constant potential is a linear function of adsorbed anionic charge density for a variety of anions including Cl^-, Br^-, ClO_4^-, NO_3^-, and N_3^-. They concluded, on the basis of the magnitude of the double layer effects, that the reaction site is in the inner layer. They also discussed discreteness-of-charge effects for these reactions but did not give a detailed analysis of the kinetic data. In the present paper, the hexamminocobalt(III) system is reexamined for nitrate anions adsorbed on the electrode in order to determine more carefully the extent of discreteness-of-charge effects.

Experimental and method of data analysis

The kinetic data were obtained by dc polarography as described previously (7). The drop time of the mercury electrode was controlled at 5 s and the flow rate was 0.26 mg s^{-1}. Sodium and potassium nitrate were twice recrystallized from triply distilled water and dried *in vacuo*. Sodium fluoride was twice recrystallized from purified methanol and dried *in vacuo* at 100°C in a platinum dish. A similar procedure was used for potassium fluoride, the drying being carried out at 300°C. The diffusion coefficient of the dipolarizer, $Co(NH_3)_6^{3+}$ in solutions of ionic strength = 0.2 *M* was 7.35×10^{-6} cm^2 s^{-1}; its concentration was kept constant for all experiments at 5×10^{-4} *M*. The rate constant was calculated from the ratio of the observed current to its diffusion limited value according to the theory of Koutecky for an irreversible electrode process with inclusion of the correction for electrode sphericity (12). The reference electrode was a saturated calomel electrode, and the counter electrode a Pt cylinder. All experiments were carried out at 25°C.

The potential drop across the diffuse layer, ϕ^d was estimated on the basis of the equation

$$[1] \quad (\sigma_m + \sigma_a)^2 = \theta^2 \sum_i c_i[\exp(-z_i f \phi^d) - 1]$$

where σ_m is the charge density on the electrode, σ_a, that due to adsorbed anions, c_i, the concentration of ion i with valence z_i, and $f = F/RT$. θ^2 is equal to $2RT\epsilon\epsilon_0$ where ϵ is the dielectric constant of the solvent and ϵ_0, the permittivity of free space. The necessary double layer data for the system

$$x\ M\ NaNO_3 + (0.2 - x)\ M\ NaF$$

were obtained earlier (13). In the present case, the kinetic data are obtained close to the point of zero charge in the 0.2 *M* NaF system. As a result, the concentrations of the reactant and product in the diffuse layer are significant and must be taken into account in the estimation of ϕ^d. Setting $\Phi = \exp(-f\phi^d)$ and $\Sigma = (\sigma_m + \sigma_a)^2/\theta^2$, eq. [1] may be written as

$$[2] \quad \Sigma = c_s\Phi + c_2\Phi^2 + c_3\Phi^3 + (c_s + 3c_d)/\Phi - 2c_s - 4c_d$$

where c_s is the base electrolyte concentration (c_s = 0.2 *M*), c_d,

[1] On leave from Šafárik University, Košice, Czechoslovakia.

Can. J. Chem. Downloaded from www.nrcresearchpress.com by 210.87.254.6 on 09/06/12
For personal use only.

Can. J. Chem. Downloaded from www.nrcresearchpress.com by 210.87.254.6 on 09/06/12
For personal use only.

the depolarizer concentration in the bulk ($c_d = 5 \times 10^{-4}$ *M*), c_2, the concentration of divalent (product) cations at the boundary of the diffusion layer diffusing away from the electrode, and c_3, the concentration of trivalent cations at the boundary of the diffusion layer close to the electrode ($c_2 + c_3 = c_d$). In general, c_2 and c_3 vary with variation in current density, and therefore, with electrode potential. In the present case, it was assumed that $c_2 = c_d i/i_d$ where i is the current at the end of drop life and i_d its diffusion limited value. When $\Phi > 1$, eq. [2] is most easily solved by neglecting the term in $1/\Phi$ and obtaining an analytical solution of the resulting cubic equation; the estimate of Φ and thus ϕ^d is improved with the inclusion of the term in $1/\Phi$ by iteration. When $\Phi < 1$, eq. [2] can be solved by neglecting the terms in Φ, Φ^2, and Φ^3 and solving the resulting linear equation in $1/\Phi$; improved estimates are obtained by iteration with inclusion of the terms in Φ, Φ^2, and Φ^3 as constants calculated on the basis of the previous estimate. It should be noted that when both reactant and product concentrations are considered in the estimation of ϕ^d, the result is very little different than the result obtained when the concentration of multivalent cations in the diffuse layer is assumed to be determined only by the concentration of depolarizer in the bulk ($c_3 = c_d$ and $c_2 = 0$). Therefore, it is concluded that the above method of estimating ϕ^d using the Gouy–Chapman model is reasonable even though one recognizes that the estimates of c_2 and c_3 are approximate.

If ion pairing of the reactant $Co(NH_3)_6^{3+}$ with the anion of the supporting electrolyte is significant, as suggested previously for the case of F^- (11), then the charge on the reactant is 2+. The product cation which is substitutionally labile has the same charge. In this case, eq. [1] becomes

$$[3] \quad \Sigma = c_s\Phi + c_d + (c_s + 2c_d)/\Phi - 2c_s - 3c_d$$

The techniques outlined above are used to solve this equation for Φ, and thus, ϕ^d. When $\Phi > 1$, the term in $1/\Phi$ is initially neglected and the resulting quadratic equation in Φ solved. The initial estimate is improved by iteration with inclusion of the term in $1/\Phi$ calculated on the basis of the previous estimate. Similarly, when $\Phi < 1$, the linear equation in $1/\Phi$ is solved initially neglecting the terms in Φ and Φ^2, and subsequently by iteration.

Results

Kinetic data were obtained in eighteen different electrolyte solutions of composition

$$x\ M\ NaNO_3 + (0.2 - x)\ M\ NaF$$

and

$$x\ M\ KNO_3 + (0.2 - x)\ M\ KF$$

where $x = 0$, 0.01, 0.016, 0.025, 0.04, 0.063, 0.10, 0.14, and 0.2. Data obtained in 0.2 *M* solutions of NaF, $NaNO_3$, KF, and KNO_3 are shown in Fig. 1. As one would anticipate, the rate constant increases with increase in NO_3^- concentration at constant electrode potential and ionic strength for solutions containing a given cation. The acceleration is attributed to the shift in the potential drop across the diffuse layer in the negative direction with increase in the extent of NO_3^- ion adsorption, and the corresponding increase in the rate of reduction of the positively charged reactant. No significant difference between the data obtained in the Na^+ and K^+ systems was observed. The experimental transfer coefficients obtained in 0.2 *M* NaF and KF are 0.98 and 1.00, respectively. These results agree well with those obtained by Satterberg and Weaver (11), namely, 0.88 in 1.0 *M* KF and 0.98 in 0.1 *M* NaF; as the ionic strength increases, the double layer effect is reduced and its influence on the transfer coefficient becomes smaller. In 0.2 *M* $NaNO_3$ and KNO_3, the experimental transfer coefficient is 0.67. As a result of adsorption of the nitrate anion, the potential drop across the diffuse layer changes much less with electrode potential so that the transfer coefficient is less than that in the fluoride systems.

Satterberg and Weaver (11) argued that $Co(NH_3)_6^{3+}$ is predominantly present in fluoride solutions as the outersphere ion pair $Co(NH_3)_6^{3+} \cdots F^-$, and presented convincing evidence that the ion pair is the predominant reacting species when the potential drop across the diffuse layer is positive. Since ϕ^d is approximately a linear function of electrode potential in the present systems, the method proposed earlier (14) to estimate the charge on the reactant cannot be used. This method was introduced in order to avoid estimating the reactant charge on the basis of kinetic data obtained in different electrolyte solutions, either with a constant electrolyte at varying ionic strength as was common in early work (15, 16), or at constant ionic strength with variation in the nature of the ions as in the present investigation. When the methods developed by Frumkin (15) and Gierst (16) are used to determine the charge on the reactant, the change in the local activity coefficient of the reactant at the reaction site due to changes in ionic strength and composition is ignored. If it is assumed that the reaction site is on the outer Helmholtz plane (o.H.p.), then the experimental transfer coefficient is given by

$$[4] \quad \alpha_{ex} = \alpha_a - (\alpha_a - z)\frac{d\phi^d}{d\phi^m}$$

where α_a is the apparent transfer coefficient, z, the charge on the reactant, and ϕ^m, the electrode potential on the rational potential scale. In the case of 0.2 *M* NaF and KF, ϕ^d is positive over most of the available potential range, and therefore, independent of whether one assumes the charge on the reactant is 2+ or 3+ when this quantity is estimated on the basis of the Gouy–Chapman model. The value of $d\phi^d/d\phi^m$ in this potential range is 0.22. If z is assumed to be 3+, the corresponding value of α_a is 0.42; on the other hand, assuming $z = 2+$, the estimated value of α_a is 0.71. In the case of 0.2 *M* $NaNO_3$ and KNO_3, ϕ^d is negative. The magnitude of ϕ^d is slightly higher when z is assumed to be 2 rather than 3 but the coefficient $d\phi^d/d\phi^m$ is independent of this assumption and equal to 0.028. When z is set equal to 3+, the value of α_a from eq. [4] is 0.60, whereas it is 0.63 when z is assumed to be 2+. Keeping in mind that the contributions of discreteness-of-charge and coverage effects are neglected on the basis of eq. [4], the best agreement between estimated values of α_a in the presence and absence of adsorption occurs when the charge on the reactant is set equal to 2+. In the absence of discreteness-of-charge effects, attractive ion–ion interactions and surface coverage effects, the apparent transfer coefficient is related to the true or intrinsic transfer coefficient α by the equation (17, 18)

$$[5] \quad \alpha_a = \alpha - \lambda(\alpha - z)$$

where λ is a dimensionless fraction determined by the distance between the reaction plane (r.p.) and o.H.p., and the dielectric permittivity of the medium between these planes. When the reaction site is in the inner layer, λ is positive and α_a is greater than α in the case of cationic reactants. In previous studies of

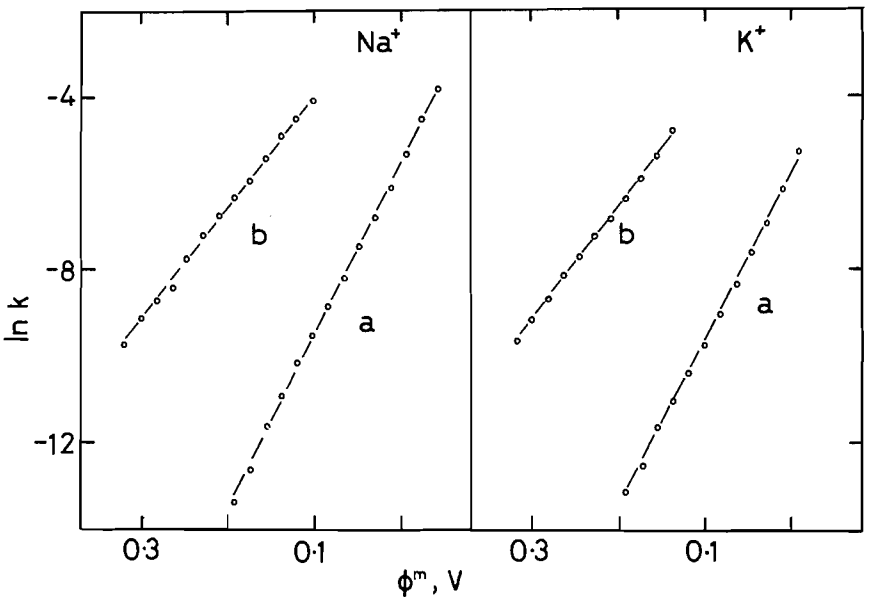

FIG. 1. Plots of the logarithm of the rate constant for reduction of $Co(NH_3)_6^{3+}$ at mercury against electrode potential on the rational scale, ϕ^m in solutions of 0.2 *M* NaF (*a*, Na^+), 0.2 *M* $NaNO_3$ (*b*, Na^+), 0.2 *M* KF (*a*, K^+), and 0.2 *M* KNO_3 (*b*, K^+).

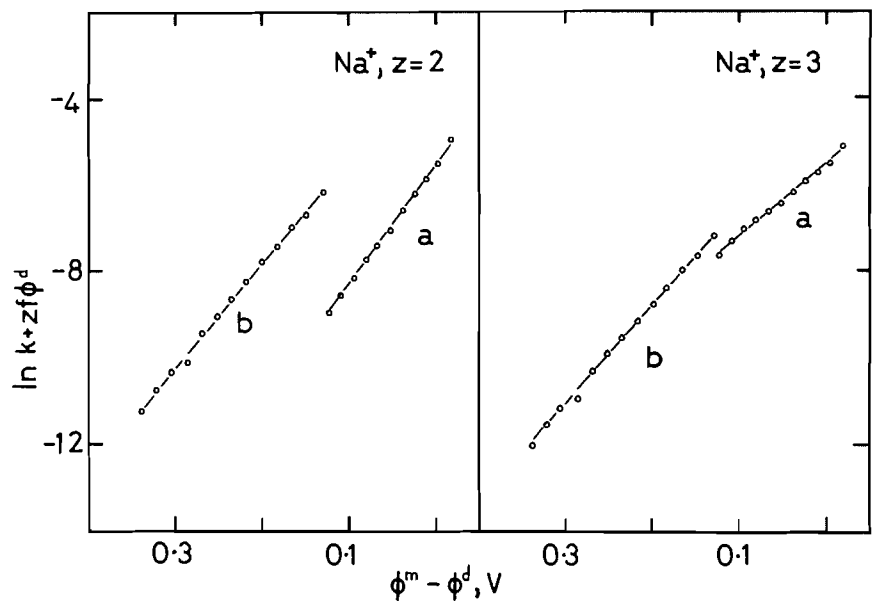

FIG. 2. Plots of the logarithm of the corrected rate constant, $\ln k + zf\phi^d$ for reduction of $Co(NH_3)_6^{3+}$ at mercury against the potential drop across the inner layer, $\phi^m - \phi^d$ in solutions of 0.2 *M* NaF (*a*) and 0.2 *M* $NaNO_3$ (*b*). The corrected rate constants for the plots on the left hand side were calculated assuming a reactant charge, $z = 2+$, whereas those on the right hand side were calculated assuming $z = 3+$.

the ammine complexes of both Co(III) (11) and Cr(III) (19), it was concluded that the reaction site for reactants not adsorbed on the electrode is in the inner layer in aqueous solutions. In this case, α_a is anticipated to be greater than 0.5, and the effect of the adsorbed anions rather large. These conclusions are consistent with the present results if the charge on the reactant is assumed to be 2+.

Corrected Tafel plots (cTp) for the data obtained in the Na^+ systems are shown in Fig. 2 for the cases that z is set equal to 2+ and 3+. Neglecting discreteness-of-charge effects, the corrected rate of reaction is given by

$$[6] \quad \ln k + zf\phi^d = \ln k_0 - \alpha_a f(\phi^m - \phi^d)$$

where k is the rate constant for the reduction reaction, and k_0, its value when both ϕ^m and ϕ^d are zero. The cTp were constructed using values of ϕ^d estimated as described above with consideration of the presence of the reactant and product in the double layer. When z is assumed to be 2+, the corrected rate constant in the presence of 0.2 *M* $NaNO_3$ is an order of magnitude greater than that in the presence of 0.2 *M* NaF. A large acceleration of the reaction rate above that predicted by the classical theory is expected when the reaction site is in the inner layer and attractive interaction between the reactant and adsorbed anions is strong. On the other hand, if z is set equal to 3+, the corrected rate constant in $NaNO_3$ is only slightly greater than that in NaF, but the slope of the c.T.p. in the former system is significantly higher. This analysis demonstrates that determination of z by the classical methods (15, 16) would have

Can. J. Chem. Downloaded from www.nrcresearchpress.com by 210.87.254.6 on 09/06/12
For personal use only.

Can. J. Chem. Downloaded from www.nrcresearchpress.com by 210.87.254.6 on 09/06/12
For personal use only.

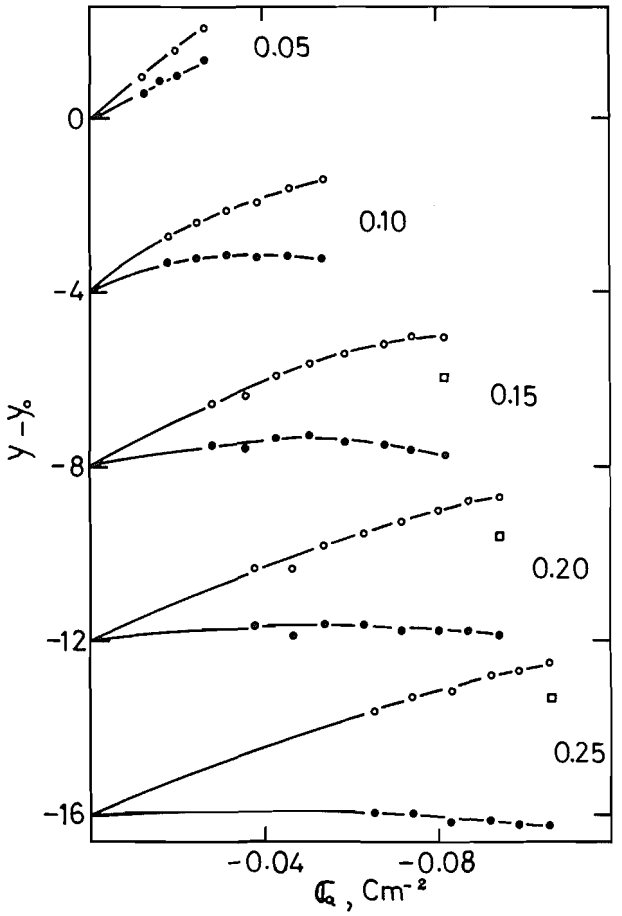

FIG. 3. Plots of the logarithm of the corrected rate constant, $y = \ln k + zf\phi^d$ for reduction of $Co(NH_3)_6^{3+}$ at mercury in mixed $NaNO_3$–NaF solutions with respect to that in pure NaF, y_0 against adsorbed charge density due to nitrate anions, σ_a for constant potential drop across the inner layer, $\phi^m - \phi^d$. The points (●) were calculated assuming $z = 3+$ whereas those marked (○) were calculated assuming $z = 2+$. The single points (□) give the values of y for $z = 3+$ with respect to y_0 for $z = 2+$. The values of $\phi^m - \phi^d$ in volts are indicated adjacent to each group of curves. The ordinate scale is correct for the data at $\phi^m - \phi^d = 0.05$ V whereas the data at 0.10, 0.15, 0.20, and 0.25 V have been shifted down by 4, 8, 12, and 16 units, respectively.

given a value of 3+ when discreteness-of-charge effects are neglected, and the reaction site assumed to be the o.H.p. However, the classical analysis ignores possible variation in α_a with change in solution composition; in the present case, α_a changes significantly with solution composition when z is set equal to 3+ (Fig. 2). Furthermore, if discreteness-of-charge effects are truly negligible, the r.p. must be sufficiently far from the inner Helmholtz plane (i.H.p.) that attractive interaction between adsorbed nitrate ions and the reactant is not possible. In the analysis of the adsorption data for NO_3^- at Hg (13), it was concluded that i.H.p. is very close to the o.H.p., so that interactions with the reactant even when it is on the o.H.p. or slightly further away in the diffuse layer are highly probable. Thus, the present analysis of the kinetic data indicates strongly that the average charge on the reactant is less than 3+. The c.T.p. obtained for the K^+ system are qualitatively similar when z is assumed to be 2+. However, when z is set equal to 3+, the corrected rate constant in the KF system is greater than that in KNO_3 for more positive values of $\phi^m - \phi^d$. The latter result is entirely unexpected and lends further support to the assumption that ion pairs play a role in the electrode reaction.

The change in the corrected rate constant, $y = \ln k + zf\phi^d$ with solution composition at constant $\phi^m - \phi^d$ is illustrated in Fig. 3 for the Na^+ system with z set equal to 2+ or 3+. When $z = 3+$, y increases with the extent of NO_3^- adsorption for $\phi^m - \phi^d = 0.05$ V, but the change in y with σ_a at more positive potentials is negligible. On the other hand, when z is assumed to be 2+, y increases smoothly with the amount of NO_3^- adsorbed and a significant discreteness-of-charge effect is observed at all potentials where data were obtained. When the results for the Na^+ system presented in Figs. 1 and 2 are examined, it is clear that approximately one half of the double layer effect due to adsorbed nitrate ions is accounted for by the classical Frumkin theory when it is assumed that only ion pairs react. Accordingly, the reaction site is assumed to be the o.H.p., and the local potential at this site to be the average potential on the o.H.p., ϕ^d. The portion of the double layer effect not accounted for by the classical model is attributed to non-coincidence of the r.p. and o.H.p., non-equality of the local potential at the reaction site and the average potential on the r.p., local ion pairing due to attractive ion–ion interactions, and coverage of the electrode by adsorbed nitrate ions.

In order to assess further the double layer effects and the role of ion pairs in the reaction, the magnitude of the discreteness-of-charge effects are now considered. On the basis of the theory presented earlier (18), the change in y with respect to its value in the absence of adsorbed nitrate ions, y_0, is given by

$$[7] \quad y - y_0 = \frac{(\alpha - z)f(1-\lambda)(1-g)\sigma_a}{K_2} + \frac{(a_{\neq}\sigma_d)_0}{RT} - \frac{a_{\neq}\sigma_r}{RT} + p_{\neq}\ln(1 - \sigma_a/\sigma_{am})$$

The first term accounts for the departure of the local potential at the reaction site from its average value; the dimensionless parameter g is related to the degree that repulsive interactions between adsorbed anions are screened by their electrostatic environment and is given by

$$[8] \quad g = (C_d + K_2)/(C_d + K_i)$$

where C_d is the differential capacity of the diffuse layer, K_i, the integral capacity of the inner layer, and K_2, the integral capacity of the region between the i.H.p. and o.H.p. The second and third terms account for attractive interactions between the cationic reactant and anions on the r.p., and in the vicinity of the reaction site in the diffuse layer. The first of these refers to interaction in pure NaF; σ_d is anionic charge density in the diffuse layer and $a_{\neq}$, the interaction parameter in the activated state (18). When nitrate ion adsorption is present, attractive ion–ion interactions are possible with both the adsorbed anions and anions in the vicinity of the o.H.p. in the diffuse layer when the potential drop across the region is positive, or when the same potential drop is negative but the anion concentration in the vicinity of the o.H.p. is still significant. σ_r refers to the anionic charge density in the vicinity of the reaction site and includes contributions from both the inner and diffuse layers; on the other hand, σ_d refers to the corresponding anionic charge density in the diffuse layer only (18). The last term accounts for surface coverage by adsorbed nitrate ions, σ_{am} being the maximum adsorbed charge density and $p_{\neq}$, the number of solvent molecules displaced by the reactant at the surface in the transition state.

Can. J. Chem. Downloaded from www.nrcresearchpress.com by 210.87.254.6 on 09/06/12
For personal use only.

The quantitative contribution of two of the effects discussed above may be estimated on the basis of the double layer data obtained earlier for the nitrate system (13). From the value of α_a obtained in 0.2 *M* NaF (0.71), $(\alpha - z)(1 - \lambda)$ is equal to -1.29 when $z = 2+$. In the case of $NaNO_3$ – NaF systems, g was found to be 1.3 and $K_2 \simeq 2.0$ F m^{-2} (13). It follows that $(\alpha - z)f(1 - \lambda)(1 - g)/K_2$ is equal to 7.5 m C^{-1}, and that $y - y_0$ should decrease with increasing $|\sigma_a|$. This result reflects the fact that the accelerating effect of adsorbed nitrate is overestimated when the discrete nature of these anions is ignored (18). The coverage term also leads to a decrease in $y - y_0$ with increase in $|\sigma_a|$. Setting σ_{am} equal to -0.25 C m^{-2} (13) and assuming $p_\neq$ is unity, $p_\neq \ln (1 - \sigma_a/\sigma_{am})$ is equal to -0.51 when $\sigma_a = -0.1$ C m^{-2}. Considering these two terms only, $y - y_0$ is expected to decrease by 1.26 when σ_a reaches -0.1 C m^{-2}. However, experimentally, $y - y_0$ increases by at least 2.4 units under these conditions for the case $z = 2+$. It follows that the influence of attractive interaction between the reactant and adsorbed anions, accounted for by the term $-a_\neq \sigma_r/RT$, would have to be very large and positive to account for the discreteness-of-charge effect estimated when $z = 2+$. Although attempts have been made to calculate $a_\neq$ (8–10), the models proposed are not very sophisticated, and therefore no attempt is made here to estimate $a_\neq$. Alternatively, when z is assumed to be 3+, α_a is 0.42 and $(\alpha - z)f(1 - \lambda)(1 - g)/K_2$ is approximately equal to 15.1 m^2 C^{-1}. With consideration of coverage, $y - y_0$ is expected to decrease by 2.02 when σ_a reaches -0.1 C m^{-2}. In this case, the attractive interaction on the reaction plane is approximately equal and opposite to the effects of ion shielding and coverage. Whether z is assumed to be 2+ or 3+, there is considerable variation in the magnitude of the non-classical contribution to y with the potential drop $\phi^m - \phi^d$. This can be attributed to the large variation in the inner layer parameters for the NaF – $NaNO_3$ system (13) which results in a corresponding variation in the degree of ion screening and interaction.

Discussion

Analysis of the double layer effects in the present case is complicated by the fact that the nature of the ionic atmosphere in the diffuse layer changes from an anionic environment to a cationic one when the electrolyte is changed from fluoride to nitrate. For example, in the presence of 0.2 *M* NaF, the kinetic data are obtained positive of the point of zero charge (p.z.c.) where the predominant ion at the o.H.p. is the flouride anion. On the other hand, in the presence of 0.2 *M* $NaNO_3$, the potential drop across the diffuse layer is negative and the reaction occurs in an ionic atmosphere composed chiefly of sodium cations in the diffuse layer together with adsorbed nitrate ions in the inner layer. Thus, the nature of the double layer effects undoubtedly changes with the change in solution composition. The analysis is further complicated by the fact that the reactant is expected to pair with anions in the bulk of the solution. The influence of the ion pair on the electrode kinetics is expected to change with the nature of the anion in the bulk and with the potential drop across the diffuse layer. On the basis of existing data (20, 21), $Co(NH_3)_6^{+}$ is expected to ion pair relatively strongly with the F^- anion and to a somewhat lesser extent with the NO_3^- ion (13). Thus, in 0.2 *M* NaF, the reactant is predominantly the ion pair $Co(NH_3)_6^{3+} \cdots F^-$, the unpaired species being more strongly repelled from the r.p. when the value of ϕ^r, the average potential on that plane, is positive. The double layer effect under these circumstances is classified as Type II (18), some attractive interaction between the reactant and the F^- anions on the o.H.p. being expected. Neglecting the effect of these interactions on α_a, the value of λ in eq. [5] is 0.14; accordingly, the r.p. is slightly closer to the electrode than the o.H.p. In 0.2 *M* $NaNO_3$, the reactant is predominantly the trivalent cation. This conclusion is based on the facts that ion pairing is weaker in the nitrate solution, and that the trivalent species is predominant on the r.p. because the potential drop across the diffuse layer is negative in the range where the kinetic data are obtained. Under these circumstances, the kinetics are very strongly influenced by attractive interactions between the reactant and the nitrate ions adsorbed on the i.H.p. In fact, on the basis of the previous analysis of the equilibrium data for the NO_3^- – F^- system (13), the i.H.p. is estimated to be quite close to the o.H.p., and thus, also to the r.p. The lower value of α_a in 0.2 *M* $NaNO_3$ (0.60) is assumed to reflect the decrease in attractive ion–ion interactions with change in electrode potential in the negative direction, and the corresponding decrease in the value of σ_a. It follows that the kinetic data in mixed electrolyte solutions are for a parallel reaction involving both unpaired and paired reactants. The apparent rate constant is then given by (22)

$$[9] \quad k = k_M \rho_M \exp(-3f\phi^d) + k_{MA}(1 - \rho_M) \exp(-2f\phi^d)$$

when discreteness-of-charge effects are neglected and the classical model assumed. k_M and k_{MA} are the rate constants for the unpaired and ion paired species, respectively, and ρ_M, the fraction of unpaired cobalt cations in the bulk. The rate constant for either species may be written

$$[10] \quad k_i = k_{0i} \exp[\alpha_{ai} f(\phi^d - \phi^m)]$$

where k_{0i} and α_{ai} are quantities analogous to those defined in eq. [6]. No attempt is made to analyze the present data with respect to a parallel reaction mechanism but such an analysis could be carried out if equilibrium data for the bulk of the solution were available.

If the above assumptions regarding the charge on the reactant in 0.2 *M* NaF and $NaNO_3$ are correct, then the analysis of discreteness-of-charge effects presented in Fig. 3 should be modified. More specifically, the value of y with $z = 3+$ in 0.2 *M* $NaNO_3$ should be compared with y_0 using $z = 2+$ in 0.2 *M* NaF. Values of $y - y_0$ for three higher values of $\phi^m - \phi^d$ are also shown in Fig. 3. It is apparent that the discreteness-of-charge effect is still very large when the data are examined in this fashion. The calculation of y when a parallel reaction is involved is not a simple matter and would require separate estimates of k_M and k_{MA} (eq. [9]). In this case, y is given by

$$[11] \quad y = \rho_M(\ln k_M + 3f\phi^d) + (1 - \rho_M)(\ln k_{MA} + 2f\phi^d)$$

Although our data are not sufficiently detailed to estimate y in this case, it seems clear that it would vary smoothly with σ_a and indicate a strong influence of local ion pairing on the reaction plane.

As pointed out above, there are no great differences in the results obtained in the Na^+ and K^+ systems. A small increase in $\ln k$ (0.12) is observed in going from 0.2 *M* KF to 0.2 *M* NaF. This may reflect a small double layer effect caused by the potential at the reaction site being more positive at the Hg/aqueous KF interface but it could also be due to a change in the activity of the reactant in the bulk of the solution. In the case of pure nitrate solutions, $\ln k$ is slightly higher in KNO_3 (0.01). Although the above factors must also be considered, in the case of the nitrate systems, the anion is more strongly

adsorbed from KNO_3 solutions (13) so that the effects observed with NaF and KF are reversed. Because the inner layer parameters differ in KNO_3 and $NaNO_3$, the magnitude of the discreteness-of-charge contribution is also expected to change but the magnitude of this change is not very large.

The analysis of discreteness-of-charge effects presented here relies heavily on the Gouy–Chapman theory of the diffuse layer and its estimate of the potential drop ϕ^d. Deficiencies in this model with respect to the analysis of kinetic data for reactions involving highly charged species which are attracted into the double layer have been discussed in detail in the literature (11, 19, 23, 24). The present data were obtained at a lower ionic strength than most of those presented earlier, where less severe problems with the Gouy–Chapman model are expected. In addition, the effect of the presence of the reactant and product on the value of ϕ^d, which is not negligible, was taken into consideration. The influence of the highly charged species is even more important on estimates of $d\phi^d/d\phi^m$, a quantity which plays an important role in the analysis used in previous work (11, 19, 23, 24). In fact estimates of this quantity given by Satterberg and Weaver (11) are significantly higher than those calculated here. In view of the complex nature of the double layer effect for the present system it is not possible to comment further on the reliability of the Gouy–Chapman results. However, recent estimates of ϕ^d based on more sophisticated models (25, 26) are in serious disagreement with the classical results when multivalent ions are involved. In conclusion, double layer effects for highly charged reactants must be examined in more detail in the absence of ion pairing in order to elucidate the problem further.

Acknowledgement

The financial assistance of the Natural Sciences and Engineering Research Council of Canada is gratefully acknowledged.

1. R. PARSONS. J. Electroanal. Chem. **21**, 35 (1969).
2. W. R. FAWCETT and S. LEVINE. J. Electroanal. Chem. **43**, 175 (1973).
3. R. GUIDELLI and M. L. FORESTI. Electrochim. Acta, **18**, 301 (1973).
4. V. S. KRYLOV, V. A. KIR'YANOV, and I. F. FISHTIK. J. Electroanal. Chem. **109**, 115 (1980).
5. M. L. FORESTI and R. GUIDELLI. J. Electroanal. Chem. **53**, 219 (1974).
6. I. ŽEŽULA, V. RYCHNAVSKÁ, and E. ALEXYOVÁ. J. Electroanal. Chem. **86**, 433 (1978).
7. W. R. FAWCETT and K. MARKUŠOVÁ. Can. J. Chem. **60**, 2038 (1982).
8. W. R. FAWCETT and S. LEVINE. J. Electroanal. Chem. **65**, 505 (1975).
9. R. GUIDELLI. J. Electroanal. Chem. **74**, 347 (1976).
10. I. F. FISHTIK and V. S. KRYLOV. Elektrokhimiya, **16**, 636 (1980); **16**, 641 (1980).
11. T. L. SATTERBERG and M. J. WEAVER. J. Phys. Chem. **82**, 1784 (1978).
12. J. KOUTECKÝ and J. ČIŽEK. Coll. Czech. Chem. Commun. **21**, 836 (1956).
13. W. R. FAWCETT and J. B. SELLAN. Can. J. Chem. **55**, 3871 (1977).
14. W. R. FAWCETT, J. E. KENT, and Y. C. KUOLEE. J. Electroanal. Chem. **20**, 357 (1969).
15. A. N. FRUMKIN, O. A. PETRII, and N. V. NIKOLAEVA-FEDOROVICH. Electrochim. Acta, **8**, 177 (1963).
16. L. GIERST. Trans. Symposium on electrode processes. *Edited by* E. Yeager. Wiley, New York. 1961. pp. 109–138.
17. W. R. FAWCETT. J. Electroanal. Chem. **22**, 19 (1969).
18. W. R. FAWCETT. Can. J. Chem. **59**, 1844 (1981).
19. M. J. WEAVER and T. L. SATTERBERG. J. Phys. Chem. **81**, 1772 (1977).
20. V. A. FEDOROV, V. E. MIRONOV, and F. YA. KUL'BA. Zhur. Neorg. Khim. Zhur. Neorgan. Khim. **7**, 2528 (1962).
21. M. J. WEAVER. Unpublished results (private communication).
22. D. J. BIEMAN and W. R. FAWCETT. J. Electroanal. Chem. **34**, 27 (1972).
23. M. J. WEAVER and F. C. ANSON. J. Electroanal. Chem. **65**, 711 (1975).
24. M. J. WEAVER. J. Electroanal. Chem. **93**, 231 (1978).
25. D. HENDERSON and L. BLUM. Can. J. Chem. **59**, 1906 (1981).
26. M. LOZADA-CASSON, R. SAAVEDRA-BARRERA, and D. HENDERSON. J. Chem. Phys. **77**, 1550 (1982).

Can. J. Chem. Downloaded from www.nrcresearchpress.com by 210.87.254.6 on 09/06/12
For personal use only.

COMMUNICATION

Theoretical study on the gas-phase solvation of acetone and dimethylsulfoxide toward the proton

SHINICHI YAMABE[1] and TSUTOMU MINATO
Department of Chemistry, Nara University of Education, Takabatake-cho, Nara 630, Japan

AND

KIMIHIKO HIRAO
Department of Chemistry, College of General Education, Nagoya University, Chikusa-ku, Nagoya 464, Japan

Received May 18, 1983

SHINICHI YAMABE, TSUTOMU MINATO, and KIMIHIKO HIRAO. Can. J. Chem. **61**, 2827 (1983).

An *ab initio* MO calculation is made for the $H^+(acetone)_n$ and $H^+(DMSO)_n$ gas-phase clusters. In the "shells" of $n = 2$, the cationic nature for the attack of the third solvent molecule is dispersed to the methyl hydrogens and the S atom (in DMSO) as well as to the proton. This leads to the small difference of stability for several geometries of $n = 3$. A noticeable disagreement between experimental and calculated energies for $n = 1 \rightarrow 2$ in $H^+(DMSO)_n$ is discussed.

SHINICHI YAMABE, TSUTOMU MINATO et KIMIHIKO HIRAO. Can. J. Chem. **61**, 2827 (1983).

On a effectué des calculs "*ab initio*" des OM pour des aggrégats de H^+(acétone)$_n$ et de $H^+(DMSO)_n$ en phase gazeuse. Dans les "couches" de $n = 2$, la nature cationique pour l'attaque de la troisième molécule de solvant se répartit sur les hydrogènes du méthyle et sur l'atome de S (dans le DMSO) ainsi que sur le proton. Ceci conduit à une légère différence de stabilité pour les géométries de $n = 3$. On discute d'une différence assez significative qui existe entre les énergies calculées et expérimentales pour $n = 1 \rightarrow 2$ du $H^+(DMSO)_n$.

[Traduit par le journal]

High ion source pressure mass spectrometer measurements can provide thermochemical data for gas-phase clustering of ions through measurements of the temperature variation of the equilibrium constant of the clustering reaction (1). Also we have established that satisfactory agreement can be obtained between the observed enthalpy change ($\Delta H^0_{n-1,n}$) and the calculated stabilizing energy ($\Delta E_{n-1,n}$) (2). Here we present a theoretical analysis of the protonated clusters of two dipolar aprotic solvents, acetone and dimethylsulfoxide (DMSO). Experimental measurements have been reported for these two clusters which led to the suggestion of some interesting structural differences (3).

In Fig. 1, the optimized geometries are displayed together with the net electronic charges. The basis sets used for the MO calculation are 4-31G for $H^+(acetone)_n$ and 3-21G(*) (4) for $H^+(DMSO)_n$. For $H^+(DMSO)_3$ only, the minimal basis set STO-3G* is used due to the vast size of the system. Up to $n = 2$, the same types of the cluster structures are obtained. The cluster of $n = 2$ is regarded as a shell, and the third solvent molecule attacks it weakly. The stable geometry of $H^+(acetone)_3$ is found to be different from that of $H^+(DMSO)_3$.

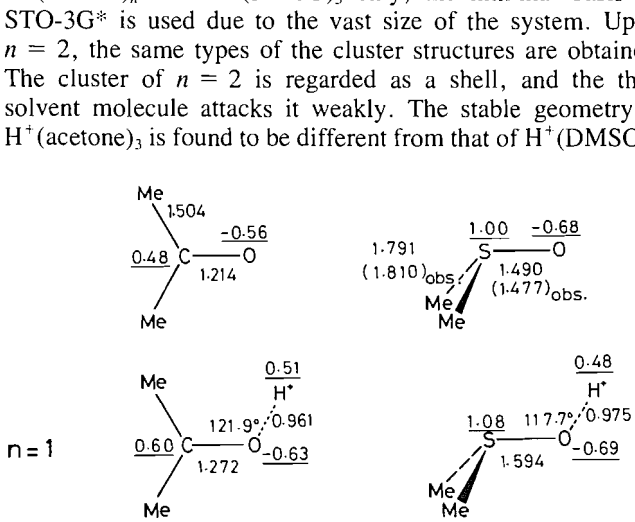

[1]To whom all correspondence should be addressed.

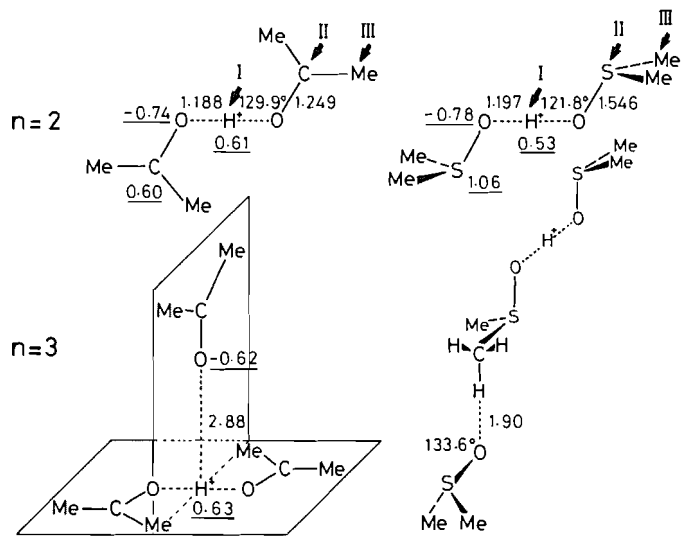

FIG. 1. Geometries of $H^+(acetone)_n$ and $H^+(DMSO)_n$ clusters optimized with the 4-31G and 3-21G(*) basis sets, respectively. The geometries of acetone and DMSO are fully optimized. For $n = 1$ and 2, the internal freedoms are optimized except the methyl part taken from the neutral molecules. For $n = 3$, only the orientation and the distance between the $n = 2$ cluster and the neutral molecule are optimized. For $n = 2$, another model of the "head-to-tail" type is examined and is found to be less stable than that shown in the figure. The bond length is in Å. Underlined numbers denote the net charges where negative values correspond to the electron-rich atoms. The geometry of $H^+(DMSO)_3$ is obtained by the STO-3G* basis set. The bold arrows indicated in $n = 2$ mean the cationic sites for the attack of the third solvent molecule.

In the former system, the proton is attacked by the third molecule in the direction perpendicular to the shell plane. Due to the large distance ($R_{H^+\cdots O} = 2.88$ Å), the third acetone can rotate freely around the $H^+\cdots O{=}C$ axis. In the latter system, type III

Can. J. Chem. Downloaded from www.nrcresearchpress.com by 210.87.254.105 on 09/06/12
For personal use only.

TABLE 1. (*a*) The basis set dependence of total energies (in au) and dipole moments (in debye)

	Acetone			DMSO			
	4-31G	STO-4G		DZ+p‡	4-31G(*)‡	3-21G(*)	STO-3G*
Energy (+190 au)	−1.6776	−0.8969	Energy (+545 au)	−6.5078	−5.9159	−3.8467	−0.3881
Dipole moment (2.85)†	3.55	1.99	Dipole moment (3.96)†	5.24	4.91	4.27	2.81

(*b*) Stabilization energies ($\Delta E_{n-1,n}$ in kcal/mol) and experimental enthalpy change ($\Delta H^0_{n-1,n}$ in kcal/mol)

		$\Delta E_{n-1,n}$					$\Delta E_{n-1,n}$	
n	$\Delta H^0_{n-1,n}$	4-31G	STO-4G	n	$\Delta H^0_{n-1,n}$	DZ+p‡	4-31G(*)‡	3-21G(*)
1	−198.6§	−203.5	−247.0	1	−214.4§	−226.8	−229.0	−230.1
2	−30.1§	−35.0	−46.5	2	−30.8§	—	−41.5	−47.4
3	−12.2‖	−9.1	+1.4	3	−21.3§	—	—	—

†Observed dipole moment.
‡The geometries obtained by 3-21G(*) are used.
§Taken from ref. 3.
‖K.Hiraoka. Private communication.

is the best among three possible stable geometries shown by three bold arrows in Fig. 1 (III > II > I). Apparently, type II is favorable in view of the cationic character of the S atom, but the exchange repulsion between the lone-pair electrons on the sulfur atom and that on the oxygen atom of the third DMSO decreases the stability of II. The larger stability of III arises both from the protonic net atomic charges on the methyl hydrogen (*0.22* in the neutral molecule and *0.25* in $n = 2$) of DMSO and from the absence of the exchange repulsion. However, the energy differences between the three types are only a few kcal/mol, and it is seen that H^+, S, and methyl H are all favorable sites for the third DMSO. Similarly, type III in $H^+(acetone)_3$ is only slightly less stable (~2 kcal/mol) than type I shown in Fig. 1. In this respect, the cluster size would be enlarged readily through the attachment of solvent molecules toward various moderately cationic sites in the shells of $n = 2$. Comparison between the energies, $\Delta E_{n-1,n}$ and $\Delta H^0_{n-1,n}$ is given in Table 1. While good agreement is obtained for $H^+(acetone)_n$, a somewhat noticeable discrepancy is observed for $H^+(DMSO)_n$. The 3-21G(*) MO calculation is found to overestimate $\Delta E_{n-1,n}$ by 1~6 kcal/mol relative to that of 4-31G(*). The latter may yet overestimate $\Delta E_{n-1,n}$ to some extent (4~5 kcal/mol at most), according to our experience. On the other hand, $\Delta H^0_{1,2}$ for $H^+(DMSO)_n$ seems to be too small in view of $\Delta H^0_{0,1}$ and $\Delta H^0_{1,2}$ for $H^+(acetone)_n$ and $H^+(acetonitrile)_n$. The $\Delta H^0_{1,2}$ values for the three clusters have been reported to be almost the same (~−30 kcal/mol) (3). The electron-rich oxygen of DMSO would result in a larger $\Delta H^0_{1,2}$ (probably −34~35 kcal/mol) than those of the latter systems. In proton bound dimers of n-donor oxygens, the systems with a hypervalent bond, $=S \rightarrow O$ and $\equiv N \rightarrow O$, would give the larger hydrogen bond energies. Further experiment on $H^+(DMSO)_n$ seems to be desirable.

Acknowledgment

The authors thank the Institute for Molecular Science for the allotment of CPU time on the HITAC M-200H computer.

1. P. KEBARLE. Ann. Rev. Phys. Chem. **28**, 445 (1977).
2. K. HIRAO, M. SANO, and S. YAMABE. Chem. Phys. Lett. **87**, 181 (1982); M. D. NEWTON. J. Chem. Phys. **67**, 5535 (1977); H. KISTENMACHER, H. POPKIE, and E. CLEMENTI. J. Chem. Phys. **61**, 799 (1974); W. P. KRAEMER and G. H. F. DIERCKSEN. Theoret. Chim. Acta, **27**, 265 (1972); **23**, 393 (1972); **23**, 398 (1972); Chem. Phys. Lett. **5**, 463 (1970); **5**, 570 (1970).
3. Y. K. LAU, P. P. S. SALUJA, and P. KEBARLE. J. Am. Chem. Soc. **102**, 7429 (1980).
4. W. J. PIETRO, M. M. FRANCL, W. J. HEHRE, D. J. DEFREES, J. A. POPLE, and J. S. BINKLEY. J. Am. Chem. Soc. **104**, 5039 (1982).

Can. J. Chem. Downloaded from www.nrcresearchpress.com by 210.87.254.105 on 09/06/12
For personal use only.

ADDITIONS AND CORRECTIONS / AJOUTS ET CORRECTIONS

Vol. 61, 1983

George I. Birnbaum, Wayne J. P. Blonski, and Frank E. Hruska. Structure and conformation of the anticodon nucleoside 5-methoxyuridine in the solid state and in solution

Page 2299. Table 5 was inadvertently omitted from the original article and Fig. 4 was printed incorrectly.

TABLE 5. ^1H and ^{13}C chemical shifts (δH, δC) and $^1H-^1H$ coupling constants J(H,H) for uridine (U) and 5-methoxyuridine (mo^5U) in D_2O[a,b]

δ(H)	mo^5U	U	J(H,H)	mo^5U	U	δ(C)	mo^5U	U
H5	—	5.96	1′2′	4.2	4.8	C2	151.2	152.9
H6	7.61	7.88	2′3′	5.4	5.2	C4	162.7	167.3
H1′	5.96	5.93	3′4′	5.7	5.4	C5	137.9	103.6
H2′	4.36	4.37	4′5′	2.8	2.9	C6	120.7	143.1
H3′	4.29	4.25	4′5″	3.1	4.4	C1′	90.6	90.7
H4′	4.15	4.16	5′5″	−12.8	−12.7	C2′	75.2	74.9
H5′	3.97	3.94	—	—	—	C3′	70.5	70.8
H5″	3.86	3.83	—	—	—	C4′	85.3	85.4
OCH_3	3.75	—	—	—	—	C5′	61.4	62.1
						OCH_3	58.4	—

[a]Proton data (relative to TSP): 0.01 *M* mo^5U at 270 MHz, 298 K, pH = 4.5; and 0.1 *M* U at 220 MHz, 296 K, pH = 6.8; ref. 30.

[b]Carbon data obtained on a Bruker WH 90DS spectrometer at 305 K; 0.2 *M* mo^5U, pH = 4.0 and 0.4 *M* U, pH = 7.0; δ(C) measured relative to internal dioxane and converted to TMS scale; δ(TMS) = δ(dioxane) + 67.86 ppm.

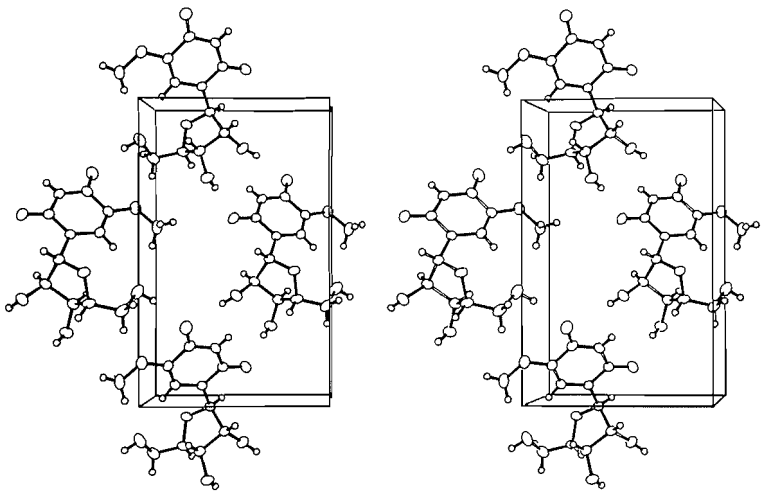

FIG. 4. Stereoscopic view along *z* of the molecular packing in the crystal.

Can. J. Chem. Downloaded from www.nrcresearchpress.com by 210.87.254.42 on 09/06/12
For personal use only.